Volcanism in Hawaii

Edited by Robert W. Decker, Thomas L. Wright, *and* Peter H. Stauffer

Volume 1

- Physiography, Tectonics, and Submarine Geology
- Geology of the Island of Hawaii
- Petrogenesis and Volcanic Gases

U.S. GEOLOGICAL SURVEY PROFESSIONAL PAPER 1350

UNITED STATES GOVERNMENT PRINTING OFFICE, WASHINGTON : 1987

DEPARTMENT OF THE INTERIOR

DONALD PAUL HODEL, *Secretary*

U.S. GEOLOGICAL SURVEY

Dallas L. Peck, *Director*

Library of Congress Cataloging-in-Publication Data

Volcanism in Hawaii.

(U.S. Geological Survey Professional Paper 1350)
Contents: v.1. Physiography, tectonics, and submarine geology; Geology of the Island of Hawaii; Petrogenesis and volcanic gases. v.2. Structure; Dynamics; History of investigations of Hawaiian volcanism.
Supt. of Docs. no.: I 19.16:1350
1. Volcanism—Hawaii. 2. Volcanic ash, tuff, etc.—Hawaii. I. Decker, Robert Wayne, 1927–. II. Wright, Thomas Llewellyn, 1935–. III. Stauffer, Peter Herman, 1935–. IV. Series: United States. Geological Survey. Professional Paper 1350.
QE524.V65 1987 551.2'2'09969 86–600292

**For sale by the Books and Open-File Reports Section,
U.S. Geological Survey, Federal Center, Box 25425, Denver, CO 80225**

FOREWORD

When Thomas A. Jaggar established the Hawaiian Volcano Observatory (HVO) in 1912, he could not have imagined the extent to which his pioneering studies would expand in the next 75 years. He demonstrated great foresight in setting two major research goals for the observatory: (1) the conduct of systematic, scientific studies to understand more about volcanic processes, both during and between eruptions; and (2) the practical application of research results for mitigating hazards—the forecast of impending eruptions and paths of destructive lava flows and the evaluation of all other types of volcanic hazard. The results of studies by HVO staff and other scientists have been shared with the National Park Service since 1917, when Hawaii National Park was created by Congress, and I want to emphasize that the cooperation and support of the Park Service over the ensuing years have been exceptionally helpful for our scientific work and for the benefit of the public.

During these 75 years following the founding of HVO, scientists have pursued Jaggar's original goals with great success. In addition to developing volcano-monitoring techniques now used worldwide, the observatory also has served as a training center for volcanologists from many countries, as well as for the postgraduate training of a great number and variety of USGS scientists, myself included. The lessons learned at HVO became especially valuable when Mount St. Helens erupted catastrophically in 1980, and our cadre of HVO staffers past and present were able to provide monitoring and forecasting information for that volcano, resulting in the saving of many lives.

The papers in this volume reflect the greatly improved understanding of the behavior of Kilauea and Mauna Loa Volcanoes that has been developed since the early studies in Hawaii. The structure and tectonic setting of the volcanoes, the physical and chemical properties of the eruptive products, and the history of eruptive activity over the past several thousand years have all been investigated in great detail, and the results are summarized in this book. These volcanoes have served as unique natural laboratories for the study of volcanic phenomena and the development of new monitoring instruments, and the new methods and instruments in time became standards for monitoring in most other observatories around the world. The use of sophisticated instruments led to dramatic improvements in our ability to forecast the activity of Kilauea and Mauna Loa over the past 75 years. In particular, our ability to precisely monitor inflation-deflation cycles, the location of magma-generated microearthquakes, and volcanic tremor has moved from the subjective, intuitive stage to the level of being a science in itself. In recent decades, new technology for laser distance measuring, real-time analysis of telemetered seismic signals, and volcanic-gas analysis have greatly improved our forecasting capability. Currently we are pursuing new applications of computers to all the problems of volcano monitoring, including the generation of three-dimensional models of the volcanic "plumbing systems" for Kilauea and Mauna Loa.

All these exciting scientific accomplishments, though nourished by improved technology, have in fact been linked by a continuing thread of human ingenuity and dedication to science such as characterized the earliest work of Thomas Jaggar. His achievements and those of the people who succeeded him demonstrate the critical importance of individual imagination and creativity in earth-science research. I take great pride and personal pleasure in presenting these results of 75 years of research in Hawaiian volcanism to the scientific community and the public.

Dallas L. Peck
Director, U.S. Geological Survey

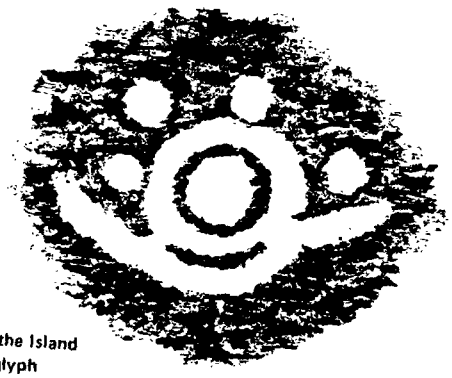

A Trip Around the Island
Hawaiian Petroglyph

PREFACE

"Stones rot; only the chants remain." This ancient Polynesian saying reflects the rapid changes that occur on volcanic islands. Young lava flows are soon covered by lush vegetation, and only the stories of their eruption, passed from generation to generation, survive. This collection of articles on Hawaiian volcanism commemorating the 75th anniversary of the Hawaiian Volcano Observatory is a chant to future generations. Much has been learned in these past 75 years, but much more is still to be discovered.

Scientific literature serves at least two purposes. From the standpoint of data it is, or should be, an archive of the truth. The data in these volumes are as close to the truth as is humanly possible. Interpretation of the data is another matter, and from this standpoint scientific literature should be a forum for debate. Readers of chapter 1, part I, and chapter 2 will discover that the authors reach different interpretations concerning the volume and propagation rates of Hawaiian volcanism during the past few million years. These authors base their respective conclusions largely on the same data. Eventually, additional data, strength of arguments, and the consideration and consensus of the readers may lead to acceptance of some interpretations and rejection of others. That is something for the scientific community, not the editors, to decide.

The staff and guest investigators at the Hawaiian Volcano Observatory over the past 75 years have represented many diverse scientific disciplines and backgrounds. There is great strength in this diversity. Working closely together on common problems, geologists, geochemists, geophysicists, biologists, oceanographers, meteorologists, and general scientific practitioners have learned a great deal about Hawaiian volcanoes as well as about the scientific methods of their colleagues. The whole has greatly exceeded the sum of the parts. Close cooperation among scientists with different backgrounds has led to conceptual models of volcanism that satisfy not only the geologic and geophysical field observations, but also the theoretical constraints of thermodynamics and rock mechanics.

The scope of articles in these volumes, and the many publications by guest investigators at the observatory during recent years, reflect the view that volcanoes can best be studied from a multidisciplinary approach. We hope that seismologists will read the chapters on Hawaiian petrology and volcanic gases and that, in turn, gas geochemists will read about the distribution and causes of earthquakes beneath the Island of Hawaii. The Hawaiian Volcano Observatory has made important gains in the cross-fertilization of science in the past, and as science becomes more and more specialized in the future, this role will become even more important.

Most place names in the Hawaiian Islands, and several geographical and descriptive terms used in volcanology, derive from the Hawaiian language. In the standard written form of that language, diacritical marks are used; these diacritical marks not only indicate the pronunciation, but in many cases are essential to distinguish between otherwise similar words of different meanings. However, the volcanological terms of Hawaiian origin (such as "aa" and "pahoehoe") are spelled in the English language without the diacritical marks, and the Board on Geographic Names in Washington, whose rulings the USGS follows, does not recognize such marks for Hawaiian place names. Hence no diacritical marks are used on Hawaiian words in the chapters of the present work. In order to acquaint those interested with the original Hawaiian spelling and pronunciation of these words, however, a pronunciation guide for Hawaiian words is included at the end of volume 2.

A work of the scale and complexity of the present one, compiled and produced with the aim of meeting short time deadlines, is clearly the product of many willing and skilled hands, from the authors to the printers. In the USGS Branch of Western Technical Reports, special contributions were made by Derrick Hirsch in editing, Jeff Troll in coordination and layout, Jim Pinkerton in overseeing the editing of figures, and Al Earnest and the entire drafting staff in preparing the hundreds of illustrations. The cooperation of the Branch of Eastern Technical Reports in helping prepare illustrations for certain chapters is also appreciated.

These volumes, readers, may be chants, but they are also intended to be steppingstones. The trail is yours.

Robert W. Decker, Thomas L. Wright, and Peter H. Stauffer
Editors

CONTENTS

VOLUME I

PHYSIOGRAPHY, TECTONICS, AND SUBMARINE GEOLOGY

Chapter 1. The Hawaiian-Emperor volcanic chain
- Part I. Geologic evolution *5*
  David A. Clague and G. Brent Dalrymple
- Part II. Stratigraphic framework of volcanic rocks of the Hawaiian Islands *55*
  Virginia A.M. Langenheim and David A. Clague

2. Subsidence of the Hawaiian Ridge *85*
   James G. Moore

3. Slopes of the Hawaiian Ridge *101*
   Robert K. Mark and James G. Moore

4. Submarine topography around the Hawaiian Islands *109*
   Daniel J. Fornari and J. Frisbee Campbell

5. The geomorphic and structural development of Hawaiian submarine rift zones *125*
   Daniel J. Fornari

6. Geology of the summit of Loihi submarine volcano *133*
   Alexander Malahoff

GEOLOGY OF THE ISLAND OF HAWAII

Chapter 7. Geologic history and evolution of geologic concepts, Island of Hawaii *149*
Donald W. Peterson and Richard B. Moore

8. Hawaii: The view from space *191*
   George E. Ulrich, Peter J. Mouginis-Mark, and Jo-Ann Bowell

9. Effects of volcanic emanations on carbon-isotope content of modern plants near Kilauea Volcano *209*
   Meyer Rubin, John P. Lockwood, and Irving Friedman

10. Hawaiian radiocarbon dates *213*
    Meyer Rubin, Lea Kelley Gargulinski, and John P. McGeehin

11. Stratigraphy of Kilauea Volcano *243*
    R. Michael Easton

12. Eruptive history and long-term behavior of Kilauea Volcano *261*
    Robin T. Holcomb

Chapter 13. Stratigraphy and petrology of the Uwekahuna Bluff section, Kilauea caldera *351*
Thomas J. Casadevall and Daniel Dzurisin

14. Intrusive rocks of Kilauea caldera *377*
Thomas J. Casadevall and Daniel Dzurisin

15. An early 19th century reticulite pumice from Kilauea Volcano *395*
Robert P. Sharp, Daniel Dzurisin, and Michael C. Malin

16. The 1972–1974 Mauna Ulu eruption, Kilauea Volcano: An example of quasi-steady-state magma transfer *405*
Robert I. Tilling, Robert L. Christiansen, Wendell A. Duffield, Elliott T. Endo, Robin T. Holcomb, Robert Y. Koyanagi, Donald W. Peterson, and John D. Unger

17. The Puu Oo eruption of Kilauea Volcano, episodes 1–20, January 3, 1983, to June 8, 1984 *471*
Edward W. Wolfe, Michael O. Garcia, Dallas B. Jackson, Robert Y. Koyanagi, Christina A. Neal, and Arnold T. Okamura

18. Holocene eruptive history of Mauna Loa Volcano *509*
John P. Lockwood and Peter W. Lipman

19. Mauna Loa 1974–1984: A decade of intrusive and extrusive activity *537*
John P. Lockwood, John J. Dvorak, Thomas T. English, Robert Y. Koyanagi, Arnold T. Okamura, Marjorie L. Summers, and Wilfred R. Tanigawa

20. Hualalai Volcano: A preliminary summary of geologic, petrologic, and geophysical data *571*
Richard B. Moore, David A. Clague, Meyer Rubin, and Wendy A. Bohrson

21. Pleistocene subglacial eruptions on Mauna Kea *587*
Stephen C. Porter

22. Volcanic hazards in the Hawaiian Islands *599*
Donal R. Mullineaux, Donald W. Peterson, and Dwight R. Crandell

PETROGENESIS AND VOLCANIC GASES

Chapter 23. Recent advances in Hawaiian petrology and geochemistry *625*
Thomas L. Wright and Rosalind T. Helz

24. Trace-element chemistry of Kilauea and Mauna Loa lava in space and time: A reconnaissance *641*
Robert I. Tilling, Thomas L. Wright, and Hugh T. Millard, Jr.

25. Diverse olivine types in lava of the 1959 eruption of Kilauea Volcano and their bearing on eruption dynamics *691*
Rosalind Tuthill Helz

Chapter 26. Origin of the West Maui volcanic rocks inferred from Pb, Sr, and Nd isotopes and a multicomponent model for oceanic basalts *723*
Mitsunobu Tatsumoto, Ernst Hegner, and Daniel M. Unruh

27. Constraints on the characteristics of magma sources for Hawaiian volcanoes based on noble-gas systematics *745*
Ichiro Kaneoka

28. Hawaiian eruptive gases *759*
L. Paul Greenland

29. SO_2 and CO_2 emission rates at Kilauea Volcano, 1979–1984 *771*
Thomas J. Casadevall, J. Barry Stokes, L. Paul Greenland, Lawrence L. Malinconico, John R. Casadevall, and Bruce T. Furukawa

30. Composition of gases from the 1984 eruption of Mauna Loa Volcano *781*
L. Paul Greenland

31. Sulfur and carbon abundances in Hawaiian tholeiite lavas: 1972–1975 eruptions of Kilauea and 1975 eruption of Mauna Loa *791*
Karen J. Franczyk, Everett K. Gibson, Jr., and Robert I. Tilling

32. Variation of $\delta^{13}C$ in fumarolic gases from Kilauea Volcano *805*
Irving Friedman, Jim Gleason, and Trevor Jackson

33. Helium at Kilauea Volcano
Part I. Spatial and temporal variations at Sulphur Bank *809*
Irving Friedman and G. Michael Reimer
Part II. Distribution in the summit region *815*
G. Michael Reimer

34. Use of satellite telemetry for monitoring active volcanoes, with a case study of a gas-emission event at Kilauea Volcano, December 1982 *821*
Kenneth A. McGee, A. Jefferson Sutton, and Motoaki Sato

35. Hawaiian volcanoes and the biogeology of mercury *827*
Barbara Z. Siegel and Sanford M. Siegel

VOLUME 2

STRUCTURE
DYNAMICS
HISTORY OF INVESTIGATIONS OF HAWAIIAN VOLCANISM

Any use of trade names and trademarks in this publication is for descriptive purposes only and does not constitute endorsement by the U.S. Geological Survey.

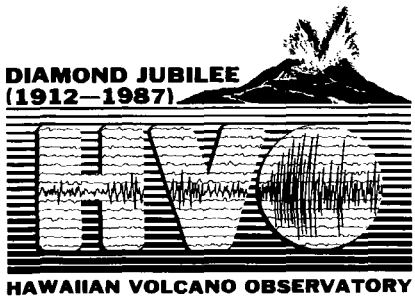

Volcanism in Hawaii

Papers to commemorate the 75th anniversary of the founding of the Hawaiian Volcano Observatory

---

Overleaf: Morphology of the sea floor in the northern Pacific Ocean, showing prominence and central position of Hawaiian-Emperor volcanic chain (compare with slope map in front of volume 2). From the map "World Ocean Floor" by Bruce C. Heezen and Marie Tharp, published 1977 by United States Navy (Office of Naval Research). Copyright 1977 by Marie Tharp, 1 Washington Avenue, South Nyack, NY 10960.

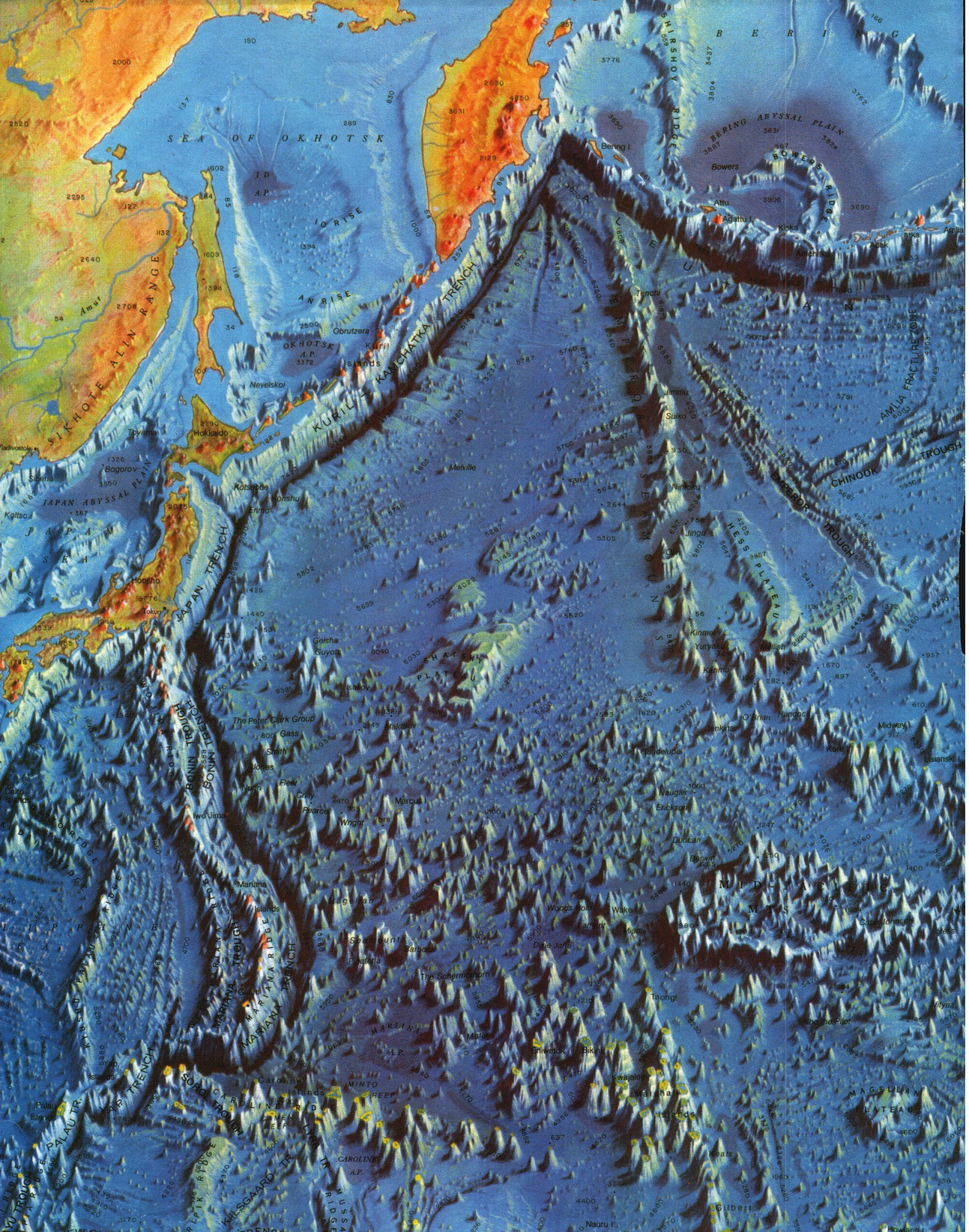
SEA OF OKHOTSK
BERING ABYSSAL PLAIN
BOWERS RIDGE
Bering I.
Bowers
Attu
Agattu I.
Kiska
Amlia
Atka
Adak
Amchitka
SHIRSHOV RIDGE
Tenchi
Jimmu
Suiko
Nintoku
Jingu
Kinmei
Yuryaku
Ojin
Hancock
Midway
Lisianski I.
Gardner
Pinnacles
Laysan
Maro Reef
Lisianski
Pearl & Hermes Reef
Necker I.
Nihoa
Kauai
Oahu
Molokai
Maui
Hawaii
Kaena Ridge
Hawaiian Ridge
Pensacola
Mauna Kea
Mauna Loa
Kilauea
Snowdon
Wilkes
Stanford
Hinds
Mahukona
Kaena Point
Hawaiian Arch
Hawaiian Swell
Hawaiian Terrace
Hawaiian Moat
Hawaiian Outer Rise
Hawaiian Trough
Hawaiian Deep
Hawaiian Fracture Zone
Hawaiian Lineament
Hawaiian Seamount Province
Hawaiian Volcanic Province
Hawaiian Hotspot
Hawaiian Plume
Hawaiian Mantle Plume
Hawaiian Mantle Upwelling
Hawaiian Mantle Downwelling
Hawaiian Mantle Convection
Hawaiian Mantle Plume Head
Hawaiian Mantle Plume Tail
Hawaiian Mantle Plume Stem
Hawaiian Mantle Plume Root
Hawaiian Mantle Plume Base
Hawaiian Mantle Plume Top
Hawaiian Mantle Plume Flank
Hawaiian Mantle Plume Core
Hawaiian Mantle Plume Boundary
Hawaiian Mantle Plume Interface
Hawaiian Mantle Plume Transition
Hawaiian Mantle Plume Zone
Hawaiian Mantle Plume Region
Hawaiian Mantle Plume Province
Hawaiian Mantle Plume Belt
Hawaiian Mantle Plume Chain
Hawaiian Mantle Plume Trail
Hawaiian Mantle Plume Track
Hawaiian Mantle Plume Path
Hawaiian Mantle Plume Line
Hawaiian Mantle Plume Row
Hawaiian Mantle Plume Series
Hawaiian Mantle Plume Sequence
Hawaiian Mantle Plume Succession
Hawaiian Mantle Plume Progression
Hawaiian Mantle Plume Migration
Hawaiian Mantle Plume Movement
Hawaiian Mantle Plume Drift
Hawaiian Mantle Plume Displacement
Hawaiian Mantle Plume Translation
Hawaiian Mantle Plume Rotation
Hawaiian Mantle Plume Pole
Hawaiian Mantle Plume Euler Pole
Hawaiian Mantle Plume Euler Vector
Hawaiian Mantle Plume Euler Rotation
Hawaiian Mantle Plume Euler Angle
Hawaiian Mantle Plume Euler Parameter
Hawaiian Mantle Plume Euler Constant
Hawaiian Mantle Plume Euler Coefficient
Hawaiian Mantle Plume Euler Matrix
Hawaiian Mantle Plume Euler Quaternion
Hawaiian Mantle Plume Euler Axis

Aerial view of Laysan Island, the largest island in the northwestern (leeward) Hawaiian Chain. Photograph by George H. Balazs, National Marine Fisheries Service.

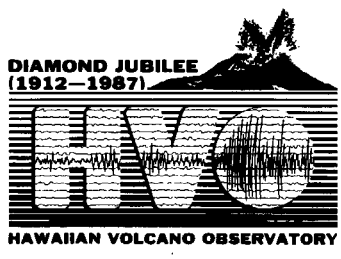
DIAMOND JUBILEE
(1912—1987)
HVO
HAWAIIAN VOLCANO OBSERVATORY

Volume 1

Mother and Child
Hawaiian Petroglyph
Puako, Hawaii

PHYSIOGRAPHY, TECTONICS, AND SUBMARINE GEOLOGY

The Hawaiian-Emperor volcanic chain is a dogleg ridge, largely submarine, that stretches nearly 6,000 km across the floor of the north Pacific Ocean. At the southeast end is the Island of Hawaii; from there it extends northwestward along the Hawaiian Ridge to a major bend beyond Kure Atoll. North of the bend the chain continues as the submarine ridge of the Emperor Seamounts. Volcanoes are active at the southeast end of the chain and become progressively older northwestward, reaching ages of 75–80 Ma at the north end of the Emperor Seamounts.

Nearly all of this volcanic chain, with an estimated total area of 1.2 million km^2, lies under water. Only the Hawaiian Islands and a few atolls of the Hawaiian Ridge, totaling some 16,878 km^2, rise above the ocean surface. Understandably, the chain has been explored largely by oceanographers. However, because many of the seamounts are similar to the island volcanoes of Hawaii, much has been learned by comparative studies.

The six chapters in this section deal with the origin and evolution of the Hawaiian-Emperor volcanic chain and the submarine geology of the Hawaiian Ridge. They begin with considering the entire chain and narrow down to the undersea summit of Loihi Volcano off the southeast coast of the Island of Hawaii.

THE HAWAIIAN-EMPEROR VOLCANIC CHAIN
Part I
Geologic Evolution

By David A. Clague *and* G. Brent Dalrymple

ABSTRACT

The Hawaiian-Emperor volcanic chain stretches nearly 6,000 km across the North Pacific Ocean and consists of at least 107 individual volcanoes with a total volume of about 1 million km^3. The chain is age progressive with still-active volcanoes at the southeast end and 80–75-Ma volcanoes at the northwest end. The bend between the Hawaiian and Emperor Chains reflects a major change in Pacific plate motion at 43.1±1.4 Ma and probably was caused by collision of the Indian subcontinent into Eurasia and the resulting reorganization of oceanic spreading centers and initiation of subduction zones in the western Pacific. The volcanoes of the chain were erupted onto the floor of the Pacific Ocean without regard for the age or preexisting structure of the ocean crust.

Hawaiian volcanoes erupt lava of distinct chemical compositions during four major stages in their evolution and growth. The earliest stage is a submarine alkalic preshield stage, which is followed by the tholeiitic shield stage. The shield stage probably accounts for >95 percent of the volume of each volcano. The shield stage is followed by an alkalic postshield stage during which a thin cap of alkalic basalt and associated differentiated lava covers the tholeiitic shield. After several million years of erosion, alkalic rejuvenated-stage lava erupts from isolated vents. An individual volcano may become extinct before the sequence is complete. The alkalic preshield stage is only known from recent study of Loihi Seamount. Lava from later eruptive stages has been identified from numerous submerged volcanoes located west of the principal Hawaiian Islands.

Volcanic propagation rates along the chain are 9.2±0.3 cm/yr for the Hawaiian Chain and 7.2±1.1 cm/yr for the Emperor Chain. A best fit through all the age data for both chains gives 8.6±0.2 cm/yr. Alkalic rejuvenated-stage lava erupts on an older shield during the formation of a new large shield volcano 190±30 km to the east. The duration of the quiescent period preceding eruption of rejuvenated-stage lava decreases systematically from 2.5 m.y. on Niihau to <0.4 m.y. at Haleakala, reflecting an increase in the rate of volcanic propagation during the last few million years. Rejuvenated-stage lava is generated during the rapid change from subsidence to uplift as the volcanoes override a flexural arch created by loading the new shield volcano on the ocean lithosphere.

Paleomagnetic data indicate that the Hawaiian hot spot has remained fixed during the last 40 m.y., but prior to that time the hot spot was apparently located at a more northerly latitude. The most reliable data suggest about 7° of southward movement of the hot spot between 65 and 40 Ma.

The numerous hypotheses to explain the mechanism of the hot spot fall into four types: propagating fracture hypotheses, thermal or chemical convection hypotheses, shear melting hypotheses, and heat injection hypotheses. A successful hypothesis must explain the propagation of volcanism along the chain, the near-fixity of the hot spot, the chemistry and timing of the eruptions from individual volcanoes, and the detailed geometry of volcanism. None of the geophysical hypotheses proposed to date are fully satisfactory. However, the existence of the Hawaiian swell suggests that hot spots are indeed hot. In addition, both geophysical and geochemical hypotheses suggest that primitive undegassed mantle material ascends beneath Hawaii. Petrologic models suggest that this primitive material reacts with the ocean lithosphere to produce the compositional range of Hawaiian lava.

INTRODUCTION

The Hawaiian Islands; the seamounts, banks, and islands of the Hawaiian Ridge; and the chain of Emperor Seamounts form an array of shield volcanoes that stretches nearly 6,000 km across the north Pacific Ocean (fig. 1.1). This unique geologic feature consists of more than 107 individual volcanoes with a combined volume slightly greater than 1 million km^3 (Bargar and Jackson, 1974). The chain is age progressive with still-active volcanoes at the southeast end whereas those at the northwest end have ages of about 75–80 Ma. The volcanic ridge is surrounded by a symmetrical depression, the Hawaiian Deep, as much as 0.7 km deeper than the adjacent ocean floor (Hamilton, 1957). The Hawaiian Deep is in turn surrounded by the broad Hawaiian Arch.

At the southeast end of the chain lie the eight principal Hawaiian Islands. Place names for the islands and seamounts in the chain are shown in figure 1.1 (see also table 1.2). The Island of Hawaii includes the active volcanoes of Mauna Loa, which erupted in 1984, and Kilauea, which erupted in 1986. Loihi Seamount, located about 30 km off the southeast coast of Hawaii, is also active and considered to be an embryonic Hawaiian volcano (Malahoff, chapter 6; Moore and others, 1979, 1982). Hualalai Volcano on Hawaii and Haleakala Volcano on Maui have erupted in historical times. Between Niihau and Kure Island only a few of the volcanoes rise above the sea as small volcanic islets and coral atolls. Beyond Kure the volcanoes are entirely submerged beneath the sea. Approximately 3,450 km northwest of Kilauea, the Hawaiian Chain bends sharply to the north and becomes the Emperor Seamounts, which continue northward another 2,300 km.

It is now clear that this remarkable feature was formed during the past 70 m.y. or so as the Pacific lithospheric plate moved north and then west relative to a melting anomaly, called the Hawaiian hot spot, located in the asthenosphere. According to this hot-spot hypothesis, a trail of volcanoes was formed and left on the ocean

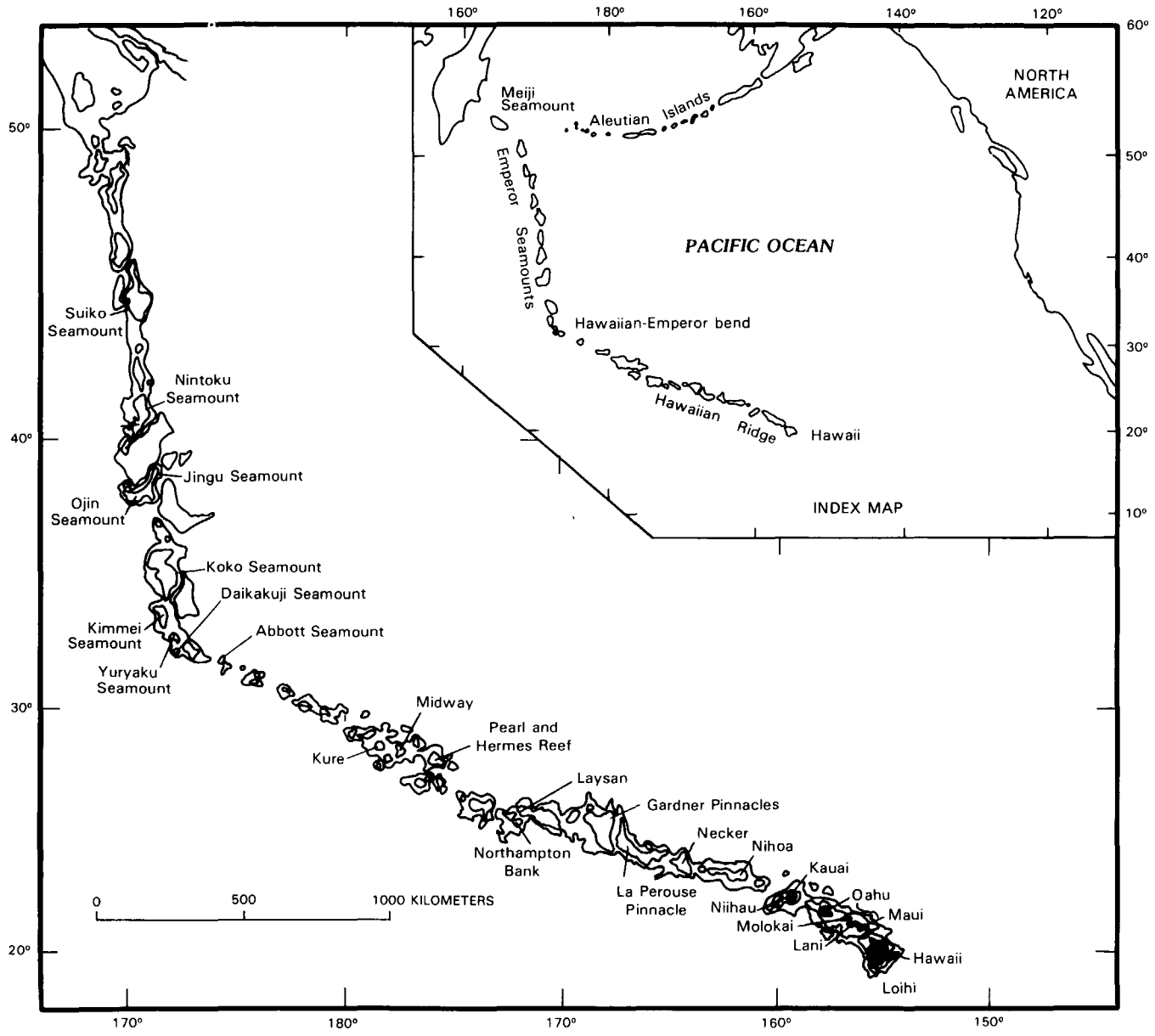

FIGURE 1.1.—Bathymetry of Hawaiian-Emperor volcanic chain modified from Chase and others (1970). Contours at 1-km and 2-km depths shown in area of the chain only. Inset shows location of chain (outlined by 2-km depth contour) in central North Pacific.

floor as each volcano was progressively cut off from its source of lava and a new volcano was born behind it.

Wilson (1963a, c) was the first to propose that the Hawaiian Islands and other parallel volcanic chains in the Pacific were formed by movement of the sea floor over sources of lava in the asthenosphere. Although the Emperor Chain was recognized as a northward continuation of the Hawaiian Chain by Bezrukov and Udintsev (1955) shortly after the Emperor Seamounts were first described by Tayama (1952) and Dietz (1954), Wilson confined his hypothesis to the volcanoes of the Hawaiian Islands and the Hawaiian Ridge. Christofferson (1968), who also coined the term "hot spot," extended Wilson's idea to include the Emperor Seamounts and suggested that the Hawaiian-Emperor bend represents a major change in the direction of sea-floor spreading from northward to westward. Morgan (1972a, b) proposed that the Hawaiian and other hot spots are thermal plumes of material rising from the deep mantle and that the worldwide system of hot spots constitutes a reference frame that is fixed relative to Earth's spin axis.

Although experimental testing of the various hypotheses proposed to explain hot spots has so far proven unproductive, the hot-

spot hypothesis has several important corollaries that can and have been tested to varying degrees. Foremost among these is that the volcanoes should become progressively older to the west and north as a function of distance from the hot spot. This progressive aging should be measurable with radiometric methods and also should be evident in the degree of erosion, subsidence, and geological evolution of the volcanoes along the chain. A second important corollary is that the latitude of formation of the volcanoes, as recorded in the magnetization of their lava flows, should reflect the present latitude of the hot spot rather than the present latitude of the volcanoes. Third, because the active mechanism is beneath the lithosphere, the Hawaiian-Emperor Chain should show no relation to the structure of the sea floor. Finally, the volcanic rocks of the volcanoes should be similar in both chemistry and sequence of eruption for each volcano along the chain, or should change in a systematic and coherent way.

In this paper we describe the Hawaiian-Emperor volcanic chain and those individual volcanoes that have been sampled and studied. We review the evidence that indicates that all of the corollaries mentioned above are true and, therefore, that the hot-spot hypothesis is a viable explanation of the origin of the chain. We will also describe the various hypotheses that have been proposed to explain the hot-spot mechanism and discuss their strengths and weaknesses.

ACKNOWLEDGMENTS

We thank Tom Wright and Jim Natland for their reviews, Kay McDaniel for her patience in typing it all, and Brigitta Fulop for drafting the figures.

STRUCTURE AND AGE OF THE UNDERLYING CRUST

The volcanoes of the Hawaiian-Emperor Chain were formed by eruption of lava onto the floor of the Pacific Ocean without regard for the age or preexisting structure of the ocean crust, or for the presence of preexisting volcanoes. The precise age of the ocean crust beneath much of the chain is poorly known because of the paucity of magnetic anomalies in the area (fig. 1.2). The Hawaiian Islands and Ridge east of about Midway Island lie on crust older than anomaly 34 but younger than anomaly M0. In a general way, both the Hawaiian seamounts and the underlying crust increase in age to the west so that the age of the crust beneath each volcano at the time it was built was between 80 and 90 m.y. (fig. 1.3). Volcanoes between Midway and the Hawaiian-Emperor bend and in the Emperor Seamounts south of Jingu Seamount are all built on crust whose age is between that of anomalies M0 and M3. Because the seamounts increase in age to the northwest but the underlying crust is roughly the same age, the age of the crust when the overlying volcano was built decreases systematically from about 80 m.y. at the bend to about 55 m.y. at Jingu Seamount. North of Jingu Seamount the age of the crust is not known, but plate reconstructions imply decreasing crustal ages to the north (Scientific Party DSDP 55, 1978; Byrne, 1979).

Northward from Jingu Seamount, we estimate that the crustal age at Suiko was roughly 40 m.y. and at the northernmost seamount, Meiji, was <20 m.y. when those volcanoes formed. If this extrapolation is extended beyond Meiji Seamount to hypothetical seamounts we presume existed once but which have been subducted or accreted in the Kuril Trench, we conclude that the Hawaiian hot spot was located, and perhaps originated, beneath the Kula-Pacific spreading axis at about 100–90 Ma.

Preexisting structures in and on the underlying crust appear to have had little or no influence on the formation of the Hawaiian-Emperor Chain (fig. 1.2). Several fracture zones, including the Mendocino, Murray, and Molokai, cross the chain, but none appears to have greatly affected the orientation of the chain, the rate of propagation of volcanism, or the volume of eruptive products. Likewise, the chain has overridden at least one Late Cretaceous seamount, again without obviously affecting the orientation, rate of propagation of volcanism, or the volumes of eruptive products (Clague and Dalrymple, 1975).

ERUPTIVE SEQUENCE

Hawaiian volcanoes erupt lava of distinct chemical compositions during four different stages in their evolution and growth (table 1.1). The three later stages are well studied and documented (Stearns, 1940a, b, c; Macdonald and Katsura, 1964; Macdonald, 1968), but the first (preshield) stage, which includes the early phase of the submarine history of the volcano, has only been examined recently (Moore and others, 1979, 1982).

The tholeiitic eruptive stage includes a long period of submarine eruption that forms a volcanic edifice with steep slopes and a subaerial eruptive phase that forms the shield-shaped volcano (Peterson and Moore, chapter 7). In this paper we refer to this entire stage of tholeiitic volcanism as the shield stage. In the shield stage, tholeiitic basalt flows construct the main volcanic edifice in the relatively short span of perhaps 1 m.y. or less (Jackson and others, 1972). Wright and others (1979) independently propose 200,000 yr as the duration of tholeiitic volcanism. Most of the mass of an individual volcano (95–98 percent) is formed from these voluminous eruptions. The shield stage usually includes caldera collapse and eruption of caldera-filling tholeiitic basalt. During the next stage, the alkalic postshield stage, alkalic basalt also may fill the caldera and form a thin cap of alkalic basalt and associated differentiated lava that covers the main shield. This alkalic lava accounts for less than 1 percent of the total volume of the volcano. After as much as a few million years of volcanic quiescence and erosion, very small amounts of SiO_2-poor lava may erupt from isolated vents; this stage is commonly called the posterosional stage; we refer to it here as the alkalic rejuvenated stage. An individual volcano may become extinct before this eruptive cycle is complete, but the general sequence is typical of the well-studied Hawaiian volcanoes (table 1.2). Some of these ideas are more than half a century old. Cross (1915) recognized that each of the Hawaiian volcanoes built a shield of lava, comparable to Kilauea flows, during a period of frequent voluminous eruptions. He also noted that this period was followed by a period of erosion and declining activity that produced cinder cones

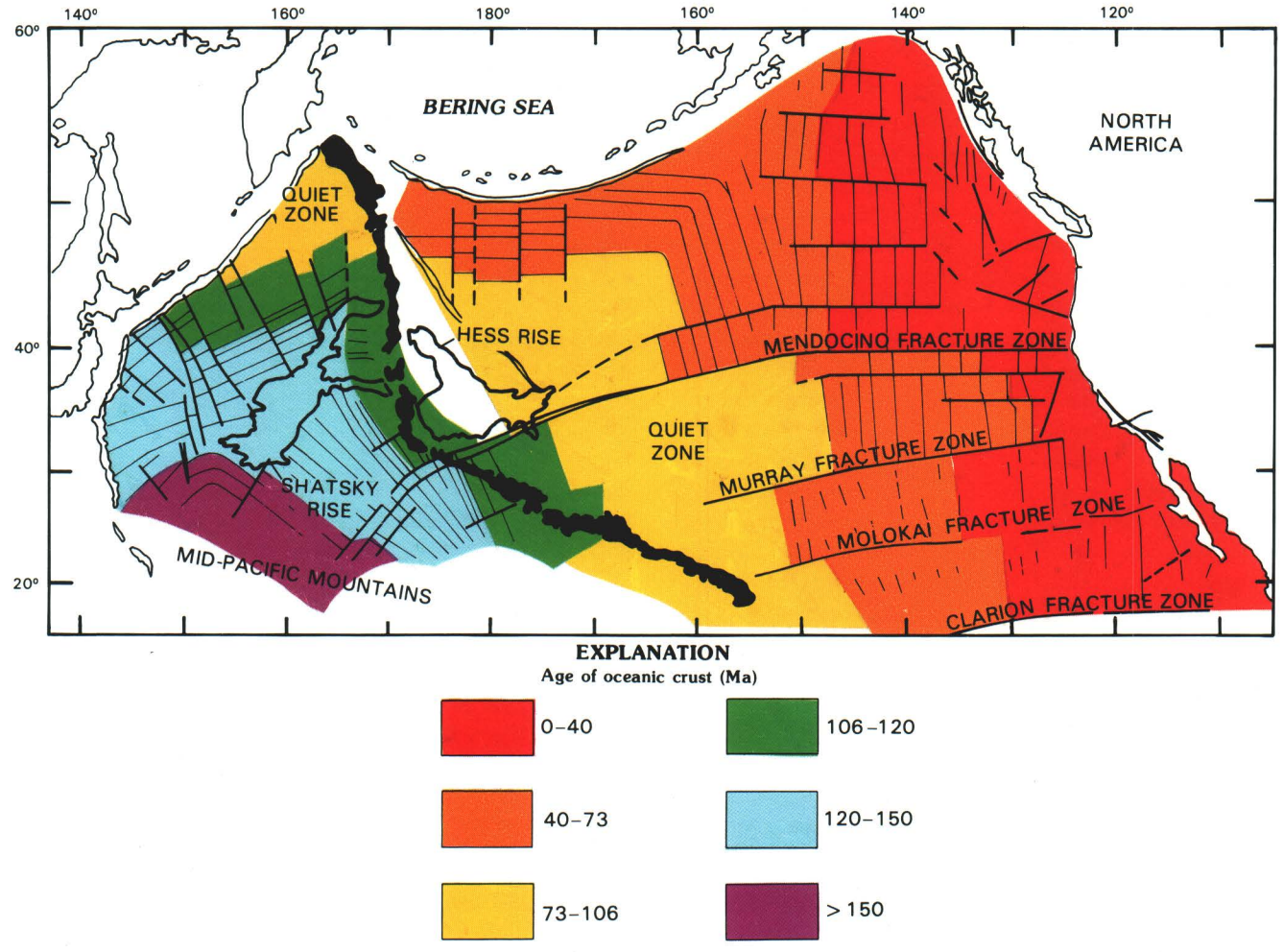

FIGURE 1.2.—Magnetic anomalies and structure of ocean floor crust in North Pacific modified from Hilde and others (1976). Hawaiian-Emperor Chain (black) crosscuts preexisting fracture zones and Mesozoic magnetic-anomaly sequence.

and small flows of lava richer in SiO_2 and FeO (these are the hawaiite and mugearite that characterize the alkalic postshield stage). S. Powers (1920) noted that eruptive centers of nepheline basalt on Kauai, Oahu, Molokai, and Maui were active long after the main volcano became quiet; he appears to have been the first to associate nepheline basalt with late-stage eruptions following an erosional hiatus.

New insight into the preshield stage has come from recent studies of Loihi Seamount, a small submarine volcano located about 30 km off the southeast coast of Hawaii. Its location, small size, seismic activity, and fresh, glassy lava all indicate that Loihi is an active volcano and the youngest in the Hawaiian-Emperor Chain. Some of the older lava samples recovered from Loihi Seamount are alkalic basalt and basanite, whereas the youngest lava samples recovered are tholeiitic and transitional basalt. This observation led Moore and others (1982) to conclude that Loihi Seamount, and perhaps all Hawaiian volcanoes, initially erupt alkalic basalt. Later, the bulk of the shield is built of tholeiitic basalt, but during declining activity the magma compositions revert to alkalic basalt. The alkalic preshield stage, like the alkalic postshield stage, produces only small volumes of lava, probably totaling less than a few percent of the volcano.

We have omitted the main caldera-collapse stage of Stearns (1966) from the eruption sequence because it can occur either during the shield stage or near the beginning of the alkalic postshield stage. The lava erupted may therefore be tholeiitic or alkalic basalt, or of both types.

GEOLOGY OF THE HAWAIIAN ISLANDS

Descriptions of volcanoes and their eruptions were made by nearly all the earliest visitors to the Hawaiian Islands. Descriptions of particular note are those of William Ellis (1823), George, Lord Byron (1826), Joseph Goodrich (1826, 1834), and Titus Coan

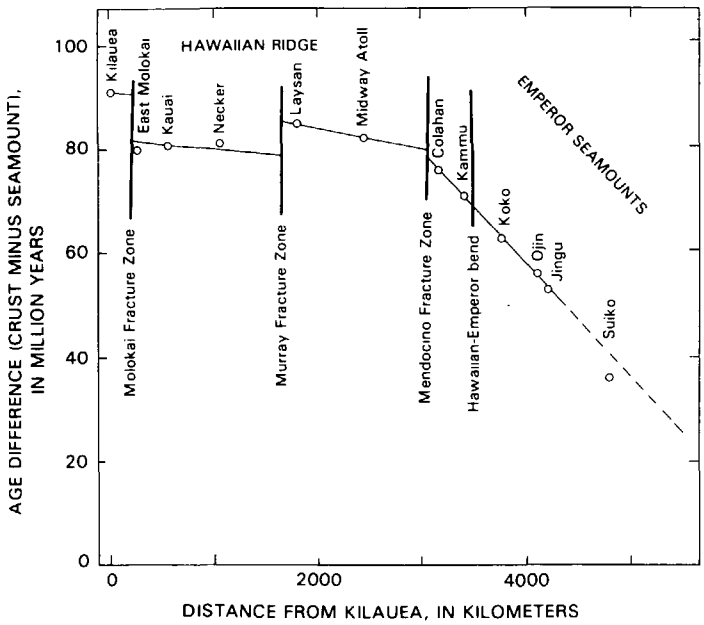

FIGURE 1.3.—Age of oceanic crust when overlying volcano formed, as a function of distance from Kilauea, for selected volcanoes in Hawaiian-Emperor Chain. Note offsets at fracture zones. Along Hawaiian Ridge both crust and volcanoes increase in age to west so crustal age when volcanoes formed is roughly constant. On the other hand, Emperor Seamounts increase in age to north but crust decreases in age; thus age of crust when seamounts formed decreases from roughly 75 Ma at the bend to less than 40 Ma at Suiko Seamount.

TABLE 1.1.—*Hawaiian eruptive products*

Eruptive stage	Rock types	Eruption rate	Volume (percent)
Rejuvenated --	alkalic basalt basanite nephelinite nepheline melilitite	Very low	<1
Postshield ---	alkalic basalt transitional basalt ankaramite hawaiite mugearite benmoreite trachyte phonolite	Low	~1
Shield -------	tholeiitic basalt olivine tholeiitic basalt picritic tholeiitic basalt icelandite (rare) rhyodacite (rare) [1]alkalic basalt (?)	High	95-98
Preshield ----	basanite alkalic basalt transitional basalt [1]tholeiitic basalt (?)	Low	~3

[1]Wright and Helz (chapter 23) suggest that the shield stage may include rare intercalated alkalic basalt and that the preshield stage includes tholeiitic basalt. We suspect that tholeiitic and alkalic basalt occur intercalated during the transitions from preshield to shield stage and from shield stage to postshield stage but that during the main shield stage only tholeiitic lava is erupted.

(1840 and other letters until 1882). Many of their letters describing the volcanoes were published in the American Journal of Science. Goodrich, in particular, provided detailed descriptions of the volcanoes on the Island of Hawaii. None of the earliest descriptions however, included information about the mineralogy or petrology of the lava.

The United States Exploring Expedition visited Hawaii in 1840–41. The commander of the expedition published a narrative (Wilkes, 1845) containing descriptions of caldera activity at Kilauea and new maps of both Kilauea and Mauna Loa calderas. James D. Dana, the geologist of the expedition, published a detailed report on the geology of the areas visited by the expedition (Dana, 1849). This report contains descriptions of lava flows including their mineralogy and flow morphology, in addition to numerous other observations on the active and inactive volcanoes that make up the islands. Later reports by Dutton (1884), J.D. Dana (1887, 1888, 1889), Green (1887), and Brigham (1909) added details on eruptions and expanded the geologic observations to other islands.

E.S. Dana (1877), Cross (1904), and Hitchcock (1911) presented detailed petrographic descriptions of lava from the islands. Daly (1911) and Cross (1915) described the mineralogy and petrology of Hawaiian lava flows at the time the Hawaiian Volcano Observatory was established, and Jagger (1917) described activity in Halemaumau lava lake. The paper by Cross (1915) is a milestone because it added detailed descriptions and chemical analyses of rocks from Hawaiian volcanoes other than Kilauea and Mauna Loa.

More detailed petrographic descriptions of lava from the islands were published by S. Powers (1920). Soon afterward, papers appeared by Washington (1923a, b, c) and Washington and Keyes (1926, 1928) with detailed accounts of the geology and petrology, new high-quality chemical analyses of lava from Hawaii and Maui, and a classification of Hawaiian volcanic rocks. Palmer (1927, 1936) added geologic descriptions and petrography of lava from Kaula and Lehua Islands, both of which are tuff cones of the alkalic rejuvenated stage. Lehua Island is just one of several rejuvenated-stage vents associated with Niihau, whereas Kaula Island sits atop a completely submerged shield.

These early, mainly descriptive and reconnaissance studies were superseded by detailed mapping of the islands beginning in the 1930's. H.T. Stearns and his coworkers, in a remarkable series of bulletins published by the Hawaii Division of Hydrography, published geologic maps and descriptions of Oahu (Stearns and Vaksvik, 1935; Stearns, 1939, 1940b), Lanai and Kahoolawe (Stearns, 1940c), Maui (Stearns and Macdonald, 1942), Hawaii (Stearns and Macdonald, 1946), Niihau (Stearns, 1947), and Molokai (Stearns and Macdonald, 1947). The bulletin on Kauai by Macdonald and others (1960) completed the monumental mapping job begun by Stearns; though Stearns did not coauthor the report, he did much of the mapping and is an author of the map. These maps and bulletins provide the geologic framework for all

TABLE 1.2.—*Eruptive stages represented on volcanoes of the Hawaiian-Emperor Chain*

[Volcano numbers from Bargar and Jackson (1974); numbers 0 and 65A added for consistency. Presence of stages: M, major unit; R, rare or of small volume; X, present but extent unknown; A, known to be absent; -, unknown. (T), transitional lava probably erupted during late shield stage or caldera-collapse phase of that stage. For volcanoes from Kilauea through Necker, data from detailed mapping and sampling; for remaining volcanoes, primarily from dredge and drill samples]

Volcano Number	Volcano Name	Eruptive Stages: Preshield (alkalic)	Shield (tholeiitic)	Postshield (alkalic)	Rejuvenated (alkalic)
	Hawaiian Islands				
0	Loihi	M	M	-	-
1	Kilauea	-	M	A	A
2	Mauna Loa	-	M	A	A
3	Mauna Kea	-	M	M	A
4	Hualalai	-	M	M	A
5	Kohala	-	M	M	A
6	East Maui	-	M	M	M
7	Kahoolawe	-	M	R	R
8	West Maui	-	M	R	R
9	Lanai	-	M	A	A
10	East Molokai	-	M	M	R
11	West Molokai	-	M	R	A
12	Koolau	-	M	A	M
13	Waianae	-	M	M	R
14	Kauai	-	M	R	M
15	Niihau	-	M	R	M
15A	Kaula	-	X	X	X
	Northwestern Hawaiian Islands and Hawaiian Ridge				
17	Nihoa	-	M	-	-
19	(Unnamed Seamount)	-	X(T)	-	-
20	(Unnamed Seamount)	-	X	-	X
21	(Unnamed Seamount)	-	X	-	-
23	Necker	-	M	X	X
26	La Perouse Pinnacles	-	X	-	-
28	Brooks Bank	-	X(T)	X	-
29	St. Rogatien Bank	-	-	X	-
30	Gardner Pinnacles	-	X	X	-
36	Laysan	-	-	X	-
37	Northampton Bank	-	X	-	-
39	Pioneer Bank	-	X	-	-
50	Pearl and Hermes Reef	-	-	X	-
51	Ladd Bank	-	-	-	X
52	Midway	-	M	X	-
53	Nero Bank	-	X	-	-
57	(Unnamed Seamount)	-	-	X	-
63	(Unnamed Seamount)	-	-	-	X
65	Colahan	-	X	-	X
65A	Abbott	-	X(T)	-	-
	Emperor Seamounts				
67	Daikakuji	-	X	-	-
69	Yuryaku	-	X	X	-
72	Kimmei	-	-	X	-
74	Koko (southern)	-	X	M	-
76	Koko (northwest)	-	X	-	-
81	Ojin	-	X	X	-
83	Jingu	-	-	X	-
86	Nintoku	-	-	X	-
90	Suiko (southern)	-	-	X	-
91	Suiko (central)	-	M	X	-
108	Meiji	-	M	-	-

subsequent studies of the islands and can also be used to put many of the earlier descriptions into a broader geological context. A number of derivative publications include summaries of the geology of the islands by Stearns (1946, 1966), an overview of the petrography of lava from the islands by Macdonald (1949), and a summary of the geology of the Hawaiian Islands by Macdonald and others (1983). The brief geologic summaries in appendix 1.1 have largely been extracted from the above publications. Additional unpublished observations by ourselves are included for Hualalai, East and West Molokai, Koolau, Kauai, and Niihau.

The maps of Stearns and coworkers separate rejuvenated-stage lava from earlier lava, but do not subdivide shield and postshield lava on the basis of chemical composition. The eruptive stages that are known to occur in each of the volcanoes of the Hawaiian Islands are summarized in table 1.2. Evidence for the alkalic preshield stage exists only at Loihi Seamount. If this stage is present in all Hawaiian volcanoes, it is completely buried by later, shield-stage tholeiitic lava. The tholeiitic shield stage is known to form the major portion of the subaerial and, we assume, the submarine part of each volcano. On the main islands, only Hualalai Volcano and Kaula Island do not have subaerial exposures of tholeiitic lava. Alkalic lava of the alkalic postshield stage occurs relatively late in the eruptive sequence and has not yet developed on Loihi Seamount or Kilauea and Mauna Loa Volcanoes. To the northwest of there it occurs on all volcanoes except Lanai and Koolau, although the volumes present on Kauai, Niihau, Kahoolawe, and West Molokai are small. Some volcanoes have predominantly mugearite, whereas others have predominantly hawaiite; these are called Kohala type and Haleakala type, respectively, by Macdonald and Katsura (1962). Wright and Clague (in press) propose two additional types: a Hualalai type with a bimodal trachyte-alkalic basalt lava distribution and a Koolau type with little or no alkalic postshield lava present.

Hawaiian volcanoes commonly have summit calderas and elongate curved rift zones from which much of the lava issues. Summit calderas exist on Loihi Seamount (Malahoff, chapter 6; Malahoff and others, 1982), Kilauea, and Mauna Loa. Each of these calderas is connected to two prominent rift zones. Not all Hawaiian volcanoes, however, had a summit caldera. West Molokai Volcano, in particular, shows no evidence of ever having had a caldera. Flat-lying lava ponded inside a caldera is not exposed on Hualalai, Mauna Kea, Kohala, or Niihau, but former calderas are inferred at those volcanoes from geophysical data (see Macdonald and others, 1983).

The formation and structure of the rift zones have been examined in an elegant paper by Fiske and Jackson (1972), who concluded that the orientation of the rift zones reflects local gravitational stresses within the volcanoes. Isolated shields such as Kauai and West Molokai had nearly symmetrical stress fields represented by generally radial dikes and thus have only poorly defined rift zones. The rift zones of these isolated volcanoes tend to align parallel to the orientation of the chain, suggesting the influence of a more regional stress field that also controls the orientation of the chain. In contrast, the rift zones of the other volcanoes tend to be aligned parallel to the flanks of the preexisting shields against which they abut.

GEOLOGY OF THE HAWAIIAN RIDGE

The Northwestern Hawaiian Islands were the focus of all geologic investigations along the Hawaiian Ridge west of Kauai until oceanographic techniques were applied to the area in the 1950's. Geological descriptions of the leeward islands include those of S. Powers (1920) for Nihoa and Necker Islands, and Washington and Keyes (1926) and Palmer (1927) for Nihoa, Necker, Gardner Pinnacles, and French Frigates Shoal (LaPerouse Pinnacles). These reports cite earlier sketchy descriptions. Macdonald (1949) reexamined Palmer's samples and added more detailed petrography. The petrology of the basaltic basement of Midway Atoll is described from two drill cores by Macdonald (1969) and Dalrymple and others (1974, 1977), whereas the geology of the site is detailed by Ladd and others (1967, 1969). Paleomagnetic data on flows and dikes from Nihoa and Necker Islands are given by Doell (1972), whereas similar data from the Midway drill core are given by Gromme and Vine (1972).

Marine geologic investigations of the Hawaiian Ridge began with Hamilton's pioneering work in 1957. Much subsequent work has focused on the structure of the oceanic crust in the vicinity of the chain, but few cruises have actually been conducted that dealt mainly with the geology of the Hawaiian Ridge. In the early 1970's, Scripps Institution of Oceanography and the Hawaii Institute of Geophysics conducted cruises to the Hawaiian Ridge. Samples collected by these cruises are described in Clague (1974a, 1974b) and Garcia, Grooms, and Naughton (in press). Subsequent cruises to the area by the Hawaii Institute of Geophysics and the U.S. Geological Survey are cited in appendix 1.1.

Lava samples recovered from the Hawaiian Ridge and Emperor Seamounts are more difficult to assign to volcanic stages because they are recovered by dredging and drilling or are collected from small islets and the field relations are usually unknown or only poorly known. Table 1.2 summarizes the available data from the Hawaiian Ridge. Based on the sequence and volumes of lava in the Hawaiian Islands, we have assumed that tholeiitic basalt always represents the shield stage and that strongly alkalic, SiO_2-poor lava represents the alkalic rejuvenated stage. Differentiated alkalic lava has been assigned to the alkalic postshield stage. Some alkalic basalt occurrences could be assigned to either the alkalic postshield or rejuvenated stages; they have been assigned on the basis of trace-element signatures and mineral chemistry using criteria outlined in a later section of this paper. No lava samples have been assigned to the alkalic preshield stage because we assume that the small volumes of such early lava have been buried by the later voluminous tholeiitic lava of the shield stage.

The samples recovered by dredging are probably not representative of the lava forming the bulk of the individual seamounts, but instead represent the youngest lava types erupted on the volcanoes. This natural sampling bias should result in an overrepresentation of alkalic lava from both the postshield and rejuvenated stages. In addition, selection of recovered samples for further study introduces another bias because the freshest samples are commonly alkalic lava, particularly hawaiite, mugearite, and trachyte. With these biases in mind, it is still possible to note general trends along the entire chain.

Tholeiitic basalt and picritic tholeiitic basalt, similar to those of the shield stage of subaerial Hawaiian volcanoes, have been recovered from 11 seamounts, banks, and islands in the Hawaiian Ridge west of Kauai and Niihau (table 1.2; appendix 1.1). The abundance of tholeiitic basalt from the Hawaiian Ridge implies that these volcanoes are genetically related to the Hawaiian Islands and that the general sequence of Hawaiian volcanism, in which tholeiitic basalt forms a major portion of each volcano, has occurred along the entire Hawaiian Chain.

GEOLOGY OF THE EMPEROR SEAMOUNTS

Little was known of the geology of the Emperor Seamounts until quite recently. The chain was recognized as the continuation of the Hawaiian Ridge by Bezrukov and Udintsev (1955), but not until 1968 were the first samples recovered from Suiko Seamount (Ozima and others, 1970). These samples are dominantly, if not completely, ice-rafted detritus. Subsequent studies included a cruise to the southern part of the chain by Scripps Institution of Oceanography in 1971 (ARIES Leg VII; Davies and others, 1971, 1972), Deep Sea Drilling Project (DSDP) Site 192 on Meiji Seamount (Creager and Scholl, 1973), DSDP Sites 308 and 309 on Koko Seamount (Larson and others, 1975), a cruise by the Hawaii Institute of Geophysics (Dalrymple and Garcia, 1980), a cruise by the U.S. Geological Survey in 1976 that surveyed the sites for Leg 55 of DSDP (Dalrymple and others, 1980a), and Leg 55 DSDP Sites 430, 431, 432, and 433 in the central part of the chain (Jackson and others, 1980). The Scripps Institution of Oceanography cruise ARIES VII in 1971 and the Leg 55 DSDP cruise in 1977 were particularly successful, and most of our knowledge of the Emperor Seamounts is derived from these two cruises.

The petrology of lava samples recovered by these two cruises is described in Clague (1974a) and Kirkpatrick and others (1980), respectively. A detailed seismic interpretation of the carbonate caps of many of the seamounts is given by Greene and others (1980), and overviews of the results of DSDP Leg 55 are given by Jackson and others (1980) and Clague (1981).

Table 1.2 summarizes the available data on eruptive stages represented by samples from the Emperor Seamounts, and details are given in appendix 1.1 for individual volcanoes. We have assumed that tholeiitic basalt represents the shield stage and that alkalic lava postdates the tholeiitic shield stage; only at Ojin and Suiko Seamounts does drilling show that the alkalic lava overlies the tholeiitic flows.

Tholeiitic basalt and picritic tholeiitic basalt similar to those of the shield stage of subaerial Hawaiian volcanoes have been recovered by drilling and dredging from six volcanic edifices in the Emperor Seamounts. The abundance of tholeiitic lava from the Emperor Seamounts is strong evidence that these volcanoes are genetically related to the Hawaiian Islands and Hawaiian Ridge. Likewise, the general eruptive model for the Hawaiian Islands is apparently applicable to the Emperor Seamounts.

Alkalic postshield-stage lava has been recovered by dredging and drilling from nine seamounts in the chain. In general these samples are alkalic basalt, hawaiite, mugearite, and trachyte similar to lava erupted in the Hawaiian Islands, but lava from Koko Seamount includes anorthoclase trachyte and phonolite that are interpreted to have erupted during the alkalic postshield stage (Clague, 1974a). Lava of the rejuvenated alkalic stage has not been identified from any of the Emperor Seamounts.

SUBSIDENCE OF THE VOLCANOES

Charles Darwin (1837, 1842) was the first to suggest that coral atolls might grow on subsiding platforms and that drowned atolls and certain deeply submerged banks with level tops could be explained by subsidence. Hess (1946) recognized that flat-topped submarine peaks, which he named guyots, were drowned islands. He thought that they were volcanic, bare of sediments and coral, and had been planed off by erosion at sea level. He attributed their depth to rising sea level caused by sediment deposition in the oceans. Menard and Dietz (1951) agreed with Hess that submergence was primarily due to a rise in sea level, but they thought that local subsidence might also play a role. Hamilton (1956), in his classic study of the Mid-Pacific Mountains, which included a program of dredging and coring, concluded that those (and other) guyots were formerly basaltic islands that had been wave and stream eroded and on which coral reefs subsequently grew. Their eventual submergence, he thought, was primarily caused by regional subsidence of the sea floor. It is now known that Darwin and Hamilton were basically correct about the steps leading to the formation of guyots, and about the predominant role of subsidence in the process.

The Hawaiian-Emperor volcanic chain is an excellent example of the gradual transformation of volcanic islands to guyots. From southeast to northwest there is a continuous progression from the active volcanoes such as Mauna Loa and Kilauea through the eroded remnants of Niihau, Nihoa, and Necker, through growing atolls like French Frigates Shoal and Midway Islands, to deeply submerged guyots like Ojin and Suiko. The progression can be observed not only along the chain but within the stratigraphy of individual seamounts. Drilling, dredging, and seismic observations have shown conclusively that the atolls and guyots of the chain are capped by carbonate deposits that overlie subaerial lava flows (see, for example, Ladd and others, 1967; Davies and others, 1971, 1972; Greene and others, 1980; Jackson and others, 1980).

The subsidence of Hawaiian volcanoes with time results from thermal aging of the lithosphere and isostatic response to local loading. The depth of the sea floor (and of volcanoes sitting upon it) increases away from spreading ridges because the lithosphere cools, thickens, and subsides as it moves away from the source of heat beneath the ridge (Parsons and Sclater, 1977; Schroeder, 1984). Detrick and Crough (1978) pointed out that the subsidence of many islands and seamounts, including those along the Hawaiian-Emperor Chain, was far in excess of that which could be accounted for by this normal lithospheric aging or by lithospheric loading. They proposed that the lithosphere is thermally reset locally as it passes over a hot spot and that the excess subsidence is largely a consequence of renewed lithospheric aging.

The Hawaiian-Emperor Chain rests on crust of Cretaceous age (circa 120–80 Ma) for which the depth should be about 5.5–5.9 km. The depth near Hawaii, however, is less than 4.5 km (fig. 1.4). The depth increases along the chain to about 5.3 km near the Hawaiian-Emperor bend in a manner consistent with the thermal resetting hypothesis. Thus, the subsidence of Hawaiian volcanoes as they move away from the hot spot is in part a function of their distance from the hot spot, that is, of the reset thermal age of the lithosphere beneath the chain. The volcanoes are passively riding away from the Hawaiian hot spot on cooling and thickening lithosphere that is subsiding at about 0.02 mm/yr.

Superimposed on the effect of crustal aging is subsidence caused by the immense and rapid loading of the lithosphere by the growing volcanoes (Moore, chapter 2). This effect is local, but while the volcano is active the rate of subsidence caused by loading may exceed that from lithospheric aging by more than two orders of magnitude. Moore (1970) found, from a study of tide-gage records in the Hawaiian Islands and on the west coast of North America, that Hilo on the Island of Hawaii has been subsiding at an absolute rate of 4.8 mm/yr since 1946. Recent data on drowned coral reefs near Kealakekua Bay indicate an absolute subsidence rate for the western side of Hawaii of 1.8 to 3+ mm/yr averaged over the past 300,000 yr and also indicate that the rate may have accelerated during that time (Moore and Fornari, 1984). Moore's (1970) tide-gage data also show that absolute subsidence decreases systematically away from the Island of Hawaii, with rates for Maui and Oahu of 1.7 mm/yr and 0 mm/yr, respectively. Some of this decrease in subsidence may be due to compensating uplift as the volcanoes are carried over the Hawaiian Arch, but an analysis of gravity data indicates that there is no appreciable viscous reaction to the seamount loads over time (Watts, 1978). Thus, it is probable that the volcanoes are isostatically compensated within a few million years of their birth, and that thermal aging of the lithosphere is the major cause of subsidence along the chain.

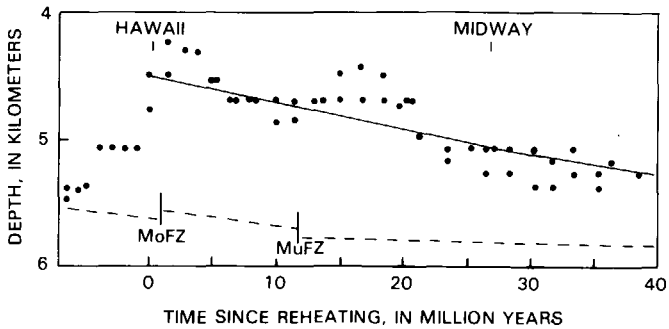

FIGURE 1.4.—Minimum depth to sea-floor swell as a function of time since reheating (or age of volcanoes along chain). Dashed line is predicted depth for normal aging of lithosphere away from spreading ridge. Solid line is predicted depth for thermally reset lithosphere 45 km thick. MoFZ and MuFZ, Molokai and Murray Fracture Zones, respectively. Modified from Detrick and Crough (1978) and Crough (1983).

GEOCHRONOLOGY AND PROPAGATION OF VOLCANISM

EARLY WORK: LEGENDS AND DEGREE OF EROSION

According to Hawaiian legend, the goddess Pele first inhabited Kauai, but then moved southeastward island by island to Kilauea Volcano, where she now resides (Bryan, 1915). The reasoning behind this legend is unknown, but it was probably based in large part on the relative appearance of age of the various volcanoes. Many centuries after this legend originated, J.D. Dana (1849) rendered the first scientific opinion confirming the general age progression implied by the legend.

Dana was not only the first geologist to conclude that the order of extinction of Hawaiian volcanoes was approximately from northwest to southeast, he also recognized that the Hawaiian Chain included the islets, atolls, and banks that stretch for some distance to the northwest of Kauai. Dana saw no reason to think that the volcanoes of the chain did not originate simultaneously: "No facts can be pointed to, which render it even probable that Hawaii is of more recent origin than Kauai" (Dana, 1849, p. 280). Their relative degree of erosion, however, provided ample evidence to indicate their order of extinction: "From Kauai to Mount Loa all may thus have simultaneously commenced their ejections, and have continued in operation during the same epoch till one after another became extinct. Now, the only burning summits out of the thirteen which were once in action from Niihau to Hawaii, are those of Loa and Hualalai: we might say farther that these are all out of a number unknown, which stretched along for fifteen hundred miles, the length of the whole range. This appears to be a correct view of the Hawaiian Islands" (Dana, 1849, p. 280). Subsequent workers agreed with Dana on the general order of extinction (for example, Brigham, 1868; Dutton, 1884; Hillebrand, 1888; Hitchcock, 1911; Cross, 1915; Martin and Pierce, 1915; Wentworth, 1927; Hinds, 1931; Stearns, 1946), although the sequences they proposed invariably differed in detail (table 1.3). Of these various workers only Stearns (1946), who studied the Hawaiian Islands in more detail than any of his predecessors, had the sequence exactly correct as judged by present data.

The idea that the volcanoes of the Hawaiian Chain originated simultaneously and only became extinct progressively seems to have persisted until a few decades ago. Stearns (1946), for example, mentions the lack of evidence to indicate when any of the Hawaiian volcanoes began but shows all of the main shields except Hualalai and Kilauea erupting simultaneously at the end of the Pliocene (Stearns, 1946, p. 97, fig. 25). Two exceptions were Cross (1904) and Wentworth (1927), who thought that the degree of erosion was probably a function of when the volcanoes emerged above the sea as well as of the elapsed time since they ceased to erupt. Cross (1904, p. 518) states: "It appears to me plausible to assume that the earliest eruptions occurred at or near the western limit of this zone (the more than 1000 mile expanse of the island chain), and that in a general way at least, the centers of activity have developed successively farther and farther to the east or southeast, until now the only active loci of eruption are those of Mauna Loa and Kilauea on the island of

TABLE 1.3.—*Early estimates of the order of extinction of the principal Hawaiian volcanoes*

[Criteria used are given beneath each source; volcanoes listed in proposed order of extinction, oldest at top]

Dana (1849) Erosion	Brigham (1868) Erosion	Dana (1888) Erosion	Hillebrand (1888) Floral diversity	Wentworth (1927) Erosion	Hinds (1931) Erosion	Stearns (1946) Erosion and stratigraphy
Kauai	West Kauai, Niihau	Kauai	West Oahu, Kauai	Koolau	Waianae	Kauai
Waianae	Waianae	Waianae	Molokai, East Oahu	Kauai	Koolau	Waianae
West Maui	East Kauai	West Maui	Kohala, West Maui	East Molokai	Niihau	Koolau
Koolau	West Molokai	Kohala	Mauna Kea	West Maui	Kauai	West Molokai
Mauna Kea	West Maui	Koolau	East Maui	Mauna Kea	West Molokai	East Molokai
East Maui	Kohala	East Maui	Hualalai	Waianae	East Molokai	West Maui, Lanai
Mauna Loa	Koolau	Mauna Kea	Mauna Loa, Kilauea	East Maui	Lanai	Kahoolawe
	East Molokai	Hualalai		Lanai	West Maui, Kohala	East Maui
	Mauna Kea	Mauna Loa, Kilauea		Niihau, West Molokai	Kahoolawe	Kohala
	Lanai, Kahoolawe			Kahoolawe	East Maui	Mauna Kea
	East Maui			Kohala	Mauna Kea	Haulalai, Mauna Loa, Kilauea
	Hualalai			Hualalai, Mauna Loa, Kilauea	Hualalai	
	Mauna Loa, Kilauea				Mauna Loa, Kilauea	

Hawaii." He specifically noted the difference between his hypothesis and that of Dana.

Estimates of the geologic ages of the Hawaiian volcanoes varied considerably among those early workers willing to hazard a guess on the basis of the meager data then available. Dana (1849) thought it likely that the eruptions commenced as early as early Carboniferous or Silurian time; this estimate was based on the concept that the Earth had cooled from a molten globe producing fissuring and volcanism, the apparent lack of post-Silurian volcanism in the interior of the North American continent, and the presumption that the oceans would cool after the continents. Cross (1904) speculated that the western part of the leeward islands formed in the early part of the Tertiary. Wentworth (1925, 1927) attempted to quantify erosion rates for several of the islands and estimated the extinction ages of some of the volcanoes as follows:

Lanai	0.15 Ma
Kohala	0.22 Ma
Koolau	1.00 Ma
Kauai	2.09 Ma

On the basis of physiographic evidence, Wentworth doubted that any part of the Hawaiian group emerged above sea level before late Tertiary time. Hinds (1931), like Cross (1904), recognized that the atolls and banks of the leeward islands were the remnants of once-larger volcanoes: "The landscapes of the leeward group—the volcanic stacks, the reef limestone and calcareous sand islands rising from submarine platforms, and submerged platforms from which no islands rise, represent the final stages in the destruction of a volcanic archipelago. Such a fate awaits the windward islands unless they be rejuvenated by volcanic or diastrophic forces" (Hinds, 1931, p. 196). He recognized that the amount of erosion and subsidence required to reduce a mammoth Hawaiian volcano to a coral atoll was probably considerable and concluded: "The complete or nearly complete destruction of the Leeward islands suggests that volcanism ceased there well back in the Tertiary, hence the mountains must have risen above the ocean long before, perhaps even in Mesozoic time" (Hinds, 1931, p. 205). On the basis of geomorphic considerations, Stearns (1946) thought that the volcanoes of the main Hawaiian Islands rose above sea level in the Tertiary.

RADIOMETRIC AND FOSSIL AGES

The first radiometric ages for Hawaiian volcanoes were determined by McDougall (1963), who measured ages of 2.8 to 3.6 Ma for his Middle and Upper Waianae Series on Oahu (all K-Ar ages have been converted to the new constants; Steiger and Jaeger, 1977). He also reported an age of 8.6 Ma for what he called the Mauna Kuwale Trachyte of the Lower Waianae Series(?), an age that later proved to be incorrect, probably because of excess argon in the biotite analyzed (Funkhouser and others, 1968). In subsequent studies McDougall and Tarling (1963) and (primarily) McDougall (1964) reported K-Ar ages of lava from 7 of the principal Hawaiian volcanoes and concluded that the ages of the shield stages were approximately:

Kauai	5.8–3.9 Ma
Waianae	3.5–2.8 Ma
Koolau	2.6–2.3 Ma
West Molokai	1.8 Ma
East Molokai	1.5–1.3 Ma
West Maui	1.3–1.15 Ma
East Maui	0.8 Ma
Hawaii (all 5 volcanoes)	<1 Ma

McDougall thus confirmed Stearns' extinction sequence and also suggested that the main shield stage of a Hawaiian volcano essentially was complete before the next volcano rose above the sea.

Since the pioneering work of McDougall, many additional radiometric ages have been determined for the volcanoes of the main islands, and the dating has been extended to the volcanoes of the

leeward islands, the western Hawaiian Ridge, and the Emperor Seamounts. In total, there are now reasonably precise radiometric age data for 35 of the volcanoes in the Hawaiian-Emperor Chain (see appendix 1.1). Radiometric ages of two volcanoes on the Hawaiian Ridge are not included in appendix 1.1 because it is probable that the samples are not from Hawaiian volcanoes (Clague and Dalrymple, 1975). These include a minimum age of 71 ± 5 Ma for altered basalt from Wentworth Seamount, 80 km northwest of Midway, and an age of 77.6 ± 1.7 Ma for a sample of rhyolite (probably an erratic, see appendix 1.1) dredged from the northern slope of Necker Island.

In addition to the radiometric age data, there are paleontologic ages for several of the Hawaiian-Emperor volcanoes based on material recovered by dredging and drilling programs. In general, these ages postdate volcanic activity and are consistent with the radiometric data. From southeast to northwest they include (1) an age of 28–31 Ma for late Oligocene nannofossils in volcanogenic sediments at DSDP Site 311 on the archipelagic sediment apron of an unnamed seamount (no. 58 of Bargar and Jackson, 1974) 240 km northwest of Midway (Bukry, 1975); (2) an age of 15–32 Ma (East Indies Tertiary stage Te) for larger foraminifers (Cole, 1969) and smaller foraminifers (Todd and Low, 1970) in reef limestone above basalt in a drill hole at Midway Atoll; (3) an age of 39–41 Ma for dredged late Eocene larger foraminifers from Kammu Seamount (Sachs, quoted in Clague and Jarrard, 1973); (4) an age of 50.5 ± 3.5 Ma for early Eocene coccoliths in volcanogenic sediments cored at DSDP Site 308 atop Koko Seamount (Bukry, 1975); (5) an age of 57–59 Ma for late Paleocene calcareous nannofossils (Takayama, 1980) and pelagic foraminifers (Hagn and others, 1980) in sediments above basalt at DSDP Site 430 on Ojin Seamount; (6) late Paleocene planktonic foraminifers and probable early Eocene benthic foraminifers in sediments above basalt at DSDP Site 432 on Nintoku Seamount (Butt, 1980); (7) an age of 59–61 Ma for middle Paleocene calcareous nannofossils in sediments above basalt at DSDP Site 433 on Suiko Seamount (Takayama, 1980); and (8) an age of 70–73 Ma for lower Maestrichtian nannofossils from sediments above basalt at DSDP Site 192 on Meiji Seamount at the northern end of the Emperor Seamounts (Worsley, 1973). None of these fossil ages is in conflict with the radiometric data.

On the other hand, Menard and others (1962) describe Miocene corals and pelagic foraminifers dredged from a submarine terrace 10 km southwest of Oahu. The authors note the difficulty in assigning an age to these samples and state that the "planktonic foraminifera *Globigerinoides quadralobates* [=*G. trilobus auct.*] *plexus* suggest a lower limit of early Miocene. The upper age limit is less definitive" (Menard and others, 1962, p. 896). Present nomenclature would identify these samples as *Globigerinoides triloba*, which ranges in age from early Miocene to Pleistocene (Kenneth and Srinivasan, 1983). Menard and others (1962) cite as additional evidence of the Miocene age of the sample the 60 percent of extinct coral species in the sample. We conclude that none of these criteria unequivocally supports a Miocene age and no conflict exists between the ages of the reef and that of the underlying volcanic basement of 1.8–2.7 Ma.

Two samples of Eocene terrigenous sediment recovered 250 km east of Hawaii and 100 km south of Kauai (Schreiber, 1969) are also anomalous. These samples were probably derived from volcanoes that predate the Hawaiian Chain, or they may have been reworked from sediment on the sea floor during formation of the Hawaiian volcanoes.

The available radiometric data are summarized in table 1.4 and plotted in figure 1.5 as a function of distance measured from Kilauea Volcano along the Hawaiian-Emperor trend. Because some of the volcanoes are unnamed and some seamounts and islands consist of more than one major volcanic edifice, each dated volcanic center is identified in the table with the number assigned to it by Bargar and Jackson (1974). The exceptions are Abbott Seamount, a small volcano between Colahan and Kammu Seamounts, and Kaula Island, which were not previously numbered and to which we have assigned numbers 65A and 15A, respectively.

As can be seen from figure 1.5, the age data confirm the general age progression along the chain as first suggested by Dana (1849) and required by the hot-spot hypothesis of Wilson (1963a), and they show that the progression is continuous from Kilauea at least to Suiko Seamount, more than half way up the Emperor Seamounts Chain and nearly 5,000 km from the active volcanoes of Mauna Loa and Kilauea. The data also substantiate the hypothesis that the Emperor Seamounts are a continuation of the Hawaiian Chain, as proposed by Christofferson (1968) and Morgan (1972a, b).

RATES OF VOLCANIC PROPAGATION

In order to determine accurately the rate of volcanic propagation along the Hawaiian-Emperor Chain, we would like to know the time that each tholeiitic shield volcano first erupted onto the sea floor, but such data clearly are not obtainable. What is available for the dated volcanoes is one or more radiometric age on lava flows erupted during one or more stage of volcanic activity (see appendix 1.1). In order to calculate propagation rates, therefore, it is necessary to adopt some consistent strategy for selecting the numerical age used to represent the age of each dated volcano. Different authors have approached this problem in different ways. McDougall (1971) used the youngest age of tholeiitic basalt as representing the time of cessation of volcanism for each dated volcano in the principal Hawaiian Islands. In contrast, Jackson and others (1972) and Dalrymple and others (1980b, 1981) used the oldest age for tholeiitic volcanism as the best available approximation of the age of the volcanoes. McDougall (1979) and McDougall and Duncan (1980) adopted yet another approach and used the average age of tholeiitic shield volcanism. For table 1.4, we have chosen the oldest reliable ages for tholeiitic volcanism available, but the choice of which ages to use is probably not critical when considering the data for the chain as a whole. The reason is that the existing data on the rate of formation of Hawaiian volcanoes indicate that the tholeiitic shields are probably built up from the sea floor in as little as 0.5–1.5 m.y. (see summary in Jackson and others, 1972). This amount of time is within the analytical uncertainty of the K-Ar ages at about 20 Ma, or less than one-third of the way along the dated

TABLE 1.4.—*Summary of K-Ar geochronology along the Hawaiian-Emperor volcanic chain*

[Volcano number and distance from Bargar and Jackson (1974) and K.E. Bargar (written commun., 1978). Best K-Ar age is oldest reliable age of tholeiitic basalt, where available; all data converted to new constants $\lambda\varepsilon+\lambda\varepsilon' = 0.581\times10^{-10}$/yr, $\lambda\beta = 4.962\times10^{-10}$/yr, $^{40}K/K = 1.167\times10^{-4}$ mol/mol]

Volcano Number	Volcano Name	Distance from Kilauea along trend of chain (km)	Best K-Ar age (Ma)	Data source	Remarks
1	Kilauea	0	0-0.4	--	Historical tholeiitic eruptions
3	Mauna Kea	54	0.375±0.05	1	Samples from tholeiitic shield (Hamakua Volcanics)
5	Kohala	100	0.43±0.02	2	Samples from tholeiitic shield (Pololu Basalt)
6	Haleakala	182	0.75±0.04	3	Samples from tholeiitic shield (Honomanu Basalt)
7	Kahoolawe	185	>1.03±0.18	3	Samples from alkalic postshield stage (upper part of Kanapou Volcanics)
8	West Maui	221	1.32±0.04	4	Samples from tholeiitic shield (Wailuku Basalt)
9	Lanai	226	1.28±0.04	5	Samples from tholeiitic shield (Lanai Basalt)
10	East Molokai	256	1.76±0.07	3	Samples from tholeiitic shield (lower member of East Molokai Volcanics)
11	West Molokai	280	1.90±0.06	3	Samples from tholeiitic shield (lower part of West Molokai Volcanics)
12	Koolau	339	2.6±0.1	4,6	Samples from tholeiitic shield (Koolau Basalt)
13	Waianae	374	3.7±0.1	6	Samples from tholeiitic shield (lower member of Waianae Volcanics)
14	Kauai	519	5.1±0.20	7	Sample from tholeiitic shield (Napali Member of Waimea Canyon Basalt)
15	Niihau	565	4.89±0.11	8	Samples from tholeiitic shield (Paniau Basalt)
15A	Kaula	600	4.0±0.2	21	Phonolite from postshield stage (?)
17	Nihoa	780	7.2±0.3	9	Samples from tholeiitic shield
20	Unnamed	913	9.2±0.8	20	Dredged samples of alkalic basalt
23	Necker	1,058	10.3±0.4	9	Samples from tholeiitic shield
26	La Perouse Pinnacles	1,209	12.0±0.4	9	Samples from tholeiitic shield
27	Brooks Bank	1,256	13.0±0.6	20	Dredged samples of hawaiite and alkalic basalt
30	Gardner Pinnacles	1,435	12.3±1.0	20	Dredged samples of alkalic and tholeiitic basalt
36	Laysan	1,818	19.9±0.3	10	Dredged samples of hawaiite and mugearite
37	Northampton Bank	1,841	26.6±2.7	10	Dredged samples of tholeiitic basalt
50	Pearl and Hermes Reef	2,281	20.6±0.5	11	Dredged samples of phonolite, hawaiite, and alkalic basalt
52	Midway	2,432	27.7±0.6	12	Samples of mugearite and hawaiite from conglomerate overlying tholeiitic basalt in drill hole
57	Unnamed	2,600	28.0±0.4	11	Dredged samples of alkalic basalt
63	Unnamed	2,825	27.4±0.5	11	Dredged samples of alkalic basalt
65	Colahan	3,128	38.6±0.3	13	Dredged samples of alkalic basalt
65A	Abbott	3,280	38.7±0.9	13	Dredged samples of tholeiitic (?) basalt
67	Daikakuji	3,493	42.4±2.3	14	Dredged samples of alkalic basalt
69	Yuryaku	3,520	43.4±1.6	11	Dredged samples of alkalic basalt
72	Kimmei	3,668	39.9±1.2	14	Dredged samples of alkalic basalt
74	Koko (southern)	3,758	48.1±0.8	14,15	Dredged samples of alkalic basalt, trachyte, and phonolite
81	Ojin	4,102	55.2±0.7	16	Samples of hawaiite and tholeiitic basalt from DSDP Site 430
83	Jingu	4,175	55.4±0.9	17	Dredged samples of hawaiite and mugearite
86	Nintoku	4,452	56.2±0.6	16	Samples of alkalic basalt from DSDP Site 432.
90	Suiko (southern)	4,794	59.6±0.6	18,19	Single dredged sample of mugearite
91	Suiko (central)	4,860	64.7±1.1	16	Samples of alkalic and tholeiitic basalt from DSDP Site 433

Data sources:

1. Porter and others (1977)
2. McDougall and Swanson (1972)
3. Naughton and others (1980)
4. McDougall (1964)
5. Bonhommet and others (1977)
6. Doell and Dalrymple (1973)
7. McDougall (1979)
8. G.B. Dalrymple (unpub. data, 1982)
9. Dalrymple and others (1974)
10. Dalrymple and others (1981)
11. Clague and others (1975)
12. Dalrymple and others (1977)
13. Duncan and Clague (1984)
14. Dalrymple and Clague (1976)
15. Clague and Dalrymple (1973)
16. Dalrymple and others (1980a)
17. Dalrymple and Garcia (1980)
18. Saito and Ozima (1975)
19. Saito and Ozima (1977)
20. Garcia and others (1986b)
21. Garcia and others (1986a)

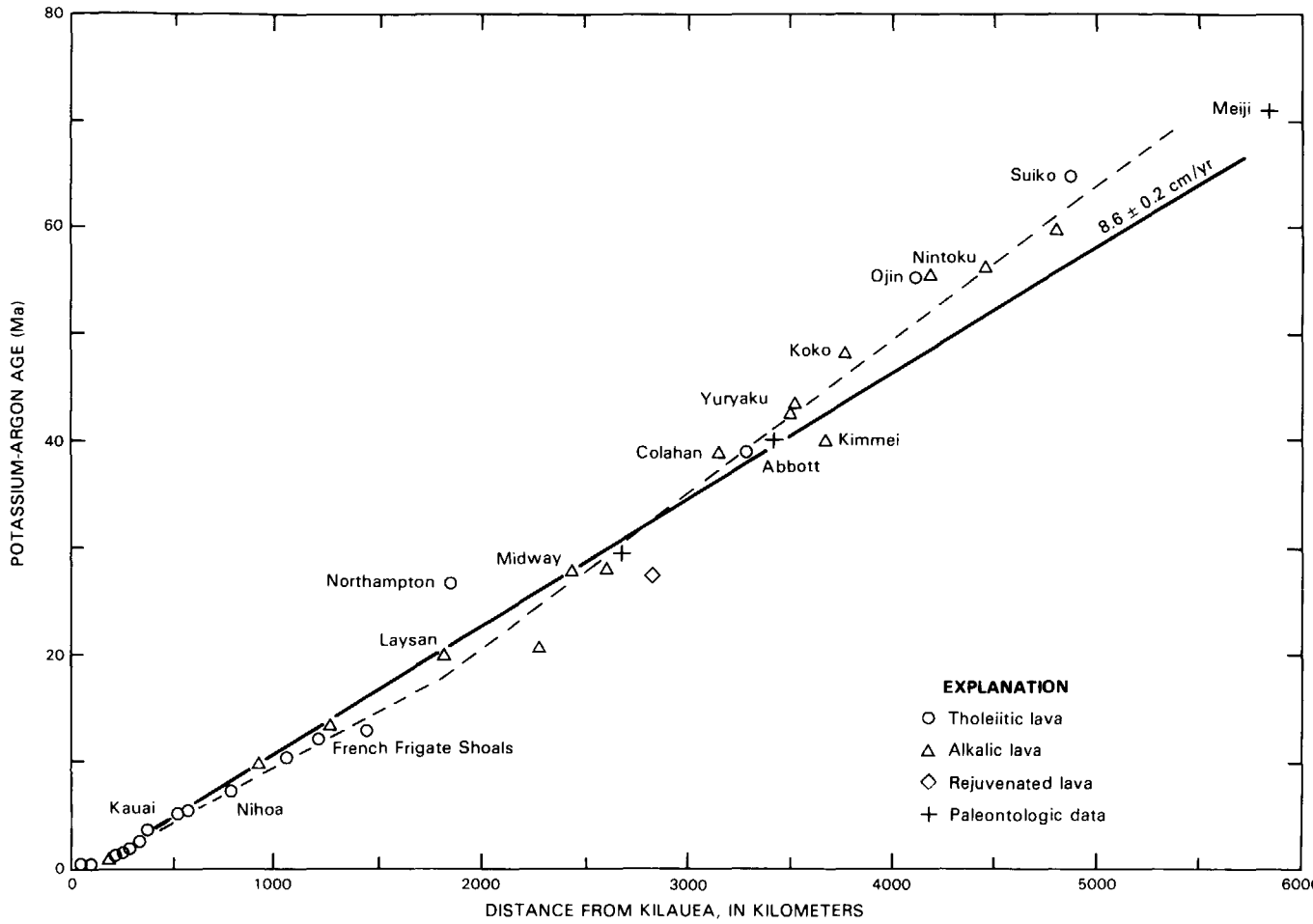

FIGURE 1.5.—Age of volcanoes in Hawaiian-Emperor Chain as a function of distance from Kilauea. Solid line is least-squares cubic fit (York 2) from table 1.5 and represents average rate of propagation of volcanism of 8.6 ± 0.2 cm/yr. Dashed line is two-segment fit using data from Kilauea to Gardner and Laysan to Suiko (table 1.5). Radiometric data from table 1.4, paleontologic data discussed in text.

part of the chain. The question of which ages to use is in any case moot for most of the volcanoes west of Kauai because so few suitable samples have been recovered that there is rarely a choice to make.

A majority of the age data from islands and seamounts west of French Frigates Shoal were obtained on alkalic rocks rather than on tholeiitic basalt. This is because the alkalic rocks, being younger than the tholeiitic basalt, are more likely to be recovered by dredging and drilling and are more resistant to submarine alteration than tholeiitic basalt. This bias toward ages of alkalic lava also probably makes very little difference because the difference between the ages of the postshield alkalic and youngest tholeiitic rocks is only a few hundred thousand years in the Hawaiian Islands (McDougall, 1964, 1969; Funkhouser and others, 1968; McDougall and Swanson, 1972; Doell and Dalrymple, 1973) and, presumably, in the other volcanoes of the Hawaiian-Emperor Chain. For one unnamed volcano on the western Hawaiian Ridge (63 in appendix 1.1 and table 1.4) the only data available are from lava erupted during the alkalic rejuvenated stage. In the principal Hawaiian Islands, lava erupted during the rejuvenated stage may postdate the tholeiitic shield and alkalic postshield stages by more than 4 m.y. (McDougall, 1964; G.B. Dalrymple, unpublished data, 1985), so the main shield of volcano 63 may be several million years older than indicated in table 1.4.

Previously, age-distance data along the Hawaiian-Emperor Chain have been regressed using a simple linear regression of age (dependent variable) on distance (independent variable), either unconstrained (for example, McDougall, 1971, 1979; Jackson and others, 1972; McDougall and Duncan, 1980) or forced through the origin (for example, Dalrymple and others, 1980b, 1981). The resulting volcanic propagation rates for the Hawaiian segment of the chain have ranged from as little as 6 cm/yr (Jackson and others, 1975) to as much as 15 cm/yr (McDougall, 1971; Jackson and others, 1972), although most recent estimates have been between 8 and 10 cm/yr (McDougall, 1979; McDougall and Duncan, 1980;

Dalrymple and others, 1981). Simple linear regression models have the disadvantages that they presume no error in distance and they do not take into account the experimental errors of individual determinations.

We have treated the data in table 1.4 using a two-error cubic fit (York 2), which allows for errors in both age and distance and weights the data accordingly (York, 1969). Errors for the age determinations are straightforward and are either provided in the original references or have been estimated by us from the array of data available on an individual volcano. Jackson and others (1975) estimated the cumulative errors in distance to be about 1.5 km at Kilauea to as much as 20 km near the western end of the Hawaiian Chain. We have interpolated and extrapolated these values to find errors for the distances in table 1.4. The results of both the York 2 regressions and the two simpler regression models for various segments of the Hawaiian-Emperor Chain are given in table 1.5. For the entire chain, the average rate of volcanic propagation is 8.6 ± 0.2 cm/yr with an intersection (that is, theoretical zero time) 89 km northwest of Kilauea using the York 2 regression. The simple regression models yield similar, though slightly lower, values of propagation rate.

Rates of propagation for the Hawaiian segment of the chain, that is, Kilauea through Abbott, have been calculated using both the maximum and minimum ages of tholeiitic volcanism. The results do not vary with model and range from 8.6 to 9.2 cm/yr. For comparison, we have included comparable calculations using the average ages of McDougall (1979). The resulting rates are somewhat higher than the rates calculated from either the maximum or

TABLE 1.5.—*Rates of propagation of volcanism along segments of the Hawaiian-Emperor Chain for several linear-regression models*

[Rates are in centimeters per year. Intercept, in kilometers, and correlation coefficient, r, given in parentheses where relevant. Simple regression is of age on distance, unweighted data; York 2 fit is two-error cubic, weighted data]

Chain segment	Data source	Simple regression		York 2 fit
		Unconstructed	Forced through origin	
Hawaiian-Emperor ---	table 1.4	7.8±0.2 (175, 0.992)	8.2±0.1	8.6±0.2 (89)
Hawaiian ----------	table 1.4 (maximum ages)	8.6±0.3 (102, 0.985)	9.1±0.2	9.2±0.3 (80)
	McDougall, 1979 (average ages)	9.4±0.3 (91, 0.994)	9.9±0.2	11.3±0.1 (3)
	appendix 1.1 (minimum ages)	8.6±0.3 (119, 0.986)	9.1±0.2	9.1±0.3 (97)
Emperor ----------	table 1.4	6.5±0.8	7.9±0.2	7.2±1.1
Kilauea to Gardner -	table 1.4	9.9±0.3 (57, 0.992)	10.6±0.3	9.6±0.4 (73)
Laysan to Suiko ----	table 1.4	6.9±0.4 (0.971)	8.1±0.2	6.8±0.3
Gardner to Waianae -	table 1.4	9.5±0.4 (54, 0.993)	10.1±0.2	10.1±0.8 (9)

minimum data, but the difference is largely a consequence of differences in the data sets, the ones in table 1.4 and appendix 1.1 being more current.

Rates calculated for the Emperor Chain, that is, Daikakuji through Suiko, are markedly lower than for the Hawaiian Chain, ranging from 6.5 to 7.2 cm/yr when not forced through the origin. Separate rates for these two major segments of the chain are only meaningful, however, if there was a rate change at the time of formation of the bend. This hypothesis can be tested by using the linear equations found from the York 2 regressions to predict the age of the bend, which we estimate to be 3,451 km from Kilauea at the position of volcano 68. The predicted ages for the bend are 36.7 Ma and and 43.0 Ma for the Hawaiian and Emperor segments, respectively. The Hawaiian prediction, which is similar to the value of 37.8 Ma found by McDougall (1979), differs significantly from the measured bend age of 43.1 ± 1.4 Ma as determined from the ages of Daikakuji and Yuryaku Seamounts. This suggests that if there was a significant change in volcanic propagation rate it did not occur at bend time, but some time after, a conclusion also reached by Epp (1978).

For some time, it has been apparent to us that a change in rate near or before the time of formation of Midway is consistent with the available data (Dalrymple and others, 1980b). For example, the fits of the data for the chain segments Kilauea-Gardner and Laysan-Suiko are slightly better than the fits for the Hawaiian and Emperor segments (table 1.5; fig. 1.5). The two former lines intersect near Gardner Pinnacles at an age of about 18 Ma. Epp (1978) concluded that a rate change occurred around 20–25 Ma. We have tried various ways to determine the most likely time for a change in the rate of volcanic propagation, including correlation with eruption volumes along the chain (see section below on eruption rates) and age-predictive models for the central parts of the chain, but we are not convinced that the results are meaningful. We can only conclude that the data imply, but do not require, a change of rate sometime after the formation of the Hawaiian-Emperor bend and before or near the time of formation of Laysan Volcano.

In addition to the possibility of a major change in the volcanic propagation rate, as discussed above, there are also indications of short-term departures from linearity. Short-term changes in the volcanic propagation rate were first proposed by Jackson and others (1972) to explain the apparent acceleration of propagation during the past 5 m.y. or so. They did not suggest that short-term variations in propagation rate reflected variations in relative motion of hot spot and plate. Shaw (1973) and Walcott (1976) proposed thermal feedback mechanisms to account for such variations without varying the relative rate of motion between the hot spot and the Pacific plate (see section below on models). Nonlinear models have been disputed by McDougall (1979) and McDougall and Duncan (1980), who argue that linear regressions fit the Hawaiian data so well that no other model needs to be considered.

It seems obvious to us from the geometry alone, however, that the volcanic propagation rates must be nonlinear in detail. If this were not so, then either the volcanism would have formed a ridge rather than individual volcanoes, or the volcanoes in the chain would be spaced in proportion to their ages along a single line. Neither is the case; the volcanoes are irregularly spaced within a band some 200–300 km wide, indicating clearly that volcanic propagation is irregular.

Although some of the irregularities in the age-distance data no doubt reflect dating errors and differences in the stage of volcanism sampled, some of the deviations appear to be larger than can reasonably be attributed to these causes. For example, the ages of Laysan and Northampton Bank should differ by only about 0.3 m.y. rather than the 6.7 m.y. indicated by their measured ages. A similar discrepancy occurs in the ages of volcanoes near the bend (table 1.4; fig. 1.5). There are also volcanoes in the chain that appear to have been active simultaneously even though they were separated by distances of hundreds of kilometers. Examples include Laysan, and Pearl and Hermes, as well as Midway and Northampton. Indeed, Mauna Loa, Kilauea, and Loihi are currently active, erupting tholeiitic basalt, and are separated by more than 80 km.

The primary reason that Jackson and others (1972) suggested short-term nonlinearities in propagation rates was the pronounced curvature in the age-distance data from the volcanoes of the principal Hawaiian Islands. When plotted as a function of distance from Kilauea, the ages for these volcanoes clearly indicate an acceleration of volcanic propagation over the past 5 m.y. (Jackson and others, 1972). This curvature is also one reason that virtually all regressions intersect the distance axis northwest of Kilauea (table 1.5) and predict a negative age for that volcano. McDougall (1979) has argued that the curvature is caused by a bias toward young ages for the less eroded volcanoes, but this cannot be so. Even though Kohala Mountain is relatively uneroded, it is deeply incised on the windward side by several canyons whose floors are near sea level, and it is unlikely that further erosion will expose lava significantly older than is now exposed. In addition, the rapid subsidence of Hawaii (Moore, 1970) may carry the oldest subaerial lava flows below sea level before they can be exposed by erosion. Similar arguments can be made for West Maui, Lanai, Kahoolawe, East Molokai, and Koolau Volcanoes, where lava deep within the subaerial part of the tholeiitic shield has been exposed by marine or stream erosion or by faulting.

We have plotted the known age range for tholeiitic shield, alkalic postshield, and alkalic rejuvenated-stage volcanism for the principal Hawaiian volcanoes in figure 1.6, from which the acceleration of volcanic propagation over the past 3–5 m.y. is evident. It is also clear from this figure that the curvature in the age-distance data is not a function of which eruption stage, tholeiitic shield or alkalic postshield, is chosen to represent the age of the volcanoes. Furthermore, a bias toward younger ages for the less eroded volcanoes, taken to include Kilauea through Haleakala, cannot produce the curvature because older ages for these volcanoes would exaggerate, not lessen, the apparent acceleration. Thus, the acceleration of volcanic propagation in the principal islands, as proposed by Jackson and others (1972), appears to us to be real.

While the overall rate of propagation of volcanism along the chain (or at least major segments of it) may be linear and reflect the relative motion between the Pacific plate and the Hawaiian hot spot, there also appears to be ample justification for retaining nonlinear

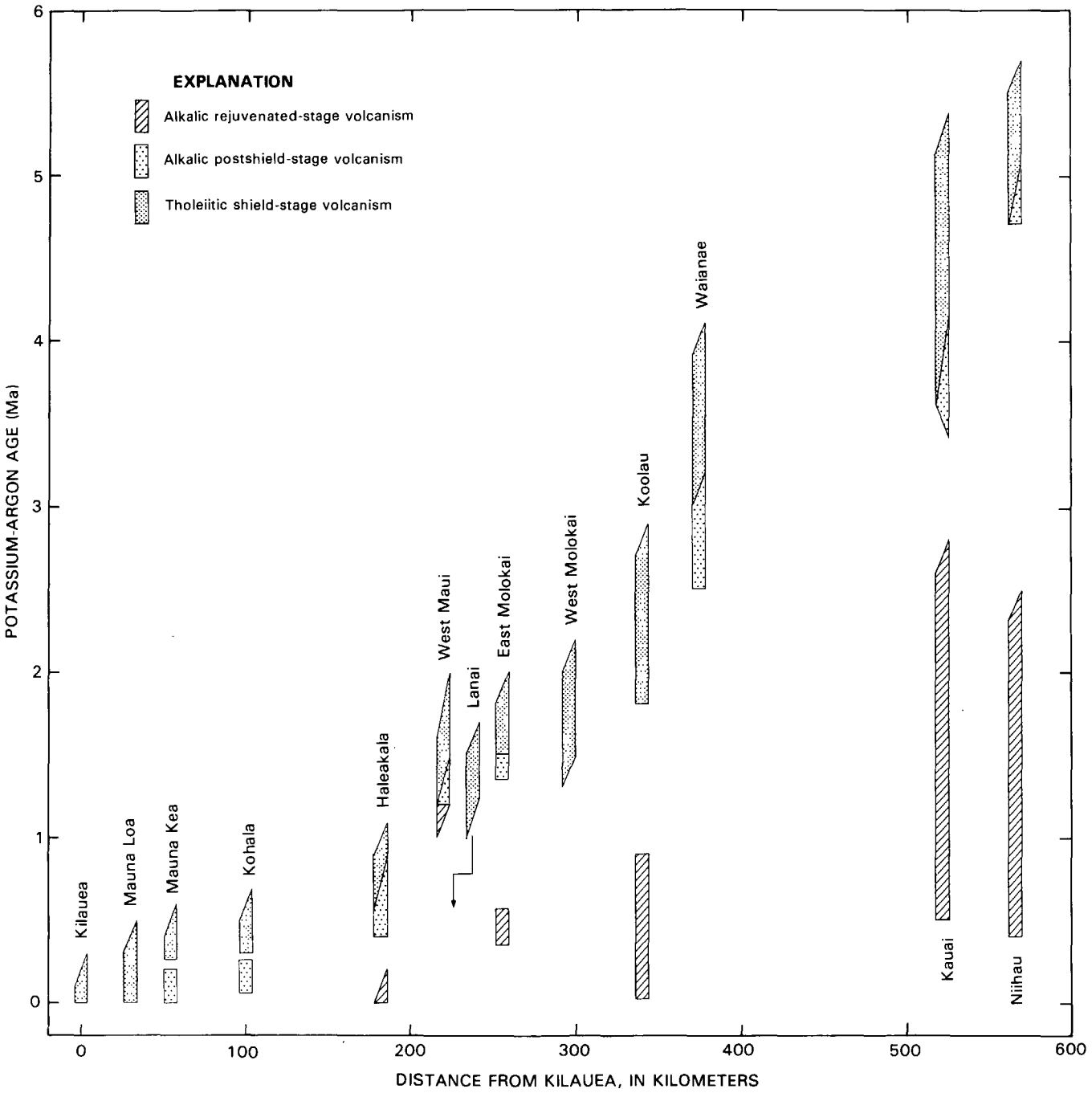

FIGURE 1.6.—Known durations of tholeiitic shield, alkalic postshield, and alkalic rejuvenated-stage volcanism for dated volcanoes of principal Hawaiian Islands. Angled lines indicate overlapping or uncertain ages or overlapping volcanism. Data from sources discussed in appendix 1.1. Data for Niihau and for Kauai (Koloa Volcanics) are from G.B. Dalrymple (unpublished data, 1985).

propagation on a small scale as a working hypothesis. It is unlikely that the cause of this nonlinear propagation, if real, will be known until more is learned about the hot-spot mechanism.

ERUPTION RATES ALONG THE CHAIN

The bathymetry of the chain as a whole is not well known, particularly for the western Hawaiian Ridge, and the 1970 charts for the North Pacific (Chase and others, 1970) and their 1973 derivative (Chase and others, 1973) are probably still the best published sources available. An updated bathymetric chart for the Emperor Seamounts (Clague and others, 1980) was based on the data used by Chase and others (1970) and additional geophysical profiles collected between 1970 and 1979; recently published bathymetry for much of the central part of the Emperor Seamounts (Smoot, 1982) is based on previously classified Navy multibeam

data. The gross structure of the Emperor Seamounts is little changed in the later charts, but the shapes and locations of some individual volcanoes changed dramatically (fig. 1.7).

Bargar and Jackson (1974) compiled volume data along the chain and identified individual volcanic centers and their rift systems using the bathymetry of Chase and others (1970). From the more accurate multibeam data it is clear that many of the volcanic centers and rift zones identified by Bargar and Jackson are incorrect in detail. Because the number and general sizes of the volcanoes change little on the later charts, we have used Bargar and Jackson's volume estimates rather than engage in the laborious process of calculating new ones from the newer data. We suspect that the volumes based on multibeam data would vary relatively little from those of Bargar and Jackson.

The cumulative volume of the volcanoes is plotted in figure 1.8 against distance from Kilauea beginning at Tenchi Seamount, 500 km north of Suiko. It is clear that the volume of eruptive products per unit distance along the chain has not been constant over the past 70 million years.

We have calculated dV/dx, where V is volume and x is distance, for segments of the chain, which are summarized in table 1.6. Also listed are dx/dt, where t is time, calculated from the age relations along the chain, and the derived quantity dV/dt for segments along the chain. These calculations clearly show that the volumes erupted per unit distance along the chain and per unit time increase from the Emperor Seamounts to the Hawaiian Ridge and to the Hawaiian Islands. The present-day eruption rate for Kilauea alone, when compared to eruption rates along the Hawaiian Ridge and Emperor Seamounts, demonstrates that the Hawaiian hot spot is presently producing large volumes of lava at the greatest eruption rates in its known history. The average eruption rate from Hualalai to Kilauea is 5 times that for the islands as a whole and nearly 22 times the rate for the entire chain. The only section of the chain where volumes do not increase toward the present is the westernmost section of the Hawaiian Ridge, which formed immediately following the change in plate motion recorded as the Hawaiian-Emperor bend. This change in plate motion was followed by a virtual cessation of volcanic activity that lasted for nearly 10 m.y.

PETROLOGY OF THE HAWAIIAN-EMPEROR VOLCANIC CHAIN

EARLY WORK: LAVA SERIES AND DIFFERENTIATES

Early observers of Hawaiian eruptions rather uniformly agreed that the lava originated "in the bowels of the earth." As time progressed this view was expanded upon, but it was not until the 1950's and 1960's that the lava source and the processes generating the various lava types were discussed in detail. S. Powers (1920) proposed that nepheline basalt and trachyte were formed by differentiation of basaltic magma because of their occurrence late in the eruptive sequence. He wrote (S. Powers, 1920, p. 280): "Each volcano has arisen at an intersection in a fracture system in the earth's crust, has been fed from the same primal source, and has finally lost connection with that source. When this takes place differentiation may proceed in the magma chambers of large volcanoes and the extreme products of Hawaiian volcanism, nepheline basalt and trachyte, may appear either at the close of the main volcanism or in a later phase after extensive erosion."

This viewpoint, that there was a single primary Hawaiian magma from which the varieties of lava evolved by means of differentiation, was popular well into the 1960's. H. Powers (1935) expressed a similar view, although he showed that fractional crystallization alone could not explain the differentiation of Hawaiian basalt. Macdonald (1949) proposed that the sole primary Hawaiian lava was olivine basalt, although his calculated average included both alkalic and tholeiitic olivine basalt analyses (which he did not distinguish at that time). He also proposed that andesine andesite (hawaiite), oligoclase andesite (mugearite), and trachyte were successive differentiates from an olivine basalt parental lava. This view is now known to be incorrect because Macdonald's calculated olivine basalt was basically a tholeiitic basalt in composition. He further inferred that picritic basalt of the oceanite type (here termed picritic tholeiitic basalt) formed by the accumulation of olivine and that ankaramite was not an oceanite that simply accumulated clinopyroxene. This last idea is correct, ankaramite being alkalic in composition whereas picritic basalt of the oceanite type is tholeiitic. In order to differentiate ankaramite and nepheline basalt from the parental olivine basalt, Macdonald (1949) proposed that limestone assimilation and selective remelting (wall-rock assimilation) were important processes. He correctly inferred that the dunite xenoliths so common in alkalic lava from the postshield and rejuvenated stages formed by accumulation of olivine followed by recrystallization.

Tilley (1950) recognized that the bulk of the primitive shields was made of tholeiitic basalt and that alkalic rocks erupted only during the declining stages of activity. He proposed that alkalic olivine basalt was derived from tholeiitic basalt by crystal fractionation. H. Powers (1935) had, however, earlier noted that primitive lava was silica saturated, whereas the late differentiated lava was silica undersaturated; he argued that these lavas could therefore not be simply related to one another by crystal fractionation.

New concepts important to understanding the origin of Hawaiian lava were introduced by H. Powers (1955). He clearly established that the abundant rocks termed olivine basalt in the shields are silica saturated and noted that they are compositionally distinct for individual volcanoes. He proposed the concept of magma batches to account for the subtle differences between the lava of different shields. He also reiterated that olivine basalt erupted during the declining stages of activity is silica undersaturated. His discussion of fractionation trends for tholeiitic and alkalic basalt is nearly identical to present-day views. He further recognized that earthquakes associated with volcanic activity gave a minimum depth of magma generation which he took to be 48–56 km (30–35 miles). His estimates of the source rocks that could be melted to produce basalt and of the causes of melting provided a framework for experimental research for many years. In particular, he noted that basalt could be generated at depth by wholesale melting of rocks of basaltic composition or by partial melting of peridotite. The models of melting he considered all assumed that it was caused by an increase in temperature. He dismissed exothermic nuclear processes

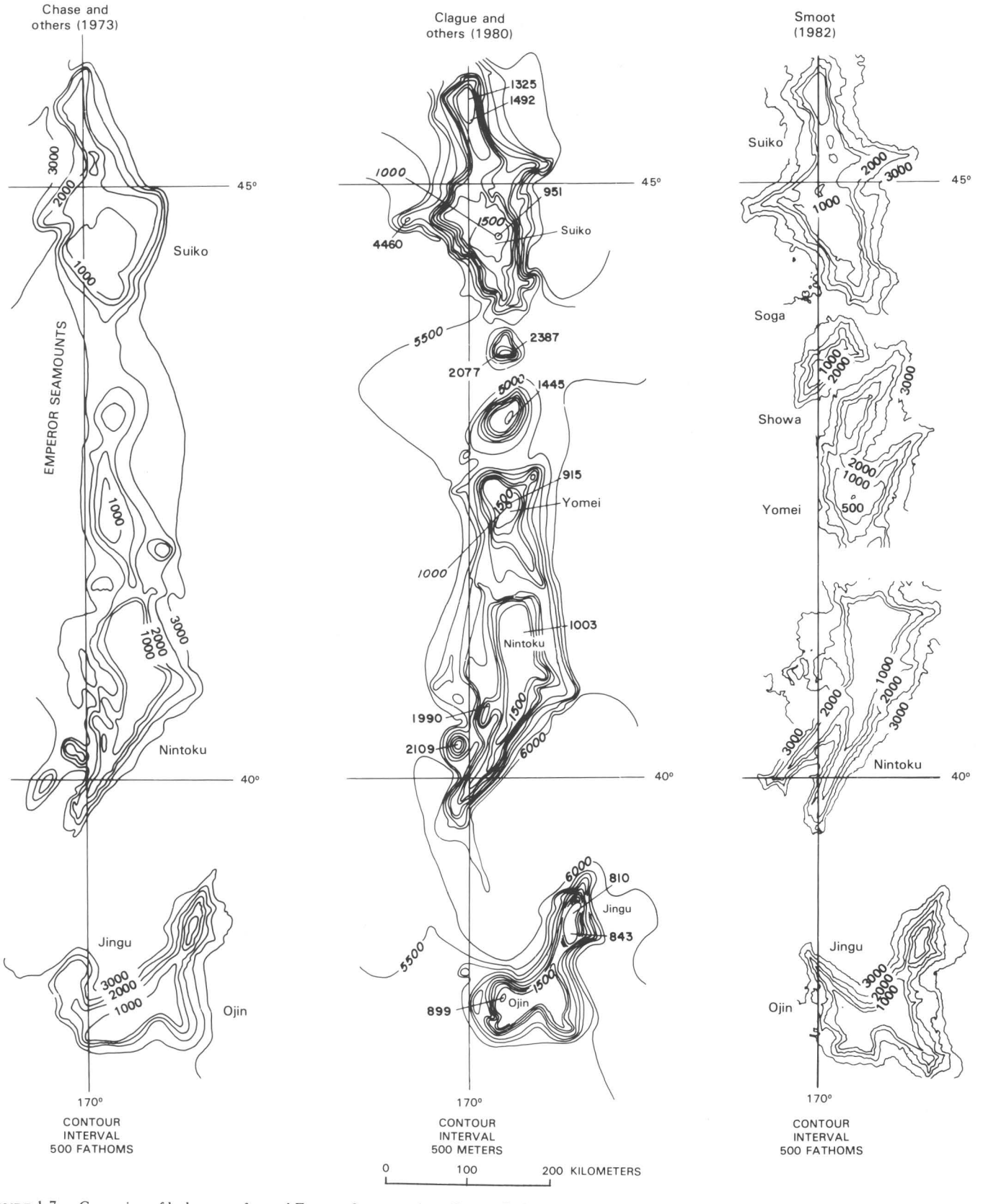

FIGURE 1.7.—Comparison of bathymetry of central Emperor Seamounts from Chase and others (1973; left), Clague and others (1980b; center) and Smoot (1982; right). General size and shape of seamounts were fairly well mapped by bathymetric sounding (left and center), but multibeam bathymetry (right) adds wealth of detail. Contour intervals are 500 fathoms for left and right figures and 500 m for center figure.

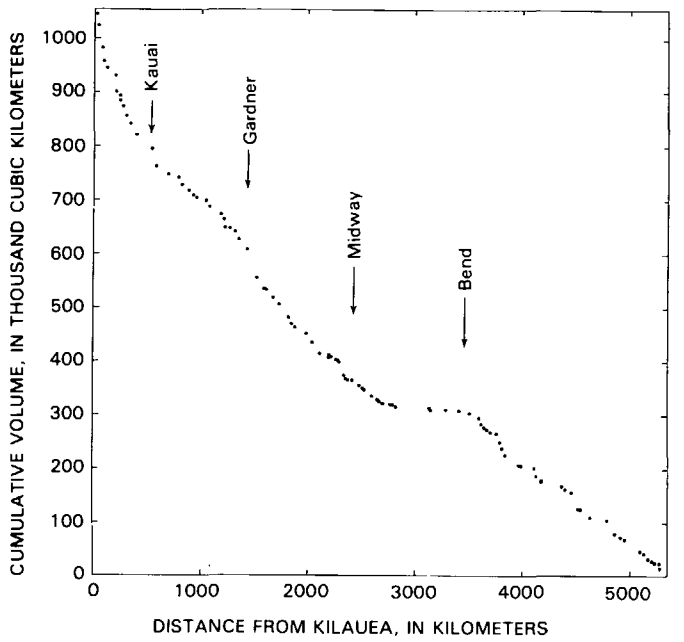

FIGURE 1.8.—Cumulative volcanic volume along Hawaiian-Emperor Chain plotted as a function of distance from Kilauea (along trend of chain). Average volume increment rate (dV/dx) for Emperor Chain is 0.16×10^3 km^3/km. Just east (left) of the bend there is a segment of very low volcanic productivity, in which only 0.02×10^3 km^3/km was erupted. Remainder of submarine portion of the Hawaiian Chain has an average dV/dx of 0.20×10^3 km^3/km. In Hawaiian Islands section from Kauai to Haleakala can be fit by 0.40×10^3 km^3/km and that from Haleakala to Kilauea by 1.1×10^3 km^3/km.

in the crust because Hawaiian lava is not enriched in U, Th, or K. He emphasized convection from hotter regions deep in the mantle and friction produced by dynamic processes (he proposed tides). His convection model is very similar to later plume models and his friction model to at least a part of later thermal-feedback models, both of which are discussed more thoroughly later in this paper.

Kuno and others (1957) clearly demonstrated that closed-system crystal fractionation of tholeiitic basalt led to generation of granophyre in the differentiation of thick lava bodies. They related picritic tholeiitic basalt, olivine tholeiitic basalt, tholeiitic basalt, and granophyre as one differentiation sequence and alkali olivine basalt, picrite basalt of ankaramite type (here called ankaramite), hawaiite, mugearite, and trachyte as another differentiation sequence. They presented trace-element data, which they used to evaluate the proposed fractionation trends. Most importantly, they dismissed any fractionation relation between tholeiitic and alkalic basalt and proposed that they originated independently "through melting of the earth's material under different sets of physical conditions" (Kuno and others, 1957, p. 214). They argued that both lava types were generated by partial melting of peridotite, but that alkalic basalt was derived at greater depth. Their discussion implies that the source rocks were homogeneous and that only the physical conditions of melting varied. In addition, the alkali-silica diagram, widely used to distinguish between tholeiitic and alkalic lava, was first presented in this paper.

Eaton and Murata (1960) published a detailed study locating earthquake epicenters as deep as 60 km beneath Kilauea using basically the same data cited by Powers (1955). These observations establish a minimum depth of magma generation for tholeiitic shield lava of greater than 60 km, although they still allow for selective melting (wall-rock reaction) at shallower depths (Macdonald, 1968).

Macdonald and Katsura (1962, 1964) established the tholeiitic character of the early lava on Kohala and West Maui, where the known late-stage lava is alkalic. They also demonstrated that the subtle variations in composition of the tholeiitic basalt from different volcanoes were unrelated to the type of alkalic cap that followed (Kohala or Haleakala type). In contrast to the interpretations of Tilley (1950), H. Powers (1955), and Kuno and others (1957), Macdonald and Katsura (1964) proposed that alkalic basalt formed by differentiation of tholeiitic basalt. They cited as evidence the interbedded sequence of tholeiitic and alkalic flows, including some of transitional composition, that occur in Haleakala-

TABLE 1.6.—*Eruptive rates along the Hawaiian-Emperor Chain*

[Volume/distance data from figure 1.8; propagation rate data from table 1.5, except for Kilauea to Hualalai; recent data for Kilauea from Dzurisin and others (1984), based on combined eruption-intrusion rate]

Segment	Volume/distance, dV/dx (10^3 km^3/km)	Propagation rate, dx/dt (km/m.y.)	Eruption rate dV/dt (10^3 km^3/m.y.)
Kilauea (1956-1983)	---	---	86
Kilauea to Hualalai	1,500	250	290
Hualalai to Waianae	400	101	40
Hawaiian Islands (0-5.5 Ma)	---	---	56
Waianae to Gardner Pinnacles	190	101	19
Gardner Pinnacles to volcano 57	200	68	14
Volcano 57 to Hawaiian-Emperor bend	20	68	1
Emperor Seamounts	160	72	12
Average for entire chain	---	---	13

type volcanoes between the tholeiitic shield lava and the later alkalic postshield-stage lava and proposed that volatile transfer might be an important differentiation process. They discussed thoroughly the fractionation sequences of both alkalic and tholeiitic lava and related the Mauna Kuwale rhyodacite to tholeiitic lava of the Waianae Range.

The years 1964–68 produced new insights from a variety of studies. The first isotopic data from Hawaiian lava (Lessing and Catanzaro, 1964; Hamilton, 1965; Powell and DeLong, 1966; Tatsumoto, 1966) clearly demonstrated that the source rocks for Hawaiian lava were heterogeneous. Experimental studies at high pressure and temperature (for example, O'Hara, 1965; Green and Ringwood, 1967) added new data bearing on the mineralogy of potential source rocks and the physical conditions of melting. At the same time, trace-element data began to be used to evaluate Hawaiian petrogenetic processes (Schilling and Winchester, 1966; Gast, 1968). Studies of Hawaiian xenoliths (White, 1966) added to the abundant new data being used to evaluate the petrogenesis of Hawaiian lava and the nature of the source rocks. This period marks a transition from relatively qualitative models of petrogenesis to modern quantitive modeling and testing of basalt petrogenesis. To a great degree present day petrogenic models are based on these same types of data and similar quantitative modeling techniques. However, because modern isotopic and trace-element data are more accurate and precise, the models proposed are more refined and complex.

Macdonald (1968) followed Green and Ringwood (1967) and proposed that the tholeiitic, alkalic, and nephelinitic lava types were derived from a single parent magma of olivine tholeiitic basalt composition. He proposed that the compositional variations reflect the depth at which fractional crystallization occurred with tholeiitic basalt fractionated at shallow depths, alkalic basalt at moderate depths, and nephelinitic lava at depths of several tens of kilometers. He further argued that the primary magma is olivine tholeiitic basalt rather than tholeiitic basalt because most lava has lost olivine, which accumulated within the magma chambers to form the high-density masses discovered by gravity surveys (summary and references in Jackson and others, 1972). Macdonald (1968) noted that the highest temperature lava from the Kilauea Iki eruption contained 27–30 percent olivine and proposed that this closely approximated primary magma. Wright (1973) calculated the bulk composition of the same eruption and proposed it as a representative parental (but not necessarily primary) composition for Kilauea tholeiitic basalt. Macdonald (1968) presented quantitative models showing that ankaramite is alkalic basalt plus olivine and clinopyroxene and that hawaiite is alkalic basalt minus olivine, clinopyroxene, plagioclase, and magnetite. This type of mass-balance approach was later refined by Wright (1971) and Wright and Fiske (1971) to demonstrate the roles of fractionation and hybridization in generating basalt at Kilauea and Mauna Loa. The debate about whether primary tholeiitic magma is olivine rich or olivine poor continues today (see Wright and Helz, chapter 23; Wright, 1984; Budahn and Schmitt, 1984). Extreme compositions are liquids with 20 percent MgO (Wright, 1984) and average tholeiitic basalt with 9 percent MgO (Powers, 1955).

Macdonald (1968) also calculated average compositions of Hawaiian lava from the different eruptive stages. His average compositions, recalculated on a dry-reduced normalized basis, are presented in table 1.7. These averages clearly show that lava of the tholeiitic shield stage is silica saturated and that of alkalic postshield and rejuvenated stages is silica undersaturated. The presence of normative hypersthene in the mugearite, benmoreite, and trachyte, which are derived from undersaturated alkalic basalt, reflects fractionation of Fe-Ti oxides, which enriches the residual melt in silica. Rejuvenated-stage alkalic basalt contains greater than 5 percent normative nepheline, and average nephelinite and nepheline melilitite contain normative leucite. Alkalic basalt of the preshield and rejuvenated stages are similar in composition. The preshield Loihi Seamount averages are calculated from Moore and others (1982), Frey and Clague (1983), and D.A. Clague (unpub. data, 1985).

XENOLITH DISTRIBUTIONS

In a detailed analysis of the xenolith populations in Hawaiian lava, Jackson (1968) subdivided the xenoliths into dikes and sills, cumulates, and metamorphic rocks. His breakdown of the relative abundances and types of xenoliths is given in table 1.8, modified to include xenoliths found in Loihi Seamount alkalic preshield lava. Jackson noted that only those xenoliths with metamorphic textures could represent either mantle source rocks or mantle residua left after partial melting. The dikes, sills, and some, but not all, of the cumulate rocks are cognate or from shallow depths. The cumulate xenoliths from Hualalai Volcano appear to come from a variety of sources, including cumulates formed as part of oceanic crustal layer 3, cumulates of tholeiitic Hawaiian shield lava, and cumulates of lava from the alkalic postshield stage (D.A. Clague, unpub. data, 1985). The single cumulate xenolith from Loihi Seamount presumably represents a cumulate of ocean crustal layer 3.

Jackson and Wright (1971) proposed that the abundant dunite xenoliths in the Honolulu Volcanics represent residue left after melting the mantle to form Koolau shield tholeiite, an interpretation with which we disagree. Jackson and Wright (1971) inferred that the garnet lherzolite and lherzolite found only in alkalic lava from the rejuvenated stage were potential mantle source rocks. The difference in xenolith populations for the three alkalic eruptive stages is striking since only the lava from the preshield stage and rejuvenated stage contain xenoliths that formed at depths greater than about 20 km. Although it would be useful if these xenolith populations reflected the mantle through which the lava ascends, it seems more likely that they reflect the development of shallow magma storage reservoirs, which act as hydraulic filters and remove xenoliths carried up from greater depths in much the same way as lakes remove sediment from rivers.

Lava stored in a shallow magma reservoir, either within a few kilometers of the surface or at the base of the oceanic crust, lose any xenoliths they may have acquired during ascent and from this point can only entrain xenoliths that occur at shallower levels in the volcanic system. However, lava of the preshield and rejuvenated stages erupts in small volumes at infrequent intervals and probably no shallow magma storage reservoirs exist. During the shield stage, tholeiitic lava erupts in large volumes at frequent intervals from a

TABLE 1.7.—*Average compositions and norms of major Hawaiian lava types*

[All figures in weight percent; -- not present. Normative components calculated with original FeO/Fe_2O_3 ratios. See Macdonald (1968) for remainder of norms for all but the alkalic preshield stage. Data for alkalic preshield stage from Frey and Clague (1983) and D.A. Clague (unpub. data, 1985)]

Stage	Alkalic preshield				Tholeiitic shield		Alkalic postshield						Alkalic rejuvenated			
Lava type	Tholeiite and olivine tholeiitic basalt	Transitional basalt	Alkalic basalt	Basanite	Picritic tholeiitic basalt	Tholeiitic and olivine tholeiitic basalt	Ankaramite	Alkalic basalt	Hawaiite	Mugearite	Benmoreite	Trachyte	Alkalic basalt	Basanite	Nephelinite	Melilitite
Chemical composition																
SiO_2 ------	48.4	48.3	45.6	43.5	46.7	50.0	44.6	45.9	48.6	52.1	58.3	62.8	45.2	44.6	40.6	37.8
Al_2O_3 -----	12.2	13.6	11.6	11.1	8.5	14.1	12.2	14.9	16.1	17.1	18.0	18.3	12.8	12.8	11.6	11.2
FeO* ------	12.0	12.3	12.4	13.6	12.1	11.3	12.6	13.0	12.2	10.0	7.5	4.5	12.4	12.5	13.3	14.6
MgO -------	11.2	7.5	13.5	12.2	20.9	8.5	13.1	7.9	4.9	3.3	1.6	.4	11.5	11.3	12.4	13.0
CaO -------	11.0	11.4	10.4	11.4	7.4	10.4	11.6	10.6	8.1	6.2	3.6	1.2	11.5	10.7	13.1	14.1
Na_2O ------	2.1	2.7	2.5	3.2	1.6	2.2	1.9	3.0	4.3	5.5	6.0	7.5	2.7	3.6	3.9	4.2
K_2O -------	.4	.7	.8	1.3	.3	.4	.7	1.0	1.5	2.1	2.9	4.3	.9	1.0	1.2	1.0
TiO_2 ------	2.3	3.1	2.7	3.1	2.0	2.5	2.7	3.0	3.4	2.4	1.2	.5	2.3	2.6	2.9	2.9
P_2O_5 ------	.2	.3	.3	.5	.2	.3	.3	.4	.7	1.1	.7	.2	.5	.5	.9	1.1
MnO -------	.2	.2	.2	.2	.2	.2	.2	.2	.2	0.2	.2	.2	.2	.2	.2	.1
Normative composition																
Q --------	--	--	--	--	--	2.2	--	--	--	--	--	--	--	--	--	--
Ne --------	--	--	2.7	11.8	--	--	2.6	2.6	0.3	--	--	--	6.0	10.5	17.3	18.7
Lc --------	--	--	--	--	--	--	--	--	--	--	--	--	--	--	5.7	4.8
Hy --------	14.3	6.3	--	--	15.9	21.5	--	--	--	2.7	4.0	.4	--	--	--	--
Ol --------	10.5	5.9	23.1	17.7	29.5	--	22.2	13.2	6.7	2.1	--	--	19.3	17.9	14.9	20.2

shallow magma storage reservoir and perhaps a deeper staging zone (see review by Decker, chapter 42). During the alkalic postshield stage, lava erupts in small volumes at infrequent intervals, though in larger volumes and at more frequent intervals than during the alkalic preshield or rejuvenated stages. During this stage, lava apparently resides in reservoirs below the base of the oceanic crust (Clague and others, 1981) for time periods sufficient for the dense peridotite xenoliths to settle out. Tholeiitic lava at Kilauea passes through two such filters, one an intermediate-depth (20–30 km) staging area, the second a well-defined and complex shallow reservoir system 3–7 km beneath the surface. After passing through these filters, the lava can only incorporate as xenoliths the wall rocks occurring at depths shallower than the shallowest reservoir (dikes, sills, and olivine cumulates). Alkalic lava of the postshield stage contains abundant xenoliths of dunite, which have CO_2 inclusions that were trapped at depths of at least 15 km, and cumulate xenoliths of rocks from oceanic crustal layer 3 (Roedder, 1965; D.A. Clague, unpub. data, 1985). These observations suggest that in the postshield stage any shallow magma chamber of the shield stage no longer exists but an intermediate staging area at 20–30 km, similar to that beneath Kilauea, acts as an effective filter that removes any lherzolite or garnet peridotite xenoliths. Lava may fractionate in this zone and, upon movement to the surface, entrain xenoliths of ocean crust rocks and cumulates formed in earlier volcanic stages at shallow depth. The presence of xenoliths that originate at great depth in alkalic lava of both the preshield and rejuvenated stages implies that neither shallow nor intermediate staging area acts as an effective filter in these stages. The near-primary character of the host lava also indicates that the lava was not stored at shallow depths but rather moved from its source region to the surface in short time periods (Clague and Frey, 1982).

This analysis leads us back to Jackson's (1968) conclusion that only the xenoliths with metamorphic textures could possibly be mantle source rocks or residua. We conclude that only the lherzolite and garnet peridotite xenoliths represent mantle rocks from below the magma storage zone that appears to have existed beneath Hawaiian shield volcanoes at depths of 20–30 km. The dunite and wehrlite xenoliths are either deformed cumulates formed during

TABLE 1.8.—*Distribution of Hawaiian xenolith types*

[Data from Jackson (1968) except the alkalic preshield stage which is from D.A. Clague (unpub. data, 1985)]

		Xenolith type (percent)		
Eruptive stage	Lava type	Dike rocks and vein fillings	Cumulates	Metamorphic rocks
Alkalic rejuvenated	alkalic basalt basanite nephelinite nepheline melilitite	(<1)	(1) olivine cumulates dominant	(99) dunite ≅ wehrlite ≅ lherzolite> harzburgite, garnet peridotite locally
Alkalic postshield	alkalic basalt	(3) veins dominant	(35) olivine cumulates> pyroxene cumulates	(62) dunite>> wehrlite
	ankaramite	(14) dikes and sills dominant	(53) pyroxene cumulates> olivine cumulates	(33) dunite>> wehrlite
	hawaiite mugeartie trachyte	(14) dikes and sills dominant	(57) pyroxene cumulates> olivine cumulates	(29) dunite>> wehrlite
Tholeiitic shield	tholeiitic basalt	(75) dikes and sills dominant	(25) olivine cumulates dominant	none
Alkalic preshield (Loihi)	alkalic basalt basanite	none	(1) olivine cumulates	(99) dunite>> lherzolite

earlier stages in the volcano's growth or cumulates formed during formation of oceanic crust (see Sen, 1983, 1985; Kurz and others, 1983; Sen and Presnall, 1985).

The remaining xenoliths of spinel lherzolite, rare harzburgite, and rare garnet peridotite that occur in alkalic lava of the rejuvenated stage and even more rarely in alkalic lava of the preshield stage therefore are the only xenoliths of deeper mantle material. Spinel lherzolite xenoliths have many characteristics that imply a close genetic relationship to midocean-ridge basalt; however, both the Sr-isotopic and rare-earth data indicate that these xenoliths have been enriched by mixing between residua left after formation of midocean-ridge basalt and an enriched magma or vapor (Frey 1980, 1984; Wright, 1984; Frey and Roden, in press). These xenoliths probably represent depleted oceanic lithosphere modified by processes related to Hawaiian magmatism.

The final group of xenoliths consists of pyroxenite, websterite, and garnet-bearing pyroxenite and websterite. These occur in only a few vents of the alkalic rejuvenated stage in the Honolulu Volcanics (Jackson and Wright, 1970) and on Kaula Island (Garcia, Frey, and Grooms, in press). These rocks occur both as separate xenoliths and as layers in xenoliths. Some of these xenoliths have been called garnet lherzolite (Jackson and Wright, 1970), but they are not merely a higher pressure assemblage of spinel lherzolite because their bulk compositions are distinct (Jackson and Wright, 1970; Sen, 1983). The iron-rich olivine in all the xenoliths of this group led Sen (1983) to argue that they represent neither source rocks nor residua related to Hawaiian lava. Frey (1980, 1984) has argued that they may represent crystal accumulates from alkaline Hawaiian magma. We conclude that none of the xenoliths found in Hawaiian lava represent mantle source rocks or residua related to Hawaiian volcanism. They do, however, provide insight into the conduit systems through which much of this lava passed.

Jackson and Wright (1970) demonstrated that xenoliths in the Honolulu Volcanics were compositionally zoned in a geographic sense with respect to the Koolau caldera; abundant dunite near the caldera grades into lherzolite and finally garnet-bearing websterite and pyroxenite away from the caldera. Jackson and Wright (1970) combined these observations with experimental petrologic and geophysical data to construct a cross section through the mantle and crust beneath Oahu (fig. 1.9). Their cross section emphasizes the mineralogic and compositional heterogeneity of the mantle beneath Hawaiian volcanoes. However, the origins of many of the rock types are now thought to be different from those proposed by Jackson and Wright (1970). A more recent model by Sen (1983) shows plagioclase lherzolite beneath the oceanic crust to a depth of about 30 km (defined by the limit of plagioclase stability), spinel lherzolite from 30 to nearly 50 km, and garnet lherzolite below about 50 km. The zone beneath the volcanoes includes cumulate dunite to depths

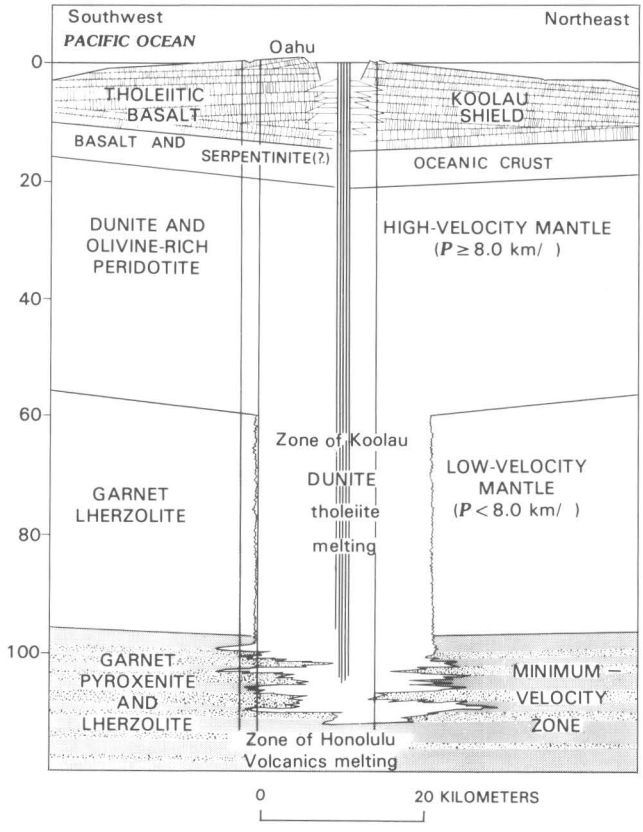

FIGURE 1.9.—Cross section beneath Oahu from Jackson and Wright (1970). Dunite zone inferred to be mantle residue left behind from partial melting that forms Koolau tholeiitic shield lava. Configuration of rock types and their mode of origin are far different from those shown in figure 1.10.

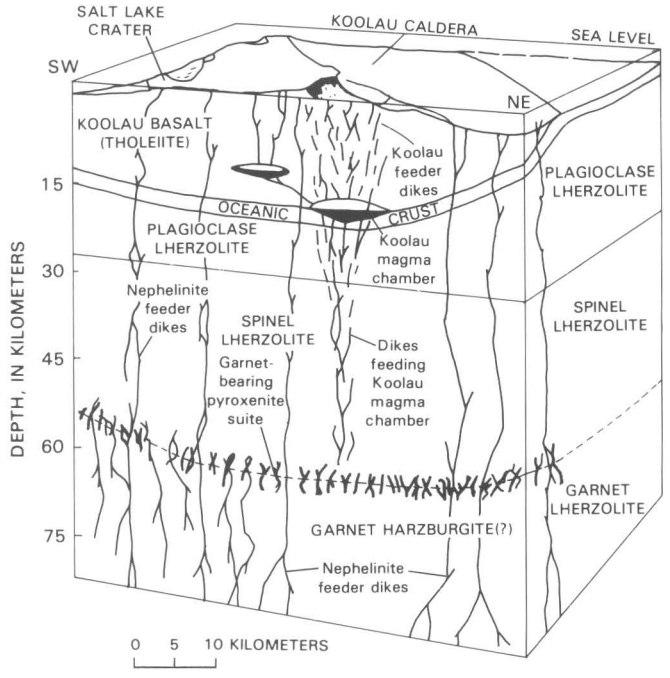

FIGURE 1.10.—Cross section beneath Oahu from Sen (1983) showing configuration of various mantle source and residual rocks brought to surface as xenoliths of abundant dunite, lherzolite, and garnet peridotite by rejuvenated-stage Honolulu Volcanics.

of about 15 km (fig. 1.10). The areal distribution of xenoliths observed by Jackson and Wright (1970) reflects passage of the Honolulu Volcanics lava through the zone of dunite cumulates.

PETROLOGY OF LAVAS ALONG THE VOLCANIC CHAIN

In the middle to late 1970's new studies added data to the already complex data array on Hawaiian volcanoes. Studies on lava recovered from the older submarine portions of the chain (Clague, 1974; Dalrymple and others, 1974, 1977, 1981; Clague and others, 1975; Dalrymple and Clague, 1976; Kirkpatrick and others, 1980; Clague and Frey, 1980; Lanphere and others, 1980; Dalrymple and Garcia, 1980; Garcia, Grooms, and Naughton, in press) clearly demonstrate that the volcanoes of the entire Hawaiian-Emperor volcanic chain erupted tholeiitic basalt and picritic tholeiitic basalt similar to those of the shield stage in the Hawaiian Islands. In addition, alkalic lava similar to that erupted during the postshield stage in the Hawaiian Islands, including hawaiite, mugearite and trachyte, is commonly recovered from the older volcanoes. In the drill holes on Ojin and Suiko, tholeiitic lava occurs below alkalic lava, as in the Hawaiian Islands. Some samples are chemically and mineralogically similar to alkalic rejuvenated-stage lava from the Hawaiian Islands (table 1.2). The identification of which dredged or drilled lava samples erupted during which eruptive stage relies on comparison of the major-element compositions to those of the various Hawaiian lava types (table 1.7) in conjunction with trace-element ratios (Clague and Beeson, 1980; Clague and others, 1980c; Frey and Clague, 1983) and mineral compositions (Keil and others, 1972; Fodor and others, 1975; Clague and others, 1980a). In particular, we have found that the composition of groundmass pyroxene and the K/Ba and P_2O_5/Zr ratios seem to separate alkalic basalt of the postshield and rejuvenated stages. Rejuvenated-stage alkalic basalt has lower K/Ba and higher P_2O_5/Zr ratios and pyroxene with more calcic compositions and higher concentrations of Na, Ti, and Al than postshield-stage alkalic basalt. Lava samples recovered from the volcanoes west of the principal Hawaiian Islands are discussed in appendix 1.1 and summarized in table 1.9.

Several conclusions may be drawn from these studies of samples from along the Hawaiian-Emperor Chain. The first conclusion is that the Hawaiian hot spot has produced very similar lava types in the same eruptive sequence for at least the last 65 m.y. (table 1.10). Samples from the same eruptive stage are similar to one another in both major- and trace-element compositions, including rare-earth elements (Clague and Frey, 1980; Frey and Roden, in press). Isotopic studies indicate, however, that small systematic changes occur over time (Lanphere and others, 1980; Unruh and

TABLE 1.9.—*Rock types and inferred volcanic stages represented along the Hawaiian-Emperor Chain*

[X, present; --, not present or not known; (T), transitional; volcano numbers from Bargar and Jackson (1974)]

Volcano		Shield stage			Alkalic postshield stage						Alkalic rejuvenated stage				
Number	Name	Tholeiitic basalt	Picritic tholeiitic basalt	Rhyodacite	Alkalic basalt	Ankaramite	Hawaiite	Mugearite	Trachyte	Phonolite	Alkalic basalt	Basanite	Nephelinite	Melilitite	Tephrite
1	Kilauea	X	X	--	--	--	--	--	--	--	--	--	--	--	--
2	Mauna Loa	X	X	--	--	--	--	--	--	--	--	--	--	--	--
4	Hualalai	X	X	--	X	X	--	--	X	--	--	--	--	--	--
3	Mauna Kea	X	X	--	X	X	X	--	--	--	--	--	--	--	--
5	Kohala	X	--	--	--	--	--	X	X	--	--	--	--	--	--
6	Haleakala	X	--	--	X	X	X	X	--	--	X	X	--	--	--
7	Kahoolowe	X	X	--	--	X	--	--	--	--	X?	--	--	--	--
8	West Maui	X	X	--	X	X	--	X	X	--	--	X	--	--	--
10	East Molokai	X	X	--	X	X	X	X	X	--	X	X	--	--	--
9	Lanai	X	X	--	--	--	--	--	--	--	--	--	--	--	--
11	West Molokai	X	X	--	X	--	X	--	--	--	--	--	--	--	--
12	Koolau	X	X	--	--	--	--	--	--	--	X	X	X	X	--
13	Waianae	X	X	X	--	--	X	--	--	--	--	--	--	--	--
14	Kauai	X	X	--	--	--	X	--	--	--	X	X	X	X	--
15	Niihau	X	X	--	X	--	--	--	--	--	X	--	--	--	--
15A	Kaula	X	--	--	--	--	--	--	--	X	--	X	--	--	--
17	Nihoa	X	X	--	--	--	--	--	--	--	--	--	--	--	--
19	Unnamed Seamount	--	X	--	--	--	--	--	--	--	--	--	--	--	--
20	Unnamed Seamount	X	--	--	--	--	--	--	--	--	--	X	--	--	--
21	Unnamed Seamount	--	X	--	--	--	--	--	--	--	--	--	--	--	--
23	Necker	--	X	X?	--	--	X	--	--	--	--	--	--	--	X?
26	La Perouse Pinnacles	--	X	--	--	--	--	--	--	--	--	--	--	--	--
30	Gardner Pinnacles	--	X	--	X	--	--	--	--	--	--	--	--	--	--
38	Brooks Bank	X	--	--	--	--	X	--	--	--	--	--	--	--	--
29	St. Rogatein Bank	--	--	--	--	--	X	--	--	--	--	--	--	--	--
36	Laysan	--	--	--	--	--	X	X	--	--	--	--	--	--	--
37	Northampton Bank	X	X	--	--	--	--	--	--	--	--	--	--	--	--
39	Pioneer Bank	X	--	--	--	--	--	--	--	--	--	--	--	--	--
50	Pearl and Hermes Reef	--	--	--	X	--	X	--	--	X	--	--	--	--	--
51	Ladd Bank	--	--	--	--	--	--	--	--	--	--	--	X	--	--
52	Midway Island	X	--	--	--	--	X	X	--	--	--	--	--	--	--
53	Nero Bank	--	X	--	--	--	--	--	--	--	--	--	--	--	--
57	Unnamed Seamount	--	--	--	X	--	--	--	--	--	--	--	--	--	--
63	Unnamed Seamount	--	--	--	--	--	--	--	--	--	--	--	--	--	[1]X
65	Colahan Seamount	(T)	--	--	--	--	--	--	--	--	--	--	--	--	[1]X
65A	Abbott Seamount	(T)	--	--	--	--	--	--	--	--	--	--	--	--	--
67	Daikakiyi Seamount	X	--	--	X	--	--	--	--	--	--	--	--	--	--
69	Yuryaku Seamount	--	--	--	X	--	--	--	--	--	--	--	--	--	--
72	Kimmei Seamount	--	--	--	X	--	--	--	--	--	--	--	--	--	--
74	Koko Seamount (southeast)	X	--	--	X	--	X	X	X	X	--	--	--	--	--
76	Koko Seamount (northwest)	X	--	--	--	--	--	--	--	--	--	--	--	--	--
81	Ojin Seamount	X	--	--	--	--	X	--	--	--	--	--	--	--	--
89	Jingu Seamount	--	--	--	--	--	X	X	--	--	--	--	--	--	--
86	Nintoku Seamount	--	--	--	X	--	--	--	--	--	--	--	--	--	--
90	Suiko Seamount (southern)	--	--	--	--	--	--	X?	--	--	--	--	--	--	--
91	Suiko Seamount (central)	X	X	--	X	--	--	--	--	--	--	--	--	--	--
108	Meiji Seamount	X	--	--	--	--	--	--	--	--	--	--	--	--	--

[1]Dredges from unnamed seamount (63) and Colahan Seamount recovered ankaramite, tephrite, and amphibole-bearing hawaiite that are probably rejuvenated stage lava.

TABLE 1.10.—*Composition of tholeiitic basalt from volcanoes of the Hawaiian-Emperor Chain*

[All figures in weight percent, dry reduced normalized average analyses; olivine added or subtracted so that Mg/(Mg+0.85 Fe) = 0.70; --, not analyzed; P_2O_5 value in parentheses is high due to marine phosphatization]

Volcano	Kilauea	Mauna Loa	Mauna Kea	Hualalai	Kohala	East Maui	West Maui	Lanai	East Molokai	West Molokai	Koolau	Waianae (upper)	Waianae (lower)
SiO_2 --	48.9	50.5	46.4	49.4	48.2	49.7	47.3	49.0	46.4	49.2	51.5	46.9	47.9
Al_2O_3 -	12.1	12.2	12.8	11.8	13.5	13.3	12.6	12.8	12.9	11.8	13.2	13.4	14.1
FeO ---	11.4	11.0	12.3	11.9	11.8	10.9	12.2	11.0	12.4	11.9	10.4	11.9	11.2
MgO ---	12.7	12.3	13.6	13.4	13.1	12.1	13.7	12.3	13.8	13.2	11.7	13.2	12.5
CaO ---	9.7	9.2	9.9	9.2	9.4	9.6	9.8	8.8	9.7	8.9	8.3	9.1	9.6
Na_2O --	1.99	1.98	1.82	1.84	1.62	1.76	1.66	2.13	1.89	2.42	2.47	2.07	1.86
K_2O ---	.44	.36	.28	.28	.10	.33	.23	.11	.20	.18	.27	.53	.26
TiO_2 --	2.34	1.85	2.40	1.75	1.93	2.01	2.14	1.66	2.22	2.08	1.68	2.46	2.20
P_2O_5 --	.22	.21	.23	.16	.20	.13	.20	.18	.25	--	.22	.35	.25
MnO ---	.17	.16	.17	.15	.18	.18	.17	.14	.18	.19	.15	.15	.17

Volcano	Kauai	Niihau	Nihoa	Unnamed (20)	Unnamed (21)	Necker Island	La Perouse Pinnacles	Gardner Pinnacles	Northampton Bank	Pioneer	Daikakiji	Suiko high TiO_2	Suiko low TiO_2
SiO_2 --	48.4	48.4	47.4	46.9	47.1	47.15	47.5	47.6	48.7	48.2	49.7	47.6	47.9
Al_2O_3 -	12.5	12.1	11.5	11.2	11.3	11.1	11.7	12.5	11.4	11.2	11.5	12.7	13.0
FeO ---	11.9	12.1	12.4	12.6	12.4	12.8	11.8	11.3	11.7	11.9	11.5	12.3	11.9
MgO ---	13.3	13.6	13.8	14.0	13.8	14.1	13.1	12.6	13.0	13.3	12.9	13.7	13.2
CaO ---	9.2	8.1	9.4	9.6	9.2	9.8	10.7	10.3	10.1	9.8	9.05	8.7	9.3
Na_2O --	1.93	2.28	1.77	2.06	2.25	1.59	1.82	2.06	2.00	2.20	2.08	2.26	2.26
K_2O ---	.30	.49	.26	.24	.64	.38	.39	.16	.32	.67	.43	.28	.14
TiO_2 --	2.06	2.49	2.59	2.97	2.72	2.47	2.44	1.98	2.26	2.36	2.32	2.10	1.86
P_2O_5 --	.23	.31	(.70)	.28	.35	.36	.34	.26	.23	.17	.36	.22	.16
MnO ---	.17	.16	.15	.15	.15	.17	.20	.16	.16	.14	.16	.18	.18

others, 1983). The lower $^{87}Sr/^{86}Sr$ ratios and higher $^{143}Nd/^{144}Nd$ ratios of lava from the central Emperor Seamounts compared to those of lava from the Hawaiian Islands and Ridge imply that tholeiitic lava erupted 65 m.y. ago was derived from a more depleted source than that erupting today. Lanphere and others (1980) correlated this observation with the data shown in figure 1.3 to suggest that the chemistry of Hawaiian tholeiitic lava has varied as a function of the age and thickness of the oceanic lithosphere beneath each volcano when it was constructed. The correlation suggests that the oceanic lithosphere forms at least part of the source material for Hawaiian tholeiitic magma, or that the magma partially reequilibrates with the oceanic lithosphere. Wright (1984) proposes that Hawaiian magma originates from oceanic lithosphere converted to asthenosphere.

STRATIGRAPHIC STUDIES IN THE HAWAIIAN ISLANDS

Studies of stratigraphically controlled samples (Beeson, 1976; Clague and Beeson, 1980; Chen and Frey, 1983; Clague and others, 1983; Feigenson, 1984; Lanphere and Frey, 1985) have shown that major-element, trace-element, and isotopic ratios change systematically as a function of time at some Hawaiian volcanoes. These observations are not universal (Stille and others, 1983; Frey and others, 1984) in as much as Waianae and Mauna Kea erupted isotopically similar lava during the tholeiitic shield and alkalic postshield stages. Chen and Frey (1983) observed systematic stratigraphic trends in $^{87}Sr/^{86}Sr$, Rb/Sr, $^{143}Nd/^{144}Nd$, and Sm/Nd ratios in samples from East Maui Volcano. Their data indicate that the tholeiitic lava had higher $^{87}Sr/^{86}Sr$ and Sm/Nd ratios and lower $^{143}/Nd$ ^{144}Nd and Rb/Sr ratios than the later alkalic lava from the postshield and rejuvenated stages. They proposed a complex mixing model to explain the apparent paradox of having more radiogenic isotopic ratios combined with more depleted trace-element ratios in the same rocks. Their model proposes two sources, a primitive mantle-plume source and a depleted oceanic-lithosphere source, which can mix before melting or can produce partial melts which then mix. They argue that small amounts of small-percentage melts from the oceanic lithosphere (midocean-ridge source) are mixed with enriched mantle or with melts derived from enriched mantle. This model is similar to earlier selective-melting models qualitatively proposed by Green and Ringwood (1967) and Macdonald (1968). It would also be possible to mix small-percentage melts of enriched mantle with the oceanic-lithosphere source (basically an enrichment model) to create the source rocks for Hawaiian magma (Clague and others, 1983; Chen and Frey, 1985), although the measured and calculated compositions do not match as closely as in the model of Chen and Frey (1983). All these models predict a range of source compositions from which the lava is generated.

Other studies emphasize the bulk composition of the source rocks and the processes and physical conditions of the melting process. For example, Clague and Frey (1982), from a detailed trace-element analysis of the rejuvenated stage Honolulu Volcanics on Oahu, concluded that lava ranging from nepheline melilitite to alkalic basalt was generated by 2–11 percent partial melting of a homogeneous garnet (<10 percent) lherzolite source that was carbon bearing. The source had been recently enriched and had a chondrite-normalized La/Yb ratio of 4.4. During melting, phlo-

gopite, amphibole, and a Ti-rich phase (oxide?) remained in the residua, but apatite was completely melted. This model can be combined with the model of Chen and Frey (1983) to generate the source composition indicated for the Honolulu Volcanics (see Roden and others, 1984). The homogeneous composition of the mantle source for the Honolulu Volcanics implies that the recent enrichment event affects a large volume of depleted mantle from which the lava is then generated by partial melting. This is not the same process espoused in the model preferred by Chen and Frey (1983) in which enriched mantle or partial melts of enriched mantle mix with partial melts of depleted mantle. Note that all these models consider only two mixing end members, whereas the isotopic data clearly indicate that at least three distinct source compositions are required (Tatsumoto, 1978; Staudigel and others, 1984). Feigenson (1984) proposed three-end-member mixing models for Kauai lava but did not identify the trace-element signatures of the source components.

The generation of large volumes of tholeiitic lava has been the focus of recent studies by Wright (1984) and Budahn and Schmitt (1984), who used different approaches and reached dramatically different conclusions. Wright (1984) used mass-balance considerations to calculate the components and abundance of material that must be added to depleted lithosphere to generate Hawaiian tholeiitic basalt by large percentages of partial melting (35–42 percent melting). His models did not attempt to calculate the variations in source composition for tholeiitic basalt from the different volcanoes (Leeman and others, 1977, 1980; Basaltic Volcanism Study Project, 1981). Budahn and Schmitt (1984) used inverse procedures to estimate the variations in source composition required to generate the tholeiitic basalt from a number of Hawaiian volcanoes. Their estimated sources had 74–86 percent olivine plus orthopyroxene, 11–21 percent clinopyroxene, and 3–5 percent garnet. All the calculated sources had slightly enriched light-rare-earth-element contents, and low heavy-rare-earth abundances (0.9 to 1.6 times chondrites). They calculated the partial melting at 2–10 percent for these sources. Budahn and Schmitt (1984) did not address the processes that led to creation of these different source compositions, nor did they consider the volumes of mantle source regions required, or the constraints on the production of partial melts provided by Kilauea's magma supply and eruption processes. Wright's (1984) model follows from consideration of these additional constraints. The large difference between the models of Wright (1984) and Budahn and Schmitt (1984) emphasizes the uncertainties concerning the compositions and processes that create the source rocks and the lava of the Hawaiian Islands.

PETROLOGIC STUDIES OF LOIHI SEAMOUNT

Studies of Loihi Seamount have provided new insight in magma genesis in the Hawaiian Islands. Trace-element and isotopic studies demonstrate that the source rocks beneath a single volcano are heterogeneous and require at least three mantle components (Frey and Clague, 1983; Lanphere, 1983; Staudigel and others, 1984). Perhaps more important is the observation of very high $^3He/^4He$ ratios, which imply a primitive undegassed source of volatiles (Kaneoka, chapter 27; Kurz and others, 1983; Rison and Craig, 1983; Kaneoka and others, 1983). The ratio of $^3He/^4He$ is inversely related to the volume of the volcanoes on the Island of Hawaii (Kaneoka, chapter 27; Kurz and others, 1983), suggesting that at smaller volcanoes lava is generated from sources that are largely primitive and not degassed. Another observation is that Hawaiian volcanoes initially erupt alkalic lava generated from heterogeneous source compositions by rather small percentages of partial melting (Moore and others, 1982; Frey and Clague, 1983). The evolutionary sequence at a Hawaiian volcano is therefore from small-volume, infrequent eruptions of small-percentage melts to large-volume, frequent eruptions of large-percentage melts, and then back to small-volume, infrequent eruptions of small-percentage melts (Wise, 1982).

PETROLOGIC OVERVIEW

In summary, the petrology of lava from along the Hawaiian-Emperor Chain indicates that at least three source materials are involved in the generation of Hawaiian lava; one of these sources is apparently the depleted ocean lithosphere, whereas another is relatively primitive undegassed mantle. The third component is less well defined. Since multiple sources are required, mixing of these sources or of melts generated from these sources must occur. The compositions of lava along the chain apparently are related to the age (thickness) of the underlying oceanic lithosphere; the volcanoes formed on younger and thinner oceanic lithosphere were generated from a source with a larger component of the depleted ocean lithosphere. Detailed overviews of the petrology of Hawaiian tholeiitic lava and Hawaiian alkalic lava are presented in Wright and Helz (chapter 23) and Clague (in press), respectively.

Volcano volume reflects the degree of melting of the tholeiitic basalt and probably also the size and frequency of intrusion of magma batches. The inverse correlation of volcano volume with $^3He/^4He$ ratio in tholeiitic basalt indicates that smaller percentage melts are derived from sources with more of the primitive component and larger percentage melts are derived from sources with less of the primitive component. Volcano volumes and compositions of the shield tholeiitic basalt are also related, less-enriched tholeiitic basalt forms larger shields and more-enriched tholeiitic basalt forms smaller shields (Clague and Frey 1979), although this correlation is imperfect. Models developed in the future should address the problem of characterizing the isotopic and trace-element compositions of the three mantle components and address the timing and processes of mixing of these sources. The source volumes inferred from different melting models must be considered. Wright's (1984) model requires only modest source volumes, whereas the model of Budahn and Schmitt (1984) requires partial melting of a mantle zone 100 km thick and 100 km wide to generate the volcanoes of the principal Hawaiian Islands. Such enormous inferred volumes of mantle source rock pose numerous problems for models advocating small-percentage melting to generate the tholeiitic shields.

A separate problem is the cause of the alkalic rejuvenated stage. Jackson and Wright (1970) used tide-gage data from Moore (1970) to suggest that generation of the rejuvenated-stage Honolulu Volcanics might be caused by uplift as Oahu has passed over the

Hawaiian Arch. They argued that the Hawaiian Arch, an isostatic response to volcanic loading on the oceanic crust, follows the progression of active volcanic centers by several hundred kilometers and several million years. Clague and others (1982) showed that the duration of the quiescent period preceding eruption of the rejuvenated-stage lava has decreased systematically from nearly 2.5 m.y. on Niihau to <0.4 m.y. at Haleakala (see fig. 1.6). They suggested that a new mechanism should be sought to explain the age data. We have reexamined the data and conclude that they are consistent with the model proposed by Jackson and Wright (1970) because the rate of volcanic migration is increasing. The rejuvenated stage follows the formation of the shield not by a constant time but by a constant distance. The rejuvenated-stage Koloa Volcanics on Kauai and Kiekie Basalt on Niihau began erupting during formation of the Koolau shield located 180–225 km to the southeast. Likewise, the Honolulu Volcanics on the Koolau Range of Oahu began erupting during formation of the East Maui shield located 160 km to the southeast. The rejuvenated-stage Kalaupapa Volcanics on East Molokai erupted during formation of the Mauna Kea shield located 200 km to the southeast. Finally, the rejuvenated-stage Hana Volcanics on East Maui began erupting during formation of the Mauna Loa shield, located 160 km to the southeast. In each case, the lava of the rejuvenated stage began erupting during formation of a large shield 190 ± 30 km to the southeast. The Hawaiian Arch is about 250 km from the center of the volcanic ridge, but only 210 km to the east-southeast of Hawaii (Walcott, 1970). It is therefore likely that a factor in magma generation during the rejuvenated stage is the rapid change from subsidence to uplift as the volcanoes override the flexural arch created by formation of large shields. To the northwest of the Hawaiian Islands the rates of volcanic propagation were slower and more constant; we predict that lava of the rejuvenated stage will postdate the shield stage by 2–3 m.y. We also suggest that the apparent paucity of lava from the rejuvenated stage to the northwest of the Hawaiian Islands may reflect the absence of large volcanic edifices capable of flexing the lithosphere sufficiently. Likewise, the absence of any lava samples of the rejuvenated stage from the Emperor Seamounts may result from the rather wide spacing between volcanic edifices: by the time the next younger volcano formed, the previously constructed volcano was already beyond the arch. The fact that the Emperor volcanoes were constructed on young, thin lithosphere would amplify this effect because the distance from the load to the flexural arch decreases as the lithosphere becomes less rigid.

FIXITY OF THE HAWAIIAN HOT SPOT

Wilson's original hypothesis for the origin of the Hawaiian and other island chains by passage of the crust over a source of lava in the mantle (Wilson, 1963a, b, c) did not require that the hot spot be fixed, only that it have some motion relative to the crust above it. Morgan (1972a, b), on the other hand, specified that a worldwide system of thermal plumes (hot spots) was fixed in the mantle and that the relative movement between them was small or negligible. Several workers (for example, Minster and others, 1974; Gordon and Cape, 1981; Morgan, 1981) have shown from relative plate motions and paleomagnetic and other data that Morgan's hypothesis of relative hot-spot fixity is basically correct, but that the fixity of the hot-spot frame of reference with respect to the spin axis, particularly in early Cenozoic and Late Cretaceous times, is not established.

PALEOMAGNETIC TESTS OF HOT-SPOT FIXITY

Age data along the chain have shown that there has been more or less continuous relative motion between the Hawaiian hot spot and the Pacific plate, thereby proving the kinematic aspect of the hot-spot hypothesis, but these data have little or no bearing on the question of hot-spot fixity. The lava flows that form volcanoes of the Hawaiian-Emperor Chain, however, contain a nearly continuous magnetic record of the latitude of the Hawaiian hot spot for the entire Cenozoic and the latest Cretaceous. Although only a small fraction of this magnetic record has been read, there are now sufficient data to provide a partial test of the fixity hypothesis for the Hawaiian hot spot. Paleomagnetic data from volcanoes along the chain show that the Hawaiian hot spot (and thus presumably the worldwide hot-spot frame) has been, to a first approximation, fixed with respect to the spin axis since the time of formation of the Hawaiian-Emperor bend. The limited data indicate, however, that there was motion between the hot spot and the spin axis, that is, true polar wander, before that time.

The paleolatitudes of several Hawaiian-Emperor volcanoes, as determined from paleomagnetic studies on individual rock samples and from shipboard magnetic surveys, are given in table 1.11 and plotted in figure 1.11 as a function of volcano age. In general, the data indicate that the Hawaiian-Emperor volcanoes formed not at their present latitudes but at a latitude near the present latitude of Hawaii. Thus, the latitude of the Hawaiian hot spot has been approximately fixed throughout the Cenozoic. The data are not of uniform quality, however, and some care must be exercised in their interpretation.

The paleomagnetic data have been discussed and evaluated by Jackson and others (1980), Kono (1980), and Sager (1984), who point out that the paleomagnetic sampling of Meiji, Nintoku, Ojin, Midway, Nihoa, and the Island of Hawaii involved a small number of lava flows, making it doubtful that the secular variation is adequately averaged out. The errors for the Ojin and Nintoku sites reflect this uncertainty, but there is reason to suspect that the errors assigned to the paleolatitudes of Midway, Meiji, and Nihoa are too small. This is because of the unusually low dispersions and the likelihood of serial correlation of some of the flows, which further decreases the number of independent measurements from the sites.

The paleolatitude of 17.5° ± 5°, determined for Suiko by Kodama and others (1978) from magnetic survey data, is suspect for several reasons. First, the magnetic anomaly over Suiko is complex, resulting in a low statistical test of fit ($R = 1.1$) for the inversion. Second, it is likely that Suiko is constructed from several coalesced volcanoes (Bargar and Jackson, 1974), possibly of different ages, and the necessary assumption of uniform magnetization is probably invalid for this seamount. In addition, the paleolatitude is inconsistent with that obtained from the paleomagnetic study of

TABLE 1.11.—*Paleolatitudes determined for volcanoes of the Hawaiian-Emperor Chain*

[From paleomagnetic measurements on lava flows and from shipboard magnetic surveys (SM). Data from compilations by Kono (1980) and Sager (1984); the more reliable data (Sager, 1984) underlined; uncertainties are the values of α_{95}]

Volcano Number	Volcano Name	Number of flows determined	Present latitude (degrees north)	Paleolatitude (degrees north)
1,2,4,	Kilauea, Mauna Loa Hualalai (historical)	17	19.5	19.6±1.4
1,2,3	Kilauea, Mauna Loa Mauna Kea(^{14}C dated)	8	19.5	17.7±10.7
12	Koolau	33	21.4	16.8±3.6
13	Waianae	55	21.5	15.7±3.3
14	Kauai (Makaweli Member, Waimea Canyon Basalt)	25	22.0	15.6±3.1
14	Kauai (Napali Member, Waimea Canyon Basalt)	46	22.1	14.9±3.1
17	Nihoa	14	23.1	21.0±6.6
52	Midway	13	28.2	15.4±5.4
65A	Abbott	(SM)	31.8	17.5±2.4
81	Ojin	6	38.0	17.6±13.2
86	Nintoku	4	41.3	36.0±24.6
91	Suiko	(SM)	44.8	16.7±5
91	Suiko	65	44.8	27.1±3.5
108	Meiji	6	53.0	19.2±4.1

Suiko (Kono, 1980), which is the best study of its kind for any of the volcanoes in the chain.

Sager (1984) included in his compilation two additional determinations from the principal Hawaiian Islands that we have chosen to omit from table 1.11. These include a group of 129 flows from the Islands of Hawaii and Niihau, and a second group of 19 flows from Kauai. Both groups include flows from the rejuvenated stage that were erupted several million years after the hot spot had moved (relatively) southeastward to form new tholeiitic shields. Although both of these determinations were included by Sager in his list of more reliable paleolatitudes, they are so close to the present position of the hot spot that their elimination has no significant impact on the conclusions drawn from the data.

Taken at face value, the more reliable paleolatitude data (fig. 1.11) indicate that the Hawaiian hot spot may have been a few degrees south of its present position during the late Cenozoic, near its present position when Abbott Seamount formed at about 39 Ma, and 7° north of its present position at Suiko time, 65 Ma. Analyses of paleoequator (Sager, 1984) and worldwide paleomagnetic data (Livermore and others, 1983), however, show that there has been little or no motion of the spin axis relative to the worldwide hot-spot frame during the past 40 m.y. or so. From this comparison of independent data Sager (1984) concluded that the apparent southward displacement of the Hawaiian hot spot shown by the data from younger volcanoes in the chain (fig. 1.11) reflected changes in the magnetic field rather than relative movement between the hot spot and the spin axis.

The apparent displacement indicated by the Suiko data, however, is probably real. The Suiko paleolatitude is based on analysis of a large number of flows (table 1.11) recovered by coring over an interval of 550 m (Kono, 1980). Even when certain flows thought to represent a very short time interval are grouped, there are still a minimum of 40 independent data. There are also 12 places in the cores where the inclination changes by more than 15°, which indicates that at least 13 secular variation cycles have been sampled, making it likely that secular variation has been adequately averaged out. Other paleomagnetic stability indices indicate that 27.1°±3.5° is a highly reliable measure of the latitude of formation of Suiko Seamount (Kono, 1980).

BIOFACIES AND TEMPERATURE DATA FROM THE HAWAIIAN-EMPEROR CHAIN

Although northward displacement of the Hawaiian hot spot relative to the spin axis is only indicated by the single paleolatitude from Suiko, it is supported by a variety of additional data. Analysis of Pacific deep-sea sediment cores, for example, shows that the paleoequator was 10°–16° farther north than at present between about 75 Ma and 65 Ma (Sager, 1984).

Biofacies data from DSDP Leg 55 drilling in the Emperor Seamounts provide semiquantitative substantiation of the Suiko paleolatitude. The bioclastic sediment on Suiko, Nintoku, and Ojin Seamounts consists primarily of coralline algae and bryozoans with ostracodes, foraminifers, and assorted shell fragments typical of a shallow-water, high-energy environment (Jackson and others, 1980). Only a single coral was found in the Suiko material, and none was recovered from either Ojin or Nintoku, indicating that corals were not significant contributors to the carbonate buildups.

Schlanger and Konishi (1975) have pointed out that carbonate buildups in the Pacific can be divided into bryozoan-algal and coral-algal facies, the distribution of which depends largely on water temperature and solar insolation and thus is, to a large degree, a function of latitude. They observe that in the modern Pacific, the coral-algal facies dominates at latitudes less than about 20°, whereas the bryozoan-algal facies is predominant above about 30° latitude. They locate the boundary between these facies at about 25° latitude, but emphasize that the transition is gradual. In the central Pacific, the annual surface-water temperature at 25° latitude is about 22 °C (Muromtsev, 1958), which is usually considered the minimum for active coral-algal reef growth (Vaughn and Wells, 1943; Heckel, 1974). The optimum temperature for vigorous reef growth is 25–29 °C. Thus, the existence of carbonate buildups of the bryozoan-algal facies atop Ojin, Nintoku, and Suiko Seamounts indicates that the reefs atop the volcanoes formed in water temperatures less than about 22 °C.

Using the oxygen-isotope temperature data of Savin and others (1975) for the North Pacific, Greene and others (1978) reconstructed the approximate latitude variation through time for the 20 °C and 22 °C isotherms (fig. 1.12). They showed that if the Hawaiian hot spot were fixed, then Suiko Seamount would have formed in water warm enough to have developed active coral-algal reefs. Following the analysis of Greene and others (1978), Jackson and others (1980) showed that the Paleocene water temperature at the latitude determined by the paleomagnetic data from Suiko was appropriate for the bryozoan-algal carbonates that occur immediately above the basalt.

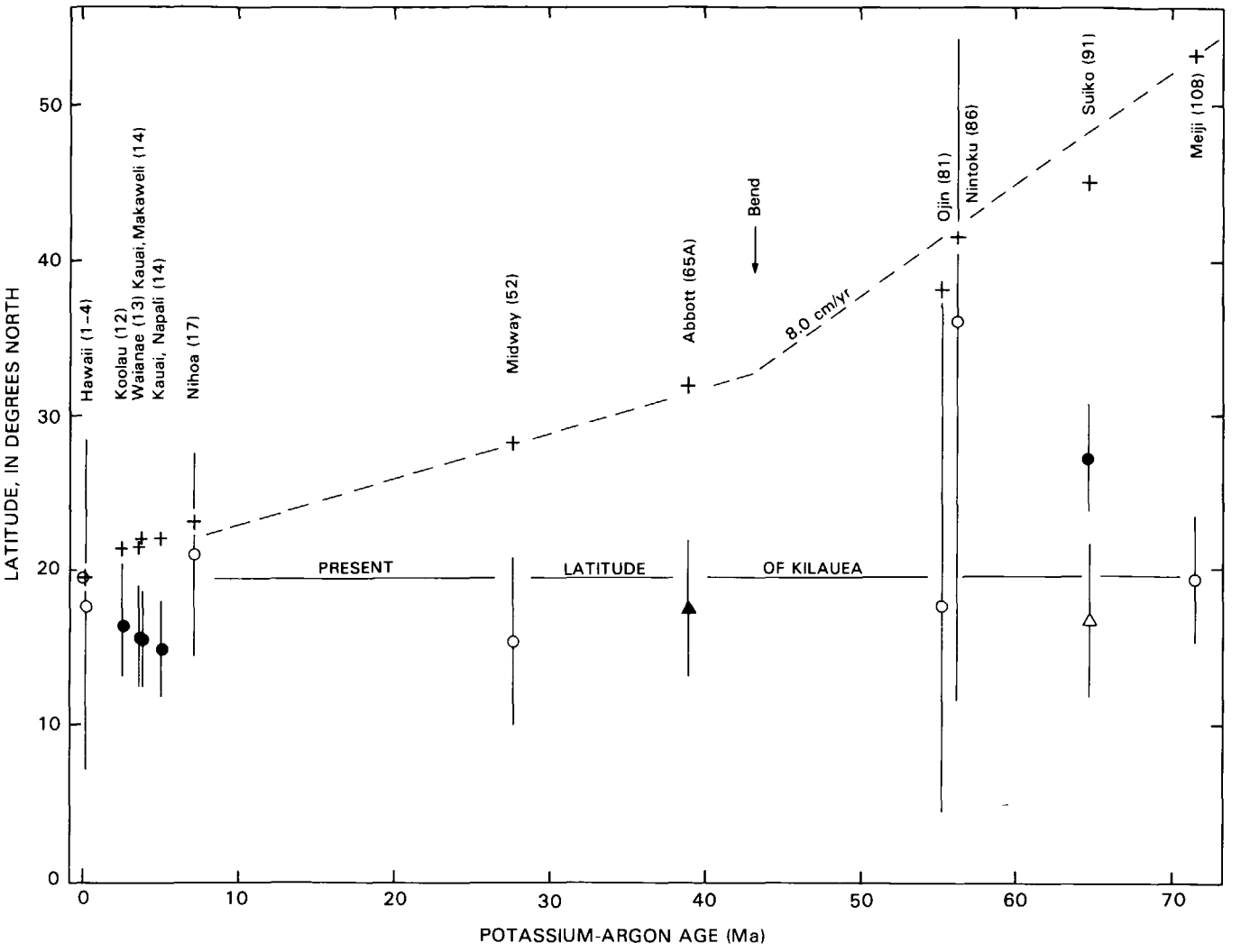

FIGURE 1.11.—Paleolatitude plotted against age for volcanoes along Hawaiian-Emperor Chain. Crosses, present latitude; dots and circles, paleolatitudes determined from paleomagnetic data; triangles, paleolatitudes determined from shipboard magnetic surveys. More reliable data indicated by solid symbols. Error bars show α_{95}. Dashed reference line is backtracked position of hot spot relative to Pacific plate assuming a constant velocity of 8 cm/yr. Paleomagnetic data from table 1.11, age data from table 1.4 and appendix 1.1.

The paucity of coral material on seamounts in the central Emperor Chain is in contrast to Koko and the seamounts on the bend, where corals are more common but still less abundant than in a region of vigorous coral reef growth (Davies and others, 1971, 1972; Matter and Gardner, 1975). Oxygen-isotope temperatures of carbonate diagenesis for Suiko, Nintoku, Ojin, and Kammu Seamounts (McKenzie and others, 1980) show a gradual warming from Suiko to Koko, at least in part caused by southward migration of the hot spot (Jackson and others, 1980). Thus, the biofacies and paleotemperature data from Leg 55 are consistent with the paleomagnetic data, indicating a latitude of 27° for the hot spot at Suiko time. The data are also consistent with Sager's (1984) suggestion that the hot spot had reached its approximate present latitude by the time Abbott Seamount formed just after formation of the Hawaiian-Emperor bend; the slightly cooler temperatures indicated by the carbonate facies and temperature data from the bend seamounts are probably related to the sudden drop in ocean temperature in the late Eocene rather than to a more northerly hot spot.

Thus, the paleomagnetic data from Suiko, the biofacies and temperature data from the central and southern Emperor Seamounts, and the Pacific paleoequator data all indicate southward migration of the Hawaiian hot spot in the early Tertiary and Late Cretaceous. This conclusion is consistent with previous findings, based on analysis of worldwide paleomagnetic data in the hot-spot frame of reference, of about 10° of southward movement of the hot-spot frame relative to the spin axis (that is, true polar wander)

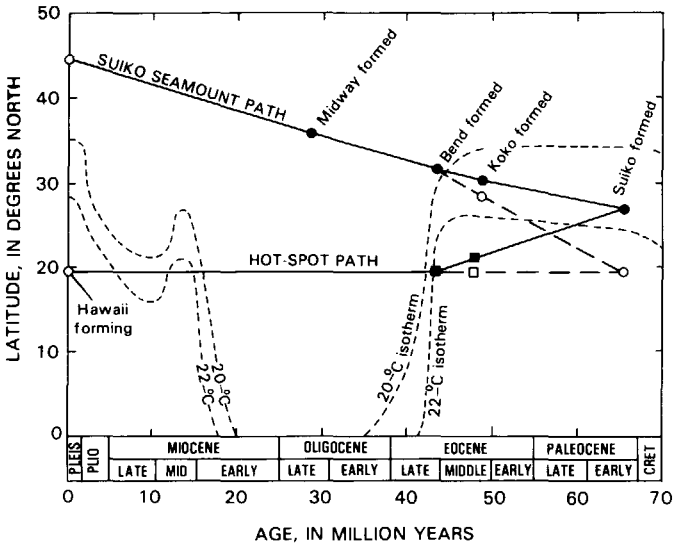

FIGURE 1.12.—Approximate position of 20 °C and 22 °C surface-water isotherms in north-central Pacific during Cenozoic, modified from Greene and others (1978), based on data of Savin and others (1975). Dots, paleolatitudes of Suiko Seamount assuming that Suiko formed at 27° N. and that hot spot has been fixed since time of bend formation. Circles, paleolatitudes for Suiko assuming a fixed hot spot for past 65 m.y. Squares, positions of formation of Koko Seamount and bend under same assumptions. Backtracking was about an Emperor pole at lat 17° N., long 107° W. and a Hawaiian pole at lat 69° N., long 68° W. (Clague and Jarrard, 1973). The 22 °C isotherm is approximate boundary between coral-algal (warmer) and bryozoan-algal (colder) facies of Schlanger and Konishi (1975).

during the latest Cretaceous and earliest Tertiary (for example, Gordon and Cape, 1981; Jurdy, 1981, 1983; Morgan, 1981; Gordon, 1982).

The paleolatitude of 17.5°±4.4° N. found for Abbott Seamount puts the Hawaiian hot spot at about its present latitude by 40 Ma, which is consistent with the conclusion of Livermore and others (1983) that true polar wander did not occur during the past 35 m.y. The paleoequator analysis of Sager (1984) suggests that there was no true polar wander after formation of the bend, that is, after 43 Ma. This requires approximately 7.6° of southward latitudinal motion of the hot spot between 65 Ma and 43 Ma and 5° of northward motion of the Pacific plate in order to satisfy the relative motion of about 0.65° latitude per million years indicated by the age-distance data.

COMPARISON TO OTHER PACIFIC LINEAR ISLAND CHAINS

Another way of evaluating the movement of hot spots is to compare the orientation and age progression quantitatively along volcanic chains formed during the same time period on the same plate. Several studies (Clague and Jarrard, 1973; Jackson, 1976; Jarrard and Clague, 1977; Epp, 1978; McDougall and Duncan, 1980; Turner and others, 1980; and Duncan and Clague, 1985) have attempted such evaluations for the Pacific plate since Morgan (1971) first proposed the technique. Most of the linear volcanic chains in the Pacific basin are oriented roughly west-northwest and apparently formed sequentially over nearly stationary hot spots during the last 43 m.y. as the Pacific plate rotated clockwise about a pole located near lat 69° N., long 68° W. (Clague and Jarrard, 1973). Another group of linear chains exhibit roughly north-trending orientations and apparently formed by the same mechanism between at least 80 Ma and 43 Ma as the Pacific plate rotated clockwise about a pole located near lat 17° N., long 107° W. (Clague and Jarrard, 1973).

The hot spots that formed the Hawaiian, Austral-Cook, Society, Marquesas, Caroline, Pitcairn-Gambier, Samoan, and Islas Revilla Gigedos island chains and the Pratt-Welker and Cobb-Eickelberg seamount chains moved very little with respect to one another (Duncan and Clague, 1985). The most convincing evidence that hot spots move with respect to one another comes from the orientation of the Marquesas Islands, which is discordant by about 25° with that predicted, implying motion of the Marquesas hot spot to the northeast with respect to the hot-spot reference frame at several centimeters per year (Jarrard and Clague, 1977) during the last 5 m.y. The rates of volcanic migration along the chains younger than 43 Ma fit a pole of rotation at lat 68° N., long 75° W. and an angular rotation rate of 0.95°±0.02°/m.y. (Duncan and Clague, 1985).

CAUSE OF THE HAWAIIAN-EMPEROR BEND

An especially knotty problem over the past decade has been the relationship between Pacific sea-floor spreading, worldwide plate motion, and the Hawaiian-Emperor bend. Since there is now firm evidence that the motion of the hot-spot frame was small during the early Cenozoic and has been negligible since then, the 120° angle in the Hawaiian-Emperor bend must represent a major (circa 60°) change in the absolute motion of the Pacific plate. Since the motions of individual plates are not independent, we would expect such a significant change to be part of a worldwide reorganization of both absolute and relative plate motions. Various authors have suggested that the bend might correlate with circum-Pacific tectonic events (Jackson and others, 1972; Clague and Jarrard, 1973; Moore, 1984), that it may be caused by the collision of India and Eurasia (Dalrymple and Clague, 1976), or that it may be the result of new subduction zones along the southwestern margin of the Pacific plate (Gordon and others, 1978). However, completely satisfactory correlations have not been achieved.

A major feature of the northeast Pacific magnetic-anomaly pattern is the major change in the trend of the magnetic anomalies, that is, the magnetic bight, between anomalies 24 and 21. Reconstruction of the Pacific plate shows that this change in the anomaly pattern is the result of a change in spreading about the Pacific-Kula-Farallon triple junction, in particular the cessation of spreading on the Kula Ridge (Scientific Party DSDP 55, 1978; Byrne, 1979). This occurred perhaps as early as anomaly 24 but no later than the time of anomaly 21, which is approximately the time of the major change in spreading direction between Greenland and Europe (Vogt

and Avery, 1974) and shortly before an apparent increase in the frequency of geomagnetic reversals (Jacobs, 1984). The change in anomaly orientation can also be correlated with numerous events associated with worldwide reorganization of plate motions (Rona and Richardson, 1978).

The early magnetic time scales of Heirtzler and others (1968) and LaBreque and others (1977) put anomaly 21 at about 54–53 Ma and 52–51 Ma (corrected for new K decay and abundance constants), respectively, which implies a lag of at least 10 m.y. between the reorganization of Pacific magnetic anomalies and the formation of the Hawaiian-Emperor bend at 43.1 ± 1.4 Ma (Dalrymple and Clague, 1976). More recent time scales, however, have narrowed this somewhat awkward gap. Ness and others (1980) put anomaly 21 at about 49–48 Ma, Lowrie and Alvarez (1981) at about 48.5–47.5 Ma, and Butler and Coney (1981) at about 47–46 Ma. As suggested by Butler and Coney, a lag of 3–4 m.y. is close enough to suggest a causal relationship between the relative motion change represented by the magnetic bight and the absolute change represented by the Hawaiian-Emperor bend.

Gordon and others (1978) suggested that the change in direction of the Pacific plate at ~43 Ma was caused by the development of new trenches along the southwestern boundary of the plate. These new trenches, which replaced an earlier set of ridges and transform faults, were the result of rifting of Australia from Antarctica and the accompanying convergence of the Australia-Indian and Pacific plates. Gordon and others (1978) suggest that some time would have elapsed before the subducting plate would have been long enough and dense enough to exert sufficient torque on the Pacific plate to change its direction of motion. This could explain the lag between the timing of reorientation of the magnetic anomalies, which record the change in relative plate motion, and the age of the Hawaiian-Emperor bend, which records the change in absolute plate motion. The duration of the lag time would depend on the rate of plate convergence. As noted by Gordon and others (1978) a lag time of perhaps as much as 10 m.y. might be explained if convergence were sufficiently slow. Their mechanism is more plausible, however, if the lag can be shortened to a few million years, as now seems likely.

HAWAIIAN HOT-SPOT MODELS

Although there is now little doubt that the Hawaiian-Emperor Chain owes its origin to a hot spot that has been approximately fixed with respect to the Earth's spin axis throughout the Cenozoic, there is scant information concerning the exact mechanism involved. Even the term "hot spot" may be misleading, for excess heat is not necessarily involved. Alternatively, it could be the result of pressure release in a mantle source area (Green, 1971; McDougall, 1971; Jackson and others, 1972).

A successful hypothesis for the Hawaiian hot-spot mechanism must explain the propagation of volcanism along the chain, the near-fixity of the hot spot, the chemistry and timing of the eruptions from individual volcanoes, and the detailed geometry of volcanism, including volcano spacing and departures from absolute linearity. Over the past decade or so several mechanisms have been advanced to explain how a linear chain of volcanoes might be progressively erupted onto the sea floor, but most are highly generalized and suffer from lack of detail. Few of the hypotheses address all of the kinematic and petrological issues, and none seems to be amenable to experimental test. Nonetheless, they are interesting speculations on solutions to an extremely difficult problem.

All of the proposed mechanisms can be grouped into four basic types:

1. Propagating fracture driven by lithospheric stresses.
2. Thermally or chemically driven convection.
3. Melting caused by shear between the lithosphere and the asthenosphere.
4. Mechanical injection of heat into the lithosphere.

PROPAGATING-FRACTURE HYPOTHESES

Dana (1849) was the first to associate the Hawaiian volcanic chain with crustal fracturing. He proposed that the Hawaiian and other volcanic chains in the Pacific were each emplaced along a series of short echelon fractures (or "rents") that were widest at the southeast end where volcanism was the most prolonged. He considered these fractures to be part of a worldwide system reflecting tension in the crust resulting from cooling of the Earth from an initially molten state. S. Powers (1917) agreed that the eruptions occurred through a superficial set of echelon fractures following the trend of the chain, but he attributed the trend to some deeper seated lines of weakness. Chubb (1934) thought that the Hawaiian swell represented the surface manifestation of a broad anticline trending in the direction of the chain and produced by compression oriented north-northeast and south-southwest. He proposed that the Hawaiian volcanoes erupted along strike faults and dip faults atop and aligned with the anticline.

Betz and Hess (1942) found no evidence of vertical displacement along fault scarps but thought that the chain might be the manifestation of a great transcurrent strike-slip fault resulting from crustal shortening within the Pacific basin caused by Tertiary volcanism along the margins of the basin. In view of the Earth's sphericity, the straightness of the chain indicated to them that the fault plane was essentially vertical. Considering the strength and thickness of the ocean crust, they thought that an anticline the dimensions of the Hawaiian swell was unlikely and proposed instead that the swell represented a thick lava pile related to the presumed fault zone. Dietz and Menard (1953) thought this idea improbable because of the enormous volume of lava that would be required to produce the swell.

Other early authors subscribed to the idea that the Hawaiian Chain developed atop a propagating fracture (for example, Stearns, 1946; Eaton and Murata, 1960; Jackson and Wright, 1970), but they were vague or noncommital as to the cause of the rupture.

Most recent authors who have advanced propagating-fracture hypotheses have attempted to relate the cause of the fracture to either local or regional stress fields within the Pacific plate. Green (1971) suggested that divergent flow vectors caused by the movement of the plate over an imperfect sphere, that is, an uneven upper mantle

surface, caused local tension and intermittent failure of the lithosphere. The fracturing would allow rapid upwelling and partial melting of material from the low-velocity zone. One problem with this hypothesis is the means by which the irregularities on the asthenosphere are maintained, but Menard (1973) suggested that such persistent asthenospheric "bumps" might be caused by a rising thermal plume in the mantle.

McDougall (1971), following the ideas of Green (1971), proposed that the physical feature that subjected the plate to local tension might be either a thermal high or an incipient upwelling caused by a local concentration of heat-producing radioisotopes. According to McDougall's model, fracturing results in the diapiric rise of peridotitic material from the asthenosphere into the lithosphere (fig. 1.13*A*, *B*), where partial melting then generates tholeiitic magma. Movement of the plate and counterflow of the asthenosphere eventually decapitate the diapir, but replacement of material from deeper levels of the asthenosphere perpetuates the high and a new diapir is created (fig. 1.13*C*, *D*). Noting that the rate of propagation of volcanism along the Hawaiian Chain is slightly more than twice the half-spreading rate of the East Pacific Rise, McDougall concluded that there must be counterflow of material in the asthenosphere in a zone of thickness comparable to that of the lithosphere. Jackson and others (1980) showed that it was not possible to reconcile equal-but-opposite hot-spot motion with the paleolatitude of Suiko Seamount if the counterflow had persisted throughout the history of the Hawaiian-Emperor Chain. Hot-spot countermovement until the time of the bend followed by latitudinal stability from then to the present is, however, kinematically permissible.

Another mechanism for producing a local stress field and lithospheric rupture was proposed by Walcott (1976), who related the stress to the volcanic load on the lithosphere. He suggested that large volcanoes will produce lithospheric stresses during growth that may be large enough to cause disruption of the plate. If the plate is under a normal state of horizontal compression, then the failure of the lithosphere will occur preferentially parallel to the direction of the compressive stress. The direction of rupture will remain linear as long as the ambient stress direction remains constant, and the rate of propagation will depend on the speed of formation of the load. Noting the rapidity with which Hawaiian volcanoes form, Walcott concluded that the propagation of volcanism along the Hawaiian chain must be limited by the availability of magma source material. Thus, the mechanism would be self-perpetuating and self-regulating. Although this mechanism will result in a line of volcanoes, it does not explain the observed age progression nor does it account for hot-spot fixity, but it might be locally important and explain the detailed distribution of volcanoes within the Hawaiian Chain (Walcott, 1976).

Expanding on the original idea of Dana (1849), Jackson and others (1972) observed that the individual volcanic centers of the Hawaiian-Emperor Chain appear to lie on short, sigmoidal, overlapping loci that are echelon in a clockwise sense in the Hawaiian Chain and in a counterclockwise sense in the Emperor Chain (fig. 1.14), although the latter was based on inadequate bathymetric data. They proposed that the pattern of loci may be caused by

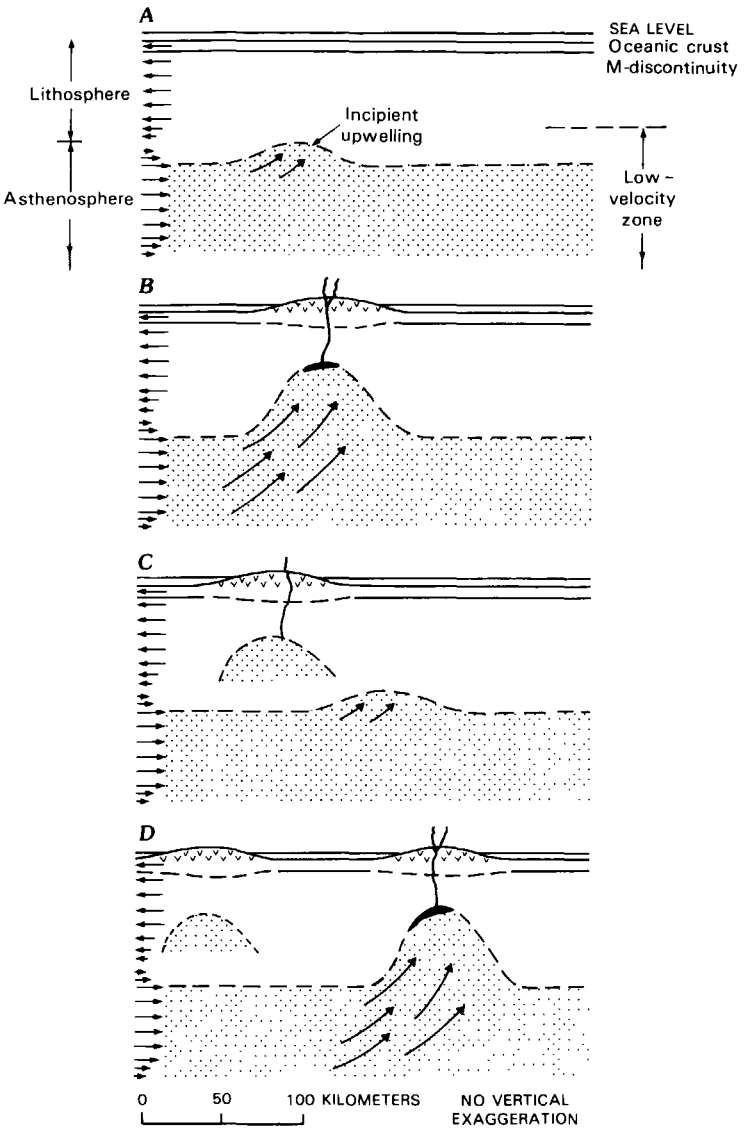

FIGURE 1.13.—Schematic diagram of McDougall's (1971) propagating-fracture hypothesis. Propagating tensional fracture allows diapiric upwelling from asthenosphere (***A***) and partial melting (***B***). Relative motion between lithosphere and asthenosphere (arrow along left margin) eventually decapitates diapir (***C***) and cycle begins at a new position (***D***). The shaded zone represents peridotitic material that is the source rock of the lava. From McDougall.

extensional strain resulting from tension within the Pacific plate, but they did not speculate on the ultimate cause of the stresses. Jackson and Shaw (1975) developed this idea more fully and extended it to other chains in the Pacific. They argued that linear hot-spot chains track and record the states of stress in the Pacific plate as a function of time, and that the stress was reflected in the detailed geometry of volcanoes within a chain, that is, in the orientation of the volcanic loci, which represent the injection of magma along lines perpendicular to least principal stress directions. On the basis of their analysis of the Hawaiian-Emperor, Pratt-Welker, Tuamotu, and

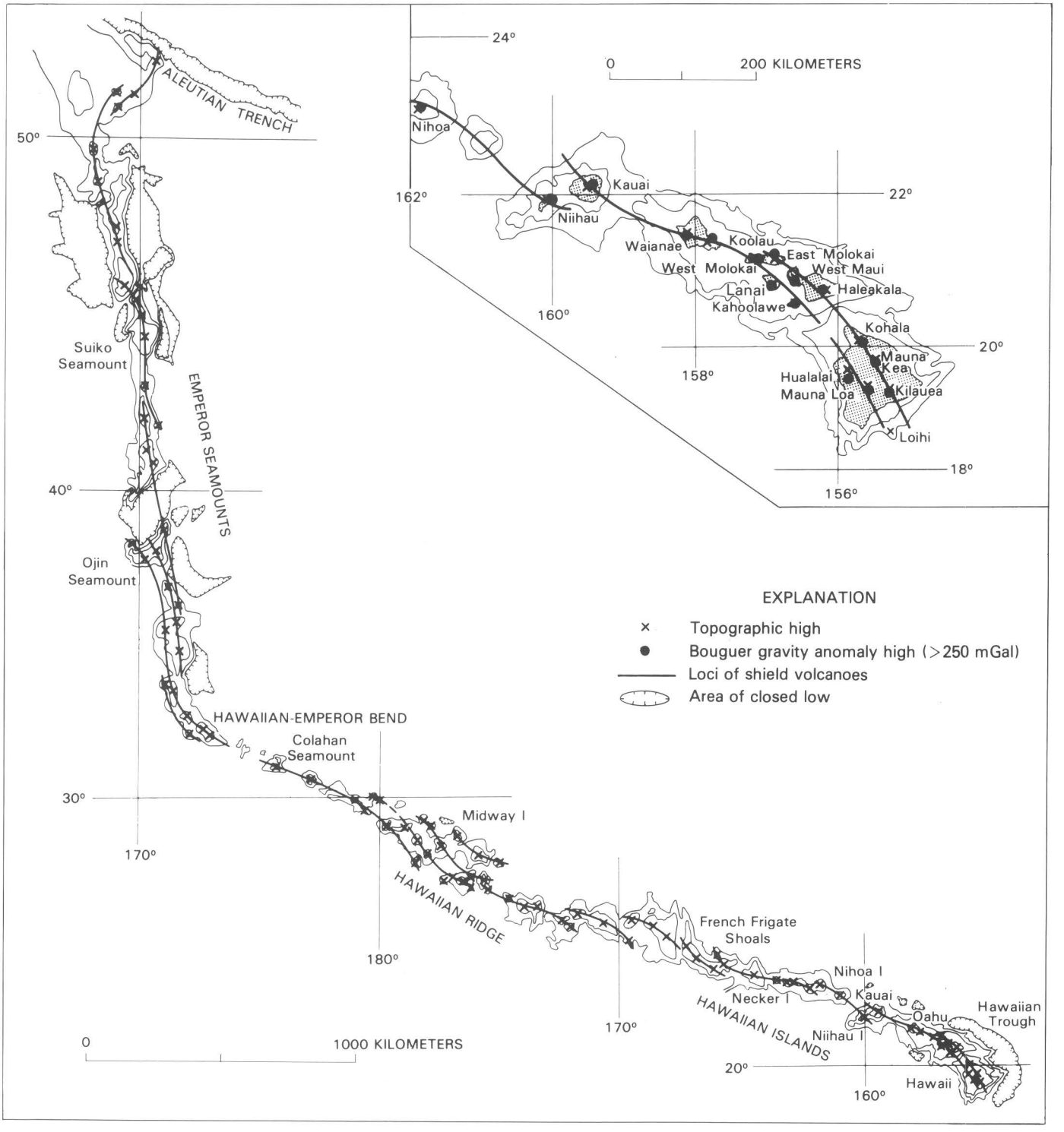

FIGURE 1.14.—Loci of shield volcanoes in Hawaiian-Emperor Chain according to Jackson and others (1972). Inset shows detailed relation between topographic highs, Bouguer gravity anomaly highs, and loci for principal Hawaiian Islands. Contour interval is 1 km; hachures indicate area of closed low.

Austral-Ellice-Gilbert-Marshall Chains, they concluded that the stress orientations since the time of formation of the Hawaiian-Emperor bend were caused by a right-lateral rotational couple acting within the plane of the Pacific plate. This couple resulted in the minimum principal stress oriented in a northeast-southwest direction. Before the time of the bend, the rotational couple was left-lateral and the minimum stress was oriented north-northwest and south-southeast. The curvature in the volcanic loci, they proposed, reflects episodic swings of the minimum-stress directions that averaged about 12 m.y. per episode and were perhaps a consequence of episodic changes in the force vectors at plate boundaries. Jackson and Shaw (1975) were uncertain about the exact causes of the stress field within the Pacific plate, but noted that possible contributors included convergence and divergence at plate boundaries, varying convection rates in the asthenosphere, and volume changes within the plate resulting from changing pressure and temperature.

On the basis of an analysis of volcano spacing and the relation of volcanic chains to preexisting plate structures, Vogt (1974) suggested that the factors that controlled the path of hot-spot chains are not clearly of one origin, but included simple shear, reactivated sea-floor-spreading structures, and local stresses. He concluded that the sigmoidal loci (fractures) postulated by Jackson and others (1972) for the Hawaiian Chain had no counterpart in other chains, although Jackson and Shaw (1975) claimed to have found a similar pattern on other chains in the Pacific.

Solomon and Sleep (1974) preferred the propagating-fracture hypothesis, in part because it avoided the necessity of an abnormal and unknown source of heat in the asthenosphere. They emphasized that the stresses in the Pacific plate can be explained entirely in terms of the forces acting on plate boundaries, and that such mechanisms have the attractive feature of being amenable to numerical treatment. They proposed that the continued motion of the plate with respect to the boundary force field and to secondary convection cells in the asthenosphere might cause a linear propagating fracture as new parts of the plate moved into zones of tension, and that such a tensional fracture would permit the passive upwelling of volcanic material from below. This model offers no explanation why Hawaii is located where it is. In addition, passive mantle upwelling seems inadequate to produce the enormous volume of lava that comprises the Hawaiian Islands.

Turcotte and Oxburgh (1973, 1976, 1978) also subscribed to propagating tensional fractures as a possible cause of linear midplate volcanism. They noted that although brittle failure may occur at the surface of a plate, plastic failure is more likely at depth where lithostatic pressure is large compared with the yield stress. Theoretically, plastic and brittle failure will occur at angles of 35° and 45°, respectively, to the direction of tension (fig. 1.15*A*). Possible causes of tension include thermal stresses in the cooling and thickening plate as it moves outward from the spreading ridge and membrane stresses caused by the movement of plates on the surface of the nonspherical Earth (fig. 1.15*B*, *C*). Turcotte and Oxburgh note that the angle between the Hawaiian Chain and the direction of sea-floor spreading, as deduced from magnetic anomalies and fracture zones, is 34°, in good agreement with the predicted value. They also note that the angle between the trend of the chain and the

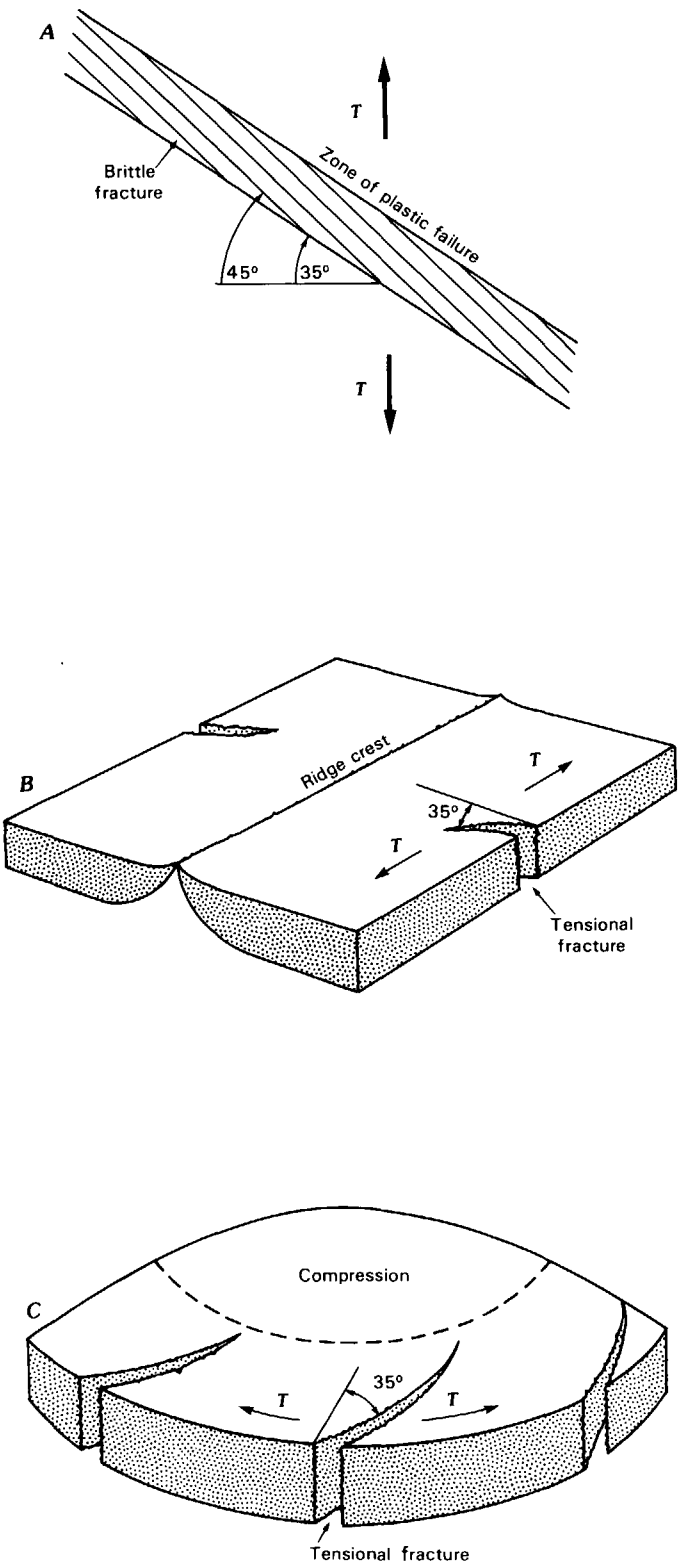

FIGURE 1.15.—Tensional stresses as a possible cause of propagating fractures in lithospheric plates. ***A***, Orientation of plastic and brittle failure in thin plate under tension (*T*) according to Turcotte and Oxburgh (1973, 1976, 1978). ***B***, Fracture in lithospheric plate from tensional stress caused by cooling and thickening of plate away from spreading ridge. ***C***, Fracture caused by membrane stresses in northward-moving plate on oblate Earth.

loci of Jackson and others (1972) is approximately correct for brittle fracture. The Cook-Austral, Tuamoto-Pitcairn, and Kodiak-Bowie Chains also lie at angles of between 31° and 42° to spreading directions, but the angle made by the Marquesas is 60°, which is much larger than that predicted by Turcotte and Oxburgh (1978).

Both plastic and brittle failure, as proposed by Turcotte and Oxburgh, provide a means of propagating a fracture as a function of plate motion and might account for some degree of hot-spot fixity. The thermal mechanism relies on cooling and thickening of the plate as a function of time and distance from the spreading ridge. Once started, the fracture will propagate from a point that remains at a fixed crustal age from the ridge. As these authors point out, fractures due to membrane stresses would be most likely in middle latitudes because the change in the radius of curvature of the Earth is a maximum at a latitude of about 45°. For a plate in the northern hemisphere moving northward, the fracture would propagate southward from a point that remains latitudinally fixed. This mechanism does not, however, account for the great variety of latitudes of active Pacific hot spots, the parallelism of Pacific volcanic chains, or the Hawaiian-Emperor bend (Solomon and Sleep, 1974).

Handschumacher (1973) advanced three fracture-related explanations for the Emperor Seamount Chain, but he did not extend them to include the Hawaiian Chain. Two of the mechanisms, extrusion along a strike-slip fault and interaction between a stable part of the Pacific plate on the west and a spreading ridge on the east, have since been disproved by the age progression (younger southward) of the Emperor volcanoes. The third mechanism, secondary activity along a zone of weakness between eastern and western parts of the plate, invokes preexisting structural control, but, like all propagating fracture hypotheses, does not provide any insight into the lava-producing mechanism.

THERMAL AND CHEMICAL CONVECTION HYPOTHESES

Numerous authors have associated the Hawaiian Chain with thermally driven convection in the asthenosphere. Among the earliest were Dietz and Menard (1953) and Menard (1955), who hypothesized that the Hawaiian Arch or swell occurred over the intersection of two upwelling and diverging convection cells. This would put the lithosphere under tension and produce fracturing as the volcanic load increased, providing a reasonable explanation for the geometry and form of the Hawaiian Arch, Ridge, and Deep. It does not, however, account for the constant rate of propagation of volcanism along the chain, although in 1955 this was poorly known. Although he did not discuss the Hawaiian Chain, Wilson (1962) showed it to be coincident with an early Tertiary ridge which he suggested formed by diverging convection cells.

Wilson (1963a, b, c, d) was the first to suggest a thermal convection mechanism that specifically addressed the age progression in the Hawaiian and eight other parallel chains in the Pacific. He speculated that the source of lava resided in the stagnant, or at least more slowly moving, region of a mantle convection cell (fig. 1.16). Spreading of the sea floor above this fixed source would result in an age-progressive chain of volcanoes. Wilson (1963a) tentatively put the source at a depth of about 200 km, below the low-velocity zone, but did not speculate on the ultimate cause of the lava source.

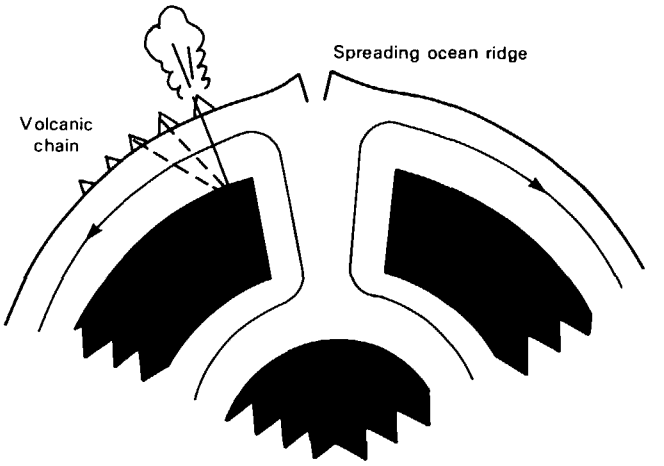

FIGURE 1.16.—Wilson's proposed possible origin of Hawaiian Chain. If lava is generated in stable core of mantle convection cell and surface is carried along by plate motion, then one source can give rise to a chain of successively extinct volcanoes. Modified from Wilson (1963), by permission of the National Research Council of Canada.

The hypothesis that has undoubtedly received the most attention since Wilson's is that of Morgan (1971, 1972a, b) who proposed that the Hawaiian and other Pacific hot spots were narrow thermal zones of upwelling, which he termed "plumes," that originate deep within the Earth's mantle, possibly near the core. They arise because of thermal instabilities (excess heat), which cause upward convection of hot plumes of mantle rock in much the same way that thermal instabilities in the atmosphere cause thunderhead clouds. According to this hypothesis, the plumes are of relatively low viscosity, about 150 km in diameter, and convect upward at a rate of about 2 m/yr. In addition to providing lava for volcanic chains, plumes are considered by Morgan to be a driving force of plate tectonics, to be capable of rifting continents, and to occur on midocean ridges as well as in the middle of plates. Morgan identified about 20 hot spots, but subsequent authors have tended to be more generous (for example, Burke and Wilson, 1976; Crough, 1983).

One aspect of Morgan's hypothesis that has proven extremely important to the study of plate tectonics, whether or not hot spots are actually plumes, is the concept that hot spots are fixed relative to one another and to the Earth's spin axis. As we discussed earlier, hot-spot fixity appears to be generally true for long periods of geologic time, and thus hot spots provide a stable reference frame for studies of absolute plate motions.

Morgan (1972a, 1972b) observed that most hot spots were characterized by a positive gravity anomaly and a topographic high, both of which, he said, are symptomatic of rising thermal currents in the mantle. Morgan calculated that as few as 20 plumes could bring up from depth an estimated 500 km^3/yr of mantle material and half of the total heat flow from the Earth.

Wilson (1973) endorsed the plume hypothesis and likened plumes to other natural diapiric mechanisms such as salt domes, thunderheads, and volcanic pipes. Menard (1973) noted that the Hawaiian, Austral-Cook (Macdonald Seamount), and Gulf of Alaska hot spots all lie on the updrift side of asthenospheric bumps and concluded that equally persistent rising plumes were required to sustain the asthenospheric relief at sites not associated with hot spots. Strong (1974) noted that the compositions of Kilauea and Mauna Loa lava were not the same, concluded that the Hawaiian plume was probably not the direct source of lava, and questioned whether Morgan's plumes were necessarily zones of mass transport. Alternatively, he suggested they might be zones of high thermal conductivity or concentrated diffusion.

Morgan (1972b) proposed four tests of the plume hypothesis, including seismic detection, prediction of plate motions from plume dynamics, evaluation of the necessity of plumes for heat transport from the deep mantle, and correlation of changes in Cenozoic and Cretaceous spreading patterns with the disappearance or emergence of new hot spots. Of the four, only the seismic test had any real potential for yielding a conclusive answer. Davies and Sheppard (1972), Kanasewich and others (1972, 1973), and Kanasewich and Gutowski (1975) analyzed seismic rays passing beneath the Hawaiian Islands from earthquakes in the southwest Pacific. They concluded that there is a zone of abnormally high velocities near the core-mantle boundary beneath Hawaii and that the seismic data are generally consistent with Morgan's plume hypothesis, although there were no data indicating an extension of the velocity anomaly upward through the upper mantle. The interpretation of the seismic data was questioned by Wright (1975) and Green (1975), who concluded that the observed travel time anomalies were most likely the result of upper mantle inhomogeneities beneath the seismic detector arrays in western North America. From a study of teleseismic arrivals from 55 earthquakes recorded at 21 stations on Hawaii, however, Ellsworth and others (1975) found evidence of lower than average velocities at depths of 30–50 km beneath the island. Whether this anomaly extends into the asthenosphere is unknown. Thus, the seismic evidence for a thermal plume beneath Hawaii appears to be, at best, inconclusive.

One difficulty with the plume hypothesis is that narrowly confined convection is unstable in fluids with high Prandtl numbers (kinematic viscosity divided by thermal diffusivity) such as mantle material (Turcotte and Oxburgh, 1978). Narrow plumes might be sustained, however, if confined to the upper mantle and heated from below by a lower mantle source (Turcotte and Oxburgh, 1978). Another problem is that the amount of partial melting that would result from the adiabatic decompression of mantle material rising from the core-mantle boundary is much too high to result in Hawaiian basalt (Turcotte and Oxburgh, 1978). This objection might not apply if mantle plumes are a source of heat for melting of the lower lithosphere or the uppermost asthenosphere rather than a direct source of magma.

An alternative to thermal plumes, proposed by Anderson (1975), is that the plumes are relict compositional conduits. According to Anderson's hypothesis, the Earth accreted inhomogeneously and in the sequence in which compounds would condense from a cooling nebula. Thus, the primitive deep mantle was a material enriched in Ca, Al, Ti, and the refractory trace elements, including U and Th. This material, being less dense than the overlying layers, rose as chemical plumes through buoyancy early in Earth's history and partially melted to yield anorthosites. Present-day hot spots occur above the mantle residua of this partial melting. These plumes provide heat to the base of the lithosphere because they are enriched in heat-producing elements, principally U and Th, and so constitute what could be called radioactive hot spots. Chemical plumes might explain both asthenospheric bumps and also the episodic nature of volcanism. Anderson proposed that the rapid withdrawal of heat by magma could periodically outstrip heat production and therefore temporarily halt magma generation. However, one would think that the chemical inhomogeneities should be seismically detectable.

Richter (1973) and Richter and Parsons (1975) have suggested that the Hawaiian-Emperor Chain and other linear chains might be a consequence of the nonlinear interaction of two different scales of mantle convection, one involving sea-floor spreading and the return flow necessary to conserve mass, and the other a Rayleigh-Benard convection reaching to depths of about 650 km. This latter convection forms rolls whose axes initially are aligned perpendicular to the spreading direction. In time, however, the latitudinal rolls give way to longitudinal rolls with axes parallel to the direction of plate motion (fig. 1.17). The time for the transition to occur depends on the spreading velocity, but may be as short as about 20 m.y. for a fast (about 10 cm/yr) plate like the Pacific plate. Longitudinal rolls will generate alternating bands of tension and compression in the overlying plate. Linear volcanic chains might form along the zones of tension and, either because of modulation of convection amplitude along the roll or because of the fracture properties of the plate, could propagate opposite to the direction of spreading. A feature of this mechanism is that ages out of order can occur. In addition, an age gap of some tens of millions of years could occur near the bend in the Hawaiian-Emperor Chain because of the time required for a new set of longitudinal rolls to be established

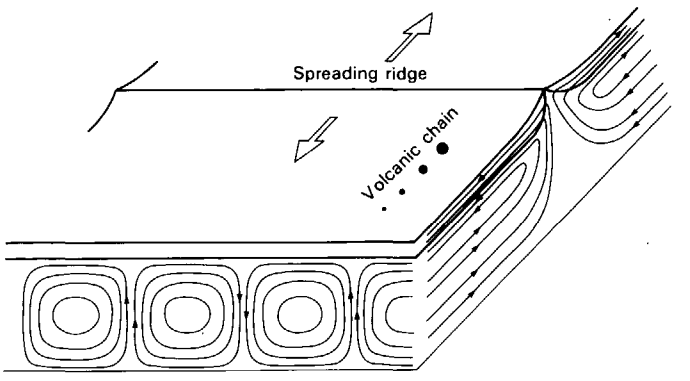

FIGURE 1.17.—Schematic diagram of large-scale asthenospheric flow related to sea-floor spreading and superimposed small-scale longitudinal rolls. Volcanic chain might occur in zone of tension between diverging rolls and would propagate opposite to direction of spreading. From Richter and Parsons (1975).

following a change in spreading direction. The age data for the Hawaiian-Emperor Chain (fig. 1.5), however, show that the propagation is continuous around the bend, although seamounts are sparse on the westernmost Hawaiian Ridge. Another feature of the longitudinal roll model is that parallel volcanic chains should be spaced at some multiple of twice the depth of the convecting layer, which is in accord with the geometry of the major Pacific chains for a convecting depth of about 600 km (Richter, 1973).

SHEAR-MELTING HYPOTHESES

Shear melting with thermal feedback to regulate the propagation rate was proposed by Shaw (1973) to explain the nonlinear time-distance-volume relations along the Hawaiian Chain noted by Jackson and others (1972) and Swanson (1972) (fig. 1.18). According to his hypothesis, the hot spot is the result of a delicately balanced thermomechanical process that derives energy from plate motion and is regulated by a feedback process inherent in the physical properties of the rocks involved. In principle, the idea is quite simple and is based on the observation that a viscous medium will rise in temperature when sheared. Shear occurs within a finite zone between the lower lithosphere and the upper asthenosphere because of their relative motion. As shear proceeds the temperature rises and the viscosity decreases within the shear zone. This allows an increase in the rate of shearing, which in turn produces a further increase in temperature. The increasing temperature eventually results in partial melting and the formation of magma, which rises to the surface to form the volcanoes. The magma carries off excess heat, the temperature decreases rapidly, viscosity increases, and melting stops temporarily as a new cycle is initiated. Each cycle lasts a few million years and is characterized by accelerating propagation of volcanism and eruption volume followed by a sudden halt.

A means of localizing shear melting and fixing the resulting hot spot relative to the mantle was advanced by Shaw and Jackson (1973). They proposed that once partial melting began the residua sinks, forming a type of gravitational anchor that reaches down into the mantle, perhaps to the core-mantle boundary (fig. 1.19). The downwelling anchor not only forms a geographic pinning point for the hot spot but also results in the inflow of fresh mantle material beneath the hot spot, which thus is not limited by supply. There is strong evidence, however, that the depleted residua from partial melting of the most likely parent rocks are less dense than the parent material and would not sink (see, for example, O'Hara, 1975; Boyd and McCallister, 1976; Jordan, 1979). Thus, unless the source of Hawaiian basalt is something quite unusual, the formation of a gravitational anchor seems unlikely, and the shear-melting hypothesis suffers from the lack of both a starting mechanism and a means of localization.

HEAT-INJECTION HYPOTHESIS

It has long been known that the Hawaiian hot spot, among others, is associated with a broad topographic anomaly on the ocean floor, the Hawaiian swell, which has been attributed to some sort of thermal anomaly for more than three decades (see, for example, Dietz and Menard, 1953; Menard, 1955). Only recently, however, has it become clear that the swell may be the result of thermal resetting and thinning of the aging and thickening lithosphere. Detrick and Crough (1978) observed that long-term rates of subsidence of volcanoes in the Pacific are higher than can be accounted for by the subsidence that accompanies the cooling and thickening of the lithosphere as it moves away from the spreading ridge (Parsons and Sclater, 1977; Schroeder, 1984). They proposed that the excess subsidence is the result of thermal resetting of the lithosphere as the aging plate rides over the hot spot. The resetting is accompanied by lithospheric thinning and a rise in the elevation of the sea floor. The rapid subsequent subsidence then represents a gradual return of these shallow areas to normal depths, that is, depths commensurate with the age of the sea floor (see also Crough, 1979, 1983; Epp, 1984). The hypothesis of thermal resetting is supported by anomalously high heat flow along the

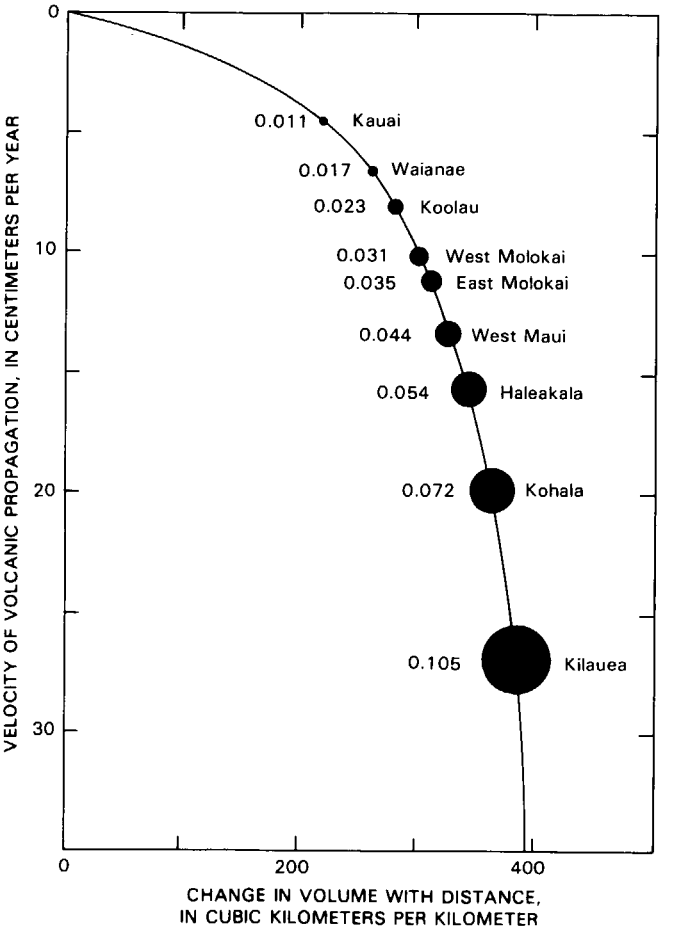

FIGURE 1.18.—Change in volume of lava with respect to unit distance versus change in distance with respect to time (velocity of volcanic propagation) for principal Hawaiian Islands. Diameter of circles approximately proportional to apparent eruption rates, which are also given (in cubic kilometers per year) next to circles. From Shaw (1973).

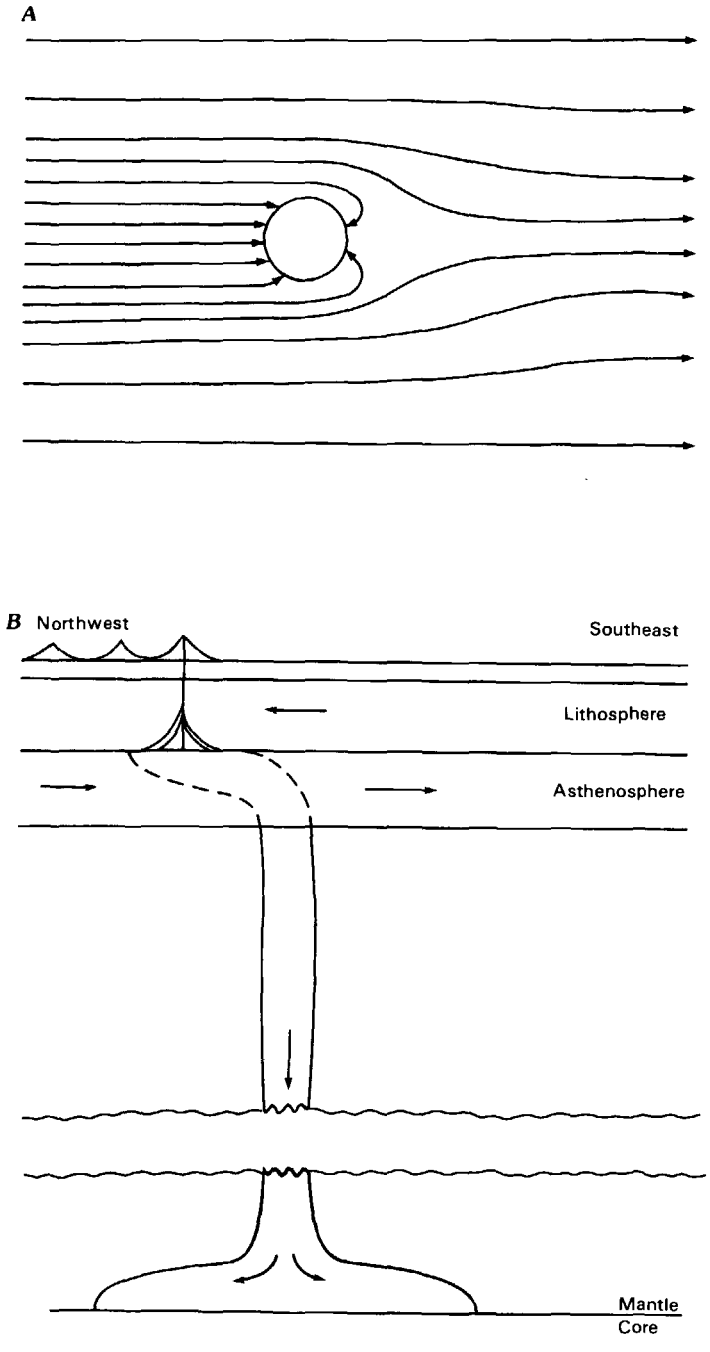

FIGURE 1.19.—Schematic views of possible downwelling of dense residua from tholeiitic melting. *A*, Plan view showing hypothetical flow lines in asthenosphere along horizontal plane taken at time near culmination of melting episode. *B*, Vertical section showing proposed gravitational anchor. From Shaw and Jackson (1973).

Hawaiian Ridge (Detrick and others, 1981). The concept of lithospheric thinning over hot spots is substantiated by the flexural data, which indicate that the lithosphere over hot spots is much thinner than that of comparable age flexed at subduction zones (McNutt, 1984).

Detrick and Crough (1978) recognized that the major problem with their thermal model for the Hawaiian swell is that it requires extremely rapid heating of the lithosphere; a heat flux more than 40 times normal is indicated, if the heating is entirely by conduction. This is because the kinematics of plate motion relative to the hot spot requires the swell to rise in only a few million years, whereas it would take about 100 m.y. at twice the normal heat flux to raise the swell. This problem, however, may not be as serious as it once seemed. More recent modeling by Nakiboglu and Lambeck (1985) demonstrates the sensitivity of these calculations to the lower boundary condition. They argue that most of the Hawaiian swell can be produced by thermal conduction, but a small dynamic component may also be required to support the swell. Another potential solution to this problem, proposed by McNutt (1984), is lithospheric delamination, a process invoked by Bird (1979) to explain volcanism in continental interiors. According to this hypothesis, a strip of the lower lithosphere separates from the upper lithosphere and descends into the asthenosphere. This produces the sudden rise in temperature at the base of the remaining lithosphere required to produce the swell without invoking an unreasonable heat flux. The lateral resistance of the descending strip might also provide the necessary stability of the hot spot with respect to the mantle. It is unclear how delamination might begin, but once started theory suggests that it can propagate at plate velocities (Bird and Baumgardner, 1981).

One problem with delamination is that it requires the sinking into the asthenosphere of the lower lithosphere, which is thought to be one component of the source of ocean-island basalt. For Hawaii the proposed depth of delamination, that is, the thickness of the lithosphere over the hot spot, is slightly less than 30 km (McNutt, 1984), a depth considered to be well above the source region of Hawaiian basalt. It is also clear from pressure-temperature relations that the descending slab would not melt (and if it did the residua would rise rather than sink). Therefore, Hawaiian basalt would have to be generated from the material of the upper asthenosphere, although at lower lithosphere depths, and the lithosphere-asthenosphere boundary would be a purely mechanical one (that is, with no compositional differences across the boundary).

In summary, geophysical models for the Hawaiian hot spot tend to be highly generalized and difficult if not impossible to test. None has yet been advanced that satisfactorily explains all of the geometric, kinematic, physical, and chemical observations from the Hawaiian-Emperor Chain. Although many intriguing and clever ideas have been advanced, the hot-spot mechanism is still somewhat mysterious. Detrick and Crough's (1978) idea that the Hawaiian swell is caused by thermal resetting of the aging ocean crust implies that hot spots are indeed hot. In addition, the possibility that the swell is dynamically supported (Detrick and Crough, 1978) implies that material wells up beneath the lithosphere. Petrologic studies indicate that Hawaiian lava is generated from mantle sources consisting of at least 3 geochemical components; one of these is a primitive undegassed component. The cause of the Hawaiian hot spot is still unknown, but present hypotheses are consistent with Morgan's plume hypothesis in which hot primitive mantle material ascends beneath the ocean lithosphere below Hawaii and reacts with

the lithosphere to produce the compositional range of Hawaiian lava.

REFERENCES

Anderson, D.L., 1975, Chemical plumes in the mantle: Geological Society of America Bulletin, v. 86, p. 1593-1600.

Bargar, K.E., and Jackson, E.D., 1974, Calculated volumes of individual shield volcanoes along the Hawaiian-Emperor Chain: U.S. Geological Survey Journal of Research, v. 2, p. 545-550.

Bargar, K.E., Marshall, M., and Trumbull, J.V.A., 1975, Bathymetry and ice-rafted pebbles from the northern end of the Emperor Seamount Chain: U.S. Geological Survey Open-File Report 75–609, 18 p.

Basaltic Volcanism Study Project, 1981, Basaltic Volcanism on the Terrestrial Planets: New York, Permagon Press, Inc., 1286 p.

Beeson, M.H., 1976, Petrology, mineralogy and geochemistry of the East Molokai Volcanic Series, Hawaii: U.S. Geological Survey Professional Paper 961, 53 p.

Betz, F., Jr., and Hess, H.H., 1942, The floor of the North Pacific Ocean: The Geographical Review, v. 32, p. 99-116.

Bezrukov, P.L., and Udintsev, G.B., 1955, The northern end of the Hawaiian suboceanic ridge: Doklady Akademiya Nauk, v. 103, no. 6, p. 1077-1080.

Bird, P., 1979, Continental delamination and the Colorado Plateau: Journal of Geophysical Research, v. 84, p. 7561-7571.

Bird, P., and Baumgardner, J., 1981, Steady propagation of delamination events: Journal of Geophysical Research, v. 86, p. 4891-4903.

Bonhommet, N., Beeson, M.H., and Dalrymple, G.B., 1977, A contribution to the geochronology and petrology of the Island of Lanai, Hawaii: Geological Society of America Bulletin, v. 88, p. 1282-1286.

Boyd, F.R., and McCallister, R.A., 1976, Densities of fertile and sterile garnet peridotite: Geophysical Research Letters, v. 3, p. 509-512.

Brigham, W.T., 1868, Notes on the Volcanic phenomena of the Hawaiian Islands: Boston, Society of Natural History, Memoir, 1, p. 341-472.

———1909, The volcanoes of Kilauea and Mauna Loa: Bernice Pauahi Bishop Museum, Memoir 2, no. 4, 222 p.

Bryan, W.A., 1915, Natural History of Hawaii: Honolulu, Hawaiian Gazette Co., 569 p.

Budahn, J.R., and Schmitt, R.A., 1984, Petrogenetic modelling of Hawaiian tholeiitic basalts: A geochemical approach: Geochimica et Cosmochimica Acta, v. 49, p. 67-87.

Bukry, D., 1975, Coccolith and silicoflagellate stratigraphy, northwestern Pacific Ocean, Deep Sea Drilling Project, Leg 32, *in* Larson, R.L., Moberly, R., and others, Initial Reports of the Deep Sea Drilling Project, v. 32: Washington, U.S. Government Printing Office, p. 677-701.

Burke, K.C., and Wilson, J.T., 1976, Hot spots on the Earth's surface: Scientific American, v. 235, no. 2, p. 46-57.

Butler, R. F., and Coney, P. J., 1981, A revised magnetic polarity time scale for the Paleocene and early Eocene and implications for Pacific plate motion: Geophysical Research Letters, v. 8, p. 301-304.

Butt, A., 1980, Biostratigraphic and paleoenvironment analyses of the sediments at the Emperor Seamounts, DSDP Leg 55, northwestern Pacific: Cenozoic foraminifers, *in* Jackson, E.D., Koizumi, I., and others, Initial Reports of the Deep Sea Drilling Project, v. 55: Washington, U.S. Government Printing Office, p. 289-325.

Byron, G., 1826, Voyage of the 'Blonde' to the Sandwich Islands: London, 260 p.

Byrne, T., 1979, Late Paleocene demise of the Kula-Pacific spreading center: Geology, v. 7, p. 341-344.

Campbell, F., DeCarlo, E., McMurtry, G., and Kroenke, L., 1984, Preliminary report on the assessment of the resource potential of selected seamounts in the Exclusive Economic Zone surrounding the Hawaiian Archipelago: Hawaii Institute of Geophysics Report, October 1984, 45 p.

Chase, T.E., Menard, H.W., and Mammerickx, J., 1970, Bathymetry of the North Pacific: La Jolla, Scripps Institution of Oceanography Charts 2, 7, 8.

———1973, Bathymetric atlas of the North Pacific Ocean, N.O. Pub. No. 1301-2-3.

Chen, C.-Y., and Frey, F.A, 1983, Origin of Hawaiian tholeiites and alkalic basalt: Nature, v. 302, p. 785-789.

———1985, Trace element and isotope geochemistry of lavas from Haleakala Volcano, East Maui: Implications for the origin of Hawaiian basalts: Journal Geophysical Research, v. 90, p. 8743-8768.

Christofferson, E., 1968, The relationship of sea-floor spreading in the Pacific to the origin of the Emperor Seamounts and the Hawaiian Island Chain [abs.]: American Geophysical Union Transactions, v. 49, p. 214.

Chubb, L.J., 1934, The structure of the Pacific basin: Geological Magazine, v. 71, p. 289-302.

Clague, D.A., 1974a, The Hawaiian-Emperor Seamount Chain: Its origin, petrology, and implications for plate tectonics: University of California, San Diego, Ph.D. thesis, 319 p.

———1974b, Nephelinic lavas dredged from the western Hawaiian Ridge: Geological Society of America Abstracts 6 (3), p. 156.

———1981, Linear island and seamount chains, aseismic ridges and intraplate volcanism: Results from DSDP: Society Economic Paleontologists and Mineralogists Special Publication No. 32, p. 7-22.

———1982, Petrology of tholeiitic basalt dredged from Hualalai Volcano, Hawaii: Eos, Transactions, American Geophysical Union, v. 63, p. 1138.

———in press, Hawaiian alkaline volcanism: Journal of the Geological Society of London.

Clague, D.A., and Beeson, M.H., 1980, Trace element geochemistry of the East Molokai Volcanic Series, Hawaii: American Journal of Science, v. 280-A, p. 820-844.

Clague, D.A., and Dalrymple, G.B., 1973, Age of Koko Seamount, Emperor Seamount Chain: Earth and Planetary Science Letters, v. 17, p. 411-415.

———1975, Cretaceous K-Ar ages of volcanic rocks from the Musicians Seamounts and the Hawaiian Ridge: Geophysical Research Letters, v. 2, p. 305-308.

Clague, D.A., Dalrymple, G.B., Greene, H.G., Wald, D., Kono, M., and Kroenke, L., 1980b, Bathymetry of the Emperor Seamounts, *in* Jackson, E.D., Koisumi, I., and others, Initial Reports of the Deep Sea Drilling Project, v. 55: Washington, U.S. Government Printing Office, p. 845-849.

Clague, D. A., Dalrymple, G. B., and Moberly, R., 1975, Petrography and K-Ar ages of dredged volcanic rocks from the western Hawaiian ridge and the southern Emperor Seamount Chain: Geological Society of America Bulletin, v. 86, p. 991-998.

Clague, D.A., Dao-Gong, C., Murnane, R., Beeson, M.H., Lanphere, M.A., Dalrymple, G.B., Friesen, W. and Holcomb, R.T., 1982, Age and petrology of the Kalaupapa Basalt, Molokai, Hawaii: Pacific Science, v. 36, p. 411-420.

Clague, D.A., Fisk, M.R., and Bence, A.E., 1980a, Mineral chemistry of basalts from Ojin, Nintoku, and Suiko Seamounts, Leg 55 DSDP, *in* Jackson, E.D., Koisumi, I., and others, Initial Reports of the Deep Sea Drilling Project, v. 55: Washington, U.S. Government Printing Office, p. 607-637.

Clague, D.A., and Frey, F.A., 1979, Petrology of the Hawaiian-Emperor volcanic chain: Hawaii Symposium on Intraplate volcanism and submarine volcanism, Abstracts Volume, p. 118.

———1980, Trace element geochemistry of tholeiitic basalts from site 433C, Suiko Seamount, *in* Jackson, E.D., Koisumi, I., and others, Initial Reports of the Deep Sea Drilling Project v. 55: Washington, U.S. Government Printing Office, p. 559-569

———1982, Petrology and trace element geochemistry of the Honolulu Volcanics, Oahu: Implications of the oceanic mantle beneath Hawaii: Journal of Petrology, v. 23, 447-504.

Clague, D.A., Frey, F.A., and Beeson, M.H., 1983, Rare-earth element and Sr isotopic evidence for the origin of the East Molokai volcanics, Hawaii: Eos, Transactions, American Geophysical Union, v. 64, p. 902.

Clague, D.A., Jackson, E.D., and Wright, T.L., 1980c, Petrology of Hualalai volcano, Hawaii: Implication for mantle composition: Bulletin Volcanologique, v. 43-4, p. 641-656.

Clague, D.A., and Jarrard, R.D., 1973, Tertiary Pacific plate motion deduced from the Hawaiian-Emperor Chain: Geological Society of America Bulletin, v. 84, p. 1135-1154.

Coan, T., 1840, Missionary Herald, xxxvii, p. 283.

Cole, W.S., 1969, Larger foraminifera from deep drill holes on Midway Atoll: U.S. Geological Survey Professional Paper 680-C, 15 p.

Creager, J.S., Scholl, D.W., 1973, Geological synthesis of Leg 19, Deep Sea Drilling Project, results: Far North Pacific, and Aleutian Ridge, and Bering Sea, *in* Creager, J.S., Scholl, D.W., and others, Initial Reports of the Deep Sea Drilling Project, v. 19: Washington, U.S. Government Printing Office, p. 897-913.

Cross, W., 1904, An occurrence of trachyte on the Island of Hawaii: Journal of Geology, v. 12, p. 510-523.

———1915, Lavas of Hawaii and their relations: U.S. Geological Survey Professional Paper 88, 97 p.

Crough, S.T., 1979, Hotspot epeirogeny: Tectonophysics, v. 61, p. 321-333.

———1983, Hotspot swells: Annual Reviews of Earth and Planetary Sciences, v. 11, p. 165-193.

Dalrymple, G.B., 1971, Potassium-argon ages from the Pololu Volcanic Series, Kohala Volcano, Hawaii: Geological Society of America Bulletin, v. 82, p. 1997-2000.

Dalrymple, G.B., and Clague, D.A., 1976, Age of the Hawaiian-Emperor bend: Earth and Planetary Science Letters, v. 31, p. 313-329.

Dalrymple, G.B., Clague, D.A., Garcia, M.O., and Bright, S.W., 1981, Petrology and K-Ar ages of dredged samples from Laysan Island and Northampton Bank volcanoes, Hawaiian Ridge, and evolution of the Hawaiian-Emperor Chain: Geological Society of America Bulletin Part II, v. 92, p. 884-933 (Summary in Part I, v. 92, p. 315-318).

Dalrymple, G.B., Clague, D.A., and Lanphere, M.A., 1977, Revised age for Midway volcano, Hawaiian volcanic chain: Earth and Planetary Science Letters, v. 37, p. 107-116.

Dalrymple, G.B., and Garcia, M.O., 1980, Age and chemistry of volcanic rocks dredged from Jingu Seamount, Emperor Seamount Chain, *in* Jackson, E.D., Koisumi, I., and others, Initial Reports of the Deep Sea Drilling Project, v. 55: Washington, U. S. Government Printing Office, p. 685-693.

Dalrymple, G.B., Greene, H.G., Ruppel, B.D., Bear, T.E., and Clague, D.A., 1980a, Pre-leg 55 site survey geophysical data from the Research Vessel S.P. *Lee* cruise LEE 8-76-NP, *in* Jackson, E.D., Koisumi, I., and others, Initial Reports of the Deep Sea Drilling Project, v. 55: Washington, U.S. Government Printing Office, p. 801-844.

Dalrymple, G.B., Lanphere, M.A., and Clague, D.A., 1980b, Conventional and $^{40}Ar/^{39}Ar$ K-Ar ages of volcanic rocks from Ojin (Site 430), Nintoku (Site 432), and Suiko (Site 433) Seamounts and the chronology of volcanic propagation along the Hawaiian-Emperor Chain, *in* Jackson, E.D., Koisumi, I., and others, Initial Reports of the Deep Sea Drilling Project, v. 55: Washington, U.S. Government Printing Office, p. 659-676.

Dalrymple, G.B., Lanphere, M.A., and Jackson, E.D., 1974, Contributions to the petrography and geochronology of volcanic rocks from the leeward Hawaiian Islands: Geological Society of America Bulletin, v. 85, p. 727-738.

Dalrymple, G.B., Lanphere, M.A., and Natland, J.H., 1980c, K-Ar minimum age for Meiji Guyot, Emperor Seamount Chain, *in* Jackson, E.D., Koisumi, I., and others, Initial Reports of the Deep Sea Drilling Project: v. 55: Washington, U.S. Government Printing Office, p. 677-683.

Dalrymple, G.B., Silver, E.A., and Jackson, E.D., 1973, Origin of the Hawaiian Islands: American Scientist, v. 61, p. 294-308.

Daly, R.A., 1911, The nature of volcanic action: American Academy of Arts and Sciences Proceedings, v. 47, no. 3, p. 45-122.

Dana, E.S., 1877, Contributions to the petrography of the Sandwich Islands: American Journal of Science, series 3, v. 37, p. 441-467.

Dana, J.D., 1849, United States Exploring Expedition During the Years 1838, 1839, 1840, 1841, 1842: New York, George P. Putnam, 756 p.

———1887, History of the changes in the Mt. Loa Craters, on Hawaii: American Journal of Sciences, series 3, v. 33, p. 433-451; v. 34, p. 81-97, p. 349-364.

———1888, History of the changes in the Mt. Loa Craters, on Hawaii: American Journal of Sciences, series 3, v. 35, p. 15-34, p. 213-228, p. 282-289; v. 36, p. 14-32, p. 81-112, p. 167-175.

———1889, Points on the geologic history of the islands Maui and Oahu: American Journal of Sciences, series 3, v. 37, p. 81-103.

Darwin, C. 1837, On certain areas of elevation and subsidence in the Pacific and Indian Oceans, as deduced from the study of coral formations: Proceedings of the Geological Society of London, v. 2, p. 552-554.

———1842, The Structure and Distribution of Coral Reefs: New York, Appleton.

Davies, D., and Sheppard, R.M., 1972, Lateral heterogeneity in the Earth's Mantle: Nature v. 239, p. 318-323.

Davies, T.A., Clague, D.A., and Wilde, P., 1971, Preliminary report on Leg VII of Aries expedition: Geological investigations in the western North Pacific: Scripps Institution of Oceanography Reference Series, No. 71-27.

Davies, T.A., Wilde, P., and Clague, D.A. 1972, Koko Seamount: A major guyot at the southern end of the Emperor Seamounts: Marine Geology, v. 13, p. 311-321.

Detrick, R.S., and Crough, S.T., 1978, Island subsidence, hot spots, and lithospheric thinning: Journal of Geophysical Research v. 83, p.1236-1244.

Detrick, R.S., von Herzen, R.P., Crough, S.T., Epp, D. and Felin, U., 1981, Heat flow on the Hawaiian swell and lithosphere reheating: Nature, v. 292, p. 142-143.

Dietz, R.S., 1954, Marine geology of northwestern Pacific: description of Japanese bathymetric chart 6901: Geological Society of America Bulletin, v. 65, p. 1199-1224.

Dietz, R.S., and Menard, H.W., 1953, Hawaiian swell, deep, and arch, and subsidence of the Hawaiian Islands: The Journal of Geology, v. 61, p. 99-113.

Doell, R.R., 1972, Paleomagnetism of volcanic rocks from Niihau, Nihoa, and Necker Islands, Hawaii: Journal of Geophysical Research, v. 77, p. 3725-3730.

Doell, R.R., and Dalrymple, G.B., 1973, Potassium-argon ages and paleomagnetism of the Waianae and Koolau Volcanic Series, Oahu, Hawaii: Geological Society of America Bulletin, v. 84, p. 1217-1242.

Duncan, R.A., and Clague, D.A., 1984, The earliest volcanism on the Hawaiian Ridge: Eos, Transactions, American Geophysical Union, v. 65, p. 1076.

———1985, Pacific plate motion recorded by linear volcanic chains, *in* Nairn, A.E.M., Stehli, F.G., and Uyeda, S., eds., The ocean basins and margins, v. 7A: New York, Plenum, p. 89-121.

Dutton, C.E., 1884, Hawaiian volcanoes: U.S. Geological Survey Annual Report, v. 4, p. 75-219.

Dzurisin, D., Koyanagi, R.Y., and English, T.T., 1984, Magma supply and storage at Kilauea Volcano, Hawaii, 1956-1983: Journal of Volcanology and Geothermal Research, v. 21, p. 177-206.

Eaton, J.P., and Murata, K.J., 1960, How volcanoes grow: Science, v. 132, p. 925-938.

Ellis, W., 1823, A narrative of tour through Hawaii: London, 367 p., reprinted Honolulu, 1917.

Ellsworth, W.L., Cipar, J.J., Ward, P.L., Aki, R., Koyanagi, R., and Unger, J., 1975, Crust and upper mantle structure of Kilauea Volcano, Hawaii: Grenoble, Abstracts of papers presented at the Interdisciplinary Symposia, International Union of Geodesy and Geophysics, XVI General Assembly, p. 109-110.

Epp, D., 1978, Age and tectonic relationships among volcanic chains on the Pacific plate: University of Hawaii, Ph.D. thesis, 199 p.

———1984, Implications of volcano and swell heights for thinning of the lithosphere by hotspots: Journal of Geophysical Research, v. 89, p. 9991-9996.

Evernden, J.F., Savage, D.E., Curtis, G.H., and James, G.T., 1964, Potassium-argon dates and the Cenozoic mammalian chronology of North America: American Journal of Science v. 262, p. 145-198.

Feigenson, M.D., 1984, Geochemistry of Kauai Volcanics and a mixing model for the origin of Hawaiian alkalic basalts: Contributions to Mineralogy and Petrology, v. 87, p. 109-119.

Feigenson, M.D., Hofmann, A.W. and Spera, F.J., 1983, Case studies on the origin of basalt II. The transition from tholeiitic to alkalic volcanism on Kohala Volcano, Hawaii: Contributions to Mineralogy and Petrology, v. 84, p. 390-405.

Fiske, R.S., and Jackson, E.D., 1972, Orientation and growth of Hawaiian volcanic rifts—the effect of regional structure and gravitational stresses: Royal Society of London, Proceedings, series A, v. 329, p. 299-326.

Fodor, R.V., Keil, K., and Bunch, T.E., 1975, Contributions to the mineral chemistry of Hawaiian rocks IV. Pyroxenes in rocks from Haleakala and West Maui Volcanoes, Maui, Hawaii: Contributions to Mineralogy and Petrology, v. 50, p. 173-195.

Frey, F.A., 1980, The origin of pyroxenites and garnet pyroxenites from Salt Lake Crater, Oahu, Hawaii: Trace element evidence: American Journal of Science, v. 280-A, 427-449.

———1984, Rare earth element abundances in upper mantle rocks, *in* Henderson, P., ed., Rare earth element geochemistry: Amsterdam, Elsevier, p. 153-203.

Frey, F.A., and Clague, D.A, 1983, Geochemistry of diverse basalt types from Loihi Seamount, Hawaii: Petrogenetic implications: Earth and Planetary Science Letters, v. 66, 337-355.

Frey, F.A., Kennedy, A., Garcia, M.O. West, H.B., Wise, W.S. and Kwon, S.-T., 1984, Mauna Kea Volcano, Hawaii: Lava compositions and their evolution: Eos, Transactions, American Geophysical Union, v. 65, p. 300.

Frey, F.A., and Roden, M.F., in press, The mantle source for the Hawaiian Islands: Constraints from the lavas and ultramafic inclusions, *in* Menzies, M., and Hawkesworth, C., eds., Mantle metasomatism.

Funkhouser, J.G., Barnes, I.L., and Naughton, J.J., 1968, The determination of a series of ages of Hawaiian volcanoes by the potassium-argon method: Pacific Science, v. 22, p. 369-372.

Garcia, M.O., Frey, F.A., and Grooms, D.G., in press, Petrology of volcanic rocks from Kaula Island, Hawaii: Implications for the origin of Hawaiian phonolites: Contributions to Mineralogy and Petrology.

Garcia, M.O., Grooms, D.G., and Naughton, J.J., in press, Petrology and geochronology of volcanic rocks from seamounts along and near the Hawaiian Ridge: Contributions to Mineralogy and Petrology.

Gast, P.W. 1968, Trace element fractionation and the origin of tholeiitic and alkaline magma types: Geochimica Cosmochimica Acta, v. 32, p. 1057-1086.

Goodrich, J., 1826, Notice of the volcanic character of the Island of Hawaii: American Journal of Science, v. 1, p. 1-36.

———1834, Letters of Rev. Joseph Goodrich: American Journal of Science, XXV, p. 199.

Gordon, R.G., 1982, The late Maastrichtian palaeomagnetic pole of the Pacific plate: Geophysical Journal of the Royal Astronomical Society, v. 70, p. 129-140.

Gordon, R.G., and Cape, C.D., 1981, Cenozoic latitudinal shift of the Hawaiian hotspot and its implications for true polar wander: Earth and Planetary Science Letters, v. 55, p. 37-47.

Gordon, R.G., Cox, A., and Harter, C.E., 1978, Absolute motion of an individual plate estimated from its ridge and trench boundaries: Nature, v. 274, p. 752-755.

Gramlich, J.W., Lewis, V.A., and Naughton, J.J., 1971, Potassium-argon dating of Holocene basalts of the Honolulu Volcanic Series: Geological Society of America Bulletin, v. 82, p. 1399-1404.

Green, A.G., 1975, On the postulated Hawaiian plume with emphasis on the limitations of seismic arrays for detecting deep mantle structure: Journal of Geophysical Research v. 80, p. 4028-4036.

Green, D.H., 1971, Composition of basaltic magmas as indicators of origin: Application to oceanic volcanism: Philosophical Transactions of the Royal Society of London, Series A, v. 268, p. 707-725.

Green, D.H., and Ringwood, A.E., 1967, The genesis of basaltic magmas: Contributions to Mineralogy and Petrology, v. 15, p. 103-190.

Green, W.L., 1887, Vestiges of the molten globe, pt. 2, The Earth's surface features and volcanic phenomena: Honolulu, 337 p.

Greene, H.G., Clague, D.A. and Dalrymple, G.B., 1980, Seismic stratigraphy and vertical tectonics of the Emperor Seamounts, DSDP Leg 55, *in* Jackson, E.D., Koisumi, I., and others, Initial Reports of the Deep Sea Drilling Project, v. 55: Washington, U.S. Government Printing Office, p. 759-788.

Greene, H.G., Dalrymple, G.B., and Clague, D.A., 1978, Evidence for northward movement of the Emperor Seamounts: Geology, v. 6, p. 70-74.

Gromme, S., and Vine, F.J., 1972, Paleomagnetism of Midway Atoll lavas and northward movement of the Pacific plate: Earth and Planetary Science Letters, v. 17, p. 159-168.

Hagn, H., Butt, A., and Malz, H., 1980, Paleocene shallow-water facies at Emperor Seamounts: DSDP Leg 55, Northwest Pacific, *in* Jackson, E.D., Koisumi, I., and others, Initial Reports of the Deep Sea Drilling Project, v. 55: Washington, U. S. Government Printing Office, p. 327-347.

Hamilton, E.I., 1965, Distribution of some trace elements and the isotopic composition of strontium in Hawaiian lavas: Nature, v. 206, no. 4981, p. 251-253.

Hamilton, E.L., 1956, Sunken Islands of the Mid-Pacific Mountains: Geological Society of America Memoir 64, 97 p.

———1957, Marine geology of the southern Hawaiian Ridge: Geological Society of America Bulletin, v. 68, p. 1011-1026.

Handschumacher, D., 1973, Formation of the Emperor Seamount Chain: Nature, v. 244, p. 150-152.

Heckel, P.H., 1974, Carbonate buildups in the geologic record: A review *in* Laporte, L.F., ed., Reefs in time and space: Society of Economic Paleontologists and Mineralogists, Special Publication no. 18, p. 90-154.

Heirtzler, J.R., Dickson, G.O., Herron, E.M., Pitman, W.C., III, and LePichon, X., 1968, Marine magnetic anomalies, geomagnetic reversals, and motions of the ocean floor and continents: Journal of Geophysical Research, v. 73, p. 2119-2136.

Hess, H.H., 1946, Drowned ancient islands of the Pacific basin: American Journal of Science, v. 244, p. 772-791.

Hilde, T.W.C., Isezaki, N. and Wageman, J.M., 1976, Mesozoic seafloor spreading in the North Pacific, *in* Sutton, G.H., Manghmani, M.H., and Moberly, R., American Geophysical Union, Geophysical Monogram, no. 19, p. 205-226.

Hillebrand, W., 1888, Flora of the Hawaiian Islands: London, Williams and Norgate, 673 p.

Hinds, N.E.A., 1931, The relative ages of the Hawaiian landscapes: University of California Publications in the Geological Sciences, v. 20, no. 6, p. 143-260.

Hitchcock, C.H., 1911, Hawaii and Its Volcanoes: Honolulu, The Hawaiian Gazette Co., 314 p.

Horibe, Y., Kim, K. and Craig, H., 1983, Off-ridge submarine hydrothermal vents: Back-arc spreading centers and hotspot seamounts: Eos, Transactions, American Geophysical Union, v. 64, p. 724.

Jackson, E.D., 1968, The character of the lower crust and upper mantle beneath the Hawaiian Islands: Prague, 23rd International Geological Conference, Proceeding 1, p. 135-150.

———1976, Linear volcanic chains on the Pacific plate, *in* Sutton, G.H., Manghnani, M.H., and Moberly, R., eds., The Geophysics of the Pacific Ocean Basin and its Margin: Washington, D.C., American Geophysical Union Monograph 19, p. 319-335.

Jackson, E.D., Koisumi, I., Dalrymple, G.B., Clague, D.A., Kirkpatrick, R.J., and Greene, H.G., 1980, Introduction and summary of results from DSDP Leg 55, the Hawaiian-Emperor Hot-Spot experiment, *in* Jackson, E.D., Koisumi, I., and others, Initial Reports of the Deep Sea Drilling Project, v. 55: Washington, U. S. Government Printing Office, p. 5-31.

Jackson, E.D., and Shaw, H.R., 1975, Stress fields in central portions of the Pacific plate: deliniated in time by linear volcanic chains: Journal of Geophysical Research, v. 80, p. 1861-1874.

Jackson, E.D., Shaw, H.R., and Bargar, K.E., 1975, Calculated geochronology and stress field orientations along the Hawaiian Chain: Earth and Planetary Science Letters, v. 26, p. 145-155.

Jackson, E.D., Silver, E.A., and Dalrymple, G.B., 1972, Hawaiian-Emperor Chain and its relation to Cenozoic circumpacific tectonics: Geological Society of America Bulletin, v. 83, p. 601-618.

Jackson, E.D., and Wright, T.L., 1970, Xenoliths in the Honolulu Volcanic Series, Hawaii: Journal of Petrology, v. 11, p. 405-430.

Jacobs, J.A., 1984, Reversals of the Earth's magnetic field: Bristol, Adam Hilger Ltd., 230 p.

Jaggar, T.A., 1917, Volcanological investigations at Kilauea: American Journal of Science, Series 4, v. 44, p. 161-220.

Jarrard, R.D., and Clague, D.A., 1977, Implications of Pacific Island and seamount ages for the origin of volcanic chains: Reviews of Geophysics and Space Physics, v. 15, p. 57-76.

Jordan, T.H., 1979, Mineralogies, densities, and seismic velocities of garnet

lherzolites and their geophysical applications, *in* Boyd, F.K., and Meyer, H.D.A., eds., The mantle sample: Inclusions in kimberlites and other volcanics: American Geophysical Union, Washington D.C., p. 1-14.

Jurdy, D.M., 1981, True polar wander: Tectonophysics, v. 74, p. 1-16.

———1983, Early Tertiary subduction zones and hot spots: Journal of Geophysical Research, v. 88, p. 6395-6402.

Kanasewich, E.R., Ellis, R.M., Chapman, C.H., and Gutowski, P.R., 1972, Teleseismic array evidence for inhomogeneities in the lower mantle and the origin of the Hawaiian Islands: Nature Physical Science, v. 239, p. 99-100.

———1973, Seismic array evidence of a core boundary source for the Hawaiian linear volcanic chain: Journal of Geophysical Research, v. 78, p. 1361-1371.

Kanasewich, E.R., and Gutowski, P.R., 1975, Detailed seismic analysis of a lateral mantle inhomogeneity: Earth and Planetary Science Letters v. 25, p. 379-384.

Kaneoka, I., Takaoka, N., and Clague, D.A. 1983, Nobel gas systematics for coexisting glass and olivine crystals in basalts and dunite xenoliths from Loihi Seamount: Earth and Planetary Science Letters, v. 66, p. 427-437.

Keil, K., Fodor, R.V., and Bunch T.E., 1972, Contribution to the mineral chemistry of Hawaiian rocks II. Feldspars and interstitial material in rocks from Haleakala and West Maui volcanoes, Maui, Hawaii: Contributions to Mineralogy and Petrology, v. 37, p. 253-276.

Kenneth, J.P. and Srinivasan, 1983, Neogene planktonic foraminifera: Strousber, Penn., Hutchinson Ross Publishing Co., p. 62-66.

Kim, K., and Craig, H., 1983, Methane: A "real-time" tracer for submarine hydrothermal systems: Eos, Transactions, American Geophysical Union, v. 64, p. 724.

Kirkpatrick, R.J., Clague, D.A., and Friesen, W., 1980, Petrology and geochemistry of volcanic rocks, DSDP Leg 55, Emperor Seamount Chain, *in* Jackson, E.D., Koisumi, I., and others, Initial Reports of the Deep Sea Drilling Project, v. 55: Washington, U.S. Government Printing Office, p. 509-557.

Klein, F.W., 1982, Earthquakes at Loihi Submarine volcano and the Hawaiian hot spot: Journal of Geophysical Research, v. 87, p. 7719-7726.

Klein, F.W., and Koyanagi, R.Y. 1979, Seismicity of Kilauea and Loihi Volcanoes, Hawaii: Hawaii Symposium on Intraplate Volcanism and Submarine Volcanism, Abstracts, p. 127.

Kodama, K., Uyeda, S., and Isezaki, N., 1978, Paleomagnetism of Suiko Seamount, Emperor Seamount Chain: Geophysical Research Letters, v. 5, p. 165-168.

Kono, M., 1980, Paleomagnetism of DSDP Leg 55 basalts and implications for the tectonics of the Pacific plate, *in* Jackson, E.D., Koisumi, I., and others, Initial Reports of the Deep Sea Drilling Project, v. 55: Washington, U.S. Government Printing Office, p. 737-758.

Kuno, H., Yamasaki, K., Iida, C., and Nagashima, K., 1957, Differentiation of Hawaiian magmas: Japanese Journal of Geology and Geography, v. 28, p. 179-218.

Kurz, M.D., Jenkins, W.J., Hart, S.R., and Clague, D., 1983, Helium isotopic variations in volcanic rocks from Loihi Seamount and the Island of Hawaii: Earth and Planetary Science Letters, v. 66, p. 388-406.

LaBrecque, J.L., Kent, D.V., and Cande, S.C., 1977, Revised magnetic polarity time scale for Late Cretaceous and Cenozoic time: Geology, v. 5, p. 330-335.

Ladd, H.S., Tracey, J.I., Jr., and Gross, M.G., 1967, Drilling on Midway Atoll, Hawaii: Science, v. 156, p. 1088-1094.

———1970, Deep drilling on Midway Atoll: U.S. Geological Survey Professional Paper 680–A, 22 p.

Lanphere, M.A., 1983, $^{87}Sr/^{86}Sr$ ratios for basalt from Loihi Seamount, Hawaii: Earth and Planetary Science Letters, v. 66, p. 380-387.

Lanphere, M.A., and Dalrymple, G.B., 1980, Age and strontium isotopic composition of the Honolulu Volcanic Series, Oahu, Hawaii: American Journal of Science, v. 280–A (Jackson Volume), p. 736-751.

Lanphere, M.A., Dalrymple, G.B., and Clague, D.A., 1980, Rb-Sr systematics of basalts from the Hawaiian-Emperor volcanic chain, *in* Jackson, E.D., Koisumi, I., and others, Initial Reports of the Deep Sea Drilling Project, v. 55: Washington, U.S. Government Printing Office, p. 695-706.

Lanphere, M.A., and Frey, F.A., in press, Geochemical Evolution of Kohala Volcano, Hawaii: Contributions to Mineralogy and Petrology.

Larson, R.L., Moberly, R., and others, 1975a, Initial Reports of the Deep Sea Drilling Project, v. 32: Washington, U.S. Government Printing Office.

———1975b, Site 311: Hawaiian magnetic lineations: Initial Reports of the Deep Sea Drilling Project, v. 32, Washington, U.S. Government Printing Office, p. 295-309.

Leeman, W.P., Budahn, J.R., Gerlach, D.C., Smith, D.R., and Powell, B.N., 1980, Origin of Hawaiian tholeiites: Trace element constraints: American Journal of Science, v. 280-A, p. 794-819.

Leeman, W.P., Murali, A.V., Ma, M.-S., and Schmitt, R.A., 1977, Mineral constitution of mantle source regions for Hawaiian basalts-rare earth element evidence for mantle heterogeneity, *in* Dick, H.J.B., ed., Magma genesis: Bulletin, Oregon Department of Geology and Mineral Industries, v. 96, p. 169-183.

Lessing, P., and Catanzaro, E.J., 1964, Sr^{87}/Sr^{86} ratios in Hawaiian lavas: Journal of Geophysical Research, v. 69, p. 1599-1601.

Livermore, R. A., Vine, F. J., and Smith, A. G., 1983, Plate motion and the geomagnetic field, I, Quaternary and late Tertiary: Geophysical Journal of the Royal Astronomical Society, v. 73, p. 151-171.

Lowrie, W., and Alvarez, W., 1981, One hundred million years of geomagnetic polarity history: Geology, v. 9, p. 392-397.

Macdonald, G.A., 1949, Hawaiian petrographic province: Geological Society of America Bulletin, v. 60, p. 1541-1596.

———1968, Composition and origin of Hawaiian lavas, *in* Coats, R.E., Hay, R.L., and Anderson, C.A., eds., Studies in volcanology: Geological Society of America Memoir, v. 116, p. 477-522.

———1969, Petrology of the basalt cores from Midway Atoll: U.S. Geological Survey Professional Paper 680–B, p. B1-B10.

Macdonald, G.A., Abbott, A.T., and Cox, D.C., 1983, Volcanoes in the Sea: Honolulu, University of Hawaii Press, 517 p.

Macdonald, G.A., Davis, D.A., and Cox, D.C., 1960, Geology and groundwater resources of the Island of Kauai, Hawaii (geologic map of Kauai enclosed): Hawaii Division of Hydrography, Bulletin 13, 207 p.

Macdonald, G.A., and Katsura, T., 1962, Relationship of petrographic suites in Hawaii: The crust of the Pacific Basin: American Geophysical Union, Geophysical Monograph 6, p. 187-195.

———1964, Chemical composition of Hawaiian lavas: Journal of Petrology, v. 5, p. 82-133.

Malahoff, A., McMurtry, G.M., Wiltshire, J.C., and Yeh, H.-W., 1982, Geology and geochemistry of hydrothermal deposits from active submarine volcano Loihi, Hawaii: Nature, v. 289, p. 234-239.

Martin, W.F., and Pierce, C.H., 1915, Water resources of Hawaii: U. S. Geological Survey Water Supply Paper 318.

Matter, A., and Gardner, J.V., 1975, Carbonate diagenesis at Site 308, Koko Guyot, *in* Larson, R.L., Moberly, R., and others, Initial Reports of the Deep Sea Drilling Project, v. 32: Washington, U. S. Government Printing Office, p. 521-535.

McDougall, I., 1963, Potassium-argon ages from western Oahu, Hawaii: Nature, v. 197, p. 344-345.

———1964, Potassium-argon ages from lavas of the Hawaiian Islands: Geological Society of America Bulletin, v. 75, p. 107-128.

———1969, Potassium-argon ages on lavas of Kohala Volcano, Hawaii: Geological Society of America Bulletin, v. 80, p. 2597-2600.

———1971, Volcanic island chains and sea floor spreading: Nature, v. 231, p. 141-144.

———1979, Age of shield-building volcanism of Kauai and linear migration of volcanism in the Hawaiian Island chain: Earth and Planetary Science Letters, v. 46, p. 31-42.

McDougall, I., and Duncan, R.A., 1980, Linear volcanic chains recording plate motions?: Tectonophysics, v. 63, p. 275-295.

McDougall, I., and Swanson, D.A., 1972, Potassium-argon ages of lavas from the Hawi and Pololu Volcanic Series, Kohala Volcano, Hawaii: Geological Society of America Bulletin, v. 83, p. 3731-3738.

McDougall, I., and Tarling, D.H., 1963, Dating of polarity zones in the Hawaiian Islands: Nature, v. 200, p. 54-56.

McDougall, I., and Ur-Rahman, A., 1972, Age of the Gauss-Matuyama boundary and the Kaena and Mammoth events: Earth and Planetary Science Letters, v. 14, p. 367-380.

McKenzie, J., Bernoulli, D., and Schlanger, S. O., 1980, Shallow-water carbonate sediments from the Emperor Seamounts: Their diagenesis and paleogeographic significance, *in* Jackson, E. D., Koisumi, I., and others, Initial Reports of the Deep Sea Drilling Project, v. 55: Washington, U.S. Government Printing Office, p. 415-455.

McNutt, M.K., 1984, Lithospheric flexure and thermal anomalies: Journal of Geophysical Research, v. 89, p. 11,180-11,194.

Menard, H.W., 1955, Deformation of the northeastern Pacific basin and the west coast of North America: Geological Society of America Bulletin, v. 66, p. 1149-1198.

———1973, Depth anomalies and the bobbing motion of drifting islands: Journal of Geophysical Research, v. 78, p. 5128-5137.

Menard, H.W., Allison, E.C., and Durham, J.W., 1962, A drowned Miocene terrace in the Hawaiian Islands: Science, v. 138, p. 896-897.

Menard, H.W., and Dietz, R.S., 1951, Submarine geology of the Gulf of Alaska: Geological Society of America Bulletin, v. 62, p. 1263-1286.

Minster, J.B., Jordan, T.H., Molnar, P., and Haines, E., 1974, Numerical modelling of instantaneous plate tectonics: Geophysical Journal of the Royal Astronomical Society, v. 36, p. 541-576.

Moore, G.W., 1984, Tertiary dismemberment of western North America: Proceedings of the Third Circum-Pacific Energy and Mineral Resources Conference, p. 607-612.

Moore, J.G., 1970, Relationship between subsidence and volcanic load, Hawaii: Bulletin Volcanologique, v. 34, p. 562-576.

Moore, J.G., Clague, D.A., and Normark, W.R., 1982, Diverse basalt types from Loihi Seamount, Hawaii: Geology, v. 10, p. 88-92.

Moore, J.G., and Fornari, D.J., 1984, Drowned reefs as indicators of the rate of subsidence of the Island of Hawaii: Journal of Geology, v. 92, p. 752-759.

Moore, J.G., Normark, W.R., and Lipman, P.W., 1979, Loihi Seamount—A young submarine Hawaiian volcano: Hawaii Symposium on Intraplate Volcanism and Submarine Volcanism, Abstracts, p. 127.

Morgan, W.J., 1971, Convection plumes in the lower mantle: Nature, v. 230, p. 42-43.

———1972a, Deep mantle convection plumes and plate motions: American Association of Petroleum Geologists Bulletin, v. 56, p. 203-213.

———1972b, Plate motions and deep mantle convection, *in* Shagam, R., and others, eds., Studies in Earth and Space Sciences: Geological Society of America Memoir 132 (Hess Volume), p. 7-22.

———1981, Hotspot tracks and the opening of the Atlantic and Indian Oceans, *in* Emiliani, C., ed., The Sea, v. 7, The Oceanic Lithosphere: New York, John Wiley and Sons, p. 443-487.

Muromtsev, A.M., 1958, The principal hydrologic features of the Pacific Ocean: Leningrad (Gidrometerologicheskoe Isdatel'stov)(from Russian, Jerusalem, 1963, Israel Prog. Sci. Trans.), 417 p.

Nakiboglu, S.M., and Lambeck, K., 1985, Thermal response of a moving lithosphere over a mantle heat source: Journal of Geophysical Research, v. 90, p. 2985-2994.

Naughton, J.J., Macdonald, G.A., and Greenberg, V.A., 1980, Some additional potassium-argon ages of Hawaiian rocks: the Maui volcanic complex of Molokai, Maui, Lanai, and Kahoolawe: Journal of Volcanology and Geothermal Research, v. 7, p. 339-355.

Ness, G., Levi, S., and Couch, R., 1980, Marine magnetic anomaly timescales for the Cenozoic and Late Cretaceous: A precise, critique and synthesis: Reviews of Geophysics and Space Physics, v. 19, p. 753-770.

O'Hara, M.J., 1965, Primary magmas and the origin of basalts: Scottish Journal of Geology, v. 1, p. 19-40.

———1975, Is there an Icelandic mantle plume?: Nature, v. 253, p. 708-710.

Oostdam, B.L., 1965, Age of lava flows on Haleakala, Maui, Hawaii: Geological Society of America Bulletin, v. 76, p. 393-394.

Ozima, M., Kaneoka, I., and Aramaki, S., 1970, K-Ar ages of submarine basalts dredged from seamounts in the western Pacific area and discussion of oceanic crust: Earth and Planetary Science Letters, v. 8, p. 237-249.

Palmer, H.S., 1927, Geology of Kaula, Nihoa, Necker, and Gardner Islands, and French Frigate Shoals: Bernice Pauhi Bishop Museum Bulletin 5 (Tanager Expedition Publication Number 4), 35 p.

———1936, Geology of Lehua and Kaula Islands: Bernice Pauhi Bishop Museum Occasional Papers, v. 12, no. 13, 36 p.

Parsons, B., and Sclater, J.G., 1977, An analysis of the variation of ocean floor bathymetry and heat flow with age: Journal of Geophysical Research v. 82, p. 803-827.

Porter, S.C., Stuvier, M., and Yang, I.C., 1977, Chronology of Hawaiian glaciations: Science, v. 195, p. 61-63.

Powell, J.L., and DeLong, S.E., 1966, Isotopic composition of strontium in volcanic rocks from Oahu: Science, v. 153, no. 3741, p. 1239-1242.

Powers, H.A., 1935, Differentiation of Hawaiian lavas: American Journal of Science 5th Series, v. 30, no. 175, p. 57-71.

———1955, Composition and origin of basaltic magma of the Hawaiian Islands: Geochimica et Cosmochimica Acta, v. 7. p. 77-107.

Powers, S., 1917, Tectonic lines in the Hawaiian Islands: Geological Society of America Bulletin, v. 28, p. 501-514.

———1920, Notes on Hawaiian petrology: American Journal of Science, 4th Series, v. 50, p. 256-280.

Richter, F.M., 1973, Convection and the large-scale circulation of the mantle: Journal of Geophysical Research, v. 78, p. 8735-8745.

Richter, F.M., and Parsons, B., 1975, On the interaction of two scales of convection in the mantle: Journal of Geophysical Research, v. 80, p. 2529-2541.

Rison, W., and Craig, H., 1983, Helium isotopes and mantle volatiles in Loihi Seamount and Hawaiian Island basalts and xenoliths: Earth and Planetary Science Letters, v. 66, p. 407-426.

Roden, M.F., Frey, F.A., and Clague, D.A., 1984, Geochemistry of tholeiitic and alkalic lavas from the Koolau Range, Oahu, Hawaii: Implications for Hawaiian Volcanism: Earth and Planetary Science Letters, v. 69, p. 141-158.

Roedder, E., 1965, Liquid CO_2 inclusions in olivine-bearing nodules and phenocrysts from basalts. American Mineralogist, v. 50, p. 1746-1782.

Rona, P.A., and Richardson, E. S., 1978, Early Cenozoic global plate reorganization: Earth and Planetary Science Letters, v. 40, p. 1-11.

Sager, W.W., 1984, Paleomagnetism of Abbott Seamount and implications for the latitudinal drift of the Hawaiian hot spot: Journal of Geophysical Research, v. 89, p. 6271-6284.

Saito, K., and Ozima, M., 1975, ^{40}Ar-^{39}Ar isochron age of a mugearite dredged from Suiko Seamount in the Emperor Chain: Rock Magnetism and Paleogeophysics, v. 3, p. 81-84.

———1977, ^{40}Ar-^{39}Ar geochronological studies on submarine rocks from the western Pacific area: Earth and Planetary Science Letters, v. 33, p. 353-369.

Savin, S.M., Douglas, R.G., and Stehli, F.G., 1975, Tertiary marine paleotemperatures: Geological Society of America Bulletin, v. 86, p. 1499-1510.

Schilling, J., and Winchester, J.W., 1966, Rare earths in Hawaiian basalts: Science, v. 153, p. 867-869.

Schlanger, S.O., and Konishi, K., 1975, The geographic boundary between the coral-algal and the bryozoan-algal limestone facies: A paleolatitude indicator: IX International Geological Congress of Sedimentology, Nice, Theme 1, Sedimentologic Indicators, p. 187-190.

Schreiber, B.C., 1969, New evidence concerning the age of the Hawaiian Ridge: Geological Society of America Bulletin, v. 80, p. 2601-2604.

Schroeder, W., 1984, The empirical age-depth relation and depth anomalies in the Pacific Ocean basin: Journal of Geophysical Research, v. 89, p. 9873-9883.

Scientific Party DSDP 55, 1978, Drilling confirms hot spot origins: Geotimes, v. 23, no. 2, p. 23-26.

Sen, G., 1983, A petrologic model for the constitution of the upper mantle and crust of the Koolau Shield, Oahu, Hawaii, and Hawaiian magmatism: Earth and Planetary Science Letters, v. 62, p. 215-228.

Sen, G., and Presnall, D.C., 1986, Petrogenesis of dunite xenoliths from Koolau Volcano, Oahu, Hawaii: Implications for Hawaiian Volcanism: Journal of Petrology, v. 27, p. 197-217.

Shaw, H.R., 1973, Mantle convection and volcanic peridocity in the Pacific;

evidence from Hawaii: Geological Society of America Bulletin, v. 84, p. 1505-1526.

Shaw, H.R., and Jackson, E.D., 1973, Linear island chains in the Pacific: Result of thermal plumes or gravitational anchors?: Journal of Geophysical Research, v. 78, p. 8634-8652.

Smoot, N.C., 1982, Guyots of the mid-Emperor Chain mapped with multibeam sonar: Marine Geology, v. 47, p. 153-163.

Solomon, S.C., and Sleep, N.H., 1974, Some simple physical models for absolute plate motions: Journal of Geophysical Research, v. 79, p. 2557-2567.

Staudigel, H., Zindler, A., Hart, S.R., Leslie, T., Chen, C.Y. and Clague, D., 1984, The isotope systematics of a juvenile intraplate volcano: Pb, Nd, and Sr isotope ratios of basalts from Loihi Seamount, Hawaii: Earth and Planetary Science Letters, v. 69, p. 13-29.

Stearns, H.T., 1939, Geologic map and guide of the Island of Oahu, Hawaii (geologic map of Oahu enclosed): Hawaiian Division of Hydrography, Bulletin 2, 75 p.

Stearns, H.T., 1940a, Four-phase volcanism in Hawaii [abs.]: Geological Society of America Bulletin, v. 51, p. 1947-1948.

———1940b, Supplement to the geology and ground-water resources of the Island of Oahu, Hawaii (includes chapters on geophysical investigations by J.H. Swartz, and petrography by G.A. Macdonald): Hawaii Division of Hydrography, Bulletin 5, 164 p.

———1940c, Geology and ground-water resources of the Islands of Lanai and Kahoolawe, Hawaii (includes chapters on geophysical investigations by J.H. Swartz, and petrography by G.A. Macdonald; geologic map of Lanai enclosed): Hawaii Division of Hydrography, Bulletin 6, 177 p.

———1946, Geology of the Hawaiian Islands: Hawaii Division of Hydrography Bulletin 8, 106 p.

———1947, Geology and ground-water resources of the Island of Niihau, Hawaii; also Macdonald, G.A. 1947. Petrography of Niihau (geologic map of Niihau enclosed): Hawaii Division of Hydrography, Bulletin 12, 51 p.

———1966, Geology of the State of Hawaii: Palo Alto, Pacific Books, 266 p.

Stearns, H.T., and Dalrymple, G.B., 1978, The K-Ar age of the Black Point dike on Oahu, Hawaii, and its relation to the Yarmouth Interglaciation: Occasional Papers of the Bernice Pauhi Bishop Museum, v. 24, p.307-313.

Stearns, H.T., and Macdonald, G.A., 1942, Geology and ground-water resources of the Island of Maui, Hawaii (geologic map of Maui enclosed): Hawaii Division of Hydrography, Bulletin 7, 344 p.

———1946, Geology and ground-water resources of the Island of Hawaii (geologic map of Hawaii enclosed): Hawaii Division of Hydrography, Bulletin, 9, 363 p.

———1947, Geology and ground-water resources of the Island of Molokai, Hawaii (geologic map of Molokai enclosed): Hawaii Division of Hydrography, Bulletin 11, 113 p.

Stearns, H.T., and Vaksvik, K.N., 1935, Geology and ground-water resources of the Island of Oahu, Hawaii: Hawaii Division of Hydrography, Bulletin 1, 479 p.

Steiger, R.H., and Jager, E., 1977, Subcommission on geochronology: Convention on the use of decay constants in geo and cosmochronlogy: Earth and Planetary Science Letters, v. 36, p. 359-362.

Stille, P., Unruh, D.M., and Tatsumoto, M., 1983, Pb, Sr, Nd, and Hf isotopic evidence of multiple sources for Oahu, Hawaii basalts: Nature, v. 304, p. 25-29.

Strong, D.F., 1974, Volcanic couples and deep mantle plumes: Nature, v. 247, p. 191-193.

Swanson, D.A., 1972, Magma supply note at Kilauea Volcano, 1952-1971: Science, v. 175, p. 169-170.

Takayama, T., 1980, Calcareous nannofossil biostratigraphy, Leg 55 of the Deep Sea Drilling Project, *in* Jackson, E. D., Koisumi, I., and others, Initial Reports of the Deep Sea Drilling Project, v. 55: Washington, U.S. Government Printing Office, p. 349-364.

Tatsumoto, M., 1966, Isotopic composition of lead in volcanic rocks from Hawaii, Iwo Jima, and Japan: Journal Geophysical Research, v. 71, p. 1721-1733.

———1978, Isotopic composition of lead in oceanic basalt and its implication to mantle evolution: Earth and Planetary Science Letters, v. 38, p. 63-87.

Tayama, R., 1952, On the near-Japan bathymetric chart (introduction to the submarine geography of the northwest Pacific): Hydrographic Magazine, no. 32, p. 160-167 and 201 (in Japanese).

Tilley, C.E., 1950, Some aspects of magmatic evolution: Geological Society of London Quarterly Journal, v. 106, p. 37-61.

Todd, R., and Low, D., 1970, Smaller foraminifera from Midway drill holes: U. S. Geological Survey Professional Paper 680–E, 46 p.

Turcotte, D.L., and Oxburgh, E.R., 1973, Mid-plate tectonics: Nature, v. 244, p. 337-339.

———1976, Stress accumulation in the lithosphere: Tectonophysics, v. 35, p. 183-199.

———1978, Intra-plate volcanism: Philosophical Transactions of the Royal Society of London, Series A, v. 288, p. 561-579.

Turner, D.L., Jarrard, R.D., and Forbes, R.S., 1980, Geochronology and origin of the Pratt-Welker Seamount Chain, Gulf of Alaska: a new pole of rotation for the Pacific Plate: Journal Geophysical Research, v. 85, p. 6547-6556.

Unruh, D.M., Stille, P., and Tatsumoto, M., 1983, Isotopic heterogeneity among Hawaiian-Emperor basalts: Eos, Transactions, American Geophysical Union, v. 64, 347-348.

Vaughan, T.W., and Wells, J.W., 1943, Revision of the suborders, families, and genera of the Scleractinia: Geological Society of America, Special Paper no. 44, 363 p.

Vogt, P.R., 1974, Volcano spacing, fracture, and thickness of the lithosphere: Earth and Planetary Science Letters, v. 21, p. 235-252.

Vogt, P. R., and Avery, O. E., 1974, Detailed magnetic surveys in the northeast Atlantic and Labrador Sea: Journal of Geophysical Research, v. 79, p. 363-389.

Walcott, R.I., 1970, Flexure of the lithosphere at Hawaii: Tectonophysics, v. 9, p. 435-446.

———1976, Lithospheric flexure, analysis of gravity anomalies, and the propagation of seamount chains, *in* Sutton, G.H., Manghnani, M.H., and Moberly, R., The Geophysics of the Pacific Ocean Basin and its margin: American Geophysical Union Monograph 19, p. 431-438.

Washington, H.S., 1923a, Petrology of the Hawaiian Islands; I. Kohala and Mauna Kea, Hawaii: American Journal of Science, Series 5, v. 5, p. 465-502.

———1923b, Petrology of the Hawaiian Islands; II Hualalai and Mauna Loa: American Journal of Science, Series 5, v. 6, p. 100-126.

———1923c, Petrology of the Hawaiian Islands; III, Kilauea and general petrology of Hawaii: American Journal of Science, Series 5, v. 6, p. 338-367.

Washington, H.S., and Keyes, M.G., 1926, Petrology of the Hawaiian Islands: V. The Leeward Islands: American Journal of Science, Series 5, v. 12, p. 336-352.

———1928, Petrology of the Hawaiian Islands: VI Maui: American Journal of Science, Series 5, v. 15, p. 199-220.

Watts, A.B., 1978, An analysis of isostacy in the world's oceans 1. Hawaiian-Emperor Seamount Chain: Journal of Geophysical Research, v. 83, p. 5989-6004.

Wentworth, C.K., 1925, The geology of Lanai: Bernice Pauhi Bishop Museum, Bulletin 24, 72 pp.

———1927, Estimates of marine and fluvial erosion in Hawaii: Journal of Geology v. 35, p. 117-133.

West, H.B., and Garcia, M.O., 1982, Composition and evolution of the alkalic cap stage lavas from Mauna Kea Volcano, Hawaii: Eos, Transactions, American Geophysical Union, v. 63, p. 1138.

White, R.W., 1966, Ultramafic inclusions in basaltic rocks from Hawaii: Mineralogie und Petrographie Mitt., v. 12, p. 245-314.

White, W.M., and Hofmann, A.W., 1982, Sr and Nd isotope geochemistry of oceanic basalts and mantle evolution: Nature, v. 296, p. 821-825.

Wilkes, C., 1845, Narrative of the United States Exploring Expedition, 1838-1842, *4*: Philadelphia, 539 p.

Wilson, J.T., 1962, Cabot Fault, an Appalachian equivalent of the San Andreas and Great Glen faults and some implications for continental displacement: Nature v. 195, p. 135-138.

———1963a, A possible origin of the Hawaiian Islands: Canadian Journal of Physics, v. 41, p. 863-870.

———1963b, Continental drift: Scientific American, v. 208, no. 4, p. 86-100.

———1963c, Evidence from islands on the spreading of ocean floors: Nature, v.

197, p. 536-538.
———1963d, Hypothesis of Earth's behavior: Nature, v. 198, p. 925-929.
———1973, Mantle plumes and plate motions: Tectonophysics, v. 19. p. 149-164.
Wise, W.S., 1982, A volume-time framework for the evolution of Mauna Kea Volcano, Hawaii: Eos, Transactions, American Geophysical Union, v. 63, p. 1137.
Worsley, J.R., 1973, Calcareous nannofossils: Leg 19 of the Deep Sea Drilling Project, *in* Creager, J.S., Scholl, D.W., and others, Initial Reports of the Deep Sea Drilling Project, v. 19: Washington, U.S. Government Printing Office, p. 741-750.
Wright, C., 1975, Comments on 'Seismic array evidence of a core boundary source for the Hawaiian linear volcanic chain' by E.R. Kanasewich and others: Journal of Geophysical Research v. 80, p. 1915-1919.
Wright, T.L., 1971, Chemistry of Kilauea and Mauna Loa lava in space and time: U.S. Geological Survey Professional Paper 735, 40 p.
———1973, Magma mixing as illustrated by the 1959 eruption, Kilauea Volcano, Hawaii: Geological Society of America Bulletin, v. 84, p. 849-858.
———1984, Origin of Hawaiian tholeiite: A metasomatic model: Journal of Geophysical Research, v. 89, p. 3233-3252.
Wright, T.L., and Clague, D.A., in press, Petrology of Hawaiian lava: Geologic Society of America, Decade of North American Geology, the Eastern Pacific Region.
Wright, T.L., and Fiske, R.S., 1971, Origin of the differentiated and hybrid lavas of Kilauea Volcano, Hawaii: Journal of Petrology, v. 12, p. 1-65.
Wright, T.L., Shaw, H.R., Tilling, R.I., and Fiske, R.S., 1979, Origin of Hawaiian tholeiitic basalt: a quantitative model: Hawaii Symposium on Intraplate Volcanism and Submarine Volcanism, Abstracts, p. 104.
York, D., 1969, Least squares fitting of a straight line with correlated errors: Earth and Planetrary Science Letters, v. 5, p. 320-324.

APPENDIX 1.1

NOTES ON THE GEOLOGY AND GEOCHRONOLOGY OF INDIVIDUAL VOLCANOES IN THE HAWAIIAN-EMPEROR CHAIN

Following are brief descriptions and comments on the geology and geochronology of all volcanoes in the Hawaiian-Emperor Chain that have been mapped or sampled. References to sources of data are included in the reference list of the main text of the paper. The radiometric ages are conventional K-Ar age determinations unless otherwise indicated; errors are the estimated standard deviations of precision. Volcanoes are discussed from southeast to northwest, that is, from youngest to oldest, using the numbering system (in parentheses) of Bargar and Jackson (1974). Stratigraphic nomenclature used here is from Langenheim and Clague (chapter 1, part II).

Loihi Seamount (no number).—Loihi Seamount is inferred to be the youngest Hawaiian volcano on the basis of its location and seismic activity, the presence of fresh glassy pillow lava, and the occurrence of hydrothermal discharge into the water column. Loihi is located on the southeast flank of Kilauea on the Island of Hawaii and is 30 km offshore and 60 km south-southeast from the summit of Mauna Loa. The seamount rises to 950 m below sea level and has a distinct north-south orientation, delineating two rift zones that extend from the roughly 2.8-km by 3.7-km summit caldera (Malahoff and others, 1982). The volcano is active seismically; persistent swarms of shallow earthquakes that are probably caused by volcanic intrusion or submarine eruptions (Klein, 1982) occur periodically near the summit (Klein and Koyanagi, 1979). Moore and others (1982) describe fresh glassy pillow lava recovered from Loihi Seamount that includes basanite, alkalic basalt, basalt transitional between alkalic and tholeiitic basalt, and tholeiitic basalt. They also demonstrated that the alkalic lava is generally older than the tholeiitic lava and suggested that Loihi Seamount, and presumably all Hawaiian volcanoes, have a stage of alkalic volcanism before the tholeiitic shield stage that is characterized by infrequent, small-volume eruptions of alkalic lava. Further evidence that Loihi Seamount is an active volcano is provided by the discovery of a plume of hydrothermal methane and helium in the water column above Loihi (Horibe and others, 1983; Kim and Craig, 1983) and the presence of water-temperature anomalies recorded by the ANGUS camera sled (Malahoff and others, 1982).

Kilauea Volcano (1).—The lava of Kilauea, currently active and historically the most active volcano in Hawaii, can be divided into the older Hilina Basalt and the younger Puna Basalt, which are separated by the Pahala Ash. The exposed lava consists of tholeiitic basalt and picritic tholeiitic basalt that issued from the 3-km by 5-km summit caldera and the two rift zones. The rift zones extend to the east and the southwest, with the east rift zone extending nearly 50 km from the summit caldera to Cape Kumikahi at the northeast corner of the island and for at least an additional 90 km beneath the sea.

Mauna Loa Volcano (2).—The lava of Mauna Loa is divided into the Ninole Basalt (oldest), the Kahuku Basalt, and the Kau Basalt (youngest). The Kahuku and Kau are separated by the Pahala Ash and are thought to be coeval with the Hilina Basalt and Puna Basalt, respectively, of Kilauea. The exposed lava is all tholeiitic basalt and picritic tholeiitic basalt that issued from the 2.5-km by 4-km summit caldera, named Mokuaweoweo, and two rift zones. The rift zones extend southwest and east-northeast. The southeastern and the southwestern slopes of Mauna Loa are steepened by downfaulting along the Kaoiki and Kealakakua fault systems. Mauna Loa last erupted in 1984. Possible remnants of two earlier shield volcanoes are exposed in the Ninole Hills (Ninole Basalt) and in the vicinity of Kulani. Neither of these earlier shield volcanoes is well delineated and both may be merely deeper parts of the Mauna Loa shield uplifted along normal faults in a manner analogous to that in the Hilina fault system near Puu Kapukapu. With the exception of numerous ^{14}C ages, the sole published age data for Mauna Loa were obtained by Evernden and others (1964) on two samples from the Ninole Basalt. One sample contained negligible radiogenic ^{40}Ar. The other sample had a radiogenic ^{40}Ar content of 2.5 percent and a calculated age of 0.54 Ma. No uncertainty was given for the age, but from the quality of the data we estimate a standard deviation of approximately 0.4 m.y. It seems unlikely that the Ninole Basalt is more than a few hundred thousand years old.

Mauna Kea Volcano (3).—Mauna Kea Volcano last erupted some 3,600 years ago (Porter and others, 1977). The volcano has a well exposed section of shield lava capped by postshield alkalic lava. The rocks are divided into the older Hamakua Volcanics and the younger Laupahoehoe Volcanics. The Hamakua Volcanics consists of shield-stage tholeiitic basalt, olivine tholeiitic basalt, and picritic tholeiitic basalt, and overlying postshield-stage alkalic basalt, ankaramite, and hawaiite. There is no clear boundary between the shield and postshield lavas; tholeiitic and alkalic lavas are intercalated near the boundary (Frey and others, 1984). Most of the surface of Mauna Kea is blanketed by the younger Laupahoehoe Volcanics which is mostly hawaiite, with much less ankaramite and alkalic basalt (West and Garcia, 1982). The Hamakua Volcanics is exposed only in deep erosional canyons.

The rift zones of Mauna Kea are not well defined, but cinder cones are roughly aligned in westerly and southerly directions from the summit. A nearly buried east rift zone is still clearly delineated by a submarine ridge extending nearly 40 km to sea. It is uncertain if a summit caldera existed, but the crude arcuate alignment of some cinder cones, coupled with a large gravity high just south of the summit, indicate that a former caldera may be buried beneath the Laupahoehoe Volcanics.

Porter and others (1977) obtained K-Ar ages on three samples from the Hamakua Volcanics. The two younger flows gave ages of 0.27 ± 0.04 Ma, whereas the older flow gave an age of 0.375 ± 0.050 Ma. K-Ar and ^{14}C ages for flows from the Laupahoehoe Volcanics range from about 0.19 Ma to 4.5 ka. Funkhouser and others (1968) reported a K-Ar age of 0.6 ± 0.3 Ma for a single sample of hawaiite from the Laupahoehoe Volcanics.

Hualalai Volcano (4).—Hualalai Volcano was last active in 1800-01 when two major and several smaller flows issued from a series of vents on the northwest rift zone. With the exception of a large trachyte cone and flow at Puu Waawaa (Waawaa Trachyte Member), the entire subaerial surface of the volcano consists of alkalic basalt flows of the alkalic postshield stage. All subaerial rocks of Hualalai are called the Hualalai Volcanics. A detailed study of the volcano (Moore and others, chapter 20) shows that nearly all the lava is alkalic basalt, with only a few flows that are

gradational to hawaiite. Some ^{14}C ages of charcoal from beneath many of these flows demonstrate the youth of the alkalic basalt surface. The structure of the volcano is poorly known, although the northwest and south rift zones are well defined. It is unknown if a summit caldera existed in the past. Recent studies on the submarine northwest rift zone recovered tholeiitic basalt and picritic tholeiitic basalt (Clague, 1982), indicating that Hualalai, like all other Hawaiian volcanoes, had a tholeiitic shield stage. The submarine portion of the rift is overlain by terrace deposits that are inferred to be as old as 120 ka (Moore and Fornari, 1984), which indicates that the tholeiitic shield stage had ended by this time.

Funkhouser and others (1968) reported an age of 0.4 ± 0.3 Ma for the Waawaa Trachyte Member of the Hualalai Volcanics; recent K-Ar results indicate the trachyte is about 105 ka (G.B. Dalrymple, unpub. data, 1985).

Kohala Volcano (5).—Kohala Volcano is composed of the older Pololu Basalt and the younger Hawi Volcanics. The Pololu Basalt is a succession of thin flows of tholeiitic basalt, olivine tholeiitic basalt, and picritic tholeiitic basalt except near the top of the section, where alkalic basalt occurs. Most of the Pololu Basalt represents the shield stage, whereas the uppermost, alkalic part represents the alkalic postshield stage. The younger Hawi Volcanics formed during the alkalic postshield stage and is separated from the Pololu Basalt by an erosional unconformity. Most of the Hawi lava is mugearite, but benmoreite and hawaiite are also present. Cinder cones of the Hawi Volcanics align along two rift zones trending northwest and southeast. Arcuate faults near the summit indicate that a caldera probably formed during eruption of Pololu lava, but Hawi lava has entirely buried it. A gravity high located southeast of the summit may correspond to the approximate location of this inferred caldera. Hawi lava is absent from an 11-km section on the northwest side of the volcano. Flows are deflected from this zone by a series of fault scarps in the summit region that bounds a northwest-trending graben 10 km long and 2–5 km wide. Lava erupted inside the graben, filled it, flowed to the northwest and southeast ends, and overflowed most of the southwest rim. Feigenson and others (1983) made a detailed petrologic study of stratigraphically controlled lava samples from the Pololu Volcanics, and Lanphere and Frey (1985) made a similar study of samples from the Pololu Basalt and Hawi Volcanics.

Evernden and others (1964) obtained an age of 0.43 Ma for one sample of tholeiitic basalt from the Pololu Basalt. Dalrymple (1971) obtained scattered age results that averaged 0.7 ± 0.15 Ma on five samples from the Pololu Basalt. The best data for lava of the Pololu is from McDougall and Swanson (1972), who dated nine flows ranging in age from 0.459 ± 0.028 to 0.304 ± 0.091 Ma. The average of the three oldest flows is 0.43 ± 0.02 Ma. Ages on 12 samples from the Hawi Volcanics (McDougall, 1969; McDougall and Swanson, 1972) range from 0.261 ± 0.005 to 0.061 ± 0.001 Ma.

East Maui Volcano (6).—East Maui Volcano is the youngest volcano in the Hawaiian Islands having rejuvenated-stage volcanics. The volcano was last active in about 1790 (Oostdam, 1965). The oldest unit is the Honomanu Basalt, a series of tholeiitic basalt, olivine tholeiitic basalt, and picritic tholeiitic basalt flows that represents the shield stage. Above sea level these flows are nearly completely buried by those of the overlying Kula Volcanics and Hana Volcanics. The Kula Volcanics is composed predominantly of hawaiite with some ankaramite and alkalic basalt and represents the alkalic postshield stage. There is little evidence of extensive erosion between the shield and postshield lavas. The Hana Volcanics is composed mostly of the same rock types as the Kula Volcanics, but it erupted after an erosional period; it represents an alkalic rejuvenated stage of volcanism. Three rift zones are delineated by the location of vents for the Kula and Hana Volcanics. The east and southwest rifts are characterized by vents of both these units, whereas the north rift has only Kula Volcanics vents. The Hana Volcanics is unique among Hawaiian rejuvenated stage volcanic rocks in that its vents are aligned along the preexisting rift zones, the duration of the erosional period is rather short (<0.4 m.y.), and ankaramite and hawaiite are present. Chen and Frey (1983, 1985) present a detailed geochemical study of lava from all three eruptive stages.

Naughton and others (1980) reported ages for 7 samples of the Honomanu Basalt from three localities. The individual sample ages range from 0.54 to 0.91 Ma. Probably the best age for the Honomanu Basalt is the mean of 0.75 ± 0.04 Ma of the four measurements on samples from the so-called crater of Haleakala. McDougall (1964) dated two samples of the Kula Volcanics at 0.46 and 0.86 Ma, whereas the mean of four samples from the Kula Volcanics dated by Naughton and others (1980) is 0.41 ± 0.09 Ma. No ages have been determined for the Hana Volcanics.

Kahoolawe (7).—The volcanic rocks of Kahoolawe have not been subdivided. The only formation, the Kanapou Volcanics, includes tholeiitic basalt and olivine tholeiitic basalt of the shield stage, tholeiitic and alkalic basalt of the caldera-filling phase, and alkalic basalt and hawaiite of the alkalic postshield stage. Five vents along the seacliff in Kanapou Bay erupted alkalic basalt following an extended period of volcanic quiescence; these vents presumably represent an alkalic rejuvenated stage. The volcano was built by eruptions along a prominent west-southwest rift zone and two less pronounced rifts trending east and north. Most of the vents have been removed by erosion, but remnants of about six vents remain. The caldera of 5 km diameter lies at the eastern end of the island and has been breached by the sea.

Naughton and others (1980) dated two samples collected by H.S. Palmer in 1925 from the upper (alkalic) part of the Kanapou Volcanics. The mean of the two measurements is 1.03 ± 0.18 Ma.

West Maui Volcano (8).—The volcanic rocks of West Maui are divided into the Wailuku Basalt, Honolua Volcanics, and Lahaina Volcanics. The Wailuku Basalt consists of tholeiitic basalt, olivine tholeiitic basalt, and picritic tholeiitic basalt of the shield stage and of alkalic basalt of a caldera-filling phase. The Honolua Volcanics, which represents an alkalic postshield stage, consists of a thin discontinuous cap of mugearite with some trachyte and hawaiite. The Lahaina Volcanics followed a long period of erosion and consists of the cones and flows of four small eruptions of basanite and olivine-rich basanite. The Lahaina Volcanics represents the alkalic rejuvenated stage. The volcano has ill-defined rift zones delineated by dike swarms trending northeast and south and by vents of the Honolua Volcanics trending north and south from the small central caldera. The caldera-filling lava is severely altered by late gases; erosion has preferentially removed these altered rocks in Iao Valley.

McDougall (1964) dated three samples of the Wailuku Basalt, and the ages all fall within the narrow range of 1.30–1.33 Ma with a mean of 1.32 ± 0.04 Ma. Naughton and others (1980) obtained ages of 1.58 and 1.97 Ma on two samples from the Wailuku, but the precision of the measurements is poor. The samples dated by Naughton and his colleagues may be from an older part of the shield than those dated by McDougall (Naughton and others, 1980). McDougall's results for four samples of the Honolua Volcanics range only from 1.18 to 1.20 Ma, whereas Naughton and others (1980) measured an age of 1.50 ± 0.13 Ma for a single sample of the Honolua Volcanics. Naughton and others (1980) dated one sample from the Lahaina Volcanics at 1.30 ± 0.10 Ma, an age which appears to be too old on stratigraphic grounds.

Lanai (9).—Only tholeiitic lava was erupted during the shield stage and caldera-collapse phase of Lanai Volcano; no later alkalic lava is known. The Lanai Basalt consists of tholeiitic basalt, olivine tholeiitic basalt, and picritic tholeiitic basalt that erupted from the northwest, southwest, and southeast rift zones and from the summit caldera underlying the present-day Palawai Basin. An extensive dike swarm marking the southwest rift crops out along the Kaholo Pali. Most of the dikes are nearly vertical and are about 30 cm thick.

Bonhommet and others (1977) measured ages for six samples of the Lanai Basalt that were collected on the southern part of the Lanai shield. The data fit a K-Ar isochron indicating an age for the Lanai Basalt of 1.28 ± 0.04 Ma. Naughton and others (1980) obtained ages of 0.71 ± 1.27 to 0.86 ± 0.55 Ma for three samples from the northeastern part of the island. They speculate that the northeastern part of the shield may be somewhat younger than the southern part, but the mean of their three ages (0.81 ± 0.66 Ma) is not significantly different from the more precise isochron age of Bonhommet and others (1977) at the 95-percent level of confidence.

East Molokai Volcano (10).—The lava of East Molokai is subdivided informally into an upper and a lower member of the East Molokai Volcanics. The lower member consists of tholeiitic basalt, olivine tholeiitic basalt, and picritic tholeiitic basalt characteristic of the shield stage, but alkalic basalt of the postshield stage occurs in the upper part of the lower member. Beeson (1976) and Clague and Beeson (1980) have shown that tholeiitic and alkalic basalt are intercalated in the upper part of the lower unit. The upper member consists predominantly of mugearite,

with smaller amounts of hawaiite and trachyte and represents the alkalic postshield stage. Following an extended erosional period, during which the 1,200-m cliffs on the north side of the island formed, alkalic basalt and basanite of the rejuvenated stage Kalaupapa Volcanics erupted to form the Kalaupapa Peninsula and Mokuhooniki Island, a tuff cone located offshore of the east end of the island. East Molokai Volcano was built by eruptions along eastward- and west-northwestward-extending rift zones and from a summit caldera about 2.5 km by 7 km in size. The caldera-filling lava flows are similar to those of the lower member except that they are horizontal, more massive, and more extensively altered.

McDougall (1964) dated two samples from the lower member of the East Molokai Volcanics. Both ages agree at 1.52 Ma. Naughton and others (1980) obtained an age of 1.76 ± 0.07 Ma based on several analyses of a single sample. McDougall also dated three samples of the upper member and obtained ages of 1.35 to 1.49 Ma. A basalt sample from the Kalaupapa Peninsula was dated at 1.24 ± 0.16 Ma by Naughton and others (1980), but this appears to be too old in view of the younger ages (0.35 ± 0.03 to 0.57 ± 0.02) obtained for three samples of the Kalaupapa Volcanics by Clague and others (1982).

West Molokai Volcano (11).—The volcanic rocks of West Molokai belong to the West Molokai Volcanics. Most of the exposed lava is tholeiitic basalt of the shield stage. This lava erupted from an east-northeast rift zone that crosses the summit area. A less pronounced rift trends toward the northwest. There is no evidence of a summit caldera. Alkalic lava of the postshield stage, predominately hawaiite with subordinate alkalic basalt, erupted from a series of cinder and spatter cones located mainly on the northwest rift zone. No rejuvenated-stage lava is known. A shoal area extends beneath the sea to the west-southwest nearly 65 km and includes Penguin Bank. This bank probably represents a separate volcanic center, but it has not been studied and little is known of its history.

McDougall (1964) dated one sample from the summit of the West Molokai shield at 1.89 Ma. From the sample locality, we conclude that it is from the tholeiitic shield (lower part of West Molokai Volcanics). Naughton and others (1980) dated six samples of the lower part of the West Molokai Volcanics from three localities. The three localities gave mean ages of 1.84 ± 0.07, 1.90 ± 0.06, and 1.52 ± 0.06 Ma.

Koolau Volcano (12).—Koolau Volcano on Oahu is composed of tholeiitic basalt, olivine tholeiitic basalt, and rather rare picritic tholeiitic basalt that erupted from a long rift system oriented northwest-southeast. These shield-building flows make up the Koolau Basalt. Lava that ponded in the 16-km by 13-km caldera is also tholeiitic and is called the Kailua Member of Koolau Basalt. The rift zones are identified by an extensive dike complex consisting of hundreds of nearly vertical dikes that average 60–90 cm thick. A few of the youngest flows of the Koolau Basalt appear to be transitional between tholeiitic and alkalic basalt. The rejuvenated-stage Honolulu Volcanics erupted from about 36 groups of vents following a long period of volcanic quiescence and erosion. The lava is strongly alkalic and ranges in composition from alkalic basalt, basanite, and nephelinite, to melilitite. The vents from which these rocks erupted show no relationship to the preexisting rift zones or caldera-bounding faults. Many of the vents formed by violent hydromagmatic eruptions that formed tuff cones commonly containing accidental blocks of Koolau Basalt and coral limestone. Clague and Frey (1982) presented a detailed trace-element geochemical study of the lava and summarized the geology of the Honolulu Volcanics.

K-Ar ages have been reported for a large number of samples from the Koolau Basalt by McDougall (1964), Funkhouser and others (1968), McDougall and Ur-Rahman (1972), and Doell and Dalrymple (1973), who also summarized and evaluated the ages. The best ages for the Koolau Basalt range from 1.8 to 2.7 Ma. Ages for lava of the rejuvenated-stage Honolulu Volcanics range from about 0.03 to 0.9 Ma (Funkhouser and others, 1968; Gramlich and others, 1971; Stearns and Dalrymple, 1978; Lanphere and Dalrymple, 1980).

Waianae Volcano (13).—Waianae Volcano is divided into the older Waianae Volcanics and the younger Kolekole Volcanics. The Waianae Volcanics is subdivided into the Lualualei, Kamaileunu, and Palehua Members. The Lualualei Member consists of tholeiitic basalt, olivine tholeiitic basalt, and picritic tholeiitic basalt of the shield stage. The Kamaileunu Member consists of rocks that accumulated inside the 14-km-wide caldera and is also composed mostly of tholeiitic lava, although alkalic rocks are present near the top. The Kamaileunu Member also includes the only occurrence of icelandite and rhyodacite (Mauna Kuwale-Rhyodacite Flow) in the Hawaiian Islands. The Palehua Member consists mainly of hawaiite with rather rare alkalic basalt flows; it represents the alkalic postshield stage. The Kolekole Volcanics represents the group of young cones near the southwest end of the island and a single flow of alkalic lava erupted in Kolekole Pass. The tholeiitic shield lava erupted from three rift zones trending northwest, south-southeast, and northeast. There is no unconformity between tholeiitic and alkalic lava within the caldera; the boundary is transitional and may be similar to the one on East Molokai. K-Ar ages have been determined for a large number of samples from the Waianae Volcanics by McDougall (1964), Funkhouser and others (1968), McDougall and Ur-Rahman (1972), and Doell and Dalrymple (1973), who also summarized and evaluated all of the data. Ages from the Lualualei and Kamaileunu Members range from about 3.0 to 3.9 Ma. Ages from the Palehua Member range from about 2.5 to 3.2 Ma.

Kauai (14).—The Island of Kauai consists of a single large shield volcano with a summit caldera 16–19 km across. The Waimea Canyon Basalt has been divided into four members, but all consist of tholeiitic basalt, olivine tholeiitic basalt, and abundant picritic tholeiitic basalt. The Napali Member represents the shield stage, whereas the Olokele and Makaweli Members represent the caldera-filling phase, having filled the summit caldera and a 6-km-wide graben on the south flank, respectively. Two other calderas formed on the flanks of the Kauai shield volcano: the Lihue depression, 11–16 km across, was apparently not filled by tholeiitic lava; the Haupu caldera, roughly 3 km across was filled with thick ponded flows called the Haupu Member of the Waimea Canyon Basalt. These are the only flank calderas known in the Hawaiian Islands. Near the top of the Olokele and Makaweli Members, a single flow of hawaiite rests on a soil 30–60 cm thick. This single flow apparently represents the alkalic postshield stage on Kauai. Unlike most Hawaiian volcanoes, Kauai has no well-defined rift zones; dikes radiate from the summit caldera in all directions, although they are more concentrated in the northeast and west-southwest directions.

Following a long period of volcanic quiescence and deep erosion, the alkalic rejuvenated stage Koloa Volcanics erupted from at least 40 vents concentrated on the south and east flanks of the shield. The lava ranges from alkalic basalt, basanite, and nephelinite, to melilitite. The abundant vents located along the southeast coast erupted almost entirely alkalic basalt.

McDougall (1964) reported ages for three samples from the Napali Member ranging from 3.63 to 5.77 Ma. Evernden and others (1964) obtained an age of 3.43 Ma for a single sample from the Napali. In a more recent study, McDougall (1979) reported K-Ar ages ranging from 3.81 ± 0.06 to 5.14 ± 0.20 Ma for 16 samples of the Napali collected from three localities. He concluded that some of the variation was probably due to differential Ar loss, that the Napali Member was erupted between about 5.1 and 4.3 Ma, and that the Napali lava in Waipio Valley was erupted over a short time interval at about 5.1 ± 0.2 Ma.

Ages of 4 samples from the Makaweli Member range from 3.60 to 4.15 Ma (McDougall, 1964). Only three samples from the Koloa Volcanics (rejuvenated stage) have been dated; two samples have ages of 0.62 and 1.21 Ma (Evernden and others, 1964) and another an age of 1.46 Ma (McDougall, 1964).

Niihau (15).—The Island of Niihau consists of a deeply eroded shield volcano mantled by lava of the alkalic rejuvenated stage on the north, west, and south sides. The Paniau Basalt consists of tholeiitic basalt and olivine tholeiitic basalt of the shield stage and the remnants of a single alkalic postshield stage vent at Kaeo. Several dikes exposed near the eastern coastline are also of alkalic basalt and presumably fed vents that have been completely removed by erosion. A magnificent dike swarm is exposed in the eastern seacliff (Dalrymple and others, 1973, fig. 5); these dikes trend southwest and represent a rift zone. The summit of the volcano was northeast of the present-day island, and the eastern side of the volcano has been removed by erosion or downfaulting. The period of volcanic quiescence and marine erosion that removed the eastern side of the shield was followed by eruption of the alkalic rejuvenated-stage lava of the Kiekie Basalt, which is entirely alkalic basalt. Lehua Island off the north shore is a breached tuff cone of the Kiekie Basalt.

Ages for Niihau have not been published, but data for 11 tholeiitic flows and dikes of the Paniau Basalt fit a K-Ar isochron with an age of 4.89 ± 0.11 Ma (G.B. Dalrymple, unpub. data, 1983).

Kaula Island (15A).—Kaula Island is a small tuff cone on a large submarine edifice. The edifice almost surely represents a separate shield volcano related to the Hawaiian Islands, but it has not been sampled. The tuff cone is probably a vent of the alkalic rejuvenated stage. Garcia, Frey and Grooms (in press) described accidental blocks of tholeiitic basalt, basanite, phonolite, and ultramafic xenoliths that occur in the tuff.

Garcia, Grooms, and Naughton (in press) obtained K-Ar ages for two phonolite blocks and a basanite from the tuff; they determined ages of 4.00 ± 0.09 and 4.22 ± 0.25 Ma for phonolite samples, 3.98 ± 0.70 Ma for a biotite separated from the phonolite, and 1.8 ± 0.2 Ma for the basanite.

On the basis of the composition and age of the phonolite, we propose that the phonolite is from the alkalic postshield stage, the basanite blocks are from rejuvenated-stage flows underlying the tuff cone (Garcia, Frey, and Grooms, in press), and tholeiitic basalt represents the shield stage.

Nihoa Island (17).—Nihoa Island is a remnant of a large tholeiitic shield with flows dipping 5°–10° to the southwest. All the flows exposed on Nihoa are of tholeiitic basalt, and they range from aphyric to porphyritic in texture (Dalrymple and others, 1974).

Funkhouser and others (1968) obtained an age of 7.5 ± 0.4 Ma for a single sample from Nihoa Island. Dalrymple and others (1974) reported a best weighted mean age of 7.2 ± 0.3 Ma for six samples of tholeiitic basalt from the island.

Unnamed Seamount (19).—A single sample dredged by the Hawaii Institute of Geophysics from this seamount has been analyzed (Garcia, Frey, and Naughton, in press). The samples in dredge 9-11 are moderately altered picritic tholeiitic to transitional basalt with about 30 percent olivine phenocrysts. These probably erupted during the late shield stage or the caldera-filling phase. The seamount is undated.

Unnamed Seamount (20).—On the second leg of the Hawaii Institute of Geophysics cruise 72-07-02, dredge 51 recovered tholeiitic basalt with 20 percent phenocrysts of augite, plagioclase, and olivine, and aphyric alkalic lava of basanite composition (Clague, 1974a; Garcia, Frey, and Naughton, in press). These rocks probably erupted during the shield and the alkalic rejuvenated stages, respectively. Garcia, Frey, and Naughton (in press) obtained a weighted mean age of 9.6 ± 0.8 Ma for four analyses of two of the dredged alkalic basalt samples.

Unnamed Seamount (21).—On the second leg of the Hawaii Institute of Geophysics cruise 72-07-02, dredge 49 recovered tholeiitic to transitional basalt containing 20 percent phenocrysts of olivine and augite (Clague, 1974a). This lava probably erupted during the shield stage. The volcano is undated.

Necker Island (23).—Samples have been collected from Necker Island (Dalrymple and others, 1974), and others have been dredged from the submarine flanks of the volcano during Hawaii Institute of Geophysics cruises 72-07-02 (second leg, dredge 48) and KK84-08-06-01 (Clague, 1974a; Campbell and others, 1984). The subaerial samples are mostly picritic tholeiitic basalt collected from flows dipping 5°–10° to the north-northwest. Palmer (1927) described two dikes that are alkalic lava. One is highly altered, but on the basis of chemical analysis appears to be a nephelinite; the other is described as a hawaiite. These two dikes probably fed vents during the alkalic rejuvenated stage and alkalic postshield stage, respectively. The single lava sample dredged in 1972 is a rhyolite porphyry (Clague and Dalrymple, 1975). This rock type is unknown from elsewhere in the Hawaiian-Emperor Chain, and we suspect that it is either an ice-rafted erratic or a piece of ship's ballast. The 1984 dredges have not yet been analyzed but contain calcareous sediment, volcaniclastic breccia, basalt, and hyaloclastite.

Funkhouser and others (1968) reported an age of 11.3 ± 0.6 Ma for a single sample of subaerial basalt. Dalrymple and others (1974) dated two samples of tholeiitic basalt from the island; they gave a mean age of 10.3 ± 0.4 Ma. The rhyolite porphyry has a Cretaceous age (Clague and Dalrymple, 1975).

La Perouse Pinnacle (French Frigates Shoal) (26).—La Perouse Pinnacle and an even smaller adjacent rock are the only subaerial exposures of volcanic rock within French Frigates Shoal, a coral atoll consisting of 15 or 16 small sand islets. La Perouse Pinnacle is a stack of lava flows that dip 1°–2° to the northwest. The subaerial flows are picritic tholeiitic basalt (Dalrymple and others, 1974) that probably erupted during the shield stage. Four dated samples have a mean age of 12.0 ± 0.4 Ma.

Brooks Bank (28).—Three samples have been analyzed from dredge 41 of the second leg of the Hawaii Institute of Geophysics cruise 72-07-02 (Clague, 1974a; Garcia, Frey, and Naughton, in press). Two of these samples are hawaiite, probably from the same flow, and the third sample is an olivine basalt transitional between tholeiitic and alkalic basalt. The hawaiite probably erupted during the alkalic postshield stage and the transitional basalt during either the late shield stage or the caldera-collapse phase. The hawaiite and alkalic basalt have a mean age of 13.0 ± 0.06 Ma.

St. Rogatien Bank (29).—A single sample has been analyzed from dredge 44 of the second leg of the Hawaii Institute of Geophysics cruise 72-07-02 (Clague, 1974a). The sample is an aphyric hawaiite that probably erupted during the alkalic postshield stage; it has not been dated.

Gardner Pinnacles (30).—The two rocks that constitute Gardner Pinnacles are the westernmost subaerial exposures of volcanic rock in the Hawaiian Chain. The alkalic basalt flows that make up the rocks dip 15° to the west and are cut by several east-trending dikes (Dalrymple and others, 1974). Dredged samples of geochemically similar, though less differentiated, alkalic basalt were recovered in dredge 37 from the second leg of the Hawaii Institute of Geophysics cruise 72-07-02 (Clague, 1974; Garcia, Frey, and Naughton, in press). A later dredge on the flank of Gardner Pinnacles (HIG dredge 6-7; see Garcia, Frey, and Naughton, in press) recovered largely unaltered picritic tholeiitic basalt. We infer that the picritic tholeiitic basalt erupted during the shield stage and the alkalic basalt flows during the postshield stage. Additional samples have recently been recovered during Hawaii Institute of Geophysics cruise KK84-04-28-05 from a number of dredge stations on Gardner Pinnacles, but these have yet to be analyzed (Campbell and others, 1984).

Samples from the island were too altered for dating (Dalrymple and others, 1974), but Garcia, Frey, and Naughton (in press) obtained a weighted mean age of 12.3 ± 1.0 Ma for two dredged samples of alkalic basalt and one of tholeiitic basalt.

Laysan Island (36).—A single dredge during U.S. Geological Survey cruise LEE8-76-NP recovered a variety of hawaiite and mugearite pebbles (Dalrymple and others, 1981) that probably erupted during the alkalic postshield stage. Conventional K-Ar and ^{40}Ar-^{39}Ar measurements on five of the samples fall within the range 18.8–21.4 Ma, and ^{40}Ar-^{39}Ar incremental heating experiments on three samples gave a mean age of 19.9 ± 0.3 Ma.

Northampton Bank (37).—A Hawaii Institute of Geophysics cruise sampled the south side of Northampton Bank and recovered coral-reef debris, picritic tholeiitic basalt, and olivine tholeiitic basalt that probably erupted during the shield stage. Dalrymple and others (1981) reported conventional K-Ar and ^{40}Ar-^{39}Ar age data for three dredged samples of tholeiitic basalt. Only one of the samples gave a ^{40}Ar-^{39}Ar age spectrum plateau. The inferred age for that sample is 26.6 ± 2.7 Ma.

Pioneer Bank (39).—On the second leg of the Hawaii Institute of Geophysics cruise 72-07-02, dredge 25 recovered pillow breccia of olivine tholeiitic basalt (Clague, 1974a) that probably erupted during the shield stage. The volcano is undated.

Pearl and Hermes Reef (50).—On the second leg of the Hawaii Institute of Geophysics cruise 72-07-02, dredge 24 recovered round clasts of alkalic basalt, hawaiite, and nepheline phonolite (Clague and others, 1975) that probably erupted during the alkalic postshield stage. It is possible that the phonolite sample erupted during an alkalic rejuvenated stage, although other phonolite samples from Koko Seamount in the Emperor Seamounts are all interpreted to have erupted during the alkalic postshield stage (Clague, 1974a). The weighted mean age of phonolite, hawaiite, and alkalic basalt is 20.6 ± 0.5 Ma.

Ladd Bank (51).—On the second leg of the Hawaii Institute of Geophysics cruise 72-07-02, dredge 23 recovered a single fresh clast of ankaramite vitrophyre that is compositionally similar to a basanite or nephelinite (Clague, 1974a). This sample probably erupted during an alkalic rejuvenated stage; it is undated.

Midway Island (52).—In 1965, two holes were drilled through the reef on Midway and into flows of tholeiitic basalt (Ladd and others, 1967). Analyses of the tholeiitic flows are presented in Dalrymple and others (1974) and of hawaiite and mugearite cobbles from a conglomerate overlying the flows in Dalrymple and others (1977). We infer that the tholeiitic flows erupted during the shield stage and the hawaiite and mugearite during an alkalic postshield stage.

Dalrymple and others (1974) reported ages for four samples of tholeiitic basalt from the reef drill hole at Midway. The ages ranged from 10.8 to 18.2 Ma. In the later study, Dalrymple and others (1977) reported an age for Midway of 27.7 ± 0.6 Ma based on conventional K-Ar and ^{40}Ar-^{39}Ar analyses of two unaltered samples of hawaiite and mugearite from the conglomerate. Incremental heating experiments showed that the conventional K-Ar ages obtained earlier for the tholeiitic basalt samples do not represent crystallization ages.

Nero Bank (53).—Scripps Institution of Oceanography cruise TASADAY III recovered a vitrophyre of picritic tholeiitic basalt that probably erupted during the shield stage (Clague, 1974a); it is undated.

Unnamed Seamount (57).—On the second leg of the Hawaii Institute of Geophysics cruise 72-07-02, dredge 20 recovered several samples of open-textured alkalic basalt that probably erupted during an alkalic postshield stage (Clague and others, 1975). Three samples of the basalt have concordant K-Ar ages with a mean of 28.0 ± 0.04 Ma.

Unnamed Seamount (58).—DSDP Site 311, located 240 km west of Midway Island, recovered volcanogenic deposits from the archipelagic apron of this volcano (Larson and others, 1975) that yielded a nannoplankton age of 31–28 Ma (Bukry, 1975).

Unnamed Seamount (63).—Scripps Institution of Oceanography cruise TASADAY III recovered a wide range of alkalic lava types including ankaramite, analcime tephrite, amphibole-bearing tephrite, and amphibole-bearing hawaiite (Clague, 1974a, 1974b; Clague and others, 1975). These strongly alkalic rocks probably originated by crystal fractionation from alkalic rejuvenated-stage basanitic parental magma. Clague and others (1975) obtained concordant K-Ar results from three samples of the alkalic lava; the mean age is 27.4 ± 0.05 Ma.

Hancock Seamount (64).—Hawaii Institute of Geophysics cruise KK84-04-28-05 recently recovered samples in a number of dredges from Hancock Seamount; these samples have not been analyzed or dated (Campbell and others, 1984).

Colahan Seamount (65).—On U.S. Geological Survey cruise L8-82-NP, dredge 4 recovered samples of transitional basalt, tephrite, and amphibole-bearing hawaiite (Duncan and Clague, 1984; D.A. Clague, unpub. data, 1983) that probably erupted during an alkalic rejuvenated stage. Analysis of these samples is still in progress; therefore the identification of eruptive stage is less certain than for the other seamounts. Duncan and Clague (1984) have reported ^{40}Ar-^{39}Ar total-fusion ages of 37.5 ± 0.3 and 39.8 ± 0.2 Ma for two alkalic basalt samples.

Abbott Seamount (65A).—On U.S. Geological Survey cruise L8-82-NP, dredges 2 and 3 recovered samples of transitional to alkalic basalt that probably erupted during the late shield stage or caldera-collapse phase (Duncan and Clague, 1984). Analysis of these samples is still in progress. Duncan and Clague (1984) reported ^{40}Ar-^{39}Ar total-fusion ages of 40.4 ± 0.5 and 36.3 ± 0.3 Ma for two of the samples.

Kammu Seamount (66).—On Scripps Institution of Oceanography cruise AIRES VII, dredge 54 recovered abundant carbonate reef debris but no volcanic rocks. N. Sachs (quoted in Clague and Jarrard, 1973) identified *Spiroclypeus variablis* Tan., a large foraminifer of late Eocene age.

Daikakuji Seamount (67).—On Scripps Institution of Oceanography cruise AIRES VII, dredge 55 recovered a range of lava samples including hypersthene-bearing tholeiitic basalt, basalt transitional between tholeiitic and alkalic basalt, and alkalic basalt (Clague, 1974a; Dalrymple and Clague, 1976). Microprobe analyses of glass rinds on some of these samples are in agreement with the published analyses on altered whole-rock samples. The tholeiitic basalt is interpreted to have erupted during the shield stage, the transitional basalt during the late shield stage or caldera-filling phase, and the alkalic basalt during the alkalic postshield stage.

Dalrymple and Clague (1976) made conventional K-Ar and ^{40}Ar-^{39}Ar age determinations on tholeiitic and alkalic basalt and on plagioclase separates. On the basis of ^{40}Ar-^{39}Ar incremental-heating results from the alkalic basalt and ^{40}Ar-^{39}Ar total-fusion analyses of the plagioclases samples, they concluded that the best age for the seamount was 42.4 ± 2.3 Ma.

Yuryaku Seamount (69).—On Scripps Institution of Oceanography cruise AIRES VII, dredge 53 recovered several fairly fresh pebbles of alkalic basalt (Clague, 1974a; Clague and others, 1975; Dalrymple and Clague, 1976). These samples probably erupted during the alkalic postshield stage.

Clague and others (1975) determined an age of 43.4 ± 1.6 Ma for Yuryaku on the basis of ^{40}Ar-^{39}Ar incremental-heating experiments on two dredged samples of alkalic basalt.

Kimmei Seamount (72).—On Scripps Institution of Oceanography cruise AIRES VII, dredges 51 and 52 recovered several samples of alkalic basalt that have been analyzed (Clague, 1974a; Dalrymple and Clague, 1976). Two of these samples are rather severely phosphatized, but all three probably erupted during the alkalic postshield stage.

Dalrymple and Clague concluded that the best age for Kimmei was 39.9 ± 1.2 Ma from ^{40}Ar-^{39}Ar incremental-heating experiments on three dredged samples of alkalic basalt.

Koko Seamount, southeast part (74).—On Scripps Institution of Oceanography cruise AIRES VII, dredge 43 recovered a large collection of rounded volcanic beach cobbles and abundant coral fragments. The volcanic cobbles include tholeiitic basalt, alkalic basalt, hawaiite, mugearite, trachyte, and phonolite (Clague, 1974a). The tholeiitic basalt probably erupted during the shield stage and the entire suite of related alkalic lava types probably erupted during the alkalic postshield stage. DSDP Leg 32 drilled two shallow holes on Koko Seamount, but neither reached volcanic basement (Larson and others, 1975). The structure and seismic stratigraphy of the seamount are described by Davies and others (1972) and Greene and others (1980).

Clague and Dalrymple (1973) obtained conventional K-Ar and ^{40}Ar-^{39}Ar total fusion data on seven dredged samples of sanidine trachyte, alkalic basalt, and phonolite. Krummenacher (cited in Clague and Jarrard, 1973) obtained K-Ar ages of sanidine from two trachyte samples. The data are concordant and have a mean of 48.1 ± 0.8 Ma (Dalrymple and Clague, 1976).

Koko Seamount, northwest flank (76).—On Scripps Institution of Oceanography cruise AIRES VII, dredge 44 recovered pillow fragments of differentiated tholeiitic basalt from the northwest flank of Koko Seamount (Clague and Dalrymple, 1972; Clague 1974a). This lava probably erupted from a rift zone during the shield stage.

Ojin Seamount (81).—DSDP Leg 55 drilled site 430 through a lagoonal sediment pond near the center of Ojin Seamount (Jackson and others, 1980). Five lava flows were penetrated, including four flows of aphyric to sparsely porphyritic hawaiite and an underlying flow of tholeiitic basalt (Kirkpatrick and others, 1980). The overlying sediment consists of shallow-water carbonate reef or bank deposits. The flows were clearly erupted subaerially: a red soil zone was recovered between two of them. The four hawaiite flows were apparently erupted rather rapidly, because their paleomagnetic inclinations are very similar (Kono, 1980). The lowermost tholeiitic flow probably erupted during the shield stage, whereas the hawaiite flows probably erupted during an alkalic postshield stage.

Dalrymple and others (1980) obtained an age of 55.2 ± 0.7 Ma for Ojin on the basis of ^{40}Ar-^{39}Ar incremental-heating results from two samples of hawaiite and one sample of tholeiitic basalt recovered during drilling of DSDP site 430.

Jingu Seamount (83).—A Hawaii Institute of Geophysics cruise in July 1977 recovered several fresh samples and abundant moderately altered samples of hawaiite and mugearite (Dalrymple and Garcia, 1980) that probably erupted during an

alkalic postshield stage.

Dalrymple and Garcia (1980) reported an age of 55.4±0.9 Ma for Jingu based on ^{40}Ar-^{39}Ar incremental-heating experiments on three of these dredged samples of hawaiite and mugearite.

Nintoku Seamount (86).—DSDP Leg 55 drilled site 432 into a lagoonal sediment pond on the top of Nintoku Seamount (Jackson and others, 1980). Samples of three lava flows were recovered from beneath sandstone, conglomerate, and a thin red clay horizon. The flows are all alkalic lava. The top two flows are identical feldspar-porphyritic alkalic basalt, and the bottom flow is transitional between alkalic basalt and hawaiite. All three flows probably erupted during the alkalic postshield stage. As on Ojin Seamount, these flows were clearly erupted subaerially.

Dalrymple and others (1980) obtained ^{40}Ar-^{39}Ar data from two samples recovered during drilling of DSDP site 432. Only one of the samples gave easily interpretable results, and that one indicated an age of 56.2±0.6 Ma.

Yomei Seamount (88).—DSDP Leg 55 drilled two holes at site 431 on a faulted terrace (Jackson and others, 1980). Neither hole reached volcanic basement. The upper 7.5 m consisted of fragments of manganese-oxide crust, authigenic silicates, phosphate, ice-rafted pebbles, and calcareous sand of Quaternary age. The lower 9.5 m consisted of authigenic silicates, manganese-oxide crust fragments, altered basalt clasts, and calcareous sand of middle Eocene age.

Suiko Seamount, southern part (90).—Saito and Ozima (1975, 1977) obtained a ^{40}Ar-^{39}Ar incremental-heating isochron age of 59.6±0.6 Ma for a single sample of mugearite dredged from the southern part of Suiko. The reliability of this age has been questioned, however, on the basis of (1) selection of the sample from a variety of ice-rafted material dredged from Suiko and (2) the unorthodox and potentially misleading treatment of the ^{40}Ar-^{39}Ar data (Dalrymple and others, 1980). Three conventional K-Ar determinations ranging from 22 Ma to 43 Ma on samples from the same dredged material (Ozima and others, 1970) are unreliable because of severe sample alteration. The sample of mugearite could represent lava of an alkalic postshield stage; however, the presence of abundant ice-rafted material (Ozima and others, 1970) creates obvious difficulties in identifying an indigenous sample from among the erratics.

Suiko Seamount, central part (91).—DSDP Leg 55 drilled a deep reentry hole (433C) in a lagoonal sediment pond (Jackson and others, 1980) on top of Suiko Seamount. The hole penetrated 550.5 m, the lower 387.5 m entirely in basalt. Samples of more than 100 flows or flow lobes were recovered, of which the upper three flow units are alkalic basalt and the remainder are tholeiitic basalt and picritic tholeiitic basalt. The three alkalic flows probably erupted during a postshield stage, whereas the thick sequence of tholeiitic lava represents the shield stage.

Dalrymple and others (1980) determined an age of 64.7±1.1 Ma for two samples of alkalic and tholeiitic basalt recovered during drilling of DSDP site 433C. The data were obtained by ^{40}Ar-^{39}Ar incremental heating.

Tenji Seamount (98).—A single dredge was obtained from Tenji Seamount by the U.S. Coast Guard Cutter *Glacier* in September 1971 (Bargar and others, 1975). The small group of rocks recovered included samples of basalt, crystal tuff, volcaniclastic sandstone, mudstone, graywacke, and a manganese nodule. Some of the lava samples could be derived from the seamount, but the rest are clearly glacial erratics. None of the samples was dated because of the uncertainty of their origin.

Meiji Seamount (108).—DSDP Leg 19 drilled site 192 on top of Meiji Seamount. A thickness of 13 m of pillow basalt with glassy margins was recovered; the rocks are highly altered, but interpretation of the immobile trace elements suggests that they are tholeiitic basalt erupted during the shield stage (Dalrymple and others, 1980b).

The only radiometric data available for Meiji is a minimum age of 61.9±5.0 Ma for highly altered basalt recovered during drilling of DSDP site 192 (Dalrymple and others, 1980b). This age is considerably less than the 70–68 Ma for overlying sediments based on nannoflora (Worsley, 1973).

THE HAWAIIAN-EMPEROR VOLCANIC CHAIN
Part II
Stratigraphic Framework of Volcanic Rocks of the Hawaiian Islands

By Virginia A.M. Lanĝenheim *and* David A. Clague

ABSTRACT

Stratigraphy is an important tool for understanding the geologic history of the volcanoes of the Hawaiian Islands, providing a framework for much information from other geologic and related fields. Three major eruptive stages in a Hawaiian volcano's life—shield stage (tholeiitic), postshield stage (alkalic), and rejuvenated stage (alkalic)—have generally provided a basis for dividing the volcanic rocks into stratigraphic units. Such units are basic to stratigraphy, and suitable nomenclature for them helps promote unambiguous scientific communication regarding the spatial and temporal relations of rocks. The stratigraphic nomenclature of the Hawaiian Islands is herein reviewed and updated to reflect current scientific needs and to be consistent with the most recent (1983) North American Stratigraphic Code.

The major divisions of volcanic rocks on each island formerly called "Volcanic Series" are all considered to be of formational rank and renamed accordingly. Their names reflect either a predominant commonly accepted lithologic type (such as "Basalt") or the variety of volcanic lithologies in the unit (those units are called "Volcanics"). Only those subdivisions of the major units that are currently considered to be useful as formally named units of member or lesser rank are retained; others are considered to be informal. Principal and other reference localities are designated for those well-established units for which a type locality was not previously specified.

We give in tabular form a brief summary of each stratigraphic unit, including its lithology, occurrence, thickness, type and reference localities, stratigraphic relations, age, and any stratigraphic changes made herein.

INTRODUCTION

Stratigraphy is an important tool for understanding the geologic history of the Hawaiian Islands, providing a framework into which much of the scientific information contributed by other geologic and related fields can be fit in an organized manner.

The purpose of this paper is to present a brief summary of the volcanic stratigraphy of the islands, and, because the discrimination of stratigraphic units is basic to stratigraphy, to review the stratigraphic nomenclature for these rocks and update it as far as possible to reflect current scientific needs and to conform to the most recent North American Stratigraphic Code (North American Commission on Stratigraphic Nomenclature, 1983). In order to present a better view of the stratigraphy of the volcanic rocks of the islands, we begin with a short discussion of the geologic setting.

ACKNOWLEDGMENTS

We thank R.L. Christiansen and R.W. Decker for their constructive critical reviews. We also gratefully acknowledge the following persons for their helpful comments and suggestions: D.A. Brew, E.E. Brabb, T.J. Casadevall, G.B. Dalrymple, R.M. Easton, M.O. Garcia, R.T. Holcomb, P.W. Lipman, J.P. Lockwood, J.G. Moore, R.B. Moore, D.W. Peterson, S.C. Porter, J.M. Sinton, D.A. Swanson, G.P.L. Walker, and E.W. Wolfe.

We are deeply grateful to Cynthia Barclay and William Fedasko for their assistance in searching the literature and with the preparation of the typescript.

GEOLOGIC SETTING

The Hawaiian Islands consist of a chain of volcanoes that stretches about 2,700 km (1,700 mi) across the northern Pacific Ocean in a northwesterly direction from the Island of Hawaii to Kure Island (fig. 1.20). The principal (so-called Windward) Hawaiian Islands of Hawaii, Maui, Kahoolawe, Lanai, Molokai, Oahu, Kauai, Niihau, and Kaula lie at the southeastern end of the chain. All of these islands are formed by large volcanoes, though Kaula is only a small crescent-shaped erosional remnant of a tuff cone, presumably resting on a large submerged volcano. Some of the islands are formed by a single volcano, others by two or more coalesced volcanoes. The subaerial part of these volcanoes, which constitutes only a small fraction of the total mass of each volcano, is typically shield shaped. In older volcanoes, this shield shape is largely modified by erosion. The rocks of the southeastern islands are almost entirely of volcanic origin; only minor amounts of sedimentary rocks occur. Northwest of the Windward Islands lie the so-called Leeward Hawaiian Islands (fig. 1.20), which consist of small volcanic islets and atolls; only few of the volcanoes there rise above the sea.

The age of the volcanoes increases progressively from the southeast end, where the volcanoes are still active, to the northwest end, where the volcanoes are about 30 Ma. Most of the volcanoes have been extinct for millions of years. The only historical eruptions have been at East Maui (Haleakala) Volcano on the Island of Maui, and Hualalai, Mauna Loa, and Kilauea Volcanoes on the Island of Hawaii; Mauna Loa and Kilauea are frequently active.

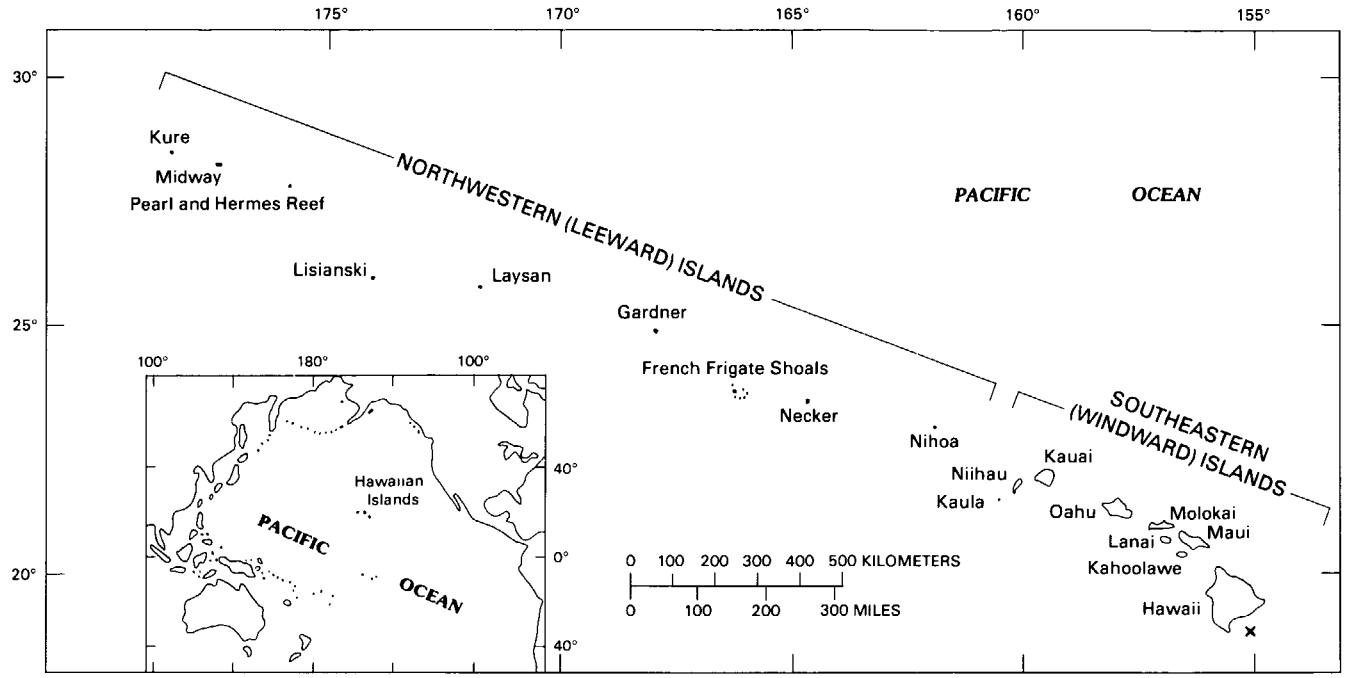

FIGURE 1.20.—Index map of Hawaiian Islands. x, Loihi Seamount.

Hawaiian volcanoes go through four major eruptive stages—preshield, shield, postshield, and rejuvenated stages—in their evolution and growth, and each stage is represented by rocks of distinct chemical and mineralogical composition. The stages used in this report are from Clague and Dalrymple (chapter 1, part I); see also Peterson and Moore (chapter 7) for discussion of alternative nomenclature. All but the preshield stage are well studied and documented (Stearns, 1940b; Macdonald and Katsura, 1964; Macdonald, 1968). Although an individual volcano may become extinct before all the stages are complete, the general sequence of stages is typical of well studied Hawaiian volcanoes.

Very little is known about the preshield stage, which includes the earliest phase of submarine activity and, in the one known example (Loihi Seamount, fig. 1.20), apparently consists of alkalic basalt and basanite (Moore and others, 1982). The main volcanic edifice (more than 95 percent of the total volume of the volcano) is constructed, in perhaps a million years or less, by voluminous eruptions of silica-rich tholeiitic basalt (and rare rhyodacite and icelandite) during the shield stage. The shield stage, as used here, includes the submarine eruption of tholeiitic basalt, which precedes the subaerial shield-forming eruptions. During the shield stage or at the beginning of the next stage, the postshield stage, a caldera may form and be filled with tholeiitic and (or) alkalic basalt. This process of caldera formation and filling was previously referred to as the caldera-filling or caldera-collapse stage, but is here considered to be a phase of the shield stage or postshield stage. During the postshield stage, a relatively thin cap of alkalic basalt and associated differentiated lava (ankaramite, hawaiite, mugearite, benmoreite, and trachyte) covers the main shield. This alkalic lava makes up less than 1 percent of the total volume of the volcano. Later, after a relatively long period of volcanic quiescence and erosion, a very small amount of silica-poor lava (alkalic basalt, basanite, nephelinite, and nepheline melilitite; rare ankaramite and hawaiite known on East Maui Volcano only) erupts from isolated vents; this stage is referred to here as the rejuvenated stage.

During the shield and postshield stages, eruptions are not confined to the summit area of a volcano, but also occur along extensive zones of fissures, called rift zones, that extend down the flanks of the volcano. These zones are usually marked at the surface by collapse craters, cinder and spatter cones, and grabens, and below the surface by large numbers of dikes. During the rejuvenated stage, however, eruptions occur at vents unassociated with the preexisting rift zones, with the exception of rejuvenated-stage lava on East Maui Volcano.

The shield stage is represented by lava that is dark colored and forms relatively long and thin flows. Most of these flows have sparse to abundant olivine phenocrysts, and some have abundant large phenocrysts of plagioclase. Pyroclastic deposits are minor components during the shield stage.

The postshield stage is represented by lava that is commonly lighter colored than shield-stage lava and contains pyroxene, olivine, and plagioclase phenocrysts. This lava forms shorter and thicker flows. Pyroclastic deposits are more abundant during the postshield stage. There is little evidence of erosion between the eruption of shield-stage lava and postshield-stage lava.

The lava that ponds in a caldera during the shield stage or at the beginning of the postshield stage is usually massive and may show columnar structure.

Rejuvenated-stage lava is also dark colored, but usually forms thick flows with few or no phenocrysts; pyroclastic deposits are

common during this stage.

The shield, postshield, and rejuvenated stages have generally formed the basis for the major stratigraphic divisions or subdivisions of the rocks of the Hawaiian volcanoes (fig. 1.21).

PREVIOUS STUDIES

The geology of the Hawaiian Islands has been studied for more than a hundred years (see Clague and Dalrymple, chapter 1, part I, and Peterson and Moore, chapter 7, for summaries of geologic investigations). Early geologic investigations concentrated on the main southeastern islands and were mainly reconnaissance and general descriptive studies. These early studies were superseded by detailed mapping of the eight major southeastern islands beginning in the 1930's and continuing for nearly 30 years. H.T. Stearns and his coworkers, in a series of bulletins published by the Hawaii Division of Hydrography, produced detailed geologic maps (at scale of 1:62,500, except Hawaii at 1:125,000) and descriptions of the Islands of Oahu (Stearns and Vaksvik, 1935; Stearns, 1939, 1940a), Lanai and Kahoolawe (Stearns, 1940b), Maui (Stearns and Macdonald, 1942), Hawaii (Stearns and Macdonald, 1946), Niihau (Stearns, 1947b), Molokai (Stearns and Macdonald, 1947), and Kauai (Macdonald and others, 1960; Stearns was not a coauthor of this report, but did much of the geologic mapping).

These bulletins have provided the basic stratigraphic framework for subsequent petrologic, mineralogic, geochemical, and geophysical investigations of the islands. Only a few stratigraphic studies have been done since publication of the bulletins, and those studies and detailed geologic mapping have been mainly on the Island of Hawaii.

STRATIGRAPHIC NOMENCLATURE

The classification and naming of stratigraphic units (used here as synonomous with lithostratigraphic units), although to some extent arbitrary and artificial, helps promote concise and unambiguous scientific communication as to the spatial and temporal relations of rocks. Stratigraphic units can be formally or informally named; both are useful in stratigraphic work. Formally named units, however, are named and defined in accordance with procedures outlined in the Code, and any major changes made to them, such as boundary or rank changes, need to be justified.

In the Hawaiian Islands, formal stratigraphic names have been applied only to rock units on the eight main southeastern Hawaiian Islands (Hawaii, Maui, Kahoolawe, Lanai, Molokai, Oahu, Kauai, and Niihau), and these names are almost entirely restricted to volcanic rocks and the sedimentary rocks closely associated with them. Other sedimentary units, such as beach and reef deposits, have been formally named, but they are not discussed here.

Stearns and his coworkers divided the rocks of each volcano into one or more major units that they formally named as "Volcanic Series" (see remarks column in table 1.12). These "Series" consisted of rocks resulting from a succession of extensive eruptions. Some of the "Series" consisted entirely of volcanic rocks, whereas others consisted of volcanic rocks, related intrusions, and their weathering products. Some of the "Series" were not subdivided, whereas others were subdivided either into formations or into members. Although the use of "Volcanic Series" as part of a formal name conformed to the "stratigraphic code" in use at the time the unit was named (Ashley and others, 1933), it does not conform to later codes, including the present (1983) code (American Commission on Stratigraphic Nomenclature, 1961, 1970; North American Commission on Stratigraphic Nomenclature, 1983), which restricts the use of the term "Series" to chronostratigraphic units.

The above inconsistencies, plus recent petrologic, mineralogical, and geochemical studies, have necessitated changes in the stratigraphic nomenclature for the volcanic rocks of the Hawaiian Islands[1] because (1) the lithic or descriptive terms of the names do not conform to the current stratigraphic code or do not reflect modern petrologic classification; (2) the ranks of the units are unclear or inappropriate; and (3) formalization of some names is not now considered to be necessary or useful.

The basic guidelines used in this report for updating the stratigraphic usage in the Hawaiian Islands are those recommended by the 1983 North American Stratigraphic Code (North American Commission of Stratigraphic Nomenclature, 1983). Any changes to the stratigraphic nomenclature made in this report, such as revision (change of rank or lower or upper boundary), redefinition (change of name), and abandonment of formally named stratigraphic units, have been approached as follows:

(1) Formal names are retained only for units that serve a useful purpose and require the stability of nomenclature that formalization affords. As stratigraphic units of any rank become established by repeated demonstration of their usefulness, those formal names that have not been used for a few decades or are currently not thought to serve a useful purpose are abandoned as formal names, but the geographic term of their name may be used informally to identify particular flows (and their associated cones) or beds.

(2) Major stratigraphic units on each volcano are all considered to be of formational rank, and are all formally named units. The ranks of stratigraphic units are important in that they give some concept of the scale of the units in relation to other units. Some of these units could have been considered to be units of group rank, but this does not seem necessary. The volcanic products of one volcano (except for some ash deposits) do not occur on other volcanoes, although they may overlap or interfinger at their boundaries where two or more volcanoes coalesce. Therefore, the units of a volcano can be considered to be essentially confined to one large "mountain," and group rank does not seem appropriate. This approach would also give some consistency to the stratigraphic nomenclature of all the islands.

(3) Formally named subdivisions of the major stratigraphic units are those units of member or lesser rank that are distinctive and (or) extensive. Many of the major units of the Hawaiian volcanoes are very often difficult to subdivide because of rapid lateral changes and lack of key beds.

[1]G.A. Macdonald had planned to revise the stratigraphic nomenclature of the Hawaiian Islands (written commun. to R.W. Kopf, 1976, 1977) before his untimely death in 1978.

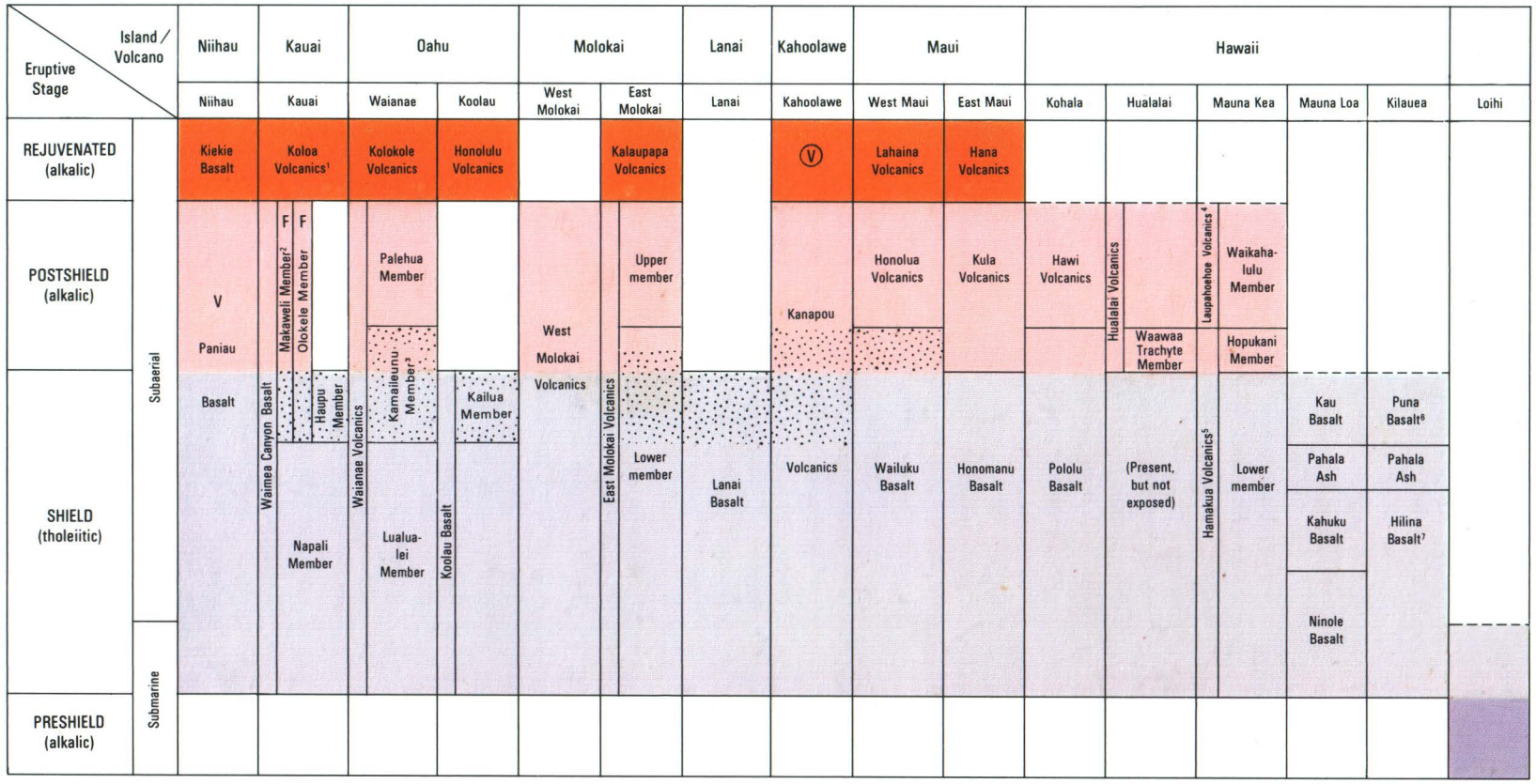

FIGURE 1.21.—Chart showing relations of eruptive stages to volcanoes and stratigraphic units, southeastern Hawaiian Islands, arranged approximately from northwest (left) to southeast (right) (see fig. 1.20 for location). No age correlation between units on different volcanoes implied. Dashed lines indicate end of stage not implied. Base of oldest unit on each volcano (except Loihi) assumed to be at the base of the shield stage.

(4) Formal names of the major stratigraphic units consist of a unique geographic term followed by a simple and generally accepted lithic term, such as "Basalt," or by the term "Volcanics." The initial letter of each term is capitalized. "Basalt" is used for units that consist entirely or almost entirely of basalt, whether tholeiitic or alkalic. An example is the Puna Basalt. The general term "Volcanics" (equivalent to the term "Formation") is used for units that do not have a predominant rock type or are composed of rock types such as hawaiite, mugearite, trachyte and basanite. Examples are the Lahaina Volcanics, Hamakua Volcanics, and Honolulu Volcanics (table 1.12).

The term "Formation" was not used because it does not convey that the unit is composed of volcanic rocks. The term "Volcanic Complex," which indicates a diverse assemblage of extrusive volcanic rocks, related intrusions, and their weathering products, could have been used for some units. However, we tentatively have opted for the term "Volcanics," because it is a shorter term, has precedence of use in the Hawaiian Islands, and does not introduce a new term until the need is confirmed by future investigations.

In general, the term "Basalt" is used for units that represent all or part of the shield stage, although a minor part of the postshield stage may also be represented. The term "Volcanics" is used for units that represent all or part of the postshield stage and for units that represent both shield stage and postshield stage. All units that represent the rejuvenated stage, with the exception of the Kiekie Basalt of Niihau Volcano, are termed "Volcanics."

(5) Formal names of subdivisions of the major units consist of a unique geographic term followed by the appropriate rank term—"Member," "Flow(s)," or "Bed(s)." An intervening lithic or descriptive term may be used in member names and is used in bed and flow names. The initial letter of each term is capitalized. Examples include the Napali Member, Kahele Ash Member, Makanaka Glacial Member, Mokuone Breccia Beds, and Mauna Kuwale Rhyodacite Flow.

Members, flows, and beds can also be informally named. Informal members are designated solely by their lithology or by their stratigraphic position, and none of the initial letters of their names is capitalized. Examples are ash member and lower member. The terms "historic member" and "prehistoric member" are not used in this report because age should play no part in differentiating lithostratigraphic units. Informal flows and beds are similarly designated, such as lower flow, upper flows, ash bed, and breccia beds, but may also combine a geographic term with the unit term or terms; only the initial letter of the geographic term is capitalized. Examples are the Kona ash beds, Kilea flow, and Makapipi flows. With one exception (see Waianae Volcano), all named flows in the Hawaiian Islands are considered to be informal in this report.

(6) A principal reference locality is herein designated for some well established units for which a type locality was never specified. For units that previously had more than one type locality specified, the one here considered to be the more accessible is retained as the type, and the other localities are redesignated as reference localities.

A designated stratotype (type section or type locality) is essential in the definition of a formal stratigraphic unit because it serves as the standard for the unit and constitutes the basis for its recognition. It should therefore be representative of the concept of the unit. Because of the nature of Hawaiian volcanic activity, the stratotype for many of the Hawaiian volcanic units is not truly representative of those units, and reference sections or localities become invaluable in illustrating the lithologic diversity within a unit or the stratigraphic relations with other units. We have not attempted to specify additional reference sections or localities in this report, but we hope this will be done in future stratigraphic studies.

STRATIGRAPHIC SUMMARY

The stratigraphy of the eight main Hawaiian Islands is briefly discussed below by island and volcano from southeast to northwest.

A summary of the formally named stratigraphic units used in this report is given in table 1.12, including a brief description of the lithology, occurrence, thickness, type and reference localities, stratigraphic relations, and age of each. The descriptions of the units were largely taken from the sources cited in the remarks column. Informal units are listed if they were previously formally named. Type localities are used throughout the table, even though some of the units have specified type sections.

Almost all of the isotopic ages shown in the table are K-Ar ages. Numerous radiocarbon ages have been determined for the youngest volcanoes but, with a few exceptions, are not shown. For a summary of radiocarbon ages for the Island of Hawaii, see Rubin and others (chapter 10). The relative ages assigned to the stratigraphic units are based on the Decade of North American Geology time scale (Palmer, 1983), which has the following epoch boundaries: Miocene-Pliocene, 5.3 Ma; Pliocene-Pleistocene, 1.6 Ma; and Pleistocene-Holocene, 10 ka. A correlation diagram of the major stratigraphic units is presented as figure 1.22.

Stratigraphic changes that are made in this report, using the guidelines of the Code and the approach discussed previously, are indicated in the remarks column and discussed below. Former names that have been applied to the units are also indicated in the remarks column. We have not used glottal stops in the geographic part of lithostratigraphic-unit names, although some authors have used them in other publications.

HAWAII

The Island of Hawaii, the largest of the Hawaiian Islands, consists of five coalesced volcanoes: Kilauea, Mauna Loa, Mauna Kea, Hualalai, and Kohala (fig. 1.23). Mauna Kea is the highest of these volcanoes; Mauna Loa is the largest by volume. Little erosion has occurred on these volcanoes except on the northeastern sides of Kohala and Mauna Kea.

KILAUEA VOLCANO

Kilauea, the youngest volcano of the island and still very active, consists entirely of shield-stage tholeiitic lava that issued from the summit caldera and the east and southwest rift zones. The rocks of the volcano are divided into the Hilina Basalt (older) and the

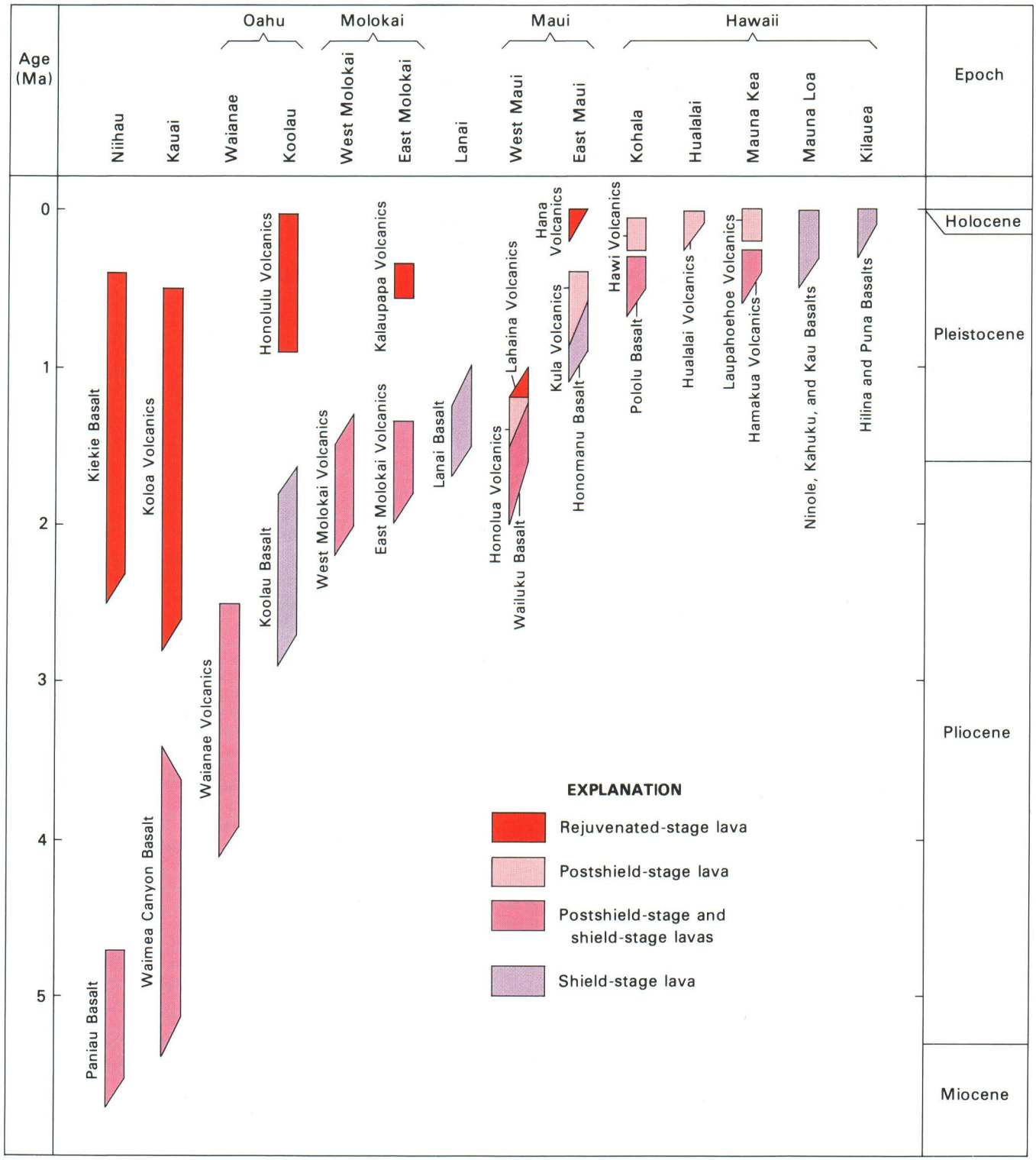

FIGURE 1.22.—Correlation diagram of isotopically dated major volcanic stratigraphic units of southeastern Hawaiian volcanoes. Modified from Clague and Dalrymple (chapter 1, part I, fig. 1.6). Diagonal lines indicate overlapping or uncertain ages. Epoch boundaries from Palmer (1983).

Puna Basalt (younger), generally separated from one another by the Pahala Ash (see subsection "Mauna Loa Volcano"; see also Easton, chapter 11). The Hilina Basalt is exposed only in fault scarps located along the south flank of the volcano. The Hilina Basalt includes the Halape (oldest), Kahele, Pohakaa, and Moo (youngest) Ash Members (Easton, chapter 11). The Puna Basalt covers almost the entire surface of Kilauea and essentially consists of all post-Pahala lava (see discussion below). The Puna includes the prehistoric Uwekahuna (older) and historical Keanakakoi (younger) Ash Members.

The ages of the Hilina and Puna Basalts are not well known. The Hilina Basalt is probably older than the approximately 31-ka

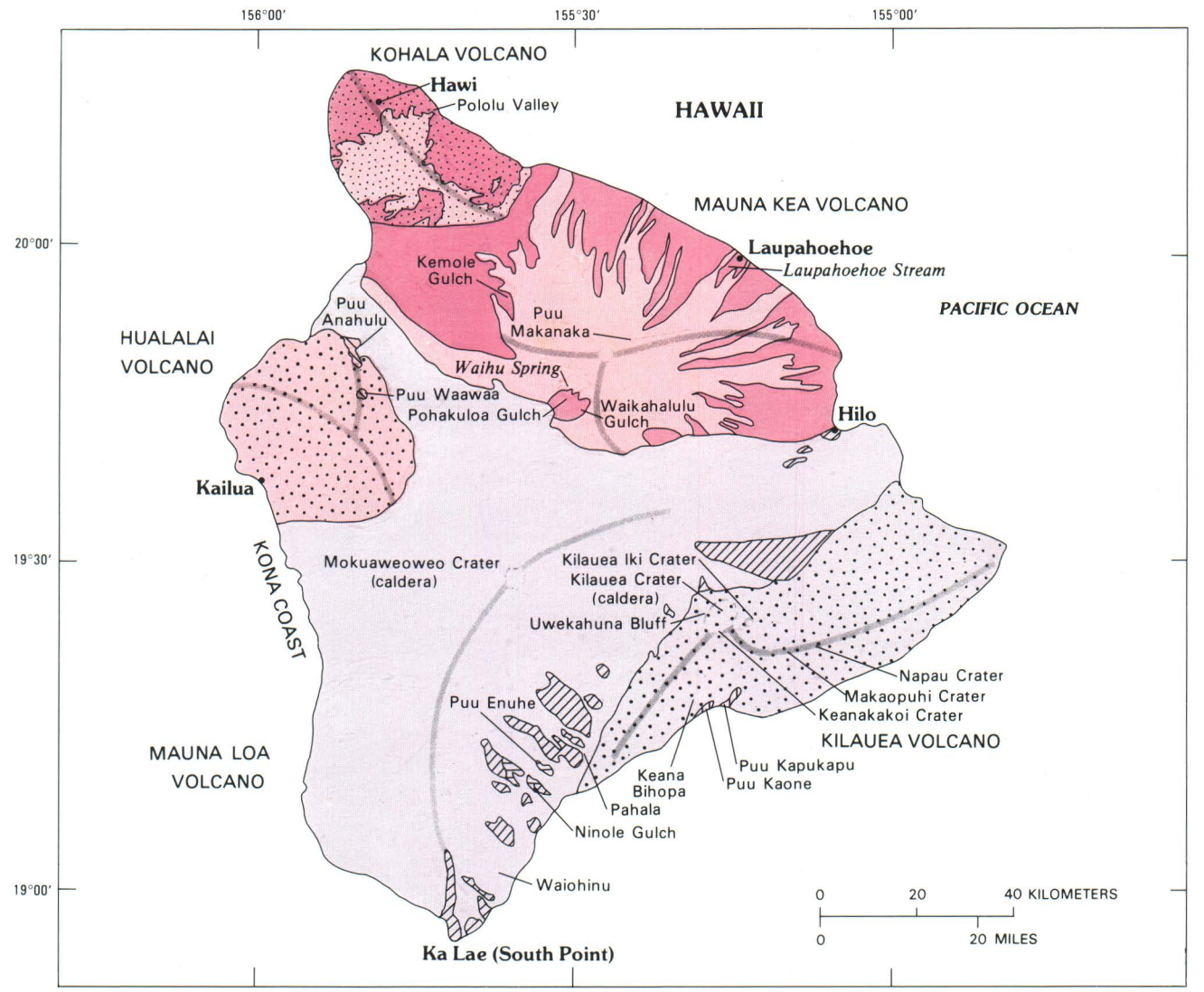

EXPLANATION

KOHALA

- Hawi Volcanics (Pleistocene)
- Pololu Basalt (Pleistocene)

HUALALAI

- Hualalai Volcanics (Holocene and Pleistocene)
- Waawaa Trachyte Member (Pleistocene)

MAUNA KEA

- Laupahoehoe Volcanics (Holocene and Pleistocene) (Waikahalulu Volcanic and Makanaka and Waihu Glacial Members, undivided
- Hamakua Volcanics (Pleistocene) (Hopukani Volcanic and Pohakuloa Glacial Members and lower member, undivided)

MAUNA LOA

- Kau Basalt (Holocene and Pleistocene)
- Kahuku Basalt (Pleistocene)
- Ninole Basalt (Pleistocene)

KILAUEA

- Puna Basalt (Holocene and Pleistocene) (includes Keanakakoi and Uwekahuna Ash Members) (Pahala Ash, not shown)
- Hilina Basalt (Pleistocene) (includes Moo, Pohakaa, Kahele, and Halape Ash Members

Contact — Caldera boundary — Rift zone

FIGURE 1.23.—Generalized geologic map of the Island of Hawaii, showing localities mentioned in text. Modified from Macdonald and others (1983), Easton (chapter 11), and Porter (1979a, 1979b). Rift zones from Fiske and Jackson (1972). Caldera boundary of Mauna Kea Volcano is inferred to be buried beneath younger lava (see Porter, 1972).

radiocarbon age obtained from the base of the Pahala Ash on Mauna Loa, and the oldest exposed Hilina flows are estimated to be about 100 ka (Easton, chapter 11). Most of the Puna Basalt was erupted during the last 10,000 years, but a Puna flow intercalated with the Pahala Ash at Puu Kaone was radiocarbon dated at about 22 ka (see Easton, chapter 11). The Uwekahuna Ash Member of the Puna Basalt has radiocarbon ages ranging from 2.17 ka to 1.04 ka; however, the age of the eruption or eruptions is uncertain. The ash could have been deposited about 2.1 ka (Casadevall and Dzurisin, chapter 13; Lockwood and Rubin, 1986) or about 1.5 ka (Holcomb, chapter 12).

MAUNA LOA VOLCANO

The lava of Mauna Loa, like that of Kilauea, is all shield-stage tholeiitic lava that has mostly issued from the summit caldera and southwest and northeast rift zones.

The oldest exposed rocks belong to the Ninole Basalt, which forms a series of steep-sided hills on the southeast flank of the volcano. The Ninole, which was originally named the Ninole Basalt by Stearns (1926), was later called the Ninole Volcanic Series by Stearns and Macdonald (1946). Recently, Lipman (1980) used the name Ninole Volcanics. As the Ninole is all tholeiitic basalt, the term used by Stearns (1926) is more informative and is used here. The Ninole was thought to represent remnants of an earlier shield volcano mostly buried by lavas from Mauna Loa (Stearns and Macdonald, 1946), but recent studies indicate that it may merely be deeper parts of the Mauna Loa shield, no more than a few hundred thousand years old, that have been uplifted along normal faults (Lipman, 1980).

Unconformably overlying the Ninole are the Kahuku Basalt (older) and Kau Basalt (younger) (table 1.12), which are separated by the Pahala Ash. Lipman (1980) recently used the terms Kahuku Volcanics and Kau Volcanics, but as these units are composed entirely of basalt, they are here renamed the Kahuku Basalt and Kau Basalt, respectively. The Kahuku Basalt crops out on the east and south sides of the volcano. The Kau Basalt covers most of the surface of Mauna Loa and consists of all post-Pahala lava.

The Pahala Ash is a distinctive yellowish vitric ash that has been largely altered by weathering to a reddish brown mixture of clay minerals and hydrated oxides. The thickness of the unit varies considerably, but it is locally more than 15 m thick (Easton, chapter 11).

These ash deposits were originally the uppermost part of what Noble and Clark (in Washington, 1923) called the Pahala Series, which also included the underlying flows. Stone (1926) used the term Pre-Kilauea Series for the uppermost ash and underlying flows, and restricted the name Pahala to the uppermost ash deposits, calling them the Pahala Ash. He applied the name Pahala Ash to ash deposits of Mauna Loa and Kilauea, but not to those of Mauna Kea. Stearns and Clark (1930) used the name Pahala Basalt for both the uppermost ash deposits and the underlying flows. The flows of their Pahala Basalt are herein called the Kahuku Basalt on Mauna Loa and the Hilina Basalt on Kilauea. Wentworth (1938) used the term Pahala Tuff in the same general sense as the Pahala Ash of Stone (1926), but also used the term Waiau Formation (recently abandoned by Porter, 1973) for equivalent ash on Mauna Kea and the term Glenwood Tuff for equivalent ash on parts of the east slope of Mauna Loa. Stearns and Macdonald (1946) and Davis and Macdonald (in Avias and others, 1956), however, considered the Pahala Ash to be a persistent ash formation that was derived from several sources. They believed the Pahala occurred on all the volcanoes, separating their major units on Kilauea (Hilina and Puna Volcanic Series), Mauna Loa (Kahuku and Kau Volcanic Series), and Mauna Kea (Hamakua and Laupahoehoe Volcanic Series) and capping the older unit (Pololu Volcanic Series) of Kohala and a member (Waawaa Volcanics) of the Hualalai Volcanic Series of Hualalai.

Current mapping on Mauna Kea, Hualalai, and Kohala indicates that the extensive surficial ash deposits on these volcanoes were locally derived and are genetically distinct from the Pahala Ash on Kilauea and Mauna Loa (E.W. Wolfe, oral commun., 1986). Therefore, we are geographically limiting the Pahala to the occurrences on Kilauea and Mauna Loa.

The age of the Ninole Basalt is considered to be no more than a few hundred thousand years. The single published K-Ar age of 0.54 Ma has an estimated uncertainty of 0.4 m.y. (see Clague and Dalrymple, chapter 1, part I). The Kahuku Basalt and the Kau Basalt are approximately coeval with the Hilina Basalt and Puna Basalt, respectively, of Kilauea. The Pahala Ash on Mauna Loa and Kilauea is considered by Easton (chapter 11) to be entirely of Pleistocene age (between about 30 ka and 10 ka).

MAUNA KEA VOLCANO

Mauna Kea last erupted about 3.6 ka (Porter, 1979a). The volcano passed through the shield stage into the postshield stage and produced a cap of differentiated lava that almost completely buried the original subaerial shield. It is uncertain if a summit caldera existed; however, a small caldera has been inferred to lie buried beneath the younger lava (Porter, 1972). Rift zones are less pronounced than on Kilauea and Mauna Loa, but westerly, southerly, and easterly rifts are suggested by alignments of cinder cones. The lower northeastern slope of the volcano has gulches cut into it, whereas the other slopes are generally little affected by erosion. The upper slopes of the volcano were glaciated during the Pleistocene.

The rocks of the volcano were divided into the Hamakua Volcanic Series and the overlying Laupahoehoe Volcanic Series by Stearns and Macdonald (1946). The Hamakua represents the shield stage and part of the postshield stage; the Laupahoehoe represents the rest of the postshield stage. These units, considered to be of formational rank by Stearns and Macdonald (1946), were subdivided by them into informal members.

Recently, Porter (1979a, 1979b; see also Porter, 1973, 1974; Porter and others, 1977) formally redefined the Hamakua and Laupahoehoe to include glacial deposits, raised them to group rank, and subdivided both units into formally named volcanic and glacial formations. They subdivided the upper part of the Hamakua Group into the Hopukani Formation (volcanic) and the Pohakuloa Formation (glacial), but Porter (1979a, 1979b) called the lower part of

the group the "lower member of Stearns and Macdonald (1946)." Porter and others (1977; see also Porter, 1973, 1974) originally subdivided their Laupahoehoe Group into three volcanic formations—Liloe (oldest), Hanaipoe, and Waikahalulu (youngest) Formations—and two interstratified glacial formations—Waihu and Makanaka Formations. The Makanaka included the Kemole Member, a volcanic unit. This usage was superseded by a threefold subdivision of the Laupahoehoe Group (Porter, 1979a, b), in which all of the volcanic rocks were assigned to the Waikahalulu Formation; the names Liloe, Hanaipoe, and Kemole were abandoned as formal names of lithostratigraphic units and were formally applied to chronostratigraphic units—the Liloean, Hanaipoean, and Kemolean Stages.

Because the use of the Hamakua and Laupahoehoe as units of group rank is not consistent with the approach used here for the rest of the volcanoes of the Hawaiian Islands, these units are here reduced to formation rank and renamed the Hamakua Volcanics and Laupahoehoe Volcanics. Their subdivisions are reduced to member rank and renamed to reflect the overall nature of their lithologies (see table 1.12).

The Hamakua is considered to be of Pleistocene age and the Laupahoehoe of Pleistocene and Holocene age on the basis of K-Ar and radiocarbon dating (Porter, 1979a) (table 1.12).

HUALALAI VOLCANO

Hualalai Volcano last erupted in 1800–1801, when several flows issued from the well-defined northwest rift zone. Less well defined rift zones trending north and southeast are marked by numerous cinder and spatter cones. It is not known whether the volcano had a summit caldera. Shield-stage tholeiitic lava is not exposed on Hualalai Volcano, but tholeiitic rocks are known to occur in the subsurface and in the submarine part of the volcano (Moore and others, chapter 20; Clague, 1982).

The entire subaerial surface of the volcano consists of postshield-stage alkalic basalt, with minor hawaiite and trachyte, named the Hualalai Volcanic Series by Stearns and Macdonald (1946). They included within the Hualalai a trachyte cone and flow, which they called the Waawaa Volcanics. Though they gave the Waawaa what is now considered to be a formational rank name, they clearly considered it to be a member of the Hualalai (Stearns and Macdonald, 1946, p. 143), and it is so considered here (table 1.12).

Stearns and Macdonald (1946) did not apply a name to the ash deposits that mantle the slopes of the volcano, although Wentworth (1938) had earlier called these deposits the Kona Tuff Formation. Later, Davis and Macdonald (in Avias and others, 1956) presumably included the Kona Tuff Formation within the Hualalai, effectively giving the Hualalai group status. R.B. Moore (oral commun., 1986) suggests that this unit should never have been formally named; it is here abandoned as a formal name and the unit is informally called the Kona ash beds. Thus, the Hualalai is here reduced to formational rank and renamed the Hualalai Volcanics.

The Hualalai Volcanics is largely of Holocene age, but the oldest flows are of Pleistocene age (Moore and others, chapter 20). The Waawaa Trachyte Member has a published K-Ar age of 0.4 ± 0.3 Ma (Funkhouser and others, 1968), but recent unpublished K-Ar determinations by G.B. Dalrymple (oral commun., 1986) indicate the trachyte is about 0.105 Ma.

KOHALA VOLCANO

Kohala Volcano is an oval volcano built up around northwest and southeast rift zones. It is deeply dissected on its northeast side. Arcuate faults near the summit of the volcano suggest that a caldera formed during the shield stage but was later buried by the younger lava in the postshield stage.

The volcanic rocks of Kohala Volcano were originally divided by Stearns and Macdonald (1946) into the Pololu Volcanic Series (older), composed of shield-stage tholeiitic basalt with caldera-filling postshield-stage alkalic basalt near the top, and the Hawi Volcanic Series (younger), consisting of differentiated alkalic lava of the postshield stage (table 1.12). Neither of these units has been subdivided, and they are here renamed the Pololu Basalt and Hawi Volcanics, respectively, to reflect their lithologies. The Pololu Basalt and Hawi Volcanics are of Pleistocene age on the basis of K-Ar determinations (McDougall, 1969; McDougall and Swanson, 1972) (table 1.12).

MAUI

The Island of Maui (fig. 1.24), the second largest of the Hawaiian Islands, consists of two large coalesced volcanoes, East Maui (or Haleakala) Volcano and West Maui Volcano, connected to one another by an isthmus formed when lava of East Maui banked against the already existing West Maui Volcano. The Maui volcanoes are more dissected than the volcanoes of the Island of Hawaii.

EAST MAUI (OR HALEAKALA) VOLCANO

East Maui Volcano last erupted about 200 years ago and has a large summit crater called Haleakala Crater, which is primarily of erosional origin (Macdonald and others, 1983). East Maui is the youngest Hawaiian volcano to have rejuvenated-stage lava.

The rocks of the volcano were originally divided by Stearns and Macdonald (1942) into the Honomanu Volcanic Series (oldest), Kula Volcanic Series, and Hana Volcanic Series (youngest), representing the shield, postshield, and rejuvenated stages, respectively (table 1.12). The Kula eruptions took place along southwest, east, and northwest rift zones. The Hana eruptions are unique among Hawaiian rejuvenated-stage eruptions because their vents are aligned along preexisting rift zones (southwest and northwest rift zones), the erosional period preceding these eruptions was rather short (<0.4 m.y.), and ankaramite and hawaiite are present.

The Honomanu Volcanic Series is almost completely buried by later lava and is only exposed in the seacliffs along part of the north coast. The Honomanu Volcanic Series was not subdivided by Stearns and Macdonald (1942), and it was more recently called the Honomanu Formation in the Haleakala Crater area by Macdonald

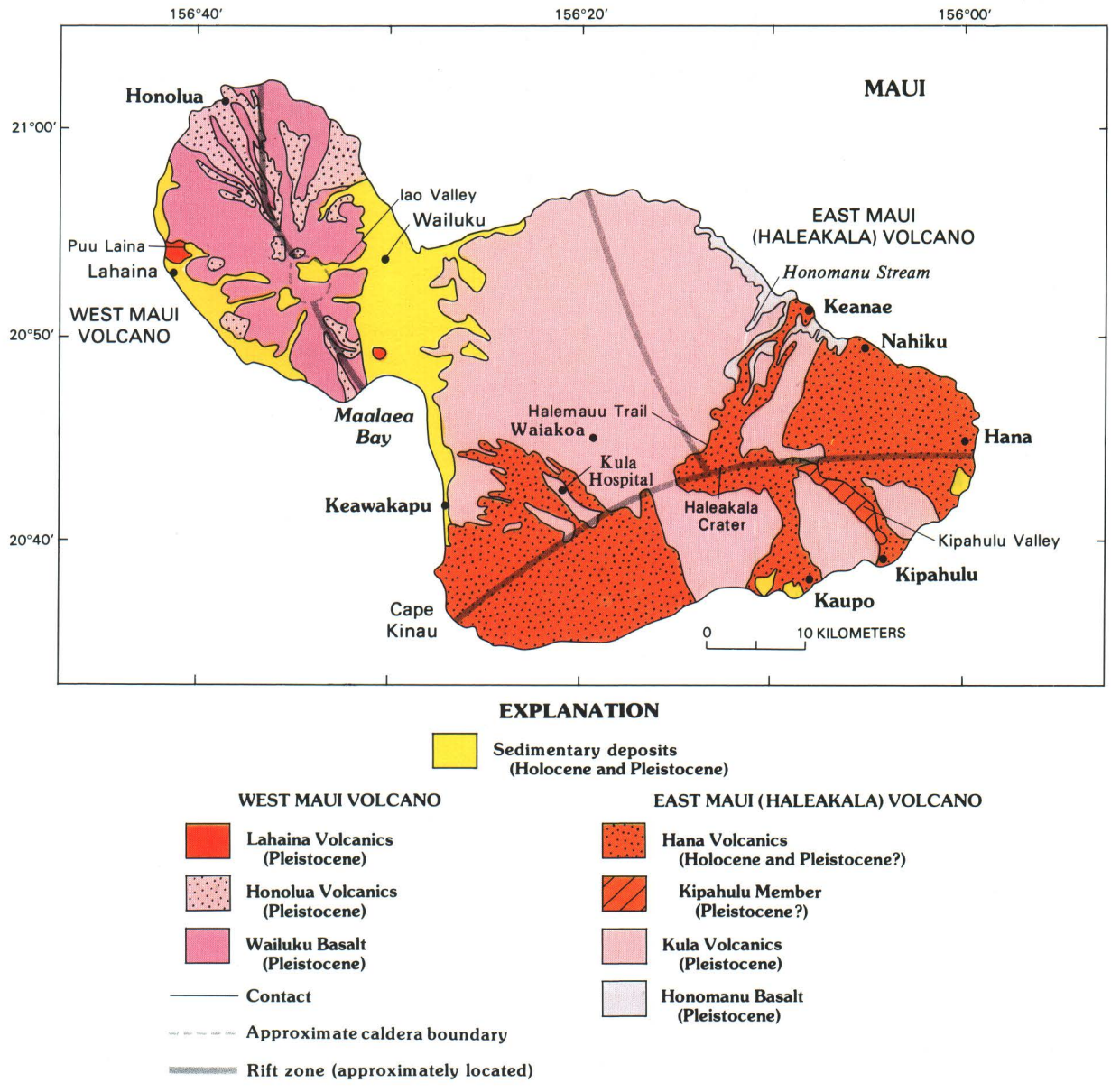

FIGURE 1.24.—Generalized geologic map of Maui, showing localities mentioned in text. Modified from Macdonald and others (1983). Rift zones from Fiske and Jackson (1972). West Maui Volcano caldera boundary from Macdonald and others (1983, fig. 20.4).

(1978). As it consists entirely of tholeiitic basalt, it is here renamed everywhere the Honomanu Basalt.

The Kula Volcanic Series of Stearns and Macdonald (1942), which was later called the Kula Formation by Macdonald (1978), is here renamed the Kula Volcanics to reflect its varied lithology. Rocks in the lower part of the south wall of Haleakala Crater that Stearns and Macdonald (1942) had originally assigned to the Honomanu were excluded from the Honomanu and named the Kumuiliahi Formation by Macdonald (1978). As these rocks appear more properly to belong to the Kula (Macdonald and others, 1983, p. 391), they are here tentatively included in the Kula, and the name Kumuiliahi Formation is not used.

The Kula was named by Stearns (1942) for the settlement of Kula (now called Waiakoa) along the roads leading to the Kula Sanatorium or Hospital on the west slope of the volcano, but he did not designate a type locality. Macdonald and Davis (in Avias and others, 1956), however, did specify the type locality as "Kula, a district on the west slope of East Maui Mountain." This "locality" is here considered to be along Highway 37 near Waiakoa (Kula Post Office), about 7 km northeast of Kula Hospital. Other accessible

sections of the Kula, according to Stearns, are along the Kaupo-Kipahulu road near Kipahulu and along Halemauu Trail in the Haleakala Crater area; these are here considered to be reference localities.

Stearns and Macdonald (1942) subdivided the Hana Volcanic Series into many local formally named units in the Keanae and Nahiku areas along the northeast coast. It was not clear whether they intended these units to be of member or formation rank (see Stearns and Macdonald, 1942, p. 94, 95), but they applied formational-rank names to these units. Macdonald and Davis (in Avias and others, 1956) considered them to be formations. In Kipahulu Valley in the southeastern part of the island, however, Stearns and Macdonald (1942) included only the Kipahulu Member within the Hana. The Kipahulu was later raised in rank by Macdonald and Davis (in Avias and others, 1956) to Kipahulu Formation, though in later publications by Macdonald and Abbott (1970), Macdonald and others (1983), and Stearns (1985) the term Kipahulu Member is used. Thus the Hana had previously been considered to be of group rank. Macdonald (1978) did reduce the rank of the Hana in the Haleakala Crater area, using the name Hana Formation, but he did not address the status of the formational rank units in the Keanae and Nahiku areas.

Therefore, the following changes are here made to the Hana: The Hana is reduced to formational rank everywhere and renamed the Hana Volcanics. Its subdivisions in the Keanae and Nahiku areas, being mainly single flows of very limited extent, are abandoned as formally named units and are used informally (table 1.12). The Kipahulu is retained as a member of the Hana because it is a fairly extensive unit and is separated from earlier Hana flows by an erosional unconformity. The historical lava flow of about 1790 in the Cape Kinau area (Oostdam, 1965) is considered to be part of the Hana, although it was not included in the Hana by Stearns and Macdonald (1942), and they gave "1750?" as the date of the flow. Finally, to correct an error in Keroher and others (1966, p. 1976), the Hana does not include the Kaupo Mudflow.

The Pleistocene age of the Honomanu Basalt and Kula Volcanics is well documented by K-Ar determinations (Naughton and others, 1980) (table 1.12). No isotopic ages have been determined for the Hana Volcanics, but it is here considered to be Pleistocene(?) and Holocene. The Kipahulu Member is probably Pleistocene, judging by its relations to older units.

WEST MAUI VOLCANO

West Maui Volcano is incised by deep valleys and is considered to be extinct. Lava was erupted from a small central caldera and from the north and southeast rift zones.

The rocks of West Maui Volcano were divided by Stearns and Macdonald (1942) into three major units—Wailuku Volcanic Series (oldest), Honolua Volcanic Series, and Lahaina Volcanic Series (youngest). These units represent the shield stage and postshield caldera-filling phase, the postshield stage, and the rejuvenated stage, respectively.

Stearns and Macdonald did not subdivide the Wailuku and Honolua, which are here renamed the Wailuku Basalt and Honolua Volcanics, respectively. They did, however, include two formational-rank units, the Kilea Volcanics and the Laina Volcanics, within their Lahaina Volcanic Series. The Lahaina was recently reduced to formational rank and renamed the Lahaina Volcanics by Clague and others (1982), but they did not address the status of the Kilea and Laina. The Kilea Volcanics and Laina Volcanics are two small flow units with associated cinder cones; because they are of such limited extent, they are here abandoned as formally named units and their names used informally (table 1.12). The name Lahaina Volcanics of Clague and others (1982) is retained here.

Isotopic age determinations of the Wailuku Basalt and Honolua Volcanics (McDougall, 1964; Naughton and others, 1980) (table 1.12) indicate a Pleistocene age for both units. The Lahaina Volcanics is less well dated, but it is also considered to be Pleistocene. The single K-Ar age of 1.30 ± 0.10 Ma (Naughton and others, 1980) is considered to be too old on stratigraphic grounds.

KAHOOLAWE AND LANAI

Each of these islands consists of a single shield volcano with a summit caldera, and each has been little dissected.

KAHOOLAWE VOLCANO

The lava of Kahoolawe Volcano was erupted along a prominent southwest rift zone (fig. 1.25). The caldera was almost completely buried beneath a cap of later lava.

The rocks that form essentially all of the Island of Kahoolawe, the smallest of the major islands, were called the Kanapou Volcanic Series by Stearns (1946). The Kanapou, which is not subdivided and is here renamed the Kanapou Volcanics, represents the shield stage, a caldera-filling phase of both the shield and postshield stages, and the postshield stage. The small rejuvenated-stage vents that occur in the sea cliffs on the west side of Kanapou Bay were not considered by Stearns (1946) to be part of the Kanapou, and they are not so considered here.

The alkalic part of the Kanapou Volcanics has been dated at about 1 Ma (Naughton and others, 1980); the tholeiitic part is undated, but is presumed here to be Pleistocene also. The rejuvenated-stage vents are not isotopically dated. They were considered to be of Holocene age by Macdonald and others (1983), but this age is probably too young.

LANAI VOLCANO

The Island of Lanai was built by eruptions from the summit and along northwest, southwest, and southeast rift zones (fig. 1.26). The caldera was mostly filled by lava flows, but its remnant is now covered by alluvium.

The volcanic rocks of Lanai represent the shield stage, including the caldera-filling phase, and they were called the Lanai Volcanic Series by Stearns (1946). Wentworth (1925) had originally applied the name Lanai Basalt to the lava flows of Lanai Volcano and the name Manele Basalt to the small crater remnant

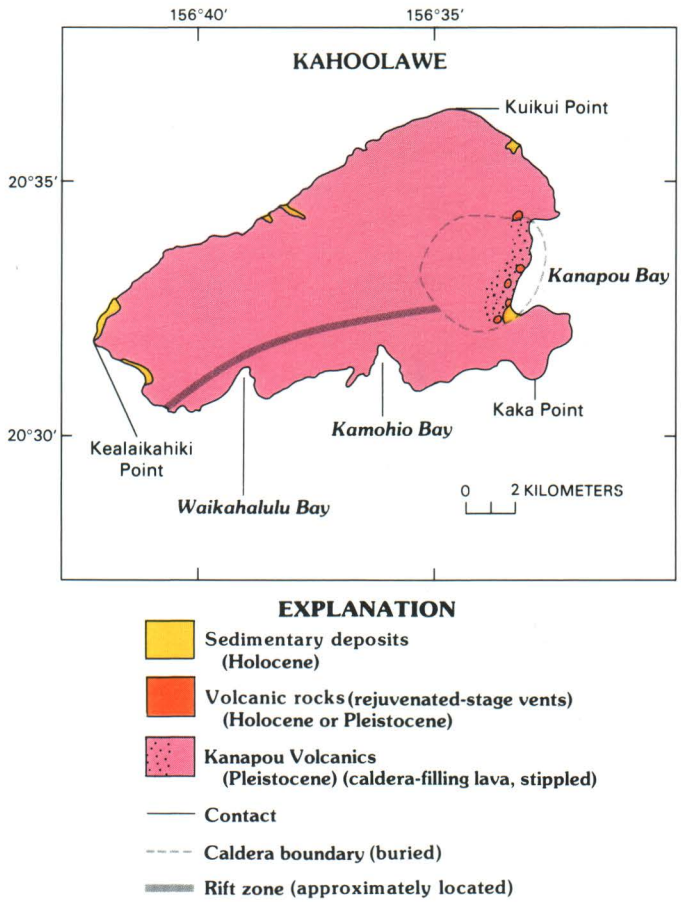

FIGURE 1.25.—Generalized geologic map of Kahoolawe, showing localities mentioned in text. Modified from Macdonald and others (1983). Rift zone from Fiske and Jackson (1972).

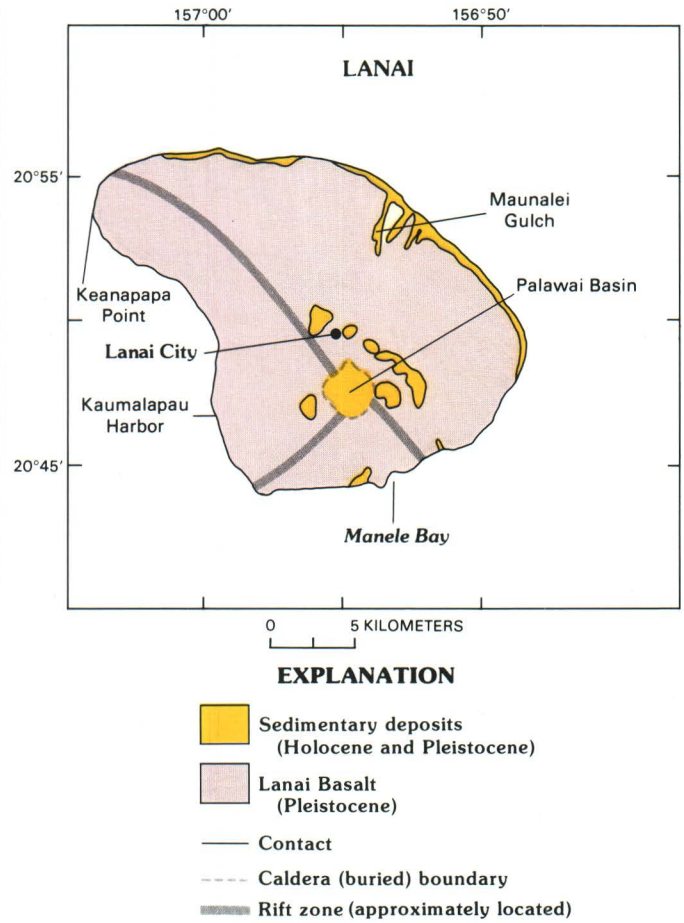

FIGURE 1.26.—Generalized geologic map of Lanai, showing localities mentioned in text. Modified from Macdonald and others (1983). Rift zones from Fiske and Jackson (1972). Caldera boundary inferred to be largely coincident with Palawai Basin.

that forms the headland southwest of Manele Bay. Stearns (1946) redefined the Lanai to include not only the lava flows but also other associated rocks (pyroclastic and intrusive rocks) in a unit he called the Lanai Volcanic Series; he did not include Wentworth's terms Lanai and Manele Basalts as part of the Lanai Volcanic Series. However, Macdonald and Davis (in Avias and others, 1956) included (improperly) the Lanai Basalt, which included Manele Basalt, in the Lanai Volcanic Series, seemingly giving group status to the later unit.

The Lanai Volcanic Series of Stearns (1946) is here reduced to formational rank and renamed the Lanai Basalt. Though there is a chance of confusion with the Lanai Basalt of Wentworth, which consisted only of the lava flows, it would be more misleading to call the unit "Lanai Volcanics" because it consists totally of shield-stage tholeiitic basalt.

The term Manele Basalt is here abandoned as a formal name because it has essentially the same lithology and same age as the Lanai Basalt, as used here, and is of extremely limited extent and the term has been applied to a former high stand of the sea.

The Lanai Basalt is of Pleistocene age based on a K-Ar isochron age of 1.28±0.4 Ma (Bonhommet and others, 1977) (table 1.12).

MOLOKAI

The Island of Molokai is another volcanic doublet, made up of two coalesced volcanoes—East Molokai and West Molokai Volcanoes (fig. 1.27). East Molokai Volcano had a summit caldera; there is no evidence that West Molokai Volcano had one. Both volcanoes are deeply dissected along their northern coasts.

EAST MOLOKAI VOLCANO

East Molokai Volcano was built principally by eruptions from the summit caldera and along east and northwest rift zones.

The volcanic rocks of East Molokai Volcano were divided by Stearns (1946, 1947a) into the East Molokai Volcanic Series (older) and the Kalaupapa Basalt (younger).

The East Molokai Volcanic Series, here renamed the East Molokai Volcanics, was subdivided by Stearns into two informal members—lower and upper members. The lower member represents the shield stage and part of the postshield stage; both stages include a caldera-filling phase. The upper member represents the rest of the postshield stage.

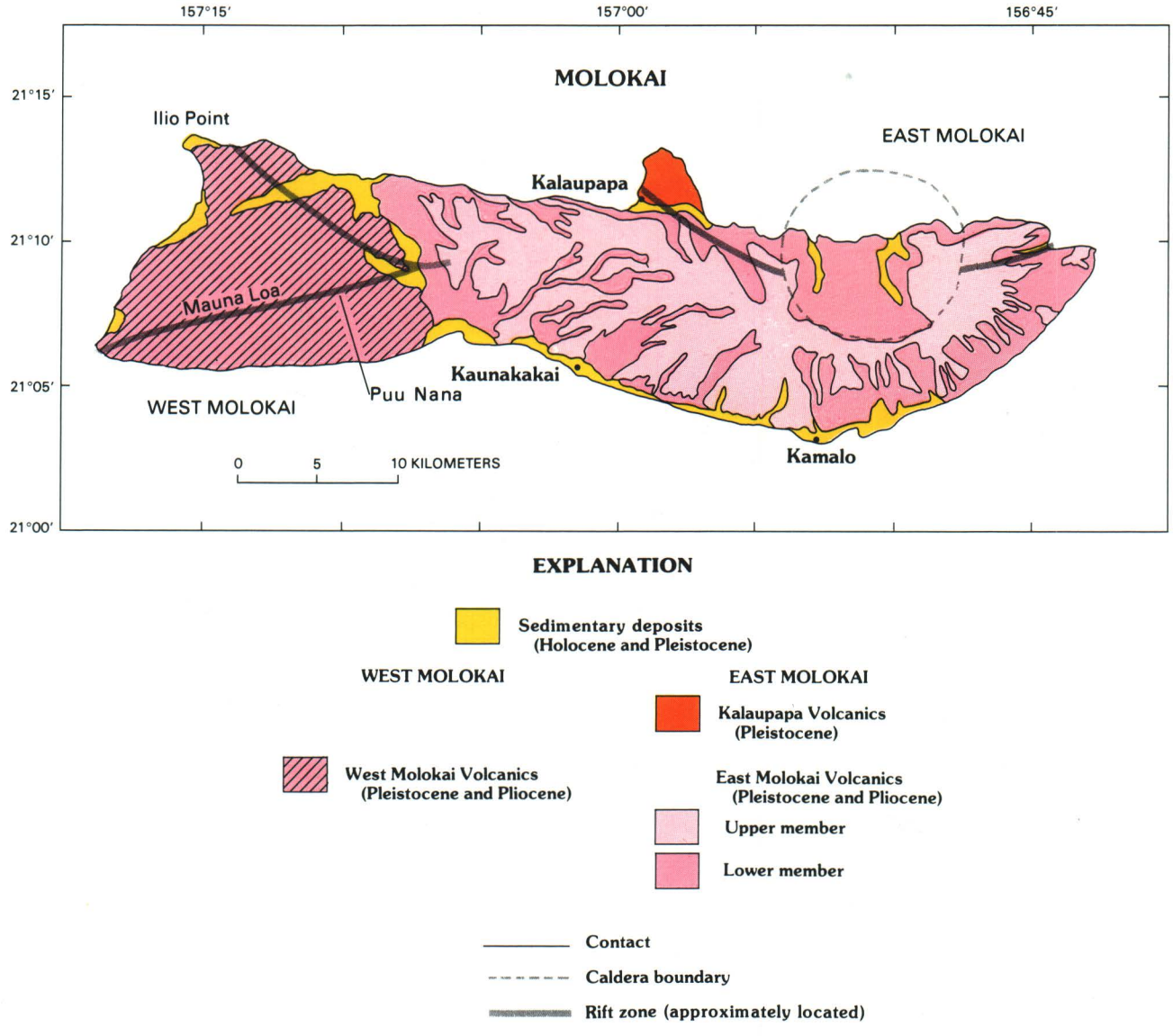

FIGURE 1.27.—Generalized geologic map of Molokai, showing localities mentioned in text. Modified from Macdonald and others (1983). Rift zones from Fiske and Jackson (1972). East Molokai Volcano caldera boundary from Holcomb (1985).

The Kalaupapa Basalt, which consists of alkalic basalt and basanite, is here renamed the Kalaupapa Volcanics to reflect the range of compositions present. The Kalaupapa has been proposed as a separate shield (see Macdonald and others, 1983; Holcomb, 1985), but it is here considered to represent a rejuvenated-stage vent associated with East Molokai Volcano on the basis of its age and chemistry (see Clague and others, 1982).

The East Molokai Volcanics is largely Pleistocene, but its lowermost flows are Pliocene on the basis of K-Ar age determinations on its lower and upper members (McDougall, 1964; Naughton and others, 1980) (table 1.12). The Kalaupapa Volcanics has a Pleistocene age based on K-Ar determinations of 0.57 ± 0.02 and 0.35 ± 0.03 Ma (Clague and others, 1982).

WEST MOLOKAI VOLCANO

West Molokai Volcano was built by eruptions principally along a northeast rift zone that crosses the summit area (Puu Nana) and along a northwest rift zone. There is no evidence of a summit caldera.

All of the volcanic rocks of West Molokai Volcano were called the West Molokai Volcanic Series by Stearns (1946, 1947a). The West Molokai Volcanic Series, which was not subdivided by Stearns, is here renamed the West Molokai Volcanics to reflect its varied rock types. The West Molokai Volcanics represents the shield and postshield eruptive stages.

The age of the West Molokai Volcanics is considered to be

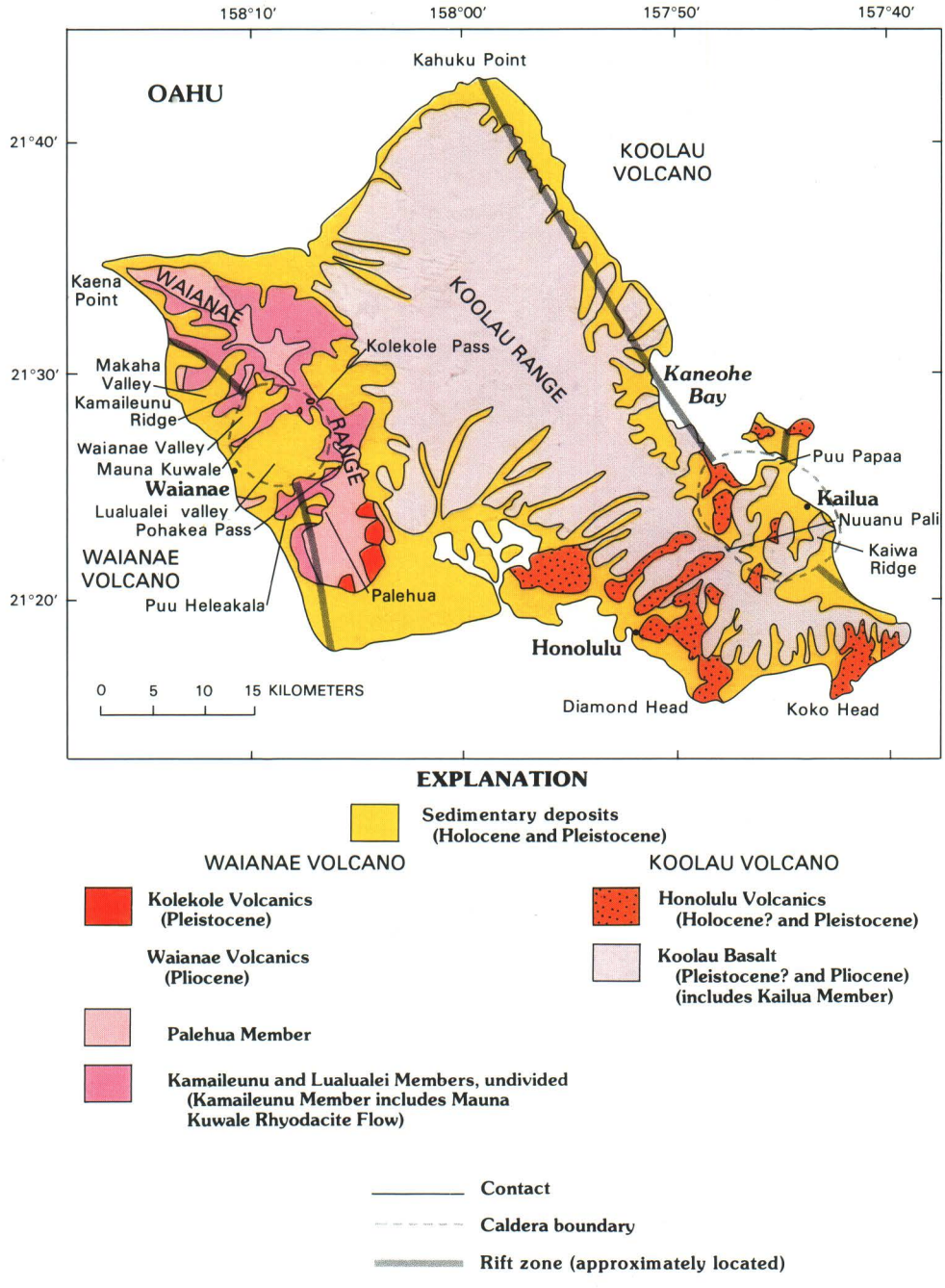

FIGURE 1.28.—Generalized geologic map of Oahu, showing localities mentioned in text. Modified from Macdonald and others (1983) and Sinton (in press). Rift zones from Fiske and Jackson (1972). Koolau Volcano caldera boundary from Clague and Frey (1982); Waianae Volcano caldera boundary from Sinton (in press).

Pliocene and Pleistocene on the basis of K-Ar determinations by Naughton and others (1980) (table 1.12).

OAHU

This island is made up of the highly dissected remnants of two shield volcanoes—Koolau Volcano (east) and Waianae Volcano (west) (fig. 1.28)—that have lost their original shield outline and are now two northwest-trending ridges shaped mainly by erosion. Both volcanoes had summit calderas.

KOOLAU VOLCANO

The lava of Koolau Volcano was principally erupted from the caldera and along the northwest and southeast rift zones. A major dike complex occurs in the rift zones (Walker, chapter 41). The vents

for the youngest lava (rejuvenated stage) show no relationship to the preexisting rift zones.

The rocks of this volcano were originally divided by Stearns (1935, 1939) into three major volcanic units—the Kailua Volcanic Series (oldest), the Koolau Volcanic Series, and the Honolulu Volcanic Series (youngest). The Koolau and the Honolulu represent the shield stage and rejuvenated stage, respectively. Stearns originally believed the Kailua Volcanic Series represented an older lava series that was under or close by the summit caldera of Koolau Volcano, but that it was not part of Koolau Volcano. He later (Stearns, 1940a) recognized that the Kailua was part of the Koolau Volcano, representing the caldera complex. Macdonald and Davis (in Avias and others, 1956) included (improperly) the Kailua Volcanic Series in the Koolau Volcanic Series. Although the ranks they intended for these units are not clear, it is here presumed that the Kailua Volcanic Series was of formational rank.

More recently the Koolau has been considered to be of formational rank. It was called the Koolau Formation by Wentworth (1951) and the Koolau Volcanics by Lanphere and Dalrymple (1979) (table 1.12). It is here renamed the Koolau Basalt because it consists entirely of shield-stage tholeiitic basalt. Although Wentworth (1926, fig. 15) also used the term "Koolau basalt" in the explanation of a page-size geologic map of a small area of Oahu, he did not describe the unit and there does not seem much chance of confusion with the Koolau Basalt as used here. The Kailua Volcanic Series is here reduced in rank and renamed the Kailua Member of the Koolau Basalt.

The Honolulu Volcanic Series was defined by Stearns (1935) to consist of rejuvenated-stage lava that erupted from more than 35 vents on the southern slopes of the volcano. These lavas are strongly alkalic and form a variety of cones (tuff, cinder, spatter), many with associated lava flows. The eruptions presumably did not come in rapid succession, but occurred over a long period of time. Their general sequence (Macdonald and others, 1983) (table 1.12) has been based largely on the relative degree of weathering and erosion and on relations to stands of the sea because few superpositional relations are known and isotopic ages are considered unreliable.

The Honolulu Volcanic Series was of group rank as defined by Stearns (1935, 1939) because it was made up of numerous formally named units of formational rank (table 1.12). Hay and Iijima (1968) and Clague and others (1982) also considered the Honolulu to be of group rank. Lanphere and Dalrymple (1979) and Clague and Frey (1982) used the formational-rank term Honolulu Volcanics, but did not address the status of its formally named subdivisions. The Honolulu is here considered to be of formational rank, and the term Honolulu Volcanics is retained to reflect its range of lithologic compositions.

The formally named eruptive units that make up the Honolulu could have been reduced in rank and retained as formally named members, but, because most are single flows of very limited extent, this seems unnecessary; they are here all considered to be informal units (table 1.12).

The age of the Koolau Basalt is Pliocene based on K-Ar ages ranging from 2.7 to 1.8 Ma (Doell and Dalrymple, 1973); however, a Pleistocene age cannot be ruled out for the youngest flows (table 1.12). The Kailua Member has not been isotopically dated, but is probably Pleistocene.

The K-Ar ages reported for the Honolulu Volcanics range from about 0.9 to about 0.03 Ma, but there are large differences (sometimes a factor of ten) in the ages reported by different investigators for the same eruptive units (see Clague and Dalrymple, chapter 1, part I; Macdonald and others, 1983). The Honolulu is certainly in part Pleistocene on the basis of published K-Ar ages, but because of the unreliability of some of the ages, a Holocene age cannot be ruled out for the youngest flows.

WAIANAE VOLCANO

Waianae Volcano was built by eruptions from the summit caldera and along the principal northwest and southeast rift zones.

The rocks of the volcano are divided into the Waianae Volcanics, representing the shield and postshield stages (both including a caldera- filling phase), and the Kolekole Volcanics, representing the rejuvenated stage (Sinton, in press). The Waianae was originally named the Waianae Volcanic Series and subdivided into three informal members (lower, middle, and upper) by Stearns (1935). He described these members but did not map them separately (Stearns, 1939). The Waianae has recently been subdivided by Sinton (in press) into three formally named members—the Lualualei (oldest), Kamaileunu, and Palehua (youngest) Members. These members are, for the most part, equivalent to Stearns' lower, middle, and upper members, respectively (table 1.12; see Sinton, in press). The Kamaileunu Member includes the Mauna Kuwale Rhyodacite Flow and several icelandite flows. These are the only known occurrences of rhyodacite and icelandite in the Hawaiian Islands. The rhyodacite flow was given formal status by Sinton (in press), and because it is of such distinctive lithology it is also considered to be formal here.

A Pliocene age for the Waianae Volcanics is inferred from K-Ar determinations ranging from 3.9 to 2.5 Ma (Doell and Dalrymple, 1973) (table 1.12). Funkhouser and others (1968) reported an average K-Ar age of about 2.4 Ma for the Mauna Kuwale Rhyodacite Flow, but this age is inconsistent with their reported ages for the overlying lava flow (4.3 Ma) and dikes (about 3 Ma) cutting the rhyodacite. According to Sinton (in press), the Mauna Kuwale probably has a minimum age of 3.2 Ma. The Kolekole Volcanics has not been isotopically dated but is tentatively considered by Sinton (in press) to be Pleistocene.

KAUAI

KAUAI VOLCANO

The Island of Kauai (fig. 1.29) consists of a single deeply eroded shield volcano with a summit caldera 15-20 km across, the largest in the Hawaiian Islands, and at least two flank calderas, the only ones known in the islands. Lava erupted not only in the calderas, but also from northwest and southeast rift zones. After a period of erosion, rejuvenated-stage lava erupted from about 40

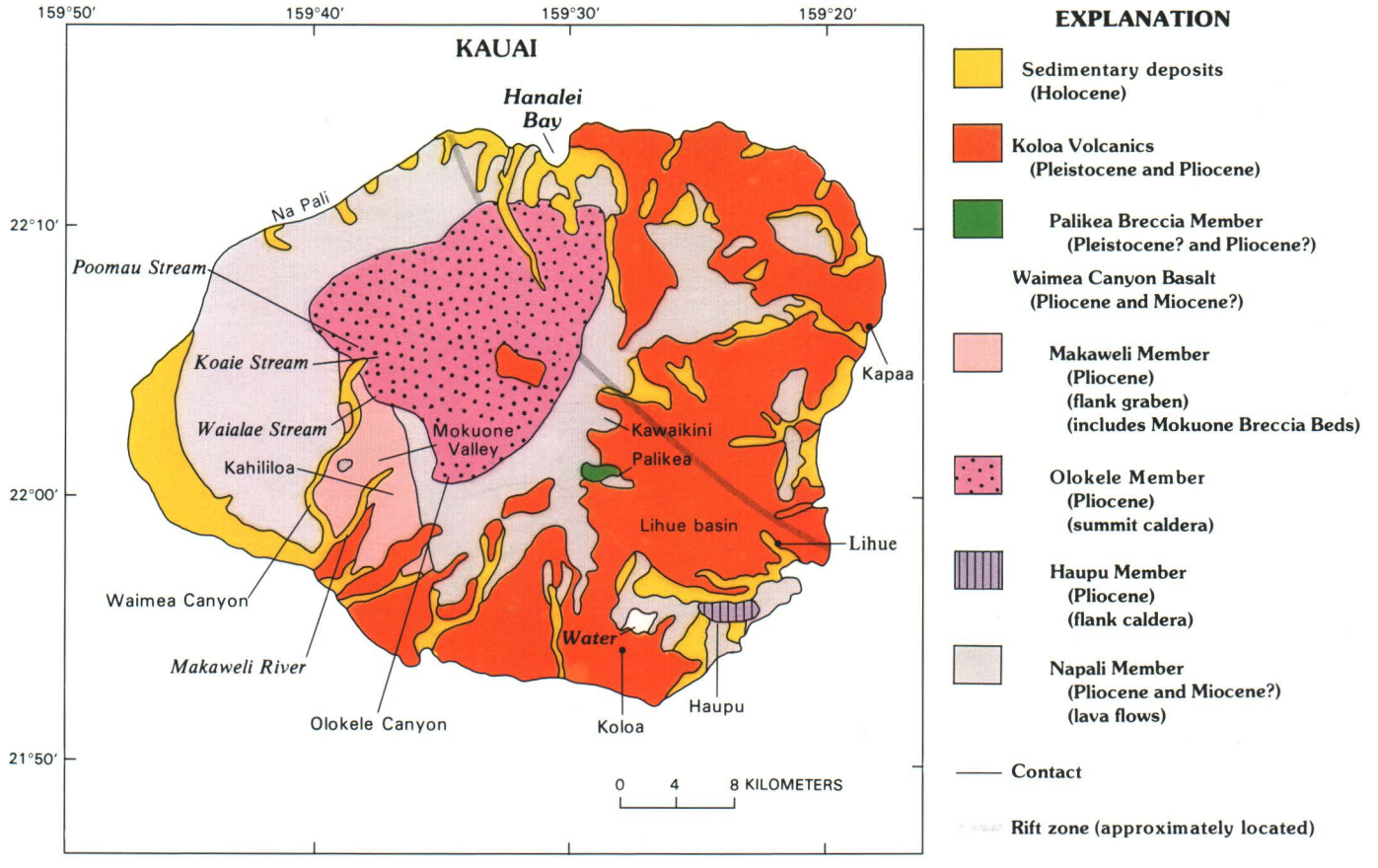

FIGURE 1.29.—Generalized geologic map of Kauai, showing localities mentioned in text. Modified from Macdonald and others (1983). Rift zones from Fiske and Jackson (1972). Summit caldera and southeast flank caldera are represented by Olokele Member and Haupu Member, respectively. Another flank caldera is represented by Lihue basin, a subcircular basin 10-15 km wide, which is almost bisected by southeast rift zone. There is no evidence that shield-stage or postshield-stage lava poured into this caldera, but it was later filled with rejuvenated-stage lava (Koloa Volcanics).

vents scattered over the eastern two-thirds of the island; these vents show no relation to the older rift zones.

The rocks of Kauai Volcano were originally divided by Stearns (1946) into the Waimea Volcanic Series (older), later renamed the Waimea Canyon Volcanic Series (Macdonald, 1949), and the Koloa Volcanic Series (younger). The Waimea Canyon represents the shield stage including the caldera-filling phase. Postshield-stage hawaiite is rare and occurs only at the top of the Waimea Canyon (fig. 1.21, table 1.12). The Koloa represents the rejuvenated stage.

The Waimea Canyon Volcanic Series was subdivided by Macdonald and others (1954, 1960) into four formally named formations—the Napali, Haupu, Olokele, and Makaweli Formations. The Makaweli Formation as defined by Macdonald and others (1960) included associated sedimentary deposits, which were called the Mokuone Member.

In order to have a nomenclature consistent with the other volcanoes of the Hawaiian Islands, the following changes are here made to the Waimea Canyon Volcanic Series: The Waimea Canyon is reduced to formational rank and renamed the Waimea Canyon Basalt to reflect its predominant lithology. Its subdivisions are reduced to member rank and called the Napali, Haupu, Olokele, and Makaweli Members. The sedimentary unit included within the Makaweli is reduced in rank and renamed the Mokuone Breccia Beds (table 1.12).

Although the Napali, Haupu, Olokele, and Makaweli Members consist of essentially the same rock types, they are distinguishable and extensive units. The Napali Member consists of thin-bedded flank flows, whereas the Olokele and Makaweli Members consist of massive or thick-bedded flows. The Olokele is separated from the Makaweli and from the Napali by faults. The Haupu, which presumably represents a small caldera on the southeast flank of the volcano, also consists of thick-bedded flows, but it is isolated from the Olokele and Makaweli Members and is surrounded by older thin-bedded flows of the Napali Member.

The Napali, Olokele, and Makaweli Members had more than one type locality specified by Davis and Macdonald (in Avias and others, 1956) and Macdonald and others (1960). One of the localities is here retained as the type locality for each unit, and the other localities are redesignated as reference localities (table 1.12.).

The Koloa Volcanic Series, as defined by Stearns (1946) and Macdonald and others (1960), included within it a sedimentary unit that they named the Palikea Formation. The Palikea Formation consists largely of breccia underlying and interbedded with Koloa lava flows. The breccia, which grades laterally in some places into stream-laid conglomerate, is primarily made up of fragments of the Waimea Canyon Basalt and represents the rapid shedding of debris from the steep slopes of the volcano before and during Koloa time. Clague and others (1982) reduced the Koloa Volcanic Series to formational rank and renamed it the Koloa Volcanics, but they did not discuss the status of the Palikea Formation. The Palikea is here reduced in rank and renamed the Palikea Breccia Member of the Koloa Volcanics.

The Waimea Canyon Basalt is largely of Pliocene age, but the oldest flows may be Miocene, as indicated by K-Ar ages ranging from about 5.1 to 3.6 Ma (McDougall, 1964; 1979). The age relations between the caldera-filling-phase members are not known, but the Olokele Member is considered to be older than the Makaweli Member, and the Haupu Member is thought to be coeval with the Olokele.

The Koloa Volcanics is largely Pleistocene, an age indicated by all the published K-Ar ages, but unpublished K-Ar ages of 2.59 and 2.01 Ma (G.B. Dalrymple, oral commun., 1986) suggest that the oldest flows are Pliocene. The age of the Palikea Breccia Member is not known, but it is probably Pliocene and Pleistocene on the basis of its stratigraphic relations to Koloa lava flows.

NIIHAU

NIIHAU VOLCANO

The Island of Niihau (fig. 1.30) is the deeply eroded remnant of a shield volcano. The central highland area, which consists of shield-stage tholeiitic lava, is fringed by a low coastal platform, which consists of rejuvenated-stage lava. The shield-stage lava was erupted from a southwest rift zone; the summit of the shield (and former caldera?) was presumably northeast of the present island.

The rocks of the volcano were divided by Stearns (1946, 1947b) into two major units—the Paniau Volcanic Series (older) and the Kiekie Volcanic Series (younger). The Paniau almost entirely represents the shield stage; a single postshield-stage vent that occurs at Kaeo and a couple postshield alkalic basalt dikes along the east coast of the island are also considered in this report to be part of the Paniau Basalt. These units are here renamed the Paniau Basalt and Kiekie Basalt, respectively. Although all of the rejuvenated-stage units on the other islands are called "Volcanics," the name Kiekie Volcanics is not used here because the Kiekie consists entirely of alkalic basalt.

No isotopic ages for the Island of Niihau have been published. However, unpublished K-Ar data for 11 flows of the Paniau indicate a Miocene and Pliocene age (G.B. Dalrymple, oral commun., 1986). The Kiekie Basalt was considered to be of Pleistocene age by Stearns (1947b) on the basis of its relations to Pleistocene shorelines, but unpublished K-Ar ages (G.B. Dalrymple, oral commun., 1986) indicate a Pliocene and Pleistocene age.

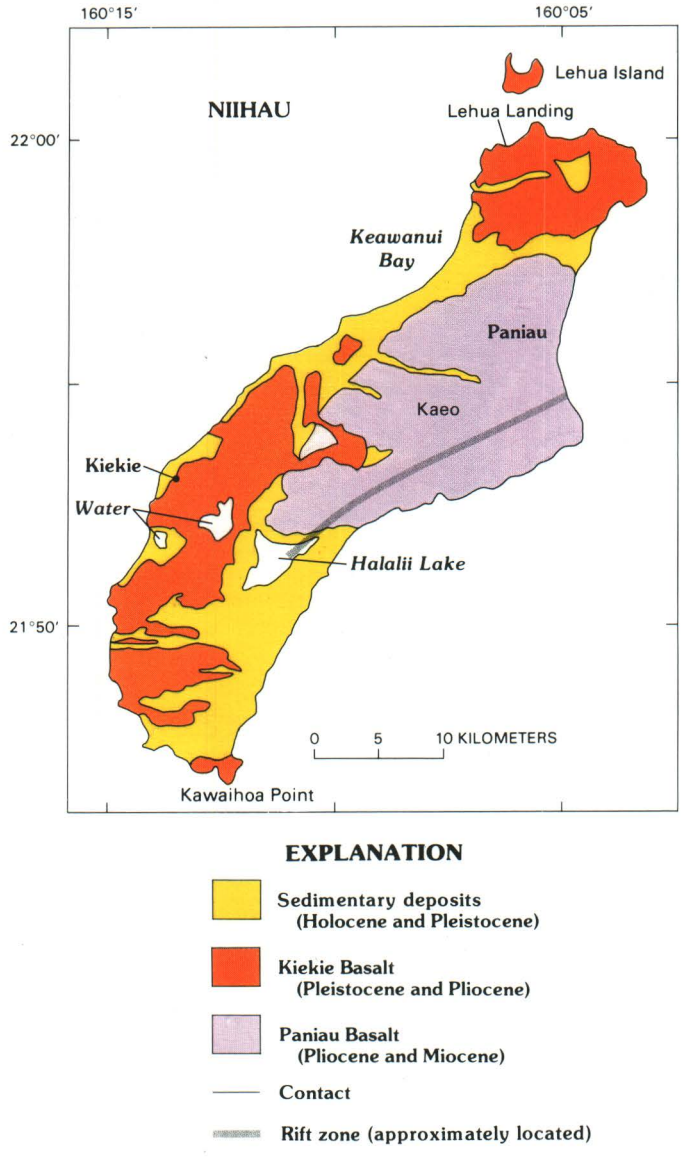

FIGURE 1.30.—Generalized geologic map of Niihau, showing localities mentioned in text. Modified from Macdonald and others (1983). Rift zone approximately follows dike swarm mapped by Stearns (1947b).

REFERENCES

American Commission on Stratigraphic Nomenclature, 1961, Code of Stratigraphic Nomenclature: American Association of Petroleum Geologists Bulletin, v. 45, no. 5, p. 645-665.

———1970, Code of Stratigraphic Nomenclature (revised): Tulsa, Oklahoma, American Association of Petroleum Geologists, 45 p.

Ashley, G.H., Cheney, M.G., Galloway, J.J., Gould, C.N., Hares, C.J., Howell, B.F., Levorsen, A.I., Miser, H.D., Moore, R.C., Reeside, J.B., Jr., Rubey, W.W., Stanton, T.W., Stose, G.W., and Twenhofel, W.H., 1933, Classification and nomenclature of rock units: Geological Society of America Bulletin, v. 44, p. 423-459.

Avias, J., Davis, D.A., Hanzawa, S., Ladd, H.S., Macdonald, G.A., and Obellianne, J.M., 1956, Oceanie proprement dite [Oceania properly speaking], pt. 2 of Oceanie, v. 6 of Lexique Stratigraphique International [International Stratigraphic Lexicon]: Paris, Centre National de la Recherche Scientifique, 286 p.

Bonhommet, N., Beeson, M.H., and Dalrymple, G.B., 1977, A contribution to the geochronology and petrology of the island of Lanai, Hawaii: Geological Society of America Bulletin, v. 88, p. 1282-1286.

Clague, D.A., 1982, Petrology of tholeiitic basalt dredged from Hualalai Volcano, Hawaii: Eos, Transactions American Geophysical Union, v. 63, p. 1138.

Clague, D.A., Dao-Gong, C., Murnane, R., Beeson, M.H., Lanphere, M.A., Dalrymple, G.B., Friesen, W., and Holcomb, R.T., 1982, Age and petrology of the Kalaupapa Basalt, Molokai, Hawaii: Pacific Science, v. 36, p. 411-420.

Clague, D.A., and Frey, F.A., 1982, Petrology and trace element geochemistry of the Honolulu Volcanics, Oahu: Implications for the oceanic mantle beneath Hawaii: Journal of Petrology, v. 23, p. 447-504.

Decker, R.W., and Christiansen, R.L., 1984, Explosive eruptions of Kilauea Volcano, Hawaii, *in* Explosive volcanism: Inception, evolution, and hazards (National Research Council Studies in Geophysics): Washington, National Academy Press, p. 122-132.

Doell, R.R., and Dalrymple, G.B., 1973, Potassium-argon ages and paleomagnetism of the Waianae and Koolau Volcanic Series, Oahu, Hawaii: Geological Society of America Bulletin, v. 84, p. 1217-1242.

Easton, R.M., and Garcia, M.O., 1980, Petrology of the Hilina Formation, Kilauea Volcano, Hawaii: Bulletin Volcanologique, v. 43-4, p. 657-673.

Fiske, R.S., and Jackson, E.D., 1972, Orientation and growth of Hawaiian volcanic rifts: The effect of regional structure and gravitational stresses: Proceedings of the Royal Society of London, ser. A. v. 329, p. 299-326.

Funkhouser, J.G., Barnes, I.L., and Naughton, J.J., 1968, The determination of a series of ages of Hawaiian volcanoes by the potassium-argon method: Pacific Science, v. 22, p. 369-372.

Hay, R.L., and Iijima, A., 1968, Nature and origin of palagonite tuffs of the Honolulu Group of Oahu, Hawaii, *in* Coats, R.R., Hay, R.L., and Anderson, C.A., eds., Studies in volcanology: Geological Society of America Memoir 116, p. 331-376.

Hinds, N.E.A., 1930, The geology of Kauai and Niihau: Bernice P.Bishop Museum Bulletin 71, 103 p.

Holcomb, R.T., 1985, The caldera of East Molokai Volcano, Hawaii: National Geographic Society Research Reports, v. 21, p. 81-87.

Keroher, G.C., and others, 1966, Lexicon of geologic names of the United States for 1936-1960: U.S. Geological Survey Bulletin 1200, p. 1449-2886.

Lanphere, M.A., and Dalrymple, G.B., 1979, Age and strontium isotopic composition of the Honolulu Volcanics, *in* Geological Survey Research 1979: U.S. Geological Survey Professional Paper 1150, p. 180.

Lipman, P.W., 1980, Rates of volcanic activity along the southwest rift zone of Mauna Loa Volcano, Hawaii: Bulletin Volcanologique, v. 43-4, p. 703-725.

Lockwood, J.P., and Rubin, Meyer, 1986, Distribution and age of the Uwekahuna Ash, Kilauea Volcano, Hawaii (abstract): International Volcanological Congress Feb. 1-9, 1986, New Zealand Abstracts, p. 112.

Macdonald, G.A., 1942, Geology and ground-water resources of the Nahiku area, East Maui: Hawaii Division of Hydrography Bulletin 7 (part 2), p. 223-274.

———1945, Ring structures at Mauna Kea, Hawaii: American Journal of Science, v. 243, no. 4, p. 210-217.

———1949, Hawaiian petrographic province: Geological Society of America Bulletin, v. 60, p. 1541-1595.

———1968, Composition and origin of Hawaiian lavas *in* Coats, R.E., Hay, R.L., and Anderson, C.A., eds., Studies in volcanology: Geological Society of America Memoir 116, p. 477-522.

———1978, Geologic map of the crater section of Haleakala National Park, Maui, Hawaii: U.S. Geological Survey Miscellaneous Investigations Series Map I-1088, scale 1:24,000.

Macdonald, G.A., and Abbott, A.T., 1970, Volcanoes in the sea: Honolulu, University of Hawaii Press, 441 p.

Macdonald, G.A., Abbott, A.T., and Peterson, F.L., 1983, Volcanoes in the sea: The geology of Hawaii (2nd ed.): Honolulu, University of Hawaii Press, 517 p.

Macdonald, G.A., Davis, D.A., and Cox, D.C., 1954, Kauai, an ancient Hawaiian volcano: The Volcano Letter, no. 526, p. 1-3.

———1960, Geology and ground-water resources of the Island of Kauai, Hawaii: Hawaii Division of Hydrography Bulletin 13, 212 p.

Macdonald, G.A., and Katsura, T., 1964, Chemical composition of Hawaiian lavas: Journal of Petrology, v. 5, pt. 1, p. 82-133.

Malin, M.C., Dzurisin, Daniel, and Sharp, R.P., 1983, Stripping of Keanakakoi tephra in Kilauea Volcano, Hawaii: Geological Society of America Bulletin, v. 94, p. 1148-1158.

McDougall, Ian, 1963, Potassium-argon ages from western Oahu, Hawaii: Nature, v. 197, p. 344-345.

———1964, Potassium-argon ages from lavas of the Hawaiian Islands: Geological Society of America Bulletin, v. 75, p. 107-128.

———1969, Potassium-argon ages on lavas of Kohala Volcano, Hawaii: Geological Society of America Bulletin, v. 80, p. 2597-2600.

———1979, Age of shield-building volcanism of Kauai and linear migration of volcanism in the Hawaiian Island chain: Earth and Planetary Science Letters, v. 46, p. 31-42.

McDougall, Ian, and Swanson, D.A., 1972, Potassium-argon ages of lavas from the Hawi and Pololu Volcanic Series, Kohala Volcano, Hawaii: Geological Society of America Bulletin, v. 83, p. 3731-3738.

Moore, J.G., Clague, D.A., and Normark, W.R., 1982, Diverse basalt types from Loihi seamount, Hawaii: Geology, v. 10, p. 88-92.

Naughton, J.J., Macdonald, G.A., and Greenberg, V.A., 1980, Some additional potassium-argon ages of Hawaiian rocks: the Maui volcanic complex of Molokai, Maui, Lanai, and Kahoolawe: Journal of Volcanology and Geothermal Research, v. 7, p. 339-355.

North American Commission on Stratigraphic Nomenclature, 1983, North American Stratigraphic Code: American Association of Petroleum Geologists Bulletin, v. 67, no. 5, p. 841-875.

Oostdam, B.L., 1965, Age of lava flows on Haleakala, Maui, Hawaii: Geological Society of America Bulletin, v. 76, p. 393-394.

Palmer, A.R., 1983, The Decade of North American Geology 1983 Time Scale: Geology, v. 11, p. 503-504.

Porter, S.C., 1971, Holocene eruptions of Mauna Kea Volcano: Science, v. 172, p. 375-377.

———1972, Buried caldera of Mauna Kea Volcano, Hawaii: Science, v. 175, p. 1458-1460.

———1973, Stratigraphy and chronology of late Quaternary tephra along the south rift zone of Mauna Kea Volcano, Hawaii: Geological Society of America Bulletin v. 84, p. 1923-1940.

———1974, Mauna Kea *in* Greely, R., ed., Guidebook to the Hawaiian Planetology Conference: Moffett Field, California, Ames Research Center (NASA), p. 239-246.

———1979a, Quaternary stratigraphy and chronology of Mauna Kea, Hawaii: A 380,000 year record of mid-Pacific volcanism and ice-cap glaciation: Geological Society of America Bulletin, v. 90, no. 7, pt. 1, p. 609-611; pt. 2, p. 980-1093.

———1979b, Geologic map of Mauna Kea Volcano, Hawaii: Geological Society of America Map and Chart Series, MC-30, scale 1:50,000.

Porter, S.C., Stuiver, Minze, and Yang, I.C., 1977, Chronology of Hawaiian glaciations: Science, v. 195, no. 1, p. 61-63.

Powers, H.A., 1948, A chronology of the explosive eruptions of Kilauea: Pacific Science, v. 2, no. 4, p. 278-292.

Sinton, J.M., in press, Revision of stratigraphic nomenclature of Waianae Volcano, Oahu, Hawaii: U.S. Geological Survey Bulletin 1775-A.

Stearns, H.T., 1926, Origin of the volcanoes of Mauna Loa and Kilauea (abstract): Geological Society of America Bulletin, v. 37, p. 150.

———1930, Geography and geology (part 1), *in* Stearns, H.T., and Clark, W.O., Geology and water resources of the Kau district: U.S. Geological Survey Water-Supply Paper 616, p. 29-165.

———1935, Geography and geology, *in* Stearns, H.T., and Vaksvik, K.N., Geology and ground-water resources of the Island of Oahu, Hawaii: Hawaii Division of Hydrography Bulletin 1, p.1-198.

———1939, Geologic map and guide of the Island of Oahu, Hawaii: Hawaii Division of Hydrography Bulletin 2, 75 p.

———1940a, Supplement to the geology and ground-water resources of the Island of Oahu, Hawaii: Hawaii Division of Hydrography Bulletin 5, 160 p.

———1940b, Geology and ground-water resources of the Islands of Lanai and Kahoolawe, Hawaii: Hawaii Division of Hydrography Bulletin 6, 177 p.

———1942, General geology and ground-water resources of Maui: Hawaii Division of Hydrography Bulletin 7 (part 1), p. 1-222.

———1945, Glaciation of Mauna Kea, Hawaii: Geological Society of America Bulletin, v. 56, p. 267-274.

———1946, Geology of the Hawaiian Islands (1st ed.): Hawaii Division of Hydrography Bulletin 8, 112 p.

———1947a, Geology (part 1) *in* Stearns, H.T., and Macdonald, G.A., Geology and ground-water resources of the Island of Molokai, Hawaii: Hawaii Division of Hydrography Bulletin, v. 11, p. 1-35.

———1947b, Geology and ground-water resources of the Island of Niihau, Hawaii: Hawaii Division of Hydrography Bulletin 12, p. 1-38.

———1967, Geology of the Hawaiian Islands (2nd ed.): Hawaii Division of Hydrography Bulletin 8, 112 p.

———1985, Geology of the State of Hawaii (2nd ed.): Palo Alto, Pacific Books, 335 p.

Stearns, H.T., and Clark, W.O., 1930, Geology and water resources of the Kau district, Hawaii: U.S. Geological Survey Water-Supply Paper 616, 194 p.

Stearns, H.T., and Macdonald, G.A., 1942, Geology and ground-water resources of the Island of Maui, Hawaii: Hawaii Division of Hydrography Bulletin 7, 344 p.

———1946, Geology and ground-water resources of the Island of Hawaii: Hawaii Division of Hydrography Bulletin 9, 363 p.

———1947, Geology and ground-water resources of the Island of Molokai, Hawaii: Hawaii Division of Hydrography Bulletin 11, 113 p.

Stearns, H.T., and Vaksvik, K.N., 1935, Geology and ground-water resources of the Island of Oahu, Hawaii: Hawaii Division of Hydrography Bulletin 1, 474 p.

Stone, J.B., 1926, The products and structure of Kilauea: Bernice P. Bishop Museum Bulletin 33, 60 p.

Washington, H.S., 1923, Petrology of the Hawaiian Islands: II, Hualalai and Mauna Loa: American Journal of Science, 5th series, v. 6, art. 10, p. 100-126.

Wentworth, C.K., 1925, The geology of Lanai: Bernice P. Bishop Museum Bulletin 24, 72 p.

———1926, Pyroclastic geology of Oahu: Bernice P. Bishop Museum Bulletin 30, 121 p.

———1938, Ash formations of the Island of Hawaii: Hawaiian Volcano Observatory, Special Report 3, 183 p.

———1951, Geology and ground-water resources of the Honolulu - Pearl Harbor area, Hawaii: Honolulu, Hawaii Board of Water Supply, 111 p.

Wentworth, C.K., and Jones, A.E., 1940, Intrusive rocks of the leeward slope of the Koolau Range, Oahu: Journal of Geology, v. 8, p. 975-1006.

Wentworth, C.K., and Powers, W.E., 1941, Multiple glaciations of Mauna Kea, Hawaii: Geological Society of America Bulletin, v. 52, p. 1193-1218.

Wentworth, C.K., and Winchell, Horace, 1947, Koolau Basalt Series, Oahu Hawaii: Geological Society of America Bulletin, v. 58, p. 49-78.

Winchell, Horace, 1947, Honolulu Series, Oahu, Hawaii: Geological Society of America Bulletin, v. 58, p. 1-48.

TABLE 1.12.—*Summary of stratigraphic units for main southeastern Hawaiian Islands*

[Volcanic rocks and closely associated intrusive rocks and sedimentary deposits only. Units on each volcano are listed from youngest to oldest; see text for further explanation. All isotopic ages (in parentheses) and K-Ar ages (in millions of years), recalculated from new decay constants, unless otherwise noted; see summary by Clague and Dalrymple (chapter 1, part I). The term "partly" (in parentheses) preceding a former name indicates that the unit as then defined is equivalent to only part of the unit as used here; the term "part" (in parentheses) following a former name indicates that the unit as used here is equivalent to only part of the unit as then defined]

Unit (this report)	Description	Age	Remarks
	HAWAII		
	Kilauea Volcano		
Puna Basalt	Shield-stage lava of tholeiitic basalt and picritic tholeiitic basalt. Historic and prehistoric lava flows and minor intercalated pyroclastic deposits. Exposed over most of surface of Kilauea. Maximum exposed thickness: > 100 m. Type locality: Uwekahuna Bluff at Kilauea Crater (caldera). Reference localities: at Napau, Makaopuhi, and Kilauea Iki Craters, and near Keana Bihopa (see Easton, chapter 11). Overlies and is locally intercalated with Pahala Ash; interfingers with Kau Basalt of Mauna Loa Volcano. Includes Keanakakoi Ash Member and Uwekahuna Ash Member:	Holocene and Pleistocene (^{14}C, 1.13-22.6 ka) (see text)	Puna Basalt (Easton, chapter 11). Formerly: Kamehame Basalt (part) (Stearns, 1926, 1930); Puna Volcanic Series (Stearns and Macdonald, 1946); Puna Formation (Easton and Garcia, 1980).
Keanakakoi Ash Member	Lithic and vitric ash. Pyroclastic surge and minor airfall deposits. Mainly represents explosive eruption of A.D. 1790, but has slightly older reticulite pumice at base and post-1790 but pre-1823 reticulite pumice at top. Occurs around Kilauea Crater (caldera). Maximum exposed thickness: ~11 m. Type locality: just southwest of Keanakakoi Crater. Is interbedded with historic Puna lava flows.	Holocene	Keanakakoi Ash Member (Easton, chapter 11). Formerly: Keanakakoi Formation (part) (Wentworth, 1938; Powers, 1948); "aa" [erroneously for ash?] member (part) of Puna Volcanic Series (Stearns and Macdonald 1946, p. 108); Keanakakoi Formation (part) of Puna Volcanic Series (Davis and Macdonald in Avias and others, 1956); Keanakakoi Member (part) of Puna Formation (Easton and Garcia, 1980); (partly) Keanakakoi Formation (Malin and others, 1983).
Uwekahuna Ash Member	Mostly ash. Mainly pyroclastic surge deposits Exposed near base of Kilauea Crater (caldera) and on southeast flank of Mauna Loa. Maximum exposed thickness: ~5 m. Type locality: Uwekahuna Bluff. Interbedded with prehistoric Puna lava flows.	Holocene (^{14}C, see text)	Uwekahuna Ash Member (Easton, chapter 11). Formerly: Uwekahuna Ash of Kilauea Series (Stone, 1926); Uwekahuna Formation (Wentworth, 1938; Powers, 1948); Uwekahuna Tuff of Puna Volcanic Series (Stearns and Macdonald, 1946, p. 194); Uwekahuna Ash of Puna Volcanic Series (Macdonald, 1949, p. 65, 67; Davis and Macdonald in Avias and others, 1956); Uwekahuna Member of Puna Formation (Easton and Garcia, 1980).
Pahala Ash	Vitric ash, largely palagonitized. Occurs on Mauna Loa and Kilauea Volcanoes (see text). Maximum exposed thickness: ~15 m. No type locality designated; named for exposures near town of Pahala on south slope of Mauna Loa. Principal reference locality: Moolelo, just southwest of Keana Bihopa; reference localities: Puu Kapukapu and Puu Kaone, all on Kilauea Volcano (see Easton, chapter 11). Overlies Hilina Basalt on Kilauea and Kahuku Basalt on Mauna Loa.	Pleistocene	Geographically restricted (see text). Pahala Ash (Easton, chapter 11). Formerly: Pahala Series (part) (Noble and Clark in Washington, 1923); Pahala Ash of Pre-Kilauea Series (Stone, 1926); Pahala Basalt or Formation (part) (Stearns, 1930); Pahala Tuff (Wentworth, 1938); Pahala Ash (part) (Stearns and Macdonald, 1946; Davis and Macdonald in Avias and others, 1956); Pahala Formation (Easton and Garcia, 1980).

TABLE 1.12.—*Summary of stratigraphic units for main southeastern Hawaiian Islands*—Continued

Unit (this report)	Description	Age	Remarks
	HAWAII--Continued		
	Kilauea Volcano--Continued		
Hilina Basalt	Shield-stage lava of tholeiitic basalt, olivine tholeiitic basalt, and picritic tholeiitic basalt. Predominantly flows with associated pyroclastic deposits. Exposed in Hilina fault system escarpments along south flank of volcano. Maximum exposed thickness: ~300 m. Type locality: just south of Keana Bihopa. Reference localities: Keana Bihopa and Puu Kapukapu. Base not exposed. Includes Moo, Pohakaa, Kahele, and Halepe Ash Members, all intercalated with Hilina lava flows.	Pleistocene (see text)	Hilina Basalt (Easton, chapter 11). Formerly: Pahala Basalt (part) (Stearns and Clark, 1930); Hilina Volcanic Series (Stearns and Macdonald, 1946); Hilina Formation (Easton and Garcia, 1980; Decker and Christiansen, 1984).
Moo Ash Member	Mostly yellow-brown ash and palagonite. Maximum exposed thickness: ~3 m. Type locality: Keana Bihopa. Reference locality: Puu Kapukapu.	Pleistocene	Moo Ash Member of Hilina Basalt (Easton, chapter 11). Formerly: Moo Member of Hilina Formation (Easton and Garcia, 1980).
Pohakaa Ash Member	Thickest of ash members. Yellow- to reddish-brown-weathering palagonite, vitric ash, and soil. Exposed thickness: 1-4 m. Type locality: Pohakaa Arroyo, about 3 km southwest of Keana Bihopa. Reference locality: Puu Kapukapu.	Pleistocene	Pohakaa Ash Member of Hilina Basalt (Easton, chapter 11). Formerly: Pohakaa Member of Hilina Formation (Easton and Garcia, 1980).
Kahele Ash Member	Crudely bedded red clay with palagonite. Exposed thickness: 10-125 cm. Type locality: Pohakaa Arroyo, about 3 km southwest of Keana Bihopa. Reference locality: Puu Kapukapu.	Pleistocene	Kahele Ash Member of Hilina Basalt (Easton, chapter 11). Formerly: Kahele Member of Hilina Formation (Easton and Garcia, 1980).
Halape Ash Member	Palagonite and poorly bedded clay. Exposed thickness: 10-50 cm. Type locality: Keana Bihopa. Reference locality: Puu Kapukapu.	Pleistocene	Halape Ash Member of Hilina Basalt (Easton, chapter 11). Formerly: Halape Member of Hilina Formation (Easton and Garcia, 1980).
	Mauna Loa Volcano		
Kau Basalt	Shield-stage lava of tholeiitic basalt, olivine tholeiitic basalt, and picritic tholeiitic basalt. Historic and prehistoric lava flows and minor intercalated pyroclastic deposits. Exposed over most of surface of Mauna Loa. Maximum exposed thickness: > 185 m. Type locality: west wall of Mokuaweoweo Crater (caldera). Overlies Pahala Ash and Kahuku Basalt; interfingers with Puna Basalt of Kilauea Volcano.	Holocene and Pleistocene	Renamed. Formerly: Kamehame Basalt (part) (Stearns, 1926, 1930); Kau Volcanic Series (Stearns and Macdonald, 1946); Kau Formation (Porter, 1971, 1974); Kau Volcanics (Lipman, 1980).
Pahala Ash	See description under Kilauea.	Pleistocene	See "Remarks" under Kilauea; see also text under Mauna Loa.
Kahuku Basalt	Shield-stage lava of tholeiitic basalt, olivine tholeiitic basalt, and picritic tholeiitic basalt. Lava flows and minor intercalated pyroclastic deposits. Exposed on east and south sides of Mauna Loa. Maximum exposed thickness: 180 m. Type locality: Kahuku Pali, a fault escarpment running north of Ka Lae. Overlies (fault or unconformity) Ninole Basalt.	Pleistocene	Renamed. Formerly: lower member of Pahala Basalt (part) (Stearns 1930); Kahuku Volcanic Series (Stearns and Macdonald, 1946); Kahuku Volcanics (Lipman, 1980).
Ninole Basalt	Shield-stage lava of tholeiitic basalt, olivine tholeiitic basalt, and picritic tholeiitic basalt. Lava flows with pyroclastic deposit near top. Exposed north of Waiohinu on southeast slope of Mauna Loa. Maximum exposed thickness: ~600 m. Type locality: walls of valley at Puu Enuhe, near Ninole Gulch. Base not exposed.	Pleistocene (0.54±0.4) (see text)	Ninole Basalt (Stearns, 1926, 1930) (see text). Formerly: (partly) Ninole Tuff (Wentworth, 1938); Ninole Volcanic Series (Stearns and Macdonald, 1946); Ninole Volcanics (Lipman, 1980).

TABLE 1.12.—*Summary of stratigraphic units for main southeastern Hawaiian Islands*—Continued

Unit (this report)	Description	Age	Remarks
	HAWAII--Continued		
	Mauna Kea Volcano		
Laupahoehoe Volcanics	Postshield-stage alkalic lava flows and associated volcanic and sedimentary deposits. Occurs on most of surface of Mauna Kea. Typical exposed thickness: 50-100 m. Type locality: near town of Laupahoehoe. Reference localities: in Waikahalulu and Pohakuloa Gulches. Conformably overlies Hamakua Volcanics. Divided into Waikahalulu Volcanic Member, and Makanaka and Waihu Glacial Members:	Holocene and Pleistocene	Reduced in rank and renamed (see text). Formerly: (partly) Laupahoehoe Volcanic Series (Macdonald, 1945; Stearns and Macdonald, 1946); Laupahoehoe Series (Porter, 1971); Laupahoehoe Group (Porter, 1973, 1974, 1979a, 1979b; Porter and others, 1977).
Waikahalulu Volcanic Member	Postshield-stage lava predominantly of hawaiite, but some alkalic basalt and ankaramite. Flows and associated pyroclastic deposits. Occurs on upper and lower slopes of volcano. Typical exposed thickness: 50-100 m. Type locality: in Waikahalulu Gulch. Reference locality: in Pohakuloa Gulch. Conformably, and locally unconformably, overlies Hamakua Volcanics. Interstratified with Makanaka and Waihu Glacial Members.	Holocene and Pleistocene (^{14}C and K-Ar, 0.0045-0.19)	Reduced in rank and renamed (see text). Formerly: (partly) Laupahoehoe Volcanic Series (Stearns and Macdonald, 1946); (partly) Waikahalulu Formation of Laupahoehoe Group (Porter, 1974, Porter and others, 1977); Waikahalulu Formation of Laupahoehoe Group (Porter, 1979a, 1979b).
Makanaka Glacial Member	Gravel and diamicton. Exposed on upper slopes of volcano. Exposed thickness: > 10 m. Type locality: Puu Makanaka. Reference localities: in Waikahalulu and Kemole Gulches. Intercalated with Waikahalulu lavas. Younger than Waihu Glacial Member.	Pleistocene	Reduced in rank and renamed (see text). Formerly: Makanaka Drift (Wentworth and Powers, 1941; see also Stearns, 1945); Makanaka Formation (part) of Laupahoehoe Group (Porter, 1974; Porter and others, 1977); Makanaka Formation of Laupahoehoe Group (Porter, 1979a, 1979b).
Waihu Glacial Member	Mainly conglomerate and diamictite. Exposed mainly on upper slopes below summit of Mauna Kea. Exposed thickness: generally $\leq$ 30 m. Type locality: near Waihu Spring. Reference localities: in Pohakuloa Gulch and near Waihu Spring.	Pleistocene	Reduced in rank and renamed (see text). Formerly: Waihu Drift (Wentworth and Powers, 1941); Waihu Fanglomerate (Stearns, 1945); Waihu Formation of Laupahoehoe Group (Porter and others, 1977; Porter, 1974, 1979a, 1979b).
Hamakua Volcanics	Divided into three members: upper two formally-named members represent postshield-stage lava flows and pyroclastic cones and associated sedimentary (glacial) deposits; informal lower member represents shield-stage lava flows. Type locality: in south wall of Laupahoehoe Stream gulch. Reference locality: Pohakuloa Gulch.	Pleistocene	Reduced in rank and renamed (see text). Formerly: (partly) Hamakua Volcanic Series (Stearns and Macdonald, 1946); Hamakua Group (Porter, 1973, 1974, 1979a, 1979b; Porter and others, 1977) (see text).
Pohakuloa Glacial Member	Gravel and diamicton. Exposed mainly in Pohakuloa and Waikahalulu Gulches. Maximum exposed thickness: ~40 m. Type locality: west wall of upper Pohakuloa Gulch. Reference locality: in Waikahalulu Gulch. Locally overlies upper flows of Hopukani Volcanic Member.	Pleistocene	Reduced in rank and renamed (see text). Formerly: Pohakuloa Drift (Wentworth and Powers, 1941); Pohakuloa Formation of Hamakua Group (Porter, 1974, 1979a, 1979b; Porter and others, 1977)
Hopukani Volcanic Member	Postshield-stage lava of alkalic basalt, ankaramite, and hawaiite. Flows and cinder cones. Exposed mainly in gulches on lower windward slopes of Mauna Kea and in saddle between Mauna Kea and Kohala Volcanoes. Exposed thickness: ~25 m. Type locality: in south wall of Laupahoehoe Stream gulch. Reference localities: in Pohakuloa and Waikahalulu Gulches. Overlies lower member.	Pleistocene (0.27±0.04, 0.375±0.050)	Reduced in rank and renamed (see text). Formerly: upper member of Hamakua Volcanic Series (Stearns and Macdonald, 1946); Hopukani Formation of Hamakua Group (Porter, 1974, 1979a, 1979b; Porter and others, 1977).

TABLE 1.12.—*Summary of stratigraphic units for main southeastern Hawaiian Islands*—Continued

Unit (this report)	Description	Age	Remarks
	HAWAII--Continued		
	Mauna Kea Volcano--Continued		
lower member	Shield-stage lava of tholeiitic basalt, olivine tholeiitic basalt, and picritic tholeiitic basalt. Exposed in sea cliffs and gulches along northeast coast of Mauna Kea (so-called Hamakua coast) and near mouths of valleys between Hilo and Laupahoehoe. Exposed thickness: probably ~150 m. Base not exposed.	Pleistocene	Formerly: lower member of Hamakua Volcanic Series (Stearns and Macdonald, 1946, p. 154, fig. 31) (see text).
	Hualalai Volcano		
Hualalai Volcanics	Postshield-stage lava of alkalic basalt and rare hawaiite. Historic and prehistoric lava flows and associated pyroclastic deposits. Covers entire surface of Hualalai Volcano. Maximum exposed thickness: ~150 m. Type locality: around town of Kailua. Interfingers with Kau Basalt of Mauna Loa Volcano. Base not exposed. Includes Kona ash beds (informal) and Waawaa Trachyte Member (formal) (see text).	Holocene and Pleistocene	Reduced in rank and renamed (see text). Formerly: Hualalai Volcanic Series (Stearns and Macdonald, 1946).
	Kona ash beds		Abandoned as formally named unit (see text). Formerly: Kona Tuff Formation (Wentworth, 1938); unnamed unit of Hualalai Volcanic Series (Stearns and Macdonald, 1946); Kona Tuff Formation of Hualalai Volcanic Series (Davis and Macdonald in Avias and others, 1956).
Waawaa Trachyte Member	Trachyte cone and flow. Occurs in Puu Waawaa-Puu Anahulu area. Exposed thickness: ~275 m. Type locality: Puu Waawaa. Base not exposed.	Pleistocene (0.105, see text)	Renamed. Formerly Waawaa Volcanics [Member] of Hualalai Volcanic Series (Stearns and Macdonald, 1946, p. 143) (see text).
	Kohala Volcano		
Hawi Volcanics	Postshield-stage lava of mostly mugearite and hawaiite with some trachyte and benmoreite. Lava flows and associated pyroclastic deposits. Occurs in summit area and parts of slopes of Kohala Volcano. Exposed thickness of flows: ~30 m. Type locality: in Kumakua Gulch, about 1 km east of Hawi. Underlies Quaternary surficial deposits. Conformably, locally unconformably, overlies Pololu Basalt. Basalt.	Pleistocene (0.061±0.001, 0.261±0.005)	Renamed. Formerly: Hawi Volcanic Series (Stearns and Macdonald, 1946).
Pololu Basalt	Shield-stage lava of tholeiitic basalt, olivine tholeiitic basalt, and picritic tholeiitic basalt; postshield-stage caldera-filling alkalic basalt near top. Thin lava flows and associated pyroclastic deposits. Occurs on upper and lower slopes of Kohala. Maximum exposed thickness: ~900 m. Type locality: on northwest side of Pololu Valley. Base not exposed.	Pleistocene (0.304±0.091-0.459±0.028)	Renamed. Formerly: Pololu Volcanic Series (Stearns and Macdonald, 1946).

TABLE 1.12.—*Summary of stratigraphic units for main southeastern Hawaiian Islands*—Continued

Unit (this report)	Description	Age	Remarks
	MAUI		
	East Maui (Haleakala) Volcano		
Hana Volcanics	Rejuvenated-stage lava of alkalic basalt and basanite; rare ankaramite and hawaiite. Lava flows and associated intrusive rocks and pyroclastic and sedimentary deposits. Exposed in summit region and on eastern and southwestern slopes. Exposed thickness: > 300 m. Type locality: village of Hana. Unconformably overlies Kula Volcanics. Includes Kipahulu Member in Kipahulu Valley. Also includes historic flow of A.D. 1790 in Cape Kinau area and numerous informal flows in Nahiku and Keanae areas (see text) that are listed below in sequence (youngest to oldest) from Stearns and Macdonald (1942):	Holocene and Pleistocene(?)	Reduced in rank, revised to include historic (A.D. 1790) flow, and renamed (see text). Formerly: Hana Volcanic Series (Stearns, 1942); Hana Formation (Macdonald, 1978); Hana Group (Clague and others, 1982).
			Abandoned as formally named units (see text). Formerly all in Hana Volcanic Series (see Macdonald, 1942; Macdonald and Davis in Avias and others, 1956):
	Nahiku area: Hanawi flow Paakea flow Kuhiwa flow Mossman flow Kapaula flow Makaino flow Waiaaka flow Makapipi flows Big Falls flows		Hanawi Basaltic Andesite Paakea Basalt Kuhiwa Basaltic Andesite Mossman Picritic Basalt Kapaula Basaltic Andesite Makaino Basaltic Andesite Waiaaka Basaltic Andesite Makapipi Basalt(s) Big Falls Picritic Basalt(s)
			Formerly all in Hana Volcanic Series (see Stearns, 1942):
	Keanae area: Keanae flow Waiokamilo flow Piinaau flow Ohia flow Wailuanui flow Pauwalu flow		Keanae Basalt Waiokamilo Basalt Piinaau Basalt Ohia Basalt Wailuanui Basalt Pauwalu Basalt
Kipahulu Member	Late alkalic rejuvenated-stage lava of alkalic basalt and basanite; rare ankaramite and hawaiite. Lava flows. Exposed thickness: > 400 m. Type locality: Kipahulu Valley. Unconformably overlies Hana Volcanics (older flows), Kula Volcanics, and Honomanu Basalt.	Pleistocene(?)	See text. Formerly: Kipahulu Member of Hana Volcanic Series (Stearns, 1942); Kipahulu Formation of Hana Volcanic Series (Macdonald and Davis in Avias and others, 1956); Kipahulu Member of Hana Volcanic Series (Macdonald and Abbott, 1970; Macdonald and others, 1983; Stearns, 1985).
Kula Volcanics	Postshield-stage lava of hawaiite with some ankaramite and alkalic basalt. Lava flows with associated intrusive rocks and pyroclastic and sedimentary deposits. Exposed in summit region and on all slopes. Maximum exposed thickness: ~600 m. Type locality: near Waiakoa, on west slope of volcano; reference localities: near Kipahulu and along Halemauu Trail (see text). Overlies Honomanu Basalt.	Pleistocene (0.46-0.86, 0.41±0.09)	Renamed. Formerly: Kula Volcanic Series (Stearns, 1942); (partly) Kula Formation (Macdonald, 1978). Includes rocks formerly called Kumuiliahi Formation by Macdonald (1978) (see text).
Honomanu Basalt	Shield-stage lava of tholeiitic basalt, olivine tholeiitic basalt, and picritic tholeiitic basalt. Lava flows and associated intrusive rocks and rare pyroclastic deposits. Exposed in summit region and on north, northeast, and southwest slopes. Maximum exposed thickness: ~250 m. Type locality: in Honomanu Stream valley. Base not exposed.	Pleistocene (0.75±0.04)	Renamed. Formerly: Honomanu Volcanic Series (Stearns, 1942); (partly) Honomanu Formation (Macdonald, 1978).

TABLE 1.12.—*Summary of stratigraphic units for main southeastern Hawaiian Islands*—Continued

Unit (this report)	Description	Age	Remarks
	MAUI--Continued		
	West Maui Volcano		
Lahaina Volcanics	Rejuvenated-stage lava of basanite and picritic basanite. Lava flows and associated pyroclastic deposits. Exposed in small areas on west and southeast sides of West Maui. Exposed thickness of flows: 3-20 m; cones, ~45 m. No type locality designated. Principal reference locality[1]: Puu Laina. Unconformably overlies Honolua Volcanics. Locally includes two informal flows: Laina flows and cinder cone Kilea flow and cinder cone	Pleistocene (1.30±0.10, see text)	Lahaina Volcanics (Clague and others, 1982) (see text). Formerly: Lahaina Volcanic Series of Stearns (1942); Lahaina Group (Naughton and others, 1980). Abandoned as formally named units. Formerly of Lahaina Volcanic Series (Stearns, 1942): Laina Volcanics Kilea Volcanics
Honolua Volcanics	Postshield-stage lava of mugearite, trachyte, and hawaiite. Lava flows and associated domes dikes, and pyroclastic deposits. Caps ridges on all flanks of volcano. Maximum exposed thickness: ~300 m. Type locality: village of Honolua. Overlies Wailuku Volcanics.	Pleistocene (1.18-1.20, 1.50±0.13)	Renamed. Formerly: Honolua Volcanic Series (Stearns, 1942).
Wailuku Basalt	Shield-stage lava of tholeiitic basalt, olivine tholeiitic basalt, and picritic tholeiitic basalt, and postshield-stage caldera-filling lava of alkalic basalt. Lava flows with associated intrusive rocks and pyroclastic and sedimentary deposits. Widely exposed on West Maui Volcano. Maximum exposed thickness: > 1,500 m. Type locality: south wall of Iao Valley. Base not exposed.	Pleistocene (1.32±0.04, 1.58-1.97)	Renamed. Formerly: Waikulu Volcanic Series (Stearns, 1942).
	KAHOOLAWE		
	Kahoolawe Volcano		
Kanapou Volcanics	Postshield-stage lava of alkalic basalt and hawaiite; postshield-stage caldera-filling lava of alkalic basalt; shield-stage caldera-filling lava of tholeiitic basalt; shield-stage lava of tholeiitic basalt and olivine tholeiitic basalt. Lava flows and associated pyroclastic deposits and intrusive rocks. Forms essentially all of island. Maximum exposed thickness: ~450 m. Type locality: cliffs of Kanapou Bay. Base not exposed.	Pleistocene (upper alkalic part, 1.03±0.18)	Renamed. Formerly: Kanapou Volcanic Series (Stearns, 1946; Macdonald and Davis in Avias and others, 1956).
	LANAI		
	Lanai Volcano		
Lanai Basalt	Shield-stage (including caldera-filling phase) lava of tholeiitic basalt, olivine tholeiitic basalt, and picritic tholeiitic basalt. Lava flows and associated pyroclastic deposits and intrusive rocks. Forms almost all of island. Maximum exposed thickness: > 1,000 m. No type locality designated. Principal reference locality[1]: Maunalei Gulch on northeast side of island (J.G. Moore, oral commun., 1986). Base not exposed.	Pleistocene (1.28±0.4)	Reduced in rank and renamed (see text). Formerly: (partly) Lanai Basalt and Manele Basalt (Wentworth, 1925); Lanai Volcanic Series (Stearns, 1946); Lanai Volcanic Series (which [improperly] included Lanai Basalt, and Lanai Basalt [improperly] included Manele Basalt) Macdonald and Davis in Avias and others, 1956).

TABLE 1.12.—*Summary of stratigraphic units for main southeastern Hawaiian Islands*—Continued

Unit (this report)	Description	Age	Remarks
	LANAI--Continued		
	Lanai Volcano--Continued		
	(Manele crater remnant)		Abandoned as formally named unit (see text). Formerly: Manele Basalt (Wentworth, 1925); Manele Basalt of Lanai Basalt of Lanai Volcanic Series (Macdonald and Davis in Avias and others, 1956).
	MOLOKAI		
	East Molokai Volcano		
Kalaupapa Volcanics	Rejuvenated-stage lava of alkalic basalt and basanite. Lava flows and associated cone. Makes up Kalaupapa peninsula. Maximum exposed thickness: ~125 m. Type locality: Kalaupapa peninsula. Unconformably overlies East Molokai Volcanics.	Pleistocene (0.35±0.03, 0.57±0.02)	Renamed. Formerly: Kalaupapa Basalt (Stearns, 1946, 1947a; Clague and Frey, 1982).
East Molokai Volcanics	Divided into two informal members. Upper member: postshield-stage lava of mugearite, with lesser amounts of hawaiite and trachyte. Lava flows and associated pyroclastic deposits and intrusive rocks. Lower member: shield-stage (including caldera-filling phase) lava of tholeiitic basalt, olivine tholeiitic basalt, and picritic tholeiitic basalt, and postshield-stage (including caldera-filling phase) alkalic basalt. Lava flows and associated intrusive rocks and pyroclastic and sedimentary deposits. Makes up almost all of East Molokai. Maximum exposed thickness: > 1,500 m. Type locality: cliff south of Kalaupapa peninsula. Locally overlies West Molokai Volcanics of West Molokai Volcano. Base not exposed.	Pleistocene and Pliocene (1.35-1.49, upper member; 1.52 and 1.76±0.07, lower member)	Renamed. Formerly: East Molokai Volcanic Series (Stearns, 1946, 1947a).
	West Molokai Volcano		
West Molokai Volcanics	Postshield-stage lava of hawaiite and alkalic basalt; shield-stage lava of tholeiitic basalt. Lava flows and associated intrusive rocks and pyroclastic deposits. Forms most of West Molokai. Maximum exposed thickness: > 400 m. Type locality: West Molokai mountain (Mauna Loa). Locally overlapped by East Molokai Volcanics. Base not exposed.	Pleistocene and Pliocene 1.52±0.6, 1.89, 1.84±0.7, 1.90±0.06)	Renamed. Formerly: West Molokai Volcanic Series (Stearns, 1946; 1947a)
	OAHU		
	Koolau Volcano		
Honolulu Volcanics	Rejuvenated-stage lava, ranging from alkalic basalt, basanite, and nephelinite to melilitite. Exposed on southwest and northeast flanks of Koolau Range. No type locality designated; named for exposures in city and county of Honolulu. Honolulu Volcanics consists of an assemblage of local informally named lava flows, cinder, spatter, and tuff cones, and ash deposits (see text and below; sequence listed below from Macdonald and others, 1983). Unconformably overlies Koolau Basalt.	Holocene(?) and Pleistocene (0.03-0.9) (see text)	Honolulu Volcanics (Clague and Frey, 1982) [also Lanphere and Dalrymple, 1979]. Formerly: Honolulu Volcanic Series (Stearns, 1935, 1939); Honolulu Series (Winchell, 1947); Honolulu Group (Hay and Iijima, 1968; Clague and others, 1982).

TABLE 1.12.—*Summary of stratigraphic units for main southeastern Hawaiian Islands*—Continued

Unit (this report)	Description	Age	Remarks
	OAHU--Continued		
	Koolau Volcano--Continued		
			Abandoned as formally named units see text). Formerly all in Honolulu Volcanic Series (Stearns, 1935, 1939, 1940a; see also Avias and others, 1956, for other former names):
	Hawaiiloa flow (and associated cone)		Hawaiiloa Volcanics
	Pali Kilo flow (and associated cone?)		
	Pyramid Rock flow		Pyramid Rock Basalt
	Moku Manu tuff cone		Moku Manu Volcanics
	Ulupau tuff cone (and flow?)		Ulupau Tuff (also Ulupau Head Tuff); Mokapu Basalt (part)
	Mokolea flow		Mokolea [misspelled Mokulea by Stearns (1935)] Basalt; Mokapu Basalt (part)
	Kalihi flow (and associated cone)		Kalihi Volcanics
	Haiku flow (and associated cone)		Haiku Volcanics
	Rocky Hill flow (and associated cones)		Rocky Hill Volcanics (Basalt)
	Manoa cinder cone (and lava flow?)		
	Aliamanu flow (and associated cone)		Aliamanu Tuff (Basalt)
	Kaneohe flow (and associated cones)		Kaneohe Volcanics
	Luakaha flow (and associated cone)		Nuuanu Volcanics (Basalt) (part)
	Makuku flow (and associated cone)		Nuuanu Volcanics (Basalt) (part)
	Pali flow (and associated cone)		Pali Volcanics
	Makawao tuff and breccia deposits		Makawao Breccia
	Kaau flows (and associated tuff and mudflow deposits)		Kaau Volcanics (Basalt, Tuff)
	Mauumae flow (and associated cone)		Mauumae Volcanics
	Salt Lake tuff cone		Salt Lake Tuff
	Makalapa tuff cone		Makalapa Tuff
	Ainoni flow (and associated cone)		Ainoni Volcanics
	Castle flow (and associated cone)		Castle Volcanics
	Maunawili flow (and associated cone)		Maunawili Volcanics
	Training School flow (and associated cone)		Training School Volcanics
	Diamond Head tuff cone		Diamond Head Tuff [also Diamond Head Black Ash; Black Point Ash]
	Kaimuki flows		Kaimuki Volcanics (Basalt)
	Black Point flow		Black Point Basalt
	Kamanaiki flows		Kamanaiki Basalt
	Punchbowl flows (and associated cone)		Punchbowl Volcanics
	Manana tuff cone		Manana Tuff
	Koko Crater tuff cone		Koko Volcanics (part)
	Kahauloa flows (and associated cone)		
	Hanauma tuff cone		Koko Volcanics (part)
	Koko Head flow (and associated cone)		Koko Volcanics (part)
	Kalama flow (and associated cone)		Kalama Volcanics
	Kaohikaipu flow (and associated cone)		Kaohikaipu Volcanics
	Kaupo flow (and associated conelet)		Kaupo Basalt
	Round Top cinder and ash deposits		
	Sugarloaf flow (and associated cinder cone and ash deposits)		Sugar Loaf Basalt
	Tantalus flow (and associated cinder cone and ash deposits)		Tantalus Basalt
Koolau Basalt	Shield-stage lava of tholeiitic basalt, olivine tholeiitic basalt, and rare picritic tholeiitic basalt; near top, rocks transitional between tholeiitic and alkalic basalt. Lava flows (typically thin-bedded) with associated intrusive rocks (dikes) and minor pyroclastic and sedimentary deposits. Widely exposed in Koolau Range. Maximum exposed thickness of flows: probably > 1,000 m. No type locality designated. Principal reference locality[1]: Nuuanu Pali. Locally unconformably overlies Waianae Volcanics of Waianae Volcano. Base not exposed. Includes Kailua Member:	Pleistocene(?) and Pliocene (1.8-2.7)	Renamed (see text). Formerly: Koolau Basalt (Wentworth, 1926); Koolau Volcanic Series (Stearns, 1935); Koolau Series (Wentworth and Jones, 1940; Winchell, 1947); Koolau Basalt Series (Wentworth and Winchell, 1947); Koolau Formation (Wentworth, 1951); Koolau Volcanics (Lanphere and Dalrymple, 1979).

TABLE 1.12.—*Summary of stratigraphic units for main southeastern Hawaiian Islands*—Continued

Unit (this report)	Description	Age	Remarks
	OAHU--Continued		
	Koolau Volcano--Continued		
Kailua Member	Shield-stage caldera-filling tholeiitic basalt and olivine tholeiitic basalt. Thick-bedded lava flows and dikes cutting them. Exposed near town of Kailua. Exposed thickness: ~500 m. No type locality specified. Principal reference locality[1]: Kaiwa Ridge. Reference locality[1]: east side of Puu Papaa. In fault(?) contact with Koolau extracaldera flows. Base not exposed.	Pleistocene(?)	Reduced in rank (see text). Formerly: Kailua Volcanic Series (Stearns, 1935); Kailua Volcanic Series of Koolau Volcanic Series [improperly] (Macdonald and Davis in Avias and others, 1956).
	Waianae Volcano		
Kolekole Volcanics	Rejuvenated-stage alkalic lava. Flows and cones. Occurs near Kolekole Pass and at south end of Waianae Range. Thickness at type locality: ~2 m. Type locality: Kolekole Pass. Unconformably overlies flows of Waianae Volcanics and alluvium.	Pleistocene	Kolekole Volcanics (Sinton, in press). Formerly: (partly) Kolekole Volcanics (Stearns, 1946; Macdonald and Davis in Avias and others, 1956).
Waianae Volcanics	Postshield-stage lava of hawaiite with rare alkalic basalt and mugearite; postshield-stage caldera-filling lava of alkalic basalt; shield-stage caldera-filling lava of tholeiitic basalt; shield-stage lava of tholeiitic basalt, olivine tholeiitic basalt, and picritic tholeiitic basalt. Flows and associated intrusive, pyroclastic, and sedimentary rocks. Exposed over most of Waianae Range. Base not exposed. Divided into Palehua (youngest), Kamaileunu, and Lualualei (oldest) Members.	Pliocene	Waianae Volcanics (Sinton, in press) (see text). Formerly: Waianae Volcanic Series (part) (Stearns, 1935); Waianae Volcanic Series (Stearns, 1946).
Palehua Member	Postshield-stage lava of hawaiite with minor alkalic basalt and mugearite. Flows and associated pyroclastic deposits. Occurs at higher elevations throughout Waianae Range. Maximum exposed thickness: > 300 m. Type locality: near Palehua. Conformably, locally unconformably, overlies Kamaileunu Member.	Pliocene (2.5-3.2)	Palehua Member of Waianae Volcanics (Sinton, in press). Formerly: upper member (part) of Waianae Volcanic Series (Stearns, 1935); upper member of Waianae Volcanic Series (Stearns, 1946).
Kamaileunu Member	Postshield-stage caldera-filling lava of alkalic basalt, hawaiite, and rare ankaramite, grading down into shield-stage caldera-filling lava of tholeiitic basalt and rare icelandite. Thick flows and associated rocks. Well exposed in ridges bounding Waianae, Lualualei, and Makaha Valleys. Maximum exposed thickness: > 600 m. Type locality: Kamaileunu Ridge. Reference localities: near Puu Heleakala and Pohakea Pass. Conformably, locally unconformably, overlies Lualualei Member. Includes formally named Mauna Kuwale Rhyodacite Flow:	Pliocene (3.0-3.5)	Kamaileunu Member of Waianae Volcanics (Sinton, in press). Formerly: lower member (part) and middle member (part) of Waianae Volcanic Series (Stearns, 1935).
Mauna Kuwale Rhyodacite Flow	Rhyodacite. Exposed on Mauna Kuwale and Kauaopuu ridges. Exposed thickness: ~135 m. Type locality: Mauna Kuwale. Underlies hawaiite and overlies icelandite of Kamaileunu Member.	Pliocene (see text)	Mauna Kuwale Rhyodacite Flow of Kamaileunu Member (Sinton, in press). Formerly: part of lower member of Waianae Volcanic Series (Stearns, 1935); part of upper member of Waianae Volcanic Series (Stearns, 1940a); Mauna Kuwale Trachyte (McDougall, 1963, 1964); Mauna Kuwale Rhyodacite of upper Waianae Volcanic Series (Funkhouser and others, 1968).
Lualualei Member	Shield-stage lava of tholeiitic basalt, olivine tholeiitic basalt, and picritic tholeiitic basalt. Thin-bedded flows and associated rocks. Occurs mainly in Lualualei Valley. Exposed thickness: > 450 m. Type locality: Puu Heleakala. Base not exposed.	Pliocene (3.0-3.9)	Lualualei Member of Waianae Volcanics (Sinton, in press). Formerly: lower member (part) and middle member (part) of Waianae Volcanic Series (Stearns, 1935).

TABLE 1.12.—*Summary of stratigraphic units for main southeastern Hawaiian Islands*—Continued

Unit (this report)	Description	Age	Remarks
	KAUAI		
	Kauai Volcano		
Koloa Volcanics	Rejuvenated-stage lava of alkalic basalt, basanite, nephelinite, and melilitite. Lava flows and associated pyroclastic deposits. Widely exposed over eastern two-thirds of island. Maximum exposed thickness: ~650 m. Type locality: vicinity of town of Koloa. Unconformably overlies Waimea Canyon Basalt. Locally includes Palikea Breccia Member, which underlies and is intercalated with Koloa lava flows.	Pleistocene and Pliocene (0.62, 1.21, 1.46, 2.01, 2.59) (see text)	Koloa Volcanics (Clague and others, 1982) (see text). Formerly: Koloa Series (Hinds, 1930); Koloa Volcanic Series (Stearns, 1946; Macdonald, 1949; Macdonald and others, 1954, 1960; Macdonald and Davis in Avias and others, 1956).
Palikea Breccia Member	Breccia and lesser conglomerate. Exposed in narrow bands over eastern two-thirds of island. Maximum exposed thickness: ~215 m. Type locality: Palikea ridge, about 5 km southeast of Kawaikini peak.	Pleistocene(?) and Pliocene(?)	Reduced in rank and renamed (see text). Formerly: Palikea Formation of Koloa Volcanic Series Macdonald and others, 1954, 1960; Davis and Macdonald in Avias and others, 1956).
Waimea Canyon Basalt	Shield-stage lava of tholeiitic basalt, olivine tholeiitic basalt, and picritic tholeiitic basalt; rare postshield-stage hawaiite near top. Lava flows and minor pyroclastic deposits. Widely exposed. Total exposed thickness: ~800 m. Type locality: walls of Waimea Canyon. Divided into Makaweli, Olokele, Haupu, and Napali Members.	Pliocene and Miocene(?) (3.6-5.1)	Reduced in rank and renamed (see text). Formerly: Kauai Lavas (Hinds, 1930); Waimea Volcanic Series (Stearns, 1946); Waimea Canyon Volcanic Series (Macdonald, 1949; Macdonald and others, 1954, 1960; Davis and Macdonald in Avias and others, 1956; Stearns, 1967).
Makaweli Member	Shield-stage caldera-filling lava of tholeiitic basalt, olivine tholeiitic basalt, and picritic tholeiitic basalt; postshield-stage hawaiite flow near top of unit. Represents south flank graben. Predominantly thick-bedded flows. Exposed in southwestern part of island. Maximum exposed thickness: ~450 m. Type locality[1]: West wall of Makaweli River canyon. Reference locality[1]: east wall of lower Waimea Canyon. Includes Mokuone Breccia Beds at base of and intercalated with flows. In fault contact with Olokele and Napali Members.	Pliocene (3.60-4.15)	Reduced in rank (see text). Formerly: Makaweli Formation of Waimea Canyon Volcanic Series (Macdonald and others, 1954, 1960; Davis and Macdonald in Avias and others, 1956).
Mokuone Breccia Beds	Breccia with lesser conglomerate. Exposed in narrow bands in southwestern part of island. Maximum exposed thickness: ~300 m. Type locality: walls of Mokuone Valley, west of Kahililoa.	Pliocene	Reduced in rank and renamed (see text). Formerly: Mokuone Formation (Macdonald and others, 1954); Mokuone Member of Makaweli Formation (Davis and Macdonald in Avias and others, 1956; Macdonald and others, 1960).
Olokele Member	Shield-stage caldera-filling lava of tholeiitic basalt, olivine tholeiitic basalt, and picritic tholeiitic basalt; postshield-stage hawaiite flow near top. Represents large summit caldera. Thick-bedded flows and associated pyroclastic deposits. Exposed in central part of island. Maximum exposed thickness: ~800 m. Type locality[1]: walls of upper Olokele Canyon. Reference localities[1]: walls of Poomaa, Koaie, and Waialae Streams. In fault contact with Makaweli and Napali Members.	Pliocene	Reduced in rank (see text). Formerly: Olokele Formation of Waimea Canyon Volcanic Series (Macdonald and others, 1954, 1960; Davis and Macdonald in Avias and others, 1956).
Haupu Member	Shield-stage caldera-filling lava of tholeiitic basalt, olivine tholeiitic basalt, and picritic tholeiitic basalt. Represents southeast flank caldera. Thick-bedded flows exposed on Haupu ridge. Maximum exposed thickness: ~500 m. Type locality: south side of Haupu ridge. Separated from Napali Member by buried caldera faults(?).	Pliocene	Reduced in rank (see text) Formerly: Haupu Volcanic Series (part) (Stearns, 1946); Haupu Formation of Waimea Canyon Volcanic Series (Macdonald and others, 1954, 1960).

TABLE 1.12.—*Summary of stratigraphic units for main southeastern Hawaiian Islands*—Continued

Unit (this report)	Description	Age	Remarks
	KAUAI--Continued		
	Kauai Volcano--Continued		
Napali Member	Shield-stage lava of tholeiitic basalt, olivine tholeiitic basalt, and picritic tholeiitic basalt. Mostly thin-bedded flows and associated pyroclastic deposits. Widely exposed. Maximum exposed thickness: ~800 m. Type locality : west wall of Waimea Canyon. Reference locality : northwest coast of island (Napali coast). Base not exposed.	Pliocene and Miocene(?) (4.3-5.1)	Reduced in rank (see text). Formerly: Napali Formation of Waimea Canyon Volcanic Series (Macdonald and others, 1954, 1960).
	NIIHAU		
	Niihau Volcano		
Kiekie Basalt	Rejuvenated-stage lava of alkalic basalt. Lava flows and pyroclastic deposits. Forms low coastal plain. Maximum exposed thickness: ~90 m. Type locality: town of Kiekie. Unconformably overlies Paniau Basalt.	Pleistocene and Pliocene (see text)	Renamed. Formerly: Kiekie Volcanic Series (Stearns, 1946, 1947b); Kiekie Volcanics (Clague and others, 1982).
Paniau Basalt	Shield-stage lava of tholeiitic basalt, olivine tholeiitic basalt, and rare postshield-stage alkalic basalt. Lava flows and associated intrusive rocks, minor ash. Single post-caldera stage alkalic vent at Kaeo. Comprises central highlands of island. Maximum exposed thickness: ~350 m. Type locality: east side of Paniau hill. Base not exposed.	Pliocene and Miocene (see text)	Renamed. Formerly: Paniau Volcanic Series (Stearns, 1946, 1947b).

[1]Here designated.

Addendum

Some units on the Islands of Hawaii, Maui, and Oahu listed in table 1.12 and discussed in the text were also formerly called "Formations" as follows (listed in alphabetical order): Hana Formation (East Maui Volcano, Maui); Hawi Formation (Kohala Volcano, Hawaii); Honolua Formation (West Maui Volcano, Maui); Honolulu Formation (Koolau Volcano, Oahu); Honomanu Formation (East Maui Volcano, Maui); Hualalai Formation (Hualalai Volcano, Hawaii); Kahuku Formation (Mauna Loa Volcano, Hawaii); Kau Formation (Mauna Loa Volcano, Hawaii); Kolekole Formation (Waianae Volcano, Oahu); Koolau Formation (Koolau Volcano, Oahu); Kula Formation (East Maui Volcano, Maui); Lahaina Formation (West Maui Volcano, Maui); Ninole Formation (Mauna Loa Volcano, Hawaii); Pololu Formation (Kohala Volcano, Hawaii); Waawaa Formation (Hualalai Volcano, Hawaii); Waianae Formation (Waianae Volcano, Oahu); and Wailuku Formation (West Maui Volcano, Maui). See Easton, R.M., and Gaiswinkler-Easton, M., 1983, A guide to the geology of the Hawaiian Islands--Hawaii, Maui, and Oahu: Joint Annual Meeting of the Geological Association of Canada, Mineralogical Association of Canada, and Canadian Geophysical Union, Field Guidebook, v. 2, p. 1-91.

SUBSIDENCE OF THE HAWAIIAN RIDGE

By James G. Moore

ABSTRACT

The great load placed on the ocean floor by the Hawaiian volcanoes, combined with the removal of magma from depth to build the volcanoes, has caused the lithosphere to sag and the Hawaiian Ridge to subside. Constraints on the amount and age of subsidence have been derived from tide gauge measurements, geophysical measurements, and studies of submarine canyons, submerged carbonate reefs, drill holes, and dredge hauls. Most of the volcanoes have subsided 2–4 km since reaching the sea surface, and the bases of the volcanoes have subsided 5–8 km. The bulk of subsidence is complete about 1 m.y. after initiation of volcanism on the sea floor, and about one-half of the upbuilding of the volcanoes is reduced by subsidence. A substantial but unknown part of volcanic growth results from intrusion of dikes and sills into the volcanic edifice, and hence the subsidence of different parts of the volcanoes varies.

Major sea-level terraces form while the volcanoes are actively growing above sea level. As the site of volcanism and subsidence migrates toward the southeast, these terraces become tilted toward the point of active volcanic loading. This tilting makes it difficult to correlate terraces from volcano to volcano along the Hawaiian Ridge by use of depth alone.

The young volcanoes at the southeast end of the Hawaiian Ridge have not yet completed their growth and subsidence. Hence volcanic ages derived from them provide estimates of volcanic propagation rates that are too high. Likewise, volumes measured for the volcanoes only above the level of the ocean floor indicate eruption rates for the older, subsided volcanoes that are too low. These factors raise doubts about inferred increases in volcanic propagation rates and eruption rates during the last few million years.

Volcanic centers on the Hawaiian Ridge are commonly aligned along two or more curved loci roughly parallel to the ridge and approximately 40 km apart. These loci may mark the edges of downbending of the two sides of the lithospheric subsidence trough, where fracturing conducts magma to the surface. The curved map trends along the loci may be the result of interference in these subsidence-induced fractures by major pre-Hawaiian seamounts rafted into the area of active volcanism.

Some of the intense seismic activity concentrated at the southeastern end of the Hawaiian Ridge may result from bending and dislocation of the volcanic pile as its southeastern part subsides more rapidly than the part adjacent on the northwest.

INTRODUCTION

The Hawaiian Ridge is formed by the most vigorous volcanic center on Earth and consequently is one of the youngest, highest, and steepest topographic features on the planet. Northwestward movement of the Pacific plate relative to the mantle hot spot that produces the volcanic center carries the volcanic products away at a rate of about 10 cm/yr, thus forming the ridge. The combination of the weight of erupted material and the removal of material from depth to feed the volcanoes causes the lithosphere to flex downward and the volcanic islands to subside. Subsidence is also partly caused by cooling and contraction of the lithosphere as it moves away from the mantle hot spot.

The subsiding ridge has depressed the adjacent ocean floor more than one hundred kilometers away from the ridge axis. The volcanic products of the ridge fill the inner part of this depression, but the outer part remains a moat-like depression called the Hawaiian Deep. The axis of this deep parallels the ridge on each side and forms an arc around the southeast end of the ridge with a radius of about 140 km (fig. 2.1). The center of curvature falls on the island of Hawaii between the summits of Mauna Loa and Mauna Kea Volcanoes.

Outside of the Hawaiian Deep is a broad low upbowing of the ocean floor called the Hawaiian Arch. The arch probably formed mainly because mantle material squeezed out from beneath the sinking ridge and buoyed up the fairly rigid bend beyond the deep, but also perhaps partly through heating and uplift of mantle rocks as they encountered the Hawaiian hot spot.

The Hawaiian Ridge extends from its active southeast end at Kilauea, Mauna Loa, and Loihi Volcanoes nearly 3,500 km northwest across the central Pacific to the bend where the Emperor Seamounts begin. From this bend the seamount chain continues north for another 2,500 km to its end near the Aleutian Trench. The ages of volcanoes increase systematically from Kilauea toward the northwest; the age is about 43 Ma at the Hawaiian-Emperor bend and about 70 Ma at the north end of the Emperor Seamounts (Clague and Dalrymple, chapter 1). Across this same span of distance the volcano peaks become systematically lower in elevation (fig. 2.2): the highest at the young southeast end are more than 4 km above sea level; a large group located 1,000–3,000 km northwest are close to sea level; and the northern Emperor Seamounts are commonly about 3 km deep. Although the shape and height of the volcanoes have been modified by erosion and by growth of carbonate reefs, these elevation differences result mainly from subsidence.

ACKNOWLEDGMENTS

I thank Brent Dalrymple, David Clague, Donald Peterson, and Harold Stearns for helpful reviews. Thanks also to the many

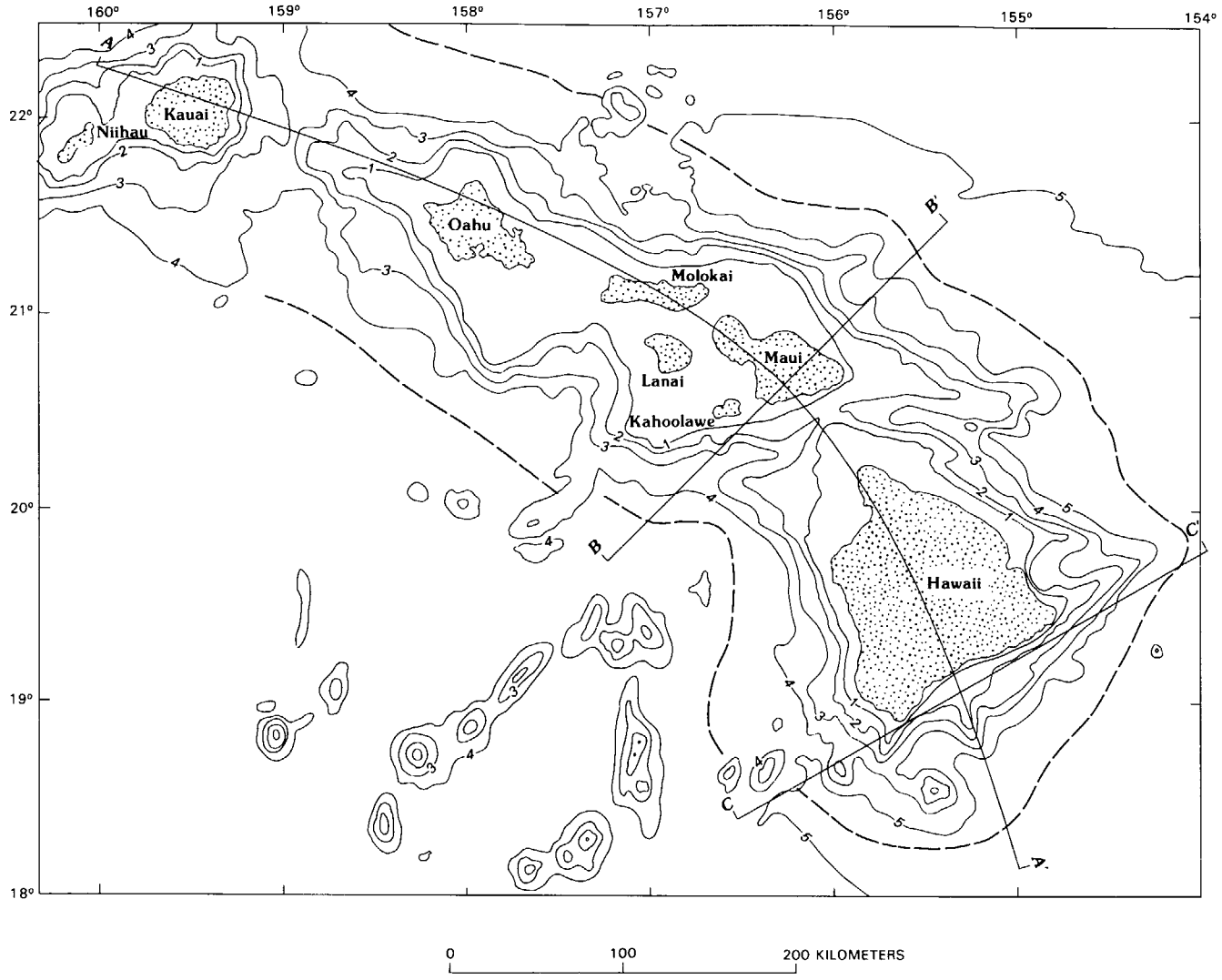

FIGURE 2.1.—Map of southeastern part of the Hawaiian Ridge showing axis of the Hawaiian Deep (dashed line) and section lines of figure 2.6. Depth contours in kilometers.

colleagues who have guided me through the intricacies and excitement of Hawaiian geology. The earliest and most effective of these were Donald Richter, Jerry Eaton, and Chester Wentworth.

TIDE GAUGE MEASUREMENTS

An analysis of tide-gauge data indicated that Honolulu on Oahu is approximately stable, because sea level at Honolulu is rising at a rate similar to that reported by many other stations that apparently reflect the worldwide eustatic rise (Moore, 1970). A reanalysis of Honolulu tidal data for the period 1935–83 indicates that sea level is rising there at a rate of 1.2 mm/yr. The close comparison of this rate with a recent estimate of global sea level increase of 1.5 mm/yr (Barnett, 1983) supports the notion that Honolulu is practically stable.

Some of the scatter inherent in tidal observations can be eliminated by comparing tide levels at other Hawaiian stations with those at the apparently stable Honolulu. Factors such as eustatic sea-level rise, barometric pressure, and sea temperature affect both Honolulu and other neighboring stations in the same way and hence are eliminated by using the differences in annual mean water levels for Honolulu and the neighboring stations. Such an analysis of measurements through 1967 indicated that sea level was rising at Hilo, Hawaii, at 4.1 mm/yr and at Kahului, Maui, at 1.7 mm/yr *relative to the assumed stable Honolulu* (Moore, 1970). Hence Hawaii and Maui were presumed to be undergoing absolute subsidence at those rates.

However, precise determination of sea level trends requires a long period of measurement. The 16 years of record for Kahului and the 21 years for Hilo utilized for the previous estimates were

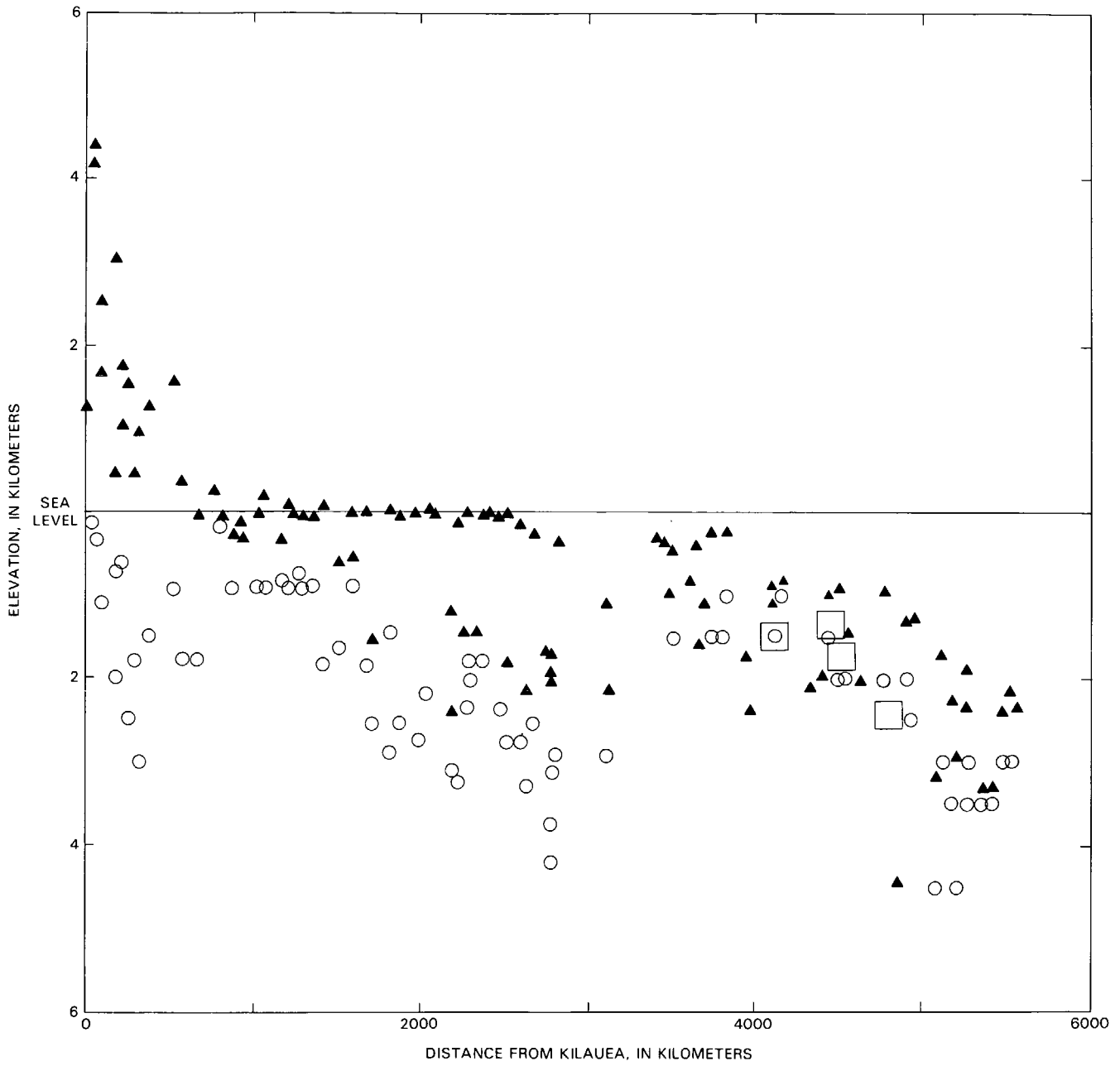

FIGURE 2.2.—Elevation and depth of volcanic features of the Hawaiian Ridge-Emperor Seamounts area. Triangles, tops of individual volcanoes; circles, depths of prominent terraces believed to have formed at sea level; squares, depth of penetration of drill holes on seamounts that encountered only subaerially erupted lava.

minimal. A reanalysis using the 17 additional years of measurements since 1967 provide a better data base for estimation of longer term trends in subsidence rates (fig. 2.3).

The primary measurement used is the annual mean of sea level at the various stations as reported by the U.S. National Ocean Survey. This annual mean is the stand of sea level relative to a fixed datum measured every hour and averaged for one year. The trends of differences of the annual mean of Hilo minus Honolulu and of Kahului minus Honolulu have been determined through 1983. Linear regression fits of this data indicate that Hilo is subsiding relative to Honolulu (assumed stable) at 2.4 mm/yr and Kahului at 0.3 mm/yr. The reason for the differences between the older estimates and these revised estimates is clear from the plot of annual means of sea level (fig. 2.3). The trend through 1967 was steeper than the longer trend through 1984. This change affects both the Kahului and Hilo stations, but is not a worldwide effect because the Honolulu means have been subtracted from the plotted data. The reason for this change in slope is unknown; it may reflect regional

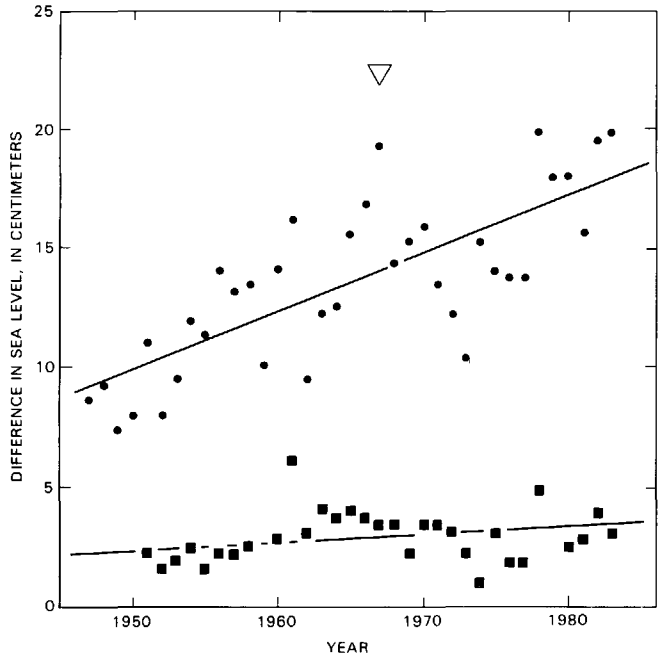

FIGURE 2.3.—Differences in annual means of sea level through 1983. Dots, means at Hilo, Hawaii, minus means at Honolulu, Oahu; squares, means at Kahului, Maui, minus means at Honolulu, Oahu. Open triangle, limit of data (1967) for analysis of Moore (1970).

variations in atmospheric or marine conditions on sea level or a real pulsation in subsidence rates.

In evaluating the subsidence of coastal stations such as Kahului and Hilo, the location of these stations relative to the deep subsiding trough underlying the Hawaiian Ridge must be considered (fig. 2.4). Subsidence varies between different locations on the island of Hawaii and probably reaches a maximum near the island center, where the base of the crust is depressed about three times as much as it is at Hilo on the coast. The surface subsidence at the island center may not actually be three times greater than it is at Hilo, however, because other processes taking place between the surface and the base of the crust, such as intrusion and variations in magma storage within shallow magma chambers, may affect surface subsidence.

DRILLING AND DREDGING

Many holes have been drilled on the Hawaiian Islands principally for the purpose of developing fresh water supplies. Most of these holes penetrate only a short distance below sea level, but a few deep research holes have been particularly valuable in providing information on the history of subsidence as well as on variations in sea level caused by other factors.

A hole drilled on the Ewa coastal plain, Oahu, reached a depth of 337 m and bottomed in red clinker and weathered vesicular subaerial basalt of the Koolau Volcano. The hole records a long period of subsidence and deposition of shallow marine and lagoonal muds, marsh deposits (lignite), and coral reefs, with intermittent periods of erosion and weathering (Stearns and Chamberlain, 1967).

Two holes were drilled on Midway Atoll in 1965. The deeper one penetrated limestone reef material until it encountered weathered basalt, overlain by basaltic conglomerate, at a depth of 384 m. The hole then went through a series of basaltic lava flows to the bottom at 504 m below sea level. The high vesicularity of these lavas (fig. 2.5) indicates that all were erupted subaerially.

A geothermal test well was drilled at an elevation of 182 m on the east rift zone of Kilauea Volcano in early 1976. This hole was 1,962 m deep and bottomed 1,780 m below sea level. The drill cuttings reveal the first appearance of pillow-like glass at 348 m below sea level, and the apparent transition zone between subaerially erupted and subaqueously erupted basalt is placed between 275 and 382 m below sea level (Stone, 1977). We will assume the change to be at 348 m. The age of the lavas encountered in the hole is not known, but it is evident that since the time the drill-hole region was at sea level, 182 + 348 = 530 m has been added to the upper surface of Kilauea Volcano. If the sea-level stand were the same then as now, the volcano has subsided 348 m. However, sea level may have been as much as 100 m below its present stand, in which case the volcano may have subsided only 248 m. One-half to two-thirds of the volcanic buildup of this part of the volcano has therefore been lost by subsidence. This ratio is similar to that for the southeastern Hawaiian Ridge as a whole. It now stands 5–6 km above the old ocean floor, which is depressed 5–8 km below the ridge axis (fig. 2.6). Hence about one-half of the buildup of the ridge has been lost by subsidence.

During Leg 55 of the Deep Sea Drilling Project (DSDP), holes were drilled on the tops of four seamounts of the Emperor chain (Jackson, Koisumi, and others, 1980). All of the core material recovered from these holes indicates that the lava flows were erupted subaerially and that the sediments are of shallow-water origin. Evidence for the subaerial nature of the lava flows is the presence of coarsely vesicular flow tops, red oxidized flow tops and bases, interbedded red tropical soils, and absence of pillow lavas; the sediments above the basalts contain shallow reef and littoral organisms and structures.

Because the water depth was great where these DSDP holes were started, they provide information on subsidence that is deeper than holes drilled on land (fig. 2.2). Hole 430 on Ojin Seamount (lat 37°59′ N.) reached 1,566 m below sea level and bottomed in material of subaerial origin. Hole 432 on Nintoku Seamount (lat 41°20′ N.) reached 1,327 m below sea level in lava flows with red oxidized tops interbedded with red tropical soil. Hole 433 on Suiko Seamount (lat 44°30′ N.) reached 2,422 m below sea level and penetrated a considerable thickness of reef limestone overlying subaerially erupted basalt. The Emperor DSDP holes document minimum subsidence of nearly 2.5 km after the volcanoes reached sea level and produced subaerially erupted lava.

Dredging of the submarine flanks of the Hawaiian volcanoes can also provide information on the amount of subsidence. Four dredge hauls from the submarine east rift zone of Mauna Kea Volcano recovered lavas that are much more vesicular than similar

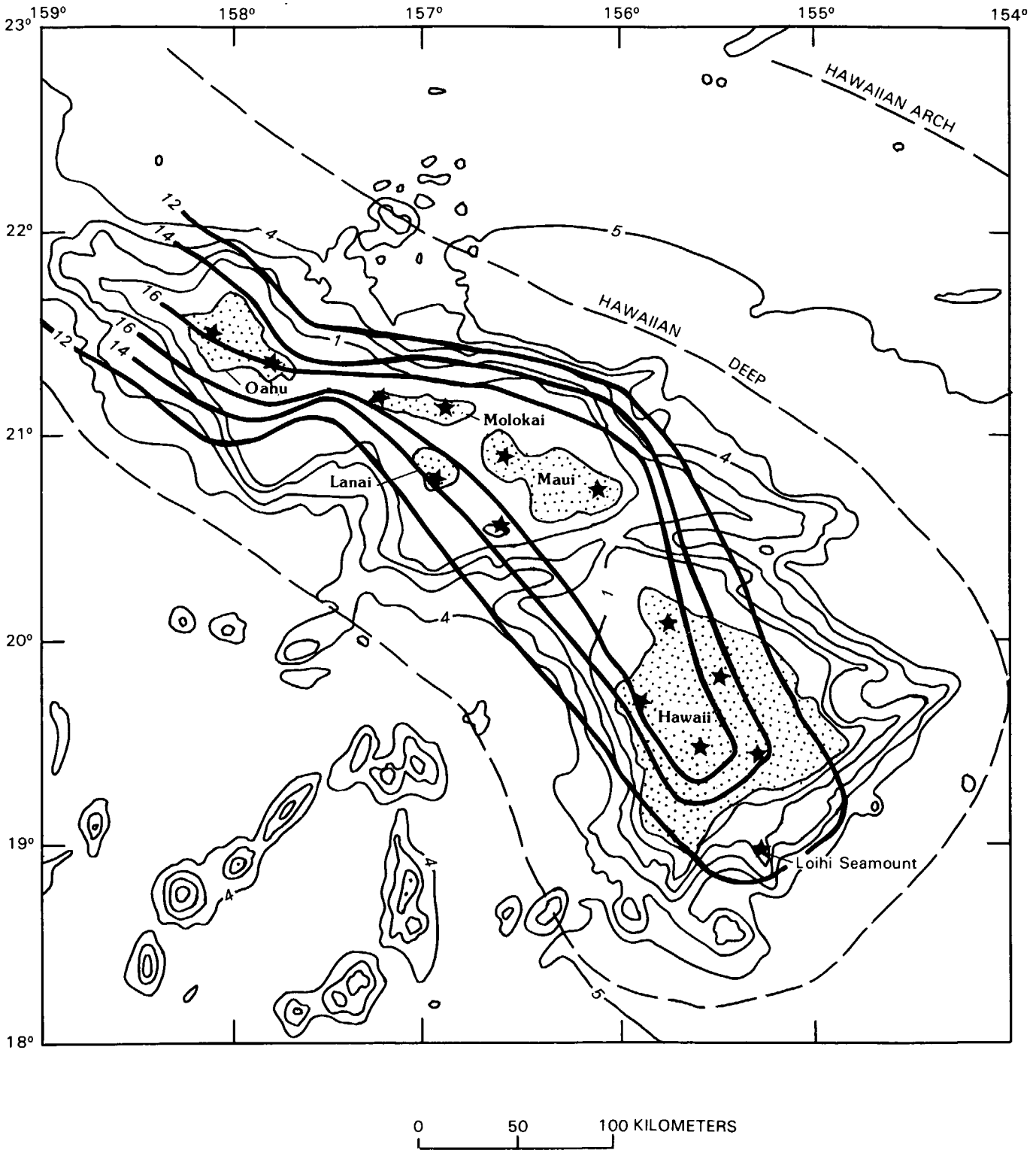

FIGURE 2.4.—Structure contours (heavy lines), in kilometers below sea level on the base of the crust, as determined by seismic refraction for the southeastern part of the Hawaiian Ridge. Data from Shor (1960), Furumoto and others (1973), and Zucca and others (1982). Depth contours in kilometers. Stars, volcanic centers.

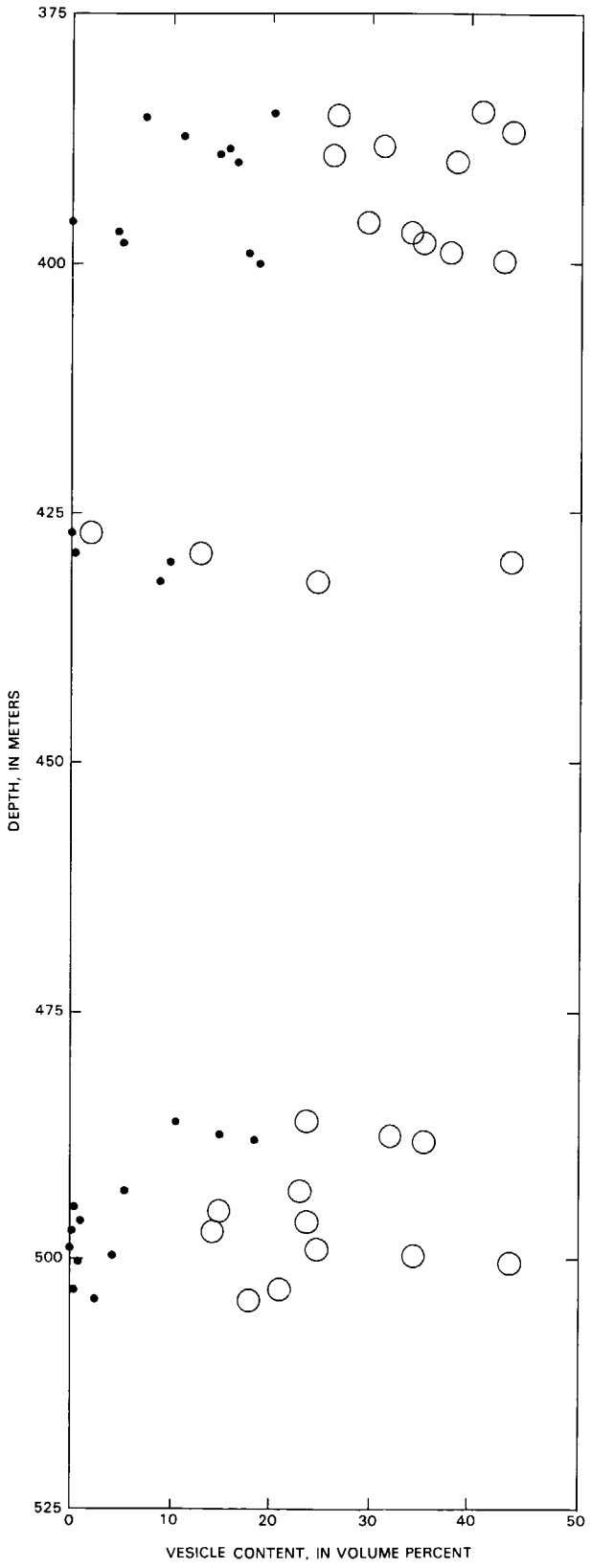

FIGURE 2.5.—Vesicularity of lava samples from 1965 drillhole on Midway Island. Open circles, volume percent of all vesicles; dots, volume percent of unfilled, open vesicles.

lavas collected from the same depth on the currently active rift zones of Kilauea and Mauna Loa Volcanoes. Comparison of vesicularity indicates that Mauna Kea has subsided about 1,000 m since extrusion of these lavas (Moore and Peck, 1965).

On the northwest rift of Hualalai Volcano, sulfur-poor degassed lavas have been dredged from depths down to 1,750 m. The low sulfur content of these lavas indicates that they were erupted under subaerial conditions and therefore that the volcano has subsided more than 1.7 km since their eruption (D.A. Clague, written commun., 1985).

ZONE OF ONGOING SUBSIDENCE

The southeast end of the Hawaiian Ridge, including the Island of Hawaii, is currently undergoing the most rapid subsidence. Tide gauge measurements indicate that Hilo has subsided at a rate of 2.4 mm/yr during the last 36 years. An analysis of the depth of reefs off the northwest coast in comparison with eustatic sea-level curves indicates that subsidence there has ranged from 1.8 to more than 3 mm/yr and has increased over the last 0.3 m.y. (Moore and Fornari, 1984). A study of submerged Hawaiian artifacts carved in lava flows indicates that Honaunau on the Kona coast of Hawaii is submerging at about 3 mm/yr (Apple and Macdonald, 1966). Photographs of the Kealakekua Bay region of west Hawaii taken in 1929 show a distinct sea-level algae line which is now 18.5 cm lower than the present-day line of the same character at the same place, indicating a submergence rate of 3.4 mm/yr (Moore and Fornari, 1984). Assuming that the current rise of sea level is 1.5 mm/yr, then these submergence rates translate to subsidence rates of 1.5 mm/yr for Honaunau and 1.9 mm/yr for Kealakekua Bay.

A growing body of data indicates that in addition to the general long-term subsidence, parts of the ridge are subject to landsliding and other forms of rapid subsidence. Such processes are an effective means of moving material to a lower elevation and of reducing the slope of the Hawaiian Ridge. During the November 1975 magnitude 7.2 earthquake, a 25-km-long zone along the southeast coast of Hawaii subsided as much as 3.5 m (Tilling and others, 1976). Such processes can be an efficient way of accommodating the rapid and dramatic subsidence that must be occurring on the southeast end of the ridge (fig. 2.6).

The Kalaupapa Peninsula on the north coast of Molokai is the exposed part of a small shield volcano that initially erupted below sea level, at the base of the giant northern sea cliff of the island. The vent in the center of the present peninsula erupted lava that covers a total area of about 20 km^2, half of which is now above sea level. Radiometric dating indicates that this activity occurred at 0.34–0.57 Ma (Clague and others, 1982). Available bathymetry (Mathewson, 1970) demonstrates that the submarine part of the shield has a markedly steeper slope below a depth of about 50 m (fig. 2.7). This slope break apparently marks the level of the sea at the time of volcanism (Mark and Moore, chapter 3). Therefore sea level is presently 50 m above its level during Kalaupapa volcanism. Sea level now stands relatively high compared to much of the Pleistocene when it probably averaged about 50 m below the present level. If we assume that sea level was at its present level

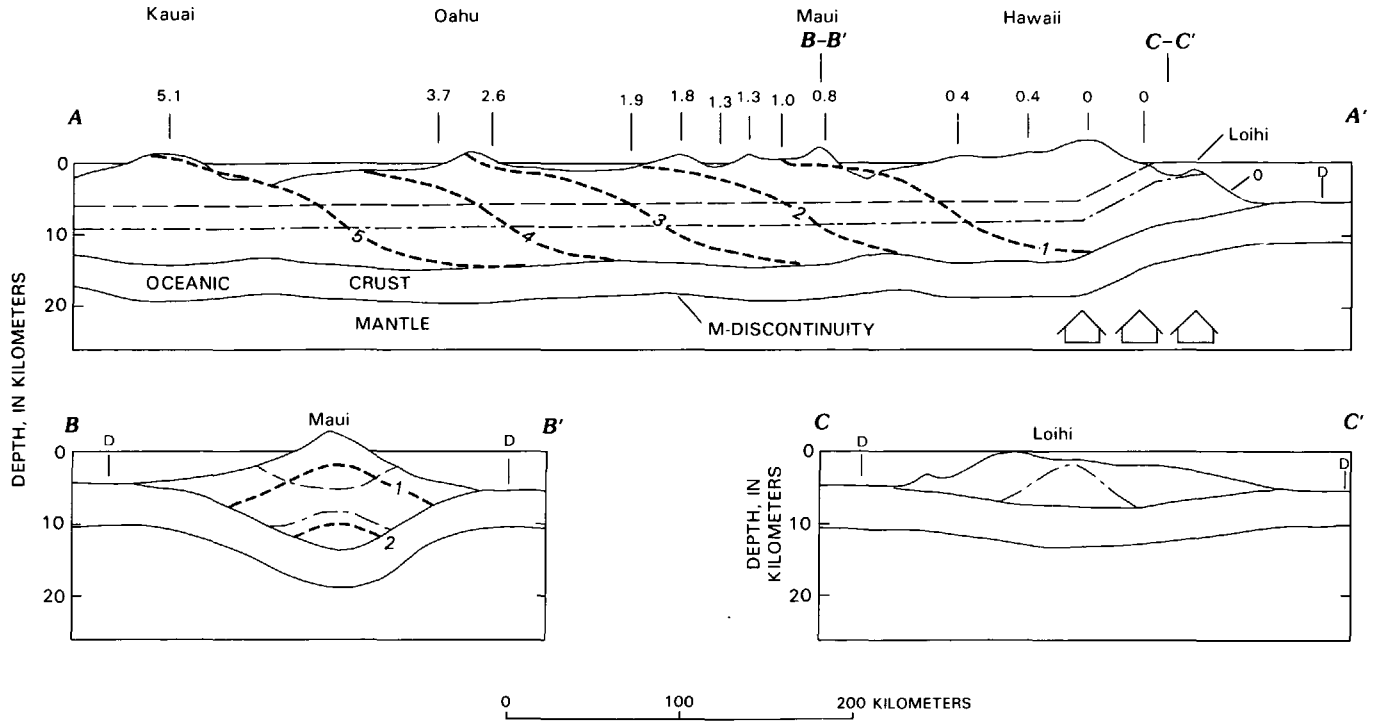

FIGURE 2.6.—Diagrammatic sections of the Hawaiian Ridge based primarily on seismic refraction and gravity measurements (Zucca and others, 1982). Location of sections shown in figure 2.1: *A–A'*, curved longitudinal crustal section along the length of the ridge; *B–B'*, transverse section through Haleakala Volcano on Maui; *C–C'*, transverse section through Loihi Volcano south of Hawaii. Radiometric ages of volcanic rock series in Ma (Clague and Dalrymple, chapter 1) are shown above section *A–A'*. Heavy dashed lines, isochrons of volcanic products in Ma (note that the zero isochron is the present southeastern slope of the ridge); dashed line, boundary between subaerially and subaqueously erupted lava; dash-dot line, boundary between tholeiitic basalt above and early alkalic basalt below. D, axis of Hawaiian Deep. Vertical exaggeration, ×4. Magma chambers and volcanic conduits are omitted for clarity, but position of mantle hot-spot area shown by arrows in *A–A'*.

during growth of the Kalaupapa shield, then subsidence occurred at the low rate of about 0.1 mm/yr. If sea level was below its present level, as it was during much of the Pleistocene, then subsidence would be even less. The Kalaupapa evidence, therefore, indicates that subsidence of central Molokai has been 0.1 mm/yr or less during the last one-half million years.

The presence of coral reefs above sea level provides constraints on the timing and amount of subsidence of the Hawaiian Ridge, and this evidence consequently is critical to an understanding of the subsidence history. Recent studies have shown that coral deposits, previously believed to have been reefs uplifted hundreds of meters, were actually laid down by a giant wave that swept up on land more than 300 m high about 115,000 years ago (Moore and Moore, 1984; Moore and others, 1984). This evidence removes the need for the volcanoes to have risen tectonically hundreds of meters, as previously proposed (Stearns, 1978). Instead, rapid subsidence during volcano growth, and continuing perhaps 1 m.y. after growth, is consistent with most evidence.

Oahu is the southeasternmost island on which extensive coral reefs, clearly in growth position, occur above sea level. These reefs include the Waimanalo reef at 7.5 m above sea level dated at 125 ka, the Laie reef at 21.5 m, and the Kaena reef at 29–30 m dated at about 650 ka (Stearns, 1978). These reefs presumably grew and developed when sea level was higher than today owing to glacioeustatic causes, and they testify to the stability of Oahu and the lack of significant present-day subsidence. However, the presence of important terraces below sea level on Oahu, especially those below 150 m (fig. 2.8), which is commonly considered to be the lowest glacioeustatic stand of the sea, indicates that Oahu, like the other islands, subsided before the growth of reefs that now occur above sea level.

Available evidence therefore indicates that contemporary subsidence at rates of a few millimeters per year can be documented at several sites on the island of Hawaii, including Hilo and the west (Kona) coast. Subsidence on Maui, if occurring, is an order of magnitude less, and Molokai and Oahu have been virtually stable for a long period.

SUBMARINE TERRACES

A large number of submarine benches, terraces, and flat-topped ridges or seamounts appear on large- and small-scale bathymetric maps of parts of the Hawaiian Ridge. Many are rather subtle features, only visible on detailed bathymetric charts. Several

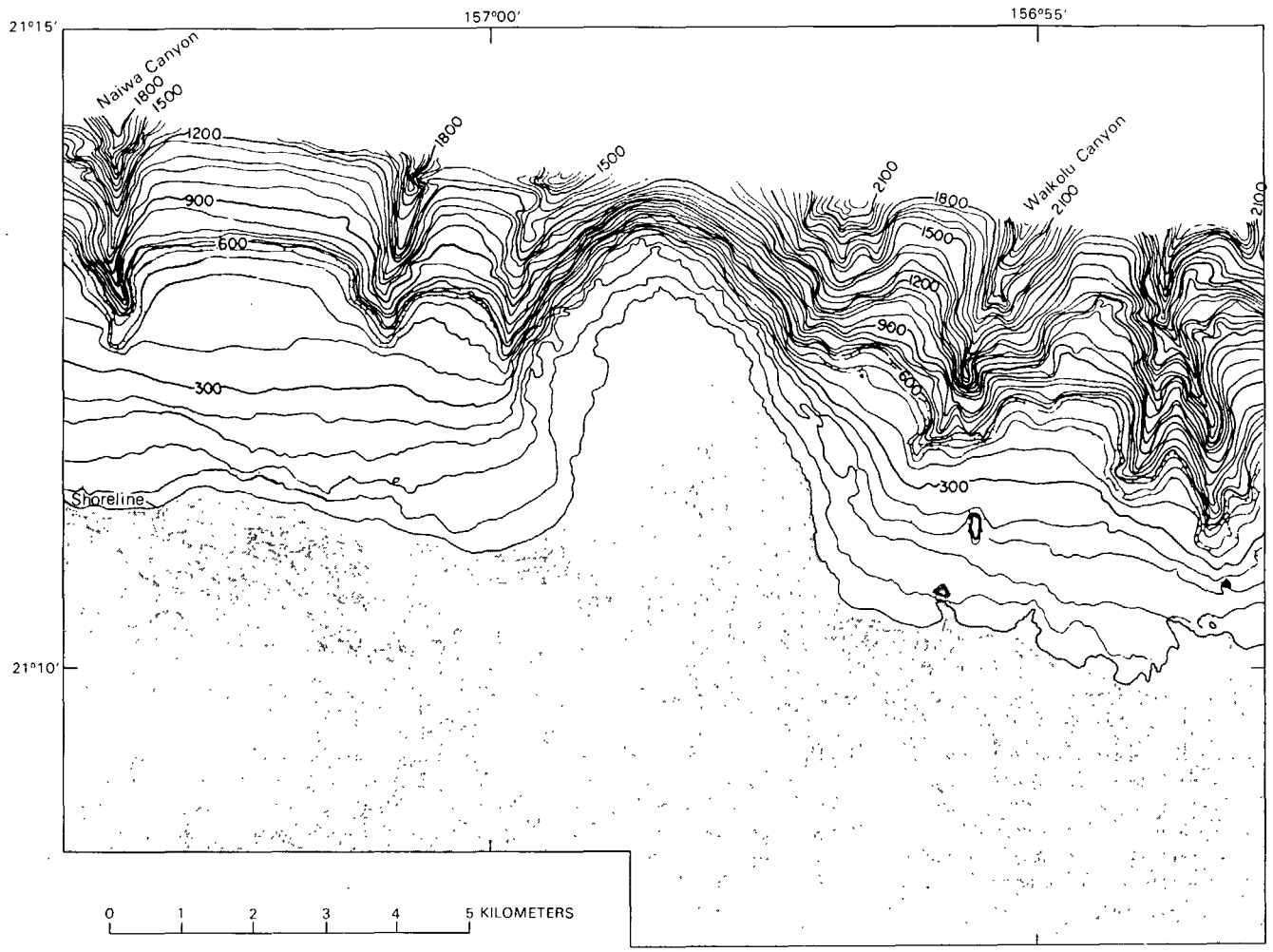

FIGURE 2.7.—Map of the Kalaupapa Peninsula on northern Molokai. Bathymetry after Mathewson (1970). Elevations and depths in feet; bathymetric contour interval, 60 ft.

of these that have been investigated by diving, dredging, and photography proved to be submerged coral reefs. A study of detailed nearshore bathymetric charts indicates that submarine terraces are common off several of the chief Hawaiian Islands at depths of 100–150 m. Curiously, deeper terraces in the depth range 200–500 m seem to be present only off the Island of Hawaii (fig. 2.8*A*). A prominent terrace at about 150-m depth occurs off west Hawaii on Kohala, Mauna Kea, and Hualalai Volcanoes, but younger lavas from Mauna Loa Volcano flood it south of lat 19°15' N. Submersible dives reveal that it is a well-developed coral reef. Radiocarbon ages of the reef limestone show that the reef drowned 13,250 years ago (Moore and Fornari, 1984).

A second major reef terrace occurs at about 400-m depth off northwest Hawaii (Campbell, 1984) and is almost certainly correlative with the terrace at that depth off the northeast coast of Mauna Kea Volcano (figs. 2.1, 2.8). Submersible dives in 1985 off northwest Hawaii recovered reef limestone samples which yielded preliminary uranium-series ages of about 115 ka (B. Szabo, written commun., 1985).

These shallow reef terraces apparently deepen and become separated toward the southeast, forming an imbricate pattern tilted southeast (fig. 2.8). The terraces, which were presumably formed horizontally at sea level, have since been depressed more toward the southeast where subsequent subsidence has been greater. Toward the northwest, where Pleistocene subsidence occurred at only a very low rate, terraces of many different ages formed atop one another at the lower limit of the eustatically shifting sea, 100–150 m below present sea level.

Small-scale bathymetric charts of the Hawaiian Ridge show a series of large and prominent benches and terraces bounded below by a steep slope (fig. 2.9). The shapes of these abrupt slope changes indicate that they formed at the subaerial-subaqueous lava transition zone during island growth by grading of lava flows to sea level (Mark and Moore, chapter 3). A compilation of the depths of such

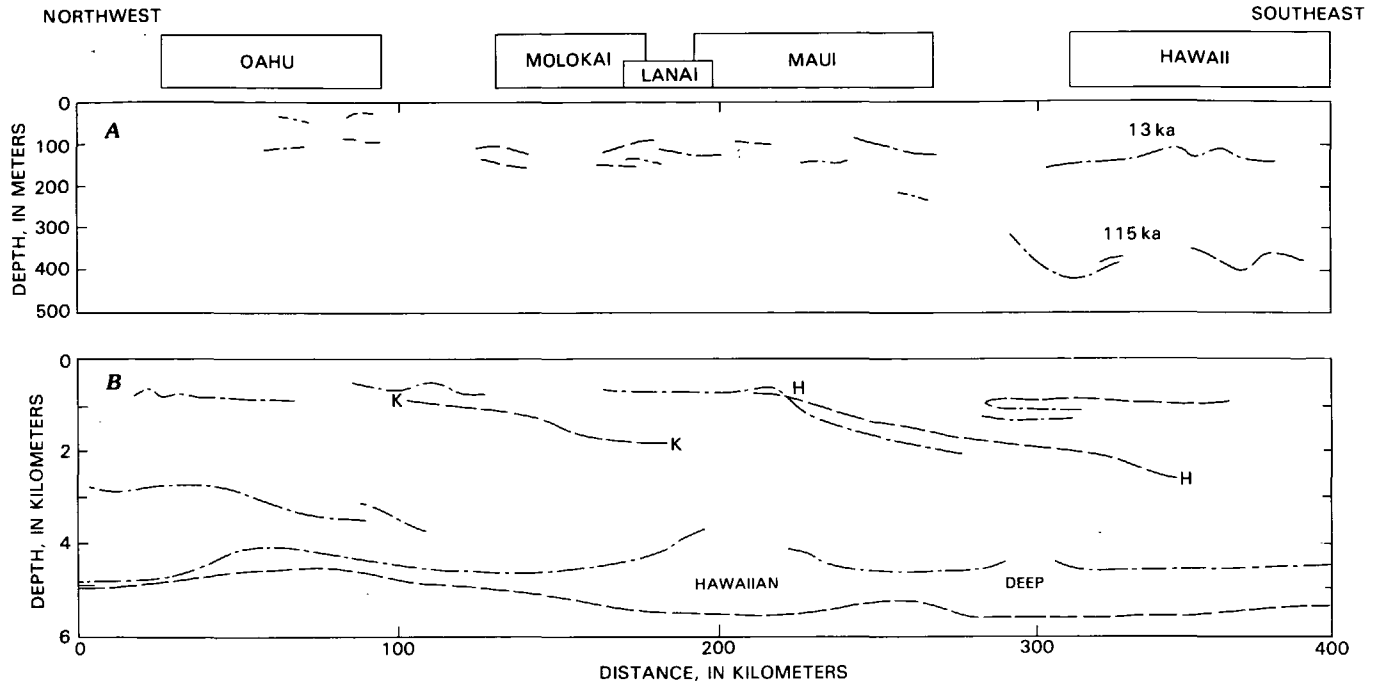

FIGURE 2.8.—Depths of terraces and axes of Hawaiian Deep projected onto a vertical plane striking N. 45° W. ***A***, Terraces in upper 500 m, including two dated terraces off west Hawaii. ***B***, All major terraces above Hawaiian Deep, including the tilted H and K terraces shown in figure 2.9. Dashed line, features on northeast side of ridge; dash-dot line, features on southwest side of ridge.

benches on the entire Hawaiian-Emperor chain indicates that they range from 1 to 4 km but are commonly 2–3 km (fig. 2.2). These depths, coupled with drill-hole evidence, suggest that the Hawaiian volcanoes have generally subsided 2–3 km after they had grown above sea level and could be marked by such sea-level features.

One of the more prominent benches surmounts the east Maui Ridge (called the Haleakala Ridge by Wilde and others, 1980). This terrace, here called the H terrace, is tilted down to the southeast and can be traced more than 150 km from north of west Maui at about 400-m depth to north of the Island of Hawaii at 2,000-m depth (figs. 2.8, 2.9). The terrace slopes about 1 km per 100 km, or about one-half degree, but it is believed to have been an original horizontal feature that has since tilted down toward the Hawaiian hot spot. A second such tilted terrace off north Molokai projects down beneath the H terrace and consequently is believed to be older (figs. 2.8, 2.9). This second feature, called the K terrace, can be traced nearly 100 km from about 900-m depth northwest of Molokai to 1,800-m depth northeast of Molokai. The K terrace is clearly younger than the proposed giant submarine landslide north of Molokai (Moore, 1964), but older than the Kalaupapa Volcano of north Molokai (0.34–0.57 Ma). The Molokai submarine canyons (see section "Submarine Canyons") could have been cut subaerially when the K terrace was about at sea level.

The ages of these tilted terraces are unknown, but they can be crudely approximated by comparing their depths with those of terraces of known ages in the same general area, assuming generally uniform rates of subsidence that are more rapid in the center than at the edge of the ridge. The H terrace, which was probably formed during the period when the present surface of Haleakala Volcano was developing, is about five times as deep as the 400-m terrace of Hawaii dated at 115 ka (fig. 2.8). Considering the lateral position of the H terrace, its age is probably 0.5–1.0 Ma. The K terrace, about twice as deep (and old) as the H terrace, probably formed when volcanism was active on Molokai at 1.8–1.9 Ma (Clague and Dalrymple, chapter 1). When the K terrace formed, the unsubsided Molokai volcanoes were more than 3 km above the sea, a height that may have led to gravitational instability and landsliding of the island's north flank.

SUBMARINE CANYONS

Submarine canyons have been identified off Kauai, Oahu, Molokai (Shepard and Dill, 1966), and Hawaii (this report), and doubtless many more will be found as improved bathymetric data become available. The Kauai submarine canyons head about 3.5 km offshore on the northwest coast and can be traced to depths of more than 2,200 m. The canyons are steep walled; Honopu Canyon has walls about 750 m high at an axial depth of 1,500 m.

Canyons off the northeast coast of Oahu head 3–4 km offshore and can be traced downward to depths exceeding 2,000 m. These canyons have been extensively filled by sediment in their upper parts, and they also passed sediment to fan deposits near the Hawaiian

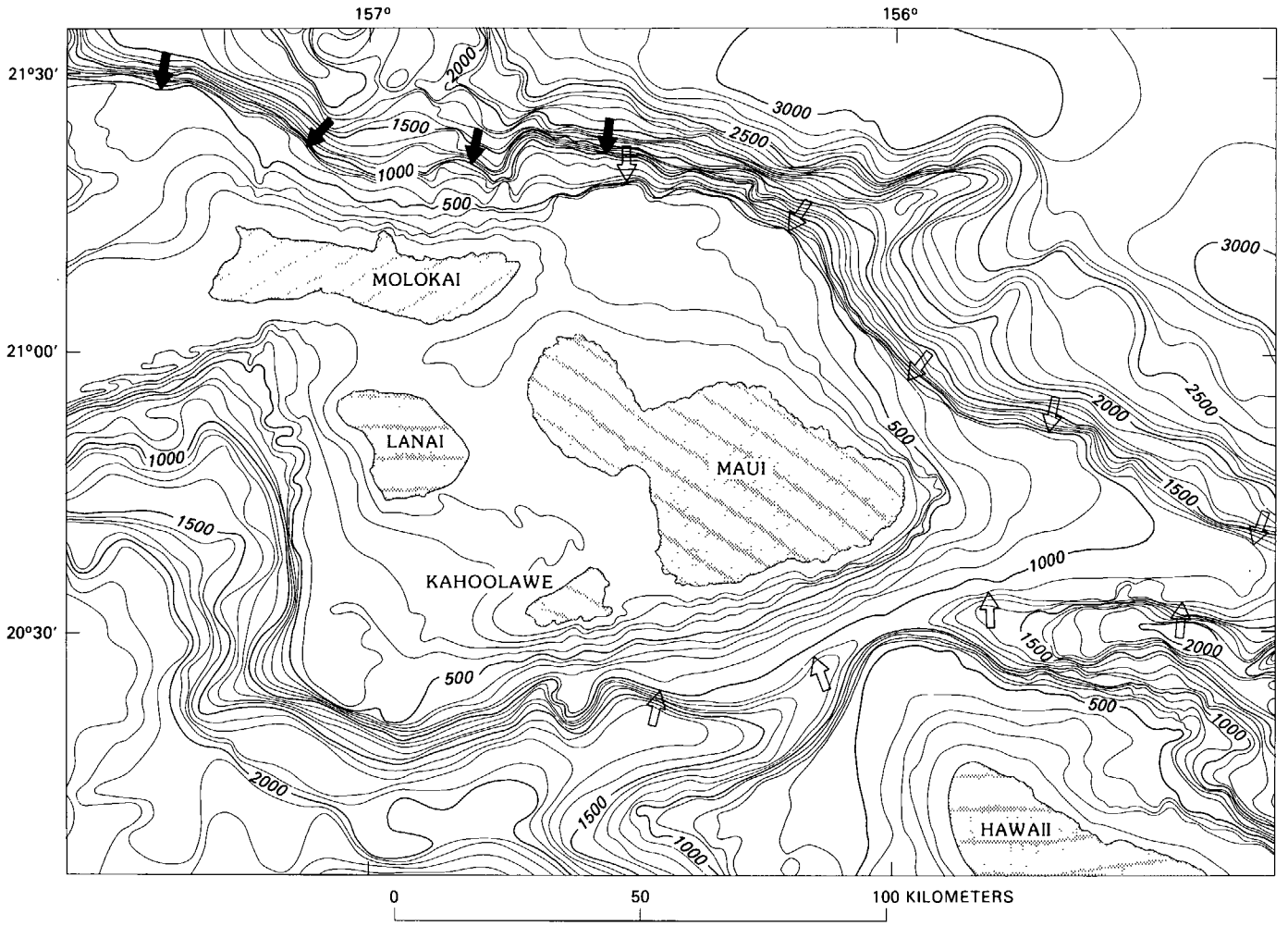

FIGURE 2.9.—Major tilted submarine terraces on southeastern Hawaiian Ridge. Open arrows, H terrace; solid arrows, K terrace. Contour interval, 100 fathoms (600 ft).

Deep (Andrews and Bainbridge, 1972). Ponds of such sediments occur between the blocky seamounts northeast of Oahu downslope from the canyons and indicate that these seamounts (variously interpreted as volcanoes or landslide blocks) predate canyon cutting.

The upper parts of 12 submarine canyons have been mapped in detail by Mathewson (1970) off the north coast of Molokai (fig. 2.7). Several of these canyons are directly offshore from major subaerial canyons and they head 1–2 km from shore. It is likely that the submarine canyons that flank the Kalaupapa Peninsula were cut before the peninsula was built at about 0.4 Ma (fig. 2.7).

A recent compilation of unpublished NOAA charts reveals three submarine canyons off windward Kohala Volcano (fig. 2.10). These canyons head less than 1 km from shore and can be traced downslope only to the limit of available bathymetry at a depth of 440 m. These submarine canyons are 40–80 m deep and hence are much less deeply incised than the 600-m-deep land canyons. This contrast can be attributed to the fact that the tops of the submarine canyons, as well as the upper part of the terrain between the canyons, has been planed off by erosional recession of the 400-m-high seacliff during subsidence. The canyons are offshore from major and minor subaerial canyons cut in Kohala Volcano. However, no submarine canyon lies offshore from Waipio Valley, the most southern Kohala canyon. This absence probably results from filling of the submarine continuation of Waipio Valley by lava from the younger, adjacent Mauna Kea Volcano (Stearns, 1966, p. 125).

Detailed bathymetric mapping off western Hawaii to locate anchor sites for an ocean thermal-energy conversion test platform has revealed a system of submarine canyons that generally head at depths greater than 1,000 m (Campbell and Erlandson, 1979). The western limit of this detailed mapping does not show the lower limit of these canyons, but several descend to depths greater than 1,600 m.

All who have investigated the Hawaiian submarine canyons note that they commonly align with present-day subaerial valleys but generally show little or no bathymetric expression across the near-

shore zone down to depths of about 100 m or more. Seismic-reflection profiling off windward Oahu (Coulbourn and others, 1974) shows that submarine troughs, filled and concealed by young sediments nearshore, connect the subaerial valleys with the visible submarine canyons. This fact provides support for a subaerial origin of at least some submarine canyons.

Hamilton (1957) and Macdonald and Abbott (1970) proposed erosion below sea level by submarine processes as the major cause of the Molokai submarine canyons, because the canyons extend deeper than any previously postulated estimate of submergence. On the other hand, other workers support subaerial erosion for the carving of all the canyons. Stearns (1966) believes submarine erosion simply could not cut such canyons in hard basalt; Mathewson (1970) points to the continuity of subaerial-submarine stream profiles to make the case for subaerial canyon cutting and later subsidence. Comparison of the depths of the lower ends of canyons with depths of major terraces believed to be sea-level features, as well as the evidence from drillholes (fig. 2.2). leaves little doubt that subsidence has been adequate to permit all of the canyons to have been cut by subaerial processes, although post-subsidence modification of the canyons by submarine processes is likely.

CRUSTAL STRUCTURE

Measurements of gravity and determinations of crustal structure by seismic refraction and reflection experiments have provided important constraints on the structure of the Hawaiian Ridge. This work shows that the depth to the base of the crust as marked by the M-discontinuity increases from about 10 km far from the ridge to as much as 20 km beneath the ridge. A 100-km-long seismic-refraction profile shot in 1978 offshore from the west coast of Hawaii indicates that the base of the crust has been depressed about 8 km beneath Mauna Loa Volcano (Zucca and others, 1982; Hill and Zucca, chapter 37). The base of the crust, normally 10–11 km below sea level away from the ridge, has been depressed to a depth of 13–14 km on both the west and south coasts of the island and down to 18.5 km beneath Mauna Loa (fig. 2.6). Seismic-refraction data farther northwest indicate that the M-discontinuity south of Oahu is about 20 km below sea level (Furumoto and Wollard, 1965; Watts and others, 1985).

The inferred lowering of the base of the crust beneath the ridge may be caused in part by injection of relatively low-density basaltic dikes and sills into the mantle beneath the original crustal layer. Such basaltic material would reduce the density and seismic velocity of the the upper mantle, convert it to a crustlike material, and cause a downward migration of the M-discontinuity. An interpretation based on seismic, gravity, and geoid data suggests that the lower 4 km of the depressed oceanic crust south of Oahu is composed of such a dense intrusive complex (Watts and others, 1985). This work also indicates that the old ocean floor on top of the oceanic crust has been warped down 5–7 km beneath the ridge to depths as great as 12 km below sea level.

Seismic refraction and gravity measurements have also shown that a significant mass fraction of the Mauna Loa and Kilauea volcanic edifices above the oceanic crust is composed of intrusive cores beneath the summit region and rift zones (Hill and Zucca, chapter 37). Intrusion of such material will add weight to the crust and cause subsidence of the volcano base, but will not cause the same degree of subsidence of the top of the volcanoes as it would if erupted subaerially as lava flows.

Depression of the top of the oceanic crust is 5–7 km near Oahu, and depression of the base of the oceanic crust is about 8 km beneath Mauna Loa, as revealed by seismic experiments. Despite the possibility that some of the apparent depression of the base of the crust is caused by intrusive activity, subsidence of the base of the volcanoes is probably 5–7 km and may be greater.

The major depression of the crust caused by the weight of the growing volcanoes atop the Hawaiian hot spot forms a giant trough or canoe-like crustal warp (fig. 2.4). This southeast-trending trough underlies the Hawaiian Ridge and terminates about 50 km southeast of the Island of Hawaii near the area where the Hawaiian Deep curves around the end of the ridge (fig. 2.1). The propagation of the Hawaiian Ridge and its underlying trough onto new virgin crust toward the southeast can be compared to the movement of a massive caterpillar tread over muddy ground (fig. 2.6). The sharp downflexing of the crust and lithosphere at the head of the caterpillar is probably the cause of some of the earthquakes concentrated around the volcanic front (fig. 2.11).

The edges of the deepest part of the downbowed crust are roughly coincident with the two or more loci, commonly about 40 km apart, that connect individual volcanic centers (fig. 2.4). Sharp bending of the crust and mantle on the two sides of the base of this trough may cause fractures that tap magmas from the hot spot and are related to the formation and progagation of these volcano loci. The changes in trend of these loci along the ridge (Shaw and others, 1980) are perhaps caused by the presence of major pre-Hawaiian volcanic seamounts that were rafted over the hot-spot area. Such seamounts and their underlying subsidence troughs could affect the downflexing of the lithosphere caused by the new volcanic load and perturb the positions of the fractures that conduct magma from the hot spot to the surface to feed the new volcanoes.

The prevolcanic sea floor underlying the Hawaiian Ridge is, like the underlying base of the crust, warped down into a trough. This trough, which is filled with material erupted from the volcanoes, extends beneath the level of the old ocean floor about as far down as the largest volcanoes presently rise above that level. The cross-sectional area of this trough beneath the level of the old ocean floor is about 750–1,000 km^2, equal to or somewhat greater than the cross-sectional area of the volcanic ridge above the old ocean floor. If the rate of plate motion is assumed to be 10 cm/yr, 0.075–0.1 km^3 of volcanic material subsides beneath the level of the old ocean floor per year. This volume is similar to or slightly less than the current measured output of Kilauea Volcano of 0.11 km^3/yr (Swanson, 1972). Hence the bulk of the material erupted from the Hawaiian hot spot is not only deeply buried, but has subsided below the general level of the surface on which it was originally deposited (the old ocean floor). Models considering the origin and structure of the ridge, and of the magmas that formed it, need take this fact into account.

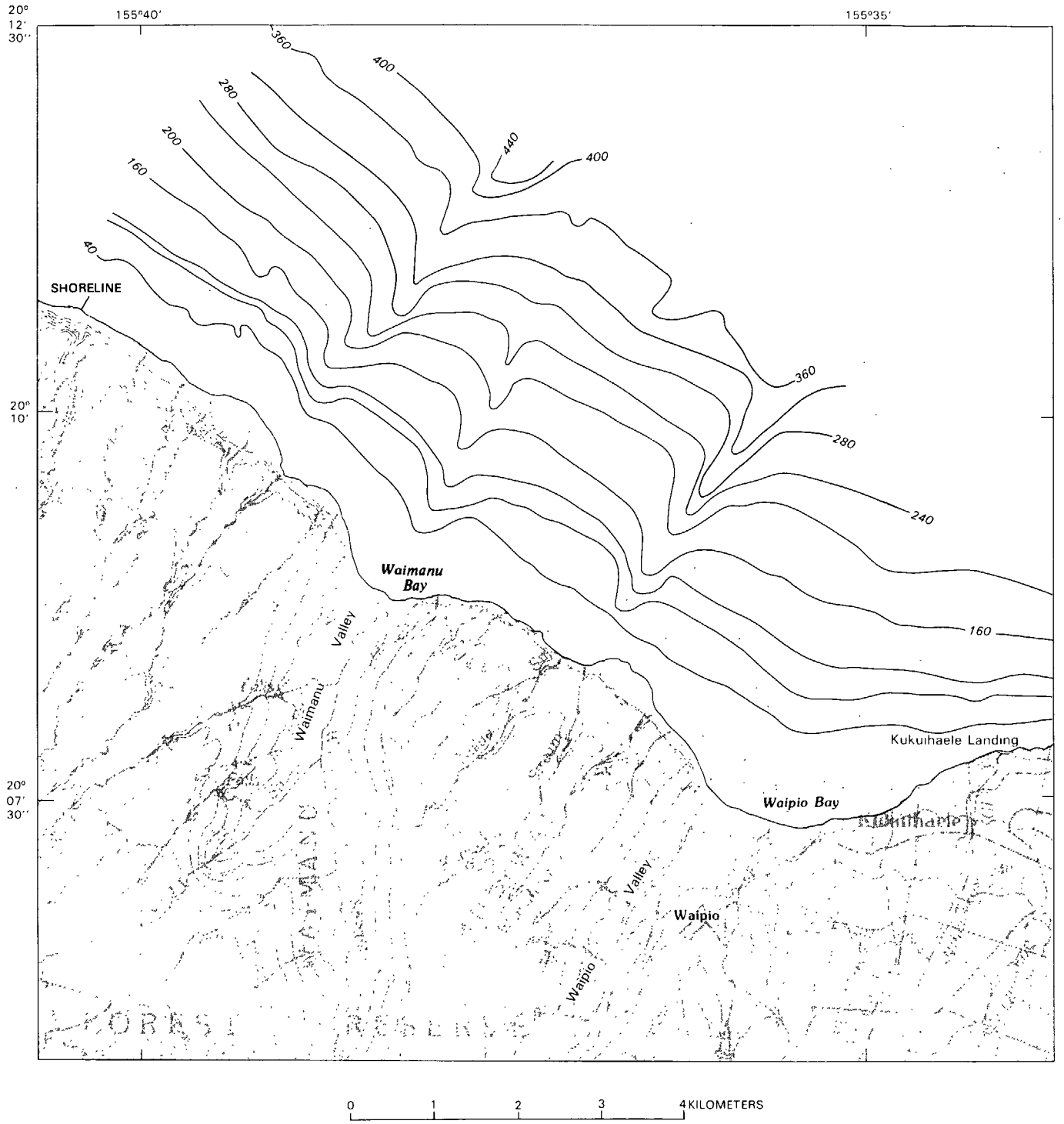

FIGURE 2.10.—Map of northeastern Kohala showing subaerial and submarine canyons. Bathymetric contour interval, 40 m.

The axis of the trough beneath the ridge has undergone most of its subsidence within a short distance (and hence time) from the unsubsided oceanic crust to the southeast. The base of the crust (and presumably also the old ocean floor) has subsided 7.5 km in the 100 km from the beginning of downwarping to the region beneath Mauna Loa (fig. 2.6). This is equivalent to a subsidence of 7.5 mm/yr if we assume that the volcanic system propagates laterally at a rate of 10 cm/yr relative to the crust.

The axis of the Hawaiian Deep becomes deeper northwest of the hot spot because of continued subsidence of the ridge and crust in

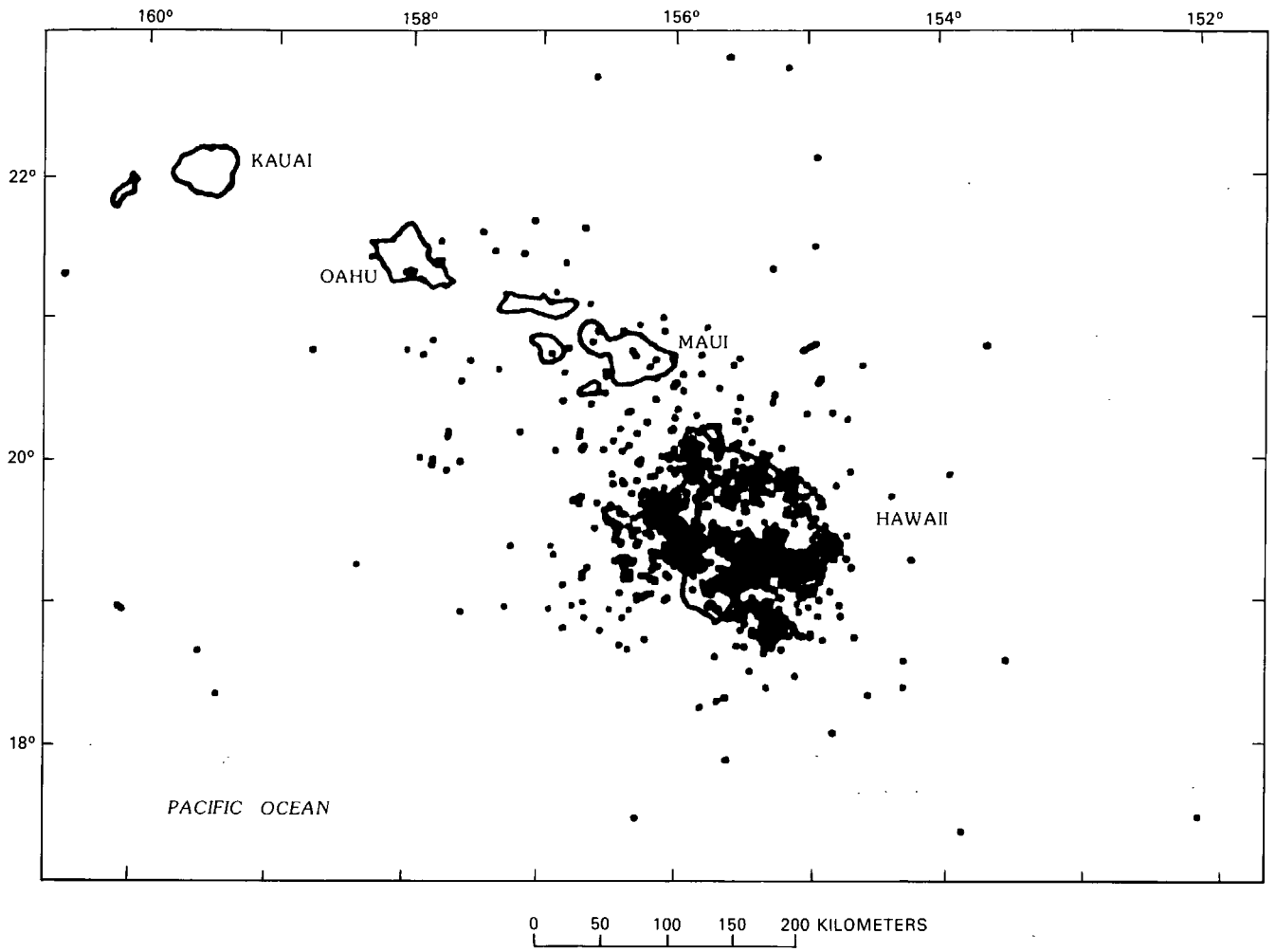

FIGURE 2.11.—Epicentral locations of earthquakes with magnitude 3 or larger in the Hawaiian region during 1968–83 (F.W. Klein, written commun., 1985).

response to the weight of erupted products. In addition, the lithosphere may have been reheated, and hence elevated adjacent to the hot spot to partly create the Hawaiian Arch (Von Herzen and others, 1982). Cooling and subsidence of the lithosphere northwest of the hot spot adds to the depression of the trough axis. Seismic refraction experiments indicating that the depth to the base of the crust south of Oahu is 20–23 km (Furumoto and Woollard, 1965) suggest the possibility of minor continued subsidence from Mauna Loa to Oahu.

CHARACTER OF SUBSIDENCE

The extent of the depression of the M-discontinuity from unaffected crust southeast of the ridge, through Kilauea, and northwestward to the older volcanoes provides information on the history and character of subsidence (fig. 2.6). Assuming a volcanic propagation rate of 10 cm/yr, each 100 km represents 1 m.y.

The bulk of subsidence occurred in about 1 m.y. The center of the base of the volcanic ridge subsides about 8 km, and the part of the volcano that first broke the sea surface subsides about 5 km. However, the sides of a volcano undergo considerably smaller amounts of subsidence than the center, producing a trough-like shape to the boundary between subaerially and submarine erupted basalt (fig. 2.6, section *B-B'*).

The southeast end of the ridge is downshearing against that part to the northwest because ongoing subsidence is greater to the southeast (fig. 2.6). This southeasterly dislocation probably occurs at all scales in southeast Hawaii and no doubt produces some of the seismic activity (fig. 2.11). Moreover, it must be an important process in shaping the geometry of volcanic conduits, magma chambers, and rift zones. Major fault systems such as the Kaoiki, which separates Mauna Loa from Kilauea, and the Hilina, on the south flank of Kilauea, are probably related to this process.

The general pattern of subsidence permits an estimate of the volume proportions of certain divisions of the volcanoes. A section

through the embryonic part of the ridge at Loihi Volcano (fig. 2.6) indicates a cross-sectional area of the ridge here of about 880 km^2 of basalt, all subaqueously erupted or intrusive. Petrologic studies (Moore and others, 1982) indicate that Loihi has recently undergone a transition from eruption of early alkalic lava to eruption of tholeiitic lava, and the section suggests that about 30 percent of the ridge here is composed of the early alkalic material. This estimate does not consider the possibility that much of the basal part of the volcano is composed of intrusive rock, possibly of a different composition. At this early stage already about 40 percent of the volume of the volcano has subsided beneath the level of the prevolcanic ocean floor.

In contrast, Haleakala Volcano on Maui has virtually completed its volcanic cycle, except for lingering small-scale eruption of late alkalic lavas. The cross-sectional area of the volcanic ridge here is about 1,450 km^2, of which about 16 percent is the early alkalic lava and only a few percent is late alkalic lava. Presently only 4 percent of the volcanic pile is above sea level, but 25 percent of the volume of the ridge here was erupted above sea level and built shield volcanoes largely of tholeiitic basalt. The other 75 percent of the volcanic ridge, although also composed principally of tholeiitic basalt, was erupted beneath the sea and is composed largely of pillowed lavas that predate the growth of the subaerial shield volcanoes and have steeper slopes (Moore and Fiske, 1969). About 53 percent of the volume of volcanic materials here has subsided beneath the level of the prevolcanic ocean floor.

The primary constraint on the measured rate of volcanic propagation along the Hawaiian Ridge is the body of radiometric ages of rocks collected from the volcanoes (Clague and Dalrymple, chapter 1). It is evident that virtually all of these samples are from near the top of the volcanoes. Wherever possible, tholeiitic lavas rather than the later alkalic lavas were collected and dated, so the ages more nearly define the age of the major shield-building stage of volcano growth.

Time-distance plots of the age data show an apparent acceleration of the volcanic propagation rate (as well as the volcanic eruption rate) in the last approximately one million years. Shaw and others (1980) find that the average rate of volcanic progression from the Hawaiian-Emperor bend to West Maui Volcano is 7.9 cm/yr, and the average rate from West Maui Volcano to Kilauea is 17.8 cm/yr. Clague and Dalrymple (chapter 1) support the notion of a relatively recent acceleration in the volcanic propagation rate and note that otherwise the curvature of the time-distance plot causes it to intersect the distance axis northwest of Kilauea and predict a negative age for that volcano.

However, the fact that the southeast end of the ridge has not undergone all of its subsidence is an important limitation to the use of unqualified time-distance plots to determine the propagation rate. The exposed and dated parts of the southeastern volcanoes will clearly submerge beneath the sea and be covered with younger lavas. When the first phase of rapid subsidence is complete for Kilauea, the present summit will be 1 km or more below sea level. Loihi Volcano (figs. 2.1 and 2.6), now 1 km below sea level, will have to grow more than 2 km up before it breaks the sea surface because more than one-half of its volcanic growth is offset by subsidence. In order for the ages of Kilauea and Mauna Loa to be comparable with those of the northwestern volcanoes, one must obtain samples of yet unerupted lavas that will mantle the presently exposed surface. Hence, if such unerupted future lava could be dated now it would have a negative age as suggested by Clague and Dalrymple. Until more is known about the volume and age of the submarine volcanic products, it seems premature to propose a dramatic increase in the rate of volcanic propagation in the last million years or so. Assuming that the rate has remained constant, then straight-line projection of age-distance data to Kilauea and on to Loihi suggests a negative (future) age for Loihi of 1–1.5 m.y. (Clague and Dalrymple, chapter 1). Since Loihi is already of finite age, the duration of the chief period of volcano growth is about 1.5–2 m.y. (fig. 2.6)

The proposed increase in the volume of volcanic products and hence eruption rates at the young end of the ridge (Clague and Dalrymple, chapter 1; Shaw and others, 1980) is also uncertain, because all of the previously measured volcanic volumes include only that part of the ridge above the level of the flat ocean floor surrounding the Hawaiian Ridge. The volume of volcanic material in the trough underlying the ridge has not been considered. Because the old ocean floor is fully depressed beneath the entire length of the ridge except at the extreme southeast end, it is not surprising that larger apparent volumes (and higher eruption rates) have been calculated for the unsubsided region.

The base of the volcanic material erupted between 1 Ma and the present is not depressed as much as that erupted between 2 and 1 or 3 and 2 Ma (fig. 2.6). The volume between the 1 Ma and zero isochrons is even further reduced if we consider the fact that the sides of the depressed zone loop around the end of the ridge (compare with fig. 2.4). This part of the ridge will subside many kilometers within the next one million years.

As the Hawaiian Ridge propagates southeasterly in the lithosphere by the northwesterly movement of the Pacific plate, the southeast end of the ridge and the surrounding ocean floor bend down toward the hot-spot area or toward the youngest volcano. Movement of the lithospheric plate away from the hot spot progressively removes a given island or volcano from the subsiding zone adjacent to the hot spot. At the present time Kahului, Maui, which is 180 km from Mauna Loa (near the hot-spot center), is not subsiding rapidly (fig. 2.3). and Molokai and Oahu appear to be stable. Hence the rapidly subsiding zone is largely in the vicinity of the Island of Hawaii, and it may be outlined by the concentration of recent earthquakes (fig. 2.11). Downwarping of the base of the crust begins about 100 km both southeast and southwest of Mauna Loa (Zucca and others, 1982). and available evidence suggests that the downwarping zone is roughly circular with a 100-km radius. The center of downwarping as defined by the curvature of the Hawaiian Deep (fig. 2.4) is about midway between the summits of Mauna Loa and Mauna Kea Volcanoes.

The manner of tilting of pre-existing terraces is clarified if we trace the history of a horizontal surface affected by this downwarping sag (fig. 2.12). Close to the center of the sag, assumed to be cone-like, the terrace will subside faster than on its edges where no subsidence occurs. As the terrace moves relatively northwest from the sag, progressively all subsidence will stop and the tilt will be

"frozen in" on the terrace. If we assume that the sag moves 10 cm/yr southeast relative to the crust, and that subsidence is 2.5 mm/yr at the cone center, then an original horizontal surface will finally end tilted toward the sag at about 1.5 km/100 km (fig. 2.12). This tilt is similar to that of the H terrace off east Maui (fig. 2.8).

The depression of the M-discontinuity beneath the Hawaiian Ridge is a measure of subsidence of the volcanoes. The high proportion of the volcanic pile that is below the level of the prevolcanic ocean floor even at the youngest, southeasternmost volcanoes indicates that subsidence is very rapid. Much of the subsidence occurs while the volcanoes are growing. A large part of the total subsidence has occurred by the time the volcanoes reach sea level; Loihi Volcano, still 1 km below sea level, has already subsided more than 1 km (fig. 2.6) and will presumably subside an additional 6 km if it grows to the size of Mauna Loa. However, subsidence is much more rapid after the volcanic products are deposited above sea level because the buoyancy of water does not affect this material and its effective weight is 1 g/cm^3 greater. This fact is demonstrated by the slope of the depressed M-discontinuity at the volcanic front. This slope becomes abruptly steeper beneath the southeast shoreline of Hawaii (fig. 2.6). These slopes (assuming a volcanic propagation rate of 10 cm/yr) indicate subsidence rates of 4 mm/yr for the submarine part of the volcano, and 12 mm/yr for the subaerial part of the volcano. Comparison of these slopes at the base of the crust with volcanic profiles at the top of the crust (fig. 2.6) indicates that downbowing of the crust is an almost immediate response to volcanic loading.

Through the life of the growing volcano, new material deposited on top undergoes progressively less subsidence than the older material below it. Hence when the volcano achieves enough mass above sea level to be marked by sea-level terraces, these features will undergo only a small part of the total subsidence experienced by the older, lower parts of the volcano.

CONCLUSIONS

Subsidence of the Hawaiian Ridge can be constrained by tide-gauge measurements, geophysical measurements of crustal structure, and information gained from submarine canyons, submerged carbonate reefs, deep drilling, and dredging. An analysis of these data indicates the following:

1. The Hawaiian Ridge has undergone rapid and dramatic subsidence. Most volcanoes have subsided 2–4 km since reaching the sea surface, and the bases of the volcanoes have subsided 5–8 km.

2. Between one-half and two-thirds of the upbuilding of the volcanoes is offset by subsidence.

3. Major sea-level terraces formed during the chief periods of volcanic growth above sea level tend to tilt toward the point of active volcanic loading, that is toward the southeast. Hence depth correlation of terraces along the island chain may be misleading.

4. Because the young volcanoes at the southeast end of the Hawaiian Ridge have not completed their subsidence and growth, volcanic ages derived from them provide estimates of volcanic propagation rates that are too high. Likewise, volumes measured for the volcanoes only above the level of the ocean floor indicate eruption rates for the older, subsided volcanoes that are too low. These factors raise doubts about both the proposed increase in volcanic propagation rate and eruption rate during the last few million years.

5. The alignment of volcanoes along two or more curving loci about 40 km apart and parallel to the Hawaiian Ridge may result from sharp bending of the crust and mantle on the two sides of the base of the subsided trough underlying the ridge. Such bending may

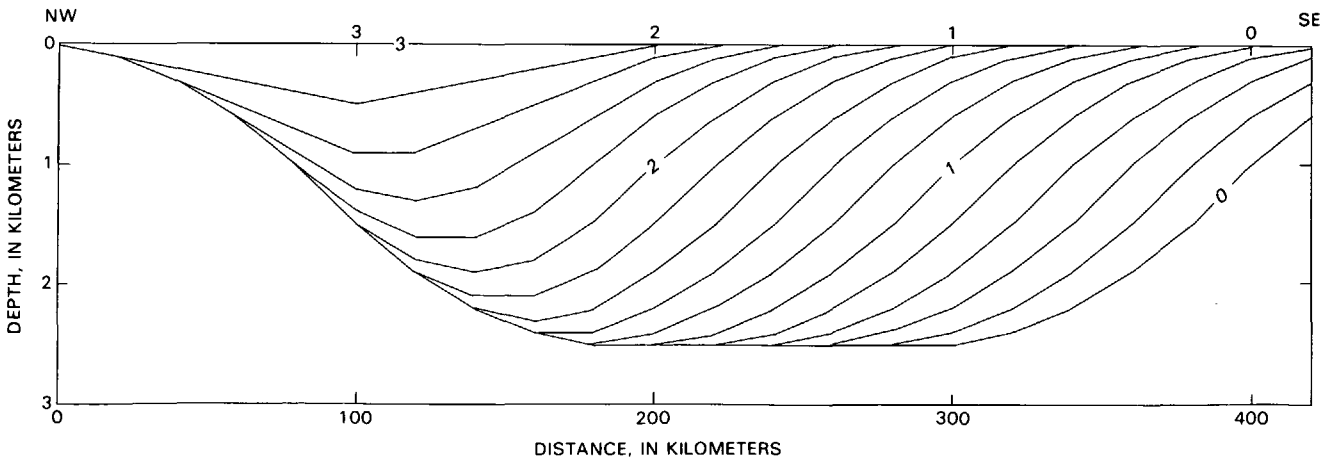

FIGURE 2.12.—Vertical section passing through center of migrating cone-like subsidence zone (100-km radius) that migrates southeast at 10 cm/yr; position of the center of the cone at specific times (Ma) is shown at top. The center of the cone subsides 2.5 mm/yr and subsidence and migration have occurred for 3 m.y. Profiles show successive shapes of a warped surface that was horizontal at 3 Ma; numbers give ages in Ma. Note the formation of a tilted terrace sloping about 1.5 km/100 km to the southeast that is left behind in the wake of the migrating subsidence zone. This model can apply to the deformation either of a sea-level terrace or of the ocean floor at the beginning of the propagation of the subsiding Hawaiian Ridge.

initiate fractures that tap magmas from the hot spot and feed the volcanoes. The changes in mapped trend of the loci may be caused by the rafting of pre-Hawaiian seamounts over the hot spot area, where they perturbed this downflexing of the lithosphere and the location of the conduit fractures.

6. An estimate of volumes based on patterns of subsidence indicate that as much as 16 percent of the volume of the ridge is early alkalic lava, about 25 percent was erupted subaerially, and about 53 percent has subsided beneath the level of the old ocean floor. These estimates may be reduced if a substantial volume of the volcanoes is composed of intrusive rather than extrusive rocks.

7. A part of the seismic activity that is centered at the southeastern end of the Ridge may result from bending and dislocation of the volcanic pile as the southeastern part subsides relative to that adjacent on the northwest.

REFERENCES CITED

Andrews, J.E., and Bainbridge, C., 1972, Submarine canyons off eastern Oahu: Pacific Science, v. 26, no. 1, p. 108–113.

Apple, R.A., and Macdonald, G.A., 1966, The rise of sea level in contemporary times at Honaunau, Kona, Hawaii: Pacific Science, v. 20, p. 125–136.

Barnett, T.P., 1983, Recent changes in sea level and their possible causes: Climate Change, v. 5, p. 15–38.

Campbell, J.F., 1984, Rapid subsidence of Kohala volcano and its effect on coral reef growth: Geo-Marine Letters, v. 4, p. 31–36.

Campbell, J.F., and Erlandson, D., 1979, OTEC-1 anchor site survey: Hawaii Institute of Geophysics, v. HIG-79-6, 55 p.

Clague, D.A., Dalrymple, G.B., Green, H.G., Wald, D., Kono, M., and Kröenke, L.W., 1980, Bathymetry of the Emperor Seamounts, Leg 55 of the Deep Sea Drilling Project, *in* Jackson, E.D., Koisumi, I., and others, Initial reports of the Deep Sea Drilling Project, v. 55: Washington, U.S. Government Printing Office, p. 845–855.

Clague, D.A., Dao-gong, C., Murnane, R., Beeson, M.H., Lanphere, M.A., Dalrymple, G.B., Friesen, W., and Holcomb, R.T., 1982, Age and petrology of the Kalaupapa Basalt, Molokai, Hawaii: Pacific Science, v. 36, no. 4, p. 411–420.

Coulbourn, W.T., Campbell, J.F., and Moberly, R., 1974, Hawaiian submarine terraces, canyons, and Quaternary history evaluated by seismic-reflection profiling: Marine Geology, v. 17, p. 215–234.

Furumoto, A.S., Wiebenga, W.A., Webb, J.P., and Sutton, G.H., 1973, Crustal structure of the Hawaiian archipelago, northern Melanesia, and the central Pacific basin by seismic refraction methods: Tectonophysics, v. 20, p. 153–164.

Furumoto, A.S., and Woollard, G.P., 1965, Seismic refraction studies of the crustal structure of the Hawaiian archipelago: Pacific Science, v. 19, no. 3, p. 315–319.

Hamilton, E.L., 1957, Marine geology of the southern Hawaiian Ridge: Geological Society of America Bulletin, v. 68, p. 1011–1026.

Hill, D.P., 1969, Crustal structure of the island of Hawaii from seismic-refraction measurements: Bulletin of the Seismological Society of America, v. 59, no. 1, p. 101–130.

Jackson, E.D., and Koisumi, I., and others, 1980, Initial reports of the Deep Sea Drilling Project, v. 55: Washington, U.S. Government Printing Office.

Macdonald, G.A., and Abbott, A.T., 1970, Volcanoes in the sea: University of Hawaii Press, 441 p.

Mathewson, C.C., 1970, Submarine canyons and the shelf along the north coast of Molokai Island, Hawaiian ridge: Pacific Science, v. 24, p. 141–144.

Moore, J.G., 1964, Giant submarine landslides on the Hawaiian Ridge: U.S. Geological Survey Professional Paper 501-D, p. D95-D98.

———1970, Relationship between subsidence and volcanic load, Hawaii: Bulletin Volcanologique, v. 34, p. 562–576.

Moore, J.G., Clague, D.A., and Normark, W.R., 1982, Diverse basalt types from Loihi seamount, Hawaii: Geology, v. 10, p. 88–92.

Moore, J.G., and Fiske, R.S., 1969, Volcanic substructure inferred from dredge samples and ocean-bottom photographs, Hawaii: Geological Society of America Bulletin, v. 80, p. 1191–1202.

Moore J.G., and Fornari, D.J., 1984, Drowned reefs as indicators of the rate of subsidence of the Island of Hawaii: Journal of Geology, v. 92, p. 752–759.

Moore, J.G., and Moore, G.W., 1984, Deposit from a giant wave on the Island of Lanai, Hawaii: Science, v. 226, p. 1312–1315.

Moore, J.G., Moore, G.W., Szabo, B.J., 1984, Age of debris from a huge Pleistocene wave on Lanai, Hawaii [abs.]: EOS, v. 65, n. 45f, p. 1082.

Moore, J.G., and Peck, D.L., 1965, Submarine lavas from the east rift zone of Mauna Kea, Hawaii [abs.]: Geological Society of America Abstracts with Program, Cordilleran Section, Fresno, CA.

Shaw, H.R., Jackson, E.D., and Bargar, K.E., 1980, Volcanic periodicity along the Hawaiian-Emperor Chain: American Journal of Science, v. 280-A, p. 667–708.

Shepard, F.P., and Dill, R.F., 1966, Submarine canyons and other sea valleys: Chicago, Rand McNally and Company, 381 p.

Shor, G.G., 1960, Crustal structure of the Hawaiian ridge near Gardner Pinnacles: Bulletin of the Seismological Society of America, v. 50, no. 4, p. 563–573.

Stearns, H.T., 1966, Geology of the State of Hawaii: Palo Alto, California, Pacific Books, 266 p.

———1978, Quaternary shorelines in the Hawaiian Islands: Bernice P. Bishop Museum Bulletin 237, 57 p.

Stearns, H.T., and Chamberlain, T.K., 1967, Deep cores of Oahu, Hawaii and their bearing on the geologic history of the central Pacific basin: Pacific Science, v. 21, no. 2, p. 153–165.

Stone, C., 1977, Chemistry, petrography, and hydrothermal alteration of basalts from Hawaii geothermal project well-A, Kilauea, Hawaii: University of Hawaii Masters thesis, 84 p.

Stone, C., and Fan, P., 1978, Hydrothermal alteration of basalts from Hawaii geothermal project well-A, Hawaii: Geology, v. 6, p. 401–404.

Swanson, D.A., 1972, Magma supply rate at Kilauea Volcano, 1952-1971: Science, v. 175, p. 169–170.

Tilling, R.I., Koyanagi, R.Y., Lipman, P.W., Lockwood, J.P., Moore, J.G., and Swanson, D.A., 1976, Earthquakes and related catastrophic events, Island of Hawaii, November 29, 1975: A preliminary report: U.S. Geological Survey Circular 740, 33 p.

Von Herzen, R.P, Detrick, R.S., Crough, S.T., Epp, D., and Fehn, U., 1982, Thermal origin of the Hawaiian Swell: heat flow evidence and thermal models: Journal of Geophysical Research, v. 87, no. 8, p. 6711–6723.

Watts, A.B., Ten Brink, U.S., Buhl, P., and Brocher, T.M., 1985, A multichannel seismic study of lithospheric flexure across the Hawaiian-Emperor seamount chain: Nature v. 315, no. 6015, p. 105–111.

Wilde, P., Chase, T.E., Normark, W.R., Thomas, J.A., and Young, J.D., 1980, Oceanographic data off the southern Hawaiian Islands: Lawrence Berkeley Laboratory Publication 359, Lawrence Berkeley Laboratory, University of California, Berkeley.

Zucca, J.J., Hill, D.P., and Kovach, R.L., 1982, Crustal structure of Mauna Loa Volcano, Hawaii, from seismic refraction and gravity data: Bulletin of the Seismological Society of America, v. 72, no. 5, p. 1535–1550.

SLOPES OF THE HAWAIIAN RIDGE

By Robert K. Mark *and* James G. Moore

ABSTRACT

Slopes of the southeastern Hawaiian Ridge have been computed from elevation and bathymetric data digitized at 750-m spacing. Maps derived from these data show that most of the subaerial slopes of Mauna Loa shield volcano, built of tholeiitic basalt, are 3° to 6° and the steepest average slope is 8° at 3,300-m elevation. The lower slopes of much of Mauna Kea, capped by alkalic basalt, are also 3° to 6°, but they steepen to 6° to 9° on the east side, and the steepest average slope is 13° at 3,000-m elevation.

Submarine slopes are generally steeper than subaerial slopes on an active marine volcano, but both submarine and subaerial slopes become gentler downward. Consequently, submarine slopes are steepest slightly below sea level and merge upslope with the gentlest subaerial slopes. On Kilauea and Mauna Loa the average subaerial slope below 2,000-m elevation is 4°, but 500 m below sea level the slope increases to 13°. This sharp downward-slope increase at the subaerial-subaqueous transition results from several processes, but perhaps the most important depends on the buoyant effect of water on propagation of a lava flow. A flow cannot move downhill as readily underwater because gravity exerts less force on it, and so the flow will thicken, spread laterally, and build up the slope. Depression of this slope change in older volcanoes is a measure of subsidence of the volcano that has occurred since termination of the major period of shield growth.

Major submarine landslides commonly head in regions with regional slopes of 14° to 17°, but are flanked by slopes as great as 19°, the landslide having reduced the slope at its head. Arcs of anomalously steeper slopes at intermediate depths apparently mark gravitationally induced creep zones that bulge the volcano flank seaward.

INTRODUCTION

The present slope of landforms results from the equilibrium attained between the processes that built up the landform and those gravitationally induced processes that operate to reduce it to a flat plane. Volcanic activity, first on the sea floor and eventually on island peaks, is the chief process that built up the Hawaiian Ridge. Concurrently the ridge has undergone reduction by erosion, mass wasting, landsliding, and isostatic subsidence. An insight into all of these processes can be attained by analysis of slope.

Digitized topographic and bathymetric data (fig. 3.1) were employed to generate slope maps and plots of the southeast Hawaiian Ridge (figs. 3.2, 3.3). This proprietary data set, which includes over 42,000 scattered elevation values, was provided by Dynamic Graphics, Inc. Using the Surface Gridding Library (Dynamic Graphics, Inc., 1978), we computed a grid of 751 rows and 931 columns, with 750-m spacing, from the scattered data. Slopes were computed by fitting a quadratic surface to the three-by-three array around each grid point. Color separation negatives for publication were produced on the Scitex Response 280 System laser drum plotter.

The computer slope calculations determine the tangent of the angle of slope as measured from the horizontal. The color boundaries on the slope maps (figs. 3.2, 3.3) are in even increments of slope-angle tangent, which multiplied by 100 is equal to the percent grade. The equivalent angle in degrees is shown in table 3.1. Degrees are used in discussing slopes in the text because this is probably more meaningful to the average map user.

Rapid computer techniques were employed to determine the area-averaged slope for each 100-m interval of depth and elevation for the six segments of the age-progressive Hawaiian Ridge shown in figure 3.1. These average slopes were smoothed using RSMOOTH (Velleman and Hoagun, 1981) and plotted against depth (fig. 3.4). The slope-depth plots of the six segments, which are systematically older to the northwest, permit analysis of the changes in slope that occur through time.

ACKNOWLEDGMENTS

The digitized version of the topographic and bathymetric data used to generate the slope map and plots was provided by Dynamic Graphics, Inc. Careful reviews of the manuscript were made by D.A. Clague and M.A. Clynne. We are grateful for this help.

SUBAERIAL SLOPES

The unmodified subaerial slopes of Mauna Loa shield volcano are mostly very gentle (fig. 3.2). Substantial parts of the the lower slopes are between 3° and 6°, and slopes near the summit are rarely steeper than 11°. The steepest average slope is 8° and occurs at 3,300-m elevation (fig. 3.4). Flatter surfaces occur in saddles between Mauna Loa and the neighboring volcanoes Mauna Kea and Hualalai, where lavas are ponded. The smaller tholeiitic shield of Kilauea, which is built on the south side of Mauna Loa, shows gentle slopes generally less than 3°. In part this gentle slope is probably caused by ponding of both Mauna Loa and Kilauea lavas between the southeast flank of Mauna Loa and the summit and east rift zone of Kilauea. The flat area that covers much of the southeast part of the island (Puna) results from such lava flows ponded north of the east-rift-zone ridge of Kilauea. This area generally slopes less than 3° and is the largest such gently sloping area on the Hawaiian Islands.

The southern coastal part of Kilauea shows anomalously steep slopes exceeding 9° and locally exceeding 17°. These steep areas are clearly related to the Hilina fault system, in which steep fault scarps are common. A similar coastal region of steep terrain occurs on the west side of Mauna Loa and probably represents lava-mantled fault scarps (Normark and others, 1979).

In contrast to Mauna Loa and Kilauea, the central part of Mauna Kea Volcano is capped by alkalic lava that produces steeper slopes. Though much of the lower parts of this volcano has slopes between 3° and 6°, they steepen to 6° to 9° on the east side. The upper central part, however, commonly reaches a maximum slope of 14°. The steepest average slope is 13° and occurs at an elevation of 3,000 m (fig. 3.4).

This steeper central region of Mauna Kea is a result of several factors. Firstly, the alkalic lava flows, particularly hawaiite that erupted from vents on the upper slopes, are generally somewhat richer in SiO_2 and hence more viscous than the alkali basalt flows of the lower slopes or the tholeiitic basalt flows of Mauna Loa. Consequently the flows are thicker and pile up closer to the vent. Secondly, many of the alkalic flows are of smaller volume than tholeiitic flows and hence flow a shorter distance, thereby piling up near the summit. Thirdly, the younger lava flows of Mauna Kea were not erupted from long rift zones as on Mauna Loa, but from vents clustered near the summit. Finally, the alkalic lava of Mauna Kea is apparently rich in gas and has built dozens of rather large cinder cones on the upper parts of the volcano. These steep pyroclastic cones are concentrated on the upper part of the volcano and, with the lava flows that pond between them and cover them, tend to produce a steep cap to the volcano.

Haleakala Volcano on East Maui (fig. 3.3) is steep like Mauna Kea, also in part because of its cap of alkalic lava. The volcano is asymmetric, being steeper on the south side, both above and below sea level. This steep south side may result from faulting or landsliding. Slopes on the upper part of the volcano commonly exceed 17° and parts of the south slope exceed 19°. The steepest average slope is 14° and occurs at 1,700-m elevation (fig. 3.4).

Some of the localized areas of steep subaerial slope result from erosion of deep canyons. The young volcanoes of the Island of Hawaii are little eroded except for Kohala. Steep slopes on northeast Kohala result from several major stream-cut canyons. The canyons of north Kauai and east Molokai also generate moderate areas of steep slope (fig. 3.3).

SUBMARINE SLOPES

On average, submarine slopes on the Hawaiian volcanoes are steeper than subaerial slopes but, like their subaerial counterparts, generally flatten downward. Consequently the submarine slopes are steepest slightly below sea level on a young volcano, and near sea level this steep subaqueous slope meets the more gentle subaerial slope. The average subaerial slope from the shoreline of Kilauea and Mauna Loa up to about 2,000-m elevation is about 4°. Below sea level this slope steepens abruptly to an average of 13° at 500-m depth (fig. 3.4).

Not only does the slope angle increase when a lava flow passes from land to sea, but a similar phenomenon occurs where a rift zone crosses the shoreline. Even though individual lava flows issue at many points along the rift zone, both above and below sea level, the axial crest of the rift-zone ridge plunges more steeply below sea level. The crest of the east rift zone of Kilauea plunges an average of 1.5° for 50 km from the summit caldera to the east cape of the island. Below sea level the rift zone extends another 80 km to its end at 5,500 m depth, and over this distance the crest plunges at an average angle of about 4°.

This marked slope change at the subaerial-subaqueous transition zone is the result of several processes, primarily volcanic. Regional slopes are modified at sea level by erosion and by growth of coral reefs. However, development of the steepening just below sea level on the young, active volcanoes Mauna Loa and Kilauea, where erosion and reef growth are minimal, indicates that volcanic processes must be the dominant cause. One process is the chilling effect of water on flowing lava. This tends to increase the flow's effective viscosity and cause it to thicken or divide into pillowed flow lobes and hence flow a shorter distance, thus steepening the general slope angle. A second process is the disturbance of a lava flow crossing the shoreline by vigorous surf action, which disrupts flow channels and lava tubes and causes the flow to divide, spread, and flow a shorter distance over a broader front. Both of these processes can cause a flow to break up into solid fragmental material, producing a flow-foot breccia (Moore and Fiske, 1969). A third, and perhaps the most important, process depends on the buoyant effect of water on the propagation of a lava flow. When a flow crosses the shoreline and enters the sea, its effective density drops by 1 g/cm^3. The flow cannot move downhill on the same slope as readily, because gravity exerts less force on it, and so the flow will thicken and spread laterally.

The net effect of these processes that inhibit flow of lava under water is to cause the shoreline to be extended seaward with a gentle subaerial slope and to pile lava up below sea level at shallow depth, thus creating a steep slope below sea level. This marked slope change caused by the subaerial-subaqueous lava transition can be identified on older volcanoes, where it occurs at considerable depth (fig. 3.4). The depth of the slope change is a measure of the subsidence that the volcano has undergone since the slope change was created. One of the more striking feaures of the slope map of the Hawaiian Ridge is the presence of a zone of steep slope surrounding all of the islands. The steep slope surrounding the islands of Maui, Kahoolawe, Lanai, Molokai, and Oahu marks the former shoreline of a giant island more than twice the size of the present Island of Hawaii (fig. 3.3).

LANDSLIDES

Because of its youth, great height, and steep slopes, the Hawaiian Ridge is the site of numerous landslides that occur at widely different scales. Many landslides head in the exceptionally steep zone originally formed just below sea level. Because lava flows apparently do not propagate readily underwater, mass movement

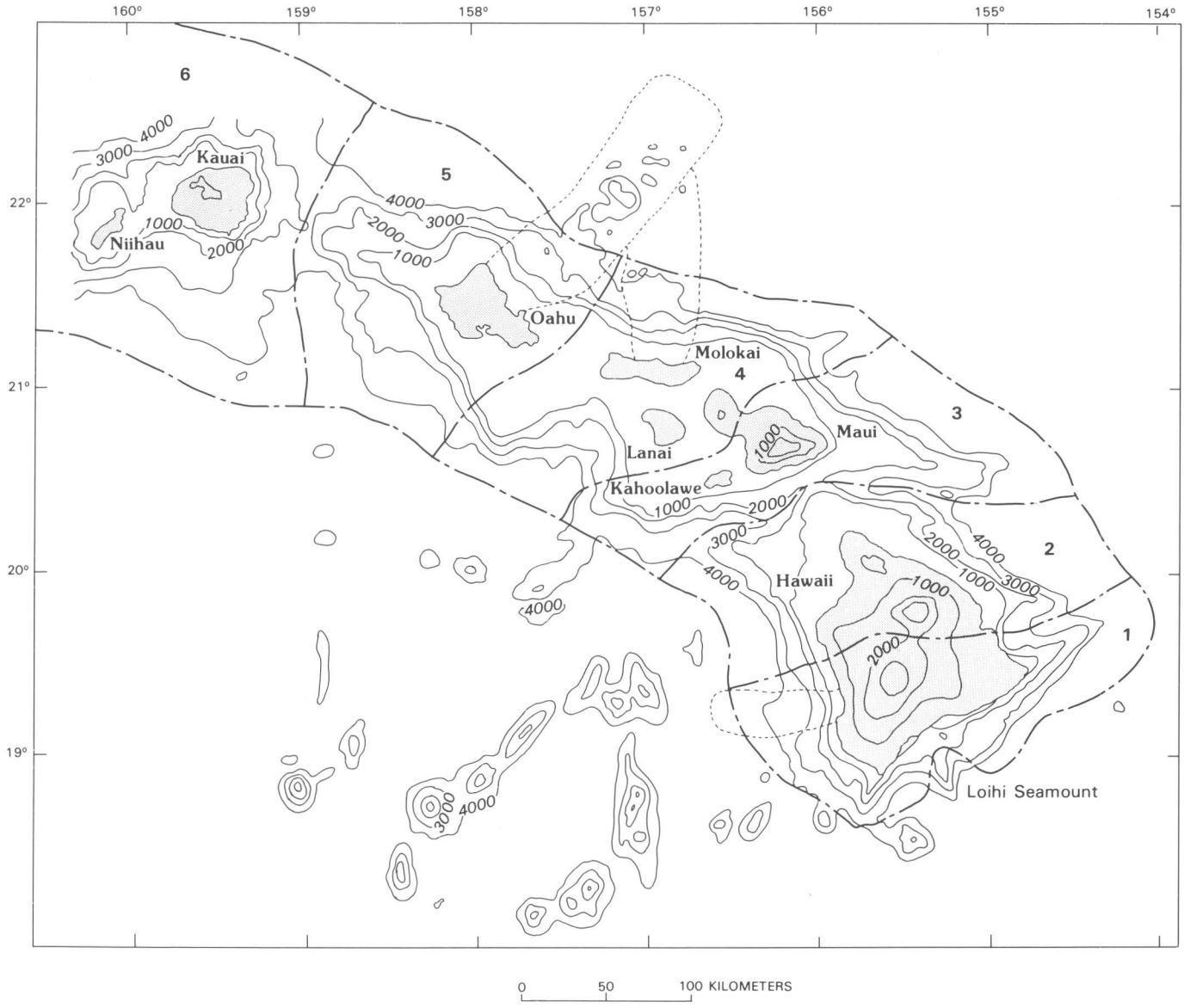

FIGURE 3.1.—Generalized topography and bathymetry of southeastern part of the Hawaiian Ridge. Contours in meters. Dotted lines bound major landslides; dash-dot lines bound age-progressive segments of ridge, numbered 1–6 (1 is youngest).

must be an important process in carrying volcanic material from near the shoreline to depth in order to maintain a slope in equilibrium.

Major landslides are suggested by two features of the slope map: They generally head on a particularly steep segment of the subaerial-subaqueous transition zone, but they are flanked by even steeper zones, the landslide having reduced the slope at its head. These relations are evident for the proposed landslides off the north coasts of Molokai and Oahu (fig. 3.1; Moore, 1964), and for the Alika landslide off the west coast of Hawaii. The landslide north of Molokai heads in a region where the maximum regional slope is about 17°, but it is flanked by steeper slopes exceeding 19°. The landslide northeast of Oahu likewise heads in a region with maximum slopes generally less than 14° but is flanked by slopes as steep as 19°. The Alika landslide off west Hawaii heads in a region with average slopes somewhat exceeding 14°, but it is flanked by slopes exceeding 19°. Additional steep offshore regions of Hawaii, prone to massive submarine landslides such as these three, are the east coast of Kilauea Volcano north of the the east cape of the island, and the south coast of Mauna Loa Volcano northeast of the south cape of the island (fig. 3.3).

Aside from these major landslides, other curious features of the slope map are probably related to downslope movement. These are arcs of steep slope at moderate depths that are separated from the main steep subaerial-subaqueous transition zone by a region of

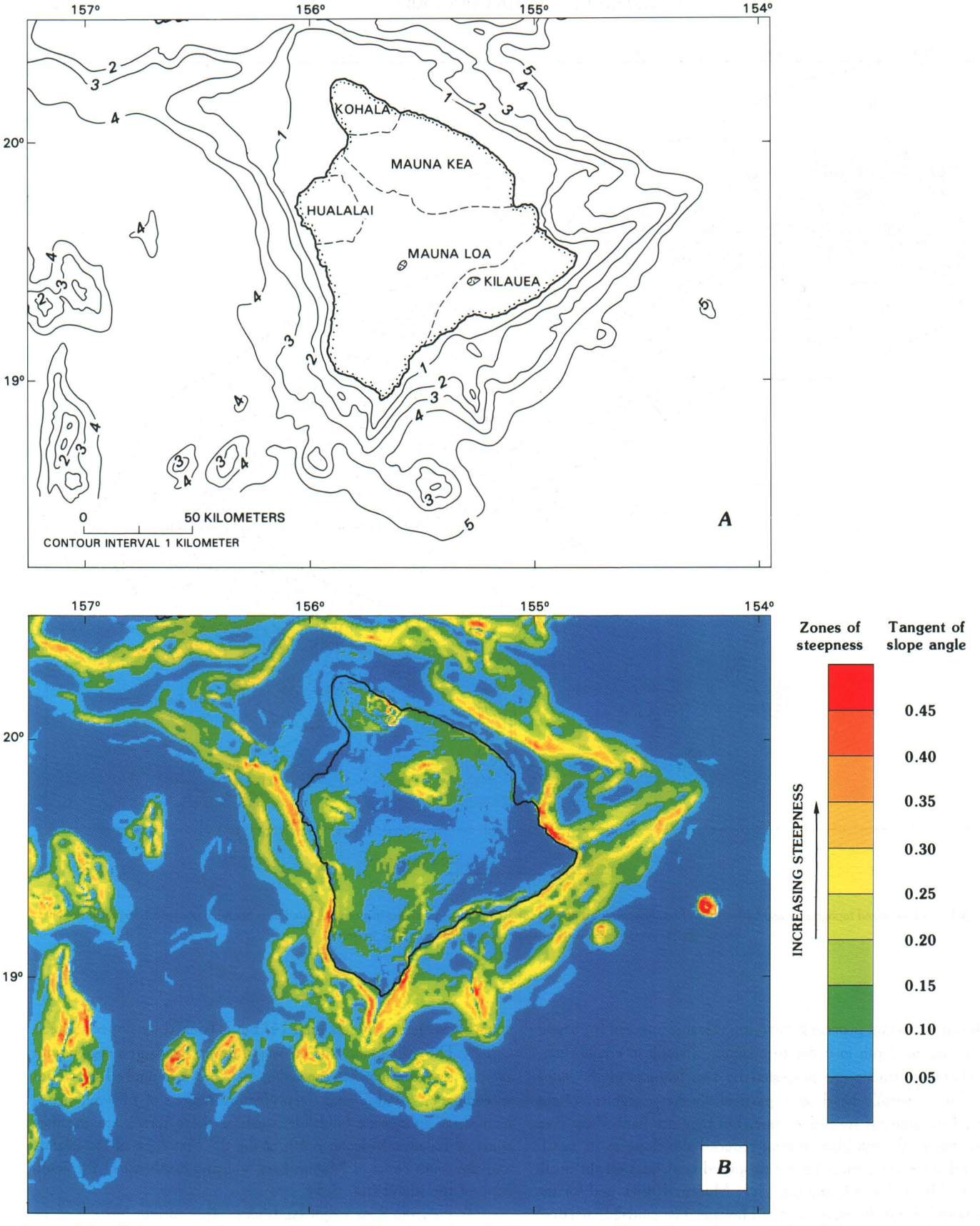

FIGURE 3.2.—Bathymetry and slopes around the Island of Hawaii. ***A***, Generalized bathymetric map. Dashed lines on the island are boundaries between the five volcanoes. ***B***, Computer-generated slope map of same region (including land areas). Slope steepness represented by color-coded intervals defined by tangents of slope angle measured from horizontal. Each color represents a slope-angle range of about 2.5° (see also table 3.1).

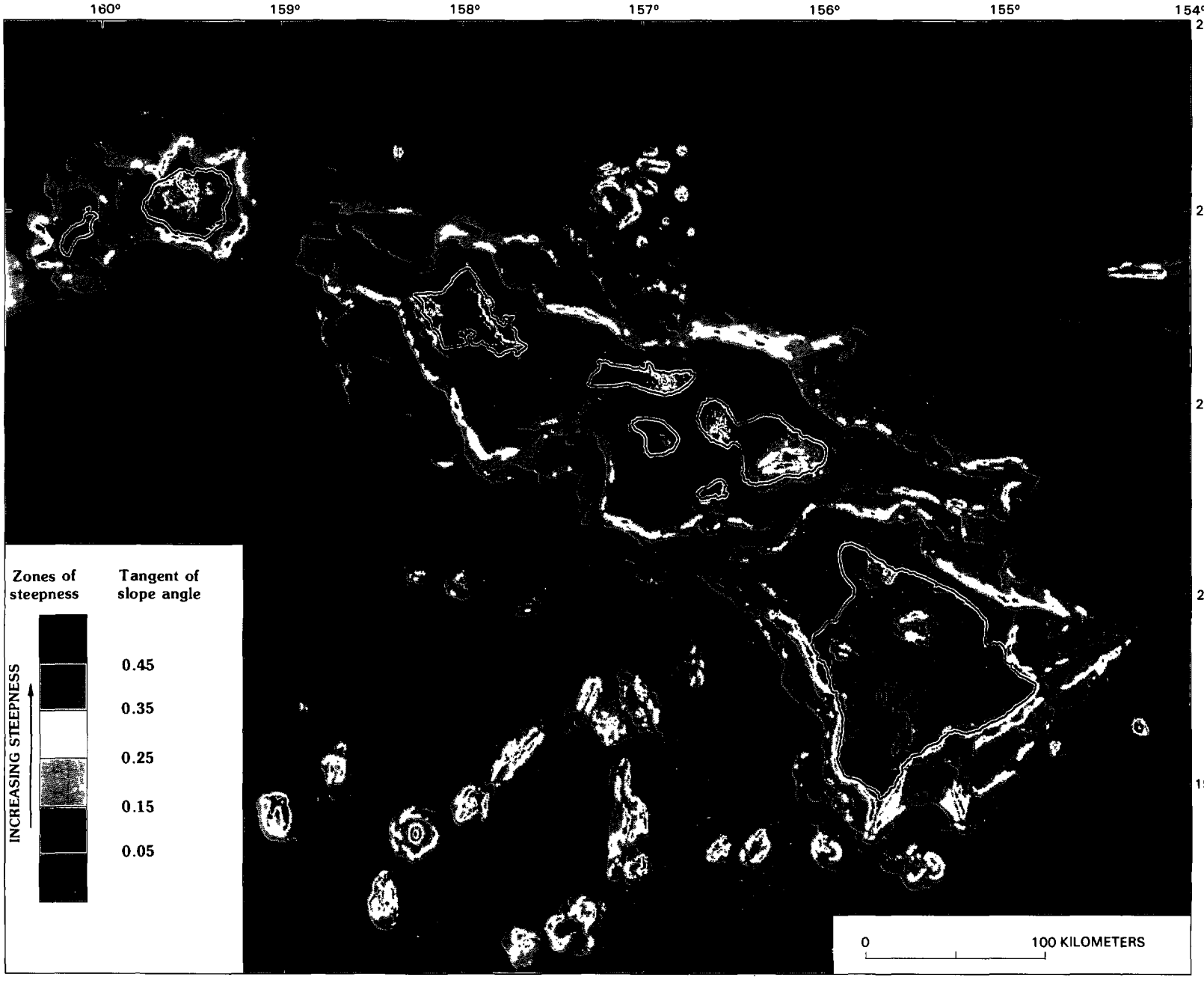

FIGURE 3.3.—Computer-generated slope map of southeastern part of the Hawaiian Ridge. Slope steepness represented by color-coded intervals defined by tangents of angle of slope. Each color represents a slope-angle range of about 5° (see also table 3.1).

TABLE 3.1.—*Angles of slope equivalent to values of tangent used as interval boundaries*

Tangent	Slope angle (degrees)
0.55	28.8
.50	26.6
.45	24.2
.40	21.8
.35	19.3
.30	16.7
.25	14.0
.20	11.3
.15	8.5
.10	5.7
.05	2.9

gentler slope. A prime example is the steep band at about 3,000-m depth that extends from Loihi Seamount off the south coast of the Island of Hawaii to near the east cape of the island (fig. 3.2). Others appear both north and south of the Alika landslide off west Hawaii. These arcs of anomalously steep terrane seem to mark gravitationally induced creep zones where the volcano flank is markedly bulged seaward. The probability of such bulges failing and producing major submarine landslides is not known.

SLOPE CHANGES WITH AGE

The bathymetric data have been compartmentalized into six segments (fig. 3.1) representing a volcanic age sequence becoming progressively older toward the northwest. The southeasternmost segment (number 1) includes Kilauea and Mauna Loa Volcanoes on the southern part of the Island of Hawaii. This segment is considered typical of youthful marine volcanoes because it includes the youngest, and currently most active, volcanic systems. The remaining segments with their included islands and general age of completion of major volcanic growth are, from southeast to northwest: (2) north Hawaii, 0.4 Ma; (3) east Maui and Kahoolawe, 0.8 Ma; (4) Molokai, Lanai, and west Maui, 1 Ma; (5) Oahu, 2.5 Ma and (6) Kauai and Niihau, 5 Ma. The slope-depth plot of each of these segments is compared to that of segment 1 so that departures from the assumed original volcanic condition can be evaluated (fig. 3.4). These departures apparently result from subsidence of the volcanoes and from erosional degradation.

The most extreme slope change of all the segments occurs in segment 1 near sea level and results from the subaerial-subaqueous lava transition. The average slope changes from about 4° at 200 m above sea level to 13° at 500 m below sea level. A similar abrupt change can be recognized in the other segments, although it is generally deeper and less distinct. The center of the slope change in segment 2 is 1.3 km below sea level; in 3, 2.1 km; in 4, 1.3 km; in 5, 1.3 km; and in 6, 1.0 km. These variations of the depth of the slope change from that in segment 1 are believed to be a measure of volcano subsidence since extension of the shoreline during a major period of volcano growth. Many of the areas of slope change are less distinct than that of segment 1. This results from the fact that the averaging technique includes different shorelines of different ages and

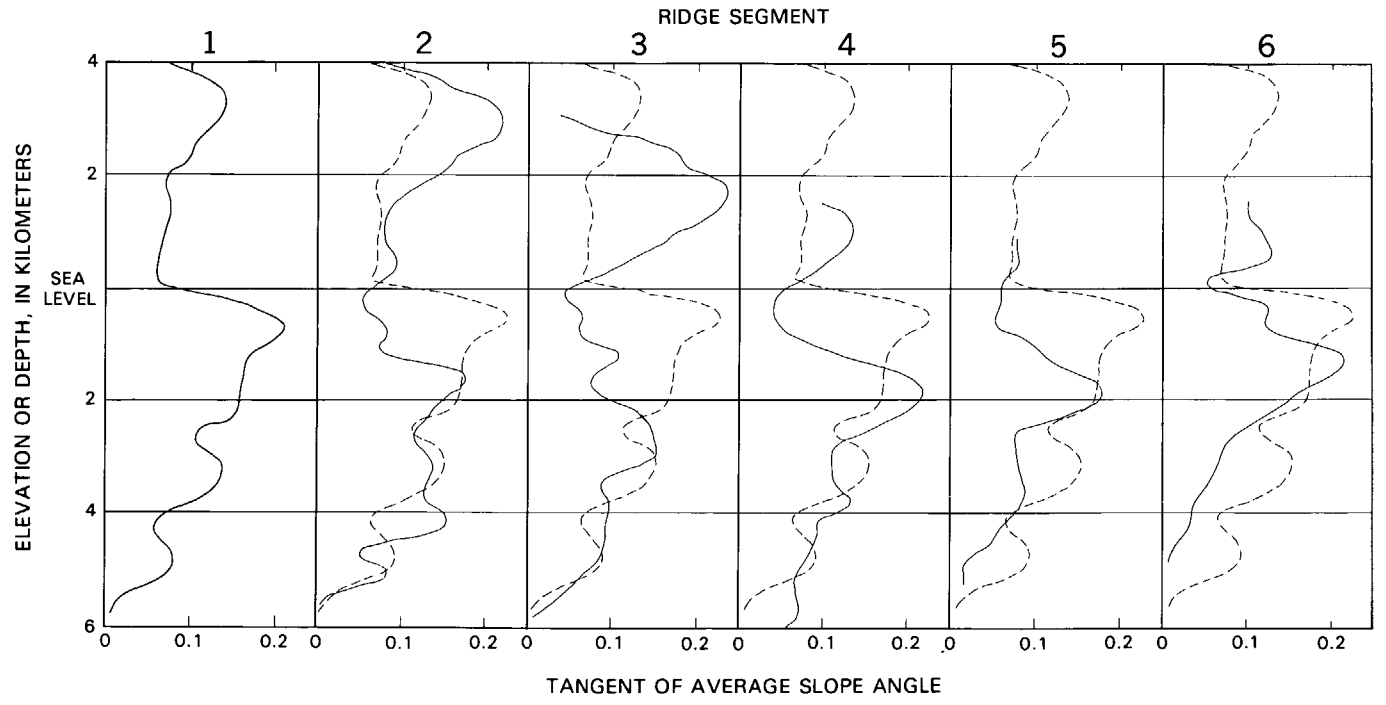

FIGURE 3.4.—Smoothed profiles of area-averaged slope against elevation for six segments of the Hawaiian Ridge (see figure 3.1). The trend of segment 1 (south Hawaii) is repeated as dashed line on the other five plots.

the same shoreline which has been warped and has subsided different amounts (Moore, chapter 2).

A marked smoothing of the lower submarine flanks of the volcanoes appears to proceed with age. On segment 1 the slope below the subaerial-subaqueous transition undergoes a general decrease with depth, which is interrupted twice by changes toward steeper slopes which are the bulges previously described. The first slope change increases the average slope 2.3° and the second about 1.7°. On segment 2 the slope decrease is interrupted 3 times by slope increases of 1.3°, 1.7°, and 2°. Segment 4 shows three zones of slope increase of 1.3°, 0.2°, and 0.4°. Segment 5 has only one, of 0.6°, and segment 6 has no zones of increase in slope below the transition zone.

Smoothing of the lower flanks is, moreover, accompanied by a general reduction of slope, so that all the zones of steep slope seem to have been removed (see segment 6 area on figures 3.3 and 3.4). The arcuate zones of steep slopes on the mid-depth submarine slopes of the younger volcanoes are missing on the older ones. Some form of mass wasting, requiring several million years to be effective, seems to smooth and flatten the lower slopes of these giant volcanoes.

REFERENCES CITED

Dynamic Graphics, Inc., 1978, User manual for the surface gridding library: 129 p.

Moore, J.G., 1964, Giant submarine landslides on the Hawaiian Ridge: U.S. Geological Survey Professional Paper 501–D, p. D95–D98.

Moore, J.G., and Fiske, R.S., 1969, Volcanic substructure inferred from dredge samples and ocean-bottom photographs, Hawaii: Geological Society of America Bulletin, v. 80, p. 1191–1202.

Normark, W.R., Lipman, P.W., and Moore, J.G., 1979, Regional slump structures on the west flank of Mauna Loa Volcano, Hawaii: [abs.]: Hawaii Symposium on Intraplate Volcanism and Submarine Volcanism, Hilo, Hawaii, July 16–22, 1979, Abstracts with Program, p. 72.

Velleman, P.G., and Hoagun, D.C., 1981, Applications, basics, and computing of exploratory data analysis: Boston, Mass., Duxbury Press, 354 p.

SUBMARINE TOPOGRAPHY AROUND THE HAWAIIAN ISLANDS

By Daniel J. Fornari[1] *and* J. Frisbee Campbell[2]

ABSTRACT

The submarine topography around the Hawaiian Islands reflects the time-integrated effects of volcanism, Pacific-plate tectonic fabric, island subsidence, sedimentation, gravitational collapse of unbuttressed volcano sides, and low-relief debris flows that transport shallow-water carbonate and volcanogenic sediment to greater depths on the submarine slope. First-order topographic relief around the islands is created by the submarine extensions of volcanic rift zones. The height above the surrounding abyssal sea floor and the topographic roughness of these rifts are inversely proportional to the age of the adjacent volcano. Second-order sea-floor relief around Hawaii is typified by Cretaceous seamounts that lie west of Hawaii and a few young volcanoes, including Loihi Seamount, direcly south of Hawaii. In addition to these obvious volcanic seamounts, a group of flat-topped mounts and small cones (Oahu Seamounts) extends to the northeast from the Island of Oahu. More subtle relief on the slumping of large sections of unbuttressed volcano flanks. These slumps form prominent steps on the otherwise regular, steep submarine slopes. Relief created by localized debris flows of surficial sediment and carbonate/volcanic rubble is usually less than 50 m; however, this process appears to be active on all Hawaiian submarine slopes investigated with Sea MARC II side-scan sonar and may be the principal agent for downslope sediment transport. Finally, reef development on the shallow parts of older, subsided volcanic foundations forms wide, low-gradient platforms that have karst-like microtopography.

INTRODUCTION

The strategic location of the Hawaiian Islands for oceanic exploration and the commerce that followed has resulted in the study of their natural history and geologic evolution since the 1700's. They have been a focus of marine research for the past 50 years, and much literature has been devoted to various aspects of Hawaiian marine geology and geophysics. The principal aim of this paper is to summarize the major topographic elements of the sea floor around Hawaii and to present new graphical and remote-sensing images of the sea floor around several of the islands. Only brief background information is offered, because much of the detailed information has already been discussed in the references we cite. In addition, other papers in this volume discuss specific topics that bear upon the development of the sea floor topography around the Hawaiian Islands. In particular, questions relating to island subsidence, carbonate-platform development, and submarine canyons are discussed in papers by Mark and Moore (chapter 3) and Moore (chapter 2). Data on Loihi Seamount is discussed by Malahoff (chapter 6), and the evolution of Hawaiian submarine rift zones is presented by Fornari (chapter 5).

ACKNOWLEDGMENTS

We thank the reviewers W. Dudley, R. Moberly, J.G. Moore, R. Pujalet, U. ten Brink, and A.B. Watts for their constructive comments. Paul White and Edwin Katibah of Dynamic Graphics Inc. were instrumental in providing the sea-floor graphics used to illustrate the paper. The management of Dynamic Graphics kindly provided all machine and personnel time needed to produce the images. M.A. Luckman expertly drafted and assisted in the preparation of all the figures. Support for Fornari was provided by the Office of Naval Research under contract number N00014-80-C-0098MM to the Lamont-Doherty Geological Observatory. Sea MARC II data in the Alenuihaha Channel were collected during the Hawaii Deep Water Cable Program, a project funded by the U.S. Department of Energy, grant number DE-AC01--82CE76214 to the Hawaiian Electric Company. Lamont-Doherty Geological Observatory Contribution No. 3841. Hawaii Institute of Geophysics Contribution No. 1592.

REGIONAL BATHYMETRY

The regional bathymetry around the Hawaiian Islands (fig. 4.1) has been mapped by numerous oceanographic institutions, the U.S. National Ocean Survey, and the U.S. Navy (see, for example, Chase and and others, 1971; Chase and others, 1980; Wilde and others, 1980, and references therein). The principal regional bathymetric features are the Hawaiian Deep and the Hawaiian Arch (fig. 4.2), which are topographic manifestations of lithospheric flexure, superimposed on the regional swell of the Hawaiian Ridge, that result from the load of the volcanic islands on the oceanic lithosphere (Betz and Hess, 1942; Dietz and Menard, 1953; Hamilton, 1957; Menard, 1964; Watts, 1976; Watts and others, 1985). The Molokai Fracture Zone (fig. 4.2) represents a diffuse zone of elongate troughs that reach depths below 5,000 m to

[1]Lamont-Doherty Geological Observatory of Columbia University, Palisades, New York 10964.
[2]Hawaii Institute of Geophysics, University of Hawaii, Honolulu, Hawaii 96822.

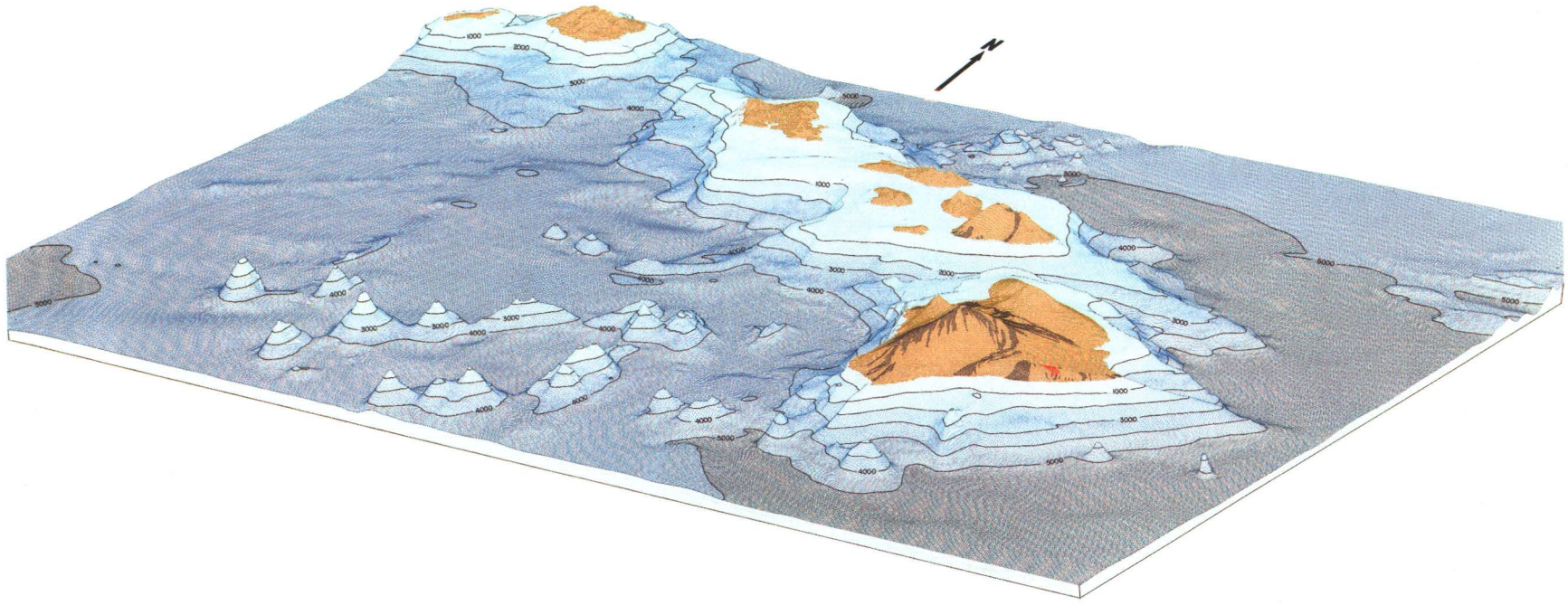

FIGURE 4.1.—Computer-drawn perspective model of the ocean floor around the Hawaiian Islands. Data base from Chase and others (1980) and Wilde and others (1980) and bathymetric charts of the U.S. National Ocean Survey (Nautical Chart Catalog No. 2, Panels, B, C, E). Bathymetric contour interval 1,000 m; grid spacings between nodal points (E.-W.) 1,667.18 m, and (N.-S.) 1,674.87 m. Subaerial contours from U.S. Geological Survey topographic map series. Black areas on land, historical lava flows (drawn from U.S. Geological Survey 1:100,000 series maps and Scientific Event Alert Network Bulletin, Smithsonian Institution, June 30, 1983). Red areas on land, 1983 lava flows from the east rift zone of Kilauea. Green areas, older slopes of inactive volcanoes. See figure 4.2 for geographic names. Vertical exaggeration × 5. Provided by Dynamic Graphics Inc., Berkeley, Calif.

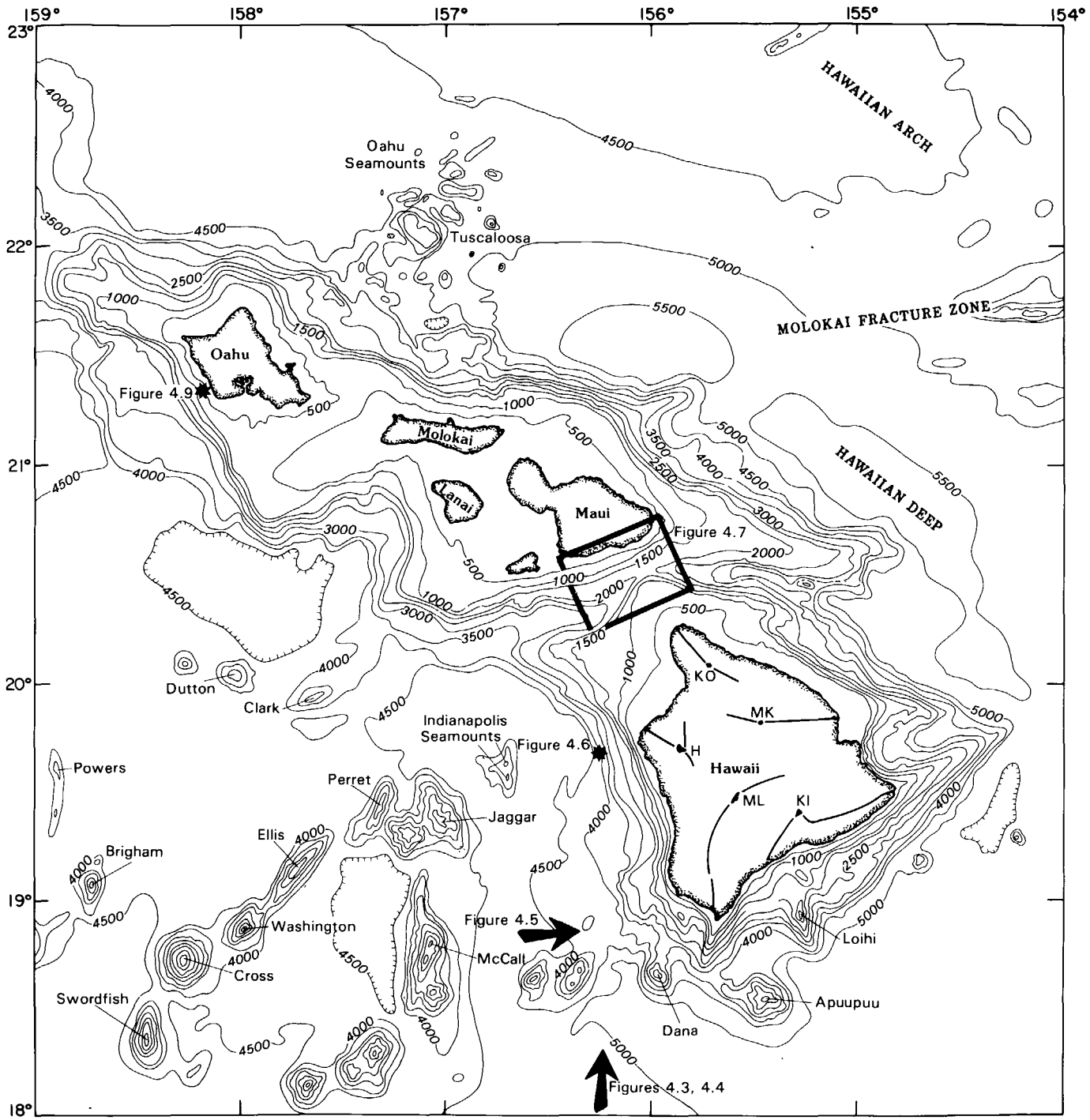

FIGURE 4.2.—Bathymetry around the principal Hawaiian Islands. Contour interval 500 m, simplified from Wilde and others (1980). Sites, viewing directions, and areas covered in some other figures are also indicated. Volcanoes on the Island of Hawaii: KO, Kohala; MK, Mauna Kea; H, Hualalai; ML, Mauna Loa; KI, Kilauea.

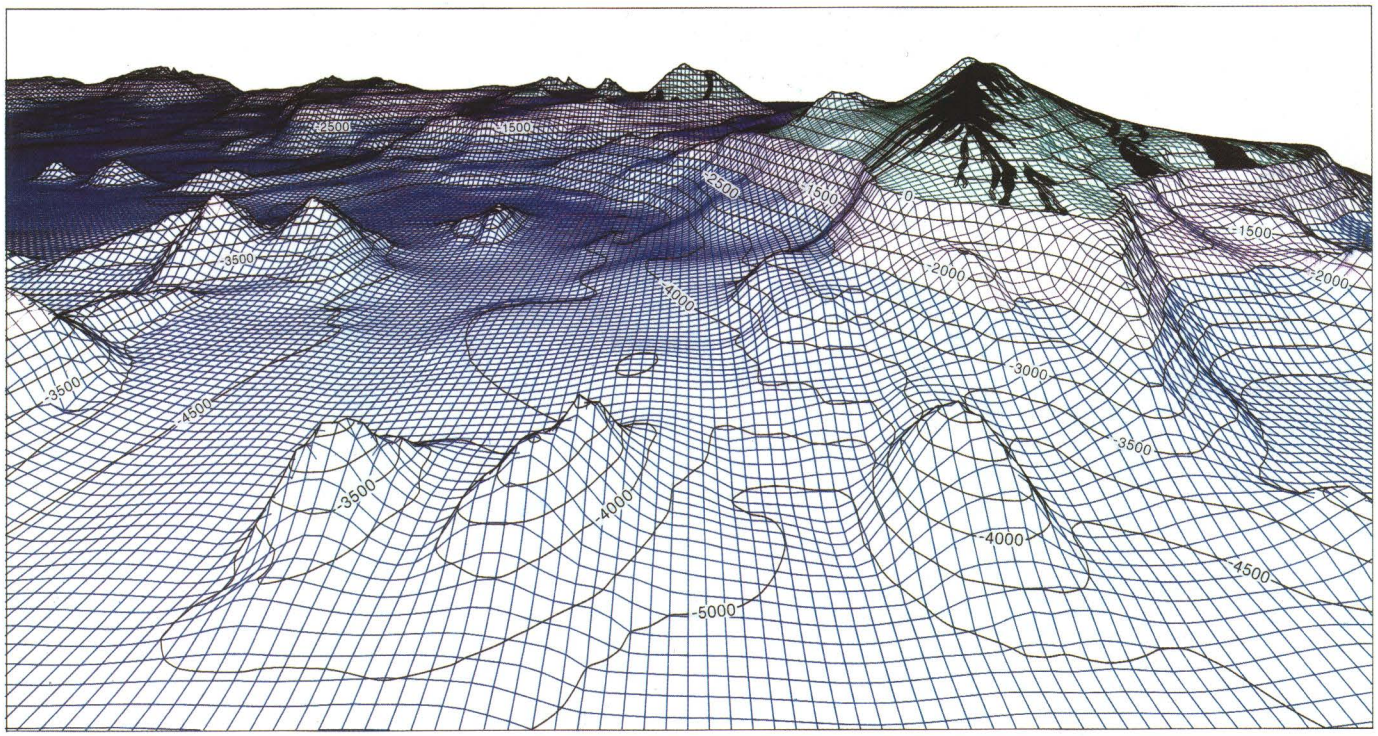

FIGURE 4.3.—Computer-drawn perspective model of the sea floor on western flank of Hawaiian Ridge from Hawaii to Oahu, looking approximately north. Contour interval 500 m. View point and direction marked on figure 4.2. Elevation of view point is 5,285 m above sea level. Data base is same as for figure 4.1. Vertical exaggeration ×5. Provided by Dynamic Graphics Inc., Berkeley, Calif.

the east of the Hawaiian Arch. The fracture zone topography narrows considerably within the arch and is likely to be responsible for the lineated contour pattern, trending west-northwest, found on the carbonate platform east of Molokai. Indeed, the principal trends of the subaerial and submarine rift zones of the East and West Molokai Volcanoes are subparallel to the fracture-zone trend and are likely to have been partly controlled by it (Furumoto and Woollard, 1965; Strange and others, 1965; Moberly and McCoy, 1966; Malahoff and Woollard, 1968).

DETAILED SEA-FLOOR TOPOGRAPHY, HAWAII TO OAHU

A computer-drawn perspective model of the sea floor around the southern Hawaiian Islands (produced by Dynamic Graphics Inc., of Berkeley, California) is shown in figure 4.1. The data base used to generate this figure is from Chase and others (1980), Wilde and others (1980), and bathymetric charts of the U.S. National Ocean Survey. The bathymetric data were gridded, digitized as a set of 43,000 x, y, and z coordinates, and then used to calculate a surface model of least tension in the form of a rectangular grid. The grid model contains 480,000 grid points (800 × 600) and was calculated by the Surface Gridding Library program of DGI. The bathymetric map in figure 4.2 shows the plan-view contours of most of the area of figure 4.1 and serves to locate the islands and seamounts, the starting points and azimuths of the perspective views shown in figures 4.3–4.5, and the location of other figure areas.

Three principal topographic elements are present on the sea floor shown in figure 4.1. They are (1) the submarine extensions of subaerial volcanic rift zones; (2) old and young seamounts; and (3) carbonate platforms. In addition to these major topographic features, there are several subtle steps in the western submarine slope of Hawaii (see figs. 4.3-4.5) that we interpret to be large-scale gravitational slumps of parts of Mauna Loa and Hualalai Volcanoes. One of these features is the already recognized Alika slide of Normark and others (1979).

SUBMARINE RIFT ZONES

Each principal island within the Hawaiian chain is composed of several volcanoes; consequently, the submarine flanks of each island are dominated by rift-zone ridges that may have as much as 3,000 m of relief above the surrounding abyssal sea floor. These submarine ridges are oriented in three principal directions: east to northeast, south-southwest, and northwest. A detailed discussion of the submarine topography and structure of the submarine rifts of Hawaii is presented in Fornari (chapter 5). In general, however, the total relief and topographic roughness of Hawaiian submarine rifts is

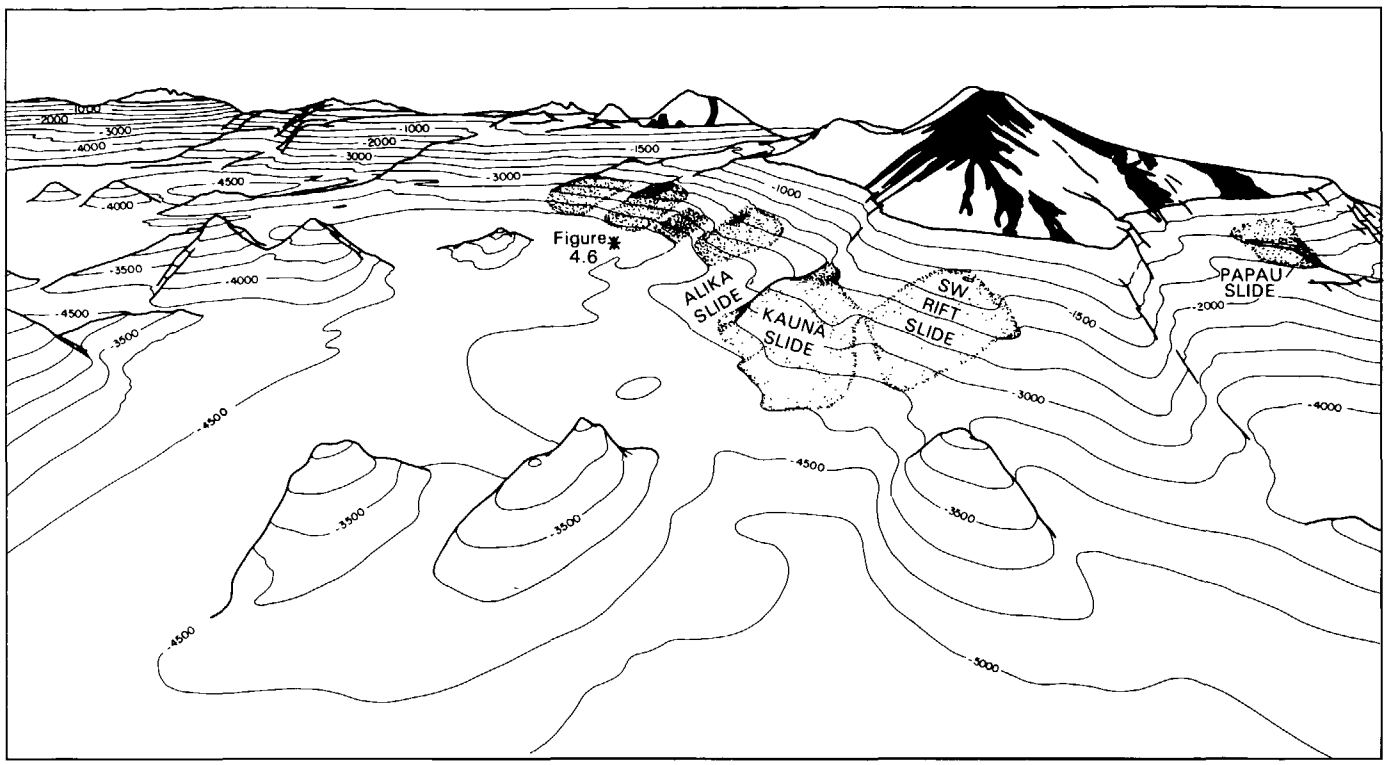

FIGURE 4.4.—Interpretative sketch of view seen in figure 4.3 showing positions of large gravitational slide blocks on the west flank of Island of Hawaii. Contour interval 500 m.

greatest next to the most active volcanic centers. The prominent asymmetry in the across-strike profiles of some of these submarine ridges can be directly attributed to the mobility of ridge flanks that are not buttressed by an adjacent volcano (Fornari, chapter 5; Stearns and Macdonald, 1946; Fiske and Kinoshita, 1969; Fiske and Jackson, 1972; Koyanagi and others, 1972; Swanson and others, 1976; Lockwood, 1979; Lipman, 1980).

The nearshore morphology of the submarine rifts changes as the islands subside (figs. 4.1, 4.2; Moore, chapter 2; Moore, 1970; Moore and Fornari, 1984). The shape and development of the carbonate platform that surrounds and lies between the Islands of Maui and Oahu have been largely controlled by the rift topography of East and West Molokai Volcanoes, as well as that of Waianae, Koolau and Penguin Banks(?) Volcanoes, parts of which now lie buried beneath a carbonate and sediment cover (Gregory and Kroenke, 1982). Off northwestern Hawaii, the northwest rift zone of Hualalai forms the southern boundary of the Kohala terrace, the wide platform that extends northwestward between Hualalai and Kohala Volcanoes. Flows ponded between Hualalai's rift and Kohala's northern rift zone created a broad, buttressed volcanic foundation that gradually subsided but was not subject to large-scale gravitational slumping; hence this was an ideal environment for reef buildup and platform development (Campbell and Erlandson, 1979, 1981; Campbell, 1984). For a further discussion of the subsidence history of the Hawaiian Islands and the development of carbonate platforms and reef terraces the reader is referred to Moore (chapter 2).

SEAMOUNTS

Important second-order topography around the Hawaiian Islands that is created by seamounts is also depicted in figures 4.1 and 4.2. Most of the seamounts that lie west of Hawaii are older features (see, for example, Moore, 1965; Francheteau and others, 1970), generally considered to be approximately Cretaceous in age, that were probably created at or near a ridge axis. The alignment of the main cluster of seamounts is generally northeast-southwest; however, two separate lineaments appear to meet at Perret and Jagger Seamounts to form a V shape pointing northeast. This V shape and the curious butterfly-like shape of Perret-Jagger Seamounts (fig. 4.2) imply a possible tectonic control on volcanism (the lineation is oblique to the trend of the Molokai Fracture Zone). These seamounts have not been studied in great detail, however, and their precise origin and volcanic history are unknown.

A few seamounts south of Hawaii (Dana and Apuupuu) may be genetically related to Hawaiian volcanism. Loihi Seamount, located 35 km south of Kilauea's south flank, is clearly a Hawaiian volcano and has been the subject of several deep-sea camera, dredging, and bathymetric surveys, and earthquake studies (Malahoff, chapter 6; Moore and others, 1979; Malahoff and others,

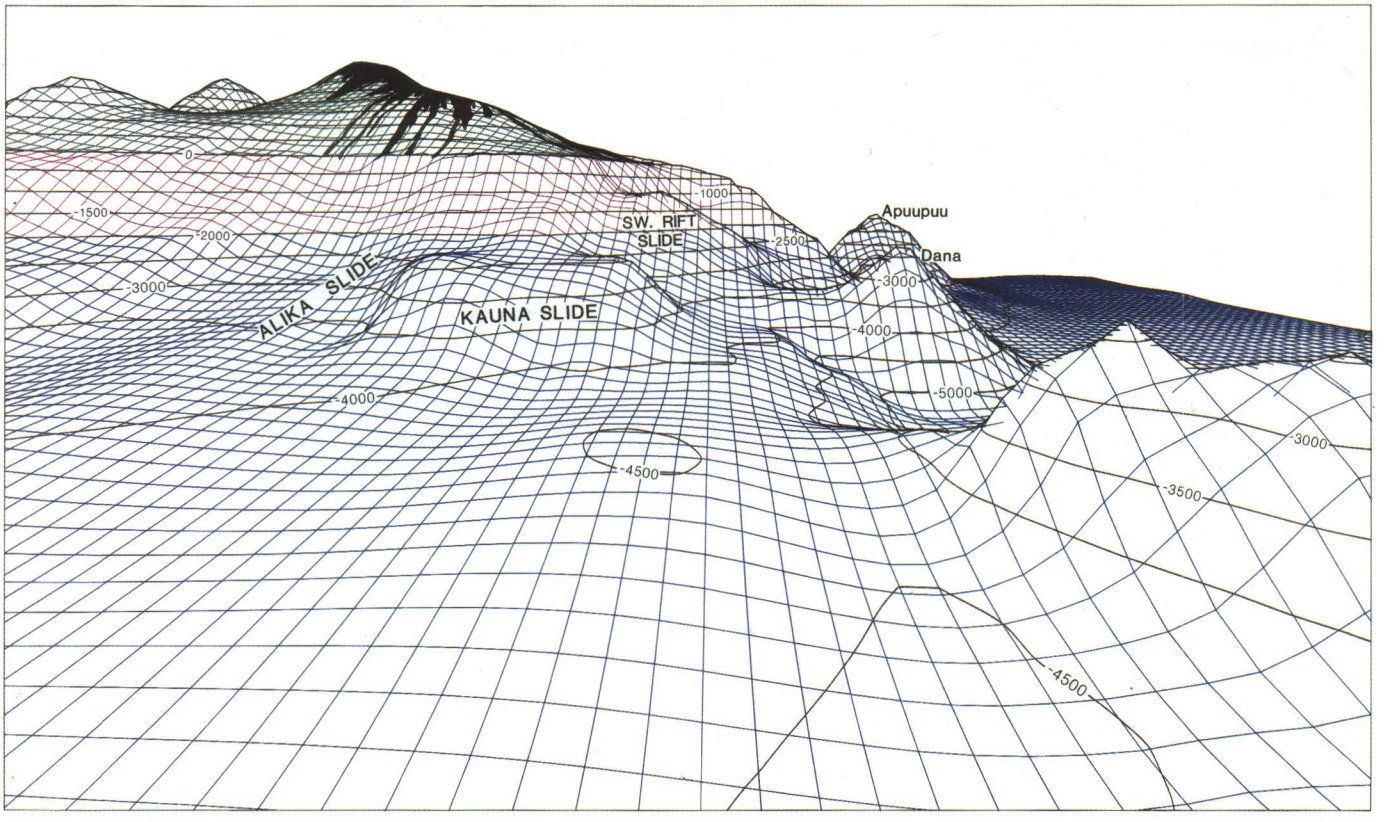

FIGURE 4.5.—Computer-drawn model of sea floor off southwestern part of Island of Hawaii, showing prominent step and bulge in the slope created by the Kauna slide. Alika slide of Normark and others (1979) is low, broad bulge to north of Kauna block. Contour interval 500 m. View point of perspective located 1,162 m below sea level; it and direction of view marked on figure 4.2. Apuupuu Seamount in background. Loihi Seamount hidden behind ridge created by submarine continuation of Mauna Loa's southwest rift zone. Vertical exaggeration ×5. Provided by Dynamic Graphics Inc., Berkeley, Calif.

1982; Moore and others, 1982; Klein, 1982). This submarine volcano rises 4,000 m above the surrounding abyssal floor and its topography is dominated by an elongate rift-zone ridge that extends to the south from summit pit craters. The diverse suite of alkalic to tholeiitic pillow basalts recovered from Loihi has led to new perspectives on the classical so-called thoeliitic shield-building stage of Hawaiian volcanism, and the chemistry of mafic inclusions recovered in the dredge hauls promises to further refine models of Hawaiian petrogenesis and volcanic history (Moore and others, 1982; Staudigel and others, 1984). Detailed U.S. Navy SASS multibeam bathymetry and ANGUS camera tows over Loihi (Malahoff, chapter 6; Malahoff and others, 1982) reveal that most constructional volcanism is restricted to the summit pit craters and shallower parts of the southern and northern rift zones, whereas most of the flanks are covered by clastic volcanic rocks and hemipelagic sediment. These data suggest that Hawaiian volcanoes develop submarine rift zones and shallow-level magma reservoirs early in their development. Additionally, the north-south elongation of Loihi appears to be partially controlled by the presence of Mauna Loa's southwest rift zone to the west. This physiography agrees with the predictions made by Fiske and Jackson (1972) regarding volcano shape and rift zone orientation and the genetic dependence of these two parameters on the locations of preexisting edifices.

A group of flat-topped seamounts of more problematic origin is located northeast of Oahu (Oahu seamounts, see figs. 4.1, 4.2). After analyzing bathymetric charts of this area, Moore (1964) suggested that these topographic highs are landslide blocks created by large slumps that affected the northeastern slope of Oahu and, to a lesser extent, the northern slope of Molokai. A close inspection of the sea-floor topography in figure 4.1 and the contours in figure 4.2 shows two prominent tongue-like features at the base of the northeast slopes of Oahu and Molokai. One feature extends northeast from Oahu at depths between 2,000 m and 4,000 m, and the other extends north from Molokai at depths between 3,000 m and 4,000 m. At the head of each tongue is an amphitheater-like reentrant in the regional slope contours (fig. 4.2). These bathymetric features could represent large gravitational slides that have affected the unbuttressed parts of volcanoes on each island. This area has been resurveyed using sparker and air-gun reflection profiling equipment (Andrews and Bainbridge, 1972) and more recently with multichannel seismic reflection methods (A.B. Watts, oral commun., 1985). Andrews and Bainbridge (1972) concluded that the lobate

structures at the base of Oahu's northeast slope resulted from transport of detrital sediment by turbidity currents that were channelled down submarine canyons and deposited their load over preexisting basement highs.

We agree with Moore (1964) that these basement highs could be large slump blocks. The prominent disruption of bathymetric contour trends along the northeast coast of Oahu and north coast of Molokai indicates that these island flanks have probably been subjected to gravitational mass-wasting processes and that surficial sediment has been transported downslope by rubble slides and turbidity currents (Mathewson, 1970; Andrews and Bainbridge, 1972).

The origin of the seamounts that extend seaward from the edges of these probable slump blocks is, however, quite different. Available bathymetric data indicate that several of the smaller topographic highs form well-developed closed-contour peaks similar to many small volcanic seamounts that dot the Pacific Basin. The larger features seem to have been formed by two volcanoes coalescing together to form a crude figure 8 or bow-tie shape. The prominent flat top of Tuscaloosa Seamount, the principal topographic high in the group, is rather large but not unusually so in the context of Pacific guyots (see, for example, Menard, 1984; Vogt and Smoot, 1984). In addition, Andrews and Bainbridge (1972) determined that the topographic highs in the Oahu Seamount group have controlled sediment deposition around the seamounts and that the sedimentary layers seen on seismic reflection records are not distorted or chaotic, as would be expected if they had been emplaced by slumping or sliding. Unpublished multichannel seismic records from north and east of Oahu (A.B. Watts, oral commun., 1985) do not show any evidence of lystric or other faults between the seamounts or of distortion of sedimentary layers. In addition, the large distance between Tuscaloosa Seamount and the Oahu shelf (approx. 85 km) decreases, in our opinion, the probability that such large volumes of material could be transported across the slope.

Whereas the topography at the southwest end of the Oahu seamounts is likely to have been created by large landslides, we suggest (along with Andrews and Bainbridge, 1972) that the isolated topographic highs in the central and northeastern part of the group are older (Cretaceous?), partially buried volcanic edifices and that some may be guyots. These seamounts are not aligned along any known rift zone that extends from Oahu. In fact, the trend of the group is perpendicular to the strike of the Koolau volcanic range. The Oahu seamounts have summit depths and shapes that are similar to those of seamounts in the Musicians Seamount group, located north of Oahu (Rea and Naugler, 1970).

GRAVITATIONAL SLUMP BLOCKS

A model produced by DGI of the west flank of the Hawaiian Ridge is shown in figure 4.3. The starting viewpoint and azimuth of the perspective shown in figure 4.3 are marked on figure 4.2. The most interesting features displayed by this bathymetric compilation are the pronounced steps in the morphology of the basal slope of the ridge. These prominent steps in the otherwise steep slopes of the Hawaiian Ridge are likely to reflect large-scale gravitational slumping of parts of the volcanoes that have not been buttressed during their growth and development. A line drawing of the model shown in figure 4.3 appears as figure 4.4 on which the most obvious slump blocks have been shaded. It is apparent from these graphical representations of bathymetry that the tops of most slide blocks lie at depths of 2,000–2,500 m. The exception is the southwest-rift slide (fig. 4.3), which is much shallower (1,000–1,500 m) and is probably the youngest feature of this kind on the western flank of Hawaii. The shallower depth of the southwest-rift slide is likely to result from its position near the submarine extension of Mauna Loa's southwest rift zone and the short time over which it could have subsided since its formation. The coincidence in top depths of most of the slide blocks shown in figure 4.4 may be a function of the integrated effects of volcano growth, island subsidence, and oversteepening of the flanks to a critical point after which they are gravitationally unstable.

The Alika slide (Normark and others, 1979) is the best studied slump in this area; it shows up on figures 4.3–4.5 as a broad, low bulge in the lower southwest flank of Hawaii. This feature covers a depth range between 2,000 m and the base of the island slope at 4,000 m. Normark and others (1979) have mapped the entire area of the slide using airgun, 3.5-kHz echo-sounder, and gravity measurements and found that it is approximately 200 m thick at the toe and covers an area 20–25 km wide and nearly 80 km long.

The Kauna slide is a more prominent bulge to the south of the Alika slide and has nearly 2,000 m of relief from the top of the step to the foot of the block (figs. 4.3–4.5). Emplacement of the Kauna block most likely predated the movement of the Alika slide, because it appears to have channelled the Alika flow along its northern margin.

A similar but much less prominent step is present on the central south flank of Hawaii, between 2,500-m and 3,000-m depth (figs. 4.1, 4.2; see also, Moore, chapter 2), southeast of the Papau slide (Fornari and others, 1979b). On the southwest side of Oahu (figs. 4.1, 4.2), a prominent break in the slope at 2,500-m depth is likely to represent the top of a major slump block or group of blocks that developed on the unbuttressed southwest flank of the Waianae Range. Alternatively this feature may be the top of an older volcano that is now partially buried by the Waianae Range.

The development of these large slump-block features on the flanks of Hawaiian volcanoes suggests that gravitational failure of the slopes is an important process that alters the original constructional slopes of volcanoes during the early and mature shield-building stages. This process restabilizes the edifice, widening its base, and creates prominent steps in the steep submarine slopes. It is not known if the gravitational failures take place principally subaqueously or subaerially, nor whether the relief created by these features represents the aggregate of many episodes of slumping and mass-wasting or only a few events of enormous proportions.

A possible answer to these questions may be found through the study of the Hilina fault system, a series of subparallel and echelon faults that trend northeast on the south flank of Kilauea Volcano. Swanson and others (1976) and Tilling and others (1976) have demonstrated that the Hilina faults result from gravitational slumping

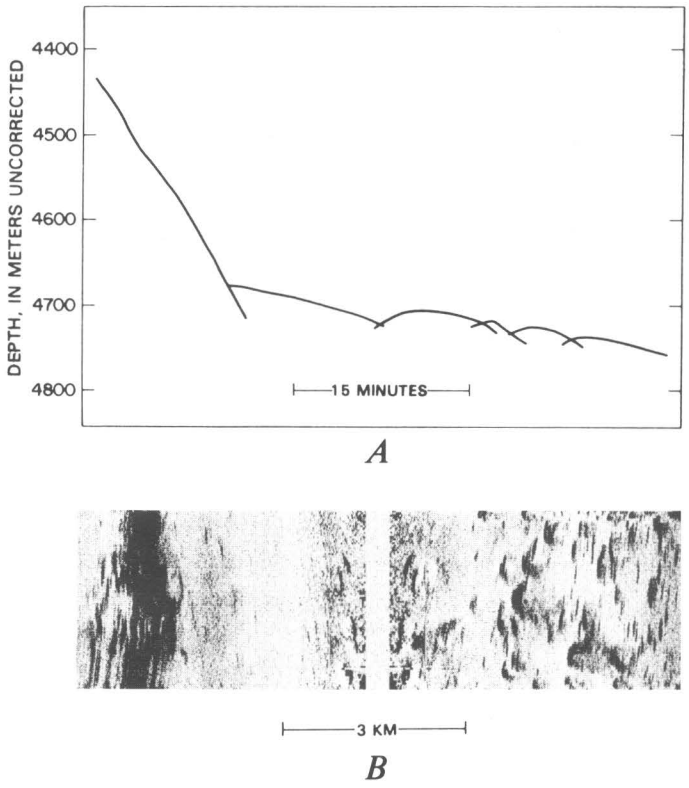

FIGURE 4.6.—Character of sea bottom off west coast of Island of Hawaii. ***A***, Tracing of 3.5-kHz echo-sounding profile (see figures 4.2 and 4.4 for location). Steep slope at left is base of Hualalai Volcano. Just seaward of slope is smooth sediment pond that appears to cover large blocks, represented by hyperbolic echos, that appear farther offshore. Horizontal scale is time; ship was moving at approximately 10 knots. ***B***, Sea MARC II side-scan sonar record of approximate area shown in *A*. Steep slope is represented by strong reflection at left of image, the large blocks as discrete reflections to right.

of the south flank of Kilauea. The slumping is induced by injection of magma into the east rift zone, thereby dilating the rift and forcing it to expand southward, in the direction it is not buttressed. These faults are a part of the initial stage of synconstructional edifice modification; they are known to continue out onto the submarine slope and have probably localized subsequent gravitational failures along their fault planes. The total relief created by the Hilina fault system is approximately 600 m, and the relief on a few individual scarps is as high as 300–450 m (Macdonald and others, 1983). The faults of the Hilina system may be viewed as modern-day analogs of faults (and fault systems) that now lie buried on the west flank of the Island of Hawaii whose cumulative activity and relief have created the large-scale gravitational slumps mapped on figures 4.3–4.5. Smaller scale features such as the Alika slide and Papau slide are likely to represent individual slide events in an area prone to gravitational collapse.

The development of prominent steps on the basal flanks of many of the Hawaiian Islands (and probably other volcanic oceanic islands) is controlled by the distribution of buttressing rift zones and gravitational mass-wasting of unbuttressed volcano sides. Clearly, large-scale gravitational mass-wasting of volcano flanks is responsible for the development of subtle but nonetheless important bathymetric features around Hawaii and probably around other oceanic volcanic islands as well (for example, Reunion Island, Duffield and others, 1982; Dallas Jackson, written commun., 1985).

LOW-RELIEF SUBMARINE RUBBLE AND DEBRIS FLOWS

The large-scale topographic features of the sea floor around Hawaii that are discussed above are easily resolved with standard bathymetric sonar tools. The investigation of smaller relief features and the microtopography of the sea floor has necessitated the development and use of sophisticated side-looking sonar systems that measure the acoustic reflectivity of the sea floor. The most successful system of this kind is the Sea MARC system, developed by International Submarine Technology of Redmond, Washington.

The Sea MARC II system, operated by the Hawaii Institute of Geophysics of the University of Hawaii, has been used in several surveys of the submarine flanks of Hawaiian volcanoes (Blackinton and others, 1983; Campbell, 1983; Campbell and Hussong, 1983; Fornari, 1984; Niedoroda and others, 1985). The technical details of the system have been described by Kosalos and others (1982) and Blackinton and others (1983). This system operates at 12 kHz, can insonify a swath of sea floor as large as 10 km wide, and can resolve linear sea floor topopgraphic features as small as 5–10 m high and several tens of meters long at survey speeds as great as 8 knots. Lateral changes in sea-floor reflectivity can be mapped and correlated to possible structural, morphologic, and sedimentologic facies.

An example of the use of the Sea MARC II system is presented in figure 4.6, which shows a 5-km-wide swath of sea floor in the Hawaiian Deep, west of Keahole Point on the Island of Hawaii. The Sea MARC II data show blocks as large as one kilometer in length and several tens of meters high that appear to be randomly scattered on the bottom. A dive made near this location by the Navy submersible *Trieste* found blocks reported to be the size of houses scattered on the bottom. These blocks are likely to be the deposits that were generated by one of the large gravitational slides located along this unbuttressed part of Hualalai Volcano.

Another principal result of the Sea MARC II surveys around the Hawaiian Islands has been the recognition of extensive rubble and debris flows and their deposits on the steep submarine flanks of the volcanoes. A mosaic of Sea MARC II side-scan sonar images (fig. 4.7) shows part of the Alenuihaha Channel and the deep channel that separates the Island of Maui from Hawaii, and an interpretative geologic sketch map of the principal features of this sonar mosaic is shown in figure 4.8.

Three major bathymetric features are present in the area shown in figure 4.8. These are the Kohala terrace, the northern slope of Kohala Volcano, and the southern slope of Haleakala Volcano on Maui. As can be seen on figure 4.7, nearly the entire submarine slope of Haleakala is covered by sinuous and branching patterns of high reflectivity, separated by linear acoustic shadows, which we have interpreted as being debris flow-lobes and channels. In several

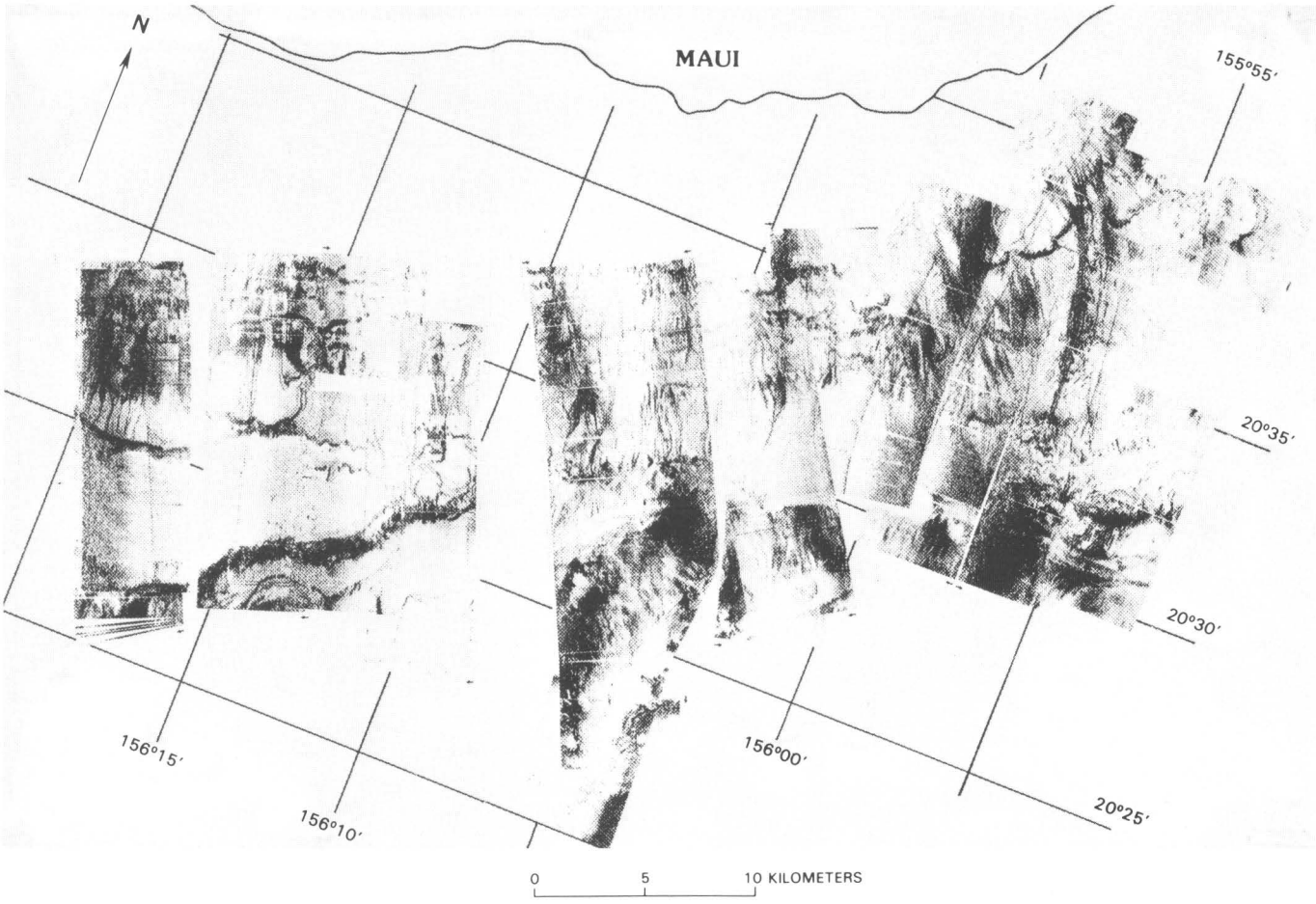

FIGURE 4.7.—Sea MARC II side-scan sonar image of the Alenuihaha Channel to south of Island of Maui. Dark areas on records are reflections from either hard, reverberant sea floor (such as volcanic rock or pavements with little sediment cover), or from linear relief that rises above surrounding sea floor. Light areas are acoustically less reflective and represent sediment-covered bottom or sea floor in complete or partial acoustic shadow (varied shades of gray). See figure 4.8 for interpretative map and Campbell (1983) for detailed description of this sea-floor area.

cases one can see that debris flows have been channelled by cuts and reentrants in flow fronts or scarps that trend across the slope. These flow fronts or scarps create strong reflections on the sonar images, implying that they have vertical or near-vertical faces. The total relief of these features may be as much as 100–200 m; the relief on individual flow fronts or scarps, however, is likely to be on the order of a few tens of meters, given the width of the returned signal and the difficulty in resolving these narrow features by conventional echo sounding. In comparison, the Sea MARC II image of the northern submarine flank of Kohala consists principally of strong returns suggestive of volcanic sea floor (Campbell, 1983), with very little dendritic fabric that could represent reflections from debris slides or channels. The northwestern edge of the Kohala terrace (Campbell and Erlandson, 1981; Campbell, 1984) has low reflectivity similar to the Alenuihaha Channel axis and other areas with gentle slopes that are covered with sediment. It is likely that the axis of the Alenuihaha Channel is largely filled with volcanic and coralline debris shed from Haleakala's southern slope. These sediments have been transported in fluvial erosional channels on land, in shallow submarine canyons on the upper slopes, and by debris flows and turbidity currents down the middle and lower submarine slopes (Campbell, 1983).

A Sea MARC II side-scan sonar mosaic of the sea floor off southwestern Oahu is shown in figure 4.9. There are several prominent morphological features in this area, including (1) the shelf-terrace area that lies between the shoreline and the top edge of the carbonate escarpment; (2) the continuous steep carbonate escarpment, which marks the western edge of a relict carbonate platform; (3) reflective ridge-and-gully terrain that lies seaward of the base of the escarpment; (4) highly reflective swaths of terrain that trend up and down the slope and are located seaward of the base of the escarpment; and (5) digitate lobes of alternating high- and low-reflectivity sea floor, located near the break in the slope between 1,500 m and 2,250 m at the downslope ends of the highly reflective

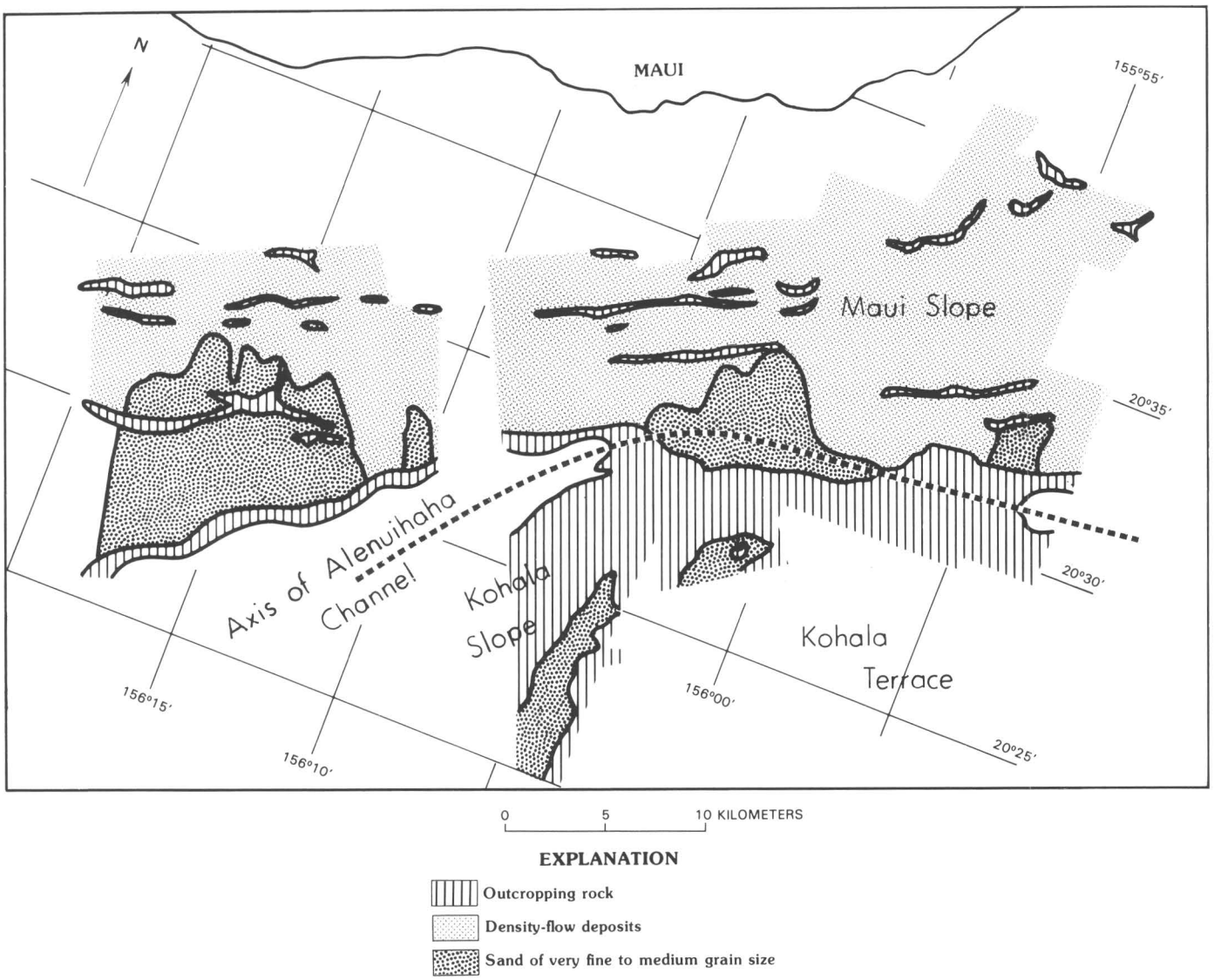

FIGURE 4.8.—Interpretative map of area of Sea MARC II images shown in figure 4.7. Note extensive linear, branching reflections and intervening acoustic shadows on south flank of Maui that we interpret as debris flows. Northern flank of Kohala Volcano forms a distinctly separate acoustic province. Samples, deep-sea photography, and Sea MARC II survey indicate that this submarine slope consists largely of outcropping volcanic flows and flow fronts with some volcanogenic and carbonate sediment on small terraces.

swaths, that are likely to represent localized landslide lobes (Fornari, 1983, 1984). The details of the sea-floor geology in this area have been studied with marine geophysical methods (Normark and others, 1982; Niedoroda and others, 1985) and with submersibles (Coles, 1982; Fornari, 1982, 1983, 1984).

The mosaic image in figure 4.9 and the interpretative maps in figures 4.10 and 4.11 provide an insight into the contemporary processes that act to shape the submarine shelf and slope areas on an older Hawaiian island such as Oahu. Also indicated on figure 4.10 are the telephone cable breaks that occurred during a hurricane on November 23, 1982. The reader is referred to Noda (1983), Fornari (1983), and Hollister (1984) for a detailed treatment of the cable-break data and the relation between cable breaks, sea-floor topography, and ocean-floor sediment dynamics.

Seaward of the base of the carbonate escarpment shown in figures 4.9 and 4.10 there are numerous zones of slightly higher reflectivity (fig. 4.10, unit C) that form crudely fan-shaped swaths of terrain interpreted to be more cobbly sea floor within the ridge-and-gully terrain identified on DSV *Turtle* dives (Fornari, 1982; 1983). These swaths of sea floor are characterized by linear patterns on the side-scan sonar records, and some swaths trend into the axes of the bathymetric reentrants typical along this southwestern coast of Oahu (Niedoroda and others, 1985). Seaward of these unit C acoustic reflectivity zones, swaths of terrain with much higher reflectivity (fig.

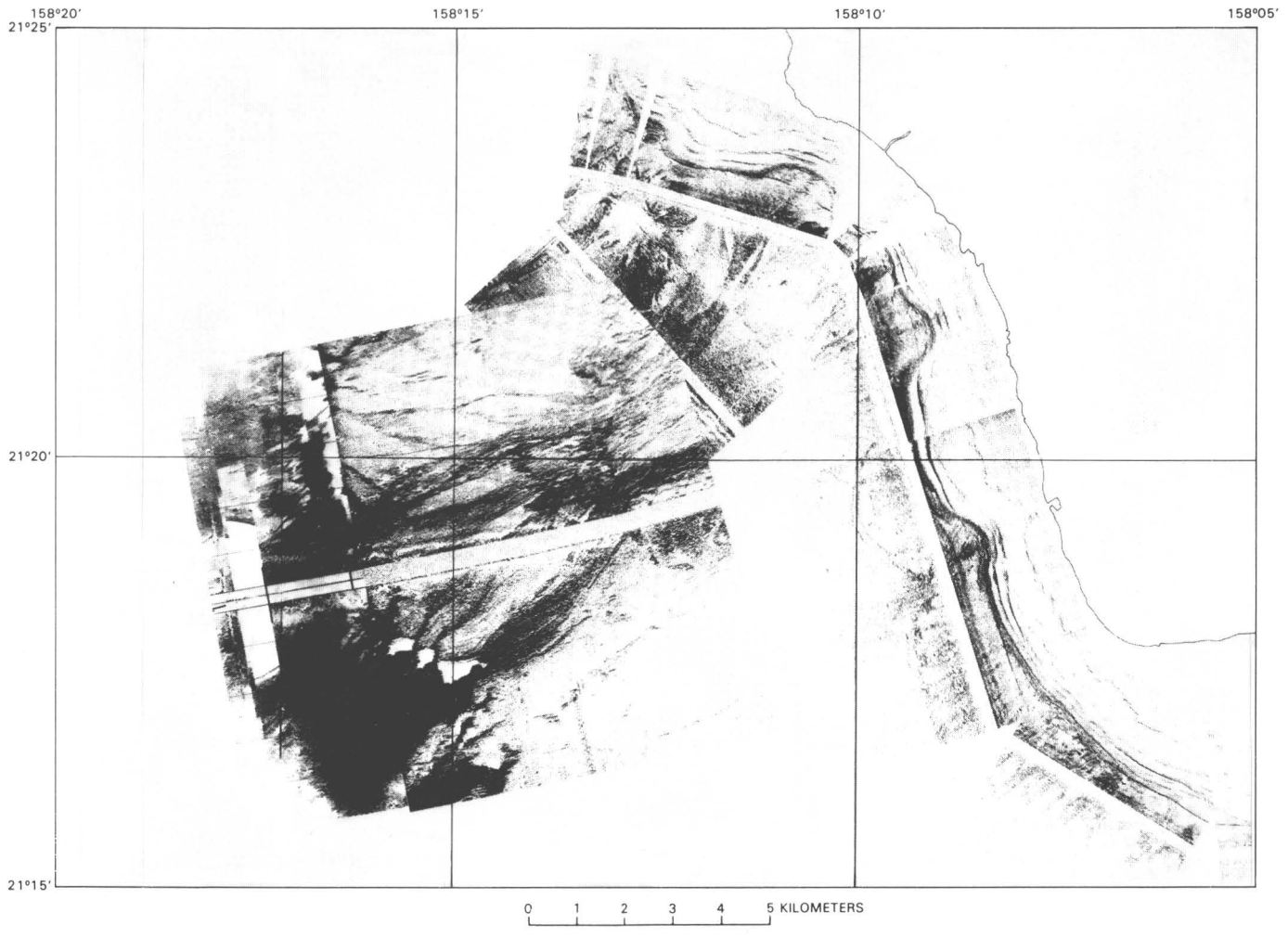

FIGURE 4.9.—Sea MARC II side-scan sonar image of the sea floor off Kahe Point, Oahu. See figure 4.10 for interpretation and Fornari (1984) for complete discussion of these data.

4.10, unit R) are likely to be areas of sea floor consisting of either gravelly or hard sediment (possibly indurated, cemented carbonate or manganese pavement). The acoustic contrast between the R and C zones is easily seen on figure 4.9, as is the higher reflectivity of these areas compared to the N zones (nonreflective). Near the southwestern edge of the sonar image in figure 4.9 there are several finger-like zones of sea floor characterized by narrow, alternating swaths of high and low reflectivity that create prominent acoustic shadows (figs. 4.9 and 4.10). These zones have been mapped by the symbol L on figure 4.10, and they appear to lie directly downslope from the R acoustic-facies zones.

A comparison between the Sea MARC II image in figure 4.7 and that in figure 4.9 points to the similarity in acoustic character of the sea-floor areas affected by low-relief rubble and debris flows. The importance of downslope transport of sediment by these processes on the flanks of Hawaiian volcanoes (Fornari and others, 1979b; Campbell, 1983; Campbell and Hussong, 1983) is suggested by the sinuous outline of the flow lobes and the delicate branching reflectors separated by intervening areas of low reflectivity that are likely to represent dendritic flow lobes and channels. Relief created by the debris flows is not great, usually on the order of a few tens of meters or less above the surrounding sea floor (Niedoroda and others, 1985). In most cases these features cannot be resolved with standard bathymetric echo sounding from the sea surface.

Thick wedges of clastic sediment, transported by debris flows and deposited on the submarine flanks of volcanoes, are important components of the gross stratigraphy of oceanic volcanoes and result from gravitational mass-wasting of large sections of unbuttressed volcano flanks and downslope movement of sediment in rubble and debris flows.

CARBONATE ESCARPMENTS

An interpretative sketch is shown in figure 4.12 of the stratigraphy viewed from the submersible *Makali'i* during several dives on

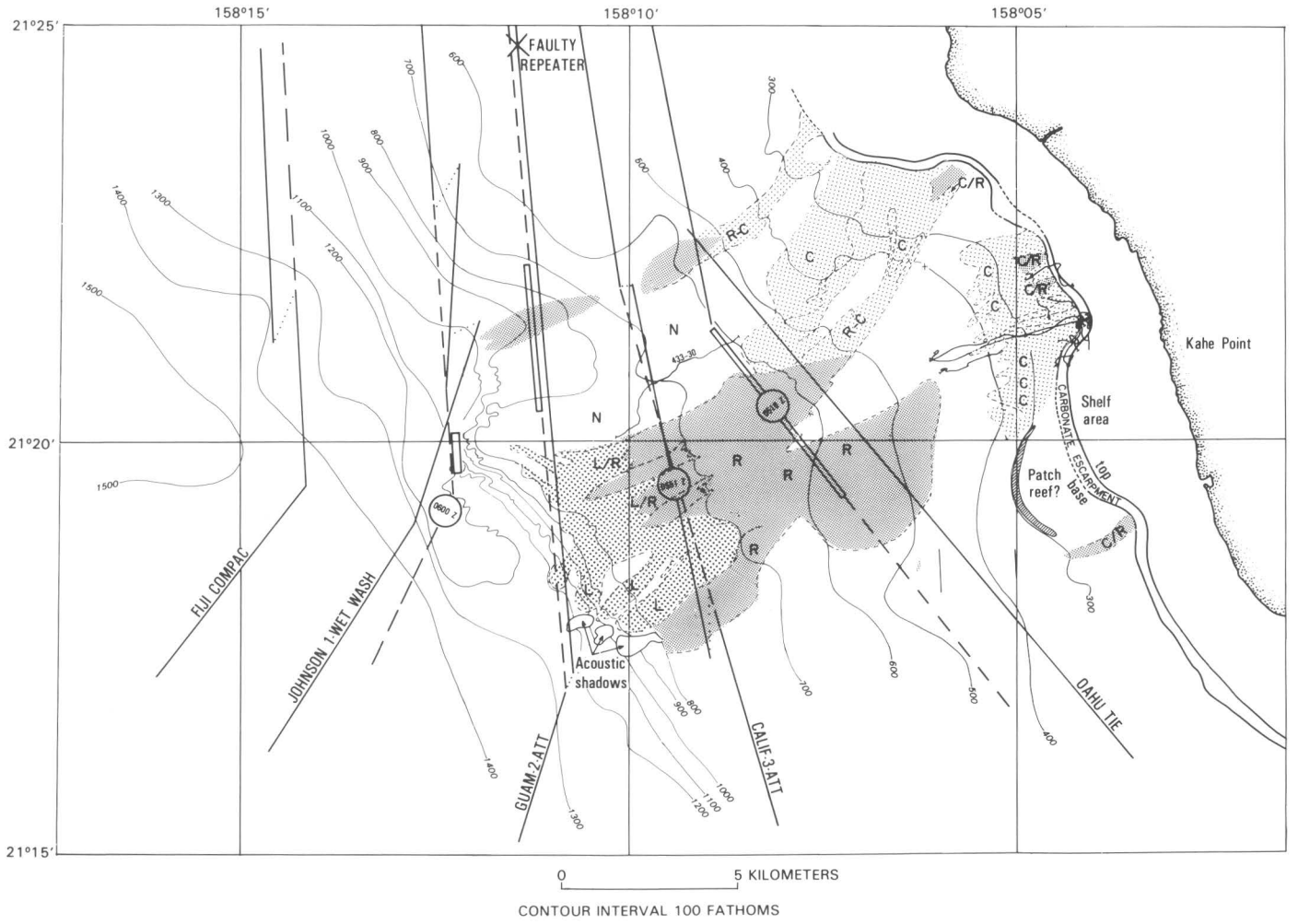

FIGURE 4.10.—Interpretative map of area of Sea MARC II image shown in figure 4.9. Major changes in acoustic reflectance relate to changes in surface sediment and depositional process. Prominent landslide lobes show analogous acoustic character to similar features on the south flank of Maui (see fig. 4.7). Reflective cobbly zones coincide with probable areas of active downslope transport of coarse volcanic and coralline rubble in traction carpets or rubble streams. See Fornari (1983, 1984) for further details and discussion of cable-break data.

the carbonate escarpment that is located just seaward of Kealakekua Bay, Hawaii (Moore and Fornari, 1984). During the traverse of *Makali'i* dive 164 (Moore and Fornari, 1984) a prominent cliff 3–10 m high was found in depths between 350 and 360 m. This cliff is continuous in a northwest direction along a contour-parallel trend, is subparallel to the escarpment, and exposes a volcanic conglomerate (fig. 4.12). The conglomerate consists of angular to subangular volcanic clasts that range in size from 0.5 cm to 0.5 m, with the median size being 0.5–2 cm, in a matrix of finer volcanic and biogenic carbonate silt and sand. Few bedding planes or graded beds were observed in the exposures; however, abundant fractures parallel to the original depositional surface indicate that crude bedding is probably present in the deposit and that it was laid down in successive episodes. Outcrops of the reef carbonate on the

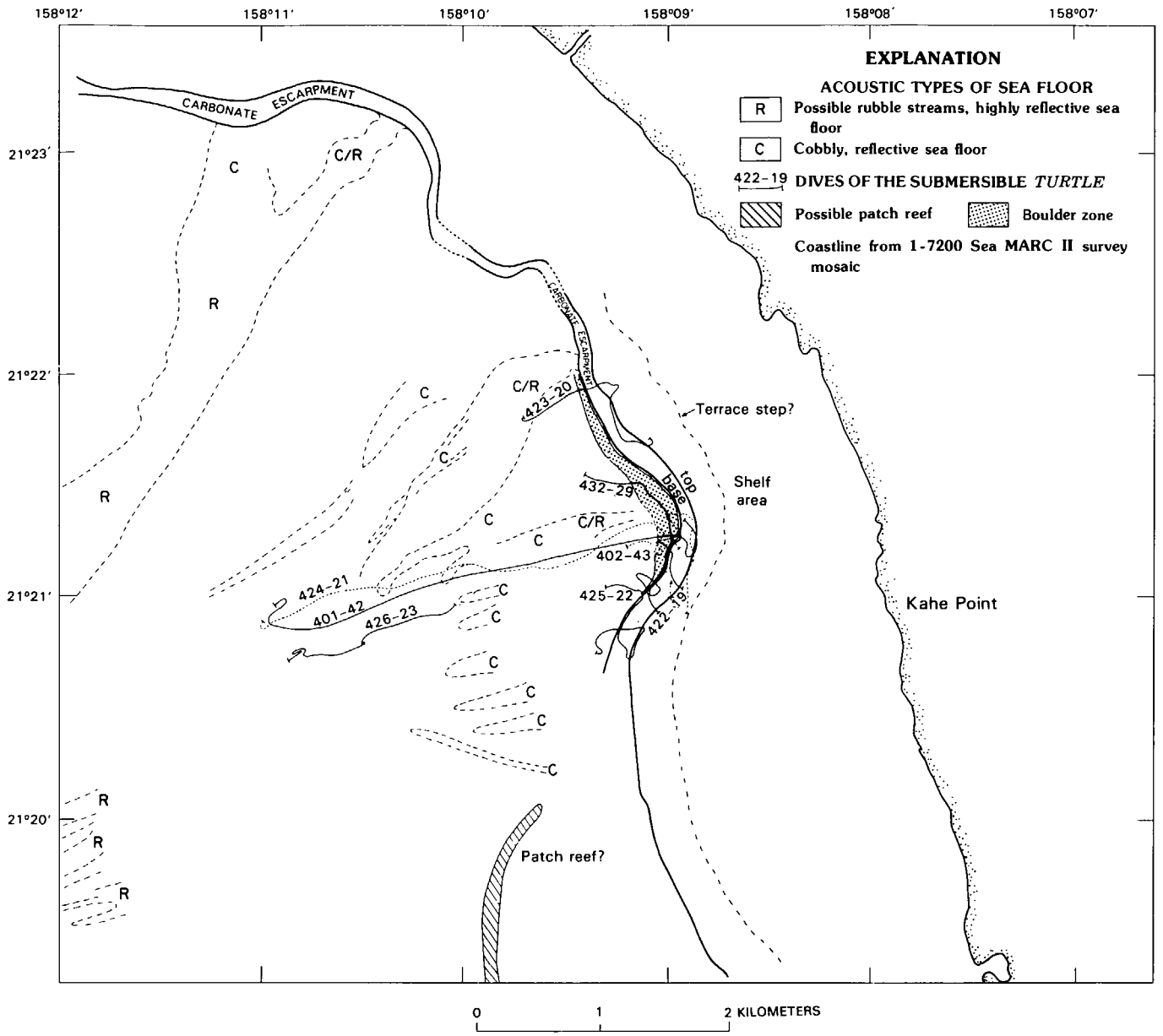

FIGURE 4.11.—Schematic map of nearshore part of area covered by Sea MARC II image off Kahe Point, Oahu, shown in figure 4.10. Submersible dive tracks and details of the sonar image have been mapped. See Fornari (1983, 1984) for further details.

escarpment above this cliff indicate that the conglomeratic deposit underlies and is the foundation for the massive limestone terrace (fig. 4.12). The instability of the volcaniclastic deposit in Kealakekua Bay is suggested by the common occurrence of large tabular blocks of the conglomerate on the sea floor immediately west of the cliff that were probably spalled off the vertical face. In some cases the base of the cliff was observed to have been undercut by as much as several meters, a process that certainly must accelerate the shedding of blocks from the escarpment.

This volcaniclastic deposit and exposures of other similar sedimentary sequences along the shallow submarine slope of Hawaii (Fornari and Perfit, unpub. data) indicate that erosion of the volcanic foundation takes place at a rapid rate. Deposition of clastic volcanogenic sediment by debris flows down the slopes leads to seaward-thinning wedges of mechanically weak clastic deposits that, when covered by successive sequences of lava, may provide an ideal surface on which seismically induced gravitational slumping can occur. This notion is supported by earthquake studies (Crosson and

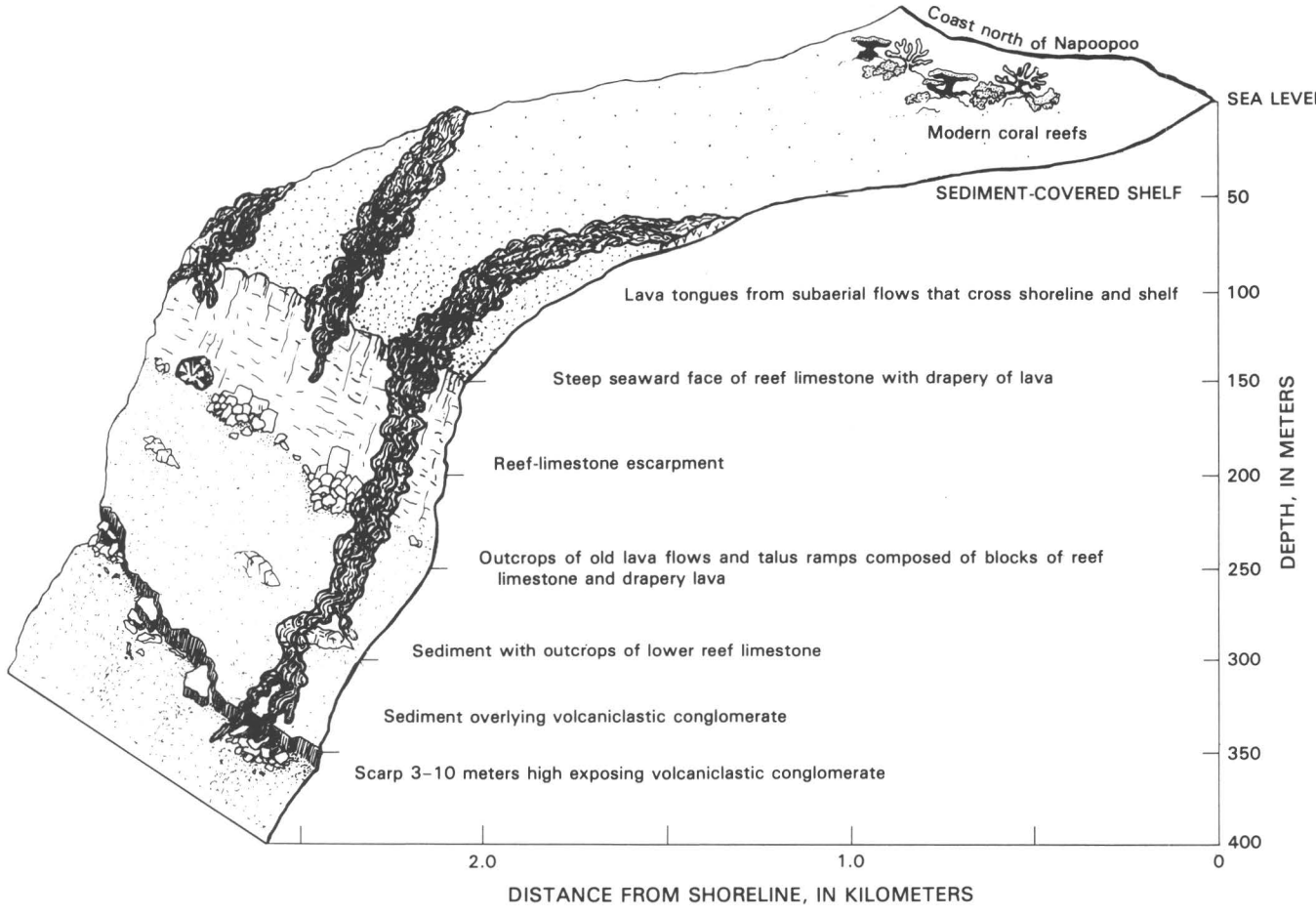

FIGURE 4.12.—Interpretative drawing of sea floor to 400-m depth off Kealakekua Bay, Hawaii, based on *Makali'i* dives (Moore and Fornari, 1984). Lava at base of carbonate escarpment is surrounded by reef limestone. This type of intercalation results from flows crossing an actively growing reef and being covered by later reef growth as subsidence occurs. Note volcaniclastic conglomerate bed 3–10 m thick that forms a continuous scarp along the base of the subsided reef terrace. This deposit was created by erosion of volcanic and carbonate outcrops on the slope and shore and deposited by rubble flows. Drawn by C.L. Fornari.

Endo, 1982) that indicate that focal mechanisms associated with nonvolcanic earthquakes on Kilauea's south flank occur within a slip plane that is coincident with a weak layer above old oceanic crust.

CONCLUSIONS

The sea floor around the Hawaiian Islands comprises several major classes of topography that are intimately related to (1) constructional volcanism that built the islands; (2) the preexisting fabric of the oceanic crust upon which the islands are built; (3) island subsidence; (4) gravitational collapse of unbuttressed volcano sides; and (5) low-relief debris flows that transport clastic sediment down the submarine slopes. The submarine continuations of subaerial rift zones create the most prominent relief around the islands. The topographic roughness and regional slope of each submarine rift is directly proportional to the age of the adjacent volcano. Seamounts around the Hawaiian Islands are largely older (Cretaceous) volcanoes that have been been partially buried by sediment. Some of these features may be drowned guyots. Several young seamounts that are genetically related to Hawaiian volcanism lie south of the Island of Hawaii. More subtle topographic features are present on the basal flanks of the Hawaiian Ridge and form steps and bulges in the lower slopes. These features were created by large-scale gravitational mass wasting of volcano flanks not buttressed by adjacent edifices. Low-relief debris flows appear to be the principal mechanism whereby clastic sediment is transported down the submarine flanks of oceanic volcanoes.

REFERENCES CITED

Andrews, J.E., and Bainbridge, C., 1972, Submarine canyons off eastern Oahu: Pacific Science, v. 26, p. 108–113.

Betz, F., and Hess, H.H., 1942, The floor of the north Pacific Ocean: Geographical Review, v. 32, p. 99–116.

Blackinton, J.G., Hussong, D.M., and Kosalos, J.G., 1983, First results from a combination side-scan sonar and seafloor mapping system (Sea MARC II):

Offshore Technology Conference, 15th, Houston, May 2-5, 1983, Appendix A, Proceedings, p. 309–314.

Campbell, J.F., 1983, Hawaii deep water cable program, phase II—at sea route surveys: Hawaii Institute of Geophysics Report, HIG–83-4, 50 p.

———1984, Rapid subsidence of Kohala Volcano and its effect on coral reef growth: Geo-Marine Letters, v. 4, p. 31–36.

Campbell, J.F., and Erlandson, D.L., 1979, Ocean Thermal Energy Conversion–1 (OTEC–1) Anchor site survey: Hawaii Institute of Geophysics Report, HIG–79-6, pp. 55.

———1981, Geology of Kohala submarine terrace, Hawaii: Marine Geology, v. 4, p. 63–72.

Campbell, J.F., and Hussong, D.M., 1983, Submarine geology of the Alenuihaha channel, the results of a Sea MARC II survey [abst.]: Eos, Transactions, American Geophysical Union, v. 64, p. 1032.

Chase, T.E., Menard, H.W., and Mammerickx, J., 1971, Bathymetric atlas of the north-central Pacific: Washington, H.O. Publication 1302, U.S. Naval Oceanographic Office.

———1980, Bathymetry of the North Pacific: La Jolla, Scripps Institution of Oceanography and Institute of Marine Resources, Chart No. 8.

Coles, S.L., 1982, A visual reconnaissance of the bottom between 20 and 365 m depth offshore of Kahe Point, Oahu for the purpose of OTEC pipeline/cable routing: unpublished report prepared for the Hawaiian Electric Co., Honolulu.

Crosson, R.S., and Endo, E.T., 1982, Focal mechanisms and locations of earthquakes in the vicinity of the 1975 Kalapana earthquake aftershock zone 1970–1979: implications for tectonics of the south flank of Kilauea Volcano, Island of Hawaii: Tectonics, v. 1, no. 6, p. 495–542.

Dietz, R.S., and Menard, H.W., 1953, Hawaiian swell, deep and arch, and subsidence of the Hawaiian Islands: Journal of Geology v. 61, p. 314–333.

Duffield, W.A., Stieltjes, L., and Varet, J., 1982, Huge landslide blocks in the growth of Piton de la Fournaise, La Reunion and Kilauea Volcano, Hawaii: Journal of Volcanology and Geothermal Research, v. 12, p. 147–160.

Fiske, R.S., and Jackson, E.D., 1972, Orientation and growth of Hawaiian rifts: the effects of regional structure and gravitational stresses: Royal Society of London, Proceedings, Series A., v. 329, p. 299–326.

Fiske, R.S., and Kinoshita, W.T., 1969, Rift dilation and seaward displacement of the south flank of Kilauea Volcano, Hawaii [abs.]: Symposium on volcanoes and their roots, Oxford, International Association of Volcanology and Chemistry of the Earth's Interior, p. 53–54.

Fornari, D.J., 1982, Deep-Submergence Vehicle *Turtle* dives off Keahole Pt., Hawaii, geological investigations of submarine slope micromorphology: baseline studies to assist in future OTEC cold-water pipe designs and deployments: Canoga Park, Ca; Rockwell International Energy Systems Group Technical Report.

———1983, Final Report, Deep-Submergence Vehicle *Turtle* dives off Kahe Point, Oahu, Hawaii: Chatham, N.Y., unpublished technical report, Offshore Investigations Limited, 60 p.

———1984, Preliminary Report, Sea MARC II side scan sonar image of the seafloor off Kahe Point, Oahu, Hawaii: Chatham, N.Y. unpublished technical report, Offshore Investigations Limited, 19 p.

Fornari, D.J., Malahoff, A., and Heezen, B.C., 1979a, Submarine slope micromorphology and volcanic substructure of the Island of Hawaii inferred from visual observations made from U.S. Navy Deep-Submergence Vehicle (DSV) *Sea Cliff*: Marine Geology v. 32, p. 1–20.

Fornari, D.J., Moore, J.G., and Calk, L., 1979b, A large submarine sand-rubble flow on Kilauea Volcano, Hawaii: Journal of Volcanology and Geothermal Research, v. 5, p. 239–256.

Francheteau, J., Harrison, C.G.H., Sclater, J.G., and Richards, M.L., 1970, Magnetizations of Pacific seamounts: A preliminary polar curve for the northeastern Pacific: Journal of Geophysical Research, v. 75, p. 2035–2061.

Furumoto, A., and Woollard, G.P., 1965, Seismic refraction studies of the crustal structure of the Hawaiian Archipelago: Pacific Science, v. 19, p. 315–319.

Gregory, A.E., and Kroenke, L.W., 1982, Reef development on a mid-oceanic island: Reflection profiling studies of the 500-meter shelf south of Oahu: American Association of Petroleum Geologists Bulletin, v. 66, p. 843–859.

Hamilton, E.L., 1957, Marine geology of the southern Hawaiian ridge: Geological Society of America Bulletin, v. 68, p. 1011–1026.

Hollister, C.D., 1984, Cable failures off Oahu caused by Hurricane Iwa: AT&T Communications, unpublished technical report.

Klein, F., 1982, Earthquakes at Loihi submarine volcano and the Hawaiian hot spot: Journal of Geophysical Research, v. 87, p. 7719–7726.

Kosalos, J.G., Blakinton, J.G., Hussong, D.M., and Fryer, P., 1982, The Sea MARC II seafloor reconnaissance system [abs.]: Eos, Transactions, American Geophysical Union, v. 63, p. 983.

Koyanagi, R.I., Swanson, D.A., and Endo, E.T., 1972, Distribution of earthquakes related to mobility of the south flank of Kilauea Volcano, Hawaii: U.S. Geological Survey Professional Paper 800–D, p. D89–D97.

Lipman, P., 1980, The southwest rift zone of Mauna Loa: implications for structural evolution of Hawaiian volcanoes: American Journal of Science, v. 280–A, p. 752–776.

Lockwood, J.P., 1979, Geologic asymmetry of the northeast rift zone of Mauna Loa Volcano, Hawaii—evidence for a mobile south flank [abs.]: Hilo, Hawaii Symposium on Intraplate Volcanism, p. 170.

Macdonald, G.A., Abbott, A.T., and Peterson, F.L., 1983, Volcanoes in the Sea, The Geology of Hawaii (2d ed.): Honolulu, University of Hawaii Press, pp. 517.

Malahoff, A., McMurtry, G., Wiltshire, J., and Yeh, H., 1982, Geology and chemistry of hydrothermal deposits from active submarine volcano Loihi, Hawaii: Nature, no. 298, p. 234–239.

Malahoff, A., and Woollard, G.P., 1968, Magnetic and tectonic trends over the Hawaiian Ridge, *in* Knopoff, L., Drake, C.L., and Hart, P.J., eds., The crust and upper mantle of the Pacific area: American Geophysical Union Monograph 12, p. 241–276.

Mathewson, C.C., 1970, Submarine canyons and the shelf along the north coast of Molokai Island, Hawaiian ridge: Pacific Science, v. 24, p. 235–244.

Menard, H.W., 1964, Marine Geology of the Pacific: New York, McGraw-Hill, 271 p.

———1984, Origin of guyots: the Beagle to Seabeam: Journal of Geophysical Research, v. 89, p. 11,117–11,123.

Moberly, R., and McCoy, F.W., 1966, The sea floor north of the eastern Hawaiian Islands, Marine Geology, v. 4, p. 21–48.

Moore, J.G., 1964, Giant submarine landslides on the Hawaiian ridge: U.S. Geological Survey Professional Paper 501–D, p. D95–D98.

———1965, Petrology of deep-sea basalt near Hawaii: American Journal of Science, v. 263, p. 40–52.

———1970, Relationship between subsidence and volcanic load, Hawaii: Bulletin Volcanologique, v. 34, p. 562–576.

Moore, J.G., Clague, D., and Normark, W.R., 1982, Diverse basalt types from Loihi Seamount, Hawaii: Geology, v. 10, p. 88–92.

Moore, J.G., and Fiske, R.S., 1969, Volcanic substructure inferred from dredge samples and ocean bottom photographs: Geological Society of America Bulletin, v. 80, p. 1191–1202.

Moore, J.G., and Fornari, D.J., 1984, Drowned reefs as indicators of the rate of subsidence of the Island of Hawaii: Journal of Geology, v. 92, p. 752–759.

Moore, J.G., Normark, W.R., and Lipman, P.W., 1979, Loihi Seamount—a young submarine Hawaiian volcano [abs.]: Hilo, Hawaii Symposium on Intraplate Volcanism, p. 127.

Niedoroda, A.W., Palmer, A.C., Pittman, J.R., Vandermeulen, J.P., and Campbell, J.F., in press, Oahu OTEC preliminary design: sea floor surveys: Proceedings of Offshore Site Investigations 1985.

Noda, E., 1983, Effects of Hurricane Iwa, November 23, 1982, offshore Kahe Point, Hawaii: (unpublished report submitted to RCUH, University of Hawaii).

Normark, W.R., Chase, T.E., Wilde, P., Hampton, C.E., Butmacher, B., Seekins, A., and Johnson, K.H., 1982, Geologic report for the O'OTEC site off Kahe Point, Oahu, Hawaii: U.S. Geological Survey Open-File Report 82–468A, 9 p.

Normark, W.R., Lipman, P., and Moore, J.G., 1979, Regional slump structures on the west flank of Mauna Loa Volcano, Hawaii [abs.]: Hawaii Symposium on Intraplate and Submarine Volcanism, Abstract volume, p. 172.

Rea, D.K., and Naugler, F.P., 1970, Musicians seamount province and related crustal structures north of the Hawaiian Ridge: Marine Geology, v. 10, p. 89–111.

Staudigel, H., Zindler, A., Hart, S.R., Leslie, T., Chen, C.-Y., and Clague, D.A., 1984, The isotope systematics of a juvenile intraplate volcano: Pb, Nd, and Sr isotope ratios of basalts from Loihi Seamount, Hawaii: Earth and Planetary Science Letters, v. 69, p. 13–29.

Stearns, H.T., and Macdonald, G.A., 1946, Geology and groundwater resources of the Island of Hawaii: Hawaii Division of Hydrography Bulletin, v. 9, 363p.

Strange, W.E., Woollard, G.P., and Rose, J.C., 1965, An analysis of the gravity field over the Hawaiian Islands in terms of crustal structure: Pacific Science, v. 19, p. 381–389.

Swanson, D.A., Duffield, W.A., and Fiske, R.S., 1976, Displacement of the south flank of Kilauea Volcano: the result of forceful intrusion of magma into the rift zones: U.S. Geological Survey Professional Paper 963, 39 p.

Tilling, R.I., Koyanagi, R.Y., Lipman, P.W., Lockwood, J.P., Moore, J.G., and Swanson, D.A., 1976, Earthquake and related catastrophic events, Island of Hawaii, November 29, 1975: a preliminary report: U.S. Geological Survey Circular 740, 33 p.

Vogt, P.R. and Smoot, N.C., 1984, The Geisha Guyots: multibeam bathymetry and morphometric interpretation: Journal of Geophysical Research, v. 89, p. 11,085–11,107.

Watts, A.B., 1976, Gravity and bathymetry in the central Pacific Ocean: Journal of Geophysical Research, v. 81, p. 1533–1553.

Watts, A.B., ten Brink, U.S., Buhl, P., and Brocher, T.M., 1985, A multichannel seismic study of lithospheric flexure across the Hawaiian-Emperor Seamount Chain: Nature, v. 315, p. 105–111.

Wilde, P., Chase, T.E., Normark, W.R., Thomas, J.A., and Young, J.D., 1980, Oceanographic data off the southern Hawaiian Islands: Berkeley, Lawrence Berkeley Laboratory, University of California, LBL Publication No. 359.

THE GEOMORPHIC AND STRUCTURAL DEVELOPMENT OF HAWAIIAN SUBMARINE RIFT ZONES

By Daniel J. Fornari[1]

ABSTRACT

The structure and morphology of Hawaiian submarine rift zones reflect the time-integrated effects of constructional volcanic processes, island subsidence, destructive gravitational slumping of unbuttressed volcano sides, and reef buildup and sedimentation. Structural modification of submarine rift flanks begins during initial stages of eruptive history and reaches a maximum during the shield-building stage. This process is exemplified by faults on the south submarine flank of Kilauea's east rift zone, debris slides like the Papau slide on the south flank of Hawaii, and large gravitational slump features, like the Kauna and Alika slides, on the southwest flank of Mauna Loa. The submarine northwest rift of Hualalai and Mauna Kea's submarine east rift have morphological characteristics indicating that their structural evolution is largely complete. Further changes to these evolved submarine rift zones and to older Hawaiian submarine slopes will be caused principally by subsidence, burial beneath carbonate platforms and sediments, and erosion and redeposition of hemipelagic and volcanogenic sediments by rubble flows and debris slides that transport sediments down steep submarine slopes.

INTRODUCTION

The submarine slopes of three shield volcanoes on the Island of Hawaii have been investigated since 1974 using the U.S. Navy submersibles DSV *Turtle* and DSV *Sea Cliff* (Fornari and others, 1979a). The resulting data have increased our understanding of volcanic and morphologic features on the submarine slopes of Kilauea, Mauna Loa, and Hualalai Volcanoes, and have led to the development of basic models of oceanic-island structure using submarine flank terrains as modern analogs of past volcanic episodes and processes (Fornari and others, 1979a).

The east rift of Kilauea (known offshore as the Puna Ridge) (Fornari and others, 1978) and the southwest rift of Mauna Loa (figs. 5.1, 5.2; Fornari and others, 1979b) were studied previously using U.S. Navy submersibles. With the analysis of data from seven dives on the south flank of the northwest rift of Hualalai Volcano (Schwartz and Fornari, 1982) and additional dredge and surface-ship (remote sensing) studies (Campbell and Erlandson, 1981; Clague, 1982), it has been possible to compare the morphological and structural evolution of these submarine features. That comparison forms the focus of this paper; it is especially interesting because of the age difference among the three Hawaiian submarine rifts, Hualalai's being the oldest and Kilauea's the youngest.

ACKNOWLEDGMENTS

E. Wolfe, R. Moore, J.G. Moore, D. Clague and G.P.L. Walker read various drafts of an earlier manucript and their constructive comments greatly improved this paper. I thank D. Christie, R. Decker, B. Decker and A. Malahoff for constructive comments on the final draft. D. Schwartz provided valuable assistance in reducing data from submersible dives on Hualalai. M.A. Luckman drafted the figures. Field and laboratory studies that were the basis for this synthesis have been supported by the U.S. Navy Office of Naval Research, Grant N00014-80-C-0098MM to the Lamont-Doherty Geological Observatory. Lamont-Doherty Geological Observatory Contribution No. 3840.

HAWAIIAN RIFT ZONES

SUBAERIAL PORTIONS

Hawaiian rift zones form swaths of tectonically disrupted terrain with rugged topography that consists of eruptive fissures, spatter ramparts and cones, and open cracks and collapse features (Stearns and Macdonald, 1946; Macdonald and Abbott, 1970; Lipman, 1980). The surficial expression of rift zone volcanism is usually a zone 3–4 km wide showing constructional and extensional features and normally coincident with a topographic ridge.

Geophysical anomalies (principally Bouguer gravity and magnetic anomalies) are useful in delineating the width of the intrusion zone, a steeply dipping plexus of dikes through which magma rises to the surface from shallow reservoirs located 2–6 km beneath the summit area (Swanson and others 1976; Ryan and others, 1981). Gravity and magnetic studies indicate that the intrusive dike complex beneath the narrow zone of surface rifting may be as wide as 12–17 km at depths of 3–4 km (Malahoff and Woollard, 1968; Broyles and others, 1979).

The positions of individual rift zones with respect to their volcanic centers and to neighboring volcanoes were investigated by Fiske and Jackson (1972) and in later field studies by Broyles and others (1979) and Lipman (1980a, b). Their conclusions are that

[1]Lamont-Doherty Geological Observatory of Columbia University, Palisades, New York 10964

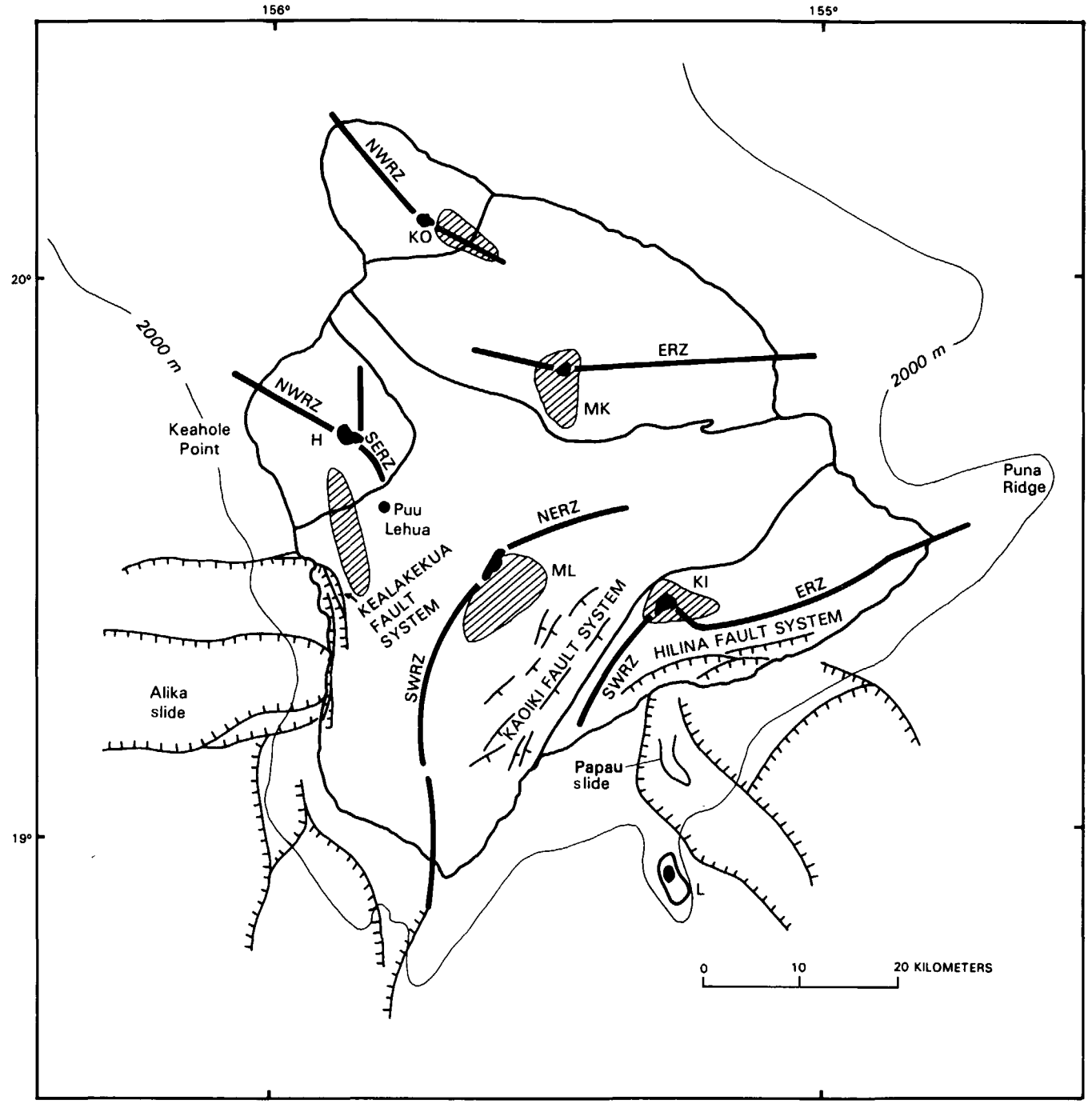

FIGURE 5.1.—Island of Hawaii showing boundaries between volcanoes, traces of rift zones, some fault systems, and areas of closed-contour Bouguer gravity highs (lined) from Kinoshita and others (1963). Volcanoes: KI, Kilauea; ML, Mauna Loa; H, Hualalai; MK, Mauna Kea; KO, Kohala; L, Loihi Seamount. Boundaries of submarine slump structures (ticks on downthrown side) are from Normark and others (1979). NWRZ, northwest rift zone; SWRZ, southwest rift zone; SERZ, southeast rift zone; ERZ, east rift zone; NERZ, northeast rift zone.

Hawaiian rift zones are shallow-level features whose locations are principally dictated by gravitational stresses within an edifice, but also indirectly by the shapes and positions of preexisting shields whose flanks have served as foundations for nascent volcanoes. As a result, the rifts vary in length; Kilauea's east rift zone and Mauna Loa's southwest rift zone are more than 100 km long including their submarine portions. Variation in rift-zone length may be attributed to the distribution of surrounding edifices that are large enough to inhibit or attenuate the development of a young rift zone. For example, Kilauea's southwest rift zone is sandwiched between Loihi

FIGURE 5.2.—Island of Hawaii showing 500-m submarine contours (from Wilde and others, 1980), traces of principal subaerial rift zones from each volcano, and locations of profiles shown in figures 5.3 and 5.4. Volcanoes: KI, Kilauea; ML, Mauna Loa; H, Hualalai; MK, Mauna Kea; KO, Kohala. NWRZ, northwest rift zone; SWRZ, southwest rift zone; SERZ, southeast rift zone; ERZ, east rift zone; NERZ, northeast rift zone.

Seamount to the south and Mauna Loa's southwest rift zone to the north and west, and its evolution and growth have thus been hindered. As a result, the southwest rift zone of Kilauea is rather short (~25 km, on land) and has no substantive morphologic expression on the sea floor south of Hawaii (see Fornari and Campbell, Chapter 4). Fiske and Jackson (1972) have pointed out that a basic understanding of the temporal and spatial growth of individual volcanoes within a composite shield can be achieved by

studying the lengths and relative positions of each volcano's rift zones.

SUBMARINE PORTIONS

PUNA RIDGE

Surface ship studies (Malahoff and McCoy, 1967; Moore and Fiske, 1969) and submersible investigations (Fornari and others, 1978) have shown that Puna Ridge (the submarine continuation of Kilauea's east rift zone; figures 5.1, 5.2) consists of purely constructional volcanic terrain on its crest and upper flanks. This terrain is characterized by steep flow-front escarpments separated by constructional benches on the upper flanks and narrow, linear volcanic ridges (pillow walls) and subparallel tensional and eruptive fissures on the ridge crest. All these features strike N. 45° E., parallel to the trend of the ridge (Fornari and others, 1978). The flank and ridge-crest terrains differ significantly. At the ridge crest there is an almost total absence of sediment and a dominance of constructional volcanic features. The flank areas, in contrast, have progressively more sediment with increasing depth, extrusive features that appear slightly more weathered and older (glassy crusts on extrusive forms that are starting to devitrify and spall off), and more common evidence of contemporary faulting and disruption of the volcanic sea floor. On the southern flank of Puna Ridge, at depths shallower than about 500 m, there are southeast-dipping normal faults that appear to be continuations of fault-line scarps of the Hilina fault system (fig. 5.1; Malahoff and McCoy, 1967). The subaerial Hilina scarps represent headwalls of major landslide blocks (Swanson and others, 1976), and the shallow submarine scarps probably also reflect lateral, slump-block readjustment of the unbuttressed flank of Kilauea caused by magma injection and dilation.

The slumping and mass-wasting that affects Hawaii's south flank leads to a fault-block-like submarine topography having alternating linear highs and lows that generally trend in a northeast direction. One major result of the tectonic and erosional processes is the redeposition of large quantities of sediment on the lower south flank of Puna Ridge and on the island's submarine south flank. This sediment is augmented by coarse basaltic debris derived through wave erosion of lava flows along the south coast and by the downslope transport of this material by tidal currents and debris flows and slides such as the Papau slide (Moore and Fiske, 1969; Fornari and others, 1979c).

MAUNA LOA'S SOUTHWEST RIFT ZONE

The southwest rift zone of Mauna Loa (figs. 5.1, 5.2) has also been investigated by submersibles and by remote-sensing from surface ships. Geophysical data show the gross structure of the rift as a series of scarps with steep west-facing walls that have vertical relief of 100 m to nearly 2,000 m (Fornari and others, 1979b). The principal linear scarp continues out to sea for about 50 km, and its asymmetric and faulted morphology has been interpreted to be a result of gravitational slumping of the unbuttressed west flank of Mauna Loa (Fornari and Campbell, chapter 4; Fornari and others, 1979b; Normark and others, 1979; Lipman, 1980a). The face of this scarp was acsended on three submersible dives and found to be composed of pillow-lava sequences, exposed in steeply (60°–70°) sloping outcrops and surrounded by volcaniclastic sediment. Less steep benches (10°–30° slopes) separate the outcrops. The tops of the outcrops are often capped by vertical walls, 1–3 m wide and 10–60 m high, formed by exposed dikes that have been stripped of their surrounding volcanic cover (Fornari and others, 1979b, fig. 6). Mass wasting of scarps must be very active because the steeply sloping outcrops and vertical dikes are highly unstable and prone to collapse. During the dives, extensive evidence of undercutting and erosion was seen in the form of toppled dike walls and faceted blocks of diabase dike rock strewn around the sea floor at the base of the walls and on the sediment (Fornari and others, 1979b).

Geophysical records of the sea floor to the west of the main scarp (Fornari and others, 1979b, fig. 4) suggest that thick deposits of clastic sediment lie in structural fault-bounded basins created by gravitational slump tectonics. Farther offshore, along the southern part of Hawaii's west coast, similar large slump-block features (for example, the Kauna and Alika slides) have been recognized on bathymetric compilations and geophysical records (Fornari and Campbell, chapter 4; Normark and others, 1979).

HUALALAI'S NORTHWEST RIFT ZONE

The submarine extension of Hualalai's northwest rift zone (figs. 5.1, 5.2) has been previously studied using conventional echo sounding (Campbell and Erlandson, 1981), dredging (Clague, 1982), and submersible diving (Schwartz and Fornari, 1982). These studies revealed the gross bathymetric character of the rift, the morphology and structure of parts of the submarine slope, and also determined that the exposed volcanic rocks are largely tholeiite and picritic, tholeiitic pillow basalt. The geochemistry of these rocks indicate that they have probably been derived from mantle sources separate from those feeding the other volcanoes on Hawaii (Clague, 1982).

The northern submarine flank of the rift zone has a regional slope of 3°–7° (the Puna Ridge has an average slope of 10°; Moore, 1971) and rugged topography created by constructional volcanism operating principally on the crest and north flank of the rift (Campbell and Erlandson, 1981). The data of Campbell and Erlandson (1981) clearly show that volcanic flows coming from the north flank are ponded against the preexisting terrace topography of the Kohala shelf.

The south flank of the rift zone, as seen in profile C of Campbell and Erlandson (1981, fig. 4) and in unpublished profiles recorded by the Hawaii Institute of Geophysics, differs from the north flank in having a steeper regional slope (16°–26°) and smoother acoustic reflectivity with fewer hyperbolae.

The southeastern part of the rift zone's south flank forms the submarine slope west of Keahole Point (figs. 5.1, 5.2) and has been observed during three previously reported DSV *Turtle* dives (Fornari, 1982). This area has microtopographic relief of 1–3 m; however, at shallower depths (less than 300 m) the outcrops have relief of as much as 7 m. Much of this relief is created by the downslope ends or edges of subaerially derived lava flows. Average slope

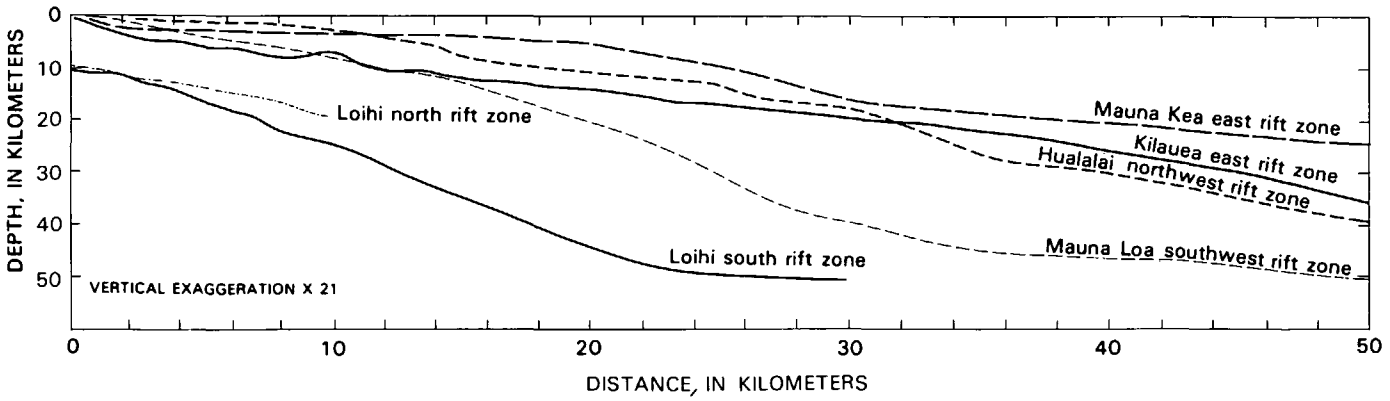

FIGURE 5.3.—Profiles of Hawaiian submarine rift zones taken along their strike. Drawn from published bathymetric maps (see references in text) and plotted following the axis of minimum depth of each rift. Data points were taken every 100 m of depth change. Horizontal distance is from the shoreline except for Loihi's rifts. Profile locations shown on figure 5.2.

angles for various segments of each dive traverse show that an abrupt increase in slope from approximately 15° to 27° occurs at about 750 m depth. This depth roughly conforms to the upslope onset of a ridge-and-gully terrain that is the principal sea-floor morphology in this area and apparently also occurs in similar depth ranges on other Hawaiian submarine slopes investigated with submersibles. The ridges and gullies are oriented parallel to the slope and usually have relief of 1–5 m (amplitude) and varied wavelengths. These features are likely to represent consequent topography developed over buried flow lobes (probably subaerial ones that have since subsided, although some may have originated from shallow submarine vents), which have subsequently served to channel tidal scouring in between the highs, thereby maintaining the troughs while sediment continued to accumulate on the low ridges.

This slope transition may be the result of basement faults, now largely buried, associated with earlier episodes of gravitational slumping of the west flank of Hualalai and its northwest rift zone. Only small fault scarps were observed during the submersible dives in this area, however, and those scarps are largely confined to depths below 1,000 m and have relief of 3–6 m. The scarp faces are smooth, in contrast to the rough, jagged flow fronts, and expose massive lava with occasional intercalations of carbonate, either as blocks or lenses several tens of centimeters thick (Fornari, 1982; Schwartz and Fornari, 1982). Alternatively, this slope change may reflect the general paleodepth to which subaerial flows were able to move. Historical subaerial flows (ranging in date from 1801 to 1950) that have flowed into the sea on the west flank of Hawaii have been mapped using a submersible, and they are known to have only reached depths of approximately 250 m (D.J. Fornari and M.R. Perfit, unpublished data).

Wide expanses of the sea floor in this area are covered by volcanic and carbonate clastic debris and sediment. These deposits bury most evidence of flow fronts and fault scarps; however, several southwest-facing ramps with 5–10 m of relief were traversed and are thought to have been formed by depositional draping over a preexisting basement structure. Much of the area examined during the dives between depths of 350 m and 1,000 m is covered by these clastic deposits. South of latitude 19° 48′ N. and below 1,500 m depth, the spacing between isobaths increases and the regional slope decreases to about 10° (fig. 5.2).

Extrapolation of dive observations, echo sounding, and bathymetric data indicate that the lower south flank of Hualalai's northwest rift zone is largely covered by volcanic and carbonate erosional debris and hemipelagic sediment. The net geomorphic effect has been to smooth and obscure nearly all of the constructional volcanic morphology through mass-wasting of flow fronts and scarp faces, resulting in deposition of talus and in downslope transport of erosional products. While indications of downslope movement of talus are present, no slump scars or discrete slump deposits were observed during the *Turtle* dives. The north flank of Hualalai's northwest rift zone, on the other hand, consists primarily of pillow lava and constructional volcanic topography that is variably covered by hemipelagic sediment.

DISCUSSION

Profiles drawn along the strike and across strike of several Hawaiian submarine rift zones are shown in figures 5.3 and 5.4, respectively. These profiles were constructed from 100-m bathymetric contour data (Chase and others, 1971; Moore, 1971; Wilde and others, 1980; Campbell and Erlandson, 1981; Malahoff and others, 1982; Moore and others, 1982). The differences between rift-zone profiles can largely be explained by age differences and differences in structural evolution. The profiles shown in figure 5.3 clearly show the differences in plunge angle as well as the localized effects of constructional volcanism along the crests of the youngest rifts (Puna Ridge and Loihi Seamount's north and south rifts).

The profile of Mauna Kea's east rift zone shows the effects of the carbonate reef buildup that has constructed a 20-km-wide shelf

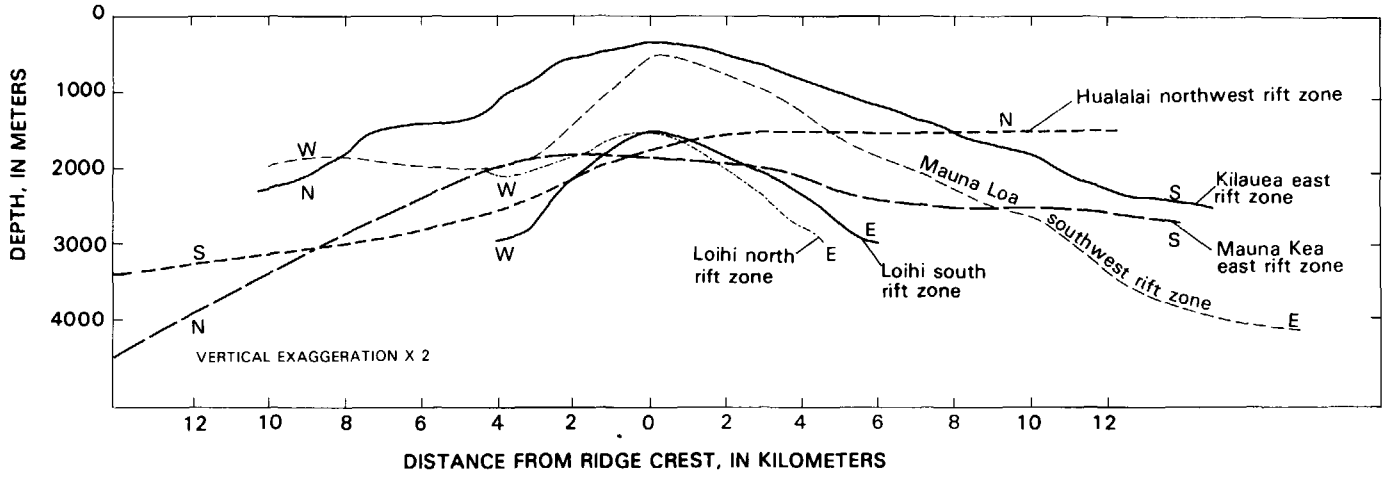

FIGURE 5.4.—Profiles of Hawaiian submarine rift zones taken across their strike. Drawn from same data set used in figure 5.3. Horizontal distance is centered on the topographic crest of each rift. Profile locations shown in figure 5.2. Approximate compass orientations of profiles indicated by labels on ends (N, north; E, east; S, south; W, west).

over the nearshore segment of this rift. Because volcanic activity has been absent along this rift for tens of thousands of years, the rough constructional topography of the rift has been buried by clastic and hemipelagic sediment and a coralline mantle. Mauna Kea's east rift zone shows two prominent slope transitions. The shallower one reflects the change from carbonate platform to a steeper slope that probably more closely reflects the original constructional rift slope. Farther seaward, the slope of the rift axis decreases abruptly about 30 km from the shoreline and then continues at this lower value past the end of the profile shown in figure 5.3. If the profile were extended (see fig. 5.2 for contours), one would see that Mauna Kea's profile consists of several steeper sections separated by wide, lower gradient benches that eventually merge onto the abyssal sea floor at approximately 5 km depth. This characteristic old-rift topography is similar to that of Hualalai's northwest rift zone, although the steeper ramp sections are smaller on Hualalai, possibly reflecting the smaller size of Hualalai Volcano compared to Mauna Kea.

Hualalai's northwest rift zone has a slightly steeper profile than Mauna Kea's east rift zone, but it also shows the effects of reef growth and carbonate terrace development. Along Hualalai's rift the terrace extends about 8 km from the shoreline; however, the Kohala terrace to the north is a much broader feature, whose morphology and development reflect the extended period of volcanic quiescence along the northwest coast of Hawaii and the older age of this portion of the island (Campbell and Erlandson, 1981). Hualalai's rift profile also appears rather smooth; but this is most likely a result of the use of wide-beam echo sounders to survey this area. A detailed inspection of echo-sounder records from the crest of Hualalai's northwest rift zone shows an abundance of overlapping hyperbolae suggestive of constructional volcanic sea floor (Campbell and Erlandson, 1981).

Mauna Loa's southwest rift zone also has a smooth profile, but its regional slope is greater than that of all other rifts except Loihi's (fig. 5.2). The smoothness of this profile does reflect a general absence of recent constructional volcanism on the rift-zone crest; however, young-looking volcanic flow fronts and outcrops are present on the west flank of the rift (Fornari and others, 1979b). The absence of a carbonate shelf on Mauna Loa's southwest rift zone indicates that this part of the island is still too young (volcanically active) and gravitationally unstable to allow carbonate reef terraces to grow and develop.

Kilauea's east rift zone (Puna Ridge) shows much more local irregularity than do the rifts of Mauna Kea, Hualalai, and Mauna Loa (fig. 5.3), undoubtedly because it is linked to the most active volcano and subaerial rift zone on Hawaii. Because of its young age, Puna Ridge does not possess a carbonate terrace (fig. 5.3). The rather constant gradient of this rift zone out to 50 km from shore and its greater elevation above the surrounding sea floor (for corresponding distances from shore) compared to Mauna Loa's southwest rift zone, probably result from the buoyant effects of magma intrusion and lack of subsidence, similar to the manner in which the crest of the East Pacific Rise is supported and elevated by accretionary magmatism (see Macdonald and others, 1984, and references therein).

Loihi Seamount's north and south rift zones are excellent examples of juvenile Hawaiian submarine rift zones. Both have steep plunge angles and local topographic roughness created by constructional volcanism on the rift crests. The north rift is not as steep as the south rift because of the constraining effects of Kilauea's south flank and southwest rift on its development. The crests of Loihi's rifts are known from deep-sea photography (Malahoff and others, 1982) to consist of pillow-lava flows, while the flanks of the rift zones and much of the volcano sides are covered with coarse pillow-lava talus.

Profiles across the strikes of these Hawaiian rifts are shown in figure 5.4. The most important feature of these profiles is the

consistently asymmetric character of the rifts. In all cases the rift flank that is not buttressed is steeper, indicating that gravitational slumping of rift flanks fundamentally alters the geometry of a rift zone. As exemplified by Loihi Seamount's rifts, this process is initiated at a very early stage in a rift zone's growth and continues through the volcano's early-mature stage of development.

Hence, Hawaiian rift zones initially develop and grow purely through constructional volcanism; however, early in the rift zone's active life the influence of adjacent volcanoes on its growth becomes important. The following model illustrates the importance of gravitational slumping and preexisting volcano location to the development of rift zones and volcano flank morphology and structure. In addition, this model offers an explanation for the absence of large-scale gravitational slumps on the west flank of Mauna Loa north of approximately latitude 19° 30′ N.

Fiske and Jackson (1972), who used the gravity data of Kinoshita and others (1963) to support their thesis, suggested that Hualalai's southeast rift zone has played a dominant role in the construction of the original Hualalai edifice, much of which is now buried beneath the flank of Mauna Loa (fig. 5.1, 5.2). The Bouguer gravity map of Hawaii (Kinoshita and others, 1963) shows an elongate north-south gravity high (265 mGal closed contour) that continues south of the surficial boundary between Hualalai and Mauna Loa and reaches latitude 19° 25′ N (fig. 5.1). South of the summit of Hualalai, the gravity high is west of the surface position of the rift zone, and the gravity maximum is the lowest of the five gravity highs on the island. This may be in part because the dense dike rocks are buried under 1–2 km of Mauna Loa lava and clastic deposits. The location of the gravity high, offset to the west with respect to the present surface rift, is still within the 12- to 17-km width of the dike complex proposed by Broyles and others (1979). However, the buttressing of Mauna Loa's west flank (see Lipman, 1980a, b) would lead one to expect the surface rift to lie west of the gravity high, in the direction that can most easily accommodate extensional tectonics because it is not buttressed.

I suggest that the dike complex under Hualalai's gravity high is a foundation that buttresses the northern part of the west flank of Mauna Loa. Deep-seated gravitational slumping on the west flank of Mauna Loa is, therefore, restricted to the area south of the end of the gravity high (approximate latitude 19° 25′ N. fig. 5.1). The extension of the Kealakekua fault north of latitude 19° 25′ N. may represent gravitational slump-block failure (Normark and others, 1979; Lipman, 1980a) of just the upper few kilometers of Mauna Loa's west flank that are unbuttressed by Hualalai's southern rift dike complex. In addition, the abrupt development of a carbonate terrace north of latitude 19° 30′ N. (fig. 5.2) probably results partially from the relative stability and low rate of volcanic activity along Hualalai's west flank as compared to Mauna Loa's gravitationally unstable west flank south of Kealakekua Bay.

CONCLUSION

There are several morphologic similarities between the youthful Puna Ridge and Hualalai's older northwest rift zone. Echo reflection characteristics and data from dives and dredges in the summit areas of both rifts reveal a predominance of fresh pillow lava and constructional morphology on the ridge crests. The unbuttressed south flanks of both rifts are mantled by volcaniclastic deposits resulting from mass wasting of constructional topography and from gravitational slumping. The latter process has disrupted the constructional slopes and widened the bases of the topographic ridges.

Because these two rifts are near opposite ends of the age spectrum for the Island of Hawaii, it is apparent that the processes of constructional volcanism (centered on a line source along the rift axis) and mass wasting of the unbuttressed rift flank are fundamental to the evolution of submarine rift-zone morphology and structure. The principal difference between Hualalai's northwest rift zone and Puna Ridge is the nearly complete burial of the headwalls of slump blocks on Hualalai's rift by subsequent volcaniclastic deposits that cover nearly all of the original constructional relief and fault scarps.

The morphology and structure of the submarine continuation of Mauna Loa's southwest rift zone are quite different from those of Puna Ridge and of Hualalai's northwest rift zone. The unbuttressed west flank of the southwest rift is very unstable at this stage in Mauna Loa's shield-building history, and gravitational slumping has created a prominent asymmetric scarp topography rather than a more symmetric constructional rift topography (fig. 5.4). The large vertical offsets and horizontal extent of the slumping indicate that this reconfiguration of the cross-sectional and plan-view structure and morphology of the rift zone is deep seated and extends well down into the volcanic pile. The abundance of these large-scale gravitational slump features (for example, Kauna and southwest rift slides) on the west flank of Mauna Loa attests to the predominance of this process during the mature phase of shield building (Fornari and Campbell, chapter 4). The size of gravitational slumps on volcano flanks is probably controlled by edifice size and by the constraining influence of adjacent volcanoes, which act to buttress parts of the volcanic pile.

The structure and morphology of Hawaiian submarine rift zones are primarily the result of a time-integrated sequence of volcanic constructional processes and gravitational tectonics. Initially constructional volcanism dominates, although parts of a rift may begin to be modified by gravitational slumping even during the juvenile stage. Early in a volcano's mature shield-building stage, however, the instability of the subaerial shield (whose foundation is the clastic volcanic sequences laid down during the volcano's emergence) results in the dominance of destructional gravitational slumping over constructional processes and the drastic reshaping of the submarine rift. At a still later date the combined effects of repeated slumping, minor renewed volcanism, the possible growth of a new volcano nearby, subsidence of the island, and development of a carbonate reef terrace result in a mature submarine rift like that of Mauna Kea's east rift zone or Hualalai's northwest rift zone.

REFERENCES CITED

Broyles, M.L., Suyenaga, W., and Furumoto, A.S., 1979, Structure of the lower east rift zone of Kilauea Volcano, Hawaii, from seismic and gravity data: Journal of Volcanology and Geothermal Research, v. 5, p. 317–336.

Campbell, J.F., and Erlandson, D.L., 1981, Geology of Kohala submarine terrace, Hawaii: Marine Geology, v. 4, p. 63–72.

Chase, T.E., Menard, H.W., and Mammerickx, J., 1971, Bathymetric atlas of the north-central Pacific: Washington, D.C., U.S. Naval Oceanographic Office, H.O. Publication 1302.

Clague, D.A., 1982, Petrology of tholeiitic basalt dredged from Hualalai Volcano, Hawaii [abs.]: Eos (Transactions of the American Geophysical Union),v. 63, no. 45, p. 1138.

Clague, D.A., Jackson, E.D. and Wright, T.W, 1980, Petrology of Hualalai Volcano, Hawaii: implication for mantle composition: Bulletin Volcanologique , v. 43-4, p. 641–656.

Fiske, R.S., and Jackson, E.D., 1972, Orientation and growth of Hawaiian rifts: the effects of regional structure and gravitational stresses: Proceedings of the Royal Society of London, Series A., v. 329, p. 299–326.

Fornari, D.J., Malahoff, A., and Heezen, B.C., 1978, Volcanic structure of the crest of the Puna Ridge, Hawaii: geophysical implications of submarine volcanic terrain: Geological Society of America Bulleltin, v. 89, p. 605–616.

———1979a, Submarine slope micromorphology and volcanic substructure of the Island of Hawaii inferred from visual observations made from U.S. Navy deep-submergence vehicle (DSV) *Sea Cliff*: Marine Geology, v. 32, p. 1–20.

———1979b, Submarine extension of the southwest rift zone of Mauna Loa Volcano, Hawaii: visual observations from U.S. Navy deep submergence vehicle DSV *Sea Cliff*: Geological Society of America Bulletin, v. 90, p. 435–443.

Fornari, D.J., Moore, J.G., and Calk, L., 1979c, A large submarine sand-rubble flow on Kilauea Volcano, Hawaii: Journal of Volcanology and Geothermal Research, v., 5, p. 239–256.

Fornari, D.J., 1982, DSV *Turtle* dives off Keahole Point, Hawaii, geological investigations of submarine slope micromorphology: baseline studies to assist in future OTEC cold-water pipe designs and deployments: Rockwell International Energy Systems Group Technical Report, Canoga Park, Ca.

Kinoshita, W.T., Krivoy, H.L., Mabey, D.R., and MacDonald, R.R., 1963, Gravity survey of the Island of Hawaii: U.S. Geological Survey Professional Paper 475–C, p. 114–116.

Lipman, P., 1980a, The southwest rift zone of Mauna Loa: implications for structural evolution of Hawaiian volcanoes: American Journal of Science, v. 280-A, p. 752–776.

———1980b, Rates of volcanic activity along the southwest rift zone of Mauna Loa Volcano, Hawaii: Bulletin Volcanologique, v. 43-4, p. 703–725.

Macdonald, G.A., and Abbott, A.T., 1970, Volcanoes in the Sea—the geology of Hawaii: Honolulu, University of Hawaii Press, 441 p.

Macdonald, K., Sempere, J-C., and Fox, P.J., 1984, East Pacific Rise from Siqueiros to Orozco fracture zones: Along-strike continuity of axial neovolcanic zone and structure and evolution of overlapping spreading centers: Journnal of Geophysical Research, v. 89, p. 6049–6069 and p. 6301–6305.

Malahoff, A., and McCoy, 1967, The geologic structure of the Puna submarine ridge: Journal of Geophysical Research, v. 72, p. 541–548.

Malahoff, A., McMurtry, G., Wiltshire, J., and Yeh, H., 1982, Geology and chemistry of hydrothermal deposits from active submarine volcano Loihi, Hawaii: Nature, no. 298, p. 234–239.

Malahoff, A., and Woollard, G.P., 1968, Magnetic and tectonic trends over the Hawaiian Ridge, *in* Knopoff, L., Drake, C.L., and Hart, P.J., eds., The crust and upper mantle of the Pacific area: American Geophysical Union Monograph no. 12, p. 241–276.

Moore, J.G., 1971, Bathymetry and geology—east cape of Hawaii: U.S. Geological Survey Miscellaneous Geological Investigations Map, I–677, scale 1:62,500.

Moore, J.G., Clague, D., and Normark, W. R., 1982, Diverse basalt types from Loihi Seamount, Hawaii: Geology, v. 10, p. 88–92.

Moore, J.G., and Fiske, R.S., 1969, Volcanic substructure inferred from dredge samples and ocean bottom photographs: Geological Society of America Bulletin, v, 88, p. 1191–1202.

Normark, W.R., Lipman, P., and Moore, J.G., 1979, Regional slump structures on the west flank of Mauna Loa Volcano, Hawaii [abs.]: Hawaii Symposium on Intraplate and Submarine Volcanoes, Abstract volume, p. 172.

Ryan, M.P., Koyanagi, R.Y., and Fiske, R.S., 1981, Modeling the three-dimensional structure of macroscopic magma transport systems: applications to Kilauea, Hawaii: Journal of Geophysical Research, v. 86, p. 7111–7129.

Schwartz, D., and Fornari, D.J., 1982, Submersible investigations of the northwest rift zone of Hualalai Volcano, Hawaii: Eos (Transactions of the American Geophysical Union), v. 63, p. 1138.

Stearns, H.T., and Macdonald, G.A., 1946, Geology and groundwater resources of the Island of Hawaii: Hawaii Division of Hydrography Bulletin, v. 9, 363 p.

Swanson, D.A., Duffield, W.A., and Fiske, R.S., 1976, Displacement of the south flank of Kilauea Volcano: the result of forceful intrusion of magma into the rift zones: U.S. Geological Survey Professional Paper 963, 39 p.

Wilde, P., Chase, T.E., Normark, W.R., Thomas, J.A., and Young, J.D., 1980, Oceanographic data off the southern Hawaiian Islands: Berkeley, University of California, Lawrence Berkeley Laboratory, LBL Publication 359.

GEOLOGY OF THE SUMMIT OF LOIHI SUBMARINE VOLCANO

By Alexander Malahoff[1]

ABSTRACT

Loihi submarine volcano is a seismically active seamount whose summit is at a water depth of 969 m (530 fathoms), 28 km (15 miles) southeast of the Island of Hawaii at 18°56′ N., 155°15.9′ E. Loihi is on the southernmost extension of the Kahoolawe-Hualalai-Mauna Loa volcanic line and probably marks the latest activity of the Hawaiian hot spot. The base of the volcanic edifice is 4,023 m (2,200 fathoms) below sea level. Loihi has formed through periodic volcanism along a northwest- to southeast-striking 31-km-long rift. High-resolution, shipboard hydrographic survey techniques supplemented by narrow, multibeam acoustic bottom surveys were followed by transponder-navigated bottom photography and ocean-floor dredge sampling. The combined data have produced a detailed picture of an emerging Pacific island. The summit of the volcano contains a calderalike depression 2.8 km wide and 3.7 km long with steep inner and outer walls. Within the depression, there are two pit craters; one is 0.6 km in diameter and 73 m deep, the other is 1.2 km in diameter and 146 m deep.

Shipboard and aeromagnetic studies show the presence of a 3,900-nT peak-to-peak normal bipole residual magnetic anomaly over its edifice. Superposed upon the normally polarized anomaly is a short wavelength, reversely polarized anomaly with peak-to-peak amplitude of 1,600 nT located directly over the summit of Loihi. Modeling of the reversely polarized anomaly suggests the source to be a nonmagnetic body, possibly a near-surface magma chamber below the summit of Loihi. Extensive bottom photography shows newly formed, glass-encrusted lava flows with pillow, sheet, lobate and aa forms erupted along the southeast slopes of the summit. The slopes of the volcano show evidence of recent, large-scale landslides that have scarred the volcano along its eastern and western slopes. Along the eastern edges of the summit depression, photographs show the presence of both hydrothermal activity and mineral precipitation with chimney forms similar to those mapped along the active rift systems of the East Pacific Rise and the Juan de Fuca Ridge. Orange to yellow iron-rich precipitates mark extensive hydrothermal vents around the central calderalike depression where water temperature anomalies in excess of several degrees Celsius have been detected. No exotic, hydrothermally associated, benthic animal communities have been detected in the present study. Photographic evidence suggests that forms of hydrothermal metallic precipitates found on Loihi may be similar to those found along the East Pacific Rise and that similar precipitates may be found at depths on other seamounts and volcanic islands.

INTRODUCTION

Loihi Seamount is a young (probably less than 0.5 Ma), active, submarine volcano on the southern extension of the Hawaiian hot spot (Jackson and others, 1972) along the Kahoolawe-Hualalai-Mauna Loa volcanic line; it is the youngest volcano in the Hawaiian Island chain and is the possible site for the next emerging island (fig. 6.1). The name Loihi, meaning long in Hawaiian, was first introduced by Emery (1955) to explain the elongate shape of the seamount. Loihi is seismically active, with shallow earthquake swarms that are distinct from the seismic activity of Kilauea (Klein, 1982), the nearest active volcano. A zone of deep earthquakes at a depth of 60 km between Kilauea, Loihi and Mauna Loa suggest a common deep source for the magma supply of the three volcanoes from the Hawaiian hot spot. Petrologic studies of basalt dredged from the volcanic edifice by Moore and others (1982) show these rocks to be glassy, tholeiitic pillow basalt, tholeiitic-alkalic transitional basalt, alkali basalt, and basanite. Most of the rocks sampled from the summit appear to be weakly vesicular, suggesting the possibility of mild explosive activity at the summit of Loihi (Moore and others, 1982). Extensive bottom photography and photointerpretation of surficial geology were performed by the author using the Woods Hole Oceanographic Institution's underwater camera system (ANGUS) deployed from the research vessel *Kana Keoki*. These data show the presence of fresh pillow lava, fresh sheet and lobate flows, and fresh aa and pahoehoe flows emerging from the summit of Loihi. Bottom transponder-controlled dredging (shipboard) of prospective hydrothermal deposit sites on the summit showed the presence of copper-enriched nontronite deposits (Malahoff and others, 1982). The nontronite was identified using bottom photography. The deposits were found to be associated with the freshest lava flows at several sites near the summit.

In order to map Loihi submarine volcano, detailed high-resolution bathymetric surveys were conducted over its summit by the National Oceanic and Atmospheric Administration (NOAA) vessels *Fairweather* and *Rainier*. The bathymetric surveys used shipboard traverses spaced 400 to 800 m apart. Navigation was by miniranger, with the network tied to the old Hawaiian datum. The details of the summit crater bathymetry were also mapped using the

[1]Department of Oceanography and Hawaii Institute of Geophysics, University of Hawaii, Honolulu, Hawaii 96822.

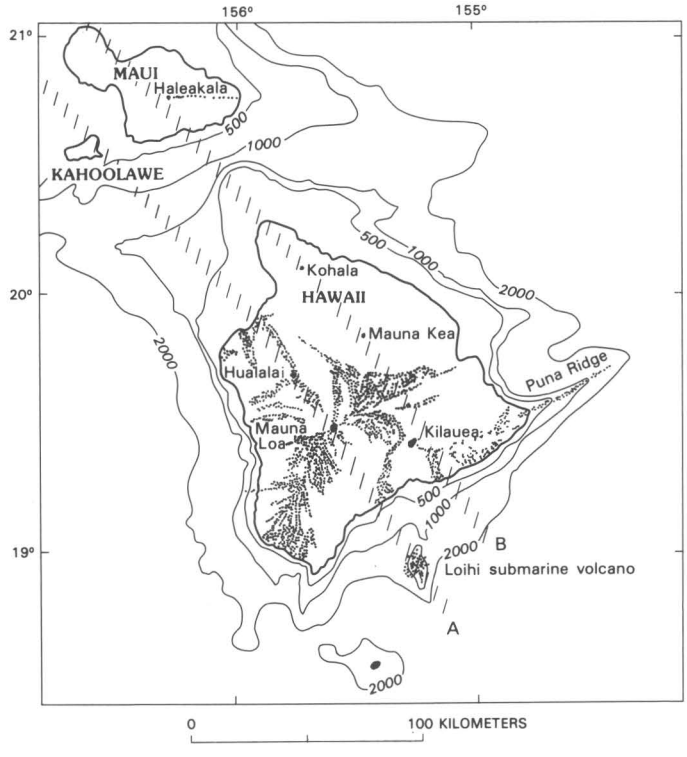

FIGURE 6.1.—Location of twin traces (hachures) of the Hawaiian hot spot showing Loihi submarine volcano at south end of Kahoolawe-Hualalai-Mauna Loa-Loihi trace (A), and the Haleakala-Kohala-Mauna Kea-Kilauea trace (B). Historical Hawaiian lava flows shown by dotted pattern. Bathymetric contours are in meters.

acoustic transponder and altimeter on the ANGUS photographic system. Bathymetric details of the whole volcanic edifice (see fig. 6.3) were determined through a U.S. Navy-conducted, high-resolution, narrow-beam, 64-beam Sonar Array Survey System (SASS) aboard the U.S. Navy (USN) ship *Hess*. All surveys were performed between 1978 and 1981. The depths for both the NOAA and the USN bathymetric surveys were plotted using fathoms as the depth unit. Airborne magnetic studies of Loihi were performed earlier by Malahoff and Woollard (1968, 1970) and were supplemented by shipboard magnetic traverses by vessels of the Hawaii Institute of Geophysics. This paper focuses on the surficial morphology and structure of Loihi as an example of the early stages of the structural development of a Hawaiian island as a submarine volcano.

ACKNOWLEDGMENTS

The research described in this paper was supported by funding from the National Ocean Survey (NOS) of the National Oceanic and Atmospheric Administration (NOAA). The United States Navy provided ship time aboard the USN ship *Hess* to conduct the multibeam, narrow-beam surveys over the flanks of Loihi. The bottom photographic surveys were performed by the ANGUS group of the Woods Hole Oceanographic Institution in October 1980 aboard the University of Hawaii's research vessel *Kana Keoki*. It was through the dedication and professionalism of the ANGUS team that such excellent photographic data were obtained during adverse weather conditions. I would like to thank Dr. Frisbee J. Campbell of the Hawaii Institute of Geophysics, University of Hawaii, and Captain William King of the research vessel *Kana Keoki* for their assistance in organizing the shipboard operations, and also the commanding officers of the NOAA ships *Rainier* and *Fairweather* for the excellent hydrographic coverage obtained over the summit of Loihi. I am grateful for the assistance and discussions offered during the cruise by Dr. Stephen Hammond and Dr. Robin Holcomb, for critical reviews of this paper by Dr. Gary McMurtry, and also for the help of Ms. Cheryl Komenaka in the preparation and compilation of the manuscript.

MORPHOLOGY OF THE VOLCANIC EDIFICE

Loihi is on the eastern flank of the southern extension of Mauna Loa volcano (fig. 6.1). Its northern base is 1,900 m below sea level, whereas the southern base is 4,755 m below sea level, showing that the edifice of Loihi was built on an original submarine slope of about 5°. The volcano apparently grows through continued volcanism, not only from a caldera or summit craters, but also from an elongate rift system consisting of a 17-km-long southern rift limb and a 7-km-long northern rift limb (fig. 6.2). The Loihi rift and crater system is not unlike those for the summits of the neighboring Mauna Loa and Kilauea Volcanoes.

The steepness of the southwestern and northeastern slopes of the volcano (35° to 40° between the water depths of 1,830 and 3,290 m) and the presence of armchairlike indentations into the edifice (at 155°14′ W., 18°47.5′ N., at 155°17.5′ W., 18°52.5′ N. and at 155°15′ W., 18°57.5′ N.) suggest that extensive erosion in the form of downslope mass wasting has occurred contemporaneously with the growth of the edifice by submarine volcanism. Bottom photographs of the upper flanks of Loihi show the development of talus slopes through the breakup of pillow basalt and sheet and lobate flows. The sheet and lobate flows frequently exhibit the photographic characteristics of pahoehoe and aa lava at the summit. The shaded areas in figure 6.2 indicate sites of talus slope and downslope mass wasting as interpreted from the study of bottom photography and bathymetry. Examination of the bathymetric data does not show the presence of any extensive flank cones on Loihi. This evidence, however, does not preclude the possible presence of flank fissures. The process of talus generation and downslope mass wasting appears to be steady and extensive. Therefore, the upward growth of the volcano is dependent upon a constant source of extrusive magma from the summit crater and the upper rift zones.

The detailed bathymetric map of the Loihi summit (fig. 6.3) was prepared from the total bathymetric data base, including the NOAA hydrographic survey, the Woods Hole Oceanographic Institution ANGUS camera data, and the USN SASS surveys. The combined bathymetric data suggest that the summit of Loihi has an oval configuration with the long axis parallel to the rift zone. A summit depression about 2,800 m wide and 3,700 m long appears

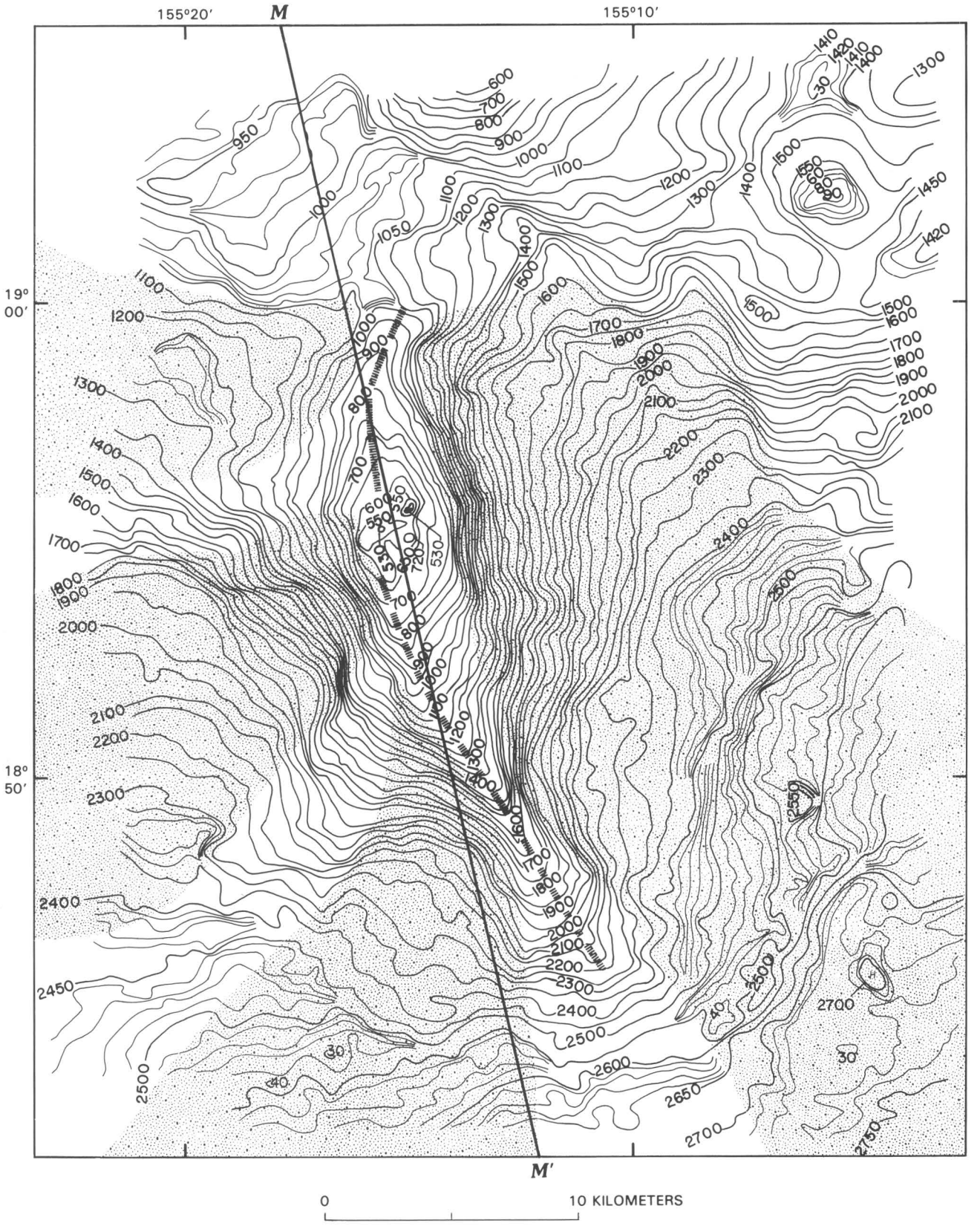

FIGURE 6.2.—Bathymetric map of Loihi, constructed from narrow-beam, multibeam surveys carried out aboard the U.S. Navy ship *Hess*. Water depth in fathoms (1 fathom = 1.83 m). Dotted pattern shows flanks of volcano that may have been subjected to mass wasting and talus formation. Heavy hachured line indicates the location of north and southeast rift zones of Loihi. Profile $M-M'$ refers to figure 6.6.

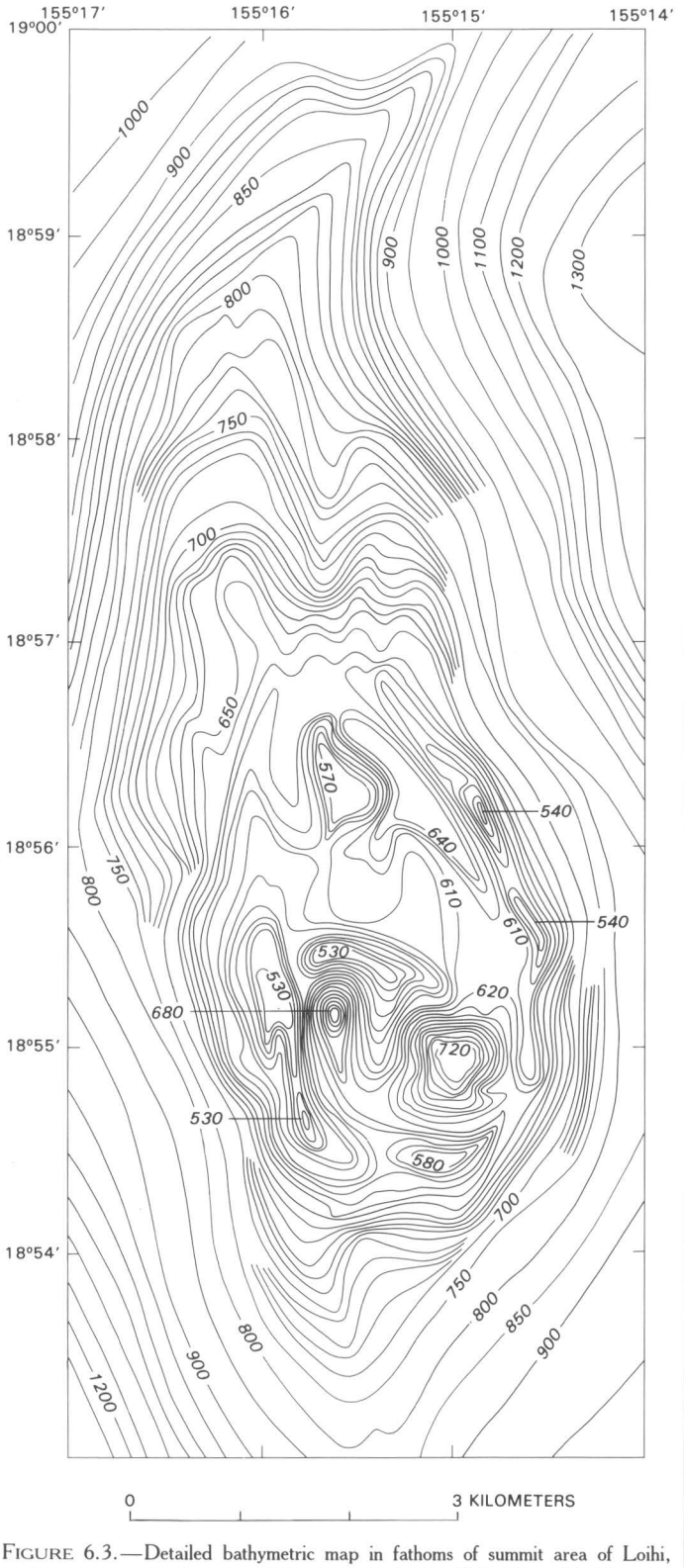

FIGURE 6.3.—Detailed bathymetric map in fathoms of summit area of Loihi, drawn from narrow-beam, multibeam surveys by the U.S. Navy ship *Hess* and narrow-beam surveys over summit area by the NOAA ships *Fairweather* and *Rainier*. Contour interval: 10 fathoms at summit and 50 fathoms on flanks.

to be structurally offset to the east of the north-south rift system. This depression, possibly a summit caldera, is approximately 128 m deep from rim to floor. The shallowest point along the rim is 969 m below sea level. Two pit craters within the caldera-like depression are 73 and 146 m deep. The Loihi summit depression may be a young caldera similar in its geologic structure to that of Kilauea caldera. Macdonald and Abbott (1970) suggest that the development of a caldera in a developing Hawaiian volcano, such as Kilauea, could begin early in the life of the volcanic edifice, which could be the case for young submarine volcanoes such as Loihi.

The geographic proximity of Kilauea and Loihi and the common deep magmatic source (Klein, 1982) suggest that both Kilauea and Loihi are in their early stages of edifice development. Indeed, the location and size of Loihi indicate that it may, in fact, be the youngest Hawaiian volcano. Therefore, the Loihi summit may be undergoing periods of swelling and shrinking as a result of shallow magmatic injection and removal through flank eruptions, similar to those that occur at Kilauea. Such magmatic processes could result in the formation of a subsidence caldera on Loihi. The summit depression of Loihi is surrounded by an oval ring of bathymetric highs (fig. 6.3) that could mark the outer rim of the caldera. Alternatively, the bathymetric highs could also mark a ring of individual volcanic cones or vents on the summit. A physiographic diagram of the summit of Loihi, based upon the high-resolution bathymetric data, was drawn by the author (fig. 6.4) to show the structural relation between the location of the summit depression and the flank rift zones (Malahoff and others, 1982). As in the case of Kilauea, the two pit craters appear to have been formed on the floor of the Loihi summit depression. The structural setting of the summit depression, based upon analyses of the bathymetric data, suggests an offset between the north flank and south flank rifts at the summit of Loihi.

STRUCTURE OF THE LOIHI EDIFICE

Studies of earthquake distribution beneath the summits of Mauna Loa, Kilauea and Loihi by Klein (1982) indicate that between the surface of the Island of Hawaii and a depth of about 40 km these volcanoes have separate volcanic conduits. Below that depth the earthquake hypocenters form a more common zone. The Hawaiian hot spot is interpreted by Klein (1982) to be at a depth of 60 km between and beneath the three volcanoes. Magmatic activity at the three volcanic sites can be explained by a dynamic model of an idealized Hawaiian volcano developed by Eaton and Murata (1960) and Eaton (1962), and by Klein (1982) from interpretation of seismic events associated with Kilauea and Loihi. This model shows the location of a magma reservoir to be 2 to 3 km beneath the summit caldera. This magma reservoir is refilled with magma from the 60-km-deep hot spot source. In this model, flank eruptions are followed by the partial emptying of the reservoir and, in the case of large flank eruptions, by the formation of pit craters at the summit. Growth of the volcanic edifice occurs as surface lava flows emanate from the summit and the flank rifts, and the intrusion of magma forms dike complexes within the rift zones. The source for these

magmatic events in the model appears to be a summit magma reservoir. It is assumed in this paper that the magmatic plumbing of Loihi is similar to that of the model.

Magnetic anomalies have been used in the past to study the size and shape of dike complexes within active and extinct volcanic centers of the Hawaiian Islands (Malahoff and Woollard 1968, 1970). Aeromagnetic studies of the active volcanoes along the Islands of Vanuatu (Malahoff 1970) showed the superposition of short-wavelength, reversed magnetic anomalies on the normally magnetized bipole anomalies located over the edifices of the volcanoes. Models based upon the wavelength of the observed magnetic anomaly, the magnetization of the volcanic edifice, and the contained dike complex were used by Malahoff and Woollard (1968, 1971) to construct calculated anomalies that were matched to those observed above the volcanic centers of Hawaii. Johnson and Malahoff (1971) conducted magnetic anomaly studies over Macdonald submarine volcano, at the southern end of the Austral Island chain. Macdonald Volcano marks the active volcanic center of the Austral Islands hot spot. A 500-nanotesla (nT), reversely polarized magnetic anomaly is superposed upon the normally polarized bipole of the volcano. In the aeromagnetic study of the Vanuatu volcanoes, Malahoff (1970) detected a similar reversely magnetized short-wavelength anomaly over the active Ambrym Volcano and interpreted that anomaly to reflect the presence of rocks having temperatures above the Curie point, approximately 578 °C for magnetite (Nagata, 1961), within the edifice of the volcano. Johnson and Malahoff (1971) interpreted the origin of the observed, reversely polarized, secondary magnetic anomaly above Macdonald Volcano to also be due to the presence of volcanic rocks heated above the Curie point within the edifice of the volcano, thus possibly marking the site of a magma reservoir.

The compilation of the residual magnetic anomaly data over the southern end of the Hawaiian Island chain is depicted in figure 6.5. All volcanoes on the Island of Hawaii show the presence of normally polarized, high-amplitude magnetic anomalies, such as 750 nT for Kohala Volcano, 1,250 nT for the east rift zone of Kilauea, 900 nT for Mauna Kea, 100 nT for Kilauea, 600 nT for Hualalai, 800 nT for Mauna Loa and 1,100 nT for Loihi. The high-amplitude anomalies are formed by the combined magnetic effects of the volcanic edifice and the intrusive dike systems within the edifice. The aeromagnetic profiles over Loihi were flown at an altitude of 2,800 m. A northwest- to southeast-oriented magnetic anomaly profile was also taken aboard the research vessel *Kana Keoki* across the summit of Loihi and approximately above the long axis of the edifice (profile *M–M'*, fig. 6.2). Figure 6.6 illustrates the wavelength and amplitude of the residual magnetic anomaly of this profile. At sea level, the total amplitude of the normally polarized, residual magnetic anomaly above Loihi is 3,900 nT (peak-to-peak). It is assumed that the normal polarity of the residual magnetic anomaly is due to the presence of flow and dike basalt younger than 0.7 Ma, the age of the present normal magnetic polarity epoch (LaBrecque and others, 1977).

It is interesting to note that superposed upon the normally polarized magnetic bipole anomaly is a reversely magnetized bipole anomaly with a peak-to-peak amplitude of 1,600 nT. As with

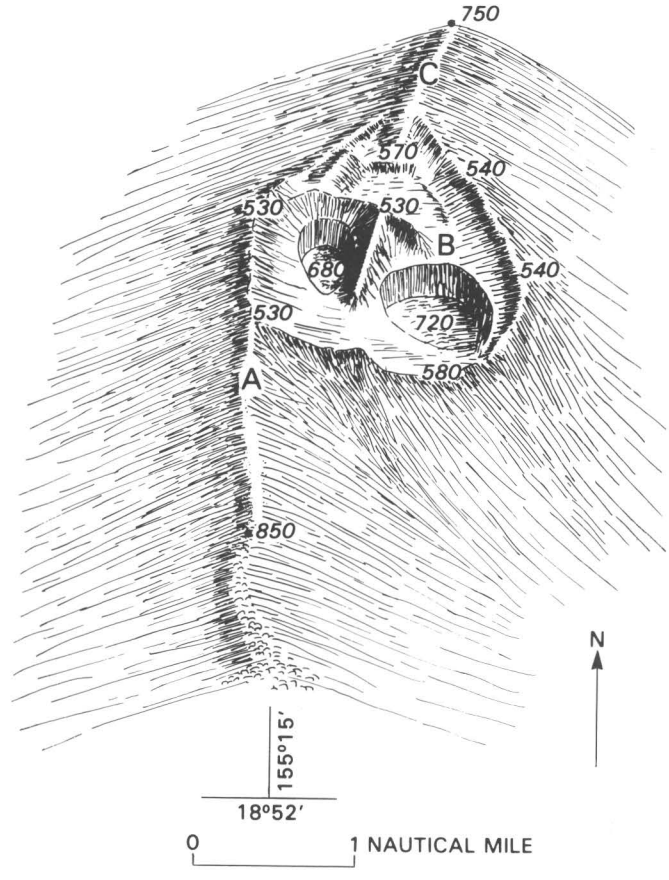

FIGURE 6.4.—Perspective physiographic drawing of summit of Loihi, constructed from bathymetric data base shown in figure 6.3. Spot depths in fathoms. Principal physiographic features: A, southeast flank rift; B, summit caldera with pit craters; C, north flank rift.

similar studies of secondary bipole residual magnetic anomalies observed over active volcanoes (Malahoff, 1970; Johnson and Malahoff, 1971), the interpretation of the observed magnetic anomaly is based upon several speculative source models. Using a two-dimensional model technique (Heirtzler and others, 1962) and the assumption of only a terrain effect for the normally magnetized bipole anomaly, a bulk rock magnetization of 75×10^{-3} emu was required to construct a calculated anomaly for the edifice of Loihi that would match the observed bipole anomaly. The assumed magnetization of 75×10^{-3} emu for the volcanic edifice of Loihi falls within the range of 20×10^{-3} emu to 150×10^{-3} emu measured by Johnson and Clague (1981) for the magnetization of samples recovered by rock dredging from Loihi. The observed anomaly can also be matched with a calculated anomaly based upon a terrain model with an associated dike complex having a magnetization contrast of 15×10^{-3} emu, extending to a depth of 40 km below the summit. In both of these terrain-effect calculations, however, the reversely magnetized, superposed bipole anomaly (fig. 6.6) is difficult to account for. As a speculation, the reversely polarized anomaly was modeled by using a nonmagnetic block (rocks heated

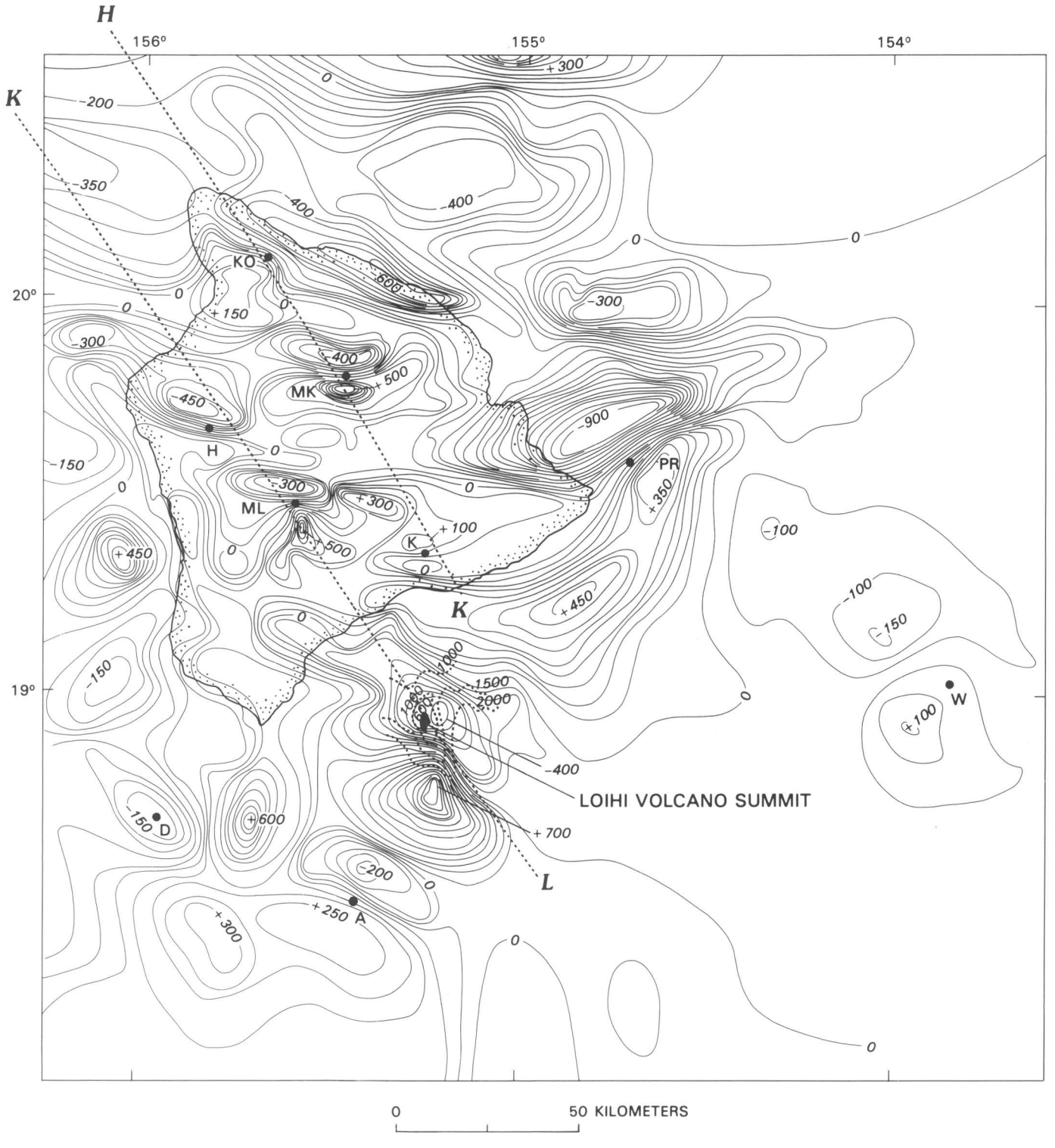

FIGURE 6.5.—Residual total-force magnetic anomaly map of Island of Hawaii and surrounding ocean areas; intensity in nanoteslas (nT). Data obtained from aeromagnetic flights, altitude 2,000 m above sea level over ocean and lower slopes of island. Flight altitude 3,000 m above Mauna Kea (MK) and Mauna Loa (ML). Other volcanic centers: KO, Kohala; H, Hualalai; K, Kilauea; PR, Puna Ridge; W, Wini Seamount; A, Apuupuu Seamount; D, Day Seamount. Dotted contour lines over Loihi summit show general bathymetry in fathoms. Haleakala-Mauna Kea-Kilauea trace of hot spot shown by line *H–K*; the Kahoolawe-Hualalai-Mauna Loa-Loihi trace shown by line *K–L*. Aeromagnetic data from Malahoff and Woollard (1970).

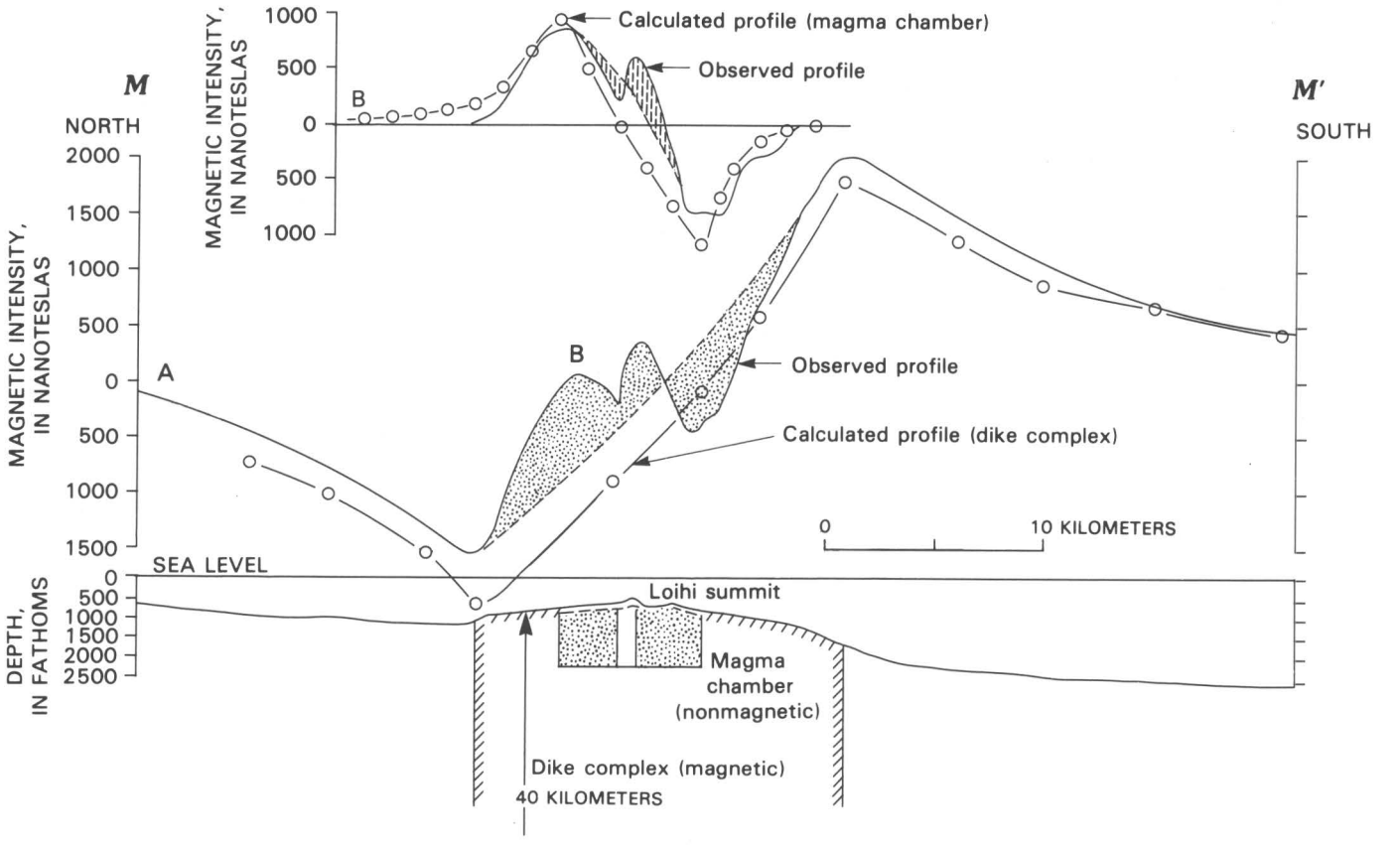

FIGURE 6.6.—Residual total-force magnetic-anomaly profile, M–M' (see location on fig. 6.2), observed at sea level above flank rifts and summit of Loihi. Magnetic intensity in nanoteslas (nT). Principal components of profile: profile A, normally polarized residual total-force magnetic anomaly; profile B, stippled area representing reversely magnetized section along profile A. Profile B also shown in upper diagram in form of residual anomaly subtracted from profile A. Calculated profile, lower diagram, based on model of surficial terrain effect and a magnetic dike complex, with assumed magnetization contrast of 15×10^{-3} emu extending to depth of 40 km. Calculated profile, upper diagram, is based on model of nonmagnetic magma chamber within Loihi edifice. Dashed area (upper diagram) represents normally polarized anomaly segment within profile B assumed to reflect small magnetic body within magma chamber.

above the Curie point) 7 km wide, possibly 3 km in vertical extent, located beneath the surface of the Loihi summit and divided in half by a vertical rock body less than 1 km wide having temperatures below the Curie point (normally polarized; fig. 6.6). This speculative interpretation of the observed residual magnetic anomaly profile over Loihi is based upon one of a number of models and suggests the presence of a heated rock body within the edifice of Loihi Volcano. This rock body could be a shallow summit magma reservoir that, as at Kilauea, may be structurally expressed at the summit by the presence of a caldera and pit craters.

NEOVOLCANIC ZONES OF THE LOIHI SUMMIT

The geologic interpretation of bottom photographic data (fig. 6.7) from the summit of Loihi shows a broad range of lava types and vents present on the summit. The photographic data were obtained using the Woods Hole Oceanographic Institution's ANGUS camera system, with a bottom-transponder navigation network and tow altitudes of 5 to 20 m above the ocean floor. The data were visually examined for the presence of geologic features such as fresh or broken pillow lava, lobate, sheet, aa and pahoehoe lava flows, talus, exposed dike systems, smooth or rippled sediment, visible structural features such as faults and fissures, and evidence of hydrothermal activity, such as yellow, orange or green precipitates (that is, nontronite; Malahoff and others, 1982), or the presence of hydrothermal chimneys. Photointerpretation techniques used in this study were similar to those used by Ballard and others (1979, 1982) and Crane and Ballard (1980) for ANGUS photographic data taken over the neovolcanic zone of the Galapagos Rift. Photographs were analyzed, frame by frame, and condensed into the interpretative geologic map shown in figure 6.7. The most interesting observation derived from the study of the photographic data over the Loihi summit is the relatively small area covered by fresh lava flows. The

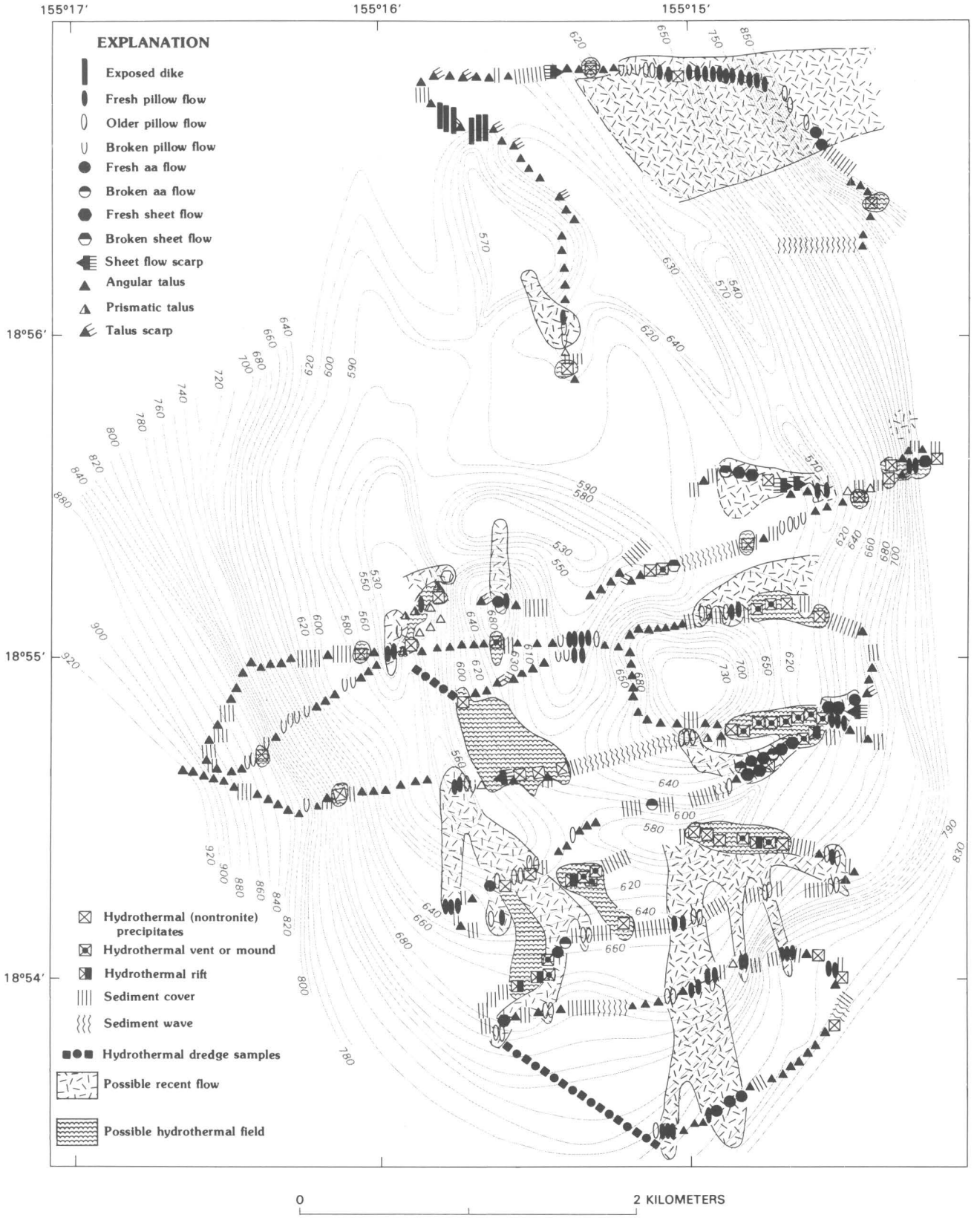

FIGURE 6.7.—Interpretive geologic map of Loihi summit area. Geologic symbols are drawn along tracklines of ANGUS camera system. Geologic data are superposed upon high-resolution bathymetric map (contour interval, 10 fathoms).

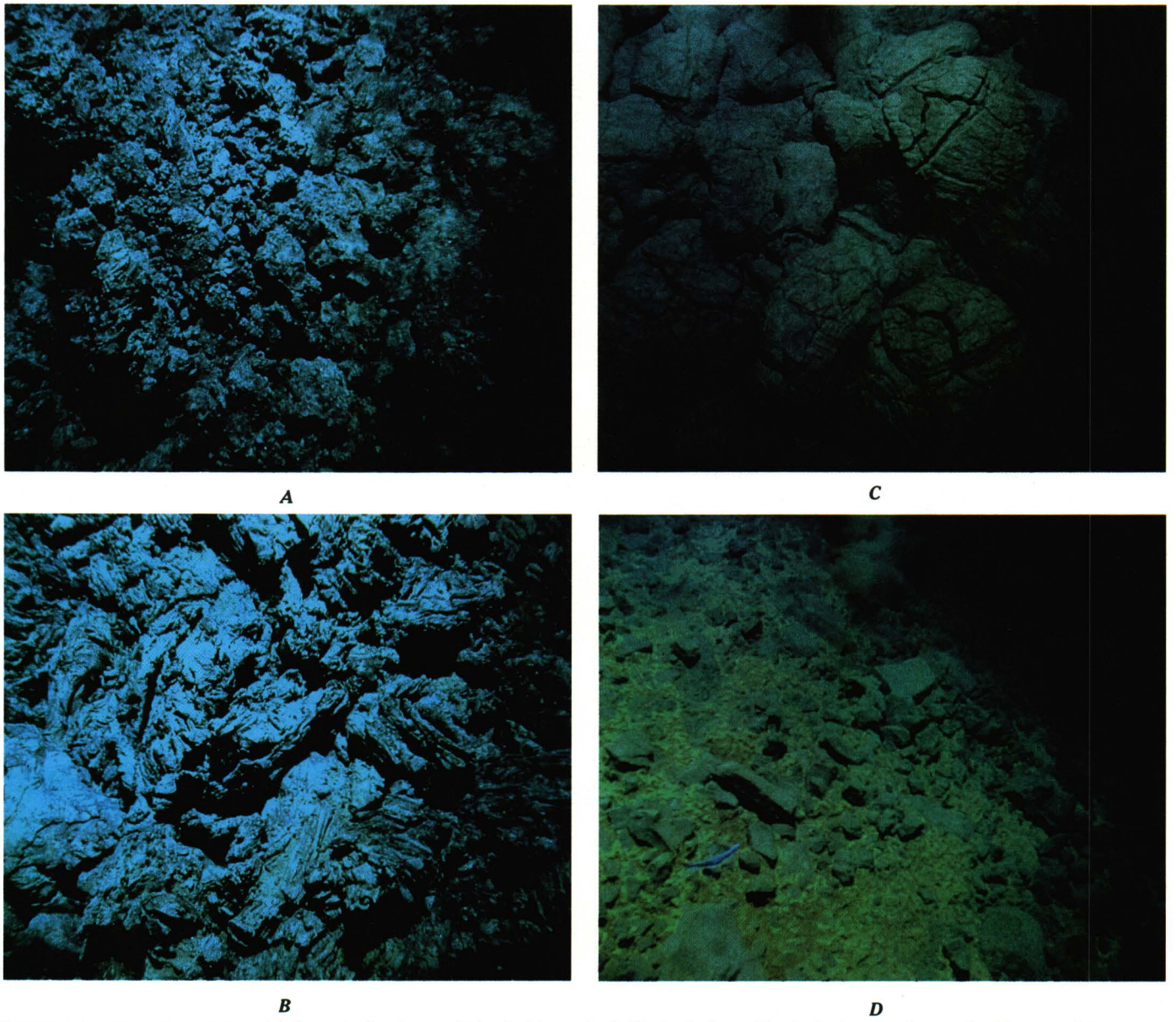

FIGURE 6.8.—Ocean-floor photographs of aa and pillow flows and talus, Loihi summit. ***A***, Blocky, fresh transitional pahoehoe to aa flow, south caldera rim; photocoverage 14 by 22 m, location at 155°14.9′ W., 18°53.7′ N. ***B***, Blocky, fresh transitional from pahoehoe to aa flow; photocoverage 7 by 11 m; location same as in 8*A*. ***C***, Fresh pillow basalt, northeast rim of Loihi caldera; photocoverage 10 by 14 m; location at 155°14.9′ W., 18°56.8′ N. ***D***,Talus along western inner margin of the summit depression; photocoverage 10 by 14 m. Yellow to orange hydrothermal nontronite covers much of central area of photograph; location at 155°15.95′ W., 18°55′ N.

freshest lava flows, those with high photoreflectivity and no visible sign of sediment coverage (fig. 6.8*A*, *B*), were found to originate from volcanic centers along the southern edge of the Loihi summit depression. The two longest lava flows appear to extend a maximum distance of 1,800 m from their sources, which are at water depths of 970 to 1,060 m. The photographic data suggest that these lava flows consist largely of pillow (fig. 6.8C) and lobate flows at the vent sites and transform into lava types similar to aa or broken sheet flows (fig. 6.8*A*, 6.9*B*) downslope from the vent site.

The steeper slopes of Loihi outside the summit depression are covered by talus, as are the steeper, inside slopes of the pit craters (fig. 6.9*B*). The floors of the two pit craters appear to be covered by sediment. Talus appears to be common in the photographic data. Sheet flows, similar in their photographic appearance to those observed by Ballard and others (1979, 1982) over the Galapagos Ridge, were photographed at several sites at the northeastern rim of the summit depression (fig. 6.9*A*). Sheet flows appear to form at the site of submarine volcanic eruptions where higher magmatic volumes and higher extrusion temperatures may have occurred. These flows occupy areas of the Loihi summit that are less than a few thousand square meters in area. They appear to undergo mechanical breakup soon after extrusion, with the downslope mass wasting resulting in the formation of talus (fig. 6.9*B*). Downslope mass-wasting talus development has apparently been extensive enough to expose the

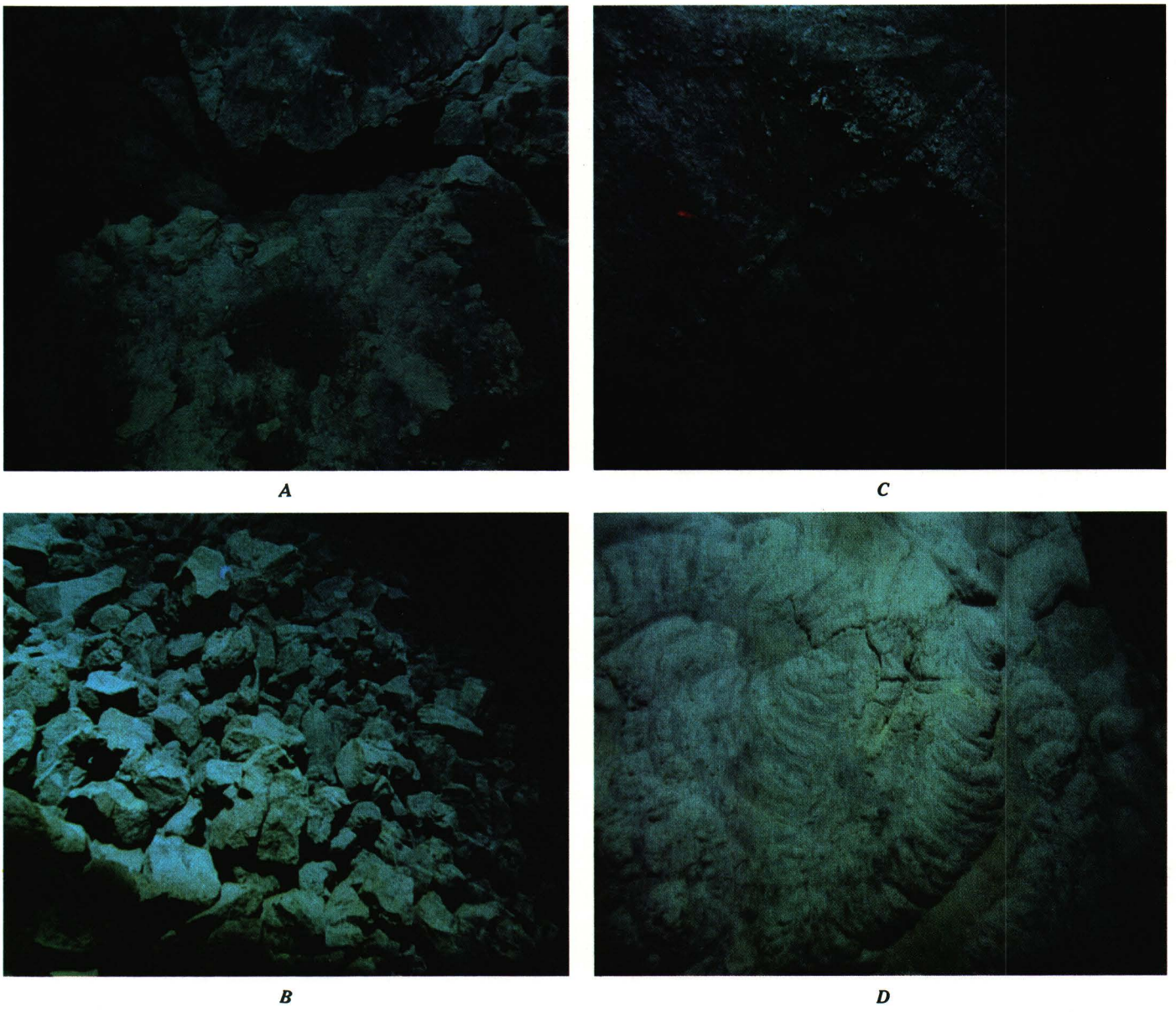

FIGURE 6.9.—Ocean-floor photographs of fresh sheet flows, broken sheet flows, exposed dikes, and lobate flows, Loihi summit. ***A***, Fresh sheet flow, showing initial stages of mechanical breakup; photocoverage 13 by 20 m; location at 155°14.8′ W., 18°54.65′ N. ***B***, Talus derived from broken sheet flow; photocoverage 10 by 14 m; location same as in 9*A*. ***C***, Exposed dike rocks, north rim Loihi caldera; photocoverage 24 by 36 m; location at 155°15.7′ W., 18°50.7′ N. ***D***, Ponded lobate and pillow flows; photocoverage 17 by 25 m, location at 155°15.4′ W., 18°56′ N.

underlying dike structure (fig. 6.9*C*) at the northern edge of the summit depression. Ponded lava is also observed (fig. 6.9*D*). Incipient lobate flows appear to have developed in association with the lateral lava drainage out of the lava ponds, that formed in flat-lying areas of the summit depression.

The slopes of the two pit craters within the summit depression appear to be covered by talus. Rippled sediment and talus cover large areas of the basaltic floor of the summit depression and the pit craters. Lava flows with the freshest appearance in the photographs are on the southern rim of the summit depression. The lava appears to have erupted from vents on the local highs that have the appearance of cones.

Extensive patches of hydrothermally precipitated yellow, red or green iron oxide and nontronite (Malahoff and others, 1982; DeCarlo and others, 1983) cover areas of the talus slopes (fig. 6.8*D*) and also form fields of individual chimneys 0.5 to 2.0 m high (fig. 6.10). Transponder-controlled shipboard dredging of two of the hydrothermal vent sites along the southern edge of the summit depression produced samples of yellow-brown goethite and nontronite, similar in composition to the iron-rich montmorillonite-nontronite recovered from the Red Sea Rift, the East Pacific Rise and the Galapagos hydrothermal mounds (Malahoff and others, 1982), as well as from the caldera of Axial Volcano on the Juan de Fuca Ridge (McMurtry and others, 1984). The shape and size of

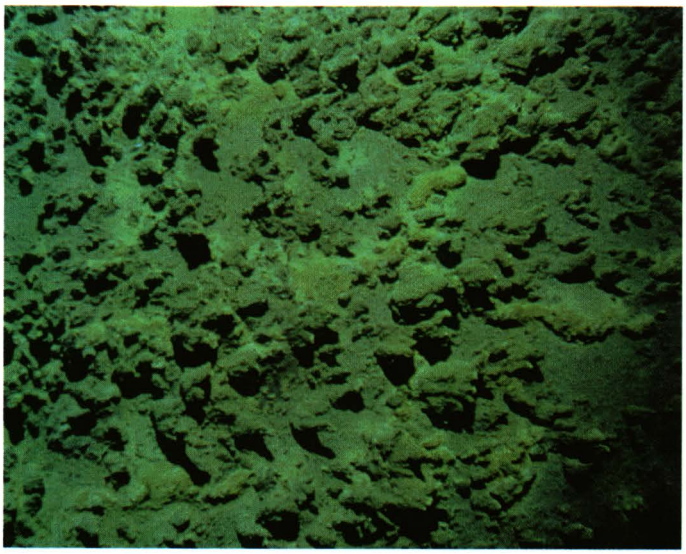

FIGURE 6.10.—Ocean-floor photograph of hydrothermal field, southeast edge, Loihi summit depression. Hydrothermal chimneys 0.5 to 2 m high. Dark areas to side of chimneys are shadows cast by camera strobe lights; photocoverage 14 by 22 m, location at 155°14.75′ W., 18°54.45′ N.

the low temperature hydrothermal chimneys of Axial caldera are similar to those photographed by the ANGUS system over Loihi. More than 100 chimneys can be counted in the photograph of figure 6.10, which covers an area of approximately 22 by 14 m.

The hydrothermal vent fields on the summit of Loihi are as long as 600 m. Malahoff and others (1982) measured water temperature anomalies of greater than 1 °C at a water depth of 10 m above the ocean floor where the nontronite-iron oxide deposits are situated, suggesting an extrapolated temperature of about 30 °C at the vent sites on the ocean floor. Most of the hydrothermal fields mapped in this study are characterized by the presence of reddish-yellow hydrothermal precipitates deposited on the surface of sediments (fig. 6.10), on talus (fig. 6.8*D*) or along cracks and fissures of sheet flows. All the hydrothermal vents with identifiable chimneys mapped in this study are adjacent to fresh lava flows (fig. 6.7). The association between fresh lava flows, visible hydrothermal vent fields and water temperature anomalies is common at midocean ridge-crest sites (Haymon and Kastner, 1980; Lonsdale and others, 1980; Ballard and others, 1981; Bäcker and others, 1985; Hekinian and Fouquet, 1985) and ridge-crest submarine volcanoes such as Axial (Malahoff and others, 1984; McMurtry and others, 1984) and along off-ridge seamounts such as the Red and Green Seamounts off the East Pacific Rise at 20°50′ N. (Lonsdale and others, 1982). At the active vent sites of Axial caldera, outer zones of disaggregated nontronite precipitates are found beyond the inner zone of sulfide precipitation and the middle zone of nontronite chimneys (McMurtry and others, 1984; Arquit and others, 1985). A similar outer zone, consisting of isolated patches of nontronite deposits, is found precipitated on the upper talus-covered slopes of Loihi, and thus probably marks the outer zones of Loihi hydrothermal fields.

The depth of the hydrothermal vent fields on Loihi mapped in this study ranges from a shallow point of 1,043 m below sea level at the southern rim of the summit depression to 1,500 m below sea level along the flanks of Loihi. Other hydrothermal vent sites may be present along the north flank and south flank rifts of Loihi.

To date, no high-temperature hydrothermal minerals, such as polymetallic sulfides, have been sampled during this or other shipboard rock-dredging expeditions on Loihi (Moore and others, 1982; DeCarlo and others, 1983), although it is possible that polymetallic sulfides may have been precipitated as chimneys (observed in the bottom photographs) or beneath the surface of Loihi (DeCarlo and others, 1983). High-temperature water anomalies were not detected over the summit of Loihi during the current studies, and no evidence for hydrothermal vent macro-organisms, such as worms or clams, has been observed in the current photographic data set taken over the summit of Loihi.

DISCUSSION

Loihi submarine volcano is a young Hawaiian volcano that is 969 m below sea level at the southern end of the Kahoolawe-Hualalai-Mauna Loa limb of the Hawaiian hot spot trace. The comprehensive bathymetric, photographic, geologic, and magnetic studies conducted over the Loihi summit show the volcano has structural similarities to the young subaerial volcanoes of Hawaii. The 2.8-km-wide summit depression, with a rim depth of 969 m below sea level and a floor depth of 1,134 m below sea level could represent the initial stages of submarine caldera development. Two pit craters within the summit depression are similar in their structural setting to craters on the summit of Kilauea Volcano. The summit depression of Loihi appears to be at the intersection of two flank rifts. Most of the volcanic extrusions that have built the edifice of Loihi probably erupted from the two flank rifts and from summit vents, thus giving Loihi its elongate shape. Although seismic studies show that the magma supply for Mauna Loa, Kilauea and Loihi originates from a common source (probably the Hawaiian hot spot) at a depth of 60 km or more beneath the surface, all three volcanoes apparently have individual conduits and seismic further showing that the magmatic cycles of the three volcanoes are largely independent of each other. A pronounced 3,900-nT peak-to-peak residual total-force magnetic anomaly is also observed over the edifice of Loihi. Within the configuration of this normally polarized, bipole anomaly, a shorter wavelength anomaly of amplitude 1,600 nT and having a reversed polarization is observed. The configuration of reversed polarization within a normally polarized magnetic anomaly profile has been observed over other active subaerial and submarine volcanoes. A speculative interpretation of the residual total-force magnetic anomaly observed over Loihi suggests the presence of a heated rock body or magma source, with temperatures above 578 °C, 7 km wide and 3 km thick located within the edifice.

Visual examination of the photographic data reveals the most common rock type to be volcanic talus. Ten fresh lava flows were mapped in this study with their vent sources traced to volcanic mounds located in and around the summit depression. The most extensively mapped lava flows with the freshest appearance are

about 2 km long and are along the southern rim of the depression; this lava appears to have erupted from 100- to 150-meter-high volcanic mounds. The lava mapped within these areas consists of sheet, lobate and pillow flows, with aa flows or broken sheet flows mapped along the steeper slopes of the summit. The freshest flows have been identified by Moore and others (1982) as tholeiitic in composition, as compared to older alkalic lava dredged from the Loihi edifice. The broken ends of fresh lava flows frequently observed directly above the talus piles on Loihi indicate that new lava is mechanically disintegrated into talus along the summit slopes shortly after formation, thereby building a submarine volcanic edifice that may be composed of alternating layers of talus and lava flows. Fields of hydrothermal precipitates consisting of blankets and chimneys are all found to be associated with fresh lava flows. No visible hydrothermal vent communities, such as the worm and clam communities observed at the East Pacific Rise or the Juan de Fuca hydrothermal vent sites, were observed in this study. Similarly, no high water temperatures were detected with the acoustic thermometer mounted on the camera sled. Bottom-transponder navigation-controlled dredging of the hydrothermal vent sites produced samples of nontronite; therefore, the hydrothermal blankets and chimneys observed in the photographs are probably constructed of nontronite, iron oxide, and other low-temperature hydrothermal precipitates. Higher temperature polymetallic sulfide deposition may have taken place within the edifice of Loihi during the upward migration of the hydrothermal fluids to the surface. The data described in these studies do not preclude the presence of unmapped high temperature smokers on Loihi. The tectonic, volcanic, and hydrothermal processes observed over the summit of Loihi probably represent submarine geologic processes that may be typical of those active along the summits of emerging hot spot volcanic islands and other major submarine basaltic volcanoes.

REFERENCES

Arquit, A., Malahoff, A., and McMurtry, G.M., 1985, Chemical and biological halos of a hydrothermal vent system, Axial caldera, Juan de Fuca Ridge: American Geophysical Union, Eos, v. 66, p. 401.

Bäcker, H., Lange, J., and Marchig, V., 1985, Hydrothermal activity and sulphide formation in axial valleys of the East Pacific Rise crest between 18 and 22° S.: Earth and Planetary Science Letters, v. 72, p. 9–22.

Ballard, R.D., Holcomb, R.T., and van Andel, T.H., 1979, The Galapagos Rift at 86° W.: 3. Sheet flows, collapse pits, and lava lakes of the rift valley: Journal of Geophysical Research, v. 84, p. 5407–5422.

Ballard, R.D., Francheteau, J., Juteau, T., Rangan, C., and Normark, W., 1981, East Pacific Rise at 21° N.: the volcanic, tectonic, and hydrothermal processes of the central axis: Earth and Planetary Science Letters, v. 55, p. 1–10.

Ballard, R.D., van Andel, T.H., and Holcomb, R.T., 1982, The Galapagos Rift at 86° W.: 5. Variations in volcanism, structure, and hydrothermal activity along a 30-kilometer segment of the rift valley: Journal of Geophysical Research, v. 87, p. 1149–1161.

Crane, K., and Ballard, R.D., 1980, The Galapagos Rift at 86° W.: 4. Structure and morphology of hydrothermal fields and their relationship to the volcanic and tectonic processes of the rift valley: Journal of Geophysical Research, v. 85, p. 1443–1454.

DeCarlo, E.H., McMurtry, G.M., and Yeh, H.-W., 1983, Geochemistry of hydrothermal deposits from Loihi submarine volcano, Hawaii: Earth and Planetary Science Letters, v. 66, p. 438–449.

Eaton, J.P., 1962, Crustal structure and volcanism in Hawaii, *in* The Crust of the Pacific Basin: American Geophysical Union Monograph 6, p. 13–29.

Eaton, J.P., and Murata, K.J., 1960, How volcanoes grow: Science, v. 132, p. 925.

Emery, K.O., 1955, Submarine topography south of Hawaii: Pacific Science, p. 286–291.

Haymon, R.M., and Kastner, M., 1980, Hot spring deposits on the East Pacific Rise at 21° N.: preliminary description of mineralogy and genesis: Earth and Planetary Science Letters, v. 53, p. 363–381.

Heirtzler, J.R., Peter, G., Talwani, M., and Zurflueh, E.G., 1962, Magnetic anomalies caused by two dimensional structure; their computation by digital computers and their interpretation: New York, Columbia University Technical Reports, v. 6, p. 6–62.

Hekinian, R., and Fouquet, Y., 1985, Volcanism and metallogenesis of axial and off-axial structures on the East Pacific Rise near 13° N.: Economic Geology, v. 80, p. 221–229.

Jackson, E.S., Silver, E.A., and Dalrymple, G.B., 1972, Hawaiian-Emperor chain and its relation to Cenozoic circum-Pacific tectonics: Geological Society of America Bulletin, v. 83, p. 601–617.

Johnson, H.P., and Clague, D.A., 1981, Magnetic properties of submarine basalt as a function of rock geochemistry: samples from Loihi Seamount, Hawaii: American Geophysical Union, Eos, v. 62, p. 1082.

Johnson, R., and Malahoff, A., 1971, Relation of Macdonald Volcano to migration of volcanism along the Austral Chain: Journal of Geophysical Research, v. 76, p. 3282–3290.

Klein, F.W., 1982, Earthquakes at Loihi submarine volcano and the Hawaiian hot spot: Journal of Geophysical Research, v. 87, p. 7719–7726.

LaBrecque, J.L., Kent, D.V., and Cande, S.C., 1977, Revised magnetic polarity time scale for the Late Cretaceous and Cenozoic time: Geology, v. 5, no. 6, p. 330–335.

Lonsdale, P.F., Batiza, R., and Simkin, T., 1982, Metallogenesis at seamounts on the East Pacific Rise: Marine Technology Society Journal, v. 16, p. 54–61.

Lonsdale, P.F., Bischoff, J.L., Burns, V.M., Kastner, M., and Sweeney, R.E., 1980, A high-temperature hydrothermal deposit on the seabed at a Gulf of California spreading center: Earth and Planetary Science Letters, v. 49, p. 8–20.

Macdonald, G.A., and Abbott, A.T., 1970, Volcanoes in the sea—the Geology of Hawaii: Honolulu, University of Hawaii Press, 441 p.

Malahoff, A., 1970, Gravity and magnetic studies of the New Hebrides Island Arc: New Hebrides, British Service, 67 p.

Malahoff, A., McMurtry, G.M., Hammond, S., and Embley, R.W., 1984, High temperature hydrothermal fields; Juan de Fuca Ridge axial volcano: American Geophysical Union, Eos, v. 65, p. 1112.

Malahoff, A., McMurtry, G.M., Wiltshire, J.C., and Yeh, H.-W., 1982, Geology and chemistry of hydrothermal deposits from active submarine volcano Loihi, Hawaii: Nature, v. 298, p. 234–239.

Malahoff, A., and Woollard, G.P., 1968, Magnetic and tectonic trends over the Hawaiian Ridge, *in* Knopoff, L., Drake, C.L., Hart, P.J., ed., The Crust and Upper Mantle of the Pacific Area: Washington, D.C., American Geophysical Union, Monograph 12, p. 241–276.

——— 1970, Geophysical studies of the Hawaiian Ridge and Murray Fracture Zone, *in* Maxwell, A.E., ed., The Sea-Ideas and observations on the progress in the study of the seas: New York, Interscience Publishers, p. 73–131.

McMurtry, G.M., Malahoff, A., Feely, R.A., and Massoth, G.J., 1984, Geology and chemistry of the hydrothermal nontronite deposits from the Juan de Fuca Ridge: American Geophysical Union, Eos, v. 65, p. 1112.

Moore, J.G., Clague, D.A., and Normark, W.R., 1982, Diverse basalt types from Loihi Seamount, Hawaii: Geology, v. 10, p. 88–92.

Nagata, T., 1961, Rock Magnetism: Tokyo, Maruzen Company, Ltd., 350 p.

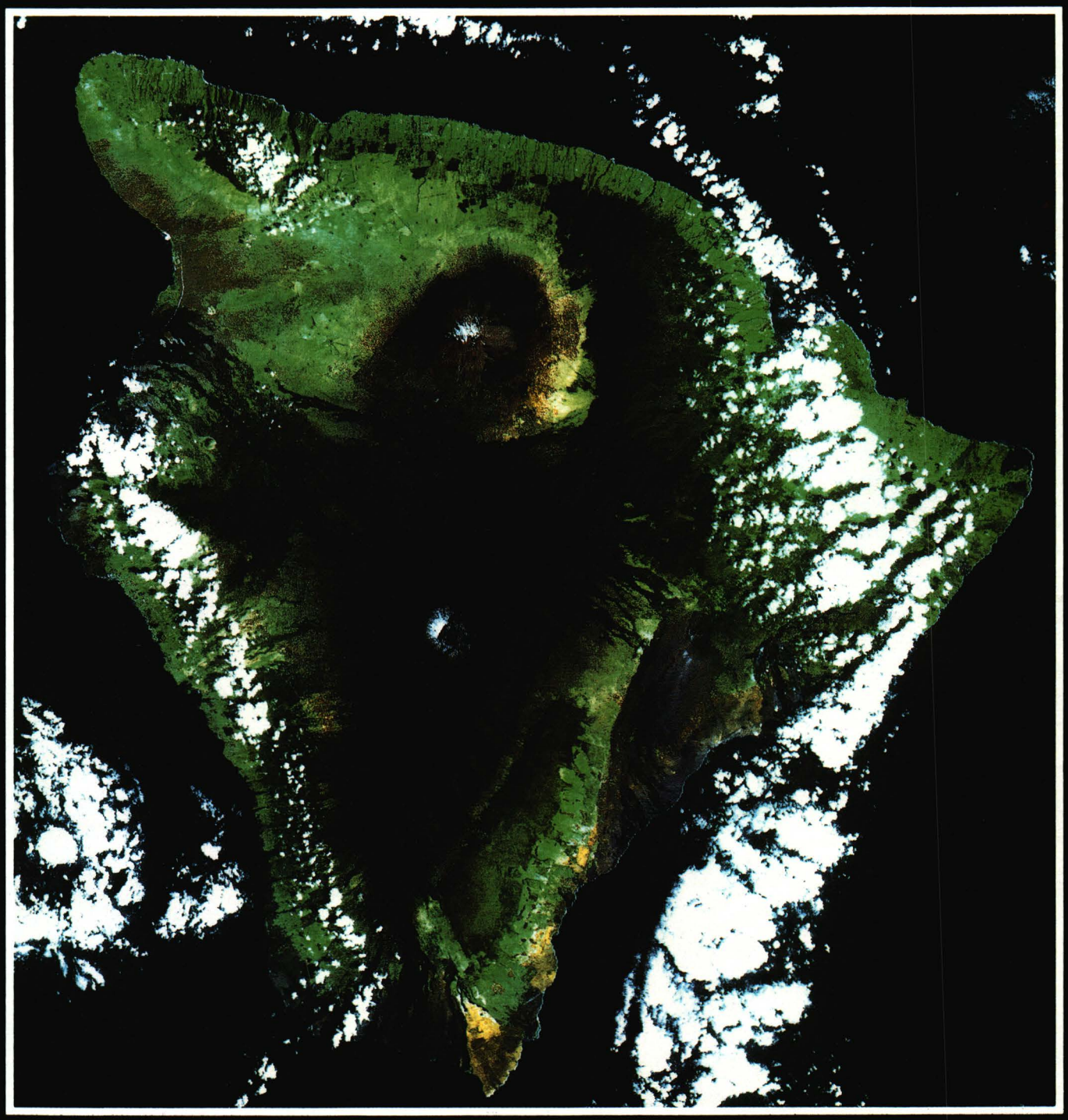

Landsat image of the Island of Hawaii, taken February 11, 1973. This rendition, made at the USGS Flagstaff image-processing facility, is a simulation of the true color; the blue component, not measured by Landsat, was artificially derived by extrapolation from the red and green channels. Clearly visible in lower center are lava flows from the southwest and northeast rift zones of Mauna Loa Volcano, radiating from its summit caldera.

Man with Paddle
Hawaiian Petroglyph
Puna, Hawaii

GEOLOGY OF THE ISLAND OF HAWAII

The Island of Hawaii, aptly termed the "Big Island," is the setting for all current and most historical volcanic activity in the Hawaiian Chain, and the work of the Hawaiian Volcano Observatory has of necessity been concerned largely with the active volcanoes. Modern volcanism can only be understood, however, through study of past volcanic activity. Accordingly, many workers at HVO have participated in mapping projects that extend our knowledge of Hawaiian volcanic history at least back to the emergence of the volcanoes above sea level.

The latest geologic map of the Island of Hawaii was published by Harold Stearns and Gordon Macdonald in 1946 as part of a series of maps and descriptive bulletins for all the Hawaiian Islands. A revision of that map currently being prepared by a consortium of USGS and university geologists will incorporate information from a number of chapters in this section.

The section begins with a broad view of where we are now and where we have been in our understanding of the geology of Hawaii. With modern satellites we no longer have to confine ourselves to earthbound observation—chapter 8 gives us a view from space. Chapters 9 and 10 treat radiocarbon dating, a technique that has been essential in unraveling the prehistoric record of Hawaiian volcanism. Kilauea is the most active Hawaiian volcano in recent times, and chapters 11 through 17 discuss its activity from the most recent to the most ancient. Two following chapters on Mauna Loa provide comparable insight into both the historical and prehistoric behavior of that largest volcano in the Hawaiian Chain. The third volcano on the Big Island that can be considered active is Hualalai; chapter 20 provides the first modern assessment of its geologic history. Mauna Kea, dormant for about 4,000 years, underwent Pleistocene glaciation as well as volcanic activity—the relation between the two is discussed in chapter 21.

The section concludes with a revised assessment of volcanic hazards in the Hawaiian Islands; such hazards are mostly associated with the active volcanoes on the Island of Hawaii. Revised hazard-zone maps should be of value to all concerned with use of the precious and fragile land resources on the Big Island.

GEOLOGIC HISTORY AND EVOLUTION OF GEOLOGIC CONCEPTS, ISLAND OF HAWAII

By Donald W. Peterson *and* Richard B. Moore

ABSTRACT

The Island of Hawaii consists of five Quaternary shield volcanoes: Kohala, Mauna Kea, Hualalai, Mauna Loa, and Kilauea, in order of latest activity. Loihi Seamount, an active volcano 25–30 km south of the island, may eventually grow to merge with the Island of Hawaii.

Early Polynesian settlers on Hawaii kept no written records, and the visits of the earliest European explorers were too brief to contribute much information about the volcanoes. Systematic observations of Hawaiian volcanic activity began in the 1820's, and records by missionaries, explorers, botanists, and geologists described the general characteristics of Hawaiian eruptions and the morphology of the volcanoes. During the 19th century, the geologists J.D. Dana and C.E. Dutton developed basic concepts of Hawaiian volcanic processes that differed considerably from ideas then commonly held about volcanism. The Hawaiian Volcano Observatory, founded in 1912 under the direction of T.A. Jaggar, launched a program of continuous, systematic surveillance of Kilauea and Mauna Loa Volcanoes, which has continued until the present time.

During the first half of the 20th century, understanding of the geologic history of the island advanced by means of frequent observations of eruptions, recognition and study of contrasting rock types, and comprehensive reconnaissance mapping that charted the distribution of rock types and the structure of the volcanoes. More recently, additional understanding has been achieved through geophysical studies, offshore submarine investigations, numerical dating of rocks, advances in petrology and geochemistry, continuous surveillance and monitoring of eruptions, and more detailed geologic mapping.

These continuing advances have permitted earlier concepts on the evolution of Hawaiian volcanoes to be gradually modified, and the order of events, as currently understood, follows this sequence:

1. Initial stage. Basanite, alkalic basalt, and lava transitional to tholeiite build a moderately steep-sided edifice from the deep ocean floor.
2. Shield-building stage. Principal development of shield volcano; eruptions are frequent and voluminous from vents in summit area and along radial rift zones; repeated cycles of caldera formation and filling; weight of growing edifice causes regional subsidence. Three substages: (a) submarine—pillow lavas build moderately sloping submarine edifice; (b) sea-level—vigorous interaction between degassing molten lava and ocean waves, lava-steam explosions, hyaloclastite deposits; (c) subaerial—pahoehoe and aa lava flows build gently sloping shield volcano; processes of substages a and b may continue below and at sea level.
3. Capping stage. Alkalic basalt and related differentiated rocks build steeply sloping cap over tholeiitic shield; eruption frequency diminishes, explosive eruptions increase; final caldera buried.
4. Erosional stage. Frequency of eruptions declines to zero; stream and wave erosion cuts valleys and cliffs; coral reefs may form offshore.
5. Renewed volcanism stage. After long quiescence, highly differentiated lava and tephra erupt intermittently; erosion and reef building continue.
6. Atoll stage. Volcano is eroded to sea level abetted by regional subsidence; structure encircled and capped by coral reefs.
7. Late seamount stage. Regional subsidence eventually causes edifice to sink below sea level where it quietly remains as a seamount.

The volcanoes of the Island of Hawaii represent only the first four stages. Loihi is at stage 1 or 2a, Kilauea and Mauna Loa are at 2c, Hualalai and Mauna Kea at 3, and Kohala at 4.

The petrologic history of each Hawaiian volcano is summarized by silica- and magnesia-variation diagrams. These diagrams also illustrate chemical differences and similarities among the volcanoes, the differentiation trends of basaltic magmas, and the major role played by olivine in controlling basalt composition.

Though volcanic activity has dominated the development of the island, other geologic agents have also been at work. Subsidence caused by volcanic loading occurs at a rate of a few millimeters per year. Eustatic changes of sea level, chiefly during the Pleistocene, gave rise to marine terraces, most of which are below the modern strandline. High rainfall on the windward side has caused erosion of deep canyons having thick deposits of sediment in their lower reaches. Pleistocene glacial deposits cap Mauna Kea. Fault scarps are common on the active volcanoes Mauna Loa and Kilauea. Tsunamis generated by local and distant earthquakes have caused coastline erosion and redeposition every few decades through historical time and, by inference, throughout the entire life of the island.

INTRODUCTION

Hawaii, one of the world's largest volcanic islands, lies at the southeastern end of the Hawaiian Ridge, a linear chain of mostly submarine volcanic mountains that extends for 3,500 km through the central Pacific Ocean (fig. 7.1). The eight main Hawaiian islands span about 640 km from southeast to northwest; numerous small islands, atolls, reefs, and shoals lie farther northwest, extending the archipelago proper to about 2,600 km. The exclusively submarine portion of the Hawaiian Ridge continues northwestward for another

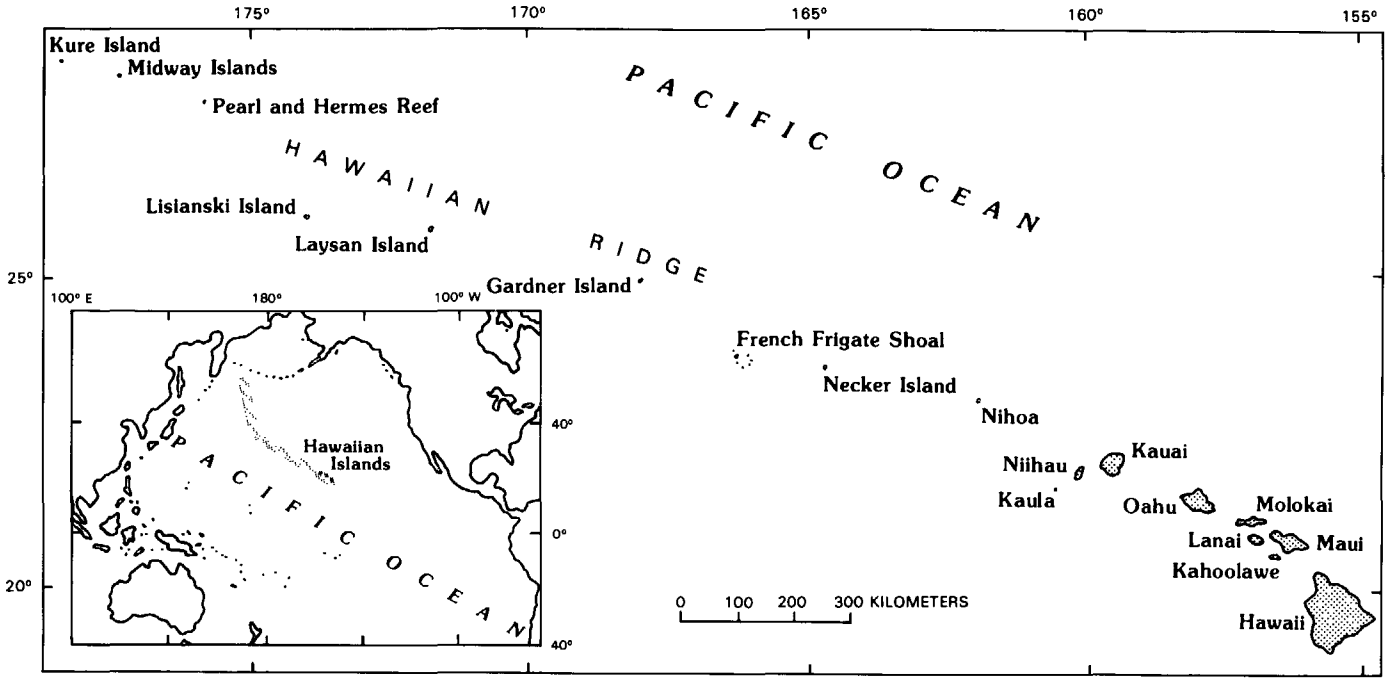

FIGURE 7.1.—Hawaiian archipelago showing location of eight main Hawaiian Islands at southeast end and small islands, atolls, and reefs that extend northwestward along Hawaiian Ridge. Pattern of inset shows location of Hawaiian-Emperor Chain.

900 km, then bends sharply northward to become the Emperor Seamounts, a similar linear chain that extends for another 2,500 km as far as the Aleutian Trench (fig. 7.1). The combined Hawaiian-Emperor volcanic chain is thought to record the persistent movement of the Pacific plate over a stationary melting spot beneath the crust (Dalrymple and others, 1973). The magma generated erupts to build volcanoes at the surface of the plate above the melting spot; as the plate moves on, these volcanoes cease growing but new ones begin. The Island of Hawaii is now thought to lie just north of the melting spot. The origin of the Hawaiian-Emperor Chain is reviewed by Clague and Dalrymple (chapter 1, part I).

Hawaii consists of five individual volcanoes: Kohala, Mauna Kea, Hualalai, Mauna Loa, and Kilauea (fig. 7.2; table 7.1). They rise from the sea floor, which lies here at a depth of about 5–6 km; the island is only their uppermost part, and by far the greatest part of their bulk lies beneath the ocean surface (table 7.2). The subaerial part of each volcano is typically shield shaped, though some have been modified by erosion.

Of the five volcanoes, Kohala, which forms the northernmost part of the island (fig. 7.2), has been inactive the longest. Stream erosion has deeply incised its northeastern flank, though the other flanks are less dissected. Cinder cones stud the upper part of the shield. Kohala last erupted at about 60 ka (McDougall and Swanson, 1972). Adjoining Kohala on the southeast is Mauna Kea, whose summit (4206 m) is the highest point on the island. Cinder cones are abundant on Mauna Kea; its most recent eruptions were at about 3.6 ka (Porter and others, 1979b). Several canyons incise the lower portions of its northeastern flank, whereas the remainder of the volcano has been little affected by erosion.

South of Mauna Kea is Mauna Loa, whose surface accounts for more than half the area of the island (table 7.1). A caldera occupies its summit, several pit craters indent the surface near the summit, and prominent rift zones, consisting of cinder and spatter cones, spatter ramparts, fissures, and small craters, extend northeast and southwest from the summit. Mauna Loa has erupted frequently in historical time, most recently in 1984 (Lockwood and others, chapter 19, 1985), and most of its surface is not eroded. Northwest of Mauna Loa is Hualalai, a relatively steep-sided shield with many cinder cones on its upper parts; it is essentially undissected by erosion. It has erupted once in historical time (1800–1801), from vents along its northwest rift zone. Abutting Mauna Loa's southeast flank is Kilauea, the most readily accessible and best studied of Hawaii's volcanoes. A caldera occupies its summit area, and several large pit craters indent the summit area and upper east rift zone. Rift zones extend from the caldera to beyond the shoreline both east and southwest from the summit. Kilauea, like Mauna Loa, has erupted frequently throughout historical time; the eruptions of these two volcanoes have provided much significant information about processes of basaltic volcanism.

Loihi is a seamount located 30 km south of the south coast of Hawaii (figs. 7.2, 7.8). Its highest point reaches to within about 950 m of the ocean surface. Ongoing studies have revealed evidence of its recent eruptive activity and demonstrate that it is a growing submarine volcano (Malahoff, chapter 6; Malahoff and others, 1982; Moore and others, 1982).

The geologic history of a basaltic volcanic island superficially may appear to be quite simple—a long sequence of repeated lava flows has constructed a broad, layered volcanic edifice. The wide

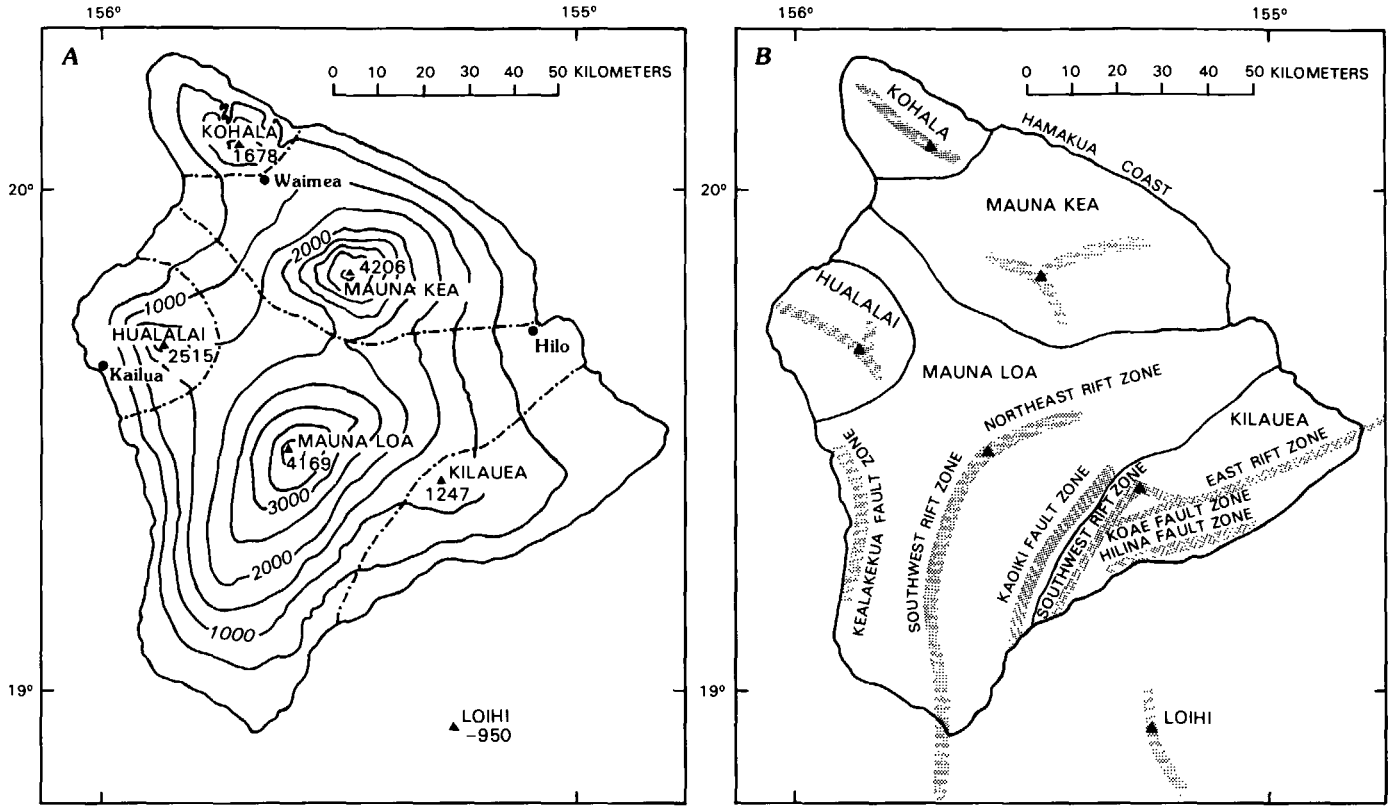

FIGURE 7.2.—Island of Hawaii and Loihi Seamount showing major geographic and geologic features. ***A***, Generalized topography and boundaries of five volcanoes. Contours and summit elevations in meters. ***B***, Major rift zones and fault zones; those on Kilauea and Mauna Loa are named.

TABLE 7.1.—*Physical dimensions of the subaerial portions of Hawaii's volcanoes*

[Adapted from Stearns and Macdonald, 1946, p. 24]

Volcano	Elevation of highest point (m)	Area (km^2)	Percent of area of island
Mauna Loa	4,169	5,271	50.5
Kilauea	1,247	1,430	13.7
Hualalai	2,521	751	7.2
Mauna Kea	4,206	2,380	22.8
Kohala	1,670	606	5.8
Entire island	4,206	10,438	100

TABLE 7.2.—*Volume and relative percentages of subaerial and submarine mass of each volcano and for entire Island of Hawaii*

[Volumetric data from Bargar and Jackson, 1974, table 1; sea floor assumed approximately level at depth of 5 km below sea level]

	Subaerial part		Submarine part		Total	
Volcano	Volume above sea level (10^3 km)	Fraction above sea level (percent)	Volume below sea level (10^3 km)	Fraction below sea level (percent)	Volume above plus below sea level (10^3 km)	Fraction of entire island mass (percent)
Mauna Loa	7.5	17.6	35.0	82.4	42.5	38
Kilauea	0.7	3.6	18.7	96.4	19.4	17
Hualalai	0.6	4.8	11.8	95.2	12.4	11
Mauna Kea	3.1	12.5	21.7	87.5	24.8	22
Kohala	0.4	2.9	13.6	97.1	14.0	12
Entire Island	12.3	10.9	100.8	89.1	113.1	100

variety of subjects covered by the succeeding papers in this section, however, demonstrates that such a view is oversimplified, and the geologic history actually includes a rich diversity of processes and events that were deciphered through the efforts of a long succession of geologists and other workers. Hence the geologic history of the Island of Hawaii will here be related from the point of view of how the concepts evolved during the last two centuries—in essence, a history of the development of the understanding of Hawaii's geologic history.

ACKNOWLEDGMENTS

Ideas summarized in this paper stem from the long progression of geologists who have worked on Hawaii, far too numerous to mention individually, but who merit sincere gratitude and are here collectively recognized. Special thanks are given to R.W. Decker, who stimulated the production of the paper, and to R.T. Holcomb, who served as a ready source of information, ideas, and constructive criticism. We also particularly thank R.I. Tilling and W. A. Duffield, who greatly improved the paper by their incisive and thorough reviews.

DEVELOPMENT OF CONCEPTS OF THE GEOLOGIC HISTORY OF HAWAII

PROGRESS FROM THE LATE 18TH CENTURY TO THE MID-20TH CENTURY

It is possible to summarize simplistically the geologic history of Hawaii in a single sentence: Hawaii has been built of adjacent and partly overlapping mounds of basaltic lava flows and small amounts of tephra, which originated on the ocean floor and successively grew above the sea to form the five distinct volcanoes that compose the still-evolving island. However, such a condensed history does not consider related processes and conditions that have shaped these volcanoes, such as changes in composition of the magma, shifts in vent location, causes and manifestations of stresses within the volcanoes, diversity of eruptive style and flow behavior, variations in duration of inactive intervals, and interactions between eruptive products and sea water. Underlying the development of the island, however, is the fundamental process of volcanism, for without countless and repeated volcanic eruptions, the Island of Hawaii would not exist.

Evidence of recent volcanism was noticed by even the earliest European visitors. The journals of Captain James Cook, who was the first European to visit Hawaii in 1778, emphasized navigation, geographic discovery, flora, fauna, and the nature of the endemic people, noted the volcanic characteristics of the island (Beaglehole, 1967, p. 486): "The coast of the Kau district presents a prospect of the most horrid and dreary kind: the whole country appearing to have undergone a dreadful convulsion. The ground is covered with cinders and intersected with black streaks which mark the course of lava that has flowed, not many ages back, from the mountain to the sea. The southern promontory looks like the dregs of a volcano." One of Cook's sailors, John Ledyard, led a field party to the interior of the island, where fresh lava flows and other signs of recent volcanic activity were encountered. Ledyard (1783) expressed the astute opinion that the entire island was of volcanic origin. However, members of the Cook expedition seemed unaware that the island included active volcanoes. Captain George Vancouver, on an expedition to Hawaii in 1793–94, was the first to record volcanic activity on the island (Vancouver, 1798, p. 8). Archibald Menzies, the botanist on the Vancouver expedition, explored part of the interior of the island and led ascents of Hualalai and Mauna Loa. Menzies' account of this first recorded ascent of Mauna Loa is a fascinating tale of hardship and persistence (see Hitchcock, 1909, p. 63–79). Menzies described the volcanic character of Mauna Loa, particularly the summit region, and he noted fume clouds and ash issuing from Kilauea.

The first detailed descriptions of Hawaiian volcanic activity were written by missionaries and were based in particular on a notable trip around the island trip in 1823. William Ellis (1827) described the characteristics of rocks and landforms and provided sketches and vivid impressions of the vigorous behavior of lava lakes and vents on the floor of Kilauea caldera. Joseph Goodrich (1826), an American missionary stationed at Hilo, wrote to Benjamin Silliman, editor of the American Journal of Science, with information about Kilauea; his earliest letter recounted the same journey described by Ellis. Based on the volcanic activity and the landforms they observed throughout the trip, these missionaries ascribed the origin of the entire island to volcanism. Ellis summarized this conclusion as follows (Ellis, 1827, p. 181): "The whole island of Hawaii, covering a space of four thousand square miles, from the summits of its lofty mountains * * * down to the beach, is, according to every observation we could make, one complete mass of lava, or other volcanic matter, in different stages of decomposition. Perforated with innumerable apertures in the shape of craters, the island forms a hollow cone over one vast furnace, situated in the heart of a stupendous submarine mountain, rising from the bottom of the sea * * *."

During the following years, sporadic visits to the volcanoes were reported by missionaries, sea captains, and a few other persons. The accounts of most of these visits are conveniently summarized by Dana (1890), Brigham (1909), and Hitchcock (1909). The accounts of several missionaries of this period, notably Goodrich and C.S. Stewart, were published in the American Journal of Science, the Missionary Herald, and a few other journals (see Macdonald, 1947). The botanist David Douglas described his visits to Kilauea and Mauna Loa in 1834 (Douglas, 1914; Harvey, 1947, p. 220-231). These accounts document the major changes in the morphology of Kilauea caldera and the persistent action of the lava lake and other vents on the caldera floor during the early and middle decades of the nineteenth century.

The first systematic exploration of the Hawaiian volcanoes was carried out by members of the Wilkes expedition during 1840–41. Wilkes' (1845) own narrative includes fascinating accounts of the exploration and of specific trips to the volcanoes, but J.D. Dana (1849) provided geological insight into the volcanoes and their role in the development of the island (Appleman, chapter 60). Dana noted the generally quiet behavior of Hawaiian volcanoes, their gently sloping flanks, and the scarcity of products from explosive eruptions. He correctly ascribed these features to the high fluidity of the Hawaiian lava in contrast to the more viscous lava of steeper sided volcanoes with more explosive habits. He also described the concentration of vents in the summit areas and along narrow linear zones radiating from the summits (the concept of the rift zone), and he correlated flank eruptions of Kilauea with concurrent subsidence of the lava lake and caldera floor—evidence of possible connection between flank and summit magma conduits. Even so, Dana regarded Kilauea as only a vent of Mauna Loa, rather than an independent volcano. For example, he described the island of Hawaii as being made up of three volcanoes, "Mount" Kea, "Mount" Loa, and Hualalai (Dana, 1849, p. 159), and he stated that volcanic activity was "confined to Loa and Hualalai" (p. 168). Furthermore, he included his general discussion of Kilauea (p. 171–206) in the section on Mauna Loa (p. 168–214). Nevertheless, he wondered about the lack of correlation in their activity and was puzzled that lava could be elevated to erupt at the summit of Mauna Loa while nearly 10,000 feet lower an open, constantly active conduit fed the lava lake at Kilauea. Although he proposed a separation of conduits (p. 218–221), he did not suggest that Kilauea might be an independent volcano. Finally, he described Kohala as a ridge separated from Mauna Kea by a scarp, but he

did not define it as a separate volcano or even as part of the three volcanoes making up the island.

The eruptive activity of Kilauea and Mauna Loa during the next four decades (1840–1880) was reasonably well documented, in spite of only irregular visits and the lack of an established system of surveillance. This documentation is chiefly owing to Titus Coan, a missionary stationed at Hilo and a perceptive and dedicated volcano observer. His missionary duties required frequent trips past Kilauea, and from 1840 to the early 1880's he recorded the volcano's activity. From the 1850's he summarized his observations in letters to his friend, J.D. Dana, who became the editor of the American Journal of Science, and Coan's graphic descriptions regularly found their way into the pages of that journal. He also observed the activity of Mauna Loa, although access there was much more difficult; he recorded the dates of eruption, and for most of the significant ones was able to visit the scene of the action. Several other missionaries, a few scientists, and an occasional tourist also made observations that were published. These reports were compiled by Dana (1890), Hitchcock (1909), Brigham (1909), and Macdonald (1947). Nearly all accounts from those of the Wilkes expedition to Dutton's study in 1882 were purely descriptive, but the record they chronicled provided evidence supporting the concept that the long-term growth of the island was the product of episodic lava flows from the active volcanoes.

C.E. Dutton carried out the most extensive geologic studies of Hawaii in the 19th century (Dutton, 1884). He described the surface morphology and structure of the five volcanoes. He recognized that Kilauea is a separate volcano, distinct from Mauna Loa (Dutton, 1884, p. 120–121) for the following reasons: (1) The distance between Kilauea and Mauna Loa is about the same as the distance between other pairs of adjacent volcanoes of the island; (2) according to hydrostatic principles, the difference in elevation between lava lakes at Kilauea and the summit of Mauna Loa is too great to permit liquid continuity; (3) Kilauea caldera "is situated on a totally distinct mountain pile," the top of which stands topographically above a saddle that separates the two volcanoes. Dutton observed that flows from the two volcanoes are intercalated and thus that the two volcanoes are intergrown. He concurred with Dana that Hawaiian volcanoes have gentler flanks than many other well-known volcanoes. Dutton emphasized the immense size of Mauna Loa, especially in view of its apparently huge submarine part, and he reasoned that Mauna Kea, which rises higher than Mauna Loa but has steeper sides and a smaller base, is considerably smaller in volume.

The distinction between the basaltic lava types of pahoehoe and aa commonly is credited to Dutton (1884 cited by Macdonald, 1972, p. 71; Peterson and Tilling, 1980, p. 272), although Dana (1849, p. 161–163) accurately described "pahoihoi" and "clinkers" several decades earlier. However, Dutton (1884, p. 95) apparently first introduced the Hawaiian term aa for the slaggy, rough, clinkery type. After Dutton's report, the terms aa and pahoehoe came into common use. Dutton (1884) suggested that the two lava types form because of contrasts in the dimensions of the lava flows and in the relations among lava movement, cooling, and solidification. He also (p. 105) proposed that the term caldera is more appropriate than the term crater to describe the large depressions at the summits of Kilauea and Mauna Loa.

During the 19th century, Kilauea's intracaldera lava lake, which was active for many decades, received the most attention. Dutton described his own observations and quoted extensively from the writings of others in summarizing activity that included vigorous fountaining and lava flows, quiet circulation within multiple lava lakes, updoming of portions of the caldera floor, and noisy and sometimes spattering "blowing cones," all of which were interspersed with major episodes of lava withdrawal and partial collapse of the solid floor of the caldera (Dutton, 1884, p. 106–119). Such behavior led him to speculate (p. 126) that the caldera formed as a consequence of repeated fluctuations in the height of the lava column. He reasoned that when the column was high, wall rocks were softened or melted by magmatic heat, and when the column lowered, such weakened rock spalled off and sank; thus repeated oscillations of the lava-column height caused the depression to enlarge. He seems to have visualized a magma column nearly as wide as the caldera. While not every facet of his explanation finds favor today, Dutton deserves credit for recognizing the process of collapse as essential to the development of the caldera. Like Dana, he recognized that linear zones of weakness (now called rift zones) radiate from the summit and noted that eruptions along these zones were accompanied by lowering of the lava column in the caldera.

Dutton (1884) visited the source of the 1880–81 eruption of lava from the northeast flank of Mauna Loa, and he accurately described the structure and character of the rift zone there. He was impressed by the large volume of lava produced during this 11-month-long eruption and by the small proportion that remained near the vents. He identified vent areas of earlier eruptions and thus gained considerable insight into the manner in which the volcano, and indeed the island, grew from rift eruptions. A brief excerpt is appropriate to summarize the concept he visualized (Dutton, 1884, p. 134–135):

> There is a strange fascination in wandering over this vast expanse of desolation. No doubt the dominant idea is the immensity of it. The best conception of the magnitude of Mauna Loa is to be obtained by attempting to traverse any limited district of it on foot. Mile after mile may be traversed but the landscape seems ever the same. All the great landmarks seem to stand just where they stood an hour before * * *. The only alternations are from aa to pahoehoe. Traces of recent eruptions are seen everywhere, but all the views are fragmentary. So extensive has each and every one of them been that the greater portions of them always reach far beyond the limits of vision, and mingling together are lost in the confusion of multitude. The imagination is discouraged at the thought that this colossal pile has been built up by thousands upon thousands of these eruptions.

Dutton himself saw no eruption in Mokuaweoweo, the summit caldera of Mauna Loa. However, from his review of the observations of others, he concluded that activity at the summit generally preceded flank eruptions and that summit activity declined and ended when lava broke out on the flanks, suggesting hydraulic connections among various vents of the volcano. As he had for the caldera of Kilauea, Dutton advocated for Mokuaweoweo an origin by collapse, citing a lack of evidence for explosive origin and the abundance of partly subsided blocks. He speculated that a caldera would tend to develop at the summit of a volcano when it grew large

enough for flank eruptions to occur and draw lava from a summit magma reservoir, thus reducing support beneath the central orifice. He therefore proposed that summit depressions could have existed at both Mauna Loa and Kilauea throughout much of their development (Dutton, 1884, p. 142–143).

Dutton concluded that Mauna Kea had long been inactive, because the rocks are deeply weathered, soil cover is common, and ravines and canyons disrupt the profile of the flanks, particularly on the northeastern, windward side (Dutton, 1884, p. 160, 168–170). He described the abundant cinder cones in the summit area of Mauna Kea and took note of the nearby flows of unusually hard and flinty lava that was used by Hawaiians for tools and weapons (p. 163–164). In recent years these distinctive rocks have been recognized as products of magmatic differentiation, but the idea of differentiation was spawned long after Dutton's time and he did not speculate on the cause of the somewhat unusual character of the quarried rock.

Dutton mentioned Kohala only briefly, recognizing it as the volcano longest inactive on the island, as demonstrated by its deeply incised canyons and its thick soil (Dutton, 1884, p. 171). He described Kohala lava as basalt with a tendency toward andesite, and he noted its many cinder cones. Similarly, his description of Hualalai is brief; he noted the abundant cinder cones in its summit region, the basaltic character of its lava, and the common occurrence of olivine (p. 173–174). He stated (p. 83) that Hualalai erupted three times in the early 19th century, later giving dates of 1801 (p. 181) and of 1805 and 1811 (p. 173), but he did not cite a source for these dates, which are in part at variance with the now commonly accepted time of eruption during 1800–1801 (Moore and others, chapter 20; Ellis, 1827, p. 38; Stearns and Macdonald, 1946, p. 146).

Stimulated by his participation in the Wilkes expedition, Professor James Dwight Dana of Yale University maintained a lively interest in Hawaii throughout his long and distinguished career. He kept himself informed about virtually every reliable observation of activity at Kilauea and Mauna Loa and published many accounts of it in the American Journal of Science. Dana made his second journey to the islands in 1887 at the age of 74 and later published a book (Dana, 1890) that served for years as the definitive work on Hawaiian volcanoes. Dana's general ideas on the geologic history of the volcanoes remained similar to those he developed on the Wilkes expedition, which were summarized above. However, he ultimately accepted the evidence offered by Dutton and others that Kilauea is a separate volcano and not part of Mauna Loa. This change in opinion was evidently not easy for him, as in the process of acquiescing he devoted several pages (Dana, 1890, p. 258–264) to recounting the virtues of his original views.

About two decades later, two major volumes were published about the volcanoes of Hawaii (Brigham, 1909; Hitchcock, 1909); each includes a chronological narrative of the activity of Kilauea and Mauna Loa, and each includes many photographs of volcanic features, as well as maps that illustrate the changes in caldera morphology through the years. Brigham's work also contains many of his own personal observations and experiences. Hitchcock's personal observations are fewer, but he was particularly diligent in documenting information, and the usefulness of his volume is enhanced because of extensive quotations from sources now hard to find. Although neither author developed new concepts on volcano development, their descriptive chronologies are very valuable. The timing of their publication was serendipitous, as these unique reference volumes appeared just before the establishment of the Hawaiian Volcano Observatory (HVO) in January 1912.

The founding of the HVO by T.A. Jaggar began the modern era of continuous surveillance and systematic documentation of the Hawaiian volcanoes (Apple, chapter 61). Jaggar and other HVO staff members made detailed daily observations of Halemaumau, and various scientific instruments were introduced to complement the regular program of observation. The easily accessible lava lake at Halemaumau offered abundant opportunities for observation and experimentation, and Jaggar collaborated with visiting scientists to build a new understanding of the behavior of Hawaiian volcanoes. Vast amounts of data were collected on the circulation and the rise and fall of the lava lake, composition of lava, character of seismicity, ground deformation, gas chemistry, and lava temperatures. In addition to the activities of the lava lake, all eruptions of Mauna Loa and Kilauea were thoroughly documented. Jaggar made several successful long-range forecasts of Mauna Loa activity.

Jaggar was a geologist and a geophysicist; he was a keen observer of eruptive phenomena, and he was much interested in experimentation and development of instruments. He and his collaborators led volcanology from a science of description to a science of quantitative measurement, experimentation, and interpretation. He wrote prolifically (see, for example, Jaggar, 1947); a convenient summary of his major writings appears in Macdonald (1947, p. 83–103).

Jaggar proposed that the magma column of Halemaumau consists of (1) hypomagma, a homogeneous, aphyric fluid from a source deep within the Earth, with gas contained in solution; (2) pyromagma, a vesiculating gas-rich foam, which constitutes the highly fluid portion of lava lakes and includes the lava of erupting fountains and; (3) epimagma, which he also called bench magma, a highly crystalline, pasty, largely degassed but still-incandescent lava forming the floor and lining of lava lakes; he visualized epimagma as forming the contact sheath of the magma conduit. Although Jaggar's terms are chiefly applicable to active lava lakes and have been but little used, they help to illustrate his key concept that the rate and amount of gas vesiculation determine the behavior of erupting lava.

Jaggar postulated a tidal influence on the behavior of Halemaumau lava lake, which led him to propose that activity peaked at solar equinoxes and solstices. Subsequent workers have found little evidence to substantiate the latter proposal, although investigations continue into the possibility that tidal maxima serve as a trigger for some eruptions (Shimozuru, chapter 49; Dzurisin, 1980). Jaggar sought diligently for evidence of cyclicity in eruptive behavior, and he was convinced that changes in behavior were governed by the 11.1-yr sunspot cycle, upon which was superimposed a 134-year cycle defined by the interval between the explosive eruptions of Kilauea in 1790 and 1924. Reexamination of his evidence and the timing of subsequent eruptions have failed to support his concepts regarding the sunspot cycle.

He was impressed by certain coincidences of eruptive events at Mauna Loa and Kilauea; although they rarely erupted simultaneously, Jaggar thought he recognized lowering of the Halemaumau lava lake during eruptions of Mauna Loa. Hence he advocated the view that Kilauea and Mauna Loa are closely interconnected (Jaggar, 1947, p. 90, 200), even though he clearly regarded them as independent systems. He interpreted the island to be arranged as a cross (Jaggar, 1920, p. 193–195; 1947, p. 90), in which the north-northeast-trending upright extends from Mauna Kea summit through the summit and along the southwest rift zone of Mauna Loa to South Point. The transverse arm of the cross extends between Hualalai and Kilauea summits, which are symmetrical about the upright, and the summit of Mauna Loa lies near the intersection of the two elements. Kohala is not part of this structure. (This cross pattern can be recognized by noting the geographical relations of the four volcanoes, see fig. 7.2). The supposed geographic symmetry of Hualalai and Kilauea, the record of occasional explosive eruptions of Kilauea, and Kilauea's lesser output of lava than Mauna Loa convinced Jaggar that Kilauea is older than Mauna Loa and that it is approaching the same state of "decadence" as Hualalai has achieved (Jaggar, 1920, p. 191–198).

Stearns and Macdonald (1946, p. 135) demonstrated that Kilauea and Hualalai behave quite independently of one another. Kilauea's many eruptions since the 1950's, as well as petrogenetic considerations developed after Jaggar's time and discussed later herein, refute any suggestion that the volcano is in late decline. Even though not all of Jaggar's hypotheses have withstood the test of time, his contributions remain monumental. His many observations and thorough documentation of the activity of Kilauea and Mauna Loa constitute a permanent record of the growth processes of Hawaiian volcanoes.

Other scientists made many contributions in studies of Hawaiian volcanism during the decades of the 1910's to 1940's. The petrologic studies of Daly (1911, 1914, 1933, 1944), Cross (1915), and Washington (1923a, b, c) demonstrated the near-constant composition of highly fluid lava throughout most of the subaerial growth of the volcanoes and the variable composition of the late differentiated lava. Through integrated field and laboratory studies, Sidney Powers (1916, 1920) helped document the relations between lava composition and eruptive behavior. Stone (1926) reviewed published reports of Kilauea and was perhaps the first to describe the geology and geologic history of the whole of Kilauea. H.A. Powers (1935) evaluated the differentiation processes and pointed out that crystal fractionation alone could not account for Hawaiian differentiated rocks. Wentworth (1938) examined geomorphic processes and the products of explosive eruptions. Harold T. Stearns and colleagues began systematic geologic mapping in the 1920's, which led to the first geologic map of a part of the island (Stearns and Clark, 1930) and eventually to a comprehensive geologic report about the entire island (Stearns and Macdonald, 1946). Their geologic map of the island (scale 1:125,000) established a consistent stratigraphic nomenclature and thus provided a basis for examining the stratigraphic relations among the five volcanoes (figs. 7.3 and 7.4). The mapping was complemented by petrologic and petrographic studies (Macdonald, 1949a, b). The combined results are the foundation upon which all further geologic investigations of Hawaii have been built.

From his studies throughout the islands, Stearns (1940) defined a progression of four stages of volcanism, which he later (1946, p. 17–20; 1966) expanded to a series of eight stages that describe the growth, erosion, submergence, reef development and posterosion volcanism of the Hawaiian and other islands of the central Pacific (fig. 7.5). The following summary reviews Stearns' ideas as expressed in 1946; their subsequent modifications are discussed later.

Stage 1 involves building the volcano from the ocean floor to sea level. The volcano produces mostly pillow lava, and Stearns believed then that the submarine deposits include extensive tuff from explosive interaction between molten lava and seawater. The first material to emerge above sea level is poorly consolidated ash that erodes rapidly. Eventually subaerial lava flows veneer this material, reducing the rate of wave erosion.

Stage 2 is the subaerial growth of the volcano. Countless thin sheets of highly fluid, compositionally uniform primitive olivine basalt erupt from rift zones and a central crater to build the volcano; Stearns (1946, p. 17) described the edifice as a shield-shaped dome. Eruptions are closely spaced in time; because of this and the high surface porosity that minimizes runoff, virtually no stream erosion occurs. Rare explosive eruptions may occur. All the volcanoes on Hawaii have already passed through this youthful stage.

Stage 3 of Stearns is characterized by collapse around the summit vent areas to form a caldera and subsidence along the rift zones to form craters and grabens. Eruptions continue to be frequent, and the lava continues to be of uniform composition. Explosive eruptions may occur slightly more frequently than during stage 2. Caldera walls prevent overflows of lava onto the flanks behind them, and so localized erosion and stream drainage may develop on sectors of the volcano not frequently covered by new lava. Kilauea and Mauna Loa are now in this stage.

Stage 4 is characterized by change in lava composition from primitive basalt to more alkalic types such as andesite and trachyte. These more viscous lavas fill any caldera, craters, and grabens and build a steeper sided cap. Explosive eruptions are common, ash is interbedded with lava, and cinder cones may be abundant. Intervals between eruptions are longer, and erosion increases; disconformities may separate successive flows and ash layers. Stearns (1946, p. 19) regarded Hualalai, Mauna Kea, and Kohala to be in this stage.

Stage 5 is dominated by stream and marine erosion. Local climate and exposure to prevailing winds and ocean currents determine the rate of erosion. The subsequent stages 6 (subsidence and reef building), 7 (emergence and renewed volcanism), and 8 (atoll and resubmergence) (fig. 7.5) have not yet been reached by the volcanoes of Hawaii; they are represented by volcanoes on other islands to the northwest.

This order of stages as proposed by Stearns (1946, 1966) culminated a century and a half of gradually improved understanding of the processes of growth and development of Hawaii and its sister islands. Subsequent studies have modified or redefined some of the stages, but much of the early foundation remains firm to the present day.

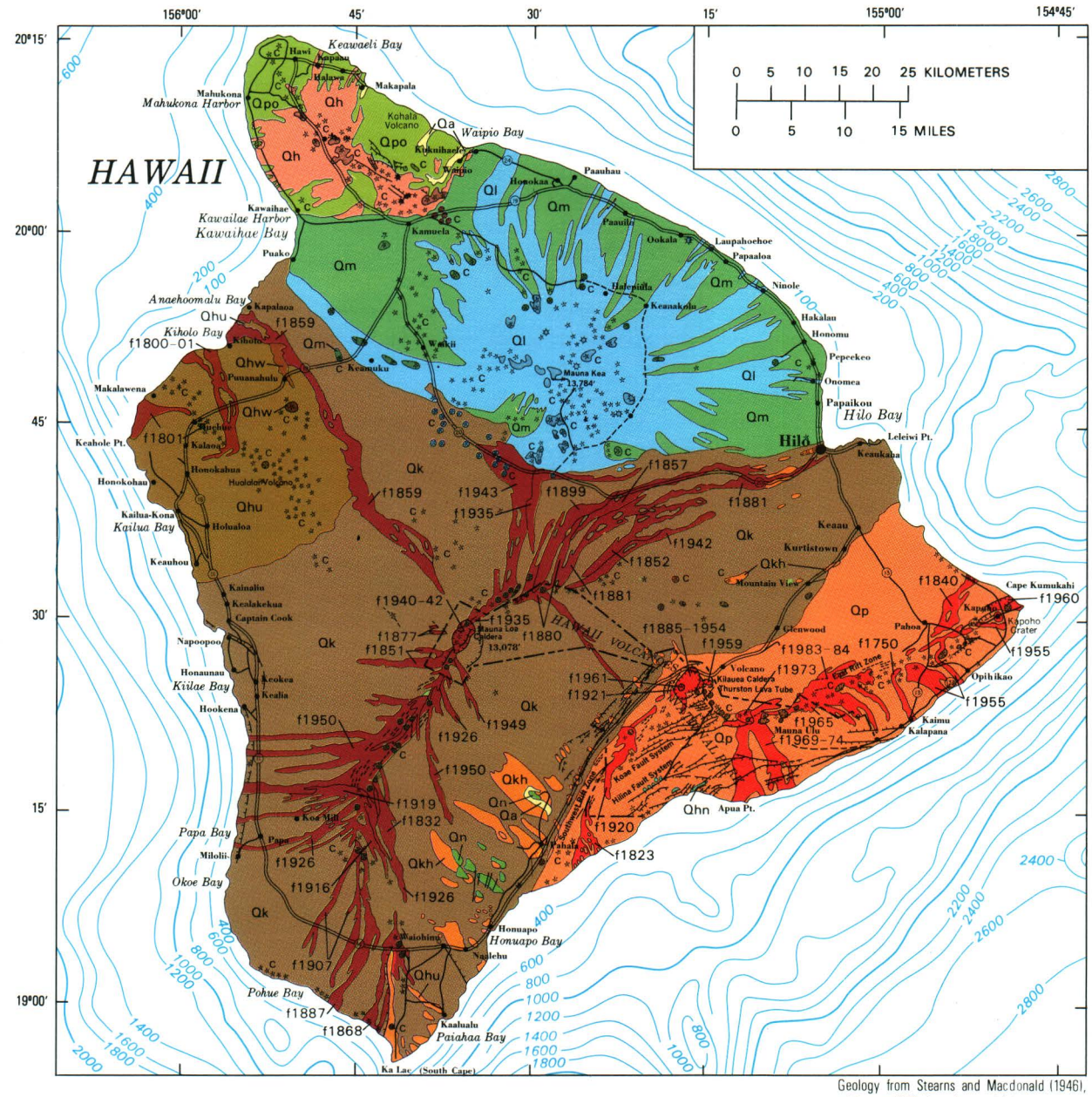

FIGURE 7.3.—Geologic map of Island of Hawaii. Geology from Stearns and Macdonald (1946), with lava flows from 1946 to 1984 added. Taken from American Association of Petroleum Geologists Geological Highway Map: Alaska and Hawaii (Circum-Pacific Edition, 1974); modified with permission from the American Association of Petroleum Geologists. Stratigraphic nomenclature from Langenheim and Clague (chapter 1, part II). Figure 7.4 shows correlation of geologic units among several volcanoes.

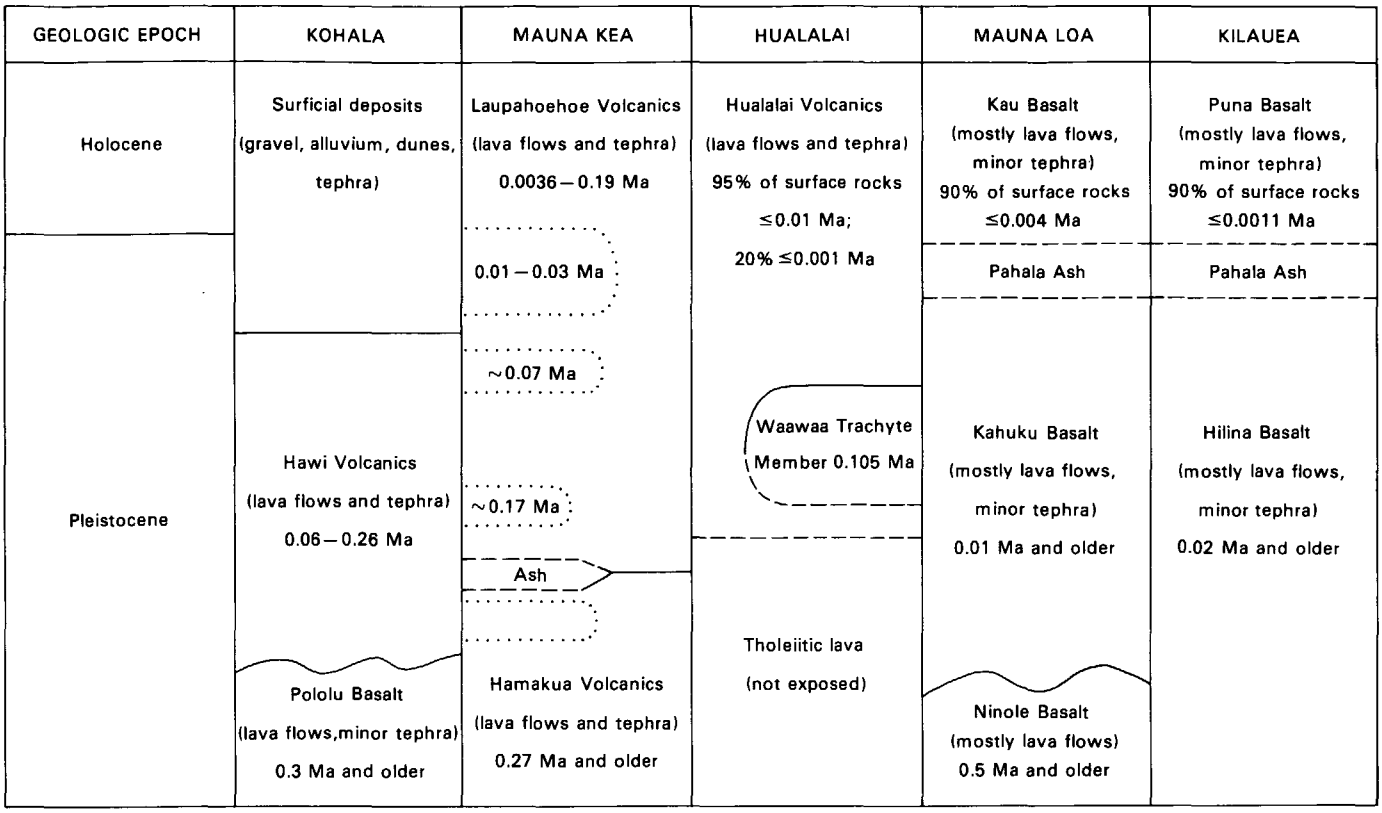

FIGURE 7.4.—Correlation chart showing major rock units on Island of Hawaii and their relative stratigraphic positions. Most names established initially by Stearns and Macdonald (1946), some units redefined by subsequent authors; relations shown here and nomenclature from Langenheim and Clague (chapter 1, part II). Numerical ages generalized from radiometric values given by various references cited in text. Dashed lines: indefinite, gradational, or controversial boundaries; dotted lines: glacial deposits (at Mauna Kea; from Porter, 1979a, 1979b); wavy lines: distinct hiatus.

DEVELOPMENTS SINCE THE MID-20TH CENTURY

The recognition and definition of the stages of island growth by Stearns (1946, 1966) were achieved in spite of severe limitations in the available evidence bearing on geologic history. The most significant limitations were these: (1) The submarine part of each volcano, which records the early geologic history, was inaccessible. (2) Present exposures reveal only the youngest rocks on most of the island's volcanoes. (3) Precise methods for dating basaltic lava had not been developed. We will consider the consequences of each of these limitations.

(1) Volcanoes are roughly conical in shape, so most of the volume of volcanic islands in the deep ocean lies below sea level. Bargar and Jackson (1974) used topography and bathymetry to measure the volumes of subaerial and submarine portions of the volcanoes of the Hawaiian-Emperor Chain; their results for the Island of Hawaii are shown in table 7.2. Only about 11 percent of the volume of the volcanoes of the island is above sea level, yet only the rocks and surface morphology of this part were available to Stearns and his associates for study. It is this small fraction that provided the evidence for Stearns' scheme of growth stages.

(2) Of this small subaerial fraction, erosion has penetrated the surface lavas only slightly or not at all on most volcanoes of the island. Even on Kohala and Mauna Kea, the most deeply eroded volcanoes, the exposed sections reveal but a small fraction of the geologic history. Hence the growth stages have been inferred chiefly from the most recent events as recorded by surface lavas and by analogy to the older, more deeply eroded volcanoes on the other islands. Even on older islands, however, erosion has only partly uncovered the subsurface rocks.

(3) Until the mid-20th century, fossils were the chief tool for determining rock ages, and few Hawaiian rocks contain fossils. Hence the only rocks that could be dated with much confidence were flows that had been emplaced during historical time. The dates of other geologic events were estimated by extrapolation of recurrence intervals of historical eruptions or inferred from rates of weathering, relative amounts of vegetation growing on old lava, degree and estimated rates of erosion, and stratigraphic relations among the exposed rocks. Even though such methods permitted conclusions to be reached, the lack of a way to measure numerical ages of basalt placed severe constraints on many geologic interpretations.

Since the time of the reports by Stearns (1946) and Stearns and Macdonald (1946), the gaps in knowledge have been narrowed through advances in a variety of disciplines, including geophysics, petrology, submarine geology, and radiometric and other dating techniques. Additional insights have been achieved through detailed

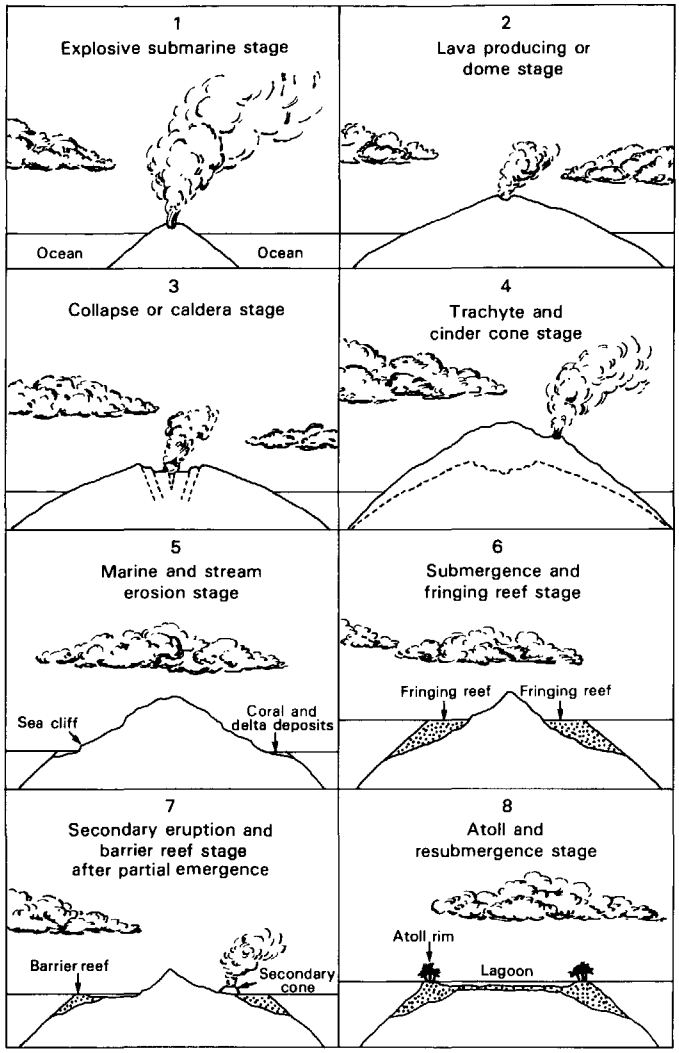

FIGURE 7.5.—Eight stages proposed by Stearns (1946) for geologic history of a volcanic island in the central Pacific.

geologic mapping of many areas, sophisticated applications of aerial photography, and sustained critical observations of a wide variety of eruptive activity. Findings at Loihi Seamount, 30 km offshore from the south coast of Hawaii, and its recognition as an active volcano have been of special value.

SUBMARINE INVESTIGATIONS

Investigations of submarine volcanism around Hawaii, including sea bottom photographs and studies of dredged samples, were begun in the 1960's. J.G. Moore and collaborators showed, for example, that at depths from 490 m to 5,190 m along the submarine extension of the east rift zone of Kilauea, virtually all the sea-floor material is fresh pillow lava, some of which is fragmental; nearby seamounts are composed of similar material, although most is less fresh and mantled with sediment (Moore and Reed, 1963; Moore, 1965). These studies found no indication of chemical exchange between erupting lava and sea water; rock composition, including water content, did not vary with depth. A progressive decrease in vesicle size, however, was observed to a depth of about 800 m, below which only microscopic vesicles were found. These findings confirmed the long-held inference that pillow lava is the dominant product of undersea basaltic eruptions of Hawaiian volcanoes. Pillow lava may also form when subaerially erupted lava enters the sea (Moore, 1975). The systematic relation between water depth and vesicle size apparently provided a tool by which the depth of eruption of submarine lava might be estimated. It was later found, however, that alkalic basalt dredged from Loihi at depths of 1–2 km has high vesicularity in comparison with tholeiitic samples collected at comparable depth (Moore and others, 1982, p. 91), demonstrating that vesicle size is a function of more than just depth of eruption.

The restricted development of vesicles in submarine tholeiites suggests that hydrostatic pressure of sea water inhibits vesiculation and explosive eruptions at depths below a few hundred meters (Moore, 1965). In contrast, explosive activity is common at the shoreline and in shallow depths, and it produces a zone of clastic debris intermixed with lava that extends from sea level to depths of several hundred meters (fig. 7.6). Explosive interactions occur between molten lava and sea water during shallow-water eruptions and also when subaerial lava flows enter the sea; the fragmented material may then be transported to cover deeper slopes. Fragmentation processes of explosion, implosion, thermal shock, and wave abrasion were observed at Kilauea from 1969 to 1973 during flows into the sea from Mauna Ulu (Moore and others, 1973; Peterson, 1976); the fragmented products are interleaved with coherent subaqueous lava flows, including pillow lava. Constructional submarine slopes are steep enough that slumping and landslides are common processes (Moore, chapter 2); near Oahu and Molokai, evidence has been found for truly huge submarine landslides (Moore, 1964). Slopes of the subaerial shields of the volcanoes are more gentle, in distinct contrast to steeper submarine slopes (Moore and Fiske, 1969). As the edifice grows through continuing eruptions, the clastic zone is covered by subaerially erupted lava, and it forms a layer between the submarine and subaerial lava that is a marker horizon extending through the volcano, preserving a record of the littoral and shallow-water processes and of subsidence of the island (fig. 7.6).

These and other investigations helped to characterize the submarine platform upon which the island rests and the behavior of lava in the presence of seawater. They are limited, however, to the exposed carapace and so do not give direct information about the internal core and the early history of the volcanoes. The recent recognition of Loihi Seamount as an active volcano, however, has furnished an opportunity to study an earlier stage in the growth of a Hawaiian shield volcano.

PETROLOGIC INVESTIGATIONS

Studies of Hawaiian lavas have made major contributions to igneous petrology during recent decades. The lavas are ideal for detailed investigations, because they reflect magma-generation and

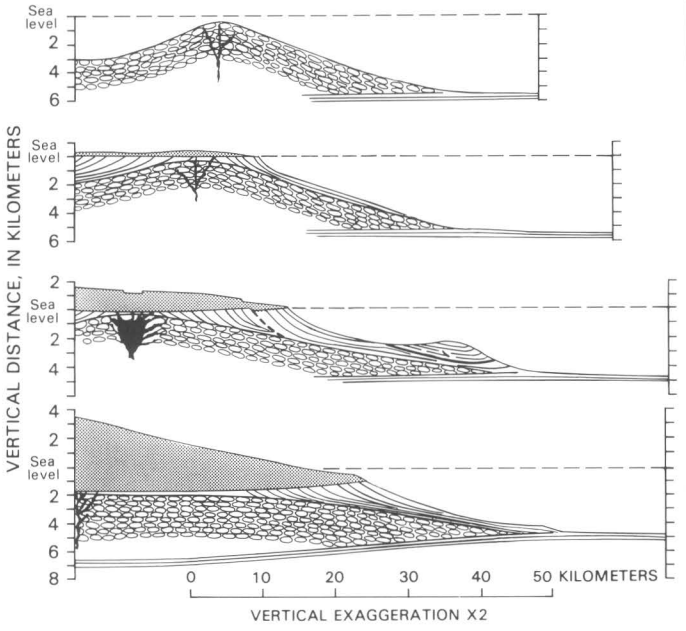

FIGURE 7.6.—Cross sections illustrating oceanic volcanic islands in submarine, sea-level, and subaerial stages of evolution (reproduced from Moore and Fiske, 1969, fig. 3, p. 1200). Patterns indicate rock types: ovals, pillow lavas with included pillow fragments and sediment; lined pattern, clastic rocks, including phreatic-explosion ash, littoral-cone ash, and flow-foot breccia and including some pillowed flows and pillow breccias; dark pattern, subaerial lava flows with minor ash; solid black, intrusive rock. Note contrast between submarine and subaerial slopes, continuation of clastic layer beneath subaerial shield, and downbowing of sea floor by subsidence caused by volcanic loading. Depth and elevation figures left side are in feet.

petrogenetic processes uncontaminated by assimilation of continental crustal rocks. Recent petrologic investigations of Hawaiian lavas are discussed in several papers elsewhere in this work (for example, Wright and Helz, chapter 23; Tilling and others, chapter 24), and the general petrologic development of the individual volcanoes of Hawaii is summarized later in this paper. Here we relate the growth stages established by Stearns (1946, 1966) to modern petrologic concepts and terminology.

The terminology applied to the lavas of Hawaii has shifted considerably during recent decades. In this paper we use the terms tholeiite and alkalic basalt and names for the other more differentiated lavas according to the usage adopted by Macdonald (1960) and Macdonald and Katsura (1961, 1962, 1964). They concurred with Powers (1935, 1955) that crystal fractionation alone cannot explain all of the chemical variation in rocks of the alkalic suite. Because no source materials for assimilation are available, Macdonald and Katsura (1961, 1962) suggested that volatile transfer and thermodiffusion might play a role in the differentiation processes. Another proposal was that wholly independent parent magmas produced the tholeiitic and alkalic suites (Kuno and others, 1957), but Macdonald and Katsura (1962) opposed this idea because of the small proportion of rocks representing alkalic magma. These and subsequent studies have retained the concept that voluminous and frequent eruptions of tholeiitic lava build a shield volcano (stage 2 of Stearns, 1946), with or without a summit caldera, and that this is followed by a transition to less frequent and less voluminous eruptions of more alkalic lava and tephra, which build a steeper sided carapace atop the shield (stage 4 of Stearns, 1946).

Petrologists have long sought to explain the origin of these two suites of lava. Samples of lava erupted at Kilauea Volcano from the 1950's to the present have helped relate eruptive behavior to the petrogenesis of tholeiitic magma (for example, Macdonald and Katsura, 1961; Murata and Richter, 1966; and Wright, 1973). Lava of the tholeiitic suite exhibits small but distinct chemical and mineralogical variations; most of these variations can be explained by the addition or subtraction of olivine, and hence such lava is referred to as olivine-controlled lava.

Powers (1955) first proposed the concept of distinct batches of magma derived from different parts of the mantle to explain variations other than those caused by olivine control. It was subsequently shown that olivine-controlled tholeiites of Mauna Loa appear to have been derived from a single batch of magma, whereas olivine-controlled tholeiites of Kilauea seem to have come from several separate batches (Wright, 1971; Wright and Fiske, 1971). Later work identified ten different chemical variants (magma batches) of Kilauea magma, which are mixed in varying proportions to produce the lavas erupted between 1968 and 1974 (Wright and others, 1975; Wright and Tilling, 1980). Trace-element contents of the tholeiites of Mauna Loa and Kilauea indicate derivation from more than one parent magma, confirming Powers' (1955) earlier deduction; the magma for each volcano was generated by distinctive partial-melting processes in different mantle source regions (Leeman and others, 1980). More recently, trace-element data suggest that olivine-controlled lavas of Mauna Loa, like those of Kilauea, also exhibit long-term compositional changes with time (Tilling and others, chapter 24; Budahn and Schmitt, 1985).

Wright (1984) proposed that Hawaiian tholeiite is the product of partial melting of mantle material that is residual from the material that earlier yielded midocean-ridge tholeiite and to which new components have been metasomatically added from a deeper melting source beneath Hawaii. This proposal is consistent with the distribution of trace elements and isotopes in the different tholeiites. These concepts provide a sound basis for the astute inferences by early workers that most of the volcano's volume, including much of the hidden portion of the shield, is constructed of tholeiite.

The subtle but significant compositional variations in Hawaiian tholeiites now provide problems and challenges that earlier workers, such as Cross (1915) and Washington (1923a, b, c) never anticipated, but the petrogenesis of the more alkalic lava poses a continuing challenge. Although much of the work on problems of alkalic magma has centered on other islands where more highly differentiated rocks are well represented, three of the volcanoes of the Island of Hawaii include alkalic rocks. Macdonald (1968) has provided a useful summary of the evidence that the alkalic and later suites of lava could be derived from the tholeiitic suite and that such derivation is compatible with the overall patterns of eruptive behavior. These and subsequently developed concepts on the origin of the alkalic suite are summarized by Clague (in press).

Samples dredged from Loihi provided some information with surprising implications for the composition of the deep interior of Hawaiian volcanoes. In addition to the anticipated tholeiite, the dredge hauls included transitional basalt, alkalic basalt, and basanite (Moore and others, 1982; Frey and Clague, 1983). Geochemical studies have led to the inference that the earliest erupted material was alkalic basalt; the initial melted material marking the onset of a new volcano may normally be of that composition (Frey and Clague, 1983). The wide compositional variety of dredge samples suggests that a transition from alkalic volcanism to the tholeiitic volcanism typical of the main growth stage of the shield may now be in progress. Palagonite coatings on the samples of alkalic basalt are thicker than coatings on tholeiite, suggesting that alkalic basalt is the older (Frey and Clague, 1983). Frequent seismic swarms (Klein and Koyanagi, 1979) suggest that Loihi is actively growing. Stratigraphic relations cannot be examined, and an alternate interpretation is that Loihi may now be at the end of the tholeiitic stage and only now is passing into the alkalic stage. The frequent seismicity however, as well as the relative thickness of palagonite, render this less likely. Still further implications of the geochemistry and petrogenesis of Loihi are discussed by Clague (in press). If Loihi is indeed passing from an initial alkalic stage to a tholeiitic stage, as proposed by Frey and Clague (1983), then alkalic volcanism is not solely confined to the waning stages of the life cycle of Hawaiian volcanoes. Even though it now serves as but a single example, findings at Loihi Seamount suggest that the hidden inner cores of Hawaiian volcanoes may record histories more complex than previously assumed.

AGE DETERMINATIONS

Until very recently, the lack of a method to date young basalts, the difficulty of correlating laterally discontinuous lava flows, and the scarcity of marker horizons placed severe limitations on stratigraphic studies in Hawaii. Even when radiometric dating techniques began to be developed and applied in the 1950's and 1960's, their usefulness on Hawaii appeared to be limited. The utility of the K-Ar method is constrained because Hawaiian rocks are very young and very low in potassium. As recently as the early 1970's, radiocarbon dating appeared to be applicable only to the few pyroclastic layers, because they contained the only obvious organic material intercalated among the lava flows. In spite of the difficulties, however, these and other radiometric techniques have subsequently been utilized to obtain numerical ages for many of the prehistoric lavas.

McDougall (1964) obtained K-Ar ages for rocks from several of the older Hawaiian Islands, but his initial effort to date samples from Hawaii (Kohala Volcano) was unsuccessful. However, refined sample preparation and improved techniques enabled a later study to succeed (McDougall and Swanson, 1972). The ages of Kohala rocks in the exposed part of the tholeiitic suite range from about 0.46 to 0.30 Ma, and ages of rocks in the alkalic suite range from about 0.26 to 0.06 Ma. These results established a position in the geologic time scale for the subaerial portion of Kohala Volcano, providing information on its growth rate, the interval between tholeiitic and alkalic volcanism, the duration of alkalic volcanism, and the date of last activity. Perhaps the only other exposed basaltic rocks on Hawaii old enough to be within the range of the K-Ar method are those of the Ninole Basalt on the south flank of Mauna Loa; these have yielded K-Ar ages from more than 0.5 to less than 0.1 Ma (Evernden and others, 1964, p. 156–158). A chronology for both volcanism and glaciation on Mauna Kea was established with the aid of K-Ar and radiocarbon techniques (fig. 7.4; Porter, chapter 21, 1979a, 1979b; Porter and others, 1977).

Initial attempts at radiocarbon dating of Hawaiian samples in the 1960's were confined to carbonized residues found in ash layers; results were not then published. During the early systematic geologic mapping of Mauna Loa in the mid-1970's, methods for finding carbonized organic remains beneath lava flows were improved, providing considerable material for radiocarbon dating (Lockwood and Lipman, 1980). This led to many successful radiocarbon age determinations for lava flows on the volcanoes of Hawaii (Rubin and others, chapter 10; Kelley, 1979; Kelley and others, 1979). However, application of the radiocarbon method is constrained both by its upper limit of 30–40 ka, depending on sample characteristics, and by the restricted distribution of datable carbon associated with lava flows. Woody residues are confined to zones near the margins of lava flows that have invaded vegetated areas, so the method cannot be used for flows above the tree line or in other barren areas nor for portions of lava flows that do not lie near a margin.

Many lavas of Hawaii are too old for radiocarbon dating and too young for K-Ar age determination. A technique that may provide ages within this gap is thermoluminescence (TL). This technique relies on an incompletely understood phenomenon in which light is emitted by certain minerals as they are heated toward the point of incandescence (Berry, 1973; May, 1979). Berry (1973) conducted experiments testing the feasibility of TL as a dating technique for Hawaiian rocks and concluded that the method holds promise. Subsequently more elaborate experiments yielded reasonably consistent results for feldspar from rocks of the alkalic suite for ages from about 250 to 2.5 ka (May, 1979, p. 40). Results for feldspar-poor tholeiitic rocks were not as consistent, but May (1979, p. 41) expressed the belief that a dating technique using TL could ultimately be developed for tholeiites through a range from about 100 to 10 ka.

Another method of dating uses the secular variation of the earth's magnetic field. As iron-titanium oxides in newly erupted lava cool through the Curie temperature, they assume and preserve the direction of magnetism of the earth's field at that time and place. Geomagnetic studies take advantage of this characteristic to construct a history of the changes in orientation of the magnetic field, using rocks that can be dated independently. By matching the magnetic direction of a rock of unknown age to the local geomagnetic history, the possible age(s) of the unknown rock can be determined. Working with lavas already dated by the radiocarbon method, Holcomb (1980) derived the history of the secular variation of the magnetic field in Hawaii for the past 2,500 yr and in turn has applied it to obtain ages for most of the surface flows of Kilauea Volcano. Although this method ultimately depends on radiocarbon

ages, samples for study are not restricted to the vegetated zones where datable carbon may occur. The dates obtained through this approach enabled Holcomb (chapter 12, 1980) to determine that 90 percent of the surface rocks of Kilauea are younger than 1.1 ka.

The increasing degree of weathering with increasing age has long been used to estimate visually the relative ages of lava flows. To see if weathering could be used to derive numerical ages, Halbig and others (1979) correlated the thickness of alteration rinds on basaltic glass with radiocarbon ages of the same lavas. They found that the rind thickens at an average rate of about 1.05 mm/100 yr during the first 1,000 years; thereafter rates become unreliable because of mechanical attrition and spalling. They recognized the potential effects of variations in climate and glass composition but did not study those effects. This technique, even with its probable limitations, has the advantages of being quicker, simpler, and less expensive than radiometric and paleomagnetic age determination, and it may prove useful for qualitative and semiquantitative estimates of age.

CALDERAS AS RELATED TO VOLCANO DEVELOPMENT

Dutton (1884, p. 142–143) suggested that caldera formation was a recurring process during the growth of Hawaiian volcanoes, but the proposal by Stearns (1940, 1946) that a single caldera forms at the end of shield growth was tacitly accepted by most workers until recently (Holcomb, chapter 12, 1976, 1980). Macdonald (1965) reviewed possible mechanisms for the formation of Hawaiian calderas and concluded that most commonly piecemeal collapse occurs above a shallow magma reservoir when magma is withdrawn by either voluminous eruption or intrusion along a rift zone. Macdonald further reasoned, in accord with the ideas of Stearns, that a volcano must achieve a state of maturity for a magma reservoir to have grown to a sufficiently large size for magma withdrawal to be able to trigger collapse. Calderas exposed by erosion at older volcanoes, such as Kohala on Hawaii as well as some on other islands, formed originally within tholeiitic lavas but were later filled by transitional or alkalic lavas. Although such evidence is permissive only, it supports the idea that calderas form at the conclusion of tholeiitic shield building (Stearns, 1940, 1946, 1966; Macdonald, 1965).

Macdonald (1965) considered many hypotheses before selecting a preferred mechanism for caldera formation, but he did not explicitly consider the possibility that such formation might occur more than once. Powers (1948) had suggested the existence of an earlier caldera at Kilauea on the basis of discrepant elevations of young ash beds and partially obscured surface structures. Using additional evidence, Holcomb (chapter 12, 1976, 1980, p. 194) concluded that the present caldera of Kilauea is nested within a prehistoric caldera that had been filled and nearly buried. He also noted evidence for an earlier caldera at the summit of Mauna Loa (Holcomb, 1976). If his conclusions are correct, the presence of a caldera is neither a sufficient nor necessary condition to infer a specific stage in the life cycle of a volcano, and the possibility exists, within any Hawaiian volcano, that a succession of calderas may lie buried.

This viewpoint is supported by results from Loihi, where a bathymetric survey revealed a summit depression approximately 70 m deep, and measuring about 2.8 km by 3.7 km, which includes two pit craters of about 0.8 and 1.2 km in diameter, each of which is more than 250 m deep (Malahoff, chapter 6; Malahoff and others, 1982; summarized by Macdonald and others, 1983, p. 117–118). If Loihi is accepted as a volcano in an early stage of its evolution (see section "Petrologic Investigations"), it provides an additional example of caldera formation at a stage other than near the end of the main growth of a Hawaiian volcano.

This change in thinking is reflected by Macdonald and others (1983, p. 146–149), who no longer specify the development of a caldera as an individual stage in the development of a volcano, but rather include it simply as an event that may happen during the shield-building stage. We concur with this usage and further advocate avoiding the characterization of the transition from tholeiitic to alkalic magmatism by the use of terms such as "caldera-filling" and "post-caldera." These shifts in viewpoints are incorporated in our proposed modifications to the scheme of growth stages for Hawaiian volcanoes, outlined in a subsequent section.

STRUCTURAL DEVELOPMENT OF HAWAIIAN VOLCANOES

The shield volcanoes of Hawaii have broad bases in relation to their height and subaerial slopes in the tholeiitic stage, unmodified by faulting or erosion, generally of 3°–10° and averaging about 6°. Volcanoes with a steeper sided alkalic cap have summit slopes that locally approach 20° and average about 12°. The subaerial part of each volcano is built of tens or hundreds of thousands of discrete, overlapping lava flows of pahoehoe and aa that radiate outward from a central summit vent area and from two or more linear rift zones. Beds of tephra may be interlayered sporadically with the tholeiitic lava, and the proportion of tephra to lava increases during the growth of the alkalic cap.

Some descriptions state that lava flows have the form of sheets (see Stearns, 1946, p. 17; Stearns and Macdonald, 1946, p. 24), an impression easy to derive because their thickness is small compared to their lateral dimensions. However, the geologic map (fig. 7.3; Stearns and Macdonald, 1946, plate 1) shows that for most flows the ratio of length to width is large, and it seems preferable to visualize flows as elongated tongues or lobes (Peterson, 1971, p. 163–164). This visualization helps emphasize the across-flow discontinuity of Hawaiian flows, which is one of the major problems in efforts to establish consistent stratigraphic correlations. Adjacent volcanoes generally grow contemporaneously, and their flows are commonly interdigitated.

Slopes on the submarine part of the volcano are steeper than on the subaerial part; they are commonly 10°–20° (fig. 7.6). Submarine flows are dominantly of pillow lava and are assumed also to be tongue-shaped, like subaerial flows. Superimposed upon and incorporated within this primary edifice of overlapping lava flows and sporadic tephra layers are a number of structures that develop throughout the growth of the shield, including rift zones, faults, landslides, calderas, craters, and tephra and spatter cones.

Rift zones have long been recognized as integral structural elements of Hawaiian volcanoes (Dana, 1849; Dutton, 1884). The summit areas and rift zones include almost all vents through which lava is erupted, and the surfaces of the rift zones of Kilauea and Mauna Loa are marked by spatter cones, spatter ramparts, pit craters, grabens, faults, cracks, and fissures, which constitute a record of repeated active volcanism and related ground dislocations. Where the subsurface portions of rift zones have been exposed by erosion on the older islands, they are marked by abundant closely spaced subparallel dikes, which demonstrate that rift zones tend to maintain consistent orientation and position throughout the growth of a shield.

Fiske and Jackson (1972) proposed that the orientations of rift zones on volcanoes that grew from the ocean floor, distant from other volcanoes, is determined by regional stress patterns; at volcanoes that grew on the flank of an already existing edifice, the orientation of the rift zones is determined by the gravitational stress field influenced by the buttressing effect of the older volcano. Their hypothesis is supported by results of experiments with gelatin models and is basically consistent with the progression of development of the volcanoes on all the islands from Kauai to Hawaii (see, for example, Moore, chapter 2, fig. 2.6). Their analysis yields the following sequence of origin for the volcanoes of Hawaii: Kohala, Hualalai, Mauna Kea, Mauna Loa, and Kilauea (fig. 7. 7). This sequence of origin is not necessarily the same as either the order of petrogenetic development or the time progression of known eruptions; for example, hawaiite on Mauna Kea is more differentiated than alkalic basalt on Hualalai, and historical activity has occurred at Hualalai but not at Mauna Kea. These relations suggest that Mauna Kea has passed through the petrogenetic development sequence more rapidly than Hualalai.

The model of Fiske and Jackson (1972) provides a generally consistent explanation for the orientations of rift zones and for many aspects of the behavior of the different volcanoes. As adjacent volcanoes commonly grow contemporaneously, however, fluctuations of eruption rates and shifts of vent sites from summit to rift zone in one volcano may cause changes in slope direction or in the influence of buttressing, thereby affecting the prevailing stress fields of an adjacent volcano and influencing the development of its rift zones. Stearns and Clark (1930) noted, for example, that the growth of Kilauea against the southeast flank of Mauna Loa caused a change in the pattern of behavior of the nearby fault systems of Mauna Loa. Lipman (1980) concluded that the growth of Kilauea has, in effect, squeezed the northeast rift zone of Mauna Loa and effectively sealed off its lower, easternmost extension and that it has caused the

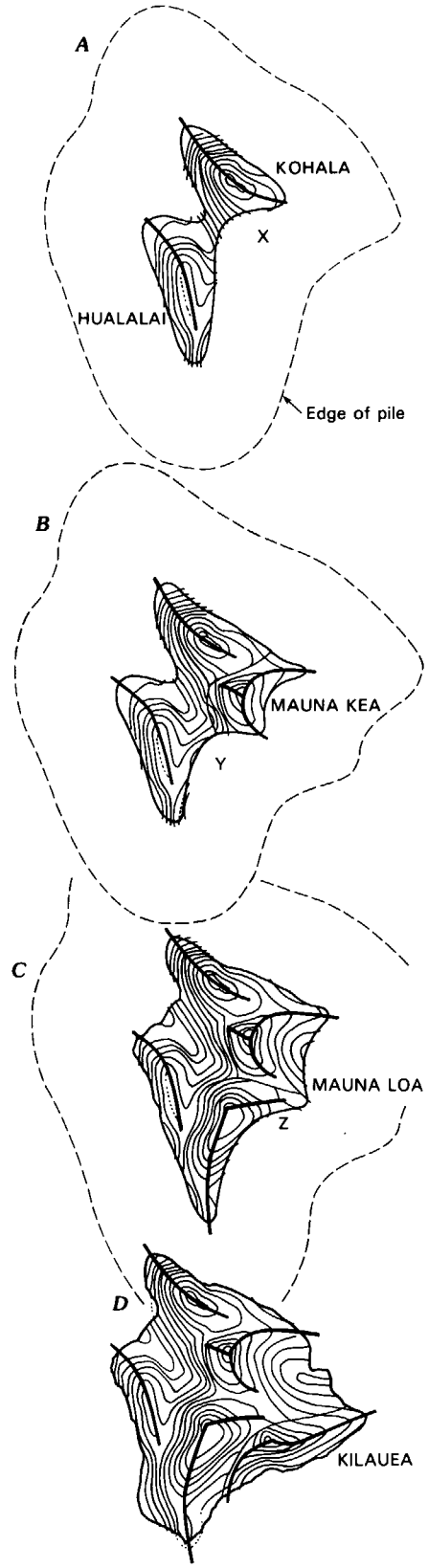

FIGURE 7.7.—Growth of Island of Hawaii as proposed by Fiske and Jackson (1972, fig. 11, p. 315). Reproduced by permission. ***A***, Early formed Kohala-Hualalai edifice; X marks site of future Mauna Kea. ***B***, Later stage; Y marks site of future Mauna Loa. ***C***, Still later stage; Z marks site of future Kilauea. ***D***, Present configuration. Each sketch shows orientations of rift zones, which developed in accord with prevailing regional or gravitational stress patterns.

southwest rift zone of Mauna Loa to migrate gradually westward. Such changes support the basic concept of Fiske and Jackson (1972) that rift zones develop in accord with the prevailing stress field, although they require modification of the idea that the rift zones remain fixed in position and orientation.

Pertinent to these issues is the orientation of the rift zones of Loihi Volcano. The bathymetric contours along the south flank of the island are oriented about N. 60° E. (fig. 7.8*A*); according to the concept of Fiske and Jackson (1972), the rift zones of Loihi should lie approximately parallel to this direction. Instead, the orientation of the elongate ridges inferred to mark the rift zones is mostly about N. 30° W., varying locally to due north and N. 10° E. (fig. 7.8*B*); it thus is chiefly almost at right angles to the expected orientation (Malahoff, chapter 6; Malahoff and others, 1982; Moore and others, 1982). Too little is known about the details of the structure and morphology of Loihi to fully evaluate this apparent discrepancy, but it may be noted that the rift zones of Loihi are approximately parallel to the line of the major loci of volcanoes to the northwest (fig. 7.8*A*; Malahoff, chapter 6). The central vent of Loihi lies approximately along the projection of the 4,000-m depth contour, approximately 1,000 m above the level of the regional ocean floor (fig. 7.8*A*). It may be that during the early growth of Loihi, the influence of the regional stress pattern predominated over that of the gravitational stress field on the flanks of the older volcanoes, or perhaps Loihi began before the submarine slopes of Kilauea and Mauna Loa had advanced to the Loihi site. As Loihi grows, it will offer a variety of tests for the Fiske-Jackson (1972) hypothesis and will be a fascinating subject for study by future generations of scientists.

The gravitational stress field on volcano flanks influences the structure in still another important way. Landslides have long been recognized as a hazard in Hawaii, occurring chiefly on steep slopes such as seacliffs and stream-cut valley walls; they are commonly induced by saturation of the ground by heavy rains, by shaking from earthquakes, or especially by the two in combination. In contrast to these relatively small, frequent landslides, Moore (1964) advocated large-scale landsliding as the origin for extensive areas of irregular submarine topography offshore from several islands, including Hawaii. Masses covering several thousand square kilometers north of Molokai and north of Oahu are inferred to be two immense landslides that moved more than 100 km along slide planes with an average slope of about 2°. As more detailed bathymetry has become available for offshore areas around Hawaii, it has been recognized that landslides are common on the submarine flanks of volcanoes. Some large-scale slumping events may be related to step-faulting on the subaerial seaward flanks of volcanoes, such as in the Hilina fault system on the south flank of Kilauea (Moore and Fiske, 1969, p. 1199–1200). Certain bathymetric details of Loihi are also inferred to be the result of submarine landslides (Malahoff, chapter 6).

Moore and Krivoy (1964) proposed that gravity-induced seaward movement of the south flank of Kilauea caused dilation of its east rift zone, leading to permissive emplacement of dikes by magma from the summit reservoir. This idea was tested when detailed analyses of the displacements of points on the east rift zone, the

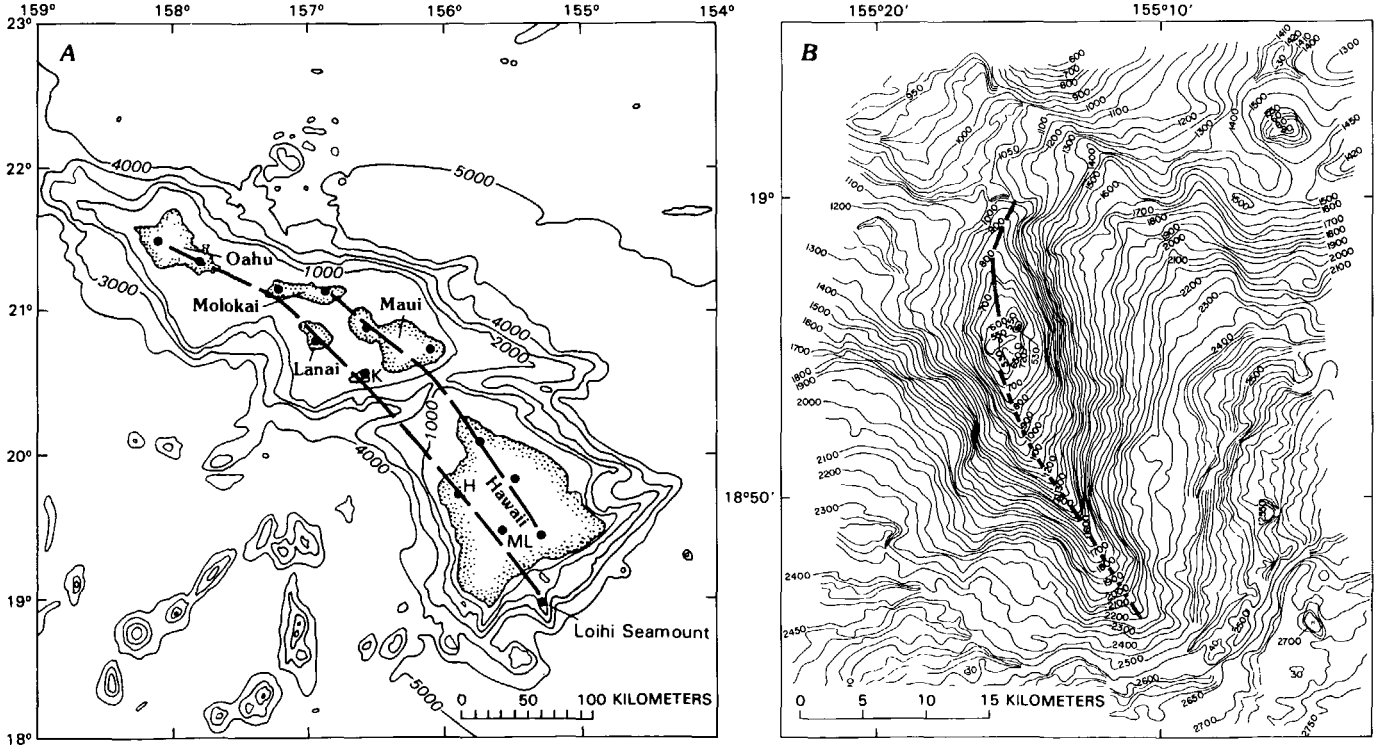

FIGURE 7.8.—Loihi Seamount. ***A***, Position along regional curved locus extending through western line of volcanoes from Oahu to Hawaii, including Hualalai and Mauna Loa Volcanoes (after Moore and others, 1982). Bathymetric contours in meters. ***B***, Bathymetric map (after Malahoff and others, 1982). Elongate ridges extending south-southeast and north from summit are major rift zones of volcano. They lie subparallel to volcano locus shown in *A* instead of parallel to submarine contours of island platform. Depth contours in fathoms (1 fathom = 1.83 m).

Koae and Hilina fault systems, and other parts of the south flank were made by Duffield (1975) and Swanson and others (1976a). They examined the amount, direction, and time of displacement as related to the time and place of eruptions and concluded that displacements on the rift zone and south flank were caused by forcible injection of magma into the rift zone, rather than the rift zone being dilated as a result of faulting and sliding of the south flank and permissively allowing magma to enter. Nevertheless, gravity plays an important role, because displacements are toward the sea in the unbuttressed direction. Hence these findings are compatible with those of Fiske and Jackson (1972) concerning the role of gravity in the development of the east rift zone.

The $M=7.2$ earthquake at Kilauea on November 29, 1975, was probably related to strains accumulated throughout the south flank from intrusion of dikes into the rift zone (Swanson and others, 1976a; Tilling and others, 1976). However, the earthquake itself has been determined to be the result of abrupt southward movement of the south flank edifice across the underlying oceanic crust (Ando, 1979; Furumoto and Kovach, 1979; Crosson and Endo, 1981, 1982). This movement induced extensive displacements throughout the Hilina and other fault systems (Tilling and others, 1976).

Marine terraces positioned both above and below sea level (Stearns and Macdonald, 1946) have long suggested that the level of the sea fluctuated over extended periods of time; they have been interpreted both as eustatic and as related to local crustal movements. Submergence of cultural artifacts of the early Hawaiian people indicates that Hawaii is currently subsiding (Apple and Macdonald, 1966). This inference was supported by a study of tide-gage records, which yielded a rate of subsidence at the Hilo tide gage of about 4.1 mm/yr, implying an annual volume rate of subsidence of the east end of the Hawaiian Ridge of about 0.27 km^3/yr (Moore, 1970). The rate of subsidence at Hilo has subsequently been redetermined to be 2.4 mm/yr, giving a recalculated volume rate of subsidence of 0.075–0.1 km^3/yr (Moore, chapter 2). The sinking of Hawaii is interpreted to be the result of crustal loading by the erupted products. The new volume rate of subsidence agrees closely with the figure of 0.11 km^3/yr, which recently has been the average annual volume of lava erupted by Kilauea (Swanson, 1972).

Marine deposits now above sea level are difficult to explain if progressive subsidence is the result of eruption and crustal loading. However, recent reinterpretation of such deposits as resulting from a giant ocean wave permits the interpretation that Hawaii, instead of alternately rising and sinking, has indeed been sinking persistently in response to long-sustained crustal loading (Moore and Moore, 1984).

Moore (chapter 2) demonstrates that the constructional volcanic edifices, instead of merely resting on the deep ocean floor at a depth of 5–6 km as previously believed, have bowed the crust downward during and after their growth, that most of their bases have subsided about 8–10 km, and that since reaching the sea surface the volcanoes have subsided 2–5 km. Hence a substantial part of their mass that is now below sea level was erupted subaerially.

HISTORICAL ACTIVITY

Among Hawaii's volcanoes, only Kilauea and Mauna Loa have erupted since the time of the missionaries, but they have in that interval been among the world's most active volcanoes. A summary of their activity is provided in tables 7.3 and 7.4.

When first known to the outside world, Kilauea became famous for its long-lasting lava lake in the crater and vent complex of Halemaumau inside the summit caldera. Lava in the lake circulated, fountained, and alternately rose and fell within Halemaumau Crater. The lake episodically overflowed onto the caldera floor and, during its 101-year life span, added about 2 km^3 of lava to the caldera, raising the floor several hundred meters. This lava constructed a gently sloping shield volcano inside the caldera, with the summit at Halemaumau. A few eruptions also occurred during this time along the east and southwest rift zones of Kilauea, but most activity was concentrated in the summit caldera. The lava-lake activity ended in 1924 with subsidence and explosive eruptions at Halemaumau, which left the pit crater more than 400 m deep.

During the next few years, brief episodic eruptions occurred at Halemaumau and partly filled the pit crater formed in 1924, but a period of repose followed from the mid-1930's to 1952. Since then, Kilauea has had more than two dozen eruptions within the caldera and nearby summit area as well as along both rift zones, extruded more than 1.3 km^3 of lava, and exhibited a very wide variety of behavior (see references in table 7.3). Most eruptions since the 1960's have occurred along the east rift zone. Individual eruptions have lasted from less than a day to more than two years. Episodic activity at Puu Oo, in the central east rift zone, began in January 1983 and continues as of early 1986 (Wolfe and others, chapter 17).

Mauna Loa erupted 35 times between 1832 and 1950 (table 7.4), an average of one eruption every 3.4 years. Eruptions showed a tendency to alternate between the summit area and either the northeast or southwest rift zone. Intervals between eruptions ranged from as brief as 4 months to as long as 11 years, and eruptions lasted from less than a day to 547 days. The native Hawaiians had no traditions or stories about Mauna Loa eruptions, so the length of the period of quiescence preceding 1832 is not known. Because the summit and upper rift zones are remote from Hawaiian villages, small eruptions may have gone unobserved; alternatively, a prolonged period of actual quiet may have prevailed. The latter seems much more likely, as eruptions of the type occurring in the nineteenth and twentieth centuries would have been obvious to the Hawaiians and would have influenced their activities. Following the eruption of 1950, the volcano did not erupt again until 1975, when a one-day-long eruption ended the longest period of quiet in historical time (Lockwood and others, chapter 19, 1976). The most recent activity occurred in 1984, when a 22-day-long eruption sent lava flows to within 18 km of the waterfront at Hilo and 6 km of the outskirts of the city (Lockwood and others, chapter 19, 1985)

The frequent activity of both these volcanoes suggests that similar patterns of behavior are likely to continue during the near future. Holcomb (chapter 12, 1980), however, has analyzed the long-range shifts in type and location of activity of Kilauea and has

developed a model indicating major shifts from summit growth and caldera filling to rift-zone growth and summit collapse. Equivalent patterns of shifting behavior at Mauna Loa are being reconstructed by Lockwood and Lipman (chapter 18).

REVISED SCHEME OF EVOLUTIONARY STAGES FOR HAWAIIAN VOLCANOES

The evolutionary stages defined by Stearns (1946) have served as a basic framework for Hawaiian geologic history for about four decades. Macdonald and Abbott (1970, p. 138) modified the stage boundaries to reflect improved knowledge of submarine processes and subdivided the first stage of Stearns into deep and shallow submarine stages. Later, Macdonald and others (1983, p. 147–149) recognized that calderas are not necessarily unique to a specific stage in the growth of the volcano, and their updated classification omitted the caldera stage.

Other investigators have emphasized four stages that are of significance in the petrologic evolution of Hawaiian volcanoes, roughly patterned after the initial definitions by Stearns (1940). Although the various workers have been consistent in designating four stages, they have selected different ways of defining their progression. Stearns (1940) initially defined them as (1) youthful, shield-building (chiefly olivine-bearing basalt); (2) mature, caldera formation (also olivine-bearing basalt); (3) old age, caldera filling (differentiated rocks); and (4) rejuvenated or post erosion (highly differentiated rocks); Stearns later (1946, 1966) added non-eruptive developmental stages. Tilley (1950) reiterated the same four stages of Hawaiian volcanism. Leeman and others (1980) redefined them as (1) shield-building stage (tholeiitic lava); (2) caldera-filling stage (tholeiitic, transitional, and mildly alkalic lava); (3) postcaldera stage (including alkali olivine basalt and related differentiates); and (4) posterosional stage (including basanitic and nephelinitic lavas). The chief difference in their scheme is that the formation of calderas has been included with shield building, and a caldera-filling stage has been substituted for the second stage and serves as the transition from tholeiitic to alkalic basalt. A different variant is offered by Clague and Dalrymple (chapter 1, part I, table 1.1). Their four stages are (1) preshield stage (including basanite, alkalic and transitional basalt); (2) shield stage (tholeiitic basalt and picritic tholeiitic basalt); (3) postshield alkalic stage (alkalic lavas of assorted composition); and (4) rejuvenated stage (alkalic lava and highly differentiated types such as basanite and nephelinite). Their stage (1) reflects the new findings at Loihi, and their stage (3) is equivalent to the latter part of stage (2) and all of stage (3) of Leeman and others (1980). The scheme of evolution to be offered here utilizes the four stages as defined by Clague and Dalrymple (chapter 1, part I), although the terms used for some of the stages are different, and additional stages are defined.

Earlier discussion (see section "Calderas as Related to Volcano Development") established our view that it is not appropriate to retain a separate stage of caldera formation. By the same arguments it is also inappropriate to designate another stage as postcaldera. For example, if either Kilauea or Loihi caldera is filled by new lava in the future, as seems quite likely, the subsequent activity in reality would be postcaldera, but the composition will most likely still be tholeiitic. This lava would certainly not meet the essential evolutionary criteria required of the so-called postcaldera stage, which some of the above authors have specified as reflecting the differentiation to alkalic magma. It is also possible for the magma of a volcano to undergo differentiation to the alkalic suite without the volcano having had a caldera (for example, no evidence has yet been found for a caldera at Hualalai, though it is possible that unknown filled calderas lie within the edifice). In view of these several considerations, we feel the name "postcaldera stage" is a misnomer and its use should be avoided.

Our intention is to propose a scheme of evolution with the same purpose as that by Stearns (1946) and subsequently modified by Macdonald and Abbott (1970) and Macdonald and others (1983)—to outline in simple form the major steps in development of a typical Hawaiian volcano. Such schemes are of necessity oversimplified because of the variations and exceptions followed by individual volcanoes, yet they are useful as a framework or standard of comparison, and most importantly they can serve as a spur in the search for improved understanding. The stages here include not only the growth of the volcano as reflected by petrogenetic developments reviewed just above, but they also include other significant geologic processes and environmental conditions. Some of the terms used by preceding authors have been retained, but others have been revised, either because of redefinition of a stage reflecting a modified current concept or simply because another term seemed more appropriate. The terms adopted avoid rock names because we find it difficult to apply a petrologic term without introducing some ambiguity. Furthermore, all reference to a caldera in the terms and in the definitions of stages has been removed because we hold the opinion that calderas may repeatedly form and be refilled at various times during the rapid growth of a shield; thus their development and filling is not sufficient to define a distinct stage. The terms here also avoid the prefixes pre- and post-, as associated with a process or a feature, because their use implies, sometimes erroneously, that this process or feature does not operate or exist at all during the designated stage. We wish to emphasize that the successive stages may overlap and intergrade, and the processes characteristic of two or more stages may be operating at different places on a volcano at the same time. Furthermore, volcanoes do not necessarily pass through every stage, nor do different volcanoes necessarily progress through stages at similar or consistent rates.

In spite of the advances since 1946, such as new geophysical and geochemical tools, improved investigative techniques, and extensive offshore submarine exploration, our concepts of volcano development are still based on facts derived from only a thin outer shell of the Hawaiian volcanoes. Petrological theories have made exciting and possibly valid inferences about the petrogenesis of magma and the growth of the volcanoes, but until these ideas can be tested by actually probing the deep interior and the base of several volcanoes, the concepts must remain speculative. So although the scheme proposed here represents an effort to reflect currently prevailing ideas as unabiguously as possible, it still suffers from some

TABLE 7.3.—*Historical eruptions of Kilauea through May 1985*

[Dashes (---), no data; query (?), questionable data]

Date eruption began Year	Month and day	Duration (days)	Location of major vent(s)	Approximate area (km^2)	Approximate volume ($m^3 \times 10^6$)	References
1750(?)	---	---	East rift	4.1	14.9	Holcomb, chapter 12, 1980.
1790(?)	---	---	-- do ----------	7.9	28.8	Holcomb, chapter 12, 1980.
1790	November (?)	---	Caldera (explosive)	(Blocks lapilli, ash)	---	Brigham, 1909, p. 36–39; Hitchcock, 1909, p. 165–167; Swanson and Christiansen, 1973; Decker and Christiansen, 1984.
1823	---	---	Southwest rift	10.0	11.5	Hitchcock, 1909, p. 163; Stearns, 1926.
1823	---	101 yr (intermittent)	Caldera, Halemaumau	8.2	2,000.0	Ellis, 1827, p. 163–176; Brigham, 1909, p. 40–222; Hitchcock, 1909, p. 179–182, 186–188, 191–194, 198–206, 210–260; Jaggar, 1947, p. 9–169, 216–314.
1832	January 14	---	East rim of caldera	---	---	Brigham, 1909, p. 46; Hitchcock, 1909, p. 182–185.
1840	May 30	26	East rift	17.1	215.0	Coan, 1841; Brigham, 1909, p. 50–55; Hitchcock, 1909, p. 188–190.
1868	April 2	---	Kilauea Iki	.2	---	Brigham, 1909, p. 106–110; Hitchcock, 1909, p. 207.
1868	April 2	---	Southwest rift	.1	.2	Brigham, 1909, p. 109–119; Hitchcock, 1909, p. 207–210; Coan, 1869.
1877	May 4	1	Caldera wall	---	---	Brigham, 1909, p. 131–132; Hitchcock, 1909, p. 217.
1877	May 21 (?)	---	Keanakakoi	.1	---	Brigham, 1909, p. 132; Hitchock, 1909, p. 217.
1884	January 22	1	East rift (submarine)	---	---	Stearns and Macdonald, 1946, p. 111; Macdonald and Abbott, 1970, p. 75.
1879	July 14	1 (?)	Distinct episodes of Halemaumau overflows and (or) caldera fissure outbreaks. These are part of the 1823 101-year-long summit eruption. Earlier lava buried; lava from those episodes locally exposed in caldera.	---	---	Brigham, 1909, p. 133, 140; Hitchcock, 1909, p. 219.
1882	September	3 yr		---	---	Brigham, 1909, p. 156–158; Hitchcock, 1909, p. 221–226.
1888	July	310		---	---	Dana, 1890, p. 123.
1892	April	730 (intermittent)		---	---	Brigham, 1909, p. 184–191.
1918	February 23	14		.1	.2	Jaggar, 1947, p. 112.
1919	February 7	294		4.1	26.0	Jaggar, 1947, p. 118–125.
1921	January	60 (approx)		2.0	6.7	Jaggar, 1947, p. 149–151.
1919	December 15	221	Southwest rift (Mauna Iki)	13.0	47.0	Jaggar, 1947, p. 137–146.
1922	May 28	2	East rift (Makaopuhi, Napau)	.1	---	Jaggar, 1947, p. 155–157.
1923	August 25	7	East rift	.5	.1	Jaggar, 1947, p. 161.
1924	May 10	17	Caldera (explosive)	(Blocks)	---	Jaggar and Finch, 1924; Jaggar, 1947, p. 162–168, 205–259; Decker and Christiansen, 1984.
1924	July 19	11	Halemaumau	.05	.24	Jaggar, 1947, p. 168–169.
1927	July 7	13	-- do ----------	.1	2.42	Jaggar, 1947, p. 175–176.
1929	February 20	2	-- do ----------	.15	1.47	Jaggar, 1947, p. 180–181.
1929	July 25	4	-- do ----------	.2	2.75	Jaggar, 1947, p. 181–182.
1930	November 19	19	-- do ----------	.23	6.48	Jaggar, 1947, p. 185–186.
1931	December 23	14	-- do ----------	.3	7.37	Jaggar, 1947, p. 186–189.
1934	September 6	33	-- do ----------	.4	7.26	Jaggar, 1947, p. 197.
1952	June 27	136	-- do ----------	.6	49.0	Macdonald, 1955, 1959.
1954	May 31	3	Halemaumau, caldera	1.1	6.5	Macdonald, 1959; Macdonald and Eaton, 1957.
1955	February 28	88	East rift	15.8	92.0	Macdonald, 1959; Macdonald and Eaton, 1964.
1959	November 14	36	Kilauea Iki	.6	51.0	Richter and Eaton, 1960; Macdonald, 1962; Richter and others, 1970.
1960	January 13	36	East rift	10.6	120.0	Do.
1961	February 24	1	Halemaumau	.05	.02	Richter and others, 1964.
1961	March 3	22	-- do ----------	.8	.27	Do.
1961	July 10	7	-- do ----------	1.0	13.2	Do.
1961	September 22	3	East rift	.8	2.3	Do.
1962	December 7	2	-- do ----------	.05	.33	Moore and Krivoy, 1964.
1963	August 21	2	East rift (Alae)	.2	.04	Peck and Kinoshita, 1976.
1963	October 5	1	East rift	3.4	6.9	Moore and Koyanagi, 1969.
1965	March 5	10	East rift (Makaopuhi, Napau)	7.8	18.0	Wright and others, 1968.
1965	December 24	1	East rift (Alae and vicinity)	.6	.9	Fiske and Koyanagi, 1968.
1967	November 5	251	Halemaumau	.65	84.1	Kinoshita and others, 1969.
1968	August 22	5	East rift	.03	.04	Jackson and others, 1975.
1968	October 7	15	-- do ----------	2.1	7.0	Do.
1969	February 22	6	-- do ----------	6.0	17.0	Swanson and others, 1976b.
1969	May 24	875	East rift (Mauna Ulu)	50.0	185.0	Swanson and others, 1971, 1979; Peterson and others, 1976, p. 647–648.
1971	August 14	1	Caldera	2.0	10.0	Peterson and others, 1976, p. 649–650; Duffield and others, 1982.
1971	September 24	5	Halemaumau, caldera, southwest rift	4.0	8.0	Peterson and others, 1976, p. 650; Duffield and others, 1982.
1972	February 3	455	East rift (Mauna Ulu)	35.0	125.0	Peterson and others, 1976, p. 651–652; Tilling and others, chapter 16.
1973	May 5	1	East rift (Pauahi, Hiiaka)	.14	1.0	Peterson and others, 1976, p. 651–652; Tilling and others, chapter 16.
1973	May 7	187	East rift (Mauna Ulu)	.5	2.5	Peterson and others, 1976, p. 652; Tilling and others, chapter 16.
1973	November 10	30	East rift (Pauahi and vicinity)	1.5	3.0	Peterson and others, 1976, p. 652–653; Tilling and others, chapter 16.

TABLE 7.3.—*Historical eruptions of Kilauea through May 1985*—Continued

Date eruption began Year	Month and day	Duration (days)	Location of major vent(s)	Approximate area (km^2)	Approximate volume ($m^3 \times 10^6$)	References
1973	December 12	222	East rift (Mauna Ulu)	8.0	30.0	Peterson and others, 1976, p. 653–654; Tilling and others, chapter 16.
1974	July 19	3	Caldera, Keanakakoi, and vicinity)	3.2	10.0	Peterson and others, 1976, p. 656; Lockwood and others, chapter 19.
1974	September 19	1	Halemaumau, caldera	1.1	11.0	Do.
1974	December 31	1	Southwest rift, Koae fault system	7.5	15.0	Do.
1975	November 29	1	Halemaumau, caldera	---	.25	Tilling and others, 1976, p. 15–17.
1977	September 12	20	East rift	8.0	35.0	Moore and others, 1980.
1979	November 16	1	East rift (Pauahi and vicinity)	.17	.7	Banks and others, 1981.
1980	March 11	1	East rift (near Mauna Ulu)	.0001	.000003	
1982	April 30	1	Halemaumau, caldera	.25	.5	Banks and others, 1983.
1982	September 23	1	South outer caldera	.75	4.0	Banks and others, 1983.
1983	January 3	continuing (August 1986)	East rift, Puu Oo	40 (approx)	350 (approx)	Wolfe and others, chapter 17.

of the same basic limitations as did that of Stearns (1946). New facts, as they become available, will inevitably modify current concepts, and we hope the progress will be at a rate such that this new scheme will require early revision.

We propose the following scheme of evolution for Hawaiian volcanoes (see fig. 7.9 and table 7.5)

1. Initial stage. Although little known, products apparently include a variety of differentiated, alkalic-type lavas. Calderas are possible.
2. Shield-building stage. Products are tholeiitic basalt and tholeiitic picrite, and major growth of the shield volcano occurs. Eruptions are frequent and voluminous. Three substages are recognized according to physical environment:
   a. Submarine substage; dominantly pillow lava and derivatives, relatively steep slopes.
   b. Sea-level substage; development of hyaloclastite rocks chiefly by explosive interaction between molten lava and seawater and by wave abrasion.
   c. Subaerial substage; pahoehoe and aa build gently sloping shield-shaped edifice; small percentage of tephra.

   Calderas and pit craters may form and be filled repeatedly during any of these substages.
3. Capping stage. Magma becomes differentiated to yield alkalic basalt and other alkalic rocks. Eruptions become less frequent, lava becomes more viscous and is interspersed with explosive products, and a steeper sided cap is built. Any existing caldera is filled. Eruptions decline and finally end.
4. Erosional stage. Erosion by streams and waves carves valleys, canyons, and seacliffs. Although erosion operates during stages (2) and (3), affecting any portion of the volcano not frequently covered by new eruptive products, it becomes the dominant process when eruptions end. Corals grow in the shallow water around the islands and may build large reefs when undisturbed by new lava.
5. Renewed volcanism stage. After long quiescence of hundreds of thousands to perhaps more than a million years, alkalic basalt and more highly differentiated lavas, such as basanite and nephelinite, may erupt intermittently, both as lava and tephra, through a span of perhaps thousands of years. Erosion and reef building continue in unaffected areas.
6. Atoll stage. After stream and wave erosion, coupled with subsidence induced by volcanic loading, have reduced the volcano to sea level, the former island typically is encircled by coral reefs. If subsidence continues, coral may build an edifice atop the eroded volcanic rock to thicknesses of hundreds of meters.
7. Late seamount stage. Rate of regional subsidence eventually exceeds rate of reef building; island sinks below sea level to become a seamount; pelagic sediments mantle edifice, which may survive quietly for millions of years.

Each Hawaiian volcano begins growing in a deep-ocean environment, but only a single example, Loihi, has provided clues to the composition and characteristics of the lava of the deep-sea stage. Loihi is as yet little explored, but it is already a large volcano, rising at least 3,000 m above its base. A wealth of petrologic information has been extracted from the dredged samples from Loihi, an innovative petrogenetic evolution has been suggested (Frey and Clague, 1983), and it is tempting to assume that all or most Hawaiian volcanoes have undergone this same petrogenesis. The assumption is reasonable, but the characteristics of later stages are all derived from the study of several or many volcanoes. Hence, until rocks similar to those of Loihi are found at other new seamounts or are encountered by deep drilling into the core of older volcanoes, the details and implications of stage (1) should be considered provisional.

Stage 1 begins with fissures or single vents erupting lava onto the ocean floor. Repeated flows build a submarine edifice (fig. 7.9), which consists mostly of pillow lava. If of alkalic composition, the edifice may have sides that are quite steep; the bathymetry of Loihi (Malahoff, chapter 6; Malahoff and others, 1982) shows some slopes approaching 45°. The first embryonic volcano in a region would grow independently of any influence by neighboring edifices. However, when one or more additional volcanoes develop nearby,

TABLE 7.4.—*Historical eruptions of Mauna Loa through 1985*

[Dashes (---), no data; query (?), questionable data]

Date eruption began Year	Month and day	Duration (days)	Location of major vent(s)	Approximate area (km^2)	Approximate volume ($m^3 \times 10^6$)	References
1832	June 20	21 (?)	Caldera	---	---	Stearns and Macdonald, 1946, p. 79.
1843	January 9	95	Northeast rift	53	191	Brigham, 1909, p. 63–65; Hitchcock, 1909, p. 84–85.
1849	May 15	15	Caldera	---	---	Coan, 1851; Brigham, 1909, p. 65; Hitchcock, 1909, p. 85
1851	August 8	21	-- do ----------	18	69	Brigham, 1909, p. 65; Hitchcock, 1909, p. 85–86.
1852	February 17	21	Caldera, northeast rift	28	107	Coan, 1852; Brigham, 1909, p. 65–68; Hitchcock, 1909, p. 86–94.
1855	August 11	450	Northeast rift	31	115	Brigham, 1909, p. 68–71; Hitchcock, 1909, p. 94–100.
1859	January 23	300	North flank	85	459	Davis, 1859; Dana, 1859, 1860; Brigham, 1909, p. 75–80; Green, 1887; Hitchcock, 1909, p. 100–104.
1865	December 30	120	Caldera	---	---	Hitchcock, 1909, p. 104.
1868	March 27	16	Southwest rift	24	145	Coan, 1869; Brigham, 1909, p. 100–116; Hitchcock, 1909, p. 104–111; Moore and Ault, 1965, p. 5–7; Fisher, 1968.
1871	August 1	30	Caldera	---	---	Coan, 1871, p. 456.
1872	August 10	60	-- do ----------	---	---	Brigham, 1909, p. 125; Hitchcock, 1909, p. 111–112.
1873	January 6	2 (?)	-- do ----------	---	---	Brigham, 1909, p. 126; Hitchcock, 1909, p. 112–114.
1873	April 20	547	-- do ----------	---	---	Brigham, 1909, p. 122–127; Hitchcock, 1909, p. 114–115.
1875	January 10	30	-- do ----------	---	---	Brigham, 1909, p. 127; Hitchcock, 1909, p. 115; Coan, 1877.
1875	August 11	7	-- do ----------	---	---	Do.
1876	February 13	1	-- do ----------	---	---	Brigham, 1909, p. 127; Coan, 1877.
1877	February 14	11	Caldera, west flank (offshore)	---	---	Brigham, 1909, 127–128; Hitchcock, 1909, p. 115–116; Coan, 1877.
1880	May 1	6	Caldera	---	---	Brigham, 1909, p. 133, 145; Hitchcock, 1909, p. 116.
1880	November 1	280	Northeast rift	62	230	Brigham, 1909, p. 145–155; Hitchcock, 1909, p. 116–119.
1887	January 16	10	Southwest rift	29	230	Brigham, 1909, p. 165–168; Hitchcock, 1909, p. 123–127.
1892	November 30	3	Caldera	---	---	Brigham, 1909, p. 185.
1896	April 21	16	-- do ----------	---	---	Brigham, 1909, p. 192–196; Hitchcock, 1909, p. 128–130.
1899	July 4	23	Caldera, northeast rift	42	153	Brigham, 1909, p. 196–199; Hitchcock, 1909, p. 132–138.
1903	October 6	60	Caldera	---	---	Brigham, 1909, p. 202–204; Hitchcock, 1909, p. 138–139.
1907	January 9	15	Caldera, southwest rift	21	76	Brigham, 1909, p. 206–209; Hitchcock, 1909, p. 142–146.
1914	November 25	48	Caldera	---	---	Jaggar, 1947, p. 99.
1916	May 19	14	Southwest rift	17	61	Jaggar, 1947, p. 104.
1919	September 26	42	Caldera, southwest rift	24	268	Jaggar, 1919, 1947, p. 125–133; Moore and Ault, 1965, p. 7.
1926	April 10	15	-- do ----------	35	115	Jaggar, 1926, 1947, p. 171–173.
1933	December 2	17	Caldera	5	76	Jaggar, 1947, p. 195–196.
1935	November 21	42	Caldera, northeast rift	36	122	Jaggar, 1947, p. 197–200.
1940	April 7	133	Caldera	10	76	Macdonald, 1954; Macdonald and Abbott, 1970, p. 57–60.
1942	April 26	15	Caldera, northeast rift	28	76	Macdonald, 1954; Macdonald and Abbott, 1970, p. 60–65.
1949	January 6	145	Caldera	15	59	Macdonald and Orr, 1950; Finch and Macdonald, 1951; Macdonald and Abbott, 1970, p. 65–67.
1950	June 1	23	Southwest	91	460	Finch and Macdonald, 1953; Macdonald, 1954; Macdonald and Abbott, 1970, p. 9–11.
1975	July 5	1	Caldera, southwest and northeast rifts	14	30	Lockwood and others, chapter 19, 1976.
1984	March 25	22	Caldera, southwest rift, and, primarily, northeast rift	48	220	Lockwood and others, chapter 19, 1985.

the flows from two or more sources begin to interfinger, and the presence of each volcano would influence the path of flows from its neighbor. Linear rift zones develop, with their orientations determined by stress fields influenced both by regional tectonics and local gravitational forces (Fiske and Jackson, 1972).

The shield-building stage (2) includes the principal growth of the volcano; products consist almost exclusively of tholeiitic basalt and tholeiitic picrite (olivine-rich tholeiite). By far the greatest proportion of Hawaiian volcanoes consists of tholeiite erupted during the shield-building stage (fig. 7.9, table 7.5). Three substages have been designated submarine (2a), sea level (2b), and subaerial (2c); the behavior of the erupted products and their physical character is largely determined by which of these three environments they encounter.

The submarine substage (2a) involves the repeated voluminous extrusion of tholeiite, which assumes the form of pillow lava;

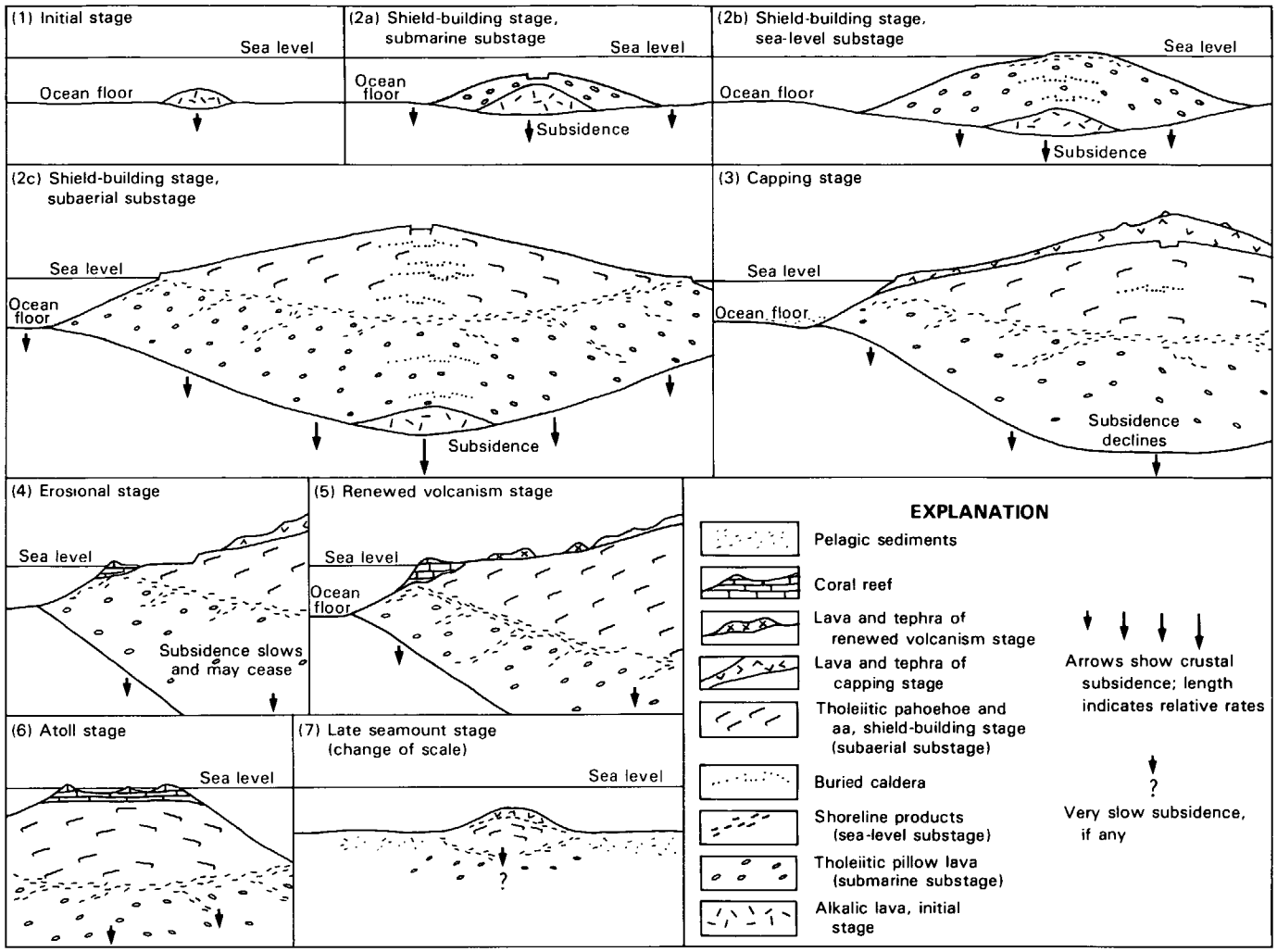

FIGURE 7.9.—Diagrams showing successive stages in evolution of a Hawaiian volcano as proposed in this paper. Changes between stages normally are transitional and gradational. For simplicity, feeder conduits and rift zones are omitted. Substantial crustal subsidence caused by volcanic loading occurs throughout growth stages (1) through (3); subsequent sea-level changes may be sporadic, but net subsidence continues into stage (7). Vertical exaggeration varies from approximately 2× to approximately 4×. Only stages (1) through (4) are represented on Hawaii. See text for additional details.

countless repeated flows build a submarine shield volcano. Lava issues from both summit vents and rift zones, and submarine eruptions probably exhibit as wide a variety of flow behavior as do subaerial eruptions, except that below a few hundred meters depth the pressure is sufficient to inhibit explosive activity, and any vesicles are only of microscopic size. Slopes of the edifice are generally 10° to 20°. The crust beneath the volcano subsides during rapid growth and volcanic loading; thus the length of time required for the summit to reach sea level is longer than previously thought, perhaps approaching a million years (Moore, chapter 2).

As the summit of the growing submarine shield approaches sea level, the sea-level substage (2b) begins. The hydrostatic head declines enough to allow the ocean water to boil when encountered by vesiculating molten lava. The abrupt production of steam disrupts the lava, sometimes explosively, and it is shattered to form tephra and hyaloclastite material (Moore and Fiske, 1969). As the process continues, a broad mound of mixed tephra and lava eventually emerges above sea level. Waves immediately begin to erode the tephra and fragment the lava, and initially the new island may be transitory. But if the supply of new material is steady and sufficiently large, the volcanic pile grows fast enough to keep ahead of wave erosion, and the new island enlarges. When the vent is sufficiently protected from sea water, explosions decline and coherent flows form a resistant veneer over the fragmental material, reducing the rate of wave erosion. The island of Surtsey, south of Iceland, is a well-observed example of the process by which a basaltic volcano initially emerges above the sea (Thorarinsson, 1967). Although the process has not been observed in Hawaii, basaltic volcanoes there would

TABLE 7.5.—*Revised evolutionary scheme for Hawaiian volcanoes*

Stage	Dominant composition of magma	Dominant geologic processes and characteristics[1]
(1) Initial	Alkalic basalt, basanite, transitional basalt	Initial activity of new volcano; rates and frequency of eruption and duration of stage not known; edifice may be steep sided (because only a single example is recognized, this stage is considered provisional).
(2) Shield-building	Tholeiitic basalt, tholeiitic picrite	Frequent voluminous eruptions from central vent and rift zones, historic examples suggest eruptive rates of 1–3 km^3/100 yr, frequency about 5–50 eruptions/100 yr; shield-shaped edifice built; caldera may form and be refilled repeatedly during any substage.
(2a) Submarine	-- do ----------	Products pillow lava and pillow fragments; moderately steeply sloping edifice.
(2b) Sea level	-- do ----------	Products hyaloclastites—the result of explosive interaction between sea water and molten lava, and wave abrasion.
(2c) Subaerial	-- do ----------	Products chiefly pahoehoe and aa lava flows, interspersed with sporadic tephra produced by occasional explosions; dominantly fluid lava builds gently sloping edifice; processes of 2a and 2b continue.
(3) Capping	Alkalic basalt, transitional basalt, other alkalic rocks[2]	Products initially pahoehoe and aa lava flows, increasing proportions of tephra-built cinder cones, gradual or abrupt change to smaller briefer eruptions; increasing lava viscosity (block flows); declining eruptive rates and frequency of eruptions, eventually at intervals exceeding 10^3 yr; capping structure steeper sided than stage 2c.
(4) Erosional	None	Lack of eruptions allows fluvial and marine erosion to carve valleys, canyons, cliffs, and so on; reefs may develop along some shorelines (erosion operates during all stages, but effects offset by repeated eruptions).
(5) Renewed volcanism	Alkalic basalt, basanite, nephelinite, nephiline melilitite	Sporadic eruptions, generally from vents not related to central conduit or rift zones, commonly explosive though some are effusive. Eruptions are of low volume and widely spaced in time. Erosion and reef building continue.
(6) Atoll	None	Abetted by regional subsidence, fluvial and marine erosion reduce volcano to sea level. Reef building continues, may form ring-shaped group of islands with interior lagoon.
(7) Late seamount	None	Rate of regional subsidence eventually exceeds rate of reef building and island sinks below sea level to become a seamount; gradually mantled by pelagic sediments; subdued edifice may survive for millions of years.

[1]In addition to processes listed, regional crustal subsidence caused by weight of growing volcanoes is nearly continuous, resulting in apparent rise in sea level. Episodes of glaciation cause a worldwide drop in sea level, temporarily offsetting steady regional subsidence.
[2]Other alkalic rocks may include hawaiite, mugearite, benmoreite, ankaramite, trachyte.

presumably emerge above the ocean in a like manner. The zone of tephra, fragmental lava, and hyaloclastite forms a distinctive horizon marking the transition from submarine to subaerial lava (Moore and Fiske, 1969). The behavior of lava at and below sea level was further reviewed above in the section "Submarine Investigations."

Once an island is established, the subaerial substage (2c) begins, which involves further growth of the shield by continued eruptions. The lava issues both from central vents and rift zones radial to the summit, and in composition the lava continues to be tholeiitic basalt. Slopes are generally from 3° to 10°, and they contrast distinctly with the steeper submarine slopes. Rate of growth is rapid, demonstrated by a general lack of both erosion and soils between successive flows. This substage is exemplified by frequent and well documented eruptions of Kilauea and Mauna Loa. As the subaerial shield grows, the processes of substages 2a and 2b continue below and at sea level as the volcano expands outward. Crustal subsidence continues (Moore, chapter 2), so that much of the subaerially erupted lava becomes part of the submarine edifice, and the hyaloclastite horizon assumes a broad, sagging profile (fig. 7.9). Calderas may form and be filled repeatedly throughout the tholeiitic lava stage.

The capping stage (3) begins as the magma eventually differentiates to yield alkalic basalt; at some volcanoes, lava transitional between tholeiitic and alkalic basalt is erupted (fig. 7.9, table 7.5). If a caldera is present, lava that fills it may be either tholeiite, transitional lava, or alkalic basalt. There is no theoretical reason why a caldera could not form during stage 3; calderas do occur in volcanoes of alkalic basaltic composition elsewhere in the world. However, they have not been observed to form during this stage in Hawaii, and in view of the declining volume rate of eruption characteristic of stage 3, caldera formation seems highly unlikely. With the change in composition, explosive eruptions become more common, and a steeper sided cap with slopes of as much as 20° is built over the shield. Differentiation may proceed further to yield one or more of the following: hawaiite, mugearite, benmoreite, trachyte, and ankaramite. Alkalic basalt, like tholeiite, forms pahoehoe and aa; the more differentiated lavas become increasingly viscous and may form block lava. Eruptions gradually become separated by progressively longer time intervals and finally end. Subsequent evolution of the volcanoes through the erosional stage (4), renewed volcanism stage (5), atoll stage (6), and late seamount stage (7) are briefly reviewed above, illustrated in figure 7.9, and outlined in table 7.5.

Of the volcanoes of Hawaii, Loihi seems to be at the end of stage 1, entering into stage 2a; Kilauea and Mauna Loa are in stage 2c; Hualalai is in stage 3; Mauna Kea is further along in stage 3, perhaps very late in the stage, and the processes of stage 4 are becoming dominant; and Kohala is in stage 4. None of these volcanoes has progressed beyond stage 4; the volcanoes of the other islands to the northwest are in various parts of stages 4 and 5, whereas stages 6 and 7 are represented by atolls, islets, and seamounts along the Hawaiian Ridge northwest of the main group of islands. Our stages 1, 2, 3, and 5 correspond to the four stages defined by Clague and Dalrymple (chapter 1, part I), although they are designated by different terms.

PETROLOGIC HISTORY OF INDIVIDUAL VOLCANOES

Though the volcanoes of Hawaii are broadly similar to one another in certain respects, each has achieved a specific position

within the hierarchy of growth stages by means of an individual course of petrologic development. Each volcano is basically a tholeiitic shield, but Kohala, Mauna Kea, and Hualalai Volcanoes have passed into or beyond the capping stage (3), whereas Mauna Loa and Kilauea are in the subaerial part of the shield-building stage (2c). Loihi cannot yet be termed a tholeiitic shield, though it appears to have completed the initial stage (1) and is entering the submarine part of the shield-building stage (2a). Among the volcanoes with alkalic caps, tholeiitic lavas of Kohala and Mauna Kea are exposed in a few canyons on the Hamakua coast, whereas Hualalai tholeiites are not exposed on the subaerial surface but have been found in a few water wells and along the submarine extension of the northwest rift zone (Clague, 1982).

The petrologic development is summarized here by showing (1) chemical variations and similarities among tholeiitic and alkalic basalts of the five island volcanoes plus Loihi; (2) differentiation processes by which basaltic magma produces rocks of other compositions; and (3) effects of olivine control on related lavas. To illustrate these processes we have selected five basic variation diagrams as follows: $Na_2O + K_2O$ vs. SiO_2 (fig. 7.10), CaO vs. SiO_2 (fig. 7.11), CaO vs. MgO (fig. 7.12), TiO_2 vs. MgO (fig. 7.13), and Na_2O vs. MgO (fig. 7.14). These diagrams are derived from 834 chemical analyses of rocks from Hawaii, distributed among the volcanoes as follows: Kohala, 36 analyses; Mauna Kea, 36; Hualalai, 293; Mauna Loa, 117; Kilauea, 340; Loihi, 12. Most analyses are from references listed in table 7.6; some are unpublished data of E.D. Jackson (Hualalai), T.L. Wright (Hualalai), and R.B. Moore (Hualalai and Kilauea).

In spite of documented long-term storage of Hawaiian tholeiitic magma in rift zone reservoirs, fractionation of such magma has rarely produced compositions more silicic than basalt (boundary at 52 percent SiO_2). The sole known exception is the Yellow Cone scoria (Kilauea southwest rift zone) with 55 percent SiO_2, which was produced by mixing of a differentiate with 60 percent SiO_2 and 2 percent MgO with a more olivine-rich magma (Wright and Fiske, 1971). Otherwise, andesitic or more silicic compositions of tholeiitic parentage are unknown on the Island of Hawaii, although rhyodacite occurs on Oahu (Macdonald and others, 1983).

Most of the subaerial part of Kohala and Mauna Kea and all of Hualalai are composed of alkali olivine basalt and its differentiates, and the average recurrence interval for eruptions on Hualalai in the Holocene has been about 50 yr, as evidenced by radiocarbon age data (Moore and others, chapter 20). These facts suggest that alkali olivine basalt has been generated frequently during late Pleistocene and Holocene time. Fractionation of alkali olivine basalt magma has been extensive; the most differentiated rocks at each volcano include trachyte on Hualalai, benmoreite and trachyte on Kohala, and a single reported occurrence of mugearite on Mauna Kea.

Macdonald and Katsura (1964) described separate compositional fields for alkalic and tholeiitic basalts for the whole Hawaiian island chain, and these fields for the Island of Hawaii are illustrated in the alkali-silica variation diagrams of figure 7.10. A few basalts from each volcano straddle the boundary between the fields. The alkali-silica diagrams further show that slightly andesitic melts are the most SiO_2-rich erupted from the tholeiitic suite on the island, and that trachyte is the most silicic rock produced by fractionation of the alkalic suite.

The lime-silica variation diagrams (fig. 7.11) show rather diverse trends among the different volcanoes. Kohala, Mauna Kea, Hualalai, and Loihi illustrate the general alkalic trend of decreasing CaO with increasing SiO_2, whereas the data for the tholeiitic Mauna Loa and Kilauea volcanoes produce bell-shaped curves that peak at about 50–51 percent SiO_2.

The lime-magnesia variation diagrams (fig. 7.12) document the major role played by olivine in the tholeiitic suite for MgO content above about 6.8 percent (Powers, 1955; Wright 1971; Wright and others, 1975; Wright and Tilling, 1980). The change in slope of the curves below this point indicates departure from olivine control and the coprecipitation of pyroxenes and plagioclase. Curves for the alkalic rocks of Kohala, Mauna Kea, and Hualalai change slope at about the same point as those of the tholeiitic suite, suggesting that olivine-controlled fractionation is also important among some basaltic rocks of the alkalic suite. Wide scatter in most of the plots at contents of MgO greater than 6.8 percent indicates that considerable mixing of different batches of olivine-controlled magma, or differentiation involving phases in addition to olivine, has occurred in both suites (except on Mauna Loa; see Rhodes, 1983).

The titania-magnesia variation diagrams (fig. 7.13) show considerable scatter, even at relatively high MgO values, reflecting the effects of possible mixing of magma in shallow storage chambers as well as temporal variations at given contents of MgO. The reason for the change in slope among the alkalic rocks at 5–6 percent MgO, instead of the more usual 6.8 percent in the tholeiitic suite (Wright and Fiske, 1971), is not clear, but this change may reflect the accumulation of titaniferous clinopyroxene in magmas that have fractionated olivine nearly to its possible limit. Olivine-controlled lavas of Mauna Kea and Kilauea generally are higher in TiO_2 than those of the other volcanoes; the differences do not seem to be related to differences between the alkalic and tholeiitic suites.

The soda-magnesia variation diagram for all volcanoes together (fig. 7.14) shows again the importance of olivine-controlled fractionation and of mixing in shallow magma chambers (the part of the plotted data showing the latter is dominated by analyses of Kilauea rocks). The diagram also demonstrates the generally higher soda values in alkalic rocks (dominated by analyses of Hualalai rocks).

Relatively recent reports on the petrology of individual Hawaiian volcanoes and on models for generation of tholeiitic and alkalic magmas are given in table 7.6. These studies are summarized by Wright and Helz (chapter 23) and will be treated only briefly here. Most workers, beginning with Stearns and Macdonald (1946), have suggested that alkalic rocks are related to tholeiitic basalts either by protracted fractional crystallization of tholeiitic magma or by varying degrees of partial melting of the mantle source. This conclusion was based partly on the small volume of alkalic rocks compared to tholeiites and on field relations, notably the occurrence of basalts of transitional composition stratigraphically between tholeiitic and alkalic basalts on Kohala and Mauna Kea and on other islands in the Hawaiian Chain. More recently,

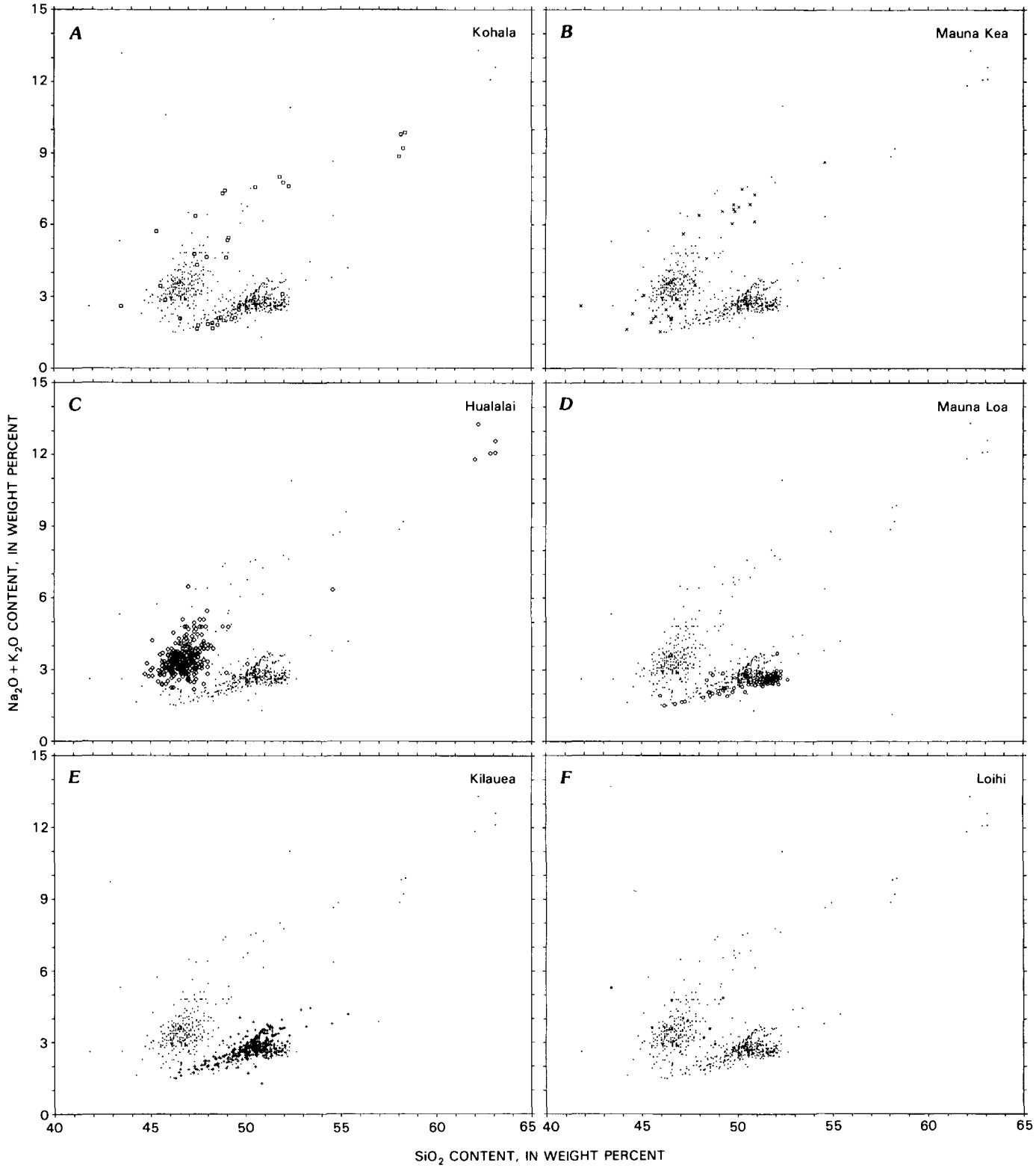

FIGURE 7.10.—Alkali-silica variation diagrams (Na_2O+K_2O vs. SiO_2) for volcanic rocks of Hawaii. ***A–F***, Plots for individual volcanoes as indicated. ***G***, Data for all six volcanoes combined. Individual diagrams show data for that volcano by heavy symbols and for comparison data for the other volcanoes by light dots. Analyses from published and unpublished sources.

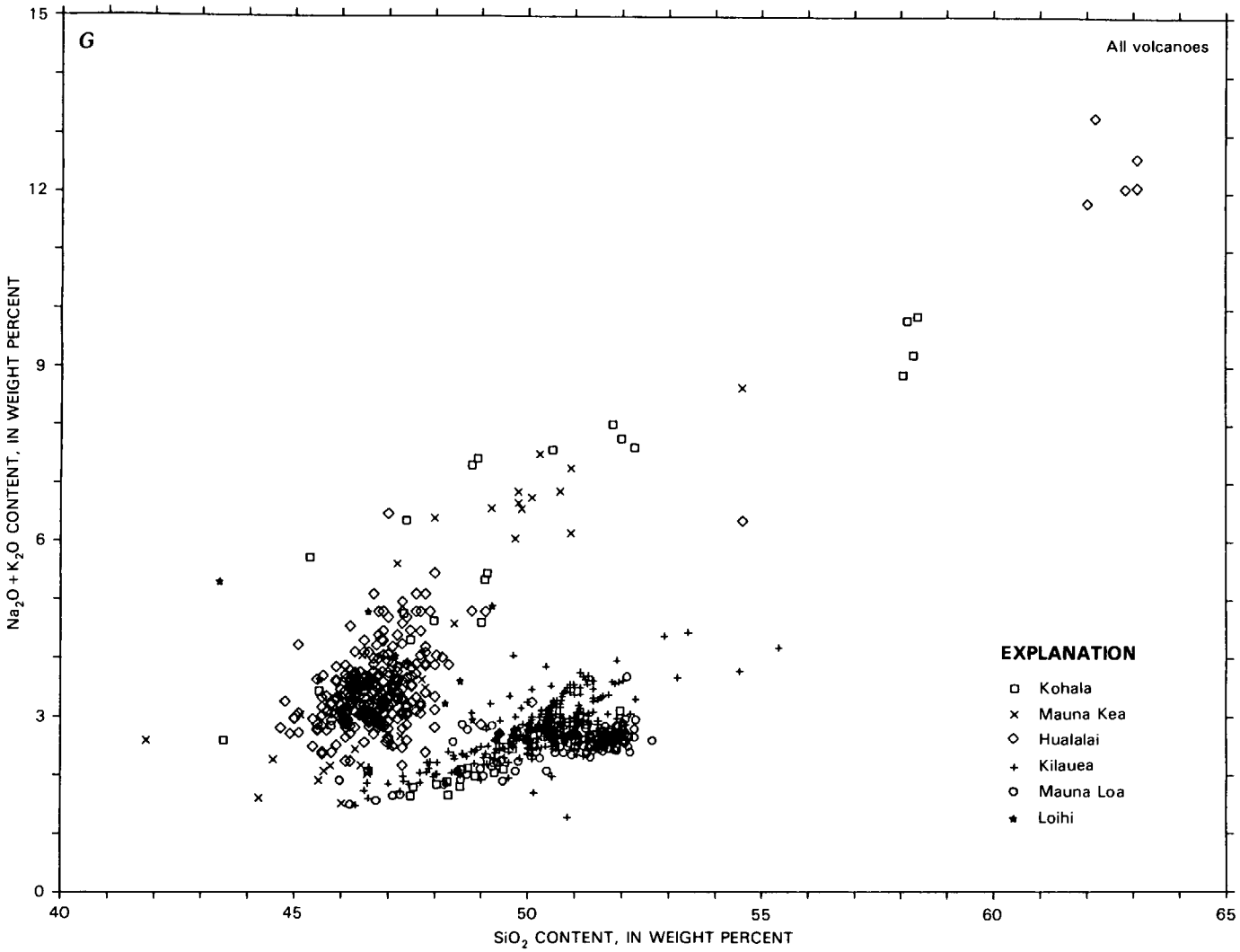

FIGURE 7.10.—Continued.

Lanphere and others (1980) concluded that alkalic and tholeiitic rocks are slightly different in terms of Rb and Sr abundances and isotopic compositions, suggesting intrinsic differences in mantle source regions. Lanphere (1983) has presented $^{87}Sr/^{86}Sr$ data for Loihi Seamount and concluded that the source materials for its divergent lavas are also isotopically distinct. Wright (1984) presented a metasomatic model for the origin of Hawaiian tholeiite that involves partial melting of a mantle source from which some mid-ocean-ridge basaltic liquid has been removed and to which has been added a nephelinitic fluid, amphibole, apatite, iron sulfide, and magnetite/ilmenite.

KOHALA

Kohala is the longest inactive and likely the oldest volcano on the Island of Hawaii, although, as noted by Lipman (1980), ages of basalts in the Ninole Hills in the south flank of Mauna Loa are similar to those of the oldest dated Kohala lavas (0.7–0.45 Ma; see Evernden and others, 1964; Dalrymple, 1971).

The geology of Kohala was mapped in reconnaissance by Stearns and Macdonald (1946); detailed mapping by M.O. Garcia and S.C. Porter is in progress. Stearns and Macdonald recognized two major groups of volcanic units; they termed the older of these the Pololu Volcanic Series, which they considered to be Pliocene to early Pleistocene in age, and the younger the Hawi Volcanic Series, which they considered middle Pleistocene. These units have been renamed the Pololu Basalt and the Hawi Volcanics by Langenheim and Clague (chapter 1, part II). Subsequent K-Ar dating (McDougall, 1964; Dalrymple, 1971; McDougall and Swanson, 1972) has established a Pleistocene age (0.7–0.06 Ma) for all of the subaerially exposed part of Kohala. McDougall and Swanson (1972) concluded that the Pololu shield-building stage ended at

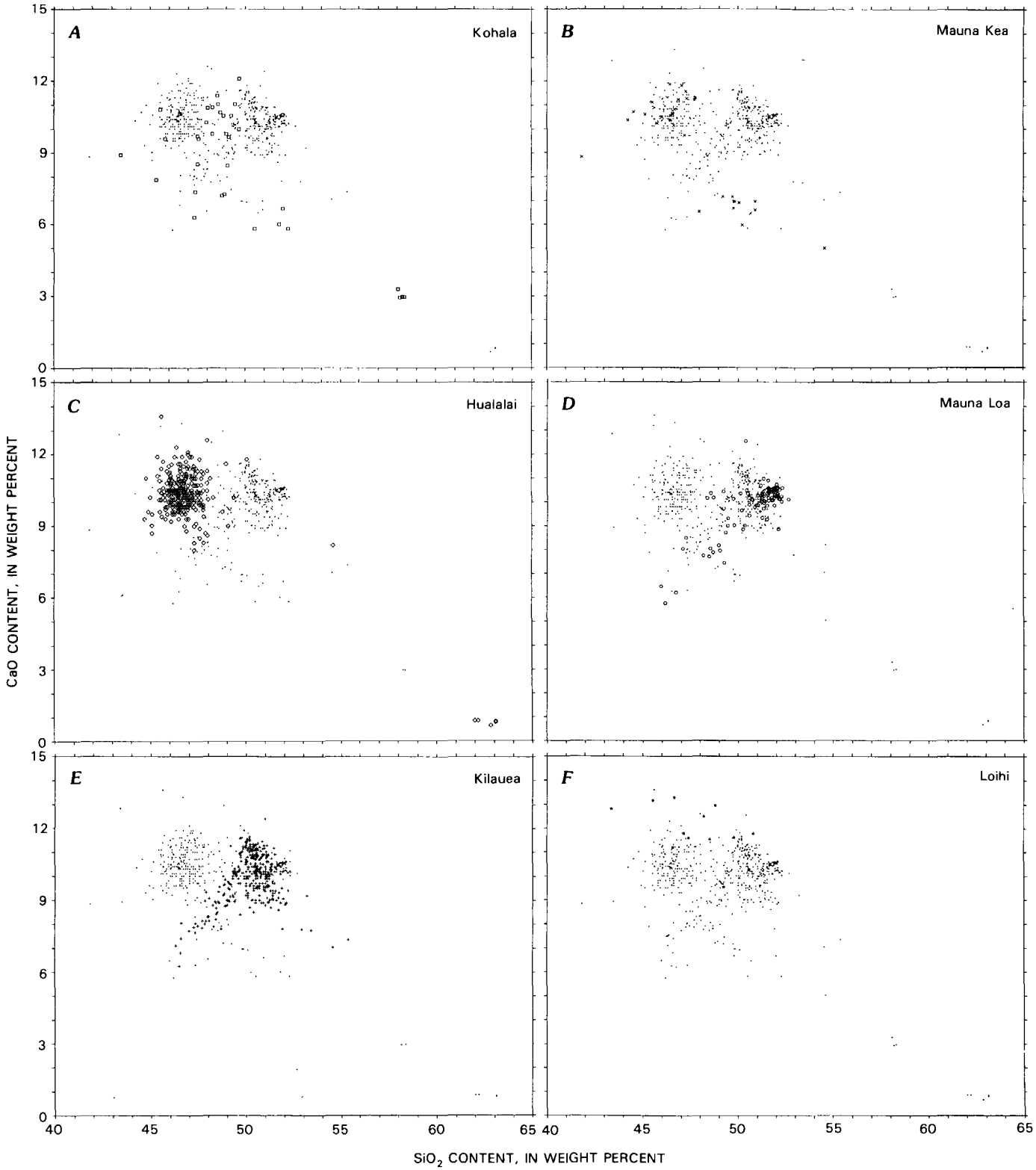

FIGURE 7.11.—Lime-silica variation diagrams (CaO vs. SiO_2) for volcanic rocks of Hawaii. ***A–F***, Plots for individual volcanoes, as indicated. **G**, Data for all six volcanoes combined. Individual diagrams show data for that volcano by heavy symbols and for comparison data for other volcanoes by light dots. Analyses from published and unpublished sources.

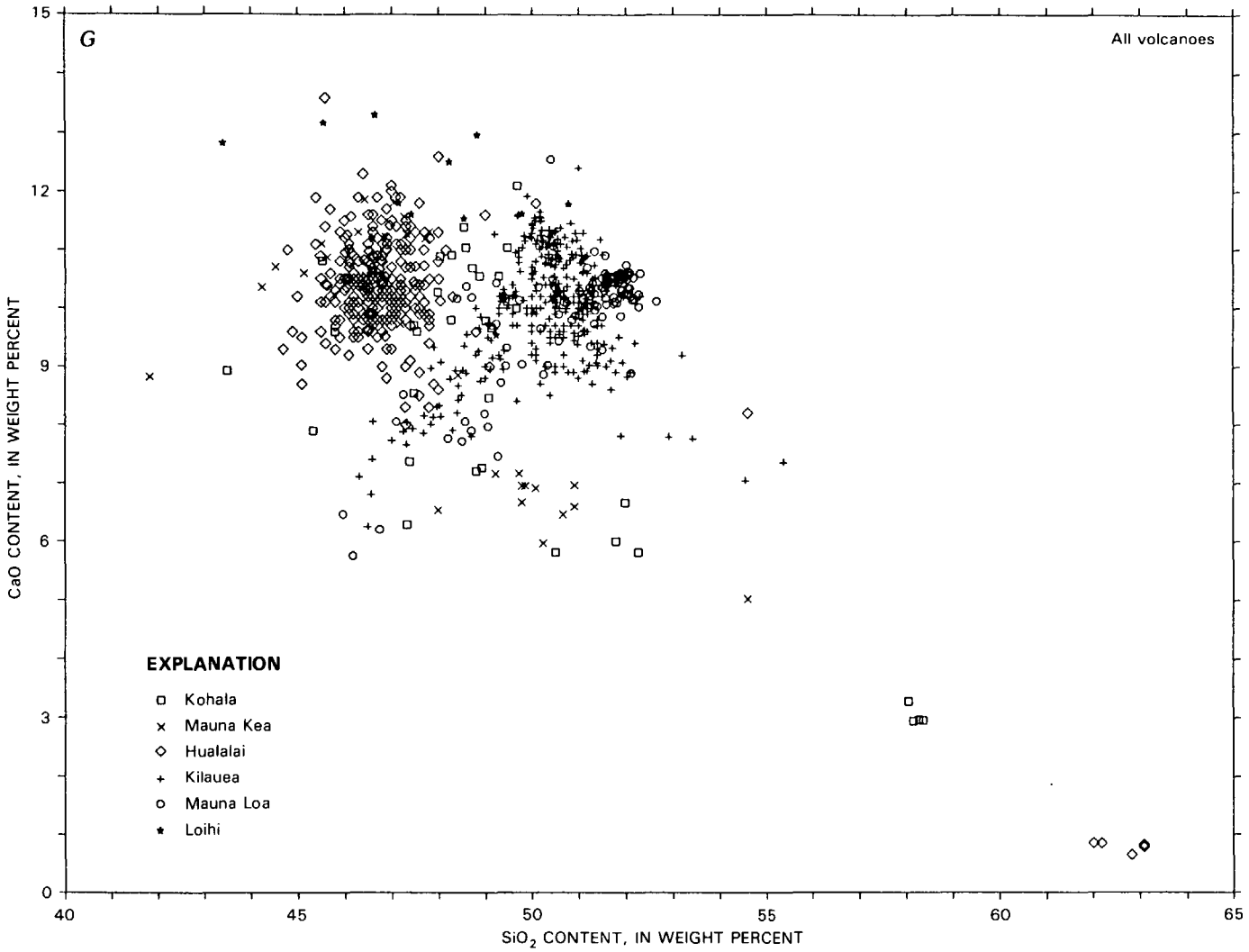

FIGURE 7.11.—Continued.

about 0.3 Ma and that the Hawi alkalic cap was formed by eruptions at 0.25–0.06 Ma (see fig. 7.4).

The lower part of the Pololu Basalt is tholeiitic (Macdonald and Katsura, 1964) and was extruded during the shield-building stage of the volcano; the younger volcanic materials are alkalic and characterized by larger proportions of intercalated cinders and ash. Variation diagrams (figures 7.10–7.14) suggest that some transitional basalts occur in the upper part of the Pololu Basalt.

The Hawi Volcanics is entirely alkalic and ranges in composition from alkali olivine basalt to benmoreite. Mugearites are particularly abundant, and more mafic rocks are rare. Feigenson and others (1983) report the occurrence of dunite xenoliths in some alkali basalt flows. Most of the Hawi vents are along Kohala's northwest-southeast-trending rift zone; the relation of this rift to the geometry of the tholeiitic shield is unknown, although probably the modern rift zone approximately coincides with the ancient one. A caldera that probably formed during Pololu time was buried by Hawi lavas (Stearns and Macdonald, 1946).

Variation diagrams (fig. 7.10–7.14) for Kohala rocks show that they generally are similar to rocks from Mauna Kea. Rocks of Kohala are somewhat more evolved, however; a single mugearite has been reported from Mauna Kea, whose subaerial lavas are dominated by hawaiite, ankaramite, and alkali olivine basalt.

The alkali-silica variation diagram for Kohala rocks (fig. 7.10*A*) shows the fields of tholeiitic and alkalic rocks and the differentiation products of alkali olivine basalt that include hawaiite, mugearite, and benmoreite. The lime-silica variation diagram for Kohala (fig. 7.11*A*) shows considerable scatter in the basalt range,

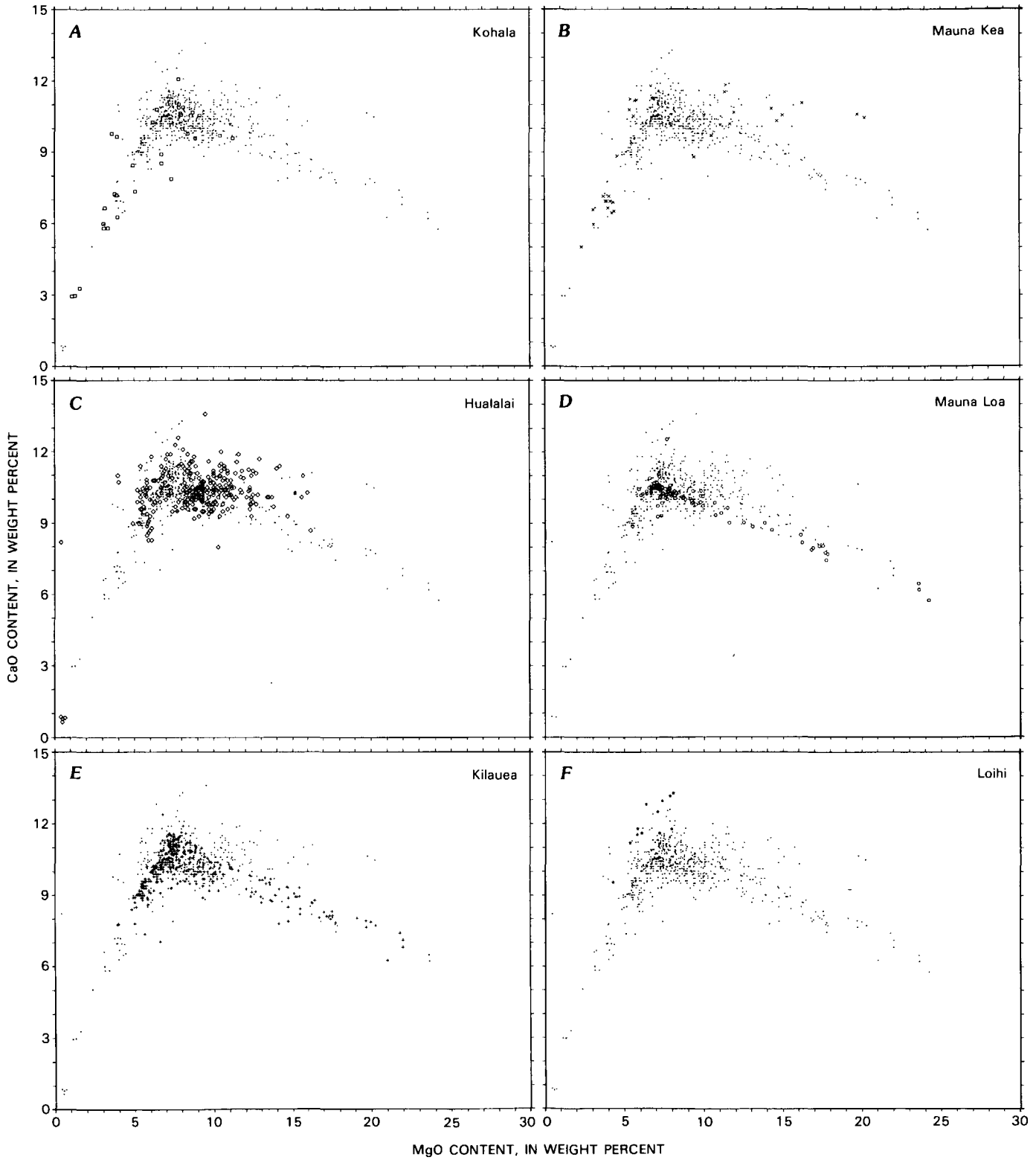

FIGURE 7.12.—Lime-magnesia variation diagrams (CaO vs. MgO) for volcanic rocks of Hawaii. ***A–F***, Plots for individual volcanoes, as indicated. **G**, Data for all six volcanoes combined. Individual diagrams show data for that volcano by heavy symbols and for comparison data for other volcanoes by light dots. Analyses from published and unpublished sources.

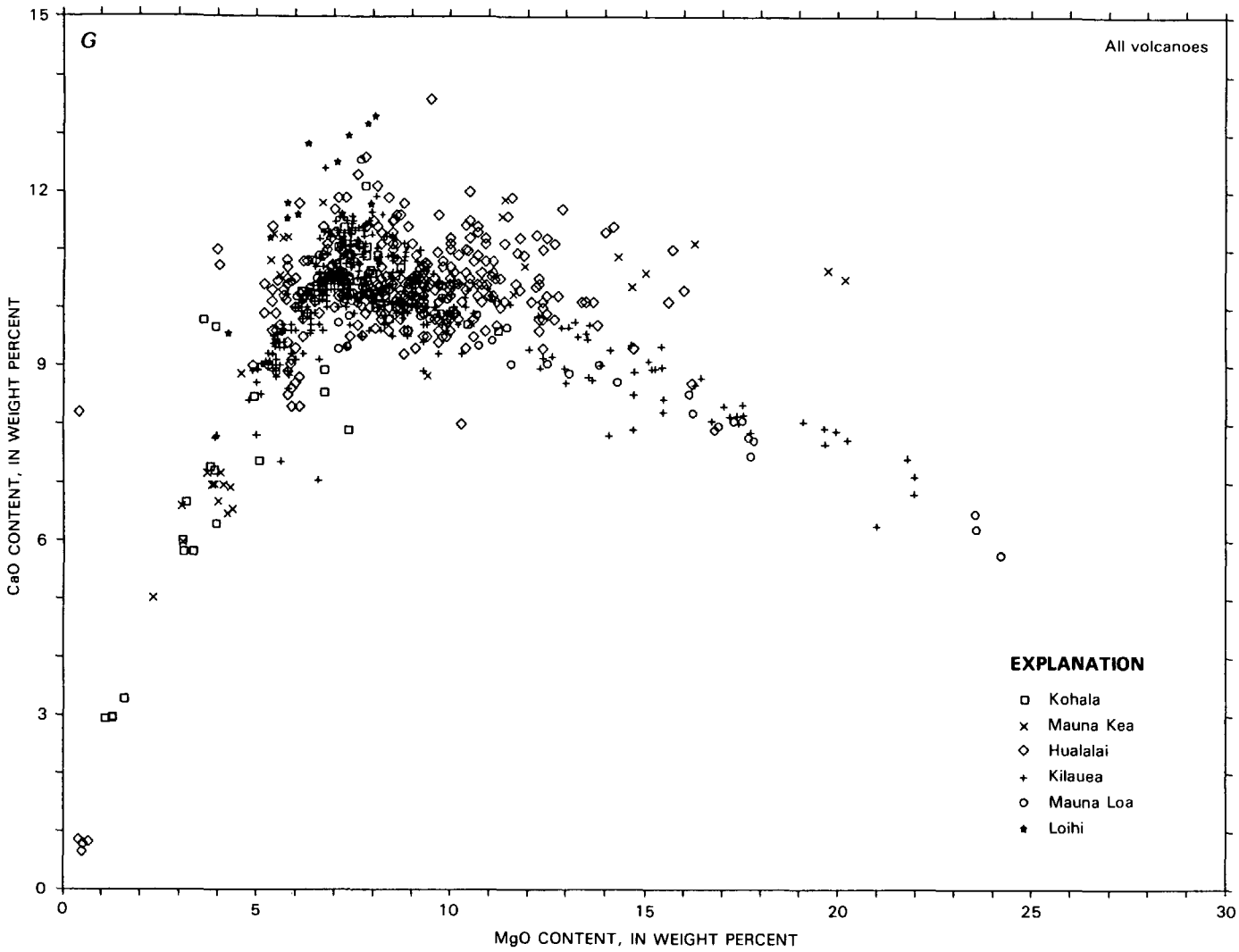

FIGURE 7.12.—Continued.

probably resulting from highly variable proportions of plagioclase and clinopyroxene phenocrysts. Mugearites and benmoreites of Kohala fall on a smooth trend. The lime-magnesia diagram (fig. 7.12 *A*) shows that Kohala tholeiites are similar to those from Hualalai, Mauna Loa, and Kilauea. The titania-magnesia diagram (fig. 7.13*A*) shows broad scatter among the Kohala rocks, suggesting that considerable mixing (Feigenson, 1984) and accumulation of Ti-rich phases (ilmenite, titanomagnetite, Ti-rich clinopyroxene) have occurred. Figure 7.14 (soda-magnesia diagram) further suggests that Kohala tholeiites are similar to those from Kilauea and Mauna Loa and that its alkalic rocks are generally similar to those from Hualalai and Mauna Kea.

MAUNA KEA

Mauna Kea has been inactive the second longest among volcanoes on the island of Hawaii. Some Mauna Kea lavas overlie rocks of Kohala on the east and south sides of Kohala; interlayering of lavas from the two sources likely occurs at depth. Stearns and Macdonald (1946) divided Mauna Kea lavas into the older Hamakua Volcanic Series (Pleistocene) and the younger Laupahoehoe Volcanic Series (Pleistocene and Holocene), now called the Hamakua Volcanics and Laupahoehoe Volcanics, respectively (fig. 7.4; Langenheim and Clague, chapter 1, part II). The two units locally are separated by as much as 5 m of weathered ash (originally called the Pahala Ash), most of which probably originated from proximal vents on Mauna Kea.

K-Ar ages reported by Porter and others (1977) range from 375±50 ka to 270±35 ka for the Hamakua Volcanics and 188±15 ka to 54.9±8.5 ka for the Laupahoehoe Volcanics. Radiocarbon ages by the same authors indicate that some Laupahoehoe lavas are as young as about 4.5 ka, and ash is as young as 3.6 ka (Porter, 1979b).

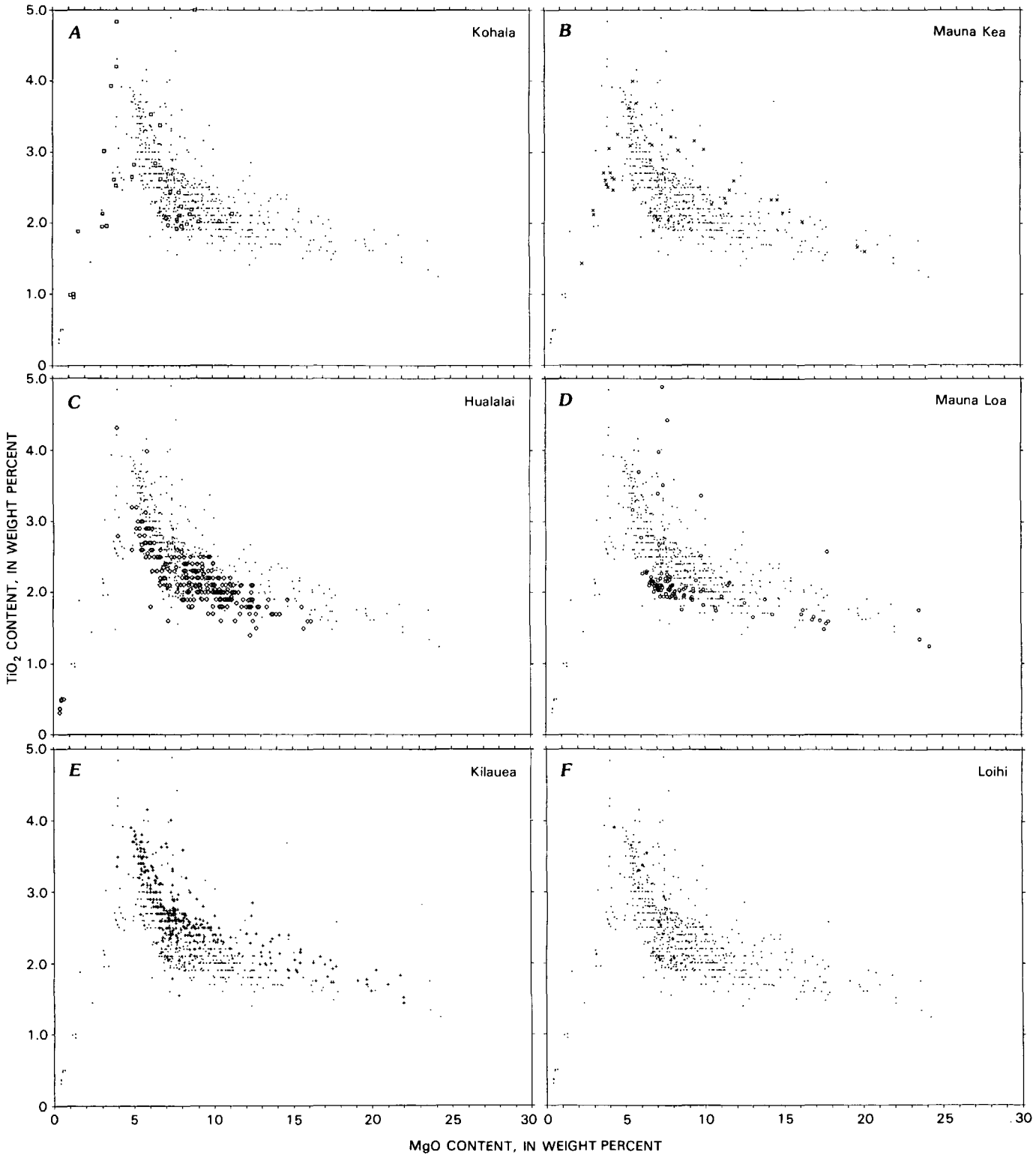

FIGURE 7.13.—Titania-magnesia variation diagrams (TiO_2 vs. MgO) for volcanic rocks of Hawaii. ***A–F***, Plots for individual volcanoes as indicated. ***G***, Data for all six volcanoes combined. Individual diagrams show data for that volcano by heavy symbols and for comparison data for volcanoes by light dots. Analyses from published and unpublished sources.

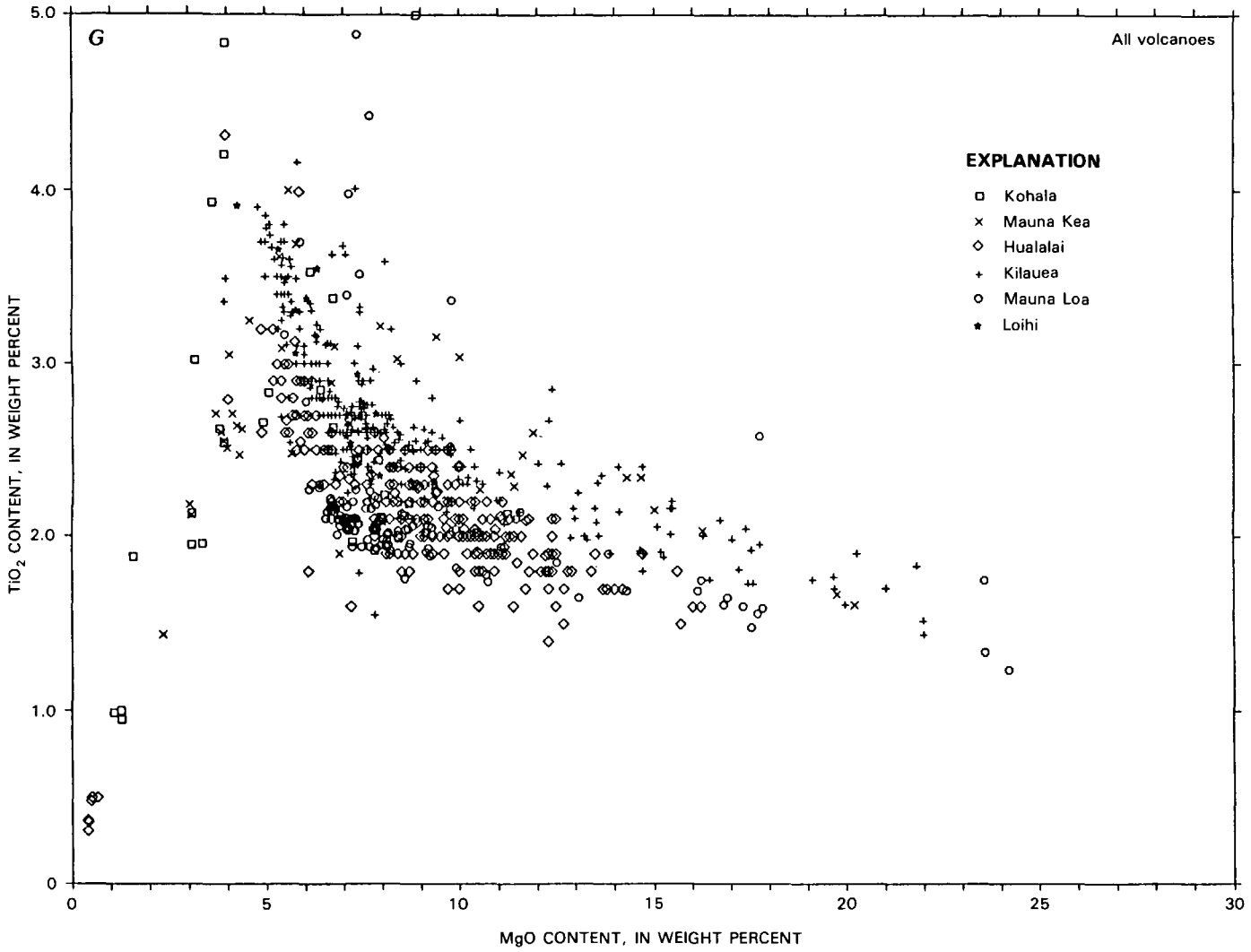

FIGURE 7.13.—Continued.

Tholeiitic basalts of the Hamakua Volcanics crop out only locally on the Hamakua (northeastern) coast of the island, where they commonly are interbedded with transitional and alkalic basalts (Macdonald and Katsura, 1964; Macdonald, 1968). The bulk of the subaerial part of the volcano, including all of the Laupahoehoe Volcanics, consists of transitional basalts, alkali olivine basalts, ankaramites, hawaiites, and a single known mugearite (Macdonald, 1968). Eruptions of alkali olivine basalt and derivative lavas produced cinder cones and lava flows (chiefly aa), widely distributed on the flanks and summit area of the volcano. Xenoliths of mafic and ultramafic rocks, commonly of cumulus origin, occur in several cones and flows (Jackson and others, 1982).

The early structural and eruptive history of Mauna Kea is conjectural, because alkalic lavas that constitute its cap have buried most structures. Porter (1972) recognized diffuse rift zones trending west, south-southeast, and east-northeast from an inferred buried caldera beneath the summit. It is not known whether these alignments of vents were inherited from the early tholeiitic, shield-building stage of the volcano.

As noted above, lavas of Mauna Kea are quite similar to, but generally less evolved than, those of Kohala (fig. 7.10–7.14). The alkali-silica variation diagram for Mauna Kea rocks (fig. 7.10*B*) indicates that virtually all analyzed lavas are alkalic. Fig. 7.11*B* shows that CaO decreases with increasing SiO_2, as with alkalic rocks from the other volcanoes. Wide scatter at the low-SiO_2 end suggests highly variable proportions of plagioclase and clinopyroxene phenocrysts. Figure 7.12*B* indicates that ankaramites from Mauna Kea with MgO greater than 11 percent are similar only to a few ankaramites from Hualalai. Fig. 7.13*B* shows that high-MgO Mauna Kea ankaramites and Kilauea tholeiites have similarly high

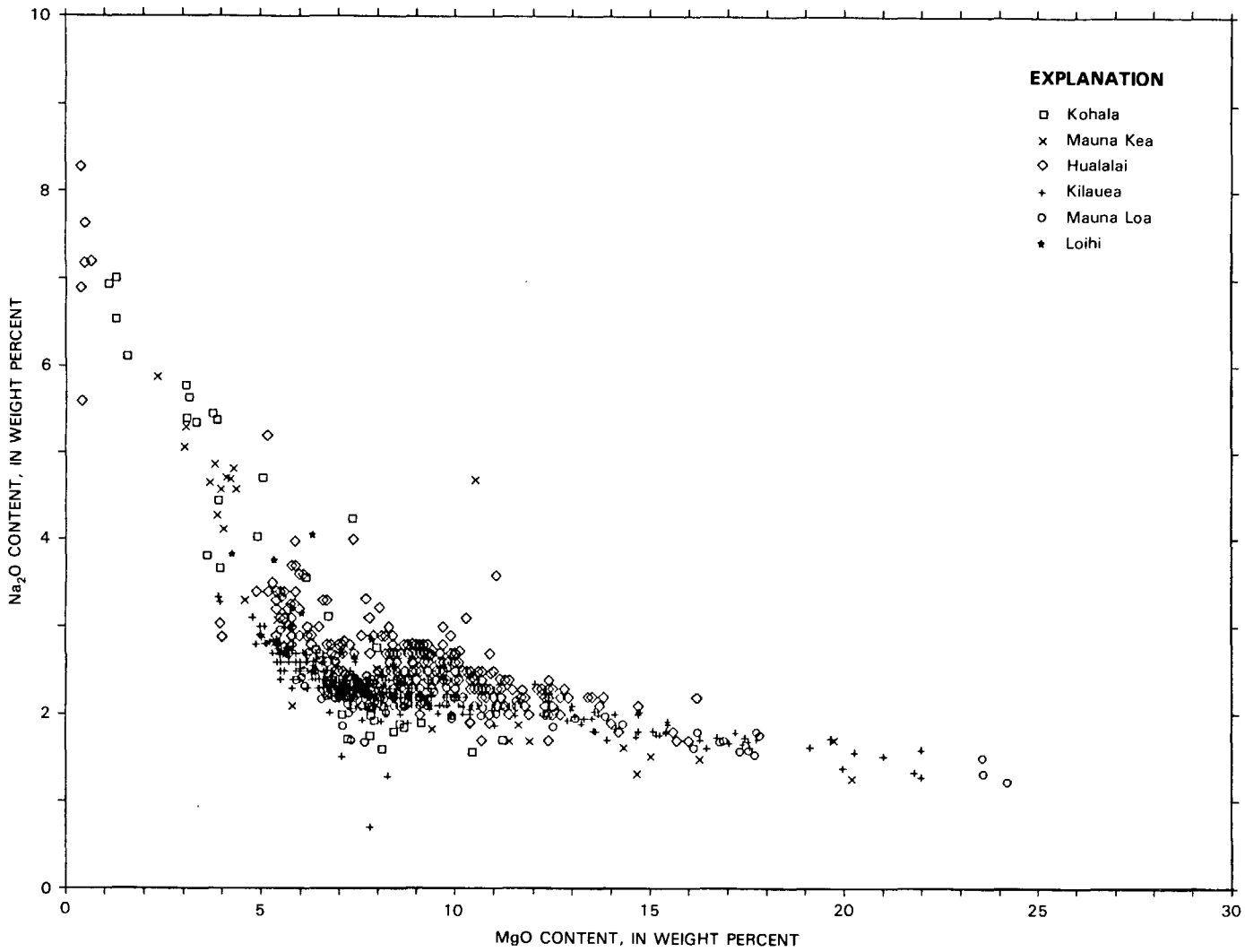

FIGURE 7.14.—Soda-magnesia variation diagram (Na_2O vs. MgO) for volcanic rocks of Hawaii. Analyses from published and unpublished sources.

TiO_2 contents; the two are distinct from the rocks of the other volcanoes. On figure 7.14 Mauna Kea rocks are seen to be similar to those of the other alkalic suites.

HUALALAI

Hualalai consists of a cap of alkalic lavas crowning an older tholeiitic shield (Moore and others, chapter 20). Exposed subaerial lavas are all alkalic; tholeiite has been recovered only from the submarine portion of the prominent northwest rift zone and (Clague, 1982) the bottoms of a few water wells. The geology of Hualalai was mapped in reconnaissance by Stearns and Macdonald (1946); detailed maps have been completed recently by D.A. Clague and by R.B. Moore.

About 5 km east of Hualalai's summit, a diffuse rift zone trends north from the principal northwest rift zone, which bends here and continues 13 km south-southeast. The subaerial portion of the northwest rift zone, 2–4 km wide, is 24 km long from the junction east of the summit to the ocean; bathymetry suggests that its submarine extension may be 70 km long. The north rift zone, about 10 km long and 5 km wide, contains less than 5 percent of the vents and has been inactive during the past 2,000 years. No ancient or modern caldera is evident, but there is, as on Mauna Kea, a concentration of vents in the summit area.

Trachyte, the most SiO_2-rich rock on the Island of Hawaii, crops out on the north rift zone of Hualalai at the Puu Waawaa cone and Puu Anahulu flow. Trachyte and microsyenite occur as xenoliths in basaltic deposits from four vents on the northwest and south-

TABLE 7.6.—*Selected references on the petrology and geochemistry of individual volcanoes of Hawaii*

Volcano	References
Kohala	Stearns and Macdonald (1946), Macdonald and Katsura (1964), Macdonald (1968), Feigenson and others (1983).
Mauna Kea	Stearns and Macdonald (1946), Macdonald and Katsura (1964), Macdonald (1968).
Hualalai	Moore and others (chapter 20), Stearns and Macdonald (1946), Macdonald (1968), Clague and others (1980).
Mauna Loa	Stearns and Macdonald (1946), Macdonald and Katsura (1964), Macdonald (1968), Wright (1971), Rhodes (1983).
Kilauea	Stearns and Macdonald (1946), Macdonald and Katsura (1964), Macdonald (1968), Wright (1971), Wright and Fiske (1971), Wright and others (1975), Wright and Tilling (1980), Wright 1984).
Loihi	Moore and others (1982), Frey and Clague (1983), Lanphere (1983).

southeast rift zones, and trachyte just above sea level was encountered in a drillhole on the northwest rift. A rather uncertain age for Puu Waawaa of 0.4 ± 0.3 Ma was obtained by Funkhouser and others (1968), but subsequently G.B. Dalrymple (written commun., 1985) determined an age of $0.106 \pm .006$ Ma. The steep topographic gradients in the area of the northwest rift zone suggest that other trachyte bodies may underlie a thin draping of more mafic lavas. Trachytes were produced during the Pleistocene, when magmatic activity was apparently much greater than it has been during the Holocene and much larger volumes of parental alkali olivine basalt were available for fractionation in shallow magma chambers.

Stearns and Macdonald (1946) mapped the alkalic rocks of Hualalai as the Hualalai Volcanic Series, which included the Waawaa Volcanics. These units are now called the Hualalai Volcanics and the Waawaa Trachyte Member, respectively (fig. 7.4; Langenheim and Clague, chapter 1, part II). Subsequent mapping and radiocarbon dating (Moore and others, chapter 20) have shown that about 95 percent of the surface is younger than 10 ka, and about 20 percent is younger than 1 ka. About 200 vents have erupted during Holocene time; the latest eruptions occurred in 1800–1801 (Stearns and Macdonald, 1946).

Hawaiite is the other differentiated lava that has been erupted by Hualalai; neither mugearite nor benmoreite, common on Kohala, has been found. The more silicic lavas are relatively old; during the last 5,000 years, most eruptions have produced olivine-controlled and differentiated alkali olivine basalt. Xenoliths include mafic and ultramafic rocks and are common in more than two dozen vents and associated flows. They are generally either rocks cognate to the volcano or fragments of oceanic crustal layer 3 (Jackson and others, 1981).

The alkali-silica variation diagram for Hualalai rocks (fig. 7.10C) shows that differentiation of alkalic magmas has produced the most silica-rich rocks on the island. It is possible that mugearites and benmoreites were formed during the period of trachyte volcanism, but they have never been found as flows, cones, or xenoliths.

Figure 7.11C shows the typical alkalic trend of decreasing CaO with increasing SiO_2, but it includes wide scatter at the basaltic end and a huge Daly gap (no lavas of intermediate silica content).

Figure 7.12C shows a wide scatter of CaO contents in the MgO range 5–15 percent, indicating that mixing of magmas has been an important process within Hualalai and reflecting the fact that phenocrysts of clinopyroxene and plagioclase locally are common. Figure 7.14 shows the higher soda content in alkalic rocks (analyses dominantly from Hualalai) vs. tholeiites.

MAUNA LOA

If the structurally high lavas in the Ninole Hills are considered to be part of Mauna Loa (Lipman, 1980), this volcano has been erupting above sea level for at least 400,000 years. Most of its surface, however, is Holocene, as mapped by Stearns and Macdonald (1946), Lipman and Swenson (1984), and Lockwood and others (1984, and unpublished data). Stearns and Macdonald (1946) divided Mauna Loa rocks into (1) the Pliocene Ninole Volcanic Series, shown by subsequent K-Ar dating (Evernden and others, 1964; Dalrymple, 1971) to be late Pleistocene; (2) the Pleistocene Kahuku Volcanic Series; and (3) the latest Pleistocene and Holocene Kau Volcanic Series. These units are now called the Ninole Basalt, the Kahuku Basalt, and the Kau Basalt (see fig. 7.4; Langenheim and Clague, chapter 1, part II). The Kahuku and Kau are separated by the Pahala Ash.

All known subaerial lavas of Mauna Loa are tholeiites, and most lavas are olivine controlled. Differentiated lavas are rare, in contrast to Kilauea (Wright, 1971). Figure 7.10*D* shows that a few of the more differentiated lavas plot close to the line separating alkalic from tholeiitic basalts (Macdonald and Katsura, 1964).

Figure 7.11*D* shows that CaO generally increases with increasing SiO_2 in Mauna Loa rocks, but begins to decrease as andesitic (52 percent SiO_2) compositions are approached. This trend reflects the removal of olivine (low in silica and lime) from tholeiitic melts. As andesitic compositions are approached, CaO begins to decrease, reflecting coprecipitation of pyroxene and (or) plagioclase, as in the alkalic trend.

Figure 7.12*D* (CaO vs. MgO) shows that most Mauna Loa tholeiites are olivine-controlled, as noted by Wright (1971) and Rhodes (1983). In a few cases, differentiated magmas (<6.8 percent MgO; Wright, 1971) have been mixed with olivine-controlled magmas to produce hybrid lavas whose compositions plot off the olivine-control line.

Figure 7.13*D* (TiO_2 vs. MgO) suggests that there are two trends among the Mauna Loa rocks. One has relatively low TiO_2 at specific MgO abundances and may reflect accumulation of ilmenite and (or) titanomagnetite.

KILAUEA

The oldest subaerial rocks of Kilauea were mapped as the Hilina Volcanic Series by Stearns and Macdonald (1946). The rocks in their lowermost exposures are thought to date from 100–70 ka (Easton and Garcia, 1980). Holcomb (1980) has determined

that 90 percent of the surface of Kilauea is younger than 1.1 ka, and 70 percent is younger than 0.5 ka. The youngest rocks of Kilauea were mapped as the Puna Volcanic Series by Stearns and Macdonald (1946). The Puna is of latest Pleistocene and Holocene age. These units have been renamed the Hilina Basalt and the Puna Basalt by Easton (chapter 11). The Hilina and the Puna are separated by the Pahala Ash (see fig. 7.4).

The known eruptive vents of Kilauea are confined to its summit caldera (3 km by 5 km in size) and two rift zones that extend east and southwest from the summit. The east rift zone, which initially trends southeast for 6 km from the summit and then turns east-northeastward and extends another 45 km, is the longer and historically more frequently active of the two (Duffield and others, 1982). It extends below sea level another 70 km beyond the eastern end of the island (Moore and Reed, 1963; Fornari and others, 1978). The subaerial part of the southwest rift zone is about 32 km long, and no extension has been identified offshore.

The south flank of Kilauea is unbuttressed, in contrast to its north side, and thus it is free to move southward in response to repeated injection of magma into storage chambers beneath the summit and rift zones (Swanson and others, 1976a). The large earthquakes of 1868 and 1975 were possibly related to accumulated stress caused by rift deformation. The normal fault scarps of the Hilina system record cumulative displacements of at least 300 m.

Eruptions of Kilauea and Mauna Loa are normally placid and nonexplosive, but Mauna Loa has had minor phreatic eruptions in Holocene time and Kilauea experienced violent explosive eruptions in 1790 and 1924 and doubtless many times previously (Swanson and Christiansen, 1973; Decker and Christiansen, 1984). The 1790 event was probably phreatomagmatic and may have been associated with a major collapse that formed the modern caldera (Holcomb, 1980). Lavas of that age cover much of the lower east rift zone (Moore, 1981, 1983); draining of the summit magma reservoir to feed the eruptions on the rift zone likely induced the collapse. The 1924 phreatic eruption was preceded by the injection of magma from the summit reservoir into the east rift zone, accompanied by ground subsidence at Kapoho, near the subaerial terminus of the rift; a submarine eruption may have occurred to the east-northeast. The event climaxed with a series of steam explosions at Halemaumau over the course of several days. The combination of lava withdrawal, explosions, and collapse of the walls greatly increased both the diameter and depth of Halemaumau Crater.

Other large explosive eruptions on Kilauea built the Kapoho cone, only 20 m above sea level, a few hundred years ago, and were associated with collapse of the three largest pit craters on the lower east rift zone in the time interval 1.3 to 0.2 ka (Moore, 1981, 1983).

Many historical eruptions of Kilauea have lasted only a few days to a few weeks, but three relatively long-lived eruptions have built satellitic shields and associated cones (Mauna Iki, Mauna Ulu, and Puu Oo) since 1919. Two late prehistoric satellitic shields (Kane Nui o Hamo and Heiheiahulu) lie along the east rift zone; similar shields probably formed throughout the growth of the volcano and now the older ones lie buried. Long-lived eruptions from central vents along rift zones apparently were less common during most of the last 1,500 years than they have been during historical (post-1820) time.

All known Kilauea lavas are only tholeiitic basalt; olivine-controlled, differentiated, and hybrid lavas have been erupted from its rift zones, while summit lavas are all olivine-controlled (Wright and Fiske, 1971). As with a few Mauna Loa lavas, a few Kilauea lavas fall in the transition zone between tholeiitic and alkalic Hawaiian rocks on the alkali-silica variation diagram (fig. 7.10*E*). It can also be seen from figure 7.10*E* that, despite its relative youth, Kilauea has erupted a few lavas that are somewhat more differentiated than any that have been found on Mauna Loa. It is not known why the rift zones of Kilauea are able to accommodate long-lived magma chambers whereas those of Mauna Loa do not, but the reason may be related to the different heights of the two volcanoes.

The variation diagram of CaO vs. SiO_2 shows that Kilauea tholeiites are similar to those from Mauna Loa. CaO increases with increasing SiO_2 until andesitic compositions are approached and then decreases with further increase of SiO_2. The lime content of Kilauea tholeiitic differentiates is markedly higher than that in alkalic differentiates of the other volcanoes.

Plots of the variation of CaO and TiO_2 with MgO (figs. 7.12*E*, 7.13*E*) show olivine-controlled differentiation down to MgO abundances of about 6.8 percent; departures from the straight trend reflect magma mixing in rift-zone storage chambers (Wright and Fiske, 1971). Melts erupted on the rift zones range as low as 4.1 percent MgO and include both differentiated and hybrid lavas (Wright and Fiske, 1971). TiO_2 is generally higher in MgO-rich Kilauea lavas than in those from Hualalai and Mauna Loa.

LOIHI

Because of its early stage of development, Loihi Seamount was expected to consist exclusively of tholeiitic rocks, but dredged samples included alkali olivine basalts and basanites, some with abundant ultramafic xenoliths, as well as tholeiites (Moore and others, 1982). From this it has been concluded that limited partial melting of mantle source material during the initial stages of formation of Hawaiian volcanoes may result in generation of alkalic basalts (Moore and others, 1982; Frey and Clague, 1983). With increased partial melting, tholeiitic melts would form, and Loihi appears to be in a transitional stage between the generation of these two types of basalt.

It is also possible, however, that the rocks of Loihi represent more than one mantle source. Lanphere (1983) reported $^{87}Sr/^{86}Sr$ ratios for the different groups of basalts recovered from Loihi and concluded that their mantle sources had different Sr-isotope compositions.

Analytical data reported by Moore and others (1982) are incorporated here in figures 7.10–7.14. The variation diagram of $Na_20 + K_20$ vs. SiO_2 (fig. 7.10*F*) shows that Loihi alkalic and tholeiitic basalts are similar to those from other volcanoes on the Island of Hawaii, but no other basanites have been reported.

The field of high-CaO Loihi rocks is evident on figures 7.11*F* and 7.12*F*. Figures 7.13*F* and 7.14 further indicate that analyzed Loihi rocks are generally similar to those from other Hawaiian

volcanoes and that olivine-controlled differentiation and mixing of magmas have occurred.

NONERUPTIVE GEOLOGIC PROCESSES

Hawaii is the youngest island of the archipelago and the only one with appreciable historical volcanic activity, and any review of its geologic history necessarily deals chiefly with the growth and construction processes related to volcanism. However, geologic agents other than volcanism have also been at work, some constantly and others sporadically. During the active growth stages of a volcano their effects are commonly outstripped or covered by the effects of volcanism, but during the later evolutionary stages, when the frequency and volume rate of eruptions decline, the effects of these other geologic agents become more apparent.

EROSION AND SEDIMENTATION

Extensive discussions of the effects of erosion and sedimentation on the Island of Hawaii are given elsewhere, chiefly in Stearns and Macdonald (1946) and Macdonald and others (1983); we present only a brief summary here.

Annual rainfall on the windward side of Hawaii (east and northeast) is high, as much as 7,600 mm (300 inches). Erosion has been effective in cutting canyons on the windward slopes of the older volcanoes, Kohala and Mauna Kea, and to some extent in the old Ninole Hills on the south flank of Mauna Loa. In these areas of steep topography, soil creep and mudflows locally contribute to the process of erosion. The leeward (west and southwest) side of the island receives much less rainfall, locally as little as 250 mm (10 inches). As a consequence, the western flanks of Kohala and Mauna Kea are little dissected by streams. Hualalai, Kilauea, and most of Mauna Loa show little evidence of stream erosion, because the surface has been frequently renewed by Holocene volcanic activity. Another important factor inhibiting stream erosion is the porous nature of young volcanic rocks. Even heavy rain infiltrates young lava flows quickly, and surface runoff is minimal.

As noted by Stearns and Macdonald (1946), Macdonald and others (1983), and other workers, the locations of canyons on the northeastern side of Kohala are partly fault-controlled and partly consequent, initially cut near the edges of lava flows. Their local relief is as much as 500 m. Submergence of the island during latest Pleistocene and Holocene time has drowned the valley mouths, and the major canyons, including Waipio, Waimanu, Honokane Nui, and Pololu, contain thick sedimentary fill.

Canyons cut into the windward flank of Mauna Kea are not as deep (maximum 200 m) as those on Kohala, because the surface of Mauna Kea is younger. Radial drainage consequent upon the lava-flow topography dominates; slopes are thinly mantled by locally derived cinders, and the effect of structures, such as buried faults, appears to be minimal. The Wailuku River, which flows through part of Hilo, is primarily a consequent stream cut near the edges of Mauna Loa flows that lapped onto the flank of Mauna Kea.

The Ninole Hills, on the south flank of Mauna Loa, are either structurally high (Lipman, 1980) or erosional (Stearns and Macdonald, 1946) remnants of early Mauna Loa. Gulches that separate the hills are likely inherited from Pleistocene time; their positions can still be identified even though they have been buried by flows of the younger Kahuku and Kau Basalts.

Marine erosion has been vigorous, primarily on the windward sides of the island, and has formed sea cliffs as high as 400 m on Kohala and 100 m on Mauna Kea (Macdonald and others, 1983). Sea stacks and caves are common on the Hamakua coast. Wave action along the southeastern coast has formed sea cliffs several meters high on historic and prehistoric flows from vents on Kilauea's east rift zone. Erosion along this coast is so vigorous that a wave-cut face 1–3 m high was maintained even while lava from the east rift zone of Kilauea was still actively flowing into the sea (Peterson, 1976); within months of the cessation of activity, the newly created shoreline had been worn back appreciably. In contrast, marine erosion of flows from Kohala, Mauna Kea, Hualalai, and Mauna Loa on the western (leeward) side of the island has been slight, and sea cliffs higher than a few meters are rare, even on the older (Pleistocene) flows.

Eolian erosion and sedimentation have been of local importance on the island. Extensive areas on the west flank of Mauna Kea are covered by eolian silt, which originated chiefly as ash at vents and perhaps as glacial debris blown from the summit area. Dunes consisting of reworked Pahala ash are common in the South Point area on the southern flank of Mauna Loa. The Kau Desert, on the southwest flank of Kilauea, has many small active dunes that consist primarily of wind-blown pyroclastic debris originally ejected during the explosive eruptions of 1790 and 1924.

CHANGES OF SEA LEVEL

Many workers have studied changes of sea level in the Hawaiian Islands, especially H.T. Stearns and more recently J.G. Moore. The major controls on sea level have been (1) worldwide eustatic fluctuations caused by Quaternary climatic changes resulting in varying amounts of water stored in glaciers and (2) subsidence of the islands as a result of volcanic load (Moore, chapter 2, 1969).

Ancient shorelines have been identified throughout the Hawaiian Islands by wavecut terraces below and near sea level and by deposits above sea level inferred to represent marine terraces (Stearns, 1946, 1966, 1978; Macdonald and others, 1983). These widely separated stands of the sea suggested to Stearns that the crust has repeatedly oscillated up and down throughout Quaternary time. In view of the ongoing subsidence of the southeastern end of the island chain, readily shown to be caused by the persistent process of volcanic loading (Moore, chapter 2; Apple and Macdonald, 1966; Moore, 1970; Moore and Fornari, 1984), such large-amplitude fluctuations were puzzling. Moore and Moore (1984), however, have provided evidence showing that most or all of the supposed subaerial terrace deposits have instead resulted from a giant catastrophic wave, which avoids the need to explain high stands of sea level by crustal oscillation. Moore (chapter 2) discusses the subsidence processes in detail.

If, however, another major global glaciation occurs, sea level may drop faster than the ongoing subsidence. Canyon-cutting on the

Island of Hawaii would then become more vigorous, as streams become graded to the new lower sea level.

GLACIATION

Mauna Kea was glaciated during Pleistocene time, and the resulting deposits were studied by Wentworth and Powers (1941), Porter and others (1977), and Porter (1979a, b). These workers recognized the effects of four separate glaciations that occurred during the period 280–10 ka. Typical glacial features such as striated boulders, roches moutonnees, ground moraine, and lateral and terminal moraines are visible in the summit area of Mauna Kea. Porter (1979b) estimated that the maximum thickness of ice was 150–170 m.

Glaciers may have formed on Mauna Loa also, but any evidence of them has been buried by Holocene lavas (Macdonald and others, 1983).

EARTHQUAKES AND FLANK DISPLACEMENTS

Most earthquakes on and near the Island of Hawaii are the consequence of volcanic activity. Some are induced as magma moves into storage chambers beneath the summits of Mauna Loa and Kilauea, others as magma is intruded into the rift zones that radiate from the summit calderas. The intrusion of magma results in an accumulation of stress that must eventually be relieved. Some earthquakes occur when magma moves out of an area, resulting in local foundering of overlying rocks.

Large earthquakes (magnitude 6 or greater) in Hawaii have been concentrated in three principal areas: (1) the Kealakekua fault system on the west flank of Mauna Loa, (2) the Kaoiki fault system on the southeast flank of Mauna Loa, and (3) the Hilina fault system on the south flank of Kilauea. Each of these areas has experienced at least one earthquake of magnitude (M) greater than 6 since 1950. In addition, a deep (48-km) $M=6.2$ earthquake struck the east flank of Mauna Kea in 1973 and apparently triggered sympathetic crustal aftershocks on the north flank of Mauna Kea, an area that has experienced occasional swarms for decades (Unger and Ward, 1979).

Earthquakes that occur on the Kealakekua and Hilina fault systems are, in large part, the result of gravitational sliding of parts of the volcanic edifices toward the sea. In these areas, there is no adjoining volcano to provide a buttress against such sliding; thus, when the volcano is overinflated (as Mauna Loa was in the aftermath of the great 1950 eruption and as the east rift zone of Kilauea was by the end of the 1969–1974 Mauna Ulu eruption), a condition of accumulated strain analogous to oversteepening results in failure of the volcano's flank (Swanson and others, 1976a).

Large earthquakes in the Kaoiki region probably are largely the result of inflation of the summit region and upper northeast rift zone of Mauna Loa. Here the strain release is accommodated by strike-slip faulting (Endo, 1985) rather than by normal faulting, because the presence of Kilauea provides a buttress resisting downward slippage of Mauna Loa's southeast flank.

Large fault scarps, as high as about 300 m, are the major surface expression of repeated faulting along the Hilina and Kealakekua systems. The Kaoiki system consists of upper and lower parts. The lower part is inactive seismically, and fault scarps there have been buried by lava flows as old as 9 ka (Lipman, 1980). The upper part, where modern seismicity is concentrated, is characterized by extensive ground cracking, but fault scarps of large displacement are absent (Endo, 1985).

TSUNAMIS

Tsunamis (seismic-induced sea waves) are the most dangerous and destructive natural hazards that affect Hawaii and its residents. Hawaiian tsunamis usually are caused by earthquakes of local or circum-Pacific origin that displace the ocean bottom; this displacement in turn generates a wave in the overlying water. These low-amplitude waves travel at speeds of several hundred kilometers per hour in deep ocean, but when they approach land masses they are slowed and build up to heights of many meters. The greatest recorded height of a wave striking the Island of Hawaii was 16.8 m at the mouth of Pololu Valley in 1946, although greater (but unmeasured) heights may have been reached in 1868 and at other times (Macdonald and others, 1983).

Tsunamis that have struck Hawaii since 1819 are listed in table 7.7. The average interval between tsunamis has been about five years, but the average interval separating the seven that have caused severe damage has been about 22 years. However, their recurrence interval has no regular pattern.

TABLE 7.7.—*Principal tsunamis observed in Hawaii during historical time*

[Adapted from Macdonald and others, 1947, 1983]

Date	Source	Damage in Hawaii
1819, April 12	Unknown	Unknown
1837, November 7	South America	SEVERE
1841, May 17	Kamchatka	Slight
1868, April 2	Hawaii	SEVERE
1868, August 13	South America	SEVERE
1869, July 25	South America (?)	Moderate
1872, August 23	Hawaii	Slight
1877, May 10	South America	SEVERE
1883, August 26	East Indies	Slight
1896, June 15	Japan	None
1901, August 9	Japan (?)	None
1906, January 31	Unknown	None
1906, August 16	South America	Slight
1918, September 7	Kamchatka	Slight
1919, April 30	Unknown	None
1922, November 11	South America	None
1923, February 3	Kamchatka	Moderate
1923, April 13	Kamchatka	None
1927, November 4	California	None
1927, December 28	Kamchatka	None
1928, June 16	Mexico	None
1929, March 6	Aleutian Islands	None
1931, October 3	Solomon Islands	None
1933, March 2	Japan	Slight
1938, November 10	Alaska	None
1944, December 7	Japan	None
1946, April 1	Aleutian Islands	SEVERE
1952, November 4	Kamchatka	Slight
1957, March 9	Aleutian Islands	Slight
1960, May 22	South America	SEVERE
1964, March 28	Alaska	None
1975, November 29	Hawaii	SEVERE

The effects of tsunamis are not likely to be preserved in the geologic record for very long. Vegetation generally grows rapidly in Hawaii and would mask debris. Boulders are thrown up on the tops of low sea cliffs also by severe storms, and these would be indistinguishable from those washed up by tsunamis. Deep narrow canyons (Pololu, Laupahoehoe) on the northeastern coast, which are most vulnerable to severe tsunami damage, are rapidly filled with new fluvial sediments. On the other hand, Moore and Moore (1984) interpreted a widespread gravel on Lanai, Maui, and northwest Hawaii as a deposit from a giant wave, possibly generated by a submarine landslide south of Lanai dating from about 100 ka. This event, however, was much larger and rarer than ordinary tsunamis.

FUTURE DEVELOPMENT

KOHALA

Kohala Volcano is generally considered extinct, because its last known eruption occurred at about 60 ka (McDougall and Swanson, 1972). However, renewed volcanism on other Hawaiian volcanoes has begun one million or more years after cessation of alkalic cap activity (Clague and Dalrymple, chapter 1, part I). Future eruptions of Kohala thus are possible; they might be alkalic basaltic, basanitic, or nephelinitic in composition.

Erosion is probably the major geologic process that will affect Kohala in the future. Unless parts are rebuilt by renewed volcanic activity, sustained fluvial and coastal erosion for millions of years will wear Kohala down to sea level. If regional subsidence continues in the future as it has in the past (Moore, chapter 2), subsidence will supplement the erosion process. Kohala will become a separate island long before it is leveled by erosion, if subsidence causes the saddle between it and Mauna Kea to be submerged.

MAUNA KEA

Mauna Kea may well erupt again, since it has been only about 4,500 years since it last erupted (Porter and others, 1977). The next eruptions may be similar in composition to the most recent (hawaiite), although it is possible that mugearite, benmoreite, or trachyte will appear in the future. Mauna Kea is still considered to be in the capping stage (3) although unless additional eruptions of alkalic rocks occur, it will have quietly completed the transition to the erosional stage (4).

As on Kohala, erosion will be the major geologic process occurring on Mauna Kea. Over the next few millions of years, erosion and subsidence probably will reduce the volcano to sea level.

HUALALAI

The average recurrence interval for eruptions of Hualalai in the Holocene has been about 50 yr (200 events in 10,000 yr), but clusters of eruptions separated by gaps of hundreds of years have apparently occurred. A few satellitic shields that probably took several years to form are present. Most of the recent eruptions have been of high volume (>0.25 km^3). Phreatic explosions have occurred at two vents within the past 700 years; the products of one covered an area of at least 10 km^2. Eruptions since at least 100 ka have been exclusively of alkali olivine basalt and its differentiates; no major change in chemical composition is expected for tens of thousands of years. Perhaps in hundreds of thousands of years Hualalai will erupt basanite and (or) nephelinite. An intense swarm of earthquakes beneath Hualalai in 1929 is believed to have been associated with underground movement of magma (Macdonald and Abbott, 1970, p. 53–54), and the volcano may have been close to having an eruption (Moore and others, chapter 20). Since 1929, however, neither ground deformation nor swarms of earthquakes have been detected on Hualalai, so it cannot be estimated when the next magmatic activity will occur.

Hualalai is virtually undissected, although a few intermittent streams are subject to flash flooding. Heavy rain in 1980 and 1981 resulted in deposition of several hundred cubic meters of debris in alluvial fans near the summit and downcutting of gullies by as much as 5 m. On the southwest flank of the volcano, gullying locally occurs on flows that are relatively old (13–5 ka). The surface renewal rate (18 km^2 per 100 yr for the last 3,000 yr) suggests that erosion will not have a pronounced effect on Hualalai's morphology for a long time, possibly tens of thousands of years.

MAUNA LOA

Mauna Loa has been active about 6 percent of the time since 1835, and a similar rate of activity likely will continue in the foreseeable future. Mauna Loa has erupted an average of 2.9 km^3 of lava per century during historical time, and most of its surface is younger than 4 ka (Lockwood and Lipman, chapter 18). Historical Mauna Loa eruptions have ranged in duration from a few hours to 450 days, and future eruptions from the summit, rift zones, and north and west flanks probably will be similar. Mauna Loa does not seem to build satellitic shields, in contrast to Kilauea. In view of the prevailing rate of crustal subsidence (Moore, chapter 2), it seems unlikely that the height of Mauna Loa above sea level will increase much more than a few tens or hundreds of meters; however, repeated filling and collapse of Mokuaweoweo Crater seems likely to occur.

If Mauna Loa follows the pattern of most other Hawaiian volcanoes, thousands to hundreds of thousands of years in the future, it will erupt alkalic basalts and their differentiates. As noted earlier, a few basalts of Mauna Loa already appear to be transitional in their chemical composition.

Mauna Loa is nearly undissected; until the output of the volcano decreases markedly, erosion will have negligible effect on its constructional landforms.

KILAUEA

Kilauea has been active about 60 percent of historical time and has extruded more than 1.2 km^3 of tholeiitic basalt since 1952. Three satellitic shields have formed during this century, and two others during the past few hundred years. In contrast to Mauna Loa, Kilauea has sustained long-term eruptions (at least 5 years). Magma will continue to be stored in its rift zones, where it will differentiate; perhaps more differentiates as extreme as the Yellow

Cone scoria will form and be erupted. Eventually, basalts more transitional in composition will be erupted, although Kilauea seems unlikely to erupt alkalic rocks until its present rate of magma production declines. That may be hundreds of thousands of years in the future.

Kilauea also is little eroded, although a few intermittent streams flood during heavy rains. Kilauea's historical output of about 2.2 km^3/100 yr seems likely to ensure that its surface will be frequently renewed; at present, 90 percent of its surface is younger than 1.1 ka (Holcomb, chapter 12).

LOIHI

If Loihi erupts in the future at a rate comparable to those of Kilauea and Mauna Loa, its summit will reach the ocean's surface in a few tens of thousands of years. Moore and others (1982) suggested that Loihi has been or may soon begin erupting tholeiitic basalt exclusively as the amount of partial melting of the mantle source increases. If it reaches sea level, it will initially form a separate island, but if eruptions continue, it could ultimately be joined with Hawaii. Loihi likely will follow the same eruptive pattern as other volcanoes along the island chain.

REFERENCES CITED

Ando, M., 1979, The Hawaii earthquake of November 29, 1975: low dip angle faulting due to forceful injection of magma: Journal of Geophysical Research, v. 84, no. B 13, p. 7616–7626.

Apple, R.A., and Macdonald, G.A., 1966, The rise of sea level in contemporary times at Honaunau, Kona, Hawaii: Pacific Science, v. 20, p. 125–136.

Banks, N.G., Klein, F.W., Moore, R.B., Jackson, D.B., and Okamura, A.T., 1981, Kilauea Volcano November 1979 eruption [abs]: Eos (American Geophysical Union Transactions), v. 62, no. 45, p. 1072.

Banks, N.G., Wolfe, E.W., Duggan, T.A., Okamura, A.T., Koyanagi, R.Y., Greenland, L.P., and Jackson, D.B., 1983, Magmatic events at Kilauea Volcano, Hawaii, 1982 [abs.]: Eos (American Geophysical Union Transactions), v. 64, no. 45, p. 901–902.

Bargar, K.E., and Jackson, E.D., 1974, Calculated volumes of individual shield volcanoes along the Hawaiian-Emperor Chain: U.S. Geological Survey Journal of Research, v. 2, p. 545–550.

Beaglehole, J.C., 1967, The journals of Captain Cook on his voyages of discovery; Volume III: The voyage of the Resolution and Discovery, 1776–1780: Cambridge University Press, 1647 p.

Berry, A.L., 1973, Thermoluminescence of Hawaiian basalts: Journal of Geophysical Research, v. 78, p. 6863–6867.

Brigham, W.T., 1909, The volcanoes of Kilauea and Mauna Loa: B.P. Bishop Museum Memoir, v. 2, no. 4, 222 p.

Budahn, J.R., and Schmitt, R.A., 1985, Petrogenetic modeling of Hawaiian tholeiitic basalts: a geochemical approach: Geochimica et Cosmochimica Acta, v. 49, p. 67–87.

Clague, D.A., 1982, Petrology of tholeiitic basalt dredged from Hualalai Volcano, Hawaii: Eos (American Geophysical Union Transactions), v. 63, p. 1138.

———in press, Hawaiian alkaline volcanism: Quarterly Journal, Geological Society of London.

Clague, D.A., Jackson, E.D., and Wright, T.L., 1980, Petrology of Hualalai Volcano, Hawaii: implication for mantle composition: Bulletin Volcanologique, v. 43, no. 4, p. 641–656.

Coan, T., 1841, Great eruption of the volcano of Kilauea: Missionary Herald, v. 37, p. 283–285.

———1851, Mauna Loa eruption of 1849: American Journal of Science, 2d ser., v. 12, p. 82.

———1852, On the eruption of Mauna Loa, Hawaii, February 1852: American Journal of Science, 2nd ser., v. 14, p. 106–107, 219–224.

———1869, Notes on the recent volcanic disturbances of Hawaii: American Journal of Science, 2nd ser., v. 47, p. 89–98.

———1871, On Kilauea and Mauna Loa: American Journal of Science, 3d ser., v. 2, p. 454–456.

———1877, Volcanic eruptions on Hawaii: American Journal of Science, 3d ser., v. 14, p. 68–69.

Cross, Whitman, 1915, Lavas of Hawaii and their relations: U.S. Geological Survey Professional Paper 88, 97 p.

Crosson, R.S., and Endo, E.T., 1981, Focal mechanisms of earthquakes related to the 29 November 1975 Kalapana, Hawaii, earthquake: the effect of structure models: Bulletin of the Seismological Society of America, v. 71, no. 3, p. 713–729.

———1982, Focal mechansims and locations of earthquakes in the vicinity of the 1975 Kalapana earthquake aftershock zone 1970–1979: implications for tectonics of the south flank of Kilauea Volcano, Island of Hawaii: Tectonics, v. 1, p. 495–542.

Dalrymple, G.B., 1971, Potassium-argon ages from the Pololu Volcanic Series, Kohala Volcano, Hawaii: Geological Society of America Bulletin, v. 82, p. 1997–1999.

Dalrymple, G.B., Silver, E.A., and Jackson, E.D., 1973, Origin of the Hawaiian Islands: American Scientist, v. 61, p. 294–308.

Daly, R.A., 1911, The nature of volcanic action: American Academy of Arts and Sciences, Proceedings, v. 47, p. 47–122.

———1914, Igneous rocks and their origin: New York, McGraw-Hill Book Co., 563 p.

———1933, Igneous rocks and the depths of the earth: New York, McGraw-Hill Book Co., Inc., 598 p.

———1944, Volcanism and petrogenesis as illustrated in the Hawaiian Islands: Geological Society of America Bulletin, v. 55, p. 1363–1400.

Dana, J.D., 1849, Geology: U.S. Exploring Expedition, under the command of Charles Wilkes, U.S.N., 1838–1842: v. 10, p. 156–226.

———1859, Eruption of Mauna Loa, Hawaii: American Journal of Science, 2d ser., v. 27, p. 410–415.

———1860, Eruption of Mauna Loa, Sandwich Islands: American Journal of Science, 2d ser., v. 29, p. 301–302.

———1890, Characteristics of Volcanoes: New York, Dodd, Mead Co., 399 p.

Davis, J.B., 1859, Great eruption of the volcano Mauna Loa, in the Island of Hawaii: Edinburgh New Philosophical Journal, new ser., v. 10, p. 94–97.

Decker, R.W., and Christiansen, R.L., 1984, Explosive eruptions of Kilauea Volcano, Hawaii: *in* Explosive volcanism: inception, evolution, and hazards: Washington, D.C., National Academy Press, p. 122–132.

Douglas, D., 1914, Journal kept by David Douglas during his travels in North America, 1833–1837, London, p. 298–317.

Duffield, W.A., 1975, Structure and origin of the Koae fault system, Kilauea Volcano, Hawaii: U.S. Geological Survey Professional Paper 856, 12 p.

Duffield, W.A., Christiansen, R.L., Koyanagi, R.Y., and Peterson, D.W., 1982, Storage, migration, and eruption of magma at Kilauea Volcano, Hawaii, 1971–1972: Journal of Volcanology and Geothermal Research, v. 13, p. 273–307.

Dutton, C.E., 1884, Hawaiian volcanoes: U.S. Geological Survey, 4th Annual Report, p. 75–219.

Dzurisin, Daniel, 1980, Influence of fortnightly earth tides at Kilauea Volcano, Hawaii: Geophysical Research Letters, v. 7, p. 925–928.

Easton, R.M., and Garcia, M.O., 1980, Petrology of the Hilina Formation, Kilauea Volcano, Hawaii: Bulletin Volcanologique, v. 43, p. 657–673.

Ellis, William, 1827, Journal of William Ellis, Narrative of a tour of Hawaii, with remarks on the history, traditions, manners, customs, and language of the inhabitants of the Sandwich Islands: Honolulu (1963), Advertiser Publishing Co., Ltd., reprint of the London 1827 edition, 342 p.

Endo, E.T., 1985, Seismotectonic framework for the southeast flank of Mauna Loa Volcano, Hawaii: Seattle, University of Washington, Ph.D. dissertation, 327 p.

Evernden, J.F., Savage, D.E., Curtis, G.H., and James, G.T., 1964, Potassium-argon dates and the Cenozoic mammalian chronology of North America:

American Journal of Science, v. 262, p. 145–198.

Feigenson, M.D., Hofmann, A.W., and Spera, F.J., 1983, Case studies on the origin of basalt, II. The transition from tholeiitic to alkalic volcanism on Kohala Volcano, Hawaii: Contributions to Mineralogy and Petrology, v. 84, p. 390–405.

Finch, R.H., and Macdonald, G.A., 1951, Report of the Hawaiian Volcano Observatory for 1948 and 1949: U.S. Geological Survey Bulletin 974–D, p. 103–133.

———1953, Hawaiian volcanoes during 1950: U.S. Geological Survey Bulletin 996–B, p. 27–89.

Fisher, R.V., 1968, Puu Hou littoral cones, Hawaii: Geologisches Rundschau, v. 57, p. 837–864.

Fiske, R.S., and Jackson, E.D., 1972, Orientation and growth of Hawaiian volcanic rifts: the effect of regional structure and gravitational stresses: Proceedings of the Royal Society of London, v. 329, p. 299–326.

Fiske, R.S., and Koyanagi, R.Y., 1968, The December 1965 eruption of Kilauea Volcano, Hawaii: U.S. Geological Survey Professional Paper 607, 21 p.

Fornari, D.J., Malahoff, A., and Heezen, B.C., 1978, Volcanic structure of the crest of the Puna Ridge, Hawaii: geophysical implications of submarine volcanic terrain: Geological Society of America Bulletin, v. 89, p. 605–616.

Frey, F.A., and Clague, D.A., 1983, Geochemistry of diverse basalt types from Loihi Seamount, Hawaii: petrogenetic implications: Earth and Planetary Science Letters, v. 66, p. 337–355.

Funkhouser, J.G., Barnes, I.L., and Naughton, J.J., 1968, The determination of a series of ages of Hawaiian volcanoes by the potassium-argon method: Pacific Science, v. 22, p. 369–372.

Furumoto, A.S., and Kovach, R.L., 1979, The Kalapana earthquake of November 29, 1975: an intra-plate earthquake and its relations to geothermal processes: Physics of the Earth and Planetary Interiors, v. 29, p. 355–364.

Goodrich, Joseph, 1826, Notice of the volcanic character of the Island of Hawaii: American Journal of Science, lst series, v. 11, p. 2–7.

Green, W.L., 1887, Vestiges of the molten globe, Pt. 2 of the Earth's surface features and volcanic phenomena: Honolulu, 377 p.

Halbig, J.B., Orr, J.B., and Lockwood, J.P., 1979, Use of alteration rind thickness to date prehistoric Hawaiian lavas: Hawaii Symposium on Intraplate Volcanism and Submarine Volcanism, Hilo, Hawaii, Abstract Volume, p. 163.

Harvey, A.G., 1947, Douglas of the fir, A biography of David Douglas, Botanist: Cambridge, Mass., Harvard University Press, 290 p.

Hitchcock, C.H., 1909, Hawaii and its volcanoes: Honolulu, The Hawaiian Gazette Co., Ltd., 314 p. (2nd edition with supplement, 1911).

Holcomb, R.T., 1976, Complexity and hazards of Hawaiian shield volcanoes [abs]: Geological Society of America, Abstracts with Program, v. 8, no. 6, p. 920–921.

———1980, Kilauea Volcano, Hawaii: chronology and morphology of the surficial lava flows: Stanford University, Ph.D. dissertation, 321 p., also U.S. Geological Survey Open-File Report 81–354, 1981.

Jackson, D.B., Swanson, D.A., Koyanagi, R.Y., and Wright, T.L., 1975, The August and October 1968 east rift eruptions of Kilauea Volcano, Hawaii: U.S. Geological Survey Professional Paper 890, 33 p.

Jackson, E.D., Beeson, M.H., and Clague, D.A., 1982, Xenoliths in volcanic rocks from Mauna Kea Volcano, Hawaii: U.S. Geological Survey Open-File Report 82–201, 19 p.

Jackson, E.D., Clague, D.A., Engleman, E., Friesen, W.B., and Norton, D., 1981, Xenoliths in the alkalic basalt flows from Hualalai Volcano, Hawaii: U.S. Geological Survey Open-File Report 81–1031, 32 p.

Jaggar, T.A., 1919, Activity of Mauna Loa: Hawaiian Volcano Observatory Bulletin, v. 7, no. 10, p. 128–158.

———1920, Seismometric investigation of the Hawaiian lava column: Seismological Society of America Bulletin, v. 10, p. 155–275.

———1926, Journal of Mauna Loa eruption: Hawaiian Volcano Observatory Bulletin, v. 14, p. 31–47, 54–57.

———1947, Origin and development of craters: Geological Society of America Memoir 21, 508 p.

Jaggar, T.A., and Finch, R.H., 1924, The explosive eruption of Kilauea in Hawaii, 1924: American Journal of Science, ser. 5, v. 8, p. 353–374.

Kelley, M.L., 1979, Radiocarbon dates from the Hawaiian Islands—a compilation: U.S. Geological Survey Open File Report 79–1700, 37 p.

Kelley, M.L., Spiker, E.C., Lipman, P.W., Lockwood, J.P., Holcomb, R.T., and Rubin, M., 1979, U.S. Geological Survey, Reston, Virginia, Radiocarbon dates XV: Mauna Loa and Kilauea Volcanoes, Hawaii: Radiocarbon, v. 21, p. 306–320.

Kinoshita, W.T., Koyanagi, R.Y., Wright, T.L., and Fiske, R.S., 1969, Kilauea Volcano; the 1967–1968 summit eruption: Science, v. 166, p. 459–468.

Klein, F.W., and Koyanagi, R.Y., 1979, Seismicity of Kilauea and Loihi Volcanoes, Hawaii: Hawaii Symposium on Intraplate Volcanism and Submarine Volcanism, Hilo, Hawaii, Abstract Volume, p. 124.

Kuno, H., Yamasake, K., Iida, C., and Nagashima, K., 1957, Differentiation of Hawaiian magmas: Japan Journal of Geology and Geography, v. 28, p. 179–218.

Lanphere, M.A., 1983, $^{87}Sr/^{86}Sr$ ratios for basalt from Loihi Seamount, Hawaii: Earth and Planetary Science Letters, v. 66, p. 380–387.

Lanphere, M.A., Dalrymple, G.B., and Clague, D.A., 1980, Rb-Sr systematics of basalts from the Hawaiian-Emporer volcanic chain: Initial Reports of the Deep Sea Drilling Project, 55, p. 695–706.

Ledyard, John, 1783, A journal of Captain Cook's last voyage to the Pacific Ocean and in quest of a northwest passage between Asia and America: Hartford, Conn., Nathaniel Patkon.

Leeman, W.P., Budahn, J.R., Gerlach, D.C., Smith, D.R., and Powell, B.N., 1980, Origin of Hawaiian tholeiites: Trace element constraints: American Journal of Science, v. 280-A, p. 794–819.

Lipman, P.W., 1980, The southwest rift zone of Mauna Loa: implications for structural evolution of Hawaiian volcanoes: American Journal of Science, v. 280-A, p. 752–776.

Lipman, P.W., and Swenson, Alan, 1984, Generalized geologic map of the southwest rift zone of Mauna Loa Volcano, Hawaii: U.S. Geological Survey Miscellaneous Investigations Series Map I– 1323, scale 1:100,000.

Lockwood, J.P., Banks, N.G., English, T.T., Greenland, L.P., Jackson, D.B., Johnson, D.J., Koyanagi, R.Y., McGee, K.A., Okamura, A.T., and Rhodes, J.M., 1985, The 1984 eruption of Mauna Loa Volcano, Hawaii: Eos, Transactions, American Geophysical Union, v. 66, no. 16, p. 169–171.

Lockwood, J.P., Koyanagi, R.Y., Tilling, R.I., Holcomb, R.T., and Peterson, D.W., 1976, Mauna Loa threatening: Geotimes, v. 21, no. 6, p. 12–15.

Lockwood, J.P., and Lipman, P.W., 1980, Recovery of datable charcoal beneath young lavas: lessons from Hawaii: Bulletin Volcanologique, v. 43, no. 3, p. 609–615.

Macdonald, G.A., 1947, Bibliography of the geology and water resources of the Island of Hawaii: Hawaii Division of Hydrography, Bulletin 10, 191 p.

———1949a, Petrography of the Island of Hawaii: U.S. Geological Survey Professional Paper 214–D, p. 51–95.

———1949b, Hawaiian Petrographic Province: Geological Society of America Bulletin, v. 60, p. 1541–1596.

———1954, Activity of Hawaiian volcanoes during the years 1940–1950: Bulletin Volcanologique, ser. 2, v. 15, p. 120–179.

———1955, Hawaiian Islands: Catalog of the active volcanoes of the world including solfatara fields, Part III, International Volcanological Association, Naples, Italy, 37 p.

———1959, The activity of Hawaiian volcanoes during the years 1951–1956: Bulletin Volcanologique, ser. 2, v. 22, p. 3–70.

———1960, Dissimilarity of continental and oceanic rock types: Journal of Petrology, v. 1, p. 172–177.

———1962, The 1959 and 1960 eruptions of Kilauea Volcano, Hawaii, and the construction of walls to restrict the spread of the lava flows: Bulletin Volcanologique, v. 24, p. 249–294.

———1965, Hawaiian calderas: Pacific Science, v. 19, p. 320–334.

———1968, Composition and origin of Hawaiian lavas: Geological Society of America Memoir 116, p. 477–522.

———1972, Volcanoes: Englewood Cliffs, N.J., Prentice-Hall, Inc., 510 p.

Macdonald, G.A., and Abbott, A.T., 1970, Volcanoes in the sea: Honolulu, University of Hawaii Press, 441 p.

Macdonald, G.A., Abbott, A.T., and Peterson, F.L., 1983, Volcanoes in the sea, second edition: Honolulu, University of Hawaii Press, 517 p.

Macdonald, G.A., and Eaton, J.P., 1957, Hawaiian volcanoes during 1954: U.S. Geological Survey Bulletin 1061–B, 17–72.

———1964, Hawaiian volcanoes during 1955: U.S. Geological Survey Bulletin 1171, 170 p.

Macdonald, G.A., and Katsura, T., 1961, Variations in the lava of the 1959 eruption in Kilauea Iki: Pacific Science, v. 15, p. 358–369.

———1962, Relationship of petrographic suites in Hawaii: Crust of the Pacific Basin, Geophysical Monograph no. 6, p. 187–195.

———1964, Chemical composition of Hawaiian lavas: Journal of Petrology, v. 5, p. 82–133.

Macdonald, G.A., and Orr, J.B., 1950, The 1949 summit eruption of Mauna Loa, Hawaii: U.S. Geological Survey Bulletin 974–A, p. 1–31.

Malahoff, A., McMurtry, G.M., Wiltshire, J.C., and Yeh, H.W., 1982, Geology and chemistry of hydrothermal deposits from active submarine volcano Loihi, Hawaii: Nature, v. 298, p. 234–239.

May, R.J., 1979, Thermoluminescence dating of Hawaiian basalt: U.S. Geological Survey Professional Paper 1095, 47 p.

McDougall, Ian, 1964, Potassium-argon ages from lavas of the Hawaiian Islands: Geological Society of America Bulletin, v. 75, p. 107–128.

McDougall, Ian, and Swanson, D.A., 1972, Potassium-argon ages of lavas from the Hawi and Pololu Volcanic Series, Kohala Volcano, Hawaii: Geological Society of America Bulletin, v. 83, p. 3731–3738.

Moore, J.G., 1964, Giant submarine landslides on the Hawaiian Ridge: U.S. Geological Survey Professional Paper 501–D, p. D95–D98.

———1965, Petrology of deep-sea basalt near Hawaii: American Journal of Science, v. 263, p. 40–52.

———1970, Relationship between subsidence and volcanic load, Hawaii: Bulletin Volcanologique, v. 34, p. 562–576.

———1975, Mechanism of formation of pillow lava: American Scientist, v. 63, p. 269–277.

Moore, J.G., and Ault, W.U., 1965, Historic littoral cones in Hawaii: Pacific Science, v. 19, p. 3–11.

Moore, J.G., Clague, D.A., and Normark, W.R., 1982, Diverse basalt types from Loihi Seamount, Hawaii: Geology, v. 10, p. 88–92.

Moore, J.G., and Fiske, R.S., 1969, Volcanic substructure inferred from dredge samples and ocean-bottom photographs, Hawaii: Geological Society of America Bulletin, v. 80, p. 1191–1202.

Moore, J.G., and Fornari, D.J., 1984, Drowned reefs as indicators of the rate of subsidence of the island of Hawaii: Journal of Geology, v. 92, p. 752–759.

Moore, J.G., and Koyanagi, R.Y., 1969, The October 1963 eruption of Kilauea Volcano, Hawaii: U.S. Geological Survey Professional Paper 614-C, 13 p.

Moore, J.G., and Krivoy, H.L., 1964, The 1962 flank eruption of Kilauea Volcano and structure of the east rift zone: Journal of Geophysical Research, v. 69, p. 2033–2045.

Moore, J.G., and Moore, G.W., 1984, Deposit from a giant wave on the Island of Lanai, Hawaii: Science, v. 226, p. 1312–1315.

Moore, J.G., Phillips, R.L., Grigg, R.W., Peterson, D.W., and Swanson, D. A., 1973, Flow of lava into the sea, 1969–1971, Kilauea Volcano, Hawaii: Geological Society of America Bulletin, v. 84, p. 537–546.

Moore, J.G., and Reed, R.K., 1963, Pillow structures of submarine basalts east of Hawaii: U.S. Geological Survey Professional Paper 475–B, p. B153–B157.

Moore, R.B., 1981, Preliminary geologic map of the Kapoho quadrangle, Hawaii: U.S. Geological Survey Open-File Report 81–947, scale 1:24,000.

———1983, Distribution of differentiated tholeiitic basalt on the lower east rift zone of Kilauea Volcano, Hawaii: a possible guide to geothermal exploration: Geology, v. 11, p. 136–140.

Moore, R.B., Helz, R.T., Dzurisin, D., Eaton, G.P., Koyanagi, R.Y., Lipman, P.W., Lockwood, J.P., and Puniwai, G.S., 1980, The 1977 eruption of Kilauea Volcano, Hawaii: Journal of Volcanology and Geothermal Research, v. 7, p. 189–210.

Murata, K.J., and Richter, D.H., 1966, Chemistry of the lavas of the 1959–60 eruption of Kilauea Volcano, Hawaii: U.S. Geological Survey Professional Paper 537–A, 26 p.

Peck, D.L., and Kinoshita, W.T., 1976, The eruption of August 1963 and the formation of Alae lava lake, Hawaii: U.S. Geological Survey Professional Paper 935–A, 33 p.

Peterson, D.W., 1971, Petroleum potential of Hawaii, *in* Cram, I. H., ed., Future Petroleum Provinces of the United States: American Association of Petroleum Geologists Memoir 15, p. 161–169.

———1976, Processes of volcanic island growth, Kilauea Volcano, Hawaii: International Association of Volcanology and Chemistry of the Earth's Interior, Proceedings of the Symposium on Andean and Antarctic Volcanology Problems, Special Series, p. 172–189.

Peterson, D.W., Christiansen, R.L., Duffield, W.A., Holcomb, R.T., and Tilling, R.I., 1976, Recent activity of Kilauea Volcano, Hawaii, *in* Gonzales-Ferran, O., ed., International Association Volcanology and Chemistry of the Earth's Interior, Symposium on Andean and Antarctic Volcanology Problems, 1974, Santiago, Chile, Proceedings: p. 646–656.

Peterson, D.W., and Tilling, R.I., 1980, Transition of basaltic lava from pahoehoe to aa, Kilauea Volcano, Hawaii: field observations and key factors: Journal of Volcanology and Geothermal Research, v. 7, p. 271–293.

Porter, S.C., 1972, Buried caldera of Mauna Kea Volcano, Hawaii: Science, v. 175, p. 1458–1460.

———1979a, Hawaiian glacial ages: Quaternary Research, v. 12, p. 161–187.

———1979b, Quaternary stratigraphy and chronology of Mauna Kea, Hawaii: a 380,000-yr record of mid-Pacific volcanism and ice-cap glaciation: Geological Society of America Bulletin, Part II, v. 90, p. 980–1093.

Porter, S.C., Stuiver, M., and Yang, I.C., 1977, Chronology of Hawaiian glaciations: Science, v. 195, p. 61–63.

Powers, H.A., 1935, Differentiation of Hawaiian lavas: American Journal of Science, 5th series, v. 30, p. 57–71.

———1948, A chronology of the explosive eruptions of Kilauea: Pacific Science, v. 2, p. 278–292.

———1955, Composition and origin of basaltic magma of the Hawaiian islands: Geochimica et Cosmochimica Acta, v. 7, p. 77–107.

Powers, Sidney, 1916, Explosive ejectamenta of Kilauea: American Journal of Science, 4th series, v. 41, p. 227–244.

———1920, Notes on Hawaiian petrology: American Journal of Science, 4th series, v.50, p. 256–280.

Rhodes, J.M., 1983, Homogeneity of lava flows: chemical data for historic Mauna Loan eruptions: Journal of Geophysical Research, v. 88, suppl. (2), p. A869–A879.

Richter, D.H., Ault, W.U., Eaton, J.P., and Moore, J.G., 1964, The 1961 eruption of Kilauea Volcano, Hawaii: U.S. Geological Survey Professional Paper 474–D, 34 p.

Richter, D.H., and Eaton, J.P., 1960, The 1959–60 eruption of Kilauea Volcano: New Scientist, v. 7, p. 994–997.

Richter, D.H., Eaton, J.P., Murata, K.J., Ault, W.U., and, Krivoy, H.L., 1970, Chronological narrative of the 1959–60 eruption of Kilauea Volcano, Hawaii: U.S. Geological Survey Professional Paper 539–E, 73 p.

Stearns, H.T., 1926, the Keaiwa or 1823 lava flow from Kilauea Volcano, Hawaii: Journal of Geology, v. 34, p. 336–351.

———1940, Four-phase volcanism in Hawaii [abs]: Geological Society of America Bulletin, v.51, p. 1947–1948.

———1946, Geology of the Hawaiian Islands: Hawaii Division of Hydrography, Bulletin 8, 105 p. (2nd printing, 1967, with supplement, 112 p.).

———1966, Geology of the State of Hawaii: Palo Alto, Ca., Pacific Books, 266 p.

———1978, Quaternary shorelines in the Hawaiian Islands: Bernice P. Bishop Museum Bulletin 237, 57 p.

Stearns, H.T., and Clark, W.O., 1930, Geology and water resources of the Kau District, Hawaii: U.S. Geological Survey Water-Supply Paper 616, 194 p.

Stearns, H.T., and Macdonald, G.A., 1946, Geology and ground-water resources of the Island of Hawaii: Hawaii Division of Hydrography, Bulletin 9, 363 p.

Stone, J.B., 1926, The products and structure of Kilauea: B.P. Bishop Museum, Bulletin 33, 59 p.

Swanson, D.A., 1972, Magma supply rate at Kilauea Volcano, 1952–1971: Science v. 175, p. 169–170.

Swanson, D.A., and Christiansen, R.L., 1973, Tragic base surge in 1790 at

Kilauea Volcano: Geology, v. 1, p. 83–86.

Swanson, D.A., Duffield, W.A., and Fiske, R. S., 1976a, Displacement of the south flank of Kilauea Volcano: the result of forceful intrusion of magma into the rift zones: U.S. Geological Survey Professional Paper 963, 39 p.

Swanson, D.A., Duffield, W.A., Jackson, D.B., and Peterson, D.W., 1979, Chronological narrative of the 1969–71 Mauna Ulu eruption of Kilauea Volcano, Hawaii: U.S. Geological Survey Professional Paper 1056, 55 p.

Swanson, D.A., Jackson, D.B., Duffield, W.A., and Peterson, D.W., 1971, Mauna Ulu eruption, Kilauea Volcano: Geotimes, v. 16, no. 5, p. 12–16.

Swanson, D.A., Jackson, D.B., Koyanagi, R.Y., and Wright, T.L., 1976b, The February 1969 east rift eruption of Kilauea Volcano, Hawaii: U.S. Geological Survey Professional Paper 891, 30 p.

Tilley, C.E., 1950, Some aspects of magmatic evolution: Quarterly Journal of the Geological Society of London, v. 106, p. 37–61.

Tilling, R.I., Koyanagi, R.Y., Lipman, P.W., Lockwood, J.P., Moore, J.G., and Swanson, D.A., 1976, Earthquake and related catastrophic events, Island of Hawaii, November 29, 1975: A preliminary report: U.S. Geological Survey Circular 740, 33 p.

Thorarinsson, S., 1967, Surtsey: New York, Viking Press, 47 p.

Unger, J.D., and Ward, P.L., 1979, A large, deep Hawaiian earthquake—the Honomu, Hawaii event of April 26, 1973: Seismological Society of America Bulletin, v. 69, p. 1771–1781.

Vancouver, G., 1798, A voyage of discovery to the north Pacific Ocean: New York, Da Capo Press (reprinted 1967), v. 3.

Washington, H.S., 1923a, Petrology of the Hawaiian Islands: I. Kohala and Mauna Kea, Hawaii: American Journal of Science, 5th series, v. 5, p. 465–502.

———1923b, Petrology of the Hawaiian Islands: II. Hualalai and Mauna Loa: American Journal of Science, 5th series, v. 6, p. 100–126.

———1923c, Petrology of the Hawaiian Islands: III. Kilauea and general petrology of Hawaii: American Journal of Science, 5th series, v. 6, p. 338–367.

Wentworth, C.K., 1938, Ash formations of the island Hawaii: Hawaiian Volcano Observatory, 3rd Special Report, 173 p.

Wentworth, C.K., and Powers, W.E., 1941, Multiple glaciation of Mauna Kea, Hawaii: Geological Society of America Bulletin, v. 52, p. 1193–1218.

Wilkes, C., 1845, Narrative of the U.S. Exploring Expedition, 1838–1842, Philadelphia, Lea and Blanchard, v. 4, p. 87–231.

Wright, T.L., 1971, Chemistry of Kilauea and Mauna Loa lava in space and time: U.S. Geological Survey Professional Paper 735, 39 p.

———1973, Magma mixing as illustrated by the 1959 eruption, Kilauea Volcano, Hawaii: Geological Society of America Bulletin, v. 84, p. 849–858.

———1984, Origin of Hawaiian tholeiite: a metasomatic model: Journal of Geophysical Research, v. 89, p. 3233–3252.

Wright, T.L., and Fiske, R.S., 1971, Origin of the differentiated and hybrid lavas of Kilauea Volcano, Hawaii: Journal of Petrology, v. 12, p. 1–65.

Wright, T.L., Kinoshita, W.T., and Peck, D.L., 1968, March 1965 eruption of Kilauea Volcano and the formation of Makaopuhi lava lake: Journal of Geophysical Research, v. 73, p. 3181–3205.

Wright, T.L., Swanson, D.A., and Duffield, W.A., 1975, Chemical compositions of Kilauea east-rift lava, 1968–1971: Journal of Petrology, v. 16, p. 110–133.

Wright, T.L., and Tilling, R.I., 1980, Chemical variations in Kilauea eruptions 1971–1974: American Journal of Science, v. 280-A, p. 777–793.

HAWAII: THE VIEW FROM SPACE

By George E. Ulrich, Peter J. Mouginis-Mark,[1] *and* Jo-Ann Bowell

ABSTRACT

Aerial portrayal of Hawaii has advanced dramatically in the 20th century through the use of aircraft, mapping cameras, and photogrammetric instruments. In the past two decades, Earth-orbiting spacecraft have added new dimensions to the study of Hawaii's volcanoes, including synoptic views of all or most of the Island of Hawaii from hundreds of kilometers above the surface and repetitive coverage from automated satellites that record changes on the Earth's surface with time.

Astronaut crews in Apollo, Skylab, and Shuttle spacecraft have taken valuable photographs of short-lived events such as the 1983–84 eruptions on Kilauea and Mauna Loa. Landsat satellites have provided several digital images of high quality, and improved sensors now in use on Landsat for many parts of the world may be transmitting pictures of Hawaii in the near future. Multispectral scanners and a synthetic aperture radar system have been used on recent Shuttle missions and have provided digital images showing subtle volcanic features and even textural differences between lava flows from orbital altitudes of 230 to 290 km. Radar is particularly attractive for Hawaiian volcanoes because it is independent of surface illumination and weather and thus is useful day or night and in cloud-covered areas. Experimentation during the next several years on the Space Shuttle flights will improve present coverage even more as new improved methods continue to be developed.

INTRODUCTION

Since man first arrived in the Hawaiian Islands, his understanding of them has progressed, along with his technology, to new and improved perspectives. Early Polynesian canoes from the Markesa Islands carried the first humans to within sight of the broad volcanic shields and eroded seacliffs. Their view from the sea—a profile on the horizon commonly shrouded in clouds and mist—was a local view, constantly changing with location and lighting. Songs and chants were the basis for description of the islands; early cartographic definition was very unlike the accurate maps and charts of today.

For several centuries after their discovery, the islands were charted by ships' navigators with only the stars and Earth's magnetic field as control. Early maps depended on the artistic talents of the mapmakers while onboard ship or, as likely as not, back in their home ports of Europe and America. More precise definition of the land was achieved when surveyors marked points at the shorelines, on the mountain tops, and along the valleys and ridges between. Before the advent of modern transportation, these surveys were accomplished only with tremendous physical effort and endurance, and they required years of labor to complete.

In the 20th century, the use of aircraft and aerial photography has revolutionized the cartographic profession. The birdseye view of the Hawaiian Islands could be recorded on film at selected scales and over large areas in several days of flying. These photographs were then systematically converted by photogrammetric methods to accurate topographic maps, as a basis for displaying present and future use of the land, and, on the Island of Hawaii for frequent revision, showing new volcanic deposits as they occurred.

In the last two decades, the mapping of Hawaii has been both a stimulus to and a beneficiary of space exploration. The volcanic history and landforms of Hawaii have served as analogs for the study of similar features on other planets. For example, a comparison with analogous features on Mars was the basis for presenting the many excellent examples of oblique and vertical photographic views of the volcanic shields of Hawaii by Greeley (1974) and Carr and Greeley (1980). These photographs were taken between 1942 and 1975 from various altitudes, none of which approached orbital heights.

In spite of the tremendous advances in mapping accuracy made possible by aerial photography, drawbacks remain. Many standard aerial photographs are required to cover the island. The distortion introduced by terrain relief and the inability of aircraft to remain perfectly horizontal preclude the use of these photographs as accurate planimetric maps. Stereoscopic models of overlapping photographs permit precise three-dimensional contour mapping, but the numerous models required are expensive and consume many months of labor.

The view from space adds a totally new perspective to the utility of aerial photography. If there is a single most important aspect of images taken from Earth orbit, it is probably the synoptic view it offers, namely the broad view of a large part of the Earth's surface at one moment in time. Though standard aerial photographs provide high-resolution coverage, they are necessarily limited in the size of the area shown; the view from space is valuable in its instantaneous portrayal of a much larger area albeit in less detail. A second important aspect of space images, the possibility of repeated coverage on subsequent orbits, has many useful applications. A sequence of photographs or digital pictures of phenomena that change with time intervals of days, months, or years can be produced at relatively low cost, once the spacecraft is available. Obvious examples are volcanic eruptions, weather systems, forest

[1]Planetary Geosciences Division, Hawaii Institute of Geophysics, University of Hawaii 96822.

fires, and agricultural conditions. Furthermore, special spectrometers can also view large areas in both the visible and infrared wavelengths to scan for zones of surface alteration, permitting concentrations of economically important minerals or potential geothermal resources to be identified.

The purpose of this paper is threefold: (1) to demonstrate some applications of space images for the improvement of existing maps; (2) to illustrate some aspects of the geology and structure of the Island of Hawaii, using a few examples of available photographs, satellite images, and radar data; and (3) to provide a selective listing of the better images available for the Hawaiian Island chain. Tables 8.1 and 8.2 list those images considered most useful based on minimum cloud coverage, geologic interest, and availabilty from the Earth Resources Observation Systems (EROS) Data Center as of this writing.

ACKNOWLEDGMENTS

Appreciation goes to Charles A. Wood for reviewing and recommending additions to the photographs listed in table 8.1. The authors are indebted to William R. Muehlberger for advice and information on the Skylab and Shuttle photographs, to Ellen M. Sanchez and Kathleen Edwards for direction in the processing of the Landsat images, and to Mary Ann Hager for copies of several important photographs. James D. Griggs provided valuable and always dependable advice and assistance on numerous photographic matters. Christina A. Neal and Ray M. Batson provided very helpful critical reviews of the manuscript, improving it significantly. P.J. Mouginis-Mark received support from NASA's Non-Renewable Resources Branch under NASA/JPL Grant No. 956925.

APOLLO, SKYLAB, AND SHUTTLE PHOTOGRAPHY

Early photographs of Hawaii from space, taken on the Apollo 9 mission in March 1969, formed a panoramic series of four oblique views showing mostly clouds and were published as a mosaic in Dalrymple and others (1973). One of the better photographs of the island was taken from the Skylab spacecraft at an altitude of 435 km (270 mi; see figure 8.1). This vertical view provided an excellent cartographic delineation of the island's shoreline. More recent photographs, from the Space Shuttle missions since 1983, have normally been taken from lower altitudes (230–300 km; 143–186 mi), although Shuttle mission 41–C in April 1984 returned photographs from orbits as high as 500 km (310 mi).

All photographs cited were taken with hand-held NASA-modified cameras, primarily the Hasselblad 500 EL/M, using 70-mm (2.75-in) Kodak Ektachrome film. Advantages in the use of hand-held cameras to view the Earth include the ability to point the lens at targets of opportunity and the flexibility to interchange lenses of different focal lengths. A majority of the hand-held photographs of Hawaii taken from space to date have been taken through a telephoto lens (see table 8.1). The nominal ground resolution from a typical Space Shuttle altitude (284 km; 177 mi) using a 250-mm focal-length lens is about 25 m; the resolution using a 100-mm lens is about 60 m (Mohler, 1983). An example of a telephoto view of Mauna Loa Volcano's summit caldera and most of its two rift zones is shown in figure 8.2 for comparison with the wider angle view of figure 8.3.

The documentation of volcanic activity during and following an eruption is an obvious application of remote-sensing techniques on Hawaii. The beginning of the March–April 1984 eruption of Mauna Loa was precisely marked by a thermal sensor on a military satellite. On the shorter, manned Space Shuttle missions, special events can be targeted for photographic coverage, but the combined requirements of timing and good visibility are largely a matter of luck and perseverance on the part of the flight crews. One such opportunity permitted the plumes from the Mauna Loa eruption of 1984 to be photographed on four different days (table 8.1; fig. 8.3). Less prominent but quite visible was the plume from an eruption on Kilauea Volcano in late 1983 (fig. 8.4).

Perhaps the most photogenic of the five shield volcanoes on the Island of Hawaii is Mauna Kea, the most cited example of a tholeiitic shield capped by alkalic cones and flows in its later stages of development. The distribution of cinder cones on the summit and flanks of this symmetrical shield are shown in figure 8.5. The diversion of younger lava flows from Mauna Loa to the east and west around the base of Mauna Kea is also illustrated.

TABLE 8.1.—*Selected photographs of the Hawaiian Island chain taken by Gemini, Apollo, Skylab, and Space Shuttle missions*

[Data for Shuttle missions are taken mainly from NASA documents (Nowakowski, 1984a, b; Palmer, 1984; and Nowakowski and Palmer, 1984) but are modified where more information was available]

Mo	Da	Yr	Space-craft	Mission	Scene identification	Orbit	Feature	Quality	Percent clouds	Center of scene Lat.	Long.
02	11	73	Landsat	1	8120320180500	67-46	North Hawaii	8888	30	20.22	155.43
02	11	73	Landsat	1	8120320182500	67-47	South Hawaii	8888	20	18.78	155.16
03	01	73	Landsat	1	8122120181500	67-46	North Hawaii	8888	20	20.28	155.50
03	01	73	Landsat	1	8122120183500	67-47	South Hawaii	8882	20	18.84	155.85
10	09	77	Landsat	2	8299119392500	67-47	South Hawaii	8888	30	18.83	155.72
01	07	78	Landsat	2	82108119354X0	67-46	North Hawaii	8888	20	20.18	155.39
01	07	78	Landsat	2	82108119360X0	67-47	South Hawaii	8888	30	18.74	155.74
09	07	78	Landsat	3	83018620064X0	67-46	North Hawaii	8888	30	20.18	155.37

1 Image quality is scaled from 1 (poorest) to 8 (best). Columns under Quality represent, in order, Multispectral Scanner bands 4 (wavelength 0.5 to 0.6 microns), 5 (0.6-0.7), 6 (0.7-0.8), and 7 (0.8-1.1).

Cloud patterns and ocean roughness are remarkably well portrayed in the synoptic view from space. The typical cloud pile-up on the windward side of Hawaii in contrast with the open sky and smoother ocean surface on the leeward or Kona side (fig. 8.6) produces the illusion of an island sailing northeastward across the Pacific. The disturbance of windflow (orographic effect) across and around the five volcanic shields provides a fruitful area of research for atmospheric scientists.

LANDSAT AND OTHER MULTISPECTRAL SATELLITE IMAGES

Digital images transmitted from Landsat, originally called Earth Resources Technology Satellite (or ERTS), provide repetitive coverage of the Earth from polar orbit using a scanner system that includes spectral bands from near infrared through the visible wavelengths. Landsats 1, 2, and 3 recorded scenes of Hawaii on four bands over the wavelength range of 0.5 to 1.1 microns. A typical image is approximately 185 km (115 mi) on each side and has a nominal resolution per picture element (pixel) of 80 m (Short and others, 1976). The amount of area included within Landsat images compared with photographs taken on Skylab and Shuttle missions is shown in figure 8.7.

In comparison with photographs taken from aircraft and manned spacecraft, the shortcomings of digital images from satellites are mainly their lower spatial resolution, their rigid format and direction of view, and the acquisition of data at only one lighting geometry (due to the sun-synchronous nature of the Landsat orbits; Short and others, 1976). The advantages of digital images recorded by satellites are: (1) they cover larger areas, (2) they have uniform resolution across the entire image, and (3) they include various spectral bands that can be filtered or enhanced after the image is recorded to delete atmospheric haze or to emphasize the surface distribution of different natural materials. In contrast, improvements to aerial photographs are normally made as the pictures are taken, requiring extensive experience and know-how. Corrections for haze, color, and lighting are difficult to apply in the photographic laboratory, but are generally possible for digital images via computer processing.

Image processing and enhancement of digital scenes such as from Landsat can be helpful in geologic interpretation and illustration of regional features on Earth as well as other planets. The Landsat scene shown in figure 8.8 was recorded in 1978. Other scenes (until late 1978; table 8.2) can be purchased from EROS in several formats. Repetitive overflights could eventually make it possible to acquire near-perfect images of the entire island chain, although the current spacecraft configuration prohibits the transmission of new images from Landsats 4 and 5.

Cartographic applications of Landsat data require that scenes be fitted to standard map projections and existing map products. Figure 8.8 has been geometrically adjusted to the universal transverse mercator projection, and the red and green color bands have been combined with an artificially generated blue band to create a simulated true-color rendition of Hawaii as described by Eliason and others (1974). Landsat scenes can be modified by computer to increase their interpretability. One example is the superposition of the scene on a digital elevation model (obtained from the U.S. Defense Mapping Agency) derived from the 1:250,000-scale map series. The registration procedure, whereby every pixel of the image is assigned a corresponding elevation value, is the most labor-intensive part of this technique.

The composite data set thus produced can be digitally rotated to an oblique aerial view. The vertical exaggeration, the vertical angle of the perspective view, and the look-azimuth desired can all be adjusted by an analyst for maximum interpretability. We chose the northwestward view shown in figure 8.9 to look across the rift structures of Mauna Loa and Kilauea Volcanoes. If one wanted to look for subtle structures (for example, parallel to a rift zone), the down-structure view could be generated just as easily. A three-times vertical exaggeration appears to best illustrate the relief of the volcanoes in this case. An additional processing technique, not developed in time for this report, is the removal of cloud cover from the image while retaining the terrain information from the elevation model. This effect can be created by digitally stenciling out the white pixels in the scene and replacing them with a digital shading of the elevation model.

A further enhancement of the oblique aerial view could include a second oblique view—slightly offset in azimuth but with other variables held constant—to provide a stereo pair. An example of this technique for another volcanic area is illustrated elsewhere (Anonymous, 1984a, 1984b). Subtle structures such as shallow craters and small cones and shields can be more easily recognized and interpreted in the stereoscopic view.

Unfortunately the number of geologically useful Landsat images of Hawaii is small due to the frequent canopy of clouds that cover much of the island. The Thematic Mappers on Landsats 4 and 5 have better spectral and spatial resolution than any previous Landsat. These spacecraft do not carry tape recorders, however, and the only areas on the Earth's surface that can be acquired are those in direct line of sight with a receiving station. As of this writing (1985) and because of the inability to record, there are no images of Hawaii yet available from these spacecraft (Landsats 4 or 5). This problem may be resolved when a tracking and data-relay satellite (TDRS-west) is launched in the near future. (Note: The TDRS satellite was lost in the shuttle *Challenger* accident in 1986, and its replacement and launching will be significantly delayed. Until that time, new Landsat images for the Hawaiian Islands will not be available.)

While Landsat is an established standard for orbital-digital images of the Earth, other sensors are under development, many of them using the Space Shuttle as a platform. One such experiment, the German MOMS–1 (Modular Optoelectronic Multispectral Scanner), was flown on the Shuttle in February 1984 and recorded the image of Hawaii reproduced in figure 8.10. The image has a spatial resolution of approximately 20 m in two spectral channels (0.60 and 0.90 microns), sufficient to identify features such as the new lava flows of the 1983–85 east-rift eruptions on Kilauea. Obvious applications for these images lie in their potential for mapping recent eruption areas, portraying patterns of flow distribu-

TABLE 8.2.—*Selected Landsat scenes of the Island of Hawaii*

[Images and photographs listed can be purchased from EROS Data Center, Sioux Falls, SD 57198]

Mo	Da	Yr	Space-craft	Mission identificat.	Scene identification [1]	Orbit	Feature	Focal length	Percent clouds [2]	Perspective [3]	Direction	Stereo [4]	Center of scene Lat [5]	Long
08	24	65	Gemini	V	S-65-45616	51	Hawaii to Kauai	80	80	Oblique	SW	No	20.0	154.0
10	15	68	Apollo	7	AS7-7-1740	51	Niihau	80	--	---do---	NE	No	23.0	160.5
10	15	68	Apollo	7	AS7-7-1741	51	Oahu	80	--	---do---	NE	Yes	23.0	158.5
10	15	68	Apollo	7	AS7-7-1742	51	Oahu, Maui	80	--	---do---	NE	Yes	23.0	157.0
10	15	68	Apollo	7	AS7-7-1743	51	--do---------	80	--	---do---	NE	Yes	22.0	157.0
10	15	68	Apollo	7	AS7-7-1744	51	Maui, Hawaii	80	--	---do---	NE	Yes	22.0	156.5
10	15	68	Apollo	7	AS7-7-1745	51	Maui,Kahoolawe,Haw	80	--	---do---	NE	Yes	21.5	156.0
10	15	68	Apollo	7	AS7-7-1746	51	--do---------	80	--	---do---	NE	Yes	20.0	155.5
10	15	68	Apollo	7	AS7-7-1747	51	Hawaii	80	--	---do---	NE	Yes	21.5	155.0
02	03	69	Apollo	9	AS9-3505 to-8	--	Hawaii to Niihau	100(?)	50	---do---	SW	Yes	20.0	154.0
12	07	73	Skylab	4	SL4-139-3997	--	Hawaii	100	10	Vertical	--	No	19.6	155.5
04	05	83	Shuttle	STS-6, S-06	40-745	22	Mauna Loa	250	85	---do---	--	Yes	19.5	155.5
06	18	83	--do---	STS-7, S-07	20-1029	5	Oahu,Molakai,Lanai	100	30	Oblique	N	Yes	22.5	158.0
06	18	83	--do---	----do-----	20-1030	5	Molokai,Maui,Lanai	100	30	---do---	N	Yes	23.0	157.0
06	18	83	--do---	----do-----	22-1134	6	Niihau	250	30	---do---	NE	No	22.0	160.0
06	18	83	--do---	----do-----	22-1135	6	Kauai	250	20	---do---	E	No	22.0	159.5
06	18	83	--do---	----do-----	22-1136	6	Oahu	250	20	---do---	E	No	21.5	158.0
06	18	83	--do---	----do-----	22-1137	6	Molak,Lanai,Kahool	250	15	---do---	E	Yes	21.0	157.0
06	18	83	--do---	----do-----	22-1138	6	--do---------	250	25	---do---	E	Yes	21.0	157.0
06	18	83	--do---	----do-----	22-1139	6	Maui, Lanai	250	30	---do---	E	Yes	21.0	156.5
06	18	83	--do---	----do-----	22-1141	6	Hawaii	250	30	---do---	SE	Yes	20.0	155.5
06	18	83	--do---	----do-----	22-1142	6	--do---------	250	30	---do---	SE	Yes	19.5	155.5
06	18	83	--do---	----do-----	22-1144	6	Hawaii, Maui	250	506	---do---	NE	Yes	19.5	156.0
06	19	83	--do---	----do-----	03-0084	22	Niihau	250	10	Vertical	--	No	22.0	160.0
06	19	83	--do---	----do-----	03-0085	22	Kauai	250	20	---do---	--	No	22.0	160.0
06	19	83	--do---	----do-----	03-0886	22	Pearl Harbor	250	25	---do---	--	No	21.5	158.0
06	19	83	--do---	----do-----	03-0087	22	Molokai, Lanai	250	15	---do---	--	Yes	21.0	157.0
06	19	83	--do---	----do-----	03-0088	22	Maui, Kahoolawe	250	15	---do---	--	Yes	21.0	157.0
06	19	83	--do---	----do-----	03-0089	22	--do---------	250	15	---do---	--	Yes	21.0	156.5
06	19	83	--do---	----do-----	03-0090	22	Mauna Loa Volcano	250	15	---do---	--	Yes	19.5	155.5
06	19	83	--do---	----do-----	03-0091	22	--do---------	250	15	---do---	--	Yes	19.5	155.5
06	19	83	--do---	----do-----	03-0092	22	--do---------	250	15	---do---	--	Yes	19.5	155.5
06	19	83	--do---	----do-----	03-0093	22	--do---------	250	15	---do--	--	Yes	19.5	155.5
06	19	83	--do---	----do-----	03-0094	22	--do---------	250	15	---do---	--	Yes	19.5	155.5
06	19	83	--do---	----do-----	19-0874	22	Kauai	100	10	---do---	--	No	22.0	160.0
06	19	83	--do---	----do-----	19-0875	22	Molokai & adjacent	100	10	Oblique	N	No	21.0	157.5
06	19	83	--do---	----do-----	19-0876	22	Maui & adjacent	100	15	Vertical	--	Yes	20.5	156.5
06	19	83	--do---	----do-----	19-0877	22	--do---------	100	15	---do---	--	Yes	20.5	156.0
06	19	83	--do---	----do-----	19-0878	22	Hawaii	100	15	---do---	--	Yes	20.0	155.5
06	19	83	--do---	----do-----	19-0879	22	--do---------	100	15	---do---	--	Yes	19.5	155.5
06	19	83	--do---	----do-----	19-0880	22	--do---------	100	15	---do---	--	Yes	19.5	155.5
06	20	83	--do---	----do-----	03-0114	37	Mauna Kea Volcano	250	30	Oblique	SW	No	19.5	155.5
06	20	83	--do---	----do-----	03-0115	37	--do---------	250	30	---do---	SW	No	19.5	155.5
11	28	83	--do---	STS-9, 41-A	31-1015	4	Mauna Loa Volcano	250	05	Vertical	--	No	19.5	155.5
11	28	83	--do---	----do-----	31-1016	4	--do---------	250	10	---do---	--	Yes	19.0	155.5
11	28	83	--do---	----do-----	31-1017	4	--do---------	250	20	---do---	--	Yes	19.5	155.5
11	28	83	--do---	----do-----	31-1018	4	M. Kea, Hilo Bay	250	20	Oblique	S	Yes	20.0	155.5
11	28	83	--do---	----do-----	31-1019	4	Hawaii coast	250	10	Vertical	--	Yes	20.0	155.5
11	28	83	--do---	----do-----	31-1020	4	Mauna Loa Volcano	250	10	Oblique	SW	Yes	19.5	155.5
11	28	83	--do---	----do-----	31-1021	4	--do---------	250	10	---do---	SW	Yes	19.5	155.5
11	28	83	--do---	----do-----	31-1022	4	Hawaii	250	10	---do---	SW	Yes	19.5	155.5
11	28	83	--do---	----do-----	31-1023	4	--do---------	250	10	---do---	SW	No	20.0	155.5
11	28	83	--do---	----do-----	31-1024	4	--do---------	250	10	---do---	SW	No	20.0	155.5
11	28	83	--do---	----do-----	32-1118	4	--do---------	100	20	---do---	SW	No	19.5	155.5
11	28	83	--do---	----do-----	32-1119	4	--do---------	100	20	---do---	SW	No	19.5	155.5
11	28	83	--do---	----do-----	32-1120	4	--do---------	100	20	---do---	SW	No	19.5	155.5
11	29	83	--do---	----do-----	35-1596	20	Hawaii, Maui	100	15	---do---	SE	Yes	20.0	156.0
11	29	83	Shuttle	STS-9, 41-A	35-1597	20	Haw,Maui,Molok,Lan	100	20	Oblique	E	Yes	21.0	156.5
11	29	83	--do---	----do-----	35-1598	20	Lanai,Molok,Maui	100	20	---do---	E	Yes	21.0	157.0
11	29	83	--do---	----do-----	35-1599	20	Molok,Oahu,Kahool	100	20	---do---	W	Yes	21.5	158.0
11	29	83	--do---	----do-----	35-1600	20	Kauai, Niihau	100	20	---do---	W	No	22.0	159.5
11	29	83	--do---	----do-----	46-1836	20	Haw,Maui,Lan,Molok	250	30	---do---	NE	No	21.0	156.5
11	29	83	--do---	----do-----	46-1837	20	Hawaii	250	20	---do---	NE	No	19.5	156.0
11	29	83	--do--	----do-----	46-1838	20	Molokai,Lanai,Maui	250	40	---do---	NE	No	21.0	157.0
11	29	83	--do---	----do-----	46-1840	20	SE Haw, Kil. plume	250	20	---do---	NE	Right	19.0	155.5
11	29	83	--do---	----do-----	46-1841	20	Hawaii, Kil. plume	250	20	---do---	NE	Ctr	19.5	155.5
11	29	83	--do---	----do-----	46-1842	20	NW Haw, Kohala	250	20	---do---	NE	Left	20.0	155.5
11	29	83	--do---	----do-----	46-1843	20	Maui, Kahoolawe	250	30	---do---	NE	No	20.5	156.5
11	29	83	--do---	----do-----	46-1844	20	Maui, Lanai	250	30	---do---	NE	No	21.0	156.5
11	29	83	--do---	----do-----	46-1845	20	Lanai, Maui, Molok	250	30	Vertical	--	No	21.0	156.5
11	29	83	--do---	----do-----	46-1846	20	Molokai, Lanai	250	30	---do---	--	No	21.0	157.0
11	29	83	--do---	----do-----	46-1848	20	Kauai	250	40	---do---	--	No	22.0	159.5
02	04	84	--do---	STS-11, 41-B	41-2351	22	Honolulu, Oahu	250	10	Oblique	--	Yes	21.5	158.0
02	04	84	--do---	----do-----	41-2352	22	--do---------	250	10	---do---	--	Yes	21.5	158.0
02	04	84	--do---	----do-----	41-2353	22	Molokai,Lanai,Maui	250	0	---do---	--	Yes	21.0	157.0
02	04	84	--do---	----do-----	41-2354	22	Mol,Lan,Kahoo,Maui	250	10	---do---	--	Yes	21.0	157.0
02	04	84	--do---	----do-----	41-2355	22	Maui, Kahoolawe	250	10	---do---	--	Yes	21.0	156.5

TABLE 8.2.— *Selected Landsat scenes of the Island of Hawaii*— Continued

Mo	Da	Yr	Space-craft	Mission identificat.	Scene identi-fication [1]	Orbit	Feature	Focal length	Percent clouds [2]	Perspec-tive [3]	Direc-tion	Stereo [4]	Center of scene Lat	Long [5]
02	04	84	--do---	----do------	41-2356	22	Hawaii	250	30	---do---	--	Yes	19.5	155.5
02	06	84	--do---	----do------	33-1458	53	Kauai	100	30	Vertical	--	No	22.0	156.5
02	06	84	--do---	----do------	33-1459	53	Maui,Kahool,Lanai	100	30	---do---	--	No	21.0	156.5
02	06	84	--do---	----do------	33-1460	53	Hawaii	100	30	---do---	--	Yes	19.5	155.5
02	06	84	--do---	----do------	33-1461	53	--do----------	100	30	---do---	--	Yes	20.0	155.5
02	06	84	--do---	----do------	34-1554	53	Niihau	250	30	---do---	--	Yes	22.0	160.0
02	06	84	--do---	----do------	34-1555	53	Kauai	250	30	---do---	--	Yes	22.0	159.5
02	06	84	--do---	----do------	34-1556	53	Oahu	250	30	---do---	--	Yes	21.5	158.0
02	06	84	--do---	----do------	34-1557	53	--do----------	250	20	---do---	--	Yes	21.5	158.0
02	06	84	--do---	----do------	34-1558	53	--do----------	250	20	---do---	--	Yes	21.5	158.0
02	06	84	--do---	----do------	34-1561	53	Maui	250	30	---do---	--	Yes	21.0	156.5
02	06	84	--do---	----do------	34-1562	53	--do----------	250	20	---do---	--	Yes	21.0	156.5
02	06	84	--do---	----do------	34-1563	53	Hawaii	250	5	---do---	--	Yes	19.5	155.5
02	06	84	--do---	----do------	34-1564	53	--do----------	250	30	---do---	--	Yes	20.0	155.5
02	06	84	--do---	----do------	34-1565	53	--do----------	250	30	---do---	--	Yes	20.0	155.5
02	06	84	--do---	----do------	34-1566	53	--do----------	250	1	---do---	--	Yes	19.5	155.5
02	06	84	--do---	----do------	34-1567	53	--do----------	250	5	---do---	--	Yes	19.0	155.5
02	06	84	--do---	----do------	34-1568	53	--do----------	250	5	---do---	--	Yes	19.5	155.5
02	06	84	--do---	----do------	34-1569	53	--do----------	250	15	---do---	--	Yes	19.5	155.5
02	08	84	--do---	----do------	43-2625	84	Kauai	250	30	Oblique	--	No	22.0	159.5
02	08	84	--do---	----do------	43-2626	84	Oahu	250	20	---do---	--	No	21.5	158.5
02	08	84	--do---	----do------	43-2627	84	Molokai, Lanai	250	30	---do---	--	No	21.0	157.0
02	08	84	--do---	----do------	43-2629	84	Hawaii	250	30	---do---	--	Yes	19.5	155.5
02	08	84	--do---	----do------	43-2630	84	--do----------	250	30	---do---	--	Yes	19.5	155.5
02	09	84	--do---	----do------	45-2794	100	Hawaii Isl. chain	100	30	---do---	NW	No	19.5	155.5
02	09	84	--do---	----do------	45-2795	100	Hawaii	100	30	---do---	--	No	19.5	155.5
02	09	84	--do---	----do------	45-2796	100	--do----------	100	30	---do---	--	No	19.5	155.5
02	09	84	--do---	----do------	46-2923	100	--do----------	250	60	---do---	N	Yes	19.5	155.5
02	09	84	--do---	----do------	46-2924	100	--do----------	250	60	---do---	N	Yes	19.5	155.5
02	09	84	--do---	----do------	46-2925	100	--do----------	250	60	---do---	N	Yes	19.5	155.5
04	06	84	--do---	STS-13, 41-C	31-0968	6	Niihau	250	25	Vertical	--	No	22.0	160.0
04	06	84	--do---	----do------	31-0969	6	Kauai	250	25	---do---	--	No	22.0	159.5
04	06	84	--do---	----do------	31-0974	6	Mauna Loa plumes	250	80	Oblique	SW	Yes	19.5	155.5
04	06	84	--do---	----do------	31-0975	6	--do----------	250	80	---do---	SW	Yes	19.5	155.5
04	06	84	--do---	----do------	32-1087	6	--do----------	50	40	Vertical	--	No	22.0	160.0
04	06	84	--do---	----do------	51-2264	6	Kauai, Niihau	250	30	---do---	--	No	22.0	160.0
04	06	84	--do---	----do------	51-2265	6	Oahu	250	25	---do---	--	No	22.0	158.0
04	07	84	Shuttle	STS-13, 41-C	35-1538	21	Mauna Loa plumes	250	25	Oblique	SE	Yes	19.5	155.5
04	07	84	--do---	----do------	35-1539	21	--do----------	250	25	---do---	SE	Yes	19.5	155.5
04	07	84	--do---	----do------	35-1540	21	Mauna Loa plumes	250	25	Oblique	S?	Yes	19.5	155.5
04	07	84	--do---	----do------	36-1633	21	M. Loa plume, Maui	50	40	Vertical	--	No	22.0	160.0
04	07	84	--do---	----do------	36-1686	37	Mauna Loa plumes	50	60	Oblique	SW	No	21.0	155.0
04	08	84	--do---	----do------	34-1411	37	--do----------	250	30	---do---	NE	Yes	19.5	155.5
04	09	84	--do---	----do------	52-2537	51	--do----------	250	50	---do---	SE	No	20.5	157.0
04	09	84	--do---	----do------	52-2538	51	--do----------	250	50	---do---	SE	No	20.0	156.5
04	12	84	--do---	----do------	37-1807	96	--do----------	250	40	---do---	E	No	19.5	155.5
04	12	84	--do---	----do------	37-1808	96	--do----------	250	40	--do----	S	No	19.9	155.5
04	12	84	--do---	----do------	37-1809	96	Oahu	250	25	---do---	SW	No	21.5	158.0
04	12	84	--do---	----do------	37-1810	96	Hawaii	250	35	---do---	SW	No	19.5	155.5
04	12	84	--do---	----do------	52-2726	97	Mauna Loa plumes	250	40	---do---	NE	No	20.0	155.0
04	12	84	--do---	----do------	52-2727	97	--do----------	250	40	---do---	NE	No	19.5	155.0
04	12	84	--do---	----do------	52-2728	97	--do----------	250	40	---do---	NE	No	20.0	155.0
09	02	84	--do---	S84-14, 41-D	34-0075	53	--do----------	250	30	---do---	--	No	20.0	155.5
09	02	84	--do---	----do------	34-0076	53	--do----------	250	30	---do---	--	No	19.5	155.5
09	02	84	--do---	----do------	44-0093	84	Mauna Kea	250	10	Vertical	--	No	20.0	155.5
11	10	84	--do---	51-A	35-0013	38	Mauna Loa	250	15	Oblique	NE	Yes	19.5	155.5
11	10	84	--do---	----do------	35-0014	38	--do----------	250	15	---do---	NE	Yes	19.5	155.5
11	10	84	--do---	----do------	35-0015	38	--do----------	250	20	---do---	NE	Yes	19.5	155.5
11	10	84	--do---	----do------	35-0016	38	Hawaii	250	20	---do---	NW	Yes	19.5	155.5
11	10	84	--do---	----do------	35-0017	38	--do----------	250	20	---do---	NW	Yes	19.0	155.5
11	10	84	--do---	----do------	36-0016	38	Mauna Loa, M. Kea	100	15	---do---	NE	Yes	19.5	156.0
11	10	84	--do---	----do------	36-0017	38	--do----------	100	15	---do---	NE	Yes	19.0	155.5
04	14	85	--do---	51D	S85-23-40-62	35	Kauai, Niihau	250	40	---do---	SE	No	26.0	160.0
04	14	85	--do---	51D	S85-23-40-82	36	Hawaii, west side	250	40	Vertical	--	Yes	17.0	156.0
04	14	85	--do---	51D	S85-23-40-83	36	--do----------	250	40	---do---	--	Yes	17.0	156.0
04	16	85	--do---	51D	S85-23-42-98	66	Niihau, west Kauai	250	20	---do---	--	No		59.0
04	16	85	--do---	51D	S85-23-42-100	66	Hawaii, M. Loa	250	40	---do---	--	No	22.0	155.5
04	18	85	--do---	51D	S85-23-46-43	97	Hawaii to Oahu	250	50	---do---	--	No	16.0	152.0
06	21	85	--do---	51G	51G-47-13	100	Hawaii to Niihau	100	50	Oblique	E	Yes	----	-----
06	21	85	--do---	51G	51G-48-15	100	--do----------	100	50	--do----	E	Yes	----	-----

1 Numbers to left of hyphen indicate magazines; numbers to right of hyphen indicate frames.

2 Photos with ›30 percent cloud cover are not included except where known to have useful information. Percent areas covered by clouds are mainly from NASA documents and generally cover a higher percentage of the land area within a scene. Some estimates have been revised slightly.

3 Some photographs designated as vertical are slightly inclined from true vertical.

4 Stereo "yes" indicates some overlap with adjacent photograph on left or right.

5 Longitude values are west of the Greenwich Meridian. Latitudes are north.

tion, and measuring areas covered by new lava flows (compare figs. 8.10*B* and 8.10*C*).

RADAR IMAGES

Additional studies of part of Kilauea Volcano from space have been conducted using an imaging radar system (SIR-B) that was flown on board the Shuttle in October 1984. Data were acquired across the southeastern part of the Island of Hawaii, extending from South Point, across Kilauea caldera to Hilo Bay (fig. 8.11).

The SIR-B radar operated at a wavelength of 23 cm, complementing information gained at visible and near infrared wavelengths by Landsat and MOMS–1. It was similar to the synthetic aperture radars flown on the Seasat satellite in 1978 described by Elachi (1980), and the Shuttle Imaging Radar (SIR-A) experiment flown on the Space Shuttle in 1981 (Elachi and others, 1982).

However, unlike these earlier orbital radar systems, SIR-B had the capability to vary the angle at which the radar beam encountered the surface, and obtained images of Hawaii at incidence angles of 28 and 48 degrees. Because orbital radars provide their own illuminating energy and are capable of penetrating clouds, they can provide useful images at all times (day or night) as well as in areas of frequently poor weather, such as Kilauea's east rift zone. Because of the choice of spacecraft orbits and the short duration (8 days) of the mission, only two SIR-B radar images (swathwidths of approximately 20 and 30 km on the ground) were obtained during the Shuttle flight. More complete coverage is anticipated on the reflight of the SIR-B experiment (SIR-B′) scheduled for early 1987.

Radar images display, in part, variations in surface roughness at a scale of a few centimeters to a few decimeters with a pixel size of about 15–20 meters, and many of the individual pit craters and lava flows can be recognized within the national park (fig. 8.12). In particular, variations in the surface texture of lava flows is clearly seen in the SIR-B images. Two examples are identified in figure 8.12; the December 1974 lava flow and the multiple flows within Kilauea caldera show diverse radar backscatter properties. The December 1974 flow erupted as pahoehoe close to Kilauea caldera, but at a distance of approximately 5 km from the vent the flow passed through the transition to aa. This transition (at point A in fig. 8.12) is indicated by an increase in radar brightness associated with the greater backscatter from the rough aa surface. In comparison, the near-vent pahoehoe surface produces a dark radar signal because of its smooth, specular surface.

Kilauea caldera provides further insights into the capability of the SIR-B radar system to distinguish between different surface materials. The caldera rim and the edge of Kilauea Iki pit crater are distinctive (B in fig. 8.12) due to the contrast between the crater floor (low radar return) and the surrounding rain forest (high radar return). Less obvious are the September 1982 pahoehoe flow (C) and other pahoehoe flows within the caldera, due to the uniformly low radar returns from those features as viewed at an incidence angle of 48 degrees.

Such a variation in the radar signature of the different flows is attributed to the decimeter-scale roughness of the lava flow surfaces. Similarly, brightness variations around Halemaumau pit crater (D in fig. 8.12) are attributed to variations in the number and size of boulders (decimeters to meters in diameter) scattered across the caldera floor during the 1924 phreatic eruption.

SUMMARY

Images from space of active or young volcanic areas like Hawaii provide graphic information having several advantages over typical aerial and surface photographs. Considering the larger areas covered and the greater applicability of image-enhancement techniques, views from Earth-orbital altitudes have proved to be a relatively economical form of cartographic data having significant value for the earth sciences. Furthermore, the choice of spaceborne sensor (photography, digital multispectral images, or synthetic aperture radar) permits different physical and compositional attributes of the Earth's surface to be studied. Thus with future Space Shuttle flights and the orbiting of new and currently planned automated satellites (having names like TOPEX, ERS–1, SPOT–1, and Radarsat), the volcanoes of Hawaii will come under more detailed scrutiny from space in the next few years.

REFERENCES CITED

Anonymous, 1984a, Landsat vertical image yields a stereo oblique: Geotimes, v. 29, no. 4, p. 10–11.

———1984b, Image yields stereo oblique: Earth science, v. 37, no. 4, p.18–19.

Carr, M.H., and Greeley, Ronald, 1980, Volcanic features of Hawaii—a basis for comparison with Mars: National Aeronautics and Space Administration Special Paper, NASA SP–403, 211 p.

Dalrymple, G.B., Silver, E.A., and Jackson, E.D., 1973, Origin of the Hawaiian Islands: American Scientist, v. 61, p. 294–308.

Elachi, Charles, 1980, Spaceborne imaging radar: geologic and oceanographic applications: Science, v. 209, no. 4461, p. 1073–1082.

Elachi, Charles, Brown, W.E., Cimino, J.B., Dixon, T., Evans, D.L., Ford, J.P., Saunders, R.S., Breed, C., Masursky, H., McCauley, J.F., Schaber, G., Delwig, L., England, A., MacDonald, H., Martin-Kaye, P., and Sabins, F., 1982, Shuttle imaging radar experiment: Science, v. 218, p. 996–1003.

Eliason, E.M., Chavez, P.S., and Soderblom, L.A., 1974, Simulated "true color" images from ERTS data: Geology, v.2, no. 5, p. 231–234.

Greeley, Ronald, 1974, Aerial reconnaissance of the geology over the Island of Hawaii, *in* Greeley, Ronald, ed., Geologic Guide to the Island of Hawaii: National Aeronautics and Space Administration CR15 2416, p. 113–183.

Mohler, R.R.J., 1983, Catalog of Space Shuttle Earth observation hand-held photography: Space Transportation System 6 Mission: National Technical Information Service Report JSC–18897, 28 p.

Nowakowski, B.S., 1984a, Catalog of Space Shuttle Earth observation hand-held photography: Space Transportation System 7 Mission: National Technical Information Service Report JSC–18913, 31 p.

———1984b, Catalog of Space Shuttle Earth observations hand-held photography: Space Transportation System 9 Mission: National Technical Information Service Report JSC–20175, 51 p.

Nowakowski, B.S., and Palmer, W.F., 1984, Catalog of Space Shuttle Earth observations hand-held photography: Space Transportation System 41–C Mission: National Technical Information Service Report JSC–20056, 46 p.

Palmer, W.F., 1984, Catalog of Space Shuttle Earth observations hand-held photography: Space Transportation System 41–B Mission: National Technical Information Service Report JSC–20690, 44 p.

Short, N.M., Lowman, P.D., Freden, S.C., and Finch, W.A., 1976, Mission to Earth: Landsat views the world: National Aeronautics and Space Administration Special Publication SP–360, 459 p.

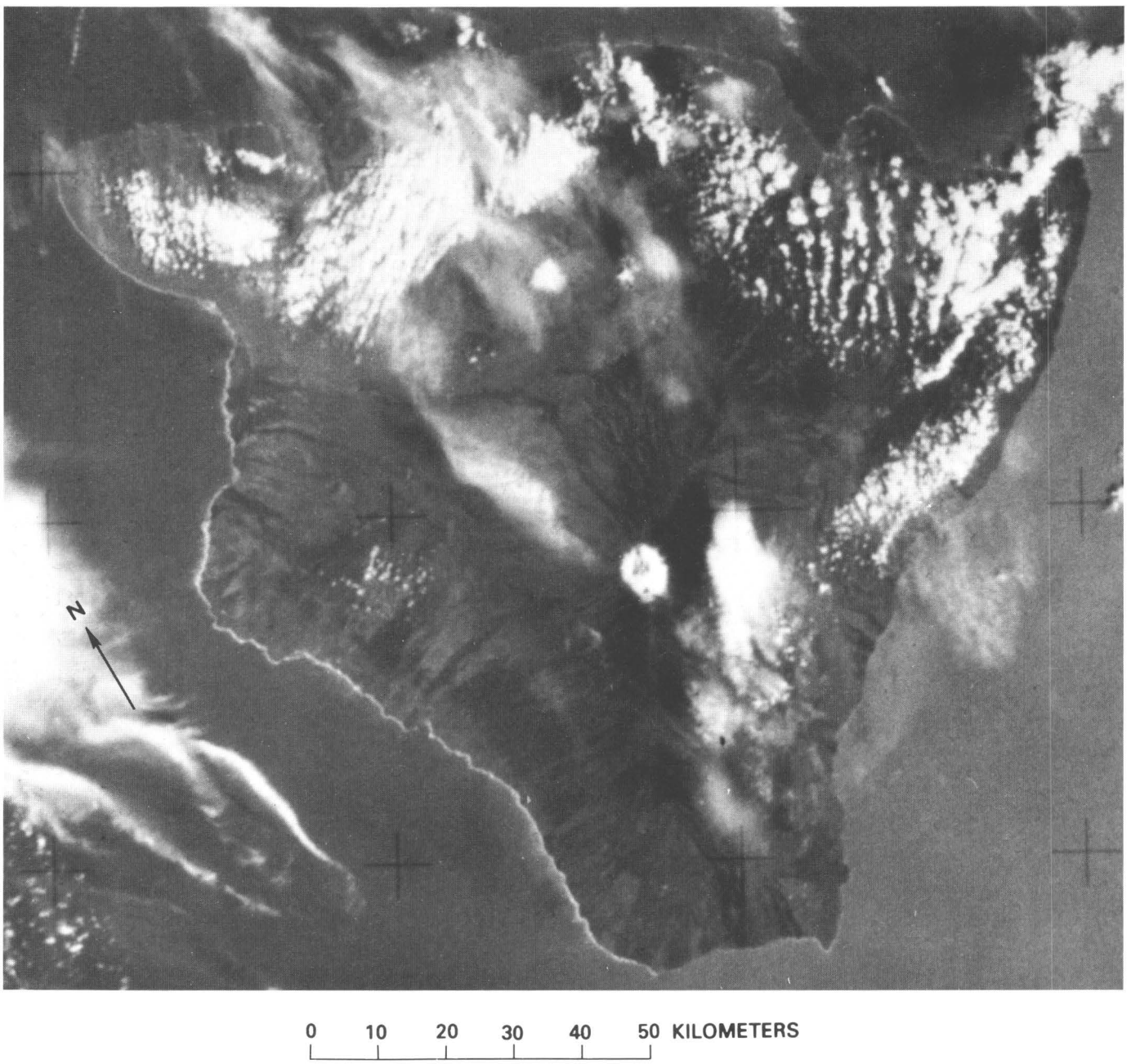

FIGURE 8.1.—View of Island of Hawaii taken on December 7, 1973, during Skylab 4 mission from altitude of about 435 km (270 mi). Snow-capped summits of Mauna Loa (4,170 m; 13,677 ft; center) and Mauna Kea (4,205 m; 13,796 ft; northeast) are 40 km (25 mi) apart. Reseau crosses provide calibration for photogrammetric applications. (NASA photograph SL4–139-3997; lens focal length, 100 mm).

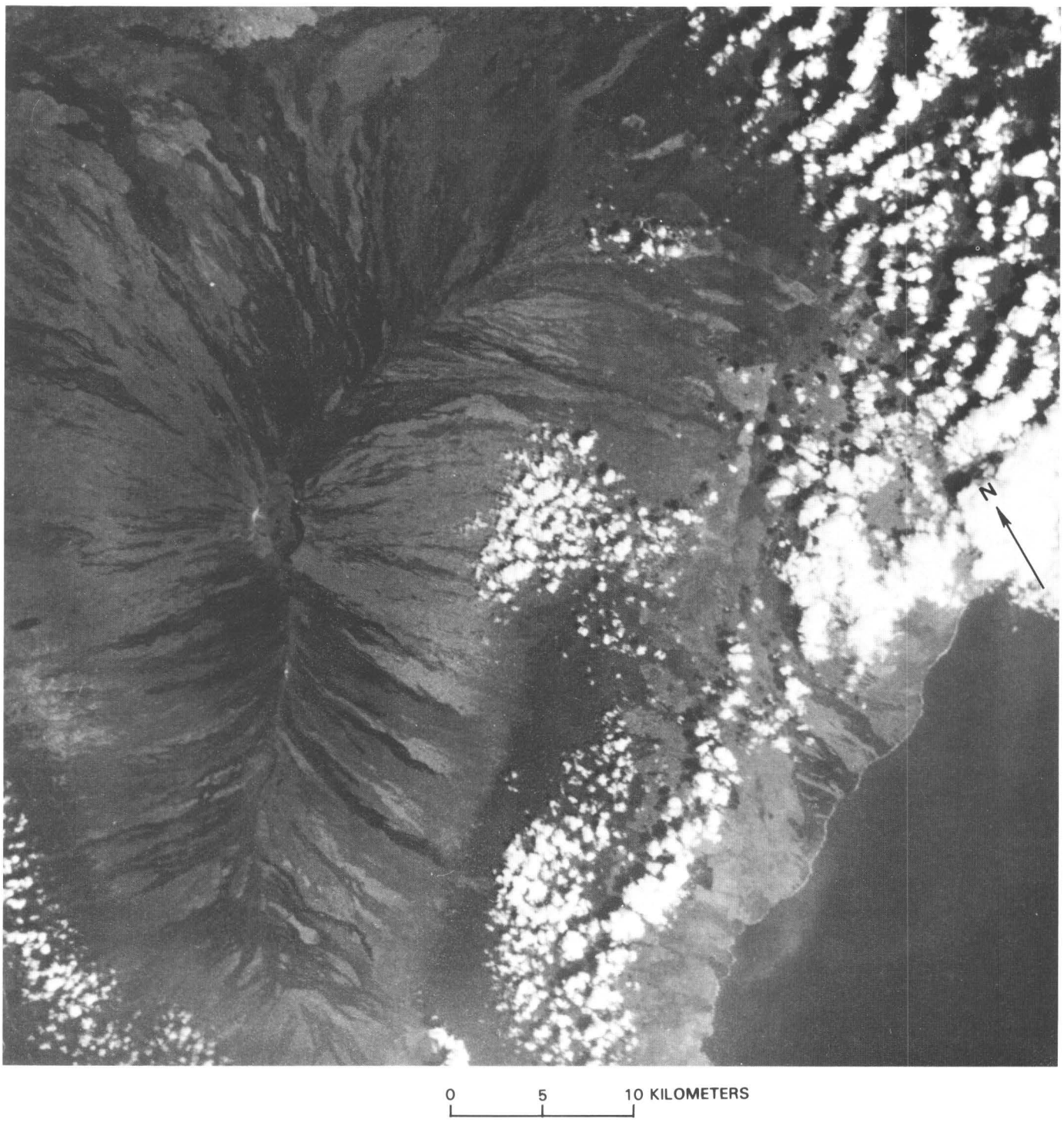

FIGURE 8.2.—Near-vertical view from Space Shuttle of Mauna Loa Volcano showing Mokuaweoweo caldera and young lava flows from northeast and southwest rift zones. (NASA photograph 41A–31-1017; lens focal length, 250 mm; November 1983).

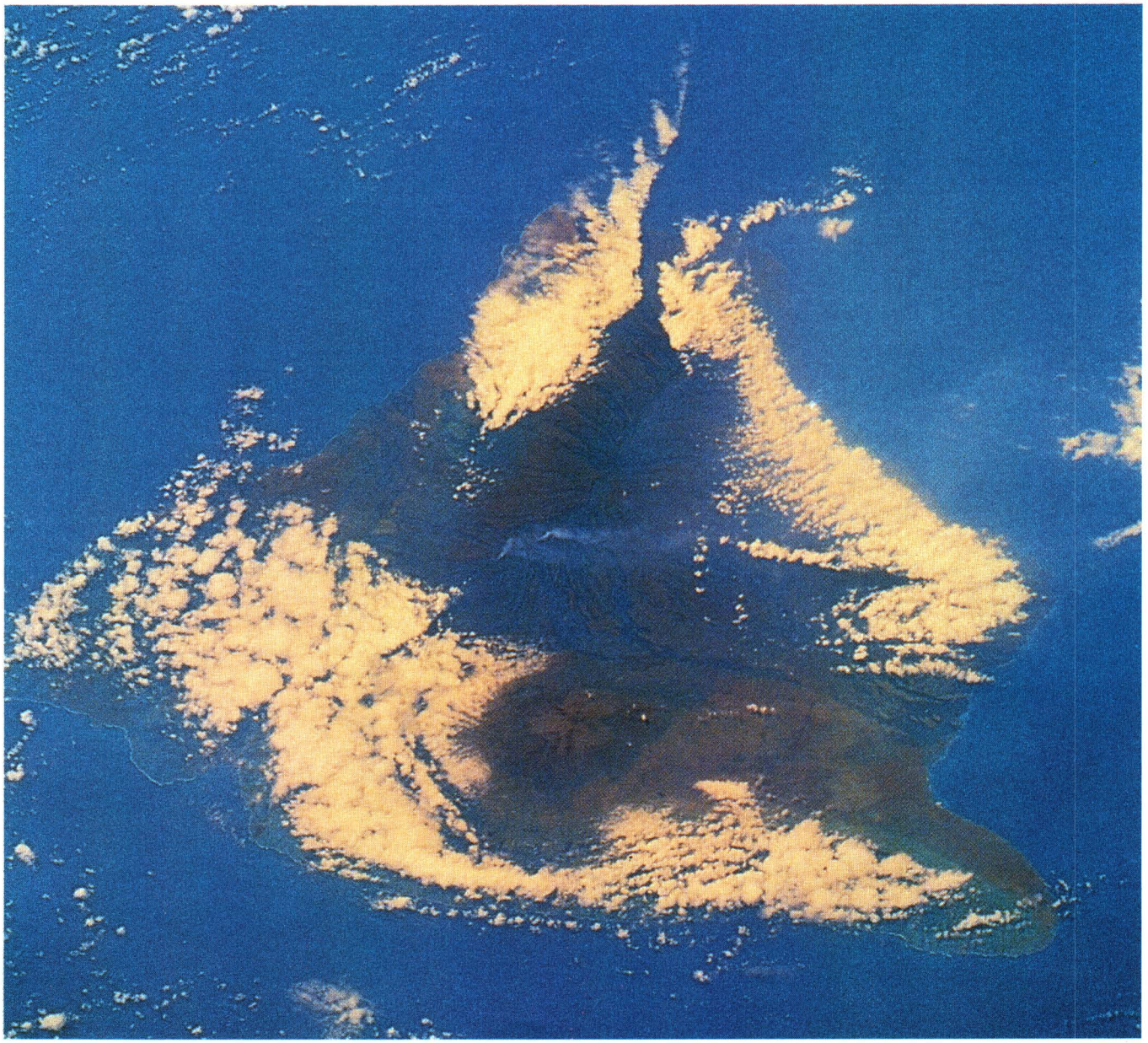

FIGURE 8.3.—Oblique view from Space Shuttle of Island of Hawaii showing eruption plumes from Mauna Loa on April 7, 1984, twelve days after start of eruption. Higher plume (on right) is from degassing vent. Lower plume is from lava-producing vent (J.P. Lockwood, oral commun., 1985). Upper parts of new lava flows are visible as they move toward Hilo Bay (large reentrant on lower left). Active flow front is below clouds, lower on northeast rift. Often-present cloud bank obscures northeast rift zone of Mauna Loa and most of Kilauea Volcano to left. Mauna Kea Volcano is in central near-field. View southwest. (NASA photograph 41C–43-1539).

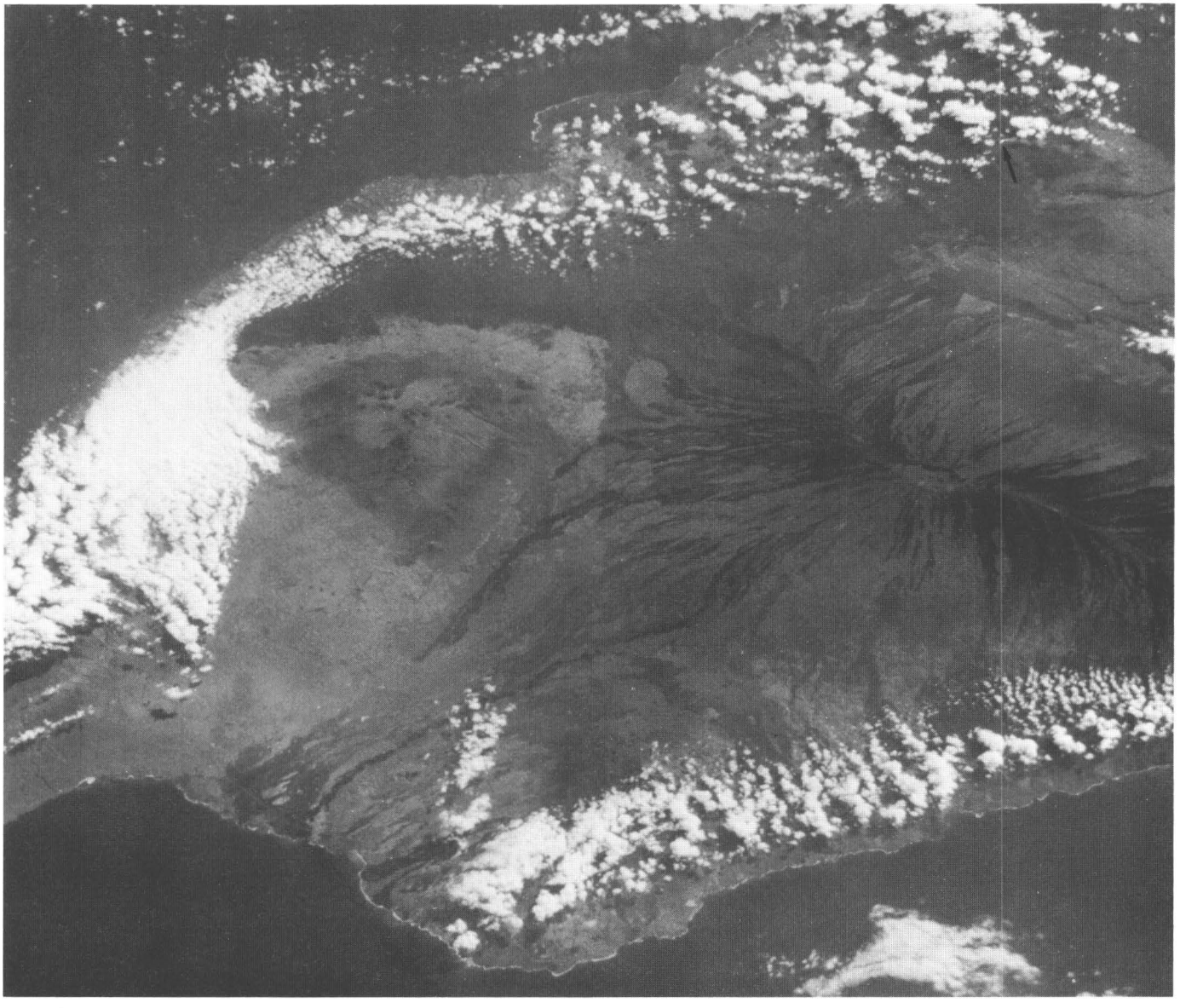

FIGURE 8.4.—Oblique view from Space Shuttle of Island of Hawaii, including Mauna Loa Volcano (right center), Kilauea Volcano and plume from phase 12 eruption of Puu Oo on the east rift zone (top right, arrow), Mauna Kea Volcano (left of center) with numerous cinder cones, Kohala Volcano (left edge), and Hualalai Volcano (bottom center, partly obscured by clouds), also with cinder cones. Note many young (dark) lava flows from Mauna Loa and Hualalai that have reached North Kona and South Kohala coasts. View east. (NASA photograph 41A–46-1841, November 30, 1983).

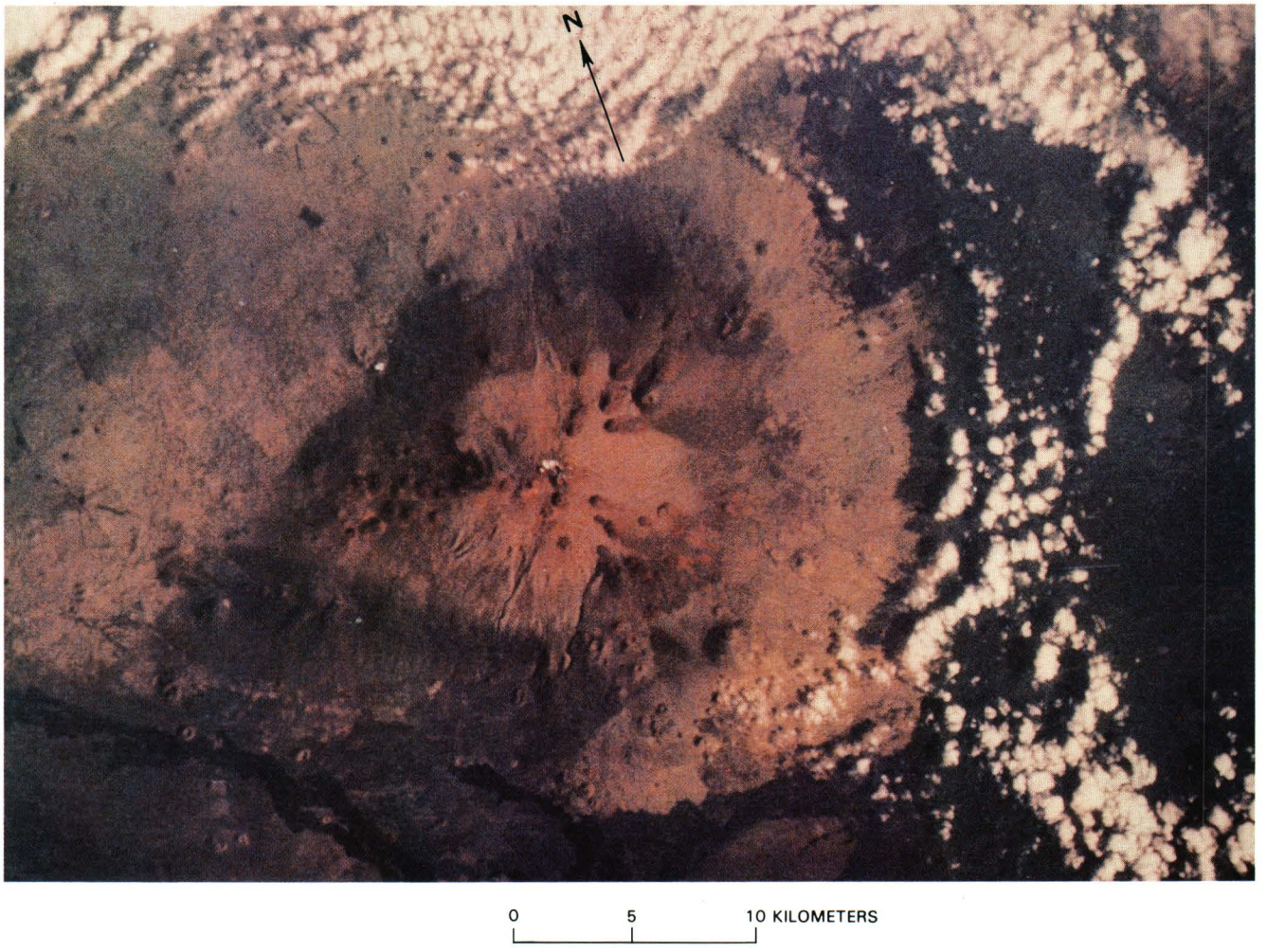

FIGURE 8.5.—View from Space Shuttle of Mauna Kea, showing distribution of alkalic cinder cones capping older tholeiitic shield. Young (dark) lava flows at bottom of photograph are from Mauna Loa. (NASA photograph 41B–34-1565, February 1984).

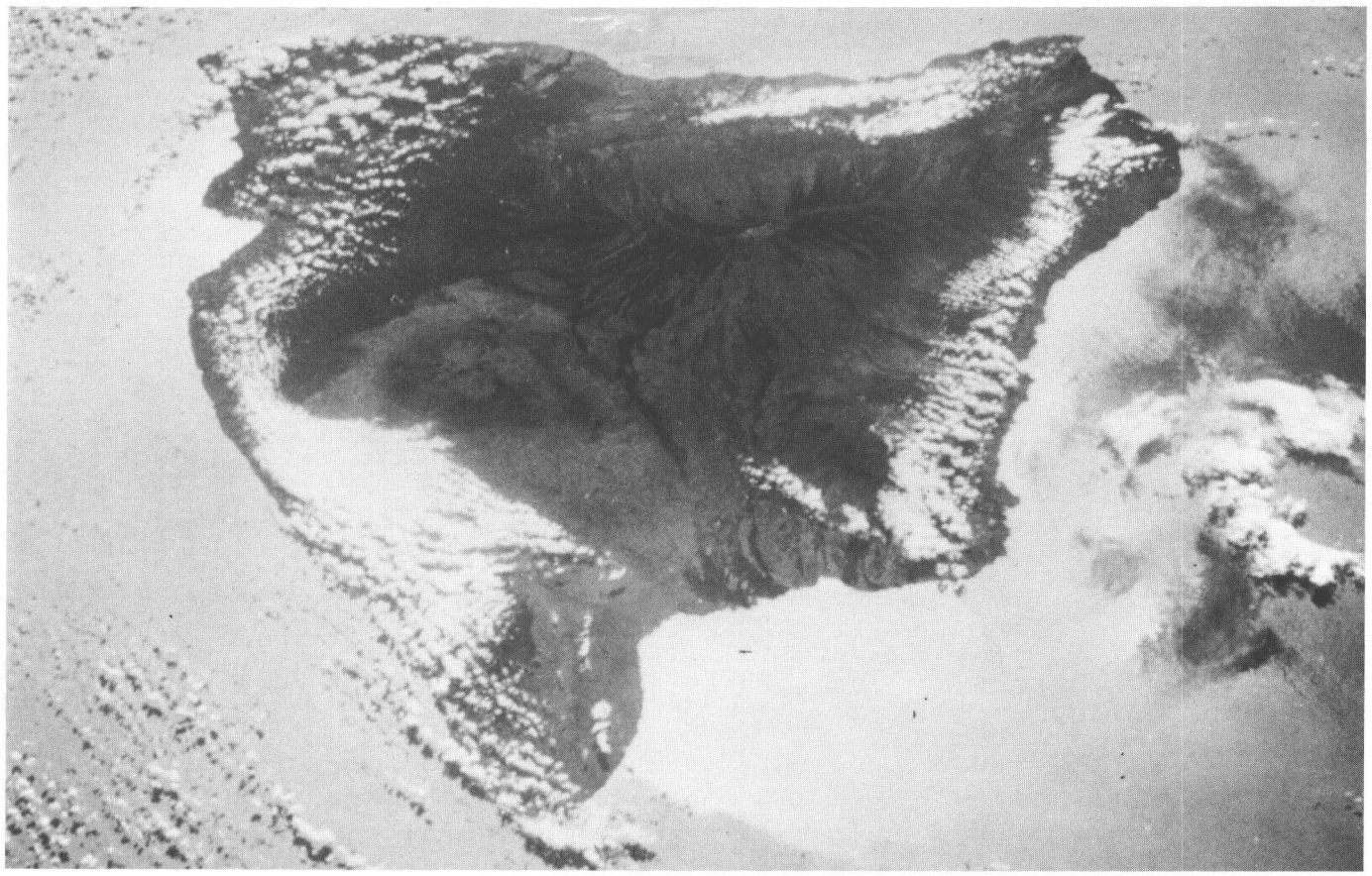

FIGURE 8.6.—Oblique view of Hawaii taken from Space Shuttle on December 3, 1983, at altitude of 240 km (150 mi). Cloud concentration is caused by northeasterly tradewinds against shield volcanoes, in contrast to clear sky and calm seas on leeward (Kona) side of island. Difference in ocean-surface texture is enhanced by sun illumination with respect to spacecraft. View southeast. (NASA photograph 41A–35-1596).

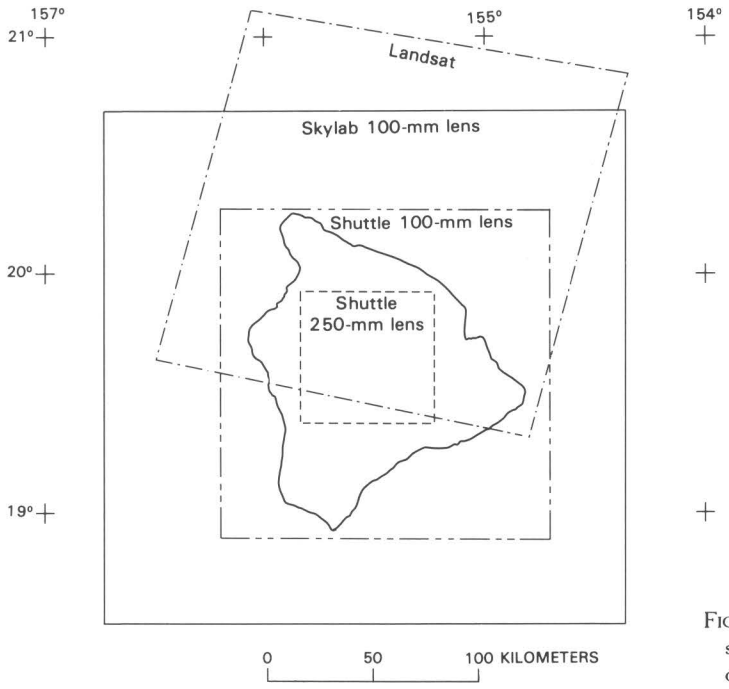

FIGURE 8.7.—Areas covered by typical Landsat, Skylab, and Space Shuttle scenes. The Skylab and Shuttle footprints are for a Hasselblad camera at altitudes of 435 km (270 mi) and 300 km (185 mi) respectively.

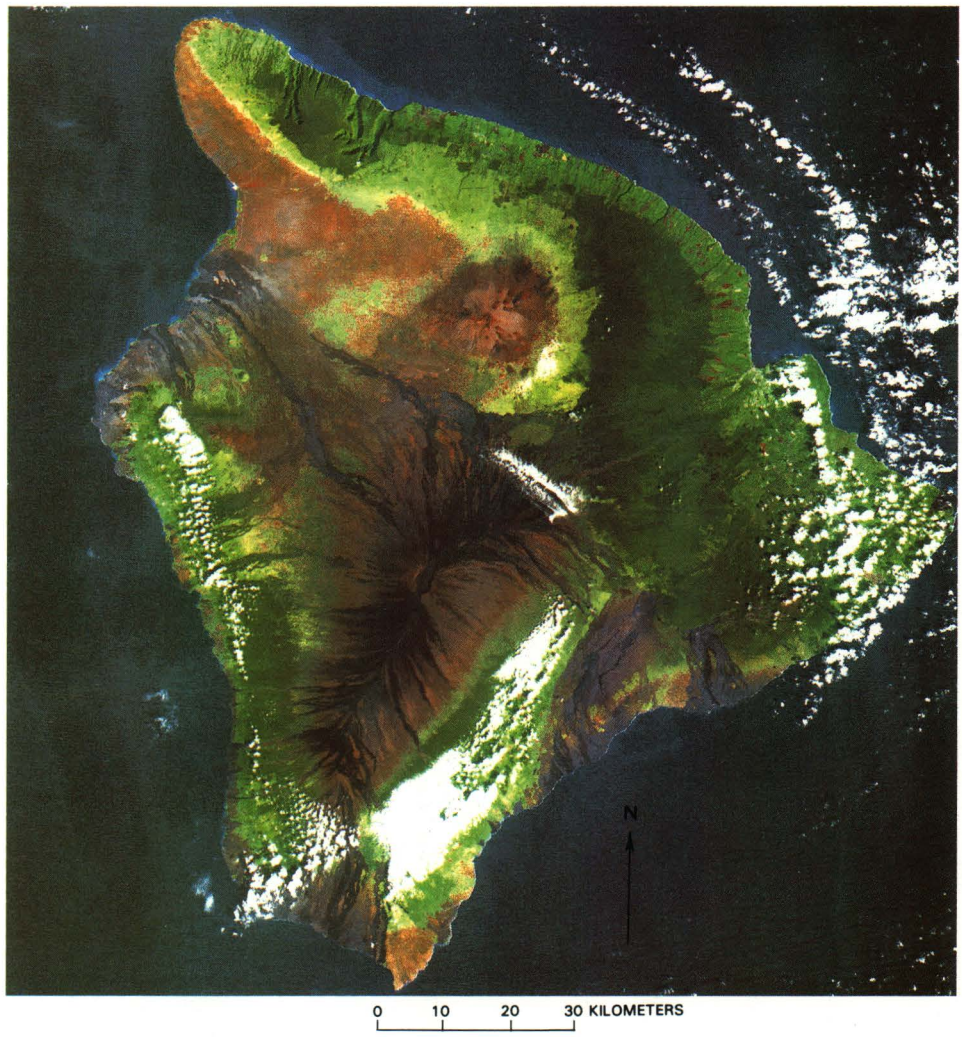

FIGURE 8.8.—Composite Landsat image of Island of Hawaii recorded on January 7, 1978, at altitude of about 915 km (570 mi). Image was geometrically corrected and processed to simulate true color by U.S. Geological Survey's Image Processing Facility at Flagstaff, Ariz. (Scene identification numbers 821081193-54X0 and -60X0).

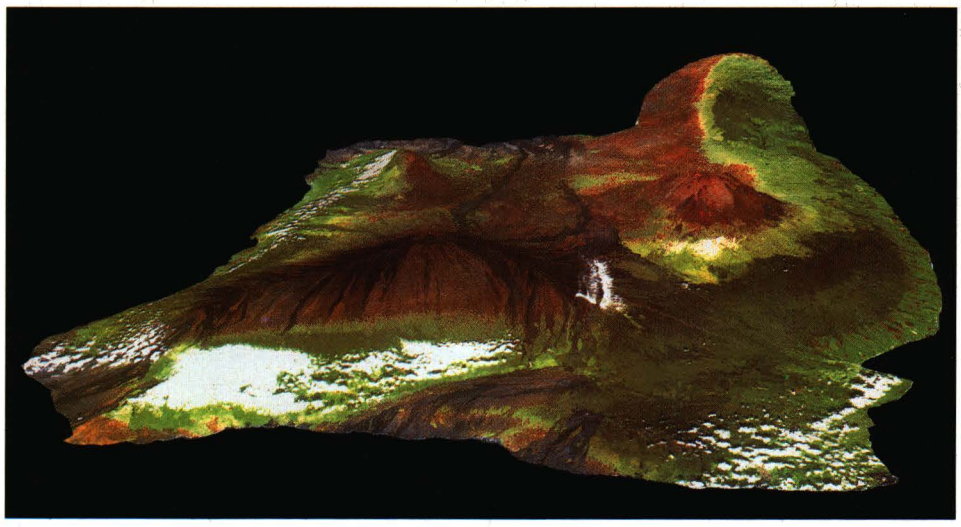

FIGURE 8.9.—Landsat image (same as fig. 8.8) digitally converted to oblique view looking northwest to illustrate Mauna Loa and Kilauea basaltic shields. Prepared by U.S. Geological Survey Image Processing Facility at Flagstaff, Ariz.

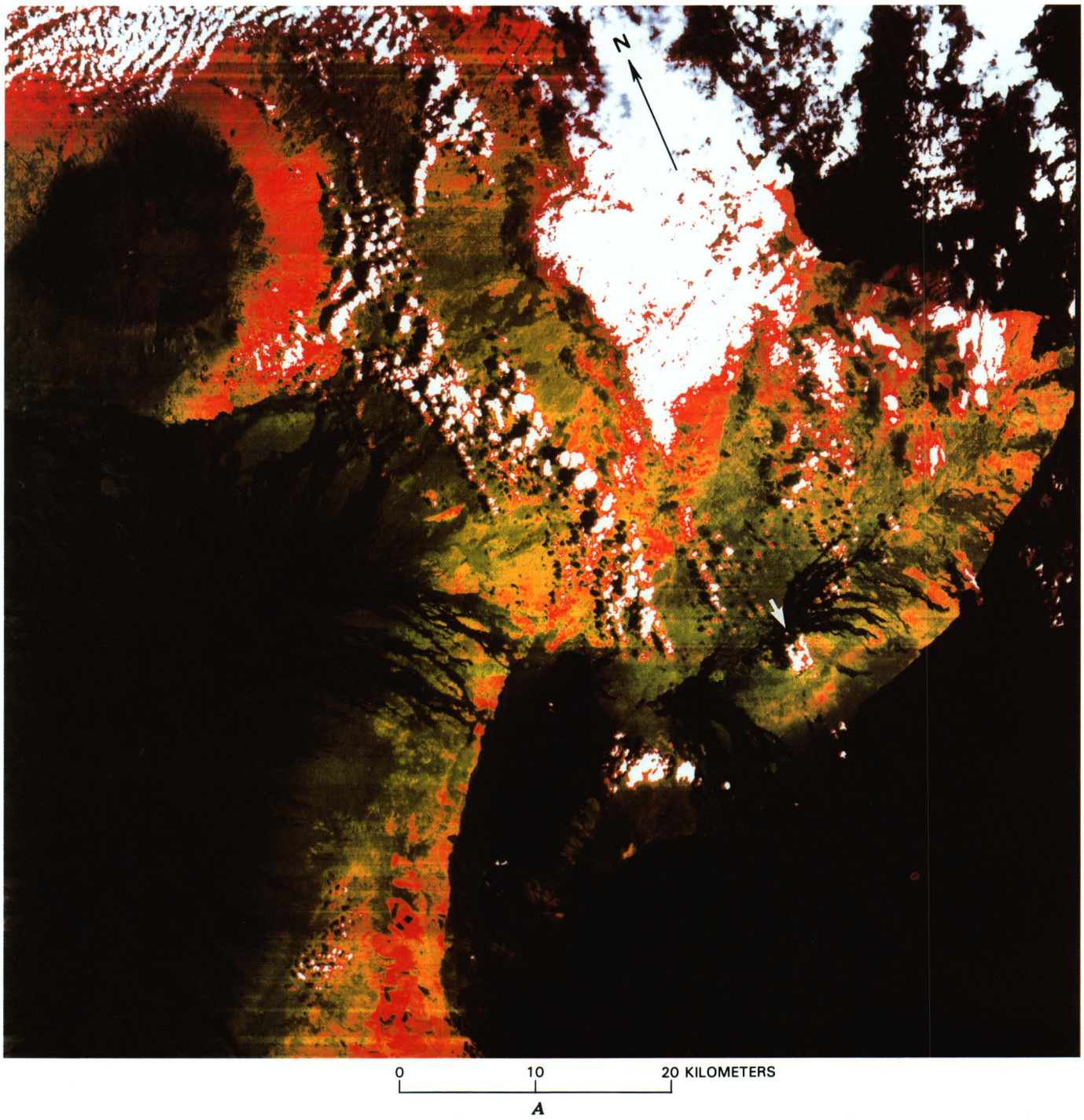

FIGURE 8.10.—Scene of eastern Hawaii from German MOMS–1 experiment on February 6, 1984, at 0930 H.s.t. from Space Shuttle. Lava flows are from Puu Oo vent (arrow in *A*). Color representation for two channels of MOMS–1 instrument is based on image-enhancement technique using HSI display mode (hue, saturation, and intensity shown in blue, green, and red channels of display system). Ratio between two channels (at 0.60 and 0.90 microns), combined with the HSI display mode, enhances weak variations in image contrast. White features are clouds. ***A***, Northeast quarter of original scene. ***B***, Enlarged subscene (750 by 750 pixels) of Puu Oo eruption area. ***C***, Eruption area (E.W. Wolfe, written commun.) showing new flows through episode 14 in January 1984, that can be directly compared with *B*.

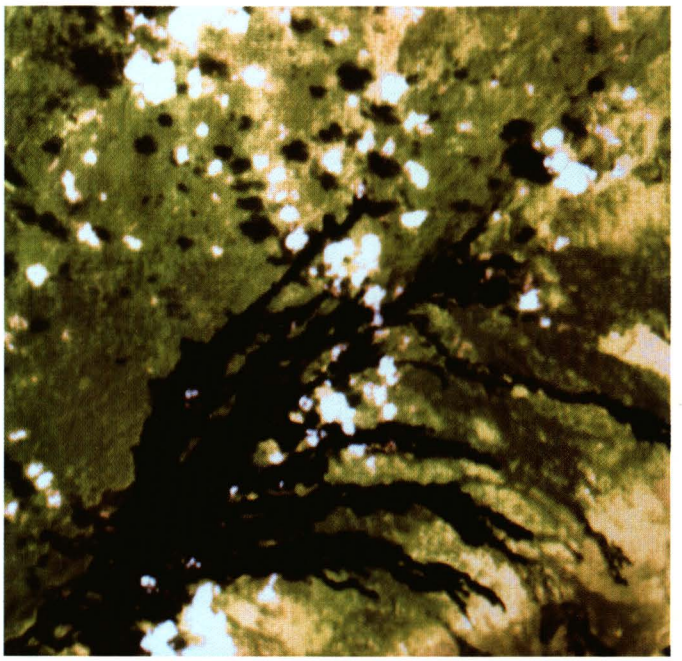

B

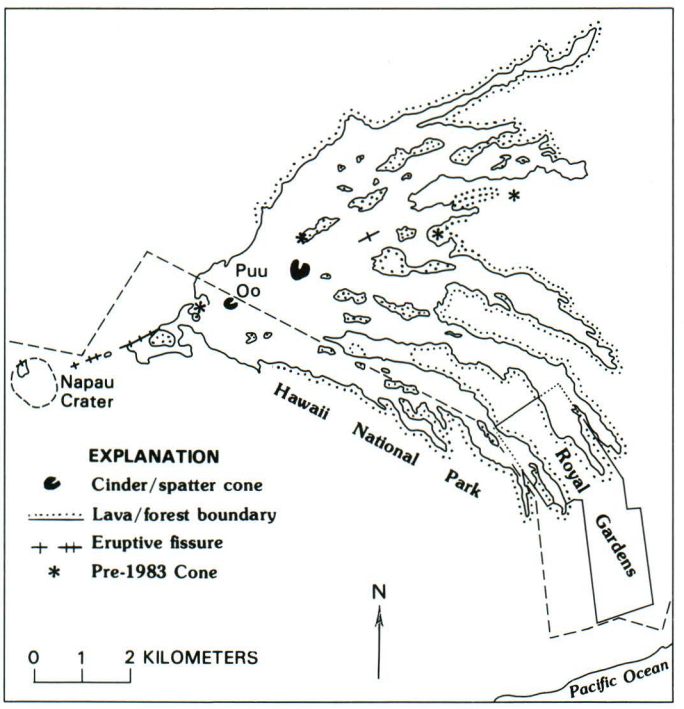

C

FIGURE 8.10.—Continued.

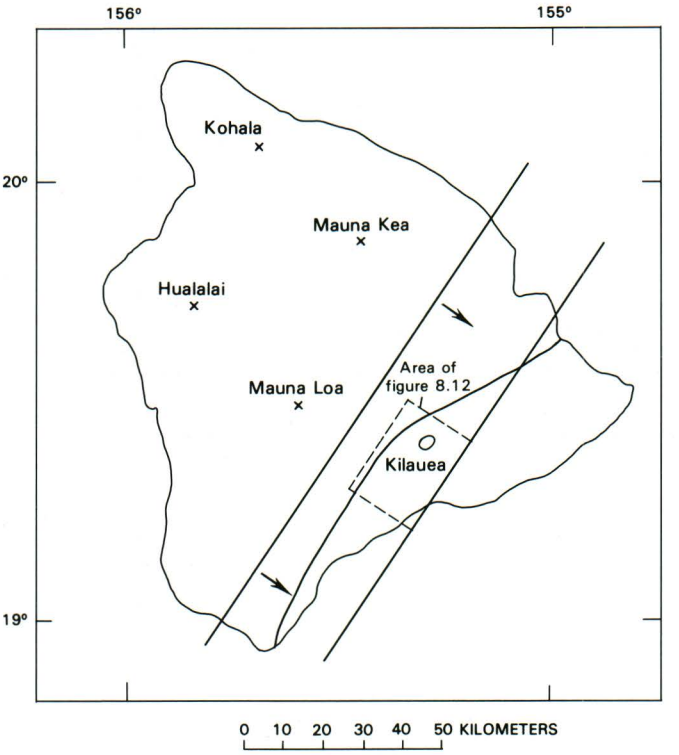

FIGURE 8.11.—Location of SIR-B radar images (area between parallel lines) that were acquired over southeast Hawaii in October 1984. Radar look-direction (arrowed) was toward southeast, and Shuttle flew from southwest to northeast on both data takes.

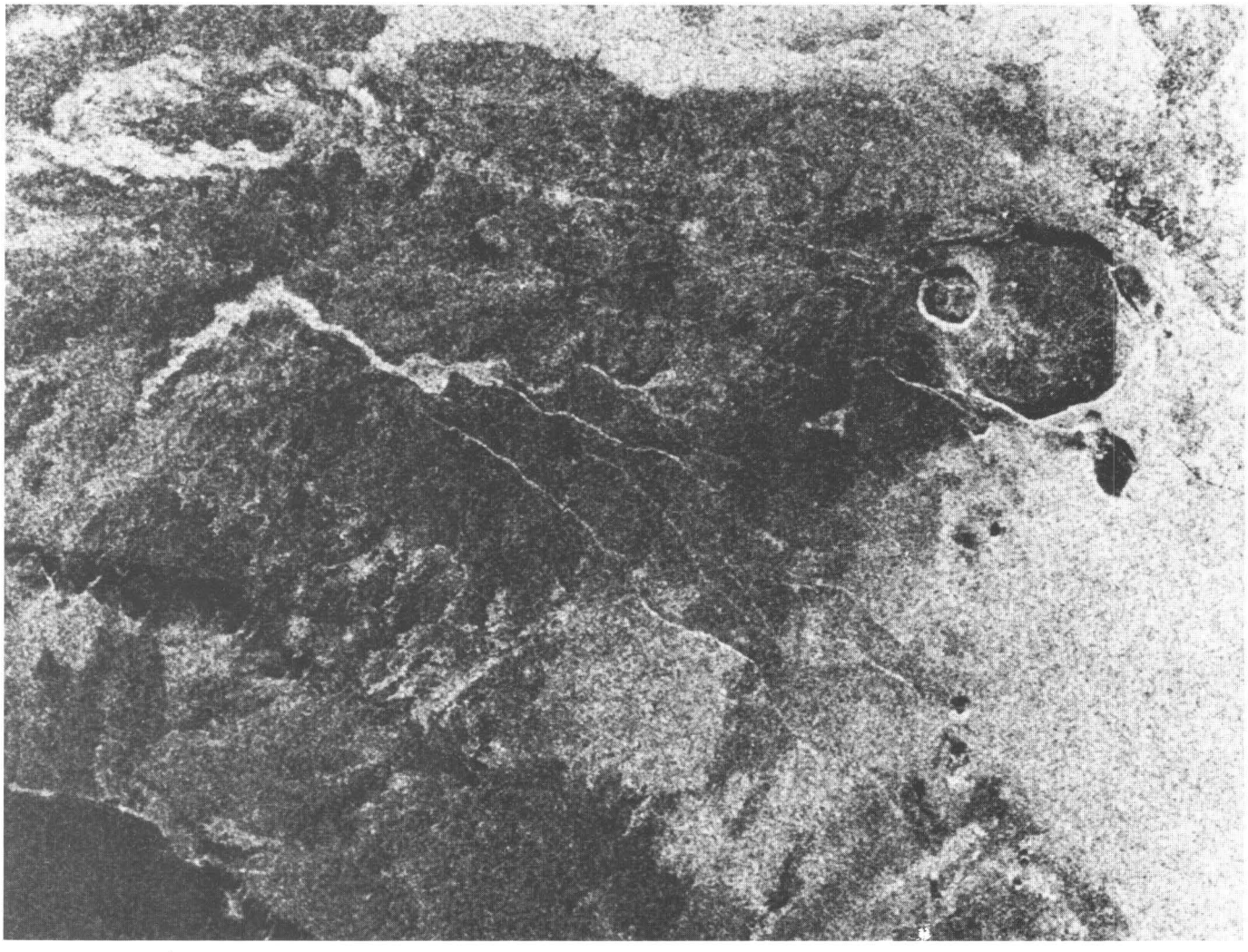

A

FIGURE 8.12.—Radar image and map of Kilauea summit area (see fig. 8.11 for location. ***A***, Subscene of SIR-B Data Take number 115.2, acquired at incidence angle of 48 degrees. Nominal image resolution is approximately 20 meters per pixel. ***B***, Same area indicating location of prominent lava flows, craters, and pali. A, transition from aa to pahoehoe on December 1974 lava flow; B, Kilauea Iki pit crater; C, September 1982 pahoehoe flows where low radar returns are evident; D, variations in radar brightness around Halemaumau pit crater (dotted line) are attributed to spatial variations in size and number of boulders ejected onto surrounding terrain by 1924 phreatic eruption of Halemaumau.

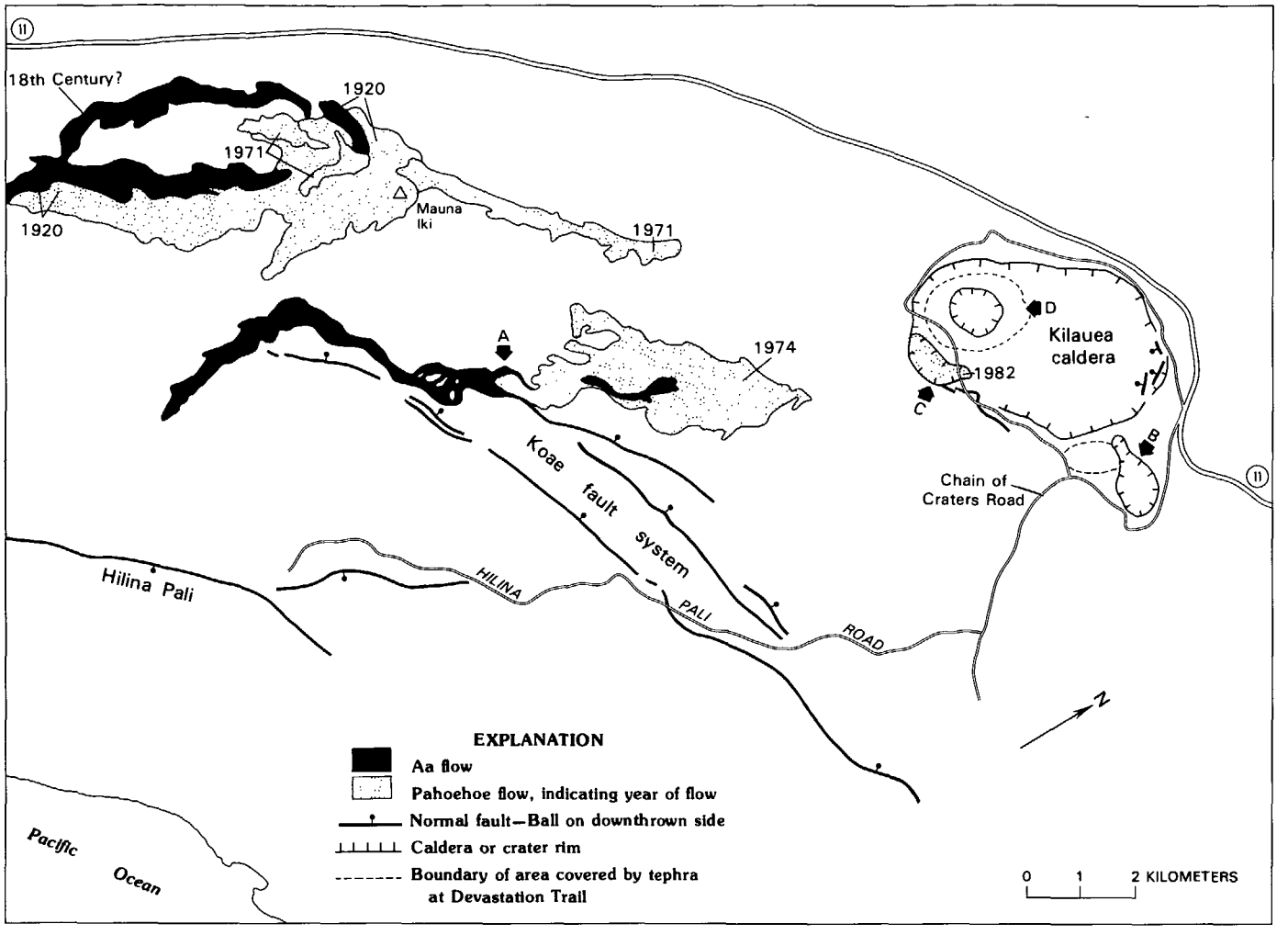

B

FIGURE 8.12.—Continued.

EFFECTS OF VOLCANIC EMANATIONS ON CARBON-ISOTOPE CONTENT OF MODERN PLANTS NEAR KILAUEA VOLCANO

By Meyer Rubin, John P. Lockwood, *and* Irving Friedman

ABSTRACT

Measurement of stable and unstable carbon isotopes were made on growing plants at various distances from fumarolic volcanic vents on the Island of Hawaii. Samples of CO_2 from volcanic gas vents were also measured, as well as control samples of unaffected atmosphere and plants. Results indicate that the proximity of the sample to the source of volcanic emanation does affect the ^{14}C concentration as anticipated, but for a variety of reasons the $^{13}C/^{12}C$ ratio, although significantly altered, does not relate directly to ^{14}C activity. Depending on how close a plant grows to fumaroles, the radiocarbon age can appear to be 1,400 years too old, with extremes of 4,000 years not unlikely.

INTRODUCTION

During investigations of the age of a pyroclastic ash on Kilauea (the mostly A.D. 1790 Keanakakoi Ash Member of the Puna Basalt) using buried charcoal, a negative correlation was observed between the radiocarbon age and the collection distance from the caldera (fig. 9.1). In order to test whether a $^{13}C/^{12}C$ ratio on the charcoal could give an indication of how much, or if any, non-radiogenic, juvenile carbon from volcanic vents was incorporated in the plants during growth, a series of samples was collected from living plants at various distances from active vents as well as control samples that could not have incorporated volcanic CO_2. From previous work

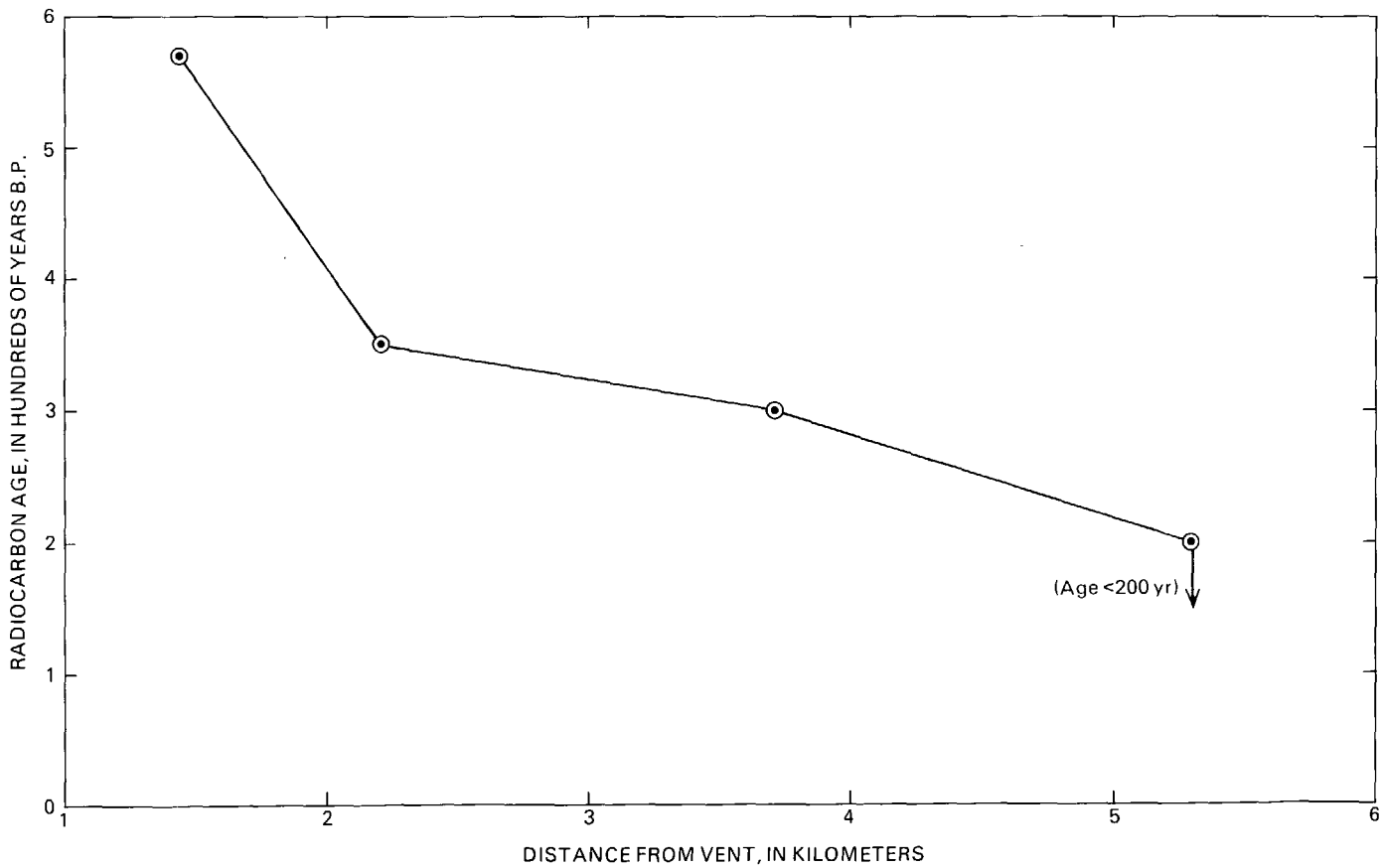

FIGURE 9.1.—Carbon-14 ages on charcoal from the mostly A.D. 1790 Keanakakoi Ash Member of the Puna Basalt as a function of collection distance from steam vents.

TABLE 9.1.—*Isotopic composition of Hawaiian plants*

Lab number	Description	$\delta^{13}C$ PDB (in permil)[1]	^{14}C (percent of modern)[2]	Apparent age (in ka)[3]
W-5476	Ohia[4] leaves from living trees overhanging the ocean on the windward Hamakua coast, Kukui Point.	-28.9	124	0
W-5477	Ohia leaves from anomalous kipuka south of Bird Park.	-24.5	124	0
W-5474	Ohia leaves from Puhimau Thermal Area.	-25.8	108	1.4
W-5482	Root of living Ohia tree at edge of fumarole at margin of Puhimau Thermal Area.	-26.3	108	1.4
W-5480	Fern[5] growing directly in hot steam at margin of fumarole at Puhimau Thermal Area.	-26.8	82	4.3
3464-6	Gas sample, Puhimau vent.	-3.0	--	--
3464-7	Gas sample, Halemaumau.	-3.5	--	--
W-1957	Gas sample, Sulfur Bank no. 2, Kilauea 1966.	-3.6	.1	>45
W-1958	Gas sample, Sulfur Bank no. 1.	--	.0	>45
W-3983	Gas sample, Sulfur Bank, 1971.	--	.2	>40
W-3989	Gas sample, 1971 fissure, Kilauea.	--	.5	>40

[1] CO_2 from samples of air collected weekly for 4 yr on Mauna Loa at 3,048 m elevation range from -7.1 to -8.4 permil.

$$\delta^{13}C_{PDB} = \left(\frac{R\ sample}{R\ standard}\right) - 1 \quad 1{,}000, \text{ where R = the ratio } {}^{13}C/{}^{12}C.$$

[2] Measured in comparison to the National Bureau of Standards 1960 oxalic acid standard. Modern equals 95 percent of the activity of this standard.

[3] Using present-day wood activity as 124 percent of modern.

[4] *Metrosideros polymorpha.*

[5] *Nephrolepsis exaltata.*

(Chatters and others, 1969; Sulerhitzky, 1970; Libby and Libby, 1972; Panichi and Tongiorgi, 1975; Michael, 1978; Weinstein and Betancourt, 1978; Puchelt and Hubberten, 1979; Bruns and others, 1980; Saupe and others, 1980), juvenile CO_2 from volcanic vents was found to be "dead" (contains no ^{14}C), and plants growing immediately adjacent to the vents could give anomalous ages as much as several thousand years too old. What was not known, however, was whether the ^{13}C measurements could help in determining possible old carbon contamination in the hundreds of previously dated samples from Hawaii.

METHODS

Grab samples were collected of living, native vegetation growing under different conditions of exposure to volcanic gases, from the worst case of ferns growing directly in the hot steam of a fumarole to leaves of trees overhanging the Hamakua coast bathed in the uncontaminated northeast trade winds (table 9.1). Samples were taken of first-year leafy growth to verify that the biologically fixed carbon was obtained from the atmosphere in the year of sampling (1983). The $^{13}C/^{12}C$ measurements were made in Denver, Colorado, on an aliquot of the same samples that were dated by ^{14}C measurements in Reston, Virginia. The dried plant material was oxidized at 900 °C and the purified CO_2 was analyzed on a 12-inch triple-collector magnetic-sector mass spectrometer. The analytical precision is ± 0.1 percent (2 sigma). All $^{13}C/^{12}C$ ratios are reported in permil relative to the Peedee belemnite (PDB) standard. A value of -28.1 permil was obtained for NBS–21 graphite. The Sulfur Bank gas samples were collected in 1966 by Bruce

Hanshaw and Meyer Rubin and measured by the same methods. The 1971 gas samples were collected by Meyer Rubin and Elliott Spiker. The gas for ^{14}C determinations was collected by absorption in NaOH. The leaves, collected from several growing plants in a localized area, were only given a hot water wash as a pretreatment, then counted in gas proportional counters as acetylene.

DISCUSSION

As anticipated, the ^{14}C data show the dilution effect of the "dead" CO_2 of juvenile volcanic origin. The Sulfur Bank gas has a ^{14}C activity of juvenile gas. Within our background error of ± 1 percent, there is no measurable ^{14}C. The gas samples from Puhimau vent and Halemaumau crater as well as from Sulfur Bank and the 1971 fissure have $\delta^{13}C$ values ranging from -3.0 to -3.6 permil. Pure air has a $\delta^{13}C$ of approximately -8 ± 0.3 permil. This 5 permil difference between the pure air and the volcanic gas should show up in the $\delta^{13}C$ of the leaves if the plants incorporated the isotopically heavier volcanic gas. The Kilauea samples are about 2 permil heavier than those from a tree growing on the seacliff remote from volcanic CO_2. If 40 percent of the CO_2 assimilated by the plants was of volcanic origin, we would expect the $\delta^{13}C$ of the plant material to be heavier by about 2 permil. Inasmuch as Puhimau gas contains 1 to 5 percent CO_2 (L.P. Greenland, oral commun., 1985) only 1 percent of this gas mixed with 99 percent air (0.035 percent CO_2) could account for this change in $\delta^{13}C$. However, the $\delta^{13}C$ values of the leaves and roots are probably affected by factors such as moisture availability and temperature as well as the $\delta^{13}C$ of the ingested CO_2, and the $\delta^{13}C$ values of the samples collected on Kilauea do not relate directly to the ^{14}C activity, as can be seen in table 9.1.

The ^{14}C results (table 9.1) may appear slightly confusing because they are compared to 0.95 times the activity of an oxalic acid standard, which gives the modern or present-day atmospheric activity if there had been no bomb testing. The ^{14}C produced by the nuclear weapons tests since 1953 first elevated the activity to 200 percent of the 95 percent oxalic acid standard; absorption by the oceans and other buffering mechanisms has subsequently lowered it to approximately 124 percent (as of 1985).

If the present-day activity is represented by the two samples at 124 percent ^{14}C activity, then the samples growing in a thermal area are depressed by 16 percent, giving the plants an initial age of approximately 1.4 ka. The fern leaves growing at the very edge of a fumarole, a worst case situation, were depressed approximately 42 percent, differing from normal living plants by 4,300 years.

Thus, the charcoal from plants buried by an ash or lava flow could have an initial built-in age of as much as 4.3 ka, but more likely not more than 1.4 ka, depending on how close to a volcanic fumarole the plants grew at the time of burial. This dilution is also possible near central volcanic areas, particularly downwind, decreasing in effect rapidly away from the source of the dead CO_2 (fig 9.1). Nonmeteoric CO_2 is higher in abundance at Kilauea summit fumaroles, but decreases in abundance away from the caldera, along both the east and southwest rift zones (L.P. Greenland, written commun., 1985).

CONCLUSIONS

Carbonaceous samples dating volcanic activity are probably usually correct to within twice the stated one-sigma counting error. However, because one cannot always reconstruct the locations of volcanic fumaroles or determine the original juvenile CO_2 gas activity, radiocarbon samples from volcanic areas may appear too old by about 1,400 years. In rare situations samples may date 4,300 years too old.

Most contaminants of charcoal collected for radiocarbon chronology studies result in geologically young ages (modern rootlets, humic acids, and so on). Our studies show that samples collected from the immediate vicinity of CO_2-emitting volcanic fumaroles can also incorporate contaminants that result in radiocarbon ages that are too old. Considerable caution should be used in the evaluation of ages from central volcanic areas. Given the present sparse data one cannot use $\delta^{13}C$ to predict possible old carbon contamination.

REFERENCES CITED

Bruns, Michael, Levin, Ingeborg, Munnich, K.O., Hubberten, H.W., Fillipakis, S., 1980, Regional sources of volcanic carbon dioxide and their influence on ^{14}C content of present-day plant material: Radiocarbon, v. 22, no. 2, p. 532–536.

Chatters, R.M., Crosby, J.W., and Engstrand, L.G., 1969, Fumarole gaseous emanations their influence on carbon-14 dates: Washington State University College of Engineering Circular 32, 9 p.

Libby, L.M., and Libby, W.F., 1972, Volcanism and radiocarbon dates, *in* Rafter, T.A., and Grant-Taylor, T. eds., International Radiocarbon Conference, 8th, Proceedings: Wellington, Royal Society of New Zealand, v. 1, p. A72–A75.

Michael, H.N., 1978, Radiocarbon dates from Akrotiri, Thera, 1967–1977, *in* Doumas, D., ed., Thera and the Aegean World, I: International Science Conference, London, 2nd, Papers, p. 791–795.

Panichi, Costanzo, and Tongiorgi, Ezio, 1975, Carbon isotopic composition of CO_2 from springs, fumaroles, mofettes, and travertines of central and southern Italy: a preliminary prospection method of geothermal area: United Nations Symposium on Development and Use of Geothermal Resources, 2nd, Proceedings, San Francisco, Lawrence Berkeley Laboratory, University of California.

Puchelt, H., and Hubberten, H.W., 1979, Vulkanogenes Kohlendioxid: Aussagen und Herkunft aufgrund von Isotopenuntersuchungen, *in* Arbeitstagung, Isotope in der Natur., Leipzig, 1979, 2nd, Proceedings.

Saupe, Francis, Strappa, Osvaldo, Coppens. Rene, Guillet, Bernard, and Jaegy, Robert, 1980, A possible source of error in ^{14}C dates: volcanic emanations (examples from the Monte Amiata district, Provinces of Grosseto and Sienna, Italy): Radiocarbon, v. 22, no. 2, p. 525–531.

Sulerzhitzky, C.D., 1970, Radiocarbon dating of volcanoes: Bulletin Volcanologique, v. 35, p. 85–94.

Weinstein, G.A., and Betancourt, P.P., 1978, Problems of interpretation of the Akrotiri radiocarbon dates, *in* Doumas, C., ed., Thera and the Aegean World, I: International Science Congress, 2nd, London, Papers, p. 805–814.

HAWAIIAN RADIOCARBON DATES

By Meyer Rubin, Lea Kelley Gargulinski, *and* John P. McGeehin

ABSTRACT

Radiocarbon dates have been obtained from 306 geologic samples collected from the Island of Hawaii and analyzed by the U.S. Geological Survey laboratory at Reston, Virginia. The dates range from modern (present-day carbon) to greater than 38 ka. For convenience, the tabulated dates are grouped by volcano: 185 from Mauna Loa, 90 from Kilauea, 30 from Hualalai, and 1 from Mauna Kea. Maps show sample locations, and a selected bibliography of articles covers aspects of Hawaiian radiocarbon dates.

INTRODUCTION

Understanding the history of volcanism in Hawaii requires an understanding of the timing of the volcanic events. This article lists the radiocarbon dates from the Island of Hawaii, giving their sample locations, ages, significance, and stratigraphic relations in tabular form. Dates from each volcano on Hawaii are grouped in a separate table. These tables and the accompanying bibliography provide a comprehensive source of information on Hawaiian radiocarbon dates.

HISTORY OF ^{14}C DATING IN THE HAWAIIAN ISLANDS

Although radiocarbon dating methods have been available since the late 1940's, only a handful of dates were determined on material from Hawaiian lava flows before 1976. This was not because of lack of interest but because samples of datable organic material were not available. With improved understanding of the conditions of charcoal formation and preservation beneath basaltic lavas, opportunities for discovery increased. Lockwood and Lipman (1979) pioneered the recovery of such material, allowing the dating of many new samples. Dates from Hawaii before 1979 are listed in Kelley (1979) and Kelley and others (1979). In the present paper, we list all dates from Hawaii analyzed for volcano-stratigraphic purposes at the U.S. Geological Survey radiocarbon laboratory at Reston, Va. Many dates obtained for other purposes, such as archaeologic dates, geochemical dates related to volcanic gases and volcanic emanations affecting the biosphere, and dates on ground water are not listed here, as they are beyond the scope of this article.

A curve depicting the number of radiocarbon dates by year since 1950 would be a steeply rising one. The development of the new technique of tandem-accelerator mass spectrometry, with its attendant thousandfold decrease in the required sample size, will undoubtedly cause this curve to rise even more steeply. Many sites yield charcoal in insufficient quantity for a conventional radiocarbon age without large-scale quarrying operations, but the new method can provide a reliable date from a few milligrams of carbon. The experience of volcanologists indicates that many additional flows can be dated, now that the sample requirements have been reduced significantly.

Radiocarbon dates from Hawaii have revolutionized our understanding of the island's volcanic history. Previous workers had to be satisfied with relative ages, rather than numerical dates. In addition to directly dating the geologic deposit, ^{14}C dating has helped to calibrate other forms of dating, which then could be used as a substitute dating technique where carbon is not available. These alternate methods include paleomagnetic-age curves of various types and individual weathering indices developed by several workers. All of these are calibrated on ^{14}C-dated flows.

CARBON SOURCES

The ideal sample for radiocarbon dating of a flow would be a sample from a short-lived plant converted to vitreous charcoal by the heat of the advancing lava (Lockwood and Lipman, 1979). The plant should have been growing away from the influence of volcanic-source CO_2, which lacks the ^{14}C present in atmospheric CO_2, should be buried too deeply for surface rootlet penetration, and should not be soaked in ground water rich in organic components. Poor samples would be those from buried soils, poor in organic matter, having modern rootlets, or lying under the water table. Various enrichment and purification techniques for removing contaminants have been developed to analyze such poor-quality samples, but the results are not always reliable. Charcoal from post-flow fires commonly trickles down through the flow (most easily with aa) and can give the appearance of having been formed during the flow's advance, but such material will not date the actual flow.

VALIDITY OF THE DATES

The uncertainty given for the dates in the tables (the figure after the $\pm$) is the standard deviation (one sigma) based only on the counting statistics and not on analysis of replicate samples from the field. This counting error does not include variable factors, such as contamination, isotopic fractionation, and other laboratory uncertainties. Experience has shown that these factors raise the uncertainty to more than twice the quoted error.

Another type of error encountered in some samples taken from volcanic areas is that caused by dilution of the normal ^{14}C content in atmospheric CO_2 by volcanic emanations that contain no ^{14}C.

Plants take up this ^{14}C-poor CO_2 in their metabolism and therefore have an initial apparent age because of such deficient initial activity. This error in extreme cases can produce an apparent age of 3 ka in living plants (Rubin and others, chapter 9). However, common practice suggests that unless a plant is known to be growing immediately adjacent to a vent, it can be assumed to give a reasonably correct age.

HOW ^{14}C DATING HAS AFFECTED THE THINKING OF HAWAIIAN GEOLOGISTS

What surprises have been produced by the numerous ^{14}C dates obtained in recent years? In general, geologists did not have to revise greatly their age estimates for flows younger than 1 ka. By extrapolation of historical weathering rates, they had been able to estimate fairly accurately the ages of the younger flows. Flows having a very weathered appearance, however, had been estimated to be much older than the dates ultimately derived by ^{14}C measurements.

SUMMARY OF HAWAIIAN RADIOCARBON DATES AND THEIR SIGNIFICANCE

Sample locations, laboratory numbers, and ages of Hawaiian radiocarbon dates have been plotted (figs. 10.2–10.5; see also fig. 10.1) and are also listed by volcano (tables 10.1–10.4). The tables list samples in order of increasing age and also give additional information on location, geologic section, altitude and flow name. Only those samples that were processed at the U.S. Geological Survey radiocarbon laboratory at Reston, Va., and that have geologic significance are included in this compilation.

Much further information for each sample, including the complete geologic section and significance, the date of collection, and the collector's judgment as to whether the sample age appears to be a valid age for the overlying flow or ash is available from the U.S. Geological Survey laboratory at Reston or from the collector. All collectors are or were members of the U.S. Geological Survey. Other chapters in the present work make use of the dates collected here in their studies of separate volcanic areas, and they constitute prime sources of information on Hawaiian chronology.

MAUNA LOA

The numerous samples dating the flows of Mauna Loa (table 10.1; figs. 10.2–10.4) serve only to establish a foundation for further work. Of the hundreds of individual flows that have been mapped, many have been dated, but there are still many more flows to be dated. Where carbon is not available, or the age is beyond the range of ^{14}C dating, observational methods of relative dating will be used, with the radiocarbon dates as a calibration where possible.

Some tentative statements as to the activities of the various volcanoes can be made. Mauna Loa appears to have been more active during the brief period of its recorded history than during the several centuries immediately preceding 1840. Activity was also higher around 0.8–1.0 ka (800–1,000 years before present). Surface flows on Mauna Loa appear to be older than those of Kilauea. Areal percentages covered by various ages of flows are discussed by Lockwood and Lipman (chapter 18). Flows several thousand years old are common on Mauna Loa, but flows more than a few hundred years old are rare on Kilauea. About 30 percent of the surface of the southwest side of Mauna Loa has been covered by lava in the past 1,000 years, but about 90 percent of Kilauea's surface is younger than 1 ka.

Ages of Mauna Loa flows range from very recent to greater than 38 ka, the very oldest flows being exposed along deeply incised river channels and fault scarps.

KILAUEA

As is evident from the dates (table 10.2; fig. 10.5), Kilauea is a young, active volcano. Kilauea's surface is only about one-tenth as old as was thought previously. The northeast rift zone appears to be the same age as the southwest rift zone but has more bulk, erupting more often and with greater volume. The older rocks are, in general, found farther away from the rift zone. About 90 percent of the surface flows are younger than 1.1 ka (Holcomb, chapter 12). Kilauea is the youngest volcano on the Island of Hawaii, with dated eruptions from the present time back to about 23 ka.

HUALALAI

Although the flows of Hualalai (table 10.3; fig. 10.2) have not been as frequent as Kilauea in historical time, the flows in the past 1,500 years have been very large and cover 10–20 percent of the area. All of the approximately 200 cones on Hualalai are of Holocene age (less than 10 ka) and 95 percent of the surface flows are also Holocene in age. As much as 50 percent of the area is covered by flows younger than 5 ka. Hualalai is still an active volcano, with an average of one eruption every 50 years during Holocene time, and the last known eruption occurred in 1801. Ages range from less than 200 years to 13 ka.

MAUNA KEA

Mauna Kea is, next to Kohala Volcano, the oldest and least active of the Hawaiian volcanoes. The date from Mauna Kea (table 10.4; fig. 10.3) is Holocene in age, but this does not reflect the age of the majority of deposits (see Porter, chapter 21).

SELECTED BIBLIOGRAPHY

DATE LISTS

Buckley, J.D., 1973, Isotopes' radiocarbon measurements X: Radiocarbon, v. 15, p. 280–298.

Buckley, J.D., and Willis, E.H., 1969, Isotopes' radiocarbon measurements VII: Radiocarbon, v. 11, p. 53–105.

———1972, Isotopes' radiocarbon measurements IX: Radiocarbon, v. 14, p. 114–139.

Buddemeier, R.W., and Hufen, T.H., 1978, Hawaii Institute of Geophysics radiocarbon dates: Radiocarbon, v. 15, p. 68–74.

Crane, H.R., 1956, University of Michigan radiocarbon dates I: Science, v. 124, p. 664–672.

Crane, H.R., and Griffin, J.B., 1958, University of Michigan radiocarbon dates II: Science, v. 127, p. 1098–1105.

———1959, University of Michigan radiocarbon dates IV: Radiocarbon, v. 1, p. 173–198.

———1960, University of Michigan radiocarbon dates V: Radiocarbon, v. 2, p. 31–48.

———1962, University of Michigan radiocarbon dates VII: Radiocarbon, v. 4, p. 183–203.

———1963, University of Michigan radiocarbon dates VIII: Radiocarbon, v. 5, p. 228–253.

Fairhall, A.W., Young, A.W., and Erickson, J.L., 1976, University of Washington dates IV: Radiocarbon, v. 18, p. 221–239.

Hubbs, C.L., Bien, G.S., and Suess, H.E., 1962, La Jolla natural radiocarbon measurements II: Radiocarbon, v. 4, p. 204–238.

———1965, La Jolla natural radiocarbon measurements IV: Radiocarbon, v. 7, p. 66–117.

Ives, P.C., Levin, Betsy, Oman, C.L., and Rubin, Meyer, 1967, U.S. Geological Survey radiocarbon dates IX: Radiocarbon, v. 9, p. 505–529.

Ives, P.C., Levin, Betsy, Robinson, R.D., and Rubin, Meyer, 1964, U.S. Geological Survey radiocarbon dates VII: Radiocarbon, v. 6, p. 37–76.

Kelley, M.L., 1979, Radiocarbon dates from the Hawaiian Islands: A compilation: U.S. Geological Survey Open-File Report 79-1700, 39 p.

Kelley, M.L., Spiker, E.C., Lipman, P.W., Lockwood, J.P., Holcomb, R.T., and Rubin, Meyer, 1979, U.S. Geological Survey, Reston, Virginia, radiocarbon dates XV: Mauna Loa and Kilauea Volcanoes, Hawaii: Radiocarbon, v. 21, p. 306–320.

Kigoshi, Kunihiko, Tomikura, Yoshio, and Endo, Kunihiko, 1962, Gakushuin natural radiocarbon measurements I: Radiocarbon, v. 4, p. 84–94.

Krueger, H.W., and Weeks, C.E., 1966, Geochron Laboratories, Inc. radiocarbon measurements II: Radiocarbon, v. 8, p. 142–160.

Levin, Betsy, Ives, P.C., Oman, C.L., and Rubin, Meyer, 1965, U.S. Geological Survey radiocarbon dates VIII: Radiocarbon, v. 7, p. 372–398.

Libby, W.F., 1951, Radiocarbon dates III: Science, v. 114, p. 291–296.

———1954, Chicago radiocarbon dates V: Science, v. 120, p. 733–742.

Marsters, Beverly, Spiker, Elliott, and Rubin, Meyer, 1969, U.S. Geological Survey radiocarbon dates X: Radiocarbon, v. 11, p. 210–227.

Rubin, Meyer, and Alexander, Corrinne, 1958, U.S. Geological Survey radiocarbon dates IV: Science, v. 127, p. 1476–1487.

———1960, U.S. Geological Survey radiocarbon dates V: Radiocarbon, v. 2, p. 129–185.

Rubin, Meyer, and Berthold, S.M., 1961, U.S. Geological Survey radiocarbon dates VI: Radiocarbon, v. 3, p. 86–98.

Rubin, Meyer, and Suess, H.E., 1956, U.S. Geological Survey radiocarbon dates III: Science, v. 123, p. 442–448.

Stuckenrath, Jr., Robert, 1967, University of Pennsylvania radiocarbon dates X: Radiocarbon, v. 9, p. 333–345.

Sullivan, B.M., Spiker, Elliott, and Rubin, Meyer, 1970, U.S. Geological Survey radiocarbon dates XI: Radiocarbon, v. 12, p. 319–334.

Vogel, J.C., and Waterbolk, H.T., 1964, Groningen radiocarbon dates V: Radiocarbon, v. 6, p. 349–369.

SPECIFIC USES

Berry, A.L., 1973, Thermoluminescence of Hawaiian basalts: Journal of Geophysical Research, v. 78, p. 6863–6867.

Coe, R.S., Groome, Sherman, and Mankinen, E.A., 1978, Geomagnetic paleointensities from radiocarbon-dated lava flows on Hawaii and the question of the Pacific nondipole low: Journal of Geophysical Research, v. 83, no. B4, p. 1740–1756.

Doell, R.R., and Cox, Allan, 1965, Paleomagnetism of Hawaiian lava flows: Journal of Geophysical Research, v. 70, no. 14, p. 3377–3405.

May, R.J., 1975, Thermoluminescence dating of Hawaiian basalts: Palo Alto, Stanford University, Ph.D. dissertation, 156 p.

———1977, Thermoluminescence dating of Hawaiian alkalic basalts: Journal of Geophysical Research, v. 82, p. 3023–3029.

———1979, Thermoluminescence dating of Hawaiian basalt: U.S. Geological Survey Professional Paper 1095, 47 p.

McWilliams, M.O., Holcomb, R.T., and Champion, D.E., 1979, Holocene geomagnetic secular variation for Hawaii: Eos (American Geophysical Union, Trans.), v. 60, no. 18, 244 p.

———1982, Geomagnetic secular variation from ^{14}C-dated lava flows on Hawaii and the question of the Pacific non-dipole low, *in* Runcorn, S.K., Creer, K.M., and Jacobs, J.H., eds., The Earth's core: Its structure, evolution, and magnetic fields: Royal Society of London Series A, v. 306, p. 211–222.

Morgenstein, M., Riley, T.J., 1975, Hydration-rind dating of basaltic glass: A new method for archaeological chronologies: Hawaii University, Institute of Geophysics, Contributions, p. 1–18.

GENERAL TOPICS

Easton, R.M., 1978, The stratigraphy and petrology of the Hilina Formation: The oldest exposed lavas of Kilauea Volcano, Hawaii: Honolulu, University of Hawaii, m.s. thesis.

Holcomb, R.T., 1981, Kilauea Volcano, Hawaii: Chronology and morphology of the surficial lava flows: U.S. Geological Survey Open-File Report 81-0354, 383 p.

Inman, D.L., and Veeh, H.H., 1966, Dating the 10-fathom terrace off Hawaii [abs.]: American Geophysical Union Transactions: v. 47, p. 125.

Lockwood, J.P., and Lipman, P.W., 1979, Recovery of charcoal for ^{14}C dating from beneath lava—lessons from Hawaii: Journal of Volcanology and Geothermal Research, v. 4.

Macdonald, G.A., and Abbott, A.T., 1970, Volcanoes in the Sea: Honolulu, University of Hawaii Press, 441 p.

Macdonald, G.A., and Eaton, J.P., 1964, Hawaiian volcanoes during 1955: U.S. Geological Survey Bulletin 1171, p. 156–157.

Peterson, D.W., 1967, Geologic map of Kilauea Crater Quadrangle: U.S. Geological Survey GQ Map 667, scale 1:24,000.

Porter, S.C., 1971, Holocene eruptions of Mauna Kea Volcano, Hawaii: Science, v. 172, p. 375–377.

———1972, Buried caldera of Mauna Kea Volcano, Hawaii: Science, v. 175, p. 1458–1460.

———1973, Stratigraphy and chronology of late Quaternary tephra along the south rift zone of Mauna Kea Volcano, Hawaii: Geological Society of America Bulletin, v. 84, p. 1923–1940.

———1975, Late Quaternary glaciation and tephrochronology of Mauna Kea, Hawaii: Royal Society of New Zealand Bulletin 13, p. 247–251.

———1979, Quaternary stratigraphy and chronology of Mauna Kea, Hawaii: A 380,000-yr record of mid-Pacific volcanism and ice-cap glaciation: Summary: Geological Society of America Bulletin, v. 90, p. 609–611.

———1979, Hawaiian glacial ages: Quaternary Research, v. 12, p. 161–187.

Porter, S.C., Stuiver, Minze, and Yang, I.C., 1977, Chronology of Hawaiian glaciations: Science, v. 195, p. 61–63.

Woodcock, A.H., Rubin, Meyer, and Duce, R.A., 1966, Deep layer of sediments in alpine lake in the tropical mid-Pacific: Science, v. 154, p. 647–648

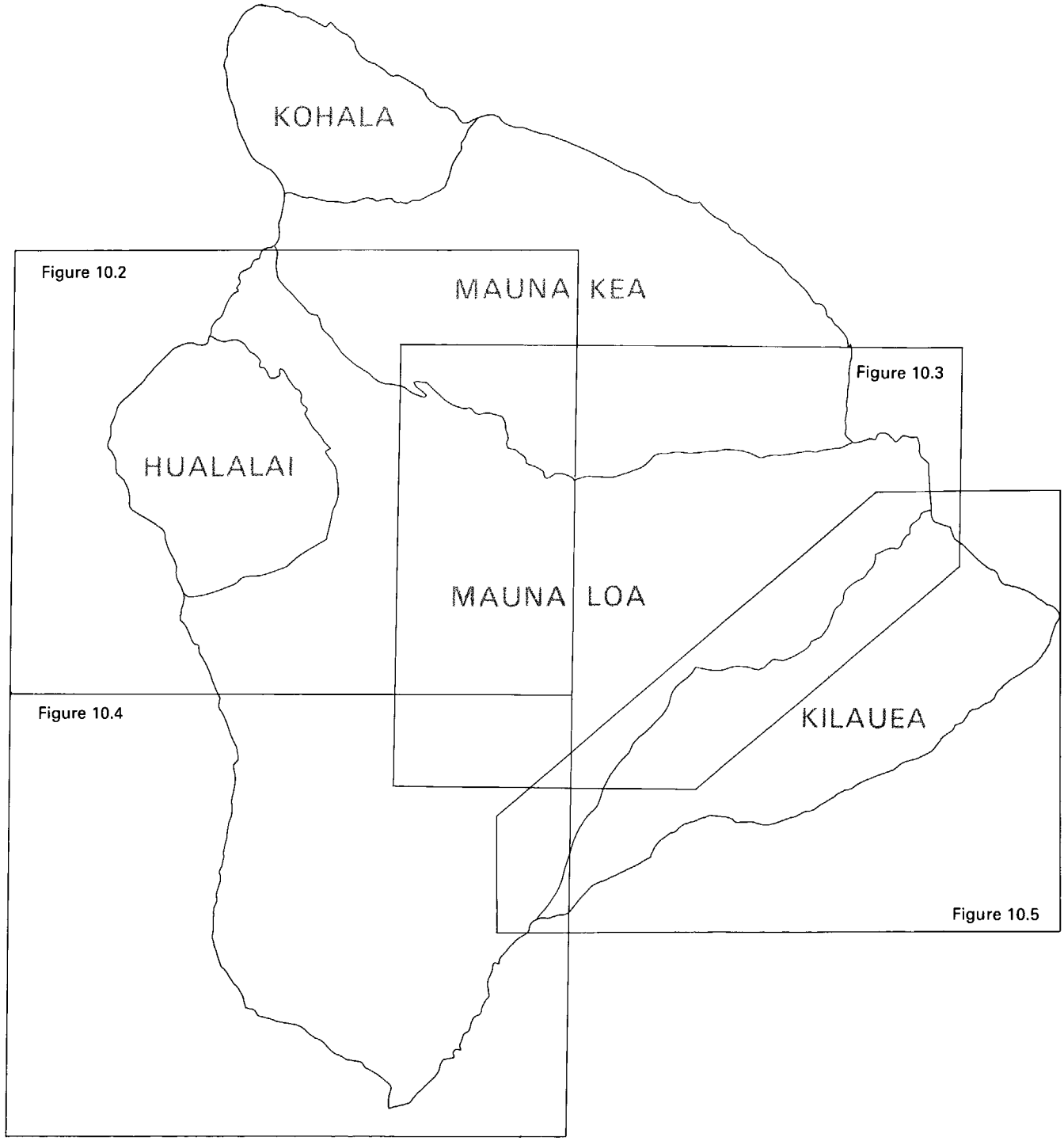

FIGURE 10.1.—Index map of Island of Hawaii showing areas covered by locality maps, figures 10.2.–10.5.

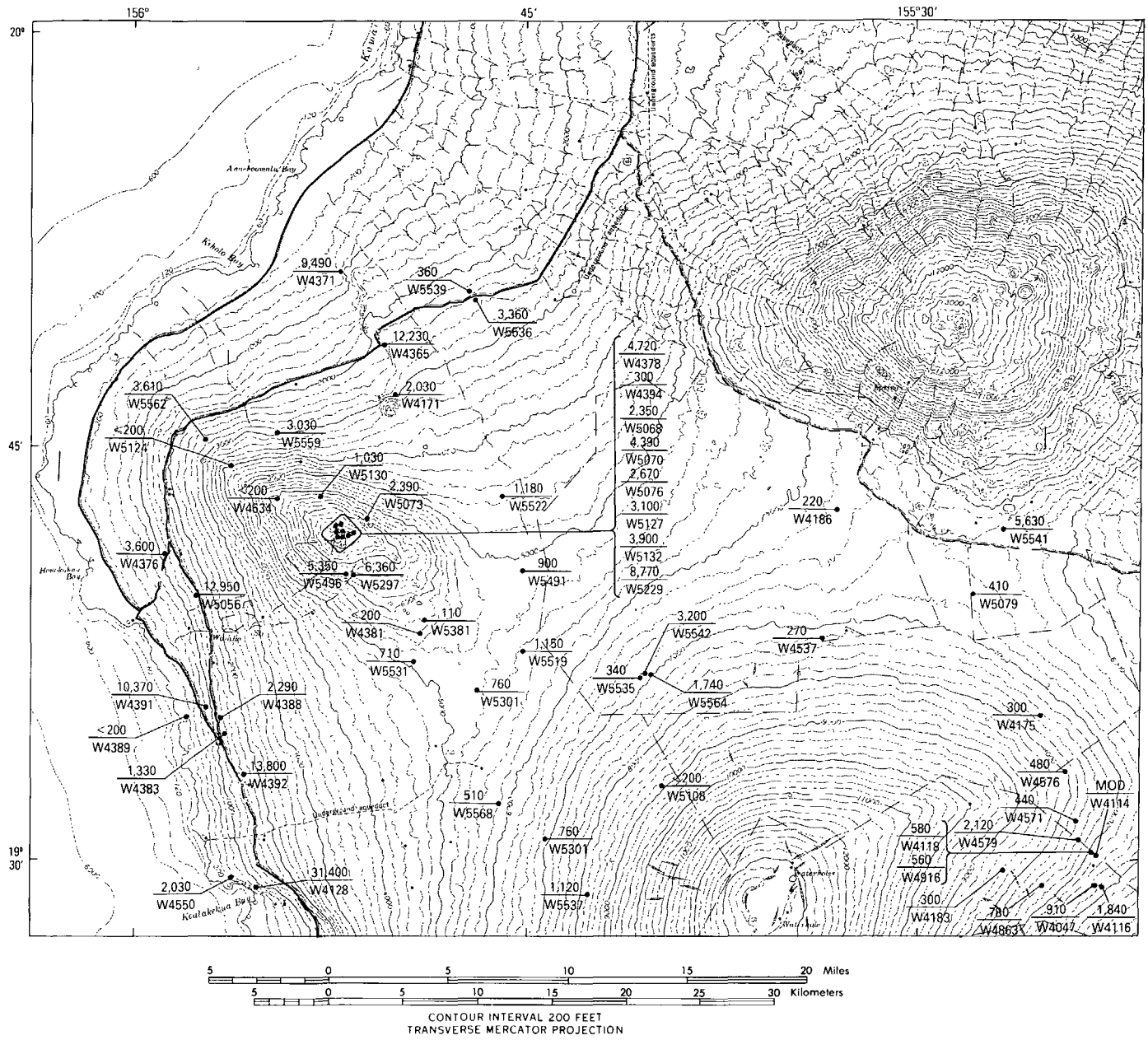

FIGURE 10.2.—Localities and ages of ^{14}C-dated samples on Hualalai Volcano and the northwestern part of Mauna Loa Volcano. Dots, sample localities; for each locality the ^{14}C age in years B.P. (blue) and the sample number (red) are given. For details of samples, see tables 10.1 and 10.3. MOD, modern.

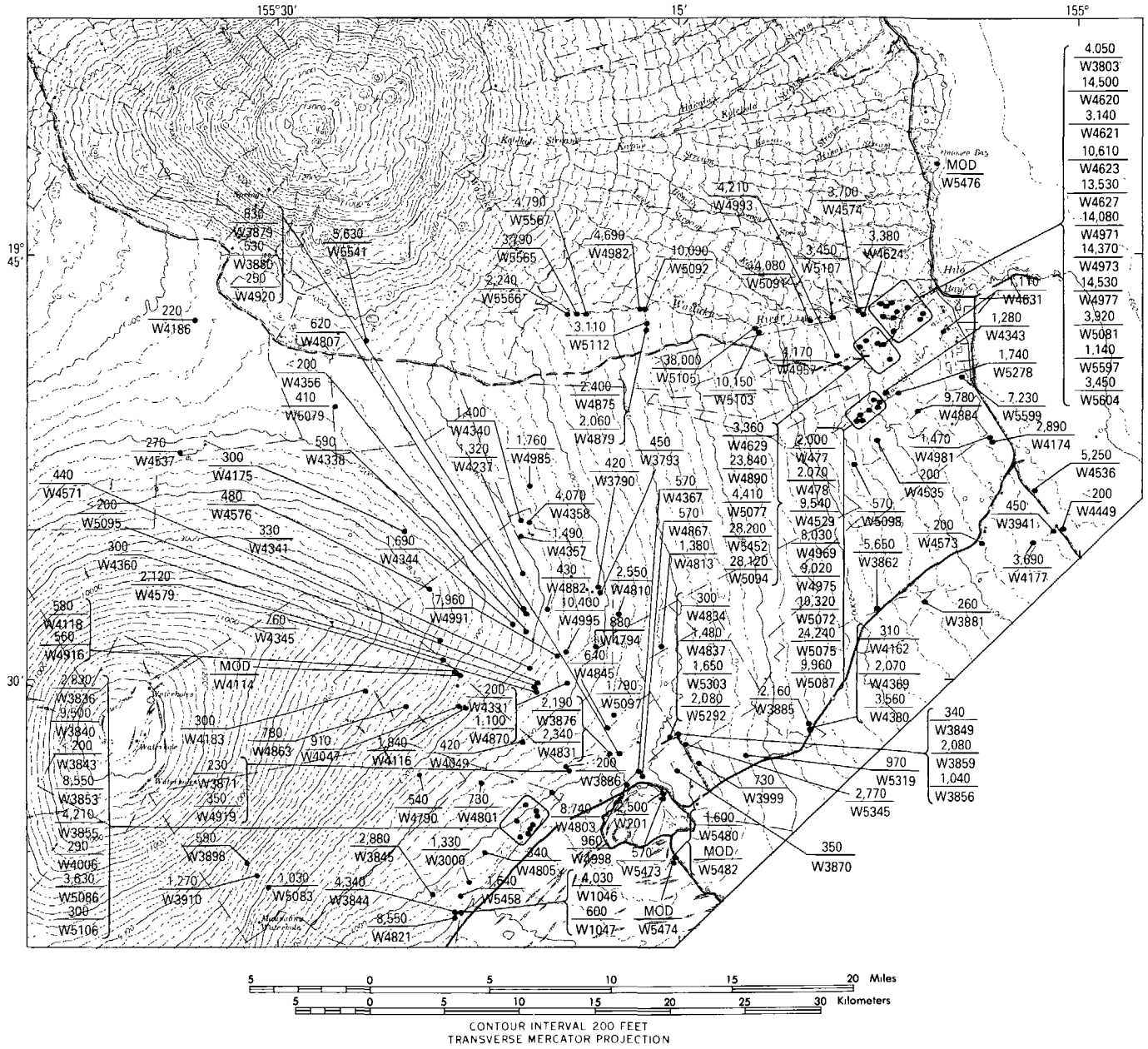

FIGURE 10.3.—Localities and ages of ^{14}C-dated samples on Mauna Kea Volcano, eastern part of Mauna Loa Volcano, and northwestern part of Kilauea Volcano. Dots, sample localities; for each locality the ^{14}C age in years B.P. (blue) and the sample number (red) are given. For details of samples, see tables 10.1, 10.2, and 10.4.

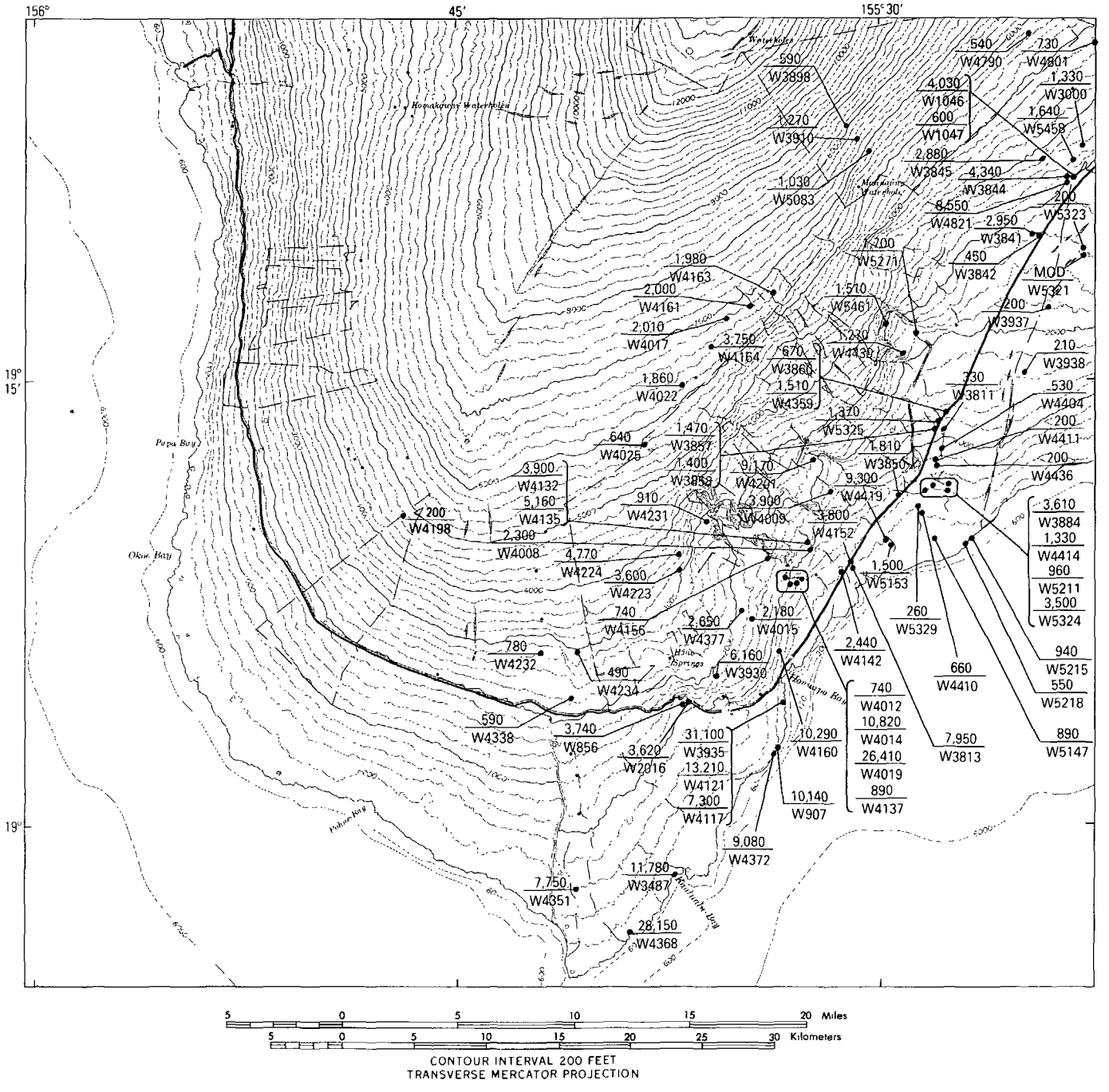

FIGURE 10.4.—Localities and ages of ^{14}C-dated samples on southwestern part of Mauna Loa Volcano. Dots, sample localities; for each locality the ^{14}C age in years B.P. (blue) and the sample number (red) are given. For details of samples, see table 10.1.

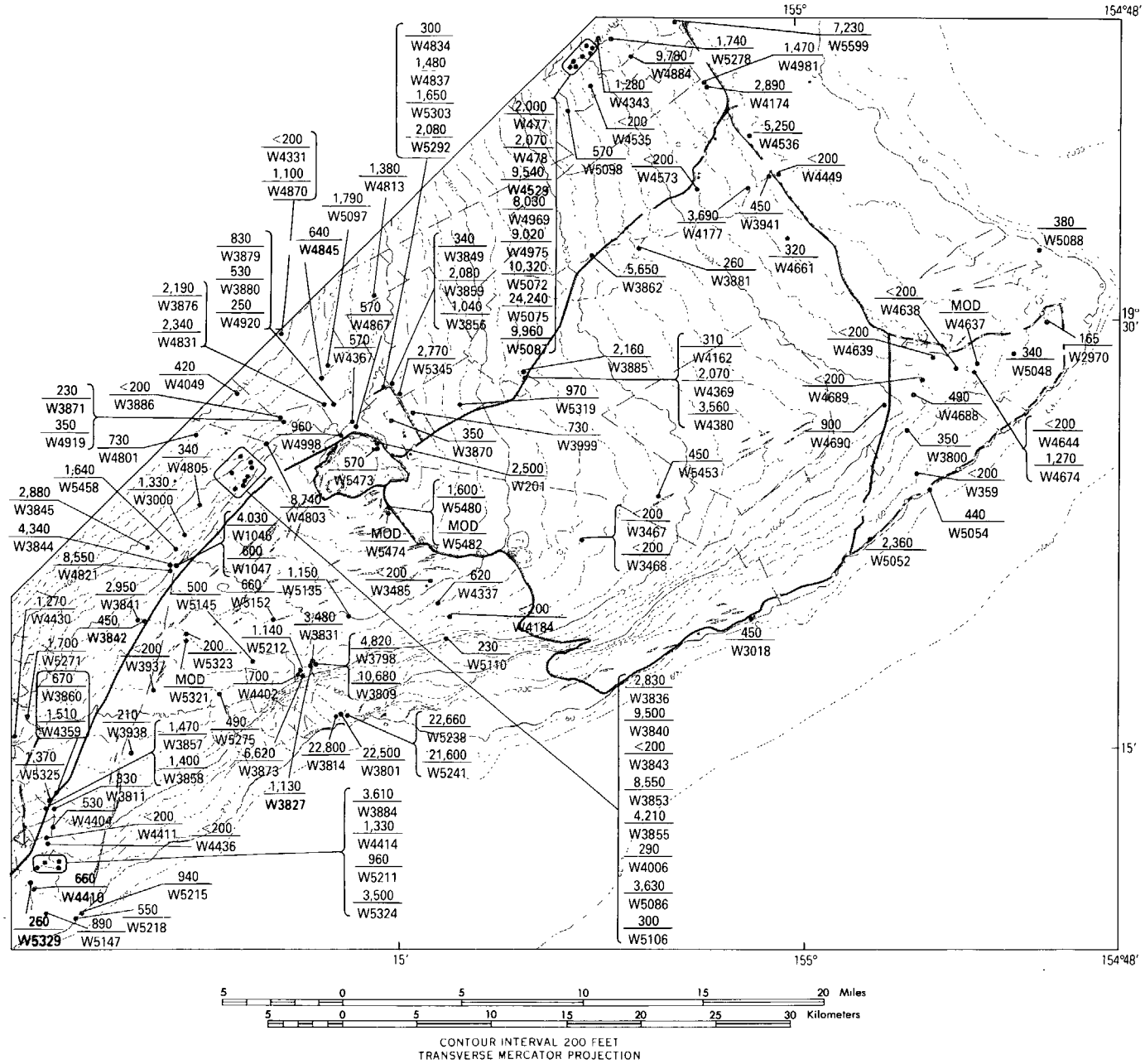

FIGURE 10.5.—Localities and ages of ^{14}C-dated samples on Kilauea Volcano and southeastern part of Mauna Loa Volcano. Dots, sample localities; for each locality the ^{14}C age in years B.P. (blue) and the sample number (red) are given. For details of samples, see tables 10.1 and 10.2.

TABLE 10.1—*Radiocarbon dates from Mauna Loa Volcano, Island of Hawaii*

[Samples listed in order of increasing age; uncertainty is one standard deviation, ± 1σ; modern age means sample is younger than AD 1950; ML = Mauna Loa; MK = Mauna Kea; mauka = toward the mountain, makai = toward the sea; see figs. 10.2–10.4 for localities. Stratigraphic nomenclature from Langenheim and Clague (chapter 1, part II)]

Sample	Radiocarbon age (years before present)	Location (latitude, longitude, quadrangle)	Elevation (m)	Sample and site description	Collector
W4114	Modern	19°30'09" 155°23'10" Puu Ulaula	2,070	Root fragments under margin of aa, Keamoku flow, 800 m N. of end of Strip Rd., 300 m E. of Puu Ulaula Trail.	J. P. Lockwood
W3843	<200	19°24'32" 155°20'37" Kilauea Crater	1,050	Charcoal root fragments from Pahala Ash below flow of Kipuka Maunaiu, at head of gully, along contact with Keamoku flow, Ohaikea Rd.	P. W. Lipman
W4198	<200	19°10'28" 155°46'37" Papa	1,481	Charcoal fragments along basal aa, at edge of Manuka flow, resting on pumice blanket from Hapaimanu, N. end of prominent kipuka, NW. of Pohakuloa.	P. W. Lipman
W4331	<200	19°29'52" 155°19'07" Kilauea Crater	1,542	Charcoal rootlets, in soil at base of pahoehoe, E. Keamoku flow, overlain by grey tube-fed pahoehoe, Puu Oo Trail, Keauhou Ranch Rd. pit, 4 km SE. of Keawewai Camp.	J. P. Lockwood
W4356	<200	19°32'20" 155°20'44" Kulani	1,913	Charcoal, at base of large tree mold, Solomon's Water Hole flow, overlain by aphanitic tube-fed pahoehoe, Powerline Rd., between pole 103 and 104.	J. P. Lockwood
W4411	<200	19°12'22" 155°28'02" Pahala	238	Charcoal roots under aa clinkers at edge of flow, SE. of Highway 11, NE. of Paauau Gulch.	N. G. Banks
W4535	<200	19°38'31" 155°07'35" Piihonua	337	Charcoal roots, in red-orange sub-laterite soil, young Ainaola pahoehoe flow, overlain by very fine crystalline, near aphanitic dark grey pahoehoe, drainage ditch 10 m S. of Ainaola Dr.	J. P. Lockwood
W5095	<200	19°29'46" 155°20'39" Kilauea Crater	1,684	Charcoal rootlets from edge of Keamoku flow, NW. of Kipuka Kekake, Powerline Rd., pole 140.	J. P. Lockwood
W5108	<200	19°30'42" 155°44'24" Puu O Uo	2,082	Charcoal twigs from Puu O Uo flow, along S. margin of the flow near uppermost ohia forest, 5 km WNW. from summit of Puu O Uo.	J. P. Lockwood
W4186	220±60	19°42'41" 155°33'09" Puu Koli	1,914	Charcoal, beneath thin pahoehoe toes at contact with old MK aa around small kipuka, Red Leg Trail, 5 km SSE. of Pohakuloa cabins.	J. P. Lockwood
W3871	230±60	19°26'44" 155°19'07" Kilauea Crater	1,281	Charcoal roots in ash below Keamoku aa flow, from roadcuts in Kipuka Ki.	J. P. Lockwood
W4920	250±70	19°27'48" 155°17'04" Kilauea Crater	1,250	Charcoal (rerun of W-3879, age 830±60).	J. P. Lockwood
W5329	260±200	19°10'52" 155°28'41" Pahala	85	Charcoal, from soil beneath pahoehoe overlying Pahala Ash, top of Pahala section, at base of cliff below Puu Kalea.	N. G. Banks
W4537	270±60	19°37'49" 155°33'43" Puu Koli	2,243	Charcoal roots beneath aa margin of Keamuku flow, 3 km NNE. of Puu Kokoolau.	J. P. Lockwood

TABLE 10.1.—*Radiocarbon dates from Mauna Loa Volcano, Island of Hawaii*—Continued

Sample	Radiocarbon age (years before present)	Location (latitude, longitude, quadrangle)	Elevation (m)	Sample and site description	Collector
W4006	290±70	19°24'44" 155°20'33" Kilauea Crater	1,095	Charcoal roots in Pahala Ash, underlying Kipuka Maunaiu flow, Ohaikea Rd.	P. W. Lipman
W4183	300±60	19°29'44" 155°26'40" Kipuka Pakekake	2,550	Charcoal, SW. margin of prominent red pahoehoe kipuka on W. margin of Kau 1880 flow.	J. P. Lockwood
W4360	300±60	19°39'37" 155°20'41" Kilauea Crater	1,676	Charcoal underlying marginal blocks of aa, Keamoku flow, Powerline Rd., pole 142.	J. P. Lockwood
W4175	300±50	19°35'12" 155°25'17" Puu Ulaula	2,292	Charcoal underlying dark grey aa, Puu Kupanaha flow, overlain by 1880 lavas, Kulani-Mauna Loa Observatory Rd.	J. P. Lockwood
W5106	300±80	19°24'58" 155°20'59" Kilauea Crater	1,166	Coarse charcoal roots, beneath tree mold in base of flow, Lacey Cesspool picrite-rich flow overlain by basalt of Kipuka Maunaiu, Peter Lee Rd.	J. P. Lockwood
W4238	300±70	19°04'17" 155°40'57" Kahuku Ranch	688	Charcoal root fragments in olivine-rich pahoehoe, Puu Lokuana.	P. W. Lipman
W4341	330±60	19°30'29" 155°20'36" Kulani	1,766	Charcoal rootlets under aa at margin of pahoehoe flow, Puu Kulua flow, lowest unit in Keamoku suite, Powerline Rd., 1.6 km S. of Keawewai Camp.	J. P. Lockwood
W4805	340±60	19°23'50" 155°22'16" Kilauea Crater	1,155	Charcoal rootlets beneath thin edge of fresh pahoehoe flow, Ke A Poomoku Ohaikea, 3 m mauka of Powerline Rd.	J. P. Lockwood
W5535	340±150	19°36'14" 155°40'36" Puu O Uo	2,137	Charcoal roots at margin of loose shelly pahoehoe, under radial vent surrounded by 1859 lava.	J. P. Lockwood
W4919	350±70	19°26'44" 155°19'07" Kilauea Crater	1,281	Charcoal (rerun of W-3871, age 230±60).	P. W. Lipman
W5539	360±150	19°50'23" 155°47'23" Puu Anahulu	710	Bush fragments at basal contact of 1859 aa flow, Mamalahoa Highway, 37 km NE. of Kailua.	J. P. Lockwood
W5079	410±60	19°32'37" 155°27'56" Puu Oo	2,059	Charcoal roots in pocket of ash beneath thin pahoehoe toe above picrite, Humuulu flow, overlain by 1855 flow, 1 km E. of Mauna Loa Observatory Rd.	J. P. Lockwood
W4049	420±70	19°27'47" 155°20'48" Kilauea Crater	1,498	Vitreous charcoal from Keamoku flow, upper unit, underlying thin outlier of aa.	J. P. Lockwood
W3790	420±70	19°33'15" 155°18'04" Kulani	1,574	Charcoal from thin soil, developed on old spatter, underlying Kulani picrite, on high-standing dry hillock.	J. P. Lockwood
W4882	430±70	19°32'28" 155°19'54" Kulani	1,795	Coarse charcoal fragments in a horizontal tree mold at margin of tube-fed pahoehoe Kulaloa flow, Kilauea Forest Reserve lobe, overlain by Kulani picrite, 200 m SW. of Kilauea Forest Reserve Boundary Rd.	J. P. Lockwood

TABLE 10.1.—*Radiocarbon dates from Mauna Loa Volcano, Island of Hawaii*—Continued

Sample	Radiocarbon age (years before present)	Location (latitude, longitude, quadrangle)	Elevation (m)	Sample and site description	Collector
W4571	440±70	19°31'08" 155°23'42" Puu Ulaula	2,268	Charcoal rootlets beneath margin of aa breccia, W. Keamoku flow, 1.3 km NE. of Puu Ulaula Trail.	J. P. Lockwood
W3793	450±60	19°33'15" 155°18'07" Kulani	1,574	Charcoal from water-saturated spatter underlying 2 m of Kulani picrite.	J. P. Lockwood
W4576	480±60	19°33'19" 155°24'15" Puu Ulaula	2,414	Charcoal roots beneath Mauna Loa Boys' School flow, at crescent-shaped spatter cone, 1 km ENE. of Puu Kulua.	J. P. Lockwood
W4243	490±80	19°05'49" 155°40'43" Kahuku Ranch	829	Charcoal fragments in dirt and ash adjacent to flow margin, underlying aa containing small phenocrysts of plagioclase and olivine, Akihi.	J. P. Lockwood
W5568	510±150	19°31'52" 155°46'08" Puu Lehua	1,762	Vitreous twigs and fine rootlets, under slabby pahoehoe fragments at outer margin of thin pahoehoe squeeze-out, N. margin of Puu O Uo flow, 250 m NW. of prominent kipuka.	J. P. Lockwood
W3880	530±60	19°27'48" 155°17'04" Kilauea Crater	1,250	Organic debris and sooty soil directly underlying ropy pahoehoe.	J. P. Lockwood
W4790	540±70	19°26'25" 155°24'07" Kipuka Pakekake	1,609	Charcoal rootlets, Ke A Poomoku pahoehoe flow, W. edge of fresh flow, 1.3 km S. of National Park boundary, 700 m SE. of prominent rockwall.	J. P. Lockwood
W4916	560±70	19°30'11" 155°23'10" Puu Ulaula	2,079	Charcoal (rerun of W-4118, age 580±80).	J. P. Lockwood
W5098	570±60	19°37'37" 155°08'28" Piihonua	463	Charcoal twigs and roots, in muddy ash layer between Kulaloa and Panaewa pahoehoe flows, off Kulaloa Rd., Waiakea Homesteads.	J. P. Lockwood
W4367	570±70	19°26'33" 155°16'29" Kilauea Crater	1,238	Charcoal under basalt flow on Volcano Golf Course, Keamoku flow, 50 m W. of third green on golf course.	R. B. Moore
W4118	580±80	19°30'11" 155°23'10" Puu Ulaula	2,079	Charcoal from younger phase of Keamoku flow.	J. P. Lockwood
W4338	590±50	19°31'43" 155°20'48" Kulani	1,887	Coarse charcoal fragments from tree mold at margin of aa flow, Keawewai Camp flow, Powerline Rd., pole 112.	J. P. Lockwood
W3898	590±70	19°23'25" 155°30'53" Mauna Loa	2,428	Charcoal from pocket of baked ash, very young precaldera aa flow, Ainapo Trail.	J. P. Lockwood
W1047	600±250	19°21'54" 155°23'06" Wood Valley	910	Charcoal fragments in sandy ash, top of Pahala Ash, just below black sandy ash, Kaoiki Pali.	G. A. Macdonald
W4807	620±70	19°32'22" 155°20'44" Kulani	1,917	Charcoal roots in ash pockets of picrite-rich aa, at contact with aphanitic pahoehoe, Solomon's Water-hole flow, Powerline Rd., between pole 103 and 104, Puu Oo Trail.	J. P. Lockwood
W4025	640±45	19°13'09" 155°37'54" Puu Keokeo	1,774	Charcoal fragments at base of Pohina flow, where it rests on Pahala Ash at edge of Na Manua Haalou Swamp.	J. P. Lockwood

TABLE 10.1.—*Radiocarbon dates from Mauna Loa Volcano, Island of Hawaii*—Continued

Sample	Radiocarbon age (years before present)	Location (latitude, longitude, quadrangle)	Elevation (m)	Sample and site description	Collector
W4845	640±70	19°28'17" 155°17'44" Kilauea Crater	1,349	Charcoal rootlets in soot, beneath thick pahoehoe toe, Keamoku flow, Keauhou Ranch, Golf Course lobe.	J. P. Lockwood
W4410	660±70	19°10'37" 155°28'37" Pahala	53	Charcoal roots in Pahala Ash just below lava basalt flow, stream bed, Kanenelu flat, Hionamoa Gulch.	N. G. Banks
W4801	730±70	19°26'20" 155°22'21" Kilauea Crater	1,442	Charcoal fragments and soot, from small bush molds, upper part of deep ash below pahoehoe toe, picrite-rich Kipuka Maunaiu pahoehoe, overlying Ke A Poomoku flow, 1.5 km mauka of Powerline Rd.	J. P. Lockwood
W4156	740±60	19°09'02" 155°33'56" Punaluu	473	Charcoal roots from ash at base of Kipuka Nene flow, exposed in pothole along Hilea Gulch.	P. W. Lipman
W4012	740±60	19°08'17" 155°33'08" Punaluu	305	Charcoal roots from ash underlying thin variable-olivine pahoehoe flow at Kipuka Nene, Hilea Gulch.	P. W. Lipman
W5301	760±100	19°35'46" 155°47'11" Puu Lehua	1,561	Charcoal in soil on Hualalai cinder cone, overrun by picritic ML flow, 1 km NE. of Kanahaha.	R. B. Moore
W4345	760±70	19°29'34" 155°20'37" Kilauea Crater	1,661	Charcoal rootlets beneath thin pahoehoe lobe, Powerline Rd., pole 142.	J. P. Lockwood
W4232	780±70	19°05'41" 155°42'09" Kahuku Ranch	780	Small sparse hard charcoal, in thin marginal aa near its base, where lapping onto pumice from Kahuku picrite cone.	P. W. Lipman
W4863	780±70	19°29'12" 155°25'08" Kipuka Pakekake	2,254	Charcoal roots in discontinuous soil above picrite-rich aa where overlain by thin aphanitic tube-fed pahoehoe and vesicular aa, overlain by 1880 and Ke A Poomoku flows, E. margin of small kipuka 400 m ESE. of 1880 lobe distal end.	J. P. Lockwood
W3879	830±60	19°27'48" 155°17'04" Kilauea Crater	1,250	Charcoal from flaky roots in Pahala Ash, 15 cm beneath ropy pahoehoe.	J. P. Lockwood
W4794	880±60	19°31'11" 155°18'06" Kulani	1,533	Tiny vitreous fragments of ohia leaves and twigs in soot, from overlying tree canopy knocked off by falling spatter, Olaa Uka flow, dense rain forest in gully on S. edge of Kulani Cone.	J. P. Lockwood
W4137	890±60	19°08'30" 155°33'17" Punaluu	381	Charcoal roots from lens of Pahala-like ash, below thin olivine-rich pahoehoe, Kipuka Nene flow, Hilea Gulch.	P. W. Lipman
W4047	910±70	19°29'15" 155°23'11" Kipuka Pakekake	1,934	Charcoal under olivine-rich aa flow.	J. P. Lockwood
W4231	910±60	19°10'17" 155°36'05" Punaluu	878	Charcoal roots in Pahala Ash, underlying olivine-rich pahoehoe, and overlying phenocryst-poor aa, stream bed, Hilea Gulch gauging station.	P. W. Lipman

TABLE 10.1.—*Radiocarbon dates from Mauna Loa Volcano, Island of Hawaii*—Continued

Sample	Radiocarbon age (years before present)	Location (latitude, longitude, quadrangle)	Elevation (m)	Sample and site description	Collector
W5083	1,030±60	19°22'50" 155°30'17" Mauna Loa	2,091	Elongate charcoal fragments, beneath thin Keamoku pahoehoe toes, overlying discontinuous ash, Lower Ainapo Trail.	J. P. Lockwood
W4870	1,100±70	19°29'52" 155°19'07" Kilauea Crater	1,542	Coarse charcoal root fragments underlying thick pahoehoe, overlain by Keamoku flow, Puu Oo Trail, Keauhou Ranch Rd.	J. P. Lockwood
W4631	1,110±60	19°42'23" 155°05'10" Hilo	41	Charcoal roots underlying pahoehoe with round vesicles, at top of stream deposit, overlying thin Kulaloa pahoehoe flow, Waiakea Stream, S. of Kumakoa St. bridge.	J. M. Buchanan-Banks
W5537	1,120±200	19°28'44" 155°42'38" Sulphur Cone	2,499	Charcoal rootlets in small ash pocket below narrow young aphanitic pahoehoe toes, 2.8 km SW. of Puu O Uo.	J. P. Lockwood
W5597	1,140±300	19°42'50" 155°05'56" Hilo	67	Scattered charcoal fragments in ash deposit, overlain by Kinoole aa, Alenaio Stream at tributary E. of Komohana Street.	J. M. Buchanan-Banks
W5519	1,150±200	19°37'28" 155°45'22" Puu Lehua	1,649	Charcoal in soil on picritic pahoehoe, under young pahoehoe, SE. of Ahu a Umi Heiau.	R. B. Moore
W3910	1,270±60	19°23'22" 155°33'45" Mauna Loa	2,318	Charcoal in ash pocket underlying tree mold in tube-fed late prehistoric pahoehoe flow, Ainapo Trail, ML S. flank.	J. P. Lockwood
W4430	1,270±70	19°16'03" 155°29'06" Wood Valley	689	Charcoal roots in soil and ash below lava flow, overlain by crystal-poor pahoehoe, Pelelilii Gulch.	N. G. Banks
W4343	1,280±70	19°40'11" 155°07'20" Hilo	232	Charcoal roots beneath thin pahoehoe flow, young Waiakea-Uka pahoehoe, Waiakea-Uka School.	J. P. Lockwood
W4237	1,320±50	19°33'47" 155°20'42" Kulani	1,884	Vitreous narrow rootlets under pahoehoe toes, overlying weathered phenocryst-rich aa kipuka, and overlain by Kulani picrite.	J. P. Lockwood
W3000	1,330±70	19°22'29" 155°22'33" Wood Valley	915	Organic debris and charcoal, at uppermost part of yellow ash section, overridden by ML pahoehoe, Kaoiki Pali.	R. I. Tilling
W5325	1,370±200	19°13'55" 155°27'59" Pahala	389	Charcoal roots in soil and in ash and pahoehoe, Highway 11, Piukea Gulch.	N. G. Banks
W4813	1,380±60	19°31'08" 155°15'53" Kulani	1,297	Soot with scattered fragments of fern leaves, in deep ash above old spatter, under fresh spatter covered by fountain-fed pahoehoe, Olaa Uka flow, one day's hike S. of Stainback Highway.	J. P. Lockwood
W3858	1,400±60	19°13'26" 155°27'56" Pahala	457	Carbonized wood fragments (ohia lehu) in Pahala Ash, beneath young prehistoric ML pahoehoe flow, Kaalaala Gulch.	P. W. Lipman

TABLE 10.1.—*Radiocarbon dates from Mauna Loa Volcano, Island of Hawaii*—Continued

Sample	Radiocarbon age (years before present)	Location (latitude, longitude, quadrangle)	Elevation (m)	Sample and site description	Collector
W4340	1,400±70	19°35'43" 155°20'52" Kulani	1,779	Charcoal rootlets imbedded in soot at base of pahoehoe, overlain by nearly aphanitic tube-fed pahoehoe, overlain by 1942 aa, 1 km NW. of Mauna Loa Boys' School.	J. P. Lockwood
W4981	1,470±50	19°38'34" 155°03'23" Hilo	110	Charcoal rootlets in unoxidized pocket of older, coarse grey-black aa at base of Panaewa picrite flow, Allied Aggregates Quarry.	J. P. Lockwood
W3857	1,470±60	19°13'26" 155°27'56" Pahala	457	Charcoal fragments beneath young prehistoric ML pahoehoe flow, Kaalaala Gulch.	P. W. Lipman
W4357	1,490±50	19°35'03" 155°20'52" Kulani	1,812	Charcoal roots in soil beneath aphanitic pahoehoe, with uniform-size, spherical vesicles, 1 km E. of Mauna Loa Boys' School.	J. P. Lockwood
W5153	1,500±70	19°09'48" 155°27'46" Pahala	53	Charcoal roots in soil and ash under pahoehoe, Punaluu Gulch.	N. G. Banks
W5461	1,510±110	19°17'02" 155°29'50" Wood Valley	963	Charcoal roots in sooty zone at top of Pahala Ash, young Upper Wood Valley pahoehoe, overlies section exposed on Wood Valley headwall, Kapapala Ranch Water Tunnel Trail.	J. P. Lockwood
W5458	1,640±150	19°22'16" 155°22'49" Wood Valley	920	Charcoal roots in black sooty ash at top of Pahala Ash, Halfway House olivine-rich pahoehoe, Peter Lee Rd. and Highway 11 junction, 2 m above base of Kaoiki Pali, in fresh slump.	J. P. Lockwood
W4344	1,690±70	19°31'57" 155°21'13" Kulani	1,963	Large charcoal roots underlying marginal blocks of aa above old spatter on this mostly buried spatter cone, Powerline Rd., 5.5 km SW. of Kulani Prison Headquarters.	J. P. Lockwood
W5271	1,700±80	19°27'58" 155°48'14" Wood Valley	?	Charcoal rootlets in ash under pahoehoe, upper crossover of water-course along E. edge of Wood Valley.	N. G. Banks
W5278	1,740±100	19°40'12" 155°36'52" Hilo	201	Charcoal twigs and roots in pockets at top of ash deposit overlying aa, overlain by young pahoehoe flow, Kukuau flow, Waiakea Stream, N. of Hoaka Rd.	J. M. Buchanan-Banks
W5564	1,740±250	19°36'36" 155°40'17" Puu O Uo	2,140	Charcoal roots beneath thin pahoehoe sheets, W. of eastern 1859 lobe, 500 m SE. of P.T.A. Bobcat Trail.	J. P. Lockwood
W4985	1,760±60	19°36'49" 155°20'26" Kulani	1,666	Charcoal fragments beneath pahoehoe toes in ash pockets of aa, overlain by Punahoa flow, N. of 1942 flow, Powerline Rd.	J. P. Lockwood
W3850	1,810±80	19°11'14" 155°29'09" Pahala	137	Charcoal in Pahala Ash, overlain by phenocryst-poor ML pahoehoe from SW. rift zone, Moaula Gulch.	P. W. Lipman
W4116	1,840±60	19°29'10" 155°23'08" Kipuka Pakekake	1,940	Charcoal from thin soil at contact of pahoehoe and aa.	J. P. Lockwood

TABLE 10.1.—*Radiocarbon dates from Mauna Loa Volcano, Island of Hawaii*—Continued

Sample	Radiocarbon age (years before present)	Location (latitude, longitude, quadrangle)	Elevation (m)	Sample and site description	Collector
W4022	1,860±70	19°14'56" 155°36'50" Punaluu	1,891	Charcoal fragments at base of plagioclase porphyritic aa flow, Punaluu Kahawai.	P. W. Lipman
W4163	1,980±80	19°18'01" 155°33'43" Keaiwa Reservoir	2,036	Charcoal roots in Pahala Ash, at base of flow, underlying phenocryst-poor aa flow, collected where aa cascaded through small lava tube, Kauhuhuula Gulch.	P. W. Lipman
W4161	2,000±70	19°17'47" 155°34'12" Keaiwa Reservoir	2,060	Charcoal fragments from basal Hionamoa flow, a large phenocryst-poor unit, head of Makaka Ravine.	P. W. Lipman
W477	2,000±250	19°39'45" 155°08'06" Hilo	244	Charcoal of ohia buried in cinders of prehistoric vent of the last group of lavas of ML, Kau volcanic series, Waiakea Homesteads.	G. A. Macdonald
W4017	2,010±70	19°17'10" 155°35'24" Keaiwa Reservoir	2,074	Charcoal fragments from Pahala-like ash, underlying weathered phenocryst-poor pahoehoe, Hionamoa Gulch.	P. W. Lipman
W4550	2,030±60	19°29'13" 155°56'17" Honaunau	61	Carbonaceous soil underlying glassy pahoehoe flow and overlying the entire Kealakekua Pali sequence, Captain Cook Monument, Kaawaloa, Kealakekua Bay.	J. P. Lockwood
W478	2,070±250	19°39'45" 155°08'06" Hilo	244	Charcoal of tree fern, Kau Basalt, Waiakea Homesteads.	G. A. Macdonald
W4579	2,120±70	19°30'32" 155°23'45" Puu Ulaula	2,213	Charcoal roots beneath pahoehoe toes, overlain by all Keamoku flow units, Upper Strip Rd. pahoehoe, 250 m NE. of Puu Ulaula.	J. P. Lockwood
W4015	2,180±60	19°07'04" 155°34'28" Naalehu	534	Charred log, base of young aa flow containing large olivine phenocrysts.	P. W. Lipman
W3876	2,190±70	19°27'50" 155°17'36" Kilauea Crater	1,256	Charcoal from root underlying ML NE. rift aa flow, covering Pahala Ash on E. extension of Kaoiki fault, Puu Oo Trail.	J. P. Lockwood
W5566	2,240±150	19°42'07" 155°23'25" Puu Oo	1,742	Charcoal root fragments overlain by Puu Kahiliku picrite-rich flow, deep gully in ash along cow path, 50 m E. of Puu Oo Ranch access road.	J. P. Lockwood
W4008	2,300±60	19°09'23" 155°32'26" Punaluu	316	Carbonized wood fragments in ash at base of the plagioclase-porphyritic aa flow in the Ninole Gulch area, one of the last flows from this sector of ML to flow into ocean.	P. W. Lipman
W4831	2,340±70	19°27'50" 155°17'36" Kilauea Crater	1,256	Charcoal root in sooty ash, under Keauhou Ranch aa flow, overlain by all Keamoku flows, junction of Puu Oo Rd. and Kaoiki Pali.	J. P. Lockwood
W4142	2,440±60	19°08'36" 155°31'19" Punaluu	53	Charcoal fragments in Pahala-like ash, base of Ninole aa flow, Ninole Gulch.	P. W. Lipman

TABLE 10.1.—*Radiocarbon dates from Mauna Loa Volcano, Island of Hawaii*—Continued

Sample	Radiocarbon age (years before present)	Location (latitude, longitude, quadrangle)	Elevation (m)	Sample and site description	Collector
W4810	2,550±80	19°32'06" 155°17'20" Kulani	1,448	Charcoal and rootlets in organic mat at base of pahoehoe toes, overlain by dense tube-fed pahoehoe, N. of Kulani Cone, 2.5 km S. of Stainback Highway, Kulani Prison boundary road, S. of prominent picrite exposures.	J. P. Lockwood
W4377	2,650±50	19°07'04" 155°34'28" Naalehu	533	Carbonized wood fragment at base of olivine-rich aa flow, Kaalaiki quarry.	P. W. Lipman
W3836	2,830±60	19°26'28" 155°20'38" Kilauea Crater	1,064	Carbonaceous soil below aa of the Keamoku flow.	P. W. Lipman
W3845	2,880±70	19°22'20" 155°23'56" Wood Valley	1,083	Charcoal root fragments, top of Pahala Ash below olivine-rich ML pahoehoe flow, where draped over Kaoiki fault scarp, Kaoiki Pali.	P. W. Lipman
W4174	2,890±70	19°38'34" 155°02'53" Hilo	111	Amorphous sooty material underlying Panaewa flow, Hilo side of Allied Aggregates quarry.	J. P. Lockwood
W3841	2,950±80	19°20'02" 155°24'29" Wood Valley	793	Charcoal root fragments from Pahala Ash, overlain by olivine-rich pahoehoe, Puu Kuanene area.	P. W. Lipman
W5112	3,110±60	19°42'34" 155°16'22" Upper Piihonua	1,105	Charcoal rootlets in ash mixed with aa clasts at base of pahoehoe, overlain by upper Piihonua Punahoa flow, Wailuku River.	J. P. Lockwood
W4621	3,140±70	19°42'17" 155°07'01" Hilo	169	Charcoal root at contact between lava flow and ash deposit, overlain by pahoehoe with spherical vesicles, 698 Kaumana Dr.	J. M. Buchanan-Banks
W5542	3,200±200	19°36'25" 155°40'21" Puu O Uo	2,131	Charcoal roots beneath thick pahoehoe toes, overlain by Kaniku flow, Naiomamani Kipuka.	J. P. Lockwood
W4629	3,360±80	19°41'52" 155°07'29" Hilo	216	Charcoal roots beneath thin pahoehoe flow at contact with thick ash deposit, underlies 1880 flow and overlies ash, Waipahoehoe Stream, Ponahawai Homesteads, N. of Kaumana Dr.	J. M. Buchanan-Banks
W5536	3,360±200	19°50'47" 155°47'12" Puu Anahulu	756	Charcoal roots in basal aa breccia, under Mamalahoa Highway, Kaniku euhedral olivine laths with aa, Highway 190, E. of 1859 contact.	J. P. Lockwood
W4624	3,380±80	19°43'00" 155°08'08" Piihonua	256	Charcoal tree trunk in sealed tree mold, overlain by KPUA pahoehoe, Wailuku-Alenaio diversion canal, N. of Waianuenue Ave.	J. M. Buchanan-Banks
W5107	3,450±60	19°42'56" 155°09'11" Piihonua	299	Charcoal root at base of tree mold, Lauiole Falls pahoehoe, overlain by Waianuenue pahoehoe, Wailuku River, 20 m E. of Hilo County Water Department gauging ladder.	J. P. Lockwood
W5604	3,450±200	19°42'50" 155°05'56" Hilo	67	Charcoal (rerun of W-5081, age 3920±80).	J. M. Buchanan-Banks

TABLE 10.1.—*Radiocarbon dates from Mauna Loa Volcano, Island of Hawaii*—Continued

Sample	Radiocarbon age (years before present)	Location (latitude, longitude, quadrangle)	Elevation (m)	Sample and site description	Collector
W4223	3,600±70	19°08'41" 155°36'58" Punaluu	983	Charcoal roots in Pahala Ash, overlain by transitional aa-pahoehoe containing sparse large olivine and plagioclase phenocrysts, roadcut, Mountain House tunnel road.	P. W. Lipman
W2016	3,620±250	19°04'15" 155°36'52" Naalehu	326	Charcoal, depth 417 cm, underlying surface pahoehoe lava flow, Bishop Museum cesspool excavation, Waiohinu.	R. R. Doell
W5086	3,630±80	19°25'25" 155°20'50" Kilauea Crater	1,244	Charcoal roots in patches in unconsolidated oxidized ash, overlain by Upper Strip Rd. phenocryst-picrite pahoehoe, 1.9 km N. of Kapapala Ranch corral.	J. P. Lockwood
W4574	3,700±70	19°43'05" 155°08'18" Piihonua	263	Charcoal roots beneath young tube-fed pahoehoe, overlying massive olivine-rich aa, KPUA flow, Wailuku River, across from KPUA.	J. P. Lockwood
W856	3,740±250	19°04'00" 155°37'00" Naalehu	326	Charcoal, under pahoehoe flow in churchyard, Waiohinu.	K. J. Murata
W4164	3,750±70	19°16'02" 155°36'38" Keaiwa Reservoir	1,996	Charcoal fragments, base of aa flow which contains abundant small plagioclase phenocrysts, Puu Kinikini.	P. W. Lipman
W5565	3,790±200	19°42'56" 155°18'53" Upper Piihonua	1,314	Charcoal root fragments, at base of Wailuku River olivine-pahoehoe flow, S. bank of river, 500 m upstream from Water Gauging Station Trail.	J. P. Lockwood
W4152	3,800±90	19°08'53" 155°30'58" Punaluu	84	Charcoal fragments from thin lens of Pahala-like ash below transitional hummocky pahoehoe-aa flow, Highway 11 roadcut.	P. W. Lipman
W4009	3,900±80	19°11'22" 155°31'42" Punaluu	488	Carbonized wood, base of Punaluu aa flow, Punaluu Gulch.	P. W. Lipman
W4132	3,900±90	19°09'39" 155°32'33" Punaluu	372	Charcoal roots from thin lens of Pahala-like ash, below pahoehoe flow, Ninole Gulch.	P. W. Lipman
W5081	3,920±80	19°42'50" 155°05'56" Hilo	67	Charcoal from stream deposit between two pahoehoe flows, overlain by Kulaloa flow, Alenaio Stream at Komohana St.	J. M. Buchanan-Banks
W1046	4,030±350	19°21'54" 155°23'06" Wood Valley	911	Charcoal in sandy silty ash, top of Pahala Ash, Mamalahoa Highway, Kaoiki Pali.	G. A. Macdonald
W3803	4,050±50	19°42'48" 155°07'05" Hilo	152	Soil, rich in organic matter and containing bits of charcoal, from cesspool excavation, Kaumana area of Hilo.	J. P. Lockwood
W4358	4,070±70	19°35'41" 155°20'41" Kulani	1,762	Fine charcoal rootlets in sooty organic layer at base of Kulani pahoehoe, underlying thick lobe of pahoehoe, 1.2 km NW. of Mauna Loa Boys' School.	J. P. Lockwood
W4957	4,170±90	19°41'06" 155°08'46" Piihonua	354	Charcoal atop orange ash, Wilder Rd. pahoehoe, under Kulaloa flow, 400 m S. of Humuulu Saddle Rd.	J. P. Lockwood

TABLE 10.1.—*Radiocarbon dates from Mauna Loa Volcano, Island of Hawaii*—Continued

Sample	Radiocarbon age (years before present)	Location (latitude, longitude, quadrangle)	Elevation (m)	Sample and site description	Collector
W4993	4,210±80	19°41'29" 155°09'08" Piihonua	372	Charcoal exposed at base of pahoehoe by slumping of underlying ash along streambed, under Piihonua pahoehoe, W. of Akolea Rd., Kaliuiki Stream.	J. P. Lockwood
W3855	4,210±90	19°25'25" 155°20'22" Kilauea Crater	?	Charcoal from Pahala Ash, below phenocryst-poor aa flow draped on Kaoiki fault scarp.	P. W. Lipman
W3844	4,340±80	19°21'52" 155°23'16" Wood Valley	920	Charcoal fragments from soil zone below aa flow, draped over Kaoiki fault scarp.	P. W. Lipman
W5077	4,410±120	19°41'24" 155°07'12" Hilo	183	Vegetative mat beneath surficial pahoehoe at contact with underlying ash, overlain by Wilder Rd. pahoehoe, Brilhante property, Edita Rd.	J. M. Buchanan-Banks
W4982	4,690±60	19°43'07" 155°16'30" Piihonua	1,160	Charcoal from yellow-brown ash overlain by aa of MK hawaiite, N. bank of Wailuku River.	J. P. Lockwood
W4224	4,770±90	19°09'14" 155°36'59" Punaluu	1,044	Charcoal roots in Pahala Ash, overlain by phenocryst-poor pahoehoe flow, roadcut on Mountain House tunnel road.	P. W. Lipman
W5567	4,790±250	19°42'56" 155°18'30" Upper Piihonua	1,292	Charcoal root fragments in scattered pockets of soft MK ash at base of dense aphanitic aa of Upper Wailuku River, S. bank of river.	J. P. Lockwood
W4135	5,160±100	19°09'38" 155°32'33" Punaluu	369	Charcoal roots from thin layer of Pahala-like ash, overlain by phenocryst-poor pahoehoe flow, Ninole Gulch.	P. W. Lipman
W4536	5,250±100	19°36'40" 155°01'55" Mountain View	98	Large charcoal root, Puna Sugar Picrite aa, overlying yellow-red ash, 700 m SW. of plantation house, Keaau-Pahoa Rd.	J. P. Lockwood
W3862	5,650±90	19°32'34" 155°07'28" Mountain View	528	Charcoal fragments, top of Pahala-type ash overlain by young ML aa flow, SW. of Mountain View.	P. W. Lipman
W3930	6,160±110	19°25'05" 155°35'42" Naalehu	567	Charcoal root fragments in ash, overlain by transitional pahoehoe-aa ML flow, Alapai Gulch.	P. W. Lipman
W5599	7,230±230	19°40'48" 155°04'31" Hilo	76	Carbonaceous roots at top of ash layer, overlain by Malaai aa, Hilo Golf Course, drainage ditch N. of Haihai St.	J. M. Buchanan-Banks
W4117	7,300±100	19°04'19" 155°33'26" Naalehu	21	Carbonaceous soil from ash at base of top ML flow, bay S. of Kahukupoko Point.	P. W. Lipman
W4351	7,750±70	18°56'37" 155°40'48" Ka Lae	98	Charcoal and soil from top of Pahala Ash, along contact with flow in Kahawai Kolano gully, 0.6 km ENE. of Pacific Missile Range Facility.	J. P. Lockwood

TABLE 10.1.—*Radiocarbon dates from Mauna Loa Volcano, Island of Hawaii*—Continued

Sample	Radiocarbon age (years before present)	Location (latitude, longitude, quadrangle)	Elevation (m)	Sample and site description	Collector
W3813	7,950±110	19°08'45" 155°30'58" Punaluu	76	Black carbonaceous soil at top of Pahala Ash, Puehu quarry.	J. P. Lockwood
W4991	7,960±110	19°30'44" 155°19'36" Kulani	1,658	Charcoal rootlets at contact between Keauhou Ranch picrite and nearly buried spatter cone, middle of logging road, 900 m W. of Puu Lalaau.	J. P. Lockwood
W4969	8,030±70	19°39'16" 155°08'21" Piihonua	372	Organic matter in zones around aa clasts at base of D. Smith flow, Waiakea Stream, 1.9 km above Hoaka Rd. Bridge.	J. P. Lockwood
W4821	8,550±90	19°21'49" 155°23'18" Wood Valley	930	Rootlets and carbonaceous sooty ash, top of Pahala Ash, Halfway House picrite-rich pahoehoe that mantles Kaoiki Pali here, halfway up prominent gully at Old Halfway House.	J. P. Lockwood
W3853	8,550±100	19°25'11" 155°20'20" Kilauea Crater	1,122	Charcoal root fragments from soil zone, overlain by ML pahoehoe flow, interbedded with Pahala Ash, or reworked ash, Kaoiki Pali.	P. W. Lipman
W4803	8,740±100	19°26'08" 155°19'45" Kilauea Crater	1,219	Soft charcoal rootlets in soot below thick Strip Rd. pahoehoe, in prominent deep gully near National Park SW. boundary fence, 1.5 km SW. of Strip Rd. in Kipuku Ki.	J. P. Lockwood
W4975	9,020±130	19°39'38" 155°07'40" Piihonua	274	Charcoal rootlets in thin ash at base of flow, overlain by Puu Hoakalei picrite flow, Waiakea Stream, 500 m upstream from Hoaka Rd. bridge.	J. P. Lockwood
W4372	9,080±80	19°02'45" 155°33'32" Naalehu	37	Sooty soil at top of ash zone, Maniania Pali, overlain by olivine -rich pahoehoe, top of seacliff, 100 m NE. of contact with plagioclase -phyric flow.	P. W. Lipman
W4201	9,170±100	19°12'26" 155°32'17" Punaluu	652	Charcoal roots in Pahala Ash, overlain by phenocryst-poor pahoehoe flow, part of flow sequence from ML that laps out against eroded Ninole Hills, Upper Moaula Gulch.	P. W. Lipman
W4419	9,300±130	19°09'46" 155°29'51" Pahala	64	Charcoal roots in soil and ash below lava flow, under crystal-poor ML flow, in kipuka, Punaluu Gulch.	N. G. Banks
W3840	9,500±140	19°25'05" 155°24'29" Kilauea Crater	1,144	Charcoal rootlets and carbonaceous soil from Pahala Ash between two ML aa flows, draped over Kaoiki fault scarp, Kaoiki Pali.	P. W. Lipman
W4529	9,540±110	19°39'14" 155°08'22" Piihonua	379	Charcoal roots and wood fragments beneath capped tree mold, Old Waiakea Uka aphanitic pahoehoe, Waiakea Stream, between Hoaka and Ainaole Rds.	J. P. Lockwood
W4884	9,780±140	19°39'32" 155°06'03" Hilo	201	Charcoal tree root in thin ash deposit under plagioclase phyric pahoehoe, Waiakea Homesteads, streambed, Alaloa Rd.	J. M. Buchanan-Banks

TABLE 10.1.—*Radiocarbon dates from Mauna Loa Volcano, Island of Hawaii*—Continued

Sample	Radiocarbon age (years before present)	Location (latitude, longitude, quadrangle)	Elevation (m)	Sample and site description	Collector
W5087	9,960±70	19°39'19" 155°08'17" Piihonua	360	Charcoal in brown layer of thick yellow ash at base of pahoehoe, under very old pahoehoe of Waiakea Stream, 1.7 km upstream from Hoaka Rd. bridge.	J. P. Lockwood
W5092	10,090±120	19°43'06" 155°16'23" Upper Piihonua	1,097	Charcoal roots at base of Wailuku River pahoehoe, in ash deposit which overlies MK rocks, S. bank of Wailuku River.	J. P. Lockwood
W907	10,140±300	19°03'00" 155°35'00" Naalehu	61	Carbonaceous ash exposed in sea cliff, S. of Honuapu, top of Pahala Ash, which is underlain and overlain by basalt, Maniani Pali.	G. D. Fraser
W5103	10,150±80	19°42'23" 155°12'02" Piihonua	663	Coarse charcoal at base of tree mold, Upper Wailuku River young pahoehoe, under Punahoa flow, Wailuku River, 70 m above waterfall.	J. P. Lockwood
W4160	10,290±150	19°06'01" 155°33'34" Naalehu	186	Charcoal roots in Pahala Ash, overlain by phenocryst-poor pahoehoe flow, Honuapu.	P. W. Lipman
W5072	10,320±70	19°39'32" 155°07'51" Piihonua	305	Charcoal root beneath pahoehoe at contact with underlying ash deposit, overlain by D. Smith and University of Hawaii flows, Waiakea Stream in Waiakea-Uka, Kalana Place.	J. M. Buchanan-Banks
W4995	10,400±150	19°30'53" 155°19'11" Kulani	1,635	Root fragments under pahoehoe flow that overlies Puu Lalaau olivine-rich spatter, N. bank of water hole, 50 m NW. of Puu Lalaau.	J. P. Lockwood
W4623	10,610±150	19°43'24" 155°06'59" Hilo	140	Charcoal root at contact between lava rubble and ash, under Wailuku River channel aa, W. of Rainbow Falls.	J. M. Buchanan-Banks
W4014	10,820±90	19°08'18" 155°32'56" Punaluu	229	Charcoal roots in uppermost main Pahala Ash, near tree molds in overlying pahoehoe flow sequence, Hilea Gulch.	P. W. Lipman
W3487	11,780±100	18°58'18" 155°37'18" Ka Lae	5	Charcoal fragments in Pahala Ash overlain by an intercalated basalt flow, W. side of Kaaluala Bay, 9.2 km NE. of South Point.	J. P. Lockwood
W4121	13,210±190	19°04'20" 155°33'25" Naalehu	15	Carbonaceous soil from ash at base of middle flow sequence, bay S. of Kahukupoko Point.	P. W. Lipman
W4627	13,530±180	19°43'12" 155°06'32" Hilo	99	Crumbly rootlets at top of ash deposit at contact with overlying pahoehoe, Rainbow Falls intersection, Waianuenue Ave. and Kaumana Dr.	J. M. Buchanan-Banks
W4392	13,800±300	19°32'51" 155°55'57" Kealakekua	439	Charcoal from shrub in soil, on picritic basalt flow, under basalt flow from Hualalai in Honalo, E. side of Mamalahoa Highway.	R. B. Moore
W4971	14,080±150	19°43'14" 155°07'13" Hilo	162	Tree charcoal at contact between pahoehoe flow and basal ash, underlying picrite-porphyritic pahoehoe, parking lot of First Protestant Church, Waianuenue Ave.	J. M. Buchanan-Banks

TABLE 10.1.—*Radiocarbon dates from Mauna Loa Volcano, Island of Hawaii*—Continued

Sample	Radiocarbon age (years before present)	Location (latitude, longitude, quadrangle)	Elevation (m)	Sample and site description	Collector
W5091	14,080±160	19°42'41" 155°10'05" Piihonua	451	Charcoal roots at base of pahoehoe in kipuka of yellow ash, underlying Punahoa flow, Kahoama Stream, upstream from Wailuku River.	J. P. Lockwood
W4973	14,370±190	19°42'58" 155°07'25" Hilo	186	Charcoal tree root beneath pahoehoe flow at contact with underlying ash, overlain by porphyritic pahoehoe, Ainaloa Subdivision, Kaeokulani St.	J. M. Buchanan-Banks
W4620	14,500±200	19°45'20" 155°07'27" Hilo	163	Charcoal root at contact between ash unit and pahoehoe flows sequence, which underlies thick ash, saprolite, and lava from MK, Wailuku River.	J. M. Buchanan-Banks
W4977	14,530±120	19°43'05" 155°07'01" Hilo	146	Charcoal roots at contact between pahoehoe flow and underlying ash, overlain by picrite-porphyritic pahoehoe, Kaumana Springs, Waianuenue Ave.	J. M. Buchanan-Banks
W4894	21,900±270	19°39'32" 155°07'51" Piihonua	305	Charcoal root beneath pahoehoe in ash deposit, underlying picrite-rich and olivine-poor pahoehoe, Waiakea Stream in Waiakea-Uka, Kalana Place.	J. M. Buchanan-Banks
W4890	23,840±600	19°41'50" 155°07'25" Hilo	207	Charcoal root in ash deposit, between pahoehoe flows, Waipahoehoe Stream, Chong's Bridge.	J. M. Buchanan-Banks
W5075	24,240±500	19°39'40" 155°07'38" Piihonua	268	Charcoal roots beneath pahoehoe at contact with underlying ash deposit, underlies University of Hawaii and D. Smith aa flows, Waiakea Stream in Waiakea-Uka, Hoaka Rd.	J. M. Buchanan-Banks
W4019	26,410±390	19°08'19" 155°32'53" Punaluu	183	Thin carbonaceous mat, scraped from base of pahoehoe flow of the Ninole volcanic rocks, Hilea Gulch.	P. W. Lipman
W5094	28,120±400	19°41'53" 155°08'06" Piihonua	256	Charcoal rootlets at top of yellow ash, overlain by Punahoa flow, overlies old picrite-rich flow, Lower Kaluiiki Stream, 600 m W. of Chong's Bridge.	J. P. Lockwood
W4368	28,150±800	18°56'20" 155°38'50" Ka Lae	9	Carbonaceous soil under pahoehoe flow interlayered with main unit of Pahala Ash, sea cliff exposure, 75 m SW. of margin of Puu O Mahaua Cone.	P. W. Lipman
W5452	28,200±600	19°41'50" 155°08'14" Piihonua	287	Charcoal roots under aphanitic pahoehoe flow, Kaluiiki Stream.	J. P. Lockwood
W3935	31,100±900	19°04'16" 155°33'24" Naalehu	1.5	Charcoal roots in Pahala-like ash, at base of tree mold in overlying ML aa flow, base of sea cliff in bay S. of Kahukupoko Point.	P. W. Lipman
W4128	31,400±1,600	19°29'07" 155°55'53" Honaunau	5	Charcoal fragments in ash, overlain by small pahoehoe lobe of mainly aa flow, along prominent main ash bed exposed along Pali Kapu Keoua, Kealakekua scarp.	P. W. Lipman
W5105	>38,000	19°42'25" 155°12'06" Piihonua	664	Charcoal fragments at top of thick ash, overlain by Homelani ash, in turn overlain by Punahoa aphanitic pahoehoe, Upper Wailuku River.	J. P. Lockwood

TABLE 10.2—*Radiocarbon dates from Kilauea Volcano, Island of Hawaii*

[Samples listed in order of increasing age; uncertainty is one standard deviation, ± 1σ; modern age means sample is younger than AD 1950; ML = Mauna Loa; MK = Mauna Kea; mauka = toward the mountain, makai = toward the sea; see figs. 10.2–10.4 for localities. Stratigraphic nomenclature from Langenheim and Clague (chapter 1, part II)]

Sample	Radiocarbon age (years before present)	Location (latitude, longitude, quadrangle)	Elevation (m)	Sample and site description	Collector
W2999	Modern	19°24'18" 155°14'53" Volcano	1,166	Humus layer in yellow ash, overlying pahoehoe flow of prehistoric age, Thurston Lava Tube.	R. I. Tilling
W3481	Modern	19°24'00" 155°20'00" Kilauea Crater	1,076	Wood (ohia) from fallen tree in ohia-koa forest, in aa and ash.	J. P. Lockwood
W3486	Modern	19°22'00" 155°18'00" Kilauea Crater	1,257	Wood (ohia) from fallen tree in kipuka, overlying pahoehoe.	J. P. Lockwood
W4122	Modern	19°26'37" 155°15'05" Kilauea Crater	1,196	Charcoal, 60-80 cm above base in lithic ash of upper Keanakoi, makai side of Iiwi Road across from Lockwood house.	J. P. Lockwood
W4637	Modern	19°28'36" 154°53'25" Pahoa South	177	Charcoal rootlets, underlying thin Puu Pilau flow, W. side of quarry.	R. B. Moore
W5321	Modern	19°19'21" 155°22'46" Wood Valley	786	Wood and charcoal roots below tree mold underlying historical but undescribed shield, N. of 1920 lava flow.	N. G. Banks
W2970	<200	19°30'06" 154°51'48" Kapoho	61	Wood from Kapoho Cone, E. rift zone.	R. I. Tilling
W3467	<200	19°22'27" 155°08'10" Makaopuhi Crater	765	Charcoal underlying fountain-fed pahoehoe flow, SE. side of small crater SE. of Napau, E. rift zone.	R. T. Holcomb
W3468	<200	19°22'27" 155°08'10" Makaopuhi Crater	765	Charcoal in root mold where lava flowed into crack, underlying fountain-fed pahoehoe, E. rift zone.	R. T. Holcomb
W3480	<200	19°24'00" 155°20'00" Kilauea Crater	1,079	Wood (ohia) from kipuka of older aa lava surrounded by finer, fresher aa of the Keamoku flow.	J. P. Lockwood
W3483	<200	19°24'00" 155°20'00" Kilauea Crater	1,076	Wood (ohia) from standing tree in ohia-koa forest.	J. P. Lockwood
W3485	<200	19°21'00" 155°14'00" Makaopuhi Crater	920	Wood (ohia) from standing tall tree, in Ainahou Ranch pahoehoe.	J. P. Lockwood
W3886	<200	19°26'48" 155°19'09" Kilauea Crater	1,283	Charcoal fragments in Keanakakoi ash, from pit, Kipuka Ki.	P. W. Lipman
W359	<200	19°24'55" 154°55'50" Pahoa South	69	Charcoal in tree mold in prehistoric pahoehoe, E. rift zone, Puna.	G. A. Macdonald
W3937	<200	19°17'37" 155°24'24" Wood Valley	?	Charcoal from tree mold where lava ponded rapidly against the base of a fault scarp.	R. T. Holcomb
W4184	<200	19°19'48" 155°12'59" Makaopuhi Crater	765	Charcoal underlying tube-fed pahoehoe in large kipuka, E. rift zone, Ainahou Range.	J. P. Lockwood
W4436	<200	19°12'13" 155°27'58" Pahala	218	Charcoal roots in soil layer underlying young pahoehoe, 671 m E. of benchmark 803 on Highway 11 just N. of Pahala turnoff.	N. G. Banks

TABLE 10.2.—*Radiocarbon dates from Kilauea Volcano, Island of Hawaii*—Continued

Sample	Radiocarbon age (years before present)	Location (latitude, longitude, quadrangle)	Elevation (m)	Sample and site description	Collector
W4449	<200	19°35'16" 155°01'01" Mountain View	96	Charcoal roots in baked ash beneath surficial lava flow at Waipahoehoe Gulch, E. rift zone, S. bank of gulch along S. margin of Puna Sugar Co. field 20.	R. T. Holcomb
W4452	<200	19°15'35" 155°24'37" Wood Valley	530	Charred wood from within the hollow interior of sealed lava tree protruding from surface of Red Cone flow, along gaping eruptive fissures about 1 km uprift from Red Cones, along the SW. rift zone.	R. T. Holcomb
W4573	<200	19°34'53" 155°03'43" Mountain View	244	Charcoal roots in ash beneath thin tube-fed pahoehoe of the Kurtistown Kilauea flow, 400 m SW. of Kurtistown Assembly of God Church.	J. P. Lockwood
W4638	<200	19°28'28" 154°54'01" Pahoa South	204	Charcoal rootlets in young flow overlying Kiapu Cone in Leilani Estates.	R. B. Moore
W4639	<200	19°28'55" 154°55'00" Pahoa South	229	Charcoal under tree mold beneath pre-1790 flow in Leilani Estates, roadcut on Kahukai St., N. side of intersection with Kupono St.	R. B. Moore
W4644	<200	19°28'19" 154°53'31" Pahoa South	171	Charcoal roots in soil under surface lava flow, in roadcut W. side of Malama Homesteads road, 80 m S. of old Pohoiki Rd.	R. B. Moore
W4689	<200	19°28'03" 154°55'24" Pahoa South	242	Charcoal roots in thin soil underlying pre-1790 flow, roadcut, S. Pomaikai St., Leilani Estates.	R. B. Moore
W5323	<200	19°19'43" 155°22'49" Wood Valley	792	Wood and charcoal at edge of tree mold and in underlying roots, beneath 1920 lava flow, 700 m N. of 81-6 geodimeter station.	N. G. Banks
W3938	210±60	19°15'35" 155°24'37" Wood Valley	?	Charcoal in tree mold, 3 m from eruptive fissure.	R. T. Holcomb
W5110	230±60	19°19'01" 155°13'07" Makaopuhi Crater	512	Charcoal roots along vertical contact between Kamapuaa flow and pahoehoe at W. flow contact, at base of Poliokeawe Pali, below cascade drapery 125 m NE. of easternmost switchback in Ainahou Ranch.	J. P. Lockwood
W3881	260±70	19°32'47" 155°05'53" Mountain View	415	Charcoal root fragments in ash below phenocryst-poor Kilauea pahoehoe, in Fern Acres.	P. W. Lipman
W4834	300±70	19°27'55" 155°15'25" Kilauea Crater	1,187	Charcoal in thick organic mat underlying Keanakakoi Ash Member of Puna Basalt on east-west section of Wright Road.	J. P. Lockwood
W4162	310±70	19°28'17" 155°10'10" Volcano	784	Charcoal roots from ash at base of Kilauea pahoehoe flow, SE. side of Wung Ranch quarry.	P. W. Lipman
W4470	310±70	19°13'02" 155°27'42" Pahala	341	Charcoal root in ash underlying young pahoehoe lava flow exposed in gully, NE. edge of macadamia orchard.	R. T. Holcomb

TABLE 10.2.—*Radiocarbon dates from Kilauea Volcano, Island of Hawaii*—Continued

Sample	Radiocarbon age (years before present)	Location (latitude, longitude, quadrangle)	Elevation (m)	Sample and site description	Collector
W4661	320±70	19°33'09" 155°01'23" Mountain View	151	Charcoal in tree mold, enclosed in pahoehoe flow in Iki-Thurston lava tube area, located near private home 100 m W. of Melia St. in Orchid Land Estates.	R. B. Moore
W3811	330±60	19°13'02" 155°27'42" Pahala	341	Charcoal fragments from Kilauea pahoehoe flow, beneath young prehistoric ML pahoehoe flow exposed in gully.	J. P. Lockwood
W3849	340±60	19°28'02" 155°15'05" Kilauea Crater	1,177	Carbonaceous soil and charcoal, base of pyroclastic sequence, underlying basal reticulite of Keanakakoi Ash, Member of Puna Basalt in pit in Olaa Forest Reserve, depth 50 cm, Wright Rd.	P. W. Lipman
W5048	340±60	19°29'00" 154°52'05" Kapoho	110	Charcoal in tree mold underlying Honuaula flow, in new papaya field 100 m mauka of road connecting Pohoiki and Kapoho Rds.	R. B. Moore
W3800	350±150	19°26'14" 154°56'07" Pahoa South	174	Carbonaceous debris under prehistoric aa flow, depth 2 m, in cesspool excavation, Puna.	J. P. Lockwood
W3870	350±60	19°26'38" 155°15'07" Kilauea Crater	?	Clay, rich in organic matter and containing charcoal fragments near base of Keanakakoi Ash.	J. P. Lockwood
W5054	440±60	19°24'05" 154°55'15" Pahoa South	15	Charcoal fragments in soil underlying Kehena Beach Section, 50 m N. of small old quarry on makai side of Highway 137.	R. B. Moore
W3842	450±60	19°19'59" 155°24'20" Wood Valley	792	Charcoal fragments from soil below phenocryst-poor pahoehoe flow from Kilauea along base of Kaoiki Pali, old quarry, SW. rift zone.	P. W. Lipman
W3941	450±60	19°35'16" 155°01'06" Mountain View	518	Charcoal from top of ash layer beneath tube-fed pahoehoe flow partly filling old stream channel between two kipukas of ash-covered aa apparently derived from Mauna Loa.	R. T. Holcomb
W5453	450±110	19°24'00" 155°05'23" Kalalua	677	Charcoal roots overlain by prehistoric flow SE. of Puu Kahaualea, 250 m E. of crack that consumed January 1983 eruption.	J. P. Lockwood
W4688	490±60	19°27'26" 154°55'43" Pahoa South	274	Charcoal underlying young flow W. of Kaliu, Leilani Estates, South Kumakahi St., 40 m S. of intersection with Malama St.	R. B. Moore
W5275	490±150	19°17'17" 155°21'11" Kau Desert	640	Charcoal in soil layer recording old fire, buried by Keanakakoi Ash, Member of Puna Basalt, 15 km SW. of crater.	N. G. Banks
W5145	500±100	19°18'09" 155°20'29" Kau Desert	724	Charcoal roots in soil-ash pockets underlying Puu Koae aa.	N. G. Banks
W4404	530±70	19°12'48" 155°27'44" Pahala	271	Charcoal roots in soil beneath pahoehoe flow, 0.7 km SE. of Highway 11 in gulch that parallels the highway.	N. G. Banks

TABLE 10.2.—*Radiocarbon dates from Kilauea Volcano, Island of Hawaii*—Continued

Sample	Radiocarbon age (years before present)	Location (latitude, longitude, quadrangle)	Elevation (m)	Sample and site description	Collector
W5218	550±70	19°09'36" 155°26'50" Pahala	15	Charcoal in soil pockets underlying Ulekuwale Pueo.	N. G. Banks
W4867	570±70	19°26'35" 155°16'24" Kilauea Crater	1,238	Vitreous fern and ohia leaves in organic black soot lens, underlying Keanakakoi Ash, Member of Puna Basalt near cesspool excavation at SE. end of Dahlberg residence, 150 m NW. of golf course number 3 green.	J. P. Lockwood
W5423	570±100	19°25'58" 155°15'52 Kilauea Crater	1,201	Charcoal rootlets in soil developed within Keanakakoi surge deposit, on Sandalwood Trail between steaming bluff and Volcano House.	J. M. Buchanan-Banks
W4337	620±70	19°20'11" 155°13'25" Makaopuhi Crater	815	Charcoal rootlets at base of tube-fed Ainahou flow located 1.5 km SSE. of Ainahou Ranch House, Kamapuaa flow, 20 m E. of Poliokuwe Pali Rd.	J. P. Lockwood
W5152	660±70	19°19'41" 155°19'47" Kau Desert	853	Charcoal roots in mixed ash and eolian sand under pahoehoe.	N. G. Banks
W3860	670±60	19°13'02" 155°27'35" Pahala	399	Charcoal in Pahala Ash, below thin pahoehoe (one of the last major prehistoric flows on Kilauea SW. rift zone), along small gully, tributary to Kaalaala Gulch.	P. W. Lipman
W4402	700±70	19°17'44" 155°08'41" Kau Desert	658	Charcoal roots in soil and ash underlying pahoehoe flow, 325 m SW. of Hilina Pali Rd. end.	N. G. Banks
W3999	730±80	19°27'04" 155°14'19" Volcano	1,134	Carbonaceous soil containing small charcoal fragments from beneath toe of pahoehoe flow.	P. W. Lipman
W5147	890±70	19°09'52" 155°28'04" Pahala	45	Charcoal roots in ash pockets underlying pahoehoe, E. side of Puu Pili Rd., NW. of Puu Pili.	N. G. Banks
W4690	900±70	19°27'07" 154°56'55" Pahoa South	348	Charcoal underlying rootless lava flow located in cinder pit 500 m W. of Highway 13 in Kamaili Homesteads, SE. part of Norona Quarry.	R. B. Moore
W5215	940±70	19°09'79" 155°26'44" Pahala	46	Charcoal roots in discontinuous soil-ash layer under pahoehoe, E. of Ulekuwale Pueo.	N. G. Banks
W4998	960±60	19°26'11" 155°16'59" Kilauea Crater	1,225	Carbonized leaves in vitric ash rich in organic material, within Uwekahuna Ash Member of Puna Basalt 50 m E. of easternmost point of Tree Molds visitor area road.	J. P. Lockwood
W5211	960±70	19°11'34" 155°27'26" Pahala	145	Charcoal roots in soil and ash under pahoehoe, E. side of flood control ditch makai of aa gravel borrow pits.	N. G. Banks
W5319	970±120	19°27'20" 155°12'25" Volcano	968	Charcoal twigs and rootlets in black sooty soil at base of pahoehoe flow underlying Keanakakoi Ash Member of Puna Basalt located at Volcano Dump off Highway 11.	J. P. Lockwood
W3856	1,040±70	19°28'02" 155°15'05" Kilauea Crater	1,177	Carbonaceous clay and ash at base of pyroclastic base-surge sequence, Uwekahuna Ash Member of Puna Basalt just N. of Kilauea summit, in pit of Olaa Forest Reserve, depth 80 cm, Wright Rd.	P. W. Lipman

TABLE 10.2.—*Radiocarbon dates from Kilauea Volcano, Island of Hawaii*—Continued

Sample	Radiocarbon age (years before present)	Location (latitude, longitude, quadrangle)	Elevation (m)	Sample and site description	Collector
W3827	1,130±60	19°18'06" 155°18'23" Kau Desert	704	Charcoal beneath Kilauea basalt flow, overlying Hilina Series rocks exposed in Poliokeawe Pali.	J. P. Lockwood
W5212	1,140±70	19°17'53" 155°18'38" Kau Desert	693	Charcoal roots in soil, makai edge of trail W. of Hilina Pali parking lot in the first gully.	N. G. Banks
W5135	1,150±70	19°19'46" 155°16'51" Kau Desert	892	Charcoal roots in soil under pahoehoe, Kipuka Nene flow, surface flow in parking lot.	N. G. Banks
W4674	1,270±70	19°28'19" 154°53'31" Pahoa South	169	Charcoal rootlets in soil underlying lava flow in roadcut, W. side of Malama Homesteads Rd., 80 m S. of old Pohoiki Rd.	R. B. Moore
W4414	1,330±60	19°11'27" 155°27'29" Pahala	146	Charcoal of one tap root below a tree mold, Cinder Hills.	N. G. Banks
W4837	1,480±60	19°27'55" 155°15'25" Kilauea Crater	1,187	Organic soot within the Uwekahuna Ash Member of Puna Basalt on the east-west section of Wright Rd.	J. P. Lockwood
W4359	1,510±60	19°13'56" 155°27'35" Pahala	399	Carbonaceous soil under thin pahoehoe of Kilauea SE. rift zone, small gully, tributary to Kaalaala Gulch, 25 km mauka of Highway 11.	P. W. Lipman
W5303	1,650±150	19°27'55" 155°15'25" Kilauea Crater	1,187	Dark sooty ash with charcoal flakes (with small modern rootlets present) underlying the Wright Road Uwekahuna Ash Member of Puna Basalt on the east-west section of Wright Rd.	J. P. Lockwood
W5097	1,790±70	19°28'40" 155°17'23" Kilauea Crater	1,347	Black sooty soil from organic layer at base of weathered ash unit, overlain by Uwekahuna Ash, Member of Puna Basalt, Keauhou Ranch, 1.4 km E. of Puu Oo Trail, 2.2 km WSW. of end of Wright Rd.	J. P. Lockwood
W4119	1,800±80	19°14'48" 155°21'09" Maliikakani Point	50	Carbonaceous baked ash containing charred root fragments beneath aa flow mantling Pahala Ash on rim of Kukalauula Pali.	R. T. Holcomb
W4369	2,070±80	19°28'17" 155°10'10" Volcano	786	Charcoal near base of tree mold under pahoehoe flow exposed in quarry on Wung Rd., NW. of Highway 11.	P. W. Lipman
W3859	2,080±70	19°28'02" 155°15'05" Kilauea Crater	1,177	Carbonaceous clay and ash, underlying base-surge sequence, Uwekahuna Ash, Member of Puna Basalt just N. of Kilauea summit, from pit in Olaa Forest Reserve, depth 130 cm.	P. W. Lipman
W5292	2,080±150	19°27'55" 155°15'25" Kilauea Crater	1,187	Dark sooty ash with charcoal flakes (cleaned of modern rootlets) underlying the Uwekahuna Ash Member of Puna Basalt on Wright Road at the same location as W-5303 (age 1,650 ± 150).	J. P. Lockwood
W3885	2,160±70	19°28'17" 155°10'10" Volcano	786	Charcoal around base of tree mold in crystal-poor Kilauea pahoehoe, Wung Ranch quarry.	P. W. Lipman
W5052	2,360±90	19°22'55" 154°57'29" Kalapana	9	Charcoal in soil underlying early Heiheiahulu pahoehoe flow with tree molds exposed at Kalapana dump on mauka side of road.	R. B. Moore

TABLE 10.2.—*Radiocarbon dates from Kilauea Volcano, Island of Hawaii*—Continued

Sample	Radiocarbon age (years before present)	Location (latitude, longitude, quadrangle)	Elevation (m)	Sample and site description	Collector
W201	2,500±250	19°25'00" 155°20'00" Kilauea Crater	1,209	Fern mold underlying basaltic pumice, excavation for N. wing of Volcano House, Keanakakoi Ash Members of Puna Basalt.	H. A. Powers
W5345	2,770±150	19°27'37" 155°14'52" Volcano	1,160	Charcoal rootlets at base of pahoehoe flow buried by Uwekahuna Ash and Keanakakoi Ash Members of Puna Basalt, located 15 m E. of Wright Rd. and 3.5 km N. of Old Volcano Highway.	J. P. Lockwood
W3831	3,480±80	19°18'06" 155°18'22" Kau Desert	703	Charcoal beneath Kilauea basalt flow overlying rocks of the Hilina Basalt, exposed in Poliokeawe Pali.	J. P. Lockwood
W5324	3,500±200	19°11'23" 155°28'20" Pahala	137	Charcoal roots in soil under pahoehoe flow at right angle bend of Old Pahala Dump Rd., W. side of road, makai of bagasse flume.	N. G. Banks
W4380	3,560±60	19°28'17" 155°10'10" Volcano	782	Carbonaceous soil and charcoal fragments within Wung Quarry ash sequence on Wung Ranch, Uwekahuna Ash, Member of Puna Basalt, of Highway 11.	P. W. Lipman
W3884	3,610±60	19°12'44" 155°28'10" Pahala	177	Charcoal in ash below olivine-rich pahoehoe flow, Pahala vent.	P. W. Lipman
W4177	3,690±70	19°34'56" 155°01'49" Mountain View	142	Charcoal beneath pahoehoe exposed in trench, Puna Sugar Field 20, SE. from Keauu.	J. P. Lockwood
W3798	4,820±90	19°28'10" 155°18'20" Kau Desert	698	Carbonized charcoal tree fern (hapuu) from ash directly above lava dated by W-3809 (age 10,680 ± 130), from new scar formed during 1975 earthquake Hilina Pali.	J. P. Lockwood
W3873	6,620±150	19°17'11" 155°18'15" Kau Desert	?	Ash rich in organic material and containing charcoal fragments from uppermost level of thick Pahala Ash sequence, W. side Keana Bihopa Arroyo, Hilina Pali.	J. P. Lockwood
W3809	10,680±130	19°18'10" 155°18'20" Kau Desert	696	Charcoal beneath basalt and ash in upper Hilina Pali section, from new scar formed during 1975 earthquake.	J. P. Lockwood
W905	17,360±650	19°20'00" 155°20'00" Kau Desert	189	Carbonaceous ash from contact of lower Pahala Ash with overlying basalt, SE. end of seaward-facing Keone fault scarp, Keone Pali.	G. D. Fraser
W5241	21,600±600	19°16'39" 155°15'30" Kau Desert	107	Charcoal roots in black ash located at the top of the second ash layer above the base of Kapukapu cliff.	N. G. Banks
W3801	22,500±300	19°16'16" 155°17'10" Kau Desert	171	Charcoal from top of Pahala Ash section on Puu Keone.	J. P. Lockwood
W5238	22,660±600	19°16'38" 155°15'30" Kau Desert	91	Charcoal roots in black soil located above lowest ash layer in Kapukapu cliff.	N. G. Banks
W3814	22,800±340	19°16'14" 155°17'20" Kau Desert	183	Charcoal exposed in fresh outcrop created by massive slumping during 1975 earthquake, Puu Keone.	J. P. Lockwood

TABLE 10.3.—*Radiocarbon dates from Hualalai Volcano, Island of Hawaii*

[Samples listed in order of increasing age; uncertainty is one standard deviation, ± 1σ; modern age means sample is younger than AD 1950; ML = Mauna Loa; MK = Mauna Kea; mauka = toward the mountain, makai = toward the sea; see figs. 10.2–10.4 for localities. Stratigraphic nomenclature from Langenheim and Clague (chapter 1, part II)]

Sample	Radiocarbon age (years before present)	Location (latitude, longitude, quadrangle)	Elevation (m)	Sample and site description	Collector
W4634	<200	19°42'55" 155°54'35" Kailua	1,841	Charcoal rootlets from high-water mark of olivine basalt flow from Kaupulahu Crater along main road up NW. flank and rift zone of Hualalai.	R. B. Moore
W4381	<200	19°37'55" 155°48'50" Hualalai	1,667	Charcoal rootlets in soil developed on Puu Ikaaka cinders, overlain by pahoehoe flow, 700 m E. of Hualalai summit road along Judd Trail, 200 m S. of trail at N. base of Puu Ikaaka.	R. B. Moore
W4389	<200	19°35'00" 155°58'33" Kealakekua	3	Charcoal in soil separating two flows at Kahaluu Beach Park, on E. side of Alii Drive, below T.K. Cook's house.	R. B. Moore
W5124	<200	19°44'08" 155°56'25" Kailua	1,250	Charcoal in soil developed on old cone, overlain by young flow on Hualalai Ranch, N. of Moanuiahea near flower nursery.	R. B. Moore
W5381	110±60	19°38'46" 155°49'00" Hualalai	1,768	Charcoal in soil under Moore Crater flow, SE. side of airstrip.	R. B. Moore
W4394	300±60	19°41'50" 155°52'44" Kailua	2,316	Charcoal from under edge of Malekule flow at end of road on N. side of cinder cones, edge of flow against cinder cone.	R. B. Moore
W5531	710±150	19°37'00" 155°49'26" Puu Lehua	1,509	Charcoal in soil under toe of Waha Pale flow at E. edge of flow, 800 m S. of Bishop experimental plot.	R. B. Moore
W5491	900±110	19°40'27" 155°45'53" Hualalai	1,545	Charcoal in cinders under toe of Moore Crater flow, one of the largest on the Big Island.	R. B. Moore
W5130	1,030±60	19°43'03" 155°52'48" Kailua	1,987	Charcoal under North Jackson Crater flow between two old cones.	R. B. Moore
W5522	1,180±200	19°43'09" 155°46'11" Hualalai	1,378	Charcoal in soil on ML flow under pahoehoe overflow from channel of Trusdell Crater flow.	R. B. Moore
W4383	1,330±50	19°34'23" 155°55'00" Kealakekua	366	Charcoal from under highest basalt flow in Tanaka's quarry, E. side of quarry.	R. B. Moore
W4171	2,030±80	19°46'52" 155°50'00" Puu Anahulu	866	Charcoal in soil zone on top of trachyte cinders under olivine-bearing basalt flow, N. flank of Puu Waawaa.	R. B. Moore
W4388	2,290±70	19°34'58" 155°56'46" Kealakekua	354	Charcoal in soil on top of aa flow under basalt flow on E. side of Mamalahoa Highway, N. of Tanaka quarry.	R. B. Moore
W5068	2,350±80	19°41'47" 155°52'31" Hualalai	2,353	Charcoal under edge of older Luamakami pahoehoe flow overlying cinders in ditch in road 300 m W. of highest saddle N. of Hualalai summit.	R. B. Moore

TABLE 10.3.—*Radiocarbon dates from Hualalai Volcano, Island of Hawaii*—Continued

Sample	Radiocarbon age (years before present)	Location (latitude, longitude, quadrangle)	Elevation (m)	Sample and site description	Collector
W5073	2,390±60	19°42'18" 155°50'44" Hualalai	2,000	Charcoal under spatter bombs at edge of deposit from NE. Mawahine Cone along road between Bishop Estate and Puu Waawaa Ranch.	R. B. Moore
W5076	2,670±80	19°41'14" 155°51'55" Hualalai	2,377	Charcoal under 0.5 m bombs from the 8001-ft. cone on S. side of lower saddle on N. side of Hualalai summit.	R. B. Moore
W5559	3,030±200	19°45'07" 155°54'47" Kiholo	1,030	Charcoal in soil under Puu Waawaa Ranch flow at ranch road.	R. B. Moore
W5127	3,100±80	19°44'15" 155°52'40" Hualalai	2,292	Charcoal in soil developed on old cone, covered by flow, transected by pit crater, on E. side of pit crater 700 m NE. of Malekule.	R. B. Moore
W4376	3,600±70	19°40'55" 155°58'44" Kailua	341	Charcoal in soil on aa flow under basalt flow near Palani Junction, in roadcut on side of Highway 19, 0.8 km S. of Palani Junction.	R. B. Moore
W5562	3,610±200	19°45'05" 155°57'29" Kiholo	817	Charcoal in soil beneath old Hualalai Ranch flow along road W. of ranch office.	R. B. Moore
W5132	3,990±70	19°41'50" 155°52'17" Hualalai	2,390	Charcoal in soil developed on older spatter, covered by younger spatter on S. side of main Hualalai summit road, 100 m W. of highest saddle.	R. B. Moore
W5070	4,390±70	19°41'44" 155°52'59" Hualalai	2,256	Charcoal in cinders under edge of slabby pahoehoe flow SW. of Malekule in gully 200 m above main road down Kaupuleku side of Hualalai.	R. B. Moore
W4378	4,720±80	19°41'50" 155°52'47" Kailua	2,292	Charcoal in soil developed on cinders underlying edge of second flow down from West Malekule on E. wall of West Malekule pit crater.	R. B. Moore
W5496	5,350±180	19°40'16" 155°51'55" Hualalai	1,905	Charcoal in cinders from extensive cinder unit S. of Hualalai summit along road near W. boundary of quad.	R. B. Moore
W5297	6,360±100	19°40'13" 155°51'41" Hualalai	1,902	Charcoal under Puu Neneakolu flow along Waiaha Stream between road and Puu Hale.	R. B. Moore
W5299	8,770±200	19°41'45" 155°52'01" Hualalai	2,390	Charcoal in red soil under cinders in canyon above recent alluvial fan at Hualalai summit.	R. B. Moore
W4371	9,490±100	19°51'21" 155°52'15" Puu Anahulu	195	Charcoal under olivine-rich basalt 4 m thick at NW. end of Puu Anahulu Cone, 200 m W. of end of trail leading N. from Mamalahoa Highway.	R. B. Moore
W4391	10,370±150	19°35'25" 155°57'26" Kealakekua	199	Carbonaceous material in yellow to red cinders overlain by basalt flow at intersection of Kuakini Highway and Kam III Rd.	R. B. Moore
W4365	12,230±150	19°48'39" 155°50'30" Puu Anahulu	677	Charcoal roots in soil zone on top of trachyte lava flow, under olivine-rich basalt flow on W. side of Puu Anahulu, roadcut, 200 m E. of Mamalahoa Highway.	R. B. Moore
W5056	12,950±150	19°39'28" 155°57'37" Kailua	439	Charcoal in soil under Keopu flow 100 m W. of Mamalahoa Highway next to Keopu subdivision road.	R. B. Moore

TABLE 10.4—*Radiocarbon date from Mauna Kea Volcano, Island of Hawaii*

[Samples listed in order of increasing age; uncertainty is one standard deviation, ± 1σ; modern age means sample is younger than AD 1950; ML = Mauna Loa; MK = Mauna Kea; mauka = toward the mountain, makai = toward the sea; see figs. 10.2–10.4 for localities. Stratigraphic nomenclature from Langenheim and Clague (chapter 1, part II)]

Sample	Radiocarbon age (years before present)	Location (latitude, longitude, quadrangle)	Elevation (m)	Sample and site description	Collector
W5541	5,630±200	19°41'53" 155°26'41" Puu Oo	1,986	Charcoal root fragments at top of deep ash overlain by Puu Kalaieha flow on Parker Ranch land off Saddle Rd.	J. P. Lockwood

STRATIGRAPHY OF KILAUEA VOLCANO

By R. Michael Easton[1]

ABSTRACT

This paper reviews and revises the lithostratigraphic nomenclature of Kilauea Volcano. The major stratigraphic units of the volcano are redefined as the Hilina Basalt (oldest), Pahala Ash, and Puna Basalt (youngest) in accordance with the stratigraphic code. Four pyroclastic units within the Hilina Basalt can be used as stratigraphic markers; these are formally proposed and described here and given member rank. These new stratigraphic units are, from oldest to youngest, the Halape, Kahele, Pohakaa and Moo Ash Members. The Pohakaa has a similar distribution and lithology to the Pahala Ash and represents a major period of ash deposition on Kilauea at about 40–50 ka. Two pyroclastic units intercalated within the Puna Basalt are the circa 1.5-ka Uwekahuna Ash Member and the mostly A.D. 1790 Keanakakoi Ash Member. The origin and source of these pyroclastic units, particularly the Pahala Ash and the Pohakaa Ash Member, is briefly discussed, in light of new rare-earth-element and petrographic data from these units.

INTRODUCTION

A stratigraphic unit, whether it be a group, formation, member, or flow, becomes established through the repeated demonstration of its utility. Since the Hawaiian Volcano Observatory was established 75 years ago, a number of stratigraphic terms have been introduced to help geologists unravel the stratigraphy of Kilauea Volcano. Some of these terms have become well established through use; others, although widely used, do not meet all of the criteria required of formal stratigraphic units as outlined in Article 3 of the North American stratigraphic code (North American Commission on Stratigraphic Nomenclature, 1983).

The purpose of this paper is to review the stratigraphic nomenclature of Kilauea Volcano and to revise it so as to be consistent with the stratigraphic code and with current needs. Some new stratigraphic terms are herein formally proposed so that they will be available to the geologic community and their utility can be tested. Stratigraphy is an important tool in aiding our understanding of Kilauea Volcano, and I hope that this revision of stratigraphic nomenclature will make this tool even more effective.

ACKNOWLEDGMENTS

R.T. Holcomb was in large part responsible for this paper through his encouragement, and this paper has benefited from discussion over the years with M.O. Garcia, R.T. Holcomb, J.P. Lockwood, and G.A. Macdonald. As a historical note, it was G.A. Macdonald's intention to revise the stratigraphy of the Island of Hawaii and Kilauea Volcano in order to make the nomenclature consistent with the recommendations of the stratigraphic code, but this work was cut short by his untimely death. This paper was reviewed by R.L. Christiansen and R.T. Holcomb, and I thank them for their careful reading and helpful comments and suggestions.

PREVIOUS WORK

The various lithostratigraphic schemes that have been applied to Kilauea Volcano and correlations between them are summarized in figure 11.1. An essential element of all these schemes is the use of the Pahala Ash as a marker horizon to divide the lava of Kilauea Volcano into pre-Pahala and post-Pahala units. This usage arose because the Pahala Ash was considered to be the only stratigraphic unit found on several (four of the five) volcanoes on the Island of Hawaii (see Stearns and Macdonald, 1946). It has therefore been used as an important stratigraphic marker. As discussed in detail later, the Pahala Ash does not always meet the criteria required of a marker horizon, and this can present local correlation problems.

Stone (1926) divided Kilauea rocks into the pre-Kilauea Series, comprising all rocks below and including the unit he called the Pahala Ash, and the Kilauea Series, comprising prehistoric and historical lavas younger than the Pahala. L.F. Noble and W.O. Clark (unpub. data, 1920, in Washington, 1923) made a similar division, but used the terms Pahala Series and post-Pahala Series; this division was later revised in Stearns and Clark (1930). In both these works, the lavas of Kilauea and Mauna Loa were not differentiated stratigraphically. Stearns and Clark (1930) included lava and tuff of both volcanoes in the Pahala Basalt (which included the upper ash member now called the Pahala Ash) and the overlying Kamehame Basalt. The Kamehame Basalt was divided into a lower prehistoric part, which included all ash units above the Pahala Basalt, and an upper part composed essentially of historic flows (fig. 11.1).

Wentworth (1938), in his examination of Kilauea pyroclastic rocks, introduced the term Pahala Tuff for what has generally been called the Pahala Ash by workers both before and since. He also introduced the terms Uwekahuna Formation and Keanakakoi Formation for ash units of Kilauea stratigraphically above his Pahala Tuff.

[1]Ontario Geological Survey, Toronto, Ontario, Canada M53 1B3.

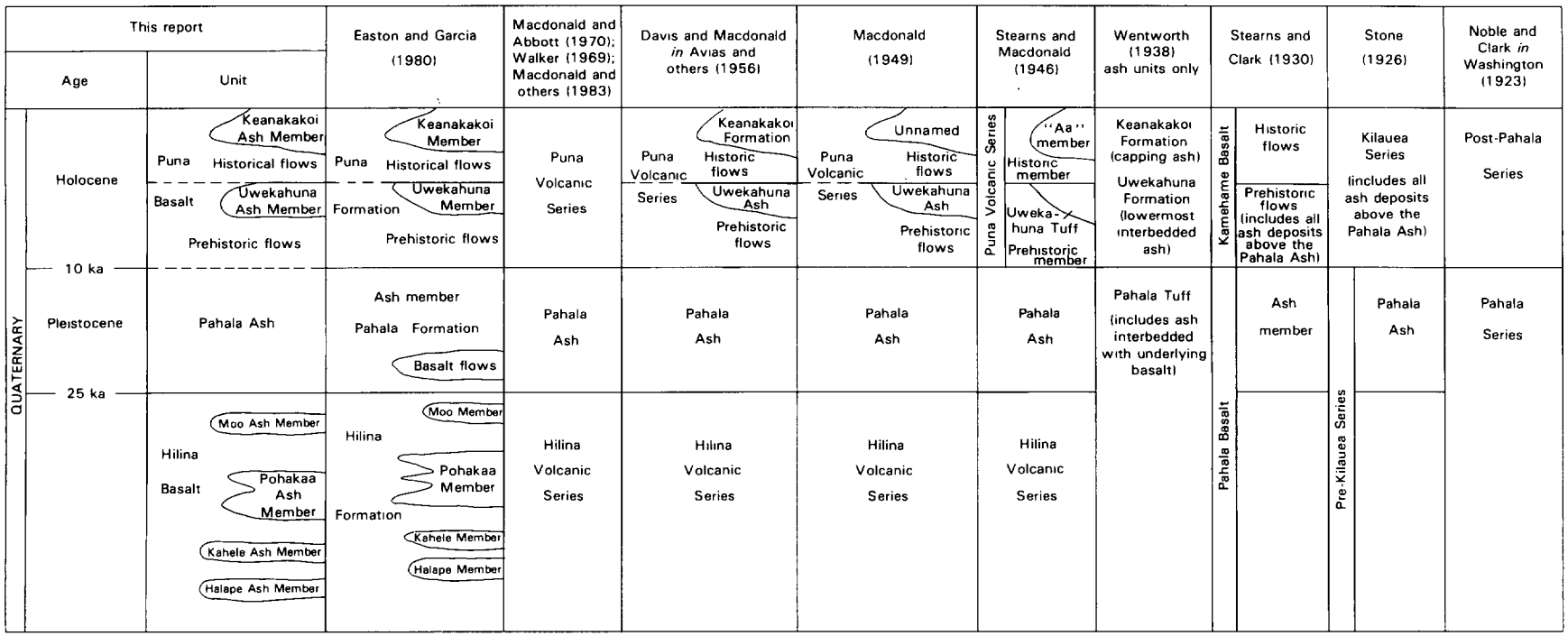

FIGURE 11.1.—Evolution of lithostratigraphic nomenclature for Kilauea Volcano. Stearns and Macdonald's (1946) "aa" member is probably erroneous for ash member. Dashed line between Puna Basalt and Pahala Ash of this report indicates that locally lowermost Puna flows are intercalated with Pahala Ash and are of Pleistocene age (see text).

Modern usage began when Stearns and Macdonald (1946) divided the rocks below the ash member of the Pahala Basalt (Stearns and Clark, 1930) into the Kahuku Volcanic Series for lava of Mauna Loa and the Hilina Volcanic Series for lava of Kilauea (fig. 11.1). In addition, they divided the rocks called the Kamehame Basalt by Stearns and Clark (1930), which overlie the Pahala on Mauna Loa and Kilauea and include the historical lava of the two volcanoes, into the Kau Volcanic Series on Mauna Loa and the Puna Volcanic Series on Kilauea (fig. 11.1), thus abandoning the term Kamehume Basalt. They included the Uwekahuna in the Puna and called it Uwekahuna Tuff, but treated rocks called the Keanakakoi Formation by Wentworth (1938) as an informal member. The Pahala Ash was used to separate these stratigraphic units. Macdonald (1949, p. 65, 67) also included the Uwekahuna in the Puna Volcanic Series but called it the Uwekahuna Ash. Davis and Macdonald (in Avias and others, 1956) included Wentworth's Keanakakoi Formation in the Puna. Walker (1969), Macdonald and Abbott (1970), and Macdonald and others (1983) essentially retained the nomenclature of Stearns and Macdonald (1946; fig. 11.1).

Easton and Garcia (1980) renamed the Hilina Volcanic Series and the Pahala Ash as the Hilina and Pahala Formations, respectively, and effectively reduced the rank of the Puna Volcanic Series (and its subdivisions) and renamed it the Puna Formation. Easton and Garcia (1980) also introduced new stratigraphic terms for several ash units within the Hilina Formation (fig. 11.1), but these terms were not formally proposed in the sense of Article 3 of the stratigraphic code.

STRATIGRAPHY OF KILAUEA VOLCANO

The revised stratigraphic nomenclature for Kilauea Volcano proposed in this paper is shown in figures 11.1 and 11.2. As the use of the term "Formation" does not indicate the predominant lithology or volcanic origin of each lithostratigraphic unit, the names Hilina Basalt, Pahala Ash, and Puna Basalt replace the names Hilina Formation, Pahala Formation, and Puna Formation of Easton and Garcia (1980), respectively. The name Pahala Ash is used in this report, although the ash is indurated and more properly could be called a tuff. However, the term ash is commonly applied to its indurated counterpart, and the name Pahala Ash is widely used.

Reference sections for each of the units are given in table 11.1; they are those of Stearns and Macdonald (1946) unless otherwise indicated. Short descriptions of the three major stratigraphic units are also given below.

In addition to the name changes of two main lithostratigraphic units of Kilauea Volcano, a number of subdivisions of these formations can be made (figs. 11.1, 11.2). These subdivisions are herein formally proposed as members and described in detail under the appropriate higher rank stratigraphic unit. Locations of reference sections for some of these units are given in table 11.1.

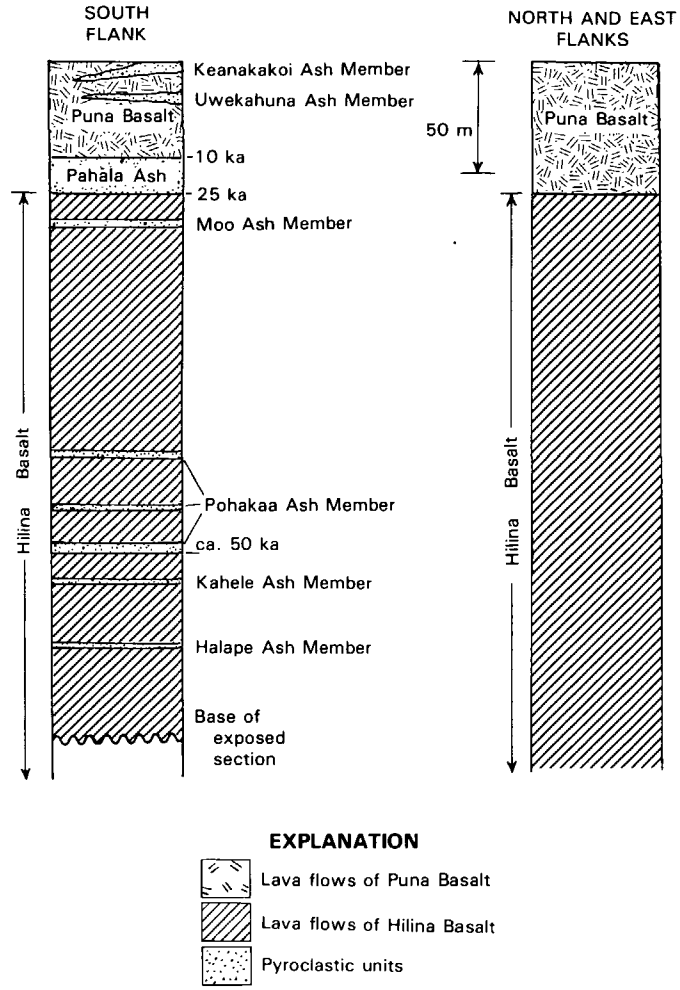

FIGURE 11.2.—Generalized stratigraphic column for south flank of Kilauea Volcano (left) based on sections measured along Hilina fault system (see fig. 11.4). Inferred stratigraphic column for north and east flanks of Kilauea Volcano shown on right. Absence of ash horizons on north flank indicated here reflects trade-wind patterns in Hawaiian region. Although Keanakakoi Ash Member of the Puna Basalt is present in Glenwood region on north flank of Kilauea, its distribution on east flank is unknown.

HILINA BASALT

The Hilina Basalt is exposed only in valleys along the Hilina fault system on the south flank of Kilauea Volcano (fig. 11.3). Exposures are limited to Puu Kapukapu, Puu Kaone, Puueo Pali, Hilina Pali, and a fault scarp north of Kalaeapuki (fig. 11.3). The Hilina Basalt consists predominantly (95 percent) of lava flows, but several major ash horizons are present.

Stone (1926) and Stearns and Clark (1930) examined the formation but gave only general descriptions. Macdonald described a section of the formation 1.6 km southwest of the end of Hilina Road (Stearns and Macdonald, 1946, appendix) and also gave brief petrographic descriptions of the lava (Macdonald, 1949).

TABLE 11.1.—*Type localities and reference localities of lithostratigraphic units, Kilauea Volcano*

[See figure 11.3 for localities]

Locality	Description
1	Type section of the Hilina Basalt (Stearns and Macdonald, 1946). 1.6 km southwest of end of Hilina Pali Road (approx. lat 19°17′00″ N., long 155°18′45″ W., Kau Desert 7.5-min quadrangle).
2a	Reference section of Hilina Basalt, Keana Bihopa, from base of pali (370 m elev) to top (640 m elev) (19°17′19″ N., 155°18′25″ W., Kau Desert 7.5-min quadrangle). 250 m south-southwest of end of Hilina Pali Road.
2b	Type section of Halape Ash Member, Hilina Basalt, Keana Bihopa, (395 m elev) (19°17′19″ N., 155°18′25″ W., Kau Desert 7.5-min quadrangle).
2c	Type section of Moo Ash Member, Hilina Basalt, Keana Bihopa (570 m elev) (19°17′19″ N., 155°18′25″ W., Kau Desert 7.5-min quadrangle).
2d	Reference section of Puna Basalt, Keana Bihopa (600–640 m elev) (19°17′19″ N., 155°18′25″ W., Kau Desert 7.5-min quadrangle).
3a	Type section of Kahele Ash member, Hilina Basalt, Pohakaa Arroyo (approx. 470 m elev) (19°16′40″ N., 155°20′00″ W., Kau Desert 7.5-min quadrangle).
3b	Type section of Pohakaa Ash Member, Hilina Basalt, Pohakaa Arroyo (approx. 425–450 m elev) (19°16′40″ N., 155°20′00″ W., Kau Desert 7.5-min quadrangle).
4a	Reference section of Hilina Basalt and Halape, Kahele, Pohakaa and Moo Ash Members, Puu Kapukapu, from base of pali (100 m elev) to top (300 m elev) (19°16′45″ N., 155°15′35″ W., Kau Desert 7.5-min quadrangle).
4b	Reference section of Pahala Ash, Puu Kapukapu (19°16′15″ N., 155°17′15″ W., Kau Desert 7.5-min quadrangle).
5	Reference section of Pahala Ash, Puu Kaone (19°16′15″ N., 155°17′15″ W., Kau Desert 7.5-min quadrangle).
6	Principal reference section of Pahala Ash, Moolelo, Hilina Pali (19°17′00″ N., 155°19′00″ W., Kau Desert 7.5-min quadrangle).
7	Reference section of Puna Basalt and Uwekahuna Ash Member, Nanahu Arroyo, Hilina Pali, 0.5 km northeast of end of Hilina Pali Road (19°18′15″ N., 155°18′34″ W., Kau Desert 7.5-min quadrangle).
8	Type sections of Puna Basalt and of Uwekahuna Ash Member, Uwekahuna Bluff, Kilauea caldera (Kilauea Crater 7.5-min quadrangle).
9	Reference section of Puna Basalt, Kilauea Iki Crater, summit lava (Volcano 7.5-min quadrangle).
10	Reference section of Puna Basalt, east-rift-zone lava, Makaopuhi Crater (Makaopuhi Crater 7.5-min quadrangle).
11	Reference section of Puna Basalt, east-rift-zone lava, Napau Crater (Volcano 7.5-min quadrangle).

Walker (1969) examined the Hilina while mapping the Kau Desert quadrangle. Easton and Garcia (1980) described the petrography and geochemistry of the Hilina lava in detail. Easton (1978) examined the Hilina in detail and measured sections through the formation at most exposures (Easton, 1978, fig. 3, appendix). The two most extensive and best exposed sections are at Keana Bihopa (Hilina Pali) and Puu Kapukapu (figs. 11.3, 11.4).

LAVA FLOWS

The exposed Hilina Basalt consists of a sequence of aa and pahoehoe flows. Individual pahoehoe flows are 0.5–3 m thick, averaging 2 m. Upper surfaces are commonly ropy and reddish to purplish, and surface crusts are rarely preserved, indicating minor erosion (1–10 cm of material removed) between flows. Pahoehoe sequences of mineralogically similar rocks 8–16 m thick are common, and it is difficult to distinguish individual flows in these sequences. These flow sequences, more abundant in the upper part of the Hilina Basalt, could represent different phases of the same eruption (much like the 1969–74 flows erupted from Mauna Ulu).

The aa flows are 1–6 m thick, averaging 4 m including the clinker zones; the core zone accounts for 20–80 percent of the flow thickness. The clinker zones are partially to totally weathered to reddish-brown clay and commonly contain soil or yellow palagonite horizons in their upper parts. The palagonite layers are probably remnants of ash pockets or lenses. Otherwise, all flow rocks are fresh, mainly because of the low rainfall in the area.

The relative amounts of aa and pahoehoe in the measured sections vary (fig. 11.4, table 11.2). In general, pahoehoe flows predominate in sections farthest away from the caldera (for example, Puueo Pali), supporting the suggestion of Swanson (1973) that only large volume, tube-fed pahoehoe eruptions are able to reach and flood large areas of Kilauea's south flank.

The relative abundances of rock types in the Hilina Basalt are also shown in table 11.2. Olivine basalt contains more than 5 percent olivine phenocrysts (Macdonald, 1949). Picrite basalt contains less than 35 percent modal plagioclase and more than 15 percent modal olivine (Macdonald, 1949; Wright, 1971). Olivine basalt is more abundant than other kinds of basalt in the sections examined (table 11.2). Hypersthene was only rarely observed in lava of the Hilina Basalt, and then only in small amounts. Picrite basalt and plagioclase porphyritic basalt are present only at Puueo Pali and Puu Kapukapu and may be derived from the nearby east rift zone (Macdonald, 1944). Further details on the petrography of Hilina Basalt lava are found in Easton and Garcia (1980).

The Hilina Basalt flows are chemically distinct from the overlying Puna Basalt flows, the former having higher FeO^t content for the same MgO content and lower K_2O/P_2O_5 ratio than the latter (Easton and Garcia, 1980). This distinction may aid in mapping the Hilina and Puna Basalts in areas where the intervening Pahala Ash is thin or absent. Easton (1978) and Easton and Garcia (1980) concluded on the basis of mapping and geochemistry that the Hilina Basalt exposed on the south flank of Kilauea was an intricately stacked sequence of flows derived from the summit caldera and from the east and southwest rift zones of Kilauea. Further details on the chemistry of Hilina Basalt lava are given in Easton and Garcia (1980).

The lower contact of the Hilina Basalt is not exposed, but at least 300 m of lava is exposed along the Hilina Pali. The upper contact of the Hilina Basalt has been defined as the base of the Pahala Ash (Stearns and Macdonald, 1946). The age of the Hilina Basalt is not well defined, but it is older than the radiocarbon age of 31 ± 0.9 ka obtained from the base of the Pahala Ash on Mauna Loa (Kelley and others, 1979). The base of the exposed Hilina Basalt lava at Puu Kapukapu may be estimated to be on the order of 100 ka from average eruption rates determined at Nanahu Arroyo[2] along the Hilina Pali (Easton, 1978).

[2]Name does not appear on current topographic map, but has recently been approved by the U.S. Board on Geographic Names (Donald J. Orth, written commun., 1986).

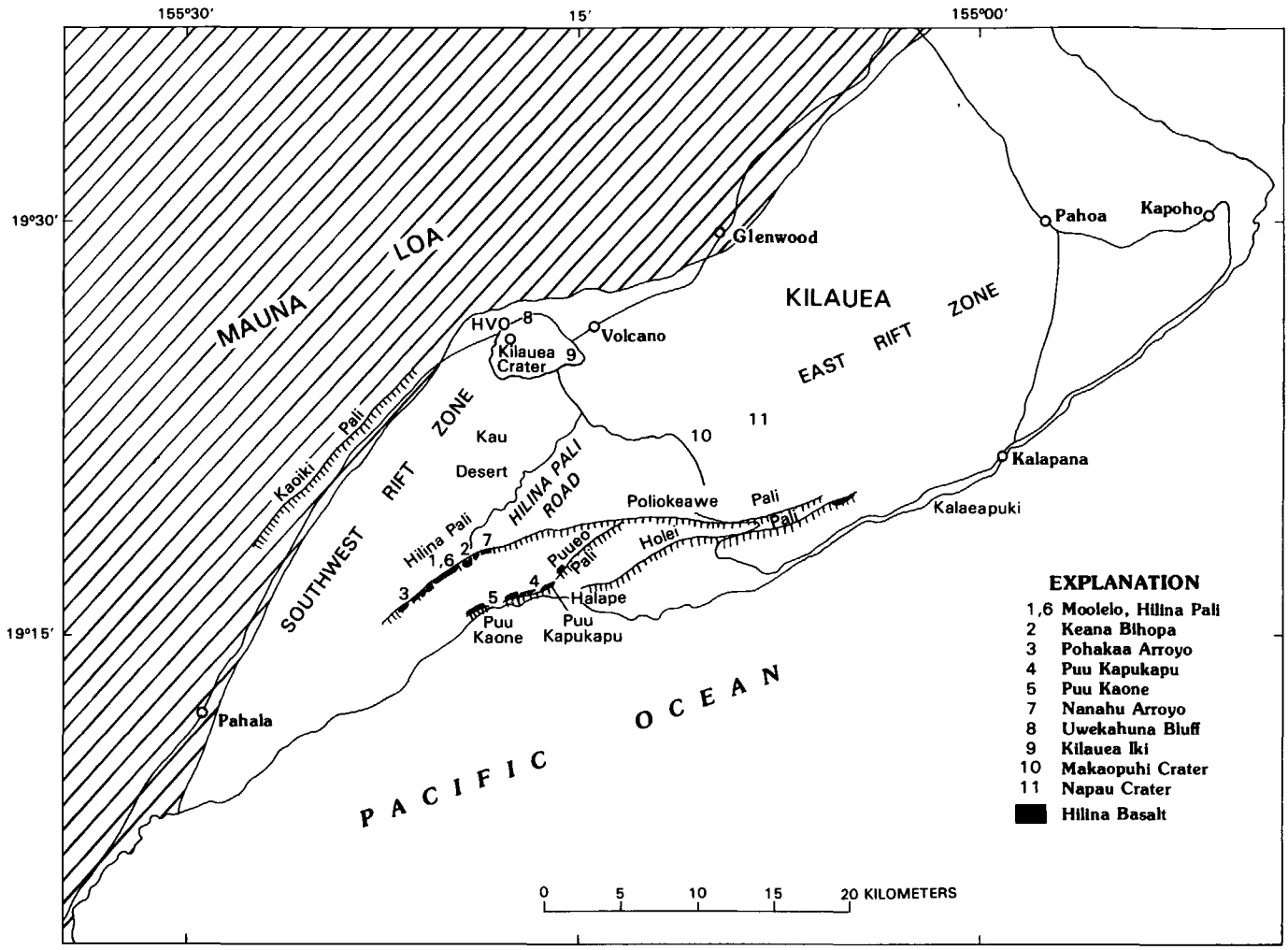

FIGURE 11.3.—Location of type and reference sections for stratigraphic units of Kilauea Volcano (see table 11.1).

PYROCLASTIC AND SEDIMENTARY DEPOSITS

The Hilina Basalt contains several altered and reworked ash horizons (fig. 11.4). The number of ash horizons varies between sections, reflecting intercalation of lava flows with the ash beds. More distal sections such as Puu Kapukapu contain fewer ash horizons because in these areas ash from occasional explosive eruptions could accumulate for longer periods without flow activity occurring. The overall thickness of the ash horizons is relatively constant in any area, but it decreases with distance from Kilauea's summit. The above features make bed-to-bed correlation difficult. Nevertheless, it is still possible to define at least three major ash events and one minor one, widely separated in space and time within the Hilina Basalt which can be correlated between sections over distances of tens of kilometers (figs. 11.2, 11.4).

HALAPE ASH MEMBER (NEW TERM)

This member is found at Puu Kapukapu and at Keana Bihopa near the base of the exposed Hilina section (figs. 11.3, 11.4). The name is derived from the Halape area at the base of Puu Kapukapu (Pukui and others, 1974). The type section is at Keana Bihopa (tables 11.1, 11.3). The unit is found at roughly the same stratigraphic level in both localities, but at each locality it varies laterally in thickness from 10 cm to 50 cm. At Puu Kapukapu, the unit grades downward into a deeply weathered aa clinker zone; at both localities it is overlain by aa flows.

The member is composed of red-weathering, poorly bedded, clayey soil and palagonite. Soil predominates at Puu Kapukapu, but at Keana Bihopa, brown beds of palagonite 0.5–1 cm thick are present. A section from Keana Bihopa is described in table 11.3.

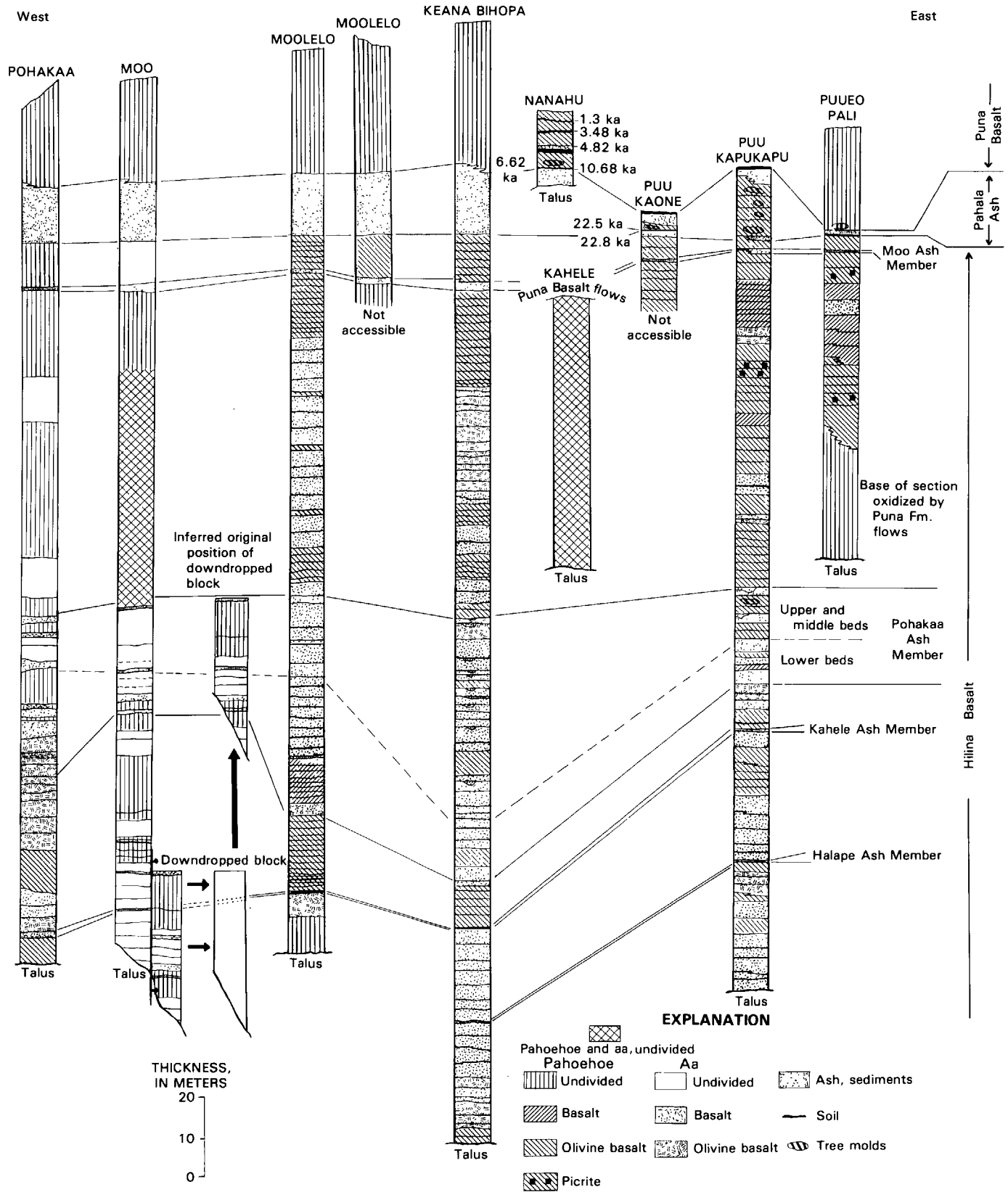

FIGURE 11.4.—Measured stratigraphic sections of Hilina Basalt along Hilina fault system, south flank of Kilauea Volcano. Data adapted from Easton (1978). Base of Hilina Basalt is nowhere exposed. Intercalated lava flows shown in sections of Pahala Ash and Pohakaa Ash Member are Puna Basalt flows and Hilina Basalt flows, respectively (see text).

TABLE 11.2.—*Abundance of rock and flow types exposed on Kilauea Volcano, in part modified from Easton and Garcia (1980)*

[All figures in percent; n.d., not determined]

Area or subdivision	Relative abundance of rock type exposed				Relative abundance of flow types exposed		Relative abundance of flow type in each rock type			
	Olivine basalt	Picrite basalt	Basalt	Hypersthene-bearing basalt	Aa	Pahoehoe	Basalt		Olivine basalt	
							Aa	Pahoehoe	Aa	Pahoehoe
Puna Basalt										
Historical flows	78	7	13	2	n.d.	[1]100	n.d.	n.d.	n.d.	n.d.
Prehistoric flows	71	5	22	2	n.d.	[1]100	n.d.	n.d.	n.d.	n.d.
Moolelo[2]	67	3	30	0	50	50	n.d.	n.d.	n.d.	n.d.
Hilina Basalt										
Keana Bihopa[3]	56	0	44	0	60	40	90	10	38	62
Pohakaa[4]	68	n.d.	32	n.d.	57	43	n.d.	n.d.	n.d.	n.d.
Kapukapu[5]	62	4	34	0	36	64	60	40	24	76
Puueo Pali[6]	67	8	25	n.d.	5	95	5	95	0	100

[1]Cliff sections, Hilina Pali and Kapukapu only.
[2]Difficult to estimate number of flows; pahoehoe, aa figures approximate. From Macdonald (1946).
[3]50 flows of olivine basalt: 20 aa, 30 pahoehoe; 40 flows of basalt: 35 aa, 5 pahoehoe.
[4]Lower half of section, top of Pohakaa Ash Member to base of section.
[5]50 flows of olivine basalt and picrite basalt: 12 aa, 30 pahoehoe, transition pahoehoe; 25 flows of basalt: 15 aa, 10 pahoehoe.
[6]Upper section, above top of the Pohakaa Ash Member: 16 flows of olivine basalt, 2 flows of picrite basalt, all pahoehoe; 6 flows of basalt, 5 pahoehoe, 1 aa.

The Halape Ash Member is lithologically similar to the better exposed Kahele Ash Member. Although the unit is thin, it can be correlated between palis (fig. 11.2). The age of the member is not known, but it is probably between 100 ka and 30 ka on the basis of the estimated age of the base of the Hilina Basalt (Easton, 1978).

KAHELE ASH MEMBER (NEW TERM)

This pyroclastic unit crops out all along the Hilina Pali and at Puu Kapukapu (fig. 11.4). The name is derived from Kahele Arroyo[2], a valley at approximately 19°18′00″ N. latitude and 155°17′10″ W. longitude located 1 km east-southeast of the Hilina Shelter. The type section is at Pohakaa Arroyo[2] (table 11.3). Thickness is variable, being only 10-50 cm at Keana Bihopa and Puu Kapukapu, but increasing along the Hilina Pali to 125 cm at Pohakaa Arroyo. Except at Pohakaa Arroyo, the unit is crudely bedded; bedding is better developed than in the Halape Ash Member. The Kahele Ash Member contains some brown and red-brown palagonite but consists mostly of a red clay; 10 to 25 percent more ash material is present than in the Halape Ash Member. At Pohakaa Arroyo the unit also includes a bed, 10–15 cm thick, of gray, coarse, crossbedded sand composed of rounded olivine and lava fragments (table 11.3; fig. 11.5). In addition, a bed of glassy, vesicular scoria and glass fragments only 2–5 cm thick is present; these materials are interpreted to be cinder-cone eruptive debris derived from the southwest rift zone of Kilauea. Eastward thinning of the Kahele Ash Member indicates a possible source in the southwest rift zone for much of this unit. A representative section of this unit is described in table 11.3. The age of this member is not known, but it is presumed to be between 100 ka and 30 ka. Both the Halape and Kahele Ash Members differ from ash units higher in the section in being more deeply weathered (possibly a result of greater age) and in consisting of red clay rather than yellow-brown palagonite. It is possible that the Halape and Kahele Ash Members may represent a period of soil development as well as ash deposition.

POHAKAA ASH MEMBER (NEW TERM)

The Pohakaa Ash Member represents a major period of ash production comparable in scale to that of the Pahala Ash. The name is derived from Pohakaa Arroyo[2] on the Hilina Pali. Pohakaa was a Hawaiian god who lived in precipitous places and who rolled down stones, frightening and injuring passersby (Kalakaua, 1888). The name is appropriate both to the exposure and to the lithology of the unit.

The Pohakaa Ash Member contains intercalated flows, but it is underlain and overlain by about 100 m of lava containing no ash units. The intercalated flows have no distinctive features and are not considered to be part of the Pohakaa Ash Member. At Pohakaa Arroyo, the member consists of six individual ash layers, each 1–4 m thick (total thickness 10–12 m), at Moolelo of five horizons (total 6.5 m), at Keana Bihopa three to five layers (total 7 m), and at Puu Kapukapu four layers (total 10 m). The Pohakaa Member is not exposed at Puueo Pali, probably because the section there is incomplete. The type section of the Pohakaa Member is at Pohakaa Arroyo (tables 11.1, 11.3), where it shows the greatest number, thickness, and lithologic variation of the ash layers; however, the member is more accessible at Keana Bihopa and Puu Kapukapu.

Although the Pohakaa Ash Member has an areal distribution on Kilauea and is lithologically similar to the Pahala Ash, it has been given member instead of formation rank for the following reasons: (1) The Pohakaa Ash Member is limited in present-day exposure and, unlike the Pahala Ash, has only been found on Kilauea Volcano; thus the unit is not as widespread as the Pahala Ash. (2) If the Pohakaa Ash Member were upgraded to formation rank, then the Hilina Basalt would need to be raised to group rank or split into an upper and lower formation separated by the Pohakaa ash layers. Such a division would cause confusion and would be unsuitable for areas where the Pohakaa Ash Member is thin or absent. As there is no compelling need to give the Pohakaa formational rank, the designation of the rank of member seems most adequate at present.

The Pohakaa Ash Member can be subdivided into lower, middle, and upper beds; however, it is not always possible locally to separate the middle and upper beds. These smaller units are not sufficiently characteristic to warrant formal designation as beds or members.

The total thickness of the member is 6–10 m at Puu Kapukapu, 7–15 m at Keana Bihopa, and 8–15 m at Pohakaa; it thus shows an eastward and southward thinning. This thinning is best defined when only the thickness of primary ash beds is included. It has been possible to distinguish reworked beds from primary ash beds within the Pohakaa Ash Member, the Pahala Ash, and younger ash horizons on Kilauea by means of the following criteria:

(1) Primary beds are regularly layered beds of palagonite, 1–30 cm thick, containing remnant small glass shards, distinct grains of pumice or accretionary lapilli, usually yellow-brown in color, and few olivine crystals or rock fragments.

TABLE 11.3.—*Descriptions of Hilina Basalt ash units, Kilauea Volcano*

[Descriptions from type sections; listed in order from oldest to youngest. Location of sections shown in figure 11.3.]

Thickness (cm)	Description
	Halape Ash Member—Keana Bihopa section
	Overlying aa flow
10–20	Red palagonite, grades downward into red-weathered clinker of underlying aa flow.
	Underlying aa flow.
	Kahele Ash Member—Pohakaa Arroyo
	Overlying lava flow.
20	Coarse, red-brown to black, glassy scoria, clinker and pumice, refractive index of glass 1.602±0.002, fragments as large as 20 mm.
40	Red-brown indurated palagonite, rare plagioclase grains, subhedral olivine phenocrysts, some glass shards with refractive index of 1.604.
5–10	Rippled, coarse-bedded, pink to white-gray pebble gravel; 40–50 percent olivine sand, rounded grains; also vesicular lava sand and gravel-size grains.
30	Yellow-red palagonite.
	Underlying lava flow.
	Pohakaa Ash Member—Keana Bihopa
	Overlying lava flow.
	Upper beds (may include parts of middle beds) (45–50 percent ash material; 1.25–1.5 m total thickness).
20	Brown palagonite, fining upward; minor clinker and pumice, mostly altered glass, refractive index of palagonite 1.548±0.002.
5–8	Gray, friable, sand-size lava fragments.
5–8	Pale red palagonite with black glassy cinders 0.5–1 mm large.
30	Gray, laminated, friable beds of fragments 2–4 mm large of rounded, red, gray, and black lava, minor rounded olivine.
35	Pale brown to yellow palagonite, cinders as large as 1 mm, some glass with refractive index 1.606±0.002.
50–100	Weathered aa clinker and red soil.
	Interstratified lava: 16 m of aa and transition pahoehoe olivine basalt and basalt flows (6 flows).
	Middle beds (30 percent ash material; 1.75 m total thickness). Unit cut by stream channels with many local unconformities.
10–20	Red-brown palagonite, with or without soil.
5	Gray, rounded, red and black lava fragments, beds of friable sand.
10	Yellow-brown palagonite.
30	Brown indurated palagonite in beds 1–2 cm thick, locally eroded and unconformably in contact with overlying flow.
8	Finely laminated, gray, friable sand-size rounded lava and olivine fragments, mantles underlying unit.
10 (locally 30–50)	Finely bedded and crossbedded; gray, rounded lava grains; fills channels cut in underlying beds.
10	Brown to red-brown palagonite, vitric cinders 1–2 mm large.
5	Coarse rounded sand-size lava fragments.
20	Brown to red-brown clay, palagonite, or soil.
20	Brown soil containing aa blocks and clinker.
	Interstratified lava: 18 m of aa and pahoehoe basalt and olivine basalt flows (6 flows).
	Lower beds (50 percent ash material; 2.75–3 m total thickness).
30	Brown to red-brown soil and palagonite.
10	Yellow-gray palagonite with black cinders as large as 3 mm.
25	Brown to red-brown palagonite with local beds of glassy cinders.
60	Beds 1–10 cm thick of gray, rounded olivine and lava fragments 2–3 mm large, locally beds 1–2 cm thick of yellow-brown palagonite.
25	Yellow-brown palagonite in beds 1–3 cm thick, brown beds contain glassy cinders 1–2 mm large.
10	Rounded lava and rock fragments, as large as 5 cm.
5	Gray to yellow-brown palagonite.
1–3	Red, black, and gray rounded lava fragments as large as 3 cm.
7	Gray-brown palagonite, bedding on 5-mm scale, vitric cinders as large as 1 mm.
12	Yellow-brown palagonite.
15	Red, black, and gray, vesicular, rounded basalt fragments.
3–7	Brown palagonite, vitric cinders 0.5–1 mm large.
20–50	Gray, finely laminated beds of olivine and lava sand and gravel.
20	Yellow-brown palagonite with rounded red and black lava fragments as large as 1 cm, weakly bedded.
5	Brown palagonite with vitric, angular cinders as large as 4 mm.
25	Brown palagonite.
30	Reddish to purplish-gray aa clinker, brown to pale yellow-brown ash and soil matrix.
	Underlying aa and pahoehoe flows.
	Moo Ash Member—Keana Bihopa (50 percent ash material, 2.5 m total thickness)
	Overlying pahoehoe flows.
10–15	Fine black sand, soil, brown palagonite.
6	Pale brown, accretionary lapilli 1–2 mm in diameter.
1	Purple-brown palagonite, vitric cinders 1–2 mm large.
5	Pink-brown palagonite, vitric cinders 1 mm large.
5	Purple-brown to brown palagonite, with red and black cinders 1 mm large, local carbonized roots.
2–3	Red-brown palagonite, pumice fragments 5–7 mm large.
5–7	Gray, rounded lava and olivine sand.
2	Purple-brown palagonite, vitric cinders 1 mm large.
2	Gray lava sand.
10	Accretionary lapilli 2–3 mm in diameter, local charcoal at base.
1–2	Reddish clay or soil.
5	Finely laminated beds (1–2 mm thick) of gray lava and olivine sand.
5	Brown accretionary lapilli.
1	Reddish soil.
25–30	Brown to purple-gray, red, and black altered flow fragments 10–25 mm large.
1–2	Reddish clay (soil?).
5	Brown, coarse, rounded lava fragments.
5	Brown, glassy, angular pahoehoe crusts 2–3 mm across.
10	Finely laminated gray lava and olivine sand.
5	Vitric black cinders 2–3 mm large.
5	Red-brown clay (soil?).
40–50	Gray, finely laminated beds of rounded flow and clinker material.
10–40	Yellow to red-brown palagonite, soil near base.
	Underlying aa flows.

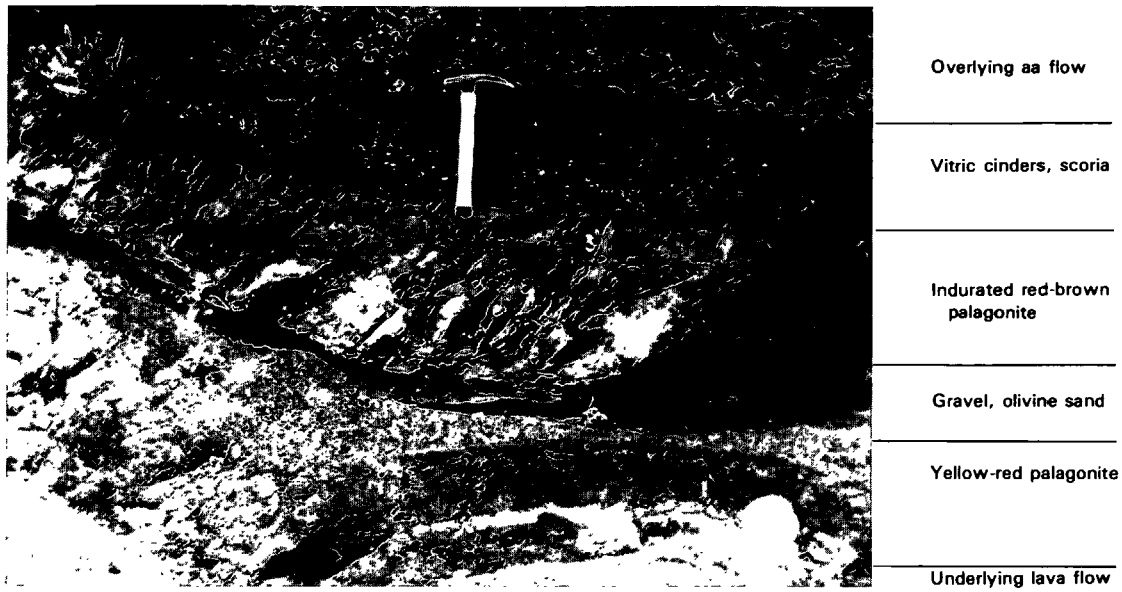

FIGURE 11.5.—Kahele Ash Member of Hilina Basalt at Pohakaa Arroyo, Hilina Pali. Entire thickness of member is shown.

(2) Reworked beds contain sedimentary and pyroclastic material, including: distinct rounded to angular fragments of flow rocks; broken pahoehoe crusts, scoria, and clinker; abundant subrounded olivine fragments (10 percent or more), commonly attached to rock; and minor plagioclase crystal fragments. The bedding layers are thin (1 mm to 5 cm), and crossbedding, undulatory bedding, truncated bedding, and local soil horizons are often present in local channels cut into palagonite. These reworked units are commonly found as friable, gray-weathering, fine-sand to granule-gravel beds.

(3) Surge deposits, which are present mainly in some of the younger ash units contain both primary and reworked layers. The characteristics of these deposits have been described by Swanson and Christiansen (1973) and Decker and Christiansen (1984). Primary and reworked material are intercalated on a fine scale, and it must be realized that most ash layers on Kilauea are a mixture of both types. Sedimentary material similar to that present in the older ash units is found on the surface throughout the Kau Desert region of Kilauea.

The lower beds of the Pohakaa Ash Member form the thickest part of the member (3–4 m) and constitute the first two ash horizons at Pohakaa, Moo, Moolelo, and Puu Kapukapu. At Keana Bihopa, these lower beds are thicker than at other localities. The lower beds consist of alternating beds (5–30 cm) of primary ash (table 11.3; fig. 11.6) and local interbeds of reworked ash and sediment. The lower beds of the Pohakaa Ash Member mark the first appearance of thick palagonitized ash horizons in the exposed Hilina Basalt; they are characterized by a greater proportion of yellow-brown palagonite than the middle and upper beds, by a greater proportion of primary ash beds (50 percent and more along the Hilina Pali, 25 percent and more at Puu Kapukapu), and by the absence of local unconformities, crossbedding, truncated beds, and large- and small-scale channels.

The middle beds of the Pohakaa Ash Member are characterized by a greater abundance of reworked ash beds and sediment (75 percent along the Hilina Pali, 90–95 percent at Puu Kapukapu), a greater abundance of brown and red-brown palagonite, more soil horizons, extensive development of small stream channels 5–50 cm deep, and the presence of crossbedding, truncated beds, channel filling by later ash beds, and filling of channels by lava flows and later primary ash beds (fig. 11.7). Local unconformities are also common in the middle beds.

The upper beds of the Pohakaa Ash Member are present only locally and are restricted almost entirely to large-scale stream channels as much as 10 m deep. These channels grade laterally into a yellow-brown palagonite matrix found in aa clinker layers (usually a red-brown soil matrix is present), indicating that eruption of ash and lava occurred concurrently, in contrast to the situation during formation of the Pahala Ash and the lower parts of the Pohakaa Ash Member. There is also more primary ash material in the upper beds than in the middle beds. Yellow-brown palagonite is more abundant in the upper beds, and small-scale channeling (less than 2 m across), crossbedding, and other sedimentary structures common to the middle beds are less pronounced in the upper beds. A section through the Pohakaa Ash Member at Pohakaa Arroyo is described in table 11.3.

The thickness of the middle and upper beds is difficult to establish. At Keana Bihopa and Pohakaa Arroyo, the middle and upper beds are thickest where located in the deepest parts of the valley chutes, central to the incised valleys. Aa flows are present locally in these channels, but they do not fill them. Along Moolelo and at Puu Kapukapu, the beds of the Pohakaa Ash Member are much more uniform in thickness, and they can be traced laterally with little variation in thickness. These latter two areas lack present-day stream channels. The presence of the thickest, best developed

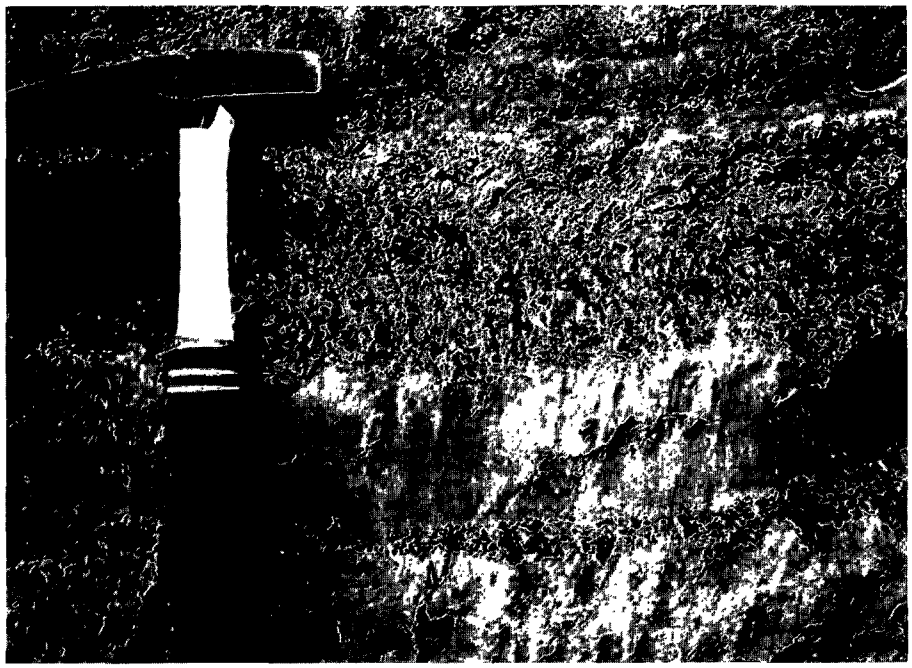

FIGURE 11.6.—Closeup view of lower beds of Pohakaa Ash Member, Keana Bihopa, showing typical bedding and lithology. Pahala Ash beds are similar to those shown here.

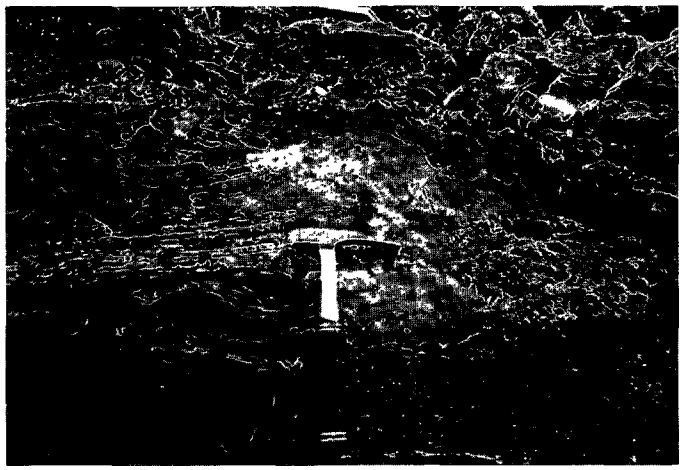

FIGURE 11.7.—Middle beds of Pohakaa Ash Member of Hilina Basalt, Keana Bihopa. Stream channel and minor crossbeds to left of hammer (30 cm long) are mantled by later ash and stream deposits. Overlying aa flow (upper right) fills later channel developed within upper beds in photograph.

sections in current valley cuts and the absence of channels elsewhere along the palis indicate that the drainage system on the south flank of Kilauea has changed very little for several thousand years.

At Pohakaa Arroyo, in the middle beds of the Pohakaa Ash Member, a crossbedded, rippled, pale-gray unit of finely laminated beds containing lithic and crystal fragments forms a horizon 10–15 cm thick that is interbedded with the typical red and yellow-brown palagonite beds (fig. 11.8). This unit closely resembles an outcrop at the Lanai Lookout on Oahu described by Fisher (1977) and attributed to base-surge deposition. Unfortunately, there are no diagnostic textures present at the Pohakaa exposure that would confirm a base-surge origin for the deposit. The proximity of this outcrop to the southwest rift zone does indicate that a base-surge deposit could be present. No similar unit was found in any of the other Hilina sections.

Abundant soils, red-brown palagonite, and extensive stream development imply a more humid climate during the deposition of the Pohakaa Ash Member than at present. This is supported by the presence of *Metrosiderus* sp. (Ohia lehua) tree molds in flows overlying the middle beds of the Pohakaa Ash Member at Puu Kapukapu and at Pohakaa Arroyo. These are the only tree molds found in the Hilina section, other than those present in flows within and overlying the Pahala Ash.

The age of the Pohakaa Ash Member is not known. The member is older than 30 ka because it underlies the Pahala Ash (Kelley and others, 1979), and it may be on the order of 40–50 ka. This age is based on lava and ash accumulation rates obtained from Nanahu Arroyo[2] by Easton (1978): 1 cm/yr for 100 m lava; 1 cm/yr for 10 m of ash and soil. No chemical data are available on ash from the Pohakaa Ash Member. Refractive-index measurements of basaltic glass from the member are similar to those of other Kilauea glass samples (fig. 11.9). A Kilauea source is thus very likely for the primary ash units in the Pohakaa Ash Member, and

FIGURE 11.8.—Middle beds of Pohakaa Ash Member of Hilina Basalt, Pohakaa Arroyo. Undulating beds near hammer may be base-surge deposit. See text for additional details.

the distribution of ash material in the member is consistent with such a source. As discussed in further detail below in the section "Pahala Ash," a Mauna Loa source for both the Pahala and the Pohakaa cannot be ruled out.

MOO ASH MEMBER (NEW TERM)

The Moo Ash Member is well exposed along the Hilina Pali and is also present at Puu Kapukapu and Puueo Pali. The name is derived from Moo Arroyo[2], where the unit is exposed; Moo is the Hawaiian word for dragon. The type section is at Keana Bihopa and is described in tables 11.1 and 11.3.

At Keana Bihopa, the Moo Ash Member underlies a sequence of olivine basalt pahoehoe flows 10–12 m thick, which are capped by Pahala Ash. At this locality, the Moo Ash Member ranges in thickness from 2.5 m on the inward (north) side of the arroyo to 1.5 m near the face of the pali. The overlying flows thicken where the ash thins. It appears that the ash has been eroded away from the lip of the pali and later covered by flows that draped the pali. The Moo Ash Member is lithologically similar to the Pohakaa Ash Member and the Pahala Ash, being composed of a mixture of palagonite and vitric ash (primary ash beds) and reworked ash and sediment.

Criteria for distinguishing the Moo Ash Member from the Pahala Ash include the following: (1) The Pahala Ash is overlain by and intercalated with flows bearing tree molds of *Cibotium* sp. (tree ferns). No tree molds are found below the base of the Pahala Ash down to the middle beds of the Pohakaa Ash Member. (2) The Moo Ash Member is a tuff and sediment horizon 1–2 m thick located 10–15 m below the Pahala and separated from it by a series of mineralogically uniform basalt flows. (3) The Moo Ash Member contains several beds of accretionary lapilli, which are absent from the Pahala Ash on Kilauea.

The Moo Ash Member may be present at Puu Kapukapu and Puueo Pali (fig. 11.4) as a bed of yellow-brown palagonite and

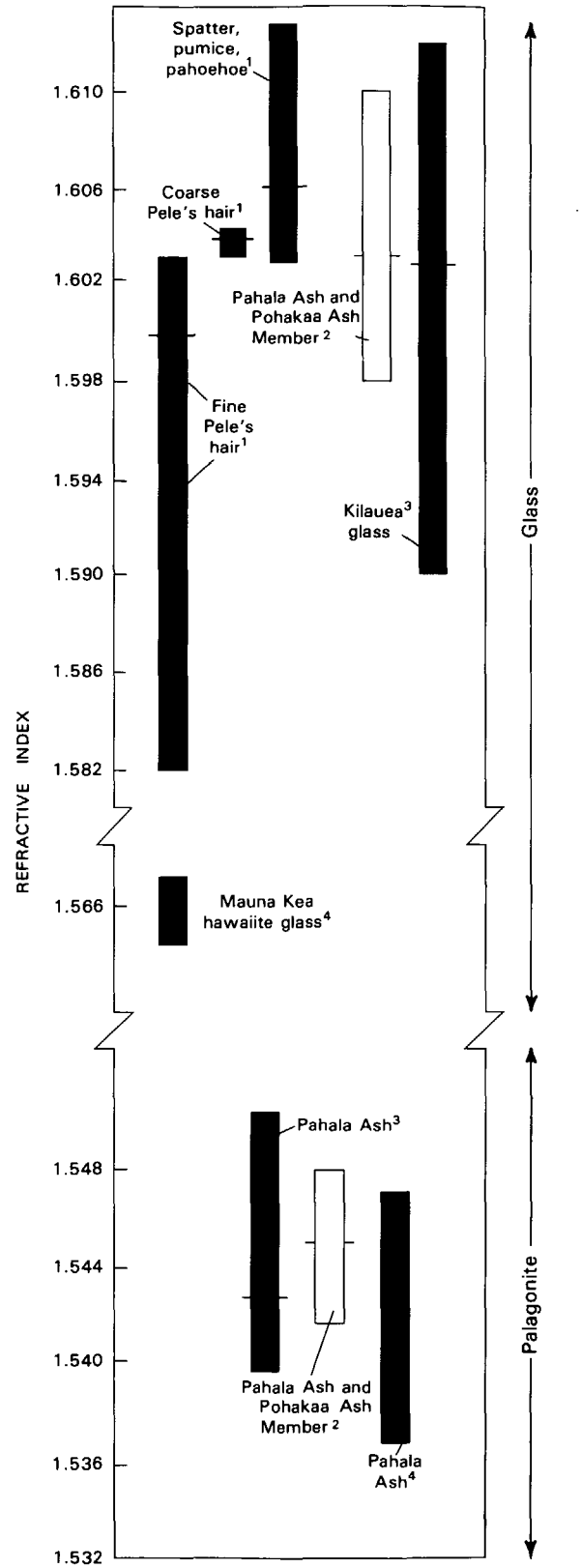

FIGURE 11.9.—Refractive-index measurements of Kilauea glass and palagonite and Mauna Kea glass showing basaltic nature of preserved glass in Pahala Ash and Pohakaa Ash Member. Sources identified by number: 1, Duffield and others (1977); 2, Easton (1978); 3, Wentworth (1938); 4, Macdonald (1949).

sediment 50–100 cm thick and located 3 m below the base of the Pahala Ash. At both these localities, and at Puu Kaone, this ash layer lacks accretionary lapilli, and its assignment to the Moo Ash Member is tentative.

In some areas the Moo Ash Member may be conformable with the lower part of the Pahala Ash, and in such instances it would be difficult to distinguish the two units without radiocarbon ages. At present, the Moo Ash Member is considered part of the Hilina Basalt, because the overlying lavas are similar chemically to those of the Hilina Basalt and distinct from Puna Basalt flows, and wherever the Moo Ash Member is exposed, it is separate from the Pahala Ash.

The age of the Moo Ash Member is not precisely known. It is older than the 24 ka age for the base of the Pahala Ash at Puu Kaone and the 30 ka age for the base of the Pahala Ash on Mauna Loa (Kelley and others, 1979). A reasonable estimate for the age of the Moo Ash Member is between 30–35 ka. Charcoal is present in the Moo Ash Member, but sufficient quantities have not yet been recovered for dating purposes. The Moo Ash Member is lithologically similar to the Pohakaa Ash Member and the Pahala Ash and probably had a similar origin and source.

PAHALA ASH

The Pahala Ash on Kilauea Volcano is only exposed atop fault scarps at Hilina Pali, Puueo Pali, Holei Pali, Puu Kapukapu, and Puu Kaone, and in the Glenwood District (figs. 11.3, 11.10). The distribution of the Pahala Ash on the Island of Hawaii is shown in figure 11.10. The Pahala Ash on Kilauea has been described by Stone (1926), Stearns and Clark (1930), Wentworth (1938), Stearns and Macdonald (1946), Fraser (1960), Walker (1969), and Easton (1978). Stearns and Macdonald (1946) review the older literature on the Pahala Ash on the Island of Hawaii, much of which is concerned with the origin and source of the ash. Wentworth (1938), Hay and Iijima (1968), and Hay and Jones (1972) present chemical analyses of the Pahala from Kilauea, although many of these samples were highly altered. Hay and Iijima (1968), Hay and Jones (1972), and Easton and Easton (1983) have examined the alteration of the Pahala Ash.

The formation was named for the town of Pahala on Mauna Loa Volcano, where the ash is exposed on the surface, but not in section (Wentworth, 1938). Stearns and Macdonald (1946) do not specify a type or reference locality but do present a section through the Pahala Ash at the base of Kaoiki Pali, 5 km southwest of Kilauea caldera. Wentworth (1938) describes a number of sections through the Pahala Ash. The Pahala Ash at Puu Kapukapu and Puu Kaone on Kilauea (fig. 11.3) is well exposed, and it is proposed that sections at these two localities be designated as reference sections for the Pahala Ash on Kilauea. A section through the Pahala Ash at Moolelo (fig. 11.11) is typical of the character of the formation on the south flank of Kilauea and is here designated as the principal reference section. It consists of a mixture of yellow-brown palagonite derived from weathered ash, and beds of reworked ash and sediment. The section at Puu Kaone (fig. 11.12) shows the presence of intercalated flows, which are present locally throughout the Pahala Ash.

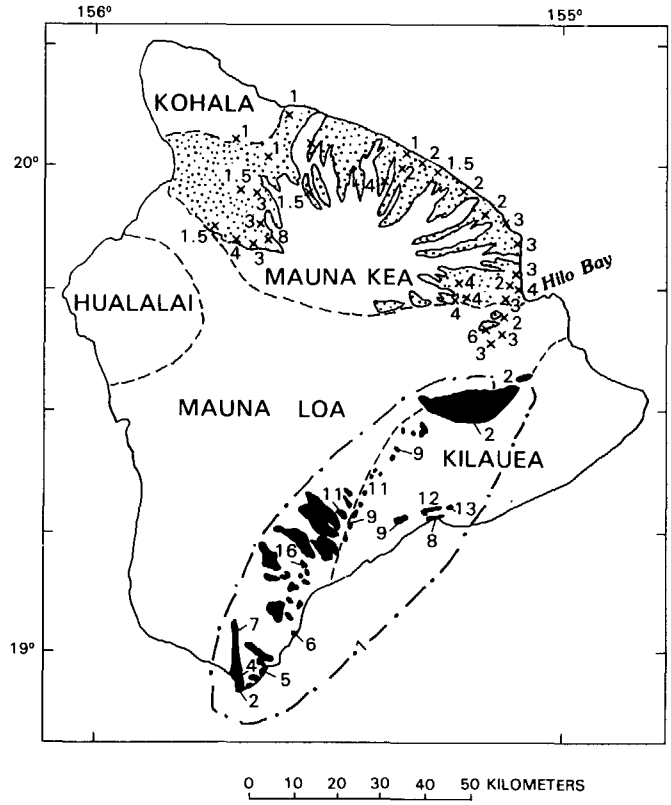

FIGURE 11.10.—Distribution of Pahala Ash on Island of Hawaii. Data from Stearns and Macdonald (1946) and Fraser (1960). The main period of Pahala Ash deposition on Kilauea and Mauna Loa was between 24 ka and 10 ka (Kelley and others, 1979). Distribution of Pahala Ash is also consistent with a Mauna Loa source instead of Kilauea source indicated here.

Flows are interbedded with or overlie the Pahala Ash at Puu Kaone, Puu Kapukapu, and in places along the Hilina Pali. Flows within the Pahala Ash are more abundant south and east of the summit area and are characterized by the presence of *Cibotium* sp. (tree fern) tree molds 15–25 cm in diameter. In addition, some flows contain hypersthene, a mineral rarely observed in the Hilina Basalt. Chemically, these lava flows are similar to Puna Basalt lava flows, and they are here considered to be part of the Puna Basalt. They are also mineralogically similar to the Puna Basalt flows, and they

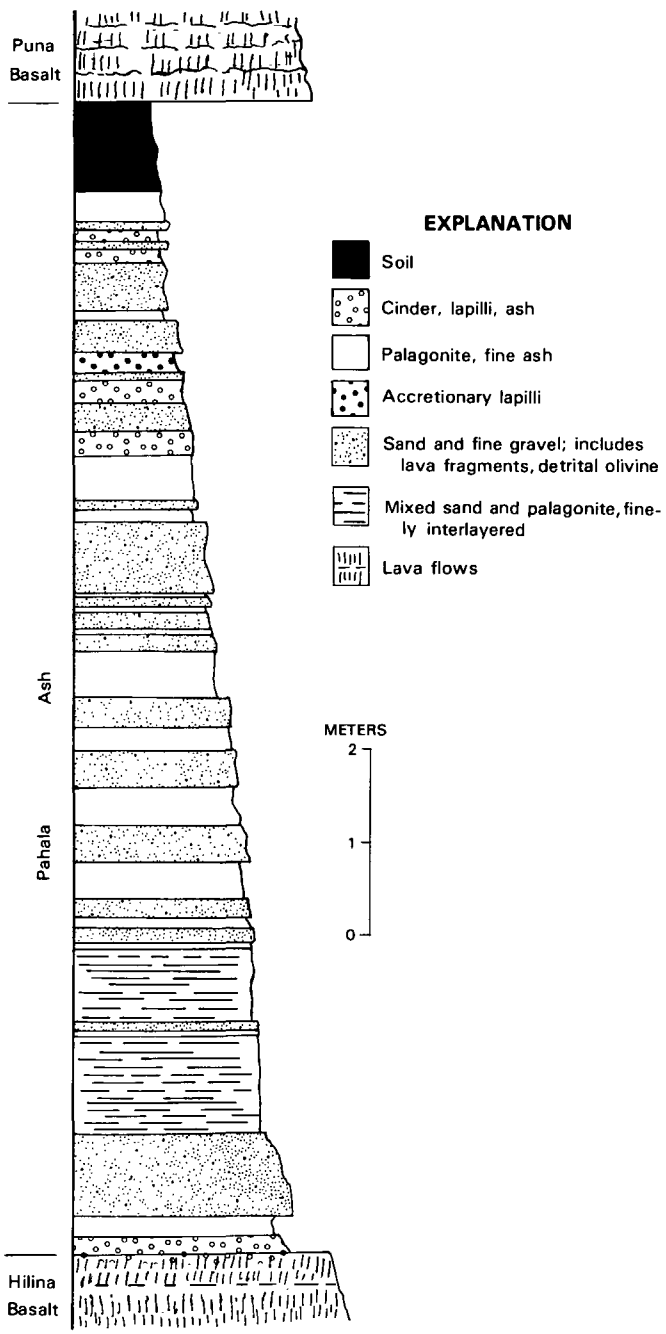

FIGURE 11.11.—Measured section of Pahala Ash exposure 14.25 m thick at Moolelo, Hilina Pali, 20 km south of Kilauea caldera (lat 19°17′ N., long 155°19′ W.), showing proportion of ash and reworked material (sand and gravel) in typical section.

differ only in the presence of tree molds. In areas where the Pahala Ash is absent, it is unlikely that these flows could be distinguished from other Puna Basalt flows. This supports the historical designation of the Pahala Ash as essentially a pyroclastic unit.

Pahala Ash beds at Puu Kapukapu are 1–2 m thick and are underlain by 6–8 m of basalt flows with *Cibotium* sp. tree molds. Farther east, the beds are 0–2 m thick and are overlain by 10–12 m of olivine basalt flows and capped by an additional 2–4 m of ash. The section at Puu Kaone (fig. 11.12) is similar in that it also contains interbedded Puna flows. At Puueo Pali, farther to the east, three 1-m-thick ash beds are interstratified with lava flows 30 m below the top of the pali. These beds contain coarser vitric fragments than are common to the west, and they may be related to fire-fountaining along the east rift zone. If this is the case, these ash beds may not be correlative with the Pahala Ash.

Widely varying thicknesses for the Pahala Ash at Puu Kaone (10–14 m) and Puu Kapukapu (6–12 m) have been reported in the literature (Stone, 1926; Stearns and Clark, 1930; Wentworth, 1938; Stearns and Macdonald, 1946), but these figures include the lava flows. Ground slumping in the area has moved blocks of ash downslope, burying underlying flows and coating flows with a thin veneer of ash. Both effects make the Pahala Ash appear thicker than it truly is.

The Pahala Ash exposed along the Hilina Pali averages 15 m in thickness. In addition, the amount of primary ash versus reworked ash and sediment is greater along the Hilina Pali (50 percent primary) than at Kapukapu (25–40 percent primary). Both effects are consistent with a source for the Pahala on Kilauea or Mauna Loa (see later discussion).

On Mauna Loa, the Pahala Ash contains fewer reworked or sedimentary beds than on Kilauea, and lapilli-size material is more common (Stearns and Macdonald, 1946). The thickness of the Pahala Ash on Mauna Loa varies (fig. 11.10), but locally it is as thick as on Kilauea. On parts of Mauna Loa, the ash resembles loess and may have been transported by wind either during or after deposition.

A charcoal sample collected by G. Fraser from the lower part of the Pahala Ash at Puu Kaone was dated at 17.36±0.65 ka (Rubin and Berthold, 1961). Resampling near this site in 1977 at the base of an olivine basalt flow (Puna Basalt) interbedded with the ash (fig. 11.12) yielded charcoal that was dated at 22.5±0.5 ka and 22.8±0.5 ka (Kelley and others, 1979). These ages are preferred over the previous age of 17.36 ka because three counters were used instead of one, and the earlier sample was diluted because of insufficient carbon (M. Rubin, written commun., 1978). The data indicate that the base of the Pahala Ash on Kilauea has an age of about 23–25 ka. An age of 31.1±0.9 ka has been reported from the base of Pahala Ash on Mauna Loa (Kelley and others, 1979). This is older than the age at Puu Kaone, and it is possible that these lowermost dated ash beds on Mauna Loa may be correlative with the Moo Ash Member of the Hilina Basalt on Kilauea.

The upper part of the Pahala Ash has been dated at several localities on Mauna Loa and Kilauea (see Kelley and others, 1979). The ages range from about 12 ka to 0.2 ka; such a range would be expected because these ages date the time the formation was first buried by lava. The oldest of these overlying flows have ages of 10–12 ka, indicating that the bulk of the ash was deposited between 24 ka and 10 ka on the two volcanoes. Little flow activity occurred on the south flank of Kilauea during this interval. The upper part of

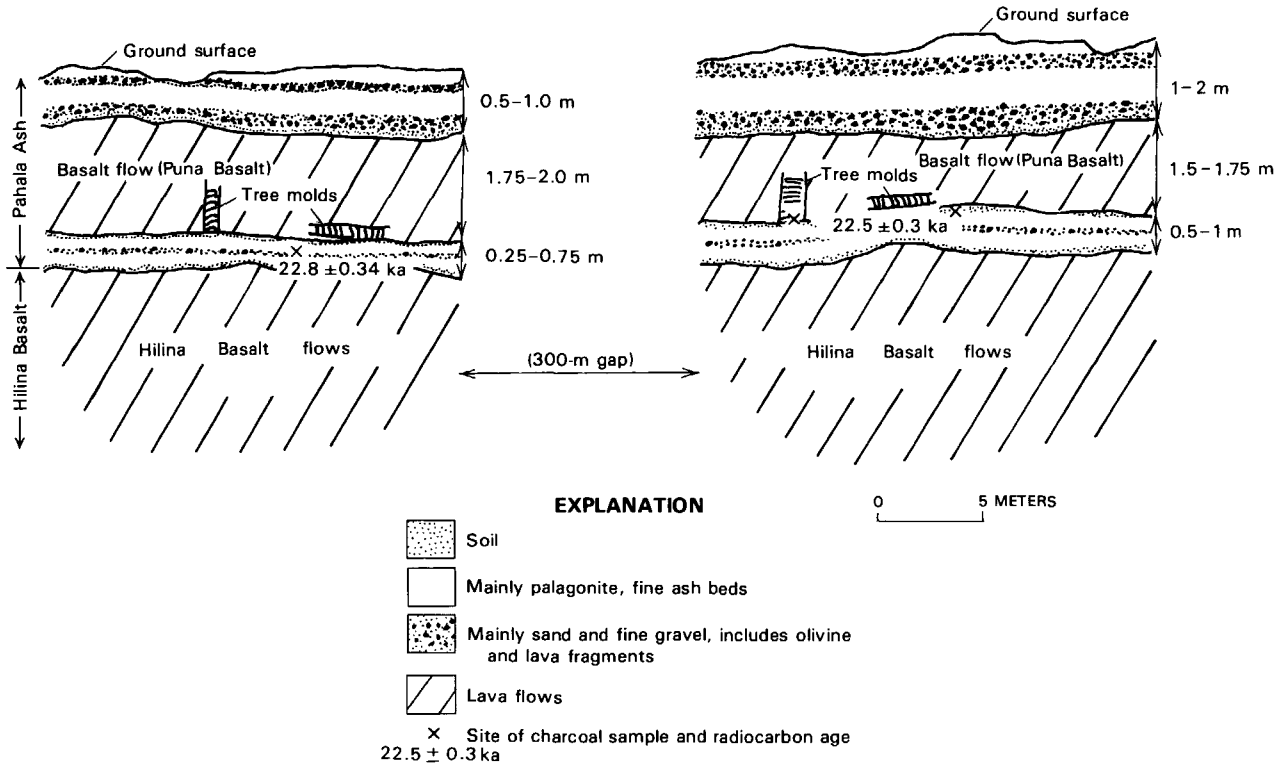

FIGURE 11.12.—Stratigraphic sections of Pahala Ash at Puu Kaone, Kilauea Volcano. Radiocarbon ages from Kelley and others (1979).

the Pahala Ash is obviously not useful as a time-stratigraphic horizon because of the long interval between deposition and burial of the ash. The base of the ash may mark a time-stratigraphic horizon, but additional ages are needed to confirm this. The origin of the ash is discussed later in the paper.

PUNA BASALT

The Puna Basalt covers most of Kilauea and was mostly erupted within the last 10,000 years following Pahala Ash deposition. Historical lava flows are included within the formation. The name is derived from the Puna District of Kilauea, where these flows are abundant (Stearns and Macdonald, 1946). Although Stearns and Macdonald defined the Puna as overlying the Pahala Ash, lava flows here considered to be part of the Puna are locally intercalated with the Pahala Ash (see section "Pahala Ash"). Thus, the base of the Puna Basalt generally overlies the Pahala, but locally may be present within the Pahala and may be as old as about 23 ka. No good sections of the prehistoric lava flows are present in the type locality designated by Stearns and Macdonald (1946, p. 193–194), in the walls of Kilauea caldera, although many surface exposures of flows are present.

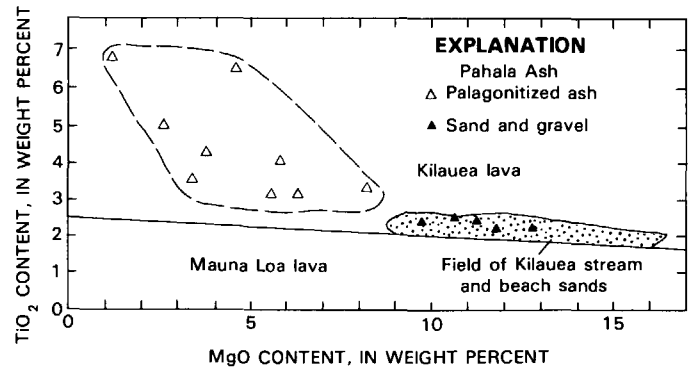

FIGURE 11.13.—TiO_2 content plotted against MgO content for two main lithologies in Pahala Ash. Palagonite beds show a wide range, in part because of in-place alteration (Hay and Jones, 1972; Easton and Easton, 1983). Detrital beds in Pahala Ash fall in field of recent Kilauea stream and beach sands and show less evidence of alteration (Easton and Easton, 1983). Straight line separates field of Kilauea and Mauna Loa lava flows (Wright, 1971; Easton and Garcia, 1980).

LAVA FLOWS

There are some slight chemical and mineralogical differences between Hilina Basalt and Puna Basalt lavas (see section above on Hilina Basalt; Easton and Garcia, 1980). Descriptions of Puna Basalt lava, particularly the historical flows, can be found in Stearns and Clark (1930), Stearns and Macdonald (1946), Easton and Garcia (1980), and Holcomb (1981). Chemical analyses of prehistoric flows of the Puna Basalt are given in Wright (1971). Sections through the prehistoric flows of the formation are present in the walls of Kilauea caldera, notably at Uwekahuna Bluff. Other sections through prehistoric flows are in pit craters along the east rift zone, including Kilauea Iki, Makaopuhi Crater, and Napau Crater; and along the Hilina Pali at the same locations as the Hilina Basalt exposures; these sections can be regarded as reference sections (table 11.1) for the Puna Basalt because they typify groups of flows originating from the summit, the east rift zone, or both areas of Kilauea.

PYROCLASTIC AND SEDIMENTARY DEPOSITS

Several prehistoric ash units are interbedded with lava flows of the Puna Basalt. Only two of these units have been given formal status as members of the Puna Basalt—the Keanakakoi Ash Member and the Uwekahuna Ash Member (renamed to indicate their dominant lithology; formerly the Keanakakoi and Uwekahuna Members of Easton and Garcia, 1980). These members are generally restricted to the summit region of Kilauea. Apart from these and several unnamed older ash layers, the products of the 1924 phreatic eruption in Kilauea crater are also present overlying the Keanakakoi Ash Member on the southwest flank of Kilauea (Decker and Christiansen, 1984). These very young deposits are considered to be part of the Puna Basalt.

Older Ash Units

At Nanahu Arroyo along the Hilina fault system (figs. 11.3, 11.14) several flow and ash units overlie the Pahala Ash. The uppermost of these units has a radiocarbon age of 1.13 ± 0.25 ka (Kelley and others, 1979) and may be correlative with the Uwekahuna Ash Member. The next lowest soil layer was overlain by lava at about 3.48 ± 0.25 ka (Kelley and others, 1979). A third unit consists of 65 cm of ash that overlies a 69-cm-thick soil horizon developed on a lava flow overlying the Pahala Ash. This ash unit was covered by lava at 4.82 ± 0.2 ka (Kelley and others, 1979).

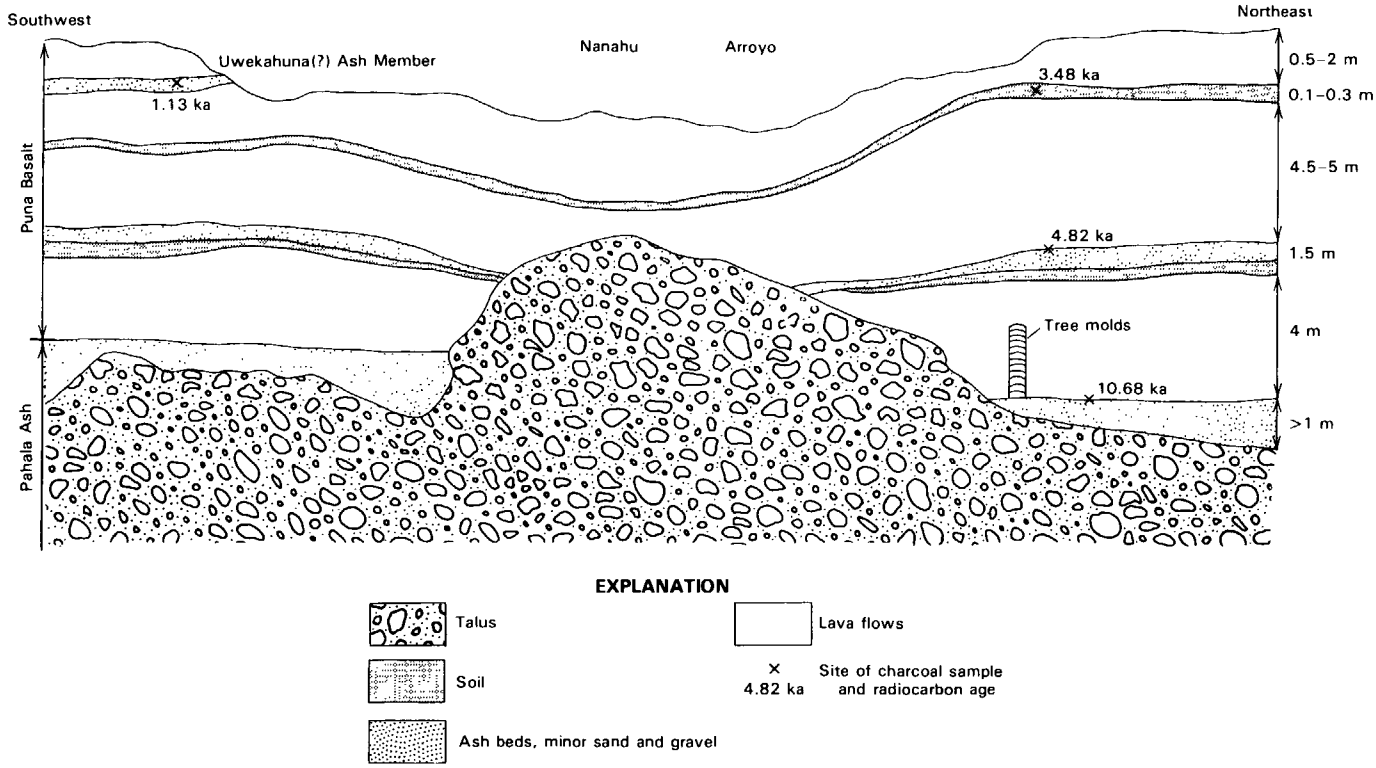

FIGURE 11.14.—Stratigraphic section through Puna Basalt at Nanahu Arroyo. Location of dated charcoal samples (Kelley and others, 1979) and Puna Basalt soil and ash units are shown. Only part of exposed Pahala Ash at this locality is shown.

Given the thick accumulation of soil beneath the ash and the minimal evidence of soil formation in the ash itself, this age may be close to the time of ash deposition. None of these older ash units is widespread enough to be given formal stratigraphic status at present, but they do indicate older explosive activity of Kilauea Volcano between the times the Pahala Ash and Uwekahuna Ash Member were deposited.

Uwekahuna Ash Member

The Uwekahuna Ash Member is a hydromagmatic deposit exposed near the base of the present caldera cliffs at Kilauea and on or near the surface of some areas on the southeast flank of Mauna Loa. The unit was named by Stone (1926) for Uwekahuna Bluff, where about 5 m was previously well exposed (see Powers, 1916). It was subsequently covered by lava and has been partly exposed (about 2 m) more recently (Casadevall and Dzurisin, chapter 13). The member has a distribution similar to that of the Keanakakoi Ash Member, and it probably had a similar origin (Decker and Christiansen, 1984). Radiocarbon ages on charcoal from overlying and underlying flows indicate an approximate age of 1.1–1.5 ka for this unit (Kelley and others, 1979). Descriptions of the unit are found in Casadevall and Dzurisin (chapter 13), and also in Powers (1916), Wentworth (1938), Stearns and Macdonald (1946), and Decker and Christiansen (1984). A reference section is here designated as shown in table 11.1.

Keanakakoi Ash Member

This unit was originally called the Keanakakoi Formation by Wentworth (1938), who considered it to comprise the whole series of ash layers southwest of Kilauea caldera, including ash of the 1790 and 1924 eruptions. The name is derived from Keanakakoi Crater near Kilauea caldera, and the unit is well exposed at its type locality along scarps southwest of Keanakakoi Crater. Powers (1948) also considered the unit to include all fragmental eruptive deposits southwest of Kilauea caldera, and he recognized that these deposits included a number of unconformities. Only the uppermost layer of the member was considered by Powers (1948) to be related to the 1790 eruption. Recent work by Swanson and Christiansen (1973), Christiansen (1979), and Decker and Christiansen (1984) indicate that the member consists of fallout, pyroclastic-surge, and reworked deposits, and were mostly deposited during the 1790 eruption. Recent radiocarbon dating has confirmed this interpretation (Kelley and others, 1979). Decker and Christiansen (1984) showed an idealized section of the member, Malin and others (1983) briefly described the member, and Stearns and Clark (1930) produced a map of its distribution.

Decker and Christiansen (1984) noted the following six major units within the Keanakakoi Ash Member, each unit separated from its neighbors by truncated surfaces: (1) Basal wind-redeposited Pele's hair and reticulite pumice. (2) Predominantly well sorted vitric ash with planar mantle bedding. (3) Less well sorted lithic-vitric ash, commonly with wavy and lenticular bedding, cross-stratification, and bedding sags beneath lithic blocks. (4) A local lava flow. (5) Lithic ash and blocks, with abundant accretionary lapilli and cross-stratification. (6) An uppermost deposit of fallout and wind-resorted pumice and Pele's hair. Units 1 and 2 correspond roughly to the "lower mixed unit" of Malin and others (1982); unit 3 is their "intermediate vitric unit"; and unit 5 is their "upper lithic unit." Malin and others (1982) suggested that the upper layer of fallout and wind-resorted pumice and Pele's hair was deposited between 1790 and 1823, but do not include it in their Keanakakoi.

The definition of the Keanakakoi in this report is that of Decker and Christiansen (1984), including both the lower and upper pumices. The Keanakakoi was mainly deposited during the 1790 eruption, but the basal pumice is slightly older (R.L. Christiansen, oral commun., 1986), and the overlying fallout and the unconformably overlying fallout and resorted pumice layer—the "golden pumice" of Sharp and others (chapter 15)— is circa A.D. 1820.

PALEOCLIMATE AND PALEOGEOGRAPHY

During the 10,000 to 15,000 years of Pahala Ash deposition on Kilauea, very few lava flows reached its south flank. This in part accounts for the thickness of the formation and is probably a result of diversion of lava away from the south flank by an incipient Kaoe fault zone, by entrapment of lava within a deep caldera, or by a prolonged period of mainly ash production at Kilauea caldera. This long period of deposition also allowed reworking of the ash and development of sheetwash plains consisting of reworked ash and broken flow material, much as is occurring today southwest of Kilauea caldera. Similar conditions probably also existed during deposition of the Pohakaa Ash Member of the Hilina Basalt.

In addition, lava flows intercalated with and immediately overlying the Pahala Ash and Pohakaa Ash Member contain abundant tree molds. The presence of *Cibotium* sp. (tree fern) molds as much as 25 cm in diameter within Pahala flows at Puu Kaone and Puu Kapukapu indicate that sufficient time elapsed between deposition of the ashes and the flows to produce forest growth (about 400 years; see Atkinson, 1971). Annual rainfall of about 200 cm is needed for the development of fern forests. The area of these molds now receives less than 50 cm of rain annually; hence a wetter climate probably existed during these periods of ash deposition. Tree molds are absent elsewhere in the Hilina Basalt. This paleoclimatic regime may also have been important in establishing conditions favorable for ash production (for example, by producing a higher ground-water table).

DISCUSSION

In the following discussion on the origin and source of the Pohakaa, Moo, and Pahala pyroclastic deposits, emphasis is placed on the better studied Pahala Ash. However, all of these units are similar in lithology and distribution, and the comments with regard to the Pahala Ash are probably applicable to the Pohakaa and Moo ashes as well.

The source of the Pahala Ash is controversial. Stearns and Clark (1930) and Wentworth (1938) attributed the ash to explosive eruptions of vents on Mauna Loa Volcano and elsewhere outside Kilauea. Stone (1926), Stearns and Macdonald (1946), Fraser

(1960), and Easton (1978) regarded the Pahala deposits southwest of Kilauea caldera as originating from Kilauea (fig. 11.10). Refractive-index measurements of Pahala Ash glass (fig. 11.9) and chemical analyses of the glass (Fraser, 1960; Hay and Iijima, 1968; Hay and Jones, 1972; Easton and Easton, 1983) confirm that the bulk of the ash is basaltic in composition; hence it is probably not derived from Mauna Kea, which would likely have glass erupted of hawaiite composition at that time (Porter, 1979). Isopach patterns of the Pahala Ash (fig. 11.10; Fraser, 1960) are also consistent with a Kilauea source, as is the greater proportion of ash versus detrital material closer to the summit of Kilauea caldera. However, the isopach data is also consistent with a Mauna Loa source for the Pahala Ash (R.T. Holcomb, written commun., 1983, 1984). Rare-earth-element data on the Pahala Ash (fig. 11.15; Easton and Easton, 1983) are inconclusive regarding the origin of the primary ash material. It is definitely basaltic in composition, but alteration makes it difficult to distinguish between a Kilauea and a Mauna Loa source (fig. 11.15). The detrital component of the Pahala Ash on Kilauea (fig. 11.13) is derived from the weathering of Kilauea lavas and is not as altered as the ash component of the formation (fig. 11.13; Easton and Easton, 1983).

Since the original nature of the Pahala Ash is difficult to decipher because of alteration, the origin of the ash has also remained controversial. Two suggested origins are as follows: (1) The ash may consist of magmatic fire-fountain debris (Stearns and Clark, 1930; Wentworth, 1938; Stearns and Macdonald, 1946); Stearns and Macdonald (1946) considered that most of the Pahala Ash was of fire-fountain origin, but allowed for the possibility of a phreatic or phreatomagmatic origin. (2) The ash may be the product of phreatic or phreatomagmatic eruptions of Kilauea that were similar to but of larger scale and duration than the 1790 and May 1924 eruptions of Kilauea's summit (Stone, 1926; Fraser, 1960).

Physical evidence for a phreatic or phreatomagmatic origin include the presence of accretionary lapilli and lithic and crystal fragments in the Pahala, Pohakaa, and Moo ashes in addition to the predominant vitric ash. Judging from the 1790 and 1924 eruptions, hydromagmatic activity at Kilauea's summit is an effective means of producing large quantities of ash; this process of origin is also consistent with a wetter climate during these periods of ash deposition. If the ash is from eruptions at Mauna Loa, then snow and ice in the summit area could also have been a significant factor in ash production (R.T Holcomb, written commun., 1983, 1984). Alternatively, G.A. Macdonald (written commun., 1978) reported that the fire-fountain debris for the 1959 Kilauea Iki eruption could be found as far south as Ka Lae (the southernmost point on the Island of Hawaii) on Mauna Loa, hence the extensive distribution of the Pahala Ash on Kilauea and Mauna Loa does not preclude a magmatic origin. However, this fire-fountain debris consists only of pumiceous shards and Pele's hair and does not include blocky shard fragments such as are common in the Pahala Ash. Possibly both origins are correct: the ash may be predominantly hydromagmatic in origin, but magmatic deposits may also be present locally within the formation.

Decker and Christiansen (1984) have discussed the significance of the number of pyroclastic deposits within the exposed Kilauea section with respect to future volcanic hazards. Holcomb (chapter 12) discusses how some of these ash deposits may be related to caldera collapse at Kilauea. The ash horizons are therefore important markers of Kilauea volcanic activity.

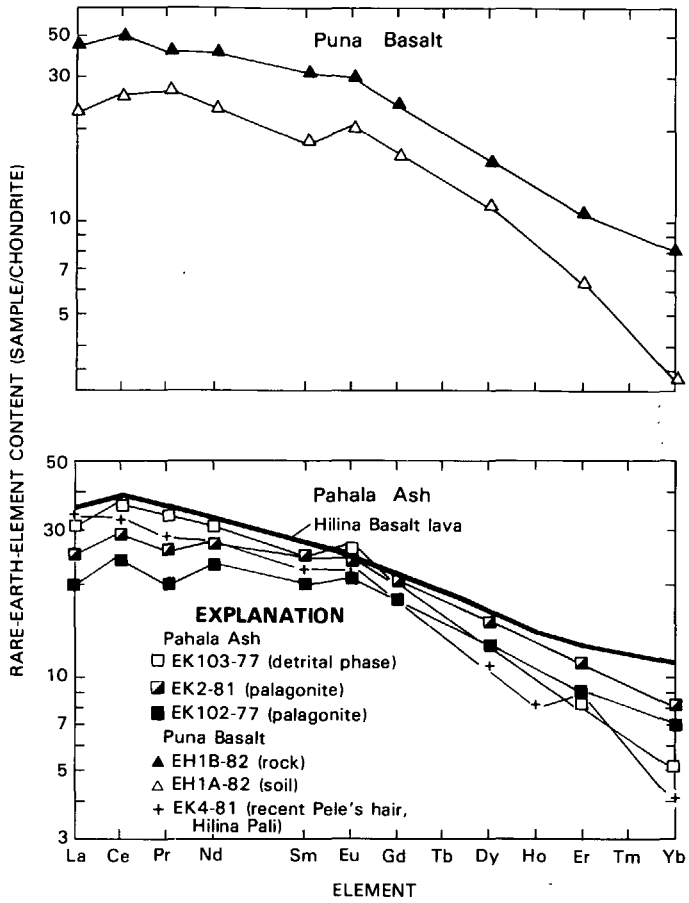

FIGURE 11.15.—Chondrite-normalized rare-earth-element (REE) data for Pahala Ash samples. Sample EK103-77 is a gray-weathering sand bed from Pahala Ash at Keana Bihopa, Hilina Pali. Its REE pattern is similar to typical Kilauea lava (for instance, Hilina Basalt lava shown) and modern Kilauea stream and sheetwash sands (not shown; Easton and Easton, 1983); low content of heavy REE in sample may be a result of presence of detrital olivine in the sample. Sample EK102-77 is palgonitized ash from Pahala Ash overlying EK103-77. Although the REE pattern is similar to that for Hilina Basalt lava, REE abundances are about 20–25 percent lower than in lava. The same is true of sample EK2-81, a Pahala Ash sample from Mauna Loa near town of Waiohinu. The REE loss in Pahala Ash palagonite is similar to that observed for soils developed over Puna Basalt lava flows from east rift zone of Kilauea (EH1A-82, EH1B-82) and is probably related to weathering and alteration. The REE data indicate a basaltic composition for Pahala Ash, but alteration, particularly with respect to light REE, prevents discrimination between Mauna Loa and Kilauea sources.

REFERENCES CITED

Atkinson, I.A.E., 1971, Successional trends in the coastal and lowland forests of Mauna Loa and Kilauea Volcano, Hawaii: Pacific Science, v. 23, p. 387–400.

Avias, J., Davis, D.A., Hanzawa, S., Ladd, H.S., Macdonald, G.A., and Obelliane, J.M., 1956, Oceanie proprement dite [Oceania properly speaking],

in Oceanie, Lexique Stratigraphique International [International Stratigraphic Lexicon], v. 6, pt. 2: Paris, Centre National de la Recherche Scientifique, 286 p.

Christiansen, R.L., 1979, Explosive eruption of Kilauea Volcano in 1790 [abs.], *in* Hawaii Symposium on Intraplate Volcanism and Submarine Volcanism, Hilo, Hawaii, July 16–22, 1979: p. 158.

Decker, R.W., and Christiansen, R.L., 1984, Explosive eruptions of Kilauea Volcano, Hawaii, *in* Explosive volcanism: Inception, evolution and hazards: Washington, National Research Council, National Academy Press, p. 122–132.

Duffield, W.A., Gibson, E.K., Jr., and Heiken, G.H., 1977, Some characteristics of Pele's hair: U.S. Geological Survey Journal of Research, v. 5, p. 93–101.

Easton, M.G., and Easton, R.M., 1983, Effects of weathering on trace and rare-earth element contents of volcanic sediments, Island of Hawaii, USA [abs.]: Geological Association of Canada Program with Abstracts, v. 8, p. A-19.

Easton, R.M., 1978, The stratigraphy and petrology of the Hilina Formation: The oldest exposed lavas of Kilauea Volcano, Hawaii: University of Hawaii, University of Hawaii, Honolulu, M.S. thesis, 274 p.

Easton, R.M., and Garcia, M.O., 1980, Petrology of the Hilina Formation, Kilauea Volcano, Hawaii: Bulletin Volcanologique, v. 43, p. 657–673.

Fisher, R.V., 1977, Erosion by volcanic base surge density currents: U-shaped channels: Geological Society of America Bulletin, v. 88, p. 1287–1297.

Fraser, G.D., 1960, Pahala Ash—an unusual deposit from Kilauea Volcano, Hawaii [art.] 163 *of* Short papers in the geological sciences: U.S. Geological Survey Professional Paper 400–B, p. B354–B355.

Hay, R.L., and Iijima, A., 1968, Nature and origin of palagonite tuffs of the Honolulu Group of Oahu, Hawaii, *in* Coats, R.R., Hay, R.L., and Anderson, C.A., eds., Studies in Volcanology: Geological Society of America Memoir 116, p. 331–376.

Hay, R.L., and Jones, B.F., 1972, Weathering of basaltic tephra on the Island of Hawaii: Geological Society of America Bulletin, v. 83, p. 317–332.

Holcomb, R.T., 1980, Preliminary geologic map of Kilauea Volcano, Hawaii: U.S. Geological Survey Open-File Report 80–796, 2 maps, 1:50,000 scale.

———1981, Kilauea Volcano, Hawaii: chronology and morphology of the surficial lava flows: U.S. Geological Survey Open-File Report 81–354, 321 p.

Kalakaua, K. D., 1888, The legends and myths of Hawaii: New York, Charles L. Webster and Co., 530 p. [reprinted 1972, Tokyo, Charles E. Tuttle Co.].

Kelley, M.L., Spiker, E.C., Lipman, P.W., Lockwood, J.P., Holcomb, R.T., and Rubin, M., 1979, U.S. Geological Survey Reston, Virginia, radiocarbon dates XV: Mauna Loa and Kilauea Volcanoes, Hawaii: Radiocarbon, v. 21, p. 306–320.

Macdonald, G.A., 1944, The 1840 eruption and crystal differentiation in the Kilauean magma column: American Journal of Science, v. 242, p. 177–189.

———1949, Petrography of the Island of Hawaii: U.S. Geological Survey Professional Paper 214–D, p. D51–D96.

Macdonald, G.A., and Abbott, A.T., 1970, Volcanoes in the Sea: Honolulu, University of Hawaii Press, 441 p.

Macdonald, G.A., Abbott, A.T., and Peterson, F.L., 1983, Volcanoes in the Sea, 2nd edition: Honolulu, University of Hawaii Press, 517 p.

Malin, M.C., Dzurisin, D., and Sharp, R.P., 1983, Stripping of Keanakakoi tephra on Kilauea Volcano, Hawaii: Geological Society of America Bulletin, v. 94, p. 1148–1158.

North American Commission on Stratigraphic Nomenclature, 1983, North American Stratigraphic Code, 1983 edition: American Association of Petroleum Geologists Bulletin, v. 67, p. 841–875.

Porter, S.C., 1979, Quaternary stratigraphy and chronology of Mauna Kea, Hawaii: A 380,000-yr record of mid-Pacific volcanism and ice-cap glaciation: Geological Society of America Bulletin, v. 90, pt. 2, p. 909–1093.

Powers, H.A., 1948, A chronology of explosive eruptions of Kilauea: Pacific Science, v. 2, p. 278–292.

Powers, S., 1916, Explosive ejectamenta of Kilauea: American Journal of Science, Series 4, v. 41, p. 227–244.

Pukui, M.K., Elbert, S.H., and Mookini, E.T., 1974, Place Names of Hawaii, 2nd edition: Honolulu, University of Hawaii Press, 289 p.

Rubin, M., and Berthold, S., 1961, U.S. Geological Survey radiocarbon dates, VI: Radiocarbon, v. 3, p. 93–94.

Stearns, H.T., and Clark, W.O., 1930, Geology and groundwater resources of the Kau District, Hawaii: U.S. Geological Survey Water Supply Paper 616, 183 p.

Stearns, H.T., and Macdonald, G.A., 1946, Geology and ground-water resources of the Island of Hawaii: Hawaii Division of Hydrography Bulletin 9, 363 p.

Stone, J.B., 1926, The products and structure of Kilauea: Honolulu, Bernice Pauhi Bishop Museum Bulletin 33, 60 p.

Swanson, D.A., 1973, Pahoehoe flows from the 1969–1971 Mauna Ulu eruption of Kilauea Volcano, Hawaii: Geological Society of America Bulletin, v. 84, p. 615–626.

Swanson, D.A., and Christiansen, R.L., 1973, Tragic base surge in 1790 at Kilauea Volcano: Geology, v. 1, p. 83–86.

Walker, G.W., 1969, Geological map of the Kau Desert quadrangle, Hawaii: U.S. Geological Survey Geologic Map GQ–827, scale 1:24,000.

Washington, H.S., 1923, Petrology of the Hawaiian Islands: II, Hualalai and Mauna Loa: American Journal of Science, 5th Series, v. 6, art. 10, p. 100–126.

Wentworth, C.K., 1938, Ash formations on the Island of Hawaii: Honolulu, 3rd Special Report of the Hawaiian Volcano Observatory, Hawaii Volcano Research Association, 183 p.

Wright, T.L., 1971, Chemistry of Kilauea and Mauna Loa in space and time: U.S. Geological Survey Professional Paper 735, 40 p.

ERUPTIVE HISTORY AND LONG-TERM BEHAVIOR OF KILAUEA VOLCANO

By Robin T. Holcomb

ABSTRACT

Long-term variations in Kilauea's eruptive behavior are revealed by mapping, paleomagnetic dating, and morphologic analysis of the surficial lava flows.

About 70 percent of Kilauea's surface is younger than 500 years, about 90 percent younger than 1,100 years. Much of its present caldera dates from the 18th century. An earlier caldera collapse about 1,500 years ago was followed by an eruptive hiatus outside the caldera until summit overflows began about 1,100 years ago.

Kilauea's surface is dominated by the products of sustained eruptions; it consists of 67 percent tube-fed pahoehoe, 14 percent surface-fed pahoehoe, and 16 percent aa. Eruptions are sustained longer at the summit and are briefer along the rift zones away from the magma reservoir beneath the summit. More than 50 percent of Kilauea is still covered by lava flows from long-sustained eruptions at the summit, despite an absence of such overflows in the last 250 years. Local variations in eruptive behavior along different rift structures probably reflect different connections to the principal reservoir.

Changes in eruptive behavior have occurred over intervals of decades and centuries. Some changes have been repeated, and some appear to have been evolutionary. Two caldera collapses and accompanying large explosive eruptions have been followed by intervals of little activity along the subaerial rift zones. Rift activity waxed as summit activity waned, and one waxing sequence resembles an evolutionary progression: rift eruptions, at first brief and widely separated in time and space, gradually became frequent along restricted segments of the rift zone and culminated in sustained activity at localities progressively farther from the summit. The current rift-zone activity resembles that which occurred in the 18th century preceding the explosive eruption of 1790.

The causes of long-term eruptive variation remain undetermined, though shifts in the sites of principal magma storage are probably involved. Slow development of integrated plumbing along the rift zones is probably interrupted by sudden subsidences of the summit and the unbuttressed south flank. Possible behavioral models are classified as evolutionary, cyclical, and stochastic; they differ greatly in their implications on long-range forecasting.

INTRODUCTION

By the early 1970's it was clear that an eruption history of Kilauea Volcano was needed for the period preceding the 19th century. The Polynesian oral history had been lost early in that century, and only a few scattered traditions had survived. During the following one hundred years Kilauea's eruptive behavior had shown little change, being nearly continuous and almost completely restricted to the caldera (fig. 12.1*A*). As a result, rift eruptions were thought rare and volcanic hazards small, and the Puna District was extensively developed (fig. 12.1*B*). However, summit activity had become episodic after collapse of Halemaumau and explosions in 1924, and a flurry of rift eruptions began in 1955. Continued rift activity through the 1960's raised the possibility of a higher long-term eruption frequency outside the caldera and of consequent greater hazard (fig. 12.1*C*). When I joined the staff of the Hawaiian Volcano Observatory in 1971 I began to reexamine the risk and the usefulness of the historical record for assessing it.

One impediment to study of long-term eruption histories had been a feeling that they could tell little about future behavior. According to the idealized life history of Hawaiian volcanoes (fig. 12.2), a shield undergoes distinct developmental stages, including a youthful growth stage and a mature caldera stage. The caldera develops when magma supply can no longer overcome a tendency for the summit to founder (Macdonald, 1965). Though eruptions may continue vigorously for some time afterward, caldera formation marks the end of shield growth. According to this view, Kilauea had recently entered its mature stage; behavior preceding caldera formation differed from that occurring now, so little could be learned about present hazards through study of precaldera events.

Powers (1948), however, had inferred that an ancient caldera was filled and buried before the present one formed. If there had been one earlier caldera there could have been many; perhaps the volcano had no distinct shield-building and caldera stages but underwent repeated caldera collapse and filling as it grew (Holcomb, 1976b). If so, Kilauea might continue to grow long into the future, and events that occurred before caldera formation might be repeated. In particular, collapses might interrupt dikes transporting magma into rift zones (Fiske and Jackson, 1972) and thereby cause changes in long-term eruption patterns. If repeated patterns occurred, they might tell much about the operation of the volcano and lead to better forecasts of its behavior. The work reported here was focused on those possibilities.

ACKNOWLEDGMENTS

Many friends and colleagues have provided assistance. R.L. Christiansen and D.W. Peterson have contributed frequent discussions since 1971. D.E. Champion and M.O. McWilliams collaborated in much of the paleomagnetic work. N.G. Banks, T.C. Casadevall, R.R. Doell, D. Dzurisin, R.M. Easton, P.W. Lipman, J.P. Lockwood, R.B. Moore, and M. Rubin provided unpublished ^{14}C ages, paleomagnetic data, and other information. Contributions were made also by many others, especially the staff of

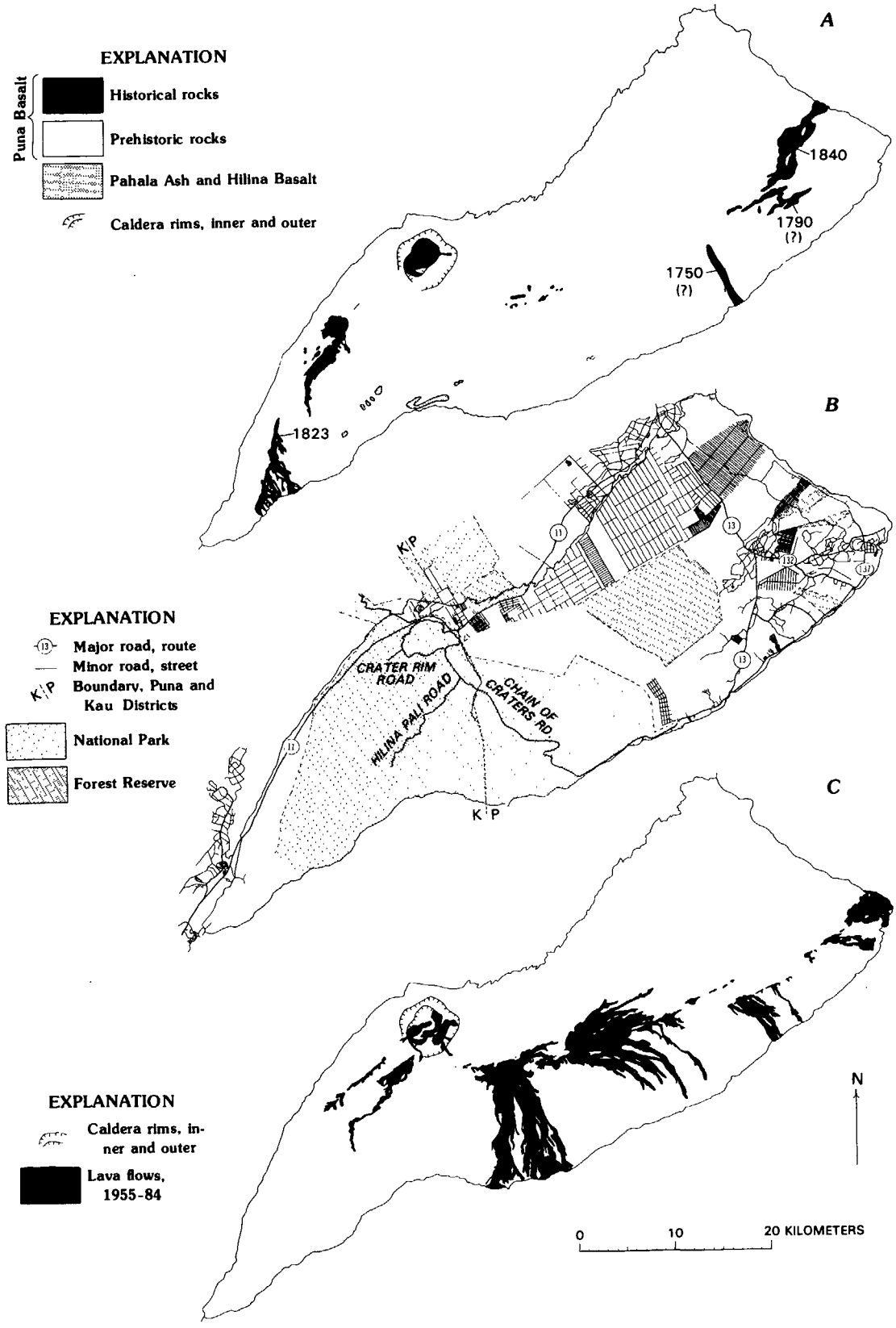

FIGURE 12.1.—Historical eruptions and property development on Kilauea Volcano. ***A***, Stratigraphy of Kilauea, showing historical lava flows erupted before 1954, with dates given for some flows, from Stearns and Macdonald (1946). ***B***, Property subdivisions, developed mostly after 1950. ***C***, Lava flows erupted during 1955–84.

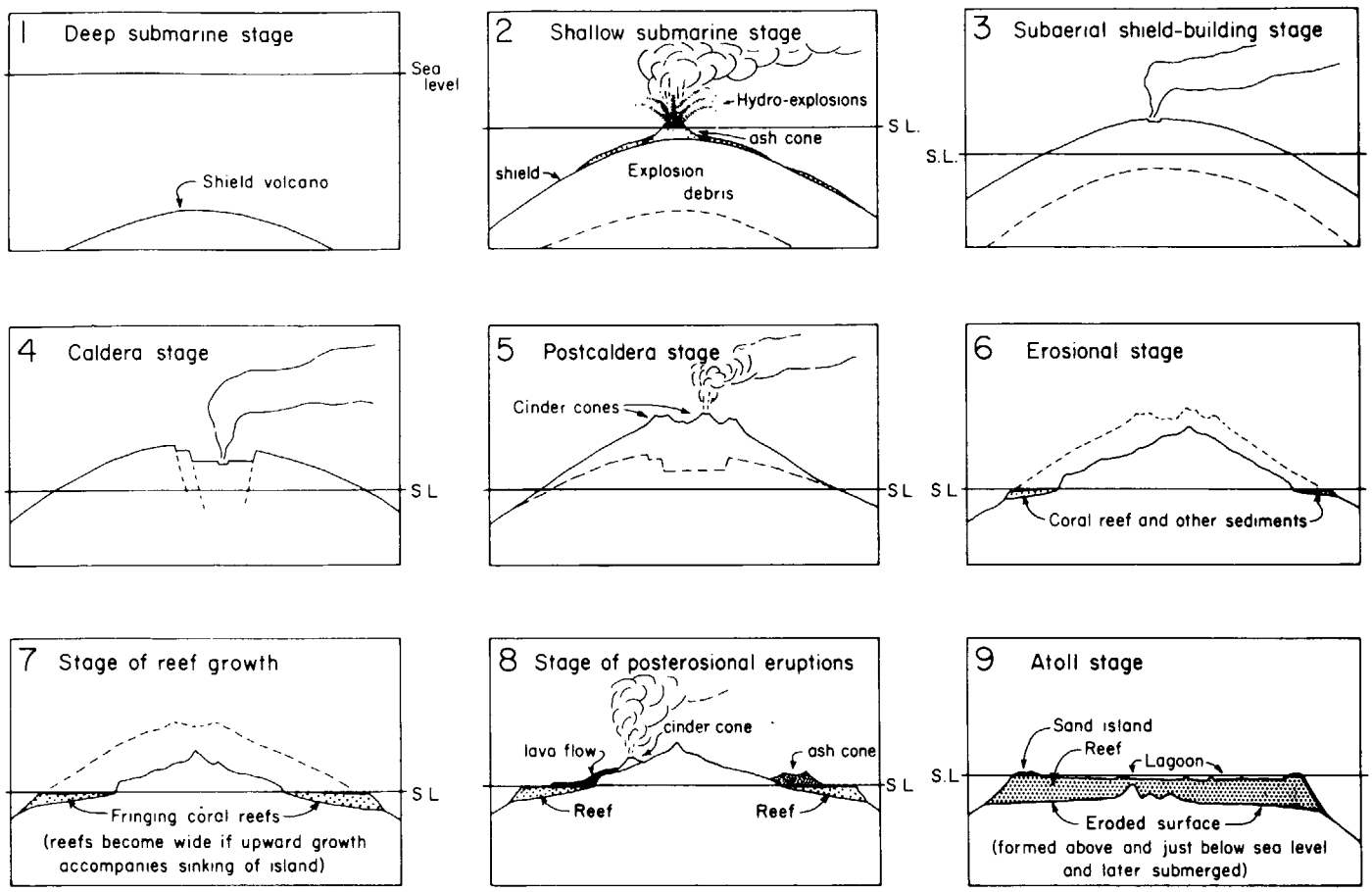

FIGURE 12.2.—Life cycle of a Hawaiian volcano, from Macdonald and Abbott (1970).

the Hawaiian Volcano Observatory, residents of Kilauea, and the faculty and students of Stanford University. Some of the work was supported by a grant from the Piton Foundation of Denver, Colorado. This report has benefited greatly from encouragement by R.W. Decker and reviews by D.E. Champion, R.L. Christiansen, D. Dzurisin, R.B. Moore, and D.W. Peterson. The maps were colored by B.M. Myers, G.R. Stoopes, and D.E. Wieprecht.

PURPOSE AND PROCEDURE

Kilauea's recent history has been surveyed to evaluate long-term eruptive changes. The work has focused on the interval recorded by the surficial lava flows; a tentative history for this interval has been derived from geologic mapping, age determinations, and morphologic analysis of eruption products (Holcomb, 1980b).

GEOLOGIC MAPPING

In order to establish stratigraphic sequences and gather other information, a reconnaissance geologic map of Kilauea's subaerial edifice was made at a scale of 1:50,000 (Holcomb, 1980a; many subsequent illustrations herein are adapted from that map, as indicated in fig. 12.3). Four years of general familiarization (1971–75) were followed by several months of systematic photograph interpretation (1975–76) and three months of ground checking (1977). Emphasis was placed on lava-flow morphology. Standard procedures were adapted to suit the particular goals of the work, time available, and characteristics of the mapped area.

The subaerial part of Kilauea is about 80 km long, averages about 20 km wide, and includes about 1,500 km^2. It is a long, domelike ridge rising to a summit elevation of about 1,240 m (fig. 12.4*A*). The orographic rainfall pattern renders it climatically and

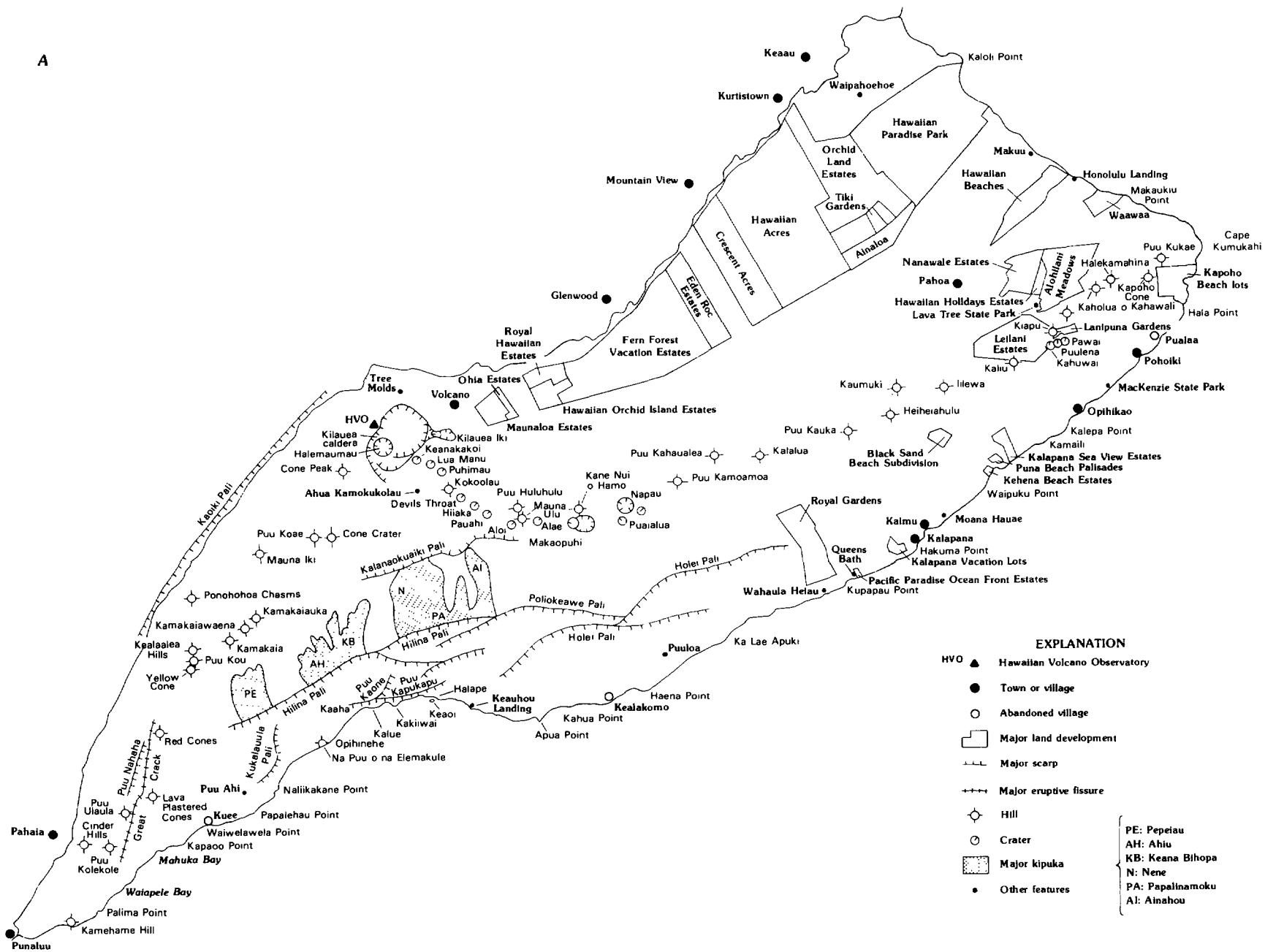

FIGURE 12.3.—Index maps for Kilauea Volcano. ***A***, Some named localities; others are shown on figure 12.5. ***B***, Coverage of map and aerial-photograph illustrations in this report; numbers refer to figure numbers.

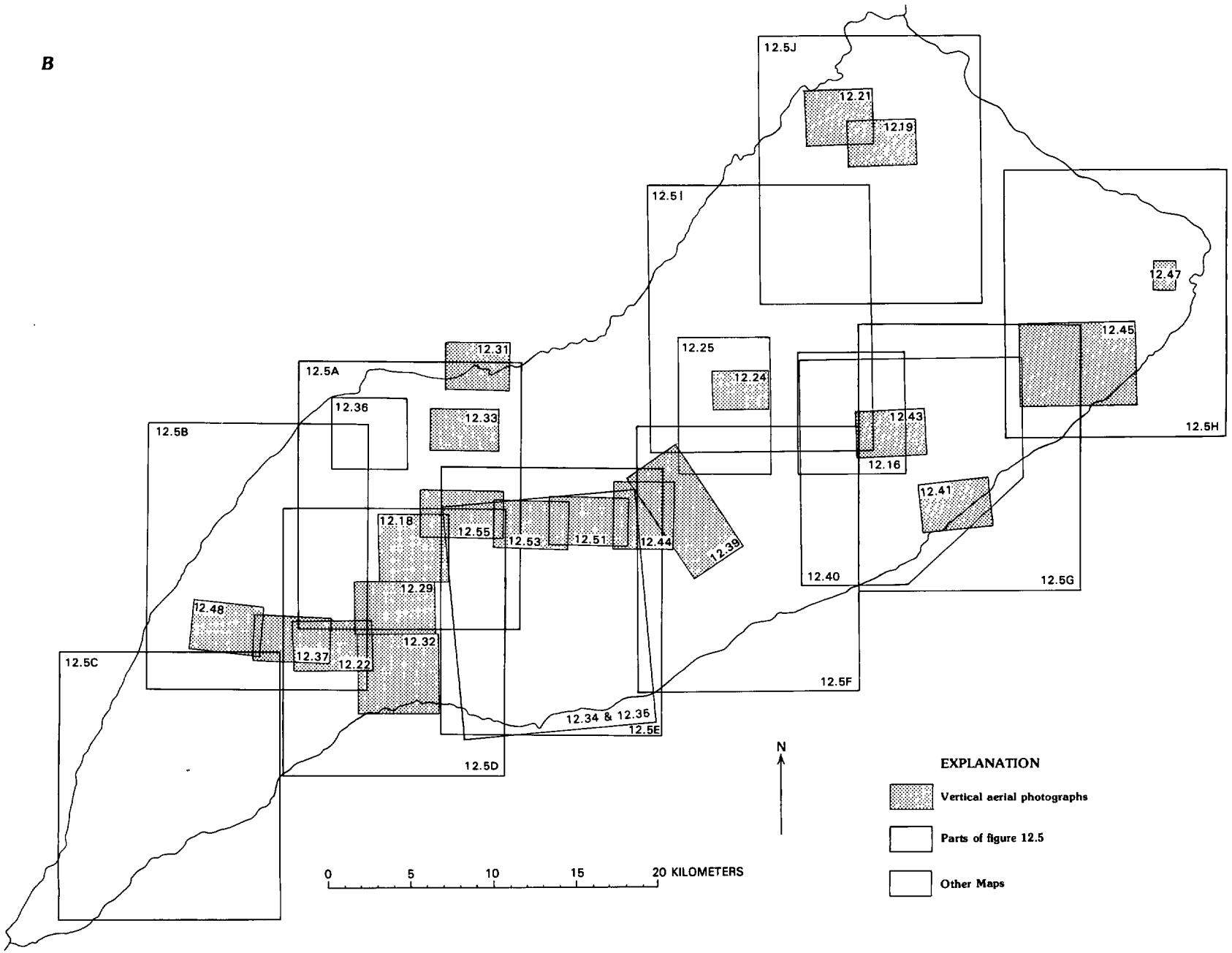

FIGURE 12.3—Continued.

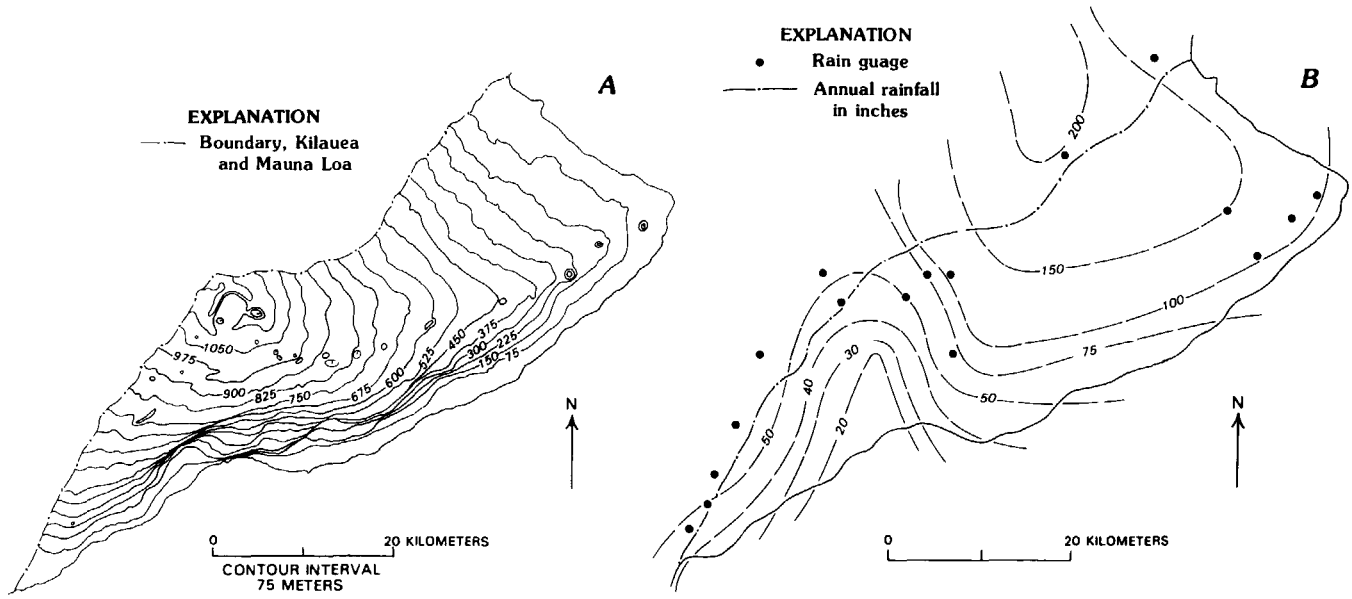

FIGURE 12.4.—Variation of geographic and mapping conditions on Kilauea Volcano. ***A***, Topography. ***B***, Annual rainfall, from Taliaferro (1959). ***C***, Vegetation, from Ripperton and Hosaka (1942). ***D***, Mapping confidence.

botanically diverse, and large parts range from tropical rain forest to barren desert (fig 12.4*B*,*C*). These variations made the mapping procedure very different from one flank to another, and as a result mapping confidence varies widely (fig. 12.4*D*).

A simplified version of the geologic map is presented here as figure 12.5. Though the original is more detailed than maps of most other shield volcanoes, it still represents merely a reconnaissance for the goal of a detailed eruption history.

CLASSIFICATION OF LAVA FLOWS AND ERUPTIONS

In order to examine more than simple eruption frequencies, the eruptions were classified according to their behavior. This was done through morphologic classification of eruption products (fig. 12.6) using interpretive principles developed during the Mauna Ulu eruptions of 1969–74. The morphology of a lava flow is influenced by the behavior of the eruption that produces it, with sustained effusion leading to a high degree of channelization and formation of lava tubes (fig. 12.7; Peterson and Swanson, 1974). Different kinds of eruptions produce different kinds of vent edifices and flow assemblages (Swanson, 1973; Holcomb, 1976a). Brief eruptions produce small edifices and simple assemblages of surface-fed pahoehoe and aa, while long-sustained eruptions produce large lava shields and assemblages dominated by tube-fed pahoehoe (table 12.1). Eruptions of intermediate duration, several weeks to a few years, typically produce small shields and complex assemblages of all three flow types. The flow assemblages and vent types were used to classify Kilauea's eruptions (fig. 12.8).

DATING

Most of the ages obtained in this work used a paleomagnetic method based on the secular variation of the Earth's magnetic field (Holcomb and others, 1986). Oriented rock samples were collected during four 2-week to 3-week trips in 1978, 1979, 1981, and 1983. Directions of remanent magnetization were measured first at 67 sites on lava flows dated previously by ^{14}C. Most of these sites were on the southeast flank of Mauna Loa (fig. 12.9), where many flows have spread over weathered ash well suited for charcoal preservation (Lockwood and Lipman, 1980). Results from these sites were used to define a history of Hawaiian secular variation during the last few thousand years (fig. 12.10). Kilauea flows of unknown age were then dated by comparing their magnetization with this history of secular variation.

Flows could not be dated precisely using this method, because of dispersion in the results between paleomagnetic sites on lava flows of similar ^{14}C age. Instead, it was necessary to infer approximate ages using a semi-quantitative classification procedure. When directions of dated flows younger than 2.5 ka were plotted on an equal-area projection, they defined fields mutually exclusive in age (fig. 12.11*A*). Undated flows were then assigned ages corresponding to fields in which they fell (fig. 12.11*B*–*F*). The chronology offered here is tentative; refinements in the history of magnetic secular variation will no doubt lead to revisions in the eruption history.

In this report the chronology of Holcomb and others (1986) has been revised using results from paleomagnetic sites not yet published. In paleomagnetic citations that follow, sites prefixed by

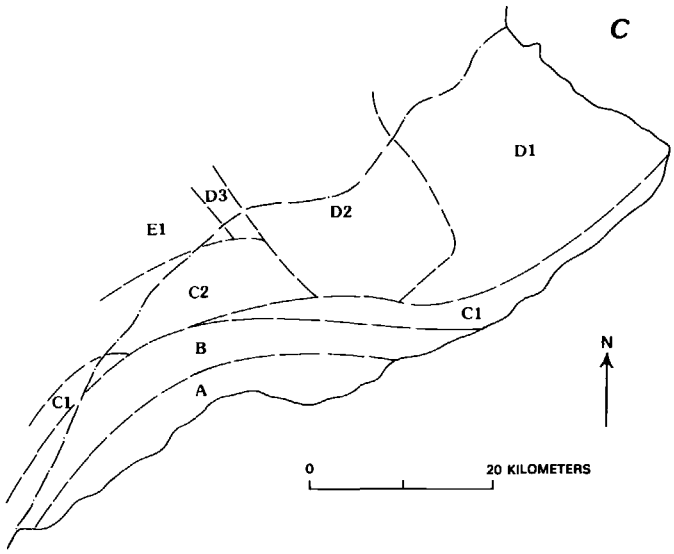

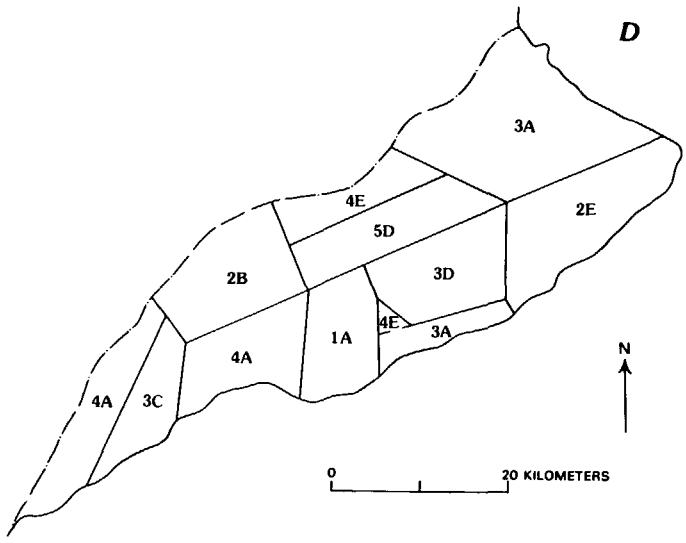

EXPLANATION

Vegetation zone	Approximate yearly rainfall (inches)	Approximate altitude limit (feet)	Characteristics of the vegetation: Natural cover	Characteristics of the vegetation: Typical plants
A	20	1,000	Xerophytic shrub with a coastal fringe of trees	Algaroba, koahaole, swollen fingergrass, feather fingergrass, piligrass, bristly foxtail
B	20-40	3,000	Xerophytic shrub with some trees in the upper part	Lantana, koahaole, klu, cactus, uhaloa, ilima, falsemallow, Natal redtop, piligrass, native panicums, kakonakona
C Low phase (C1)	40-60	2,500	Mixed open forest and shrubs	Koahaole, guava, lantana, Spanish clover, Bermudagrass, kukaipuaa, pilipiliula
High phase (C2)		2,500-4,000	Mixed open forest	Bermudagrass, Spanish clover, wild geranium, bristly-fruited mallow, plantain, rattail
D Low phase (D1)		1,500	Shrub and closed forest	Guava, sensitive plant, Boston fern, Hilograss, ricegrass, basketgrass, honohono, staghorn fern
Middle phase (D2)	60	Variable	Closed forest	Ohia lehua, tree fern, staghorn fern
High phase (D3)		4,000-7,000	Open forest	Koa, pukamole, sheepgrass, mountain pili, rattail, alapaio fern, tree fern
E Low phase (E1)	50	4,000-7,000	Open forest and shrub	Koa, mamani, heu pueo, mountain pili, large Hawaiian lovegrass, kalamaloa, sweet vernalgrass, bracken fern, alapaio fern, Kentucky bluegrass

EXPLANATION

GENERAL DEGREE OF CONFIDENCE	MAIN FACTOR LIMITING CONFIDENCE
1 Very good	A Adjacent pahoehoe flows have inherently obscure contacts
2 Good	B Tephra obscures relations between underlying units
3 Average	C Vegetal sparsity on nonadjacent flows obscures chronology based on plant succession
4 Poor	D Rain forest obscures geology
5 Very Poor	E Human forest modification obscures plant succession

FIGURE 12.4.—Continued.

8B and 9B were collected in 1978–79 and published by Holcomb and others (1986). Unpublished sites prefixed by 1B were collected by Holcomb and D.E. Champion in 1981; those prefixed by 3R were collected by Holcomb and J.D. Ward in 1983; one prefixed by 4A was collected by J.P. Lockwood in 1984.

Also used are ^{14}C ages by the U.S. Geological Survey radiocarbon laboratory in Reston, Virginia, directed by M. Rubin. Such ages are cited by their laboratory identification numbers prefixed by W. All of the cited ages are included in compilations by Kelley (1979), Kelley and others (1979), or Rubin and others (chapter 10). Though published originally with laboratory precision to the nearest 10 yr, most of the ages are expressed here only to about the nearest 100 yr. Replicate ages and comparisons with paleomagnetic data suggest that dating precision is about 200 yr

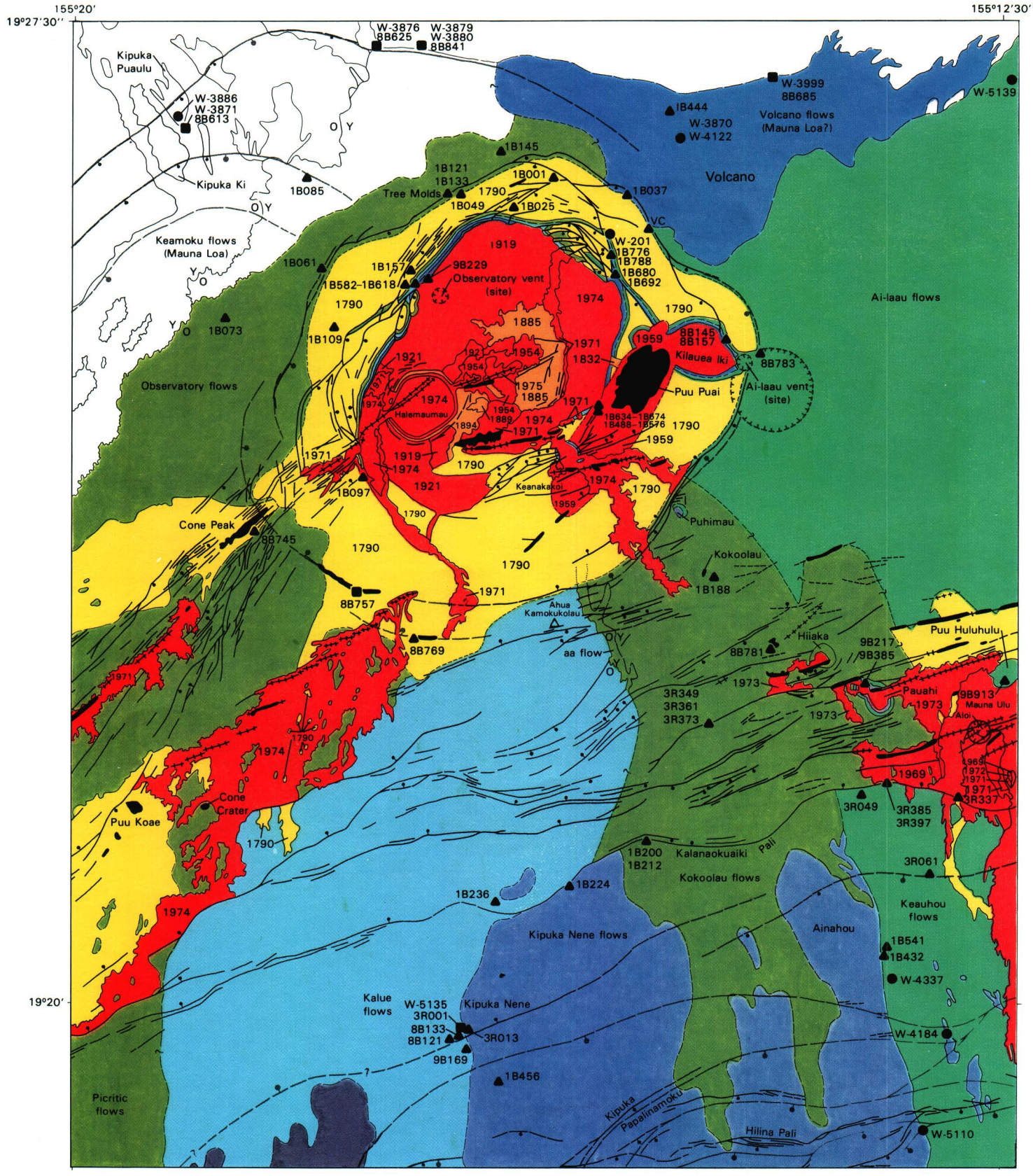

FIGURE 12.5.—Reconnaissance geologic map of Kilauea Volcano showing lavas erupted through 1977, revised and simplified from Holcomb (1980a), which also shows topography and cultural features. In this version, lava flows are classified only by age; in original map they were classified also by flow morphology and eruption type. Age uncertainties are discussed in text. Year of eruption is indicated for historical flows. ***A***, Summit region and Koae fault system. Volcano flows may have been fed by eruptions of Mauna Loa. VC, visitor center sampling site of Coe and others (1978). ***B***, Upper southwest rift zone. Some Observatory flows(?) may have been erupted

EXPLANATION

Ages of rock units

- 20th century
- 19th century

Year of eruption is indicated

- 18th century, including Keanakakoi Ash Member
- 250-350 yr B.P., including Observatory flows
- 350-500 yr B.P., including Ai-laau and Keauhou flows
- 500-750 yr B.P., including Kalue flows
- 750-1,000 yr B.P., including Volcano flows
- 1,000-1,500 yr B.P., including Kipuka Nene flows
- 1,500-10,000 yr B.P. including Uwekahuna Ash Member

Puna Basalt

- 10,000-25,000 yr B.P., including Pahala Ash
- >25,000 yr B.P., including most of Hilina Basalt

Structural and morphologic features

- Y/O ---?-- Contact; dashed where uncertain, queried where highly uncertain; older and younger units indicated by O and Y
- Fissure; dashed where uncertain
- Eruptive fissure; dashed where uncertain
- Pyroclastic cone or rampart
- Surficial fault; dashed where uncertain; ball and bar on downthrown side
- Buried fault; dashed where uncertain, queried where highly uncertain; ball and bar on downthrown side
- Buried craters; dashed where inferred

Measurement sites

- W-201 — ^{14}C age only, with no paleomagnetic samples. Code is laboratory identification number
- W-3871, 8B613 — Paleomagnetic site of this study at a ^{14}C collection site or on a flow of otherwise known age. Codes are laboratory identification numbers; see text
- 1B444 — Paleomagnetic site of this study on a flow of otherwise unknown age
- Paleomagnetic sites of previous studies; identification omitted
- Triangulation station (only a few included as geographic references)

from Mauna Loa, as mapped by Stearns and Macdonald (1946). ***C***, Lower southwest rift zone. Flows west of Great Crack may belong to more age groups than indicated here. ***D***, Flank south of summit region. Area encompasses much of Hilina and Koae fault systems, and the Papau submarine landslide (Moore and Peck, 1965; Fornari and others, 1979) occurs offshore. ***E***, Upper east rift zone and south flank. Much of this area shown also in figure 12.35, in which lava flows are classified by morphology. ***F***, Part of middle east rift zone and south flank. South flank here covered largely by lava flows from Kane Nui o Hamo. ***G***, South flank and east rift zone from Heiheiahulu to Malama. Especially prominent in this area are 18th-century lava flows of Heiheiahulu, which in figure 12.40 are classified by morphology. ***H***, East rift zone from Kaliu to Cape Kumukahi. Flows of 17th and 18th centuries not distinguished confidently in this area. Transform fault as inferred by Zablocki (1977). ***I***, Part of flank north of middle east rift zone. This heavily forested area includes poorest known part of Kilauea. ***J***, North flank southeast of Keaau. All flows older than Ai-laau shield in northern part of this area may have been erupted on Mauna Loa.

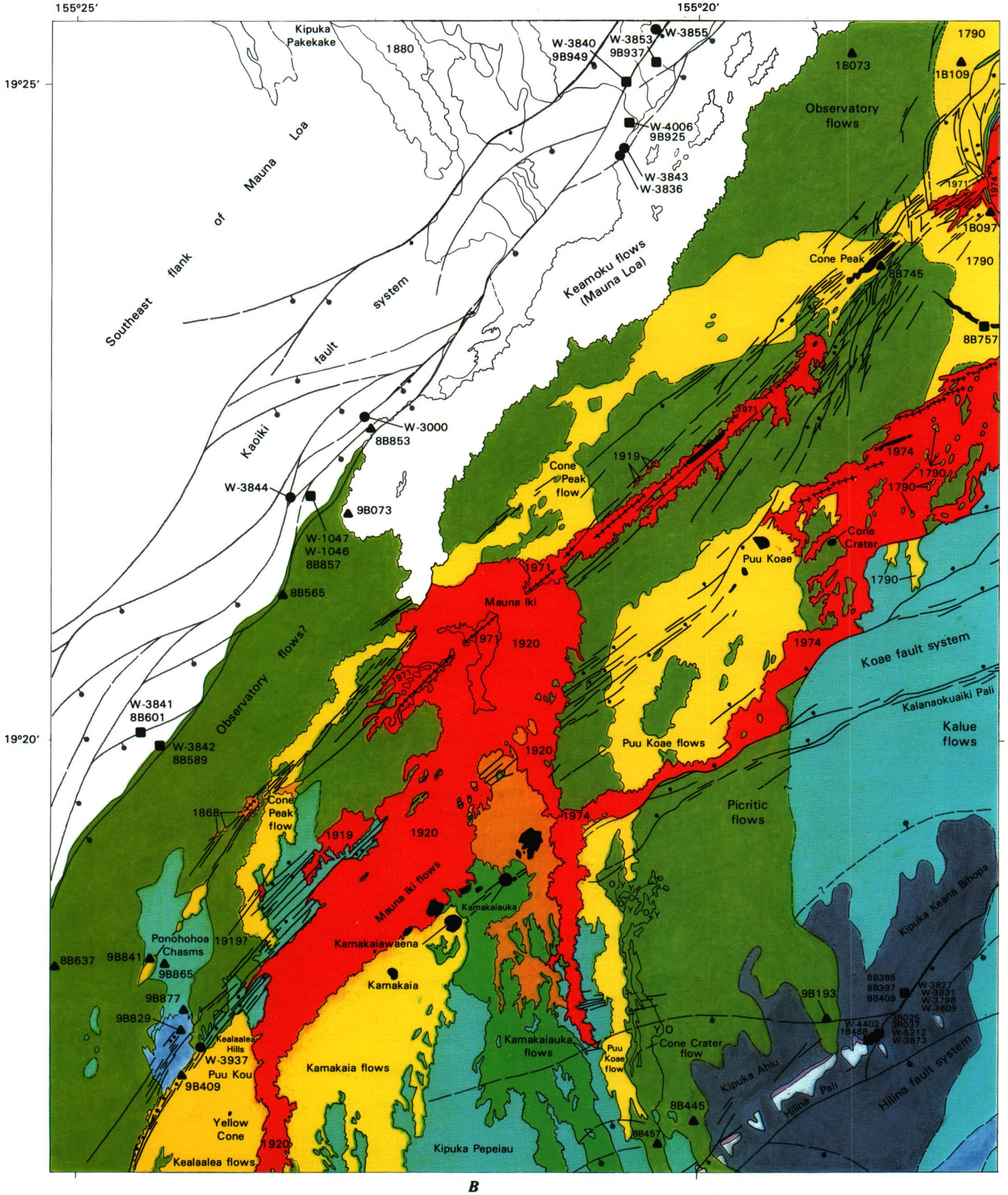

B

FIGURE 12.5.—Continued.

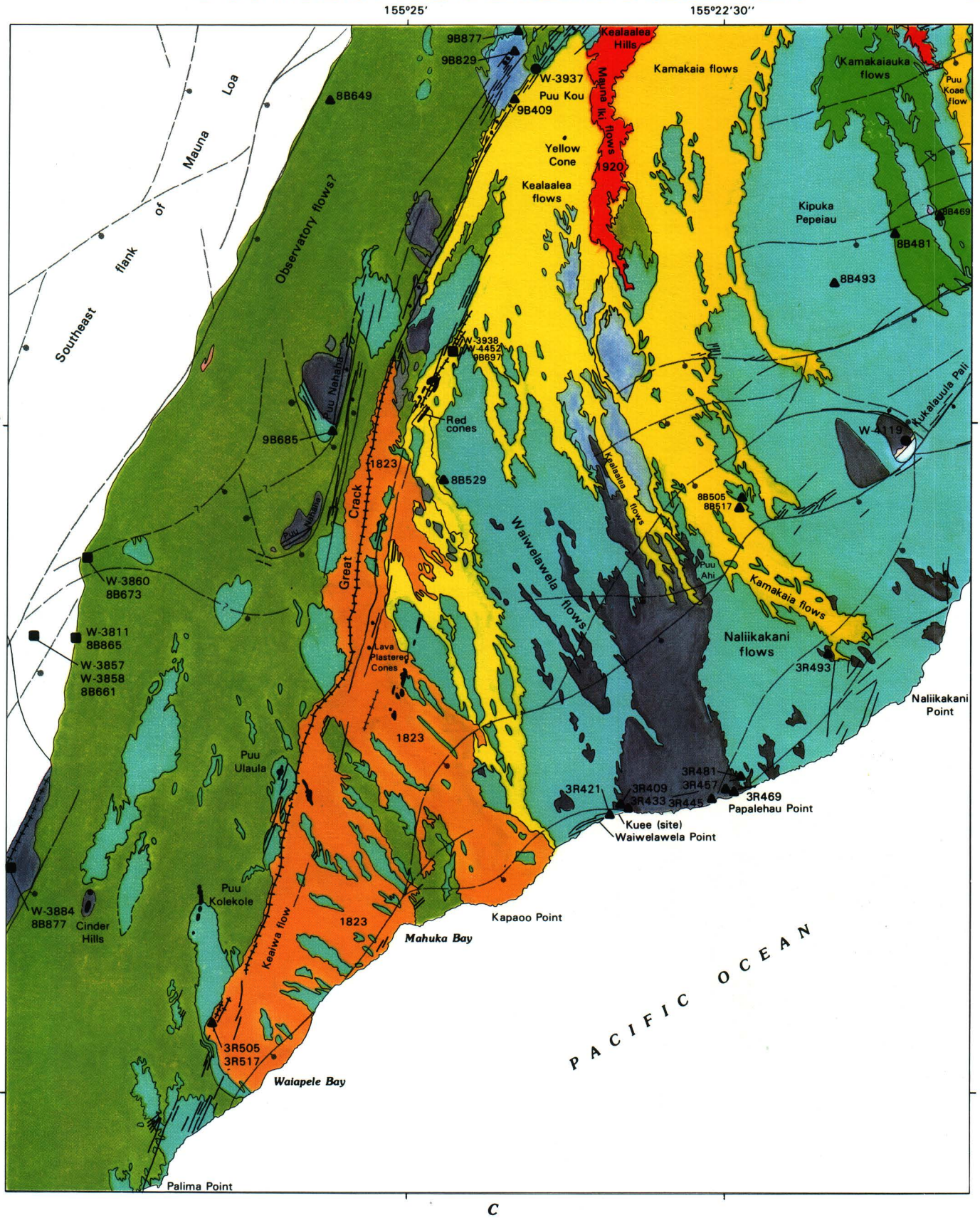

C

FIGURE 12.5.—Continued.

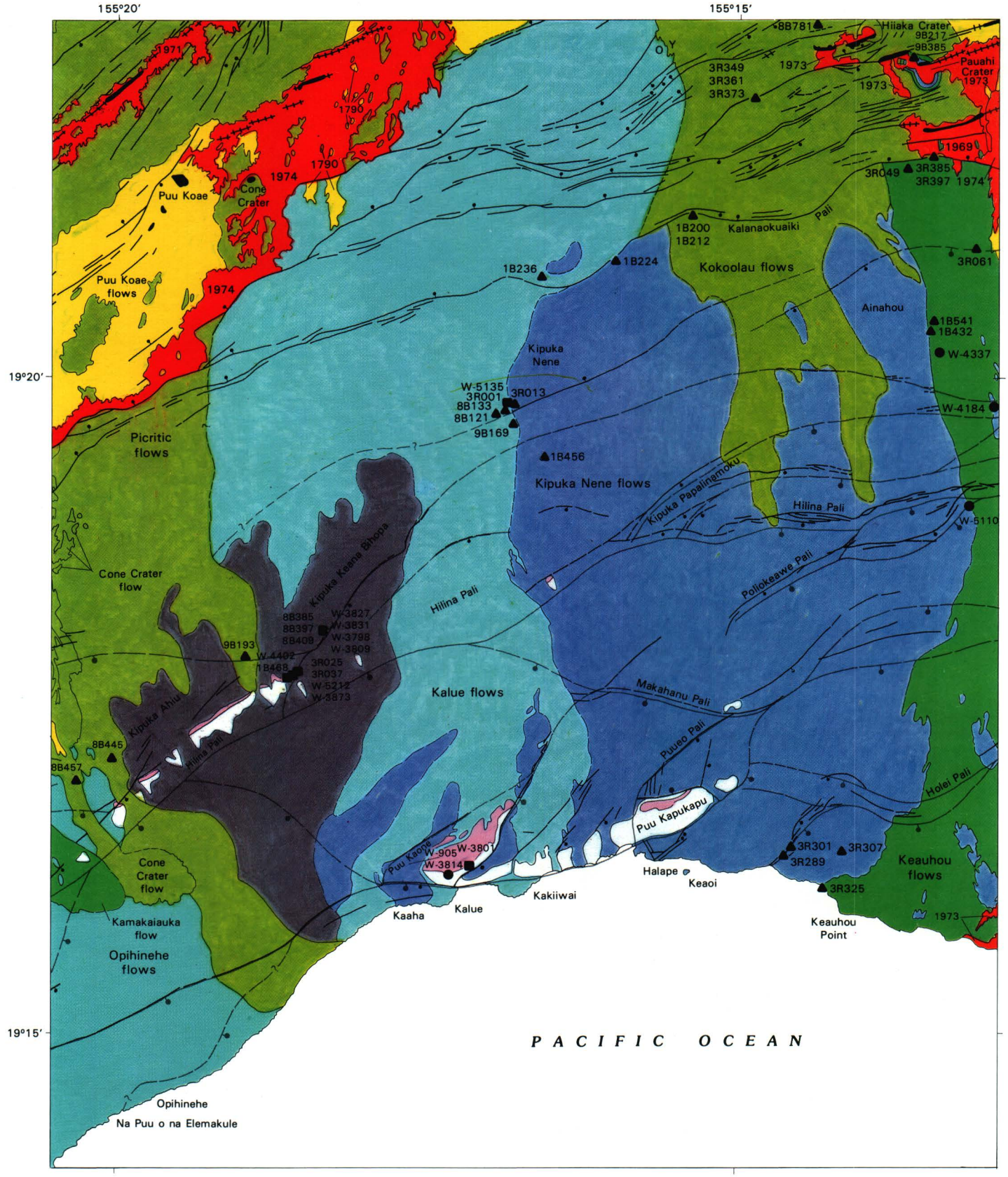

D

FIGURE 12.5.—Continued.

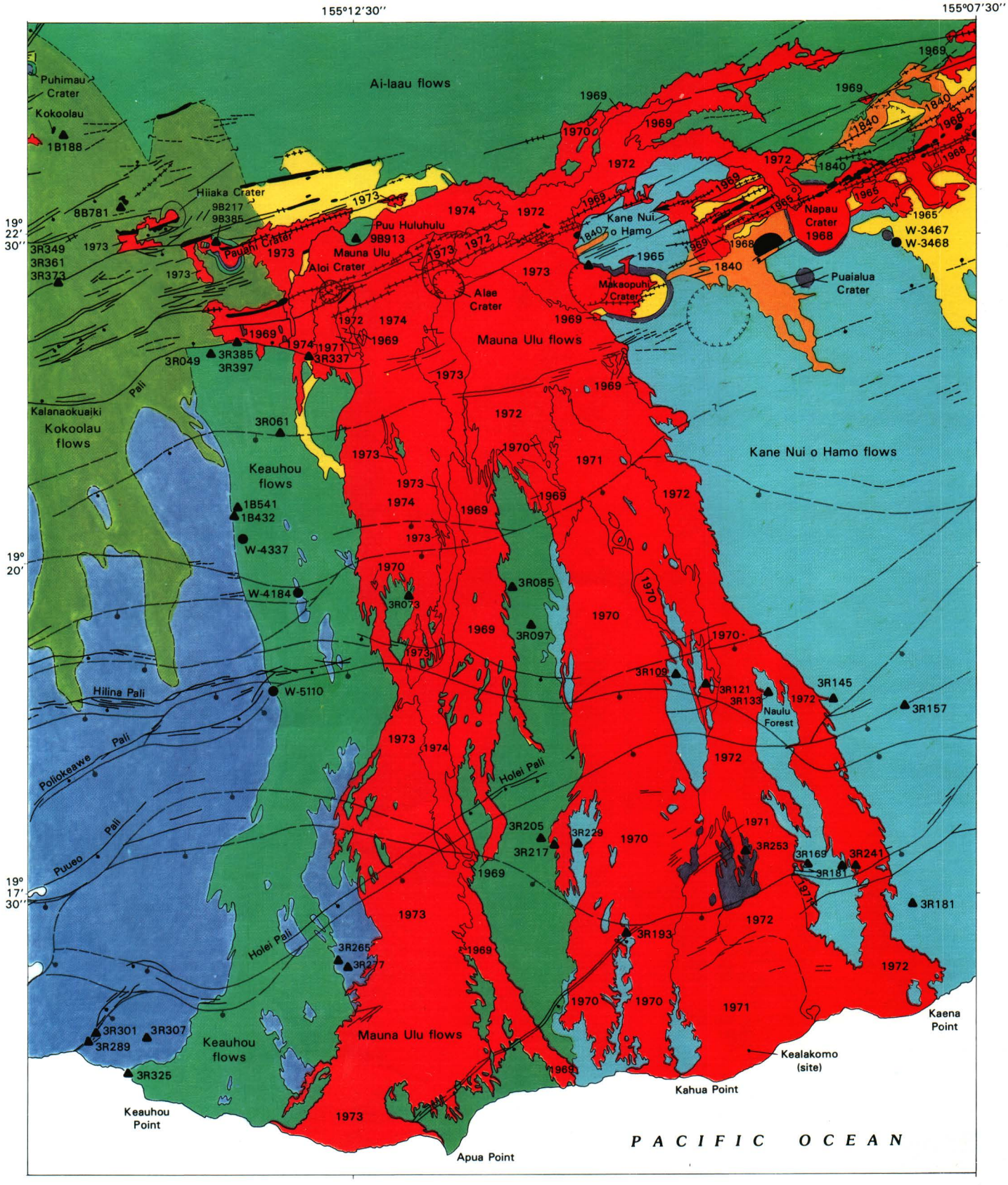

E

FIGURE 12.5.—Continued.

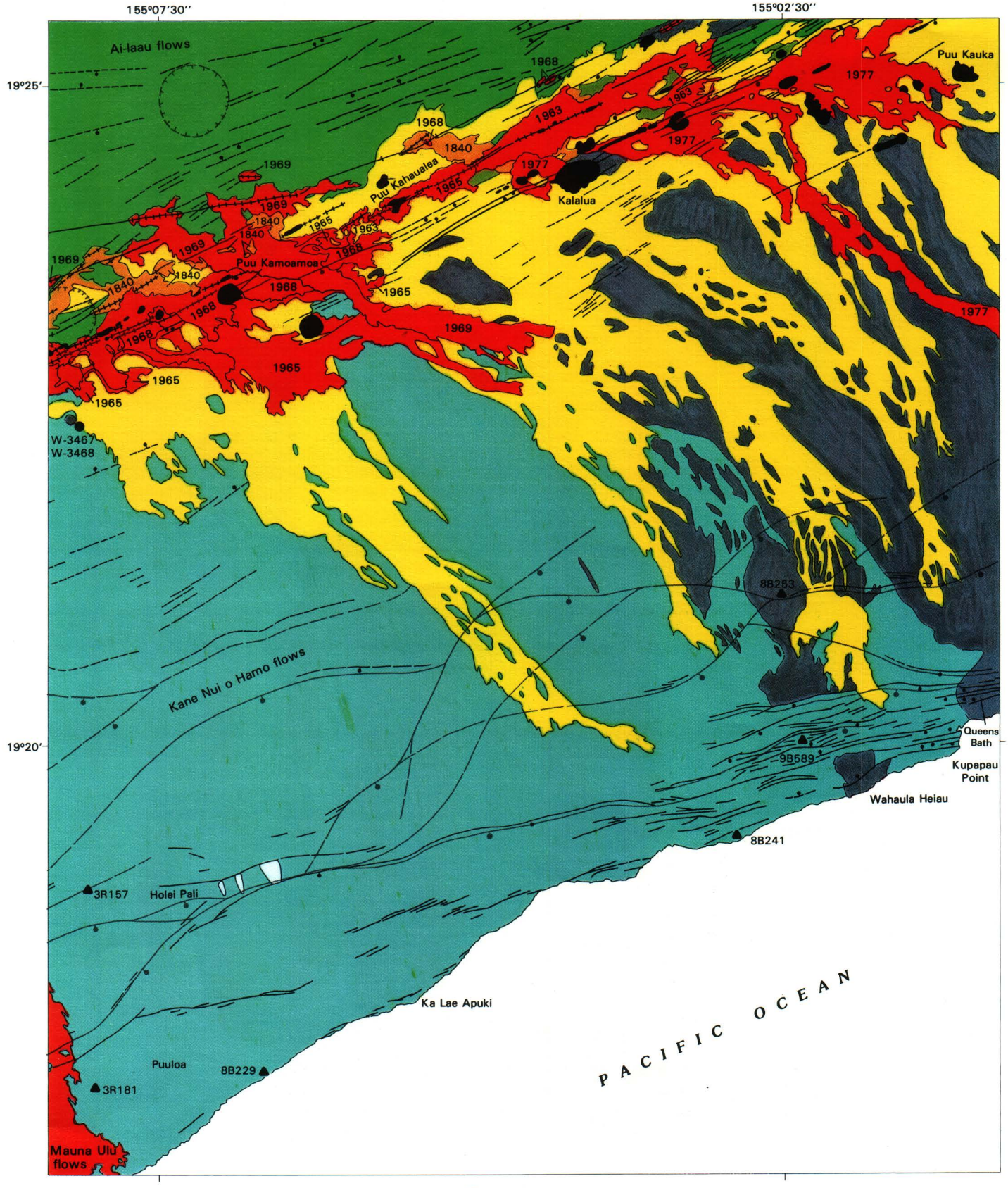

F

FIGURE 12.5—Continued.

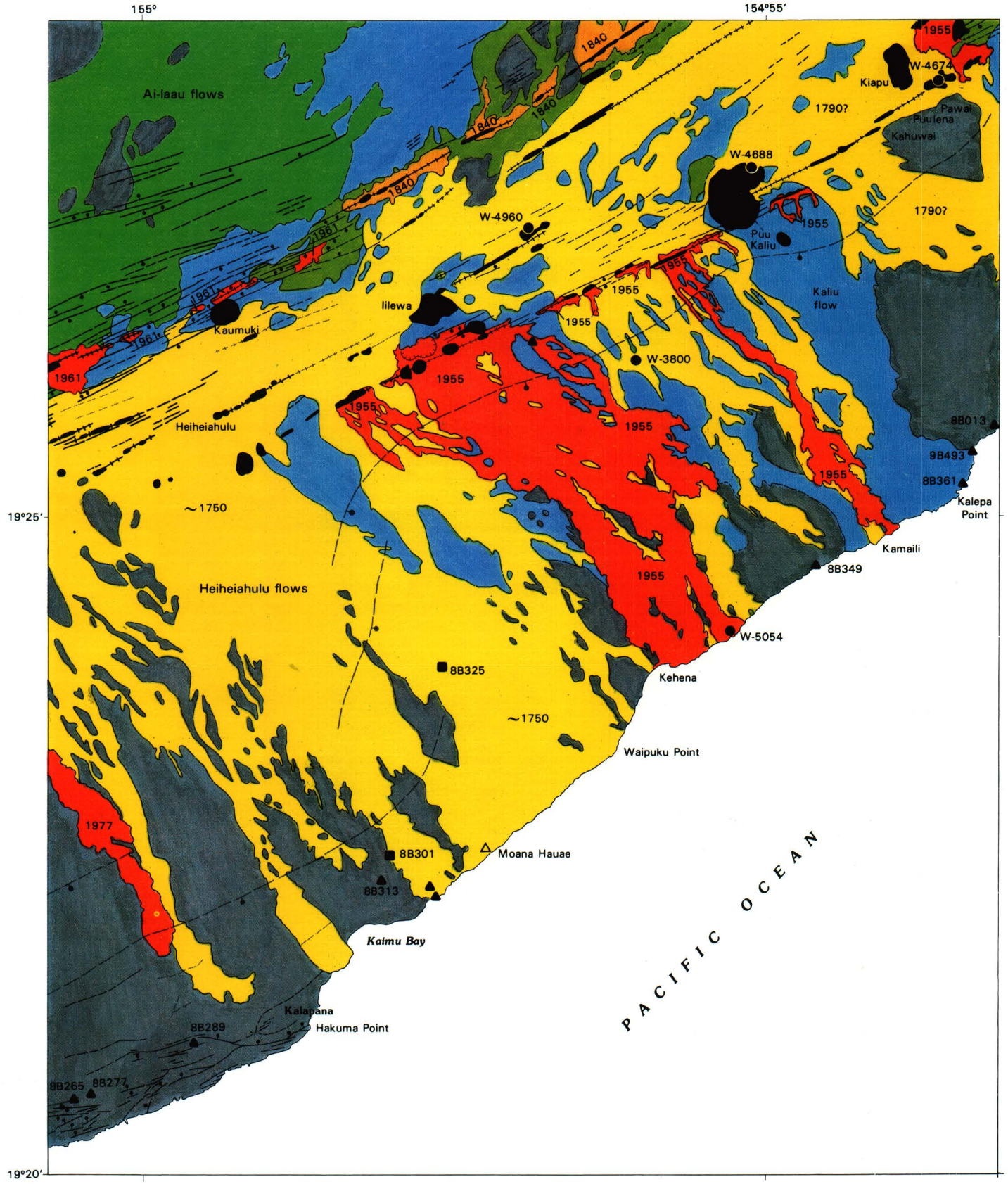

G

FIGURE 12.5—Continued.

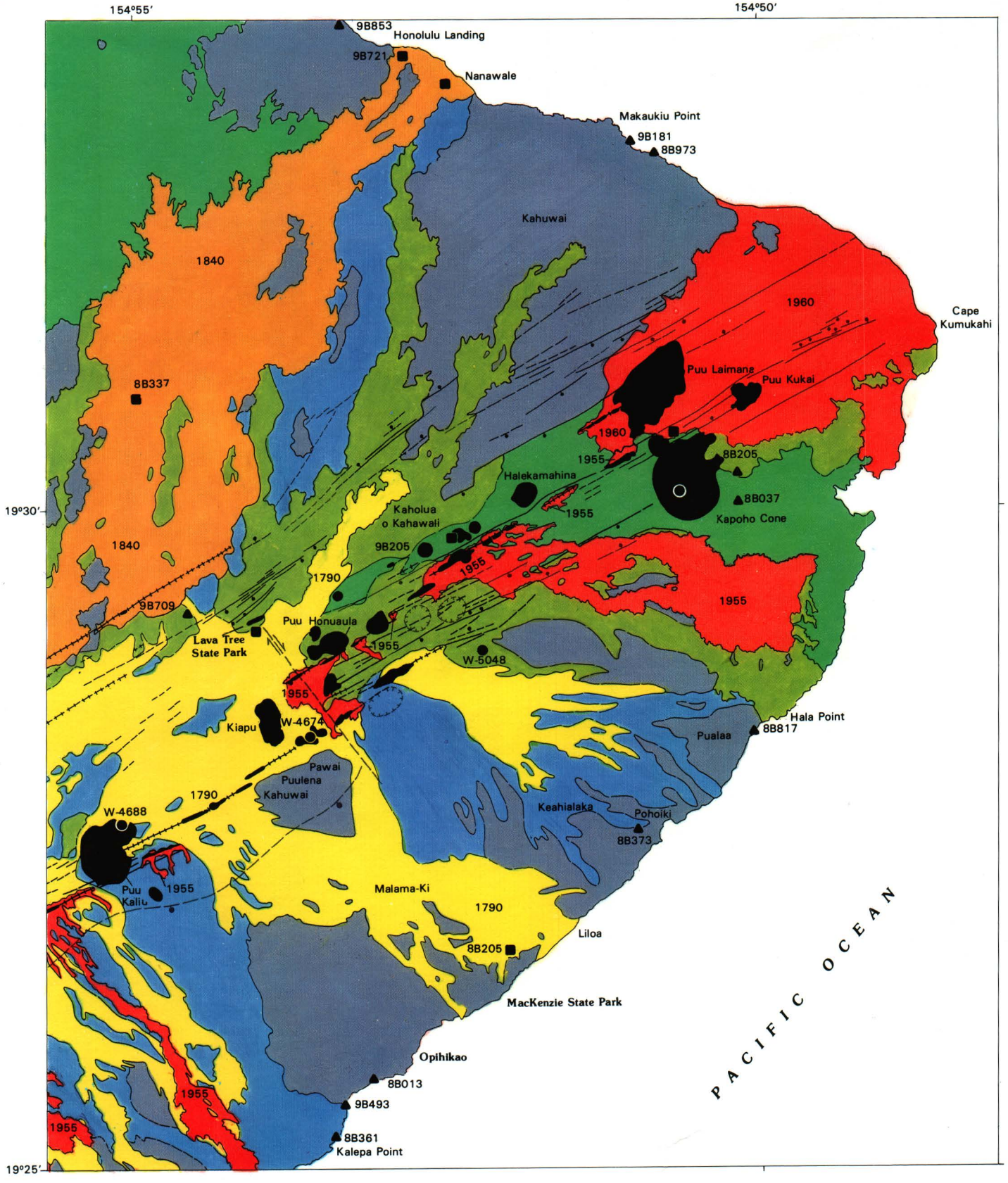

H

FIGURE 12.5—Continued.

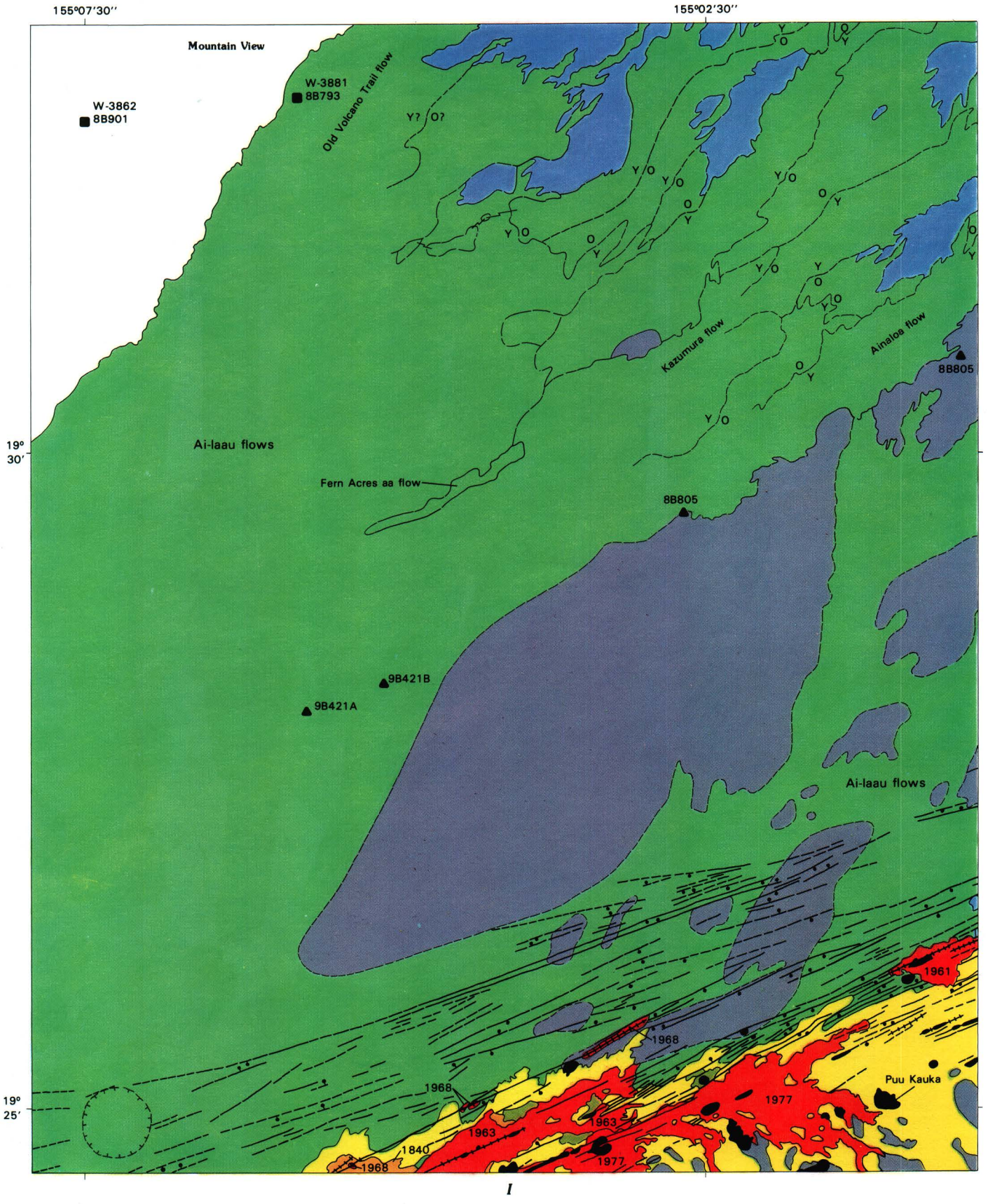

FIGURE 12.5—Continued.

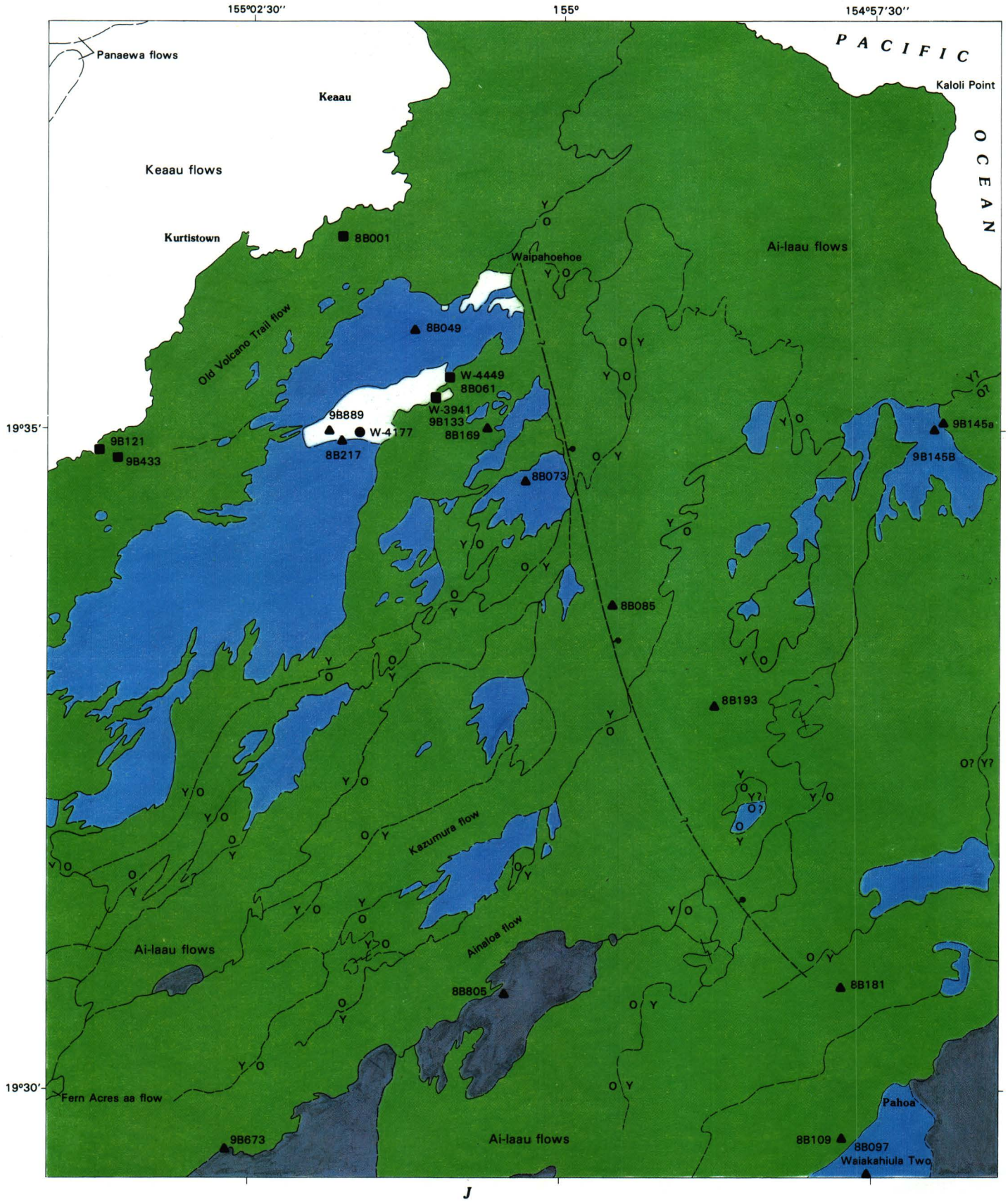

FIGURE 12.5—Continued.

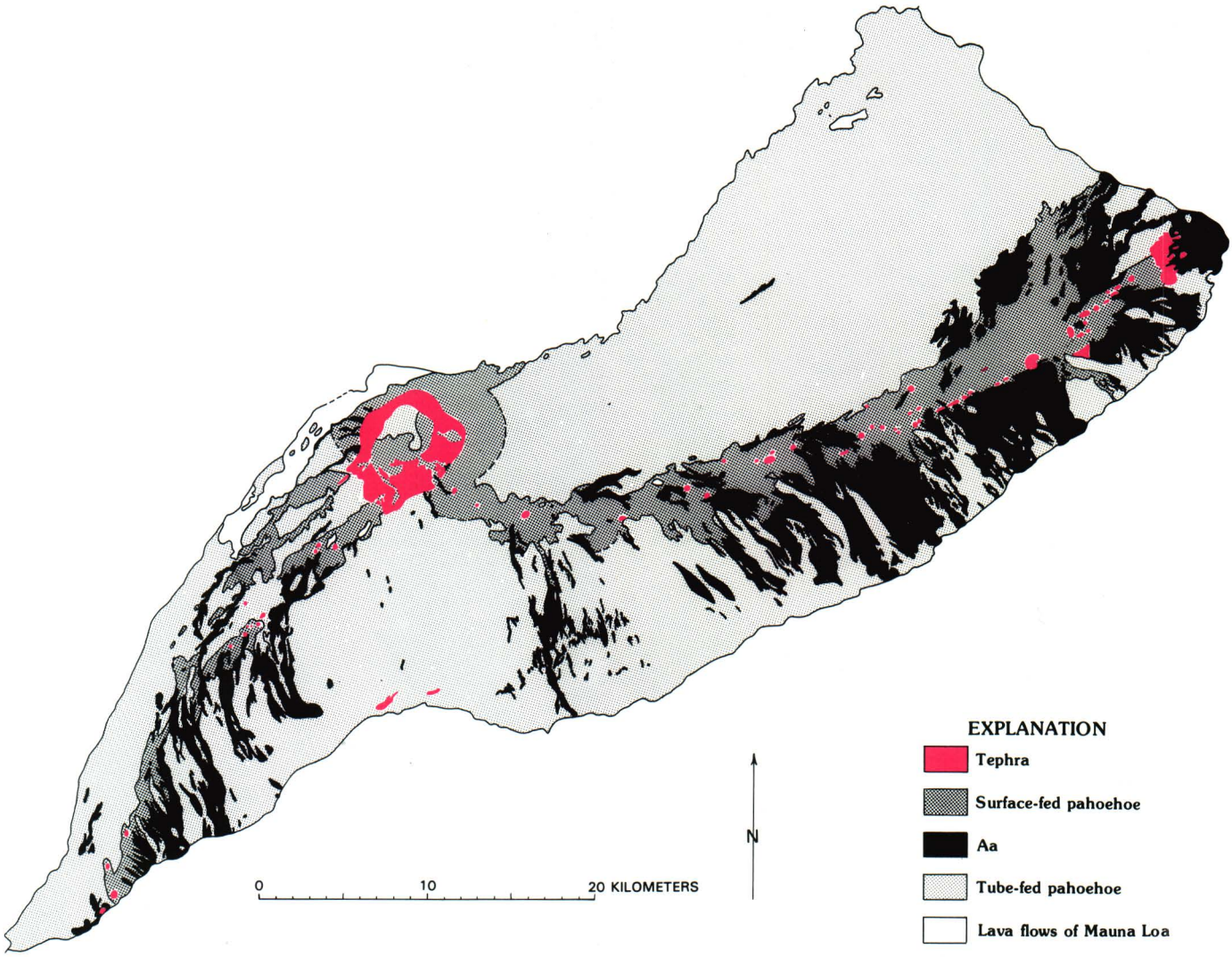

FIGURE 12.6.—Kilauea lava flows, classified by morphology; extensive tephra units are shown separately in red. Dashed lines, gradational or uncertain contacts.

(Holcomb and others, 1986). Large errors may arise from contamination by modern organisms in subtropical rainforest and by old fumarolic carbon elsewhere (Rubin and others, chapter 9).

AGE OF KILAUEA'S SURFACE

Most surficial flows have magnetization corresponding to ages of 250–1,100 yr (green hues on fig. 12.12). About 70 percent of the surface is younger than 500 yr, 90 percent younger than 1,100 yr (fig. 12.13; table 12.2). This is about ten times younger than was commonly believed as recently as a decade ago. When the mapping was begun, it was thought that a large part of Kilauea's surface was 5,000–10,000 yr old, largely because of a 2.57-ka ^{14}C age (now known to be erroneous) on the Keanakakoi Ash Member of the Puna Basalt near the rim of Kilauea'a present caldera (Rubin and Suess, 1956). The caldera is older than the ash because the ash is draped unbroken across caldera faults. Lava flows truncated by the caldera are older still; because vegetation patterns reveal clear age differences among these flows, many were thought to be much older than 2.5 ka. It was therefore puzzling when ^{14}C dating in the late 1970's found few ages older than 1 ka (Kelley and others, 1979). This dating suggested that Kilauea's surface was younger than expected, and when paleomagnetic work was planned in 1978 it was thought that a majority of surface flows were as young as 2–4 ka. The paleomagnetic results actually show that they are even younger.

This youthfulness is not inconsistent with other information about Kilauea's rate of magma supply. Assuming a supply rate of 9×10^6 m^3/mo (Swanson, 1972) and mean flow thickness of 2 m, an estimate for Kilauea's rate of surface coverage is 54,000 km^2/1,000 yr, 36 times the rate needed to cover the volcano's 1,450-km^2 subaerial surface during such an interval. This coverage rate is a

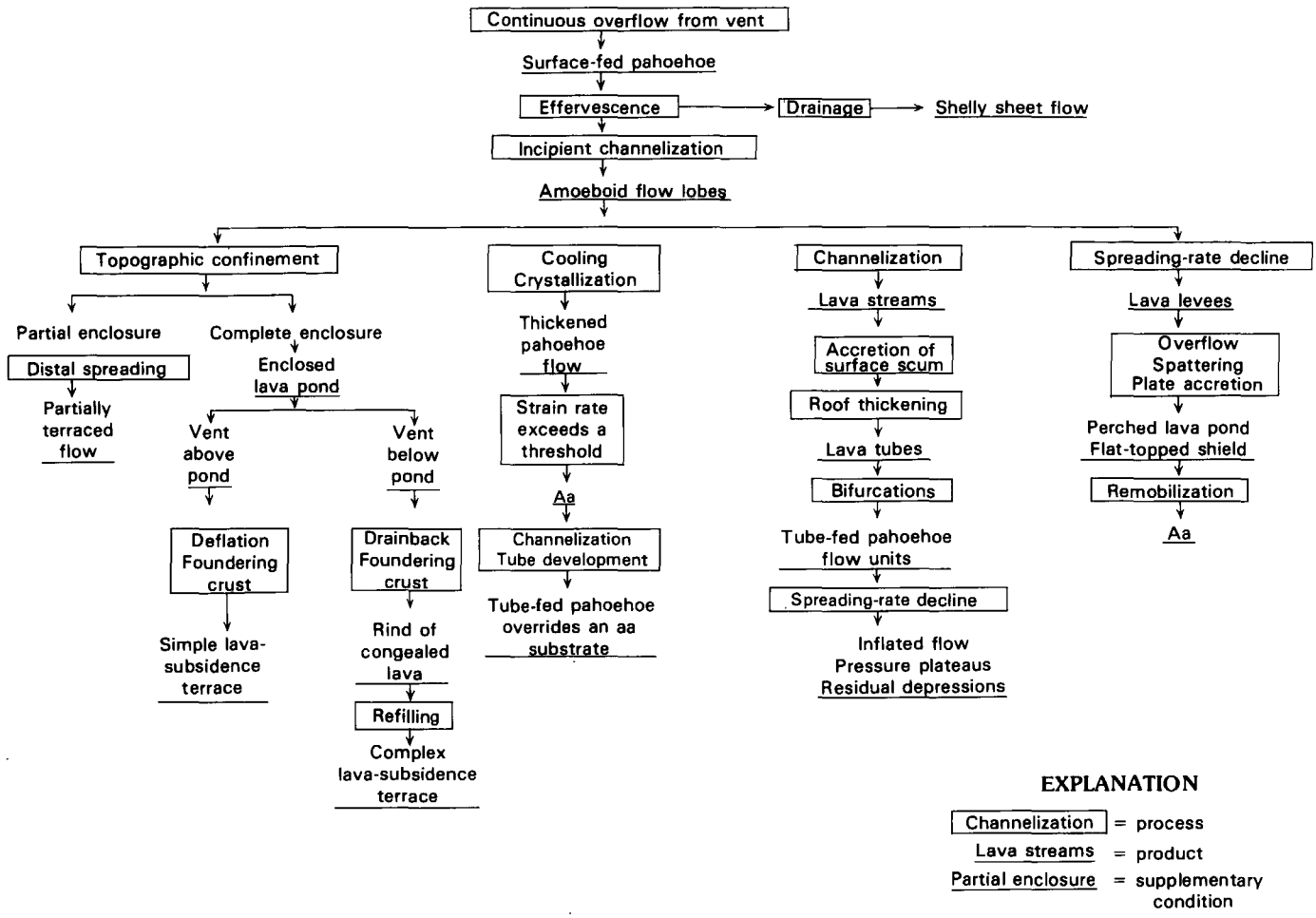

FIGURE 12.7.—Patterns of possible evolution of a lava flow. Summarized here are some processes and environmental factors affecting morphology of basaltic lava flows. In order to infer eruptive behavior it is necessary to distinguish between landforms resulting mainly from topographic influences and those resulting mainly from character of an eruption. Not all branches shown in this flow chart have been useful for interpreting eruptive behavior.

maximum value because it is not corrected for overlapping of flows or, extension of flows onto submarine flanks. Despite those omissions, however, the supply rate seems adequate to explain the rate of surface renewal graphed on figure 12.13.

STRUCTURAL SUBDIVISIONS

Different parts of Kilauea differ in eruptive behavior, so that temporal variations must be extracted from an overprint of spatial variation. Magma rises into Kilauea beneath its summit and then moves laterally for great distances along its rift zones (Fiske and Jackson, 1972). Different behaviors characterize different parts of the system, which is commonly divided into six structural subdivisions (fig. 12.14). A review of these subdivisions will provide a background for the historical account.

SUMMIT

The summit is dominated by collapse features (fig. 12.5*A*). Caldera faults form an annulus of arcuate blocks stepped downward toward an inner sink. All major displacements on caldera faults occurred before eruption of most of the Keanakakoi Ash Member in 1790 (Christiansen, 1979). Other collapse features include Kilauea Iki, Keanakakoi, and smaller prehistoric craters and the Halemaumau pit formed in 1924. Though most eruptive fissures trend east-northeast across caldera structures, other trends occur; some late prehistoric lava erupted from fissures concentric to the caldera.

Eruptions of all types occur in the summit area, but those of long duration are characteristic. Nearly continuous activity at Halemaumau for more than a century built a lava shield that filled the inner sink to overflowing by 1921. Similar eruptions buried an

earlier caldera; still preserved are parts of two lava shields, one surrounding a vent at the east end of Kilauea Iki (the Ai-laau shield), and the other centered in the northwest caldera (the Observatory shield). Tube-fed flows from these vents cover much of Kilauea. Explosive eruptions occur also at long intervals; a small one occurred in 1924, and several much larger ones occurred earlier (Decker and Christiansen, 1984).

EAST RIFT ZONE

The east rift zone forms a ridge extending more than 60 km beyond Cape Kumukahi, the easternmost point on the Island of Hawaii (fig. 12.15; Moore, 1971). Its subaerial part is 4–6 km wide and is loosely divided into an upper segment extending from the caldera to Napau Crater, a middle segment from Napau to Heiheiahulu lava shield, and a lower segment from Heiheiahulu to Cape Kumukahi. The upper segment is dominated by pit craters, and the other segments are marked by closely spaced fissures, faults, and grabens having net seaward subsidence.

The rift zone is straighter and wider than commonly portrayed. Kinks inferred in the lower segment (Skokan, 1974; Furumoto, 1976) are merely offsets in recent eruptive fissures, not in the rift zone as a whole (fig. 12.5*G*,*H*). Seaward migration of the middle segment (as suggested by Swanson and others, 1976a) has not occurred recently; historical eruptions have followed its axis, 18th-century lava having obscured the structures of its southern half (fig. 12.16). All recent flows from the middle segment have spread seaward because the rift zone has subsided below its northern margin, but some older flows of the north flank were erupted from it. The upper segment was almost entirely buried by lava from the Ai-laau vent about 400 years ago; it is probably wider and straighter than the curved chain of young pit craters, which may reflect recent localization to its southwest edge (fig. 12.5*E*). Magma intruding west along Koae faults (Unger and Koyanagi, 1979) may have produced westward widening of the rift zone.

Eruptions are briefer along the rift zone than at the summit. Flows from eruptions of moderate duration are prominent along the upper and middle rift segments, and less so along the lower segment. Brief eruptions are especially numerous along the middle and lower segments, and pyroclastic vents are more common there.

SOUTHWEST RIFT ZONE

The southwest rift zone does not form a distinct ridge like the east rift zone, its seaward subsidence is more obvious, and it does not extend far beyond the shoreline (Moore and Fiske, 1969). It parallels the Kaoiki fault system of Mauna Loa; its structures may follow buried Kaoiki faults. It consists of an inactive zone inland and an active zone seaward. The active zone contains strands of closely spaced fractures separated by unbroken blocks. The rift zone can be divided into segments where it bends near Yellow Cone; the upper segment trends about S. 50° W. and the lower segment trends about S. 15° W.

In the lower segment a seaward zone of recent rifting about 1 km wide is dominated by the Great Crack (fig. 12.5C). Other strands in the active zone extend through Puu Ulaula and Puu Kolekole (inland) and Red Cones and Lava Plastered Cones (seaward). Most faults are down to the southeast, toward the sea. More than 20 m of displacement has occurred on faults along the northwest side of the active zone; some landward blocks like Puu Nahaha stand high enough to escape draping by young flows from the rift, though they are draped by young flows from the summit. A seaward migration of eruptions may have occurred; all vents seaward of the faults appear young, while all inland vents are older than 1,000 years. But the most recently active Great Crack is inland from some other vents of the active zone.

The upper segment appears to be a broad graben or sag. It has no large pit craters, though a few small pits do occur. The seaward zone of active rifting flares from a width of 1 km in the southwest to more than 3 km in the northeast (fig. 12.5*B*). It is currently split into three strands converging downrift; each strand consists of closely spaced fractures breaking the sheet of late prehistoric summit flows.

The middle strand extends from the main center of summit tumescence (south of the caldera) through Cone Crater and Puu Koae to the lower segment of the rift zone. Eruptions from this strand have been vigorous and brief, producing spatter cones and aa flows but little tube-fed pahoehoe. The flows have olivine-controlled compositions similar to lavas erupted at the summit (Wright, 1971). This strand probably connects directly to a deeper magma reservoir and taps magma that is changed little by differentiation or loss of volatiles but cannot sustain eruption after the gas-rich fraction has escaped.

The northern strand passes from Halemaumau through Cone Peak and Mauna Iki. Its fissures end 5 km southwest of Mauna Iki without reaching the lower segment. Its historical eruptions have followed shortly after summit activity and have produced little tephra. Lava feeding the Mauna Iki eruption (1919–20) drained from Halemaumau along shallow fissures (Jaggar, 1947). This strand probably is connected to the deeper plumbing by way of Halemaumau so that its magma loses gas through summit eruptions and fumaroles. Eruptions can be sustained for months or years by drainage of degassed lava when Halemaumau acts as a shallow holding tank. (For supporting chemical and deformation data, see Duffield and others, 1982.)

The southern strand passes from the Koae faults through Kamakaia and Yellow Cone; it may intersect the middle strand where the latter bends into the lower rift segment. Its eruptions have been brief to moderately long, but they are unique on Kilauea because they produce cinder cones and viscous lava flows (fig. 12.17) of (for Kilauea) highly differentiated compositions (Wright and Fiske, 1971). This strand may have only a tenuous connection to the main plumbing, its magma residing at shallow depths for long intervals after backing up along Koae structures.

KOAE FAULT SYSTEM

The Koae fault system extends east-northeastward between the rift zones (fig. 12.5*A*,*D*). Its faults have their downthrown side mainly toward the caldera and have had recurrent movement (Duffield, 1975). Some scarps were large enough by the 18th

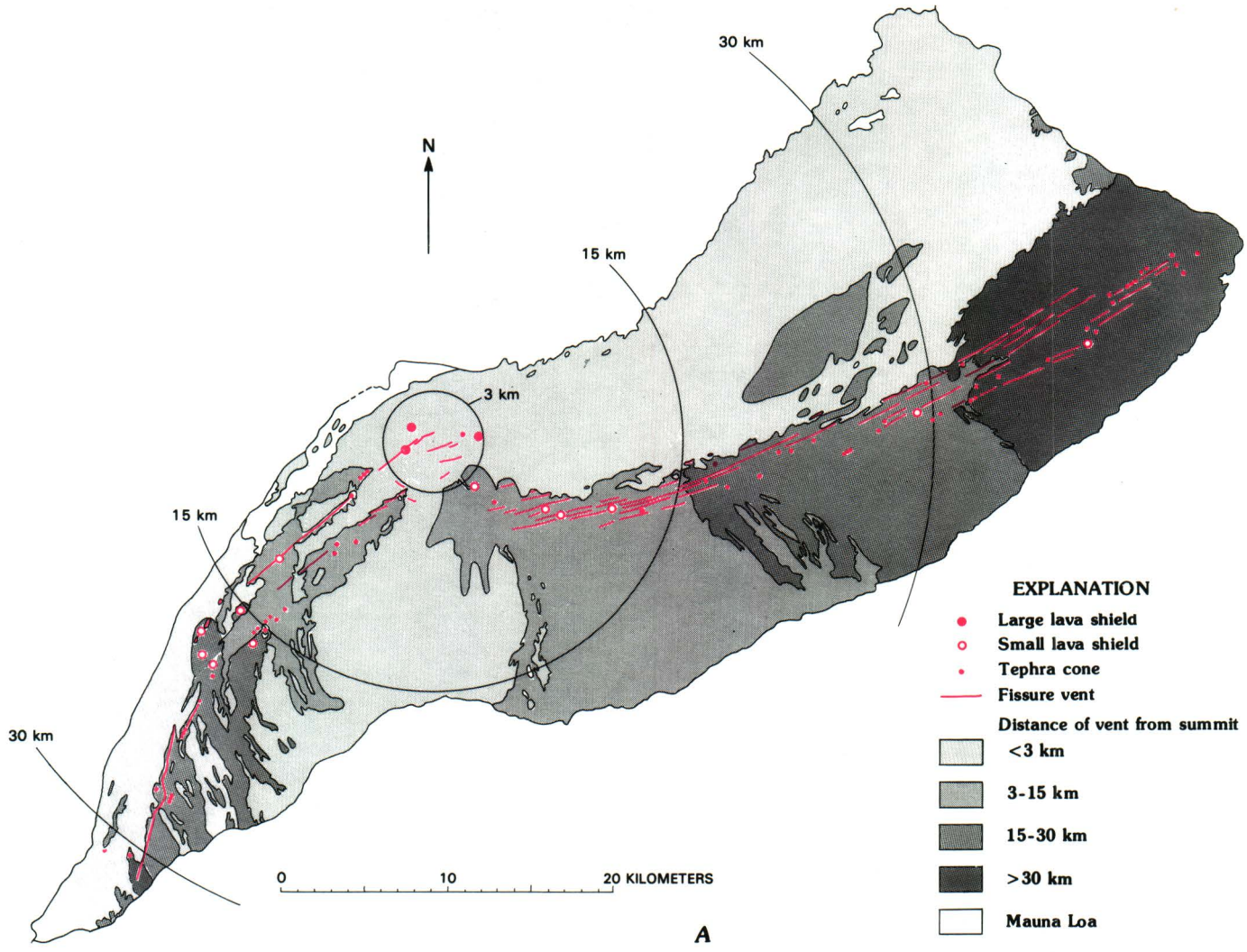

FIGURE 12.8.—Kilauea lava flows classified by location and by type of eruption. ***A***, Flows classified by location of eruption. Lava flows from summit cover large areas of north flank and southwest rift zone as well as flank south of summit. ***B***, Flows classified by eruption type. Eruptions tend to be briefer at greater distances from summit. Because it is difficult to group older flows into eruption assemblages, some older aa flows alone are inferred to represent brief eruptions and older tube-fed flows alone are inferred to represent sustained eruptions; these inferences may not always be correct.

century to deflect lava flows from Cone Crater and Puu Koae. Most present scarps postdate the Kalue flows thought to be 500–750 years old, but some scarps are older. A segment of Kalanaokuaiki Pali extending 2 km east of the Hilina Pali Road crossing is rimmed by Kipuka Nene flows thought to be about 1,100 years old (fig. 12.18); the younger Kalue flows failed to overtop the scarp, and lava tongues oozed down into the open fracture at its base. The southernmost Koae fault extending eastward from Kipuka Nene campground is overlapped by Kalue flows and has had little displacement during the subsequent 500 years.

Few eruptions are known from the Koae fault system, and most of them have been from near its intersection with the southwest rift zone. Some lava was erupted from eastern Koae structures in 1973 (Tilling and others, chapter 16). Spatter found beneath Kokoolau lava along Kalanaokuaiki Pali may be clots ejected by heated air or steam after surface flows invaded the fracture. It remains possible that true eruptions from the central Koae system have occurred and then been obscured by the younger flows from the summit.

The Koae fault system may be an ancient feature of Kilauea, or it may have been produced recently by contraction or migration of the rift zones and caldera. An anomalous area of caldera-concentric structures along the central Koae (Duffield, 1975) may reflect the buried rim of an earlier caldera, and the fault segments extending to the east and west may follow former eruptive-rift structures radial to

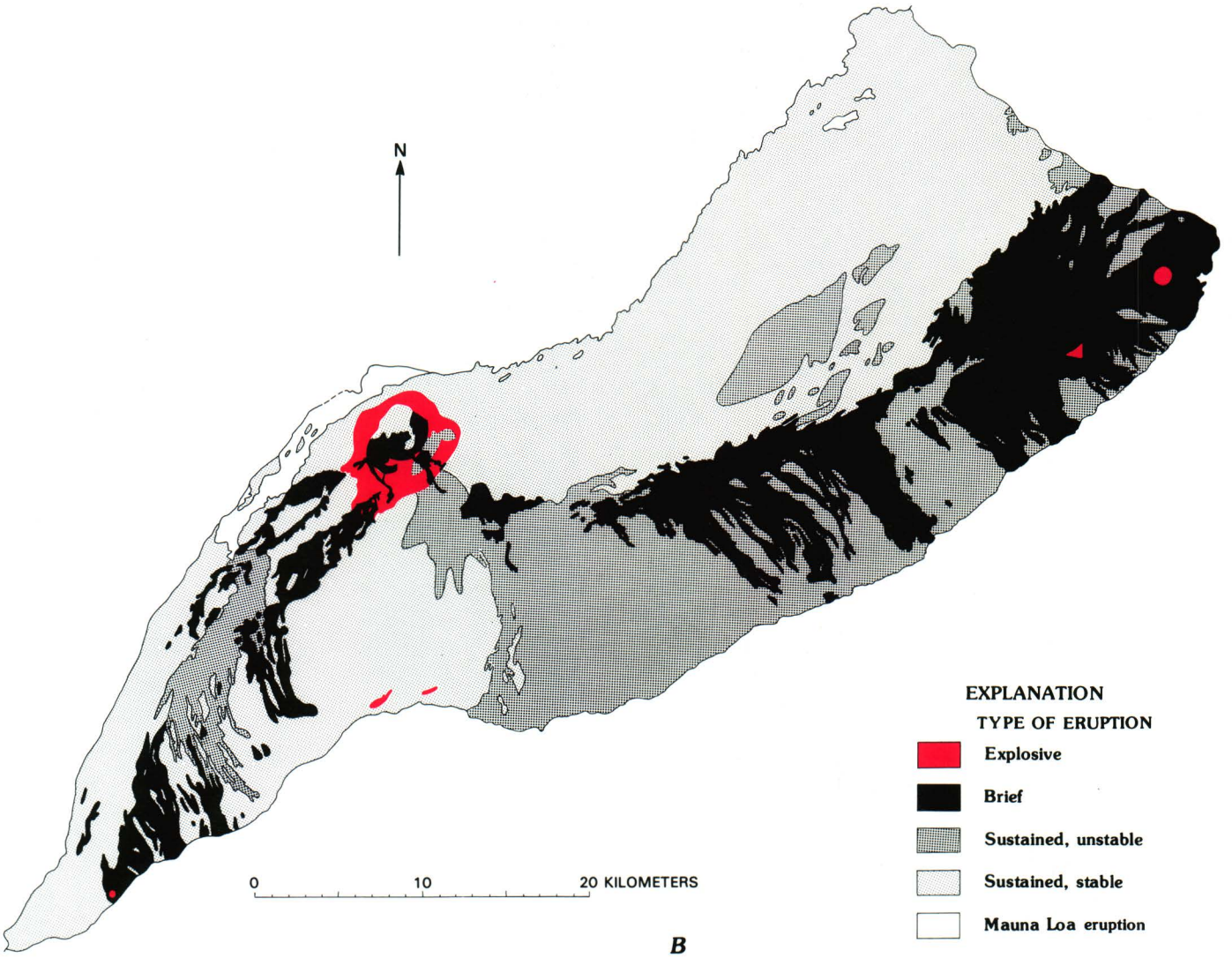

FIGURE 12.8.—Continued.

that caldera. If so, the bend in the east rift zone could have arisen from northward migration of summit collapse instead of southward migration of the rift zone.

SOUTH FLANK

The south flank is the area seaward of the rift zones and the Koae fault system. Faults of the south flank (Hilina fault system) mainly show displacement down to the south (fig. 12.5*C–F*). The most prominent faults, such as those of Hilina, Poliokeawe, and Holei Palis and of Puu Kapukapu, occur in the seaward part of the south flank; this has led to a distinction between faulted and unfaulted parts of the flank (Swanson and others, 1976a). Buried Hilina faults, however, inferred from steepened slopes, occur inland close to the Koae system and probably extend into each of the rift zones (Holcomb, 1980b). The Hilina fault system probably is not isolated from other Kilauea structures but grades into them; its apparent isolation arises from the restricted extent of its recent displacements.

The age of the Hilina system is not known. Stearns and Clark (1930) considered the faults to postdate the base of the Pahala Ash, about 23 ka (Easton, 1978), because the ash caps some blocks (Puu Kapukapu and Puu Kaone) truncated by the faults. Puu Kapukapu is about 300 m high. If the block seaward of Puu Kapukapu subsided to sea level in 3-m increments similar to the displacement of November 29, 1975 (Tilling and others, 1976), it would have required 100 such episodes recurring at intervals of about 230 years. The highest part of Hilina Pali undraped by younger lava also is about 300 m high, and the youngest Pahala Ash truncated by this fault could be as young as about 11 ka (Easton, 1978). That displacement could have been accomplished by 3-m subsidence episodes repeated every 110 years. These frequencies are reason-

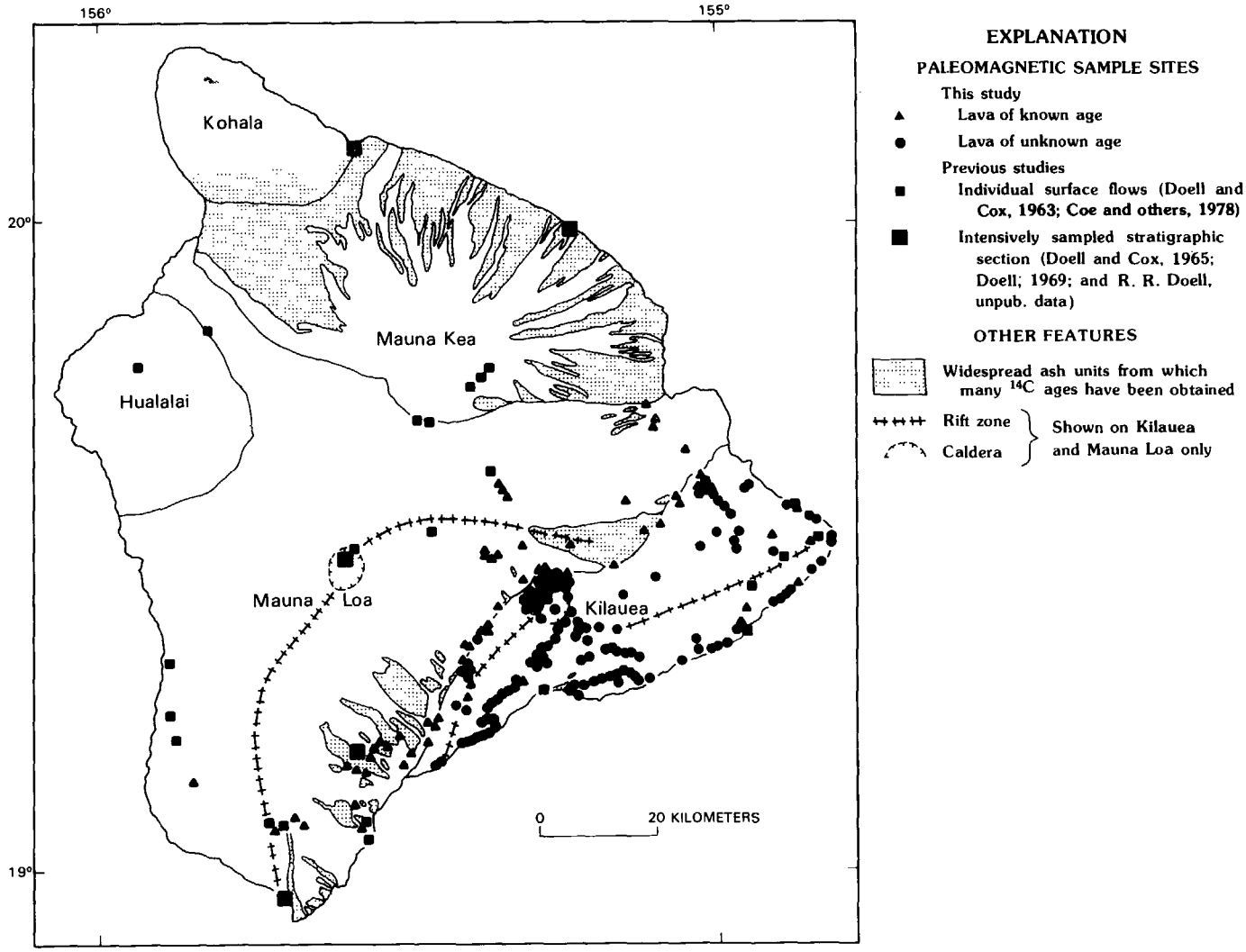

FIGURE 12.9.—Paleomagnetic sampling locations on five volcanoes that make up Hawaii. Map modified from Stearns and Macdonald (1946).

able, and the interpretation by Stearns and Clark may be correct. However, the faults could be younger and could have had large, catastrophic displacements earlier in their development, or they could be older and draped by Pahala Ash that is now buried or subsided beneath the sea. The Hilina fault system could be older than Kilauea and could have developed from seaward migration of the Kaoiki fault system as older inland faults were stabilized by the growing edifice.

No eruptions are known from the south flank; sparse dikes along Hilina Pali were fed by lava flows spreading down into open fissures (Walker, 1967; Easton and Lockwood, 1983). Nonetheless, episodes of Hilina displacement may affect Kilauea's eruptive behavior by dilating the rift zones and disrupting the magma plumbing system.

NORTH FLANK

The north flank does not show surficial structures, though inactive structures may be buried. Only one possible buried fault is inferred, with great uncertainty, subparallel to the coast at an elevation of about 60 m, 5 km inland from Kaloli Point (figs. 12.5*J*, 12.19). Several kipukas (inliers) in the youngest flows are truncated along this line, and no kipukas of older Mauna Loa lava occur seaward of it. The surface slope decreases across it from 1.6° inland to 1.0° seaward, and the seaward lava has assumed a thickened elephant-hide appearance (Stearns and Macdonald, 1946) below the break in slope. The discontinuity may be a normal fault, its downdropped eastern block buried by younger lava, or it may parallel a buried seacliff several dekameters high. Alternatively, it

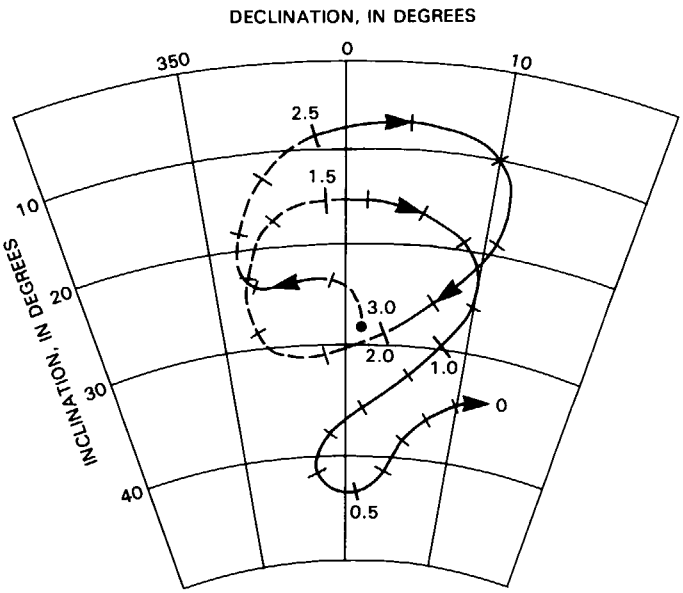

FIGURE 12.10.—Generalized history of Hawaiian geomagnetic secular variation during the last 3,000 years. Track dashed where confidence is less. Ticks are shown at approximate 100-yr intervals, and numbers indicate thousands of years before present. Unpublished data have been used to modify earlier version by Holcomb and others (1986).

could be the edge of a very broad, flat cone of lava banked against an older, steeper slope. Such a cone could develop from several causes; for example, a rise in relative sea level could have raised the baselevel to which the slope was formerly adjusted.

No eruptions are known from this flank; for at least the last few millenia it has passively accumulated lava, mostly as tube-fed flows from the summit.

EARLIER PREHISTORIC ACTIVITY

Because of incomplete exposures and dating uncertainties, a full eruption history of Kilauea is not yet possible, even for the last few thousand years. Available information does, however, permit a general history, having increased detail with younger age. The history is reviewed in the following sections, in which many dating uncertainties are discussed. Readers not interested in these details may want to skip ahead to the section entitled "Summary of Eruptive History."

PLEISTOCENE SHIELD GROWTH

Kilauea's early history was studied by Easton (chapter 11, 1978), who estimated that the volcano began to grow around 200–300 ka. Only the later subaerial part of shield growth has been available for study; it is recorded by the Hilina Basalt, Pahala Ash, and lower part of the Puna Basalt exposed in the Hilina fault scarps of the central south flank (fig. 12.20). The lowermost Hilina flows now exposed are estimated to have ages of 100 ka, and the Pahala Ash was deposited between 25 ka and 10 ka (Easton, chapter 11). Rocks below the Pahala Ash are mostly tube-fed pahoehoe flows, probably from sustained summit eruptions. Interspersed among the flows are ash layers, probably erupted at the summit in large explosions associated with successive caldera collapses. Little is known about rift-zone activity during this interval.

OLDER HOLOCENE FLOWS

About 10 percent of Kilauea's surface consists of rock older than about 1,100 years. Some of the older lava flows are veneered by ash deposits. Among these are kipukas of picritic aa of about 5.2 ka (W–4536) on the north flank southeast of Keaau (fig. 12.21), probably erupted from the northeast rift zone of Mauna Loa (Lockwood and Lipman, chapter 18). Pahoehoe above ash in one kipuka has been dated at about 3.7 ka (W–4177, fig. 12.5*J*). The source of this lava is unknown; it could have come from the summit of Kilauea or from the northeast rift zone of Mauna Loa. As discussed later, it may be coeval with flows previously thought to have been erupted 750–1,000 years ago. Buried flows resting on Pahala Ash below the rim of Hilina Pali have been dated at about 6.6 ka and 4.8 ka (W–3873 and W–3798, fig. 12.5*D*). Younger flows, separated from the older ones by thin ash and forming much of the surface in Kipuka Ahiu and Kipuka Keana Bihopa (fig. 12.22), have been dated at about 3.5 ka (W–3831, fig 12.5*D*). These flows are veneered by ash and eolian sand thick enough to support a carpet of high range grass and scattered ohia trees (*Metrosideros polymorpha*). The ash on and between these older Puna flows suggests that explosive eruptions occurred more than once between 6.6 and 1.5 ka, but the number of eruptions is not known. The flows have various directions of magnetization, but not enough ^{14}C ages are available to derive a continuous magnetic history.

Several vents still exposed in kipukas along the east rift zone may be older than 2,000 years; among them are Kapoho Crater, Kiapu, Iilewa, and Kalalua (fig. 12.5*F–H*). Some vents along the lower southwest rift zone may also be older. The Cinder Hills 2 km southeast of Pahala are overlapped by a lava flow dated by ^{14}C at about 3.5 ka (W–5324, fig. 12.5*C*). A thin lava flow issuing from a prominent fissure along the Kilauea-Mauna Loa boundary 1 km southeast of Pahala has been dated at about 3.6 ka (W–3884, fig. 12.5*C*); though Lipman and Swenson (1984) mapped this fissure as an eruptive vent, a lava flow erupted elsewhere could have flowed into it farther upslope and then overflowed its rim.

FLOWS BENEATH UWEKAHUNA ASH MEMBER OF PUNA BASALT

Much of Kilauea may have been covered by lava in a short interval preceding deposition of the Uwekahuna Ash Member. In stratigraphic sections of the summit and upper east rift zone, flows below the Uwekahuna Ash Member have remanent magnetizations (crosses, fig. 12.11*C*) distinct from those of flows of the last millenium. Examples occur in Uwekahuna Bluff (9B229A; sites 133 of Doell and Cox, 1965; 137D,E of Doell, unpublished work), Tree Molds (1B121), Kilauea Iki (8B145), and Pauahi (9B385). Surficial flows inland from Papalehau Point (3R457, fig. 12.5*C*) may have been erupted at the summit also.

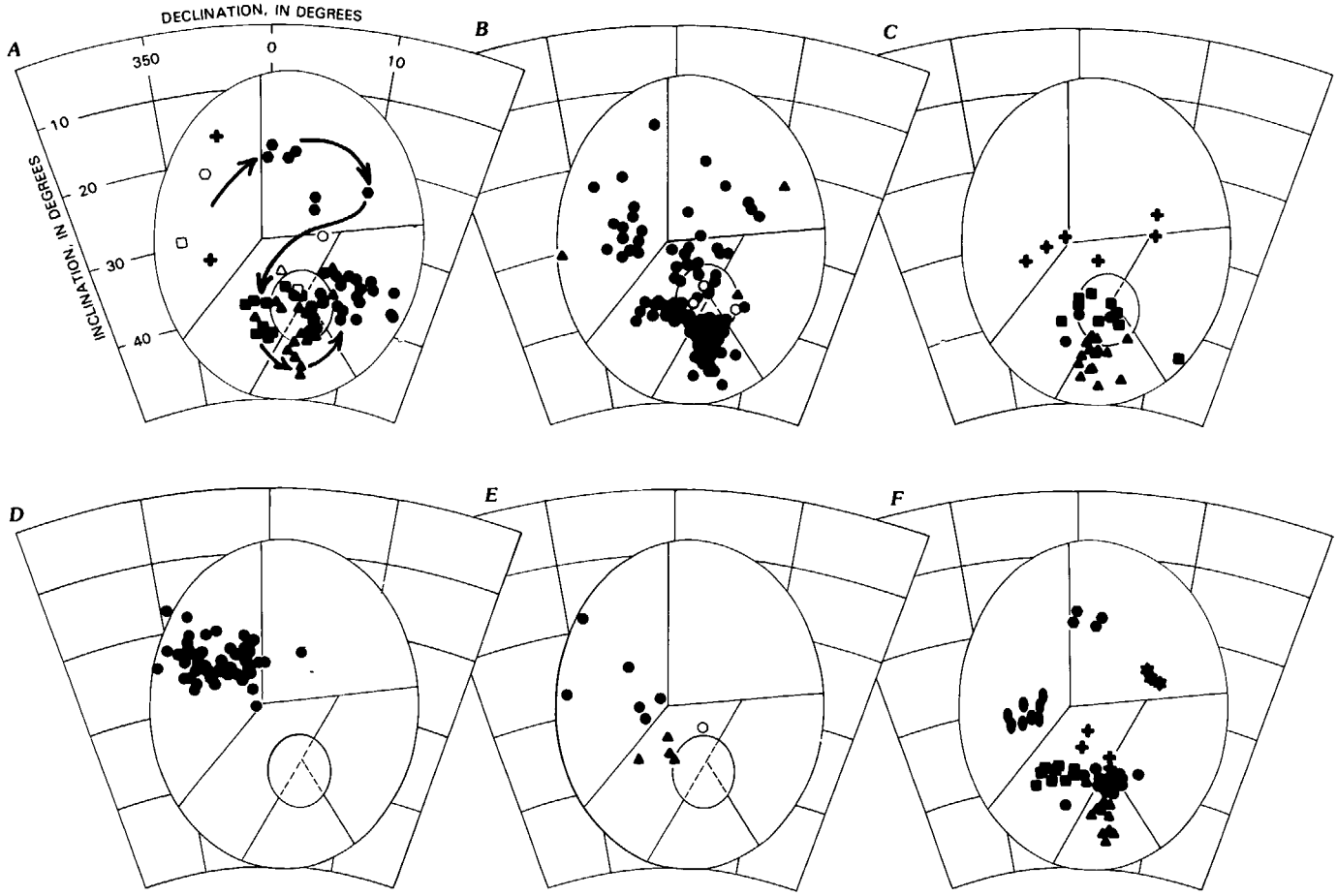

FIGURE 12.11.—Semiquantitative method used to infer ages of lava flows. Unpublished data have been used to modify version by Holcomb and others (1986). Large ellipse divided into fields containing sites of similar age; smaller ellipse is area of confusion having diverse ages clustered together. ***A***, Age classification from dated flows; symbols represent different ages: dots, younger than 250 years B.P.; triangles, 250–500 years B.P.; squares, 500–1,000 years B.P.; hexagons, 1,000–1,500 years B.P.; crosses, 1,500–2,000 years B.P. Open symbols are doubted results. Arrows approximate secular variation. ***B***, Site mean directions for undated surface flows of Kilauea. Dots, pahoehoe; triangles, aa. Open symbols indicate doubted results. ***C***, Stratigraphic section in Uwekahuna Bluff (Doell and Cox, 1965; R.R. Doell, unpublished work). Symbols denote different parts of section: crosses, below Uwekahuna Ash of Puna Basalt (nos. 131–133, 137C–137E); squares, lower section above Uwekahuna Ash Member (nos. 134–137B, 137F–137H); triangles, middle part of section; dots, upper part of section. ***D***, Stratigraphic section in west wall of Mokuaweoweo caldera, Mauna Loa Volcano (Doell, 1969). ***E***, Buried flows of Kilauea, exposed in walls of caldera and pit craters. Symbols indicate stratigraphic position: dots, below hiatus; triangles, above hiatus. Circle indicates anomalous magnetization below hiatus in Makaopuhi Crater. ***F***, Groups of surface flows thought from independent evidence to be closely similar in age: dots, Observatory; triangles, Ai-laau; squares, Kalue; crosses, Volcano; stars, Kipuka Nene; hexagons, Kukuau (Mauna Loa); ellipses, older flows of Kalapana.

Flows with similar magnetization crop out along both rift zones. Among them are a red tephra cone and lava flows (paleomagnetic site 9B345) exposed beneath a yellow tephra layer in the west wall of Pauahi Crater (fig. 12.23). Mixed flow assemblages (8B253, 8B349, 8B313, 8B289, 8B277) between Kaimu and Kupapau (fig. 12.5*F,G*; older Kalapana flows of fig. 12.11) indicate sustained eruption from the middle east rift zone near Kalalua, and other mixed flows around Kapoho (9B181, 8B973, 8B817) may represent sustained eruption from the lower east rift zone near Puu Honuaula (fig. 12.5*H*). Tube-fed flows with similar magnetization on the north flank in Hawaiian Beaches (9B853) and Ainaloa (8B805) subdivisions (fig. 12.5*H*) may have been erupted from the summit or from the middle east rift zone. This old north-flank lava supports a monotonous forest in which separate flows cannot be distinguished (figs. 12.24, 12.25); forest patchiness probably is caused by ohia dieback (Jacobi, 1983) rather than flow boundaries.

Their similar magnetizations suggest that these flows were erupted within a few centuries preceding the Uwekahuna Ash Member, but ages are not yet well constrained. Because a Mauna Loa flow (8B697) dated by ^{14}C at about 1.8 ka (W–3850) is magnetically similar, these Kilauea flows were assigned ages of 2.0–1.5 ka by Holcomb and others (1986). But Lockwood and Rubin (1986) now judge the Uwekahuna Ash Member above them

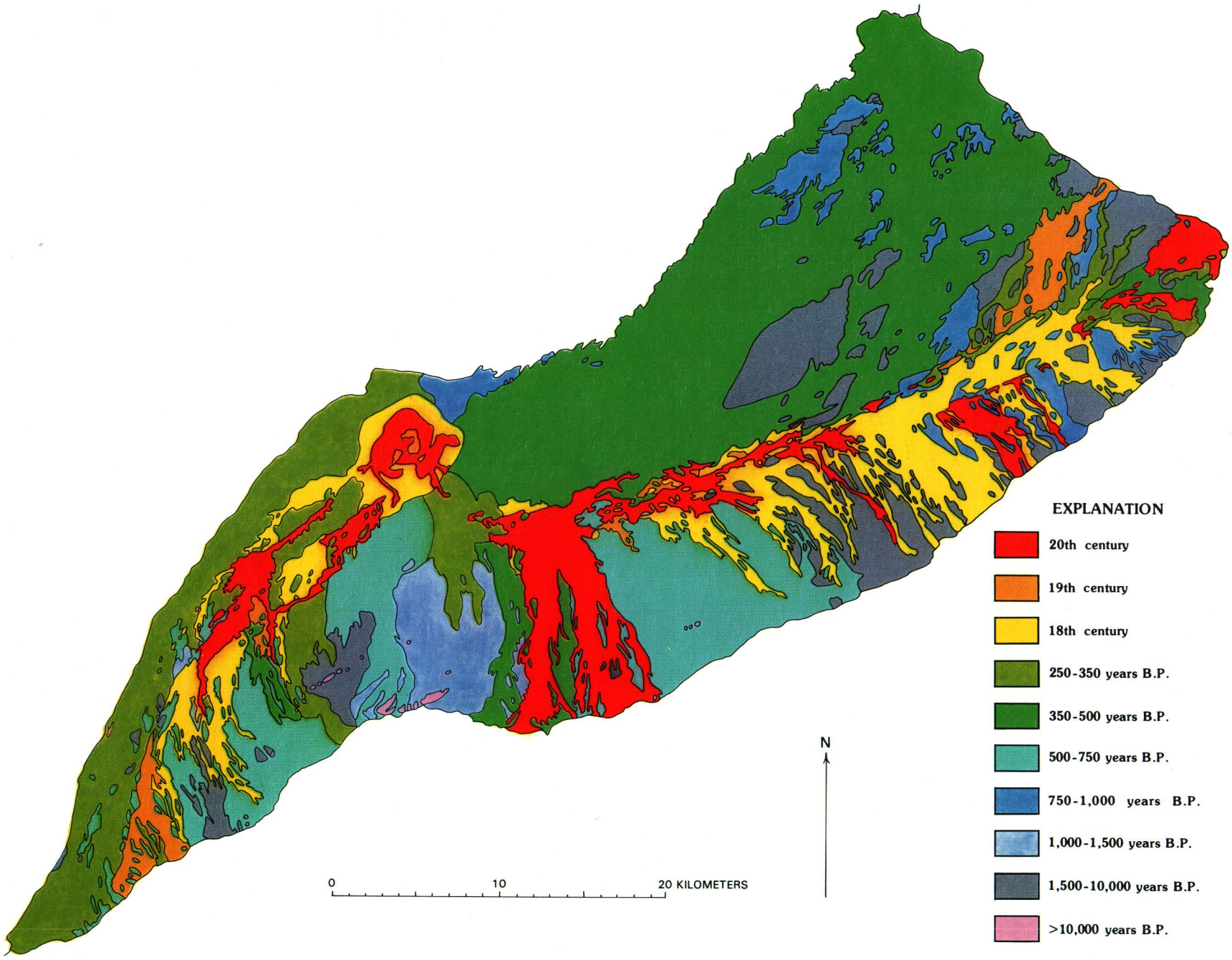

FIGURE 12.12.—Stratigraphic map of Kilauea, showing approximate ages of surficial lava flows. Modified from Holcomb (1980b).

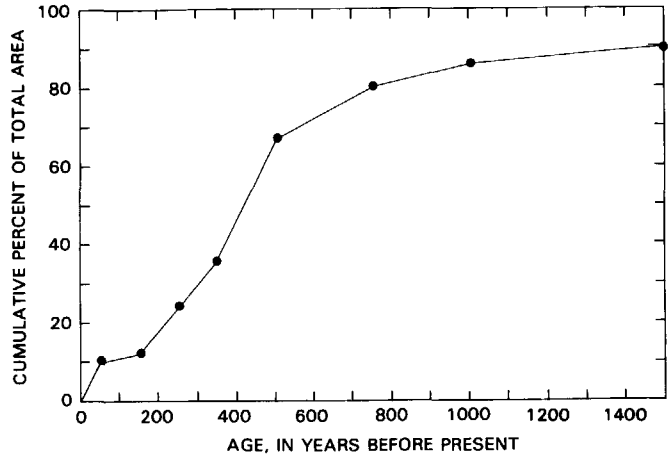

FIGURE 12.13.—Age of Kilauea's surface, a graphical presentation of data in table 12.2. Large variation is shown in rate of flooding, intervals 0–100 and 400–600 yr B.P. having high rates and intervals 100–200 and 1,000–1,500 yr B.P. having low rates. Lower apparent rates of earlier intervals arise partly from later coverage of older flows by younger lava.

to have an age of 2.1 ka, and stratigraphic relations permit most of the flows to be older. Lava east of Kaimu, possibly correlative with 8B313, has been dated at about 2.4 ka by ^{14}C (W–5052, fig. 12.5*G*). Ages of about 2.1 ka and 2.2 ka have been obtained for pahoehoe in a quarry at 786-m elevation along the northeast margin of Kilauea (W–4369 and W–3885). Ash-veneered aa on the rim of Kukalauula Pali is dated at about 1.8 ka (W–4119, fig. 12.5*C*), but its magnetization is not known. Though their ages remain uncertain, lava flows from the summit and east rift zone probably covered much of Kilauea within the few hundred years before the development of the Powers caldera.

POWERS CALDERA

That an ancient caldera was buried before the present one developed was inferred by Powers (1948) because the Uwekahuna Ash Member occurs in the base of Uwekahuna Bluff at an elevation of about 1,100 m, while at Tree Molds it occurs at about 1,220 m (Doerr, 1933). The exposure in Uwekahuna Bluff must cap an old caldera block that subsided about 120 m. This inference is confirmed by paleomagnetic data; flows above the Uwekahuna Ash Member are magnetically similar to Kilauea's surface flows (fig. 12.11*C*) and indicate rapid accumulation in the last millenium. If this thick section is coeval with the thin carapace elsewhere but is younger than higher flows beneath the Uwekahuna Ash Member at Tree Molds, it must fill a caldera.

The configuration of the Powers caldera is poorly known. A buried outer rim is inferred to coincide with the outermost structures of the modern caldera because the outer fault west of Uwekahuna predates the most recent collapse (fig. 12.5*A*). This outer rim did not bound a deep sink because it is little more than 100 m higher than older rock exposed beneath the Uwekahuna Ash Member in Uwekahuna Bluff; a shallow subsided annulus at least 1 km wide, similar to the present one, must have existed. Faulting within that annulus is suggested by draping of the Uwekahuna Ash Member over a step 30 m high formerly exposed in the face of Uwekahuna Bluff (Powers, 1948).

The age of the Powers caldera also is not yet well constrained. It is probably older than 1,300 years because its oldest overflows are thought to be about 1,100 years old, and at least a few hundred years of filling should have preceded overflow. The caldera and Uwekahuna Ash Member should be close in age if caldera collapse caused the explosive eruption. Holcomb and others (1986) inferred an age of about 1.5 ka for both caldera and ash, but they may be older. Eight ^{14}C ages currently available for the Uwekahuna Ash Member range from about 1.0 ka to about 2.2 ka. Lockwood and Rubin (1986) now believe that the younger ages reflect sample contamination and judge the age of the ash to be about 2.1 ka. An age of 1.5 ka is retained in this report; several generalizations herein may need revision if further work confirms the older age. Casadevall and Dzurisin (chapter 13) adopt the older age and discuss some of its possible consequences.

SUMMIT HIATUS

Collapse of the Powers caldera was followed by a caldera-filling interval in which no lava spread from the summit onto the flank. Dzurisin and Casadevall (1986) believe that this interval was very short (only a few years) because the uppermost pumice of the Uwekahuna Ash Member in Uwekahuna Bluff was not eroded before it was covered by lava. But the uneroded pumice could be much younger than the rest of the ash, and paleomagnetic data suggest a long interval between flows below and above the ash. Lava beneath the ash has magnetization consistent with an age greater than 1.5 ka (9B229A; sites 133, of Doell and Cox, 1965, and 137D,E of R.R. Doell, unpublished work), while lava above the ash has magnetization consistent with an age of about 0.75 ka (1B618; sites 137F,G,H of R.R. Doell, unpublished work).

A surface marking a hiatus is exposed also in three pit craters. In Kilauea Iki Crater (fig. 12.26) it lies between flows separated by a red cinder layer. In Pauahi Crater (fig. 12.27) and Makaopuhi Crater (fig. 12.28) it lies above weathered ash and debris on which a forest grew, so that tree molds were produced when the area was flooded by lava. Paleomagnetic samples have been collected from lava flows just above and just below the hiatus in each crater (Kilauea Iki, 8B145 below, 8B157 above; Pauahi, 9B385 below, 9B217 above; Makaopuhi, 9B157 below, 9B241 above). The flows above are all younger than 1.0 ka (fig. 12.11*E*). Flows below have directions indicating pre-Powers caldera ages older than 1.5 ka, except for one. The lower flow in Makaopuhi has a direction corresponding to less than 1.0 ka; if the direction is correct, it suggests only a brief hiatus and rapid forest growth there. But because no stratigraphic evidence bounds its age, the flow could be much older; alternatively, it may have been remagnetized during rapid accumulation and slow cooling of the Kane Nui o Hamo lava shield above it. With this possible exception, the hiatus is correlative

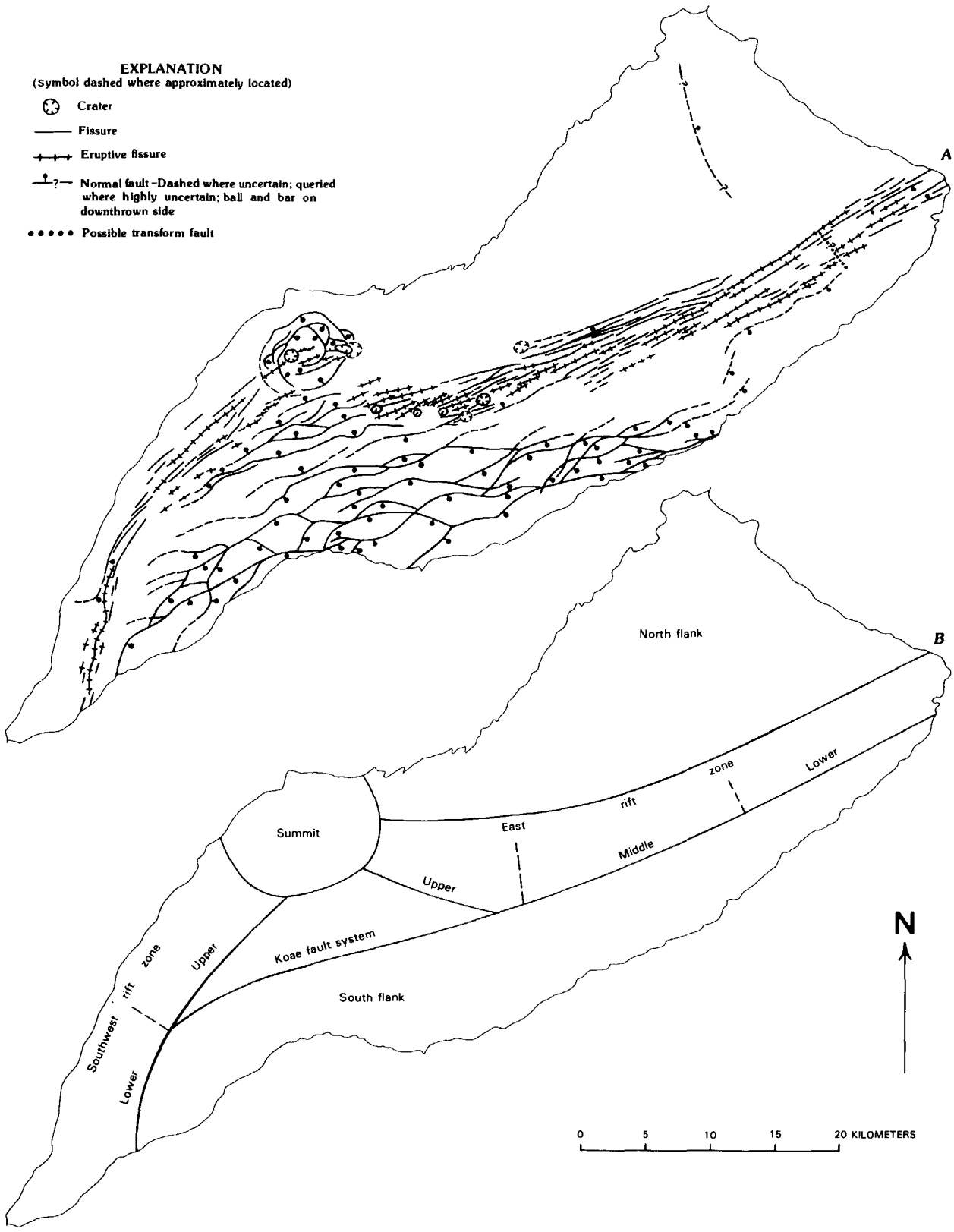

FIGURE 12.14.—Structure of Kilauea. *A*, Mapped structures, simplified from Holcomb (1980b). *B*, Structural subdivisions, modified from Swanson and others (1976a).

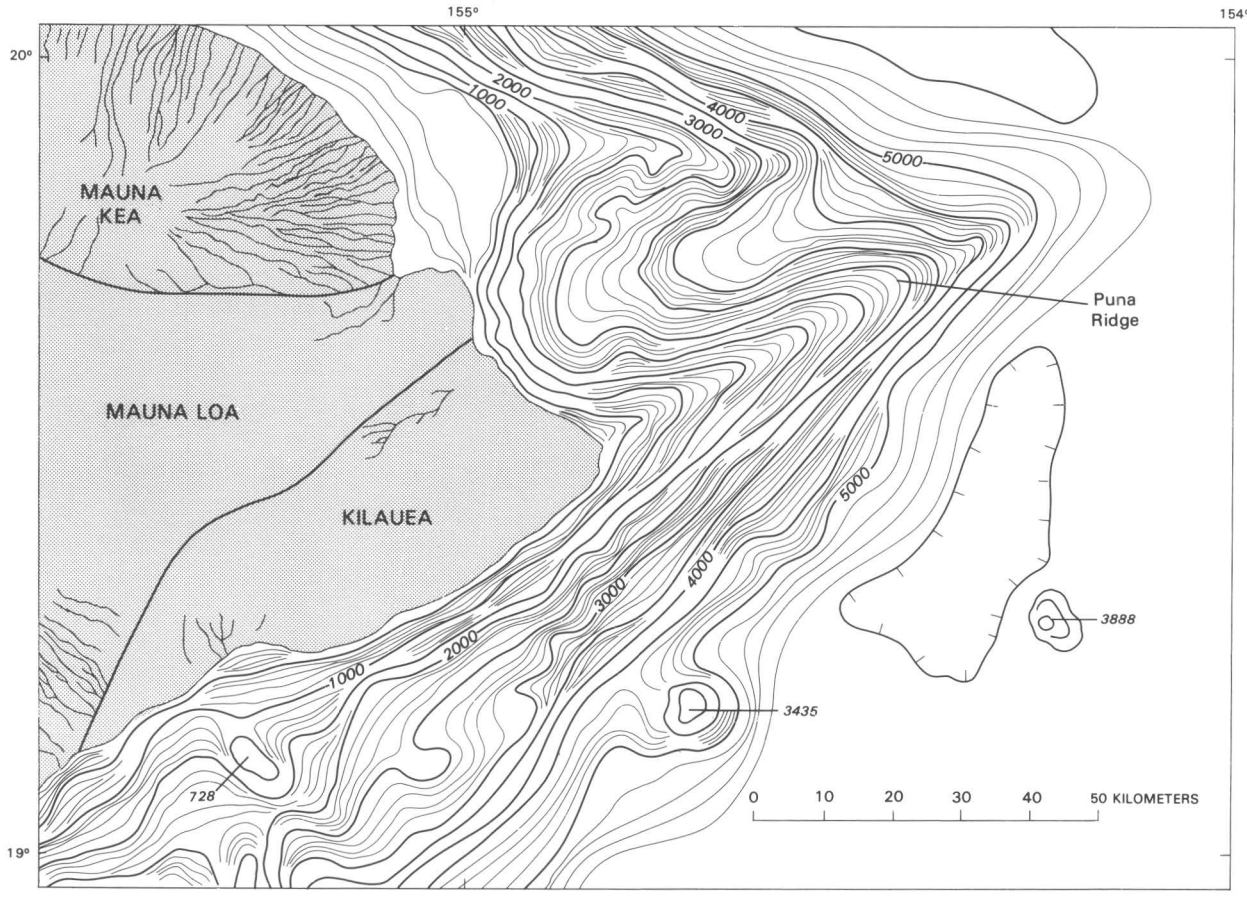

FIGURE 12.15.—Bathymetry around eastern part of Hawaii, showing Puna Ridge. From Wilde and others (1980); depths in meters; contour interval 100 m. Hachures indicate area of closed low depression.

at all sites and spans more than 500 years from more than 1.5 ka to less than 1.0 ka.

Coincident with this hiatus is a paucity of eruptions along subaerial parts of the rift zones. A small pyroclastic cone of the lower east rift zone east of Kiapu has been dated at about 1.3 ka by ^{14}C (W–4674, fig. 12.5*H*), and paleomagnetic data have suggested one group of flows (9B829, fig. 12.5*B*; 3R409, fig. 12.5C) in this interval along the southwest rift zone. No others are known, however; most eruptions in this interval were probably confined to a deep inner sink or submarine segments of the rift zones.

KIPUKA NENE FLOWS

The earliest overflows from the Powers caldera may be the tube-fed flows of Kipuka Nene and Kipuka Papalinamoku, which form much of the coast between Keauhou and Kaaha (fig. 12.5*D*). The flows have a distinctive magnetization (1B224, 1B456, 3R013; table 12.5) similar to Mauna Loa flows (4A276) dated at about 1.1 ka by ^{14}C (W–3910, 1,270 years B.P.; W–5083, 1,030 years B.P.). If the Kipuka Nene flows do postdate the Powers caldera, they are probably about 1.1 ka. Available stratigraphic evidence, however, does not require them to postdate the caldera. Additional uncertainty is caused by other nearby flows having different magnetizations but ^{14}C ages also of about 1.1 ka, as noted later in discussion of the Kalue flows.

Initial errors in dating the Kipuka Nene flows illustrate well the difficulties encountered in work of this kind. Though the Kipuka Nene flows are clearly veneered by surficial deposits and vegetation that are absent on overlying Kalue flows (fig. 12.29), it was difficult to find the exact boundary between them. Initially inferring the boundary to parallel the west side of a prominent band of trees, I collected paleomagnetic samples in 1978 from sites 8B121 and 8B133 on each side of this boundary (fig. 12.30*A*). The results revealed the same magnetization at both sites (table 12.5; fig. 12.30*B*). Wanting to make sure that I had really sampled the older flows, in 1979 I collected from site 9B169 south of a fault that extended through Kipuka Nene. This fault seemed to be overlapped to the west by the younger Kalue flows, and I reasoned that lava on the southern rim of the fault scarp must belong to the older flows. The results again gave virtually the identical magnetization, so I

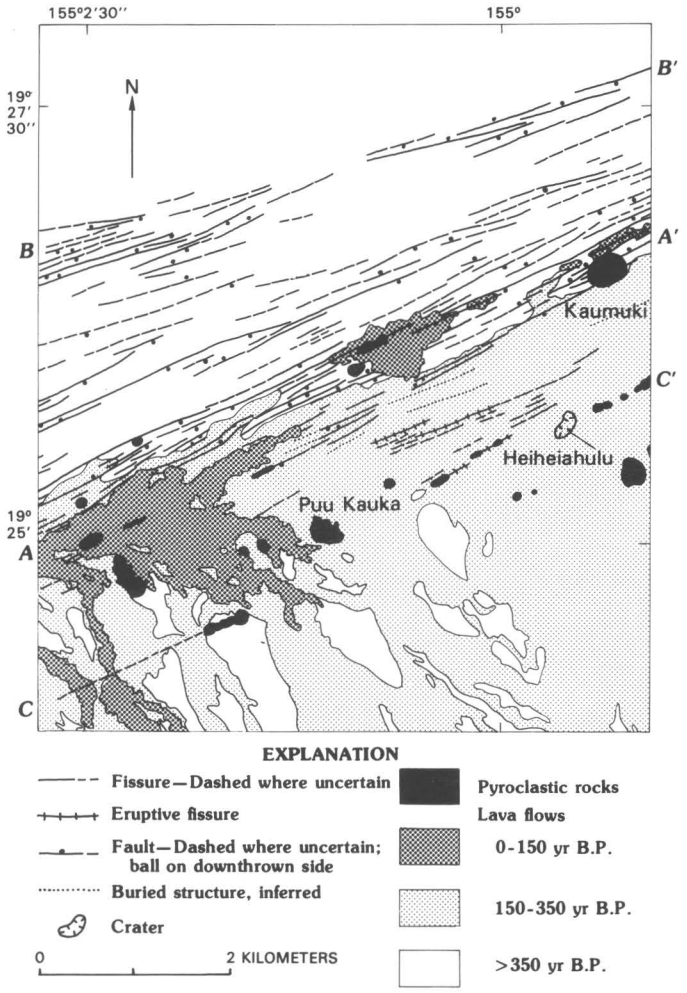

FIGURE 12.16.—Eastern part of middle east rift zone, with contrasting surficial structure north and south of active zone A–A'. North edge of rift zone is along B–B'; south edge along C–C'. Lava flows 350–500 years old north of A–A' broken by many fissures but no eruptive vents; flows 150–250 years old south of A–A' have many vents but few younger fissures. Flooding south of A–A' probably followed large dilation of rift zone a few hundred years ago.

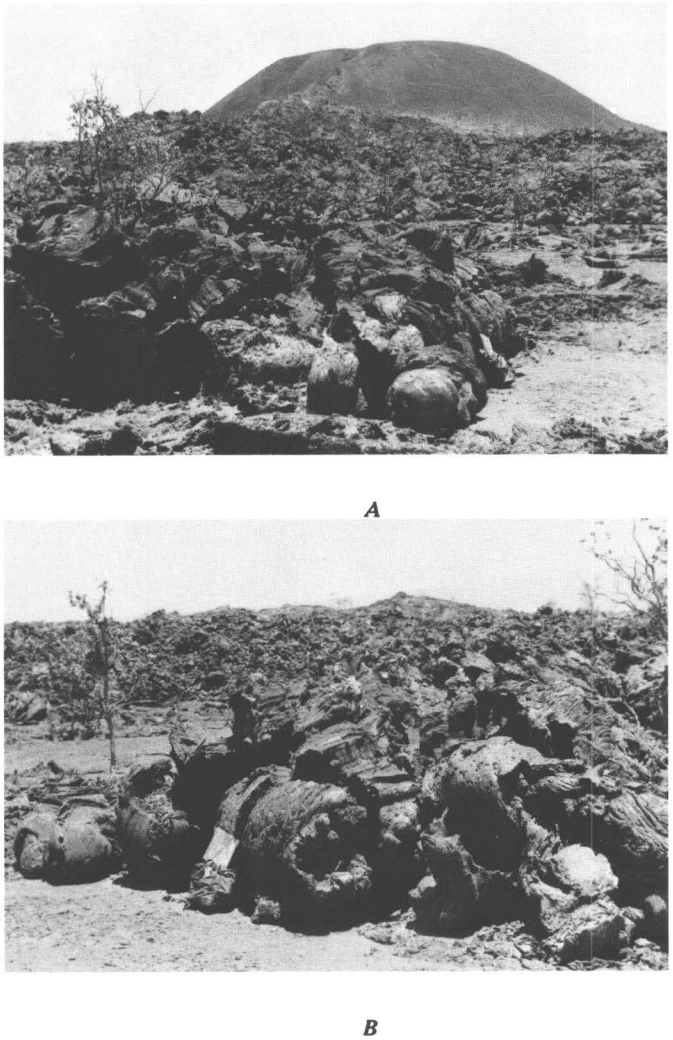

A

B

FIGURE 12.17.—Unusual eruption products of Kamakaia Hills. Photographs by R.T. Holcomb, 1977. ***A***, Kamakaiwaena, one of several cinder cones found only in this area of Kilauea, and peculiar near-vent lava flow in foreground. View northeast (see figure 12.48 for location). ***B***, Closer view, looking west, of same flow, which consists of thick, cylindrical, toothpastelike extrusions that twisted back on themselves and then broke as they cooled. These protrusions are morphologically distinct from all other flow forms seen on Kilauea and resemble some elongate pillows of submarine lava flows. Scale indicated by aerial-photograph case (about 25 cm wide) perched on day pack.

assigned the Kipuka Nene flows a young age similar to that of the Kalue flows and tried to explain the difference in surficial cover by inferring that a tephra-producing eruption at Kane Nui o Hamo (which shares the same magnetization) had occurred during a short interval between the two sets of lava flows. However, still not being satisfied, in 1981 I collected from two more sites, 1B236 on the rim of Kalanaokuaiki Pali and 1B456 deep within Kipuka Nene. This time I found a distinctly different magnetization (fig. 12.30*B*). Then N.G. Banks found beside the Kipuka Nene picnic shelter a contact between two lava flows, with a thin deposit of ash between them. In 1983 I collected 3R001 and 3R013 on each side of this contact and found two different magnetizations corresponding to the two measured previously: the boundary had finally been discovered. Though I have not traced it away from the picnic shelter, it must extend roughly as shown in fig. 12.30*A*, about 100 m east of the contact inferred initially.

The distinctive Kipuka Nene magnetization is also shared by the flows of Opihikao (8B013; fig. 12.5*H*); they may have been erupted from Puulena or Kahuwai, which are notable for their phreatomagmatic ash blanket (Moore, 1983). Other eruptions of this age are not yet known from elsewhere along the rift zones.

VOLCANO FLOWS

Volcano village is built on flows forested differently from younger Ai-laau flows (fig. 12.31). One of these older flows is dated

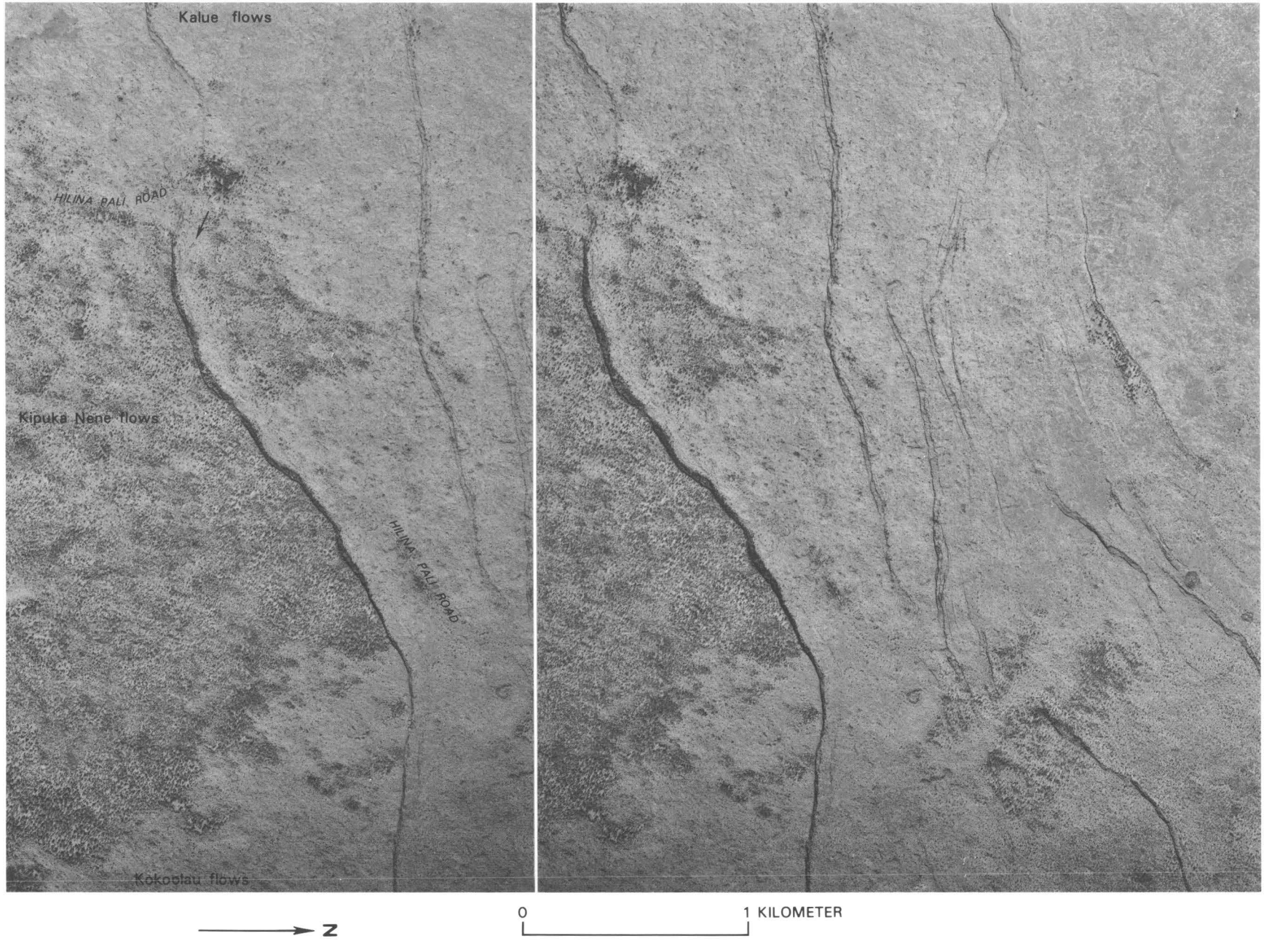

FIGURE 12.18.—Contrasting vegetation patterns along Kalanaokuaiki Pali. Barren Kalue and Kokoolau flows interpreted to postdate much of fault displacement, while tree-covered Kipuka Nene flows are thought to predate it. Pattern of polygonal plates (arrow) at base of cliff is characteristic of ponded lava. Duffield (1975, p. 10) argued against ponding because similar smooth surface is found on south side of fault, but smooth surface is not extensive there, lacks polygonal pattern, and could have formed from spreading of pond as it rose above scarp that initially held it back. Pairs of small red dots, paleomagnetic sample sites. Stereo pair prepared from frames 74, 75 of roll 14CC, USDA series EKL, 1965.

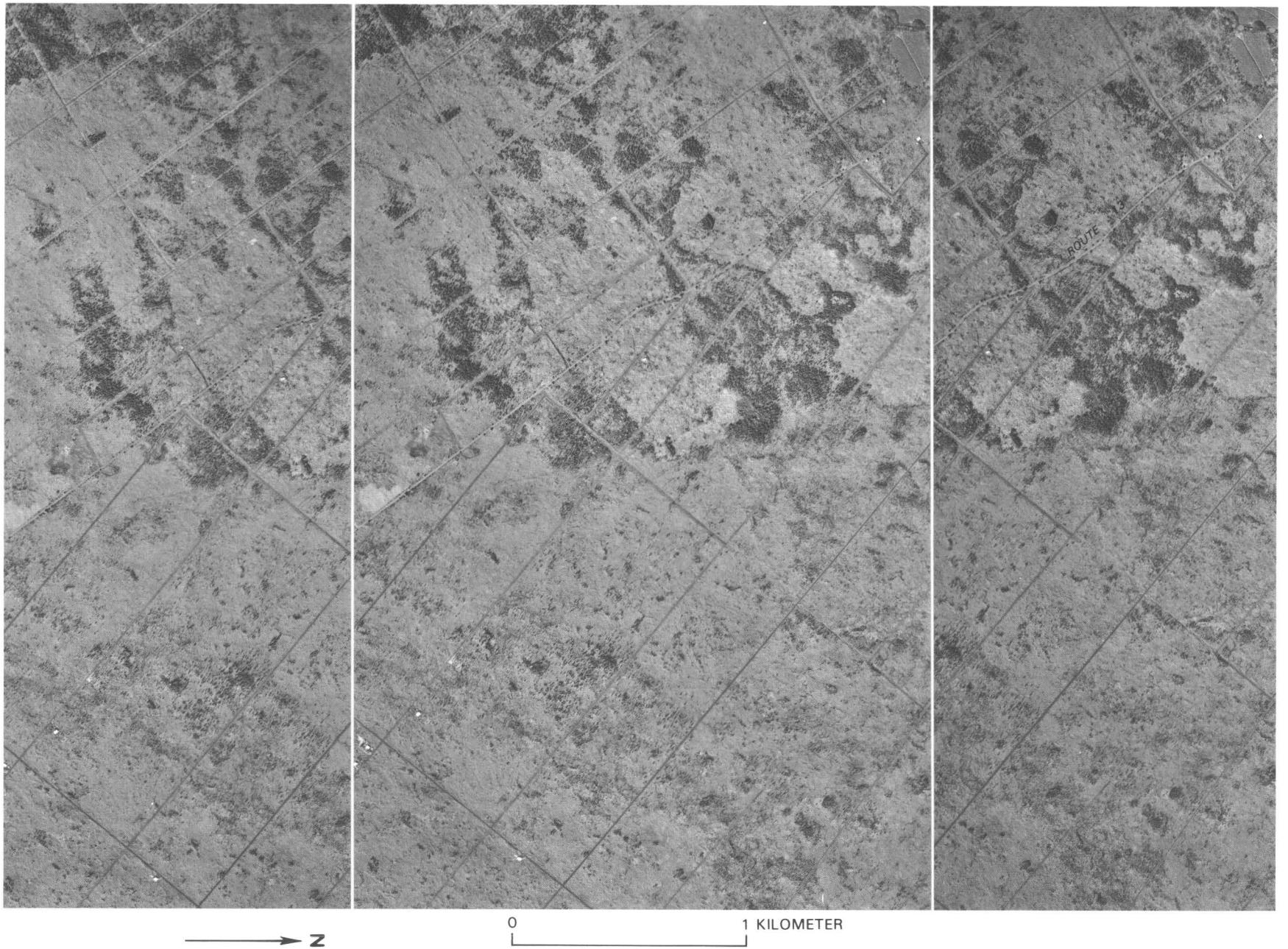

FIGURE 12.19.—Topographic and geologic discontinuity southeast of Keaau (see fig. 12.3). Sharp vegetation change extending north-south corresponds to flow boundary; young Ai-laau flows to east are highly inflated on a wide coastal plain, while older flows to west form kipukas elongate northeast-southwest between less inflated lobes of young lava extending down steeper slope to coastal plain. Pairs of small red dots, paleomagnetic sample sites; larger red dots, ^{14}C sample sites. Stereo triplet prepared from frames 64–66, roll 12CC, USDA series EKL, 1965.

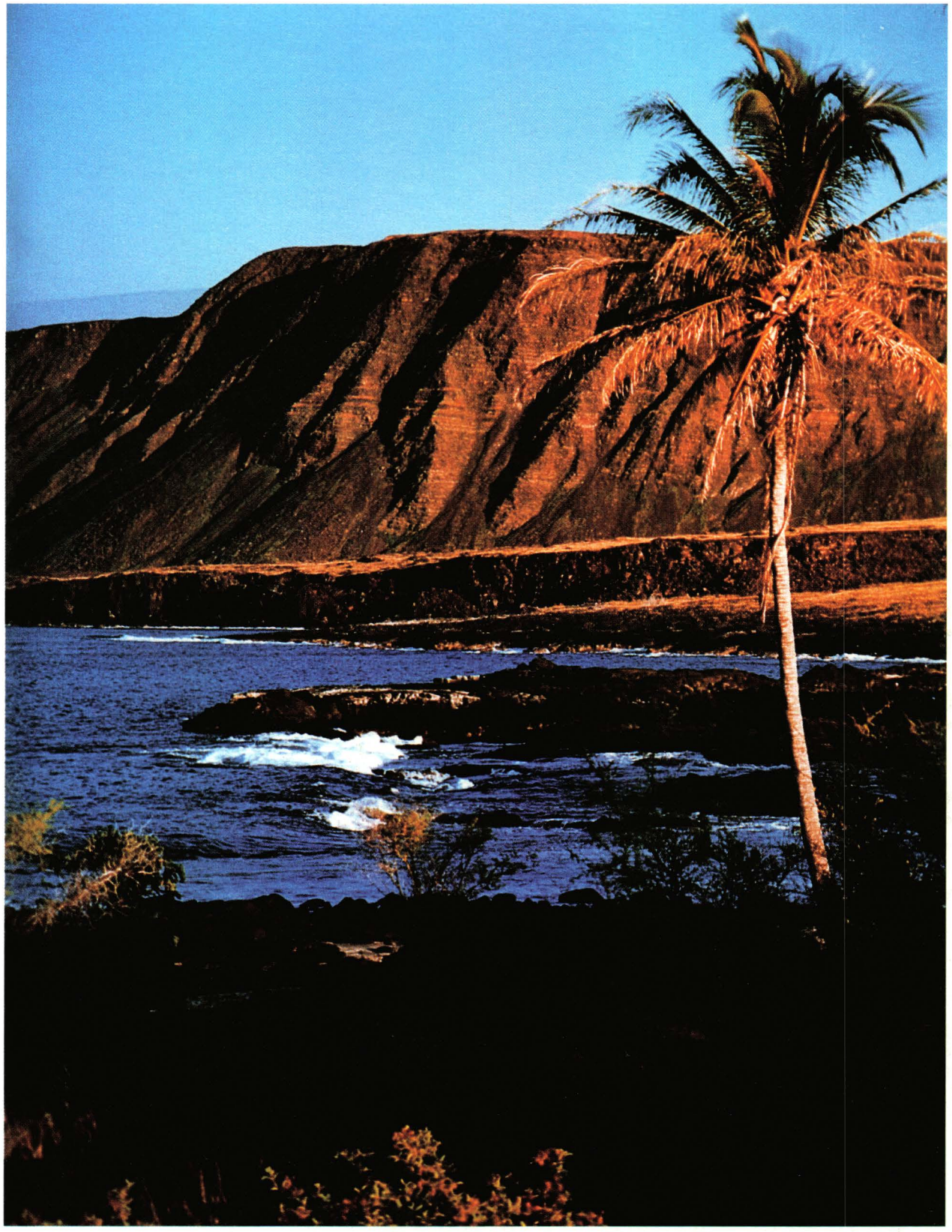

A

FIGURE 12.20.—Oldest rocks exposed on Kilauea. ***A***, Puu Kapukapu, viewed from Keauhou Landing. Most of visible stratigraphic section, about 300 m thick, is included in Hilina Basalt, with cap of Pahala Ash 10–20 m thick. Lower fault scarp in front of Puu Kapukapu displaces lava flows of Kipuka Papalinamoku thought to be about 1,100 yr old. Foreground, composed of lava 350–500 yr old, subsided beneath sea level during earthquake of November 29, 1975. Profile of Mauna Loa visible beyond Puu Kapukapu, to left. Photograph by R.T. Holcomb, April 1974. ***B***, Closer aerial view of Puu Kapukapu, showing lava flows and prominent ash layers in Hilina Basalt. Rim of Hilina Pali visible beyond Puu Kapukapu, to left. Photograph by D.A. Swanson, June 1971.

B

FIGURE 12.20—Continued.

at 730 ± 80 years B.P. by ^{14}C (W–3999), and its magnetization (8B685) is consistent with age of 750–1,000 years B.P. A flow resting above the Uwekahuna Ash Member in the Volcano rubbish dump has been dated at about 1,000 years B.P. by ^{14}C (W–5319). A source has not been established for these flows; Holcomb (1980a, b) interpreted them as caldera overflows, and this is consistent with their magnetic similarity to flows in the eastern caldera wall below Waldron Ledge (1B776, 1B788) and to the flow above the hiatus in Kilauea Iki (8B157). They could have come from the northeast rift zone of Mauna Loa, however; nearby Mauna Loa flows draped over a Kaoiki fault scarp 2 km north of Tree Molds (fig. 12.5*A*) have similar magnetization (8B841) and ^{14}C age (830 ± 60 and 530 ± 60 years B.P., W–3879 and W–3880, respectively). It is conceivable too that flows exposed in Kilauea Iki (8B157) and the eastern caldera (1B680, 1B692, 1B776, 1B788) also were erupted from Mauna Loa and flowed into the Powers caldera.

The Volcano flows may extend far down the flank of Kilauea. Much of the north flank is surfaced by younger Ai-laau flows, but older flows above the Pahala Ash are exposed in kipukas south of Keaau (fig. 12.5*J*). Aerial photographs reveal rudimentary fluvial drainage on the kipukas but not the younger flows (fig. 12.21). The

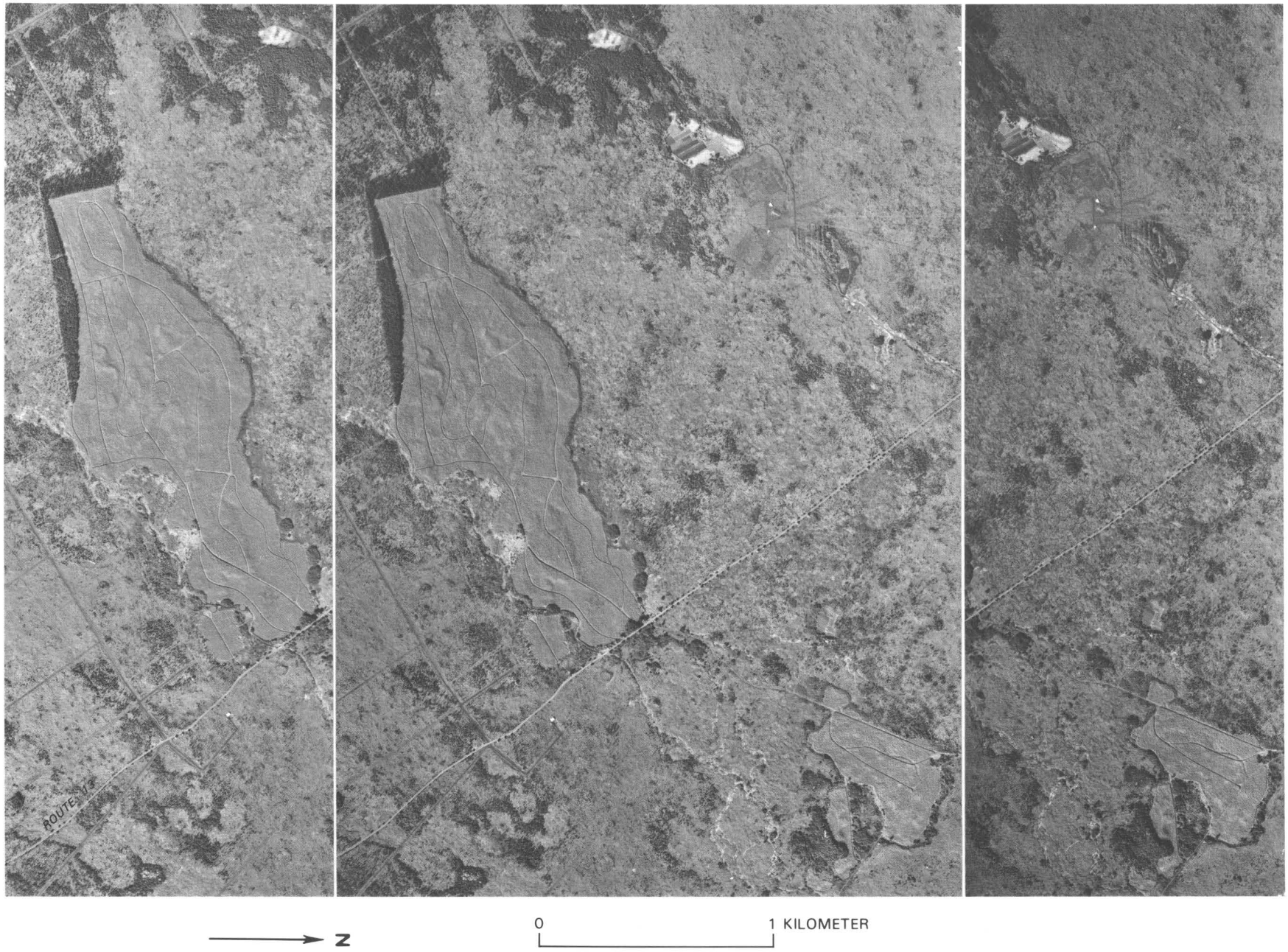

FIGURE 12.21.—Lava flows of three ages southeast of Keaau. Old ash-covered Mauna Loa flows are occupied by truck farms and fields of sugar cane, while Kilauea flows are uncultivated. Two groups of Kilauea flows differ in age and appearance: Older flows have blotchier vegetation pattern and incipient drainage channels absent on younger flows; ohia trees cluster atop younger flows near their margins. Flow groups differ in their directions of remanent magnetization. Large red dots, ^{14}C sample sites; pairs of small red dots, paleomagnetic sites. Some small clumps of ohia along axes of younger flows are known to occur above lava tubes. Thick stand of trees bordering southern and western sides of largest cane field is an artificial planting of Norfolk pines and other trees. Stereo triplet prepared from photographs 81–83, roll 12CC, USDA series EKL, 1965.

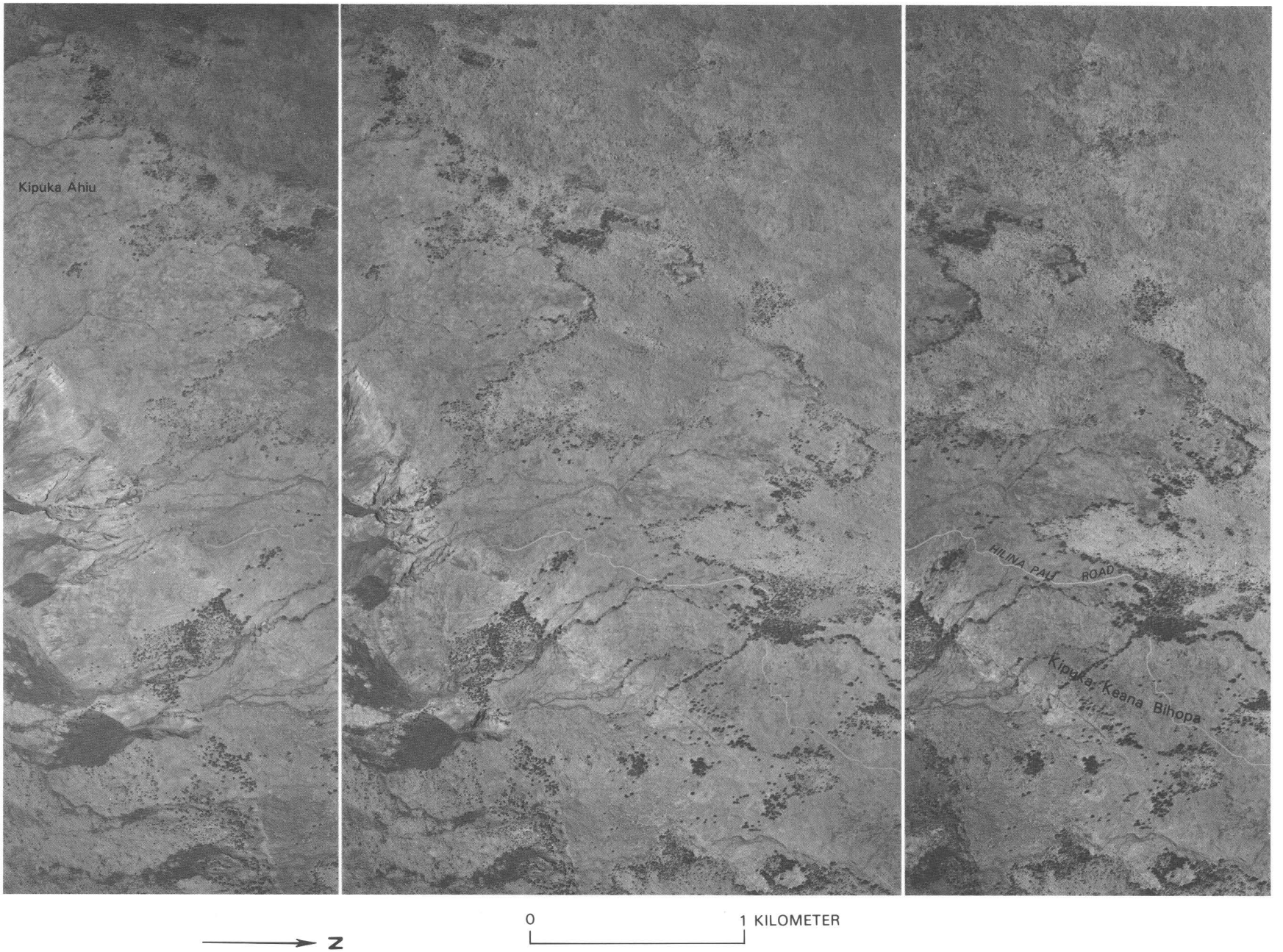

FIGURE 12.22.—Vegetation contrasts near end of Hilina Pali Road. Kipukas are carpeted by range grass on veneer of ash and sand, while barren areas to north are dotted only by low trees and shrubs. Walker (1967) thought contrasts arose from partial stripping of an ash deposit, but Holcomb (1980b) believed them to reflect lava flows of different ages. Some bare patches within kipukas may arise from stripping or nondeposition; others may be tongues of younger lava flows. N.G. Banks (unpublished work) has found lava younger than 1,000 yr at some places within kipukas. Large red dots, ^{14}C sample sites; pairs of small red dots, paleomagnetic sites. Stereo triplet prepared from frames 4–6, roll 5CC, USDA series EKL, 1965.

FIGURE 12.23.—Red tephra cone left of center exposed in west wall of Pauahi Crater. Crater of cone was choked with coarse debris and then filled by ponded lava, which cooled to produce massive block with radial jointing. Exquisitely detailed molds of tree ferns are found in lower part of pond. Yellow tephra layer of figure 12.27 occurs higher in wall on both sides of cone and dips down toward crater. Hiatus above yellow tephra is apparently correlative with hiatus beneath lava pond, and yellow tephra may be coeval with coarse debris within buried crater. People at upper left stand on overlook along Chain of Craters Road; overlook was later moved about 100 m to right. On crater floor at lower right is perched lava pond (Holcomb and others, 1974) active on this day. Workers on crater floor are measuring deformation of floor, which is crust of fresh lava lake being domed by continued injection of lava. Foreground, septum between west pit and larger central pit of Pauahi; septum is veneered by thin crustal plates of lava lake that subsided within central pit a few weeks earlier (Tilling and others, chapter 16). Lava has since broken through crust of west pit and dribbled across septum into central pit. Photograph by R.T. Holcomb, December 4, 1973.

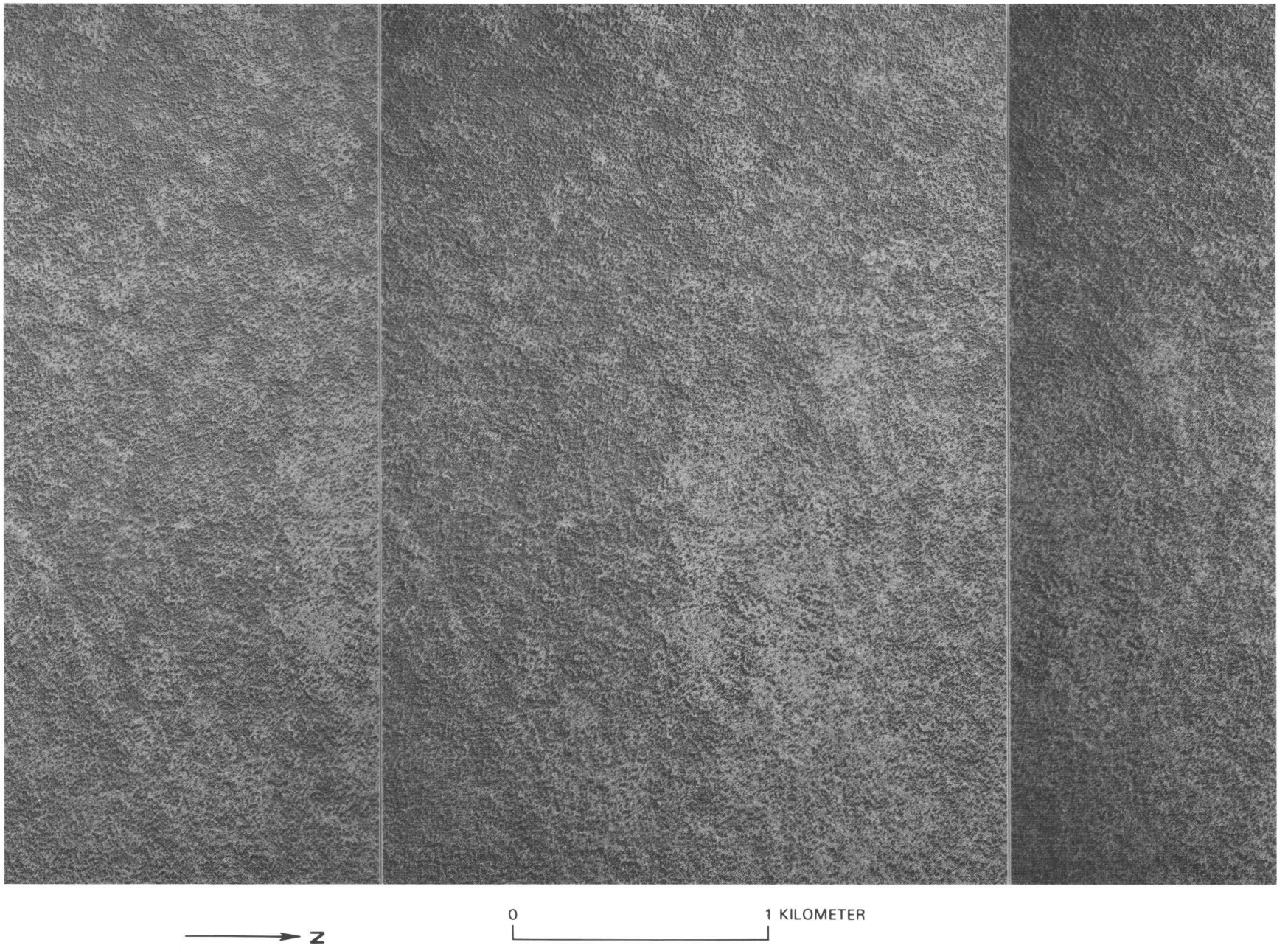

FIGURE 12.24.—Monotonous forest along north side of middle east rift zone, developed on lava flows older than 1,500 years. Aerial photographs could not be used to identify lava-flow boundaries here, but ground traverse showed that major boundaries must exist (fig. 12.25). Prominent rift structures are visible in southeast corner, and broad low swell, elongate east-northeast to west-southwest near center of this view, may be an ancient feature of rift zone. Stereo triplet prepared from frames 125–127, roll 12CC, USDA series EKL, 1965.

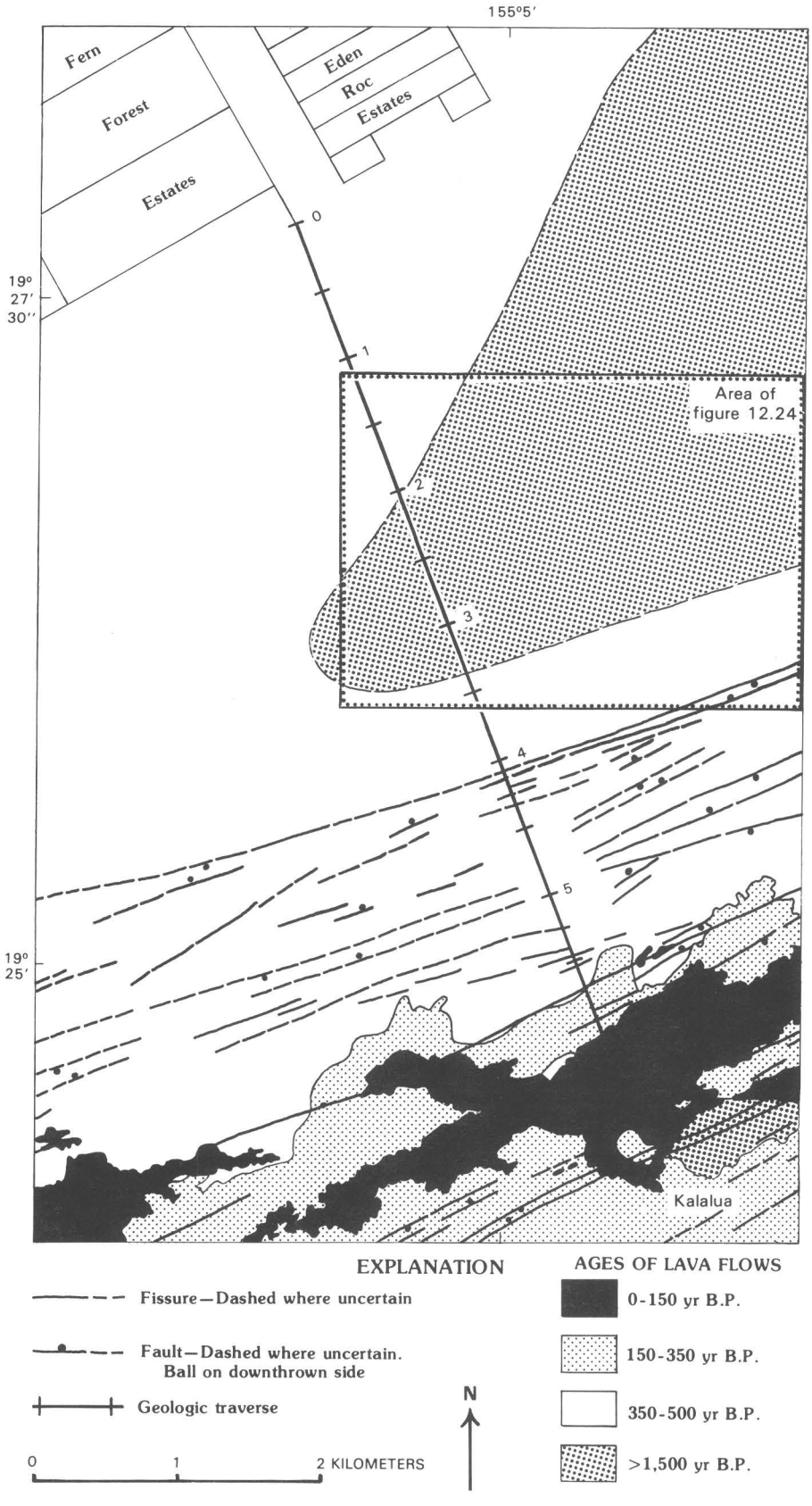

FIGURE 12.25.—Geologic map of Kilauea north flank adjacent to middle east rift zone. Contacts within area of figure 12.24 inferred from changes in rock type found along one tape-and-compass traverse through forest, indicated by heavy line marked at 0.5-km intervals.

older flows are more weathered and have a different vegetation pattern. Tree molds in the younger flows show that trees were growing on the older flows when they were flooded by the younger lava. The older flows have magnetization (8B049, 8B073, 8B217; fig. 12.11*F*, crosses) similar to those at Volcano, but they are similar also to 9B889 (fig. 12.5*J*), which is tentatively correlated with lava dated at about 3.7 ka (W–4177). They are also magnetically similar to a Mauna Loa flow (8B901) upslope from Mountain View dated at about 5.6 ka (W–3862). This magnetic direction is near that for a geocentric axial dipole; it is frequently repeated and is therefore not very diagnostic of age.

A few flows along Kilauea's rift zones are also magnetically similar. Among them is the flow above the hiatus in Pauahi Crater (9B217), which could represent an overflow from the summit. Another is the Kaliu flow (8B361 and 9B493, fig. 12.5*G,H*), which overlies the flows of Opihikao, but its measured magnetic dispersion is high and its age is therefore uncertain. Ash-covered pahoehoe of Waiakahiula Two (8B097, fig. 12.5*J*) above Pahoa also has this direction, as do flows of Keahialaka and Pohoiki (8B373, fig. 12.5*H*; Moore, 1981), but they could be older. A site (9B865, fig. 12.5*B*) on the lava shield of Ponohohoa Chasms also is similar, but here again the age is not constrained stratigraphically. An unnamed pyroclastic cone of the lower east rift zone, 2 km northeast of Iilewa Crater (fig. 12.5*G*), has been dated at about 900 years B.P. by ^{14}C (W–4690), but its magnetization is not known.

Tube-fed pahoehoe flows on the inland side of the lower southwest rift zone (fig. 12.5C) have yielded ^{14}C ages of about 900–1,000 years (W–5147, W–5211, W–5215). The source of these flows is uncertain; they could have spread down the west flank of Kilauea from a source on Mauna Loa, or they could have come from the summit of Kilauea. They may be coeval with the flows from the Observatory vent if that vent is older than the Ai-laau vent, as discussed in a later section, despite distinctly younger ^{14}C ages for the Observatory flows.

In summary, though several flows are tentatively assigned to Kilauea eruptions 750–1,000 years ago, most are equivocal. Stratigraphic uncertainty permits many to be older, and of those dated by ^{14}C, all except one could have been erupted from Mauna Loa.

KALUE FLOWS

Much of the Koae fault zone north and west of Kipuka Nene (figs. 12.18, 12.29) is surfaced by barren lava thought to have overflowed the southern caldera rim. These flows are not easily differentiated from other so-called regional pahoehoe (Walker, 1967) barren of vegetation above Hilina Pali, but they are magnetically distinct (fig. 12.11*F*, squares). Below the pali they are easily distinguished from older flows, being darker (fig. 12.32) and less green because of less weathering and less surficial cover. Between Hilina Pali and Puu Kaone they are split into four main lobes; two cascaded over the coastal cliffs to form the Kakiiwai and Kalue lava deltas, and a third forms the shoreline at Kaaha.

The magnetization of these flows is shared by others to the west (fig. 12.5C), including the pahoehoe of Kipuka Pepeiau (8B493), the Naliikakani flows (3R481), and the Waiwelawela flows (8B529; but site 3R421 on the Waiwelawela flows has yielded a different result). The Opihinehe flows (fig. 12.5*D*) are probably coeval. Because no lava shield of this age is known along the southwest rift zone, these extensive flows are inferred to come from the same summit source as the Kalue flows.

Similar magnetization is also shared by extensive pahoehoe seaward of the east rift zone (fig. 12.5*E,F*) from Kupapau to Kaena Point (8B229, 8B241, 3R157, 3R181) and beneath the eastern flows of Mauna Ulu (3R097, 3R109, 3R121, 3R133, 3R169, 3R193, 3R229). The eruption of Kane Nui o Hamo fed these flows. The size of the lava shield and large extent of its tube-fed flows suggest that this was the longest and most stable eruption of any known along either rift zone, but no other rift eruptions of similar age have been found.

The age of this group is uncertain, and because it illustrates the contradictions still existing among stratigraphic, paleomagnetic, and ^{14}C data, some details will now be given. The magnetization of this group is consistent with an age of 750–500 years, according to the preliminary chronology of Holcomb and others (1986), and the magnetically distinct Kipuka Nene flows beneath are judged from other evidence to have an age of 1.1 ka, as noted earlier. Yet charcoal from beneath one of the upper flows (3R001; fig. 12.30) in Kipuka Nene indicates an age of 1.15 ka (W–5135) for Kalue lava. The problem is compounded by two other flows in Kipuka Keana Bihopa (fig. 12.5*D*) with still different magnetizations but ^{14}C ages of 1.14 ka (W–5212) and 1.13 ka (W–3827). Though the magnetic inclinations of both latter flows (8B397, 3R025) differ from those of Kalue, their declinations are similar; they could be coeval with Kalue flows but have inclinations affected by a topographic magnetic anomaly along Hilina Pali. If so, the three ^{14}C dates would agree well in assigning an age of 1.14 ka to the Kalue flows instead of the 500–750 years adopted here. If this were true, then the magnetically distinct older flows of Kipuka Nene would have to be older than its assigned age, and possibly predate the Powers caldera.

AI-LAAU FLOWS

Much of Kilauea's north flank is covered by tube-fed flows extending northeast from the summit to the coast between Haena and Honolulu Landing. The Ainaloa, Kazumura, Old Volcano Trail, and other flows of this group are well-known for their large lava tubes. Despite high rainfall in this area, the flows are little weathered and support a juvenile forest (figs. 12.5*J*, 12.21) implying that they are young. Their vegetation was even lighter in the 19th century, eliciting comments from visitors. For example, Wilkes (1845, p. 119) observed in 1840 that "After leaving Olaa, we had no distinct path to follow; for the whole surface became a mass of lava, which retained all its metallic lustre, and appeared as if it had but just run over the ground—so small was the action of decomposition. There were only a few stunted bushes on our track." Even a critique accusing Wilkes of exaggeration (by "A.V." in the February 1, 1847, issue of a missionary journal, *The Friend*) described vegetation different from today, saying "the road from Olaa to the

A

FIGURE 12.26.—Hiatus exposed in Kilauea Iki Crater. Photographs by J.D. Griggs, December 1985. ***A***, Northeast wall of crater below Byron Ledge overlook, showing color change on face of cliff. Tree-covered recess at right is older Ai-laau part of crater. ***B***, Closer view of color change, which coincides with layer of red cinders. Debris from this layer mantles slopes below, reddening surface and supporting more plant growth than slopes above. Cinder unit is truncated at right by densely vegetated thin lava plaster on wall of Ai-laau crater; plaster may be dregs of subsided lava lake.

volcano is generally very distinct. Ohelo bushes grow much of the way, as other bushes, grass and small trees, on both sides of the road."

Of seven ^{14}C ages obtained from these lava flows (table 12.6), three that duplicate others are anomalous and are disregarded. Others range from 260 to 450 years and average 335 years B.P. They are distinctively magnetized (fig. 12.11*F*, triangles; sites 8B001, 8B061, 8B085, 8B169, 8B193, 8B421, 8B733, 8B793, 9B121, 9B133, 9B421, 9B433, 9B397, 9B673).

Ohia trees clustered along flow margins can be used to delineate individual tube-fed flows (figs. 12.5*J*, 12.21) up to elevations of about 500 m. Separate flows cannot be mapped above this; they disappear upslope into a monotonous young ohia-hapuu forest that extends to the summit region. Thurston Lava Tube and other tubes fanning eastward from the summit fed the multiple lobes distinguished at lower elevations.

The source of the flows is the eastern part of Kilauea Iki (figs. 12.5*A*, 12.33), which is an eruptive crater choked with talus. It is older than the other parts of Kilauea Iki and supports a more mature forest. It is also less deep and has lava plastered against its walls in some places. The rest of Kilauea Iki is deeper, steeper, and lacks wall plaster; it is a chain of later collapse pits. A sagged platform east of this Ai-laau vent resembles those developed above Alae and Aloi Craters after burial (Swanson and others, 1972; Holcomb and others, 1974); a buried pit crater is inferred beneath it. The presence of such a crater, filled with still-cooling lava, could explain a self-potential anomaly mapped by Zablocki (1976) in this area.

Also inferred to come from the Ai-laau vent are magnetically similar (8B109, 8B181, 9B145A) tube-fed flows extending northeast from the middle east rift zone near Kalalua to the coast around Makuu (fig. 12.5*G–J*). Initially these flows were assumed to have come from the rift zone, but no vent could be found; vents inferred by Moore and Koyanagi (1969) are younger fissures crossing the flows, while Kalalua and other pyroclastic cones are older and Puu Kahaualea is younger. Because their vegetation and magnetization are similar to those of the other flows from the Ai-laau vent, they are inferred to be of the same age and come from that same vent. If so, they must have spread east past the northeast side of Kane Nui o Hamo and along the northern part of the rift zone for several kilometers before moving northeast onto the north flank. Fissures, faults, and grabens may have prevented them from crossing the rift zone and spreading farther south. The many structures crossing them must be younger or had recurrent displacement after burial 350–500 years ago.

B

FIGURE 12.26—Continued.

The lightly vegetated Keauhou flows seaward of the upper east rift zone west of Kane Nui o Hamo (figs. 12.5*E*, 12.34, 12.35) have similar magnetization (8B541, 1B432, 3R049, 3R073, 3R085, 3R205, 3R217, 3R265, 3R325, 3R397) and ^{14}C ages (table 12.6). These flows could come from the Ai-laau vent, but they are smaller and include a more complex assemblage of flow types. They probably represent sustained, unstable eruption (table 12.1) from an upper-east-rift vent, most likely Puu Huluhulu. The spatter cone between Hiiaka and Devils Throat also has similar magnetization; this brief eruption may have preceded the sustained one (like the brief eruptions of 1968–69 that preceded the Mauna Ulu eruption of 1969–74) but a stratigraphic relationship has not been established. Some pit craters of the upper east rift zone must postdate these eruptions.

Other flank vents and flows are thought to have similar ages. Two assemblages have similar magnetization. One is the group of Kamakaiauka along the southern strand of the southwest rift zone (fig. 12.5*B*); its age assignment is tentative because only one paleomagnetic site (8B481) has been sampled from an aa flow. Another group along the lower east rift zone (fig. 12.5*H*) includes Kaholua o Kahawali (9B205) and its associated lava flows. A flow younger than Puu Kaliu but older than A.D. 1790 lava has been dated at about 500 years B.P. (W–4688), while a flow at Kehena has been dated by ^{14}C at about 450 years B.P. (W–5054). Puu Honuaula and a flow 2 km southwest of Puu Kaliu are dated at about 350 years B.P. (W–5048, W–3800).

Macdonald (1941) and Holcomb (1980a) included several other vents with Kaholua o Kahawali because the legend of Pele and Kahawali suggests that a long chain of vents erupted at the same time. But mapping by R.B. Moore (1981) has not confirmed this. Moore believes that Kaholua o Kahawali and an adjacent cone are significantly younger than Halekamahina and other nearby vents. Moore has also mapped as much older a flow having similar magnetization (8B037) east of Kapoho Crater.

One other Puna flow should be mentioned, the prominent aa flow of Makaukiu Point between Nanawale and Cape Kumukahi (fig. 12.5*H*). A ^{14}C age of 350 years B.P. (W–5088) has been obtained from charcoal beneath this flow, and chemical weathering data suggest an age of 300–350 years (Atkinson and Swindale, 1974). Moore (1981) has mapped it as one of the youngest prehistoric units in the Kapoho area because it still projects beyond the adjacent shoreline to form Makaukiu Point. However, this flow is clothed by a mature *Pandanus* forest that implies it is much older (Atkinson, 1970), and paleomagnetic data (8B973, 9B181) indicate that it and the flows beneath are older than 1.5 ka.

Dating is not yet precise enough to determine relative ages of eruptions within this interval, and it is not clear whether the rift eruptions are younger or older than the Ai-laau vent. Some Hawaiian traditions suggest a sequence: Kaholua o Kahawali and the flows seaward of Puu Huluhulu are associated with the current volcano goddess Pele (Ellis, 1827; Macdonald, 1941), while activity at Kilauea Iki is associated with Pele's predecessor, Ai-laau

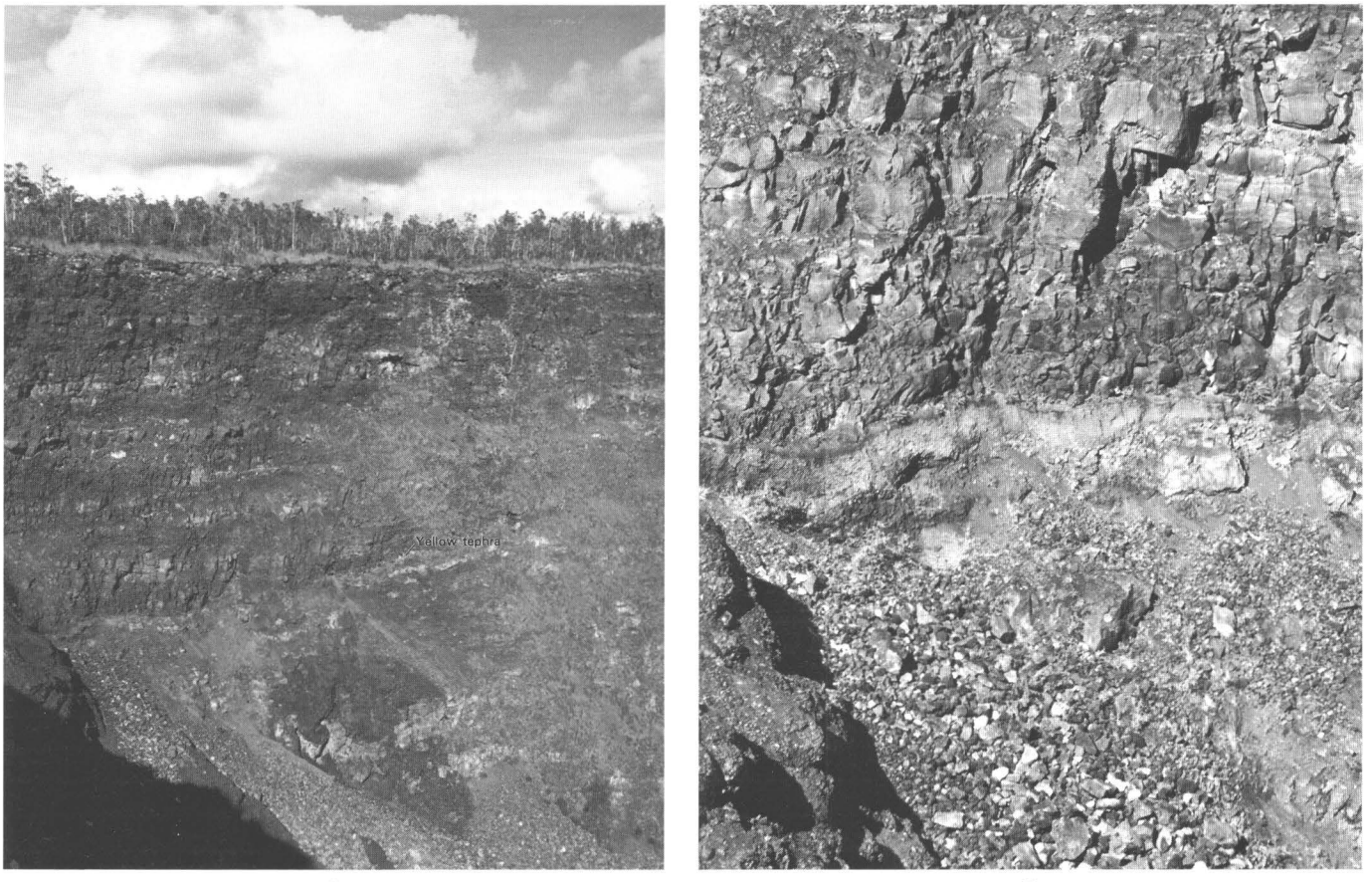

A *B*

FIGURE 12.27.—Hiatus exposed in north wall of Pauahi Crater. Photographs by J.D. Griggs, October 1985. ***A***, Northwest wall of Pauahi, viewed from overlook shown in figure 12.23. Hiatus occurs atop yellow tephra layer. ***B***, Closeup view of yellow tephra, which is mixture of blocks and ash. This tephra may consist in part of Uwekahuna Ash Member, but because it grades laterally into coarse debris in crater of buried tephra cone nearby (fig. 12.23), at least some of it may have been ejected from local source. Organic ash is abundant atop tephra, and overlying lava flow contains many tree molds.

(Westervelt, 1916). If that chronology is correct, the rift eruptions followed the summit eruption.

OBSERVATORY FLOWS

Lightly vegetated prehistoric tube-fed flows in a band 4 km wide extend down the inland side of the southwest rift zone (fig. 12.5*B*,*C*). They are buried by Keamoku, Mauna Iki, and Cone Peak flows at elevations of 800–900 m but reappear higher up; flows with similar magnetization (1B001, 1B013, 1B025, 1B037, 1B049, 1B061, 1B073, 1B109, 1B133) form the northwest rim of the present caldera (fig. 12.5*A*) and the upper section of Uwekahuna Bluff (5 flows of 1B157; sites 145–148, Doell and Cox, 1965).

Though detailed mapping may show some of these flows to have been erupted on Mauna Loa (possibly more of the lava north of Tree Molds dated by W–3879 and W–3880), the source of at least some was a long-sustained vent located in what is now the northwest caldera near Uwekahuna Bluff. A large lava shield grew around this vent; it is well expressed west and northwest of the caldera rim by ground slopes, mappable aa lobes, and flow lineations radiating from a point about 1 km east of the Hawaiian Volcano Observatory (fig. 12.36). The crater of the Observatory vent may have extended close to Uwekahuna Bluff. Though the large shield and extensive tube-fed pahoehoe indicate that activity was long-sustained at the Observatory vent, the radiating aa lobes indicate some instability toward the end of its activity, like that observed at Mauna Ulu (Tilling and others, chapter 16; Holcomb, 1976a).

Flows of apparently similar age cover the south flank north and west of Kipuka Ahiu and extend over Hilina Pali to the coast west of Kaaha (fig. 12.5*B*,*D*). They consist of multiple units, aa flows from the southwest rift zone being interbedded with pahoehoe flows from the summit. Aa mapped by Walker (1967) as one unit from Puu Koae actually consists of two flows separated by pahoehoe from the summit (fig. 12.37). The western aa flow, traceable directly to Puu Koae, was erupted in the 18th century and lies atop the pahoehoe, while the eastern aa lobe, inferred to come from Cone Crater, lies below the pahoehoe. Another pahoehoe sheet occurs beneath the Cone Crater aa flow. The pahoehoe unit between the aa flows is distinctively picritic. Though Walker (1967) did not map the contact between the picritic unit and older pahoehoe, he did show extensive distribution of picritic basalt with separate symbols,

A

FIGURE 12.28.—Hiatus exposed in Makaopuhi Crater. ***A***, Northwest wall of crater, viewed from west rim, showing lower layer of yellow tephra separated by thin lava flows from upper layer of reddish tephra. Massive lava flows above red tephra occur in flank of Kane Nui o Hamo lava shield. Photograph by R.T. Holcomb, February 6, 1973. ***B***, Closeup view of upper tephra layer, which consists of red and green cinder beds. This layer appears to have been barren of vegetation when it was covered by lava. Photograph by R.T. Holcomb, March 24, 1974. ***C***, Closeup view of lower yellow tephra layer, which consists of blocks and ash. Large size of some blocks indicates they were ejected from local source, such as nearby pit crater ancestral to Makaopuhi. Upper part of this layer is rich in organic ash, and lava flow above it contains many molds of trees and ferns, indicating hiatus in accumulation of lava flows. Photograph by R.T. Holcomb, March 24, 1974. ***D***, Southwest wall of crater, viewed from mezzanine, showing two tephra layers and small tephra cone lower in section. Photograph by R.T. Holcomb, June 30, 1972, when lava from Mauna Ulu was cascading over crater rim to build talus-and-lava cones (Holcomb and others, 1974) against crater wall.

B

C

FIGURE 12.28.—Continued.

D

FIGURE 12.28.—Continued.

and picritic lava has been traced to the southwest rim of Kilauea caldera (T.L. Wright, oral commun., 1976), where it is the top unit beneath the Keanakakoi Ash Member. The Cone Crater aa (8B457) and the picritic unit (1B097) are magnetically similar to the Observatory flows; the older pahoehoe (8B445) is magnetically more similar to the flows of Volcano.

The Observatory flows are of uncertain age. They predate Cone Peak and other 18th-century flows of the southwest rift zone, but their age relative to Ai-laau flows is not yet certain. Vegetation is sparser on Observatory flows, but this probably arises from a rainfall contrast instead of a difference in age: annual rainfall on the north flank is 380 cm (150 in.) versus 75 cm (30 in.) on the southwest flank. Observatory flows have deeper weathering (J. Lockwood, oral commun., 1985), but because they are downwind from summit vents their weathering may have been accelerated by fumarolic acids.

Four ^{14}C ages have been obtained from Observatory flows (table 12.6), but one is anomalous. Sample W–4998 was collected within the caldera near Tree Molds (fig. 12.5*A*) and is the sample most likely contaminated by fumarolic carbon (Rubin and others, chapter 9; Chatters and others, 1969). The other three ages are similar to those for Ai-laau flows. Because the Observatory flows

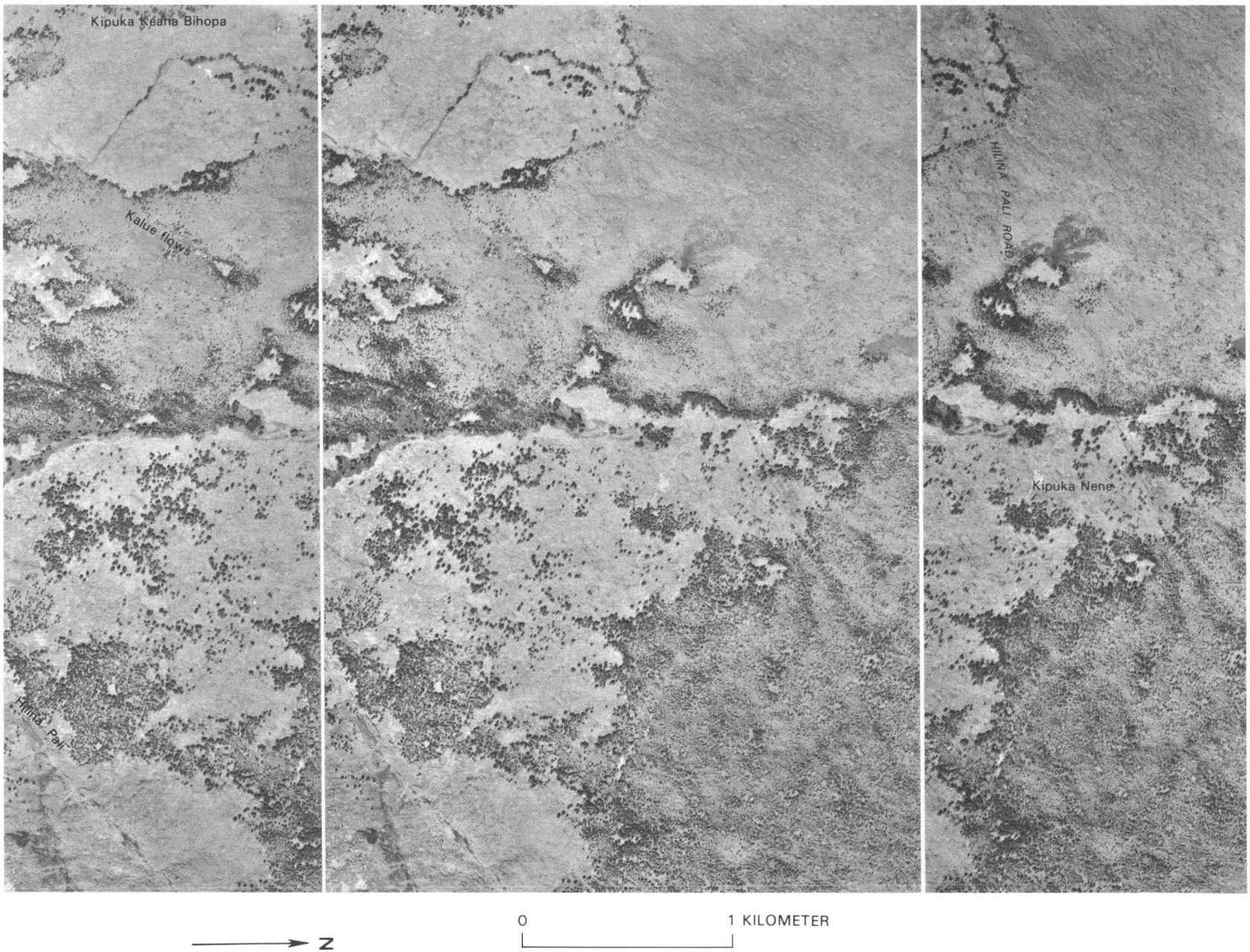

FIGURE 12.29.—Vegetation contrasts in Kipuka Nene area. Kipuka Nene and Kalue flows believed about 1,100 and 500–750 years old, respectively. Though vegetation contrasts generally seem to reflect different ages of lava flows, vegetation boundaries do not follow flow boundaries exactly, as shown in figure 12.30. Large red dot, ^{14}C sampling site; pairs of small red dots, paleomagnetic sampling sites. Stereo triplet prepared from frames 75–77, roll 14CC, USDA series EKL, 1965.

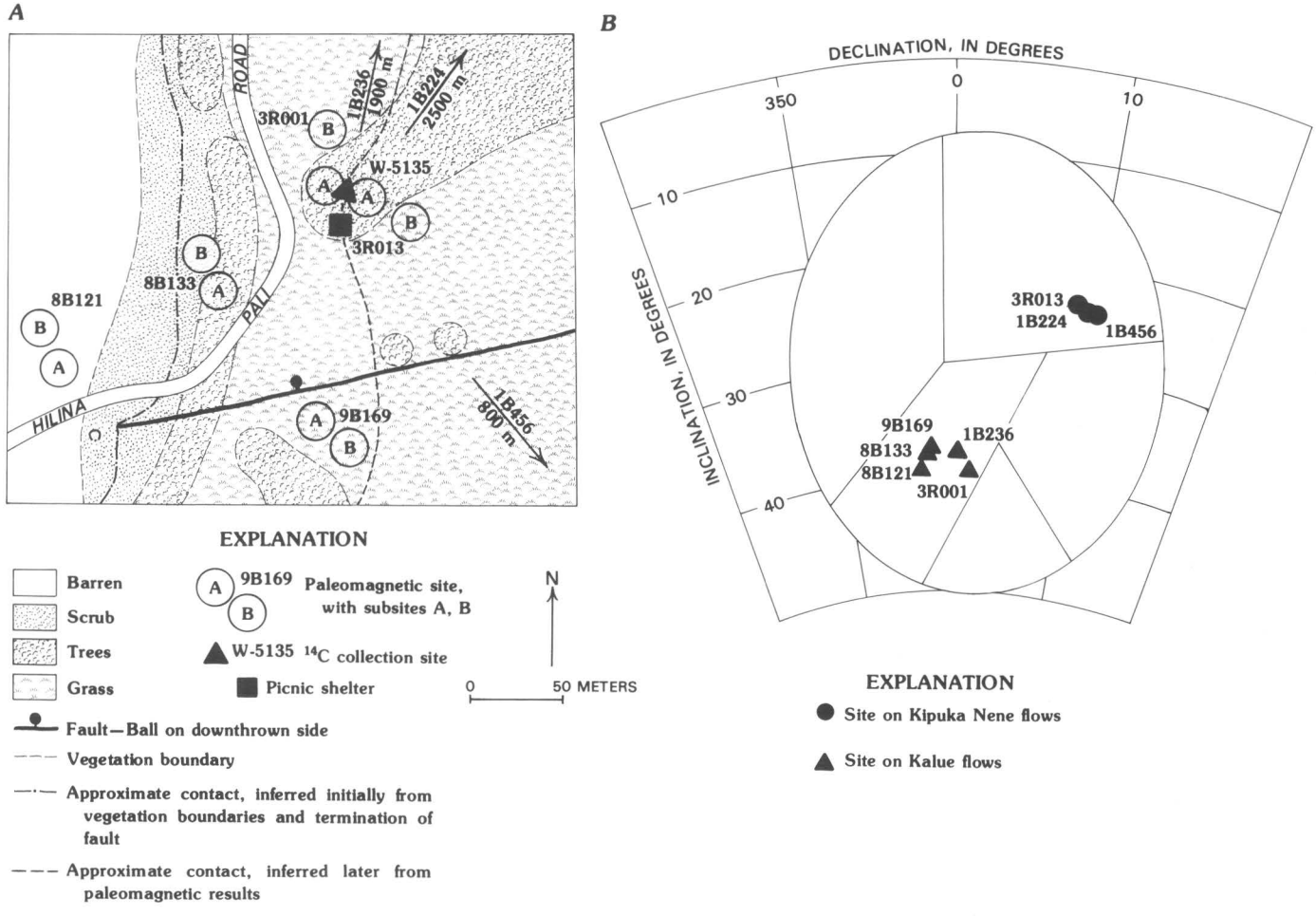

FIGURE 12.30.—Location of Kalue flow margin adjacent to Kipuka Nene. ***A***, Sketch map of Kipuka Nene picnic area, showing flow margin inferred initially and that inferred currently. Margin, traced with certainty only near picnic shelter, does not coincide exactly with vegetation boundary, causing earlier confusion about ages of Kipuka Nene and Kalue lava flows. Boundary between trees and barren lava may follow edge of thicker, inflated part of Kalue flows not easily penetrated by tree roots. Thinner marginal lobes may be penetrated easily by roots of trees but not roots of grass, and sand and soil beneath may provide water and nutrients enhancing tree growth. ***B***, Paleomagnetic results from Kipuka Nene area; Kipuka Nene and Kalue flows are magnetically distinct. Ellipse divided into fields containing sites of similar age, as defined in figure 12.11.

were sampled downwind from summit vents, their ^{14}C ages could be affected by fumarolic carbon, while samples beneath Ai-laau flows from the rainy windward flank could be contaminated by modern organisms. This suggests that the Observatory flows may be younger; but three older ages from the southwest rift zone could also represent Observatory flows (table 12.6), and they would raise the Observatory mean to more than 500 years.

The two flow groups differ magnetically (fig. 12.11*F*), the Observatory direction being intermediate between the Ai-laau and 18th century directions. However, the Observatory magnetization is not far from the axial dipole direction and alone is not diagnostic of age. Holcomb and others (1986) argued that the Observatory flows are younger than Ai-laau flows because lava in Uwekahuna Bluff beneath the Observatory flows seemed to have Ai-laau magnetization, according to the data of Doell and Cox (1965, flows 138–144) and R.R. Doell (unpublished work, flows 137I, 138A, 138B, 139A, 140A, 141A, 141B, 142A). But later sampling (1B582, 1B594, 1B606) has not confirmed the Ai-laau direction in Uwekahuna Bluff; it appears that the inferred Ai-laau samples of Doell and Cox were taken from a rotated fault block. Because the Observatory flows are magnetically not very different from the Volcano flows, they could be similar in age to the Volcano flows and thus 500 years older than judged by Holcomb and others (1986). Detailed mapping and chemical analyses should help sort out ages and sources of these various interfingered flows from Kilauea and Mauna Loa.

LATEST PREHISTORIC ERUPTIONS

Prominent widespread flows along both rift zones span a narrow range of ages. Most of them probably date from the 18th century, though some may be slightly older. This interval of frequent rift eruptions ended with a caldera collapse and explosive eruption at the summit.

FIGURE 12.31.—Vegetation contrasts between flows of Volcano, older flows of Mauna Loa, and younger flows of Ai-laau vent. Large red dot, ^{14}C sample site; pair of smaller red dots, paleomagnetic sample site. Stereo triplet prepared from frames 183–185, roll 12CC, USDA series EKL, 1965.

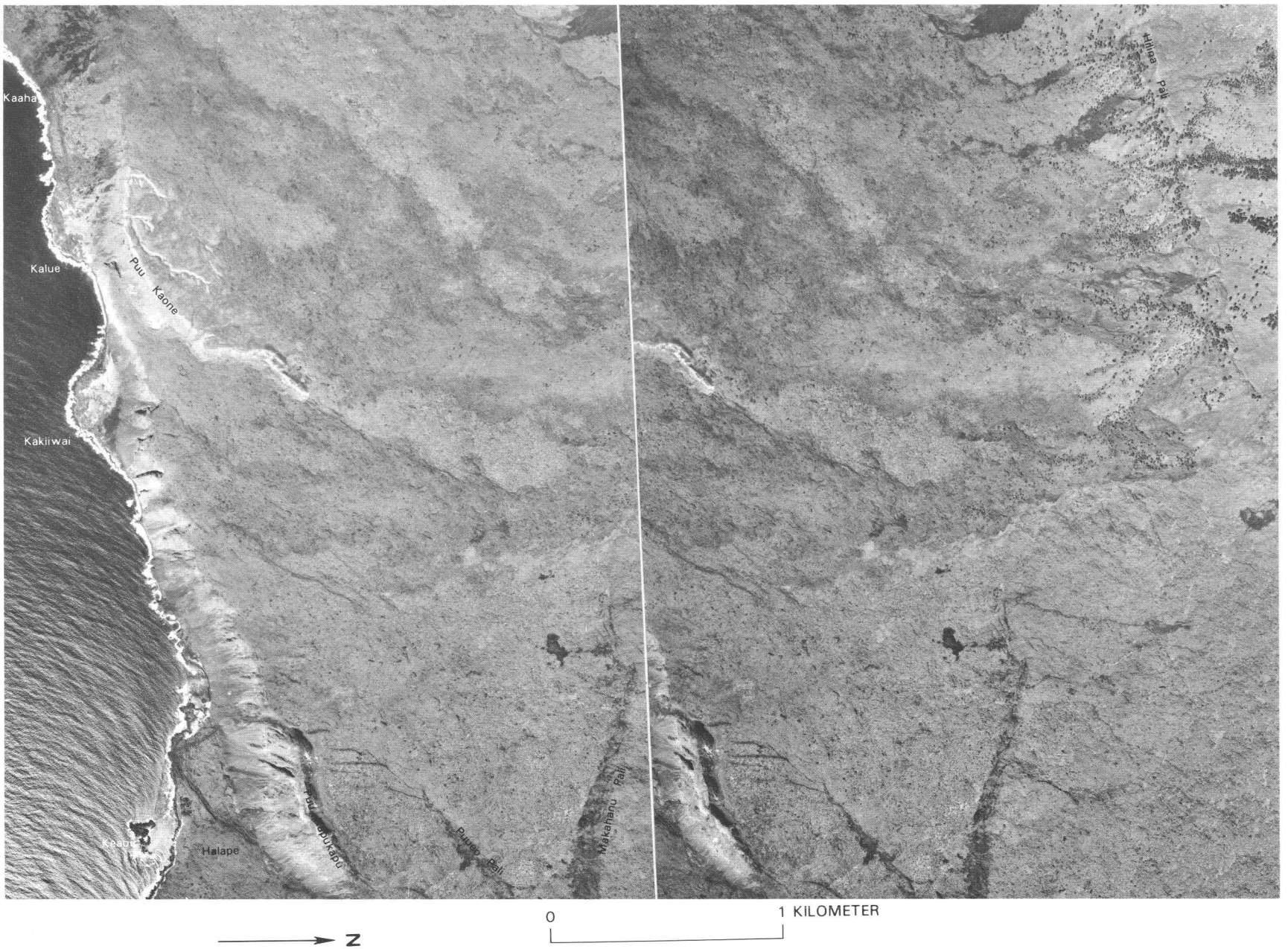

FIGURE 12.32.—Contrasting flow units in area between Hilina Pali and Puu Kaone. Two series of widespread surficial flows differ in photographic tone and surficial cover. Stereo pair prepared from frames 77, 78, roll 14CC, USDA series EKL, 1965.

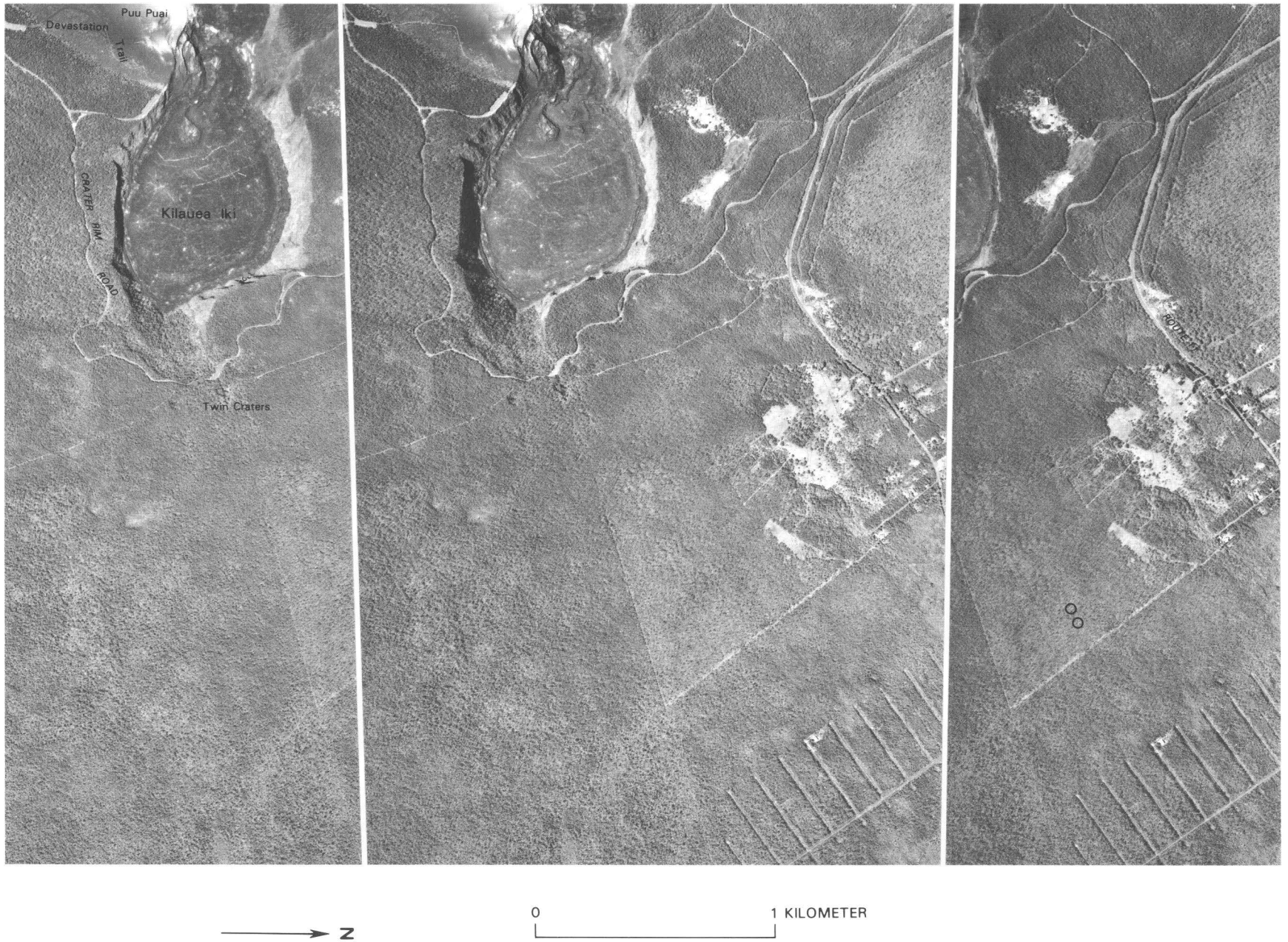

FIGURE 12.33.—Ai-laau vent and lava shield. Kilauea Iki is chain of three or four collapse structures extending eastward from inner sink of present caldera; it contains lava lake erupted in 1959. Ai-laau vent area includes east end of Kilauea Iki and small Twin Craters. Broad, shallow sag southeast of vent area is thought to overlie buried pit crater. Broad ridge with small axial pits (circled) extending northeast from vent area may represent path of major lava tube; similar ridges radiate south and southeast from broad sag, beyond this view. Paired red dots, paleomagnetic sample sites. Stereo triplet prepared from frames 185–187, roll 12CC, USDA series EKL, 1965.

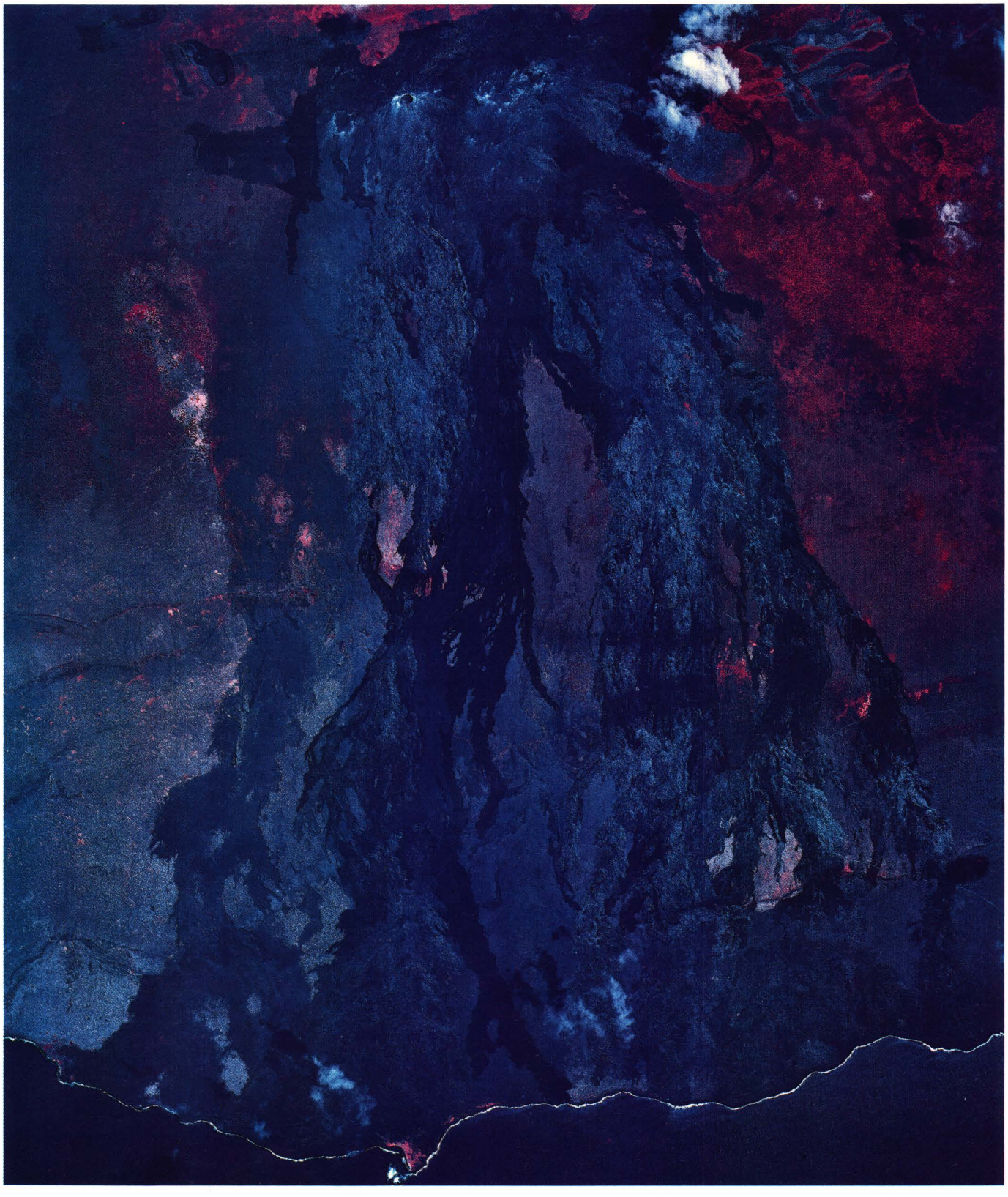

FIGURE 12.34.—Mauna Ulu region of upper east rift zone and south flank. High-altitude false-color infrared photograph showing bands of Mauna Ulu lava in center, flanked to left by Keauhou and Kipuka Nene flows, and to right by flows of Kane Nui o Hamo. Rain forest along rift zone is red; oldest grass-covered flows have very light tones. Barren lava flows are bluish gray and black. Darkest flows are aa; rest are pahoehoe. U2 photograph by NASA Ames Research Center, 1974.

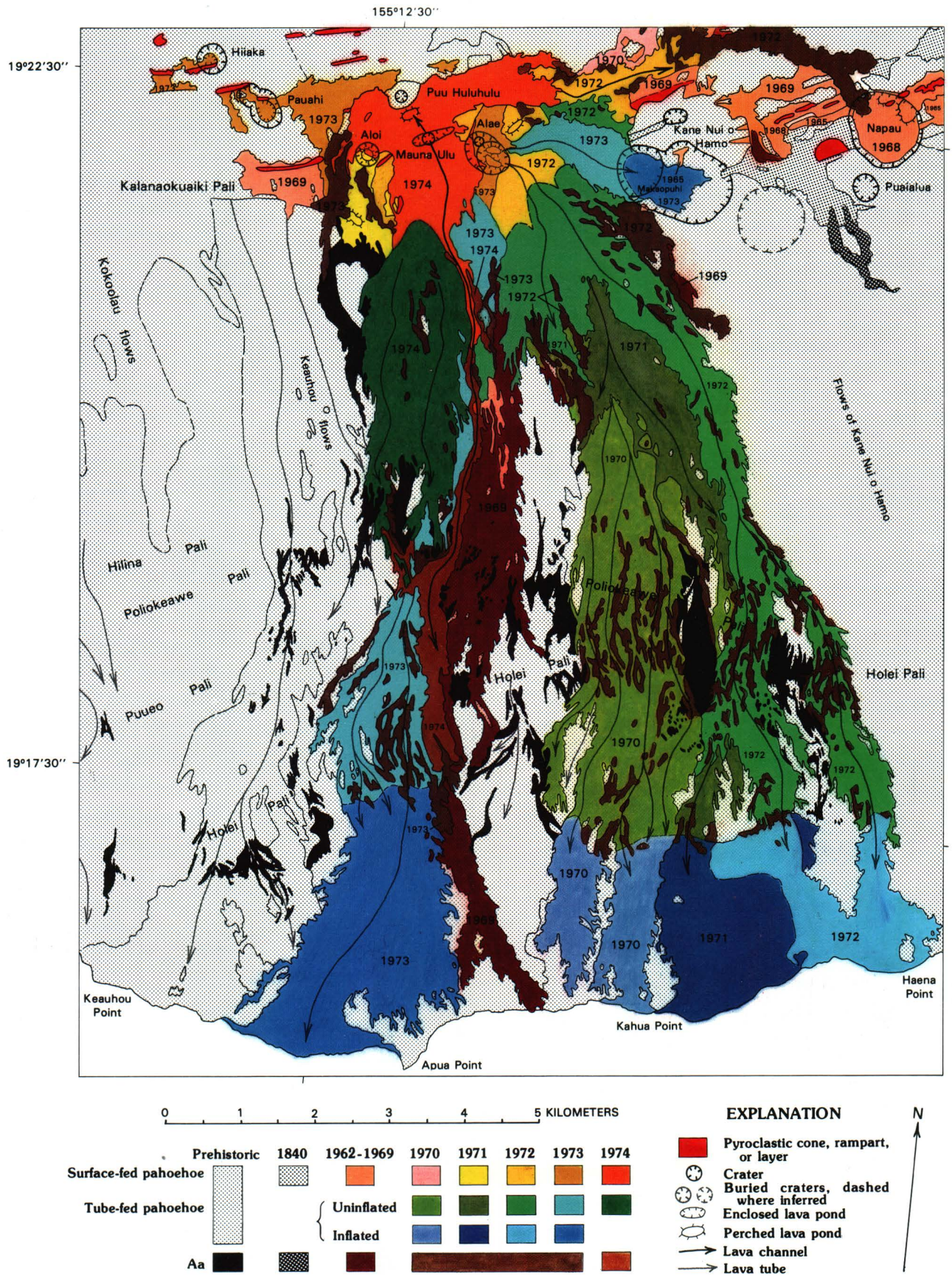

FIGURE 12.35.—Mauna Ulu region, with lava flows classified by their morphology. Shown also are boundaries between pahoehoe units of different age, as indicated on figure 12.5*E*, and eruption years of historical flows. Simplified from Holcomb (1976a, 1980a).

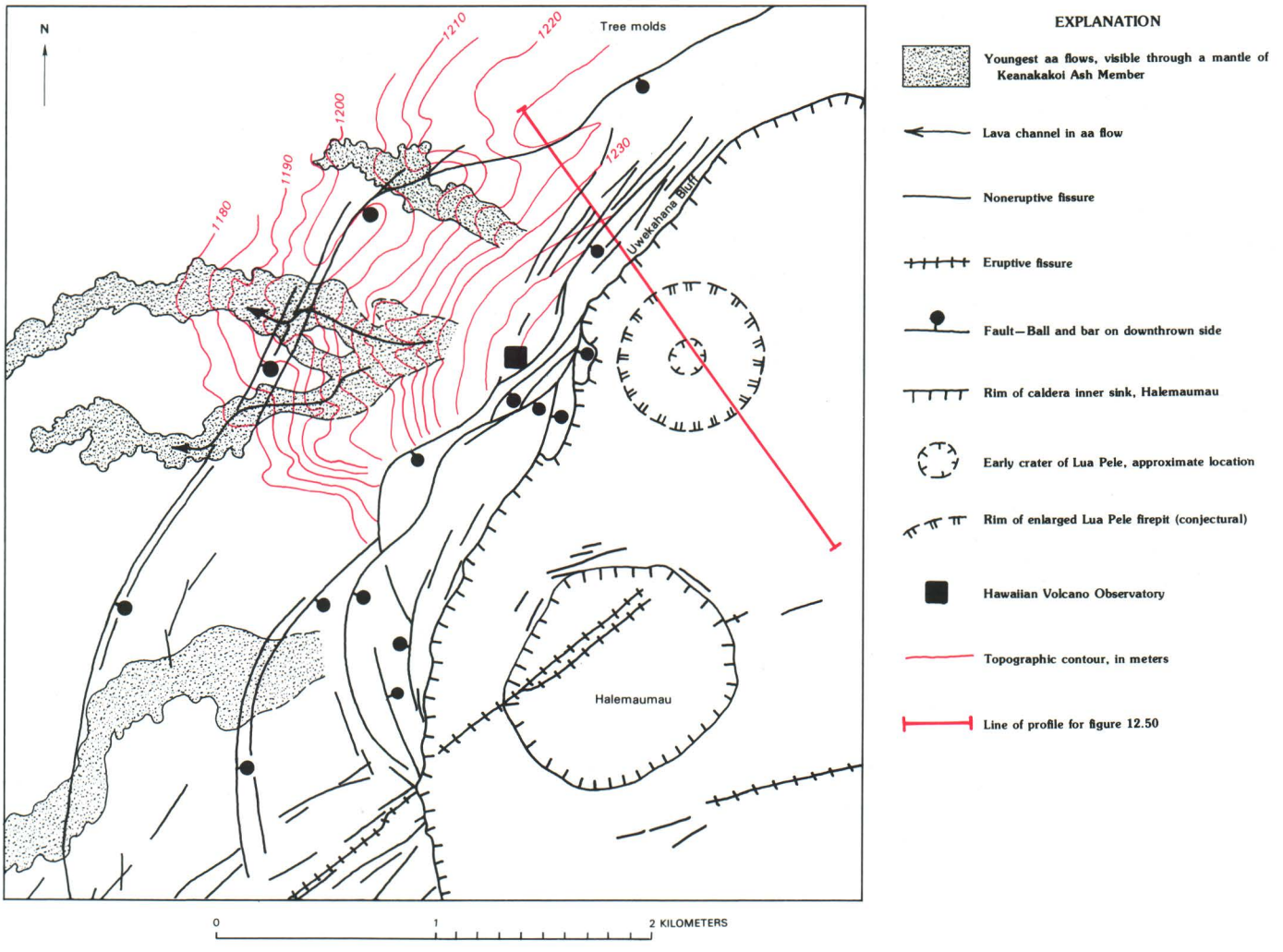

FIGURE 12.36.—Northwest sector of Kilauea caldera. Location of Observatory vent is inferred from radiating ground slopes and lava flows. Enlarged Observatory firepit is conjectural, its former existence suggested by remnants of concentric dikes on present caldera wall (fig. 12.49). Youngest aa flows and their channels (visible beneath mantle of Keanakakoi Ash Member) appear to have been deflected along fault scarp now cutting across them, indicating that displacement began before flows were erupted. This early deformation could have arisen from thermal contraction of lava filling older Powers caldera, as shown in figure 12.50.

KOKOOLAU ERUPTION

Superposition relations between Kokoolau (fig. 12.38) and surrounding lava flows are not yet clear. Holcomb (1980a) interpreted Kokoolau as a kipuka surrounded by flows from the Ai-laau vent, but paleomagnetic sites on Kokoolau (1B188, fig. 12.5*A*) and seaward flows (1B212, 3R349) extending into Kipuka Papalinamoku have shown that they are probably younger, dating from the late 17th century or early 18th century. An aa flow east of the Ahua Kamokukolau triangulation station (fig. 12.5*A*), atop Kalue lava and probably fed by a caldera-concentric vent mantled by A.D. 1790 ash south of Keanakakoi, is overlapped by pahoehoe on its east side (Peterson, 1967, and written commun., 1966). The younger pahoehoe is thought to come from Kokoolau; if so, Kokoolau is not only younger than the Kalue lava but also younger than at least one of the concentric vents. Kokoolau probably belongs to an extensive assemblage from the 17th and 18th centuries that extends the length of the east rift zone.

VEGETATION PATTERNS OF THE MIDDLE EAST RIFT ZONE

One reason for the age uncertainty of Kokoolau is a coincidental vegetation boundary caused by orographic rainfall variation. The rest of the east rift zone extends through an area of high rainfall and rapid forest growth, making it possible to differentiate lava flows using vegetation patterns (Atkinson, 1970). The latest prehistoric flows downrift from Kokoolau can be recognized from their distinctive vegetation. Although in rainy areas they are densely overgrown, their vegetal structure and floristic composition indicate that they are considerably younger than neighboring flows, including those from the Ai-laau vent (fig. 12.39).

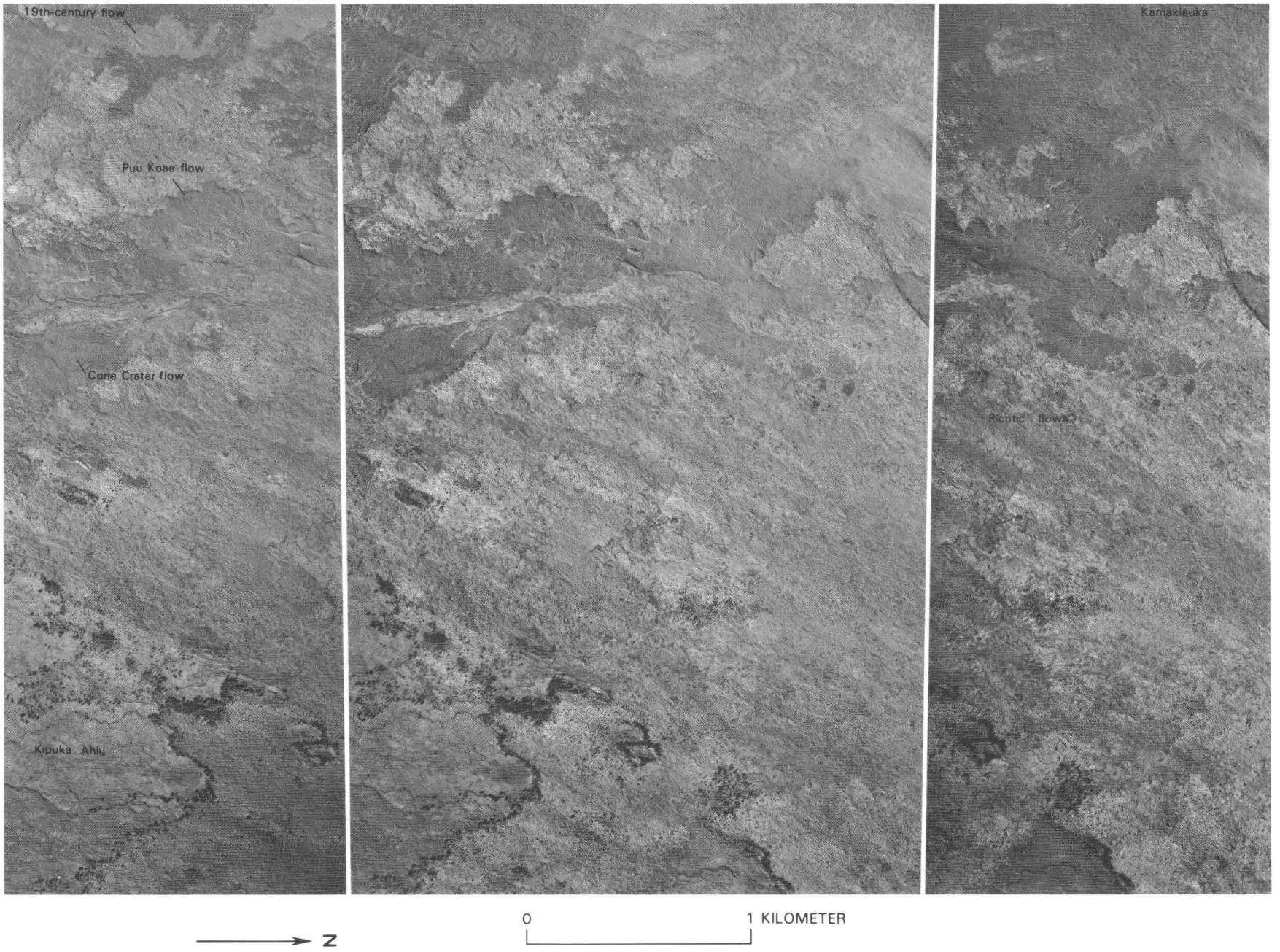

FIGURE 12.37.—Overlapping flows between Kamakaia and Kipuka Ahiu. Aa flows of two ages are present, with sheets of tube-fed pahoehoe between and beneath them. Both pahoehoe units inferred to originate from summit, upper aa from Puu Koae, lower aa from Cone Crater and chain of spatter ramparts to northeast (now covered by lava of 1974). Tonal stripes trending north-northeast to south-southwest at right represent variations in sand cover; dark bands contain more sand. Stereo triplet prepared from frames 201–203, roll 12CC, USDA series EKL, 1965.

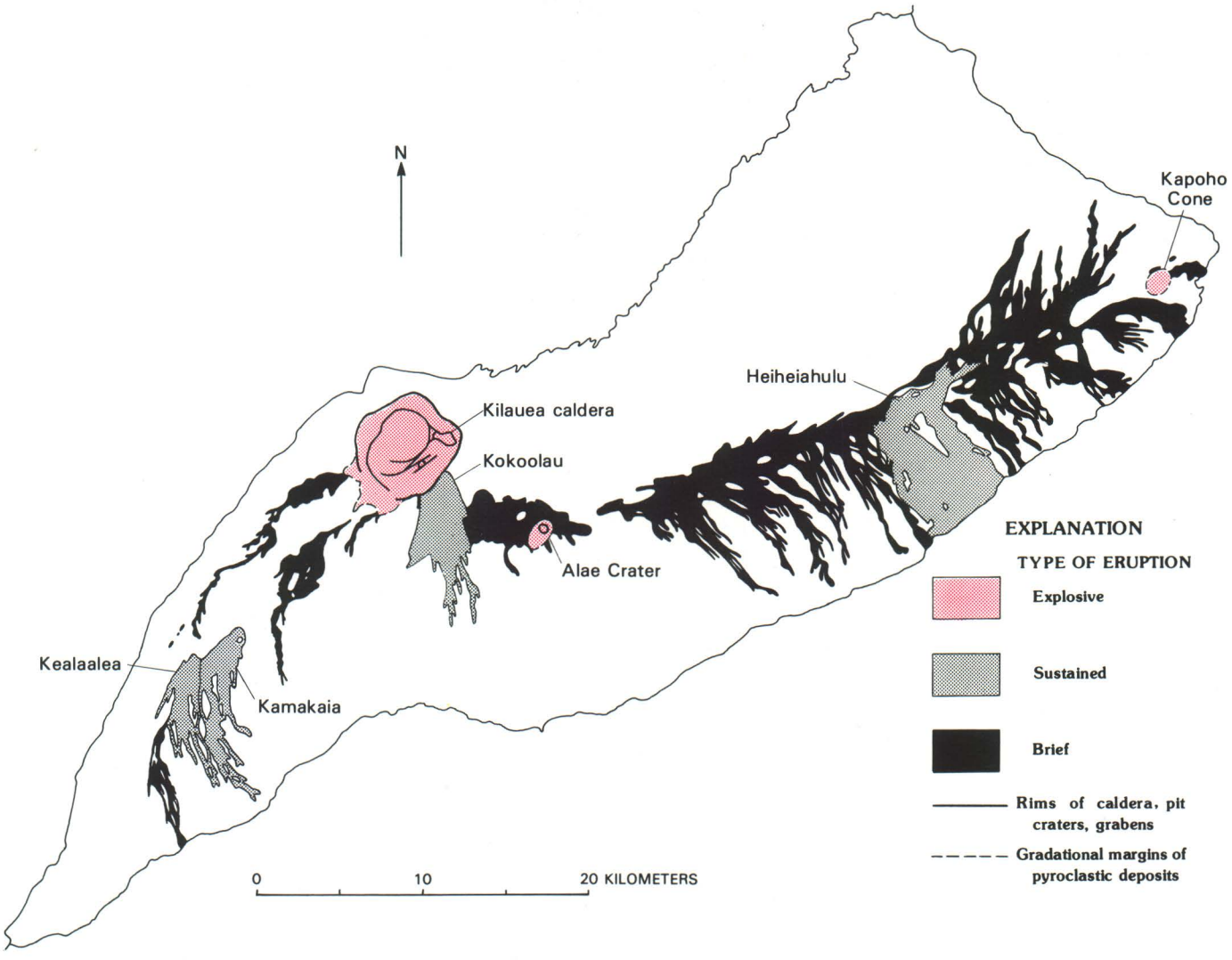

FIGURE 12.38.—Kokoolau and eruption products of 18th century.

Older flows display on aerial photographs a relatively coarse forest grain owing to greater spacing and crown heights of trees. Vegetation patterns have hectometer-scale patchiness, unrelated to flow morphology. When viewed on the ground, large ohia lehua trees (*Metrosideros polymorpha*) of older forests commonly are seen to be epiphytically rooted, indicating that they are not the first generation of trees on the flows. Older flows have more floral diversity; kukui trees (candlenut: *Aleurites moluccana*) are especially common in older forests at lower elevations and are easily detectable because of their high albedo. The younger flows possess a finer vegetation grain arising from close spacing of young trees, and the patchiness of the forest on them is closely related to flow margins and other features of the flow morphology.

Most of the younger flows date from the 18th century, though some could be slightly older. They are distinctly older than flows of 1840, which are also densely vegetated but with plants that are shorter and more closely spaced (fig. 12.39). Though they must be prehistoric, their ^{14}C ages are consistently less than 200 years B.P. (W–359, W–2970, W–3467, W–3468, W–4638, W–4639, W–4644, W–4689).

An 18th century age is indicated also by 19th-century accounts showing that the flows were then much less overgrown than now. Members of the United States Exploring Expedition in 1840–41 were able to walk the length of the middle east rift zone from Napau to Pahoa in a single day, traversing "old lava plains * * * covered with stunted shrubs" (Wilkes, 1845; see especially p. 181–183, 216). A similar trip in 1975 required two days of arduous travel through heavy forest, despite some barren areas of 20th-century lava. When Wilkes passed by the north side of Heiheiahulu lava shield (which he called "Kalalua") he could see that it was a volcanic cone surfaced by streams of pahoehoe even though he had no time to examine it at close range. Today the shield is so densely carpeted with small trees and uluhe (*Dicranopteris linearis*, a species of false staghorn fern) that its nature cannot be determined without climbing

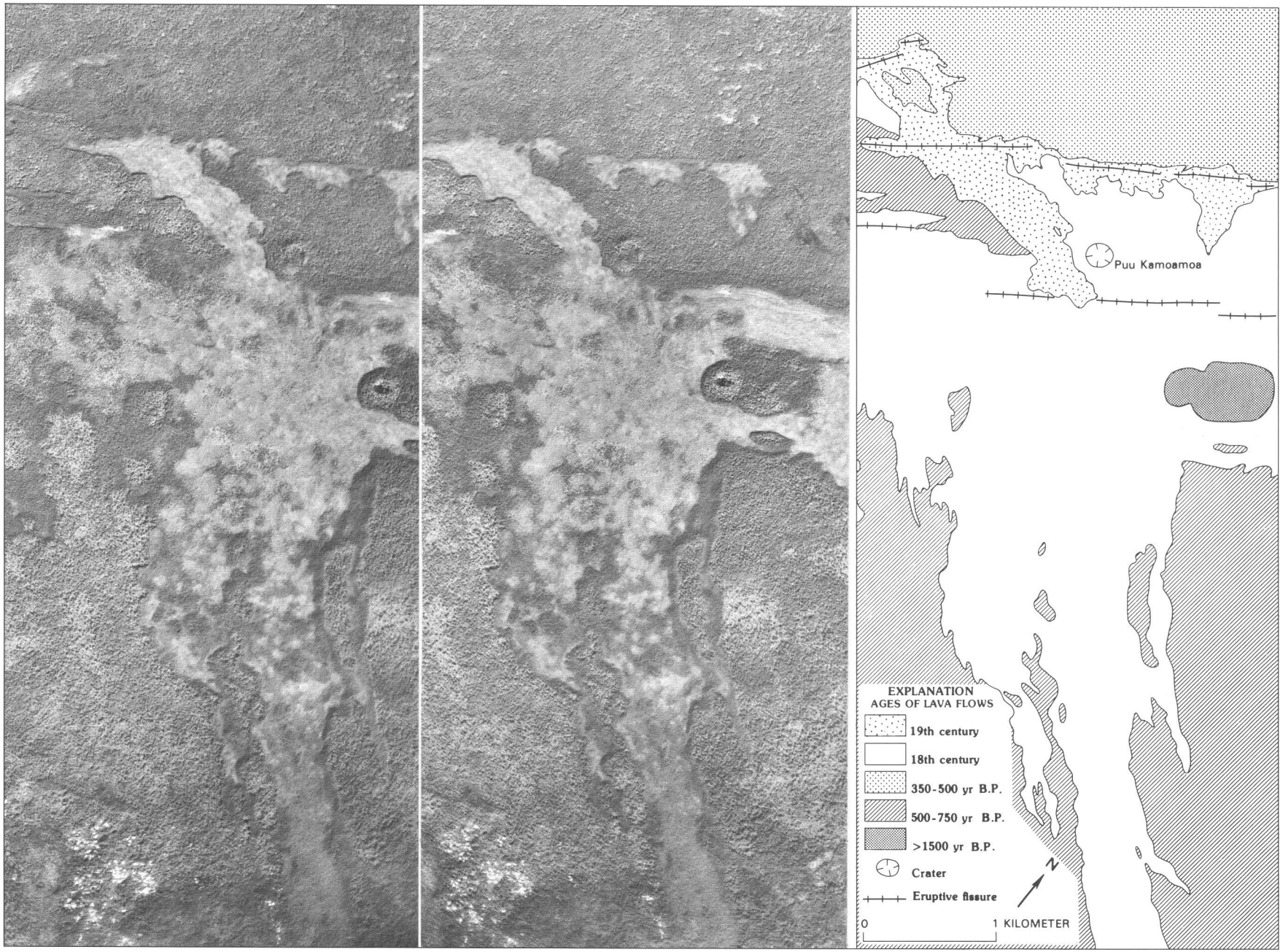

FIGURE 12.39.—Vegetation contrasts near Puu Kamoamoa before extensive flooding by 20th-century lava. All flows visible here are densely vegetated, and their forest patterns vary with age and surface morphology. Most trees are ohia, but light-toned ones in lower left are kukui on flow-mantled fault scarp. Where trees are small on young flows, unshaded understory is composed largely of uluhe; where trees are large, understory is generally dominated by hapuu. Stereo pair prepared from photographs 019, 020, roll 14, U.S. Navy series HAI, 1954.

its flank; in fact, the vegetation is so dense that Heiheiahulu and some smaller cones mentioned by Wilkes cannot even be seen from most places along the rift zone. Because of their vegetal sparsity then and dense vegetation now, most flows along the middle east rift zone must have been quite young when traversed in 1840.

In an earlier interpretation of these vegetation patterns, Moore and Koyanagi (1969) differentiated "late prehistoric" flows (older than about 300 years) from "very late prehistoric" flows older than 1840. However, the vegetation contrasts they used to differentiate the two groups arise from differences in flow morphology instead of age. This is demonstrated by vegetation patterns seaward of Heiheialulu lava shield, inland from Kaimu (fig. 12.40). Here oral history establishes the age, and ranges of climate and flow morphology reveal various rates of forest development for different conditions of rainfall and substrate.

HEIHEIAHULU ERUPTION, CIRCA A.D. 1750

In 1823 Ellis (1827) was told in Kaimu that "the district * * * was overflowed [by lava] in the days of Arapai." Because the reign of Alapai ["Arapai"] was less than a century earlier (approximately 1730–54, according to Hitchcock, 1911) this report should be reliable. Macdonald (1941) supposed the eruption of circa 1750 to be represented by a barren aa flow along the coast about 1 km east of Kaimu (fig. 12.41). Macdonald could not trace this flow directly to its source because it disappears into thick forest, but extrapolation upslope showed that its probable source was Heiheiahulu (Stearns and Macdonald, 1946).

Stratigraphic relations at the shoreline demonstrate that this flow is not the youngest one. Its eastern margin is overlain by pahoehoe of a lava delta (Moore and others, 1973) covering 3 km of shoreline eastward past the Moana Hauae triangulation station and Waipuku Point (figs. 12.41, 12.42). This delta was fed by a lava tube traceable to the upper flank of Heiheiahulu (fig. 12.43). Other tubes and channels radiate from Heiheiahulu; the shield and its flows comprise a diverse assemblage similar to that of Mauna Ulu. The Kaimu district was overflowed not by a single flow but by many, and by analogy with Mauna Ulu this 18th-century eruption was sustained for several months or a few years.

Though all of the Heiheiahulu flows are closely similar in age, their vegetation is highly diverse, varying with flow morphology and climate. The dominant trees on all flows are young ohia (*Metrosideros polymorpha*), but the flows vary widely in the size and spacing of their trees and the character of their understories. In a narrow relatively warm and dry band along the coast, the vegetation is light on all flows but is more dense on tube-fed pahoehoe than on aa. Aa is colonized only by scattered ohia and lichen, while adjacent pahoehoe has thickets of shrubs and grasses as well as more numerous ohia. The contrast is probably caused by differences in water retention; pahoehoe is less permeable and rainwater remains on it longer than on aa. Though vegetation is much more dense in wetter and cooler areas at higher elevations inland, vegetal contrast remains high between flow types. Ohia trees are taller and more closely spaced on aa flows than on pahoehoe. The broader spaces between trees on pahoehoe are generally overgrown by thick tangles of uluhe. Aa probably provides better substrate for trees where rainfall is abundant. Transitions in the vegetal cover on a single flow correspond to morphologic transitions, so that although Heiheiahulu lavas are densely forested, it is still possible to map morphologic transitions from vegetation patterns visible on aerial photographs. Trees grow faster along margins of flows than in their centers, probably because thinner margins are more easily penetrated by roots. Where flows are thick they commonly possess massive interiors that may prevent roots from reaching nutrients and moisture beneath the lava.

These vegetation patterns can be used to identify 18th-century flows along most of the east rift zone. Similar relations of vegetation to flow morphology and climate have been found on the 1868 flow of Mauna Loa (Juvik, 1976).

OTHER ERUPTIONS FROM THE EAST RIFT ZONE

A few flows have been included with the 18th-century group despite evidence that they may be somewhat older. On some flows the vegetation is slightly different, the ohia trees being taller and more widely spaced and giving the forest a coarser grain when viewed on aerial photographs. Some of these flows may be contemporaneous with the Observatory flows, but this is not yet certain; some of the flows differ for reasons other than age. An example just southeast of Napau (fig. 12.44) has a vegetation pattern coarser than most 18th-century flows, but ^{14}C samples W–3468 and W–3469 suggest an age younger than 200 years. This flow consists of surface-fed pahoehoe generally less than 1 m thick, penetrated by tree molds from which many of the present trees grow. These conditions may have permitted more diversity and rapid growth; if so, they prevent fine age distinctions based on vegetation differences.

Some age uncertainties arise from early historical descriptions. For example, the pahoehoe of Malama-Ki Forest Reserve, comprising the coastline between Lililoa and Mackenzie State Park (fig. 12.45), is included in the 18th-century group even though Ellis' (1827, p. 201, 205) account seems to preclude such an age. Ellis was told on passing through Malama that the area inland was inundated by an eruption in about A.D. 1790, but he observed that the coastal tract where he traveled "was covered with soil, and smiling with verdure." He was told later at the village of Pualaa that an eruption near the time of Cook's visit inundated much country along the lower east rift zone but was arrested by the contiguous hills of Kaliu, Malama (Kahuwai-Puulena), and Honuaula. Macdonald (1941) inferred from these accounts that the flows of circa 1790 were confined to the region north of Puu Kaliu and Malama, but aerial photographs show that Macdonald's fissure vent extending from Kaliu to Malama fed flows to the south as well as to the north. The two reports given to Ellis could have referred to two different eruptions in the late 18th century, so that the one confined north of the Kaliu-Malama complex differs from the one sending flows into the lower Malama district, resolving the apparent contradiction. But Ellis' implication that coastal Malama was not flooded is clearly inconsistent with the flow distribution shown on figure 12.45. More faith is placed here in the vegetation and flow morphology than in Ellis' inference. An 18th-century age for the Malama flow is also consistent with its direction of remanent magnetization (site 8B025). Ellis' verdant coastline may front another part of Malama, or

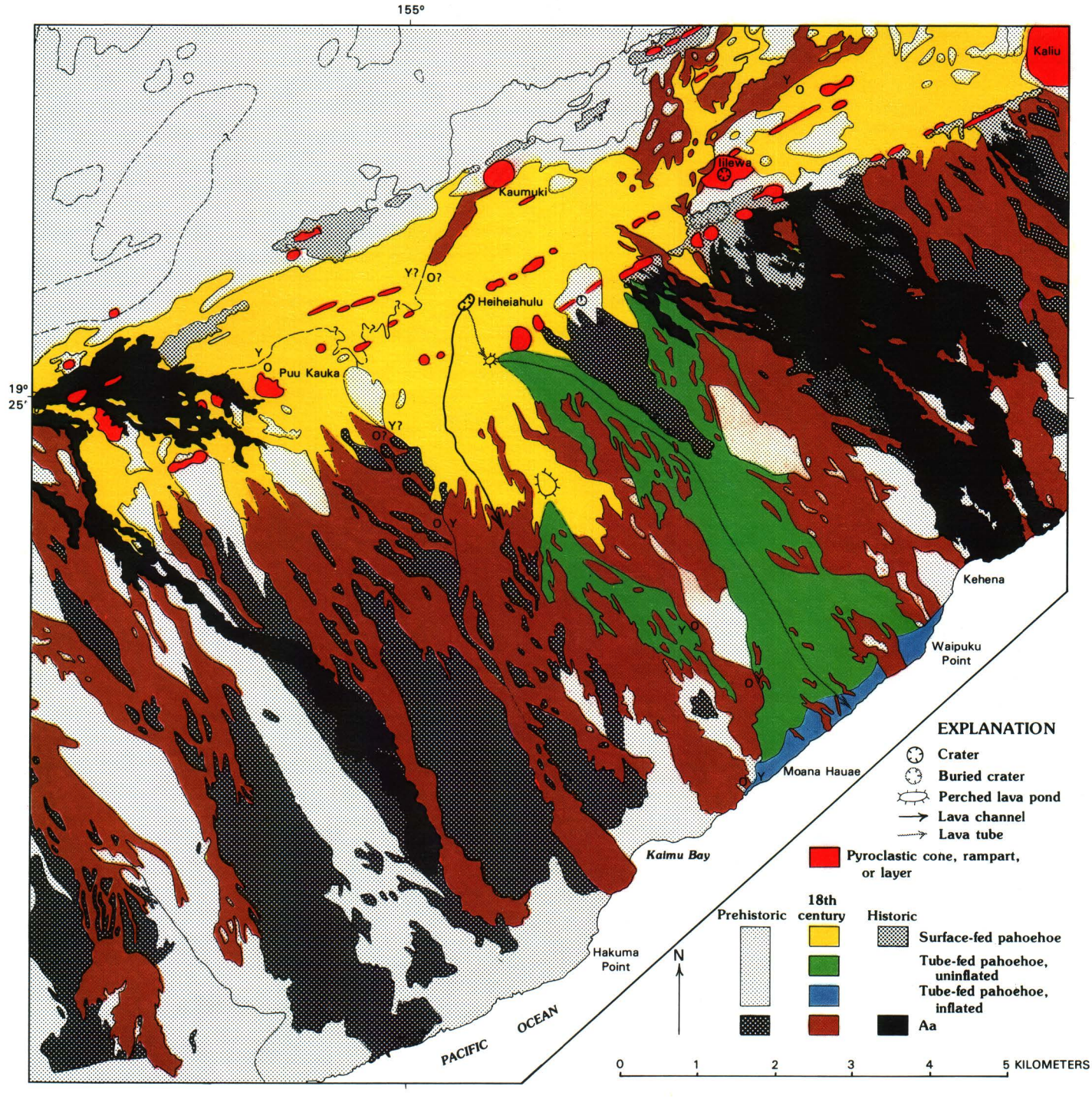

FIGURE 12.40.—Lava flows of circa 1750 eruption of Heiheiahulu, classified by their morphology. Relative ages indicated at some contacts: Y, younger; O, older; queried where uncertain.

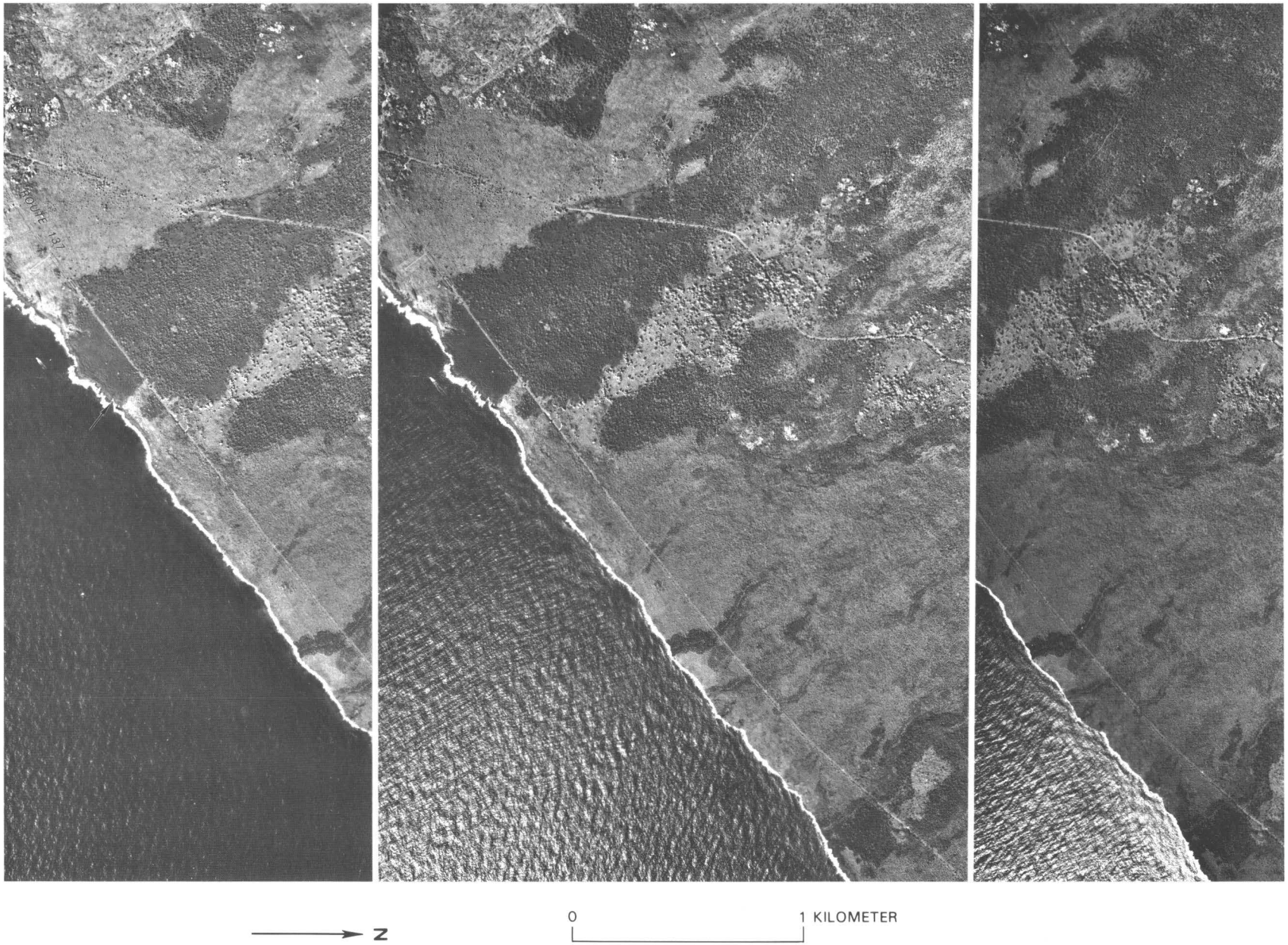

FIGURE 12.41.—Coastal flows between Kaimu and Waipuku Point. Prominent dark flow was only one designated as circa 1750 by Macdonald (1941), but flow morphology and superposition relations indicate that many other flows are of similar age and also erupted at Heiheiahulu. Spacing of ohia on 18th-century aa decreases with increasing elevation inland. Dark-gray, fine-textured tube-fed flows of 18th century are sparsely overgrown with shrubs and grasses between small ohia. Light-toned older flows are densely vegetated, with scattered large trees being prominent. Distinctive globular trees are mango; very light trees are kukui. Arrow indicates small cove whose northeast edge is shown in figure 12.42B. Pairs of red dots are paleomagnetic sample sites, each dot representing a subsite. Stereo triplet prepared from photographs 47–49, roll 12CC, USDA series EKL, 1965.

A

B

FIGURE 12.42.—Stratigraphic relation of circa 1750 flows at shoreline. ***A***, Oblique aerial view showing circa 1750 flow of Macdonald (1941) on left and tube-fed flow of Moana Hauae/Waipuku Point lava delta on right. Narrow, light-toned horn of pahoehoe extends along shoreline from delta to front of aa flow. Horns typically form when surf retards spreading of delta front but permits lava to spread along shore. Photograph by J.P. Lockwood, June 1974. ***B***, Seaward view from atop aa flow in contact with pahoehoe delta. Marine erosion has removed clinkery top of aa flow, producing small cove indicated on figure 12.41, which extends to right of this view. Rock hammer at left (circled) is on contact between flows. Pahoehoe is molded around underlying clinkers. Photograph by J.P. Lockwood, June 1976.

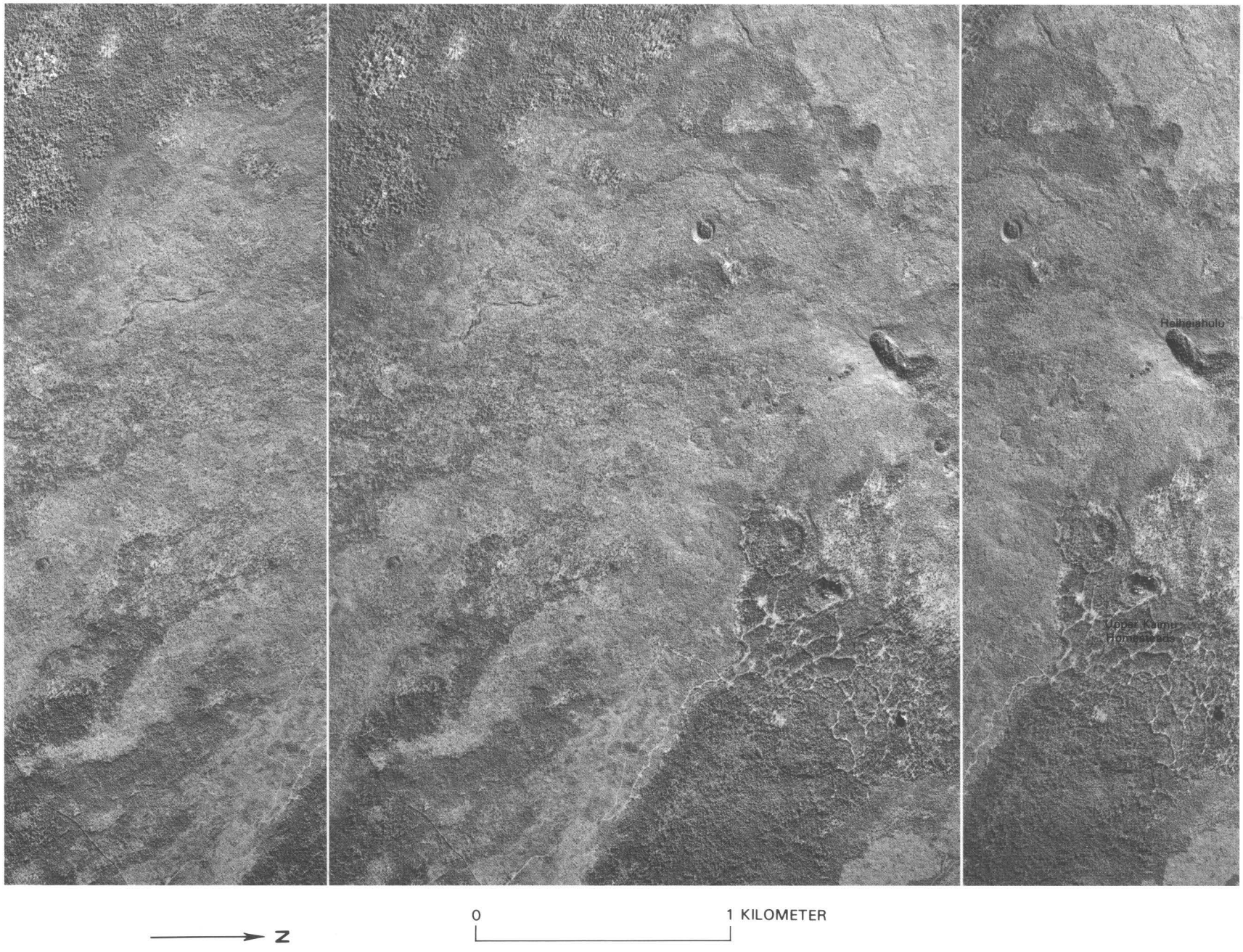

FIGURE 12.43.—Seaward flank of Heiheiahulu. Dark-toned aa supports dense ohia forest, while pahoehoe is covered by uluhe thickets and more widely spaced ohia. Stereo triplet prepared from photographs 55–57, roll 12CC, USDA series EKL, 1965.

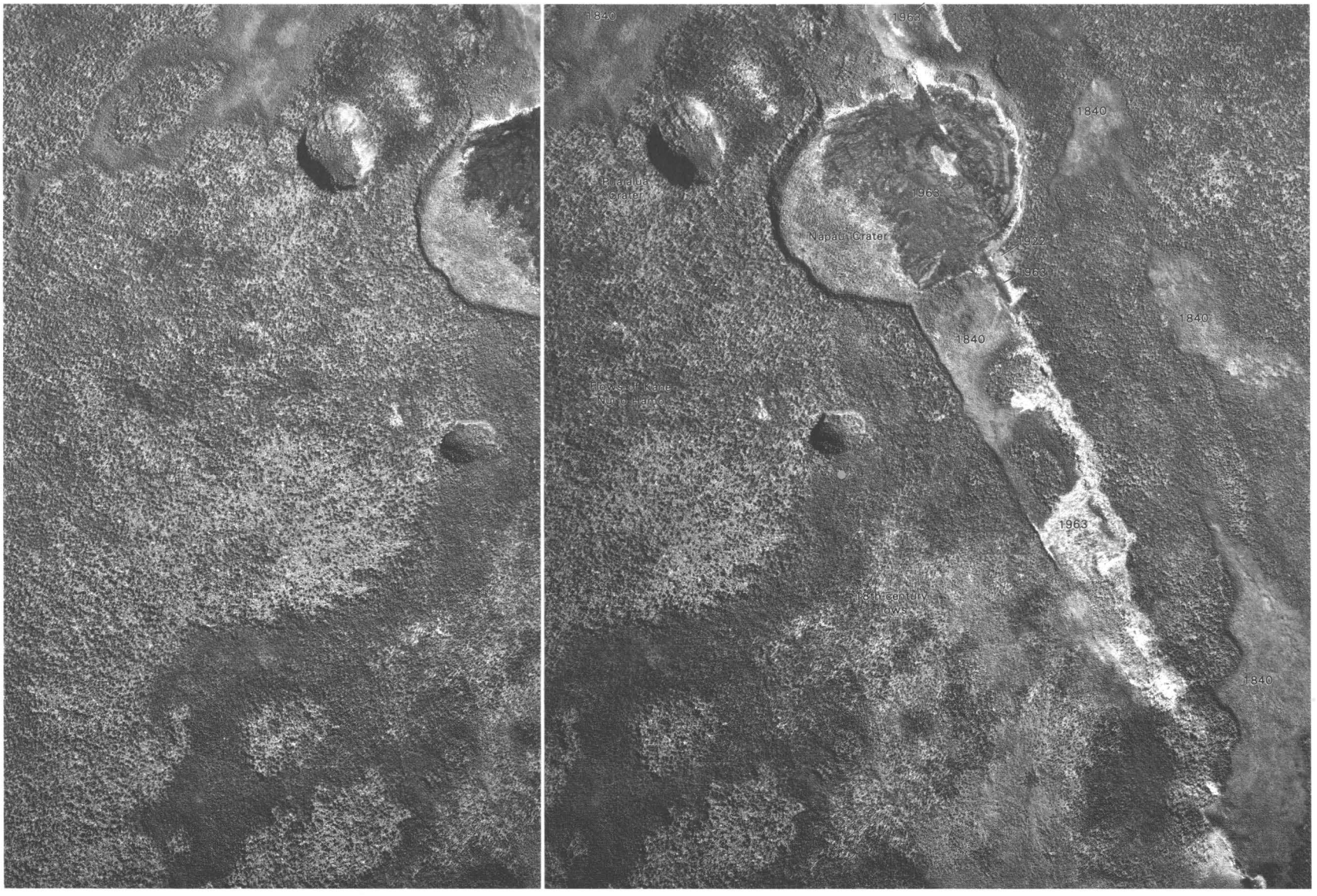

FIGURE 12.44.—Young lava flows near Napau, with years of eruption indicated. Large red dot is ^{14}C sampling site, where ages of less than 200 yr have been obtained from charred roots beneath flow. Stereo pair prepared from photographs 142, 143, roll 12CC, USDA series EKL, 1965.

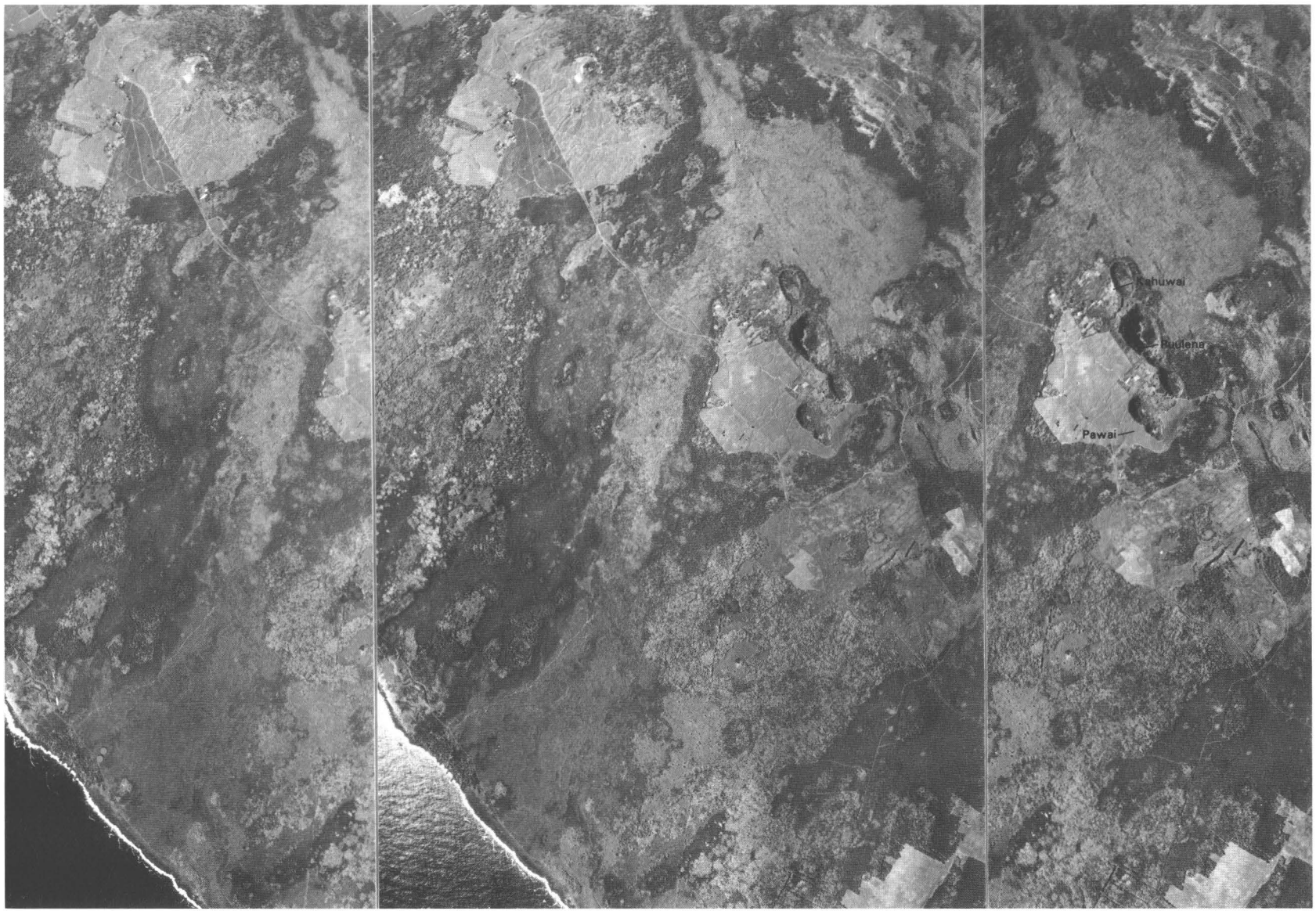

FIGURE 12.45.—Late prehistoric Malama flows, erupted from fissure extending east-northeast from Kaliu past Kahuwai and Puulena. Macdonald (1941) attributed flows inland of fissure to eruption of circa 1790, but their vegetation and morphology show that seaward flows are coeval. Open fissures and spatter ramparts occur together with a tube system; evidently criteria of table 12.1 can be contradictory in some cases. Holcomb (1980b) used vegetation differences to assign 17th-century age to flow east of Pawai Crater, but R.B. Moore (1985) has shown it to be from same eruption of circa 1790. Large red dot, ^{14}C sample site; pair of small red dots, paleomagnetic sample site. Stereo triplet prepared from photographs 128–130, roll 23, U.S. Navy series HAI, 1954.

vegetation may have been reestablished quickly along the coast. Kaliu, Malama, and Honuaula could have dammed a flood of lava and yet permitted some tongues to flow through the gaps between them.

The most recent activity in Kapoho Crater (fig. 12.46) is of uncertain age but probably occurred in the early 18th century or 17th century. An age significantly earlier than A.D. 1800 seems required by the account of Ellis (1827), who in 1823 recognized the volcanic nature of the tuff cone and questioned local residents about its last eruption. Though tradition described it as a seat of volcanism, the people living there could give no specific information about the last eruption, which suggests that it had occurred long before. There had certainly been enough time for thick vegetation to grow, because Ellis described the tuff cone as "overhung with trees, and clothed with herbage" (Ellis, 1827, p. 205–206). On the other hand, the aa flow extending east from the cone (fig. 12.47) is magnetized (8B205) in a direction similar to the Observatory flows, and a ^{14}C age of less than 200 years B.P. (W–2970) has been obtained from charcoal beneath a thick pyroclastic layer within the cone. Given the uncertainty in the ^{14}C and paleomagnetic ages, a single eruption could have produced both the flow and pyroclastics a century or so before Ellis' visit.

The morphologies of flows and vents indicate that all of these latest prehistoric eruptions, except for those of Kokoolau and Heiheiahulu, and perhaps the one of circa 1790, had high discharges and short durations. Though the flows typically extend several kilometers from their fissure vents and terminate as aa lobes, they are remarkably free of mappable lava channels.

ERUPTIONS FROM THE SOUTHWEST RIFT ZONE

The 18th century saw frequent and sustained eruptions from the southwest rift zone as well as the east rift zone, with eruptions occurring from all of its active parts.

Brief eruptions were widespread (fig. 12.5*B*). A vigorous one from the northern strand produced the Cone Peak ramparts (8B745) and flows that extended nearly to Kamakaia. Subdued eruptions near the end of the same strand built small shields and lava pads (9B841), similar to those of 1868, inland from Kamakaia; some of the pads overlap the Cone Peak aa flow. Vigorous eruption from the central strand produced Puu Koae and other spatter cones and aa flows extending to about 1 km from Hilina Pali.

Another brief eruption occurred from the lower segment about 1.3 km east of Puu Nahaha and 600 m east of the upper end of the Keaiwa flow of 1823 (fig. 12.5C). Lava flows from this eruption reached the sea between Kapaoo Point and Waiwelawela Point. They are more weathered than the overlying Keaiwa flow and have been dated by ^{14}C at about 200 years B.P. (W–3938, W–4452). The Red Cones and their aa flows, which also overlie these flows, are undated, but they too are overlapped by the Keaiwa flow. Both the Red Cones and the earlier unnamed flows probably date from the 18th century. Their eruptive fissures appear to have extended through Yellow Cone from the southern strand of the upper segment, but they cannot be traced far uprift because they are buried by other 18th-century lava flows of sustained eruptions.

The late prehistoric lava commonly termed the Kamooalii flow (see Stearns, 1926) consists of two assemblages of similar age from different strands of the rift zone. A sustained eruption from the central strand built a lava shield at Puu Kou and Kealaalea Hills (fig. 12.5*B*), and a complex flow assemblage extending seaward across the Kau Trail and past the west side of Puu Ahi (fig. 12.5C). The eastern part of the Kamooalii flow is another complex assemblage fed by vents of the southern strand, including Kamakaia and Kamakaiawaena (fig. 12.48). Kamakaia flows overlap those of Kealaalea. Magnetization of Kealaalea (9B409) and Kamakaia (8B517) flows is consistent with an 18th-century age, and the Kealaalea flows have been dated by ^{14}C as younger than 200 years B.P. (W–3937). Both flow assemblages probably represent sustained, unstable eruptions during the 18th century.

Yellow Cone is a small kipuka of pyroclastic material protruding through the flank of the Kealaalea shield (fig. 12.5*B*). It may predate the 18th century; no young flows have been found seaward of it beneath the flows of Kealaalea. While the lavas of Yellow Cone, Red Cones, Kamakaia, Kamakaiawaena, and Kamakaiauka along the southern strand of the southwest rift zone all have differentiated compositions, the analyzed flows from the Great Crack and central strand of the upper southwest rift do not (Wright and Fiske, 1971).

FIGURE 12.46.—Kapoho Crater, looking northeast from distance of about 1 km. Photograph by R.T. Holcomb, 1977.

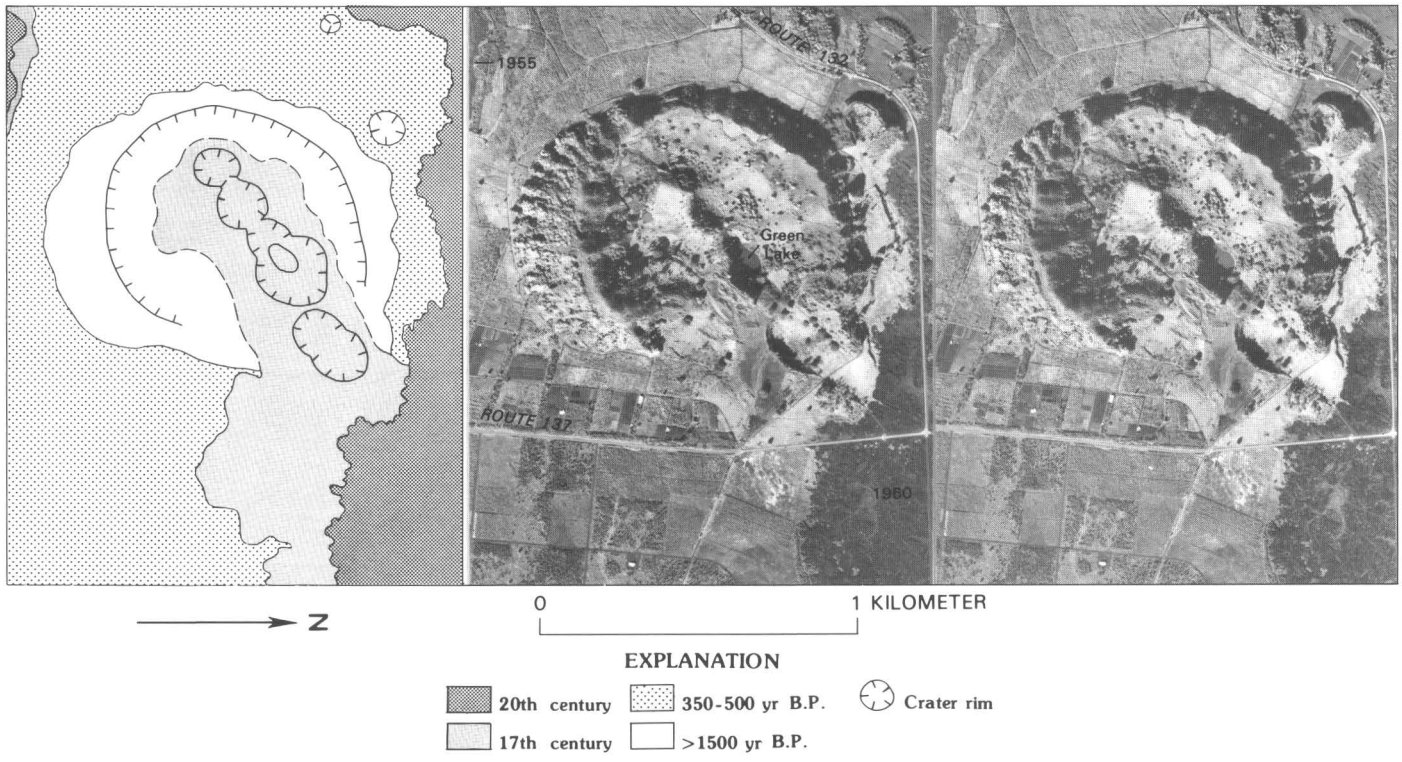

FIGURE 12.47.—Vertical view of Kapoho Crater. Tuff cone is incomplete, possessing gap on its eastern side through which thick prehistoric aa flow extends east about 1.5 km to present shoreline. This aa flow probably was erupted during 17th century and sits atop pahoehoe flows that have direction of magnetization consistent with age of 350–500 yr B.P. (pairs of small red dots, paleomagnetic sample sites). Both flows veneered by ash distributed around tuff cone, suggesting that pyroclastics postdate flows, but aa flow must be younger than cone if it has extended through gap in cone, and sharp break in slope around outer base of cone suggests that cone protrudes through pahoehoe flows and predates them as well. A ^{14}C age of less than 200 yr B.P. was obtained from charred log beneath ash on interior slope of tuff cone (large red dot). Both aa flow and its ash veneer may have been erupted during 17th century from chain of craters within cone, while bulk of cone is older than pahoehoe flows. Crater containing Green Lake is thickly rimmed by ash. Ellis (1827, p. 206) described within Kapoho Crater "a smaller circle of hills, equally verdant, and ornamented with trees" that may have comprised an inner tuff ring (not now definable as morphologic feature, possibly destroyed by quarrying). Aa flow and young ash deposits around chain of craters may be products of single eruption.

The compositions of the 18th-century flows beneath Red Cones, and of flows from other seaward vents such as the Lava Plastered Cones, are not known.

In summary, the latest prehistoric interval saw from the northern strand of the upper southwest rift zone a brief but vigorous eruption at Cone Peak followed by brief, less vigorous eruptions farther downrift. The central strand saw brief, vigorous eruption at Puu Koae and sustained, unstable eruption at Kealaalea, with their sequence not yet known. The southern strand saw a vigorous brief eruption east of Puu Nahaha followed by a smaller eruption of Red Cones and sustained eruption at Kamakaia farther uprift.

THE MODERN CALDERA

The age of the modern caldera and the timing of collapse with respect to the explosive eruption of A.D. 1790 are not yet known. There still remains much room for alternative sequences and mechanisms.

Much—maybe all—of the collapse preceded the explosive eruption, because all of the 1790 ash now exposed is draped unbroken across the modern caldera faults surrounding the inner sink (Christiansen, 1979). Within the sink, the so-called sand spit between Keanakakoi and Halemaumau and the deeply subsided blocks adjacent to Uwekahuna Bluff and Waldron Ledge also are draped by the ash. However, higher caldera walls in several places lack ashy plaster and may have seen local collapse following ash deposition. It remains possible that most of the collapse occurred only a short time (hours or days) before the onset of explosive eruption. It also remains possible that much collapse occurred within the inner sink during, or even following, the explosive eruption without continued displacement along the outer caldera structures.

Alternatively, the inner sink could have reached essentially its present diameter sometime earlier than 1790. Incipient smaller scale collapse probably did begin earlier, with alternating rise and fall of the magma column. Many dikes and other intrusive bodies are exposed along the north wall of the modern caldera (Powers, 1916); those rising high through the stratigraphic section must postdate the Observatory vent (Casadevall and Dzurisin, chapter 14). Some dikes appear to follow structures bounding the inner sink of the modern caldera: Some occurrences thought by Powers to be intru-

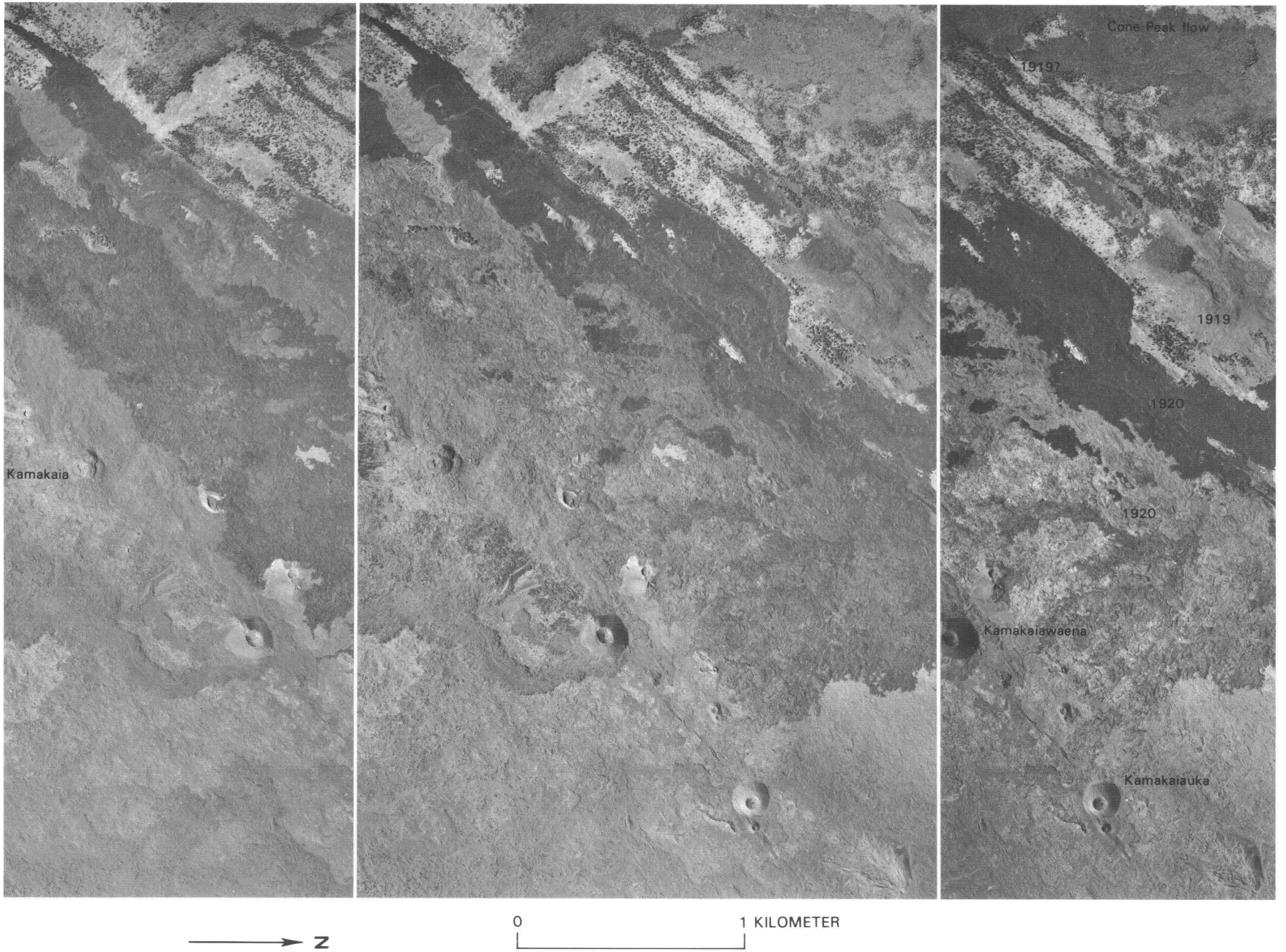

FIGURE 12.48.—Kamakaia Hills. Red dot indicates approximate viewpoint for figure 12.17. Stereo triplet prepared from frames 41–43, roll 5CC, USDA series EKL, 1965.

sions within the truncated stratigraphic section are actually veneer a few meters thick adhering to the caldera wall (fig. 12.49). These probably are remnants of dikes intruded along older fissures concentric to the Observatory vent. Some thinner dikes seem to extend irregularly into the wall away from these thicker concentric dikes instead of rising vertically through fissures radial to the caldera. The concentric fissures may have formed when the magma column subsided to produce an enlarged Observatory pit like Halemaumau, and dikes may have been intruded along these fissures later when the magma column rose again. The column could have oscillated several times, and successive collapses could have enlarged the sink to nearly its present size long before the climactic explosive eruption in 1790. (It was suggested by de St. Ours, 1979, that multiple collapses occurred at different centers; see also, de St. Ours, 1982.) An active lava lake may have been present much of the time in this sink; reticulite at the base of the Keanakakoi Ash Member shows that high lava fountains occurred near the summit sometime before the 1790 explosions (Decker and Christiansen, 1984). A hypothetical sequence showing the enlargement of an Observatory firepit followed by a larger scale collapse to form the present inner caldera sink is sketched in figure 12.50. This sequence was drawn assuming a 17th-century age for the Observatory flows, but other ages and other sequences are possible.

FIGURE 12.49.—Part of north caldera wall of Kilauea, showing light-toned rectangular rock body that Powers (1916) interpreted as sill-like intrusion projecting into cliff face. Close inspection has shown instead that it adheres like plaster on cliff face. Cliff and trees on its rim are 120 m and 10 m high, respectively. Steam in foreground rises through lava flows of 1919. Photograph by J.D. Griggs, May 1979.

Stratigraphic constraints on the age of the northwest part of the inner caldera sink turn largely on the age of the Observatory lava shield. Much of the caldera here must have developed after the Observatory shield ceased to grow, because much of the shield was engulfed by the collapse of the inner sink. If the Observatory flows do date from the 17th century, they constrain caldera development to the late 17th century and 18th century. But if the Observatory flows are older than 700 years, the caldera could have begun to grow long before the 18th century.

Neither is the age of caldera formation well constrained to the south. A few eruptions from fissures concentric to the caldera probably occurred after extensive collapse in the summit region. One flow from a concentric fissure southwest of the caldera and having 18th-century magnetization (8B757) occurs between layers of the Keanakakoi Ash Member and must date from 1790. Others predate the ash by unknown amounts; magnetization of one (8B769) south-southwest of the caldera implies that it could date from the 17th century, but its large within-site dispersion (4.7°) permits it to be a century younger. An aa flow east of the Ahua Kamokukolau triangulation station was probably fed by a concentric vent south of Keanakakoi; as discussed earlier, the east side of this flow is overlapped by pahoehoe probably from Kokoolau. Two of these flows from caldera-concentric vents were deflected by preexisting Koae fault scarps and then broken by recurrent displacements on those scarps.

PIT CRATERS OF THE UPPER EAST RIFT ZONE

Subsidence and dilation of both rift zones also occurred during the past few centuries, but the timing of these events with respect to summit collapse is not yet known. Especially prominent are several pit craters of the upper east rift zone. Some craters probably collapsed in the 18th century, though a few show signs of complex development that began earlier. Makaopuhi and Alae illustrate the complexity especially well.

The coarse ejecta exposed in the wall of Makaopuhi (fig. 12.28C) indicate that an earlier pit existed at or near the site of the present one. The present crater consists of two parts indenting the flank of Kane Nui o Hamo (figs. 12.51, 12.52; see Aramaki and Moore, 1969, fig. 7). The eastern pit may be older than 500 years; it was partly filled by a thick lava lake followed by four thinner flows (Stone, 1925). The lowermost of these flows sent dikes down into columnar joints of the lake far enough to suggest that the lake cooled for at least a few decades before it was covered (Moore and Evans, 1967). The uppermost flow may have been erupted from the southwest crater wall; its surface slopes slightly (0.3°) away from

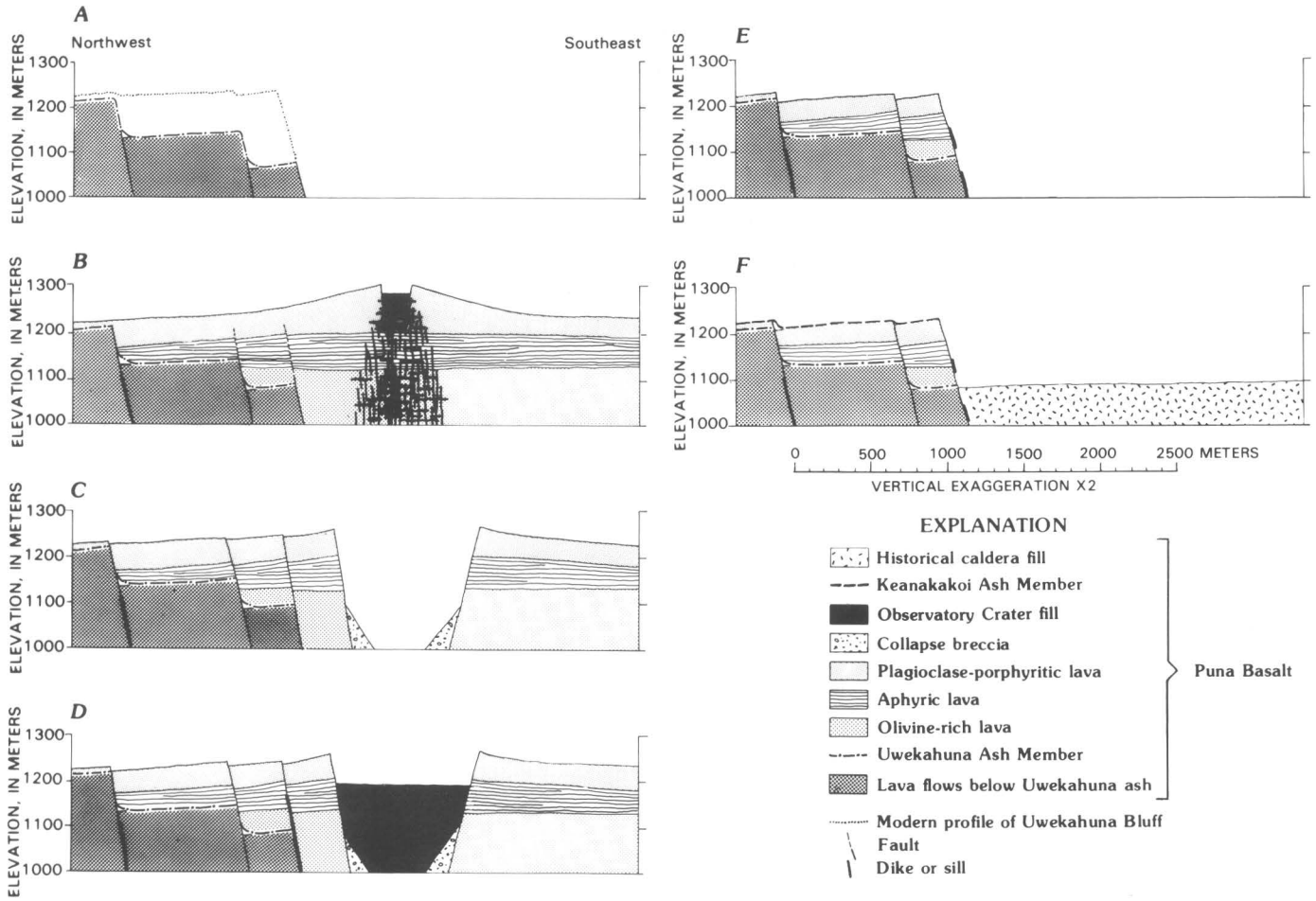

FIGURE 12.50.—Cross sections showing possible developmental sequence for Uwekahuna Bluff, assuming that Observatory shield ceased to grow during 17th century. Line of profile shown on figure 12.36. ***A***, About 1,500 years ago. Powers caldera mantled by Uwekahuna Ash Member. Profile of modern caldera shown for comparison. ***B***, About 300 years ago. Powers caldera filled by flows of three successive groups (Casadevall and Dzurisin, chapter 13). Lower fill broken by differential thermal contraction above buried fault scarps. Dikes and sills surround magma column beneath Observatory lava shield, and dikes intrude along some peripheral caldera faults. ***C***, About 275 years ago. Drainage of magma has produced enlarged firepit. Continued contraction of caldera fill has broken surficial lava flows, forming low scarps above buried faults. ***D***, About 250 years ago. Magma has risen again into firepit and has fed dikes along fractures around pit. ***E***, About 200 years ago. Inner sink rejuvenated by caldera collapse, and dike remnants adhere to its wall. ***F***, Present time. Modern caldera mantled by Keanakakoi Ash Member and partially filled by historical lava flows.

lava drapery and spatter along a fissure in the wall. Lava also issued from a fissure on the crater floor to form small pads atop the upper flow. Another collapse then produced a western pit with the older crater fill forming a mezzanine on its eastern side. The age of the western pit is not known; though it is prehistoric, it must be fairly young. Vegetation on the earlier mezzanine is similar to that developed elsewhere on lava flows of the 18th century.

Alae also was a compound crater (figs. 12.53, 12.54). It appears on aerial photographs that the older pit postdates Puu Huluhulu and the flows of Keauhou; it may therefore be younger than 350 years. The crater was partly filled by a lava lake capped by thinner flows, and then a new collapse formed an inner pit bordered by a western mezzanine. Phreatic explosions from the inner pit deposited a layer of lapilli 15 cm thick on the crater rim and ejected blocks up to 1 m in diameter, some of them to nearly 1 km west of the crater (Stearns and Clark, 1930, p. 143). The debris was partly covered by lava that extruded from a fissure on the northwest rim and flowed into the crater. This lava was overlaid by additional ejecta, possibly from the caldera eruption of 1790, which in turn was overlapped by more lava in 1840 that flowed across the mezzanine into the inner pit. On aerial photographs, the vegetation on a part of Alae mezzanine appears similar to that of 18th-century flows elsewhere, but this cannot be confirmed; the inner pit was floored by a new lava lake in 1963 (Peck and others, 1966), and the entire crater was buried in 1969–71 (Swanson and others, 1972).

Pauahi and Hiiaka are compound craters too (figs. 12.55, 12.56). Before it was buried in 1973, a small lava lake in the central pit of Pauahi supported vegetation typical of 18th-century age, while the lightly vegetated walls of the west pit appeared fresher. The outer compartment of Hiiaka is a sag instead of a sharp-rimmed

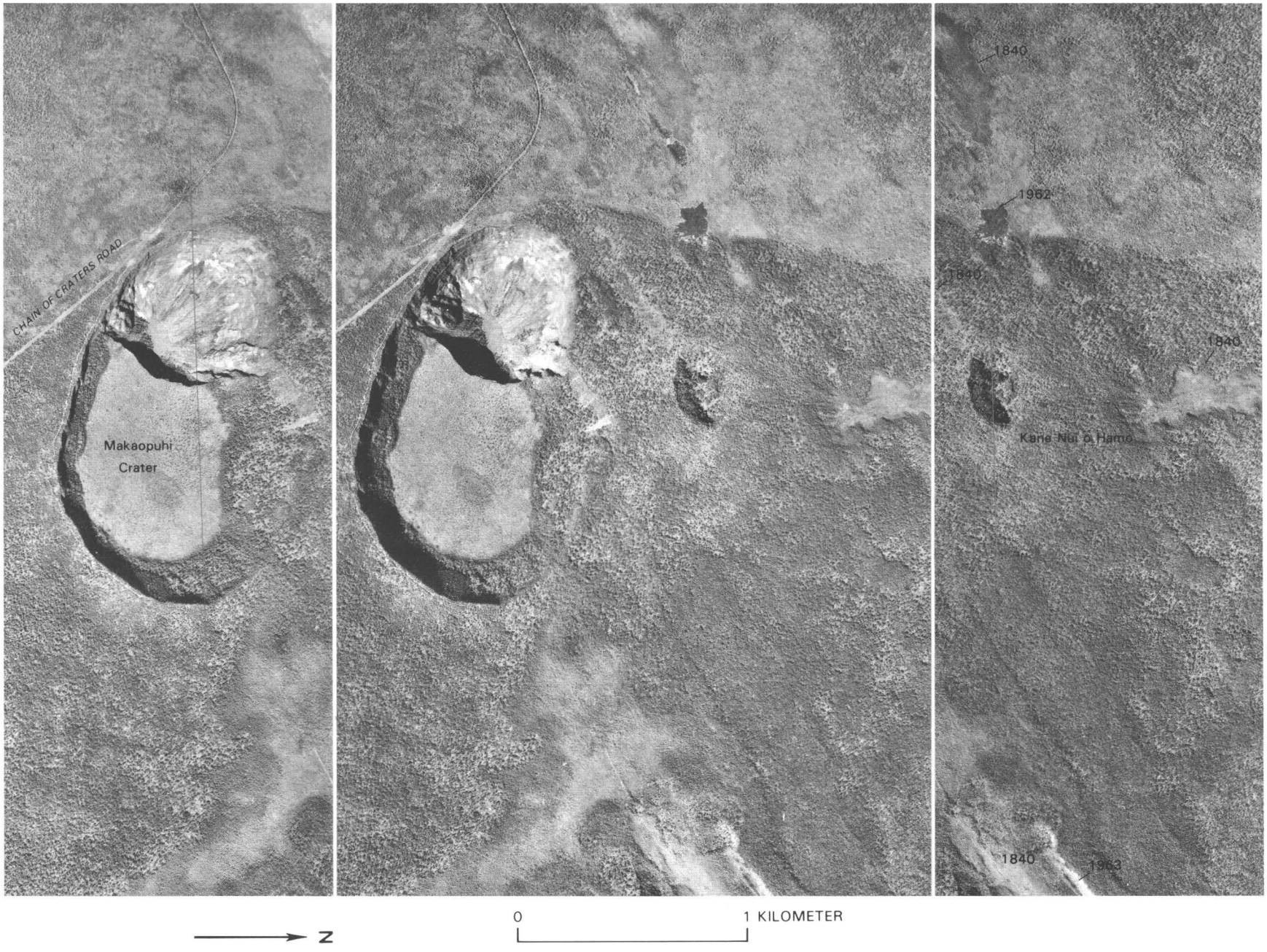

FIGURE 12.51.—Makaopuhi Crater area before much of it was covered by 20th-century lava flows. West pit of Makaopuhi in this view contains very small flat floor of ponded lava erupted in 1922; west pit was later filled and western part of mezzanine covered during eruptions from 1965 to 1974. Red dots, paleomagnetic sample sites above and below yellow tephra layer. Also shown in red are lines of profile for figure 12.52. Ovate, slightly darker area on eastern mezzanine is prehistoric lava pad extruded from fissure extending northeast across mezzanine. Northeast-trending lineament west of this pad is another fissure from which another pad was extruded in August 1972 (fig. 12.52). Stereo triplet prepared from frames 159–161, roll 12CC, USDA series EKL, 1965.

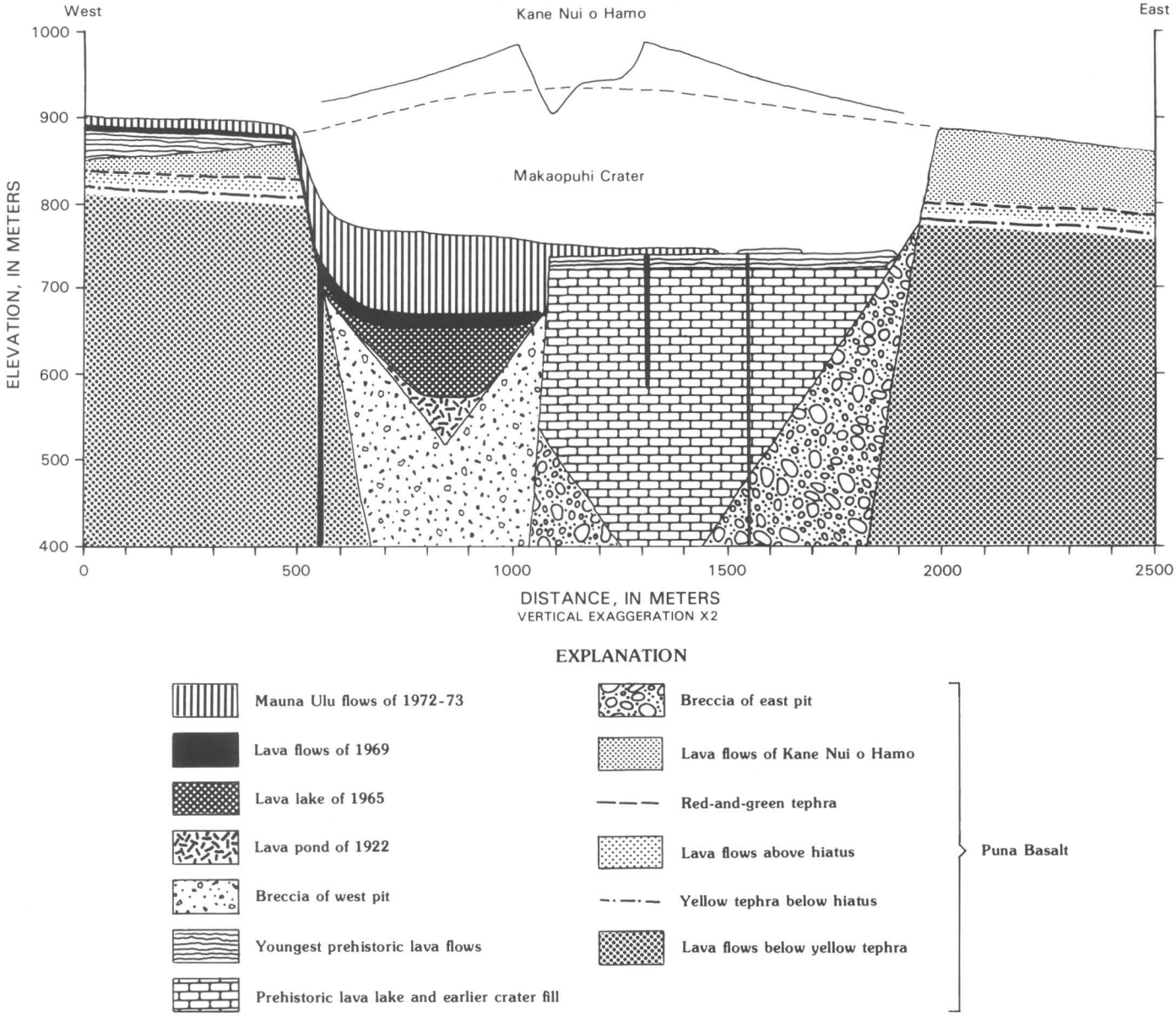

FIGURE 12.52.—Cross section of Makaopuhi Crater, along longer red line of figure 12.51. Also shown are inferred precollapse profile (dashed line) along this section, and present profile (solid line) across crater of Kane Nui o Hamo lava shield 800 m to the north (shorter red line of figure 12.51). Thick vertical lines are dikes that fed prehistoric lava pad on mezzanine (east; see fig. 12.51), eruptions of 1922 and 1965 (west), and eruption on mezzanine in August 1972 (center). Dike of 1972 is shown as rootless because it was probably fed laterally by Mauna Ulu lava ponded in west pit (Tilling and others, chapter 16).

crater (figs. 12.55, 12.56). Stearns and Clark (1930, p. 128) attributed the sagging to subsidence of an intact block preceding collapse of the inner pit, but other interpretations are possible. In the alternative shown in figure 12.56, the sag developed by thermal contraction of lava filling a buried crater, similar to the sag now developed at Alae. A buried crater of this sort could be a source of tephra now exposed in the wall of Pauahi (fig. 12.27).

The complex histories of several pit craters, and the coarse ejecta exposed in the walls of some, indicate that they have long been sites of repeated collapse and phreatic explosion. Nodes in the plumbing system may occur at these places, developed where Koae faults intersect the rift zone. Such nodes could form reservoirs for producing differentiated and hybrid magmas along the rift zone (Wright and Fiske, 1971; Swanson and others, 1976b, p. 28).

Though they are prehistoric, several of the simple craters and younger pits of the compound craters must be very young. They could have formed at the same time as a caldera collapse in or before 1790, all of them resulting from one drainage event lower along the

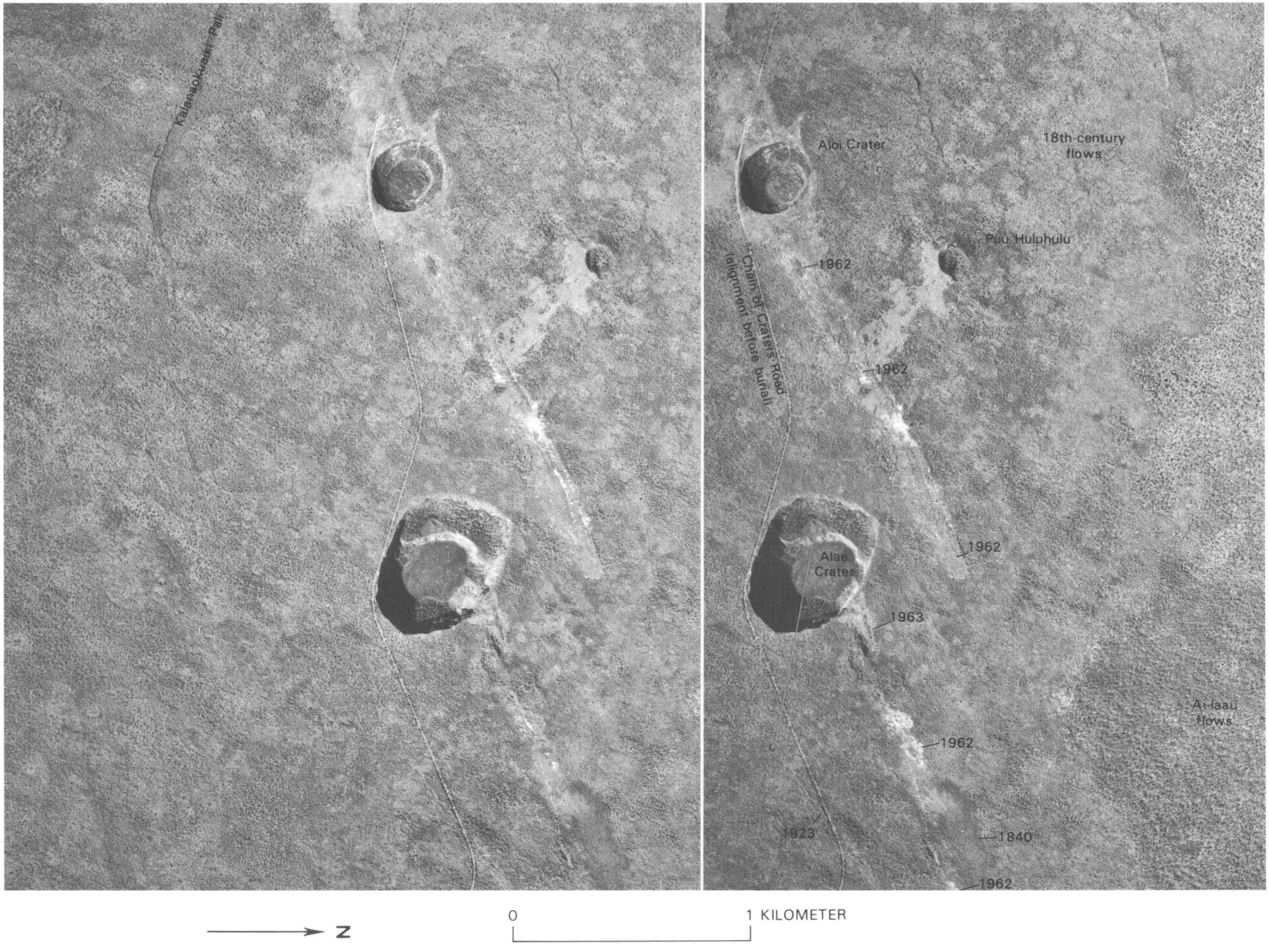

FIGURE 12.53.—Alae Crater, Aloi Crater, and Puu Huluhulu before craters were buried by growth of Mauna Ulu. Red dots, paleomagnetic sampling sites. Also shown in red is line of profile for figure 12.54. Stereo pair prepared from frames 174 and 175, roll 12CC, USDA series EKL, 1965.

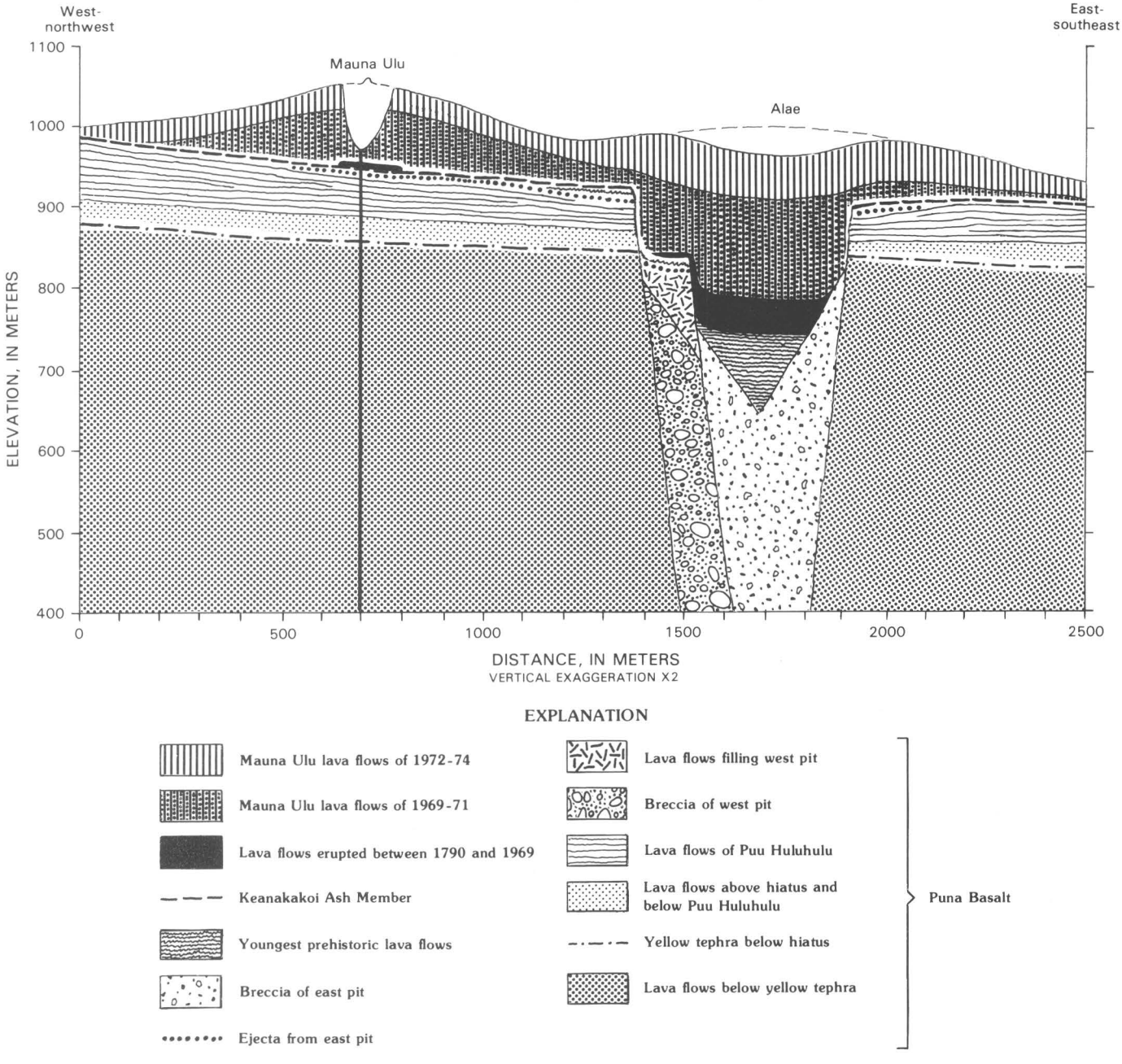

FIGURE 12.54.—Cross section of Mauna Ulu and buried Alae Crater, along line shown on figure 12.53. Dashed lines show profiles before crater formation on Mauna Ulu and sagging of lava shield above Alae Crater. Thick vertical line represents dike that fed Mauna Ulu. Hiatus and yellow tephra layer correlative with Uwekahuna Ash Member are inferred from their known occurrence in Makaopuhi Crater to east and Pauahi Crater to west. Thin layers of prehistoric ejecta and lava on rim of Alae are inferred from description by Stearns and Clark (1930); their thickness is exaggerated in this illustration.

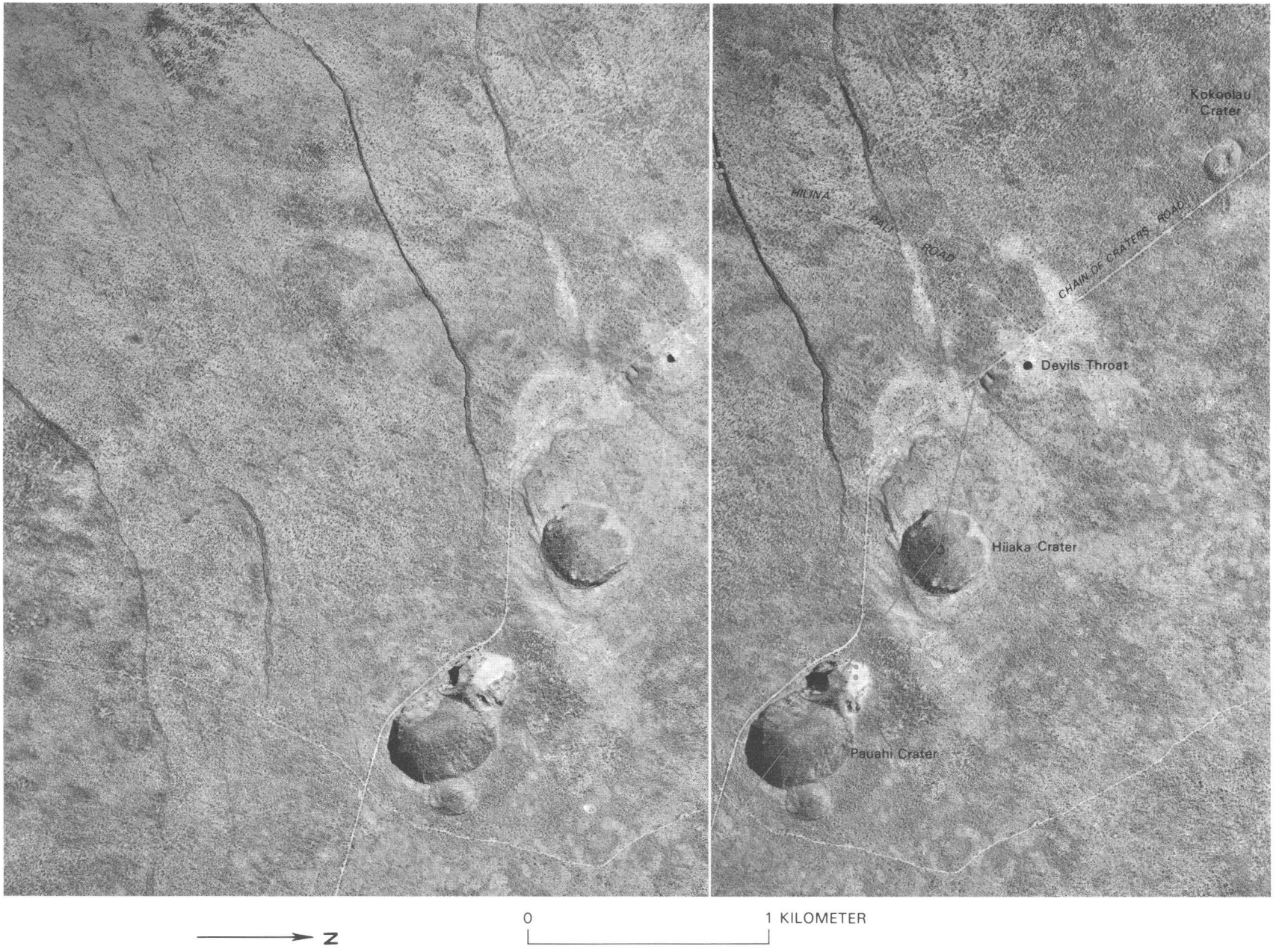

FIGURE 12.55.—Pauahi and Hiiaka before these craters were partly filled by lava during 1968–79. Larger central pit of Pauahi was floored by prehistoric lava lake. Pairs of red dots, paleomagnetic sample sites. Also shown in red is line of profile for figure 12.56. Stereo pair prepared from frames 188 and 189, roll 12CC, USDA series EKL, 1965.

east rift zone, but this has not been proved. Similar pits may form in the future, especially near sites of sustained eruption such as Mauna Ulu and Puu Oo.

SUMMIT ERUPTION OF A.D. 1790

Except for thin deposits of older and younger basaltic pumice at its base and top, the Keanakakoi Ash Member was produced by a series of explosions in 1790 (Decker and Christiansen, 1984). This eruption was still remembered well when Europeans first visited Kilauea in 1823, and it was notable for wiping out a detachment of Keoua's Puna army (Swanson and Christiansen, 1973). Deposited in quick succession were well-sorted vitric ash, less well sorted lithic-vitric ash, a local lava flow from a circumferential fissure, and poorly sorted lithic ash and blocks. Hawaiian accounts suggest that the main explosive phase continued for two or three days. The explosions were probably caused by rapid lowering of the summit magma column and entrance of subsurface water into the emptying magma conduits. Lowering of the magma column may have been associated with the voluminous eruptions of circa 1790 low on the subaerial east rift zone, but the relative timing of the summit and rift events has not been established.

It appears that the two most recent episodes of large caldera collapse and ash eruption were separated in time by about 1,500 years. Several smaller collapses and explosive eruptions could have occurred between them but have not yet been recognized.

AFTERMATH OF THE 1790 ERUPTION

More than 30 years passed between the eruption of 1790 and Ellis' visit in 1823. Little is known about this interval, but at some point eruptive activity had resumed at the summit, within the inner sink of the modern caldera. During this interval, lava fountains probably produced the golden pumice at the top of the Keanakakoi Ash Member (Sharp and others, chapter 15). By the time of Ellis' visit, the inner sink had filled with lava to within 160 m of the

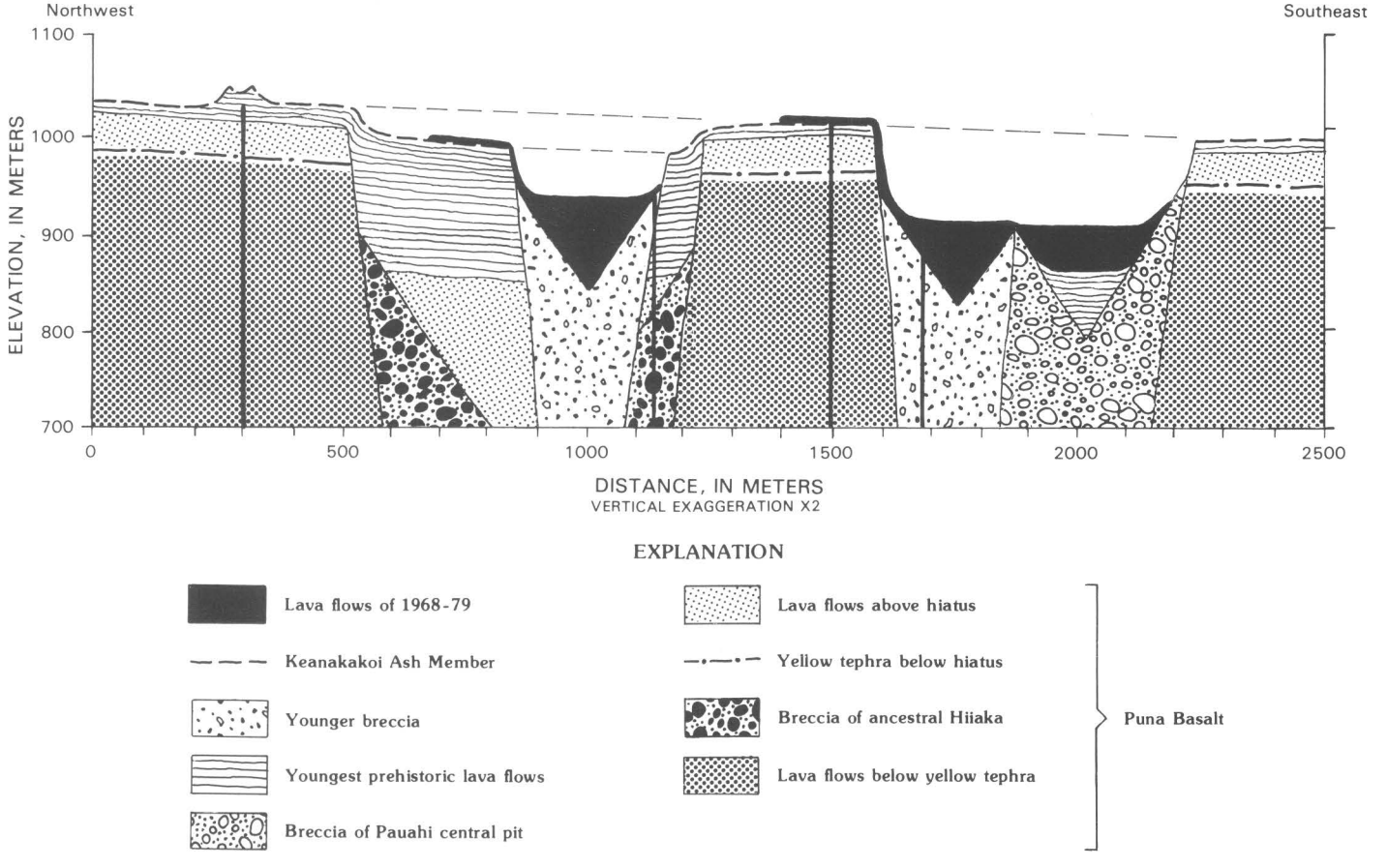

FIGURE 12.56.—Cross section through Pauahi, Hiiaka, and unnamed spatter cone near Devils Throat, along red line shown in figure 12.55. Ash and hiatus exposed in west wall of Pauahi have not been found in Hiiaka, where they are inferred to be hidden behind crater fill. Hiiaka is interpreted here as complex crater formed by two collapses, with earlier crater rim buried by prehistoric lava flows that sagged from thermal contraction. This has not been proved, however; other interpretations are possible. Ash and debris exposed in west wall of Pauahi may consist partly of Uwekahuna Ash Member ejected from Powers caldera, and partly of material ejected from local source such as older crater of Hiiaka. Dashed lines show profiles before sagging and collapse. Thick vertical lines represent dikes that fed younger lava flows.

northern rim, and then subsided again to leave a congealed terrace called the Black Ledge. This subsidence probably occurred during the southwest rift eruption of 1823, shortly before Ellis' visit. No other flank eruptions have been definitely tied to this interval, though some of the 18th-century flows may have been erupted then. Ellis' Hawaiian guides told him that several places had been overflowed by lava since the explosions of 1790. Other activity had occurred too, including a memorable earthquake and ground cracking at Kaimu.

HAWAIIAN TRADITIONS

Much of the Polynesian oral history has been lost, and many surviving fragments are contradictory, ambiguous, or unspecific. Some accounts still preserved, however, provide provocative comparisons with geologic information.

ELLIS' GENERAL ACCOUNT

The most authoritative summary was recorded in 1823 by Ellis (1827, p. 171–172) on the caldera rim. This history was given by Ellis' Hawaiian guides, according to whom Kilauea

had been burning from time immemorial, or, to use their own words, 'mai ka po mai,' from chaos till now, * * * and had overflowed some part of the country during the reign of every king that had governed Hawaii: that in earlier ages it used to boil up, overflow its banks, and inundate the adjacent country—but that, for many kings' reigns past, it had kept below the level of the surrounding plain, continually extending its surface and increasing its depth, and occasionally throwing up, with violent explosion, huge rocks or red-hot stones. These eruptions, they said, were always accompanied by dreadful earthquakes, loud claps of thunder, with vivid and quick-succeeding lightning. No great explosion, they added, had taken place since the days of Keoua [1790]; but many places near the sea had since been overflowed, on which occasions they supposed Pele went by a road underground from her house in the crater to the shore.

Confirmation of the story was provided to Ellis (1827, p. 194) a few days later at Kaimu, along the southern coast of Puna, where

the evenings we spent with the people of the place in conversation on various subjects, but principally respecting the volcano which we had recently visited. They corroborated the accounts we had before heard, by telling us it had been burning from time immemorial, and added, that eruptions from it had taken place during every king's reign, whose name was preserved in tradition, or song, from Akea, first king of the island, down to the present monarch.

This account is especially valuable because it is the earliest one known and was taken from local informants at Kilauea. As a result, it is the one least likely to have been distorted by distance, time, or Western preconceptions. But much uncertainty remains in its interpretation. It is difficult to say how much of it is a simple summary of witnessed events and how much is interpretation by Ellis of what was said to him or by Hawaiians of phenomena observed by them.

Especially troublesome is the possibility of Hawaiian interpretation, because evidence indicates that other traditions do include geologic inferences from the natural record. The Hawaiian account of Pele's successive homes agrees well with the progression of island volcanism, even though the sequence could not have been witnessed directly. Unless the agreement between fact and legend is coincidental, the legend must rest on inferences from nature by Hawaiians. If traditions could include inferences about the history of the archipelago they could also include inferences about the history of Kilauea.

Despite this uncertainty, however, Ellis' acount merits serious consideration. Hawaiians were probably living on Kilauea throughout the millenium in which most surficial lava flows were erupted, and they should have seen the eruptions. Widespread consistency in genealogies suggest that oral traditions can be very precise. It is worthwhile to compare Ellis' account with modern information.

Agreement between tradition and geologic information appears generally to be good. Tradition agrees well with the other evidence in stating that Kilauea had been active for a long time, had had frequent eruptions, had undergone a change in behavior from frequent overflows to summit confinement, and had had explosive eruptions.

Ellis' account is more specific than the other evidence in at least four ways. First, Ellis states that eruptions were so frequent as to occur during every king's reign, while the geologic record could permit dormant intervals of several decades or more. Second, Ellis says that the caldera developed gradually over some extended interval, while the geologic record permits sudden caldera development shortly before the explosive eruption of 1790. Third, Ellis says that explosive eruptions had occurred more than once and at intervals, while the geologic information requires no explosive eruptions between those of the Uwekahuna Ash Member (probably pre-Polynesian) and the Keanakakoi Ash Member in A.D. 1790 (Christiansen, 1979). Fourth, Ellis' account states that many coastal areas (on more than one occasion?) had been overflowed by lava since 1790, while the geologic evidence requires no such eruptions between 1790 and 1823. (Several flows in Puna and a few along the southwest rift zone could date from this interval, but the evidence available also permits them to be older.)

There are no definite contradictions between Ellis' account and currently available geologic evidence, but potential conflicts exist, especially in regard to the timing of the last summit overflows. While the tradition states explicitly that the summit had not overflowed "for many kings' reigns past," the paleomagnetic evidence indicates that such overflows had occurred as recently as the 17th century or even the early 18th century, within 100–150 years of Ellis' visit. This seems a rather short interval to include the reigns of many kings, and in fact Kalakaua's (1888, p. 31) history lists the reigns of only five kings of Hawaii between A.D. 1685 and 1824. Despite this potential disagreement and the uncertain derivation of Ellis' account, however, there are few concrete reasons to doubt the veracity of the tradition, and it appears to have potential value in supplying information not yet available from other kinds of evidence.

WESTERVELT'S EMBELLISHMENTS

Other traditions seem less reliable. Some cited by Westervelt (1916) give many details not included in Ellis' account. For example, Westervelt describes specific changes in the focus of summit eruptions, and particular explosive eruptions, not mentioned by Ellis. According to Westervelt (1916, p. 1–3):

When Pele came to the island Hawaii, seeking a permanent home, she found another god of fire already in possession of the territory. Ai-laau was known and feared by all the people. *Ai* means 'the one who eats or devours.' *Laau* means 'tree' or a 'forest.'

Ai-laau was, therefore, the fire-god devouring forests. Time and again he laid the districts of south Hawaii desolate by the lava he poured out from his fire-pits.

* * * * *

He lived, the legends say, for a long time in a very ancient part of Kilauea, on the large island of Hawaii, now separated by a narrow ledge from the great crater and called Kilauea-iki (Little Kilauea). This seems to be the first and greatest of a number of craters extending in a line from the great lake of fire in Kilauea to the seacoast many miles away * * *.

After a time, Ai-laau left these pit craters and went into the great crater and was said to be living there when Pele came to the seashore far below.

In one of the Pele stories is the following literal translation of the account of her taking Kilauea:

'When Pele came to the island Hawaii, she first stopped at a place called Ke-ahi-a-laka in the district of Puna. From this place she began her inland journey toward the mountains. As she passed on her way there grew within her an intense desire to go at once and see Ai-laau, the god to whom Kilauea belonged, and find a resting place with him as the end of her journey. She came up, but Ai-laau was not in his home. Of a truth he had made himself thoroughly lost. He had vanished because he knew that this one coming toward him was Pele. He had seen her toiling down by the sea at Ke-ahi-a-laka. Trembling dread and heavy fear overpowered him. He ran away and was entirely lost. When Pele came to that pit she laid out the plan for her abiding home, beginning at once to dig up the foundations. She dug day and night and found that this place fulfilled all her desires. Therefore, she fastened herself tight to Hawaii for all time'

Elsewhere in this book, after quoting Ellis' account presented above, Westervelt (1916, p. 191–192) states that

When the crater was 'boiling up, overflowing its banks, and inundating the adjacent territory,' as the natives said, it poured out lava which became solid rock. As it went westward, the character of its overflow changed, becoming explosive, hurling out cinders and ashes instead of boiling lava, so that all the land, especially toward the south and west, is covered with volcanic ash.

Westervelt's account can be interpreted in many ways, one of which is the following: Long ago much of Kilauea was forested (because of a hiatus in summit overflows?), but then frequent overflows from the summit destroyed more and more of the forest. For a long time the eruptions were focused in the vicinity of Kilauea Iki, but eventually the site of eruption shifted to the west, somewhere within the perimeter of the present caldera. Eventually a series of eruptions occurred along the east rift zone, the site of eruption progressing uprift from the coast. As these eruptions occurred, the summit was shaken by tremors and a summit pool of lava drained away, leaving behind an empty, growing crater. Following a series of explosive eruptions, lava returned to the enlarged crater, which became a new site of long-sustained activity.

This account is highly provocative, and it is tempting to relate particular events of the tradition to events inferred from geologic evidence. However, this would be dangerous because the reliability of Westervelt's account is highly uncertain, for several reasons.

First, Westervelt cites no sources, though comments elsewhere in his book suggest that he had consulted Hawaiian-language newpapers of the late 19th century in Honolulu. With the sources unknown, there is no way to judge their reliability.

It appears that some material is Westervelt's own synthesis of several different accounts, and there is a strong possibility that his own preconceptions were incorporated. For example, the westward shift in the focus of summit volcanism may not have come from tradition but from his own understanding of summit events. A few decades earlier Dutton (1884, p. 121) had used geologic evidence to infer such a shift of the eruptive focus.

Westervelt's accounts could have been earlier degraded by Hawaiian storytellers, especially if his sources were newspaper accounts from the late 19th century in Honolulu, a time and locale far removed from the Kilauea of pre-Western influence. During the disintegration of Polynesian society following Captain Cook's arrival, an apparently well-preserved oral history was adulterated and partly lost. It is possible, for example, that the westward shift in eruptive activity really was mentioned by Westervelt's sources, but that these sources themselves were influenced by Dutton's interpretation.

Finally, Westervelt's account is inconsistent with traditions given elsewhere. Other sources, for example, describe Pele's arrival in very different ways and make no mention at all of Ai-laau. Until the ancestry of Westervelt's account can be established and evaluated, it can be given little credence. This is also true of many other provocative traditions.

SOME OTHER TRADITIONS

Though specific details of most traditions cannot be taken as literal truth, some traditions probably allude to real eruptions, especially those traditions Ellis recorded as associated with specific lava flows. Examples are the late prehistoric Keauhou flows west of Kealakomo (associated with a legendary conflict between Pele and Kamapua'a; Ellis, 1827,p. 183), the vent and flows of Kaholua o Kahawali (tied to the legend of Kahawali; Ellis, 1827, p. 207–210), and a flow formerly forming Cape Kumukahi (associated with Pele's rejection by the Puna Chief Kumu-kahi; Westervelt, 1916, p. 27–28). Some traditions state a time in history for a particular lava flow, for example, that Pele's action occurred during the reign of a particular king whose dates have been inferred from well-kept genealogies. Such statements could provide especially valuable checks on the geologic evidence, but even here confusion can arise.

An example of possible contradition in the most authentic traditions concerns the age of Puu Huluhulu (fig. 12.57), which paleomagnetic evidence suggests is 350 to 500 years (9B913). Seaward of Puu Huluhulu and of similar age are the Keauhou lava flows. Ellis (1827, p. 183) notes this flood of lava as dating from Pele's struggle with Kamapua'a, which Kalakaua (1888, p. 140) attributes approximately to the year A.D. 1200 in the reign of Kamaiole. But Ellis' comments elsewhere (p. 182) suggest a different age for Puu Huluhulu:

Within a few miles of Kirauea, we passed three or four high and extinct craters. One of them, Keanakakoi, the natives told us, sent forth, in the days of Riroa, king of Hawaii about fourteen generations back, most of the lava over which we were travelling. The sides of these craters were generally covered with verdure, while the brown irregular-shaped rocks on their indented summits frowned like the battlements of an ancient castle in ruins.

The crater of Liloa's reign cannot be the pit now known as Keanakakoi because Ellis (1827, p. 179) had earlier clearly stated that the only deep crater he saw besides the caldera was Kilauea Iki; he saw no others, though his guides said there were many in the

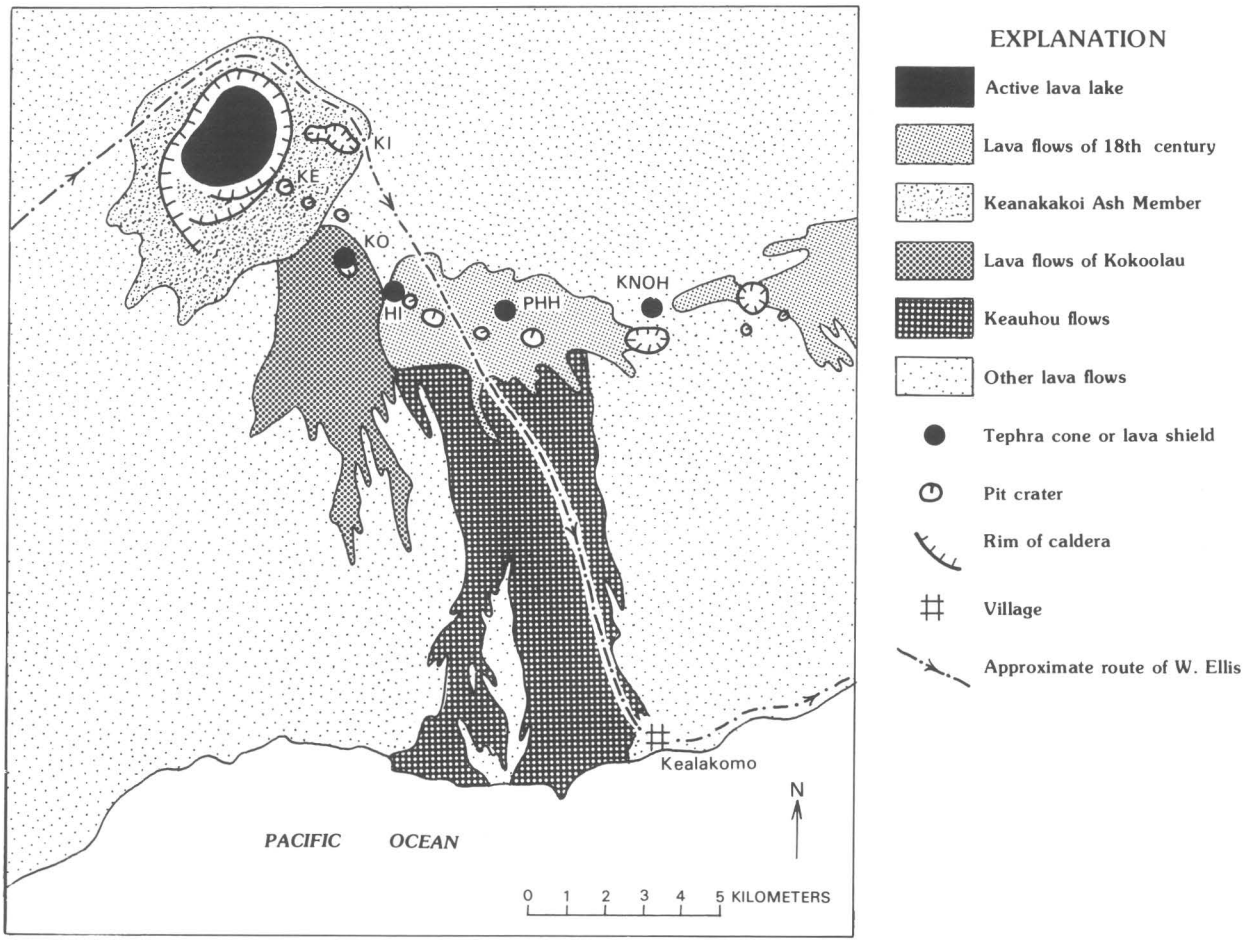

FIGURE 12.57.—Approximate route and features probably observed by William Ellis on his trek from Kilauea caldera to Kealakomo in 1823. He saw "three or four high and extinct craters" but no "deep" craters besides Kilauea Iki, though he was told that others were nearby (Ellis, 1827, p. 179, 182). Geographic features: KI, Kilauea Iki; KE, Keanakakoi; KO, Kokoolau; HI, Hiiaka; PHH, Puu Huluhulu; KNOH, Kane Nui o Hamo.

neighborhood. Moreover, Ellis described this and some other craters as high-standing edifices. Along the route that Ellis travelled from the caldera to the coast are three such features: Kokoolau, Puu Huluhulu, and the spatter cone near Devils Throat. Ellis would also have seen Kane Nui o Hamo in the distance.

If Puu Huluhulu was the crater at issue it would contradict Ellis' other comments because Liloa's reign occurred long after the inferred time of conflict between Pele and Kamapua'a. According to Kalakaua's (1888) chronology Liloa preceded Liholiho (reigning during Ellis' visit of 1823) by 14 reigns, while Kamaiole preceded Liloa by another eight reigns. Kalakaua believed Kamaiole to have reigned around A.D. 1200 and Liloa around A.D. 1475. While Liloa's reign falls into the range indicated by the paleomagnetic data (350–500 years B.P.), Kamaiole's reign does not. If Puu Huluhulu is the source of flows tied to Kamapua'a, the two traditions are in conflict. Moreover, Kane Nui o Hamo should not be the active vent of Liloa's reign because it is clearly older than Puu Huluhulu.

Other interpretatiouns are possible. The Pele-Kamapua'a tradition could refer to Kane Nui o Hamo, whose lava flows have a paleomagnetic direction consistent with the dates assigned to Kamaiole's reign. Ellis clearly stated, however, that the Pele-Kamapua'a conflict was associated with the young, dark lava flows west of Kealakomo (the Keauhou flows), and these flows could not have come from Kane Nui o Hamo; the flows from Kane Nui o Hamo are the older ones upon which Kealakomo sat.

Another alternative would have Kokoolau as the vent of Liloa's reign and Puu Huluhulu the older source of the Kamapua'a flows. This would preserve the chronology implied by the traditions; but then both Kokoolau and Puu Huluhulu would be older than expected from their paleomagnetic data, unless the reigns were briefer than believed by Kalakaua.

From the discussion above it should be clear that caution must be used in extracting eruption history from the traditions. In fact, the most useful comparisons between traditions and geologic information may proceed in the opposite direction, the geologic data providing a firmer base for reconstructing the social history.

HISTORICAL ERUPTIONS

The historical activity of Kilauea has been reviewed in detail several times previously (Dana, 1890; Brigham, 1909; Hitchcock, 1909; Stearns and Clark, 1930; Stearns and Macdonald, 1946; Macdonald and Abbott, 1970). Only a brief summary is given here.

LONG-SUSTAINED SUMMIT ERUPTIONS, 1823–1924

Though brief references to Hawaiian volcanism were recorded in the late 18th century (Ledyard, 1783; Beaglehole, 1967; Vancouver, 1798; A. Menzies, in Hitchcock, 1909), the historical record really began with Ellis' (1827) description of Kilauea in 1823. At that time a sustained eruption was in progress, and most of the inner sink was occupied by an active lava lake standing about 270 m below the north rim. About 90 m above the lake surface was the Black Ledge a terrace of freshly congealed lava thought to represent the level reached by caldera filling a short time before. The caldera floor probably had subsided in the spring of 1823, when a brief but voluminous eruption from the Great Crack flooded the western south flank with lava (the Keaiwa flow, which reached the sea from Kapaoo Point to Waiapele Bay). The subsidence of the caldera floor apparently did not generate large explosions at the summit, though small phreatic explosions deposited tephra at two places along the Great Crack (Stearns, 1926).

Continued activity after 1823 refilled the caldera to a level about 15 m above the Black Ledge by 1832, when a small eruption occurred on Byron Ledge and the caldera floor subsided again, this time about 300 m (Goodrich, 1833). Filling then recommenced, and in 1834 the caldera was much the way it had been in 1823, with an inner pit 113 m deep surrounded by a black ledge (Douglas, 1905). Continued activity filled the pit and apparently overflowed the black ledge so that it was no longer visible late in 1838 (Strzelecki, 1845). At this time the activity had become confined to 5 lava lakes, the largest of them called Hau-mau-mau in the southwestern part of the caldera on the site of the pit crater now called Halemaumau.

Vigorous summit activity in the spring of 1840 was followed by another subsidence of the caldera floor and a rapid series of brief eruptions along the east rift zone. The last eruption from the lower east rift zone was especially voluminous and sent surface-fed lava flows northeastward from the vicinity of Pahoa to the coast at Nanawale (Coan, 1841). Shortly afterward Kilauea was visited and described by members of the United States Exploring Expedition (Wilkes, 1845; Dana, 1849). The subsided inner sink at this time was about 100 m deep and was surrounded by a new black ledge about 480 m wide rising to about 180 m below the western caldera rim. By 1846 the inner basin had filled again (Dana, 1850), and by 1848 a lava shield at the site of Halemaumau had grown nearly as high as the lowest part of the caldera rim (Coan, 1851).

The next subsidence of the caldera floor occurred in 1868, when large earthquakes shook the southern part of Hawaii and simultaneous eruptions occurred from Mauna Loa and Kilauea (Coan, 1868). One Kilauea outbreak produced a chain of small lava pads near the distal end of the northern strand of the upper southwest rift zone. Another small eruption from Byron Ledge fed a lava flow that ponded on the floor of Kilauea Iki. An area about 1,900 m wide on the central caldera floor sagged about 100 m, and a deeper conical pit about 900 m wide and about 200 m deep developed at its southwest end at Halemaumau (Hitchcock, 1909). The pit again filled, and by 1874 a lava shield at Halemaumau had once again grown to about the elevation of the southern caldera rim (Coan, 1874). Minor subsidences in and around Halemaumau occurred again in 1879, 1886, 1891, and 1894 (Hitchcock, 1909). None of those episodes was associated with known eruptions from the rift zones, though some undated post-1790 flows south of Mauna Iki (fig. 12.5*B*; Holcomb, 1980b) could have been erupted at one of those times.

The subsidence of 1894 was followed by 13 years of dormancy and very subdued, episodic activity within the pit of Halemaumau (Hitchcock, 1909). In 1908 the activity once again became more vigorous, and it was nearly continuous until 1924, with minor subsidences of the lava column occurring in 1916, 1919, 1922, and 1923 (Jaggar, 1947). The 1919 subsidence was followed by the 1919–20 eruption of Mauna Iki along the southwest rift, the first sustained eruption along either rift zone during the historical interval and probably the first since the Heiheiahulu eruption of circa 1750. The 1922 subsidence was associated with small eruptions from Makaopuhi to Napau, and the 1923 event was followed by another small eruption between Makaopuhi and Alae. The summit activity once again built a broad lava shield that occupied the entire inner sink of the modern caldera, with Halemaumau at its summit.

INTERMITTENT SUMMIT AND FLANK ERUPTIONS, 1924–1968

The century-long interval of nearly continuous activity in the caldera ended in 1924 (Jaggar and Finch, 1924; Stearns, 1925). In the spring of that year an 80-m drop of the magma column was followed by a swarm of earthquakes that migrated from the summit along the east rift zone past Kapoho. Though much ground deformation developed near Kapoho, a subaerial eruption did not occur; a submarine eruption may have occurred somewhere beyond Cape Kumukahi. Renewed subsidence of the magma column at Halemaumau was then followed by 17 days of repeated phreatic explosions and collapse of the caldera floor around Halemaumau.

Lava returned to Halemaumau shortly after the 1924 explosions ceased, but instead of being sustained the activity was now episodic. A series of seven brief eruptions in the next 10 years (Jaggar, 1947) reduced the depth of Halemaumau from 390 to 150 m, and then no eruptions occurred for 18 years, from 1934 to 1952. Sustained eruption from June to November of 1952 filled Halemaumau with another 120 m of lava. A brief eruption in May–June 1954 added 6 m of lava in Halemaumau and a thin lava flow on the caldera floor to the east (Macdonald, 1955).

Then, after at least 150 years of infrequent eruption and 33 years of no eruption, the subaerial part of Kilauea's east rift zone resumed frequent activity in February–May 1955 with a series of eruptions along its lower segment (fig. 12.58*A*; Macdonald and Eaton, 1964). These were followed by a sustained eruption in Kilauea Iki in 1959 and then by eruptions from the middle and lower segments of the east rift zone in January–February 1960 (fig. 12.58*B*; Richter and others, 1970). Brief eruptions at Halemaumau in February–March 1961 were followed by a series of outbreaks at 13 places along the middle and lower east rift zone in September 1961 (Richter and others, 1964), and further eruptions from the upper and middle east rift zone occurred in December 1962, August 1963, and March and December 1965 (fig. 12.58*C*; Moore and Krivoy, 1964; Peck and others, 1966; Fiske and Koyanagi, 1968; Wright and others, 1968). A sustained eruption then occurred in Halemaumau from November 1967 to

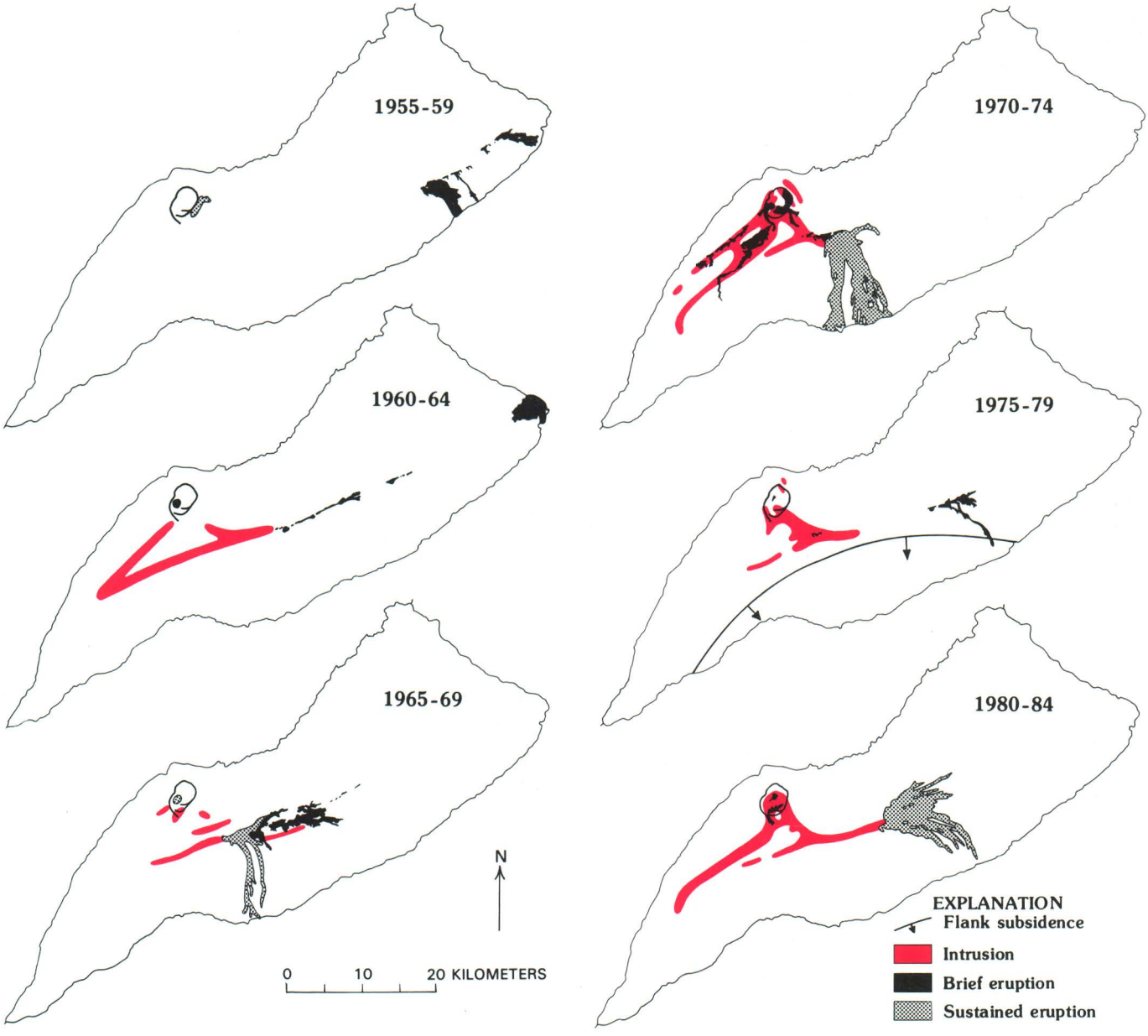

FIGURE 12.58.—Lava flows and intrusions during the interval 1955–1984 at Kilauea. Intrusions since 1962 are inferred from locations of shallow earthquake swarms compiled by Klein and others (chapter 43).

July 1968 (Kinoshita and others, 1969). This was the last sustained eruption in the summit region; sustained activity since then has occurred only along the east rift zone.

FREQUENT AND SUSTAINED FLANK ERUPTIONS, 1968–1985

The 1967–68 summit eruption was followed by a succession of brief eruptions from the upper and middle east rift zone in August and October 1968, and February 1969 (Moore and Koyanagi, 1969; Jackson and others, 1975; Swanson and others, 1976b). While the flank eruptions of 1955–1963 were widely distributed along the east rift zone and interspersed with sustained eruptions at the summit, the 1968–69 eruptions were concentrated along a short segment of the rift zone between Hiiaka and Napau pit craters. As the locus of eruptions contracted, the intervals between eruption decreased to a few months. The sequence culminated in a sustained eruption that began in May 1969 and continued, with brief interruptions, until June 1974, building the lava shield of Mauna Ulu (figs. 12.34, 12.35, 12.58*D*; Swanson and others, 1979; Tilling and others, chapter 16). An interruption in the second half of 1971 saw two brief eruptions from the summit and northern strand of the upper southwest rift zone (Duffield and others, 1982). Other interruptions saw brief eruptions higher up the east rift zone in May and November 1973 (Tilling and others, chapter 16). The final cessation of activity at Mauna Ulu in June 1974 was followed by brief eruptions from the summit and middle strand of the upper southwest rift zone in July, September, and December 1974.

A magnitude 7.2 earthquake and subsidence along the south coast on November 29, 1975 (fig. 12.58*E*; Tilling and others, 1976) was followed by episodes of summit deflation and rift intrusion in June, July, and August 1976 and February 1977 (Dzurisin and others, 1980) and then a brief eruption from the middle east rift zone in September 1977 (Moore and others, 1980). An intrusion of magma into the upper east rift zone in May 1979 was followed by a brief eruption at Pauahi and vicinity in November 1979, and five more intrusive episodes along the upper east rift zone in March (two episodes), August, October, and November 1980 (Dzurisin and others, 1984; Banks and others, 1981). Activity then shifted to the southwest rift zone, with intrusive episodes occurring there in January and August 1981 and June 1982. Brief eruptions occurred at the summit in April and September 1982 (Banks and others, 1983).

Following the 1982 summit eruptions, activity shifted once again to the east rift zone. An intrusion into the upper east rift zone in December 1982 was followed in January 1983 by an eruption near Puu Kahaualea on the middle east rift zone. That eruption was sustained, building a vent edifice called Puu Oo (Wolfe and others, chapter 17); it still continues at this writing in March 1986.

SUMMARY OF ERUPTIVE HISTORY

Kilauea saw subaerial shield growth punctuated by large explosions 100,000–10,000 years ago (Hilina Basalt and Pahala Ash); long-sustained summit eruptions and briefer rift eruptions 10,000–2,000 years ago (scattered kipukas); sustained eruptions from the summit and rift zones 2,000–1,500 years ago; caldera collapse and filling 1,500–1,100 years ago (Uwekahuna Ash Member of the Puna Basalt and hiatus); extensive caldera overflows and numerous rift eruptions, with no patterns of summit-flank interrelation yet discerned, 1,000–350 years ago (Volcano, Kalue, Ai-laau flows); sustained summit activity followed by extensive rift eruptions accompanying caldera collapse, followed by summit explosion, 350–200 years ago (Observatory flows, Keanakakoi Ash Member of Puna Basalt); and long-sustained summit eruption followed by frequent rift eruptions during the last 200 years (historical records).

The recent eruption history is summarized in figure 12.59. About 1,500 years ago the Powers caldera developed, truncating lava flows assigned paleomagnetically to the interval 2,000–1,500 years B.P. The Uwekahuna Ash Member was draped onto the rim and step faults of the caldera. Little is known about Kilauea's eruptions of about 1,500–1,100 years B.P.; only a few flows along the rift zones are known from this interval, and the summit region was remarkably devoid of eruptions outside the Powers caldera. Unless the magma supply was cut off during this interval, most of the eruptive activity must have been confined to the caldera and to submarine parts of the volcano. The Powers caldera began to overflow about 1,200–1,100 years ago and continued to do so intermittently until the 18th century. These overflows covered much of Kilauea's surface. The overflows on different flanks have different ages, indicating that activity was concentrated on one side of the summit for a few decades or centuries and then shifted to another side to cover a different sector. Progressive time relations between summit activity and rift activity are not yet resolved during this interval.

Such progressions do appear beginning about 500–350 years ago. Although paleomagnetic dating does not yet resolve a summit-rift progression at that time, traditions cited by Westervelt (1916) suggest that long-lived activity at the Ai-laau vent was followed by rift eruptions and summit collapse, which were in turn followed by sustained activity at the Observatory vent.

The Observatory activity was followed by many brief eruptions and a few sustained eruptions along both rift zones, especially the east rift zone. This flurry of flank eruptions must have been accompanied by growth of the modern caldera, much of which postdates the Observatory shield. Caldera collapse climaxed with phreatomagmatic eruption of the Keanakakoi Ash Member in A.D. 1790.

Following the 1790 eruption, Kilauea's behavior changed again, and for more than a century almost all subaerial activity was confined to the caldera. During this interval, only two large flank eruptions are known, in 1823 and 1840, wheras activity within the caldera was sustained almost continuously.

Kilauea's famous 19th-century pattern of continuous summit activity ceased in 1924, possibly following a submarine eruption from the east rift zone that coincided with summit collapse. Since then summit eruptions have been infrequent and relatively brief, while eruptions from the rift zones have become more frequent and more sustained.

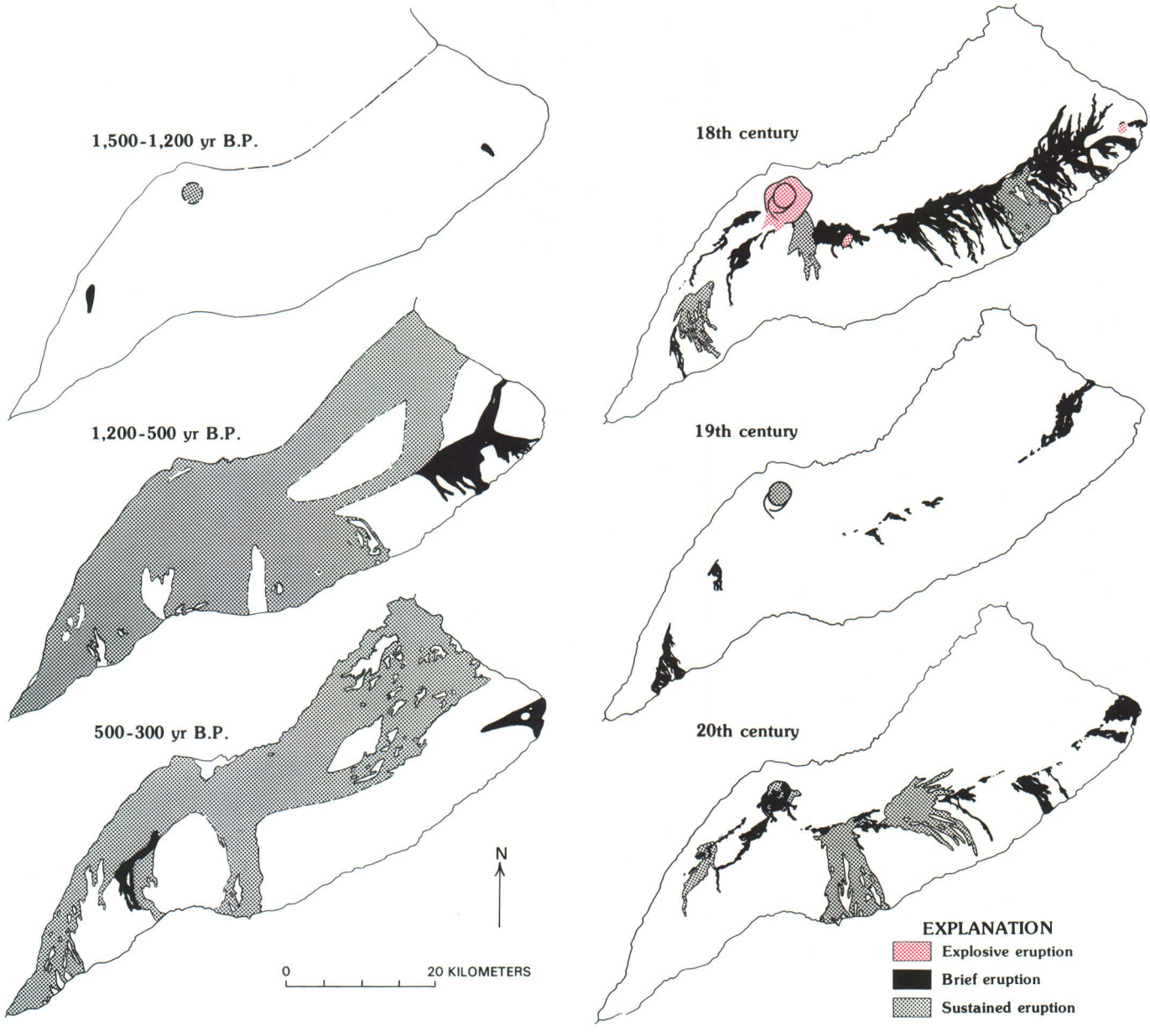

FIGURE 12.59.—Series of maps summarizing Kilauea's eruption history during the last 1,500 years, generalized from information in figures 12.5, 12.6, and 12.8.

MODELS FOR LONG-TERM BEHAVIOR

It may be useful here to speculate a little about the causes of temporal variation in eruptive behavior. Those causes will be a topic of future research because they may lead to better eruption forecasts.

Many models can be visualized, and they can be classified in various ways. For example, we can distinguish evolutionary, cyclical, and steady-state models differing in their forecasting utility.

A cyclical model is shown in figure 12.60. This caldera-dominated model features shifts in magma storage as successive calderas form and fill. In this model caldera collapse arises from changes in magma plumbing, and collapse in turn causes changes in the plumbing, acting as a feedback mechanism of an oscillatory system. Kilauea's history between about 1,500 and 200 years B.P. could represent one long cycle, and its history since 200 years B.P. could represent another shorter one, with the volcano's current state corresponding to stage 2 or stage 3 of the model (fig. 12.60).

Another cyclical model is shown in figure 12.61. This slumping-dominated model focuses on Kilauea's unbuttressed south flank, which the caldera model ignores. Eruptive behavior in this model responds to changes in magma storage arising from flank deformation. It was suggested more than 20 years ago that magma storage in the rift zones is controlled by recurrent slumping of the south flank (Moore and Krivoy, 1964). Later it was concluded from the timing

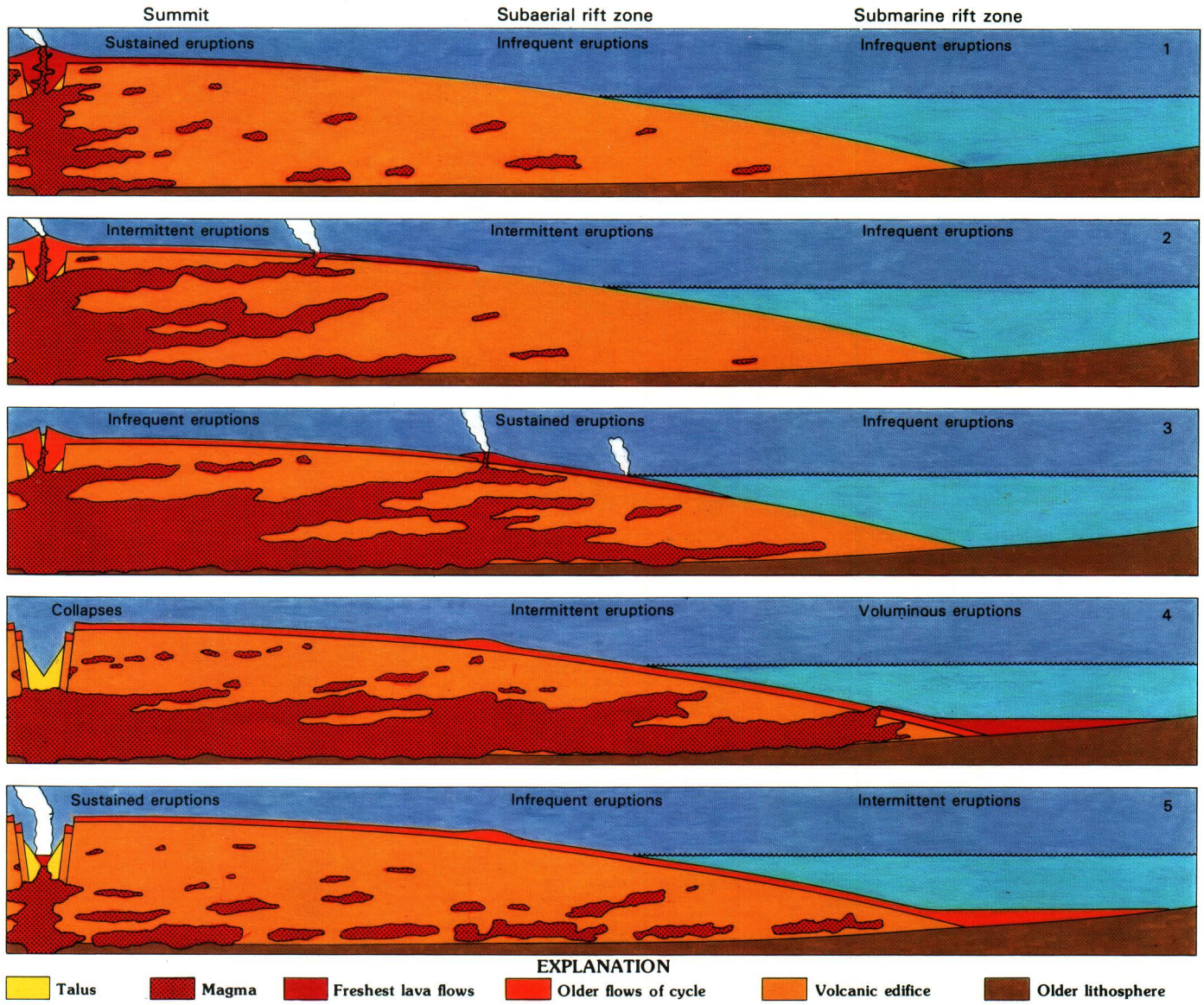

FIGURE 12.60.—Cyclical model for long-term behavior of Kilauea, based on repeated episodes of caldera collapse and filling. Schematic longitudinal profiles of rift zone show five stages in cycle, which could represent dynamic equilibrium between hydrostatic, thermal, and frictional factors. **Stage 1.** Eruptions are long-sustained and restricted to caldera, filling it so that most magma is stored beneath summit. As magma column rises, however, dikes are injected laterally under increasing head and penetrate into rift zones. **Stage 2.** Summit eruptions are less sustained and rift eruptions more frequent as more magma is diverted into rift zones. **Stage 3.** As better continuity is developed in plumbing of rift zone, longer eruptions occur farther from summit. As lava is erupted at lower elevations, magma column subsides beneath summit, and caldera-filling lava slowly cools. **Stage 4.** Voluminous eruptions from rift zones drain magma from upper parts of edifice, and collapse ensues. Collapse at summit rejuvenates caldera, and collapse along rift zones reduces continuity of their plumbing systems. **Stage 5.** Magma rising from deep beneath summit now finds its easiest escape into newly deepened caldera; activity is once again sustained within caldera, and continuity is further reduced in rift plumbing system as dikes solidify.

of flank deformation that slumping is a passive response to forceful intrusion of magma into the rift zones (Swanson and others, 1976a). But that conclusion was based on observations of just the past century; long-term changes in flank behavior might accompany long-term changes in eruptive behavior. Some intervals might be dominated by forceful intrusion and passive deformation and other intervals by active slumping and permissive intrusion. The true state of the edifice might be a quasi-equilibrium perturbable in either direction, with feedback mechanisms forcing an oscillation.

Still other models could be fundamentally cyclical but made complex from the interplay of various mechanisms. For example, slumping cycles and caldera cycles could both operate, independently or in rhythm. If episodes of slumping occurred more often than episodes of caldera collapse, with each perturbation disrupting the

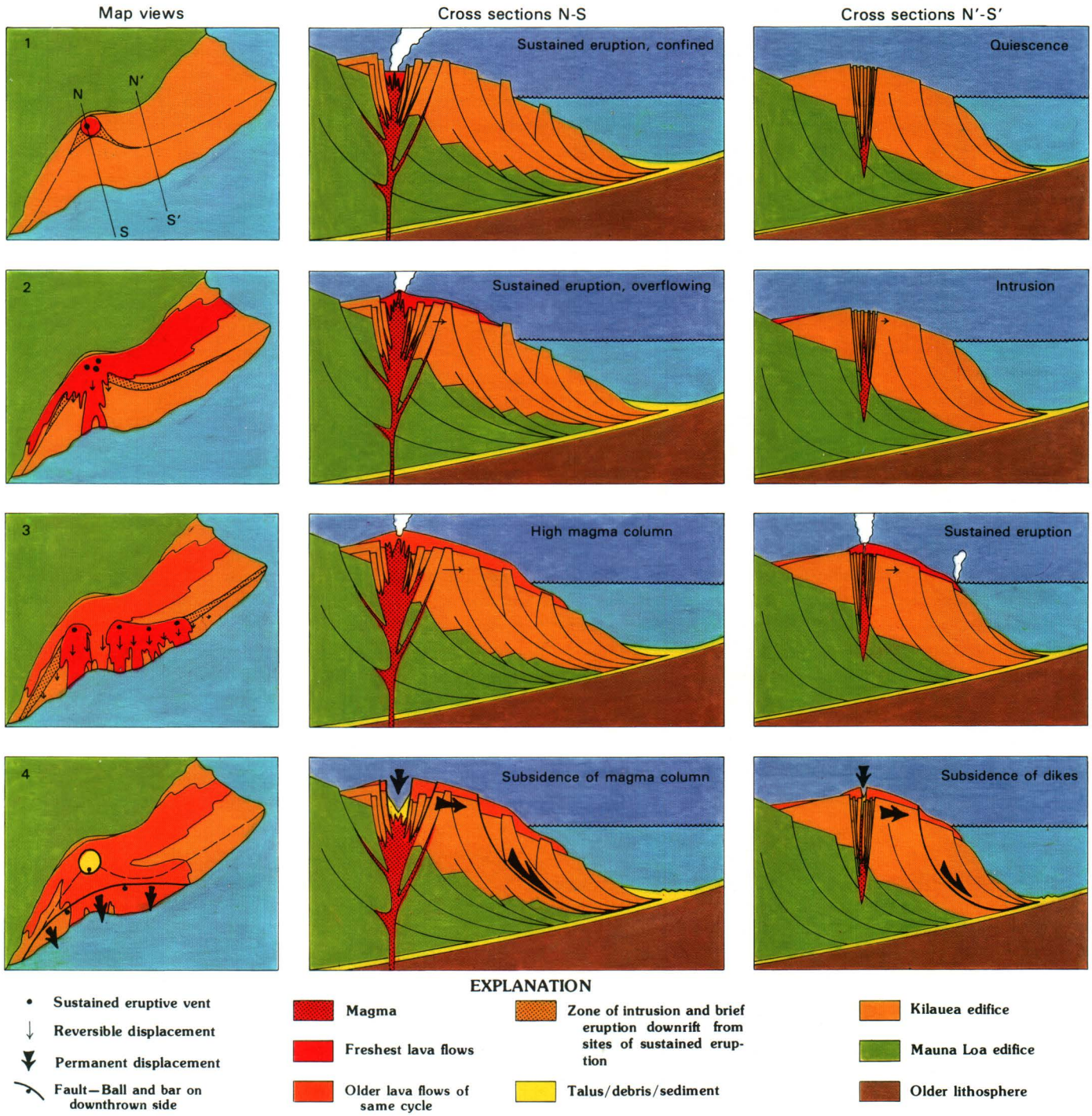

FIGURE 12.61.—Cyclical model based on seaward displacement of south flank. Schematic maps and transverse cross sections show four stages in cycle. Slumping cycles of this sort could occur over intervals as short as a few years, and they might be superimposed on long-term caldera cycles. Slumping episodes might sometimes induce caldera subsidence. Slippage might be concentrated within a layer of oceanic sediment several hundred meters thick beneath the volcano, as suggested by Nakamura (1982). **Stage 1.** Volcanic edifice is in repose as magma column rises passively to fill summit reservoir. **Stage 2.** Summit magma column rises high and overflows. Magma is forcefully intruded under rising head into rift zones, and south flank is displaced. Much of this flank deformation can be reversed if magma withdraws. **Stage 3.** Continued intrusion initiates sustained eruptions along rift zones and displaces south flank further. Flank is made increasingly unstable by steepening its slope and loading its surface, but permanent displacement does not occur until frictional threshold is overcome. **Stage 4.** Oversteepening and loading of flank by extrusion and forceful intrusion overcome sliding resistance, and permanent slumping displacement occurs along flank faults. Lateral expansion of magma reservoir causes summit magma column to subside, and head loss causes magma also to subside far out along rift zones. Magma pressure drops rapidly and stops driving permanent displacement, but slumping continues until frictional resistance overcomes inertia of sliding block. Magma resumes passive filling of space made available by slumping episode.

plumbing system and followed by evolutionary reintegration of the plumbing system, very complicated but possibly predictable harmonic patterns of eruption might ensue.

Cyclical models imply the possibility of long-range forecasts, but steady-state or stochastic models do not. By itself, stage 3 of figure 12.60 could represent such a model, with much magma always stored throughout a plumbing system that is never seriously disrupted. Eruptions of any type could occur from any part of the system at any time. In this model there would be no systematic evolution of the plumbing system over decades or centuries; instead, the variations in eruptive behavior would arise merely from chance developments such as the times when individual dikes happened to intersect the surface. If a model like this best described the volcano's behavior, it might not be possible to predict long-term changes using the previous history.

Alternative noncyclical models could blend evolutionary processes with random events. Random behavior might be superimposed upon, or reset, evolutionary progressions, and evolutionary behavior might characterize some intervals but not others. For example, the magma plumbing system might respond in a predictable, evolutionary way to a major submarine eruption or flank subsidence not caused by feedback mechanisms within the system. Although major perturbations would remain unpredictable, evolutionary trends following them might permit forecasts of long-term behavior between them. That is, we might be able to forecast long intervals of dominantly summit activity versus long intervals of dominantly rift activity. Predictive success would be achieved much of the time even though major perturbations remained unpredictable.

CONCLUSIONS

Kilauea's surface is about 10 times younger than was thought previously (table 12.2); 70 percent is younger than 500 years, 90 percent younger than 1,100 years. A major hiatus in summit overflows occurred between about 1,500 and 1,100 years ago. Much of the present caldera dates from the 18th century, but it was preceded by at least one earlier caldera that developed about 1,500 years B.P. and was later filled.

The various subdivisions of Kilauea are covered by lava flows of different types (table 12.3) produced by eruptions of different kinds from different parts of the magma plumbing system (table 12.4). Kilauea's surface is dominated by tube-fed pahoehoe (67 percent), while surface-fed pahoehoe (14 percent) is mainly limited to near vents along the rift zones, and aa (16 percent) occurs mainly on the south flank seaward of the rift zones. Surface coverage has been dominated by tube-fed lava flows from long-sustained eruptions at the summit; 51 percent of the volcano's surface still consists of such lava even though summit overflows have not occurred for the last 200 years. About 30 percent of Kilauea was covered by lava from just one long eruption at the Ai-laau vent a few hundred years ago. Surface coverage by brief eruptions is minor (22 percent), despite the high frequency of such eruptions in recent decades.

Different parts of Kilauea have differed in eruptive behavior. The most notable difference is between the summit and rift zones, with most long-sustained eruptions occurring at summit vents. Sustained unstable eruptions are more numerous along the upper parts of the rift zones than along their lower parts. Pyroclastic central vents are more common along the lower parts of the rift zones, especially below elevations of 500 m. The briefest fissure eruptions have occurred all along the rift zones and at the summit, displaying on average no obvious affinity for any part of the volcano. During particular decades or centuries, however, they have been concentrated in restricted regions. Other spatial variations appear to have been characteristic of particular localities, such as the southern strand of the southwest rift zone.

Different intervals of Kilauea's history have been dominated by different eruptive behaviors. Behavioral changes have occurred over intervals of decades and centuries. The changes include variations in both frequency and type of eruption. Some changes have been repeated at long intervals, and some may have occurred in evolutionary sequences. Two explosive eruptions large enough to produce extensive pyroclastic sheets seem to have been followed by intervals longer than a century in which most eruptive activity was confined to a summit caldera. While the caldera slowly filled, vegetation became well established on the volcano's flanks. Rift activity waxed as summit activity waned, and in the recent historical example the waxing sequence resembles an evolutionary progression: rift eruptions were at first brief and widely separated in space and time, but gradually they became frequent along a restricted segment of the rift zone and culminated in sustained activity at one locality.

During the past 500 years, when the eruptive pattern can best be defined, there has been a repeated pattern of sympathetic behavior between the summit and rift zones. Little flank activity has occurred when summit activity was sustained, and sustained summit activity has ceased when there was much activity on the rift zones. Rift activity has been accompanied by subsidence at the summit, and large summit collapses have been followed by phreatomagmatic eruption. Events following explosive eruptions, however, have displayed no consistent pattern. The large explosive eruption of 1790 was preceded by much rift activity and followed by much summit activity, but the smaller eruption of 1924 was preceded by much summit activity and followed by little such activity. The current rift activity resembles that which occurred in the 18th century before the explosive eruption of 1790.

TABLE 12.1.—*Classification of Kilauea eruptions*

[Types of lava flow: PS, surface-fed pahoehoe; PT, tube-fed pahoehoe; A, aa]

Type	Duration	Character of effusion	Vents	Lava flows
Brief, fissure	Hours to days	Simple waxing, waning; small fountains.	Open fissures, ramparts.	Few; PS and A.
Brief, localized	Days to weeks	Simple waxing, waning or pulses; large fountains.	Pyroclastic cones, mounds.	Several; PS and A.
Sustained, unstable	Months to years	Complex sequence; waxing, pulses, waning.	Small shields.	Many; PS, PT, and A.
Sustained, stable	Decades to centuries	Mainly slow, steady; some interruptions.	Large shield.	Many; mainly PT.
Explosive	Days to weeks	Successive explosions.	Crater.	Few or none.

TABLE 12.2.—*Age distribution of Kilauea's surface*

[Areas measured by digitizer on a generalized map at scale of 1:50,000]

Age (yr B.P.)	Area		Cumulative area	
	(km^2)	(percent)	(km^2)	(percent)
0–50	146.5	10.1	146.5	10.1
50–150	38.2	2.6	184.7	12.7
150–250	168.2	11.6	352.9	24.3
250–350	167.6	11.5	520.5	35.8
350–500	454.5	31.3	975.0	67.1
500–750	190.6	13.1	1,165.6	80.2
750–1,000	89.6	6.2	1,255.3	86.4
1,000–1,500	50.4	3.5	1,395.6	89.9
>1,500	146.0	10.1	[1]1,451.6	100.0

[1]A separate measurement of total area on the same map gave 1,451.0 km^2.

TABLE 12.3.—*Distribution of lava types on Kilauea's subaerial surface*

[Areas measured by digitizer on a generalized map at scale of 1:50,000. Types of lava: PS, surface-fed pahoehoe; PT, tube-fed pahoehoe; A, aa: T, pyroclastics; ML, all types erupted from Mauna Loa]

Structural subdivision	Area		Lava type	Area	
	(km^2)	Percent of Kilauea		(km^2)	Percent of subdivision
Summit	51.6	3.6	PS	19.4	37.5
			PT	5.0	9.6
			A	1.5	3.0
			T	18.3	35.6
			ML	7.4	14.3
Koae fault system	65.7	4.5	PS	7.8	11.9
			PT	51.1	77.7
			A	6.3	9.6
			T	.5	.8
Upper southwest rift zone	88.4	6.1	PS	21.3	24.1
			PT	46.6	52.7
			A	7.5	8.5
			T	1.1	1.2
			ML	11.9	13.5
Lower southwest rift zone	91.5	6.3	PS	13.8	15.1
			PT	64.0	69.9
			A	13.7	15.0
Upper east rift zone	55.1	3.8	PS	20.9	38.0
			PT	31.2	56.6
			A	2.8	5.0
			T	.2	.4
Middle east rift zone	91.5	6.3	PS	36.7	40.1
			PT	42.8	46.8
			A	10.7	11.7
			T	1.2	1.4
Lower east rift zone	81.8	5.7	PS	43.0	52.5
			PT	8.1	9.9
			A	25.9	31.7
			T	4.9	5.9
North flank	445.7	30.8	PS	19.1	4.3
			PT	403.4	90.5
			A	21.4	4.8
			ML	1.8	.4
South flank	475.9	32.9	PS	17.4	3.7
			PT	316.9	66.6
			A	141.1	29.6
			T	.6	.1
Total subaerial Kilauea	[1]1,447.3	100.0	PS	199.4	13.8
			PT	969.1	67.0
			A	230.9	16.0
			T	26.8	1.9
			ML	21.1	1.5

[1]A separate measurement of total area on the same map gave 1,447.9 km^2.

TABLE 12.4.—*Distribution of lava on Kilauea's surface from different types of eruption*

[Areas measured by digitizer on a generalized map at scale of 1:50,000]

Location of vents	Area covered by eruption type									
	Brief		Sustained, stable		Sustained, unstable		Explosive		Total	
	(km^2)	(percent)	(km^2)	(percent)	(km^2)	(percent)	(km^2)	(percent)	(km^2)	(percent)
Summit	10.2	0.7	732.9	50.6	0	0	18.5	1.3	761.6	52.6
Upper southwest rift zone	35.8	2.5	0	0	34.0	2.3	0	0	69.8	4.8
Lower southwest rift zone	28.0	1.9	0	0	0	0	.0	.0	28.0	1.9
Upper east rift zone	7.5	.5	0	0	183.3	12.6	0	0	190.8	13.1
Middle east rift zone	93.9	6.5	0	0	100.2	6.9	0	0	194.1	13.4
Lower east rift zone	154.5	10.7	0	0	25.0	1.7	.0	.0	179.5	12.4
Mauna Loa	-----	----	-----	----	-----	----	----	---	21.3	1.5
Undetermined	-----	----	-----	----	-----	----	----	---	2.6	.2
Total	329.9	22.8	732.9	50.6	342.5	23.5	18.5	1.3	[1]1,449.4	99.9

[1]A separate measurement of total area on the same map gave 1,450.4 km^2.

TABLE 12.5.—*Paleomagnetic results from lava flows in the Kipuka Nene area of Kilauea*

[D and I are respectively, mean declination and inclination, in degrees, of remanent magnetization in 12 specimens from each site. α_{95} is circle of 95-percent confidence around the mean direction]

Site	D	I	α_{95}
Kalue flows			
1B224	9.5	24.6	1.7
1B456	10.2	24.6	1.8
3R013	8.7	24.1	2.6
Kipuka Nene flows			
8B121	357.0	39.2	1.6
8B133	357.5	37.9	1.2
9B169	357.9	37.4	1.6
3R001	1.9	39.2	2.1

TABLE 12.6.—*^{14}C ages of material related to the Ai-laau and Observatory vents*

Source of flow	Sample	Age (yr B.P.)
Ai-laau vent	[1]W–4449	<200
	[2]W–4573	<200
	W–3881	260±70
	W–4162	310±70
	W–4661	320±70
	W–3941	450±60
	[2]W–3885	2,160±70
Probably Puu Huluhulu	W–4184	<200
	W–5110	230±60
	W–4337	620±70
Observatory vent	W–4470	310±70
	W–3811	330±60
	W–3852	450±60
	[3]W–4998	960±60
Possibly Observatory vent	W–4404	530±70
	W–5218	550±70
	W–3860	670±60

[1]Same prehistoric flow as W–3941; disregarded.
[2]Same prehistoric flow as W–4162; disregarded.
[3]Anomalous, possibly contaminated by fumaroles.

REFERENCES CITED

Aramaki, S., and Moore, J.G., 1969, Chemical composition of prehistoric lavas at Makaopuhi Crater, Kilauea Volcano, and periodic change in alkalai content of Hawaiian tholeiitic lavas: Tokyo, Bulletin of the Earthquake Research Institute, v. 47, p. 257–270.

Atkinson, I.A.E., 1970, Successional trends in the coastal and lowland forest of Mauna Loa and Kilauea Volcanoes, Hawaii: Pacific Science, v. 24, p. 387–400.

Atkinson, I.A.E., and Swindale, L.D., 1974, Age determinations of some prehistoric lava flows in Hawaii: Hawaii Agricultural Experiment Station Technical Bulletin 90, 43 p.

Banks, N.G., Klein, F.W., Moore, R.B., Jackson, D.B., and Okamura, A.T., 1981, Kilauea Volcano's November 1979 eruption [abs.]: Eos, American Geophysical Union Transactions, v. 62, p. 1072.

Banks, N.G., Wolfe, E.W., Duggan, T.A., Okamura, A.T., Koyanagi, R.Y., Greenland, L.P., and Jackson, D.B., 1983, Magmatic events at Kilauea Volcano, Hawaii [abs.]: Eos, American Geophysical Union Transactions, v. 64, p. 901–902.

Beaglehole, J.C., 1967, The journals of Captain James Cook on his voyages of Discovery, 1776–1780, v. 3, The voyage of the Resolution and Discovery, 1776–1780: New York, Cambridge University Press, 1,647 p.

Brigham, W.T., 1909, The volcanoes of Kilauea and Mauna Loa: Honolulu, Bernice P. Bishop Museum Memoirs, v. 2, no. 4, 222 p.

Chatters, R.M., Crosby, J.W., III, and Engstrand, L.G., 1969, Fumarole gaseous emanations: Their influence on carbon-14 dates: Washington State University, College of Engineering, Circular 93.

Christiansen, R.L., 1979, Explosive eruption of Kilauea volcano in 1790 [abs.]: Hawaii Symposium on Intraplate Volcanism and Submarine Volcanism, Hilo, Hawaii, July 16–22, 1979, Abstract volume, p. 158.

Coan, T., 1841, Great eruption of the volcano of Kilauea, Missionary Herald, v. 37, p. 283–285.

———1851, [On Kilauea]: American Journal of Science, 2nd series, v. 12, p. 80–82.

———1868, [On the earthquakes and eruption of 1868]: American Journal of Science, 2nd series, v. 46, p. 106–109.

———1874, Note on the Hawaiian volcanoes: American Journal of Science, 3rd series, v. 8, p. 467.

Coe, R.S., Grommé, C.S., and Mankinen, E.A., 1978, Geomagnetic paleointensities from radiocarbon-dated lava flows on Hawaii and the question of the Pacific nondipole low: Journal of Geophysical Research, v. 83, p. 1740–1756.

Dana, J.D., 1849, Geology, United States Exploring Expedition, during the years 1838, 1839, 1840, 1841, 1842, under the command of Charles Wilkes, U.S.N.: Philadelphia, v. 10, 756 p.

———1850, Historical account of the eruptions on Hawaii: American Journal of Science, ser. 2, v. 9, p. 347–364.

———1890, Characteristics of volcanoes: New York, Dodd, Mead, 399 p.

Decker, R.W., and Christiansen, R.L., 1984, Explosive eruptions of Kilauea Volcano, Hawaii, *in* Explosive volcanism: Inception, evolution, and hazards: Washington, D.C., National Academy Press, p. 122–132.

Doell, R.R., 1969, Paleomagnetism of the Kau volcanic series, Hawaii: Journal of Geophysical Research, v. 74, p. 4857–4868.

Doell, R.R., and Cox, A.V., 1963, The accuracy of the paleomagnetic method as evaluated from historic Hawaiian lava flows: Journal of Geophysical Research, v. 68, p. 1997–2009.

———1965, Paleomagnetism of Hawaiian lava flows: Journal of Geophysical Research, v. 70, p. 3377–3405.

Doerr, J.E., Jr., 1933, Tree molds in the Volcano golf course: Hawaii National Park Notes, v. 3, p. 3–7.

Douglas, D., 1905, Sketch of a second journey to the northwestern parts of the continent of North America and to the Sandwich Islands during the years 1829–'30–'31–'32–'33–'34, Part VI: Oregon Historical Quarterly, v. 6, p. 417–449.

Duffield, W.A., 1975, Structure and origin of the Koae fault system, Kilauea Volcano, Hawaii: U.S. Geological Survey Professional Paper 856, 12 p.

Duffield, W.A., Christiansen, R.L., Koyanagi, R.Y., and Peterson, D.W., 1982, Storage, migration, and eruption of magma at Kilauea Volcano, Hawaii, 1971–1972: Journal of Volcanology and Geothermal Research, v. 13, p. 273–307.

Dutton, C.E., 1884, Hawaiian volcanoes: U.S. Geological Survey 4th Annual Report, p. 75–219.

Dzurisin, D., Anderson, L.A., Eaton, G.P., Koyanagi, R.Y., Lipman, P.W., Lockwood, J.P., Okamura, R.T., Puniwai, G.S., Sako, M.K., and Yamashita, K.M., 1980, Geophysical observations of Kilauea Volcano, Hawaii, 2. Constraints on the magma supply during November 1975–September 1977: Journal of Volcanology and Geothermal Research, v. 7, p. 241–269.

Dzurisin, D., and Casadevall, T.C., 1986, Stratigraphy and chemistry of the Uwekahuna Ash: Product of prehistoric phreatomagmatic eruptions at Kilauea Volcano, Hawaii [abs.]: International Association of Volcanology and Chemistry of the Earth's Interior, Aukland-Hamilton-Rotorua, New Zealand, February 1–9, 1986, Abstracts, p. 100.

Dzurisin, D., Koyanagi, R.Y., and English, T.T., 1984, Magma supply and storage at Kilauea Volcano, Hawaii, 1956–1983: Journal of Volcanology and Geothermal Research, v. 21, p. 177–206.

Easton, R.M., 1978, The stratigraphy and petrology of the Hilina Formation: the oldest exposed lavas of Kilauea Volcano, Hawaii: Honolulu, University of Hawaii, M.S. thesis, 274 p.

Easton, R.M., and Lockwood, J.P., 1983, "Surface-fed dikes"—the origin of some unusual dikes along the Hilina fault zone, Kilauea Volcano, Hawaii: Bulletin Volcanologique, v. 46, p. 45–53.

Ellis, W., 1827, Journal of William Ellis, narrative of a tour of Hawaii, or Owhyhee; with remarks on the history, traditions, manners, customs and language of the inhabitants of the Sandwich Islands: Honolulu Advertiser, 342 p., reprinted 1963.

Fiske, R.S., and Jackson, E.D., 1972, Orientation and growth of Hawaiian volcanic rifts: The effect of regional structure and gravitational stresses: Royal Society of London Proceedings, v. A329, p. 299–326.

Fiske, R.S., and Koyanagi, R.Y., 1968, The December 1965 eruption of Kilauea Volcano, Hawaii: U.S. Geological Survey Professional Paper 607, 21 p.

Fornari, D.J., Moore, J.G., and Calk, L., 1979, A large submarine sand-rubble flow on Kilauea Volcano, Hawaii: Journal of Volcanology and Geothermal Research, v. 5, p. 239–256.

Furumoto, A.S., 1976, A coordinated exploration program for geothermal sources on the Island of Hawaii, *in* United Nations Symposium on the Development and Use of Geothermal Resources, 2nd, San Francisco, California, May 1975: Proceedings, v. 2, p. 993–1001.

Goodrich, J., 1833, Volcanoes and volcanic phenomena of Hawaii: American Journal of Science, v. 25, p. 199–203.

Hitchcock, C.H., 1909, Hawaii and its volcanoes: Honolulu, Hawaiian Gazette, 2nd edition 1911, 314 p.

Holcomb, R.T., 1976a, Preliminary map showing products of eruptions, 1962–1974, from the upper east rift zone of Kilauea Volcano, Hawaii: U.S. Geological Survey Miscellaneous Field Studies Map MF–811, scale 1:24,000.

———1976b, Complexity and hazards of Hawaiian shield volcanoes [abs.]: Geological Society of America, Abstracts with Programs, v. 8, no. 6, p. 920–921.

———1980a Preliminary geologic map of Kilauea Volcano, Hawaii: U.S. Geological Survey Open-File Report 80-796, 2 sheets, scale 1:50,000.

———1980b, Kilauea Volcano, Hawaii: Chronology and morphology of the surficial lava flows: Palo Alto, Stanford University, Ph.D. thesis, 321 p. Also released as U.S. Geological Survey Open-File Report 81–354.

Holcomb, R.T., Champion, D.E., and McWilliams, M.O., 1986, Dating recent Hawaiian lava flows using paleomagnetic secular variation: Geological Society of America Bulletin, v. 97, p. 829–839.

Holcomb, R.T., Peterson, D.W., and Tilling, R.I., 1974, Recent landforms at Kilauea Volcano, a selected photographic compilation, *in* Guidebook to the Hawaiian Planetology Conference: Hilo, Hawaii, October 1974, p. 49–86.

Jackson, D.B., Swanson, D.A., Koyanagi, R.Y., and Wright, T.L., 1975, The August and October, 1968, east rift eruptions of Kilauea Volcano, Hawaii: U.S. Geological Survey Professional Paper 890, 33 p.

Jacobi, J.D., 1983, *Metrosideros* dieback in Hawaii: A comparison of adjacent dieback and non-dieback rain forest stands: New Zealand Journal of Ecology, v. 6, p. 79–97.

Jaggar, T.A., 1947, Origin and development of craters: Geological Society of America Memoir 21, 508 p.

Jaggar, T.A., and Finch, R.H., 1924, The explosive eruption of Kilauea in Hawaii, 1924: American Journal of Science, ser. 5, v. 8, p. 353–374.

Juvik, J.O., 1976, A substrate control model for vegetation succession on recent volcanic deposits in the Hawaiian and Mascarene Islands: Yearbook of the Association of Pacific Coast Geographers, v. 38, p. 125.

Kalakaua, D., 1888, The legends and myths of Hawaii: New York, Charles L. Webster (reprinted 1972, Tokyo, Charles E. Tuttle), 530 p.

Kelley, M.L., 1979, Radiocarbon dates from the Hawaiian Islands—a compilation: U.S. Geological Survey Open-File Report 79–1700, 37 p.

Kelley, M.L., Spiker, E.C., Lipman, P.W., Lockwood, J.P., Holcomb, R.T., and Rubin, M., 1979, U.S. Geological Survey radiocarbon dates XV: Mauna Loa and Kilauea Volcanoes, Hawaii: Radiocarbon, v. 21, p. 306–320.

Kinoshita, W.T., Koyanagi, R.Y., Wright, T.L., and Fiske, R.S., 1969, Kilauea Volcano: the 1967–68 summit eruption: Science, v. 166, p. 459–468.

Ledyard, J., 1783, A journal of Captain Cook's last voyage to the Pacific Ocean and in quest of a northwest passage between Asia and America: Hartford, Conn., Nathaniel Patkon.

Lipman, P.W., and Swenson, A., 1984, Generalized geologic map of the southwest rift zone of Mauna Loa Volcano, Hawaii: U.S. Geological Survey Miscellaneous Investigations Map I–1323, scale 1:100,000.

Lockwood, J.P., and Lipman, P.W., 1980, Recovery of charcoal for ^{14}C dating from beneath lava—lessons from Hawaii: Bulletin Volcanologique, v. 43, p. 609–615.

Lockwood, J.P., and Rubin, M., 1986, Distribution and age of the Uwekahuna Ash, Kilauea Volcano, Hawaii [abs.]: International Association of Volcanology and Chemistry of the Earth's Interior, Aukland-Hamilton-Rotorua, New Zealand, February 1–9, 1986, Abstracts, p. 112.

Macdonald, G.A., 1941, Lava flows in eastern Puna: Volcano Letter, no. 474, p. 1–3.

———1955, Hawaiian volcanoes during 1952: U.S. Geological Survey Bulletin 1021–B, p. 15–108.

———1965, Hawaiian calderas: Pacific Science, v. 19, p. 320–331.

Macdonald, G.A., and Abbott, A.T., 1970, Volcanoes in the sea—the geology of Hawaii: Honolulu, University of Hawaii Press, 441 p.

Macdonald, G.A., and Eaton, J.P., 1964, Hawaiian volcanoes during 1955: U.S. Geological Survey Bulletin 1171, 170 p.

Moore, J.G., 1971, Bathymetry and geology—East Cape of the Island of Hawaii: U.S. Geological Survey Map I–677, scale 1:62,500.

Moore, J.G., and Evans, B.W., 1967, The role of olivine in the crystallization of the prehistoric Makaopuhi tholeiitic lava lake, Hawaii: Contributions to Mineralogy and Petrology, v. 15, p. 202–223.

Moore, J.G., and Fiske, R.S., 1969, Volcanic structure inferred from dredge samples and ocean-bottom photographs, Hawaii: Geological Society of America Bulletin, v. 80, p. 1191–1202.

Moore, J.G., and Koyanagi, R.Y., 1969, The October 1963 eruption of Kilauea Volcano, Hawaii: U.S. Geological Survey Professional Paper 614–C, 13 p.

Moore, J.G., and Krivoy, H.L., 1964, The 1962 flank eruption of Kilauea and structure of the east rift zone: Journal of Geophysical Research, v. 69, p. 2033–2045.

Moore, J.G., and Peck, D.L., 1965, Bathymetric, topographic, and structural map of the south-central flank of Kilauea Volcano, Hawaii: U.S. Geological Survey Miscellaneous Investigations Map I–456, scale 1:62,500.

Moore, J.G., Phillips, R.L., Grigg, R.W., Peterson, D.W., and Swanson, D.A., 1973, Flow of lava into the sea, 1969–1971, Kilauea Volcano, Hawaii: Geological Society of America Bulletin, v. 84, p. 537–546.

Moore, R.B., 1981, Preliminary geologic map of the Kapoho quadrangle, Hawaii: U.S. Geological Survey Open-File Report 81–947, 1 sheet, scale 1:24,000.

———1983, Distribution of differentiated tholeiitic basalts on the lower east rift zone of Kilauea Volcano, Hawaii: A possible guide to geothermal exploration: Geology, v. 11, p. 136–140.

———1985, Preliminary geologic map of the Pahoa South quadrangle, Hawaii: U.S. Geological Survey Open-File Report 85–715, 1 sheet, scale 1:24,000.

Moore, R.B., Helz, R.T., Dzurisin, D., Eaton, G.P., Koyanagi, R.Y., Lipman, P.W., Lockwood, J.P., and Puniwai, G.S., 1980, The 1977 eruption of Kilauea Volcano, Hawaii: Journal of Volcanology and Geothermal Research, v. 7, p. 189–210.

Nakamura, K., 1982, Why do long rift zones develop better in Hawaiian volcanoes—a possible role of thick sediments, *in* Proceedings, International Association of Volcanology and Chemistry of the Earth's Interior 1980 Symposium on the Activity of Ocean Volcanoes, Ponta Delgada, Azores, Universidade dos Acores, p. 59–73.

Peck, D.L., Wright, T.L., and Moore J.G., 1966, Crystallization of tholeiitic basalt in Alae lava lake, Hawaii, *in* International Symposium on Volcanology, New Zealand, 1965: Bulletin Volcanologique, v. 29, p. 629–656.

Peterson, D.W., 1967, Geologic map of the Kilauea Crater quadrangle, Hawaii: U.S. Geological Survey Geologic Quadrangle Map GQ–667, scale

1:24,000.

Peterson, D.W., and Swanson, D.A., 1974, Observed formation of lava tubes during 1970–1971 at Kilauea Volcano, Hawaii: Studies in Speleology, v. 2, p. 209–222.

Powers, H.A., 1948, A chronology of explosive eruptions of Kilauea: Pacific Science, v. 2, p. 278–292.

Powers, S., 1916, Intrusive bodies at Kilauea: Zeitschrift fur Vulkanologie, v. 3, p. 28–33.

Richter, D.H., Ault, W.U., Eaton, J.P., and Moore, J.G., 1964, The 1961 eruption of Kilauea Volcano, Hawaii: U.S. Geological Survey Professional Paper 474–D, 34 p.

Richter, D.H., Eaton, J.P., Murata, K.J., Ault, W.U., and Krivoy, H. L., 1970, Chronological narrative of the 1959–60 eruption of Kilauea Volcano, Hawaii: U.S. Geological Survey Professional Paper 537–E, 73 p.

Ripperton, J.C., and Hosaka, E.Y., 1942, Vegetation zones of Hawaii: Hawaii Agricultural Experiment Station Bulletin 89, p. 1–60.

Rubin, M., and Suess, H.E., 1956, U.S. Geological Survey radiocarbon dates, 3: Science, v. 123, p. 442–448.

de Saint Ours, P.J., 1979, Analyse morpho-structurale et surveillance tectonique d'un volcan actif: Exemple du Kilauea, Hawaii: Orsay, France, l'Universite de Paris-Sud, Centre d'Orsay, Docteur 3eme cycle [thesis], 250 p.

———1982, Map of tectonic features of Kilauea Volcano summit region, Hawaii: U.S. Geological Survey Miscellaneous Field Studies Map MF–1368.

Skokan, C.K., 1974, A time domain electromagnetic survey of the east rift zone, Kilauea Volcano, Hawaii: Golden, Colorado School of Mines, Ph.D. dissertation no. T–1700, 152 p.

Stearns, H.T., 1925, The explosive phase of Kilauea Volcano, Hawaii, in 1924: Bulletin Volcanologique, v. 2, p. 193–209.

———1926, The Keaiwa or 1823 lava flow from Kilauea volcano, Hawaii: Journal of Geology, v. 134, p. 336–351.

Stearns, H.T., and Clark, W.O., 1930, Geology and water resources of the Kau district, Hawaii: U.S. Geological Survey Water-Supply Paper 616, 194 p.

Stearns, H.T., and Macdonald, G.A., 1946, Geology and ground-water resources of the Island of Hawaii: Hawaii Division of Hydrography Bulletin 9, 363 p.

Stone, J.B., 1925, Interior of Makaopuhi Crater: The Volcano Letter, no. 47.

Strzelecki, Count, 1845, New South Wales and Van Diemen's Land: London, p. 106.

Swanson, D.A., 1972, Magma supply rate at Kilauea Volcano, 1952–1971: Science, v. 175, p. 163–170.

———1973, Pahoehoe flows from the 1969–1971 Mauna Ulu eruption, Kilauea Volcano, Hawaii: Geological Society of America Bulletin, v. 84, p. 615–626.

Swanson, D.A., and Christiansen, R.L., 1973, Tragic base surge in 1790 at Kilauea Volcano: Geology, v. 1, p. 83–86.

Swanson, D.A., Duffield, W.A., and Fiske, R.S., 1976a, Displacement of the south flank of Kilauea Volcano, Hawaii: the result of forceful intrusion of magma into rift zones: U.S. Geological Survey Professional Paper 963, 39 p.

Swanson, D.A., Duffield, W.A., Jackson, D.B., and Peterson, D.W., 1972, The complex filling of Alae Crater, Kilauea Volcano, Hawaii: Bulletin Volcanologique, v. 36, p. 105–126.

———1979, Chronological narrative of the 1969–1971 Mauna Ulu eruption of Kilauea Volcano, Hawaii: U.S. Geological Survey Professional Paper 1056, 55 p.

Swanson, D.A., Jackson, D.B., Koyanagi, R.Y., and Wright, T.L., 1976b, The February 1969 east rift eruption of Kilauea Volcano, Hawaii: U.S. Geological Survey Professional Paper 891, 30 p.

Taliaferro, W.J., 1959, Rainfall of the Hawaiian Islands: Honolulu, Hawaii Water Authority.

Tilling, R.I., Koyanagi, R.Y., Lipman, P.W., Lockwood, J.P., Moore, J.G., and Swanson, D.A., 1976, Earthquake and related catastrophic events, Island of Hawaii, November 29, 1975: A preliminary report: U.S. Geological Survey Circular 740, 33 p.

Unger, J.D., and Koyanagi, R.Y., 1979, Evidence of the effects of shallow magma intrusion in Kilauea Volcano: Hawaii Symposium on Intraplate Volcanism and Submarine Volcanism, Hilo, Hawaii, July 16–22, 1979, Abstract Volume, p. 176.

Vancouver, G., 1798, A voyage of discovery to the north Pacific Ocean: New York, Da Capo Press, reprinted 1967.

Walker, G.W., 1967, Geologic map of the Kau Desert quadrangle, Hawaii: U.S. Geological Survey Geologic Quadrangle Map GQ–827, scale 1:24,000.

Westervelt, W.D., 1916, Hawaiian legends of volcanoes: Honolulu, Charles E. Tuttle, 205 p., reprinted 1963 (Tokyo).

Wilde, P., Chase, T.E., Normark, W.R., Thomas, J.A., and Young, J.D., 1980, Oceanographic data off southern Hawaiian Islands: Lawrence Berkeley Laboratory Publication 359.

Wilkes, C., 1845, Narrative of the United States Exploring Expedition during the years 1838, 1839, 1840, 1841, 1842, v. IV: Philadelphia, Lea and Blanchard.

Wright, T.L., 1971, Chemistry of Kilauea and Mauna Loa lava in space and time: U.S. Geological Survey Professional Paper 735, 40 p.

Wright, T.L., and Fiske, R.S., 1971, Origin of the differentiated and hybrid lavas of Kilauea Volcano, Hawaii: Journal of Petrology, v. 12, p. 1–65.

Wright, T.L., Kinoshita, W.T., and Peck, D.L., 1968, March 1965 eruption of Kilauea Volcano and the formation of Makaopuhi lava lake: Journal of Geophysical Research, v. 73, p. 3181–3205.

Zablocki, C.J., 1976, Mapping thermal anomalies on an active volcano by the self-potential method, Kilauea, Hawaii,. *in* United Nations Symposium on the Development and Use of Geothermal Resources, 2nd, San Francisco, California, May 20–29, 1975, Proceedings, v. 2, p. 1299–1309.

———1977, Self-potential studies in east Puna, Hawaii, *in* Keller, G.V., Skokan, C.K., Skokan, J.J., Daniels, J., Kauahikaua, J.P., Klein, D.P., and Zablocki, C.J., Geoelectric studies on the east rift, Kilauea Volcano, Hawaii Island: Honolulu, Hawaii Institute of Geophysics, Geothermal Resources Exploration in Hawaii, Report Number 3, p. 175–195.

STRATIGRAPHY AND PETROLOGY OF THE UWEKAHUNA BLUFF SECTION, KILAUEA CALDERA

By Thomas J. Casadevall *and* Daniel Dzurisin

ABSTRACT

Samples from 63 lava flows in a 135-m vertical section at Uwekahuna Bluff within Kilauea caldera were analyzed for major oxides, trace elements, and rare-earth elements. Four stratigraphically defined suites of subaerial lava flows are present: (A) units 1–14 (youngest suite), plagioclase-porphyritic flows (6.4–7.3 weight percent MgO); (B) units 15–30, aphyric flows (6.5–8.0 weight percent MgO); (C) units 31–51, olivine-rich flows (9.0–19.7 weight percent MgO) with the Uwekahuna Ash Member of the Puna Basalt at base; (D) units 44A–52A (oldest suite), nonvesicular, aphyric flows (7.1–7.8 weight percent MgO).

Suite D flows were erupted at about 2.8 ka, probably in an ancient caldera. At about 2.1 ka, catastrophic eruption of the Uwekahuna Ash Member may have unloaded Kilauea's deep magma-transport system and triggered extrusion of olivine-porphyritic lavas of suite C. Suites A and B may be genetically related, possibly from the top of a single reservoir; the plagioclase-porphyritic flows of suite A may represent the later eruptive product of a shallow reservoir that earlier was the source for the aphyric lavas of suite B. We interpret this sequence of aphyric lavas followed by plagioclase-porphyritic lavas as indicating a two-stage drawdown of a post-Uwekahuna Ash Member magma reservoir.

Comparison of published major- and trace-element data from Kilauea and Mauna Loa with data for the Uwekahuna Bluff flows indicates the latter are all from a Kilauea source; apparently no Mauna Loa flows occur in the west wall of Kilauea caldera, although surface flows from Mauna Loa have been mapped within 1 km of the caldera rim.

INTRODUCTION

Kilauea Volcano, on the southeast flank of much larger Mauna Loa Volcano (fig. 13.1), has a broad, gently sloping summit region 1,260 m above sea level and two rift zones that extend outward from a 3 × 5-km summit caldera. The western wall of Kilauea caldera is easily accessible and contains the largest cross-sectional exposure of the summit area (fig. 13.1). This exposure comprises numerous lava flows, at least 18 dikes (Casadevall and Dzurisin, chapter 14), the Uwekahuna laccolith (Murata and Richter, 1961), and three pyroclastic units—the A.D. 1924 lithic ash and the mostly A.D. 1790 Keanakakoi and 2.1-ka Uwekahuna Ash Members of the Puna Basalt (Powers, 1948; Dzurisin and Casadevall, 1986; Lockwood and Rubin, 1986). The wall extends from the area known as the Outlet roughly 6 km northward to the Steaming Bluff area and includes the 135-m-high Uwekahuna Bluff (fig. 13.2). From Uwekahuna Bluff north to Steaming Bluff, the western wall is an unbroken and near-vertical slice through the summit area of Kilauea shield (fig. 13.1). South of Uwekahuna Bluff, however, the wall has a stepped profile attributed to normal faulting (Dutton, 1884; Peterson, 1967; Holcomb, 1981; de Saint Ours, 1982).

We report here the results of field and laboratory studies of rocks in the Uwekahuna Bluff area of Kilauea's summit caldera. Using chemistry, field occurrence, and petrography, we distinguish flows and attempt to identify systematic chemical variations in the composition of summit lava flows. We have examined the data to see whether they allow extension of the secular chemical variation recognized for historical flows (Wright, 1971) further back in time and to see whether they support the hypothesis that more than one long-lived eruptive center was active in the Kiluaea summit area during the past several thousand years (Holcomb, 1981).

Considering the proximity of Mauna Loa surface lavas to the present western rim of Kilauea caldera (Peterson, 1967; J.P. Lockwood, written commun., 1980), we have also scrutinized the data to determine if any flow at Uwekahuna Bluff might have come from Mauna Loa. Previous work has suggested that historical lavas from Kilauea and Mauna Loa can be distinguished by major-element chemistry (Powers, 1955; Wright, 1971; Basaltic Volcanism Study Project, 1981) and rare-earth-element chemistry (Leeman and others, 1977, 1980; Basaltic Volcanism Study Project, 1981).

This study is a companion to two others conducted concurrently. One focuses on the age, distribution, and eruptive mechanism of the Uwekahuna Ash Member of the Puna Basalt, a product of large phreatomagmatic eruptions in the Kilauea summit area (Dzurisin and Casadevall, 1986; Lockwood and Rubin, 1986). The other describes the distribution and petrology of intrusive bodies in Kilauea caldera and assesses the importance of intrusions to the growth of the summit region of Kilauea (Casadevall and Dzurisin, chapter 14).

PREVIOUS STUDIES

Although geologic mapping of Kilauea's summit area has focused on young surface flows (Peterson, 1967; Walker, 1969;

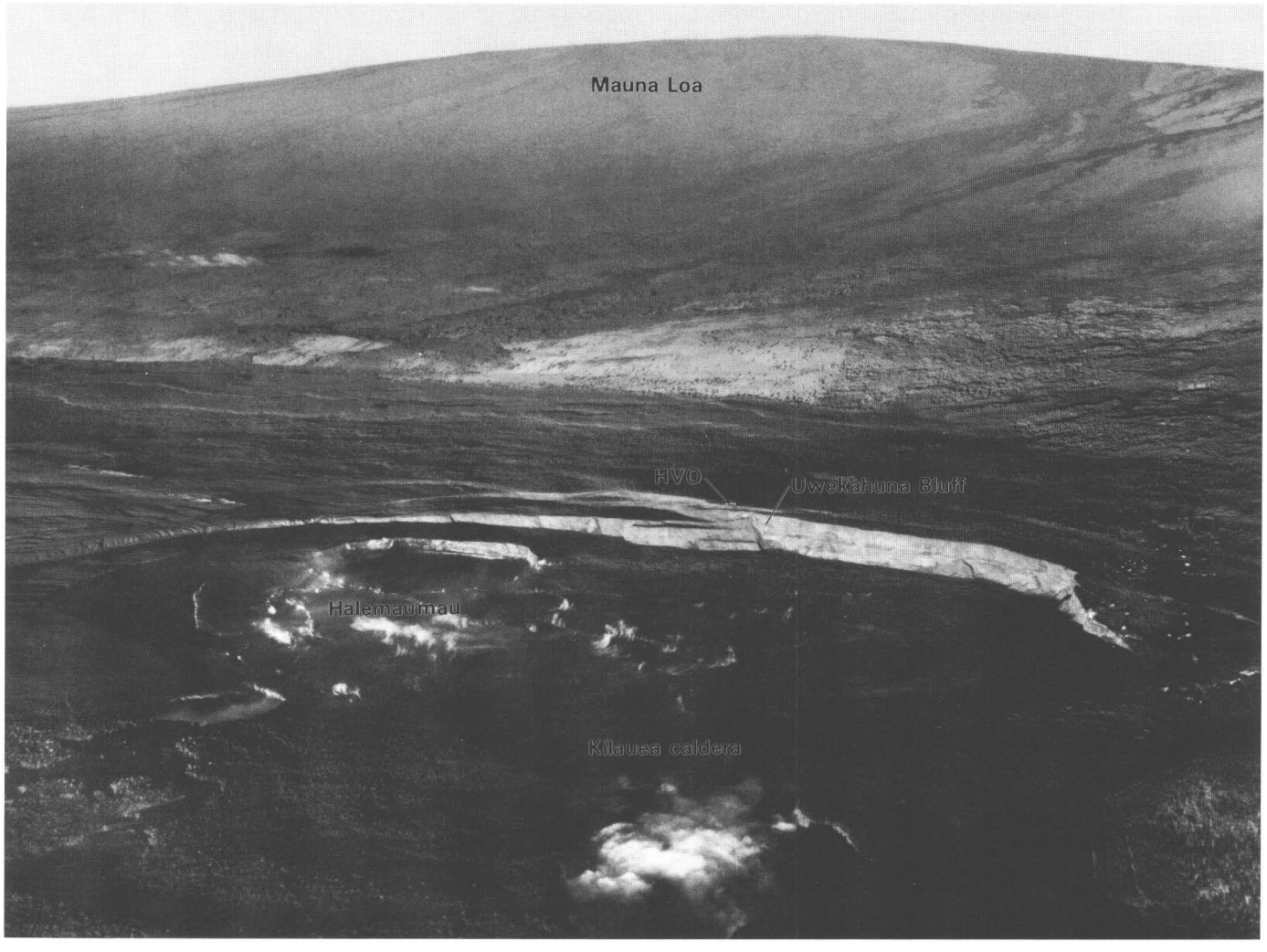

FIGURE 13.1.—Aerial view looking southwest over Kilauea caldera toward the east flank of Mauna Loa, showing location of Uwekahuna Bluff section and Hawaiian Volcano Observatory (HVO). Photograph by J.P. Lockwood, U.S. Geological Survey.

Holcomb, 1981) and on the structural setting of the summit region (de Saint Ours, 1982), some studies have concerned the walls of the caldera and nearby pit craters. Macdonald described the sequence of flows exposed at Uwekahuna Bluff (Stearns and Macdonald, 1946; Macdonald, 1949), Doell sampled the Uwekahuna section for paleomagnetic studies (Doell and Cox, 1965, 1972), and Wright (1971) reported on the chemistry of several of Doell's samples.

Stearns and Macdonald (1946, p. 99–111) placed the three widespread tephra deposits at Kilauea into a stratigraphic framework for the volcano. The Uwekahuna Ash Member of the Puna Basalt is the oldest at 2.1 ka (Lockwood and Rubin, 1986). At Uwekahuna Bluff the ash is overlain by 105–135 m of lava flows, capped by the mostly A.D. 1790 Keanakakoi Ash Member and by traces of A.D. 1924 lithic ash.

ACKNOWLEDGMENTS

We greatly appreciate the interest and advice received from many colleagues, in particular T.L. Wright, which have been helpful in clarifying our ideas. We also wish to thank J. Arth, D.E. Champion, D.A. Clague, R.T. Holcomb, J.P. Lockwood, D.W. Peterson, D.A. Swanson, and R.I. Tilling. Initial thin section descriptions and point counts for figure 13.4 were made by J.E. Ewert. Major-element chemistry was determined by J. Reid and D. Kay; instrumental neutron activation analyses were performed by L.J. Schwarz; and atomic absorption analyses were performed by D.W. Golightly and P. Aruscavage; we greatly appreciate their considerable analytical effort. M. Mangan and D. Johnson helped with computer plots of the data. Reviews of this paper by D.A. Swanson and T.L. Wright have substantially improved the presentation of our results.

METHODS OF STUDY

We sampled and described the succession of flows in the Uwekahuna Bluff section (fig. 13.3) in sequence, starting immediately below the Uwekahuna triangulation station on the caldera rim. Each flow unit was marked with a small aluminum tag bearing the appropriate unit number so that our sampling sites could be precisely revisited. We followed an existing trail near the top of the section down to about unit 12, below which we diverted to the north margin of a prominent talus cone (fig. 13.3) for the remainder of the

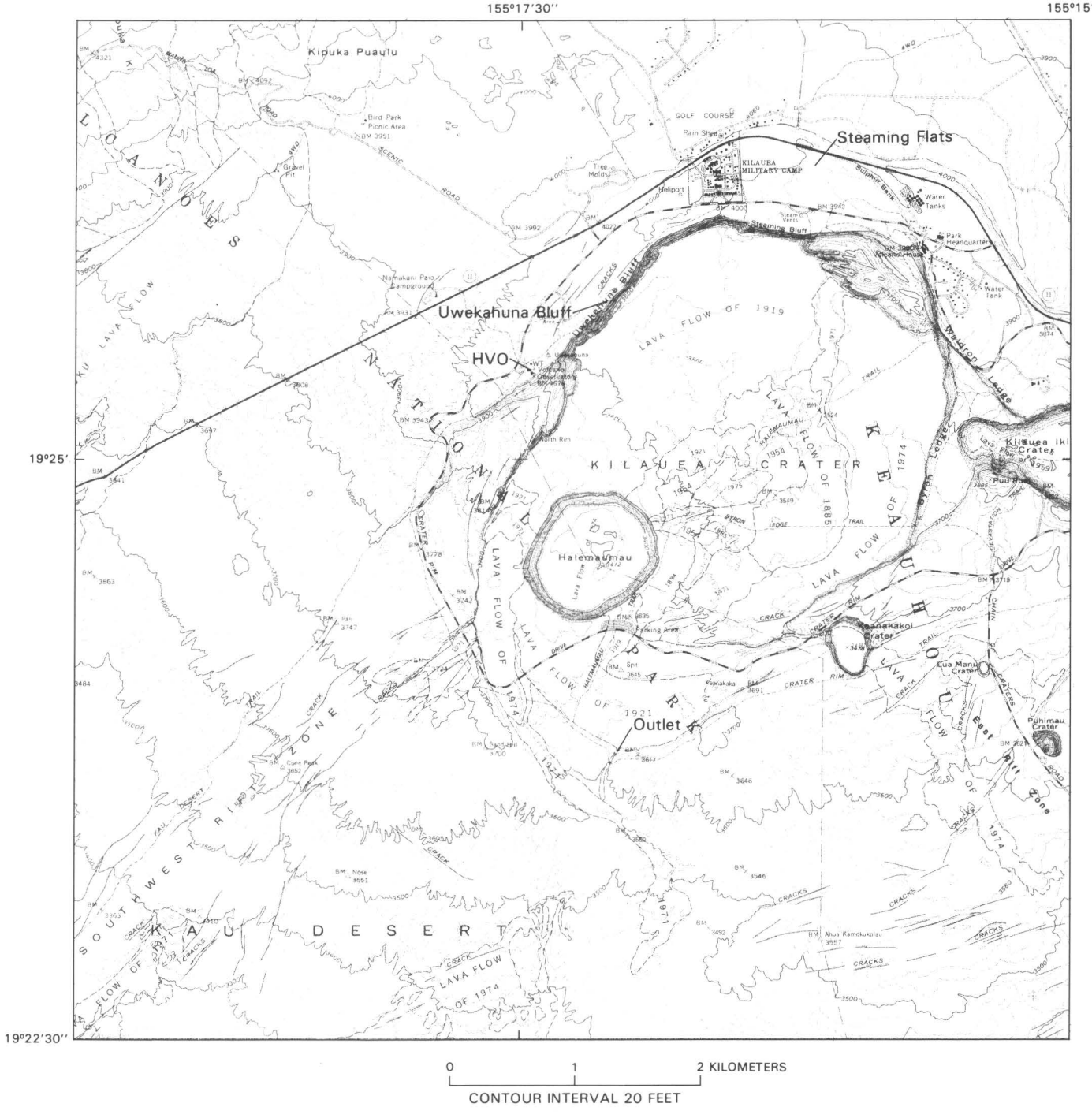

FIGURE 13.2.—Summit area of Kilauea, showing the location of segments of caldera wall examined in this study. Modified from U.S. Geological Survey Kilauea Crater 7.5-minute topographic map, 1981.

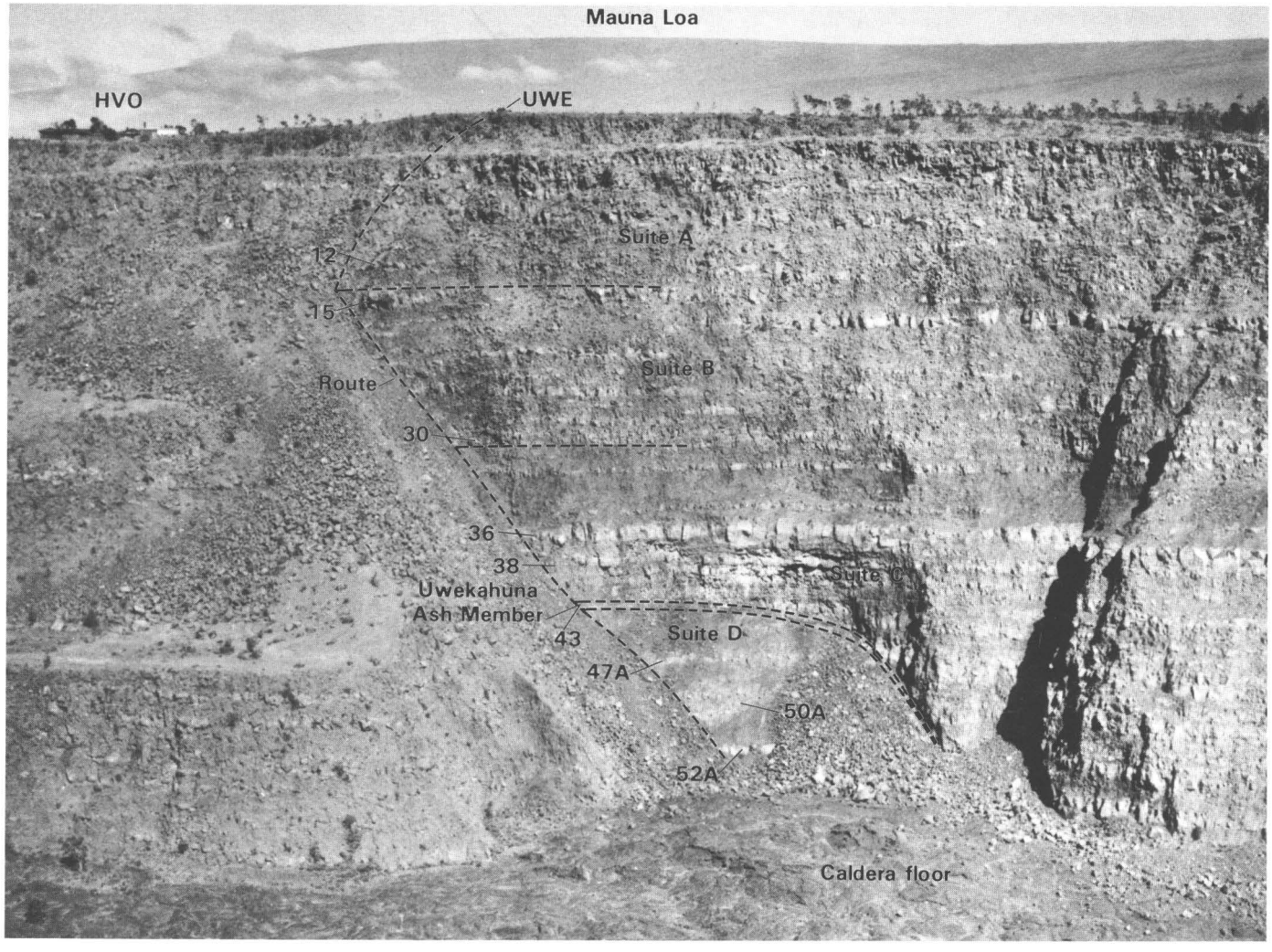

FIGURE 13.3.—Stratigraphic section exposed at Uwekahuna Bluff, with summit of Mauna Loa in distant background. Boundaries of lava suites A–D and position of the Uwekahuna Ash Member of the Puna Basalt are indicated. Selected units are labeled by number. Sampling route is shown by diagonal dashed line descending from Uwekahuna triangulation tower (UWE). HVO, Hawaiian Volcano Observatory. Height of cliff, from unit 52A up to rim, is 135 m.

section. After our sampling of the section in 1980, an earthquake in 1983 triggered rockfalls that buried the lower 50 m of the section, including all units below unit 38 (fig. 13.3).

Field criteria used to delineate lava flows and to distinguish between flows and sills include contact relations, particularly evidence for crosscutting and deformation of host rocks, and the textures of the top and bottom surfaces of a unit. Other features such as color, texture, mineralogy, and vesicle abundance and distribution, were occasionally helpful in tracing a flow unit. When viewed from a distance, the section appeared to have light-colored sills similar to the Uwekahuna laccolith. However, close examination of these suspected sills invariably revealed contact relationships that indicated an extrusive origin. We attempted to subdivide the Uwekahuna Bluff section as thoroughly as possible on the basis of field observations, while recognizing that petrologic considerations might eventually lead us to combine similar flow units into more generalized groups of flows.

The Uwekahuna Bluff section measured by Macdonald (Stearns and Macdonald, 1946, p. 193–194) differs from ours in detail, perhaps owing to different criteria used to distinguish flow units or to a different path selected for descent to the caldera floor.

FIELD OBSERVATIONS

Major features of the lava flows in the Uwekahuna Bluff section are summarized in table 13.1. The stratigraphic section at Uwekahuna Bluff consists of at least 63 flow units and 2 thick tephra deposits. The section is capped by the mostly A.D. 1790 Keanakakoi Ash Member, interpreted as the product of a large phreatomagmatic eruption possibly accompanied by partial caldera collapse (Swanson and Christiansen, 1973; Christiansen, 1979). The basal part of the Uwekahuna Ash Member exposed near the bottom of the bluff section has been assigned an age of 2.1 ka on the basis of radiocarbon dating of material from an inferred correlative

TABLE 13.1.—*Description of rock units from Uwekahuna Bluff section, Kilauea caldera, Hawaii*

[n.d., not determined]

Unit	Thickness (meters)	MgO content (wt percent)	Field description
			Keanakakoi Ash Member
0	0.3–1.0	n.d.	Ash from eruption circa A.D. 1790.
			Suite A flows
1	0.6	6.6	Flow varying in thickness from 0.3 to 1.3 m; vesicular pahoehoe with sparse olivine phenocrysts; reddish, oxidized ropy surface.
2	.9	6.6	Vesicular pahoehoe flow with sparse olivine phenocrysts.
3	4.9	6.6	Massive blocky flow with vesicular top, dense interior, and olivine phenocrysts.
4	2.75	6.8	Vesicular, ropy lava flow with red, ropy top and bottom; well-layered vesicularity; lower 0.6 m of unit is massive, dense; top and bottom flow surfaces dip toward caldera.
5	1.2	6.4	Vesicular, ropy lava flow; no layering of vesicles; similar to unit 4; flow contacts dip toward caldera.
6	4.25	6.7	Vesicular lava flow; top of flow is undulating and shows zones of vesicularity about 0.6 m wide; most of flow interior is dense.
7	.9	6.9	Vesicular flow that pinches out laterally; notably lenticular.
8	.6	6.8	Similar to flow 7.
9	1.5	7.0	Similar to flow 7.
10	3.35	6.7	Dense vesicular flow with rare zones 0.6–0.9 m thick, of dense nonvesicular material; lower 1.3 m is made of 1–3 reddish, oxidized, vesicular layers; base of unit is glassy.
11	4.1	7.3	Dense flow with rubbly, blocky aspect near top; in small gully, flow dips steeply toward crater, and measurement of true thickness is difficult.
12	5.0	6.3	Flow that dips toward caldera 27°–33°; rubble and talus cover in gully; large blocks and boulders cover this interval.
13	.3	6.6	Thin flow with glassy top and bottom.
14	.6	6.4	Thin flow with glassy top and bottom overlying reddish, highly oxidized zone.
			Suite B flows
15	1.7–10.5	7.0	Prominent red, oxidized layer with sharp upper contact; does not extend to south; may be faulted out or covered by rubble; may include several flows; oxidation occurs on fracture surfaces and in vesicles; flows dip toward caldera (maximum dip, 40°, average dip, 25°); reddish layers have a total thickness of 10.5 m; abundant loose blocks make it difficult to distinguish true bedrock.
16	.8	7.3	Distinct, thin flow unit with glassy top and bottom.
17	2.3	7.5	Light-gray rock with tiny olivine phenocrysts and irregular-shaped vesicles.
18	3.3	7.4	Massive flow with glassy top and bottom and dense zones or bands of nonvesicular material.
19	1.45	7.1	Flow with prominent irregular vesicles as large as 3 cm near top; rests on red, oxidized flow top that extends into cliff face to north.
20	.65	7.2	Thin flow, brownish gray and vesicular, that arches over an eye-shaped massive lens (tumulus?) and is overlain by prominent red, oxidized flow top.
21	2.5	7.4	Massive lens; thins rapidly to north.
22	.8	6.7	Unit composed of four thin, glassy vesicular flows with glassy tops.
23	.9–1.5	6.9	Unit of varying thickness, perhaps multiple flow units; highly vesicular with glassy flow tops and bottoms; thickens to north.
24	1.4	7.7	Vesicular flow with glassy top and red, oxidized glassy bottom; surface dips toward caldera.
25	2.1	8.0	Lens-like massive flow that thickens toward gully to south; may be an inflated pahoehoe flow.
26	4.4	7.8	Massive lens(?) of lava between two red, oxidized, vesicular flow contacts; open vugs as large as 1 cm; pipe vesicles in lower 2 m of flow.
27	4.3	7.0	Several thin (less than 1 m) red flows; highly vesicular; flow contacts dip 37°–39° and strike N. 35° E; this unit may be a tumulus.
28	2.4	7.5	Brown flow with irregular vesicles as large as 2 cm near top and dense interior with well-developed pipe vesicles; no coarse-grained zones; vesicles throughout; from a distance this unit may appear to be intrusive; to south this unit dips into gully; to north unit appears to thicken but is in cliff face and not accessible for measurement.
29	2.1	7.3	Similar in appearance to unit 28; massive, vesicular, brown, with glassy vesicular top; note 5 paleomagnetic drill holes 8X080 to 8X084; unit has prominent red, oxidized top and bottom surfaces that dip 21°–24° towards caldera and strike N. 38° E; this unit may be a tumulus.
30	1.9	7.4	Massive flow that thickens to 3.1 m in a 5-m lateral distance; vesicular throughout and highly fractured; brown-red color; a single flow with nearly horizontal top; to north along the cliff face unit appears more dense.
			Suite C flows
31	2.3	17.6	Package of thin, collapsed, shelly pahoehoe flows with excellent continuity to the north; highly vesicular with some ropy surfaces; individual flows from 4–10 cm in thickness; portions of unit contain abundant olivine phenocrysts (20 percent) as large as 5 mm.
32	1.5	18.1	Dense lava flow with obvious northward continuity and abundant olivine; paleomagnetic drill holes 8X075–8X079.
33	6.9	17.2	Prominent unit of numerous thin flows, probably collapsed shelly pahoehoe; flows highly vesicular, reddish, oxidized material, very friable; abundant olivine; flows dip about 5° away from caldera.
34	1.5	14.5	Prominent thin, dense, olivine-bearing lava flow, moderately vesicular; paleomagnetic drill holes 8X070–8X074; unit extends to north along cliff face.
35	2.5	13.7	Thin flows of collapsed shelly pahoehoe with prominent olivine phenocrysts (5–10 percent); unit dips 22° toward caldera.
36	3.3	13.2	Massive gray flow unit with lateral continuity to north; vesicular with prominent curving fractures; paleomagnetic drill holes 8X065–8X069; contains less olivine (up to 5 percent phenocrysts as large as 3 mm) than overlying units.
37	3.0	17.3	Gray-brown massive flow unit with large vesicles near top and dense interior; dips 10° toward caldera; poor lateral continuity, may be a lens; paleomagnetic drill holes 8X060–8X064.
38	2.4	9.0	Flow that interfingers with unit 37 to north, where units become difficult to distinguish; both have red, oxidized tops.
39	2.3	14.5	Unit composed of several thin horizontal layers 0.2–0.3 m thick; abundant (10 percent) olvine phenocrysts as large as 4 mm; paleomagnetic drill holes 1D070–1D075.
40	3.0	10.1	Massive, vesicular unit that becomes indistinct to north; contains abundant olivine (5 percent) as large as 2 mm but mostly less than 1 mm.
41	3.1	14.0	Vesicular unit that looks like aa flow, jumble of thin flows, and rubble; lower contact is red surface; contact with overlying flow is indistinct; contains abundant (5–10 percent) olivine as large as 3 mm.
42	1.3	19.7	Dense, vesicular flow above Uwekahuna Ash Member; paleomagnetic drill holes 1D076–1D083; abundant (10–15 percent) olivine phenocrysts with some lenses and pods containing as much as 50 percent olivine.

TABLE 13.1.—*Description of rock units from Uwekahuna Bluff section, Kilauea caldera, Hawaii*—Continued

Unit	Thickness (meters)	MgO content (wt percent)	Field description
			Beneath unit 42
43	1.5–2.2	6.5–9.7	Uwekahuna Ash Member.
			Flows of suite C ponded against Uwekahuna Ash Member
44	3.6	9.2	Upper 0.9 m, red rubble and vesicular flow with pipe vesicles; middle 1.2 m, massive flow with large, irregular vesicles; lower 1.5 m, dense, massive flow unit with finger-shaped gas vesicles.
45	7.1	13.0	Thick, massive unit overlain by 0.2–0.6 m, of reddish rubble; unit contains trains of vesicles in middle 1.5–2 m; olivine phenocrysts as large as 5 mm locally make up 10–15 percent of rock; obvious lateral continuity to north; flow has shattered or fractured appearance; bottom of unit rests on red, rubbly oxidized flow top.
46	1.8	13.3	Red, vesicular, blocky flows; several lobes of one or more flows, each with a well-preserved black glassy surface; fractured, with abundant olivine.
47	1.3	13.0	Gray-green massive flow with large irregular vesicles; olivine phenocrysts as large as 7 mm make up about 15 percent of rock; lower contact is glassy top of underlying flow unit 48.
48	3.2	9.8	Gray-green vesicular massive flow with abundant olivine as large as 3 mm.
49	.6	10.4	Olivine-rich (phenocrysts as large as 2 mm) pahoehoe flow overlying an aa flow.
50	2.7	10.1	Aa flow; top 1.5 m is rubble overlying dense interior; white sublimates on surface of blocks in rubble.
51	2.0	7.5	Dense flow overlying ash; contains portions of what may be foundered crust.
			Uwekahuna Ash Member beneath unit 51
---	4.8	---	Uwekahuna Ash Member here is 1.4 m thick; base of ash covered by 3.4 m of talus extending down to 1919 flows on caldera floor.
			Suite D flows
44A	0.6	n.d.	Scoriaceous rubble; possibly an aa flow top or scoria from nearby vent.
45A	2.4	n.d.	Massive, non-porphyritic, vesicular lava flow; lower 1.5 m forms prominent bench.
46A	1.6	n.d.	Mantled rubble, possibly infiltrated by tephra from unit 43; lower contact indistinct and highly oxidized, with some smooth, glassy (pahoehoe?) surfaces.
47A	2.4	7.1	Prominent massive flow clearly visible in fig. 13.3; fine-grained and vesicular, with weathered surface that is light colored; two paleomagnetic drill holes 1.2 m from lower contact, others may be covered by talus from the November 1975 earthquake; sample from dense lower portion of flow near paleomagnetic holes.
48A	4.2	n.d.	Rubble-covered flow; massive and vesicular; interior mostly covered by talus and ash from above, but appears to be dense and blocky; two paleomagnetic drill holes in lower portion of unit may be in an erratic boulder.
49A	1.8	n.d.	Massive, vesicular lava flow with buff weathered surface; flinty or glassy surface at top; unit contains eight paleomagnetic drill holes about 20 cm from lower contact.
50A	2.5	7.4	Massive flow unit with both vesicular and dense portions; dark gray in fresh outcop, but buff on weathered surface; sampled near base of flow.
51A	4.2	n.d.	Flow 1.5 m below base of unit 50A; surface dips 32° toward caldera; most of interval is covered by rubble and talus overlying massive, buff unit 52A.
52A	2.2	7.8	Massive, dense unit at base of section; contains unusual texture, similar to that of foundered crust from Kilauea Iki drill holes—dense non-vesicular lenses interlayed with vesicular material; samples from middle of unit.
53A	4.1	n.d.	Talus-covered slope to caldera floor, which here consists of 1919 flow.

unit outside of the caldera (Lockwood and Rubin, 1986). Based on the wider dispersal of the Uwekahuna Ash Member, its eruptions were probably more violent than eruption of the Keanakakoi (Dzurisin and Casadevall, 1986).

Flows in the Uwekahuna Bluff section can be grouped into four suites differing in hand-specimen mineralogy and field occurrence (fig. 13.3). Suite A (units 1–14), at the top of the section, includes numerous thin lenticular pahoehoe flows containing small (less than 5 mm) plagioclase laths and rare olivine phenocrysts. A few thicker and more massive flows occur in this suite, but these usually lack the lateral persistence of similar massive flows lower in the section.

Suite B (units 15–30) consists of flows that contain rare phenocrysts of olivine and plagioclase. The glassy upper surface of flow 15, the youngest in suite B, is strongly weathered and pale yellow to red-brown. The texture of this surface is preserved, and no soil was found on it. This weathered surface is the only physical evidence we discovered for a significant time break within the Uwekahuna Bluff section; it correlates with the change from the mostly aphyric flows of suite B to the porphyritic flows of suite A.

Suite C (units 31–42 and 44–51; unit 43 is the Uwekahuna Ash Member) contains flows having abundant olivine phenocrysts and little or no plagioclase visible in hand specimen. The olivine content in individual flows varies greatly and probably reflects crystal settling during flow (Fuller, 1939). We generally selected only one sample from each flow, and this is insufficient to characterize the olivine content of the entire flow. Several units consist of packages of thin (a few centimeters thick) highly vesicular layers interpreted as near-vent shelly pahoehoe flows that collapsed because of degassing and the weight of overlying flows (Swanson, 1973). A few units (for example, unit 36) are more massive and have dense interiors. These usually have appreciable lateral continuity and can be traced northward in the wall for as much as 2 km.

The Uwekahuna Ash Member (unit 43) underlies suite C. Along the south side of Uwekahuna Bluff, the ash directly underlies unit 42, about 35 m above the caldera floor (fig. 13.3). Farther north, the ash mantles an old northeast-facing slope and drops to within a few meters of the caldera floor (fig. 13.3). Ponded against this slope and overlying the ash are olivine-rich aa and pahoehoe lava flows (units 44–51), which petrographically and chemically resemble units 31–42.

Suite D (units 44A–52A) contains fairly massive and sparsely vesicular aphyric flows beneath the Uwekahuna Ash Member. Most are poorly exposed because of mantling by talus and ash from above. The near absence of olivine phenocrysts makes these flows petrographically distinct from those of suite C. Flows of suite D are

exposed in a 30-m-thick section that is cut off by a northeast-facing slope mantled by the Uwekahuna Ash Member and buried by the flows of suite C (fig. 13.3). North of Uwekahuna Bluff, the ash is essentially horizontal and extends for more than 1.5 km at a constant level above the caldera floor (Powers, 1948), which level corresponds to the lower elevation of the ash in the bluff section. The horizontal ash layer probably covered a broad, relatively flat surface, similar to that of the present caldera floor.

PETROGRAPHY

We examined 57 thin sections of rocks from Uwekahuna Bluff. Nearly all samples contain olivine phenocrysts in a holohyaline to holocrystalline groundmass. Most groundmass textures are intersertal, with brown glass between microlites. Intergranular texture is most common in the dense flow interiors, particularly in those from picritic units 44–51. Crystallinity ranges from about 25 to 85 percent. In the more crystalline samples, the groundmass consists of clinopyroxene and plagioclase in overlapping or felted microlites too small for individual crystals to be recognized. Most samples contain dark brown glass and scattered small anhedral opaque grains. Olivine is present as euhedral to subhedral phenocrysts that range in shape from stout and prismatic to elongate and lathlike. In most flows, a few olivine crystals occur in the microcrystalline groundmass. The olivine microlites and phenocrysts are in general partly resorbed and corroded. Clinopyroxene and plagioclase occur as coarse granular aggregates of subhedal crystals in which pyroxene subophitically or ophitically encloses plagioclase, as rosettes or sprays of clinopyroxene and plagioclase, and less commonly as individual phenocrysts and microlites.

Modal abundances for thin sections from 21 flows were determined by standard point-count methods (fig. 13.4). Microlites (0.05–1 mm) of plagioclase, clinopyroxene, and olivine; phenocrysts (greater than 1 mm) of plagioclase, clinopyroxene, and olivine; groundmass (microlites less than 0.05 mm); and vesicles were counted. Hypersthene was looked for but not found. Flows of suite C form a distinct cluster because of their high olivine content. Flows of suites B and D contain only sparse olivine and plagioclase, and flows of suite A are similar to the aphyric lavas except in their greater abundance of plagioclase.

CHEMISTRY

The basalt lavas of Uwekahuna Bluff are olivine tholeiite similar to other Kilauea summit flows (Macdonald, 1949; Wright, 1971; Wright and Tilling, 1980). Units 1–51 and 47A, 50A, and 52A were analyzed for major-element composition by rapid rock-analytical methods (Shapiro, 1975) and for trace-element and rare-earth-element compositions by instrumental neutron-activation (Baedecker, 1979) and atomic-absorption techniques (table 13.2). Precisions for major-element oxides (variation in percent of reported weight percent value) in rocks of basaltic composition are as follows: SiO_2 (0.3), Al_2O_3 (0.2), CaO (0.2), MgO (0.1), Na_2O (0.1), K_2O (0.1), Fe total (0.1), TiO_2 (0.05), P_2O_5 (0.04), MnO (0.04). Error limits (variation in percent of reported ppm value) for trace-element analyses for one standard deviation (one sigma) are as follows: Ba (10–20), Co (1), Cr (1), Hf (2), Rb (25–30), Ta (3), Th (6–12), Zn (2), Zr (10), Sc (1), La (1–2), Ce (2), Nd (7–17), Sm (1), Eu (1), Gd (8–25), Tb (2–3), Tm (5–15), Yb (3), Lu (3). For Cu, Co, and Ni values determined by atomic absorption methods, uncertainties are ±2 percent of reported ppm value. To facilitate comparison of chemical data, we have recalculated all analyses from table 13.2 on a dry-weight basis after converting iron to FeO_t ($FeO_t = FeO + 0.9Fe_2O_3$). The recalculated analyses are plotted on MgO variation diagrams (fig. 13.5), following Powers (1955) and Wright (1971, 1974).

MAJOR-ELEMENT CHEMISTRY

The major-element compositions of units 1–30 (suites A and B) and 47A, 50A, and 52A (suite D) are broadly similar (fig. 13.5A) and vary only slightly with stratigraphic position (fig. 13.6A). The MgO contents in all these units lie between 6.4 and 8.0 weight percent (table 13.2). Flow units 31 through 51 (suite C), however, contain various amounts of olivine, and their MgO contents range from 7.5 to 19.7 weight percent. The chemistries of units 31–51 show considerable variation with stratigraphic position (fig. 13.6A) because of differing olivine contents within each picritic flow. This wide range in olivine content for the picritic flows of suite C facilitates precise calculation of olivine-control lines by linear least-squares regression. This procedure yields equations of the form $y = ax + b$, where y is the major oxide or element, x is the MgO content, a is the slope, and b is the y intercept value at MgO = 0 weight percent (table 13.3). Most oxides correlate negatively with MgO (fig. 13.5A), indicating the diluting effect of increasing olivine content on elements that do not enter the olivine crystal structure.

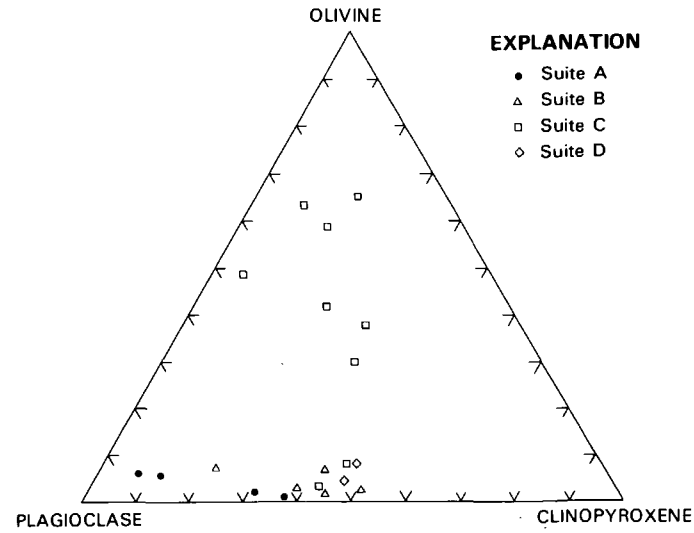

FIGURE 13.4.—Ternary diagram (clinopyroxene-olivine-plagioclase) derived from volumetric modal analyses (1,000 points per thin section) of 21 flows from Uwekahuna Bluff section.

TABLE 13.2.—*Chemical analyses of Uwekahuna Bluff samples*

[Values for oxides in weight percent; values for trace elements in parts per million. Symbols P, X, O, A, and U used to distinguish lava suites A–D and Uwekahuna Ash Member, respectively, in figs. 13.4–13.6 and 13.10. INAA, neutron-activation analysis; AA, atomic-absorption analysis; n.d., not determined; <, less than]

Sample	UWE-1	UWE-2	UWE-3	UWE-4	UWE-5	UWE-6	UWE-7	UWE-8	UWE-9	UWE-10	UWE-11	UWE-12
symbol	P	P	P	P	P	P	P	P	P	P	P	P
SiO_2	50.8	51.1	51.0	50.4	51.6	51.1	51.2	51.2	51.3	50.8	50.4	51.3
Al_2O_3	14.0	14.0	13.8	13.9	13.8	13.8	13.7	13.6	13.9	13.8	13.6	13.8
Fe_2O_3	2.5	5.7	2.9	6.7	5.3	5.2	6.6	4.3	4.1	4.5	3.2	6.7
FeO	8.9	5.9	9.1	5.8	7.4	7.2	5.6	7.5	7.7	8.0	8.4	5.7
MgO	6.6	6.6	6.6	6.8	6.4	6.7	6.9	6.8	7.0	6.7	7.3	6.3
CaO	10.5	10.7	10.6	10.5	10.6	10.7	10.7	10.7	10.5	10.7	11.2	10.7
Na_2O	2.5	2.3	2.4	2.4	2.5	2.4	2.4	2.4	2.4	2.5	2.3	2.5
K_2O	.47	.44	.47	.46	.46	.47	.44	.44	.44	.45	.42	.42
H_2O	.16	.21	.16	.18	.03	.30	.15	.10	.11	.17	.12	.29
TiO_2	2.6	2.5	2.6	2.5	2.6	2.6	2.4	2.6	2.4	2.5	2.3	2.6
P_2O_5	.31	.32	.32	.31	.32	.30	.29	.31	.30	.31	.29	.32
MnO	.22	.16	.18	.20	.18	.17	.17	.17	.18	.17	.16	.18
Ba	152	104	135	144	106	139	132	111	104	116	105	124
Co (INAA)	43	43	43	42	43	42	44	44	43	43	44	43
Co (AA)	44	44	44	46	42	44	43	46	44	42	42	44
Cr	353	336	309	338	313	327	366	331	351	313	354	235
Ni	96	100	93	91	80	91	110	98	100	87	93	82
Cu	130	120	99	130	130	95	120	130	130	120	92	140
Hf	4.06	3.93	4.05	3.85	4.13	4.00	3.85	4.02	3.92	4.00	3.57	4.05
Rb	<8	<20	16	10	9	12	15	13	13	14	<20	8
Ta	.94	.96	.95	.86	.97	.92	.88	.86	.81	.91	.83	.85
Th	.98	.84	.94	.88	.90	.83	.92	.78	.90	.89	.82	.83
U	<0.3	<0.3	<0.3	<0.3	.5	<0.3	<0.3	<0.3	<0.3	<0.3	<0.3	<0.4
Zn	112	108	111	105	118	111	108	113	110	110	109	116
Zr	152	164	181	158	152	159	138	159	151	182	145	117
Sc	31.0	31.0	30.7	30.8	32.1	30.7	30.6	31.6	31.0	31.7	33.4	33.0
La	12.7	12.7	12.9	11.9	12.8	11.8	11.7	11.8	11.6	11.8	10.8	10.9
Ce	31.6	29.9	30.3	28.5	31.3	29.5	29.5	28.9	28.2	29.7	26.5	27.8
Nd	19	21	20	12	22	20	20	21	22	24	20	18
Sm	5.83	5.76	5.89	5.66	6.09	5.66	5.68	5.81	5.57	5.80	5.28	5.80
Eu	1.93	1.89	1.91	1.83	2.04	1.88	1.90	1.92	1.89	1.92	1.78	1.93
Gd	5.8	6.6	5.8	6.1	7.4	6.4	5.8	6.4	7.1	6.9	5.9	6.0
Tb	1.02	.96	.98	.96	1.02	.95	.92	.96	.88	1.00	.88	1.01
Tm	.33	.17	.29	.29	.31	.35	.34	.39	.34	.39	.34	.41
Yb	2.22	2.25	2.18	2.26	2.48	2.17	2.25	2.31	2.09	2.18	2.08	2.48
Lu	.311	.299	.308	.301	.307	.290	.294	.309	.287	.319	.296	.340

Sample	UWE-13	UWE-14	UWE-15-1	UWE-15-2	UWE-16	UWE-17	UWE-18	UWE-19	UWE-20	UWE-21	UWE-22	UWE-23
symbol	P	P	X	X	X	X	X	X	X	X	X	X
SiO_2	51.4	50.8	51.6	51.2	50.3	51.1	51.7	50.8	50.4	51.3	50.4	50.7
Al_2O_3	13.7	14.0	13.5	13.7	13.7	13.7	13.6	13.6	13.8	13.4	13.6	13.3
Fe_2O_3	7.7	4.9	4.4	3.3	4.1	3.4	2.6	5.1	4.8	3.0	4.0	3.0
FeO	5.2	7.4	8.1	8.6	8.1	8.7	9.1	6.5	7.3	9.4	8.1	9.4
MgO	6.6	6.4	7.0	6.5	7.3	7.5	7.4	7.1	7.2	7.4	6.7	6.9
CaO	10.7	10.6	10.5	10.6	10.6	10.7	10.6	10.6	10.8	10.9	10.8	10.8
Na_2O	2.5	2.4	2.4	2.3	2.3	2.3	2.3	2.3	2.3	2.3	2.4	2.3
K_2O	.44	.43	.40	.40	.38	.38	.39	.38	.42	.42	.46	.47
H_2O	.06	.10	.05	.09	.14	.11	.07	.52	.29	.14	.25	.03
TiO_2	2.6	2.5	2.6	2.5	2.4	2.4	2.4	2.4	2.4	2.5	2.7	2.7
P_2O_5	.32	.30	.31	.28	.30	.30	.29	.28	.30	.30	.31	.30
MnO	.18	.18	.17	.17	.17	.16	.17	.17	.17	.17	.18	.17
Ba	90	97	<200	81	108	83	89	105	115	118	137	129
Co (INAA)	42	41	45	44	46	45	46	45	44	46	45	45
Co (AA)	42	42	44	44	46	48	46	48	44	46	44	48
Cr	266	235	415	287	354	386	354	351	344	316	252	265
Ni	91	84	100	96	100	110	110	100	110	110	80	87
Cu	140	140	120	110	120	100	110	120	120	98	140	120
Hf	3.74	3.76	3.68	3.81	3.67	3.48	3.66	3.67	3.59	4.00	4.05	4.06
Rb	12	9	<20	<20	<20	11	<20	<20	<20	12	11	<20
Ta	.80	.76	.74	.77	.74	.75	.77	.75	.79	.86	1.05	.99
Th	.73	.83	.66	.74	.74	.70	.77	.71	.69	.74	.91	.91
U	<0.3	0.30	<0.4	<0.4	<0.4	<0.3	<0.4	<0.4	<0.4	<0.4	0.30	<0.4
Zn	110	110	113	109	107	109	108	113	104	110	113	113
Zr	130	161	148	120	142	152	132	129	135	121	149	140
Sc	32.0	31.4	32.4	33.1	33.0	32.1	32.4	32.0	31.8	33.5	32.8	32.3
La	10.7	10.8	10.1	10.4	9.9	10.2	10.5	10.4	10.5	13.0	12.1	12.8
Ce	26.5	26.8	25.6	26.5	25.8	25.6	26.6	26.0	26.8	27.9	31.1	30.4
Nd	16	21	18	19	16	19	19	19	19	23	20	23
Sm	5.61	5.70	5.50	5.44	5.26	5.26	5.40	5.40	5.40	5.80	5.90	5.90
Eu	1.83	1.85	1.82	1.82	1.76	1.75	1.79	1.76	1.77	1.87	1.94	1.95
Gd	7.1	7.1	5.5	5.4	6.2	6.7	6.1	6.1	5.8	4.3	7.9	7.5
Tb	.93	.94	.97	.96	1.01	.91	.95	.93	.94	.98	.99	.95
Tm	.35	.39	.38	.35	.33	.32	.31	.26	.33	.30	.43	.29
Yb	2.25	2.34	2.35	2.12	2.19	2.17	2.27	2.10	2.03	2.42	2.37	2.20
Lu	.340	.319	.312	.299	.303	.301	.306	.301	.301	.300	.301	.322

Sample	UWE-24	UWE-25-1	UWE-25-2	UWE-26	UWE-27	UWE-28	UWE-29	UWE-30-1	UWE-30-2	UWE-31	UWE-32	UWE-33
symbol	X	X	X	X	X	X	X	X	X	O	O	O
SiO_2	50.0	50.7	50.6	50.9	50.6	50.5	50.8	50.5	50.8	47.6	47.7	47.7
Al_2O_3	13.4	13.5	13.3	13.3	13.7	13.5	13.2	13.3	14.0	9.9	10.2	10.1
Fe_2O_3	4.4	2.6	3.3	4.0	6.9	4.7	5.3	5.0	3.3	3.4	3.2	6.0
FeO	8.1	9.4	9.2	8.7	6.0	8.0	7.6	7.1	8.5	8.5	8.7	6.9
MgO	7.7	8.0	7.8	7.8	7.0	7.5	7.3	7.4	6.5	17.6	18.1	17.2
CaO	11.1	11.4	11.1	10.9	11.0	10.9	11.0	10.9	10.6	7.9	9.0	9.0
Na_2O	2.0	2.3	2.3	2.2	2.4	2.5	2.5	2.2	2.5	1.5	1.6	1.6

TABLE 13.2.—*Chemical analyses of Uwekahuna Bluff samples*—Continued

Sample symbol	UWE-1 P	UWE-2 P	UWE-3 P	UWE-4 P	UWE-5 P	UWE-6 P	UWE-7 P	UWE-8 P	UWE-9 P	UWE-10 P	UWE-11 P	UWE-12 P
K_2O	.45	.43	.43	.42	.44	.50	.47	.43	.45	.30	.29	.30
H_2O	.14	.08	.50	.07	.23	.24	.09	.22	.12	.41	.19	.28
TiO_2	2.1	2.4	2.4	2.4	2.6	2.5	2.6	2.5	2.5	1.8	1.8	1.9
P_2O_5	.29	.26	.28	.28	.29	.29	.31	.29	.31	.18	.21	.23
MnO	.20	.18	.17	.16	.18	.17	.18	.18	.17	.16	.15	.17
Ba	106	114	108	131	142	132	155	151	95	n.d.	140	96
Co (INAA)	46	48	47	48	44	45	46	45	43	n.d.	76	72
Co (AA)	49	49	48	49	46	46	44	44	44	n.d.	74	74
Cr	403	440	456	461	321	332	346	372	309	n.d.	1100	1040
Ni	110	120	120	130	89	96	100	110	89	n.d.	760	740
Cu	120	95	91	110	120	130	120	130	110	n.d.	90	96
Hf	3.83	3.57	3.61	3.69	3.90	3.97	3.86	3.74	4.01	n.d.	2.98	2.95
Rb	15	<20	<20	13	13	12	<20	<20	<10	n.d.	<20	14
Ta	.92	.82	.84	.94	1.01	.98	1.01	1.02	.85	n.d.	.72	.75
Th	.85	.88	.64	.88	.99	.84	.86	.85	.81	n.d.	.52	.60
U	<0.4	<0.4	<0.4	.16	<0.5	.27	.21	.24	.30	n.d.	<0.5	.27
Zn	111	110	109	107	111	109	114	109	108	n.d.	105	102
Zr	144	146	168	135	167	162	127	166	147	n.d.	131	103
Sc	31.5	32.8	32.7	32.7	32.0	31.6	32.5	33.0	31.4	n.d.	26.0	25.3
La	12.2	10.6	11.0	11.4	12.7	12.4	13.3	12.6	12.2	n.d.	8.9	9.29
Ce	28.0	26.1	26.6	27.4	30.7	30.5	30.6	30.5	29.7	n.d.	22.7	22.9
Nd	22	18	16	23	23	22	21	21	26	n.d.	18	15.8
Sm	5.84	5.30	5.40	5.50	6.10	5.80	6.00	5.85	6.00	n.d.	4.42	4.23
Eu	1.81	1.70	1.73	1.79	1.85	1.86	1.84	1.80	1.92	n.d.	1.38	1.37
Gd	6.7	5.6	6.4	5.2	5.2	6.6	5.7	5.9	7.2	n.d.	3.4	3.6
Tb	.99	.87	.87	.88	.94	.92	.97	.91	1.00	n.d.	.79	.65
Tm	.35	.35	.39	.32	.33	.31	.32	.33	.37	n.d.	.31	.213
Yb	2.03	2.02	2.11	2.09	2.19	2.05	2.07	2.00	2.47	n.d.	1.73	1.65
Lu	.299	.270	.280	.310	.313	.309	.34	.27	.317	n.d.	.26	.238

Sample symbol	UWE-34 O	UWE-35 O	UWE-36 O	UWE-37 O	UWE-38 O	UWE-39 O	UWE-40 O	UWE-41 O	UWE-42 O	UWE-43 U	UWE-44 O	UWE-45 O
SiO_2	48.6	48.6	48.8	48.0	50.5	49.0	49.4	48.9	47.2	50.8	50.8	49.2
Al_2O_3	11.2	11.4	11.6	10.0	13.2	10.8	12.4	11.6	9.4	13.2	13.0	10.7
Fe_2O_3	5.4	8.1	4.8	3.0	4.8	4.0	4.0	5.8	3.3	3.1	4.0	3.3
FeO	6.8	4.6	7.4	9.3	6.5	8.8	7.9	6.4	9.6	8.0	7.6	9.7
MgO	14.5	13.7	13.2	17.3	9.0	14.5	10.1	14.0	19.7	9.5	9.2	13.0
CaO	9.6	9.5	10.0	8.4	10.5	8.9	10.5	9.5	8.3	10.2	10.9	8.8
Na_2O	1.7	1.8	1.9	1.7	2.2	1.8	2.0	2.0	1.5	1.9	2.2	2.0
K_2O	.30	.35	.39	.34	.41	.39	.43	.37	.26	.42	.42	.46
H_2O	.11	.19	.64	.18	.30	.27	.40	.15	.27	.27	.20	.24
TiO_2	2.1	2.2	2.2	1.8	2.5	2.2	2.4	2.2	1.5	2.4	2.5	2.8
P_2O_5	.23	.25	.26	.22	.29	.25	.31	.27	.17	.29	.29	.36
MnO	.19	.15	.18	.17	.17	.16	.16	.14	.18	.16	.16	.16
Ba	99	96	<100	<200	<200	<200	86	90	<200	107	81	120
Co (INAA)	65	62	63	76	48	71	53	62	85	50	45	64
Co (AA)	66	63	66	79	50	72	58	68	85	53	50	68
Cr	961	869	887	1090	602	987	687	861	1260	535	626	790
Ni	580	490	490	790	230	600	320	490	870	230	220	500
Cu	100	95	89	78	120	100	110	110	53	110	120	120
Hf	3.06	3.26	3.43	2.72	3.8	3.30	3.61	3.32	2.33	3.30	3.7	4.15
Rb	11	10	<30	13	18	<30	11	<30	<30	8	<30	13
Ta	.79	.81	.87	.64	.91	.87	.91	.86	.56	.85	.95	1.09
Th	.67	.70	.65	.51	.75	.65	.67	.60	.52	.82	.73	.70
U	<0.5	.35	<0.4	<0.5	.23	<0.3	<0.5	.33	<0.4	.40	.44	.31
Zn	104	106	112	108	119	107	109	109	108	103	100	122
Zr	104	103	140	<100	131	<200	148	178	120	154	136	152
Sc	27.1	27.2	27.7	24.6	31.2	27.3	29.6	27.5	24.2	28.1	30.1	28.3
La	9.88	10.2	11.0	8.3	11.6	10.3	11.5	10.6	7.0	11.7	12.4	12.9
Ce	24.1	24.8	26.6	21.1	27.6	25.6	27.0	24.9	18.3	26.6	28.3	30.4
Nd	16.9	17.7	22	13	24	16	19	18	11	21	18	23
Sm	4.50	4.72	5.13	4.11	5.44	4.81	5.31	5.00	3.47	5.56	5.59	5.93
Eu	1.50	1.53	1.65	1.37	1.81	1.55	1.70	1.56	1.16	1.62	1.76	1.83
Gd	3.8	3.6	6.2	4.8	6.7	5.5	6.5	5.3	4.1	6.0	6.4	6.0
Tb	.71	.72	.88	.62	.97	.77	.85	.84	.58	.80	.96	.96
Tm	.20	.241	.27	.22	.38	.27	.31	.29	.19	.40	.29	.32
Yb	1.76	1.83	1.93	1.56	2.24	1.76	2.13	1.85	1.45	2.02	2.23	2.24
Lu	.259	.265	.287	.238	.34	.25	.299	.27	.21	.310	.30	.319

Sample symbol	UWE-46 O	UWE-47 O	UWE-48 O	UWE-49 O	UWE-50 O	UWE-51 O	UWE-47A A	UWE-50A A	UWE-52A A
SiO_2	49.0	47.4	47.5	48.4	50.0	50.1	49.8	50.0	49.6
Al_2O_3	11.5	11.5	12.4	12.4	12.8	13.1	13.6	13.2	13.5
Fe_2O_3	3.9	3.7	2.4	5.0	2.7	2.4	3.0	3.0	3.4
FeO	8.5	8.8	9.8	7.0	9.0	9.2	8.5	9.0	8.3
MgO	13.3	13.0	9.8	10.4	10.1	7.5	7.1	7.4	7.8
CaO	9.0	10.4	12.2	11.2	11.2	11.4	12.1	11.1	11.3
Na_2O	1.9	2.0	2.3	2.2	2.1	2.2	2.2	2.3	2.3
K_2O	.35	.37	.41	.42	.39	.44	.49	.50	.44
H_2O	.82	.24	.30	.08	.19	.36	.54	.36	.52
TiO_2	2.3	2.2	2.6	2.5	2.3	2.6	2.7	2.6	2.6
P_2O_5	.25	.29	.22	.33	.26	.31	.31	.29	.29
MnO	.18	.18	.20	.18	.18	.18	.18	.20	.18
Ba	<200	<200	120	133	103	123	148	128	127
Co (INAA)	68	61	51	52	54	45	44	44	45
Co (AA)	75	67	56	58	60	52	48	50	50
Cr	946	753	555	597	739	395	285	334	347

TABLE 13.2.—*Chemical analyses of Uwekahuna Bluff samples*—Continued

Sample symbol	UWE-46 O	UWE-47 O	UWE-48 O	UWE-49 O	UWE-50 O	UWE-51 O	UWE-47A A	UWE-50A A	UWE-52A A
Ni	670	460	220	240	290	120	100	110	120
Cu	71	100	130	120	98	100	91	67	110
Hf	2.99	3.5	3.8	3.68	3.4	3.9	4.01	3.98	3.8
Rb	<30	<30	<30	14	<30	15	<30	14	<20
Ta	.70	.93	1.02	.94	.85	1.03	1.10	1.13	1.08
Th	.70	.73	.80	.78	.68	.86	.97	.98	.92
U	.28	<0.5	<0.5	.29	.32	<0.6	<0.5	.30	<0.6
Zn	108	106	113	113	101	121	106	115	112
Zr	102	<200	140	130	152	154	125	202	179
Sc	25.4	27.2	29.9	30.0	30.0	31.8	31.1	31.4	31.3
La	9.6	11.1	12.7	11.7	10.7	12.4	13.4	13.8	13.3
Ce	23.9	26.9	29.8	28.3	26.3	29.3	32.4	32.7	31.3
Nd	21	18	19	20	15	20	24	21	23
Sm	4.61	5.28	5.83	5.48	5.11	5.75	5.82	5.88	5.61
Eu	1.46	1.68	1.88	1.81	1.69	1.89	1.93	1.92	1.84
Gd	4.6	6.1	6.4	6.2	5.6	7.0	7.2	6.9	5.8
Tb	.72	.80	1.00	.90	.75	.91	.95	.91	.88
Tm	.29	.28	.33	.35	.28	.34	.32	.31	.27
Yb	1.80	2.06	2.24	2.19	1.89	2.25	2.19	2.17	2.05
Lu	.244	.27	.30	.297	.27	.34	.36	.304	.297

TABLE 13.3.—*Olivine control lines*

[Coefficients for equations of the form $y = ax + b$, where y is the major oxide or element, x is the MgO content, a is the slope, and b is the y intercept value at MgO = 0 weight percent. Values for oxides in weight percent; values for trace elements in parts per million; uncertainty is one standard deviation either side of the mean slope. Data for PHKILCAL (prehistoric Kilauea caldera and Hilina flows), KIL1959 (Kilauea Iki, 1959), HISTML (historic Mauna Loa), and PPPC (prehistoric pahoehoe picrite complex flows from Wright, 1971). FeO_t, total iron oxide = $FeO + 0.9\ Fe_2O_3$; n.d., not determined]

	Suites A–D		Suite C		PPPC		PHKILCAL		KIL1959		HISTML	
Element	(*a*)	(*b*)	(*a*)	(*b*)	(*a*)	(*b*)	(*a*)	(*b*)	(*a*)	(*b*)	(*a*)	(*b*)
SiO_2	−0.315±.028	52.842	−0.248±.064	51.828	−0.289±0.023	52.894	−0.317±0.021	53.327	−0.266±0.005	51.922	−0.312±0.010	54.260
Al_2O_3	−.348±.012	16.036	−.336±.025	15.852	−.357±.010	16.643	−.354±.028	16.585	−.325±.008	15.943	−.338±.007	16.527
FeO_t	.027±.020	11.456	.071±.037	10.811	.068±.017	10.480	.081±.030	10.260	.035±.003	11.046	.025±.006	10.747
CaO	−.204±.027	12.298	−.306±.056	12.797	−.288±.017	12.184	−.266±.016	13.044	−.284±.010	12.674	−.263±.005	12.400
Na_2O	−.073±.005	2.852	−.070±.008	2.822	−.053±.007	2.691	−.065±.005	2.753	−.059±.002	2.705	−.059±.003	2.702
K_2O	−.013±.002	.524	−.015±.003	.556	−.014±.003	.561	−.012±.003	.497	−.015±.001	.658	−.006±.002	.409
TiO_2	−.060±.008	2.946	−.086±.015	3.348	−.065±.006	2.906	−.057±.012	2.843	−.072±.003	3.263	−.045±.004	2.380
P_2O_5	−.009±.001	.359	−.008±.003	.348	−.006±.001	.266	−.005±.001	.259	−.007±.001	.324	−.004±.001	.246
MnO	−.002±.001	.182	−.002±.002	.183	.000±.001	.164	n.d.		n.d.		n.d.	
Ba	−1.277±1.505	126.440	.565±2.649	100.346	n.d.		n.d.		n.d.		n.d.	
Co (INAA)	3.047±.096	22.648	3.297±.253	19.006	n.d.		n.d.		n.d.		n.d.	
Co (AA)	3.184±.144	23.350	2.772±.353	29.385	n.d.		n.d.		n.d.		n.d.	
Cr	76.943±3.049	−191.459	63.771±6.067	2.147	n.d.		n.d.		n.d.		n.d.	
Ni	63.766±1.882	−349.095	65.268±5.240	−368.050	n.d.		n.d.		n.d.		n.d.	
Cu	−3.240±.858	139.767	−3.969±1.398	151.439	n.d.		n.d.		n.d.		n.d.	
Hf	−.094±.011	4.525	−.113±.025	4.831	n.d.		n.d.		n.d.		n.d.	
Rb	.040±.202	12.028	−.289±.345	16.829	n.d.		n.d.		n.d.		n.d.	
Ta	−.015±.006	1.013	−.032±.009	1.272	n.d.		n.d.		n.d.		n.d.	
Th	−.027±.004	1.023	−.025±.005	1.001	n.d.		n.d.		n.d.		n.d.	
U	.000±.010	.282	−.005±.012	.369	n.d.		n.d.		n.d.		n.d.	
Zn	−.378±.239	113.205	−.700±.600	118.175	n.d.		n.d.		n.d.		n.d.	
Zr	−3.090±1.128	171.309	−3.137±2.066	171.211	n.d.		n.d.		n.d.		n.d.	
Sc	−.654±.052	36.464	−.635±.074	36.140	n.d.		n.d.		n.d.		n.d.	
La	−.259±.057	13.718	−.409±.079	15.931	n.d.		n.d.		n.d.		n.d.	
Ce	−.600±.110	33.117	−.800±.162	36.090	n.d.		n.d.		n.d.		n.d.	
Nd	−.421±.150	23.420	−.578±.267	25.673	n.d.		n.d.		n.d.		n.d.	
Sm	−.135±.015	6.669	−.170±.033	7.194	n.d.		n.d.		n.d.		n.d.	
Eu	−.047±.004	2.189	−.056±.008	2.333	n.d.		n.d.		n.d.		n.d.	
Gd	−.185±.054	7.549	−.291±.070	9.128	n.d.		n.d.		n.d.		n.d.	
Tb	−.025±.003	1.129	−.029±.008	1.186	n.d.		n.d.		n.d.		n.d.	
Tm	−.009±.003	.402	−.011±.004	.432	n.d.		n.d.		n.d.		n.d.	
Yb	−.054±.007	2.595	−.068±.012	2.822	n.d.		n.d.		n.d.		n.d.	
Lu	−.006±.001	.354	−.009±.002	.392	n.d.		n.d.		n.d.		n.d.	

TRACE-ELEMENT CHEMISTRY AND RARE-EARTH-ELEMENT CHEMISTRY

Nearly all flows in the section were analyzed for a suite of 22 trace elements (table 13.2). Most of the trace elements show negative linear trends when plotted against MgO (fig. 13.5*B*; table 13.3), indicating that olivine abundance exerts the principal control on trace-element content. However, several trace elements correlate positively with MgO (table 13.3). Ni and Co, which resembles Ni in its behavior, are strongly partitioned from the melt into the olivine crystal structure (Gunn, 1971; Hart and Davis, 1978). The positive correlation between Cr and MgO probably reflects the presence of inclusions of chrome spinel in olivine (Gunn, 1971). Our results for Cu differ from those of Gunn (1971), who found a significant positive correlation between MgO and Cu, probably indicating sulfide saturation in his samples. We found no correlation between Cu and MgO, and this may indicate varying levels of sulfur in the magmas supplying suite C flows (T.L. Wright, oral commun., 1985).

The rare-earth-element (REE) concentrations correlate negatively with MgO (fig. 13.5C), owing to the diluting effect of olivine crystals on the absolute concentrations of REE (Hanson, 1980). Chondrite-normalized REE data for selected flows from each suite show smooth curves with similar slopes (fig. 13.7*A*). In flows of suite C, differences in the positions of the curves reflect the large range in olivine content, whereas flows of suites A, B, and D have a smaller range in REE abundances. The shapes and slopes of the curves for all flows within the Uwekahuna Bluff section are similar, suggesting that the parent magmas had a similar origin.

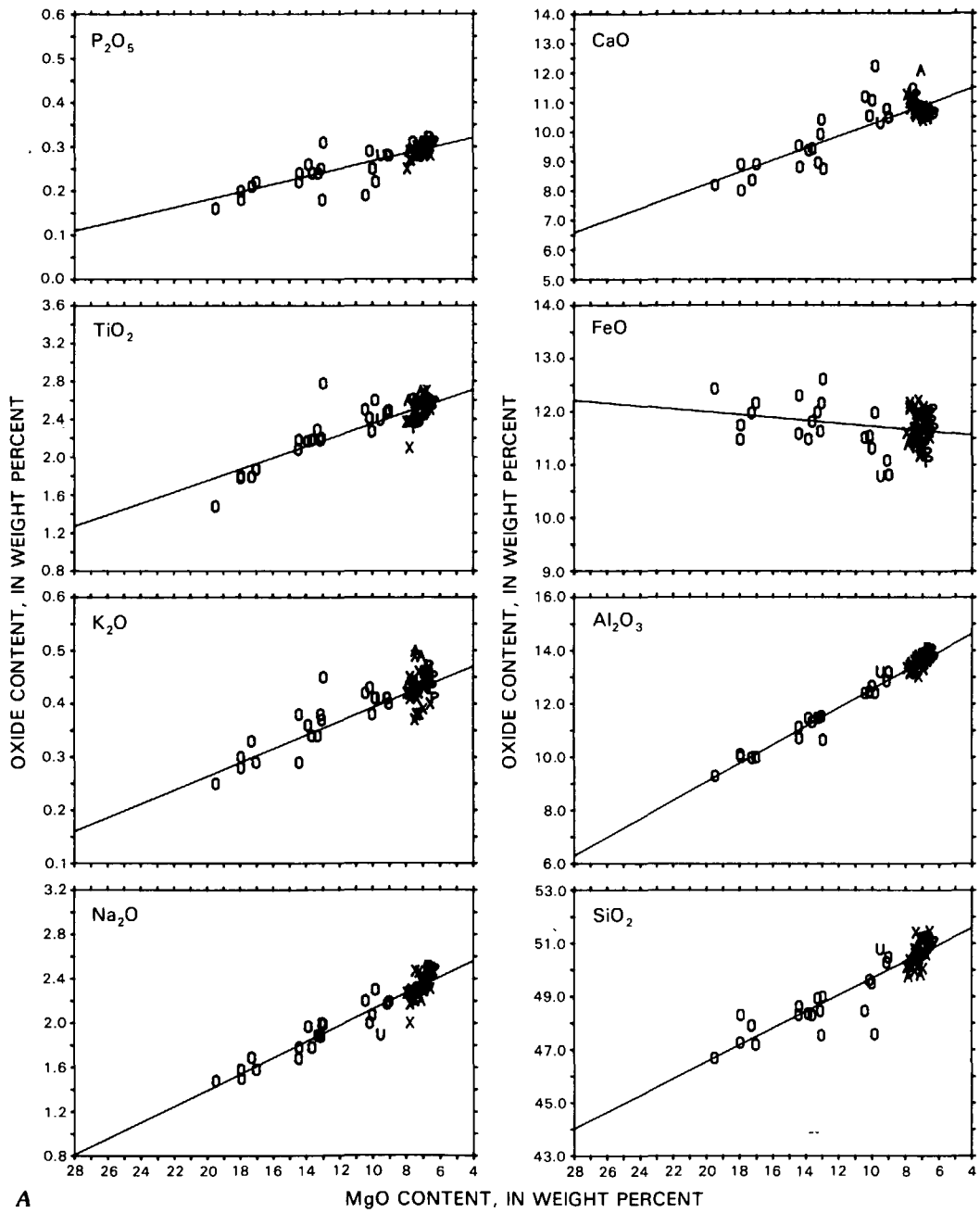

FIGURE 13.5.—MgO variation diagrams for flows of Uwekahuna Bluff section. Data symbols: P, flows of suite A, plagioclase porphyritic; X, flows of suite B, mostly aphyric; O, flows of suite C, olivine porphyritic; U, Uwekahuna Ash Member (unit 43); A, flows of suite D, aphyric. Lines are olivine-control lines for these data determined by linear least-squares regression. See table 13.3 for coefficients and figure 13.8 for comparison with olivine-control lines for other Kilauea lavas. ***A***, Plots of major-element oxides versus MgO. ***B***, Plots of trace elements versus MgO. ***C***, Plots of rare-earth elements versus MgO.

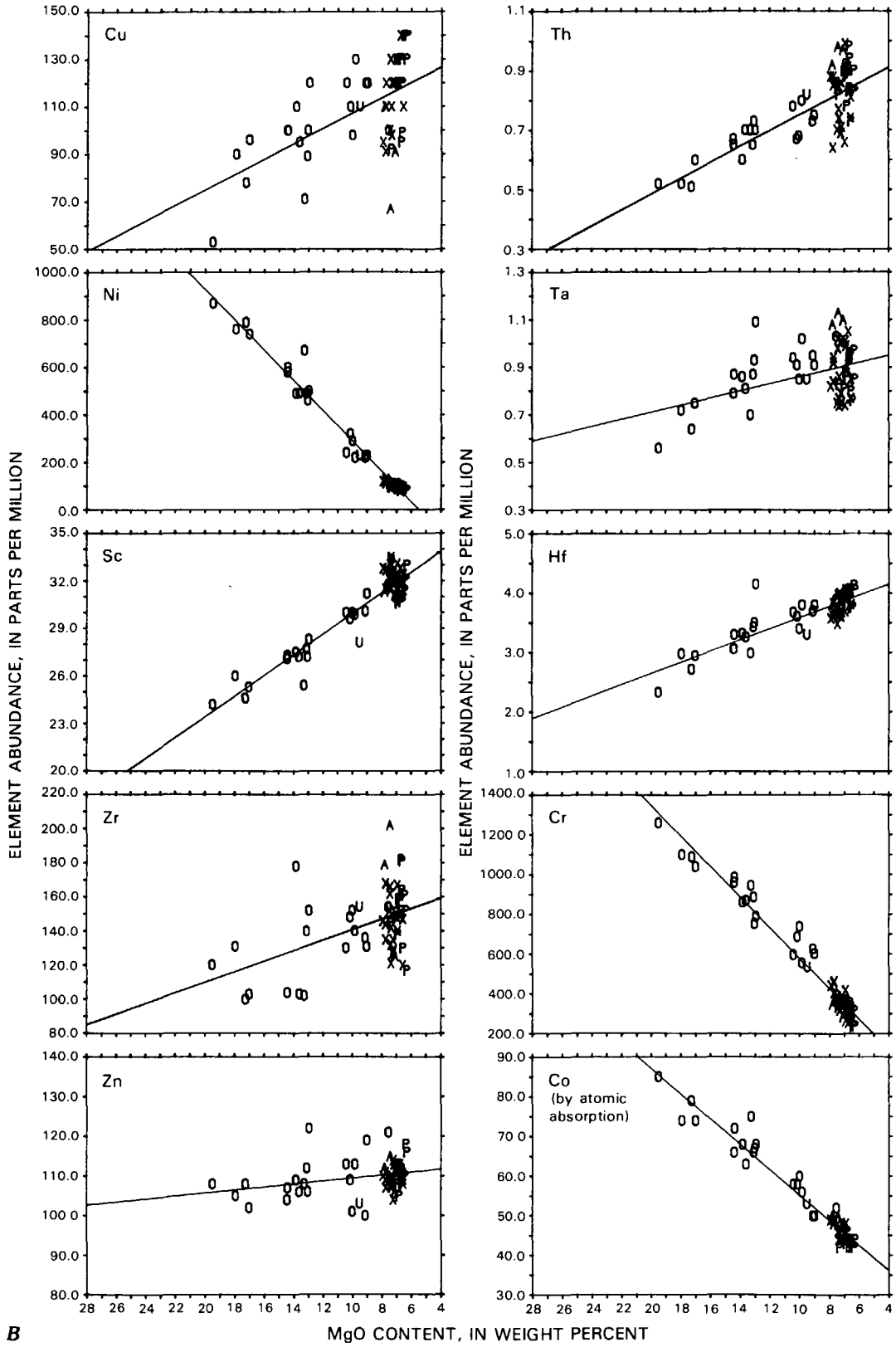

FIGURE 13.5.—Continued.

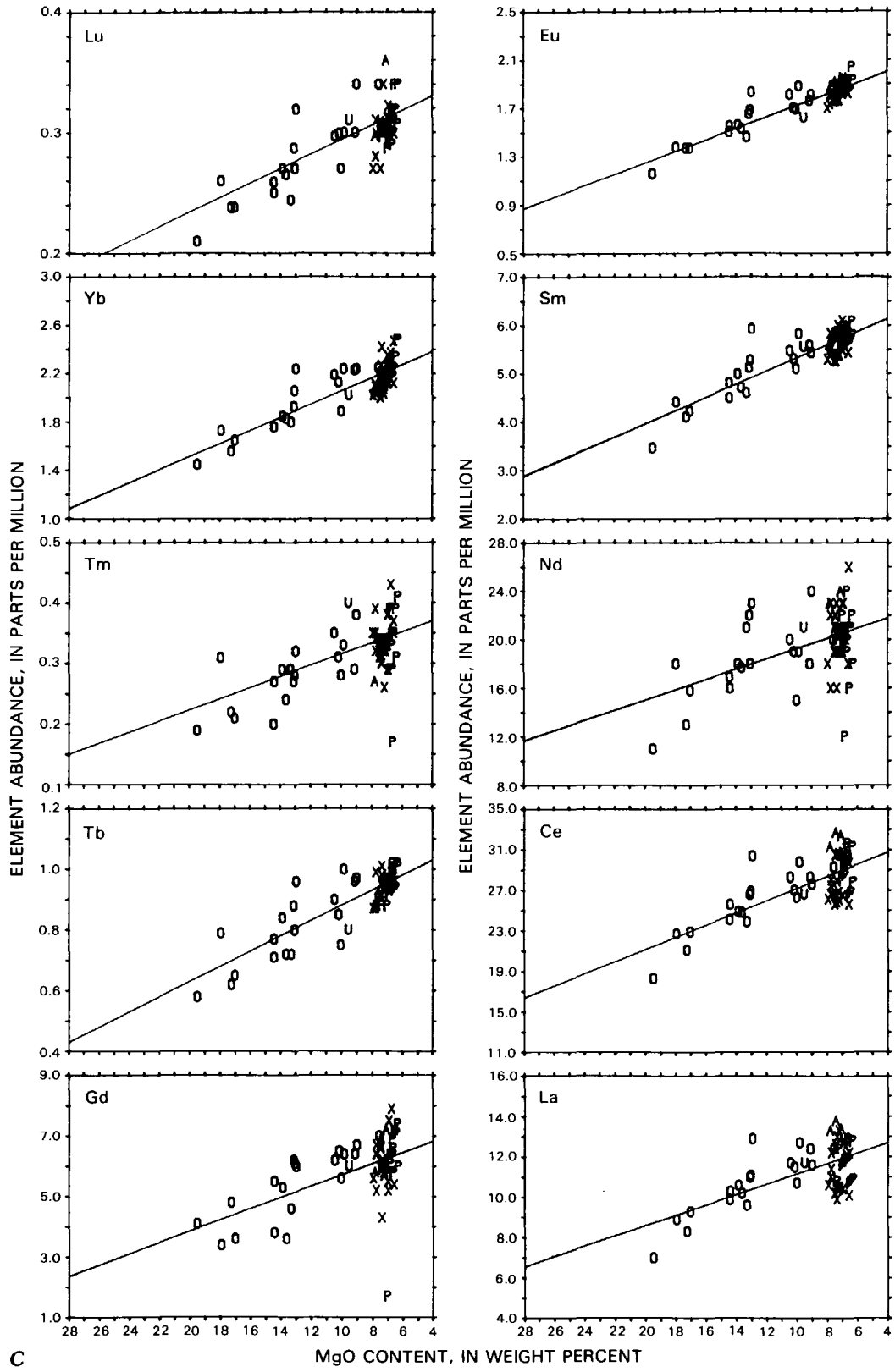

FIGURE 13.5.—Continued.

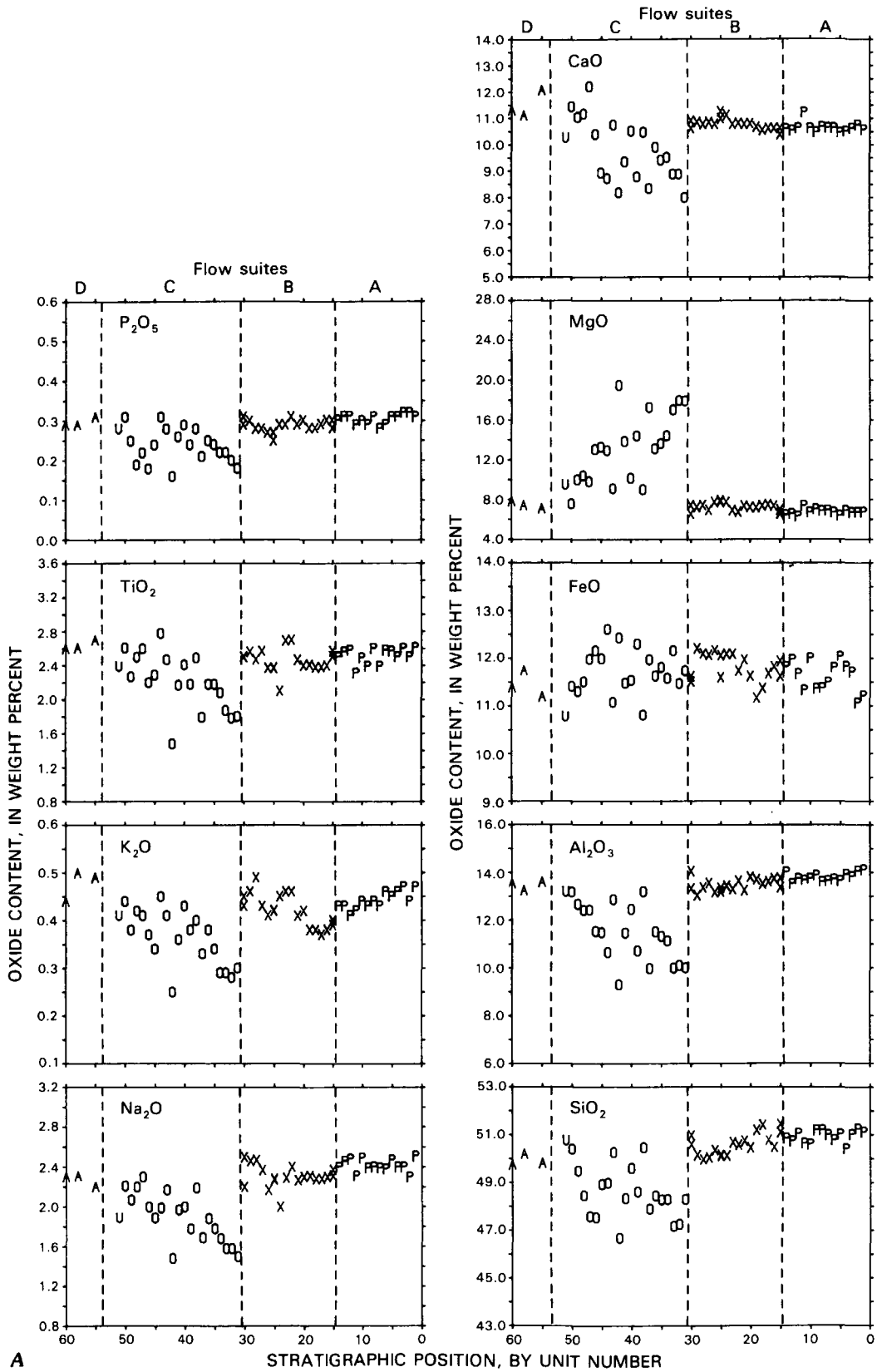

FIGURE 13.6.—Plots of chemical composition versus stratigraphic position within the Uwekahuna Bluff section. Data symbols: P, flows of suite A, plagioclase porphyritic; X, flows of suite B, mostly aphyric; O, flows of suite C, olivine porphyritic; U, Uwekahuna Ash Member (unit 43); A, flows of suite D, aphyric. Dashed lines separate suites. ***A***, Plots of major-element oxides versus MgO. ***B***, Plots of trace elements versus MgO. ***C***, Plots of rare-earth elements versus MgO.

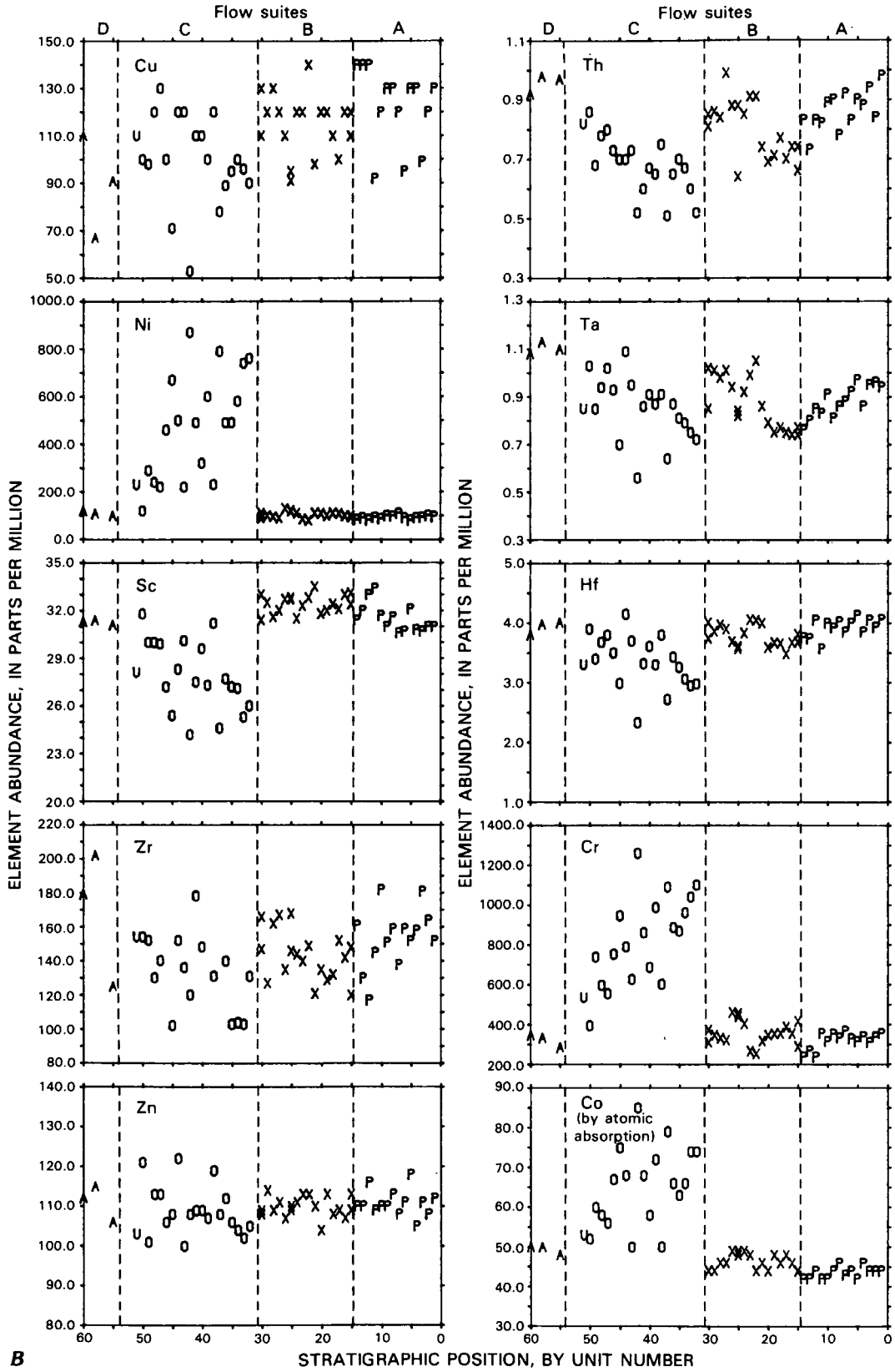

FIGURE 13.6.—Continued.

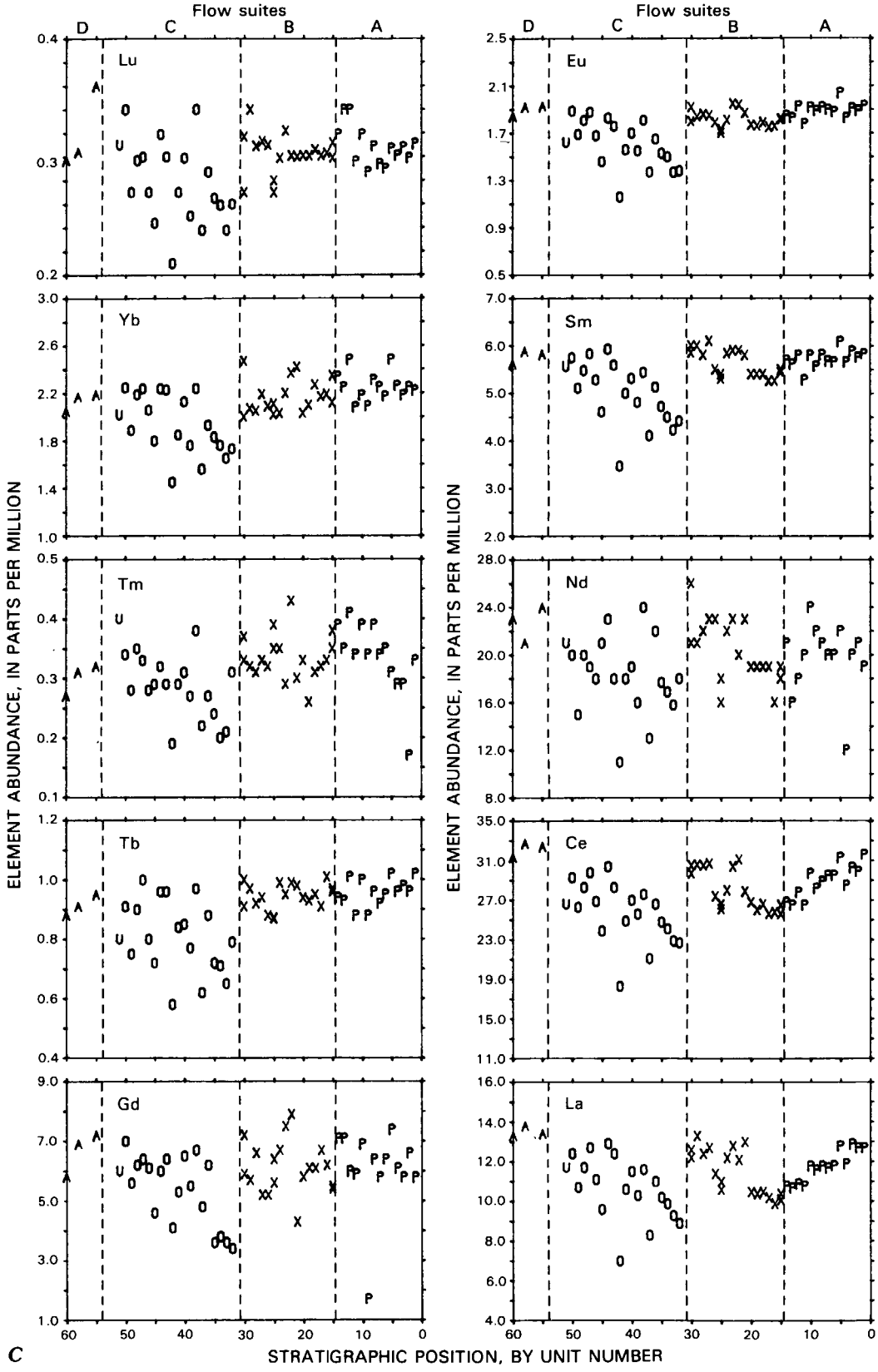

FIGURE 13.6.—Continued.

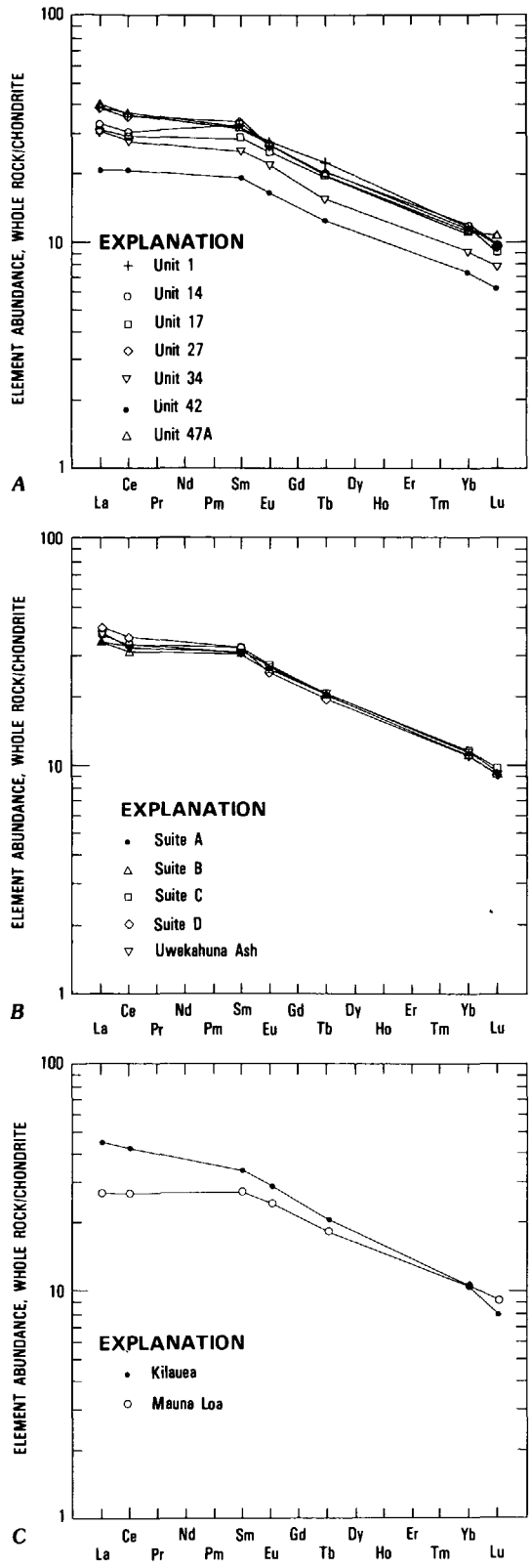

FIGURE 13.7.—Chondrite-normalized abundances of rare-earth elements in Uwekahuna Bluff samples. Abundances are normalized to chondrite values of Haskin and others (1968). Precision for most rare-earth-element (REE) abundances determined by neutron activation (Baedecker, 1979) is better than ±3 percent of reported value (see text). Precision for Nd, Gd, and Tm is poorer, and these elements are not used in plots of chondrite-normalized rare-earth abundances. ***A***, REE abundances in selected flows from Uwekahuna Bluff. ***B***, Averaged and normalized REE data for each suite of flows in Uwekahuna Bluff section and for the Uwekahuna Ash Member. ***C***, Averaged and normalized REE data for historical Mauna Loa and Kilauea flows (data from Basaltic Volcanism Study Project, 1981).

DISCUSSION

SOURCES OF MAGMAS

Flows of suites A and B have broadly similar major-element and trace-element chemistry (fig. 13.6*A*, *B*), and we detect no abrupt changes in composition such as might indicate exotic sources. The similarities in the REE patterns for these units likewise suggest a fairly homogeneous source. We interpret these data to indicate that the flows from suites A and B are comagmatic in the broad sense: they were derived from the same magma batch or from different batches with nearly identical source chemistry and crystallization histories.

Because flows of suite C contain various amounts of olivine, MgO content has a range sufficiently wide to define olivine-control lines. Wright (1971) showed that different comagmatic suites may be characterized by different olivine-control lines. The slopes and intercepts for suite C olivine-control lines are comparable to those calculated for various other suites of Kilauea lavas (Murata and Richter, 1966b; Wright, 1971). The similarity of these control lines (fig. 13.8) indicates that olivine is the only significant mineral phase affecting chemical variation in suite C flows and that the composition of that olivine is homogeneous. We interpret the flows of suite C to be derived from a Kilauea source, because their olivine-control lines resemble those of other Kilauea suites.

TRACE-ELEMENT DATA

Abundances of trace elements are similar within a restricted range among the flows from Uwekahuna Bluff and other Kilauea localities. Ba, Rb, Th, Zr, La, Ce, Sm, and Tb values fall within the ranges exhibited by historic Kilauea lavas (fig. 13.9; Basaltic Volcanism Study Project, 1981). No trace-element abundances in Uwekahuna Bluff flows are within the ranges that are unique to Mauna Loa.

The striking similarity among chondrite-normalized curves for each suite (fig. 13.7*B*) suggests that the magmas for the various suites of flows, as well as for the Uwekahuna Ash Member, are comagmatic. They may have a common parent in the upper mantle, have been affecetd by similar processes after leaving the mantle, or both.

Abundances of light REE are typically lower for Mauna Loa than for Kilauea (fig. 13.7*C*; Leeman and others, 1977, 1980; Basaltic Volcanism Study Project, 1981), whereas abundances of heavy REE are similar for Kilauea and Mauna Loa lavas. Curves for the flows in Uwekahuna Bluff more closely resemble those for Kilauea than those for Mauna Loa (fig. 13.7*B*, *C*). Thus, on the basis of major-, trace-, and rare-earth-element chemistry, it appears that no Mauna Loa flows occur in the Uwekahuna Bluff section.

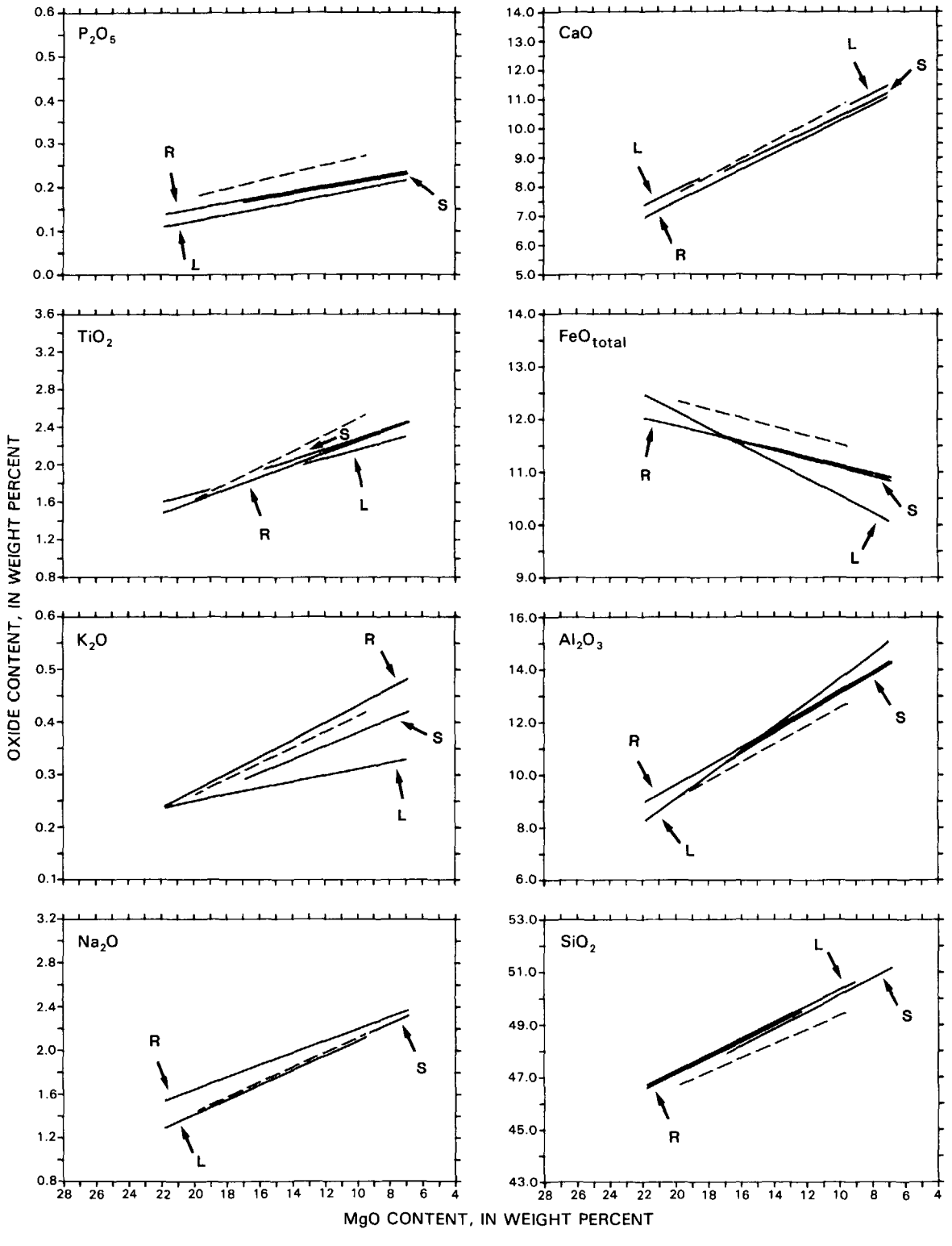

FIGURE 13.8.—Lines of olivine control for Kilauea lavas. Dashed line is for flows of picritic suite C at Uwekahuna Bluff. Other lines labeled by letters: S, Kilauea prehistoric summit lavas (Murata and Richter, 1966a; Wright, 1971); R, Kilauea southwest-rift-zone prehistoric picrites (Wright, 1971); and L, Uwekahuna laccolith (recalculated from data in Murata and Richter, 1961).

SECULAR TRENDS

Olivine control is the dominant mineral control affecting suite C flows. The flows from suites A, B, and D have MgO contents in excess of 6.4 weight percent and show no evidence of fractionation in the sense of Wright and others (1975). We assume that the minor chemical variation displayed by these flows is also olivine controlled. To look for evidence of chemical variability beyond that imposed by olivine control, we recalculated the compositions in table 13.2 to a constant 7.0 weight percent MgO by adding or subtracting olivine from the bulk compositions (Macdonald, 1944; Wright, 1971), using the composition of olivine from the Uwekahuna laccolith (Murata and Richter, 1961). That composition does not account for chrome spinel, which commonly occurs within olivine in Hawaiian lavas, and so we did not recalculate the Cr contents for the Uwekahuna Bluff samples. Listed in table 13.4 are average compositions for each of the lava suites at Uwekahuna Bluff and for juvenile material from the Uwekahuna Ash Member, all normalized to 7.0 weight percent MgO.

The following secular trends are recognized for the Uwekahuna Bluff section (fig. 13.9): (1) SiO_2 increases from 50.2 weight percent for the flows of suite D to 51.1 percent for the flows of suite A; (2) Al_2O_3, FeO_t, Na_2O, P_2O_5, and MnO remain nearly constant (table 13.4); and (3) CaO and TiO_2 decrease slightly from suite D to suite A. These secular changes differ in sense from those recognized by Wright (1971) for historical Kilauea lavas, in which SiO_2 decreases to the present and CaO and TiO_2 increase.

Historical olivine-controlled flows from Mauna Loa have more SiO_2 and less K_2O, TiO_2, and P_2O_5 than any of the flows from Uwekahuna Bluff (table 13.4; fig. 13.9). The ranges in the contents of these oxides for flows from Uwekahuna Bluff strongly resemble those for historical Kilauea flows.

CYCLIC VARIATIONS IN THE CHEMISTRY OF SUMMIT LAVAS

Plots of chemical composition versus position in the section for lavas of suites A and B (units 1–30) show essentially straight-line relationships (fig. 13.6), but small cyclic(?) departures are discernible. The olivine-rich flows of suite C display considerable scatter in MgO-variation diagrams (fig. 13.5*A*), but some evidence for cyclicity can be seen when all compositions are normalized to 7.0 weight percent MgO and plotted against stratigraphic position (fig. 13.10). Although the frequency of the apparent cycles varies from element to element, the data do suggest that cyclic variations occur in the compositions of Kilauea summit lavas.

Wright and others (1975) and Wright and Tilling (1980), on the basis of major-element chemistry, identified 10 distinct chemical variants or magma batches among the materials erupted by Kilauea in the period 1968–1974. They interpreted these variants as the unmodified products of separate partial melting events. Hofmann and others (1984) examined trace- and rare-earth-element data from Kilauea for 1968–1971; they concluded that incompatible trace-element concentrations in the lavas fit a pattern of continuous,

TABLE 13.4.—*Average chemical compositions of prehistoric lavas and ash from Uwekahuna Bluff, compared with historical Mauna Loa and prehistoric and historical Kilauea*

[Recalculated from original analyses by normalizing to 100 percent dry weight after converting all iron to FeO_{total}. Normalized to 7.0 weight percent MgO by subtracting or adding olivine of Uwekahuna laccolith composition (Murata and Richter, 1961, analysis 10). A, suite A flows; B, suite B flows; C, suite C flows; D, suite D flows; UA, Uwekahuna Ash Member, (UA = average of 5 rinds from cored bombs within Uwekahuna Ash Member (Dzurisin and Casadevall, 1986)); Kilauea A (Kil A = Kilauea summit 1911–1924) and Mauna Loa A (MLoa A) (Wright, 1971); Kilauea B (Kil B) and Mauna Loa B (MLoa B) (Basaltic Volcanism Study Project, 1981); n.d., not determined; uncertainty expressed as one standard deviation (1 sigma)]

	A	B	C	D	UA	Kil A	Kil B	MLoa B	MLoa A
SiO_2	51.10±0.23	50.90±0.39	50.60±0.78	50.23±0.25	51.08±0.35	50.33, n.d.	50.70±0.31	52.45±0.31	52.18, n.d.
Al_2O_3	13.7±0.2	13.6±0.2	13.6±0.3	13.7±0.2	13.73±0.9	14.00, n.d.	13.57±0.12	13.94±0.10	14.17, n.d.
FeO	11.7±0.3	11.8±0.3	11.3±0.5	11.4±0.3	11.63±1.00	11.09, n.d.	11.03±0.20	10.62±0.49	10.94, n.d.
MgO	7.0	7.0	7.0	7.0	7.0	7.0	7.0	7.0	7.0
CaO	10.6±0.2	10.9±0.3	11.7±0.7	11.7±0.4	11.05±0.28	11.58, n.d.	11.65±0.33	10.73±0.15	10.58, n.d.
Na_2O	2.4±0.1	2.3±0.1	2.3±0.1	2.3±0.1	2.14±0.25	2.28, n.d.	2.32±0.04	2.36±0.06	2.29, n.d.
K_2O	.44±0.02	.43±0.03	.44±0.04	.48±0.03	.45±0.02	.55, n.d.	.53±0.04	.39±0.03	.37, n.d.
TiO_2	2.51±0.08	2.49±0.12	2.62±0.21	2.68±0.04	2.51±0.09	2.72, n.d.	2.73±0.11	2.10±0.04	2.07, n.d.
P_2O_5	.30±0.01	.29±0.01	.28±0.04	.30±0.01	.26±0.06	.27, n.d.	.29±0.01	.24±0.02	.21, n.d.
MnO	.17±0.02	.17±0.01	.16±0.02	.19±0.01	.16±0.02	.17, n.d.	.17±0.01	.17±0.01	.17, n.d.
Ba	118±19	118±23	127±29	136±11	120±29	n.d.	138±18	84±14	n.d.
Cu	122±16	116±12	119±17	91±22	132±7	n.d.	n.d.	n.d.	n.d.
Hf	3.91±0.14	3.83±0.16	4.02±0.30	3.99±0.08	3.58±0.02	n.d.	4.58±0.17	3.59±0.11	n.d.
Rb	12±3	13±1	16±3	14, n.d.	13, n.d.	n.d.	11±3	6±1	n.d.
Ta	.88±0.06	.88±0.11	1.02±0.10	1.12±0.02	.93±0.05	n.d.	n.d.	n.d.	n.d.
Th	.86±0.07	.81±0.10	.80±0.06	.97±0.02	.89±0.09	n.d.	1.28±0.22	.55±0.03	n.d.
Zn	111±3	111±3	132±14	113±5	112±3	n.d.	n.d.	n.d.	n.d.
Zr	153±17	145±15	156±25	172±41	139±18	n.d.	159±20	130±5	n.d.
Sc	31.4±0.9	32.8±0.7	33.5±1.4	31.8±0.4	30.8±0.2	n.d.	33.0±2.0	31.0±1.2	n.d.
La	11.8±0.8	11.6±1.2	12.7±1.0	13.7±0.3	12.9±0.4	n.d.	15.1±1.7	8.9±0.6	n.d.
Ce	28.9±1.6	28.3±2.0	30.7±1.9	32.7±0.5	28.8±0.5	n.d.	37.5±3.2	23.9±1.4	n.d.
Nd	20±3	21±3	22±3	23±2	23±3	n.d.	n.d.	n.d.	n.d.
Sm	5.7±0.1	5.7±0.3	6.0±0.4	5.9±0.1	6.0±0.1	n.d.	6.2±0.2	5.0±0.2	n.d.
Eu	1.89±0.05	1.84±0.06	1.92±0.10	1.93±0.03	1.74±0.04	n.d.	2.00±0.07	1.69±0.04	n.d.
Gd	6.1±1.4	6.2±0.9	6.4±1.0	6.7±0.7	7.1±0.7	n.d.	n.d.	n.d.	n.d.
Tb	.96±0.04	.96±0.04	.97±0.10	.93±0.03	.90±0.02	n.d.	.96±0.03	.86±0.04	n.d.
Tm	.33±0.06	.34±0.04	.34±0.05	.31±0.02	.34±0.08	n.d.	n.d.	n.d.	n.d.
Yb	2.25±0.11	2.20±0.13	2.31±0.14	2.17±0.06	2.18±0.05	n.d.	2.05±0.03	2.10±0.04	n.d.
Lu	.31±0.02	.31±0.02	.33±0.02	.32±0.03	.31±0.01	n.d.	.26±0.10	.31±0.01	n.d.

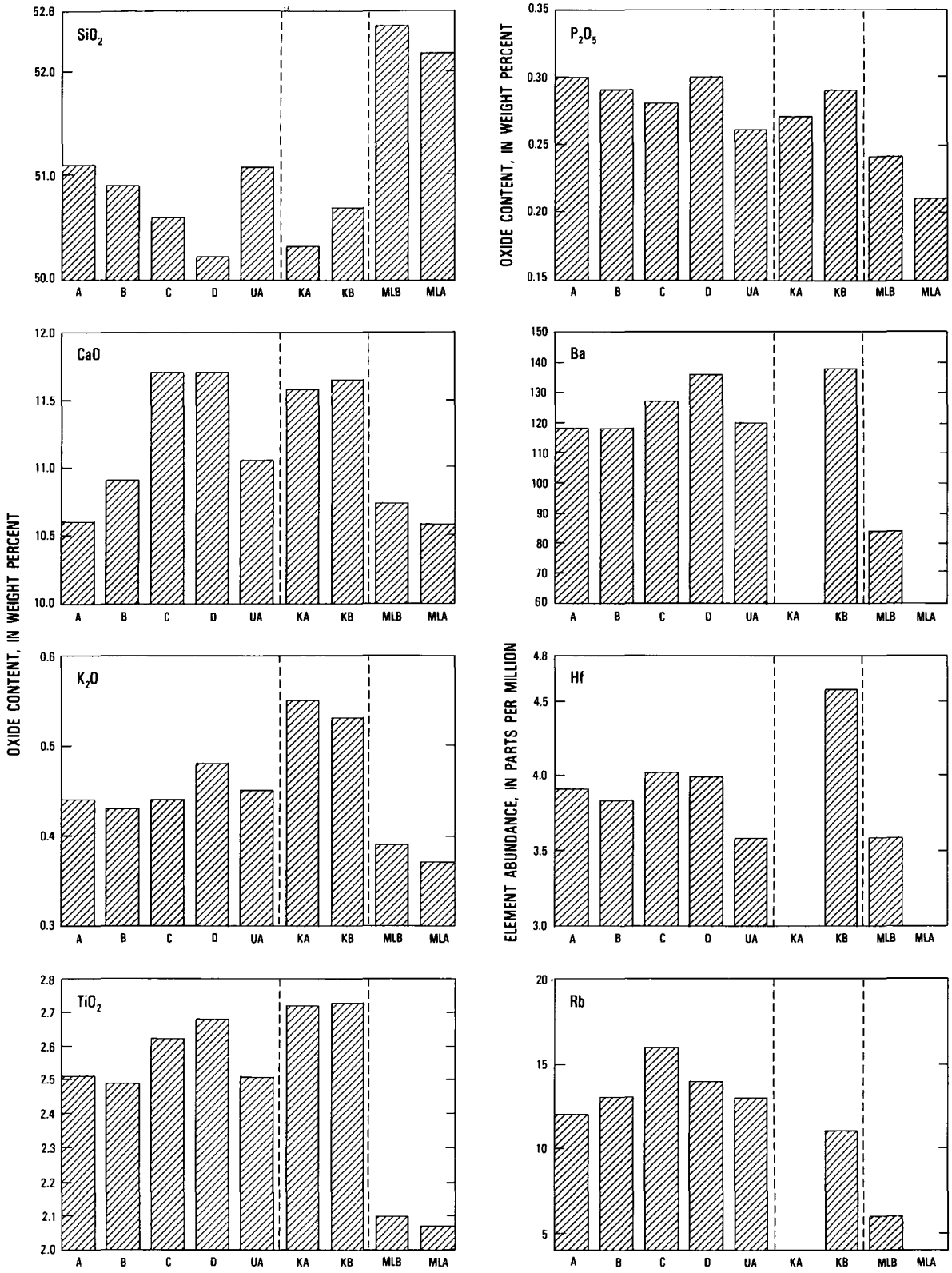

FIGURE 13.9.—Bar graphs showing averaged normalized abundances of selected major oxides and trace elements in Uwekahuna Bluff rocks and in Mauna Loa and Kilauea flows. Averages are recalculated from original analyses by normalizing to 100 percent dry weight after converting all iron to FeO. Averages have been normalized to 7.0 weight percent MgO by subtracting or adding olivine of Uwekahuna laccolith composition (Murata and Richter, 1961, analysis 10). A–D, Suites of flows from Uwekahuna Bluff; UA, Uwekahuna Ash Member; KA, Kilauea

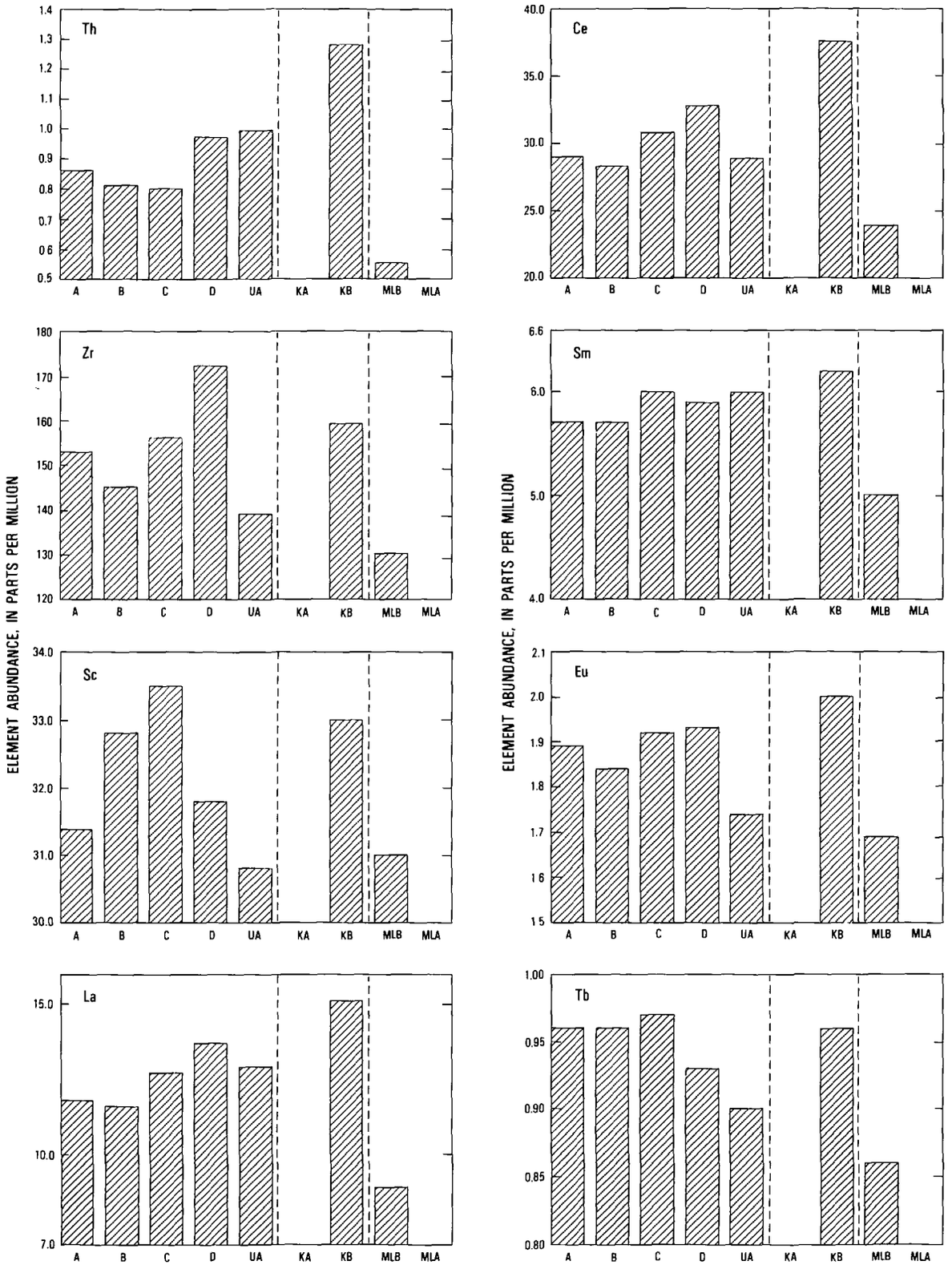

average from Wright (1971); KB, Kilauea average from Basaltic Volcanism Study Project (1981); MLB, Mauna Loa average from Basaltic Volcanism Study Project (1981); MLA, Mauna Loa average from Wright (1971). Vertical lines separate Uwekahuna Bluff data (left) from Kilauea averages (middle), and from Mauna Loa averages (right).

monotonic decrease and that "there was no longer a need to invoke the existence of distinct magma batches to explain either the trace elements or the major elements" (Hofmann and others, 1984, p. 32). Shaw (chapter 51) argues that cyclic behavior on many time scales may be the norm for Hawaiian volcanism and suggests mechanisms to account for such cycles. The apparent cycles at Uwekahuna Bluff are too pronounced to be explained by analytical uncertainty; they may reflect subtle variations in the chemistry of the parental magma stored in the shallow reservoir.

CHRONOLOGY OF UWEKAHUNA BLUFF

To appreciate more fully the significance of the various rock suites exposed at Uwekahuna Bluff, an understanding of the time

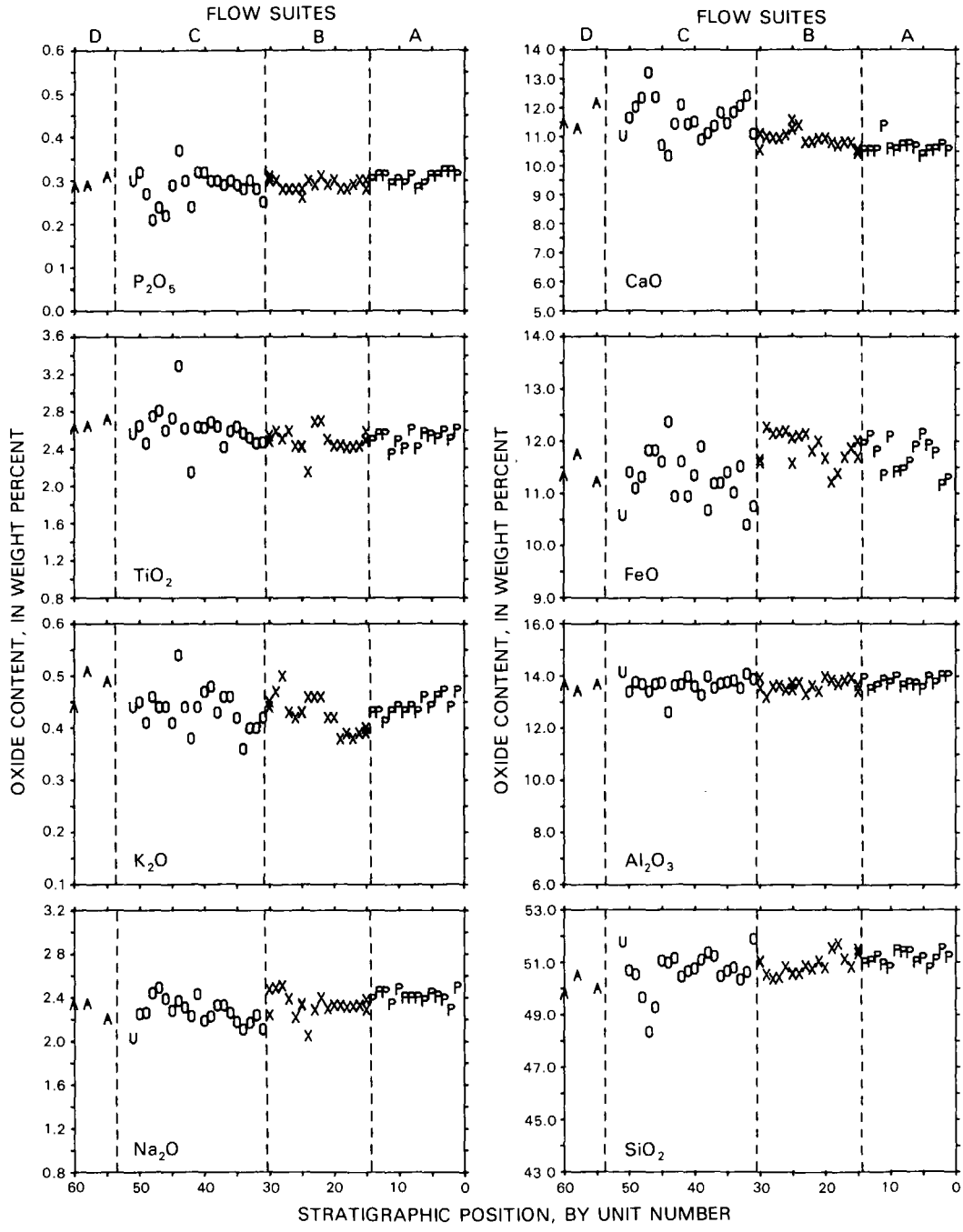

FIGURE 13.10.—Plot of recalculated major-element analyses versus stratigraphic position in the Uwekahuna Bluff section. Analyses have been recalculated to 7.0 weight percent MgO through addition or subtraction of olivine of the composition given in Murata and Richter (1961). Dashed lines separate suites of flows. U indicates sample of the Uwekahuna Ash Member. See figure 13.6 for explanation of other letter symbols.

intervals involved is essential. We offer here a tentative chronology of the sequence at Uwekahuna Bluff and a conceptual model to explain the chemical and petrologic variations observed there.

The Uwekahuna Ash Member, which underlies nearly the entire western wall of Kilauea caldera, is interpreted as the product of large explosive eruptions in the Kilauea summit region about 2.1 ka (Dzurisin and Casadevall, 1986; Lockwood and Rubin, 1986). We found no carbonaceous material within the Uwekahuna Bluff section, so no radiocarbon ages are available for the section above the Uwekahuna Ash Member. However, control on the age of flows within the various suites is available from study of paleomagnetism of the rocks from Uwekahuna Bluff.

Paleomagnetism in the flows of Uwekahuna Bluff has been studied since 1961, when 10 lava flows from the lower half of the section were sampled (Doell and Cox, 1965, 1972). We relocated those holes, which were drilled in units 29, 32, 34, 36, 37, 39, 42, 47A, 48A, and 49A (table 13.1). In 1981, nine additional flows (units 1, 2, 3, 4, 5, 15, 20, 27, and 51) were drilled (R.T. Holcomb and D.E. Champion, unpub. data).

The 1981 samples and the Doell and Cox samples record at least three distinct pole positions (D.E. Champion, oral commun., 1985). Three of the older samples of suite D (units 47A–49A) have paleomagnetic directions consistent with the directions of a lava flow that has been dated at 2.77 ± 0.15 ka (Lockwood and Rubin, 1986; sample W-5345). This age relationship is consistent with the geology of Uwekahuna Bluff, where units 47A–49A underlie the Uwekahuna Ash Member, but it implies a 600–700 yr hiatus in the Uwekahuna Bluff section between the emplacement of suite D flows and deposition of the ash.

A second time unit includes flows 15 through 51 from suites B and C. Flow 51 directly overlies the 2.1-ka Uwekahuna Ash Member. Samples from these flows show a continuous variation in paleomagnetic direction consistent with rapid and steady change of the local magnetic field vector from about 2.1 to 1.5 ka (D.E. Champion, oral commun., 1985). Field evidence indicates no major weathering surface in this sequence of flows. This consistency indicates that the flows of suites C (picrite) and B (aphyric) accumulated in roughly 600 years; no major time breaks are recognized.

The weathered top of unit 15, the uppermost flow of suite B, indicates a hiatus of unknown duration. Paleomagnetic directions within the top five flows of the section (flows of suite A) are consistent with dated field directions of about 0.35 ka (Holcomb, 1981). However, lack of paleomagnetic data for flows 6 through 14 precludes estimating the length of time represented by suite A.

Thus, five major events between 2.8 ka and 0.2 ka are recognized in the Uwekahuna Bluff section on the basis of field occurrence, radiocarbon dating of flows and tephra (Kelley and others, 1979; Lockwood and Rubin, 1986), and paleomagnetic studies (Holcomb, 1981; D.E. Champion, oral commun., 1985). We infer the following eruptive sequence for the rocks exposed at Uwekahuna Bluff:

1. Eruption of aphyric lavas of pre-Uwekahuna Ash Member age (suite D) about 2.8 ka.

2. Eruption of the Uwekahuna Ash Member about 2.1 ka.

3. Eruption of picritic lavas, replenishment of shallow reservoir, and eruption of aphyric lavas (suites C and B) about 2.1 to 1.5 ka (?).

4. Eruption of plagioclase-porphyritic lavas (suite A) about 0.8 to 0.2 ka (?).

5. Formation of present caldera and eruption of Keanakakoi Ash about 0.2 ka.

KILAUEA SUMMIT HISTORY FOR THE PAST 2,800 YEARS

Holcomb (chapter 12) has outlined one sequence of events for the recent evolution of the Kilauea summit area, but alternatives are possible. Our interpretation is generally similar, but we prefer a sequence in which some of the stratigraphic units in Uwekahuna Bluff are older than the ages assigned by Holcomb.

Holcomb (chapter 12) has used paleomagnetic data to assign an age of 2.0–1.5 ka to lava of suite D in Uwekahuna Bluff, as well as several flows outside of the caldera. A similarly magnetized lava flow on Mauna Loa has recently been dated by ^{14}C methods at 2.8 ka (D.E. Champion, oral commun., 1985). As discussed below, we believe that the Uwekahuna Ash Member is older than the 1.5 ka favored by Holcomb and others (in press), so we prefer the age of about 2.8 ka for the lava flows of suite D. These flows should be compared with pre-Uwekahuna Ash Member flows outside of the caldera to see if they may be coeval.

Holcomb (chapter 12) concludes that the present caldera of Kilauea was preceded by an older Powers caldera whose formation may have been associated with explosions that produced the Uwekahuna Ash Member in a manner similar to that proposed for the present caldera and the Keanakakoi Ash Member. The mechanism proposed for this association (Jaggar, 1947; Macdonald, 1965; Christiansen, 1979) involves large-scale summit collapse in response to rapid magma withdrawal into the volcano's rift zones, triggering phreatomagmatic explosions by providing ground water access to the volcano's plumbing system. Though the collapse of the current caldera preceded the explosive Keanakakoi eruption, the interval between collapse and explosion could have been short (Decker and Christiansen, 1983).

Several radiocarbon ages have been determined for the Uwekahuna Ash Member. When the original paleomagnetic chronology of Holcomb and others (in press) was worked out, the available measurements indicated an age of about 1.5 ka. Additional ages have been obtained since then, ranging from 1.0 ka to 2.2 ka. Lockwood and Rubin (1986) argue that the younger ages are affected by sample contamination and adopt 2.1 ka as the most representaive age for the ash. Holcomb (chapter 12) prefers to retain the earlier, younger age but we prefer the 2.1-ka ages of Lockwood and Rubin (1986).

Holcomb (chapter 12) suggests that collapse of the Powers caldera was followed by a period of caldera filling which did not affect the Uwekahuna Bluff section for about 0.75 ka, implying that the flows of suite C and suite B are younger than 0.75 ka. D.E. Champion (oral commun., 1985) believes that those flows record continuous variation in paleomagnetic field direction from about 2.1 to 1.5 ka. Dzurisin and Casadevall (1986) argue that the uppermost

pumice of the Uwekahuna Ash Member was buried quickly by picritic lava flows of suite C, because the pumice was uneroded when it was buried. We therefore assign an age of 2.1 to 1.5 ka to suite C and suite B flows and suggest that at least 30 m of suite C flows accumulated rapidly soon after the Uwekahuna Ash Member eruptions.

Our interpretation and that of Holcomb (chapter 12) converge on the age and origin of the suite A flows at Uwekahuna Bluff. These plagioclase-phyric flows are Holcomb's Observatory flows, so named because they form the substrate for the Hawaiian Volcano Observatory. He assigned them an age of 0.25–0.35 ka in figure 12.5, but also noted that they could be as old as 0.75 ka. We suggest that the weathered surface of the uppermost suite B flow records a hiatus of at least a few centuries, and adopt an age of 0.8–0.2 ka for the overlying suite A flows. Following extrusion of the suite A flows, the Uwekahuna Bluff section was capped by the Keanakakoi Ash Member.

The two main differences between our interpretation and that of Holcomb (chapter 12) are: (1) the age of the Uwekahuna Ash Member, and (2) the age and significance of the suite C and suite B lava flows. The differences are caused primarily from differing interpretations of available radiocarbon ages for summit flows and should be resolved by future work.

Our preferred interpretation is that the suite C picrites ponded in the Powers caldera soon after its formation and quickly buried the Uwekahuna Ash Member. Holcomb (chapter 12) agrees that collapse was soon followed by caldera filling, but infers that the Uwekahuna Bluff area was not covered for about 750 years. We interpret the suite C picrites as crystal cumulates or residua from a shallow magma reservoir that was rapidly drained during the Uwekahuna Ash Member eruptions, probably by a large effusive eruption low on the volcano's flank (Dzurisin and Casadevall, 1986). We infer that the lower parts of this magma reservoir were rich in olivine, because of the accumulation of settled olivine crystals (Macdonald, 1944; Murata and Richter, 1966a, b).

Murata and Richter (1966b) proposed that in the 1959 eruption of Kilauea Iki, the eruptive force mobilized olivine sludge from the depths of the shallow reservoir feeding that eruption. Helz (chapter 25) argues that the ascent rate of a juvenile component of the 1959 eruption was sufficient to entrain large olivine grains from a source in the upper mantle. We speculate that the suite C flows at Uwekahuna Bluff represent olivine sludge from the lower part of a compositionally zoned shallow magma reservoir and that unloading during the Uwekahuna Ash Member eruption was responsible for extrusion of the picrites. Preservation at the top of the Uwekahuna Ash Member of a thin pumice layer, which we tentatively assume to be related to emplacement of the ash at about 2.1 ka, indicates that at least 30 m of suite C lava flows accumulated on the floor of the Powers caldera and buried the pumice soon after it was erupted. The absence of weathered flow surfaces at the contacts of suite C flows also implies that most of their 60-m thickness accumulated rapidly after eruption of the ash. This model is attractive because it explains the presence of picrites, which are otherwise unusual in the Kilauea summit area, as a direct consequence of the equally unusual Uwekahuna Ash Member eruptions.

We speculate that the flows of suites B and A ponded within the Powers caldera and that they are genetically related. The plagioclase-porphyritic flows of suite A may represent a later eruptive product of a shallow reservoir that earlier was the source for the aphyric lavas of suite B. We tentatively interpret this sequence of aphyric lavas followed by plagioclase-porphyritic lavas as the product of a two-stage drawdown of a post-Uwekahuna Ash Member shallow magma reservoir. A possible problem with this interpretation is that paleomagnetic evidence suggests a hiatus of at least a few centuries between emplacement of the suite B and the suite A flows, and a hiatus is also indicated by the weathered contact between the suites. According to Holcomb (chapter 12), the hiatus lasted from 0.5 ka to 0.25 ka; according to D.E. Champion (oral commun., 1985) and the model proposed here, the hiatus lasted from 1.5 ka to 0.8 ka.

CONCLUSIONS

We conducted this study in an attempt to answer questions about how the summit region of Kilauea developed: (1) How important were intrusive bodies (sills, laccoliths, and dikes) to the growth of the summit region? (2) Are any lava flows from Mauna Loa exposed in the western wall of Kilauea caldera? (3) Can distinct suites of rocks be recognized in the caldera wall and give a record of the recent chemical evolution of Kilauea summit lavas? (4) Is there any evidence that distinct eruptive centers or source regions have supplied lavas to the summit region during Kilauea's recent past? In terms of these questions, we summarize our results as follows:

(1) Intrusive bodies such as sills and laccoliths are absent at Uwekahuna Bluff. The dikes and laccoliths found elsewhere in the western wall of the caldera account for less than 1 percent of the surface area of the wall (Casadevall and Dzurisin, chapter 14).

(2) The flows of Uwekahuna Bluff are similar in textural variety, phenocryst mineralogy, and major- and trace-element chemistry to prehistoric and historical Kilauea lavas. On the basis of these similarities and the lack of hypersthene, which is found in Mauna Loa flows (Macdonald, 1949), we suggest that all flows within the Uwekahuna Bluff section are from a Kilauea source.

(3) Four distinct suites of flows are recognized at Uwekahuna Bluff on the basis of field occurrence, petrography, and chemistry. Many flows represent near-vent accumulations of fluid lavas. The uniform thickness, lateral continuity, and extensive horizontality of many of the lava flows exposed in the western wall, especially above the Uwekahuna Ash Member, suggest a caldera-fill sequence.

(4) Our data do not require distinct source regions or eruptive centers for the Uwekahuna Bluff lavas, although those possibilities cannot be discounted. We attribute the petrographic differences between lava suites to processes within a single shallow magma reservoir beneath the summit area. The Uwekahuna Bluff lavas could have erupted from a single center or from several in the summit area. Our results are generally compatible with those of Holcomb (chapter 12), but remaining differences of opinion about absolute ages point out the need for additional stratigraphic study.

REFERENCES CITED

Baedecker, P.A., 1979, Instrumental neutron activation analysis program of the U.S. Geological Survey (Reston, Va.) *in* Carpenter, B.F., D'Agostino, F., and Yule, H.P., eds., Computers and activation analysis and gamma-ray spectroscopy: Contract 78042, U.S. Dept. Energy, p. 373–385.

Basaltic Volcanism Study Project, 1981, Basaltic volcanism on the terrestrial planets; New York, Pergamon Press, 1286 p.

Christiansen, R.L., 1979, Explosive eruption of Kilauea Volcano in 1790 [abs.]: International Association of Volcanology and Chemistry of the Earth's Interior, Symposium on Intraplate Volcanism and Submarine Volcanism, Hilo, Hawaii, July 1979, p. 174.

Daly, R.A., 1911, Magmatic differentiation in Hawaii: Journal of Geology, v. 19, p. 289–316.

de Saint Ours, P., 1982, Map of tectonic features of Kilauea Volcano summit region, Hawaii: U.S. Geological Survey Miscellaneous Field Studies Map, MF–1368, scale 1:24,000.

Decker, R.W., and Christiansen, R.L., 1983, Explosive eruptions of Kilauea Volcano, Hawaii, *in* Explosive Volcanism: inception, evolution, and hazards: Washington, National Academy Press, p. 122–132.

Doell, R.R.,and Cox, A.V., 1965, Paleomagnetism of Hawaiian lava flows: Journal of Geophysical Research, v. 70, p. 3377–3405.

——— 1972, The Pacific geomagnetic secular variation anomaly and the question of lateral uniformity in the lower mantle, in Robertson, E.C., ed., The nature of the solid Earth: New York, McGraw-Hill, p. 245–284.

Dutton, C.E., 1884, Hawaiian volcanoes: U.S. Geological Survey 4th Annual Report, p. 75–219.

Dzurisin, D., and Casadevall, T.J., 1986, Stratigraphy and chemistry of the Uwekahuna Ash: Product of prehistoric phreatomagmatic eruptions at Kilauea Volcano, Hawaii [abs.]: International Volcanological Congress, Auckland-Hamilton-Rotorua, New Zealand, Abstracts, February 1986, p. 100.

Dzurisin, D., Koyanagi, R.Y., and English, T.T., 1984, Magma supply and storage at Kilauea Volcano, Hawaii: Journal of Volcanology and Geothermal Research, v. 21, p. 177–206.

Fuller, R.E., 1939, Gravitational accumulation of olivine during the advance of basaltic flows: Journal of Geology, v. 47, p. 303–313.

Gunn, B.M., 1971, Trace element partition during olivine fractionation of Hawaiian basalts: Chemical Geology, v. 8, p. 1–13.

Hanson, G.N., 1980, Rare earth elements in petrogenetic studies of igneous systems: Annual Reviews of Earth and Planetary Science Letters, v. 8, p. 371–406.

Hart, S.R., and Davis, K.E., 1978, Nickel partitioning between olivine and silicate melt: Earth and Planetary Science Letters, v. 40, p. 203–219.

Haskin, L.A., Haskin, M.A., Frey, F.A., and Wildman, T.R., 1968, Relative and absolute terrestrial abundances of the rare earths, *in* Ahrens, L.H., ed., Origins and distribution of the elements: New York, Pergamon Press, p. 889–912.

Hofmann, A.W., Feigenson, M.D., and Raczek, I., 1984, Case studies on the origin of basalt: III. Petrogenesis of the Mauna Ulu eruption, Kilauea, 1969–1971: Contributions to Mineralogy and Petrology, v. 88, p. 24–35.

Holcomb, R.T., 1981, Kilauea Volcano, Hawaii: chronology and morphology of the surficial lava flows: U.S. Geological Survey Open-File Report 81–354, 321 p.

Holcomb, R.T., Champion, D.E., and McWilliams, M.O., in press, Dating recent Hawaiian lava flows using paleomagnetic secular variation: Geological Society of America Bulletin.

Jaggar, T.A., 1947, Origin and development of craters: Geological Society of America Memoir 21, 508p.

Kelley, M.L., Spiker, E.C., Lipman, P.W., Lockwood, J.P., Holcomb, R.T., and Rubin, M., 1979, U.S. Geological Survey radiocarbon dates XV: Mauna Loa and Kilauea Volcanoes, Hawaii: Radiocarbon, v. 21, p. 306–320.

Leeman, W.P., Budahn, J.R., Gerlach, D.C., Smith, D.R., and Powell, B.N., 1980, Origin of Hawaiian tholeiites: trace element constraints: American Journal of Science, v. 280–A, p. 796–821.

Leeman, W.P., Murali, A.V., Ma, M.S., and Schmitt, R.A., 1977, Mineral constitution of mantle source regions for Hawaiian basalts—rare earth element evidence for mantle heterogeneity, *in* Magma Genesis: Oregon Department of Mineral Industries Bulletin 96, p. 169–183.

Lockwood, J.P., and Rubin, M., 1986, Distribution and age of the Uwekahuna Ash, Kilauea Volcano, Hawaii [abs.]: International Volcanological Congress, Auckland-Hamilton-Rotorua, New Zealand, Abstracts, February 1986, p. 112.

Macdonald, G.A., 1944, The 1840 eruption and crystal differentiation in the Kilauean magma column: American Journal of Science, v. 242, p. 177–189.

——— 1949, Petrography of the Island of Hawaii; U. S. Geological Survey Professional Paper 214–D, 96 p.

——— 1965, Hawaiian calderas: Pacific Science, v. 19, p. 320–334.

Murata, K.J., and Richter, D.H., 1961, Magmatic differentiation in the Uwekahuna laccolith, Kilauea caldera, Hawaii: Journal of Petrology, v. 2, p. 424–437.

——— 1966a, Chemistry of the lavas of the 1959–60 eruption of Kilauea Volcano, Hawaii: U.S. Geological Survey Professional Paper 537–A, 26 p.

——— 1966b, The settling of olivine in Kilauean magma as shown by the 1959 eruption: American Journal of Science, v. 264, p. 194–203.

Peterson, D.W. 1967, Geologic map of the Kilauea Crater quadrangle, Hawaii: U.S. Geological Survey Geologic Quadrangle Map GQ–667, scale 1:24,000.

Powers, H.A., 1948, A chronology of the explosive eruptions of Kilaeua: Pacific Science, v. 2, p. 278–292.

——— 1955, Composition and origin of basaltic magma of the Hawaiian Islands: Geochimica et Cosmochimica Acta, v. 7, p. 77–107.

Powers, S., 1916, Intrusive bodies at Kilauea: Zeitschrift fur Vulkanologie, v. 3, p. 28–33.

Shapiro, Leonard, 1975, Rapid analysis of silicate, carbonate, and phosphate rocks: U.S. Geological Survey Bulletin 1401, 56 p.

Stearns, H.T., and Clark, W.O., 1930, Geology and water resources of the Kau district, Hawaii: U.S. Geological Survey Water Supply Paper 616, 194 p.

Stearns, H.T., and Macdonald, G.A., 1946, Geology and ground-water resources of the Island of Hawaii: Hawaii Division of Hydrography Bulletin 9, 363 p.

Swanson, D.A., 1973, Pahoehoe flows from the 1969–1973 Mauna Ulu eruption: Kilauea Volcano, Hawaii: Geological Society of America Bulletin, v. 84, p. 615–626.

Swanson, D.A., Christiansen, R.L. 1973, Tragic base surge in 1790 at Kilauea Volcano: Geology, v. 1, p. 83–86.

Walker, G.W., 1969, Geologic map of the Kau Desert Quadrangle, Hawaii: U.S. Geological Survey Geologic Quadrangle Map GQ–827, scale 1:24,000.

Washington, H.S., 1923, Petrology of the Hawaiian Islands, III: Kilauea and general petrology of Hawaii: American Journal of Science, v. 6, p. 338–367.

Wright, T.L., 1971, Chemistry of Kilauea and Mauna Loa in space and time: U.S. Geological Survey Professional Paper 735, 40 p.

——— 1974, Presentation and interpretation of chemical data for igneous rocks: Contribution to Mineralogy and Petrology, v. 48, p. 233–248.

——— 1984, Origin of Hawaiian tholeiite: a metasomatic model: Journal of Geophysical Research, v. 89, p. 3233–3252.

Wright, T.L., Swanson, D.A., and Duffield, W.A., 1975, Chemical composition of Kilauea east-rift lava, 1968–1971: Journal of Petrology, v. 16, p. 110–133.

INTRUSIVE ROCKS OF KILAUEA CALDERA

By Thomas J. Casadevall *and* Daniel Dzurisin

ABSTRACT

Eighteen prehistoric dikes exposed in the west wall of Kilauea caldera have been mapped and analyzed for major, trace, and volatile elements. Twelve dikes occur along Uwekahuna Bluff and to the north and east; six dikes occur south of the bluff. Alignment of many dikes approximates the northeasterly trend common for several tectonic elements at Kilauea: the 6 southern dikes generally follow the N. 48° E. strike of the southwest rift zone, and 9 of 12 dikes in the north set strike roughly parallel to the linear western wall of the caldera (N. 40° E.). Chemical analyses of the dikes show that all are tholeiitic basalts, typical of Kilauea summit flows and similar to the lava flows making up the western caldera wall.

Five dikes of the north set occupy fractures cutting the entire section of flows in the caldera wall and therefore must be fairly young. Their age relative to the A.D. 1790 Keanakakoi Ash Member of the Puna Basalt is unknown, but we suggest that they formed just before or shortly after the explosive eruption and presumed caldera collapse responsible for the ash. Dikes of the south set show a close parallelism with recent prehistoric and historical fissures in the southwest rift zone. They are also young and may be closely related to recent activity in the upper southwest rift zone. The more northerly strike of the north set of dikes may reflect the combined influences of stresses caused by flexing of Kilauea's shallow summit magma reservoir and gravitational slumping of the volcano's south flank.

PURPOSE AND BACKGROUND

At Kilauea Volcano on the Island of Hawaii, much effort has been directed to identify and understand subsurface processes responsible for eruption-related seismicity and surface deformation (Eaton and Murata, 1960). Models invariably refer to the causative bodies as dikes (Ryan and others, 1981; Duffield and others, 1982; Epp and others, 1983; Pollard and others, 1983; Dvorak and others, 1986), and the shallow magma reservoir is usually envisioned as a plexus of dikes and sills (Fiske and Kinoshita, 1969; Fiske and Jackson, 1972; Ryan and others, 1983). Despite the many references to intrusive bodies, little effort has been spent in examining those exposed in Kilauea caldera.

Kilauea is one of the youngest of the Hawaiian volcanoes, and erosional dissection of the edifice has been insufficient to expose intrusive bodies. However, the walls of the 3×5 km summit caldera are as much as 140 m high and provide a window into the upper level of the Kilauea edifice. The western caldera wall comprises numerous lava flows, at least 18 dikes, the Uwekahuna laccolith (Murata and Richter, 1961), and 3 thin pyroclastic units (the lithic ash of 1924, the Keanakakoi Ash Member of the Puna Basalt, of about A.D. 1790; and the Uwekahuna Ash Member of the Puna Basalt, of about 2.1 ka).

In this paper, we describe the distribution, form, dimensions, and chemistry of intrusive bodies exposed in the western wall of the Kilauea summit caldera. From Uwekakuna Bluff to Steaming Bluff, this wall is an unbroken, nearly vertical cliff averaging 130 m high. The wall south of Uwekahuna Bluff is lower (15–40 m) and it has a stepped profile that has been attributed to normal faulting along the caldera rim (Dutton, 1884; Peterson, 1967; Holcomb, 1981; Saint Ours, 1982). We studied the intrusive bodies exposed in the caldera walls in order to compare them petrologically with the flows that they cut, to assess their volumetric importance, and to evaluate their relationship to the structural setting and state of stress in the summit region.

PREVIOUS STUDIES

KILAUEA INTRUSIVE BODIES

The largest intrusive body exposed at Kilauea is the Uwekahuna laccolith, which Daly (1911) first described and inferred to have an intrusive origin. Powers (1916) mapped this laccolith and noted that "about 20 dikes also occur in the [caldera] walls at various points, but especially at the northeast end of the sink." Washington (1923) published two chemical analyses of a dike (11N of this report) from the wall below Steaming Bluff. Murata and Richter (1961) and Aramaki (1968) studied the petrology of the Uwekahuna laccolith, accepted its intrusive origin, and concluded that its compositional variation could be explained by gravity settling of olivine followed by filter-pressing of the residual liquid.

Walker (1969) mapped several dikes in the Hilina system of normal faults on the south flank of Kilauea, about 12 km from the summit caldera and far from any known eruptive vent. He interpreted those dikes as fillings of deep ground cracks by surface lava flows. Easton and Lockwood (1983) presented data on the volatile contents of those dikes to support that interpretation.

MECHANISMS OF INTRUSION

Several mechanisms have been proposed to explain the origin of intrusive bodies at Kilauea. One is the intrusion of magma from a deep source; in this mechanism, magmatic pressure and increasing buoyancy owing to exsolution of volatiles combine to overcome effects of gravity and lithostatic load, forcing magma upward or laterally into country rock (Ryan and others, 1981).

A second mechanism is the lateral injection of degassed lava from a ponded lava lake. Daly (1911) and Murata and Richter (1961) proposed such an origin for the Uwekahuna laccolith, and Swanson and Peterson (1973) hypothesized a similar mechanism during the filling of Alae lava lake. The driving force for such lateral injection is limited to the weight of the lava column in the lake.

A third mechanism is the filling of fractures by lava flows. Deep vertical ground cracks are common both at the summit and along the rift zones of Kilauea (de Saint Ours, 1982), and lava flows have frequently been observed cascading into these cracks (Duffield and others, 1982). Solidification of the crack filling would form a tabular body of rock indistinguishable in most respects from upwardly or laterally fed dikes. Walker (1969) and Easton and Lockwood (1983) support such an origin for the dikes in the Hilina fault system. The low volatile contents that characterize lava flows some distance from their vents (Swanson and Fabbi, 1973) aid in distinguishing such surface-fed bodies from dikes intruded from depth (Easton and Lockwood, 1983).

ACKNOWLEDGMENTS

Our appreciation of the intrusive bodies at Kilauea caldera has grown during conversations with many colleagues, particularly P.T. Delaney, R.T. Holcomb, D.W. Peterson, and D.A. Swanson. Analytical results are from the Branch of Analytical Services, U.S. Geological Survey, Reston, Va. Major-element chemistry by J. Reid and D. Kay, INAA analyses by L. Schwarz, and AA analyses by D. Golightly and P. Aruscavage were indespensible to this work. F. Brown provided rapid analyses of sulfur and chloride from the dike samples. W. Melson and T. O'Hearn (Smithsonian Institution) kindly provided the microprobe analyses of glasses from the chilled margins of several of the intrusives. The hydration-rind ages of two dike samples were measured by J. Halbig (University of Hawaii-Hilo). We greatly appreciate these considerable analytical efforts. D. Johnson assisted in computer analysis of the data. Reviews of this manuscript by D.A. Swanson and P.T. Delaney have substantially helped our presentation.

METHODS

Our work included field mapping and description, petrographic study, and chemical analysis. Most field work was done in 1979–1980 and focused on the west wall of the caldera for reasons of easy access and good exposure. We briefly examined sections of the wall near Keanakakoi, in the Byron Ledge-Waldron Ledge area, and north of Steaming Bluff (fig. 14.1), but found no dikes. Sections of these walls are covered by vegetation, talus, or young lava flows, however, so that small intrusive bodies might be obscured.

FIELD CRITERIA FOR RECOGNIZING INTRUSIONS

The Uwekahuna laccolith (fig. 14.2*A*) has a dense, blocky texture that gives it a light color and smooth, massive surface appearance. Similar light-colored, smooth-surfaced rock lenses occur throughout the western caldera wall; many have prismatic jointing similar to that in the laccolith. Based on these similarities we originally suspected that many of these bodies might be sills or laccoliths. To distinguish between surface flows and sills we focused attention on contact relations, particularly evidence for cross-cutting relations, deformation of wall rocks, and textures of the top and bottom surfaces of a unit. Textures such as pahoehoe ropes, evidence for collapsed pahoehoe shells, and the rubbly surfaces of aa flows indicate a surface flow. Internal features such as visible mineralogy and vesicle abundance and distribution were of secondary importance in mapping flow units. When these criteria were applied to the suspected sills, contact relations invariably revealed an extrusive origin. In particular, the contacts between the dikes and their wall rocks often showed signs of rapid cooling, including fine grain size and glassy margins.

Vesicles of various sizes and shapes are abundant in most flows at Uwekahuna Bluff; flows below the Uwekahuna Ash Member are generally less vesicular than those above (Casadevall and Dzurisin, chapter 13). In contrast, vesicles are rare in dikes and in the Uwekahuna laccolith. Vesicles in dike interiors are typically small (1–10 mm) and spherical. The paucity of vesicles in the dikes and laccolith suggests either that confining pressure was too large to permit formation of an extensive separate gas phase or that the intruding magma was largely degassed. Additional details of the petrography and volatile content of the intrusions are discussed later.

RESULTS

DISTRIBUTION AND DESCRIPTION OF INTRUSIVE BODIES

About 20 intrusive bodies are exposed in the western wall of the caldera. The largest and most conspicuous is the Uwekahuna laccolith (fig. 14.2*A*), which consists of two bodies having a total outcrop length of about 300 m and a maximum thickness of about 30 m. The dense, light-colored laccolith contains 15–40 percent olivine phenocrysts concentrated in its central and lower parts by gravitational settling (Murata and Richter, 1961). Similar patterns of olivine concentration occur in the thicker picritic flows of the Uwekahuna Bluff section (Casadevall and Dzurisin, chapter 13). The laccolith is the only body in the western caldera wall that visibly deformed its host rocks, except for the obvious extensions caused by dikes: 10–15 m of the overlying picritic lavas are deformed (fig. 14.2*A*).

A possible sill or low-angle dike is exposed in the western wall about 1 km north of the laccolith, but is not easily accessible from the caldera floor (fig. 14.2*B*). This massive body, which we refer to as the manta ray because of its shape, has two limbs extending outward and upward and appearing to cut across adjacent flows. We tentatively conclude that the body is an intrusion, but it could also be a flow that filled a small surface depression. The major lenticular bodies of rock in the Uwekahuna Bluff section are thick subaerial lava flows, as judged from contact relations (Casadevall and Dzurisin, chapter 13).

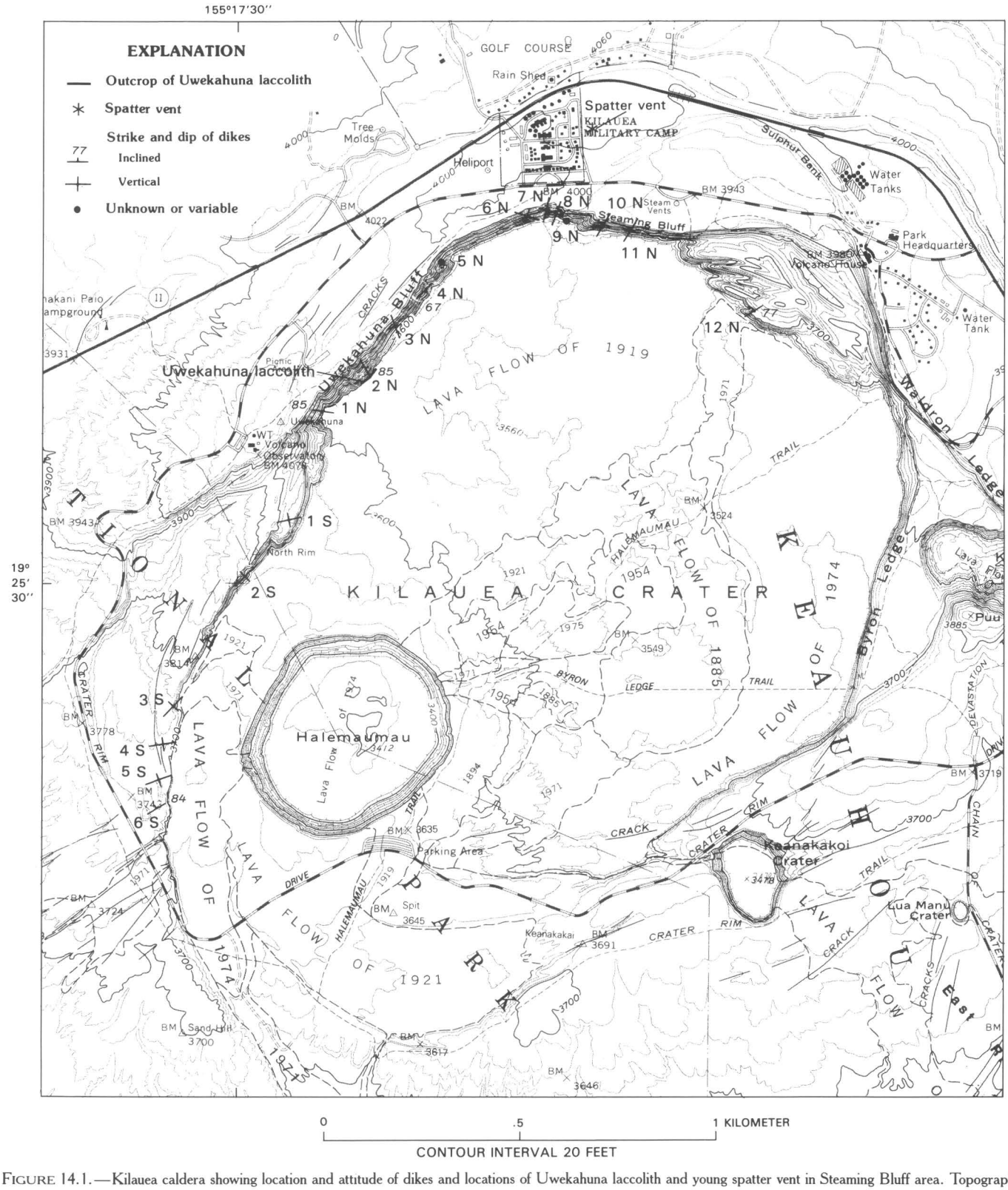

FIGURE 14.1.—Kilauea caldera showing location and attitude of dikes and locations of Uwekahuna laccolith and young spatter vent in Steaming Bluff area. Topographic map modified from U.S. Geological Survey Kilauea Crater 7.5-minute quadrangle, scale 1:24,000, 1981. Geology and structure modified from Peterson (1967) and de Saint Ours (1982). Dikes of north (N) and south (S) sets separately numbered.

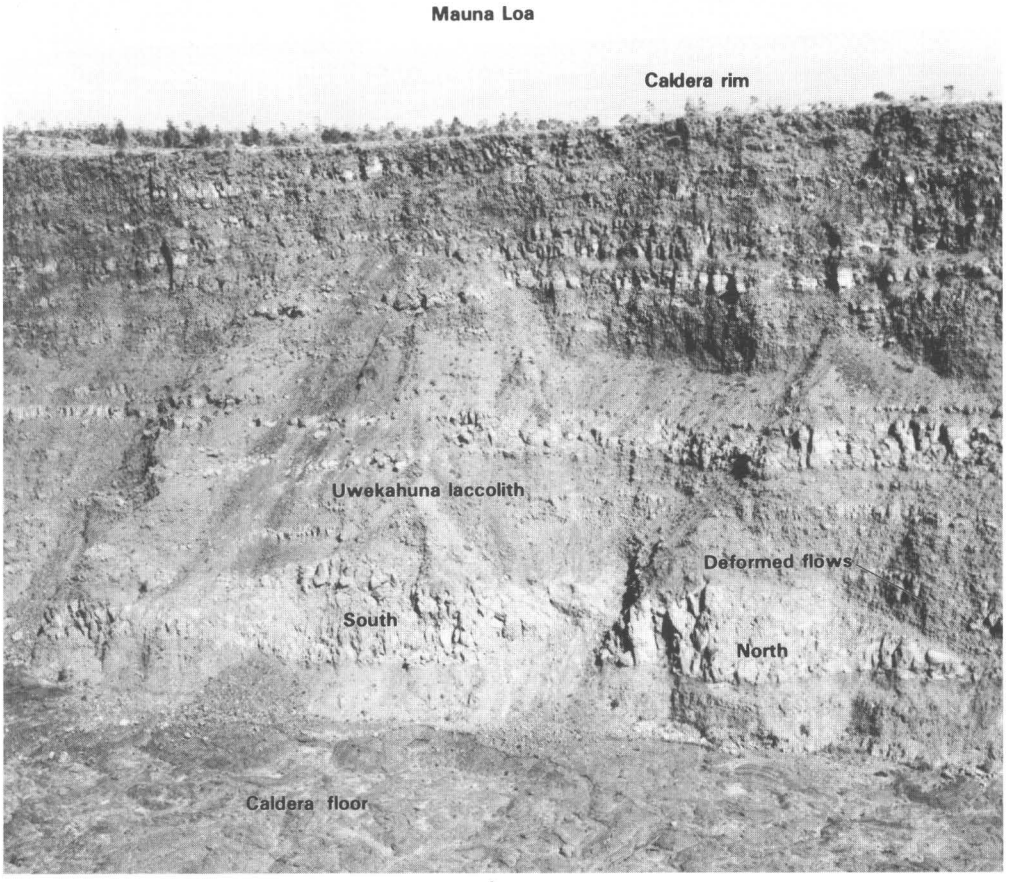
Mauna Loa
Caldera rim
Uwekahuna laccolith
Deformed flows
South
North
Caldera floor

A

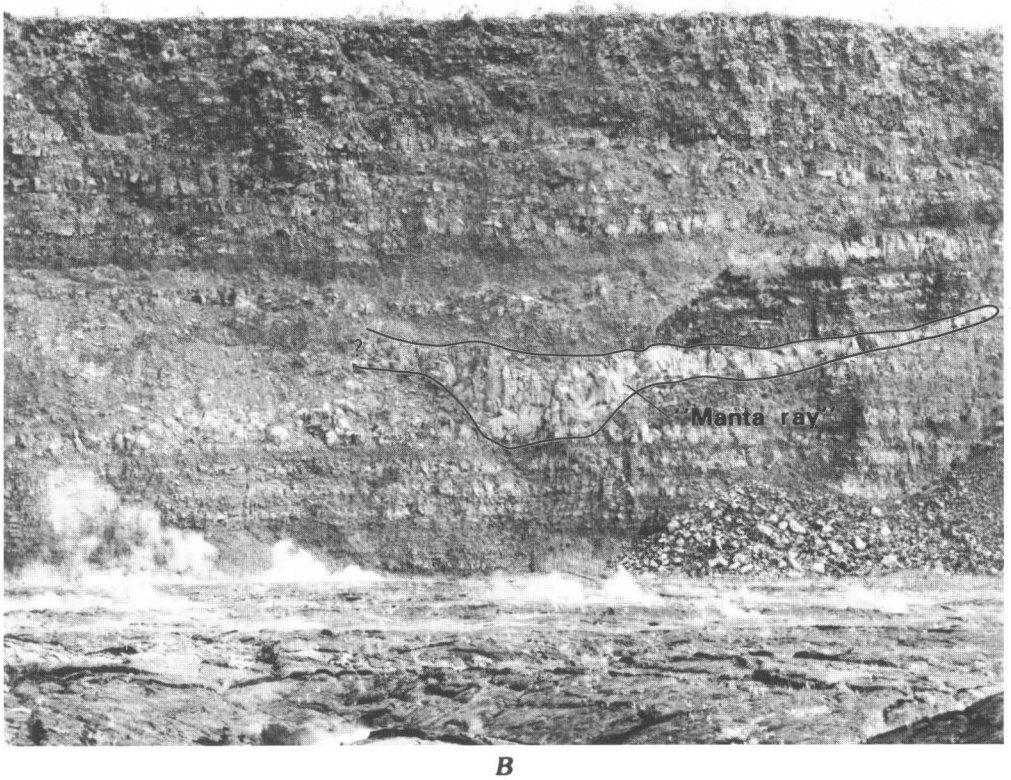
?
Manta ray

B

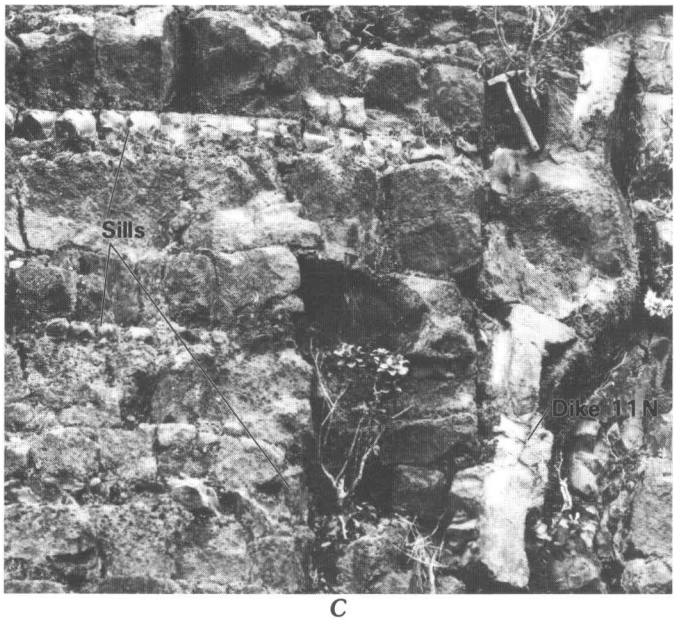

C

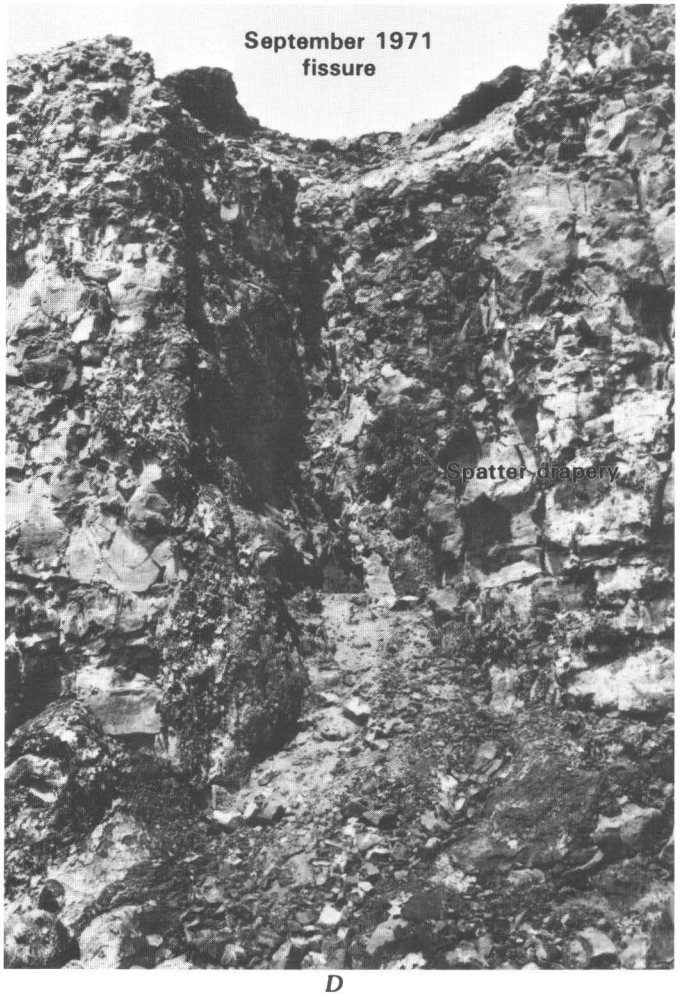

D

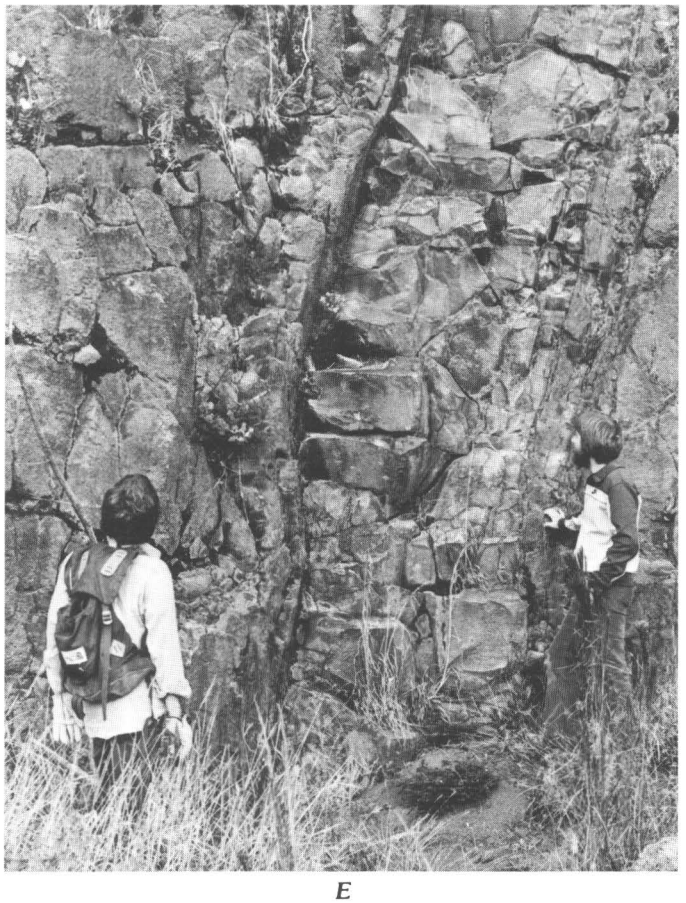

E

We identified 18 dikes in the western caldera wall that we subdivided into a north set (dikes 1N–12N) and a south set (dikes 1S–6S) based on their position relative to Uwekahuna Bluff (fig. 14.1). Most of the dikes trend northeasterly, roughly parallel to the strike of the southwest rift zone (N. 48° E.) and the linear segment of the western caldera wall (N. 40° E.; see fig. 14.6). Dike widths range from 5 cm to 2 m (table 14.1). The combined width of all dikes is only about 15 m, less than 1 percent of the length of the west wall.

DIKES OF THE NORTH SET

Dikes of the north set are oriented more northerly than those of the south set (fig. 14.1; table 14.1). Olivine-rich dikes 1N and 2N differ from other dikes of the north set in both composition and orientation (fig. 14.1); neither penetrates above the picritic lavas overlying the Uwekahuna Ash Member (Casadevall and Dzurisin, chapter 13). Dike 1N cuts the 2.1-ka Uwekahuna Ash Member and the lowermost flows of the picritic sequence at Uwekahuna

FIGURE 14.2.—Intrusive bodies in the west wall of Kilauea caldera. ***A***, Aerial view showing the two main parts (north and south) of the Uwekahuna laccolith; note tilted attitude of thin flows along northern edge of body. ***B***, Small manta ray-shaped body that is either an intrusion or formed by lava filling a surface depression. ***C***, Small sills coming off from main mass of dike 11N. ***D***, Detail of southwest caldera wall showing September 1971 eruptive fissure. ***E***, Dike 10N showing sets of prismatic joints perpendicular to dike walls.

TABLE 14.1.—*Thickness, orientation, MgO content, and brief description of dikes in the west wall of Kilauea caldera*

[n.d., not determined]

Dike	Thickness (cm)	Orientation		MgO content (weight percent)	Comments
		Strike	Dip		
North set					
1N	40–60	N. 83° W.	85° N.	6.9 (margin) 14.3 (core)	Glass margin, picritic core.
2N	85–110	N. 33° W.	85° NE.	26.6	Margin of Uwekahuna laccolith.
3N	5–10	N. 10° W.–N. 30° W.	vertical	n.d.	Thin dikelets in section of thin picritic pahoehoe flows.
4N	80 (minimum)	N. 45° E.	67° SE.	n.d.	Tabular dike; east wall is missing.
5N	8–10	n.d.	n.d.	n.d.	Thin dikelet, top of talus cone against caldera wall.
6N	20–30	N. 73° W.	vertical	6.7	Complex of dikes and dikelets with glassy margins.
7N	50	N. 17° E.	vertical	7.3	
8N	65	N. 29° E.	vertical	7.8	Glassy margins.
9N	20–30	NE. (varies)	n.d.	7.2	Complex of dikes and sills; glassy margins.
10N	60	N. 34° E.	vertical	7.0	Portion of dike by caldera floor has open, vuggy interior; glassy margins. Fills fracture that cuts entire section; dike stops 15 m below rim.
11N	100–180	N. 38° E.	vertical	7.5	Widest dike within caldera wall.
12N	100–150	N. 64° E.	77° NW.	6.9	Cuts flows in bench above 1974 flow on crater floor; glassy margins.
South set					
1S	8–12	N. 45° E.	vertical	6.7–7.7	Complex of dikelets and sills; glassy margins.
2S	75 (maximum)	N. 53° E.	vertical	6.6–7.5	Glassy margins.
3S	85–120	N. 42° E.–N. 53° E.	vertical	6.7–7.0	Above 1974 flows; glassy margins.
4S	35	N. 67° E.	vertical	7.0–7.2	Glassy margins.
5S	20–35	N. 85° E.	vertical	6.7–7.2 (margin) 20.1 (core)	Glassy margins.
6S	90 (maximum)	N. 60° E.	84° N.	n.d.	Glassy margins.

Bluff. Dike 2N occurs along the southern margin of the north part of the Uwekahuna laccolith, and it is olivine-rich throughout. It cuts several flows below the laccolith, but we did not find it above the laccolith.

The wider dikes display crude columnar jointing perpendicular to their margins. Dikes 10N and 11N have multiple cooling surfaces parallel to their walls that suggest more than one period of filling (fig. 14.2*E*). Small sills along flow contacts sprout from many dikes (fig. 14.2*C*); examples as much as 7 m long were observed.

Most samples for petrographic and chemical study were collected from the base of the exposure on the caldera floor. Along dike 10N, we rapelled from the caldera rim to collect samples and inspect the higher part of the dike about 15 m below the rim (fig. 14.3), where it terminates abruptly. This dike has fine-grained margins, 10–15 cm wide, which adhere to the walls of the fracture. The interior of the dike in its upper part is an open space about 80 cm wide, partly filled with soil and rock talus. We noted no spatter, drapery, or increased vesicularity of the dike rock to indicate eruption of the dike. The dike neither appeared to feed nor be fed from a surface flow. The host fracture, however, continued to the surface. Several factors, which we discuss later, may have prevented the magma from filling the fracture and reaching the surface, at least in the cross-section view we examined.

All but one of the 12 dikes in the north set occur in the unbroken part of the west caldera wall; dikes 6N–11N occupy fractures that cut through the entire sequence of flows in the wall (fig. 14.3). In the Steaming Flats area above these dikes, we found no evidence within several hundred meters of the rim that any dikes had vented. Where these fractures intersect the caldera rim, they are typically filled with vegetation, talus, and the Keanakakoi Ash Member. This cover obscures contact relations between the dikes and the ash.

Anecdotal evidence suggests that recent eruptive activity has occurred in the Steaming Flat area. Perret (1913, p. 615–616, fig. 6) noted that "miniature bombs or lava drops *** were discovered by the writer on the top, and surrounding the base, of several small, dome-topped cones of very scoriaceous lava situated on the northern rim of Kilauea near 'Kaniakolea', and therefore *outside* of the great pit crater, although within one of the surrounding areas of subsidence and not very far from Sulphur Banks*** ." H.A. Powers (oral commun., 1979) reported that following a large earthquake in the 1930's he found fresh spatter on the road at the western edge of Steaming Bluff, where Crater Rim Road ascends toward Kilauea Military Camp (fig. 14.1).

We did locate a spatter vent mapped by Macdonald and others (1983, fig. 19.19) (fig. 14.1). This feature is actually a series of echelon spatter ramparts that range in height from 2–8 m. They extend from the access road along the eastern boundary of Kilauea Military Camp to the northeast for approximately 150 m. The ramparts are mantled by the Keanakakoi Ash Member as much as 80 cm thick, indicating that they predate the 1790 eruption.

The area of Steaming Flats is currently aseismic (R.Y. Koyanagi, oral commun., 1979), and there is no local center of deformation in the area (A.T. Okamura, oral commun., 1984). However, nearby Sulfur Bank (fig. 14.1) is an area of active fumaroles (Casadevall and Hazlett, 1983), suggesting that a magmatic source of heat and gas is located at a shallow depth beneath the Steaming Flats area.

DIKES OF THE SOUTH SET

The six dikes south of Uwekahuna Bluff cut a thinner section of flows (15–40 m) than do the dikes north of Uwekahuna Bluff (120–140 m). Five of these southern dikes are fine grained and only

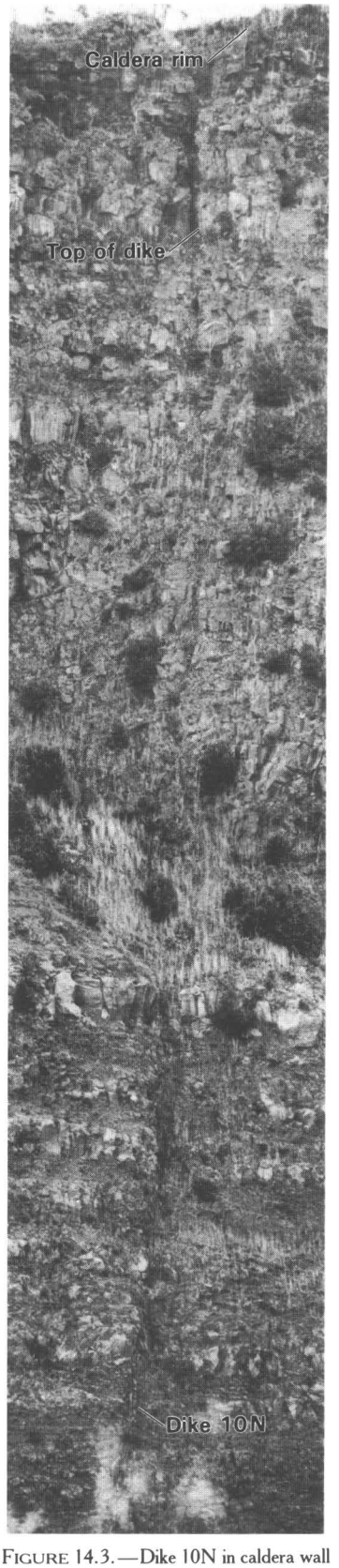

FIGURE 14.3.—Dike 10N in caldera wall below Steaming Bluff. Caldera floor at base of cliff just below bottom of view. Top of dike is about 15 m below caldera rim.

sparsely porphyritic, but dike 5S contains abundant olivine phenocrysts (tables 14.1, 14.2). Most of the dikes have open or rubble-filled interiors that resemble the 1971 eruptive fissure (Duffield and others, 1982) (fig. 14.2*D*). These dikes may have formed in a manner similar to that observed during the September 1971 eruption, in which the same fissure served first as a source of lava and later as a drain for surface flows.

The glassy margins of dikes 4S and 6S were dated by J. Halbig (written commun., 1985) using hydration-rind techniques. The hydration-rind ages have been calibrated elsewhere at Kilauea for lava flows dated by the radiocarbon method. The dikes have ages ranging from 0.55 to 0.45 ka. No ages are available for lava flows in this part of the caldera, so it is difficult to evaluate the accuracy of these ages. If, as we suspect, the flows cut by these dikes are equivalent to the upper flows exposed at Uwekahuna Bluff (suite A, 1.5–0.35 ka; see Casadevall and Dzurisin, chapter 13), the hydration-rind ages are reasonable.

PETROGRAPHY

We examined 28 thin sections from the dikes and identified three rock types on the basis of crystallinity and phenocryst content. The margins of most of the dikes and related thin sills consist of dark brown to olive glass with sparse microlites and scattered euhedral phenocrysts of olivine. The margins range from a few millimeters to several centimeters thick and pass gradually into the finely crystalline interiors of the dikes.

The cores of the thicker dikes are of two textural varieties, a porphyritic picrite (5S and 1N) with a fine- to medium-grained groundmass and an aphanitic basalt with sparse olivine phenocrysts in a groundmass of brown glass and plagioclase microlites. Olivine phenocrysts in the cores are generally corroded and resorbed, in contrast to their distinctly euhedral habit in the glassy margins. Dike 2N is medium to coarsely crystalline rock with only minor glass. It is distinct from all other dikes at Kilauea and closely resembles the Uwekahuna laccolith, which it appears to intrude and may have fed.

CHEMISTRY

MAJOR AND TRACE ELEMENTS

Fourteen dikes were analyzed for major and trace elements, including rare-earth elements, sulfur, and chlorine (table 14.2). The major-element data were determined using rapid-rock methods (Shapiro, 1975) and were supplemented by electron-microprobe analyses of glass from the margins of dikes. All analyses were recalculated on a dry-weight basis after converting iron to FeO_t ($FeO_t = FeO + 0.9Fe_2O_3$) to facilitate comparison of the data. Our objective in obtaining these data was to use chemistry, in conjunction with field occurrence and petrography, to characterize dikes or sets of dikes and to relate the dikes to the flows in the Uwekahuna Bluff section (Casadevall and Dzurisin, chapter 13). Water (H_2O^+), sulfur, and chlorine were measured to estimate the extent to which the dikes had degassed.

TABLE 14.2.—*Chemical analyses of samples from dikes in the west wall of Kilauea caldera*

[Values for oxides in weight percent; values for trace elements in parts per million. Symbols (numbers and letters) used to distinguish samples in fig. 14.4; INAA, neutron-activation analysis; AA, atomic absorption analysis; n.d., not determined; <, less than. Sources of data: for WASH-11, Washington (1923); for Uwekahuna laccolith, Murata and Richter (1961)]

Dike	1S	1S	2S	2S	3S	3S	3S	4S	4S	4S	5S
Sample	5614	W-211577	5615	W-211567	5616	5617	W-211575	5620	5621	W-211574	5618
Symbol	1	1	2	2	3	3	3	4	4	4	5
SiO_2	51.84	50.2	51.75	49.7	50.64	50.78	50.2	50.96	51.65	50.0	51.62
Al_2O_3	13.96	13.7	14.06	13.5	13.99	13.91	13.4	13.58	13.70	13.7	13.95
Fe_2O_3	n.d.	1.9	n.d.	2.2	n.d.	n.d.	2.9	n.d.	n.d.	2.0	n.d.
FeO	10.75	9.1	10.94	9.3	11.09	11.10	8.9	11.18	11.16	9.5	11.05
MgO	6.71	7.7	6.63	7.4	6.84	6.77	7.0	7.24	7.10	7.0	6.76
CaO	10.88	10.9	10.96	10.9	11.03	11.09	11.4	11.33	11.22	11.2	10.95
Na_2O	2.43	2.3	2.39	2.2	2.22	2.30	2.1	2.31	2.25	2.2	2.12
K_2O	.47	.45	.41	.40	.39	.41	.41	.45	.44	.43	.34
H_2O	n.d.	.16	n.d.	.01	n.d.	n.d.	.13	n.d.	n.d.	.04	n.d.
TiO_2	2.71	2.5	2.48	2.3	2.50	2.58	2.4	2.38	2.48	2.4	2.35
P_2O_5	.27	.26	.23	.27	.23	.24	.27	.26	.25	.27	.20
MnO	n.d.	.16	n.d.	.15	n.d.	n.d.	.18	n.d.	n.d.	.17	n.d.
CO_2	n.d.	n.d.	n.d.	n.d.	n.d.	n.d.	n.d.	n.d.	n.d.	n.d.	n.d.
Cl	n.d.	.004	n.d.	.004	n.d.	n.d.	.005	n.d.	n.d.	.006	n.d.
F	n.d.	n.d.	n.d.	n.d.	n.d.	n.d.	n.d.	n.d.	n.d.	n.d.	n.d.
S	n.d.	.042	n.d.	.049	n.d.	n.d.	.066	n.d.	n.d.	.049	n.d.
Ba	n.d.	121	n.d.	117	n.d.	n.d.	109	n.d.	n.d.	139	n.d.
Co (INAA)	n.d.	44.3	n.d.	44.5	n.d.	n.d.	43.3	n.d.	n.d.	43.6	n.d.
Co (AA)	n.d.	45	n.d.	45	n.d.	n.d.	45	n.d.	n.d.	47	n.d.
Cr	n.d.	454	n.d.	408	n.d.	n.d.	315	n.d.	n.d.	309	n.d.
Ni	n.d.	190	n.d.	140	n.d.	n.d.	100	n.d.	n.d.	100	n.d.
Cu	n.d.	120	n.d.	120	n.d.	n.d.	110	n.d.	n.d.	120	n.d.
Hf	n.d.	3.87	n.d.	3.55	n.d.	n.d.	3.99	n.d.	n.d.	3.83	n.d.
Rb	n.d.	11	n.d.	14	n.d.	n.d.	13	n.d.	n.d.	13	n.d.
Ta	n.d.	.87	n.d.	.76	n.d.	n.d.	.99	n.d.	n.d.	1.08	n.d.
Th	n.d.	.86	n.d.	.7	n.d.	n.d.	.95	n.d.	n.d.	.96	n.d.
U	n.d.	<0.6	n.d.	<0.5	n.d.	n.d.	.34	n.d.	n.d.	.37	n.d.
Zn	n.d.	111	n.d.	108	n.d.	n.d.	108	n.d.	n.d.	114	n.d.
Zr	n.d.	119	n.d.	81	n.d.	n.d.	167	n.d.	n.d.	76	n.d.
Sc	n.d.	29.9	n.d.	30.6	n.d.	n.d.	31.7	n.d.	n.d.	31.6	n.d.
La	n.d.	12.8	n.d.	10.6	n.d.	n.d.	12.3	n.d.	n.d.	12.3	n.d.
Ce	n.d.	29.0	n.d.	25.3	n.d.	n.d.	27.8	n.d.	n.d.	28.9	n.d.
Nd	n.d.	21	n.d.	21	n.d.	n.d.	9	n.d.	n.d.	23	n.d.
Sm	n.d.	5.50	n.d.	5.2	n.d.	n.d.	5.35	n.d.	n.d.	5.39	n.d.
Eu	n.d.	1.92	n.d.	1.80	n.d.	n.d.	1.74	n.d.	n.d.	1.78	n.d.
Gd	n.d.	5.1	n.d.	4.7	n.d.	n.d.	3.3	n.d.	n.d.	4.2	n.d.
Tb	n.d.	.87	n.d.	.79	n.d.	n.d.	.80	n.d.	n.d.	.83	n.d.
Tm	n.d.	.27	n.d.	.23	n.d.	n.d.	.27	n.d.	n.d.	.22	n.d.
Yb	n.d.	2.05	n.d.	2.05	n.d.	n.d.	2.10	n.d.	n.d.	2.20	n.d.
Lu	n.d.	.286	n.d.	.310	n.d.	n.d.	.302	n.d.	n.d.	.301	n.d.

Dike	5S	5S	5S	1N	1N	2N	6N	7N	8N	9N	10N
Sample	5619	W-211407	W-211573	5622	W-211408	W-211409	5623	W-211410	W-211411	W-211415	W-211412
Symbol	5	5	5	A	A	B	F	G	H	I	J
SiO_2	51.06	46.6	50.3	51.38	48.7	44.8	51.63	50.5	50.6	51.3	51.0
Al_2O_3	13.61	9.5	13.9	14.18	11.3	6.9	13.9	12.7	13.1	13.7	13.9
Fe_2O_3	n.d.	1.5	2.1	n.d.	2.0	2.8	n.d.	2.3	2.1	2.2	2.5
FeO	11.00	10.7	9.4	9.96	9.6	10.8	10.87	9.9	9.4	9.1	8.8
MgO	7.17	20.2	7.2	6.94	14.3	26.8	6.78	7.3	7.8	7.2	7.0
CaO	11.23	7.7	10.9	11.47	9.3	5.9	11.10	10.4	11.0	10.6	10.9
Na_2O	2.23	1.6	2.4	2.36	1.9	.99	2.37	2.4	2.2	2.5	2.5
K_2O	.40	.33	.44	.47	.37	.19	.41	.50	.45	.41	.44
H_2O	n.d.	.35	.33	n.d.	.13	.31	n.d.	.25	.13	.22	.16
TiO_2	2.45	1.7	2.3	2.65	2.1	1.0	2.39	2.9	2.5	2.4	2.4
P_2O_5	.19	.21	.27	.23	.25	.13	.23	.35	.28	.30	.28
MnO	n.d.	.19	.17	n.d.	.18	.20	n.d.	.20	.18	.19	.18
CO_2	n.d.	n.d.	n.d.	n.d.	n.d.	n.d.	n.d.	n.d.	n.d.	n.d.	n.d.
Cl	n.d.	.004	.005	n.d.	.004	.004	n.d.	.005	.006	.004	.004
F	n.d.	n.d.	n.d.	n.d.	n.d.	n.d.	n.d.	n.d.	n.d.	n.d.	n.d.
S	n.d.	.024	.045	n.d.	.027	.015	n.d.	.063	.068	.048	.025
Ba	n.d.	101	121	n.d.	<200	66	n.d.	148	130	103	<200
Co (INAA)	n.d.	87.9	40.5	n.d.	65.1	110	n.d.	44.6	46	42.4	41.7
Co (AA)	n.d.	89	45	n.d.	66	110	n.d.	50	52	48	48
Cr	n.d.	1220	328	n.d.	934	1620	n.d.	289	355	331	347
Ni	n.d.	980	90	n.d.	600	1400	n.d.	97	110	85	82
Cu	n.d.	68	120	n.d.	99	49	n.d.	140	120	120	100
Hf	n.d.	2.48	3.54	n.d.	3.21	1.50	n.d.	4.52	3.7	3.6	3.57
Rb	n.d.	<30	19	n.d.	<30	<30	n.d.	<30	16	<30	<30
Ta	n.d.	.66	.82	n.d.	.81	.39	n.d.	1.13	.91	.77	.77
Th	n.d.	.47	.84	n.d.	.65	<.4	n.d.	.87	.90	.68	.69
U	n.d.	.33	<.4	n.d.	.29	<.5	n.d.	.43	<.6	.31	<.6
Zn	n.d.	104	103	n.d.	106	105	n.d.	119	111	110	110
Zr	n.d.	89	168	n.d.	<100	<200	n.d.	185	157	118	<200
Sc	n.d.	20.9	29.5	n.d.	26.5	19.2	n.d.	31.9	31.2	30.1	30.5
La	n.d.	8.9	10.8	n.d.	10.2	4.6	n.d.	14.9	11.5	10.9	11.1
Ce	n.d.	21.3	25.0	n.d.	24.8	12.6	n.d.	35.5	29.0	25.8	26.0
Nd	n.d.	15	16	n.d.	18	9	n.d.	25	19	17	19
Sm	n.d.	3.92	5.22	n.d.	4.65	2.30	n.d.	6.64	5.49	5.39	5.4
Eu	n.d.	1.26	1.68	n.d.	1.54	.748	n.d.	2.17	1.78	1.81	1.72
Gd	n.d.	4.8	3.8	n.d.	5.4	3.0	n.d.	8.1	6.4	6.4	6.4
Tb	n.d.	.56	.74	n.d.	.70	.46	n.d.	1.01	.84	.86	1.05
Tm	n.d.	.17	.26	n.d.	.26	.10	n.d.	.40	.24	.34	.27
Yb	n.d.	1.40	2.15	n.d.	1.70	.91	n.d.	2.45	2.03	2.18	2.03
Lu	n.d.	.196	.298	n.d.	.253	.132	n.d.	.35	.30	.30	.29

TABLE 14.2.—*Chemical analyses of samples from dikes in the west wall of Kilauea caldera*—Continued

Dike	10N	11N	12N	11N	11N	LAC	LAC	LAC	LAC	LAC	LAC	LAC
Sample	W-211416	W-211414	W-211413	WASH-11	WASH-11	UWEMR-1	UWEMR-2	UWEMR-3	UWEMR-4	UWEMR-5	UWEMR-6	UWEMR-7
Symbol	J	K	L	K	K	U	U	U	U	U	U	U
SiO_2	51.2	50.9	51.7	51.77	50.53	48.37	48.25	46.59	46.32	48.56	49.50	52.04
Al_2O_3	14.3	13.4	13.7	13.54	13.61	11.19	10.72	7.69	8.58	11.62	12.67	13.20
Fe_2O_3	1.8	2.1	2.0	.75	1.69	3.08	2.14	2.20	1.58	2.9	4.89	2.86
FeO	9.2	9.3	9.2	9.63	9.30	8.65	9.50	10.46	10.98	8.56	6.36	8.55
MgO	7.0	7.5	6.9	7.33	7.01	15.26	16.45	21.79	21.98	14.65	11.55	5.84
CaO	10.6	10.6	10.6	10.57	10.75	8.94	8.79	7.41	7.11	9.36	10.05	8.83
Na_2O	2.3	2.4	2.4	2.18	2.16	1.76	1.61	1.33	1.28	1.74	1.99	2.79
K_2O	.43	.41	.42	.45	.35	.28	.25	.28	.21	.26	.32	.83
H_2O	.29	.10	.30	n.d.	n.d.	.13	.11	.41	.15	.17	.14	.41
TiO_2	2.4	2.4	2.3	4.01	3.68	1.88	1.75	1.83	1.44	1.92	2.14	4.16
P_2O_5	.30	.29	.30	.26	.20	.16	.16	.11	.11	.14	.18	.49
MnO	.18	.19	.17	.15	.13	.17	.17	.18	.17	.16	.16	.16
CO_2	n.d.	n.d.	n.d.	n.d.	n.d.	n.d.	n.d.	n.d.	n.d.	n.d.	n.d.	n.d.
Cl	.005	.004	.005	n.d.	n.d.	n.d.	n.d.	n.d.	n.d.	n.d.	n.d.	n.d.
F	n.d.	n.d.	n.d.	n.d.	n.d.	n.d.	n.d.	n.d.	n.d.	n.d.	n.d.	n.d.
S	.034	.027	.065	n.d.	n.d.	n.d.	n.d.	n.d.	n.d.	n.d.	n.d.	n.d.
Ba	112	99	105	n.d.	n.d.	n.d.	n.d.	n.d.	n.d.	n.d.	n.d.	n.d.
Co (INAA)	37.9	45	41.5	n.d.	n.d.	n.d.	n.d.	n.d.	n.d.	n.d.	n.d.	n.d.
Co (AA)	45	48	48	n.d.	n.d.	n.d.	n.d.	n.d.	n.d.	n.d.	n.d.	n.d.
Cr	309	370	318	n.d.	n.d.	n.d.	n.d.	n.d.	n.d.	n.d.	n.d.	n.d.
Ni	97	120	94	n.d.	n.d.	n.d.	n.d.	n.d.	n.d.	n.d.	n.d.	n.d.
Cu	120	100	120	n.d.	n.d.	n.d.	n.d.	n.d.	n.d.	n.d.	n.d.	n.d.
Hf	3.30	3.6	3.6	n.d.	n.d.	n.d.	n.d.	n.d.	n.d.	n.d.	n.d.	n.d.
Rb	<20	<30	<30	n.d.	n.d.	n.d.	n.d.	n.d.	n.d.	n.d.	n.d.	n.d.
Ta	.68	.79	.75	n.d.	n.d.	n.d.	n.d.	n.d.	n.d.	n.d.	n.d.	n.d.
Th	.68	.83	.76	n.d.	n.d.	n.d.	n.d.	n.d.	n.d.	n.d.	n.d.	n.d.
U	<.3	<.6	<.6	n.d.	n.d.	n.d.	n.d.	n.d.	n.d.	n.d.	n.d.	n.d.
Zn	98	120	115	n.d.	n.d.	n.d.	n.d.	n.d.	n.d.	n.d.	n.d.	n.d.
Zr	88	113	141	n.d.	n.d.	n.d.	n.d.	n.d.	n.d.	n.d.	n.d.	n.d.
Sc	27.5	31.0	30.1	n.d.	n.d.	n.d.	n.d.	n.d.	n.d.	n.d.	n.d.	n.d.
La	10.8	10.7	10.7	n.d.	n.d.	n.d.	n.d.	n.d.	n.d.	n.d.	n.d.	n.d.
Ce	24.1	24.9	25.5	n.d.	n.d.	n.d.	n.d.	n.d.	n.d.	n.d.	n.d.	n.d.
Nd	18	19	17	n.d.	n.d.	n.d.	n.d.	n.d.	n.d.	n.d.	n.d.	n.d.
Sm	5.34	5.24	5.24	n.d.	n.d.	n.d.	n.d.	n.d.	n.d.	n.d.	n.d.	n.d.
Eu	1.61	1.71	1.77	n.d.	n.d.	n.d.	n.d.	n.d.	n.d.	n.d.	n.d.	n.d.
Gd	6.6	6..1	5.7	n.d.	n.d.	n.d.	n.d.	n.d.	n.d.	n.d.	n.d.	n.d.
Tb	.85	.86	.83	n.d.	n.d.	n.d.	n.d.	n.d.	n.d.	n.d.	n.d.	n.d.
Tm	.23	.25	.33	n.d.	n.d.	n.d.	n.d.	n.d.	n.d.	n.d.	n.d.	n.d.
Yb	2.07	2.15	2.32	n.d.	n.d.	n.d.	n.d.	n.d.	n.d.	n.d.	n.d.	n.d.
Lu	.28	.318	.321	n.d.	n.d.	n.d.	n.d.	n.d.	n.d.	n.d.	n.d.	n.d.

The dikes are tholeiitic basalt and have compositions similar to those of typical Kilauea summit flows (Macdonald, 1949; Wright, 1971; Casadevall and Dzurisin, chapter 13), for which the main control on composition is the gain or loss of olivine (Powers, 1955; Murata and Richter, 1966a, b; Wright, 1971). Dikes of the north set and those of the south set are chemically similar. MgO variation diagrams show no obvious linear trends because most analyses cluster between 6.6 and 7.8 weight percent MgO (fig. 14.4A). The cores of the three picrite dikes (5S, 1N, and 2N) have MgO in excess of 14 weight percent; dikes 5N and 1S have glassy margins with MgO contents near 7.0 weight percent. The olivine-control lines for these two dikes are similar to those for lava flows of Uwekahuna Bluff (fig. 14.4; table 14.3; Casadevall and Dzurisin, chapter 13).

Thirteen dikes were analyzed for a suite of 24 trace elements using a combination of instrumental neutron activation (Baedecker, 1979), atomic absorption, and X-ray fluorescence methods (table 14.2). Most of the trace elements correlate negatively with MgO content (fig. 14.4*B*) but dilution by settled olivine causes Ni, Co, and Cr to show positive correlations (fig. 14.4*B*) for reasons discussed in Casadevall and Dzurisin (chapter 13). The rare-earth-element (REE) abundances and the shapes and slopes of chondrite-normalized REE plots for the dike samples (fig. 14.5) closely resemble those for Kilauea lava flows (Leeman and others, 1977, 1980; Basaltic Volcanism Study Project, 1981), including those from Uwekahuna Bluff (Casadevall and Dzurisin, chapter 13).

VOLATILE CONSTITUENTS

The dikes contain concentrations of water, sulfur, and chlorine that are higher than in typical surface-degassed lava, but lower than in primitive basaltic magma (table 14.4). Water content for glassy margins of most of the dikes is in the range of 0.13–0.35 weight percent; in dikes 2S and 4S it is considerably lower (0.01 and 0.04 weight percent, respectively). Sulfur content of glassy margins of the dikes ranges from 0.042 to 0.068 weight percent, and that of chlorine from 0.004 to 0.006 weight percent. Interiors of the dikes generally have less H_2O, S, and Cl than do their glassy margins. This difference probably reflects the fact that glassy margins quench in higher volatile contents compared to the more crystalline interior portions of the dikes. The concentrations in the glassy margins are low compared to the postulated abundances for parental Hawaiian basaltic magma (table 14.4): 0.30–0.45 weight percent H_2O; 0.10–0.15 weight percent S, and 0.008–0.011 weight percent Cl (Harris and Anderson, 1983; Gerlach and Graeber, 1985; Greenland and others, 1985; L.P. Greenland, written commun., 1985).

Gerlach and Graeber (1985) and Greenland and others (1985) have demonstrated that Hawaiian magma loses volatiles on the way to the surface as well as during eruption. Loss of carbon dioxide probably begins soon after the magma leaves the upper mantle. Significant loss of water and sulfur, on the other hand, occurs when the magma is at a confining pressure equivalent to several tens of meters of lithostatic load (Moore, 1970; Moore and Fabbi, 1971), although some is lost while the magma temporarily resides in the shallow summit reservoir (Gerlach and Graeber, 1985; Greenland and others, 1985).

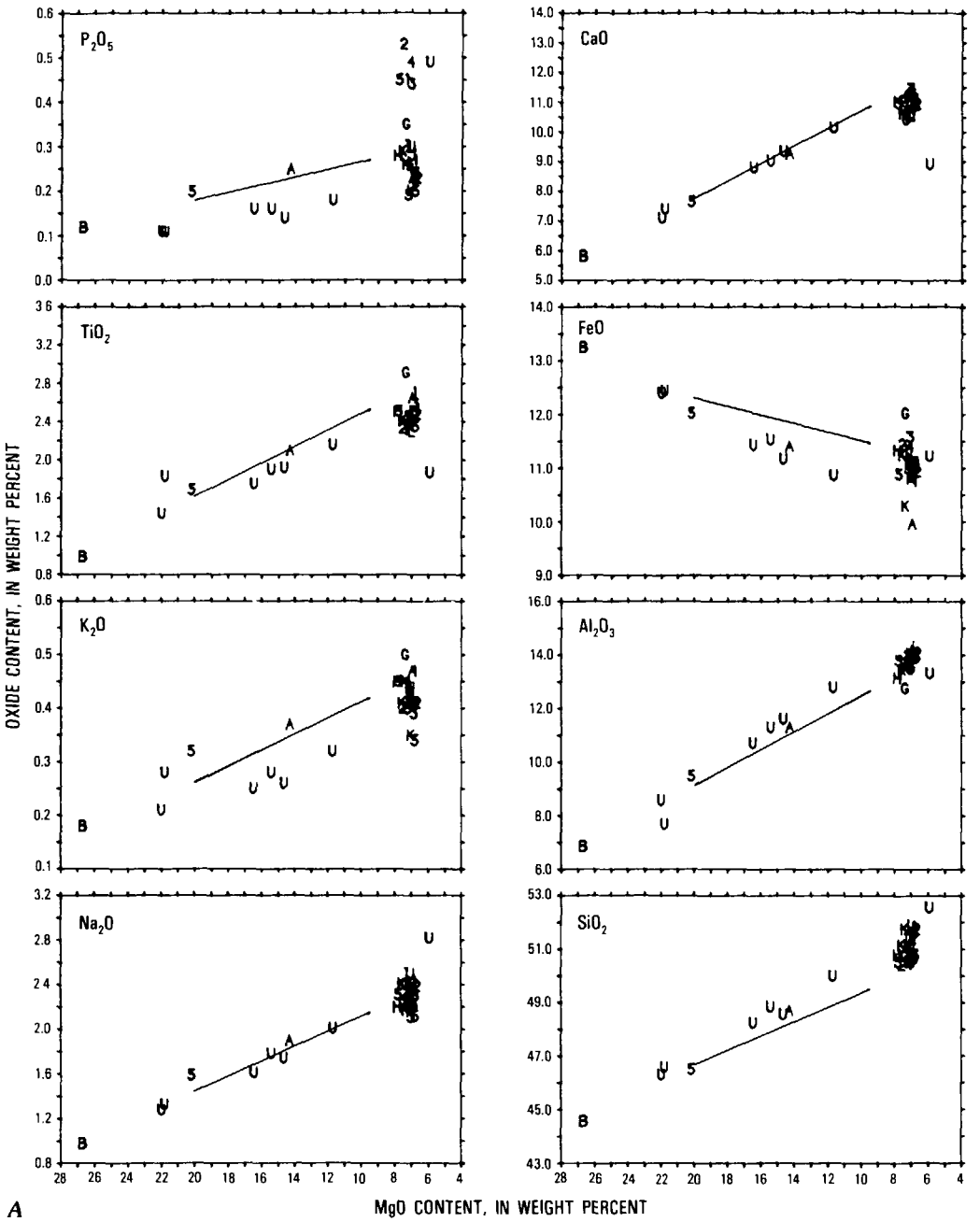

FIGURE 14.4.—MgO variation diagrams for intrusive rocks of Kilauea caldera. A, dike 1N; J, dike 10N; K, dike 11N; L, dike 12N; O, dike 10N; U, Uwekahuna laccolith. Also plotted are olivine-control lines for the picritic suite C lava flows at Uwekahuna Bluff (Casadevall and Dzurisin, chapter 13); these lines are not derived from the plotted data but instead provide a comparison between the caldera intrusions and the lava flows they intruded. Data for Uwekahuna laccolith from Murata and Richter (1961). Other number and letter symbols refer to samples listed in table 14.2. ***A***, Major-element abundances. ***B***, Trace-element abundances. ***C***, Rare-earth-element abundances.

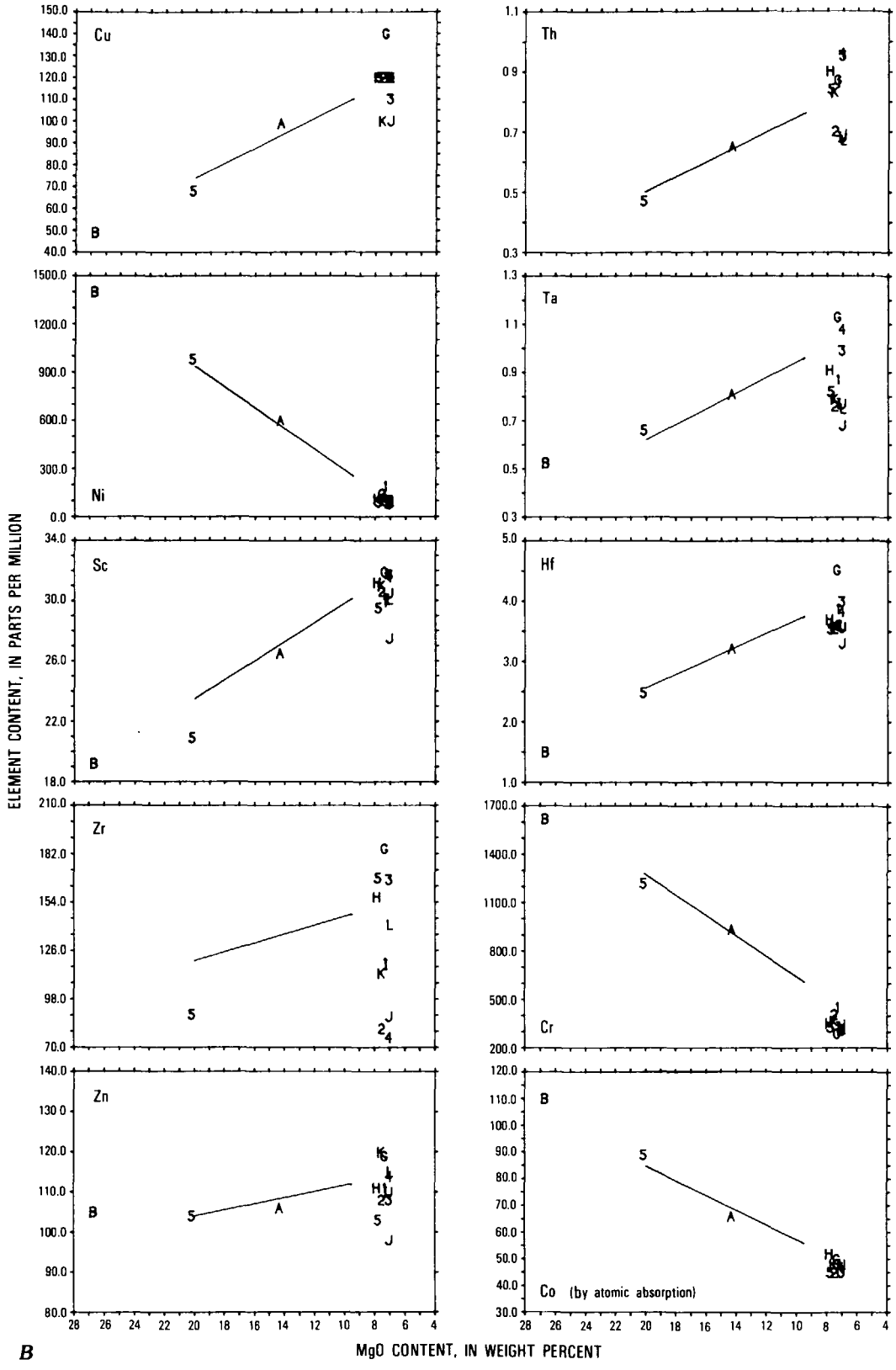

FIGURE 14.4.—Continued.

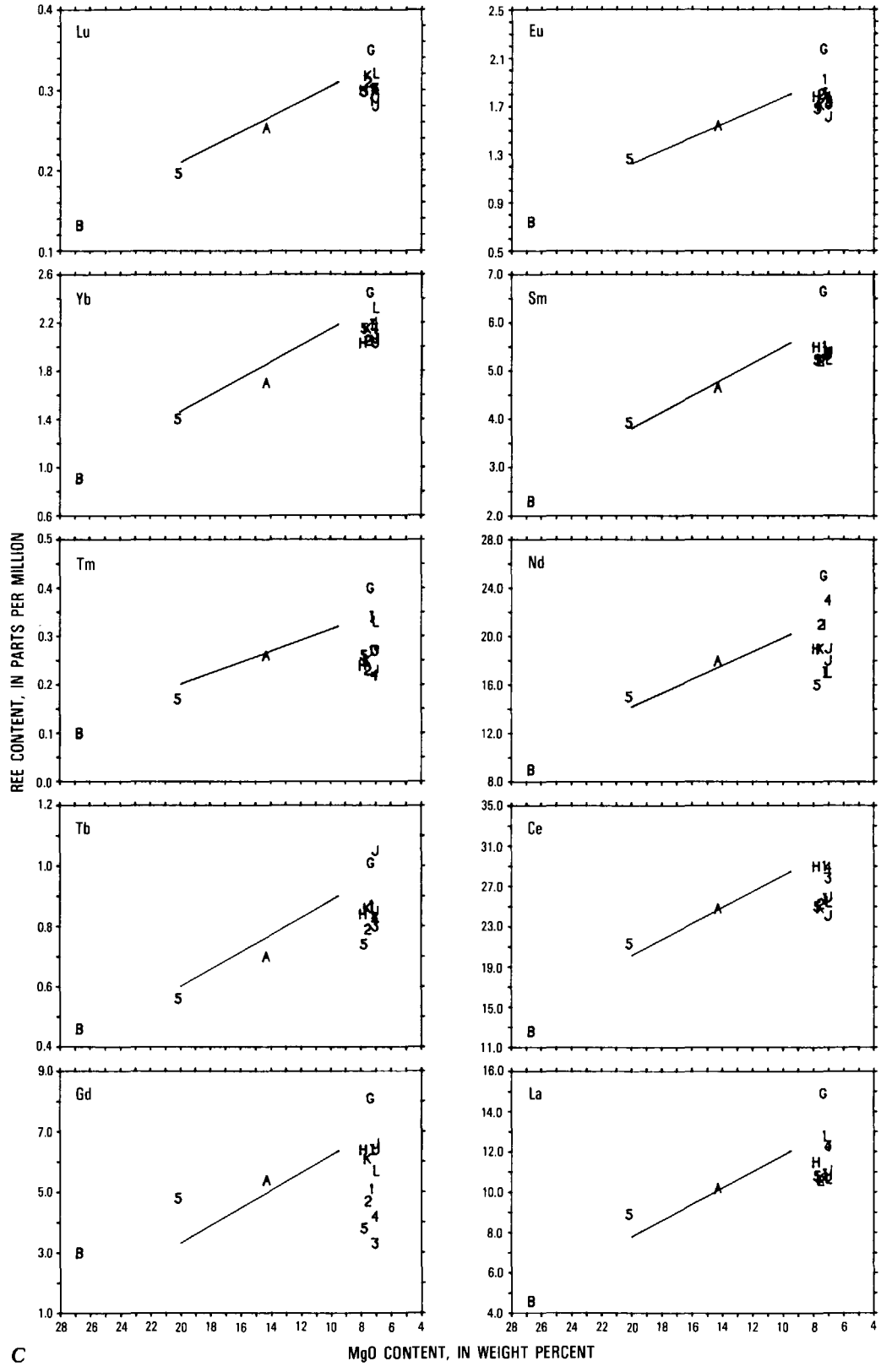

FIGURE 14.4.—Continued.

TABLE 14.3.—*Coefficients of olivine control lines (equations of the form $y = ax + b$) for Kilauea intrusive rocks and lava flows*

[y is the major oxide or element, x is the MgO content, a is the slope, and b is the y intercept value at MgO = 0 weight percent. Values for oxides in weight percent; values for trace elements in parts per million. Data sources: Dikes, this paper; Uwekahuna laccolith, Murata and Richter (1961); Uwekahuna Bluff suite C flows, Casadevall and Dzurisin (chapter 13); prehistoric pahoehoe picrite complex (PPPC) flows and prehistoric Kilauea caldera and Hilina (PHKILCAL) flows, Wright (1971). FeO_t, total iron oxide = FeO + 0.9 Fe_2O_3; n.d., not determined]

Element/oxide	Slope (a)	Uncertainty	Intercept (b)
Dike 5S			
SiO_2	−0.356	±0.047	53.651
Al_2O_3	−.332	±.024	16.181
FeO	.808	±.016	10.404
CaO	−.262	±.025	12.931
Na_2O	−.048	±.015	2.563
K_2O	−.005	±.007	.435
TiO_2	−.057	±.014	2.845
P_2O_5	−.005	±.019	.314
MnO	.002	n.d.	.148
Dike 1N			
SiO_2	−0.363	n.d.	53.898
Al_2O_3	−.391	n.d.	16.896
FeO	.196	n.d.	8.602
CaO	−.300	n.d.	13.554
Na_2O	−.063	n.d.	2.794
K_2O	−.014	n.d.	.564
TiO_2	−.075	n.d.	3.169
P_2O_5	.003	n.d.	.211
MnO	n.d.	n.d.	n.d.
Uwekahuna laccolith			
SiO_2	−0.307	±0.017	53.394
Al_2O_3	−.455	±.056	18.202
FeO	.160	±.013	8.935
CaO	−.275	±.019	13.342
Na_2O	−.066	±.005	2.744
K_2O	−.006	±.005	.367
TiO_2	−.045	±.023	2.603
P_2O_5	−.006	±.002	.253
MnO	.001	±.001	.144
Uwekahuna Bluff suite C flows			
SiO_2	−0.248	±0.064	51.828
Al_2O_3	−.336	±.025	15.852
FeO	.071	±.037	10.811
CaO	−.306	±.056	13.797
Na_2O	−.070	±.008	2.822
K_2O	−.015	±.003	.556
TiO_2	−.086	±.015	3.348
P_2O_5	−.008	±.003	.348
MnO	−.002	±.002	.183
Ba	.565	±2.649	100.346
Co (INAA)	3.297	±.253	19.006
Co (AA)	2.772	±.353	29.385
Cr	63.771	±6.067	2.147
Ni	65.268	±5.240	−368.050
Cu	−3.969	±1.398	151.439
Hf	−.113	±.025	4.831
Rb	−.289	±.345	16.829
Ta	−.032	±.009	1.272
Th	−.025	±.005	1.001
U	−.005	±.012	.369
Zn	−.700	±.600	118.175
Zr	−3.137	±2.066	171.211
Sc	−.635	±.074	36.140
La	−.409	±.079	15.931
Ce	−.800	±.162	36.090
Nd	−.578	±.267	25.673
Sm	−.170	±.033	7.194
Gd	−.291	±.070	9.128
Tb	−.029	±.008	1.186
Tm	−.011	±.004	.432
Yb	−.068	±.012	2.822
Lu	−.009	±.002	0.392
Prehistoric pahoehoe picrite complex (PPPC) flows			
SiO_2	−0.289	±0.023	52.894
Al_2O_3	−.357	±.010	16.643
FeO	.068	±.017	10.480
CaO	−.288	±.017	13.184
Na_2O	−.053	±.007	2.691
K_2O	−.014	±.003	.561
TiO_2	−.065	±.006	2.906
P_2O_5	−.006	±.001	.266
MnO	.000	n.d.	.164
Cr_2O_3	.008	.001	−.009
Prehistoric Kilauea caldera and Hilina flows (PHKILCAL)			
SiO_2	−0.317	±0.021	53.327
Al_2O_3	−.354	±.029	10.585
FeO	.081	±.030	10.260
CaO	−.266	±.016	13.044
Na_2O	−.065	±.005	2.753
K_2O	−.012	±.003	.497
TiO_2	−.057	±.012	2.843
P_2O_5	−.005	±.001	.259
MnO	n.d.	n.d.	n.d.

Lava flows from Kilauea and Mauna Loa that have traveled several kilometers from their feeding vents have low water contents of 0.01–0.10 weight percent, low total sulfur (0.004–0.007 weight percent), and chloride contents of 0.005–0.006 weight percent (Swanson and Fabbi, 1973; L.P. Greenland, written commun., 1985). These volatile contents are similar to those of surface-fed fracture fillings at Hilina Pali (Easton and Lockwood, 1983; table 14.4), but lower than most dikes in the west caldera wall. Surface flows within a few hundred meters of a vent may have higher volatile contents (0.01 weight percent S; 0.009 weight percent Cl) (Swanson and Fabbi, 1973).

DISCUSSION OF CHEMISTRY

The major- and trace-element chemistry of the dikes and Uwekahuna laccolith is similar to that of lava flows at Uwekahuna Bluff. In a companion paper (Casadevall and Dzurisin, chapter 13), we compare the composition of lava flows at Uwekahuna Bluff at a constant MgO content of 7.0 weight percent, by addition or subtraction of olivine from the bulk composition. We apply the same approach here to the intrusions. We used the olivine composition for the Uwekahuna laccolith determined by Murata and Richter (1961) and recalculated the composition for each analysis to 7.0 weight percent MgO. We then averaged the normalized magma compositions for dikes of the south set and the north set (table 14.5). The major-element and trace-element compositions of the intrusive bodies strongly resemble those of the succession of flows at Uwekahuna Bluff.

Olivine-control lines for dikes 5S and 1N, as well as for the Uwekahuna laccolith, have slopes similar to those for prehistoric Kilauea summit flows and the regional prehistoric pahoehoe picrite complex (PPPC) of the summit region (Wright, 1971), and the picritic flows (suite C) of the Uwekahuna Bluff section (table 14.3; fig. 14.4*A*; Casadevall and Dzurisin, chapter 13). These similarities indicate that the magma of the picritic dikes and the laccolith is chemically similar to other magmas of the Kilauea summit region.

TABLE 14.4.—*Volatile contents of samples from Kilauea caldera dikes and other Hawaiian intrusive and extrusive rocks*

[All values in weight percent. For Kilauea dikes, H_2O^+ content by modified Penfield method, analyses by CHN water analyzer (uncertainty ±3–5 percent of reported value); total sulfur analyses by Leco sulfur analyzer with infrared detector (uncertainty ±0.005 weight percent); total chlorine analyses using separation by Conway cell method, measured by selective ion electrode (uncertainty ±0.002 weight percent). Other samples: 1–9, Easton and Lockwood (1983), Swanson and Fabbi (1973); 10–12, L.P. Greenland, written commun. (1984); data for primitive Hawaiian magma from Greenland (in press), Greenland and others (1985), and Gerlach and Graeber (1985), also includes 0.65 weight percent CO_2]

Sample	Laboratory number	H_2O^+	Sulfur	Chloride	Total volatiles	Comments
Kilauea caldera dikes, south set						
1S	W-211577	0.16	0.042	0.004	0.206	Glass margin.
2S	W-211576	.01	.049	.004	.064	Glass margin.
3S	W-211575	.13	.066	.005	.201	Glass margin.
4S	W-211574	.04	.049	.006	.095	Glass margin.
5S	W-211573	.33	.045	.005	.380	Glass margin.
5S	W-211407	.35	.024	.004	.378	Picrite interior.
Kilauea caldera dikes, north set						
1N	W-211408	.13	.027	.004	.161	Picrite interior.
2N	W-211409	.31	.015	.004	.329	Cuts laccolith.
7N	W-211410	.25	.063	.005	.318	Glass margin.
8N	W-211411	.13	.068	.006	.204	Glass margin.
9N	W-211415	.22	.048	.004	.272	Glass margin.
10N	W-211412	.16	.025	.004	.189	Interior.
10N	W-211416	.29	.034	.005	.329	15 m below rim.
11N	W-211414	.10	.027	.004	.131	Margin.
12N	W-211413	.30	.065	.005	.370	Glass margin.
Other samples						
Field number		H_2O^+	Sulfur	Chloride	Total volatiles	Comments
(1) L-78-6B		---	0.09	0.04	0.2	0.33 Mauna Loa dike.
(2) L-78-7		.13	.05	.004	.184	Mauna Loa dike.
(3) L-78-8		.15	.03	<.05	<.23	Mauna Loa dike.
(4) L-78-9		.13	.05	.1	.28	Mauna Loa dike.
(5) L-77-35B		.05	.011	.006	.067	Hilina dike.
(6) L-77-35C		.06	.011	.007	.078	Hilina dike.
(7) --------		.09	.005	.007	.102	Uwekahuna laccolith.
(8) DAS71-1213-136		.04	.02	.009	.069	Kilauea surface flow.
(9) DAS71-1213-137		.04	.02	.009	.069	Kilauea surface flow.
(10) K 71		.13	.016	.008	.154	Puu Oo, April 1984.
(11) K 72		.16	.008	.008	.176	Puu Oo, April 1984.
(12) ML 117		.10	.016	.006	.122	Mauna Loa, April 1984.
Primitive Hawaiian magma (undegassed)						
		.30–.45	.10–.15	.008–.011	.41–.65	

The lava flows deformed by the laccolith are picritic, and we have interpreted them as ponded in an ancient caldera (Casadevall and Dzurisin, chapter 13).

The chilled margin of the Uwekahuna laccolith has a low total volatile content (table 14.4) that Easton and Lockwood (1983) attributed to degassing in a surface lake before intrusion. The picritic nature and low sulfur contents of dikes 1N (0.027 weight percent S) and 2N (0.015 weight percent S) indicate an origin similar to that of the laccolith. We concur with the interpretation of Murata and Richter (1961, p.433) that the laccolith was derived from "lateral injection during a prehistoric period of refilling of the caldera." We further suggest that dikes 1N and 2N formed by lateral injection from a picritic lava lake, since destroyed by collapse of the caldera. This lake may have been produced by eruption of the picritic lava of suite C. The intrusives may have derived from the lake and invaded its earlier overflows.

Dike 5S, on the other hand, cuts flows that are younger than the picritic flows of suite C, and therefore cannot be considered contemporaneous with either dikes 1N and 2N or with the laccolith. This dike cuts several tens of meters of lava flows in the southwest caldera wall; it may have fed a nearby olivine-rich lava flow exposed along Crater Rim Drive. That flow forms part of the regional prehistoric pahoehoe picritic complex (PPPC) of Wright (1971), as mapped by Walker (1969). R.T. Holcomb (oral commun., 1985), suggests that the PPPC probably represents a series of overflows from the summit region, a suggestion consistent with the possibility that dike 5S fed at least part of the PPPC.

The water, sulfur, and chlorine contents of the Kilauea intrusive rocks (table 14.4) indicate that about half of the parental abundance of these constituents was lost before the dikes solidified. Easton and Lockwood (1983) suggested that low total volatile content for the chilled margin of an intrusive body indicates that the body was fed by a surface flow draining into an existing fissure or by lateral injection from a surface lake, and not by intrusion from depth. The combined water, sulfur, and chlorine contents for Kilauea summit dikes (table 14.4) are high compared to those of degassed surface flows that have traveled some distance from their vent (Swanson and Fabbi, 1973) and to those of Hilina Pali crack fillings (Easton and Lockwood, 1983). However, we have no data on the volatile abundances in summit lava, which contains a higher initial volatile

TABLE 14.5.—*Chemical composition of intrusive and extrusive rocks from Uwekahuna Bluff, Kilauea compared with averages for Kilauea and Mauna Loa Volcanoes*

[Analyses recalculated to 100 percent dry weight after converting all iron to FeO_{total} and normalized to 7.0 weight percent MgO by subtracting or adding olivine of Uwekahuna laccolith composition (Murata and Richter, 1961, analysis 10). Sources of data: Kilauea caldera dike sets, this paper; Uwekahuna laccolith, Murata and Richter (1961); Uwekahuna Bluff flow suites, Casadevall and Dzurisin (chapter 13); Kilauea (1911–24 summit lavas) and Mauna Loa (historical eruptions) averages, Basaltic Volcanism Study Project (1981). n.d., not determined]

	Kilauea caldera dikes		Uwekahuna laccolith	Uwekahuna Bluff flow suites					
	North set	South set		A	B	C	D	Kilauea	Mauna Loa
SiO_2	51.31±0.44	51.14±0.50	51.20±0.17	51.10±0.23	50.90±0.39	50.60±0.78	50.23±0.25	50.70±0.31	52.45±0.31
Al_2O_3	13.8 ±0.4	13.9 ±0.2	14.0 ±0.8	13.7 ±0.2	13.6 ±0.2	13.6 ±0.3	13.7 ±0.2	13.57±0.12	13.94±0.10
FeO	11.1 ±0.6	11.2 ±0.2	10.8 ±0.4	11.7 ±0.3	11.8 ±0.3	11.3 ±0.5	11.4 ±0.3	11.03±0.20	10.62±0.49
MgO	7.0	7.0	7.0	7.0	7.0	7.0	7.0	7.0	7.0
CaO	11.0 ±0.4	11.2 ±0.2	11.6 ±0.2	10.6 ±0.2	10.9 ±0.3	11.7 ±0.7	11.7 ±0.4	11.65±0.33	10.73±0.15
Na_2O	2.3 ±0.1	2.3 ±0.1	2.2 ±0.1	2.4 ±0.1	2.3 ±0.1	2.3 ±0.1	2.3 ±0.1	2.32±0.04	2.36±0.06
K_2O	.43±0.04	.43±0.04	.37±0.05	.44±0.02	.43±0.03	.44±0.04	.48±0.03	.53±0.04	.39±0.03
TiO_2	2.68±0.58	2.45±0.12	2.46±0.24	2.51±0.08	2.49±0.12	2.62±0.21	2.68±0.04	2.73±0.11	2.10±0.04
P_2O_5	.28±0.04	.33±0.12	.19±0.02	.30±0.01	.29±0.01	.28±0.04	.30±0.01	.29±0.01	.24±0.02
MnO	.18±0.02	.17±0.01	.17±0.01	.17±0.02	.17±0.01	.16±0.02	.19±0.01	.17±0.01	.17±0.01
Ba	121 ±20	128 ±17	n.d.	118 ±19	118 ±23	127 ±29	136 ±11	138 ±18	84 ±14
Cu	117 ±13	117 ±7	n.d.	122 ±16	116 ±12	119 ±17	91 ±22	n.d.	n.d.
Hf	3.70±0.41	3.80±0.16	n.d.	3.91±0.14	3.83±0.16	4.02±0.30	3.99±0.08	4.58±0.17	3.59±0.11
Rb	16, n.d.	14 ±3	n.d.	12 ±3	13 ±1	16 ±3	14, n.d.	11 ±3	6 ±1
Ta	.86±0.15	.93±0.12	n.d.	.88±0.06	.88±0.11	1.02±0.10	1.12±0.02	n.d.	n.d.
Th	.77±0.10	.85±0.11	n.d.	.86±0.07	.81±0.10	.80±0.06	.97±0.02	1.28±0.22	.55±0.03
Zn	127 ±36	118 ±21	n.d.	111 ±3	111 ±3	132 ±14	113 ±5	n.d.	n.d.
Zr	135 ±35	126 ±41	n.d.	153 ±17	145 ±15	156 ±25	172 ±41	159 ±20	130 ±5
Sc	32.0 ±3.5	31.2 ±0.9	n.d.	31.4 ±0.9	32.8 ±0.7	33.5 ±1.4	31.8 ±0.4	33.0 ±2.0	31.0 ±1.2
La	11.5 ±1.6	12.2 ±1.1	n.d.	11.8 ±0.8	11.6 ±1.2	12.7 ±1.0	13.7 ±0.3	15.1 ±1.7	8.9 ±0.6
Ce	27.8 ±3.7	28.4 ±2.7	n.d.	28.9 ±1.6	28.3 ±2.0	30.7 ±1.9	32.7 ±0.5	37.5 ±3.2	23.9 ±1.4
Nd	20 ±3	19 ±5	n.d.	20 ±3	21 ±3	22 ±3	23 ±2	n.d.	n.d.
Sm	5.5 ±0.5	5.5 ±0.3	n.d.	5.7 ±0.1	5.7 ±0.3	6.0 ±0.4	5.9 ±0.1	6.2 ±0.2	5.0 ±0.2
Eu	1.78±0.19	1.83±0.09	n.d.	1.89±0.05	1.84±0.06	1.92±0.10	1.93±0.03	2.00±0.07	1.69±0.04
Gd	6.6 ±0.7	4.8 ±1.4	n.d.	6.1 ±1.4	6.2 ±0.9	6.4 ±1.0	6.7 ±0.7	n.d.	n.d.
Th	.91±0.08	.82±0.04	n.d.	.96±0.04	.96±0.04	.97±0.10	.93±0.03	.96±0.03	.86±0.04
Tm	.29±0.06	.25±0.02	n.d.	.33±0.06	.34±0.04	.34±0.05	.31±0.02	n.d.	n.d.
Yb	2.16±0.17	2.14±0.06	n.d.	2.25±0.11	2.20±0.13	2.31±0.14	2.17±0.06	2.05±0.03	2.10±0.04
Lu	.31	.30	n.d.	.31	.31	.33	.32	.26	.31

content than rift-zone lava (Gerlach and Graeber, 1985) or on those of any flow close to its vent. This makes it difficult to use volatile content as an indicator of origin for the dikes.

We interpret the major-, trace-, and volatile-element data for the dikes to indicate that they are composed of Kilauea magma that had an origin and evolution similar to that of the prehistoric flows of Uwekahuna Bluff. On the basis of contact relations and the higher volatile-element abundances in the dike rocks than in surface flows, we tentatively conclude that most or all of the dikes were injected from depth or laterally, not fed by surface flows.

ORIGIN OF THE DIKES

Igneous dikes are classically interpreted (Anderson, 1938) to form by forceful injection, in which magma pressure exceeds the least compressive stress acting across a potential dike plane. The extent to which existing fractures and regional structural fabric influence the propagation of dikes varies from one tectonic setting to another (Delaney and others, 1986). Most dikes in Kilauea caldera trend northeasterly, roughly parallel to major structural elements such as the southwest and east rift zones, the Hilina and Koae fault systems, and the linear west wall of the caldera. These elements were created by seaward migration of the south flank of the volcano (Fiske and Jackson, 1972; Swanson and others, 1976).

STRUCTURAL SETTING

The dikes in the summit region are confined to the west wall (fig. 14.1). Most have a northeast orientation, similar to that of surface fractures around the west rim of the caldera and to the strike of the southwest rift zone (N. 48° E.; fig. 14.6). Ground cracks extend southwestward into the southwest rift zone and northeastward only to the Steaming Flats area (de Saint Ours, 1982).

The pattern of dikes and other structural elements suggests that the dikes formed in a stress field reflecting the combined influences of the summit magma reservoir (radial) and a linear zone of weakness related to the contact between the edifices of Kilauea and Mauna Loa (N. 40° E.). That contact might be a zone of reduced compression if gravity pulls the unbuttressed Kilauea edifice seaward away from Mauna Loa (Fiske and Jackson, 1972; Swanson and others, 1976). We postulate that this zone offers a preferred path to the surface for magma in fractures in the volcano's summit region. According to this model, the southwest rift zone, the caldera rim at Uwekahuna Bluff, and the northeasterly dikes all reflect control by a structural element related to the contact between Mauna Loa and Kilauea.

SHALLOW DIKE EMPLACEMENT AT KILAUEA

The northeasterly orientation of many of the modern eruptive fissures within the Kilauea summit region (those of 1954, 1971, 1974, 1975, 1982) indicates that the northeasterly trend is still the favored orientation for fissure-fed eruptions. These fissures are typically discontinuous and in places show echelon offsets along their strike (Pollard and others, 1983). They often propagate in the form of slowly migrating surface cracks as an eruption develops (Duffield and others, 1982); seldom do these ground cracks and fissures erupt along their entire length (Pollard and others, 1983). Intrusions of

magma into the summit region and rift zones, some of which cause surface deformation and ground breakage, account for about 65 percent of the magma supplied from Kilauea's shallow magma reservoir; only about 35 percent is erupted (Dzurisin and others, 1984). Most of these intrusions probably form dikes (Swanson and others, 1976; Pollard and others, 1982; Dvorak and others, 1986) that reach shallow depths without erupting.

A number of the dikes in Kilauea caldera occupy fractures that continue to the caldera rim (fig. 14.3) but provide no evidence of having vented. We tentatively conclude that many of the dikes reached or started from very shallow depths but simply did not vent, at least not on the surface directly overlying their present host fractures in the caldera wall. We reason that the driving force of vesiculation, which increases as the dike nears the surface, is opposed by the weight of the magma, which also increases as the dike nears the surface. Partly for this reason, many shallow dikes move laterally more than vertically and vent only when their paths intersect the volcano's sloping flanks along a rift zone. Intrusions into Kilauea's rift zones commonly cause surface deformation and fractures, indicating that magma reached within a few tens to hundreds of meters of the surface without venting (Pollard and others, 1983; Dvorak and others, 1986). Once the top of a dike is shallow enough to cause ground fractures, loss of magmatic volatiles through those fractures may cause the dike's movement to stall without venting. Even if a dike succeeds in reaching the surface somewhere along its length, field observations during eruptions at Kilauea show that vents are typically separated by cracked or deformed areas that do not vent; in other words, the dike does not vent along much of its length.

We therefore conclude that (1) many shallow dikes at Kilauea do not vent; (2) dikes can stall at almost any depth because of loss of volatiles or increasing potential energy; and (3) dikes that do vent usually do so along only a part of their total length. If these inferences are correct, the lack of identifiable vent deposits above

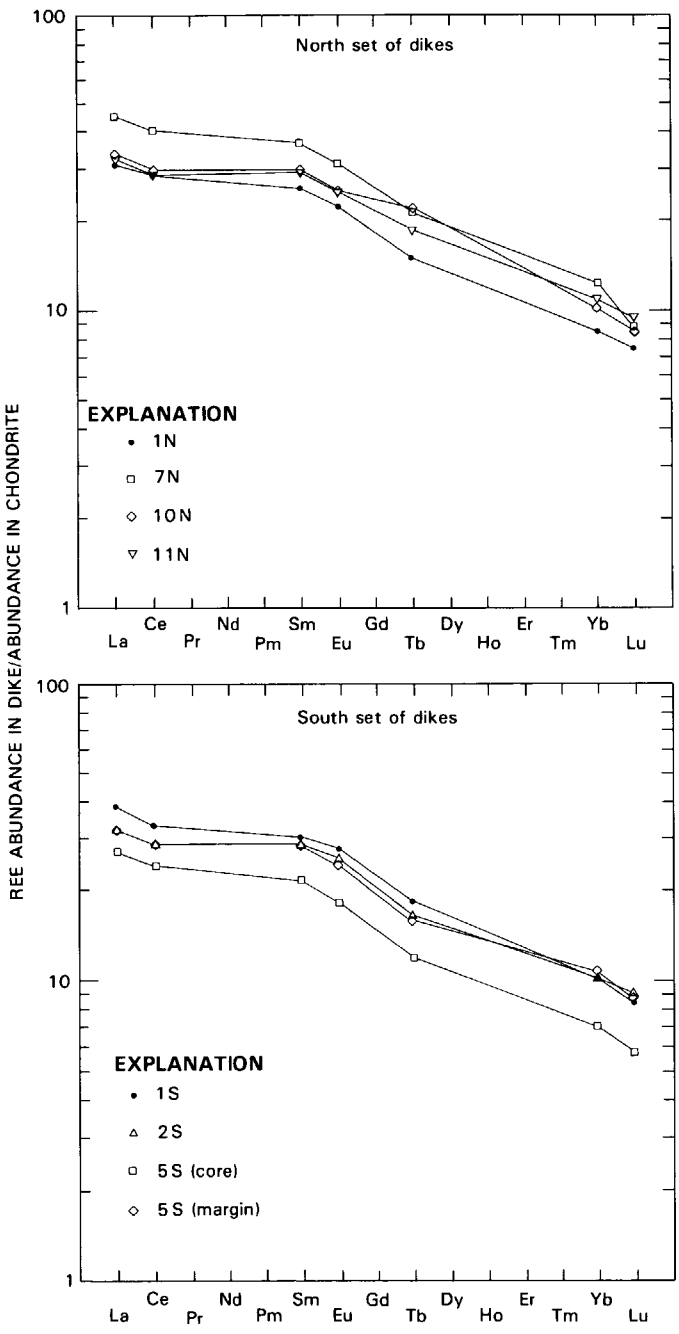

FIGURE 14.5.—Rare-earth-element (REE) plots showing chondrite-normalized abundances for north and south dike sets. Abundances are normalized to chondrite values (Haskin and others, 1968). Analytical precision for Nd, Gd, and Tm is poor (greater than ±6 percent of reported value in table 14.2), and these elements are not plotted.

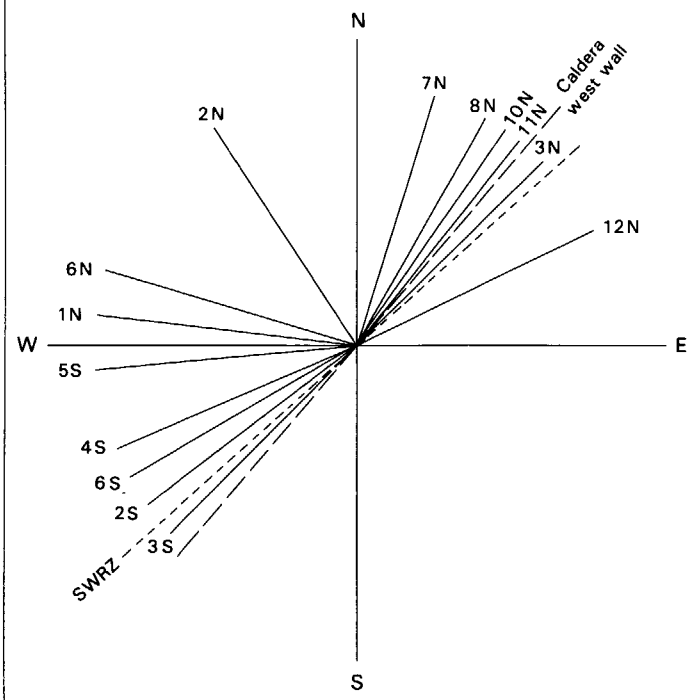

FIGURE 14.6.—Rose diagram showing orientation of dikes, west wall of Kilauea caldera. Also plotted are the orientations of the southwest rift zone (SWRZ) and the western wall of the caldera at N. 48° E. and N. 40° E., respectively.

many dikes at Kilauea caldera does not preclude an origin by forceful injection, either laterally or from below.

CONCLUSIONS

The main results of our study are the following:

(1) The Uwekahuna laccolith is the largest intrusive mass exposed in the west wall of the caldera. Contact relations indicate that most or all of the other dense lenses of rock in the wall are thick subaerial lava flows.

(2) Eighteen dikes occur in the western wall of Kilauea caldera, 12 north of and in Uwekahuna Bluff and 6 south of the bluff. The combined width of these dikes is only about 15 m and accounts for less than 1 percent of the length of the west wall.

(3) Of the 12 dikes in the north set, 5 occupy fractures cutting through the entire section of flows making up the west wall. Thus, these dikes were emplaced after all the flows had been extruded, but before the current caldera had formed.

(4) The composition of all dikes is remarkably uniform after the effects of olivine control are removed. The dikes are chemically similar to the undifferentiated summit lavas exposed at Uwekahuna Bluff and elsewhere in the Kilauea summit region.

(5) Contact relations and the volatile abundances of the dikes imply that most formed through injection, either laterally or from depth. Dikes 1N and 2N have low volatile contents and are chemically similar to the Uwekahuna laccolith and to the picritic lava flows of Uwekahuna Bluff; they may have formed by lateral injection of magma from a lava lake into a ponded sequence of picritic flows.

(6) The orientations of 15 dikes are similar to the structural grain formed by the western half of Kilauea caldera, the southwest rift zone, and the east rift zone. We conclude that the dikes formed under the combined influences of stresses caused by flexing of the summit magma reservoir and gravitational separation of Kilauea and Mauna Loa.

(7) The dikes of Kilauea caldera's west wall cut a succession of lavas that accumulated after the eruption of the Uwekahuna Ash Member, possibly as early as 2.1 ka (Dzurisin and Casadevall, 1986; Lockwood and Rubin, 1986), but before the formation of the present caldera.

FUTURE STUDIES

Several ideas about the origin of intrusive bodies at Kilauea caldera could be tested through further study. The relative ages of the dikes and the Uwekahuna laccolith could be determined by systematic paleomagnetic study supplemented by hydration-rind dating of glass from the margins of the dikes. The possible influence of regional structural fabric on dike propagation could be investigated through careful measurements of structural features such as fractures and joint sets in the vicinity of each dike (Delaney and others, 1986). More careful examination of the tops of the dikes and a thorough search for possible vent deposits could provide additional clues to their origins. Finally, additional measurements of volatile content of summit flows are necessary if the abundance of volatiles, especially sulfur and chlorine, is to be rigorously used as an indicator of dike provenance.

REFERENCES CITED

Anderson, E.M., 1938, The dynamics of sheet intrusion: Proceedings of the Royal Society of Edinburgh, v. 58, p. 242–251.

Aramaki, Shigeo, 1968, Segregation vein in the Uwekahuna laccolith, Kilauea Caldera, Hawaii: Bulletin of the Earthquake Research Institute, v. 46, p. 155–160.

Baedecker, P.A., 1979, Instrumental neutron activation analysis program of the U.S. Geological Survey (Reston, Va.) in Computers and activation analysis and gamma-ray spectroscopy, *in* Carpenter, B.F., D'Agostino, F., and Yule, H.P., eds., Contract 78042, U.S. Department of Energy, p. 373–385.

Basaltic Volcanism Study Project, 1981, Basaltic volcanism on the terrestrial planets: New York, Pergamon Press, 1286 p.

Casadevall, T.J., and Hazlett, R.W., 1983, Thermal areas of Kilauea and Mauna Loa: Journal of Volcanology and Geothermal Resources, v. 16, p. 173–188.

Daly, R.A., 1911, Magmatic differentiation in Hawaii: Journal of Geology, v. 19, p. 289–316.

de Saint Ours, P., 1982, Map of tectonic features of Kilauea Volcano summit region, Hawaii: U.S. Geological Survey Miscellansous Field Studies Map MF–1368, scale 1:24,000.

Delaney, P.T., Pollard, D.D., Ziony, J.I., and McKee, E.H., 1986, Field relations between dikes and joints: emplacement processes and paleostress analysis: Journal of Geophysical Research, v. 91, no. B5, p. 4920–4938.

Duffield, W.A., Christiansen, R.L., Koyanagi, R.Y., and Peterson, D.W., 1982, Storage, migration, and eruption of magma at Kilauea Volcano, Hawaii, 1971–1972: Journal of Volcanology and Geothermal Research, v. 13, p. 273–307.

Dutton, C.E., 1884, Hawaiian volcanoes: U.S. Geological Survey 4th Annual Report, p. 75–219.

Dvorak, J.J., Okamura, A.T., English, T.T., Koyanagi, R.Y. Nakata, J.S., Sako, M.K., Tanigawa, W.R., and Yamashita, K.M., 1986, Mechanical response of the south flank of Kilauea Volcano, Hawaii, to intrusive events along the rift zones: Tectonophysics, v. 124, p. 193–209.

Dzurisin, Daniel, and Casadevall, T.J., 1986, Stratigraphy and chemistry of the Uwekahuna Ash: Product of prehistoric phreatomagmatic eruptions at Kilauea Volcano, Hawaii [abs.]: International Volcanological Congress, Auckland-Hamilton-Rotorua, New Zealand, Abstracts, February 1986, p. 100.

Dzurisin, Daniel, Koyanagi, R.Y., and English, T.T., 1984, Magma supply and storage at Kilauea Volcano, Hawaii: Journal of Volcanology and Geothermal Resources, v. 21, p. 177–206.

Easton, R.M., and Lockwood, J.P., 1983, "Surface-fed dikes", The origin of some unusual dikes along the Hilina fault zone, Kilauea Volcano, Hawaii: Bulletin Volcanologique, v. 46, p. 45–53.

Eaton, J.P., and Murata, K.J., 1960, How volcanoes grow: Science, v. 132, p. 925–938.

Epp, D., Decker, R.W., and Okamura, A.T., 1983, Relation of summit deformation to east rift zone eruptions on Kilauea Volcano, Hawaii: Geophysical Research Letters, v. 10, p. 493–496.

Fiske, R.S., and Jackson, D.E., 1972, Orientation and growth of Hawaiian volcanic rifts: the effects of regional structure and gravitational stresses: Proceeding of the Royal Society of London, Series A, v. 329, p. 299–326.

Fiske, R.S., and Kinoshita, W.T., 1969, Inflation of Kilauea Volcano prior to its 1967–1968 eruption: Science, v. 165, p. 341–349.

Gerlach, T.M., and Graeber, E.J., 1985, Volatile budget of Kilauea Volcano: Nature, v. 313, p. 273–277.

Greenland, L.P., in press, Original volatile content of basaltic magmas: Bulletin of Volcanology.

Greenland, L.P., Rose, W.I., and Stokes, J.B., 1985, An estimate of gas emissions and magmatic gas content from Kilauea Volcano: Geochimica et Cosmochimica Acta, v. 49, p. 125–129.

Harris, D.M., and Anderson, A.T., 1983, Concentrations, sources, and losses of H_2O, CO_2, and S in Kilauean basalt: Geochimica et Cosmochimica Acta, v. 47, p. 1139–1150.

Haskin, L.A., Haskin, M.A., Frey, F.A., and Wildman, T.R., 1968, Relative and absolute terrestrial abundances of the rare earths, *in* Ahrens, L.H., ed., Origins and distribution of the elements: New York, Pergamon Press, p. 889–912.

Holcomb, R.T., 1981, Kilauea Volcano, Hawaii: chronology and morphology of the surficial lava flows: U.S. Geological Survey Open-File Report 81–354, 321 p.

Leeman, W.P., Murali, A.V., Ma, M.S., and Schmitt, R.A., 1977, Mineral constitution of mantle source regions for Hawaiian basalts—rare earth element evidence for mantle heterogeneity, *in* Magma Genesis: Oregon Department of Mineral Industries, Bulletin 96, p. 169–183.

Leeman, W.P., Budahn, J.R., Gerlach, D.C., Smith, D.R., and Powell, B.N., 1980, Origin of Hawaiian tholeiites: trace element constraints: American Journal of Science, v. 280-A, p. 796–821.

Lockwood, J.P., and Rubin, M., 1986, Distribution and age of the Uwekahuna Ash, Kilauea Volcano, Hawaii [abs.]: International Volcanological Congress, Auckland-Hamilton-Rotorua, New Zealand, Abstracts, February 1986, p. 112.

Macdonald, G.A., 1949, Petrography of the Island of Hawaii; U.S. Geological Survey Professional Paper 214–D, 96 p.

Macdonald, G.A., Abbott, A.T., and Peterson, F.L., 1983, Volcanoes in the sea: the geology of Hawaii (2d ed): Honolulu, University of Hawaii Press, 517 p.

Moore, J.G., 1970, Water content of basalt erupted on the ocean floor: Contributions to Mineralogy and Petrology, v. 28, p. 272–279.

Moore, J.G., and Fabbi, B.P., 1971, An estimate of the juvenile sulfur content of basalt: Contributions to Mineralogy and Petrology, v. 33, p. 118–127.

Murata, K.J., and Richter, D.H., 1961, Magmatic differentiation in the Uwekahuna laccolith, Kilauea caldera, Hawaii; Journal of Petrology, v. 2, p. 424–437.

——— 1966a, Chemistry of the lavas of the 1959–60 eruption of Kilauea Volcano, Hawaii; U.S. Geological Survey Professional Paper 537–A, 26 p.

——— 1966b, The settling of olivine in Kilauean magma as shown by the 1959 eruption: American Journal of Science, v. 264, p. 194–203.

Perret, F.A., 1913, Some ejectamenta from Kilauea: American Journal of Science, v. 35 p. 611–618.

Peterson, D.W., 1967, Geologic map of the Kilauea Crater quadrangle, Hawaii: U.S. Geological Survey Geologic Quadrangle Map GQ–667, scale 1:24,000.

Pollard, D.D., Delaney, P.T., Duffield, D.A., Endo, E.T., and Okamura, A.T. 1983, Surface deformation in volcanic rift zones: Tectonophysics, v. 94, p. 541–584.

Powers, H.A., 1955, Composition and origin of basaltic magma of the Hawaiian Islands: Geochimica et Cosmochimica Acta, v. 7, p. 77–107.

Powers, S., 1916, Intrusive bodies at Kilauea: Zeitschrift fur Vulkanologie, v. 3, p. 28–33.

Ryan, M.P., Koyanagi, R.Y., and Fiske, R.S., 1981, Modeling the three-dimensional structure of magma transport systems: application to Kilauea Volcano, Hawaii: Journal of Geophysical Research, v. 86, p. 7111–7129.

Ryan, M.P., Blevins, J.Y.K., Okamura, A.T., and Koyanagi, R.Y., 1983, Magma reservoir subsidence mechanics: theoretical summary and applications to Kilauea Volcano, Hawaii: Journal of Geophysical Research, v. 88, p. 4147–4188.

Shapiro, Leonard, 1975, Rapid analysis of silicate, carbonate, and phosphate rocks: U.S. Geological Survey Bulletin 1401, 56 p.

Swanson, D.A., and Fabbi, B.P., 1971, Loss of volatiles during fountaining and flowage of basaltic lava at Kilauea Volcano, Hawaii: Journal of Research of the U.S. Geological Survey, v. 1, p. 649–658.

Swanson, D.A., and Peterson, D.W., 1973, Partial draining and crustal subsidence of Alae lava lake, Kilauea Volcano, Hawaii: U.S. Geological Survey Professional Paper 800–C, p. C1–C14.

Swanson, D.A., Duffield, W.A., and Fiske, R.S., 1976, Displacement of the south flank of Kilauea Volcano: the result of forceful injection of magma into the rift zones: U.S. Geological Survey Professional Paper 963, 39 p.

Walker, G.W., 1969, Geologic map of the Kau Desert quandrangle, Hawaii: U.S. Geological Survey Geologic Quadrangle Map GQ–827, scale 1:24,000.

Washington, H.S., 1923, Petrology of the Hawaiian Islands, III: Kilauea and general petrology of Hawaii: American Journal of Science, v. 6, p. 338–367.

Wright, T.L., 1971, Chemistry of Kilauea and Mauna Loa in space and time: U.S. Geological Survey Professional Paper 735, 40 p.

——— 1984, Origin of Hawaiian tholeiite: a metasomatic model: Journal of Geophysical Research, v. 89, p. 3233–3252.

AN EARLY 19TH CENTURY RETICULITE PUMICE FROM KILAUEA VOLCANO

By Robert P. Sharp[1], Daniel Dzurisin, *and* Michael C. Malin[2]

ABSTRACT

Remnants of a fragmented reticulite pumice deposit, referred to as the golden pumice, along the southwest rim of Kilauea caldera are the product of episodes of lava fountaining of undocumented date within the caldera. At its best locality, the 2.8-m deposit consists of a basal fine-grained, well-bedded unit, 20 cm thick; an intermediate massive homogeneous unit, 1 m thick, consisting of coarse, jagged, firmly packed fragments; and an upper fine-grained unit, 1.6 m thick, of well-sorted and well-bedded pumice. The intermediate unit may be a product of massive direct fallout from lava fountains, and the finer grained upper and lower units may be pumice wind-drifted from a plume plus pumiceous debris reworked by wind. The pumice locally rests with angular unconformity on beds of 1790 pyroclastic debris and is overlain by a thin layer of 1924 lithic tephra. Layers of reworked pumiceous debris and 1790 lithic debris within the golden pumice suggest that its emplacement was episodic and may have occurred over a year or two. The stratigraphic succession and recorded observations of volcanic activity since 1823 indicate that the pumice formed between 1790 and 1823. The amount of erosion and deposition occurring between emplacement of the 1790 deposits and the pumice favors a date in the later part of this interval, possibly around 1820. We speculate that the golden pumice represents early phases in development of the lava conduit for the current fire-pit crater, Halemaumau, the most active center within Kilauea caldera during the 19th and 20th centuries.

INTRODUCTION

Surficial deposits of fragmented reticulite pumice at the southwest edge of Kilauea Crater were thought by Jaggar (1925, p. 3, 8) to be part of an underlying deposit of pyroclastic debris erupted in 1790, and they were included, by inference at least, within the Keanakakoi Formation by Wentworth (1938, p. 93). Christiansen interprets this pumice as a product of high lava fountains following an earlier episode of phreatomagmatic activity about 1790 (Christiansen, 1979; Decker and Christiansen, 1984, p. 125); Macdonald and Abbott (1970, p. 315) seemingly agree. The deposit is clearly not related to pumice at the base of the Keanakakoi Formation of Wentworth (1938, p. 95–96, 101) or to pumiceous products of post-1924 events (Wentworth, 1938, p. 149; Macdonald, 1955, p. 57; Macdonald and Abbott, 1970, p. 92–93; Richter and others, 1970, p. E5–E36). In order to distinguish this particular reticulite pumice from such older and younger deposits of similar nature, it is here informally called the golden pumice. Its stratigraphic position, between materials erupted in 1790 and 1924, was recognized by Macdonald (1949, p. 70, 72) and Macdonald and Abbott (1970, p. 315), who did not, however, discuss its origin or precise age. In this paper we present evidence that it represents a distinct event, separate from 1790 activity but early within the 1790–1924 interval, an interpretation seemingly favored, but without supporting arguments, by Finch (1947), Powers (1948, plate 3D), and Stearns (1966b, p. 40).

ACKNOWLEDGMENTS

Kilauea lies within Hawaii Volcanoes National Park, and we are indebted to park authorities for the privilege of access. The study was warmly and cooperatively supported by the U.S. Geological Survey's Hawaiian Volcano Observatory and financially aided by Grant W–13, 709 from the National Aeronautics and Space Administration. R.L. Christiansen has generously made available unpublished information from his extensive studies of the 1790 Keanakakoi Formation. Appreciation is expressed for constructive critical reviews and suggestions by Christiansen, D.A. Swanson, T.L. Wright, and R.T. Holcomb. W.G. Melson of the Smithsonian Institution kindly supplied records of a chemical analysis of 1820(?) Kilauea glass.

LOCATION AND DISTRIBUTION

Accumulations of the golden pumice are best preserved along the southwest margin of Kilauea caldera (fig. 15.1). The nearly circular, 1-km-wide pit crater of Halemaumau, last active in 1982, indents the caldera floor within 1 km of the best pumice exposures. The thickest accumulations of the golden pumice are trapped within open cracks and stream-cut gullies dissecting the southwest caldera wall and the immediately adjacent outer slope of the volcano, northwest and southeast of Crater Rim Road where it descends to the caldera floor (fig. 15.1). For convenience, the channels are termed caldera-wall gullies, although the larger ones extend headward tens of meters outside the caldera rim. The first 13 larger gullies south-southeast (fig. 15.2) of the descending reach of Crater

[1]California Institute of Technology, Pasadena, California 91125
[2]Arizona State University, Tempe, Arizona 85281

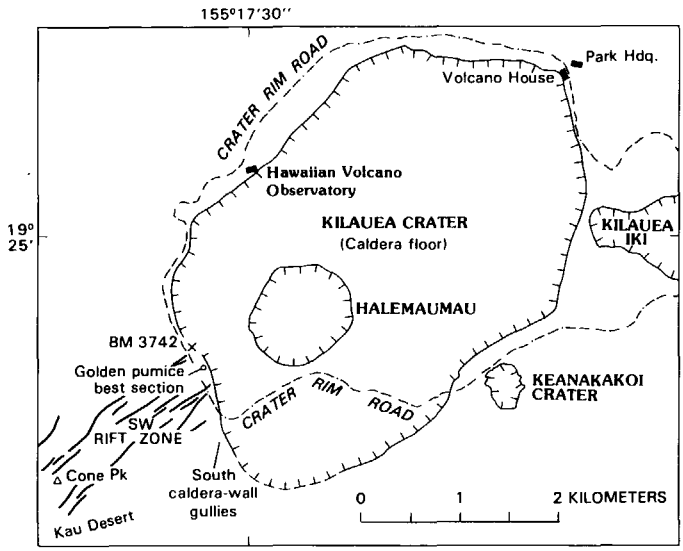

FIGURE 15.1.—Major features of Kilauea Crater and location of best section of the golden pumice.

Rim Road expose particularly informative sections. For identification, these gullies are sequentially numbered south from Crater Rim Road as 1–S, 2–S, and so on.

Remnants of the golden pumice also lie in protected places within the Kau Desert from the caldera rim southwestward more than 3 km, to and beyond Cone Peak (fig. 15.1). Their greater abundance in the northwestern part of the Kau Desert presumably reflects the direction of the dominant trade-wind flow (S. 60°–70° W.) somewhat oblique to the S. 45° W. axial trend of the desert tract.

MICROSTRATIGRAPHIC UNITS AND RELATIONS (SEE FIG. 15.3)

THE 1790 PART OF THE KEANAKAKOI FORMATION OF WENTWORTH (1938)

Stratigraphy of the Keanakakoi Formation of Wentworth (1938, p. 92–104; see also, Powers, 1948) has been most thoroughly and recently investigated by Christiansen (1979; Decker and Christiansen, 1984, p. 124–127) in a study not yet fully published. During investigation of stripping of Keanakakoi debris in Kau Desert, Malin and others (1983, p. 1149–1150) divided the 1790 part of the formation into three units: upper lithic, intermediate predominantly vitric, and lower mixed lithic and vitric; this subdivision is employed here.

Sherzer (1923, p. 460–461), Finch (1947, p. 2), and Powers (1948, p. 288) felt that only the upper lithic unit, or part of it, was emplaced by the 1790 phreatomagmatic eruptions of Kilauea, but Christiansen (1979) attributes the bulk of the Keanakakoi Formation of Wentworth (1938) to an evolutionary cycle of such activity that began around 1790. Malin and others (1983, p. 1151, 1155) favor Christiansen's interpretation, but they suggest, largely because of evidence of penecontemporaneous redistribution of tephra, that the successive eruptions occurred over a period of several years, including 1790. Easton (chapter 11) has reduced the rank of the Keanakakoi and included it in his Puna Basalt. Easton's Keanakakoi Ash Member consists mostly of deposits of the 1790 eruption, but slightly older reticulite pumice occurs at the base and the golden pumice at the top. In this paper we will use the modifier 1790 to designate that part of the Keanakakoi thought to have been formed by these explosive eruptions, without meaning to imply that all the material was necessarily emplaced within the single year 1790.

THE RETICULITE (GOLDEN) PUMICE

The thickest, most complete section of golden pumice observed (fig. 15.4) lies within the head of a gully extending outward from the caldera rim along a crack bearing S. 55° W. in the southwest rift zone (fig. 15.1). This exposure is about 30 m from the caldera brink, roughly 50 m northeast of Crater Rim Road, 78 m N. 15° E. from the SW Rift sign at the parking turnout, and 205 m S. 37° E. of BM 3742 (Kilauea Crater quadrangle). Within the 2.8-m section exposed here, upper, intermediate, and basal units are distinguished (fig. 15.3).

The basal 20 cm are well layered and consist of abraded-looking pumice fragments, mostly about 1 cm in size, in a sparse sand-size matrix of angular vitric fragments. This basal unit includes much Pele's hair and a few scattered lithic clasts as large as 6 mm, and near the top it contains a coarse sandy layer rich in lithic grains.

The massive, homogeneous intermediate unit, 1 m thick, consists of closely packed jagged pumice fragments, mostly 2–5 cm in diameter but ranging from 1 cm to 10 cm. It is nearly devoid of matrix, except for irregular vitric fragments broken from compacted pumice clasts. Tight packing has made the jagged pumice fragments interlock, giving the unit a cohesion that is expressed in a near-vertical outcrop face and in the toughness of detached pieces. No lithic fragments have been found within primary deposits of this coarse pumice, either here or in many other exposures.

The upper unit consists of 1.6 m of thinly and evenly bedded pumice, the fragments being mostly of 1-cm size. These clasts, although still angular, are consistently smaller, more regularly shaped, less jagged, and far more uniform in size than clasts of the intermediate unit. However, 53 cm above the base of the upper unit is a 5-cm layer of coarser fragments with intermediate-unit characteristics. Beds in the upper unit are mostly 3–4 cm thick, though ranging from 1 cm to 7 cm, and generally have a sparse matrix of sand-size vitric fragments. They do not display the inverse grading that typically results from flow emplacement (Sparks, 1976). Distributed throughout the upper unit are 1-cm-thick continuous beds principally composed of dense glass fragments; these layers emphasize the well-bedded aspect of this unit. Much Pele's hair is also present, especially in the lower part of the unit, and a few sparsely scattered lithic fragments, several millimeters in diameter, have been found. In the best section, a 4-cm sandy layer 10 cm from the top contains numerous lithic and crystal grains, some well worn. More

FIGURE 15.2.—View south-southeast from Crater Rim Road showing 20-m-high tephra-mantled southwest wall of Kilauea Crater, caldera-wall gullies, and 1974 lava flow along left margin. Light reflects from patches of crusted veneer on the detrital apron. U.S. Geological Survey photograph by J.D. Griggs.

and larger lithic fragments are seen within the upper unit at some other localities, where secondary reworking has clearly occurred (figs. 15.5*A*, 15.6).

In the best section, contacts between these units are sharp but conformable. Elsewhere, the contact between upper and intermediate units is unconformable (fig. 15.7) or marked by layers containing reworked lithic materials (fig. 15.5*A*). Disconformities and layers of reworked pumiceous and lithic debris also are found within the upper unit.

At the best section, the golden pumice rests with sharp contact upon coarse lithic-vitric sand, possibly dating from 1790; elsewhere it rests upon fluvial gravels, 1790 pyroclastic beds, or lava bedrock. Not all exposures of pumice display all units, the basal and intermediate units being more nearly ubiquitous and of less varying thickness than the upper unit. Remnant patches of pumice in the Kau Desert immediately southwest of the caldera rim are slablike and probably primary, but within a few hundred meters farther southwest the stratigraphy of the best section disappears and the packing and shape of pumice fragments change; preservation of these accumulations in settings protected from the northeast trade winds suggests secondary eolian reworking and redistribution. A secondary surficial crust of grayish chocolate-brown hue and irregular lumpy texture has formed on most such deposits, masking the nature of the underlying material. This crust, 2–4 mm thick, fractures easily owing to fragility of the understratum, but the crust itself is firm. Even though surficial crusts are known to form rapidly on surfaces in the Kau Desert (Malin and others, 1983, p. 1150). the thickness and firmness of this crust indicate at least slight antiquity for the deposits.

The golden pumice is primarily a reticulite (Wentworth and Williams, 1932, p. 41, 47–50) consisting of delicate, interconnected filaments of sideromelane glass (Heiken, 1974, p. 5) outlining oval and crudely polygonal patterns 0.5–2 mm in diameter. It is not as close to a perfect reticulite (Stone, 1926, p. 29; Macdonald, 1972, p. 127) as the basal Keanakakoi pumice (Wentworth, 1938, p. 95–96; Heiken, 1974, p. 5; Christiansen, 1979) or as that produced by the 1969–1974 Mauna Ulu fountains, because it has a wider range in the size and shape of openings and a more copious coating of dense black, gray, or brown glass on fragments. The golden pumice is light, having a specific gravity near 0.06 and a

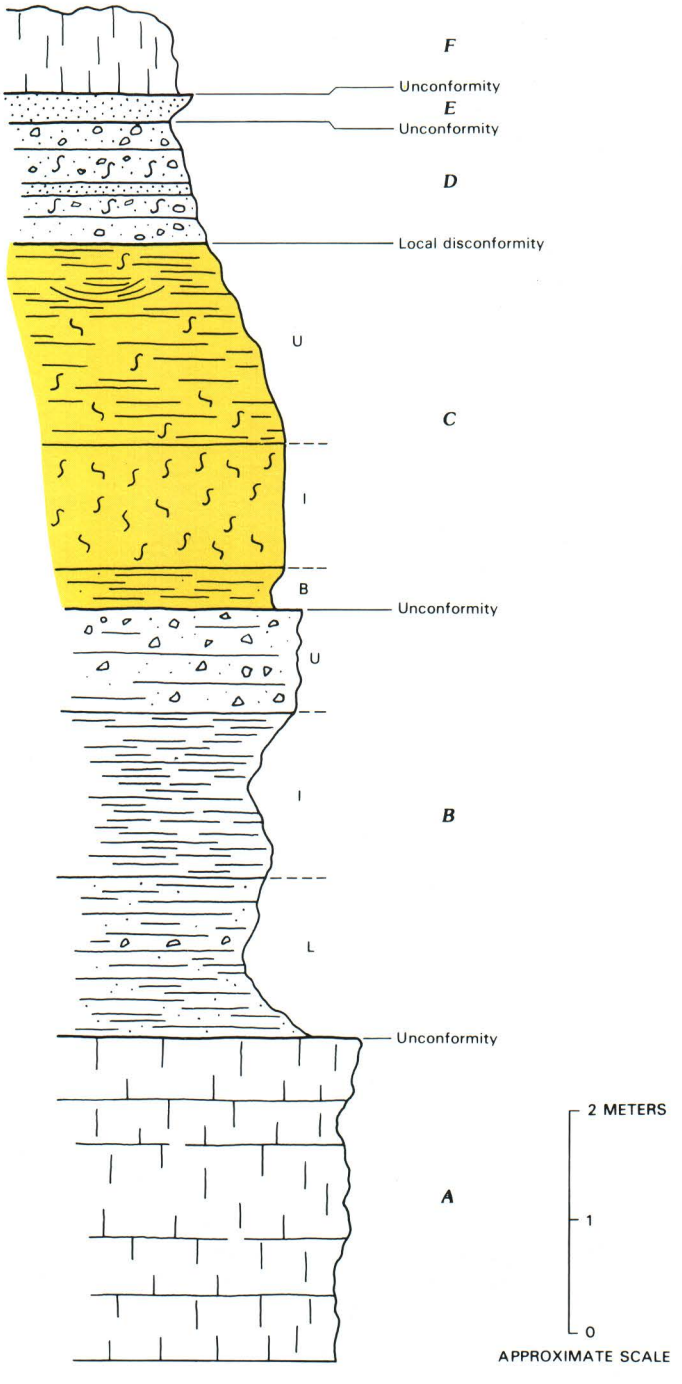

FIGURE 15.3.—Schematic columnar section, within area of southwest caldera rim. Units shown: ***A***, Crater-wall lava flows, >100 m thick, age at top 0.2–0.35 ka (Holcomb, 1980, p. 253). ***B***, ***C***, Keanakakoi Ash Member. ***B***, 1790 deposits; lower (L), intermediate (I), and upper (U) units (Malin and others, 1983), 4 m thick. ***C***, Golden pumice; basal (B), intermediate (I), and upper (U) units, 2.8 m thick, date about 1820. ***D***, Reworked mixed pumiceous and 1790 lithic debris, 1 m thick, date about 1820. ***E***, Lithic tephra, 1–7 cm thick, date 1924. ***F***, Pahoehoe lava flows, 2–3 m thick, dates 1971 and 1974.

porosity probably approaching 97 percent, and is so fragile that it crushes easily in the hand. In more perfect Hawaiian reticulite, Wentworth (1938, p. 149) measured a specific gravity of 0.043 and estimated a porosity of about 98 percent, consistent with Dana's (1891, p. 163) earlier figures. Although reticulite can form as a froth on the surface of some ponded gas-rich lava flows near vents, most Hawaiian reticulite is regarded as the product of vigorous lava fountaining.

REWORKED 1790 LITHIC DEBRIS AND PUMICE

Within the deposits constituting the detrital apron (fig. 15.8) dissected by the caldera-wall gullies are layers of reworked material derived from the adjacent tephra-mantled caldera wall. These layers, mostly 10–40 cm thick, may consist solely of 1790 lithic fragments, solely of pumice, or of mixtures of lithic and pumiceous fragments. Such layers lying below, between, and above beds composed solely of primary pumice (figs. 15.5–15.7) indicate that reworked debris was being intermittently delivered to the detrital apron before, during, and after emplacement of the golden pumice.

1924 LITHIC TEPHRA

The historically observed (Jaggar and Finch, 1924; Stearns, 1925; Jaggar, 1947, p. 205–259) explosive phreatic eruption of

FIGURE 15.4.— Best section of golden pumice exposed in gully near southwest rim of Kilauea caldera. B, bedded basal unit; I, massive intermediate unit; U, upper well-layered unit. The golden pumice is here overlain by 1924 crusted lithic tephra. U.S. Geological Survey photograph by J.D. Griggs.

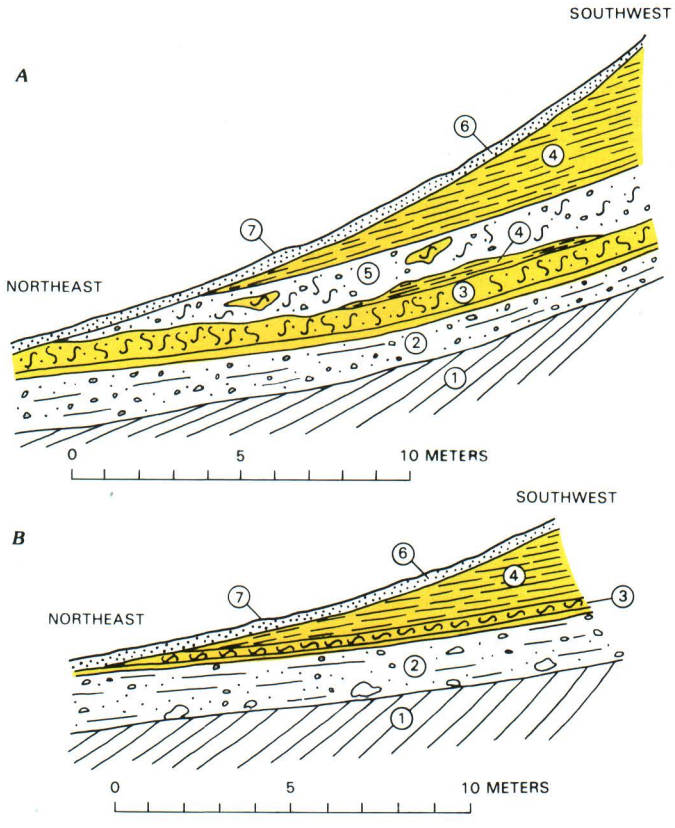

FIGURE 15.5.—Examples of angular unconformities of golden pumice and associated beds with 1790 deposits below and crusted apron veneer above. 1, 1790 beds; 2, reworked 1790 lithic debris, 20–40 cm thick; 3, basal and intermediate units of golden pumice, 45 cm; 4, upper unit of pumice, >1 m; 5, reworked mixed pumiceous and lithic debris, 60 cm; 6, apron veneer of reworked loose lithic-vitric sand, 20 cm; 7, crust on apron veneer. Angular unconformities below 2 and 6, and disconformity below 5. ***A***, South wall of caldera-wall gully 6–S. ***B***, South wall of caldera-wall gully 9–S.

Kilauea in 1924 produced a thin mantle, now crusted, of fine ash and sand- to granule-size fragments, mostly of dense lava, which covered much of the study area (Finch, 1925; Powers, 1948, plate 3D; Macdonald, 1949, p. 72; Macdonald and Abbott, 1970, p. 315). Scattered remnants of this mantle remain, filling shallow swales or forming residual scabs rising a few centimeters in relief on the present surface near and for a few hundred meters southwest of the southwest caldera rim.

Most such patches cover areas of only a few square meters or less. They are as much as 7 cm thick, but more commonly 2–4 cm. Although variable, the deposits display a reasonably consistent microstratigraphy: a basal 1–4 cm of distinctive pink, irregularly laminated fine ash, in many places containing accretionary lapilli, is succeeded by 0.3–0.5 cm of loose, matrix-free angular lithic granules, overlain by 1–2 cm of gray ash containing coarse sand and angular lithic granules, topped by a firm 1–3 mm crust in which abundant angular lithic granules are embedded. The crust has a distinctive rough texture, imparted by the projecting granules, and a medium brown color. Occasional larger lithic fragments (2–4 cm) in this crust may have been secondarily introduced from nearby exposures of 1790 lithic debris, because fragments that large do not here characterize the 1924 material beneath the crust. Lithologies of the lithic clasts in this deposit appear to duplicate those in the block field created around Halemaumau by the 1924 explosions. In the study area, the 1924 tephra rests upon golden pumice (Stone, 1926, p. 29) or, where that is lacking, directly upon the 1790 upper lithic unit.

APRON VENEER AND CRUST

A layer of loose sand and granule particles, 5–20 cm thick, capped by a firm crust, 1–3 cm thick, veneers large parts of the interfluve surface of the detrital apron in the area of caldera-wall gullies, south-southeast of Crater Rim Road (fig. 15.2). In its texture, firmness, setting, and general appearance, this crust so closely resembles the 1924 crust that it was initially and mistakenly so identified. However, it is pinkish rather than brown and lacks the characteristic underlying microstratigraphy, especially the fine ash. Furthermore, the sand and granule grains of this crust and the underlying conformable layers are a mixture of vitric and lithic particles, not solely lithic as in the 1924 deposit.

The apron veneer is a reworked deposit, which may contain 1924 debris but also includes older material, much of it vitric and probably derived from the golden pumice. It presumably dates from later than 1924, but because of its thickness and coherence perhaps only one or two decades later. It has been undermined by lateral recession of the walls of arroyo-like gullies, 1–2 m deep, cut into the alluvial apron, and so the crust may antedate that episode of dissection. In many exposures, the apron crust makes a spectacular

FIGURE 15.6.—North wall, lower reach of gully 5–S. A, reworked lithic debris. B, basal and intermediate (coarse) pumice units. C, primarily reworked lithic debris. D, reworked mixed pumiceous and lithic material. E, detrital apron crust. U.S. Geological Survey photograph by J.D. Griggs.

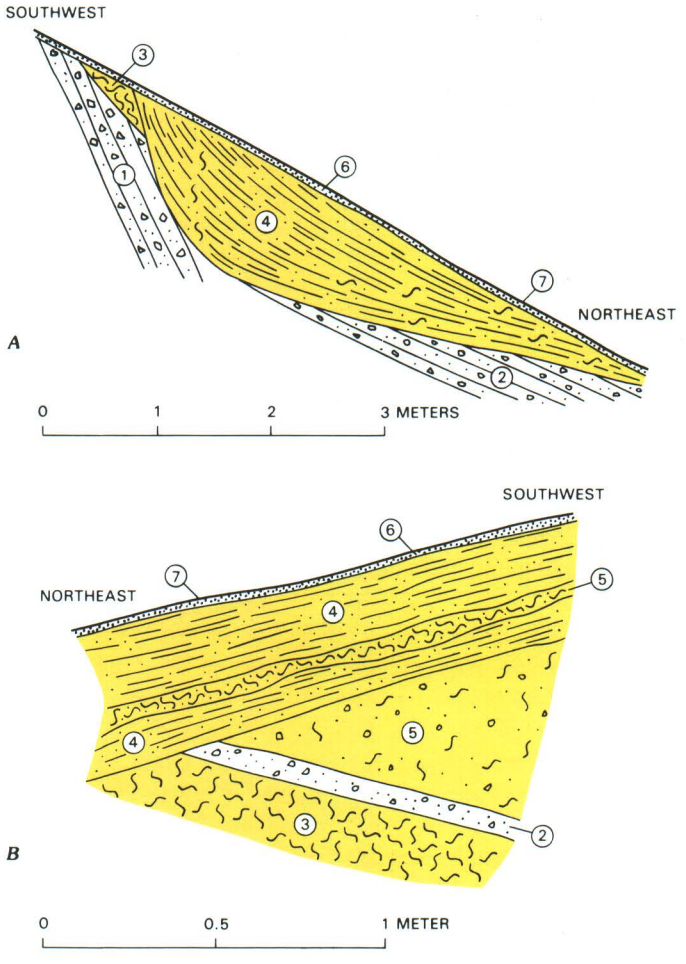

FIGURE 15.7.—Examples of unconformity between upper and intermediate units of golden pumice. 1, 1790 beds; 2, reworked 1790 lithic debris; 3, basal and intermediate units of pumice; 4, upper unit of pumice; 5, reworked coarse pumice; 6, reworked mixed pumiceous and lithic debris; 7, crusted apron veneer. ***A***, North wall of gully 8–S; ***B***, South wall of gully 1–S.

angular unconformity with the golden pumice and associated deposits (figs. 15.5, 15.7*A*).

SETTING AND RELATIONS

Microstratigraphic relations are best exposed in the first 13 major caldera-wall gullies south of Crater Rim Road. Each gully consists of a steep V-shaped upper reach indenting the caldera wall and a gentler, flat-floored arroyo-like reach cut into the detrital apron below (fig. 15.8), and each gully has experienced at least three episodes of dissection. Initially, narrow steep-walled slots, 2–3 m deep, were formed in the nearly horizontal lava flows composing the steep caldera walls, presumably by rock falls, avalanching, and fluvial erosion. These bedrock slots were subsequently partly or wholly filled by 1790 debris, forming some spectacular examples of tephra-bed draping or base-surge plastering on steep bedrock faces (fig. 15.9). Much of the 1790 debris was subsequently removed by further erosion, which locally cut through to bedrock. Deposits of pumice then partly refilled the gullies, mantled the upper gully walls, and added to the detrital apron. Such gully-wall pumice mantles form a striking large-angle unconformity with the more steeply inclined 1790 beds (fig. 15.9). Continued erosion has subsequently removed much of this caldera-wall pumice, but remnants are still seen on walls in the upper reaches of many gullies, particularly 8–S (fig. 15.10). A smaller angle unconformity between 1790 beds and the golden pumice, or associated conformable layers of reworked materials, is displayed in the walls of the lower reaches of many gullies (figs. 15.5, 15.11). A sharp angular unconformity also separates 1790 ash beds from reworked deposits of golden pumice in the Kau Desert (fig. 15.12).

Storm-water erosion within the gullies and colluvial reworking of debris mantling the caldera wall, both of which occurred contemporaneously with deposition of the upper golden pumice unit, added material to the detrital apron. Eventually most of the easily transportable debris was removed from the caldera wall, and regrading and dissection of the depositional apron occurred as the detrital load decreased. Lavas emplaced in 1971 and 1974 now bury the outer margin of the detrital apron (fig. 15.8).

ORIGIN AND EMPLACEMENT OF THE GOLDEN PUMICE

Historically, deposits of fragmented reticulite in Hawaii have been formed by high lava fountains associated with fissure eruptions on the flanks (Swanson and others, 1971) and in the summit calderas of Kilauea (Macdonald and Abbott, 1970, p. 82, 93; Richter and others, 1970) and Mauna Loa (Macdonald and Abbott, 1970, p. 62). The golden pumice has generally been regarded as the product of lava fountaining at an unidentified site or sites within Kilauea caldera. One can speculate concerning the changes that occurred at that source to produce the differences between the coarse, homoge-

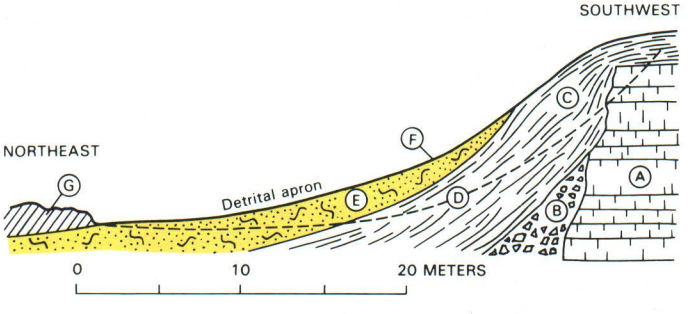

FIGURE 15.8.—Schematic cross section of detrital apron at caldera-wall gullies. A, lava flows of caldera wall; B, talus from caldera wall; C, 1790 beds; D, longitudinal profile of floor of caldera-wall gully; E, golden pumice and associated reworked pumiceous and lithic debris; F, crusted apron veneer; G, 1971 and 1974 pahoehoe lava flows.

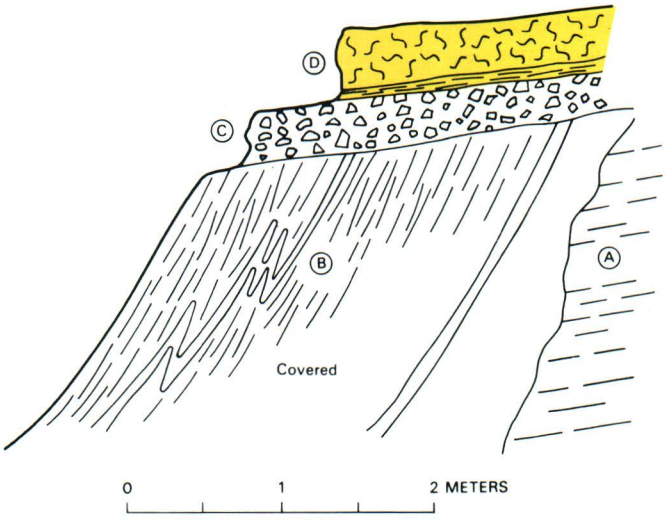

FIGURE 15.9.—Slump-deformed 1790 ash layers plastered on caldera wall and unconformably overlain by reworked lithic rubble and golden pumice, south side of caldera-wall gully 3–S. A, inferred caldera wall; B, 1790 ash beds; C, lithic-cobble rubble; D, lower and intermediate units of golden pumice.

neous, massive, tightly packed intermediate unit and the finer, well-layered, better sorted, more loosely packed basal and upper units.

Reticulite is so light that the behavior of individual fragments is strongly influenced by air currents; smaller particles, those with minimal glass coating, and those thrown highest are presumably the most strongly affected. Motion pictures of lava fountains show a central cone of debris falling back to the ground close to the fountain. This we shall term direct fallout to distinguish it from the more diaphanous plumes of material that drift for greater distances downwind (fig. 15.13). Most direct fallout follows a reasonably normal trajectory and consists largely of dense lapilli, glass, spatter and other forms of consolidated lava. A transition presumably exists between such direct fallout and drifted plume material. The coarse, closely packed pumice fragments of the intermediate unit appear to have come down directly out of the air, without significant secondary tumbling, wear or reworking. We speculate that it accumulated in the outermost part of the fallout zone and that large pumice fragments were so abundant they formed a clotted mass. We therefore refer to it as direct-fallout pumice, even though it probably drifted to some degree with the wind before coming to the ground.

Deposits of plume pumice should consist of smaller and better sorted fragments, possibly showing some evidence of attrition owing to buffeting contacts within the plume. If strong winds accompany the eruption, as commonly happens in Hawaii, such fragments may experience some eolian transport over the ground surface before coming to rest. Despite this complexity in their history, accumulations of both fallout and plume pumice are herein treated as primary. Both are highly susceptible to reworking by wind or water subsequent to their initial deposition, and such reworking imposes differences in texture, packing, coherence, fragment shape, contamination, and degree of layering that identify the resulting accumulations as of secondary origin.

Indications that much of the material composing the upper and basal units of the golden pumice has been secondarily transported by wind include the following: Good sorting; thin, even, regular layering; local cross-lamination; wear on pumice particles that has made them less jagged and removed some of the surficial glass coating; open packing; thin discrete layers of fine glass fragments; and inclusion of scattered lithic fragments, 2–3 mm in size, and thin layers rich in lithic sand. The well-bedded appearance of the upper and basal units results largely from the presence of numerous thin, continuous, even layers of fine vitric fragments that have specific gravities at least 25 times that of reticulite. These layers most likely formed as lag concentrates at times when strong trade winds removed accumulated pumice particles from the study area, leaving the smaller, denser glass fragments. Less probably, they may represent either changes in material being ejected or in the sorting of materials within plumes. Although the upper and lower units of the golden pumice contain a number of thin layers that may be primary plume pumice, and the upper unit clearly contains one 5-cm layer of primary fallout pumice, both units are inferred to be largely secondary in origin, on the basis especially of their excellent thin, regular bedding.

Deposition of fallout pumice and of plume or secondary pumice at the same site at different times could be caused by changes in the magnitude of fountaining at a fixed source or by migration of fountaining along a rift. Both are known to occur in Hawaii. Whatever the change was during the formation of the golden pumice, it was abrupt, not transitional, because the contacts between units

FIGURE 15.10.—Remnants of draped basal and intermediate units of golden pumice resting with angular unconformity on 1790 beds on northwest wall of gully 8–S. A, caldera-wall lavas; B, 1790 beds; C, golden pumice. U.S. Geological Survey photograph by J.D. Griggs.

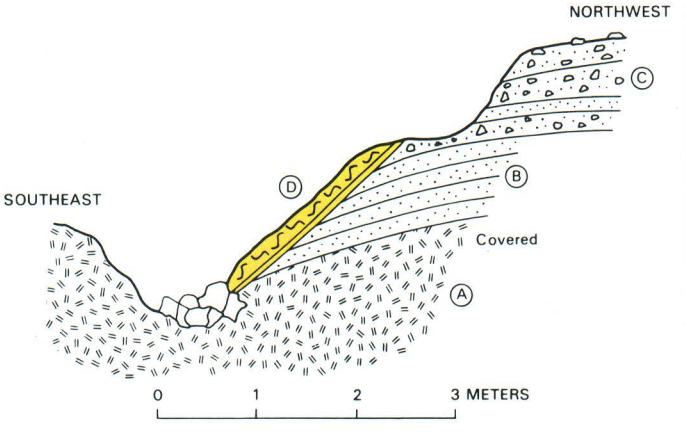

FIGURE 15.11.—Angular unconformity of draped basal and intermediate units of golden pumice on 1790 beds, north wall of gully 7–S. A, lavas; B, lower and intermediate units of 1790 deposits; C, upper lithic unit of 1790 deposits; D, basal and intermediate units of golden pumice.

are sharp. We find no compelling evidence to choose between these two alternatives, but it is perhaps simpler to imagine variations in fountaining at a fixed site, especially in accounting for the isolated 5-cm coarse fallout layer in the upper unit. The microstratigraphy of the golden pumice and associated deposits in the caldera-wall gullies (figs. 15.5–15.7) suggests that fountaining ceased completely on occasion, allowing both deposition by other processes and erosion to occur.

TEMPORAL CONSIDERATIONS

When, within the 1790–1924 period, was the golden pumice emplaced, and how much time was involved? Dana (1891, p. 43) visited Kilauea in 1877 and described deposits of reticulite along the caldera rim resting on coarse lithic conglomerate. This was almost certainly the golden pumice on the 1790 upper lithic unit. Wilkes's 1841 description (1845, p. 169–170) of coarse pumice filling open cracks of the southwest rift is almost identical to our description of the golden pumice intermediate unit. Observations of spumose lava, light as a sponge, wind-drifted, and visible all around on the surface of the Kau Desert a short walk southwest of Kilauea on August 1, 1823 (Goodrich, 1826, p. 22; Ellis, 1827, p. 162), strongly suggest that the golden pumice had been formed by that time. Probably it had formed not long before, because the pumice fragments were abundant and widely scattered and the deposits apparently not crusted, as they are now. These observations, and the improbability that lava fountaining adequate to create the golden pumice would go unrecorded after 1823 (Dana, 1891), point to the 1790–1823 interval as the likely time for the unit's origin.

A time late in that period would be particularly favored if the considerable erosion and reworking of 1790 lithic debris that occurred before pumice emplacement had been accomplished by normal fluvial and colluvial processes. However, the possibility that a more powerful process, such as base surge, might have produced the effects rather quickly deserves consideration in view of the fact that base surges are thought to have played a major role in emplacement of the 1790 deposits (Swanson and Christiansen, 1973, p. 85; Christiansen, 1979; Decker and Christiansen, 1984, p. 125). Spectacular U-shaped scour channels, local unconformities, and large bedforms within 1790 deposits for at least 0.5 km outward from the caldera rim are strong evidence for the action of base surges.

Kilauea caldera is large enough to have contained an intracaldera base surge that could have traversed the caldera floor and ascended the caldera wall. Accumulations of 1790 ash, showing base-surge characteristics, on large slump blocks on the caldera wall below Volcano House indicate to R.L. Christiansen (written commun., 1984) that this indeed happened. Likewise, the steep (60°–80°) inclination of fine 1790 ash beds (fig. 15.9) on the low southwest caldera wall is more likely to be the product of plastering of fine moist debris against the steep bedrock face by a steaming base surge than of draping by airfall deposition. These steep beds have been sharply truncated by erosion at the heads of nearly all the major caldera-wall gullies studied south of Crater Rim Road. A base surge acting in an erosive mode could have affected nearly universal truncation almost instantly. Such a surge would have had to occur late in the 1790 activity because at least part of the upper lithic unit is truncated (fig. 15.7*A*). The erosion required to form the uncomformity between golden pumice and 1790 beds might have been caused either by a base surge or by other more common surface processes.

It seems unlikely that the sandy gravel layers (figs. 15.5, 15.6) and the cobbly rubble (fig. 15.9) lying between golden pumice and the truncated 1790 beds in both the upper and lower reaches of the caldera-wall gullies are the result of base surges, because this reworked debris has been transported back toward the caldera floor rather than outward. Such debris layers were probably deposited by

FIGURE 15.12.—Angular unconformity of coarse pumice on fine-grained, well-layered 1790 ash on southwest flank of Cone Peak, about 80 m N. 16° E. from benchmark. U.S. Geological Survey photograph by J.D. Griggs.

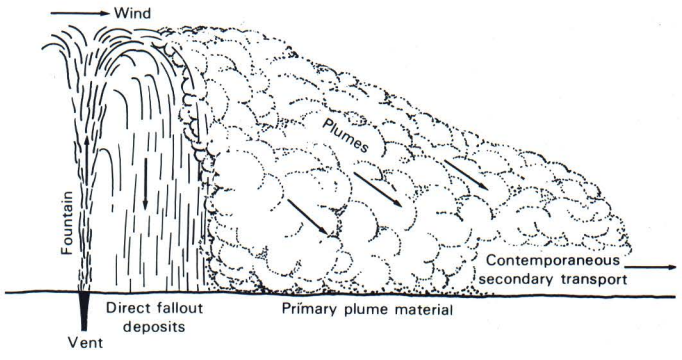

FIGURE 15.13.—Diagrammatic sketch of lava fountain, wind-drifted plumes, and related deposits. Variations in fountain height and character can produce superimposition or interlayering of different types of primary pumice deposits.

more slowly acting colluvial and fluvial processes. Relations in the caldera-wall gullies thus suggest that erosional truncation of 1790 beds could have occurred as a final gasp of the 1790 activity, but the deposition of reworked lithic layers may have occurred later and more slowly.

Pumice accumulations in the Kau Desert provide some insight on these relations. Along the western edge of the desert, a little northwest of the Kau Desert trail and about 1 km outward from the caldera rim (Kilauea Crater quadrangle), a wide fluvial arroyo 1 m deep has been eroded in 1790 deposits and older lava. Within this channel is a dissected alluvial fill of gravel, sand, and silt composed largely of reworked 1790 lithic material, capped by the golden pumice (fig. 15.14). The amount of fluvial work accomplished here before pumice deposition must have required a significant part of the 1790–1823 interval. In this same area, the golden pumice in many places rests directly upon lava bedrock from which the 1790 deposits must have been stripped before the pumice was laid down.

A favored setting for remnants of golden pumice in the Kau Desert is small niches on the flanks of little residual scabs, 30–50 cm high, on the eroded crusted surface of the 1790 upper lithic unit. Resistant overhanging ledges on such scabs make the pumice superficially appear to be interbedded with the lithic layers, and excavation is required to reveal that it is only inset (fig. 15.15). A secondary crust on the pumice, incorporating lithic fragments shed from the overhanging ledge, further obscures relations. Considerable modification of the surface of the crusted and irregularly cemented 1790 lithic layer by differential weathering, rainbeat, aqueous sapping, and probably eolian erosion had occurred to produce the scabs and their niches before the pumice was emplaced. Such modification could easily have required two or three decades. The overhanging ledges strongly suggest that erosion occurred after rather than before cementation. Even though most accumulations of golden pumice in the Kau Desert more than a few hundred meters from the caldera have probably formed by eolian reworking, such reworking likely occurred soon after pumice eruption, because newly formed pumice is very susceptible to eolian transport by the strong and prevailing northeast trade winds. Relations in the Kau Desert thus suggest pumice emplacement late in the 1790–1823 interval.

Another temporal question is the time involved in depositing the golden pumice and associated materials. The microstratigraphy of these units, as exposed in the walls of the caldera-wall gullies, strongly suggests that this was not a single brief episode. Successive eruptions of pumice were separated by intervals during which erosion created disconformities within the deposits, and stripping of detritus from the adjacent caldera wall introduced layers of pumiceous, lithic, or mixed pumiceous-lithic debris. During the period of golden pumice eruption, construction of the detrital apron at the base of that wall by colluvial, fluvial, eolian, and airfall processes was continuing.

Under current climatic conditions, the Kilauea summit is occasionally subjected to downpours of rain that create freshets and sheet floods across the surface of the detrital apron. In some years, several such events occur, in others none. Similar events probably occurred within the 1790–1823 interval and would have been capable of creating the erosional disconformities within the pumice sequence and introducing the interlayers of reworked debris. The time required to produce the golden pumice sequence may therefore have been anywhere from part of a year to several years.

Eruptive activity within Kilauea was greater than normal from about 1820 to 1832 (Hitchcock, 1911, p. 160–182; Macdonald and Abbott, 1970, p. 69–72), and it involved refilling of eruptive centers and associated lava fountaining. Native reports (Dana, 1891, p. 45) suggest that eruptive activity in Kilauea between March and June of 1823, before Ellis' visit of August 1 that year, was greater than anything occurring between 1790 and 1820

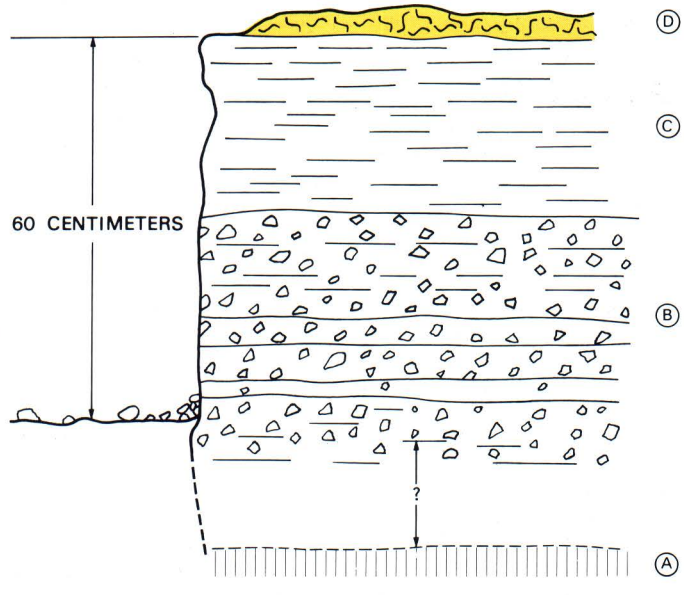

FIGURE 15.14.—Streambank exposure showing floodplain sand and silt (C) and fluvially reworked 1790 gravelly lithic debris (B) lying between coarse golden pumice (D) and the 1790 upper lithic unit or lava bedrock (A), northwest margin Kau Desert, 1 km southwest of Kilauea caldera.

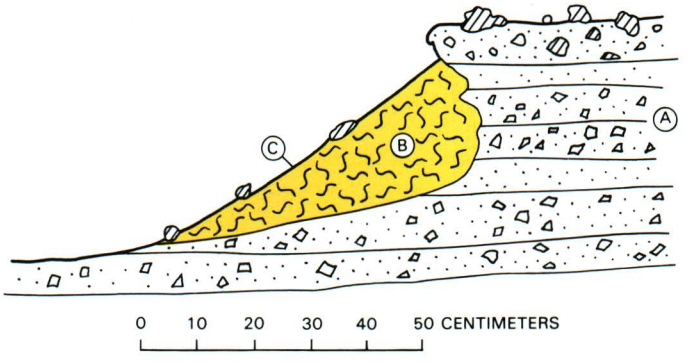

FIGURE 15.15.—Inset of crusted golden pumice within niche on flank of erosional scab on surface of upper lithic unit of 1790 deposits, Kau Desert. A, crusted upper lithic layer (1790); B, golden pumice; C, surface crust incorporating secondary lithic fragments.

(Goodrich, 1826, p. 27). The interval 1820–1823 appears adequate to accommodate the golden pumice, and the reported high degree of activity in Kilauea starting about 1820 favors that period.

Exactly when Halemaumau came into existence is not known. The crater probably did not exist as a specific topographic feature until some time after the 1790 outburst, for whose deposits it apparently was not the source (Stearns, 1966a, p. 134). A map drawn by Byron's lieutenant, Malden, in 1825 (Brigham, 1909, p. 45) shows a fairly large pit at the Halemaumau site, and various other early observers (Goodrich, 1826, p. 24; Ellis, 1827, p. 164, 170; Dana, 1891, p. 46–54; Brigham, 1909, p. 43–44) identified the southwestern part of Kilauea caldera, near the present Halemaumau, as the site of most intense activity. Although Halemaumau did not become a single crater until about 1905 (Richter and others, 1962, p. B53), we are intrigued with the speculative thought that the golden pumice may be a product of early activity of the volcanic conduit destined to determine the location of this present-day fire pit of Kilauea.

REFERENCES CITED

Brigham, W.T., 1909, The volcanoes of Kilauea and Mauna Loa: Bernice Pauahi Bishop Museum of Polynesian Ethnology and Natural History, Memoirs, v. 2, 222 p.

Christiansen, R.L., 1979, Explosive eruption of Kilauea Volcano in 1790 [abs.]: Proceedings of the Hawaii symposium on intraplate volcanism and submarine volcanism, Hilo, Hawaii, International association of volcanology and chemistry of the earth's interior, p. 158.

Dana, J.D., 1891, Characteristics of volcanoes: New York, Dodd, Mead, and Company, 399 p.

Decker, R.W., and Christiansen, R.L., 1984, Explosive eruptions of Kilauea Volcano, Hawaii: *in* Explosive volcanism: Inception, evolution and hazards: Washington, National Academy of Sciences, p. 122–132.

Ellis, William, 1827, Journal of William Ellis, Narrative of a tour of Hawaii, with remarks on the history, traditions, manners, customs, and language of the inhabitants of the Sandwich Islands: Honolulu, Hawaii, Advertiser Publishing Company, reprint of the London 1827 edition, 342 p.

Finch, R.H., 1925, The ash deposits at Kilauea Volcano: The Volcano Letter, No. 17, Hawaiian Volcano Research Association, 1 p.

———1947, Kilauea in 1790 and 1823: The Volcano letter, No. 496, Hawaiian Volcano Research Association, 2 p.

Goodrich, Joseph, 1826, Notice of the volcanic character of the Island of Hawaii: American Journal of Science, v. 11, p. 2–36.

Heiken, Grant, 1974, An atlas of volcanic ash: Smithsonian contributions to earth science, no. 12, p. 1–12.

Hitchcock, C.H., 1911, Hawaii and its volcanoes: Honolulu, Hawaiian Gazette, 314 p.

Holcomb, R.T., 1980, Kilauea Volcano, Hawaii: Chronology and morphology of the surficial lava flows: U.S. Geological Survey Open File Report 80-796, 321 p.

Jaggar, T.A., 1925, Discussion of special features: Hawaiian Volcano Observatory Monthly Bulletin, v. 13, p. 1–8.

———1947, Origin and development of craters: Geological Society of America Memoir 21, 508 p.

Jaggar, T.A., and Finch, R.H., 1924, The explosive eruption of Kilauea in Hawaii: American Journal of Science, v. 208, p. 353–374.

Macdonald, G.A., 1949, Petrography of the Island of Hawaii: U.S. Geological Survey Professional Paper 214-D, p. 51–96.

———1955, Hawaiian volcanoes during 1952: U.S. Geological Survey Bulletin 1021-B, p. 15–108.

———1972, Volcanoes: Englewood Cliffs, New Jersey, Prentice-Hall, 510 p.

Macdonald, G.A., and Abbott, A.T., 1970, Volcanoes in the sea: Honolulu, Hawaii, University of Hawaii Press, 441 p.

Malin, M.C., Dzurisin, Daniel, and Sharp, R.P., 1983, Stripping of Keanakakoi tephra on Kilauea Volcano, Hawaii: Geological Society of America Bulletin, v. 94, p. 1148–1158.

Powers, H.A., 1948, A chronology of the explosive eruptions of Kilauea: Pacific Science, v. 2, p. 278–292.

Richter, D.H., Eaton, J.P., Murata, K.J., Ault, W.U., and Krivoy, H.L., 1970, Chronological narrative: The 1959–60 eruptions of Kilauea Volcano, Hawaii: U.S. Geological Survey Professional Paper 537E, p. E1–E73.

Richter, D.H., Moore, J.G., and Haugen, R.T., 1962, Recent growth of Halemaumau, Kilauea Volcano, Hawaii: U.S. Geological Survey Professional Paper 450B, p. B53–B56.

Sherzer, W.H., 1923, Explosive eruptions of Kilauea: Science, v. 57, p. 459–461.

Sparks, R.S.J., 1976, Grain size variations in ignimbrites and implications for the transport of pyroclastic flows: Sedimentology, v. 23, no. 2, p. 147–188.

Stearns, H.T., 1925, The explosive phase of Kilauea Volcano, Hawaii, in 1924: Bulletin Volcanologique, v. 2, p. 193–209.

———1966a, Geology of the state of Hawaii: Palo Alto, California, Pacific Books, 266 p.

———1966b, Road guide to points of geologic interest in the Hawaiian Islands: Palo Alto, California, Pacific Books, 66 p.

Stone, J.B., 1926, The products and structure of Kilauea: Bishop Museum Bulletin 33, 59 p.

Swanson, D.A., and Christiansen, R.L., 1973, Tragic base surge in 1790 at Kilauea Volcano: Geology, v. 1, no. 2, p. 83–86.

Swanson, D.A., Jackson, D.B., Duffield, W.A., and Peterson, D.W., 1971, Mauna Ulu eruption, Kilauea Volcano: Geotimes, v. 16, p. 12–16.

Wentworth, C.K., 1938, Ash formations of the Isle of Hawaii: Hawaiian Volcano Observatory Third Special Report, 183 p.

Wentworth, C.K., and Williams, Howel, 1932, The classification and terminology of the pyroclastic rocks: National Research Council Bulletin 89, p. 19–53.

Wilkes, Charles, 1845, Narrative of the United States Exploring Expedition: Philadelphia, Lea and Blanchard, v. 4, 539 p.

THE 1972–1974 MAUNA ULU ERUPTION, KILAUEA VOLCANO: AN EXAMPLE OF QUASI-STEADY-STATE MAGMA TRANSFER

By Robert I. Tilling, Robert L. Christiansen, Wendell A. Duffield, Elliot T. Endo, Robin T. Holcomb, Robert Y. Koyanagi, Donald W. Peterson, *and* John D. Unger

ABSTRACT

The eruption at Mauna Ulu from February 3, 1972, to July 22, 1974, renewed the sustained activity on Kilauea's east rift zone that had previously ceased in October 1971. During 901 days of virtually continuous activity, about 162×10^6 m^3 of basaltic lava was erupted. Vent activity was confined to the Mauna Ulu-Alae area except for two short-lived outbreaks near Pauahi and Hiiaka Craters in May and November 1973. The minimum average magma production rate through April 1973 was 8×10^6 m^3/mo, comparable to rates for other periods of sustained eruptive activity at Kilauea.

The 1972–74 lava (1) covered an area of about 46 km^2; (2) raised the summit of the shield built at Mauna Ulu during the 1969–71 eruptions to a maximum height of 121 m above the pre-1969 ground surface; (3) greatly increased the size and height of the complex shield at Alae, which attained a maximum height of nearly 90 m above the pre-1969 ground surface; (4) filled the west pit of Makaopuhi Crater; and (5) entered the sea in August–October 1972 and February–May 1973 after traveling more than 12 km through well-developed lava-tube systems.

The 1972–74 eruption was dominated by active lava lakes at Mauna Ulu and Alae, their vents linked by an efficient tube system. The lava lakes exhibited a wide range of behavior, including (1) complex circulation patterns of the lake surface and low-level fountaining at drainback areas; (2) cyclic fluctuations of as much as a few tens of meters in the level of the lava column, accompanied by violent degassing during column collapse (the so-called gas-piston activity); (3) complete or partial draining of the lava lakes caused by major changes in eruptive mode or lava-supply system; (4) repeated short-duration overflows and levee construction leading to shield growth; and (5) sustained overflows and the development of lava tubes to feed long flows.

Records of Kilauea summit tilt during 1972–74, as measured at Uwekahuna vault, show two periods (February 1972 to April 1973 and December 1973 to July 1974) of oscillations within a narrow range and little or no net change in tilt. Each of these periods is interpreted to reflect a quasi-steady-state regime of magma transfer from a mantle source to Kilauea's summit reservoir and to the upper east rift zone. The first period apparently was terminated by subsurface blockage in the magma-transfer system, possibly caused by a 6.2-magnitude earthquake on April 26, 1973, which also disrupted a well-established tube system and halted lava entry into the sea. The second period marked the reestablishment of a highly efficient magma-transfer system following the November–December 1973 eruption at Pauahi. Our postulated periods of quasi-steady-state regime of magma transfer are compatible with the speculation of Daniel Dzurisin and others that the sustained eruptive activity at Mauna Ulu may be linked to increased deep magma production, as evidenced by above-average occurrence of deep harmonic tremor beneath Kilauea.

Ground deformation measured by periodic resurveying of level, ground tilt, and trilateration networks in the Kilauea summit region generally is compatible with patterns seen in continuous records of Uwekahuna tilt, seismicity, and observed eruptive activity. However, some deformation patterns during the periods of quasi-steady-state magma-transfer regime are diffuse and not amenable to simple analysis. The most coherent patterns obtained are related to the Pauahi-Hiiaka (May) and Pauahi (November) eruptions during the net inflation period of 1973; each of these was associated with a deflation at Uwekahuna of about 20 microradians. Perhaps a threshold volume or rate of change in summit magma storage must be exceeded before coherent ground-deformation patterns can be derived from geodetic surveys; the volcano may possess a characteristic yield strength, such that a finite amount of inelastic deformation must be accommodated before geodetic response can reflect elastic behavior.

INTRODUCTION

The 1969–71 Mauna Ulu eruption (figs. 16.1 and 16.2), which lasted about 2½ years and produced 185×10^6 m^3 of lava, was one of the most voluminous and long-lived historical rift eruptions of Kilauea Volcano, Hawaii (Swanson and others, 1971, 1979). The waning stage of that eruption was characterized by monotonic subsidence of the surface of a lava lake in Mauna Ulu crater, accompanied by sharp summit inflation, and was punctuated by a brief eruption within the summit caldera during August 1971 and another, in the caldera and southwest rift zone, during September 1971 (Duffield and others, 1982). The end of the 1969–71 Mauna Ulu eruption was October 15, 1971, the date when lava was last seen in the vent (Swanson and others, 1979). No eruptions occurred at Kilauea for the next 3½ months, a period of steady summit inflation.

In early February 1972, lava quietly reentered the crater of Mauna Ulu, initiating a period of sustained eruption that ultimately lasted until mid-July 1974. The 1972–74 activity was confined to the Mauna Ulu-Alae area except for an outburst from vents within and near Pauahi and Hiiaka Craters on May 5, 1973, and a month-long eruption at Pauahi in November–December 1973 (fig. 16.2). For convenience of discussion, the eruptions of Mauna Ulu (which

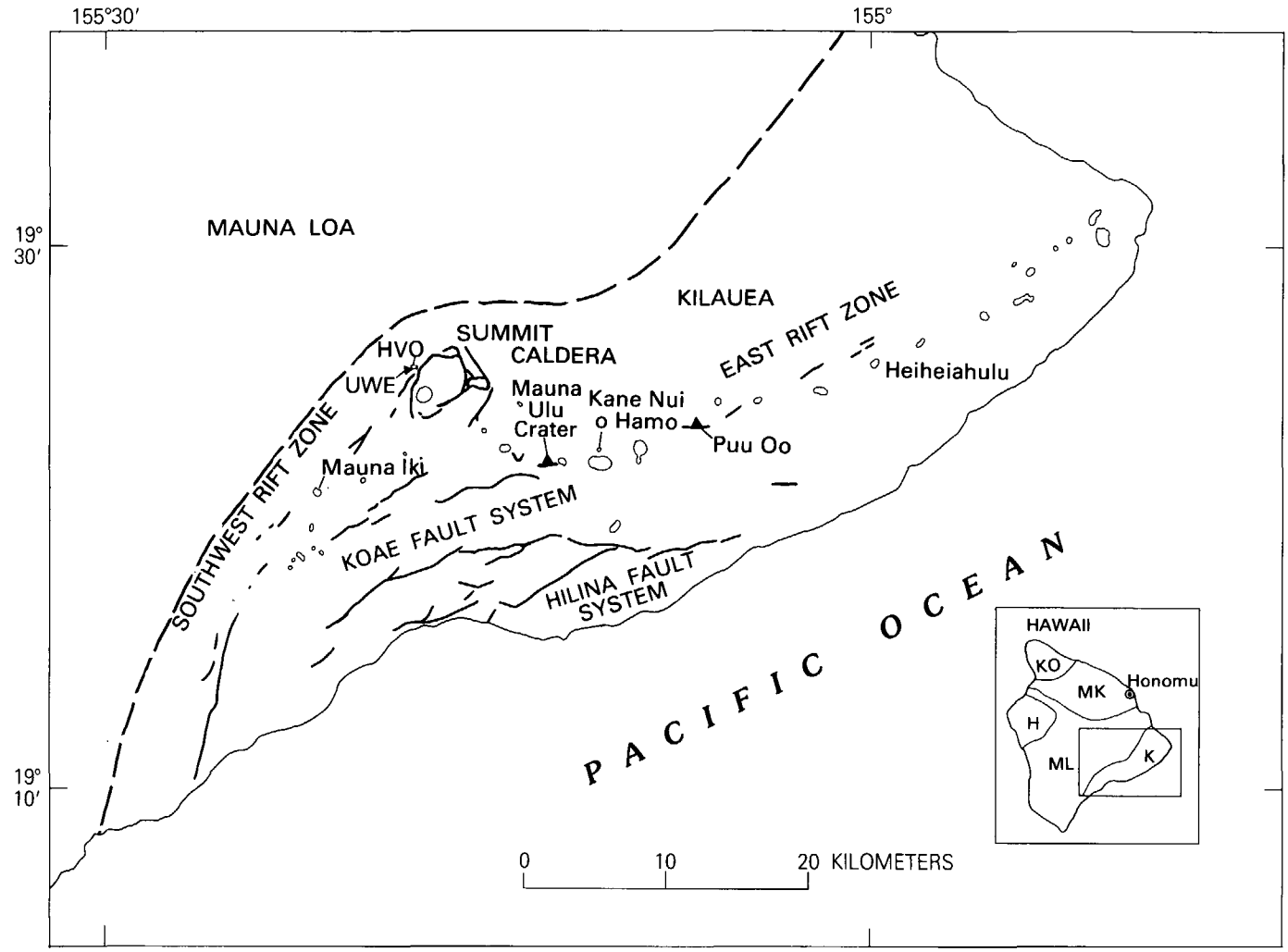

FIGURE 16.1.—Map of Kilauea Volcano showing summit caldera, rift zones, and principal fault systems; locations of the Hawaiian Volcano Observatory (HVO) and Uwekahuna vault (UWE) are also shown. Inset shows volcanoes making up Island of Hawaii: KO, Kohala; MK, Mauna Kea; H, Hualalai, ML, Mauna Loa; and K, Kilauea. Mauna Ulu eruption site (1969–1974) is on upper east rift zone, and Puu Oo eruption site (1983–present) is on middle east rift zone; these sites are indicated by solid triangles. Mauna Iki (1919–20), Heiheiahulu (1750?), and Kane Nui o Hamo (prehistoric) are volcanic shields developed on rift zones before 1969. Modified from Dzurisin and others (1984, fig. 2).

means "growing mountain" in Hawaiian), Pauahi, and Hiiaka during 1972–74 are considered collectively as the 1972–74 Mauna Ulu eruption because of their close association in space and time and the persistence of harmonic tremor thoroughout almost the entire period. The end of eruptive activity at Mauna Ulu is taken to be July 22, 1974, following a three-day summit eruption (Peterson and others, 1976), after which no molten lava could be observed at Mauna Ulu and harmonic tremor ceased.

Following the 1972–74 Mauna Ulu eruption, activity at Kilauea shifted to the summit region, where short-lived outbursts during July and September were followed by a brief eruption and intrusion in the southwest rift zone in December 1974 (Peterson and others, 1976; Dzurisin and others, 1984, table 1). Following various other short-lived eruptions and intrusions at several sites on the volcano during 1975–82 (Tilling and others, 1976b; Moore and others, 1980; Dzurisin and others, 1984), the beginning of the Puu Oo eruption in the middle east rift zone in 1983 (Wolfe and others, chapter 17) marked the return to Kilauea of a long-lived, voluminous flank eruption, like the Mauna Ulu eruptions during 1969–74.

The 1972–74 activity was particularly notable for active lava lakes that occupied the summit craters of Mauna Ulu and Alae shields for long periods of time. We consider a lava lake active if it is linked, directly or indirectly, to a feeding magma column, in contrast

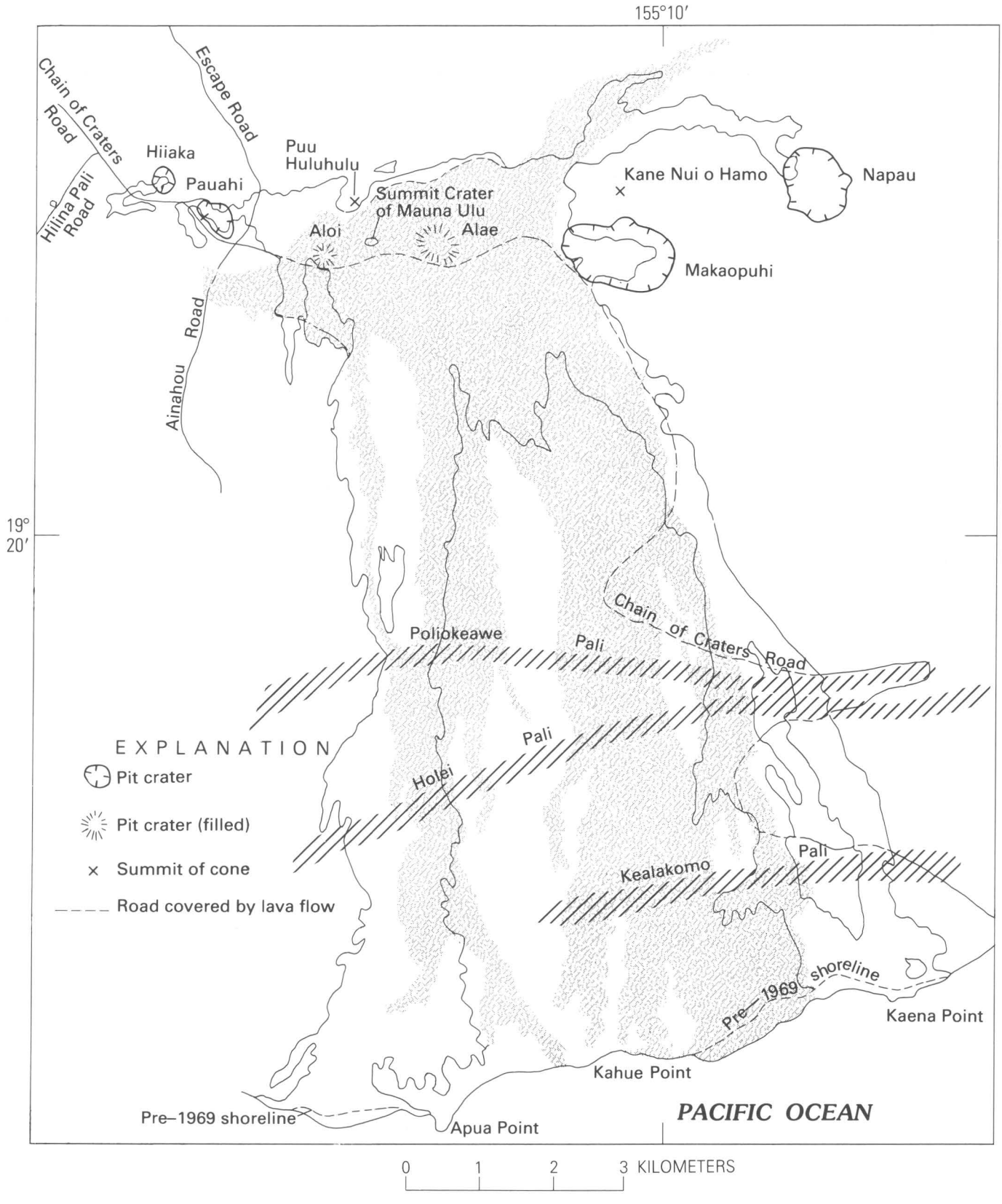

FIGURE 16.2.—Sketch map showing lava fields produced by the 1969–1971 Mauna Ulu eruption (shaded) and the 1972–74 Mauna Ulu eruption (outlined by solid line); pali means cliff in Hawaiian. Modified from Swanson and others (1979, fig. 4) and Holcomb (1976).

TABLE 16.1.—*Some published topical studies on aspects of the 1972–1974 Mauna Ulu eruption and general works on Kilauea that include data relevant to processes, products, or effects of the eruptions*

Topic	Reference
General summaries and field guidebooks.	Greeley (1974) Hazlett (1981) Macdonald and Hubbard (1982) Peterson and others (1976)
Geologic maps	Holcomb (1976) Holcomb (1980)
Lava chemistry	Wright and Tilling (1980)
Lava tubes	Peterson (1983)
Lava lakes, variations in depth to surface.	Tilling and others (1986)
Pahoehoe-aa transition	Peterson and Tilling (1980) Kilburn (1981)
Volcanic landforms	Tilling and others (1973) Holcomb (1973) Holcomb and others (1974) Tilling and others (1976b, c) Dzurisin (1978)
Lava deltas	Peterson (1976)
Lava movement under water and pillow formation.	Grigg (1973) Tepley (1975) Moore (1975)
Rockfall activity and seismicity	Tilling (1976a) Tilling and others (1975)
Pattern of historical eruptions	Klein (1982)
Ground deformation, including modeling.	Ryan and others (1983) Epp and others (1983) Dvorak and others (1983)
Magma intrusion into rift zones	Koyanagi and others (1973) Klein (1982) Dzurisin and others (1984)
Magma budget	Dzurisin and Koyanagi (1981) Dzurisin and others (1984)
Magma reservoir shape and mechanics	Ryan and others (1981) Ryan and others (1983)
Seismicity	Koyanagi and others (1976a, b) Ellesworth and Koyanagi (1977) Unger and others (1973) Unger and Ward (1979) Aki and Koyanagi (1981)
Geoelectrical studies of volcanic processes.	Zablocki (1976) Zablocki (1978)
Thermal studies	Casadevall and Hazlett (1983)
Gas and sublimate studies	Cadle and others (1973) Naughton and others (1973)
Miscellaneous	Sicks (1975) Dzurisin (1980)

to an inactive lava lake formed by passive ponding of magma within preexisting pit craters (see Swanson and others, 1979, p. 10). The long duration and easy accessibility of the 1972–74 Mauna Ulu eruption permitted frequent and numerous direct observations of the activities of these lava lakes, as well as of the development and evolution of volcanic shields, lava levees, flow channels, and lava tubes.

Many features of the 1972–74 Mauna Ulu eruption were virtually identical to those well described and illustrated by Swanson and others (1979) for the lava-lake-dominated activity of episodes 3 and 4 (called stages by them) of the 1969–71 Mauna Ulu eruption, and we refer where appropriate to those excellent descriptions rather than unnecessarily describing processes anew.

Many topical studies were undertaken during the course of the 1972–74 Mauna Ulu eruption, and several recent syntheses of Kilauea's magmatic behavior included data obtained in the 1972–74 period. A listing of some of these studies is given in table 16.1 to complement similar summaries for the 1969–71 Mauna Ulu eruption (Swanson and others, 1979, tables 1 and 2). The main purposes of this paper are to describe the eruptive phenomena in 1972–74, provide a general framework for topical studies already completed, and identify directions for possible further topical research.

ACKNOWLEDGMENTS

This paper could not have been written without the enthusiastic efforts of the many present and former members of the Hawaiian Volcano Observatory (HVO) staff who contributed to the systematic observation and monitoring of the 1972–74 Mauna Ulu eruption. Particular thanks go to John C. Forbes, William H. Francis, Kenneth T. Honma, George Kojima, John P. Lockwood, Jennifer S. Nakata, Arnold T. Okamura, Reginald T. Okamura, Marie S. Onouye, Gary S. Puniwai, James C. Ratte, Maurice K. Sako, Akira Yamamoto, and Charles J. Zablocki. Our National Park Service colleagues at Hawaii Volcanoes National Park also assisted our studies by their administrative support and additional observations of the eruptive phenomena.

During the course of the eruption, we benefited from stimulating discussions with members of the HVO staff, other U.S. Geological Survey colleagues, guest investigators, and visiting scientists, especially Michael H. Carr, Robert W. Decker, Richard S. Fiske, Ronald Greeley, John E. Guest, (the late) Everett D. Jackson, Jeffrey Judd, Peter W. Lipman, (the late) Gordon A. Macdonald, Harold Masursky, James G. Moore, Willard H. Parsons, Dallas L. Peck, Howard A. Powers, Daniel Rubel, Donald A. Swanson, Peter L. Ward, and Thomas L. Wright. Special thanks go to John Dvorak, Arnold Okamura, and Wil Tanigawa for assistance in the computer retrieval and reduction of ground-deformation data pertinent to the eruption. Support from the U.S. National Aeronautics and Space Administration (NASA) Planetology Program provided opportunities for instructive comparisons between Hawaiian and extraterrestrial volcanism and resultant landforms. Constructive reviews of an earlier draft of this paper by Donald A. Swanson and Edward W. Wolfe are greatly appreciated.

TABLE 16.2.—*Summary of east-rift eruptive activity of Kilauea Volcano, Hawaii, from February 1972 to July 1974 (modified from Peterson and others, 1976)*

Time period	Duration (days)	Location of vents (see fig. 16.3)	Esimated lava volume[1] (10^6 m^3)	Area covered by lava (km^2)
February 3, 1972 to May 4, 1973	457	Mauna Ulu and Alae	125	[2] 35
May 5, 1973	1	Pauahi and Hiiaka and nearby fissures	1	.6
May 6, 1973 to November 9, 1973	188	Mauna Ulu and Alae	2.5	.9
November 10, 1973 to December 9, 1973	30	Pauahi and nearby fissures	3	1.1
December 10, 1973 to July 22, 1974	225	Mauna Ulu	30	8
Total	901		161.5	45.6

[1]Includes only volume remaining on surface and excludes volume that drained back into fissures before eruption ended.
[2]Includes 0.47 km of new land added to south coast of Hawaii from lava entry into sea (Peterson, 1976).

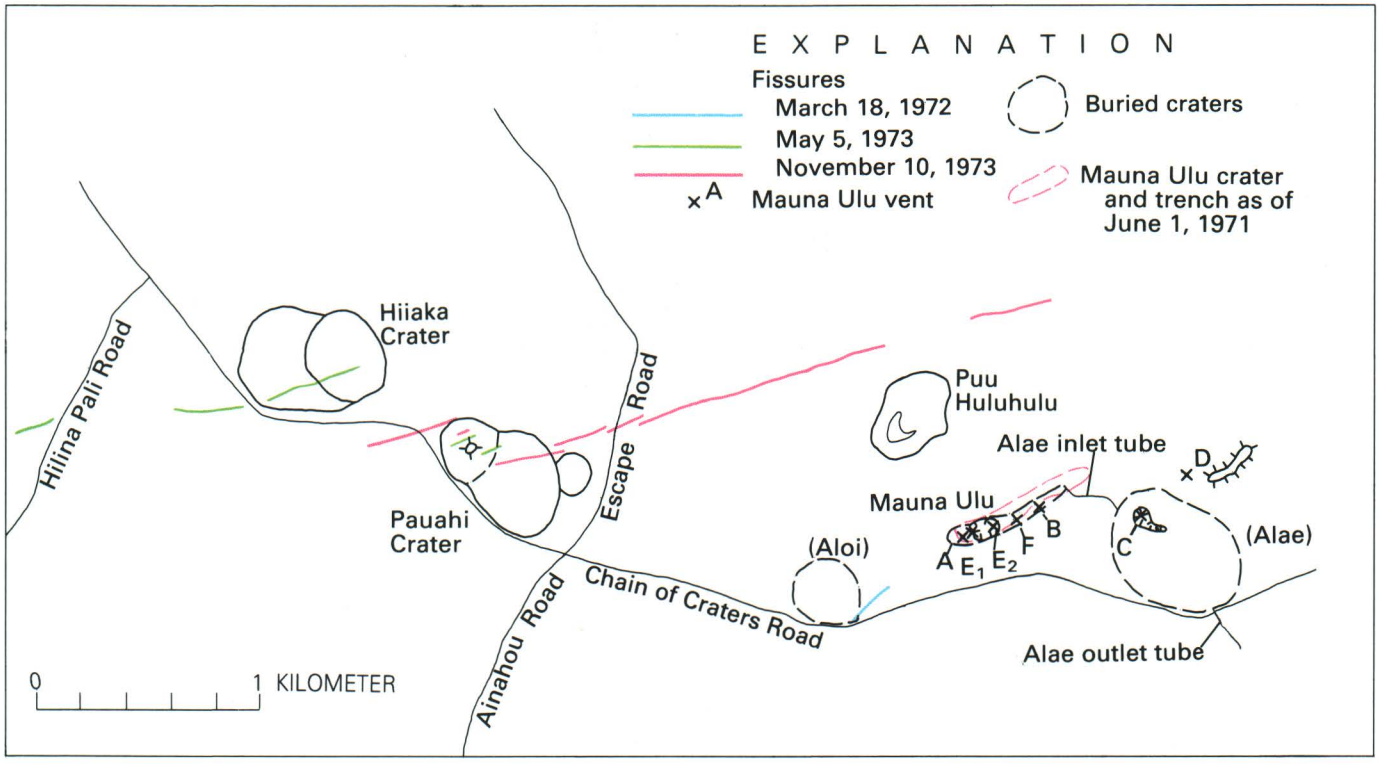

FIGURE 16.3.—Sketch map showing location of vents active during 1972–1974 eruption. The locus of 1972–74 Mauna Ulu vents (A,B,C,D,E_1,E_2, and F) essentially coincides with that of the vents active during July 1970–June 1971 (see Swanson and others, 1979, pl. 4).

OVERVIEW OF THE 1972–74 ERUPTION

Peterson and others (1976) summarized the general features of the 1972–74 eruptive activity of Kilauea Volcano; the overview given here draws on and adds to that earlier summary. The major events, locations of vents, and variation in summit tilt, as measured at Uwekahuna, throughout the 1972–74 Mauna Ulu eruption are summarized in table 16.2 and figures 16.3 and 16.4.

The eruption began in early February 1972 and was dominated through early June 1973 by active lava lakes and associated phenomena, such as overflows, lava-tube formation, and volcanic shield growth, at both Mauna Ulu and Alae (fig. 16.2). The lava lakes were clearly connected beneath the surface, but lava passageways between Mauna Ulu, Alae, and the summit reservoir are not well known. Through May 4, 1973, periodic voluminous overflows of lava from Mauna Ulu and Alae totaled 125×10^6 m^3. An unknown additional volume drained back into vents and intruded into the east rift zone. This volume of surface eruptive products, not adjusted for lava vesicularity or ground deformation, yields a minimum average magma supply rate of approximately 8×10^6 m^3/mo, comparable to the rates for the 1969–71 Mauna Ulu eruption (Swanson and others, 1979) and the 1971 summit eruptions (Duffield and others, 1982).

Many short-lived overflows from Alae, traveling only short distances, built a new shield, approximately 100 m high, abutting the eastern flank of the Mauna Ulu shield (Tilling and others, 1973, fig. 2). In contrast, long-lived overflows, instead of adding to the shield, evolved into lava tubes that were able to transport the lava for great distances from the vent. Some tube-fed lava from the Alae vent cascaded into Makaopuhi Crater and entered the sea during August–October 1972 and February–April 1973 (fig. 16.2; Tilling and others, 1973; Peterson, 1976).

The 6.2-magnitude Honomu earthquake on April 26, 1973 (Unger and others, 1973; Unger and Ward, 1979), although centered more than 60 km away (fig. 16.1, inset), apparently disrupted the well-integrated lava-tube system from Alae to the coast, and all flow into the sea stopped by about May 1. This earthquake probably also altered the magma conduit system from the summit to Mauna Ulu, as well as the lava-tube link between Mauna Ulu and Alae. Early on the morning of May 5, strong harmonic tremor and summit deflation accompanied the complete drainage of the lava lakes at Mauna Ulu and Alae. About 3½ hours later, lava fountained from a fissure in Pauahi Crater, 2 km uprift from Mauna Ulu (fig. 16.2), in the first historical eruption there. The Pauahi eruption began to wane after about 2 hours, and early in the afternoon new vent fissures opened within and near Hiiaka Crater. Near the closing stages of this activity, lava erupted briefly from a fissure in the eastern part of the Koae fault zone about 1 km west of Hiiaka, in the first historical outbreak in that area (Koyanagi and others, 1973; Duffield, 1975, p. 11–12).

By May 7, 1973, lava had quietly returned to the Mauna Ulu

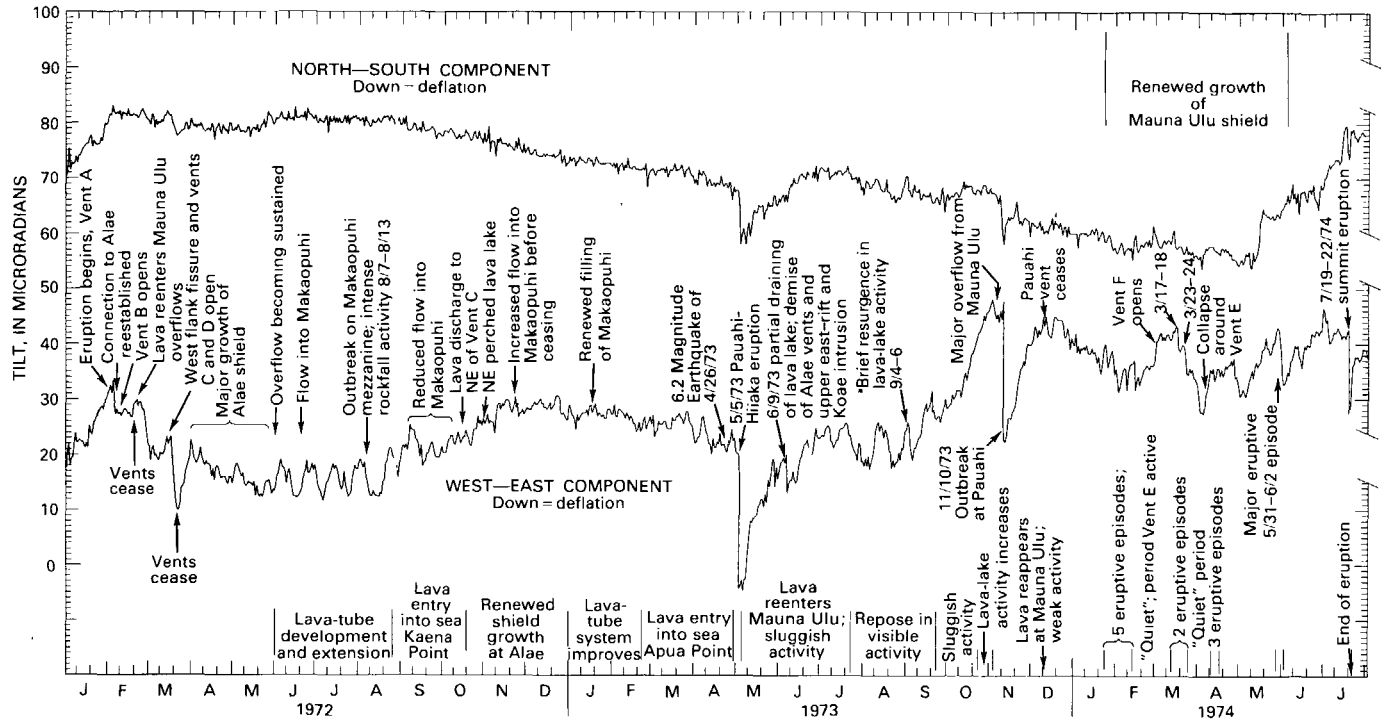

FIGURE 16.4.—Variation in Uwekahuna tilt for the period January 1972–July 1974, and its correlation with significant eruptive events (see text). Tilt data adjusted for the 18-microradian offset (east-west component) caused by the April 1973 Honomu earthquake (fig. 16.1 inset); zero point on tilt scale is arbitrary and referenced to January 1, 1972. The same data are also shown in figure 16.37 at reduced scale and not adjusted for earthquake offset.

crater. Moderate lava-lake activity had resumed at Mauna Ulu by early June, and a small lava lake reappeared at Alae. In the early hours of June 9, preceded and accompanied by harmonic tremor and abrupt summit deflation, drainage of lava partly emptied Mauna Ulu; Alae drained completely and stayed inactive for the remainder of the eruption. Almost immediately following its partial draining, Mauna Ulu lava lake began to rise again and to circulate sluggishly. Subsequent activity was summarized by Peterson and others (1976, p. 652): "Although the lava lake rose gradually with time, the surface area of the actively circulating lake steadily diminished. By mid-July the lava lake became practically stagnant, and the occasional small overflows of lava traveled only short distances on the crater floor. In late September, after nearly two months of virtual quiet, activity increased and voluminous flows flooded the crater floor."

Activity increased throughout October and early November, and Mauna Ulu lava lake rose to the crater rim, feeding voluminous overflows during November 4–8. On November 10, harmonic tremor and summit deflation again accompanied the abrupt drainage of the lake, which subsequently remained inactive for more than a month. A few hours after this sudden draining of lava from Mauna Ulu, an eruption began at Pauahi Crater (fig. 16.2) and continued vigorously for several hours, forming lava ponds in both the east and west pits fed by vents within the crater as well as by lava cascades from fissures outside Pauahi. Weak activity persisted in the west pit of Pauahi for about a month. Then, from December 9 to 12, 1973, no visible activity occurred anywhere on Kilauea.

On December 12, the seismic station located closest to the Pauahi-Mauna Ulu area began to record bursts of barely detectable harmonic tremor. By the next day, tremor had increased and become sustained, and lava quietly reentered Mauna Ulu. For the next one and one-half months, weak to moderate activity produced several short-lived flows that flooded the crusted surface of the rising lava lake.

Mauna Ulu eruptive activity in 1974 was unlike that during 1972–73. Beginning in late January, short vigorous eruptive episodes, lasting typically less than two days, produced moderately high lava fountains (40–80 m) that fed short-lived overflows. These brief eruptive periods were separated by 3-day to 5-week intervals of only feeble activity. The pattern of alternating vigorous and weak activity mimicked, albeit on a smaller scale, the episodes of high fountaining interspersed with longer periods of low activity that characterized the first stage of the 1969–71 Mauna Ulu eruption (Swanson and others, 1979).

Some overflows during the period January–June 1974 advanced as far as 9 km from the vent, but most traveled shorter distances. Consequently, the Mauna Ulu volcanic shield grew substantially in 1974, particularly during March–June, reaching a maximum height of 121 m above its pre-1969 base (Peterson and others, 1976). After June 2, the circulation of the lava lake became

increasingly sluggish, and the crusted and rubbly lake surface gradually subsided and became largely obscured by fumes. The summit region of Kilauea remained highly inflated during this period. The waning activity at Mauna Ulu apparently was unaffected by the July 19–22 summit eruption (Peterson and others, 1976), but the small, subsiding lava pool in Mauna Ulu disappeared below the rubble-covered crater bottom soon after. Harmonic tremor in the Mauna Ulu area also ceased after July 22, the arbitrary date taken for the end of the 1972–74 Mauna Ulu eruption.

The 1972–74 Mauna Ulu eruption produced a total volume of 162×10^6 m^3 of lava, 97 percent of which came from vents at Mauna Ulu and Alae, and 3 percent from vents in the Pauahi-Hiiaka area (table 16.2). During the period January–June 1974, the average magma eruption rate was about 4×10^6 m^3/mo, one-half that for the 1972–73 Mauna Ulu activity. This reduction in average magma eruption rate perhaps augured the eventual cessation of the eruption.

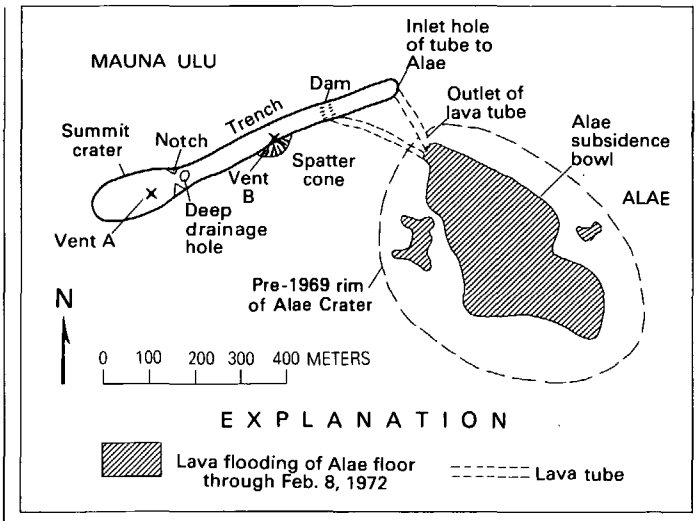

FIGURE 16.5.—Sketch map showing configuration of the summit area of Mauna Ulu shield and of Alae when the 1972–1974 eruption began in early February 1972. Summit crater, notch, trench, and lava-tube system linking Mauna Ulu and Alae had been developed by early 1971 during the 1969–71 Mauna Ulu eruption. Easternmost lava tube reopened on February 7, 1972, and fed lava onto the floor of Alae subsidence bowl, which filled to the brim by February 12.

CHRONOLOGICAL NARRATIVE

FEBRUARY 3–DECEMBER 31, 1972

REBIRTH OF MAUNA ULU LAVA LAKE

The start of the 1972–74 eruption was preceded by several months of net summit inflation and of increased seismicity from shallow sources at the summit and upper east rift. About one dozen earthquakes of magnitude 2.5 were felt by local residents between 0037 and 0200 (all times given are Hawaii standard time, H.s.t.) on January 21; these earthquakes, accompanied by shallow harmonic tremor, were centered in the caldera and Keanakakoi areas.

On the morning of February 5, 1972, a ground party discovered that lava had filled about half of the summit crater of Mauna Ulu. The reactivation of the lava lake may have occurred as early as February 2. This possible starting date is based on a telephone call from a passing motorist, who reported seeing "lava fountains on Hilina Pali" around 2130 while driving northeast from Pahala. Hilina Pali lies almost directly in line between Pahala and Mauna Ulu; thus, lava fountains or glow from Mauna Ulu might appear to issue from the pali (fig. 16.2). Though fog prevented its independent confirmation, there is little reason to doubt the February 2 eruption sighting of the motorist, a longtime resident who had witnessed many eruptions. The "bright and solid" glow witnessed by him could well have represented an early stage in refilling Mauna Ulu crater. However, seismograms for February 2 and 3 showed no unusual seismic activity or detectable harmonic tremor, which typically accompanies Kilauea eruptions.

The number of small east-rift earthquakes increased gradually about 0320 on February 4, and tremor began between 0500 and 0600. A strong storm struck the Island of Hawaii during this time, however, and the tremor recorded by several seismographs was thought at the time to be caused by high winds. The instrument at Puu Huluhulu (fig. 16.2) appeared to have been affected the most by the storm, even though some other instruments were equally exposed to the wind. In retrospect, the recorded tremor on February 4 was probably only partly due to the storm; when the storm slackened on February 5, tremor continued.

Available evidence thus indicates that lava was almost certainly flowing into Mauna Ulu crater on the morning of February 4 and possibly as early as the night of February 2. We arbitrarily use February 3 as the starting date of the 1972–74 Mauna Ulu eruption. This date is consistent with a starting time of the eruption of about 1900 on February 3, calculated by simple backward projection of the lava's rate of rise during February 5–6 (about 1.6 m/h).

REOPENING OF THE MAUNA ULU-ALAE CONNECTION

When discovered on the morning of February 5, the new lava lake had already filled about half of Mauna Ulu Crater and was slowly rising. No fountaining or surface circulation was observed. In the afternoon, the surface of the lava lake was 78 m below the crater rim, about the same elevation as the lava pool in a 30-m-diameter hole immediately east of the notch at the east end of the crater (fig. 16.5). All activity was confined to the western part of Mauna Ulu summit.

During the next two days, harmonic tremor increased, lava gradually rose, and fountaining as high as 10 m became localized at a point in the east-central part of the crater (fig. 16.5, vent A). Vent A is located in the same part of the lava lake as one of the vents active during stages 3 and 4 of the 1969–71 Mauna Ulu eruption (Swanson and others, 1979, plate 4). By 1030 on February 7, lava had risen to about 25 m below the rim of the crater and began to cascade over the notch into the pool. It flowed eastward down the

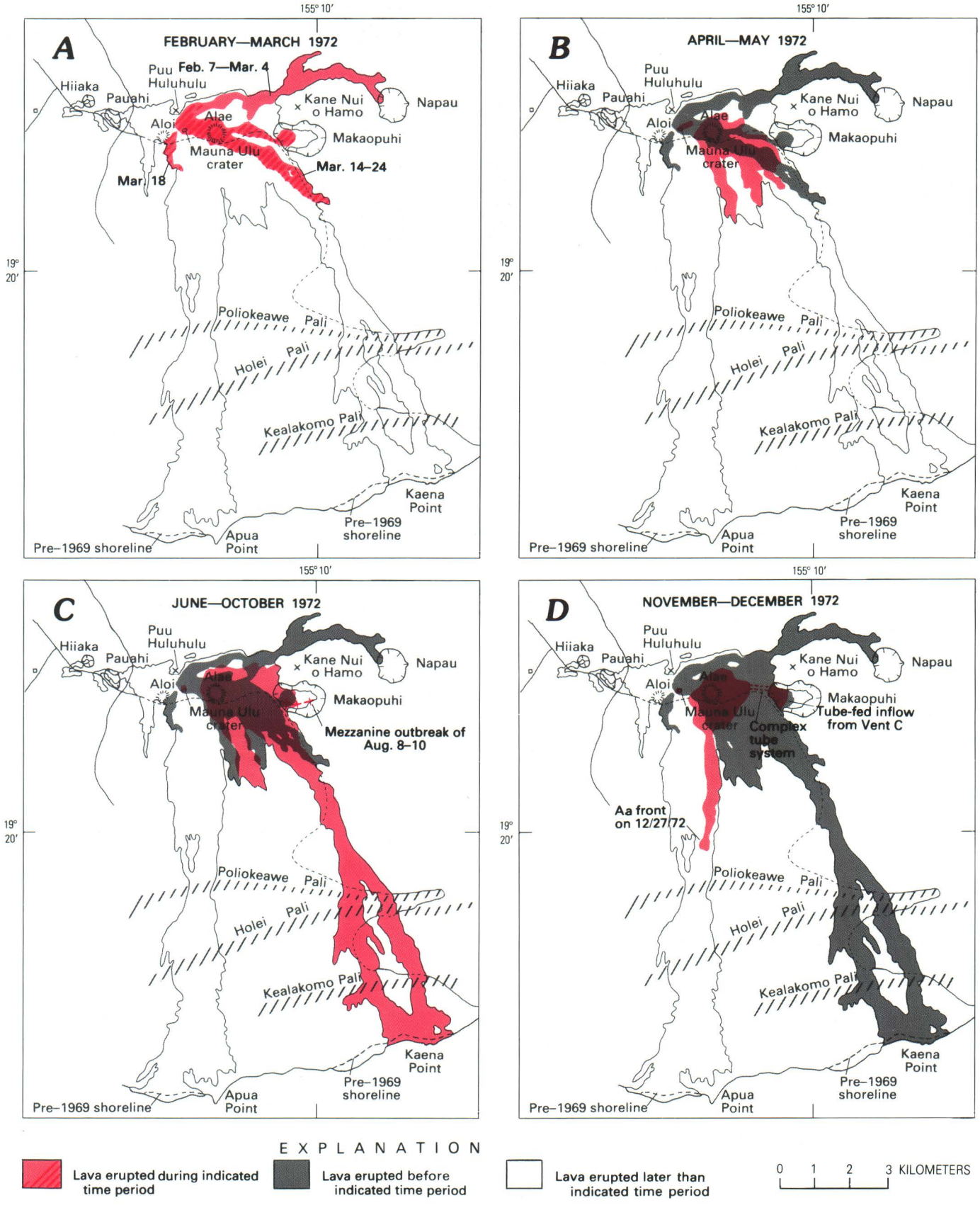
A
FEBRUARY—MARCH 1972
Feb. 7—Mar. 4
Mar. 14–24
Mar. 18
B
APRIL—MAY 1972
C
JUNE—OCTOBER 1972
Mezzanine outbreak of Aug. 8–10
D
NOVEMBER—DECEMBER 1972
Tube-fed inflow from Vent C
Complex tube system
Aa front on 12/27/72
155° 10′
19° 20′
Hiiaka
Puu Huluhulu
Pauahi
Aloi
Alae
Mauna Ulu crater
Kane Nui o Hamo
Napau
Makaopuhi
Poliokeawe Pali
Holei Pali
Kealakomo Pali
Kaena Point
Apua Point
Pre–1969 shoreline
EXPLANATION
Lava erupted during indicated time period
Lava erupted before indicated time period
Lava erupted later than indicated time period
0 1 2 3 KILOMETERS

trench, reaching the eastern end at 1200. The lave-tube system that linked Mauna Ulu and Alae during the 1969–71 eruption was still in existence, as later confirmed by thermal infra-red scanning imagery obtained during a pre-dawn flight in February 1973; lava apparently reentered this tube system and emerged at 1225 at the northwestern edge of the Alae subsidence bowl (fig. 16.5; see also Swanson and Peterson, 1972, fig. 1*B*). Activity in the lava lake continued steadily, and lava flowing in the trench developed a well-defined channel that fed directly into the Alae inlet tube(s).

LAVA-LAKE ACTIVITY AT MAUNA ULU AND ALAE AND PERIODIC OVERFLOWS

Activity on February 8 was similar to that the day before, except that rising lava now covered the notch between the summit crater and trench. Lava was overflowing a channel obstruction (the dam in fig. 16.5) that had developed about 165 m west of the end of the trench. Low fountaining continued at vent A, but a new fountain appeared near the south wall of the trench 130 m west of the dam (fig. 16.5, vent B). Vent B was to become the dominant vent for the remainder of the 1972–74 eruption.

For the next several days, activity remained much the same, with both vents A and B spurting lava fountains 10–20 m high, and a prominent spatter cone formed at vent B. Except for local variations around these two active vents, lava movement was generally eastward through the trench to the inlet for the tubes to Alae. By February 12, the Alae subsidence bowl had filled with a lava lake that remained intermittently active until early June 1973. Lava spilled over some low areas along the rim of the Alae lake but advanced only a few meters before levees developed.

During February 13–14, the vigor of vent A began to decline, while vent B produced a sustained overflow that advanced east-southeast about 1.1 km from Alae's rim toward Makaopuhi Crater (fig. 16.6*A*). Activity at vent A ceased on February 16, and the lava level at Mauna Ulu began to drop; although the fountaining at vent B temporarily increased, lava entry into Alae also ceased shortly thereafter. The surface of Alae lava lake crusted over and subsided 1–2 m, and all lava overflows stopped. For the next several days, the lava level in the summit crater continued to decline while weak fountaining persisted at vent B. By the morning of February 22, all surface activity terminated, but lava was still visible through three glowing holes at the site of vent B.

Lava reentered Mauna Ulu on February 24, and, fed by fountains 5–20 m high at vents A and B, the lake rose rapidly several tens of meters to spill over both the south and north rims of the trench. Fountains 40–75 m high at vent B were the highest observed since the eruption began. A major east-northeast-trending overflow advanced north of Kane Nui o Hamo as aa and spilled into Napau Crater on February 29 (figs. 16.6*A* and 16.7). For the next several days, numerous overflows raised the rim of the eastern part of the trench. Meanwhile, the spatter cone at vent B became the highest point on Mauna Ulu, more than 10 m higher than the rim of the summit crater (hereinafter the summit crater will be referred to simply as the crater). The episode of vigorous activity and overflows ended on March 5, when the lake surface subsided to more than 30 m below the rim of the crater (fig. 16.8). During the next several days, the lake surface continued to drop, and activity at vent B was reduced to sporadic low spurts.

Activity at vents A and B increased beginning on March 11, and on March 14 another overflow episode began. Periodic overflows, some lasting for several hours. alternated with drainbacks of 5–10 m accompanied by vigorous degassing. This cyclic activity resembled the so-called gas-piston described by Swanson and others (1979) but was larger in scale, involving the entire lake instead of a chimney-like vent. Virtually all parts of Mauna Ulu, except its extreme western end, were flooded by the overflows (fig. 16.9).

At 1800 on March 18, a new fissure vent, 200 m long, opened on the west flank of Mauna Ulu over the southeastern edge of the buried Aloi Crater (fig. 16.3). This fissure nearly coincided with that formed in April 1970 (Swanson and others, 1979, pls. 1, 3). The lava level in both the crater and trench rapidly dropped several tens of meters. Activity at the new fissure was short lived; after feeding a small flow (fig. 16.6*A*), the fountains stopped during the morning of March 19. However, accompanied by high-amplitude harmonic tremor and summit deflation, eruptive activity then shifted to the Alae area, where two new vents opened (fig. 16.11, vents C and D), each feeding fountains about 20 m high. The subsidence bowl at Alae again quickly filled; a perched lava lake soon developed by repeated overflows and levee construction, initiating the growth of a volcanic shield at Alae. During March 19–20, vents C and D fed two lava streams that advanced 2 km or more east and southeast; one of these streams poured into the deep western pit of Makaopuhi Crater (flg. 16.6*A*). Activity at the two vents then began to wane and ceased by March 24.

DOMINANT ACTIVITY SHIFTS TO ALAE: VOLCANIC SHIELD GROWTH

The opening of the vents during March 18–20 (the west-flank fissure at Mauna Ulu and vents C and D at Alae) ended the period of overflows from Mauna Ulu in 1972 (fig. 16.10): the next overflow was not to occur until early November 1973. For the remainder of 1972 and until mid-1973, generally weak activity continued intermittently at vent A within the crater, but vents C and D and various openings at or near vent B dominated the eruptive activity at Mauna

FIGURE 16.6.—Lava flows developed during 1972 in the Mauna Ulu region. Outlines of flows are approximate in this and subsequent similar figures tracing the development of lava flows during 1972–1974 Mauna Ulu eruption. Outline of the entire field, as well as the outlines of portions of lava flows not covered by younger flows, taken from geologic map of Holcomb (1976). See figure 16.3 for locations of vents. ***A***, February–March. Lava erupted during March 14–24 indicated by hachuring. ***B***, April–May. ***C***, June–October. For details about lava delta at Kaena Point, see Peterson (1976). ***D***, November–December. Except for late December flow and tube-fed inflow into western pit of Makaopuhi Crater, most flows were short-lived and accreted near vent, resulting in shield growth.

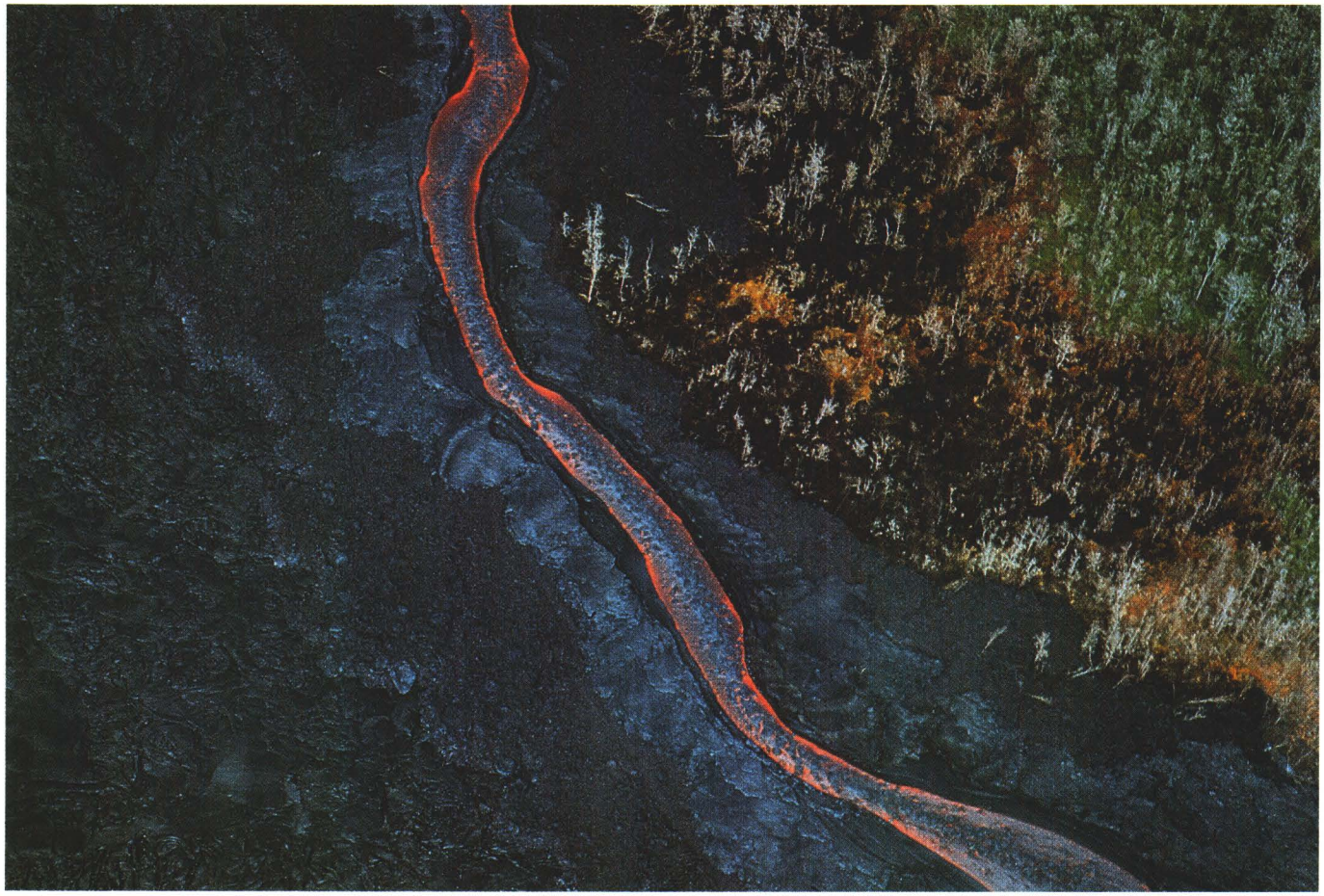

FIGURE 16.7.—View of 10-m-wide pahoehoe flow advancing through forest east of Puu Huluhulu on February 28, 1972, during overflow from Mauna Ulu (fig. 16.6*A*). Note burned vegetation adjacent to flow. Photograph taken by R.I. Tilling.

Ulu and Alae. In effect, the lava lake in Mauna Ulu's crater became mainly a passive holding tank, fluctuating in level but distinctly subordinate in activity to vents C and D, which are rootless and probably supplied from vent B through the Alae inlet tube. Whether vent B itself was a primary vent or tapped another, primary vent beneath Mauna Ulu is not known. However, we regard vent B as primary, at least for the period February 1972–April 1973 (see Tilling and others, 1973, fig. 2). All visible activity at Mauna Ulu from May 1973 on involved vents located west of vent B, and the primary vent may therefore have shifted westward at about that time.

The last week in March 1972 was marked by a lull in harmonic tremor and summit inflation; visible vent activity was restricted to weak spattering at vent A. On April 3, tremor increased and the lake in the crater rose. A new (unnamed) vent between vent B and the west end of the trench (fig. 16.3, near vent F) opened and fed a cascade of lava westward over the septum separating the trench and crater (fig. 16.11) and into the lava lake. Vent C was reactivated and began again to fill Alae lava lake. Overflows from vent D built a 20-m-high satellitic shield on the northern flank of the growing Alae shield.

For the next several months, the eruptive activity changed little. At Mauna Ulu, low fountains spouted locally from the circulating lava lake, whose level fluctuated from 20 to 30 m (generally 22–26 m) below the rim. The circulation pattern generally involved a net east-to-west movement; however, during brief episodes lasting a few minutes to half an hour, circulation reversals occurred, accompanied by turbulent disruption of the lake surface and fountaining as high as 25 m, presumably from vent A. A number of small vents and open, glowing holes in the trench, between the septum and the vent B spatter cone, intermittently ejected spatter or spawned short lava flows that covered the trench bottom. Gas-piston activity and attendant degassing were commonly observed at these vents. The lava level was generally about the same in both the crater and the trench, suggesting the existence of hydraulic connection through the septum.

The dominant vent during this period, however, was C, which quietly pumped out a virtually uninterrupted stream of lava into the

FIGURE 16.8.—Lava from the trench fed by vent B falling approximately 20 m over the septum (fig. 16.11) into the lava lake in Mauna Ulu Crater. Photograph taken by D.W. Peterson, March 5, 1972.

perched Alae lava lake, which measured about 200 m across and perhaps 5–10 m deep. Overflows from this lake fed many short lava flows, mainly to the south and southeast (fig. 16.6*B*), raised the confining levees, and accreted lava to the surroundinc areas. By May, the irregular summit area of the rapidly growing volcanic shield was more than 40 m above the mid-1971 surface of the subsidence bowl at Alae.

The generally steady and quiet output of vent C was dis-

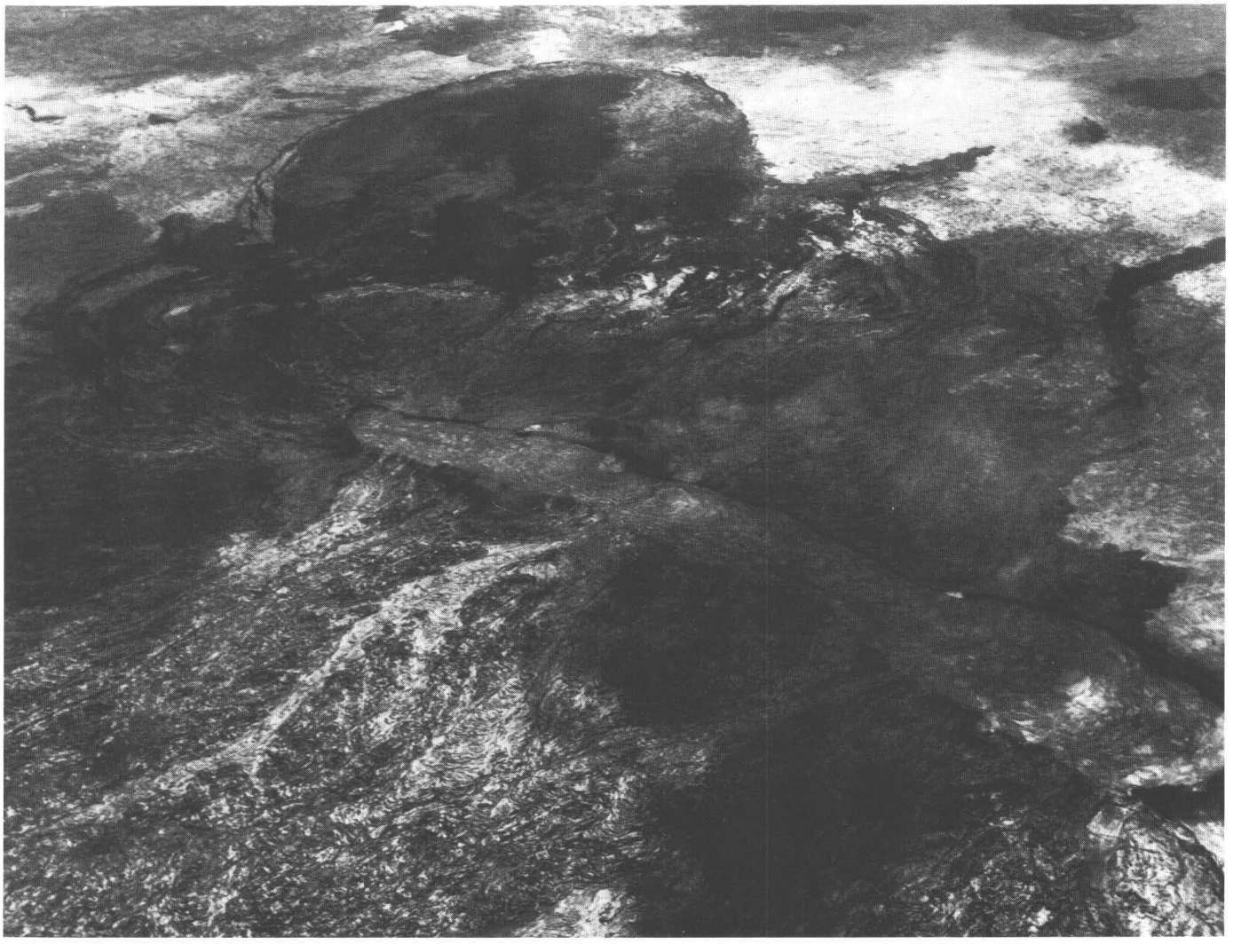

FIGURE 16.9.—Aerial view showing Mauna Ulu Crater filled with lava during March 14–24 period of overflow and shield growth. Circular structure, about 700 m across, in background is Alae subsidence bowl (fig. 16.5). Photograph taken by W.A. Duffield, March 17, 1972.

rupted, at intervals ranging from about 30 minutes to more than 2 hours, by abrupt and brief (5–30 seconds) drainbacks, causing considerable turbulence of the nearby lava-lake surface. Little or no gas was emitted during such behavior and the entire process occurred silently. Furthermore, simultaneous observations indicated that the drainback events at Alae did not correlate with gas-piston activity at Mauna Ulu.

Within Alae lava lake itself, quasi-solid but still highly mobile island-like and peninsula-like masses began to develop in late April (fig. 16.12). These islands and peninsulas eventually became fixed in position, grew, and coalesced to form a discontinuous, roughly northwest-southeast divider across the center of the lake, nearly separating it into two compartments, each of which contained lava pools (fig. 16.11). Beginning in late May, the principal inflow of lava from vent C was into the northeastern compartment; subsequent periodic overflows raised its surface about 5 m higher than that of the southwestern compartment. Spillage across the divider kept the southwestern pool active. Voluminous overflows from both compartments of the lake built the complex Alae shield to an estimated height of 80 m above the pre-1969 southeastern rim of former Alae Crater (fig. 16.13).

SUSTAINED OVERFLOWS, LAVA TUBES, AND LAVA ENTRY INTO THE SEA

Starting in June 1972, the eruption began to depart from the mode of activity characteristic of the preceding months. The level of Mauna Ulu lava lake dropped and then fluctuated between 30 and 45 m below the crater rim. Construction of the volcanic shield continued by periodic overflows around the margin of Alae lava lake, but some of the overflows were more sustained and gradually became channelized. Consequently, an integrated system of lava channels and tubes developed and carried lava great distances from

the immediate flanks of the growing shield. At times the surface of the Alae lake fell 1–10 m below the confining levees as lava drained from the lake through the tube system and emerged at the surface as far as 2 km from Alae. By June 20, surface and tube-fed lava flows from Alae again began to spill into the deep west pit of Makaopuhi Crater (fig. 16.6C).

The activity at Mauna Ulu remained essentially unchanged for the next several months. Lava entered the lake from the vent complex between vent B and the west end of the trench; surface circulation of the lava lake was predominantly from east to west; and lava fountains 5–10 m high played sporadically from various parts of the lake margin where surface lava and crust circulated downward. Meanwhile, vent C at Alae continued to feed lava through tubes into Makaopuhi's west pit. Near-vertical tubes developed around the two dominant lava cascades down the west wall of Makaopuhi and fed lava directly into the molten pool beneath the crusted floor, gradually raising it in piston-like fashion, as also happened during the filling of Alae Crater in 1969 (Swanson and others, 1972, 1979). In addition, prominent talus-and-lava cones formed against the west wall (fig. 16.14).

By early August, inflow into Makaopuhi declined, but tube-fed Pahoehoe flows accumulated in the area southeast of the Alae shield and began to advance southeastward. During August 7–13, intense rockfall activity in Makaopuhi 's west pit generated about 0.27×10^6 m^3 of rockfall debris. Many of these rockfalls were observed and photographed as they happened; correlations of field observations and seismic data suggested that this unusually energetic flurry of rockfalls was caused by eruption-induced changes in stress patterns of the crater walls (Tilling and others, 1975). The peak rockfall activity coincided with a small-volume eruption from echelon fissures on the mezzanine of Makaopuhi observed on August 9 and 10 (Tilling and others, 1975, figs. 2, 4); this eruption began between late afternoon of August 7 and early morning of August 9. Because the mezzanine vent fissures were rootless, the cause of this outbreak is problematic. It may in part be attributed to hydrofracturing induced by the weight of the lava lake and rockfall debris in the west pit exceeding the tensile strength of the mezzanine.

By mid-August, the tube-fed southeastward-flowing lava from Alae had advanced over Poliokeawe Pali and Holei Pali, buried a segment of Chain of Craters Road not covered during the 1969–71 activity, and covered flows of 1970–71 and older ages along the coastal flat. On August 23, lava reached the ocean at Kaena Point, about 1.5 km east of the lava delta of March–May 1971 (fig. 16.6C), marking the fourth time that lava had entered the sea along the south coast of Hawaii since June of 1969. The processes of lava entry into the sea and formation of lava deltas were essentially identical to those described earlier for the 1969–71 eruption of Mauna Ulu (Moore and others, 1973) and have been summarized by Peterson (1976). Substantial stretches of new black-sand beaches formed along the new shoreline when molten lava shattered upon quenching by seawater and was comminuted in the surf zone. SCUBA-diving scientists observed pillow formation and the submarine movement of lava (Grigg, 1973; Moore, 1975; Tepley, 1975).

Similar activity continued at Mauna Ulu and Alae throughout September and until mid-October. The lake level at Mauna Ulu varied between 33 and 50 m below the crater rim; the lake at Alae occasionally dropped to about 20 m below the crater rim and, at other times, briefly overflowed its levees to add to the bulk and height of the Alae shield. The volume rate of inflow of tube-fed lava into Makaopuhi Crater slackened. Temperature, flow velocity, and dimensions of lava channels were measured or estimated through openings or skylights formed by local collapse of the roof in the upstream parts of the principal tube systems (figs. 16.15, 16.16). Optical pyrometer and thermocouple measurements indicated minimum temperatures ranging between 1,130 and 1,165 °C. Average flow rates were 1.5–3.0 m/s; at times of low stands of Alae lake (for example. on October 17), flow rates in the tube systems decreased to about 0.2–0.5 m/s.

Lava flowage to the sea from Alae lake through the well developed southeast-trending tube system continued until mid-October, when lava from vent C was diverted to the east and northeast, away from the tube system. By November 8, the diverted lava had accumulated to form a well-defined lava pond, in effect a much smaller version of the Alae lake. This northeast pond periodically overflowed to construct a satellitic shield on the northeastern flank of the larger and complex Alae shield.

The diversion of vent C lava to the northeast diminished the rate of lava supply to Alae lake and to the tube system between Alae and the sea. Consequently, lava entry into the sea ceased completely by about October 20, after having formed a lava delta about 8.6×10^6 m^3 in volume and 0.18 km^2 in area (Peterson, 1976, table 1).

By early November the main lava tube draining Alae had become choked off at a point near the southeastern rim. Lava from Alae spilled into Makaopuhi again briefly in late October and more voluminously in mid-November (fig. 16.6*D*). The west pit of Makaopuhi was then virtually full of lava, the irregular surface of which sloped gently eastward from the west wall and averaged 2–3 m below the floor of the eastern mezzanine (fig. 16.17*A*).

ADDITIONAL GROWTH OF ALAE SHIELD

Activity at Mauna Ulu and Alae varied little for the remainder of 1972; the Mauna Ulu lake level fluctuated between 28 and 36 m below the crater rim, but was most commonly at about 31 m. Steady outpouring of lava from vent C through surface channels or short tubes fed numerous flows, which built the complex Alae shield higher and wider. The areas of major growth included Alae summit (around vent C) and three secondary vent areas on the southern flank of the complex shield. Accretions around these secondary vents, presumably the outlets of tubes within the shield, rose as much as 10 m above the sloping flanks of the main shield. Overflows also flooded the crusted surfaces of both compartments of the Alae lava lake, obliterating their former distinct edges.

The growth of the Alae shield was the dominant and most conspicuous activity in November–December 1972, but significant overflows to the south built a new system of lava channels and tubes,

FIGURE 16.10.—Profile of Mauna Ulu volcanic shield as seen from Alae, following February–March 1972 overflows; prominent knob is the 10-m-high

which gradually became well integrated. Toward the end of December, lava was being transported progressively greater distances from vent C through an increasingly efficient channel-tube system; as a result, shield-building processes became sporadic and subordinate. By December 27, a partly roofed, south-trending channel fed a flow that advanced to within 1 km of the edge of Poliokeawe Pali (fig. 16.6*D*). The continuing lava-lake activity at Mauna Ulu was not affected by the change of Alae's main activity from shield building to lava-tube development. In the months to come, shield building would be only an intermittent and minor eruptive process at Alae.

JANUARY 1–MAY 4, 1973

RENEWED OVERFLOWS, LAVA-TUBE FORMATION, AND LAVA ENTRY INTO SEA

Eruptive activity during January–April 1973 was dominated by continued voluminous lava output from vents at Alae, development of well-integrated lava-tube systems, and renewed entry of lava into the sea. Mauna Ulu's behavior during this interval remained basically the same as that during much of 1972; the lava-lake level was fairly steady, mostly fluctuating between 30 and 35 m below the crater rim (total range 24–41 m). Whereas during 1972 the surface movement of the lake was most commonly from east to west, in 1973 no net circulation direction prevailed.

Vent C remained the principal source of lava output at Alae during January–April 1973, and secondary nearby sources were intermittently active. Gas-piston activity became notable at vent C: a cycle consisted of the slow, quiet rise of the lava column for 15 minutes to one hour, followed by vigorous degassing and an abrupt drop of 5–20 m in the level of the column. As degassing ended, the quiet rise of lava resumed and the cycle repeated.

Associated with the steady activity at Alae during January–February, two major tube systems developed, one a south-trending system that began in December 1972 and the other a rejuvenated east-northeast-trending system toward Makaopuhi (fig. 16.18*A*). Tube-fed lava from the south-trending system spilled over Poliokeawe Pali and Holei Pali by January 12 and began to pond at the base of Holei Pali. Extension of the east-northeast-trending system resulted in renewed filling of Makaopuhi beginning on January 24. By mid-February the west pit of Makaopuhi was filled to the mezzanine level, and soon thereafter pahoehoe lava covered more than half of the mezzanine floor (fig. 16.17*B*).

Pahoehoe flows fed by the south-trending tube system continued to spread slowly over the coastal flat and on February 24 reached the ocean about 1 km west of Apua Point (fig. 16.18*A*), marking the fifth consecutive year that lava from Mauna Ulu eruptions had entered the sea. By March 20, the subaerial part of the lava delta at Apua Point had grown to about 0.18 km^2. Lava entered the sea at Apua Point throughout March and April, and the lava delta attained an area of about 0.29 km^2 and a volume of 13.0×10^6 m^3 (Peterson, 1976, table 1). As in 1972, SCUBA-diving scientists were again able to observe lava movement and pillow formation beneath the sea surface.

While inflow into Makaopuhi dwindled and finally stopped in early March, numerous overflows issued from two lava-tube skylights about 100–120 m east-northeast of vent C. These overflows and several from vent C itself resulted in a brief period of shield building at Alae summit, but the rate of flow in the south-trending system showed no decrease.

spatter cone of vent B. This profile changed little through late 1973. Composite of photographs taken by R.T. Holcomb, February 6, 1973.

Activity at Mauna Ulu and Alae through April varied little from that of earlier 1973. At times during this period, Mauna Ulu and Alae lava lakes varied roughly in concert (fig. 16.19). In mid-March, part of the east wall of Mauna Ulu crater collapsed and the lava lake lengthened eastward by about 20 m into the area of the trough. However, within about a week, the collapsed part of the wall was rebuilt and the lake perimeter retreated to near its former position. Beginning in early April, the western part of the Mauna Ulu trench subsided, and lava from vent B reached the lake in the western crater by periodic surface flows across part or all of the trench floor, rather than by flow beneath it.

EFFECT OF THE APRIL 26, 1973, HONOMU EARTHQUAKE

At 1026 on April 26, an earthquake of magnitude 6.2 shook the Island of Hawaii. The hypocenter was 48 km beneath Honomu (fig. 16.1, inset) on the northeast coast of Hawaii (Unger and others, 1973; Unger and Ward, 1979). Observations from the air and on the ground showed no appreciable immediate effect of this earthquake on the eruptive activity at Mauna Ulu and Alae, but the south-trending lava-tube system feeding the flows entering the ocean near Apua Point apparently was severely disrupted by subsurface collapse-induced obstructions that impeded and ultimately halted lava transport.

The rate of lava entering the sea showed a temporary increase immediately after the earthquake but then declined rapidly. By May 1, lava entry into the sea had ceased. Blockage of the tubes above Poliokeawe Pali caused several copious overflows from upstream skylights, which in turn fed spectacular cascades down the face of

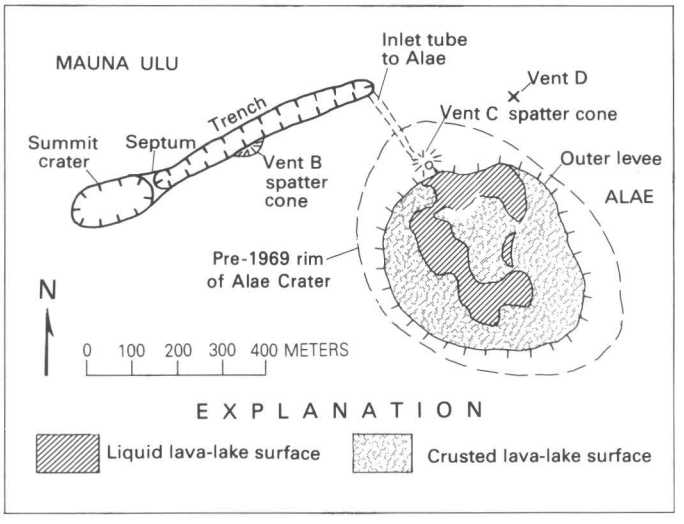

FIGURE 16.11.—Sketch map showing two compartments in lava lake at Alae and location of vents C and D. Vent C was fed through lava tubes from Mauna Ulu trench and in turn supplied vent D through surface channels and tubes. Configuration of Alae lava-lake surface varied daily, but the distinction of southwest and northeast compartments persisted for many weeks. See also Holcomb and others (1974, figs. 5-12, 5-13).

FIGURE 16.12.—View to west showing island-like masses of semisolid lava developed in Alae lava lake, which was fed by lava issuing from opening at base of fuming vent C spatter cone (center). Mauna Ulu shield, with its prominent vent B spatter cone, and Puu Huluhulu are seen in upper left. Photograph taken by D.W. Peterson, April 23, 1972.

Poliokeawe Pali and Holei Pali a few hundred meters east of the blocked tube system. These cascades continued until May 5. Tube blockage may also have caused the overflows and 5-m-high fountains on May 1 from vent C and several secondary vents on the southwest and south rim of the crusted Alae lake. By May 3, the activity at the secondary vents had nearly ended, and the lava column in vent C dropped to about 7 m below the ground surface.

We assume but cannot prove that this rather abrupt cessation in

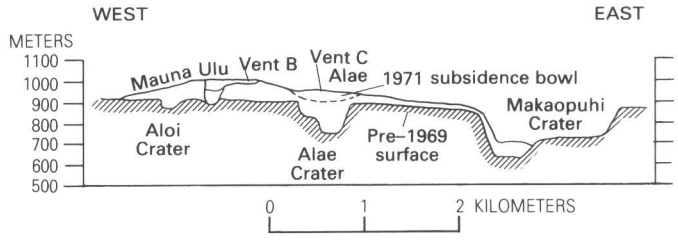

FIGURE 16.13.—Schematic cross section showing Mauna Ulu and Alae volcanic shields in late May 1972; line of section is approximately east-west but is bent at several points so as to traverse summits of Mauna Ulu and Alae, as well as Makaopuhi Crater and buried Aloi Crater. Vertical exaggeration is 2.5. Modified from Tilling and others (1973, fig. 2).

early May of the virtually continuous activity that had prevailed through April 1973 resulted from blockages in the magma conduits caused by the Honomu earthquake. A 7.2-magnitude earthquake in November 1975 (Tilling, 1976b; Tilling and others, 1976a) caused major changes in Kilauea's magma regime (Dzurisin and others, 1984). Yet, the 6.7-magnitude Kaoiki earthquake in November 1983 apparently produced no observable effects on the Puo Oo eruption (Wolfe and others, chapter 17; E.W. Wolfe, written commun., 1985). Though the coincidence in timing between cessation of activity and the Honomu earthquake may be fortuitous, we favor the working hypothesis that the disruption in magma-transfer regime perhaps was induced by the earthquake.

FIGURE 16.14.—Streams of tube-fed lava cascading down the western wall (200 m high) of Makaopuhi Crater, forming lava-and-talus cones. Photograph taken by W.A. Duffield on June 30, 1972; see Holcomb and others (1974, p. 51 and figs. 5-25, 5-26) for additional information.

FIGURE 16.15.—Geologist probing the depth of a lava stream with stainless steel pipe inserted through lava-tube skylight. Photograph taken by R.I. Tilling in January 1973.

PAUAHI-HIIAKA ERUPTION OF MAY 5, 1973

ACTIVITY WITHIN PAUAHI CRATER

At 0703 on May 5, an intense flurry of small shallow earthquakes began in the vicinity of Mauna Ulu and Alae. Subsequent smaller earthquakes were soon masked on seismograms by increasing harmonic tremor, accompanied by rapid deflation of the summit of Kilauea. Observations at 0915 showed that Mauna Ulu lava lake, whose level was 39 m below the crater rim only two days before, had completely drained to leave a very deep, rubble-choked crater, whose walls were crumbling amid thick dust clouds. The crater formerly containing the lava lake was now composed of two parts, a western pit about 180 m deep and an eastern pit about 200 m deep, both of which were entirely devoid of molten lava (figs. 16.20, 16.22*A*). The western pit approximately coincided with the general area of vent A. The empty crater extended eastward into the trench of Mauna Ulu as far as the area of the vent B spatter-and-pumice cone (fig. 16.20). Observations at 0945 showed that molten lava within the Alae volcanic edifice also had drained completely, as expressed by the collapse of the area of vent C to form a rubble-filled crater about 60 m by 100 m across and 30 m deep.

A magnitude-3 earthquake occurred at 0932 near Puu Huluhulu and was followed during the next hour by several comparable and larger shocks, some of which were felt as far away as Hilo. These earthquakes prompted inspection of the Chain of Craters Road area and a recommendation to officials of Hawaii Volcanoes National Park that the road be closed to traffic. An observer arrived at Pauahi Crater (fig. 16.18*B*) at 1020, just in time to watch the last of a series of large rockfalls from the north crater wall. At 1023 he heard a sharp loud sound and saw a dense fume cloud beginning to issue from a new opening near the deepest part of the western pit of the composite crater. At 1025 lava spurted from that opening, marking the first historical eruption in Pauahi. Within a few minutes, lava emerged from several additional openings aligned across the northern side of Pauahi, and by 1050 lava was fountaining along a 120-m-long fissure trending about N. 85° E.(figs. 16.3, 16.18*B*). At 1120 the lava fountains at the first and third vents to open on the crater floor reached their maximum height of about 20 m. Fountaining then declined rapidly along the length of the fissure, except at the two sites of maximum fountaining; drainback into the stagnant segments of the vent fissure immediately followed.

The decline of the lava fountains and increase in rate of drainback were rapid. By 1125, the remaining fountains were feeble, the level of the lava pond had dropped 17 m, and a new vent had broken out at a site a few tens of meters east-southeast of the original fissure and about 40 m above the level of the lava pond (fig. 16.18*B*). This new vent increased in vigor as the original fountains died about 1140. By then lava was draining at the two former vents on the original fissure much more rapidly than the new vent was supplying lava to the pond. Activity at the new vent soon began to weaken, and it ceased at about 1200. The lava surface in the crater had dropped to 20 m below its highest level by the time active drainback ended about 30 minutes later, leaving a pond of lava 20 m deep in the lowest part of the crater.

The total volume of lava erupted into Pauahi Crater during this first stage of the eruption was about 0.14×10^6 m^3, of which 0.12×10^6 m^3 drained back down the fissure. A few small bubbling vents were later observed to have remained intermittently active until early morning of May 6, but these contributed negligible additional volume to the lava fill within the crater.

ERUPTION SHIFTS TO HIIAKA CRATER AND NEARBY FISSURES

Earthquake activity and harmonic tremor remained high after the eruption within Pauahi. At 1255 on May 5, fountaining broke out along a set of fissures extending N. 70° E. from just east of the Chain of Craters Road to within the southeastern part of Hiiaka Crater (figs. 16.3, 16.18*B*). The highest fountains played along the fissure within the crater, reaching heights of nearly 50 m at times. Smaller fountains erupted from the fissures outside the crater and fed a spectacular cascade of lava down Hiiaka's southwestern wall. At

FIGURE 16.16.—Branch floating on lava stream bursts into flame as it encounters oxygen in the atmosphere at skylight (opening about 3 m wide) of principal lava tube leading from Alae. Passage of such branches is timed at successive downstream skylights by observers with stop watches who communicate by radio. Average rates of lava movement so determined are minimum rates, because the length of the meandering lava stream is greater than the length obtained by summing the linear distances measured between skylights and because cascades, pools, and eddies along the lava stream slow a branch's progress. Except at skylights, little oxygen is available in the lava tubes, so a branch can be carried hundreds of meters before being totally consumed. This method was used to estimate average flow velocities throughout the tube-fed stages of the 1969–71 and 1972–74 Mauna Ulu eruptions (Peterson and Swanson, 1974; this paper). Photograph taken by R.I. Tilling, September 19, 1972.

1307 lava broke out from a new fissure southwest of the Chain of Craters Road and initially ponded around the erupting vents and against one of the Koae fault scarps about 200 m farther south. The lava crossed the Chain of Craters Road at 1325 and added to the cascade down the crater wall, while fountaining continued at full force within Hiiaka.

The fissure southwest of the Chain of Craters Road, the latest near Hiiaka to open, was the first to die. Its decline was apparent by about 1500, and activity ended at about 1535. By that time, the fissures northeast of the road were erupting very gassy spatter in fountains no more than 3 or 4 m high, and the height of the lava fountains in Hiiaka had decreased as well. By 1700 the last (easternmost) vent in Hiiaka was virtually dead, spattering only feebly at long intervals, and slow drainback was underway (fig. 16.21).

At 1645, a dense fume cloud rose from a fissure 120 m west of the Hilina Pali Road (fig. 16.18*B*), 1 km southwest of its intersection with the Chain of Craters Road. Aerial observations around 1700 showed a continuous line of spattering only a few meters high along a fissure about 180 m long. A small flow was puddled around the eruptive fissure. By 1740, when this fissure was observed from the ground, it no longer was erupting lava but instead was degassing with a deafening roar and visible pale flames. The degassing gradually declined over a few hours, but the fissure fumed profusely through the next two days. This outbreak was only the second to occur within the Koae fault system in historical time, the first having been on May 24, 1969, and was much farther within the Koae system than the 1969 fissures (Koyanagi and others, 1973; Duffield, 1975; Swanson and others, 1979).

The maximum volume of the new fill in Hiiaka Crater from this

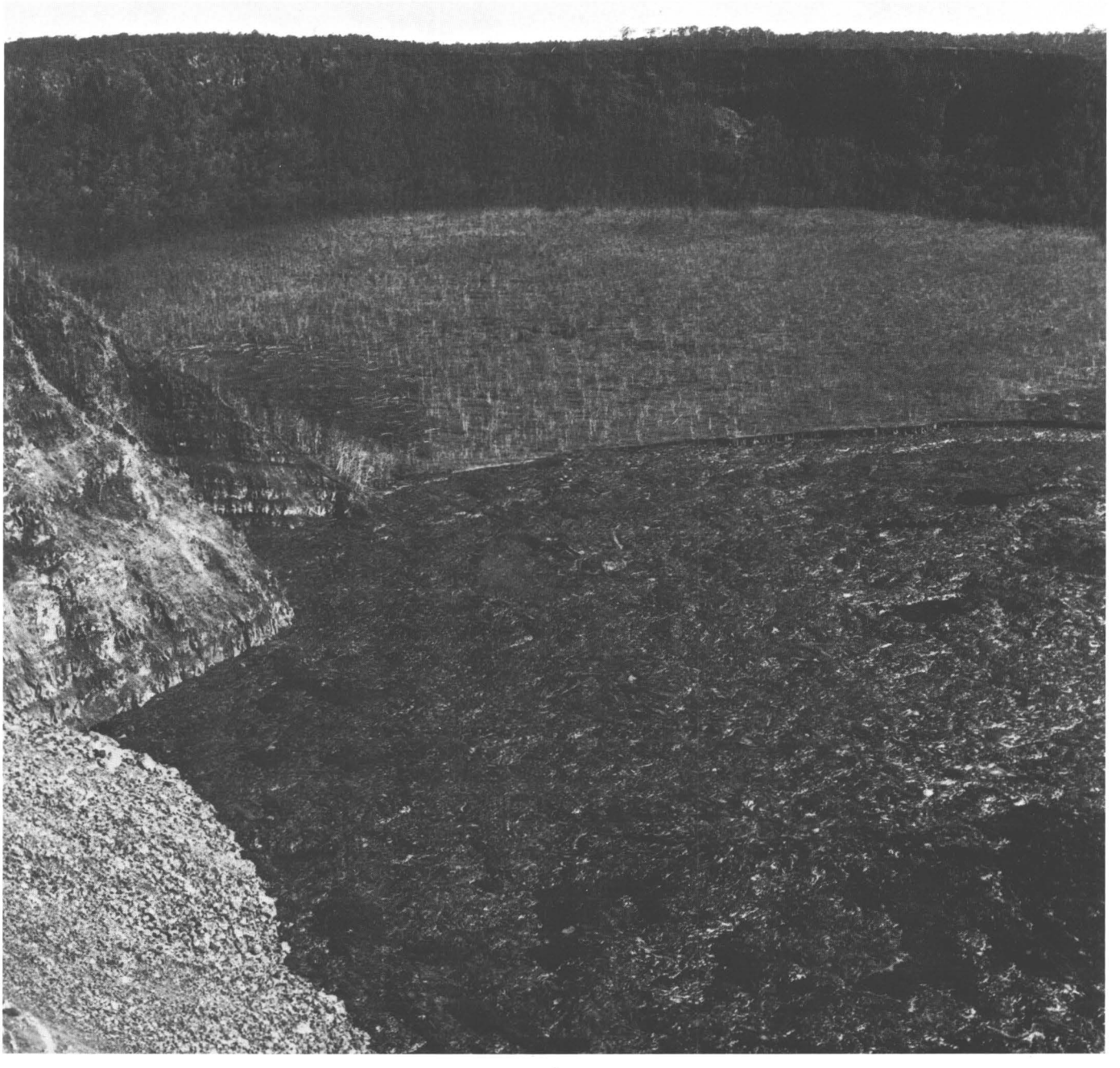

A

FIGURE 16.17.—Views of Makaopuhi Crater in early 1973. ***A,*** View on January 26, 1973, from the southwestern rim showing the west pit filled by tube-fed lava from vent C to within a few meters of the mezzanine surface. Part of 1965 lava on mezzanine (Wright and others, 1968) can still be seen (center left). Photograph taken by D.W. Peterson. ***B,*** View from nearly the same point on February 5, 1973, showing the mezzanine surface (center) more than half covered by new flow. Vegetation on mezzanine was killed earlier by fire set by the outbreak in August 1972. Photograph taken by R.T. Holcomb.

second stage of the eruption was 0.56×10^6 m^3, of which 0.12×10^6 m^3 drained back. In addition, flows covered about 0.37 km^2 of ground outside the crater, probably accounting for an additional volume of at least 0.5×10^6 m^3. Together with the 0.14×10^6 m^3 at Pauahi, these amounts make the total volume of lava erupted during the 7-hour eruption 1.2×10^6 m^3, of which 0.2×10^6 m^3 drained back into the vent fissures, resulting in a net volume remaining on the surface of about 1×10^6 m^3 (table 16.2).

MAY 6–NOVEMBER 9, 1973

The combination of the April 26 magnitude-6.2 Honomu earthquake and the May 5 Pauahi-Hiiaka eruption caused only a temporary disruption of the eruptive activity at Mauna Ulu.

B

FIGURE 16.17.—Continued.

However, these events may have been sufficient to weaken, and soon sever, the magma connection between Mauna Ulu and Alae that had operated so efficiently since February 1972.

RETURN OF LAVA TO MAUNA ULU AND ALAE

Mauna Ulu's 200-m-deep crater, emptied several hours before the Pauahi-Hiiaka eruption of May 5, was highly unstable now that its walls were no longer buttressed bv the lava lake. Rockfall dust cleared sufficiently to allow the crater floor to be seen and its level measured on the morning of May 6 (fig. 16.20), but large rockfalls continued to spall from its walls for many days, generating dust clouds that rose as high as 500 m above the crater rim (see, for example, Tilling and others, 1975, fig. 9).

Harmonic tremor as recorded on the Puu Huluhulu seismograph was at a very low level from the morning of May 6 until about 1900 on the evening of May 7, when it increased noticeably. On the morning of May 8, two small pools of lava were observed in

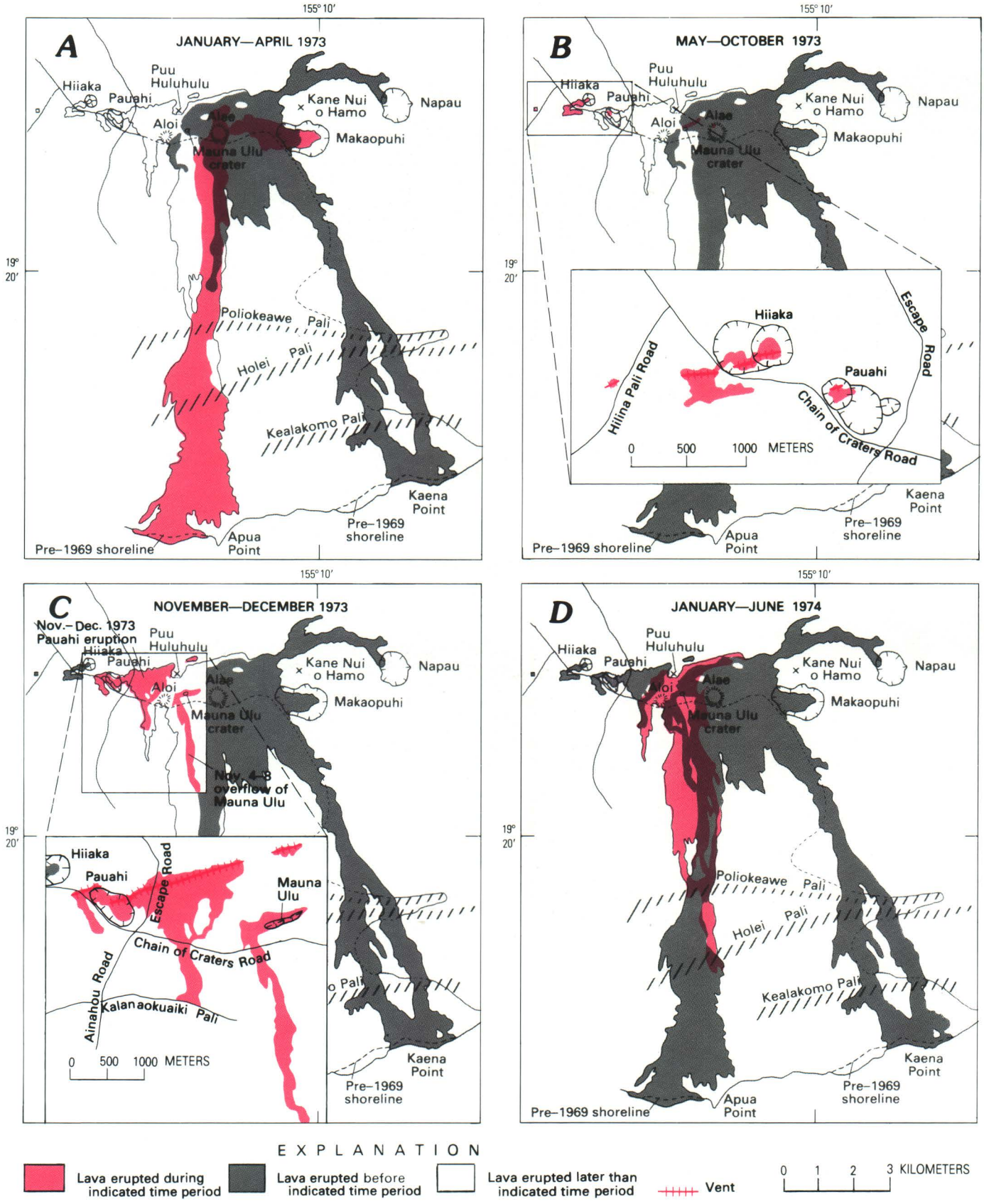
A
JANUARY—APRIL 1973
B
MAY—OCTOBER 1973
C
NOVEMBER—DECEMBER 1973
Nov.–Dec. 1973 Pauahi eruption
Nov. 4–8 overflow of Mauna Ulu
D
JANUARY—JUNE 1974
155° 10′
19° 20′
Hiiaka
Pauahi
Puu Huluhulu
Aloi
Alae
Mauna Ulu crater
Kane Nui o Hamo
Napau
Makaopuhi
Poliokeawe Pali
Holei Pali
Kealakomo Pali
Kaena Point
Apua Point
Pre–1969 shoreline
Escape Road
Chain of Craters Road
Hilina Pali Road
Ainahou Road
Kalanaokuaiki Pali
0 500 1000 METERS
EXPLANATION
Lava erupted during indicated time period
Lava erupted before indicated time period
Lava erupted later than indicated time period
Vent
0 1 2 3 KILOMETERS

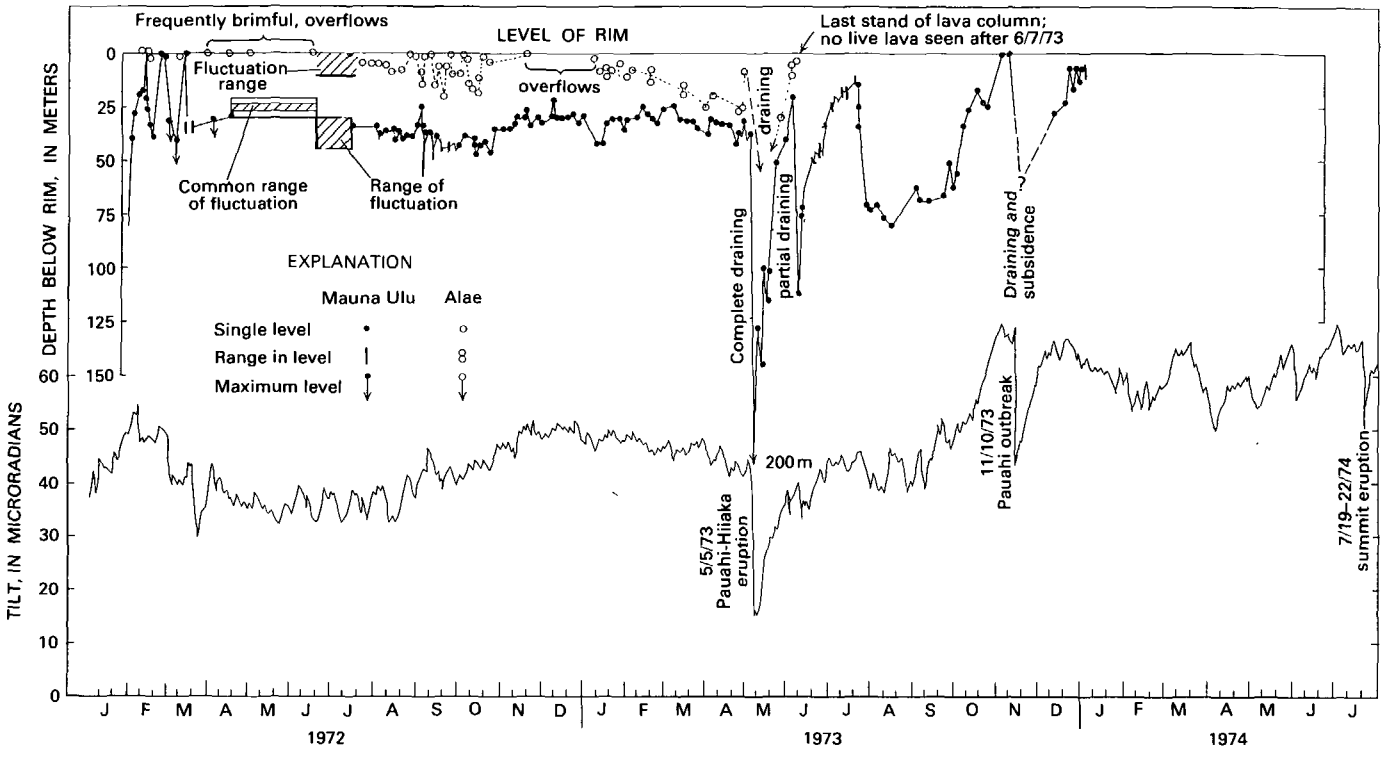

FIGURE 16.19.—Fluctuations in the depth from crater rim to the surface of lava lakes at Mauna Ulu and Alae compared with variations in the east-west component of summit tilt measured at Uwekahuna. Data plotted are from Tilling and others (1986) and figure 16.4; tilt record has been adjusted to remove the 18-microradian offset caused by the April 26, 1973 Honomu earthquake (see also figs. 16.4, 16.37).

the two deep pits of the crater; presumably lava had returned quietly during the night. Each pool rose rapidly, particularly that in the eastern deep pit. By May 15, the lava level in the eastern pit had reached as high as 97 m below the crater rim, but the level for both pits then fluctuated between 100–120 m below the rim during the next several days (fig. 16.22*B*). Then the level again rose rapidly and by May 25 the two pools had coalesced and the surface was 50 m below the crater rim. The level had risen another 10 m by May 30, and a small island of semisolid lava protruded above the surface of the lake (fig. 16.22C). This island, though changing somewhat in size and position and occasionally disappearing, persisted during much of the subsequent lava-lake activity (figs. 16.22 *D–F*). Prior to the 1972–74 Mauna Ulu eruption, the development and movement of such semisolid masses in liquid lava had only been observed at Halemaumau Crater within Kilauea's summit caldera (see, for example, Jaggar, 1920, 1947).

The lake continued to rise and on June 5 reached a level only 18 m below the rim, the highest stand since the overflows of February–March 1972, before subsiding to a depth of 23 m by June 7. Although the recovery of the lava lake was rapid, the sluggish lava circulation that prevailed throughout this time suggests that the effective viscosity of the lake lava was greater than before the May 5 draining.

On May 30, when the lava reached the 40-m level in Mauna Ulu, fresh lava was observed about 34 m below the crater rim in vent C of Alae. As the lava rose at Mauna Ulu, the level correspondingly rose at Alae, confirming the general sympathetic variation in the levels of the two lakes noted earlier (fig. 16.19). On June 5, when Mauna Ulu was at its highest level, the 100-m-diameter crater of Alae was filled to within 5 m of the rim by an active, bubbling lava lake. On June 7 the level at Alae subsided to 12 m, simultaneously with the drop at Mauna Ulu, and the lake surface became entirely crusted over.

FIGURE 16.18.—Lava flows developed during 1973 and 1974 in the Mauna Ulu region. ***A***, January–April, 1973. ***B***, May–October, 1973. Flows and vents of the May 5 Pauahi-Hiiaka eruption are shown in greater detail in the inset. No molten lava was seen at Alae after the June 9 draining of Mauna Ulu lava lake. ***C***, November–December, 1973. Major overflow from Mauna Ulu during November 4–8 and flows and vents of the November 10–11 outbreak at and near Pauahi are shown in greater detail in the inset. The flow field of Pauahi eruption was formed in less than 9 hours of activity, but weak activity associated with the vent and perched lava pond within the west pit of Pauahi persisted through December 9 (see fig. 16.29). ***D***, January–June 1974. All flows were produced in eleven relatively short-lived (no longer than 2 days) eruptive episodes: five in January–February, two in March, three in April, and one in May–June (see text). The only flow that advanced beyond Holei Pali in 1974 formed during the most voluminous eruptive episode (May 31–June 2).

FIGURE 16.20.—Aerial view looking east on May 6, 1973, showing dust-choked Mauna Ulu Crater and western half of trench (to vent B spatter cone, indicated by arrow), which collapsed during draining of lava lake on May 5 (see text). Contrast between February–March 1972 overflows (dark) and 1969–71 lava (light) is obvious in this photograph. Trail to left of crater leads to viewing platform established by the National Park Service for visitors to Hawaii Volcanoes National Park. Photograph taken by R.T. Holcomb.

JUNE 9 DRAINING OF LAVA LAKES: DEMISE OF ALAE VENT

At 2346 on June 8, strong harmonic tremor began abruptly, accompanied by rapid summit deflation and earthquakes in the eastern part of the Koae fault system. This activity ended equally abruptly at 0350 on June 9, by which time the summit had deflated by 8 microradians (fig. 16.4). When observers reached Mauna Ulu summit after daybreak, they discovered that the lava lake had fallen to about 112 m below the crater rim—a drop of 94 m from its stand

FIGURE 16.21.—Hiiaka Crater after the eruption of May 5, 1973, showing flat, crusted lava pond ringed by a lava-subsidence terrace (Holcomb, 1973), the top of which (about 6 m above pond surface) marks highest stand of lava lake during the eruption. Photograph taken by R.T. Holcomb, May 6, 1973.

just four days earlier (fig. 16.19). The large drop again triggered a rash of rockfalls from the unstable crater walls. The crusted lake at Alae also had dropped, and no molten lava could be seen anywhere on the rubble-covered floor of vent C, which was about 20 m below the crater rim. In effect, the events of June 8–9 were a smaller scale repetition of the May 5 draining of the lava lakes, but accompanied this time by intrusion into the upper east rift zone and the eastern part of the Koae fault system (Dzurisin and others, 1984, table 1) without a surface outbreak.

The lava lake at Alae never recovered from the June 9 draining, and all vent activity ceased there for the remainder of the eruption. However, the lava lake at Mauna Ulu immediately began

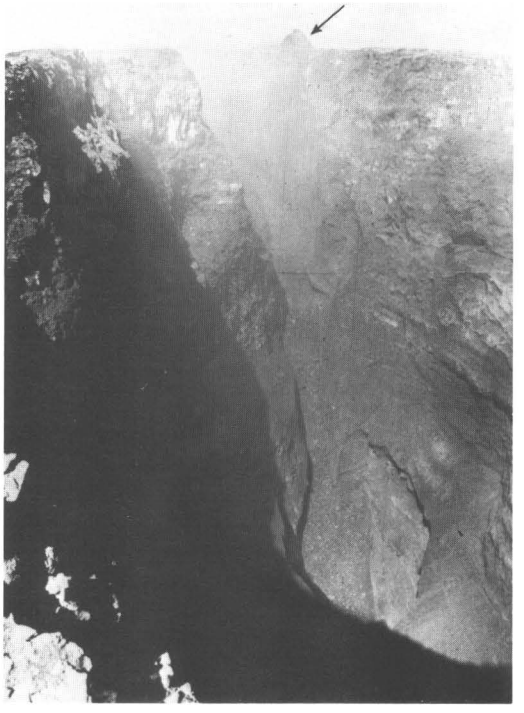

A

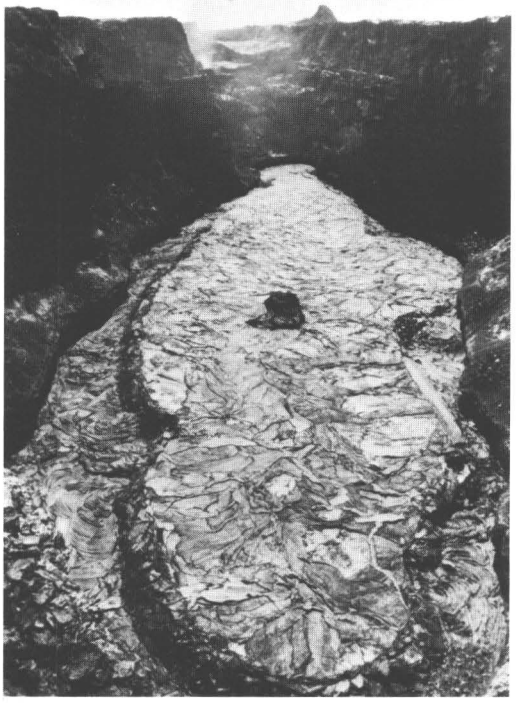

C

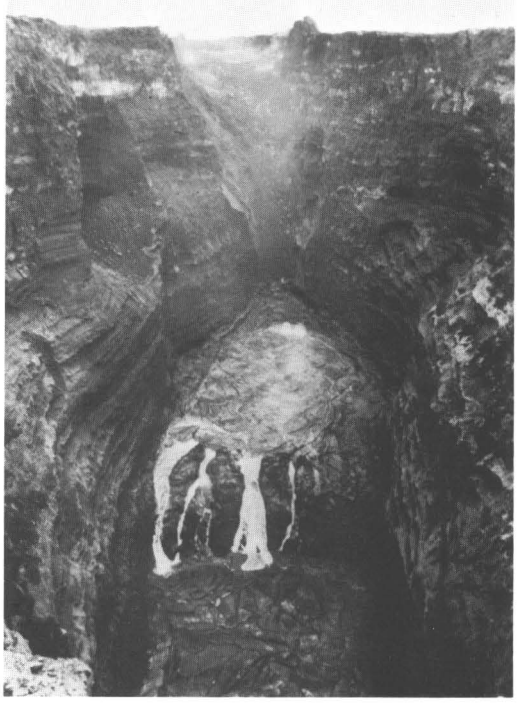

B

D

FIGURE 16.22.—Filling and draining of Mauna Ulu Crater during the period May–November 1973; all views are eastward from the western end of the crater. ***A***, Summit crater one day after the lava lake drained; crater is approximately 100 m wide and 200 m deep. Vent B spatter cone (arrow) serves as reference landmark in later views. Photograph taken by R.I. Tilling, May 6, 1973. ***B***, Renewed eruption has begun to fill the crater. Lava is shown here flowing over the levee of the lava lake in the eastern part of the crater and into deeper western part. Photograph taken by R.I. Tilling,. May 18, 1973. ***C***, Filling of the crater resumed following draining of the lava lake on June 9. Here levees confine an active lava lake that frequently overflowed into the surrounding moat. A semisolid island in center of lake, which first formed in late May and then briefly foundered following the June 9 draining, reappeared as the lake rose. Photograph taken by R.I. Tilling, June 15, 1973. ***D***, The island has grown larger, and the surface of active lake has decreased also as levees grew inward from the crater walls. Dominant flow direction of lake

E

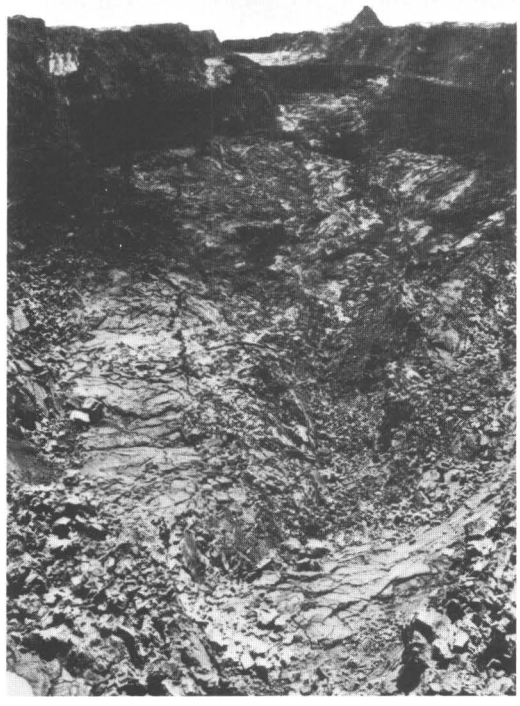

G

F

H

surface toward camera. Photograph taken by D.W. Peterson, June 21, 1973. ***E***, As lake level rose, the surface area of active lake continued to decrease. The former island has grown to become a peninsula that nearly divides the lake into two ponds. Photograph taken by R.I. Tilling, June 24, 1973. ***F***, Rise in lake surface has flooded the levees with new lava. Photograph taken by R.I. Tilling, June 28, 1973. ***G***, Gradual draining of lava during July resulted in collapse of perched lake and surrounding crust, beginning a two-month repose at Mauna Ulu (see text). Photograph taken by R.I. Tilling, July 25, 1973. ***H***, Rapid filling of the crater during October and early November produced a lava lake without levees, and the lake surface reached the lowest point on Mauna Ulu's western rim. Fountain in background fed lake and built spatter cone (fig. 16.23). Photograph taken by R.I. Tilling, November 4, 1973.

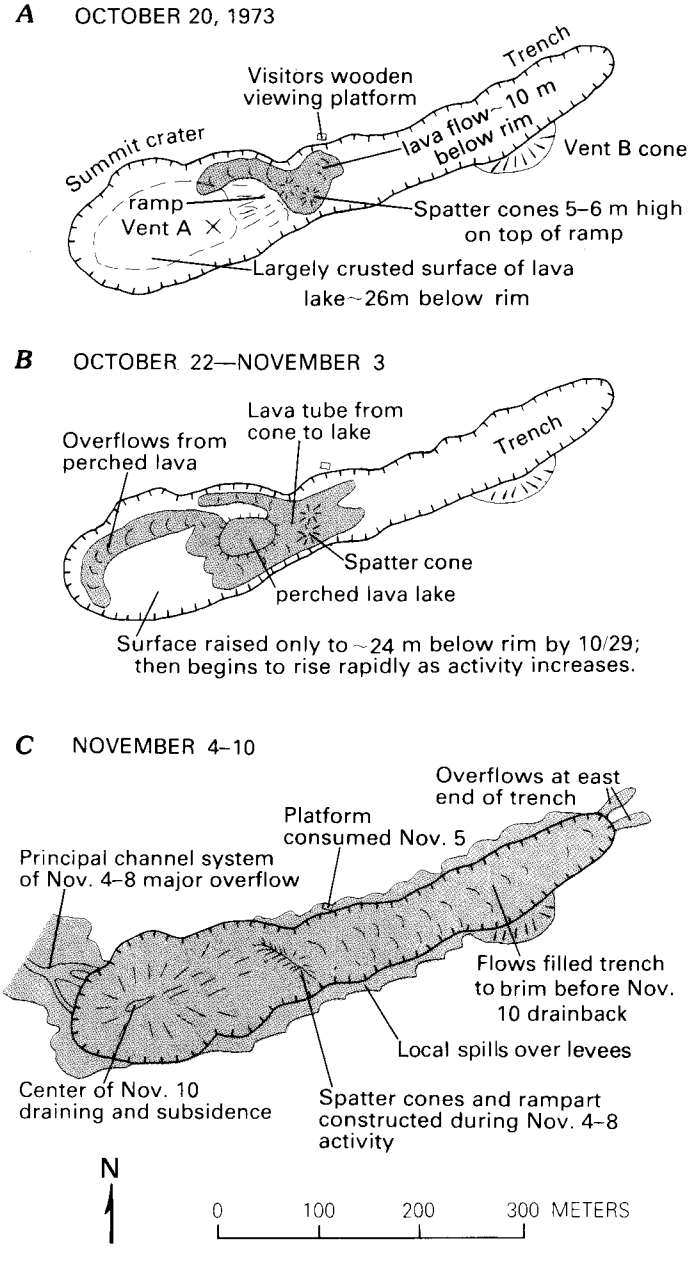

FIGURE 16.23.—Sketches showing eruptive activity at Mauna Ulu from October 20 through November 10, 1973. ***A***, October 20. ***B***, October 22–November 3. ***C***, November 4–10. Major overflow of November 4–8 was first from Mauna Ulu since March 1972.

to rise, reaching 51 m below the rim by June 19. The island of semisolid lava that first formed in late May briefly disappeared following the June 9 draining but soon reappeared and rose together with the lake surface (fig. 16.22*C–F*). The lava appeared even more viscous than following the May 5 draining. As the lava lake rose gradually, the area of sluggishly circulating lava steadily decreased. Activity was confined to a central part, perched behind natural levees and separated from the crater walls by a moat 3–20 m wide and 3–4 m deep. Periodic overflows into the moat raised the

FIGURE 16.24.—Overflow of Mauna Ulu Crater in November 1973. Lake level stabilized when overflows began on November 4, and levees again developed (compare fig. 16.22*H*), confining a perched lake at an elevation higher than the initial crater rim. Site from which photographs of figure 16.22 were taken is in foreground where stream on right overflows levee. Photograph taken by R.I. Tilling, November 7, 1973.

confining natural levees and the perched lake, as well as the level of the moat.

Sluggish lava-lake activity continued at Mauna Ulu for the next several months; lava level rose while the area of active surface lava shrank (fig. 16.22*D, E*). By mid-July, active lava was restricted to two circular areas 10–15 m in diameter, one of which included the active vent. Gas-piston cycles and associated small overflows occurred at intervals of 5–20 minutes. The declining activity, coupled with concurrent inflation at Kilauea summit, indicated that the connection between the summit reservoir and Mauna Ulu was not fully reestablished. By July 24 the lava lake had become stagnant, with the crusted surface at the vent about 15 m below the rim. No molten lava was visible, and the crusted surface began to subside (fig. 16.22*G*), beginning the longest repose in visible activity since the eruption began in February 1972. This repose period, except for the brief reappearance of lava in early September, lasted nearly two months. Subsidence was rapid for one week, averaging 5–6 m/d, and then slackened; it continued throughout August, and the lake crust fell to about 81 m below the rim. Harmonic tremor, varying from very low to moderate in intensity, persisted throughout the repose.

RESUMPTION OF LAVA-LAKE ACTIVITY AT MAUNA ULU: A MAJOR OVERFLOW

No molten lava was visible at Mauna Ulu from July 24 to September 3. Harmonic tremor markedly increased at 0435 on September 4, and observations later that morning revealed a lava lake in Mauna Ulu Crater with a few fountains up to 5 m high. The lake surface was 62 m below the crater rim, up from its 81-m level in mid-August. About 1400, tremor abruptly decreased and the low fountaining ceased. The lake persisted through September 6, by

FIGURE 16.25.—Telephoto view (300-mm lens) from Puu Huluhulu showing slabs of crust and molten material of Mauna Ulu lava lake being lifted in vortex of thermally generated whirlwind. Photograph was taken by R.I. Tilling on January 30, 1974, but similar and more vigorous activity occurred on November 8, 1973.

which time a solid, slowly subsiding crust had again developed across its entire surface.

Lava-lake activity resumed sometime between noon of September 25 and the afternoon of September 26 with the reopening of a vent in the eastern part of Mauna Ulu Crater. Lava flooded the crater floor, and within a few days the lake level rose from 68 m to 61 m below the rim; the familiar circulation pattern with periodic crustal overturns was reestablished. During the next three weeks, lava-lake activity alternated between active circulation and stagnation with the formation of crust, and the irregular surface of the lake gradually rose to 15 m below the rim in the eastern part of the crater and to 32 m in the western part.

Sharply increased summit inflation continued during October (fig. 16.4) and by October 20 the activity at Mauna Ulu was the most vigorous for many months; lava fountains from parts of the lake surface commonly attained heights of 15 m. The principal vents, whose lava columns periodically exhibited gas-piston behavior, were localized between former vents A and B, near the position of the septum that formerly separated the crater and the trench (figs. 16.11, 16.23*A*). Lava mostly flowed westward from these vents down a sloping ramp, at the base of which a perched lake developed (fig. 23*B*). Overflows from this perched lake, together with flows fed directly by the vents, flooded much of Mauna Ulu's crater floor during the next few weeks. The area of active surface greatly increased, and the lava lake continued to rise.

Mauna Ulu's activity substantially increased during the morning of November 3, when the lava surface was about 25 m below the lowest point of the western crater rim. Voluminous flows from three closely clustered vents (fig. 16.23B) raised the lava surface to 12 m below the rim by midday. The next morning fountaining was 40 m high, and modest deflation began at Kilauea summit. At 0900 on November 4, the lava level was only 3 m below the low point of the western rim, and it continued to rise at a rate of about 0.5 m/h. Soon the perched lava lake was inundated by the rising lava, and the two-level aspect (western crater and eastern trench) that had characterized the configuration of Mauna Ulu throughout much of the 1972–73 activity was lost. Mauna Ulu now resembled the brimfull lake that existed at times during February–March 1972.

By 1445 on November 4, lava had risen to the lowest point of the western rim (fig. 16.22*H*), and slow outflow commenced at 1600, marking the first overflow from the crater since March 18, 1972. This overflow, however, advanced only about 35 m, because construction of confining levees nearly kept pace with the now more slowly rising Mauna Ulu lake, whose surface area was now almost 55,000 m^2 (fig. 16.23C). Throughout the night of November 4–5, the lava lake continued to rise, and levees, typically 1–2 m high, were built along low areas of the old crater rim.

A major overflow from the western end of the crater began early on November 5, as a lava stream several meters wide flowed across a levee 8–10 m higher than the original low point on the rim (fig. 16.24). Subsequently, two or three lava streams spilled over the levees on the northwestern rim, converged into a single stream within about 30 m of the rim, and turned southward to pass east of the buried Aloi Crater (fig. 16.18C). An irregular overflow apron formed along most of the northwest crater rim, and other smaller short-lived spills occurred elsewhere, including two at the eastern end. However, voluminous outflow was confined to the south-trending stream spilling out of the western end of the crater; this flow advanced about 2.6 km before stopping in the early morning of November 8 (fig. 16.18C).

A wooden viewing platform at Mauna Ulu (fig. 16.23) was kept open to the public by the National Park Service through the night of November 4, allowing hundreds of park visitors to view the filling lava lake and 30 to 40-m-high fountains. Heat from the rising lava and continued high fountaining forced the viewing platform to be abandoned late on the night of November 4. The platform was consumed early the next morning as lava overflowed the rim.

On November 8, observers witnessed a thermally generated whirlwind that played erratically across the Mauna Ulu lava-lake surface for about 10 minutes. The whirlwind lifted crustal slabs 2–3 meters in diameter to heights of 20–30 m, and smaller pieces went much higher (fig. 16.25). Molten lava exposed beneath the vortex also was lifted high into the air and deposited, in part, as blobs of spatter and Pele's hair beyond the crater rim.

PAUAHI ERUPTION OF NOVEMBER 10–DECEMBER 9, 1973

VIGOROUS INITIAL ACTIVITY ASSOCIATED WITH FISSURE VENTS, NOVEMBER 10–11

About 1730 on November 10, seismic stations in the vicinity of Mauna Ulu and Pauahi Crater began to record a moderate to high level of harmonic tremor accompanied by a flurry of earthquakes. At the same time, a National Park Service ranger at Puu Huluhulu radioed a report to HVO that he felt ground shaking and could see greatly increased turbulence and degassing of the still brimful lava lake at Mauna Ulu. A drainback of Mauna Ulu lava lake was underway, similar to those that had occurred on May 5 and June 9. Summit deflation commenced about 15 minutes later and, combined with intensified seismic activity localized in the Pauahi-Mauna Ulu area, suggested the possibility of another eruptive outbreak.

HVO observers arrived at Mauna Ulu about 1830, in time to watch drainback; the surface of the lake in the western part of the crater had already subsided to a level of about 40 m below the rim

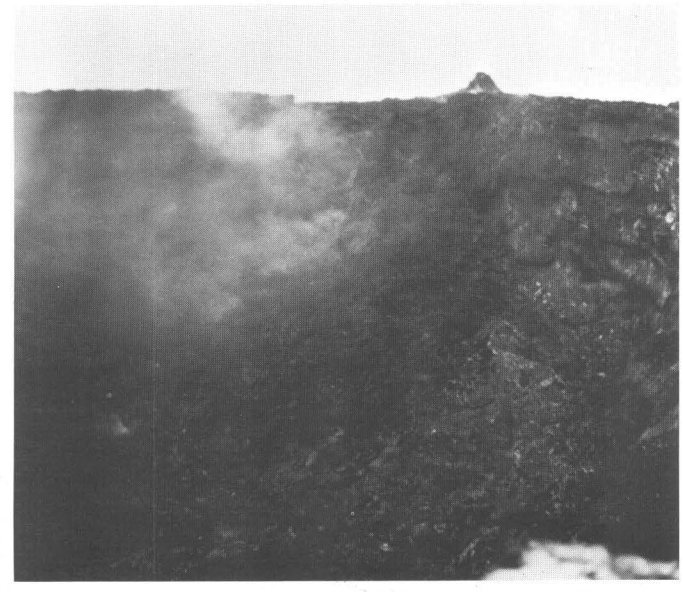

FIGURE 16.26.—Draining of lava from Mauna Ulu on November 10, 1973, left a rubble-covered crater floor about 40 m deep. During draining, the levees on the rim, left unsupported, collapsed. Photograph taken by D.W. Peterson, November 12, 1973.

(fig. 16.26). By 2100 subsidence (fig. 16.23C) had largely ceased, and partially cooled lava continued to spall from the crater walls amid showers of glowing debris. Meanwhile, rockfalls were reported in Pauahi Crater. At 2135 an earthquake was felt in the Puu Huluhulu area and triggered rockfalls at Pauahi.

At 2147, gassy lava broke out in Pauahi Crater about midway up the north wall of the east pit and began to pool at the bottom of the crater. Echelon fissures opened eastward up the wall to the crater rim. A few minutes later, a fissure trending N. 70° E., aligned with the northwest corner of the western pit, cut the Chain of Craters Road west of Pauahi (fig. 16.18C); fountaining of lava from this fissure was observed at 2200, and within minutes the road was blocked by lava. At 2215, a vent opened in the north wall of the west pit, approximately midway between the two fissures of the May 5 eruption, and lava began to pool in the west pit as well as in the east pit.

At 2245, several additional fissures opened and extended about 1.5 km east-northeast toward Puu Huluhulu; pahoehoe flows fed by fountains from these fissures ultimately covered about 1.1 km^2 of land (fig. 16.18C). Fountaining as high as 70 m continued within and outside Pauahi Crater throughout the night of November 10–11 and fed lava pools in both the east and west pits (fig. 16.27).

Shortly after midnight, lava filled the east pit to the level of the septum that separated it from the west pit and began to cascade westward and circulate clockwise (fig. 16.28). At 0135 on November 11, new lava outbreaks occurred high on the northwest wall of the west pit. Lava from these sources poured into the pit, but the rate of drainback, presumably into the May 5 fissures, was greater; the lava level in the west pit consequently began to lower. At 0150, the fissure in the east pit stopped erupting, and by 0200 flow

FIGURE 16.27.—View from the south rim of Pauahi Crater at 0015 on November 11, 1973, showing fountains 20–30 m high along fissure that cuts the north wall of the east pit of Pauahi and supplies lava to the rising lake, which at this point is still below the septum separating east and west pits. Lava fountains from other vents in the west pit (left center, near edge) feed another lava lake in the west pit. Five minutes after this photograph was taken, lava in the eastern lake had risen to the lowest point along the septum and began to spill into the west pit (see fig. 16.28). Photograph taken by R.I. Tilling.

across the septum between the pits had stopped. Soon lava was draining back into fissures in both pits, though it continued to cascade at a decreasing rate from the northwest wall of the west pit until 0545. At 0440, fountains as high as 20 m were active near the east end of the fissure system near Puu Huluhulu, but all activity along these fissures stopped by 0600.

PERSISTENT, FEEBLE ACTIVITY AT A LOCALIZED VENT WITHIN THE WEST PIT, NOVEMBER 11–DECEMBER 9

On November 12, the level of the largely crusted lava pool in the east pit of Pauahi was about 100 m below the crater rim and about 21 m below the high lava mark established before drainback. The northwest vent on the floor of the west pit of Pauahi continued to emit lava after all other activity had ceased. Lava fountains 15–35 m high still played at the vent through November 12, but four days later only a slow upwelling of lava could be seen. By November 19, a perched lava lake about 30 m in diameter had developed at the base of a spatter cone 5–10 m high situated near the west end of the northwest fissure vent (fig. 16.3). Lava level in the west pit slowly rose as the result of periodic overflows from the perched lava lake, and by November 21 it reached within 5 m of the lowest point on the septum between the two pits. On November 28, lava from the west pit trickled over the septum and descended into the east pit (fig. 16.29).

On about December 3, the activity in the west pit declined appreciably, and overflows from the perched lava lake ended. Vent activity virtually stopped, and during the next several days circulation became progressively more sluggish. By December 8, no circulation could be seen in the lake, and the crusted surface had subsided 7 m below the levees. Further subsidence of the lava crust occurred the next day, and fuming from the vent largely ceased. Cessation of tremor about noon on December 9 marked the end of the November–December Pauahi eruption.

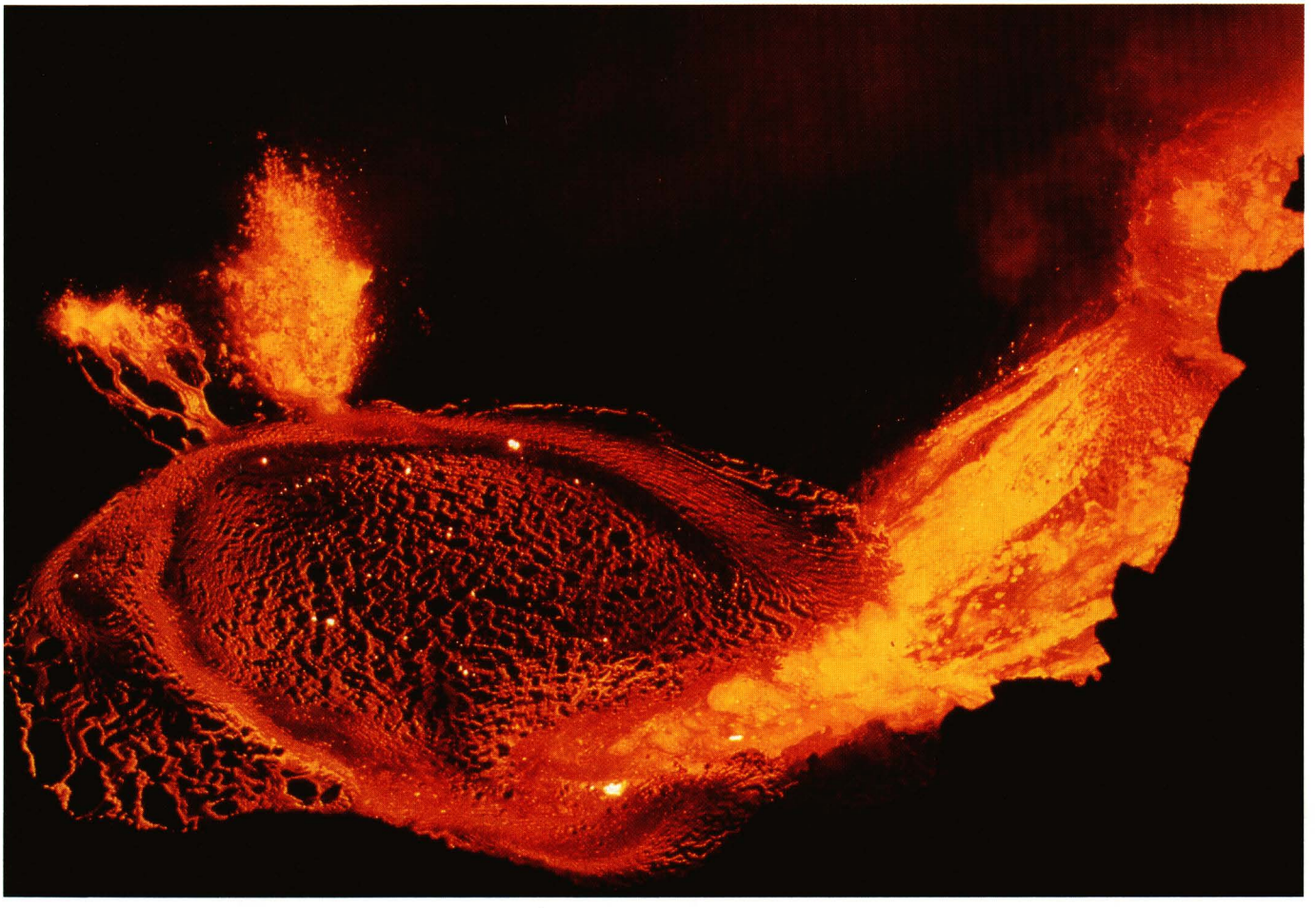

FIGURE 16.28.—View from south rim of Pauahi Crater at 0050 on November 11, 1973, showing lava from lake in east pit cascading over septum into lava lake in west pit. Two smaller vents on western wall of west pit also feed lava into the lake, which here is about 150 m across and shows clockwise circulation. Photograph taken by R.I. Tilling.

DECEMBER 10, 1973–JULY 22, 1974

REAPPEARANCE OF THE LAVA LAKE AT MAUNA ULU

No eruption occurred at Kilauea between December 9 and 12. On December 10 and 11, a portable seismometer in the Pauahi-Mauna Ulu area detected no harmonic tremor above normal background noise. Then, on December 12, the permanent seismometer closest to the Pauahi-Mauna Ulu area began sensing intermittent harmonic tremor. This tremor increased in intensity and became sustained by the next day, when lava quietly reappeared at Mauna Ulu and quickly rose to 30 m below the crater rim. Thus visible activity at Mauna Ulu resumed on December 13 (not December 12 as stated by Peterson and others, 1976). Vent activity was localized a short distance west of the vigorous vents that fed the November 4–8 overflows (fig. 16.23).

Over the next few days the lake level rose to 18–20 m below the crater rim. Initially the entire surface of the lake was active, but by December 20 activity was reduced to sporadic oozing of lava, punctuated by brief degassing bursts, from a spatter cone feeding a small perched lava lake. This low-level activity continued into mid-January 1974, and the floor of Mauna Ulu crater became irregular because of differential subsidence.

DEPARTURE FROM 1972–73 BEHAVIOR: RENEWED GROWTH OF MAUNA ULU SHIELD

Rather than the sustained lava-lake and associated eruptive behavior that generally prevailed during 1972–73, Mauna Ulu activity in 1974 was characterized by short eruptions (no more than two days) in which lava fountains 40–80 m high fed short-lived but voluminous overflows. Episodes of fountaining and overflow were separated by 3-day to 5-week periods of only feeble activity.

The voluminous overflows, augmented by spatter-cone growth during the quiet periods, resulted in renewed growth of the Mauna Ulu shield. Most overflows traveled only short distances, but several extended 5 km or more from the vent and one advanced about 9 km.

FIGURE 16.29.—View from Pauahi's west pit on December 5, 1973, toward Puu Huluhulu (arrow) and Mauna Ulu shield to right of it. Continued eruption in Pauahi's west pit through December 9 built a low lava shield, the small summit crater of which contains a perched pond of molten lava (lower left). Small amounts of lava from this perched pond have flowed across septum into the east pit. Also seen are the high mark of lava lake in east pit before drainback, and the fissure that fed the east-pit lake. Photograph taken by R.T. Holcomb.

The first of the 1974 eruptive episodes began on January 24 and was preceded by several days of heightened harmonic tremor, increased shallow summit earthquakes, and summit inflation (fig. 16.30). During the ensuing 36-hour burst of activity, a 60-m-high lava fountain (figs. 16.31, 16.32) fed by vent E_1 (fig. 16.3) filled Mauna Ulu to the brim, built a 15-m-high spatter cone atop the shield, and fed numerous overflows, one of which advanced more than 1 km from the vent. This episode was accompanied at Kilauea

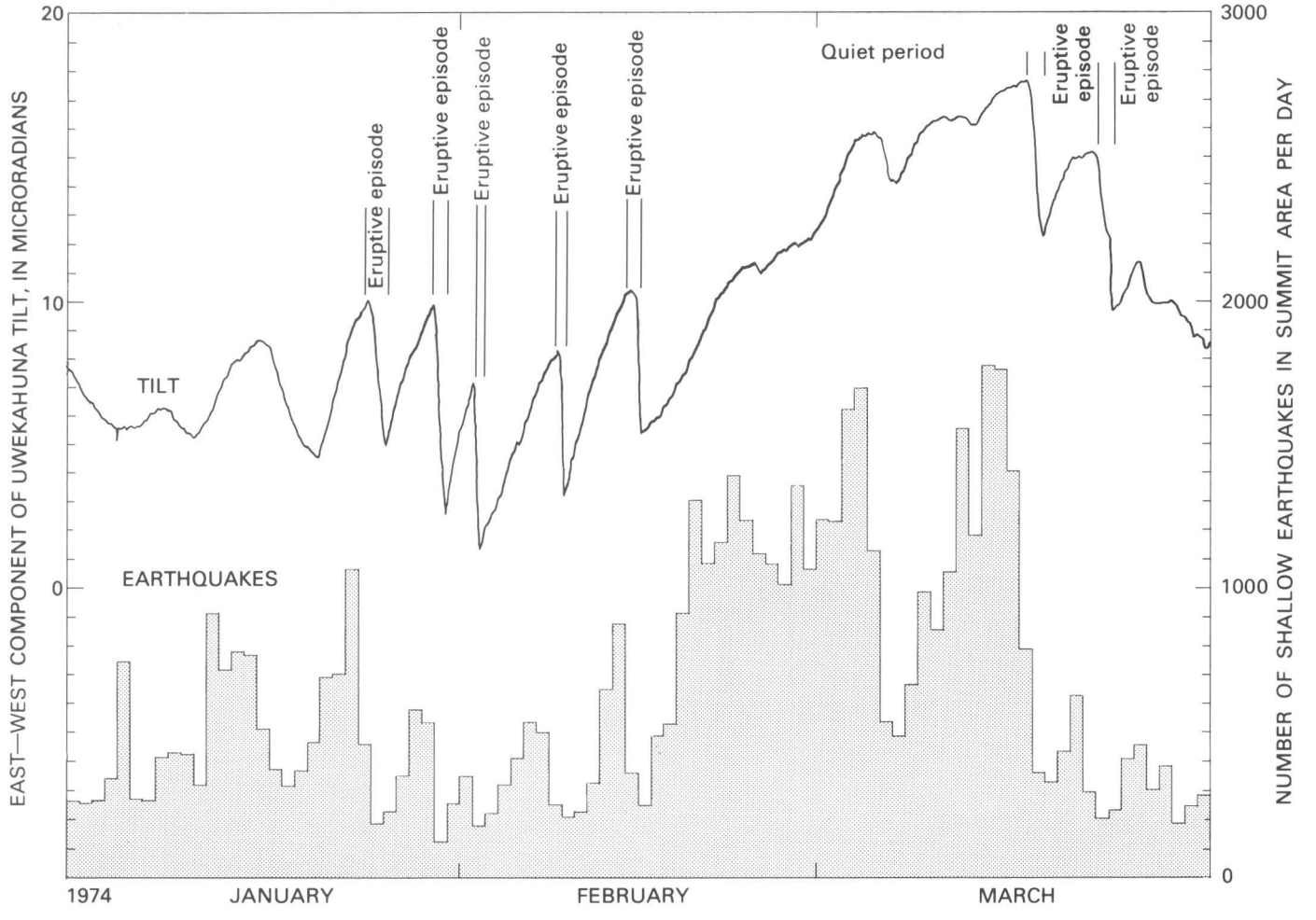

FIGURE 16.30.—Correlation of the eruptive episodes during January–March 1974, characterized by vigorous fountaining and voluminous overflows, with variations in Uwekahuna tilt and daily number of shallow (depth less than 5 km) summit earthquakes (see table 16.3 and text).

summit by abrupt but modest deflation and a decrease in seismicity. Once the episode ended, inflation began again and seismicity increased immediately, culminating in another eruptive episode on January 29. During the quiet period between the two eruptive episodes, low-level activity persisted at Mauna Ulu. The crusted lava-lake surface sagged to about 3 m below the rim, and bursts of spatter from vigorous gas-piston degassing reached heights of 20 m above the vent.

The time, duration, amount of inflation or deflation, tilt variations, and summit seismicity for five exceptionally well documented eruptive episodes during January–February 1974 are summarized in table 16.3 and figure 16.30. Lava spilled over all flanks of the Mauna Ulu shield during each episode, but the most voluminous overflows were directed northward. Much lava ponded in the saddle between Mauna Ulu and Puu Huluhulu, and a well-defined levee grew around the pond during the January 24–26 episode (fig. 16.32).

A month-long quiet period followed these January–February eruptive episodes; during the first part of this (February 15–March 5), vent activity was restricted entirely to the vent E_1 spatter cone at Mauna Ulu summit. On March 5 a new vent (designated F) opened about 140 m east-northeast of vent E_1 (fig. 16.3), accompanied by summit deflation of about 2 microradians. Both vents E_1 and F operated until March 17, and lava output from each varied within the range 2–5 m^3/s. Both vents exhibited gas-piston activity that generated spatter, enlarged their cones, and fed numerous short-lived flows. Their activities, however, could not be closely correlated in time; any connection between them was apparently complex despite their close proximity.

Two eruptive episodes occurred in March (table 16.3 and fig. 16.30). The first began in the early evening of March 17, lasted about 30 hours, and resulted in a summit deflation of about 5.5 microradians. In contrast to the January–February episodes, this one produced a maximum fountain height of only 15 m, even though lava output was equally great. South-directed overflows advanced 3 km (fig. 16.18*D*). The eruptive episode of March 23–24 (fig.

FIGURE 16.31.—Lava fountain and thermal plume produced during January 24–26 eruptive episode of Mauna Ulu viewed from Hawaiian Volcano Observatory more than 12 km away. Photograph taken by R.T. Holcomb, January 24, 1974.

16.30) produced copious overflows mainly directed southward and built the vent E_1 spatter cone even higher (fig. 16.33). This episode also included strong rockfall activity at Pauahi Crater. These frequent and large rockfalls, combined with high-amplitude tremor and rapid deflation, were reminiscent of the precursors to the May 1973 and November 1973 eruptions in the Pauahi area. This time, however, the movement of magma into the Pauahi area remained entirely underground and fed a brief intrusion into Kilauea's east rift

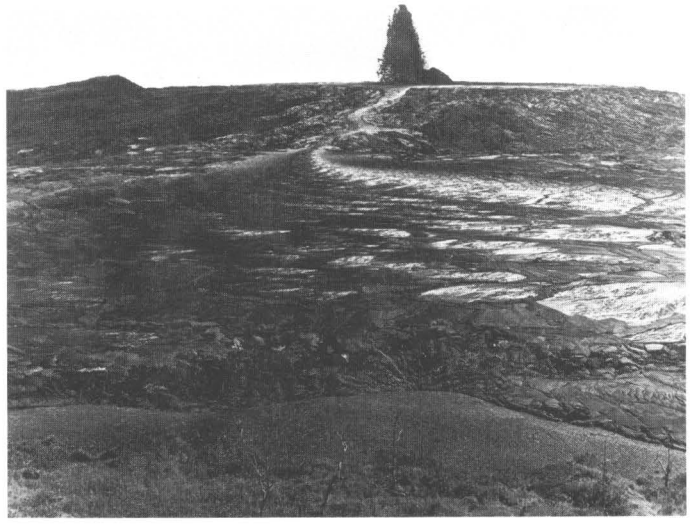

FIGURE 16.32.—View from the summit of Puu Huluhulu on January 25, 1974, during first of a series of brief eruptive episodes that were interspersed with longer quiet periods of only feeble visible activity. The lava fountain was about 60 m high. The lava lake surrounding the vent overflowed the confining levee and fed a copious flow that ponded in the saddle between Mauna Ulu and Puu Huluhulu (middle foreground). Ponded flow developed levees and evolved into a perched lava pond. Topographic feature to the left of lava fountain is the spatter cone of vent B. Photograph taken by R.T. Holcomb.

zone (Dzurisin and others, 1984, table 1), which had no observable effect on activity at Mauna Ulu. The sharp deflation ceased at 0700 on March 24, signaling the end of the episode. However, even though vigorous vent activity and voluminous surface overflows had largely ended by the morning of March 24, lava primarily from vent F continued to feed a south-moving flow through a channel-tube system. This flow cascaded over Poliokeawe Pali on April 3 and stopped several hundred meters farther two days later. During March, the southeastern flank of Mauna Ulu became underlain by a complex maze of anastomosing lava tubes, and there were abundant opportunities to observe lava-tube processes.

During the first half of April, relatively quiet activity prevailed at Mauna Ulu. The spatter cone at vent E_1 (fig. 16.33) collapsed on April 2, and continuing collapse resulted in a small (20 m by 15 m) active lava lake, which commonly exhibited gas-piston behavior. This activity apparently was confined to the area of the Mauna Ulu vents, as it was not reflected by Kilauea summit deflation or inflation. However, three larger eruptive episodes in mid-April (Apirl 13–14, 16–17, and 18–19) were accompanied by summit deflations of 5, 1.5, and 2 microradians, respectively. These episodes produced overflows, which moved down all sides of Mauna Ulu but did not enter the eastern part of the trench. The April 13–14 overflows continued virtually nonstop for 16 hours, and a dome fountain 5–10 m high played for many hours from an opening between vents E_1 and F (an excellent example of a dome fountain is shown by Swanson and others, 1979, fig. 28).

No well-defined eruptive episodes occurred during late April, but activity during this time was nonetheless fairly strong. All vent activity was confined to E_1 and a 2-m-wide new opening (designated E_2) 30 m farther east (fig. 16.3); vent F became inactive.

TABLE 16.3.—*Date and time of beginning and end of eruptive and associated premonitory quiet periods, and duration and amplitude of Kilauea summit deflation and inflation as measured by Uwekahuna mercury-pool tiltmeter January 20 to February 15, 1974*

[All times given are in Hawaii standard time]

Quiet periods				Eruptive episodes							
Inflation					Activity			Deflation			
Beginning	End	Duration (hours)	Amount (microradians)	No.	Beginning intermittent	Beginning continuous	End	Beginning	End	Duration (hours)	Amount (microradians)
1/20, 2200	1/24, 1900	93	5.6	I	1/24, 0800	1/24, 1400	1/26, 0500	1/24, 1900	1/26, 0530	35	5.1
1/26, 0530	1/29, 1400	90	5.0	II	1/29, 1800	1/29, 2400	1/30, 2400	1/29, 2400	1/30, 2400	24	7.3
1/30, 2400	2/2, 0400	52	4.5	III	2/1, 1100	Not observed, but continuous by 2/2, 0545	2/2, 1607	2/2, 0400	2/2, 1600	12	5.8
2/2, 1600	2/8, 2000	148	6.9	IV	2/8, 1900	2/9, 0100	2/9, 0600	2/8, 2000	2/9, 0700	11	5.0
2/9, 0700	2/14, 2000	133	6.8	V	2/14, 0300	Never continuous, but intermittent fountaining became strongest on 2/14, 2200	2/15, 0830	2/14, 2000	2/15, 0900	13	4.9

FIGURE 16.33.—View of Mauna Ulu shield from the west on March 27, 1974, showing steep-sided spatter cone of vent E_1, which collapsed on April 2. Flank of Puu Huluhulu is seen center left; Alae shield is behind and to right of Mauna Ulu. Photograph taken by R.I. Tilling.

Many brief but copious overflows from E_1 and E_2 added to the shield, burying vent F in the process. By the end of April, the height of the Mauna Ulu shield had increased about 15 m, to 117 m above the pre-1969 base, and its width increased proportionately. During the period of rapid shield growth, a sustained flow fed by vent E_2 formed a tube system that extended southward. Lava spilled over Poliokeawe Pali on April 30, and on May 7 the flow front reached the lip of Holei Pali before stopping the next day.

Gas-piston processes dominated the behavior of the overflows: a strong overflow would issue from vent E_1 or E_2 for a period of 5 minutes to more than one hour; then a brief but spectacular burst of degassing would abruptly terminate the overflow, and the lava column would drop 10–20 m. The lava column would then rise slowly over a period of 15 minutes to several hours. When the lava reached the rim of the vent, a new overflow would begin. The gas-piston cycles of vents E_1 and E_2 apparently operated independently.

During May, the eruptive activity at Mauna Ulu progressively declined: overflows stopped, lava in channels and tubes solidified, and the lava column dropped several meters. Piecemeal wall collapse enlarged vents E_1 and E_2; by May 12 the two openings coalesced to form an elongate crater, which measured approximately 40 m by 90 m on May 20. The lava lake within the western part of this crater was about 15–20 m below the rim. Lava circulated from west to east and then plunged over a septum into a pit at least 50 m deep in the eastern part of the crater.

During late May, lava-lake circulation became increasingly sluggish until the late evening of May 29, when summit deflation began and harmonic tremor increased. By the next morning the summit crater at Mauna Ulu had refilled, and low fountains were active along much of the lake margin. Lava was spilling over at two points on the southeast rim, and a flow already had advanced nearly 2 km southward. As the day progressed, the activity increased, as did the rate of summit deflation. During the night of May 30, gassy fountains at the lava lake threw spatter about 20 m high, and voluminous overflows began to cascade down all sides of the Mauna Ulu shield.

Fountains and overflows continued until June 1, when weather conditions permitted excellent aerial photography during peak activity (fig. 16.34). Most of the lava traveled southward, and the main flow poured over Poliokeawe Pali and Holei Pali (fig. 16.35). At about midnight the summit deflation stopped and inflation resumed; overflows ended about 0200 on June 2.

The May 29–June 2 eruptive episode was the largest of 1974 and was accompanied by about 10 microradians of summit deflation. It added another 4 m of lava to the Mauna Ulu shield to raise its summit to the maximum height reached during the 1972–74 eruption, 121 m above the pre-1969 ground surface (Peterson and others, 1976), and sent lava over Holei Pali for the first time in 1974

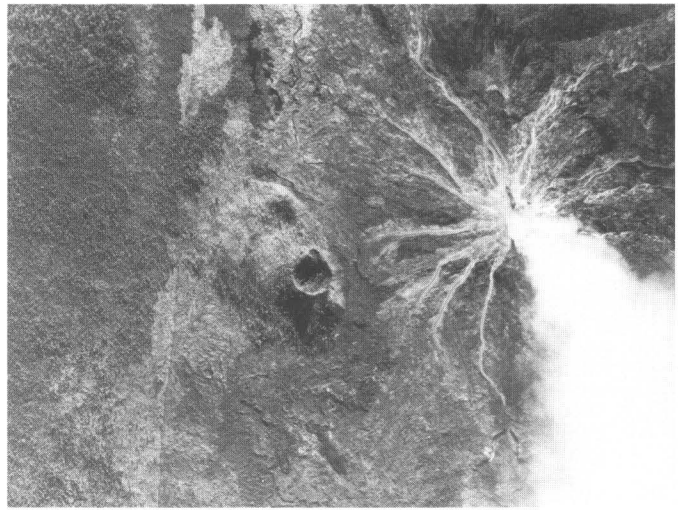

FIGURE 16.34.—Vertical aerial photograph (north is to left) taken June 1, 1974, showing active radial overflows from Mauna Ulu lava lake during the May–June eruptive episode. Also shown (center) are summit crater of Puu Huluhulu and lava pond in saddle between Mauna Ulu and Puu Huluhulu, which first formed in January 1974 (fig. 16.32) and was reactivated during several later eruptive episodes. Photograph taken by R.M. Towill Corporation.

(fig. 16.18*D*). This episode, as it turned out, also knelled the end of the 1972–74 Mauna Ulu eruption.

CESSATION OF THE 1972–74 MAUNA ULU ERUPTION

Soon after the May–June eruptive episode, Mauna Ulu's summit lake subsided, and lava circulated sluggishly 20–32 m below the crater rim. In response to the lower lake level, numerous rockfalls from steep and overhanging walls enlarged the crater at its rim from 40 m by 90 m on May 20 to 107 m by 147 m by June 20. Lava activity declined through June and much of July; the lava lake changed little in configuration and was largely obscured by fumes. Circulation became increasingly sluggish, and the crusted and rubbly lake surface continued to subside gradually, approaching about 40 m below the rim by mid-July.

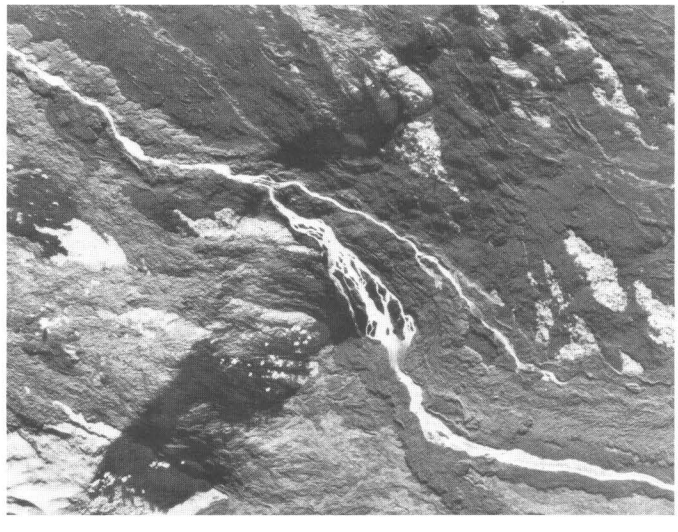

FIGURE 16.35.—Lava stream of May–June 1974 eruptive episode becomes braided during cascade over Poliokeawe Pali (about 165 m high). Northwest is to left; lava flows from upper left to lower right. Vertical aerial photograph taken by R.M. Towill Corporation on June 1, 1974.

As Mauna Ulu activy waned, the summit region of Kilauea remained highly inflated, the tilt at Uwekahuna fluctuating within a range of 4 microradians. A summit eruption on July 19–22 (Peterson and others, 1976) caused no observable changes in the already feeble activity at Mauna Ulu. Following the summit eruption, however, the small, subsiding lava pool disappeared beneath the rubble-covered crater bottom. After July 22, no molten lava was visible anywhere on Kilauea, and harmonic tremor in the Mauna Ulu area ceased.

Months after July 22, Mauna Ulu Crater was obscured by extremely heavy emission of fumes. Visible observations of the crater were impossible, but sounds of rockfalls were commonly heard, indicating continued piecemeal collapse of the walls and possible subsidence of its rubbly floor. During November 1974, attempts were made to determine the depth of the crater by hurling percussion-impact, noise-emitting probes into the crater and measuring the time elapsed between release and impact. These measurements yielded six depth estimates ranging from 56 m below the rim in the shallow northwestern part of the crater to 133 m in the considerably deeper eastern part. Large uncertainties are attached to these measurements, but they nevertheless suggest that the deepest parts of Mauna Ulu Crater in November 1974 (averaging perhaps 130 m) were considerably shallower than the maximum depth of 200 m measured following the complete drainage of the lake in May 1973. The decrease in depth presumably reflected solidification of residual lava and partial filling of the crater by rockfall debris. The depth of the Mauna Ulu crater at the end of the 1969–71 eruption was 145 m (Swanson and others, 1979, fig. 7).

GROUND DEFORMATION AND SEISMICITY

The general relations between eruption, intrusion, ground deformation, and seismicity at Kilauea Volcano have been well documented from systematic studies by scientists of the Hawaiian Volcano Observatory since its founding in 1912. A comprehensive model that integrates the data on subsurface structure, magma storage and transport, and eruptive processes was first described in the early 1960's (see Eaton and Murata, 1960; Eaton, 1962); many subsequent studies have refined and increasingly quantified this model (for example, Fiske and Kinoshita, 1969; Swanson, 1972; Kinoshita and others, 1974; Koyanagi and others, 1976a, b; Swanson and others, 1976b; Ryan and others, 1981, 1983; Aki and Koyanagi, 1981: Dvorak and others, 1983; Dzurisin and others, 1984). In the discussion to follow, we assume that the reader is familiar with the well-documented behavior typically observed for Kilauea rift activity: between eruptions, summit inflation occurs as

TABLE 16.4.—*Dates of reoccupations of the ground-deformation networks of Kilauea summit pertinent to 1972–74 Mauna Ulu eruption*

[Measurements obtained during these reoccupations provide the data for figures 16.38–16.43. Some reoccupation periods were prolonged because of inclement weather. Reoccupations of two or more types of networks during a closely bracketed time period are indicated by an asterisk (*). Data are stored on magnetic tapes at the Hawaiian Volcano Observatory]

	Level	Tilt	Trilateration
		Inflation period before eruption	
*	9/29-30/71	10/1-7/71	10/4-7/71
		10/20-22/71	
		11/1-2/71	
		11/11-12/71	
		11/19-24/71	
*	11/30-12/1/71	11/29-12/1/71	
		12/13-14/71	
*		12/27-30/71	12/20-23/71
		1/10-11/72	
*	1/17-20/72	1/26-28/72	1/26-28/72
		During the 1972-74 Mauna Ulu eruption	
		2/7-9/72	
		2/22-25/72	
		3/7-9/72	
		4/3-7/72	
		4/17-18/72	
*	6/12-13/72	6/5-8/72	6/5-14/72
		7/17-20/72	
		8/21-29/72	
		9/27-29/72	
*	12/4-13/72	12/4-11/72	12/5-29/72
		3/13-26/73	
*	5/10-11-73	5/7-14/73	5/7-10/73
		5/21-6/1/73	5/29-6/1/73
		6/26-28/73	(partial)
*	9/19-20/73	9/20-10/3/73	9/24-27/73
*	11/13-14/73	11/11-14/73	11/15-21/73
		12/10-20/73	
		1/14-29/74	
		3/12-25/74	
*	4/4-5/74		4/1-3/74
		5/22-30/74	
*	7/26-31/74	7/22-26/74	7/22-25/74

magma is supplied from the upper mantle to a reservoir 2–4 km deep; during flank eruptions, summit deflation occurs as magma moves into a rift zone.

Ground-deformation and seismic data for the 1972–74 Mauna Ulu eruption are summarized in table 16.4 and figures 16.4 and 16.36–16.46. In general, crustal deformation and seismicity during the 1972–74 Mauna Ulu eruption were typical for Kilauea east-rift eruptions. Periods of weak or no vent activity generally correlated with net inflation and increased number of shallow earthquakes in the summit region, whereas vigorous eruptive activity correlated with deflation and reduced summit seismicity.

VARIATION IN SUMMIT TILT MEASURED AT UWEKAHUNA

Tilt at Kilauea summit, especially as measured daily by the 3-m-base, water-tube tiltmeters at Uwekahuna vault (fig. 16.1) to a precision of about 1 μrad (1 microradian), provides a sensitive and continuous record of the inflation-deflation state of the shallow magma reservoir. These daily measurements are augmented by continuously recording mercury-pool capacitance tiltmeters at the same site; data from these instruments correlate well with the daily water-tube measurements. In addition to these tilt-measurement instruments, Kilauea caldera is laced by the summit electronic-distance-measurement (EDM) monitor (fig. 16.36). The five EDM lines of the summit monitor are measured on a fairly frequent basis between periodic occupations of the entire summit trilateration network of 47 lines (Kinoshita and others, 1974, fig. 9). In general, summit inflation is indicated by extensions on these EDM lines and deflation by contractions.

Summit tilt measured at Uwekahuna (figs. 16.4, 16.37) generally correlates systematically with evidence of inflation and deflation from leveling, trilateration, and gravimetric data (Dzurisin and others, 1980, 1984; Dvorak and others, 1983). Because the locus of maximum uplift most commonly lies southeast of the Uwekahuna site, northward down tilt on the north-south axis or westward-down tilt on the east-west axis almost always indicates inflation; similarly, opposite senses of relative tilt of the two components generally indicate deflation. As will be seen, however, exceptions to this general relationship sometimes occur.

For the 1972–74 Mauna Ulu eruption, the east-west component of the Uwekahuna tilt shows the variations more clearly than does the north-south component; for convenience we discuss the summit tilt in terms of change in microradians (+, apparent inflation; −, apparent deflation) only in this east-west component (fig. 16.4). Whether the apparent inflation or deflation registered by the Uwekahuna tilt corresponds to actual inflation or deflation of the entire summit region can be evaluated by comparison of level, ground tilt, and trilateration surveys. With the exception of those related to non-elastic rotation of tectonic blocks, large changes in Uwekahuna tilt indicate true summit inflation or deflation, but small changes may not be amenable to simple interpretation. Like Dzurisin and others (1984, p. 191), we assume that net summit inflation reflects increased summit storage and cumulative summit deflation reflects increased rift-zone storage, which can be manifested as eruptive activity, intrusive activity, or both.

The variation curve for Uwekahuna tilt during 1972–74 shows two plateau-like segments (fig. 16.37), each of which is characterized by variations in tilt of less than 25 μrad during periods of at least 8 months. The first of these segments encompasses the period from the start of the eruption through April 1973, and the second period from December 1973 to the end of the eruption.

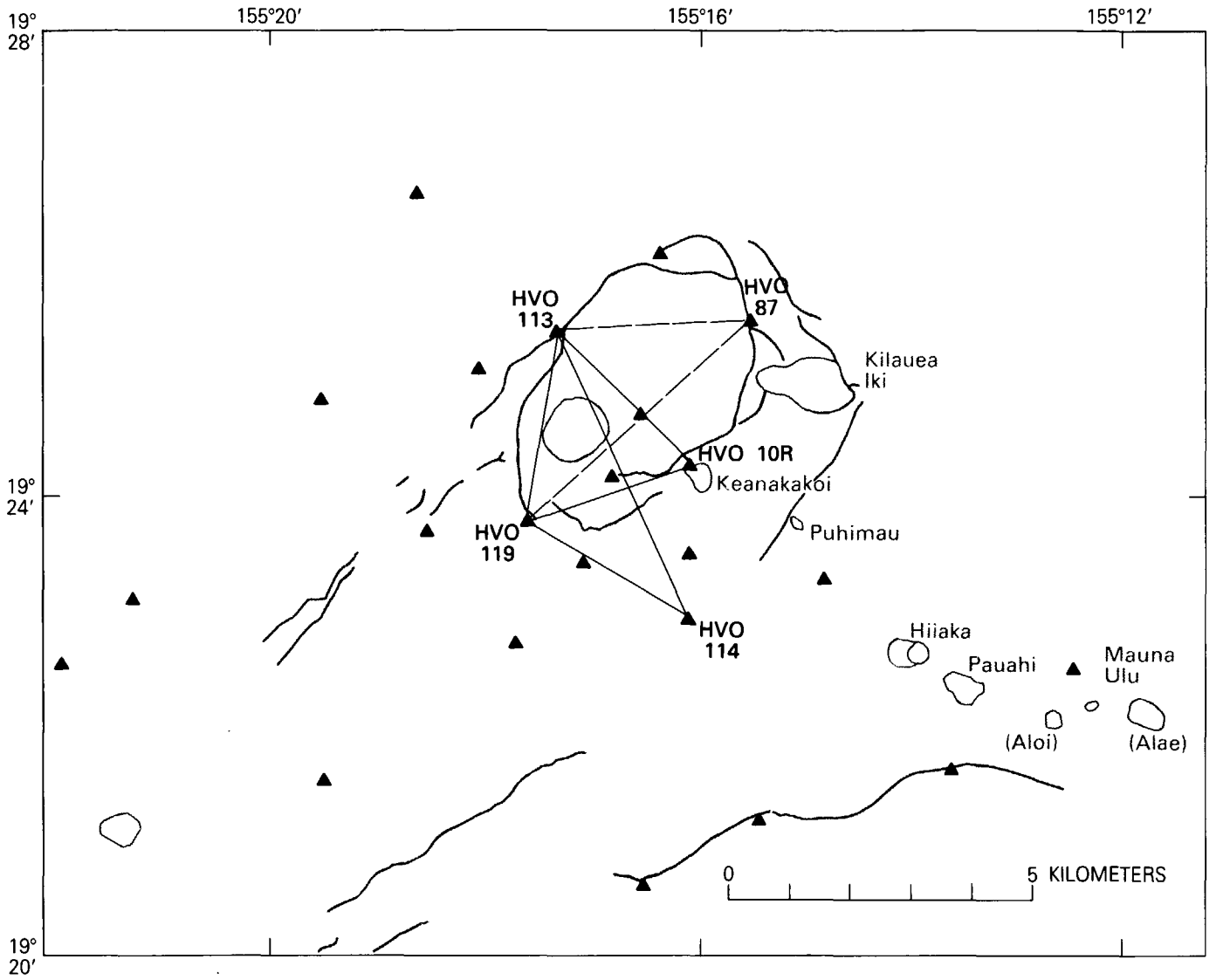

FIGURE 16.36.—Map showing location of the electronic-distance-measurement (EDM) bench marks (triangles) of the Kilauea summit trilateration network. The straight lines shown make up the so-called summit EDM monitor: solid lines are remeasured more frequently than dashed lines (see fig. 16.39). Distances between all other bench marks in the summit network (Kinoshita and others, 1974, fig. 9) are remeasured periodically depending on eruptive activity. Craters, the summit caldera, and faults in the rift zones shown for reference. HVO, Hawaiian Volcano Observatory.

These two prolonged periods of little net change in summit tilt suggest that a quasi-steady-state regime prevailed in the summit magma reservoir: supply of magma to the reservoir was counterbalanced by migration of magma into the east rift zone. This delicate balance was upset in early May 1973, possibly as a consequence of the Honomu earthquake (April 26, 1973), after which magma entered the reservoir faster than it was transferred to the rift zone, and net summit inflation occurred for the next seven months. December 1973 marked the reestablishment of open communication between the summit reservoir and the Pauahi-Mauna Ulu area, and the second period of quasi-steady state magma transfer began.

The amount of summit deflation during the May 1973 and November 1973 eruptions, about 20 μrad for each (fig. 16.37), is similar to the range of tilt oscillations during the various stages of the 1972–74 Mauna Ulu eruption (variation within the shaded bands in fig. 16.37). We suggest that the gross equivalence of the ranges of tilt changes reflects transfer of magma from the summit reservoir to the rift zone in increments just sufficient to maintain a quasi-steady-state condition that prevailed during most of the eruptive period.

A more detailed plot of the Uwekahuna tilt record for the 1972–74 Mauna Ulu eruption (fig. 16.4), adjusted for the 18-μrad tectonic offset caused by the April 1973 Honomu earthquake, reveals interesting second-order variations. The reappearance of lava at Mauna Ulu on February 3, 1972, did not appreciably disrupt the marked trend of net inflation that began in mid-1971. On February 5, the summit tilt reached a maximum since

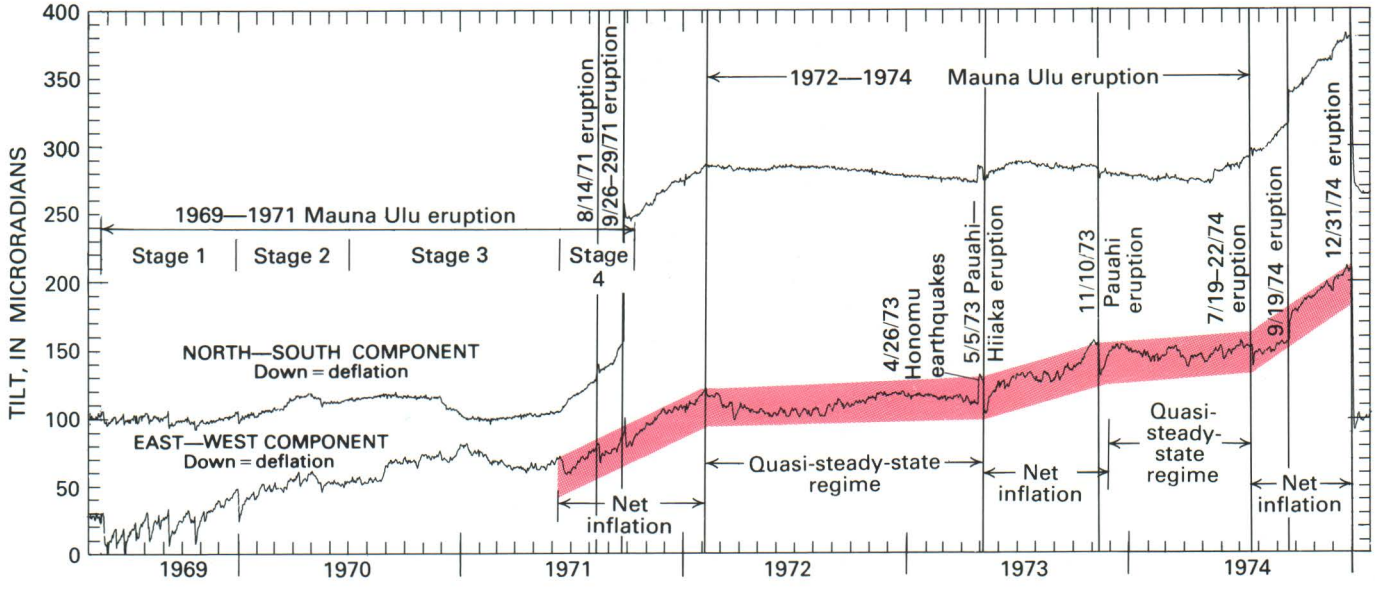

FIGURE 16.37.—Variation in Kilauea summit tilt for the period May 1969–January 1975, as measured by short-base water-tube tiltmeter at Uwekahuna vault; microradian scale arbitrary, with value at May 1, 1969, taken as zero. The magnitude-6.2 Honomu earthquake (April 26, 1973) caused an 18-microradian offset of the east-west component of tilt. Tilt record for 1972–1974 Mauna Ulu eruption is characterized by two distinctive plateau-like segments separated by period of net inflation (see text).

daily measurements were initiated at Uwekahuna in July 1956. This inflationary trend then was terminated by a 6-μrad deflation during the next two days as the lava lake rose rapidly in Mauna Ulu Crater. Thereafter, most of the larger variations in summit tilt can be related to significant changes in observed surface activity, the most prominent of which are annotated in figure 16.4.

Even many of the smaller tilt oscillations (5 μrad or less) can be correlated with changes in lava-lake level or episodes of vigorous vent activity, such as above-average lava fountaining or overflows from the vent. One of the best documented examples of such correlation is associated with the five eruptive episodes during January–February 1974 (table 16.3, fig. 16.30). Other good, but less well documented, examples are evident in figure 16.4.

Parts of the summit (Uwekahuna) tilt record cannot, however, be readily correlated with eruptive behavior. Possible reasons for such lack of correlation include: (1) Diagnostic field observations are lacking. (2) The tilt reflects subsurface magma migration processes that caused no visible change in eruptive activity, such as intrusion or leakage into secondary storage reservoirs in the rift zone(s). (3) Unrecognized time lags exist between changes in summit tilt and changes at the site of eruption. Some particularly intriguing tilt oscillations, larger than usual and more periodic and cyclical in amplitude, cannot be fully accounted for by changes in visible activity. The June–August 1972 oscillations (figs. 16.4, 16.37) occurred during a quasi-steady-state period when a well-integrated tube system supplied sustained overflows. Similar oscillations in late July–September 1973 occurred during a two-month repose in visible activity (fig. 16.4) when the summit was inflating.

These cyclical oscillations have a period of 20 to 21 days and are therefore unlikely to be related to fortnightly earth tides. They may reflect pulses of magma entry into shallow secondary reservoirs within the east rift zone, which caused localized intrusion and associated ground deformation rather than observable changes in surface activity at Mauna Ulu or Alae. Dzurisin and others (1984, fig. 4) demonstrated that similar oscillations (though more variable in amplitude), in April–August 1980 reflected periodic leakage of magma from the summit reservoir into the east rift zone. Unfortunately, the Mauna Ulu flows during 1969–74 repeatedly destroyed instrument sites and buried much of the established geodetic network in Kilauea's upper east rift zone. Periodic reoccupations that had been planned for these sites might have provided critical data on the possible existence of subsidiary magma storage reservoirs between the summit and the Mauna Ulu-Alae area or even farther downrift. Evidence for a secondary reservoir near Makaopuhi Crater before May 1969 was presented by Jackson and others (1975) and by Swanson and others (1976a).

If adjusted for the offset caused by the April 1973 Honomu earthquake, the net change in summit tilt during the entire eruption, February 3, 1972 to July 22, 1974, was no more than +8 μrad. Thus the 1972–74 Mauna Ulu eruption, despite the tilt excursions related to the two 1973 outbreaks near Pauahi (figs. 16.4, 16.37), resulted in negligible net inflation in terms of Uwekahuna tilt.

Throughout the eruption, the east-west component of summit tilt and the north-south component varied sympathetically, except during two intervals: August–December 1972 and June–October 1973. Individual tilt peaks during these intervals can be correlated, but the east-west component indicates apparent net inflation and the north-south component shows apparent net deflation (figs. 16.4, 16.37). Such a pattern can be produced either by an inflation center northeast of the Uwekahuna vault or by a subsidence center

southwest of it. Abundant studies of other historical Kilauea eruptions (for example, Fiske and Kinoshita, 1969; Duffield and others, 1982) provide no support for the possibility of an inflation center northeast of Uwekahuna. Although the alternative interpretation seems to be more plausible, given the well-documented and wide-ranging lateral shifts in inflation centers in the southern part of the summit, it too is unsatisfactory (see section below titled "Results of level, tilt, and trilateration surveys"). A departure from the general correspondence between the east-west and north-south components also characterized the period September 1970–April 1971 (Swanson and others, 1979, fig. 2) during stage 3 of the 1969–71 Mauna Ulu eruption, when lava-lake and associated processes were well developed and dominated the eruptive activity.

RESULTS OF LEVEL, TILT, AND TRILATERATION SURVEYS

Variations in Uwekhuna tilt provide a useful guide to the behavior of the summit magma reservoir, but they only represent measurements at a single locality and should be interpreted within the context of other geodetic data from ground-deformation networks spanning the entire summit of Kilauea.

SEPTEMBER 1971–JANUARY 1972: PRE-ERUPTION INFLATION

Ground-deformation networks in the summit region of Kilauea were reoccupied periodically before and during the 1972–74 Mauna Ulu eruption (table 16.4). Particularly useful are the results of closely bracketed surveys that included the reoccupation of the level or trilateration network in addition to the more frequently measured tilt network (tilt surveys were made by the spirit-level tilting or dry-tilt technique described by Kinoshita and others, 1974, p. 91). These data allow comparison of the geodetic response of the entire summit region with the tilt changes observed at Uwekahuna. For example, the 4-month net inflation (+43 μrad) preceding the 1972–74 Mauna Ulu eruption was clearly recorded by all three types of surveys, which delineated a well-defined center of inflation located about 1 km south-southeast of Halemaumau Crater (fig. 16.38*A*; Duffield and others, 1982, fig. 10*B*).

FEBRUARY 1972–APRIL 1973: QUASI-STEADY-STATE ACTIVITY

Only data from tilt surveys are available for the first several months of the eruption, a period of relatively small tilt changes at Uwekahuna but substantial visible activity at Mauna Ulu and Alae. The pre-eruption inflation, which during January 1972 resulted in a net Uwekahuna tilt change of about +15 μrad, is well expressed by plots of tilt vectors determined from measurements during January 26–28, about a week before resumption of activity at Mauna Ulu, and during the next survey on February 7–9 (fig. 16.38*B*). The period bracketed by these two surveys, though it included the start of eruption on February 3 and the tilt peak on February 5, showed virtually no net change in the east-west component of Uwekahuna tilt (figs. 16.4, 16.37). Given the measurement uncertainty of 2–3 μrad, the solid line vectors in figure 16.38*B* should have been essentially random in direction, if the Uwekahuna tilt was representative of the entire summit region. However, the vectors for the field surveys yield a fairly well-defined pattern consistent with slight summit inflation. Moreover, vectors calculated from the east-west and north-south components of Uwekahuna tilt are compatible with this inflation pattern (fig. 16.38*B*).

During the next survey period, the net Uwekahuna tilt change was negligibly small (+3 μrad), and the almost random array of vectors was not amenable to simple interpretation (fig. 16.38C). The next period, February 22–25 to March 7–9, encompassed major overflow activity at Mauna Ulu and net Uwekahuna deflation of about 9 μrad. The resulting tilt vectors for this period show a weak but nevertheless coherent deflation pattern (fig. 16.38*D*), in agreement with tilt data from Uwekahuna.

These results indiate that the measurable geodetic response of the entire summit region may not correspond to that at Uwekahuna vault during periods of minor inflation or deflation. Indeed, these observations in turn raise intriguing questions about the magma-conduit system: Is there some threshold value in the rate or volume of magma transport that must be exceeded before surface response becomes coherent over the entire summit region? Because Kilauea does not deform purely elastically (see Davis and others, 1974) but possesses a finite yield strength, must time elapse to accommodate inelastic deformation before elastic behavior dominates and integrated geodetic response is established?

It is difficult, perhaps impossible, to answer such questions with existing data, because the tilt surveys are significantly less precise than the water-tube tilt measurements at Uwekahuna. In addition, some ground displacements considerably larger than those discussed show widely diverse geodetic responses of the summit region: the center of inflation or deflation can migrate as much as 3 km in any direction within weeks; deflation generally is not a simple reversal of the preceding inflation; and the complexity of Kilauea's overall magma reservoir system allows local behavior to be almost independent for short periods of time (Fiske and Kinoshita, 1969; Swanson and others, 1976a; Duffield and others, 1982; Ryan and others, 1983; Dzurisin and others, 1984).

No appropriately paired deformation surveys are available to evaluate the effects of the mid-March deflation (13 μrad at Uwekahuna), the largest during 1972 (figs. 16.4, 16.37), which accompanied the opening of the west-flank fissure at Mauna Ulu and of Alae vents C and D that fed voluminous overflows. However, this deflation is reflected in the frequently measured lines of the summit EDM monitor (fig. 16.39).

Through May 1972 the eruption was characterized by a net Uwekahuna tilt change of −20 μrad, associated with a broad, kidney-shaped area of subsidence across the eastern part of the summit region (fig. 16.40*A*). The tilt vectors are consistent with the vertical displacements. However, similarly paired trilateration surveys (table 16.4) yield a pattern of vectors of horizontal ground displacements that is incompatible with the deflation pattern derived from tilt and level data. The reasons for this incompatibility are unknown but are under study. In addition, net summit deflations of

small magnitude, especially those involving several wider oscillations in summit tilt may in general yield less simple patterns than summit inflations.

The period June–December 1972, an interval of nearly continuous eruptive activity at Mauna Ulu and Alae, was characterized by a few months of periodic tilt oscillations (fig. 16.19) with virtually no net change in Uwekahuna tilt, followed by modest apparent net inflation of +15 μrad. However, during part of this period, the north-south component of Uwekahuna tilt indicated apparent net deflation. Perhaps these tilt data are best interpreted as indicating deflation localized south and west of Uwekahuna, as suggested by the vector calculated from the east-west and north-south tilt components (fig. 16.40*B*, vector UWE). Such deflation accords with the results of level and tilt surveys, which also suggest minor subsidence east of Pauahi (fig. 16.40*B*), but the azimuth of vector UWE appears to be incompatible with the deflation center defined by level data and vectors for other tilt sites. This incompatibility demonstrates that during the second half of 1972 Uwekahuna tilt changes were not representative of Kilauea summit as a whole. The trilateration data for the same period also yield a pattern of horizontal ground displacements that, despite being locally aberrant, can be reconciled with a model of complex net deflation (fig. 16.40C).

Comparing the surveys bracketing the entire period from mid-January to mid-December 1972 accumulates the effects of small changes and results in a coherent pattern of net deflation; the secondary low in the Pauahi-Mauna Ulu area is also reasonably defined (fig. 16.40*D*). The azimuth of the tilt vector for UWE, however, still appears anomalous with respect to the well-defined deflation center south of Halemaumau.

A weak trend of net deflation through April 1973 was expressed by both east-west and north-south components of Uwekahuna tilt and the summit EDM lines (figs. 16.37, 16.39). Remeasurement of the summit tilt network during mid-March 1973 yielded tilt vectors of about 15 μrad or less relative to the previous survey in mid-December 1972; these small changes yield a diffuse pattern (not shown) similar to those obtained during 1972.

Collectively, these data demonstrate the difficulty in making an internally consistent interpretation of ground displacements during a period dominated by quasi-steady-state eruptive activity and attendant subsurface magma transfer. In the absence of major shifts of magma from summit to rift, the geodetic response of the ground surface to small changes affecting the volcanic conduit system is apparently influenced by independent adjustments to local stresses. In addition, the Uwekahuna tilt changes, especially during June–December 1972, seem aberrant and permit interpretations incompatible with deformation patterns derived from tilt, level, and trilateration surveys.

The April 1973 Honomu earthquake, which perhaps caused or accelerated the termination of the quasi-steady-state activity, seemingly produced only minor dislocations of the volcano's surface. Other than the 18-μrad earthquake-induced offset of the Uwekahuna tiltmeter (fig. 16.37) and a 2-cm dilation of a crack at the rim of Mauna Ulu crater (Tilling, 1976a, fig. 3), no data exist to suggest other measurable geodetic response to the April 26 main shock and the 57 located aftershocks.

MAY–NOVEMBER 1973: NET SUMMIT INFLATION AND CHANGE IN ERUPTIVE MODE

The May–November 1973 period was characterized by substantial net inflation at Uwekahuna (+30 μrad) and encompassed the short-lived outbreaks at Pauahi-Hiiaka in May and at Pauahi in November, as well the partial draining of Mauna Ulu lava lake on June 9.

The May 5 Pauahi-Hiiaka eruption was accompanied by deflation of about 20 μrad at Uwekahuna. Posteruption ground-deformation surveys (table 16.4) yield a pattern typical for Kilauean east-rift eruptions or intrusions (for example, Jackson and others, 1975, figs. 13, 32; Swanson and others, 1976a, fig. 20): a distinct deflation at the summit coupled with uplift and associated local collapse at the eruption site (fig. 16.41*A*). The level data indicate maximum subsidence of 209 mm centered southeast of Halemaumau, slightly north of the center of inflation during the quasi-steady-state activity of 1972. The May 5 eruption was accompanied by intrusion in the Pauahi-Hiiaka area and into the Koae fault system, resulting in maximum measured uplift as great as 117 mm. Geodetic control is not good, but contours of equal vertical displacement can be drawn that reflect dike intrusion into the Koae fault system indicated by seismicity (Koyanagi and others, 1973). Within the uplifted area, graben-like collapse occurred along existing and new cracks in the vicinity of the eruptive fissures and resulted in vertical displacements as great as 250 mm (fig. 16.41*A*). Some ground cracks widened by as much as 0.5 m.

The results of tilt and trilateration surveys are consistent with the deformation pattern derived from the level data (figs. 16.41*A*, *B*). The tilts associated with the May 5 eruption are an order of magnitude greater than those recorded during 1972. The large horizontal displacements near Pauahi and Hiiaka reflect distension related to eruptive fissures and inferred intrusion into the Koae fault system (fig. 16.41*B*). However, the displacement vectors for benchmarks in the western part of the network, which are far removed from the sites of eruption and intrusion, appear anomalous and are not understood at present.

The summit reinflated rapidly following the May 5 eruption, and by early June the Uwekahuna tilt had essentialy recovered from its 20-μrad deflation. This rapid inflation is well shown by tilt surveys, which indicate a broad area of uplift east and south of Halemaumau (fig. 16.41C). Tilt site Escape Road No. 2 (fig. 16.41C), however, shows downtilting toward the eruption area; apparently this site had not fully recovered from the localized collapse and ground cracking of the May 5 eruption (figs. 16.41*A*, *B*). A few horizontal displacements (not shown) obtained from partial reoccupation of the trilateration network are compatible with the summit-inflation pattern defined by the tilt.

Partial draining of Mauna Ulu lava lake and related minor intrusion on June 9 were marked by a deflation of 7 μrad at Uwekahuna. The two tilt surveys that bracket this event (table

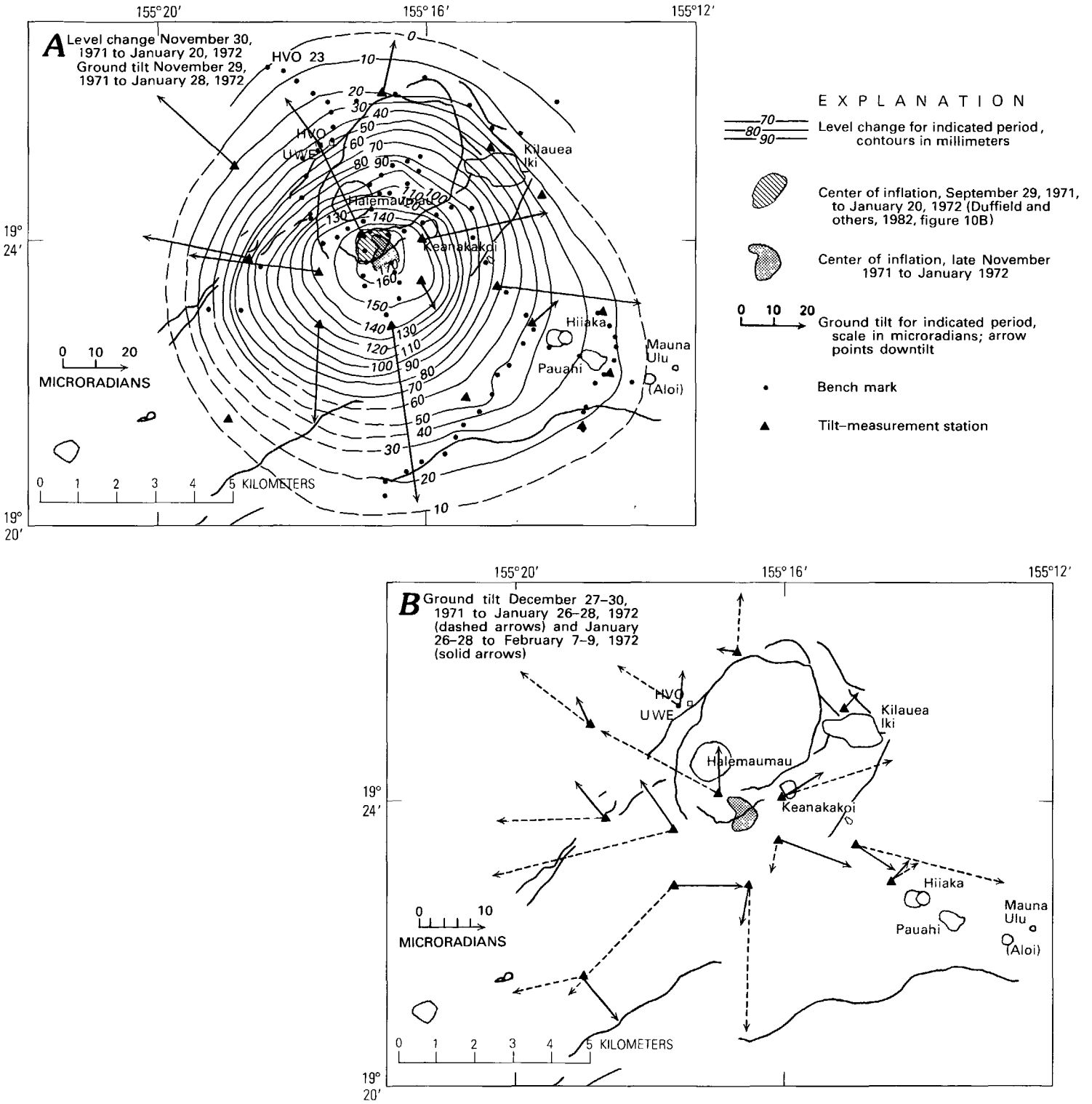

FIGURE 16.38.—Results of level and tilt surveys on Kilauea before and during first two months of the 1972–74 Mauna Ulu eruption. Vector UWE (red) calculated from east-west and north-south components of Uwekahuna tilt. Contours of level data referenced to bench mark HVO 23, assumed to be stable. ***A***, Well-defined pre-eruption inflation between November 1971 and January 1972. Inflation center defined for this 2-month period is virtually coincident with that obtained by Duffield and others (1982, fig. 10) for the 4-month period building toward the 1972–1974 Mauna Ulu eruption. ***B***, Tilt for periods spanning the final month of pre-eruption inflation (dashed vectors) and first days of the eruption beginning on February 3, 1972 (solid vectors). Survey period bracketing the start of eruption involved no net change in Uwekahuna tilt (see text). ***C***, Tilt vectors between February 7–9 and February 22–25, 1972, an interval with only about +3 microradians net change in Uwekahuna tilt (apparent inflation). ***D***, Tilt vectors between February 22–25 and March 7–9, 1972; net change in Uwekahuna tilt was about −9 microradians (apparent deflation), consistent with deflation indicated by vectors.

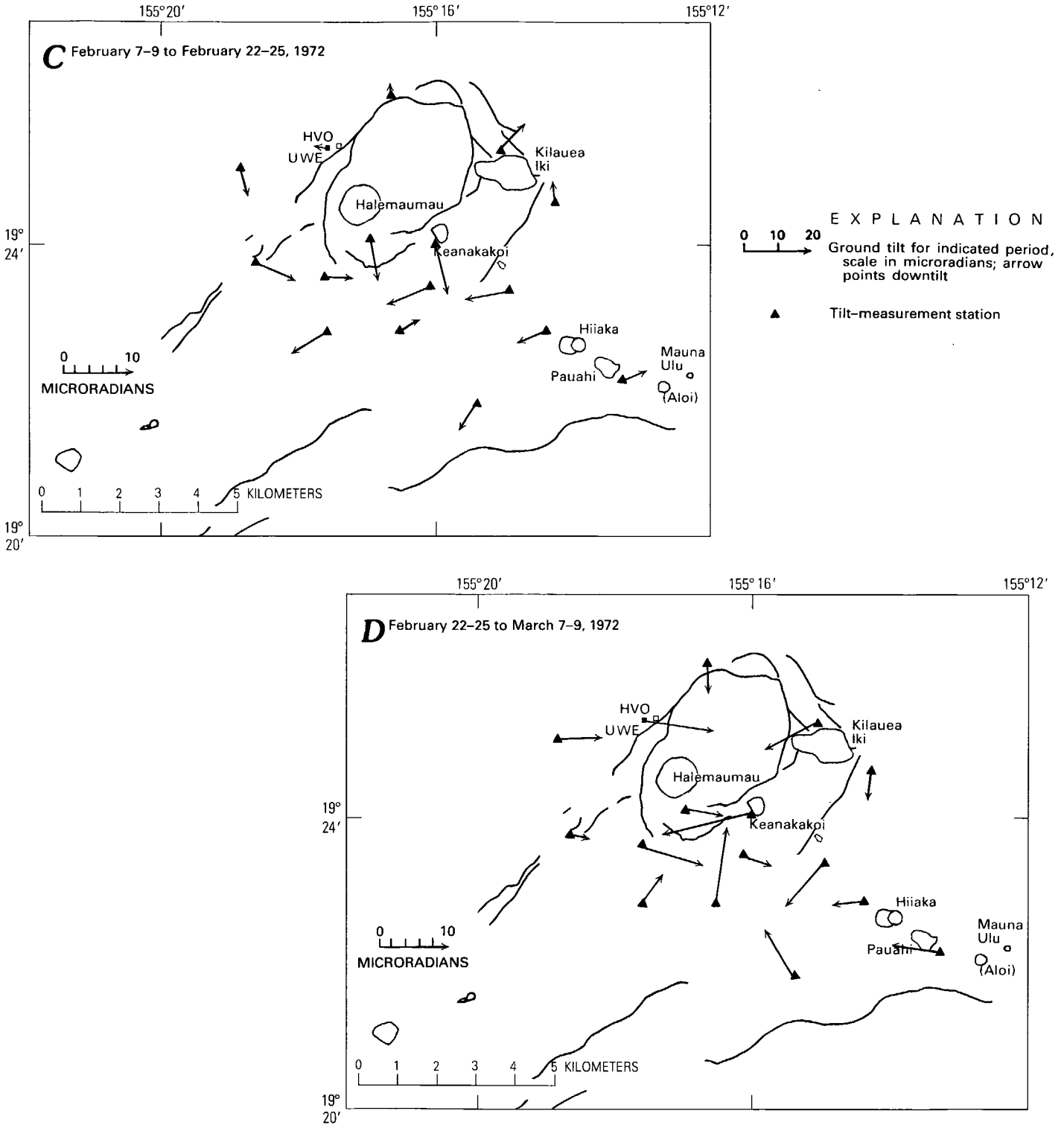

FIGURE 16.38.—Continued.

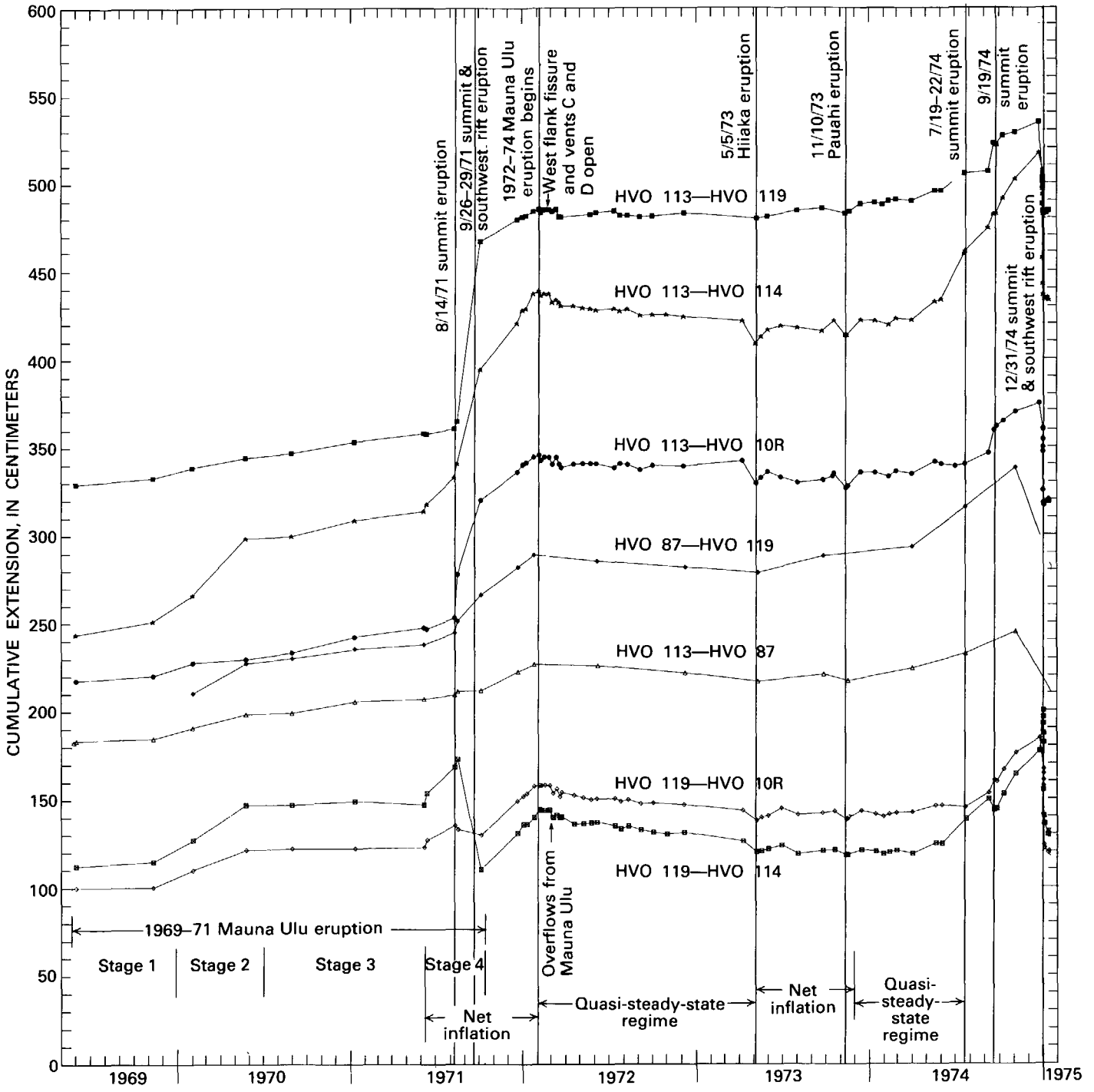

FIGURE 16.39.—Variations of distances within the summit EDM monitor between May 1969 and January 1975; locations of lines are shown in figure 16.36. Cumulative extension scale (in centimeters) is arbitrary. Frequent measurements detected small deflations in February and March 1972 related to overflows from Mauna Ulu and opening of new vents, respectively. Dotted parts of the curves for the 1973–74 period show probable variations if more frequent measurements had been made. Frequency of measurement during 1969–71 was about same as during 1972–75 (see Swanson and others, 1979, fig. 2; Duffield and others, 1982, fig. 2) but not all data plotted here.

16.4) yielded a diffuse net inflation pattern similar in shape but of slightly smaller magnitude to that obtained for the preceding survey period (see figs. 16.41*C*, *D*). Measurable geodetic response to the events of June 9, if any, apparently was largely masked by the net inflation and continued localized adjustments to the May 5 eruption that prevailed during May and June.

The reoccupation of all summit deformation networks beginning in mid-September provided data documenting the complex reinflation process following the May 5 eruption. Level and tilt data suggest a very broad zone of posteruption uplift, including the southeastern sector of the caldera and the upper part of the east rift zone (fig. 16.42*A*). The maximum vertical displacements occurred adjacent to the periphery of the eruption site on the north and southeast. The area of least vertical displacement coincides with the eruption site, indicating incomplete recovery from the localized collapse associated with the eruption (compare figs. 16.41 and 16.42). The pattern of horizontal ground displacements for the same survey period (fig. 16.42*B*) is expectedly complex but reasonably compatible with that derived from ground tilt and level data.

Net inflation during the May–October 1973 period was ended by the eruption at Pauahi on November 10 and the associated Uwekahuna deflation of about 21 μrad. All summit deformation networks were reoccupied in mid-November (table 16.4), when weak vent activity was continuing within Pauahi Crater. The previous reoccupation was completed on October 3, which was during the inflation (fig. 16.37). The differences between the surveys therefore record only about 25 percent of the total Uwekahuna deflation: the maximum measured subsidence in the summit deflation area barely exceeded 40 mm at two distinct centers (fig. 16.42*C*). Otherwise, the deformation pattern accompanying the November eruption—weak summit deflation coupled with stronger uplift and associated local collapse at the eruption site—closely resembles that for the May 1973 Pauahi-Hiiaka outbreak (see figs. 16.41, 16.42). As in May, the results of the level, tilt, and trilateration surveys bracketing the November eruption are mutually consistent.

Rapid reinflation of the summit began as soon as the peak eruptive activity of November 10–11 had dwindled to weak vent activity that persisted for nearly a month. This inflation was expressed by a tilt survey in mid-December, which shows a relatively well-defined inflation center east of Halemaumau, as well as local tilt changes presumably reflecting weak vent activity in December (fig. 16.42*D*).

DECEMBER 1973–JULY 1974: RETURN TO QUASI-STEADY-STATE REGIME AND DEPARTURE FROM 1972–73 ERUPTIVE BEHAVIOR

Kilauea apparently returned to quasi-steady-state activity in December, following rapid recovery from the November 10 outbreak at Pauahi. This is inferred from variations in Uwekahuna tilt, which showed little net change for the December 1973–July 1974 period, even though the tilt oscillations were larger than those in the quasi-steady-state period in 1972–73. The existence at this time of a highly efficient hydraulic connection between the summit reservoir and Mauna Ulu is illustrated by the close correlation between minor variations in summit tilt and visible activity during the eruptive episodes, especially the well-documented episodes during January–February 1974 (fig. 16.30). However, because of inclement weather and instrument breakdown, few deformation surveys were conducted during 1974, and we do not know whether slight shifts from equilibrium might have been detected by more frequent remeasurements.

The tilt network was remeasured in January 1974 and again in March (table 16.4). Deviations in Uwekahuna tilt were small (no more than 5 μrad), and the survey periods were prolonged by bad weather and instrument problems; the results obtained do not permit good definition of patterns. Nonetheless, tilt vectors for the December 1973–January 1974 period can be interpreted as indicating weak deflation, and those for the January–March 1974 survey, as slight inflation (patterns not shown). For both survey periods the measured tilts were 15 μrad or less, and most of the larger values were at sites near Hiiaka and Pauahi, probably because of continuing adjustments to the November–December Pauahi eruption, or possibly reflecting the influence of the eruptive activity at Mauna Ulu itself.

The level and trilateration networks in the summit area were reoccupied in early April (table 16.4). The level data indicate summit inflation (fig. 16.43*A*), consistent with the net tilt change at Uwekahuna of about +5 μrad for the period November 1973–April 1974. Residual effects of local uplift and associated collapse during November–December 1973 were still evident in April near Pauahi. The location of the inflation center, about 1 km northeast of Halemaumau indicates a substantial northward shift from the pre-eruption inflation center and the net 1972 deflation center (fig. 16.43*A*). The deformation pattern (not shown) obtained from the trilateration data is not diagnostic, but it is compatible with that shown in figure 16.43*A*. No tilt-survey data exist for April 1974 for comparison with level and trilateration measurements. However, tilt vectors for the period between November 1973–May 1974 also indicate net inflation with a center northeast of Halemaumau (fig. 16.43*B*).

Dvorak and others (1983, table 2, fig. 3) used a least-squares inversion technique and a point-source elastic model to analyze the surface displacements for the November 1973–April 1974 period. They found that: (1) the inflation centers determined separately for level and trilateration data coincide reasonably well; and (2) the model depth to the point source (summit magma reservoir) ranges from 2.2 to 2.6 km, depending on whether level data, trilateration data, or both are used.

Following the July 19–22 summit eruption, which terminated the 1972–74 Mauna Ulu eruption on the east rift, geodetic surveys were run in late July (figs. 16.43*C*, *D*). Their results reflect the prolonged inflation that preceded the July summit eruption but are complicated by the 15-μrad deflation at Uwekahuna that accompanied the eruption (Peterson and others, 1976). Level and tilt surveys were not completed until July 31 and thus bracketed part of the summit reinflation. As is typical of Kilauea summit eruptions, the area of maximum displacement coincided with the loci of eruptive fissures in the southeastern part of the caldera and in and near Keanakakoi and Lua Manu Craters (figs. 16.43*C*, *D*). The complex area of weak subsidence along the east rift zone between Hiiaka and Mauna Ulu reflects lingering effects of the November 1973 Pauahi eruption.

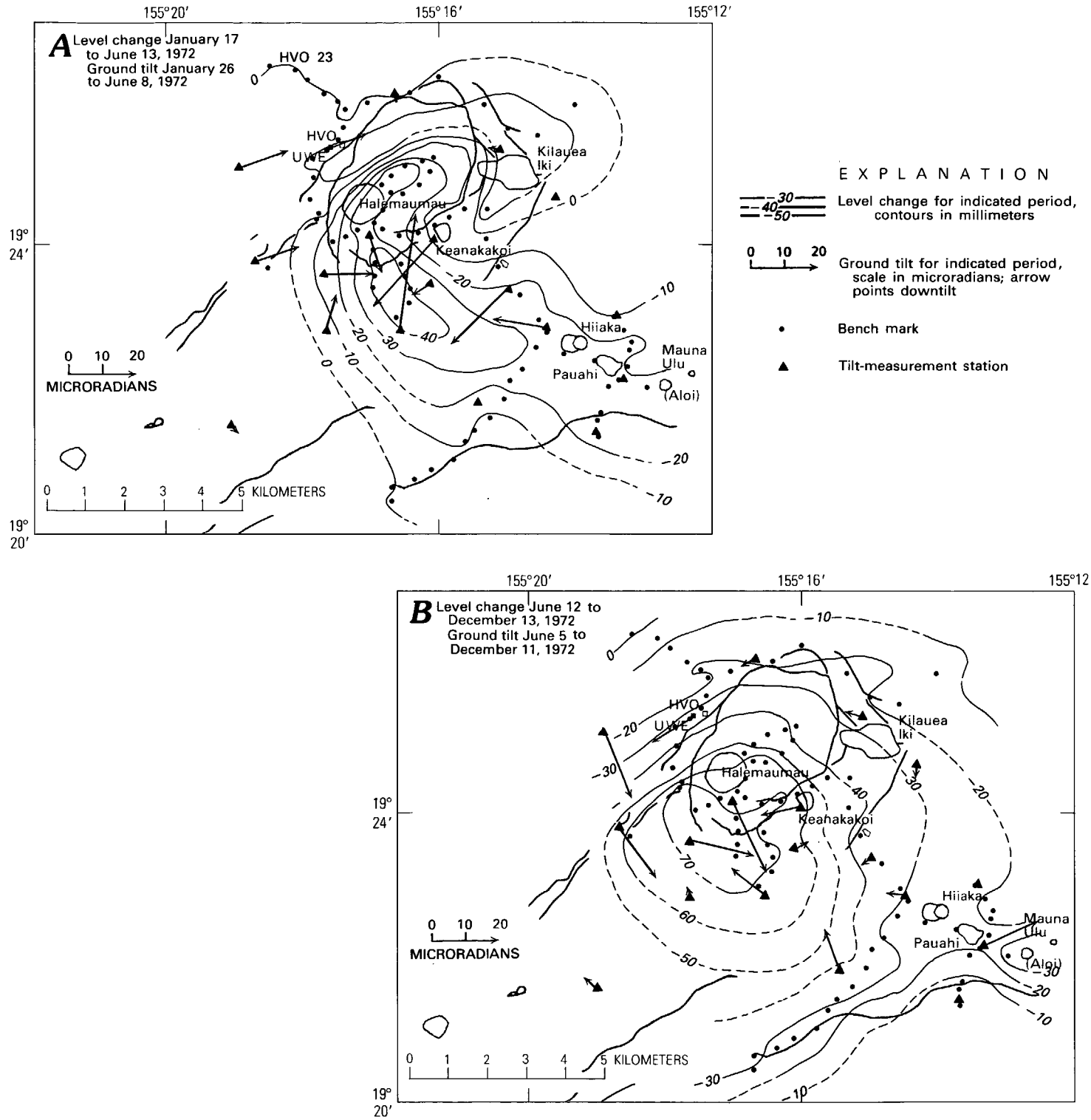

FIGURE 16.40.—Results of level, tilt, and trilateration surveys during 1972. Vector UWE (red) calculated from east-west and north-south components of Uwekahuna tilt. Contours of level data referenced to bench mark HVO 23, assumed to be stable. ***A***, Changes in elevation and tilt between January and June 1972; note change in vector scale from figures 16.38*B–D*. ***B***, Changes in elevation and tilt between June and December 1972, showing a weak but relatively well-defined pattern of net deflation; azimuth of vector UWE appears anomalous. ***C***, Horizontal displacements from trilateration surveys of Kilauea summit between June and December 1972. Displacement vectors determined by reference to assumed stable bench marks on southeastern flank of Mauna Loa Volcano (see Kinoshita and others, 1974). ***D***, Changes in elevation and tilt between January and December 1972. Combining the two survey periods shown in *A* and *B* yields a coherent deflation pattern; the azimuth of vector UWE is still anomalous. Note secondary area of subsidence in Pauahi-Mauna Ulu area.

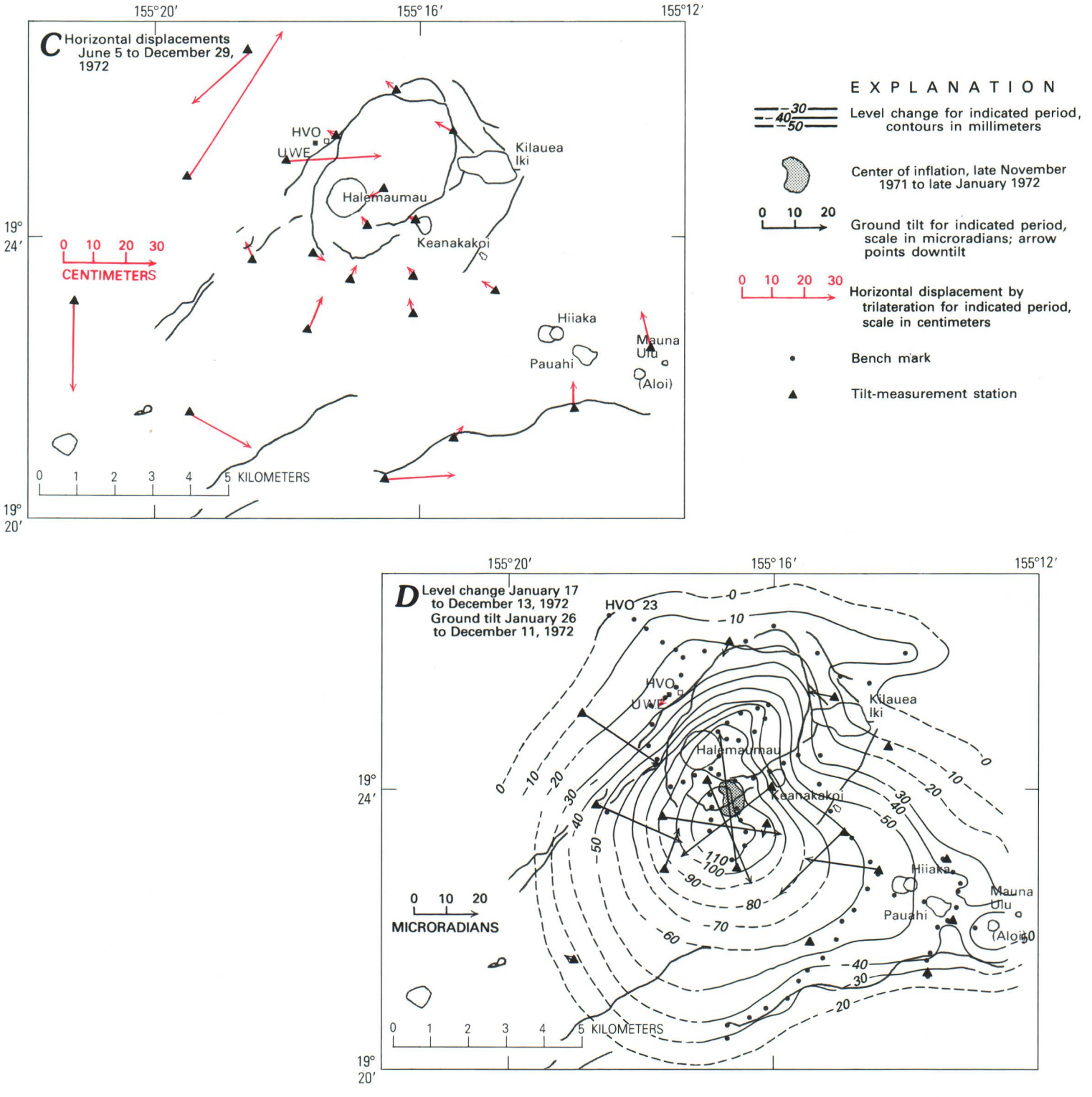

FIGURE 16.40.—Continued.

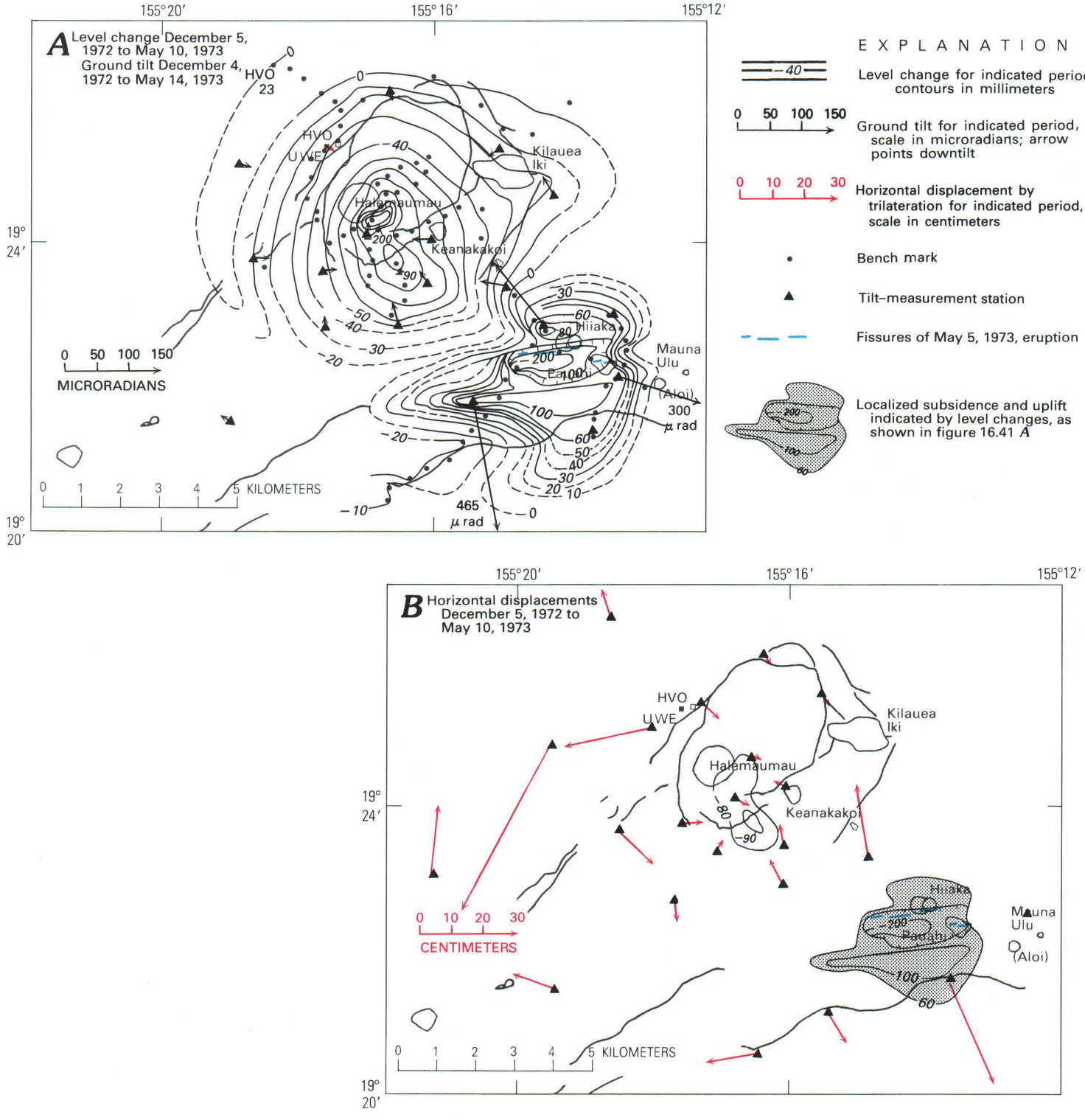

FIGURE 16.41.—Results of level, tilt, and trilateration surveys from December 1972 to June 1973. Vector UWE (red) calculated from east-west and north-south components of Uwekahuna tilt. Contours of level data referenced to bench mark HVO 23, assumed to be stable. ***A***, Changes in elevation and tilt between December 1972 and May 1973, showing the effect of the May 5 Pauahi-Hiiaka eruption and intrusion into eastern end of the Koae fault system (see text for discussion). Magnitude of tilt vectors and vertical displacements considerably larger than those in 1972 (compare with figs. 16.38 and 16.40). ***B***, Horizontal displacements from trilateration surveys between December 1972 and May 1973. Also shown are areas of localized subsidence and uplift determined from level data (see *A*). ***C***, Changes in tilt between May 7 and June 1, 1973, showing relatively small changes (note change in vector scale from *A*) that generally reflect summit inflation following May 5 eruption. Tilt in Pauahi-Hiiaka area reflects local adjustments (see text). ***D***, Changes in tilt between May 21 and June 28, 1973; this period includes the June 9 partial draining of the lava lake at Mauna Ulu. Effect of partial draining and associated intrusion is apparently masked by net inflation. Note change in vector scale from *A* and *C*.

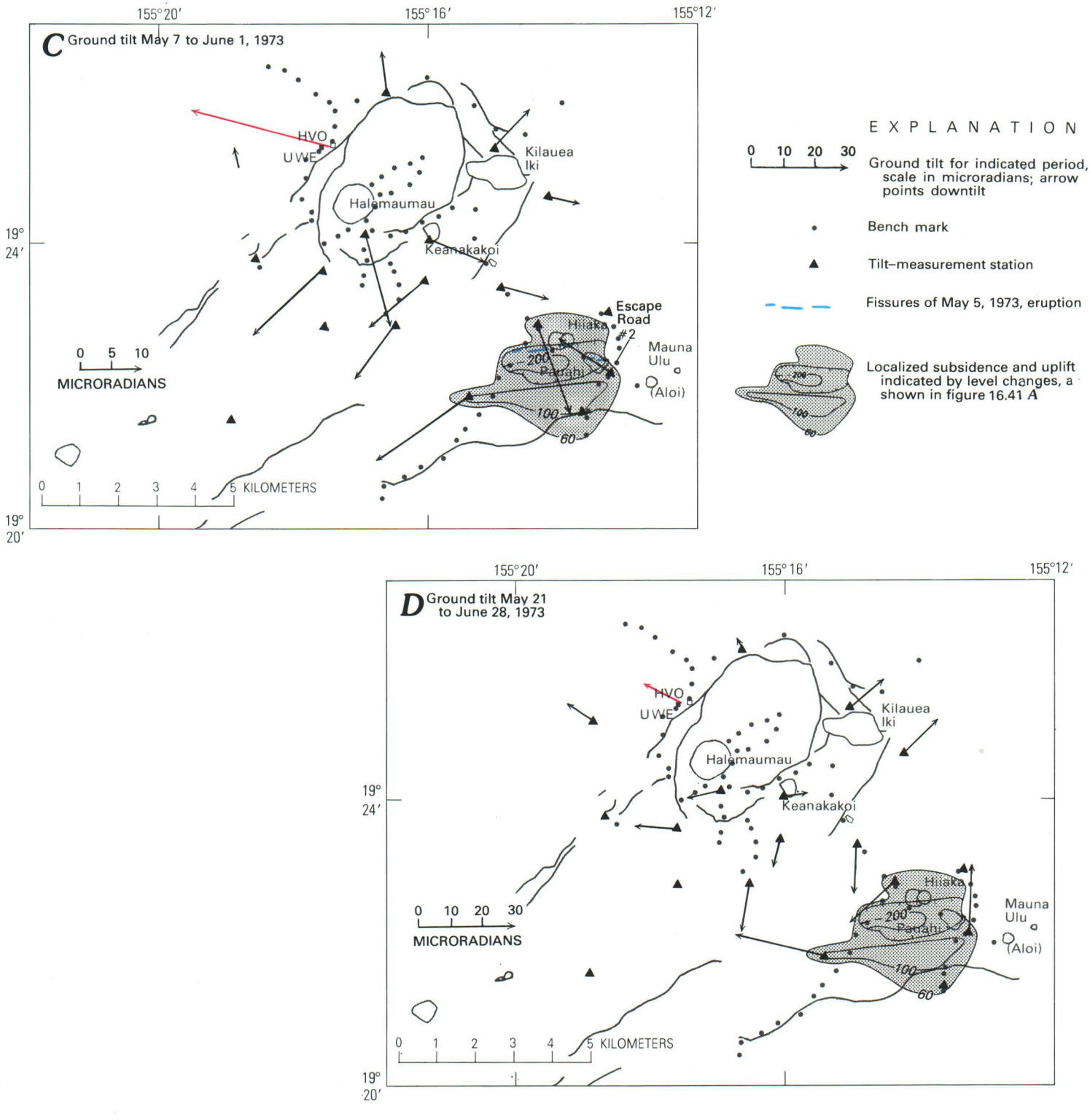

FIGURE 16.41.—Continued.

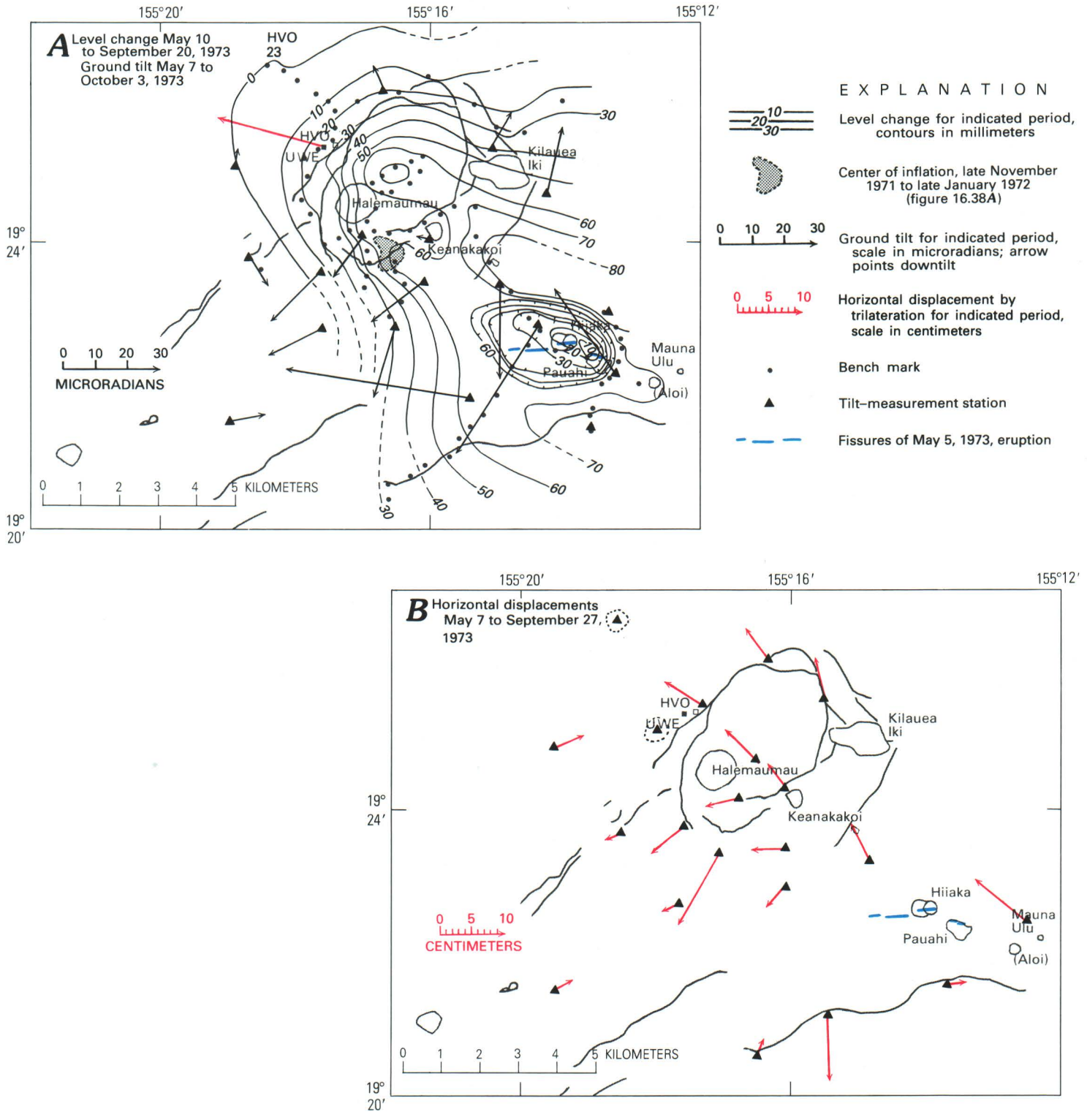

FIGURE 16.42.—Results of level, tilt, and trilateraton surveys from May to December 1973. Vector UWE (red) calculated from east-west and north-south components of Uwekahuna tilt. Contours of level data referenced to bench mark HVO 23, assumed to be stable. ***A***, Changes in elevation and tilt between May and September 1973. Effects of May 5 eruption and intrusion still evident. Elongate uplifted area shifted northward from previous inflation and deflation centers. ***B***, Horizontal displacements from trilateration surveys between May and December 1973. Changes are relatively small and resulting pattern diffuse; bench marks in dotted circles show northerly vectors that are masked by plot symbols (triangles). ***C***, Changes in elevation and tilt between September and November 1973, showing deformation associated with November 10–11 eruption at Pauahi. Deformation pattern generally similar to that for the May 5 eruption and other eruptions in Kilauea's upper east-rift zone (see text). ***D***, Changes in tilt between November and December 1973, reflecting summit inflation following the November 10–11 Pauahi eruption, which persisted feebly until December 9.

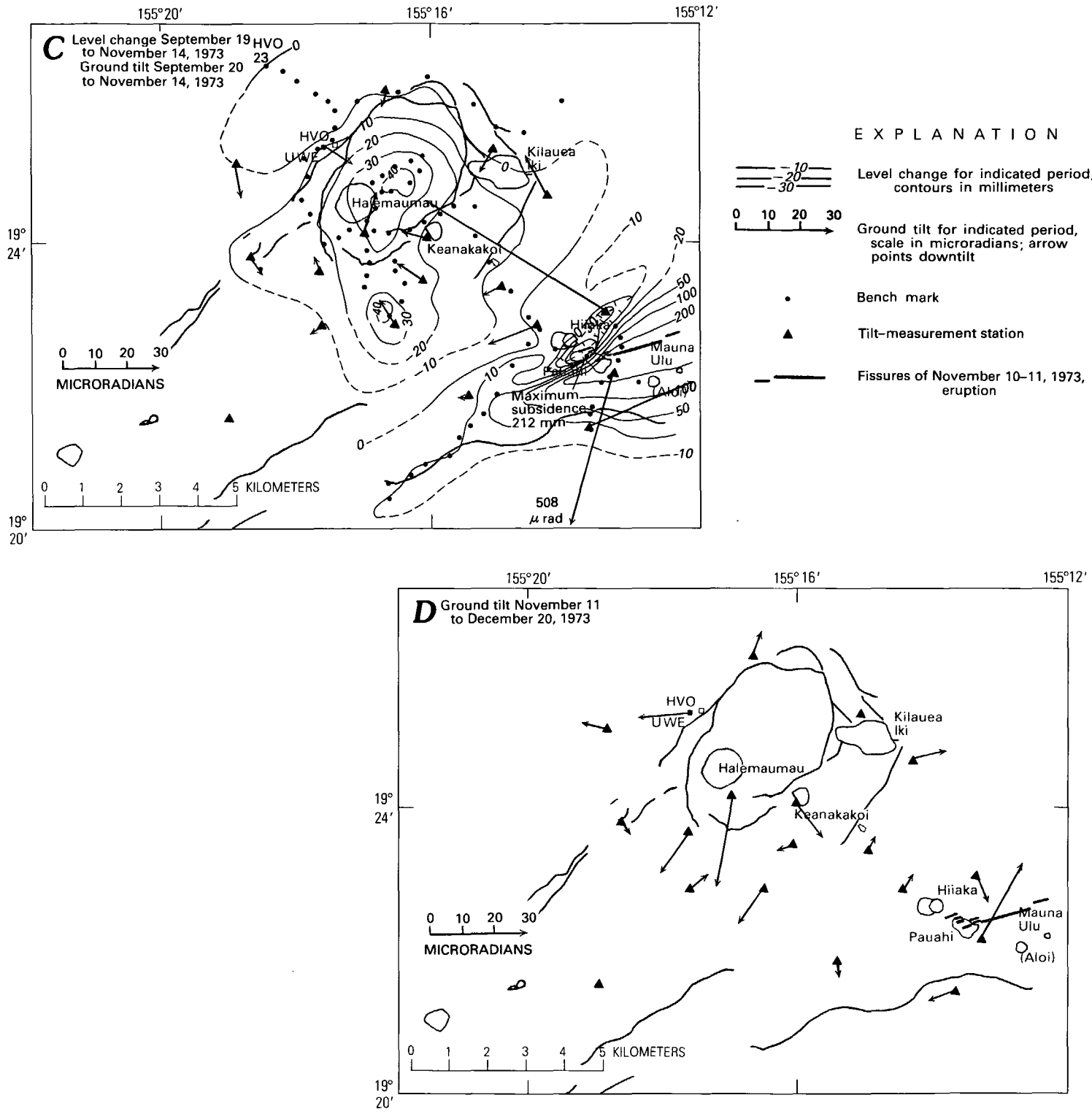

FIGURE 16.42.—Continued.

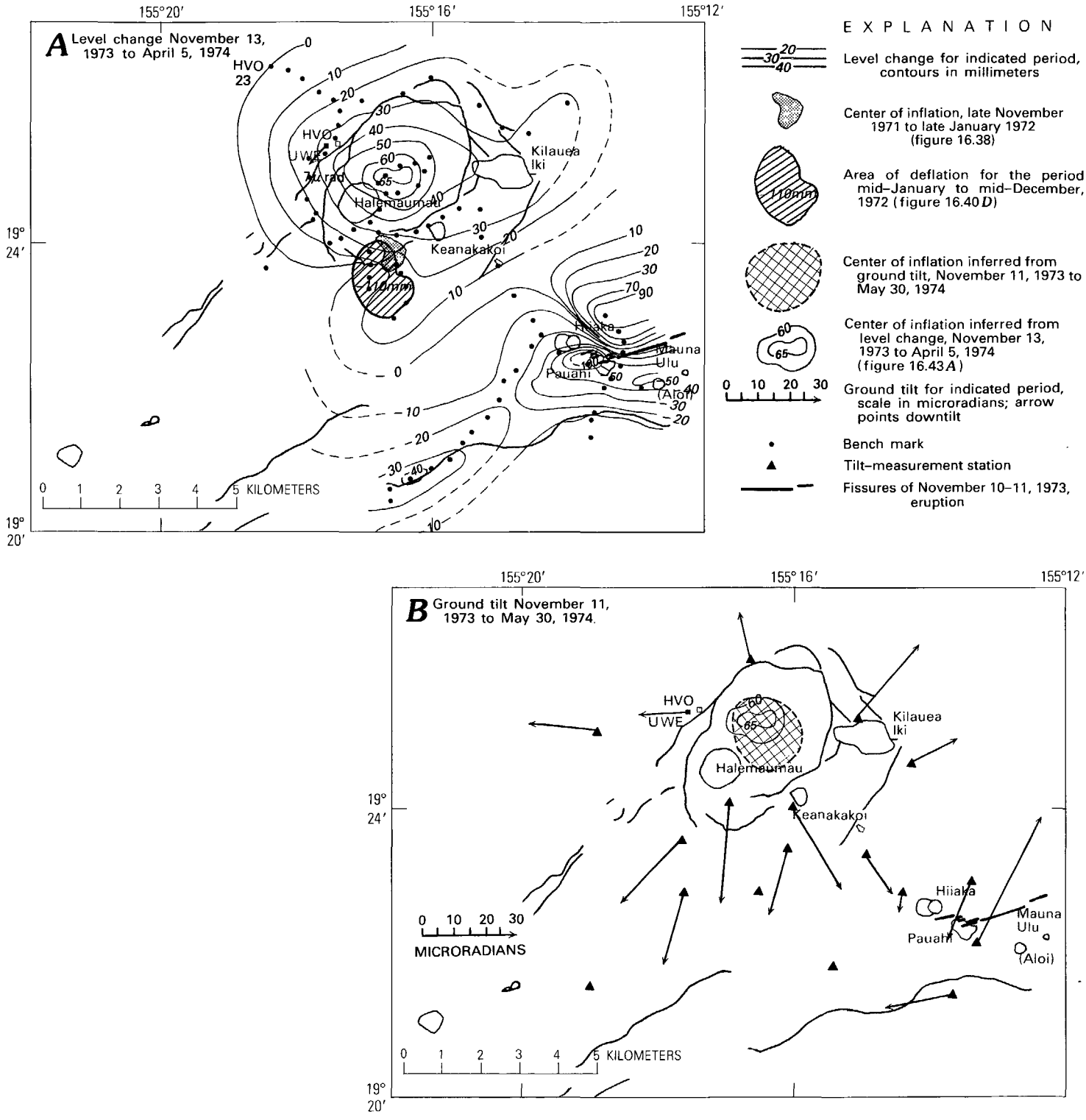

FIGURE 16.43.—Results of level, tilt, and trilateration surveys from November 1973 to July 1974. Vector UWE (red) calculated from east-west and north-south components of Uwekahuna tilt. Contours of level data referenced to bench mark HVO 23, assumed to be stable. ***A***, Changes in elevation between November 1973 and April 1974. Pattern of vertical displacements is complex and shows: (a) well-defined inflation center near northern end of uplifted area shown in figure 16.42*A*; (b) area of greater uplift north of Pauahi that perhaps reflects continued adjustments to November–December eruption; and (c) subsidence at and east of Pauahi, as well as in the eastern part of the Koae fault system. No corresponding data from tilt surveys available, but see *B*; azimuth of vector UWE appears anomalous. ***B***, Tilt vectors between November 1973 and May 1974. Broad inflation center corresponds well with previous centers determined from level data (see figs. 16.41, 16.42). Vector UWE is incompatible with radial pattern of vectors from tilt surveys. ***C***, Changes in elevation and tilt between March and July 1974, the period that includes the July 19–22 summit eruption and the end of the 1972–74 Mauna Ulu eruption on July 22. Well-defined uplift area coincides with active fissures of eruption in southern part of caldera near Keanakakoi and Lua Manu Craters. Bench mark at rim of Lua Manu (shown in red) collapsed about 2 m and not considered in contouring of the level data. ***D***, Horizontal displacements from trilateration surveys between March and July 1974. Displacement vectors point away from the eruptive fissures.

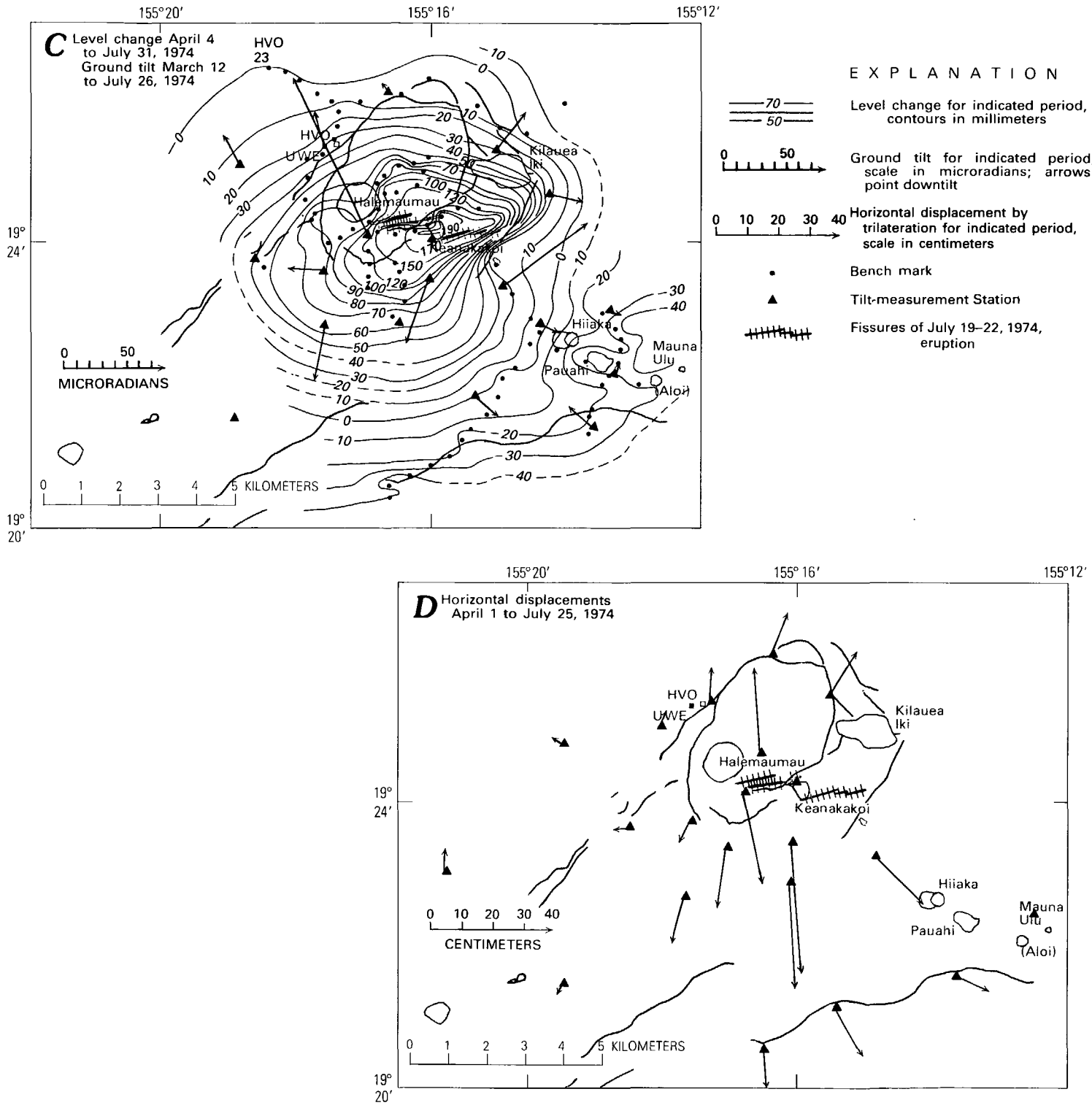

FIGURE 16.43.—Continued.

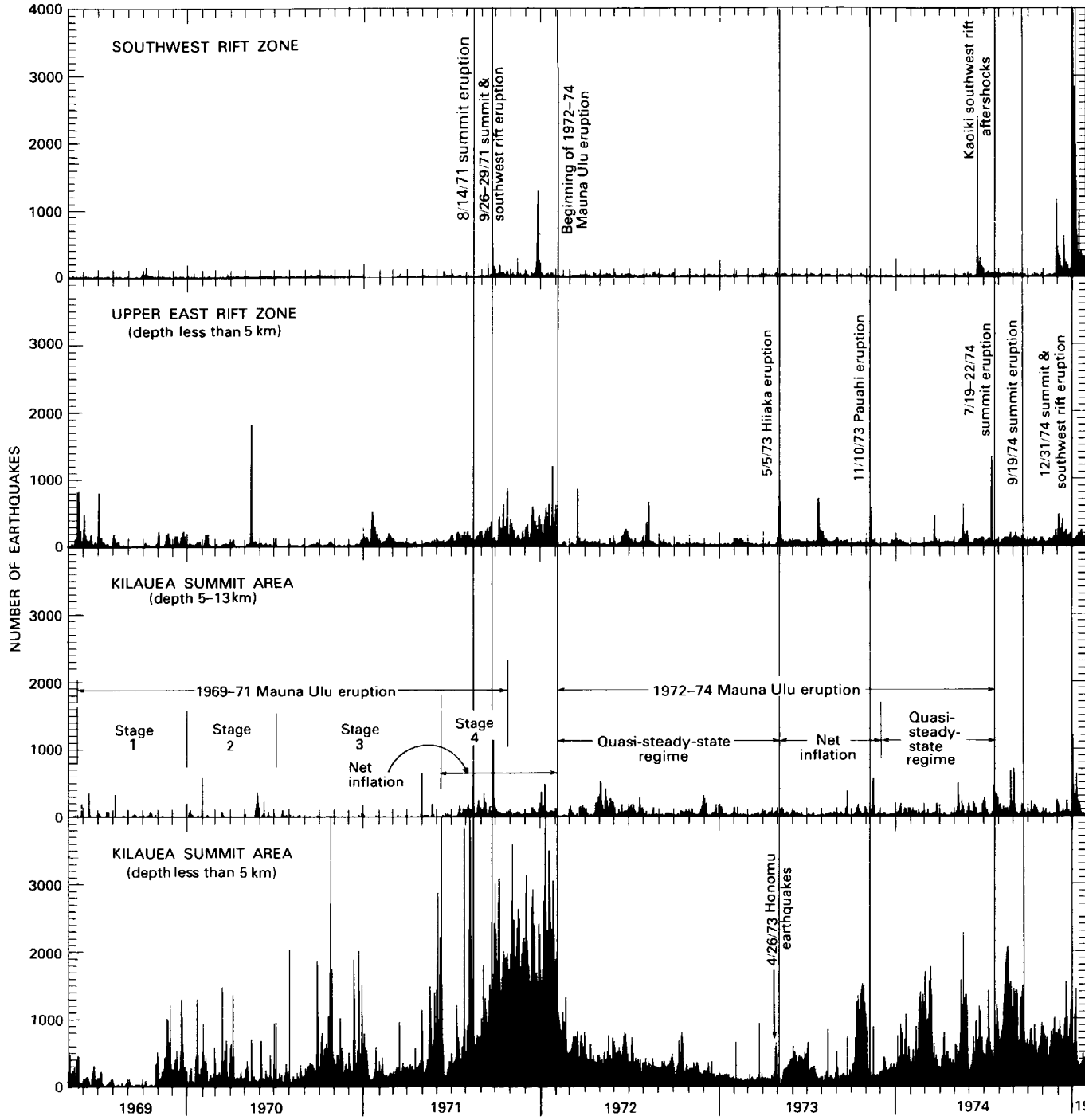

FIGURE 16.44.—Numbers of earthquakes in summit area (shallow and crustal depth), upper east rift zone, and southwest rift zone of Kilauea from May 1969 to January 1975. All events are counted, whether or not their hypocenters are well determined; counts for the southwest rift earthquakes include those in the Kaoiki fault system.

VARIATION IN SEISMICITY

Tabulations of earthquake counts and located events for 1972–74, as well as descriptions of the seismic network and instruments, have been published in summary form (Hawaiian Volcano Observatory, 1977a, 1977b, 1977c, 1977d, 1977e, 1977f, 1977g, 1977h, 1978). Some aspects of seismic activity during the 1972–74 period were discussed elsewhere (Koyanagi and others, 1973; Tilling and others, 1975; Koyanagi and others, 1976a, 1976b; Ellsworth and Koyanagi, 1977; Unger and Ward, 1979; and Aki and Koyanagi, 1981). We present in this paper a

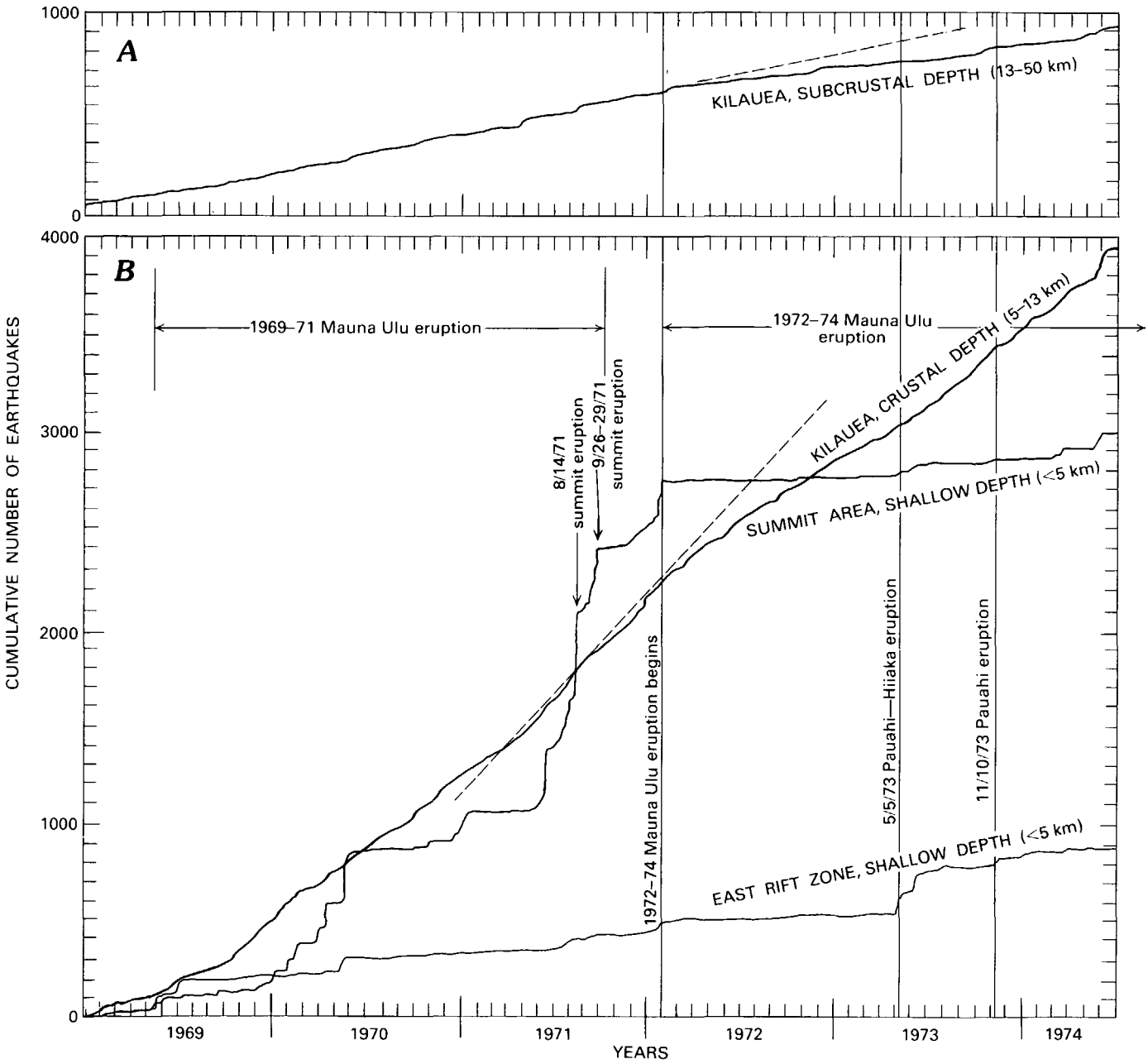

FIGURE 16.45.—Cumulative numbers of earthquakes with well-determined hypocenters, magnitude 1 or greater, at Kilauea from January 1969 to June 1974. ***A***, Subcrustal earthquakes (reference area: lat 19°11′ to 19°33′ N., long 154°48′ to 155°20′ W.). Dashed line is extrapolation of slope for period before onset of 1972–74 Mauna Ulu eruption. ***B***, Earthquakes of crustal depth (reference area: same as for subcrustal earthquakes) and shallow earthquakes in the summit area and east rift zone (reference areas: lat 19°23′ to 19°27′ N., long 155°13′ to 155°19′ W. and lat 19°20′ to 19°23′ N., long 155°06′ to 155°15′ W., respectively). Dashed line is extrapolation of slope of crustal-earthquake plot for pre-eruption net summit inflation beginning in mid-June 1971 (fig. 16.37); slope decreases after onset of 1972–74 eruption and then is similar to that during the 1969–71 Mauna Ulu eruption.

brief overview of the variation in seismicity (figs. 16.44–16.46) within the framework of the chronological narrative of volcanic activity. Systematic, more quantitative studies of the seismicity associated with the 1972–74 Mauna Ulu eruption are pending.

SEISMICITY BEFORE AND AFTER THE 1972–74 MAUNA ULU ERUPTION

Seismicity during the 1972–74 Mauna Ulu eruption was moderate relative to that of the preceding and subsequent periods.

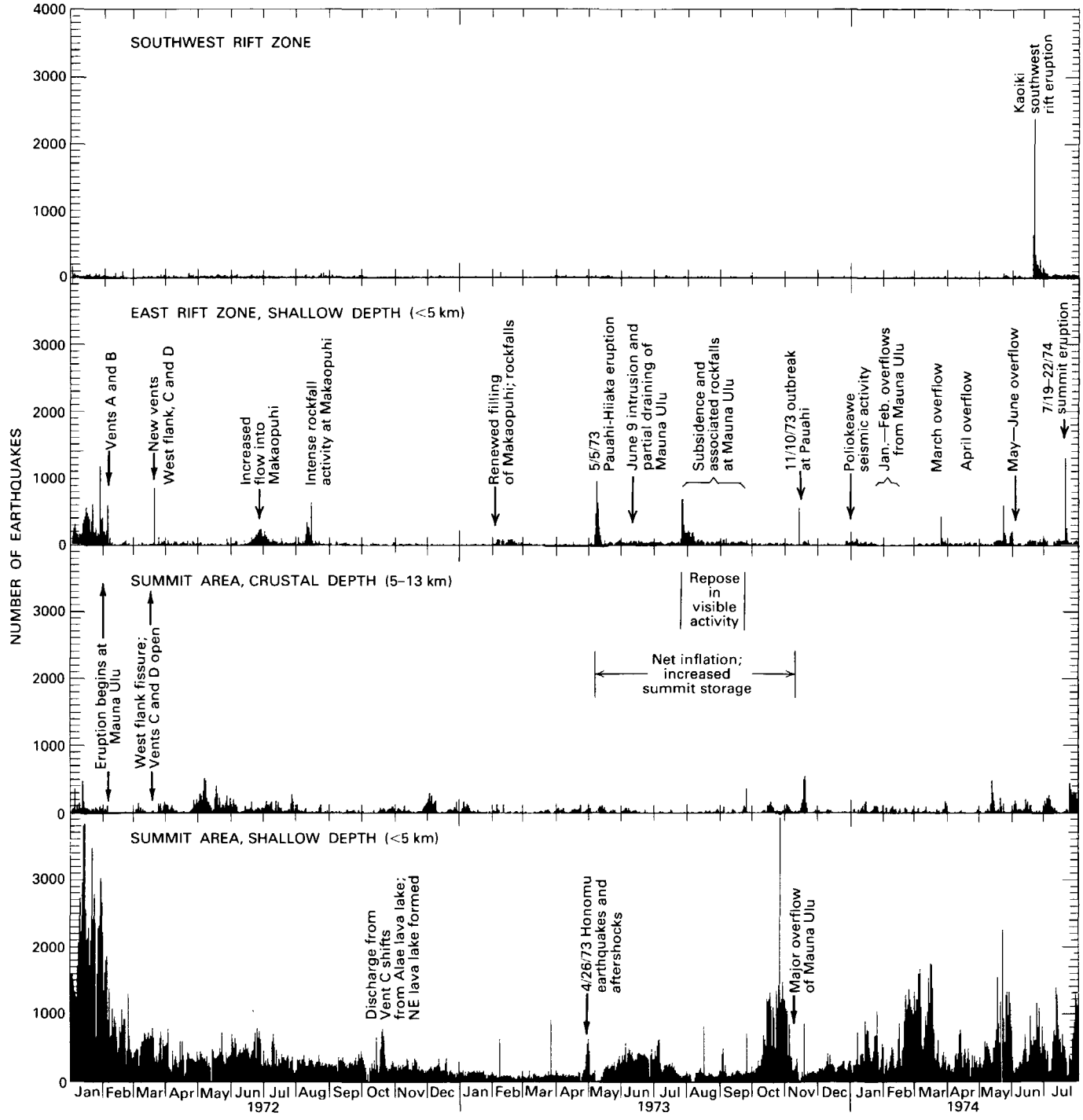

FIGURE 16.46.—Variation in seismicity during 1972–1974 Mauna Ulu eruption. Data also shown at smaller scale in figure 16.44. Significant changes in eruptive activity correlate with increased seismicity. Shallow summit-area earthquakes for the period January to March 1974 are shown in greater detail in figure 16.30.

Occurrence of long-period earthquakes at crustal depths (5–13 km) beneath Kilauea's summit became more frequent beginning in June 1971 (figs. 16.44, 16.45*B*), at about the same time as summit inflation. The generally reduced level of seismicity during the 1972–74 Mauna Ulu eruption, particularly of shallow (short-period) summit and east-rift earthquakes (depth less than 5 km), is especially evident during the first period of quasi-steady-state activity during February 1972–April 1973. Moreover, the occurrence of deeper Kilauea earthquakes (13–50 km) during the 1972–74 Mauna Ulu eruption decreased, as compared with that

during the 1969–71 Mauna Ulu eruption (fig. 16.44*A*).

As commonly observed at Kilauea, variations in the number of shallow summit earthquakes correlate closely with variations in tilt measured at Uwekahuna (see figs. 16.4, 16.37, 16.44–16.46). This correlation is well exhibited during the June 1971–January 1972 period, when the 1969–71 Mauna Ulu eruption gradually ended and the summit inflated in response to increased storage of magma in the summit reservoir (Duffield and others, 1982). A similar correlation exists between net inflation and incidence of upper-east-rift earthquakes during this period, implying periodic leakage of magma into the rift zone as the stressed summit reservoir failed repeatedly during reestablishment of the magma conduit system leading to Mauna Ulu. Within this context, the August 1971 summit eruption and the September 1971 southwest-rift eruption may be considered as massive and rather abrupt leakages by surface venting, inasmuch as the strong net summit inflation was only briefly interrupted by these events (Duffield and others, 1982).

SEISMICITY DURING THE ERUPTION

Sporadic bursts of low-level harmonic tremor in the summit region and upper east rift were recorded throughout the September 1971–January 1972 period of summit inflation. However, tremor increased in amplitude and became sustained in the early morning of February 4, 1972, only a day after the start of renewed eruption at Mauna Ulu. Within the next two days, as the new lava lake rose rapidly and vent activity increased, the numbers of shallow summit and upper-east-rift earthquakes decreased dramatically and thereafter remained low through April 1973 (fig. 16.46). This prolonged period of low seismicity implies the existence of a highly efficient and open system of magma transfer between the summit reservoir and the eruption site. We interpret the gradual net decline of shallow summit earthquakes during this period as reflecting a progressive improvement in the ability of the conduit system to transfer magma freely. Most of the conspicuous departures from the prevailing background of low seismicity can be correlated with changes in eruptive and associated activity and are so annotated in figure 16.46. Perhaps the most notable seismic events in 1972, however, were those associated with the continuous lava inflow into Makaopuhi in June–July and with the intense rockfall activity at Makaopuhi in August (Tilling and others, 1975), rather than with vent activity at Mauna Ulu or Alae.

An abrupt change in the magma-transfer regime, beginning in early May 1973, is clearly reflected in a seismic signature that that is distinct from that for the previous 15 months (figs. 16.44, 16.46). We correlate this change with obstruction of the magma transfer conduit caused by the April 26, 1973, Honomu earthquake, although we concede that their coincidence in timing could be fortuitous. Whatever the cause, the changed magma regime was expressed initially by an immediate increase in the number of shallow summit earthquakes, followed by increased east-rift seismicity in early May that preceded and accompanied the May 5 draining of Mauna Ulu and Alae lava lakes, the Pauahi-Hiiaka eruption, and the associated intrusion into the Koae fault system. After the eruption, the level of earthquake activity and harmonic tremor remained high until the early morning hours of May 6. Most of the earthquakes during this time occurred in the upper east rift zone and in the middle and eastern portions of the Koae fault system, with a secondary zone of seismicity around the summit caldera. Weak tremor, fluctuating in intensity, continued for about a week afterward.

Lava returned to Mauna Ulu's crater on May 7 and to Alae on May 30. Alae was probably entirely tube fed from Mauna Ulu, although local, limited feeding by dikes could also have occurred. The posteruption reinflation and related increase in the number of shallow summit earthquakes suggest that the reestablished link between the summit reservoir and Mauna Ulu and Alae was not a good conductor of magma. Alternatively, the increase in seismicity may reflect adjustment in brittle rock of the summit region and east rift zone during reinflation of the magma reservoir. After May 5, both the east-rift and summit seismicity were characterized by higher background levels than previously (fig. 16.46). The partial draining of Mauna Ulu lava lake and the demise of the Alae vent in early June are not clearly recognizable in the record of east-rift seismicity, though they are reflected by brief deflation at Uwekahuna and associated slight decrease in summit seismicity. The next significant increase in east-rift seismicity after the May 5 eruption occurred in late July 1973 (fig. 16.46), when collapse of the Mauna Ulu Crater floor triggered a flurry of rockfalls.

The month-long dramatic increase in the number of shallow summit earthquakes during October 1973 was the most noteworthy seismic activity since late 1971 and coincided with a period of strong inflation. The heightened seismicity began to wane in late October, when renewed vigorous activity in the rapidly rising Mauna Ulu lava lake indicated increased east-rift magma storage, and returned to background levels with the onset of the overflow from Mauna Ulu during November 4–8. Curiously, the east-rift seismicity preceding and accompanying the draining of Mauna Ulu lava lake and the November 10 outbreak at Pauahi was relatively weak and short-lived compared to that for similar events in May 1973 (fig. 16.46). The reappearance of Mauna Ulu lava lake on December 13 was heralded by increased local harmonic tremor, but otherwise it was not expressed seismically, either at the summit or the east rift zone.

We have postulated a period of quasi-steady-state activity from December 1973 to July 1974, largely on the basis of the small net change in Uwekahuna tilt. However, we have shown that this period differs from the quasi-steady-state period of February 1972–April 1973 in eruptive style. It also has a different seismic signature, characterized by significantly greater variation in the number of shallow summit earthquakes, which generally can be correlated with more variable oscillations in Uwekahuna tilt. The variations in both seismicity and Uwekahuna tilt during the final 8 months of the eruption bear a crude resemblance to those during stages 2 and 3 (January 1970–June 1971) of the 1969–71 Mauna Ulu eruption (fig. 16.44; Swanson and others, 1979, pl. 2).

The irregular increase in the number of shallow summit earthquakes following the November 10, 1973, Pauahi outbreak is inferred to reflect increased summit storage, even while the conduit

system between the summit and Mauna Ulu was gradually becoming more open and efficient in magma transfer. By mid-January 1974, the magma pathway between the summit reservoir and Mauna Ulu was fully reestablished, as evidenced by the precise correlation among the bursts of high fountaining and overflows, summit seismicity, and minor changes in Uwekahuna tilt during the five closely spaced eruptive episodes during January–February 1974 (figs. 16.30, 16.46; table 16.3). We believe that such an exact correlation can be achieved only if the magma transfer system between the summit reservoir and Mauna Ulu is fully engorged in order to maintain hydraulic equilibrium.

Shallow summit earthquakes typically increased in number before observed eruptive episodes during January–June 1974, but summit seismicity dropped abruptly and summit deflation began immediately before the high lava fountaining and voluminous overflows of the eruptions. As the summit deflated and magma moved to the eruption site during most such episodes, east-rift seismicity increased and summit seismicity decreased, in a manner like that during some of the high-fountaining events in stage 1 of the 1969–71 Mauna Ulu eruption (Swanson and others, 1979, pl. 2) and the well-documented example of summit to east rift magma transfers during April–August 1980 (Dzurisin and others, 1984, fig. 4).

VARIATION IN HARMONIC TREMOR

At Kilauea and well-monitored volcanoes elsewhere in the world, harmonic tremor has been shown to be linked to magma movement, surficial as well as subterranean, and to commonly precede and accompany intrusions and eruptions (Aki and Koyanagi, 1981). As during the 1969–71 Mauna Ulu eruption, shallow harmonic tremor in the upper east rift zone and summit area occurred at varying intensities throughout the 1972–74 Mauna Ulu eruption. Harmonic tremor typically increased in intensity and (or) became sustained shortly before and during changes in loci of energetic vent activity, including the opening of new vents. When visible activity was feeble or absent, harmonic tremor typically was more sporadic and barely detectable; on rare occasions, for as long as a few days, tremor decreased to levels too low to be discerned from background with normal gain settings of the seismic instruments.

Of perhaps greater significance is the increased occurrence of the so-called deep harmonic tremor during the period 1969–75 (Dzurisin and others, 1984). Such tremor is believed to originate in Kilauea's deep magma source region at a depth of approximately 40–50 km and to reflect the production and ascent of magma supplying Kilauea's shallow summit reservoir. A marked increase in the amplitude and duration of recorded deep tremor was observed coincident with the onset of the 1969–71 Mauna Ulu eruption.

The trend of increasing deep tremor peaked at the end of 1972, but occurrence remained much above average through 1975 (Dzurisin and others, 1984, fig. 10). We suggest that the period of maximum deep tremor correlates with the February 1972–April 1973 period of quasi-steady-state activity at Mauna Ulu. However, the increased occurrence in deep tremor apparently was not accompanied by concomitant increase in deep or crustal earthquakes at Kilauea (fig. 16.45). The foci of Kilauea crustal earthquakes (depth 5–13 km) are interpreted to define the feeding conduits from the deep magma source region to the shallow summit reservoir (Koyanagi and others, 1976a, fig. 5). Thus, our data may corroborate the speculation of Dzurisin and others (1984, p. 203) that "the rates of deep magma production and shallow supply to Kilauea may be closely linked" and that "a pulse of relatively rapid magma supply during 1968–1975 may have been responsible for the sustained eruptions at Mauna Ulu during 1969–1971 and 1972–1974." We recognize, however, that the correlation between deep tremor, magma supply, and eruptive activity is imperfect. For example, the 1967–68 Halemaumau eruption (Kinoshita and others, 1969) had the same magma supply rate as the 1969–1971 Mauna Ulu eruption (Swanson, 1972) but there was little associated deep tremor (Dzurisin and others, 1984, fig. 10).

SIGNIFICANCE OF THE 1972–74 MAUNA ULU ERUPTION

During the 1969–71 eruption, volcanic shield development was greatest during periods characterized by numerous short-distance and short-duration overflows from the main vents at Mauna Ulu. Swanson and others (1979, fig. 6) traced in detail the growth of Mauna Ulu shield, whose height grew at an average rate of about 6 m/mo and reached 80 m above the pre-eruption ground surface by the end of the major overflow activity in July 1970. At Alae, the complex filling, overflows, and draining of the lava lake between February 1969 and April 1971 resulted in net accretion of 29–40 m of lava above the rim of buried Alae Crater (Swanson and Peterson, 1972, fig. 2; Swanson and others, 1972, fig. 10). However, when activity ended in 1971, the altitude of the lowest point on the Alae lake surface, which rose or dropped by much as 19 m in response to the individual episodes of filling and subsidence, was determined in June 1971, after final settling, to be about 6 m higher than the pre-1969 datum (Swanson and Peterson, 1972, table 1).

During the 1972–74 eruption, countless overflows from vent C and subsidiary vents at Alae again filled the shallow subsidence bowl formed in 1971, and they accreted approximately another 60 m onto the complex Alae shield, increasing its height to about 100 m above the pre-1969 datum (the pre-eruption southeast rim of Alae Crater at 915 m above sea level, the same datum used by Swanson and Peterson, 1972).

At Mauna Ulu, the shield grew only slightly and irregularly from many small overflows during February–March 1972 and again during early November 1973. Vigorous growth comparable to that during 1969–70 occurred only during voluminous but short-lived eruptive episodes in 1974. By the end of April 1974, the height of the Mauna Ulu shield was 117 m above the pre-May 1969 ground surface (datum is 951 m above sea level, the same as used by Swanson and others, 1979, fig. 6) and its width increased proportionately. The final and most voluminous overflow of May 29–June 2, 1974, added another 4 m to the summit of the shield, resulting in its maximum height of 121 m above the pre-May 1969 base at the

end of the eruption. The May 1972 configuration of Mauna Ulu and Alae shields in May 1972 and of a mound filling the deep west pit of Makaopuhi Crater is schematically shown in figure 16.13. This configuration essentially persisted throughout the 1972–74 Mauna Ulu eruption, but the elevations of the landforms were modified by posteruption settling.

A comparison of the 1963 1:24,000 topographic map (based on 1954 aerial photographs) and the 1981 topographic map (based on 1977 aerial photographs) shows the following changes associated with the 1969–74 Mauna Ulu eruptions:

(1) The summit area of Mauna Ulu shield in 1977 is about 111 m above the pre-eruption ground surface, and the summit crater is deeper than 30 m.

(2) The site of buried Aloi Crater is well expressed topographically by a crudely circular area of minor subsidence (not more than 5 m) on the west flank of Mauna Ulu shield.

(3) The highest areas on the complex Alae shield, which rim the small collapse pit in the area of the (former) vent C, are nearly 90 m above the pre-1969 datum. The subsidence bowl that existed in 1971 is still reflected by a broad area of subsidence roughly coincident with the deeper compartment of the buried Alae Crater.

(4) Benchmarks not buried by 1969–74 flows have been raised or lowered a few meters, presumably in response to complex ground deformation related to eruptions during the period 1954–1977, principally the Mauna Ulu eruptions.

(5) Comparison of the maximum heights attained by Mauna Ulu and Alae during the eruption (121 m and 100 m, respectively) with their heights in 1977, as indicated by the 1981 topographic map (111 m and 90 m, respectively), demonstrates posteruption settling of about 10 m.

SUSTAINED OVERFLOWS: DEVELOPMENT OF LAVA-TUBE SYSTEMS

The 1969–74 Mauna Ulu eruptions afforded the opportunity, for the first time at Kilauea, to study the formation and evolution of lava tubes (see Greeley, 1971, 1972; Cruikshank and Wood, 1972; Peterson and Swanson, 1974; Peterson, 1983). Lava-tube and related flow processes have been described in detail by these geologists; we wish here only to outline some general observations especially pertinent to the 1972–74 eruption:

This paper is in general a sequel to the study by Swanson and others (1979) of the 1969–71 Mauna Ulu eruption. Indeed, we have presented our observations and inferences on the 1972–74 Mauna Ulu eruption in a format parallel to theirs in order to emphasize the continuity of similar eruptive processes and to facilitate the comparison of these two eruptions, separated by about 3½ months of inactivity, in the same area of Kilauea's east rift zone. Not surprisingly, much of Swanson and others' (1979) perception of the significance of the 1969–71 Mauna Ulu eruption applies also to the 1972–74 eruption.

LONG-LIVED FLANK ACTIVITY

It has previously been noted (Peterson and others, 1976; Swanson and others, 1979) that the Mauna Ulu eruptions were the longest nearly continuous rift activity at Kilauea in historical times (that is, since about A.D. 1750): the 1969–71 eruption lasted 875 days and the 1972–74 eruption lasted 901 days. Most historical flank eruptions of Kilauea have lasted a few weeks at most and more typically a few days or less. The Mauna Ulu eruptions of 1969–74 included several prolonged periods of remarkably continuous lava-lake activity, previously observed only at Halemaumau within the summit caldera during the 19th and early 20th centuries.

CONTINUOUS LAVA-LAKE ACTIVITY

Throughout much of the 1972–74 Mauna Ulu eruption, active lava lakes operated within the summit crater of Mauna Ulu and at Alae. Mauna Ulu lava lake was apparently fed directly by the magma conduit leading from the summit reservoir, whereas Alae lava lake was supplied through a very efficient tube system connected to Mauna Ulu. Lake circulation patterns and persistent vent activity suggest that magma from Kilauea summit most likely entered the Mauna Ulu system at an intricately branched inlet located beneath the area between vents A and B (fig. 16.3). The magma was directed from there through complex branches westward to feed Mauna Ulu lava lake and eastward to supply Alae lake, generally through vent C. We speculate that from mid-March 1972 through April 1973, eastward shunting of lava from the inlet dominated and resulted in vigorous activity at or near Alae and relatively sluggish activity at Mauna Ulu lava lake. The tube system connecting Mauna Ulu and Alae never fully recovered from its disruption in early May 1973, and vent C at Alae was severed from the inlet by early June. Magma thereafter was shunted westward from the inlet area to feed activity at Mauna Ulu for the remainder of the eruption.

Gas-piston activity associated with rises and falls of lava columns at Mauna Ulu and Alae was commonly observed during the 1969–74 eruptive activity. Short-term minor fluctuations in level of Mauna Ulu and Alae lava lakes may simply be due to larger scale gas-piston activity of a magma column of greater volume and lateral extent. However, large variations in lake levels over a period of time probably reflect major changes affecting either the magma-transfer system linking the Kilauea summit reservoir and the eruption site, or possibly even changes in the reservoir itself. The levels of Mauna Ulu and Alae lava lakes often varied sympathetically (fig. 16.19); at no time during 1972 did a drop in level at Mauna Ulu correlate with a rise in level at Alae or vice versa, but this correlation was weaker in early 1973. Moreover, the variations in lake level at times exhibited an unmistakable positive correlation with summit tilt (fig. 16.19). These observations suggest that a hydrostatic balance existed between the Kilauea summit reservoir, the Mauna Ulu holding tank, and the vent at Alae, compatible with the postulated quasi-steady-state magma regime operating during two long periods of the 1972–74 eruption. Detailed study of the hydrodynamics and evolution of active lava lakes at Mauna Ulu and Alae should bear importantly on the overall magma-transfer regime of Kilauea during sustained rift activity.

SHORT-DURATION OVERFLOWS: VOLCANIC SHIELD DEVELOPMENT

Volcanic shields are built by repeated eruptions of fluid lava from centralized vents. A number of small shields dot the flanks of Kilauea Volcano; examples include Kane Nui o Hamo (prehistoric) and Heiheiahulu (circa A.D. 1750?) on the east rift zone, and Mauna Iki (1919–20) on the southwest rift zone (fig. 16.1). However, it was not until the 1969–74 Mauna Ulu eruptions that shield development at Kilauea could be systematically observed and documented.

(1) Steady lava output from the vent over a long period of time (weeks to months) is the most important prerequisite in the development of channelized flows and, ultimately, lava tubes. Short-lived or erratic vent activity, even if of high volume, does not allow the formation of lava tubes.

(2) As shown in the chronological narrative, periods of sustained overflows leading to lava-tube development and periods of frequent short-duration overflows leading to shield growth generally are not coincident. On occasion, however, these two types of eruptive activity may grade from one into the other over a transition interval of several weeks; thus, both activities may go on concurrently for short periods of time.

(3) Systematic field observations of the transition of pahoehoe to aa during the sustained overflows permitted the documentation of several modes of transition and demonstrated that moving lava flows function as natural viscometers. Peterson and Tilling (1980) proposed the concept of a transition threshold zone to portray the observed inverse critical relation between viscosity and shear rate in the transition from pahoehoe to aa; this model was refined by Kilburn (1981).

(4) Sustained overflows and development of well-integrated tube systems enabled lava to be transported as far as 12 km from vents at Mauna Ulu and Alae. Flows that filled the deep west pit of Makaopuhi Crater were tube fed, as were those that entered the sea in August–October 1972 and in February–May 1973.

(5) Lava-tube systems are efficient but fragile conductors of lava and can be easily blocked or disrupted, as evidenced by the apparent drastic effect of the April 26, 1973, Honomu earthquake on the tube system feeding lava into the sea. By May 1, earthquake-induced impediments and blockage caused all flow to cease.

CHEMICAL VARIATIONS (MAGMA BATCHES)

The long-lived Mauna Ulu eruptions provided a unique opportunity to study and model subtle variations in major-element chemistry during the course of a lengthy eruption. Using the chemical composition of the lava from the 1967–68 summit eruption at Halemaumau (Kinoshita and others, 1969) as the reference analysis, Wright and others (1975) identified, after adjusting for olivine control, five chemical variants (magma batches) for the 1969–71 Mauna Ulu lava. Identification of these subtly different chemical variants in turn enabled Wright and others (1975) to demonstrate that the lava from a new fissure cutting Aloi Crater and the adjacent west flank of Mauna Ulu shield in early April 1970 was identical to that erupted by Mauna Ulu on the same date but distinct from that in preceding Mauna Ulu eruptions. Swanson and others (1979, p. 38–39) concluded that "a batch of new magma entered both the Mauna Ulu and Aloi plumbing systems just before the outbreak, implying that the systems were interconnected at some unknown depth." Hoffman and others (1984) contend, however, that the variations in the composition of the 1969–71 Mauna Ulu lava can be interpreted in terms of a partial melting model without resort to different magma batches from the mantle.

Wright and Tilling (1980) extended such chemical studies to include lava erupted during the two 1971 summit eruptions, the 1972–74 Mauna Ulu eruption, and the eruptions of July, September, and December 1974. They recognized five new magma batches (chemical variants) and concluded that the following processes were common to all eruptions in the period 1969–1974 (Wright and Tilling, 1980, p. 786):

"1. appearance of new chemically distinct batches of magma,
2. mixing of two or more of these batches prior to eruption,
3. subordinate isolation and cooling of magma followed by flow differentiation leading to eruption of differentiated compositions."

Analysis of the distribution in time and space of the chemically distinct magma batches makes it possible to estimate the residence times and volumes of these batches. For example, on the basis of such information, Wright and Tilling (1980, p. 777) suggest that the appearance of fractionated magma in July 1974 can be related to the isolation and cooling of magma introduced into shallow storage 2½ to 4 years before.

QUASI-STEADY-STATE ACTIVITY

The small amount of net summit inflation observed, together with other evidence presented earlier in this paper, suggests that a quasi-steady-state magma-transfer regime prevailed throughout much of the 1972–74 eruption. If our concept of quasi-steady-state activity is valid, then the magma influx from the deep source region must be approximately constant, at least on a time-averaged basis, and nearly equal to the increments transferred into the rift zone.

The ground-deformation patterns derived from level, ground tilt, and trilateration surveys during the periods of quasi-steady-state magma transfer, which show little net summit inflation or deflation between surveys, are not always in good agreement with the variations in Uwekahuna tilt (see section titled "Results of level, tilt, and trilateration surveys"). In contrast, deformation patterns during the period of net summit inflation related to the 1973 eruptions in the Pauahi-Hiiaka area, are more coherent. These observations suggest that a threshold amount or rate of summit tilt change must be exceeded in order for the results of ground-deformation surveys encompassing the entire summit region to yield definitive interpretations. This in turn implies that the volcanic edifice has a yield strength and that a finite amount of inelastic deformation must be accommodated before elastic behavior sets in.

COMPARISON WITH 1969–71 MAUNA ULU ERUPTION

The 1972–74 Mauna Ulu eruption shares many characteristics with the 1969–71 eruption. It differs, however, in the following aspects:

(1) The later eruption lacked the high-fountaining episodes (maximum 540 m) and associated larger summit deflation (maximum about 30 μrad) of the 1969 activity (stage 1 of Swanson and others, 1979). Although the behavior in 1974—brief eruptive episodes separated by longer intervals of weak vent activity—was qualitatively reminiscent of the stage 1 activity, fountain heights were smaller by an order of magnitude (40–80 m).

(2) The 1972–74 eruption occurred with practically no net summit inflation, whereas the 1969–71 activity resulted in a net summit inflation of approximately 60 μrad, suggesting that a more efficient magma-transfer regime existed during 1972–74.

(3) The February 1972–April 1973 period of low seismicity on the summit and east rift has no counterpart in the 1969–71 Mauna Ulu eruption.

SUMMARY REMARKS

The 1969–71 and 1972–74 Mauna Ulu eruptions provided an unparalleled opportunity to conduct systematic studies of ongoing eruptive processes associated with long-lived active lava lakes. Many of these studies have already been published (table 16.1; Swanson and others, 1979, table 1), others are in progress. Long-lived lava lakes were commonly active within or near Halemaumau Crater during the 19th and early 20th centuries, but it was not until the Mauna Ulu eruptions that such lava lakes were observed in a flank eruption. As of this writing (June 1985), the current long-lived eruption at Puu Oo in Kilauea's middle east (Wolfe and others, chapter 17) resembles activity during stage 1 of the 1969–71 Mauna Ulu eruption. Will it later evolve into a subsequent stage dominated by one or more active lava lakes? Our experience at Mauna Ulu suggests that it is possible.

REFERENCES

Aki, Keiiti, and Koyanagi, R.Y., 1981, Deep volcanic tremor and magma ascent mechanism under Kilauea, Hawaii: Journal of Geophysical Research, v. 86, no. B8, p. 7095–7109.

Cadle, R.D., Wartburg, A.F., Pollock, W.H., Gandrum, B.W., and Shedlovksy, J.P., 1973, Trace constituents emitted to the atmosphere by Hawaiian volcanoes: Chemosphere, v. 6, p. 231–234.

Casadevall, T.J., and Hazlett, R.W., 1983, Thermal areas on Kilauea and Mauna Loa Volcanoes, Hawaii: Journal of Volcanology and Geothermal Research, v. 16, p. 173–188.

Cruikshank, D.P., and Wood, C.A., 1972, Lunar rilles and Hawaiian volcanic features: possible analogues: The Moon, v. 3. no. 4, p. 412–447.

Davis, P.M., Hastie, L.M., and Stacey, F.D., 1974, Stresses within an active volcano—with particular reference to Kilauea: Tectonophysics, v. 22. no. 3-4, p. 355–362.

Duffield, W.A., 1975, Structure and origin of the Koae fault system, Kilauea Volcano, Hawaii: U.S. Geological Survey Professional Paper 856, 12 p.

Duffield, W.A., Christiansen, R.L., Koyanagi, R.Y., and Peterson, D.W., 1982, Storage, migration, and eruption of magma at Kilauea Volcano, Hawaii, 1971–72: Journal of Volcanology and Geothermal Research, v. 13, p. 273–307.

Dvorak, John, Okamura, Arnold, and Dietrich, J.H., 1983, Analysis of surface deformation data, Kilauea Volcano, Hawaii, October 1966 to September 1970: Journal of Geophysical Research, v. 88, no. B11, p. 9295–9304.

Dzurisin, Daniel, 1978, Planetary studies of Kilauea Volcano, Hawaii: the role of satellitic shields in Kilauea's recent evolution, *in* Strom, Robert and Boyce, Joseph, compilers, Reports of Planetary Geology Program 1977–1978 : NASA Technical Memorandum 79729, p. 192–193.

———1980, Influence of fortnightly earth tides at Kilauea Volcano, Hawaii: Geophysical Research Letters, v. 7, no. 11, p. 925–928.

Dzurisin, Daniel, Anderson, L.A., Eaton, G.P., Koyanagi, R.Y., Lipman, P.W., Lockwood, J.P., Okamura, R.T., Puniwai, G.S., Sako, M.K., and Yamashita, K.M., 1980, Geophysical observations of Kilauea Volcano, Hawaii, 2. Constraints on the magma supply during November 1975–September 1977: Journal of Volcanology and Geothermal Research, v. 7, p. 241–269.

Dzurisin, Daniel, and Koyanagi, R.Y., 1981, Changed magma budget since 1975 at Kilauea Volcano, Hawaii: U.S. Geological Survey Open-File Report 81–571, 46 p.

Dzurisin, Daniel, Koyanagi, R.Y., and English, T.T., 1984, Magma supply and storage at Kilauea Volcano, Hawaii, 1956–1983: Journal of Volcanology and Geothermal Research, v. 21, p. 177–206.

Eaton, J.P., 1962, Crustal structure and volcanism in Hawaii: American Geophysical Union, Geophysical Monograph 6, p. 13–29.

Eaton, J.P., and Murata, K.J., 1960, How volcanoes grow: Science, v. 132, no. 3432, p. 925–938.

Ellsworth, W.L., and Koyanagi, R.Y., 1977, Three-dimensional crust and mantle structure of Kilauea Volcano, Hawaii: Journal of Geophysical Research, v. 82, no. 33, p. 5379–5394.

Epp, David, Decker, R.W., and Okamura, A.T., 1983, Relation of summit deformation to east rift zone eruptions on Kilauea Volcano, Hawaii: Geophysical Research Letters, v. 10, no. 7, p. 493–496.

Fiske, R.S., and Kinoshita, W.T., 1969, Inflation of Kilauea Volcano prior to the 1967–68 eruption: Science, v. 165, no. 3891, p. 341–349.

Greeley, Ronald, 1971, Observations of actively forming lava tubes and associated structures, Hawaii: Modern Geology, v. 2, no. 3, p. 207–223.

———1972, Additional observations of actively forming lava tubes and associated structures, Hawaii: Modern Geology, v. 3, no. 3, p. 157–160.

———1974, editor, Guidebook to the Hawaiian Planetology Conference: NASA TMX 62362, Washington, D.C., 257 p.

Grigg, Rick, 1973, Fire under the sea: Oceans, v. 6, no. 2, p. 6–11.

Hawaiian Volcano Observatory, 1977a, Summary 65: January, February, and March 1972: Menlo Park, California, U.S. Geological Survey, 54 p.

———1977b, Summary 66: April, May, and June 1972: Menlo Park, California, U.S. Geological Survey, 44 p.

———1977c, Summary 67: July, August, and September 1972: Menlo Park, California, U.S. Geological Survey, 27 p.

———1977d, Summary 68: October, November, and December 1972: Menlo Park, California, U.S. Geological Survey, 29 p.

———1977e, Summary 69: January, February, and March 1973: Menlo Park, California, U.S. Geological Survey, 24 p.

———1977f, Summary 70: April, May, and June 1973: Menlo Park, California, U.S. Geological Survey, 61 p.

———1977g, Summary 71: July, August, and September 1973: Menlo Park, California, U.S. Geological Survey, 38 p.

———1977h, Summary 72: October, November, and December 1973: Menlo Park, California, U.S. Geological Survey, 42 p.

———1978, Summary 74: January to December, 1974: Menlo Park, California, U.S. Geological Survey, 164 p.

Hazlett, R.W., 1981, Guide to points of geologic interest in Hawaii Volcanoes National Park, Hawaii: Circum-Pacific Energy and Mineral Resources Conference, 55 p.

Hoffman, A.W., Feigenson, M.D., and Raczek, Ingrid, 1984, Case studies on the

origin of basalt: III. Petrogenesis of the Mauna Ulu eruption, Kilauea, 1969–71: Contributions to Mineralogy and Petrology, v. 88, p. 24–35.

Holcomb, R.T., 1973, Lava-subsidence terraces of Kilauea Volcano, Hawaii: International Union for Quaternary Research, Christchurch, New Zealand, Dec. 2–10, 1973, Ninth Congress Program, p. 152–153 (extended abstract).

———1976, Preliminary map showing products of eruptions, 1962–1974 from the upper east rift zone of Kilauea Volcano, Hawaii: U.S. Geological Survey Miscellaneous Field Studies Map MF–811, scale 1:24,000.

———1980, Preliminary geologic map of Kilauea Volcano, Hawaii: U.S. Geological Survey Open-File Report 80–796, scale 1:50,000, 2 sheets.

Holcomb, R.T., Peterson, D.W., and Tilling, R.I., 1974, Recent landforms at Kilauea Volcano, a selected photographic compilation, *in* Greeley, R.W., ed., Guidebook to the Hawaiian Planetology Conference, Washington, D.C., NASA TMX 62362, p. 49–86.

Jackson, D.B., Swanson, D.A., Koyanagi, R.Y., and Wright, T.L., 1975, The August and October 1968 east rift eruptions of Kilauea Volcano, Hawaii: U.S. Geological Survey Professional Paper 890, 33 p.

Jaggar, T.A., 1920, Seismometric investigation of the Hawaiian lava column: Seismological Society of America Bulletin, v. 10, no. 4, p. 155–275.

———1947, Origin and development of craters: Geological Society of America Memoir 21, 508 p.

Kilburn, C.R.J., 1981, Pahoehoe and aa lavas: a discussion and continuation of the model of Peterson and Tilling: Journal of Volcanology and Geothermal Research, v. 11, no. 2-4, p. 373–382.

Kinoshita, W.T, Koyanagi, R.Y., Wright, T.L., and Fiske, R.S., 1969, Kilauea Volcano—The 1967–68 summit eruption: Science (AAAS), v. 166, no. 3904, p. 459–468.

Kinoshita, W.T., Swanson, D.A., and Jackson, D.B., 1974, The measurement of crustal deformation related to volcanic activity at Kilauea Volcano, Hawaii, *in* Civetta, L., Luongo, G., and Rapolla, A., eds., Physical Volcanology, Developments in solid earth Geophysics: Amsterdam, Elsevier Publishers, v. 6, p. 87–116.

Klein, F.W., 1982, Patterns of historical eruptions at Hawaiian volcanoes: Journal of Volcanology and Geothermal Research, v. 12, p. 1–35.

Koyanagi, R.Y., Endo, E.T., and Ward, P.L., 1976a, Seismic activity on the island of Hawaii, 1970 to 1973, *in* Sutton, G.H., Manghnani, M.H., and Moberly, Ralph, eds., The Geophysics of the Pacific Ocean Basin and its margin: Geophysical Monograph 19, American Geophysical Union, Washington, D.C., p. 169–172.

Koyanagi, R.Y., Unger, J.D., and Endo, E.T., 1973, Seismic evidence for magma intrusion in the eastern Koae fault system, Kilauea Volcano, Hawaii [abs.]: Eos. American Geophysical Union Transaction, v. 54, no. 11, p. 1216.

Koyanagi, R.Y., Unger, J.D., Endo, E.T., and Okamura, A.T., 1976b, Shallow earthquakes associated with inflation episodes at the summit of Kilauea Volcano, Hawaii: International Association of Volcanology and Chemistry of the Earth's Interior, Symposium on Andean and Antarctic Volcanology Problems, p. 621–631.

Lipman, P.W., 1980, Rates of volcanic activity along the southwest rift zone of Mauna Loa Volcano, Hawaii: Bulletin Volcanologique, v. 43-4, p. 703–725.

Macdonald, G.A., and Hubbard, D.H., 1982, Volcanoes of the National Parks in Hawaii (8th ed.): Hawaii, Hawaii Natural History Association, Hawaii Volcanoes National Park, 64 p.

Moore, J.G., 1975, Mechanism of formation of pillow lava: American Scientist, v. 63, p. 269–277.

Moore, J.G., Phillips, R.L., Grigg, R.W., Peterson, D.W., and Swanson, D.A., 1973, Flow of lava into the sea, 1969–1971, Kilauea Volcano, Hawaii: Geological Society of America Bulletin, v. 84, no. 2, p. 537–546.

Moore, R.B., Helz, R.T., Dzurisin, Daniel, Eaton, G.P., Koyanagi, R.Y., Lipman, P.W., Lockwood, J.P., and Puniwai, G.S., 1980, The 1977 eruption of Kilauea Volcano, Hawaii: Journal of Volcanology and Geothermal Research, v. 7, p. 189–210.

Naughton, J.J., Lee, J.H., Keeling, D., Finlayson, J.B., and Dority, G., 1973, Helium flux from the Earth's mantle as estimated from Hawaiian fumarolic degassing: Science (AAAS), v. 180, no. 4081, p. 55–57.

Peterson, D.W., 1976, Processes of volcanic island growth, Kilauea Volcano, Hawaii, 1969–1973: International Association of Volcanology and Chemistry of the Earth's Interior, Symposium on Andean and Antarctic Volcanology Problems, Proceedings, p. 172–189.

———1983, Processes of development of lava tubes at Mauna Ulu, Kilauea Volcano, Hawaii [abs.]: The NSS Bulletin (Quarterly Journal of the National Spelelogical Society), v. 45, no. 1, unpaginated insert following p. 8.

Peterson, D.W., Christiansen, R.L., Duffield, W.A., Holcomb, R.T., and Tilling, R.I., 1976, Recent activity of Kilauea Volcano, Hawaii: International Association of Volcanology and Chemistry of the Earth's Interior, Symposium on Andean and Antarctic Volcanology Problems, Proceedings, p. 646–656.

Peterson, D.W., and Swanson, D.A., 1974, Observed formation of lava tubes during 1970–71 at Kilauea Volcano, Hawaii: Studies in Speleology, v. 2, part 6, p. 209–222.

Peterson, D.W., and Tilling, R.I., 1980, Transition of basaltic lava from pahoehoe to aa, Kilauea Volcano, Hawaii: field observataions and key factors: Journal of Volcanology and Geothermal Research, v. 7, p. 271–293.

Ryan, M.P., Blevins, J.Y.K., Okamura, A.T., and Koyanagi, R.Y., 1983, Magma reservoir subsidence mechanics: theoretical summary and application to Kilauea Volcano, Hawaii: Journal of Geophysical Research, v. 88, no. B5. p. 4147–4181.

Ryan, M.P., Koyanagi, R.Y., and Fiske, R.S., 1981, Modeling the three-dimensional structure of macroscopic magma transport systems: application to Kilauea Volcano, Hawaii: Journal of Geophysical Research, v. 86, no. B8, p. 7111–7129.

Sicks, G.C., 1975, The kinetics of silica dissolution from volcanic glass in the marine environment: HIG–75–23, Hawaii Institute of Geophysics, University of Hawaii, 82 p.

Swanson, D.A., 1972, Magma supply rate of Kilauea Volcano, 1952–1971: Science (AAAS), v. 175, no. 4018, p. 169–170.

Swanson, D.A., Duffield, W.A., and Fiske, R.S., 1976b, Displacement of the south flank of Kilauea Volcano: the result of forceful intrusion of magma into the rift zones: U.S. Geological Survey Professional Paper 963, 39 p.

Swanson, D.A., Duffield, W.A., Jackson, D.B., and Peterson, D.W., 1972, The complex filling of Alae Crater, Kilauea Volcano, Hawaii: Bulletin Volcanologique, v. 36, no. 1, p. 105–126.

———1979, Chronological narrative of the 1969–71 Mauna Ulu eruption of Kilauea Volcano, Hawaii: U.S. Geological Survey Professional Paper 1056, 55 p.

Swanson, D.A., Jackson, D.B., Duffield, W.A., and Peterson, D.W., 1971, Mauna Ulu eruption, Kilauea Volcano: Geotimes, v. 16, no. 5, p. 12–16.

Swanson, D.A., Jackson, D.B., Koyanagi, R.Y., and Wright, T.L., 1976a, The February 1969 east rift eruption of Kilauea Volcano, Hawaii: U.S. Geological Survey Professional Paper 891, 30 p.

Swanson, D.A., and Peterson, D.W., 1972, Partial draining and crustal subsidence of Alae lava lake, Kilauea Volcano, Hawaii: U.S. Geological Survey Professional Paper 800–C, p. C1–C14.

Tepley, Lee, 1975, Fireworks erupt when hot lava pours into the sea, 1975, Smithsonian, v. 6, no. 8. p. 70–75.

Tilling, R.I., 1976a, Rockfall activity in pit craters, Kilauea Volcano, Hawaii: International Association of Volcanology and Chemistry of the Earth's Interior, Symposium on Andean and Antarctic Volcanology Problems, Proceedings, p. 518–528.

———1976b, The 7.2 magnitude earthquake, November 1975, Island of Hawaii: Earthquake Information Bulletin, v. 8, no. 6, p. 5–13.

Tilling, R.I., Christiansen, R.L., Duffield, W.A., Holcomb, R.T., and Peterson, D.W., 1986, Determinations of the depth to the surfaces of active lava lakes at Mauna Ulu and Alae, Kilauea Volcano, Hawaii: U.S. Geological Survey Open-File Report 86–367, 16 p.

Tilling, R.I., Holcomb, R.T., Lipman, P.W., and Lockwood, J.P., 1976b, Rates of structural and landform evolution of Hawaiian volcanoes: role of short-lived and catastrophic processes: NASA Technical Memorandum X–3364, p. 157–158.

Tilling, R.I., Holcomb, R.T., Lockwood, J.P., and Peterson, D.W., 1976c,

Recent eruptions of Hawaiian volcanoes and the evolution of basaltic landforms: Geologica Romana, v. 15, p. 519–521.

Tilling, R.I., Koyanagi, R.Y., and Holcomb, R.T., 1975, Rockfall seismicity: correlation with field observations, Makaopuhi Crater, Kilauea Volcano, Hawaii: Journal of Research, U.S. Geological Survey, v. 3, no. 3, p. 345–361.

Tilling, R.I., Koyanagi, R.Y., Lipman, P.W., Lockwood, J.P., Moore, J.G., and Swanson, D.A., 1976a, Earthquake and related catastrophic events, Island of Hawaii, November 29. 1975: a preliminary report: U.S. Geological Survey Circular 740, 33 p.

Tilling, R.I., Peterson, D.W., Christiansen, R.L., and Holcomb, R.T., 1973, Development of new volcanic shields at Kilauea Volcano, Hawaii, 1969–1973: International Union for Quaternary Research, Christchurch, New Zealand, December 2–10, 1973, Ninth Congress Program, p. 366–367 (extended abstract).

Unger, J.D., Koyanagi, R.Y., and Ward, P.L., 1973, An important Hawaiian earthquake [abs.]: Eos, Transaction American Geophysical Union, v. 54, no. 11. p. 1136.

Unger, J.D., and Ward, P.L., 1979, A large, deep Hawaiian earthquake—the Honomu, Hawaii event of April 26, 1973: Bulletin of the Seismological Society of America, v. 69, no. 6, p. 1771–1781.

Wright, T.L., Kinoshita, W.T., and Peck, D.L., 1968, March 1965 eruption of Kilauea Volcano and the formation of Makaopuhi lava lake: Journal of Geophysical Research, v. 73, p. 3181–3205.

Wright, T.L., Swanson, D.A., and Duffield, W.A., 1975, Chemical compositions of Kilauea east-rift lava, 1968–1971: Journal of Petrology, v. 16, no. 1, p. 110–133.

Wright, T.L., and Tilling, R.I., 1980, Chemical variation in Kilauea eruptions 1971–74: American Journal of Science, v. 280–A, part 2, p. 777–793.

Zablocki, C.J., 1976, Mapping thermal anomalies on an active volcano by the self-potential method, Kilauea, Hawaii, *in* United Nations Symposium on the Development and Use of Geothermal Resources, 2nd, San Francisco, California, May 1975, Proceedings, v. 2, p. 1299–1309.

———1978, Applications of the VLF induction method for studying some volcanic processes of Kilauea Volcano, Hawaii: Journal of Volcanology and Geothermal Research. v. 3, p. 155–195.

THE PUU OO ERUPTION OF KILAUEA VOLCANO, EPISODES 1–20, JANUARY 3, 1983, TO JUNE 8, 1984

By Edward W. Wolfe, Michael O. Garcia[1], Dallas B. Jackson, Robert Y. Koyanagi, Christina A. Neal, *and* Arnold T. Okamura

ABSTRACT

The Puu Oo eruption began at Napau Crater in the east rift zone of Kilauea Volcano on January 3, 1983. After an initial series of intermittent fissure eruptions, the style changed to one of episodic central-vent eruptions. By early June 1984, 20 eruptive episodes had occurred, including the initial fissure-eruption episode, and approximately 240×10^6 m^3 of new basalt covered an area of more than 30 km^2. Fountains ranging up to nearly 400 m high built large cones at the central vents.

The eruption occurred in a part of the rift zone that had a long history as a locus for intrusions. Tilt changes and flurries of shallow earthquakes recorded accumulation of magma from 1978 through 1980 and again in late 1982. We interpret geodetic and seismic evidence to indicate a shallow magma reservoir in the area before emplacement of the feeder dike in early January 1983. Lava erupted during the first several months was differentiated beyond olivine control and was apparently derived from magma that had undergone prolonged storage and crystal fractionation in the rift zone.

The central-vent eruptive episodes, which began in February 1983 with episode 2, lasted from 9 hours to 12 days. They were characterized by high-volume discharge of lava, vigorous fountaining, rapid summit subsidence, and strong harmonic tremor in the vent area. The repose periods lasted from 8 to 65 days and were characterized by gradual reinflation of Kilauea's summit and persistence of weak harmonic tremor in the vent area. Alternating inflation and deflation in the summit and vent areas occurred sympathetically, suggesting that reservoirs in the rift zone and summit area were hydraulically linked.

After the initial episode, lava was erupted at an average rate of 13.4×10^6 m^3/mo. Long-term tilt change in the summit region was minimal, and, following the approach of Swanson (1972), we have calculated an average magma-supply rate of approximately 10×10^6 m^3/mo after correction for 25 percent porosity. This rate is higher than some estimates for long-term supply to the volcano, but evidence from SO_2-emission rates in the summit region also indicates that the Puu Oo eruption may have coincided with a period of increased magma supply.

After Puu Oo became established as the sole vent, olivine-controlled lava was erupted. Beneath Puu Oo, a column of magma, which may have been nearly vertical and several kilometers long, underwent short-term compositional changes during repose periods that apparently reflected fractionation of olivine. This process repeatedly produced a finite volume of MgO-depleted magma, which would be exhausted whenever the volume of the next eruptive episode exceeded that of MgO-depleted melt. A long-term compositional change manifested by gradually increasing CaO and MgO may have been a consequence either of gradually decreasing contamination of fresh summit melt by differentiated magma present in the rift zone or of gradually changing composition of the melt generated in the mantle.

INTRODUCTION

The Puu Oo eruption began at Napau Crater in the east rift zone of Kilauea Volcano (fig. 17.1) on January 3, 1983. An initial series of intermittent fissure eruptions was followed by a long and continuing series of central-vent eruptions. In the 17-month period reviewed in this paper, twenty major eruptive episodes occurred. Because it is difficult to maintain terminology that is both concise and consistent, for eruptive activity, we apply the term eruption both collectively to the entire series of related eruptive events in the east rift zone during 1983–84 and singly to individual periods of significant lava discharge within that series. Following the usage of Swanson and others (1979), we use the term episode to identify occurrences of fountaining and lava-flow production separated by relatively long quiescent periods during which Kilauea's summit reservoir inflated. Many of the eruptive episodes consisted of single fountaining and flow-production events. Others, however, such as episodes 1, 13, and 19, consisted of two or more such events separated by relatively brief quiescent periods. Thus, some of the episodes were, themselves, series of episodic events.

During those 17 months of activity, nearly 240×10^6 m^3 of basalt was erupted, covering more than 30 km^2 of largely forested country in the middle part of the rift zone and the adjacent part of the south flank of the volcano. Several flows entered sparsely populated areas and destroyed a total of 18 dwellings. Spatter falling from fountains that ranged up to nearly 400 m in height built large cones at the central vents. A 60-m-high cone, Puu Halulu, was formed within the first three months of the eruption; by the end of the twentieth episode, Puu Oo, the cone at the principal vent, stood about 130 m above the preeruption ground surface. At the time of writing (June 1985), the Puu Oo eruption continues unabated and has become the most voluminous historical eruption of Kilauea.

[1]Hawaii Institute of Geophysics, University of Hawaii, Honolulu.

Observational, instrumental, and laboratory results from the first one and one-half years of the Puu Oo eruption are presented in detail in separate papers covering geologic observations (Wolfe and others, in press), data on temperature and composition of sampled lavas (Neal and others, in press), gas studies (Greenland, in press; Greenland and others, in press), seismology (Koyanagi and others, in press), deformation studies (Okamura and others, in press), geoelectric studies (Jackson, in press), and petrology (Garcia and Wolfe, in press). Those papers provide a detailed foundation for this synthesis, and we refer the reader to them for details of topics treated here in summary fashion. Hereinafter, we draw on those papers extensively without further citation except as needed for clarity.

ACKNOWLEDGMENTS

In monitoring this long-lived eruption and organizing and analyzing the data, we received intensive and dedicated help from many associates. We especially thank geologic colleagues N.G. Banks, J. Buchanan-Banks, J.P. Lockwood, R.B. Moore, and G.E. Ulrich, who often joined or relieved us in observing eruptive activity and sampling the lavas. We also thank the staff of the Hawaiian Volcano Observatory for excellent and sustained support in all aspects of the work. John P. Hoffmann called our attention to the relation, illustrated in figure 17.27, between changes in effusion and changes in tilt rate during episode 19. Constructive reviews by T.L. Wright and D.A. Swanson are gratefully acknowledged.

GEOLOGIC SETTING FOR THE PUU OO ERUPTION

STRUCTURE AND MAGMATIC PLUMBING OF KILAUEA

A consistent generalized model of the geologic structure and magmatic plumbing of Kilauea Volcano has been developed from geologic and geophysical studies, particularly over the last three decades. This model has been recently reviewed and expanded by Ryan and others (1981, 1983), and additional recent reviews are given by Duffield and others (1982) and Dzurisin and others (1984). A brief summary of the model follows.

Basaltic magma generated at a probable depth of 60–90 km (Wright, 1984) rises through a system of fractures from deep in the mantle below Kilauea and accumulates within a relatively aseismic reservoir zone (Koyanagi and others, 1974) that lies approximately 2–6 km below the southern part of Kilauea caldera. Most likely the reservoir is a complex of interconnected sills and dikes. Continuing accumulation of magma causes inflation of the reservoir, which is manifested by uplift and distention of the crust that overlies it. Episodic relief from the magmatic stress that develops during filling of the reservoir is provided by summit eruptions and by intrusions that transfer magma from the summit to the rift zones of the volcano. During rift-zone intrusions and eruptions, subsidence and contraction occur in the crust overlying the reservoir; subsidence does not necessarily accompany summit eruptions. Inflations and deflations of the summit reservoir cause measurable tilts on the flanks of the zone of uplift or subsidence. The east-west component of such ground tilt, measured with a sensitivity better than 1 microradian by a continuously recording Hg-capacitance tiltmeter at the Uwekahuna vault (fig. 17.1), approximately 3 km northwest of the center of uplift and subsidence, is used to track the episodes of inflation and deflation. The frequency of shallow earthquakes in the vicinity of the summit reservoir also provides a continuous record of strain manifested as adjustments in the brittle country rock during eposides of inflation and deflation.

Intrusions into a rift zone are commonly accompanied by harmonic tremor and by swarms of shallow (depth <5 km) earthquakes that reflect fracturing of brittle rocks in response to dike emplacement or to volume changes in the magmatic conduit. Dike emplacement is commonly accompanied by ground cracking, extension perpendicular to the rift-zone axis, and vertically directed displacement above and flanking the dike (Pollard and others, 1983). Propagation of a dike to the surface results in an eruption. The close association of subsidence at the summit with intrusion in the rift zone implies a hydraulic link between the summit and the rift zone.

In some cases, either an aseismic zone separates the area of rift intrusion from the summit-reservoir region, or an intrusion occurs without generating an earthquake swarm in the rift zone. In the latter case, the intrusion is manifested by subsidence and related shallow earthquakes at the summit, geodetic and possibly electrical potential-field disturbances in the rift zone, and harmonic tremor. Aseismic transfers of magma, which are common, imply the presence of a preexisting magmatic conduit (Swanson and others, 1976b).

Kilauea abuts the seaward-sloping southeast flank of Mauna Loa, a much larger shield volcano that forms a massive buttress on Kilauea's northwest flank. Kilauea's summit is approximately 5 km above the adjacent sea floor, and its unbuttressed southeast flank is gravitationally unstable. Fiske and Jackson (1972) showed that this geometric arrangement results in orientation of the axis of least compressive stress perpendicular to the boundary between Mauna Loa and Kilauea. Consequently, extension and dike emplacement occur along two steeply dipping zones (the east and southwest rift zones) that approximately parallel the Kilauea-Mauna Loa boundary.

Repeated intrusion, extension, surface cracking, and extrusion have created, in each of the rift zones, a broad, gentle topographic ridge with numerous open cracks, normal faults of small throw, and linear vents, all aligned perpendicular to the direction of least compressive stress. The upper few kilometers of a rift zone must be laced by a complex of dikes that strike parallel to the rift-zone axis. The currently active part of the rift zone, as indicated by the distribution of historical (the last 200 yr) eruptive vents (Holcomb, 1980) is as much as about 2 km wide.

Geophysical evidence, including recognition of local inflation centers (see, for example, Jackson and others, 1975) and the occurrence of aseismic intrusions, indicates that magma persists along at least parts of the rift-zone interior for extended periods of time. This inference is supported by petrologic evidence, which

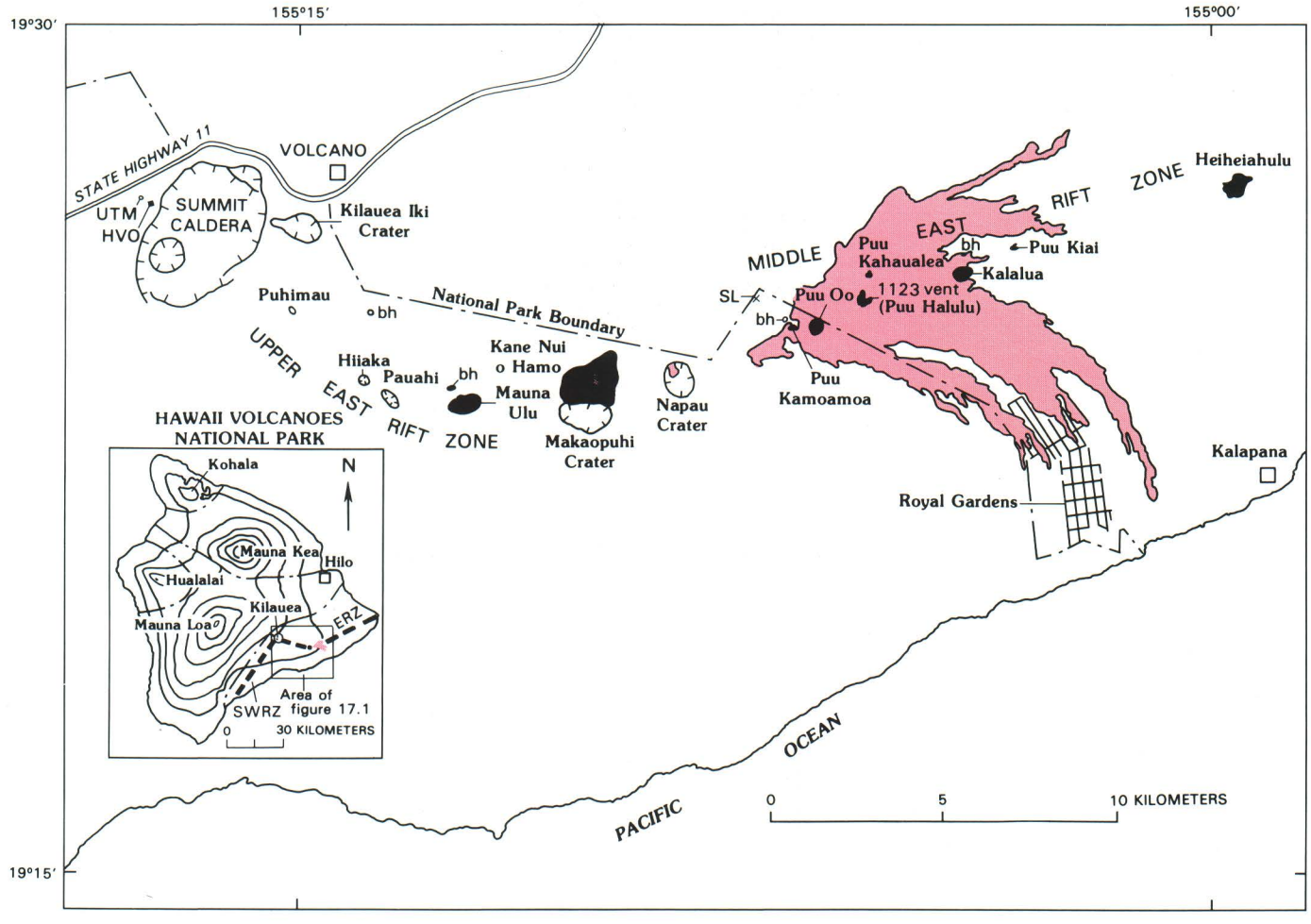

FIGURE 17.1.—Kilauea summit, upper and middle parts of east rift zone, and features discussed in text. HVO, Hawaiian Volcano Observatory; UTM, Uwekahuna tiltmeter; bh, borehole tiltmeter; SL, spirit-level tilt station. Red, flows of episodes 1–20, Puu Oo eruption. Black, shields and large cinder and spatter cones; all except Puu Oo and Puu Halulu predate the Puu Oo eruption. Inset shows location of area and outlines of volcanoes on Island of Hawaii. ERZ, east rift zone of Kilauea; SWRZ, southwest rift zone of Kilauea.

shows that melt of differentiated composition has been a significant component of rift-zone eruptions. Wright and Fiske (1971) have interpreted the differentiated melt as the product of cooling and partial crystallization of magma intruded into the rift zones from the summit region. Furthermore, geologic mapping in the lower east rift zone (Moore, 1983) has revealed areas where repeated eruption of differentiated melt has occurred, implying that local zones favorable to storage of intruded magma have persisted for hundreds of years.

Kilauea's seaward flank, generally called the south flank, is detached from the rest of the volcano along the rift zones, and it undergoes compression and seaward dislocation in response to intrusive activity in the rift zones (Swanson and others, 1976a). The approximate base of the mobile block is recorded by a zone of earthquake hypocenters, 8–9 km deep, that forms a belt parallel to the rift-zone axis but displaced southeastward from it (see fig. 17.8). Focal mechanisms indicate that fault movements occur parallel to a plane dipping 2–3° northwestward (Crosson and Endo, 1982); this subhorizontal zone of decoupling may correspond to a sediment-bearing layer at the interface between the young volcanic rocks that comprise the Island of Hawaii and the isostatically downbowed older sea floor beneath the island (Swanson and others, 1976a; Crosson and Endo, 1982).

The magma supplied to Kilauea from the mantle, then, is accommodated in summit storage, summit and rift-zone eruptions, and rift-zone intrusions. Growth of the volcano results primarily from addition of erupted basalt to its surface and from intrusion accompanied by seaward dislocation of the south flank. Dzurisin and others (1984) concluded that between 1956 and 1983 more than 2×10^9 m^3 of magma had entered Kilauea, at an average rate of about 7×10^6 m^3/mo. Approximately 35 percent of this magma was extruded during that period; the rest was stored in the rift zones, 55 percent in the east rift zone and 10 percent in the southwest rift zone. Apparently the summit reservoir has functioned in recent years, at least, mainly as a temporary holding tank.

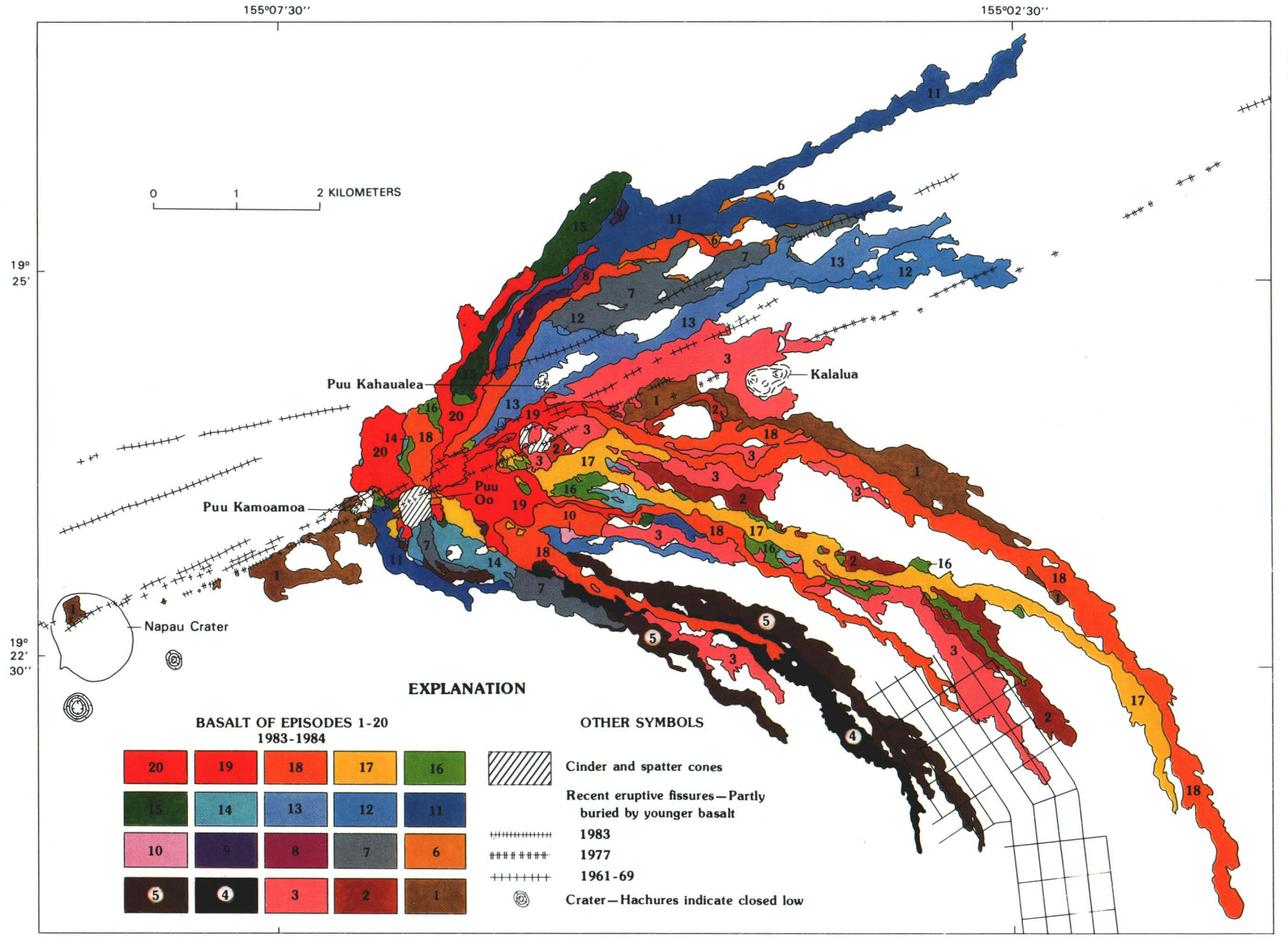

FIGURE 17.2.—Simplified geologic map of vents and flows for episodes 1–20 of the Puu Oo eruption. Also shows traces of recent pre-1983 fissure vents, which include 1977 vents (Moore and others, 1980; R.B. Moore, written commun., 1985) and 1961-69 vents (Moore and Koyanagi, 1969; Swanson and others, 1976b; Swanson and others, 1979). Flows were mapped and field checked using aerial photographs taken, when possible, after each eruptive episode.

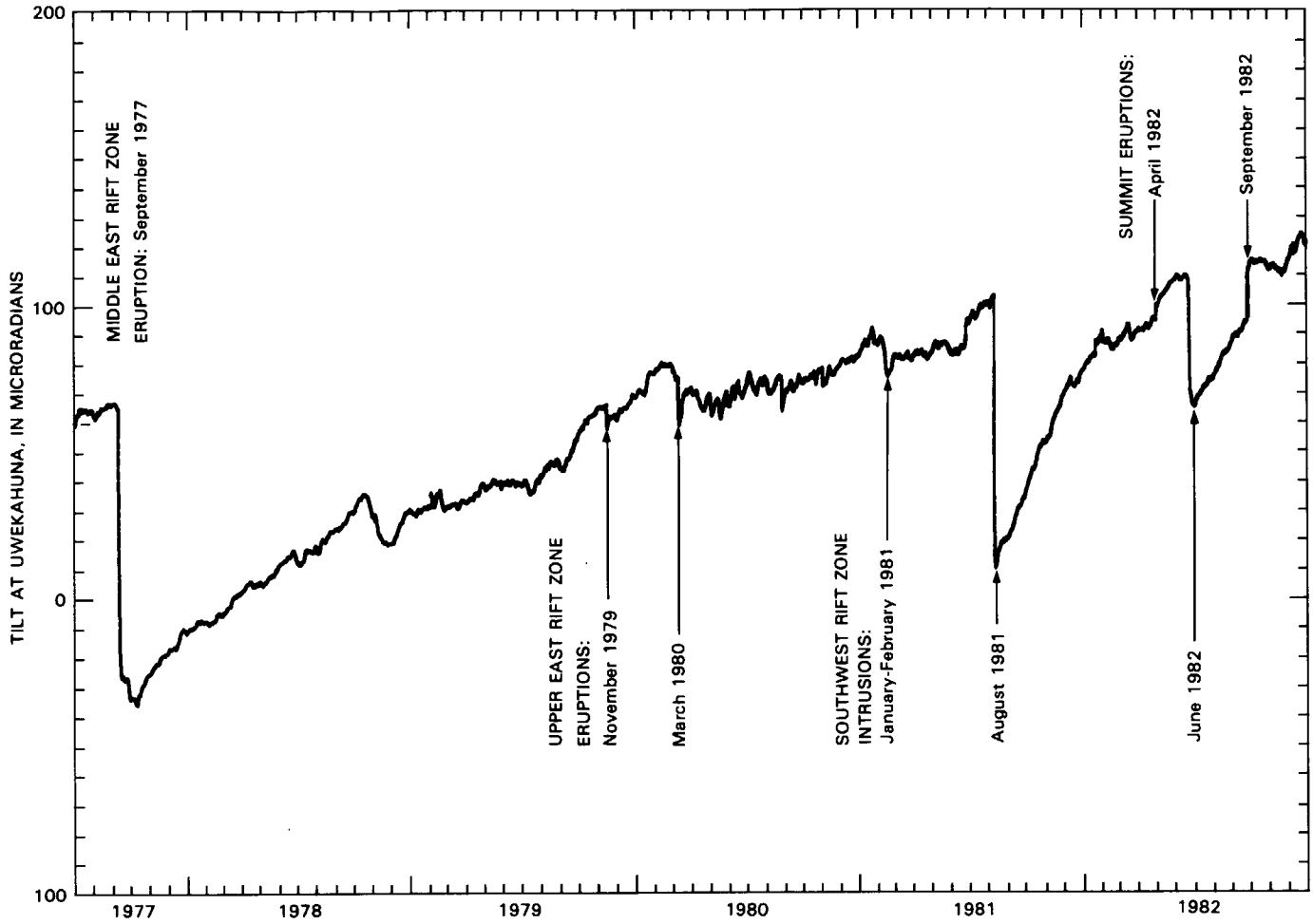

FIGURE 17.3.—East-west summit tilt at Uwekahuna, late 1977 to end of 1982. Increasing values indicate westward-directed (inflationary) tilt change; decreasing values indicate eastward-directed (deflationary) tilt change.

RECENT ACTIVITY IN THE EAST RIFT ZONE, 1955–1982

Eruptions occurred along the lower east rift zone of Kilauea in 1955 and 1960, following a virtual hiatus of 115 years (Macdonald and others, 1983). Thereafter, eruptive activity was confined to the upper and middle parts of the east rift zone. Since 1960, the frequency of earthquake occurrence has been low in the lower east rift and in the adjacent part of the volcano's south flank. Much higher seismicity, in both the rift zone and the south flank, west of the longitude of Heiheiahulu (fig. 17.1) indicates that post-1960 intrusive activity in the east rift zone has been confined to the upper and middle parts.

Fissure eruptions occurred repeatedly in the middle east rift zone from 1961 through 1969 (fig. 17.2). From 1969 through 1974, the two upper-east-rift eruptions at Mauna Ulu (Tilling and others, chapter 16; Swanson and others, 1979) dominated activity at Kilauea. Seaward displacement of Kilauea's south flank and consequent dilation of the rift zone during and after the large ($M = 7.2$) Kalapana earthquake on November 29, 1975, apparently changed the conduit system so that thereafter intrusions dominated rather than eruptions (Dzurisin and others, 1980). Dzurisin and others (1984) identified nine small but distinct intrusions that occurred in the east rift zone from 1976 through 1980. During that period, two minor eruptions (fig. 17.3) occurred in the upper part of the east rift zone, and a relatively voluminous ($35 \times 10^6 m^3$) eruption (Moore and others, 1980) occurred in the middle part (figs. 17.2 and 17.3) in September 1977.

The intrusions in the middle east rift zone were documented in part by tilt measurements. Except where covered by new flows, the middle east rift zone is heavily forested, access is difficult, and deformation data are limited. During the years between the later (1972–74) Mauna Ulu eruption and the 1977 eruption, spirit-level tilt stations in the east rift zone were largely limited to the upper part of the zone and to the part from Heiheiahulu eastward. In that eastern area, tilt measurements in early and mid-1977 showed a middle-east-rift inflation center near Heiheiahulu (Dzurisin and others, 1980). We do not know how far uprift the inflation extended. Following the 1977 eruption and through 1980, an expanded

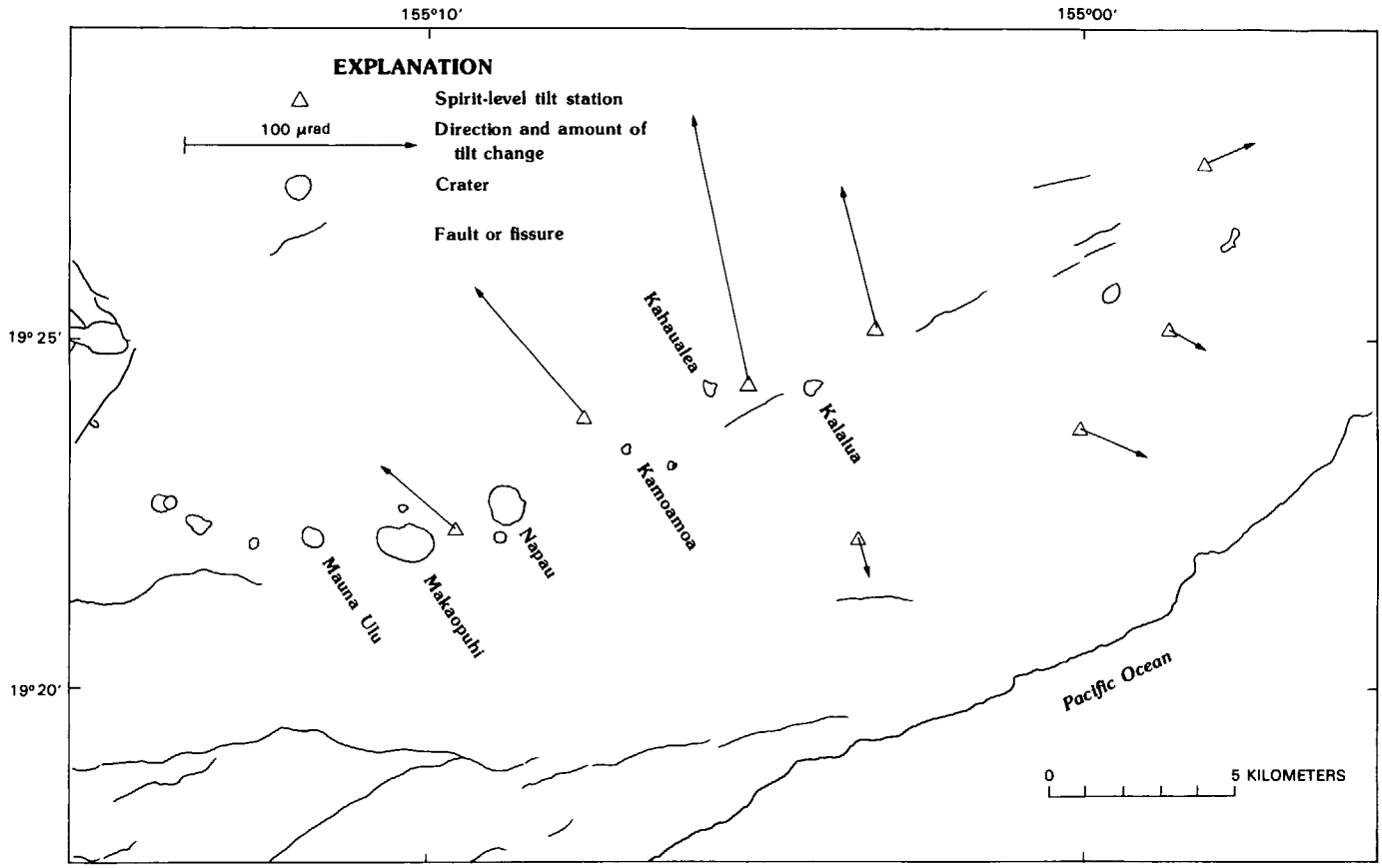

FIGURE 17.4.—Spirit-level tilt results, middle east rift zone, Kilauea Volcano, January 1978 through March 1981.

network of spirit-level tilt stations showed a broad inflationary zone approximately centered on the Puu Kamoamoa-Kalalua area (fig. 17.4).

Intermittent flurries of shallow earthquakes were recorded in the Puu Kamoamoa-Puu Kahaualea region between late 1978 and late 1980 (figs. 17.5*A*, 17.6). The flurries often occurred during or near the ends of episodes of gradual summit deflation. They may identify intrusive pulses that added magma to storage in the middle east rift zone as reflected by the increasing tumescence (fig. 17.4).

Intrusions into the east rift zone virtually ceased early in 1981 at the beginning of a series of southwest-rift-zone intrusions that continued intermittently through June 1982 (figs. 17.3, 17.5*B*). In addition to the seismic quiescence in the east rift zone during that time, there was an almost total absence of deformation, as shown by the borehole tiltmeter near Puu Kamoamoa (fig. 17.1), between early 1981 and late 1982.

Between 1956 and 1983, therefore, at least $1 \times 10^9 m^3$ of magma was added to east-rift-zone storage, according to the calculations of Dzurisin and others (1984). Earthquake distribution patterns indicate that magma accumulated only in the upper and middle parts of the rift zone after the eruption of 1960. Tilt measurements begun in the middle east rift zone after the 1975 Kalapana earthquake show that it was inflating through 1980 and was thus a major locus of magma storage. Magma reservoirs apparently became engorged, and the middle east rift zone became primed for the eruptive activity that began in 1983. The distribution of earthquake epicenters between late 1978 and late 1980 (fig. 17.5*A*) further indicates that intermittent intrusions were adding magma to a reservoir near the future main vents for the Puu Oo eruption.

IMMEDIATE PRECURSORS TO THE PUU OO ERUPTION

After a major intrusion in the southwest rift zone in August 1981, fairly sustained inflation of Kilauea's summit prevailed until late September 1982. A small summit eruption on April 30–May 1, 1982, and a second large southwest-rift intrusion in June 1982 punctuated the inflationary episode. An abrupt intrusion in the already inflated summit region on September 25 caused pronounced uplift (fig. 17.3) and led to a minor eruption in the southernmost part of Kilauea caldera. During the eruption and immediately following it, a swarm of shallow earthquakes migrated into the uppermost part of the east rift zone in the vicinity of Puhimau Crater (fig. 17.5*C*), and concomitant geoelectrical disturbances were meas-

ured in that area and also 4 km farther southeast near Pauahi Crater. However, no measurable surface deformation was detected at that time in the upper east rift, which suggests that no shallow dike was emplaced. Therefore, we infer that a surge of supply within the upper east-rift-zone conduit system led to fracturing of the shallow crustal rocks and development of an electrical anomaly.

Shallow earthquakes continued in the area between Puhimau and Pauahi Craters through early November, but with diminishing frequency after mid-October. A slow tilt change recorded by automatic tiltmeters along the upper east rift zone began on October 6, together with changes in self-potential near Pauahi. These events, which continued until about the end of the month, indicated that a gradual intrusion was under way in the upper east rift zone. Beginning about October 8, additional shallow earthquakes migrated from the upper east rift zone downrift as far as the Napau Crater area, where intermittent shallow earthquakes occurred in late October and early November (fig. 17.7). A gradual tilt change at the automatic tiltmeter near Puu Kamoamoa, beyond the downrift end of the flurry of earthquakes, began on November 8 and continued until about the middle of the month, indicating renewed accumulation of magma in the middle east rift zone.

A second intense earthquake swarm occurred in the upper east rift zone on December 9 and 10, 1982. Geoelectric response to this event was indistinct. However, a 70-mm subsidence northwest of Puhimau Crater, detected by leveling, may have been a response to emplacement of a dike within 2 km of the surface sometime between October 29 and December 9. As in the previous earthquake swarm, the shallow hypocenters once again migrated downrift to the vicinity of Napau Crater (fig. 17.7), where seismic activity continued through the end of the month. No tiltmeter disturbances occurred during early December in the upper east rift zone or near Puu Kamoamoa, but gradual tilt changes in the upper east rift and at Puu Kamoamoa began in both areas on December 20 and continued to the end of the year. The inferred intrusions during the last quarter of 1982 apparently reactivated the upper- and middle-east-rift-zone conduit system and set the stage for the Puu Oo eruption.

EMPLACEMENT OF THE FEEDER DIKE AND FISSURE ERUPTIONS OF THE FIRST EPISODE

The premonitory seismic swarm, accompanied by weak harmonic tremor, began about 1 km west of Makaopuhi Crater (fig. 17.8) at approximately 0030 (H.s.t.) January 2, 1983. When compared to the late-December seismicity, the swarm appears as an intensification of the already established earthquake pattern (fig. 17.9). However, tiltmeters located 2–4 km uprift near Mauna Ulu and Puhimau showed tilt changes virtually coincident with the onset of the swarm. Neither shallow earthquakes nor electrical changes occurred uprift in conjunction with the tiltmeter disturbances. Thus, the swarm was apparently initiated in response to a new surge of magma through melt-filled passages in which a pressure change could be transmitted rapidly and easily. An hour after the beginning of the swarm, the Uwekahuna tiltmeter began to register subsidence of the summit of Kilauea (fig. 17.10).

The located earthquakes of the swarm, mostly 2–4 km deep, formed a narrow band, 1–2 km wide, that apparently recorded magma intrusion in the form of a dike. The swarm elongated northeastward as its tip migrated downrift at a rate of approximately 0.7 km/h (fig. 17.11). The northeast end of the swarm had extended downrift nearly to Napau Crater by about 0400 January 2. Characterized by a sharply defined leading edge, the swarm continued downrift toward Puu Kamoamoa until about 0600. From then until the onset of eruptive activity early the next morning, the swarm lost its distinct leading edge (fig. 17.11) and was largely localized between Napau Crater and Puu Kamoamoa.

Surface deformation caused by the northeastward-migrating dike was detected by tiltmeters in the rift zone near both Puu Kamomoa and Kalalua while the earthquake swarm was still between Napau and Puu Kamoamoa. At 0430 January 2, the Puu Kamoamoa instrument, located north of the rift axis, started to detect a southeastward tilt of the ground, and two hours later, at 0630, the instrument north of Kalalua responded to a southward tilt. At 1030 at Puu Kamoamoa, the east-west tilt component, which was nearly parallel to the strike of the dike and thus more sensitive to passage of the dike tip (Maruyama, 1964), reversed direction from east down to west down; this reversal probably indicated the passing of the dike tip. In 10 hours, the dike tip had migrated slightly more than 7 km from the assumed starting point near Makaopuhi Crater. The migration rate based on the tilt reversal at the Puu Kamoamoa station, 0.7 km/h, agrees with the rate of downrift migration of the earthquake swarm.

The vertical surface-displacement field caused by the dike tip is expected to migrate downrift ahead of the tip, but the two should travel at the same rate (Maruyama, 1964), 0.7 km/h in this case. The initial tiltmeter disturbance at Kalalua, however, occurred at 0630, only 2 hours after that at Puu Kamoamoa, 5.4 km uprift, and nearly 6 hours earlier than predicted by downrift migration at 0.7 km/h.

This anomalous early arrival could have resulted from passage of a hydraulically induced surge of magma when the dike tip encountered another magma body. If that was the case, the migration of the pressure-induced surge from the dike tip to Kalalua may have been nearly instantaneous. At 0630, when the Kalalua tiltmeter first recorded movement, the dike tip should have been 4.2 km (0.7 km/h times 6 h) from the point of origin of the earthquake swarm. Thus it would have been between Napau Crater and Puu Kamoamoa, in the area where the leading edge of the swarm lost its definition (fig. 17.11).

About 20 hours after passage of the leading edge of the earthquake swarm, lava fountaining began at Napau Crater at 0031 January 3. The initial outbreak continued for 9.5 hours; it produced a 6-km-long, discontinuous line of erupting fissures that extended progressively downrift from Napau Crater and reached its temporary eastern limit, south of Puu Kahaualea, at 0740 (fig. 17.12). The overall migration of the vent system was downrift (fig. 17.13), but the sequence of vent opening was complicated in detail; at times, new vents opened uprift of already active ones. The sequence of

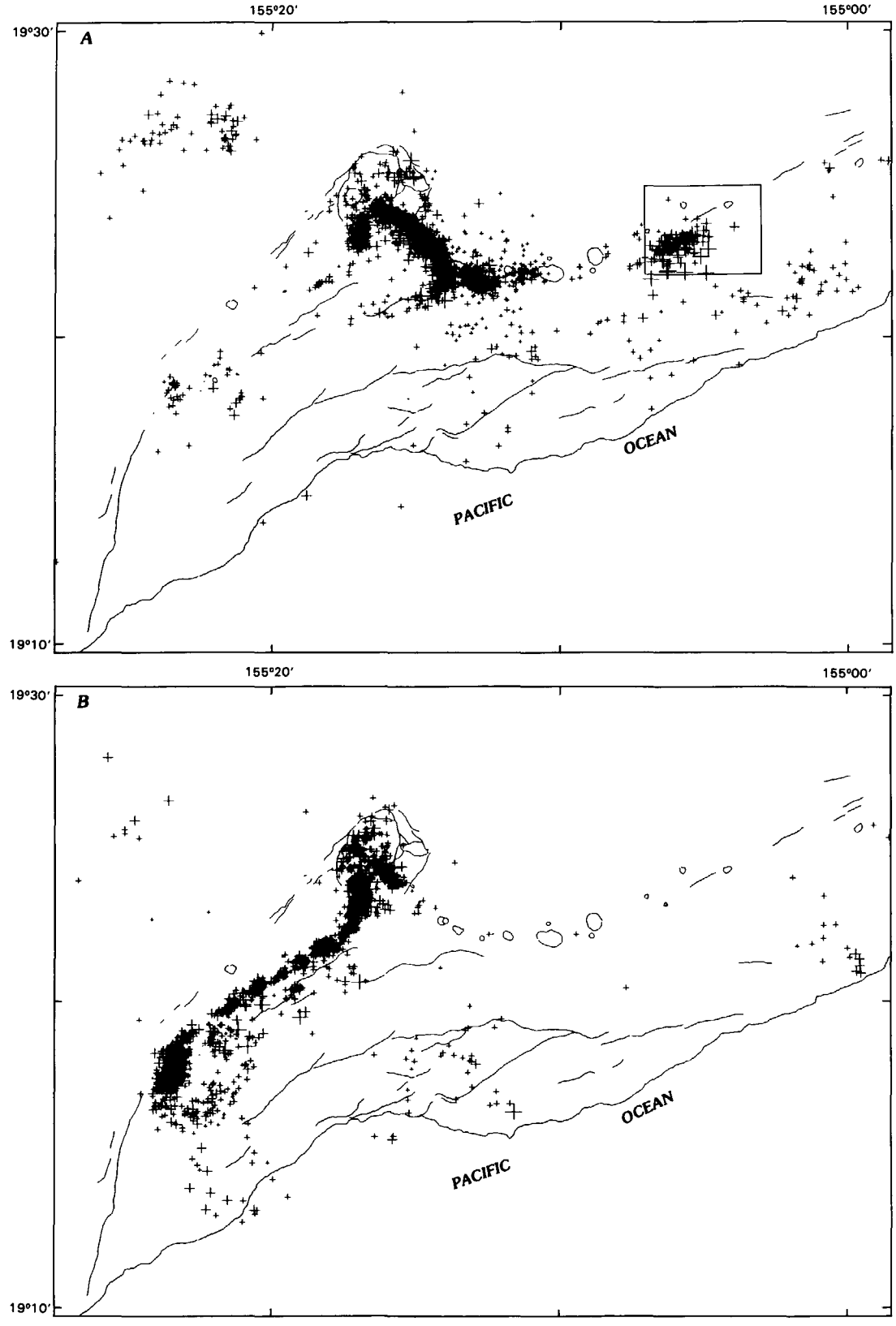

FIGURE 17.5.—Located shallow (<5-km depth) earthquakes at Kilauea from November 1978 through December 1982. ***A***, November 1978 through December 1980. Box shows location of earthquakes plotted in figure 17.6. ***B***, January 1981 through September 24, 1982. ***C***, September 25, 1982, through December 1982.

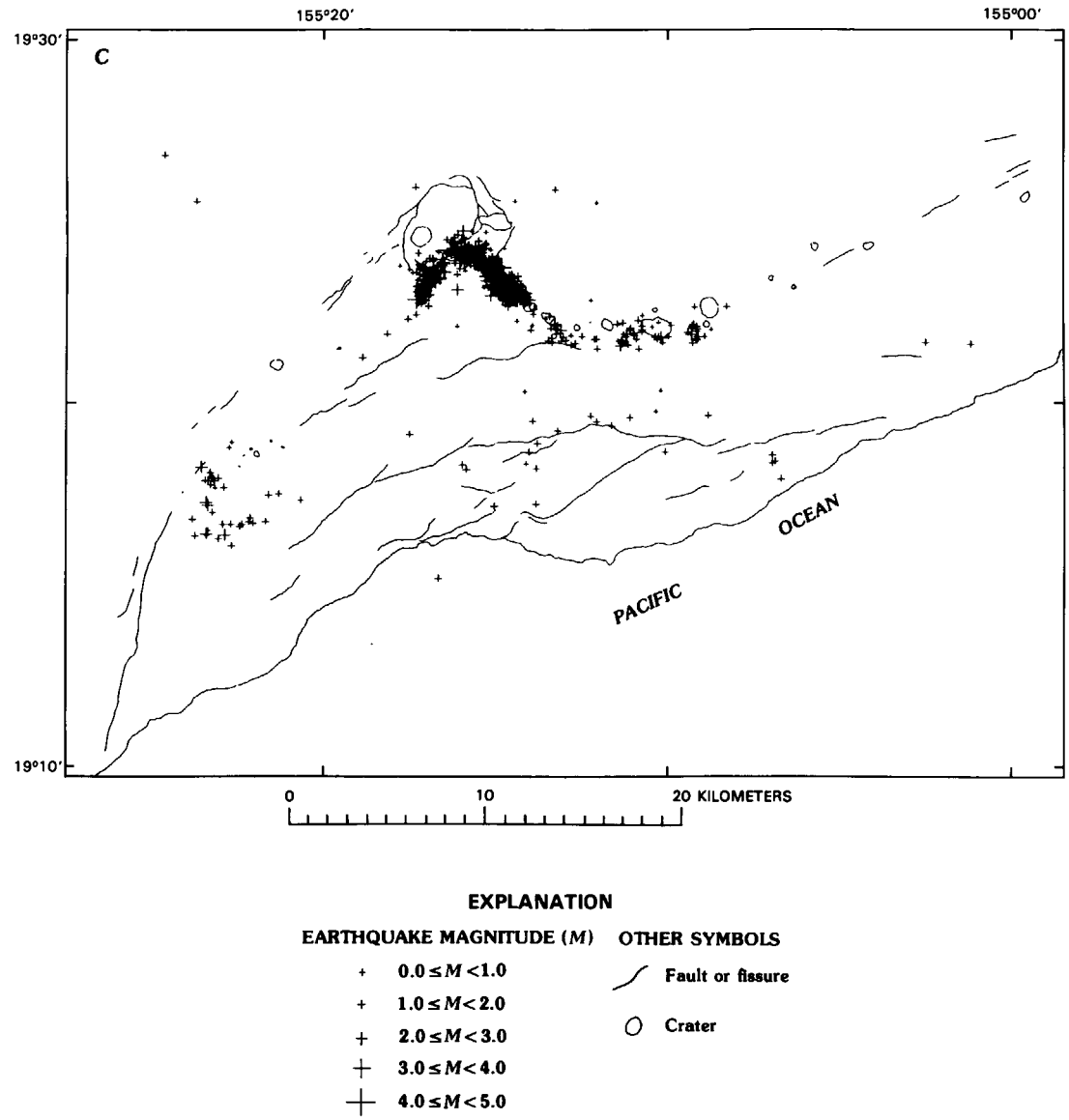

FIGURE 17.5.—Continued.

termination of eruption was also complex. The last vents to shut down, at 1000 that morning, were those at the middle of the fissure system, near Puu Kamoamoa.

Except for brief fountaining later that afternoon of the easternmost vent, which had opened at 0740, the initial outbreak was over; no further eruption occurred for approximately 2 days. Rapid subsidence of the summit stopped abruptly when extrusion stopped at 1000 January 3, and the summit reinflated until late on January 4, at which time subsidence resumed (fig. 17.10). During the respite in eruption from January 3 to January 5, shallow seismicity was distributed in a zone that extended nearly from Napau Crater to Kalalua (fig. 17.11).

Fountaining resumed at 1123 January 5, and nearly continuous fissure eruptions occurred alternately or sometimes simultaneously through January 5 and 6 at this 1123 vent, the previously active 0740 vent, and a third nearby vent that opened at 1708 January 5. Intermittent minor fissure eruptions also occurred during this period in the vicinity of Puu Kamoamoa.

Extension manifested by ground-cracking occurred on January 5 and 6 along zones that flanked the 0740-1123-1708 vent alignment (fig. 17.12). An estimated 0.5×10^6 m^3 of lava poured into an open crack south of the 0740 vent. On strike with the open crack, widening of 2–3 m occurred on cracks cutting a flow that was emplaced sometime on January 5–6; flows erupted on January 8–9

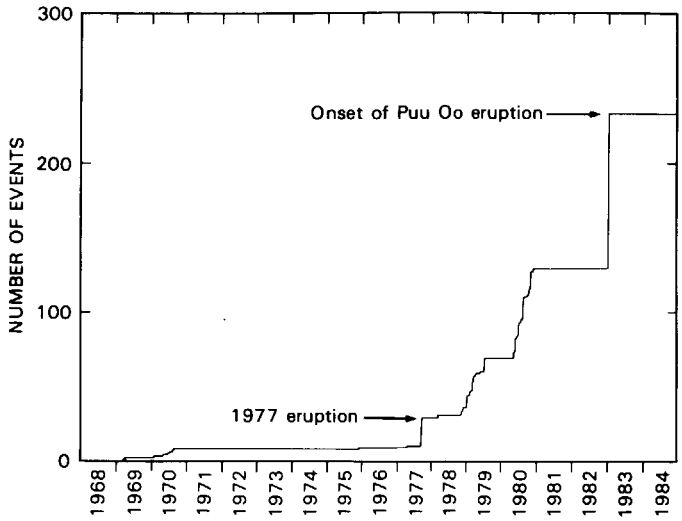

FIGURE 17.6.—Cumulative frequency of located shallow (<5-km depth) earthquakes in the Puu Kamoamoa-Puu Kahaualea area, 1978 through 1982. See figure 17.5A for location.

buried the cracks and showed no subsequent displacement.

Shallow earthquakes, sufficiently large to be well located, persisted in the eruption area between January 2 and 7. Early on January 7, seismicity increased markedly to form a renewed earthquake swarm near Kalalua, farther downrift than it had previously extended (fig. 17.11). Accelerated surface deformation in the same general area began during the evening of January 6 and, by midnight, had caused a large disturbance of the borehole tiltmeter about 300 m north of Kalalua. This event also perturbed the self potential in the same area. Daylight on January 7 showed the tiltmeter to be within a northeast-trending zone of new cracks that bounded a shallow graben. Immediate remeasurement of a horizontal distance across the zone of cracks north of Kalalua indicated that about 1.8 m of extension normal to the trend of the rift zone had occurred since the previous measurement on January 5 (Dvorak and others, in press; an additional 0.4 m of extension of the line was measured on January 11, after which there were no further changes). These events apparently recorded emplacement of the easternmost segment of the new dike system that had been delivering magma to the surface since January 3. Fountaining and flow production began on this segment of the dike at 1030 January 7 and continued for about 18 hours (fig. 17.13).

Forcible emplacement of a shallow dike apparently occurred near Kalalua on late January 6 and early January 7, but the effects of magmatic activity were evident earlier. An aseismic dislocation of the tiltmeter, discussed above, occurred at 0630 January 2, approximately 6 hours after the onset of the seismic swarm. Reoccupation, on the afternoon of January 3, of a self-potential measurement line crossing the rift zone near the tiltmeter showed a voltage increase, which contrasted with a previous long-term trend of generally decreasing self-potential. At the same time, production of profuse, hot, SO_2-rich fume was observed along newly lengthening cracks about 1 km east of the 0740 vent, where new vents would erupt four days later on January 7.

The earthquake swarm ended late on January 7. Thereafter, through at least the 20 eruptive episodes summarized here, no further concentrations of locatable shallow earthquakes occurred in the eruptive zone. The major subsidence of Kilauea's summit ended at about 0700 January 8. Thereafter, intermittent fissure eruptions, accompanied by sporadic minor tilt changes at the summit, occurred through January 15 at the 1123 and 1708 vents. An additional small eruption occurred near Puu Kamoamoa on January 23.

Fissure vents were dominant during the first episode of the Puu Oo eruption. They produced linear fountains as long as several hundred meters. Spatter from the fountains built low ramparts adjacent to the fissures, and thin fluid flows of pahoehoe, which changed locally to aa, normally spread near the erupting vents. A major exception occurred on January 7, when particularly intense effusion generated a fluid lava flow that rapidly moved 5.5 km down Kilauea's south flank at a rate that reached about 2 km/h. At the peak of that event, the discharge rate was greater than $1 \times 10^6 m^3/h$. Normal discharge in episode 1 was much lower, usually by an order of magnitude. In approximately 99 hours of actual eruption, episode 1 produced about $14 \times 10^6 m^3$ of new flows and vent deposits.

Subsidence related to the dike emplacement and the January eruptions occurred in Kilauea's summit area (fig. 17.14). The maximum vertical displacement, at least 55 cm, was in the southern part of the caldera, southeast of Halemaumau. The topographic volume loss, calculated from levelling data, was approximately $60 \times 10^6 m^3$ (Dvorak and others, in press). A concentration of shallow earthquakes in the southern caldera region (fig. 17.8) recorded brittle-fracture events coincident with the subsidence.

The earthquake swarm was approximately 16 km long (fig. 17.8), and its base was about 3–4 km deep. The feeder dike intersected the ground surface along an 8-km-long part of the earthquake zone. Using an 8-km length, 2.2-m width (from the measured extension near Kalalua), and average 3.5-km distance from top to bottom, we calculate an approximate volume of $60 \times 10^6 m^3$ for the dike, a value that is almost certainly an underestimate. Using the full 16-km length gives $120 \times 10^6 m^3$, twice as much as the topographic volume change in the summit area and probably an overestimate because the dike did not reach the surface over the full length of the earthquake swarm.

Horizontal distance measurements over the period from January–May 1982 to September–October 1983 indicated a seaward displacement of Kalalua, with respect to reference points on Mauna Loa, of more than 3 m (Hawaiian Volcano Observatory data). During the same period, stations in the upper east rift zone and downrift at Heiheiahulu showed no movement. Stations on the south flank, near the coast, were displaced seaward approximately 0.5–1 m; maximum movement was in the same sector as the earthquake swarm and diminished to the northeast and southwest. The large disparity between the apparent displacements of Kalalua and the stations closer to the coast indicates that substantial compression of the south flank resulted from intrusion of the dike. Modeling a theoretical dike that would best account for the measured horizontal displacements, Dvorak and others (in press) found that the best fit

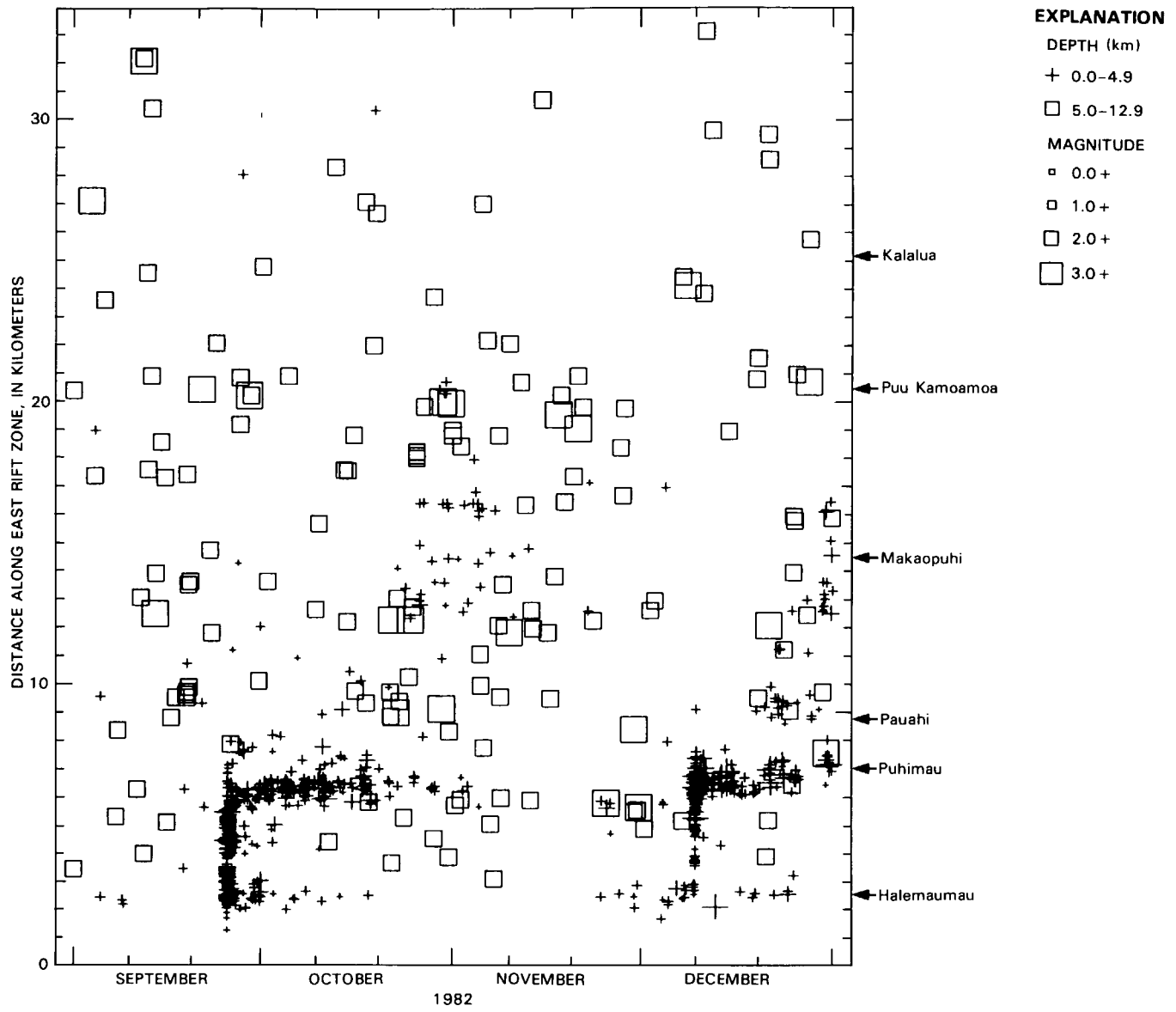

FIGURE 17.7.—Space-time diagram of earthquake epicenters in the summit, upper and middle east rift zone, and adjacent part of the south flank, Kilauea Volcano, from September through December 1982. Epicenters projected onto an east-west line.

was for a dike 11.4 km long, 2.4 km from top to bottom, and 3.6 m wide. These dimensions yield a volume of about $100 \times 10^6 m^3$, which is probably a reasonable approximation.

During the earthquake swarm, the area from Puu Kamoamoa to between Puu Kahaualea and Kalalua (fig. 17.8) showed a lower concentration of seismic activity. This area contains the major vents of the Puu Oo eruption: the 0740-1123-1708-vent complex south of Puu Kahaualea and the Puu Oo vent northeast of Puu Kamoamoa. It also coincides closely with the zone of shallow earthquake flurries that recurred repeatedly from late 1978 to late 1980 (figs. 17.5*A*, 17.6). Furthermore, the initial displacement field migrating downrift ahead of the dike tip passed through this area at a higher speed than in its passage farther uprift and produced the anomalous early tilt near Kalalua. Taken together, these data suggest that the major vents overlie a local magma reservoir established before the eruption started. The lower seismicity may record upward propagation of the dike through crust that, because of the magma reservoir, was more distended, fractured, and hotter than normal when dike emplacement occurred.

A zone of low seismicity was also found farther south in the same sector of the south flank (fig. 17.8), where it had been a persistent feature since at least the early 1960's (Hawaiian Volcano Observatory data). The quiet zone in the south flank may be related to the one in the 1983 earthquake swarm. If so, the persistence of

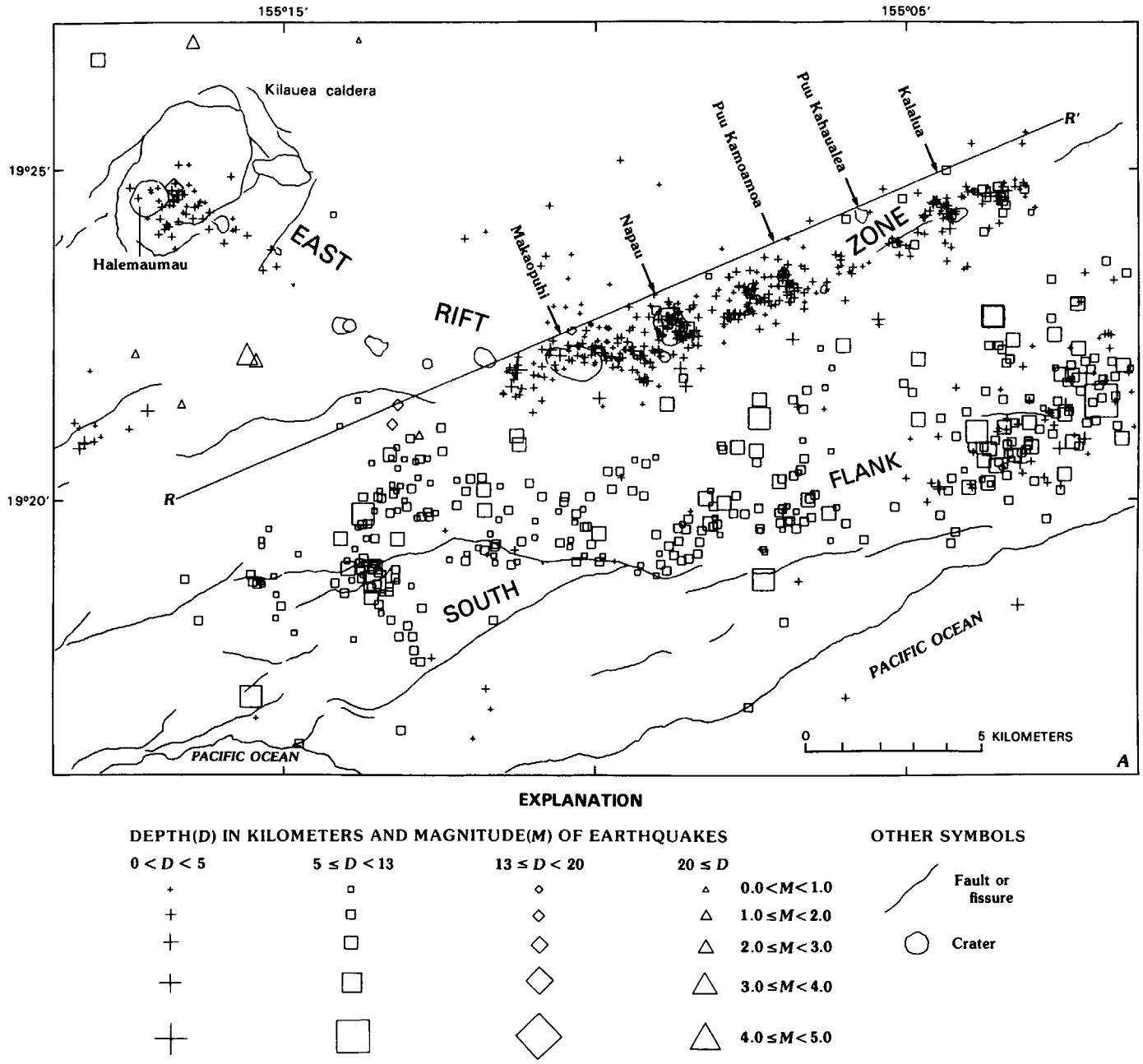

FIGURE 17.8.—Located earthquakes, January 1983, Kilauea caldera, east rift zone, and south flank. ***A***, Distribution of epicenters. Cross section *R-R'* shown in figure 17.8*B*. ***B***, Depth-distance distribution of hypocenters, projected onto line *R-R'*.

the south-flank feature may indicate that the Puu Kamoamoa-Puu Kahaualea area has had a magma reservoir for two decades or more. Two alternative explanations are that the south-flank seismic gap represents either a zone of aseismic slip or a locked zone that could yield abruptly to cause a large earthquake. Neither of these alternatives has a genetic or predictive relationship to the region of postulated magma storage in the rift zone.

EPISODIC CENTRAL-VENT ERUPTIONS: EPISODES 2–20

LOCATION, EPISODICITY, AND LAVA-DISCHARGE RATE

During episodes 2 and 3, the 1123 vent was the main eruptive vent, producing major flows that extended northeast within the rift

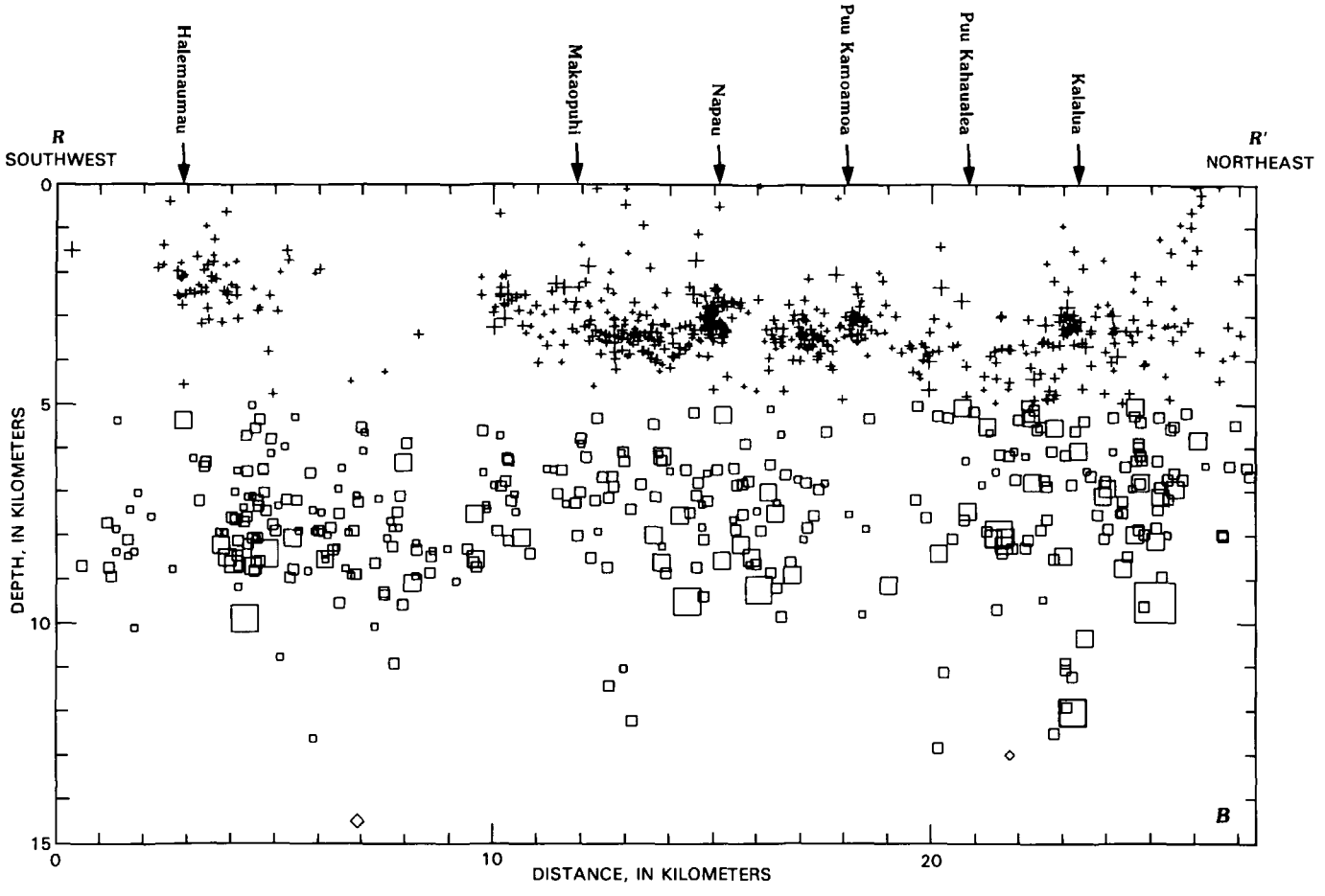

FIGURE 17.8.—Continued.

zone and southeast to the Royal Gardens subdivision (fig. 17.2). Less voluminous eruption also occurred in the area where Puu Oo would subsequently grow. Beginning with episode 4, the Puu Oo vent, supplemented on a few occasions by nearby local fissure vents, was the sole eruptive locus. During episodes 4 and 5, the major flows emerged from the south flank of Puu Oo and traveled southeast toward Royal Gardens. Thereafter, the major flows emerged from the northeast flank of Puu Oo. Many extended into dense forest north of Puu Kahaualea; others turned southeastward and advanced down the south flank toward the ocean.

An episodic pattern quickly developed (table 17.1, fig. 17.15). Eruptive episodes, which ranged in length from 9 hours to 12 days, were characterized by high-volume discharge of lava flows, vigorous fountaining, rapid summit subsidence, and strong harmonic tremor in the vent area. Repose periods, which ranged in length from 8 to 65 days, were characterized by reinflation of Kilauea's summit and weak harmonic tremor in the vent area; at times the upper surface of a magma column was evident in the conduit beneath the vent. The pattern was strikingly similar to that of the first 7 months (May–December 1969) of the 1969–71 Mauna Ulu eruption (Swanson and others, 1979). However, after 12 episodes with rapid discharge and high or sustained fountaining, the style of eruption at Mauna Ulu changed to one dominated by steady slow discharge that built the Mauna Ulu shield and transported large volumes of pahoehoe great distances from the vent through lava tubes (Tilling and others, chapter 16; Peterson and Swanson, 1974; Peterson, 1976; Swanson and others, 1979). In contrast, the episodic Puu Oo eruption has continued through episode 20 and beyond (33 episodes as of June 1985), producing one of the largest vent structures at Kilauea Volcano and creating an extraordinary complex of interleaved aa flows (fig. 17.2).

Both the duration of repose between eruptive episodes and the volume discharged during eruptive episodes varied significantly. Nevertheless, a striking regularity developed (fig. 17.16) that was particularly pronounced during episodes 4–12 and 13–17. During those two intervals, the time from the end of one eruptive episode to the end of the next varied from 9 to 31 days (from data of table 17.1) and averaged 19 ± 7 (1 standard deviation) days; erupted volumes of lava ranged from 6 to $14 \times 10^6 m^3$ and averaged $10 \pm 3 \times 10^6$ (1 standard deviation) m^3. These intervals were times of slightly higher than normal supply of lava, averaging about $15.7 \times 10^6 m^3$/mo. This difference is due largely to abnormally

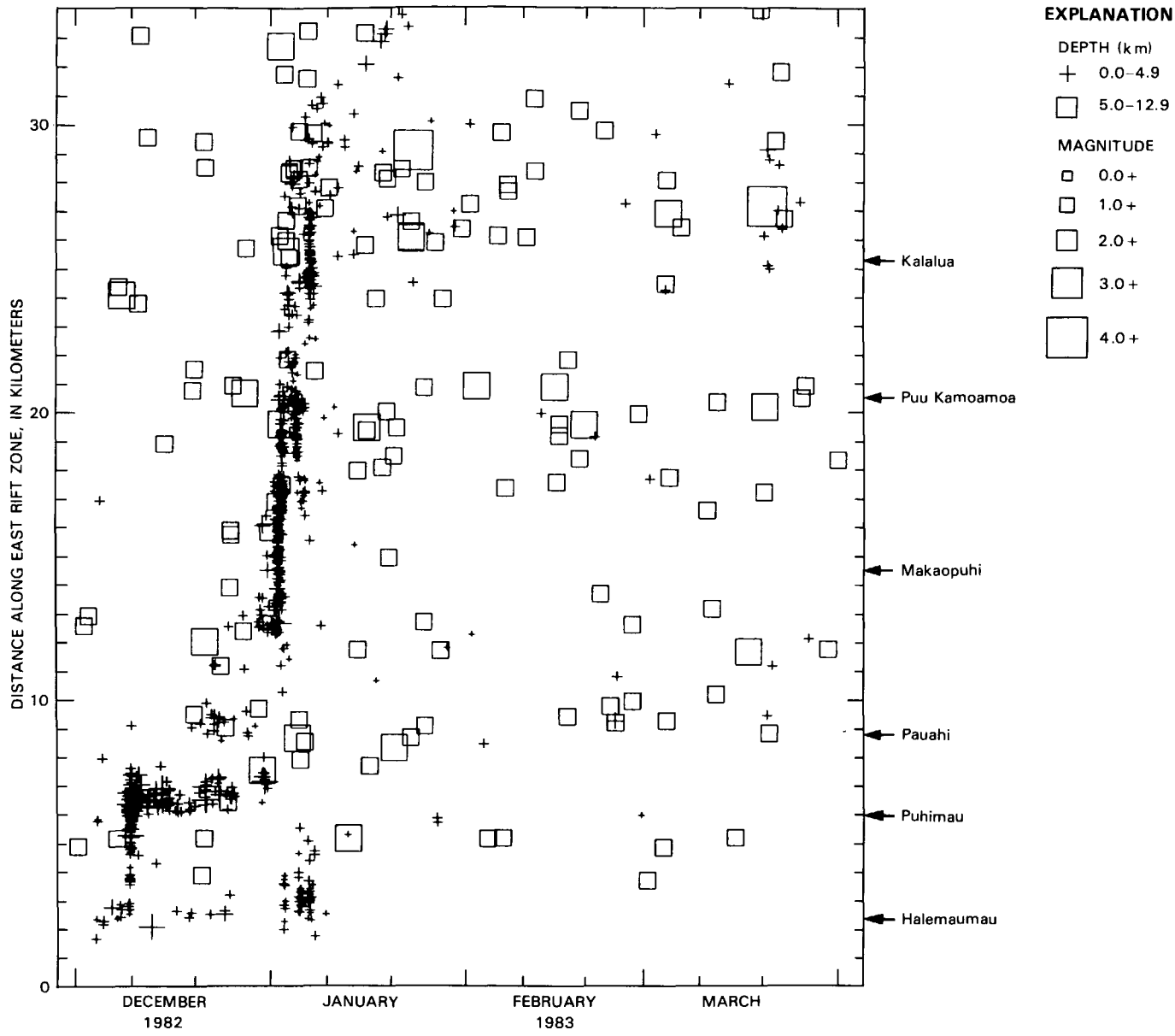

FIGURE 17.9.—Space-time diagram of earthquake epicenters in the summit, upper and middle east rift zone, and adjacent part of the south flank, Kilauea Volcano, for December 1982 through March 1983. Epicenters projected onto an east-west line.

prolonged repose before episodes 4 and 13. For comparison, during the 12 episodes of sustained fountaining that occurred in the early months of the 1969–71 Mauna Ulu eruption, lava was delivered to the surface at an approximate rate of 10×10^6 m^3/mo. During that period, average erupted volumes and average recurrence intervals at Mauna Ulu were also smaller than for the Puu Oo eruption (fig. 17.16).

As the Puu Oo eruption went on, the durations of individual episodes tended to decrease and the discharge rates to increase (table 17.1, fig. 17.17); thus comparable volumes of lava were delivered more rapidly in successive episodes. Presumably this reflected progressive enlargement and streamlining of the conduit system between the summit reservoir and the vent area.

MAGMA SUPPLY TO THE VOLCANO

Swanson (1972) examined the rate of lava production during three long eruptions of Kilauea—the 1952 Halemaumau eruption, the 1967–68 Halemaumau eruption, and the 1969–71 Mauna Ulu eruption—that were characterized by minimal net change in the degree of summit inflation as indicated by the summit tilt record. Assuming that minimal net tilt change at the summit implied minimal

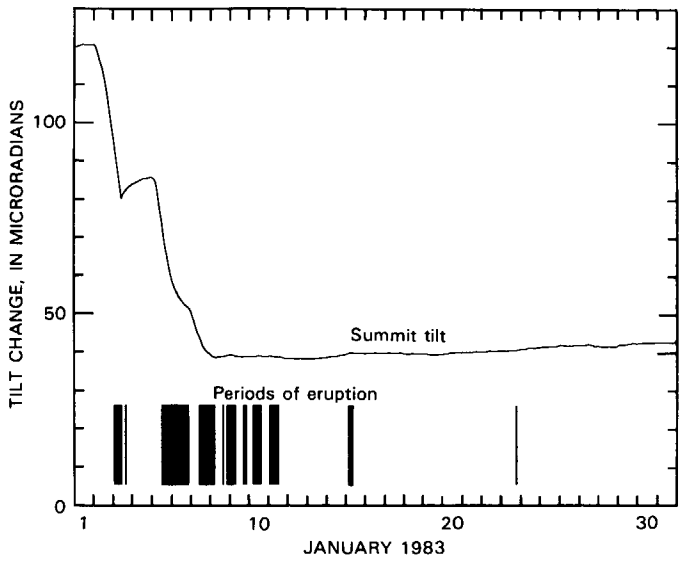

FIGURE 17.10.—East-west summit tilt record (Hg-capacitance tiltmeter at Uwekahuna) and episode 1 eruptive periods, Puu Oo eruption, January 1983. Increasing values indicate westward-directed (inflationary) tilt change; decreasing values indicate eastward-directed (deflationary) tilt change. Full magnitude of tilt change from January 5 through January 7 is greater than shown because of nonlinear response of tiltmeter to tilt change during that period.

change in the stored volume, he concluded that the erupted volumes approximated the supply of magma from the mantle. Correcting for an estimated 15 percent vesicularity, he calculated a magma-supply rate of approximately $9 \times 10^6 m^3$/mo for the three sustained eruptions. Before applying Swanson's technique to infer magma supply from the rate of lava delivery during the Puu Oo eruption, we evaluate several factors, including the large subsidence related to dike emplacement in episode 1, a long-term decrease in average tilt value, and the correction for vesicularity.

A large subsidence of Kilauea's summit occurred at the beginning of the Puu Oo eruption, and we infer that a large volume of magma, on the order of $100 \times 10^6 m^3$, remained in the intruded dike and this was not accounted for in the measured volume of episode 1 lava. After episode 1, the much smaller, alternately inflationary and deflationary tilt changes were roughly similar in magnitude and nearly cancelled each other. However, they were superimposed on a gradual, long-term decrease in average tilt that amounted to about 30 microradians by the end of episode 20 (fig. 17.15) after correction for the offset caused by the November 1983 Mauna Loa earthquake. This tilt change is equivalent to an apparent volume decrease of about $10 \times 10^6 m^3$ of magma over 17 months (see discussion in subsequent section titled "Relation of Summit Tilt Changes to Rift-Zone Activity"), which is within the uncertainty of our volume measurements. Furthermore, in an analysis of deformation and gravity data for the caldera region, Johnson (chapter 47) found that cross-caldera distances measured perpendicular to the coast have been steadily increasing at a rate of about 2 microstrain (parts per million) per month. Thus the subsidence indicated by gradually decreasing average tilt values may not reflect

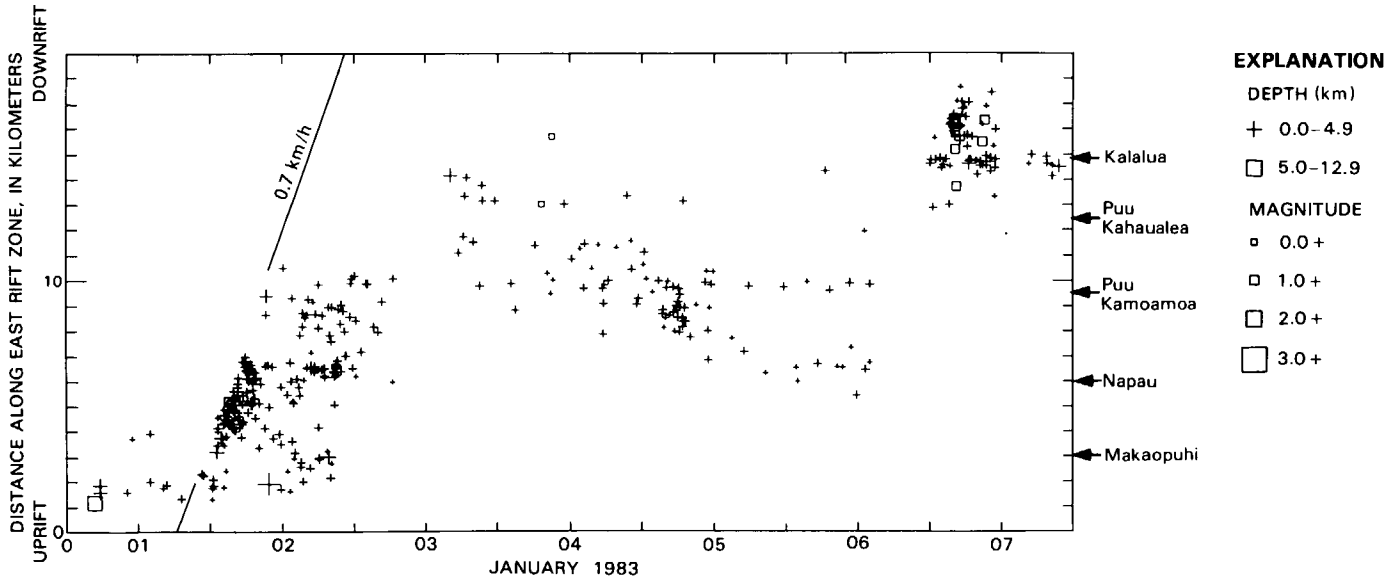

FIGURE 17.11.—Expanded space-time diagram of earthquake epicenters in upper and middle east rift zone, Kilauea Volcano, during the period January 1–7, 1983. Epicenters projected onto a line parallel to the axis of the middle east rift zone. A downrift migration rate of 0.7 km/h is inferred for the leading edge of the concentrated zone of shallow earthquakes during the morning of January 2. Location accuracy, based on horizontal and vertical standard error (Klein, 1978) for these earthquakes, is ±1 km.

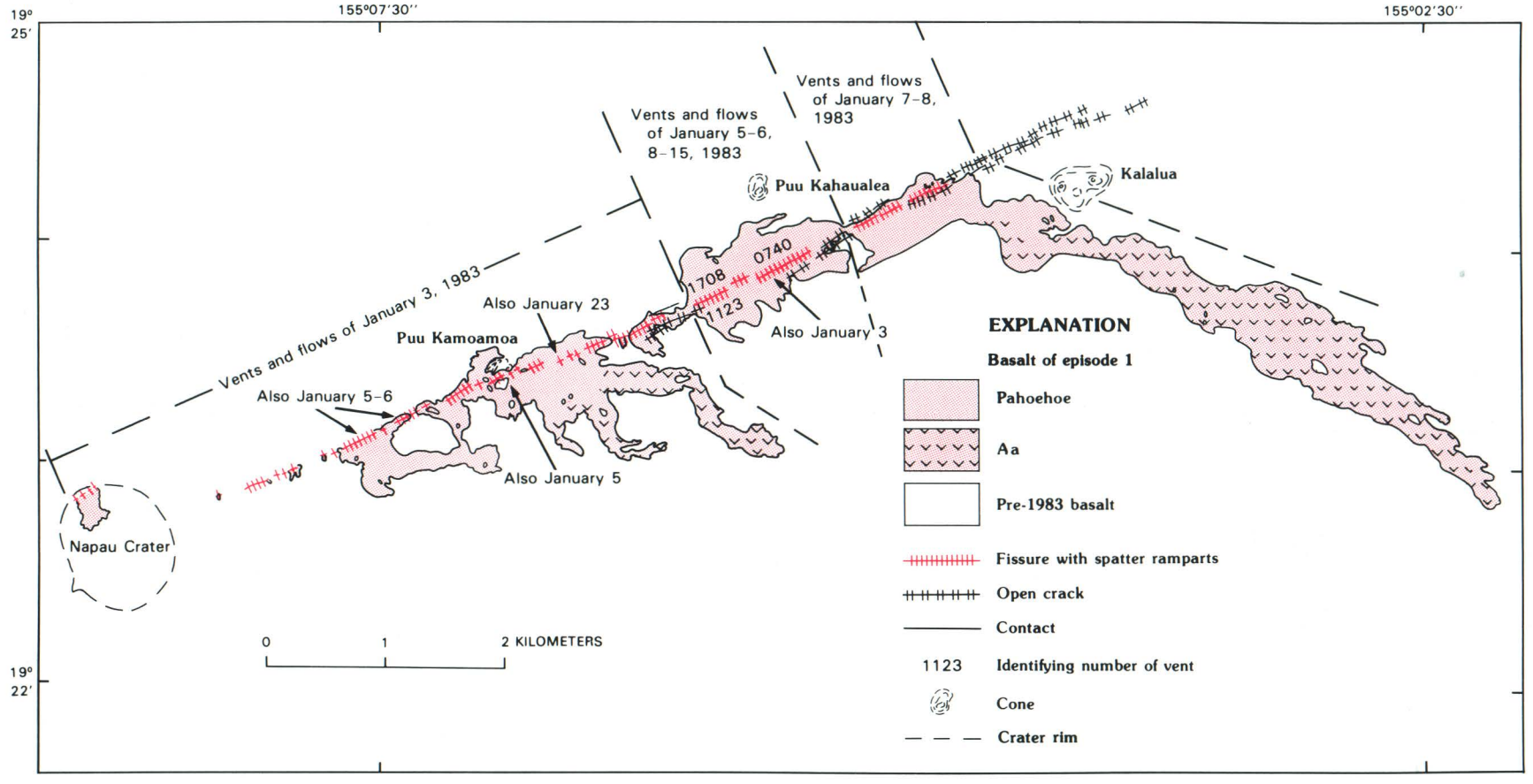

FIGURE 17.12.—Vents and flows of episode 1, Puu Oo eruption, Kilauea Volcano, January 1983.

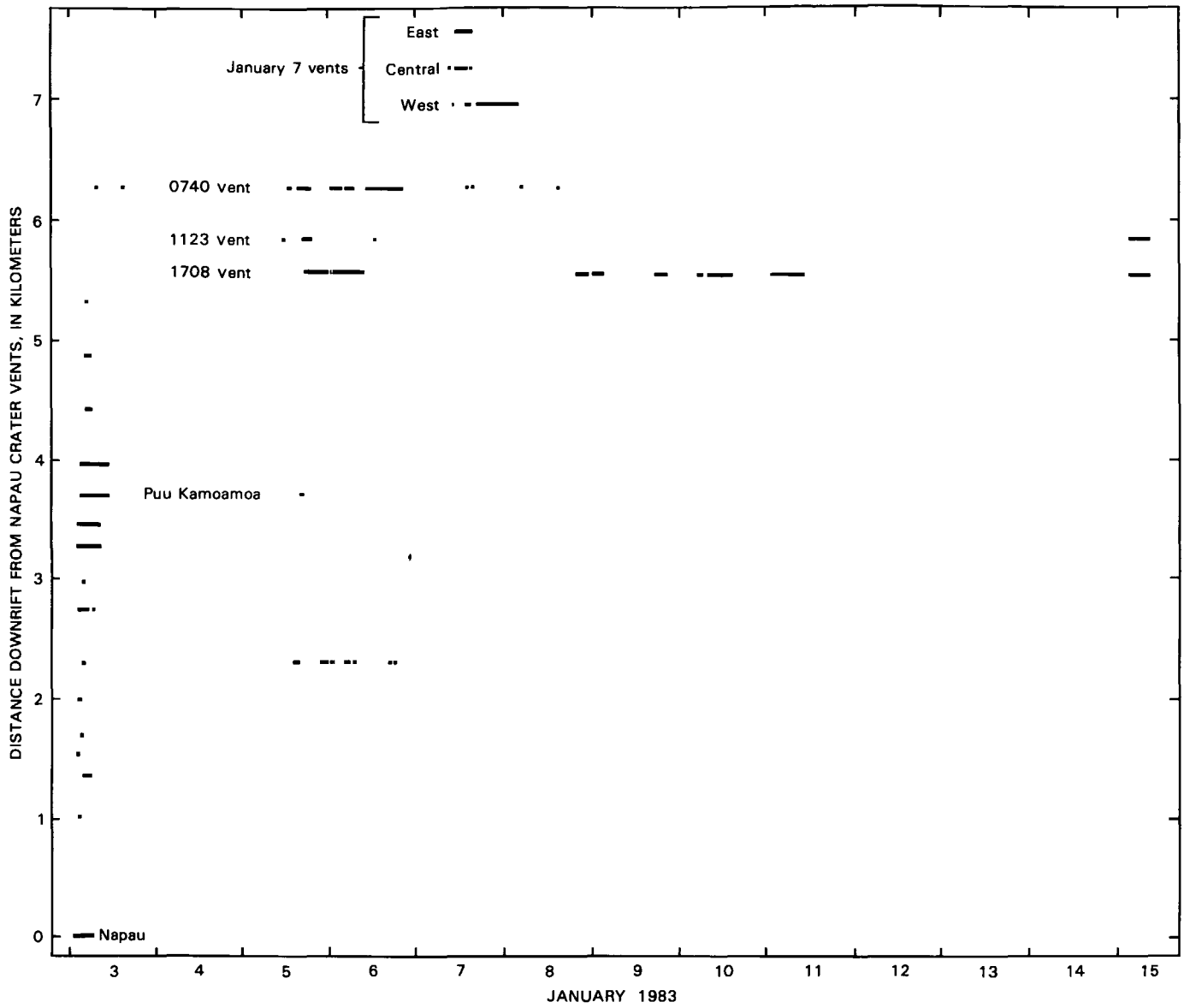

FIGURE 17.13.—Space-time diagram showing vent activity for January 3–15, episode 1 of the Puu Oo eruption. Approximate locations of centers of individual eruptive-fissure segments shown by distance downrift from the Napau Crater vents.

a reduction in reservoir magma volume but rather a gradual change in shape resulting from southeastward extension of the summit region. In addition, repeated gravity surveys from the beginning of 1984 through the time of writing (May 1985) have shown no long-term change in mass in the summit region, indicating that the average reservoir magma volume remained constant. We ignore both this gradual long-term subsidence and episode 1 with its dike emplacement in applying Swanson's technique for determining magma supply to the Puu Oo eruption.

The Puu Oo flows are dominantly vesicular rubbly aa. Average bulk densities of 1.94 and 2.17 g/cm^3 were determined from the results of two gravimeter and spirit-level profiles across the surface of an episode 3 aa flow where it overlies paved streets in a subdivision (D.J. Johnson, written commun., December 1984). These values suggest that the porosity is approximately 25 percent. Multiplying the average monthly lava supply of 13.4×10^6 m^3 by 0.75 to correct it to its dense-rock equivalent gives a rate of 10×10^6 m^3/mo of void-free lava. Thus, we infer an average magma-supply rate for episodes

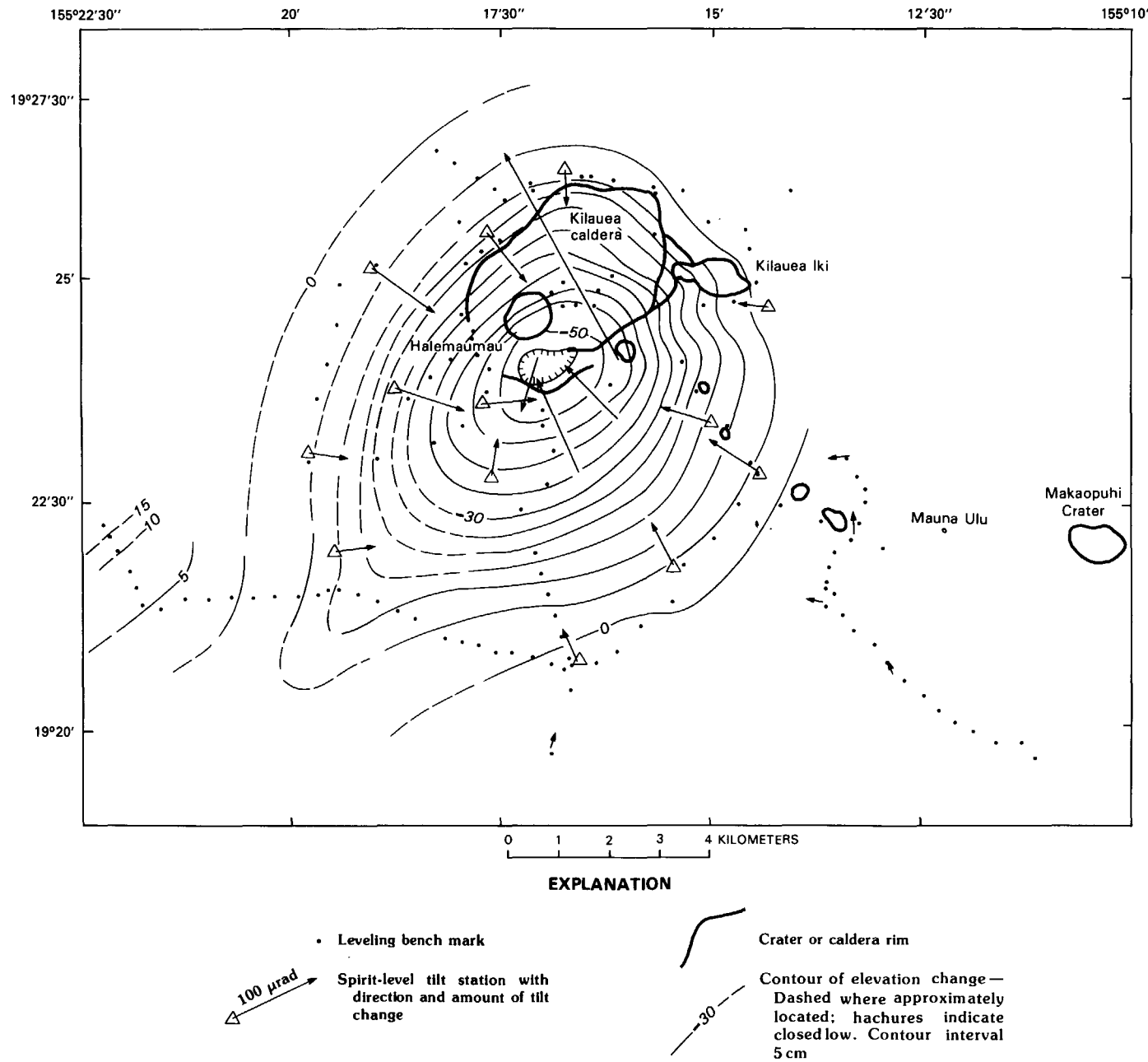

FIGURE 17.14.—Subsidence and tilt in the Kilauea summit region during the period from September 27–October 5, 1982, to February 7–11, 1983. Contours show relative elevation change.

2–20 of approximately $10 \times 10^6 m^3$/mo. Because volume-measurement errors may amount to 10 percent, this supply rate for the Puu Oo eruption is compatible with the rate determined by Swanson (1972) for other periods of sustained eruption. A slightly higher rate, approximately $11.8 \times 10^6 m^3$/mo, may be represented by the intervals encompassing episodes 4–12 and 13–17. The limited variation in recurrence interval and erupted volume (fig. 17.16) during those intervals indicates that an approximately steady-state condition had developed in the magma supply and transport system.

The question remains whether the Puu Oo magma-supply rate of at least $10 \times 10^6 m^3$/mo represents a period of elevated supply. Dzurisin and others (1984) reviewed magma-supply estimates more recent than Swanson's (Dzurisin and others, 1980; Duffield and others, 1982; Dvorak and others, 1983). They found a range of from 6×10^6 to $9 \times 10^6 m^3$/mo and concluded, from their analysis of the summit tilt record, that $7.2 \times 10^6 m^3$/mo is a reasonable minimum value for the average supply of magma from 1956 through 1983. Uncertainty arises from the possible addition of undetected

TABLE 17.1.—*Eruption data for episodes 1–20, Puu Oo eruption, Kilauea*

[All times are in Hawaii standard time (H.s.t.). ___, did not occur or was not observed]

Episode	First report of low-level eruption[1]		Beginning of vigorous eruption[2]		End of vigorous eruption[3]		Duration of vigorous eruption (hours)	Area covered (10^6 m^2)	Erupted volume (10^6 m^3)	Discharge rate[4] (10^3 m^3/h)
	Day	Hour	Day	Hour	Day	Hour				
1983										
1	___		Jan 3	0031		[5]	[5]	4.8	14	[5]
[6]2	Feb 10	1030	Feb 25	0900	Mar 4	1451	174	2.7	14	80
3	Mar 21	0600	Mar 28	0100	Apr 9	0257	290	7.9	38	130
4	___		Jun 13	1025	Jun 17	1413	100	2.2	11	110
5	Jun 29	1000	Jun 29	1251	Jul 3	0715	90	3.4	13	140
6	Jul 21	0600	Jul 22	1530	Jul 25	1630	73	2.0	9	120
7	Aug 8	0610	Aug 15	0741	Aug 17	1600	56	3.7	14	250
8	Sep 2	0900	Sep 6	0511	Sep 7	0526	24	[7]2.0	[7]8	[7]330
9	Sep 14	0009	Sep 15	1541	Sep 17	1920	52	[7]2.1	[7]8	[7]150
10	Oct 2	0800	Oct 5	0106	Oct 7	1650	64	2.7	14	220
11	___		Nov 5	2350	Nov 7	1845	43	4.3	12	280
12	Nov 29	1600	Nov 30	0447	Dec 1	1545	35	3.0	8	230
1984										
[8]13	Jan 20	1100	Jan 20	1724	Jan 22	1123	42	[7]2.6	[7]10	[7]230
[7]14	Jan 22	1123	Jan 30	1745	Jan 31	1318	19	[7]2.1	[7]6	[7]320
15	Feb 3	1000	Feb 14	1940	Feb 15	1501	19	2.2	8	420
16	Feb 27	1900	Mar 3	1450	Mar 4	2231	32	3.2	12	380
17	Mar 20	0910	Mar 30	0448	Mar 31	0324	23	3.0	10	430
18	Apr 5	1340	Apr 18	1800	Apr 21	0533	60	6.6	24	410
[9]19	Apr 23	0830	May 16	0500	May 18	0050	44	1.4	2	50
20	May 18	0800	Jun 7	2104	Jun 8	0625	9	1.6	4	480

[1]For episode 2, low-level eruption refers to a period of prolonged slow extrusion (averaging approximately 1,400 m^3/h) from February 10 to 25, 1983. For episodes 3–20, it refers to a period, preceding major eruption, during which any or all of the following phenomena were observed at the active vent: intermittent gas-piston activity, intermittent spattering, occasional extrusion of small pahoehoe flows, occurrence of a visible lava surface (sometimes partly crusted) in the conduit extending downward from the crater floor. Normally, low-level eruptive activity was confined to the interior of the crater, but on rare occasions short-lived pahoehoe flows spilled from Puu Oo.

[2]Normally, the onset of vigorous eruption was recognized in the following ways (order indicates priority): (1) direct observation of continuous emission of lava from the crater; (2) time-lapse camera record of beginning of continuous emission of lava from crater; (3) where spillway activity was not recorded, time-lapse camera record of first appearance of fountaining above the crater rim; (4) beginning of rapid increase in harmonic-tremor amplitude.

[3]The end of vigorous eruption was recognized in the following ways (order indicates priority): (1) direct observation of the cessation of lava discharge; (2) time-lapse camera record of cessation of fountaining; (3) rapid decay of harmonic-tremor amplitude.

[4]Discharge rate is calculated only for period of vigorous eruption. Except for episode 2, the volume of lava erupted during periods of low-level activity was negligible.

[5]Episode 1 was characterized by intermittent eruptive activity for nearly three weeks. Periods of active eruption totalled approximately 99 hours. The last sizeable event occurred on January 15; a minor one occurred on January 23.

[6]During episode 2, approximately 0.5×10^6 m^3 of basalt was discharged during low-level eruption from February 10 to 25. The remaining 13.6×10^6 m^3 was discharged during the period of vigorous eruption at a rate of approximately 70,000 m^3/h.

[7]Flow was partly buried by younger basalt before it could be mapped. Thus uncertainty is increased in estimates of area, volume, and discharge rate.

[8]Fountaining and flow production during episode 13 occurred in two main periods. The first, approximately 31 hours long, was separated by about 5 hours from the 6-hour-long second period.

[9]Episode 19 was characterized by low fountain activity and intermittent low-volume overflows from the lava pond within the crater of Puu Oo. This activity was interrupted by four periods 1–3 h long, totalling about 7 hours altogether, of higher fountaining and increased lava discharge estimated as about $100–200\times10^3$ m^3/hr.

magma to rift-zone storage. Furthermore, Tilling and others (chapter 16) recognized two distinct episodes during the latter part of the Mauna Ulu eruption, February 1972 through April 1973 and December 1973 through July 1974, in which sustained lava extrusion coincided with negligible summit-tilt change. During the earlier episode, the lava-extrusion rate was about 8×10^6 m^3/mo; during the later one, it was 4×10^6 m^3/mo. Neither value is corrected for vesicularity. R.I. Tilling (oral commun., May 1985) regards the values as minimum estimates of magma-supply rate because of the unevaluated possibility that magma was being stored in the upper east rift zone during the 1972–74 Mauna Ulu eruption.

The data summarized above are only permissive evidence that the Puu Oo eruption coincided with a period of greater than normal magma supply. More substantial support may come from measurement of SO_2 flux to the atmosphere in the Kilauea summit area. The average flux increased abruptly after the beginning of the eruption in January 1983 from 130 t/d to 250 t/d; the elevated flux was maintained through at least episode 20 (fig. 17.18; Greenland and others, 1985). The near coincidence of the SO_2-flux change with the beginning of the Puu Oo eruption strongly suggests that the two events were related. The increased SO_2 flux may have been a direct and rapid response to an increased rate of supply of new magma to the summit reservoir; if so, the Puu Oo eruption coincided with a period of increased magma supply.

CHARACTER OF THE CENTRAL-VENT ERUPTIONS

Central-vent eruptions occurred during episodes 2 through 20. A nearly vertical pipe-like conduit delivered a spray of gas and fragmented vesiculating magma through a vent in the floor of a broad crater within a growing pyroclastic cone. Directed upward as a jet, the spray formed the fountain that was invariably present in the central-vent eruptions. Initial fallout from the fountain built a spatter ring, which, in repeated eruptive episodes, grew upward and outward by the addition of spatter, rootless flows, and unconsolidated lapilli and bombs.

The crater of Puu Oo evolved to a broad bowl mostly enclosed by steep walls. The diameter of its gently sloping floor gradually increased from about 20 m to 100 m. A deep breach that developed in the crater wall provided a passage through which lava left the

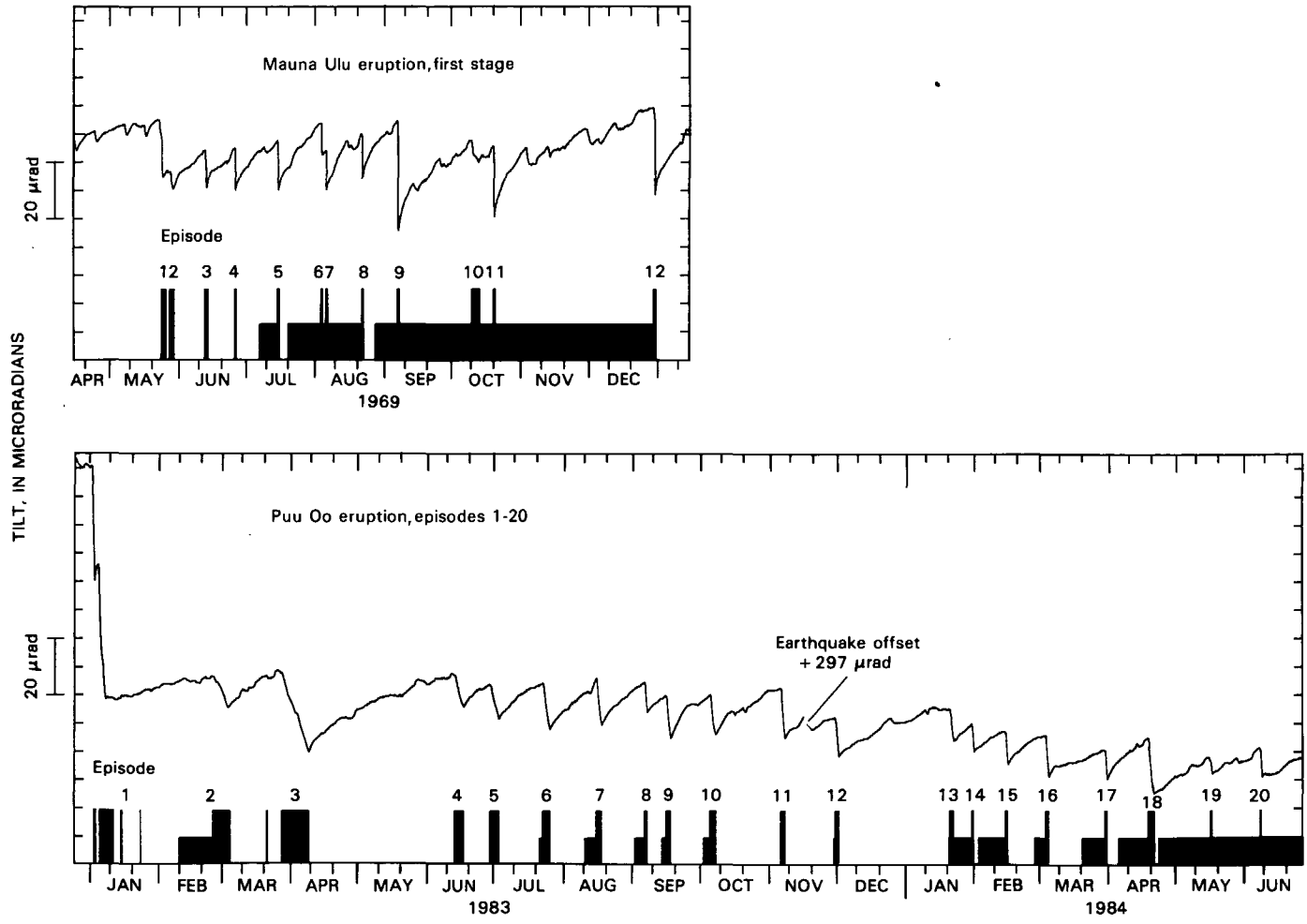

FIGURE 17.15.—East-west tilt at Kilauea summit (measured by the Uwekahuna Hg-capacitance tiltmeter), eruptive episodes (full- height bars), and observed repose-period eruptive activity (half- height bars) during episodes 1–20 of the Puu Oo eruption and the first stage of the 1969–71 Mauna Ulu eruption (Swanson and others, 1979).

crater. The floor of the breach was generally 5–15 m higher than the crater floor.

Before episode 13, rubble on the crater floor concealed the feeder conduit during most periods of repose. From episode 13 on, a persisting vertical and nearly cylindrical conduit about 20 m in diameter was revealed. Its walls exposed crudely layered platy to rubbly basalt; at its top, the pipe flared upward to meet the crater floor and was commonly draped with pahoehoe.

During eruptive episodes, the crater contained a lava pond and one or more fountains. The pond overflowed at the breach in the crater rim. Normally the spillway at the breach was fairly constricted, so that the surface of the hydraulically-dammed pond was several meters higher than the floor of the spillway. We estimate that the pond was normally at least 10–20 m deep. When high, broad fountains seemed to fill the crater, we could not see the pond, but continuing flow of lava over the spillway indicated its presence. However, flows produced during such periods were sometimes more sluggish than when a well-developed pond was seen to be present.

Though the pond shared the crater with a vigorous fountain, it maintained a fairly smooth surface that was commonly marked by a thin, flexible skin of slightly cooled lava undisrupted by effervescence. We infer that the pond consisted of mostly degassed lava that had coalesced from fragmented melt in the crater and the upper part of the conduit.

Fountains at the central vents during episodes 2–20 ranged in height from a few meters during periods of slow discharge to a maximum of nearly 400 m. In some of the eruptive episodes at Puu Oo, as, for example, episode 16, the fountain was highest in the early hours (fig. 17.19); this suggests that volatiles may have become more highly concentrated in the upper part of the conduit beneath the vent during periods of repose.

Fountain height was related at least in part to the rate of discharge. During both episodes 2 and 3, fountain height at the 1123 vent approximately doubled in concert with 2- to 3-fold increases in lava output. From episode 4 on, at Puu Oo, we normally saw no abrupt changes in discharge during an eruptive

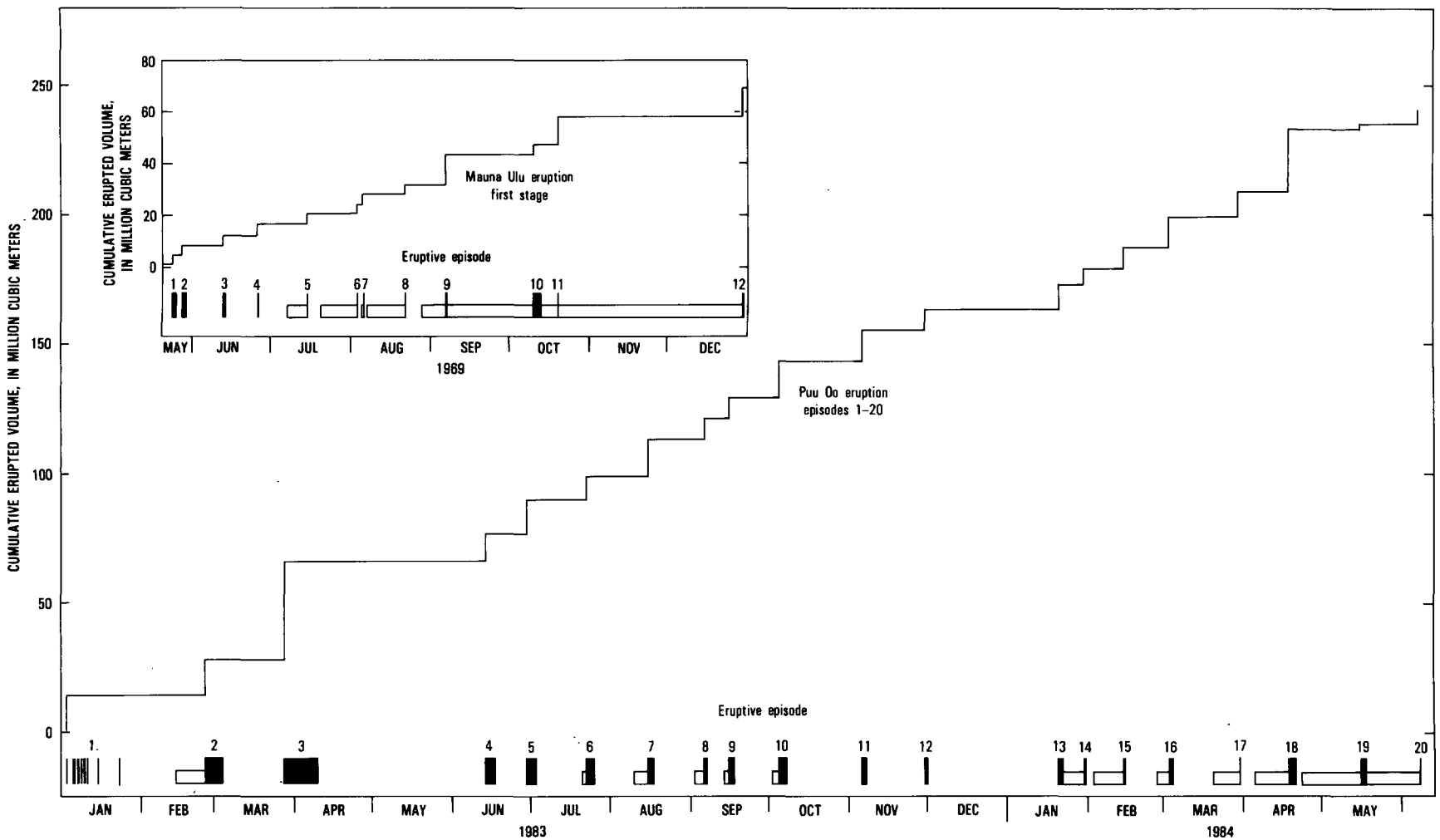

FIGURE 17.16.—Cumulative erupted volumes during episodes 1–20 of the Puu Oo eruption and the first stage of the Mauna Ulu eruption (Swanson and others, 1979). Solid full-height bar, eruptive episodes; open half-height bar, observed repose-period activity. Basalt volumes for Puu Oo eruption were determined by mapping flows and vent deposits of the individual episodes, measuring thicknesses by hand level at the flow edges, and measuring mapped area on a computerized digitizing tablet.

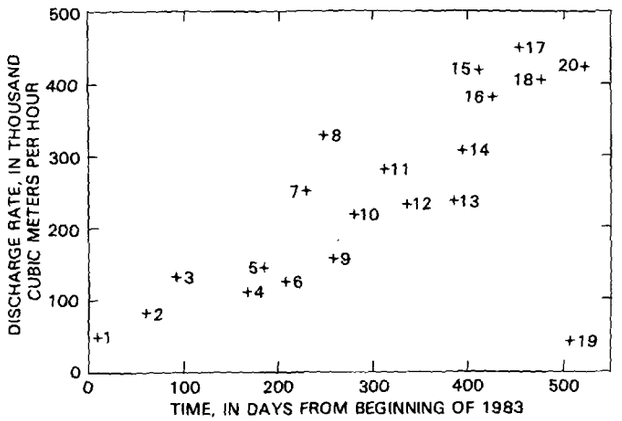

FIGURE 17.17.—Average lava-discharge rate for each of episodes 1-20, Puu Oo eruption, plotted against time.

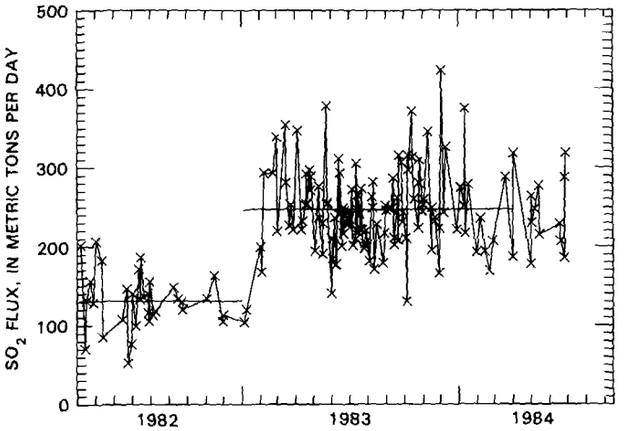

FIGURE 17.18.—Total sulfur dioxide (SO_2) flux from summit fumaroles of Kilauea Volcano, April 1982 through June 1984, based on ground measurements. Horizontal lines show change in average flux after the beginning of the Puu Oo eruption in January 1983. Modified from Greenland and others (1985); data extended through June 1984 by L.P. Greenland.

episode, but the rate was greater in successive episodes (fig. 17.17). Average fountain height at Puu Oo correlated roughly with average discharge (fig. 17.20), but appreciable scatter resulted from effects that may have included changing conduit conditions, enrichment of gas during repose periods, and damping of fountains by coalesced melt within the crater and upper part of the conduit.

Normally, each central-vent fountain episode produced one or more major elongate aa flows supplied by a river of fluid pahoehoe that originated from the steady overflow of the pond. Subordinate flows originated mainly from persistent near-vent overflows of the river and from mobilization of molten spatter that accumulated either rapidly or persistently on the flanks of the cone.

The river-fed flows evolved downstream through a similar progression of zones as that recognized in the aa lobes of the 1984 Mauna Loa eruption (Lipman and Banks, chapter 57). As at Mauna Loa, fluid channelized lava near the vent was inflated by gas but rapidly deflated downstream. The sustained cascade of spatter and the turbulence where the fountain burst from the pond apparently churned vent gases, including air, into the lava supplying the pond. Thus the pond was a continuing source of gas-rich fluid melt and was apparently fundamental in developing the long river-fed aa flows at Kilauea. Minimal development of the pond, such as during periods of high fountaining, was associated at times with production of less fluid flows. Furthermore, supply from a fountain with no basin or pond often produced thick, slow-moving aa directly.

Generally, the major flows were 4–8 km long and from 100–500 m wide. A few flows were significantly longer; the longest, produced during episode 18, extended more than 13 km from the vent (fig. 17.2). The average thickness of most of the river-fed aa flows was between approximately 3 and 5 m. However, the range of measured thicknesses was greater; locally, the distal parts of some flows were as thick as 10 m. The major river-fed flows advanced at average rates of 50–500 m/h. Surges of fluid lava at the flow fronts (Neal and Decker, 1983) resulted in more rapid advances that were sustained for tens of minutes at rates of as much as 2 km/h. Significant flow movement stopped when the lava supply was cut, generally at the vent but sometimes by diversion to a new flow. After the supply was terminated, however, slow creeping of the front sometimes continued for hours.

Low-level eruptive activity was evident during many repose periods. At Puu Oo, it was dominated by two phenomena: the gradual ascent of the magma column toward the surface and gas-piston activity much like that seen at Mauna Ulu (Swanson and others, 1979). After the open conduit descending from the crater floor became a permanent feature following episode 13, we could see that the magma-column surface rose gradually and sometimes spasmodically toward the crater floor during each repose period. If visibility was good, we would first see the top of the column when it was about 50 m down the conduit; the first sighting usually occurred at least 5 days and sometimes more than 3 weeks before the next major episode (fig. 17.15).

We were able to watch the beginnings of several of the fountaining episodes at Puu Oo. First the crater filled with lava, which steadily overflowed the spillway. Gas-piston activity, if it had been occurring, gave way to an open, roiled pond with a low dome fountain. Over a period ranging from tens of minutes to about two hours, the rate of overflow progressively increased from $1–10\times10^3$ m^3/h to normal discharge rates of 100×10^3 m^3/h or more. At the same time, the height of the fountain increased from less than 10 m to tens or hundreds of meters.

Central-vent activity at the 1123 vent during episodes 2 and 3 died gradually, as indicated by progressive decrease of fountain vigor during the last day of each episode. In contrast, eruptive episodes at the Puu Oo vent ended more abruptly. Sometimes the eruption suddenly stopped with no warning. More often, the fountain diminished and became less steady in the last 3–10 minutes

of the episode; during that brief period, we sometimes saw pauses of a few seconds or tens of seconds in fountain and flow production. Normally the output of lava from Puu Oo was steady until the terminating moments of fountain activity, after which no further discharge occurred.

SEISMIC EFFECTS IN THE ERUPTION ZONE

Intense harmonic tremor occurred in the vent area coincident with vigorous eruption. However, the amplitude of the harmonic tremor did not vary systematically with major changes in fountain height during individual eruptive episodes (fig. 17.19). Throughout the central-vent activity, the amplitude showed a positive correlation with discharge (fig. 17.21) but not with the average fountain height (fig. 17.22). Thus, the recorded tremor reflected primarily processes at levels deeper than those from which fountaining originated. The symmetry, with respect to Puu Oo, of tremor-attenuation patterns implies that the tremor source and the vent were vertically aligned, but the depth of the tremor source is uncertain.

Harmonic tremor continued at low amplitude throughout repose periods and increased rapidly at the beginning of each episode of fountaining. Relatively deep south-flank earthquakes continued throughout the period of central-vent activity, but there was no shallow seismic swarm like that during emplacement of the dike in episode 1. We infer from the absence of seismic swarms after episode 1 and also from the continuous harmonic tremor and visible evidence of magmatic activity during repose periods that a continuous magma-filled conduit between the summit reservoir and the vents persisted after episode 1.

GEODETIC EFFECTS IN THE ERUPTION ZONE

Geodetic measurements in the eruption zone were limited by the difficulty and expense of obtaining access and by burial of measurement stations by new lava flows. However, two major inferences for the period of central-vent activity can be made from the available data: (1) over the long term, slight net deflation occurred; (2) over the short term, gradual inflation accompanied repose periods, and abrupt deflation accompanied eruptive episodes.

Measurements at a spirit-level tilt station about 1.5 km northwest of Puu Kamoamoa showed that the ground tilted northwestward, away from the rift-zone axis, during the early part of the eruption (table 17.2). The major change between December 15, 1982, and January 18, 1983, undoubtedly reflects deformation resulting from emplacement of the dike in early January. A smaller change between January 18 and March 8, 1983, may record inflation of the rift zone; a measured distance across the eruptive fissure farther downrift near Puu Kahaualea gradually lengthened during the same period. During episode 3, however, the ground tilted 12 μrad southeastward toward the rift axis, consistent with subsidence there. Measurements made after episode 3 and again 16 months later after episode 24 show an additional 19 μrad of tilt toward the rift-zone axis.

The automatic borehole tiltmeter 250 m northwest of Puu Kamoamoa operated during episodes 1–10 and from shortly after episode 15 through episode 20. No recognizable tilt change was associated with episode 2. However, beginning with southeast-directed tilt during episode 3, the ground normally tilted gradually northwest during repose periods and rapidly southeast during periods of fountaining (fig. 17.23). These opposed tilt changes were commonly of similar magnitude, in the range of 3–9 μrad, and were directed approximately normal to the rift-zone axis. They presumably recorded alternating inflation and deflation in the rift zone near Puu Kamoamoa. The largest deflations occurred during episodes 3 and 18, which were the most voluminous eruptions (table 17.1). No detectable tilt change occurred during episode 19.

SUMMIT BEHAVIOR

Repeated uplift and subsidence of Kilauea's summit region, recorded by the rising and falling trace of the Uwekahuna tiltmeter (fig. 17.15), dominated summit response to the episodic eruptions. Summit inflation occurred during repose periods and was accompanied by increasing numbers of shallow, short-period earthquakes beneath Kilauea caldera (fig. 17.24). Daily frequency of earthquakes generally increased to a maximum of 100–200 in the latter part of each repose period, then decreased sharply during and following the deflation. The earthquakes apparently recorded fracturing of country rock as it adjusted to distention of the summit reservoir.

Shallow long-period earthquakes, intergradational with related harmonic tremor, were abundant beneath the caldera during the later parts of summit subsidence and the early parts of the repose periods. Before episode 8, the daily number of long-period earthquakes seldom exceeded 100, but thereafter peak counts of many hundreds of events per day were normal (fig. 17.24). Greater intensity of long-period-earthquake activity was associated with higher rates of sustained deflation. Thus the long-period events and associated tremor in the caldera area were apparently responses to rapid evacuation of magma from the summit reservoir.

RELATION OF SUMMIT TILT CHANGES TO RIFT-ZONE ACTIVITY

COMPARISON OF SUBSIDENCE AND LAVA-DISCHARGE RATES

The average rate of summit subsidence as reflected in tilt changes at Uwekahuna (fig. 17.25) increased steadily from episode 2 through episode 8. Unlike the lava-discharge rate, which continued to increase thereafter (fig. 17.17), the subsidence rate later was variable and appeared to peak at an upper limit of about 0.5 μrad/h. In the following section we discuss some possible reasons for such a variable relationship between summit tilt change and erupted volume. Dvorak and Okamura (in press) attribute the early increase in deflation rate to progressive decrease of flow resistance in the conduit system. We agree and interpret the continued increase in effusion rate to indicate that the efficiency of magma delivery to the

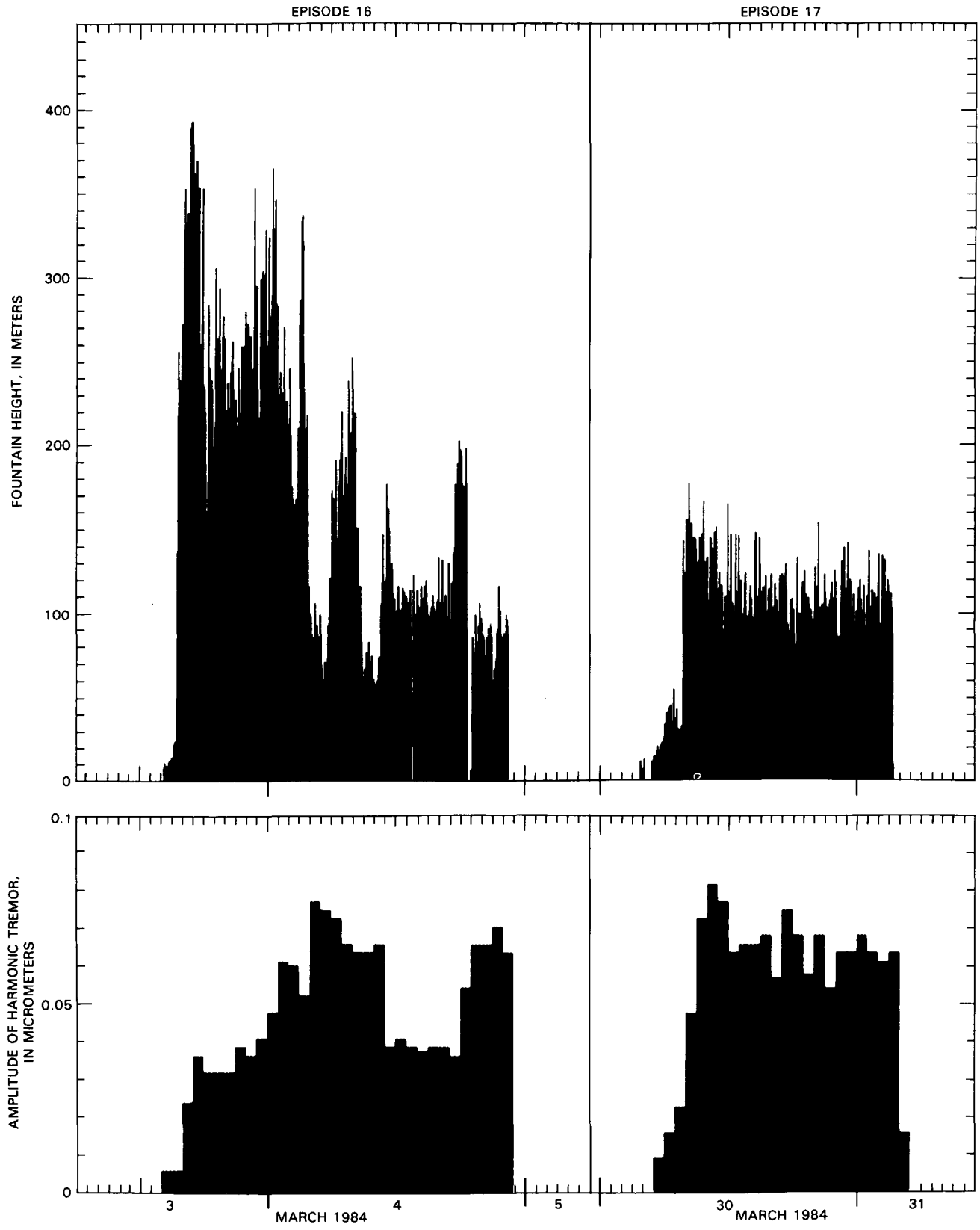

FIGURE 17.19.—Fountain height and amplitude of vent-area harmonic tremor recorded by seismometer at Makaopuhi Crater, episodes 16 and 17, Puu Oo eruption. Fountain height was measured from time-lapse film records. Gaps in fountain-height data record periods of poor visibility or inoperative camera.

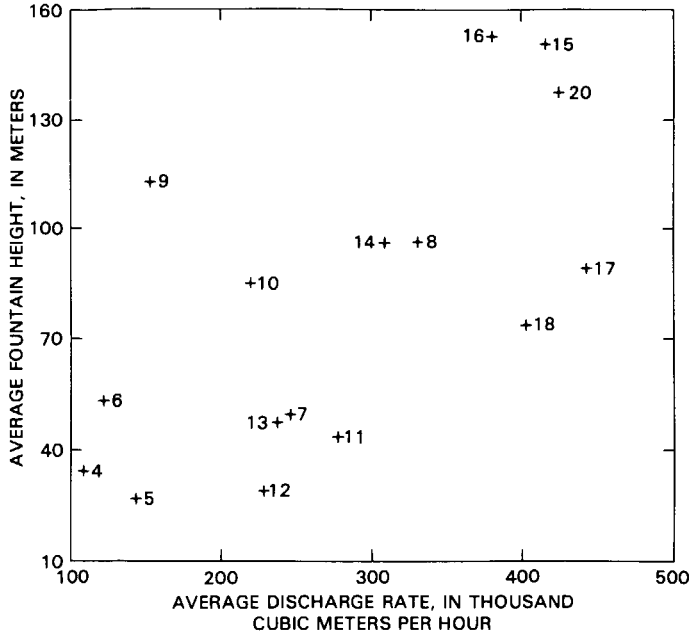

FIGURE 17.20.—Average fountain height versus average discharge rate at Puu Oo, episodes 4–18 and 20, Puu Oo eruption. Episode 19 is excluded because its intermittent fountaining yields a meaningless average.

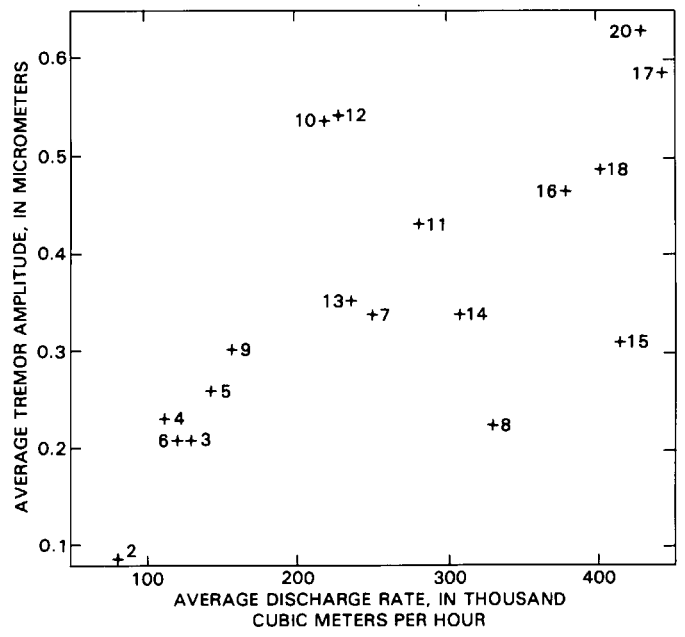

FIGURE 17.21.—Average harmonic-tremor amplitude, measured as ground displacement at the Makaopuhi Crater seismometer, versus average discharge rate at Puu Oo, episodes 2–18 and 20, Puu Oo eruption.

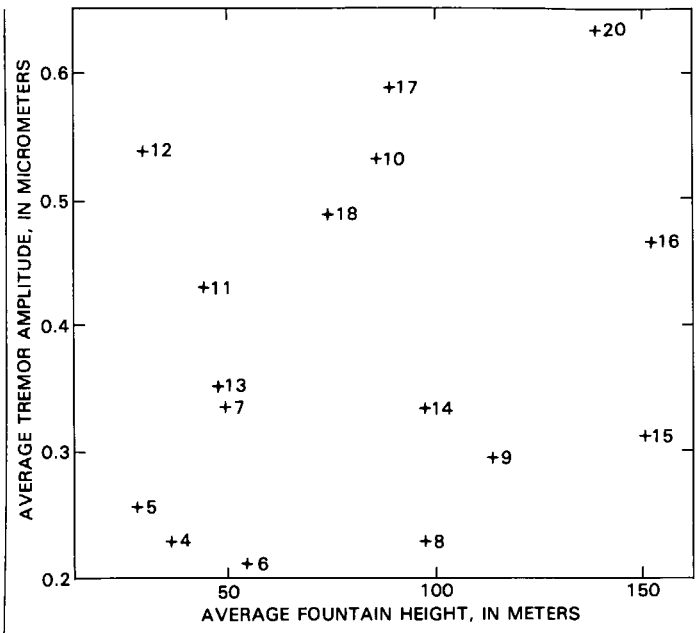

FIGURE 17.22.—Average harmonic-tremor amplitude, measured as ground displacement at the Makaopuhi Crater seismometer, versus average fountain height at Puu Oo, episodes 4–18 and 20, Puu Oo eruption. Fountain height value is a time-averaged arithmetic mean of fountain heights measured from time-lapse film records.

vent continued to increase after episode 8, even though the rate of tilt change at Uwekahuna did not.

VOLUMETRIC CONSIDERATIONS

The volume of lava erupted in each episode, adjusted for 25 percent porosity, ranged from approximately 0.3 to $1.0 \times 10^6 m^3$ per microradian of summit subsidence (table 17.3) measured on the east-west component of Uwekahuna tilt during episodes 2–20. The average value is 0.63 ± 0.21 (1 standard deviation) $\times 10^6 m^3/\mu rad$. The large variation may reflect several factors, including variable inequality between duration of eruption (table 17.1) and duration of subsidence (table 17.3), nonuniform summit response to reservoir-volume changes, variable rate of magma transfer from the summit reservoir to the rift zone during repose periods, and shifting position of the center of inflation and deflation with respect to the tiltmeter. The center of deflation did in fact shift within the region from east to

TABLE 17.2.—*Spirit-level tilt measurements at station 1.5 km northwest of Puu Kamoamoa*

[Vector azimuth gives direction of downward tilt]

Survey period	Vector magnitude (μrad)	Vector azimuth (degrees)
12/15/82–1/18/83	48	292
1/18/83–3/8/83	14	310
3/8/83–4/21/83	12	148
4/21/83–8/23/84	19	155

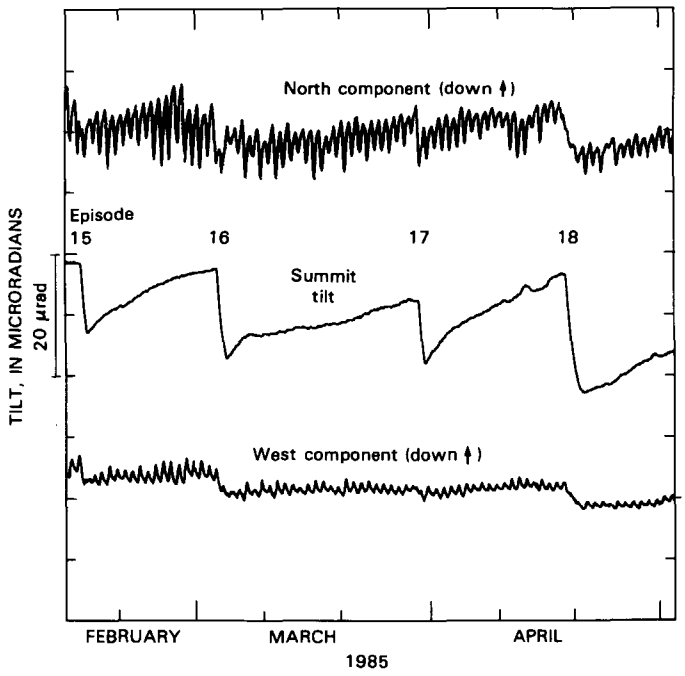

FIGURE 17.23.—East-west summit tilt and Kamoamoa borehole tilt (north and west components), episodes 15–18, Puu Oo eruption.

south of Halemaumau, as shown by levelling and spirit-level tilt surveys for the periods from February 7 to December 28, 1983, and December 28, 1983, to July 23, 1984 (fig. 17.26).

The first 12 fountaining episodes of the 1969–71 Mauna Ulu eruption produced lava at the rate of $0.34 \pm 0.09 \times 10^6 m^3/\mu rad$ of tilt change for a N. 60° W. vector calculated from Uwekahuna water-tube tilt data (Dzurisin and others, 1984). The first episode had a much lower than normal ratio of erupted volume to tilt change and was accompanied by an east-rift earthquake swarm (Swanson and others, 1979, plate 2). Thus, some of the volume of magma involved in the initial episode apparently formed a dike and is not represented at the surface. Eliminating the first episode from consideration, correcting for porosity (15 percent; Swanson, 1972), and adjusting the vector from N. 60° W. to east-west, we calculate a ratio for episodes 2–12 of the 1969–71 Mauna Ulu eruption of $0.35 \pm 0.08 \times 10^6 m^3$ of magma per microradian of east-west tilt change. This is slightly more than 50 percent of the value for episodes 2–20 of the Puu Oo eruption.

The ratio of volume change to tilt change has also been estimated by considering surficial volume change at the summit, determined from leveling surveys, as a measure of reservoir-volume change. Recent calculations of the ratio of surficial volume change to east-west Uwekahuna tilt change are $0.38 \pm 0.07 \times 10^6 m^3/\mu rad$ by Dzurisin and others (1984; value adjusted from N. 60° W. vector) and $0.45 \pm 0.13 \times 10^6 m^3/\mu rad$ by Dvorak and others (in press).

Johnson (chapter 47) attempts to relate elevation changes, Uwekahuna tilt changes, and summit-reservoir volume changes estimated from gravity measurements made from episodes 13–32 of the Puu Oo eruption, and he concludes that changes in reservoir volume may have been appreciably larger (perhaps 2.5 times) than measured surface-volume changes. If this is true, it could account for the high ratio of erupted-magma volume to tilt change for the Puu Oo eruption (0.63) compared to the lower ratio for the early Mauna Ulu episodes (0.35) and to the lower ratio calculated for surface--volume changes (0.38–0.45). We note that the ratio of erupted volume to tilt change for Mauna Ulu is slightly lower than the ratio of surface volume to tilt change; this relation implies that average reservoir-volume changes did not exceed surface-volume changes during the early Mauna Ulu episodes.

As an alternative, we suggest that the higher ratio for the Puu Oo eruption may have resulted from alternating additions to and subtractions from rift-zone storage. The rift zone, at least in the Puu Kamoamoa region, apparently inflated and deflated in tandem with Kilauea's summit (fig. 17.23). Thus we infer that successively accumulated and extruded volumes were accommodated in hydraulically connected summit and rift-zone reservoirs. If this is true, the volume of magma supplied to Kilauea during repose periods was accommodated by volume increases in both the summit and rift-zone reservoirs, and the volume of magma erupted during fountaining episodes was accommodated by volume decreases in both the summit and rift-zone reservoirs. Because part of the volume accommodation occurred in the rift-zone reservoir during Puu Oo eruptive episodes, surficial volume changes at the summit and related Uwekahuna tilt changes are insufficient measures of erupted volume.

The generally similar average ratios of volume to tilt change determined for the early Mauna Ulu episodes (0.35) and for surficial volume changes (0.38–0.45) represent about 55–70 percent of the average ratio of erupted volume to tilt change (0.63) for episodes 2–20 of the Puu Oo eruption. If the Mauna Ulu and surficial volume ratios are applied to Puu Oo episodes as a measure of summit-reservoir volume change, 55–70 percent, on the average, of the erupted volume (considered vesicle-free) was accommodated by summit-reservoir volume changes. The remaining 30–45 percent could have been accommodated by changes in the volume of rift-zone storage.

We emphasize that, because of large scatter in the ratios of erupted volume to tilt change for specific episodes (table 17.3), estimates of reservoir-volume change are at best generalized approximations. Furthermore, variations in summit-inflation rate (compare summit tilt-change patterns preceding episodes 16 and 17, fig. 17.24), including occasional deflationary episodes during repose periods, suggest that transfer of magma from the summit to the rift zone may have occurred during repose periods in an irregular and unpredictable pattern. Thus, we cannot predict the volume of rift-zone accommodation or the erupted volume for a single episode with reasonable precision from the Uwekahuna tilt record.

TIMING OF TILT CHANGES AND ERUPTIVE ACTIVITY

During eruptive episodes, changes in tilt rate or direction at the summit were often closely related to changes in eruptive activity.

Once the vent became established at Puu Oo, the tilt changes tended to lag behind the changes at the vent (table 17.3).

Typically, such changes occurred only at the beginnings and endings of eruptive episodes. However, discharge stopped and then resumed once during episode 13 and three times during episode 19. The rate of tilt change at the summit responded to each of these changes at the vent (fig. 17.27), emphasizing the effectiveness of the connection between vent and summit areas. In each case, however, the rate of summit tilt change reached a minimum several hours after the end of the related fountaining event. Similarly, the rate of tilt change reached a maximum in each case several hours after fountaining resumed.

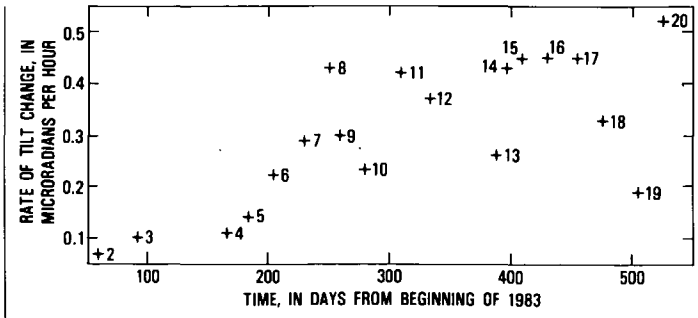

FIGURE 17.25.—Average rate of deflationary, east-west tilt change at Uwekahuna tiltmeter, episodes 2–20, Puu Oo eruption.

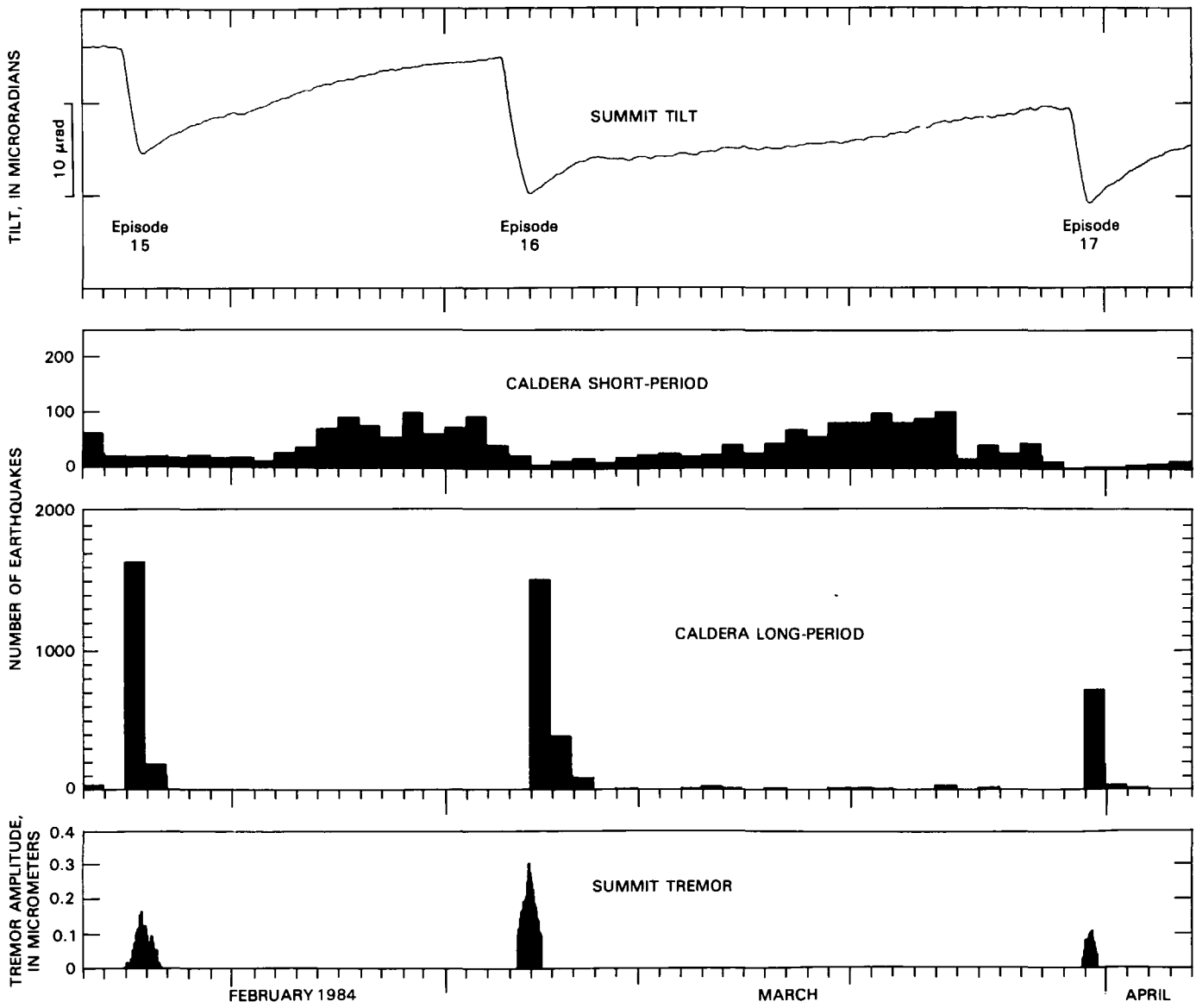

FIGURE 17.24.—East-west summit tilt, daily frequency of short-period and long-period caldera earthquakes, and amplitude of shallow harmonic tremor beneath Kilauea caldera, episodes 15–17, Puu Oo eruption.

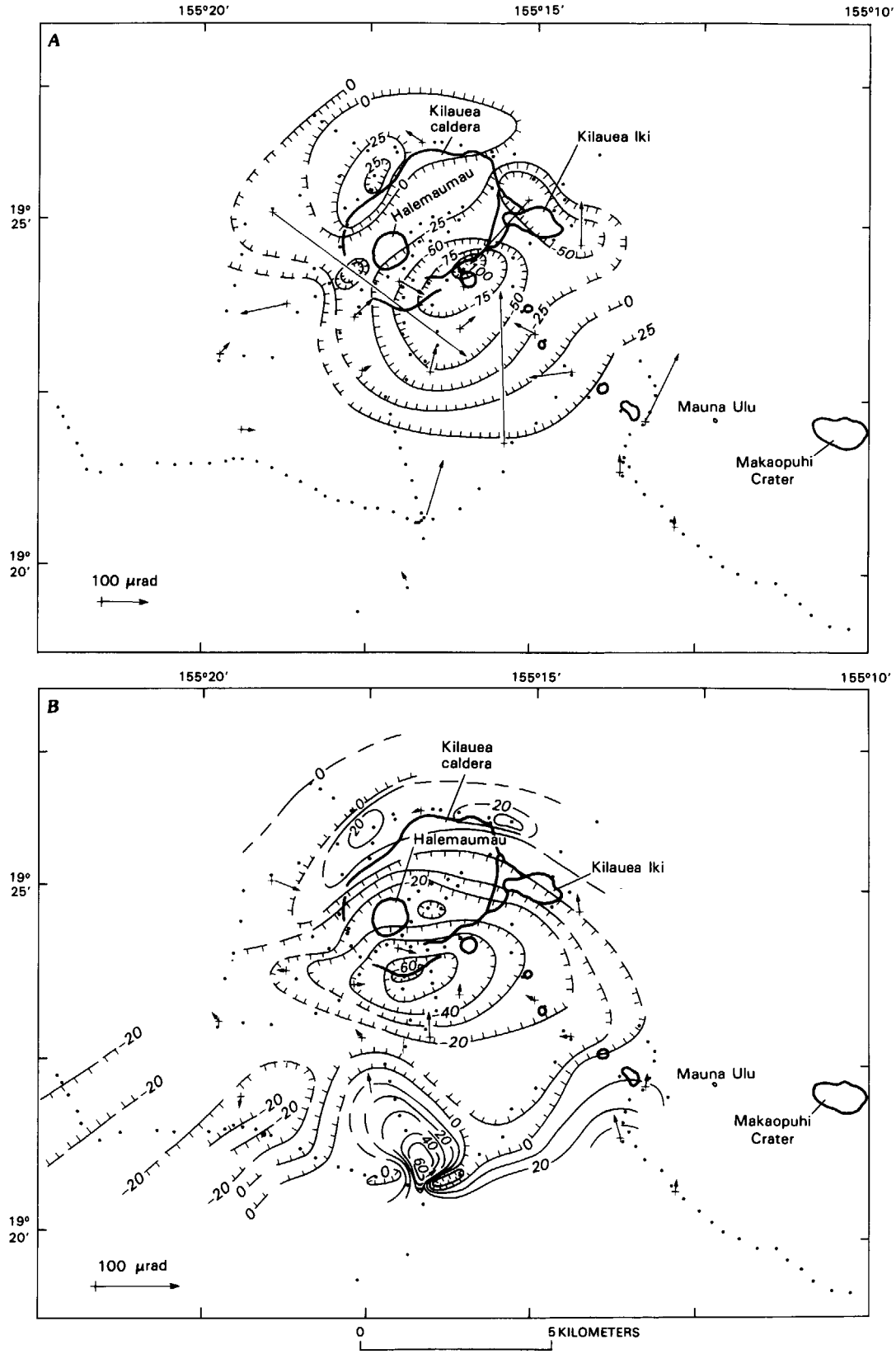

FIGURE 17.26.—Kilauea summit level change and tilt change during two periods of the Puu Oo eruption. ***A***, February 7 to December 28, 1983. ***B***, December 28, 1983, to July 23, 1984.

TABLE 17.3.—*Subsidence and relation to erupted volume, episodes 2–20, Puu Oo eruption, Kilauea*

[Tilt change is eastward on the east-west component of Uwekahuna tilt. Beginning lag is the time from start of eruption to start of accelerated, sustained deflation. For some episodes, uncertainty arises from the gradual nature of the onset of eruption or deflationary tilt change and from the absence of direct observation of the onset of eruption. Ending lag is the time from end of eruption to end of deflationary tilt change. Erupted volume corrected to remove 25 percent porosity.]

Episode	Tilt change (μrad)	Subsidence			Erupted volume/ tilt change ($10^6 m^3/\mu rad$)
		Duration (h)	Beginning lag (h)	Ending lag (h)	
2	10.9	151	−2.0	−24.8	.964
3	28.1	292	−1.0	1.0	1.014
4	11.2	98	4.6	3.3	.735
5	11.9	86	6.7	2.2	.819
6	16.2	72	3.5	2.5	.416
7	16.7	57	2.3	3.0	.630
8	10.0	23	5.8	4.5	.601
9	14.9	50	3.3	1.7	.402
10	14.1	60	3.9	.2	.745
11	17.4	41	2.2	.2	.517
12	13.8	37	.2	2.3	.434
13	11.1	43	3.6	4.6	.676
14	9.8	23	2.3	5.7	.458
15	11.3	25	.3	6.0	.531
16	14.8	33	1.2	2.5	.609
17	10.2	23	3.2	3.6	.732
18	19.4	58	2.0	.5	.928
19	4.1	21	6.0	[1]−16.8	.366
20	9.4	18	.9	9.6	.318

[1]Episode 19 included lava-pond activity and low-volume overflows that continued for a day after the end of intermittent fountaining and high-volume flow production. Ending lag = 6.6 h when considered with respect to end of high fountains and high-volume flow production.

From episode 3 on, summit deflation continued for as long as several hours beyond the end of lava production (table 17.3). From episode 4 on, the beginning of sustained rapid deflation lagged behind the beginning of steady lava production. In contrast, we note that, during episode 2, lava production continued for a full day after summit deflation had stopped. The starts of episodes 2 and 3 were gradual and the time relations therefore somewhat subjective (table 17.3), but our interpretation is that vigorous discharge lagged slightly behind the onset of rapid deflation.

The approximate balance between Uwekahuna tilt changes during repose periods and during fountaining periods for episodes 2–20 (fig. 17.15) implies that eruptive episodes began and ended in response to increased and decreased pressure in the reservoir system. However, the abrupt terminations of fountaining from episode 4 on and the delayed response of summit tilt to eruptive changes suggest that a valve nearer to the vent than to the summit reservoir was the immediate control over the timing of fountaining.

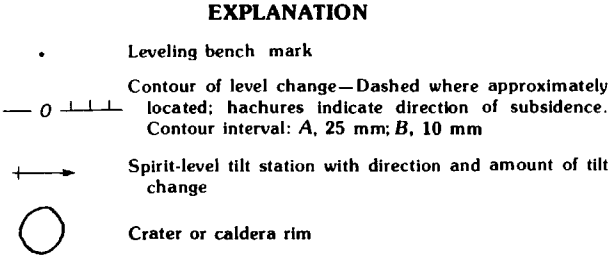

FIGURE 17.26.— Continued.

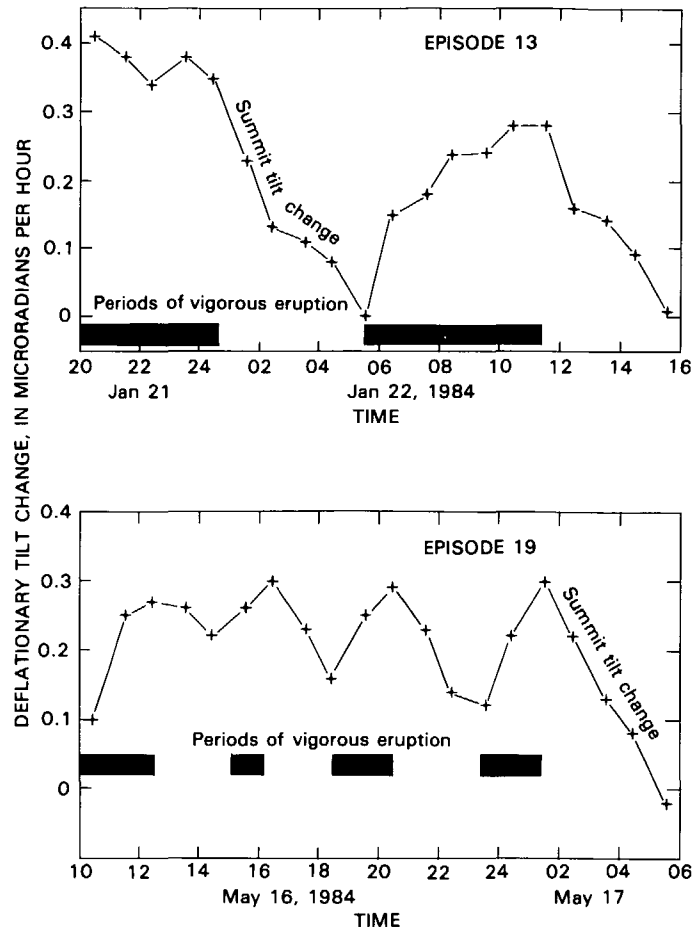

FIGURE 17.27.—Periods of vigorous discharge and variations in rate of summit tilt change for parts of episodes 13 and 19, Puu Oo eruption.

PETROLOGY

EPISODES 1–3

Samples of lava erupted during episodes 1–3 contain less than 6.8 percent MgO (figs. 17.28, 17.29) and thus represent differentiated basalt in the terminology of Wright and Fiske (1971) and Wright (1971). They are also depleted in CaO and enriched in FeO_t ($FeO_t = FeO + 0.9Fe_2O_3$) and in the incompatible elements. Following Wright and Fiske (1971), we interpret this lava as having resulted from fractionation of clinopyroxene and plagioclase as well as olivine from magma that had partly cooled and crystallized during prolonged storage within the rift zone.

The lava of episodes 1–3 is compositionally heterogeneous, even among samples collected during a limited time from a small geographic area. For example, nearly the full compositional range of lava sampled during episodes 1–3 was produced during episode 1 within the relatively restricted area of the 0740 and 1123 vents. Thus the lava apparently originated from several magma bodies that had differentiated to varying degrees within the rift zone. Partly resorbed xenocrysts and reversely zoned phenocrysts are present in

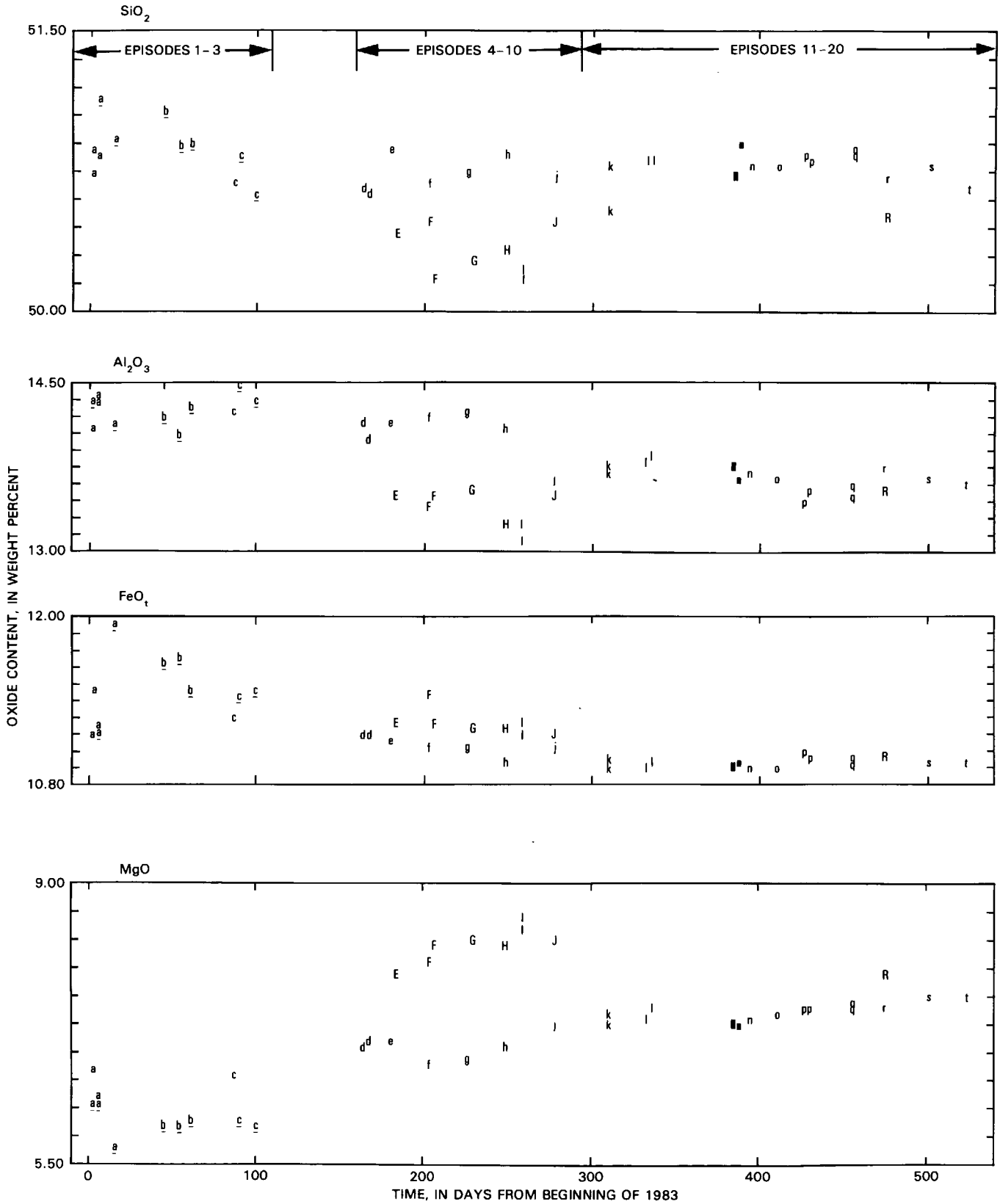

FIGURE 17.28.—Major-oxide concentrations in samples from Puu Oo eruption versus time of eruption. Letters identify episodes: a, episode 1; b, 2; c, 3; d, 4; e, 5; f, 6; g, 7; h, 8; i, 9; j, 10; k, 11; l, 12; m, 13; n, 14; o, 15; p, 16; q, 17; r, 18; s, 19; t, 20.

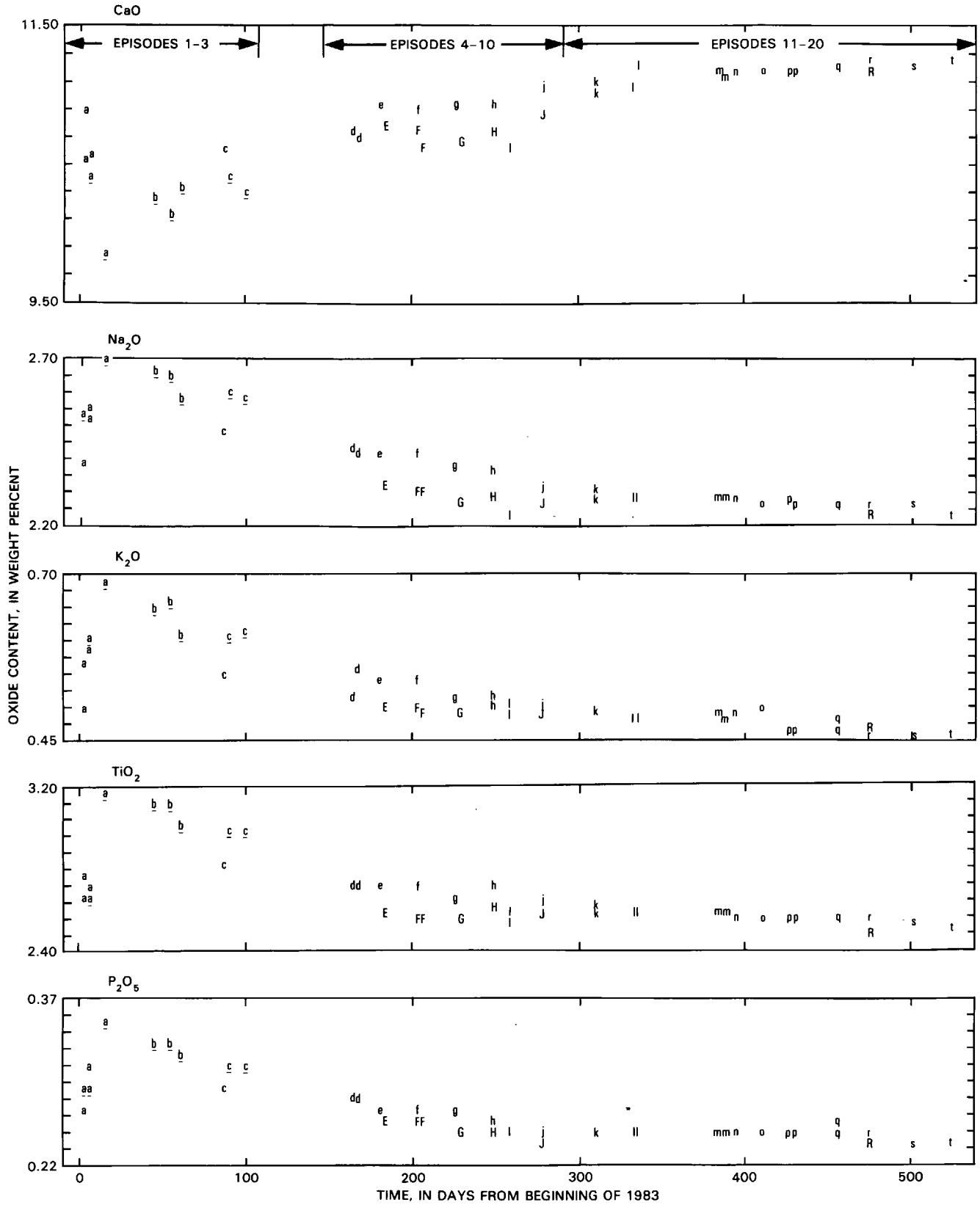

Capital letters designate MgO-rich lava erupted late in episodes 5–10 and 18. Underlined letters indicate samples from 0740 and 1123 vents (see fig. 17.12 for location). Compositions are from classical wet chemical analyses (see Neal and others, in press).

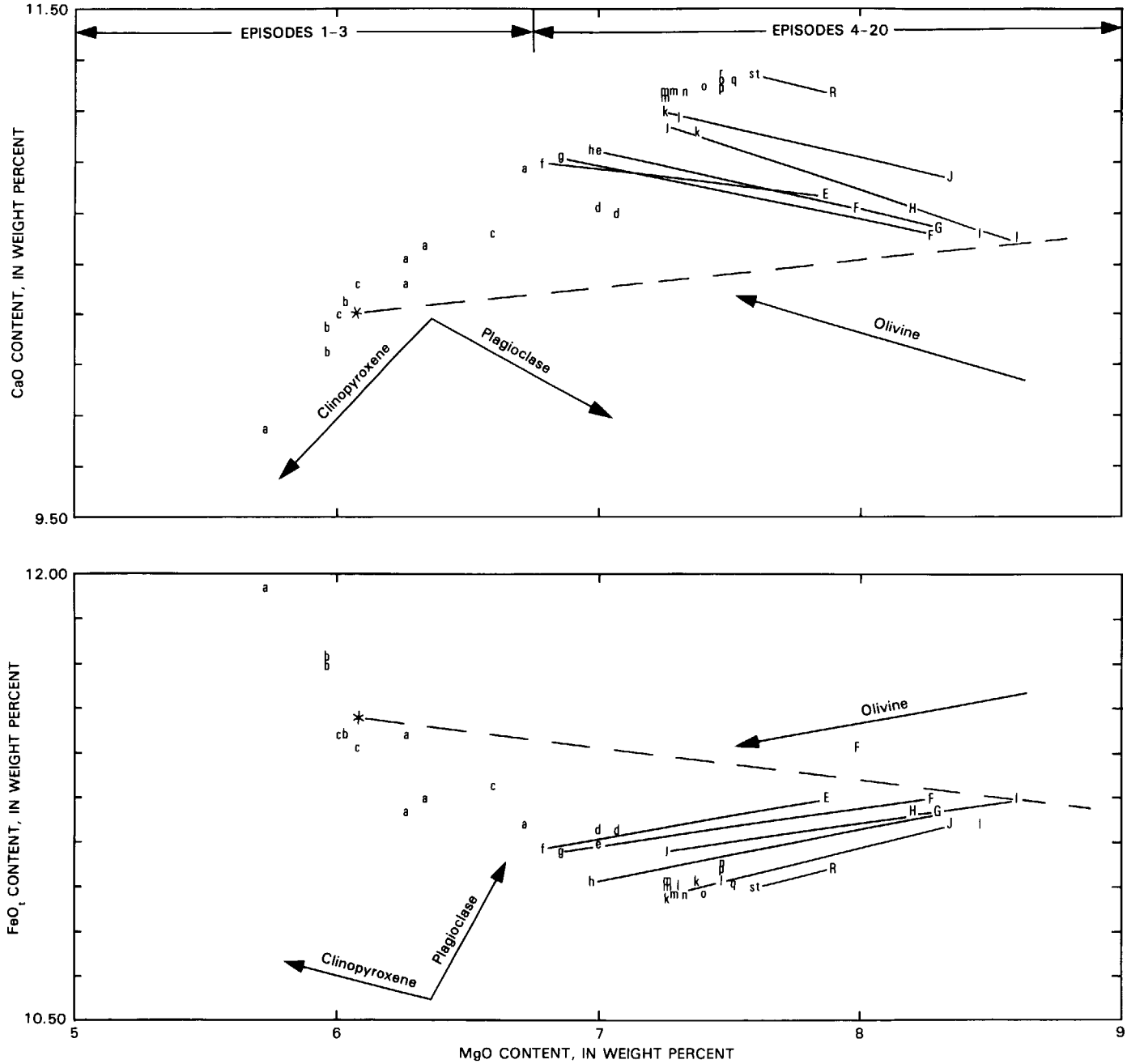

FIGURE 17.29.—CaO versus MgO and total iron (FeO_t) as FeO versus MgO for samples from Puu Oo eruption. Arrows show mineral-control lines calculated for samples with the same MgO content as the origins for the control lines (control lines have been shifted vertically to separate them from the other plotted data). Solid lines connect composition of MgO-rich lava erupted late in an episode with composition of MgO-poor lava erupted early in the succeeding episode. Long-dashed line connects average composition (*) for episode 1–3 lava (excluding the two most MgO-rich samples) and the most MgO-rich Puu Oo lava composition and is an approximate mixing line. Letters indicate episodes and capital letters MgO-rich lavas as in figure 17.28.

some of the samples, evidence that magma mixing had occurred to produce hybrid magmas.

EPISODES 4–20

Lava from episodes 4–20, all of which erupted from Puu Oo, contains 6.8 percent or more MgO. The most conspicuous compositional variation, which occurred within individual episodes 5 through 10 and to a lesser degree during episode 18, can be largely explained as a consequence of olivine fractionation; thus the lava is olivine-controlled in the terminology of Wright and Fiske (1971) and Wright (1971). An additional subtle long-term compositional change is not related to olivine control.

TABLE 17.4.—*Comparison of early episode 10 basalt and composition calculated by subtracting 3.74 percent late episode 9 olivine from late episode 9 basalt*

[Values given are in weight percent]

Oxide	(a) Early episode 10 basalt	(b) Calculated composition	Residual (a minus b)
SiO_2	50.91	50.88	0.03
Al_2O_3	13.71	13.70	.01
FeO_t	11.11	11.10	.01
MgO	7.30	7.30	.00
CaO	11.09	11.07	.02
Na_2O	2.32	2.33	−.01
K_2O	.50	.51	−.01
TiO_2	2.64	2.68	−.04
P_2O_5	.25	.26	−.01
MnO	.17	.18	−.01

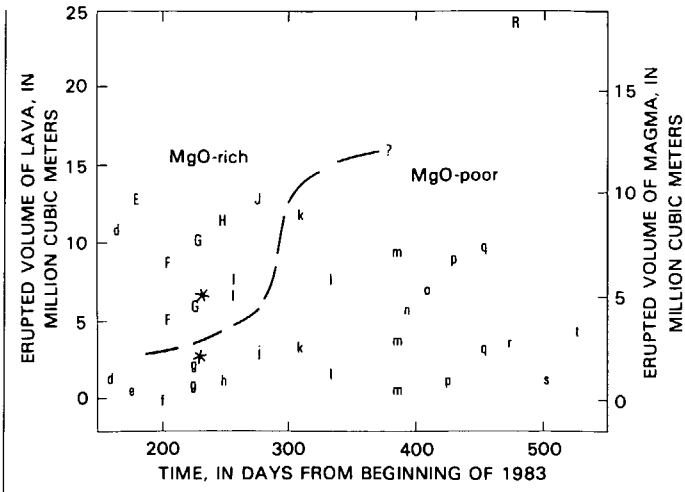

FIGURE 17.30.—Volume of lava (left axis) or magma (right axis) erupted in each episode (4–20) of the Puu Oo eruption at the time of collection of each analyzed sample. Letters indicate episodes and capital letters MgO-rich lavas as in figure 17.28. *, composition from microprobe analysis. Volume erupted by time of collection was estimated by multiplying the subsequently determined discharge rate by the time elapsed from the beginning of the eruptive episode.

During episodes 5–10 and 18, a transition to more MgO-rich lava occurred as the eruptive episode progressed, and all of the other oxides decreased in abundance as MgO increased (figs. 17.28, 17.29). Thus, eruption from a zoned body produced relatively MgO-poor lava early in an episode, and MgO-rich lava was erupted late. Samples for classical analyses represented in figures 17.28 and 17.29 were usually taken in the early and late parts of each eruptive episode. Additional analyses by electron microprobe, from episode 7 (not shown in figures 17.28, 17.29), indicate that the compositional change during the fountaining episode was gradational. Lava sampled during the period of small intracrater pahoehoe flows and pond activity that commonly preceded the major eruptive episodes was similar in composition to the early, MgO-poor lava of the following fountaining episode. Apparently magma in the column beneath the Puu Oo crater floor underwent a compositional change from MgO-rich to MgO-poor during some of the repose periods. Extension of the trends for the MgO-poor lava of episodes 5–10 indicates that only the MgO-poor variety was erupted during episodes 11–17 and 19–20.

Even though the repose periods were brief, crystal fractionation within the magma column seems the most plausible explanation for the compositional change that occurred between eruptive episodes. The most compelling example is the change from MgO-rich lava at the end of episode 9 to MgO-poor lava early in episode 10; it can be precisely accounted for by removal of 3.74 percent of late episode 9 olivine from late episode 9 basalt (table 17.4). Other repose-period compositional changes are fit less precisely by olivine fractionation alone. Nevertheless, the joins connecting the compositions of MgO-rich lava from late in one episode and MgO-poor lava from early in the next (fig. 17.29) are nearly parallel to the olivine-control line (calculated for late episode 9 basalt and its contained olivine). This near coincidence suggests that subtraction of olivine was the dominant cause of the compositional variation during single eruptive episodes. Petrographic data show that the higher MgO content of lava erupted late in a fountain episode does not reflect increased abundance of olivine crystals.

Episode 4 lava did not show the compositional change typical of episodes 5–10. Perhaps the specific magma-column geometry that led to fractionation of a limited melt volume during repose periods originated during episode 4. Thus, the fractionation occurred only during later repose periods.

The MgO-depleted magma in the zoned body was completely erupted in each of episodes 5 through 10. Thereafter, the MgO-depleted volume was too large to be exhausted in an eruptive episode, except for episode 18, which produced an appreciably greater volume than its predecessors at Puu Oo (table 17.1).

We have estimated the volume of lava that had been erupted in each episode at the time that each analyzed sample was collected (fig. 17.30). The first occurrence of both MgO-poor and MgO-rich lava in a single episode was during episode 5, but the volume of early MgO-poor lava is not well constrained. During episodes 6 through 9, MgO-poor lava gave way to MgO-rich lava after about 2.3×10^6 to $5.2\times10^6\,m^3$ of lava had been produced. The volume of MgO-poor lava in episode 10 is poorly constrained but it was less than $12.7\times10^6\,m^3$. Episode 11 produced $12\times10^6\,m^3$ of lava that was all MgO-poor, as was the lava of subsequent episodes except for 18. Lava collected at the end of episode 18, after eruption of $24\times10^6\,m^3$, was richer in MgO than early episode 18 lava but less so than most of the other MgO-rich lavas.

The volumes of MgO-poor lava, considered void-free so as to approximate magma volumes, indicate that about $3\times10^6\,m^3$ of MgO-poor magma was available in the reservoir during the early parts of episodes 5 through 9. Between episodes 9 and 11, this increased to more than $9\times10^6\,m^3$, but episode 18 indicates it did not exceed $18\times10^6\,m^3$.

Subsidence of the Puu Oo crater floor and collapse of the crater walls occurred late in episode 10. In the next two episodes, fountain heights were dramatically lower, and lava issued from several vents

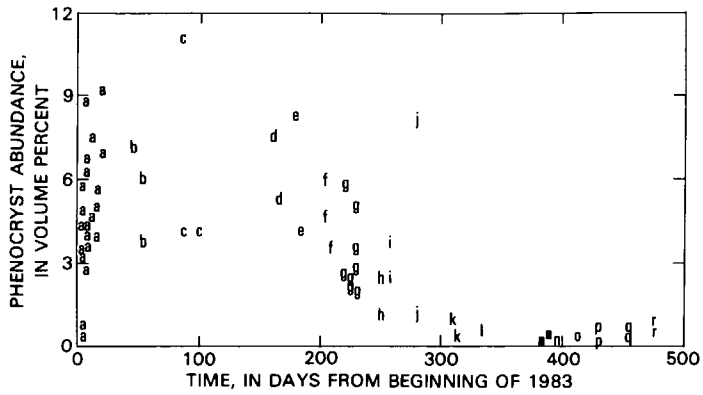

FIGURE 17.31.—Total percentage of olivine, augite, and plagioclase phenocrysts versus time of collection of lava samples from Puu Oo eruption. Letters indicate episodes as in figure 17.28.

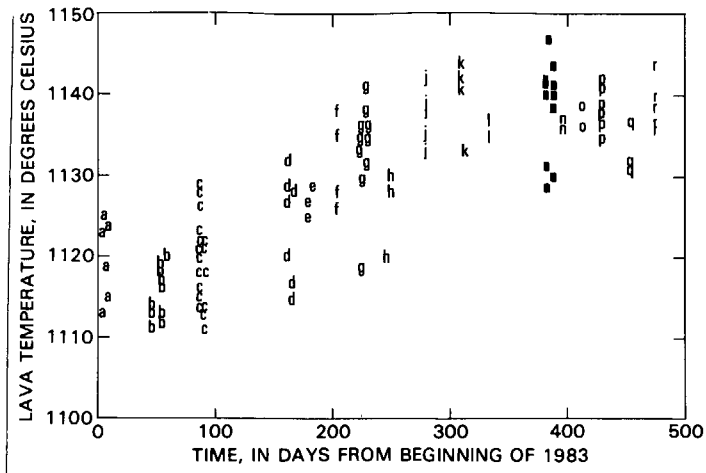

FIGURE 17.32.—Lava temperatures measured by chromel-alumel thermocouple, episodes 1–20 of Puu Oo eruption. Letters indicate episodes as in figure 17.28.

both within and outside the crater. These observations suggest that collapse in the conduit had partly blocked access to the normal vent. The marked increase in the erupted volume of MgO-depleted magma between episodes 9 and 11 may have recorded enlargement of the subcrater reservoir by the same event that caused crater collapse and disrupted the fountains.

If our hypothesis that MgO-depleted magma originated by crystal fractionation of MgO-rich magma in the magma-filled conduit beneath Puu Oo is correct, then the volume of MgO-depleted magma represents a minimum value for the volume of the magma column. We have no direct measure of the column length. However, we inferred previously from the distribution of earthquakes in the shallow swarm associated with episode 1 that the feeder dike was intruded upward to the surface from an aseismic zone at a depth of 3–4 km. If the aseismic zone persisted through the subsequent fountaining episodes as the subhorizontal zone of magma supply from the summit reservoir to the vent region, we can surmise that the magma column beneath Puu Oo was 3–4 km long. Using a 3.5-km length and the volume estimate of $3\times10^6\,m^3$ for episodes 5–9, we calculate a minimum average diameter for the magma column of about 30 m. For the volume estimates for the later episodes (9×10^6 to $18\times10^6\,m^3$), the calculated minimum average diameter is 60–80 m. These values are in close agreement with estimates of average conduit diameters of 40–70 m inferred from volumes of gas-enriched melt that caused high fountains early in some episodes (Wolfe and others, in press) and 50 ± 30 m inferred from interpretation of gas-flux and geodetic measurements (Greenland and others, in press).

The lava of episodes 4–20 shows a long-term compositional change marked by gradual increase in CaO and MgO and decrease in FeO_t and incompatible elements (figs. 17.28, 17.29). The changes are small, and the progression is imperfect. Nevertheless, figure 17.29 shows unmistakably that, in both the MgO-poor and MgO-rich lavas, CaO and MgO gradually increased together through time and FeO_t concomitantly decreased through time. Imposition of this progressive compositional change on both lava types supports our interpretation that each volume of MgO-depleted magma was derived from an associated volume of MgO-rich magma. In a sense, the two share a common fingerprint imposed by the gradual long-term compositional change.

Two possible reasons for the long-term compositional trend involve rift-zone mixing (see, for example, Wright and Fiske, 1971; Wright and others, 1975) and gradual compositional change of the melt produced in the mantle (see, for example, Hofmann and others, 1984). If mixing is the reason, fresh magma from the summit would become contaminated to progressively decreasing degrees from contact during its passage through the rift zone with older CaO- and MgO-depleted magma still in storage. We do not know the possible end-member compositions, but for illustration we have drawn an approximate mixing line (fig. 17.29) connecting the most MgO-rich sample (late episode 9) and an average composition that includes all analyzed lava from episodes 1–3 except for two samples that have significantly higher MgO contents (6.59 and 6.72 wt percent) and may reflect more recent involvement of summit magma than do other lavas of episodes 1–3.

If changing parent composition is the reason, then the progressive increase in CaO and depletion of incompatible elements, emphasized when the compositions from episodes 5–20 are normalized to a common MgO value by adjusting for olivine control, may have resulted from increasing melting of clinopyroxene in the mantle.

Reversely zoned phenocrysts in some samples from episodes 4–10 suggest magma mixing. Lava of episodes 11–20 was nearly aphyric (fig. 17.31), and no phenocrysts suggestive of disequilibrium were found. Lava-temperature measurements show much scatter (fig. 17.32) but suggest that the temperature increased through the early episodes, perhaps through episode 11, and then leveled off. This increase could have been a consequence of decreasing contamination of hotter summit melt by cooler rift-zone melt. We note that the change in phenocryst content and the change in measured temperatures through time roughly mimic the compositional changes

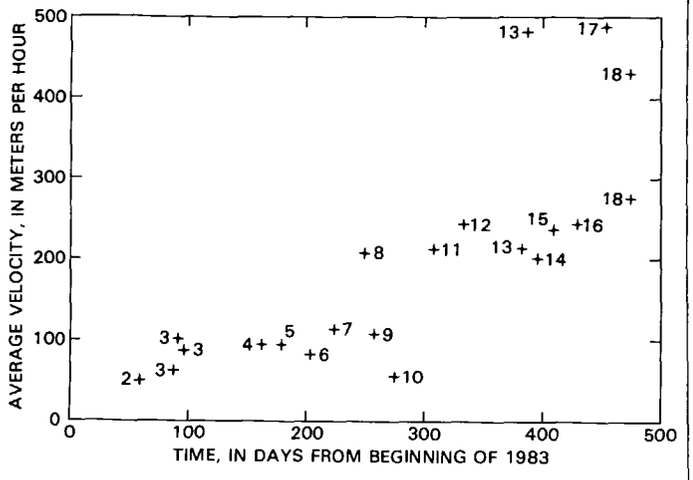

FIGURE 17.33.—Average flow-advance rate versus time of eruption for the major river-fed flow(s) of eruptive episodes 2–18, Puu Oo eruption. Flow-advance velocity was determined by periodic mapping of flow-front position.

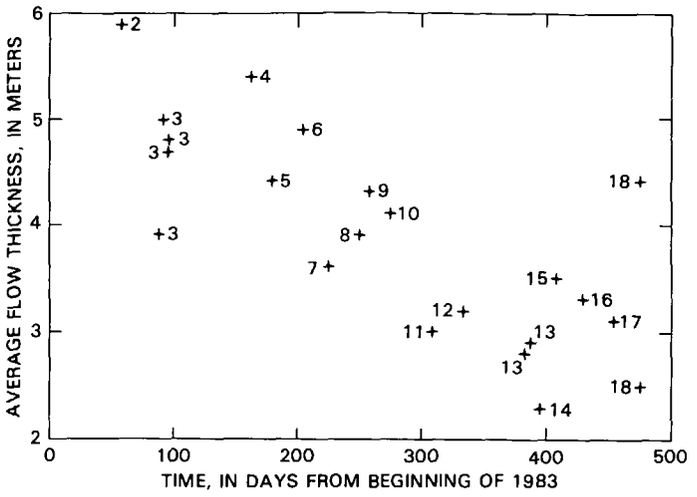

FIGURE 17.34.—Average flow thickness versus time of eruption, episodes 2–18 of Puu Oo eruption. Thickness was measured at numerous localities along flow margin. Average thickness was obtained from calculated volume/measured area.

recorded from episode 4 through 20. Average velocity and average thickness of the major river-fed lava flows (figs. 17.33 and 17.34) also roughly mimic these patterns. Velocity was greater and thickness less during episodes 11–20, suggesting that lava viscosity decreased, in accord with changing lava composition, petrography, and temperature.

NEGLIGIBLE EFFECTS OF MAUNA LOA EARTHQUAKE AND ERUPTION

A large ($M = 6.7$) earthquake (Buchanan-Banks, chapter 44; Koyanagi and others, 1984) occurred beneath Mauna Loa's southeast flank on November 16, 1983, between episodes 11 and 12 of the Puu Oo eruption. The earthquake caused an abrupt tilt change of nearly 300 μrad at the Uwekahuna tiltmeter (fig. 17.15), but it produced no recognizable change in the continuing events at Puu Oo.

A Mauna Loa eruption occurred from March 25 to April 15, 1984 (Lockwood and others, 1985); for the first time since 1919, Kilauea and Mauna Loa were in eruption simultaneously. Episode 17 of the Puu Oo eruption occurred on March 30–31, during the Mauna Loa eruption, and episode 18 on April 18–21 following the Mauna Loa eruption. The volume of episode 18 was larger than usual (table 17.1), but otherwise Puu Oo activity during and immediately after the Mauna Loa eruption was normal.

INTERPRETIVE SUMMARY

The east rift zone of Kilauea has been a major locus of magma storage as well as eruption; Dzurisin and others (1984) estimated that at least $1 \times 10^9 m^3$ of magma was added to east-rift-zone storage between 1956 and 1983. From late 1978 through 1980, the Puu Kamoamoa-Puu Kahaualea area, where the major vents of the Puu Oo eruption are located, was the site of repeated intrusions that caused flurries of shallow earthquakes and increasing tumescence of that part of the rift zone.

After a period of quiescence during 1981 and part of 1982, small intrusions into the Puu Kamoamoa area resumed following a summit intrusion and eruption on September 25–26, 1982. In early January 1983 a voluminous east-rift intrusion resulted in large subsidence of the previously distended summit reservoir, emplacement of a new feeder dike, and onset of the Puu Oo eruption.

The intrusion was initiated by an aseismic magmatic surge through magma-filled passages in the uppermost part of the east rift zone and by the onset of dike emplacement near Makaopuhi Crater. The distribution of shallow earthquakes indicates that the dike propagated upward from an aseismic region at a depth of 3–4 km within the rift zone, and its tip migrated downrift as intrusion continued. The upper edge of the dike eventually intersected the ground surface from Napau Crater to Kalalua, initiating nearly two weeks of intermittent fissure eruptions.

Over most of its length, the fissure system soon stopped erupting. Intermittent fissure eruptions during episode 1 of the series, in January 1983, became localized primarily south of Puu Kahaualea. During episodes 2 and 3, a central vent south of Puu Kahaualea, the 1123 vent, was the dominant eruptive locus, and a lesser one was located 1.5 km uprift in the area where Puu Oo was to develop. From episode 4 on, the Puu Oo vent was the main locus, and, except for fissures in the immediate vicinity of Puu Oo that were briefly active a few times, eruption has never recurred elsewhere along the fissure system (as of June 1985).

After episode 1, low harmonic tremor continued during repose periods, and subsequent fountaining episodes began without shallow earthquake swarms. Both these observations indicate that an active magma conduit was maintained between the summit and vent areas.

As the eruptive series progressed, the rift-zone conduit became more efficient in transporting magma, as indicated by the general increase in average lava-discharge rate. Factors that may have contributed to more rapid magma transport include enlargement and streamlining of passageways and reduction of melt viscosity as a consequence of increased temperature or decreased crystallinity. We have no direct means of evaluating the character of the magma-filled passageways, but enlargement or streamlining seem likely consequences of repeated passage of melt through them. We note that the lava generally became hotter and less porphyritic as the Puu Oo eruption progressed.

Several different phenomena, considered together, suggest that the main vents, located in the general Puu Kamoamoa-Puu Kahaualea area, overlay a zone of magma storage that antedated the beginning of the eruption. Effects specifically related to such a zone include: (1) anomalously rapid downrift passage of surface deformation preceding the tip of the dike; (2) dissipation of the tightly clustered concentration of shallow earthquakes that farther uprift recorded a systematic, steady downrift advance of the dike tip; (3) decreased concentration of shallow earthquakes associated with dike emplacement and establishment of the new vents; and (4) localization of repeated small intrusions from late 1978 through 1980.

The petrologic evidence suggests that a magma-storage zone had existed for a long time beneath the Puu Kamoamoa-Puu Kahaualea area. Lava erupted from the inferred storage zone during episodes 1–3 was differentiated beyond olivine control and was significantly cooler than olivine-controlled lava erupted later from Puu Oo. Following Wright and Fiske (1971), we infer that the lava of episodes 1–3 evolved as a consequence of crystal fractionation resulting from cooling and partial crystallization during prolonged storage in the rift zone. Additional compositional modification apparently resulted from magma mixing, as indicated by partly resorbed xenocrysts and reversely zoned phenocrysts. Approximately $50 \times 10^6\,m^3$ of such differentiated and hybrid magma was erupted in episodes 1–3, and perhaps an additional $100 \times 10^6\,m^3$ of this magma remained in the new dike.

Once the Puu Oo vent became established, the composition of lava was within the range of olivine control. Magma in the conduit beneath Puu Oo underwent a compositional change during repose periods that can be largely or entirely explained by fractionation of a few percent olivine. This produced MgO-depleted magma that was exhausted whenever the volume of the next eruptive episode exceeded the volume of MgO-depleted magma. During episodes 5–9, such MgO-poor magma gave way to MgO-rich magma after about $3 \times 10^6\,m^3$ of magma had been erupted; in episodes 11–20, the volume of MgO-depleted magma available in each eruptive episode was between $9 \times 10^6\,m^3$ and $18 \times 10^6\,m^3$. The reservoir in which fractionation occurred during repose periods apparently was significantly enlarged between episodes 9 and 11.

Gradual enrichment of both CaO and MgO in the olivine-controlled magma erupted during episodes 4–20 may imply either decreasing levels of contamination of olivine-controlled summit magma by differentiated magma stored in the rift zone or gradually changing composition of magma generated in the mantle. The occurrence of reversely zoned phenocrysts in some of the lava of episodes 4–10 and the progressive increase in lava temperature through those episodes support the hypothesis that the lava composition was affected by magma mixing at least through episode 10.

Intrusion of summit magma into the rift zone apparently displaced differentiated magma already in storage, causing it to erupt during episodes 1–3. If olivine-controlled magma from the summit was contaminated thereafter by differentiated magma from the rift zone, the rift-zone conduit must have intersected one or more bodies of differentiated magma. Such magma bodies were possibly stored below the zone of brittle fracture indicated by shallow earthquakes generated during upward propagation of the dike. Thus, the bodies of stored magma and the rift-zone conduit were most likely at a depth of at least 3–4 km, within the normally aseismic deeper part of the rift zone.

Symmetry of patterns of attenuation of harmonic tremor with respect to Puu Oo indicates that, although the depth is uncertain, the tremor source and the vent were in vertical alignment. Furthermore, rift-zone dikes are generally near vertical (Pollard and others, 1983), and local, approximately cylindrical conduits that transport magma upward at higher flow rates and with lower heat loss than do dikes, can evolve from dikes by local erosion of wallrock as adjacent dike segments solidify and become inactive (Delaney and Pollard, 1981, 1982). These considerations suggest that a nearly vertical conduit descended from the Puu Oo vent in the plane of the initial dike. We suppose that the junction between the approximately vertical feeder conduit and the subhorizontal rift-zone conduit was located near the base of the episode 1 dike at a depth of 3–4 km. The mouth of the conduit, about 20 m in diameter, was nearly continuously visible in the crater floor after episode 13. The diameter may have increased downward. Erupted volumes of MgO-depleted melt were too large to have been accommodated in a conduit only 20 m in diameter and 3–4 km long; average diameters of 30 m for episodes 5–9 and 60–80 m for episodes 11–20 are implied if all of the inferred fractionation took place within this vertical magma column.

As eruptive activity became localized at Puu Oo, the presence of a nearby magma reservoir became evident from rift-zone tilt changes. Beginning with a subsidence during episode 3, rift-zone tumescence developed gradually during repose periods and rift-zone subsidence occurred rapidly during eruptive episodes, as indicated by a borehole tiltmeter northwest of Puu Kamoamoa. This deformation was congruent with tilt changes at the summit. Thus an approximate hydraulic equilibrium with the summit reservoir was continually maintained along the rift-zone conduit.

The limited range and approximate equivalence of opposed inflationary and deflationary tilt changes at the summit and also in the rift zone indicate that eruptive episodes began and ended in response to magmatic pressure in the reservoir system. The secondary reservoir in the rift zone apparently acted as a valve, controlling eruptive activity from the rift zone rather than from the summit. Thus, from the end of episode 3, starts and stops of vigorous eruption normally preceded, respectively, the onset of rapid summit deflation or the resumption of summit inflation as recorded by the

Uwekahuna tiltmeter. Summit response also lagged behind pauses and resumptions of lava discharge during individual eruptive episodes.

Eruptive episodes started gradually, possibly reflecting non-Newtonian behavior of the magma in the conduit system (Hardee, chapter 54). Reservoir pressure had to build sufficiently to overcome the yield strength of the melt, after which flow of magma accelerated.

The central-vent episodes at the 1123 vent died gradually, fountain height decreasing apparently in response to gradually diminishing magmatic pressure. However, lava discharge at Puu Oo normally stopped abruptly, without the gradual decay that characterized the earlier episodes. Perhaps this change was related to development of the rift-zone reservoir. Progressive depletion of the rift-zone reservoir, reflected by subsidence in the rift zone during eruptive episodes at Puu Oo, apparently led to abrupt termination of the eruption when pressure in the near-vent part of the reservoir system fell below a critical level sufficient to maintain the supply of fresh, nonvesiculated magma to the column below the vent. Summit deflation continued briefly as pressure was equalized in the linked summit and rift-zone reservoir systems.

We calculate an overall magma-supply rate of $10 \times 10^6 m^3$/mo for episodes 2–20. Allowing for errors in volume measurement, this value is not different from the rate of $9 \times 10^6 m^3$/mo determined by Swanson (1972) for earlier periods of prolonged eruption for which the relationships between volume change in the summit reservoir and the volume erupted could be evaluated. Higher rates, nearly $12 \times 10^6 m^3$/mo, prevailed at Puu Oo during episodes 4–12 and 13–17. In these two sequences, recurrence intervals and erupted volumes had a miniminal range, indicating that an approximately steady relationship was maintained between magma supply to the reservoir system and frequency and volume of eruption. Each of these periods of elevated supply of magma to the vent was preceded by an unusually long repose period. Thus, the long-term supply rate was less.

Inferred magma-supply rates during the Puu Oo eruption equal or exceed estimates of long-term supply given by Dzurisin and others (1984), causing us to speculate that the Puu Oo eruption may coincide with a period of increased magma supply to Kilauea. A marked increase in SO_2 flux to the atmosphere in the Kilauea caldera region occurred about one month after the beginning of the eruption and may reflect increased rate of supply of magma to the summit reservoir. We are unable to evaluate the rate of percolation of exsolved gas from the reservior region to the surface, and we have no other independent, short-term measure of supply to the reservoir. Thus, like Dzurisin and others (1984), we cannot distinguish whether the Puu Oo eruption was a response to possible increase in magma supply rate or whether it may have triggered increased supply. Nevertheless, a substantial rate of supply was apparently maintained through and beyond episode 20. It led to establishment of a comparatively unimpeded transport system from the summit reservoir to the vent at Puu Oo that is likely to remain open until disrupted by a tectonic event or until diminution of supply to the rift-zone conduit allows cooling, crystallization, and eventual termination of magma transport to the vent.

REFERENCES

Crosson, R.S., and Endo, E.T., 1982, Focal mechanisms and locations of earthquakes in the vicinity of the 1975 Kalapana earthquake aftershock zone of 1970–1979: implications for tectonics of the south flank of Kilauea Volcano, Island of Hawaii: Tectonics, v. 1, p. 495–542.

Delaney, P.T., and Pollard, D.D., 1981, Deformation of host rocks and flow of magma during growth of minette dikes and breccia-bearing intrusions near Ship Rock, New Mexico: U.S. Geological Survey Professional Paper 1202, 61 p.

———1982, Solidification of basaltic magma during flow in a dike: American Journal of Science, v. 282, p. 856–885.

Duffield, W.A., Christiansen, R.L., Koyanagi, R.Y., and Peterson, D.W., 1982, Storage, migration, and eruption of magma at Kilauea Volcano, Hawaii: Journal of Volcanology and Geothermal Research, v. 13, p. 273–307.

Dvorak, J.J., and Okamura, A.T., 1985, Variations in tilt rate and harmonic tremor during the January-August 1983 east rift eruptions of Kilauea Volcano, Hawaii: Journal of Volcanology and Geothermal Research, v. 25, p. 249–258.

Dvorak, J.J., Okamura, A.T., and Dietrich, J.H., 1983, Analysis of surface deformation data, Kilauea Volcano, Hawaii: October 1966 to September 1970: Journal of Geophysical Research, v. 88, p. 9295–9304.

Dvorak, J.J., Okamura, A.T., English, T.T., Koyanagi, R.Y., Nakata, J.S., Sako, M.K., Tanigawa, W.R., and Yamashita, K.M., in press, Mechanical response of the south flank of Kilauea Volcano, Hawaii, to intrusive events along the rift zones: Tectonophysics.

Dzurisin, D., Anderson, L.A., Eaton, G.P., Koyanagi, R.Y., Lipman, P.W., Lockwood, J.P., Okamura, R.T., Puniwai, G.S., Sako, M.K., and Yamashita, K.M., 1980, Geophysical observations of Kilauea Volcano, Hawaii, 2. Constraints on the magma supply during November 1975–September 1977: Journal of Volcanology and Geothermal Research, v. 7, p. 241–269.

Dzurisin, D., Koyanagi, R.Y., and English, T.T., 1984, Magma supply and storage at Kilauea Volcano, Hawaii, 1956–1983: Journal of Volcanology and Geothermal Research, v. 21, p. 177–206.

Fiske, R.S., and Jackson, E.D., 1972, Orientation and growth of Hawaiian volcanic rifts: the effect of regional structure and gravitational stresses: Royal Society [London] Proceedings, v. 329, p. 299–326.

Garcia, M.O., and Wolfe, E.W., *in* press, Petrology of the lavas from the Puu Oo eruption of Kilauea Volcano, Hawaii: episodes 1–20, in Wolfe, E.W., ed., The Puu Oo eruption of Kilauea Volcano, Hawaii: the first 1½ years: U.S. Geological Survey Professional Paper.

Greenland, L.P., in press, Gases from the 1983–84 east rift eruption of Kilauea Volcano, *in* Wolfe, E.W., ed., The Puu Oo eruption of Kilauea Volcano, Hawaii: the first 1½ years: U.S. Geological Survey Professional Paper.

Greenland, L. P., Okamura, A. T., and Stokes, J. B., in press, Constraints on the mechanics of eruption of Puu Oo, *in* Wolfe, E.W., ed., The Puu Oo eruption of Kilauea Volcano, Hawaii: the first 1½ years: U.S. Geological Survey Professional Paper.

Greenland, L.P., Rose, W.I., and Stokes, J.B., 1985, An estimate of gas emissions and magmatic gas content from Kilauea Volcano: Geochimica et Cosmochimica Acta, v. 49, p. 125–129.

Hofmann, A.W., Feigenson, M.D., and Raczek, I., 1984, Case studies on the origin of basalt: III, Petrogenesis of the Mauna Ulu eruption, Kilauea, 1969–71: Contributions to Mineralogy and Petrology, v. 88, p. 24–35.

Holcomb, R.T., 1980, Preliminary geologic map of Kilauea Volcano, Hawaii: U.S. Geological Survey open-file report 80–796, scale 1:50,000.

Jackson, D.B., in press, Geoelectric observations: September 1982 summit eruption and the first year of the 3 January 1983 east rift zone eruption, Kilauea volcano, Hawaii, *in* Wolfe, E.W., ed., The Puu Oo eruption of Kilauea Volcano, Hawaii: the first 1½ years: U.S. Geological Survey Professional Paper.

Jackson, D.B., Swanson, D.A., Koyanagi, R.Y., and Wright, T.L., 1975, The August and October 1968 east rift eruptions of Kilauea Volcano, Hawaii: U.S. Geological Survey Professional Paper 890, 33 p.

Klein, F.W., 1978, Hypocenter location program HYPOINVERSE, part 1: user's guide to versions 1, 2, 3, and 4: U.S. Geological Survey Open-File Report 78–694, 113 p.

Koyanagi, R.Y., Endo, E.T., Tanigawa, W.R., Nakata, J.S., Tomori, A.H., and Tamura, P.N., 1984, Kaoiki, Hawaii earthquake of November 16, 1983: a preliminary compilation of seismographic data at the Hawaiian Volcano Observatory, U.S. Geological Survey Open-File Report 84–798, 35p.

Koyanagi, R.Y., Tanigawa, W.R., and Nakata, J.S., in press, Seismicity associated with the eruption of Kilauea Volcano from January 1983 to July 1984, *in* Wolfe, E.W., ed., The Puu Oo eruption of Kilauea Volcano, Hawaii: the first 1½ years: U.S. Geological Survey Professional Paper.

Koyanagi, R.Y., Unger, J.D., Endo, E.T., and Okamura, A.T., 1974, Shallow earthquakes associated with inflation episodes at the summit of Kilauea Volcano, Hawaii, *in* Gonzales-Ferran, O., ed., Proceedings of the symposium on Andean and Antarctic volanology problems, Santiago, Chile, September 1974, International Association of Volcanology and Chemistry of the Earth's Interior, Special Series.

Lockwood, J.P., Banks, N.G., English, T.T., Greenland, L.P., Jackson, D.B., Johnson, D.J., Koyanagi, R.Y., McGee, K.A., Okamura, A.T., and Rhodes, J.M., 1985, The 1984 eruption of Mauna Loa Volcano, Hawaii: Eos, Transactions of the American Geophysical Union, v. 66, p. 169–171.

Macdonald, G.A., Abbott, A.T., and Peterson, F.L., 1983, Volcanoes in the sea: the geology of Hawaii, second edition: Honolulu, University of Hawaii Press, 517 p.

Maruyama, T., 1964, Statical elastic dislocations in an infinite and semi-infinite medium: Bulletin of the Earthquake Research Institute, v. 42, p. 289–368.

Moore, J.G., and Koyanagi, R.Y., 1969, The October 1963 eruption of Kilauea Volcano, Hawaii: U.S. Geological Survey Professional Paper 614–C, 13 p.

Moore, R.B., 1983, Distribution of differentiated tholeiitic basalts on the lower east rift zone of Kilauea Volcano, Hawaii: a possible guide to geothermal exploration: Geology, v. 11, p. 136–140.

Moore, R.B., Helz, R.T., Dzurisin, D., Eaton, G.P., Koyanagi, R.Y., Lipman, P.W., Lockwood, J.P., and Puniwai, G.S., 1980, The 1977 eruption of Kilauea Volcano, Hawaii: Journal of Volcanology and Geothermal Research, vol 7, p. 189–210.

Neal C.A., and Decker, R.W., 1983, Surging of lava flows at Kilauea Volcano, Hawaii [abstract]: Eos, Transactions of the American Geophysical Union, v. 64, no. 5, p. 904.

Neal, C.A., Duggan, T.J., Wolfe, E.W., and Brandt, E.L., in press, Lava samples, temperatures, and compositions, Puu Oo eruption of Kilauea Volcano, Hawaii, episodes 1–20, January 3, 1983–June 8, 1984, *in* Wolfe, E.W., ed., The Puu Oo eruption of Kilauea Volcano, Hawaii: the first 1½ years: U.S. Geological Survey Professional Paper.

Okamura, A.T., Dvorak, J.J., Koyanagi, R.Y., and Tanigawa, W.R., in press, Surface deformation associated with the 1983 Kilauea eruption, *in* Wolfe, E.W., ed., The Puu Oo eruption of Kilauea Volcano, Hawaii: the first 1½ years: U.S. Geological Survey Professional Paper.

Peterson, D.W., 1976, Processes of volcanic island growth, Kilauea Volcano, Hawaii, 1969–1973: International Association of Volcanology and Chemistry of the Earth's Interior, Symposium on Andean and Antarctic Volcanology Problems, Proceedings, p. 172–189.

Peterson, D.W., and Swanson, D.A., 1974, Observed formation of lava tubes during 1970-71 at Kilauea Volcano, Hawaii: Studies in Speleology, v. 2, p. 209–222.

Pollard, D.D., Delaney, P.T., Duffield, W.A., Endo, E.T., and Okamura, A.T., 1983, Surface deformation in volcanic rift zones: Tectonyphysics, v. 94, p. 541–584.

Ryan, M.P., Blevins, J.Y., Okamura, A.T., and Koyanagi, R.Y., 1983, Magma reservoir subsidence mechanics: theoretical summary and application to Kilauea Volcano, Hawaii: Journal of Geophysical Research, v. 88, p. 4147–4181.

Ryan, M.P., Koyanagi, R.Y., and Fiske, R.S., 1981, Modeling the three-dimensional structure of macroscopic magma transport systems: application to Kilauea Volcano, Hawaii: Journal of Geophysical Research, v. 86, p. 7111–7129.

Swanson, D.A., 1972, Magma supply rate at Kilauea Volcano, 1952–1971: Science, v. 175, p. 169–170.

Swanson, D.A., Duffield, W.A., and Fiske, R.S., 1976a, Displacement of the south flank of Kilauea Volcano: the result of forceful intrusion of magma into the rift zones: U.S. Geological Survey Professional Paper 963, 39 p.

Swanson, D.A., Duffield, W.A., Jackson, D.B., and Peterson, D.W., 1979, Chronological narrative of the 1969-71 Mauna Ulu eruption of Kilauea Volcano, Hawaii: U.S. Geological Survey Professional Paper 1056, 55 p.

Swanson, D.A., Jackson, D.B., Koyanagi, R.Y., and Wright, T.L., 1976b, The February 1969 east rift eruption of Kilauea Volcano, Hawaii: U.S. Geological Survey Professional Paper 891, 30 p.

Wolfe, E.W., Neal, C.A., Banks, N.G., and Duggan, T.J., in press, Geologic observations and chronology of eruptive events during the first 20 episodes of the Puu Oo eruption, January 3, 1983 through June 8, 1984, *in* Wolfe, E.W., ed., The Puu Oo eruption of Kilauea Volcano, Hawaii: the first 1½ years: U.S. Geological Survey Professional Paper.

Wright, T.L., 1971, Chemistry of Kilauea and Mauna Loa lava in space and time: U.S. Geological Survey Professional Paper 735, 40 p.

———1984, Origin of Hawaiian tholeiite: a metasomatic model: Journal of Geophysical Research, v. 89, p. 3233–3252.

Wright, T.L., and Fiske, R.S., 1971, Origin of the differentiated and hybrid lavas of Kilauea Volcano, Hawaii: Journal of Petrology, v. 12, p. 1–65.

Wright, T.L., Swanson, D.A., and Duffield, W.A., 1975, Chemical composition of Kilauea east rift lava, 1968–1971: Journal of Petrology, v. 16, p. 110–133.

HOLOCENE ERUPTIVE HISTORY OF MAUNA LOA VOLCANO

By John P. Lockwood *and* Peter W. Lipman

ABSTRACT

In order to evaluate the Holocene eruptive history of Mauna Loa, surface lava flows have been classified by age and a semiquantitative analysis made of their mapped areas. A new map depicting the age distribution of these surface lavas shows that flows are generally older at lower elevations and at greater distances from eruptive sources as a consequence of the fact that there are fewer long flows than short ones. Earlier estimates of the areas and volumes of historical eruptive products have been revised on the basis of new mapping and study of written records.

Lavas of known historical age (1843 and later) cover 13 percent of Mauna Loa's surface; their total volume is about 4 km^3. This figure includes extensive buried lavas, especially within Mokuaweoweo, Mauna Loa's summit caldera. The historical lavas were erupted at an average rate of 45×10^6 m^3/yr from 1843–76, but at less than half that rate since 1877. This change in eruptive rate coincides with an abrupt change in lava chemistry and may be related to effects of the magnitude-7.5 1868 earthquake.

The average historical (1843 and later) production rate of 29×10^6 m^3/yr is higher than average rates for the preceding six and one-half centuries, as reflected by lava-flow areal coverage rates. That period, from about A.D. 1200 to 1843, began shortly before the formation of the present Mokuaweoweo and was characterized by low levels of rift-zone activity and an increased incidence of eruption from northwest flank vents radial to the summit. The preceding period of about 750 years was characterized by voluminous pahoehoe overflows from a summit lava lake—over one-fourth of the volcano is covered with these lavas. The record becomes increasingly fragmentary with age, as over one-half of Mauna Loa has been buried during the past 1,500 years (since the arrival of man on Hawaii); almost 90 percent of the surface is covered with rocks of age less than 4 ka.

Pahoehoe and aa are present in nearly equal amounts at Mauna Loa's surface, but aa is more typical of rift than of summit eruptions. The ratio of aa to pahoehoe commonly increases with transport distance, and it appears to increase with time in the Holocene, aa being more common among lavas younger than about 750 years than among older flows.

INTRODUCTION

> I have not yet discovered any native traditions respecting eruptions from the larger volcano [Mauna Loa]. It is uninhabitable, and therefore its eruptions would not usually be frought with disaster to the inhabitants, and thus would be scarcely mentioned in the traditions. When Hawaii shall have been studied carefully it will be possible to give the sequence of several pre-historic eruptions.
>
> —*C.H. Hitchcock, 1909, p. 56–57.*

Mauna Loa, which rises nearly 9 km above the isostatically depressed floor of the central Pacific (to 4,167 m above sea level), is the largest volcano on Earth; its volume has been estimated at about 40,000 km^3 (Macdonald, 1972, p. 258). That volume is probably too high, however, because older, separate volcanoes are likely buried at depth. Mauna Loa's lavas cover about 5,125 km^2 of the Island of Hawaii (fig. 18.1). These subaerial lava flows preserve the most readily accessible record of the volcano's prehistoric eruptive activity, and evidence yielded by them forms the principal basis of this report. Limited exploration of the approximately 4,000 km^2 of Mauna Loa beneath sea level has also begun (Fornari and Campbell, chapter 4; Fornari and others, 1979; Moore and others, 1985).

PREVIOUS WORK

The first systematic geologic study of any part of Mauna Loa was that of Stearns and Clark (1930), who mapped the southwestern part of the volcano. They recognized the widespread pyroclastic deposit called the Pahala Ash and proposed the name "Kamehame basalt" for lavas of both Mauna Loa and Kilauea that overlie the ash and the name "Pahala formation" for underlying flows. Stearns and Macdonald (1946) refined the stratigraphic nomenclature and proposed the terms "Kau volcanic series" (now Kau Basalt) for Mauna Loa flows overlying the Pahala Ash and "Kahuku volcanic series" (now Kahuku Volcanics) for underlying flows. Individual prehistoric lava flows were not differentiated in these previous studies, nor was the chronology of prehistoric eruptive activity examined. Modern detailed mapping of Mauna Loa is limited to the northeast and southwest rift zones of the volcano (Lipman and Swenson, 1984; Lockwood, 1984); Lipman (1980b) has made an analysis of eruptive activity for the southwest rift zone.

METHODS

To reconstruct the eruptive history of Mauna Loa, a reconnaissance geologic map of the entire volcano was compiled at 1:24,000 scale (47 7½-minute quadrangles) utilizing unpublished mapping, aerial photographic interpretation, aerial inspection, and spot field checking. For quantitative analysis of flow distribution, the map was later divided into 164 subregions on the basis of elevation, quadrangle, and eruptive subdivision (see following section entitled "Geography"). The surface areas (in square kilometers) of all geologic map units in each subregion were then determined by

tracing geologic contacts on a digitizing tablet, and the resulting areal information was entered into a computer database for sorting and analysis. A highly generalized version of the map at about 1:500,000 scale (fig. 18.2) shows the gross distribution of lava flows of different ages.

Computation of historical eruptive volumes (table 18.1) is based on estimates of original flow areas (before burial by later flows) and average flow thicknesses. Detailed planetable topographic maps made for Mauna Loa between 1912 and 1927 (U.S. Geological Survey Advance Sheets, 1:31,680 scale) proved invaluable in interpreting the distribution of pre-1930 lava flows, and aerial photographs taken in 1942, 1965, and 1977 were studied to determine original extent of flows later buried. Thicknesses of flows outside Mokuaweoweo were determined by estimates from aircraft and by scattered ground measurements. Volumes of lava erupted within Mokuaweoweo were evaluated from the decreasing caldera depths and changing caldera configurations determined since the earliest accurate measurements by Wilkes (1845, p. 157). This progressive infilling was then compared with eyewitness accounts of the duration and vigor of summit activity to apportion cumulative volumes among the various eruptions. Most accounts are vague, and for eruptions before 1933 the volumes of erupted lavas within the caldera were generally prorated to fit the observed decreases of caldera volume between surveys. Although estimates from individual flows within Mokuaweoweo may involve possible errors of more than 40 percent, cumulative totals are much more accurate owing to occasional constraints provided by various topographic surveys.

Systematic recovery of organic material from beneath prehistoric lava flows and subsequent radiocarbon dating has been one of our key methods. An improved understanding of the conditions under which charcoal is formed and preserved under lava flows (Lockwood and Lipman, 1980) has enabled us to collect charcoal for radiocarbon dating from beneath most flows that extend to vegetated areas. A total of 174 radiocarbon ages has been obtained for Mauna Loa lava flows (Rubin and others, chapter 10; Kelley and others, 1979), and these data have revolutionized our understanding of prehistoric Mauna Loa eruptive chronology.

LIMITATIONS

The data summarized in the following text and figures are only as good as the generalized, preliminary geologic mapping on which they are based. Furthermore, 10 percent of Mauna Loa remains unmapped, even in reconnaissance; most of this unmapped area is covered by dense rain forest, which is concentrated at middle elevations of the east, south, and west flanks of Mauna Loa (see figs. 18.2, 18.21). As future detailed mapping becomes available, revision of the data and interpretations presented in this report can be expected.

ACKNOWLEDGMENTS

History described without chronology would be an empty shell of conjecture, and this paper could not have been written were it not for the careful radiocarbon age determinations by Meyer Rubin and his colleagues at the USGS Radiocarbon Laboratory in Reston, Va. Our gratitude to Meyer is deep, for both lab work and field discussions.

Our quantitative summary of areal and volume relations is based on a reconnaissance geologic map of Mauna Loa that was compiled by Lisa Petersen. The Mauna Loa mapping program has been aided greatly by Duane Champion and J.M. Rhodes, whose numerous paleomagnetic determinations and chemical analyses have assisted in the correlation of prehistoric lava flows. Dan Fornari provided unpublished observations on historical submarine lava flows, and Doak Cox provided information on the previously unreported brief summit eruption of September 1, 1903. Joan Blandett provided copies of important planetable maps from the USGS Western Mapping Center historical Archives, and Bill Sanders and others at the USGS Menlo Park library went to extraordinary efforts to ferret out obscure Mauna Loa literature. Jim Hutton, Marti Lockwood, Marjorie Summers, and Rick Warschauer contributed to many aspects of this paper. The careful reviews of D.R. Mullineaux and F.W. Klein are much appreciated. All photographs in this paper were taken by the senior author.

GEOGRAPHY

Mauna Loa's summit is occupied by Mokuaweoweo, a 3-km by 5-km collapse caldera elongate northeast-southwest (see figs. 18.1, 18.27). Rift zones, which are the loci of numerous linear eruptive vents, trend from Mokuaweoweo to the east-northeast (northeast rift zone—NERZ) and to the southwest (southwest rift zone—SWRZ). The subaerial part of the SWRZ is 65 km long, but it extends about 35 km farther to the south below sea level. The SWRZ is marked by a conspicuous bend in its middle, probably a result of westward migration of the middle part of the rift zone (Lipman, 1980a). Only 50 km of the NERZ is exposed, and historical eruptive activity has been limited to the upper 19 km of the rift. This rift zone becomes progressively wider and more diffuse eastward to the point where it is buried by younger Kilauea lavas; it may be traced geophysically at least 50 km farther east beneath the Kilauea flows (Flannigan and Long, chapter 39). A north rift zone, proposed by Stearns and Macdonald (1946, p. 96, fig. 6) does not exist; instead, isolated eruptive vents, oriented radially to Mokuaweoweo, are spread rather homogeneously over the entire northwest flank (see fig. 18.17).

Mauna Loa's historical activity has long been divided into (1) *summit eruptions*, which are restricted to the immediate area of Mokuaweoweo, and (2) *flank eruptions*, which begin with summit activity but erupt most of their volume at lower altitude vents (Dutton, 1884, p. 140; Stearns and Macdonald, 1946, p. 82; Klein, 1982, p. 21–24). For this report we consider flows derived from vents below 3,660 m (12,000 ft) elevation to be products of flank eruptions, and those from vents above 3,660 m to be from summit activity. This classification of Mauna Loa flows (fig. 18.3) also allows consistent separation of summit and flank phases of typical historical eruptions (for example, 1942, 1950, 1984), which

begin with summit activity and terminate with flank extrusion. Flows referred to as northeast- or southwest-rift-zone flows are those on Mauna Loa's flanks erupted from vents below 3,660 m elevation.

HISTORICAL ERUPTIVE ACTIVITY

Polynesian settlers, who first reached Hawaii about 1,500 years ago, preserved no record of Mauna Loa's eruptive activity, and the earliest references are fragmentary accounts of activity in the late 18th and earliest 19th centuries (Hitchcock, 1909, p. 80; Colnett, 1940). The first extended account of a Mauna Loa eruption was by the Rev. Joseph Goodrich, who witnessed the June 1832 eruption from Lahaina, Maui, 190 km away. The 1832 flows have not been identified, although a possible candidate is the young flow underlying the U.S. National Oceanic and Atmospheric Administration (NOAA) Mauna Loa Observatory, on the north side of the upper NERZ (Lockwood, 1978). The paucity of eruption reports between the time of Hawaii's discovery by Europeans in 1778 and the year 1832 suggests the correctness of Hitchcock's statement: "It is very probable that Mokuaweoweo showed less activity after 1780 and before 1832 than in the decades since" (Hitchcock, 1909, p. 80).

The oldest Mauna Loa lava flows to be positively associated with a specific dated eruption are those of 1843 (fig. 18.4), which were derived from both the upper NERZ and a north-flank radial vent. The 1843 eruption was well documented by the Rev. Titus Coan, who during this eruption climbed to the upper active vent in a perilous winter journey and provided the first published description of active lava tubes (Coan, 1844). Coan sent many eruption descriptions to his friend James Dana, editor of the Silliman Journal (later the American Journal of Science) over the next 40 years, and these letters, published by Dana, form much of the basis for the excellent accounts of 19th century eruptive activity later summarized by Dana (1890), Hitchcock (1909), and Brigham (1909). Largely owing to Coan's observations, more is perhaps known about Mauna Loa's eruptions between 1843 and 1881 than is known about the following 40 years of activity! Jaggar (1947) described Mauna Loa's activity in the first four decades of this century, and Macdonald published descriptions of the eruptions of 1940, 1942, and 1950 (for references, see Macdonald and Abbott, 1970). The eruptions of 1975 and 1984 are described by Lockwood and others (chapter 19).

AREAL AND VOLUMETRIC RELATIONS AND SURFACE COVERAGE RATES

Fourteen percent of Mauna Loa's mapped surface (12.5 percent of the total area) is covered by lava flows of the 1843 and later eruptions (see figs. 18.5, 18.10). Since 1859, the rate of coverage has been about seven percent per century, although it was much higher (about 17 percent per century) in the period between 1843 and 1859 (fig. 18.5). A contemporary observation of the decrease in "copiousness of the subaerial discharges [of Mauna Loa] since 1859" was made by J.D. Dana (1888, p. 85). This historical eruptive activity has been concentrated along the two rift zones; coverage rates on the flanks of these two rift zones are similar and since 1843 have averaged about 13 percent per century for their combined totals (fig. 18.6). Our calculated areas and volumes of some individual flows (table 18.1) differ substantially from values reported by Macdonald and Abbot (1970, table 2), but our value for the cumulative volume of all historical lavas exposed outside Mokuaweoweo is similiar to theirs.

Large volumes of lava that have accumulated within Mokuaweoweo (including South Pit and North Bay) since 1843 were previously ignored or greatly underestimated (Stearns and Macdonald, 1946, p. 88). On the basis of an evaluation of changing caldera dimensions, we estimate that about 1 km^3 of lava has accumulated within the caldera since 1843.

Mauna Loa erupted approximately 4.2 km^3 of lava in the period 1843–1984 at an average extrusion rate of 30×10^6 m^3/yr, a rate substantially lower than recently inferred magmatic production rates at Kilauea (120×10^6 m^3/yr: Swanson, 1972a; Dzurisin and others, 1984). The Mauna Loa values, which have not been adjusted for density, are considered accurate to about ±20 percent.

Lava production rates are clearly different before and after 1877 (fig. 18.7). The rate was approximately 47×10^6 m^3/yr in the 34 years prior to 1877, but it dramatically lowered after that time to about 21×10^6 m^3/yr (averaged over 107 years). This abrupt rate change approximately coincided in time with a major shift in minor-element composition of Mauna Loa lava which occurred sometime between 1868 and 1877 (Rhodes and others, 1982). We propose that these changes in eruption rate and composition may be related to the great ($M = 7.5$) 1868 earthquake (Wood, 1914).

FREQUENCY AND DURATION OF ERUPTIONS

Virtually all historical eruptions have begun with activity within or near Mokuaweoweo, and so the greatest frequency of activity is at the summit (fig. 18.4; Klein, 1982). Half the historical summit eruptions have been followed within a few days by more voluminous flank eruptions, of which there have been 17: 8 on the NERZ, 7 on the SWRZ, and 2 on the north flank.

The duration of individual eruptions has varied from less than one day for several summit eruptions (table 18.1) to the 4½ years of almost continual activity during the summit eruption of 1872–77. Flank eruptions have varied in duration from 5 days (1868) to about 450 days (1855–56). Historical NERZ eruptions have mostly been of longer duration (mean 117 days) than those of the SWRZ (mean 16 days). The cumulative volume of historically erupted lava on the NERZ (1.3×10^6 m^3 is also greater than is that of the SWRZ (0.86×10^6 m^3, but the rift zone eruption with the greatest volume (1950) occurred on the SWRZ.

PREHISTORIC ERUPTIVE ACTIVITY

PROBLEMS

Our understanding of Mauna Loa's prehistoric activity is

based almost entirely on the rocks exposed on land, thus ignoring the near-equal area of the volcanic edifice beneath the sea. The eruptive record becomes less complete as one goes back in time, owing both to burial of older flows by younger lavas and to deeper weathering. Better exposures on the northwest flank bias the data toward that area relative to the largely unmapped southeast flank.

RADIOCARBON DATING

Of 174 radiocarbon ages obtained from carbonaceous matter beneath Mauna Loa flows, 143 are considered geologically reasonable for the overlying flows. The 31 rejected ages were regarded as invalid because of conflicting stratigraphic relationships. These incompatible ages are mostly caused by contamination of the sampled material by young charcoal derived from later forest fires or by old carbonaceous material in sooty soils, or by contamination of the original plant material by juvenile CO_2 devoid of ^{14}C (Rubin and others, chapter 9). The data from 143 samples give ages for 94 separate lava flows (fig. 18.8). Radiocarbon ages are most numerous for the NERZ; 44 of the 108 surface flows mapped in that area have been dated.

AGE UNITS

During our early mapping we assigned relative ages to surface lava flows on the basis of their degree of weathering (Lipman, 1980b, table 2). Flows were divided into five groups (from oldest to youngest: I to V). As radiocarbon ages became available, approximate limits were defined for each of these weathering categories.

Radiocarbon ages are presently available for almost 20 percent of the 463 surface lava flows recognized to date on Mauna Loa. The remaining undated flows were subdivided on the basis of the previously defined weathering categories and on their stratigraphic relationships with adjoining dated flows. In this paper, group V (undated flows of historical and latest prehistoric age) was combined with group IV. The age boundaries of the four groups were slightly changed from those given by Lipman (1980b) and are as follows:

Group	^{14}C age (ka)
IV	0.75–0.107 (the interval just before A.D. 1843)
III	1.5–0.75
II	4.0–1.5
I	>4.0

ERUPTIVE FREQUENCY

A total of 463 individual surface lava flows have been mapped to date on Mauna Loa. The age distribution of these flows (fig. 18.9) shows the low level of eruptive activity during group IV time relative to earlier and later periods.

The actual number of group IV flows is probably even lower than shown because (1) several small, unweathered flows of probable 19th century age high on Mauna Loa were counted with group IV flows because they could not be assigned to specific historical eruptions, (2) geographically extensive historical flows (such as those of 1950 and 1984) were only counted once but would likely have been counted as separate flows if they were of prehistoric age, and were preserved as widely separated remnants beneath younger flows, and (3) group IV flows erupted from more than one vent may have been counted more than once, in contrast to multiple-vent historic flows. As an example, 1926 lavas were only counted once, although they are exposed at isolated sites along more than 20 km of the SWRZ (Lipman and Swenson, 1984); they would likely have been counted as three separate flows if of prehistoric age.

Complete burial by younger lavas has not substantially lowered the total number of group IV flows, but does significantly lower the recognized number of older flows. Because of this, the increased number of group III flows (1.5–0.75 ka) documents a genuine increase in eruptive frequency during this period.

AREAL DISTRIBUTION

The distribution of surface flows of the various age categories in the principal geographic subdivisions (fig. 18.10) shows that flows of historical age are equal in areal extent to flows of group IV for Mauna Loa as a whole and nearly equal in each geographic subdivision. The historical flows were, however, formed in a 141-year period (1843–1984), whereas age IV flows accumulated in about 650 years before 1843. The increased extrusion rate for the historical period is also evident in figure 18.11, where the rates of surface coverage are shown as a function of time. An increased rate of historical flow coverage relative to the preceding 650 years is clear, demonstrating that such an increase, inferred by Lipman (1980b) for the SWRZ applies to the entire volcano. Additionally, small areas of probable 19th century flows of uncertain age (originally mapped as group V) were counted as group IV flows; their classification as historical flows would further accentuate the areal differences between these two groups.

More than one-fourth of Mauna Loa's surface is covered by group III lava flows, which accumulated in only about 750 years. These flows are concentrated on the northwest and southeast flanks of Mauna Loa (figs. 18.2, 18.10); most are tube-fed pahoehoe flows derived from steady overflows of a persistent lava lake at the summit.

Group I and II lava flows are substantially buried by younger lavas, so that their original coverage rates cannot be determined. Age I flows are exposed over only 10 percent of the mapped area; approximately 90 percent of Mauna Loa's surface has thus been buried in the past 4,000 years. An extrapolation of average coverage rates to earlier times, assuming steady eruption rates (fig. 18.11), suggests that flows older than 10 ka should be exposed on less than 2 percent of the volcano's surface.

As expected, average flow ages are younger at higher elevations and at lesser distances from source vents (figs. 18.12, 18.13). Most flows are relatively short and do not travel far from eruptive vents, and most eruptive vents are located high on the volcano. Because the short flows accumulate in a small area near the summit,

they eventually bury almost all of the older flows in that area. Longer flows that reach the larger flank areas are less frequent, the rate of burial at lower elevations is consequently less, and the older flows cover a larger surface area there. The classic shield shape of Mauna Loa is maintained by the overall balance between short and long flows. The more numerous short flows accumulate near the summit and tend to make the volcano's overall slope steeper, whereas the long flows are thicker at their distal ends and thus tend to flatten Mauna Loa's profile.

COMPARISON OF ACTIVITY ON THE NORTHEAST AND SOUTHWEST RIFT ZONES

The age distribution of flows derived from the NERZ and SWRZ is generally similiar (fig. 18.14), although the proportion of group II flows is higher on the SWRZ (Lipman, 1980b, p. 722). Group I flows are more extensive on the flanks of the NERZ, but this is probably due to geometric differences between the two rift zones: because of the proximity of the ocean to the SWRZ, older, long-traveled flows there are not exposed subaerially, whereas older, long flows tend to be preserved along the flanks of the NERZ (fig. 18.13). The proportion of older lavas on the NERZ would be even greater if the northeast continuation of the rift (Flannigan and Long, chapter 39, fig. 39.6) were not buried by young Kilauea lavas. The percentage of the surface downslope from each rift zone covered by historical and group IV flows is about the same.

Lipman (1980b, fig. 10) noted that there were substantial differences between the lava-flow age distribution on either flank of the SWRZ; lava coverage rates on the east flank of that rift zone are uniformly less than those on the west flank. There are no such systematic differences on opposite sides of the NERZ (fig. 18.15), although historical flows have preferentially been directed north of that rift zone, whereas group IV flows have preferentially flowed to the south. This pattern may be about to change again, however, as shown by the southward migration of historical vents (Lockwood and others, chapter 19).

DISTRIBUTION OF ERUPTIVE VENTS

Eruptive vents are found in four areas of Mauna Loa: Mokuaweoweo, the northeast and southwest rift zones, and the northwest flank. Vents are most numerous between 2,500 and 3,500 m (fig. 18.16), and the concentration of eruptive activity at these elevations has created topographic highs along both rift zones, near Puu Ulaula on the NERZ, and near Puu O Keokeo on the southwest rift zone (Lockwood and others, chapter 19, fig. 19.23; Lipman, 1980b, fig. 11, p. 714–715).

The northwest flank, buttressed by Mauna Kea and Hualalai, is cut by numerous linear eruptive fissures oriented radially to the Mauna Loa summit (fig. 18.17). Sixty-six of these radial vents have been recognized to date. Most of them are marked by linear curtain-of-fire spatter ramparts and one or more horseshoe-shaped spatter cones (fig. 18.18), although thirteen of them lack near-vent structures and are represented only by inconspicuous cracks from which voluminous, highly fluid flows quietly issued (fig. 18.19). Lava that fed these spatterless vents was apparently derived from degassed magma in shallow storage areas or from high-standing lava lakes at Mauna Loa's summit. Most of these spatterless radial vents are of group III age, a period characterized by summit lava-lake activity.

Two major radial vents have formed in historical time (1859, 1877), and two NERZ eruptions have developed radial vents after initial eruption within the rift zone (1843, 1935). Few prehistoric radial vents have yet been dated radiometrically, but the relations of their flows to adjoining lavas allows age classification (fig. 18.20). Radial vents of group IV age are most abundant; that was a time of diminished eruptive activity elsewhere on Mauna Loa and of an increased rate of formation of radial vents on the northwest flank. The rate has remained high into historical time.

DISTRIBUTION OF AA AND PAHOEHOE

The distribution of aa and pahoehoe on Mauna Loa reflects the volatile content of source eruptions, the length of individual flows, and the steepness of the terrain over which the lava flows traveled. Flow over steep slopes can cause pahoehoe to convert to aa, as well as travel for long distances. Aa and pahoehoe are merely different textures of otherwise identical lava and will form from the same material depending principally on temperature and flowage strain rates (Peterson and Tilling, 1980). Aa is produced from eruptions characterized by high fountaining of relatively volatile-rich lava, whereas extensive pahoehoe flows are derived from the stable upwelling of volatile-poor lava. Many Mauna Loa vents that are initially characterized by aa-producing high fountains later evolve to sustained pahoehoe production, resulting in the common occurrence of pahoehoe overlying aa of the same eruptive sequence. Because of differential weathering rates, the overlying pahoehoe commonly looks younger than the related aa and may easily be mistaken for an unrelated flow, especially in older terranes.

The proportions of aa and pahoehoe on Mauna Loa are about equal for the entire volcano, but they vary greatly for flows derived from the rift zones and the summit area (fig. 18.21). The greater abundance of aa flows on both rift zones reflects the dominance of fountain-fed lavas in those areas. Aa is nearly twice as abundant as pahoehoe on the SWRZ, whose slopes are steeper than those of the NERZ. Pahoehoe is much more characteristic of flows derived from Mauna Loa's summit area, where sustained lava lake activity occurred before the formation of the present Mokuaweoweo caldera.

Length of flow transport also affects the ratio of aa to pahoehoe: aa is more abundant at greater distances from eruptive sources (fig. 18.22). The proportions of aa and pahoehoe also vary with age (fig. 18.23): pahoehoe is more typical of older flows and aa more typical of group IV and historical lavas.

RELATIONS WITH ADJOINING VOLCANOES

The oldest lavas in contact with surface Mauna Loa flows are

the deeply eroded Ninole lavas on its south flank. Only 19 km^2 of the Ninole flows remain exposed; they are preserved as steep-walled, isolated ridges that rise above encroaching Mauna Loa lavas (fig. 18.24).

Radiometric dating of the Ninole flows (G.B. Dalrymple, written commun., 1978) suggests an age of about 200 ka. Stearns and Macdonald (1946, p. 66–68) considered them remnants of an older, pre-Mauna Loa volcano, but Lipman (1980a, p. 767) suggested they could be block-faulted remnants of earlier Mauna Loa lavas. Despite their age, the Ninole lavas have primary dips parallel to the younger Mauna Loa flows that surround them, indicating a source near the present upper SWRZ. We mapped them as a separate unit, since they are separated from adjacent Mauna Loa lavas by a major erosional unconformity, but we consider them most likely to be derived from the same magmatic system that fed younger Mauna Loa flows. The proposed Mohokea caldera in the area of the Ninole Hills (Hitchcock, 1906) appears to be only an erosional feature.

Late Mauna Kea cinder cones and flows overlie group I Mauna Loa lavas on the Humuula Saddle between the two volcanoes (fig. 18.25), although the contacts are mostly covered by younger Mauna Loa flows. Numerous kipukas (inliers) of Mauna Kea flows, not shown on earlier maps, are surrounded by Mauna Loa flows near the Mauna Kea–Mauna Loa contact (fig. 18.2). The total area of these kipukas is about 10 km^2.

Hualalai and Kilauea Volcanos differ greatly from Mauna Loa in their Holocene coverage rates, as is reflected by the distribution of kipukas of each volcano within the other. Four km^2 of Hualalai lava flows and cinder cones are preserved as kipukas surrounded by Mauna Loa lavas, but only 0.4 km^2 of Kilauea lavas are so surrounded. The eastern flank of Mauna Loa is covered by thin Kilauea flows, and 1.2 km^2 of Mauna Loa lavas are exposed as kipukas surrounded by Kilauea flows (fig. 18.26). The rate of coverage of Kilauea's surface (90 percent per 1,000 years; Holcomb, chapter 12, fig. 12.12) is much greater than Mauna Loa's rate, whereas Hualalai's average Holocene rate is less than Mauna Loa's (Moore and others, chapter 20, fig. 20.18). Because of Mauna Loa's larger size, however, the total area covered by Mauna Loa lava per unit time is greater than the area covered by Kilauea and Hualalai lavas combined.

GENERALIZED HISTORICAL NARRATIVE

OBSCURED EARLY HISTORY

We do not know when Mauna Loa began to form, or if the first lava was erupted on land or beneath the sea, but we can conjecture by extrapolation of Holocene activity rates that this happened more than 500,000 years ago. We do know that Kohala Volcano was then a large active structure, probably a separate island, to the north. Mauna Kea was also actively growing immediately to the north. Hualalai Volcano, to the west, has surface lavas as old as 200 ka (R.B. Moore, oral commun., 1985) and was probably also growing at the time of Mauna Loa's birth. Because Mauna Loa grew contemporaneously with Mauna Kea and Hualalai, flows of these three volcanoes interfingered. Kilauea began to grow on Mauna Loa's south flank, possibly beneath the sea, after Mauna Loa had already reached large size, perhaps before 100 ka. Lava flows and pyroclastic deposits from Kilauea also began to interlayer with flows from Mauna Loa along their contact.

RECORDED EARLY HISTORY

Flows older than 30 ka are exposed along fault scarps or river banks, or rarely as ash-mantled surface flows; these flows were derived from the same source directions as the flows that overlie them. Thus, the lower subaerial slopes of Mauna Loa existed in essentially the present shape by that time. It is probable that the present Mauna Loa geometry of a central feeder area and northeast and southwest rift zones also existed far back into Mauna Loa's unrecorded past.

The central feeder area, presently marked by Mokuaweoweo caldera (fig. 18.27), has long been the locus of multiple collapse structures. The buried rim of an earlier caldera lies to Mokuaweoweo's south and is marked by a low fault scarp (fig. 18.28), and other collapse structures at various scales have typified the Mauna Loa summit for a long period (see figs. 18.29, 18.34). Pit craters have formed and filled repeatedly at Mauna Loa's summit; cross sections of filled, dissected pit craters are well exposed in Mokuaweoweo's west wall (fig. 18.30). During the period of about 1.5–0.75 ka Mauna Loa's summit was marked by a sustained lava lake, which quietly supplied the tube-fed pahoehoe flows that now mantle the northwest and southeast flanks (figs. 18.10, 18.21).

Mauna Loa's two rift zones continued to erupt lava in nearly equal amounts as summit growth proceeded, although rates of eruptive activity have varied slightly between them, as indicated by a comparison of the areas covered downslope from each rift zone as a function of time (fig. 18.14). Because more than half the eruptive vents along the SWRZ are within 20 km of the coast, many flows from eruptions on this rift zone reached the sea, including flows from five of its seven historical eruptions. In contrast, the distance between most NERZ eruptive vents and the sea is more than 40 km, and flows from them rarely reached the ocean; none has in historical time. Flows from the NERZ did frequently enter streams on the wet windward side of the Island of Hawaii, however, and pillow lavas are well developed at the bases of several of these flows (Takahashi and Griggs, chapter 36, fig. 36.50). Prehistoric flows from the NERZ repeatedly dammed and diverted the Wailuku River (fig. 18.1).

The long flows that reached the sea enlarged Mauna Loa's surface area, in competition with subsidence and the forces of wave erosion. Where aa lava flows reached the sea, explosive contact between lava and sea water threw large amounts of lava and ash skyward, commonly forming littoral cones (fig. 18.31). Scores of these rootless cones are found along the shoreline west of the SWRZ, where the steep upland slopes have caused aa flows to predominate (fig. 18.21). Where fluid pahoehoe flows entered the

sea they commonly formed large deltalike additions to the land (fig. 18.32). Diving along the Mauna Loa coast has shown that many of these pahoehoe flows continued underwater through the formation of self-insulating conduits, as described by Moore and others (1973).

EVOLUTION OF MOKUAWEOWEO

Lava flows as young as 0.59 ± 0.07 ka are truncated by the edge of Mokuaweoweo (fig. 18.33). These fountain-fed pahoehoe flows were in part derived from arcuate fractures parallel to Mokuaweoweo's present rim and predate formation of the present caldera. Remnants of the dikes which fed these fountains are preserved along the caldera's northwest wall. Collapse of the caldera involved complex block subsidence (fig. 18.34) and was apparently accompanied by small phreatic explosions which showered blocks of hornfelsed basalt as far as 150 m beyond the present caldera rim (fig. 18.35).

Mokuaweoweo formed shortly after the beginning of group IV time, ending a period marked by the copious production of summit-fed pahoehoe flows. Group IV time was characterized by reduced output of surface lava flows from Mauna Loa's rift zones and increased activity on northwest flank radial vents. A great amount of group IV lava may have been erupted into a deep Mokuaweoweo (one-fourth of the historical lava has been erupted there), and would thus not be preserved as surface flows; this may account for some of the variations in recorded output over the past 600–700 years. Holcomb (chapter 12) suggests that a similar period of low surface coverage on Kilauea (1.5–1.0 ka) also coincided with a period of Kilauea caldera filling.

The original maximum depth of Mokuaweoweo cannot be known, although it was described as "about 400 yards" deep when first viewed by Archibald Menzies in 1794 (Wilson, 1920, p. 128). The first accurate survey of Mokuaweoweo was made in 1841 (Wilkes, 1845), when the maximum depth of the inner pit was 240 m below the summit. Major collapse of the inner pit occurred later; when next surveyed by Lydgate in 1874 (Brigham, 1909; Jaggar, 1931), it had a maximum depth of 320 m and was being rapidly filled by near-continuous lava-lake activity. By 1885, however, the inner pit had filled to 244 m below the summit (Alexander, 1888). The inner pit first overflowed in 1914, and the maximum depth of the caldera floor was 210 m below the summit by 1922 (Stearns and Clark, 1930, plate 2). In 1985 the caldera floor lay 183 m below the summit.

SUMMARY AND CONCLUSIONS

We have evaluated semiquantitatively the rates of Mauna Loa's volcanic activity over the past 10,000 years and have documented the range of behavior responsible for the formation of its surficial lavas. One can assume that similar behavior will typify the future. Mauna Loa has generated 22 flows outside Mokuaweoweo over the past 150 years, but at substantially lower production rates after 1876. There was less activity on the flanks of the volcano in the several centuries before 1843, and much of that lava output was apparently confined to Mokuaweoweo. In the preceding period, 1.5–0.75 ka, summit overflows blanketed much of the upper flanks with pahoehoe. About 40 percent of the Mauna Loa surface has been covered in the past 1,000 years (fig. 18.11), though coverage rates have varied during this period. This contrasts with coverage rates of 90 percent per 1,000 years for Kilauea (Holcomb, chapter 12) and 20 percent per 1,000 years for Hualalai (Moore and others, chapter 20). The record before 1.5 ka is fragmentary and will require much more work to refine.

The Mauna Loa coverage rate for the historical period has averaged 9 percent per 100 years. We do not know how much longer this relatively high rate of activity will persist, but we note no indication of abatement. Mauna Loa eruptions will of course continue to be a source of concern on the Island of Hawaii, but residents can take comfort in the knowledge that lava flows infrequently reach heavily populated coastal areas. Continuing investigations will provide more detailed knowledge of the varying frequency with which lava flows have covered various parts of the Mauna Loa surface. Such studies of the past provide the best guide to future volcanic behavior, behavior that will continue to impact human activities on the slopes of this great volcano.

REFERENCES

Alexander, J.M., 1888, On the summit crater in October, 1885, and its survey: American Journal of Science (3d ser.), v. 36, p. 5–39.

Brigham, W.T., 1909, The volcanoes of Kilauea and Mauna Loa on the Island of Hawaii: Bishop Museum Memoirs, v. 2, no. 4, 222 p.

Coan, T.M., 1844, Journey to Mauna Loa: The Missionary Herald (Boston), v. 40, no. 2, p. 44–47.

Colnett, James, 1940, The Journal of Captain James Colnett aboard the Argonaut from April 26, 1789 to Nov. 3, 1791: The Champlain Society (Toronto) Pub. 26, 328 p. [Reprinted 1968 by the Greenwood Press, New York].

Dana, J.D., 1888, History of changes in the Mt. Loa craters, pt. 2, on Mokuaweoweo: American Journal of Science (3d ser.), v. 36, no. 212, p. 81–112.

——— 1890, Characteristics of volcanoes, with contributions of facts and principles from the Hawaiian Islands: New York, Dodd, Mead, & Co., 339 p.

Dutton, C.E., 1884, Hawaiian volcanoes: U.S. Geological Survey 4th Annual Report, p. 79–219.

Dzurisin, Daniel, Koyanagi, R.Y., and English, T.T., 1984, Magma supply and storage at Kilauea Volcano, Hawaii, 1956–1983: Journal of Volcanology and Geothermal Research, v. 21, p. 177–206.

Fornari, D.J., Peterson, D.W., Lockwood, J.P., Malahoff, Alexander, and Heezen, B.C., 1979, Submarine extension of the southwest rift zone of Mauna Loa Volcano, Hawaii—visual observations from the U.S. Navy Deep Submergence Vehicle DSV *Sea Cliff*: Geological Society of America Bulletin, v. 90, p. 435–443.

Hitchcock, C.H., 1906, Mohokea caldera: Geological Society of America Bulletin, v. 17, p. 485–496.

——— 1909, Hawaii and its volcanoes: Honolulu, The Hawaiian Gazette Co., 314 p.

Jaggar, T.A., 1931, The crater of Mauna Loa: Hawaiian Volcano Observatory Volcano Letter 360, p. 1–4.

——— 1947, Origin and development of craters: Geological Society of America Memoir 21, 508 p.

Kelley, M.L., Spiker, E.C., Lipman, P.W., Lockwood, J.P., Holcomb, R.T.,

and Rubin, Meyer, 1979, U.S. Geological Survey, Reston, Virginia, radiocarbon dates XV—Mauna Loa and Kilauea Volcanoes, Hawaii: Radiocarbon, v. 21, no. 2, p. 306–320.

Klein, F.W., 1982, Patterns of historical eruptions at Hawaiian volcanoes: Journal of Volcanology and Geothermal Research, v. 12, no. 1, p 1–35.

Lipman, P.W., 1980a, The southwest rift zone of Mauna Loa—implications for structural evolution of Hawaiian volcanoes: American Journal of Science, v. 280-A, p. 752–776.

——— 1980b, Rates of volcanic activity along the southwest rift zone of Mauna Loa Volcano, Hawaii: Bulletin Volcanologique, v. 43, n. 4, p. 703–725.

Lipman, P.W., and Swenson, Alan, 1984, Generalized geologic map of the southwest rift zone of Mauna Loa Volcano, Hawaii: U.S. Geological Survey Miscellaneous Investigations Map I–1323, scale 1:100,000.

Lockwood, J.P., 1978, The volcanic environment of Mauna Loa Observatory, Hawaii—history and prospects, *in* Miller, John, ed., Mauna Loa Observatory—a 20th Anniversary Report: National Oceanic and Atmospheric Administration (NOAA) Special Report, p. 28–34.

——— 1984, Geologic map of the Kulani quadrangle, Hawaii (preliminary): U.S. Geological Survey Open-File Report 84–12, scale 1:24,000.

Lockwood, J.P.,and Lipman, P.W., 1980, Recovery of datable charcoal beneath young lavas—lessons from Hawaii: Bulletin Volcanologique, v. 43, no. 3, p. 609–615.

Macdonald, G.A., 1972, Volcanoes: Englewood Cliffs, N.J., Prentice-Hall, 510 p.

Macdonald, G.A., and Abbott, A.T., 1970, Volcanoes in the sea—the geology of Hawaii: Honolulu, University of Hawaii Press, 441 p.

Moore, J.G., Fornari, D.J., and Clague, D.A., 1985, Basalts from the 1877 submarine eruption of Mauna Loa, Hawaii: new data on the variation of palagonitization rate with temperature: U.S. Geological Survey Bulletin 1663, 11 p.

Moore, J.G., Phillips, R.L., Griggs, R.W., Peterson, D.W., and Swanson, D.A., 1973, Flow of lava into the sea, 1969—1971, Kilauea Volcano, Hawaii: Geological Society of America Bulletin, v. 84, p. 537–546.

Peterson, D.W., and Tilling, R.I., 1980, Transition of basaltic lava from pahoehoe to a'a, Kilauea Volcano, Hawaii—field observations and key factors: Journal of Volcanology and Geothermal Research, v. 7, p. 271–293.

Rhodes, J.M., Lockwood, J.P., and Lipman, P.W., 1982, Episodic variations in magma chemistry, Mauna Loa Volcano, Hawaii [abs.]: IAVCEI-IAGC Science Assembly, Generation of major basaltic types Reykjavik, Aug. 15–22, 1982, Abstracts Volume, p. 43.

Stearns, H.T., and Clark, W.O., 1930, Geology and water resources of the Kau District, Hawaii: U.S. Geological Survey Water-Supply Paper 616, 194 p.

Stearns, H.T., and Macdonald, G.A., 1946, Geology and ground-water resources of the Island of Hawaii: Hawaii Division of Hydrography Bulletin 9, 363 p.

Swanson, D.A., 1972a, Magma supply rate of Kilauea Volcano, 1952–1971: Science, v. 175, p. 169–170.

——— 1972b, Pahoehoe flows from the 1969–1971 Mauna Ulu eruption, Kilauea Volcano, Hawaii: Geological Society of America Bulletin, v. 84, p. 615–626.

Wilkes, Charles, 1845, Narrative of the United States Exploring Expedition during the years 1838–1842: Philadelphia, Lea and Blanchard, v. 4, 539 p.

Wilson, W.F., 1920, Hawaii nei 128 years ago—the journal of Archibald Menzies: Honolulu, private publication, 199 p.

Wood, H.O., 1914, On the earthquakes of 1868 in Hawaii: Seismological Society of America Bulletin, v. 4, no. 4, p. 169–203.

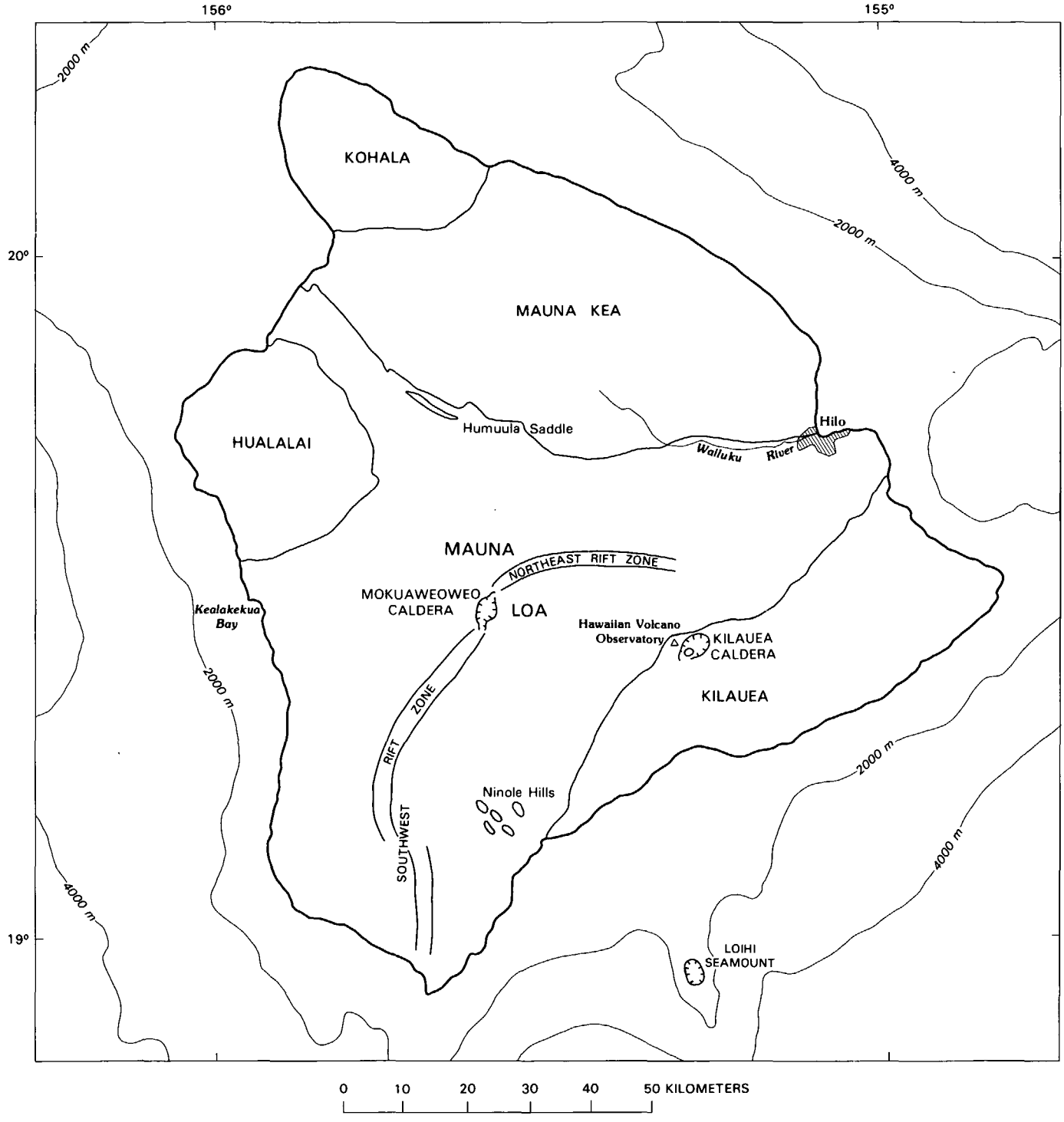

FIGURE 18.1.—Island of Hawaii, showing five volcanoes, some major structural and geographic features, and bathymetry of adjacent sea. Bathymetric contour interval 2,000 m.

TABLE 18.1.—*Ages, durations, areas, and volumes of historical Mauna Loa eruptions 1843–1984*

[Eruptive subdivisions: S, summit; NE, northeast rift zone; SW, southwest rift zone; NF, north flank. Estimated errors: 1, ±20 percent; 2, ±20–40 percent; 3, greater than ±40 percent; n.d., no data]

Date of start		Duration (days)		Eruptive subdivision(s)	Area (km^2)					Volume ($m^3 \times 10^6$)				Estimated error
(yr)	(mo-d)	Summit	Flank		Exposed outside Mokuaweoweo	Buried outside Mokuaweoweo	Original outside Mokuaweoweo	Original inside Mokuaweoweo	Total	Subaerial outside Mokuaweoweo	Estimated inside Mokuaweoweo	Estimated beneath sea level	Total	
1984	3-26	<1	22	S, NE	42	0	42	6	48	208	12	0	220	1
1975	7-05	1	0	S	3	4	7	6	13	18	12	0	30	1
1950	6-01	1	23	S, SW	112	0	112	0	112	306	0	70	376	2
1949	1-06	145	0	S	15	2	17	4	22	86	30	0	116	1
1942	4-26	2	13	S, NE	28	5	33	1	34	169	7	0	176	1
1940	4-17	134	0	S	1	5	6	7	13	14	96	0	110	1
1935	11-21	6	40	S, NE, NF	30	1	31	2	33	81	6	0	87	2
1933	12-02	17	0	S	0	1	1	5	6	2	98	0	100	2
1926	4-10	<1	14	S, SW	25	10	35	0	35	116	0	5	121	2
1919	9-26	<1	38	S, SW	21	7	28	0	28	83	0	100	183	2
1916	5-19	0	12	SW	14	3	17	0	17	31	0	0	31	2
1914	11-25	48	0	S	0	0	0	5	5	0	55	0	55	2
1907	1-09	<1	15	S, SW	25	0	25	3	28	116	5	0	121	2
1903	10-06	61	0	S	0	0	0	5	5	0	70	0	70	3
1903	9-01	<1	0	S	0	0	0	1	1	0	3	0	3	n.d.
1899	7-01	4	21	S, NE	21	0	21	2	23	73	8	0	81	2
1896	4-21	16	0	S	0	0	0	5	5	0	25	0	25	3
1892	11-30	3	0	S	0	0	0	3	3	0	12	0	12	3
1887	1-16	<1	7	S, SW	28	0	28	1	29	115	3	10	128	2
1880	11-05	0	280	NE	50	1	51	0	51	130	0	0	130	2
1880	5-01	6	0	S	0	0	0	5	5	0	10	0	10	n.d.
1879	3-09	<1	0	S	0	0	0	1	1	0	1	0	1	n.d.
1877	2-14	<1	<1	S,NF	1	0	1	0	1	1	0	7	8	3
1872	8-09	~1,200 (near -continuous)	0	S	0	0	0	5	5	0	630	0	630	2
1871	8-10	~20	0	S	0	0	0	3	3	0	20	0	20	n.d.
1868	3-27	<1	5	S, SW	23	0	23	1	24	73	0	50	123	2
1865	12-30	~125	0	S	0	0	0	5	5	0	50	0	50	n.d.
1859	1-23	<1	~300	S, NF	90	0	90	1	91	287	1	95	383	3
1855	8-11	<1	~450	S, NE	62	4	66	0	66	280	0	0	280	3
1852	2-17	1	20	S, NE	18	15	33	0	33	182	0	0	182	2
1851	8-08	4	0	S	5	7	12	0	12	35	0	0	35	2
1849	5(?)	~15	0	S	0	0	0	5	5	0	25	0	25	n.d.
1843	1-10	5	~90	S, NE, NF	37	8	45	0	45	202	0	0	202	3
Total					651	73	724	82	806	2,608	1,179	337	4,124	

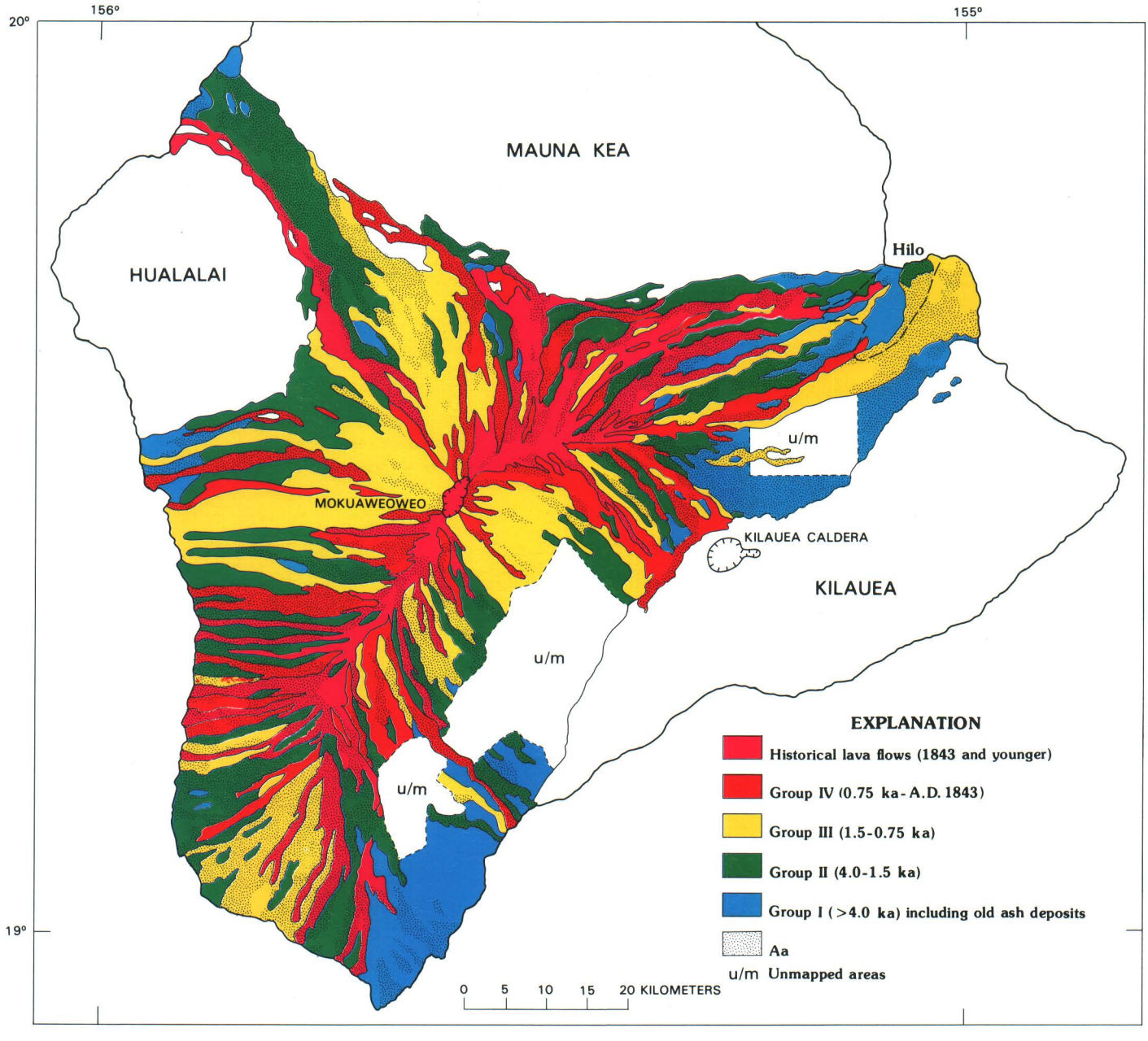

FIGURE 18.2.—Age-distribution map of Mauna Loa lava flows, greatly generalized from 1:24,000 mapping, including unpublished work in Hilo area by J.M. Buchanan-Banks.

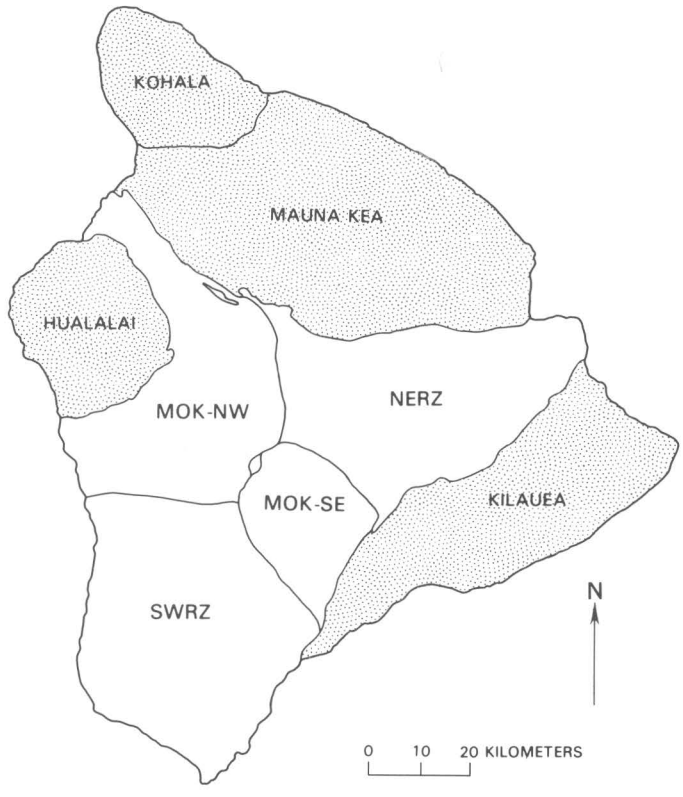

FIGURE 18.3.—Geographic subdivisions of Mauna Loa lava flows used in this paper. MOK-NW, northwest flank summit flows; MOK-SE, southeast flank summit flows; NERZ, northeast rift zone flows; SWRZ, southwest rift zone flows. Shaded areas show Island of Hawaii's other four volcanoes.

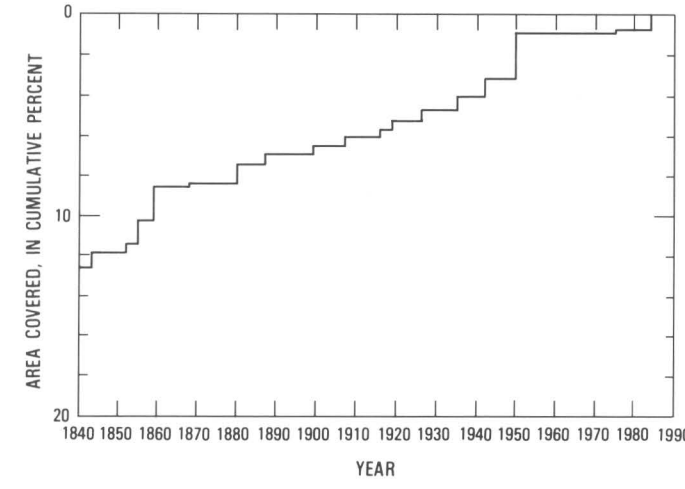

FIGURE 18.5.—Cumulative percentages of Mauna Loa's mapped surface covered by flows of historical age. Percentage given for a particular year is that covered by flows of that age or younger.

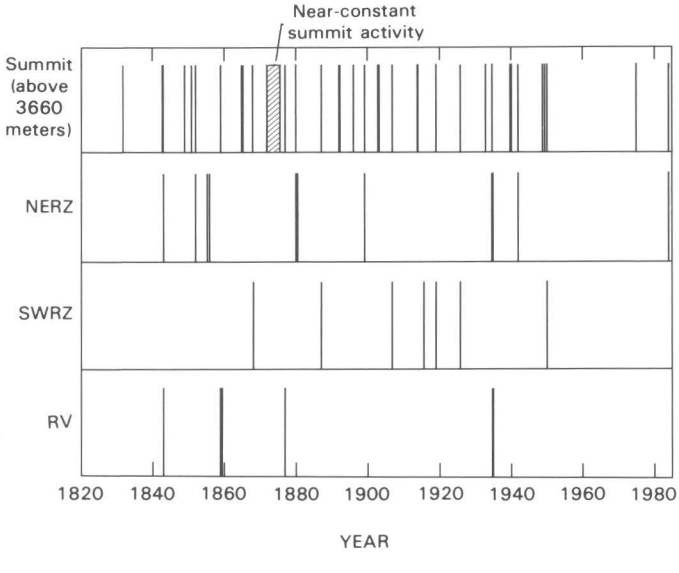

FIGURE 18.4.—Chronology of historical Mauna Loa eruptions. NERZ, northeast rift zone; SWRZ, southwest rift zone; RV, northwest flank radial vent eruptions.

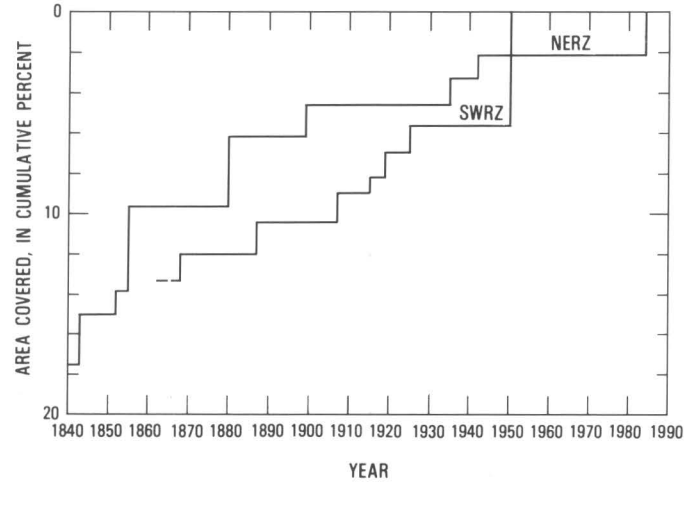

FIGURE 18.6.—Cumulative percentages of Mauna Loa's northeast and southwest rift zone flanks covered by flows of historical age. Percentage given for a particular year is that covered by flows of that age or younger.

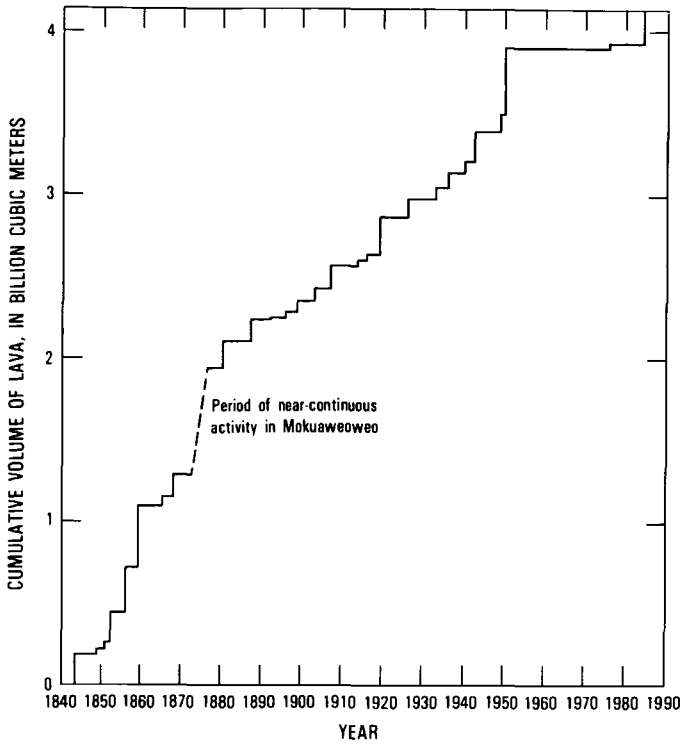

FIGURE 18.7.—Mauna Loa lava production, 1843 to 1984.

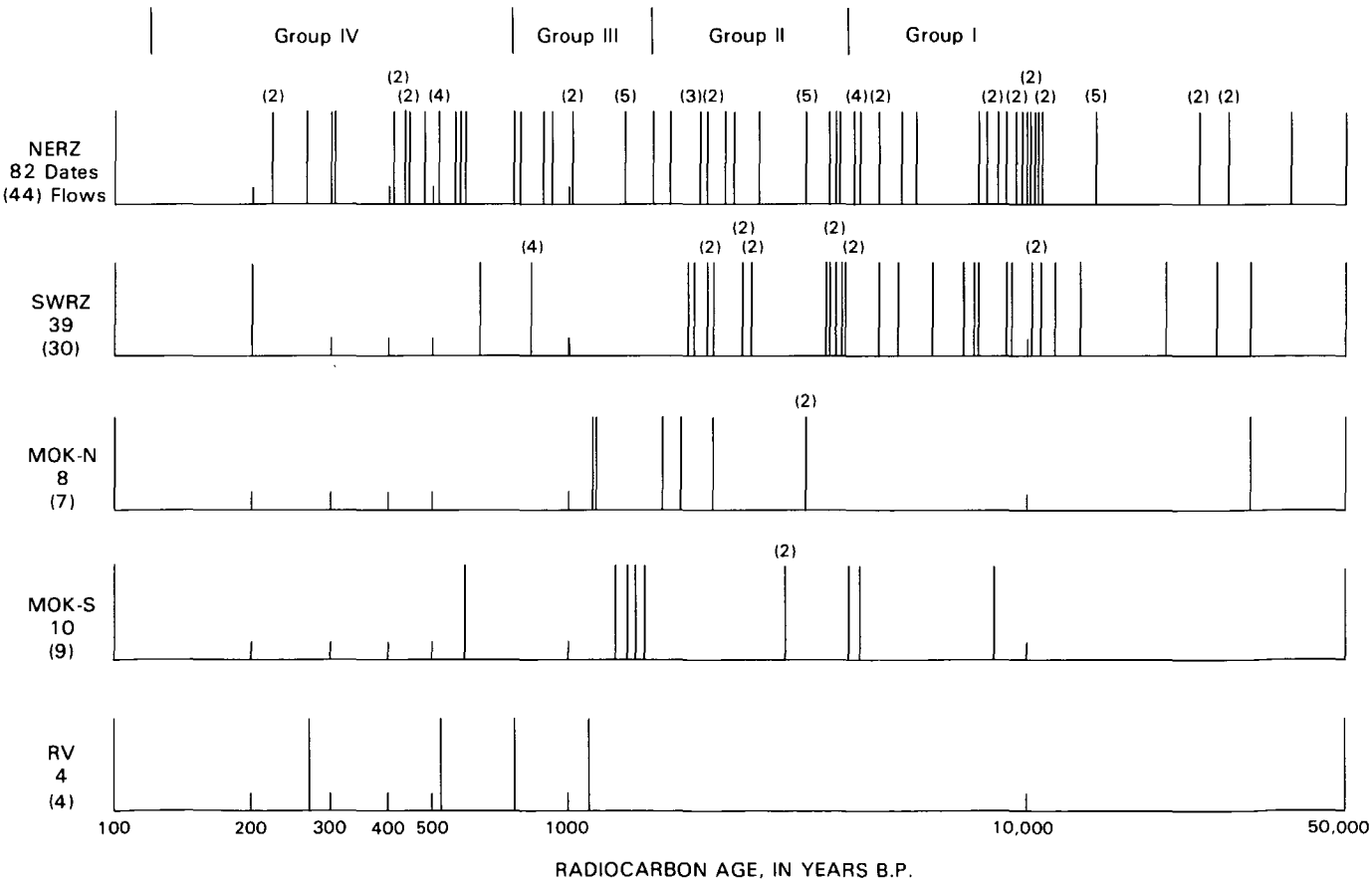

FIGURE 18.8.—Age distribution of radiocarbon-dated Mauna Loa lava flows, plotted on a logarithmic scale of time. Where multiple ages are available for individual flows, the number of these ages is plotted above bar at the mean value. All ages by Meyer Rubin. Flow sources: NERZ, northeast rift zone; SWRZ, southwest rift zone; MOK-NW, Mokuaweoweo overflows to the northwest; MOK-SE, Mokuaweoweo overflows to the southeast; RV, radial vents on northwest flank.

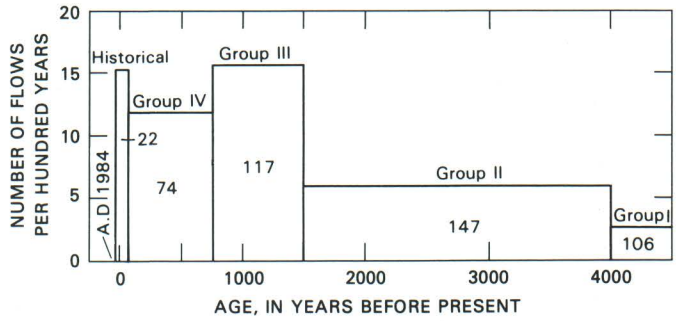

FIGURE 18.9.—Average number of flows per century for various age categories. Numbers within boxes give total numbers of flows in each age group.

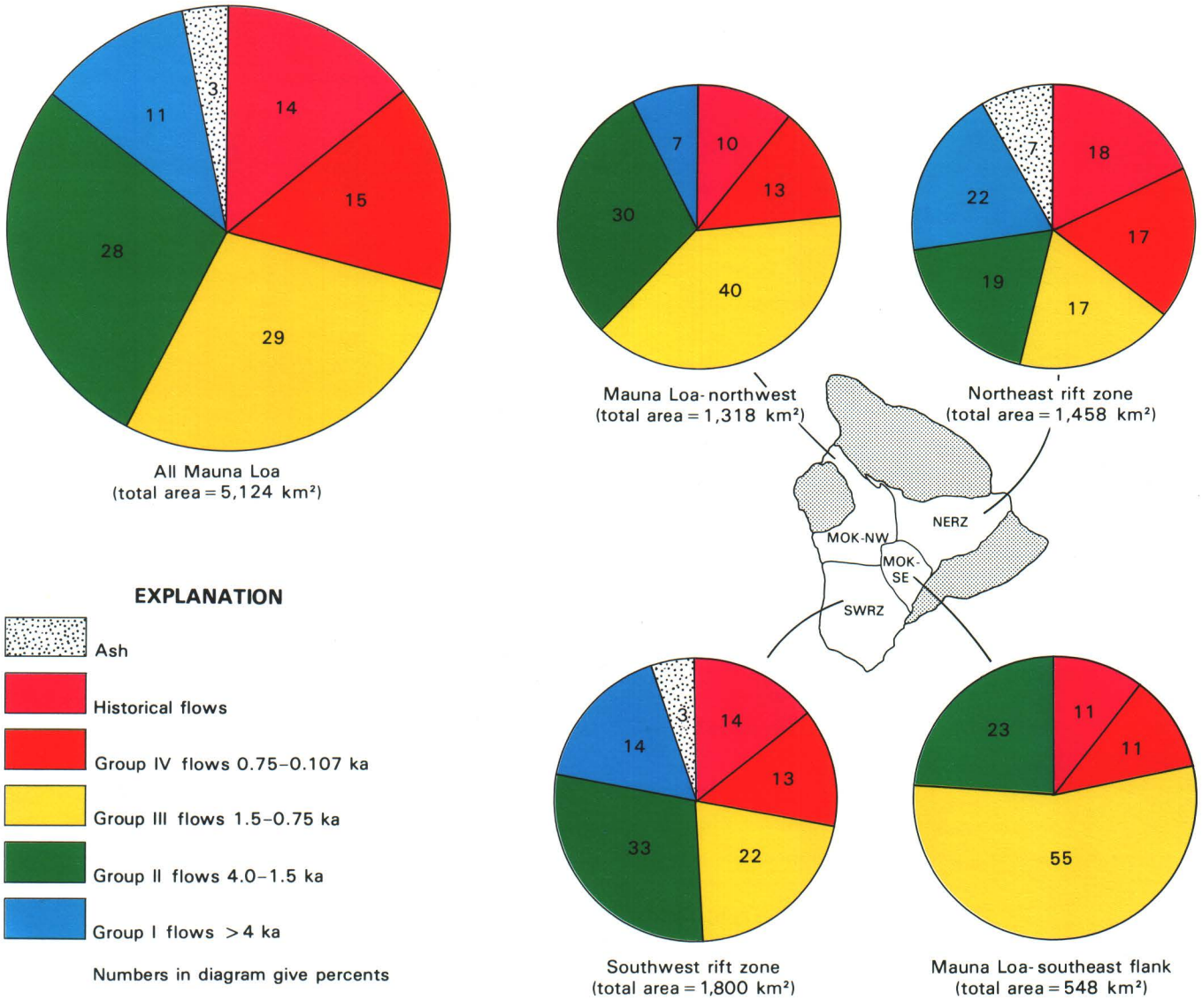

FIGURE 18.10.—Age and geographic distribution of Mauna Loa lava flows, recalculated to exclude unmapped areas. Percentages of excluded unmapped areas shown in figure 18.21.

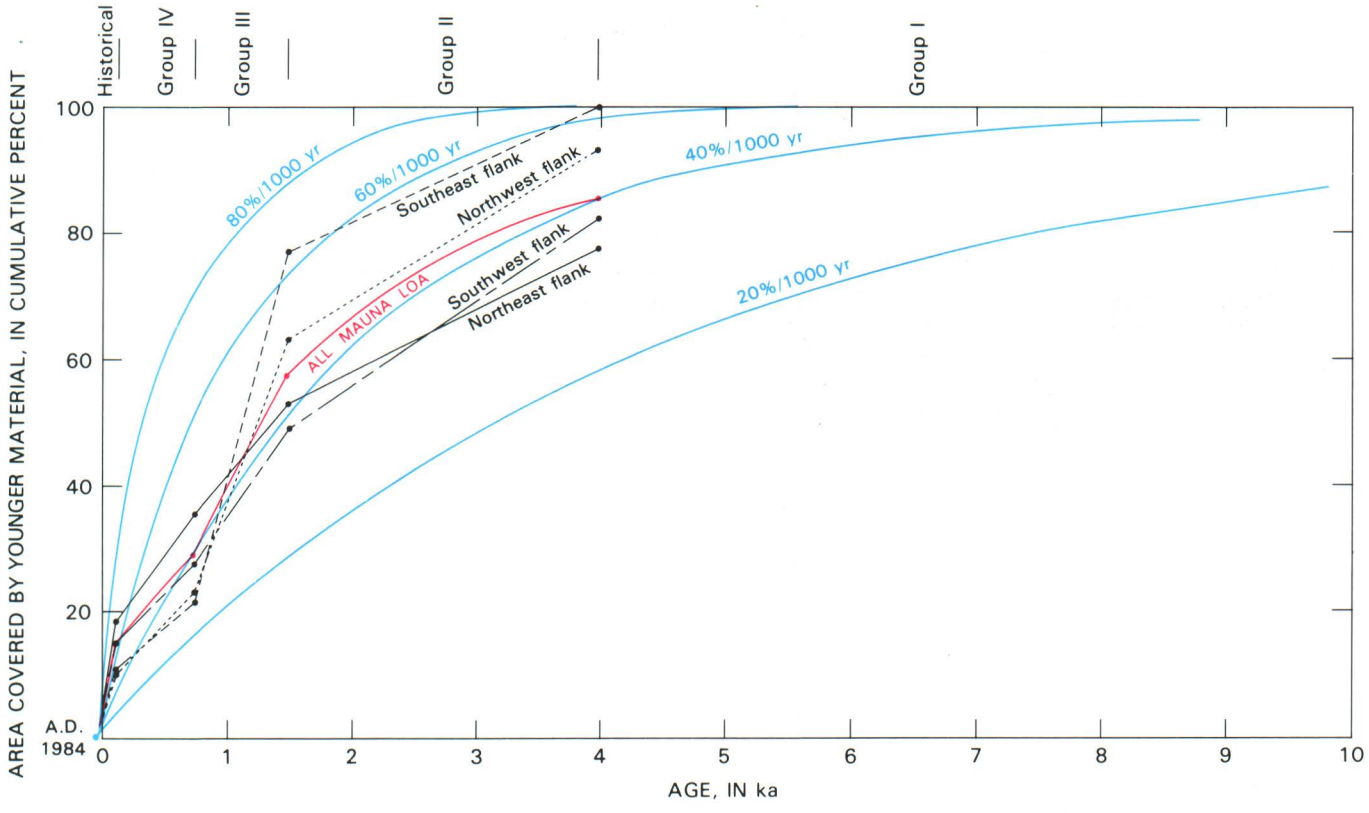

FIGURE 18.11.—Coverage of Mauna Loa's mapped surface as a function of time. Curves for areal subdivisions defined in figure 18.3 and for all areas combined (red curve) show actual age distribution of present surface. Ash deposits are included with group I lavas. Southeast flank plot is dashed because of the large areas unmapped in that region. Numbered curves (blue) are from Lipman (1980b, fig. 9A) and show expected cumulative areal coverage for indicated uniform coverage rate in percent per per 1,000 years.

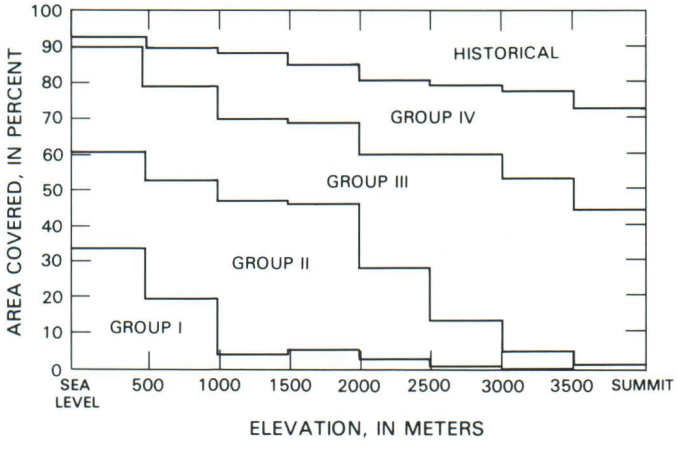

FIGURE 18.12.—Age distribution of Mauna Loa surface flows as a function of elevation.

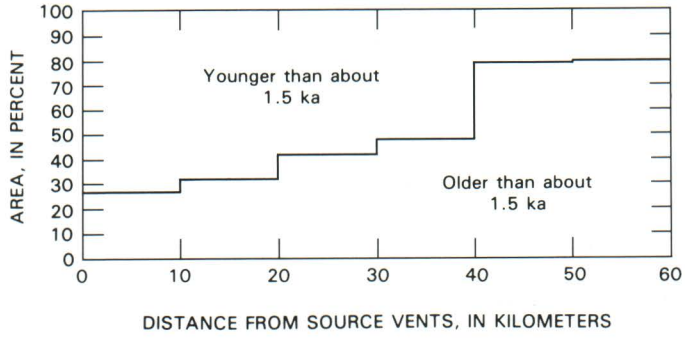

FIGURE 18.13.—Age distribution of Mauna Loa surface flows as a function of transport distance from eruptive sources.

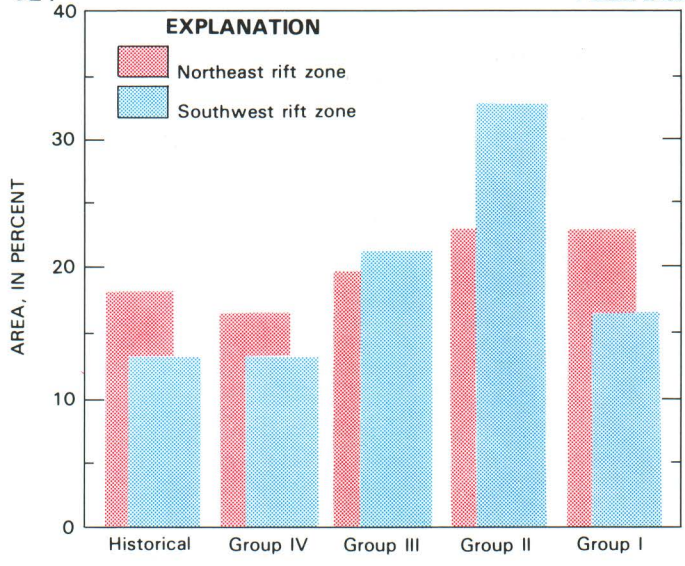

FIGURE 18.14.—Comparison of ages of flows from northeast and southwest rift zones, showing percentages of each flank covered by flows of different ages.

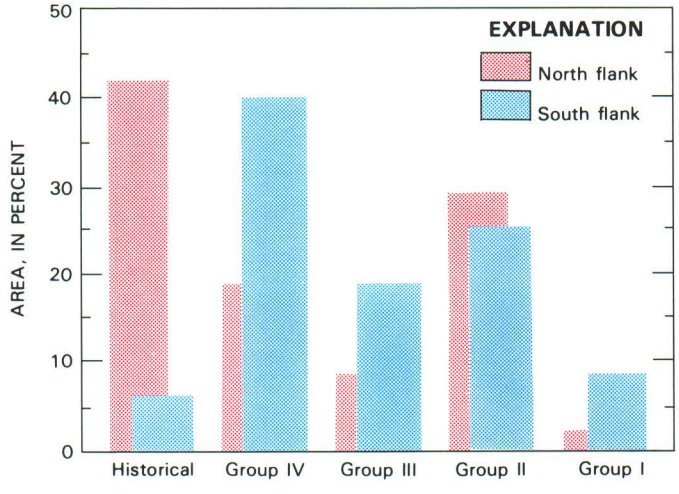

FIGURE 18.15.—Age distribution of lava flows on north and south flanks of northeast rift zone, above 1,500 m elevation, showing areal percentages of each flank covered by flows of different ages.

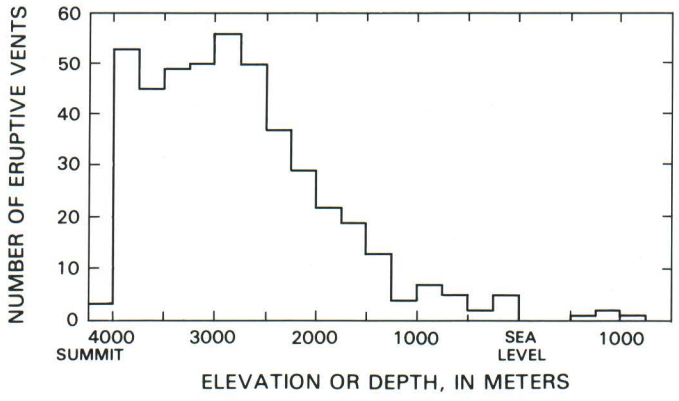

FIGURE 18.16.—Elevation distribution of Mauna Loa eruptive vents, showing total number of eruptive vents recognized within each 250-m-elevation interval of Mauna Loa. Vents on NERZ, SWRZ, and northwest flank are summed together for each elevation interval. Long vents that extend across elevation boundaries are counted in each interval.

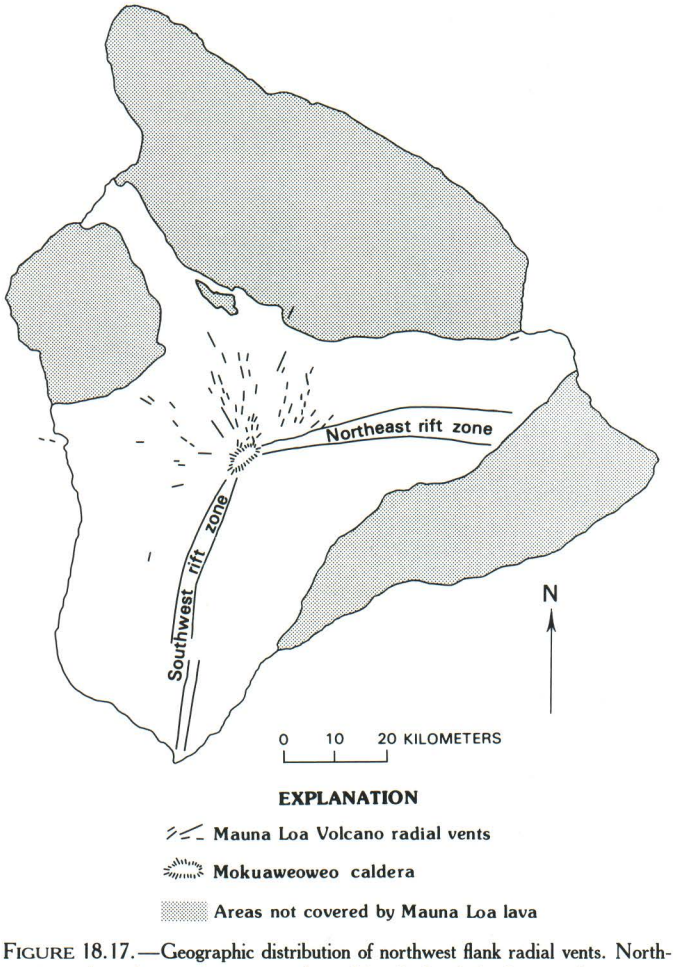

FIGURE 18.17.—Geographic distribution of northwest flank radial vents. Northeast and southwest rift zones are loci of hundreds of closely spaced vents, not shown here.

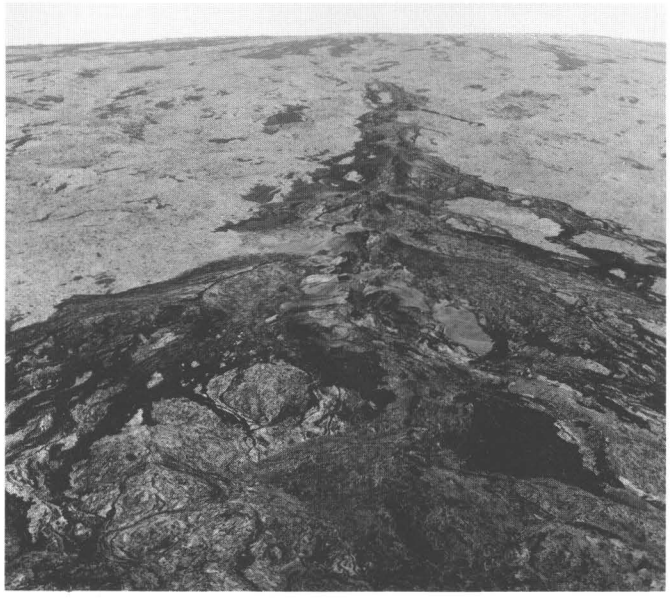

FIGURE 18.18.—Aerial view of spatter cones along a typical radial vent (1859). View to south. Strongly foreshortened view, about 500 m wide at bottom.

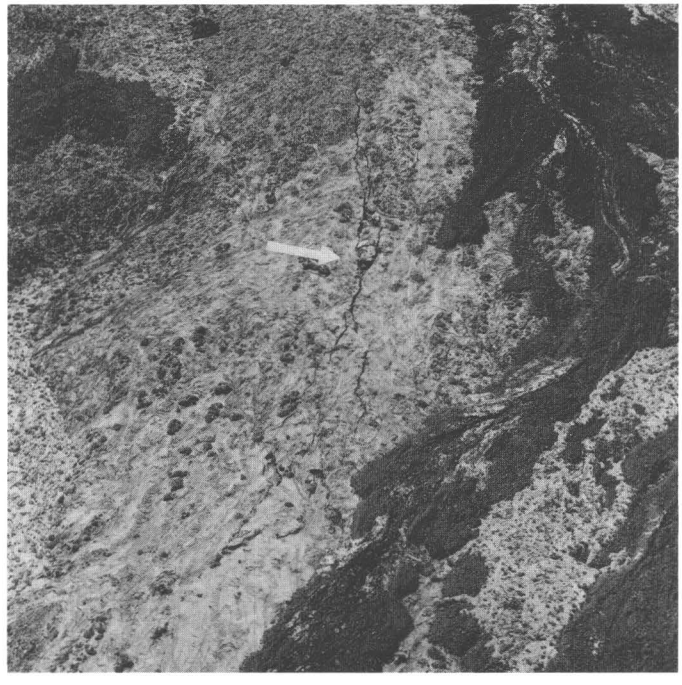

FIGURE 18.19.—Aerial view of radial vent (arrow) along which no spatter ramparts or cones developed. Top to bottom about 400 m.

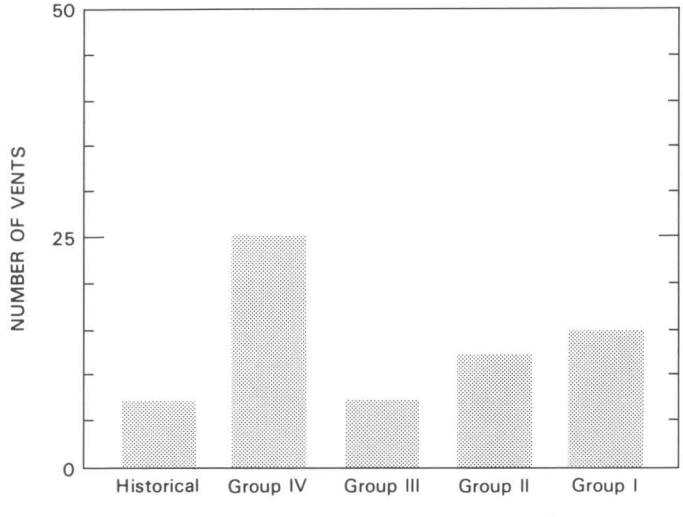

FIGURE 18.20.—Age distribution of northwest flank radial vents.

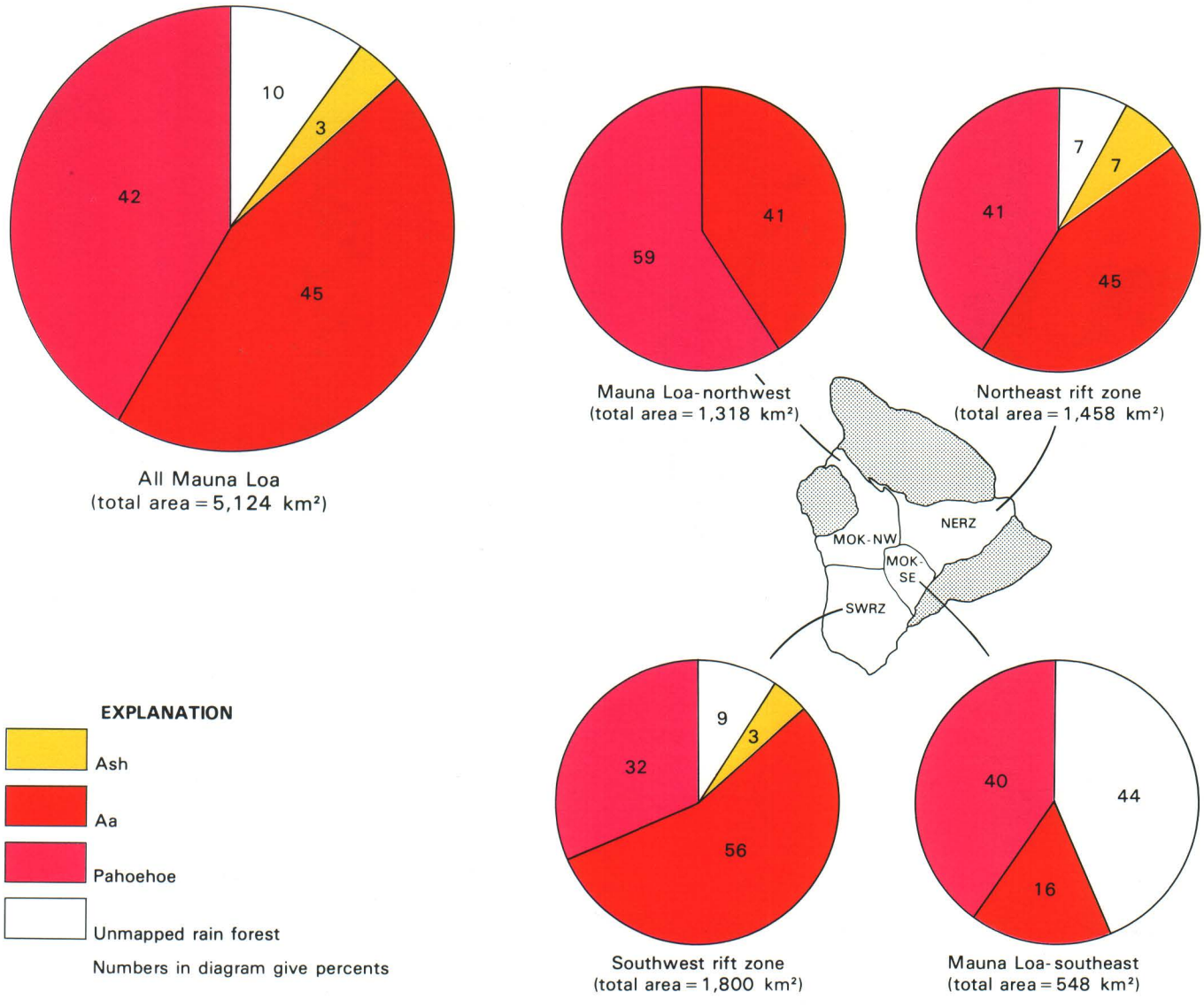

FIGURE 18.21.—Distribution of aa, pahoehoe, and unmapped areas on Mauna Loa.

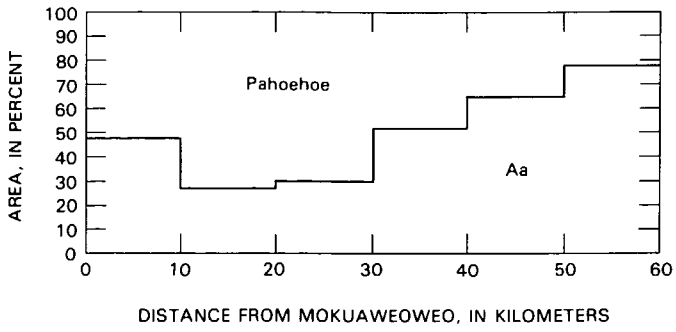

FIGURE 18.22.—Distribution of aa and pahoehoe on Mauna Loa's northwest flank as a function of transport distance from Mokuaweoweo; 1859 flows excluded.

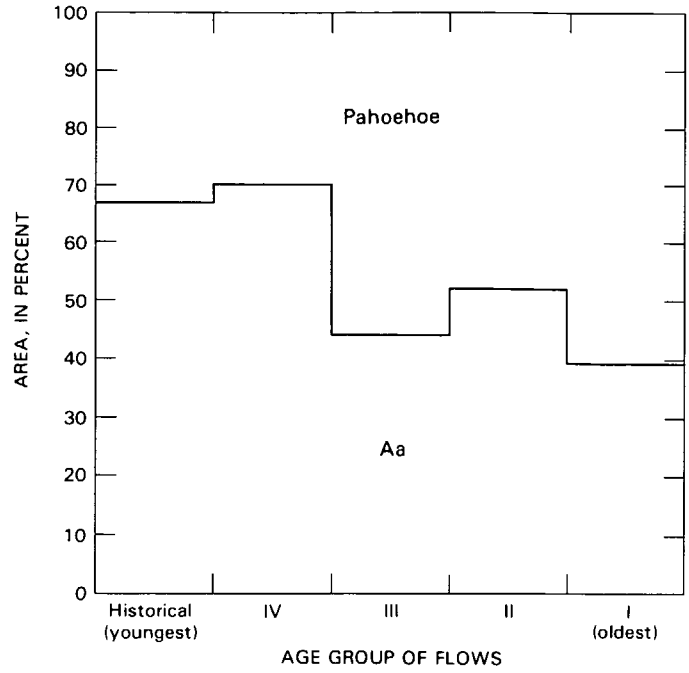

FIGURE 18.23.—Distribution of aa and pahoehoe on Mauna Loa's surface as a function of age.

FIGURE 18.24.—Aerial view of Ninole Hills from southwest, showing remnants of older Ninole flows rising above encroaching Mauna Loa lava flows north of town of Pahala.

FIGURE 18.25.—Aerial view of Mauna Loa's north flank, in Humuulu Saddle. View to south. Mauna Kea vents cut this flank of Mauna Loa and formed prominent cinder cones 20,000 to 8,000 years ago. These cones and their flows are preserved as kipukas (inliers) surrounded by younger Mauna Loa lavas.

FIGURE 18.26.—Aerial view of Mauna Loa's east flank near town of Keaau, showing kipukas (inliers) of Mauna Loa lava surrounded by young flows from Kilauea Volcano. View to southwest. Ash-covered, older kipukas support sugarcane fields.

FIGURE 18.27.—Aerial view of Mokuaweoweo caldera at summit of Mauna Loa, looking northeast. South Pit in foreground, Mauna Kea in background. Most of caldera floor is covered by pahoehoe erupted in March 1984.

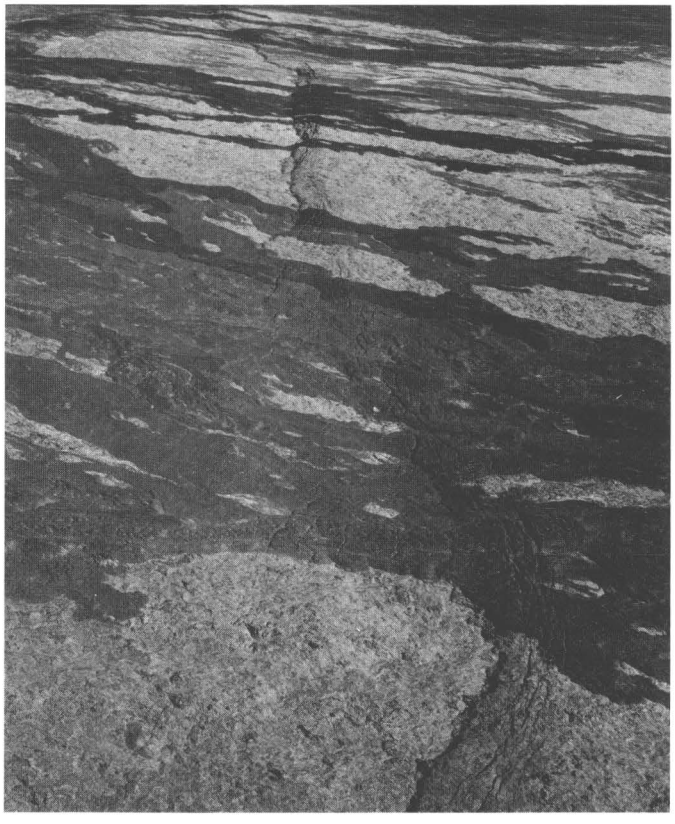

FIGURE 18.28.—Aerial view of Mauna Loa's summit area from south, showing fault developed along inferred eastern boundary of old caldera. Fault cuts group III pahoehoe (light) and group IV aa (dark).

FIGURE 18.29.—Aerial view of Lua Poholo from north. This pit crater, in northeast corner of Mokuaweoweo, has a volume of about 7×10^6 m^3 and formed about 1880, probably during flank eruption of that year. Precollapse ground surface is preserved on rotated block at bottom of crater.

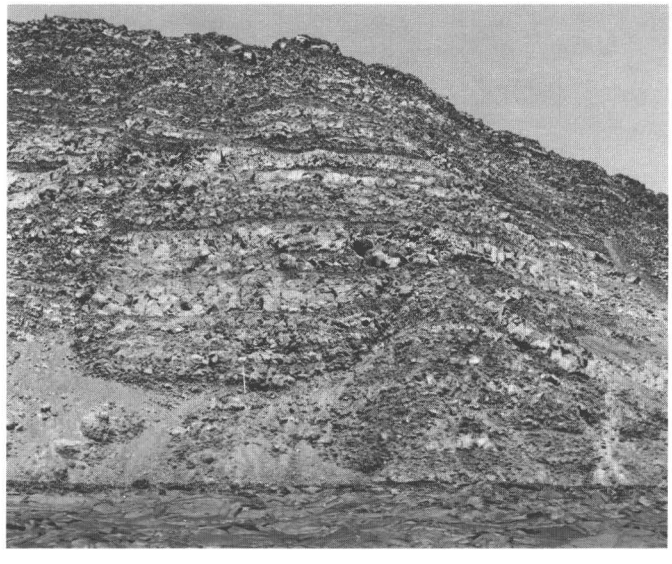

FIGURE 18.30.—Cross section of filled pit crater exposed on west wall of Mokuaweoweo caldera. Lowest of thick flows that fill crater overlies basal talus breccia (marked by a 4-meter rod). Filled crater is informally called "Lua Piha" (filled pit). Note crosscutting lopolith on right.

FIGURE 18.31.—Aerial view of Puu Hou, an 85-m-high littoral cone formed where 1868 SWRZ flow entered the sea near south tip of Hawaii Island.

FIGURE 18.32.—Aerial view of Kaawaloa Point, where a group III pahoehoe flow from Mauna Loa's summit mantles Kealakekua fault scarp and forms a typical lava delta.

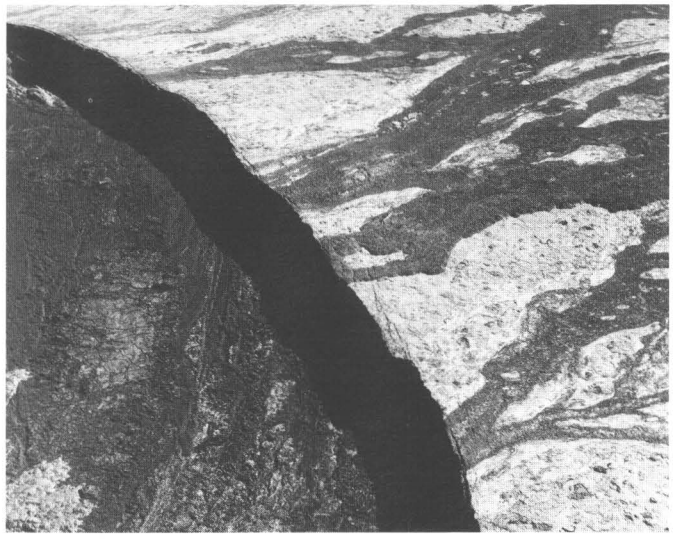

FIGURE 18.33.—Aerial view of southeast rim of Mokuaweoweo, showing truncation of group IV aa flows (dark) and underlying group III pahoehoe. Caldera rim here is 50 m high.

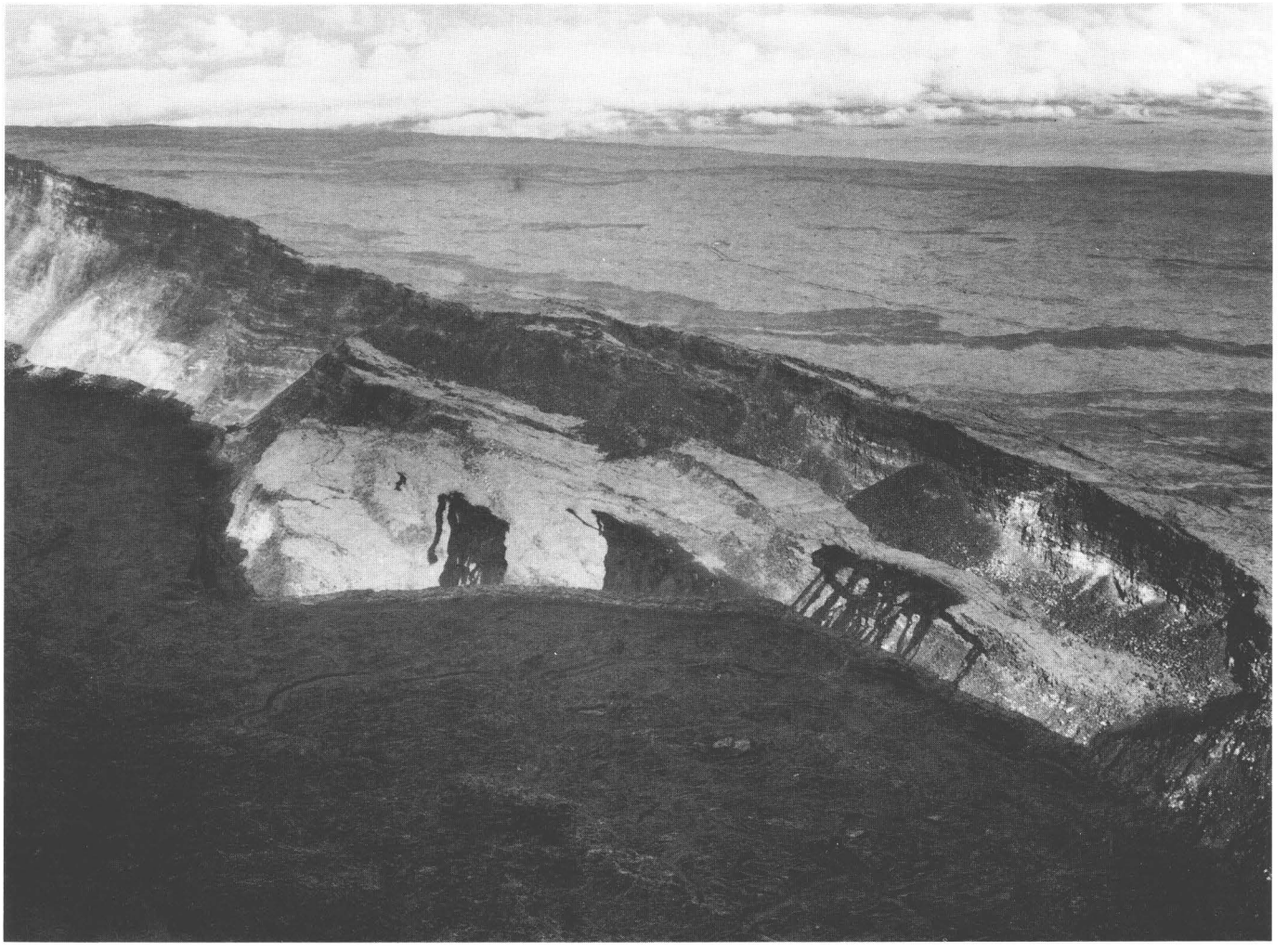

FIGURE 18.34.—Aerial view of north wall of Mokuaweoweo caldera, showing details of caldera subsidence fractures. Slump blocks are cut by summit lavas of 1942 eruption. Caldera floor is covered by lavas erupted in July 1975.

FIGURE 18.35.—Phreatic-explosion breccia fragments 100 m north of Mokuaweoweo caldera's north rim. These angular blocks of hornfelsic textured basalt here overlie a group IV aa flow.

MAUNA LOA 1974–1984: A DECADE OF INTRUSIVE AND EXTRUSIVE ACTIVITY

By John P. Lockwood, John J. Dvorak, Thomas T. English, Robert Y. Koyanagi, Arnold T. Okamura, Marjorie L. Summers, *and* Wilfred R. Tanigawa

ABSTRACT

The 1975 and 1984 eruptions of Mauna Loa Volcano were both related to a decade-long period of seismic and geodetic unrest (inflation) that was first detected in April 1974. The 1975 eruption, the first of Mauna Loa in 25 years, began just before midnight on July 5, but lasted less than 19 hours. Eruptive vents were confined to the summit region and produced about 30 million cubic meters of uniform tholeiite, which covered nearly 14 square kilometers of the summit area and north flank. Intense seismic activity continued in a localized area along the middle northeast rift zone (NERZ) for a week following the eruption and was accompanied by extensions across the rift, which suggested the intrusion of magma into this area. This led to a forecast of renewed activity on the NERZ sometime before the summer of 1978. The forecast timing proved erroneous, but the scenario was correct as to the place and character of the subsequent eruption.

The Mauna Loa summit inflated rapidly during the first two years after the 1975 eruption, but at lesser rates after 1977. Modeling of geodetic data showed that this inflation was caused by magma accumulation in a shallow storage reservoir beneath the southern edge of the summit caldera. Seismic activity was steady, although rates of intermediate-depth earthquakes began to increase in 1980, as did rates of summit deformation, resulting in a renewed forecast (1983) for an eruption of Mauna Loa within the next two years.

The 1984 summit-flank eruption began at 0125 H.s.t., March 25 (during a fortnightly earth tidal minimum). Eruptive fissures, which initially opened in the southwest corner of Mokuaweoweo, quickly propagated down the upper southwest rift and northeast rift zones, but eruptive activity was soon limited to the NERZ. A dike propagated down the NERZ at an average rate of 1.2 km/h during the day and was marked at the surface by discontinuous echelon eruptive fissures and earth cracks. The lowest eruptive vents were 15 km from the edge of Mokuaweoweo, between 2,770 and 2,930 m elevation; activity was restricted to these vents for the last three weeks of the eruption. Eruptive temperatures throughout this period remained constant at about 1,140 °C. Lava production began to diminish by early April, and lava steadily became more viscous, blocking supply channels at higher and higher elevations. When the eruption ended on April 15, approximately 220 million cubic meters of uniform tholeiite had been erupted, covering about 48 square kilometers of the Mauna Loa surface. Aa lava flowed as far as 27 km from eruptive vents to the 900-m elevation, to within 6 km of the nearest buildings in the city of Hilo.

Repeated geodetic and gravity measurements made throughout the eruption documented a substantial deflation of the Mauna Loa summit. The maximum measured subsidence, in the southern part of the summit, was 630 mm, and typical trilateration survey lines across Mokuaweoweo contracted an average of 300 mm, after initial dike-related extensions of about 600 mm. The summit area of Mauna Loa began to re-inflate immediately after the 1984 eruption, indicating the recharge processes for the volcano's next eruption have already begun.

INTRODUCTION

Mauna Loa, the largest active volcano on Earth, is a classic basaltic shield on the Island of Hawaii and rises to 4,170 m above the north-central Pacific Ocean. Mauna Loa erupted in July 1975 for the first time in 25 years. Another much larger summit and flank eruption followed in March and April 1984. Both eruptions were clearly related to a continuum of seismicity and deformation that began in 1974. This paper documents some of the events of this decade, but is only preliminary to more detailed analyses.

At the beginning of 1974 Mauna Loa had not erupted since the large eruption of June 1950 (Macdonald, 1954). Geophysical monitoring of Mauna Loa was provided principally by Hawaiian Volcano Observatory (HVO) instruments located on Kilauea prior to 1964, when the first modern seismometer was installed at the summit. Thomas A. Jaggar had previously placed seismographs at the summit at various times, but telemetry logistics limited their utility. R.W. Decker established a single EDM (Electronic Distance Measurement) survey line across Mokuaweoweo caldera in 1964, and annual reoccupation of this line (expanded to three lines by 1973) provided the only geodetic control. These transcaldera lines showed no significant changes prior to 1974. Earthquake activity was at low levels, as it had been for the previous 24 years.

The historical record of Mauna Loa's past eruptive behavior is lamentably brief—the first specific account describes the eruption of 1832, viewed from 150 km away. From 1832 to 1950 Mauna Loa had erupted an average of once every four years; the 24 years of quiescence from 1950 to 1974 was the longest noneruptive period in the volcano's brief recorded history. At the beginning of 1974 there were no premonitory indications of the decade of volcanic unrest and eruption which was soon to begin.

ACKNOWLEDGMENTS

Data and observations presented in this report came from the

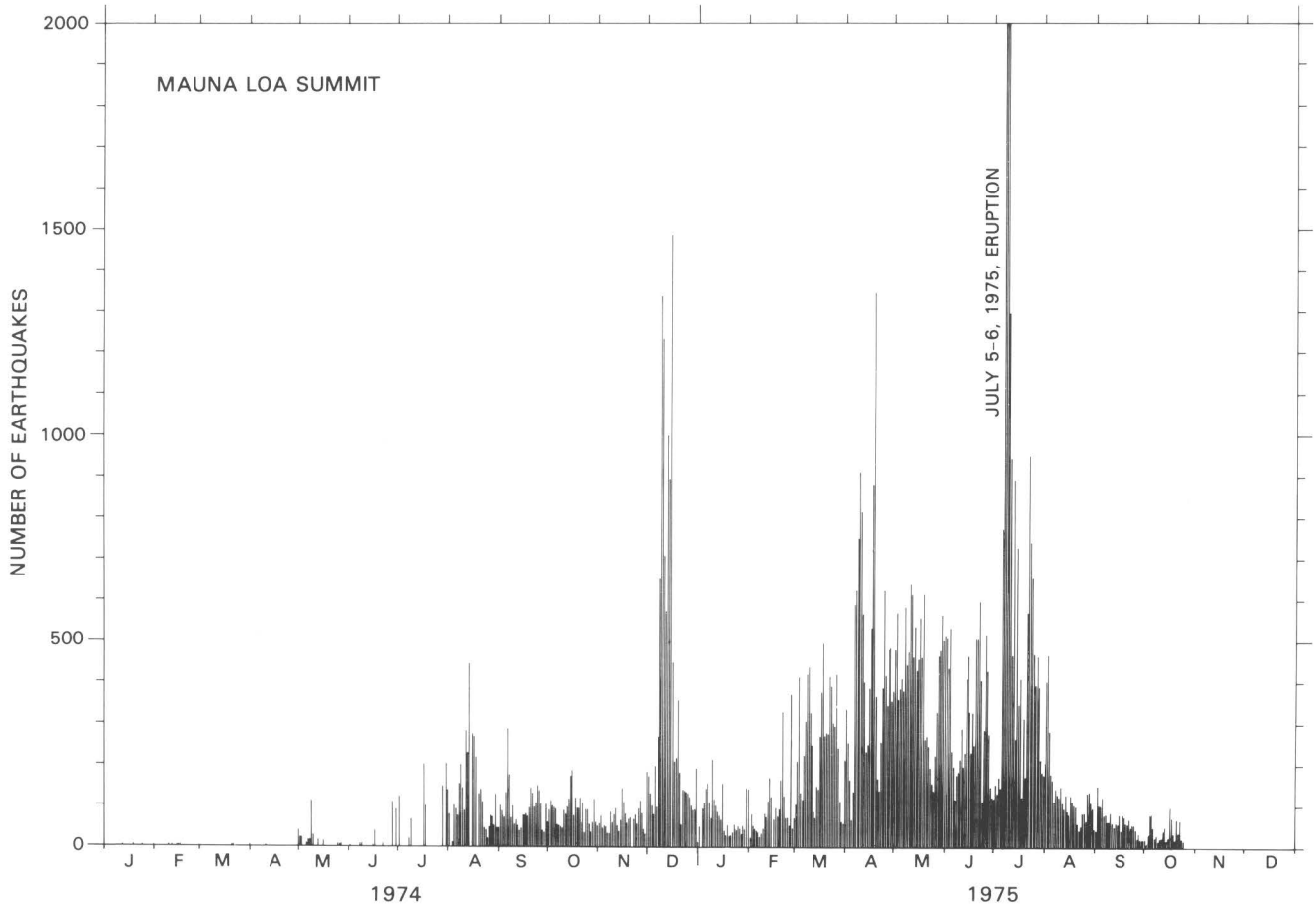

FIGURE 19.1.—Daily frequency of Mauna Loa short-period summit earthquakes ($M>0.1$), January 1974 to October 1975 (modified from Lockwood and others, 1976, fig. 5).

field and laboratory efforts of the entire staff of the Hawaiian Volcano Observatory from 1974 to 1984. This article incorporates previously published data of N.G. Banks, L.P. Greenland, D.B. Jackson, D.J. Johnson, K.A. McGee, Motoaki Sato, and J.M. Rhodes (see Lockwood and others, 1985). The careful review and thoughtful comments of P.W. Lipman greatly improved the manuscript as did review comments by T.L. Wright.

BEGINNING OF UNREST

An increase in the number of summit microearthquakes was detected in April 1974. The seismic activity continued to increase into the summer, and the possibility of future eruptive activity was noted (Koyanagi and others, 1975). Efforts to monitor the Mauna Loa activity more closely were frustrated by the fact that Kilauea was in near-continuous eruption at the Mauna Ulu eruptive vent during the first half of the year (Tilling and others, chapter 16), and brief Kilauea summit eruptions occurred in July, September, and December.

Trilateration measurements across Mokuaweoweo caldera in August 1974 revealed that significant dilation of the summit caldera had occurred since the previous measurements in 1973. This finding, together with continued increase in seismicity in the summit area, prompted expansion of the trilateration network to eight lines and the addition of two seismometers, placed around the rim of the caldera. Civil authorities were briefed on the situation, and through extensive news media interest, the island populace was alerted to the possibility of Mauna Loa eruptive activity. In mid-December 1974 the microearthquake rate ($M>0.1$) increased to 1,500 per day (fig. 19.1), and the conclusion that Mauna Loa was awakening was unescapable.

Trilateration measurements at the summit on December 14 showed significant dilation (to 4 cm) had occurred since August. On the morning of December 15, an earthquake of magnitude 4.6 below the southeastern part of the summit area was felt widely on the Island of Hawaii, and public concern was intensified.

From late December 1974 to February 1975 heavy snowfall blanketed Mauna Loa down to the 2,800-m elevation and covered all survey stations, preventing their reoccupation until early June. Aerial inspection of the summit area in April showed possibly

FIGURE 19.2.—Pit craters along upper southwest rift zone of Mauna Loa showing possibly anomalous melting of snow in April 1975. Lua Hou is in lower right corner. Photograph by J.P. Lockwood.

anomalous melting of snow in two pit craters on the upper southwest rift zone and along parts of the caldera floor (fig. 19.2).

In early spring of 1975 additional trilateration survey networks were established at lower elevations in order to measure strain across Mauna Loa's southwest rift zone (SWRZ) and northeast rift zone (NERZ). The Mokuaweoweo trilateration network was occupied on June 4 and showed as much as 10 cm of dilation of the summit since December.

Earthquakes between January 1974 and June 1975 occurred at intermediate depths (5–13 km) northwest of the summit and at shallow depths (<5 km) beneath and to the southwest of Mokuaweoweo (fig. 19.3). The number of intermediate-depth earthquakes increased first and was soon followed by an increase in the number of shallow earthquakes, commonly exceeding several hundred per day. Intense swarms occurred in August and December 1974, and again from February through June 1975.

During the week of June 30 to July 4 three borehole tiltmeters were installed on Mauna Loa's summit and north flank. One of these tiltmeters was to be destroyed by a lava flow in a few hours, before final adjustments could be made.

THE ERUPTION OF JULY 5–6, 1975

No unusual activity was noted on the Mauna Loa seismograms during the early evening of July 5; seismicity was at relatively low levels. At 2318 H.s.t. (all times given in Hawaii standard time), however, seismic alarms, signifying prolonged high-amplitude volcanic tremor, were activated in homes of HVO staff. The tremor had been first recorded by three seismometers (stations MOK,

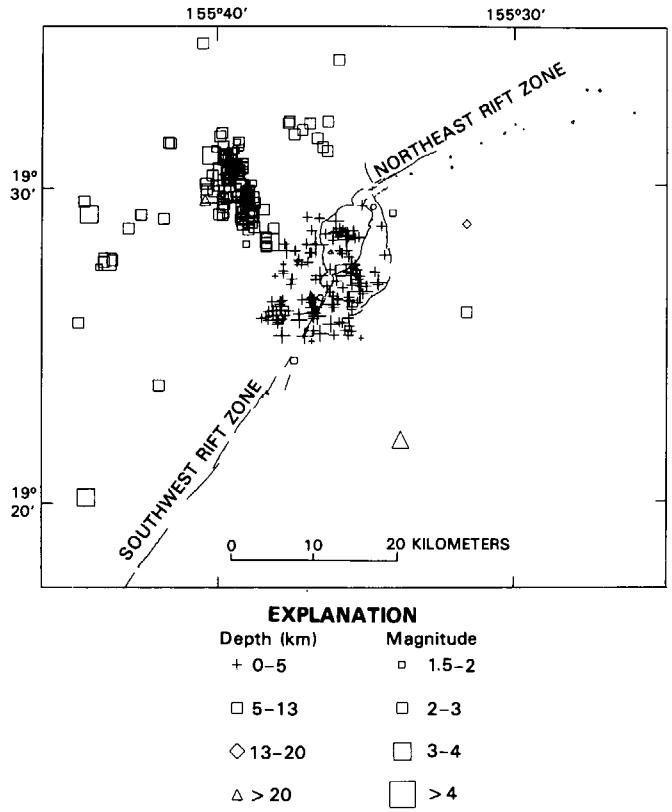

FIGURE 19.3.—Earthquake foci ($M \geq 1.5$) beneath Mauna Loa summit region in 18-month period prior to 1975 eruption (January 1, 1974, to June 30, 1975).

SWR, and WIL, see fig. 19.19) near Mokuaweoweo at 2251. Staff reached HVO at 2330 and saw that harmonic tremor was being recorded on all Mauna Loa and Kilauea seismographs. National Park and civil defense authorities were alerted to the imminent probability of a Mauna Loa eruption, and at 2342 a small glow was noted above the southwest end of Mokuaweoweo. Within one minute the glow extended across the entire summit area, and a fume cloud more than one thousand meters high was illuminated with a bright orange-red glow from the unseen lava fountains on the caldera floor.

A light airplane with two HVO staff members aboard reached the summit area at 0148; a line of fountains 20–50 m high crossed the entire floor of Mokuaweoweo at this time and extended about 1 km down the SWRZ. Lava cascades 90 m high were pouring into the three pit craters on the upper SWRZ (fig. 19.4). Flows were rapidly advancing to the west and southeast from the SWRZ vents. The eruptive fissures extended rapidly northeastward, across North Pit, and into the upper NERZ at 0225. At 0245 lava from the North Pit vents began cascading into another summit pit crater, Lua Poholo (see fig. 19.6). By 0315, the lava fountains on the SWRZ and within Mokuaweoweo were waning, and the lava flows moving to the west and southeast had stagnated. Fountains continued to migrate eastward along the NERZ, but by dawn eruptive activity was largely restricted to echelon vents near the NERZ 3,700-m level (fig. 19.5).

A voluminous aa flow moved about 2 km/h down Mauna Loa's north flank and threatened to cut the paved access road and powerlines to the Mauna Loa Observatory (an atmospheric research station operated by the National Oceanic and Atmospheric Administration, fig. 19.6). At about 0715 fountains feeding this aa flow subsided, and it soon stopped about 100 m from the Observatory road, having traveled 5.2 km. Fountaining continued at greatly diminished levels throughout the day, but ceased by nightfall. Approximately 30×10^6 m^3 of lava had been erupted, and 13.5 km^2 of the Mauna Loa summit area had been covered (fig. 19.6).

The erupted lava includes both aa and pahoehoe. This lava consists of dense pahoehoe within the caldera and mostly highly vesicular, shelly pahoehoe near eruptive vents on the rift zones. The flows are mostly blocky aa more than 500 m from eruptive vents and become more dense toward the distal ends of flows. The rock is nearly aphyric tholeiite (table 19.1), with sparse (<1 percent) olivine phenocrysts to 3 mm diameter. About 90 percent of these flows were subsequently buried by 1984 lava (see fig. 19.33).

A trilateration survey on July 7 showed that individual survey lines across Mokuaweoweo had extended by as much as 760 mm since the previous measurements in 1974, principally reflecting the July 5 intrusion of a dike across the caldera.

THE POSSIBILITY OF RENEWED ACTIVITY

July 7–12 was a period of great public concern, as an outbreak of lava lower along the NERZ seemed possible, in light of both the on-going seismicity and the numerous historical examples of brief summit eruptions followed within a few days by flank outbreaks (for example, April 1942, see Macdonald, 1954). Magma was clearly being intruded into the middle NERZ from July 6–12, as harmonic tremor continued, and several hundred small earthquakes occurred daily within the NERZ. Epicenters of these earthquakes, dozens of which were felt, were concentrated near the 2,900-m level on the NERZ, just southeast of Puu Ulaula (fig. 19.7). A trilateration network near Puu Ulaula was reoccupied on July 8 and showed significant dilation since installation of the network on May 28. On July 9, the network was again reoccupied and indicated continued dilation (as much as 4 cm extension on individual survey lines). Also on July 9, an earthquake of magnitude 4.5 near Puu Ulaula was felt throughout the island. Trilateration measurements at the summit on July 10 showed that the caldera had contracted since July 7 (as much as 5 cm of negative extension on some lines), presumably as magma drained into the NERZ. Harmonic tremor began to diminish in amplitude on July 10, and between July 9 and 12 the geodimeter lines near Puu Ulaula also contracted as much as 5 cm. With this information, the week-long 24-hour alert ended.

The historical record of Mauna Loa activity shows that isolated eruptions similar to that of July 1975 (those not followed within a few days by flank outbreaks) are nearly always followed by more voluminous flank eruptions after a period of 2–3 years (Dutton, 1882, p. 140; Stearns and Macdonald, 1946, p. 82). On

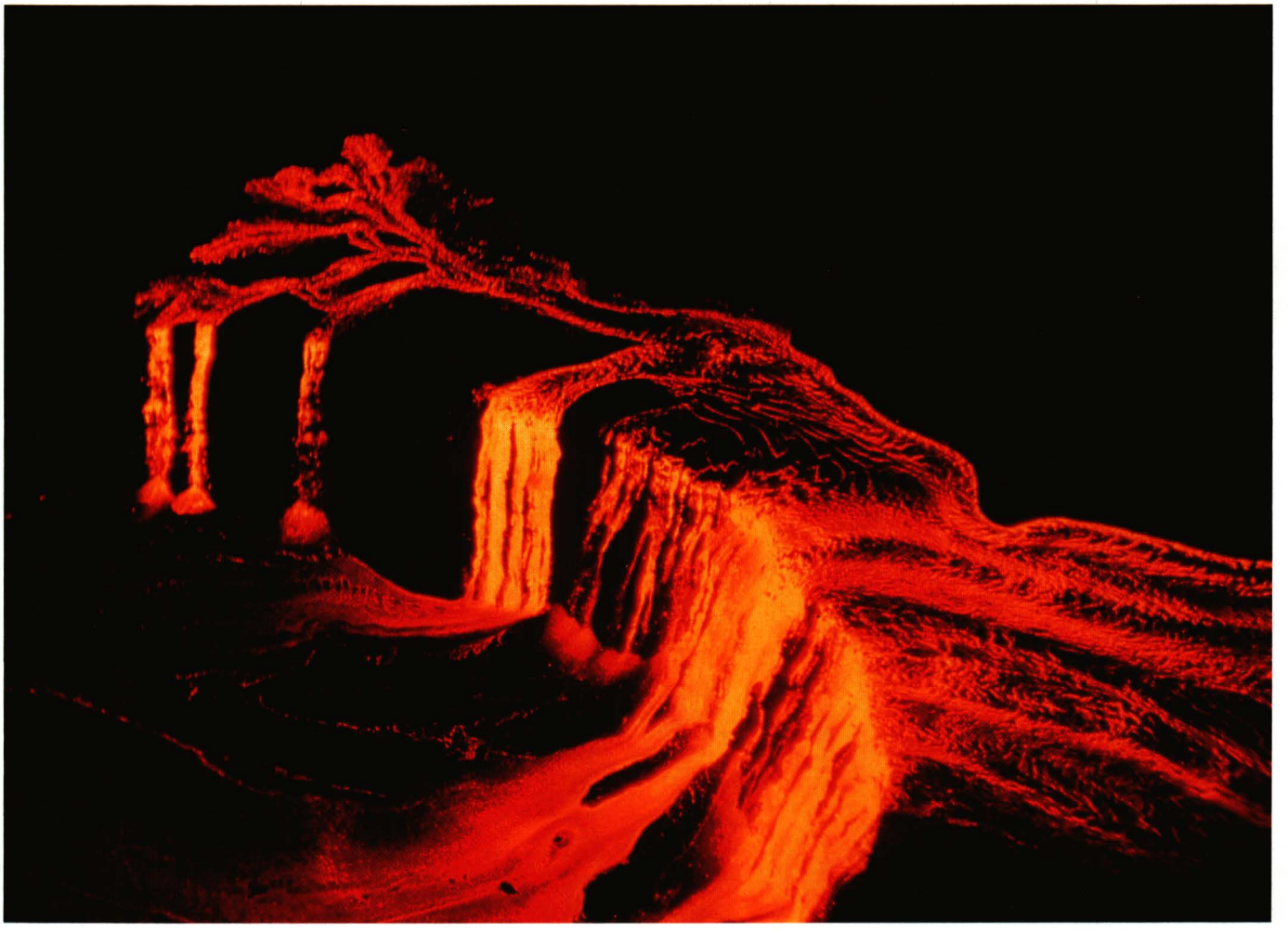

FIGURE 19.4.—Aerial view of lava cascades into Lua Hou, upper southwest rift zone, July 6, 1975, 0240 H.s.t. Cascade height about 90 m. Photograph by R.T. Holcomb.

FIGURE 19.5.—Oblique aerial view, looking west, of echelon eruptive fissures in Pohaku Hanalei area at dawn on July 6, 1975. Photograph by D.W. Peterson.

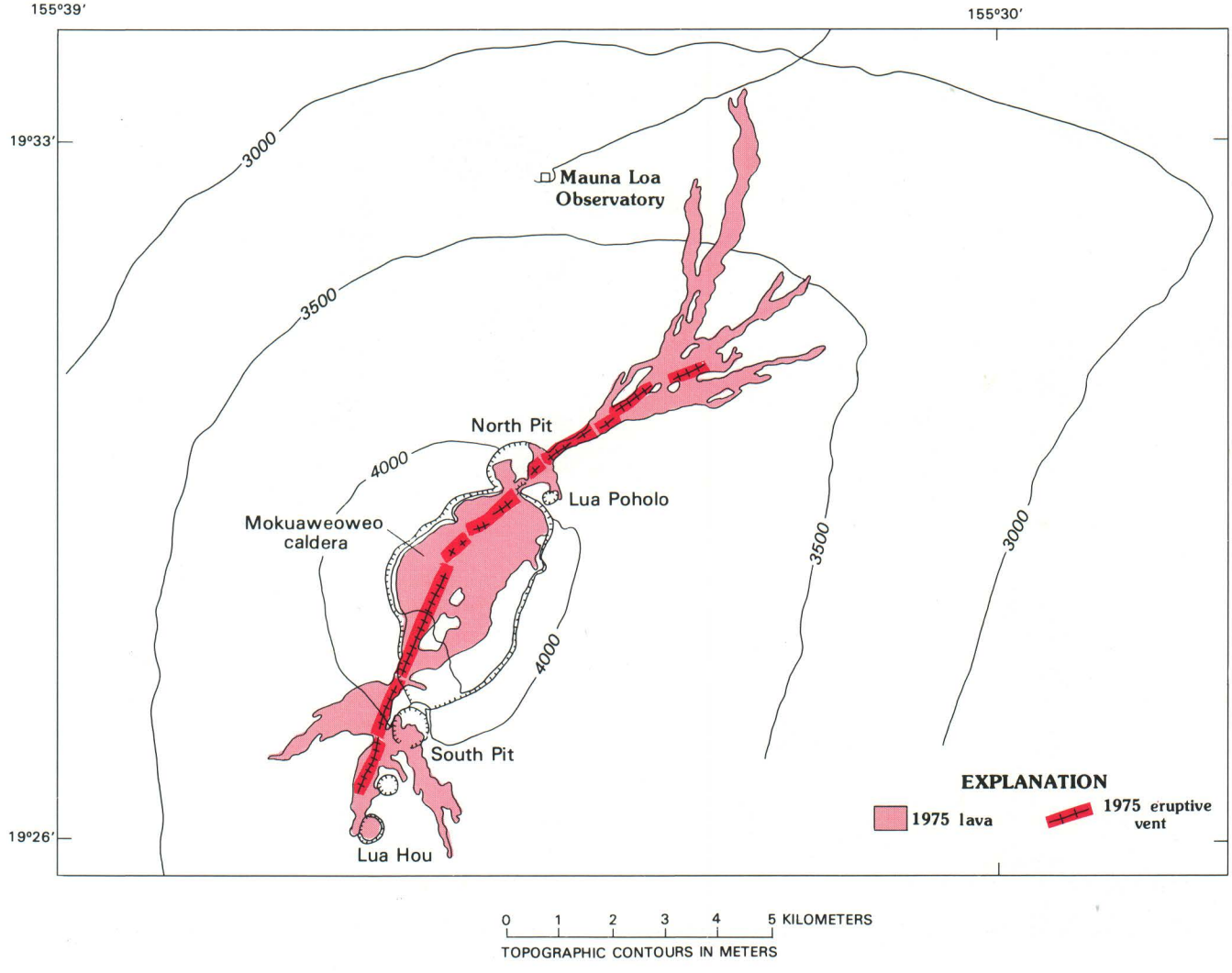

FIGURE 19.6.—Distribution of July 5–6, 1975 lava and geographic features of Mauna Loa summit area. Map by R.T. Holcomb, U.S. Geological Survey, 1975.

TABLE 19.1.—*Major-element compositions of 1975 Mauna Loa lava*

[NERZ, northeast rift zone; SWRZ, southwest rift zone; MOK, Mokuaweoweo. ML775-1 to -27, conventional rock analyses by V.C. Smith; ML-4 to -127, X-ray fluorescence analyses by J.M. Rhodes, reported on volatile-free basis, with total iron reported as Fe_2O_3. --, data not available]

Sample	ML775-1	ML775-17	ML775-21	ML775-22	ML775-23	ML775-24	ML775-26	ML775-27	ML-4	ML-5	ML-76	ML-78	ML-126	ML-127
Location	NERZ	MOK	NERZ	MOK	SWRZ	SWRZ	NERZ	SWRZ	MOK	NERZ	MOK	SWRZ	NERZ	SWRZ
Rock	aa	spatter	spatter	spatter	spatter	pahoehoe	spatter	aa	spatter	spatter	spatter	spatter	aa	spatter
SiO_2	52.04	52.01	52.13	52.31	52.13	52.15	52.11	51.93	51.76	51.64	51.81	51.54	51.87	51.58
TiO_2	2.09	2.07	2.14	2.23	2.19	2.19	2.19	2.19	2.11	2.11	2.10	2.09	2.11	2.10
Al_2O_3	14.26	14.32	14.04	13.96	14.26	14.21	14.22	14.16	13.72	13.76	13.72	13.73	13.72	13.77
Fe_2O_3	2.81	1.49	1.44	1.44	1.34	1.46	1.33	4.95	12.18	12.24	13.30	12.22	12.38	12.34
FeO	8.55	9.64	9.84	9.88	9.76	9.70	9.79	6.57	--	--	--	--	--	--
MnO	.18	.17	.17	.18	.17	.17	.17	.17	.16	.16	.17	.16	.18	.17
MgO	6.65	6.64	6.61	6.40	6.67	6.65	6.65	6.65	6.53	6.61	6.55	6.50	6.50	6.56
CaO	10.60	10.63	10.58	10.46	10.61	10.63	10.60	10.60	10.55	10.53	10.48	10.49	10.53	10.61
Na_2O	2.34	2.34	2.34	2.60	2.38	2.34	2.33	2.40	2.33	2.09	2.11	2.19	2.19	2.29
K_2O	.37	.36	.34	.40	.38	.38	.38	.38	.39	.39	.38	.39	.39	.39
P_2O_5	.23	.23	.23	.25	.23	.23	.22	.22	.26	.24	.23	.22	.24	.23
Cl	.01	0	.01	.01	0	0	.01	.01	--	--	--	--	--	--
F	.03	.03	.03	.03	.03	.03	.03	.03	--	--	--	--	--	--
S	.01	.02	.01	.02	.02	.04	.02	.01	--	--	--	--	--	--
CO_2	.01	0	.01	.01	.01	.01	.01	.01	--	--	--	--	--	--
H_2O^+	.01	0	.02	.01	.04	.04	.07	.05	--	--	--	--	--	--
H_2O^-	.07	.15	.04	.06	.01	0	0	0	--	--	--	--	--	--
Total	100.26	100.10	99.98	100.25	100.23	100.23	100.13	100.33	99.99	99.77	99.85	99.53	100.11	100.04

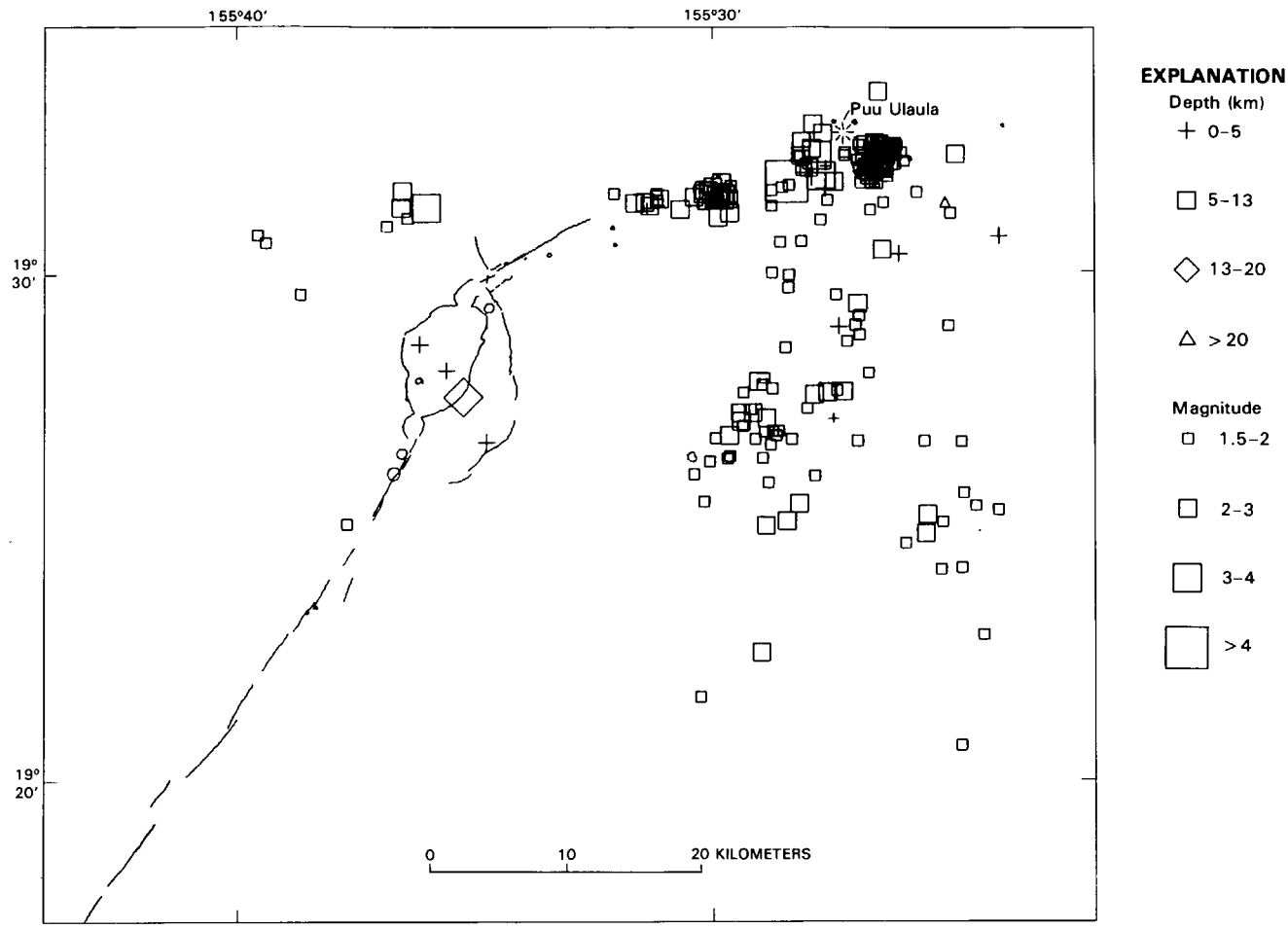

FIGURE 19.7.—Earthquake foci ($M \geq 1.5$) July 1–31, 1975. Earthquakes west of long 155° 34′ W. occurred before eruption, those to east occurred after July 5, mostly during critical period July 6–12.

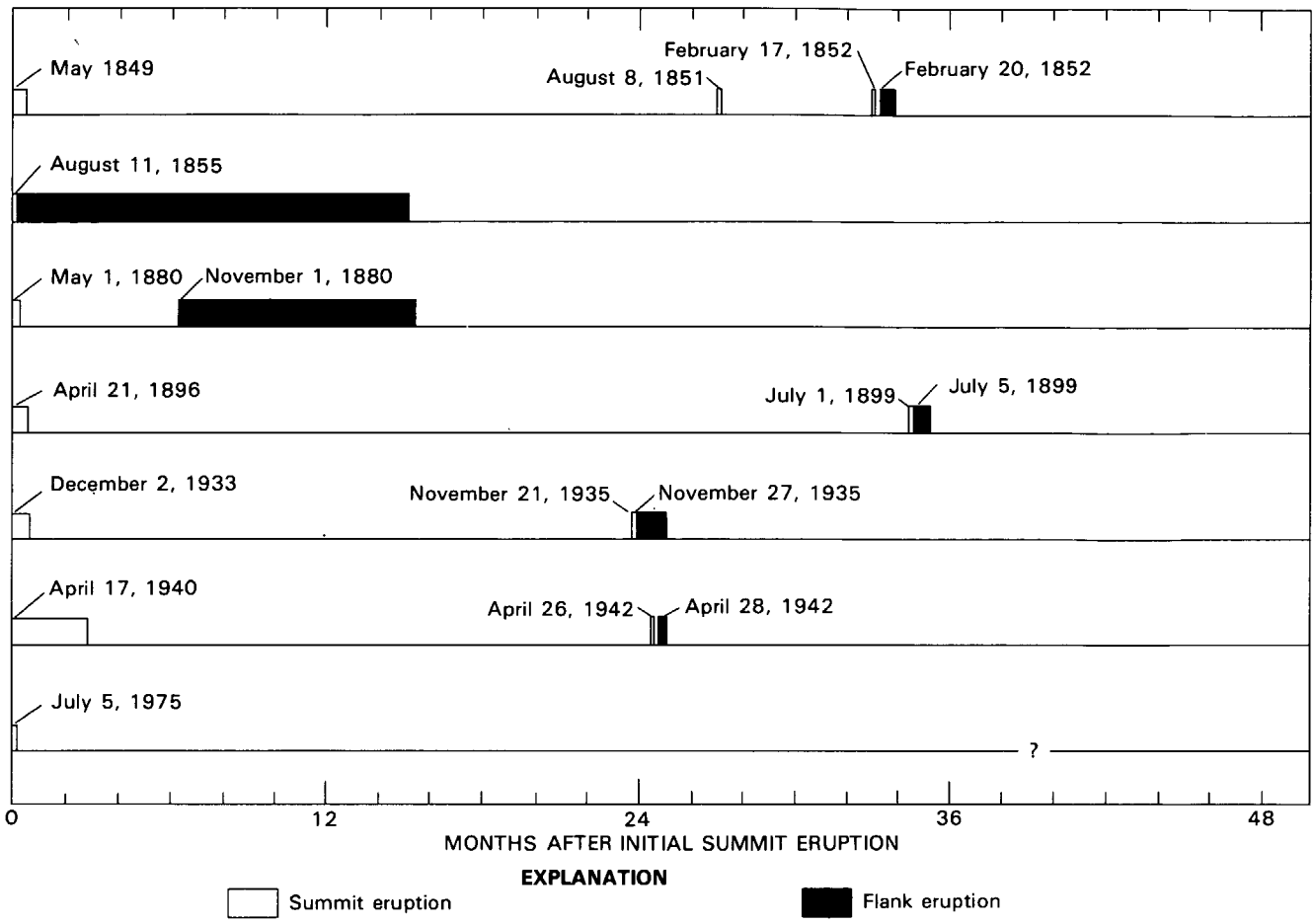

FIGURE 19.8.—Chronology of summit and northeast rift zone flank eruptions, 1849 to 1975 (modified from Lockwood and others, 1976, fig. 4).

the basis of this pattern (fig. 19.8), and the accumulating geophysical information on Mauna Loa's post-eruptive inflation, the 1975 eruption was recognized as the forerunner of future activity (Lockwood and others, 1976, p. 15):

> The historical record thus suggests that the summit eruption of July 1975 was the first phase of an eruptive sequence that will culminate with a major eruption on the flanks of Mauna Loa sometime before the summer of 1978. This flank eruption will likely be closely preceded by brief summit activity. If the Mauna Loa activity of July 6–10 is a reliable indicator, we can expect the flank vents to open between 2,800 and 3,000 m on the northeast rift zone in the vicinity of Puu Ulaula. On the basis of the historical record, we can expect relatively low fountains (50–75 m high) to form a 'curtain of fire' extending 1 to 3 km along the rift zone. The initial rate of lava production will be high, as are slope gradients high on Mauna Loa, so that lava may travel up to 10 km from eruptive vents during the first 24–48 hours. Because the rate of lava production should diminish, because the slopes of Mauna Loa become more gentle at lower elevations, and because lava will be farther from its supply vents, the flow rate will soon slow dramatically.

This scenario proved to be correct in all details, except for the timing, which was in error by almost six years (!).

THE INTERERUPTIVE PERIOD: 1975–1984

During this period the number of earthquakes beneath Mauna Loa's summit gradually increased in frequency. Geodetic monitoring showed that Mauna Loa continued to inflate at an essentially continuous, but irregular rate, reflecting the rise of magma into a shallow reservoir beneath Mokuaweoweo. The seismic and deformation data together allowed definition of the general location and depth of this reservoir (Decker and others, 1983). Civil authorities were kept apprised of Mauna Loa's inflation and the potential threat to the city of Hilo, and contingency plans were prepared for the diversion of lava flows above Hilo should that prove necessary (Lockwood and Torgerson, 1980; U.S. Army, 1980).

SEISMICITY

Over the 22-year period 1962–1984 shallow earthquakes (<5 km deep) were concentrated beneath Mokuaweoweo and the

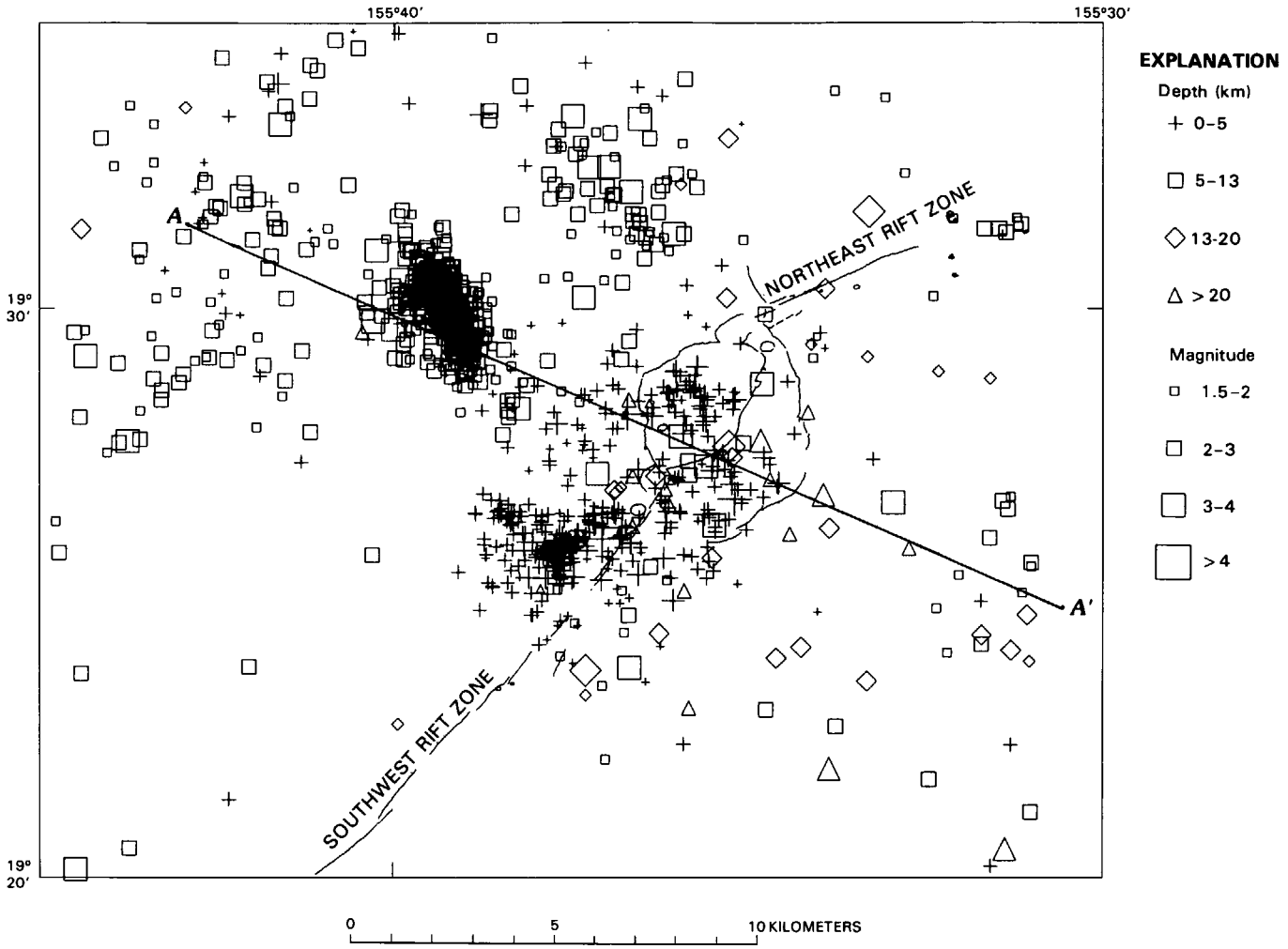

FIGURE 19.9.—Earthquake foci ($M \geq 1.5$) beneath Mauna Loa summit region from January 1, 1962, to December 31, 1984. A–A', line of cross section in figure 19.10. The earthquake foci have been obtained from a network of about 50 seismic stations covering the entire Island of Hawaii. To eliminate any bias from increasing number of earthquakes processed, owing to the increased density of seismometers over this period, only earthquakes of magnitude equal to or larger than 1.5 with horizontal and vertical location uncertainties of less than 2 km are plotted.

upper SWRZ, whereas intermediate depth earthquakes (5–13 km deep) were concentrated beneath the northwest flank (figs. 19.9, 19.10). After the 1975 eruption and the posteruption swarm of intrusion-related earthquakes in the NERZ (fig. 19.7), shallow earthquakes ceased beneath the summit, but 2–3 intermediate-depth earthquakes were noted each year until 1977, when they increased to about 20 per year (fig. 19.11). The number of deeper earthquakes (>13 km) per year was unchanged over the entire intereruptive period. Shallow earthquakes began again in 1977, and their rate generally continued to increase until the 1984 eruption (fig. 19.12).

SEISMIC INTERPRETATION

The shallow earthquakes are believed to occur in brittle rocks capping a magma storage reservoir. The intermediate-depth earthquakes northwest of the summit are of tectonic origin (E. Endo, written commun., 1983) and may be related to stresses built up in response to the wedging effects of shallow dikes emplaced along the summit caldera and rift zones. The deeper earthquakes may be caused by the opening of deep feeder conduits between the mantle magma source and the higher magma storage reservoirs.

DEFORMATION

Following the large dike-related dilation of Mokuaweoweo on July 5, 1975, and the subsequent slight contraction, trilateration lines across the caldera continued to extend (fig. 19.13). Repeated trilateration measurements between the summits of Mauna Loa, Mauna Kea, and Hualalai revealed that the extensions across Mokuaweoweo were mostly accommodated by southeastward translation of Mauna Loa's southeast flank. The northwest flank was only slightly compressed by the Mauna Loa inflation. The summit inflation is also indicated by spirit-level (dry-tilt) measurements (fig. 19.14). Spirit-level measurements were made by precise, repeated

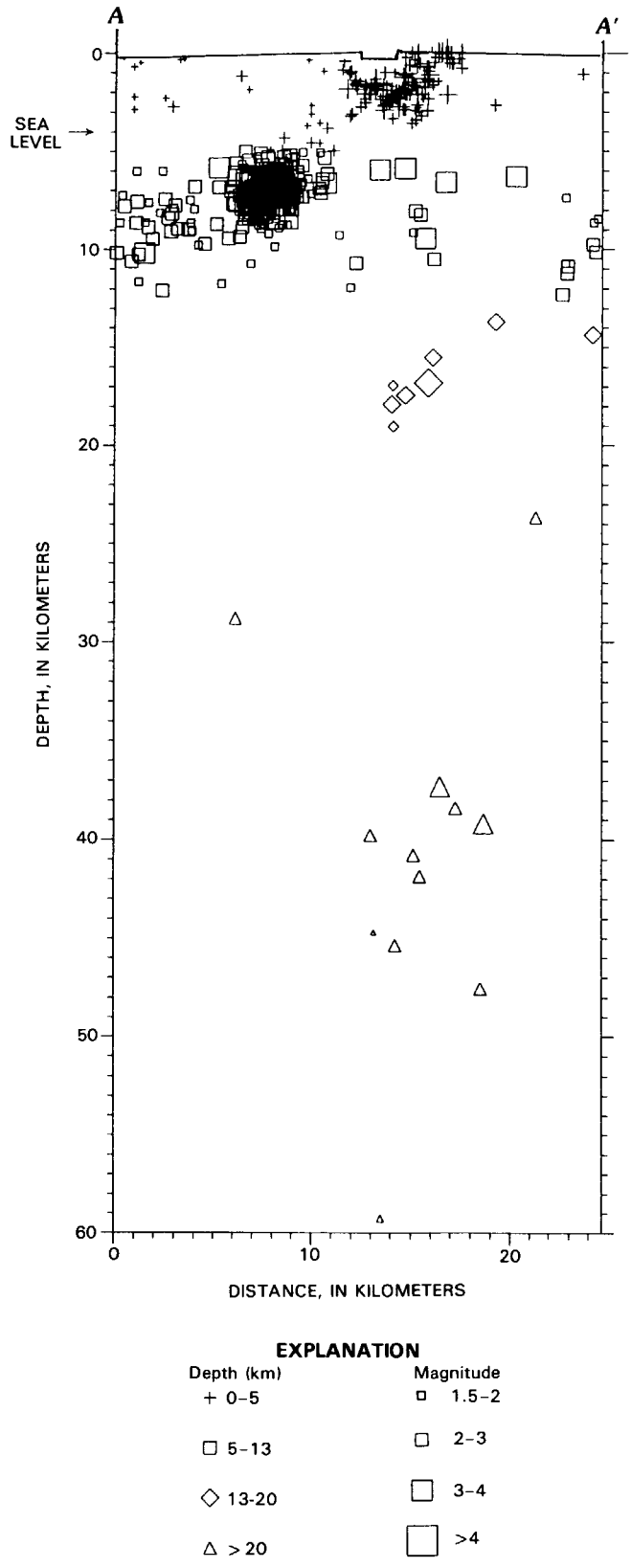

FIGURE 19.10.—Cross section of earthquake hypocenters within 2.5 km of line *A*–*A'* of fig. 19.9.

optical levels on stadia rods placed at bench marks arranged in a triangle with approximately 30- to 40-m base legs (Yamashita, 1981). Rapid outward tilt rates (inflation) persisted for one year after the 1975 eruption, followed by more moderate, though continuous, inflation after 1976. Level data for the summit region show greatest vertical uplift near the summit. The uplift profile (fig. 19.15) fits the theoretical uplift (Mogi, 1958) calculated for a pressure point source at 3.1 km depth.

DEFORMATION INTERPRETATION

Simultaneous inversion of horizontal, vertical, and tilt data for the period 1977–1981, using the methods of Dvorak and others (1983), further refined the location of the shallow inflation source (table 19.2; see fig. 19.19). In table 19.2 the longitude and latitude of the apex of inflation are x and y, respectively, and z is the depth to the point pressure source beneath the apex of inflation, referred to the elevation of the caldera floor. The volume values show, for each data source, the total volume of swelling, which represents the minimum volume of increased magma storage at depths of 3 to 4 km. The bulk rigidity and compressibility of the system are not known; thus magma-volume changes cannot be estimated. The base values show the amounts of theoretical uplift of the reference bench mark required to make the elastic model best fit the observations. The sigma values show the quality of fit between the least-squares model and the observations.

It is clear from all the deformation measurements that they fit a point-source elastic model reasonably well and that they define a common center of uplift and a surprisingly shallow pressure source. The similarity between the surface-deformation pattern of the summit areas of Mauna Loa and Kilauea Volcanoes is striking. On Kilauea, the pressure source is about 3 km deep (Fiske and Kinoshita, 1969; Swanson and others, 1976), and inflations and deflations of the summit area show similar patterns to those measured on Mauna Loa. Even though the lower zones of the magma chambers beneath Mauna Loa and Kilauea reach to several kilometers depth on the basis of seismic evidence (Koyanagi and others, 1975; Ryan and others, 1981), the changes in surface deformation on both volcanoes indicate that the zone of active magma input and removal is quite shallow, near the upper portion of the aseismic zones underlying both calderas.

The injection of magma into Mauna Loa's shallow storage reservoir over the 1977–1981 period caused an average surface-volume change of about 4×10^6 m^3/yr. This value is only 14 percent of the average historical Mauna Loa effusion rate of 29×10^6 m^3/yr (Lockwood and Lipman, chapter 18), and if characteristic of the entire 1975–1984 inter-eruptive period the cumulative amount intruded would account for only 16 percent of the volume erupted in 1984. For these reasons it is probable that magma was also accumulting at deeper levels within Mauna Loa during the 1975–1984 period. A schematic cross section of one possible model for the shallow magma-reservoir system beneath Mauna Loa shows the top of this shallow reservoir to be at about sea level (fig. 19.16).

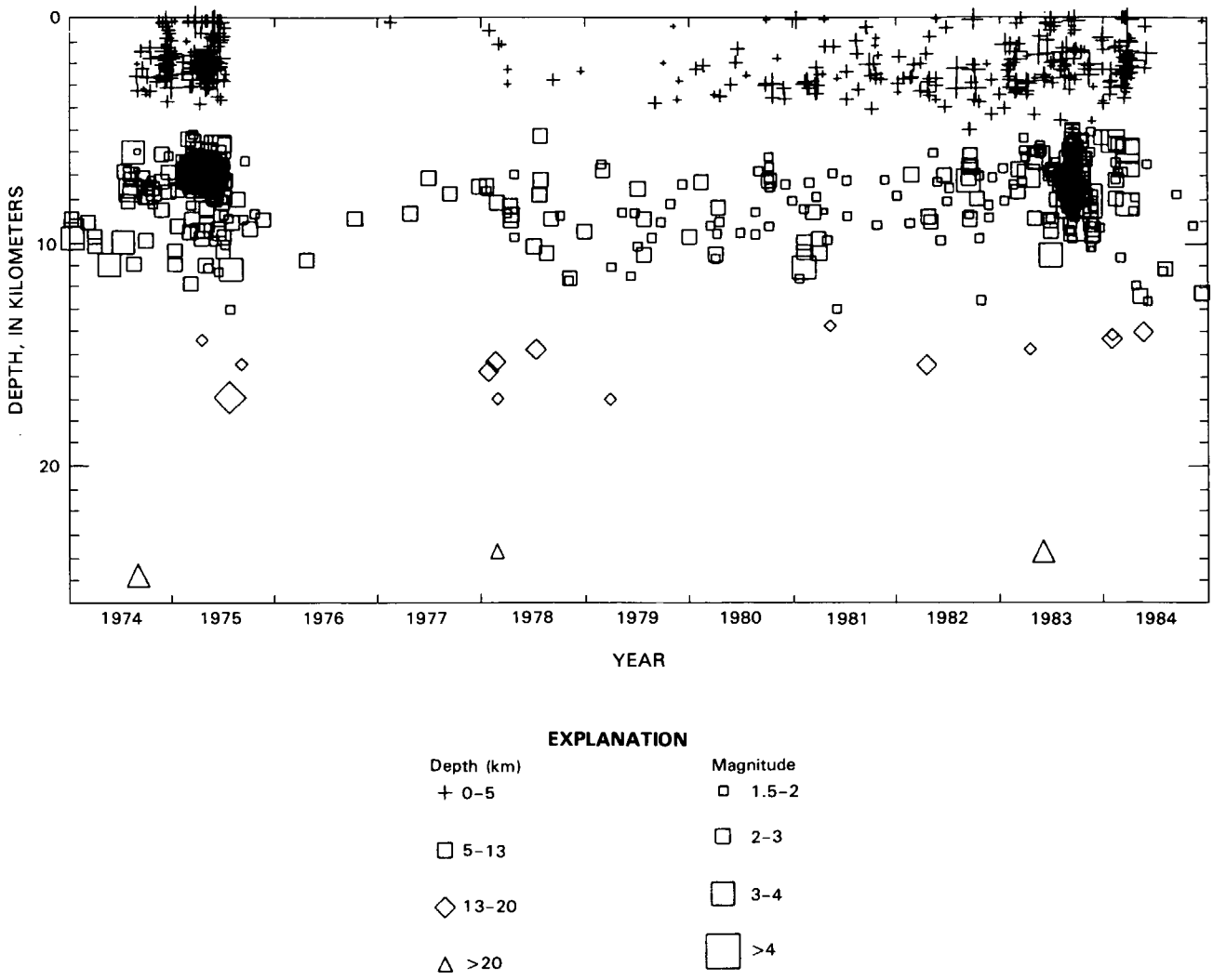

FIGURE 19.11.—Time, magnitude, and depth distribution of Mauna Loa earthquakes for period January 1, 1974, to December 31, 1984. Earthquakes plotted are those with $M>1.5$ located in area shown in fig. 19.9. Absence of earthquakes between 3 and 6 km depth suggests location of Mauna Loa's shallow magma storage reservoir.

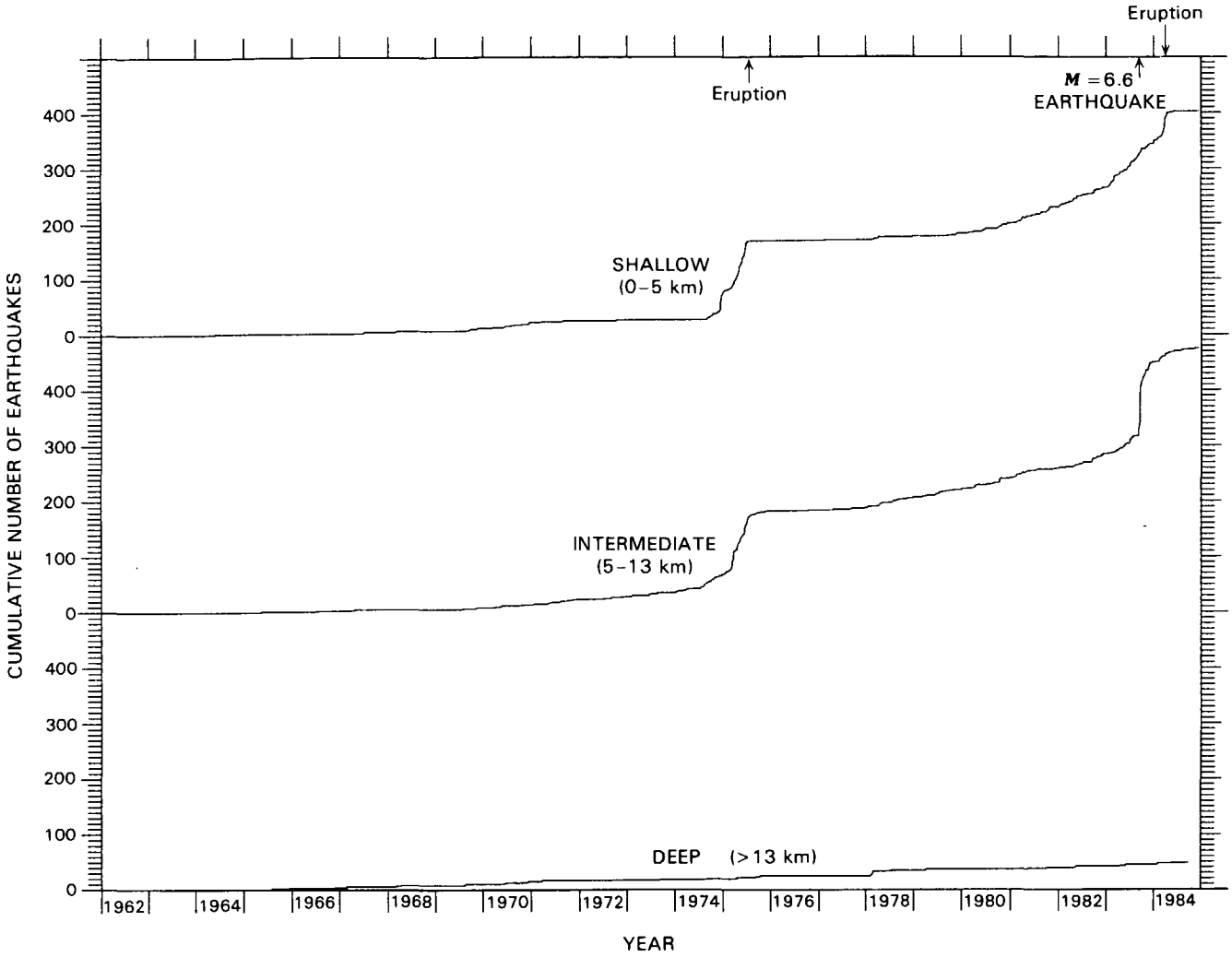

FIGURE 19.12.—Cumulative frequency plot of all earthquakes of magnitude equal to or greater than 1.5 beneath Mauna Loa summit region, from January 1, 1962, to December 31, 1984. Area included shown in figure 19.9. Note increase in intermediate depth earthquakes associated with $M = 6.6$ earthquake of November 16,1983, and its aftershocks.

Zone A, the part of the magma-reservoir system that most influences summit geodetic changes, is probably a region that inflates slowly between eruptions and deflates rapidly during eruptive activity. Zone B may also be a region of magma storage, but is less active than zone A; it has less impact on surface deformation monitors. Both zones are inferred to be plexi of molten intrusions separated by screens of hot but more solid rock.

High-temperature (to 350 °C) fumaroles were continuously active along the central part of the 1975 eruptive fissures during the entire nine-year inter-eruptive period. These fumaroles produced visible fume (fig. 19.17) in dry as well as in humid weather and commonly produced a dense blue haze on Mauna Loa's upper north flank, especially during morning hours. This fume, mostly of atmospheric composition, contained relatively high concentrations of CO_2, which was frequently detected at the NOAA Mauna Loa Observatory during morning hours of downslope air movement (Miller and Chin, 1978). This fuming ceased immediately after cessation of the 1984 eruptive activity, and the Mauna Loa summit is now clear of visible fume (see Lockwood and Lipman, chapter 18, fig. 18.27).

Kilauea erupted more than six times during the 1975–1984 inter-eruptive period (1977, 1979, 1980, twice in 1982, and multiple episodes in 1983–1984). Mauna Loa exhibited no known sympathetic behavior with any of the Kilauea activity, suggesting the independence of their magma storage systems.

THE 1984 ERUPTION

Based on the post-1975 deformation and seismic data, Decker and others (1983) forecast an "increased probability for an eruption

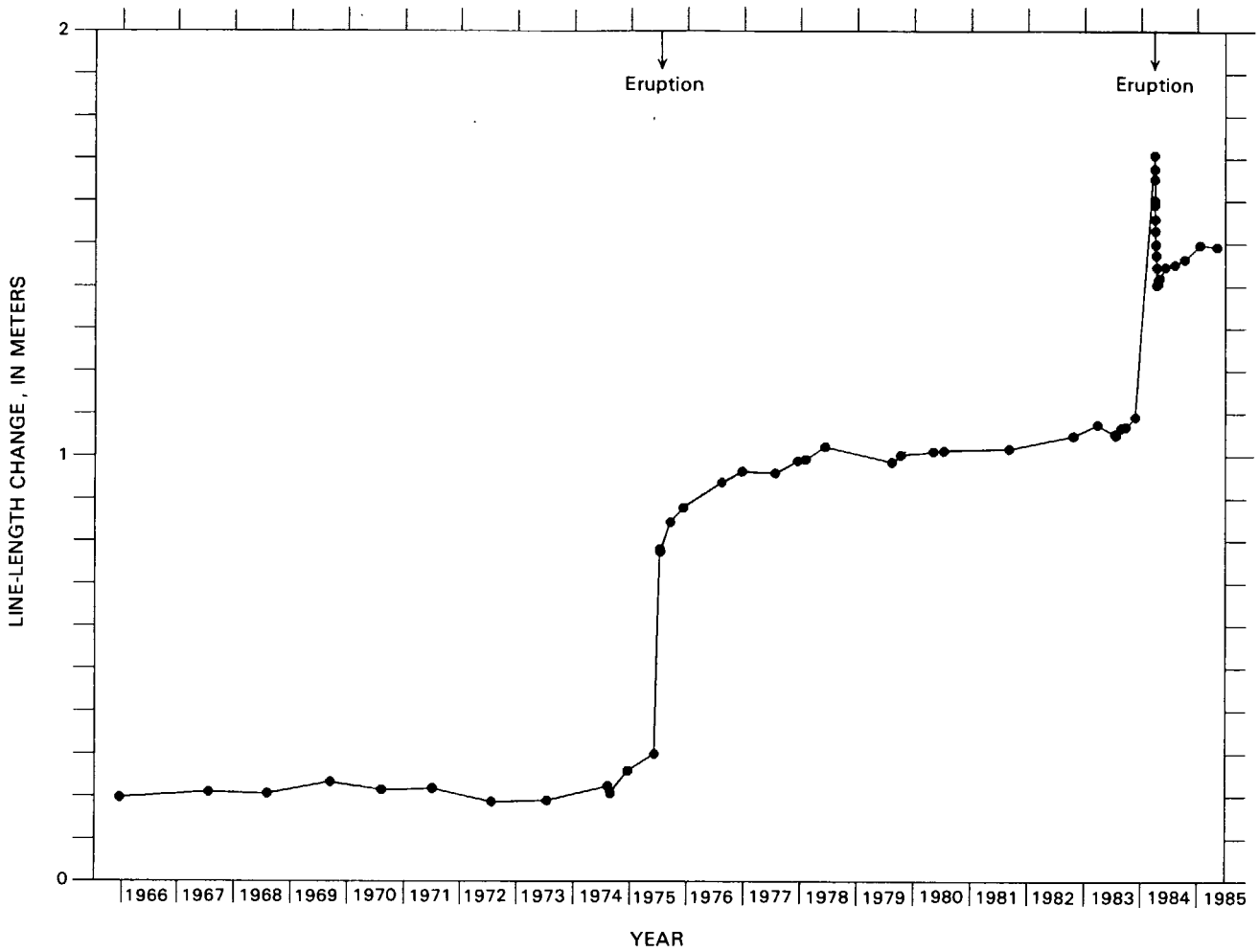

FIGURE 19.13.—Dilation of Mokuaweoweo, December 1965 to May 1985, as measured by trilateration surveys between stations HVO 92 and HVO 93 (station locations shown on fig. 19.19). Abrupt extensions on July 5, 1975, and on March 25, 1984, were associated with dike emplacement during 1975 and 1984 eruptions.

of Mauna Loa during the next two years." The inflation center was determined to underlie the south rim of Mokuaweoweo, and it was suggested that the eruption would follow historical patterns by beginning in the summit area.

PREMONITORY PHENOMENA

PREERUPTION SEISMICITY

Shallow- and intermediate-depth earthquakes increased in frequency beneath Mauna Loa from 1980 to 1983, culminating with a swarm of intermediate-depth earthquakes (5–13 km deep) beneath the northwest flank in mid-September 1983 (fig. 19.18). First-motion analyses suggest that these September earthquakes resulted from increasing lateral stresses generated in the summit and upper SWRZ, possibly as a consequence of intrusion of magma beneath the summit and upper rift zones (E. Endo, written commun., 1983).

At 0613 H.s.t. November 16, 1983, a damaging $M=6.6$ earthquake occurred beneath Mauna Loa's southeast flank (fig. 19.19). The earthquake generated an extensive aftershock sequence 20 km across, with the northern perimeter bordering Mauna Loa's NERZ. Seismicity remained high in the vicinity of Puu Ulaula until merging with eruptive seismicity on March 25, 1984.

The number of larger earthquakes ($M>1.5$) rose persistently as the time of eruption approached (figs. 19.11, 19.12). The daily frequency of smaller earthquakes ($M<1.5$) showed a more episodic increase, peaking one week before the eruption but decreasing to below average on the day before the outbreak (fig. 19.20). The overall distribution of earthquakes in the 16 months before the eruption (fig. 19.18) is remarkably similar to distribution of earthquakes in the 16 month period before the July 5, 1975, eruption (fig. 19.3).

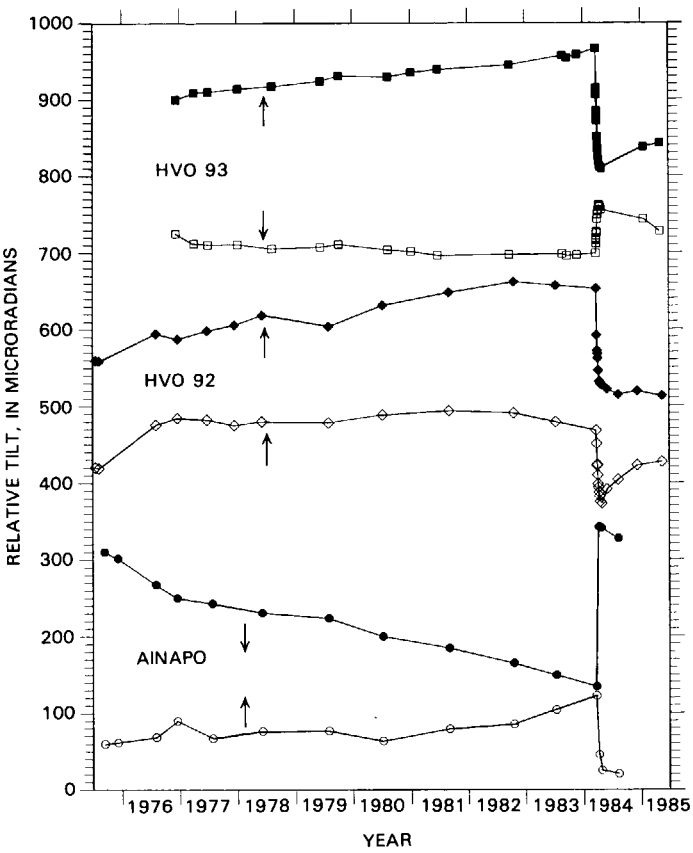

FIGURE 19.14.—Spirit-level tilt changes at three Mauna Loa summit stations, 1975 to 1985 (see fig. 19.19 for station locations). Darkened symbols are north-south component; open symbols are east-west component. Positive tilt changes indicate north or east down. Arrows show inflation direction for individual tilt components. Summit inflation is recorded at all stations prior to and after March 25 to April 15, 1984 eruption.

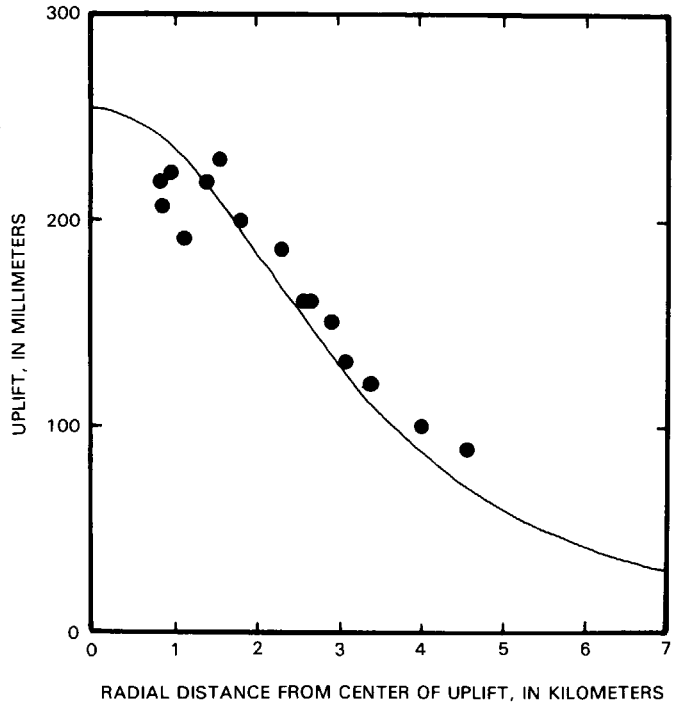

FIGURE 19.15.—Comparison of observed elevation changes in summit area (from 1977 to 1981 leveling surveys) with best-fit elastic deformation model (solid curve); see figure 19.19 for level station locations and calculated uplift center (from Decker and others, 1983, fig. 10).

TABLE 19.2.—*Mauna Loa geodetic data, 1977–1981*

[From Decker and others, 1983]

Data	x		y		z	Volume	Base	σ	σ EDM		σ Tilt
	Longitude (West)	(km)	Latitude (North)	(km)	(km)	(10^6 m^3)	(mm)	Level (mm)	mm	μ strain	(μrad)
Leveling	155°34.5′	±0.2	19°27.5′	±0.2	3.1±0.5	17±3	59±24	4	--	--	--
Tilt	155°35.2′	±0.6	19°27.5′	±0.6	2.6±1.2	8±5	--	--	--	--	27
EDM	155°35.1′	±0.7	19°27.2′	±0.4	3.2±1.2	19±8	--	--	37	25	--
All	155°35.0′	±0.4	19°27.3′	±0.3	3.9±0.8	22±6	88±50	16	40	26	30

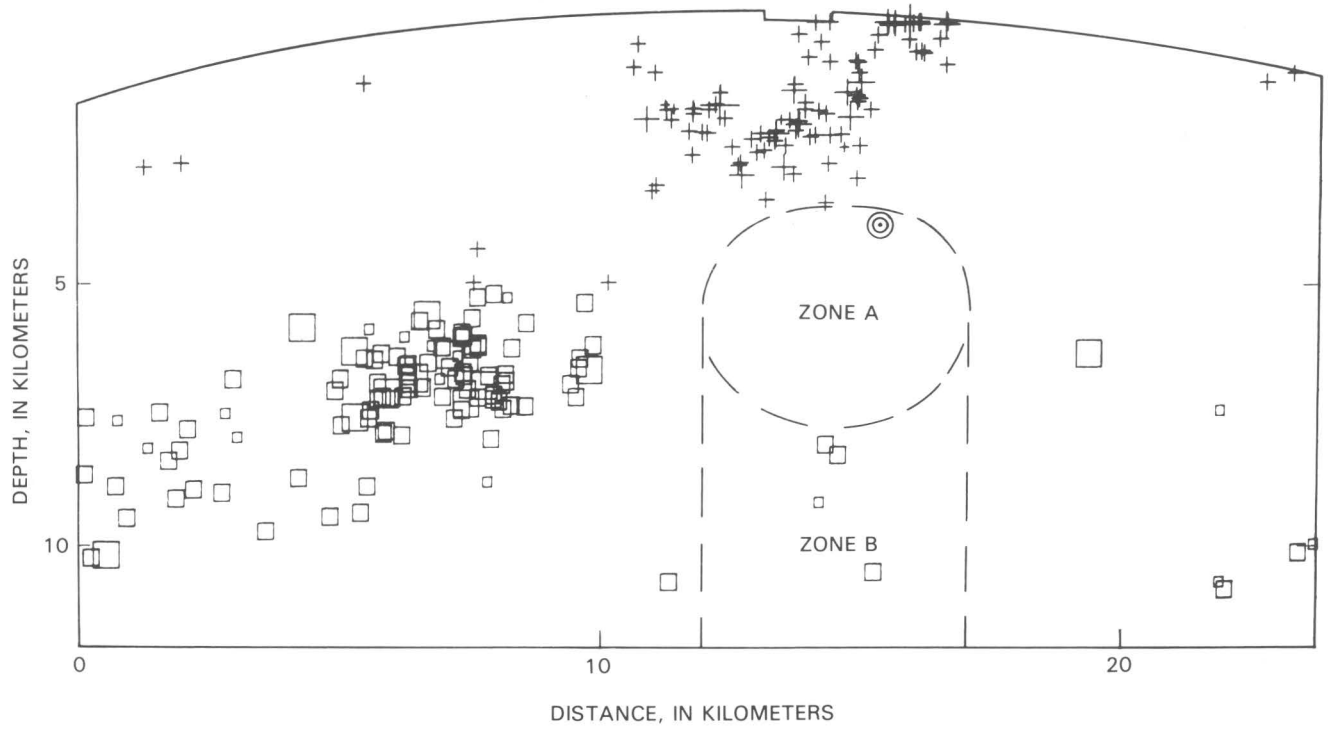

FIGURE 19.16.—Approximately true-scale schematic cross section of proposed magma reservoir system beneath Mokuaweoweo defined by an aseismic zone. Cross section and earthquake hypocenters same as in upper 12 km of figure 19.10, except earthquakes after May 1983 omitted. Double circle in zone A shows point-source inflation center calculated with 1977–81 deformation data (from Decker and others, 1983, fig. 14).

FIGURE 19.17.—Fumaroles along 1975 eruptive fissures in Mokuaweoweo caldera, view to north-northeast. 1940 cone in lower left, Mauna Kea in background. Photograph taken December 1977 by J.P. Lockwood.

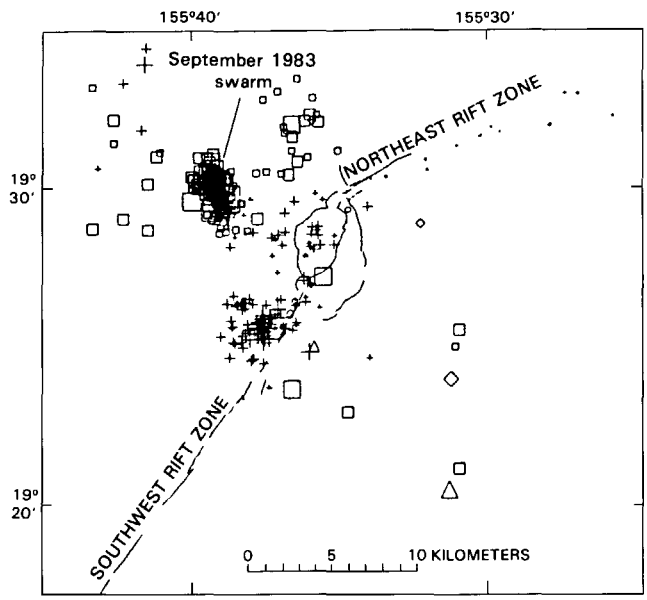

EXPLANATION

Depth (km)	Magnitude
+ 0–5	○ 1.5–2
□ 5–13	□ 2–3
◇ 13–20	□ 3–4
△ >20	□ >4

FIGURE 19.18.—Earthquake locations in summit region for 16-month period before 1984 eruption (September 24, 1982, to March 24, 1984). Compare with figure 19.3.

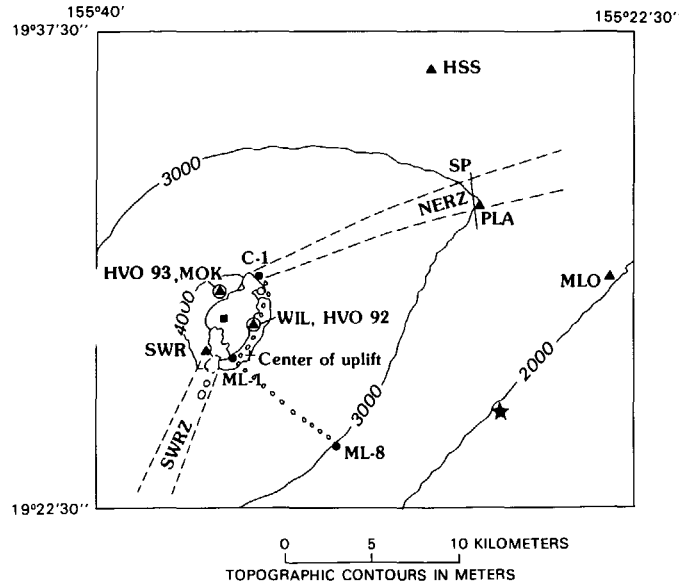

EXPLANATION

- Gravity station
- Seismic station
- Seismic, tilt, and EDM station
- Fumarole monitor
- Epicenter of November 16, 1983, $M = 6.6$ earthquake
- Level survey line

FIGURE 19.19.—Mauna Loa summit area, showing location of stations and features. NERZ, northeast rift zone; SWRZ, southwest rift zone; SP, electrical self-potential survey line.

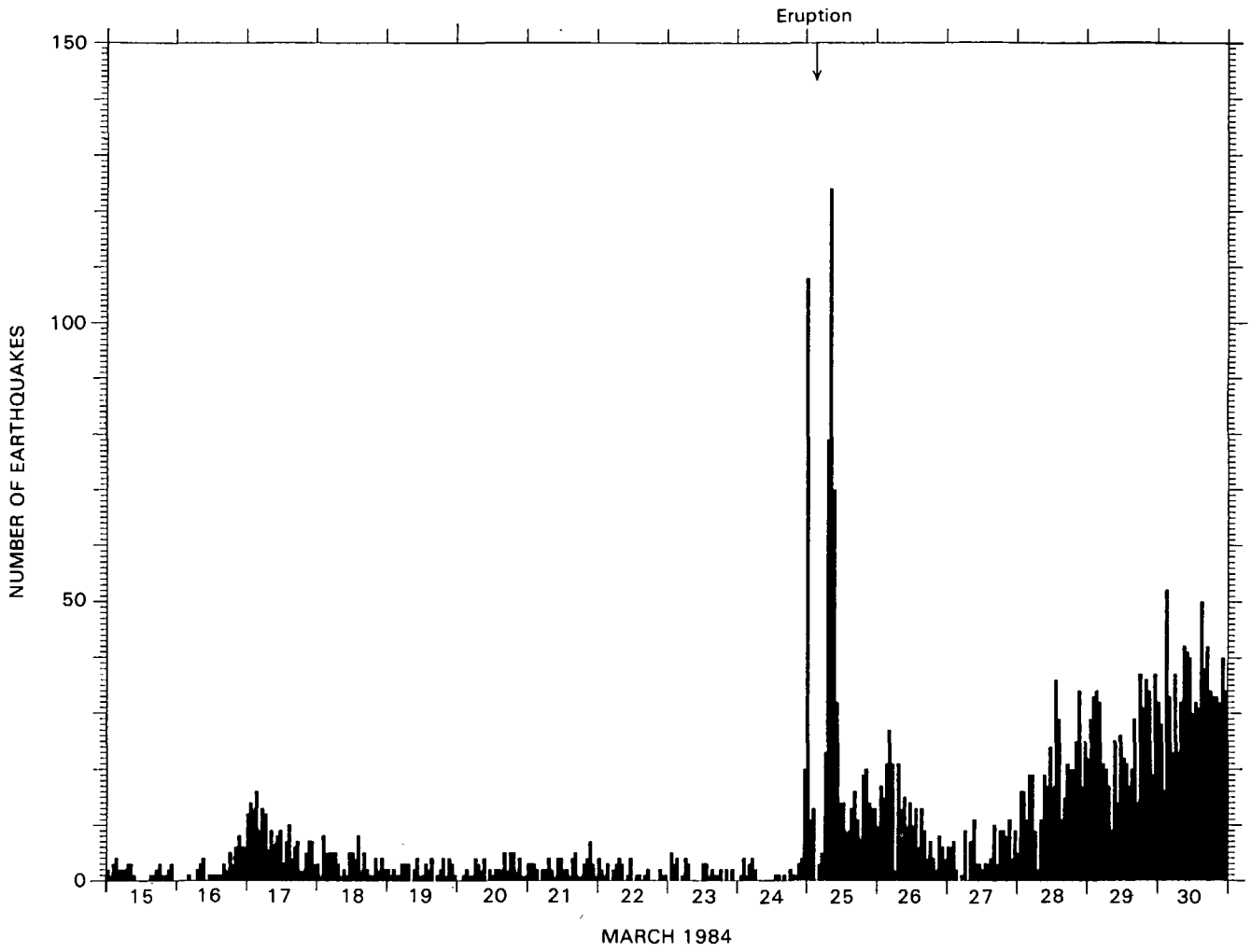

FIGURE 19.20.—Hourly counts of Mauna Loa short-period summit earthquakes for period March 15–30, 1984. Increase in earthquake frequency after March 27 accompanied deflation of Mauna Loa summit. Low counts on the morning of March 25 reflect period of masking by background of high-amplitude tremor.

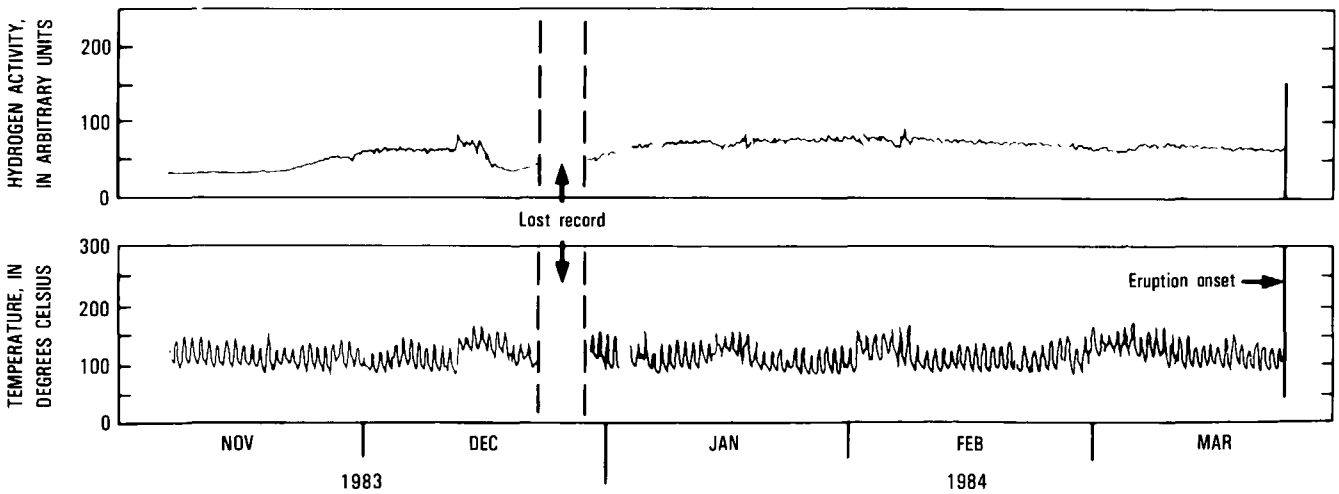

FIGURE 19.21.—Variation of temperature (t) and hydrogen (H_2) activity in a fumarole on 1975 eruptive fissure, Mokuaweoweo caldera, between November 5, 1983, and March 24, 1984. Temperature values are not field calibrated. Large diurnal temperature variations may be caused by artificial instrumental amplification. Hydrogen activity is referenced to a nonquantitative instrumental standard. Data from M. Sato and K. McGee, U.S. Geological Survey (from Lockwood and others, 1985, fig. 3).

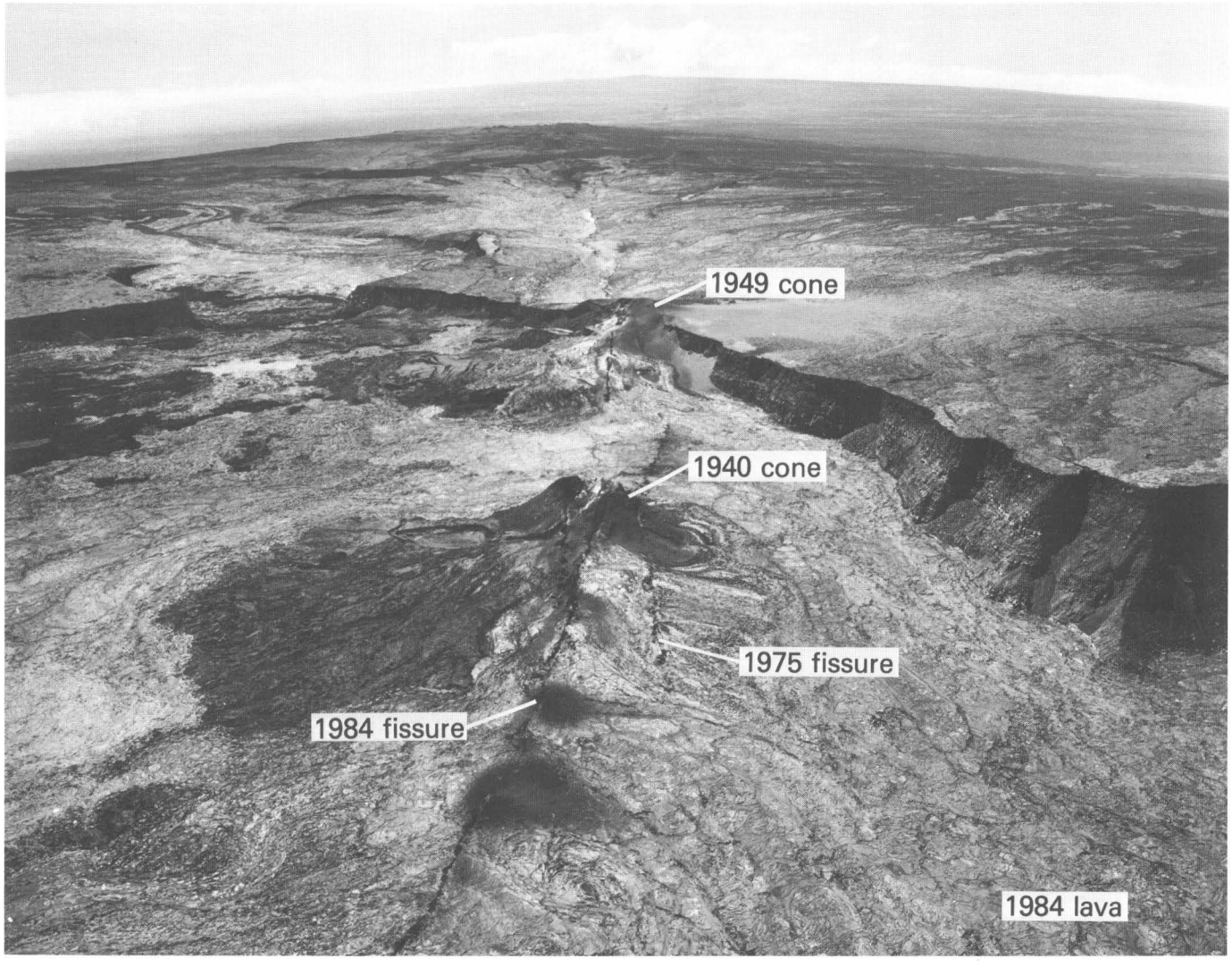

FIGURE 19.22.—Oblique aerial view, looking southwest, of 1984 eruptive fissure at southwest edge of Mokuaweoweo. Fissure extends across Mokuaweoweo, across 1940 and 1949 cones, and down the southwest rift zone. Reflective pahoehoe flows on caldera floor and down upper southwest rift were all erupted on March 25. Note 1975 eruptive fissure at northwest base of 1940 cone. Photograph by F.R. Warshauer.

PRE-ERUPTION DEFORMATION

Trilateration and tilt surveys showed that the inflation continued at a steady, but nonincreasing rate almost to the 1984 outbreak and gave no cause for alarm (figs. 19.13, 19.14).

FUMAROLE MONITORING

A remote station for monitoring H_2 activity and temperature was installed in a fumarole situated along a 1975 eruptive fissure in Mokuaweoweo on November 5, 1983 (Lockwood and others,' 1985). The first rise in temperature above the diurnal fluctuations was observed in the afternoon of November 18, 1983 (fig. 19.21).

A brief, small increase in H_2, as measured by activity of an H_2-O_2 fuel cell, was recorded concurrently with this temperature increase. The H_2 level had been stable before then, but gradually began to rise on November 21. Could these November changes have been related to the $M=6.6$ earthquake of November 16? Both temperature and H_2 increased on December 13, and on December 14 an anomalous steam cloud was seen rising to about 1 km above Mokuaweoweo. The fumaroles were visited on December 17, but temperatures and fuming were normal.

The H_2 level gradually increased again through late December and early January. Three thermal events lasted for 4 to 9 days in mid-January, early February, and early March. The H_2 levels showed concurrent changes, but the correlations were negative in 1984, contrary to the positive correlations observed in 1983. The reversal may indicate a change in the nature of emitted gases from reducing (H_2-rich) to more oxidized (H_2O, O_2-rich). The last data

FIGURE 19.23.—Echelon eruptive fissures in Pohaku Hanalei area, northeast rift zone at dawn on March 25, 1984. Compare with 1975 vent locations (fig. 19.5). View to west. Photograph by J.D. Griggs.

transmission (1 h before the sensors were destroyed at the eruption onset) showed normal background levels with no portent of the imminent events.

VISUAL OBSERVATIONS

On March 18, 1984, dull red glow was spotted along a crack (1975 fissures?) on the Mokuaweoweo floor by a hiker, but his report did not reach HVO until after the eruption began. On March 23, several observers spotted "steam clouds" rising above Mokuaweoweo. On March 24, the day before the eruption, M.M. Godchaux of Mount Holyoke College reportedly saw rocks and steam being ejected from the 1975 fissures, near the center of Mokuaweoweo, but there was no means to alert HVO.

ERUPTION NARRATIVE

Seismic stations MOK, WIL, and SWR along the rim of Mokuaweoweo (fig. 19.19) began to record an increase of shallow earthquakes at 2255 H.s.t., March 24 (fig. 19.20). Earthquakes less than $M=0.1$ were recorded at a rate of 2–3 per minute after this time. At 2330 an increase in seismic background marked the onset of harmonic tremor. The onset of tremor, which presumably recorded the beginning of magma ascent to the surface, coincided with a fortnightly earth tidal minimum. A correlation between eruptive activity and fortnightly tidal minima was also noted at a 19th century eruption of a volcano in El Salvador (Golombek and Carr, 1978), but this is not a general characteristic of Mauna Loa eruptions (Dzurisin, 1980). The earthquake swarm and tremor strengthened rapidly just before 0100, March 25. At 0056 it became impossible to stabilize astronomical telescopes on the summit of Mauna Kea, 42 km to the northwest, owing to ground oscillations, and observations were impossible for the next 2 hours.

An infrared sensor in a military satellite recorded a "strong signal" from Mauna Loa at 0125:16 on March 25; this signal indicated the first surface outbreak of the eruption. At 0130 observers at the Mauna Kea summit and at Puu Ulaula spotted a red glow reflected off fume clouds above the southwest part of Mokuaweoweo (at about 4,015 m elevation). Eruptive fissures migrated rapidly down the upper SWRZ to 3,890 m, across the 1940 cone, and to the northeast across Mokuaweoweo, a few meters southeast of the 1975 fissures (fig. 19.22). At 0357 fountains extended into the upper NERZ and migrated in a series of south-stepping echelon fissures eastward (fig. 19.23), south of the 1975 fissures (compare with fig. 19.5). At about this time the fountains died out on the SWRZ and began to wane within Mokuaweoweo. By 0700 the fountaining was restricted to a zone on the NERZ between 3,700 and 3,780 m. At 0910, however, new fountains appeared 7 km farther east, at 3,410 m. The fissure feeding this new outbreak migrated rapidly uprift and downrift, and by 0930 a 2-km-long "curtain of fire" was active between 3,400 and 3,470 m elevation. Fountains were 10–50 m high along this fissure, and lava output was estimated at $1–2\times10^6$ m^3/h. A narrow flow moved about 5 km down the southeast flank from these vents, southwest of the 1880 flow. At 1030, profuse steaming was noted along a 1-km-long fracture system between 3,260 and 3,170 m, but there was no further downrift migration of fountains for several hours, and lava production again waned.

At 1641 a new eruptive fissure opened below Puu Ulaula at about 2,850 m elevation, 19 km east of the original outbreak point within Mokuaweoweo. These vents opened south and slightly uprift from the principal vent of the previous NERZ eruption, that of 1942 (fig. 19.24). The dike feeding these vents had migrated down the NERZ at an average rate of 1,200 m/h (fig. 19.25). The new eruptive fissure migrated rapidly both uprift and downrift, and by 1830 a 1,700-m-long "curtain of fire" was active between 2,770 and 2,930 m elevation. All fountains farther uprift quickly waned, and for the next three weeks eruptive activity was confined to these lower vents, hereafter called the 2,900 m vents. Six principal structures eventually formed around localized vents along this fissure, including a cinder cone at the uprift end and a lava shield at the downrift end (fig. 19.26). Lava fountains were low and never exceeded 50 m in height. By daybreak on March 26, a fast-moving flow from the 2,900 m vents had traveled 9 km to the northeast, and three shorter flows moved eastward. These latter flows directly threatened two penal facilities at 1,600 m elevation—the abandoned Mauna Loa Boy's School and the Kulani Honor Camp (figs. 19.27, 19.28). Inmates were prepared for evacuation on March 26 but the flows ceased forward movement within 48 hours and never crossed the Powerline Road above these facilities (fig. 19.28). On March 28 a 100-m-long east-west steaming fissure was noted on the north side of a prehistoric spatter cone at 2,435 m elevation, 4 km east of the lowest eruptive vents. A dike may have been intruded below this area, but if so it never broke the surface. The principal flow (flow 1 on fig. 19.28) advanced as a narrow, well-channelized

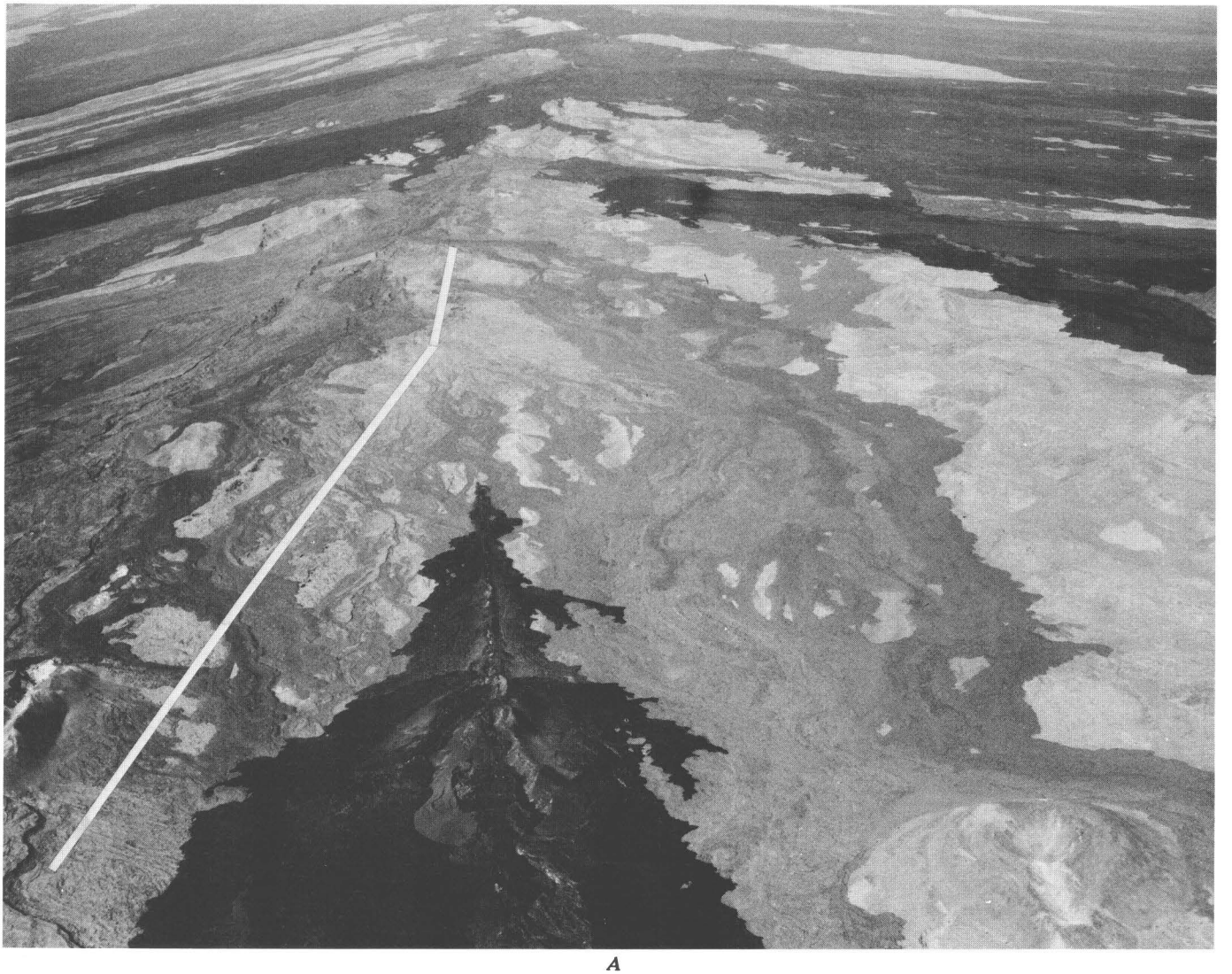

A

FIGURE 19.24.—Oblique views of middle northeast rift in area of 2,900-m vents. ***A***, Area before eruptive activity; photograph taken on September 6, 1978. ***B***, Area after March 25, 1984 eruption; photograph taken on May 5, 1984. Location where 1984 eruptive fissure later opened shown by white line in *A*. Note 1984 lava shield (arrow) at left margin of *B*. Photographs by J.P. Lockwood.

aa flow on top of and between the flows of 1852 and 1942. Although flow-advance rates slowed as the lava moved farther from the 2,900 m vents, the flow had traveled 25 km by March 29, reaching the 915 m elevation and causing concern in the city of Hilo, whose nearest buildings were then 6 km away. Several square kilometers of native rainforest were destroyed, and the copious smoke from burning vegetation (fig. 19.29), as well as large explosions from accumulations of methane gas near flow margins, accentuated the apprehension of Hilo residents.

On the morning of March 29, however, a channel levee on flow 1 collapsed at the 1,740 m elevation, 13 km upstream from the flow front. Here lava was diverted to form a second flow parallel to the first, and most of the supply to the initial lava flow was cut off. The new flow (flow 1A on fig. 19.28) also moved rapidly downslope, but did not overtake flow 1 until April 4. Another channel collapse and diversion occurred on April 5 at 2,070 m elevation, cut off the supply to flow 1A, and started a new branch (flow 1B). Lava production at the 2,900 m vents had begun to decrease in late March (Lipman and Banks, chapter 57, table 57.3) and rates of flow within the feeder channels clearly decreased (fig. 19.30). Lava in the channels became steadily more viscous (see section "Lava Petrography and Temperatures"), and channel blockages and levee

B

FIGURE 19.24.—Continued.

collapses occurred more and more frequently. These collapses restricted lava supply to the lower flow fronts, and the elevation of the lowest active flows moved steadily upslope (fig. 19.31), easing the threat to Hilo. By April 14 no active lava flows extended more than 2 km below the 2,900 m vents; the eruption ended on April 15.

On April 2 the north margin of flow 1A abutted against a 40-m-long segment of a lava diversion test barrier constructed at the 1,150 m elevation in 1977. The 4- to 5-m-high barrier impeded advance of this 10- to 12-m-thick portion of flow 1A for 6 days, but was finally overtopped by a short aa tongue on April 8, as the flow, now cut off from fresh lava supply, continued to creep forward because of gravitational downslope movement of its molten core (fig. 19.32).

The 1984 lava covered an area of about 48 km^2 (figs. 19.28, 19.33), and about 220×10^6 m^3 of lava was erupted. About 90 percent of the total volume was erupted from the 2,900 m vents. Flow thicknesses ranged from less than 1 m near short-lived vents to as much as 18 m at the distal ends of major aa flows.

As the flows cooled, a thin sublimate coating of *thenardite* (Na_2SO_4), as identified by T.E.C. Keith (written commun., 1984), formed on protected surfaces, and in late April many flows at higher, dry areas looked as if they had been dusted by a light snow.

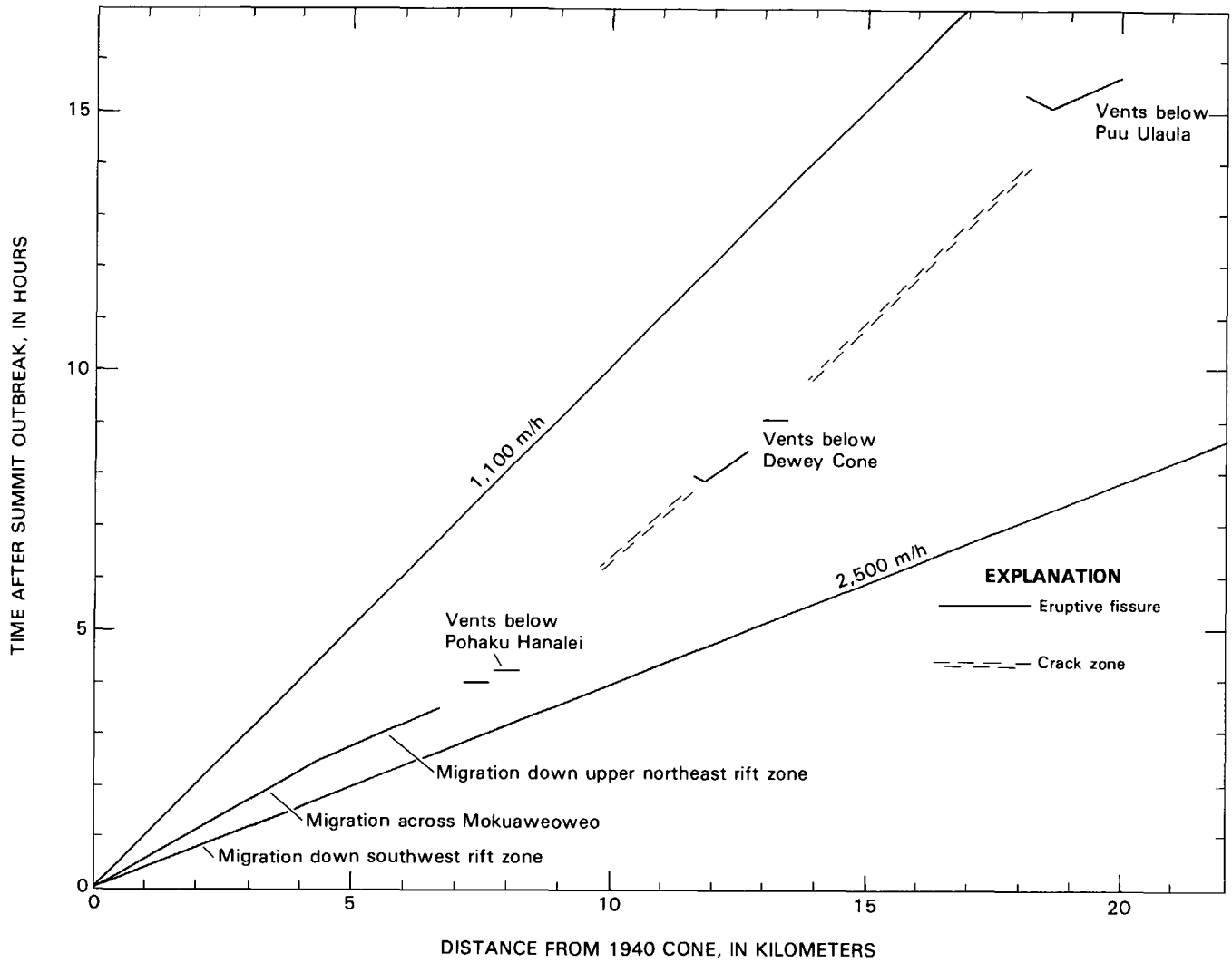

FIGURE 19.25.—Eruptive fissure (dike propagation) rates on March 25, 1984. Upside-down chevron fissure plots indicate propagation both uprift and downrift after initial surface rupture.

The thenardite was as thick as 5 mm as a mat of very fine, acicular crystals and formed after the rocks cooled below incandescence, but while still at over 100 °C. The mineral was especially common on low density (more permeable ?) aa blocks. This mineral is fragile, and water soluble, and was easily blown away by high winds; it was not seen after light rains in early May. This occurrence has apparently not been previously reported on Hawaiian lavas, although it is likely a common, but ephemeral mineral on cooling aa flows. It has also been reported as a high-temperature sublimate on the growing andesite dome of Mount St. Helens volcano (Keith and others, 1981).

A brief but spectacular eruption of Kilauea Volcano on March 30 (episode 17 of a protracted east rift zone eruption) had no effect on activity at Mauna Loa. These were the first simultaneous eruptions of Mauna Loa and Kilauea since 1919 and served to demonstrate the magmatic independence of these two volcanoes.

SEISMIC OBSERVATIONS

Although lava did not reach the surface until 0126, seismic activity had reached high levels earlier, and seven moderate earthquakes of 3.0–4.2 magnitude occurred between 0050 and 0210. This intrusion-related earthquake swarm and harmonic tremor at the summit decreased at 0215, marking the beginning of about 5 h of comparatively low seismicity (fig. 19.20), as magma migrated into the NERZ. Perhaps the elevated NERZ seismicity associated with aftershocks of the November 16, 1983, $M=6.6$ earthquake (Koyanagi and others, 1984) caused a substantial decrease in stress, which facilitated the subsequent rapid and relatively aseismic migration of magma from the summit into and along the NERZ on this morning. Or, perhaps the magma that intruded into the middle NERZ on July 6–10, 1975, was still liquid and capable of maintaining open conduits.

Between 0700 and 0915 the frequency of small earthquakes

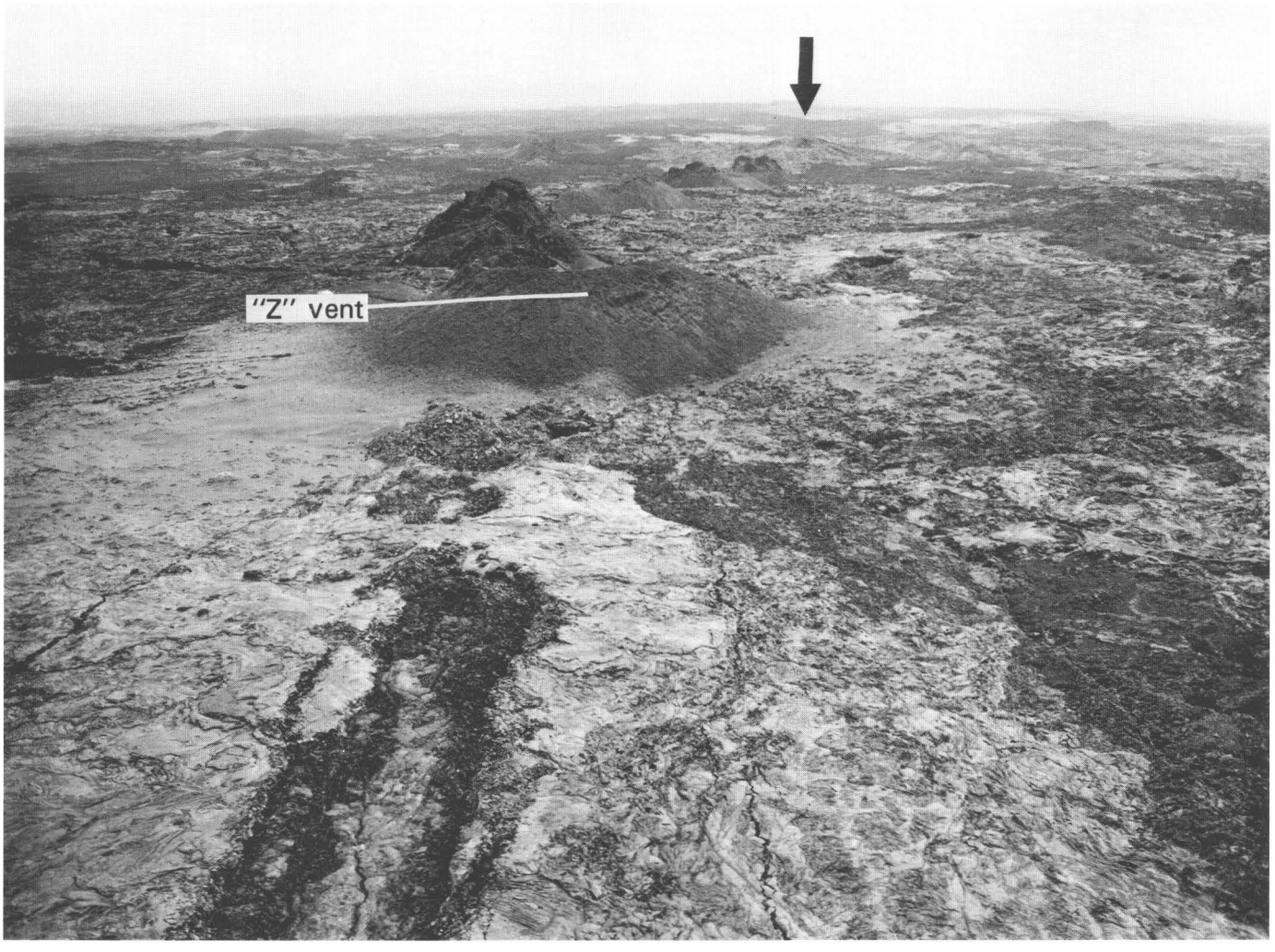

FIGURE 19.26.—Oblique view of 2,900-m vents looking downrift, with 25-m-high "Z" vent cinder cone and its tephra blanket at uprift end of vent system. This cone formed on April 8–12, and was the only vent to produce reticulite. Note lava shield at lower end of vent system (dark arrow). Cracks in foreground converge on "Z" vent and mark subsurface position of feeder dike. Note 20° bend in 1984 eruptive fissure. Photograph by J. P. Lockwood, April 30, 1985.

increased beneath the summit (fig. 19.20) and the NERZ midway between Mokuaweoweo and Puu Ulaula (fig. 19.28). At 0917 harmonic tremor increased in the NERZ, and high tremor was recorded on stations more than 30 km away. For the remainder of the vigorous eruption, tremor was centered along the NERZ and generally decreased in amplitude as a function of distance from Puu Ulaula. The dominant period of the tremor signals varied from about 0.2 to 0.7 s and also varied with recording distance from the eruption zone. Shorter period tremor dominated at stations within a few kilometers of the eruptive center. Short-period tremor was also dominant during the pre-eruptive and early eruptive stages. Tremor remained consistently strong on the seismometer nearest the eruptive site (PLA) until April 12, and after several days of low activity decayed to nearly background levels on April 15. The more distant stations MLO and HSS, located about 8 km from the center of eruption, showed highest tremor from March 25–28, followed by a lower level until April 2 and a gradual decay until the end of the eruption on April 15 (fig. 19.34).

The frequency of shallow, short-period earthquakes associated with summit subsidence started to increase on March 28. Counts peaked at 50–100 per hour on April 5–8, and they remained relatively high throughout April. These events decreased slowly thereafter and reached nearly average pre-eruption levels by mid-May. Earthquakes related to summit subsidence were mostly smaller than magnitude 1, shallower than 5 km, and centered in the caldera region. An exceptionally large earthquake on April 9, which measured $M = 3.9$, was located 2 km beneath the caldera.

Numerous small, short- and long-period earthquakes near the active vents on the northeast rift followed the cessation of eruptive activity. These events (mostly $M < 0.1$), which numbered many

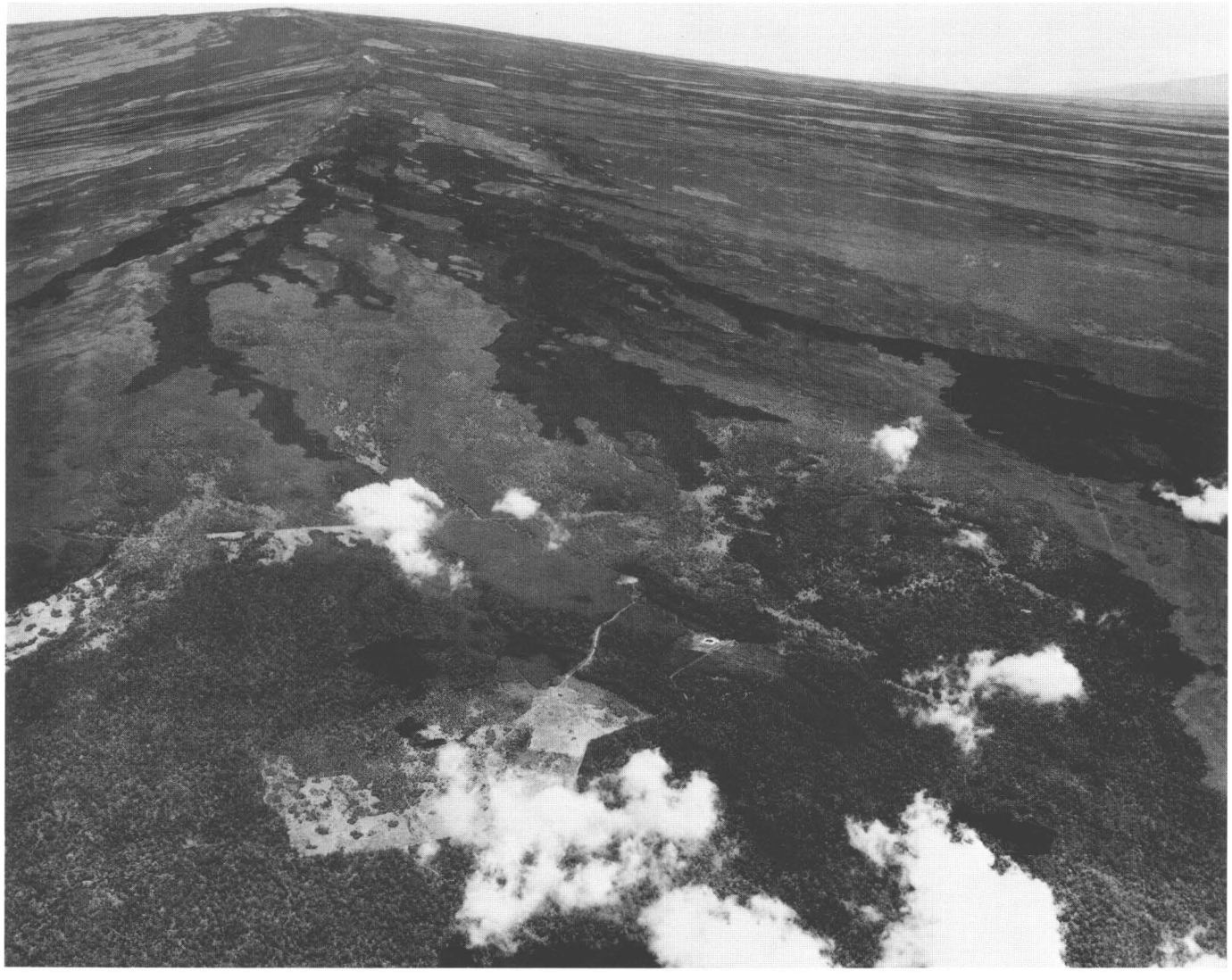

FIGURE 19.27.—Oblique aerial view of northeast rift zone showing 1984 lava (dark areas) between 2,000 and 3,000 m. Mauna Loa Boy's School is in right foreground. Kulani Honor Camp is located left of photograph margin. Lineament across center of photograph is Powerline Road. View is to west. Photograph by J.P. Lockwood.

hundreds per day in late April and throughout May 1984, were apparently caused by vent degassing activity as well as by local stresses induced by gravitational and thermal gradients; they gradually decreased to background levels (fig. 19.34).

GEODETIC OBSERVATIONS

An automatic tiltmeter located near the seismic station MOK at Mauna Loa's summit (fig. 19.19) recorded rapid surface displacements beginning at 0100 on March 25 (fig. 19.35). The initial tilt change, a sharp downward deflection to the north and west, indicated uplift of the summit region, probably caused by the sudden upward migration of magma.

A reversal in tilt direction at 0150 marked the beginning of summit subsidence and may also have corresponded to the eastward migration of eruptive vents. Subsequent spirit-level measurements at several dry tilt stations around the summit (network shown in Decker and others, 1983, fig. 13) indicated that subsidence of the summit region continued, though at a decreasing rate, for the duration of the eruption (fig. 19.36). A similar pattern of summit subsidence—contraction of several horizontal lines across the caldera—was indicated by trilateration surveys (fig. 19.37). The curves shown in figure 19.37 are similar to the decreasing lava production rate determined at the 2,900 m vents (Lipman and Banks, chapter 57, fig. 57.17). Net tilt changes between July 1983 and May 1984

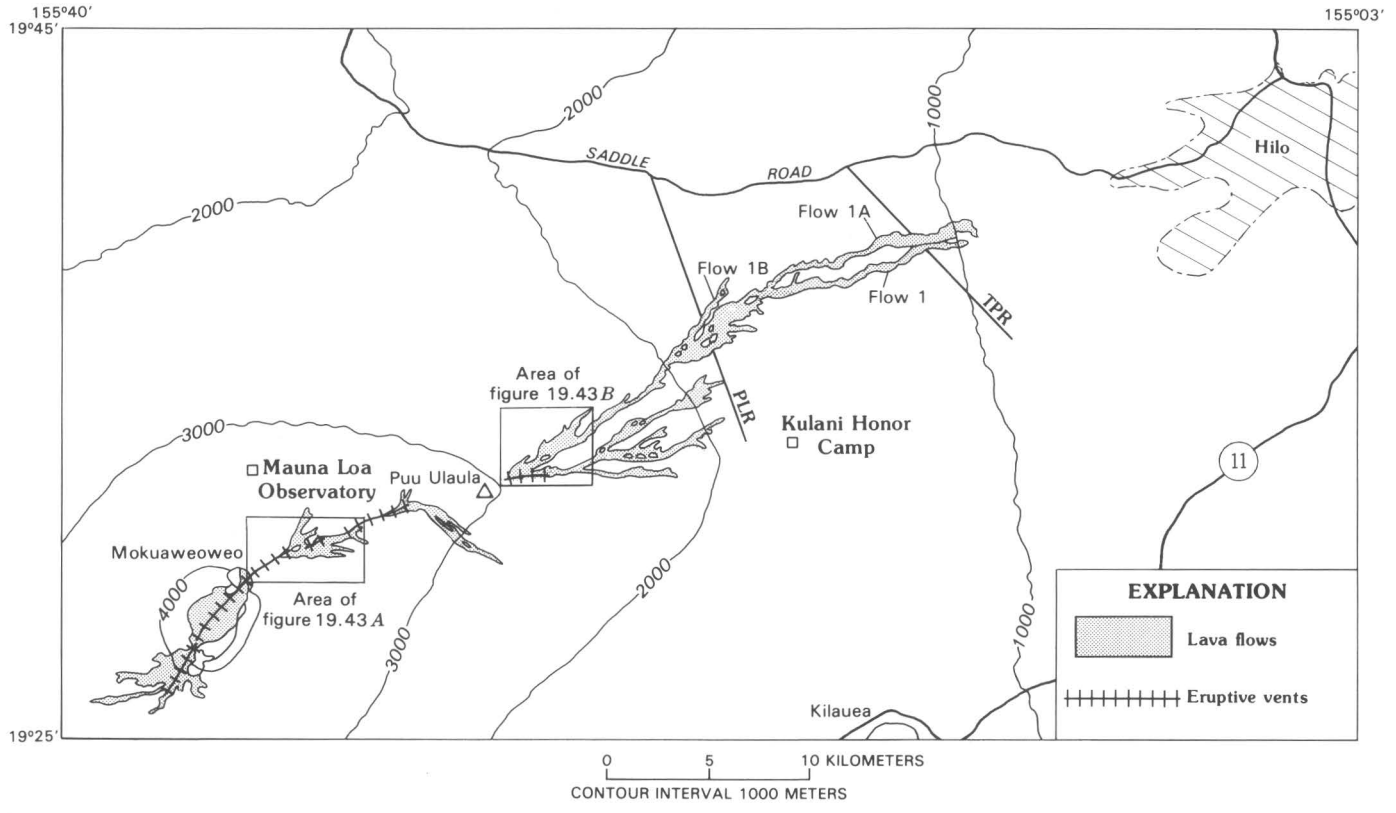

FIGURE 19.28.—Distribution of 1984 eruptive vents and lava flows and locations of figures 19.43*A*, *B*. PLR, Powerline Road; TPR, Tree-planting Road. (Modified from Lockwood and others, 1985, fig. 5.)

were 100–300 microradians at summit dry-tilt stations (fig. 19.38). The computed center of subsidence was in the southeastern area of the summit, a position identical to the center of uplift identified in 1977–1983 geodetic surveys (Decker and others, 1983). The volume of subsidence since July 1983, determined from the tilt vectors, was at least 100×10^6 m^3. Reoccupation of a 14-km-long level line that passes within 1.2 km of the subsidence center indicated that the Mauna Loa summit subsided at least 630 mm during the eruption. A resurvey of an extensive trilateration network (about 200 lines) that encompasses much of Mauna Loa indicated extension of more than 800 mm across the NERZ and compression of the adjacent flanks, which reflects dike emplacement. The dilation of the summit region was mostly accommodated by southeastward translation of the upper southeast flank, as revealed by distance measurements between the northwest summit of Mauna Loa and the summits of Mauna Kea and Hualalai Volcanoes.

GRAVITY OBSERVATIONS

A network of gravity stations on the upper slopes and summit of Mauna Loa was partly reoccupied on February 13–14, 1984. This survey, which preceded the 1984 eruption by 40 days, provided a precise datum for subsequent major changes and showed that a gravity change of only -20 ± 10 microgals (uplift) had occurred at station C-1 (fig. 19.19) in the preceding 8 years. Gravity values were determined to a precision of 10 microgals relative to a base station located 14 km distant, using two LaCoste and Romberg Model G gravimeters transported by helicopter between readings.

Reoccupation of station ML-1 (fig. 19.19) was begun within 10 h of the eruption onset and was continued on a near-daily basis. Gravity increased about 150 microgals at ML-1 during the eruption, at an exponentially decreasing rate (fig. 19.39). Because the gravity change is a function of both elevation and mass transfer changes, the exact amount of subsidence is not known.

The rate of gravity change is very similar to the exponentially diminishing rates of tilt change and horizontal strain (figs. 19.36, 19.37), which implies that the elevation change was closely tracking mass transfer changes with time. Processes such as incomplete summit collapse or extensive subaerial vesiculation are thus unlikely.

Gravity increases at C-1 (5 km from the deformation center) and ML-8 (7 km) were 61 and 19 microgals, respectively. Measurements at gravity stations on Mauna Loa's northeast flank (9, 13, and 27 km from the summit subsidence center) showed no significant changes. The rapid decay of the gravity changes with distance is consistent with a relatively shallow pressure source, as suggested by geodetic measurements.

FIGURE 19.29.—Lava flow advancing through rain forest at 950-m elevation on March 30. Flow is covering 1852 lava; more heavily forested area in lower left corner is underlain by prehistorical lava. View is to southeast. Photograph by J.P. Lockwood.

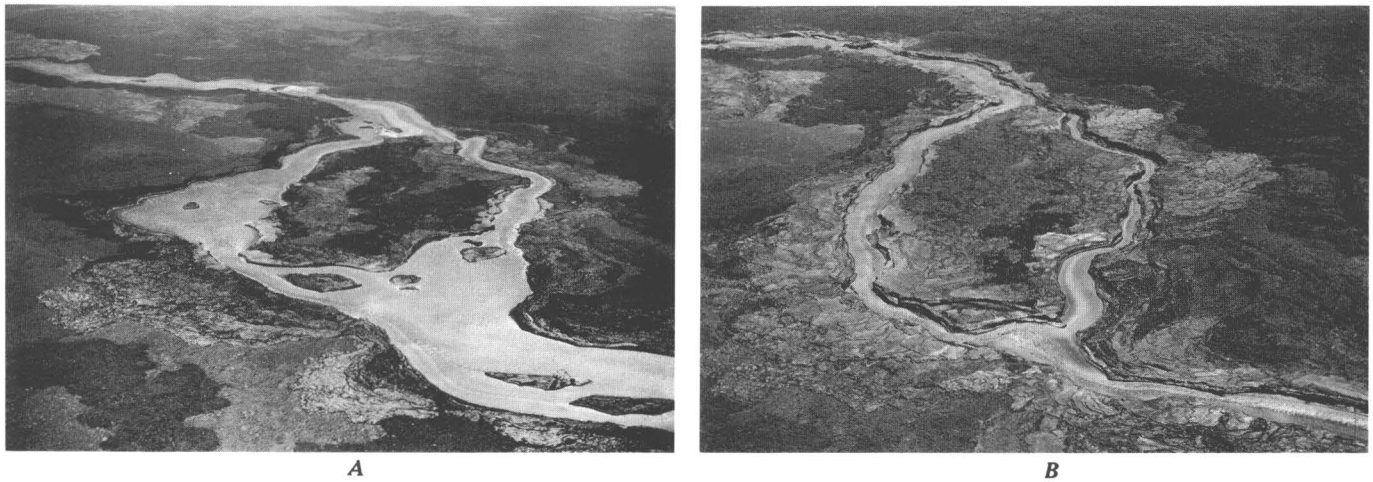

A ***B***

FIGURE 19.30.—Lava channel at 2,500 m, showing changing eruptive volumes from second to tenth day. View to east, 1852 spatter cone to left of channel. ***A***, March 26, 1984. ***B***, April 4, 1984. Photographs by J.D. Griggs.

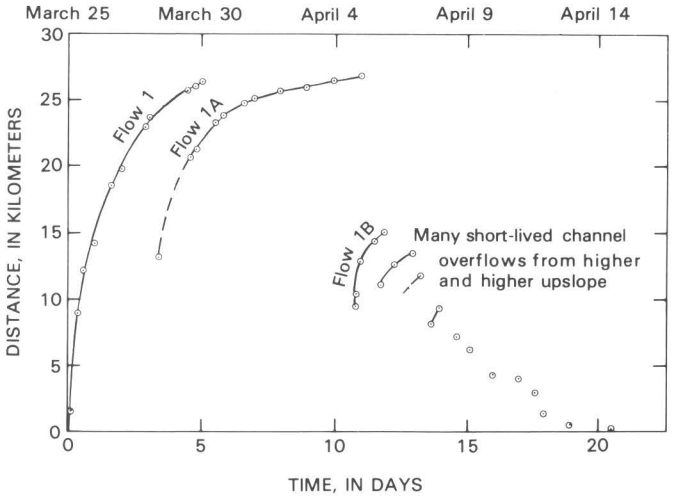

FIGURE 19.31.—Advance rates of lava flows from 2,900-m vents. Time plotted as days after initial outbreak on afternoon of March 25, 1984 (from Lockwood and others, 1985, fig. 4).

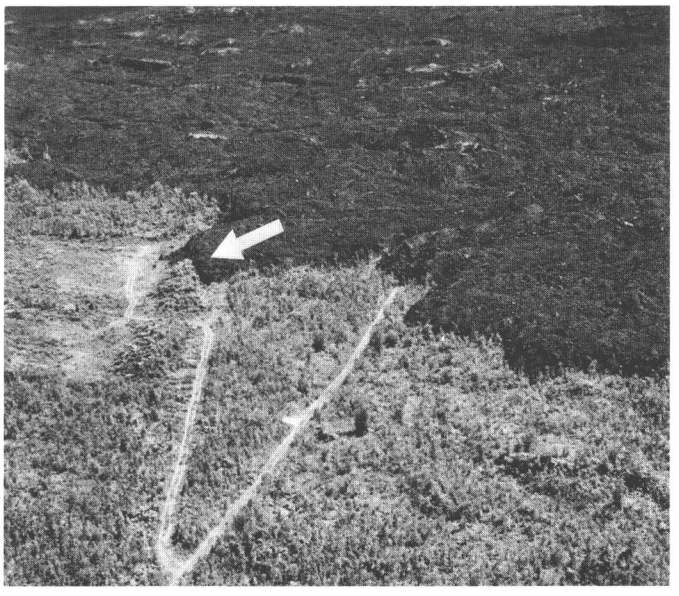

FIGURE 19.32.—Diversion of 1984 lava by U.S. Army Corps of Engineers test barriers constructed in 1977. The 4- to 5-m-high earthen barrier temporarily impeded the 1984 flows, here 14 m thick, but eventually was overtopped (arrow). View is to southeast.

GEOELECTRICAL OBSERVATIONS

A 3.8-km-long SP (electrical self-potential) line normal to the NERZ of Mauna Loa was established at about 3,000 m elevation (fig. 19.19) 9 months before the 1984 eruption. The pre-eruption SP data (fig. 19.40) show an anomaly centered over the area of the July 6–10, 1975, intrusion (Lockwood and others, 1976, p. 15). The relatively large data noise is attributed to the lack of soil or ash cover and low rainfall in this area, which produce very high electrode contact resistances.

This anomaly may indicate a zone of structural weakness that allowed upward transfer of heat. A profile along the same line on March 27, 2 days after the eruption began, shows a general increase of potentials, highest near the center of the traverse and coincident with a zone of ground cracks formed on the afternoon of March 25 (fig. 19.40).

Five days after the eruption began, VLF (very low frequency) measurements of tilt angle and ellipticity of the electromagnetic field, from a high-powered U.S. Navy radio transmitter at Lualualei, Oahu, were made along the SP profile (fig. 19.41). The steepest gradients on both the percent tilt angle and percent ellipticity curves occur approximately where they intersect at the zero crossover, a point that is nearly over the center of the anomaly-producing body.

The form of the curves suggests that the VLF anomaly is caused by a good conductor, probably with a high-angle tabular shape, directly beneath the SP high and near the center of the ground-crack zone. VLF resistivity measurements away from the conductive anomaly show high resistivity values (8,000–12,000 ohm/m); these values suggest, from an estimate of plane-wave penetration at the radio frequency used, that the depth to the top of the conductive zone is 100–150 m. The conductive body could be magma or a zone of hot, moist rocks leading to a heat source at greater depth. No emission of either steam or fume was noted from the ground cracks in this area, however, suggesting that a nonbrittle zone may have been present between the top of the shallow intrusion and the bottom of the ground cracks.

LAVA PETROGRAPHY AND TEMPERATURES

The 1984 lava consists of uniform, sparsely porphyritic tholeiitic basalt. Phenocrysts (generally less than 1 percent by volume) are euhedral to anhedral, 1- to 3-mm-diameter kinked olivine of forsteritic composition (Fo_{88-90}; M. Garcia, University of Hawaii, written commun., 1984) that is slightly to strongly resorbed, with granular pyroxene-plagioclase coronas. Similar kinked olivine in the 1959 Kilauea Iki lava has been interpreted to be of mantle origin (Helz, chapter 25). Rare clots of olivine and olivine-clinopyroxene-plagioclase intergrowths are also present. Microphenocrysts (3–30 percent) consist mostly of plagioclase laths, with slightly less abundant clinopyroxene and some olivine; all are generally less than 0.3 mm in maximum dimension. The groundmass consists of brown glass with plagioclase, granular clinopyroxene, and opaque minerals. The size and abundance of microphenocrysts increased steadily over the course of the eruption, apparently causing a concurrent increase in lava viscosity (Lipman and Banks, chapter 57; Lipman and others, 1986).

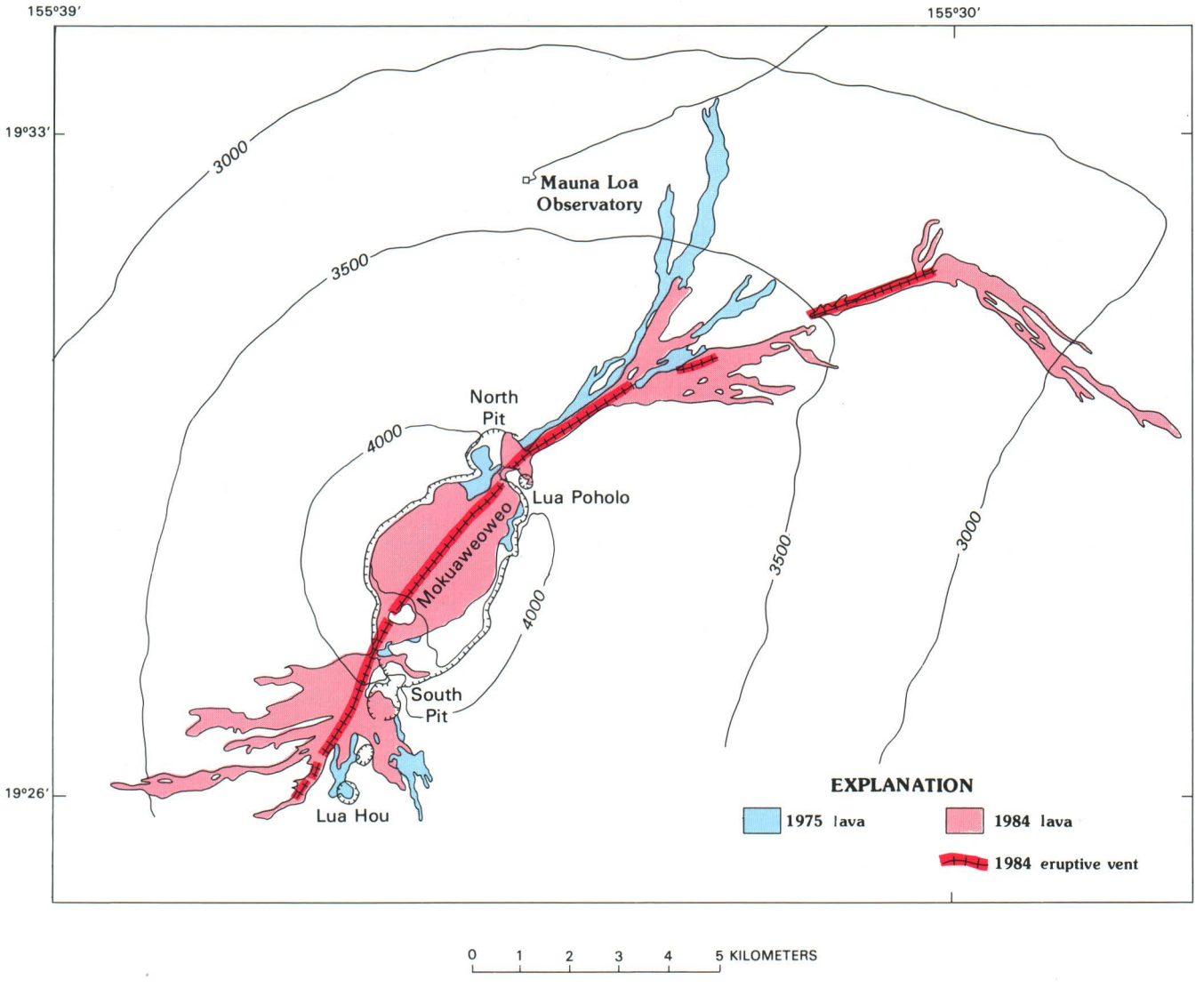

FIGURE 19.33.—Distribution of March 25, 1984, lava in summit region, showing relation to 1975 lava.

Lava temperatures were monitored throughout the eruption by Chromel/Alumel thermocouples and digital meters; the total range measured was between 1,120 °C and 1,144 °C. Fountain temperatures, measured by 2-color infrared radiometer, were generally in close agreement with the highest thermocouple temperatures obtained adjacent to the vents (Lipman and Banks, chapter 57). No changes were observed in either the fountain temperatures or in the temperatures of lava in the uppermost supply channels over the course of the eruption. The highest temperatures were obtained in lava tubes that issued from the base of spatter ramparts, although similar temperatures were obtained several kilometers downstream in the main lava channels or in overflows immediately adjacent to these channels. The lowest temperatures were obtained in thin sheet flows and in lava that appeared to have been stored for many hours or days in lava tubes. Temperatures measured in the main distributary channels decreased less than 20 °C over a total distance of 11 km downstream from the vents.

LAVA CHEMISTRY

Major-element analyses by X-ray fluorescence (table 19.3) show that the 1984 lava is remarkably uniform in composition except for one significantly more evolved sample from the SWRZ. This anomalous sample, which apparently represents contamination by older, stored magma, is not included in the analytical averages of table 19.3. With this exception, and the exception of small fluctuations in MgO content of lava erupted from the lower NERZ vents between March 25 and 30, there is little apparent difference between lava erupted along the upper SWRZ, the summit caldera, and the upper, middle, and lower segments of the NERZ. Such

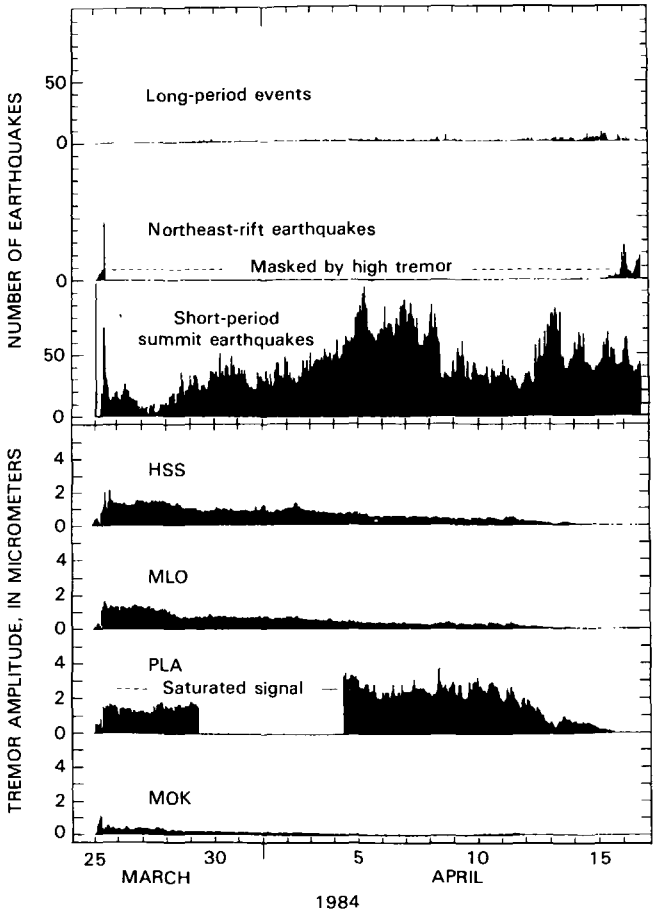

FIGURE 19.34.—Earthquake frequency (upper three plots) and tremor amplitude (lower four plots), March 25–April 16, 1984. Earthquakes as small as $M = -1$ were plotted when not masked by harmonic tremor. Harmonic tremor was read hourly at four seismic stations and plotted as micrometers of ground motion. Signals from PLA station (fig. 19.19) were saturated until April 4, when instrument sensitivity was lowered (from Lockwood and others, 1985, fig. 6).

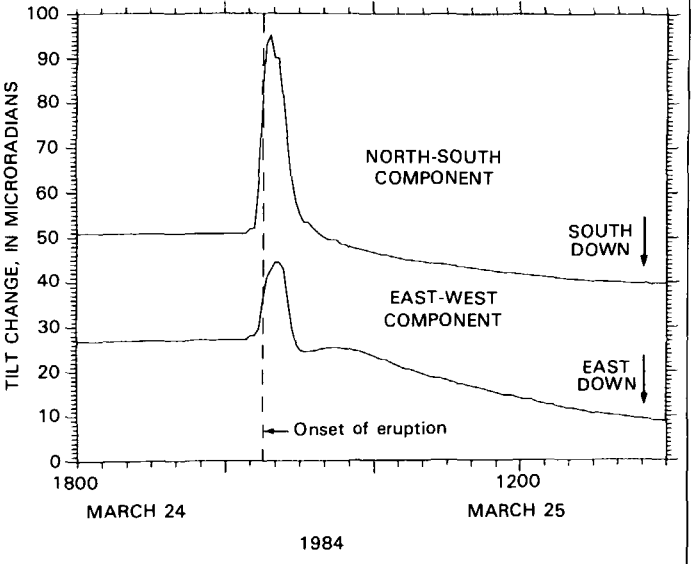

FIGURE 19.35.—Continuously recording tiltmeter record from MOK instrument for a 24-hour period beginning at 1800 H.s.t. on March 24. A positive tilt change (inflation) corresponds to a downward deflection in north and west directions (modified from Lockwood and others, 1985, fig. 7).

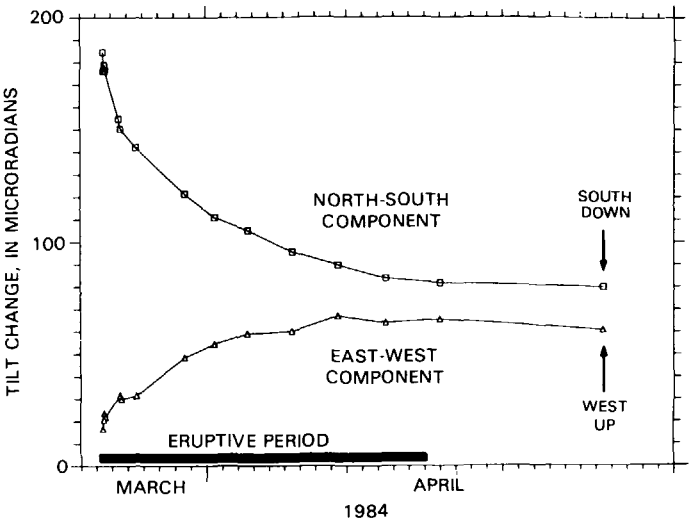

FIGURE 19.36.—Summit deflation curve determined from spirit-level (dry-tilt) measurements made near MOK station. A positive tilt change corresponds to a downward deflection in north and east directions (modified from Lockwood and others, 1985, fig. 8).

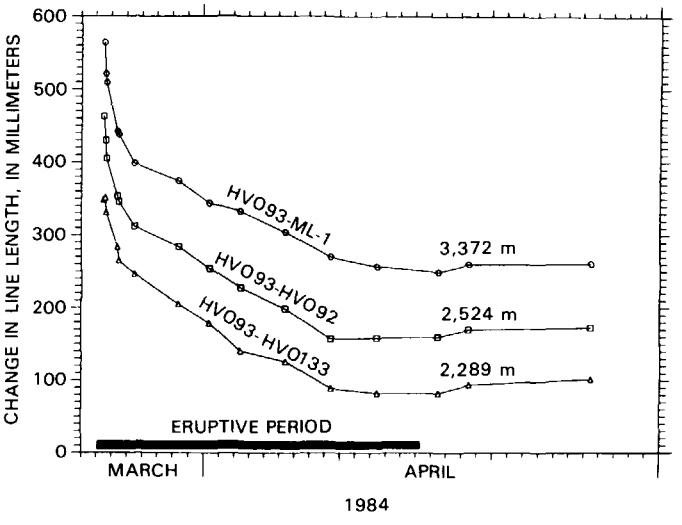

FIGURE 19.37.—Summit deflation curve determined from measurement of horizontal distances across Mokuaweoweo. Locations of survey lines are shown in Decker and others (1983, fig. 7). Line lengths from Lockwood and others (1985, fig. 9).

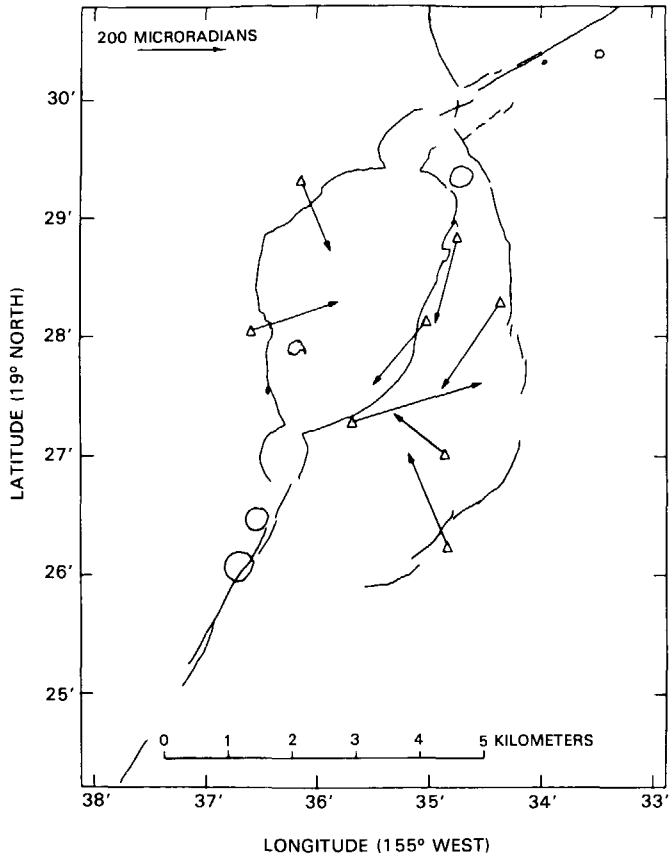

FIGURE 19.38.—Net tilt changes in summit region of Mauna Loa between June 1983 and May 1984. Triangles indicate location of spirit-level (dry tilt) stations. Vectors are drawn in direction of downward deflection of surface; length of vector shows amount of deflection (from Lockwood and others, 1985, fig. 10).

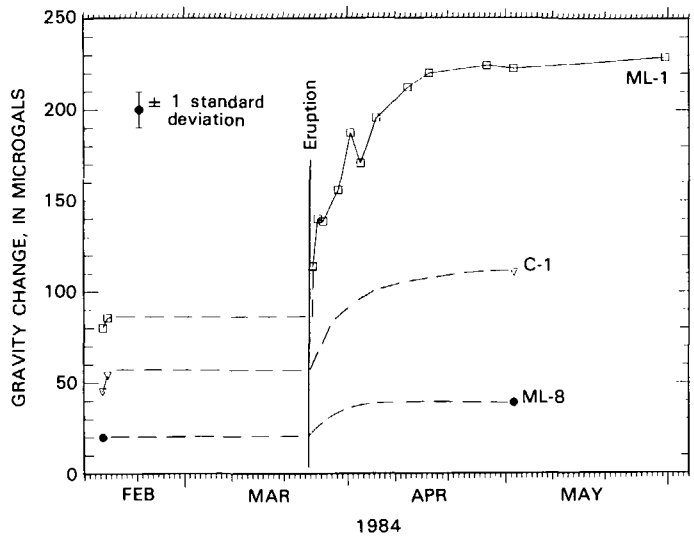

FIGURE 19.39.—Relative gravity changes at stations ML-1, C-1, and ML-8 from February 13 to May 28, 1984. Values plotted are not absolute, but only relative to February 13 datum. Dashed lines where data inferred. Data from D.J. Johnson, U.S. Geological Survey (modified from Lockwood and others, 1985, fig. 11).

homogeneity in lava composition is typical of historical Mauna Loa eruptions (Wright, 1971; Rhodes, 1983) and is consistent with the uniform lava temperature measurements.

The 1984 lava, which is slightly lower in MgO content compared with most historical Mauna Loa lava, has a composition indicative of multiple saturation with respect to olivine, clinopyroxene, and plagioclase. This lava is somewhat less evolved than the 1975 lava (table 19.1); it contains slightly less K_2O and TiO_2 and more MgO. Consequently, the 1984 lava cannot simply be residual magma remaining in shallow storage following the 1975 eruption, unless any magma stored in 1975 was less evolved than the lava erupted at that time. The combination of remarkably uniform lava composition and large eruptive volume over a 21-day period points to the ultimate derivation of this lava from a deeper reservoir of substantial size.

ERUPTIVE GASES

The 1984 eruption has yielded the first analyses ever reported for eruptive gases from Mauna Loa (Greenland, chapter 30). The gases are similar to those collected from the adjacent Kilauea Volcano, although they are lower in water and halogen content relative to sulfur (table 19.4). The low atomic C/S ratio (0.2, as at Kilauea) is attributed to pre-eruptive degassing of the magma during storage in a shallow (3–4 km deep) summit reservoir.

Thermodynamic calculations show that most samples contain excess water above that required for equilibrium with other species. Subtracting excess water from the analyses results in a calculated pO_2-temperature relation close to one directly measured in a Kilauea lava lake by Sato and Wright (1966). The excess water over that required for equilibrium in these analyses is not a meteoric contaminant but is believed to be magmatic water that has not equilibrated with the other gases because of the rapid magma rise rate.

Geographic factors had considerable influence on lava degassing. Much of the lava erupted at the 2,900 m vents was apparently partially degassed through high-temperature fumaroles along the March 25 vents between 3,400 and 3,470 m (Greenland, chapter 30). Aerial correlation spectrometer (COSPEC) monitoring showed this area of incandescent fumaroles to be a voluminous source of magmatic gas for the duration of the eruption; these fumaroles were the only source of detectable SO_2 after the end of lava production at the 2,900 m vents (J.B. Stokes, written commun., 1984). At the 2,900 m vents, high fountaining (high gas production) was most characteristic of the farthest uprift vents (including a reticulite-producing cinder cone, see fig. 19.26). At the lower end of this 1,700-m-long vent system, largely degassed pahoehoe issued continuously from a vent with almost no fountaining, constructing a 45-m-high lava shield (fig. 19.24*B*). Visible

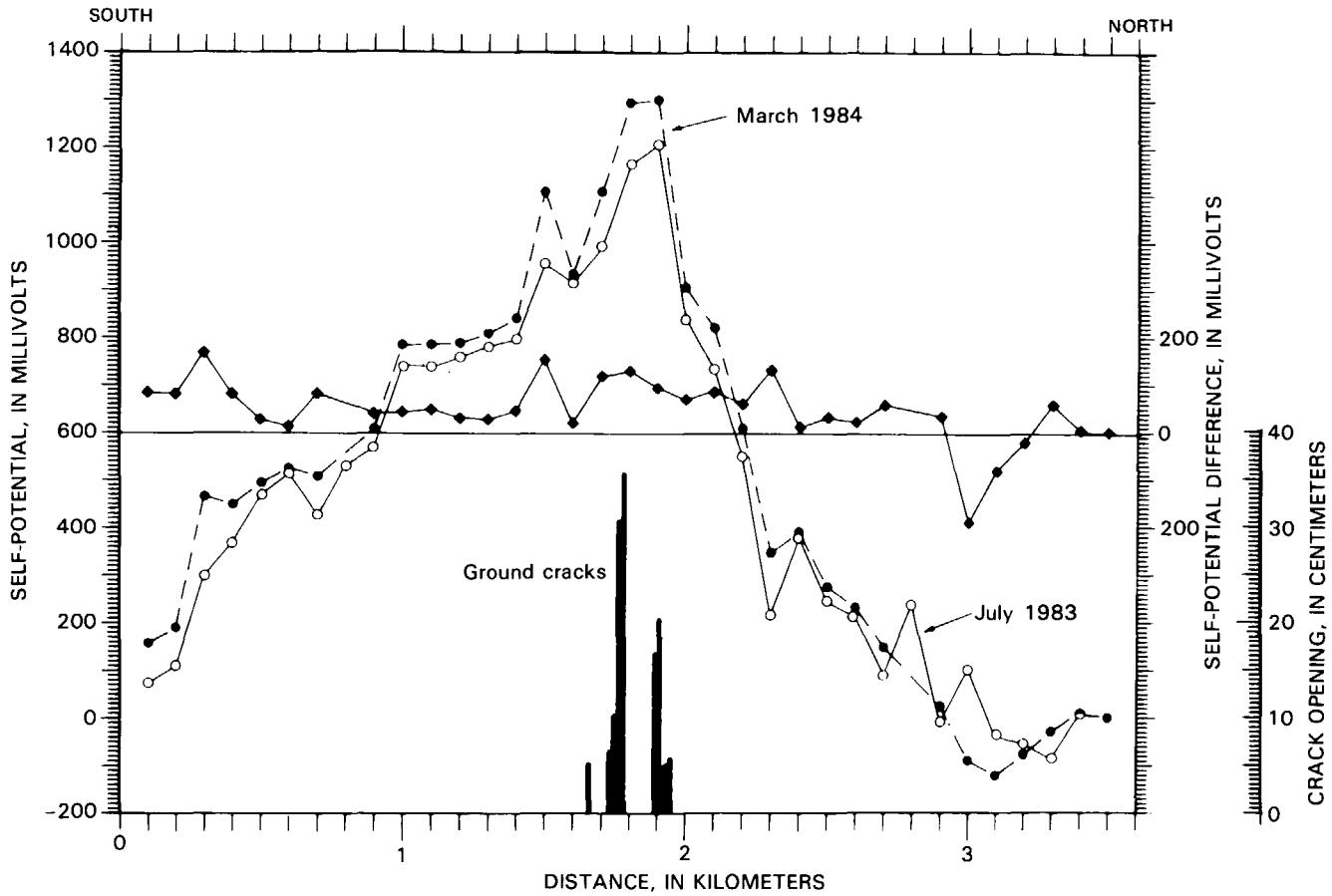

FIGURE 19.40.—Electrical self-potential (SP) profiles normal to northeast rift zone of Mauna Loa at about 3,000-m elevation, taken 9 months before 1984 eruption, and 2 days after eruption began. Locations of ground cracks that opened along profile line on March 25, 1984, are plotted on abscissa. SP data July 14, 1983 (solid lines and open circles), SP data March 27, 1984 (dashed lines and solid circles), differences between 1984 and 1983 SP data (solid lines and diamonds). Data from D.B. Jackson, U.S. Geological Survey (from Lockwood and others, 1985, fig. 12).

fume was also largely restricted to the farthest uprift of the 2,900 m vents. These circumstances may be due to vertical stratification of gas within laterally transported magma (fig. 19.42).

CONCLUSIONS: THE FUTURE

The 1975–1984 Mauna Loa eruptive sequence was the first for which extensive observations of geodetic, geoelectrical, geochemical, gravity, and temperature phenomena were possible; more has been learned about Mauna Loa inflation and eruption processes during this period than in all earlier historical eruptions.

This was Mauna Loa's first eruptive sequence since 1950 and involved the first flank eruption on the northeast rift zone since 1942. Intervals between NERZ flank eruptions have, however, been as short as 41 months (1852–1855), and posteruption geodetic measurements (figs. 19.13, 19.14) suggest inflation of Mauna Loa for her *next* eruption has already begun. As regards the volcano's long-term future behavior, we must look to the record of the past. Lava has covered the subaerial Mauna Loa surface during Holocene time at an average rate of about 40 percent per 1,000 years (Lockwood and Lipman, chapter 18, fig. 18.11). This coverage rate is likely to also characterize the long-term future, although substantial variations from this average are to be expected for shorter periods.

Most of the 32 eruptions since 1832 began with initial activity above 3,000 m elevation; 15 eruptions were limited to the summit area. The other 17 eruptions involved flank extrusion: 2 principally on the northwest flank, 7 on the southwest rift zone, and 8 primarily on the northeast rift zone. This general spatial distribution of flank eruptions will probably also characterize future activity.

Southwest rift zone eruptive loci generally migrated uprift from 1868 to 1950 (Lipman, 1980). Eruptive loci on the northeast rift zone have shown no such longitudinal distribution pattern, but have instead shown a strong tendency for southward migration with time, especially in the 20th century (fig. 19.43). The common pattern of south-stepping offset of echelon vents (fig. 19.23) is another apparent indication of this tendency for southward migration. Although

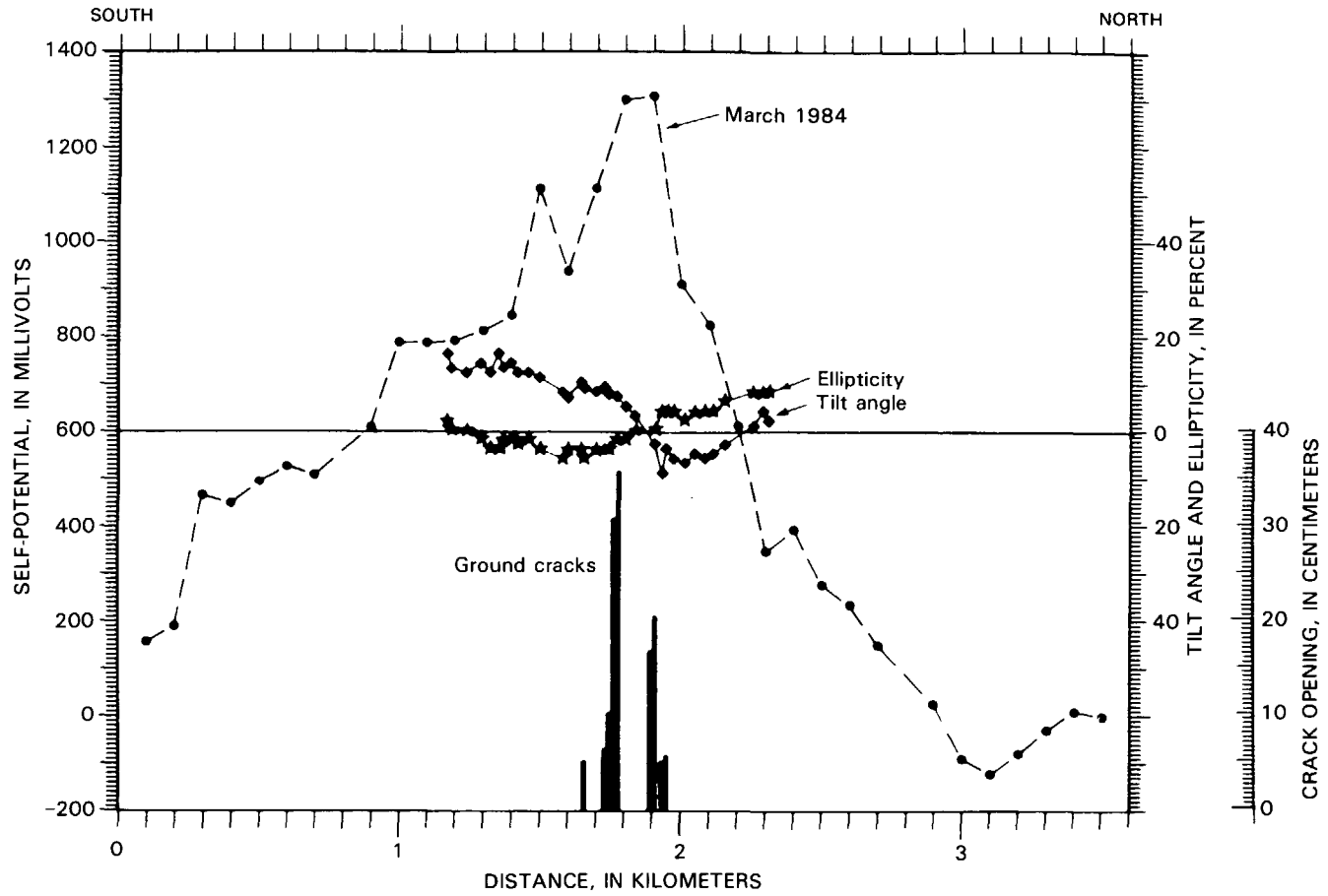

FIGURE 19.41.—Very low frequency profiles across northeast rift zone of Mauna Loa obtained on March 30, 1984. Ellipticity (stars) and tilt angle (diamonds) are shown with March 27, 1984, SP profile and ground cracks along same survey line. Data from D.B. Jackson, U.S. Geological Survey (from Lockwood and others, 1985, fig. 13).

TABLE 19.3.—*Average major-element compositions of 1984 Mauna Loa lava*

[X-ray fluorescence analyses by J.M. Rhodes. Analyses reported on volatile-free basis, with total iron reported as Fe_2O_3. *n*, sample size]

	Upper SWRZ *n*=5	Summit caldera *n*=9	Upper NERZ *n*=5	Middle NERZ *n*=5	Lower NERZ *n*=10	1975 Lava *n*=6
SiO_2	51.37	51.37	51.82	51.59	51.63	51.70
TiO_2	2.06	2.08	2.09	2.07	2.09	2.10
Al_2O_3	13.59	13.65	13.72	13.64	13.65	13.73
FeO†	11.97	12.06	12.14	12.05	12.09	12.23
MnO	.19	.18	.18	.19	.19	.16
MgO	6.75	6.73	6.68	6.66	6.81	6.55
CaO	10.54	10.51	10.55	10.48	10.51	10.51
Na_2O	2.55	2.59	2.52	2.53	2.48	2.18
K_2O	.38	.38	.38	.38	.38	.39
P_2O_5	.24	.24	.24	.24	.24	.24
Total	99.55	99.79	100.32	99.84	100.05	99.79

TABLE 19.4.—*Relative atomic compositions of Mauna Loa and Kilauea eruptive gases*

[Values shown are the ratios of atoms of the indicated elements per atoms of sulfur. Analyses by L.P. Greenland]

	Mauna Loa	Kilauea
H	6.4	16
C	.21	.26
O	5.4	10
S	1.0	1.0
Cl	.0036	.021
F	.0035	.023

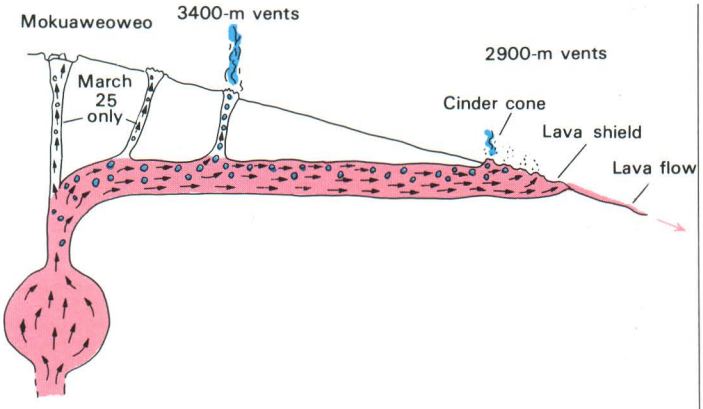

FIGURE 19.42.—Schematic longitudinal section of northeast rift zone, showing proposed degassing processes in laterally transported magma during period March 25 to April 15, 1984. Scale not internally consistent.

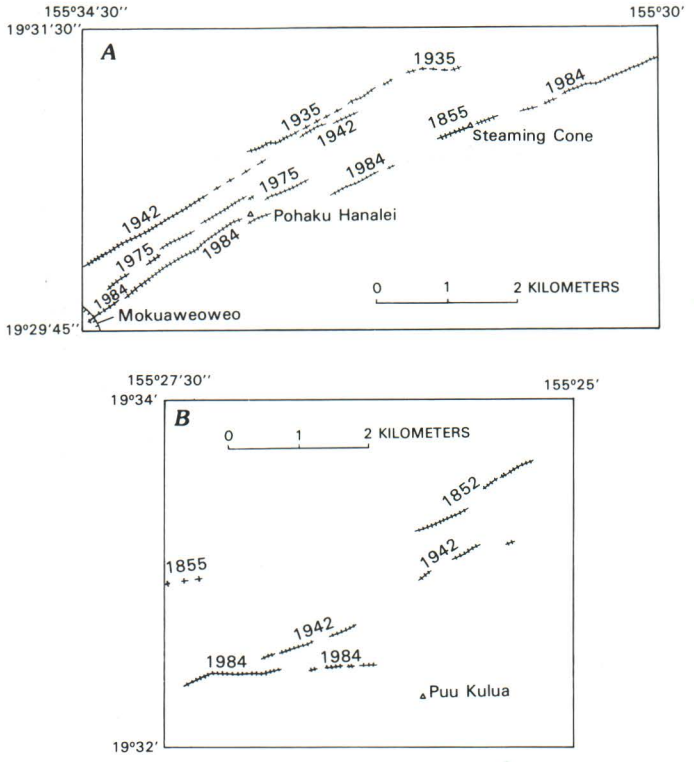

FIGURE 19.43.—Loci of historical eruptive vents at two localities on northeast rift zone. ***A***, Upper northeast rift zone, near Pohaku Hanalei. ***B***, Middle northeast rift zone, below Puu Ulaula. Figure locations shown on figure 19.28.

volumetrically more than 90 percent of historical lava flows have moved down the north side of the northeast rift zone (Lockwood and Lipman, chapter 18, fig. 18.15), future flows will preferentially flow down the south flank if the southward migration of eruptive vents continues.

REFERENCES CITED

Decker, R.W., Koyanagi, R.Y., Dvorak, J.J., Lockwood, J.P., Okamura, A.T., Yamashita, K.M., and Tanigawa, W.R., 1983, Seismicity and surface deformation of Mauna Loa Volcano, Hawaii: American Geophysical Union Transactions, Eos, v. 64, no. 37, p. 545–547.

Dutton, C.E., 1882, Hawaiian volcanoes, *in* U.S. Geological Survey Annual Report, 4th, p. 79–219.

Dvorak, J.J., Okamura, A.T., and Dieterich, James, 1983, Analysis of surface deformation data, Kilauea Volcano, Hawaii: Journal of Geophysical Research, v. 88, no. B11, p. 9295–9304.

Dzurisin, Daniel, 1980, Influence of fortnightly Earth tides at Kilauea Volcano, Hawaii: Geophysical Research Letters, v. 7, no. 11, p. 925–928.

Fiske, R.S., and Kinoshita, W.T., 1969, Inflation of Kilauea Volcano prior to its 1967–1968 eruption: Science, v. 165, p. 341–349.

Golombek, M.P., and Carr, M.J., 1978, Tidal triggering of seismic and volcanic phenomena during the 1879–1880 eruption of Islas Quemadas Volcano in El Salvador, Central America: Journal of Volcanology and Geothermal Research, v. 3, no. 3–4, p. 299–307.

Keith, T.E.C., Casadevall, T., and Johnson, D. , 1981, Fumarole encrustations—occurrence, mineralogy, and chemistry, *in* Lipman, P.W., and Mullineaux, D.L., eds., The 1980 eruptions of Mount St. Helens, Washington: U.S. Geological Survey Professional Paper 1250, p. 239–250.

Koyanagi, R.Y., Endo, E.T., and Ebisu, J.S., 1975, Reawakening of Mauna Loa Volcano, Hawaii: A preliminary evaluation of seismic evidence: Geophysical Research Letters, v. 2, no. 9, p. 405–408.

Koyanagi, R.Y., Endo, E.T., Tanigawa, W.R., Nakata, J.S., Tomori, A.H., and Tamura, P.N., 1984, Kaoiki earthquake of November 16, 1983—a preliminary compilation of seismographic data at the Hawaiian Volcano Observatory: U.S. Geological Survey Open-File Report 84–798, 30 p.

Lipman, P.W., 1980, The southwest rift zone of Mauna Loa—implications for structural evolution of Hawaiian volcanoes: American Journal of Science, v. 280-A, p. 752–776.

Lipman, P.W., Banks, N.G., Rhodes, J.M., 1985, Degassing—induced crystallization of basaltic magma and effects on lava rheology: Nature, v. 317, p. 604–607.

Lockwood, J.P., Banks, N.G., English, T.T., Greenland, L.P., Jackson, D.B., Johnson, D.J., Koyanagi, R.Y., McGee, K.A., Okamura, A.T., and Rhodes, J.M., 1985, The 1984 eruption of Mauna Loa Volcano, Hawaii: American Geophysical Union Transactions, Eos, v. 66, no. 16, p. 169–171.

Lockwood, J.P., Koyanagi, R.Y., Tilling, R.I., Holcomb, R.T., and Peterson, D.W., 1976, Mauna Loa threatening: Geotimes, v. 21, no.6, p. 12–15.

Lockwood, J.P., and Torgerson, F.A., 1980, Diversion of lava flows by aerial bombing—lessons from Mauna Loa Volcano, Hawaii: Bulletin Volcanologique, v. 43, no. 4, p. 727–741.

Macdonald, G.A., 1954, Activity of Hawaiian volcanoes during the years 1940–1950: Bulletin Volcanologique, Series 2, v. 15, p. 119–179.

Miller, J.M., and Chin, J.F.S., 1978, Short-term disturbances in the carbon dioxide record at Mauna Loa Observatory: Geophsical Research Letters, v. 5, no. 8, p. 669–671.

Mogi, K., 1958, Relations between the eruptions of various volcanoes and the deformation of the ground surface around them: Tokyo University, Earthquake Research Institute Bulletin, v. 36, p. 99–134.

Rhodes, J.M., 1983, Homogeneity of lava flows: chemical data for historic Mauna Loan eruptions: Journal of Geophysical Research, v. 88, p. A869–A879.

Ryan, M.P., Koyanagi, R.Y., and Fiske, R.S., 1981, Modeling the three-dimensional structure of macroscopic magma transport systems—application to Kilauea Volcano, Hawaii: Journal of Geophysical Research, v. 86, p. 7111–7129.

Sato, Motoaki, and Wright, T.L., 1966, Oxygen fugacities of magmatic gases from crystallizing Hawaiian tholeiite [abs.]: American Geophysical Union Transactions, Eos, v. 17, no. 1, p. 209.

Stearns, H., and Macdonald, G.A., 1946, Geology and ground-water resources of the Island of Hawaii: Hawaii Division of Hydrography Bulletin 9, 363 p.

Swanson, D.A., Duffield, W.A., and Fiske, R.S., 1976, Displacement of the south flank of Kilauea Volcano—the result of forceful intrusion of magma into the rift zones: U.S. Geological Survey Professional Paper 963, 39 p.

U.S. Army Corps of Engineers, 1980, Lava flow control, Island of Hawaii: U.S. Army Engineer District, Pacific Division [Honolulu] Review Report and Environmental Impact Statement, May 1980, 116 p.

Wright, T.L., 1971, Chemistry of Kilauea and Mauna Loa lavas in space and time: U.S. Geological Survey Professional Paper 735, p. 1–45.

Yamashita, K.M., 1981, Dry tilt—a ground deformation monitor as applied to active volcanoes in Hawaii: U.S. Geological Survey Open-File Report 81–523, 14 p.

HUALALAI VOLCANO: A PRELIMINARY SUMMARY OF GEOLOGIC, PETROLOGIC, AND GEOPHYSICAL DATA

By Richard B. Moore, David A. Clague, Meyer Rubin, *and* Wendy A. Bohrson

ABSTRACT

Hualalai Volcano is the third youngest on the Island of Hawaii. Three rift zones striking northwest, north, and south-southeast have been the loci of all late Pleistocene and Holocene eruptions. Recent detailed and reconnaissance geologic mapping and ^{14}C age determinations indicate that about 95 percent of Hualalai's surface is Holocene, about 55 percent is less than 3,000 years old, and 25 percent is less than 1,000 years old.

Tholeiitic basalt does not occur on the subaerial surface of Hualalai, but has been encountered in a few drillholes and has been dredged from the submarine portion of the northwest rift zone. We infer that Hualalai, like other Hawaiian volcanoes, is dominantly tholeiitic lava and has a thin cap of alkalic lava. The available tholeiitic basalt is mostly olivine-controlled lava that has as much as 30.8 percent MgO. Major-element, trace-element, and isotopic data indicate that Hualalai tholeiitic basalt is most similar to that of Mauna Loa but that their garnet-bearing mantle sources are different.

The subaerial alkalic lava is chiefly alkali olivine basalt with minor hawaiite and trachyte. The alkalic basalt contains varied amounts of olivine, clinopyroxene, and plagioclase phenocrysts and has as much as 16 percent MgO (ankaramite); much is differentiated beyond olivine control. Xenoliths of mafic and ultramafic rocks are common in many alkalic vent deposits and flows. The alkalic basalt of Hualalai can be produced by 5–10 percent partial melting of a source enriched in the light rare-earth elements.

Trachyte occurs in one large cone and its associated flow, as xenoliths in several basaltic vents, and in one drillhole. Gravity and aeromagnetic data support the interpretation that these rocks, the most silicic lava on the Island of Hawaii, were erupted in significant amounts during the late Pleistocene and subsequently have been thinly mantled by alkalic basalt lava flows.

Seismic studies indicate that seismicity within Hualalai is low, and there is no evidence of current magmatic movement such as occurs on Kilauea and Mauna Loa. An intrusion probably occurred in 1929, when earthquakes shook the region for more than a month. Resistivity and electrical self-potential surveys indicate that residual heat from magmatic intrusions may lie at shallow levels. We believe that Hualalai may well erupt again within the next few decades and that precursory seismic activity may be short.

INTRODUCTION

LOCATION AND GEOLOGIC SETTING

Hualalai Volcano occupies the western part of the Island of Hawaii (fig. 20.1) and makes up about half of the area commonly referred to as the Kona district. Hualalai rises to a height of 2,523 m (8,271 ft) above sea level, covers an area of about 850 km^2 (about 325 mi^2), and has a subaerial volume of about 600 km^3 (about 144 mi^3). Alkalic lava on its southern, eastern, and northeastern flanks is interbedded with tholeiitic Mauna Loa lava.

Hualalai has three rift zones that strike northwest, north, and south-southeast from a point about 5 km east of its summit. The subaerial part of the prominent northwest rift zone, 2–4 km wide (fig. 20.2), is 24 km long to the ocean; bathymetry suggests that it may continue another 70 km offshore. The ill-defined north rift zone (fig. 20.3), about 10 km long and 5 km wide, contains less than 5 percent of the vents and has been inactive during the last 2,000 years. The south-southeast-trending rift zone (fig 20.4), 3–5 km wide, is about 13 km long and, like the others, is marked by prominent cinder and spatter cones.

This progress report summarizes recent work by the U.S. Geological Survey on Hualalai, including geologic mapping, ^{14}C age determinations, petrographic studies, major-element chemical analyses, trace-element analyses, and geophysical studies.

PREVIOUS WORK

Stearns and Macdonald (1946) mapped Hualalai in reconnaissance fashion, and named all of the alkalic rocks the Hualalai Volcanic Series, which included the Waawaa Volcanics (trachyte cone and flow) at its base. These units are currently called the Hualalai Volcanics and Waawaa Trachyte Member. Macdonald (1968) noted that most of the surface vents and flows are alkali olivine basalt. Richter and Murata (1961) and Jackson and others (1981) studied xenoliths in a lava flow erupted in 1800.

Clague and others (1980) discussed the petrology of 19 prehistoric and historical alkali basalt flows of Hualalai. Clague

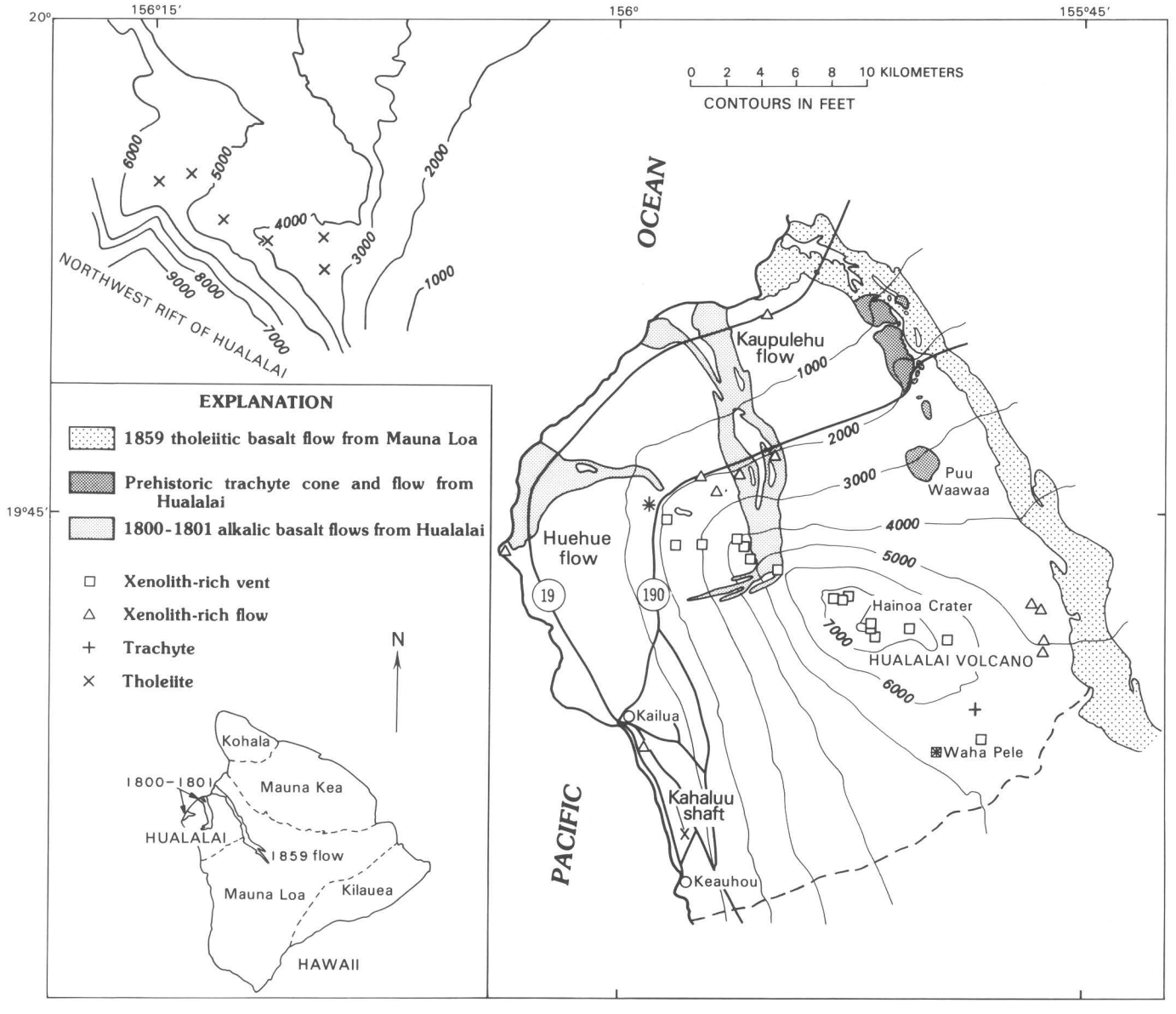

FIGURE 20.1.—Hualalai Volcano, including part of submarine northwest rift zone. Inset shows location of Hualalai on Island of Hawaii. Samples dredged from northwest rift are all tholeiitic basalt and picritic tholeiitic basalt. Symbol at Waha Pele indicates picritic tholeiitic basalt and trachyte blocks in maar deposit and xenoliths in flow from same vent. Other location with both trachyte and tholeiitic basalt, 1 km southwest of 1801 vent, is water well that encountered trachyte overlying tholeiitic basalt, both beneath more than 300 m (1,000 ft) of alkalic basalt flows. Third tholeiitic basalt location is from Kahaluu water shaft, where tholeiitic basalt occurs as shallow as 75 m (229 ft) below surface. Bathymetry from Campbell and Erlandson (1979). Dashed line marks approximate southern edge of Hualalai.

(1982) described tholeiitic basalt from the submarine northwest rift zone; much of our discussion of the tholeiitic shield lying hidden beneath the surficial alkali basalt flows is based on that study.

ACKNOWLEDGMENTS

We thank the B.P. Bishop Estate, Puu Waawaa Ranch, Huehue Ranch, Palani Ranch, and Hualalai Ranch for access to their land. Debby Kay of the USGS in Reston, Va., did the rapid-rock chemical analyses. Frank Trusdell, Jacqueline Eaby Dixon, and Richard Murnane assisted in the field. Dallas Jackson and Thomas Wright reviewed the manuscript.

STRATIGRAPHY

We have mapped all of Hualalai Volcano in reconnaissance fashion and have completed detailed mapping of lava flows and vent deposits in most of the area, including five of the eight 7½-minute

FIGURE 20.2.—Aerial view looking southeast over part of northwest rift zone of Hualalai Volcano. Mauna Loa is in background. Main 1800 vent is in center (no light-colored grass on flow), and another previously unmapped 1800 vent and flow are in lower right corner. Cone slightly to left of main 1800 vent and in front of it was nearly buried by 1800 flow.

FIGURE 20.3.—Aerial view of Hualalai Volcano from north. Dark flow in foreground is 1859 Mauna Loa flow. Large cone with pronounced radial drainage is Puu Waawaa, consisting of trachyte. A trachyte flow from that cone forms steep hummocky topography, partly casting a shadow, in center of photograph. Dark flow in front of Puu Waawaa is dated at 2,030 ± 80 yr B.P. A few small basaltic cones of the diffuse north rift zone are visible behind Puu Waawaa.

quadrangles that cover Hualalai. The mapping has been supplemented by ^{14}C ages presented in table 20.1. The generalized age-distribution map that summarizes this effort is shown in figure 20.5, and data on areas covered by lava of different age are given in table 20.2. Paleomagnetic studies (D.E. Champion, unpub. data, 1985) and future ^{14}C ages may modify these numbers slightly. The data in table 20.2 show that about 95 percent of Hualalai's surface is Holocene, as noted by Stearns and Macdonald (1946), and 25 percent is covered by lava that is <1,000 years old.

FIGURE 20.4.—Aerial view looking north-northwest across upper south-southeast rift zone of Hualalai Volcano. Most visible cones and flows are Holocene in age. Haleakala Volcano on Maui is in distance.

Hualalai has erupted about 0.2 km^3 of basalt per century during the last 3,000 years. This figure is an order of magnitude less than the 2.9 and 2.2 km^3 erupted per century by Mauna Loa and Kilauea, respectively, during historical (post-1820) time (Lockwood and Lipman, chapter 18; Macdonald, 1955).

PLEISTOCENE UNITS

Rocks of Pleistocene age that crop out on the subaerial surface of Hualalai include the Waawaa Trachyte Member (fig. 20.3), a few vent deposits and associated short flows of hawaiite, and a few alkalic basalt lava flows. Funkhouser and others (1968) reported a K-Ar age of 0.4 ± 0.3 Ma for the Waawaa Trachyte Member; more recent K-Ar determinations suggest that the trachyte is about 105 ka (G.B. Dalrymple, written commun., 1985). The volume of the Waawaa cone and flow is about 5.5 km^3, the largest volume single eruption known on the island.

The oldest dated basaltic flows on Hualalai are three flows of age 12–13 ka; each overlies another basalt flow of limited areal extent. We consider it unlikely that any older large flows will be discovered.

A cluster of cones that are mostly Pleistocene in age occurs in the summit area of the volcano (fig. 20.6). Lava dated at 12,950 ± 150 yr B.P. underlies the northeastern part of the village of Kailua and could have come only from the summit area. The summit crater (fig. 20.6) exposes dozens of flow units that suggest eruption on a satellitic shield, like Mauna Ulu on Kilauea Volcano. Near the end of the shield-building eruption, phreatic explosions ejected blocks of gabbro and diabase from a subsurface intrusion. Overlying the resulting tuff is a thin (≤1 m) lava flow of mixed hawaiite and alkali olivine basalt. A cone that overlies all of these deposits has been dated at 8,770 ± 200 yr B.P.

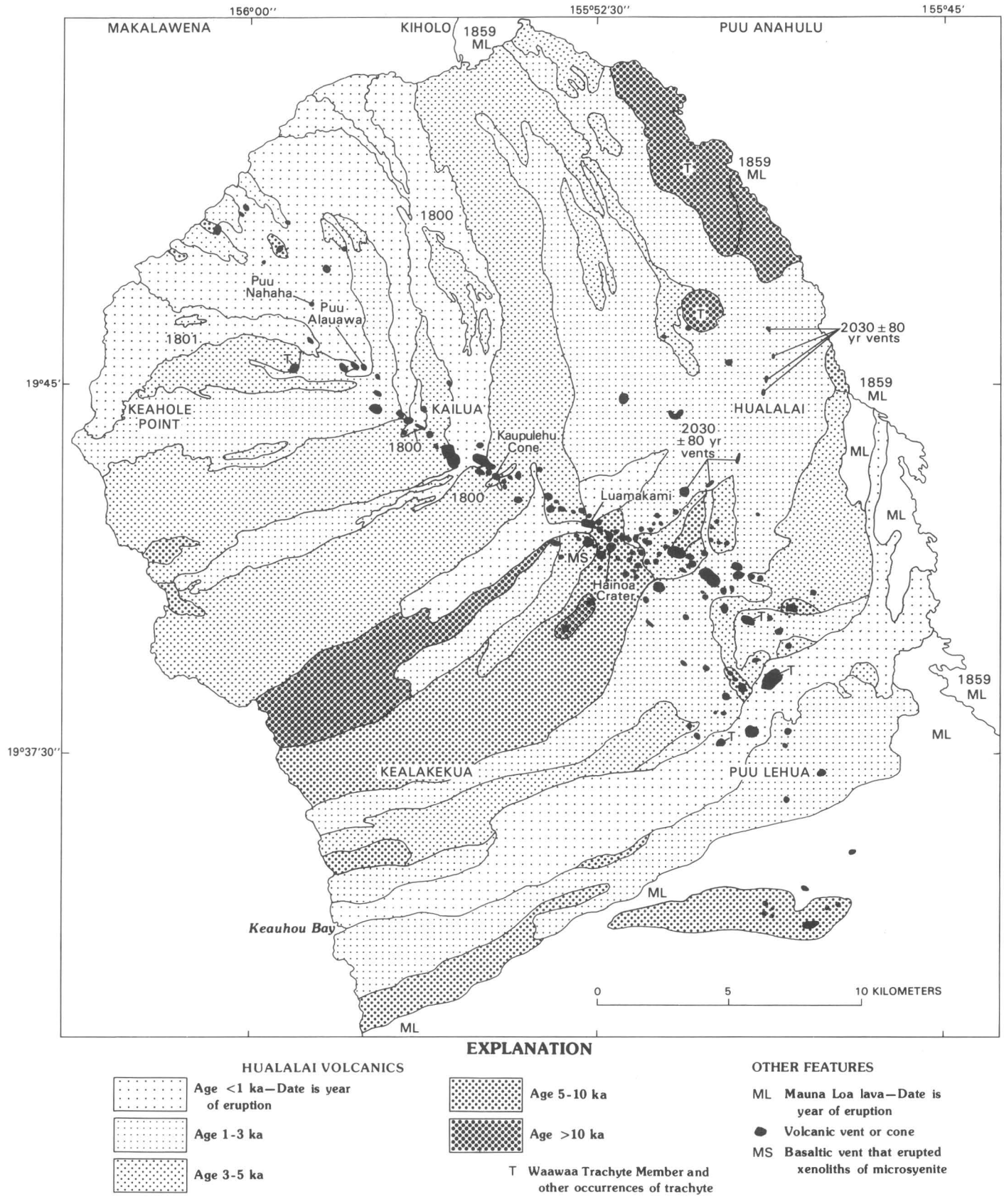

FIGURE 20.5.—Generalized geologic map of Hualalai Volcano showing age distribution of lava and locations of vents. Not all smaller vents are shown. Names of USGS 7½-minute topographic quadrangles used in mapping are shown in all capital letters.

TABLE 20.1.—*Carbon-14 ages of samples from Hualalai Volcano*

Sample	Laboratory Number	Age (yr B.P.)	Unit from which sample taken
79-15	W-4634	<200	An A.D. 1800 lava flow
82-75	W-5124	<200	An A.D. 1800 lava flow
79-8	W-4394	300±60	Young Luamakami flow
84-175	W-5531	710±150	Waha Pele flow
84-150	W-5491	900±110	Flow from large vent 3 km northeast of Waha Pele
82-129	W-5130	1030±60	Flow from cone 2 km northwest of Luamakami
84-170	W-5522	1180±200	Flow from vent 4.5 km north-northwest of Waha Pele
78-2	W-4171	2030±80	Flow from vent 3 km southeast of Puu Waawaa
79-3	W-4388	2290±70	Flow from vent 1 km west of Waha Pele
82-20	W-5068	2350±80	Old Luamakami flow
82-8	W-5073	2390±60	Cone 3 km northeast of Hainoa Crater
82-19	W-5076	2670±80	Cone 700 m east-northeast of Hainoa Crater
84-115	W-5559	3030±200	Flow 8 km northwest of Hainoa Crater
82-113	W-5127	3100±80	Cone 700 m northwest of Luamakami
78-12	W-4376	3600±70	Flow along Highway 190 4 km north-northwest of Kailua
84-119	W-5562	3610±200	Flow 900 m west of Puu Waawaa
82-131	W-5132	3990±70	Spatter 300 m northwest of Hainoa Crater
82-23	W-5070	4390±70	Flow from cone 1 km west of Hainoa Crater
79-10	W-4378	4720±80	Second highest flow in west Malekule pit crater
83-9	W-5297	6360±100	Flow from cone 1.6 km southeast of Hainoa Crater
83-14	W-5299	8770±200	Cone 60 m north of Hainoa Crater
78-5	W-4371	9490±100	Flow 10 km north-northwest of Puu Waawaa
78-11	W-4391	10,370±150	Flow 3 km north-northwest of Keauhou Bay
79-1	W-4365	12,230±150	Flow 4 km north of Puu Waawaa
82-1	W-5056	12,950±150	Flow 3 km east northeast of Kailua

TABLE 20.2.—*Areas of Hualalai Volcano's surface covered by lava of different ages*

[Quadrangle names refer to USGS 7½-minute topographic map sheets; percent figures give the percentage of the Hualalai part of each quadrangle covered by lava of that age group]

Quadrangle	Age group of lava: <1 ka		1-3 ka		3-5 ka		5-10 ka		>10 ka	
	(km^2)	(percent)	(km^2)	(percent)	(km^2)	(percent)	(km^2)	(percent)	(km^2)	(percent)
Makalawena -----	22	68.3	5	15.5	5	15.5	0.2	0.6	0	0
Kiholo ---------	95	59.2	25	15.6	40	24.9	0.5	0.3	0	0
Puu Anahulu ----	0	0	48	57.5	8	9.6	0.5	0.6	27	32.3
Hualalai -------	29	18.1	72	45.0	42	26.3	17	10.6	0	0
Kailua ---------	16	8.8	27	14.8	78	42.9	44	24.2	17	9.3
Keahole Point --	2	3.6	16	28.6	36	64.3	2	3.6	0	0
Kealakekua -----	21	27.3	24	31.2	10	13.0	22	28.6	0	0
Puu Lehua ------	16	27.1	25	42.4	2	3.4	16	27.1	0	0
Total ----------	201	24.8	242	30.0	221	27.3	102.2	12.6	44	5.4
Cumulative Percent -------		24.8		54.8		82.1		94.7		100.1

HOLOCENE UNITS

We have divided the Holocene lava flows of Hualalai into four age groups, based on our detailed and reconnaissance mapping and on ^{14}C ages: 10–5 ka, 5–3 ka, 3–1 ka, and <1 ka. About 55 percent of the surface has an age of less than 3 ka and 25 percent less than 1 ka. In contrast, Holcomb (1981) determined that 90 percent of the surface of Kilauea Volcano is younger than 1 ka, and Lockwood and Lipman (chapter 18) found that 40 percent of Mauna Loa is younger than 1 ka.

Inspection of figure 20.5 suggests that locations of vents of different ages are generally random; however, two important aspects of the volcano's overall morphology require discussion. First, the coastal part of the volcano north of the town of Kailua (figs. 20.5, 20.7) is a lava delta that has been built mostly in the last 3,000 years. The northwest rift zone, marked by spatter cones and ramparts, forms the axis of this feature; lava has built the volcanic pile nearly equally on both sides of the rift zone.

Second, the coast south of Kailua is relatively straight (fig. 20.7), and lava deltas are fewer. Some of the oldest subaerial flows on the volcano occur in this area; marine erosion typically has straightened the shoreline, whereas farther north erosion has not overcome the constructional landforms.

Several vent deposits and associated flows of Holocene age merit individual description. The eruptions of 1800–01 occurred from five separate vent areas (fig. 20.5) and extruded more than

FIGURE 20.6.—Aerial view looking north over summit area of Hualalai Volcano. Actual summit at elevation 2,521 m (8,271 ft) is between two large craters in center of photograph. Small crater barely visible just beyond Hainoa Crater (largest crater) is dated at 8,770 ± 200 yr B.P.; cone in right middle distance is dated at 2,670 ± 80 yr B.P.

FIGURE 20.7.—Aerial view looking north along western coast of Hualalai Volcano. Keauhou Bay is in foreground, dark flow from Waha Pele forming its north side. Town of Kailua is in middle distance. Lava flow of 1801 is large dark patch in distance.

300×10^6 m^3 of alkali olivine basalt. The main 1800 flow swept more than 30 m up a cone 450 m north of the vent (fig. 20.2), carried hundreds of thousands of large mafic and ultramafic xenoliths (fig. 20.8) farther downslope, and destroyed fishing villages when it reached the sea (Brigham, 1909).

The 1801 vents of the Huehue flow form a spatter rampart aligned down the slope of the volcano. This orientation caused the lava to flow longitudinally within the rampart. The flows are almost entirely tube-fed pahoehoe. A second vent slightly uphill and south of the main 1801 vents fed a small flow that overlies the main 1801 flows. This younger 1801 vent must have had extremely gentle eruptive activity because no rampart or cone was constructed along the eruptive fissure. A previously undiscovered 1800–01 vent at 1,296-m (4,250 ft) elevation on the northwest rift zone fed small aa flows down both the north and west flanks of the rift system. The fifth 1800–01 vent occurs within the much older Kaupulehu cone. The eruption veneered part of the cone and fed small flows in three directions. The eruptive sequence of the five vents is not known, but the main activity of the eruptive sequence appears generally to have migrated downslope.

The next youngest major eruption apparently occurred from Luamakami, 1 km northwest of the summit, at 300 ± 60 yr B.P., and produced flows that swept down both the north and southwest flanks of Hualalai. After extrusion of about 200×10^6 m^3 of alkali olivine basalt, collapse at one vent caused a minor phreatic explosion that deposited fragments of contact-metamorphosed basalts derived from the walls of the conduit (fig. 20.9).

The next youngest major eruption occurred at Waha Pele, on the south-southeast rift zone (figs. 20.10, 20.11), at 710 ± 150 yr B.P. As basaltic magma approached the surface, it apparently intersected a perched water table, resulting in massive phreatic explosions. Fragments of trachyte and basalt as large as 0.4 m in diameter were distributed over an area of at least 10 km^2. Later in the eruption, basaltic magma reached the surface, vigorous Strombolian activity built a wide low cone of spatter, and a large flow was extruded. This flow, which has a subaerial volume of at least 400×106 m^3, entered the sea, forming the north side of Keauhou Bay (fig. 20.7), and continued underwater for less than 1 km (J.G. Moore and D.A. Clague, unpublished data). Xenoliths of gabbro and dunite are locally common in the flow.

Another sequence of eruptions occurred on the northwest rift about 800 years ago. The vents formed then include Puu Nahaha, Puu Alauawa, and an unnamed vent about 200 m uprift from Puu Alauawa. Puu Nahaha is the oldest of these three vents and erupted mainly olivine-poor aa that flowed to the ocean on a broad front. Puu Alauawa is the next youngest and erupted plagioclase-rich pahoehoe that formed a large channel and tube system on the steep

FIGURE 20.8.—Xenoliths of 1800 Hualalai flow. Note that most of host basalt has drained away.

FIGURE 20.9.—East rim of Luamakami, Hualalai Volcano. Light-colored rocks, mainly on right, are thermally metamorphosed basalt ejected during phreatic explosion at end of eruption 300 ± 60 yr B.P.

slopes near the vent. Finally, the unnamed vent erupted and formed both pahoehoe and aa flows of olivine-rich lava. A perched lava pond formed above the eruptive fissure; no rampart or cone exists. These flows were dominantly constrained within the channel and tube system developed during the eruption of Puu Alauawa, and the result was a large flow that traveled about 10 km (northwestward) to the ocean, forming a lava delta about 3 km wide. Most of the short flows near the vent are dense aa flows, whereas the main flow is pahoehoe that partly transforms to a slabby aa near the ocean. These eruptive vents migrated uprift during the eruptive sequence. The ages of their flows are constrained by identical and unique paleomagnetic orientations for the earliest and latest flows (D.E. Champion, written commun., 1985).

FIGURE 20.10.—Waha Pele area of Hualalai Volcano from the east. Waha Pele, dated at 710 ± 150 yr B.P., is in center of photograph (arrow); dark flow from it extends to left out of photograph. Cone and flow just beyond it is dated at 2,290 ± 70 yr B.P. Light-colored areas in foreground and middle distance are underlain by trachytic debris ejected during phreatic first phase of Waha Pele eruption. Cone in right foreground consists of ankaramite with abundant mafic and ultramafic xenoliths. Part of Kailua is visible in distance.

FIGURE 20.11.—Aerial view north across part of the south-southeast rift zone of Hualalai Volcano. Waha Pele and its flow are in foreground; grassy light-colored areas just beyond Waha Pele are underlain by explosively ejected trachyte debris. Flow in right middle distance is dated at 900 ± 110 yr B.P. Large lava channel below horizon in center is part of extensive flow dated at 1,180 ± 200 yr B.P. Sharp cone on left horizon probably is about 3,000 years old; note prominent pahoehoe channel issuing from it. Part of Kohala Volcano is in distance.

An unnamed vent 3 km northeast of Waha Pele (fig. 20.12) erupted about 900 ± 110 years ago. Initial high fountaining distributed basaltic cinders and small xenoliths of trachyte over a wide area and built a large low spatter cone about 1 km in diameter and 40–60 m high. Continued voluminous production of lava constructed a satellitic shield within the older cone, and floods of lava

FIGURE 20.12.—Unnamed vent 3 km northeast of Waha Pele. This vent, dated at 900 ± 110 yr B.P., is source of flow on right side of figure 20.10. Note partly collapsed satellitic shield in lower left corner; shield fills crater of older spatter cone that formed during early stages of eruption.

rafted away parts of the cone. The flow, which has an estimated volume of 800×10^6 m^3 (one of the largest in Hawaii), moved 4 km south and 12 km north-northeast of the vent. The final events in the eruptive history of this remarkable vent were collapse of the summit of the shield to form small nested pit craters and a small eruption of alkali olivine basalt, richer in olivine and plagioclase phenocrysts than the previously erupted material, that built a small cone and flow within one of the pit craters.

Underlying part of the previously described flow are the products of another large eruption that occurred at 1,180 ± 200 yr B.P. The vent for this eruption, again unnamed, is 4.5 km north-northeast of Waha Pele. High fountaining distributed basaltic cinders and xenoliths of trachyte over a wide area. Voluminous pahoehoe flows spread northeast and southeast. These flows, which we have not yet finished mapping, are thinner than those of the 900-year-old eruption but still have a volume in excess of 400×10^6 m^3.

The youngest eruption on the diffuse north-trending rift zone occurred at about 2,030 ± 80 yr B.P. This eruption was unusual in that left-stepping echelon eruptive vents, which occur over a distance of 8 km, cut obliquely across the general strike of the rift zone, changing orientation from N. 10° W. at the northern end to N. 50° E. at the southwestern end (fig. 20.5). Similar changes in vent alignment occur over shorter distances on the northeast rift zone of Mauna Loa. It appears that the eruptive dike was fed from a reservoir beneath Hualalai's summit and followed a radial fracture extending northeastward. When it reached the northeast flank of Hualalai, a stress field probably induced by Mauna Kea caused a change in strike of the eruptive vents until they were parallel to the edge of the Mauna Kea edifice. Lava erupted at the lower elevation (1,130 m; about 3,700 ft) first and gradually broke out higher on the volcano's flank to the south and southwest as the eruption progressed, reaching elevations around 1,830 m (about 6,000 ft). We estimate the volume of this eruption to be at least 400×10^6 m^3.

PETROLOGY

THOLEIITIC SHIELD STAGE

Flows of tholeiitic basalt and picritic tholeiitic basalt of the shield stage are not exposed on the subaerial surface of Hualalai. However, the presence of a tholeiitic shield beneath the subaerial alkalic flows is confirmed by the recovery of tholeiitic basalt by dredging on the submarine northwest rift zone (Clague, 1982). In addition, tholeiitic basalt has been recovered in several water wells, and picritic tholeiitic basalt occurs as xenoliths at Waha Pele; these rocks probably are from subsurface parts of Hualalai.

The locations where tholeiitic lava has been found are shown in figure 20.1, and chemical analyses of several samples are presented in table 20.3. The discovery of tholeiitic basalt from Hualalai indicates, as with other Hawaiian volcanoes, that the vast bulk of the volcano is made of tholeiitic lava and that alkalic lava occurs in relatively small volume in the late stages of volcano growth (Clague, 1982).

The submarine tholeiitic basalt samples contain only olivine and spinel phenocrysts with the exception of two samples that also contain plagioclase and clinopyroxene. The picritic tholeiitic basalt samples contain euhedral olivine phenocrysts, subhedral to anhedral kink-banded olivine xenocrysts, extremely rare orthopyroxene

TABLE 20.3.—*Compositions of tholeiitic basalt samples from Hualalai Volcano*

[Major elements analyzed by X-ray fluorescence by J.S. Wahlberg, J. Taggart, and J. Baker; partial chemistry by B. Lai, H. Neiman, and E. Engleman, trace elements by X-ray fluorescence by H.J. Rose, J. Lindsay, B. McCall, G. Sellers, and R. Johnson; all of the USGS. KK7812–11 and KK9–2 are submarine samples from the northwest rift zone; K–11 and K–13 are from the Kahaluu water shaft (fig. 20.1)]

Sample	KK7812-11	K-13	K-11	KK9-2
	Major elements (weight percent)			
SiO_2	46.8	51.1	51.4	50.8
Al_2O_3	8.48	13.0	13.8	13.3
Fe_2O_3	1.29	3.03	5.67	2.33
FeO	10.4	8.16	5.79	8.43
MgO	23.0	9.79	7.86	7.57
CaO	6.49	10.3	10.6	10.6
Na_2O	1.36	2.01	2.05	2.15
K_2O	.20	.25	.22	.33
H_2O^+	.20	.04	.17	.36
H_2O^-	.08	.07	.27	.05
TiO_2	1.33	1.95	1.97	2.14
P_2O_5	.14	.18	.16	.24
MnO	.12	.17	.17	.16
CO_2	.04	.03	.28	<.01
Total	100.0	100.1	100.4	98.4
	Trace elements (ppm)			
Rb	4	3	<2	8
Sr	168	244	244	296
Y	14	22	25	24
Zr	77	100	97	131
Nb	<5	<5	7	12

xenocrysts, and rare small gabbroic xenoliths. The olivine-porphyritic and picritic samples plot on olivine-control lines and can be related by fractionation and accumulation of olivine of variable forsterite content. Hualalai tholeiitic basalt has trace-element and isotopic ratios distinct from Mauna Loa, Kilauea, and Loihi tholeiitic basalt and is also isotopically distinct from the overlying alkalic basalt (Clague, 1982). These differences are illustrated in table 20.4, which shows that Hualalai tholeiitic basalt is most similar to that of Mauna Loa, but that the trace-element and isotopic differences between tholeiitic basalt from the different volcanoes require that the source regions be different compositionally. The large variations in La/Yb and La/Y ratios indicate a major role for garnet in the generation of Hawaiian tholeiitic basalt. Further modeling of the major-element, trace-element, and isotopic data is in progress and will be presented elsewhere.

TABLE 20.4.—*Elemental and isotopic ratios in tholeiitic lava from Hualalai and other Hawaiian volcanoes*

[Helium data from Kurz and others (1983); other data from Clague (1982)]

	Hualalai	Mauna Loa	Kilauea	Loihi
La/Sm	2.2	1.8-2.0	2.2-2.8	2.4
La/Yb	3.6	4-5	6-8	6.0
La/Y	.36	.4	.5- .7	.55
K_2O/P_2O_5	1.7	1.8	2.0	1.5
$^{87}Sr/^{86}Sr$	.70373	.70374-.70386	.70348-.70379	.70347-.70357
$(^3He/^4He)_{Atm}$	14.4-17.6	8.0-8.6	13.4-14.7	24.4-31.9

TABLE 20.5.—*Compositions of trachyte samples from Hualalai Volcano*

[Data for HAW-15 from Basaltic Volcanism Study Project (1981). Samples 67-101A and 67-104 are accidental blocks collected by T. Wright. Analyses are classical wet chemistry by G. Riddle of the USGS; --, not determined]

Vent	Pau Waawaa	Waha Pele	Unnamed vent 3 km northeast of Waha Pele
Sample	HAW-15	67-101A	67-104
	Major elements (weight percent)		
SiO_2	62.99	63.10	62.84
Al_2O_3	18.04	17.79	17.86
Fe_2O_3	4.42	2.24	2.67
FeO	0	1.35	.90
MnO	.32	.52	.49
CaO	.71	0.79	.66
Na_2O	7.19	7.63	7.18
K_2O	4.87	4.97	4.90
H_2O^+	1.31	.26	.67
H_2O^-	1.31	.04	.16
TiO_2	.45	.50	.48
P_2O_5	.13	.12	.13
MnO	.29	.30	.27
CO_2	.11	.00	.00
Cl	--	.06	.01
F	--	.09	.08
Total	100.8	99.71	99.27
	Trace elements (ppm)		
Rb	108	--	--
Sr	48	--	--
Y	23	--	--
Zr	905	--	--
Nb	127	--	--

ALKALIC STAGE

The surficial flows of Hualalai Volcano are alkali olivine basalt or basalt transitional to hawaiite, with the exception of the Waawaa Trachyte Member cone and its flow. Trachyte also occurs as blocks in the maar deposit at Waha Pele, as a subsurface flow (drilled near the 1801 vents, figs. 20.1, 20.5), and as small chips in the cinder deposits of two other vents. These occurrences suggest that trachyte is relatively widespread on Hualalai, but that most exposures have been buried beneath subsequent alkalic basalt flows. Chemical analyses of trachyte from three of these locations are presented in table 20.5, and the locations are shown in figure 20.1. Some of the trachyte samples contain rare (<2 percent) modal nepheline.

Clague and others (1980) presented geochemical data for 17 samples of prehistoric alkali basalt flows and 15 samples from the 01 eruptions. They reached the following conclusions: (1) The historical flows are nearly homogeneous, although several samples reflect accumulation and resorption of olivine, plagioclase, and clinopyroxene xenocrysts. (2) The prehistoric flows are chemically similar to the historical flows, although they include lava that underwent fractionation leading to hawaiite. (3) The alkalic basalt magma can be derived by 5–10 percent partial melting of a garnet-bearing source that is enriched in the light rare-earth elements. (4) The source region for alkalic basalt beneath Hualalai is particularly rich in K_2O compared to that beneath other Hawaiian volcanoes.

Some of the alkali basalt vent deposits are aphyric, whereas others contain phenocrysts of olivine, olivine and plagioclase, or olivine, clinopyroxene, and plagioclase (table 20.6). The most abundant lava type is olivine-porphyritic basalt. There is no clear correlation of phenocryst mineralogy with either age or location of the vents on the volcano; however, as noted earlier, clusters of vents with similar mineralogy occur locally.

TABLE 20.6.—*Comparative abundance of phenocryst assemblages in samples of alkali basalt from Hualalai Volcano*

[Based on study of 256 samples of vent deposits, bombs, and cognate blocks]

Phenocryst assemblage	Percent of samples
Olivine	37
Olivine + plagioclase	24
Olivine + pyroxene	8
Olivine + plagioclase + pyroxene	24
Plagioclase	2
Aphyric	5

We now have analyses of about 300 samples of alkalic lava representing all the vents and many flows on the modern surface. Chemical analyses of 21 dated flows are presented in table 20.7. The analyses of alkalic basalt, trachyte, and tholeiitic basalt from tables 20.3, 20.5, and 20.6 and other unpublished analyses are plotted on the Macdonald-Katsura alkali-silica diagram in figure 20.13. We have also plotted magnesium-variation diagrams (fig. 20.14) using all available analyses of Hualalai lava. In addition, Peterson and Moore (chapter 7) compare Hualalai analyses with those from other Hawaiian volcanoes. Most of the plots display wide scatter that partly reflects varied phenocryst populations. The plot of Al_2O_3 against MgO has the tightest cluster of data and best shows the importance of olivine control; some scatter occurs at the low-magnesia end, as differentiation has proceeded beyond olivine control. Alkalic lava is olivine-controlled only at relatively high MgO contents.

Part of this study was designed to evaluate changes in lava chemistry through time. Because we have not yet completed mapping all of the volcano, we cannot at this time construct a detailed stratigraphic history of the surface flows. However, we have analyses of 18 alkalic basalt flows dated by ^{14}C that range in age from 12,950 yr B.P. to the historical 1800–01 flows. These samples can be used to evaluate time-dependent compositional changes. The major- and trace-element data from these samples are given in table 20.6, arranged from oldest to youngest. We have examined K_2O/P_2O_5, Zr/Nb, Zr/Y, Rb/Sr, and K/Rb ratios as a function of time and find no correlations that indicate systematic chemical changes through the last 13,000 years of volcanic history. In addition, we have analyzed samples from the 1800 flow, the 1801 flow, and one prehistoric vent deposit for $^{87}Sr/^{86}Sr$ ratio, and all are within analytical precision at 0.70362 ± 0.00001.

The data for the younger alkalic lava, combined with that for the much older tholeiitic lava recovered from the submarine northwest rift zone, display the same inverse correlation between $^{87}Sr/^{87}Sr$ and Rb/Sr (or La/Sm) ratios seen at other Hawaiian volcanoes (Chen and Frey, 1983; Clague and others, 1983; Feigenson, 1984; Roden and others, 1984). More detailed analysis of the alkalic basalt erupted during the last 13,000 yr may show subtle time-dependent chemical variations. However, at the present time we can only compare the groups of tholeiitic and alkalic lava flows to evaluate chemical changes over long time periods. As at Haleakala, East Molokai, Kauai, and Oahu, the samples with the most enriched trace-element ratios and the least radiogenic isotopic ratios are of younger alkalic basalt. These data can be explained by mixing of melts derived from several sources (see Chen and Frey, 1983), but they imply a complex petrogenesis of the lava.

XENOLITHS

The A.D. 1800 Kaupulehu flow on Hualalai Volcano is well known for its abundant coarse-grained xenoliths (Richter and Murata, 1961; Jackson, 1968; Jackson and others, 1981), and many prehistoric vent deposits and flows also contain abundant

TABLE 20.7—*Composition of alkali basalt samples from historical and prehistoric dated flows of Hualalai Volcano*

[All ages given in years B.P. and derived from ^{14}C determinations, except for historical 1800–01 flows. Major element data from rapid wet-chemical analyses by D. Kobilis, except those for sample 67–101, average 1800, 1801 toe, and vent, which are classical wet chemical analyses from Clague and others (1980). Trace elements analyzed by energy-dispersive X-ray flourescence by W. Bohrson; except those from the historical 1800–flows, which are from Clague and others (1980). --, not determined]

Sample	82-1A	79-1	78-11	78-5	79-10	82-23	82-131	78-12	81-22	82-7	81-92	81-47	81-86	82-129	81-152	81-153	67-101	81-91	Avg 1800	Toe 1801	Vent 1801
Age	12,950	12,230	10,370	9,490	4,720	4,390	3,990	3,600	2,670	2,390	2,350	2,290	1,180	1,030	900	900	710	300	150	149	149
Major elements (weight percent)																					
SiO_2	45.6	46.2	47.0	46.0	46.5	46.1	46.3	47.7	46.9	47.9	46.7	47.5	45.9	47.1	46.6	47.3	46.74	47.3	46.55	46.10	46.48
Al_2O_3	13.7	11.8	10.9	12.8	13.2	12.9	13.9	15.2	14.8	15.4	14.1	13.8	13.9	14.4	14.9	13.9	14.60	16.2	14.64	13.18	14.67
Fe_2O_3	3.8	1.5	1.8	2.9	3.2	2.6	5.7	2.6	7.9	2.8	2.5	5.5	4.6	2.1	3.0	3.4	2.12	1.8	2.97	3.30	2.36
FeO	8.4	10.4	10.4	9.1	9.1	9.6	6.8	10.1	5.2	10.3	9.5	7.0	8.1	10.7	9.6	9.7	10.35	10.3	9.80	8.86	10.24
MgO	10.8	13.5	14.7	10.5	10.7	11.2	11.3	5.4	6.7	6.0	9.6	10.0	9.7	9.7	8.7	10.3	9.20	6.1	9.04	11.86	9.17
CaO	10.4	10.1	9.3	11.5	10.2	10.1	10.0	10.1	10.3	8.7	10.3	10.4	9.8	10.4	10.2	8.0	10.67	8.3	10.15	11.41	10.35
Na_2O	2.2	2.2	2.1	2.3	2.5	2.3	2.4	3.2	3.3	3.6	2.5	2.5	2.4	2.6	2.8	3.0	2.71	3.6	2.90	2.26	2.77
K_2O	.65	.65	.56	.78	.83	.76	.69	1.27	1.17	1.2	.69	1.03	1.21	.9	.85	1.15	.811	1.37	.91	.66	.87
H_2O^+	.99	.99	.21	.25	.13	.67	.83	.22	.46	.57	.20	.22	.19	.65	.38	.48	.10	.16	.07	.02	.09
H_2O^-	--	--	.21	.03	.05	--	--	.12	.10	--	.07	.19	.22	--	.09	--	.06	.19	.05	.02	.05
TiO_2	2.1	2.1	1.9	1.9	2.0	1.9	2.0	2.9	2.5	2.7	1.9	2.2	2.3	2.3	2.2	2.2	2.06	2.6	2.40	1.82	2.27
P_2O_5	.24	.24	.22	.20	.27	.28	.25	.27	.38	.37	.43	.27	.32	.33	.31	.36	.25	.47	.28	.22	.28
MnO	.19	.19	.20	.18	.21	.14	.16	.20	.18	.17	.17	.19	.18	.18	.23	.21	.18	.19	.19	.18	.19
CO_2	.01	.01	.02	.02	.02	.02	.02	.02	.02	.02	.02	.02	.02	.04	.02	.02	.01	.02	.01	.02	.01
Cl	--	--	--	--	--	--	--	--	--	--	--	--	--	--	--	--	.02	--	.03	.03	.03
F	--	--	--	--	--	--	--	--	--	--	--	--	--	--	--	--	.06	--	.05	.04	.06
Total	99.1	99.0	99.3	98.7	98.9	98.5	100.4	99.4	99.9	99.8	98.5	100.9	98.9	101.4	99.9	100.0	99.94	98.6	100.04	99.98	99.89
Trace elements (ppm)																					
Rb	15	11	14	--	16	30	28	28	32	37	19	25	32	35	24	21	18	40	34	31	34
Sr	380	340	267	--	411	408	412	510	487	599	347	425	468	430	441	438	424	582	456	360	417
Y	19	21	14	--	21	21	22	29	28	25	21	20	22	22	21	19	23	31	21	17	18
Zr	114	113	87	--	123	119	122	181	177	202	121	138	144	151	134	134	137	215	147	115	143
Nb	15	18	13	--	22	19	20	35	31	32	16	18	24	22	18	18	22	38	--	--	--
Ni	252	420	533	--	312	331	330	58	101	71	229	210	233	206	166	134	187	76	152	520	290

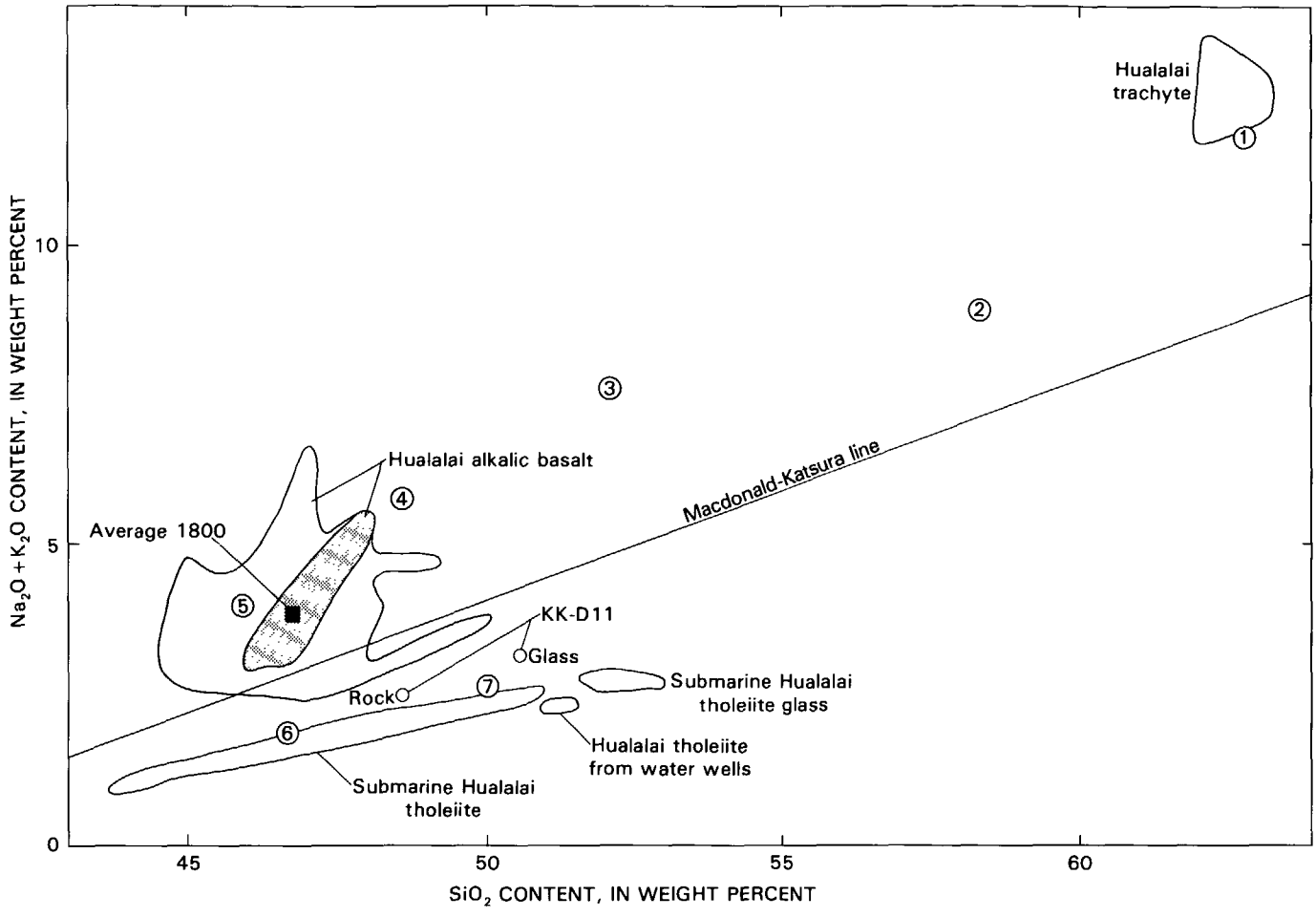

FIGURE 20.13.—Alkali-silica diagram showing the fields for Hualalai lava groups. Shaded Hualalai alkalic basalt field is from Clague and others (1980) and large unshaded field is based on about 300 new analyses. Sample KK–D11, dredged from northwest rift zone, is chemically distinct from other dredged or drilled tholeiitic samples in that it has higher alkali contents and has trace-element signature intermediate between tholeiitic basalt and alkalic basalt. Circled numbers are average Hawaiian compositions from Macdonald (1968): 1, trachyte; 2, benmoreite; 3, mugearite; 4, hawaiite; 5, alkalic basalt; 6, picritic tholeiitic basalt; 7, tholeiitic basalt.

xenoliths. Richter and Murata (1961) briefly described the remarkable occurrence of xenoliths in discrete cobble beds at about 950 m elevation in the Kaupulehu flow. More recently, Jackson and Clague (1982) presented a detailed plane-table map of this site, and Jackson and others (1981) presented data on the lithology, size, shape, density, mineralogy, and chemistry of xenoliths from the site. During our detailed mapping of Hualalai Volcano we have discovered numerous additional vents and flows and several pyroclastic deposits that contain xenoliths, commonly in great numbers. These sites are shown on figure 20.1. With a few exceptions, these new sites, like those described previously, contain dunite and gabbro xenoliths; no lherzolite or garnet-bearing xenoliths have been found. A few vents and flows have either nearly all dunite or nearly all gabbro.

Three sites are distinctive in that the coarse-grained xenoliths occur in pyroclastic deposits; these include the gabbro and diabase xenoliths in a tuff at Hainoa Crater (fig. 20.1), angular blocks of gabbro and syenite as loose blocks on the surface in the vicinity of Malekule (fig. 20.5), and a lag deposit of mainly dunite with less common wehrlite and gabbro from just east of Hainoa Crater. The lag deposit apparently formed as a wind-winnowed cinder deposit, but the other two deposits resulted from phreatic eruptions. The xenoliths in the tuff surrounding Hainoa Crater are mostly diabase with accumulated olivine and clinopyroxene; they probably formed as cumulates in a lava lake within the crater. The xenoliths in the area of Malekule include gabbro and varieties of syenite bearing biotite, apatite, or zircon. These samples apparently represent the cumulates formed in a shallow magma reservoir associated with trachyte erupted early in the alkalic stage at Puu Waawaa and other locations.

Xenoliths in the 1800 Kaupulehu flow are dominantly dunite and wehrlite with metamorphic textures (Kirby and Green, 1980). Only five percent of the xenoliths are dikes, sills, and veins, whereas about one-third are cumulates ranging from dunite, wehrlite, troctolite, clinopyroxene gabbro, and olivine-clinopyroxene gabbro to anorthosite. Orthopyroxene-bearing xenoliths are rare but include

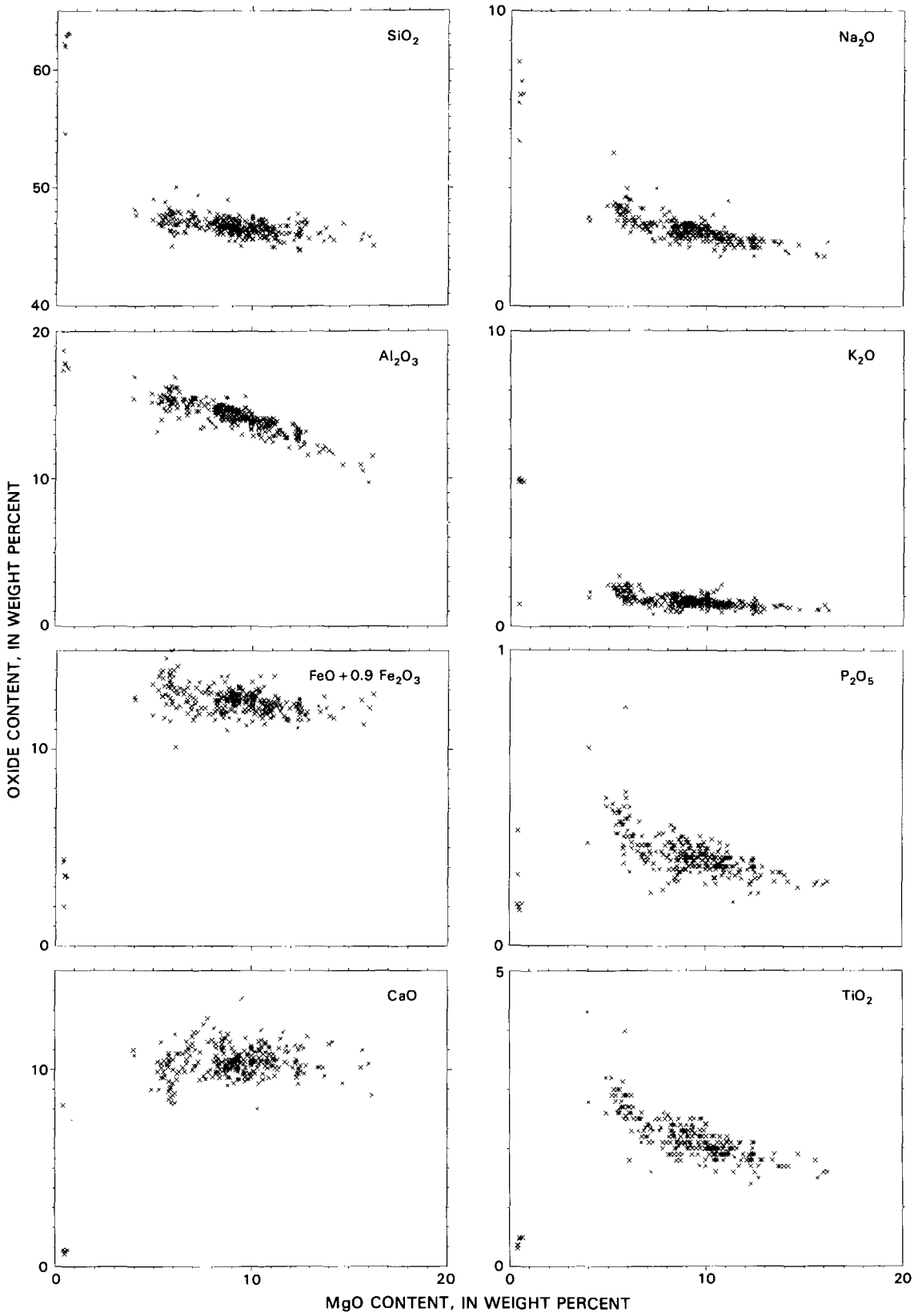

FIGURE 20.14.—Magnesia-variation diagrams for alkalic lava samples from Hualalai Volcano.

websterite and norite. Preliminary analysis of these samples indicates that some are probably cumulates related to the alkalic and tholeiitic lava of Hualalai Volcano, whereas others are related to tholeiitic basalt of the underlying oceanic crust (D.A. Clague, unpub. data, 1985).

The presence of rocks from the oceanic crust, and the pressure inferred from CO_2 inclusions in olivine (Roedder, 1965) in the dunite xenoliths, indicate that the host lava rose rapidly from a depth of about 15–20 km. Clague and others (1980) infer from the lava compositions that some fractionation occurred prior to incorporation of the xenoliths and suggest that the magma fractionated at depth. We propose that this fractionation occurred near the base of the oceanic crust at a depth of about 20 km.

The few rare xenoliths found in the tholeiitic lava dredged from the northwest rift zone are shallow level cumulates similar to those that occur in tholeiitic lava from other Hawaiian volcanoes (Jackson, 1968).

GEOPHYSICAL STUDIES AND GEOTHERMAL POTENTIAL

SEISMICITY

The Hawaiian Volcano Observatory (HVO) has maintained a seismic station 3 km east of Hualalai's summit since 1971. During the last 16 years, no swarms of microearthquakes nor any harmonic tremor from a source beneath Hualalai were recorded. Each year, however, several magnitude-4 earthquakes occur on Hualalai, most commonly from a fairly deep source just off the coast near the northwest rift zone (HVO, unpub. data). This seismicity apparently is not related to magmatic movement within the volcano.

In 1929, an intense swarm of earthquakes, lasting over a month, occurred beneath Hualalai (Macdonald and others, 1983). It seems likely that magma was intruded close to the surface at that time.

GRAVITY

Hualalai is unique among the five volcanoes on the Island of Hawaii in having a gravity high of rather low amplitude that is offset from its summit and rift zones (Kinoshita and others, 1963). The amplitude of this anomaly is 50–60 mGal less than the anomalies over the other four volcanoes. The closed high is nearly 20 km south of Hualalai's summit and appears to be more related to the Kealakekua fault system on the west flank of Mauna Loa than to Hualalai. We suggest that the relatively low gravity (250 mGal) over Hualalai's summit and rift zones reflects the presence of relatively low density trachyte that is thinly mantled with mafic lava.

AEROMAGNETICS

The aeromagnetic data for Hualalai (Godson and others, 1981) are even more striking than the gravity data. Hualalai is the only one of Hawaii's five volcanoes with a pronounced aeromagnetic low over its rift zones and summit area. We interpret these results in the same manner as the gravity data: Hualalai's rift zones and summit are underlain by relatively nonmagnetic material, that is, trachyte. The alternative view, that there is abundant magma above the Curie temperature at shallow levels, seems less likely, given the relative lack of seismicity or significant ground deformation.

ELECTRICAL GEOPHYSICAL STUDIES

Jackson and Sako (1982) have run numerous electrical self-potential traverses across the rift zones and summit area of Hualalai. They report that Hualalai has anomalies similar to those over known heat sources on Kilauea Volcano. They estimate that the depths to the tops of the sources of anomalies near the 1800 vents and near the summit are 200 m and 500 m, respectively. We suggest that the heat probably is residual and associated with a cooling magma body emplaced in 1800.

Kauahikaua and Mattice (1981) carried out resistivity surveys on Hualalai; they found low-resistivity layers beneath the summit and near the 1801 vents and suggested that they might be targets for future geothermal exploration. We suggest that further exploration of the entire northwest rift zone for potential geothermal resources is warranted. The infrequency of eruptions combined with the significant self-potential and resistivity anomalies make Hualalai an attractive target.

VOLCANIC HAZARDS

The stratigraphic and geochronologic data that we have obtained permit a preliminary assessment of the hazards that future eruptions of Hualalai pose to the burgeoning population in the Kona district. These hazards are of two general types, caused by pyroclastic materials and by lava flows.

Pyroclastic deposits on Hualalai generally are of two types: the dominant type is cinders and spatter associated with cone or rampart building at vents; less abundant is debris resulting from explosive phreatic eruptions. The latter are quite rare, although two of the last three major eruptions (those of Luamakami about 300 years ago and Waha Pele about 700 yr ago) included explosive events. At Luamakami (fig. 20.8), phreatic explosions near the end of the eruption ejected blocks of thermally metamorphosed basalt as much as 1 m in diameter at least 100 m from the vent. The affected area was quite small, however; probably less than 0.5 km^2 was devastated.

Explosive phreatic eruptions that preceded basaltic effusion at Waha Pele were more significant. As mentioned earlier, ascending basaltic magma caused violent steam eruptions that ejected blocks of trachyte, picritic tholeiite, and alkali basalt as large as 0.4 m in diameter; fine ash covered an area of at least 10 km^2. This eruption likely would have destroyed anything living nearby, but its effects did not extend to the coast 16 km away, where both ancient and modern people as well as commerce have been concentrated.

Eruptions near sea level on the lower northwest rift zone, by analogy with the 1960 eruption of Kilauea (Richter and others, 1970), could result in local phreatic explosions during dominant Strombolian and effusive activity. Most vent deposits on Hualalai have formed typical cinder-and-spatter cones and spatter ramparts. Although the wide dispersal of cinders from some vents indicates that the eruptions may have been sub-Plinian, it seems unlikely that such eruptions would threaten populated areas.

Lava flows pose by far the greater danger. Hualalai's summit is only 15 km from Kailua; the average topographic gradient across the distance is 168 m/km, corresponding to a 9.5° slope. A flow as voluminous and fluid as that of 1800 could cover that distance in a few hours. Recent (younger than 3,000 yr B.P.) flows have originated at vents that are fairly evenly spaced along the northwest and south-southeast rift zones (fig. 20.5). Thus we cannot predict on that basis where the next activity will occur. On the other hand, the youthfulness of the terrain north of Kailua and the presence of the large self-potential anomaly near the 1800 vents imply that the next eruption may occur on the northwest rift zone. The location of the vent relative to the topographic axis of the rift is critical; a few tens or hundreds of meters to the north or south may determine whether the flows go north over relatively unpopulated ranchland or southwest into populated, industrialized areas. A flow from the southeast rift zone, if it gets within one or two kilometers of the sea, could also be devastating; total property values on the 700-year-old Waha Pele flow are approaching $1 billion. It seems unlikely that mitigating measures, such as diversion barriers, would be effective—the Waha Pele flow locally is more than 15 m thick and is 1.3 km wide at the ocean. Depending on the speed and size of any future flow, evacuation may be the only feasible measure.

The eruptive recurrence interval of Hualalai for all of Holocene time is on the order of 50 years (about 200 eruptions in 10,000 yr), though much longer for any specific point on it. However, our mapping and ^{14}C dating indicate that eruptions have occurred in clusters (groups of several eruptions over a few hundred years, separated by several centuries of inactivity). The current lack of magma-related seismicity and deformation provides no information about when the next eruption might occur. In 1800 the magma ascended quite rapidly from a depth of 15–20 km (Clague and others, 1980), judging from the size and abundance of the mafic and ultramafic xenoliths that it carried up from that depth. This rapid ascent implies that seismic detection of shallow, magmatic movement may precede actual eruptive activity by only a short time. The intervals between the latest Holocene eruptions, including the 186 years since the last one, lead us to suggest that a Hualalai eruption is highly probable within the next 200 years and could well occur during the next few decades.

REFERENCES CITED

Basaltic Volcanism Study Project, 1981, Basaltic volcanism of the terrestrial planets: New York, Permagon Press, 1,286 p.

Brigham, W.T., 1909, The volcanoes of Kilauea and Mauna Loa: B.P. Bishop Museum Memoir, v. 2, no. 4, 222 p.

Campbell, J.F., and Erlandson, D., 1979, OTEC-1 anchor site survey: Hawaii Institute of Geophysics Report, 55 p.

Chen, C.-Y., and Frey, F.A., 1983, Origin of Hawaiian tholeiites and alkalic basalts: Nature, v. 302, p. 785–789.

Clague, D.A., 1982, Petrology of tholeiitic basalt dredged from Hualalai Volcano, Hawaii [abs.]: Eos, American Geophysical Union Transactions, v. 63, p. 1138.

Clague, D.A., Frey, F.A., and Beeson, M., 1983, Rare-earth element and Sr isotopic evidence for the origin of the East Molokai Volcanics, Hawaii: Eos, American Geophysical Union Transactions, v. 64, p. 902.

Clague, D.A., Jackson, E.D., and Wright, T.L., 1980, Petrology of Hualalai Volcano, Hawaii: Implications for mantle composition: Bulletin Volcanologique, v. 43–4, p. 641–656.

Feigenson, M.D., 1984, Geochemistry of Kauai Volcanics and a mixing model for the origin of Hawaiian alkalic basalts: Contributions to Mineralogy and Petrology, v. 87, p. 109–119.

Funkhouser, J.G., Barnes, I.L., and Naughton, J.J., 1968, The determination of a series of ages of Hawaiian volcanoes by the potassium-argon method: Pacific Science, v. 22, p. 369–372.

Godson, R.H., Zablocki, C.J., Pierce, H.A., Frayser, J.B., Mitchell, C.M., and Sneddon, R.A., 1981, Aeromagnetic map of the Island of Hawaii: U.S. Geological Survey Geophysical Investigations Map GP–946, scale 1:250,000.

Holcomb, R.T., 1981, Kilauea Volcano, Hawaii: chronology and morphology of the surficial lava flows: U.S. Geological Survey Open-File Report 81–0354, 321 p.

Jackson, D.B., and Sako, M.K., 1982, Self-potential surveys related to probable geothermal anomalies, Hualalai Volcano, Hawaii: U.S. Geological Survey Open-File Report 82–127, 10 p.

Jackson, E.D., 1968, The character of the lower crust and upper mantle beneath the Hawaiian Islands: International Geological Congress, Prague, 23d, Proceedings, p. 135–150.

Jackson, E.D., and Clague, D.A., 1982, Map showing distribution of the nodule beds of the 1800–1801 Kaupulehu flow of Hualalai Volcano, Island of Hawaii: U.S. Geological Survey Miscellaneous Field Studies Map MF–1355, scale 1:1200.

Jackson, E.D., Clague, D.A., Engleman, E., Friesen, W.F., and Norton, D., 1981, Xenoliths in the alkalic basalt flows of Hualalai Volcano, Hawaii: U.S. Geological Survey Open-File Report 81–1031, 33 p.

Kauahikaua, J.P., and Mattice, M., 1981, Geophysical reconnaissance of prospective geothermal areas on the Island of Hawaii using electrical methods: U.S. Geological Survey Open-File Report 81–1044, 50 p.

Kinoshita, W.T., Krivoy, H.L., Mabey, D.R., and Macdonald, R.R., 1963, Gravity survey of the Island of Hawaii: U.S. Geological Survey Professional Paper 475–C, p. C114–C116.

Kirby, S.H., and Green, H.W., 1980, Dunite xenoliths from Hualalai Volcano: Evidence for mantle diapiric flow beneath the Island of Hawaii: American Journal of Sciences, v. 280-A, p. 550–575.

Kurz, M.D., Jenkin W.J., Hart, S.R., and Clague, D.A., 1983, Helium isotopic

variations in volcanic rocks from Loihi Seamount and the Island of Hawaii: Earth and Planetary Science Letters, v. 66, p. 388–406.

Macdonald, G.A., 1955, Hawaiian Islands: Catalog of the active volcanoes of the world including solfatara fields, Part III: International Volcanological Association, Naples, Italy, 37 p.

———1968, Composition and origin of Hawaiian lavas: Geological Society of America Memoir 116, pp. 477–522.

Macdonald, G.A., Abbott, A.T., and Peterson, F.L., 1983, Volcanoes in the sea (2nd ed.): Honolulu, University of Hawaii Press, 517 p.

Richter, D.H., Eaton, J.P., Murata, K.J., Ault, W.U., and Krivoy, H.L., 1970, Chronological narrative of the 1959–60 eruption of Kilauea Volcano, Hawaii: U.S. Geological Survey Professional Paper 537–E, 73 p.

Richter, D.H., and Murata, K.J., 1961, Xenolithic nodules in the 1800–1801 Kaupulehu flow of Hualalai Volcano, Hawaii: U.S. Geological Survey Professional Paper 424–B, p. B215–B217.

Roden, M.F., Frey, F.A., and Clague, D.A., 1984, Geochemistry of tholeiitic and alkalic lavas from the Koolau Range, Oahu, Hawaii: Implications for Hawaiian volcanism: Earth and Planetary Science Letters, v. 69, p. 144 158.

Roedder, E., 1965, Liquid CO_2 inclusions in olivine-bearing nodules and phenocrysts from basalts: American Mineralogist, v. 50, p. 1746–1782.

Stearns, H.T., and Macdonald, G.A., 1946, Geology and ground-water resources of the Island of Hawaii: Hawaii Division of Hydrography Bulletin 9, 363 p.

PLEISTOCENE SUBGLACIAL ERUPTIONS ON MAUNA KEA

By Stephen C. Porter[1]

ABSTRACT

A distinctive assemblage of pyroclastic cones and lava flows inside the limit of Pleistocene glaciation on the upper slopes of Mauna Kea Volcano is attributed to subglacial eruptions during two intervals when an ice cap mantled the summit of the mountain. During the Waihu glaciation, when an ice cap of about 140 km² formed, eruptions built two pyroclastic cones composed of hyaloclastite tuff capped by subaerially erupted bomb-bearing cinder deposits. Associated lava flows have steep embayed margins and glassy surfaces, and are locally palagonitized. A bouldery conglomerate on the southwestern flank of the volcano is inferred to have resulted from floods caused by failure of glacier-impounded lakes that formed over the erupting vents.

A younger group of cones and lava flows was erupted during the Makanaka glaciation, when a smaller ice cap (70 km²) mantled the summit. A seismic discontinuity in one of these cones may mark a boundary between a hyaloclastite core and overlying hydrothermally altered cinders that are exposed locally. Associated lavas are characterized by steep margins, pillows, glassy surfaces, spiracles, and palagonitized zones. The morphology of flow margins suggests that ice was thin along rift zones but thickened away from them.

Stratigraphic relations and radiometric ages show that the Waihu-age eruptions occurred during marine isotope stage 6 and the Makanaka-age eruptions took place either during stage 3 or near the end of stage 4. Although firm evidence of subglacial eruptions earlier than the Waihu glaciation is lacking, such events are likely to have occurred during the Pohakuloa glaciation (isotope stage 8) at the close of the tholeiitic shield-building phase of Mauna Kea's growth.

INTRODUCTION

The phenomenon of subglacial volcanic eruptions has been well documented through studies of distinctive ice-contact volcanic rocks and landforms in Iceland, western Canada, and Antarctica. In each of these regions volcanoes have erupted in environments subjected to repeated and widespread glaciation. In tropical latitudes, where modern and former snowlines lie at high elevations and evidence of past glaciation is far more restricted, the opportunities for glacier-volcano interaction are less common. One of the best-documented records of such activity is from the upper slopes of Mauna Kea, the only Hawaiian volcano on which evidence of past glaciation has been found (fig. 21.1).

Glacial features on Mauna Kea were first reported by Daly (1910) and investigated more fully by Wentworth and Powers (1941) and by Stearns (1945) and Stearns and Macdonald (1946). Although Stearns speculated that a distinctive conglomerate on the south slope of the mountain may have resulted from floods caused by eruptions that melted an ice cap, supportive evidence for such events has been forthcoming only during recent stratigraphic and sedimentologic studies of the glacial and volcanic succession on the upper slopes of the mountain (Porter, 1979a, b). This evidence points to subglacial volcanic activity during at least two intervals when the summit region was mantled with an extensive ice cap. The resulting landforms and deposits, which are analogous to subglacial phenomena described from higher latitudes, are unique in Hawaii and are confined to the area within the defined limits of successive Pleistocene glaciers.

Stratigraphic nomenclature used in this chapter is that of Langenheim and Clague (chapter 1, part II).

ACKNOWLEDGMENTS

Critical reviews and constructive suggestions by William E. Scott and William S. Wise are gratefully acknowledged. This research was supported by the Earth Sciences Section, National Science Foundation through Grants GA–20320 and DES74–16379.

GLACIAL RECORD

STRATIGRAPHIC SEQUENCE ON MAUNA KEA

Exposed volcanic rocks and sediments on Mauna Kea are divided into two major lithologic successions (fig. 21.2). The Hamakua Volcanics includes a thick tholeiitic assemblage, which forms the main volcanic shield, and the overlying Hopukani Volcanic Member and the Pohakuloa Glacial Member. The Hopukani Volcanic Member comprises lavas and related pyroclastic cones exposed mainly below an elevation of 1,000 m, where they are discontinuously mantled by younger lavas.

The sediments of the Pohakuloa Glacial Member lie at or near the top of the Hopukani lavas, which were their source rocks. Although the Pohakuloa sediments were inferred by Stearns (1945) to be an explosion breccia, a variety of characteristics, including

[1]Quaternary Research Center, University of Washington, Seattle, Washington 98195.

sedimentary facies (till and outwash), grain-size distribution, clast fabric and angularity, faceted clasts, presence of striated lava surfaces underlying the unit, and absence of bomb sags, point to a glacial origin (Porter, 1979a). Exposed only in several gulches that indent the upper south slope of the volcano, the Pohakuloa Glacial Member constitutes the oldest exposed evidence of glaciation on Mauna Kea.

The overlying Laupahoehoe Volcanics consists of a widely exposed sequence of alkalic lavas and pyroclastic layers (Waikahalulu Volcanic Member), and sedimentary strata; it is much thinner than the Hamakua Volcanics. Lavas are predominantly blocky hawaiite aa flows that issued from vents near the summit and along the rift zones. On the upper slopes, a succession of superimposed flows reaches a thickness of 100 m or more, but on the lower slopes, where commonly only a single flow overlies lavas of the Hamakua Volcanics, thicknesses of 30 m or less are typical. Associated pyroclastic cones are composed of dark-gray or reddish cinders, scoria, and bombs.

Three layers of glacial drift are interstratified with lavas of the Laupahoehoe Volcanics. The Waihu Glacial Member is exposed mainly in kipukas (inliers) on the southwest slope of the volcano below an elevation of about 3,350 m. Elsewhere it is largely covered by younger lava flows and glacial deposits. A belt of Waihu moraines west of Waikahalulu Gulch is overlapped by younger lavas that pass upslope beneath post-Waihu end moraines. Where the Waihu drift is exposed at the surface, it has been substantially modified by weathering and erosion. Commonly the drift is highly indurated and forms steep cliffs along gulches. End moraines,

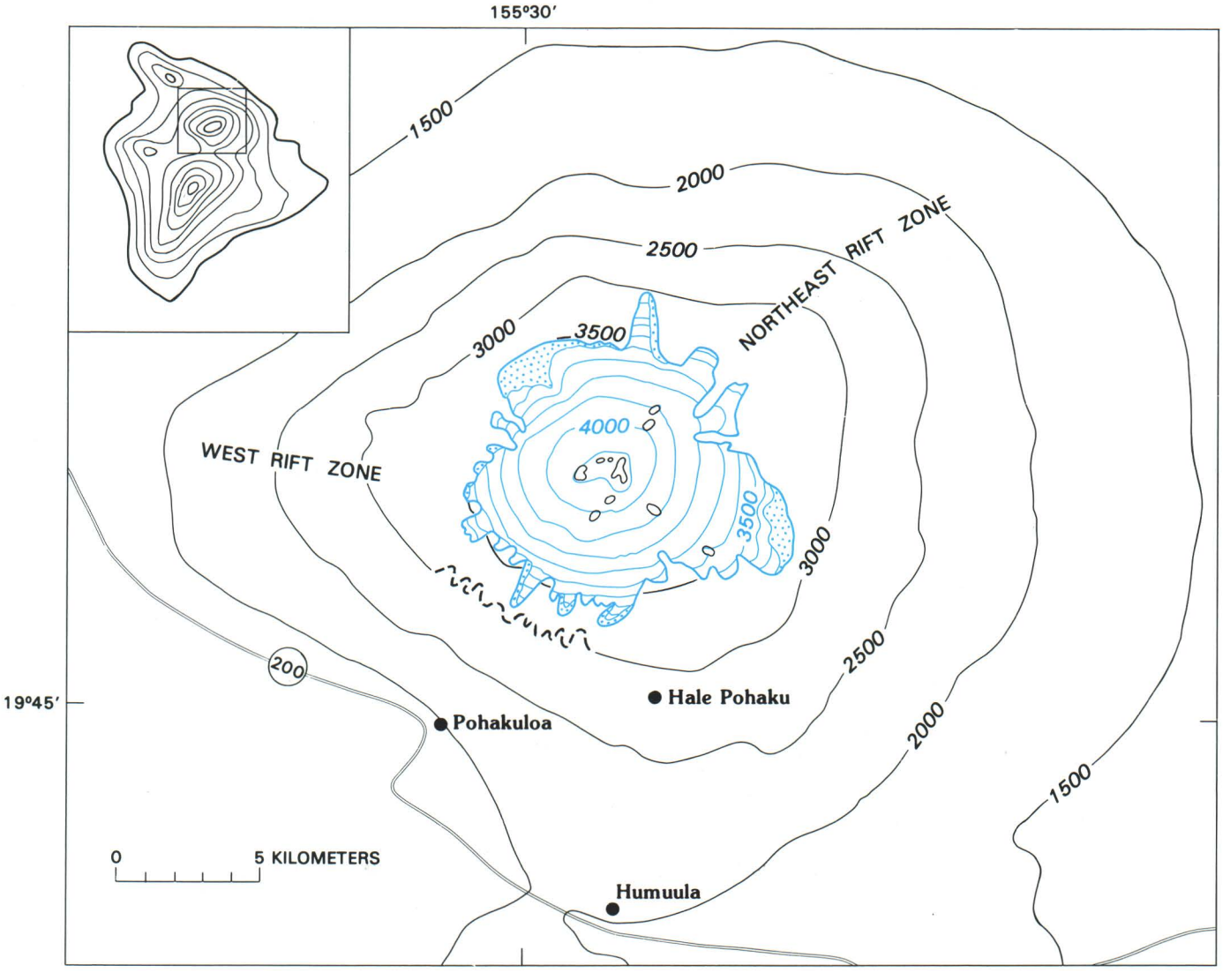

FIGURE 21.1.—Map of upper slopes of Mauna Kea showing reconstructed ice cap (blue) of the late Makanaka glaciation and the nunataks (white) that rose above it. Contour interval 500 m, with 100-m interval for ice cap. Shaded pattern shows extent of early Makanaka drift beyond late Makanaka ice limit. Known extent of more-extensive Waihu glacier is shown by heavy dashed line on the southwest flank.

however, are subdued. In places, tor-like pinnacles of drift standing up to 3 m high indicate the minimum erosion that has occurred since the moraines were deposited. Associated outwash gravels mantle the lower southwest slope of the mountain below the belt of moraines, and a dissected outwash fan lies at the base of Waikahalulu Gulch. Surface stones tend to be deeply pitted or spalled, and most have brownish oxidation rinds 1–2 mm thick.

The Makanaka Glacial Member includes two bodies of drift, the older of which is bordered by end moraines that are exposed discontinuously around the summit area. The older Makanaka drift is less indurated than Waihu drift, and surface stones are stained light yellowish brown. In many places it is buried by younger lavas or by younger drift of late Makanaka age. The younger drift forms conspicuous arcuate moraines around much of the summit area at about the 3,500-m level, as well as prominent lateral moraines along several major gulches. Above the drift limit, low recessional moraines are found, especially on the southeast and southwest slopes of the mountain. Striated lava surfaces are widespread on the summit plateau above about 3,600 m. The younger drift is little weathered, and soil profiles are thin and weakly developed. Associated meltwater sediments are confined largely to the floors of gulches and to the plain at the south base of the mountain.

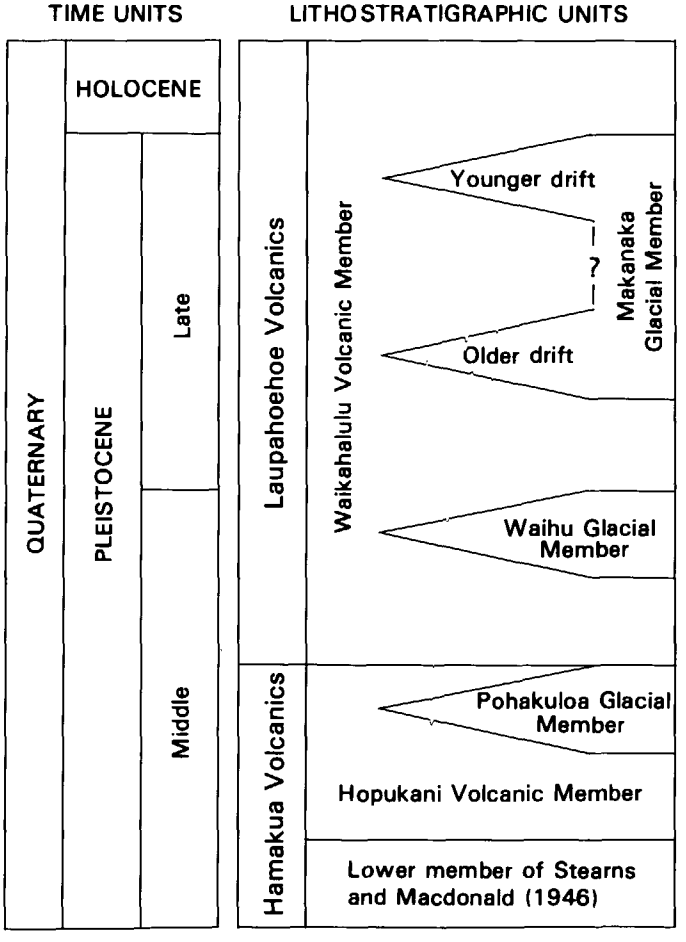

FIGURE 21.2.—Lithostratigraphic units on upper slopes of Mauna Kea, showing relation to geologic time scale (modified from Porter, 1979a).

PLEISTOCENE ICE CAPS

The ice cap of late Makanaka time can be reconstructed in considerable detail using abundant ice-limit data in the summit region (Porter, 1979b). Radial profiles, based on end moraines and on upper limits of erratic stones on cinder cones within the drift limit, were constructed along various flow lines, as inferred from striations and other ice-flow directional indicators. The profiles were then extrapolated to the summit less than 2 km away. Using these as a basis for contouring, the topographic configuration of the former ice cap was obtained (fig. 21.1). At its maximum advance, the glacier measured about 10.5 km in diameter, had an area of 70.5 km^2, and averaged about 75 m thick. Its volume is estimated to have been close to 5 km^3. The glacier margin was irregular, especially along the rift zones, where high-standing cinder cones caused divergence of ice flow. Tongues of ice flowing down the deepest gulches extended as low as 3,160 m, while broad lobes occupied the slopes between rift zones. Although the ice cap was broadly symmetrical about the summit region, its margin averaged somewhat higher in the northwest and northeast quadrants (3,570 m and 3,510 m, respectively) than in the southwest and southeast quadrants (3,465 m and 3,420 m, respectively), implying a southerly or southeasterly source of moisture (Porter, 1979b).

The early Makanaka ice cap apparently was only slightly larger than the younger ice cap, for in those places where the older drift limit can be mapped or inferred from stratigraphic data it lies no more than 100–200 m downslope from the late Makanaka limit. However, because early Makanaka moraines were not positively identified through some sectors on the eastern slope of the mountain (fig. 21.1), the exact shape of the glacier is not known. Although it probably was broadly similar to the late Makanaka ice cap, in detail it must have differed; during the period between the two advances, lava flows and cinder cones were erupted in the summit area, thereby causing local reorientation of glacier flow lines. During the earlier ice advance, the bedrock surface beneath the glacier must have been, on average, at least several tens of meters lower than during the later glaciation.

Less is known about the still-older Waihu ice cap, for few deposits or erosional features are exposed. In the southwestern quadrant of the mountain, the Waihu glacier deposited a belt of moraines that lie about 1.5 km beyond the Makanaka moraines and close to 3,000-m elevation (fig. 21.3). Assuming a symmetrical distribution of ice about the summit, the glacier covered an estimated area of 140 km^2. The estimated minimum ice thickness in the summit region was at least 150 m, based on analogy with the better-constrained late Makanaka glacier. The average diameter of the ice cap was between 12 and 13 km. Assuming an average thickness of 100 m, the total ice volume would have been close to 14 km^3. Because no large pyroclastic cones had yet been built near the summit, few, if any, nunataks rose above the glacier surface during the initial part of this glaciation. The glacier terminus apparently was less irregular than that of subsequent ice caps, probably because deep gulches had not yet been eroded into the flanks of the mountain and there were no prominent cinder cones that would have produced a lobate margin. Ice flow, inferred from preserved striations and

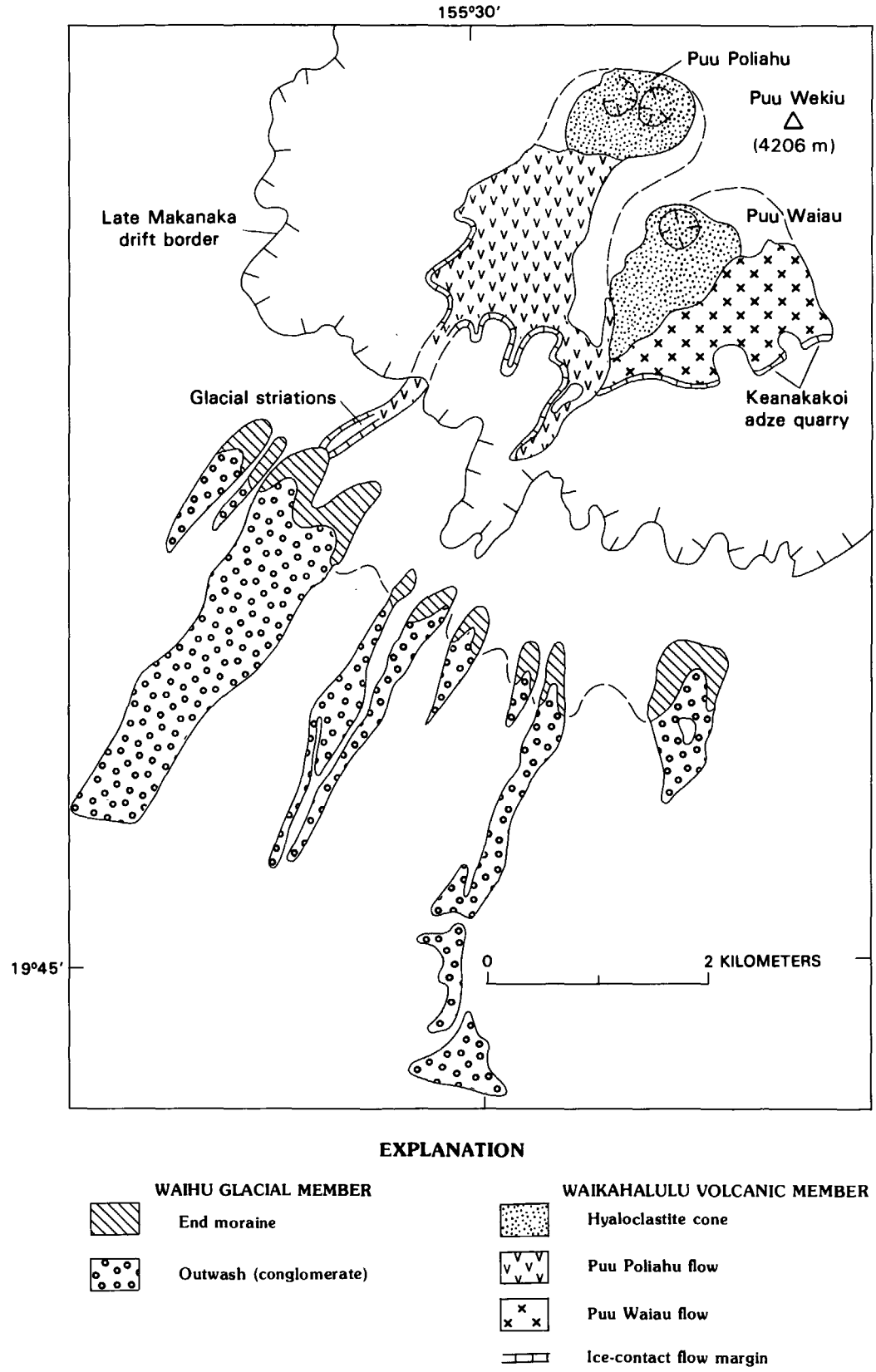

FIGURE 21.3.—Map of upper southwest slope of Mauna Kea showing distribution of intra-Waihu cones and flows with respect to Waihu end moraines and outwash deposits and to late Makanaka drift border. Dashed lines show possible extent of Waihu lava flows and moraine belt beneath younger lavas and glacial deposits.

from till fabrics, was approximately radial from the summit region.

Pohakuloa drift is seen only in several gulches on the southwest slope of the volcano, where the thickest exposures lie beneath early Waikahalulu lavas under the Waihu moraine belt. Accordingly, the Pohakuloa glacier is inferred to have been comparable in size to the Waihu ice cap, again assuming that it was symmetrically distributed about the summit region. On this basis, its areal extent was probably 130–150 km^2.

SUBGLACIAL ERUPTIONS

A distinctive assemblage of volcanic units found within the mapped limits of glaciation on Mauna Kea is unique in the Hawaiian Islands. It includes both lava flows and pyroclastic cones, built during the interval of alkalic eruptive activity, as well as associated fluvial sediments that have no known counterpart on other Hawaiian volcanoes. Detailed mapping has shown that these rocks are coeval with the Waihu and Makanaka Glacial Members, rather than with Waikahalulu volcanic rocks erupted during nonglacial intervals. Their stratigraphic association, distinctive morphology, and similarity to subglacially erupted volcanic assemblages in other parts of the world imply that they were emplaced during Pleistocene glacial episodes on Mauna Kea.

WAIHU GLACIATION

PYROCLASTIC CONES

Nearly two dozen pyroclastic cones and cone complexes lie inside the limit of the last ice cap in the summit region. Most are older than late Makanaka drift, as shown by their glacially eroded and oversteepened flanks, by erratic blocks strewn about their flanks, or by drift filling their craters. Most also are composed of dark-grayish or dark-reddish cinders, vitric ash, and bombs, as are the numerous cinder cones that lie below the limit of glaciation on the mountain.

Two cones near the summit, however, have surface morphologies and internal characteristics that are distinctly different from those of nearby cones. Puu Waiau has been largely buried by lavas on all but its southern flank, while Puu Poliahu is partly covered by younger lavas on its north, east, and southeast sides (fig. 21.3). Puu Waiau has a single crater, which contains Lake Waiau (3,968 m; fig. 21.4), whereas Puu Poliahu has two juxtaposed craters lying along an east-west axis. The slopes of nonglaciated cinder cones on Mauna Kea have angles of as great as 26°, the typical repose angle of the cinders (Porter, 1972), but the glacially eroded flanks of Puu Waiau and Puu Poliahu reach angles as great as 36° (fig. 21.5).

The uppermost 25–35 m of each of these two cones consists of typical subaerially erupted dark-gray cinders and ash containing numerous spindle bombs. Below this, however, the tephra changes character rather abruptly into a light-yellowish-brown or varicolored hyaloclastite tuff consisting of waxy, vitric particles as much as 2 cm in diameter and having concoidally fractured surfaces. The <2-mm size fraction averages 55 percent sand, 35 percent silt, and 10 percent clay. This well-bedded tuff dips 18°–20° in Puu Waiau and 20°–26° in Puu Poliahu (fig. 21.6). Bombs scattered throughout the tuff in Puu Waiau average about 50 cm in diameter, but some have diameters as great as 3 m; such bombs are less plentiful in exposed parts of Puu Poliahu. Some bombs have glassy surfaces, and some are palagonitized. Being less erodible than the enclosing tuff, bombs often remain as caps on pillars of tuff up to 2 m high.

FIGURE 21.4.—Summit region of Mauna Kea showing Puu Waiau (foreground) overlapped by steep ice-contact margin of Puu Hau Kea flow rising above Lake Waiau. Behind Puu Hau Kea (right, middle distance) rises Puu Wekiu, showing the roadcut along which hydrothermal alteration is exposed. Upper part of flow north of Puu Poliahu is visible to left of Puu Wekiu. Photograph by Agatin T. Abbott. Reprinted, by permission of University of Hawaii Press, from *Volcanoes in the Sea: The Geology of Hawaii*, second edition, by Gordon A. Macdonald, Agatin T. Abbott, and Frank L. Peterson.

FIGURE 21.5.—Puu Poliahu rising above surface of Puu Hau Kea flow; view looking north. Glacially oversteepened slope of cone facing camera has angle of 36°.

LAVA FLOWS

Distinctive hawaiite lava flows adjacent to Puu Waiau and Puu Poliahu are believed to represent later phases of the eruptions that built the cones (fig. 21.3). However, the stratigraphic relationships at the head of each flow are obscured by overlapping younger lavas and by colluvium. Their alkalic composition and their position beneath younger lavas that are coeval with Makanaka glaciation indicate that these flows are broadly post-Pohakuloa and pre-Makanaka in age (Porter, 1979a).

The front margin of the flow southwest of Puu Poliahu is marked by a steep cliff, locally up to 80 m high. In places it is deeply embayed, in contrast to the lobate fronts of most hawaiite flows. Where erosion has been slight, the flow margin has a glassy zone near its surface and is locally palagonitized. A similar flow lying south and east of Puu Waiau has similar characteristics. Associated with this latter flow, especially along its abrupt front that rises in a cliff 15–25 m high (fig. 21.7), are many prehistoric lithic workshops where early Hawaiians mined the stone for making adzes. The flow, which is very fine grained and hard, fractures into slabs appropriate for such artifacts and apparently was ideal for stone working. Its glassy groundmass contains randomly oriented microlites of plagioclase, rather than fully developed crystals, making the rock tougher than other flows and therefore easier to shape. Although the flow is remote and lies at a high elevation, the large number of adze quarries on this unit implies that the Hawaiians found its attributes to be uniquely valuable.

The high, steep margins of the Puu Waiau and Puu Poliahu flows are unlike those of most other hawaiite lavas on the mountain, which tend to be both lower and lobate. Elsewhere on the island (for example, Kohala volcano, Puu Waawaa), steep flow fronts occur in viscous lavas and on associated domes that consist of more alkalic rocks (mugearite, benmoreite, trachyte), but such flows lack embayed margins, glassy surfaces, and palagonite.

FIGURE 21.6.—Hyaloclastite tuff on northwest flank of Puu Waiau, with interbedded bombs standing in relief above eroded surface of cone.

CONGLOMERATE

A bouldery conglomerate on the south flank of Mauna Kea is traceable from the belt of Waihu end moraines to the base of the mountain in the Mauna Kea-Mauna Loa saddle. Stearns (1945), who described its occurrence and character, referred to it as the "Waihu fanglomerate" and attributed it to possible floods caused by eruptions that melted an ice cap. The deposit consists of bouldery gravel, so indurated that clasts are difficult to dislodge with a hammer (fig. 21.8). Where buried by lavas, the deposit is less indurated and resembles outwash gravels of Makanaka age. Its stratigraphic position is demonstrable in deep gulches on the south flank of the mountain, where it lies above Pohakuloa drift and early Waikahalulu lavas but below late Waikahalulu lavas and the lower drift of the Makanaka Glacial Member. Where exposed at the

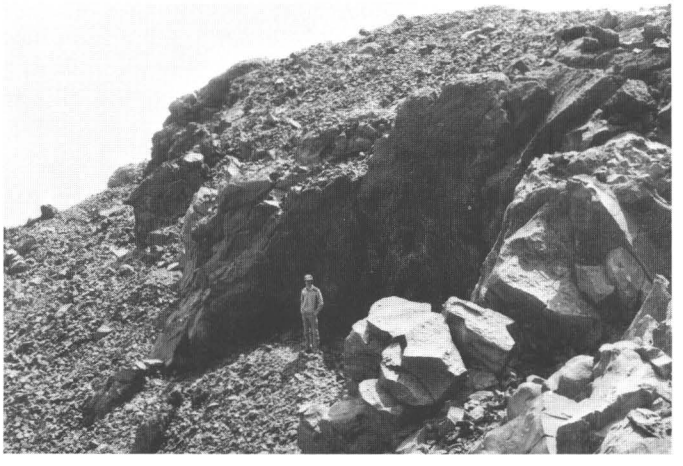

FIGURE 21.7.—Ice-contact margin of Puu Waiau flow at Keanakakoi adze quarry (elevation 3,770 m) on south slope of Mauna Kea. Debris from prehistoric quarrying operations litters surface below and above steep, embayed margin of flow.

FIGURE 21.8.—Poorly sorted conglomerate facies of Waihu Glacial Member exposed in a shallow gulch on the upper southwest slope of Mauna Kea.

surface, boulders of the conglomerate are oxidized to yellowish brown and have weathering rinds 1–2 mm thick; many are spalled, pitted, or fractured. Where it meets the Waihu moraine belt the deposit has a thickness of 10–20 m, but it thins progressively downslope and is seldom more than 1 m thick near the base of the mountain.

INTERPRETATION

The assemblage of volcanic features that formed at the time of Waihu glaciation are adequately explained by attributing them to subglacial eruptions. The thick pile of hyaloclastite forming the bulk of Puu Waiau and Puu Poliahu imply eruption under water. The cones stand 100–170 m above the surrounding terrain at the crest of the mountain, and therefore the topography offers no means of ponding a body of water. In addition, the volcanic rocks that comprise the summit region are porous. If magma reached the surface beneath a summit ice cap, however, melting of ice above the vent would likely have generated a meltwater lake in which the bedded hyaloclastite could have accumulated. The observed thickness of eruptive products (about 170 m) is consistent with the reconstructed thickness of an ice cap over the summit having the areal extent indicated by the Waihu drift limit. When the accumulating hyaloclastite deposit reached the level of the lake surface and kept water from reaching the vent, subaerial eruptive activity would have commenced and produced cinders and bombs like those seen capping the hyaloclastite in both cones. The explosive character of the early phases of activity that produced Puu Waiau is suggested by the large number of spindle-shaped bombs that are interbedded with the hyaloclastite; evidently pieces of fluid lava were ejected above the surface of the postulated lake, acquired their distinctive aerodynamic shapes as they fell back to the surface, and settled through the water onto the accumulating pyroclastic pile.

Similar subglacially erupted volcanic units in Iceland have been described by Jones (1970), who inferred deposition of a basal pillow sequence in meltwater lakes as deep as 500 m. A change to explosive volcanism occurred as the water depth over the accumulating volcanic pile decreased to less than 200 m. Hyaloclastite tuff, characteristic of basaltic eruptions from vents in shallow water, then piled up above the pillow lavas as water interacted with lava rising rapidly through the conduit. In neither of the Mauna Kea cones are the lowermost eruptive products exposed, so the presence or absence of basal pillow lavas cannot be confirmed. However, the inferred water depth of less than 200 m suggests that the lower parts of the cones consist mostly or entirely of hyaloclastite.

As explosive activity waned, lava that was erupted from the Puu Poliahu and Puu Waiau vents is inferred to have flowed downslope, melting the glacier in the process. The unusual thickness and steep embayed fronts of the flows, their abundant pillow structures, the fine grain size and glassy margins of the dense flow rock, and the presence of zones of palagonite are all consistent with such an interpretation.

The exact number and sequence of eruptive events remains uncertain, largely because the flows and cones have been partly buried by younger volcanic units and partly eroded during subsequent glaciations. Puu Waiau appears to be a simple cone with a crater at its apex; however, its north side is not exposed. Related to it is a single lava flow that lies along its east and southeast sides. The source area for the flow is not evident, but it may lie near the highest exposed part of the flow. The source could also be buried beneath younger lava on the north or northeast side of the cone, in which case the lava would have issued from the upslope side of the cone and flowed downslope around its eastern side.

Puu Poliahu, by contrast, is a complex cone consisting of two adjacent craters. The two vents may have given rise to separate lava flows that coalesced downslope, as suggested by the dashed lines in figure 21.3, or possibly only one of the vents produced a flow. Alternatively, lava may have emerged from a vent unrelated to the hyaloclastite eruption, but in the same general area. Possible source areas are now covered by younger lavas that surround Puu Poliahu on all but the southwestern side.

The map pattern south of Puu Waiau suggests that the Poliahu flow may overlap the margin of the Waiau flow (fig. 21.3), but the field relations are not diagnostic. In any event, the period of time separating the eruptions is not known.

The subglacial eruptions would have melted a substantial body of ice from the glacier. The minimum areas covered by Puu Poliahu and Puu Waiau and their associated flows are 4 km^2 and 2.8 km^2, respectively. Assuming a mean ice thickness of 150 m for areas of the glacier directly affected by the eruptions, the volume of ice melted amounted to at least 1 km^3, or about 7 percent of the estimated volume of the entire ice cap. Some of the water would have interacted explosively with the erupting magma and escaped as steam, but the bulk is likely to have been ponded in one or more lakes within the ice cap, from which it would eventually have drained downslope either slowly or catastrophically. The fluvial conglomerate facies of the Waihu Glacial Member (the "Waihu fanglomerate" of Stearns, 1945) is exposed downslope from Puu Poliahu and Puu Waiau (fig. 21.3), principally along primary drainage routes that would have channeled meltwater from the summit region. The bulk of the coarse conglomeratic outwash facies is likely to have been deposited by floods resulting from sudden dumping of glacially impounded lakes that contained nearly 1 km^3 of meltwater, a mechanism consistent with Stearns' hypothesis for the origin of the conglomerate.

EVIDENCE OF RENEWED GLACIATION

Two lines of evidence suggest that the Waihu glacier reformed following the Puu Poliahu eruption and advanced across the Poliahu flow. Fragments of glassy flow margin and palagonitized hawaiite lava have been found in the Waihu end moraine system. A tongue of the Poliahu flow that emerges from beneath the Makanaka moraine belt and retains remnants of glacially chilled margins is a possible source of these fragments. The flow tongue apparently reached or nearly reached the glacier margin at the 3,200-m level. Glacial striations on the top surface of the flow (fig. 21.3) indicate that the glacier must have readvanced across the cooled lava tongue, abrading its surface and eroding fragments of the chilled margin. Because the striated flow surface lies well beyond the limit reached by Makanaka ice advances, the readvance must have occurred either

shortly after the eruptions, as the melted part of the ice cap reformed, or during a subsequent stadial advance. In either case the glacier must have achieved nearly the same size it had at the time of the Poliahu eruption.

MAKANAKA GLACIATION

LAVA FLOWS

Four additional lava flows that originated at vents near the summit possess features indicating that they also were erupted while glacier ice mantled the upper slopes of Mauna Kea. These flows lie stratigraphically above the Waihu-age eruptive units and the lavas that were extruded before the Makanaka glaciation, but they are stratigraphically lower than post-Makanaka flows and pyroclastic cones on the upper south flank of the mountain. Accordingly, these lavas must have been erupted sometime during the Makanaka glaciation.

The flows are associated with an arcuate cluster of pyroclastic cones from which they radiate in a nearly symmetrical pattern (fig. 21.9). Like the two older intraglacial lava flows, they possess locally steep and abrupt margins that rise as much as 30 m above surrounding rock surfaces (fig. 21.4) and that in places are strongly embayed. The marginal scarps are lowest on flows erupted along the topographically prominent rift zones, and highest on thicker flows that moved down slopes between rift zones. If the eruptions were contemporaneous, these relations imply that ice was relatively thin along the rift zones and thicker in the broad regions between, an interpretation consistent with reconstructed isopachs for the late Makanaka glacier (Porter, 1979b).

Each flow has been glacially abraded and quarried since it formed, but substantial sectors of the flow margins are relatively intact. The flow north of Puu Poliahu, which originates near a cone ("McCrae Cone" in earlier reports) just west of Puu Hauoki, displays a typical array of distinctive features along its southern margin that point to an ice-contact origin. Here the flow margin forms a steep scarp 3–10 m high marked by numerous pillows as much as 3 m in diameter (figs. 21.10 and 21.11). The pillows display radial jointing, have knobby surfaces that are often glassy to depths as great as 5 mm, and are locally palagonitized. Where pillows are lacking, flow margins frequently are marked by palagonitized vitric breccias.

Spiracles are also visible along the margins of some flows. Those developed in the flow north of Puu Poliahu rise as high as 2 m above the flow base, where they are as much as 60 cm wide (fig. 21.12). The longer ones tend to narrow upward and to bend in the downflow direction, implying that the flow was mobile during their formation.

PYROCLASTIC CONES

Pyroclastic cones associated with the four intra-Makanaka lava flows displaying ice-contact features resemble typical cinder cones on the upper slopes of Mauna Kea (fig. 21.4). Their flanks have been steepened by glacial erosion, but their surfaces are mantled with colluvium consisting of loose cinders and bombs. Hyaloclastite tuff like that composing the Waihu-age cones is not visible. However, seismic surveys of Puu Wekiu ("Summit Cone" in earlier reports) conducted before construction of the large astronomical observatory there provide important evidence of the internal structure of the cone.

Furomoto and Adams (1968) identified three zones within Puu Wekiu characterized by different seismic velocities (fig. 21.13). The uppermost, having a velocity of 0.49 km/s, was interpreted as a layer of loose colluvial cinders on the flank of the cone. A second zone, having a velocity of 0.76 km/s, underlies most of the surface of the cone to a depth of as much as 150 m. The deepest zone, with a velocity of 1.83 km/s, forms the core of the cone. Its measured velocity is well below that of weathered basalt (2.74 km/s) and it must therefore be formed of a less rigid material. Furomoto and Adams inferred that this zone probably consisted of "scoriae compressed by the overburden," but the proposed subglacial origin of the eruption makes it more likely that the seismic properties of the deepest zone indicate a hyaloclastite core, which is likely to have a rigidity intermediate between those of weathered basalt and consolidated cinders. If this interpretation is correct, then the hyaloclastite extends to an elevation of about 4,040 m within the cone, a level that is consistent with the thickness of the glacier at the time of the eruption, based on the height of the ice-contact flow margins downslope.

Exposures along the summit access road, which has been excavated several meters into the southwest flank of Puu Wekiu (fig. 21.4), display evidence of extensive hydrothermal alteration beneath the surface (fig. 21.14). The altered clay-rich zone also is enriched in phyllosilicates and has a redder color than pedogenic profiles of typical cinder cones outside the glacial limit (Ugolini, 1974). Those profiles generally extend no deeper than about 15 cm. The deep and extensive subsurface reddish zone of alteration therefore cannot be attributed to normal soil-forming processes. It is instead interpreted as having resulted from the upward movement of hot solutions into the cinder- and bomb-rich superstructure of the cone during the waning phase of the subglacial eruption. The presence of alteration products in the upper part of the cone may explain the greater seismic velocity there than in thin surficial layer of unconsolidated cinders mantling the outer slope.

OUTWASH DEPOSITS

Unlike the Waihu conglomerate, which forms a broad sheet across the southwestern side of the mountain below the moraine belt, outwash related to the Makanaka ice advances is confined mainly to gulches that indent the mountain side and to fans at the south base of the volcano. If floods were generated by the Makanaka subglacial eruptions, they apparently were confined to the preexisting drainage channels and were of smaller magnitude than those of Waihu time. In contrast to the postulated Waihu floods, which appear to have been concentrated on the southwest side of the volcano, meltwater flows during Makanaka eruptions were more dispersed, having been directed primarily down gulches that descend the mountain flanks beyond the lava tongues (fig. 21.9).

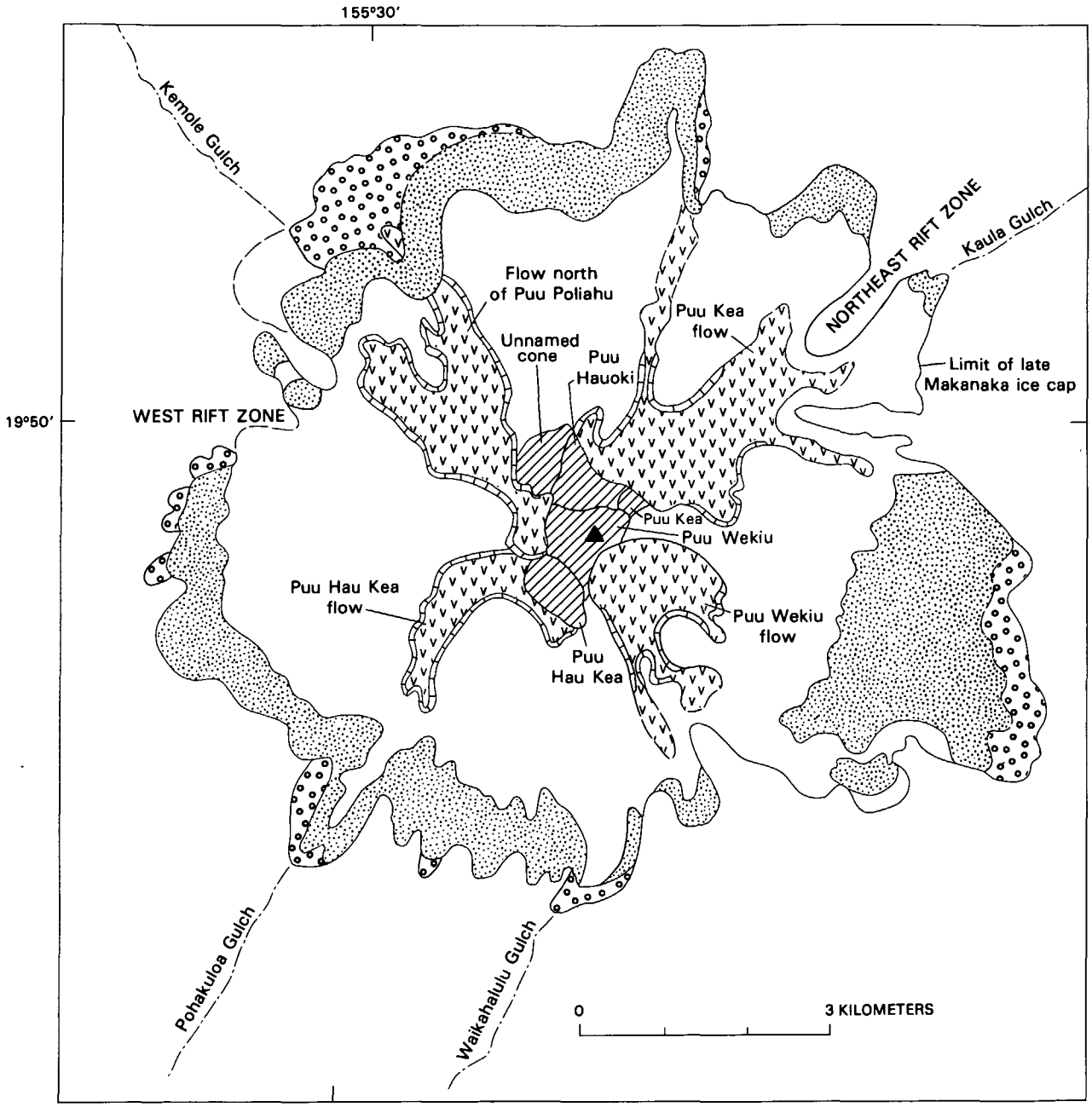

EXPLANATION

WAIKAHALULU VOLCANIC MEMBER

- Intraglacial lava flow
- Intraglacial pyroclastic cone
- Ice-contact flow margin

MAKANAKA GLACIAL MEMBER

- Late Makanaka end moraine
- Early Makanaka end moraine
- Contact—Dashed where approximately located; dotted where concealed or inferred
- ▲ Summit of Mauna Kea (4206 m)

FIGURE 21.9.—Map of summit region of Mauna Kea showing relationship of intra-Makanaka ice-contact lava flows and pyroclastic cones to early and late Makanaka end moraines.

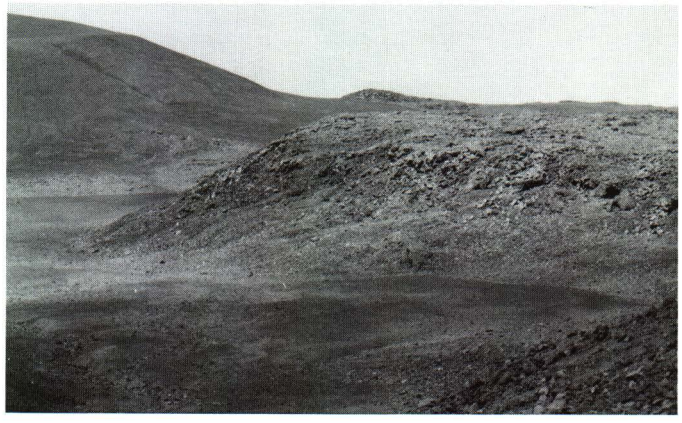

FIGURE 21.10.—Ice-contact margin of flow exposed along north side of Puu Poliahu (off picture to right). The steep margin (10–15 m high) is marked by pillow structures with radial jointing, palagonitized zones, and well-developed spiracles that rise into the flow from its base.

FIGURE 21.11.—Pillow structure at margin of flow north of Puu Poliahu. The pillow is about 1 m in diameter and marked by glassy margin, palagonite, and radial jointing.

FIGURE 21.12.—Spiracles exposed at lateral margin of flow along north side of Puu Poliahu. Interior surfaces are glassy. Spiracles are bent toward left, in direction lava flowed.

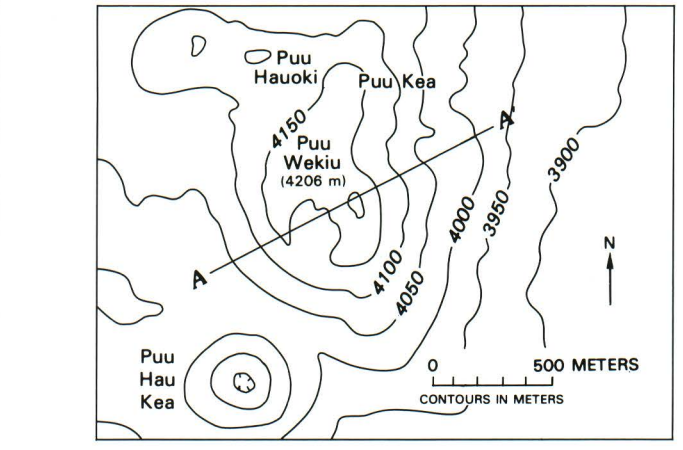

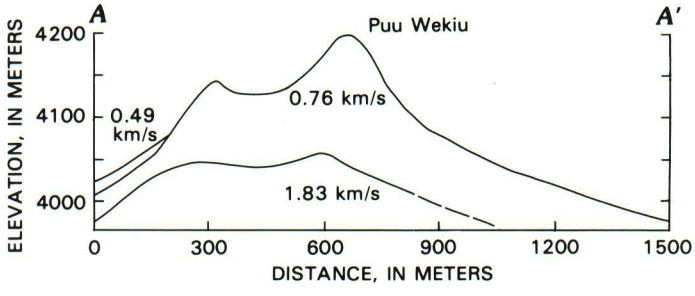

FIGURE 21.13.—Map and structure section of Puu Wekiu showing seismic-velocity zones defined by Furomoto and Adams (1968). Zone of highest velocity (1.83 km/s) is inferred to represent a core of hyaloclastite that is mantled by hydrothermally altered cinders forming a zone of lower velocity (0.76 km/s). A surficial layer of unconsolidated colluvium on the southwest slope forms a zone of still lower velocity (0.49 km/s).

FIGURE 21.14.—Hydrothermally altered pyroclastic deposits exposed along access road on south slope of Puu Wekiu (see fig. 21.4). Reddish rock is enriched in clay and phyllosilicates.

STRATIGRAPHIC RELATIONS

Stratigraphic relations and glacial features in the summit region provide constraints on the age of the subglacial eruptions. An unglaciated tongue of the flow north of Puu Poliahu emerges from beneath the late Makanaka end moraine near the head of Kemole Gulch (fig. 21.9) and overlies drift of the early Makanaka advance. These relationships imply that the flow postdates the early Makanaka maximum and antedates the late Makanaka maximum. Fragments of the chilled flow margins can be found in the late Makanaka end moraines, and the slopes of cones associated with the intra-Makanaka lavas have been glacially eroded and oversteepened. The slight erosional modification of the flows, in comparison to the erosion of the Waihu-age lavas, suggests only a single overriding advance, rather than two. These relationships imply that the eruptions date to an interval between the glacial maxima, when the ice cap was present but in a somewhat contracted state. The ice-contact flow margins can be followed downslope nearly to the late Makanaka moraine belt (fig. 21.15), but they generally are lower than the Waihu flow margins and so imply thinner ice; the size of the postulated hyaloclastite core of Puu Wekiu also points to thinner ice than during the late Makanaka glacial maximum. Because the extent and height of the several flow margins are similar, the geometry of the ice cap apparently was nearly the same during each eruptive event. The eruptions, therefore, may have been synchronous or nearly so.

CHRONOLOGY OF GLACIATIONS AND SUBGLACIAL ERUPTIONS

The timing of the Hawaiian glaciations is constrained by K-Ar ages of lava flows and radiocarbon ages of organic matter related stratigraphically to the glacial and interglacial units (Porter, 1979a). These ages show that the Pohakuloa glaciation occurred after, but probably not long after, a flow dated at 278.5 ± 68.5 ka. Thus this earliest glaciation is very likely correlative with marine oxygen-isotope stage 8, which culminated between about 276 ka and 247 ka (Hays and others, 1976). K-Ar ages of samples of the Puu Waiau and Puu Poliahu flows, and of a bomb collected from the top of Puu Waiau, cluster between 170 ka and 175 ka (171.9 ± 2.8, 174 ± 37.4, and 174.4 ± 26.5 ka), implying correlation of the Waihu glaciation with marine isotope stage 6 (190–127 ka; fig.

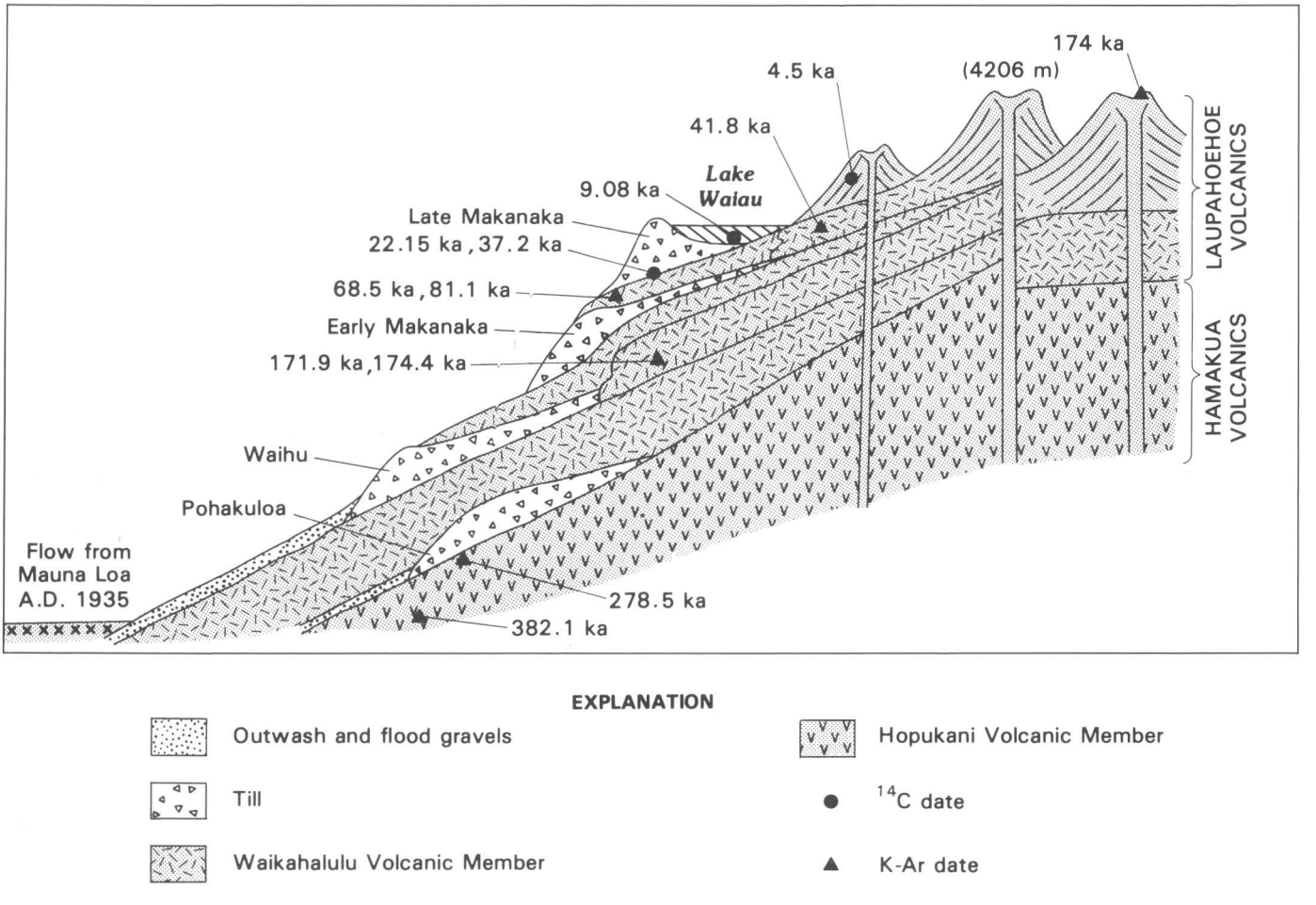

FIGURE 21.15.—Diagrammatic section showing stratigraphic relations and radiometric ages for glacial and volcanic units on upper slopes of Mauna Kea.

21.16). The early Makanaka glaciation occurred after 69.6±2.6 ka (K-Ar age) and before 37.2±1.4 ka (^{14}C age), making it a probable correlative of isotope stage 4 (73–61 ka). The late Makanaka advance culminated sometime between 29.75±0.5 (or possibly 22.15±0.25) ka and 9.08±0.2 ka (^{14}C ages), indicating equivalence to isotope stage 2 (29–10 ka).

A lava sample collected from the ice-contact margin of the flow north of Puu Poliahu has a K-Ar age of 41.3±8.3 ka. This would place it within isotope stage 3 (61–29 ka; fig. 21.16). However, the downslope extent of the ice-contact flow margins implies a large ice cap at the time of the eruptions; the subglacial eruptions may therefore have occurred either late in isotope stage 4 or early in stage 2, when the ice cover probably was more extensive. Calculations suggest that the snowline must be lowered at least 400 m before a glacier can begin to form at the summit of Mauna Kea (Porter, 1979b), and the extent of the intra-Makanaka ice-contact flows indicates snowline depression nearly as great then as during the late Makanaka maximum. It is therefore less likely that the eruptions occurred during isotope stage 3, which was an interstade marked by reduced global ice volume and general glacier recession (see, for example, Nilsson, 1983), than during either stage 4 or stage 2. These correlations are based on a single K-Ar age; dating other intra-Makanaka subglacially erupted flow units on Mauna Kea could help to resolve the present uncertainty.

Inasmuch as there is evidence for summit eruptions during the Waihu and Makanaka glaciations, might there also have been such activity during the Pohakuloa glaciation? Because the recurrence interval of eruptions is shorter during the tholeiitic shield-building phase, it seems unlikely that an ice cap as large as that of Pohakuloa time (130–150 km^2) could have existed for thousands of years without at least some eruptions occurring subglacially. The exposed Pohakuloa deposits provide no firm evidence of such activity, but the abundance of Pohakuloa meltwater sediments exposed in Waikahalulu and Pohakuloa gulches and their coarseness and poor sorting suggest that they may be related to subglacial eruptions that generated floods like those of Waihu time. Although the very limited outcrops of Pohakuloa drift make it unlikely that definitive evidence will be found, such eruptions remain a possibility.

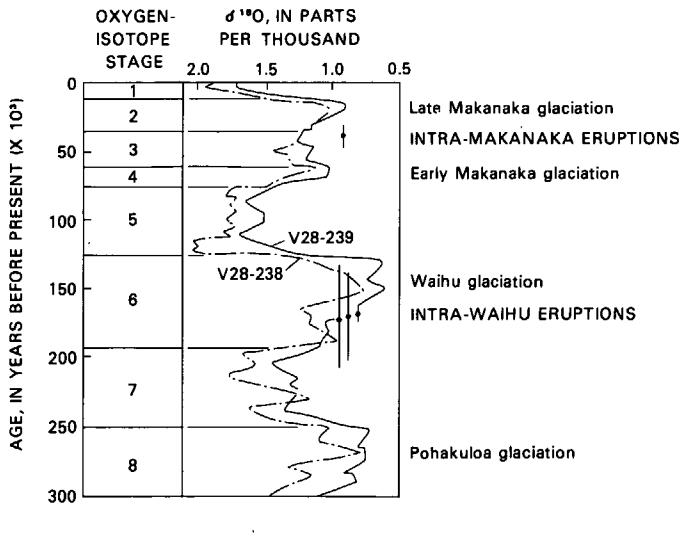

FIGURE 21.16.—Oxygen-isotopic variations in Pacific deep-sea cores V28–238 and V28–239 (Shackleton and Opdyke, 1976), showing isotope stages 1–8; inferred correlation with Mauna Kea glaciations; and K-Ar ages (dots), with error range of one standard deviation (bars), of products of subglacial eruptive activity.

REFERENCES CITED

Daly, R.A., 1910, Pleistocene glaciation and the coral reef problem: American Journal of Science, v. 298, p. 297–308.

Furomoto, A.A., and Adams, W.M., 1968, Seismic refraction study of the internal structure of a volcanic cinder cone, *in* Knopoff, Leon, Drake, C.L., and Hart, P.J., eds., The crust and upper mantle of the Pacific area: American Geophysical Union Geophysical Monograph 12, p. 112–121.

Hays, J.D., Imbrie, J., and Shackleton, N.J., 1976, Variations in the Earth's orbit: pacemaker of the Ice Ages: Science, v. 194, p. 1121–1132.

Jones, J.G., 1970, Intraglacial volcanoes of the Laugarvatn region, southwest Iceland, II: Journal of Geology, v. 78, p. 127–140.

Porter, S.C., 1972a Distribution, morphology, and size frequency of cinder cones on Mauna Kea Volcano, Hawaii: Geological Society of America Bulletin, v. 83, p. 3607–3612.

———1972b, Buried caldera of Mauna Kea Volcano, Hawaii: Science, v. 175, p. 1458–1460.

———1979a, Quaternary stratigraphy and chronology of Mauna Kea, Hawaii: a 380,000-year record of mid-Pacific volcanism and ice-cap glaciation: Geological Society of America Bulletin, Part II, v. 90, p. 980–1093.

———1979b, Hawaiian glacial ages: Quaternary Research, v. 12, p. 161–187.

Shackleton, N.J., and Opdyke, N.D, 1976, Oxygen-isotope and paleomagnetic stratigraphy of Pacific core V28–239, late Pliocene to latest Pleistocene, *in* Cline, R.M., and Hays, J.D., eds., Investigation of Late Quaternary paleoceanography and paleoclimatology: Geological Society of America Memoir 145, p. 449–464.

Stearns, H.T., 1945, Glaciation of Mauna Kea, Hawaii: Geological Society of America Bulletin, v. 56, p. 267–1526.

Stearns, H.T., and Macdonald, G.A., 1946, Geology and ground-water resources of the Island of Hawaii: Hawaii Division of Hydrography Bulletin 9, 363 p.

Ugolini, F.C., 1974, Hydrothermal origin of the clays from the upper slopes of Mauna Kea, Hawaii: Clays and Clay Minerals, v. 22, p. 189–194.

Wentworth, C.K., and Powers, W.E., 1941, Multiple glaciation of Mauna Kea, Hawaii: Geological Society of America Bulletin, v. 52, p. 1193–1218.

VOLCANIC HAZARDS IN THE HAWAIIAN ISLANDS

By Donal R. Mullineaux, Donald W. Peterson, *and* Dwight R. Crandell

ABSTRACT

Volcanic eruptions have built the Hawaiian Islands, and similar eruptions in the future will affect many areas in them, especially on Kilauea and Mauna Loa Volcanoes on the Island of Hawaii. Some of those eruptions will endanger people and property. Hazards that result directly from eruptions include lava flows, tephra falls, volcanic gases, and pyroclastic surges. Less direct hazards associated with eruptions include ground fractures and subsidence, earthquakes, and tsunamis.

The Islands of Hawaii and Maui have been subdivided on maps, for some kinds of hazards, into various zones of differing magnitude of hazard. These hazard-zone maps can be used for making land-use decisions before eruptions occur and for responding to actual or threatened eruptions. Hazard-zone maps for earthquakes and tsunamis are not included in this report; however, earthquakes of both volcanic and nonvolcanic origin can affect extensive areas in the islands, and tsunamis can be highly damaging in narrow coastal zones.

Because most volcanic events cannot be effectively controlled, volcanic hazards are best avoided by land-use planning before eruptions occur and by evacuation when they do occur. Mitigation measures to reduce effects from lava flows can be effective, at least temporarily, but such measures are generally more effective for some other hazards such as tephra falls and volcanic gases.

INTRODUCTION

All the Hawaiian Islands have been built by volcanic eruptions over a period of millions of years. Similar eruptions have continued into historical time on the islands of Hawaii and Maui and undoubtedly will occur in the future, especially on Kilauea and Mauna Loa Volcanoes. Most Hawaiian eruptions form lava flows that endanger chiefly property; explosive eruptions are relatively rare but are more likely to threaten people. As intensive land development expands toward areas of relatively high hazard, the threat to life and property will increase accordingly.

This report discusses the characteristics, frequency, location, and extent of various hazardous phenomena typical of Hawaiian volcanoes, assesses the likely future extent, frequency, and relative severity of these phenomena, and shows distribution of some hazards on hazard-zone maps. Although they have distinct limitations, these maps can be useful for planning long-range mitigation of volcanic hazards and for organizing short-term response to eruptions.

The character of volcanic eruptions in Hawaii has been described at length in many previous reports (for example, Macdonald and Abbott, 1970; Macdonald, 1972) and is treated at length elsewhere in this volume. Brief descriptions of volcanic activity in this assessment are intended to emphasize certain characteristics that can help the public and public officials to understand volcanic hazards and ways of mitigating them. Hazards resulting from eruptions that bring rock materials to or above the ground surface are here termed direct hazards. Hazards termed indirect are events that accompany such eruptions, or are secondary effects of eruptions, or result from movement of magma that does not reach the ground surface.

The term hazard in this report refers either to a hazardous event or to its products; examples are an explosive eruption or a lava flow. The term risk refers to the likelihood of losses to people, such as the loss of life, homes, or productive land. Volcanic hazards in the nearly uninhabited upper part of the east rift zone of Kilauea, for example, are of about the same frequency and severity as those in the lower, more highly populated part of the rift zone. Risk, however, is much higher in the lower part because of its greater population and more intensive land use. The potential hazards from volcanic eruptions in the islands will remain about the same in the foreseeable future, but increased risk from those eruptions will accompany growth in population and economic development.

ACKNOWLEDGMENTS

This report has been based in large part on information published by past and present scientists at the Hawaiian Volcano Observatory, on pre-1970 mapping by H.T. Stearns and G.A. Macdonald, and on more recent published and unpublished mapping and interpretations of R.T. Holcomb, P.W. Lipman, J.P. Lockwood, and R.B. Moore. In addition, much information has been provided by many other scientists who have carried on investigations at the volcano observatory. This report includes additions to and modifications of reports on volcanic hazards on the Island of Hawaii by Mullineaux and Peterson (1974), and on Oahu and Maui by Crandell (1975 and 1983).

HAWAIIAN VOLCANIC ACTIVITY

The Hawaiian Islands (fig. 22.1) lie at the southeastern end of a largely submerged volcanic chain about 6,000 km long, which extends from the Emperor Seamounts to the Island of Hawaii (Dalrymple and others, 1973). This chain consists of volcanoes that are progressively younger toward the southeast; Kilauea and Mauna Loa Volcanoes on the southeastern part of the Island of Hawaii (fig.

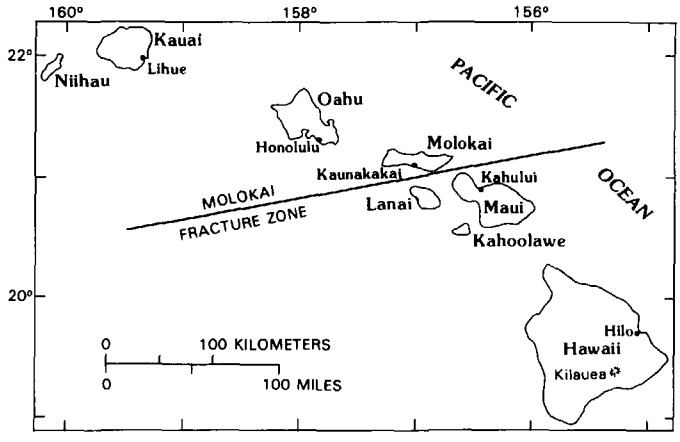

FIGURE 22.1.—Index map of the Hawaiian Islands, showing location of the Molokai fracture zone.

22.2) are now the most active in the chain. Another volcano, Loihi, is growing on the ocean floor off the southeast coast of Hawaii (Moore and others, 1982; fig. 22.2), though it probably will not rise above the ocean surface for many thousands of years.

Hawaiian volcanoes consist largely of basaltic lava flows that were highly fluid and traveled as much as tens of kilometers from their source vents. Their cones typically are broad in comparison to their height and are called shield volcanoes. During their growth, many of these volcanoes developed elongate systems of near-vertical fractures along zones of weakness called rifts or rift zones, which lead from the volcano centers outward through their flanks. Magma moving up into a volcano rises along the central conduit, and much is erupted from vents at the summit, but some magma may spread outward into the rift zones and be erupted there. In addition, a few eruptions occur at vents on the volcanoes' flanks outside the rift zones.

Hawaiian volcanoes typically follow an evolutionary pattern. In an early stage, during which the main shield is built, eruptions of highly fluid lava are frequent and voluminous; Kilauea and Mauna Loa on the Island of Hawaii are in such a stage now. Later, eruptions become less frequent but commonly are more explosive. Hualalai and Mauna Kea on the Island of Hawaii are now in this stage and probably also Haleakala on the Island of Maui; none of these volcanoes can be regarded as extinct. Sporadic eruptions can occur on Hawaiian volcanoes for many tens of thousands of years after their shield building stage has ended.

Most eruptions that build the volcanoes are not explosive, but activity at the onset of an eruption often is vigorous enough to produce fountains of molten lava that reach tens to hundreds of meters above the vent. Large lava clots fall back and may be included in spatter ramparts or lava flows, but small particles of molten and solidified lava from the fountains are carried by wind away from the vent area and fall to produce deposits of tephra. Continued and less vigorous emission of lava produces lava streams that flow away from the vent. Lava that flows into the sea can be explosively disrupted by steam, producing mounds of lava fragments called littoral cones along the shore.

Explosive eruptions are not as frequent as lava flows, but they have occurred repeatedly in Hawaii and produce a variety of products. Large clots of lava and solid rock fragments thrown high into the air by explosions fall back close to the vent to form cinder cones. Finer particles are carried away by wind, forming ash deposits that can be as much as a few meters thick near the cone. Explosions can also create cloudlike mixtures of rock fragments and gases, called pyroclastic surges, which typically spread from vents outward along the ground surface at high speed. Ash-laden clouds that rise above pyroclastic surges can also be carried away by winds and form beds of ash.

Volcanic gases are emitted during every kind of eruption and at many vents during intervening dormant periods. Gases generally are quickly diluted by air as they are dispersed downwind, although their odor may be detectable for many tens of kilometers.

Eruptions have been frequent in historical time, about the last 200 years. Kilauea and Mauna Loa have each erupted dozens of times during this period, and Hualalai erupted as recently as A.D. 1801 (Moore and others, chapter 20; Macdonald and Abbott, 1970). Haleakala Volcano on Maui last erupted about 1790 and

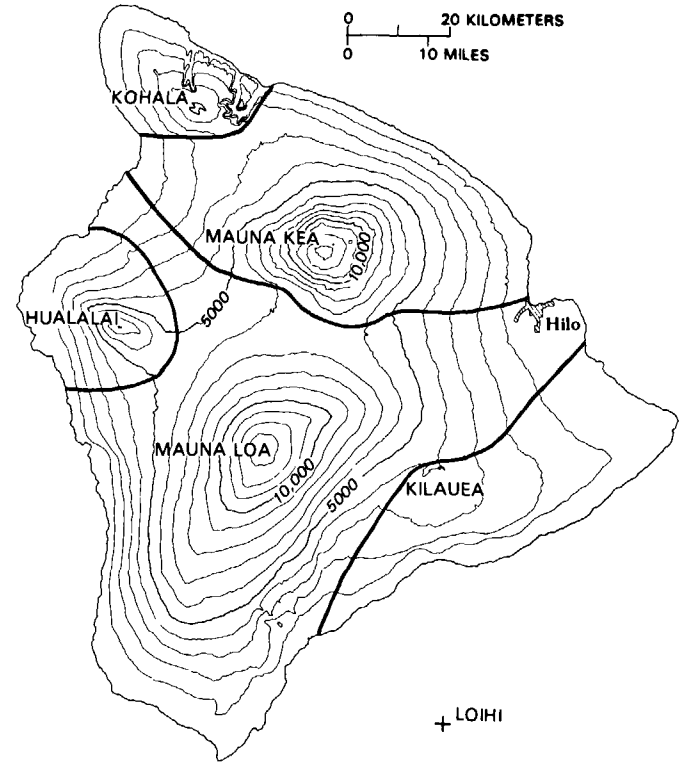

FIGURE 22.2.—Location and topography of the five volcanoes that form the Island of Hawaii, and location of the still-submerged offshore volcano Loihi. Contour interval 1,000 feet (approx. 300 m). Heavy solid lines mark boundaries of the five volcanoes.

has been active at least 10 times within the last 1,000 years (Crandell, 1983).

Several other volcanoes, though dormant during the last 200 years, are not extinct. Mauna Kea has erupted several times within the last 10,000 years (Porter, 1973) and, among those other volcanoes, has the highest eruptive probability. Other potentially active volcanic areas, such as the southeastern part of Oahu, apparently have not erupted for more than 10,000 years. The possibility of future eruptions in those areas should be recognized, even though specific preparation for such eruptions may not be economically or socially practical.

DIRECT VOLCANIC HAZARDS

Among direct volcanic hazards, lava flows occur most frequently and are the greatest hazard to property. Eruptions of tephra are also frequent but do not represent a severe hazard to people or property. Although pyroclastic surges are relatively infrequent, they can be a great danger to human life. Volcanic-gas emissions, in contrast, are common and continuous but represent relatively little danger to people or property.

LAVA FLOWS

Lava is erupted from single vents and from long fissures, and typically forms tongue-shaped to broadly lobate flows that extend downslope from the vent (fig. 22.3). The size, extent, and kind of movement of lava flows vary greatly, depending on such factors as the rate and volume of eruption and the topography over which the lava moves.

Hawaiian lava flows generally advance more slowly than the speeds at which people normally walk (3–5 km/h) but some may move much faster. Fronts of voluminous flows on steep ground have advanced as rapidly as 9 km/h, and lava streams in well-established channels on steep slopes may reach speeds of 55 km/h (Macdonald and Abbott, 1970, p. 23). Contrasting flow behavior and surface features divide most lava flows in Hawaii into two types, termed pahoehoe and aa. Pahoehoe lava is relatively fluid and forms flows that are thinner than the more viscous aa flows, and pahoehoe flows are more strongly controlled by minor topographic features. Individual pahoehoe flows range in thickness from a few tens of centimeters to as much as 3 m. During the course of a single eruption, however, successive pahoehoe flows moving along the same path may build up thicknesses of many tens of meters. Individual aa flows are generally 2–8 m thick, but locally they can be as thick as 20 m.

Hawaiian lava flows range from a few meters to more than 50 km in length, and from a meter or two to about 3 km in width. A critical factor in assessing hazards from future lava flows is the maximum distance they can be expected to extend. Although the majority of past flows from Mauna Loa have not extended more than 10–15 km from their vents, some have reached much farther in only one or a few days. The longest lava flows apparently reached their maximum extents quickly, before the loss of heat or gases caused their fluidity to decrease, or they formed lava tubes that minimized loss of heat and gases. Of many factors that influence the length of lava flows, Walker (1973) proposed that rate of eruption of the lava is most important, and that it could be used to predict the distance a lava flow will travel. Malin (1980), however, pointed out that rate of lava eruption does not correlate well with length of lava flows from Kilauea or Mauna Loa; those flows correlate more closely to volume. In 1984, a lava flow from Mauna Loa extended more than 25 km toward Hilo in less than 5 days (Lipman and Banks, chapter 57). Decreases in eruption rate then triggered channel blockages and branching of the flow (Lipman and Banks, chapter 57), and the flow did not reach closer to the city. A high sustained rate of lava eruption clearly indicates that a lava flow could reach far from the vent. The most useful clues to the probable final length of such a flow may be determination of whether the rate of eruption is constant or changing, and whether or not the flow forms a lava tube.

The paths followed by lava flows are generally downslope, but they may vary in detail. Because parts of a flow are continually cooling and becoming more viscous, the flow may not move directly into the lowest available ground as would a stream of water. Lava flows may move diagonally down slopes or even cross low ridges.

The chief threat presented by lava flows is to property that cannot be removed. They burn, crush, bury, or surround structures that lie in their paths, and reduce the value of land that is covered. Although most lava flows move so slowly that they do not threaten

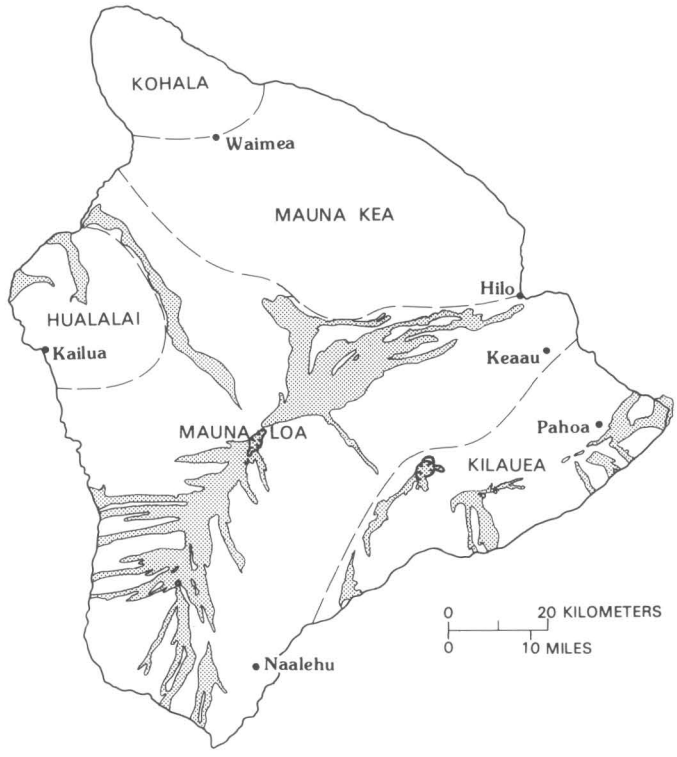

FIGURE 22.3.—The Island of Hawaii, showing approximate areas covered by pre-1975 historical and some prehistorical lava flows (stippled). Dashed lines mark the boundaries of the five volcanoes that form the island.

lives, voluminous flows, especially those on steep slopes, can move rapidly enough to endanger people.

TEPHRA FALLS

Tephra, which consists of volcanic ash and coarser fragments, is produced most frequently in Hawaii by lava fountains, but it can also be formed by explosive magmatic eruptions and by steam-blast (phreatic) explosions, both of which throw large and small fragments of molten and solid rock into the air. Large clots of lava erupted in fountains may still be molten when they fall to the ground, where they may become part of a flow or form spatter cones and ridges near the vents. Fragments ejected during eruptions that are more vigorous, and often more continuous, partly or wholly solidify before they fall back to the ground surface, and these form cinder cones around the vent. Tephra produced by steam explosions generally consists of pieces of previously solidified rock. Steam-blast eruptions such as those at Kilauea in 1924 probably resulted when ground water entered hot zones inside the volcano (Macdonald, 1972, p. 245; Decker and Christiansen, 1984). Locally, mounds of tephra (littoral cones) can be built by steam explosions where lava flows enter the ocean.

Large tephra fragments fall close to their source vents, but smaller particles commonly are carried away by winds to form widespread ash deposits. Tephra deposits are also thick near source vents, and thin rapidly with increasing distance. Tephra from lava fountains at Kilauea Iki in 1959, for example, is more than 3 m thick at 0.5 km from the vent, but thins to about 15 cm and 3 cm at distances of 2 km and 4 km, respectively (Richter and others, 1970; figs. 22.4, 22.5). Tephra from eruptions that built cinder cones on Mauna Kea is as much as a meter thick at distances of 1–2 km and 10 cm thick at about 5 km (Porter, 1973). An ash layer about 2,500 years old on the west flank of Haleakala on Maui is as much as 10 cm thick at about 9 km from the crater. Repeated eruptions of tephra from the same or nearby vents can result in even thicker deposits; widespread, prehistoric ash deposits on the Island of Hawaii are locally nearly 20 m thick (Stearns and Macdonald, 1946), and similar deposits as thick as 6 m blanket a large area on the upper northwest flank of Haleakala. Traces of ash from lava fountains commonly have been seen at distances of 40–50 km during historical eruptions of Kilauea and Mauna Loa. Tephra from steam-blast eruptions generally is coarse-grained and no more than a few tens of centimeters thick. Large fragments from the 1924 eruption at Kilauea, some weighing several tons, were thrown hundreds of meters, and smaller rocks were thrown as far as about 2 km (Jaggar, 1947; Macdonald and Abbott, 1970).

Lava fountains and eruptions that form cinder cones are spectacular but seldom endanger people or animals, who can move upwind or out of the range of the falling material. No human deaths or serious injuries from such eruptions have been reported in Hawaii during the 19th or 20th centuries. Steam-blast eruptions, however, can occur abruptly and eject large fragments that represent a distinct threat to people and animals. At least one person, in 1924, has been struck and killed by large fragments ejected in an explosive eruption (Macdonald and Abbott, 1970).

Tephra can seriously affect vegetation and manmade structures and machinery. Property may be burned and abraded by airborne particles, damaged by impact of large fragments, or buried by a blanket of ash. Ash can also cause discomfort and even injury to eyes and respiratory systems, and can smother vegetation, clog water and sewage systems, and damage machinery.

Tephra from eruptions during historical time that is thick enough to have caused severe damage has been limited to areas less than about 2 km from active vents. Tephra deposits from eruptions of Kilauea and Mauna Loa have covered the ground to thicknesses of more than 15 cm only within about 2 km from the vents. The thickness of tephra and the damage it causes gradually decrease at progressively greater distances.

PYROCLASTIC SURGES

Some explosive eruptions produce pyroclastic surges, which are clouds of ash, rock fragments, and gases that move at high speed outward from a source vent. Although pyroclastic surges move along the ground surface, they may or may not follow topographic depressions. The temperature of rock material in some surges is higher than the boiling point of water, but in others can be lower. Pyroclastic surges are commonly caused by steam explosions or by explosions of magma and steam. These explosions can originate in at least four ways: (1) interaction between ground water and molten rock in a fluctuating magma column; (2) sudden depressurization of a shallow hydrothermal system; (3) intrusion by magma into water-saturated rocks; and (4) movement of sea water directly into a conduit during submarine eruptions. Prehistoric explosive eruptions of Kilauea have been attributed to the first two causes (Decker and Christiansen, 1984).

Explosive eruptions can produce, in their early stages, a primary surge that moves laterally away from the explosion site in all directions, as well as a vertical eruption column. Secondary pyroclastic surges can develop when material falls back to the ground from the vertical column. Although velocities of 50 km/h to as much as 300 km/h can be inferred for some surges, they decelerate rapidly and typically stop less than 10 km from their source (Crandell and others, 1984).

Pyroclastic surges formed by eruptions at basaltic volcanoes have affected areas as far as 10 km from their source vents (Crandell, 1983; Dzurisin and others, in press). The probability that an area will be affected by a surge, as well as the severity of the effects, decrease progressively away from a vent. Because surges do not necessarily follow topographic lows, high areas may not be safe. Pyroclastic surges formed by eruptions at Rotomahana-Waimangu, New Zealand, in 1886 extended at least 6 km from their source area and surmounted steep hills as high as 360 m above the vents and 200 m above the adjacent land surface (Nairn, 1979).

A series of explosive eruptions at the summit of Kilauea about 2,000 years ago produced at least three pyroclastic surges (Dzurisin and others, in press). The first two were separated by lava-fountain

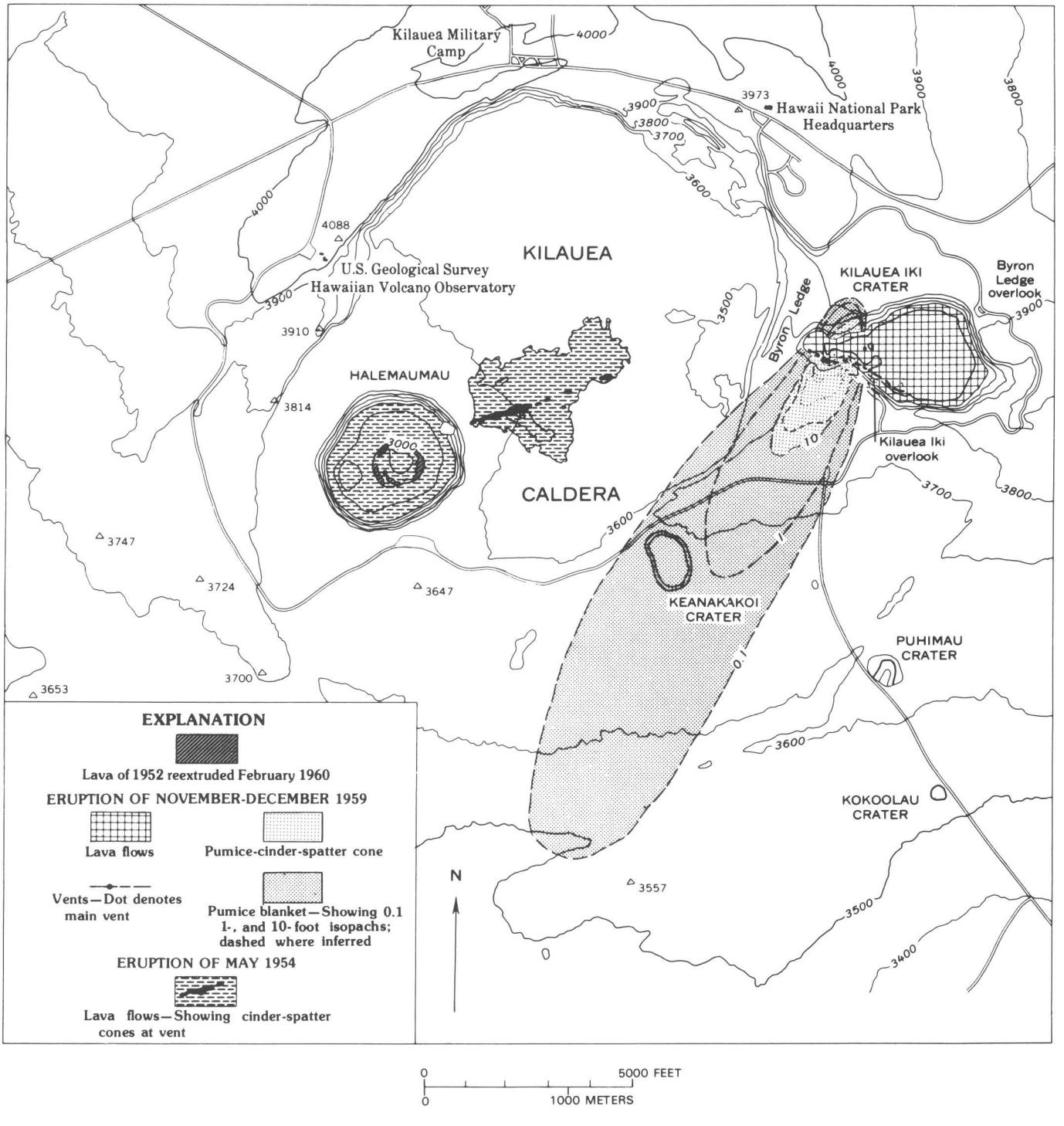

FIGURE 22.4.—The summit area of Kilauea, showing extent of tephra (pumice) blanket from Kilauea Iki vent in 1959. From Richter and others (1970). Topographic contours in feet.

eruptions, and the second and third by lava fountaining and an explosion that produced a shower of rock fragments. The last surge was followed by more fountains and by lava flows. These surges affected areas at least 10 kilometers from the vent area. Pyroclastic surges originating in the same area about 1790 left deposits of rock debris locally more than 10 m thick near Kilauea's summit caldera (Decker and Christiansen, 1984; fig. 22.6) and may have affected areas as far as 9 km from the vent. Prehistoric pyroclastic-surge

FIGURE 22.5.—Tephra (pumice) blanket in former picnic area 1 km southwest of Kilauea Iki vent, on November 30, 1959. Small shelter after 3rd phase of activity; about 1 m of tephra covers ground. From Richter and others (1970).

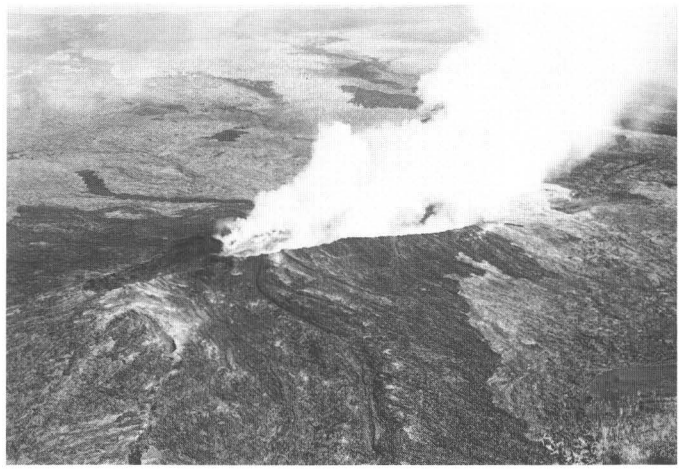

FIGURE 22.7.—Volcanic gases issuing from the Mauna Ulu vent on the upper east rift zone of Kilauea in about 1972. Distance across the photograph from left to right, through the vent, is about 2 km.

deposits also have been recognized at many localities on the southeastern part of Oahu, and on the islet of Molokini off the southwest coast of Maui.

Although less frequent than lava flows, explosive eruptions that produce pyroclastic surges represent a severe hazard to lives. The chief hazards to people are from asphyxiation by hot ash, impact by rock fragments traveling at high speed, and burns from hot and perhaps wet, clinging ash. The positions and condition of bodies of persons killed by pyroclastic surges during the 1790 eruptions of Kilauea indicated that asphyxiation and heat caused the deaths, rather than injuries resulting from impact by rock fragments (Swanson and Christiansen, 1973). The chief hazards of pyroclastic surges to property are impact and blast effects; vegetation as well as structures can also be burned, buried, and abraded.

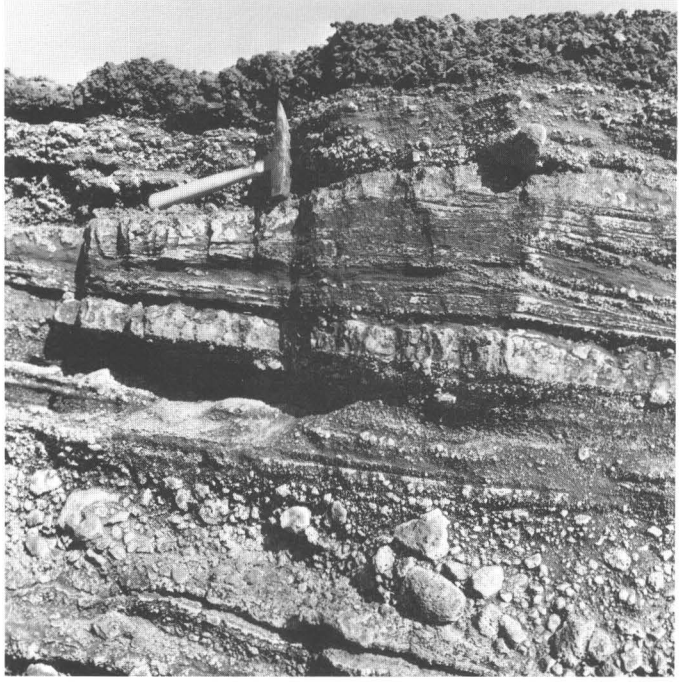

FIGURE 22.6.—Interbedded tephra-fall deposits and pyroclastic-surge deposits (with inclined bedding) that were explosively erupted from Kilauea caldera in 1790. Photograph by R.L. Christiansen, U.S. Geological Survey.

VOLCANIC GASES

Volcanic gases are emitted during all types of eruptions (fig. 22.7) and can continue to be released for many years after other eruptive activity ceases. Gas can also be expelled at vents that have never erupted lava; some fumaroles have produced gases for more than a century. The most abundant constituents of volcanic gas in Hawaii are water vapor, sulfur dioxide, and carbon dioxide, but many other gases have been detected (Macdonald, 1972, p. 50). The gases of most concern to human health are various combinations of sulfur, oxygen, and hydrogen, such as hydrogen sulfide and sulfur dioxide; other dangerous gases include chlorine, fluorine, and carbon monoxide. Carbon dioxide can collect in closed depressions and cause asphyxiation. Small amounts of mercury have also been detected in gases emitted from vents along the east rift zone of Kilauea (Siegel and Siegel, chapter 35; Siegel and Siegel, 1978).

No deaths from volcanic gases have been reported on Hawaii, although gases have killed people elsewhere, notably in Indonesia (LeGuern and others, 1982). Brief exposure to gases generally does not harm otherwise healthy persons, but it can endanger people with heart and lung ailments. The hazard is greatest downwind from and near active vents, and it may persist at vents that continue to fume during inactive periods. Gases mix with air as they drift downwind, and their concentrations and effects diminish with increasing distance from the source. Even small concentrations of sulfur-bearing gases

can affect the lungs, eyes, and skin, and may cause gastric upsets. Furthermore, these gases can combine with water to form sulfuric acid, which can damage live tissue, cloth, metal, and other materials. Many types of vegetation cannot survive near gas-emitting vents, and many varieties may be killed as far as 30 km from the source vents. Some volcanic gases, such as carbon monoxide and carbon dioxide, are odorless and heavier than air, and during windless periods they may become concentrated in topographic depressions and present an invisible danger of asphyxiation. The presence of sulfur-bearing volcanic gases generally can be detected by their odor.

INDIRECT VOLCANIC HAZARDS

Ground fractures, subsidence, and earthquakes commonly occur together as a result of magma movement. They are especially common in the summit areas and rift zones of Kilauea and Mauna Loa but are generally not severe. These hazards also occur on a larger scale along the flanks of Kilauea and Mauna Loa as a result of massive landslides (Lipman and others, 1985), and tsunamis accompanying earthquakes may affect coastlines of the islands. Such earthquakes endanger property, and the tsunamis are a great threat to lives. Earthquakes that affect Hawaii are also caused by crustal movements underneath the volcanoes, and many tsunamis that affect the islands are generated elsewhere in the Pacific Ocean.

GROUND FRACTURES

Ground fractures in rock and soil are caused when the mass on one side shifts away from or slides past an adjacent mass along a crack. Fractures may form scarps where one mass moves up or down relative to another. Cracks as much as several meters across can remain open for long periods, and some are many kilometers in length.

Cracks can form rapidly or slowly, and by repeated discrete movements or by slow, more continuous movements. Repeated vertical displacements along the same fracture can produce a scarp as high as several hundred meters.

Most fractures in the Hawaiian Islands result from magma movement, subsidence of landslide blocks, or earthquake shaking. Fractures of historical age caused by magma movement are very abundant in summit areas and rift zones on Kilauea and Mauna Loa (fig. 22.8), and prehistoric fractures, probably of similar origin, are common along the southwest rift zone of Haleakala. The gravitational subsidence of large landslide blocks on the flanks of Kilauea and Mauna Loa also creates fractures.

Earthquakes cause fractures by ground vibration and also by triggering landslides, especially in loose soils. The earthquakes of April 26, 1973, November 29, 1975, and November 16, 1983, for example, caused cracks at many places on the Island of Hawaii.

Ground fractures are a minor but persistent hazard to people and animals. Cracks that open suddenly could trap them, and a danger would remain for as long as the cracks stayed open, especially where they are hidden by thick vegetation. Ground fractures also threaten property: they can disrupt roads and buildings as well as water, sewer, power, and telephone lines.

FIGURE 22.8.—Subsidence of a graben in the Kapoho area on the lower east rift zone of Kilauea, on January 13, 1960, prior to outbreak of eruption in the area. View eastward along the Kapoho fault scarp in the village of Kapoho. Maximum vertical displacement is about 1 m (3.5 feet). Photography by R.T. Haugen, National Park Service.

GROUND SUBSIDENCE

Ground subsidence consists mainly of four kinds that differ greatly in scale: (1) subsidence of entire islands, (2) subsidence of parts of a volcano's flanks, (3) settling of small areas as a result of underground movement of magma, and (4) local collapse of the roofs of lava tubes.

Subsidence of some islands is slow but continuous, and the resulting submergence along shorelines is augmented by slow, worldwide rise of sea level. The rate of subsidence for the Island of Hawaii, which differs from place to place on the island, has been calculated as 1.4–4.1 mm/yr (Moore, chapter 2; Apple and Macdonald, 1966; Moore and Fornari, 1984). The worldwide rise of sea level is 1–2 mm/yr, thus the island is being submerged at approximately 3–6 mm/yr, equivalent to 1–2 feet per century. At Kahului, Maui, the rate of island subsidence may be as much as 1.7 mm/yr (Moore, chapter 2; Moore, 1970) and the overall submergence about 3 mm/yr, equivalent to 1 foot per century. Subsidence of such large areas is believed to result from depression of the sea floor under the weight of the islands. Coral reefs, beach rock, and soils encountered in drill holes on Oahu at depths as much as 336 m below sea level (Stearns, 1966, p. 21) indicate that the Island of Oahu also has subsided in the past. Tide-gauge records indicate that the island is now being submerged at the same rate as the worldwide rise in sea level, thus it apparently is stable now (Moore, chapter 2; Moore and Fornari, 1984).

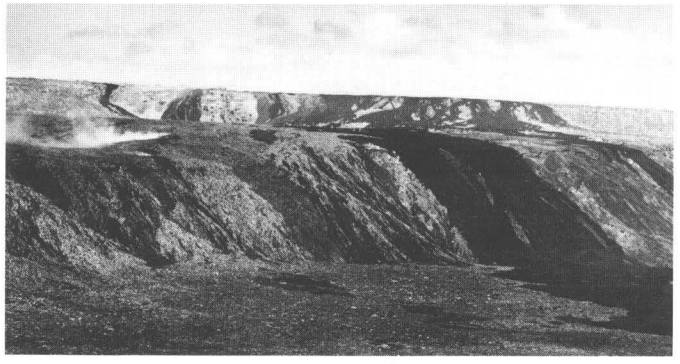

FIGURE 22.9.—Stepped topography produced by subsidence of large landslide blocks on the south flank of Kilauea. The scarps are formed by repeated downward movement of blocks south of faults. Each episode of movement develops new ground cracks; such cracks are visible on face of scarp in foreground. Scarps are partly mantled with lava erupted from Mauna Ulu in 1969–74. Photograph by R.I. Tilling, U.S. Geological Survey.

Submergence from slow, continuous subsidence and sea-level rise will eventually endanger shoreline facilities. Low-lying coastal sites will become increasingly threatened by damage from storm waves and tsunamis, and eventually by inundation. Submergence is thus a factor to be considered in long-range plans for buildings and other facilities in all coastal areas of the Hawaiian Islands, and especially on the Islands of Hawaii and Maui.

Most other types of subsidence are more rapid. Large parts of the flanks of Kilauea and Mauna Loa, for example, sometimes subside abruptly. The areas affected may be several tens of kilometers long and involve hundreds of square kilometers of land (Lipman and others, 1985). Steep scarps and stair-step topography along fault zones on the flanks of both volcanoes were formed by repeated movements during the recent geologic past (fig. 22.9). These movements result from instability of the volcanoes' flanks caused in part by intrusion of magma into rift zones and in part by the load of the unbuttressed seaward flanks of the growing volcanoes (Moore and Fiske, 1969; Swanson and others, 1976).

Rapid subsidence can damage or destroy manmade structures by tilting, shaking, and fracturing the ground. It endangers areas along shorelines because they may suddenly become inundated or lowered enough to be vulnerable to damage from storm waves and tsunamis.

Shallow underground movements of magma can also cause subsidence. Withdrawal of magma from beneath summit areas and rift zones may remove support from tracts of land and cause them to subside. Such movements may be no more than a few meters, but the summation of repeated settling can amount to tens or hundreds of meters. This process produced the summit calderas and pit craters of Mauna Loa and Kilauea, which are as much as several hundred meters deep.

Subsidence caused by withdrawal of magma is restricted to summit areas and rift zones; manmade structures in those areas can be damaged or destroyed by tilting or by differential settling of underlying rock. Some depressed areas may become more vulnerable to inundation by water or lava flows. This type of subsidence is so commonly associated with eruptions and so restricted to summit and rift-zone areas that its effects are overshadowed by those caused directly by eruptions.

Collapse of roofs of lava tubes is a minor subsidence hazard. Roof collapse can occur while lava is still moving through a tube, or later, especially if new loads are added by construction or heavy equipment. This hazard can be minimized by investigating for the presence of lava tubes at construction sites and along paths to be followed by heavy construction equipment. The hazard is highest on young pahoehoe lava flows of Mauna Loa and Kilauea, but it may also exist along the southwest rift zone of Maui and on the Kalaupapa Peninsula of Molokai.

EARTHQUAKES

Thousands of earthquakes occur each year in the Hawaiian Islands; most of them originate on the Island of Hawaii and result from the movement of magma at shallow depths (see Klein and others, chapter 43). These earthquakes commonly are associated with volcanic eruptions, but they also accompany movements of magma that does not reach the surface. The greatest number of earthquakes on the Island of Hawaii originate beneath the summit areas and along or near the rift zones of Kilauea and Mauna Loa. Most are so small that they can only be detected by instruments and cause no damage, but some are strong enough to be felt, and a few cause minor to moderate damage.

Some earthquakes are less directly associated with volcanic activity, and a few of these cause major damage (Klein and others, chapter 43). Such earthquakes originate every few years under the Island of Hawaii and are less frequent beneath and between other islands of the Hawaii group. Some of these earthquakes probably originate within or at the base of the volcanoes (Lipman and others, 1985) and others in the Earth's crust beneath the volcanoes. A major zone of structural weakness, the Molokai fracture zone, extends westward from North America and intersects the Hawaiian Islands (fig. 22.1). It has been the site of occasional strong earthquakes, some of which were centered close enough to the islands to be damaging. This structural zone holds the potential for generating major, though infrequent, earthquakes in the future.

The two largest earthquakes in Hawaii, in 1868 and 1975, had magnitudes greater than 7 and probably were caused indirectly by movement of magma into rift zones of Mauna Loa and Kilauea, respectively. Magma forced the flanks of the volcanoes outward, and the earthquakes resulted from the abrupt subsidence of part of the south flank (Swanson and others, 1976; Tilling and others, 1976; Lipman and others, 1985).

Earthquakes endanger people and property directly by shaking structures and by causing ground fractures, ground settling, and landslides. Earthquakes can also be associated with tsunamis when

both result from the sudden subsidence of a volcano's flank. Strong earthquakes in the past have damaged buildings, water tanks, and bridges, and have disrupted water, sewer, and telephone lines. Locally, such damage can be intensified where soft, saturated sediments amplify earthquake ground motions. Earthquakes also trigger rockfalls and other kinds of landslides, fracture the ground, and cause confined bodies of water to slosh back and forth. Indirect effects from shaking, such as fire, can be even more severe than direct effects.

Only a few earthquakes in Hawaii have been strong enough to cause severe and widespread damage. The frequent earthquakes caused directly by magma movement do not seriously endanger life or property; most damage resulting from the strongest earthquakes of this type has been related to the falling of loose objects. The strongest historical earthquake, in 1868, was centered beneath the south coast of the Island of Hawaii (Wood, 1914). It caused widespread and locally major damage across the entire island, triggered a destructive mudflow near the community of Pahala, and was accompanied by a devastating tsunami. The combined effects of this earthquake claimed 40–50 lives. A similar earthquake in 1975 caused widespread damage, and an accompanying tsunami claimed two lives (Tilling and others, 1976).

TSUNAMIS

Tsunamis, also called seismic sea waves or tidal waves, are large, rapidly moving ocean waves. Most tsunamis are associated with earthquakes and are generated when an abrupt movement of the ocean floor displaces a large mass of water. Tsunamis also have resulted directly from volcanism and from landsliding. Tsunamis that have originated around the rim of the Pacific Ocean at great distances from Hawaii have destructive effects similar to those that originate locally, and they are discussed along with locally generated tsunamis.

Tsunamis reportedly have swept onshore to heights as great as 40 m above sea level at some localities in the world, but the maximum recorded height reached by such a wave anywhere in Hawaii has been 16–17 m (Tilling and others, 1976). The heights and distances inland reached by different tsunamis, and on different coasts by the same tsunami, however, have varied greatly. The tsunami of November 29, 1975, reached as high as 14.6 m on the south coast of the Island of Hawaii (Tilling and others, 1976), but waves were only 1–2.4 m high on other parts of that island and less than 1 m high on the other islands. Recently, Moore and Moore (1984) have suggested that coral-bearing gravel deposits on some of the islands, formerly interpreted as beaches formed during high stands of sea level, are actually the result of a truly giant wave possibly generated by a submarine landslide.

Although the effects of tsunamis that originate at great distances are similar to those generated locally, the latter are potentially more dangerous because the time between their origin and arrival at the shoreline may be too brief to warn and evacuate people or property.

Tsunamis sometimes move onshore as turbulent waves that can damage or destroy virtually everything in their paths. People may be battered or drowned, buildings moved off their foundations or knocked over, trees uprooted, and boats carried inland. As the waves recede, they may carry people and property out to sea. Tsunamis can also rise quietly as they move onshore and inundate nearshore areas. The salt water can kill crops, poison soil, corrode metal, and damage objects and structures in other ways. The actual effects of a tsunami at any specific site will be determined by the details of local topography, both offshore and onshore, and the direction of approach of the wave, and they are difficult to predict.

The locally generated tsunami of April 2, 1868, destroyed most villages along the south coast of the Island of Hawaii and killed an estimated 46 people (Brigham, 1909, p. 495–496; Hitchcock, 1909; Wood, 1914). Five successive tsunamis that accompanied the earthquake of November 29, 1975, caused the loss of two lives and about $1.4 million in property damage.

Tsunamis have been reported in Hawaii about 50 times since the early 19th century (Macdonald and others, 1947). Those of 1837, 1868, 1877, 1946, 1960, and 1975 caused major damage. The tsunaumi of 1946 originated in Alaska and reached the islands without warning; it caused 150 deaths and $25 million damage (Macdonald and others, 1947; Shepard and others, 1950). Although adequate warnings accompanied the 1960 tsunami, which originated in Chile, they were not fully heeded, and the toll included 61 deaths as well as millions of dollars of property damage (Eaton and others, 1961).

HAZARD ZONES

Volcanic-hazard zonation maps have been prepared only for the Islands of Hawaii and Maui. Volcanic eruptions on the other islands are so unlikely in the near future that similar hazard zonation is not warranted. Likewise, no hazard-zone maps have been drawn for earthquakes or tsunamis. The threat from earthquakes is widespread across the islands, and earthquake effects are strongly influenced by local conditions. The danger from tsunamis exists only along the coasts of the islands in a narrow zone whose width depends on local topographic conditions. The danger from large tsunamis is somewhat greater along the southeast and southwest coastlines of the Island of Hawaii, because highly destructive tsunamis are occasionally generated there by large landslides.

The hazard-zone maps distinguish areas in which the general level of hazard is different from that of adjacent areas. However, the level of hazard can vary considerably within any hazard zone, either gradually or abruptly. Direct volcanic hazards, for example, decrease in magnitude gradually across zones away from active vents. For such hazards as lava flows, the frequency with which a specific site is affected decreases with increasing distance; for other hazards such as tephra and gases, the severity of effects diminishes gradually with increasing distance. Such gradational changes in the hazard may extend across an entire zone. Abrupt changes in magnitude of hazard within a zone commonly occur along sharp topographic features, and local topographic features in a zone may have a magnitude of hazard very different from that of the zone as

whole. The hills behind Ninole, for example, stand well above the adjacent slopes of modern Mauna Loa and so have a much lower lava-flow hazard than do those slopes. Consequently, the magnitude of hazard assigned to a zone applies only to that zone as a whole, and differences within it are not shown. Such differences can best be determined by specific site studies.

The change in degree of hazard across most zone boundaries is gradual rather than abrupt, and it may be apparent only over a distance of a few kilometers or more. Boundaries between many zones are approximations that serve chiefly as guidelines to show that a difference in hazard does exist and to facilitate description of the zones. Although adjacent hazard zones are separated on the maps by single lines, changes in the degree of hazard across most zone boundaries are so gradational that they might better be shown by numerous lines or a continuous change in shading.

Some zones that theoretically exist are not shown on the hazard maps. For example, in an area south of Kilauea caldera, the distribution of lava flows indicates that the hazard from future flows is much less than on the nearby southeast flank of the volcano. Zones intermediate between the two hazard zones that are shown must exist, but these intermediate zones are not drawn on the map because multiple narrow zones would suggest greater accuracy than is warranted.

Hazard zones are based chiefly on the assumption that future eruptions will be like those in the past that are known from oral and written histories and from geologic investigations. Some kinds and scales of eruptive events could occur that are not foreseen by these hazards assessments.

ISLAND OF HAWAII

HAZARD ZONES FOR LAVA FLOWS

Hazard zones for lava flows are based chiefly on lava-flow coverage of different areas during specific time periods. The zones are also based partly on the current structural conditions within the volcanoes, on fault scarps and other topographic features that would limit the distribution of lava flows, and on the frequency of past eruptive events. Recent studies of Kilauea by Holcomb (chapter 12), Mauna Loa by Lockwood and Lipman (chapter 18), and Hualalai by Moore and others (chapter 20) provide most of the data on lava-flow coverage for the time periods on which hazard zones are based. Similar data for Mauna Kea are from Porter (1973). Hazard zones and definitions used for the Island of Hawaii in this report are modified from those used for a previous volcanic-hazards assessment of the island (Mullineaux and Peterson, 1974; U.S. Geological Survey, 1976).

To facilitate comparison of the hazard from place to place across the Island of Hawaii, lava-flow hazard zones for its five volcanoes have been fit into a single scale of decreasing hazard. The overlap of hazard zones shown for Kilauea and Mauna Loa is approximate, in part because both volcanoes have changed their eruptive patterns within the past several hundred years, and their future patterns are only partly predictable. Between A.D. 1200 and A.D. 1800, for example, Kilauea erupted voluminous lava flows from precaldera summit vents; the flows covered more than 80 percent of the volcano, including its northeast and northwest flanks (Holcomb, chapter 12, fig. 12.42). Since 1800, lava has covered significant areas of its flanks only south of its east rift zone. In contrast, lava flows on Mauna Loa since about A.D. 1840 have covered more area than those of the previous several hundred years (Lipman, 1980). Neither volcano shows signs of changing its current pattern. The hazard zones shown on fig. 22.10 are based on the assumption that present kinds and rates of activity at both volcanoes will continue unchanged for at least the next few years and probably for the next few decades.

Zone 1 (fig. 22.10) consists of the summit areas and active parts of the rift zones of Kilauea and Mauna Loa; in those areas, 25 percent or more of the land surface has been covered by lava within historical time, during the 19th and 20th centuries. These areas contain the sites of most historical eruptions, and a large majority of the lava flows that will affect other zones on Kilauea and Mauna Loa in the near future probably will originate in zone 1.

Zone 2 consists of several areas that are adjacent to and downslope from the active rift zones of Kilauea and Mauna Loa and therefore are subject to burial by lava flows of even small volume erupted in those rift zones. On Kilauea south of its east rift zone, as much as 25 percent of the land surface has been covered by lava during historical time, and 10–15 percent has been covered since 1950. Lava flows have covered parts of this area as recently as January 1986, and the history of Kilauea suggests that they will continue until some significant change occurs within the volcano. Although very little of the area in zone 2 north of the lower east rift zone of Kilauea has been affected by lava since 1950, about 15 percent of that surface has been covered during historical time. On Mauna Loa, long and voluminous lava flows have repeatedly entered the areas included in zone 2, covering about 5 percent of those areas since 1950 and about 20 percent within historical time.

Zone 3 includes other areas on Kilauea and Mauna Loa in which the hazard is gradationally lower than that in zone 2. On Kilauea, less than 5 percent of the areas in zone 3 has been covered with lava during historical time. However, more than 75 percent of those areas has been covered by lava flows within the last 750 years. The hazard is less in zone 3 on the flanks of Kilauea than in zone 2 because ground subsidence within much of Kilauea's rift zones prevents lava flows of small volume from extending beyond those rift zones. On Mauna Loa, only about 1-3 percent of the land surface in most of zone 3 has been covered by lava during historical time; however, a single lava flow during the 19th century covered about 10 percent of the area in zone 3 on the northwest flank of the volcano. During the last 750 years, lava flows have covered about 15-20 percent of the flanks of Mauna Loa within zone 3. The hazard on Mauna Loa decreases progressively downslope from its summit and

FIGURE 22.10.—Hazard zones for lava flows on the Island of Hawaii. See text for explanation of numbered zones. Thin, solid line marks boundary between Mauna Loa and Kilauea Volcanoes. Stipple pattern indicates areas covered by pre-1975 historical lava flows.

rift zones across zones 2 and 3. The hazard is lower in zone 3 because lava flows on Mauna Loa typically do not extend all the way from the source vents to the coastline; only about half of the flows on this volcano during the last 1,500 years have reached its lower flanks (Lockwood and Lipman, chapter 18). Within zone 3 on Mauna Loa, the hazard is currently less in the part that lies southeast of the rift zones than on the northwest flank of the volcano and should remain so in the near future. The hills behind Ninole, east of the southwest rift zone, are not identified on the hazard-zone map. They may be an upthrown block of Mauna Loa or part of an older volcano (Lipman, 1980), and they stand as much as a hundred meters above the younger surface of Mauna Loa. The lava-flow hazard on these hills decreases with height and is about as low as that in zone 8 at their highest points.

Zone 4 embraces only Haulalai Volcano, where a few percent of the land surface was covered by lava flows in A.D. 1800-1801, but less than 15 percent has been covered during the last 750 years. Recent prehistoric as well as historical eruptions on Haulalai have been less frequent than on Kilauea and Mauna Loa. Lava flows on Hualalai have typically covered large areas, and the rift zones of the volcano do not seem to have a distinctly higher degree of hazard than do its flanks.

Zone 5, on the lower flank of Kilauea south of its caldera, has been almost unaffected by lava flows during historical time, although nearly half of this area has been covered within the last 750 years. This flank of Kilauea is currently protected by the presence of the Kilauea summit caldera and by fault scarps in the Koae fault zone that face upslope. Zone 5 seems to be relatively safe from lava-flow burial under present conditions, but it could be threatened by a new episode of voluminous eruption of lava that spilled southward from the summit caldera.

Zone 6 includes one area on the flank of Mauna Loa south-southeast of its caldera and another that is east of the lower part of its southwest rift zone. The age and extent of flows in these areas are not well known, but the oldest flows at the surface of Mauna Loa are on this flank (Lipman, 1980). These areas seem relatively unlikely to be affected by lava flows in the near future. The magnitude of the hazard south-southeast of the summit could change significantly, however, if the caldera of Mauna Loa were to fill with lava.

Zone 7 includes the summit and upper flanks of Mauna Kea; this is an area in which no eruptions have occurred since about 3,500 years ago, but lava covered about 20 percent of the land surface between 5,000 and 3,500 years ago.

Zone 8 is a large area on the lower flanks of Mauna Kea that has not been affected by lava flows for at least 10,000 years. However, zone 8 could be affected by an unusually long lava flow issuing from a vent higher on Mauna Kea.

Zone 9 consists of Kohala Volcano. No eruption has occurred there for about 60,000 years, but even though the hazard there is extremely low the volcano cannot be regarded as extinct.

HAZARD ZONES FOR TEPHRA FALLS

Hazard zones for tephra (fig. 22.11) are based on eruption frequency, proximity to potential vents, and wind directions. Frequency and proximity largely control the location of tephra hazard zones on the Island of Hawaii, because the potential hazard diminishes rapidly in severity with increasing distance from vents as both fragment size and thickness of deposits decrease. Winds have less influence on the distribution of these hazard zones because the prevailing northeasterly trade winds are not dominant over the entire Island of Hawaii; antitrade and storm winds, especially at the altitudes of vents high on Mauna Loa, and upslope and downslope winds as well as sea and land breezes result in great variations from trade-wind directions. However, antitrade winds seldom blow from Kilauea, Mauna Loa, or Hualalai across Mauna Kea or Kohala, and storm winds blowing in those directions are infrequent.

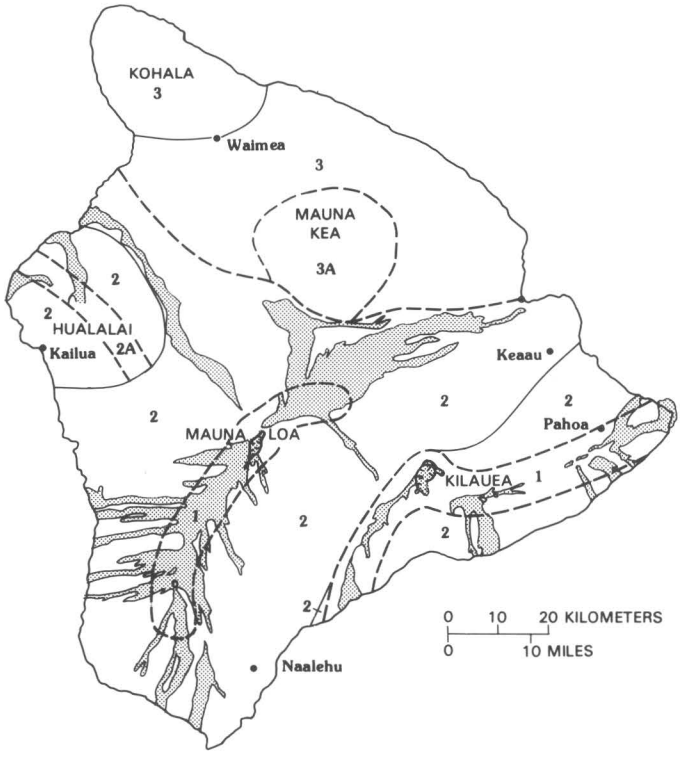

FIGURE 22.11.—Hazard zones for tephra on the Island of Hawaii. See text for explanation of numbered zones. Thin, solid lines mark boundaries between volcanoes. Stipple pattern indicates areas covered by pre-1975 historical lava flows.

Tephra is produced most frequently by lava fountains in the summit areas and rift zones of Kilauea and Mauna Loa. Such eruptions have occurred at least once every few years in historical time, and they have produced tephra as much as 1 m thick at a distance of 1 km from the vents and 10 cm thick at about 2 km (Richter and others, 1970). Steam-blast explosions have occurred at the summits of Kilauea and Mauna Loa and where the east rift zone of Kilauea intersects the shoreline. Tephra-fall deposits from steam-blast eruptions have included large rock fragments, but such eruptions rarely produce layers more than about 1 cm thick at localities

more than about 2 km from the source vents. Outside those zones, a few historical eruptions on the upper north slope of Mauna Loa suggest that tephra could be produced there by future lava fountains. Tephra mounds (littoral cones) can also be formed wherever lava flows enter the ocean; thus, they are limited to the seacoast, mostly on Kilauea and Mauna Loa. The hazard from tephra of this origin is not identified on a hazard map, inasmuch as it accompanies and is inseparable from the lava-flow hazard along the shoreline.

Tephra eruptions have been much less frequent on Hualalai; none are known in historical time. Such eruptions have been even less frequent on Mauna Kea and Kohala. The youngest eruptions on Mauna Kea occurred more than 3,500 years ago, but they produced tephra layers as thick as 5 m about 1 km from the source vents, 1 m at 2 km, and 10 cm at 4 km (Porter, 1973). No eruptions have occurred on Kohala for several tens of thousands of years.

Tephra-hazard zone 1 includes the summit areas and rift zones of Kilauea and Mauna Loa, the areas of highest eruption frequency, and extends about 2 km beyond the rift-zone boundaries. Tephra more than 10 cm thick, as well as large fragments, will likely be restricted to this zone during virtually all future eruptions from the summits and rift zones of Kilauea and Mauna Kea.

Tephra-hazard zone 2, in which tephra falls from lava fountains should be frequent but thin, includes the flanks of Kilauea and Mauna Loa and all of Hualalai. The potential hazard within this zone is locally somewhat greater on the upper north flank of Mauna Loa, where there are several vents along minor fractures. A subzone, 2A, of somewhat different character exists on Hualalai. In addition to the hazard there represented by thin tephra erupted from within zone 1, a potential exists for burial by cinder cones and thinner, more widespread tephra 10 cm or more thick from infrequent eruptions of Hualalai. This subzone includes the rift zone on Hualalai and the areas within about 4 km on both sides of the rift zone.

Tephra hazard zone 3 includes areas in which only thin deposits of tephra erupted from Kilauea, Mauna Loa, or Hualalai are likely to fall. The low frequency of winds that blow northward across Mauna Kea and Kohala from the three more active volcanoes indicates that even thin ash is likely from only a minority of eruptions. The subzone 3A marks an area of Mauna Kea above about a 2,000-m elevation in which cinder-cone eruptions could produce locally thick tephra deposits; although such eruptions have a very low probability, their effects could be locally severe.

HAZARD ZONES FOR PYROCLASTIC SURGES

On the Island of Hawaii, the deposits of pyroclastic surges have been recognized only adjacent to the caldera of Kilauea. The single hazard zone for pyroclastic surges surrounds the caldera and extends to a distance of 10 km from its center.

Pyroclastic surges conceivably could be initiated at other places where ground water or sea water can interact with magma. Magma could encounter ground water under the rift zones of Kilauea and the summit and rift zones of Mauna Loa and possibly at scattered sites elsewhere on Mauna Loa and on Hualalai. Magma and sea water could interact where both rift zones of Kilauea and the southwest rift zone of Mauna Loa meet the coastline.

HAZARD ZONES FOR VOLCANIC GASES

Hazard zones for volcanic gases are the same as hazard zones for tephra (fig. 22.11); like tephra, gases are emitted chiefly from the summit areas and rift zones of Kilauea and Mauna Loa; they are distributed by winds and their effects decrease with distance. Hazard zone 1 consists of the summit areas and rift zones of Kilauea and Mauna Loa, and extends about 2 km beyond the rift-zone boundaries.

Hazard zone 2 for gases includes Hualalai as well as the other parts of Kilauea and Mauna Loa. Although the hazard is less in zone 2, historical events show that gas effects can be significant far beyond the source vents. In 1977, gases from eruptions on Kilauea killed vegetation as far as 30 km from their source (J.P. Lockwood, written commun., 1978). From 1967 to 1974, trade winds carried gases from Kilauea's summit and east rift zone southwestward into the Kau District, reportedly causing a decline in sugar yields. Fumes then drifted around to the Kona District on the west coast and were blamed for the decline of other crops.

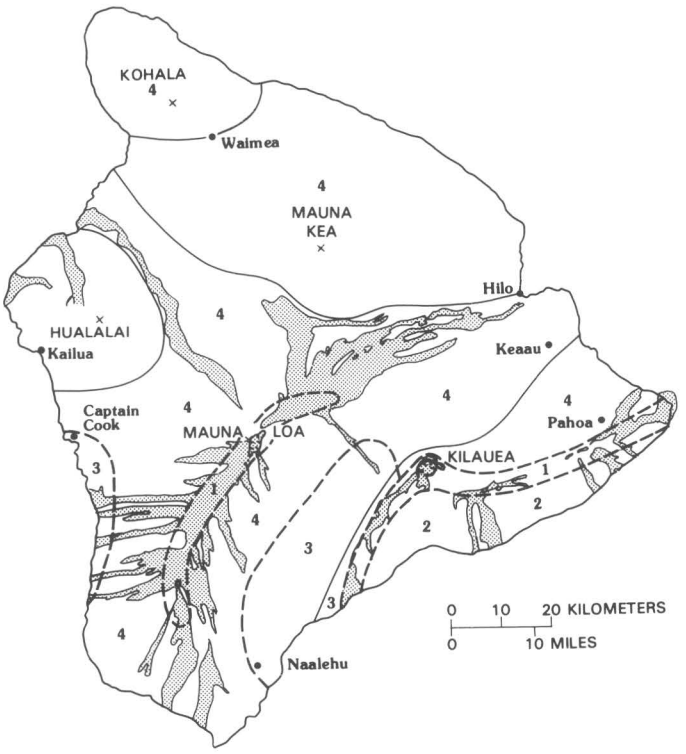

FIGURE 22.12.—Hazard zones for ground fractures and subsidence on the Island of Hawaii. See text for explanation of numbered zones. Location of areas subject to fracture and subsidence on flanks of Mauna Loa from Lipman (1980). Thin, solid lines mark boundaries between volcanoes. Stipple pattern indicates areas covered by pre-1975 historical lava flows.

Hazard zone 3 covers Mauna Kea and Kohala, which are subject to a lower degree of hazard because of their distance from vent areas and the infrequency of winds that blow across them from the south.

HAZARD ZONES FOR GROUND FRACTURES AND SUBSIDENCE

The Island of Hawaii is divided into four hazard zones for ground fracture and small-scale subsidence (fig. 22.12). The zone of highest hazard, zone 1, includes the summit areas and rift zones of Mauna Loa and Kilauea, where fractures and subsidence occur most frequently. Zone 2 consists of the south flank of Kilauea, where fracturing and subsidence occur somewhat less frequently than in the summit and rift zone areas. Fracturing and subsidence of the south flank occur chiefly along the Koae and Hilina fault zones but are not limited to them (Holcomb, chapter 12; Duffield, 1975; Lipman and others, 1985.

Hazard zone 3 embraces the areas of the Kaoiki and Kealakekua fault systems on Mauna Loa, where fractures and subsidence caused by magma movement are less frequent than on Kilauea. Zone 4, in which these hazards are least, includes the remainder of the island.

Abrupt large-scale subsidence of fault blocks causes an additional hazard from inundation along the coast seaward of the Kaoiki and Kealakekua fault systems on the flanks of Kilauea and Mauna Loa. Subsidence-induced tsunamis, however, can be a more serious hazard than the abrupt inundation. In addition, inundation hazard from slow regional subsidence exists along the entire shoreline of the island.

MAUI

The Island of Maui comprises two volcanoes, West Maui and Haleakala (Stearns and Macdonald, 1942; fig. 22.13). Potassium-argon ages of lavas of the West Maui volcano range from about 1.97 to 1.3 million years before present (McDougall, 1964; Naughton and others, 1980), and Crandell (1983) concluded that even the youngest lava flows on the volcano are more than 25,000 years old. The likelihood of a future eruption on West Maui seems remote.

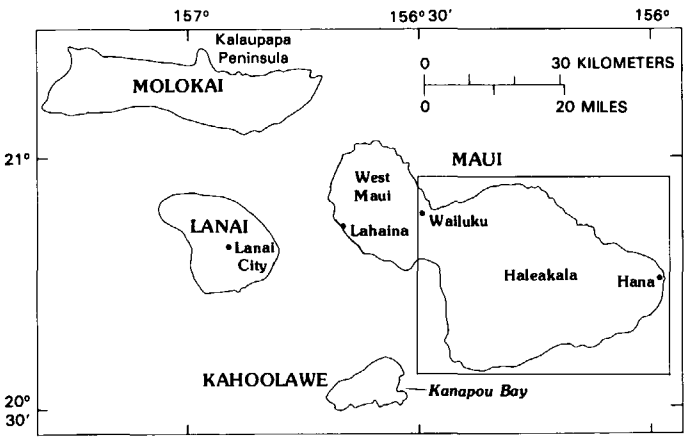

FIGURE 22.13.—The Islands of Maui, Molokai, Lanai, and Kahoolawe. Rectangle indicates area on Maui shown in figures 22.14 and 22.16.

Potassium-argon ages on lava flows of Haleakala volcano range from about 0.91 to 0.36 million years before present (McDougall, 1964; Naughton and others, 1980). Radiocarbon ages ranging from about 26,800 to 200 years before present have been reported on more recent ash deposits and lava flows (Crandell, 1983). Crandell inferred that the average frequency of eruptions on the volcano as a whole has been nearly one per 100 years during the last 1,000 years. The latest eruption occurred about 1790 at a vent in the lower part of the southwest rift zone, and it produced a 3-km-long lava flow.

HAZARD ZONES FOR LAVA FLOWS

Five zones of differing lava-flow hazard proposed by Crandell (1983) on Haleakala were based on the inferred frequency of eruptions and the ages of recent lava flows. The geologically recent eruptive history of Haleakala differs in many respects from that of the volcanoes on the Island of Hawaii. Because of these differences, lava-flow hazard zones recognized on Haleakala do not correspond exactly to hazard zones on Hawaii, and they are defined here from highest (1) to lowest (5) degree of hazard. The zones described here are the same as those outlined on a previous lava-flow hazard map of Haleakala (Crandell, 1983), but the definitions of some zones have been modified.

On Maui, lava-flow hazard zone 1 includes areas in which about 50 percent of the land surface has been covered by lava flows during the last 1,000 years, and it covers the crater of Haleakala and the southwest rift zone (fig. 22.14). The inferred frequency of lava flows has been at least one per 120 years in the crater during the last 2,500 years, and at least one per 150–200 years in the southwest rift zone during the last 1,000 years.

Zone 2 includes two areas in which 10–30 percent of the land surface has been covered by lava flows during the last 1,000 years. These areas are situated south of the southwest rift zone, where about 10 percent of the surface has been covered during the last 1,000 years, and north of the east rift zone, where lava flows have covered about 30 percent of the land surface during the same period. Lava flows are inferred to have occurred within these areas at an average rate of at least one per 500 years, and the last flow occurred less than 1,000 years ago.

Zone 3 includes areas in which eruptions have not occurred for more than 1,000 years, but where much of the land surface has been covered by lava flows within the last 20,000 years. The best evidence of rate of coverage in this zone on Haleakala is north of the southwest rift zone, where lava flows inferred to be less than 20,000 years old have covered about 75 percent of the land surface. Flows have occurred at an average rate of at least one per 2,000 years in this area, although the last flow was erupted about 4,000 years ago. The valleys that extend from the crater northward and southward to

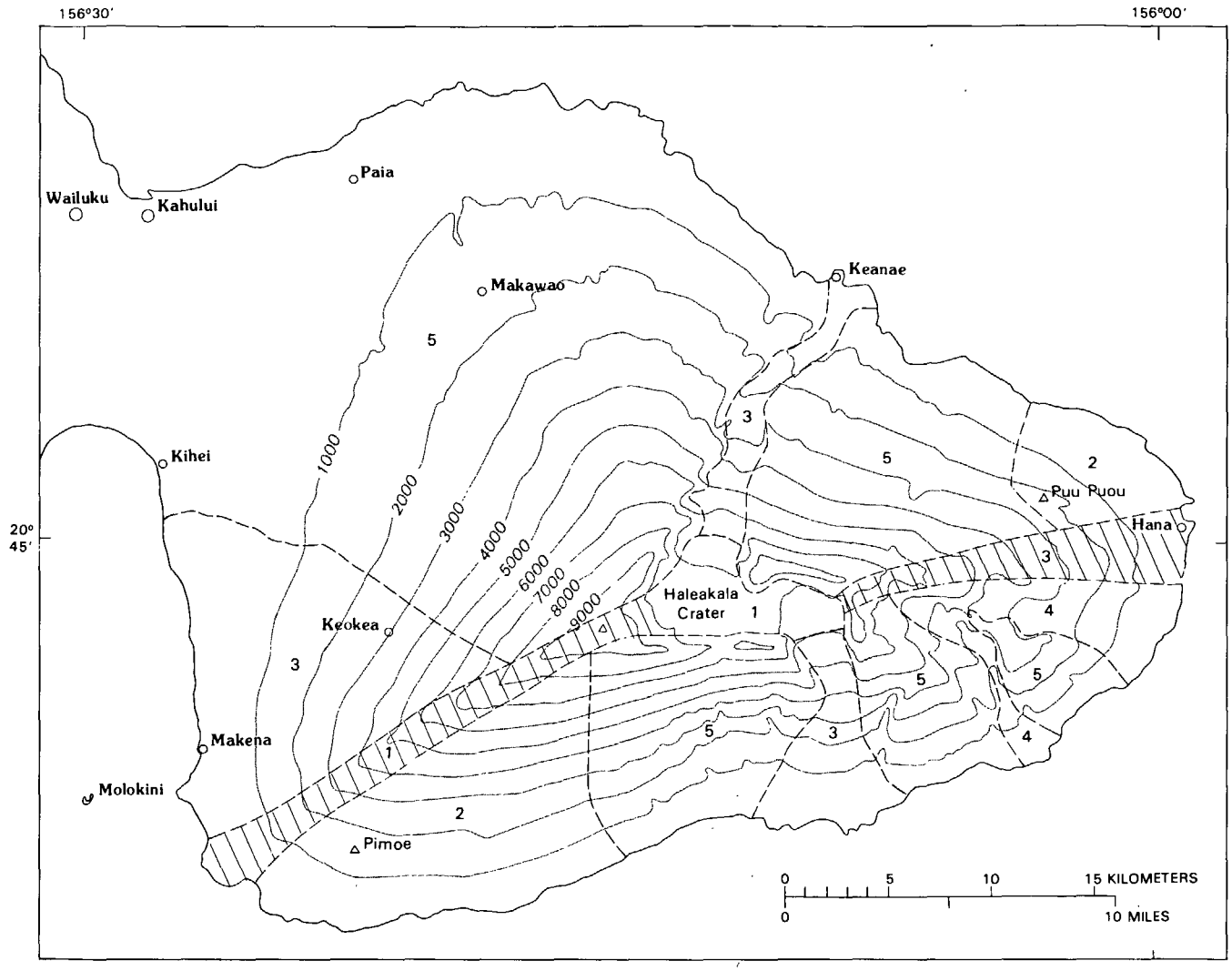

FIGURE 22.14.—Lava-flow hazard zones on Haleakala Volcano, eastern Maui. See text for description of the numbered zones. Lined areas indicate the southwest and east rift zones of the volcano. Topographic contours at 1,000-ft intervals.

the coasts, as well as the east rift zone, are included in zone 3. The two youngest flows recognized in the lower part of the southern valley were tentatively assigned an age of more than 1,000 but less than 10,000 years by Crandell (1983). A flow in the upper part of the east rift zone is radiocarbon dated at about 9,400 years before present, and one in the lower part of the rift zone is dated at 12,760 years before present. The rate of lava flow eruptions along the east rift zone probably is less than one per 2,000 years.

Zone 4 is defined solely from the average frequency of lava flows, which is inferred to be less than one per 10,000 years, but is at least one per 20,000 years. The last lava flows in these areas probably were formed more than 10,000 years ago. The rate of lava coverage is not known, but probably less than 10 percent of the area has been covered in the last 20,000 years.

Zone 5 includes areas that have not been affected by lava flows for at least 20,000 years.

Lava-flow hazard zones on Maui are compared with those on the Island of Hawaii in table 1, but the frequency of eruptions or the percentage of lava-flow cover during a specified period on one island may correspond only approximately with similar data on the other island.

TABLE 22.1.—*Comparison of lava-flow hazard zones on the Islands of Maui and Hawaii*

[N.R., not represented]

Lava-flow hazard zone on Hawaii	Lava-flow hazard zone on Maui
1	N.R.
2	N.R.
3	1 (?)
4	2
5	N.R.
6	N.R.
7	3
8	4
9	5

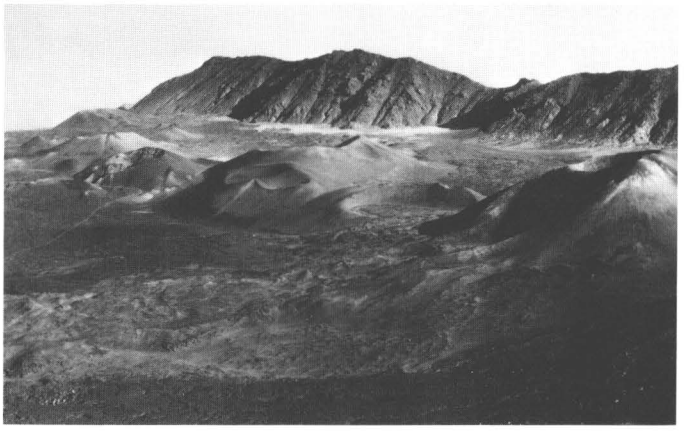

FIGURE 22.15.—View southeastward across lava flows (foreground) and cinder cones in the crater of Haleakala Volcano, eastern Maui. Cone at right side of photograph is about 150 m (500 feet) high. Average rate of eruptions in the crater during the last 2,500 years may be at least one per 100 years, but the age of the last eruption is not known.

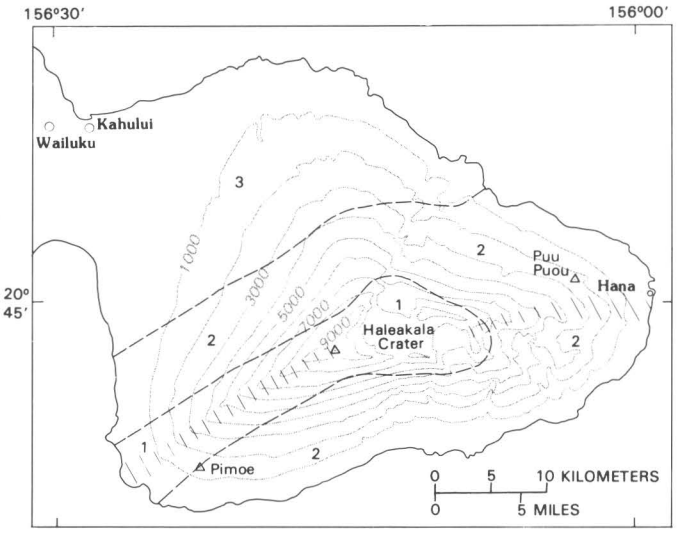

FIGURE 22.16.—Ashfall-hazard zones on Haleakala Volcano, eastern Maui. See text for description of the three zones. Lined areas indicate the southwest and east rift zones of the volcano. Topographic contours at 1,000-ft intervals.

HAZARD ZONES FOR TEPHRA FALLS

Because of the low frequency of eruptions on Maui in comparison with the Island of Hawaii, the likelihood of areas being affected by ashfall is much lower. If an ash-producing eruption does occur, the active vent probably will be within the crater (fig. 22.15) or somewhere along the southwest rift zone. Such an eruption might also occur at a flank vent, such as that represented by the Pimoe cone on the southwest side of Haleakala. Cindery ash on the northeast flank of Haleakala, northwest of Hana, probably came from a vent at or near Puu Puou (fig. 22.16). This ash is older than a 500-year-old lava flow and may be several thousand years old.

Three zones of different ashfall hazard on Maui (fig. 22.16) are based on the estimated frequency and range of thickness of future ashfalls. Within each ashfall-hazard zone, maximum thicknesses should be expected near the source vent, with rapidly decreasing thicknesses at increasing distance downwind. Zone 1 includes areas that could be affected at a rate of one ashfall per 200–500 years with thicknesss of 1–100 cm. Zone 2 includes areas in which 1–100 cm of ash could fall less often than once per 500 years but more often than once per 1,000 years and in which less than 1 cm of ash is expected once per 200–500 years. Zone 3 includes areas in which less than 1 cm of ash is expected to fall at an average rate of once per 1,000 years. This zone also includes areas in which 10 cm or more of ash may fall at least once per 3,000 years.

OTHER VOLCANIC HAZARDS

Hazard zones are not designated on Maui for pyroclastic surges, volcanic gases, ground fracture and subsidence, or earthquakes, but a few general statements can be made.

For the purpose of pyroclastic-surge hazard assessment, vents near or beneath sea level, and those in areas of high ground-water table, are regarded as areas of potential hazard from pyroclastic surges during eruptions. The most likely locations of such vents are near the coastline along the two rift zones of Haleakala. In addition, eruptions elsewhere on the windward, relatively wet, northeast side of Haleakala are more likely to be accompanied by explosions and pyroclastic surges than are eruptions at vents on drier parts of the island. The deposits of pyroclastic surges are present on the islet of Molokini, but have not been recognized on Maui.

The area of greatest potential danger to human health from volcanic gases probably is within the crater of Haleakala, because the crater is a natural basin in which heavier-than-air gases may be trapped. The crater floor would be a zone of relatively high gas hazard during an eruption. Gases erupted within the crater could also be carried by tradewinds toward the southwest and west slopes of the volcano.

Most future destructive earthquakes on Maui probably will be generated along the Molokai fracture zone (fig. 22.1) and thus could affect all or most parts of the island. For example, the earthquake of 1938, which had an epicenter about 40 km north of the island, damaged roads and structures on both Maui and Molokai (Macdonald and Abbott, 1970, p. 252; Furumoto and others, 1973).

The most likely area of ground fracture and subsidence in the future coincides with the crater and southwest rift zone of Haleakala, and these events would most likely be associated with an eruption. In addition, regional subsidence of possibly 1.7 mm/yr is occurring on Maui (Moore, chapter 2; Moore and Fornari, 1984), but this directly creates a hazard only along a narrow shoreline zone.

VOLCANIC HAZARDS ON THE OTHER ISLANDS

On islands other than Hawaii and Maui, the likelihood of an

eruption in the foreseeable future is so low that no preparation seems warranted unless premonitory signs indicate an approaching eruption. Each of these other islands is briefly discussed in the following sections.

KAHOOLAWE

The uninhabited Island of Kahoolawe is a single shield volcano with an erosionally breached caldera at its east end (Stearns, 1940; fig. 22.13). Deep weathering of rocks at the ground surface across the island (Macdonald and Abbott, 1970) and a potassium-argon age (Naughton and others, 1980) both indicate that Kahoolawe lava flows are one million or more years old. The most recent activity on the island, which is undated but much younger, produced small amounts of cinders and lava in the area of the breached caldera at Kanapou Bay (Macdonald and Abbott, 1970). The likelihood of a future eruption on Kahoolawe seems very low, but if an eruption should occur, it probably would produce a small amount of ash and lava in the Kanapou Bay area.

LANAI

Lanai also is a single shield volcano (fig. 22.13). Potassium-argon ages of lava flows reported from the island range from about 1.46 million years before present (Bonhommet and others, 1977) to 700,000 years before present (Naughton and others, 1980). More recent volcanism has not been recognized, and the likelihood of future eruptions on Lanai seems to be extremely low.

MOLOKAI

The Island of Molokai is formed chiefly by two large volcanoes, both of which are more than 1 million years old on the basis of potassium-argon ages (McDougall, 1964; fig. 22.13). The Kalaupapa Peninsula, which projects 4 km from the north side of the island, is a younger lava cone. Stearns and Macdonald (1947) noted that the lava flows on the peninsula are locally overlain by gravel which they thought was deposited by a stream graded to a stand of sea level 7.6 m higher than the present. This higher sea level has been dated at 120,000 years before present on Oahu (Ku and others, 1974); thus, the lava flows that form the peninsula seem to be older than 120,000 years before present. Three recent potassium-argon ages on the Kalaupapa lava flows, between 570,000 and 344,000 years before present, support that age assessment (Clague and others, 1982). Another vent appeared, perhaps at about the same time, off the east coast of the island. Explosions initially built a small tuff cone, but they were followed by the extrusion of lava flows (Macdonald and Abbott, 1970, p. 348).

Despite evidence cited above that the lava flows of the Kalaupapa peninsula are more than 100,000 years old, depth of weathering on the flows is less than that on some flows on the southwest flank of Haleakala that are younger than 25,000 years before present. This apparent discrepancy has not yet been resolved.

The probability of future volcanism on Molokai seems extremely low. If eruptions do occur, they probably would originate at vents at or near the Kalaupapa Peninsula or off the east end of the island.

OAHU

The eruptive activity that built Oahu occurred during three major periods. Potassium-argon age determinations on lavas from the shield volcano that forms western Oahu (fig. 22.17) range from about 3.5 to 2.74 million years before present, and lavas from the Koolau Volcano of eastern Oahu range in age from about 2.5 to 2 million years before present (McDougall, 1964). A third eruptive period began not long after 1 million years ago, and intermittent volcanism continued at least until about 30,000 years ago (Gramlich and others, 1971). All the vents active during the youngest period lie southeast of a line between Pearl Harbor and the Mokapu Peninsula (figs. 22.17, 22.18). Some of these eruptions formed such well-known features as Punchbowl and Diamond Head and produced airfall ash, lava flows, and pyroclastic-surge deposits that now underlie parts of the Honolulu metropolitan area. One flow of this period originated at the Sugar Loaf Crater on a ridge about 3 km east-northeast of Punchbowl and extended eastward into Manoa Valley, where it now underlies the University of Hawaii campus and the Honolulu suburb of Moiliili (Stearns and Vaksvik, 1935, p. 158). The ages of these events are not well known. Despite previously reported potassium-argon ages of about 900,000 and 100,000 years before present on the flow, Macdonald and Abbott (1970, p. 269) pointed out that the small amount of weathering and erosion on it suggest an age of only a few thousand years before present. Subsequent age determinations, however, gave ages of 68,000 and 66,000 years before present (Gramlich and others, 1971).

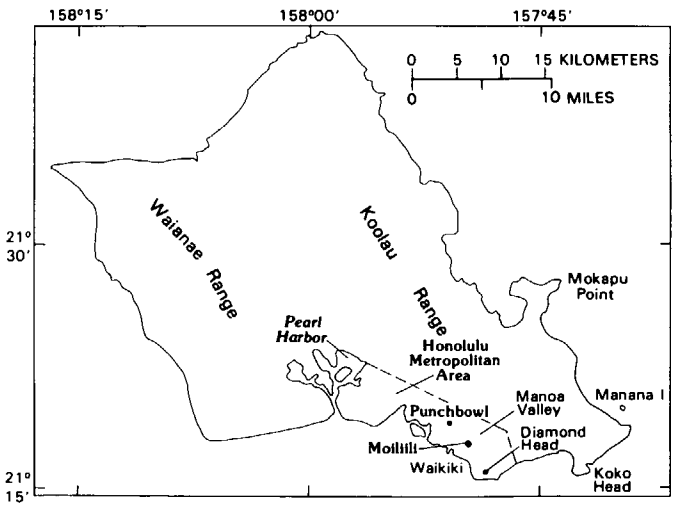

FIGURE 22.17.—The Island of Oahu. The Wainae and Koolau Ranges are each deeply eroded shield volcanoes more than 2 million years old. The most recent eruptions on Oahu originated at vents located between Koko Head and Manana Island.

FIGURE 22.18.—Aerial view southeastward across Koko Crater (center) and Koko Head (right center) on the southeast coast of Oahu. The most recent eruptions on Oahu, between about 43,000 and 31,000 years ago, occurred in the area between Koko Head and Manana Island, which is out of view 4 km to the left of the photograph.

The most recent dated eruptive activity on Oahu, between about 43,000 and 31,000 years ago, was concentrated along the shoreline in the southeasternmost part of the island between Koko Head (figs. 22.17, 22.18) and Manana (Rabbit) Island.

The restriction of the most recent eruptions to that part of the island suggests that if volcanic activity recurs, it will be located in the same general area, although not necessarily at the same vents as before. Eruptions there, if not affected by sea water, probably would produce cindery ash, whose distribution would be predominantly to the west and southwest, and perhaps lava flows. Eruptions in areas at or near sea level, or offshore, probably would be explosive and throw large rock fragments to distances of as much as several kilometers, produce airfall ash that would be carried downwind, and create pyroclastic surges (referred to as lateral blasts by Crandell, 1975). The specific areas that could be affected by these events cannot be predicted now and would not be known until an eruption began.

KAUAI AND NIIHAU

The bulk of the Island of Kauai (fig. 22.1) is formed of lava flows whose potassium-argon ages range from 5.7 to 3.8 million years before present (McDougall, 1964). The most recent eruptive activity occurred at about 40 vents scattered over the eastern two thirds of the island. These eruptions probably were spread over a long period of time, and all probably are older than 100,000 years before present (McDougall, 1964).

Ages of the lava flows that form Niihau (fig. 22.1) are not known, but even the youngest volcanic rocks on the island are older than the stand of sea level that was 7.6 m above that of the present (Macdonald and Abbott, 1970), and that evidently dates from about 120,000 years ago (Ku and others, 1974).

The absence of any eruptive activity on Kauai and Niihau for more than 100,000 years indicates that the likelihood of future eruptions on these islands is virtually nil.

MITIGATION OF VOLCANIC HAZARDS

Volcanic hazards can be mitigated chiefly by avoiding or controlling the hazards and by minimizing their effects. Hazards can be avoided on a long-term basis by land-use zoning that prevents building of structures in areas of high danger. On a short-term basis, people can be evacuated and some property removed from threatened areas when an eruption is imminent or even underway. Control

of hazardous volcanic events generally is not feasible, although diversion of some lava flows has been at least partly successful. Minimizing effects by protective measures generally is less useful for lava flows than for other volcanic hazards such as tephra and volcanic gases.

Predictions of future eruptions can also help people prepare for and respond effectively to those events. Long-range forecasts can include hazard assessments stating the probable frequency of hazardous events and areas they could affect, based on eruptions of the past. These forecasts can be accompanied by hazard-zonation maps such as those in this report, which show the relative magnitudes of certain hazards in different areas. This information can be used for making decisions regarding both long-term land use and short-term response to eruptions threatened or in progress.

Short-range forecasts are based chiefly on geophysical monitoring that measures the effects, especially earthquakes and deformation, of magma rising into the volcano. Such forecasts probably will provide warning of impending eruptions for most if not all lava-flow eruptions in Hawaii. Premonitory signs of explosive eruptions are less well known, but sudden or major lowering of magma levels, especially at the Kilauea caldera, should be regarded as a strong danger signal.

LAVA FLOWS

Avoidance through land-use zoning and evacuation is virtually the only way to reduce losses from lava flows. Areas in which lava-flow hazard is high can be zoned to restrict use. Even after eruptions have begun, flows can generally be avoided by people, and enough time often is available to remove some property from threatened localities.

Lava flows generally cannot be controlled. Although some diversions of lava flows have been successful, they can raise legal and social problems, and they require favorable conditions.

Diversion or control of flowing lava can be attempted by (1) construction of barriers and diversion channels; (2) use of explosives to block or divert lava streams, including those in lava tubes; and (3) use of water to cool and solidify lava flows. Each of these methods can be temporarily effective, and its success will ultimately depend on an early end to the eruption. The first two methods have been tried in Hawaii with limited success, and diversion barriers have recently been used successfully on Mount Etna in Italy (Lockwood and Romano, 1985). The third method was employed in 1973 at Heimaey, Iceland, and helped prevent destruction of parts of a town and harbor.

Generally, the larger and more rapidly moving the lava flows are, the more difficult it is to control or divert them. Moreover, decisions to attempt to control lava flows should be based on many factors, such as the path and other characteristics of the flow, the type of topography toward which it is moving, the economic and engineering feasibility of control measures, and the social and economic value of areas from which and toward which the lava would be diverted.

BARRIERS AND DIVERSION CHANNELS

Even small obstructions such as rock walls have changed the course of lava flows; thus barriers are an obvious diversion technique. During the 1955 and 1960 Kilauea eruptions, hastily erected barriers temporarily impeded lava flows, although the barriers were ultimately overwhelmed. Theoretically, structures of sufficient size and strength could be constructed to divert lava flows as large as any historic Hawaiian flows. For such barriers to be effective, however, wide and smooth channels would have to be provided as alternate paths. Without such channels, a voluminous flow could thicken behind the barrier and ultimately either overflow or break through it.

Plans have been proposed to protect the city of Hilo by systems of barriers and diversion channels (Jaggar, 1945; Macdonald, 1958, 1962). Their probable effectiveness has been debated (Wentworth and others, 1961), and costs and commitments to existing land use apparently have prevented any such projects from being carried out. The 1975 eruption of Mauna Loa renewed awareness of the lava-flow threat and led to consideration of lava diversion plans (Lockwood and Torgerson, 1980). Technical feasibility is, however, only one of the several difficult aspects of lava diversion. For example, artificial diversion of lava onto property that would otherwise have been spared could lead to complex legal and other problems.

DISRUPTION OF LAVA CHANNELS AND TUBES BY EXPLOSIVES

Attempts were made in 1935 and 1942 to divert Mauna Loa flows by bombing, because of potential threats to Hilo (Jaggar, 1936; Finch and Macdonald, 1949; Macdonald, 1958). It was reasoned that if a lava tube or channel were breached or blocked near its source, the advancing lava front would lose its source of supply, and the flow would halt. Lava issuing from any breach would then have to build a new channel and tube system before a flow would again reach the former front, and during this time the eruption might come to a stop. The bombings of 1935 and 1942 demonstrated the potential of this method, but the eruptions stopped before the method had been fully tested. New plans for use of explosives to divert lava flows were developed after the 1975 Mauna Loa eruption (Lockwood and Torgerson, 1980).

Attempts to divert high-volume, rapid flows might be ineffective, especially those which are not confined to channels or tubes, such as the voluminous flows from the southwest rift zone of Mauna Loa during the early part of the 1950 eruption.

COOLING LAVA FLOWS WITH WATER

During early 1973, lava flows on the island of Heimaey, Iceland, were advancing into the town of Vestmannaeyjar and threatening its harbor. Because a small-scale test indicated that water sprayed on the flow front cooled the lava sufficiently to impede its advance, huge pumps and large quantities of plastic pipe were used to implement the method on a large scale (Williams and Moore, 1973; Einarsson, 1974). As seawater was pumped from the harbor

and sprayed onto the flow, the chilled lava formed a barrier behind which new lava accumulated. The barrier eventually became high enough and strong enough to divert the oncoming lava into a new path, away from the town and harbor.

Such a technique might be feasible in Hawaii on relatively low-volume flows close to sea level. Plastic pipes enabled the water-delivery system on Heimaey to be moved readily in response to changing needs; such pipes, however, could not withstand the high pressures if water were to be delivered more than a few tens of meters above sea level. Even with such limitations, this technique might prove to be valuable under favorable conditions.

Protection from the effects of lava flows, other than by such methods of diversion or control, is generally not feasible. An individual lava flow will have roughly the same effects all the way from its source to its terminus, and attempts to protect buildings and other structures from the hot, crushing lava generally are not effective.

Long-term forecasts of the location of high-hazard areas can facilitate selection, before as well as during eruptions, of areas suitable for various uses, such as relatively safe evacuation routes. In addition, short-term forecasts of eruptions can almost always provide warnings. Even after lava-flow eruptions have begun, time generally is available to carry out evacuation plans.

TEPHRA FALLS

It is not possible to prevent widespread distribution of tephra, but hazard-zone maps can be used for choosing sites for specific uses that avoid areas of high hazard from tephra falls. Even after a tephra-producing eruption has begun, areas sometimes can be evacuated, and its effects can be effectively reduced for people who remain. People close to a vent during a tephra eruption should move upwind of the vent if possible; if they cannot, they should find suitable cover to prevent death or injury from falling fragments. Most other adverse effects can be decreased by placing damp or even dry cloths over noses and mouths to screen out ash particles. Structures in high-hazard zones can be designed to withstand impacts and loads imposed by falling material. In addition, airtight construction and filtering systems can reduce the likelihood that dust-sized particles will infiltrate structures and mechanized equipment.

PYROCLASTIC SURGES

The principal mitigative action for pyroclastic surges is to avoid them. Evacuation must be accomplished, however, before surge-forming eruptions occur, because pyroclastic surges move so rapidly that escape is not possible after they have begun.

Control of surges is not possible, although they can be deflected by natural barriers. Partial protection from the effects of surges is also possible but limited. Structures in areas of high hazard, for example, could be designed to withstand pyroclastic surges typical of Hawaiian volcanoes. Because many surges extend only short distances and become less severe near their margins, the chances of surviving them increase rapidly with increasing distance from the source vent. The people killed by a probable pyroclastic surge from Kilauea in 1790 were not seriously burned or battered, and they probably died from breathing hot air laden with volcanic gas and ash. People overrun by a pyroclastic surge could improve their chances of survival by finding any shelter, such as a vehicle, to reduce the effects of blast and impact. In addition, use of a filter could be critical because breathing of hot gas and ash is especially dangerous. A wet mask, clothing, or any other material that could filter ash and cool the air inhaled could be especially valuable.

VOLCANIC GASES

Effects of gas can be minimized by selecting building sites in zones of low hazard, and serious short-term effects can be avoided by evacuating some areas during periods of strong gas emission. However, gas probably cannot be completely avoided anywhere on the southern two-thirds of the Island of Hawaii. The emission or distribution of gas cannot be controlled.

For personal safety, topographic depressions near erupting vents should be avoided to eliminate the possibility of being overcome by odorless gases that are heavier than air. Persons with heart or respiratory ailments should avoid areas where concentrations of volcanic gas are possible. A filtering mask or damp cloth held over the face can reduce the effects of sulfur-bearing gas and temporarily lessen discomfort (see Wilcox, 1952, p. 443). No method is known, however, to eliminate gas damage to vegetation and mechanical equipment.

GROUND FRACTURES AND SUBSIDENCE

Ground-fracture and subsidence hazards to people or structures can be avoided only by staying away from areas in which they might occur, for the hazards cannot be controlled and generally cannot be economically minimized. The minor danger to people represented by these hazards can generally be avoided by using care in the areas affected. People living or working in fracture- and subsidence-prone areas should be wary of large open cracks, especially when leaving established trails or in heavily vegetated areas. Damage to structures rarely is catastrophic, but fractures with differential movements of more than a few tens of centimeters, or significant tilting from subsidence, could destroy some buildings. Thus, facilities that have unusual value or that are essential to public health and safety should not be built in areas where these hazards are high. Structures could be designed to resist fractures, but design to resist effects of tilting or submergence from subsidence probably is not economically practical.

The frequency of ground fracturing and subsidence and the localities that are susceptible can generally be predicted, and specific sites could be studied to determine the local magnitude of hazard.

EARTHQUAKES

Potential damage from strong earthquakes is widespread in

Hawaii and cannot be avoided, especially on the Island of Hawaii, but future damage could be reduced by land-use zoning and by earthquake-resistant design and construction. Areas can be avoided that are on or near steep slopes that could fail during earthquakes. Some areas that are underlain by materials susceptible to ground failure during earthquakes are shown on maps (Buchanan-Banks, 1983). Similarly, some areas could be identified in which structures could be damaged by the amplification of ground motion during earthquakes. Construction in such areas can be regulated by zoning or other measures where appropriate, and structures can be designed to resist damage from future earthquakes. Assessments of the magnitudes and frequency of future earthquakes, and of effects of past earthquakes (see Buchanan-Banks, chapter 44, and references therein), can contribute to decisions regarding appropriate future land-use and building requirements.

TSUNAMIS

Zoning to avoid tsunamis would require restricting land use along all the coastlines of the Hawaiian Islands, areas that are now intensively utilized for commercial, residential, and recreational purposes. Nevertheless, avoiding tsunamis through site selection for critical facilities, tsunami-resistant construction, and evacuation plans all could be effective for minimizing future losses. Zoning, for example, could restrict land uses along the coasts to those judged to be compatible with the tsunami hazard, and structures can be designed to resist the forces from tsunamis of predicted size. In addition, tsunami warnings often can be made in time to evacuate threatened coastal zones.

At present, the International Tsunami Information Center in Honolulu is alerted whenever potentially dangerous waves are generated by an earthquake anywhere in the Pacific region, and warnings are issued when appropriate. Low-lying areas generally can be evacuated before tsunamis from distant sources arrive. Tsunami-hazard zones on most islands are shown in telephone books in Hawaii, and people could choose in advance what routes to use in leaving threatened areas. People should be aware, however, that tsumanis could conceivably extend beyond some of the zones shown in telephone books, and they should be prepared to move farther inland or to higher ground if a large tsunami is predicted.

If a tsunami were generated locally, time might be too short for an official warning to be effective. Thus, any earthquake strong enough to make standing difficult can be taken as a warning that a tsunami may soon follow, and people along shorelines should immediately move inland or to higher ground.

FUTURE VOLCANIC ACTIVITY

Future eruptions can be expected at several volcanoes in Hawaii, and they will occur most frequently at Kilauea and Mauna Loa. The historical record suggests that no more than about 5 years will elapse without an eruption at one or the other of those two (Klein, 1982). Lava will be emitted chiefly from vents in the summit areas and along rift zones, but almost all parts of both volcanoes can be affected by lava flows. Based on historical records, about 5–10 percent of Kilauea and Mauna Loa could be covered during any 50-year period. Although wide fluctuations can be expected in eruptive rates from one decade to another, the overall rates likely will remain about the same. It is not possible, however, to predict where the next eruptive centers will be, how frequent or copious eruptions will be in a specific area, or which specific areas will be covered by lava.

The volcanic activity along Kilauea's east rift zone in historical time illustrates a difficulty in using the short historical record to predict future activity in a specific area. Between 1800 and 1950, approximately 2 percent of the eastern flanks of the volcano had been covered by lava from the east rift zone. In 1950, the probability based on these figures that a site in that region would be covered would have been 0.013 percent per year. However, between 1950 and 1975 about 8 percent of Kilauea's east flank was covered by lava, and so the coverage in that interval was actually about 0.32 percent per year. Estimates of future coverage may be no more accurate.

Mapping and dating of prehistoric lava flows also show that rates of burial have also varied widely in recent prehistoric time on both Kilauea and Mauna Loa. Overall rates of burial have changed markedly on Mauna Loa since 1868 (Lockwood and Lipman, chapter 18; Lipman, 1980); areas of high burial rates have switched from one flank of Kilauea to another at various times within the last 500 years (Holcomb, chapter 12; Holcomb, 1979). Accurate predictions of short-term probabilities of lava-flow coverage for any specific area clearly are not yet feasible.

Although lava flows are the most common volcanic hazard on Mauna Loa and Kilauea, explosive eruptions almost certainly will occur in the future. Two large explosive eruptions that produced pyroclastic surges have occurred within the last 2,000 years (Decker and Christiansen, 1984), and another in the future is a distinct possibility. While the hazard from such eruptions may seem small because of their infrequency, the potential threat to life should not be ignored.

Accurate statements of probabilities for frequency of eruptions or rate of burial by lava at Hualalai are not yet possible. However, at least four major eruptions have occurred at this volcano in the last 1,000 years (Moore and others, chapter 20; Moore and others, 1979). The lava flows from Hualalai in 1800–1801 were voluminous and highly fluid, but late prehistoric explosive eruptions near the summit built many large cinder and spatter cones. Future eruptions likely will originate both in the summit area and along the northwest and southeast rift zones, and some areas downslope from active vents will be buried by lava flows.

Neither Mauna Kea nor Kohala has been active during man's occupation of Hawaii. Mauna Kea has erupted within the last 5,000 years, however, most recently about 3,600 years ago (Porter, 1973), and it probably will erupt again. Future eruptions of Mauna Kea will probably be accompanied by mild to moderate explosive activity, producing ash and cinders that will build cones similar to those on its summit area and upper flanks, and produce ash deposits adjacent to the cones. Ash from such eruptions might drift for tens of kilometers downwind. If lava flows were erupted, they probably

would be relatively viscous and thick and would not travel more than a few kilometers from their sources. All the most recent eruptions have occurred at elevations above about 2,000 m, and future activity on Mauna Kea would most likely also originate on the upper part of the mountain.

Kohala is less likely to erupt in the near future than is Mauna Kea. The youngest flow of Kohala, a single flow that occurred long after the major growth of the volcano, has been dated at about 60,000 years before present (McDougall and Swanson, 1972). The probability of future activity of this volcano is very low compared to that for other volcanoes on the Island of Hawaii.

On Maui, Haleakala Volcano has been quiet for nearly two centuries, yet the inferred average rate of eruptions on the volcano as a whole has been nearly 1 per 100 years during the last 1,000 years (Crandell, 1983). This eruptive history suggests that an eruption could occur somewhere on Haleakala within the next 100 years. Recent eruptions have been most frequent within the crater and along the southwest rift zone, so one or the other of these areas seems to be the most likely location of the next eruption, but there is as yet no way to predict its specific time or place.

Future eruptions on Oahu and other islands are possible, but are likely to be so infrequent and scattered that preparation for such eruptions does not seem warranted now.

REFERENCES CITED

Apple, R.A., and Macdonald, G.A., 1966, The rise of sea level in contemporary times at Honaunau, Kona, Hawaii: Pacific Science, v. 20, no. 1, p. 125–136.

Bonhommet, Norbert, Beeson, M.H., and Dalrymple, G.B., 1977, A contribution to the geochronology of the Island of Lanai, Hawaii: Geological Society of America Bulletin, v. 88, p. 1282–1286.

Brigham, W.T., 1909, The volcanoes of Kilauea and Mauna Loa on the Island of Hawaii: Bernice Pauahi Bishop Museum Memoirs v. 2, no. 4, p. 379–608.

Clague, D.A., Dao-Gong, Chen, Murnane, Richard, Beeson, M.H., Lanphere, M.A., Dalrymple, G.B., Friesen, Walter and Holcomb, R.T., 1982, Age and petrology of the Kalaupapa Basalt, Molokai, Hawaii: Pacific Science v. 36, p. 411–420.

Crandell, D.R., 1975, Assessment of volcanic risk on the Island of Oahu, Hawaii: U.S. Geological Survey Open-File Report 75–287, 18 p.

———1983, Potential hazards from future volcanic eruptions on the Island of Maui, Hawaii: U.S. Geological Survey Miscellaneous Investigations Series Map I–1442.

Crandell, D.R., Booth, Basil, Kusumadinata, K., Shimozuru, Daisuke, Walker, G.P.L., and Westercamp, Denis, 1984, Source-book for volcanic-hazards zonation: UNESCO, 97 p.

Dalrymple, G.B., Silver, E.A., and Jackson, E.D., 1973, Origin of the Hawaiian Islands: American Scientist, v. 61, p. 294–308.

Decker, R.W., and Christiansen, R.L., 1984, Explosive eruptions of Kilauea Volcano, Hawaii, *in* Explosive volcanism: inception, evolution, and hazards: National Academy Press, p. 122–132.

Duffield, W.A., 1975, Structure and origin of the Koae fault system, Kilauea Volcano, Hawaii: U.S. Geological Survey Professional Paper 856, 12 p.

Dzurisin, Daniel, Lockwood, J.P., Casadevall, Thomas, and Rubin, Meyer, (in press), The Uwekahuna Ash: product of a large phreato-magmatic eruption of Kilauea Volcano, Hawaii: Bulletin of Volcanology.

Eaton, J.P., Richter, D.H., and Ault, W.V., 1961, The tsunami of May 23, 1960, on the Island of Hawaii: Seismological Society of America Bulletin, v. 51, p. 135–157.

Einarsson, T.M., 1974, The Heimaey eruption in words and pictures: Reykjavik, Heimskringla, 56 p.

Finch, R.H., and Macdonald, G.R., 1949, Bombing to divert lava flows: Volcano Letter 506, p. 1–30.

Furumoto, A.S., Nielsen, N.N., and Phillips, W.R., 1973, A study of past earthquakes, isoseismic zones of intensity, and recommended zones for structural design for Hawaii: Hawaii University Institute of Geophysics Report HIG–73–4, 50 p.

Gramlich, J.W., Lewis, V.A., and Naughton, J.J., 1971, Potassium-argon dating of Holocene basalts of the Honolulu volcanic series: Geological Society of America Bulletin, v. 82, p. 1399–1404.

Hitchcock, C.H., 1909, Hawaii and its volcanoes [2d ed., with supplement, 1911]: Honolulu, Hawaiian Gazette, 314 p.

Holcomb, R.T., 1979, Century-scale changes in eruptive behavior of Hawaiian volcanoes [abs.]: Hawaii Symposium on Intraplate Volcanism and Submarine Volcanism, Hilo, July 16–22, 1979, Abstract Volume, p. 164.

Jaggar, T.A., 1936, The bombing operation at Mauna Loa: Volcano Letter 431, p. 4–6.

———1945, Protection of harbors from lava flows: American Journal of Science, v. 243–A, p. 333–351.

———1947, Origin and development of craters: Geological Society of America Memoir 21, 508 p.

Klein, F.W., 1982, Patterns of historical eruptions at Hawaiian volcanoes: Journal of Volcanology and Geothermal Research, vol. 12, p. 1–35.

Ku, Teh-Lung, Kimmel, M.A., Easton, W.H., and O'Neil, T.J., 1974, Eustatic sea level 120,000 years ago on Oahu, Hawaii: Science, v. 183, p. 959–962.

LeGuern, F., Tazieff, H., and Faivre Pierret, R., 1982, An example of health hazard, people killed by gas during a phreatic eruption: Dieng Plateau (Java, Indonesia), February 20, 1979: Bulletin Volcanologique, v. 45 (2), p. 152–156.

Lipman, P.W., 1980, Rates of volcanic activity along the southwest rift zone of Mauna Loa Volcano, Hawaii: Bulletin Volcanologique, v. 43–4, p. 703–725.

Lipman, P.W., Lockwood, J.P., Okamura, R.T., Swanson, D.W., and Yamashita, K.M., 1985, Ground deformation associated with the 1975 magnitude-7.2 earthquake and resulting changes in activity of Kilauea Volcano, Hawaii: U.S. Geological Survey Professional Paper 1336, 45 p.

Lockwood, J.P., and Romano, Romolo, 1985, Lava diversion proved in 1983 test at Etna: Geotimes, v. 30, no. 5, p. 10–12.

Lockwood, J.P., and Torgerson, S.A., 1980, Diversion of lava flows by aerial bombing—lessons from Mauna Loa Volcano, Hawaii: Bulletin Volcanologique, v. 43–4, p. 727–741.

Macdonald, G.A., 1958, Barriers to protect Hilo from lava flows: Pacific Science, v. 12, p. 258–277.

———1962, The 1959 and 1960 eruptions of Kilauea Volcano, Hawaii, and the construction of walls to restrict the spread of the lava flows: Bulletin Volcanologique, v. 24, p. 249–294.

———1972, Volcanoes: Englewood Cliffs, New Jersey, Prentice-Hall, 510 p.

Macdonald, G.A., and Abbott, A. T., 1970, Volcanoes in the sea: Honolulu, University of Hawaii Press, 441 p.

Macdonald, G.A., Shepard, F.P., and Cox, D.C., 1947, The tsunami of April 1, 1946, in the Hawaiian Islands: Pacific Science, v. 1, p. 21–37.

McDougall, Ian, 1964, Potassium-argon ages from lavas in the Hawaiian Islands: Geological Society of America Bulletin, v. 75, p. 107–128.

McDougall, Ian, and Swanson, D.A., 1972, Potassium-argon ages of lavas from the Hawi and Pololu volcanic series, Kohala Volcano, Hawaii: Geological Society of America Bulletin, v. 83, p. 3731–3738.

Moore, J.G., 1970, Relationship between subsidence and volcanic load, Hawaii: Bulletin Volcanologique, v. 34, no. 2, p. 562–576.

Moore, J.G., and Fiske, R.S., 1969, Volcanic substructure inferred from dredge samples and ocean-bottom photographs, Hawaii: Geological Society of America Bulletin, v. 80, no. 7, p. 1191–1202.

Moore, J.G. and Fornari, D.J., 1984, Drowned reefs as indicators of the rate of subsidence of the Island of Hawaii: Journal of Geology, v. 92, p. 752–759.

Moore, J.G., Clague, D.A., and Normark, W.R., 1982, Diverse basalt types from Loihi Seamount, Hawaii: Geology, v. 10, no. 2, p. 88–92.

Moore, J.G., and Moore, G.W., 1984, Deposit from a giant wave on the Island of Lanai, Hawaii: Science, v. 226, p. 1312–1315.

Moore, R.B., Rubin, Meyer, and Spiker, E.C., 1979, Recent geologic investigations on Hualalai Volcano Hawaii [abs.]: Eos, v. 61, no. 6, p. 70.

Mullineaux, D.R., and Peterson, D.W., 1974, Volcanic hazards on the Island of Hawaii: U.S. Geological Survey Open-File Report 74–239, 61 p.

Nairn, I.A., 1979, Rotomahana-Waimangu eruption, 1886: base surge and basalt magma: New Zealand Journal of Geology and Geophysics, v. 22, no. 3, p. 363–378.

Naughton, J.J., Macdonald, G.A., and Greenberg, V.A., 1980, Some additional potassium-argon ages of Hawaiian rocks: the Maui volcanic complex of Molokai, Maui, Lanai and Kahoolawe: Journal of Volcanology and Geothermal Research, v. 7, p. 339–355.

Porter, S.C., 1973, Stratigraphy and chronology of late Quaternary tephra along the south rift zone of Mauna Kea Volcano, Hawaii: Geological Society of America Bulletin, v. 84, p. 1923–1940.

Richter, D.H., Eaton, J.P., Murata, K.J., Ault, W.U., and Krivoy, H.L., 1970, Chronological narrative of the 1959–60 eruption of Kilauea Volcano, Hawaii: U.S. Geological Survey Professional Paper 539–E, 73 p.

Shepard, F.P., Macdonald, G.A., and Cox, D.C., 1950, The tsunami of April 1, 1946: Scripps Institute of Oceanography Bulletin, v. 5, p. 391–528.

Siegel, B.Z., and Siegel, S.M., 1978, Mercury emission in Hawaii—aerometric study of the Kalalua eruption of 1977: Environmental Science and Technology, v. 12, no. 9, p. 1036–1039.

Stearns, H.T., 1940, Geology and ground-water resources of the Islands of Lanai and Kahoolawe, Hawaii: Hawaii Division of Hydrography, Bulletin 6, 177 p.

———1966, Geology of the State of Hawaii: Palo Alto, California, Pacific Books, 266 p.

Stearns, H.T., and Macdonald, G.A., 1942, Geology and ground-water resources of the Island of Maui, Hawaii Division of Hydrography, Bulletin 7, 344 p.

———1946, Geology and ground-water resources of the Island of Hawaii: Hawaii Division of Hydrography, Bulletin 9, 363 p.

———1947, Geology and ground-water resources of the Island of Molokai, Hawaii: Hawaii Division of Hydrography, Bulletin 11, 113 p.

Stearns, H.T., and Vaksvik, K.N., 1935, Geology and ground-water resources of the Island of Oahu, Hawaii: Hawaii Division of Hydrography, Bulletin 1, 479 p.

Swanson, D.A., and Christiansen, R.L., 1973, A tragic base surge in 1790 at Kilauea Volcano: Geology, v. 1, no. 2, p. 83–86.

Swanson, D.A., Duffield, W.A., and Fiske, R.S., 1976, Displacement of the south flank of Kilauea Volcano—the result of forceful intrusion of magma into the rift zones: U.S. Geological Survey Professional Paper 963, 39 p.

Tilling, R.I., Koyanagi, R.Y., Lipman, P.W., Lockwood, J.P., Moore, J.G., and Swanson, D.A., 1976, Earthquake and related catastrophic events, Island of Hawaii, November 29, 1975—A preliminary report: U.S. Geological Survey Circular 740, 33 p.

U.S. Geological Survey, 1976, Natural hazards on the Island of Hawaii: Washington, U.S. Government Printing Office, 15 p.

Walker, G.P.L., 1973, Lengths of lava flows: Philosophical Transactions, Royal Society of London, Series A, v. 274, p. 107–118.

Wentworth, C.K., Powers, H.A., and Eaton, J.P., 1961, Feasibility of a lava-diverting barrier at Hilo, Hawaii: Pacific Science, v. 15, no. 3, p. 352–357.

Wilcox, R.E., 1959, Some effects of recent volcanic ash falls, with especial reference to Alaska: U.S. Geological Survey Bulletin 1028–N, p. 409–476.

Williams, R.S., Jr., and Moore, J.G., 1973, Iceland chills a lava flow: Geotimes, v. 18, no. 8, p. 14–17.

Wood, H.O., 1914, On the earthquakes of 1868 in Hawaii: Seismological Society of America Bulletin, v. 4, no. 4, p. 169–203.

Fume cloud produced by eruption of Puu Oo, Kilauea east rift zone, as seen from Hawaiian Volcano Observatory. View is toward east, across Kilauea caldera, on October 21, 1985. Photograph by J.D. Griggs.

Rainbow Men
Hawaiian Petroglyph
Nuuanu, Oahu

PETROGENESIS AND VOLCANIC GASES

Petrologic and geochemical studies come alive in Hawaii because such processes as igneous differentiation and exsolution of volatile species in magma can be studied as they happen. Many igneous processes can in fact be quantitatively understood only through direct observation of igneous events. Such events, accurately delineated in time and space in turn, constrain deeper processes related to the construction of Hawaiian volcanoes. The first chapter in this section gives an overview of what we have learned about the petrogenesis of Hawaiian volcanoes, with an emphasis on the contributions made by studies of active volcanism.

The second and third chapters provide petrologic observations on recent volcanic activity; chapter 25, combined with chapter 48 in the section on dynamics, provides fascinating insights into one of Kilauea's most famous eruptions, the 1959 eruption in Kilauea Iki Crater. Chapters 26 and 27 address one of the most fundamental problems of Hawaiian petrology—the characterization of mantle sources for Hawaiian magma.

Chapters 28 through 34 treat comprehensively the study of volatile species associated with active Hawaiian volcanism, including a report on the first systematic collection of gases during an eruption of Mauna Loa. Chapter 34 outlines a new technique for rapid transmission of data from gas monitoring. The section closes with an interdisciplinary study of elemental mercury, tracing its path from volcanic emanations, through concentration in plants, to possible effects on human health.

RECENT ADVANCES IN HAWAIIAN PETROLOGY AND GEOCHEMISTRY

By Thomas L. Wright *and* Rosalind T. Helz

ABSTRACT

Hawaiian petrology continues to be a subject of great scientific interest. Several developments over the last three decades have substantially increased our knowledge of the processes by which basaltic magma is generated in the mantle, transported to storage in the crust, and erupted onto the surface. Significant areas of study include the following:

(1) Active volcanism at Kilauea Volcano, including the study of lava lakes ponded in pit craters. Lava lakes have provided natural laboratories in which numerous petrologic processes associated with cooling, crystallization, and differentiation of basaltic magma have been quantified. The detailed study of Kilauea lava chemistry in time and space has resulted in recognition of other petrologic processes, including storage of chemically distinct mantle-derived magma batches and mixing of these parental magma batches with magma stored and fractionated in the rift zones. Geodetic and seismologic studies at Kilauea have been critical in establishing a context in which the petrologic data can be evaluated. One unsolved question is the source of magma for each active volcano. Seismic evidence suggests a common staging area at 40 km depth, whereas petrologic studies show that each active volcano has unique chemical characteristics, indicating isolated storage regions.

(2) Detailed study of the recently discovered Loihi Seamount, the newest volcano in the Hawaiian Chain, has revealed a preshield alkalic stage similar, but not identical, to the postshield alkalic stages on the subaerial volcanoes.

(3) Detailed stratigraphic studies of individual volcanoes, using major element chemistry, trace-element chemistry, and radioactive-isotope systems, show diversity of chemical evolution in each volcano in the chain, particularly within the alkalic stage that follows construction of a tholeiitic shield. There is also diversity in the chemical and isotopic relations linking shield lava to postshield lava. The combined isotopic and chemical data has revealed significant complexity in the source mantle for Hawaiian lava, both within the stratigraphic record of a single volcano and among different volcanoes.

(4) The origin of Hawaiian magma, as defined by depth and degree of partial melting, enriched versus depleted sources, and mineralogy of the source mantle, is unresolved at present. The increasing amount of data indicates a need for more definition of the structure and composition of the Earth's mantle from such diverse disciplines as seismic tomography and the experimental physics of melting and melt transport.

Finally, all models that address the origin of the Hawaiian Islands, whether geochemical or geophysical, need to take into account the constraints imposed by seismic, geodetic, and petrologic studies of the active volcanoes in the chain.

INTRODUCTION

The Hawaiian Islands occupy a unique place in igneous petrology. Early in the development of the science Hawaii was recognized as a locale of petrologic significance, partly because of its active and approachable volcanoes, partly because of its location in the middle of the Pacific Ocean—uncomplicated by the presence of other kinds of terrain—and finally because of the wide variety of volcanic rock types available for study. Long before the recognition of plate tectonics, the Hawaiian Islands were recognized from the degree of erosion and the location of volcanic activity as having formed in an orderly progression from northwest to southeast. J.D. Dana saw that the islands were distributed in a way that defined parallel, but offset, segments that he related to tectonic controls (see Clague and Dalrymple, chapter 1, part I). Early visitors to Kilauea outlined in vivid descriptions the general nature of Hawaiian eruptions, and early visits to the bubbling lava at Halemaumau resulted in gas collections that still rank among the best ever obtained from an active volcano (Greenland, chapter 28).

With the advent of plate tectonics, the Hawaiian Chain became a classic example of midplate volcanism. The orderly progression of volcanism was quantified by radiometric dating, and the historical development was extended by recognition that the chain continued to the northwest past Midway Island, defined by long submerged seamounts of the Emperor Chain (see Clague and Dalrymple, chapter 1, part I). These seamounts were also sampled as part of the Deep Sea Drilling Project, and subsequent study revealed a remarkable uniformity, starting about 70 Ma, of both the rate of progression of volcanism and of the products of volcanism. For example, tholeiitic basalt from the 69-Ma Suiko Seamount (Clague and Dalrymple, chapter 1, part I) is geochemically similar to basalt presently being erupted at Kilauea and Mauna Loa (Clague and Frey, 1980; Kirkpatrick and others, 1980).

Earlier land-based studies by numerous workers, notably H.S. Stearns and G.A. Macdonald, had identified a sequence of compositional changes in the building of Hawaiian volcanoes that appeared to be the same, although not always complete, in each studied volcano (Clague and Dalrymple, chapter 1, part I; Macdonald and others, 1983). From these studies each Hawaiian volcano was inferred to pass through the following stages: (1) An early and voluminous tholeiitic stage that constructed huge shields rising from the ocean floor, exemplified by the active volcano Mauna Loa; (2) a period of much less voluminous alkalic volcanism, forming a small cap of mildly undersaturated alkalic lava on the tholeiitic shield, for example, the younger lava of Mauna Kea; (3) a period of erosion, which has been determined to be 0.5–2 m.y. long, in which the volcanic mass above sea level was thoroughly dissected; and (4) a period of basanitic or nephelinitic volcanism following the erosion of the old shield. The famous Oahu landmark Diamond Head is the product of eruption in this last period. This framework has been

modified as more volcanoes have been sampled and studied in detail. For example, work on Loihi Seamount has identified a preshield alkalic stage (Clague, in press). In no single volcano are all stages fully represented. Nephelinitic volcanism is rare, but well-developed series are presented on Kauai (Koloa Volcanics) and in the Koolau Range on Oahu (Honolulu Volcanics). The Kiekie Basalt on Niihau (which includes Lehua Island, Macdonald and others, 1983) and some of the Leeward Islands (Kaula, Macdonald and others, 1983) may include nephelinitic rocks. The latest, most undersaturated rocks to the southeast are not separated from the earlier alkalic series by nearly as long an interval of erosion (<500,000 years versus 2 m.y. for Kauai and Oahu) and are basanites, not nephelinites. The volcanoes that have a nephelinitic series show very little development of an earlier mildly alkalic series, whereas the basanites (the Lahaina Volcanics on West Maui Volcano, the Hana Volcanics on Haleakala Volcano) tend to overlie a lower, more mildly alkalic series. In this paper we will use the terms "nephelinitic series" to describe the truly posterosional rocks, bearing in mind that these rocks range in composition from alkali basalt through true nephelinites, and "upper alkalic series" for the rocks of other volcanoes that show a lesser erosional break.

The older Hawaiian volcanoes can be subdivided into groups on the basis of variations in the character of the mildly alkalic rock series present. This subdividing was first done by Macdonald and Katsura (1964), who recognized a Haleakala type and Kohala type. Further study suggests four significant variants:

(1) Haleakala type: characterized by a thick, transitional zone of interbedded tholeiite, transitional basalt, and ankaramite overlain by hawaiite and mugearite. Most analyzed alkali basalt in this type is slightly hypersthene-normative. Other volcanoes of this type are Mauna Kea (Macdonald and Katsura, 1964) and East Molokai (Beeson, 1976).

(2) Kohala type: mafic alkalic rocks are subordinate. The dominant rock types are hawaiite and mugearite, which form a thin cap of lava that was erupted from vents scattered around the tholeiitic shield. Trachyte may be present. As in the first type, alkali basalt in these alkalic series is slightly hypersthene-normative. Other examples are Waianae, West Molokai, and West Maui (Macdonald and Katsura, 1964).

(3) Hualalai type: characterized by an almost bimodal suite of nepheline-normative alkali basalt and trachyte (Macdonald, 1968; Clague and others, 1980). No other representatives of this type are known.

(4) Koolau type: mildly alkalic series is either absent, or present only as a few flows at the top of the tholeiitic sequence. Other examples are Lanai (Bonhommet and others, 1977), Kauai, Niihau, and Kahoolawe (Macdonald and others, 1983).

The distribution of these various types of Hawaiian volcanoes is not random. All the volcanoes are distributed on several locus lines (fig. 23.1). Two locus lines are defined for the southeastern islands of the Hawaiian Chain: the Loa line, passing through Mauna Loa, and the Kea line, passing through Mauna Kea (fig. 23.1). When looking at figure 23.1 with the above classification in mind, two features stand out. First, adjacent volcanoes are almost always of different types. Second, some types occur *only* on the Loa or Kea locus. For example, the Haleakala type is found only on the Kea locus, and the Koolau type only on the Loa locus. The existence of the four subtypes suggests that the groups result from significant differences in either source or plumbing, or both. The observations on the spatial array further suggest that adjacent volcano sources interact in some fashion at this stage in the volcano's development and that consistent differences in source may exist between the Loa and Kea locus lines. The latter possibility is supported by the trace-element data of Budahn and Schmitt (1985) on tholeiitic basalt from the Hawaiian volcanoes. Also, some correlation may exist between these four types and the nature of the various later alkalic rock series. In particular, the nephelinitic series has so far been observed only on Koolau-type volcanoes, found on the Loa locus. A more thorough examination of the upper alkalic series, seen mostly on Haleakala- and Kohala-type volcanoes on the Kea locus, may reveal other differences between the various late alkalic series that correlate either with volcano type or location.

In the last two decades, our understanding of Hawaiian volcanism has been greatly expanded as a result of the following important studies: (1) Detailed seismic, geodetic, and petrologic studies of Kilauea, conducted at the Hawaiian Volcano Observatory, have provided quantitative data on the processes of cooling, crystallization, and differentiation of tholeiitic basalt, and an understanding of how tholeiitic magma is transported and stored during construction of an Hawaiian shield; (2) the discovery, first by bathymetry, and secondly by seismic swarms and dredging, of an active undersea Hawaiian volcano—the Loihi Seamount—confirmed the continued southeastward progression of Hawaiian volcanism and, more importantly, overturned ideas about the uniformity of the tholeiitic stage of volcanism; (3) modern petrologic and geochemical studies of volcanoes in the Hawaiian Chain in all stages of development have been definitive in establishing the nature of oceanic midplate volcanism and the complexities that can occur in even this most simple of geologic settings; and (4) the study of xenoliths, high pressure phase relations, and seismic structure of the Earth have yielded insights into the structure of the Earth's mantle beneath the oceans. These four topics are emphasized in this overview. The first topic will be covered in detail; the others will be largely referenced to recent literature and to other comprehensive papers in these volumes.

ACKNOWLEDGMENTS

This overview has benefited from my discussions over the years with many persons. In particular, Al Hofmann and Fred Frey have kept me aware of the contribution of isotopic and trace-element data to the study of Hawaiian geologic problems, whereas my own research has been principally concerned with major-oxide mass balances as they relate to constraints provided by geologic, geodetic, and geophysical information. I appreciate correspondence and preprints from D.L. Anderson. The manuscript has benefited from reviews by Christina Heliker, Dave Clague, and Rosalind (Roz) Helz. Roz' review resulted in a substantially expanded content, much of it her own ideas; therefore, she was included here as a coauthor.

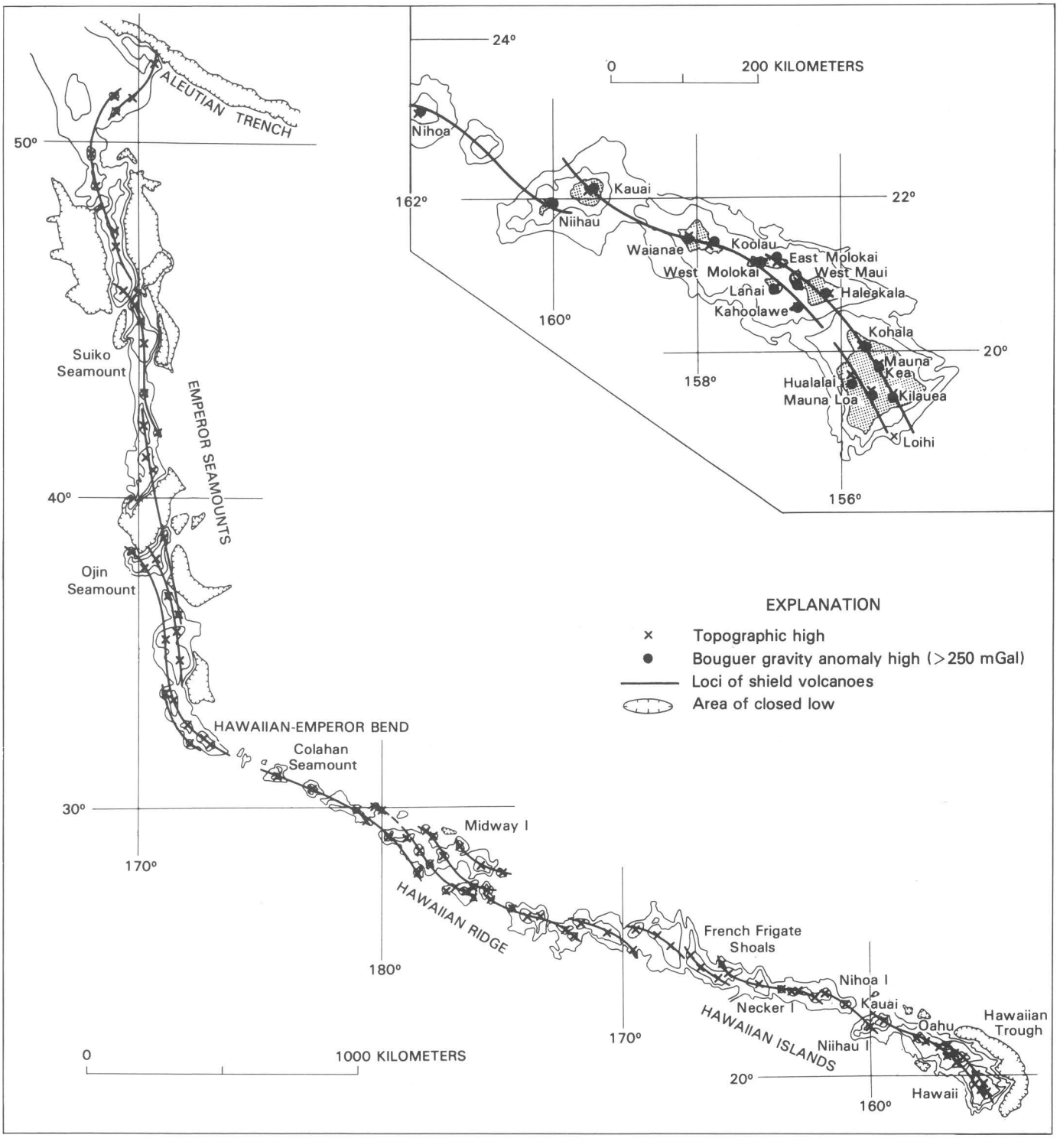

FIGURE 23.1.—Loci of shield volcanoes in the Hawaiian-Emperor Chain. Inset shows the detailed relation between topographic highs (crosses), Bouguer gravity anomaly highs (circles), and loci (heavy lines) for the principal Hawaiian Islands. From Jackson and others (1972).

THOLEIITIC VOLCANISM: WHAT HAVE WE LEARNED?

Modern petrologic study of Hawaiian volcanoes began in the 1940's and 1950's with G.A. Macdonald's work on the development of Hawaiian volcanoes and his analyses of the different lava types (Macdonald and Katsuura, 1964), with H.A. Powers' (1955) recognition that olivine played a dominant role in tholeiitic differentation, and with the work of Tilley and Scoon (1961), emphasizing chemical and mineralogic distinctions between lava from Kilauea and lava from Mauna Loa. These workers established that Hawaiian tholeiite ranges in composition from about 5.5 to 20 percent MgO, that lava with over 7 percent MgO had magnesian olivine as the dominant phenocryst, that lava with less than 7 percent MgO had augite and plagioclase in addition, and that Mauna Loa was distinguished from Kilauea by the presence of hypersthene, in combination with all three of the other silicate phases. Powers and Tilley had both demonstrated that once the chemical signature of olivine addition or subtraction has been removed, different tholeiitic volcanoes have subtly different compositions (the range of compositions related by a single set of olivine control lines are termed "magma batches") that characterized each volcano uniquely. Powers, in addition, had recognized that even more subtle variations occurred to produce separate magma batches within the products of a single tholeiitic shield.

Another level of inquiry began with modern studies at the Hawaiian Volcano Observatory, beginning about 1952, when Kilauea became active after 18 years of dormancy. From 1952 to the present (1986), every eruption has been sampled and analyzed, and eruptions that extended over periods of days, weeks, or even years, have been sampled at regular intervals to cover both the spatial and temporal distribution of eruptive products. This sampling is of critical importance because significant changes in lava composition during an eruption have occurred, and earlier (particularly the earliest) eruptive products are likely to be covered by later phases of the eruption and thus never encountered in conventional studies of older lava. This burial process is amply demonstrated, for example, by the 1983–1984 eruption of Kilauea (see Wolfe and others, chapter 17).

In another development, the occurrence of a series of eruptions in pit craters (1959, 1963, 1965) provided molten lakes of tholeiitic basalt for large, outdoor laboratory experiments in the cooling and crystallization of basalt. These studies were complementary to a study made of a prehistoric lava lake exposed in the walls of Makaopuhi Crater (Moore and Evans, 1967; Evans and Moore, 1968). In the next two subsections we address first what we have learned from the lava lakes, and secondly, we apply this information to interpret petrologic processes important to understanding the entire sequence of eruptive activity from 1952 to the present.

KILAUEA LAVA LAKES

Core drilling in the lava lakes, after they crusted over, provided a means of studying the processes of crystal-liquid movement during slow cooling. An overview of the importance of the lava-lake studies with a description of what was done on each lake, including an annotated bibliography, was written by Wright and others (1976). Subsequently, papers on the March 1965 Makaopuhi lava lake (Wright and Okamura, 1977), the August 1963 Alae lava lake (Peck and Kinoshita, 1976; Peck, 1978; Wright and Peck, 1978), and thermal-modeling studies (Peck and others, 1977; Shaw and others, 1977) have contributed further details; Peck and others (1979) demonstrated the breadth of interest in the lava lakes. Makaopuhi and Alae have both been covered by subsequent eruptions, further attesting to the value of real-time volcanic studies. The November–December 1959 Kilauea Iki lava lake, documented by Murata (1966), Murata and Richter (1966), Richter and Moore (1966), Richter and Murata (1966), and Richter and others (1970), is still being studied. Drilling programs in 1976, 1979, and 1981 were performed as a joint project of the U.S. Geological Survey and Sandia National Laboratories. Geophysical results of the 1976 drilling are given by Hermance and Colp (1982), and a description of the 1981 drilling is given by Hardee and others (1981). Thermal modeling of the lake (Hardee, 1980) and a study of the seismic structure of the lake (Chouet and Aki, 1981) have also been accomplished. Further petrologic results are reported by Helz (chapter 25; 1980) and by Helz and Wright (1983). Description of drill core is provided by Helz and Wright (1983) and by Helz and others (1984). New interpretations of the mechanics of the 1959 eruption are given by Eaton and others (chapter 48) and by Helz (chapter 25).

The studies of Alae and Makaopuhi lava lakes have quantitatively documented several processes of importance to Hawaiian petrology. These processes include the following:

(1) Settling of olivine occurs under the influence of gravity at temperatures greater than 1,150 °C. This settling is by no means as straightforward a process as that predicated by theory, as it can be shown that the observed rates of settling are far less than those predicted by Stokes' law. This difference is partly due to the presence of gas bubbles moving upward as olivine is sinking, thus impeding the progress of both, and partly to the fact that the liquid behaves as a Bingham fluid, as was discovered by direct experimentation in Makaopuhi lava lake (Shaw and others, 1968). Further study of Kilauea Iki led to the suggestion that with a large population of olivine the crystals might settle with a boundary layer of melt, decreasing the rapidity with which olivine can be segregated (Helz, 1980, p. 693–696). Helz (chapter 25) has shown, in line with earlier studies of a frozen prehistoric lava lake (Moore and Evans, 1967; Evans and Moore, 1968), that olivine, after settling, rapidly re-equilibrates to more iron-rich compositions and that the final olivine composition may be very different from that present at the time of eruption. All of these data place constraints on the interpretation of olivine abundance in natural lava.

(2) Differential separation of augite and plagioclase occurs under the influence of convective flow at temperatures between 1,150 °C and 1,080 °C This separation is a more subtle process than olivine segregation and is shown to occur at crystal sizes far smaller than those that could be gravitationally segregated in a reasonable time. Differential separation of augite and plagioclase is inferred to take place only in the absence of a separate volatile phase, because upward movement of vesicles will reverse the density gradients

needed to initiate convection in a body of molten basalt. The time at which convection in Makaopuhi lava lake was initiated has been inferred from thermal anomalies in temperature profiles taken in the melt, correlated with decreased vesicularity in core collected below a certain depth in the lake. Within months of the time at which convection was initiated, the bulk composition of the lava lake began to change in a manner reflecting loss of chemical components present in augite and plagioclase, in addition to those present in olivine (Wright and Okamura, 1977). A complementary effect of convective transfer is to enrich the margins and probably the basal parts of the lava lake in the components of augite and plagioclase, in addition to those of olivine, causing a chemical profile through a lava lake to depart from strict olivine control. The chemical effect is nicely shown in analyses from the lower part of the prehistoric Makaopuhi lava lake (Moore and Evans, 1967).

(3) Melt is physically segregated from a rigid crystal framework at temperatures below 1,080 °C. The lava lakes provide a quantitative demonstration of the process known as filter pressing, and they contribute toward an understanding of the origin of segregations of basaltic liquids with variably fractionated chemistry. Natural segregations are common in thick basaltic flows and sills throughout the world. The term "segregation vein" was applied to these bodies in the 19th century and has remained in use since. Basaltic segregations generally stand out from the host rock by their lighter color and coarser texture, and they commonly fill subhorizontal fractures. Segregation of this kind only occurs at temperatures below the critical temperature at which the lake behaves as a rigid body (see discussion in Wright and others, 1976). First demonstrated as an artifact of the drilling process (that is, melt flowing into open drill holes during thermal recovery toward predrilling temperatures), this process also results in natural segregations (segregation veins) where melt has flowed into zones of lower pressure. Most segregations have sharp contacts with the host rock, suggesting filling of an open fracture. Others have more subtle boundaries, suggesting that the wall rocks were ductile at the time of segregation. The presence of segregations is a function of the rate of cooling, and their orientation (that is, whether fillings are horizontal, vertical, or some other angle) gives important information on the stress distribution in the cooling lava. Whether segregation takes place is a function of temperature, which controls both the chemical composition and viscosity of the melt fraction, the rigidity of the crystal network, and the time during which a pressure gradient favorable to segregation is present. In the lava lakes, a combination of cooling curves and viscosity temperature relations limit the normal process of segregation to temperatures above about 1,050 °C, at which temperature melt compositions are still in the basaltic range. However, Kilauea Iki lava lake contains rare examples of small segregations of much more siliceous melt, with silica content as much as 70 percent. This mechanism may operate in basaltic intrusions to produce small bodies of rhyolite or dacite for later eruption as lava.

Several lines of evidence indicate that Hawaiian eruptions are supersaturated in volatile constituents at the time of eruption. Thus, the vesicle distribution in thick lava lakes is, in large part, a frozen record of incomplete volatile removal at high temperature. We must emphasize that lava erupted at, or under, saturation would behave very differently in terms of processes defined for the Kilauea lava lakes.

Results of the study of Makaopuhi and Alae lava lakes define classic, closed-system fractional crystallization in which mass-balance calculations document various kinds of crystal movement in liquids that vary along a regular liquid line of descent (see Wright and Peck, 1978, fig. 4). The study of processes documented by study of major oxides have been extended to show that trace elements vary consistently with major oxide relations (Lindstrom and Haskin, 1984).

Kilauea Iki, the remaining lava lake, is distinguished from Alae and Makaopuhi by its more magnesian bulk composition (average MgO content is 15–16 weight percent), larger volume, and more complex filling history. As a result, the core obtained from Kilauea Iki shows many features unlike those seen in the other lava lakes. For example, core recovered below 12 m depth has a chemistry that does not fit the olivine-controlled chemistry defined by samples collected during the eruption (Wright, 1973). Although, by definition, this lava lake also represents a closed system, the mass balances relating the chemistry of crystallizing minerals, liquid segregation, and bulk rock at different levels in the lake depart significantly from the rather straightforward relations summarized in papers on the other lava lakes. Fractionation processes identified in Kilauea Iki are listed below. Some of these processes occur at higher temperatures than in the other lakes (Nos. 1, 2, and 5), whereas others have been observed only in Kilauea Iki (Nos. 3, 4, and 6).

(1) Gravitative settling of coarse (>2 mm) olivine, resulting in a zone in which large olivine crystals are absent, occurring between 20–40 m below the surface of the lake. The composition of the moving olivine averaged Fo_{86}, that is, the chemistry of the drill core defines a set of olivine control lines on variation diagrams of Al_2O_3 versus MgO or SiO_2 versus MgO that extrapolate to an olivine composition of Fo_{86}. This composition implies that temperatures were $\geq$1,180 °C in the part of the lake through which the olivine settled (Helz, 1980; Helz and Thornber, in press).

(2) Horizontal redistribution of augite microphenocrysts, by convection. Within the olivine-depleted zone, small (1–2 mm) clots of augite microphenocrysts are present in core from near the edge of the lake and absent in the middle. This differential concentration of augite raises the CaO content of the core from 10.5 weight percent in the middle to 11.6 weight percent at the edge. In contrast to Makaopuhi, this flow differentiation has not involved plagioclase, hence it occurred only at temperatures above 1,160 °C.

(3) Diapiric upwelling of lower density melt from within the olivine-rich mush at the base of the lens of melt. The moving liquid is that present at temperatures of 1,145–1,160 °C, just below the incoming of plagioclase. This liquid is inferred to rise to the uppermost part of the lens of melt where it mixes with the melt just below the base of the upper crust. This process causes the lava below 12 m to deviate from olivine controlled chemistry. The upper mixed zone is enriched in low melting constituents such as TiO_2 and alkalis and is depleted in FeO and CaO relative to what would be expected for olivine-controlled chemistry (Helz, 1980). The source region undergoes complementary depletion in TiO_2 and alkalis relative to olivine-controlled chemistry. Helz (1980), citing data for

the upper, enriched zone only, tentatively described the enrichment to filter pressing of liquid formed during partial remelting of foundered crust deep in the lake. Recovery and analysis of deeper core has led to our present recognition that, first, this process does not require foundered crust, and second, it has affected the chemistry of the lava at virtually all levels in the lake. This process occurs only in olivine-rich rock. The requisite density inversion is much smaller in melts in bulk compositions with MgO $\leq$7.5 percent. Hence, this process would not have been expected to occur in the other lava lakes.

(4) Diapiric rise of streams of vesicles with or without entrained melt, from within the lower crust. The vesicles first entrain melt, then coarse olivine from the lower part of the lake. As the plume rises into cooler material it begins to segregate, with the vesicles and melt detaching themselves from the trail of coarse olivine. These trails remain as vertical olivine-rich bodies, which can be seen in every drill core recovered from Kilauea Iki between 40 and 58 m (Helz, 1980). These olivine-rich bodies contain excess iron-rich olivine (Fo_{77-79}) and differentiated liquid (temperature range of 1,140–1,120 °C), relative to the adjacent host rock, so they are active at lower temperatures than the diapirs in process 3. Analogous vuggy, vertical bodies also are present between 26 and 40 m, but they are much harder to spot as they lack coarse olivine (Helz, 1980). The melt- and vesicle-rich top of the vertical olivine-rich bodies looks like a segregation vein, which led Helz (1980) to suggest that segregations might be related to these bodies in some way. Similar bodies, described as "indistinct, pipe-like masses rich in olivine" occur in the lower part of the prehistoric Makaopuhi lava lake (Moore and Evans, 1967), though in that lake there was no evident connection with segregation veins.

(5) Formation of segregation veins, which are coarse-grained diabasic sills, generated by processes internal to the lava lake. Segregation veins in Kilauea Iki are more abundant than in the other lakes and form an apparently continuous set of sills, concentrated between 18 and 56 m, where they comprise 5–10 volume percent of the lake (Helz, 1980). Their bulk compositions correspond to liquids produced at 1,135–1,100 °C, using the calibration of Helz and Thornber (in press). In Kilauea Iki, segregation veins are more magnesian and presumably form at higher temperatures than those in Alae and Makaopuhi.

(6) Filling of late fractures or large vesicles by highly differentiated liquids, produced at 1,060–1,000 °C. The fractures are produced by brittle failure of the lake lava as it shrinks during crystallization and cooling. The bulk compositions of these tiny bodies are andesitic to rhyolitic (SiO_2, 56–70 weight percent, MgO, 0.5–3.0 weight percent); their existence demonstrates the mobility of interstitial liquid even when very little (<10 percent melt is present (Helz, 1984). The driving mechanism is inferred to be gas filter-pressing (Anderson and others, 1984).

In addition to these processes involving differential movement of crystals, vesicles, and liquid, Kilauea Iki illustrates very well the extent to which interstitial liquid compositions are controlled by *local* bulk composition. As discussed in Helz (1984), interstitial liquid becomes progressively depleted in FeO as olivine content increases. Other oxides (SiO_2, Al_2O_3, alkalis) increase as FeO decreases, whereas a few oxides (MgO, CaO, TiO_2) are buffered by the phase assemblage. Thus, at a given MgO content of interstitial liquid, the liquids in olivine-rich rocks are richer in SiO_2 and alkalis than liquids in olivine-poor rocks or segregation veins. Where a segregation vein occurs in an olivine-rich host, the difference in glass composition across the contact can be as great as 4 weight percent FeO within a single thin section.

The later stage mineral assemblages closely reflect these variations in interstitial melt composition. In olivine-rich rock, the low-calcium pyroxene is orthopyroxene (opx), the dominant Fe-Ti oxide is ferropseudobrookite (fpsb). With decreasing olivine content opx is replaced by pigeonite, and the oxide assemblage changes to fpsb + ilmenite, fpsb + ilmenite + magnetite, and finally ilmenite + magnetite, as observed in the low-MgO lakes 'Alae and Makaopuhi.

Thus, gravitative settling of olivine, followed by closed-system crystallization, has created a magma chamber in which different liquid lines of descent are being generated in rocks meters apart. Important implications of these observations, applied to larger differentiating chambers, are that one chamber may be capable of erupting two or more dissimilar lava series produced solely by processes operating within the chamber and not necessarily from different sources.

TIME-SPACE RELATIONS OF KILAUEA LAVA

Studies based on the chemistry of erupted lava from 1952 to 1985 have extended our knowledge of differentation processes in Hawaiian tholeiite. Interpretation of Kilauea's chemistry is also dependent on seismic and geodetic studies (Eaton and Murata, 1960; Eaton, 1962), which clearly identify a complex holding reservoir beneath the Kilauea summit through which magma for eruptions anywhere on the volcano must pass (fig. 23.2; also see Wright and Fiske, 1971, fig. 9; Ryan and others, 1981). Helz (chapter 25) presents data that supports the earlier suggestion of Wright (1973) that magma erupted in 1959 is an exception and might have bypassed storage in the normal summit-reservoir complex. Two early summaries (Wright, 1971; Wright and Fiske, 1971) document the general changes of bulk chemistry with time, quantify the concept of olivine control, describe the differentiation processes operating within Kilauea's rift zones, and treat the problem of magma batches and the mixing of liquids of different composition prior to eruption. A model was developed in Wright and Fiske (1971) in which magma batches of subtly differing bulk chemistry arrive in the storage complex beneath Kilauea summit and are displaced to higher levels in the storage complex, where they become chemically zoned due to gravitational settling of olivine as newer batches of olivine-rich magma arrive from the mantle. During eruption or intrusion within the rift zones, some portion of magma moving into the rift is separated from the main source of heat, resulting in cooling and differentiation. Rift eruptions are inferred to be fed from the lower parts of the summit reservoir complex and, more often than not, mix with fractionated magma present from previous episodes of rift intrusion to form hybrid magma. Because of

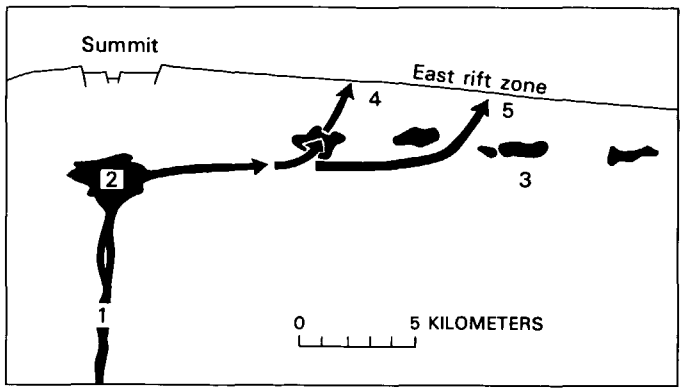

FIGURE 23.2.—Simplified model of magma storage and eruption at Kilauea (modified from Wright and Fiske, 1971, fig. 9): (1) Conduit through the oceanic crust defined seismically; (2) shallow storage reservoir, defined from both geodetic measurements and as an aseismic zone; (3) isolated pockets of magma produced by intrusions into the rift zones. Eruptions at the summit are fed directly from the top of the central reservoir. Most eruptions on the rift are also fed from lower in the central reservoir and may either become mixed with stored rift magma (4) or have direct access to the surface (5). Infrequently, stored rift magma may be erupted independently.

the compositional layering in the summit reservoir resulting from the sequence of magma batches supplied from the mantle, rift eruptions tend to be richer in olivine than summit eruptions and have a summit component in their composition that predates eruption of that component at the summit. These inferences were presented for Kilauea eruptions through 1974 in Wright and Fiske (1971), Wright and others (1975), and Wright and Tilling (1980).

In 1971 and 1974 intrusions beneath the south part of Kilauea caldera were evident (Duffield and others, 1982; HVO, unpublished data). These intrusions resulted in development of mildly differentiated lava as a component of subsequent hybrid eruptions at Kilauea summit in 1974 and 1982 (Wright and Tilling, 1980; HVO, unpublished data).

Direct eruption of fractionated lava on the east rift zone occurred in 1955, 1962, and 1968 (see Wright and Fiske, 1971; Wright and others, 1975) and again in 1977 (Moore and others, 1980) and 1983 (Wolfe and others, chapter 17; Garcia and others, in press). The parent composition, time of rift storage, and rate of crystallization in storage have been quantitatively determined for recent mildly fractionated lava (see Wright and Tilling, 1980). The processes of differentiation within the rift zone appear to be very similar to both the high-temperature and low-temperature differentiation observed in Makaopuhi and Alae lava lakes, suggesting that magma in storage is under sufficient pressure to maintain volatile components in solution, thus enabling convection to take place, and that lower temperature segregation can sometimes occur on a large scale, creating separate reservoirs of fractionated magma. The 1955 eruption requires the latter, as the early erupted lava shows an intratelluric phenocryst assemblage (hypersthene, augite, plagioclase, Fe-Ti oxides) very different from the normal assemblage of olivine and minor augite and plagioclase characterizing lava whose bulk composition is unfractionated.

In addition to study of petrologic processes demonstrated in single eruptions, it should be eventually possible to quantitatively evaluate the times of arrival of magma batches from the mantle, specify where these batches will be stored and for how long, and relate these to when and where they will be erupted to the surface. The seismic data on earthquake swarms related to magmatic intrusions (Klein and others, chapter 43), combined with detailed petrochemical study (for example, Wright and Tilling, 1980), should provide the basic data to do this within the broad framework of geodetic and geophysical observations related to magma storage (Dzurisin and others, 1984).

The processes defined at Kilauea are by no means restricted to Hawaiian tholeiite. The same processes of storage, fractionation, and mixing of magma have been amply documented for midocean ridge basalts (see, for example, Basaltic Volcanism Study Project, 1981, p. 132–160). Thus, both voluminous oceanic basalt types, whose chemistry remains fairly constant with time, behave similarly in spite of the differences in bulk chemistry. However, studies of recent Hawaiian eruptions illustrate a problem that must be considered in looking at older basaltic lava sequences in Hawaii and elsewhere; that is, samples from a single stratigraphic section may represent only a fraction of the lava from any single eruption, and significant compositional changes that occurred during the eruption may be missed. Interpreting contacts between flows to define related eruptive sequences is virtually impossible in older flows, especially in flows of small volume. In the prehistoric record, contacts preserved in a sequence of flows from Mauna Ulu (1969–1974) may look no different than a contact between lava erupted in 1961 and any one episode of Mauna Ulu that happened to cover it. This possibility underscores the fact that petrologic studies of older lava fields may lack much of the critical information that is made available when an eruption or sequence of eruptions is actually observed.

COLLECTION AND ANALYSIS OF HAWAIIAN GASES

One of the most important opportunities afforded by active volcanoes is the sampling of volatile constituents either from active fumaroles or during eruptions. Collection of usable gas samples at an active vent is far from an easy task, as it entails being able to approach an erupting fissure or lava pond, collect a sample with minimal atmospheric contamination, and analyze the sample within hours of collection in order to prevent reaction of the gas species with one another. Some of the best samples ever obtained were collected in the early 20th century from the continuously active lava lake in Kilauea caldera (Shepherd, 1921; Gerlach, 1980). Later in the century, collections were made through drill holes in Makaopuhi lava lake (Finlaysen and others, 1968) and the 1977 eruption of Kilauea (Graeber and others, 1979). In 1980, permanent gas analysis facilities were established at the Hawaiian Volcano Observatory. Greenland (chapters 28 and 30) summarizes information on extensive collections of gases from Kilauea and the first modern samples of eruptive gases from Mauna Loa. Franczyk and others (chapter 31) give complementary data on the amount of carbon and sulfur that remains in the lava after eruption.

The importance of volcanic gas analyses lies both in the estimates of primary volatile compositions of magma and in the budget of volatile species put into the Earth's atmosphere as a result of volcanic eruption. The latter subject is addressed by Casadevall and others (chapter 29) and by Gerlach and Graeber (1985). Volcanic pollutants, mainly CO_2 and SO_2, are found to be significantly less than the contribution from modern industry. The composition of gases arriving from the mantle, after storage beneath Kilauea summit, and residual gas left in erupted lava is estimated for Kilauea (table 23.1) using data of Greenland and others (1985). These estimates are close to those made by Gerlach and Graeber (1985). Estimates of volatile budgets for the 1983–1985 Kilauea eruption also provide an estimate of volatile emission rates consistent with magma supply rates obtained by seismic and geodetic methods (Gerlach and Graeber, 1985; Greenland and others, 1985). Finally, study of gases from the ongoing Kilauea east rift eruption has led to estimates of the rates of magma ascent in the conduit, the diameter of the conduit, and the vertical gradients of pressure and density within the magma column (Greenland and others, in press).

TABLE 23.1.—*H_2O-CO_2-S budget in Kilauea magma*

[Values reported are in weight percent]

	H_2O	CO_2	S
Magma arriving from mantle	0.32	0.32	0.09
Magma after storage and before eruption	.28	.03	.08
Residual volatiles in erupted lava	.05	<.01	.02

PETROLOGY IN CONTEXT: A MODEL FOR STORAGE AND TRANSPORT OF KILAUEA MAGMA

Petrologic and geochemical studies at Kilauea are not in themselves sufficient to translate chemical variations into physical processes. The framework for interpretation of time- and space-related petrologic processes at Kilauea is provided by seismic and geodetic studies. These studies provide direct evidence both for regions of magma storage and for the distribution of and relief of stress associated with magma movement at crustal and upper mantle depths (see Decker, chapter 42). A primary storage region beneath Kilauea summit is defined both seismically (Koyanagi and others, chapter 45, part I; Thurber, chapter 38; Koyanagi and others, 1976) and from ground deformation measurements (for example, Fiske and Kinoshita, 1969; Dvorak and others, 1983). Secondary, and apparently transient, areas of active storage in the rift zones are also defined by a combination of seismic and geodetic measurements (see Klein and others, chapter 43, Jackson and others, 1975; Swanson and others, 1976b). Ryan and others (1981) have incorporated both kinds of data into a generalized three-dimensional model for Kilauea.

A simplified, two-dimensional representation of magma transport and storage is shown in figure 23.2. The depth to both primary and secondary storage is from about 2 km to 6 km beneath the ground surface. The summit storage reservoir is approximately the volume of Kilauea caldera minus the lava flows of historical age that have partially filled it; massive draining of the reservoir has probably occurred during caldera formation in the past.

The rate of magma supply to the Hawaiian system, as estimated from calculated volumes of dated volcanic edifices, is greater for the Island of Hawaii than at any time past (Clague and Dalrymple, chapter 1, part I; also see Moore, chapter 2, for an alternative interpretation). The magma supply to Kilauea, estimated from geodetic and gravity data, is intruded as dikes and sills and extruded as flows in nearly equal amounts; this relation appears to be constant over periods of years (Swanson, 1972; Dzurisin and others, 1984). Recent evidence suggests that the magma supply to Kilauea has increased over the past decade (see Wolfe and others, chapter 17; Greenland and others, 1985). The passage of magma into the rift zones causes a buildup of strain in the south flank that is marked by changes in length of geodetic lines and by high seismicity. The strain is relieved when the unbuttressed south flank of Kilauea moves oceanward (Swanson and others, 1976a). Seismicity, associated both with the rift zones and the south flank, is also high during intrusion or during emplacement of a dike preceding eruption at a new location. Commonly earthquake epicenters migrate ahead of the dike tip to define the magma transport path (see Wolfe and others, chapter 17; Koyanagi and others, chapter 45, part I; Klein and others, chapter 43). Long continued eruptions such as Mauna Ulu (1969–1974) or the current Kilauea eruption at Puu Oo (Wolfe and others, chapter 17) create an open transport system in which seismicity along transport paths is greatly reduced (Koyanagi and others, chapter 45, part I).

Magma supply from the mantle during 1952–1975 was describable in terms of batches of distinct composition (Wright and others, 1975; Wright and Tilling, 1980). Following a large south flank earthquake ($M = 7.2$) in 1975 (Lipman and others, 1985), magma compositions during 1979–1984 were no longer easily divided into discrete batches. Possibly the earthquake effectively broke down internal boundaries in the storage system, so that stored magma and new magma mixed on a large scale. An earthquake of similar magnitude occurred in 1868 and had an apparent effect on both the subsequent rate of eruption and chemical composition of lava from Mauna Loa (Lockwood and Lipman, chapter 18; Tilling and others, chapter 24). This effect further emphasizes the need to know volcanotectonic constraints in order to properly interpret petrochemical data.

The high rates of magma supply from depth in the past decade are also reflected in patterns of deeper seismicity. A zone between 15 and 30 km depth (that is, in the very uppermost mantle) is less seismic than the regions above and below, perhaps defining, as with the lowered seismicity around shallow rift transport systems, a greater openness of the magma transport path (Koyanagi and others, chapter 45, part I).

The distribution in time and space of deep tremor and long-period earthquakes is of great significance, providing evidence for magma movement at depths of 40–60 km (Koyanagi and others,

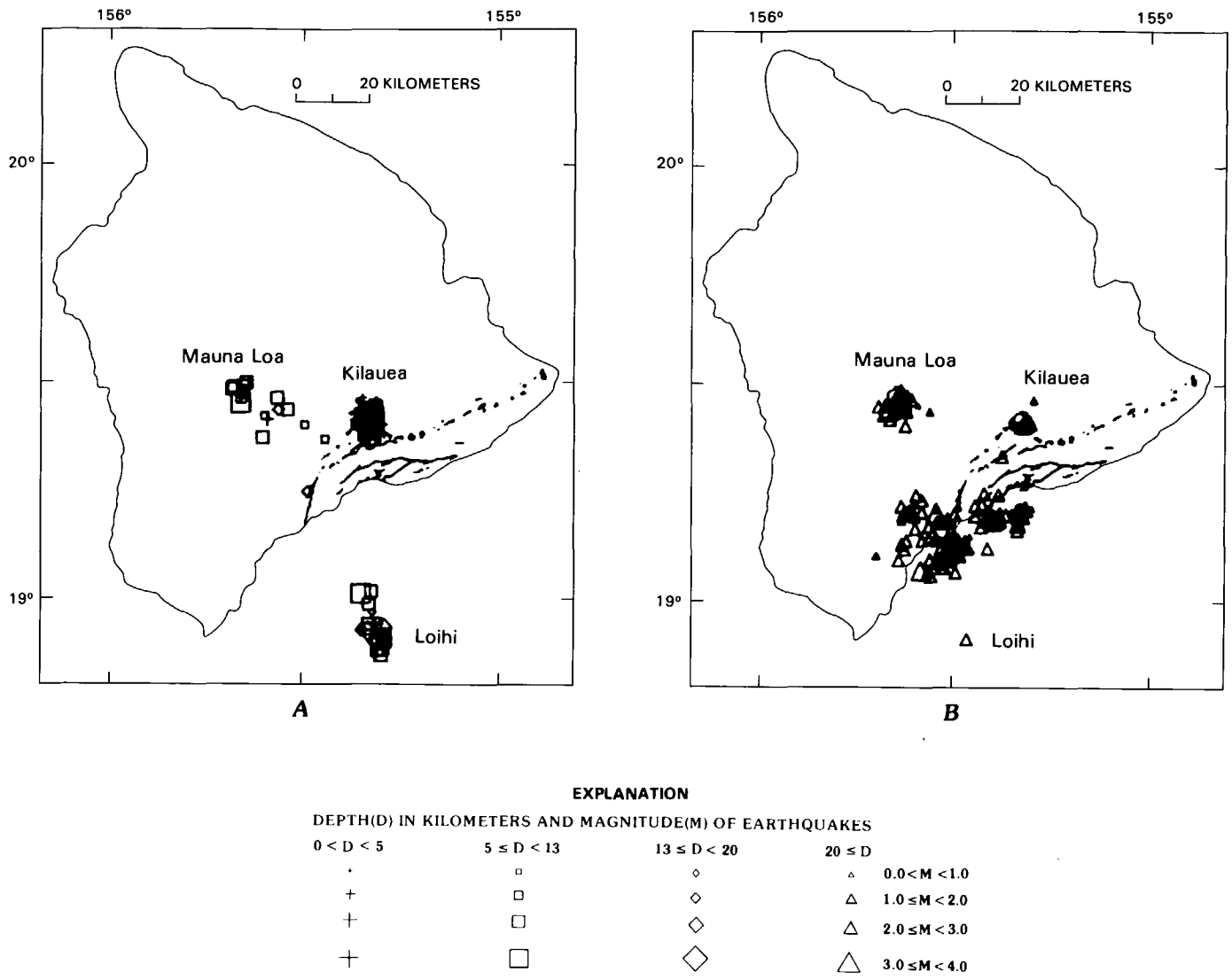

FIGURE 23.3.—Long-period seismicity of the Island of Hawaii, 1972–85. ***A***, Epicenters of long-period earthquakes with hypocenters <15 km deep. Note clustering at the three active volcanic centers. ***B***, Long-period earthquakes and locatable bursts of harmonic tremor with hypocenters >30 km deep (maximum is about 55 km). Note the dominant clustering in a broad zone between the three active volcanic centers.

chapter 45, part I; Klein, 1982). The zone of deep, long-period seismicity is centrally located with respect to all three active volcanoes—Loihi, Kilauea, and Mauna Loa—contrasting with the concentration of shallow long-period earthquakes in each volcanic edifice above and below the storage reservoir; these relations are shown in figure 23.3. The connections between deep and shallow transport systems are not clear. If, indeed, the zone shown in figure 23.3*B* defines the deeper end of magma transport systems for all three volcanoes, then it severely constrains the explanations for the distinctive chemistry and lava associations in each volcano. Either the zone of magma collection is compartmented at a scale not seen by the seismic data, or the chemical differences are produced in transit toward the surface, at much higher levels than the zone of melting. Isotopic data, as currently understood, probably rule out the latter conclusion, leaving one with a challenge to relate the observed seismicity to magma transport in a way that preserves chemical differences that originate in the melting zones (see Chen and Frey, 1985, however, for discussion of the possible influence of the transport path to the surface on chemical and isotopic variation).

Deeper yet, the zone of melting beneath Hawaii has been postulated to be within the uppermost asthenosphere, at depths greater than 60 km (see Wright, 1984). The unique chemistries of magma at the three volcanoes suggest that discrete regions of melting within the asthenosphere each have their own isotopic and trace-element signature. This problem will be discussed further in the final section.

LOIHI SEAMOUNT: A LOOK AT THE BEGINNING OF A HAWAIIAN VOLCANO

Loihi Seamount was discovered in 1955 from looking at a compilation of bathymetric data around the Hawaiian Islands (Emery, 1955). Later, with an expanded Hawaiian seismic net and a new computer system for locating earthquake foci, F.W. Klein and R.Y. Koyanagi noted swarms of shallow crustal earthquakes off the southeast coast of the Island of Hawaii (Klein and Koyanagi, 1979; Klein, 1982). Together, these observations suggested the existence of an active Hawaiian volcano in the making. Plans to dredge the seamount were carried out, samples were taken, more precise bathymetry was obtained, and preliminary results were published (Malahoff and others, 1982; Moore and others, 1982). A summary of more recent bathymetry and geophysical study is given in Malahoff (chapter 6). The dredge hauls contained both tholeiitic and alkalic basalt. Some of the latter contained xenoliths. Dating of samples showed an age range of from 0.5 to 1.6 ka, with alkalic basalt older, for the most part, than tholeiite. Thus, the newest volcano in the Hawaiian Chain showed apparent reversal in the accepted age relations of alkalic and tholeiitic basalt.

Research on Loihi was subsequently treated in a manner similar to the lunar program; we now know more about Loihi (isotopes, trace elements, major oxides) than any other single Hawaiian volcano (see Craig, 1983). Study of Loihi has generated many new questions about the growth of Hawaiian shields and the nature of the melting process(es). Workers on Loihi have concluded that the earliest stage of Hawaiian volcanism is alkalic. The Loihi data also raise the possibility that alkalic volcanism may occur at any stage in shieldbuilding, perhaps when the rate of melting in the mantle slows down for some reason. The bathymetry of the undersea portions of most Hawaiian volcanoes defines a shield shape, and this requires that the dominant shield-building lava be fluid tholeiite and that the alkalic component be at most a minor intercalation. All conclusions need to be tempered by the fact that above water we have sampled less than 10 percent of any Hawaiian shield, and the sampling at Loihi comprises only the surface lava on its shield.

Detailed petrologic and geochemical studies of Loihi (Frey and Clague, 1983; Hawkins and Melchior, 1983), combined with isotopic studies of Sr (Lanphere, 1983; Staudigel and others, 1984) and Pb and Nd (Staudigel and others, 1984), bring about the unanimous conclusions that significant heterogeneity exists within the Hawaiian hotspot and that it is difficult to relate Loihi samples with subaerial lava sequences. The tholeiite samples have a demonstrably Hawaiian chemistry that differs in small ways from both Kilauea and Mauna Loa. The alkalic samples differ from the subaerial alkalic caps on other Hawaiian volcanoes and from the nephelinitic series. Furthermore, these samples lack the garnet-bearing xenoliths of the latter series, but contain lherzolite xenoliths not found in the former series. Isotopic study of rare gases (Kaneoka and others, 1983; Kurz and others, 1983; Rison and Craig, 1983) unequivocally define the source material as primitive and undegassed mantle material, unmodified by crustal processes, relative to data from other volcanoes. Thus, the discovery and subsequent study of Loihi has provided additional constraints and new questions to be asked in relation to our understanding of Hawaiian volcanic cycles.

PUTTING IT ALL TOGETHER: INTEGRATED MODELS OF THE PETROGENESIS OF VOLCANIC SEQUENCES IN THE HAWAIIAN ISLANDS

Earlier studies of Hawaiian volcanism were based on geologic mapping and sampling stratigraphic sections for petrographic study and major-oxide chemistry. Work on trace elements and isotopes was of a reconnaissance nature confined to widely scattered samples, only some of which were tied to major-oxide study. Compilation of these data resulted in generalities about the geochemical signature of Hawaiian volcanism and recognition of the systematic differences between midplate and midocean ridge volcanism (see, for example, summaries by O'Nions and others, 1977; Lanphere and Dalrymple, 1980; Basaltic Volcanism Study Project, 1981), but contributed little to understanding the details of the evolution of individual Hawaiian shields. Recently, more concentrated studies on specific volcanoes and stratigraphically defined sequences within those volcanoes have been undertaken to establish the details of isotopic, trace-element, and major-oxide behavior. These studies have focused on Molokai (Beeson, 1976; Clague and others, 1983), Kohala (Feigenson and others, 1983; Lanphere and Frey, in press), Kilauea (Casadevall and Dzurisin, chapter 13; Hofmann and others, 1985), Haleakala (Chen and Frey, 1983, 1985), Koolau (Stille and others, 1983; Roden and others, 1984), Kauai (Feigenson, 1984), and Loihi (see above). The Honolulu Volcanics have also been studied comprehensively (Clague and Frey, 1982). The principal conclusions reached from stratigraphic studies are the following:

(1) The transition from tholeiitic basalt to alkalic basalt at the end stages of Hawaiian volcanism is commonly, but not always, gradual, with interfingering of the two rock types with rocks of transitional chemistry.

(2) Sr isotopic signatures are inversely correlated to Rb/Sr ratios and may be systematically different for the tholeiitic shield, lower alkalic lava, and uppermost alkalic lava. The progression is subtle and is best illustrated by data from Haleakala using $^{87}Sr/^{86}Sr$ ratios (Chen and Frey, 1983, 1985) for tholeiite (0.7037–0.704) through lower alkalic (0.7032–0.7035) and upper alkalic lava (0.7030–0.7033). In addition, $^{143}Nd/^{144}Nd$ ratios show a smaller variation and are inversely correlated to $^{87}Sr/^{86}Sr$ ratios. These data are interpreted to show participation of different source regions in the formation of the three series. In other volcanoes, including Waianae, West Maui, and Mauna Kea, no systematic differences exist between radiogenic-isotope signatures in the tholeiitic and alkalic stages (Hegner and others, 1986; Stille and others, in press).

(3) Pb isotopes differ for each volcano, vary independently of Sr and Nd, and appear to be related to the age and location of individual volcanoes in the Hawaiian Chain (that is, to the Loa and Kea locus lines (fig. 23.1; see also Tatsumoto, 1978; Stille and others, in press). The absolute variation of all isotopic ratios and the uncorrelated variations of Pb with Nd and Sr have led workers in Hawaii to postulate mixing of at least three kinds of variably enriched or depleted sources. Beyond defining the need for three sources, no consensus has been made as to their position in the mantle or the details of their origin (see Tatsumoto and others,

chapter 26; Tatsumoto, 1978; Staudigel and others, 1984; Kaneoka, in press; Stille and others, in press).

Other geochemical studies, using trace and major elements, address further the relations between tholeiitic and alkalic volcanism. On the basis of field mapping, petrologic study of volcanic sequences, and experimental study of basaltic phase equilibria, two hypotheses have been proposed (see Macdonald, 1968, p. 512–516, for a good summary of these hypotheses). The first hypothesis, based principally on field studies and later on high-pressure phase equilibria, is that alkalic series on Hawaiian volcanoes are derived directly by fractionation of tholeiitic magma in storage. For this process to work, pressures must be great enough to stabilize hypersthene as a liquidus phase, the crystallization of which reduces the SiO_2 of the derivative magma (see Green and Ringwood, 1964). This hypothesis is attractive from consideration of the very small volumes of the alkalic caps and was defended by Wright and others (1979) as a logical consequence of an active tholeiitic shield-building system breaking the connection with the hotspot as the plate drifts to the northwest. The second hypothesis, first presented by Kuno and others (1957), Yoder and Tilley (1962) and later, in modified form, by O'Hara (1965), all working with experimental data, postulates that alkalic magma is independently derived from a different source region at a greater depth than that which produced the tholeiite.

Evidence based on geochemistry shows that the first hypothesis is clearly untenable as a simple single-stage fractionation process, even for those volcanoes for which isotopic ratios are similar in the two rock types. Mass-balance calculations made using hypersthene as a dominant crystallizing phase satisfy major oxides, but leave minor and incompatible trace elements out of balance; that is, the alkalic basalt always has greater amounts of incompatible elements (K, P, light rare-earth elements, and so on) than can be explained by balancing SiO_2, Al_2O_3, FeO, MgO, and CaO. Chondrite-normalized rare-earth-element patterns are always steeper for alkalic basalt than for tholeiite, a relation not explainable by removal of hypersthene in which solid-liquid partition coefficients for rare-earth elements are too low to significantly steepen the patterns for derivative liquids. The mismatch between trace elements and major oxides might be rectified in a model involving a continuously replenished magma system (see O'Hara, 1977). However, replenishment does not have much appeal in explaining the waning stage of Hawaiian volcanism. Hypothesis 1 is also difficult to apply to an earlier stage of alkalic volcanism, such as Loihi, where alkalic magma is preceding, rather than following, tholeiitic magma.

Modern evidence favors the first part of hypothesis 2, that the alkalic basalt is generated independently of the tholeiite in an isotopically different source mantle. The depths at which either type of magma is generated or last equilibrated is an unresolved issue. The identification of mantle metasomatism, isotopic heterogeneity, and possible mixing of source mantle materials with each other and with basaltic melt provide little certainty as to the absolute depths of generation of any basaltic melt, with the exception that the depths are in the mantle and below the deepest earthquake foci (60 km for Hawaii). At Loihi further complications arise. The data require simultaneous eruption of magma that has equilibrated at different depths and that does not show the same isotopic relations as shown for the tholeiitic-alkalic transition at the end of Hawaiian volcanism.

The origin of the nephelinitic series, those containing modal nepheline and (or) melilite, is yet another story. Clague and Frey (1982) have exhaustively analyzed data for the Honolulu Volcanics on Oahu. They conclude that this series was produced at degrees of melting ranging from 5–11 percent and requires some premelting metasomatism of a garnet peridotite source. They specify melting at a pressure of 2.5–3.0 GPa, corresponding to a maximum depth of about 100 km. Other workers, for example Jackson and Wright (1970) and Wright (1984), favor an origin in the low velocity zone, deeper than 100 km. Because as much as 2 m.y. separates the truly nephelinitic series from underlying lava at the same locality, the nephelinite series should be only indirectly related to the thermal plume assumed to exist for the building of the large-volume Hawaiian shields. Jackson and Wright (1970, p. 427) hypothesised that post-erosional lava erupts due to release of pressure following the re-establishment of isostatic equilibrium, which was upset during the vast extrusions of shield-building lava. A more recent evaluation (Clague and Dalrymple, chapter 1, part I) finds that the time separating the shield-building lava and the uppermost alkalic lava is decreasing downchain and that the occurrence of post-erosional volcanism maintains a constant distance from contemporaneous shield-building activity. This evaluation is consistent with the Jackson-Wright model.

MELTING MODELS AND THE NATURE OF THE HAWAIIAN MANTLE

Numerous recent models for Hawaiian volcanism have been based on very different premises and data sets. Not surprisingly, the various authors come to different conclusions regarding some of the fundamental facts needed to specify the history of Hawaiian magma from its source in the mantle to its eruption at the Earth's surface. These facts are, in part, the following, each of which has been or needs to be ascertained for each major rock type or stage of volcanism, that is, shield-building tholeiite, preshield and caldera-filling alkalic basalt, and uppermost alkalic to nephelinitic rocks.

1. Mantle sources: depth, mineralogy, and bulk composition.
2. Depth of partial melting.
3 Melt fraction produced at time of melting.
4. Degree to which primary magma is changed on the way to storage in the shallow crust or to eruption, for example, loss of olivine, interaction with wall rocks, and mixing during ascent.

An excellent summary of current models to explain the Hawaiian magma system is presented by Frey and Roden (in press). The geochemical models are grouped into those based primarily on isotopic data (Kaneoka, chapter 27; Kaneoka, in press; Tatsumoto and others, chapter 26; Staudigel and others, 1984; Stille and others, in press), those based on trace-element data (Leeman and others, 1980; Clague and Frey, 1982; Hofmann and White, 1982; Budahn and Schmitt, 1985), or those based on a combination of isotopic and chemical data (Chen and Frey, 1983, 1985; Feigenson, and others, 1983; Feigensen, 1984; Roden and others, 1984;

Hofmann and others, 1984; Clague, in press; Feigensen, in press; Lanphere and Frey, in press). The geochemical models are in general formulated to fit established geochemical assumptions (such as nonfractionation of isotopes and chondritic source compositions) and pay little attention to either geophysical considerations or the constraints afforded by study of active volcanism. Some additional models (Presnall and Helsley, 1982; Sen, 1983) are based on the interpretations of geophysical data and on experimentally determined phase equilibria for basalt and for mantle rocks, but fail to apply their interpretations to actual geochemical balances. Anderson (1981) has proposed models based on seismologic data using the velocity structure of the mantle and has attempted to reconcile these models with the existing geochemical data, again without quantitative verification. Wright (1984) has considered geochemical balances consistent with the physical processes involved in constructing an Hawaiian volcano. However, the various authors find little agreement on items 1–4 above.

On item 1, disagreement arises as to the existence of a deep mantle plume, whether such a plume would supply the material to be melted (as opposed to the heat for melting at upper mantle depths), and as to the nature of the residual assemblage after melting. The $^3He/^4He$ ratios for some volcanoes support, in a striking way, the primitive nature of Hawaiian magma sources (see Kaneoka, chapter 27). Additional constraints on mantle sources, as determined by study of rare gas data, are given by Clague (in press). As noted earlier, there is agreement that several isotopically distinct sources participate at some point prior to melting and (or) storage at crustal levels. On the composition of the residual assemblage present after melting, two extreme views are presented: (1) Budahn and Schmitt (1985) use convergence of chondrite-normalized rare-earth-element patterns at the heavy end to infer the necessity of garnet in the residual assemblage for melting all Hawaiian basalt, and (2) Wright (1984) argues for a metasomatic process by which the garnet-like rare-earth-element signature is imparted to a depleted mantle source formed by melting of midocean ridge basalt before melting to produce Hawaiian tholeiite.

Most workers agree on item 2 that the actual partial melting occurs at uppermost mantle depths (that is, 100 ± 50 km) but disagree as to whether lithosphere or asthenosphere is directly melted. Presnall and Helsley (1982) and Sen (1983) favor lithospheric melting, which has been strongly criticized on both geochemical and physical grounds (see Feigenson, in press). Most authors favor primary melting of the asthenosphere. Wright (1984) differs from both in postulating that melting takes place in asthenosphere that begins as oceanic lithosphere, but through a combination of metasomatic enrichment and lithospheric thinning was converted to asthenosphere before melting. Chen and Frey (1983, 1985) propose that melts are generated in the asthenosphere and subsequently modified during passage through the lithosphere.

Arguments about item 3 follow from the consideration of residual assemblages. The geochemical models, whether using incompatible element enrichment, or garnet as a residual phase, infer small (less than 10 percent) degrees of melting, even for tholeiite. This model results in a conundrum regarding the supply of material to be melted. As aptly stated by Chen and Frey (1983, p. 789) "the entire lower lithosphere and much of the asthenosphere beneath a Hawaiian volcano must be involved in its creation." Hofmann and others (1984) in a study of short-term chemical variation at Kilauea, remain noncommittal on absolute degree of melting, although their requirement that garnet be a residual phase restricts the degree of melting to less than 20 percent, in consideration of high-pressure phase relations in ultramafic systems. O'Hara (1985) points out some important constraints on assumptions of the degree of partial melting, based on evaluation of the real shape of the melting anomaly.

Conclusions regarding item 4 are largely a consequence of inferences made for items 1–3. As stated above, isotopic data appear to require a more complicated history than one might infer from other data. The existence of magma batches at Kilauea (see Wright and others, 1975) requires heterogeneity, either inherited from the melt source or produced between initial melting and shallow storage. Even this concept (that is, magma batches at Kilauea), carefully outlined in a series of papers (Wright and Fiske, 1971; Wright and others, 1975; Wright and Tilling, 1980), has been questioned by Hofmann and others (1984), who claim that the data define a continuum in all elements. We disagree and leave this subject as a point to emphasize how difficult it is to reach a consensus of interpretation on any observations of Hawaiian volcanism.

Finally, Anderson (1984, 1985) has questioned all of the conventional ideas regarding items 1–4. He favors a source for magma in the transition region at 200–250 km depth where large scale melting is followed by processes such as eclogite fractionation during ascent and mixing with melts from enriched mantle at shallow depth, to produce the rocks forming both the oceanic crust and the oceanic islands such as Hawaii. Time will tell whether these provocative ideas can be quantified and tested against all of the geochemical and geophysical constraints provided by study of active volcanism.

One additional way of determining the composition of the mantle and the melting process is through study of xenoliths brought up with basalt. The processes by which xenoliths arrive at the surface of the earth is somewhat enigmatic. Both tholeiitic magma and alkalic magma show abundant evidence of shallow storage, although the general absence of mantle inclusions from tholeiite and their frequent association with alkalic magma remains unexplained. Clague (in press) suggests that xenoliths are filtered out of tholeiitic magma during storage in large magma chambers. Wright (1984) makes a further suggestion that the rates of tholeiitic-magma transport are too slow and the coalescing transport paths too thin to permit xenoliths to arrive at the surface. Nephelinitic magma is inferred to erupt directly from the mantle and carry the only lherzolite and garnet-bearing xenoliths. Frey and Roden (in press) provide an excellent summary of the relations of xenoliths to both basalt and mantle sources. They point out that virtually all xenoliths have undergone modification prior to their inclusion in the ascending magma in the form of interaction with fluids that may change trace-element content, isotopic ratios, or deposit hydrous minerals. Therefore, because of these factors, combined with their small size, no xenolith can be interpreted as representing the bulk mantle, or any part of the mantle large enough to be considered as a source

composition in melting models. Nonetheless, their presence is useful in assessing the depth of origin of some Hawaiian basalt.

Perhaps no single model works for all volcanoes in the chain. As Frey and Roden (in press) point out, a problem in developing a general model is that it must explain both the unique geochemical features that characterize individual Hawaiian volcanoes and simultaneously explain the geochemical variations among all Hawaiian volcanoes. As a final point, we want to reemphasize the necessity for comprehensive study of everything relevant to construction of an individual Hawaiian volcano as well as the entire volcanic chain (see Wright and others, 1979; Wright, 1984). Recent advances in our understanding of seismology (Anderson and others, 1984), phase relations of ultramafic rocks (Takahashi and Scarfe, 1985; Walker and Herzberg, 1985), and the physical processes of melt separation (MacKenzie, 1984; Richter and MacKenzie, 1984) may eventually resolve both the depth and degree of partial melting in a way that can accommodate the constraints provided by active volcanic processes.

SUGGESTIONS FOR FURTHER STUDY

The acquisition of more chemical data on Hawaiian lava has increased our qualitative and quantitative understanding of Hawaiian petrology and has also raised new questions for further study. Obviously, the location of Hawaii, in the interior of an oceanic plate far removed from influences of spreading centers or continental margins, continues to provide a setting in which possible determinations can be made as to the nature of the oceanic crust and mantle and the dynamics of plume or hotspot volcanism. Presently the heterogeneities in the hotspot magma sources are being emphasized. Yet over the long term it is important to keep in mind that the Hawaiian chain has shown an identifiable eruptive style and geochemical signature for over 70 million years. Thus, a gross uniformity must exist in the source and some unifying principles in the production of Hawaiian magma, the mechanics of its segregation from the mantle, and its transport to areas of storage within the crust. Further study of the following topics ought to bring us to a better understanding of the processes important in the formation of Hawaiian volcanoes: (1) Continued detailed geochemical study of stratigraphically constrained samples; (2) geophysical study of the mantle; (3) more detailed petrographic study (both field and thin section) of lava samples, including detailed electron probe analysis of phase chemistry; and (4) more study of the submarine portions of active or young rift zones. For example, cursory petrographic study of submarine rift samples identified mineral forms and textures such as anhedral olivine and sieved plagioclase that suggest that processes involved in submarine lava are difierent from those in subaerial equivalents on the same rift zones.

REFERENCES

Anderson, A.T., Swihart, G.H., Artioli, G., and Geiger, C.A., 1984, Segregation vesicles, gas filter-pressing, and igneous differentiation: Journal of Geology, v. 92, p. 55–72.

Anderson, D.L., 1981, Hotspots, basalts, and the evolution of the mantle: Science, v. 213, p. 82–89.

———1984, The Earth as a planet: paradigms and paradoxes: Science, v. 223, p. 347–355.

———1985, Hotspot magmas can form by fractionation and contamination of mid-ocean ridge basalt: Nature, v. 318, p. 145–149.

Basaltic Volcanism Study Project, 1981, Basaltic volcanism on the terrestrial planets: Elmsford, Pergamon Press, 1,286 p.

Beeson, M.H., 1976, Petrology, mineralogy and geochemistry of the East Molokai Volcanic Series, Hawaii: U.S. Geological Survey Professional Paper 961, 53 p.

Bonhommet. N., Beeson, M.H., and Dalrymple, G.B., 1977, A contribution to the geochronology and petrology of the Island of Lanai, Hawaii: Geological Society of America Bulletin, v. 88, p. 1281–1286.

Budahn, J.R., and Schmitt, R.A., 1985, Petrogenetic modeling of Hawaiian basalts: a geochemical approach: Geochimica et Cosmochimica Acta, v. 49, p. 67–87.

Chen, C.-Y., and Frey, F.A., 1983, Origin of Hawaiian tholeiite and alkalic basalt: Nature, v. 302, p. 785–789.

———1985, Trace element and isotopic geochemistry of lavas from Haleakala Volcano, East Maui, Hawaii: implications for the origin of Hawaiian basalts: Journal of Geophysical Research, v. 90, p. 8743–8768.

Chouet, B., and Aki, K., 1981, Seismic structure and seismicity of the cooling lava lake of Kilauea Iki, Hawaii: Journal of Volcanology and Geothermal Research, v. 9, p. 41–56.

Clague, D.A., in press, Hawaiian alkaline volcanism: Proceedings of the Royal Society of Edinburgh.

Clague, D.A., and Frey, F.A., 1980, Trace element geochemistry of tholeiitic basalts from site 433C, Suiko Seamount, *in* Shambach, J., ed., Initial reports of the Deep Sea Drilling Project [leg 55], v. 55: Washington, U.S. Government Printing Office, p. 559–569.

———1982, Petrology and trace element geochemistry of the Honolulu Volcanics, Oahu: Implications for the oceanic mantle below Hawaii: Journal of Petrology, v. 23, p. 447–504.

Clague, D.A., Frey, F.A., and Beeson, M.H., 1983, Rare-earth element and Sr isotopic evidence for the origin of the East Molokai Volcanics, Hawaii [abs.]: Eos, v. 64, p. 902.

Clague, D.A., Jackson, E.D., and Wright, T.L., 1980, Petrology of Hualalai Volcano, Hawaii: implication for mantle composition: Bulletin Volcanologique, v. 43, p. 641–656.

Craig, H., 1983, Introduction to Loihi Seamount: collected papers: Earth and Planetary Science Letters, v. 66, p. 334–336.

Duffield, W.A., Christiansen, R.L., Koyanagi, R.Y., and Peterson, D.W., 1982, Storage, migration, and eruption of magma at Kilauea Volcano, Hawaii, 1971–1972: Journal of Volcanology and Geothermal Research, v. 13, p. 273–307.

Dvorak, J.D., Okamura, A., and Dieterich, J.H., 1983, Analysis of surface deformation data, Kilauea Volcano, Hawaii: October 1966 to September 1970: Journal of Geophysical Research, v. 88, p. 9295–9304.

Dzurisin, D., Koyanagi, R.Y., and English, T.T., 1984, Magma supply and storage at Kilauea Volcano, Hawaii, 1956–1983: Journal of Volcanology and Geothermal Research, v. 21, p. 177–206.

Eaton, J.P., 1962, Crustal structure and volcanism in Hawaii, *in* Macdonald, G.A., and Kuno, H., eds., The crust of the Pacific Basin: Washington, American Geophysical Union, Monograph 6, p. 13–29.

Eaton, J.P., and Murata, K.J., 1960, How volcanoes grow: Science, v. 132, p. 925–938.

Emery, K.O., 1955, Submarine topography south of Hawaii: Pacific Science, v. 9, p. 286–291.

Evans, B.W., and Moore, J.G., 1968, Mineralogy as a function of depth in the prehistoric Makaopuhi tholeiitic lava lake, Hawaii: Contributions to Mineralogy and Petrology, v. 17, p. 85–115.

Feigenson, M.D., 1984, Geochemistry of Kauai volcanics and a mixing model for the origin of Hawaiian alkali basalts: Contributions to Mineralogy and Petrology, v. 87, p. 109–119.

———in press, Geochemical and geophysical constraints on the origin of Hawaiian lavas: Journal of Geophysical Research.

Feigenson, M.D., Hofmann, A.W., and Spera, F.J., 1983, Case studies on the origin of basalt: II. The transition from tholeiitic to alkalic volcanism on Kohala Volcano, Hawaii: Contributions to Mineralogy and Petrology, v. 84, p. 390–405.

Finlayson, J.B., Barnes, I.L.. and Naughton, J.J., 1968, Developments in volcanic gas research in Hawaii, *in* The upper crust and upper mantle of the Pacific area: American Geophysical Union Geophysics Monograph 12, p. 428–438.

Fiske, R.S., and Kinoshita, W., 1969, Inflation of Kilauea Volcano prior to its 1967–1968 eruption: Science, v. 165, p. 341–349.

Frey, F.A., 1980, The origin of pyroxenites and garnet pyroxenites from Salt Lake Crater, Oahu, Hawaii: trace element evidence, *in* Irving, J., ed., The Jackson Volume; American Journal of Science, v. 280-A, pt. 2, p. 427–449.

Frey, F.A., and Clague, D.A., 1983, Geochemistry of diverse basalt types from Loihi Seamount, Hawaii: petrogenetic implications, *in* Loihi Seamount: collected papers: Earth and Planetary Science Letters, v. 66, p. 337–355.

Frey, F.A., and Roden, M., in press, The mantle source for the Hawaiian Islands: constraints from the lavas and ultramafic inclusions, *in* Menzies, M., and Hawkesworth, C., eds., Mantle metasomatism: New York, Academic Press.

Garcia, M.O., Wolfe, E.W., and Byers, C.D., in press, Petrology of the lavas from the Puu Oo eruption of Kilauea Volcano, Hawaii: Phases 1–20, *in* Wolfe, E.W., ed., The Puu Oo eruption of Kilauea Volcano, Hawaii: the first 1½ years: U.S. Geological Survey Professional Paper.

Gerlach, T.M., 1980, Evaluation of volcanic gas analyses from Kilauea Volcano: Journal of Volcanology and Geothermal Research, v. 7, p. 295–317.

Gerlach, T.M., and Graeber, E.J., 1985, Volatile budget of Kilauea Volcano: Nature, v. 313, p. 273–277.

Graeber, E.J., Modreski, P.J., and Gerlach, T.M., 1979, Compositions of gases collected during the 1977 east rift eruption, Kilauea Volcano, Hawaii: Journal of Volcanology and Geothermal Research, v. 5, p. 337–344.

Green, D.H., and Ringwood, A.E., 1964, Fractionation of basalt magmas at high pressures: Nature, v. 201, p. 1276–1279.

Greenland, L.P., in press, Estimated mantle content of volatiles from basaltic gas compositions: Bulletin of Volcanology.

Greenland, L.P., Okamura, A.O., and Stokes, J.B., in press, Constraints on the mechanics of eruption of Puu Oo, *in* Wolfe, E.W., ed., The Puu Oo eruption of Kilauea Volcano, Hawaii: the first 1 ½ years: U.S. Geological Survey Professional Paper.

Greenland, L.P., Rose, W. I., and Stokes, J.B., 1985, An estimate of gas emissions and magmatic gas content from Kilauea Volcano: Geochimica et Cosmochimica Acta, v. 49, p. 125–129.

Hardee, H.C., 1980, Solidification in Kilauea Iki lava lake: Journal of Volcanology and Geothermal Research, v. 7, p. 211–223.

Hardee, H.C., Dunn, J.C., Hills, R.G., and Ward, R.W., 1981, Probing the melt zone of Kilauea Iki lava lake, Kilauea Volcano, Hawaii: Geophysical Research Letters, v. 8, p. 1211–1214.

Hawkins, J., and Melchior, J., 1983, Petrology of basalts from Loihi Seamount, Hawaii, *in* Loihi Seamount: collected papers: Earth and Planetary Science Letters, v. 66, p. 356–368.

Hegner, E., Unruh, D., and Tatsumoto, M., 1986, Pb, Sr, and Nd isotope evidence for the origin of the West Maui Volcanic Suite, Hawaii: Nature, v. 319, no. 6053, 478–480.

Helz, R.T., 1980, Crystallization history of Kilauea Iki lava lake as seen in drill core recovered in 1967–1979: Bulletin Volcanologique, v. 43-4, p. 675–701.

———1984, In situ fractionation of olivine tholeiite, Kilauea Iki lava lake, Hawaii [abs.]: Geological Society of America Abstracts with Programs, v. 16, p. 536–537.

Helz, R.T., Banks, N.G., Casadevall, T.J., Fiske, R.S., and Moore, R.B., 1984, A catalogue of drill core recovered from Kilauea Iki lava lake from 1967 to 1979: U.S. Geological Survey Open-File Report 84–484, 72 p.

Helz, R.T., and Thornber, C.R., in press, Geothermometry of Kilauea Iki lava lake, Hawaii: Journal of Geophysical Research.

Helz, R.T., and Wright, T.L., 1983, Drilling report and core logs for the 1981 drilling of Kilauea Iki lava lake (Kilauea Volcano, Hawaii), with comparative notes on earlier (1967–1979) drilling experiences: U.S. Geological Survey Open-File Report 83–326, 66 p.

Hermance, J.F., and Colp, J.L., 1982, Kilauea Iki lava lake: geophysical constraints on its present (1980) physical state: Journal of Volcanology and Geothermal Research, v. 13, p. 31–61.

Hofmann, A.W., Feigenson, M.D., and Raczek, I., 1984, Case studies on the origin of basalt: III. Petrogenesis of the Mauna Ulu eruption, Kilauea, 1969–1971: Contributions to Mineralogy and Petrology, v. 88, p. 24–35.

Hofmann, A.W., and White, W.M., 1982, Mantle plumes from ancient oceanic crust: Earth and Planetary Science Letters, v. 57, p. 421–436.

Jackson, D.B., Swanson, D.A., Koyanagi, R.Y., and Wright, T.L., 1975, The August and October 1968 east rift eruptions, Kilauea Volcano, Hawaii: U.S. Geological Survey Professional Paper 890, 33 p.

Jackson, E.D., Silver, E.A., and Dalrymple, G.B., 1972, Hawaiian-Emperor Chain and its relation to Cenozoic tectonics: Geological Society of America Bulletin, v. 83, p. 601–618.

Jackson, E.D., and Wright, T.L., 1970, Xenoliths in the Honolulu volcanic series, Hawaii: Journal of Petrology, v. 11, p. 405–430.

Kaneoka, I., in press, Constraints on the origin of Hawaiian basalts and evidence for a multi-component mantle: Geochimica et Cosmochimica Acta.

Kaneoka, I., Takaoka, N., and Clague, D.A., 1983, Noble gas systematics for coexisting glass and olivine crystals in basalts and dunite xenoliths from Loihi Seamount, *in* Loihi Seamount: collected papers: Earth and Planetary Science Letters, v. 66, p. 427–437.

Kirkpatrick, R.J., Clague, D.A., and Friesen, W.B., 1980, Petrology and geochemistry of volcanic rocks, *in* Initial reports of the Deep Sea Drilling Project [leg 55], v. 55: Washington, U.S. Government Printing Office, p. 509–557.

Klein, F.W., 1982, Earthquakes at Loihi Submarine Volcano and the Hawaiian hotspot: Journal of Geophysical Research, v. 87, p. 7719–7726.

Klein, F.W., and Koyanagi, R.Y., 1979, Seismicity of Kilauea and Loihi Volcanoes, Hawaii [abs.]: Hawaii Symposium on Intraplate Volcanism and Submarine Volcanism, International Association of Volcanology and Chemistry of the Earth's Interior, Hilo, Hawaii, July 16–22, 1979, Abstract Volume, p. 24.

Koyanagi, R.Y., Unger, J.D., Endo, E.T., and Okamura, A.T., 1976, Shallow earthquakes associated with inflation episodes at the summit of Kilauea Volcano, Hawaii, *in* Gonzales-Ferran, O., ed., Symposium on Andean and Antarctic Volcanology Problems, Santiago, Chile, September 1974, Proceedings, p. 621–631.

Kuno, H., Yamasaki, K., Iida, C., and Nagashima, K., 1957, Differentiation of Hawaiian magmas: Japanese Journal of Geology and Geophysics, v. 28, p. 179–218.

Kurz, M.D., Jenkins, W.J., Hart, S.R., and Clague, D., 1983, Helium isotopic variations in volcanic rocks from Loihi Seamount and the Island of Hawaii, *in* Loihi Seamount: collected papers: Earth and Planetary Science Letters, v. 66, p. 388–406.

Lanphere, N., 1983, $^{87}Sr/^{86}Sr$ ratios for basalt from Loihi Seamount, Hawaii, *in* Loihi Seamount: collected papers: Earth and Planetary Science Letters, v. 66, p. 380–387.

Lanphere, M.A., Dalrymple, G.B., and Clague, D., 1980, Rb-Sr systematics of basalts from the Hawaiian-Emperor volcanic chain, *in* Shambach, J., ed., Initial reports of the Deep Sea Drilling Project [Leg 55], v. 55: Washington, Government Printing Office, p. 695–706.

Lanphere, M.A., and Frey, F.A., in press, Geochemical evolution of Kohala Volcano, Hawaii: Contributions to Mineralogy and Petrology.

Leeman, W.P., Budahn, J.R., Gerlach, D.C., Smith, D.R., and Powell, B.N., 1980, Origin of Hawaiian tholeiites: trace element constraints, *in* Irving, A.J., ed., The Jackson Volume: American Journal of Science, v. 280-A, pt. 2, p. 794–819.

Lindstrom, M.M., and Haskin, L.H., 1984, Studies of trace element behavior during crystallization of Makaopuhi lava lake, Hawaii: National Science Foundation Final Report EAR–7904888, 5 p.

Lipman, P.W., Lockwood, J.P., Okamura, R.T., Swanson, D.A., and Yamashita, K.M., 1985, Ground deformation associated with the 1975 magnitude 7.2 earthquake and resulting changes in activity of Kilauea Volcano, Hawaii: U.S. Geological Survey Professional Paper 1276, 45 p.

Macdonald, G.A., 1968, Composition and origin of Hawaiian lavas: Geological

Society of America Memoir 116, p. 477–522.
Macdonald, G.A., Abbott, A.A., and Peterson, F.L., 1983, Volcanoes in the sea: the geology of Hawaii: Honolulu, Hawaii, University of Hawaii Press, 517 p.
Macdonald, G.A., and Katsura, T., 1964, Chemical composition of Hawaiian lavas: Journal of Petrology, v. 5, p. 82–133.
Mackenzie, D.S., 1984, The generation and compaction of partial melts: Journal of Petrology, v. 5, pt. 1, p. 82–133.
Malahoff, A., McMurtry, G.M., Wiltshire, J.C., and Yeh, H.W., 1982, Geology and chemistry of hydrothermal deposits from active submarine volcano Loihi, Hawaii: Nature, v. 298, p. 234–239.
Moore, J.G., Clague, D.A., and Normark, W.R., 1982, Diverse basalt types from Loihi Seamount, Hawaii: Geology, v. 10, p. 88–92.
Moore, J.G., and Evans, B.W., 1967, The role of olivine in the crystallization of the prehistoric Makaopuhi tholeiitic lava lake, Hawaii: Contributions to Mineralogy and Petrology, v. 15, p. 202–223.
Moore, R.B., Helz, R.T., Dzurisin, D., Eaton, G.P., Koyanagi, R.Y., Lipman, P.W., Lockwood, J.P., and Puniwai, G.P., 1980, The 1977 eruption of Kilauea Volcano, Hawaii: Journal of Volcanology and Geothermal Research, v. 7, p. 189–210.
Murata, K.J., 1966, An acid fumarolic gas from Kilauea Iki: U.S. Geological Survey Professional Paper 537–C, 6 p.
Murata, K.J., and Richter, D.H., 1966, Chemistry of the lavas of the 1959–60 eruption of Kilauea Volcano, Hawaii: U.S. Geological Survey Professional Paper 537–A, p. A1–A26.
O'Hara, M.J., 1965, Primary magmas and the origin of basalts: Scottish Journal of Geology, v. 1, p. 19–40.
———1977, Geochemical evolution during fractional crystallization of a periodically refilled magma chamber: Nature, v. 266, p. 503–507.
———1985, Importance of the "Shape" of the melting regime during partial melting of the mantle: Nature, v. 314, p. 58–60.
O'Nions, R.K., Hamilton, P.J., and Evensen N.M., 1977, Variations in $^{143}Nd/^{144}Nd$ and $^{87}Sr/^{86}Sr$ ratios in oceanic basalts: Earth and Planetary Science Letters, v. 34, p. 13–22.
Peck, D.L., 1978, Cooling and vesiculation of Alae lava lake, Hawaii: U.S. Geological Survey Professional Paper 935–B, 59 p.
Peck, D.L., Hamilton, M.S., and Shaw, H.R., 1977, Numerical analysis of lava lake cooling models: Part II, application to Alae lava lake, Hawaii: American Journal of Science, v. 277, p. 415–437.
Peck, D.L., and Kinoshita, W.T., 1976, The eruption of August 1963 and the formation of Alae lava lake, Hawaii: U.S. Geological Survey Professional Paper 935–A, 33 p.
Peck, D.L., Wright, T.L., and Decker, R.W., 1979, The lava lakes of Kilauea: Scientific American, v. 241, p. 114–129.
Powers, H.A., 1955, Composition and origin of basaltic magma of the Hawaiian Islands: Geochimica et Cosmochimica Acta, v. 7, p. 77–107.
Presnall, D.C., and Helsley, C.E.. 1982, Diapirism of depleted peridotite—a model for the origin of hot spots: Physics of the Earth and Planetary Interiors, v. 29, p. 148–160.
Richter, D.H., Eaton, J.P., Murata, K.J., Ault, W.U., and Krivoy, H.L., 1970, Chronologic narrative of the 1959–60 eruption of Kilauea Volcano, Hawaii: U.S. Geological Survey Professional Paper 537–E, 73 p.
Richter, D.H., and Moore, J.G., 1966, Petrology of the Kilauea Iki lava lake, Hawaii: U.S. Geological Survey Professional Paper 537–B, 26 p.
Richter, D.H., and Murata, K.J., 1966, Petrography of the lavas of the 1959–60 eruption of Kilauea Volcano, Hawaii: U.S. Geological Survey Professional Paper 537–D, 12 p.
Richter, F.M., and Mackenzie, D., 1984, Dynamical models for melt segregation from a deformed matrix: Journal of Geology, v. 92, p. 729–740.
Rison, W., and Craig, H., 1983, Helium isotopes and mantle volatiles in Loihi Seamount and Hawaiian Island basalts and xenoliths: Earth and Planetary Science Letters, v. 66, p. 407.
Roden, M.G., Frey, F.A., and Clague, D.A., 1984, Geochemistry of tholeiitic and alkalic lavas from the Koolau Range, Oahu, Hawaii: implications for Hawaiian volcanism: Earth and Planetary Science Letters, v. 69, p. 141–158.
Ryan, M.P., Koyanagi, R.Y., and Fiske, R.S., 1981, Modeling the three-dimensional structure of macroscopic magma transport systems: application to Kilauea Volcano, Hawaii: Journal of Geophysical Research, v. 86, p. 7111–7129.
Sen, G.A., 1983, A petrologic model for the constitution of the upper mantle and crust of the Koolau Shield, Oahu, Hawaii, and Hawaiian magmatism: Earth and Planetary Science Letters, v. 62, p. 215–228.
Sen, G., and Presnall, D.C., 1980, Dunite nodules from the Koolau shield, Hawaii: crystal cumulates from a tholeiitic magma chamber [abs.]: Geological Society of America Abstracts with Programs, v. 12, p. 519.
Shaw, H.R., Hamilton, M.S., and Peck, D.L., 1977, Numerical analysis of lava lake cooling models: Part I. Description of the method: American Journal of Science, v. 277, p. 384–414.
Shaw, H.R., Wright, T.L., Peck, D.L., and Okamura, R., 1968, The viscosity of basaltic magma: an analysis of field measurements in Makaopuhi lava lake, Hawaii: American Journal of Science, v. 266, p. 225–264.
Shepherd, E.S., 1921, Kilauea gases, 1919: Hawaiian Volcano Observatory Bulletin, v. 9, p. 83–88.
Staudigel, H., Zindler, A., Hart, S.R., Leslie, T., Chen, C.-Y., and Clague, D., 1984, The isotope systematics of a juvenile intraplate volcano. Pb, Nd, and Sr isotope ratios of basalts from Loihi Seamount, Hawaii: Earth and Planetary Science Letters, v. 69, p. 13–29.
Stille, P., Unruh, D.M., and Tatsumoto, M., 1983, Pb, Sr, Nd and Hf isotopic evidence of multiple sources for Oahu, Hawaii basalts: Nature, v. 304, p. 25–29.
———in press, Pb, Sr, Nd, and Hf isotopic constraints on the origin of Hawaiian basalts and evidence for a multi-component mantle: Geochimica et Cosmochimica Acta.
Swanson, D.A., 1972, Magma supply rate at Kilauea Volcano, 1952–1971: Science, v. 175, p. 169–170.
Swanson, D.A., Duffield, W.A., and Fiske, R.S., 1976a, Displacement of the south flank of Kilauea Volcano: the result of forceful intrusions of magma into the rift zones: U.S. Geological Survey Professsional Paper 963, 39 p.
Swanson, D.A., Jackson, D.B., Koyanagi, R.Y., and Wright, T.L., 1976b, The February 1969 east rift eruption of Kilauea Volcano, Hawaii: U.S. Geological Survey Professional Paper 891, 30 p.
Takahashi, E., and Scarfe, C.M., 1985, Melting of peridotite to 14 GPa and the genesis of Komatiite magmas [abs.] : Eos, v. 66, p. 403.
Tatsumoto, M., 1978, Isotopic composition of lead in oceanic basalt and its implication to mantle evolution: Earth and Planetary Science Letters, v. 38, p. 63–87.
Tilley, C.E., and Scoon, J.H., 1961, Differentiation of Hawaiian basalts: trends of Mauna Loa and Kilauea historic magma: American Journal of Science, v. 259, p. 60–68.
Walker, D., and Herzberg, C.T., 1985, Implications of possible liquidus-solidus convergence in mantle peridotite at high pressure [abs.]: Eos, v. 66, p. 403.
Wright. T.L., 1971, Chemistry of Kilauea and Mauna Loa lava in space and time: U.S. Geological Survey Professional Paper 735, 40 p.
———1973, Magma mixing as illustrated by the 1959 eruption, Kilauea Volcano, Hawaii: Geological Society of America Bulletin, v. 84, p. 849–858.
———1984, Origin of Hawaiian tholeiite: a metasomatic model: Journal of Geophysical Research, v. 89, p. 3233–3252.
Wright, T.L., and Fiske, R.S., 1971, Origin of the differentiated and hybrid lavas of Kilauea Volcano, Hawaii: Journal of Petrology, v. 12, p. 1–65.
Wright, T.L., and Okamura, R.T., 1977, Cooling and crystallization of tholeiitic basalt, 1965 Makaopuhi lava lake, Hawaii: U.S. Geological Survey Professional Paper 1004, 78 p.
Wright, T.L., and Peck, D.L., 1978, Crystallization and differentiation of the Alae magma, Alae lava lake, Hawaii: U.S. Geological Survey Professional Paper 935–C, 20 p.
Wright, T.L., Peck, D.L., and Shaw, H.R., 1976, Kilauea lava lakes: natural laboratories for study of cooling, crystallization and differentiation of basaltic magma, *in* The geophysics of the Pacific Ocean Basin and its margin: American Geophysical Union, Geophysical Monograph 19, p. 375–392.
Wright, T.L., Shaw, H.R., Tilling, R.I., and Fiske, R.S., 1979, Origin of Hawaiian tholeiitic basalt: a quantitative model [abs.]: Hawaii Symposium on Intrapiate Volcanism and Submarine Volcanism, International Association of

Volcanology and Chemistry of the Earth's Interior, Hilo, Hawaii, July 16–22, 1979, Abstract Volume, p. 104.

Wright, T.L., Swanson, D.A., and Duffield, W.A., 1975, Chemical composition of Kilauea east-rift lava, 1968–1971: Journal of Petrology, v. 16, p. 110–133.

Wright, T.L., and Tilling, R.I., 1980, Chemical variation in Kilauea eruptions 1971–1974, *in* Irving, A., ed., The Jackson Volume: American Journal of Science, v. 280–A, pt. 2, p. 777–793.

Yoder, H.S., Jr., and Tilley, C.E., 1962, Origin of basalt magmas—an experimental study of natural and synthetic rock systems: Journal of Petrology, v. 3, pt. 3, p. 342–532.

TRACE-ELEMENT CHEMISTRY OF KILAUEA AND MAUNA LOA LAVA IN SPACE AND TIME: A RECONNAISSANCE

By Robert I. Tilling, Thomas L. Wright, *and* Hugh T. Millard, Jr.

ABSTRACT

Rare-earth and other trace elements have been determined in 75 Kilauea and Mauna Loa tholeiite samples selected from the same rock powders previously analyzed by Wright (USGS Prof. Paper 735, 1971), to provide a representative sampling in space and time. Preliminary interpretations of the results include the following:

(1) Abundance-variation patterns for well-determined trace elements confirm the long-term temporal variation previously demonstrated by major-element data for olivine-controlled Kilauea lava. Younger lava is richer in olivine-incompatible constituents (such as K, Ti, P, LREE, Sc, and Hf): the behavior of uranium is more varied but fits the overall pattern. Results for less well determined incompatible elements provide supporting permissive evidence.

(2) Subtle systematic differences are observed between the mean compositions of olivine-controlled lava from the summit and rift-zone areas of Kilauea and, perhaps, Mauna Loa, indicating a possible, heretofore unrecognized, compositional variation with eruption locus.

(3) Our results confirm the observation of Budahn and Schmitt (Geochim et Cosmo., v. 49, 1985) that prehistoric Mauna Loa olivine-controlled lava differs systematically from its historical counterpart. Furthermore, our data demonstrate significant differences between 19th-century and 20th-century Mauna Loa lava, suggesting systematic long-term secular variation not previously detected from major-element studies alone.

(4) Mauna Loa's long-term variation trend, in contrast to Kilauea's, is characterized by decreasing abundances of olivine-incompatible constituents with time. Thus, the composition of lava from the two volcanoes diverges with time, resulting in maximum differences between them in the 20th century. The chemical distinction between Kilauea and Mauna Loa has existed for over 30,000 years.

(5) Superimposed on the long-term (centuries to millenia) variations for both volcanoes are short-term (years to decades) variations that cannot be explained by olivine control.

(6) Rhodes' (Jour. of Geophys. Res., v. 88, 1983) data for 114 analyses of Mauna Loa historical lava are interpreted to illustrate not only long-term variation, marked by an irregular decrease in the incompatible elements K, Ti, P, Nb, Zr, and Sr, but also short-term variation (<1 year). A sharp compositional break exists between the lava of the 1868 and 1880 eruptions, and we speculate that this break may reflect disruption of magmatic processes in Mauna Loa's reservoir and conduits caused by the catastrophic 1868 earthquake, the largest to strike the Island of Hawaii in historical time.

Our tentative findings have general implications for processes of intraplate (hot spot) volcanism. Specifically, any complete petrogenetic model for Hawaiian tholeiite must take into account both long-term and short-term variations in olivine-controlled lava of Kilauea and Mauna Loa.

INTRODUCTION

Kilauea and Mauna Loa Volcanoes, on the Island of Hawaii (fig. 24.1), are composed entirely of tholeiitic basalt erupted in an intraplate tectonic setting. Because of their generally nonexplosive character, the eruptions of these two volcanoes—among the most active in the world—have been systematically monitored, documented, and sampled. The papers in this volume attest to the wealth of observational data and the comparatively good general understanding of Hawaiian magmatic and eruptive mechanisms that have

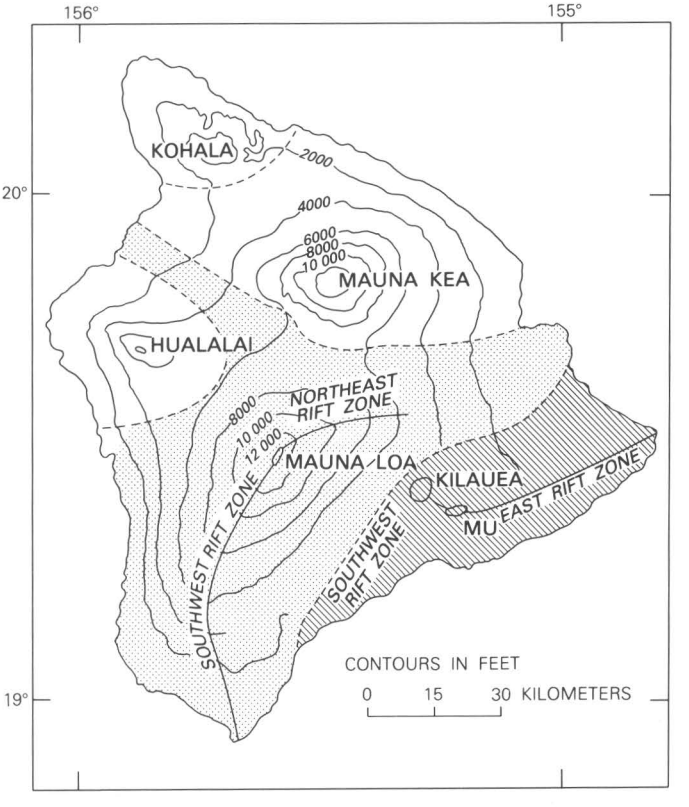

FIGURE 24.1.—Index map showing five volcanoes that make up Island of Hawaii and rift zones of Kilauea and Mauna Loa Volcanoes. MU, site of 1969–74 Mauna Ulu eruption on Kilauea's upper east rift zone. (From Wright, 1971, fig. 1).

been achieved by many decades of modern, multifaceted studies since the founding of the Hawaiian Volcano Observatory in 1912.

This paper reports results from the initial phase of a comprehensive investigation into the trace-element geochemistry of Kilauea and Mauna Loa lava undertaken as a complement to the systematic major-element geochemical study of Wright (1971). There were three primary objectives of this initial phase: (1) to conduct a reconnaissance trace-element survey of representative samples of Kilauea and Mauna Loa lava to determine possible compositional variations with location of eruptive vents or with time; (2) to improve our understanding of the distribution of trace elements in olivine-controlled lava, whose major-element variations can be explained largely by the addition or subtraction of olivine only (see, for example, Powers, 1955; Murata and Richter, 1966a,b; Wright, 1971, 1973); and (3) to identify selected trace elements whose abundances could be determined precisely and accurately to serve as the focus for subsequent, more quantitative studies of specific suites of olivine-controlled, differentiated, and hybrid lava to bear on the petrogenesis, transport and storage, and eruption of Hawaiian tholeiite.

Our study, involving 75 representative samples, considerably increases the body of trace-element data for Kilauea and Mauna Loa lava, especially lava erupted in prehistoric times (before about A.D. 1750). The analytical data we report here, though not published previously, were acquired more than a decade ago; possibly some analyses may be of lower quality than might be obtained today. Therefore, we have paid particular attention to their precision and accuracy, evaluated by comparison with more recent published analyses of Kilauea and Mauna Loa tholeiite (for example, Casadevall and Dzurisin, chapter 13; Leeman and others, 1977, 1980; Basaltic Volcanism Study Project, 1981; Rhodes, 1983; Hoffman and others, 1984; Budahn and Schmitt, 1985). As will be seen, our reconnaissance data agree well for many elements with analytical results obtained by other laboratories on similar, or, in some cases, the same samples. These data should provide a broader context for the evaluation of recent petrogenetic models of the origin of Hawaiian tholeiite (for example, Hoffman and others, 1984; Wright, 1984; Budahn and Schmitt, 1985), as well as for the design of specific, topical studies to refine our understanding of olivine-controlled basaltic lava.

ACKNOWLEDGMENTS

This study was facilitated by the cooperation, assistance, and encouragement of our colleagues at the Hawaiian Volcano Observatory as well as at the USGS centers in Denver and Reston. Philip J. Aruscavage made the fission-track spark-counting (FTSC) determinations of uranium and performed the instrumental neutron activation analyses of the samples through the gamma-counting step. The staff of the USGS Triga Reactor (Denver) were most helpful in performing neutron irradiations of the samples. Anthony F. Dorrzapf made a special effort to obtain the best possible emission-spectrographic analyses from the semi-quantitative technique used. The cheerful help of Margaret Mangan in the computer reduction and plotting of the analytical results is greatly appreciated. Joseph Arth made available his computer program for plotting chondrite-normalized rare-earth elements, and Thomas Casadevall and Daniel Dzurisin kindly provided us their analytical data on the Uwekahuna Bluff section (Kilauea caldera) prior to their publication in this volume. Rosalind T. Helz and David Gottfried, USGS, reviewed the manuscript and offered constructive criticism and useful suggestions that materially improved the paper; however, any remaining flaws rest solely with us.

PREVIOUS WORK

Pioneering petrologic and chemical studies of Kilauea and Mauna Loa lava include those of Macdonald (1949a, b; 1968), Powers (1955), Tilley and Scoon (1961), Murata and Richter (1966a, b), and Aramaki and Moore (1969). From these and other previous studies, several important conclusions developed: (1) For most of the lava from a given volcano, chemical variations can be largely explained by addition or subtraction of olivine (this is known as olivine control), although some marked exceptions have been noted; (2) systematic petrographic and chemical differences exist between the lavas of these two volcanoes; for example, orthopyroxene commonly occurs in small amounts in Mauna Loa lava but is almost totally absent in Kilauea lava; (3) composition of Kilauea lava during some eruptions varied with time; and (4) variations in composition in space and (or) time may be related to separate and chemically distinct batches of magma.

These observations, based almost exclusively on petrographic and major-element analyses, were comprehensively documented and extended not only for olivine-controlled lava, but also for differentiated and hybrid lavas, by Wright and coworkers (Wright, 1971, 1973; Wright and Fiske, 1971; Wright and others, 1975; Wright and Tilling, 1980). As defined and demonstrated empirically (Wright, 1971; Wright and Fiske, 1971), Hawaiian olivine-controlled lava characteristically has MgO contents greater than 6.80 weight percent, differentiated lava invariably contains less than 6.80, and hybrid lava varies in MgO content depending on the mixture of olivine-controlled and differentiated magmas.

Beginning in the mid-1960's, numerous trace-element and isotopic studies obtained data on Hawaiian tholeiite and other basalt types (for example, Powell and Delong, 1966; Tatsumoto, 1966,1978; Frey and others, 1968; Gast, 1968; Hubbard, 1969; Schilling and Winchester, 1969; Peterman and Hedge, 1971; DePaolo and Wasserburg, 1976; O'Nions and others, 1977). Most pertinent for our present purposes are the studies that contain analytical data on lava from Kilauea and Mauna Loa (for example, Gunn, 1971; Wright, 1971; Leeman and others, 1977, 1980; Rhodes and Lipman, 1979; Easton and Garcia, 1980; Basaltic Volcanism Study Project, 1981; Rhodes and others, 1982; Rhodes, 1983; Budahn and Schmitt, 1985). The significance of trace-element and isotopic constraints on petrogenetic models for the derivation of Hawaiian tholeiite is readily apparent from several recent papers (for example, Clague and Frey, 1982; Frey and Clague, 1983; Staudigel and others, 1984; Wright, 1984). In this paper we will touch briefly on how our reconnaissance data might bear on these models.

SAMPLE SELECTION AND ANALYTICAL TECHNIQUES

SAMPLE SELECTION

Because of the reconaissance nature of this study, the materials analyzed were selected with the following requirements in mind:

(1) Representative sampling of the eruptions of each volcano in space (summit, rift zones, flanks) and in time (prehistoric, 18th–19th centuries, 20th century).

(2) Representative sampling of the range in MgO content, if applicable, for each time-space lava group. This was done in order to compare the variations in trace-element distribution with variations expected from olivine control. Accordingly, the samples chosen for study are predominantly those demonstrated by Wright (1971) from major-element chemistry to be olivine controlled. For comparative purposes, we also selected several samples of differentiated and hybrid lava.

(3) Use of the same rock powders analyzed chemically for previous studies (Wright, 1971; Wright and Fiske, 1971). This permitted direct comparison with published major-element compositions and minimized variation stemming from sample inhomogeneity. Some samples initially chosen could not be studied because none of the original rock powder was available for analysis; where possible, suitable alternative samples meeting the other requirements were substituted. In all, 75 samples (44 from Kilauea, 31 from Mauna Loa) were analyzed by the techniques described below.

ANALYTICAL TECHNIQUES

The concentrations of 28 major, minor, and trace elements (Cs, Rb, Ba, Sr, K, Na, Th, U, La, Ce, Nd, Sm, Eu, Gd, Tb, Dy, Tm, Yb, Lu, Ta, Zr, Hf, Sb, Sc, Mn, Fe, Cr, and Co) were determined using the instrumental neutron activation analysis (INAA) procedure outlined in Zielinski and others (1977) and in Dodge and others (1982). The analytical procedure uses 1.1- to 2.3-g splits of the powdered basalt samples; USGS standard rocks G–2 and CQS–2 (a synthetic standard prepared by adding solutions of the elements of interest to a high-purity quartz powder, drying, and mixing) are used as standards. Sets of the samples and standards are irradiated for 20 min in a neutron flux of 30×10^9 n/cm^2/s, allowed to decay for 1 h: the short-lived nuclides are then gamma-counted twice on a coaxial Ge(Li) detector. The samples and standards are then reirradiated for 8 h in a flux of 3×10^{12} n/cm^2/s and counted on the coaxial Ge(Li) detector and also on a low-energy planar Ge(Li) detector. The counting conditions of our procedure are given in table 24.1. Five separate irradiations were required to analyze the 75 samples, grouped as shown in table 24.2.

A computer is used to calculate the areas under the photopeaks and apply corrections for pulse pileup, decay time, and interfering activities at the same gamma energies caused by other nuclides or by the fission of uranium and thorium. The pulse-pileup correction is computed by comparing the concentrations of iron determined by INAA to those determined by classical rock analysis or X-ray fluorescence techniques. The concentration of an element in the sample is computed by multiplying the concentration in the standard by the ratio of the corrected photopeak area in the sample to that in the standard and by the weight ratio of standard to sample. Values for the various isotopes of each element and for different decay times are weighted according to the reciprocal of the variance based on counting statistics and combined to yield a single concentration for each element.

A direct assessment of the precision and accuracy of our INAA analytical procedure is provided by results for five splits of basalt standard BCR–1 (Columbia River basalt) shown in table 24.3. The accuracy for the determinations of Rb, Sr, Th, Sm, Tb, Tm, and Sb is poor, as is the precision for Gd, Tb, Tm, Ta, and Sb (coefficient of variation >20 percent). Another diagnostic evaluation of our INAA procedure is afforded by interlaboratory comparison of results obtained for Hawaiian tholeiite (tables 24.4, 24.5, 24.6; fig. 24.2). Such comparisons indicate that our rare-earth element (REE) data agree well with published values on the same or similar samples, but the accuracy of our INAA determinations of Th and Zr is unsatisfactory, even though their precision may be acceptable. Our determination of Sm abundance is high relative to other values for the BCR–1 basalt standard (table 24.3) but systematically low compared with reported values for Kilauea and Mauna Loa lava (table 24.2; fig. 24.2). For reasons of poor accuracy and (or) precision, our INAA determinations of Rb, Sr, Zr, Th, U, Sb, Gd, Tb, and Tm are not given in the tabulations of individual analyses (tables 24.9–24.12, 24.15–24.19) despite good agreement for occasional samples (see tables 24.4, 24.5). However, possibly significant qualitative differences in the concentration ranges and averages of some of the determinations with poor precision, but with acceptable accuracy, are noted where appropriate. The INAA results for the major elements Na, K, Fe, and Mn, which accord well with values determined previously by classical rock analysis (Wright, 1971), are not reported.

The abundances of V, Ni, Cu, Mo, Zn, Ga, Nb, Y, and Pb reported were determined by a computerized emission-spectrographic (ES) technique described by Dorrzapf (1973). Even though this method is only semiquantitative in approach, results for some of the reported elements compare favorably with values determined by quantitative techniques (tables 24.4, 24.5). According to Dorrzapf (1973, p. 561), the precision of the technique "is within the range of +50 to −30 percent of the amount present***and approaches +10–15 percent for many elements***." However, strong biases were observed for some elements (for example, Nb) that exceeded this stated uncertainty.

Comparison of available data (tables 24.4, 24.5) indicates that the emission-spectrographic determinations of Zn and Pb appear to be accurate, but the values for Cu and Nb are low compared to determinations by more quantitative techniques (table 24.4; Gunn, 1971, table 1). Fair agreement exists between the available reported analyses of V, Ni, Ga, and Y, despite wide scatter in data stemming from differences in techniques, samples analyzed, possible laboratory biases, and other factors. Other than the analyses of standard BHVO–1, we know of no published data for Mo concentration in Hawaiian tholeiite to compare with our results. Thus, we have excluded the determinations of Cu and Nb in the individual analyses, but have retained the other emission-

TABLE 24.1.—*Instrumental gamma-counting conditions for neutron-activation analysis*

[Efficiency of coaxial GE(Li), 10 percent; area of planar Ge(Li), 0.785 cm²]

	Coaxial Ge(Li)			Planar Ge(Li)		
Decay time	Source-detector distance	Counting time (min)	Resolution (eV FWHM at 1,333 keV)	Source-detector distance	Counting time (min)	Resolution (eV FWHM at 122 keV)
1-5 h	6.0	16.7	2,000	--	--	500
7 d	6.0	16.7	2,000	3.0	16.7	500
14 d	3.0	33.3	2,000	3.0	33.3	500
60 d	.5	167	2,000	1.0	167	500

TABLE 24.2.—*Number of samples of spatial and temporal basalt groups irradiated and analyzed by neutron activation*

[Basalt groups: SUM, summit; ERZ, east rift zone; SWRZ, southwest rift zone; NERZ, northeast rift zone; FLKS, northwest and southwest flanks; DIFF, differentiated; P, prehistoric; T, 18th and 19th centuries; H, 20th century]

	Irradiations				
Basalt group	TIL973	TIL008	TIL694	TIL746	TIL997
			Kilauea		
SUM	1	10	1	1	7
ERZ	3	0	0	3	7
SWRZ	0	1	3	7	0
P	1	4	0	9	3
T	0	0	2	2	4
H	3	7	2	0	7
			Mauna Loa		
SUM	1	0	0	1	3
SWRZ	1	3	1	4	1
NERZ	0	0	4	0	0
FLKS	0	4	1	2	0
DIFF	1	0	4	0	0
P	2	4	3	3	1
T	1	1	5	2	2
H	0	2	2	2	1

TABLE 24.3.—*Comparison of elemental composition by neutron-activation analyses (INAA) of five splits of USGS standard rock BCR-1 and previously published values*

[--, value not given in publication]

Element	Mean (ppm)	INAA results: Coefficient of variation (percent of mean)	Published values (ppm): Gladney and others (1983)	Published values (ppm): Abbey (1983)
Cs	0.98	7	0.97	0.96
RB	62	11	47.1	47
Ba	700	7	678	680
Sr	450	4	330	330
K	14,440	9	14,000	14,000
Na	23,600	1	24,300	24,500
Th	5.6	3	6.04	6.1
U	1.95	12	1.71	1.7
La	25.6	4	25.0	27
Ce	51.9	6	53.7	53
Nd	30.8	5	28.7	--
Sm	7.6	9	6.58	6.5
Eu	2.05	4	1.96	2.0
Gd	7.3	21	6.68	--
Tb	1.3	28	1.05	1.0
Dy	5.9	11	6.35	--
Tm	.4	39	.59	--
Yb	2.9	9	3.39	3.4
Lu	.57	10	.512	--
Ta	.79	25	.79	--
Zr	220	12	191	185
Hf	4.9	7	4.9	5
Sb	.4	61	.62	.6
Sc	33	5	32.8	33
Mn	1,405	1	1,410	1,400
Fe	93,200	4	93,800	94,000
Cr	18	12	16	15
Co	36	1	36.3	36

TABLE 24.4.—*Average compositions of samples from 20th-century Kilauea summit eruptions compared with standard basalt BHVO-1 from 1919 eruption*

[MgO and K_2O reported in weight percent; other values all ppm. --, value not given in publication. Samples from 20th-century eruptions adjusted to 7.00 weight percent MgO]

	Standard basalt BHVO-1 1919 eruption, Kilauea summit				20th-century Kilauea summit eruptions			
	1	2	3	4	5 n=4	6 n=5	7 n=7	8 n=2
MgO	6.95	7.3	7.31	7.00	7.00	7.00	7.00	7.00
K_2O	.52	.46	.54	.54	.55	.55	.52	.55
Rb	15	--	10	10.1	14.4	--	11.0	9.1
Cs	--	--	* .15	.15	.19	--	--	.10
Sr	--	445	420	423	360	--	386	370
Ba	185	150	135	136	146	114	136	128
Sc	33	30	31	31.2	32.1	30	32.3	--
V	--	328	*320	322	315	--	--	--
Cr	290	266	300	279	200	--	182	--
Co	46	44	45	43.8	43.4	--	--	--
Ni	--	110	120	101	56	--	--	--
Cu	--	--	140	141	65	--	--	--
Mo	--	--	* 1	1.0	4.3	--	--	--
Zn	--	--	105	105	130	--	--	--
Ga	--	--	* 21	21.2	18.6	--	22.5	--
Zr	--	200	180	181	202	--	158	--
Hf	--	4.5	4.3	4.3	4.2	--	4.5	--
Nb	--	--	19	19.2	7.9	--	--	--
Ta	1.1	1.3	* 1.1	1.1	1.1	--	--	--
Y	--	--	* 27	27.2	18.5	--	25	--
Th	--	1.0	1.0	1.0	1.5	--	1.3	--
U	--	.3	* .4	.40	.44	--	--	--
Pb	--	--	--	--	2.1	--	[a]6	--
Sb	--	--	* .17	.17	.18	--	--	--
La	15.0	15.0	* 17	17.1	15.4	16.6	14.9	--
Ce	37	39.0	39	39.3	39.9	39.2	37.2	--
Nd	24	25.5	24	24.2	24.2	23.3	--	--
Sm	6.2	6.37	6.1	6.15	5.51	6.2	6.12	--
Eu	2.10	2.05	2.0	2.02	1.99	2.13	1.99	--
Gd	--	--	6.0	6.05	8.08	--	--	--
Tb	.9	.91	* 1.0	1.01	.74	.93	.95	--
Dy	--	5.2	* 5	5.0	5.1	5.2	5.6	--
Tm	--	--	* .3	.30	.55	--	--	--
Yb	2.08	1.97	1.9	1.92	1.93	2.03	2.04	--
Lu	.30	.28	--	--	.24	.29	.30	--

1 Frey (1980, table 1).
2 Budahn and Schmitt (1985, table 1).
3 Govindaraju (1984, appendix 1; * denotes proposed value only).
4 Values in (3) adjusted to 7.00 weight percent MgO.
5 This paper (1959 and 1967-68 eruptions).
6 Budahn and Schmitt (1985, table 2; 1924, 1952, 1954, 1961, 1967 eruptions).
7 Basaltic Volcanism Study Project (1981, tables 1.2.6.2. and 1.2.6.3; 1921, 1924, 1954, 1959, 1971, and 1974 eruptions).
8 Hoffman and others (1984, table 2; 1968 eruption).
[a]Value seems high; Tatsumoto (1978) reports isotope-dilution values of 1.32-2.03 ppm for Kilauea historical eruptions.

TABLE 24.5.—*Interlaboratory comparison of analyses of samples of Mauna Loa lava*

[MgO and K_2O reported in weight percent; other values all ppm. R, Rhodes (1983), average of n samples; BSVP, Basaltic Volcanism Study Project (1981); BS, Budahn and Schmitt (1985); T, this paper; --, not given in publication or not analyzed. For some comparisons, the same sample was analyzed, for others, different samples of the same eruption]

	Prehistoric						1859			1868		
	BS (TLW 67-29)	T	BS (TLW 67-70B)	T	BS (TLW 67-119)	T	R (n=6)	BSVP (HAW-4)	T (DPH-77)	R (n=8)	BSVP (HAW-5)	T (1868ML)
MgO	6.3	6.99	7.4	6.93	6.6	6.74	8.68	7.25	7.75	17.69	21.02	23.64
K_2O	.40	.42	.43	.46	.43	.46	.39	.42	.43	.31	.27	.26
Rb	-	16.9	21.7	-	-	-	-	6.9	-	-	4.4	9.2
Sr	349	273	361	445	383	419	324	344	461	249	213	207
Ba	85	140	91	92	120	94	-	-	147	-	70	108
Sc	28	29.4	29	30.3	29	29.3	-	29.5	28.7	-	21	20.9
V	279	311	290	297	291	293	252	-	305	200	-	202
Cr	222	224	237	248	185	183	458	350	278	1,040	1,405	1,250
Co	40	41.9	40	43.0	40	38.6	-	-	-	-	-	-
Ni	105	88	85	84	100	75	166	-	98	771	-	846
Zn	-	133	-	111	-	128	112	-	113	110	-	106
Ga	-	19.3	-	17.4	-	21.3	-	20	15.6	-	14	8.4
Zr	95	179	95	148	115	141	129	129	181	101	88	142
Hf	3.6	3.3	3.6	3.6	3.4	3.0	-	3.48	3.3	-	2.38	2.0
Nb	-	3.0	-	6.1	-	-	9.9	9	2.2	7.8	6	2.2
Ta	.6	.38	.7	.35	.7	.53	-	-	-	-	-	-
Y	-	19.2	-	19.6	-	17.1	-	23	19.6	-	15	8.5
Th	.4	.57	.4	.9	.45	.78	-	.56	.7	-	.34	.9
U	.1	.22	.1	.23	.1	.23	-		.192	-	-	-
Pb	-	1.0	-	2.4	-	2.0	-	<1	2.0	-	4	3.0
La	9.8	9.4	10.9	10.4	10.6	10.3	-	9.38	8.8	-	6.16	5.68
Ce	26.1	25.9	28.7	28.7	26.8	24.8	-	25.0	25.9	-	16.4	12.5
Nd	20	19.5	21	18.0	20	17.0	-	-	-	-	-	-
Sm	4.88	4.57	5.41	5.10	5.20	4.42	-	4.80	4.77	-	3.30	2.67
Eu	1.78	1.63	1.85	1.83	1.79	1.52	-	1.70	1.72	-	1.10	.99
Tb	.77	1.42	.80	.72	.79	1.91	-	.81	.24	-	.54	.38
Dy	4.8	5.0	5.0	5.2	4.7	4.6	-	-	-	-	-	-
Yb	1.99	1.92	1.99	1.88	2.00	2.03	-	2.00	1.75	-	-	-
Lu	.23	.23	.25	.26	.27	.29	-	.29	.25	-	.20	.15

	1887				1899		1907		1919	
	R (n=12)	BVSP HAW-6	BS (TLW 67-59)	T	R (n=5)	BS (TLW 67-65)	R (n=10)	BS (TLW 67-56)	BS (TLW 67-77)	T H-34
MgO	8.16	8.53	7.1	7.50	7.28	7.5	7.38	7.3	7.3	7.09
K_2O	.33	.33	.30	.33	.35	.35	.36	.37	0.36	0.35
Rb	-	4.9	-	-	-	-	-	-	-	6.0
Sr	281	273	294	350	299	280	305	250	305	235
Ba	-	75	65	134	-	60	-	50	80	116
Sc	-	29.5	28	30.3	-	29	-	30	29	29.6
V	248	-	261	335	263	282	258	282	280	362
Cr	378	480	285	260	310	235	300	260	240	237
Co	-	-	44	46.2	-	43	-	43	42	42.8
Ni	144	-	75	83	100	75	119	125	100	90
Zn	112	-	-	119	117	-	111	-	-	-
Ga	-	20	-	16.6	-	-	-	-	-	20.7
Zr	121	119	120	74	131	160	131	150	120	146
Hf	-	3.34	2.9	3.0	-	3.6	-	3.3	3.6	3.2
Nb	8.7	8	-	3.9	9.3	-	9.1	-	-	-
Ta	-	-	.55	.30	-	.6	-	.5	.5	.5
Y	-	23	-	21.2	-	-	-	-	-	23.9
Th	-	.50	.35	.84	-	.3	-	.4	.6	1.0
U	-	-	< .1	.148	-	.1	-	.2	.2	.286
Pb	-	6	-	2.3	-	-	-	-	-	-
La	-	7.58	8.0	7.8	-	8.5	-	8.6	8.8	8.6
Ce	-	21.0	22.1	21.4	-	23.6	-	23.5	23.4	18.8
Nd	-	-	17	16.2	-	19	-	19	20	16.0
Sm	-	4.40	4.60	-		4.87	-	4.85	4.79	4.20
Eu	-	1.60	1.64	1.51	-	1.75	-	1.75	1.70	1.45
Tb	-	.84	.74	.67	-	.74	-	.79	.76	.55
Dy	-	-	4.6	5.0	-	4.0	-	4.4	4.6	4.34
Yb	-	1.98	1.92	2.02	-	1.99	-	2.03	2.00	2.00
Lu	-	.29	.25	.28	-	.25	-	.28	.25	.26

TABLE 24.5.—*Interlaboratory comparison of analyses of samples of Mauna Loa lava*—Continued

	1926			1935		1942				1950				
	R (n=6)	BSVP HAW-8	T TLW67-67	R (n=6)	BS TLW67-67	R (n=8)	BS TLW67-62	T TLW67-62 (NE rift)	BS TLW67-68 (Summit)	R (n=12)	BSVP (HAW-10)	BS (TLW67-73)	T	T (TLW67-79)
MgO	7.39	7.90	7.82	6.99	7.1	7.10	8.8	7.21	7.1	8.17	8.99	7.0	6.87	9.22
K_2O	.37	.37	.35	.37	.37	.37	.38	.36	.32	.38	.35	.41	.37	.36
Rb	-	5.4	-	-	-	-	-	22.9	-	-	5.2	-	-	5.7
Sr	312	302	374	316	260	313	330	483	350	306	294	285	240	177
Ba	-	82	110	-	70	-	60	241	70	-	72	100	143	58
Sc	-	30.4	30.3	-	29	-	30	30.9	29	-	29.0	29.0	31.0	28.6
V	264	-	317	268	283	265	278	309	282	287	-	282	337	311
Cr	301	390	277	275	250	291	300	270	260	369	490	220	202	395
Co	-	-	47.1	-	42	-	43	45.0	43	-	-	43	44.9	49.7
Ni	112	-	145	86	90	91	75	76	85	170	-	105	82	131
Zn	117	-	104	117	-	116	-	135	-	114	-	-	114	126
Ga	-	20	19.0	-	-	-	-	20.4	-	-	19	-	20.4	18.2
Zr	134	123	185	133	120	132	200	169	-	132	121	150	174	174
Hf	-	3.45	3.0	-	3.3	-	3.6	3.3	3.3	-	3.43	3.3	2.8	2.8
Nb	9.5	8	4.5	9.4	-	9.6	-	-	-	9.6	8	-	5.4	5.4
Ta	-	-	-	-	.6	-	.6	.27	.6	-	-	.5	.40	-
Y	-	23	21	-	-		-	16.0	-	-	23	-	20.40	18.8
Th	-	.58	.59	-	.4	-	.3	1.0	.4	-	.55	.4	.60	.70
U	-	-	-	-	.1	-	.2	.160	.2	-	-	.2	.177	.194
Pb	-	3	3.1	-	-	-	-	-	-	-	5	-	3.1	2.8
La	-	8.81	8.8	-	8.8	-	8.8	8.86	8.8	-	8.52	8.9	9.00	7.5
Ce	-	23.3	23.4	-	24.5	-	24.6	22.9	23.2	-	22.5	23.8	23.3	18.8
Nd	-	-	-	-	17	-	19	16.3	19	-	-	19	16.8	16.2
Sm	-	4.97	4.44	-	4.85	-	4.86	4.53	4.88	-	4.85	5.00	4.36	3.97
Eu	-	1.61	1.61	-	1.71	-	1.73	1.57	1.68	-	1.55	1.75	1.67	1.26
Tb	-	.80	-	-	.71	-	.74	.90	.75	-	.86	.75	.56	.58
Dy	-	-	-	-	4.3	-	5.4	5.15	4.4	-		4.6	5.9	4.7
Yb	-	2.07	1.88	-	1.83	-	1.96	1.89	1.97	-	2.00	2.08	2.01	1.94
Lu	-	.30	.28	-	.27	-	.27	.25	.28	-	.29	.31	.29	.24

TABLE 24.6.—*Interlaboratory comparison of selected elements in analyses of lava samples from Kilauea Iki and Kapoho*

[MgO and K_2O reported in weight percent; other values all ppm. Gunn (1971, table I), average of n samples; BVSP, Basaltic Volcanism Study Project (1981); T, this paper. --, not given or not analyzed]

	Kilauea Iki									Kapoho	
	Iki-22, 11/18/59			Iki-42, 11/16/59		Iki-5, 11/21/59		Iki-12, 12/4/59		KP-25, 2/13/60	
	G (KI0022) (n=2)	BSVP (HAW-23)	T (S-5)	G (KI0053) (n=2)	T (S-3)	G (KI0051) (n=3)	T (S-8)	G (KI0016)	T (S-14)	BSVP (HAW-26)	T (F-17)
MgO	19.30	18.90	19.55	8.21	8.85	9.54	10.45	8.68	8.55	13.62	13.16
K_2O	.38	.38	.35	.54	.50	.51	.54	.55	.53	.49	.49
Sr	246	270	290	340	394	330	262	357	253	310	404
Ba	130	115	75	175	126	169	198	178	174	135	230
Sc	--	25.0	24.4	--	31.2	--	28.1	--	29.5	27.1	27.3
Cr	1,150	1,550	1,170	373	407	497	369	386	256	710	440
Co	95.4	--	85.1	56.7	50.8	61.4	56.6	59.6	49.8	--	65.5
Ni	812	--	542	126	168	211	170	190	149	--	269
Zn	99	--	116	102	123	100	127	105	120	--	--
Ga	11.8	--	9.3	17.4	16.9	16.2	14.6	18.9	19.6	--	15.6
Zr	--	118	145	--	--	--	--	--	--	159	158
Hf	--	3.15	3.0	--	--	--	--	--	--	4.62	3.8
Y	17.4	17	10.1	24.5	15.6	23.2	13.9	24.3	18.0	23	13.5
La	--	11.5	11.1	--	15.0	--	15.1	--	14.7	14.9	15.2
Ce	--	27.6	24.1	--	31.8	--	41.5	--	42.0	36	35.8
Sm	--	4.50	3.78	--	5.10	--	5.11	--	5.23	5.80	--
Eu	--	1.39	1.34	--	2.01	--	1.88	--	1.83	1.92	--
Yb	--	1.40	1.36	--	1.84	--	1.83	--	2.07	1.95	2.05
Lu	--	.21	.17	--	.22	--	.35	--	.21	.28	.31

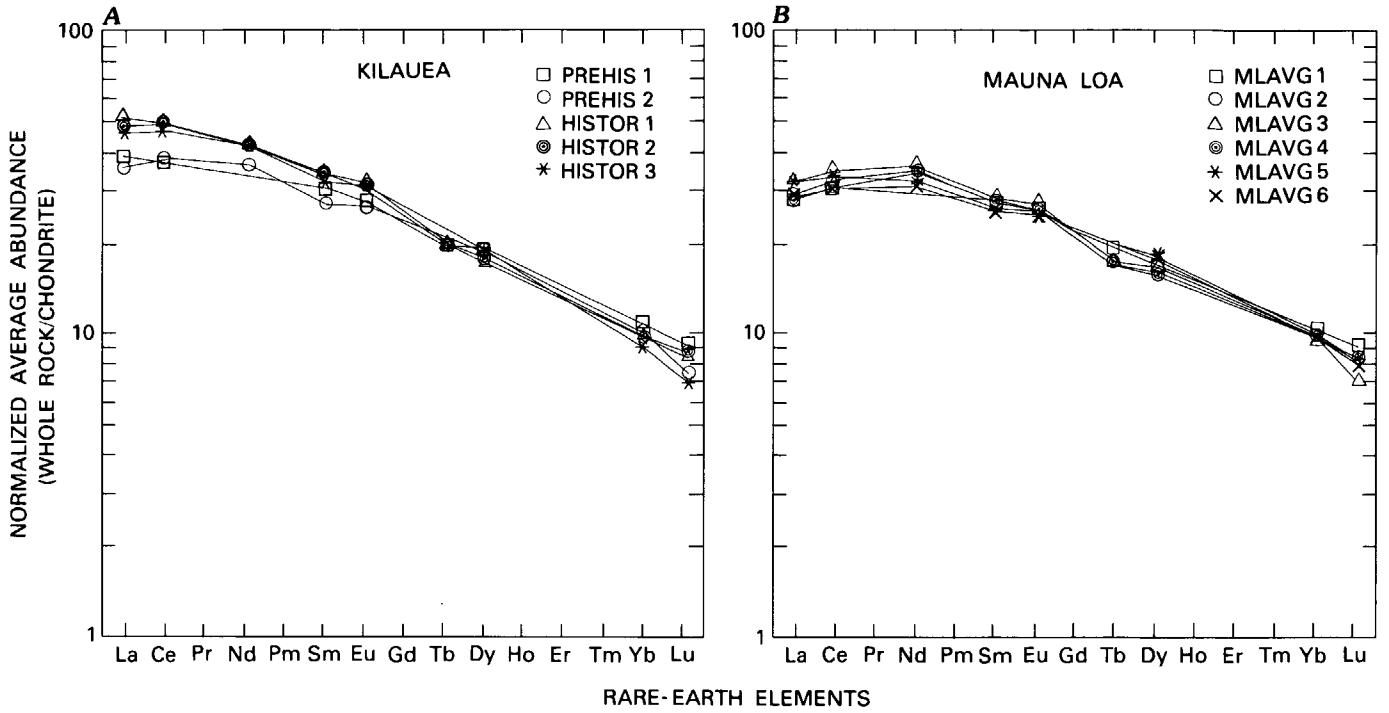

FIGURE 24.2.—Interlaboratory comparisons of MgO-adjusted average chondrite-normalized REE abundances. Patterns for data from this paper in this and subsequent figures reflect the systematic, slightly lower determination of Sm abundance in our INAA procedure relative to reported values for Hawaiian tholeiite (see table 24.4). ***A***, Kilauea samples. Prehistoric lava: PREHIS1, Budahn and Schmitt (1985); PREHIS2, this paper. Historical lava: HISTOR1, Budahn and Schmitt (1985); HISTOR2, Leeman and others (1980); HISTOR3, this paper. ***B***, Mauna Loa samples. Prehistoric lava: MLAVG3, Budahn and Schmitt, 1985; MLAVG5, this paper. Prehistoric and historical combined: MLAVG2, Leeman and others, 1980. Historical lava: MLAVG1, Basaltic Volcanism Study Project, 1981; MLAVG4, Budahn and Schmitt, 1985; MLAVG6, this paper.

spectrographic determinations (V, Ni, Mo, Zn, Ga, Y, and Pb.) In any case, systematic relative differences in the variations of some of these elements clearly reflect olivine control and suggest that their more precise determination by quantitative methods might prove to be important in subsequent studies.

Uranium concentrations we report were determined by a modification of a fission-track spark-counting technique (FTSC) first published by Cross and Tommasino (1970). Because this particular FTSC procedure has not been described previously, it is outlined in detail here. The method involves the etching of fission tracks recorded in a thin plastic detector until they become holes, which are then counted rapidly by sparking across them. A thin aluminum film is used as one of the electrodes and is destroyed behind each hole as the spark passes through, thus preventing multiple sparking through the same hole.

The specific FTSC procedure used in this study was adapted from that of Bertine and others (1970). Pellets of 0.25-inch diameter are prepared from cellulose powder (ion-exchange grade) in a pellet press. About 50 mg of sample powder is then pressed onto the top of the pellet at 34.5 MPa (5,000 psi); duplicate pellets are prepared for each sample. Standards are prepared from Dowex 1×8 anion-exchange resin that has been loaded with uranium from a $7N$ HNO_3 solution and calibrated against USGS standard basalt BCR–1 using the delayed neutron counting technique (Millard and Keaten, 1982). Double-sided adhesive tape is affixed to the top of a cellulose pellet and the resin sprinkled on top, creating a monolayer of resin beads. Pieces of 2.5×7.6 cm (1×3 in) of Lexan foil (Kimfoil, 10 μm thick) are pressed against the top of each standard and sample pellet, and this assembly is irradiated with a neutron dose of 1×10^{14} n/cm^2. This dose yields about 500 holes/ppm U and keeps the density of the holes below the upper limit for counting of 3,000 holes/cm^2. Following irradiation, the foils are etched for 30 minutes at 70 °C with $7N$ NaOH to produce holes of 2μm to 3μm diameter and then placed in the spark-counting apparatus.

The counting apparatus consists of a brass upper electrode 1 cm in diameter, an aluminum-coated Mylar lower electrode, a high voltage supply, an amplifier, and a scaler. The electrical circuit contains appropriate capacitors and resistors to shape the pulses from the sparks and to provide time for recovery after each spark. A presparking is performed at 800 V to enlarge the holes to 8 μm diameter, and then the foil is moved and the actual counting performed at 500 V. The counting is completed in less than a minute and can be repeated by simply moving to a new place on the Mylar. The accuracy and precision of the technique are shown in table 24.7 and discussed below.

The results obtained by the FTSC method proved to be considerably better than our INAA determinations for uranium. The accuracy and precision of the technique are good (table 24.7);

TABLE 24.7.—*Accuracy and precision of fission-track spark counting determination of uranium in replicates of USGS standard rocks and the Hinsdale Formation basalt*

Sample	Uranium content by fission-track spark counting			Published values (ppm)		
	Replicate analyses (ppm)	Mean (ppm)	Coefficient of variation (percent of mean)	Gladney and others (1983)	Abbey (1983)	Others
PCC-1	0.0038 .0054 .0030 .0019 .0035	0.0035	37	0.0045±0.0007	--	--
DTS-1	.0053 .0043 .0043 .0023 .0042	.0041	27	.0036±0.0005	--	--
BHVO-1	.45 .46 .50 .53	.49	8	--	--	[1].42±0.06
Basalt of Hinsdale Formation	.93 .95 .76 .69	.83	16	--	--	[2].88
BCR-1	1.66 1.76 1.76 1.68	1.72	3	1.72±0.6	1.71	1.7
GSP-1	2.42 2.45 2.20 2.34	2.35	5	2.2±0.3	2.1	--

[1]Gladney and Goode (1981).
[2]Isotope-dilution mass spectrometry (Doe and others, 1969).

the relative precision at the average level of concentration in the samples analyzed (about 0.2 ppm) should be about 10 percent or better. The mean relative difference between duplicate determinations of uranium in basalt samples of this study is 6.4 percent.

Conservative estimates of the analytical uncertainties for the concentrations of the elements analyzed in this study are given in table 24.8. The analytical data for the lava suites studied are given in tables 24.9–24.12 and 24.15–24.19 and plotted in magnesia-variation diagrams (figs. 24.4, 24.5, 24.10). Unless noted otherwise, all major-element data (water-free basis) for Kilauea and Mauna Loa lava appearing in tables and plots in this paper are from Wright (1971) or Wright and Fiske (1971), who also summarize other pertinent information on the samples studied. Our data set covers Kilauea eruptions through the 1967–68 activity at Halemaumau, and Mauna Loa eruptions through the 1950 eruption on its southwest rift zone.

TABLE 24.8.—*Estimated uncertainties of the trace-element determinations for Hawaiian basalt samples*

[Analytical methods: INAA, instrumental neutron-activation analysis; ES, emission spectrography; FTSC, fission-track spard counting. Uncertainties for INAA values based on counting statistics only. n.d., not determined]

Element	Uncertainty (percent of determined value)		
	Range	Mean	Analytical method
Rb	10-30	22	
Cs	10-30	20	INAA
Sr	10-30	15	
Ba	10-30	16	
Sc	1-5	3	INAA
V		10-15?	ES
Cr	10-25	15	INAA
Co	1-3	2	INAA
Ni			
Cu			
Mo		10-15	ES
Zn			
Ga			
Zr	1-10	3	INAA
Hf	1-10	3	INAA
Nb		10-15?	ES
Ta	1-15	6	INAA
Y		10-15?	ES
Th	5-30	9	INAA
U		<10	FTSC
Pb		10-15?	ES
Sb	10-50	28	INAA
La	1-5	3	
Ce	1-10	4	
Nd	1-15	7	
Sm	1-5	2	
Eu	1-15	4	
Gd	5-20	11	INAA
Tb	n.d.	n.d.	
Dy	1-10	3	
Tm	n.d.	n.d.	
Yb	1-10	4	
Lu	1-10	5	

KILAUEA LAVA

Trace-element determinations for Kilauea lava samples are given in tables 24.9–24.12. Most elements listed are conservatively judged to be of good accuracy and precision, but a few determinations of adequate accuracy but poorer precision (for example, Cs and Ba) are also included.

To facilitate the comparison of differences between various olivine-controlled lava suites, we utilize average compositions computed after the individual analyses are adjusted to 7.00 weight percent MgO (see appendix 24.1) to eliminate the elemental differences stemming from variation in olivine content only (fig. 24.3). In the computation of these average MgO-adjusted compositions, we omit all differentiated samples (<6.8 weight percent MgO), even though Wright (1971) and Wright and Fiske (1971) included a few whose compositions fall within the range of summit (that is, olivine-controlled) lava.

The relatively large scatter in data points in some of the MgO-variation diagrams reflects both analytical uncertainty and compositional differences not accounted for by olivine control alone. As will be seen, these compositional differences appear to vary with space and, especially, time. One of the best examples of olivine-controlled lava is afforded by the tholeiite erupted during the November–December 1959 eruption of Kilauea Iki, which, however, is not typical of Kilauea summit eruptions (see Wright, 1973). Data for the Kilauea Iki lava will be treated separately and contrasted with those of the differentiated and hybrid lavas of the January–February 1960 eruption (fig. 24.5; table 24.12).

VARIATION IN SPACE

Within analytical uncertainty, the MgO-adjusted mean trace-element compositions of the olivine-controlled lava of Kilauea's summit (SUM) and its southwest rift zone (SWRZ) are similar (table 24.13), consistent with earlier observations based on major-element data (Wright, 1971). The apparent low adjusted means for Ni and Cr for lava of Kilauea's east rift zone (ERZ), relative to those of the SUM and SWRZ (table 24.13), are inconsistent with the raw data (fig. 24.4) and reflect the unsatisfactory MgO adjustment for these two elements discussed in appendix 24.1. However, if Ni and Cr are not considered, the mean composition of the ERZ lava is characterized by generally higher abundances of olivine-incompatible elements relative to those of summit lava. Differences between many of the means are small and, strictly speaking, not statistically significant, but we are impressed by their nonrandom nature (fig. 24.6).

Because these nonrandom, subtle differences are within analytical uncertainty, it is appropriate to ask whether they might have been introduced by nonrandom grouping of samples preparatory to the five separate irradiations required to analyze the 75 samples. However, in almost all cases, samples belonging to each lava grouping—whether according to space (vent location) or to time (prehistoric, 18th–19th centuries, 20th century)—were spread over two or more irradiations, and only rarely did one irradiation contain appreciably more than half of the samples from one category

TABLE 24.9.—*Composition of olivine-controlled tholeiite of Kilauea's summit.*

[Oxide values (in weight percent) from Wright (1971, table 4), recast to 100 percent dry weight; values for elements in parts per million]

	Prehistoric						Historical					
	Hilina Basalt			Puna Basalt			18th–19th centuries		20th century			
									1959		1967–68 eruption	
Sample	57F-15	57F-17	57F-97	8X078-0	8X067-0	8X002-0	1790	1866(?)	S-1	S-2	1967HM	HM68-15
SiO_2	48.53	49.43	50.79	48.07	49.19	51.17	50.64	50.05	50.04	50.05	50.40	50.30
MgO	15.17	10.97	8.14	17.06	13.26	6.95	8.31	6.61	8.10	7.23	7.61	7.64
K_2O	.33	.38	.38	.31	.30	.46	.45	.50	.55	.60	.54	.55
TiO_2	1.91	2.21	2.51	1.98	2.00	2.44	2.64	2.70	2.63	2.75	2.66	2.62
P_2O_5	.18	.22	.24	.18	.17	.24	.25	.26	.25	.28	.26	.26
Cs	.15	.00	.16	.19	.30	.03	.12	.76	.21	.22	.00	.14
Ba	161.00	77.00	72.00	79.00	129.00	43.00	65.00	150.00	158.00	164.00	159.00	94.00
Sc	26.80	29.90	29.40	25.40	28.50	29.10	28.90	31.20	31.60	30.40	32.60	31.60
V	.00	254.00	.00	205.00	278.00	287.00	282.00	308.00	296.00	300.00	318.00	327.00
Cr	707.00	485.00	299.00	889.00	819.00	357.00	291.00	195.00	251.00	148.00	295.00	283.00
Co	75.20	61.40	45.60	79.70	65.70	41.80	47.90	43.40	45.00	44.70	46.70	46.70
Ni	.00	131.00	.00	490.00	278.00	90.00	121.00	72.00	104.00	80.00	89.00	106.00
Mo	.00	4.00	.00	4.20	6.00	4.50	3.30	3.90	4.90	4.10	3.60	4.10
Zn	.00	124.00	.00	131.00	122.00	125.00	129.00	133.00	143.00	137.00	107.00	128.00
Ga	.00	13.10	.00	10.80	13.80	17.40	18.80	17.60	16.00	18.20	19.10	19.90
Hf	2.90	3.40	3.40	3.10	3.10	3.20	3.50	4.20	3.70	4.20	4.30	4.20
Y	.00	15.40	.00	11.50	14.10	17.00	17.70	19.70	16.40	19.10	17.80	19.50
U	.41	.71	.52	.21	.33	.17	.34	.47	.48	.51	.37	.35
Pb	.00	1.20	.00	1.70	1.60	2.00	2.10	1.60	1.10	1.40	2.50	3.50
La	9.60	9.90	10.60	9.00	8.90	8.40	11.40	13.20	14.70	16.10	15.20	14.60
Ce	26.70	26.90	30.30	21.60	21.40	18.50	29.20	38.20	44.00	42.10	34.90	35.70
Nd	18.00	17.60	17.50	14.50	15.20	16.00	21.50	22.70	24.50	25.60	21.60	23.30
Sm	3.86	4.35	4.28	4.04	3.98	4.10	5.25	5.50	4.71	5.65	5.73	5.60
Eu	1.41	1.66	1.79	1.63	1.54	1.68	1.71	2.00	1.88	1.94	2.05	1.99
Dy	.00	3.60	6.00	4.60	3.90	4.30	.00	5.40	4.50	5.30	4.00	6.20
Yb	1.55	1.92	1.98	1.77	1.82	1.93	2.02	1.86	1.89	1.97	1.66	2.08
Lu	.34	.21	.29	.23	.20	.27	.27	.26	.19	.26	.28	.25

(table 24.2). Therefore, we believe that the observed minor but systematic differences (table 24.13; fig 24.6) cannot be ascribed to nonrandom sample groupings during irradiations. Such small intravolcano systematic differences between eruption loci on the volcano have not been observed or considered in previous studies (for example, Leeman and others, 1980; Budahn and Schmitt, 1985), which were based on more limited sampling and emphasized the larger intervolcano variations between Kilauea and Mauna Loa.

The relatively higher content of olivine-incompatible elements in the ERZ lava is even better illustrated by reference to the SWRZ samples (fig. 24.6) and by REE patterns (fig. 24.7*A*). The sole exception is the ratio for uranium, which is less than unity, offset from the range of other ratios, and yet varies sympathetically with them. The apparent departure in the behavior of uranium relative to other olivine-incompatible elements is not understood. Analytical bias probably is not the explanation, because the uranium appears to be as accurately determined as the other elements (see tables 24.3, 24.4, 24.7). The explanation may be related in part to unrepresentative sampling of ERZ lava, thus resulting in a biased mean. The mean computed for the ERZ is based only on data for older (prehistoric and 18th–19th centuries) lavas, which are low in uranium compared to 20th century lava (tables 24.10; fig. 24.4).

Major-element studies have shown that differentiated lava is more prevalent in the ERZ than elsewhere at Kilauea (Wright, 1971; Wright and Fiske, 1971; Moore, 1983). Our trace-element data also indicate that the olivine-controlled lava of the ERZ is more fractionated, as compared to the olivine-controlled lava of the SUM and, especially, the SWRZ. Even though eruptions in the ERZ and the SWRZ are fed from a common shallow (2–6 km deep) reservoir beneath Kilauea summit, these two rift zones intrinsically differ in topographic expression, structural setting, and eruption frequency during the past 2,000 years (see, for example, Swanson and others, 1976b; Holcomb, 1980, 1981; Duffield and others, 1982; Moore, 1983). The volume of magma intruded into and erupted in the ERZ is estimated to be more than two orders of magnitude greater than that of the SWRZ. Moreover, geophysical studies have demonstrated the existence of several secondary magma reservoirs in the ERZ (see, for example, Jackson and others, 1975; Swanson and others, 1976a; Zablocki and Koyanagi, 1979; Moore, 1983). Thus, the more differentiated and hybridized compositions of the ERZ lava may simply reflect greater opportunity for magma fractionation and mixing because of the following: (1) More voluminous and frequent transfers of magma from the summit reservoir into the ERZ relative to the SWRZ; (2) longer uninter-

TABLE 24.10.—*Composition of olivine-controlled tholeiite of Kilauea's east rift zone*

[Oxide values (in weight percent) from Wright (1971, table 6) for prehistoric samples, and from Wright and Fiske (1971, table 4) for historical samples, recast to 100 percent dry weight; values for elements in parts per million. Samples TLW67-130 and TLW68-6 fit definition of differentiated (less than 6.80 weight percent MgO) and are omitted in calculation of averages and not plotted in figure 24.4]

	Prehistoric				Historical			
					18th–19th centuries			
					1790?	1840		
Sample	TLW67130	TLW67131	TLW67132	MP-57	H-23	TLW68-5	TLW68-6	TLW68-12
SiO_2	50.72	49.45	50.37	50.12	50.96	50.62	51.21	48.08
MgO	6.13	10.05	8.08	8.73	7.16	9.35	6.03	17.54
K_2O	.51	.52	.45	.41	.44	.40	.55	.33
TiO_2	2.92	2.67	2.53	2.53	2.71	2.32	3.06	1.92
P_2O_5	.28	.25	.23	.24	.25	.25	.30	.18
Cs	.26	.28	.14	.11	.19	.17	.12	.16
Ba	137.00	140.00	157.00	163.00	189.00	130.00	165.00	110.00
Sc	30.20	29.60	31.80	27.90	32.50	31.50	32.30	25.40
V	344.00	337.00	308.00	377.00	373.00	304.00	400.00	244.00
Cr	83.00	419.00	335.00	281.00	179.00	405.00	47.00	812.00
Co	43.30	55.00	50.40	47.40	48.80	55.60	49.00	82.70
Ni	57.00	196.00	112.00	146.00	99.00	167.00	62.00	512.00
Mo	4.80	4.20	4.20	4.40	5.60	4.60	5.50	3.80
Zn	158.00	145.00	128.00	141.00	135.00	145.00	161.00	124.00
Ga	22.30	21.40	20.30	25.40	22.50	21.20	24.10	15.00
Hf	3.80	3.90	3.60	3.60	4.40	3.90	5.30	3.20
Y	23.40	22.50	21.80	21.10	24.60	18.00	25.20	13.90
U	.30	.37	.34	.36	.39	.21	.35	.19
Pb	4.80	2.50	2.70	4.10	2.90	2.10	4.40	2.60
La	13.80	13.60	11.90	11.20	12.10	11.20	15.70	9.20
Ce	35.60	33.20	30.40	31.50	36.30	30.60	42.30	24.30
Nd	24.60	24.00	22.80	21.20	24.80	22.20	32.70	17.20
Sm	6.02	5.52	4.91	4.56	5.58	5.02	6.73	3.85
Eu	1.96	1.88	1.88	1.45	2.04	1.92	2.43	1.47
Dy	6.40	6.60	5.80	5.70	7.60	5.70	7.20	.00
Yb	2.19	2.03	1.94	2.21	2.15	2.14	2.79	1.57
Lu	.31	.24	.29	.21	.28	.30	.32	.19

rupted storage of summit magma in isolated secondary reservoirs or pockets, thereby allowing greater cooling and fractionation before eruption to yield more differentiated lava; and (3) increased incidence of magma mixing to produce hybrid lava by repeated filling of the secondary reservoirs by new magma, either from storage pockets uprift or from the summit reservoir.

VARIATION IN TIME

Wright (1971) showed that for olivine-controlled Kilauea lava, at any given MgO content, three time groupings (prehistoric, 18th–19th centuries, and 20th century) could be distinguished on the basis of major-element composition. Younger lava is characterized by higher K_2O, TiO_2, and P_2O_5 and by several other chemical distinctions. One of the principal objectives of our study was to try to further document such secular variation using trace elements. Leeman and others (1980, p. 802), citing unpublished, limited data for prehistoric Kilauea lava, tentatively concluded that there is "little or no difference in trace element contents with time at Kilauea, but additional analyses are required to confirm this conclusion." More recently however, Budahn and Schmitt (1985, table 2), referring to the same unpublished data as did Leeman and others (1980), presented the ranges and means of selected trace elements (REE, Sr, Ba, and Sc) for 7 Kilauea lava samples (20th century, 5; prehistoric, 2).

Budahn and Schmitt (1985, p. 71) noted that with respect to light-rare-earth-element (LREE) abundance patterns the 20th-century and prehistoric lavas were "compositionally distinct." Our more extensive data (tables 24.9–24.11 and fig. 24.4) confirm their finding and suggest that the mean contents of Sc, Co, Hf, and the LREE of lava from the 18th–19th centuries are intermediate between those for prehistoric and 20th century lavas (table 24.13; figs. 24.7*B*, 24.8). This relation is similar to progressive changes of some major elements (for example, K_2O and TiO_2) for these three time groupings (Wright, 1971).

Some historical summit eruptions of Kilauea have chemically distinct major-element compositions (Wright, 1971, fig. 12), supporting the concept of so-called magma batches, originally suggested by Powers (1955). We are aware that, in treating our trace element data in terms of means, we overlook the differences between such chemically distinct eruptions (magma batches) within the broader space or time grouping; this problem is particularly serious in dealing with the samples of prehistoric lava, for which time relations are poorly known. For example, recent work by Easton and Garcia (1980) on the Hilina Basalt, the oldest exposed rocks of Kilauea Volcano (25 ka and older), indicates considerable chemical variation. Similarly, the study of Casadevall and Dzurisin (chapter 13),

TABLE 24.11.—*Composition of olivine-controlled tholeiite of Kilauea's southwest rift zone*

[Oxide values (in weight percent) from Wright (1971, table 5), recast to 100 percent dry weight; values for elements in parts per million. Sample TLW67-12 fits definition of differentiated and is omitted in calculation of averages and not plotted in figure 24.4]

	Prehistoric						Historical				
							19th century			20th century	
							1823	1868		1920	
Sample	TLW67140	TLW67-134	KD-32	KD-32	KD-56	TLW67-28	TLW67-24	1868-SW	TLW67-12	TLW67-4	TLW67-6
SiO_2	50.23	51.17	46.59	49.07	51.13	50.16	51.01	50.62	51.40	49.75	50.26
MgO	10.03	6.81	21.98	13.30	7.32	9.12	7.29	8.61	6.79	9.21	7.49
K_2O	.40	.47	.28	.36	.40	.36	.43	.45	.50	.49	.51
TiO_2	2.34	2.48	1.52	1.98	2.42	2.22	2.43	2.39	2.80	2.55	2.66
P_2O_5	.21	.25	.15	.19	.23	.20	.22	.27	.24	.23	.25
Cs	.03	.24	.00	.20	.00	.27	.14	.00	.18	.25	.01
Ba	152.00	126.00	429.00	76.00	152.00	61.00	53.00	103.00	168.00	71.00	202.00
Sc	26.90	31.30	21.00	22.00	30.40	29.50	31.50	31.20	29.40	30.30	33.60
V	277.00	261.00	166.00	185.00	284.00	245.00	326.00	329.00	316.00	279.00	337.00
Cr	541.00	309.00	847.00	667.00	244.00	341.00	307.00	438.00	186.00	571.00	575.00
Co	50.10	40.50	88.40	69.80	42.90	51.70	45.30	47.90	39.50	51.10	50.60
Ni	191.00	97.00	787.00	510.00	91.00	186.00	111.00	182.00	106.00	178.00	150.00
Mo	3.40	3.50	4.10	3.30	3.80	3.80	4.20	4.20	4.50	4.50	4.80
Zn	123.00	157.00	110.00	110.00	128.00	134.00	119.00	108.00	131.00	146.00	140.00
Ga	20.80	17.40	9.80	14.10	22.00	17.20	20.50	20.90	24.40	19.10	24.90
Hf	2.70	3.70	2.20	2.70	3.40	3.20	3.80	3.90	4.00	4.20	4.50
Y	16.80	17.60	8.40	10.60	18.80	15.80	19.50	22.50	20.60	14.50	18.90
U	.19	.27	.19	.21	.26	.27	.33	.22	.52	.30	.51
Pb	1.00	1.00	3.00	2.90	2.40	1.20	2.70	3.00	3.80	2.00	2.50
La	10.30	12.30	6.90	8.20	10.90	10.60	11.50	10.90	12.90	13.50	14.10
Ce	24.10	29.80	20.30	21.70	33.30	27.60	31.30	31.00	34.30	35.80	36.40
Nd	19.60	21.90	12.00	13.10	19.80	16.60	20.90	18.10	22.10	21.80	23.40
Sm	4.62	5.11	2.98	3.60	4.70	4.50	5.01	5.01	5.70	5.39	5.81
Eu	1.41	1.78	1.13	1.28	1.67	1.74	1.91	1.86	1.85	1.91	2.19
Dy	5.10	6.10	3.20	3.90	5.40	5.70	6.10	4.90	6.50	5.60	5.80
Yb	2.15	2.12	1.02	1.40	1.90	1.79	2.08	2.00	2.06	1.68	1.79
Lu	.25	.28	.14	.18	.25	.26	.30	.28	.29	.24	.20

which involves the most thorough sampling of prehistoric Kilauea lava at a single locality to date, demonstrates wide variation in the composition of prehistoric lava of the Puna Basalt (2.8 ka and younger) well exposed in the northwestern wall (Uwekahuna Bluff) of Kilauea caldera.

For prehistoric Kilauea lava in our study, we note that the uranium abundance in the three samples of the Hilina Basalt analyzed (0.41–0.71 ppm) was considerably higher than that in the Puna Basalt (0.17–0.33 ppm) with no overlap (table 24.9). However, it should be noted that Easton and Garcia (1980) suggested, on the basis of sample location, that only one of the five samples (57F–15) designated by Wright (1971, table 4) as from the Hilina Series (now Hilina Basalt) truly belonged to that stratigraphic unit. In any case, sample 8X002–0 of the Puna Basalt (table 24.9) is characterized by the lowest LREE content of any of the 15 prehistoric Kilauea lava samples we analyzed. Thus, we are keenly aware of the wide internal variations within the prehistoric Kilauea and several other lava groupings, as well as the related problems in attempting to evaluate differences between mean compositions. Indeed, our reconnaissance study is intended to identify specific petrologic and geochemical topics for subsequent systematic sampling and detailed investigations.

LAVA OF THE KILAUEA IKI AND KAPOHO ERUPTIONS

The November–December 1959 summit eruption at Kilauea Iki, the related January–February 1960 lower ERZ eruption at Kapoho, and their eruptive products have been subject of many studies (for example, Helz, chapter 25, 1980; Murata and Richter, 1966a, b; Richter and Murata, 1966; Gunn, 1971; Wright, 1973; Wright and others, 1976). The Kilauea Iki lava provides one of the best documented examples of olivine control (Murata and Richter, 1966a; Gunn, 1971; Wright, 1973), whereas the Kapoho lava has been shown to include differentiated and hybrid types (Wright and Fiske, 1971). Yet, despite the abundance of petrologic and major-element data, there are few systematic trace-element data, other than the work of Gunn (1971), for the Kilauea Iki lava. For our study, we selected a suite of samples (Kilauea Iki, 10; Kapoho, 5) that spanned the duration of the eruptions and showed a wide range in MgO content (tables 24.12, 24.14; figs. 24.5, 24.9*A*). Several of the samples we studied have also been analyzed previously, but, unfortunately, the interlaboratory agreement between the results is unsatisfactory for some of the elements determined (table 24.6).

The mean composition for the Kilauea Iki lava is distinct from those for other olivine-controlled Kilauea lavas, as evidenced by its

TABLE 24.12.—*Composition of olivine-controlled tholeiite of the Kilauea Iki eruption and of differentiated and hybrid lavas of the Kapoho eruption*

[Oxide values (in weight percent) from Murata and Richter (1966a, tables 1 and 2) recast to 100 percent dry weight; values for elements in parts per million. Samples S-1 through S-9 were erupted in November, 1959; S-14 through S-25 in December, 1959; and F-1 through F-17 during January–February, 1960]

	Kilauea Iki eruption, 1959										Kapoho eruption, 1960				
Sample	S-1	S-2	S-3	S-5	S-7	S-8	S-9	S-14	S-15	S-25	F-1	F-5	F-8	F-12	F-17
SiO_2	50.04	50.05	49.67	46.74	48.28	49.31	48.46	49.51	46.88	49.53	50.57	50.79	49.96	49.39	48.88
MgO	8.10	7.23	8.86	19.55	13.69	10.49	13.35	8.56	18.89	8.87	6.56	6.09	8.28	10.59	13.16
K_2O	.55	.60	.50	.35	.45	.54	.47	.53	.36	.53	.65	.69	.60	.54	.49
TiO_2	2.63	2.75	2.55	1.80	2.27	2.54	2.30	2.62	1.86	2.67	3.11	3.37	2.92	2.69	2.43
P_2O_5	.25	.28	.26	.18	.23	.25	.23	.26	.19	.26	.35	.36	.33	.28	.26
Cs	.21	.22	.11	.11	.00	.25	.32	.00	.23	.19	.25	.19	.19	.06	.23
Ba	158.00	164.00	126.00	75.00	172.00	198.00	151.00	174.00	95.00	132.00	144.00	347.00	149.00	353.00	230.00
Sc	31.60	30.40	31.20	24.40	27.30	28.10	26.20	29.50	24.50	29.30	29.90	31.60	31.10	29.60	27.30
V	296.00	300.00	277.00	208.00	223.00	264.00	251.00	287.00	249.00	291.00	0.00	362.00	.00	301.00	254.00
Cr	251.00	148.00	407.00	1170.00	721.00	369.00	543.00	256.00	1020.00	338.00	134.00	97.00	231.00	339.00	440.00
Co	45.00	44.70	50.80	85.10	67.60	56.60	65.50	49.80	79.80	50.60	46.10	48.60	53.30	60.10	65.50
Ni	104.00	80.00	168.00	542.00	296.00	170.00	293.00	149.00	525.00	130.00	.00	82.00	.00	191.00	269.00
Mo	4.90	4.10	4.20	4.30	3.20	4.20	3.80	5.50	4.60	4.10	.00	3.90	.00	3.60	3.60
Zn	143.00	137.00	123.00	116.00	109.00	127.00	108.00	120.00	133.00	131.00	.00	122.00	.00	114.00	111.00
Ga	16.00	18.20	16.90	9.30	12.30	14.60	14.60	19.60	14.20	20.40	.00	27.60	.00	16.70	15.60
Hf	3.70	4.20	4.20	3.00	3.20	4.10	3.60	4.20	3.00	3.90	5.50	6.00	5.20	4.70	3.80
Y	16.40	19.10	15.60	10.10	9.80	13.90	12.20	18.00	15.00	15.40	.00	25.90	.00	15.40	13.50
U	.48	.51	.60	.32	.49	.34	.43	.72	.75	.45	.55	.54	.47	.40	.64
Pb	1.10	1.40	1.90	1.00	1.10	1.60	2.20	2.40	4.60	2.30	.00	3.70	.00	1.70	1.30
La	14.70	16.10	15.00	11.10	13.70	15.10	13.30	14.70	11.90	15.90	18.60	23.00	18.10	18.30	.00
Ce	44.00	42.10	31.80	24.10	30.10	41.50	36.20	42.00	24.30	31.90	45.50	51.80	49.30	45.20	.00
Nd	24.50	25.60	21.20	16.00	.00	21.80	.00	.00	15.70	22.60	.00	34.20	32.60	32.80	.00
Sm	4.71	5.65	5.10	3.78	4.65	5.11	4.79	5.23	4.02	5.22	7.05	7.27	6.87	6.10	.00
Eu	1.83	1.94	2.01	1.34	1.63	1.88	1.74	1.83	1.40	1.94	2.48	2.78	2.36	2.19	.00
Dy	4.50	5.30	5.10	4.10	5.30	7.10	4.80	4.80	4.40	5.50	7.30	7.40	5.50	7.20	5.70
Yb	1.89	1.97	1.84	1.36	1.83	1.83	1.44	2.07	1.59	1.77	2.79	2.93	2.36	1.98	2.05
Lu	.19	.26	.22	.17	.22	.35	.21	.21	.13	.26	.35	.43	.29	.38	.31

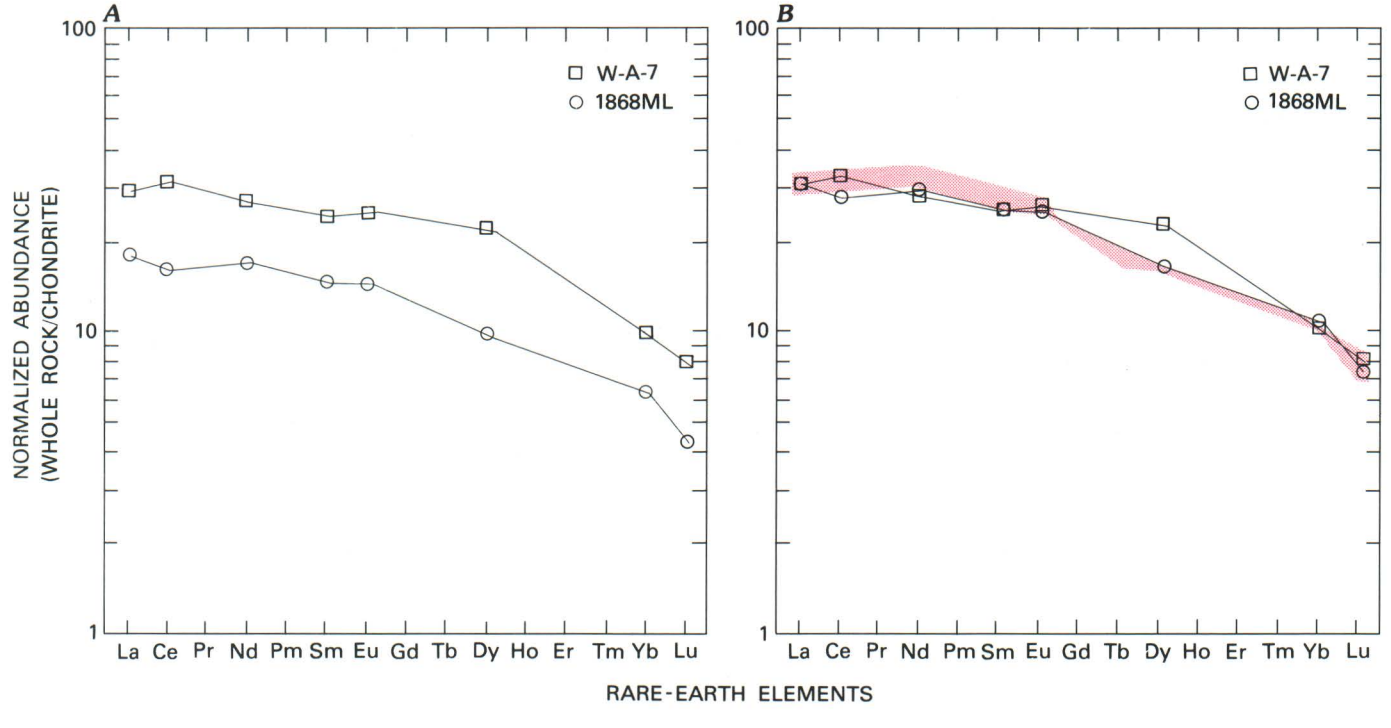

FIGURE 24.3.—Chondrite-normalized REE abundances of two samples of olivine-controlled lava of the 1868 Mauna Loa eruption plotted (***A***) from raw data (table 24.17) and (***B***) after adjustment to 7.00 weight percent MgO (see appendix 24.1), showing good convergence. Band (red) brackets the range of mean values for Mauna Loa lava plotted in figure 24.2; Dy value for sample W-A-7 and Ce value for sample 1868ML plot outside this band and may be spurious.

TABLE 24.13.—*Average compositions of spatial and temporal groups of olivine-controlled lava of Kilauea, adjusted to 7.00 weight percent MgO*

[Calculated from data in table 24.9–24.11; average for Kilauea Iki (1959) and Kapoho (1960) given in table 24.14. S.d., standard deviation. Oxide values in weight percent; values for elements in parts per million. Numbers of samples where different from numbers (n) given: summit, 7 for Cs, V, Ni, Mo, Zn, Ga, Y, Pb, and Dy (excludes Kilauea Iki eruption of 1959); east rift zone, 5 for Dy (excludes Kapoho eruption of 1960); southwest rift zone, 7 for Cs; Prehistoric, 14 for Dy, 13 for V, Ni, Mo, Zn, Ga, Y, and Pb, 12 for Cs; 18th and 19th centuries, 5 for Cs, and Dy; 20th century, 3 for Cs; historical, 8 for Cs, 9 for Dy.]

	Spatial groups						Temporal groups							
	Summit		East rift zone		Southwest rift zone		Prehistoric		18th-19th centuries		20th century		Historical (all)	
	n=9		n=6		n=10		n=15		n=6		n=4		n=10	
	Mean	S.d.	Mean	S.d.	Mean	S.d.	Mean	S.d.	Mean	S.d.	Mean	S.d.	Mean	S.d.
MgO	7.00	-	7.00	-	7.00	-	7.00	-	7.00	-	7.00	-	7.00	-
K_2O	.45	.07	.46	.05	.45	.05	.43	.05	.45	.02	.54	.02	.48	.05
TiO_2	2.56	.14	2.66	.14	2.50	.12	2.51	.15	2.58	.13	2.69	.02	2.68	.08
P_2O_5	.24	.02	.26	.01	.24	.02	.24	<.02	.26	.02	.25	.01	.25	<.02
Cs	.19	.10	.19	.06	.18	.10	.20	.09	.17	.04	.14	.12	.16	.08
Ba	114	62	161	18	[1]115	51	[1]128	53	118	52	134	60	124	53
Sc	32.1	1.8	32.5	1.9	31.3	2.3	31.5	2.4	32.5	1.7	32.8	.9	32.6	1.4
V	300	26	348	33	287	42	291	48	330	28	322	20	327	24
Cr	250	90	183	78	[2]325	110	[2]251	83	214	100	368	147	276	138
Co	43.1	1.9	44.1	2.9	[8]43.1	3.1	[8]42.7	2.5	44.4	2.6	45.0	2.6	44.6	2.5
Ni	[3]63	23	[4]39	32	[5]88	32	[7]68	42	[4]65	33	45	19	73	34
Mo	4.7	1.3	4.9	.5	3.8	1.3	4.5	1.0	4.6	.8	4.4	.6	4.5	.7
Zn	127	10	140	8	119	38	132	13	129	14	131	18	130	15
Ga	17.4	2.3	22.8	2.2	20.1	3.0	19.0	3.7	21.3	1.2	21.3	2.6	21.3	1.8
Hf	3.8	.4	4.1	.3	3.7	.5	3.6	.4	4.1	.3	4.4	.1	4.2	.3
Y	17.5	1.3	22.0	2.4	16.5	5.5	17.9	3.4	20.7	2.7	18.1	1.9	19.7	2.6
U	.42	.18	.33	.98	.30	.9	.36	.16	.30	.07	.4	.09	.34	.09
Pb	2.2	.7	3.1	.7	2.5	1.2	2.4	1.2	2.8	.5	2.7	.6	2.7	.6
La	11.9	2.1	12.6	1.1	10.8	3.6	11.4	1.4	11.9	.5	14.7	.5	13.0	1.5
Ce	30.0	5.5	33.8	2.0	31.6	4.0	29.8	4.4	32.7	2.1	36.7	1.0	34.3	2.6
Nd	20.2	2.6	24.0	1.3	19.3	4.4	20.1	2.8	22.4	2.2	23.1	.8	22.7	1.7
Sm	5.05	.59	5.34	.42	5.06	.46	4.87	.45	5.32	.19	5.78	.09	5.50	.28
Eu	1.90	.17	1.93	.21	1.83	.21	1.79	.19	1.96	.11	2.08	.09	2.01	.11
Dy	5.1	1.1	6.6	.8	5.6	.5	5.5	.9	6.2	1.0	5.6	1.0	5.9	1.0
Yb	2.06	.19	2.18	.11	1.94	.22	2.05	.22	2.15	.07	1.85	.18	2.03	.19
Lu	[6].27	.03	.27	.04	.26	.03	[6].26	.03	.29	.02	.24	.03	.27	.03

[1]Anomalously high adjusted value (702 ppm) for sample KD-32 omitted.
[2]Adjusted value for sample HD-32 is negative and omitted from average (see appendix 24.1).
[3]Three negative adjusted values (samples 57F-17, 8X078-0, and 8X067-0) omitted (see appendix 24.1).
[4]Negative adjusted value for sample TLW68-12 omitted.
[5]Two negative adjusted values (samples TLW67-140 and KD-32) omitted.
[6]Anomalously high adjusted value (0.43 ppm) for sample 57F-15 omitted.
[7]Five negative adjusted values (samples 57F-17, 8X08-0, 8X067-0, TLW67-140, and KD-32) omitted.
[8]Anomalously low value (23.7 ppm) for sample KD-32 omitted.

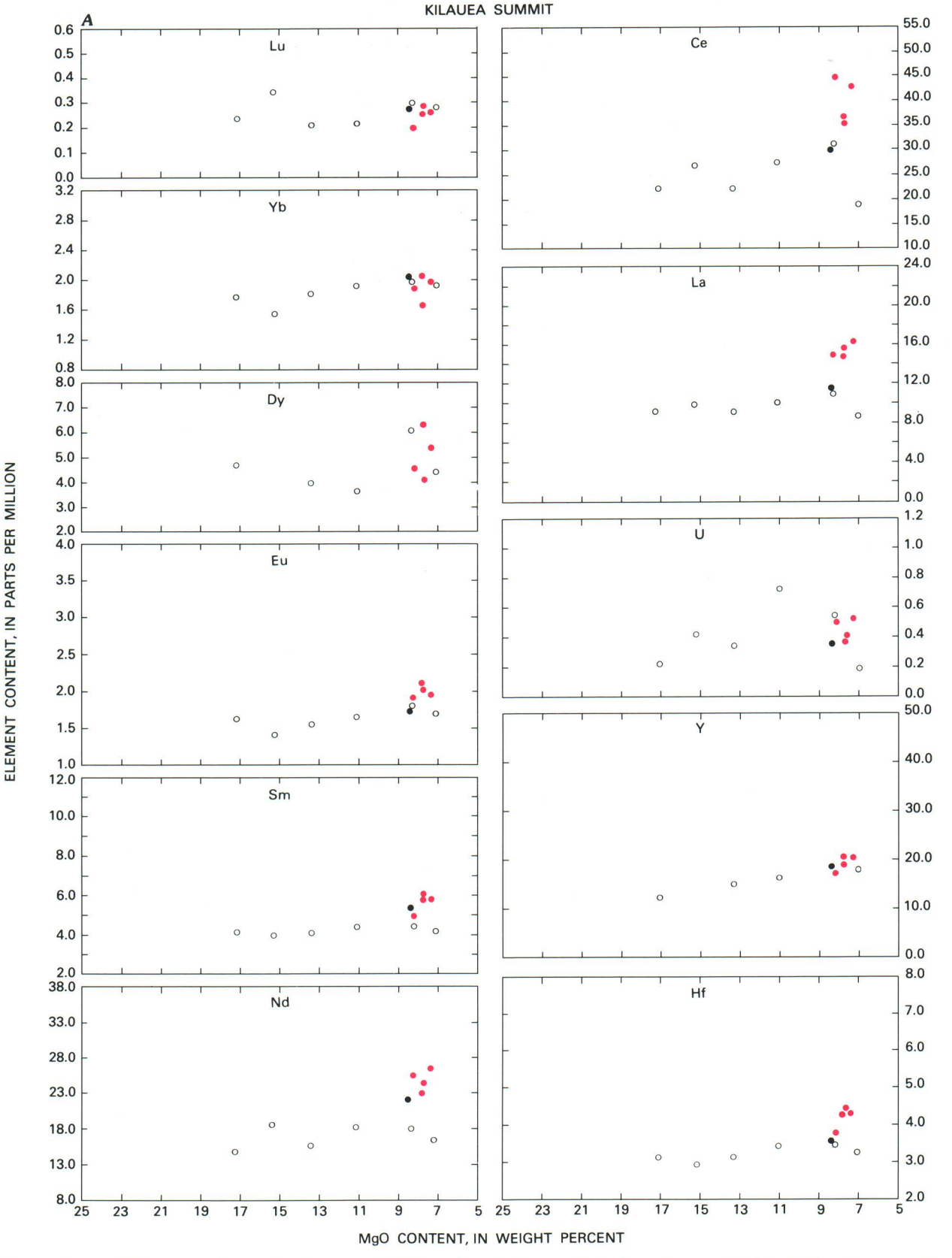

FIGURE 24.4.—MgO-variation diagrams for olivine-controlled Kilauea lava. ***A,*** Summit. ***B,*** Southwest rift zone (SWRZ). ***C,*** East rift zone (ERZ). Open symbols, prehistoric; solid black symbols, 18th–19th centuries; solid red symbols, 20th century. Data from tables 24.9–24.11; elements showing wider scatter not plotted.

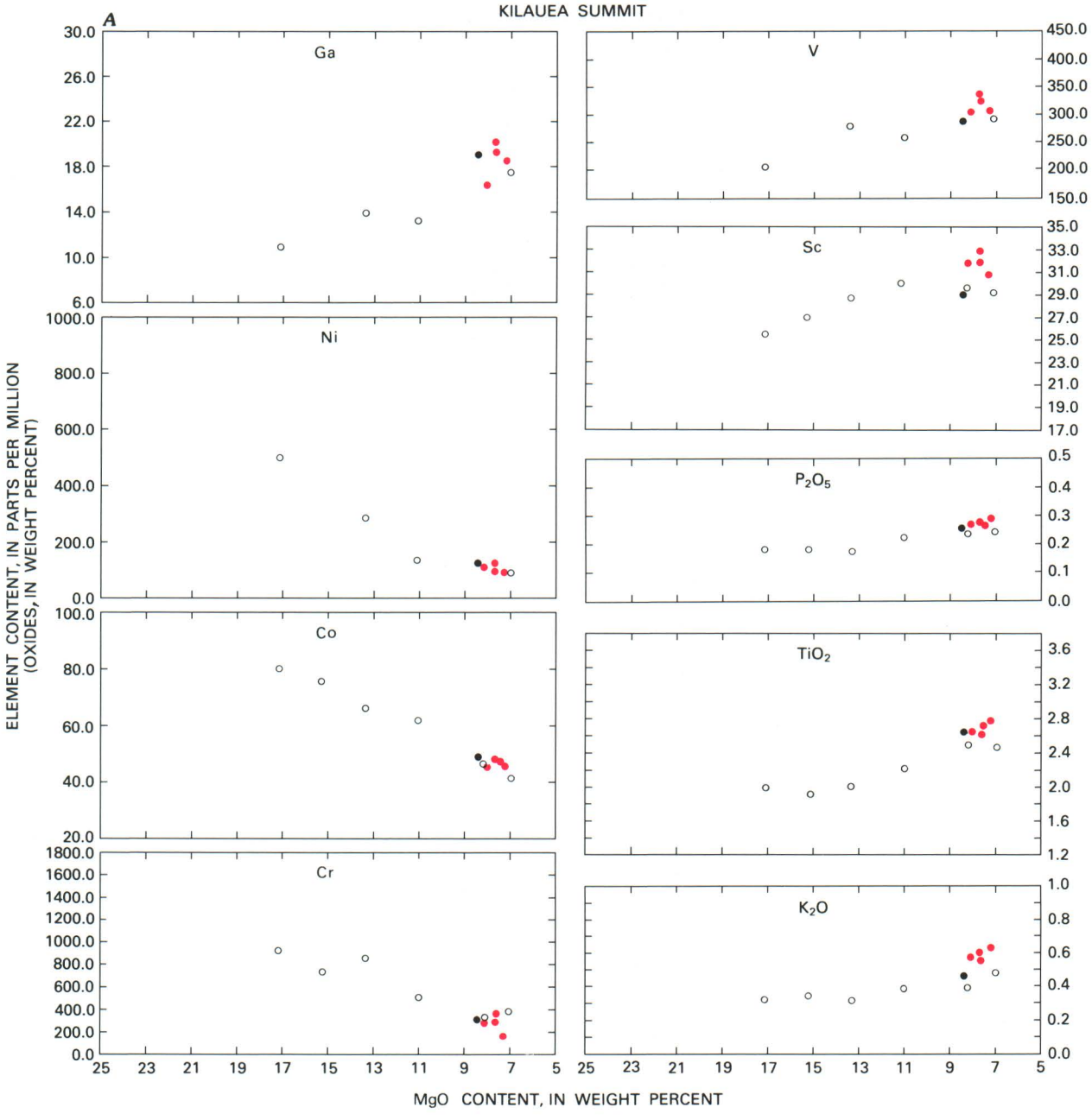

FIGURE 24.4.—Continued.

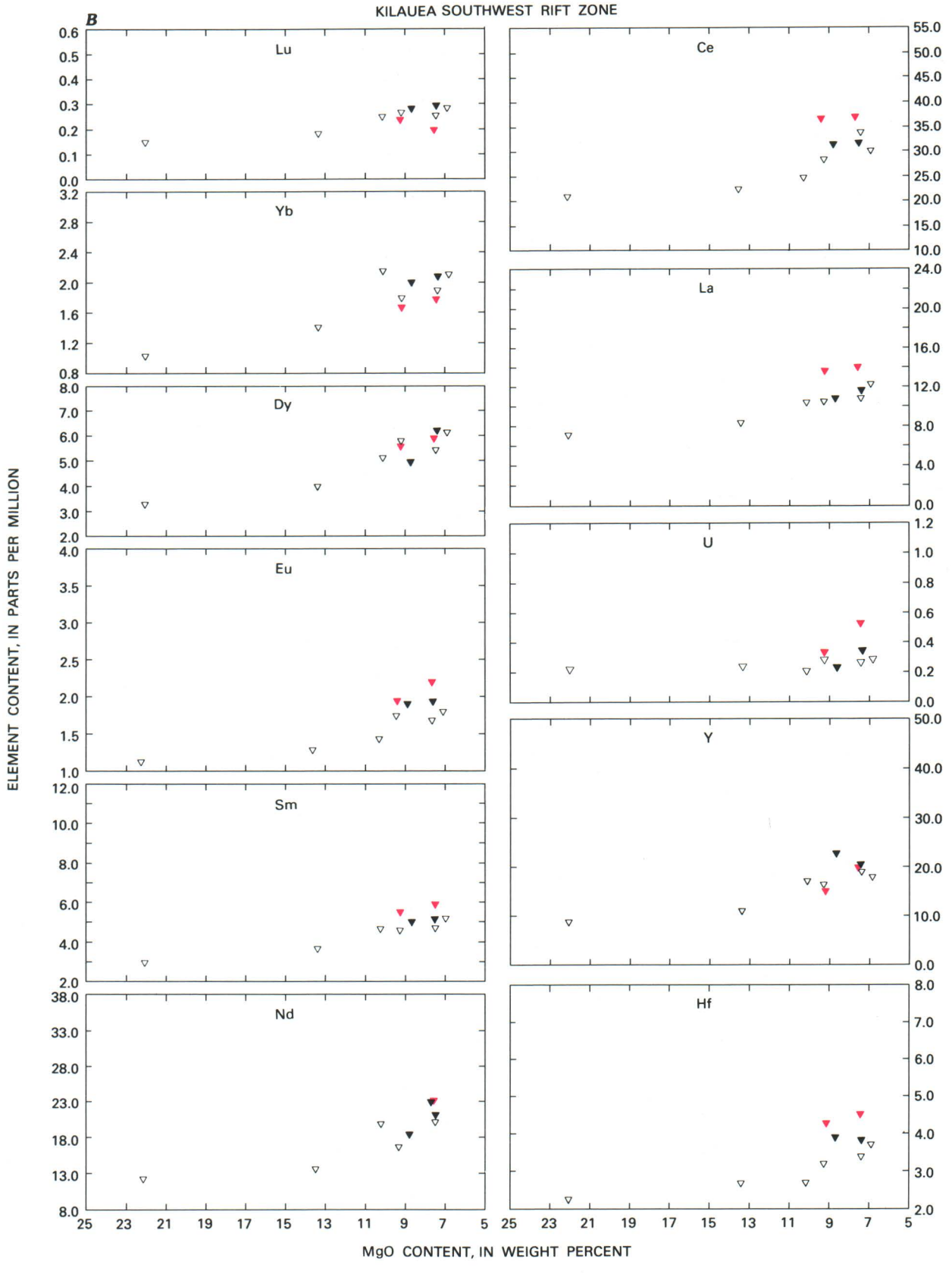

FIGURE 24.4.—Continued.

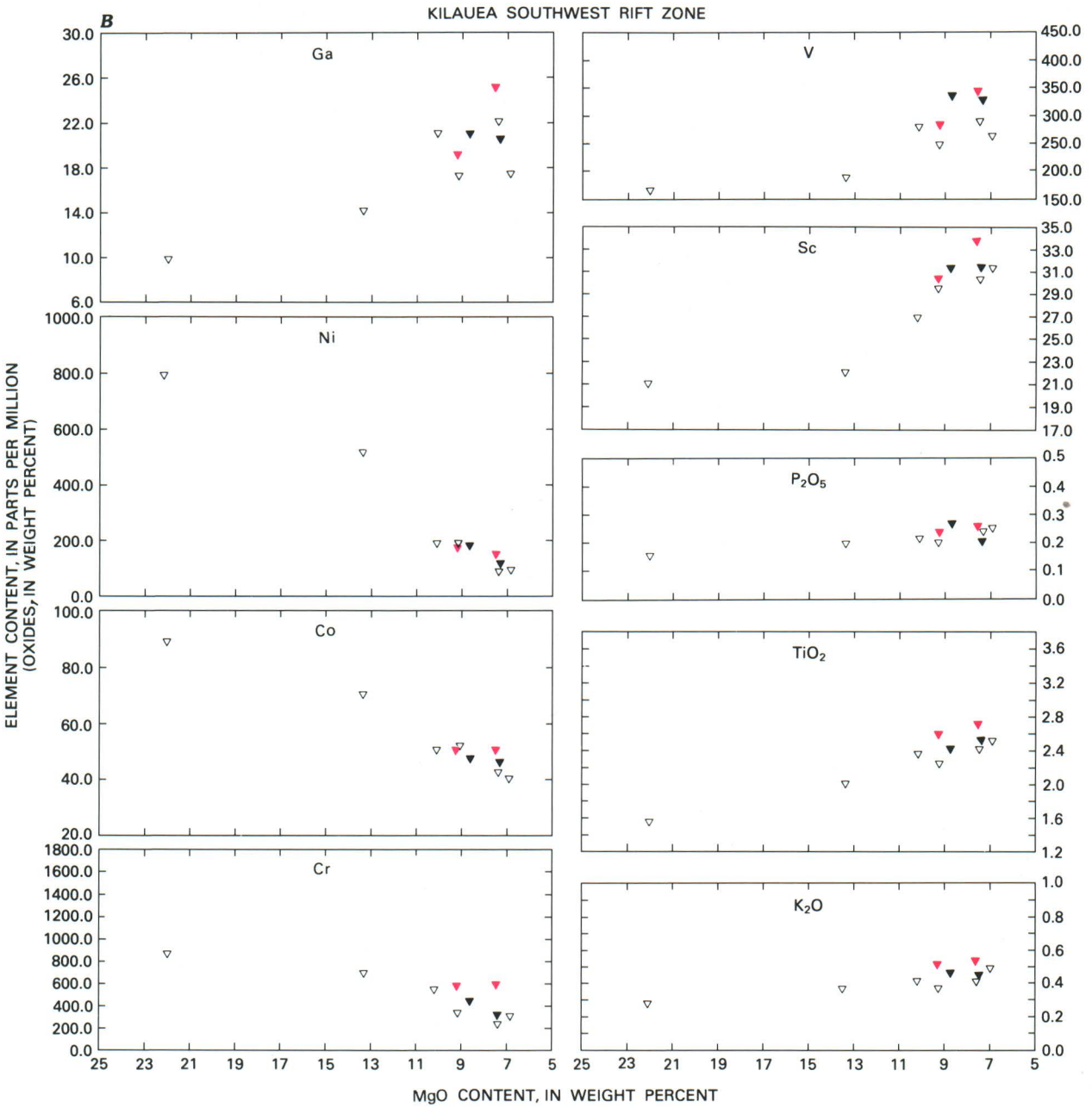

FIGURE 24.4.—Continued.

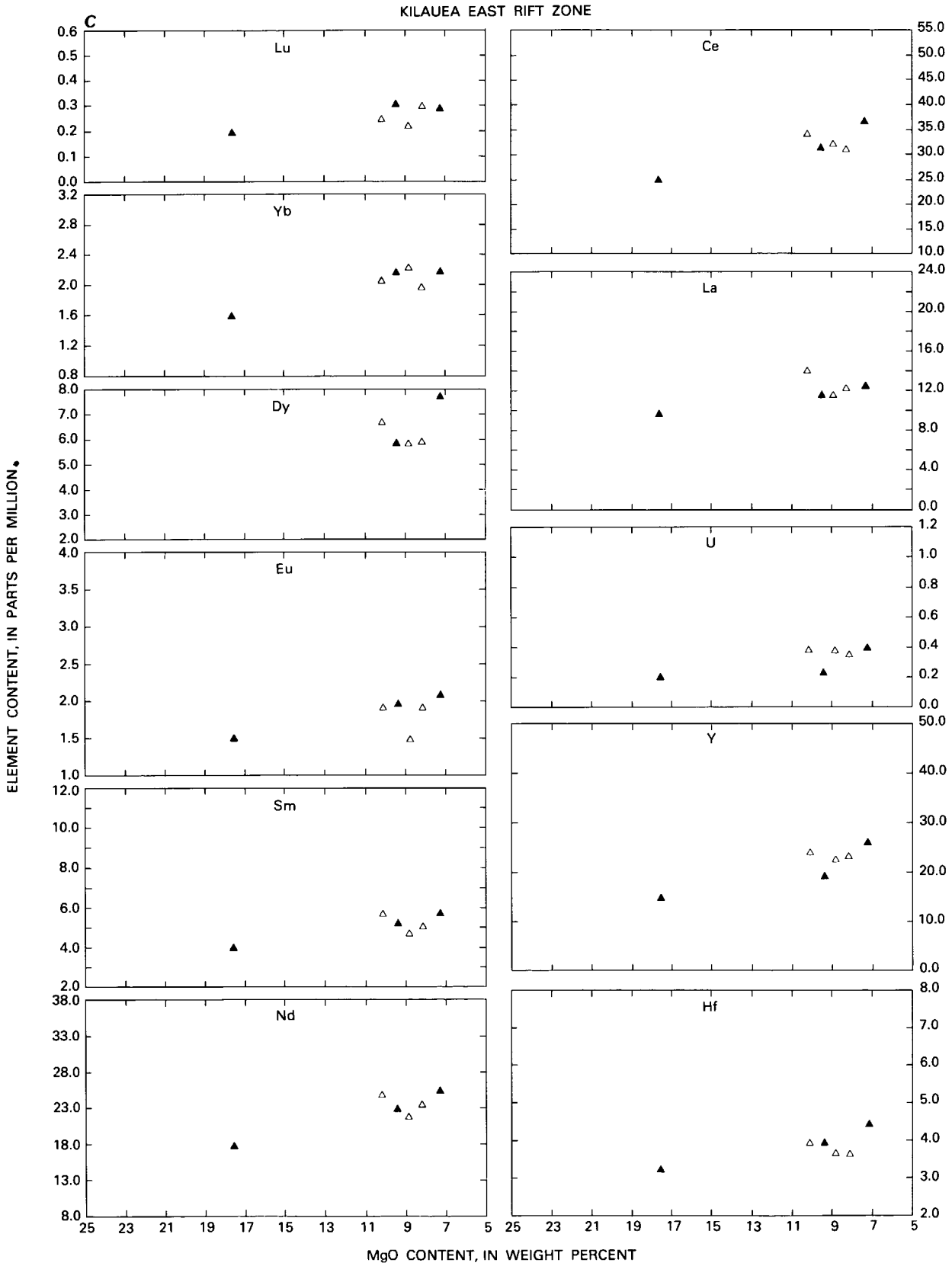

FIGURE 24.4.—Continued.

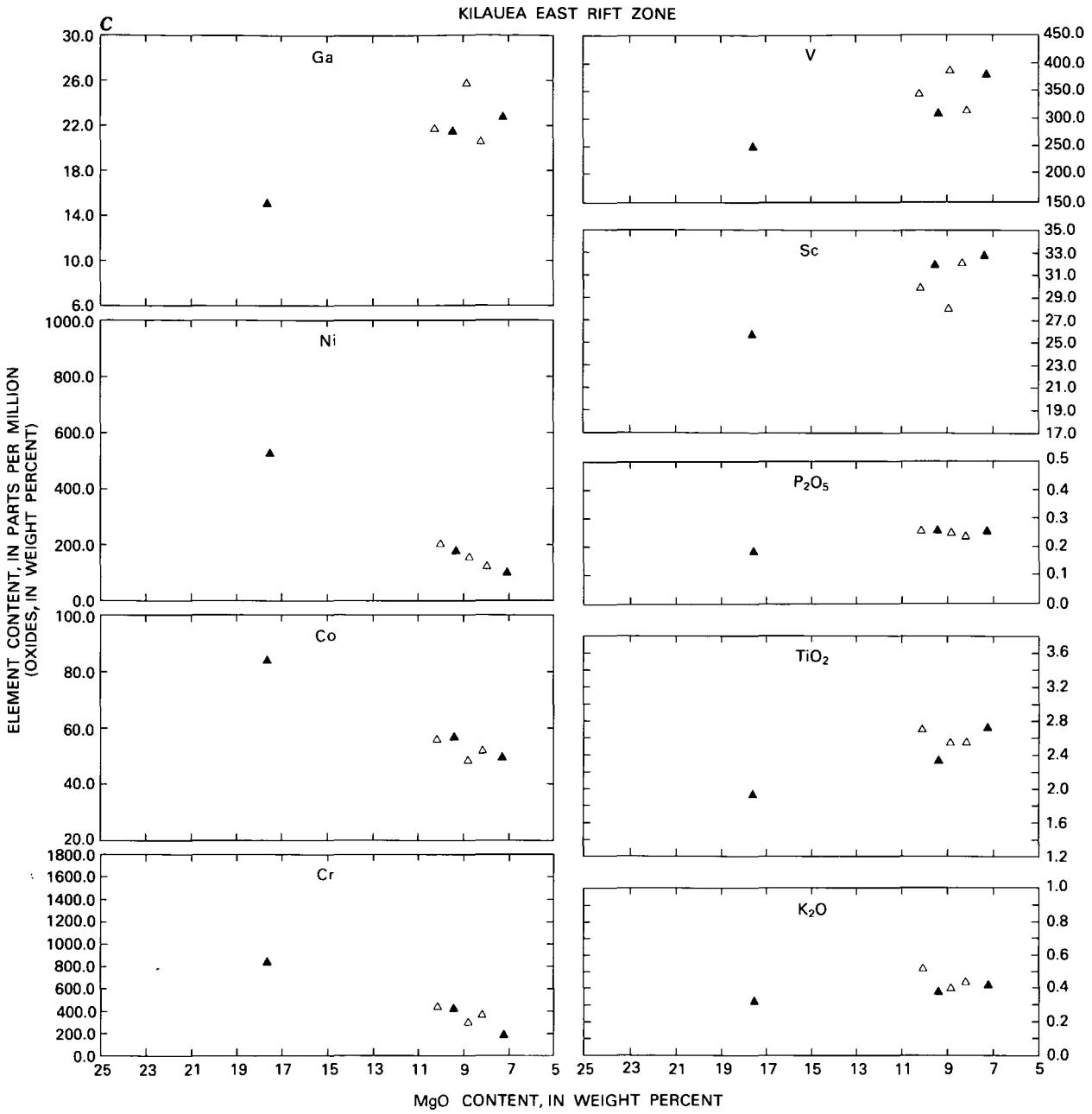

FIGURE 24.4.—Continued.

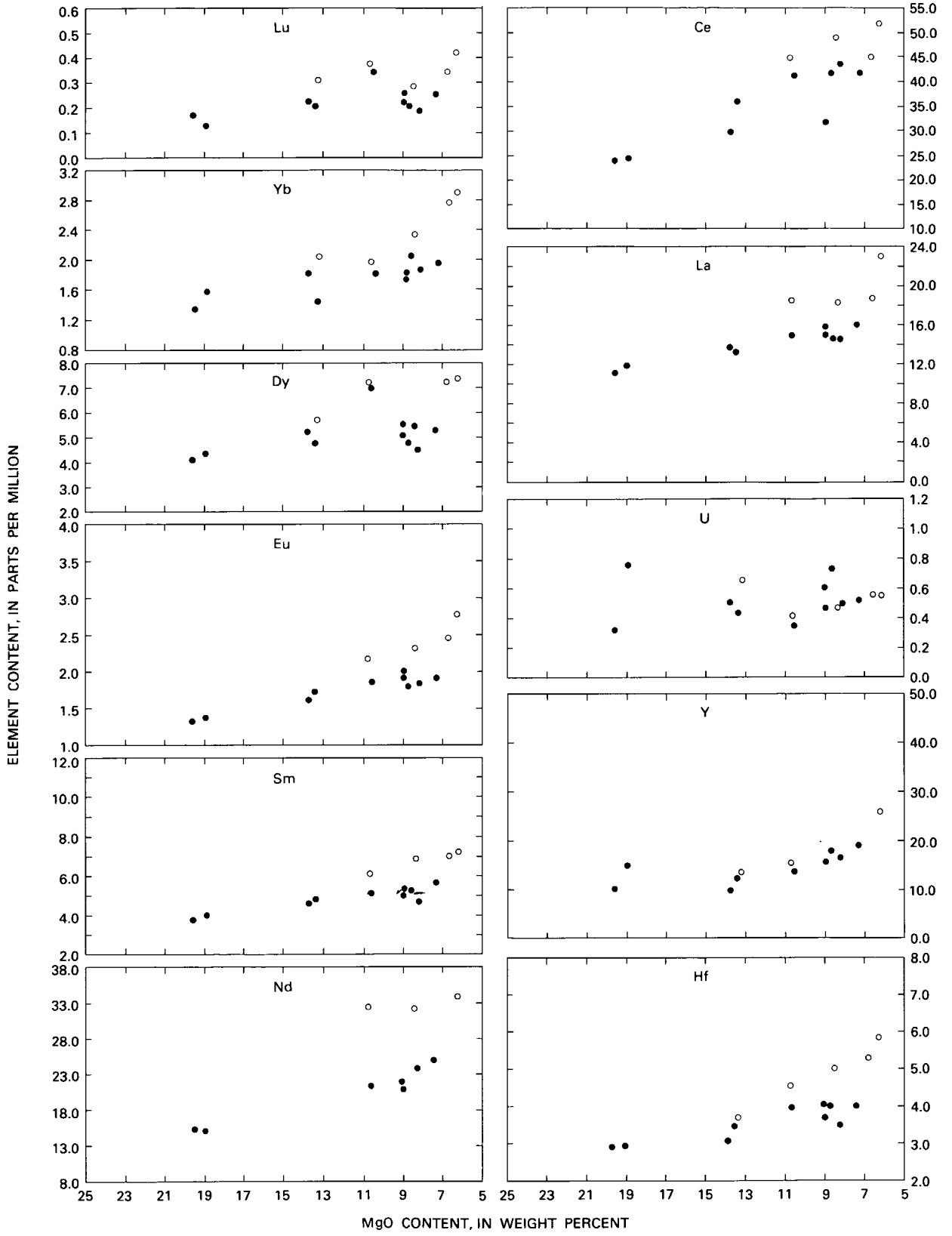

FIGURE 24.5.—MgO-variation diagrams for olivine-controlled lava of 1959 Kilauea Iki eruption (dots) and for hybrid lava of 1960 Kapoho eruption (circles). Data from table 24.12.

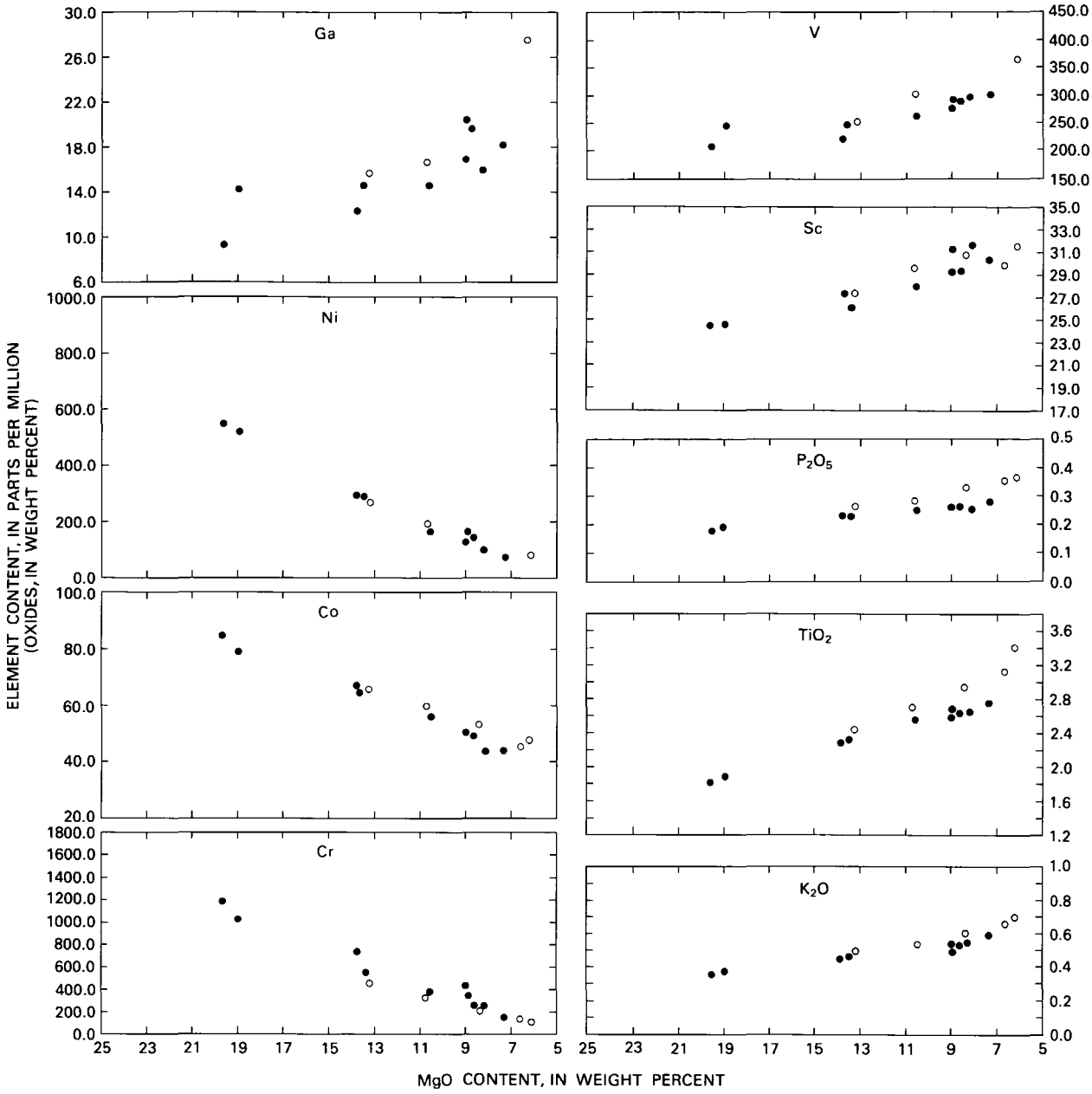

FIGURE 24.5.—Continued.

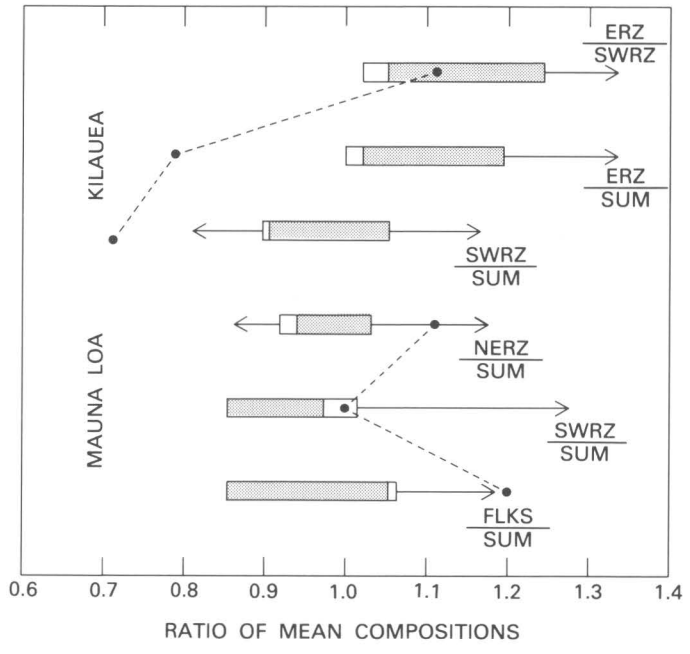

FIGURE 24.6.—Ratios of MgO-adjusted mean compositions (computed from data in tables 24.13, 24.20) of lava samples grouped according to space. SUM, summit; ERZ, east rift zone; SWRZ, southwest rift zone; NERZ, northeast rift zone; FLKS, northwest and southeast flanks. Bars show ranges of ratios for well-determined olivine-incompatible elements (K_2O, TiO_2, P_2O_5, Sc, Hf, and REE); shaded parts of bars bracket values for LREE only). Arrows indicate extension of a given range of values if less precisely determined values for V, Mo, Zn, Ga, Y, and Pb are considered; Cs and Ba are omitted because of wide scatter. Dots linked by dashed lines are ratios for uranium.

higher concentration of K_2O, TiO_2, P_2O_5, Ba, Hf, U, and the REE except for Yb and Lu (see tables 24.13, 24.14). The relatively elevated concentrations of U are especially conspicuous, and many samples contain more U than do samples of differentiated or hybrid lava. The reason for the (to date) unique composition of the Kilauea Iki lava is unknown, but major-oxide variations and other evidence prompted Wright (1973, p. 849) to suggest these lavas "were fed from a source different from that which fed other summit eruptions" in the 1952–68 period. Our trace-element data are compatible with Wright's postulation. Wright's (1973) mixing calculations show that the variations in composition of the Kilauea Iki lava can be explained by mixing olivine (plus chromite) with various proportions of two end-member magmas, represented by samples S–1 and S–2 (table 24.12) erupted the first day of the eruption.

Because of their compositional complexity and uniqueness, Kilauea Iki samples are not included in any of the space or time groupings of Kilauea lava (tables 24.9–24.11). Nor have we incorporated them in the estimate of the average composition of Kilauea Volcano as a whole (table 24.14), as was done by Leeman and others (1980, table 1 and appendix); of the ten analyses they averaged, five are of Kilauea Iki lava.

Compositional differences in the 1960 Kapoho lava are not related to olivine control alone; they were interpreted by Wright and Fiske (1971) as the result of complex mixing of undifferentiated and differentiated magmas. Their calculations showed that the lava erupted through January 26, 1960 (samples F–1 and F–5, table 24.14) can be produced by mixing undifferentiated 1961 magma and early 1955 differentiated magma, whereas lava erupted later (samples F–8, F–12, and F–17) resulted from mixing of olivine, one or more undifferentiated magmas (1959, 1961, 1967), and the early 1960 hybrid magma (Wright and Fiske, 1971, tables 10 and 11). Mixing calculations incorporating our trace-element constraints have not yet been done for the Kapoho hybrid lava, nor for any of the differentiated lava samples we analyzed, but the results of such studies should confirm or refine magma-mixing models based solely on major-element variations. For example, the decreased mean Sc contents of the differentiated and hybrid lavas (table 24.14), relative to those for olivine-controlled lava, clearly reflect the effect of pyroxenes joining olivine as phenocryst phases. In any case, the Kapoho lava (not MgO adjusted) is characterized by the highest concentrations of K, Ti, P, Ba, Hf, and REE of any of the Kilauea lava samples analyzed in this study (table 24.14; figs. 24.4, 24.5, and 24.9*A*).

MAUNA LOA LAVA

Analytical data for 31 Mauna Loa lava samples are given in tables 24.15–24.19) and plotted in magnesia-variation diagrams (fig. 24.10). The individual analyses were MgO-adjusted to a uniform MgO content of 7.00 weight percent to remove effects of olivine control (see appendix 24.1) before computation of mean compositions of samples grouped according to space or time (table 24.20). Several of the lava samples we studied also have been analyzed in previous studies, and the interlaboratory comparison of analytical results (table 24.5) indicates fair to good agreement for most elements.

POSSIBLE SPATIAL VARIATION

In comparison to Kilauea, Mauna Loa exhibits less chemical variation. Wright (1971) could not detect any significant systematic variation in major-element composition of Mauna Loa lava over space or time. More recently, Rhodes (1983), whose study represents the most thorough sampling of historical Mauna Loa lava to date, demonstrated each flow is remarkably homogeneous, despite the large areal extent and volume and the wide differences in the duration of eruptions (1–450 days). Many historical lava fields studied by Rhodes (1983, p. A869) "have compositional variability that is within, to close to, the analytical error for most elements." This observation has important implications for assessing possible systematic variation of Mauna Loa lava with time, discussed later.

Our trace-element data, within analytical uncertainty, do not indicate any obvious differences between the mean compositions of the various groupings of olivine-controlled lava (tables 24.15–24.18, 24.20). However, possible minor compositional differences as a function of space, though subtle and not significant statistically, are suggested by the comparison of ratios of mean compositions (fig. 24.6). The mean abundances of the well-deter-

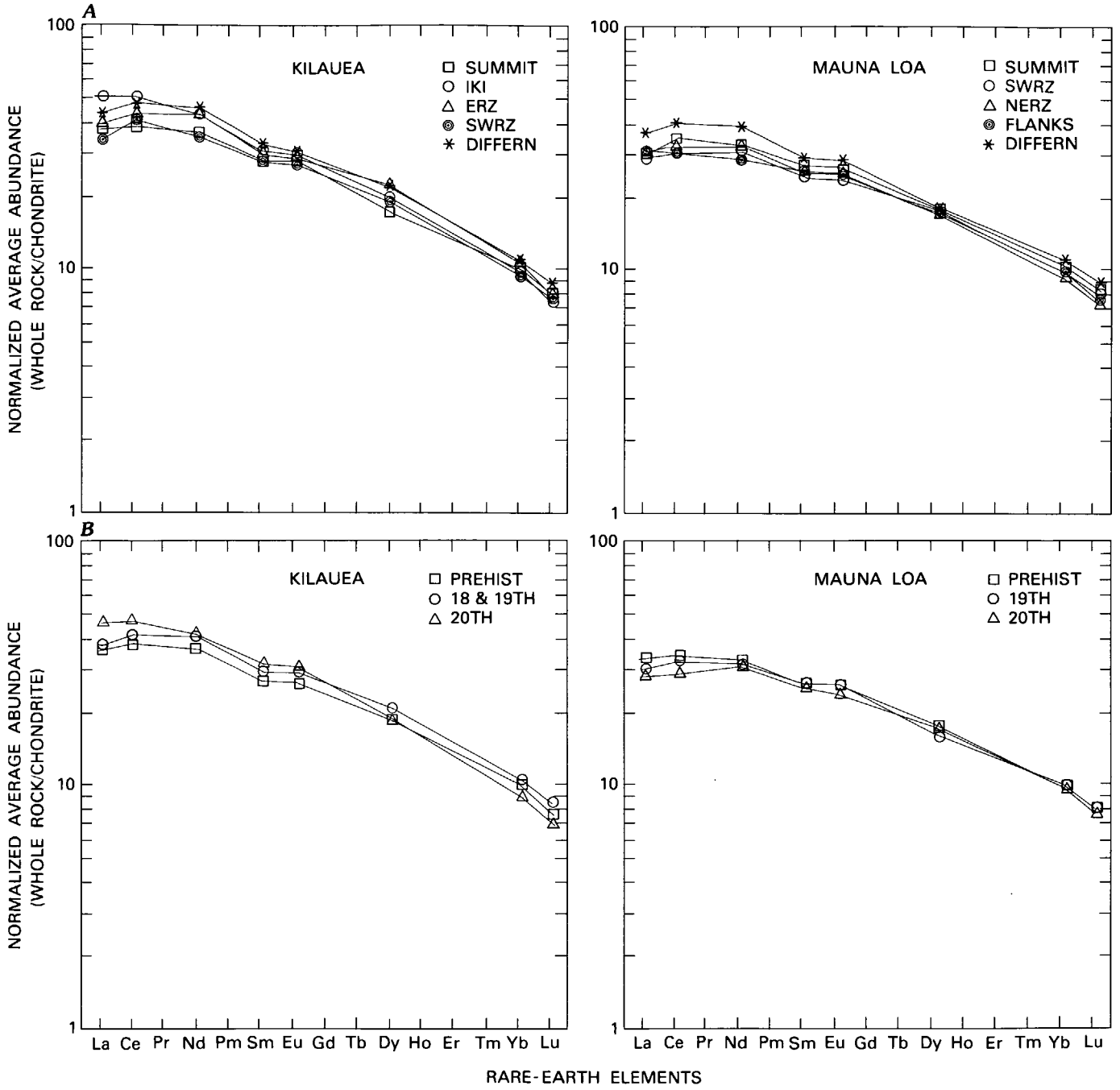

FIGURE 24.7.—Comparison of MgO-adjusted, chondrite-normalized average REE abundances of Kilauea and Mauna Loa lava samples, grouped as in tables 24.13 and 24.20 according to space (***A***) and according to time (***B***). For spatial groups, abbreviations are same as in figure 24.6; IKI, lava of 1959 Kilauea Iki eruption. Abundances of differentiated lava (DIFFERN) shown for comparison are not MgO adjusted. If DIFFERN curves are not considered, variability in space and time for Mauna Loa lava is less than Kilauea lava, which exhibits a discernible compositional gap between east rift zone (ERZ) lava and that of summit and southwest rift zone (SWRZ). Temporal variations discussed in text.

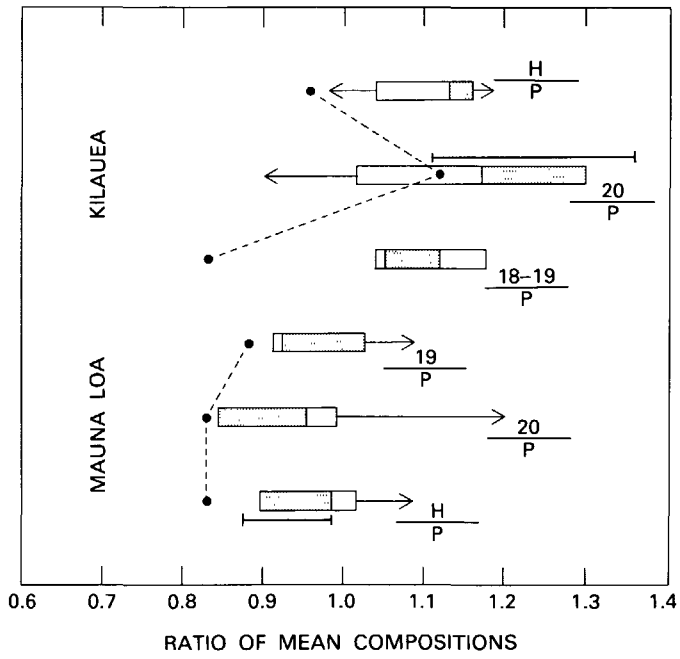

FIGURE 24.8.—Ratios of MgO-adjusted mean compositions of lava samples (listed in tables 24.13, 24.20) grouped according to time. P, prehistoric (erupted before A.D. 1750); 18 and 19, 18th and 19th centuries, respectively; 20, 20th century; H, historical undivided. Double-ended heavy line, range of ratios for LREE data of Budahn and Schmitt (1985, table 2); other symbols and explanation same as in fig. 24.6.

mined elements (K, Ti, P, Sc, Hf, and LREE) for lava of the SWRZ appear to be lower than their counterparts for SUM lava (figs. 24.6, 24.7*A*). Similar, but even more subtle, differences are hinted by the ratio shifts between the summit lava and the lava of Mauna Loa's northwest and southeast flanks (FLKS) and northeast rift zone (NERZ). Specifically, for the ratios FLKS/SUM and NERZ/SUM, the values for all REE other than La are less than unity.

We emphasize that our sampling of FLKS and NERZ lava is small and may not be representative. Furthermore, the samples of southeast-flank lava are from the Ninole Hills, whose major-element composition is unusual and highly varied (Wright, 1971, table 12). Because the Ninole lava (currently called the Ninole Basalt) comprises the oldest known rocks of Mauna Loa, as indicated by provisional K-Ar ages of 0.7 to 0.5 Ma for two dated flows (Evernden and others, 1964, table 4), it is not nearly as fresh as other Mauna Loa lava analyzed. Its chemical variability probably in part reflects posteruption weathering or possible alteration.

In any case, Rhodes and Lipman (1979) also found the Ninole Hills lava to differ compositionally from both prehistoric and historical lavas of Mauna Loa's southwest rift zone and suggested that it may be derived from a source different from that for most Mauna Loa lava. Indeed, Wright (1971, p. 18) even suggested that "The Ninole lavas may represent remnants of a separate volcano older than Mauna Loa." If so, then the apparent shift in FLKS/SUM ratios is intervolcano rather than intravolcano. Alternatively, given the wide analytical uncertainty, the apparent shifts in ratios plotted in figure 24.6 could be completely fortuitous, could represent sampling bias, or both. Nevertheless, as in the case of Kilauea lava, we are impressed by the seemingly nonrandom nature of the ratio shifts (fig. 24.6). As mentioned earlier in the discussion of Kilauea lava, such minor but nonrandom differences cannot be ascribed to grouping of samples for irradiations (table 24.2). Clearly, our speculation that the lava samples from the western sector of Mauna Loa may vary in composition as a function of space must be tested with many more precise analyses of fresher samples.

VARIATION IN TIME

Until recently, few published data on prehistoric Mauna Loa lava were available to test the possibility that it might differ compositionally from historical lava, as had been well demonstrated for Kilauea (Wright, 1971). Rhodes and his colleagues, in presenting the preliminary results of an integrated mapping and geochemical study of both prehistoric and historical lavas of Mauna Loa, concluded that "there is no evidence of major changes in compositional characteristics throughout the 31,000 years of eruptive history covered by our samples" (Rhodes and Lipman, 1979, p. 97). They recognized small "episodic" compositional variations for the historical Mauna Loa lava and suggested that processes that produced such variations "occurred episodically throughout the past 30,000 years" (Rhodes and others, 1982). However, as discussed below, we suggest that the prehistoric lava differs chemically from historical lava and that systematic minor secular variations may exist.

To our knowledge, Budahn and Schmitt (1985) were the first to report a compositional difference between the prehistoric and historical lavas of Mauna Loa. The results of our study, based on more comprehensive sampling, confirm their observation. Assuming that our mean trace-element compositions for the groupings of Mauna Loa lava are representative, our data suggest a compositional distinction between the 19th-century and 20th-century lavas as well (there are no known 18th-century eruptions). Our data suggest small but systematic relative decreases with time in the abundances of K, Ti, P, Sc, Hf, and LREE (table 24.20; figs. 24.7*B*, 24.8, 24.11). For certain of the other olivine-incompatible elements, the trend of inferred secular variation is convincingly demonstrated, we believe, by the more comprehensive and precise data of Rhodes (1983) for the historical Mauna Loa lava (table 24.21; fig. 24.12). As mentioned in the abstract by Rhodes and others (1982), the general features of the variation shown in figure 24.12 are also reflected in the variation of a few other incompatible elements and the ratios LREE/HREE, Zr/Y, and K/Ti. The striking parallelism between the variation patterns evident in figure 24.12, even at the scale of the small change between the 1949 and 1950 eruptions, attests to the high precision of Rhodes' data.

As earlier noted by Rhodes and others (1982), a significant compositional break occurs between lava erupted before and after 1870 (fig. 24.12). For this reason, we chose to lump the 1880, 1887, and 1899 eruptions with the 20th-century eruptions in computing the averages in table 24.21. However, even if the

TABLE 24.14.—*Average compositions of tholeiite samples analyzed in this study*

[Calculated from data in table 24.9–24.12 and 24.15–24.19. S.d., standard deviation. Oxide values in weight percent; values for elements in parts per million]

	Olivine-controlled lava (adjusted to 7.00 weight percent MgO)						Differentiated and hybrid lavas, (not adjusted for MgO)			
	Kilauea Iki n = 10		Kilauea[1] n = 25		Mauna Loa[2] n = 24		Differentiated[3] n = 11		Kapoho n = 5	
	Mean	S.d.	Mean	S.d.	Mean	S.d.	Mean	S.d.	Mean	S.d.
MgO	7.00	-	7.00	-	7.00	-	6.45	.42	8.94	2.95
K_2O	.55	.03	.45	.05	[4] .41	.04	.49	.09	.59	.08
TiO_2	2.73	.05	2.56	.14	2.14	.15	2.58	.41	2.90	.36
P_2O_5	.27	<.01	.24	.02	[4] .23	.02	.27	.05	.32	.04
Cs	.24	.09	.19	.08	.25	.23	.19	.20	.18	.07
Ba	164	34	[5]126	52	127	48	154	51	245	102
Sc	32.4	2.0	31.9	2.1	31.4	1.6	29.9	1.7	29.9	1.7
V	297	20	307	43	314	22	332	35	306	54
Cr	200	85	[6]261	108	[7]224	55	151	59	248	143
Co	40.7	4.6	43.5	2.6	[8]41.1	9.4	42.6	2.9	54.7	8.0
Ni	44	20	[9]68	36	[10]77	21	79	17	181	94
Mo	5.0	1.0	4.6	1.0	4.5	1.3	4.3	.7	3.7	.2
Zn	128	13	131	13	125	16	138	15	116	6
Ga	17.7	2.5	20.0	3.2	17.5	2.1	20.5	2.6	20.0	6.6
Hf	4.2	0.2	3.8	.4	3.4	.3	4.1	1.1	5.0	.8
Y	16.6	2.8	18.7	3.1	18.7	2.4	23.2	6.4	18.3	6.7
U	.59	.20	.35	.13	.22	.05	.38	.24	.52	.09
Pb	[11]1.8	.6	2.5	1.1	2.5	1.0	3.3	1.1	2.2	1.3
La	16.2	.7	12.0	1.6	9.5	1.3	12.4	1.8	19.5	2.3
Ce	39.5	5.0	31.6	4.4	24.5	3.8	33.4	8.1	48.0	3.2
Nd	23.9	1.2	21.1	2.7	17.2	1.6	23.1	6.0	33.2	.9
Sm	5.52	.27	5.12	.5	4.61	.35	5.55	1.2	6.82	.51
Eu	2.01	.07	1.88	.19	1.64	.27	1.97	.38	2.45	.25
Dy	5.8	.9	5.6	.9	5.2	.6	5.8	1.4	6.6	.9
Yb	2.01	.17	2.04	.20	2.02	.15	2.24	.42	2.42	.4
Lu	.25	.05	.26	.03	.27	.02	.31	.05	.35	.06

[1]Some trace elements not determined for all samples: n = 23 for V, Ni, Mo, Zn, Ga, Y, Pb; 22 for Dy; and 20 for Cs.

[2]Some trace elements not determined for all samples: n = 23 for Ga, Yb, and Lu; n = 23 for V, Ni, Zn, Mo, Ga, Y, U, Pb, and Sm; and 21 for Nd, 20 for Cs.

[3]So-called differentiated samples of Mauna Loa and Kilauea (MgO <6.80 weight percent include those in table 24.19 and those indicated in tables 24.9-24.11. These data are not adjusted to 7.00 weight percent MgO.

[4]Samples ID-275-2 and ID-214-2 omitted because of anomalously low values.

[5]Adjusted value for sample KD-32 (702 ppm) omitted.

[6]The adjusted value for HD-32 was negative and omitted (see appendix).

[7]Four negative adjusted values (samples TLW67-84, TLW67-89, C819, and 1868 ML) omitted.

[8]Anomalously low values (<30.0 ppm) for samples TLW67-84, C819, and 1868 ML omitted.

[9]Six negative adjusted values omitted (samples 57F-17, 8X078-0, 8X067-0, TLW68-12, TLW67-140 and KD-32).

[10]Ten negative adjusted values omitted (samples TLW67-84, TLW67-89, 65MAN-1, 1868 ML, TLW67-79, TLW67-61, TLW67-63, TLW 67-117A, ID-275-2, and ID-214-2).

[11]Anomalous value (6.6 ppm) for sample S-15 omitted.

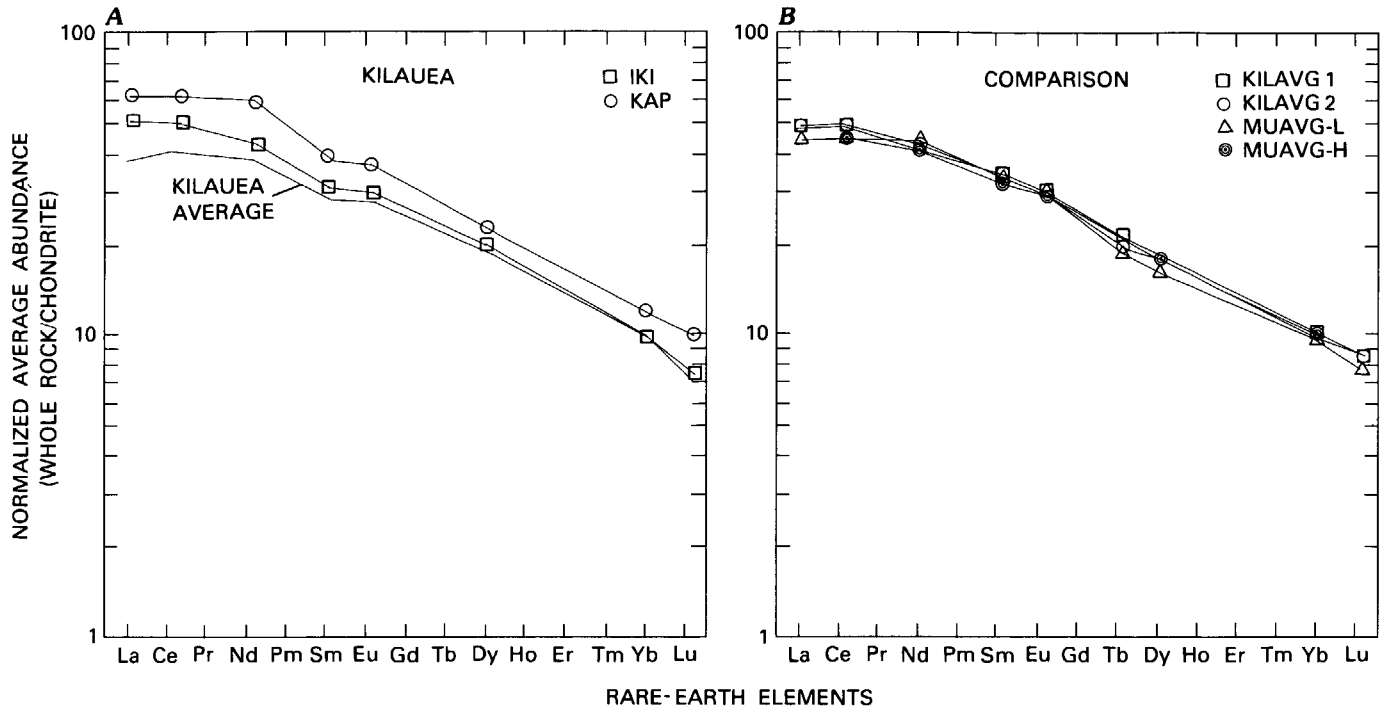

FIGURE 24.9.—Comparison of chondrite-normalized average REE abundances for groups of Kilauea lava. ***A***, Curves for MgO-adjusted Kilauea Iki lava (IKI), Kapoho lava, not MgO adjusted (KAP), and overall Kilauea average (data from table 24.14). ***B***, Curves for MgO-adjusted averages of historical Kilauea lava and averages for 1969–71 Mauna Ulu lava groups: KILAVG1 (Basaltic Volcanism Study Project, 1981), KILAVG2 and MUAVG-L (Leeman and others, 1980), and MUAVG-H (Hoffman and others, 1984). Curves for Mauna Ulu lava lie slightly below averages previously determined for historical Kilauea lava in (***B***), but slightly above our Kilauea average (***A***), which excludes data for Kilauea Iki lava (see text).

TABLE 24.15.—*Composition of olivine-controlled tholeiite of Mauna Loa's summit*

[Oxide values (in weight percent) from Wright (1971, table 8), recast to 100 percent dry weight; values for elements in parts per million]

	Prehistoric		Historical		
			19th century		20th century
			1877?	1880?	1949
Sample	TLW67-84	TLW67-70B	TLW67-88	TLW67-89	M-56-2
SiO_2	49.20	52.12	52.20	51.29	52.16
MgO	16.29	6.93	6.85	10.74	7.07
K_2O	.32	.46	.41	.30	.40
TiO_2	1.76	2.12	2.01	1.74	2.04
P_2O_5	.17	.25	.23	.23	.21
Cs	.00	.24	.05	.00	.30
Ba	67.00	92.00	86.00	157.00	94.00
Sc	25.50	30.30	32.20	30.20	32.60
V	211.00	297.00	319.00	273.00	.00
Cr	582.00	248.00	185.00	501.00	211.00
Co	59.80	43.00	46.80	64.40	50.80
Ni	565.00	84.00	80.00	149.00	.00
Mo	3.60	3.70	3.80	4.00	.00
Zn	108.00	111.00	142.00	153.00	.00
Ga	10.80	17.40	16.80	16.10	.00
Hf	2.80	3.60	3.60	3.10	3.80
Y	12.10	19.60	18.60	16.70	.00
U	.18	.23	.16	.14	.00
Pb	2.10	2.40	2.20	1.40	.00
La	7.90	10.40	10.20	7.20	8.60
Ce	23.10	28.70	27.20	21.40	.00
Nd	14.50	18.00	19.90	14.80	17.10
Sm	3.85	5.10	4.82	4.05	4.89
Eu	1.28	1.83	1.79	1.60	1.87
Dy	4.10	5.30	5.60	5.30	4.80
Yb	.00	1.88	2.34	2.02	2.16
Lu	.26	.26	.28	.26	.26

TABLE 24.16.—*Composition of olivine-controlled tholeiite of Mauna Loa's northeast rift zone*

[Oxide values (in weight percent) from Wright (1971, table 10), recast to 100 percent dry weight; values for elements in parts per million]

	Prehistoric	Historical		
		19th century		20th century
		1852	1855	1942
Sample	TLW67-29	TLW67-61	TLW67-63	TLW67-62
SiO_2	52.02	48.92	50.74	51.92
MgO	6.99	16.88	9.79	7.21
K_2O	.41	.33	.38	.36
TiO_2	2.10	1.62	2.02	2.06
P_2O_5	.24	.19	.21	.21
Cs	.11	.00	.11	.06
Ba	140.00	174.00	97.00	241.00
Sc	29.40	24.90	29.40	30.90
V	311.00	240.00	298.00	309.00
Cr	224.00	938.00	488.00	270.00
Co	41.90	76.90	53.70	45.00
Ni	88.00	472.00	179.00	76.00
Mo	3.80	4.30	5.40	4.30
Zn	133.00	108.00	145.00	135.00
Ga	19.30	11.80	19.10	20.40
Hf	3.30	2.60	3.00	3.10
Y	19.20	11.80	16.60	16.00
U	.22	.20	.22	.16
Pb	1.00	2.20	1.40	2.20
La	9.40	7.70	9.80	8.90
Ce	25.90	20.40	22.20	22.90
Nd	19.50	13.50	15.90	16.30
Sm	4.57	3.64	4.08	4.53
Eu	1.63	1.40	1.57	1.57
Dy	5.00	4.20	4.40	5.20
Yb	1.92	1.45	1.76	1.89
Lu	.23	.19	.24	.25

averages were computed using the arbitrary time groupings used elsewhere in this study for historical lava (18th and 19th centuries versus 20th century), the two resulting averages would still yield the same results, although the differences between them would be smaller.

In summary, as with the inferred secular variation in Kilauea lava, we admit that the differences observed for Mauna Loa lava also are largely within analytical uncertainty, but we attach significance to the nonrandom pattern of variations defined by the mean compositions of the prehistoric and historical lavas. If the variations were truly statistically random, then there would be no reason for the observed systematic shifts in the ratios of the mean compositions. It is also apparent from our data that the patterns of compositional variation of Mauna Loa lava in time and, possibly, space differ in trend from those for Kilauea lava, as discussed below.

DISCUSSION

DIVERGENCE IN SECULAR VARIATION PATTERNS FOR KILAUEA AND MAUNA LOA LAVAS

Systematic differences in petrographic and major-element characteristics of Kilauea and Mauna Loa lavas have been recognized in numerous previous studies, beginning with Macdonald (1949a, b), and comprehensively documented by Wright (1971). More recently, a few studies, based on limited sampling, have shown that the tholeiite lava of these two volcanoes, not surprisingly, also differ in the abundance patterns of various trace elements (Murata, 1970; Leeman and others, 1977, 1980; Basaltic Volcanism Study Project, 1981; Budahn and Schmitt, 1985). Our study reinforces the findings of these previous workers (fig. 24.13). At a given MgO content, Kilauea olivine-controlled lava has distinctly greater abundances of olivine-incompatible elements than Mauna Loa olivine-controlled lava; these distinctions are enhanced if the Kilauea Iki samples are included in the computation of average composition of Kilauea lava (table 24.14). All recent studies conclude that the chemical differences between Kilauea and Mauna Loa cannot be explained solely by shallow fractionation processes and reflect heterogeneities in the mantle source regions and (or) different melting mechanisms to produce the chemically distinct magmas (see, for example, Leeman and others, 1980; Wright, 1984; Budahn and Schmitt, 1985).

If our inferred time-space-composition relations (tables 24.13, 24.20; figs. 24.6–24.9) are valid, then an intriguing pattern emerges. For Kilauea, the MgO-adjusted mean abundances of K, Ti, P, Sc, Hf, U, and the LREE tend to increase progressively with time, whereas, for Mauna Loa, these elements tend to decrease with time (figs. 24.14, 24.15). These relations are also indicated by the data of Budahn and Schmitt (1985, table 2). The lava of the 1969–71 Mauna Ulu eruption of Kilauea shows considerable major-element variation with time and exhibits at least a temporary reversal in TiO_2 and K_2O content relative to the overall secular change for Kilauea olivine-controlled lava (Wright and others, 1975). However, the limited trace-element data for the Mauna Ulu lava (Leeman and others, 1980; Hoffman and others, 1984) and the November 1975 summit lava (one analysis, Basaltic Volcanism Study Project, 1981), if MgO-adjusted, fall close to our computed mean for 20th-century olivine-controlled Kilauea lava.

The combined effects of these two apparently diverging trends cause the difference in composition between Kilauea and Mauna Loa lava to increase with time (figs. 24.14, 24.15). Our data for other olivine-incompatible elements lack sufficient precision to define other such trends, but the limited data of Budahn and Schmitt (1985, table 2) may indicate a similar divergence of variation trends for Ba and Ta. In addition, the data of Rhodes (1983) for Nb, Zr, and Sr abundances in historical Mauna Loa lava, as discussed earlier, yields a decreasing trend with time; unfortunately, however, comparably precise data for these elements in Kilauea lava needed to fully define the diverging trends for the two volcanoes are lacking.

Samples analyzed in this study include historical eruptions through July 1968 at Kilauea and through 1950 at Mauna Loa. Only limited published trace-element data exist for Hawaiian lava erupted since then to test our observations. The few data on lava of the July 1975 summit eruption at Mauna Loa (Rhodes, 1983; Budahn and Schmitt, 1985) show that its composition falls within the range for other 20th-century eruptions.

Thus, at the present time, available trace-element data are insufficient to ascertain whether the apparent diverging secular variation trends for the two volcanoes continue in lava erupted since

TABLE 24.17.—*Composition of olivine-controlled tholeiite of Mauna Loa's southwest rift zone*

[Oxide values (in weight percent) from Wright (1971, table 9), recast to 100 percent dry weight; values for elements in parts per million. Sample C820 fits definition of differentiated and is omitted in calculation of averages and not plotted in figure 24.10]

	Prehistoric			Historical						
				19th century			20th century			
				1868		1887	1919	1926	1950	
Sample	C819	C820	65MAN-1	W-A-7	1868ML	TLW67-59	H-34	TLW-67-76	TLW67-73	TLW67-79
SiO_2	46.29	49.35	50.44	51.39	46.88	52.27	52.10	51.69	52.03	51.48
MgO	24.25	6.12	13.13	8.84	23.64	7.50	7.09	7.82	6.87	9.22
K_2O	.28	.36	.34	.41	.26	.33	.35	.35	.37	.36
TiO_2	1.24	2.82	1.66	2.07	1.34	1.95	2.12	2.05	2.10	1.93
P_2O_5	.15	.28	.19	.23	.14	.19	.21	.20	.22	.21
Cs	.54	.19	.38	.19	.45	.14	.29	.14	.10	.17
Ba	50.00	230.00	48.00	174.00	108.00	134.00	116.00	110.00	143.00	58.00
Sc	17.70	31.30	25.50	29.30	20.90	30.30	29.60	30.30	31.00	28.60
V	.00	353.00	236.00	295.00	202.00	335.00	362.00	317.00	337.00	311.00
Cr	924.00	78.00	652.00	369.00	1250.00	260.00	237.00	277.00	202.00	395.00
Co	95.70	44.90	61.70	47.00	95.40	46.20	42.80	47.10	44.90	49.70
Ni	.00	62.00	293.00	152.00	846.00	83.00	90.00	145.00	82.00	131.00
Mo	.00	4.30	4.50	4.40	4.00	3.80	5.00	4.60	4.60	5.00
Zn	.00	137.00	123.00	148.00	106.00	119.00	119.00	104.00	114.00	126.00
Ga	.00	21.40	14.80	16.10	8.40	16.60	20.70	19.00	20.40	18.20
Hf	2.00	4.40	2.40	3.20	2.00	3.00	3.20	3.00	3.60	2.80
Y	.00	25.40	15.10	16.20	8.50	21.20	23.90	21.00	20.40	18.80
U	.00	1.00	.16	.21	.16	.15	.25	.17	.18	.19
Pb	.00	3.80	1.50	2.60	3.00	2.30	2.00	3.10	2.30	2.80
La	6.70	11.50	7.20	9.30	5.70	7.80	8.60	8.80	9.00	7.50
Ce	18.20	27.10	20.80	24.40	12.50	21.40	18.80	23.40	23.30	18.80
Nd	11.40	21.80	15.10	14.80	9.50	16.20	16.00	.00	16.80	16.20
Sm	.00	4.66	3.59	4.40	2.67	.00	4.20	4.44	4.36	3.97
Eu	1.02	2.32	1.32	1.69	.99	1.51	1.45	1.61	1.67	1.26
Dy	3.00	6.00	3.80	6.50	2.90	5.00	4.30	5.40	5.90	4.70
Yb	1.21	2.63	1.47	2.00	1.30	2.02	2.00	1.88	2.01	1.94
Lu	.00	.32	.22	.27	.15	.28	.26	.28	.29	.24

TABLE 24.18.—*Composition of olivine-controlled tholeiite of Mauna Loa's northwest and southwest flanks*

[Oxide values (in weight percent) from Wright (1971, tables 11 and 12), recast to 100 percent dry weight; values for elements in parts per million. Sample TLW67-119 fits definition of differentiated and is omitted in calculation of averages and not plotted in figure 24.10]

	Northwest flank				Southwest flank		
	Prehistoric			Historical	Prehistoric (Ninole Hills)		
				1859			
Sample	TW67117A	TLW67119	TLW67125	DPH-77	ID-098-2	ID-275-2	ID-214-2
SiO_2	49.59	52.30	50.84	51.46	50.53	50.08	47.50
MgO	14.37	6.74	7.85	7.75	7.17	9.99	17.45
K_2O	.34	.46	.43	.43	.46	.09	.08
TiO_2	1.70	2.16	2.24	2.17	2.68	2.05	1.61
P_2O_5	.19	.25	.23	.25	.26	.17	.14
Cs	.00	.05	.16	.27	.10	.12	.13
Ba	101.00	94.00	117.00	147.00	138.00	93.00	73.00
Sc	24.80	29.30	29.20	28.70	31.20	30.10	24.90
V	252.00	293.00	290.00	305.00	334.00	312.00	240.00
Cr	628.00	183.00	377.00	278.00	235.00	463.00	854.00
Co	61.50	38.60	46.90	44.50	47.80	53.80	79.60
Ni	371.00	75.00	118.00	98.00	111.00	135.00	477.00
Mo	4.00	2.90	4.40	2.80	5.40	4.60	3.50
Zn	106.00	113.00	107.00	113.00	124.00	123.00	126.00
Ga	12.10	17.60	15.40	15.60	17.00	17.00	11.20
Hf	2.50	3.00	3.30	3.40	4.20	3.00	2.30
Y	12.60	17.10	20.10	19.60	21.90	17.80	12.50
U	.17	.23	.36	.19	.31	.16	.15
Pb	2.60	2.00	1.30	2.00	1.20	3.20	3.40
La	7.90	10.30	10.20	8.80	13.40	7.80	6.70
Ce	19.70	24.80	25.30	25.90	29.30	16.00	14.20
Nd	14.20	17.00	0.00	16.70	0.00	12.60	11.10
Sm	3.64	4.42	4.76	4.77	5.49	3.78	3.10
Eu	1.21	1.52	1.58	1.72	2.08	1.50	1.21
Dy	3.90	4.60	5.30	4.70	6.40	4.20	3.70
Yb	1.65	2.03	1.94	1.75	2.18	1.82	1.49
Lu	.21	.29	.27	.25	.25	.24	.19

TABLE 24.19.—*Composition of differentiated lava of Mauna Loa. These samples are not olivine-controlled in terms of major-element composition*

[Oxide values (in weight percent) from Wright (1971, table 13), recast to 100 percent dry weight; values for elements in parts per million]

	Prehistoric	Historical			
		19th century			20th century
		1843			1926
Sample	9	W-A-22	W-A-23	TLW67-66	TLW67-72
SiO_2	52.49	51.74	51.99	52.05	52.16
MgO	5.54	6.76	6.81	6.68	6.70
K_2O	.73	.46	.45	.47	.42
TiO_2	3.19	2.16	2.16	2.16	2.23
P_2O_5	.42	.25	.25	.26	.23
Cs	.19	.12	.11	.08	.02
Ba	100.00	96.00	137.00	253.00	159.00
Sc	25.90	29.30	29.30	29.30	31.60
V	375.00	299.00	309.00	.00	325.00
Cr	139.00	195.00	226.00	138.00	190.00
Co	41.20	40.50	40.90	43.20	44.50
Ni	86.00	83.00	106.00	.00	78.00
Mo	4.20	4.20	4.20	.00	4.30
Zn	128.00	152.00	131.00	.00	131.00
Ga	21.30	20.20	17.70	.00	18.90
Hf	6.70	3.10	3.30	3.30	3.50
Y	39.30	17.80	19.90	.00	23.30
U	.45	.20	.18	.25	.19
Pb	3.60	2.80	4.00	.00	2.40
La	14.90	11.00	10.30	11.60	11.00
Ce	51.10	30.40	28.50	30.70	24.10
Nd	36.00	18.70	20.20	20.00	18.40
Sm	8.50	4.77	5.22	4.59	4.95
Eu	2.76	1.65	1.70	1.76	1.77
Dy	8.95	4.80	4.60	4.50	5.20
Yb	3.01	1.81	1.73	2.19	2.33
Lu	.42	.26	.24	.37	.30

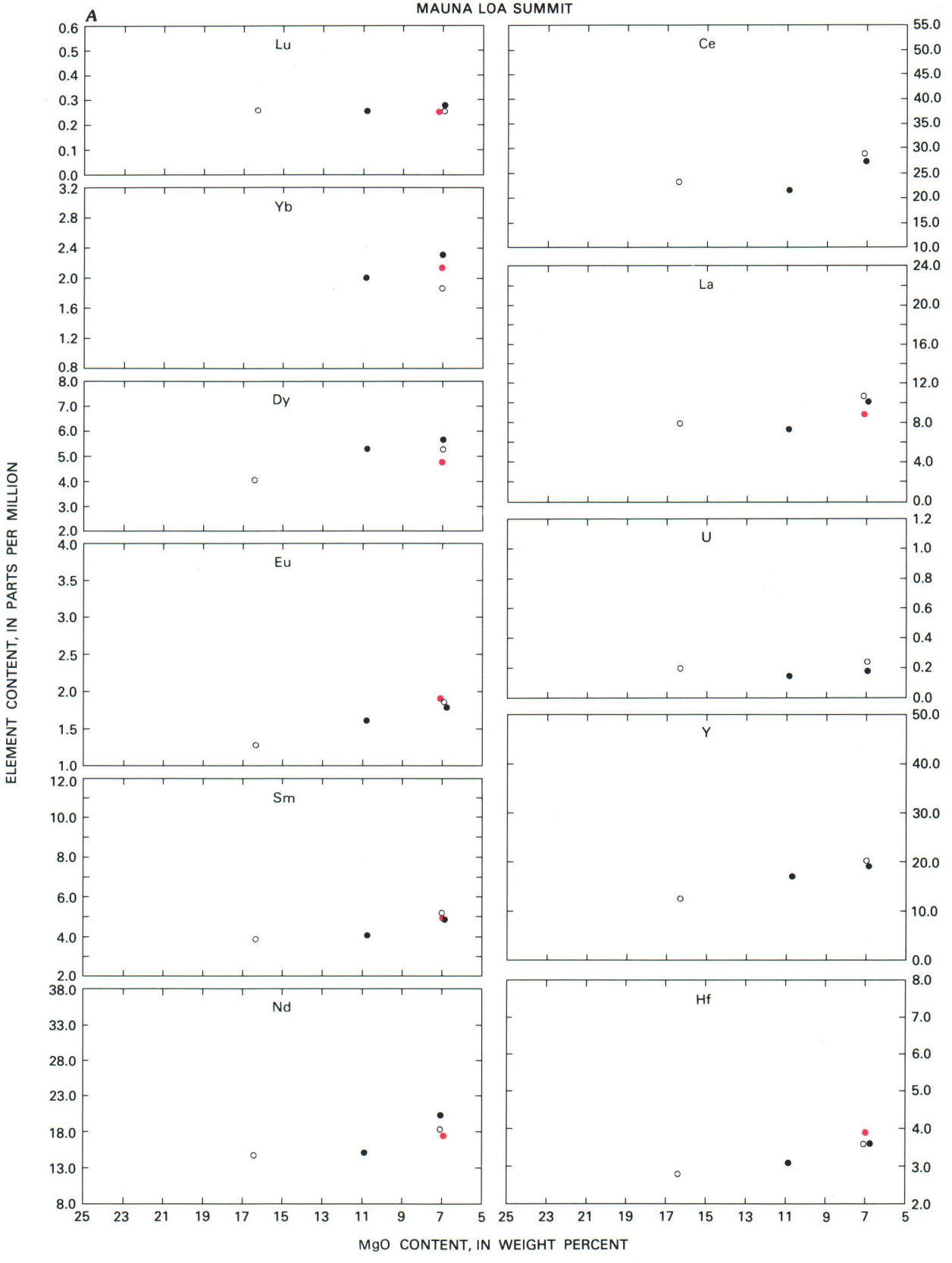

FIGURE 24.10.—MgO-variation diagrams for olivine-controlled lava of Mauna Loa. ***A,*** Summit (SUM). ***B,*** Southwest rift zone (SWRZ). ***C,*** Northeast rift zone (NERZ). ***D,*** Northwest and southeast flanks (FLKS). Open symbols, prehistoric; solid black symbols, 19th century: solid red symbols, 20th century. Differentiated lava (MgO <6.8 weight percent) of Mauna Loa (table 24.19) and of Kilauea (samples specified in headings of tables 24.9–24.11) would plot in dashed fields.

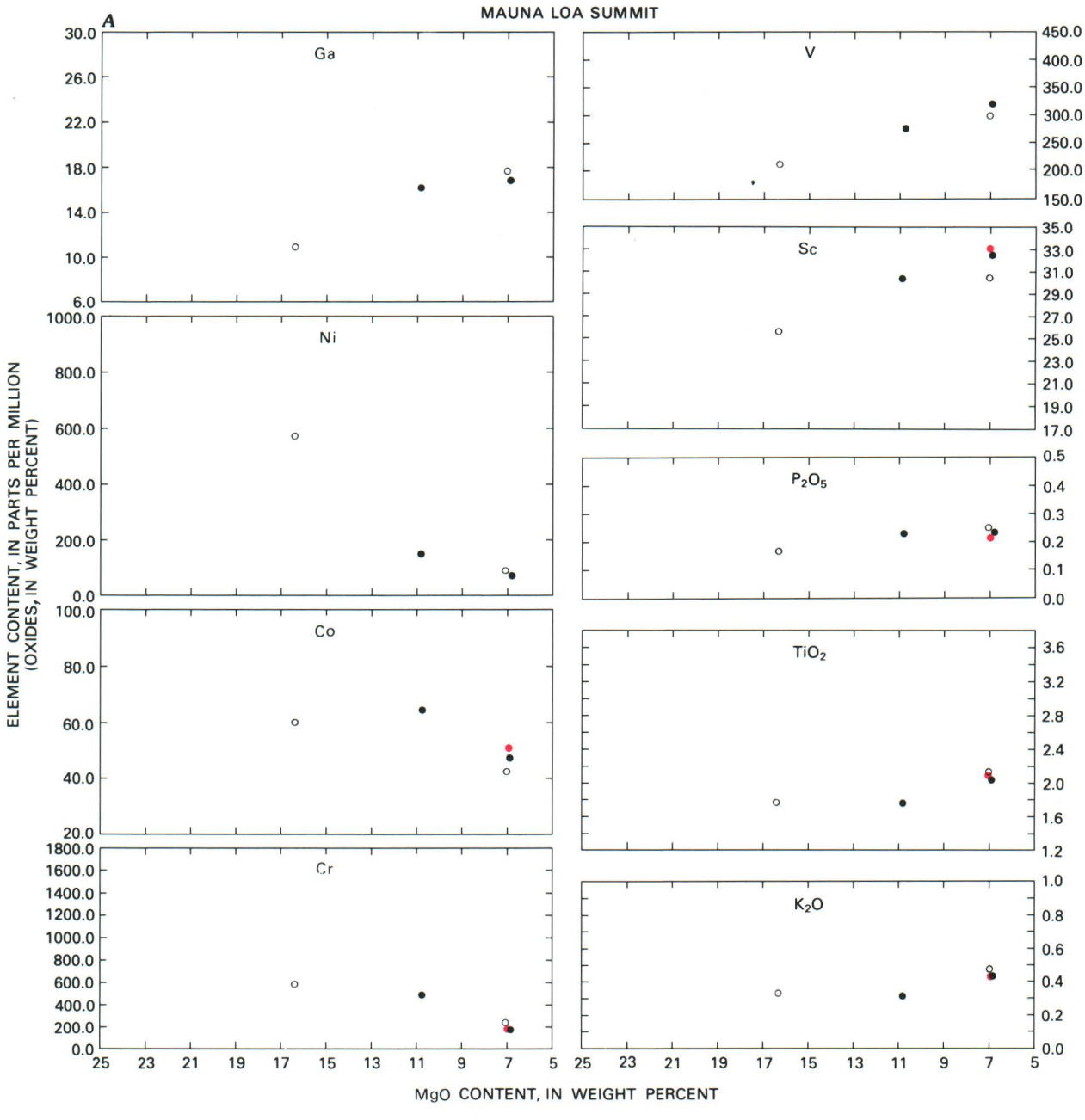

FIGURE 24.10.—Continued.

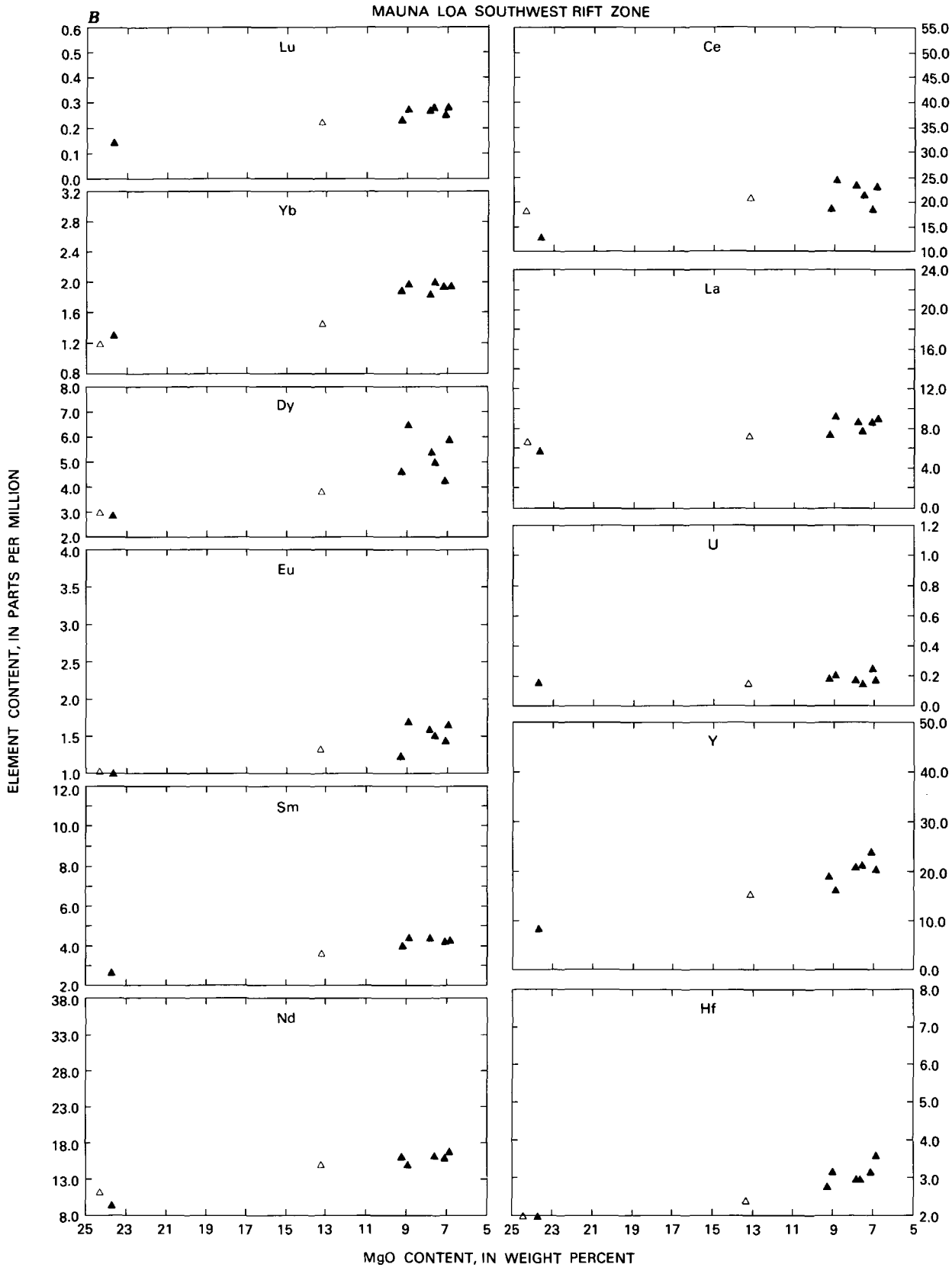

FIGURE 24.10.—Continued.

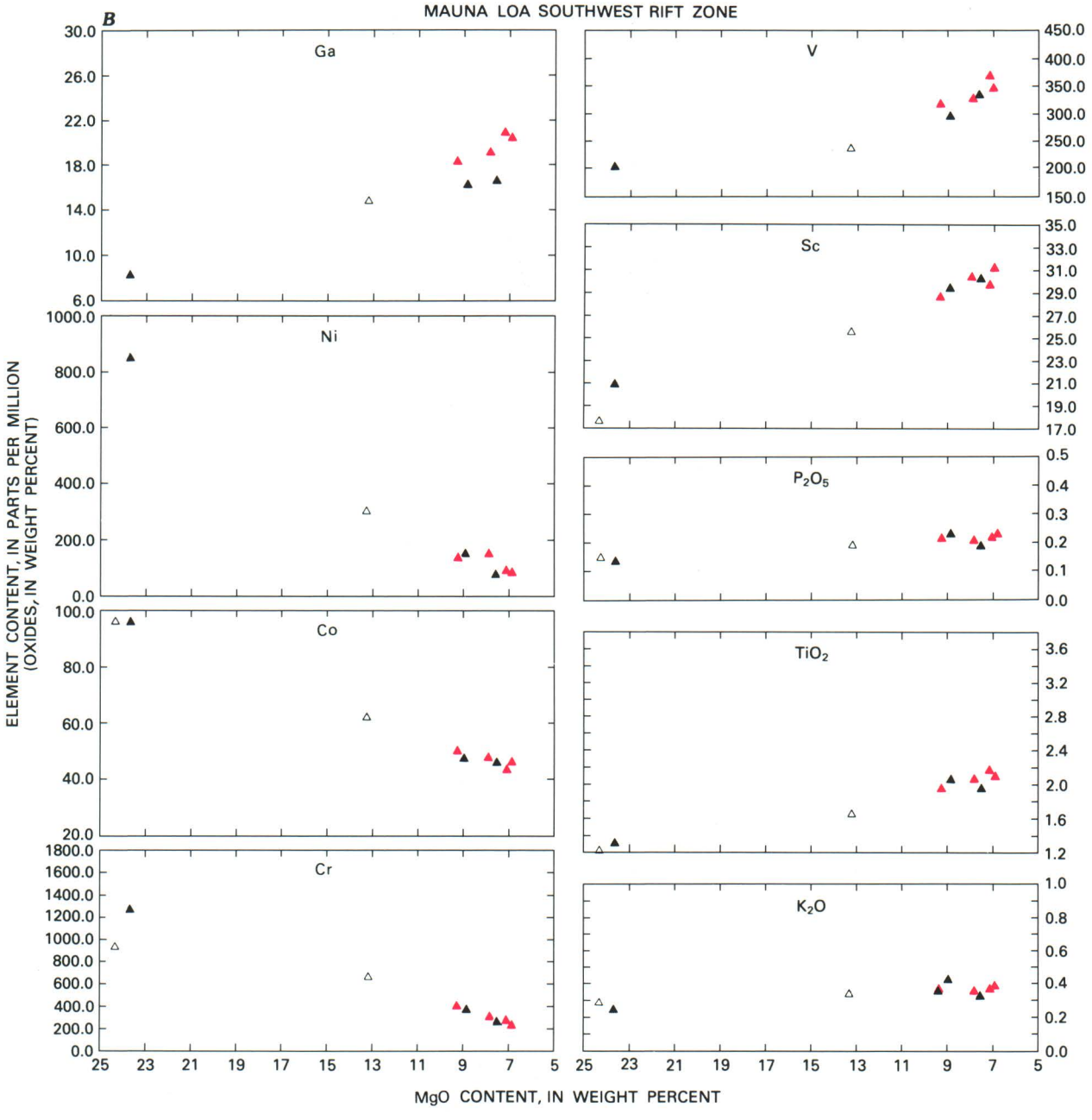

FIGURE 24.10.—Continued.

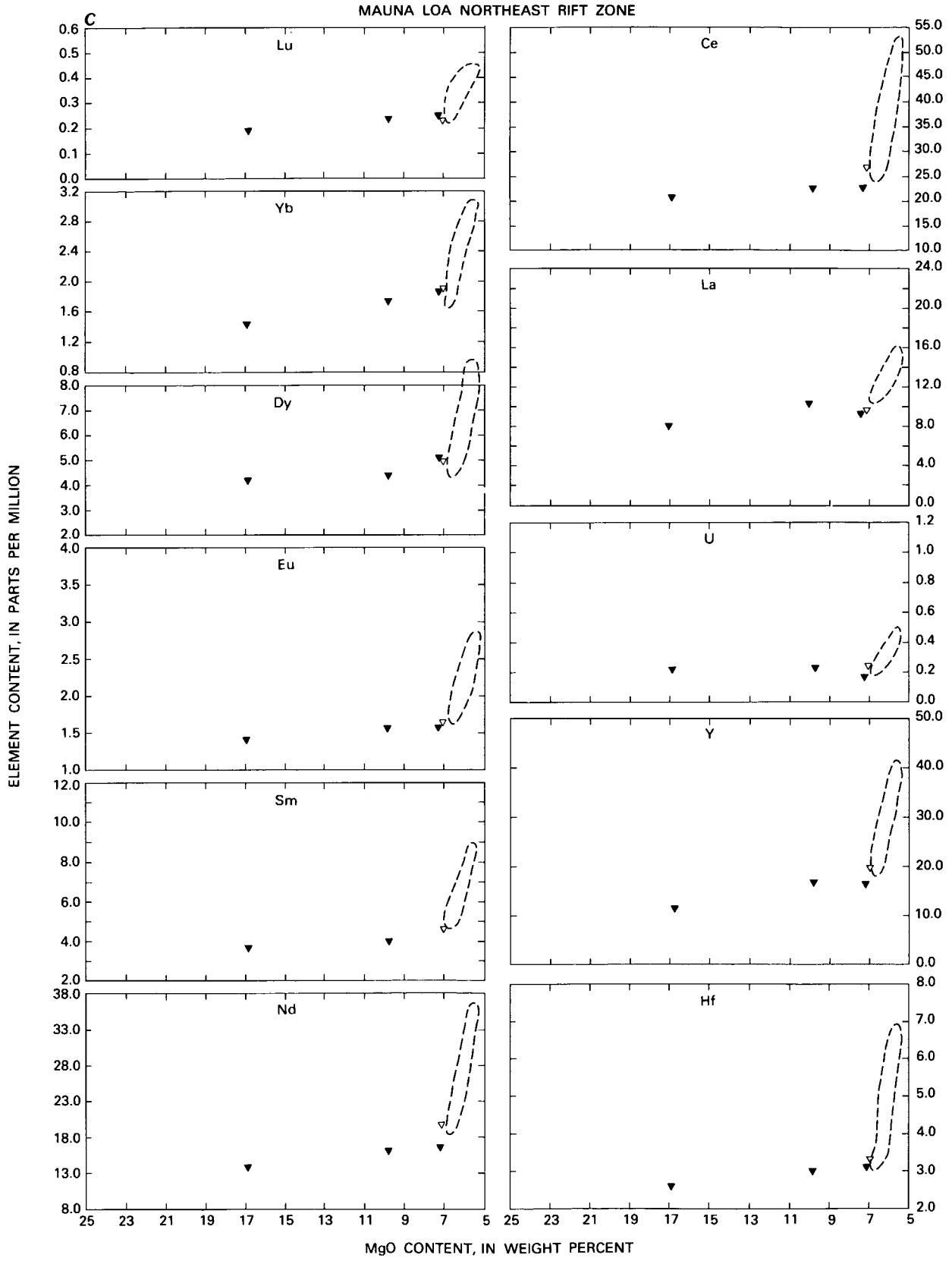

FIGURE 24.10.—Continued.

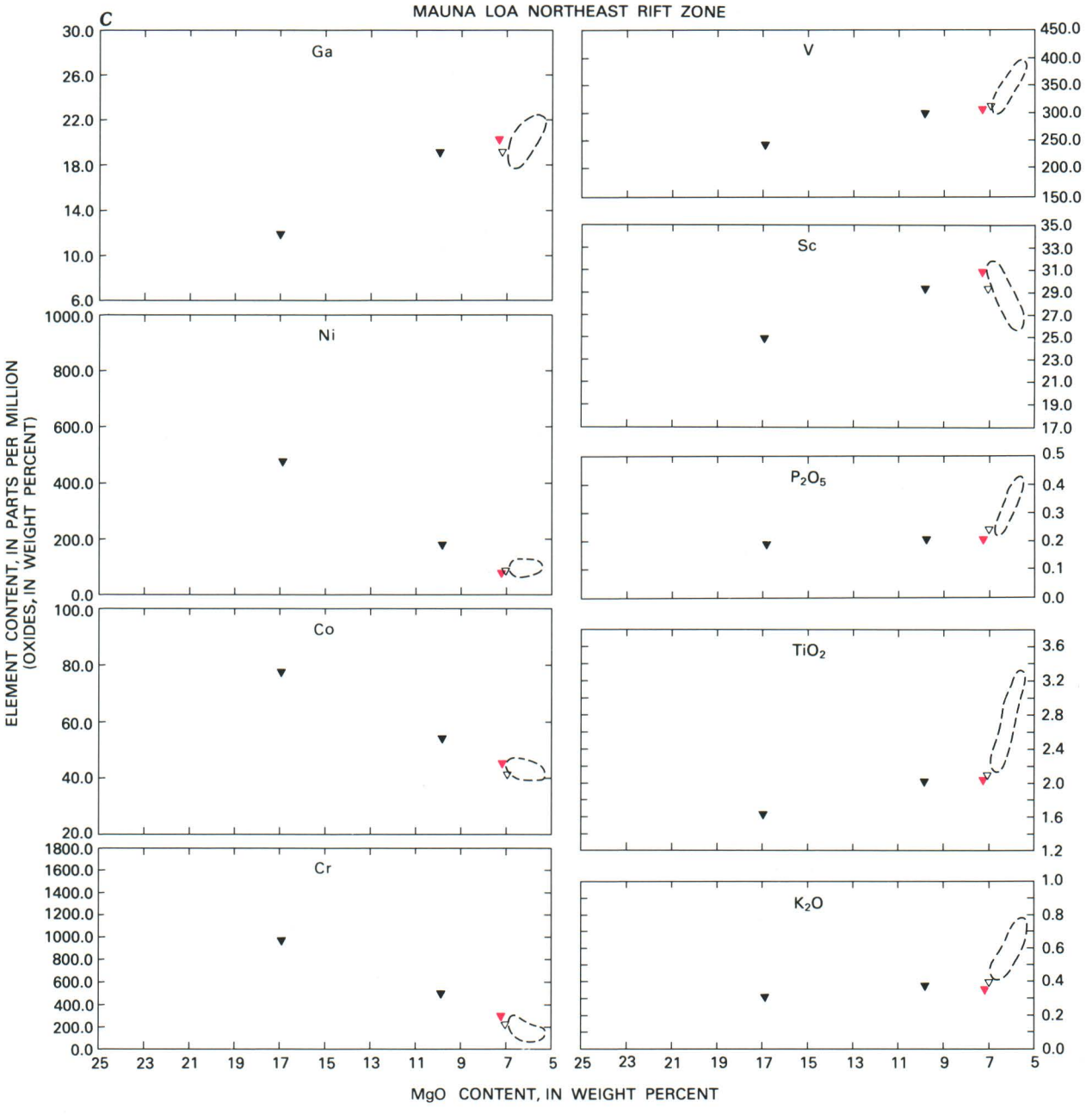

FIGURE 24.10.—Continued.

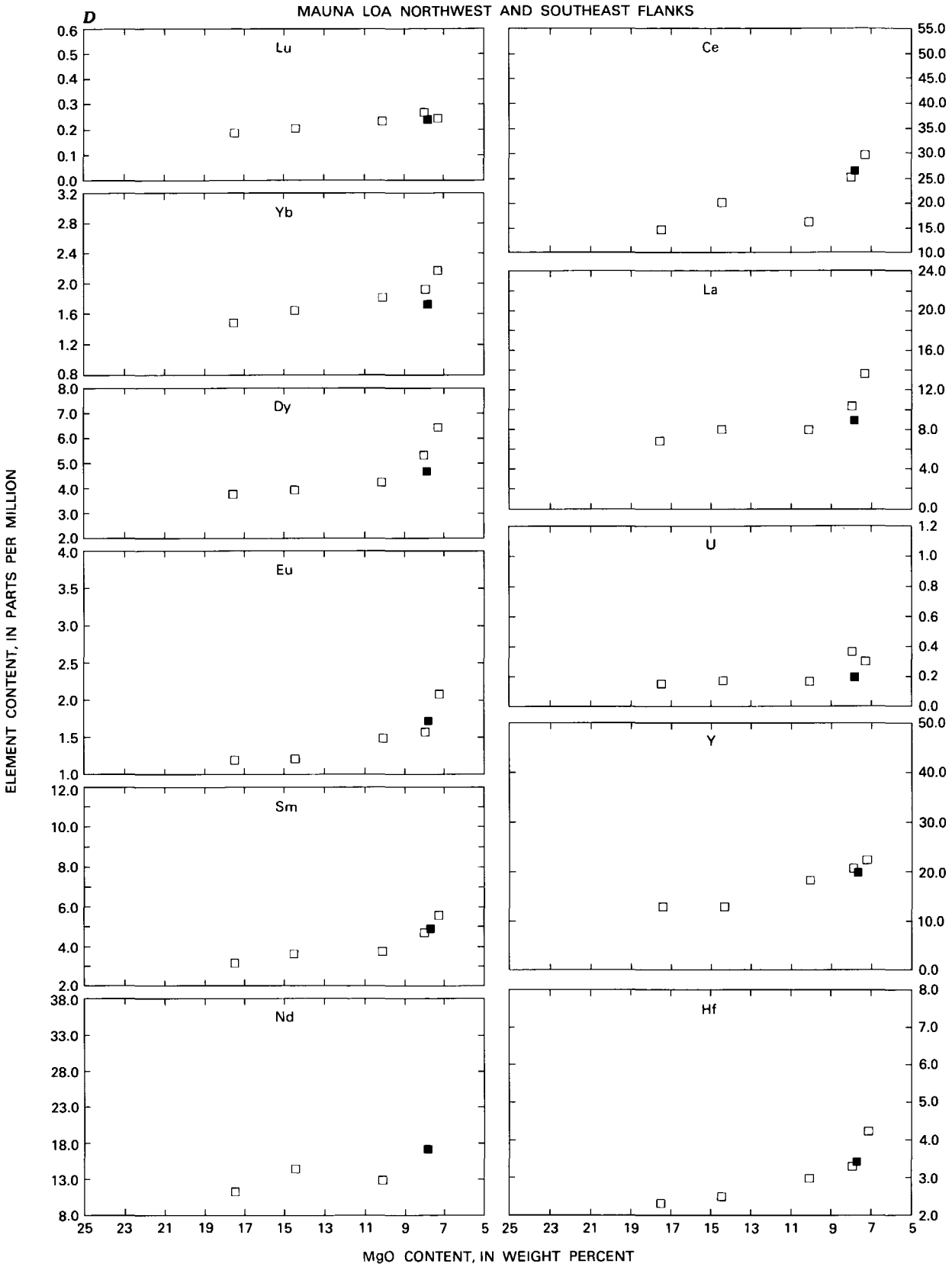

FIGURE 24.10.—Continued.

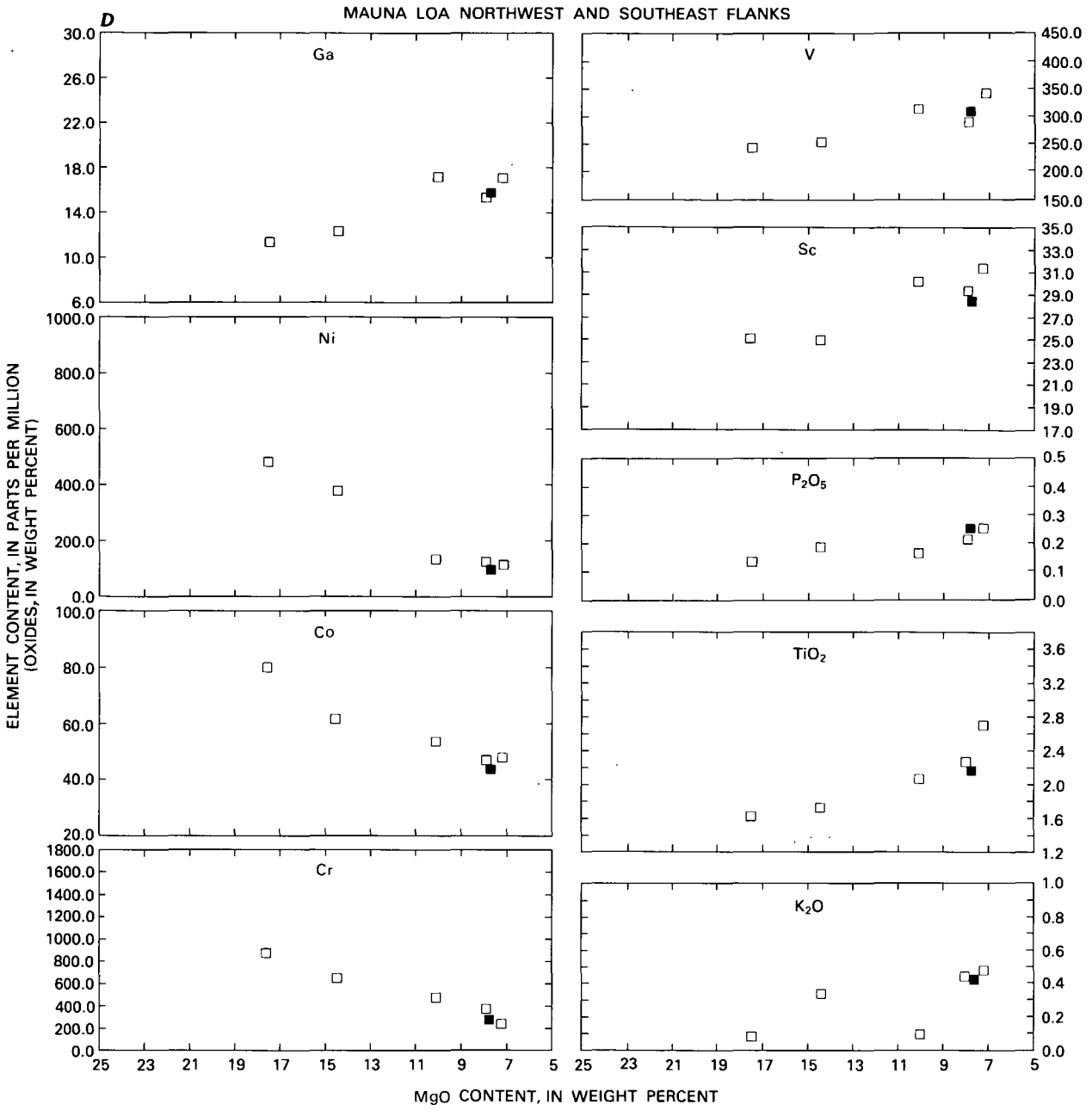

FIGURE 24.10.—Continued.

TABLE 24.20.—*Average compositions of spatial and temporal groups of olivine-controlled lava of Mauna Loa, adjusted to 7.00 weight percent MgO*

[Calculated from data in table 24.15–24.18: S.d., standard deviation. Oxide values in weight percent; values for elements in parts per million. Numbers of samples where different from numbers (n) given: summit, 3 for Cs and 4 for V, Ni, Mo, Zn, Ga, Y, U, Pb, Ce, and Yb; northeast rift zone, 3 for Cs; southwest rift zone, 8 for V, Ni, Mo, Zn, Ga, Y, U, Pb, Nd, and Lu, 7 for Sm; northwest and southeast flanks, 5 for Cs, 4 for Nd; prehistoric, 9 for V, Ni, Mo, Zn, Ga, Y, U, Pb, Sm, and Yb, 8 for Cs and Nd; 18th and 19th centuries, 7 for Sm and 6 for Cs; 20th century, 5 for V, Ni, Mo, Zn, Ga, Y, U, Pb, Ce, and Nd]

	Spatial groups								Temporal groups							
	Summit		Northeast rift zone		Southwest rift zone		Northwest and Southeast flanks		Prehistoric		18th-19th centuries		20th century		Historical (all)	
	n=5		n=4		n=9		n=6		n=10		n=8		n=6		n=14	
	Mean	S.d.	Mean	S.d.	Mean	S.d.	Mean	S.d.	Mean	S.d.	Mean	S.d.	Mean	S.d.	Mean	S.d.
MgO	7.00	-	7.00	-	7.00	-	7.00	-	7.00	-	7.00	-	7.00	-	7.00	-
P_2O	.40	.05	.40	.03	.40	.05	[1] .44	<.02	[1] .44	.03	.40	.05	.37	<.02	.39	.04
TiO_2	2.07	.14	2.12	.04	2.10	.10	[2]2.20	.08	[2]2.16	.11	2.11	.13	2.08	.03	2.10	.10
P_2O_5	.23	<.02	.23	<.02	.22	.02	.24	.01	[1] .24	<.02	.23	.02	.21	<.01	.22	.02
Cs	.20	.13	.10	.03	.36	.32	[1] .17	.07	.29	.29	.26	.26	.18	.10	.22	.20
Ba	107	37	180	68	120	47	118	22	102	25	156	47	128	62	144	54
Sc	32.3	1.3	31.3	1.6	[3]30.6	.5	31.2	1.7	31.2	1.5	[3] 31.6	1.5	30.9	1.0	31.6	1.8
V	294	22	312	5	324	26	315	16	302	24	315	12	332	20	321	17
Cr	[4]218	30	258	30	228	11	200	94	[4]210	82	[4]240	34	227	19	234	27
Co	[5]48.1	3.7	42.2	2.2	[5]42.6	3.0	41.2	5.1	[5]41.2	4.2	[5]44.1	4.4	44.7	3.2	44.5	3.
Ni	[4]88	1	[6]76	18	[7]72	25	[8]73	25	[9]86	15	[10]58	22	[11]83	14	7	
Mo	4.2	.5	4.9	1.0	5.0	.09	4.6	.9	4.7	.6	4.7	1.3	4.8	.4	4.7	1.0
Zn	131	24	132	15	123	14	119	12	121	11	133	19	121	13	128	18
Ga	16.5	1.7	19.0	2.3	18.2	2.1	16.2	1.3	16.6	1.7	16.9	1.8	20.0	.6	18.1	2.1
Hf	3.6	.1	3.3	.2	3.2	.3	3.4	.4	3.4	.4	3.4	.2	3.3	.3	3.3	.2
Y	18.1	1.6	17.2	1.6	19.6	3.0	19.0	2.4	18.5	2.2	18.0	2.2	20.3	2.8	18.9	2.6
U	.20	.05	.22	.05	.20	.04	.24	.08	.24	.06	.21	.05	.20	.04	.20	.04
Pb	2.2	.5	1.9	.8	2.8	1.1	2.6	1.4	2.4	1.2	2.5	1.2	2.5	.5	2.5	1.0
La	9.5	1.1	9.8	.7	9.2	1.2	10.0	1.8	10.2	1.5	9.4	1.0	8.7	.4	9.1	.9
Ce	27.4	2.8	25.0	1.9	23.5	3.9	23.7	4.6	25.8	4.7	24.6	2.3	21.8	2.2	23.5	2.6
Nd	18.0	1.4	17.8	1.3	17.0	1.5	15.8	1.8	17.6	2.2	17.1	1.4	16.7	.5	16.9	1.1
Sm	4.86	.24	4.59	.19	4.39	.19	4.67	.52	4.68	.48	4.66	.19	4.45	.26	4.56	.24
Eu	1.79	.08	1.69	.12	1.61	.15	1.70	.21	1.70	.17	1.73	.10	1.58	.19	1.67	.15
Dy	5.4	.4	5.1	.4	5.3	.8	5.2	.7	5.2	.6	4.8	1.7	5.1	.6	5.3	.6
Yb	2.15	.20	1.91	.02	2.03	.14	2.02	.13	1.98	.13	2.07	.19	2.00	.10	2.04	.16
Lu	.29	.03	.25	.01	.27	.01	.26	.01	.28	.03	.27	<.02	.26	<.02	<.27	<.02

[1]Anomalously low values of K_2O and TiO_2 (samples ID-275-2 and ID-214-2) omitted.
[2]High adjusted value of 2.69 ppm (sample ID-098-2) omitted.
[3]High adjusted value of 36.0 ppm (sample 1868 ML) omitted.
[4]Two negative adjusted values (samples TLW67-84 and TLW67-89) omitted. (See text, appendix 24.1).
[5]Anomalously low adjusted values (<30 ppm) (samples TLW67-84, C819, 1868 ML) omitted.
[6]Two negative adjusted values (samples TLW67-61 and TLW67-63) omitted.
[7]Two negative adjusted values (samples C819 and 1868 ML) omitted.
[8]Three negative adjusted values (samples TLW67-117A, ID-275-2, and ID-214-2) omitted.
[9]Five negative adjusted values (samples TLW67-84, 65 MAN-1, TLW67-117A, ID-275-2, and ID-214-2) omitted.
[10]Four negative adjusted values (samples TLW67-89, TLW67-61, TLW67-63, and 1868 ML) omitted.
[11]The negative adjusted value for sample TLW67-79 omitted.

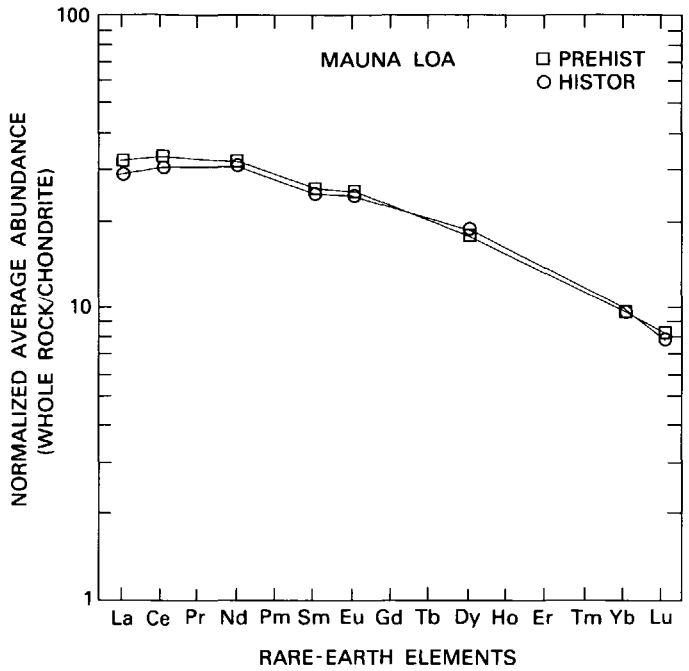

FIGURE 24.11.—Chondrite-normalized average REE abundances showing difference in LREE between prehistoric (PREHIST) and historical (HISTOR) lava of Mauna Loa (see table 24.20). Data of Budahn and Schmitt (1985, table 2) demonstrate a similar systematic difference.

TABLE 24.21.—*Averages of MgO-adjusted mean abundances of selected incompatible elements in historical lava of Mauna Loa*

[Calculated from data of Rhodes (1983, table 1), S.d., standard deviation. Oxide values in weight percent, values for trace elements in parts per million; see text and figure 24.12 for rationale in grouping eruptions]

	Average of 5 pre-1870 eruptions[1]		Average of 11 post-1870 eruptions[2]	
	Mean	S.d.	Mean	S.d.
K_2O	0.43	0.02	0.36	0.02
TiO_2	2.13	.02	2.06	.03
P_2O_5	.26	.01	.23	.01
Nb	10.5	.2	9.4	.2
Zr	140	5	131	4
Sr	350	16	309	10

[1]Total of 31 analyses for the following eruptions: 1843, 1852, 1855, 1859, and 1868 (see Rhodes, 1983, for the individual means and standard deviations of these and the eruptions listed below).

[2]Total of 83 analyses for the following eruptions: 1880, 1887, 1899, 1907, 1916, 1926, 1935, 1942, 1949, 1950, and 1975.

July 1968. It is beyond the scope of this paper to review the various petrogenetic models proposed for Hawaiian tholeiite in the light of the possible space-time-composition relations suggested by our reconnaissance study. It is clear, however, that any complete model involving partial melting and fractionation must reconcile not only the compositional differences between Mauna Loa and Kilauea lava, but also the time-space chemical variations within the lava of each volcano.

LONG-TERM AND SHORT-TERM VARIATIONS

Differences in MgO-adjusted composition within the summit (olivine-controlled) lava are interpreted to represent chemically distinct batches of magma derived from a source, or sources, whose composition evolves with time. A long-term secular major-element variation for Kilauea lava, on the scale of centuries to millenia, has been well documented by Wright (1971, p. 29), who showed that younger lava becomes progressively "richer in the olivine-incompatible constituents (K_2O, P_2O_5, TiO_2)" with time. The results of this study, as well as those of other recent studies (for example, Casadevall and Dzurisin, chapter 13; Easton and Garcia, 1980; Budahn and Schmitt, 1985) show that long-term temporal variations are also evident in trace-element abundance patterns.

Superimposed on this long-term temporal variation for Kilauea lava are shorter term (years to decades) variations, as shown by the chemically distinct MgO-adjusted lava compositions for five summit eruptions, including Kilauea Iki, during the 16-year period from 1952 to 1968 (Wright, 1971, fig. 12). An excellent recent example of short-term compositional variation at Kilauea is afforded by the olivine-controlled lava of the 1969–74 Mauna Ulu eruption (Tilling and others, chapter 16; Swanson and others, 1979). During its 5-year period, this eruption produced 10 chemically distinct variants, interpreted by Wright and others (1975) and Wright and Tilling (1980) to represent new magma batches entering Kilauea's storage reservoir. Hoffman and others (1984) confirmed the short-term secular compositional variation in the Mauna Ulu lava, defined by "monotonic decrease" in the abundances of certain elements, but interpreted it in terms of an equilibrium partial melting model not requiring magma batches. The major-element composition of the Mauna Ulu lava appears to show at least a short-term reversal of the long-term secular variation at Kilauea (Wright and others, 1975). Whether this change represents a permanent departure from the overall trend remains to be tested by systematic evaluation of the chemistry of lava erupted at Kilauea since June 1974.

Possible short-term secular variations, as expressed by compositional changes with small differences in stratigraphic position, also are apparent in recent studies on prehistoric Kilauea lava (Casadevall and Dzurisin, chapter 13; Easton and Garcia, 1980), but it is not possible to place precise time constraints on these samples. However, from detailed data on 20th-century olivine-controlled Kilauea lava, particularly from the Mauna Ulu eruption, we know that significant changes, not explainable by olivine control, can occur on a time scale of a year or less.

Perhaps the most significant conclusions from this reconnaissance study are that: (1) Mauna Loa lava, like Kilauea lava, shows long-term secular variation in composition; and (2) the trends of such variation for the two volcanoes diverge, providing additional evidence that their magmatic systems operate independently. The focus and sampling of our study were not intended to identify possible short-term variations in the MgO-adjusted olivine-controlled Mauna Loa lava. However, we believe that the comprehensive data of Rhodes (1983), in addition to confirming our suggestion of secular variation between the 19th century and 20th-century lava, also provides good evidence of short-term variation on a time scale as

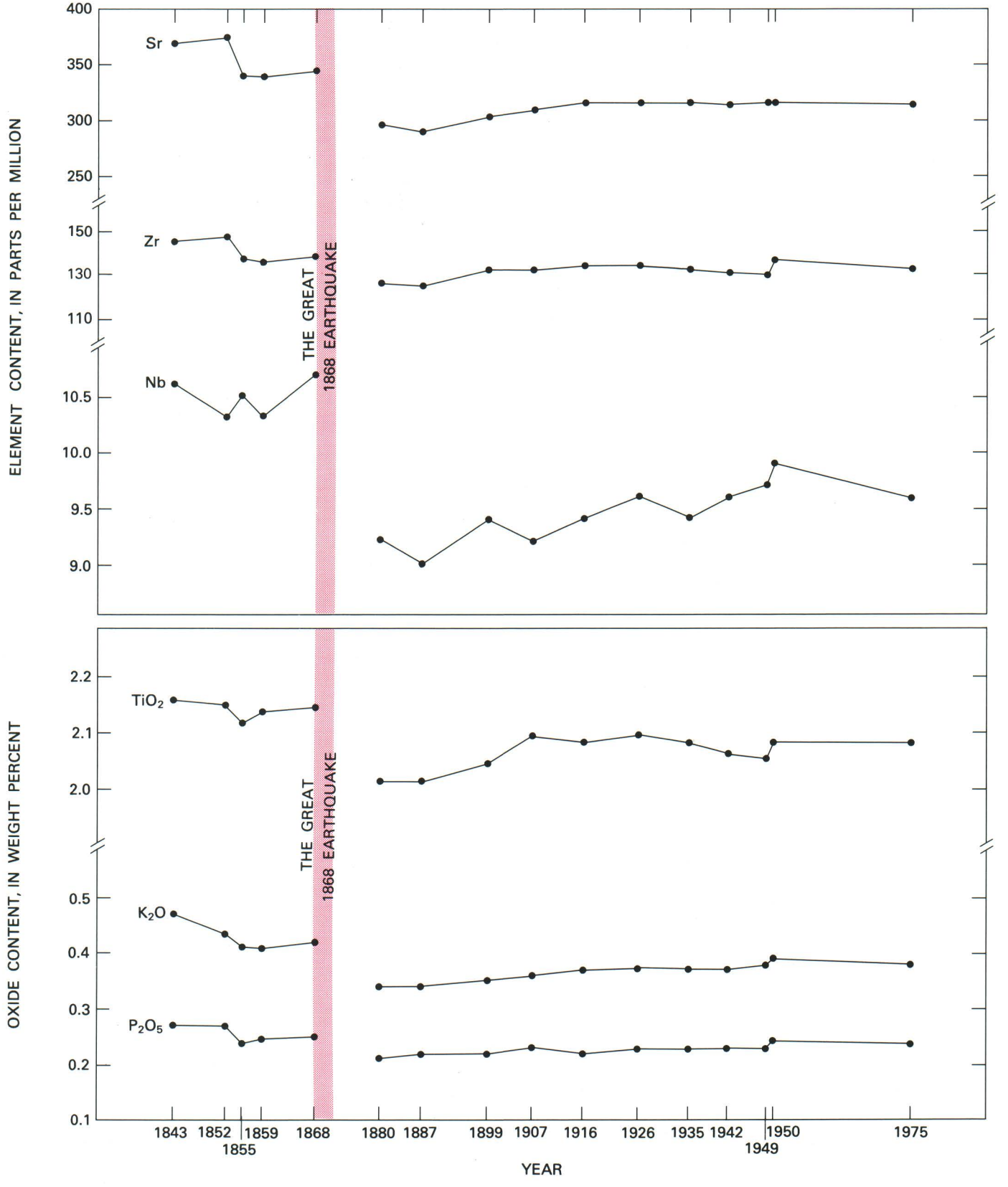

FIGURE 24.12.—MgO-adjusted average contents of olivine-incompatible elements and oxides in lava of historical Mauna Loa eruptions (data of Rhodes, 1983) plotted against year of eruption. Data published as averages; thus, individual analyses could not be adjusted for MgO content before computation of mean, as generally done in this paper (see appendix 24.1). Compositional break between 1868 and 1880 eruptions may reflect disruptive effects of catastrophic 1868 earthquake (see text).

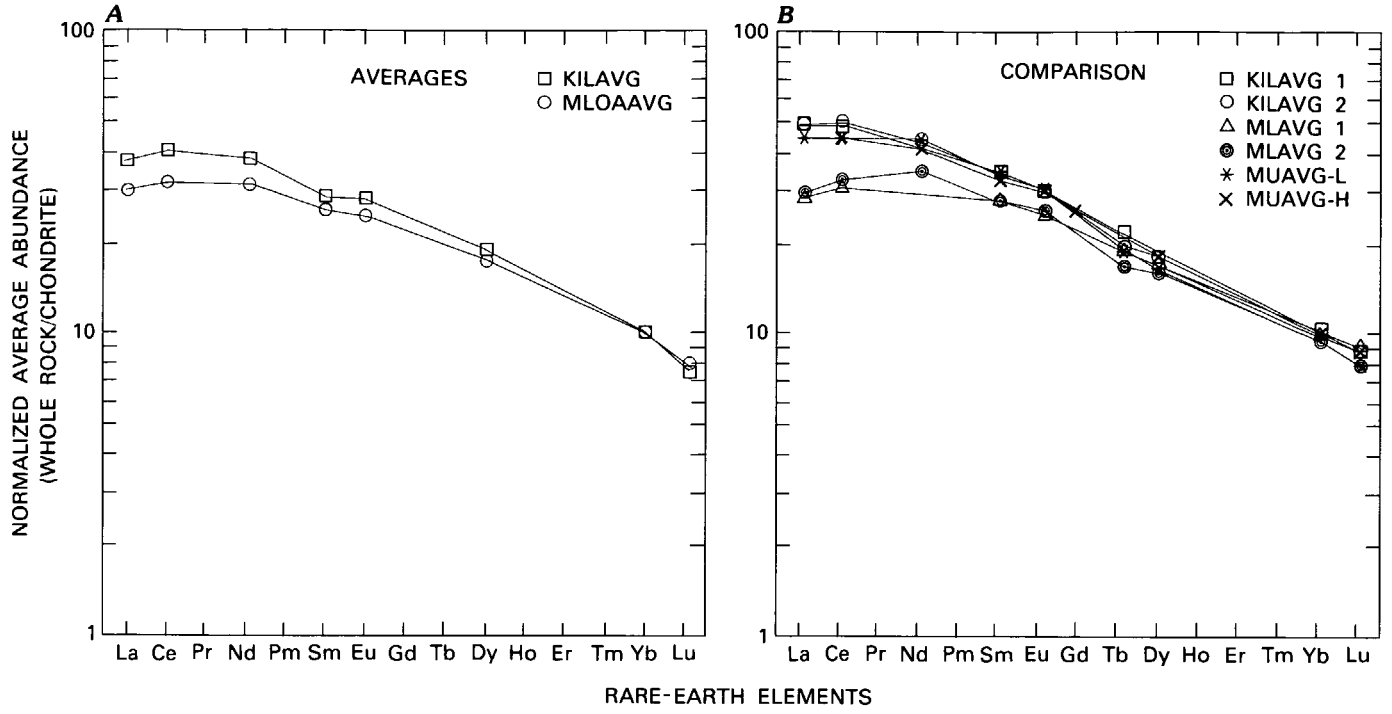

FIGURE 24.13.—Difference in MgO-adjusted average REE abundances between Kilauea (KIL), including Mauna Ulu (MU), and Mauna Loa (ML) lava samples. ***A***, Data of this paper. ***B***, Previously published data: KILAVG1 and MLAVG 1 (Basaltic Volcanism Study Project, 1981); KILAVG2 MLAVG2, and MUAVG-L (Leeman and others, 1980); MUAVG-H (Hoffman and others, 1984). See also figure 24.4 for data of Budahn and Schmitt (1985) showing compositional distinction between Mauna Loa and Kilauea.

small as one year (fig. 24.12; Rhodes and others, 1982; Rhodes, 1983). Although the variations shown in figure 24.12 may in some instances be within analytical uncertainty, the nonrandom nature of the variations and the remarkable conformity of the trends convince us that the differences shown are real. Rhodes and others (1982, abstract 43) labeled the compositional changes observed for historical Mauna Loa lava, including the "sudden drop between 1868 and 1880," as "episodic" variations. However, we interpret these compositional variations (fig. 24.12) as a segment of a long-term secular trend of decreasing abundances of the incompatible elements considered. This trend was abruptly disrupted by the processes accompanying or immediately following the 1868 eruption, but a gradual recovery afterward reestablished conformance with the general trend.

Some observations concerning the 1868 eruption are pertinent and might bear on the sharp compositional break. Some of the lava from the 1868 eruption is picritic—containing as much as 50 percent olivine phenocrysts—and has the highest mean MgO content (17.69 weight percent) of any historical Mauna Loa lava (Rhodes, 1983, table 1). This eruption began at Mauna Loa summit on March 27, 1868, and initially produced lava of moderate MgO content (~9 percent, according to Rhodes, 1983). On April 2, a catastrophic earthquake struck the Island of Hawaii; this earthquake was the largest historical earthquake in Hawaii and estimated to be greater than the magnitude-7.2 event at Kalapana on November 29, 1975 (Tilling and others, 1976). The 1868 eruptive activity shifted to the southwest rift zone on April 7, and picritic lava began to be erupted from a 5-km-long fissure, marking the first major historical activity in Mauna Loa's southwest rift zone. As noted by Lipman (1980, p. 709), the eruptive fissure was localized at the lowest elevation of any historical vent (600–900 m) in a segment of the southwest rift where "no large eruption appears to have occurred for several thousand years previously." Lipman (p. 709) suggests that the earthquake, apparently centered along the southeast flank of Mauna Loa, "may have been significant in opening up a lower part of the rift zone from which access of magma had previously been blocked for a long time."

The eruption, which ended on April 11, 1868, is interpreted to have successively tapped first the upper (olivine-poor) and then the lower (olivine-rich) part of a zoned magma reservoir developed by olivine settling (Lipman, 1980). We further suggest that the 1868 earthquake may have caused a sudden, drastic change in Mauna Loa's magma regime, as expressed by the abrupt compositional discontinuity and decades-long subsequent recovery in the long-term secular variation trend for Mauna Loa lava (fig. 24.12). Lockwood and Lipman (chapter 18, fig. 18.7) show that the average lava-production rate for Mauna Loa after 1877 was less than half that before 1877 and note that this marked change coincides with the compositional shift in historical lava (Rhodes and others, 1982). Lockwood and Lipman (chapter 18) also, independently from our study, suggest that this change in rate and composition might be related to the 1868 earthquake.

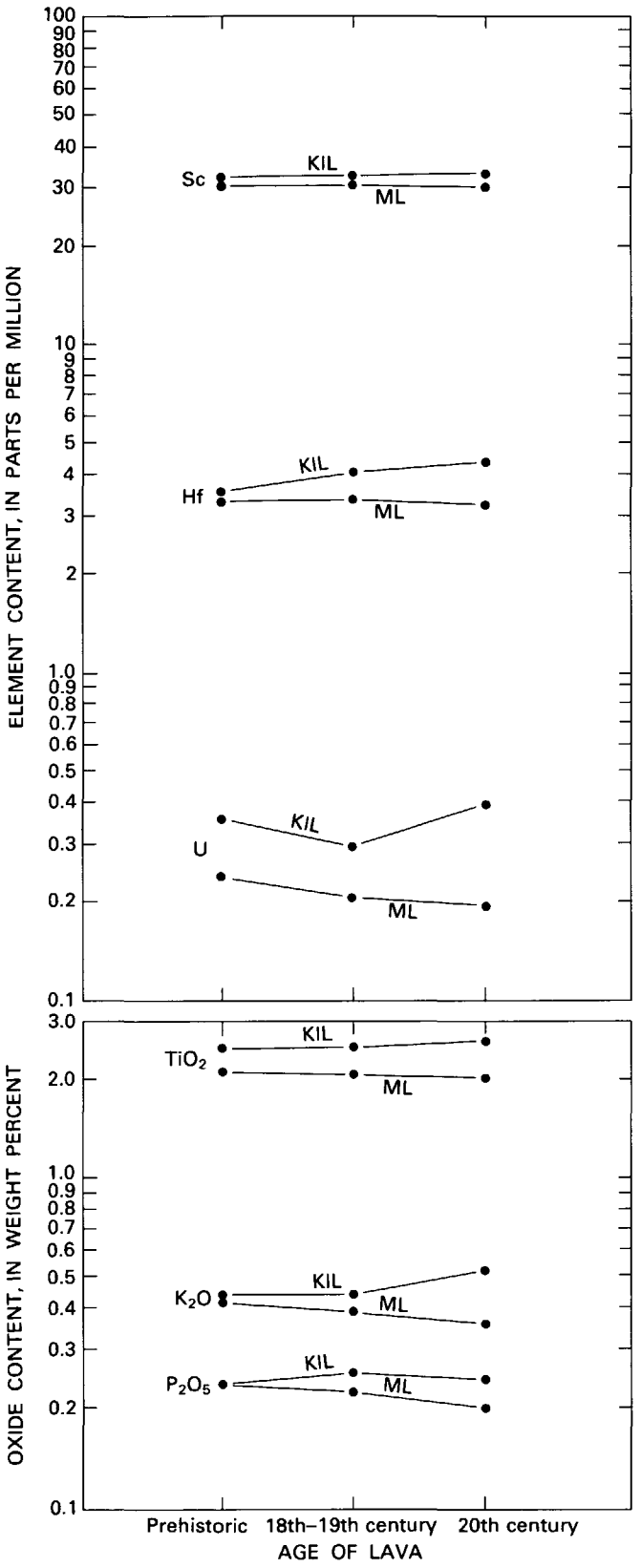

FIGURE 24.14.—Apparent diverging long-term secular compositional trends for Kilauea (KIL) and Mauna Loa (ML) olivine-controlled lava, as suggested by variations in MgO-adjusted mean contents of K, Ti, P, Sc, Hf, and U. (Data from tables 24.13 and 24.20).

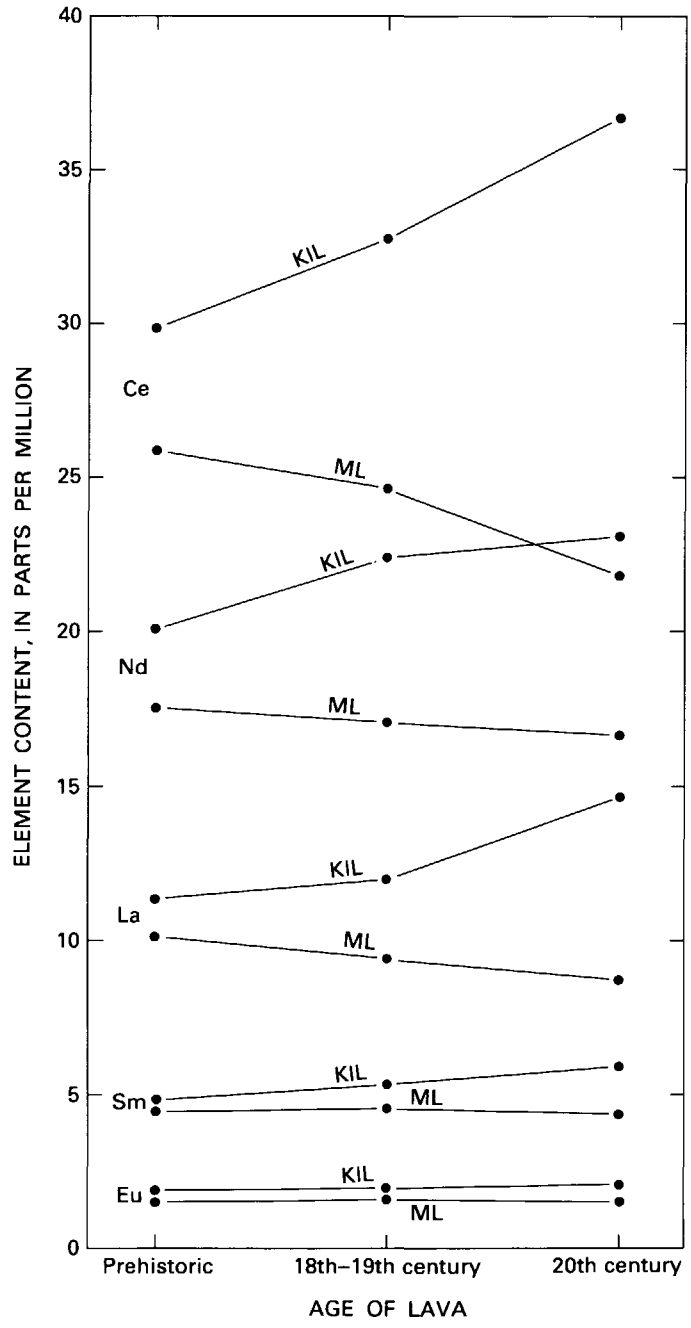

FIGURE 24.15.—Diverging long-term secular compositional trends of Kilauea (KIL) and Mauna Loa (ML) lava, as shown by variations in MgO-adjusted mean LREE abundances (data of tables 24.13 and 24.20). HREE abundance patterns of two volcanoes tend to converge, and no systematic differences are evident within analytical uncertainty.

The apparent coincidence between the compositional break, the change in lava-production rate, and the catastrophic 1868 earthquake may be purely fortuitous, but we speculate that these phenomena are at least indirectly related. If so, it would be of interest to determine whether a similar compositional break might exist for Kilauea lava, in view of the fact that the 1868 earthquake also apparently triggered, on the same day, (1) a brief eruptive outbreak at Kilauea Iki; (2) extrusion of a small amount of lava in the southwest rift zone about 15 km from the summit; and (3) approximately 100 m of subsidence of the floor of Kilauea caldera, without affecting the ongoing lava-lake activity at Halemaumau (Tilling and others, 1976; Lipman, 1980). A major change in Kilauea magma regime related to the 1975 Kalapana earthquake (magnitude 7.2) has been well documented (Dzurisin and others, 1981, 1984). Moreover, a much lower energy (magnitude 6.2) earthquake in April 1973 is interpreted to have caused substantial disruption in the magma conduit system during the 1972–74 Mauna Ulu eruption (Tilling and others, chapter 16), but the possibility that the 1973 and 1975 earthquakes might also coincide with detectable compositional changes in Kilauea lavas erupted since 1971 has not been evaluated.

DIRECTIONS FOR FUTURE STUDIES

This reconnaissance study clearly needs to be followed by more quantitative studies to confirm, refine, or reject our preliminary findings. Subsequent investigations ought to include, though not be limited to, the following.

PRECISE AND ACCURATE DETERMINATIONS OF ADDITIONAL TRACE ELEMENTS

The tentative conclusions we reached in this study are based primarily on analytical data for the well determined olivine-incompatible elements (K, Ti, P, Sc, Hf, U, and the REE), although some of the less well determined elements provide permissive evidence. It would be important to test our findings with comparably well determined abundances of other selected key incompatible elements, ideally in the same rock powders (to minimize effects of possible sample inhomogeneity) that we have analyzed. Some of the other key incompatible elements that should be investigated include Rb, Cs, Sr, Ba, Zr, Nb, Ta, and Th. In addition, the abundances of Ir, Au, and Ag in volcanic rocks, which can be precisely and accurately determined at concentrations of less than one part per billion, have been shown to be highly sensitive to differentiation processes as well as source-area effects (see, for example, Gottfried and Greenland, 1972; Bornhorst and others, 1984). Thus, systematic studies of Au, Ag, and the platinum metals, as well as studies of Cu and S to assess the effect of possible immiscible sulfide melt in tholeiite magma (for example, Skinner and Peck, 1969; Moore and Fabbi, 1971; Gottfried, 1983) should provide important trace-element data to complement the already abundant data for incompatible elements.

QUANTITATIVE OLIVINE-CONTROL LINES FOR SELECTED ELEMENTS

Excellent olivine-control lines are available for the major elements of interest, but the limited data of Rhodes (1983) and Gunn (1971) are the only systematic analytical data for both olivine-compatible and olivine-incompatible trace elements available in the published literature. Such studies should include as a critical component the analysis of olivine (and included chromite) mineral separates, preferably from the lava analyzed; however, even analysis of unrelated, but more easily concentrated, olivine separates of comparable bulk compositions could at least provide some general compositional constraints. Lava suites from the 1959 Kilauea Iki eruption, or from the 1868 Mauna Loa eruption, would serve as ideal samples for initial detailed analytical studies to establish quantitative olivine-control lines for key trace elements. It is anticipated that, with sufficiently precise determinations of olivine-compatible trace elements, several olivine-control lines could be defined for the various groupings of Mauna Loa lava, rather than only the one determined for the historical lava; in contrast, four separate control lines have already been determined for Kilauea lava in terms of major elements alone (Wright, 1971, table 3).

SYSTEMATIC STUDY OF PREHISTORIC LAVA SUITES

Studies in recent years have greatly improved our understanding of the chronology and distribution of the prehistoric lava of Kilauea and Mauna Loa (for example, Lockwood and Lipman, chapter 18; Holcomb, 1980, 1981; Lipman, 1980a, b; Moore, 1983; Lipman and Swenson, 1984). Systematic geochemical studies of these rocks now can be interpreted in a fairly well understood space and time framework. An obvious objective of further studies would be to detect temporal and spatial patterns that would better define longer term variation trends. Another important objective would be to determine how long the chemical distinction between Mauna Loa and Kilauea has been in existence. Available data suggest that the distinction has existed for more than 30,000 years (Rhodes and Lipman, 1979; Easton and Garcia, 1980).

SYSTEMATIC STUDY OF DIFFERENTIATED AND HYBRID LAVAS

The acquisition of precise data to establish quantitative control lines for olivine-controlled lava would make it possible to apply trace-element constraints to lava whose composition is determined by other major liquidus phases (clinopyroxene, orthopyroxene, and plagioclase) in addition to, or instead of, olivine. Once variation patterns are well defined for both olivine-controlled and differentiated lava, then trace-element abundances can be incorporated to provide additional variables in mixing calculations to determine the lineage of hybrid lavas. Such studies would extend the work of Wright and Fiske (1971) and serve to test their models based on major-element variations alone.

DEVELOPMENT OF COMPLETE PETROGENETIC MODELS FOR HAWAIIAN THOLEIITE

Most proposed models for the generation, transport, storage, and eruption of Hawaiian basalt are incomplete because they do not fully take into account both the long-term and the short-term secular variations in composition of the erupted lava. The preliminary results of this study, we believe, are compatible with the earlier conclusion of Wright (1971) that both the long-term and short-term variations in the MgO-adjusted composition of olivine-controlled lava reflect high-pressure fractionation processes that occur before storage in shallow magma reservoirs. However, if our speculations concerning the 1868 eruption and earthquake are valid, then the possibility that some short-term variations are produced by other processes cannot be entirely discounted.

We suggest that such complex secular chemical variation requires the magma source region(s) to be heterogeneous and possibly compositionally zoned laterally and vertically. Assuming that our inferred short-term and long-term variations, including the divergence of long-term variation trends for Kilauea and Mauna Loa, withstand the test of more data, we recommend that future petrogenetic models for Hawaiian basaltic volcanism incorporate such secular variations to furnish additional model constraints.

REFERENCES

Abbey, S., 1983, Studies in "standard samples" of silicate rocks and minerals: Geological Survey of Canada Paper 83–15, 114 p.

Aramaki, Shigeo, and Moore, J.G., 1969, Chemical composition of prehistoric lavas at Makaopuhi Crater, Kilauea Volcano, and periodic change in alkali content of Hawaiian tholeiitic lavas: Tokyo University Earthquake Research Institute Bulletin, v. 47, pt. 2, p. 257–270.

Basaltic Volcanism Study Project, 1981, Basaltic Volcanism on the Terrestrial Planets: Elmsford, N.Y., Pergamon Press, 1,286 p.

Bertine, K.K., Chan, L.H., and Turekian, K.K., 1970, Uranium determinations in deep-sea sediments and natural water using fission tracks: Geochimica et Cosmochimica Acta, v. 34, p. 641–648.

Bornhorst, T.J., Rose, WI., Jr., and Wolfe, S.P., 1984, Abundance of gold and silver in fresh calc-alkalic Quaternary volcanic rocks [abs.]: Geological Society of America Abstracts with Program, v. 16, no. 6, p. 450.

Budahn, J.R., and Schmitt. R.A., 1985, Petrogenetic modeling of Hawaiian tholeiitic basalts: A geochemical approach: Geochimica et Cosmochimica Acta, v. 49, p. 67–87.

Clague, D.A., and Frey, F.A., 1982, Petrology and trace element geochemistry of the Honolulu Volcanics, Oahu: Implications for the oceanic mantle below Hawaii: Journal of Petrology, v. 23, p. 447–504.

Cross, W.G., and Tommasino, L., 1970, A rapid reading technique for nuclear particle damage tracks in thin foils: Radiation Effects, v. 5, p. 85–89.

DePaolo, D.J., and Wasserburg, G.J., 1976, Nd isotopic variations and petrogenetic models: Geophysical Research Letters, v. 3, p. 249–252.

Dodge, F.C.W., Millard, H.T., Jr., and Elsheimer, H.N., 1982, Compositional variations and abundances of selected elements in granitoid rocks and constituent minerals, central Sierra Nevada batholith, California: U.S. Geological Survey Professional Paper 1248, 24 p.

Doe, B.R., Lipman, P.W., Hedge, C.E., and Kurasawa, H., 1969, Primitive and contaminated basalts from the southern Rocky Mountains, U.S.A.: Contributions to Mineralogy and Petrology, v. 21, p. 142–156.

Dorrzapf, A.F., Jr., 1973, Spectrochemical computer analysis—Argon-oxygen D-C arc method for silicate rocks: U.S. Geological Survey Journal of Research, v. 1, no. 5, p. 559–562.

Duffield, W.A., Christiansen, R.L., Koyanagi, R.Y., and Peterson, D.W., 1982, Storage, migration, and eruption of magma at Kilauea Volcano, Hawaii, 1971–1972: Journal of Volcanology and Geothermal Research, v. 13, p. 273–307.

Dzurisin, Daniel, and Koyanagi, R.Y., 1981, Changed magma budget since 1975 at Kilauea Volcano, Hawaii: U.S. Geological Survey Open-File Report 81–571, 46 p.

Dzurisin, Daniel, Koyangi, R.Y., and English, T.T., 1984, Magma supply and storage at Kilauea Volcano, Hawaii, 1956–1983: Journal of Volcanology and Geothermal Research, v. 21, no. 3/4, p. 177–206.

Easton, R.M., and Garcia, M.O., 1980, Petrology of the Hilina Formation, Kilauea Volcano, Hawaii: Bulletin Volcanologique, v. 43, p. 657–674.

Evernden, J.F., Savage, D.E., Curtis, G.H., and James, G.T., 1964, Potassium-argon dates and the Cenozoic mammalian chronology of North America: American Journal of Science, v. 262, p. 145–198.

Frey, F.A., 1980, The origin of pyroxenites and garnet pyroxenites from Salt Lake Crater, Oahu, Hawaii: Trace element evidence: American Journal of Science, v. 280–A, pt. 2, p. 427–449.

Frey, F.A., and Clague, D.A., 1983, Geochemistry of diverse basalt types from Loihi Seamount, Hawaii: petrogenetic implications: Earth and Planetary Science Letters, v. 66, p. 337–355.

Frey, F.A., Haskin, L.A., Poetz, J., and Haskin, M.A., 1968, Rare earth abundances in some basic rocks: Journal of Geophysical Research, v. 73, p. 6085–6098.

Gast, P.W., 1968, Trace-element fractionation and the origin of tholeiitic and alkaline magma types: Geochimica et Cosmochimica Acta, v. 32, p. 1057–1086.

Gladney, E.S., Burns, C.E., and Roelandts, I., 1983, 1982 compilation of elemental concentrations in eleven United States Geological Survey rock standards: Geostandards Newsletter, v. 7, p. 3–226.

Gladney, E.S., and Goode, W.E., 1981, Elemental concentrations in eight new United States Geological Survey rock standards: Geostandards Newsletter, v. 5, p. 31–64.

Gottfried, David, 1983, Cu, Ni, and Co fractionation patterns in Mesozoic tholeiitic magmas of eastern North America: Evidence for sulfide fractionation [abs.]: Geological Society of America Abstracts with Program, v. 15, no. 2, p. 92.

Gottfried, David, and Greenland, L.P., 1972, Variation of iridium and gold in oceanic and continental basalts: International Geological Congress, 24th, Montreal, Canada, Proceedings, Section 10, p. 135–144.

Govindaraju, K., 1984, 1984 compilation of working values and sample description for 170 international reference samples of mainly silicate rocks and minerals: Special Issue, July 1984, Geostandards Newsletter, p. 3–16 (exclusive of appendices).

Gunn, B.M., 1971, Trace element partition during olivine fractionation of Hawaiian basalts: Chemical Geology, v. 8, p. 1–13.

Helz, R. T., 1980, Crystallization history of Kilauea Iki lava lake as seen in drill core recovered in 1967–1979: Bulletin Volcanologique, v. 43, no. 4, p. 675–702.

Hoffman, A.W., Feigenson, M.D., and Raczek, Ingrid, 1984, Case studies on the origin of basalt: III. Petrogenesis of the Mauna Ulu eruption, Kilauea, 1969–1971: Contributions to Mineralogy and Petrology, v. 88, p. 24–35.

Holcomb, R.T., 1980, Preliminary geologic map of Kilauea Volcano, Hawaii: U.S. Geological Survey Open-File Report 80–796, 2 map sheets, scale 1:50,000.

———1981, Kilauea Volcano, Hawaii: Chronology and morphology of the surficial lava flows: U.S. Geological Survey Open-File Report 81–354, 321 p.

Hubbard, N. J., 1969, A chemical comparison of oceanic ridge, Hawaiian tholeiitic and Hawaiian alkalic basalts: Earth and Planetary Science Letters, v. 5, p. 346–352.

Jackson, D.B., Swanson, D.A., Koyanagi, R.Y., and Wright, T.L., 1975, The August and October 1968 east rift eruptions of Kilauea Volcano, Hawaii: U.S. Geological Survey Professional Paper 890, 33 p.

Leeman, W.P., Budahn, J.R., Gerlach, D.C., Smith, D.R., and Powell, B.N., 1980, Origin of Hawaiian tholeiites: trace element constraints: American Journal of Science, v. 280–A, part 2, p. 794–819.

Leeman, W.P., Murali, A.V., Ma, M.S., and Schmitt, R.A., 1977, Mineral

constitution of mantle source regions for Hawaiian basalts—rare earth element evidence for mantle heterogeneity, *in* Magma genesis: Oregon Department of Mineral Industries Bulletin 96, p. 169–183.

Lipman, P.W., 1980a, Rates of volcanic activity along the southwest rift zone of Mauna Loa Volcano. Hawaii: Bulletin Volcanologique, v. 43. no. 4, p. 703–726.

———1980b, The southwest rift zone of Mauna Loa: Implications for structural evolution of Hawaiian volcanoes: American Journal of Science, v. 280-A, part 2, p. 752–776.

Lipman, P.W., and Swenson, Alan, 1984, Generalized geologic map of the southwest rift zone of Mauna Loa Volcano, Hawaii: U.S. Geological Survey Miscellaneous Investigations Series Map I–1312, scale 1:100,000.

Macdonald, G.A., 1949a, Petrography of the Island of Hawaii: U.S. Geological Survey Professional Paper 214-D, p. 51–96.

———1949b, Hawaiian petrographic province: Geological Society of America Bulletin, v. 60, p. 1541–1596.

———1968, Composition and origin of Hawaiian lavas: Geological Society of America Memoir 116, p. 477–522.

Millard, H.T., Jr., and Keaten, B.A., 1982, Precision of uranium and thorium determinations by delayed neutron counting: Journal of Radioanalytical Chemistry, v. 72, p. 489–500.

Moore, J.G., and Calk, Lewis, 1971, Sulfide spherules in vesicles of dredged pillow basalt: American Mineralogist, v. 56, p. 476–488.

Moore, J.G., and Fabbi, B.P., 1971, An estimate of the juvenile sulfur content of basalt: Contributions to Mineralogy and Petrology, v. 41, p. 105–118.

Moore, R.B., 1983, Distribution of differentiated tholeiitic basalts on the lower east rift zone of Kilauea Volcano, Hawaii: A possible guide to geothermal exploration: Geology, v. 11, p. 136–140.

Murata, K.J., 1970, Tholeiitic basalt magmatism of Kilauea and Mauna Loa Volcanoes of Hawaii: Naturwissenschaften, v. 57, p. 108–113.

Murata, K. J., and Richter, D.H., 1966a, Chemistry of the lavas of the 1959–60 eruption of Kilauea Volcano, Hawaii: U.S. Geological Survey Professional Paper 537–A, 26 p.

———1966b, The settling of olivine in Kilauean magma as shown by lavas of the 1959 eruption: American Journal of Science, v. 264, p. 194–203.

O'Nions, R.K., Hamilton, P.J., and Evensen, N.M., 1977, Variations in $^{143}Nd/^{144}Nd$ and $^{87}Sr/^{86}Sr$ ratios in oceanic basalts: Earth and Planetary Science Letters, v. 34, p. 13–22.

Peterman, Z.E., and Hedge, C.E., 1971, Related strontium isotopic and chemical variations in oceanic basalts: Geological Society of America Bulletin, v. 82, p. 493–499.

Powell, J.L., and Delong, S.E., 1966, Isotopic composition of strontium in volcanic rocks from Oahu: Science. v. 153. p. 1239–1242.

Powers, H.A., 1955, Composition and origin of basaltic magma of the Hawaiian Islands: Geochimica et Cosmochimica Acta, v. 7, p. 77–107.

Rhodes, J.M., 1983, Homogeneity of lava flows: Chemical data for historic Mauna Loan eruptions: Journal of Geophysical Reserach. v. 88 (supplement), p. A869–A879.

Rhodes, J.M., and Lipman, P.W., 1979, Chemistry of prehistoric lavas erupted along the southwest rift zone of Mauna Loa [abs.]: Hawaii Symposium on Intraplate Volcanism and Submarine Volcanism, July 1979, Hilo, Hawaii, Abstract Volume, p. 97.

Rhodes, J.M., Lockwood, J.P., and Lipman, P.W., 1982, Episodic variation in magma chemistry, Mauna Loa Volcano, Hawaii [abs.]: International Association of Volcanology and Chemistry of the Earth's Interior–International Association of Geochemistry and Cosmochemistry Scientific Assembly, Generation of major basalt types, August 1982, Reykjavik, Iceland, Abstract Volume, Abstract No. 43.

Richter, D.H., Eaton, J.P., Murata, K.J., Ault, W.U., and Krivoy, H.L., 1970, Chronological narrative of the 1959–60 eruption of Kilauea Volcano, Hawaii: U.S. Geological Survey Professional Paper 537–E, 73 p.

Richter, D.H., and Murata, K.J., 1966, Petrography of the lavas of the 1959–60 eruption of Kilauea Volcano, Hawaii: U.S. Geological Survey Professional Paper 537–D, 12 p.

Schilling, J.G., and Winchester, J.W., 1969, Rare earth contribution to the origin of Hawaiian lavas: Contributions to Mineralogy and Petrology, v. 23, p. 27–37.

Skinner, B.J., and Peck, D.L., 1969, An immiscible sulfide melt from Hawaii, *in* Wilson, H.D.B., and Bateman, A.M., eds., Magmatic ore deposits—a symposium: Economic Geology Monograph, p. 310–322.

Staudigel, H., Zindler, A., Hart, S.R., Leslie, T., Chen, C.-Y., and Clague, D., 1984, The isotope systematics of a juvenile intraplate volcano: Pb, Nd, and Sr isotope ratios of basalts from Loihi Seamount, Hawaii: Earth and Planetary Science Letters, v. 69, p. 13–29.

Swanson, D.A., Duffield, W.A., and Fiske, R.S., 1976b, Displacement of the south flank of Kilauea Volcano: The result of forceful intrusion of magma into the rift zones: U.S. Geological Survey Professional Paper 963, 39 p.

Swanson, D.A., Duffield, W.A., Jackson, D.B., and Peterson, D.W., 1979, Chronological narrative of the 1969–71 Mauna Ulu eruption of Kilauea Volcano, Hawaii: U.S. Geological Survey Professional Paper 1056, 55 p.

Swanson, D.A., Jackson, D.B., Koyanagi, R.Y., and Wright, T.L., 1976a, The February 1969 east rift eruption of Kilauea Volcaho, Hawaii: U.S. Geological Survey Professional Paper 891, 30 p.

Tatsumoto, M., 1966, Isotopic composition of lead in volcanic rocks from Hawaii, Iwo Jima, and Japan: Journal of Geophysical Research, v. 71, p. 1721–1733.

———1978, Isotopic composition of lead in oceanic basalt and its implication to mantle evolution: Earth and Planetary Science Letters, v. 38, p. 63–87.

Tilley, C.E., and Scoon, J.H., 1961, Differentiation of Hawaiian basalts—trends of Mauna Loa and Kilauea historic magma: American Journal of Science, v. 259, p. 60–68.

Tilling, R.I., Koyanagi, R.Y., Lipman, P.W., Lockwood, J.P., Moore, J.G., and Swanson, D.A., 1976, Earthquake and related catastrophic events, Island of Hawaii, November 29, 1975: A preliminary report: U.S. Geological Survey Circular 740, 33 p.

Wright, T.L., 1971, Chemistry of Kilauea and Mauna Loa lava in space and time: U.S. Geological Survey Professional Paper 735, 40 p.

———1973, Magma mixing as illustrated by the 1959 eruption, Kilauea Volcano, Hawaii: Geological Society of America Bulletin, v. 84, p. 849–858.

———1984, Origin of Hawaiian tholeiite: A metasomatic model: Journal of Geophysical Research, v. 89, no. B5, p. 3233–3252.

Wright, T.L., and Fiske, R.S., 1971, Origin of the differentiated and hybrid lavas of Kilauea Volcano, Hawaii: Journal of Petrology, v. 12, p. 1–65.

Wright, T.L., Peck, D.L., and Shaw, H.R., 1976, Kilauea lava lakes: Natural laboratories for the study of cooling, crystallization, and differentiation of basaltic magma, *in* Sutton, G.H., Manghnani, and Moberly, R., eds., The Geophysics of the Pacific Ocean Basin and its margin: American Geophysical Union, Washington, D.C., Geophysical Monograph Series, v. 19, p. 375–390.

Wright, T.L., Swanson, D.A., and Duffield, W.A., 1975, Chemical compositions of Kilauea east-rift lava, 1968–1971: Journal of Petrology, v. 16, p. 110–133.

Wright, T.L., and Tilling, R.I., 1980, Chemical variation in Kilauea eruptions 1971–74: American Journal of Science, v. 280–A, pt. 2, p. 777–793.

Zablocki, C.J., and Koyanagi, R.Y., 1979, An anomalous structure in the lower east rift zone of Kilauea Volcano, Hawaii, inferred from geophysical data [abs.]: Hawaii Symposium on Intraplate Volcanism and Submarine Volcanism, July 1979, Hilo, Hawaii, Abstract Volume, p. 177.

Zielinski, R.A., Lipman, P.W., and Millard, H.T., Jr., 1977, Minor-element abundances in obsidian, perlite, and felsite of calc-alkalic rhyolites: American Mineralogist, p. 426–437.

APPENDIX 24.1

PROCEDURE TO ADJUST ANALYSES TO MgO = 7.00 WEIGHT PERCENT FOR OLIVINE-CONTROLLED LAVA

The procedure for this adjustment will be outlined briefly here. In it, we accept the average compositions of olivine (plus chromite) to be added or removed previously used by Wright (1971). For Kilauea lava, we use an olivine composition of $Fo_{86.2}$, for Mauna Loa lava, $Fo_{87.5}$ (table 24.22). The major elements in these average olivines are fairly well constrained, but their trace elements

TABLE 24.22.—*Assumed average compositions of olivine (plus chromite) used to adjust MgO to 7.00 weight percent for olivine-controlled lava of Kilauea (KAVOL) and Mauna Loa (MLAVOL)*

[KAVOL, average composition of olivine (+1.8 percent chromite) that controls composition of 1959 Kilauea Iki lava; MLAVOL, average composition of olivine (+1.5 percent chromite) that controls composition of historical flows of Mauna Loa. Oxide values (in weight percent) are from Wright (1971, table 15); Al_2O_3 primarily reflects melt inclusions of chromite. Trace-element values (in parts per million) from regression-equation estimates of: G, Gunn 1971, table 2; R, Rhodes, 1983, fig. 1]

	KAVOL ($Fo_{86.2}$)	MLAVOL ($Fo_{87.5}$)
SiO_2	39.48	39.70
Al_2O_3	1.17	.98
"FeO"	13.23	12.08
MgO	45.51	46.60
CaO	.39	.39
Na_2O	.00	.00
K_2O	.00	.00
TiO_2	.04	.03
P_2O_5	.00	.00
MnO	.22	.22
V	38 R	3 R
Cr	2,840 G	2,990 R
Co	190 G	190 G
Ni	2,430 G	2,465 R
Cu	5 G	5 G
Zn	97 G	94 G

are not. For the elements V, Cr, Co, Ni, Cu, and Zn, we use the regression-equation estimates from the olivine-control lines (Gunn, 1971; Rhodes, 1983); we assume the other trace elements to be present in negligibly small amounts or absent in olivine. However, even using significantly different assumed olivine compositions causes minimal effect on the derived adjusted values for incompatible elements and the relative differences between them.

The most convenient way to calculate the MgO-adjusted average composition of a group of related lava samples is to simply compute the mean and then adjust it to the desired MgO content. We chose, however, to adjust each individual analysis and then compute the mean and standard deviation. A comparison of these two adjustment procedures (table 24.23), using the data set showing the greatest range in MgO content (6.87 to 24.25 percent) of the lavas we studied, illustrates the following:

(1) The two mean compositions obtained are similar except for some of the transition elements, particularly Ni, which is compatible with olivine, and Cr, which is included in chromite. The significant differences in the computed mean values for Cr and Ni, however, suggest that the assumed concentrations of these elements in the olivine (table 24.22) used in the MgO adjustment are too high and (or) that the INAA and ES determinations of these elements are biased to low values in high-MgO (picritic) lava. In other words, the slope of the olivine-control line used in the adjustment procedure appears to be too steep for Cr and Ni.

In the comparison of procedures (table 24.23), MgO adjustment after the calculation of the mean occasionally results in negative adjusted values of Ni. Such negative averages are avoided by adjusting the individual analyses prior to computation of the mean; specific samples that yield negative adjusted values can then be identified and omitted from the mean. In general, lava that contains about 10 weight percent or more MgO yields negative adjusted values for Ni and, more rarely, Cr. Quantitative trace-element data are needed before the problem with the MgO adjustment of compatible elements in olivine-controlled lava can be resolved. Thus, in this study, we emphasize the variations in the olivine-incompatible elements (assumed to be negligible or absent in olivine) after MgO adjustment, because their relative differences between samples or lava suites remain valid despite the adjustment procedure.

(2) As expected, computing the average after adjustment of individual analyses substantially reduced the standard deviations of the means of the trace elements determined with relatively good precision (for example, Sc, V, Cr, Co, Ni, Ga, Hf, Eu, Sm) that show good linear correlation with MgO (see figs. 24.4, 24.5, 24.10). For the elements that show wide scatter in the MgO-variation diagrams, their standard deviations remain large regardless of the adjustment procedure used.

TABLE 24.23.—*Comparison of compositions of olivine-controlled lava of Mauna Loa's southwest rift zone (see table 24.17) after adjustment to 7.00 weight percent MgO by two different methods*

[MLAVOL olivine composition ($Fo_{87.5}$) used for adjustment; oxide values in weight percent; values for elements in parts per million]

	Adjustment after calculation of average				Adjustment of individual analyses before calculation of average		
	Range	Average (n = 9)	Standard deviation	Adjusted average	Range	Average (n = 9)	Standard deviation
MgO	6.87-24.25	12.04	7.01	7.00		7.00	0.0
K_2O	.26-.41	.34	.05	.39	.33-.50	.40	.05
[1]Rb	5.7-19.4	11.5	6.4	13.2	6.0-30.5	15.7	10.4
Cs	.10-.54	.27	.16	.31	.10-.96	.36	.32
[1]Sr	177-426	292	84	334	188-507	346	112
Ba	48-174	105	44	120	57-186	120	47
Sc	17.7-31.0	27.0	4.7	30.9	29.7-36.0	31.2	1.9
V	202-362	299	54	337	272-363	324	26
Cr	202-1250	507	364	145	211-241	228	11
Co	42.8-95.7	58.9	21.4	39.8	22.9-46.8	38.7	8.3
Ni	82-846	228	259	[3](98)	39-96	[2]72	25.3
[1]Cu	40.0-54.6	49.3	5.5	55.8	43.0-86.0	55.3	13.5
Mo	3.8-5.0	4.5	0.4	5.2	3.8-6.9	5.0	.9
Zn	104-148	120	14	138	104-151	123	14
Ga	8.4-20.7	16.8	4.0	19.2	14.5-20.7	18.2	2.1
[1]Zr	74-185	144	32	165	75-245	172	49
Hf	2.0-3.6	2.8	.6	3.2	2.8-3.6	3.2	.3
[1]Nb	2.2-7.3	4.8	1.5	5.5	3.8-7.3	5.2	1.4
[1]Ta	.30-.57	.41	.09	.47	.30-.80	.49	.16
Y	8.5-23.9	18.1	4.8	20.7	14.7-24.0	19.6	3.0
[1]Th	.6-2.7	1.0	.7	1.1	.6-4.8	1.3	1.3
U	.15-0.25	.18	.04	.21	.15-.27	.20	.04
Pb	1.5-3.1	2.4	.5	2.8	1.8-5.2	2.8	1.1
[1]Sb	.10-.18	.14	.04	.16	.10-.31	.19	.11
La	5.7-9.3	7.8	1.2	8.9	7.9-11.9	9.2	1.2
Ce	12.5-24.4	20.2	3.6	23.1	18.8-32.2	23.5	3.9
Nd	9.5-16.8	14.5	2.6	16.6	15.5-20.2	17.0	1.5
Sm	2.67-4.44	3.95	.64	4.53	4.20-4.61	4.39	.19
Eu	.99-1.69	1.39	.26	1.59	1.33-1.81	1.61	.15
[1]Gd	3.21-6.00	4.79	1.19	5.49	4.05-6.34	5.58	.73
[1]Tb	.38-.67	.55	.11	.63	.55-.68	.61	.06
Dy	2.9-6.5	4.6	1.2	5.3	4.3-6.8	5.27	.75
[1]Tm	.12-.59	.38	.17	.44	.12-.69	.47	.21
Yb	1.21-2.02	1.76	.33	2.02	1.74-2.24	2.03	.14
[1]Lu	.15-.29	.25	.05	.29	.25-.29	.27	.01

[1]Not listed in individual analyses.
[2]Negative adjusted value (see text for discussion).
[3]Three negative adjusted values for individual analyses omitted.

DIVERSE OLIVINE TYPES IN LAVA OF THE 1959 ERUPTION OF KILAUEA VOLCANO AND THEIR BEARING ON ERUPTION DYNAMICS

By Rosalind Tuthill Helz

ABSTRACT

The lava of the 1959 eruption of Kilauea Volcano, containing about 20 weight percent olivine, is the only picritic lava erupted in the summit area in historical time. The olivine population can be divided into several distinct classes: (1) irregular, blocky crystals (1–12 mm long), many of which contain multiple planar extinction discontinuities, which appear to be deformation features; (2) euhedral or skeletal crystals (0.5–5 mm long); (3) round or otherwise strongly resorbed grains; (4) angular or conchoidal fragments; and (5) subhedral crystals containing sulfide-bearing inclusions. Also present are dunitic aggregates, some with deformed or annealed textures, and rare olivine megacrysts.

Olivine in drill core from Kilauea Iki lava lake, quenched as much as 22 years after the eruption, has the same petrographic features seen in eruption samples or early lake samples. In particular, the deformation features in olivine have survived 22 years at 1,140–1,190 °C.

Olivine phenocrysts in samples of eruption pumice have core compositions of $Fo_{83.5-88.7}$ and contain 0.10–0.25 weight percent NiO. Zoning is moderate (≤3 percent Fo within most crystals); normally and reversely zoned crystals are about equally abundant. There is no correlation between petrographic class and core composition or style of zoning. This variable but moderate zoning seen in olivines in the eruption pumices is not preserved in olivines in drill core from the lake. Lake olivine is all normally zoned, varying by 5 percent Fo or more, and appears to have re-equilibrated with the melt during slow cooling.

The eruption samples are, for the most part, poorly equilibrated. Disequilibrium features observed include: (1) compositional heterogeneity in glasses (away from olivines); (2) presence of a boundary layer of MgO-poor glass near 30 percent of the olivine grains analyzed; (3) widespread occurrence of partially resorbed olivines, in all classes; (4) presence of reversely zoned, unzoned and (or) normally zoned olivines in the same thin section; (5) presence of olivines of very different core compositions in the same section; and (6) presence of olivines of different rim compositions in the same section. These features appear to record mixing immediately before or during the eruption. In particular, the resorption of olivine, seen in grains of all classes, at all but the earliest stages of the eruption, is interpreted as resulting from mixing of thermally disparate magmas, in which the hotter component was dominant.

Many aspects of this eruption are unusual for a Kilauean summit eruption, including: (1) High olivine content; (2) very magnesian glasses, recording high eruption temperatures; (3) the presence of deformed olivine, as single grains or in aggregates, like that commonly found in Hawaiian alkalic rocks; (4) occurrence of rare olivine megacrysts; (5) presence of olivine with sulfide-bearing inclusions; and, perhaps, (6) presence of reversely zoned olivines. These features can be explained by a model in which one of the two mixing components of the eruption, previously defined by Wright (1973), came directly from the mantle, without being stored for a significant time in the shallow summit reservoir. The lava component erupted from the east end of the initial fissure appears to represent this juvenile component. The ascent rate of this component from its source at a depth of 45–60 km is estimated to be 0.6–0.8 cm/s. This rate is sufficient to entrain the largest olivine grains and dunitic aggregates found in the 1959 lavas.

INTRODUCTION AND HISTORICAL BACKGROUND

The 1959 summit eruption of Kilauea Volcano was unique in the history of the Hawaiian Volcano Observatory (HVO) and of Kilauea in that it was the first major eruption for which most of the array of modern volcano-monitoring techniques now available was used. This eruption lasted from November 14 to December 20, 1959, and formed a conspicuous cinder cone (Puu Puai) and a large lava lake in Kilauea Iki pit crater (see fig. 25.1). The eruption consisted of seventeen phases of high fountaining and lava output, separated by periods of quiescence, during which some of the erupted material drained from the lake back down the throat of the main vent. HVO personnel made detailed records of this eruptive activity, its timing and patterns, including fountain heights and temperatures, and the depth of filling of the pit crater. The pumice and lava were then studied petrographically and chemically. These results were published in a series of professional papers (Murata and Richter, 1966a; Richter and Murata, 1966; Richter and others, 1970) that, taken together, give a very detailed picture of the eruption. In addition, Kilauea Volcano had been monitored seismically for several years before 1959; also, summit deformation before and during the eruption was monitored using the tiltmeter network established in 1957. Descriptions of the relationship between earthquake activity, summit deformation and the 1959–60 eruptions of Kilauea, by Eaton (1962) and Eaton and Murata (1960), constituted a quantum jump in our understanding of the physical behavior of active volcanoes.

The lava lake formed during the 1959 summit eruption has also been much studied. The upper crust of the lake has been drilled repeatedly (in 1960, 1961, 1962, 1967, 1975, 1976, 1979, and

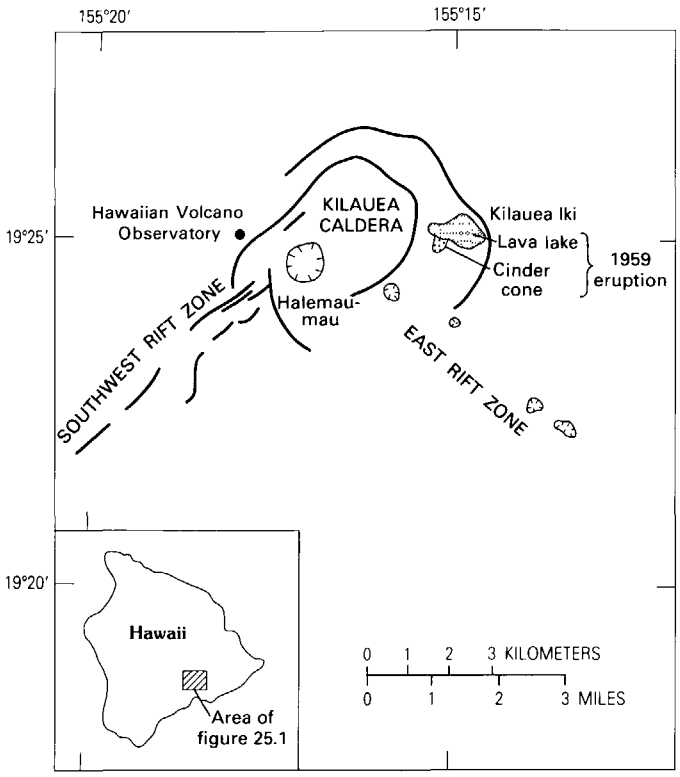

FIGURE 25.1.— Index map of the summit area of Kilauea Volcano, showing the location of Kilauea Iki lava lake and the 1959 cinder cone relative to the main caldera and the upper east rift zone of Kilauea.

1981), resulting in almost 1,200 m of drill core. Richter and Moore (1966) present a detailed petrographic and chemical description of the 1960–62 core. Partial data on petrography and (or) chemistry for the drill core recovered in 1967–1981 may be found in Helz (1980), Luth and Gerlach (1980), Luth and others (1981), Helz and Wright (1983), Helz and others (1984), and Helz (1984). The thermal history of the lake has also been monitored from the earliest days; Helz and Thornber (in press) give a partial summary of that literature. Lastly, the lake has been the object of several geophysical investigations, such as those of Zablocki and Tilling (1976), Chouet and Aki (1981), Hardee and others (1981), and Hermance and Colp (1982).

The 1959 summit lava is unique in several respects, the most conspicuous of which is its olivine content: it is the only picritic basalt erupted at or near Kilauea's summit in historical time. The average MgO content of the eruption pumice was estimated by Wright (1973) to be 15.43 percent by weight, which corresponds to about 20 percent by weight olivine crystals. Other historical eruptions with comparable olivine content have occurred on the rift zones, for example, the 1840 east-rift eruption (see analyses in Macdonald, 1944; Wright and Fiske, 1971). Other young summit eruptions have 7.0–8.5 percent MgO and correspondingly smaller amounts of phenocrystic olivine (Wright, 1971).

Consequently, the eruption pumice and the 1959 lava lake contain an enormous population of olivine crystals, occurring singly and in aggregates. This paper presents the results of a petrographic and chemical study of selected olivine crystals and aggregates, both in eruption pumice and in drill core from the lava lake. The study supplements earlier work on the eruption (cited above) by providing detailed electron microprobe data on a large suite of eruption samples. A limited amount of microprobe data on the 1959 eruption pumices has already been published (Leeman and Scheidegger, 1977; Harris and Anderson, 1983), but coverage of the eruptive suite was very incomplete.

ACKNOWLEDGMENTS

This paper builds on the past and present work of many people who have studied the 1959 eruption. In particular, I would like to thank J.G. Moore of the United States Geological Survey (USGS), Menlo Park, for access to his thin sections of submarine east-rift lava and T.L. Wright (USGS, Hawaiian Volcano Observatory) for access to his collection of thin sections of subaerial Kilauea lava. B.C. Hearn (USGS, Reston) and S.H. Kirby (USGS, Menlo Park) helped with the interpretation of the textures of the annealed olivine aggregates. In addition, I have benefited from conversations with D.A. Clague, J.P. Eaton, P. Delaney and S.W. Kieffer, all of the USGS, A.T. Anderson, Jr. of the University of Chicago, and C.-Y. Chen of the University of Illinois at Urbana. Lastly, I wish to thank B.C. Hearn and M.P. Ryan for constructive reviews of the manuscript.

SAMPLING AND ANALYTICAL PROCEDURES

SAMPLE SELECTION

The 1959 summit eruption consisted of 17 distinct phases. These phases, and the variations of lake level with time, are described in detail in Murata and Richter (1966a) and Richter and others (1970) and are summarized in figure 25.2. During each phase, eruptive materials were sampled, often both pumice from the fountain and flow material from the edge and upper crust of the lava lake. In selecting a subset of samples for this study, preference was given to pumice samples, because they were quenched much faster than flow samples, and to samples previously studied, especially those for which a bulk analysis was presented in Murata and Richter (1966). The collection dates of samples examined petrographically is indicated by the dots along the curve in figure 25.2. Although samples from only twelve of the seventeen phases were checked, they are fairly evenly distributed in time throughout the eruption.

In addition to these eruption samples, I have examined 600 thin sections of drill core from the lava lake. The drill-core sections contain all the types of olivine seen in the eruption samples. In addition, I found in the drill core two olivine megacrysts and a dozen dense polycrystalline olivine aggregates of distinctive texture. These unusual aggregates and megacrysts, of types not seen in the eruption pumice, are the only lake samples that will be discussed in detail in this paper.

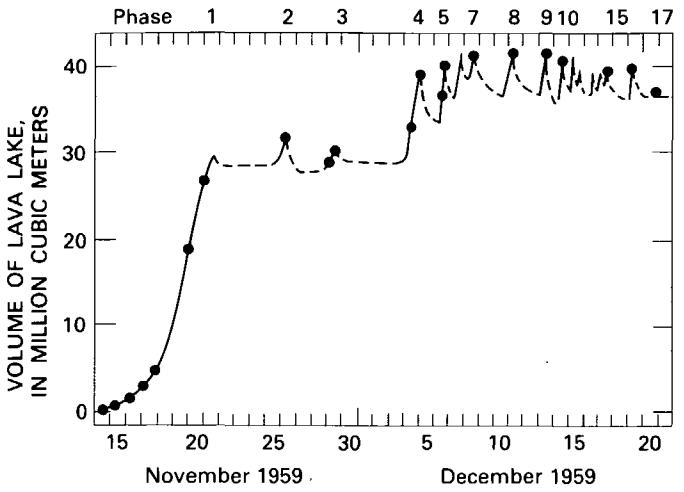

FIGURE 25.2.—Volume of Kilauea Iki lava lake versus time (after Richter and Moore, 1966, fig. 3). Decrease in lake volume at the end of each phase represents drainback down the eruptive vent. Each dot corresponds to a sample examined in this study. Phases represented in this study are numbered along the top of the diagram.

PETROGRAPHIC METHODS

All thin sections have been examined in transmitted light. All polished sections have also been checked in reflected light to verify the identification of opaque and near-opaque phases. No universal-stage work has been done.

In addition to the thin-section work, the drill core from the lake has been examined macroscopically in detail, with emphasis on the size and distribution of olivine phenocrysts. The results of this work are presented in Helz (1980), Helz and Wright (1983), and Helz and others (1984) and form part of the background to the present paper.

ANALYTICAL METHODS

Olivine and glass analyses were obtained using an ARL-SEMQ nine-channel electron microprobe. Operating conditions were an accelerating voltage of 15 kV and a beam current of 0.1 μA. Natural mafic silicates and basaltic glasses were used as standards. Counting times were 40 s for most major elements, 20 s for some of the minor elements (Ti, Cr, P, and K in glass; Ni and Cr in olivine). All data were reduced using a modified Bence-Albee routine (Bence and Albee, 1968: Albee and Ray, 1970). In addition, the glass analyses were renormalized, using a glass of known composition, following the method of Melson and others (1976). The glass selected for this was sample 69–1–22 from the 1965 Makaopuhi lava lake (Wright and Okamura, 1977). The revised analysis of Jarosewich and others (1979) was used for the renormalization procedure. This process eliminates minor day-to-day variations in analyses caused by slight shifts in the instrument and produces a data set of great internal precision. The accuracy of the analyses, which depends on the uniformity of the standards, the accuracy of the standard analyses, and of the Bence-Albee corrections, is not affected by the renormalization procedure. All analyses reported correspond to the composition of a single point unless the number of points included is specified.

CLASSIFICATION OF OLIVINES

The olivine in the lava of the 1959 Kilauea eruption is not only abundant but quite varied petrographically. The earliest description is that of Richter and Murata (1966), who described three classes of olivine: euhedral, rounded, and skeletal. The euhedral and skeletal olivine they reported to be fairly iron-rich (Fo_{82}), whereas the larger, blocky grains with rounded corners were more magnesian (Fo_{87-88}). The compositions were determined by X-ray techniques. Richter and Murata further remarked that the larger, rounded grains were obviously out of equilibrium with their present host liquid just before quenching, whereas the more iron-rich euhedral grains appeared to have the equilibrium olivine composition.

Based on examination of drill core from the lake, Helz (1980) divided the olivine phenocryst population in the lake into two groups. Type 1 were large, blocky crystals, the overall form of which was irregular. These commonly, but not always, contain multiple planar extinction discontinuities, bounding kink-bands, or subgrains with rectangular boundaries; similar features have been described by Kirby and Green (1980) in olivine in dunite xenoliths from Hualalai Volcano. Type 2 grains, in this classification, were smaller, euhedral olivines, which were free of deformation features. Type 2 olivine is more abundant than type 1 by a ratio of roughly 5:1.

Further study of samples from both the lava lake and the eruption pumice has led to the following five-fold classification:

(1) Class 1 (formerly type 1) consists of large grains (1–12 mm long), generally blocky in form, but irregular in overall outline, as described in Helz (1980). They commonly contain planar extinction discontinuities, bounding kink-bands, which extend all the way across the crystal (see figs. 25.4*A–B*, 25.5*A*). More rarely, the subgrains may be rectangular (see fig. 25.5*B*). Grains of this class rarely contain melt inclusions. Although planar extinction discontinuities may be quite abundant in a given grain, the total amount of strain involved is usually not large. The extinction position of different parts of the grains never varies by more than 15° of rotation and the usual range is 5°–10°. These grains may exhibit local rounding or resorption at their edges. If resorption is present, the subgrain boundaries are preferentially resorbed by the melt (as in figs. 25.4*A*, 25.5*A*). Olivine grains in this class are the most conspicuous in any given thin section (see fig. 25.3).

(2) Class 2, containing all euhedral and skeletal grains (see figs. 25.3, 25.4C and 25.5C), is the most abundant class of olivine. The distinguishing feature of this class is that the form of the grains suggests that they have grown from a melt in the recent past. Minor rounding of tips and corners of grains may occur, but in general class 2 olivine exhibits much less resorption than class 1 grains do. They are completely free of multiple planar extinction discontinuities. They commonly contain melt inclusions, most often a single large inclusion, of negative crystal form, in the center of the grain. Grains

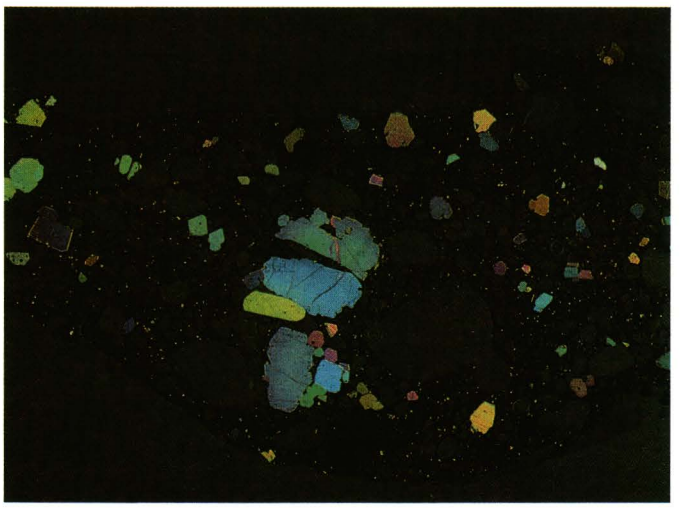

FIGURE 25.3.—Eruption sample Iki–24, from phase 9 of the 1959 eruption. All birefringent grains are olivine; matrix is moderately vesicular brown glass. Note large range in size that exists for both olivine and vesicles. Nicols partly crossed. Field of view is 2.2 cm across.

of this type are commonly 0.5–2 mm long, but they may reach 5 mm in length. A large skeletal grain is shown in figure 25.4*D*; skeletal grains of this size are rare in the 1959 lavas.

(3) Class 3 includes a small population of grains whose shapes have been so extensively modified by resorption that they cannot be assigned to group 1 or 2 on the basis of shape. Most class 3 grains are almost perfectly rounded. More rarely they may be amoeboid, but are never skeletal. These grains do not contain kink-bands; any grain with such features, even though strongly rounded, has been put in class 1.

(4) Class 4 includes rare angular or conchoidal fragments of olivine. Some care is needed to distinguish between broken pieces of olivine and crystals that have odd shapes because they have been sectioned obliquely. Nevertheless, there are a few grains of olivine that are clearly bounded by fracture surfaces. This class provides evidence for local brittle failure of olivine under conditions quite different from those under which the deformation features seen in class 1 olivine formed. Some of these angular fragments may be slightly modified by resorption (see fig. 25.4*C*). Others have survived for decades in the lake without significant resorption or overgrowth of olivine (see fig. 25.5*D*).

(5) Class 5 olivine grains are those containing swarms of inclusions of opaque minerals and pale glass, in which the opaques consist partly or entirely of sulfide. Chromite (or chromian spinel) is the other opaque phase that may be present. Class 5 grains are very rare, melt-bearing inclusions in most grains being sulfide-free. Sometimes the entire core of the olivine grain is so charged with inclusions that it looks dirty in thin section. More often, the inclusions occur only in patches within an otherwise clear grain. Inclusions also occur as a continuous necklace, separating a clear core and a clear rim. Examples of these various types are shown in figures 25.4*E* and 25.5*E*. Grains in this class are usually small (1–4 mm long) and are equant but not conspicuously euhedral in outline. A few class 5 grains contain planar extinction discontinuities, but most are undeformed. The presence of included sulfide is the crucial feature in assigning a grain to this class. Some olivine grains have inclusion swarms similar to the class 5 swarms in all respects, except that they lack sulfide. These grains have been excluded from class 5 as presently defined, though more detailed work on their inclusions might justify extending this class to include them.

This five-fold classification was first published in Helz (1983). Almost simultaneously, and quite independently, Schwindinger and others (1983) published a different classification scheme for olivine in the 1959 lava. Schwindinger and coworkers leached the olivine grains out of the glass of several samples of eruption pumice to view them in three dimensions. Their classification thus emphasizes three-dimensional form and surface morphology. Also, they worked exclusively with eruption pumice. These differences in scope and technique have led inevitably to different classification schemes. The two schemes are not in conflict, however; rather, the two studies complement each other.

The present classification scheme was developed by looking at olivine as it appears in thin section, that is, in two dimensions. I have considered chiefly the overall form of the grain (complexly blocky, euhedral, round, fragmental) and the presence of certain internal features (multiple planar extinction discontinuities, swarms of sulfide-bearing inclusions) in assigning a grain to a given class. Features not used here to classify grains include: Size of grain; presence or absence of inclusions of chromite or brown glass; and presence or absence of minor or local resorption. Certain classes do exhibit group characteristics with respect to this set of features. For example, class 1 grains tend to be larger than any other type. Inclusions of brown basaltic glass are very common in class 2 grains, and rare in all other classes. However, this clustering of additional traits is a matter of observation, and not part of the classification process.

With so many types of olivine present, the possibility obviously arises that only some classes of crystals (for example, class 2) are cognate with the host, whereas others (perhaps class 1) may be largely xenocrystic. As will become evident below, there are many gradations between cognate and xenocrystic, and so these terms will be little used in this paper. Instead, the term phenocryst is used to mean any olivine grain big enough to see with the unaided eye, without genetic implications, while the terms grain or crystal may include smaller olivine grains as well.

PETROGRAPHY OF THE ERUPTION PUMICE

The eruption samples examined in this study are listed in table 25.1, together with their dates of collection and petrographic notes on the olivine present. Two sample designations are given. The first is the collection number assigned in the field, which will be used in this paper. The second number (S-number in parentheses) is the number used in Murata and Richter (1966a) and Richter and Murata (1966); it is reproduced here to facilitate comparison with those papers. Some samples investigated here were not analyzed in

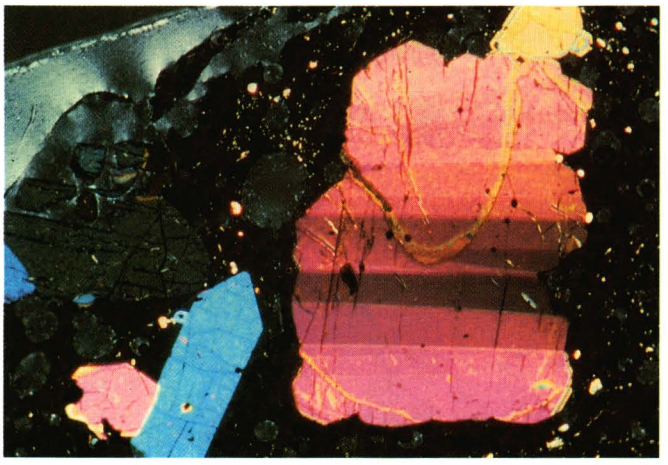

A

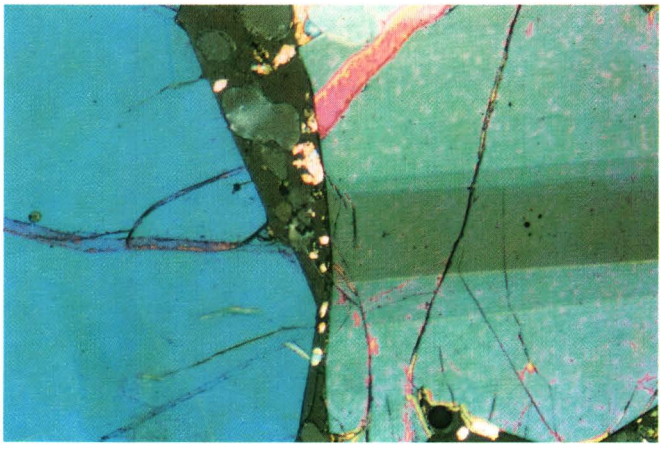

B

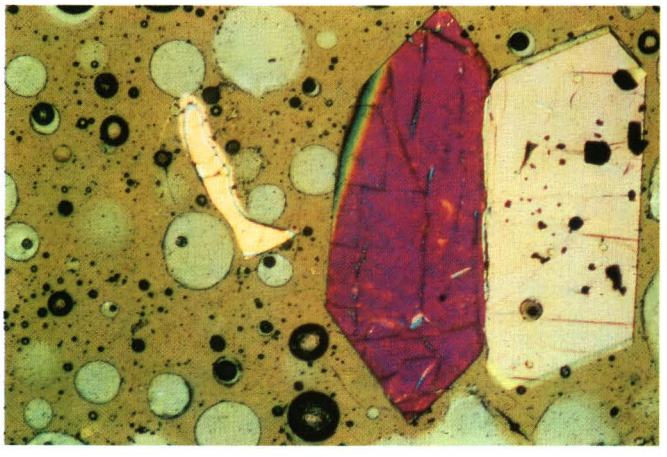

C

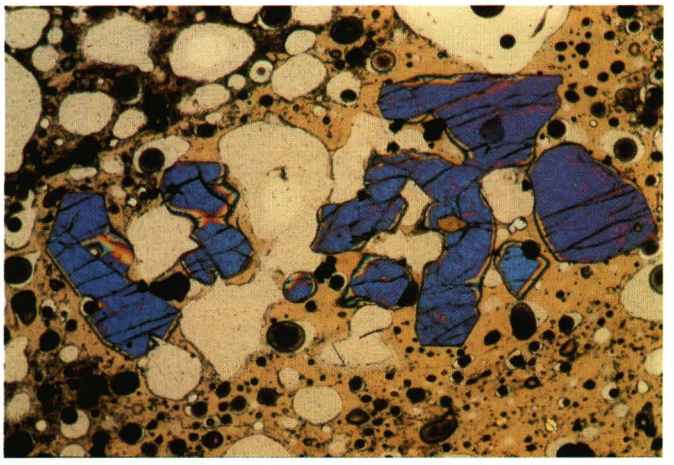

D

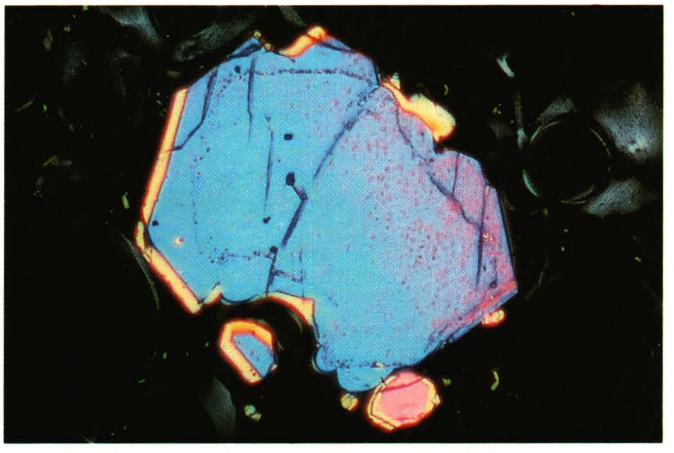

E

FIGURE 25.4.—Representative olivine grains from the eruption pumice of the 1959 Kilauea eruption. ***A***, Deformed (class 1) olivine grain, 2 mm long from Iki–21 (phase 8). The edges are resorbed and show preferential resorption along the planar extinction discontinuities bounding the kink-bands. Two euhedral (class 2) grains are visible to the left. Crossed nicols. ***B***, Deformed (class 1) olivine grain (right), showing relationship between the curved (possibly bent?) edge of the grain and the position of the extinction discontinuities, along an edge where resorption has not occurred. This grain, from Iki–24, is visible in the center of figure 25.3. Field of view 2 mm across. Crossed nicols. ***C***, Euhedral (class 2) and fragmental (class 4) olivine grains in Iki–7 (phase 1). The euhedral grains are 1 mm long. Nicols partly crossed. ***D***, Coarse skeletal (class 2) olivine grain, 3 mm in length, in Iki–21 (phase 8). Such grains are very rare in the 1959 lava. Nicols slightly crossed. ***E***, Class 5 olivine (1 mm long) with necklace of tiny inclusions, from sample Iki–32 (phase 15). The edge of this crystal shows local resorption (cuspate edges) but is euhedral elsewhere around its rim. Nicols partly crossed.

the earlier studies, and therefore have no S-numbers.

All samples in table 25.1 contain abundant brown glass, mostly very fresh and clear, but locally charged with fine-grained opaques. All glasses are quite vesicular, some of them so vesicular that less than a third of the area of the thin section is glass and crystals. A typical olivine-rich, moderately vesicular eruption sample is shown in figure 25.3. All of the birefringent material in this section is olivine; clearly the size range of olivine present is very large.

The crystalline material present in the eruption pumice consists almost entirely of olivine plus chromite. Both phases are always present; there are few chromite-free olivine grains and no chromite-free samples. Chromite occurs principally as inclusions in olivine; most crystals not included in olivine are immediately adjacent to

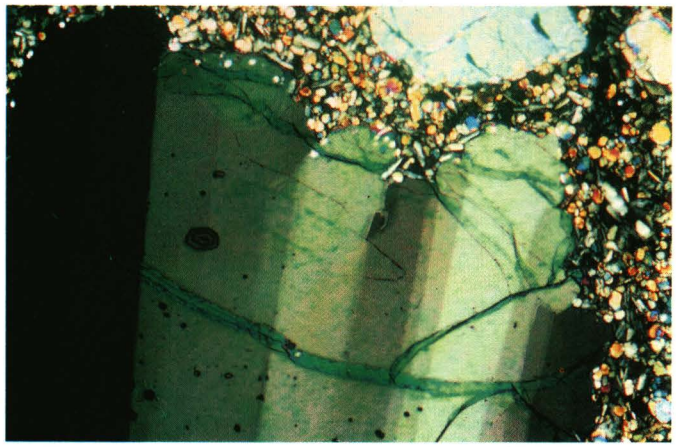

A

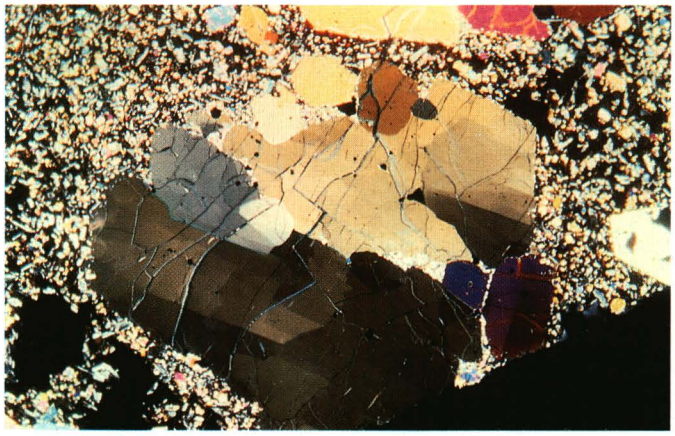

B

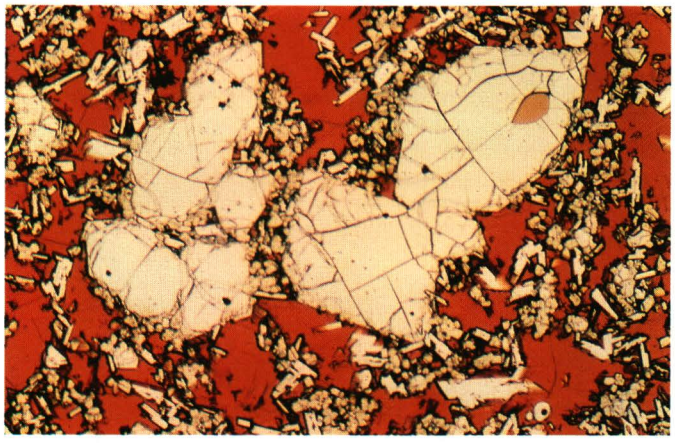

C

D

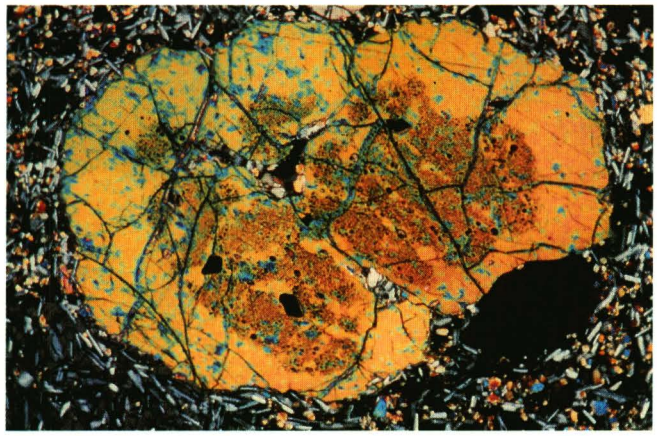

E

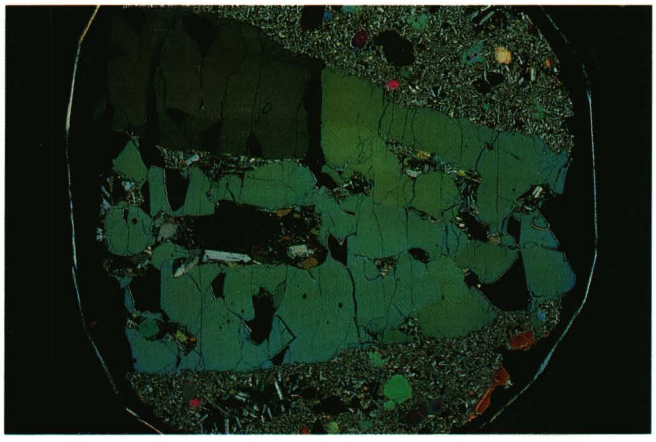

F

FIGURE 25.5.—Representative olivine from Kilauea Iki lava lake. ***A***, Deformed (class 1) olivine grain from KI81–2–226, quenched from 1,140 °C in 1981. It has multiple planar extinction discontinuities and cuspate margins like the grain in figure 25.4*A*. Part of grain visible is 2 mm long. Crossed nicols. ***B***, Deformed (class 1) grain in aggregate KI79–1–189.0(b), quenched from 1,130–1,135 °C in 1979. The olive-green grain shows rectangular subgrain boundaries instead of planar extinction discontinuities extending across the whole grain. This grain is 5 mm long. Black area at lower right is the edge of the rock section. Crossed nicols. ***C***, Euhedral (class 2) olivine grains from KI76–1–149.1, quenched from 1,105 °C in 1976. These are grouped into clusters of 2–3 grains each. Smaller crystals are groundmass phases, including olivine, augite, and plagioclase, in brown glass. Field of view 3 mm across. Plane-polarized light. ***D***, Fragmental (class 4) olivine grain from sample KI75–1–145.1, quenched from 1,120 °C in 1975. All surfaces of the pink triangular grain are slightly conchoidal. This grain is 5 mm long. Class 1 (yellow grain, lower right) and class 2 (purple grains to left) olivine phenocrysts are also visible. The glass is at extinction. Crossed nicols. ***E***, Class 5 olivine phenocryst (3 mm across) with inclusion-rich core, from sample KI81–1–306.7, quenched from 1,085 °C in 1981; smaller, attached grain is at extinction. Crossed nicols. ***F***, Olivine megacryst from sample KI76–2–20.5. It is mounted on a glass slide, just visible in the picture, which is 2.54 cm across. The grain is somewhat skeletal, with former melt inclusions now visible as areas of mesostasis. Irregular black areas within the crystal are the result of fragmentation and plucking during sectioning. Faint extinction discontinuities (visible in upper part of crystal) are present throughout the grain. Crossed nicols.

TABLE 25.1.—*Samples of 1959 eruption pumice investigated*

Sample	Phase of eruption	Date	Type of sample	Olivine classes present	Resorption observed?	Kink bands present in olivines?	Types (numbers) of sections examined
Iki-1(S-2)	1	11/14/59	Flow	2	No	No	TS, PTS
Iki-58(S-1)	1	1/14	Flow	2	No	No	TS, PTS
Iki-42	1	1/16	Flow	2	No	No	TS(2)
Iki-2(S-4)	1	11/17	Pumice	2	No	No	TS
Iki-22 (S-5)	1	11/18	Pumice	1,2,3	Yes	Yes	TS, PTS
Iki-44 (S-7)	1	11/20	Pumice	1,2,3	Yes	Yes	TS, PTS
Iki-5 (S-8)	1	11/21	Pumice	1,2	No	Yes	TS
Iki-7 (S-9)	1	11/21	Pumice	1,2,3,4	Yes	Yes	TS, PTS
Iki-8(S-10)	2	11/26	Flow	1,2	Yes	Yes	TS
Iki-11(S-11)	2	11/26	Pumice	1,2,3,5	Yes	Yes	TS, PTS
Iki-9(S-12)	3	11/28	Pumice	2	Yes	No	TS, PTS(2)
Iki-10(S-13)	3	11/29	Pumice	2	Yes	No	TS
Iki-12(S-14)	4	12/4	Flow	2	No	No	TS
Iki-13(S-15)	4	12/5	Pumice	1,2,3,4	Yes	No	TS, PTS
Iki-14(S-16)	5	12/6	Pumice	1,2,4,5	Yes	Yes	TS, PTS
Iki-15(S-17)	5	12/7	Pumice	1,2	Yes	Yes	TS
Iki-19(5-18)	7	12/8	Pumice	1,2,3,5?	Yes	Yes	TS
Iki-20	7	12/8	Pumice	2,5	Yes	No	PTS
Iki-21(S-19)	8	12/11	Pumice	1,2,4,5	Yes	Yes	TS, PTS
Iki-24	9	12/13	Pumice	1,2,4	Yes	Yes	PTS
Iki-36	9	12/13	Pond Surface	1,2,4	Yes	Yes	TS(2)
Iki-26(S-21)	10	12/14	Pumice	1,2,3	Yes	Yes	TS, PTS
Iki-32(S-22)	15	12/17	Pumice	1,2,3,5	Yes	Yes	TS, PTS
Iki-33(S-24)	16	12/19	Pumice	1,2	Yes	Yes	TS, PTS
Iki-38(S-25)	17?	12/19?	Ooze	1,2	No	No	TS

olivine. Crystals of chromite occurring in the glass, at some distance from olivine, are rare. This pattern of association of olivine and chromite suggests that spinel nucleates on olivine, whenever possible.

A few eruption samples also contain minor amounts of fine-grained augite, with or without tiny laths or plates of plagioclase. These phases occur in all of the earliest phase 1 pumice samples (Iki–58, Iki–1, Iki–42) plus some phase 2 and 3 samples (Iki–11, Iki–9). These minerals are never sufficiently coarse grained to be considered phenocrystic. They do not survive in recognizable form in the lake (Helz, 1980), but must make up part of the groundmass.

As can be seen in table 25.1, the petrographic character of the olivine in the eruption pumice varies with time. The early phase 1 samples (Iki–58, Iki–1, Iki–42, Iki–2) contain only minor amounts of euhedral class 2 olivine showing little or no resorption. Lava temperature evidently increased during this period, however, as the latest of this series of samples does not contain the tiny augite ± plagioclase crystals seen in pumice erupted on November 14–16. On November 18, 1959, the olivine content of the lava increased and the olivine assemblage became more complex, now including representatives of classes 1, 2, and 3. This situation persisted to the end of the first phase, with some fragmental olivine (class 4) occurring in the latest sample (see fig. 25.4C).

Phase 2 samples also have a complex olivine assemblage, including the earliest known class 5 olivine. Phase 3, by contrast, marks a reversion to a depleted olivine population like the early phase 1 pumice, but with more rounding of the olivine. An early phase 4 sample is similarly olivine-poor, but later phase 4 and the phase 5 samples again contain a complex olivine assemblage, which contains the first fragmental olivine seen since the end of phase 1.

Phase 6 is not represented, but phase 7 pumice continues to have a very complex olivine assemblage, containing all classes of olivine except the fragmental class 4. Phases 8 and 9 contain abundant and very variable olivine (see figs. 25.3, 25.4*A–B*), including class 4 fragments, but without any class 3 (round or strongly resorbed) grains. These are the last eruption samples known to contain fragmental olivine. In phases 10 and 15, rounded

class 3 olivine reappears, but class 4 olivine is absent. Later samples from phase 16 and 17(?) contain abundant olivine, but it is, like that in the earliest pumice, less variable in form. In the latest sample, an ooze, the olivine shows neither resorption nor kink-bands; the only other samples like it are the earliest (November 14–17) phase 1 samples.

Thus, the sequence of appearance of the different classes is: first, class 2, followed by 1 and 3, then 4, then 5. Class 3 and class 4 olivine tend not to occur in the same sample: of the eight samples with class 3 grains and 6 samples with class 4 fragmental olivine, only two (Iki–7, Iki–13) contain both classes. Class 5 olivine, the last class to appear, is found in phases 2, 5, 7, 8, and 15 and may occur in association with any of the other classes. The sequence of disappearance, as the eruption went on, was: first, 4, then 3 and 5, leaving only 1 and 2 present in the last phase.

Certain of these classes are uncommon, and it might be thought that the apparent gaps in the occurrence of classes 3, 4, and 5 would disappear, if more thin sections were examined. For many samples, however, more than one section is available already, and the olivine population is almost always the same in both sections. Thus, it appears that the occurrence of class 3, 4, and 5 olivine as reported in table 25.1 is not an accident of sectioning but a characteristic of particular samples.

PETROGRAPHY OF OLIVINE PHENOCRYSTS AND MEGACRYSTS IN THE LAVA LAKE

The same five classes of olivine that occur in the eruption pumice can be found in samples from the lake. Such samples cannot he related to individual phases, however, because of mixing in the lake, drainback between phases, and re-eruption of some of the same material in later phases. In addition to these complications, there has been significant redistribution of olivine within the lake after it crusted over, as discussed in Helz (1980). The dominant process was probably gravitative settling, as the coarser class 1 olivine grains have been affected more than the smaller class 2 phenocrysts. For these reasons, it is not possible to develop an olivine stratigraphy for the lake that would correlate with the time sequence observed in table 25.1. Posteruptive redistribution of olivine has produced essentially three zones in the lake: an upper, olivine-rich zone down to a depth of 18 m, an olivine-depleted zone from 18–40 m, and a second olivine-rich zone from 40 m down to within 2 m of the bottom of the lake (Helz, 1980; Helz and Wright, 1983; Helz and others, 1984). Both olivine-rich zones contain all five classes of olivine. The olivine-depleted zone generally contains only class 2 grains, which are commonly rounded and may be locally rimmed with pyroxene.

It might be thought that some of the features used to classify olivine in the eruption pumice would disappear during prolonged annealing in the lake. In fact, the only type of grain significantly affected is the skeletal olivine. Skeletal grains do occur in the pumice, though usually only in the microphenocryst size range (<0.5 mm). Lake samples, having cooled more slowly, contain virtually no skeletal olivine. Sample KI79–1–189.0 contains the only known example of a coarse skeletal olivine in the lake. Typical grains of class 2 lake olivine are shown in figure 25.5C. These look very much like their equivalents in the eruption pumice, as overgrowths of olivine are minor and glass inclusions tend to crystallize later than the melt outside the olivine.

Other types of olivine have also survived as much as 22 years of slow cooling unscathed. For example, figure 25.5*A* shows a class 1 olivine, with multiple planar extinction discontinuities, and strongly resorbed outline, which is virtually identical to the grain shown in figure 25.4*A*. The first grain was quenched from 1,198 °C on December 11, 1959 (see table 25.1). The second was quenched from 1,140 °C on April 22, 1981 (Helz and Wright, 1983; Helz and Thornber, in press). The extinction discontinuities have not been removed by annealing, nor have the crystallographically irrational curved surfaces of the resorbed grains healed. Apparently they are very unfavorable sites for further growth of olivine. Fragmental olivine also survives in the lake (see fig. 25.5*D*), perhaps for the same reason: the broken surfaces are not favorable growth sites, compared with the abundant rational faces and edges available on the class 2 phenocrysts and groundmass olivine.

The distribution of class 5 grains in the lake, which appears to be random, is of particular interest. These grains occur in olivine-rich samples at the edge of the lake, and in the center, at all depths, wherever class 1 grains occur. One of the best examples of this class (fig. 25.5*E*) is from the bottom of the deepest drill hole in the center of the lake. As indicated in table 25.1, class 5 grains have not yet been observed in any phase 1 samples. The bulk of the lake, however, was erupted during phase 1 and did not drain back down the vent (see fig. 25.2). Therefore, if the apparent absence of class 5 grains from phase 1 is real, the presence of grains of this class throughout the lake, including its most northerly and (or) deepest parts, implies that the bulk of the lake was very well mixed during phases 2–17, and perhaps for some time thereafter, even though there was little net increase in lava in the lake after phase 1.

OLIVINE MEGACRYSTS

The principal reason for considering lake samples in a paper on the dynamics of the 1959 eruption is that the lake contains a sparse population of very large olivine grains and aggregates of olivine, distinct from any observed in the available thin sections of eruption pumice. Perhaps the most curious are the two olivine megacrysts that have been found in the lake. One of these is shown in fig. 25.5*F*; data on both are presented in table 25.2.

The actual size of these large single crystals, or megacrysts, of olivine is unknown, but the parts of the grains visible in drill core and thin section are 20 mm by 10 mm. Though found at very different levels in the lake, the two grains are so much alike that they look like pieces of the same crystal. Both are wedge-shaped in section and contain as inclusions large areas of glass plus augite, plagioclase, and other groundmass phases. Presumably the original grains were skeletal, with irregular cavities in their cores. Their external form is not euhedral; their present grain boundaries appear to be fracture surfaces, at least in part. Both megacrysts contain abundant planar

extinction discontinuities (as in fig. 25.5*F*), but the total angle of rotation is very slight in both megacrysts. The planes are decorated with minute inclusions or voids, a style of decoration that is not commonly observed in ordinary class 1 olivine phenocrysts. Megacrysts of this sort have not previously been reported in Kilauean lava.

PETROGRAPHY OF OLIVINE AGGREGATES

Schwindinger and others (1983) reported that 95 percent of the olivine in the eruption samples studied by them occur in aggregates. This figure is not unreasonable for other eruption samples as well, but may be a little high for lake samples. Whatever the exact figure, isolated single crystals of olivine are uncommon. Large clots of crystals are also exceptional, however; most clumps of crystals appear, at least in thin section, to consist of 2–6 individual grains (see fig. 25.3).

If one considers only the largest aggregates, there are two distinct types present. The more common type of large olivine aggregates consists of relatively open or skeletal clusters of grains, like that shown in figure 25.6*A–B*. These open clusters consist of class 2 grains, rounded or otherwise, which have a common crystallographic orientation. A subordinate set, rotated 90° from the first set, is not uncommon, but other crystal orientations are rare. The crystals in these open aggregates are not sorted by size (see fig. 25.6*B* especially). These networks of crystals are open, with glass and vesicles along boundaries and at interstices. Schwindinger and others (1983) studied this type of open aggregate in some detail and recognized several subcategories. They have suggested that these aggregates form by synneusis, the swimming together of crystals suspended in a melt. Similar aggregates are common in the lake; these differ from the one shown in figure 25.6*A* chiefly in that they contain fewer crystals and less interstitial glass. The significance of these aggregates is that, whatever their exact origin, everything about them suggests that they formed in the presence of abundant melt, most probably in Kilauea's summit reservoir.

The second group of olivine aggregates differs markedly in character from the open, glomerocrystic clots described above. This group, which will be referred to as dense olivine aggregates or dunite aggregates, consists of clusters of non-euhedral olivine, for the most part very tightly interlocked or intergrown. The grains are not oriented crystallographically relative to each other. Such olivine aggregates, or dunite fragments, are uncommon; the one dozen examples known to date are described in table 25.2.

The dunitic aggregates in table 25.2 are from drill core, and so have undergone variable periods of slow cooling in the lake between eruption and quenching. Therefore, table 25.2 includes the dates on which the various samples were drilled and the temperatures from which they were quenched. The temperature estimates are based on the composition of the glass found in the groundmass of the host rock of each sample, using the empirical calibration presented in Helz and Thornber (in press) for Kilauean samples, except for sample KI76–2–20.5, which was collected long after the rock crystallized. For this sample, the temperature (about 100 °C) was determined by downhole thermocouple measurement. From these data it can be seen that individual aggregates were stored anywhere from 9 months to 22 years in the lake and quenched from temperatures ranging from 950 °C to 1,140 °C.

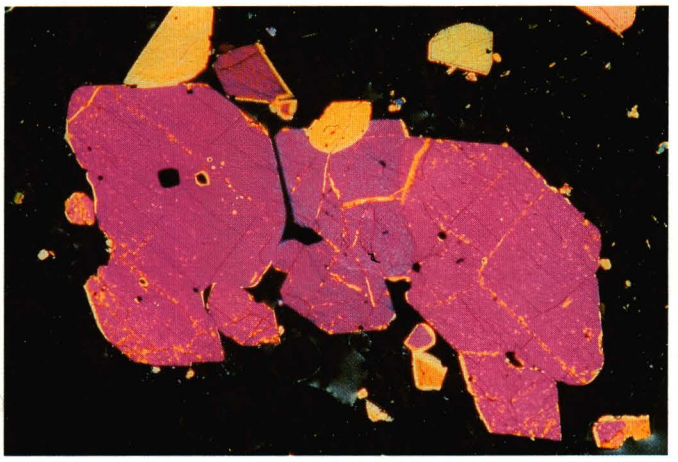

A

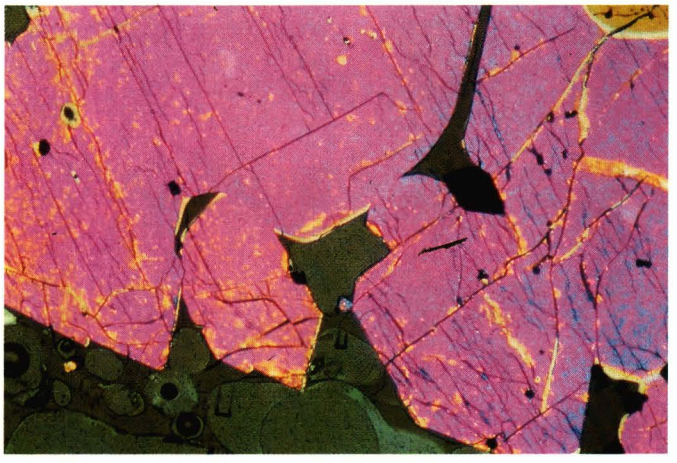

B

FIGURE 25.6.—Skeletal olivine aggregate from the 1959 Kilauea eruption. ***A***, Aggregate of euhedral grains in sample Iki–33 (phase 16). Note the strong preferred orientation of the crystals. The aggregate is 6 mm long. Crossed nicols. ***B***, Close-up of the same aggregate, showing its open nature. Interior grain margins are slightly rounded, exterior margins strictly euhedral.

It is evident from table 25.2 that these twelve dunitic aggregates are not distinctive in size; most are similar in size to the largest individual class 1 olivine grains. Even the largest are no bigger than the megacrysts described above. It is not surprising, therefore, that they occur randomly within the upper and lower olivine-rich zones, associated with the coarser olivine phenocrysts. Because the lake appears to have become very well mixed during the eruption, it is not possible to associate the aggregates and megacrysts with a particular phase or phases, even though they may have been far from random in their occurrence in the eruption samples.

This group of dense olivine aggregates can be divided into three subcategories: (1) seven aggregates consisting dominantly of

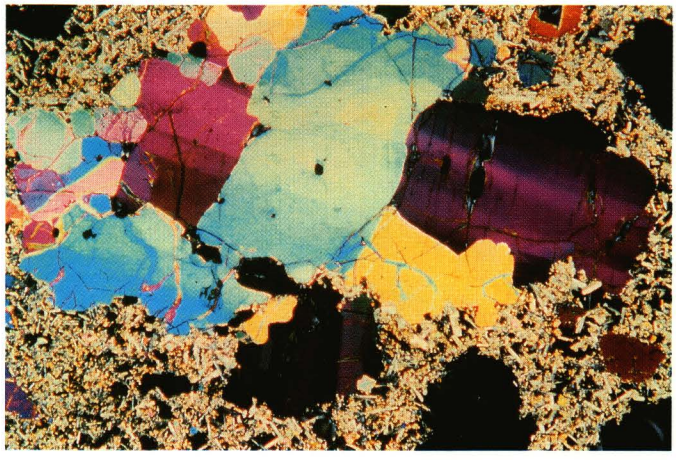

A

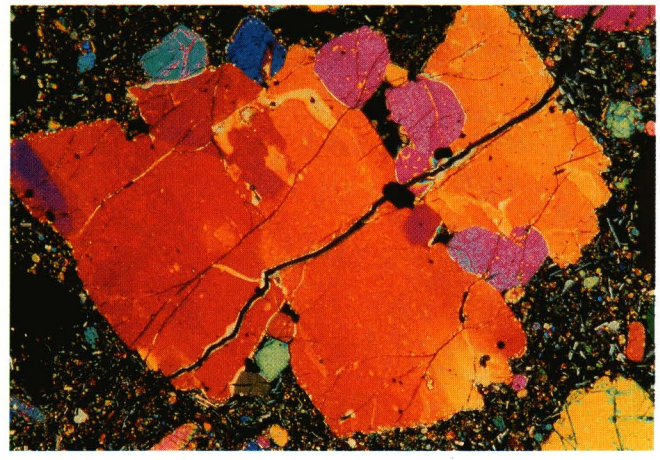

C

B

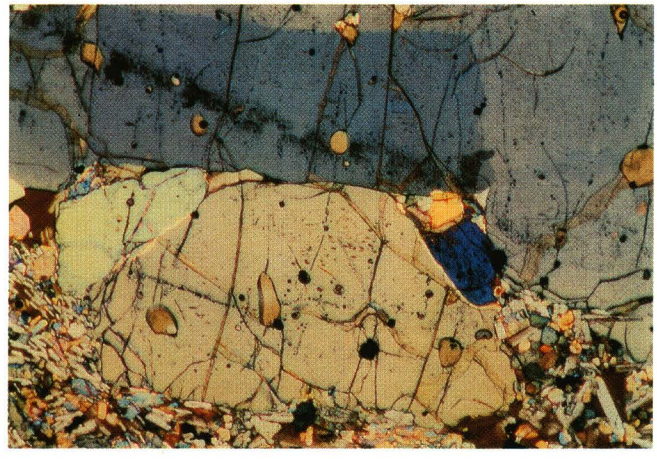

D

FIGURE 25.7.—Dunitic aggregates from Kilauea Iki lava lake. ***A***, Aggregate of deformed olivines from KI–113, quenched from 1,090 °C–1,095 °C in 1960. All but a few of the small grains are deformed. The aggregate is 8 mm across. Crossed nicols. ***B***, Close-up of a triple junction in aggregate, showing irregular grain boundaries, plus lack of 120° angles, and minimal penetration of melt from host along boundaries and at triple junction. (The black strip that intersects the triple junction is an epoxy-filled crack formed during sectioning.) Note cracks radiating from chromite inclusion in blue grain at left. Field of view 2.5 mm across. Crossed nicols. ***C***, Aggregate of class 1 olivine (6 by 5 mm), from KI81–1–230.4, quenched from 1,140 °C in 1981. The large grains contain irregular blocky subgrains, the boundaries of which are oblique to the section. Chromite (black) and smaller, strain-free olivine grains occur along the margins of the coarse olivine. Grain boundaries at triple junctions intersect at angles near 120°, and most grain boundaries are planar. Melt penetration of this aggregate is minimal, even after 22 years in the lava lake. Crossed nicols. ***D***, Aggregate of class 5 olivine in KI67–2–87.5, quenched from 1,073 °C in 1967, showing swarms of inclusions. Most inclusions are very tiny. Note densest inclusion swarm trends obliquely to grain boundaries. Field of view is 1 mm across. Partly crossed nicols.

interlocking class 1 grains: (2) two clusters of class 5 grains: and (3) three aggregates containing areas of a mosaic of unstrained olivine grains.

DENSE AGGREGATES OF CLASS 1 GRAINS

This is the commonest type of dense aggregate, with seven known examples. One of these, recovered in 1960 from a depth of 6.86 m in the lake, is shown in figure 25.7*A–B*. It consists of anhedral grains, for the most part tightly interlocked, most containing multiple planar extinction discontinuities. Some grains contain chromite inclusions, surrounded by fractures radiating from the inclusion wall into the olivine (see fig. 25.7*B*). Triple junctions, generally not intersecting at 120°, contain very small pools of glass. Two-grain boundaries can be highly irregular (fig. 25.7*A–B*) and are mostly unmarked by inclusions of vapor, glass, or other material. The aggregate contains a population of smaller, equant, usually unstrained grains that occur at the margins of the large grains but do not completely surround them. In the textural classifications developed for olivine-rich xenoliths from basalts and kimberlites, this and other aggregates in this group are transitional between the coarse and porphyroclastic categories of Harte (1977), or the protogranular and porphyroclastic categories of Mercier and Nicolas (1975).

The aggregate in KI–113 was quenched only nine months after the eruption ceased, so its texture may be presumed to be

relatively little affected by long-term storage in the lake. The other aggregates of class 1 grains, from 26–70 m below the surface of the lake, were cooled slowly from about 1,190 °C to the quenching temperature indicated in table 25.2 over periods of 8 to 22 years. However, the only textural change consistently observed in the latter aggregates is that the grain boundaries become more planar, and the angle of their intersections at triple junctions approach 120° (see figs. 25.5*D*, 25.7C). There is some tendency for greater penetration of the aggregate by melt, but, as figure 25.7C shows, this is not necessarily extensive, even after 22 years. In some of the more recently quenched samples there is a tendency for chromite to occur interstitially in the aggregate, rather than as inclusions in olivine (fig. 25.7C); but other aggregates (fig. 25.5*D*) have included chromite preserved.

Some aspects of the fabric of these seven aggregates are unaffected by annealing in the lake. For example, the aggregates are notably inequigranular, with the ratio of largest to smallest olivine grains present varying from 10 to 30 (see table 25.2). There is no tendency for the proportion of small grains to increase or decrease with time, nor does average grain size change in any other way as length of storage in the lake increases. Also, as in the isolated crystals, there is no discernable tendency for the kink bands or rectangular subgrains to disappear with time. The lack of internal reorganization of the large deformed grains suggests that the apparent expulsion of chromite to grain boundaries seen in some aggregates (fig. 25.7C) was accomplished during an earlier cycle of deformation and recrystallization. The present generation of subgrains, then, must have been produced in a second deformation event, the effects of which have not been eliminated by recrystallization during storage in the lake.

By decrease in number of adhering grains, these aggregates appear to grade into the dispersed class 1 olivine phenocrysts. It seems possible that all the class 1 grains and clusters found in the eruption samples and in the lake may have been disaggregated from rocks like this first group of dense, dunitic aggregates.

AGGREGATES OF CLASS 5 GRAINS

Three of the dense aggregates listed in table 25.2 contain olivine with sulfide-bearing inclusions. The two smaller ones (KI67–2–87.5 and KI79–1–203.6), consisting exclusively of class 5 grains, will be discussed here. The description below applies equally to rare smaller clusters of class 5 grains, containing 2 to 6 grains each.

A close-up view of the KI67–2–87.5 aggregate (fig. 25.7D) shows most of the features of this type. The grains are full of inclusions; some inclusions are large, of brown glass with or without opaques and vapor, but most are tiny and any glass present is pale. Included crystalline phases are chromite and sulfide. In some cases, the sulfide bleb appears to be too large to be a daughter phase, in the terminology of Roedder (1984), suggesting that such inclusions were polyphase initially, the melt already being saturated with an immiscible sulfide liquid (±chromite) at the time the inclusions formed. No daughter silicates have been observed. Grain shapes are irregular, but grain boundaries are tight only locally. These aggregates all show extensive penetration of melt along grain boundaries, independent of storage time in the lake. This and the abundant inclusions give these aggregates a dirty, moth-eaten appearance in thin section.

The localization of some inclusions in the KI67–2–87.5 aggregate (fig. 25.7*D*) in planar arrays suggests that they formed when melt ± sulfide, chromite, and vapor were injected into fractures in a previously existing grain or aggregate of grains. This distribution of inclusions is different from that in most class 5 grains, in which the inclusions commonly occupy either the core (as in fig. 25.5*E*) or a well-defined necklace (as in fig. 25.4*E*). The latter arrangements are more characteristic of primary inclusions, that is, inclusions incorporated during the growth of the individual olivine grain. The inclusion arrays in figure 25.7*D*, by contrast, appear to be secondary crack fillings (see Roedder, 1984, for a discussion of primary versus secondary inclusions). Sulfide-bearing inclusions also occur in irregular trails, swirls, and patches that cannot, from their geometry, be unequivocally designated as primary or secondary.

Class 5 grains are very rare, occurring in only 3 percent of the thin sections of drill core examined. The fact that aggregates of class 5 grains occur at all suggests that the single grains may formerly have been in aggregates, as it is highly improbable that these rare grains would coalesce into pure class-5 clusters after having been dispersed in the 1959 lava. Because of their rarity and in spite of the variation in distribution of inclusions, it seems likely that all these sulfide-bearing grains and aggregates came from a fairly limited source region.

DENSE AGGREGATES CONTAINING POLYGONAL MOSAICS OF OLIVINE

Three of the dunitic aggregates described in table 25.2 consist partly or entirely of a mosaic of equigranular polygonal olivine. Two of these (in KI79–5–171.4 and KI81–1–181.5) are the largest known aggregates in the lake. Each of the three is slightly different in character, having a different range of grain sizes in the mosaic areas, as follows:

KI67–2–87.9	0.6–2.5 mm
KI79–5–171.4	0.4–1.0 mm
KI81–1–181.5	0.05–0.2 mm

The grain size of the mosaics is independent of storage time in the lake, as the coarsest was quenched in 1967 and the finest grained in 1981. Mosaic textures similar to those shown in figure 25.8*A–C* have been produced experimentally by thermal annealing (Mercier, 1979, p. 200, fig. 2d). None of the grains in the mosaics show any sign of strain, suggesting that they were not produced by recrystallization during steady-state deformation of the sort studied by Ross and others (1980). The lack of correlation between mosaic grain size and time of storage in the lake suggests that none of these mosaics was produced during post-eruptive annealing in the lake.

The smallest and simplest of these three aggregates (fig. 25.8C) consists of strain-free grains with curvilinear boundaries and limited size range. This texture corresponds to the equant gran-

TABLE 25.2.—*Data on olivine aggregates and megacrysts found in Kilauea Iki lava lake*

Sample	Depth of sample (m)	Date drilled (mo/d/yr)	Quenching temperature (°C)	Location in lake	Size of aggregate in section (mm)	Crystal size range: Largest (mm)	Crystal size range: Smallest (mm)	Size ratio (largest/smallest)	Dominant crystal class
Olivine Aggregates									
KI-113	6.86	8/24/60	1090-1095	center	8 x 5	4	0.2	20	1
KI67-2-87.5	26.67	6/14/67	1073	north edge	7 x 5	6	0.5	12	5
KI67-2-87.9	26.79	7/6/67	1090	north edge	(a)[1] 12 x 7	8	0.8	10	1
					(b) 9 x 3	2.5	0.6	4	Polygonal mosaic
KI79-5-171.4	52.24	2/1/79	950-980	north edge	[1] 14 x 10	7	0.4	28	Polygonal mosaic
KI81-1-181.5	55.32	4/10/81	1010-1030	center	[1,2] 16 x 4	2	< 0.1	> 20	Polygonal mosaic
KI79-1-189.0	57.61	12/21/78	1130-1135	center	(a)[1] 8 x 6	6	0.4	15	1
					(b)[1] 6 x 6	6	0.6	10	1
KI79-6-190.3	58.00	2/14/79	1130-1135	between center and north edge	5 x 4	5	0.5	10	1
KI79-1-203.6	62.06	12/21/78	1140	center	3 x 2	2	0.3	7	5
KI81-1-224.4	68.40	4/13/81	1140	center	10 x 5	8	0.5	16	1
KI81-1-230.4	70.23	4/13/81	1140	center	6 x 5	6	0.2	30	1
Megacrysts									
KI76-2-20.5	6.25	8/30/76	~100	center	[1] 20 x 10	single crystal		-	-
KI81-1-238	72.54	4/14/81	1135-1140	center	[1] 20 x 10	single crystal		-	-

[1]Cut by edge of section. Area given is that within the section.

[2]Area of aggregate on drill core surface 16 mm x 10 mm. The section was cut perpendicular to the core surface.

uloblastic category of Harte (1977) or the mosaic equigranular category of Mercier and Nicolas (1975, fig. 6b, p. 464), a texture attributed to lengthy annealing at high temperatures. The olivines in this inclusion contain abundant healed discoid fractures similar to textures in olivines from San Carlos and elsewhere, which have been interpreted (Wanamaker and Evans, 1985) as produced by decrepitation of fluid inclusions during rapid decompression. Similar healed fractures occur in inclusions KI67–2–87.5 and KI79–1–189.0(a), but are not as common in these aggregates as in figure 25.8C.

The KI81–1–181.5 aggregate is more complex, in that it contains, in addition to the fine-grained mosaic shown in figure 25.8*B*, a population of coarser, more euhedral crystals, commonly containing a necklace of inclusions, some with sparse, tiny sulfide blebs. The coarser grains probably represent a second stage of grain coarsening, with the larger crystals having grown at the expense of smaller ones. The necklace of inclusions would correspond to impurities along former boundaries of the grains, swept up as the olivine grains grew outward. For the following reasons, this interpretation is preferred to a model in which the coarser grains would be considered to be later cumulates that attached themselves to a preexisting fine-grained substrate: First, some of the coarse grains occur within the mosaic, not at its edge. Second, the grains are very tightly intergrown and randomly oriented (unlike the open cumulate aggregates shown in fig. 25.6*A–B*). Third, the small mosaic grains contain very tiny inclusions similar in character to those in the coarser grains, suggesting that the coarse grains grew by incorporating this mosaic and its grain-boundary phases. Clearly the second-stage coarsening did not take place in the lava lake; the mosaic at the left end of the aggregate (fig. 25.8*D*) is in direct contact with the host and shows no coarsening whatever. Therefore, both stages predate incorporation in the present host.

The third of these aggregates, from sample KI79–5–171.4 (fig. 25.8*D*), is the most heterogeneous and also the most enigmatic. It contains areas where deformed class 1 grains are partly enclosed by strain-free polygonal grains, but elsewhere it contains euhedral, class-2-like grains. This aggregate also shows more extensive penetration by melt (now groundmass crystals) than any other aggregate. Of all the aggregates in table 25.2, this one appears to have the most complex history.

In contrast to the other two groups of aggregates, which correspond to one or another of the olivine classes described above, the mosaic grains do not occur as a recognizable separate class of dispersed grains. It is possible that some of the smallest class 1 and some class 3 grains might be former polygonal mosaic, but this seems unlikely: there are very few such grains in the eruption pumice. A more likely explanation is that strongly annealed dunites are simply rarer than the mildly deformed ones.

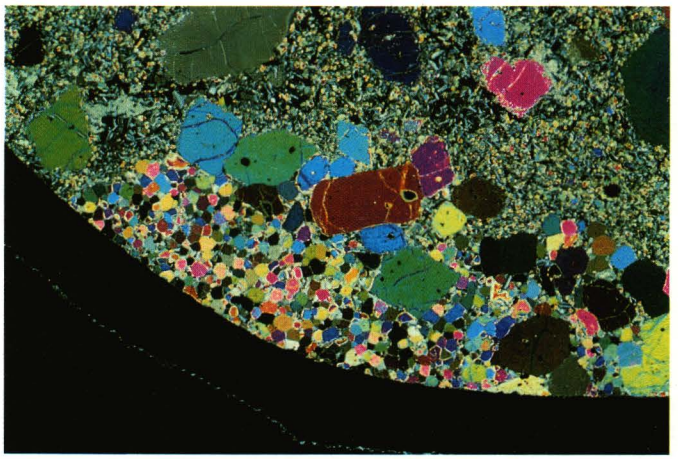

A

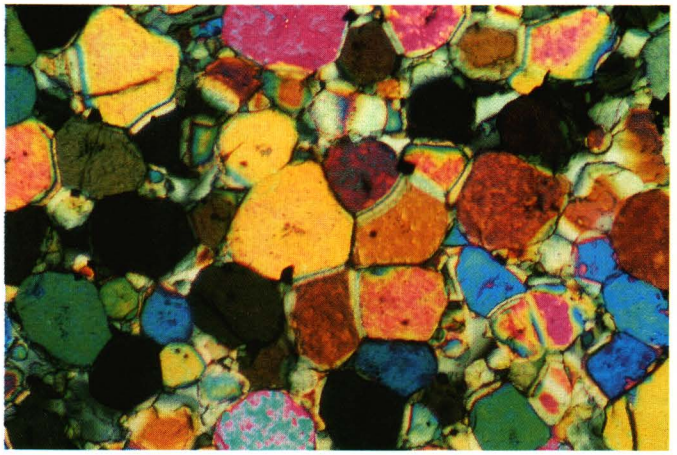

B

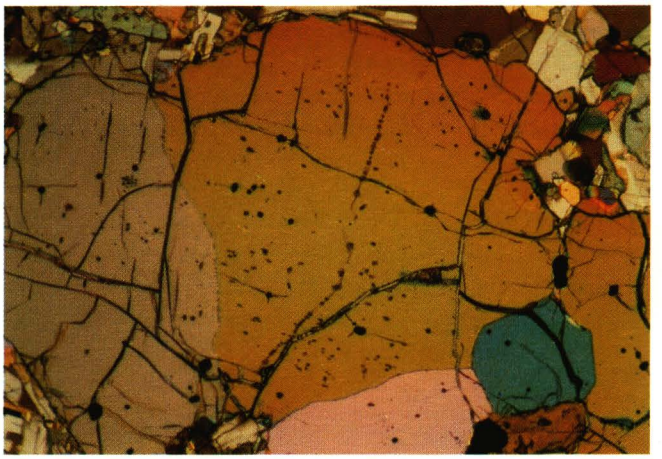

C

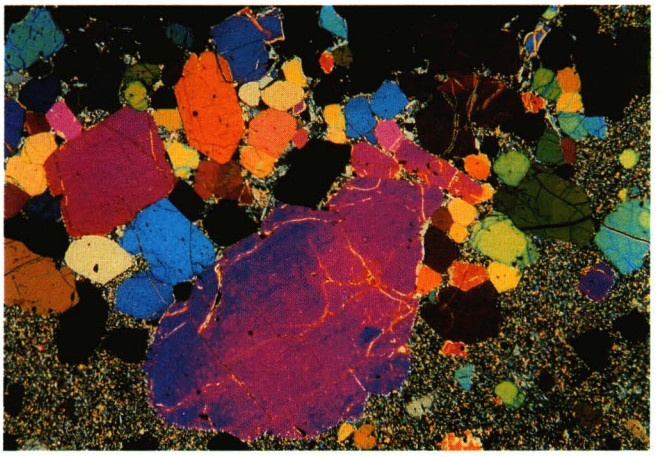

D

FIGURE 25.8.—Dunitic aggregates found in Kilauea Iki lava lake. ***A***, Olivine aggregate and host in KI81–1–181.5, quenched from 1,010–1,030 °C in 1981. Field of view is 1 cm across. The aggregate consists of areas of fine-grained polygonal mosaic of olivine, with coarser, more euhedral olivine present along the edge or (lower right) within the mosaic. At the left end of the aggregate, the mosaic is in direct contact with the groundmass of the host. Crossed nicols. ***B***, Close-up of polygonal mosaic in aggregate in KI81–1–181.5. Field of view 1 mm across. Most grains are olivine. Most of the olivine grains contain a central swarm of tiny inclusions (see yellow grains in center). Chromite grains (opaque) occur at margins of olivine. Minor interstitial plagioclase and augite are present locally. Crossed nicols. ***C***, Close up of the smaller olivine aggregate from KI67–2–87.9, quenched from 1,090 °C in 1967. Grain boundaries intersect at angles near 120° at triple junctions, but are otherwise curvilinear, so that grain shapes are irregular. The color variation seen in the tan olivine grains reflects zoning toward the host; it follows the outline of the aggregate, not of individual grains. Black grains within the aggregate are chromite. Fuzzy inclusions are healed discoid fractures containing asterisk-like inclusions of brown glass and chromite. Field of view is 4 mm across. Nicols partly crossed. ***D***, Olivine aggregate (10 by 14 mm) in sample KI79–5–171.4, quenched from 950–980 °C in 1979. This aggregate has been extensively penetrated by melt, now visible as interstitial groundmass-size crystals. It contains local areas of polygonal olivine, surrounding coarser deformed olivine (the green grains on right side), and areas of randomly oriented euhedral olivine (center and left). Crossed nicols.

In summary, then, rare dunitic aggregates have been found in Kilauea Iki lava lake. The textures of the various aggregates, which record multiple deformation events, multiple annealing events, and (or) rapid decompression, match those observed in ultramafic xenoliths of mantle origin. The fact that the history recorded in these aggregates appears to predate entirely their incorporation in the 1959 lava implies that all aggregates are xenolithic. To the extent that class 1 and class 5 olivine grains in the 1959 lava are derived by disaggregation from similar preexisting dunite, crystals in those classes may likewise be considered xenocrystic.

OLIVINE PHENOCRYSTS AND DUNITIC AGGREGATES IN OTHER HAWAIIAN ROCKS

Olivine is virtually ubiquitous as a phenocryst phase in Hawaiian tholeiites and mafic alkalic rocks. With the petrographic description of the phenocrysts, megacrysts, and dense aggregates found in the Kilauea Iki lava in hand, it is now appropriate to review the information available on the petrography of olivine from other Kilauea lava and from those of other Hawaiian volcanoes.

No comparably detailed petrographic work on Kilauea

olivines has been done previously. Even studies focused on the picritic lava of Kilauea (Macdonald, 1944; Muir and Tilley, 1957; Murata and Richter, 1966a, 1966b) have not mentioned the occurrence of kink-banded olivine, for example. Therefore I have re-examined all of the thin sections of subaerial Kilauea basalt available to me, with the present classification scheme in mind. The available sections included samples of the historical eruptions described in Wright (1971), including the 1920 eruption, the relatively magnesian 1921 summit eruption, and the 1840 east-rift picrite. In addition, samples of the 1977, April 1982, and September 1982 eruptions, and samples of phases 1–8 of the ongoing (as of January 1986) Puu Oo eruption have been examined. The earlier samples were available only as covered thin sections; for the 1977–1983 samples, polished sections were available for examination.

One good example of a kink-banded olivine phenocryst was found in this search, in TLW 67–1g, the most magnesian lava of the 1920 southwest-rift eruption (Wright, 1971). No other class 1 or probable class 5 olivine has been observed in any of them. The olivine phenocyrsts present all fall in class 2 of the present classification system, being either euhedral or skeletal. Skeletal grains are much more common, proportionately, than they are in Kilauea Iki samples. Resorbed grains, though present (in some Puu Oo samples, for instance), are rare.

The olivine-rich precaldera intrusive rocks exposed in Kilauea's caldera wall, including the Uwekahuna laccolith, were also examined, with the thought that they might represent samples of olivine-rich sludge from the bottom of Kilauea's summit reservoir. The olivine phenocrysts in these intrusives are uniform in grain size (1–5 mm long) in contrast to the more variable olivine in Kilauea Iki (see fig. 25.3). Planar extinction discontinuities were observed in very few grains. These grains are small, and the bands very faint. In about one-half the cases, the discontinuities exist only at the margin of the grain and are absent from the interior. No such grains have been observed in the 1959 lava, and it is not clear whether these marginal extinction discontinuities are deformation or growth features.

Examination of the submarine east-rift lava described by Moore (1965) turned up deformed olivine in two samples, No. 1742, from 1,400 m below sea level, and No. 1706, from 5,000 m below sea level. Another dredged sample of Kilauea east-rift lava, shown to me by M.O. Garcia (University of Hawaii) also contains good examples of blocky, deformed olivine crystals, strikingly similar to those in the 1959 lava.

In addition to these instances of kink-banded olivine in Kilauea tholeiite, such olivine has been reported from tholeiite of Hualalai, dredged from 2 km below sea level (Clague, 1982) and in one Haleakala tholeiite in the suite studied by Chen and Frey (1983) (C.-Y. Chen, written commun., 1984). Thus, the kink-banded olivine in the 1959 Kilauea tholeiite are not unique. However, they appear to be virtually absent from other subaerial Kilauea eruptions.

Dunitic aggregates containing deformed olivine and (or) mosaics of unstrained grains occur very widely in alkalic rocks in Hawaii. They have been described from Hualalai (Kirby and Green, 1980; Jackson and others, 1981), from the Honolulu Volcanics (formerly the Honolulu Volcanic Series; Jackson and Wright, 1970; Sen, 1983), and from Loihi Seamount (Moore and others, 1982; Roedder, 1983). Other reports of similar materials in Hawaiian tholeiite are lacking, however. Jackson (1968), in his very extensive survey of coarse-grained xenoliths in Hawaiian rocks, stated that all coarse-grained xenoliths he had found in tholeiitic lavas were cumulates, and that "none of the minerals is strained or deformed" (Jackson, 1968, p. 142). He further presented data showing that pure olivine rocks, containing no other cumulus or interstitial phases, were very rare in Hawaiian tholeiite. The deformed dunitic aggregates found in Kilauea Iki appear to be the first such material recognized in any Hawaiian tholeiite.

OLIVINE AND GLASS COMPOSITIONS: ERUPTION PUMICE

This section presents compositional data on olivine and glass in the eruption samples. Of particular interest are (1) variations in composition and zoning of the olivine phenocrysts as a function of petrographic class and of time, (2) variations in average glass composition with time, and (3) more detailed data on the glasses immediately adjacent to olivine phenocrysts in the eruption pumice. As will become evident, these rapidly quenched samples preserve a significant amount of internal disequilibrium, as might be expected in an eruption long-recognized as involving magma mixing (Wright, 1973).

Analyses of representative olivine grains are presented in table 25.3. These analyses cover the range of phenocryst composition observed. The forsterite contents shown are reproducible to ± 0.1 percent, MnO ± 0.02 percent, CaO to ± 0.03 percent absolute. NiO is more variable, reproducible to perhaps ± 0.05 percent absolute. The intragrain chemical variation (see table 25.3, columns 1 and 2, for example) is modest, but it exceeds the analytical uncertainty and is generally systematic, with the cores being uniform and all variation (zoning) confined to the rims. There are a few grains, especially in the later samples, where forsterite content varies more irregularly, but the total range of intragrain variation in these grains is ≤ 0.8 mol percent Fo. Therefore, it seems justifiable to document, and to interpret, the zoning patterns of most of these olivines.

Table 25.4 includes average glass compositions for the fifteen eruption samples studied. These include only glass analyses taken some distance (>1 mm) away from the olivine phenocrysts. All of the glass compositions are olivine-controlled (Powers, 1955; Wright, 1971); that is, they are related to each other chiefly by addition or removal of olivine ($\pm$chromite), the only phenocryst phase present. Hence, the most variable component is MgO, which ranges from 6.35 to 10.03 weight percent and is reproducible to ± 0.10 percent. Other oxides are less variable: total iron as FeO only varies from 11.00 to 11.65 percent, for example. As documented in Helz and Thornber (in press), the MgO content of Kilauea glass in equilibrium with olivine varies linearly with temperature and appears to be a usable geothermometer. The quenching

temperature assigned each glass in table 25.4 is based on this calibration.

OLIVINE PHENOCRYST COMPOSITION VERSUS PETROGRAPHIC CLASS

Olivine compositional data as a function of the petrographic classes established above are presented in figures 25.9*A–B* and 25.10. Figure 25.9*A* shows histograms of the forsterite content of the cores of all the olivine phenocrysts analyzed to date. Each symbol corresponds to one analyzed point. For grains showing <0.5 percent variation in forsterite, all points are plotted. Most such grains are strongly resorbed (class 3 or 1) or fragmental (class 4) and may not have any real rims preserved on them.

The most important feature of figure 25.9*A* is that there is extensive overlap in core compositions between the euhedral class 2 olivine and the less regularly shaped, kink-banded and (or) sulfide-bearing olivine in classes 1 and 5. Class 1 and 5 cores extend to higher forsterite contents (88.7 percent), and class 2 cores to lower forsterite contents (85.0 percent), but the bulk of both subsets fall between 85 and 88 percent Fo. The class 3 and 4 grains are not distinctive, with most having 86.5–87.7 percent Fo. It should be noted that the composition of olivine from phase 1 (which made up most of the lake; see fig. 25.2) is no different from that of olivine in the later phases, except that the most iron-rich class 2 grains are absent.

TABLE 25.3.—*Composition of selected olivine grains from the 1959 eruption pumice, showing extremes of composition and zoning*

[Oxide contents in weight percent]

	1	2	3	4	5
Sample	Iki-22		Iki-9		Iki-24
	core	rim	core	rim	core
Olivine class	1	1	2	2	1
Points in analysis	5	4	2	4	3
SiO_2	39.44	39.90	40.09	38.95	40.22
TiO_2	.01	.01	.05	.04	.00
Al_2O_3	.03	.02	.00	.02	.00
Cr_2O_3	.02	.00	.04	.02	.01
FeO	14.22	12.09	12.26	18.16	11.03
NiO	.10	.19	.15	.01	.17
MnO	.20	.17	.12	.20	.17
MgO	45.86	47.76	47.38	42.37	47.87
CaO	.24	.20	.24	.32	.25
Na_2O	.00	.00	.00	.02	.02
Total percent	100.12	100.34	100.33	100.11	99.74
Mol% Fo	85.2	87.6	87.3	80.6	88.6
Comments	Reverse zoning		Extreme normal zoning		Most magnesian

Most of the olivine phenocrysts in the eruption samples are zoned, and figure 25.9*B* summarizes the available data on zoning patterns for the same population of grains whose core compositions were given in figure 25.9*A*. Most grains vary over a range of 3 percent Fo or less, the zoning generally being confined to the outermost 10–30 μm of the crystal. Only two small class 2 grains are more strongly zoned, showing as much as an 8 percent decrease in Fo from core to rim. The class 3 and 4 grains are essentially unzoned.

Three features of figure 25.9*B* are particularly noteworthy. First, normally zoned and reversely zoned grains are almost equally abundant. Second, there is little difference between the euhedral class 2 grains and the class 1 and 5 grains in this respect. If anything, reverse zoning is more frequent in the class 2 population. Lastly, the olivine phenocrysts analyzed so far from phase 1 samples are mostly either reversely zoned or unzoned. Normally zoned phenocrysts do not become common until phase 2.

The variation in NiO content of olivine cores for this same population of grains is shown in figure 25.10. NiO content was of particular interest because potentially it might allow one to distinguish between cognate and xenocrystic (peridotite-derived) olivine, or perhaps between olivine that coexisted with sulfide and olivine that did not. As can be seen in figure 25.10, however, the various populations appear not to have distinctive NiO contents. The few class 5 sulfide-bearing grains in the eruption pumice tend to fall below the median NiO content for the class 1 + 5 grains overall, but even here the difference is not very marked. (It should be noted that all the sulfides in the class 5 grains in the eruption samples are tiny, hence do not unequivocally predate entrapment and therefore do not prove that the basaltic melt from which the olivine in fig. 25.10 grew was sulfide-saturated.) From the analyses in table 25.3 one might suppose that there was a positive correlation between NiO and forsterite contents, but when the entire data set is considered there is no such correlation. The NiO contents observed here (0.10–0.30 percent) are the same as reported by other workers for Kilauea basalt (Häkli and Wright, 1969; Bence and others, 1981) and other mafic rocks (Fleet and others 1977; Fleet and MacRae, 1983).

It is evident from figures 25.9*A–B* and 25.10 that the various petrographic classes of olivine described earlier are not distinct with respect to Fo content or NiO content or style of zoning. They are not distinguishable on the basis of MnO or CaO contents either. This suggests that the olivine grains formed under some continuous range of conditions and that none of the classes can be singled out on the basis of composition as being xenocrystic to their host.

The results presented above are slightly at variance with those of some earlier workers. Richter and Murata (1966) reported that large blocky olivine phenocrysts were magnesian ($Fo_{87–88}$) and small euhedral olivine crystals more iron-rich (Fo_{82}). Certainly individual crystals can be found with these characteristics, but the composition ranges of the two populations overlap almost completely. Even the microphenocrysts (not shown in figs. 25.9*A–B*, 25.10) range from Fo_{87} to Fo_{74}. Thus, the various olivine groups cannot be considered to be successive generations of crystals grown

TABLE 25.4.—*Composition of glass away from olivine phenocrysts in selected samples of the 1959 Kilauea eruption pumice*

[Oxide contents in weight percent; total iron reported as FeO]

	1	2	3	4	5	6	7	8	9	10	11	12	13	14	15
Sample No.	Iki-1	Iki-58	Iki-22	Iki-44	Iki-7	Iki-11	Iki-9	Iki-13	Iki-14	Iki-20	Iki-21	Iki-24	Iki-26	Iki-32	Iki-33
Date (mo/d) sample collected	11/14	11/15	11/18	11/20	11/21	11/26	11/28	12/5	12/6	12/8	12/11	12/13	12/14	12/17	12/19
Phase of eruption	1	1	1	1	1	2	3	4	5	7	8	9	10	15	16
SiO_2	49.91	50.23	49.18	49.46	49.62	49.32	50.46	49.84	49.43	49.81	49.76	49.88	49.26	49.65	49.63
TiO_2	2.96	2.91	2.49	2.66	2.64	2.64	2.82	2.62	2.60	2.60	2.63	2.68	2.67	2.63	2.63
Al_2O_3	13.99	13.98	12.10	12.82	12.88	12.69	13.51	12.74	12.73	13.02	12.85	13.19	12.98	12.93	13.03
Cr_2O_3	.01	.00	.08	.07	.05	.06	.01	.07	.06	.04	.07	.07	.06	.04	.06
FeO	11.40	11.65	11.33	11.27	11.25	11.15	11.00	11.14	11.27	11.28	11.21	11.04	10.92	11.08	11.22
MnO	.13	.14	.13	.14	.13	.12	.14	.13	.13	.13	.13	.13	.13	.13	.12
MgO	6.35	6.46	10.03	8.55	8.60	8.48	6.93	9.04	9.49	8.21	9.09	8.61	8.67	8.73	8.70
CaO	11.25	11.50	11.17	11.25	11.33	11.39	11.56	11.39	11.38	11.33	11.41	11.51	11.51	11.55	11.67
Na_2O	2.67	2.62	2.33	2.53	2.46	2.51	2.48	2.36	2.29	2.32	2.39	2.17	2.46	2.45	2.28
K_2O	.62	.60	.52	.54	.56	.56	.58	.55	.58	.54	.55	.58	.52	.54	.60
P_2O_5	.28	.26	.22	.26	.25	.27	.31	.23	.21	.27	.26	.24	.24	.23	.24
Total	99.57	100.35	99.58	99.55	99.77	99.19	99.80	100.11	100.17	99.51	100.35	100.10	99.42	99.96	100.18
Points in average	8	14	6	6	7	4	6	9	5	5	7	4	6	5	4
Quenching temperature (°C)	1142	1144	1216	1187	1188	1185	1154	1196	1205	1181	1197	1188	1189	1191	1190

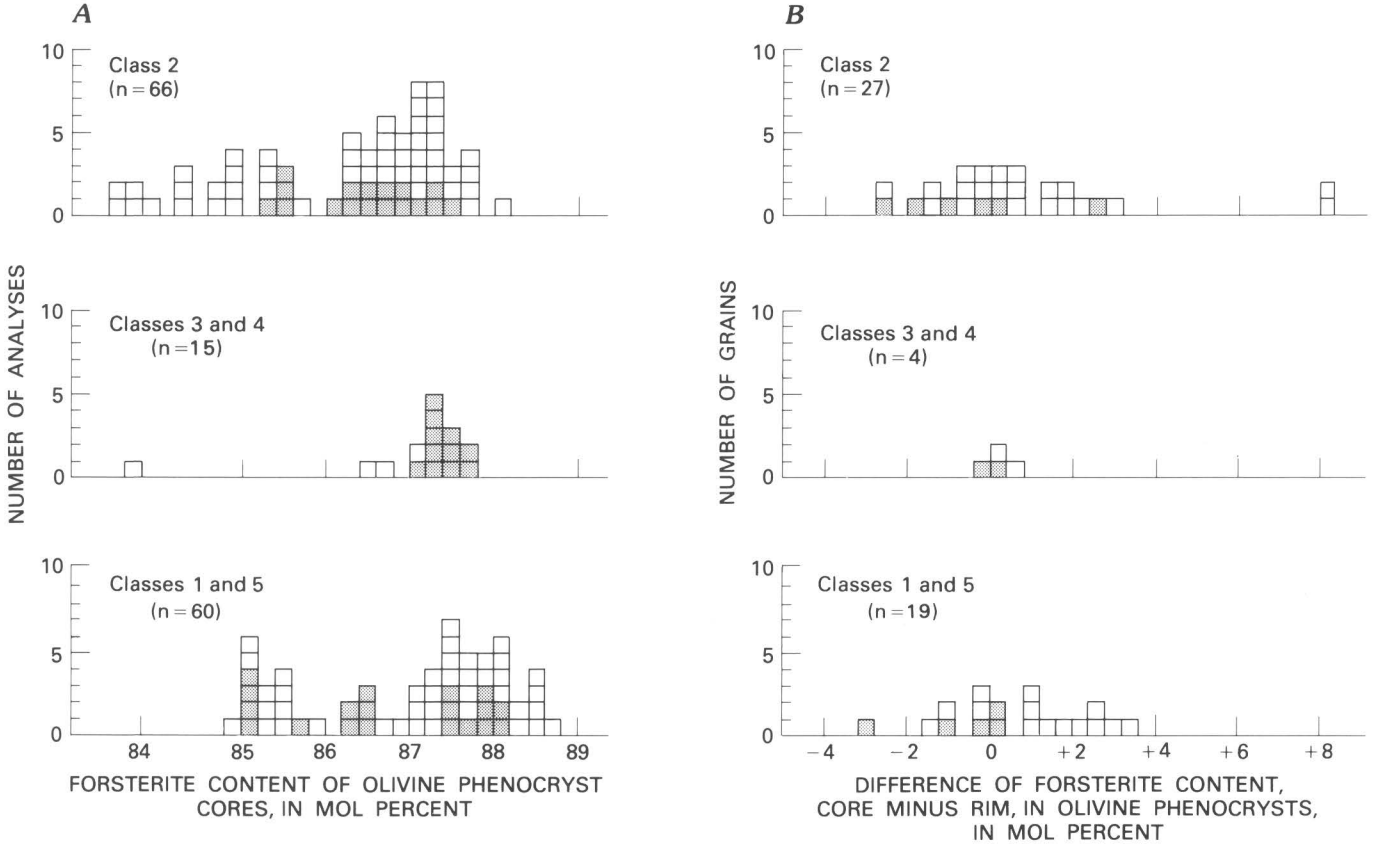

FIGURE 25.9.—Compositional data for olivine phenocrysts from the 1959 Kilauea eruption. Shaded squares, olivine from phase 1; open squares, olivine from later phases. ***A***, Frequency distribution of forsterite content of the cores of olivine phenocrysts in eruption samples. Each square represents one analyzed point. ***B***, Frequency distribution of different types of Mg-Fe zoning observed in olivine phenocrysts in eruption samples, for the same olivine population as in fig. 25.9*A*. Each square represents one grain. Negative abscissa values indicate reverse zoning.

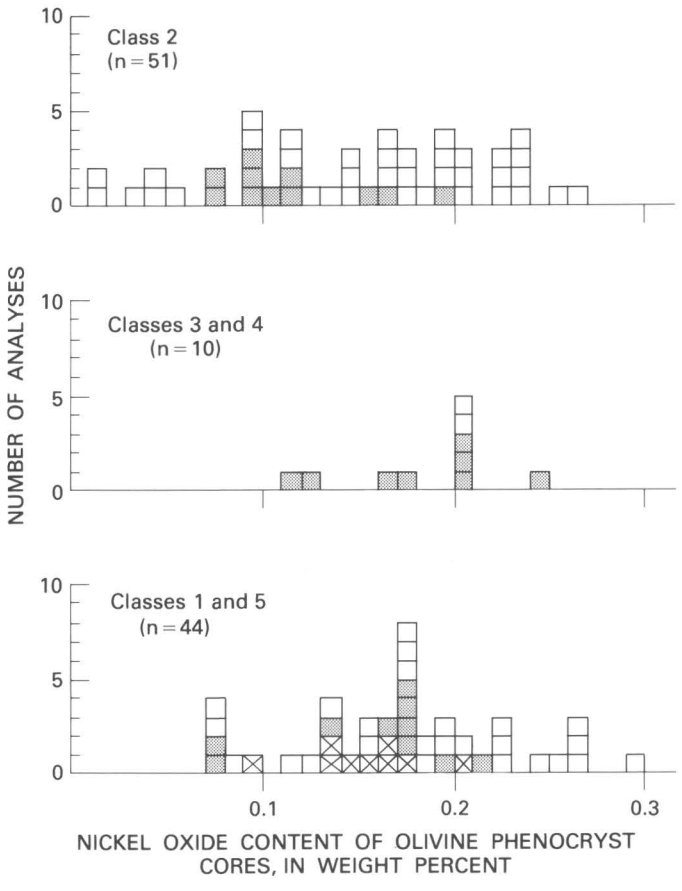

FIGURE 25.10.—NiO content of the cores of olivine phenocrysts in the 1959 Kilauea eruption samples, for the same population of olivine grains as in fig. 25.9. Each square represents one analyzed point. There are fewer points in this figure than in figure 25.9 because Ni was not always analyzed for. Shaded squares, phase 1 olivine; squares with x, class 5 olivine, from phases 2–16; open squares, other olivine from phases 2–16. The calculated limit of detection of NiO is 0.08 weight percent.

from a single batch of magma.

The data in figure 25.9*B*, showing that most olivine phenocrysts are zoned, are superficially in conflict with Leeman and Scheidegger's (1977) statement that the olivine in the 1959 eruption is not zoned. This is a question of semantics, however: Leeman and Scheidegger chose to regard any grain that varied by less than 5 percent Fo as unzoned, and it is true that strongly zoned grains are rare in the 1959 lava.

OLIVINE PHENOCRYST COMPOSITIONS VERSUS TIME

It is evident from figure 25.9*A–B* that olivine compositions and zoning patterns vary slightly from phase to phase of the eruption. These variations from sample to sample are shown in figure 25.11. Note that in this figure, in contrast to figures 25.9*A* and 25.10, symbols correspond to more than one analyzed point. For example, in sample Iki–11, three grains have been analyzed, one each from classes 1, 2, and 5. There are six analyzed core points and three rim points on the class 5 grain, but some of the core points fall on top of each other, so are not visible as separate points in figure 25.11. Average MgO content of the glass in each sample (see table 25.4) is plotted below the olivine data. The range of MgO content shown is that observed in glass more than 1 mm away from any olivine phenocryst. The fields in figure 25.11 outline the range of core compositions for the two groups of olivine.

As noted above, olivine is sparse in the cool (1,140–1,145 °C), early phase 1 samples. The olivine grains are small and euhedral, but with variable zoning. Iki–22, the first of the olivine-rich samples, has a much more magnesian glass with a quenching temperature of 1,217 °C (see table 25.4) and a phenocryst population of large, reversely zoned olivine crystals. Previous workers (Leeman and Scheidegger[1] 1977; Ford and others, 1983; Harris and Anderson, 1983) have noted that the cores of these olivine phenocrysts would be in equilibrium with the glass in the sample at about 1,250 °C. None has reported the existence of the more magnesian rims, however.

In contrast to Iki–22, Iki–44 has only fairly magnesian olivine grains in it, all virtually unzoned. The glass in this sample was quenched from a lower temperature (1,189 °C) than that in Iki–22. The glass in Iki–7 is similar to that in Iki–44 but it includes, besides magnesian, unzoned olivines like those in Iki–44, reversely zoned euhedral olivines, some of which are shown in figure 25.4C. Thus, in phase 1 we see a large range in glass composition and a significant range in olivine composition (Fo_{88} to $Fo_{84.5}$). However, there is no correlation between glass composition and olivine core composition, olivine rim composition, or the style of zoning, if any. As noted above, all large zoned olivine grains in phase 1 are reversely zoned.

Phase 2 (Iki–11) contains the first coarse, normally zoned olivine, in addition to reversely zoned crystals. The crystals do not converge on a common rim composition, however: the class 1 crystals range from $Fo_{87.8}$ (core) to Fo_{85} (rim), whereas the class 2 crystals go from Fo_{85} (core) to $Fo_{87.4}$ (rim). Further evidence of internal disequilibrium is the observation that the glass in this sample is appreciably more heterogeneous than that in any individual phase 1 sample, with MgO ranging from 8.07 to 8.60 percent, for glasses well away from olivine.

Phase 3 (Iki–9), like Iki–58 from phase 1, though olivine-poor, does not contain a uniform olivine population. Only two small class 2 olivines occur in the thin section, but they show very different zoning patterns: one ranges from $Fo_{87.4}$ to $Fo_{79.3}$ and is euhedral at the edges; the other varies from $Fo_{84.9}$ to $Fo_{83.1}$ and is resorbed at the edges. The glass in this sample was quenched from a lower temperature (1,154 °C) and is more differentiated than that in any but the earliest phase 1 samples.

Phase 4 glass (Iki–13) is again more magnesian, with a quenching temperature of 1,196 °C, and the glass is more hetero-

[1]Leeman and Scheidegger (1977) refer to Iki–22 as KI–7 and to what is probably Iki–7 as KI–22. This is a numbering mixup: Iki–22 has a unique high-MgO glass not found in any other phase 1 pumice. Ford and others (1983), using Leeman and Scheidegger's data, reproduce the same numbering error.

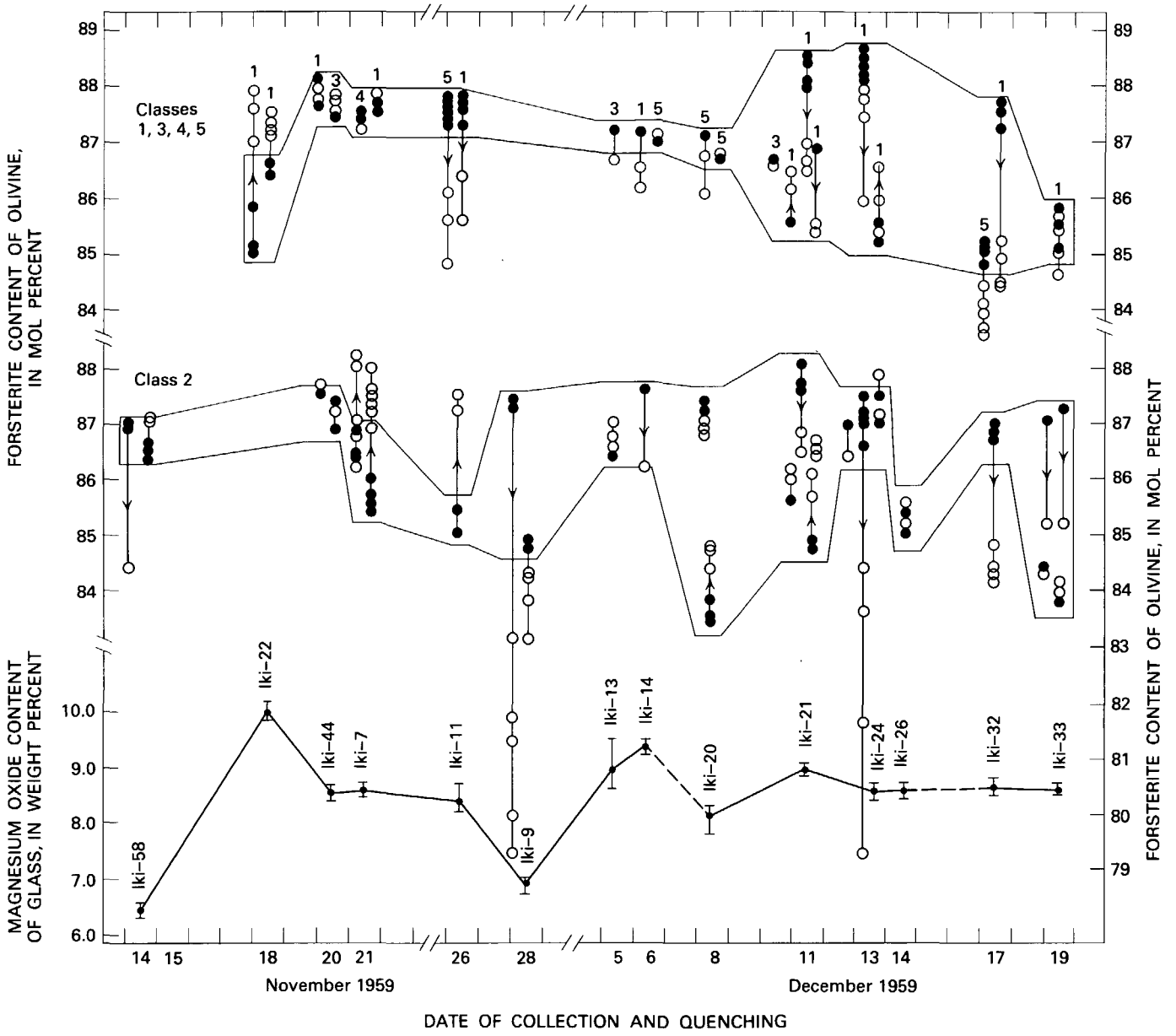

FIGURE 25.11.—Composition of olivine phenocrysts (mol percent Fo) and of glass (weight percent MgO) in samples from the 1959 eruption of Kilauea, plotted against the dates of eruption and quenching. For olivine, each symbol includes all analyzed points on a given grain having the same composition, rounded to 0.1 percent Fo. All data from a given grain are connected by a line. Solid circles, analyzed points from the cores of grains; open circles, points around the rims of the same grains. Grains in classes 1, 3, 4 and 5 are individually labeled. Arrows pointing toward rim compositions emphasize the direction of zoning. For glass, the small dots give the average MgO content of glass, from table 25.4, whereas the bar indicates the total range of MgO content observed, for glass more than 1 mm away from olivine.

geneous than any other sample, with MgO varying from 8.70 to 9.48 percent. Phase 5 (Iki–14) contains a still hotter (1,205 °C) but more uniform glass, with 9.32 to 9.55 percent MgO. In both samples, olivine phenocrysts are weakly zoned, in both normal and reverse senses, and are consistently magnesian ($Fo_{87.5}$ to $Fo_{86.0}$).

Phase 6 is not represented here. Phase 7 (Iki–20) is, again, a cooler phase (1,181 °C), though not as differentiated or olivine-poor as phase 3. The olivine population within the section is more diverse than ever: Both normally and reversely zoned grains are present, and the class 2 olivine exhibits a wide range of core compositions ($Fo_{87.5}$ to $Fo_{83.4}$). For the first time, however, the rim compositions of the different grains converge toward a common composition, as though they had been trying to equilibrate, either with each other or with a common melt.

Phase 8 (Iki–21) is hotter again (1,197 °C) and very olivine-rich, with a very heterogeneous olivine population. As in phase 7, the rims of the various class 2 grains appear to be converging on a common composition. This sample contains the most magnesian ($Fo_{88.1}$) class 2 olivine found.

Phase 9 (Iki–24, see fig. 25.3) contains a slightly cooler (1,188 °C) glass. Like Iki–21, it contains a very varied group of olivine crystals, with the class 1 grains converging on a common rim composition. It also contains the only strongly zoned grain ($Fo_{87.5}$ to $Fo_{79.3}$) found since phase 3, and the most magnesian olivine ($Fo_{88.7}$) in the whole analyzed population shown in figure 25.11.

From phase 10 through phase 16 (samples Iki–26, Iki–32, and Iki–33), glass composition is constant, implying uniform quenching temperatures of 1,188–1,190 °C. The glass is quite homogeneous, away from olivine, within each section. The olivine grains are either normally zoned or unzoned; none shows pronounced reverse zoning. Also, although core composition remains quite varied, olivine rim compositions are consistently more iron-rich ($Fo_{85.5}$ to $Fo_{83.5}$) than in all previous phases but phase 3. This trend toward simpler, better equilibrated olivine compositional variations begins earlier than the simplification in the petrographic variants, which is confined to phases 16 and 17 (see table 25.1).

COMPOSITION OF GLASS ADJACENT TO OLIVINE

The glass compositions presented in table 25.4 and discussed above are those found more than 1 mm away from any olivine phenocryst. Glass closer to olivine grains is more variable in composition, in ways that cannot be explained as the result of quench overgrowths on olivine. This section presents data on selected pairs of olivine rim and adjacent glass that illustrate both this greater variation in the glass and its apparent correlation with the condition (euhedral or resorbed) of the adjacent olivine rim.

The olivine rim compositions (shown in fig. 25.11) were taken on points within 10 μm (and usually within 3–5 μm) of the contact of the olivine with the glass. The adjacent glass analyses are taken at distances of 20–30 μm away from the contact. Most of the rim points shown in figure 25.11 have a corresponding analysis of adjacent glass. From this data set, figure 25.12 includes data on only three samples: two phase 1 samples (Iki–22, Iki–44) and the latest analyzed sample (Iki–33, from phase 16).

In Iki–22, glass adjacent to the large reversely zoned phenocrysts is less magnesian than glass elsewhere in the section. Around the edge of each crystal, glass adjacent to euhedral corners and faces is more magnesian than glass adjacent to resorbed edges. Some of this resorption is very local (fig. 25.13). It is possible that all the adjacent glass has been depleted in MgO by growth of olivine during quenching, but the variation within the adjacent glass cannot be so explained; the analyzed points are all equally far from olivine.

The glass in Iki–44 is less magnesian and the olivine more magnesian than Iki–22, as noted above. Here we see data from four different grains, two in a cluster and two isolated phenocrysts. Three of these grains have adjacent glass analyses with MgO

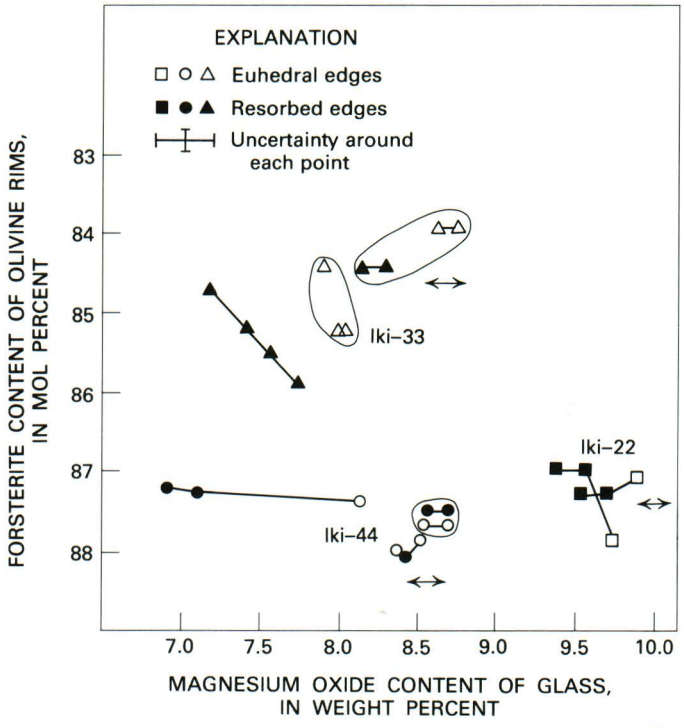

FIGURE 25.12.—Composition of rims of olivine phenocrysts (mol percent Fo) plotted against the MgO content (weight percent) of glass adjacent to the olivine rim, for three samples from the 1959 Kilauea eruption. Squares, data from Iki–22; circles, data from Iki–44; triangles, data from Iki–32. In this figure, points connected by a line are from around the periphery of a single grain. Data within a circle represents points on two or more different grains from a cluster of olivine grains. The double-ended arrow shows the range of MgO in glass more than 1 mm from olivine for each of the samples. The uncertainty in Fo and in MgO is ±0.1 percent.

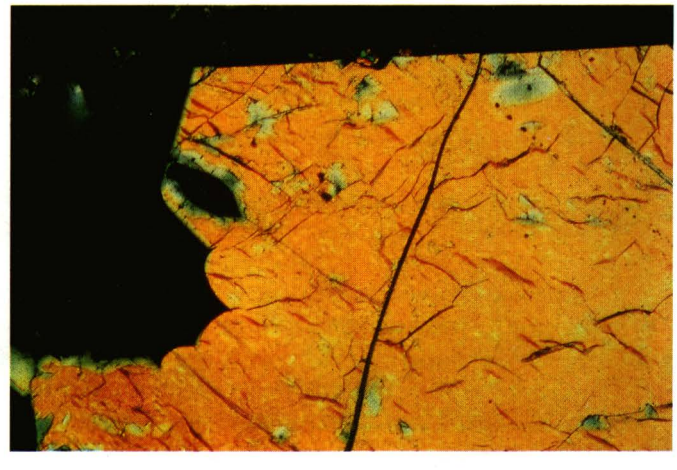

FIGURE 25.13.—Large olivine grain from Iki–22, showing euhedral form locally modified by resorption. Cuspate edges like this are also visible in figure 25.4*E*. Field of view 2 mm across. Crossed nicols.

contents close to the average MgO content of the distant glass; these glasses appear to be unaffected by any quench overgrowths on olivine. The fourth grain is surrounded by a sheath of variable, but less magnesian glass, some of which is grossly different in composition from glass elsewhere in the thin section. As in Iki–22, the euhedral parts of this crystal have relatively magnesian glass adjacent to them, while the resorbed parts are next to glass with 7 percent MgO.

Iki–33 provides evidence that this same kind of heterogeneity was present almost to the end of the eruption. One grain, completely euhedral, is surrounded by glass identical to the distant glass. An adjacent resorbed grain is surrounded by glass with significantly less MgO. The cluster of euhedral grains shown in figure 25.6*A–B* lies in a pool of glass with 8 percent MgO; these grains show only minor resorption. A last grain, of class 1, is surrounded by a sheath of glass with 7.2 to 7.7 percent MgO and is strongly resorbed on all sides.

Similar patterns occur in the other eruption samples analyzed so far. The main variants may be summarized as follows:

(1) In the first type of rim-glass relationship, the adjacent glass contains 0.2 to 1.5 weight percent less MgO than the glass more than 1 mm away from olivine. The enclosed olivine shows signs of resorption, such as rounding of corners and wavy or cuspate margins, as seen in figures 25.4*E*, 25.5*A*, and 25.13. Resorption may be partial, or the entire rim of the crystal may be affected. Glass next to resorbed surfaces is consistently less magnesian than glass adjacent to euhedral corners and edges, even on the same grain. A dozen such grains, partly or completely rimmed by low-MgO glass, have been found. They occur in samples Iki–7, 11, 9, 14, 20, 24, and 32, in addition to the samples in figure 25.12.

(2) In the second type of rim-glass relationship, the adjacent glass has a composition essentially equal (within ±0.2 weight percent MgO) to that of the more distant glass. There is no correlation between crystal form and glass composition; the grain may be locally resorbed or completely euhedral. Thirty-one such grains have been analyzed, of which 12 are essentially euhedral.

In addition, there are two small euhedral grains, one in Iki–9 and the other in Iki–32, which have skins of low-MgO glass but show little resorption, like the cluster of grains in Iki–33 (fig. 25.6*A–B*). No cases are known in which an olivine grain has a sheath of glass appreciably more magnesian (>0.2 percent MgO) than the distant glass.

The existence of these boundary layers (or sheaths) of contrasting glass composition was not evident from petrographic examination, as no color difference exists between the various compositions; their presence was only detected with the microprobe. These MgO-poor boundary layers cannot simply result from quench overgrowth on olivine, because 31 out of 46 grains do not have them. Sheathed grains are not rare, though; they make up 30 percent of the grains analyzed. The possibility that olivine (or other) crystals might carry a boundary layer of melt with them as they move has been suggested before (Helz, 1980), but the layers themselves have not previously been observed.

COMPOSITION OF OLIVINE IN THE LAKE

The rapidly quenched eruption pumice samples preserve many sorts of disequilibrium and evidence of magma mixing. Olivine phenocrysts in the lake, by contrast, have had months or years to exchange Mg for Fe with the surrounding host liquids before being quenched during drilling. Table 25.5 presents data for olivine in the aggregates and megacrysts described in table 25.2. These grains differ from isolated phenocrysts in the same samples in that core compositions may be slightly more forsteritic, but they are otherwise quite representative of phenocrystic olivine in the lake.

The shallow samples (KI–113 and KI76–2–20.5 in table 25.5) show strong normal zoning, from $Fo_{88–86}$ (cores) to $Fo_{78–72}$ (rims). Such extensive zoning, with a range of 10–14 percent Fo, is unknown so far in the eruption samples. This zoning probably developed in the lake, during crystallization of the groundmass. Note that the holocrystalline sample (KI76–2–20.5), quenched from about 100 °C, shows more extensive zoning than the KI–113 clot, which was quenched from 1,090 °C. Extensive normal zoning of this sort is common in olivine phenocrysts in older Hawaiian lava flows (Maaloe and Hansen, 1982). In the flows, some uncertainty exists over whether the narrow, iron-rich rims are overgrowths or result from exchange of Fe and Mg between preexisting olivine and the differentiating melt. In these lake samples, there is no ambiguity; the zoning is produced by re-equilibration, not by overgrowth.

Samples from deeper in the lake show progressively less zoning, always in the normal sense. In KI67–2–87.9 (table 25.5) the range in forsterite content is 10 mol percent. The intragrain color variations seen in the olivine cluster in figure 25.8*D* are produced by this zoning. It is evident that the zoning follows the outline of the whole aggregate, not of individual grains within the cluster. In the 1981 samples (table 25.5, columns 5–6 and 9–10) the range of forsterite variation is only 4–5 mol percent. In these later samples, there is a positive correlation between maximum forsterite content and core quenching temperature, as follows:

Sample	Percent Fo	Temperature (°C)
KI81–1–238	85.1	1,135–1,140
KI67–2–87.9	82.7	1,090
KI81–1–181.5	79.2	1,010–1,030

Even more extensive re-equilibration of olivine phenocrysts has been described by Moore and Evans (1967) in samples from deep within the prehistoric Makaopuhi lava lake. There, the phenocrysts were almost unzoned and had the same composition as groundmass olivine. Maaloe and Hansen (1982) present calculations showing how zoning in initially forsteritic olivine phenocrysts would be expected to change with time, as exchange of Fe for Mg proceeds. The olivine in both lava lakes follows the model very well.

The feature of these data most relevant to the present paper, however, is that they suggest that even the largest olivine aggregates and megacrysts have been affected by exchange of Fe and Mg with the melt during slow cooling. The zoning complexities present in the eruption olivine phenocrysts are gone, even in the earliest drill core.

TABLE 25.5.—*Composition of olivine megacrysts and grains in dunitic aggregates from Kilauea Iki lava lake, 1959 Kilauea eruption*

	1	2	3	4	5	6	7	8	9	10
Sample type	KI-113 class 1 aggregate		KI67-2-87.9 class 1 aggregate		KI81-1-181.5 mosaic		KI76-2-20.5 megacryst		KI81-1-238 megacryst	
Points in analysis	3	1	2	1	5	1	7	1	4	3
SiO_2	39.61	37.53	39.82	38.14	38.52	37.87	39.70	37.18	39.68	38.8
TiO_2	.00	.00	.04	.07	.00	.00	.00	.01	.00	.02
Al_2O_3	.00	.00	.04	.06	.00	.00	.00	.00	.00	.01
Cr_2O_3	.00	.00	.02	.03	.00	.00	.02	.00	.00	.00
FeO	11.93	21.95	16.20	24.83	19.54	23.26	12.88	25.08	14.12	18.19
NiO	.17	.04	-	-	.09	.11	.20	.11	.14	.02
MnO	.17	.32	.15	.21	.28	.33	.19	.34	.18	.25
MgO	47.03	39.47	43.62	36.74	41.79	38.55	46.49	37.17	45.29	42.30
CaO	.24	.24	.30	.28	.15	.17	.22	.20	.23	.29
Na_2O	.01	.00	.05	.07	.01	.01	.02	.01	.02	.02
Total percent	99.16	99.55	100.24	100.43	100.38	100.30	99.72	100.10	99.66	99.96
Mol percent Fo	87.5	77.8	82.7	72.51	79.2	74.7	86.6	72.5	85.1	80.6
Location	core	rim	core	rim	small grain, center of mosaic	rim of larger crystal at edge of aggregate	core	rim	core	rim
	largest grain in aggregate		large single crystal							
Quenching temperature (°C)	1090-1095 °C		1090 °C		1010-1030 °C		~ 100 °C		1135-1140 °C	

Only the sizes and textures of the aggregates and megacrysts may preserve information relevant to the dynamics of the 1959 eruption.

DISCUSSION

The olivine phenocryst population in the 1959 eruption samples is very heterogeneous petrographically. It is somewhat more uniform chemically, but zoning patterns are varied, with normally and reversely zoned grains almost equally abundant in the population analyzed. There is no correlation between petrographic class and chemical composition. The petrographic and chemical characteristics of this olivine phenocryst population vary from phase to phase of the eruption, supporting a model of magma mixing and progressive internal equilibration that will be advanced below.

Olivine in Kilauea Iki lava lake retains all of the textures seen in the eruption samples. In addition to abundant olivine phenocrysts, the lake contains rare olivine megacrysts and dunitic aggregates. Though textures are stable for decades in the lake, chemical composition is not. The lake olivines are all normally zoned, and their cores may be relatively Fe-rich, because of continued exchange of Fe and Mg with the melt during slow cooling of the lava lake.

Many features of this population of phenocrysts and aggregates are unusual and bear on the dynamics of the 1959 eruption. These features are (1) the presence of deformed olivine grains, (2) the presence of dense olivine aggregates of complex history, (3) the occurrence of rare olivines containing sulfide-bearing inclusions, (4) the presence of reversely zoned and of oppositely zoned crystals in a single thin section, and (5) the occurrence of resorbed olivine. The significance of these will be considered in turn.

DEFORMATION FEATURES IN OLIVINE

Olivine with multiple planar extinction discontinuities extending across the whole grain or with complex rectangular subgrains is present in the 1959 eruption pumice and in Kilauea Iki lava lake. The grains occur singly, in small clusters, or in larger aggregates.

Irregularly shaped, deformed crystals like this are common in Hawaiian alkalic rocks (see, among others, White, 1966). Similar kink-banded olivine, as isolated grains or in small clusters, has been reported from many other localities as well (Blanchard and others, 1976; Imsland, 1984; Francis, 1985). The kink-banded olivines are always among the coarsest grains present, as at Kilauea Iki. In most of these occurrences, the deformed grains are all very forsteritic (Fo_{90}), which is not the case in the 1959 pumice. Most authors consider the deformed olivine to be xenocrystic. Imsland (1984) considers it (and the chromian diopside associated with it in the ankaramites of Jan Mayen) to be mantle-level phenocrysts precipitated from the ankaramitic parental liquid.

Extinction discontinuities, or rectangular subgrain boundaries like those shown in figure 25.5*B*, have been produced experimentally in olivine at high temperatures and pressures (Raleigh, 1968; Carter and Ave Lallemant, 1970; Raleigh and Kirby, 1970). They form in olivine in a crystalline matrix, in response to non-hydrostatic stress. As yet there are no studies that investigate the minimum amount of interstitial melt necessary to prevent olivine from deforming in this manner. Kink-bands do not form under hydrostatic conditions, however; kink-banded crystals surrounded by melt (figs. 25.3, 25.4*A–B*) must have been deformed in a very different environment.

Aggregates of deformed olivine are the most numerous class of dense olivine aggregates in Kilauea Iki (table 25.2). The deformed olivine in these aggregates is similar in size and petrographic character to the isolated, deformed phenocrysts. It was suggested above that the isolated class 1 crystals were produced by disaggregation of coarse, mildly deformed dunite like the seven dense, melt-poor aggregates found in the lake. In fact, the literature on olivine deformation virtually requires such an origin for any grain with deformation features. Their depth of origin cannot be tightly constrained merely from the presence of deformation features, however, as olivine deforms readily over a wide range of pressures and temperatures. Nevertheless, minimum confining pressures of several hundred megapascals, much higher than the 100 MPa (1 kbar) in Kilauea's summit reservoir, seem indicated (Carter and Ave Lallemant, 1970).

DENSE OLIVINE AGGREGATES

Kilauea Iki lava lake contains several dense aggregates of olivine, as discussed above. Most consist of coarse, mildly deformed class 1 grains; others contain polygonal mosaics of unstrained olivine (table 25.2). Neither of these types contains significant amounts of basaltic melt, and where melt does occur, it appears to be the host melt penetrating the aggregate, rather than being indigenous to the aggregate. The mineralogy and textures of these aggregates are matched by those of the dunite tectonite xenoliths that are so common in Hawaiian mafic alkalic rocks, whether from the Honolulu Volcanics (Jackson and Wright, 1970), Hualalai (Kirby and Green, 1970), Loihi Seamount (Moore and others, 1982; Roedder, 1983), or elsewhere (White, 1966; Jackson, 1968). Similar textures occur in other types of olivine-rich xenoliths and in alpine peridotite (see, for example, Mercier and Nicolas, 1975; Mercier, 1979). Textures like those seen in the coarse, mildly deformed aggregates of table 25.2 are considered by these authors to be produced by plastic deformation in the upper mantle, the polygonal mosaics by recrystallization of deformed grains and subsequent annealing. It seems possible that the textures of the Kilauea Iki aggregates were produced the same ways.

The olivine in the dunite tectonite xenoliths from Hawaiian alkalic rocks are more iron-rich than the olivine in most peridotite. Jackson and Wright (1970) give $Fo_{87.5–84}$ and Sen (1983) gives $Fo_{90–81}$ for the olivine in the dunite xenoliths in the Honolulu Volcanics, while White (1966) reports $Fo_{89–84}$ for all dunite xenoliths from the Hawaiian Islands. This range is similar to the range of compositions seen in class 1 olivines in the pumice samples ($Fo_{88.7–85}$) and to the core compositions seen in the dunitic aggregates in the lake ($Fo_{87.5–83}$). However, the same compositional range is observed for other classes of olivine phenocrysts in this eruption (fig. 25.9*A*) and for olivine from other Hawaiian tholeiite (Maaloe and Hansen, 1982; Basaltic Volcanism Study Project, 1981).

The origin of these relatively iron-rich dunite tectonites has been controversial. Their compositions and the fact that they tend to occur in lavas that have come up near the central conduit of tholeiitic shields (Jackson and Wright, 1970) suggest a relationship with the tholeiitic series, even though the dunite is normally found in alkalic rocks. They have been considered to be residual (Jackson and Wright, 1970) cumulates from shallow crustal magma chambers (Sen, 1983) or perhaps from the mantle (Wright, 1984), or metamorphic mantle rocks of indeterminate origin (Kirby and Green, 1980). None of these ideas explains simultaneously (1) the iron-rich olivine compositions identical to those of tholeiitic phenocrysts, (2) the general scarcity of minerals other than olivine + chromite, and (3) the absence of cumulate textures and the ubiquity of deformed or annealed textures in this rock type.

The model favored here is that the dunitic inclusions in the 1959 lava are cumulates from tholeiite, as suggested by Sen (1983) and Wright (1984), but that they precipitated on conduit walls at mantle and deep crustal levels, rather than in shallow crustal reservoirs. Their composition suggests they are cumulates from tholeiite, and their limited mineralogy suggests they formed in a thermally buffered environment. Heating of the conduit wall, by frequent passage of tholeiitic liquid, seems more likely to forestall precipitation of interstitial pyroxene and other minerals than periodic replenishment of more isolated, shallow crustal reservoirs. Also, the occurrence of similar dunite inclusions in summit lava of the very young volcano Loihi suggests that they start forming early in the development of the tholeiitic shield, and that at that stage they are already located very near the main conduit. Lastly the rarity of undeformed representatives of this type implies they come from an environment where low melt fractions and a plastic response to non-hydrostatic stress are the norm. These conditions are not likely to be met in shallow magma chambers. In this model, megacrysts like those found in Kilauea Iki would be presumed to form in melt-rich pockets along the conduit wall. Disruption of these pockets by a

later batch of magma would then incorporate the megacrysts into a magma capable of erupting.

By contrast with these dunite tectonites, the cumulate-textured xenoliths described by Jackson (1968) are much more likely candidates to be cumulates from crustal magma chambers of the sort visualized by Sen (1983). This suite contains minor dunite. Most of its representatives contain appreciable pyroxene and plagioclase, as well as olivine, in contrast to the dunite tectonites, which rarely contain other minerals. Also, the members of this suite, including its rare dunite, were described by Jackson (1968) as exhibiting no deformation features.

An alternate way of producing Fe-rich dunite tectonite might be to have the spinel-lherzolite, typical of the Hawaiian upper mantle away from tholeiitic conduits (Jackson, 1968; Jackson and Wright, 1970) react completely with passing tholeiitic liquid, removing pyroxene and changing the composition of the remaining olivine + chromite. Whatever path was followed, it seems likely that the iron-rich, deformed dunite is produced at upper mantle or deep crustal levels, in the immediate vicinity of the tholeiitic conduit. The geochemistry of the included rare gases in some dunite tectonites is MORB-like (Kaneoka and others, 1983; Rison and Craig, 1983), which suggests they are associated somehow with the oceanic lithosphere that underlies all Hawaiian volcanoes, or at least, that they may have exchanged the isotopes with such material. The isotopic composition of the 1959 dunite samples is unknown, but after months or years of storage in the lake, they will not be pristine in any case.

The questions then arise of how the dunite is deformed, and what the timing of the deformation is, relative to the time of eruption. Mercier (1979) compared textures of xenoliths in kimberlite with experimentally observed rates of recrystallization for deformed olivine and concluded that at 1,400–1,600 °C the deformation textures, especially in kink-banded paleoblasts, would be entirely recrystallized within hours or days. For those xenoliths, he suggested that the textures must have been produced by the host kimberlite itself, as it moved through the mantle to the surface.

In the present case, it has been observed that deformed olivine grains have persisted for 22 years in the lava lake at 1,140–1,190 °C. The expected temperatures in the upper part of Kilauea's conduit and in the deeper parts of the shallow reservoir are probably 1,250–1,350 °C, based on estimates of parental MgO contents by Wright (1984) and the resulting liquidus temperatures suggested from the calibration of Helz and Thornber (in press). At these temperatures, the deformation features observed in single grains and in aggregates would be expected to survive for days to years, but beyond that their age cannot be constrained, as there are no data on static olivine-annealing rates in the temperature range of interest. Consequently, it is not possible to say that all of the deformation features seen in the 1959 olivine were produced by the host magma; at these lower temperatures, some may have been produced in earlier deformation events. Indeed the localization of chromite at grain boundaries in some aggregates where the coarsest olivine still contains deformation features (fig. 25.7C) may indicate that these aggregates have been subject to repeated deformation.

Nevertheless, the absence of primary igneous (cumulate) textures supports the idea that the dense aggregates come from an environment where deformation is almost unavoidable during sampling by the host, if not before. Furthermore, the scarcity of strongly deformed olivine or olivine aggregates in most Kilauea lava, including very olivine-rich shallow intrusives like the Uwekahuna laccolith, suggests that these dense aggregates have not formed in the shallow reservoir and do not survive there indefinitely. The more abundant glomerocrystic clusters of oriented, undeformed olivine, like that shown in figure 25.5*A–B*, are more likely representatives of olivine cumulates from Kilauea's shallow reservoir. The dense, deformed aggregates must have come from much deeper parts of Kilauea's plumbing.

The presence of two annealed aggregates (KI67.2–87.9b and KI81–1–181.5) containing no deformed grains complicates the picture somewhat. Their textures reflect prolonged thermal annealing in a hydrostatic environment. If the deepest parts of the conduit sampled are characterized by extremely low melt fractions and nonhydrostatic stress, these two aggregates must have been annealed at higher levels, suggesting that they were relatively high in the plumbing for some time prior to eruption.

SULFIDE-BEARING OLIVINE

Sulfides are rare in Kilauea basalt. They have been found included in, or associated with, ilmenite and titanomagnetite separates from differentiated rift lava (Desborough and others, 1968). They also occur as immiscible blebs in glass or as inclusions in augite in early scoria of the 1977. eruption (Moore and others, 1980), and as a late phase in interstitial liquid in Alae lava lake (Skinner and Peck, 1969) and in Kilauea Iki lava lake (R.T. Helz, unpub. data, 1985).

This paper reports the first known occurrence of sulfide in Kilauea summit lava. In the 1959 samples, it occurs in olivine as one phase in swarms of inclusions, which consist otherwise of chromite, glass, and vapor. This occurrence is very similar to the occurrence of sulfide as inclusions in olivine in the dunite xenoliths from Loihi (Roedder, 1983). Such grains and aggregates are very rare in the 1959 lava, and it was suggested above that they all came from the same limited source region.

The question is, where is that source? Sulfide is stable as a separate phase only at appropriate combinations of temperature, silicate melt composition, and sulfur and oxygen fugacities. The occurrence of sulfide as inclusions in some olivine phenocrysts demonstrates that the necessary combinations exist, at least locally, but the scarcity of sulfide-bearing melt inclusions in the 1959 and other summit lava suggests that the conditions are rarely met. It is known that melt composition and oxygen fugacity of Kilauea lava vary within rather narrow limits (Wright, 1971; Anderson and Wright, 1972). To the extent that magma temperatures of the 1959 lava were higher than most summit eruptions, the lava would be less likely than most to contain sulfide. One can conclude, therefore, that the sulfur fugacity was, at least locally, higher than usual. Recent studies of gases emitted from the summit area of Kilauea Volcano

show a tremendous flux of magmatic gas (CO_2, SO_2), which is lost from stored magma even between eruptions (Greenland and others, 1985; Gerlach and Graeber, 1985). Most melt inclusions in olivine are sulfide-free, suggesting that the melt in the summit reservoir generally contains much less sulfur than would be required to stabilize a separate sulfide liquid. It seems likely, therefore, that the sulfide-bearing inclusions formed at greater depth than the other melt inclusions, either in the lowest parts of the summit reservoir or deeper. Geobarometry on the sulfide-bearing olivine, using the methods of Roedder (1983) or Harris and Anderson (1983), might help constrain the depth of origin of these and other olivine xenocrysts. The observations that the sulfide-bearing, inclusion-rich olivine almost never contains deformation features and that aggregates of such olivine tend to be less densely compacted (fig. 25.7*D*) than the deformed olivine aggregates are compatible with the idea that class 5 olivine is derived from higher levels than the deformed class 1 olivine and the dense aggregates. The presence of sulfide-bearing inclusions in one of the annealed aggregates (shown in fig. 25.8*A–B*) suggests that this particular aggregate was stored and annealed at a level close to the source of the other sulfide-bearing olivine, though this very dense aggregate may have originated at still greater depths.

SIGNIFICANCE OF OLIVINE ZONING IN THE ERUPTION PUMICE

A complete evaluation of olivine zoning in the 1959 lava must wait on the availability of detailed compositional profiles of the olivine. However, the isolated point analyses presented here are sufficient to characterize the nature and extent of zoning and its gross variation with time during the eruption.

The most curious feature of the olivine zoning is the presence of a substantial number of reversely zoned crystals. Mechanisms for producing reverse zoning in olivine include magma mixing and decompression at constant temperature. Crystals entrained in a hotter magma might develop more magnesian rims eventually, but the usual effect in the 1959 lava is partial resorption. Some of the reversely zoned crystals in the 1959 lava are perfectly euhedral (fig. 25.4C) and show no sign of resorption or any other kind of hiatus in crystal growth, suggesting that some other mechanism is involved. The analysis of van Kooten and Buseck (1978) suggests that reverse zoning in olivine forms when a water-bearing melt, saturated with olivine, undergoes isothermal decompression. This results in an increase in oxygen fugacity, an increase in the Fe^{+3}/Fe^{+2} ratio, and hence an increase in the $Mg/Mg+Fe^{+2}$ ratio in olivine crystallizing from the melt. Their calculations showed that forsterite content would increase 3–5 percent for a 200-Mpa (2 kbar) drop in pressure, at 1,000 °C, for a melt containing 2.5 weight percent H_2O. The pressure effect in a dry magma has been determined by Takahashi and Kushiro (1983) and is much smaller: if Kilauea magma were completely dry, a 3 percent reversal in Fo content would record 2,500 MPa (25 kbar) of isothermal decompression. The amount of water in Hawaiian tholeiite is of the order of 0.3–0.6 weight percent H_2O (Moore, 1965), so a pressure drop of between 200–2,500 MPa (2–25 kbar) would be required to produce the maximum reverse zoning seen in the 1959 eruption.

The question arises as to what stage of decompression might be recorded in the reversely zoned phenocrysts. Every crystal in the eruption pumice was moved from the level of Kilauea's shallow reservoir, which is 2–6 km below the summit of the volcano (Eaton, 1962; Ryan and others, 1981), to the surface, and so has undergone a pressure drop of roughly 100 ± 50 MPa (1 ± 0.5 kbar). If this were sufficient to produce detectable reverse zoning, then all phenocrysts would be reversely zoned; in fact, only some of them are (see figs. 25.9*B*, 25.11). Furthermore, the number of reversely zoned olivine grains and the extent of reverse zoning tended to decline as the eruption progressed (fig. 25.14*A–B*). The trends are irregular but suggest that the reverse zoning is neither stable in shallow storage nor being produced there. Those olivine grains showing pronounced reverse zoning were probably brought up by the 1959 magma from below the level of the shallow reservoir.

Another question of interest is, how long could the variable zoning seen in the eruption samples last before internal equilibrium would be restored? Detailed calculations for each sample are beyond the scope of this paper, but the calculations of Maaloe and Hansen (1982) suggest that the time interval is between a month and a year, for zoned margins typically 10–30 μm thick. This is compatible with the observations that (1) the kind of zoning changed, and internal equilibrium in the eruption samples increased perceptibly over the 5-week period of the eruption and (2) shallow lake samples quenched as little as 9 months later show only strong normal zoning, of a sort rarely seen in the eruption samples. Thus many of the olivine grains from eruption pumice analyzed here were quenched within weeks, or at most a few months, of the time their zoning was produced.

SIGNIFICANCE OF RESORBED OLIVINES

Partial resorption of olivine is widespread in the 1959 eruption pumice and has been noted by previous workers (Richter and Murata, 1966). Resorption textures, including cuspate margins like those shown in figures 25.4*A*, *D* have been produced experimentally by Thornber and Huebner (1985); these are not simply unusual growth forms. This resorption occurs in samples quenched from 1,160–1,217 °C (see table 25.4), far above the incoming of pigeonite, which lies at 1,090–1,100 °C in the 1959 lava (Helz and Thornber, in press; unpub. data, 1985). Consequently, the resorption cannot be the result of a reaction relationship between olivine and liquid.

As discussed above, about 30 percent of the olivine grains analyzed from eruption samples are partly or completely enclosed in a sheath of glass significantly less magnesian than glass elsewhere in the same section. Glass next to resorbed edges is significantly less magnesian than glass next to euhedral parts of the same grain. That these MgO-depleted glass sheaths are not produced by quench overgrowths in olivine seems clear from the fact that 70 percent of the olivine grains are bordered by glass identical in composition to glass farther away from olivine.

These observations suggest that the resorption was produced as follows: Olivine crystals from a cooler part of the magma

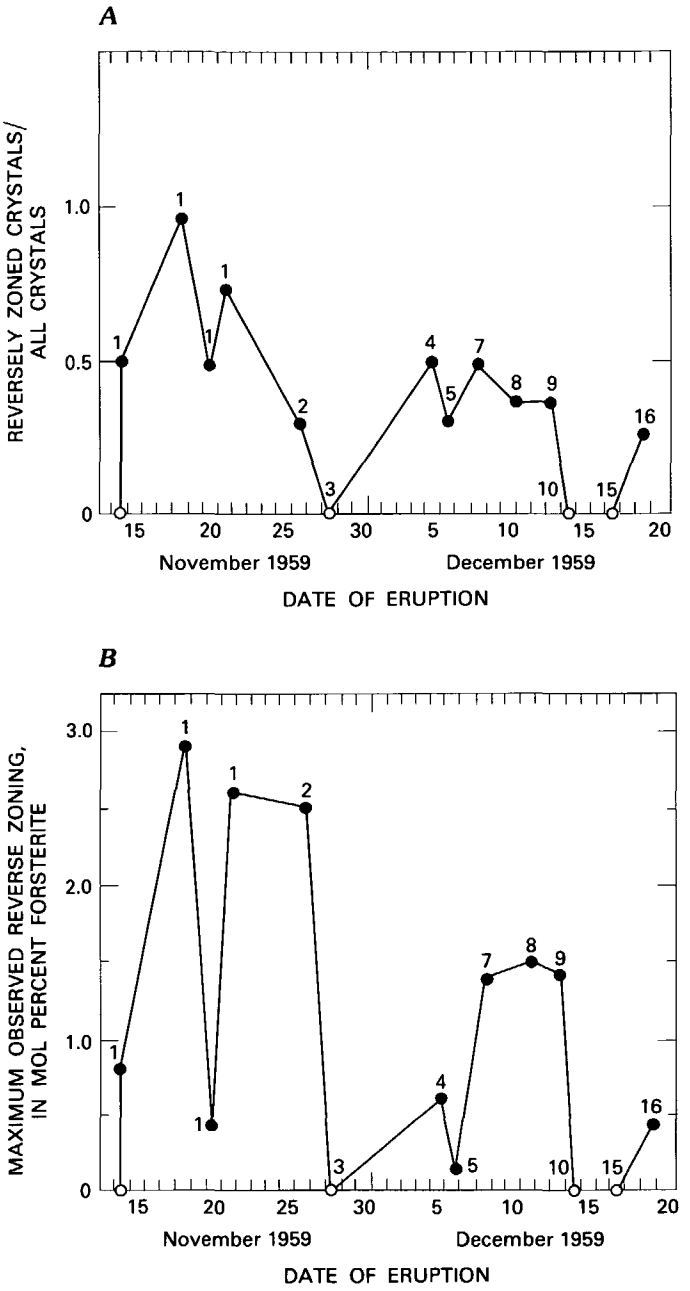

FIGURE 25.14.—Occurrence of reversely zoned olivine in 1959 eruption samples. *A*, Frequency of occurrence of reversely zoned crystals in 1959 eruption pumice, as a fraction of the total number of analyzed crystals, plotted against time of eruption. Points are labeled with the number of phase in which the sample was erupted. *B*, Maximum observed reverse zoning (as difference in mol percent Fo between core and rim) observed in 1959 eruption pumice, plotted against time of eruption. Samples containing no reversely zoned crystals plot on abscissa. Phase numbers as in figure 25.14*A*.

chamber were swept up in hotter, more mobile liquid. A thin layer of less magnesian, cooler, and hence slightly more viscous liquid moved with the crystals. (This layer might tend to gradually slough off the leading edge of the grain as it moves farther into the hotter liquid.) Thermal equilibrium between the new host and the crystal with its liquid boundary layer was established very rapidly (within minutes), at which point the melt in the boundary layer was superheated and no longer in equilibrium with olivine of any composition. The melt began to resorb the adjacent olivine, stopping when equilibrium was reached, that is, when the composition of the adjacent melt was equal to that of the rest of the melt. Once equilibrium was attained, the resulting odd-shaped grain persisted for decades without healing of the resorbed surfaces.

This model explains not only the occurrence of local resorption in olivine, but the fact that resorption is independent of rim composition or style of zoning. Of the 15 grains or clusters in low-MgO glass, 6 are normally zoned, 5 are unzoned, and 4 are reversely zoned. Rim compositions ranging from $Fo_{88.0}$ to $Fo_{80.7}$ have all been resorbed. This model also explains the occurrence of resorbed edges on 19 grains for which no compositionally distinct glass rims were found but which nevertheless show at least local resorption. Under this model, these would have had MgO-poor boundary layers at one time, but chemical equilibrium within the melt was re-established prior to quenching of the sample. The widespread occurrence of partial resorption of olivine in the 1959 samples implies that mixing of thermally disparate magmas was very common during the 1959 eruption.

These results have implications that may be important in other areas. First, resorption does not necessarily indicate that a given crystal is xenocrystic to the magma system. Second, one must be wary about calculating crystal-liquid distribution ratios in systems where magma mixing may have occurred, even where the glass is uniform in color, unless the glass has been thoroughly checked for chemical uniformity.

MODEL FOR THE 1959 ERUPTION

The physical processes preceding this eruption have been described by Eaton and Murata (1960), Eaton (1962), and Eaton and others (Chapter 48). In the late 1950's, seismic activity at Kilauea included intermittent swarms of deep (45–60 km) earthquakes. A minor swarm occurred in January 1959. The summit was inflating during the January swarm, and continued to do so thereafter, but subsided again between May and August 1959. This long period of subsidence was followed by an intense deep earthquake swarm on August 14–19. Reinflation of the summit began in late September and continued until the outbreak of the eruption on November 14, 1959 (Eaton and Murata, 1960, fig. 7). Other precursory seismic activity included weak harmonic tremor at depths of 5–15 km, presumably resulting from upward migration of magma in the conduit. Beginning in September, shallow earthquakes occurred in the northern part of the caldera. These were numerous, but very small until November 14, just before the eruption. The seismic and tilt data combined to give a picture of magma, originating at 45–60 km, migrating upward and becoming lodged slightly to the north of Halemaumau, prior to triggering an eruption. The overall magma path was not unlike that outlined in Ryan and others (1981) for the period 1961–1974 at Kilauea. The 1958–1960

period was exceptional, however, in having earthquakes at 45–60 km; such deep earthquakes have not been seen since. Also, the intense swarm of tiny earthquakes seen only on the north pit seismograph (Eaton, 1962; Eaton and others, chapter 48) are unique to the 1959 eruption.

Neither Eaton and Murata (1960) nor Eaton (1962) states specifically that the lava erupted in November and December 1959 included any of the magma liberated during the August earthquake swarm. It was not at first evident that this might be so, as can be seen by considering the usual pattern of magma storage in the summit reservoir (see Wright, 1971; and Wright and Fiske, 1971).

In these papers, it was shown that summit lava, though olivine controlled (Powers, 1955), typically lies at the olivine-depleted end of the olivine control line; that is, it contains minor phenocrystic olivine but has no fractionated augite or plagioclase. Variation in the amount of olivine, as observed in the 1959 eruption, was considered to be achieved by tapping different levels of a magma reservoir that was olivine-rich at the bottom and melt-rich at the top (Murata and Richter, 1966b; Wright, 1971).

In addition to varying in olivine content, the summit lava exhibits batch-to-batch compositional differences unrelated to olivine control. Different batches are chemically distinctive, some being unique, and can be followed through the volcanic plumbing. Wright and Fiske (1971) presented evidence that magma batches erupted at the summit in the 1950's and 1960's had appeared in flank eruptions 1–6 years earlier. They inferred that (1) magma batches arriving at the summit reservoir do not mix with each other in storage; (2) flank eruptions tap lower levels of the reservoir than summit eruptions do; and (3) summit eruptions usually tap magma that has been in storage in the shallow (2–4 km) reservoir for years, or even decades, prior to eruption.

Wright and Fiske (1971) recognized the 1959 eruption as exceptional in that neither of its two component magma batches (3a and 3b in the terminology of Wright and Fiske, 1971) had ever appeared in flank lava or as major eruptions in Halemaumau. In particular, the 1960 Kapoho eruption, which immediately followed the 1959 summit eruption, was not related chemically to the summit eruption. The picture of the summit reservoir that emerged from this work was of a highly compartmentalized magma storage zone, like that shown by Fiske and Kinoshita (1969), such that even closely spaced eruptions might drain completely unconnected parts of the reservoir. This draining of discrete reservoirs has been demonstrated to occur at Kilauea during other time periods as well, including 1967–1969 (Dvorak and others, 1983) and 1972–1973 (Ryan and others, 1983). The isolation of the 1959 magma from all other parts of Kilauea's reservoir that were active from 1955 to 1965 led Wright and Fiske to hypothesize that the 1959 magma occupied chambers "separated from the main conduits of the central reservoir" (Wright and Fiske, 1971, p. 54).

Other exceptional features of this eruption, besides its unusual seismicity, chemistry, and inferred deviant path to the surface, include its having (1) the highest lava fountains observed at the summit (580 m, or 1,900 feet, observed December 17, 1959); (2) the hottest eruption temperatures ever measured (1,192 °C on December 5, 1959); and (3) the most magnesian glass recovered for a historical Kilauea eruption. In addition, the pumice blanket produced during phase 3 is unusual in a historical Kilauea summit eruption. (All data is from Richter and others, 1970.) Thus, at least some of the 1959 lava was hotter and more gas-rich than typical Kilauea summit lava.

This paper has presented evidence that the 1959 lava contains material that appears to have originated below the level of the shallow reservoir. This includes (1) deformed olivine grains, singly and in aggregates, (2) aggregates of thermally annealed olivine, and (3) olivine megacrysts. Such materials are common in Hawaiian alkalic lava, but rare to absent in subaerial tholeiite, from Kilauea and elsewhere in Hawaii. In addition, the 1959 eruption contains rare olivine with sulfide-bearing inclusions and olivine with significant reverse zoning, neither of which appear to be produced in Kilauea's summit reservoir.

The unusual features of this eruption would be most easily explained if one of the two magmatic components erupted was the same magma that was liberated during the August earthquake swarm and reached the base of the shallow reservoir in late September. The hypothesis is that at that point the magma followed a seldom-used path to the north of the main reservoir (that is, the reservoir as located in Fiske and Kinoshita, 1969, and Ryan and others, 1981), encountering an older batch of stored magma. It broke through this older chamber to the surface on November 14, bringing some of the stored magma with it. The unusual features of the eruption are considered to be a direct consequence of the presence of the juvenile component.

THE MODEL AT MANTLE LEVELS

Kilauea tholeiite may originate as highly magnesian (>20 percent MgO) melt and fractionate appreciably, to MgO contents of 13–14 weight percent, enroute to the surface (Wright, 1984). The average MgO content of the 1959 eruption has been estimated as 15.43 percent (Wright, 1973) and hence is closer to the primitive melt than to the hypothesized parental one. Can this inferred differentiation from 20 to 15 percent MgO be made compatible with the apparent presence in the 1959 Kilauean lava of possible mantle-level material?

The answer to this potential contradiction is implicit in the theoretical model for the migration of fluid-filled cracks, as developed by Stevenson (1983), modifying earlier work by Weertman (1971a,b). In Stevenson's model, material from the lower end of the rising packet of fluid precipitates to close the crack below. In fact, healing the crack in this fashion is essential to migration of a discrete packet of melt. All that is necessary for a Kilauean tholeiite to contain mantle or deep crustal material and to differentiate is that the amount of material precipitated to seal the crack at the lower end exceed the amount picked off the walls at the upper end of the body of melt.

This model of crack migration dovetails with the hypothesized origin for the iron-rich dunite xenoliths proposed above. The dunite would correspond to this crack-healing material, because, for

TABLE 25.6.—*Calculated settling velocities of olivine phenocrysts and aggregates in Kilauea Iki lava lake, assuming Newtonian behavior*

Particle radius (cm)	Settling velocity (cm/s)
For viscosity 150 P, pressure 0.1 MPa (1 bar)	
0.25	0.05
0.5	0.21
1.0	0.85
For viscosity 50 P, pressure 1.5 GPa (15 kbar)	
0.25	0.16
0.5	0.65
1.0	2.6

tholeiite, the precipitate would be olivine + chromite. The exact composition of the olivine would vary slightly with depth, as the migrating melt fractionated enroute to the shallow reservoir. The deformation observed in the dunite xenoliths would be produced as the leading edge of a melt packet opened the crack, by analogy with the process Mercier (1979) inferred for deformed olivines in xenoliths in kimberlite. Because the Kilauea conduit is re-opened at frequent intervals, however, it is possible that some of the deformation observed in the dunitic aggregates was produced by an earlier packet of melt, not the host magma.

MAGMA ASCENT RATE

If the hypothesized model for the 1959 eruption is correct, we can calculate the average ascent velocity of the new magma package. To travel from depths of 45–60 km to the surface in the period from August 14–19 to November 14, the magma would have to move at 0.58–0.77 cm/s. This is compatible with ascent velocities for fluid-filled cracks, estimated by Stevenson (1983) to be 0.1–10 cm/s. It falls at the extreme low end of the range of ascent velocities Spera (1984) cites for xenolith-bearing lava (10^{-2} m/s to 30 m/s).

Is this velocity fast enough to entrain the largest objects found in the lake? Table 25.6 presents the results of calculating the Stokes' law settling velocities of olivine in basalt, for objects of different sizes. The first set of results is for a viscosity typical of very magnesian basalt at 0.1 MPa (1 atmosphere), the second set for the lower viscosity that the same melt would have at 1,500 MPa (15 kbar). Both viscosity estimates are taken from Kushiro and others (1976). The calculated settling rates for the largest particles found, which have average radii between 0.5 and 1.0 cm, would be 0.21–0.85 cm/s at low pressures and 0.65–2.6 cm/s at the high pressure limit. Non-Newtonian effects were neglected, on the assumptions that (1) much of the olivine phenocryst load (the very numerous class 2 olivine crystals and open aggregates) in the 1959 lava was in fact picked up from the lowest part of the older, stored magma, in Kilauea's summit reservoir and (2) the lava did not vesiculate until it was well up into the crust. The calculated Newtonian settling velocities are maximum values; to the extent that the magma was non-Newtonian, settling velocities would be lower, and the magma could more easily retain the larger olivine and olivine aggregates.

The calculated settling velocities are close to the average ascent velocity inferred above. If the eruption model is correct, this agreement means that the juvenile component was moving just fast enough to entrain the largest olivine and olivine aggregates found. It implies, further, that no significantly larger dunite inclusions will be found in the lake and that the magma never stopped moving from the time it picked up the aggregates until it began vesiculating, when non-Newtonian behavior took over. These deep-seated ascent rates are irrelevant to near-surface processes such as venting, fountaining, and so on, which involve the presence of a gas phase (see Eaton and others, chapter 48), resulting in strongly non-Newtonian behavior. The ability of the lava to entrain olivine in the shallow chamber was a function of magma discharge rate (Murata and Richter, 1966b); this rate increased during eruption, as the magma became more non-Newtonian (Wadge, 1981).

OLD VERSUS NEW MAGMA

It remains to be established which of the two recognized mixing components of the 1959 eruption was stored, old magma and which was the more juvenile. Early on it was noticed that the lava erupted from the east end of the initial fissure (Iki–58, or S–1 of Wright, 1973; or 3b of Wright and Fiske, 1971) was enriched in an augite-like component relative to west-end lavas (Iki–1 or S–2, or magma 3a). Murata and Richter (1966a) hypothesized that the former lava was derived by settling of augite phenocrysts into hotter parts of the magma chamber, where they were redissolved to give the east-end melt compositions. Calculations by Wright and Fiske (1971) supported this observation, though Wright (1973) noted that the implied physical model was very complex.

There are three problems with this augite-resorption hypothesis. First, it would require both components to be stored magma, rather than one stored and one juvenile, for if the Iki–1 (S–2) parent were not a stored component, the apparent relationship tested by the calculation would not exist, and the calculation would be meaningless. Second, the amount of augite (6 percent, Wright, 1973) required by the calculation is so small that the calculation cannot distinguish with certainty between low-pressure and high-pressure augite. Lastly, there is no petrographic evidence, in the form of phenocrystic augite, for the process. The tiny augite crystals

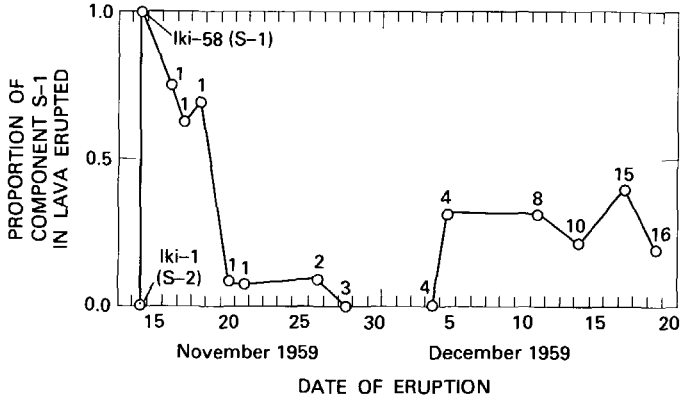

FIGURE 25.15.— Proportion of S–1 magmatic component present in various 1959 eruption samples (taken from Wright, 1973) plotted against date of eruption. The mixing components used by Wright (1973), namely samples Iki–58 (S–1) and Iki–1 (S–2), plot at 1.0 and zero respectively. Numbers by points identify the phase of the eruption.

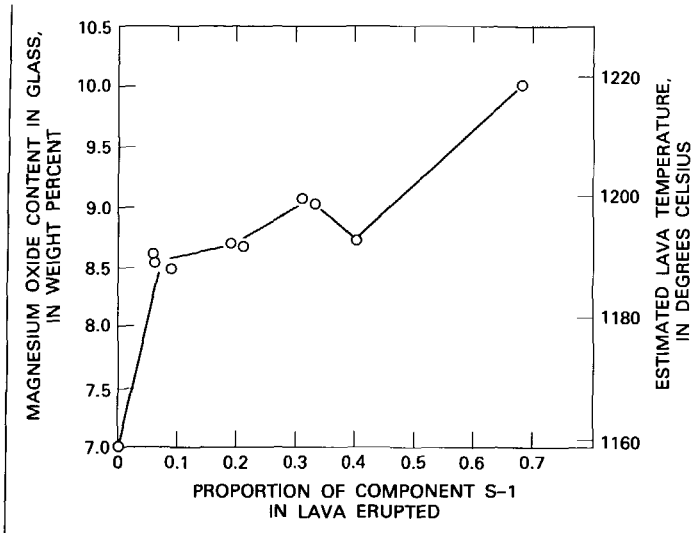

FIGURE 25.16.—MgO content of the glass (weight percent, left side) and estimated glass quenching temperature (right side) plotted against the fraction of S–1 component present for all samples erupted after November 17, for which both a bulk analysis and a glass analysis are available.

in the initial eruption samples are not phenocryst-sized and are almost always associated with plagioclase. This is a problem because plagioclase is not required by the calculation, and augite could not be readily separated from plagioclase by flow differentiation of the sort described by Wright (1973). Careful search for augite phenocrysts in the lake, including samples of foundered crust and of the basal chill zone, has failed to uncover any phenocrystic augite, resorbed or otherwise; nor does augite occur as an inclusion in olivine in any eruption sample.

Another line of evidence that must be considered is shown in figure 25.15, which plots the change in mixing ratio found by Wright (1973) against time (see also Wright, 1973, fig. 3). Early phase 1 lava is disproportionately rich in S–1 (Iki–58, the east-end component), later phases richer in S–2 (west-end). This might be interpreted as showing that stagnant S–1 magma was pushed out first, as the chamber was flooded by new, hot S–2 magma.

However, three other lines of evidence favor the east-end lava (Iki–58 or S–1 or 3b) as the new component, with the west-end lava the stored component. The first is the recognition of Wright and Fiske (1971, p. 54) that the brief 1954 Halemaumau eruption was of west-end (their 3a) type. Thus, west-end lava had been in storage near the surface for five years prior to 1959. Second is the occasional recurrence of the west-end component in almost pure (>90 percent) form after the initial curtain of fire shrank to a single vent on November 15. Figure 25.15 shows that the late phase 1 and phase 3, and early phase 4 samples are pure, or nearly pure west-end (S–2) material. The east-end component is never seen in pure form, except of course in the type sample Iki–58, where its purity is a matter of definition only. This pattern is more compatible with east-end material being the newer material, seen only as it filters through older, stored magma.

The last piece of evidence that the east-end component may be the more juvenile is shown in figure 25.16, which shows the correlation between the amount of S–1 (east-end) material and MgO content in glass (which covaries with temperature), for eruption samples from November 18 on. The more S–1, the hotter the sample, with the exception of Iki–32 from phase 15. This suggests that the S–1 component was consistently hotter than S–2 melts, hence probably more juvenile.

If one accepts that S–1 is the new and S–2 is the stored component, the above interpretation of the data in figure 25.15 must be revised. Instead of old magma being pushed out first, the new, more fluid magma must have streamed through the more stagnant material, to be erupted first. The stored magma was more prominent in later phases because it was remobilized by picking up heat and perhaps gas bubbles, from the newer, gassier material.

ERUPTION CHRONOLOGY

Using the above model and the data presented in this paper, the 1959 eruption can now be described in terms of progressively more intimate intermingling and internal equilibration of two separate types of olivine tholeiitic magma, a previously stored component and a new component that originated at 45–60 km depth and began its ascent in the August earthquake swarm.

The initial eruption fissure broke open along the south side of Kilauea Iki pit crater on November 14, 1959. Iki–1 (or S–2) was erupted at the west end, while Iki–58 (or S–1) was erupted at the east end. Initial samples of both components were relatively cool and differentiated, with a sparse population of class 2 olivine. Iki–58 is slightly hotter than Iki–1, however, and contains more phenocrystic olivine, including at least one reversely zoned grain (fig. 25.11), all features consistent with its being the new component. From November 14 to 17, lava continued to be dominantly east-end material (fig. 25.15), but gradually got hotter. On November 18, the hottest known sample, Iki–22, was erupted. This sample

contains a complex olivine assemblage that includes the most extensive reverse zoning found (tables 25.1, 25.3; figs. 25.11 and 25.14*B*).

No samples from November 19 have been analyzed, but by November 20, the lava being erupted was very nearly pure west-end material, though quite olivine-rich (fig. 25.15). The first such sample, Iki–44, contains a cooler glass than Iki–22, but the olivine is more magnesian and weakly zoned. Kink-banded olivine is present, but the banding is very faint, as the amount of deformation is slight. Compositionally, all the olivines appear to be in equilibrium with each other and (or) in equilibrium with a common melt. Such olivines might have come from the lowest (hottest) part of the west-end magma chamber.

A later sample from phase 1, Iki–7, is similar to Iki–44 in temperature in melt composition, and in the character of its class 1 olivines, but contains reversely zoned euhedral (class 2) olivines that are probably juvenile. Iki–7 also contains fragmental (class 4) olivine. Phase 2 (Iki–11) is slightly hotter and richer in the east-end component than Iki–44 and Iki–7. It contains the first normally zoned class 1 olivine found, the first sulfide-bearing class 5 olivine known, and more reversely zoned class 2 olivine. Clearly more new material was being tapped; the greater heterogeneity of the glass in Iki–11 (fig. 25.11) suggests that this mixing was very recent.

Phase 3 (Iki–9) was so extremely gas-rich that very little of it got into the lake; instead, it formed a pumice blanket downwind of the vent (Richter and others, 1970). It is pure west-end material, though slightly hotter than Iki–1 (S–2). Presumably this phase was derived from the gas-charged, differentiated upper part of the west-end magma chamber. The only puzzling feature of this phase is why this material did not erupt in phase 1. Two possible explanations are: (1) It came from an isolated cupola that was not breached by the initial fracture, or (2) the extra gas was derived from the new magma, which, after it had accumulated in a layer of differentiated west-end material near the roof, blew that material out as phase 3.

Early phase 4 lava was similar to that of phase 3. Later samples, like Iki–13, were much hotter (1,196 °C, table 25.4) and richer in east-end component (fig. 25.15) and olivine. The glass in Iki–13 is uniquely heterogeneous (fig. 25.11), suggesting that it was produced by very recent mixing of two components. Phase 5 (Iki–14) was hotter still (1,205 °C), but its glass is homogeneous, as though the disequilibrium of the Iki–13 mixing event had begun to dissipate. Both of these samples contain a complex assemblage (table 25.1) of very magnesian olivine (fig. 25.11) that shows little zoning. The combination of a change in mixing ratio of S–1 and S–2 (fig. 25.15), and the increase in temperature suggest that new material was fed into the base of the S–2 chamber about December 5. The presence of fragmental (class 4) olivine in these samples, presumably produced by brittle failure (shallow diking?), is compatible with this suggestion. The fact that both S–1/S–2 mixing ratios and glass quenching temperatures vary rather little after phase 5 suggests that this was the last significant influx of new material into the part of the chamber that was feeding the eruption.

Phase 7 (Iki–20) marks the reappearance of cooler lava (1,181 °C, see table 25.4). It also marks the first appearance of (1) very diverse, non-overlapping core compositions within a single sample, and (2) convergence of olivine rim compositions from those very different cores toward a common rim composition. Earlier eruption samples, though exhibiting great diversity of zoning pattern, generally included only a narrow range of core compositions in classes 1, 3, 4, and 5 (taken together) and class 2 (see fig. 25.11). From phase 7 through phase 16, by contrast, one or both of these olivine groups include very varied phenocryst cores within a single thin section. These varied cores must have formed initially in different parts of the magmatic plumbing. Hence, their close juxtaposition in the later samples is evidence for increasingly intimate commingling of all parts of the active magmatic system. The convergent zoning suggests that this mingling resulted in accelerated internal equilibration of the samples. Rapid fine-scale mixing was possible because both components were basaltic and quite fluid, with only minimal viscosity contrasts.

Phases 8 and 9, represented by Iki–21 and Iki–24, include the last evidence for new material entering the actively erupting part of the chamber. They contain (1) the most magnesian olivine observed; (2) the only class 1 olivine with significant reverse zoning other than those in Iki–22 (figs. 25.11, 25.14*B*); and (3) the latest known fragmental olivine (table 25.1). The thermal perturbation at the onset of phase 8 (1,197 °C, compared with 1,181 °C in phase 7) is smaller than that at phase 4 (1,196 °C vs. 1,154 °C in phase 3), and Iki–24 (phase 9) is cooler still, rather than hotter, as Iki–14 (phase 5) was. This suggests that the amount of new material introduced was rather slight and may simply represent more thorough in-mixing of the deepest part of the chamber. On the other hand, these observations do agree with evidence presented by Eaton and others (chapter 48) that the magma reservoir was being intruded by new magma from the end of phase 1 through phases 8 and 9.

Subsequent samples from phases 10, 15, and 16, show some variation in the S–1/S–2 ratio but no thermal perturbations, suggesting that thermal equilibrium within the mixed volume was complete. Reverse zoning is scarce (figs. 25.11, 25.14*A*), and olivine rims are consistently iron-rich (fig. 25.11). Chemical equilibration was still incomplete, however, as evidenced by the occurrence even in phase 16 (Iki–33) of olivine with rims of low-MgO glass.

SUMMARY

This paper documents the petrographic and chemical diversity of the olivine phenocrysts and aggregates in the 1959 lava of Kilauea Volcano. The lava contains five petrographically distinct classes of olivine, dunitic aggregates with deformed or annealed textures, and two olivine megacrysts (10×20 mm in section). Olivine cores vary from $Fo_{83.5}$ to $Fo_{88.7}$. Zoning is moderate (≤3 percent Fo within most crystals); normal and reverse zoning are about equally abundant. There is no correlation between petrographic class and core composition or style of zoning. Olivine in drill core from Kilauea Iki lava lake has the same petrographic features as olivine in the rapidly quenched eruption samples. Pre-eruption zoning and overall chemical composition is not preserved in the lake olivine, as it has

exchanged Mg for Fe with the melt.

Many features of the 1959 eruption are unusual for a historical Kilauea summit eruption and can be explained by a model in which one of the two observed magmatic components of this mixed-magma eruption came directly from the mantle, bypassing the main shallow reservoir. The component erupted from the east end of the initial fissure appears to be the juvenile component, responsible for the very hot, gas-rich, olivine-rich nature of the 1959 lava. The various components of the olivine population were picked up by the rising magma in roughly the following sequence:

(1) Deepest are the deformed olivine grains, aggregates of deformed olivine, and megacrysts, though the actual depths are poorly constrained. The thermally annealed aggregates may be strictly deep seated, or may have been annealed in shallower storage. All these materials are hypothesized to be derived originally from material lining the conduit wall at mantle or deep crustal levels. They are xenocrystic to the S–1 magma, but accumulated from earlier Kilauea tholeiite, so are not compositionally distinct.

(2) Euhedral olivine crystals with significant reverse zoning are deep-seated phenocrysts of the S–1 magma, recording large (several hundred MPa, or several kbar), but poorly constrained amounts of near-isothermal decompression. Reversely zoned class 1 olivine grains were picked off the walls deeper than unzoned class 1 olivine and erupted sooner after sampling, as this style of zoning is not stable in the shallow reservoir.

(3) Sulfide-bearing olivine grains and aggregates, rarely deformed and never showing reverse zoning, come from somewhere above the source of the deformed and (or) reversely zoned olivine, but below the shallow reservoir, where SO_2 is liberated from the magma. They may be cognate but are more probably xenocrystic to the S–1 magma.

(4) The occurrence of fragmental class 4 olivine, presumably formed by brittle failure, correlates fairly well with other indicators for episodes of influx of new S–1 liquid into the shallow chamber at the end of phase 1, and at phases 4–5 and 8–9. These fragments are hypothesized to result from fracture of old shallow olivine cumulates within the volcanic edifice.

(5) The bulk of the phenocrysts present, including most euhedral and rounded class 3 grains, unzoned or with some normal zoning, were picked up from the lower parts of the stored (S–2) magma. The widespread resorption observed in all classes of olivine is a consequence of mixing of thermally disparate melts at this stage.

(6) The small, euhedral olivine crystals with strong (8 percent Fo) normal zoning formed in the most rapidly cooled margin of the stored magma; they were only rarely sampled during the eruption.

Disequilibrium features present in the eruption samples include: (1) the presence of heterogeneous glass (away from olivine); (2) the presence of boundary layers of MgO-poor glass near olivine; (3) the presence of reversely zoned, unzoned and (or) normally zoned olivine in the same thin section; (4) the presence of olivine with very different core compositions in the same section; and (5) the presence of olivine with different rim compositions in the same section. Comparison with other data (Maaloe and Hansen, 1982) suggests that the mixing event(s) recorded by these features took place weeks before the eruption, or perhaps only within the 36 days of the eruption itself. Further analysis of these various indicators of change, or "geospeedometers," is deferred to a later paper.

The presence of kink-banded olivine is, by comparison, a relatively slow geospeedometer, as these deformation textures may last months to a few years at shallow-reservoir conditions. Their rarity in subaerial tholeiite, even picritic lava, suggests that they do not survive for decades in subsurface reservoirs, in contrast to their survival for 22 years in Kilauea Iki lava lake. However, deformed olivine occurs frequently in submarine east-rift lava of Kilauea. This suggests that some lower rift lava may move out laterally into the rift before reaching the shallow reservoir and so, like the 1959 lava, avoid prolonged shallow storage before their eruption. It would be of interest to search this submarine lava for the other types of deeper seated material found in the 1959 lava.

REFERENCES CITED

Albee, A.L., and Ray, L., 1970, Correction factors for electron probe microanalysis of silicates, oxides, carbonates, phosphates, and sulfates: Analytical Chemistry, v. 42, p. 1408–1414.

Anderson, A.T., Jr., and Wright, T.L., 1972, Phenocrysts and glass inclusions, and their bearing on oxidation and mixing of basaltic magmas, Kilauea Volcano, Hawaii: American Mineralogist, v. 57, p. 188–216.

Basaltic Volcanism Study Project, 1981, Basaltic volcanism on the terrestrial planets: New York, Pergamon Press, Inc., 1,286 p.

Bence, A.E., and Albee, A.L., 1968, Empirical correction factors for the electron microanalysis of silicates and oxides: Journal of Geology, v. 76, p. 382–403.

Bence, A.E., Brande, S., Indelicato, G., and Allen, F., 1981, Analysis of trace and minor elements in rock-forming minerals using an automated electron microprobe: Proceedings of the 8th International Conference on X-ray Optics and Microanalysis, p. 538–548.

Blanchard, D.P., Rhodes, J.M., Dungan, M.A., Rodgers, K.V., Donaldson, C.H., Brannon, J.C., Jacobs, J.W., and Gibson, E.K., 1976, The chemistry and petrology of basalts from leg 37 of the deep-sea drilling project: Journal of Geophysical Research, v. 81, p. 4231–4246.

Carter, N.L., and Avé Lallemant, H.G., 1970, High temperature flow of dunite and peridotite: Geological Society of America Bulletin, v. 81, p. 2181–2202.

Chen, C.-Y. and Frey, F.A., 1983, Origin of Hawaiian tholeiite and alkali basalt: Nature, v. 302, p. 785–789.

Chouet, B., and Aki, K., 1981, Seismic structure and seismicity of the cooling lava lake of Kilauea Iki, Hawaii: Journal of Volcanology and Geothermal Research, v. 9, p. 41–56.

Clague, D.A., 1982, Petrology of tholeiitic basalt dredged from Hualalai Volcano, Hawaii [Abs.]: Eos, v. 63, p. 1138.

Desborough, G.A., Anderson, A.T., Jr., and Wright, T.L., 1968, Mineralogy of sulfides from certain Hawaiian basalts: American Mineralogist, v. 63, p. 636–644.

Dvorak, J., Okamura, A., and Dieterich, J.H., 1983, Analysis of surface deformation data, Kilauea Volcano, Hawaii from October 1966 to September 1970: Journal of Geophysical Research, v. 88, p. 9295–9304.

Eaton, J.P., 1962, Crustal structure and volcanism in Hawaii: American Geophysical Union Geophysical Monograph, v. 6, p. 13–29.

Eaton, J.P., and Murata, K.J., 1960, How volcanoes grow: Science, v. 132, p. 925–938.

Fiske, R.S., and Kinoshita, W.T., 1969, Inflation of Kilauea Volcano prior to its 1967–1968 eruption: Science, v. 165, p. 341–349.

Fleet, M.E., and MacRae, N.D., 1983, Partition of Ni between olivine and sulfide and its application to Ni-Cu sulfide deposits: Contributions to Mineralogy and Petrology, v. 83, p. 75–81.

Fleet, M.E., MacRae, N.D., and Herzberg, C.T., 1977, Partition of nickel between olivine and sulfides: a test for immiscible sulfide liquids: Contributions to Mineralogy and Petrology, v. 65, p. 191–197.

Ford, C.E., Russell, D.G., Craven, J.A., and Fisk, M.R., 1983, Olivine-liquid equilibria: temperature, pressure, and composition dependence of the crystal/liquid cation partition coefficients for Mg, Fe^{2+}, Ca and Mn: Journal of Petrology, v. 24, p. 256–266.

Francis, D., 1985, The Baffin Bay lavas and the value of picrites as analogues of primary magmas: Contributions to Mineralogy and Petrology, v. 89, p. 144–154.

Gerlach, T.M., and Graeber, E.S., 1985, The volatile budget of Kilauea Volcano. Nature, v. 313, p. 273–277.

Greenland, L.P., Rose, W.I., and Stokes, J.B., 1985, An estimate of gas emissions and magmatic gas content from Kilauea Volcano: Geochimica et Cosmochimica Acta, v. 49, p. 125–130.

Häkli, T., and Wright, T.L., 1967, The fractionation of nickel between olivine and augite as a geothermometer: Geochimica et Cosmochimica Acta, v. 31, p. 877–884.

Hardee, H.C., Dunn, J.C., Hills, R.G., and Ward, R.W., 1981, Probing the melt zone of Kilauea Iki lava lake, Kilauea Volcano, Hawaii: Geophysical Research Letters, v. 8, p. 1211–1214.

Harris, D.M., and Anderson, A.T., Jr., 1983, Concentrations, sources and losses of H_2O, CO_2, and S in Kilauean basalt: Geochimica et Cosmochimica Acta, v. 47, p. 1139–1150.

Harte, Ben, 1977, Rock nomenclature with particular relation to deformation and recrystallization textures in olivine-bearing xenoliths: Journal of Geology, v. 85, p. 279–288.

Helz, R.T., 1980, Crystallization history of Kilauea Iki lava lake as seen in drill core recovered in 1967–1979: Bulletin Volcanologique, v. 43–4, p. 675–701.

———1983, Diverse olivine population in lavas of the 1959 eruption of Kilauea Volcano, Hawaii [abs.]: Eos, v. 64, p. 900.

———1984, In situ fractionation of olivine tholeiite: Kilauea Iki lava lake, Hawaii [abs.]: Geological Society of America Abstracts with Programs, v. 16, p. 536–537.

Helz, R.T., Banks, N.G., Casadevall, T.J., Fiske, R.S., and Moore, R.B., 1984, A catalogue of drill core recovered from Kilauea Iki lava lake from 1967–1979: U.S. Geological Survey Open File Report 84–484, 72 p.

Helz, R.T., and Thornber, C.R., in press, Geothermometry of Kilauea Iki Lava Lake, Hawaii.

Helz, R.T., and Wright, T.L., 1983, Drilling report and core logs for the 1981 drilling of Kilauea Iki lava lake (Kilauea Volcano, Hawaii) with comparative notes on earlier (1967-1979) drilling experiences: U.S. Geological Survey, Open File Report 83–326, 66 p.

Hermance, J.F., and Colp, J.L., 1982, Kilauea Iki lava lake: geophysical constraints on its present (1980) physical state: Journal of Volcanology and Geothermal Research, v. 13, p. 31–61.

Imsland, P., 1984, Petrology, mineralogy and evolution of the Jan Mayen magma system: Reykjavik, Visindafelag Islendinga, Rit 43, Prentsmidjan Oddi, 332 p.

Jackson, E.D., 1968, The character of the lower crust and upper mantle beneath the Hawaiian Islands: International Geological Congress, 23d, Prague, Proceedings, v. 1, p. 135–150.

Jackson, E.D., Clague, D.A., Engleman, E., Friesen, W.B., and Norton, D., 1981, Xenoliths in the alkalic basalt flows from Hualalai Volcano, Hawaii: U.S. Geological Survey Open-File Report 81–1031.

Jackson, E.D., and Wright, T.L., 1970, Xenoliths in the Honolulu Volcanic Series, Hawaii: Journal of Petrology, v. 11, p. 405–430.

Jarosewich, E., Nelen, J.A., and Norberg, J.A., 1979, Electron microprobe reference samples for mineral analyses: Smithsonian Contributions to the Earth Sciences, v. 22, p. 68–72.

Kaneoka, I., Takaoka, N., and Clague, D.A., 1983, Noble gas systematics for coexisting glass and olivine crystals in basalts and dunite xenoliths from Loihi Seamount: Earth and Planetary Science Letters, v. 66, p. 427–437.

Kirby, S.H., and Green, H.W., II, 1980, Dunite xenoliths from Hualalai Volcano: evidence for mantle diapiric flow beneath the Island of Hawaii: American Journal of Science, v. 280-A, p. 550–575.

Kushiro, I., Yoder, H.S., Jr., and Mysen, B.O., 1976, Viscosities of basalt and andesite melts at high presure: Journal of Geophysical Research, v. 81, p. 6351–6356.

Leeman, W.P., and Scheidegger, K.F., 1977, Olivine/liquid distribution coefficients and a test for crystal-liquid equilibrium: Earth and Planetary Science Letters, v. 35. p. 247–257.

Luth, W.C., and Gerlach, T.M., 1980, Composition and proportions of major phases in the 1959 Kilauea Iki lava lake in December 1978 [abs.]: Eos, v. 61, p. 1142.

Luth, W.C., Gerlach T.M., and Eichelberger, J.C., 1981, Kilauea Iki lava lake: April 1981 [abs.]: Eos, v. 62, p. 1073.

Maaloe, S., and Hansen, B., 1982, Olivine phenocrysts of Hawaiian olivine tholeiite and oceanite: Contributions to Mineralogy and Petrology, v. 81, p. 203–211.

Macdonald, G.A., 1944, The 1840 eruption and crystal differentiation in the Kilauean magma column: American Journal of Science, v. 242, p. 177–189.

Melson, W.G., Vallier, T.L., Wright, T.L., Byerly, G., and Nelen, J., 1976, Chemical diversity of abyssal volcanic glass erupted along Pacific, Atlantic, and Indian Ocean seafloor spreading centers: American Geophysical Union Geophysical Monograph, v. 19, p. 351–368.

Mercier, J-C.C., 1979, Peridotite xenoliths and the dynamics of kimberlite intrusion, *in* The mantle sample: inclusions in kimberlites and other volcanics: Proceedings of the Second International Kimberlite Conference, v. 2, p. 197–212.

Mercier, J-C.C., and Nicolas, A., 1975, Textures and fabrics of upper mantle peridotites as illustrated by xenoliths from basalts: Journal of Petrology, v. 16, p. 454–487.

Moore, J.G., 1965, Petrology of deep-sea basalt near Hawaii: American Journal of Science, v. 263, p. 40–52.

Moore, J.G., Clague, D.A., and Normark, W.R., 1982, Diverse basalt types from Loihi Seamount, Hawaii: Geology, v. 10, p. 88–92.

Moore, J.G., and Evans, B.W., 1967, The role of olivine in the crystallization of the prehistoric Makaopuhi lava lake, Hawaii: Contributions to Mineralogy and Petrology, v. 15, p. 202–223.

Moore, R.B., Helz, R.T., Dzurisin, D., Eaton, G.P., Koyanagi, R.Y., Lipman, P.W., Lockwood, J.P., and Puniwai, G.S., 1980, The 1977 eruption of Kilauea Volcano, Hawaii: Journal of Volcanology and Geothermal Research, v. 7, p. 189–210.

Muir, I.D., and Tilley, C.E., 1957, Contributions to the petrology of Hawaiian basalts 1. The picrite-basalts of Kilauea: American Journal of Science, v. 255, p. 241–253.

Murata, K.J., and Richter, D.H., 1966a, Chemistry of the lavas of the 1959–60 eruption of Kilauea Volcano, Hawaii: U.S. Geological Survey Professional Paper 537–A, 26 p.

———1966b, The settling of olivine in Kilauean magma as shown by lavas of the 1959 eruption: American Journal of Science, v. 264, p. 194–203.

Powers, H.A., 1955 Composition and origin of basaltic magma of the Hawaiian Islands: Geochimica et Cosmochimica Acta, v. 7, p. 77–107.

Raleigh, C.B., 1968, Mechanisms of plastic deformation in olivine: Journal of Geophysical Research, v. 73, p. 5391–5406.

Raleigh, C.B., and Kirby, S.H., 1970, Creep in the upper mantle: Mineralogical Society of America Special Paper 3, p. 113–121.

Richter, D.H., Eaton, J.P., Murata, K.J., Ault, W.U., and Krivoy, H.L., 1970, Chronological narrative of the 1959–60 eruption of Kilauea Volcano, Hawaii: U.S. Geological Survey Professional Paper 537–E, 73 p.

Richter, D.H., and Moore, J.G., 1966, Petrology of the Kilauea Iki lava lake, Hawaii: U.S. Geological Survey Professional Paper 537–B, 26 p.

Richter, D.H., and Murata, K.J., 1966, Petrography of the lavas of the 1959–60 eruption of Kilauea Volcano, Hawaii: U.S. Geological Survey Professional Paper 537–D, 12 p.

Rison, W., and Craig, H., 1983, Helium isotopes and mantle volatiles in Loihi Seamount and Hawaiian Island basalts and xenoliths: Earth and Planetary Science Letters, v. 66, p. 407–426.

Roedder, E., 1983, Geobarometry of ultramafic xenoliths from Loihi Seamount, Hawaii, on the basis of CO_2 inclusions in olivine: Earth and Planetary Science

Letters, v. 66, p. 369–379.
———1984, Fluid inclusions: Reviews in Mineralogy, v. 12, 644 p.
Ross, J.V., Avé Lallement, H.G., and Carter, N.L., 1980, Stress dependence of recrystallized-grain and subgrain size in olivine: Tectonophysics, v. 70, p. 39–61.
Ryan, M.P., Blevins, J.Y.K., Okamura, A.T., and Koyanagi, R.Y., 1983, Magma reservoir subsidence mechanics: theoretical summary and application to Kilauea Volcano, Hawaii: Journal of Geophysical Research, v. 88, p. 4147–4181.
Ryan, M.P., Koyanagi, R.Y., and Fiske, R.S., 1981, Modelling the three-dimensional structure of macroscopic magma transport systems: application to Kilauea Volcano: Journal of Geophysical Research, v. 86, p. 7111–7129.
Schwindinger, K.R., Roppo, P.S., and Anderson, A.T., Jr., 1983, Synneusis of olivine phenocrysts into glomeroporphyritic clusters [abs.]: Geological Society of America Abstracts with Programs, v. 15, p. 682.
Sen, G., 1983, A petrologic model for the constitution of the upper mantle and crust of the Koolau shield, Oahu, Hawaii, and Hawaiian magmatism: Earth and Planetary Science Letters, v. 62, p. 215–228.
Skinner, B.J., and Peck, D.L., 1969, An immiscible sulfide melt from Hawaii: Economic Geology Monograph, v. 4, p. 310–322.
Spera, F.J., 1984, Carbon dioxide in petrogenesis III: role of volatiles in the ascent of alkaline magma with special reference to xenolith bearing mafic lavas: Contributions to Mineralogy and Petrology, v. 88, p. 217–232.
Stevenson, D.J., 1983, Magmatic transport by the migration of fluid-filled cracks [abs.]: Eos, v. 64, p. 848.
Takahashi, E., and Kushiro, I., 1983, Melting of a dry peridotite at high pressures and basalt magma genesis: American Mineralogist, v. 68, p. 859–879.
Thornber, C., and Huebner, J.S., 1985, Dissolution of olivine in basaltic liquids I: Experimental observations and applications: American Mineralogist, v. 70, p. 934–945.
Van Kooten, G.K., and Buseck, P.R., 1978, Interpretation of olivine zoning: study of a maar from the San Francisco volcanic field, Arizona: Geological Society of American Bulletin, v. 89, p. 744–754.
Wadge, G., 1981, The variation of magma discharge during basaltic eruptions: Journal of Volcanology and Geothermal Research, v. 11, p. 139–168.
Wanamaker, B.J., and Evans, B., 1985, Experimental diffusional crack healing in olivine, *in* Schock, R.N., ed., American Geophysical Union Monograph 31: p. 194–210.
Weertman, J., 1971a, Theory of water-filled crevasses in glaciers applied to vertical magma transport beneath oceanic ridges: Journal of Geophysical Research, v. 76, p. 1171–1183.
———1971b, Velocity at which liquid-filled cracks move in the Earth's crust or in glaciers: Journal of Geophysical Research, v. 76, p. 8544–8553.
White, R.W., 1966, Ultramafic inclusions in basaltic rocks from Hawaii: Contributions to Mineralogy and Petrology, v. 12, p. 245–314.
Wright, T.L., 1971, Chemistry of Kilauea and Mauna Loa lava in space and time: U.S. Geological Survey Professional Paper 735, 40 p.
———1973, Magma mixing as illustrated by the 1959 eruption, Kilauea Volcano, Hawaii: Geological Society American Bulletin, v. 84, p. 849–585.
———1984, Origin of Hawaiian tholeiite: a metasomatic model: Journal of Geophysical Research, v. 89, p. 3233–3252.
Wright, T.L., and Fiske, R.S., 1971, Origin of the differentiated and hybrid lavas of Kilauea Volcano, Hawaii: Journal of Petrology, v. 12, p. 1–65.
Wright, T.L., and Okamura, R.T., 1977, Cooling and crystallization of tholeiitic basalt, 1965 Makaopuhi lava lake, Hawaii: U.S. Geological Survey Professional Paper 1004, 78 p.
Zablocki, C.J., and Tilling, R.I., 1976, Field measurements of apparent Curie temperatures in a cooling basaltic lava lake, Kilauea Iki, Hawaii: Geophysical Research Letters, v. 3, p 487–490.

ORIGIN OF THE WEST MAUI VOLCANIC ROCKS INFERRED FROM Pb, Sr, AND Nd ISOTOPES AND A MULTICOMPONENT MODEL FOR OCEANIC BASALT

By Mitsunobu Tatsumoto, Ernst Hegner,[1] *and* Daniel M. Unruh

ABSTRACT

Isotope ratios of Pb, Sr, and Nd for West Maui volcanic rocks fall within the range of those from other volcanoes of the Kea trend. Shield-building and caldera-filling rocks have indistinguishable Sr and Nd isotope ratios, but the latter rocks have slightly more radiogenic Pb. Posterosional volcanic rocks have lower $^{87}Sr/^{86}Sr$ ratios and less radiogenic Pb than underlying rocks. Isotope data for West Maui, as well as those for other Hawaiian volcanoes, are not adequately explained by binary mixing, but must be accounted for by mixing of at least three end members: the oceanic crust (Kilauea end member), the depleted upper mantle (posterosional end member). and a deep-mantle plume (Koolau end member). Isotope data thus far reported for oceanic basalt can also be described by a three-component mixing model: the depleted upper mantle (MORB source), Austral-St. Helena source, and recycled oceanic and continental crust (plumes?). However, data trends for oceanic basalt from individual areas suggest that mantle plumes may have only moderately radiogenic Pb, Sr, and Nd, requiring that such basalt was derived by mixing of these plumes with the chemically heterogeneous upper mantle (at least seven isotopically different components). Lithospheric contamination may also be involved.

INTRODUCTION

The geology and geophysics of the Hawaiian Islands have been extensively studied in order to understand intraplate volcanism and the formation of linear island chains. It has been thought for some time that the Emperor-Hawaiian Chain was formed by the northwestward motion of the Pacific plate over a fixed mantle hot spot (Wilson, 1963). It follows from the hot-spot hypothesis that the volcanoes of the chain are progressively older northwestward from the currently active volcanoes of Kilauea, Mauna Loa, and Loihi. The progression of ages has been well documented by K-Ar age measurements of Hawaiian rocks (McDougall, 1964; Dalrymple and others, 1973; Dalrymple and Clague, 1976).

The loci of the Hawaiian volcanoes follow two parallel curves (fig. 26.1): the Loa (southwestern) and Kea (northeastern) trends (Jackson and others, 1972, and references therein). From youngest to oldest, volcanoes on the Loa trend are Loihi, Mauna Loa (Hawaii), Hualalai (Hawaii), Kahoolawe, Lanai, West Molokai, Koolau (Oahu), Waiane (Oahu), and Kauai; those on the Kea trend are Kilauea (Hawaii), Mauna Kea (Hawaii), Kohala (Hawaii), Haleakala (East Maui), West Maui, and East Molokai.

Hawaiian volcanoes usually evolve in three stages: a shield-building stage, producing mostly tholeiite, a caldera-filling stage (alkalic rocks), and a posterosional stage (nephelinitic rocks) (Macdonald, 1968). However, recent studies of Loihi reveal a seamount stage in which basanite and alkali basalt with subordinate tholeiite are erupted before the shield-building tholeiitic stage (Moore and others, 1982). Although the earlier three-stage division may be too simple, subaerial Hawaiian rocks can be conveniently subdivided according to the three major stages. The two volcanoes on Maui, Haleakala in the east and the smaller West Maui Volcano, have developed to the posterosional stage. Those on the Island of Hawaii, however, 100 km to the southeast, have not yet erupted lava of posterosional type.

Strontium isotopes have been used for two decades to trace the origin of Hawaiian volcanic rocks (see, for example, Lessing and Catanzaro, 1964; Hamilton, 1965; Powell and Delong, 1966). From the Sr isotope difference between the Koolau Basalt (shield-building stage) and Honolulu Volcanics (posterosional alkalic-nephelinitic stage) on Oahu, Powell and Delong (1966) suggested that the two volcanic sequences were not derived from a common parent magma and that the upper mantle source regions are chemically and isotopically heterogeneous. Later isotope studies of Pb, Nd, Sr, and Hf (for example, Lanphere and Dalrymple, 1980; Stille and others, 1983; Roden and others, 1984) support this contention.

Chen and Frey (1983), in an extensive geochemical and isotopic study of Haleakala, found inverse correlations between $^{143}Nd/^{144}Nd$ and Sm/Nd abundance ratios and between $^{87}Sr/^{86}Sr$ and Rb/Sr abundance ratios. These findings are consistent with mixing of two kinds of melt, one derived from an enriched mantle and another formed by melting of a fraction (less than two percent of the total volume) of midocean-ridge basalt source.

[1]Department of Geological Sciences, University of Saskatchewan, Saskatoon, Saskatchewan, S7N OWO, Canada.

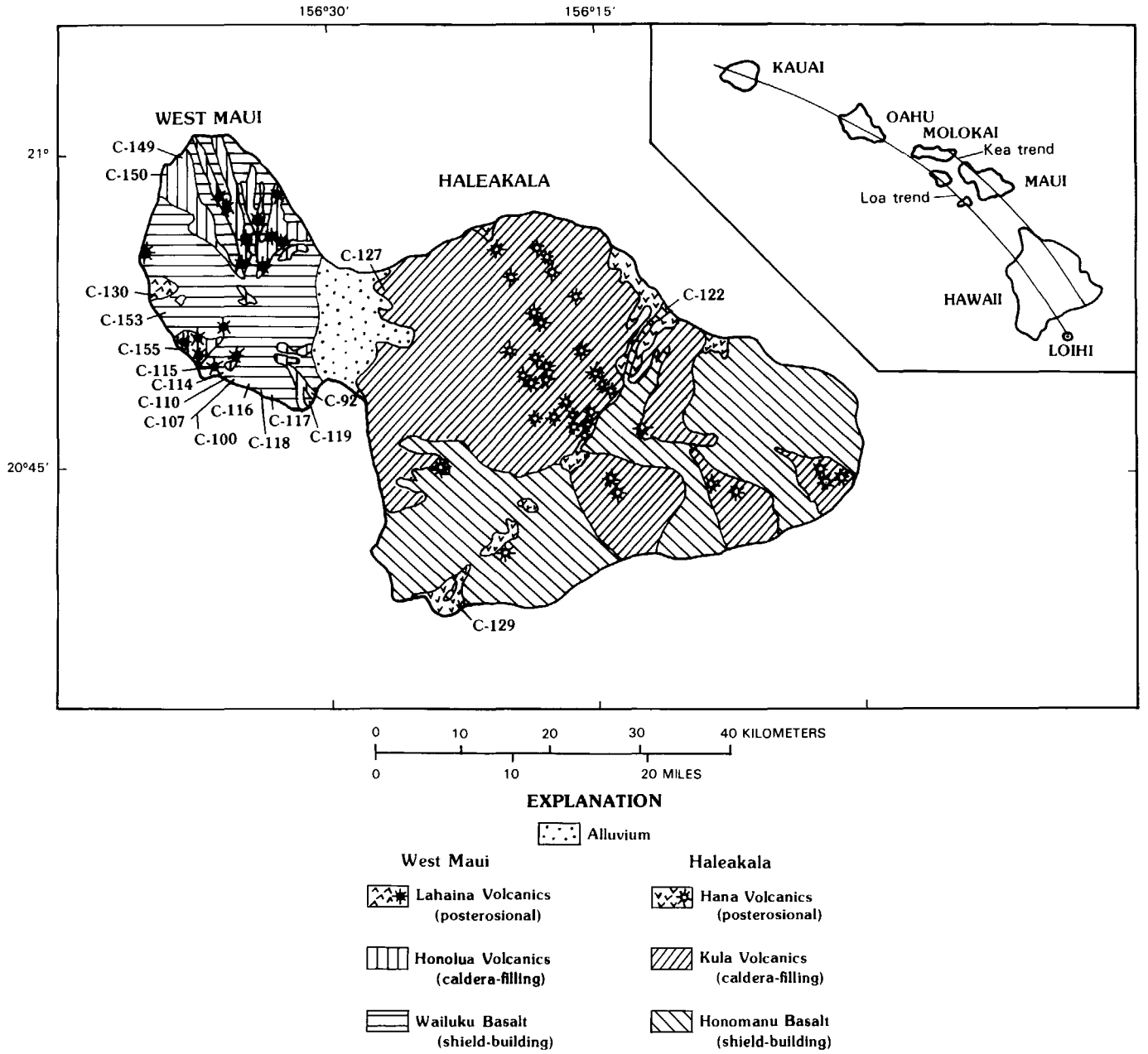

FIGURE 26.1.—Geologic map of the Island of Maui, simplified from Macdonald (1949). Sample locations are shown by numbers (for exact location, see Macdonald and Katsura, 1964, table 6 and 7; and this study). Inset shows location of Kea and Loa lineaments of volcanic centers in Hawaiian Islands.

Stille and others (1983) analyzed Pb, Sr, Nd, and Hf isotopes in volcanic rocks from Oahu and found that the isotope systematics can be best explained by a model involving mixing of three or more independent magma sources. Staudigel and others (1984) concurred with this view in an isotopic study of Loihi Seamount volcanic rocks. In order to place additional isotopic constraints on Hawaiian basalt petrogenesis, we measured Pb, Sr, and Nd isotopes in volcanic rocks from West Maui Volcano. The results were reported in brief previously (Hegner and others, 1986). In this paper we report concentrations of U, Th, Pb, Rb, Sr, Sm, and Nd, as well as Pb, Sr, and Nd isotopic ratios, in Maui volcanic rocks, and we discuss the origins of both Hawaiian volcanic rocks and oceanic basalt in general.

Stratigraphic nomenclature used in this report is that from Langenheim and Clague (chapter 1, part II).

ACKNOWLEDGMENTS

We are indebted to the late Dr. G.A. Macdonald for the C-series basalt samples. The supplemental samples were kindly

provided by Dr. J.A. Philpotts from the Macdonald collection. One of the authors (M.T.) thanks Drs. J.M. Sinton and Alan Zindler for their help with the field work.

GEOLOGY AND SAMPLES

The geology of Maui has been described in Stearns and Macdonald (1942) and Macdonald (1949). The Island of Maui comprises two volcanoes, both of which lie on the Kea trend. These volcanoes are the youngest in which post-erosional volcanics have erupted (fig. 26.1). The West Maui Volcano is wholly prehistoric and about one-fourth the size of the Haleakala (East Maui) Volcano, which last erupted in A.D. 1790. The Wailuku Basalt (formerly Wailuku Volcanic Series) represents the shield-building stage of West Maui and is composed mostly of tholeiite and intercalated alkali basalts with minor ankaramite near the top. Caldera-filling lava of the Honolua Volcanics (formerly Honolua Volcanic Series) is dominantly differentiated alkalic rock ranging from mugearite to soda trachyte in composition. After cessation of the Honolua volcanism and prolonged erosion, basanitic lava of the Lahaina Volcanics (formerly Lahaina Volcanics Series) was erupted.

The shield-building lava of Haleakala has been designated the Honomanu Basalt, and the composition of exposed rocks ranges only from tholeiitic olivine basalt to oceanite. The Honomanu Basalt is overlain by the Kula Volcanics, which are dominantly composed of hawaiite. The Hana Volcanics represents Haleakala's posterosional volcanism; this unit is less silica-saturated and consists of alkalic olivine basalt and basanitoid in contrast to the basanite-dominated Lahaina Volcanics of West Maui.

We analyzed 6 samples of tholeiitic basalt and 2 of alkali olivine basalt collected from the Wailuku Basalt (shield building), 8 samples of alkalic differentiates from the Honolua Volcanics (caldera filling), and 3 samples of basanite from the Lahaina Volcanics (posterosional). Sample numbers prefixed by a "C" were collected by the late Dr. Gordon A. Macdonald. Rock names and locations of samples C–92 to C–130 are listed by Macdonald and Katsura (1964) and are shown in figure 26.1. Samples collected by Macdonald from other sites have the following identities and places of collection (G.A. Macdonald, written commun., 1966): C–149, mugearite, transitional toward trachyte, roadcut at top of grade on west side of Pohakupule Gulch, West Maui, Honolua Volcanics; C–150, mugearite, transitional toward trachyte; dikelike body cutting mugearite flow in roadcut at berm where road starts to descend the west side of Honolua Gulch, West Maui, Honolua Volcanics; C–153, hawaiite, boulder in Kanaha Stream below Paupau Hill, just above Kelawea Village on outskirts of Lahaina, West Maui, Honolua Volcanics; C–155, mugearite, south branch of Makamakaole Gulch, 25 feet southeast of culvert under road, West Maui, Honolua Volcanics.

Samples designated "HMT" series were collected by one of us (M.T.) under the guidance of Dr. J.M. Sinton, University of Hawaii. Sample localities are the same as those of the C-series of Macdonald and Katsura (1964, tables 6 and 7), except HMT–2b, which is an alkalic olivine basalt from above an ash bed separating it from tholeiite (HMT–2a). Three samples from Haleakala Volcano were analyzed for comparison with Chen and Frey's (1983) data; they include a tholeiite from the Honomanu Basalt (shield building), a hawaiite of the Kula Volcanics (caldera filling), and a basanitoid of the Hana Volcanics (posterosional). Haleakala samples are also from the late Dr. Macdonald's collection. K-Ar ages by McDougall (1964) are 1.20 ± 0.02 Ma for olivine basalt from the upper part of the Wailuku Basalt, 1.16 ± 0.01 Ma for mugearite and trachyte of the Honolua Volcanics, and 0.44–0.86 Ma for alkalic rocks of the Kula Volcanics of Haleakala. Therefore, the isotopic data obtained from these samples require no age correction.

EXPERIMENTAL PROCEDURES

About 100 mg of each sample were dissolved in HF and HNO_3 with spike mixtures of ^{233}U-^{236}U-^{230}Th-^{205}Pb, ^{87}Rb-^{84}Sr, and ^{150}Nd-^{149}Sm in a PFA Teflon vial. First, Pb was separated in a 1*N* HBr medium using a single anion-exchange resin column of 100 µL volume (Tatsumoto and Unruh, 1976). The effluent was converted into 7*N* HNO_3 solution. The U and Th were then separated using an anion-exchange resin column of 600 µL volume. The effluent was converted into HCl solution, and Rb, Sr, and rare-earth elements (REE) were separated using a cation-exchange resin column of 4 mL volume. The Sr was purified using a 400 µL cation-exchange resin column, and the Nd and Sm were separated using 2-methyllactic acid in a 600 µL cation-exchange

TABLE 26.1.—*Standard analyses for selected elements and isotope ratios*

[Uncertainties refer to last significant figure(s) and represent 95 percent confidence level]

Sample	$^{143}Nd/^{144}Nd$	$^{87}Sr/^{86}Sr$	Rb (ppm)	Sr (ppm)	Sm (ppm)	Nd (ppm)
La Jolla standard	0.511865±10	--	--	--	--	--
NBS SRm-987 standard	--	.710255±30	--	--	--	--
BCR-1	.512654±15	.705009±20	46.47	329.6	6.64	29.06

resin column (Nakamura and others, 1976).

Pb isotopes were measured using single Re filaments with a phosphoric acid-silica gel in a NBS tandem-type mass spectrometer equipped with a 10^{11}-Ω resistor. The beam intensities of ^{206}Pb ranged from 3×10^{-12} to 1×10^{-10} A. A mass-fractionation correction of 0.12 ± 0.03 percent per atomic mass unit was applied to the raw Pb data. The U, Th, and Rb were measured using Re triple filaments in the same tandem mass spectrometer. The Sr, Nd, and Sm isotopic analyses were done in a VG 54R mass spectrometer using oxidized Ta filaments for Sr and Re-Ta triple filaments for Nd and Sm (Nakamura and others, 1976). Sr and Nd isotopic compositions of samples were deduced from the spiked runs by normalizing $^{86}Sr/^{88}Sr=0.1194$ and $^{146}Nd/^{144}Nd=0.7219$, respectively, using a linear fractionation law (Dodson, 1970). The NBS Sr standard SRM–982 and La Jolla Nd standard were measured in runs of varying (normal ^{86}Sr)/(spike ^{84}Sr) and (normal ^{144}Nd)/(spike ^{150}Nd) ratios (up to unity), and we found that spiked runs agree with unspiked runs to within 0.005 percent. Four samples (powdered) that showed somewhat high $^{87}Sr/^{86}Sr$ ratios compared to other samples were leached with 6*N* HCl at ≈80 °C for 10 h in order to eliminate alteration effects (O'Nions and others, 1977; Zindler and others, 1984). The leached samples were

TABLE 26.2.—*Selected elemental concentration and elemental and isotope ratios in samples of Maui volcanic rocks*

Sample		Rb (ppm)	Sr	Rb/Sr	Sm (ppm)	Nd	Sm/Nd	Pb (ppm)	U	Th	$\frac{^{238}U}{^{204}Pb}$	$\frac{^{232}Th}{^{238}U}$
WEST MAUI												
Lahaina Volcanics												
C-130	basanite	8.4	245	0.034	4.59	19.91	0.23	1.38	0.39	1.16	17.7	3.1
C-115	basanite	43.8	705	.062	4.82	25.94	.19	3.03	1.40	4.05	28.9	3.0
HMT 79-5	(C-115)	40.5	667	.061	7.97	39.42	.20	4.51	1.54	5.60	21.4	3.7
Honolua Volcanics												
C-155	mugearite	49.8	1,331	.037	17.62	87.05	.20	4.27	1.22	5.56	18.1	4.7
	--	--	--	--	--	--	--	1.18	5.33	--	4.7	--
C-153	hawaiite	8.7	499	.017	9.06	40.33	.22	1.59	.46	1.51	18.6	3.4
C-150	mugearite	44.1	1,149	.038	15.15	71.00	.21	4.23	1.66	78.05	24.7	4.4
C-149	mugearite	48.2	1,041	.046	14.95	64.91	.23	5.04	2.07	6.14	25.9	3.1
C-128	trachyte	59.1	400	.148	14.63	78.24	.19	7.27	1.84	7.24	16.0	4.1
C-116	trachyte	64.5	432	.149	20.33	98.84	.21	6.15	2.35	7.45	24.3	3.0
	--	--	--	--	--	--	--	2.55	8.42	--	3.4	--
C-92	trachyte	50.0	1,040	.048	15.67	81.33	.19	4.56	1.86	4.84	25.7	2.7
[1]HMT79-2b	alkali basalt	3.4	525	.006	8.58	31.05	.28	2.04	.29	1.46	8.9	5.3
Wailuku Basalt												
HMT 79-3	tholeiitic olivine basalt (C-120)	.6	360	.002	5.51	20.51	.27	.95	.11	.70	7.3	6.1
C-119	tholeiitic olivine basalt	7.7	489	.016	8.10	25.94	.31	1.16	.35	1.15	19.1	3.4
C-118	alkalic olivine basalt	1.4	254	.006	4.20	16.49	.25	1.20	.23	.61	11.8	2.8
C-117	tholeiitic olivine basalt	3.6	382	.009	4.14	16.96	.24	1.14	.22	.76	12.1	3.6
[1]C-114	alkalic olivine basalt	3.1	739	.004	6.88	27.41	.25	1.37	.27	1.23	12.5	4.7
C-110	tholeiite	4.2	319	.013	4.93	17.92	.27	2.85	.23	.62	5.0	2.8
[1]C-107	tholeiite	5.1	356	.014	6.97	25.99	.27	.96	.27	.77	17.8	2.9
C-100	tholeiite	3.1	346	.009	3.45	13.07	.26	.87	.20	.68	14.5	3.5
EAST MAUI (HALEAKALA)												
Hana Volcanics												
C-129	basanitoid	23.9	523	.046	6.16	27.58	.22	1.63	.61	2.09	23.6	3.5
[2]H65-11	alkalic basalt	18.8	582	.032	6.01	26.1	.23	--	--	2.6	--	--
Kula Volcanics												
C-127	hawaiite	29.8	831	.036	7.53	37.40	.20	2.27	.97	3.05	26.8	3.3
[2]H65-4	alkalic basalt	19.9	616	.032	6.83	30.7	.22	--	--	2.1	--	--
Honomanu Basalt												
C-122	tholeiitic olivine basalt	4.72	225	.021	4.23	14.71	.29	1.08	.20	.51	11.6	2.6
[2]C-122		4.11	207	.020	3.73	12.3	.30	--	--	.8	--	--

[1]Analyses from Unruh and others (oral commun., 1985).
[2]Chen and Frey (1983).

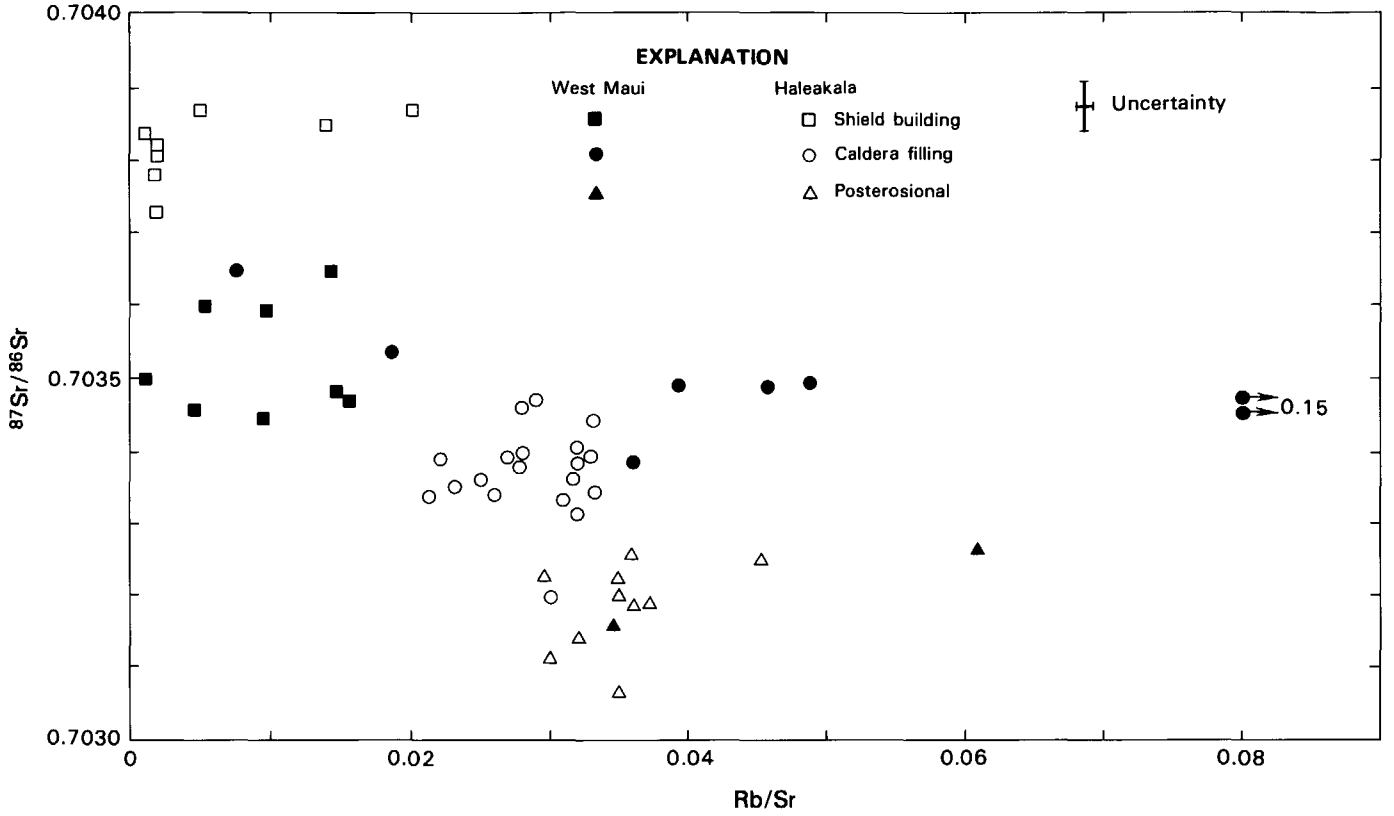

FIGURE 26.2.—Plot of $^{87}Sr/^{86}Sr$ ratio against Rb/Sr ratio for samples of volcanic rocks from Maui. Data for Haleakala from Chen and Frey (1983) included. Uncertainty bars apply to all data.

analyzed only for Sr isotopic composition. The standard runs during this study averaged $^{143}Nd/^{144}Nd = 0.511865 \pm 0.000010$ for the La Jolla Nd, and $^{87}Sr/^{86}Sr = 0.710265 \pm 0.000030$ for NBS SRM–987 (table 26.1). No instrumental bias corrections were applied to the isotope data in table 26.3. The USGS rock standard BCR–1 was analyzed once during the course of this study, and the results are listed in table 26.1. Blanks for the analyses are in ng: Pb, 0.1–0.15; U, <0.01; Th, <0.01; Rb, 0.1–0.2; Sr, 0.5–1; Sm, <0.03; Nd, <0.1.

RESULTS

TRACE-ELEMENT CONCENTRATIONS

The elemental concentration data for volcanic rocks from West Maui and Haleakala are listed in table 26.2. Data for Haleakala samples from Chen and Frey (1983) are also included. The trace-element abundances of Rb, Sr, Sm, Nd, Pb, U, and Th of West Maui and Haleakala are similar to those in other subaerial Hawaiian basalts (Tatsumoto, 1978; Clague and Frey, 1982; Roden and others, 1984).

Plots of the ratios $^{87}Sr/^{86}Sr$ versus Rb/Sr and $^{143}Nd/^{144}Nd$ versus Sm/Nd for West Maui and Haleakala samples are shown in figures 26.2 and 26.3, which include data from Haleakala obtained by Chen and Frey (1983). The variation in Rb/Sr ratios of West

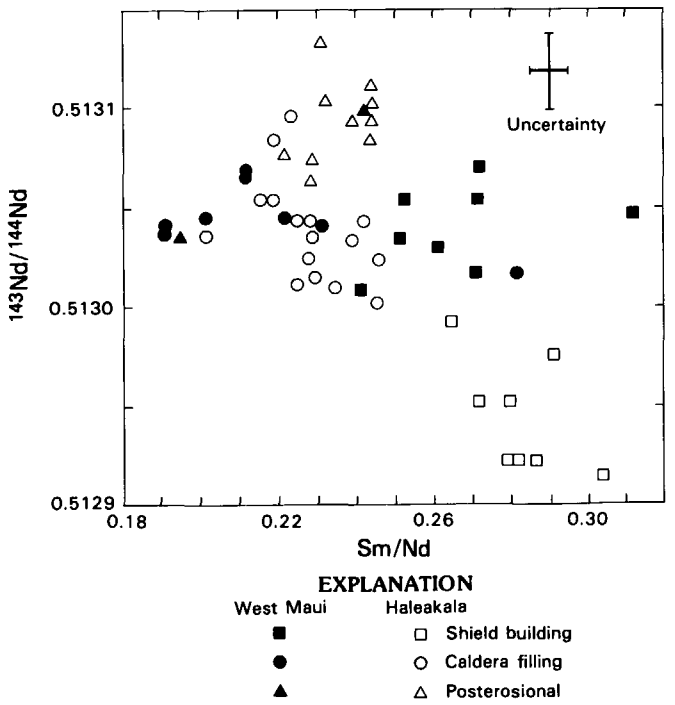

FIGURE 26.3.—Plot of $^{143}Nd/^{144}Nd$ ratio against Sm/Nd ratio for samples of volcanic rock from Maui. Uncertainty bars apply to all data.

Maui volcanic rocks (fig. 26.2) is large compared to that of the Haleakala volcanic rocks, because West Maui samples contain highly fractionated alkalic rocks such as trachyte that do not occur at Haleakala. Sm/Nd ratios (fig. 26.3) of West Maui vary from 0.31 to 0.19 and are similar to those of the Haleakala volcanic rocks. The lowest values are for trachyte and basanite, and Rb/Sr ratios of these rocks are correspondingly high. In contrast, $^{143}Nd/^{144}Nd$ values of West Maui volcanics are almost constant. Chen and Frey (1983) discovered profound negative correlations between parent/daughter abundance ratios and radiogenic isotope abundances in the

TABLE 26.3.—*Isotope data for Sr, Nd, and Pb in samples of Maui volcanic rocks*

[Uncertainties correspond to last significant figure(s) and are 95 percent confidence level. Uncertainties for lead are limited to a few values because of correction uncertainties for mass fractionation]

Sample	Rock type	$^{87}Sr/^{86}Sr$	ϵ_{Sr}	$^{143}Nd/^{144}Nd$	ϵ_{Nd}	$^{206}Pb/^{204}Pb$	$^{207}Pb/^{204}Pb$	$^{208}Pb/^{204}Pb$
WEST MAUI								
Lahaina Volcanics								
C-130	basanite	0.70315±3	-22.0	0.513086±28	8.7	18.169±11	15.452±14	37.750±49
				.513107±10				
C-115	basanite	.70326±2	-20.4	.513034±20	7.7	18.191±11	15.460±14	37.833±49
HMT79-5	(C-115)	.70325±4	--	.513031±18	--			
		.70327±3						
Honolua Volcanics								
C-155	mugearite	.70343±4	-18.0	.513043±8	7.9	18.513±11	15.494±14	38.050±49
C-153	hawaiite	.70353±3	-16.6	.513041±7	7.8	18.447±11	15.456±14	37.917±49
C-150	mugearite	.70349±3	-17.2	.513065±9	8.3	18.502±11	15.483±14	38.033±49
C-149	mugearite	.70349±3	-17.2	.513037±64	7.7	18.509±11	15.489±14	38.030±49
C-128	trachyte	.70347±3	-17.5	.513034±20	7.7	18.492±11	15.476±14	38.008±49
C-116	trachyte	.70348±5	-17.3	.513064±7	8.3	18.523±11	15.471±14	37.961±49
C-92	trachyte	.70350±3	-17.0	.513035±16	7.7	18.482±11	15.466±14	37.957±49
HMT79-1a	(C-92)	.70355±4	--	.513033±20	--	18.487±11	15.462±14	37.947±49
HMT79-2b	alkali basalt	.70354±3	--	.513033±20	7.3	18.506±11	15.560±14	38.040±49
[1]HMT79-2b		.70352±4	--	.513005±16	--	18.474±16	15.535±16	37.974±49
Wailuku Basalt								
HMT79-3	tholeiitic olivine basalt (C-120)	.70349±4	-17.2	.513014±19	7.3	18.462±11	15.456±14	37.925±50
C-119	tholeiitic olivine basalt	.70347±4	-17.5	.513044±28	7.9	18.426±11	15.472±14	37.904±49
HMT79-2A	(C-119)	.70356±3	--	.513025±20		18.462±11	15.454±14	37.899±49
C-118	alkalic olivine basalt	.70364±4	--	.513049±12	8.0	18.258±11	15.471±14	37.762±49
		[3].70359±2	-15.8					
C-117	tholeiitic olivine basalt	.70359±3	-15.8	.513007±15	7.2	18.404±15	15.429±14	37.940±49
		.70361±2						
[1]C-114	alkalic olivine basalt	.70346±4	-17.6	.513032±22	8.9	18.412±11	15.472±14	37.906±49
C-110	tholeiite	.70363±3	--	.513053±13	8.1	18.309±11	15.476±14	37.874±49
		[3].70365±3	-14.9					
[1]C-107	tholeiite	.70348±3	-17.3	.513070±12	8.1	18.438±11	15.499±14	37.948±49
C-100	tholeiite	.70361±4		.513027±13	7.5	18.365±11	15.470±14	37.877±49
		[3].70344±3	-17.9					
EAST MAUI (HALEAKALA)								
Hana Volcanics								
C-129	basanitoid	.70325±3	-20.6	.513070±13	8.4	18.259±11	15.453±14	37.828±49
[2]H65-1	alkalic basalt	.70314±4	-22.1	.51310±2	9.0	--	--	--
Kula Volcanics								
C-127	hawaiite	.70339±4	-18.6	.513030±15	7.6	18.351±11	15.468±14	37.938±49
[2]H65-4	alkalic basalt	.70334±3	-19.3	.51302±1	7.4	--	--	--
Honomanu Basalt								
C-122	tholeiite olivine basalt	.70378±3	-13.1	.512976±16	6.6	18.303±11	15.452±14	37.924±49
		.70374±4						
		.70374±3						
[2]C-122		.70387±4	-11.8	.51291±2	5.3	--	--	--

[1]Analyses from Stille and others (1985).
[2]Chen and Frey (1983).
[3]On acid leached samples (6N HCl, 10 hours).

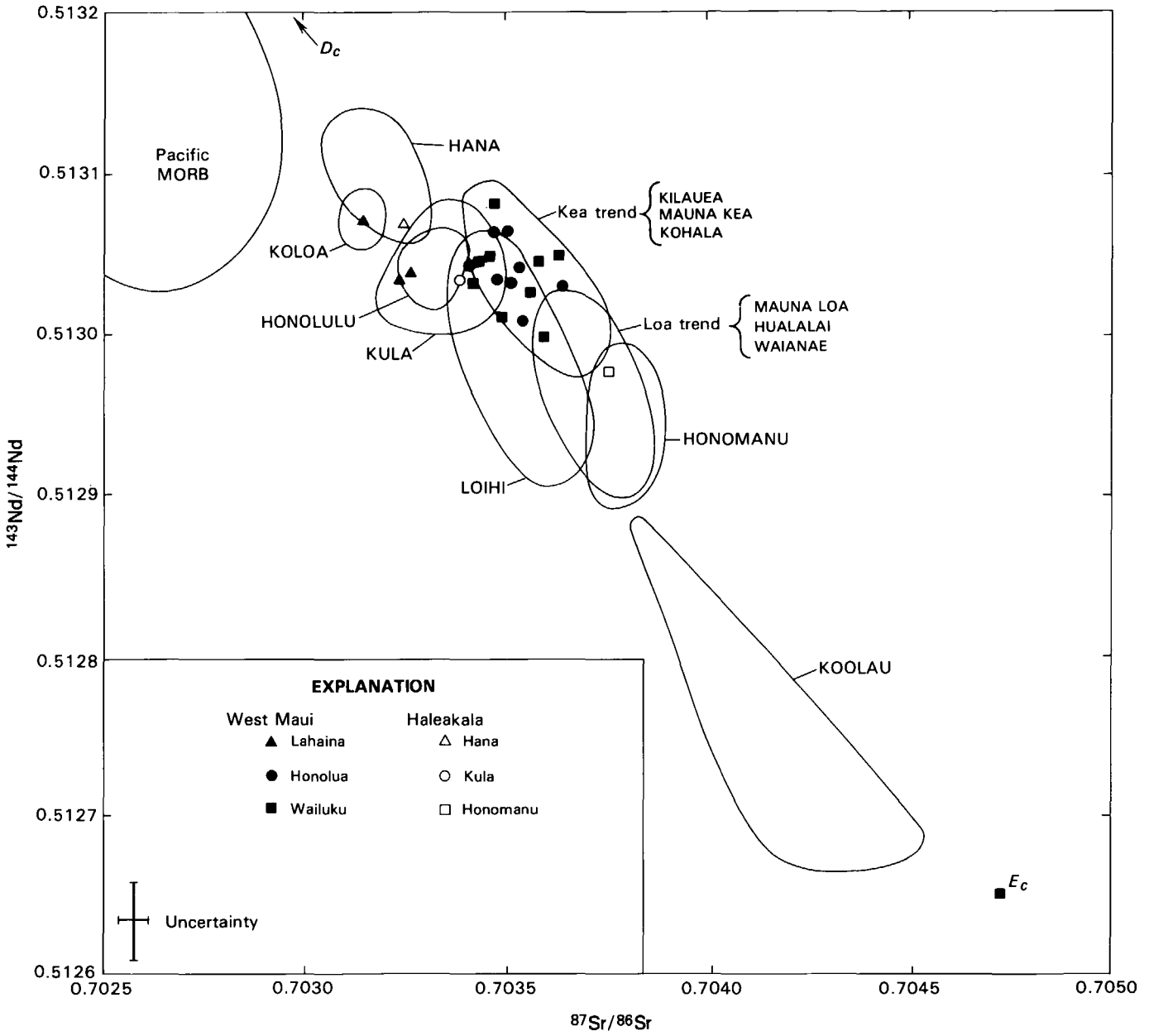

FIGURE 26.4.—Plot of $^{87}Sr/^{86}Sr$ ratio against $^{143}Nd/^{144}Nd$ ratio for Hawaiian basalt. Data for samples from Maui are shown by symbols. Data for Honomanu Basalt, Kula Volcanics, and Hana Volcanics of Haleakala from Chen and Frey (1983) are also shown. Also shown are fields for Koolau Basalt and Waianae Volcanics, Oahu; (Stille and others, 1983; Roden and others, 1984); Loihi (Staudigel and others, 1984); Koloa Volcanics, Kauai, (O'Nions and others, 1977); and volcanics from Island of Hawaii (Stille and others, in press). Data for posterosional basalt appears to be shifted slightly to left from main Hawaiian trend and close to East Pacific Ridge basalt (Pacific MORB) field. D_c and E_c, possible depleted and enriched members, respectively, in hypothetical two-component mixing model. Uncertainty bars apply to all individual symbols.

Rb-Sr and Sm-Nd systems. Although such negative correlations for West Maui samples are somewhat indistinct, our results clearly do not support the mantle-isochron concept of Brooks and others (1976), who proposed that a positive correlation of Rb/Sr with $^{87}Sr/^{86}Sr$ corresponds to an age of mantle differentiation of 1.8 Ga. The trace-element concentrations of Maui tholeiite (this study; Chen and Frey, 1983) are distinctly higher than those of normal mid-ocean-ridge basalt (N-MORB) but are comparable to those in enriched MORB (P-MORB) (see, for example, Tatsumoto and others, 1965; Cohen and O'Nions, 1982).

For seven samples from the Wailuku Basalt, West Maui, Rb and Sr concentrations and Rb/Sr ratios are similar to those of the Koolau Basalt, Oahu (Roden and others, 1984) (sample HMT 79–3 is omitted because of its weathered nature). However, the Rb concentrations and Rb/Sr ratios of Wailuku rocks appear to be distinctly lower than those of Loihi tholeiite (Frey and Clague,

1983; Staudigel and others, 1984), although their $^{87}Sr/^{86}Sr$ ratios are similar.

ISOTOPIC COMPOSITIONS

The Sr, Nd, and Pb isotopic data for West Maui and Haleakala are listed in table 26.3. The Sr and Nd data of Haleakala by Chen and Frey (1983) are also included in the table. The Nd-Sr data of West Maui basalt are plotted on a Nd-Sr correlation diagram in figure 26.4.

The C-series samples generally appear to be fresh; however, a $^{87}Sr/^{86}Sr$ value higher than 0.7036 in one of the three Wailuku samples proved to be related to alteration. Sample HMT 79–2b also shows slight alteration and a higher $^{87}Sr/^{86}Sr$ value.

The $^{87}Sr/^{86}Sr$ ratio of all samples from West Maui varies from 0.70315 to 0.70364, which correspond to an ε_{Sr} range of 7.0 (0.07 percent) and is well within the range (0.7031–0.7046; ε_{Sr} range, 21.3) of Hawaiian volcanic rocks so far reported (Lanphere and others, 1980; Chen and Frey, 1983; Stille and others, 1983, in press; Roden and others, 1984). The ε_{Sr} is the deviation in parts per ten thousand from the present day bulk earth value of $^{87}Sr/^{86}Sr = 0.7047$ (O'Nions and others, 1977). Although the bulk-earth value has been debated (for example, Zindler and others, 1982), we use the ε_{Sr} just for convenience to compare $^{87}Sr/^{86}Sr$ variations in the present paper. The variation is smaller than that for the three Haleakala volcanic sequences (0.70307–0.70387; ε_{Sr} range, 11.4) and the tholeiitic series of Koolau (0.70367–0.70458; ε_{Sr} range, 12.9), but it is similar to that for the Loihi Seamount volcanics (0.7033–0.7037; ε_{Sr} range, 5.7, Staudigel and others, 1984). Similar $^{87}Sr/^{86}Sr$ ratios (0.70346–0.70370) for West Maui volcanic rocks are also reported by Feigenson and others (1984). The shield-building Wailuku Basalt and the late-stage Honolua alkalic rocks from West Maui have an almost constant $^{87}Sr/^{86}Sr$ ratio of 0.70353 ± 0.00010, corresponding to an ε_{Sr} range of only 1.4. The $^{87}Sr/^{86}Sr$ ratios are distinctly smaller than those of Honomanu Basalt but slightly higher than those of Kula alkalic rocks from Haleakala. The $^{87}Sr/^{86}Sr$ ratio of Lahaina basanite from West Maui is distinctly smaller than that of volcanic rocks of the earlier stages, but similar to those in the Hana Volcanics at Haleakala (fig. 26.2) and in the Honolulu Volcanics on Oahu (Stille and others, 1983).

Chen and Frey (1983, fig. 1) reported that the $^{143}Nd/^{144}Nd$ ratio in Haleakala rocks varies from 0.51313 to 0.51291. This variation corresponds to an ε_{Nd} variation of 4.2, and Nd isotopic ratios are negatively correlated with Sm/Nd ratios. Like ε_{Sr}, ε_{Nd} is the deviation in parts per ten thousand from the present day bulk-earth value of $^{143}Nd/^{144}Nd = 0.51264$ (DePaolo and Wasserburg, 1976). In contrast to Haleakala, the $^{143}Nd/^{144}Nd$ ratio of all samples analyzed from West Maui exhibits almost constant values (0.51301 to 0.51309), which correspond to an ε_{Nd} range of only 1.6. Furthermore, $^{143}Nd/^{144}Nd$ ratios for shield-building Wailuku Basalt and alkalic Honolua Volcanics vary from only 0.51301 to 0.51307, these valves correspond to a narrow range of ε_{Nd} of 1.2.

The Sr and Nd ratios of West Maui volcanic rocks are inversely correlated and plot at the upper end of the Hawaiian data array shown in figure 26.4 (Stille and others, 1983, 1985; Roden and others, 1984; Staudigel and others, 1984). The Lahaina Volcanics (posterosional) has similar $^{143}Nd/^{144}Nd$ ratios to the underlying rocks but smaller $^{87}Sr/^{86}Sr$ ratios. Consequently, the Lahaina data are shifted slightly to the left, close to the MORB field, and plot in the fields of Hana (Haleakala) and Honolulu (Oahu) data.

The Pb isotopic compositions of West Maui samples are shown in a diagram plotting $^{206}Pb/^{204}Pb$ against $^{207}Pb/^{204}Pb$ and $^{208}Pb/^{204}Pb$ in figure 26.5. Note that the scale for $^{207}Pb/^{204}Pb$ is expanded five times relative to those for $^{206}Pb/^{204}Pb$ and $^{208}Pb/^{204}Pb$. The variation in Pb isotopic compositions (table 26.3) is partly caused by measurement errors associated with mass fractionation. However, the ratios of West Maui samples vary beyond measurement errors.

The Pb isotopic compositions of West Maui volcanic rocks fall within the field for Hawaiian volcanic rocks between Waianae (Oahu) and Kilauea (Hawaii); in contrast to the Sr and Nd isotopes; however, the West Maui rocks display the largest range in Pb isotopic composition of any single Hawaiian volcano so far determined except Loihi. On the other hand, Pb isotopic compositions of Honomanu, Kula, and Hana rocks from Haleakala show smaller variations compared to West Maui, although Nd and Sr show larger variations (Chen and Frey, 1983). However, only three samples from Haleakala were analyzed in the present study. The Pb data for Haleakala measured by Chen and Frey are not published and were compiled from Staudigel and others (1984, fig. 5), and the actual sample population is not known to us. The least radiogenic Pb in Wailuku samples is similar to those in the Haleakala samples, but Pb in upper Wailuku samples is more radiogenic. The Pb in the alkalic late-stage Honolua Volcanics is more radiogenic than that of the Wailuku samples showing oceanic-crust assimilation as discussed later. Alkali basalt sample HMT 79–2b has a significantly high $^{207}Pb/^{204}Pb$ ratio compared to other samples (fig. 26.5). The data fall on the "1.8-Ga MORB trend" instead of the "0.9-Ga Hawaiian trend" in the plot of $^{206}Pb/^{204}Pb$ versus $^{207}Pb/^{204}Pb$ (Tatsumoto, 1978) and indicate a Pb-isotopic diversity in Hawaiian

FIGURE 26.5.—Plots of $^{206}Pb/^{204}Pb$ ratio against $^{207}Pb/^{204}Pb$ and $^{208}Pb/^{204}Pb$ ratios for Hawaiian volcanic rocks. Data from Maui (this study), Island of Hawaii (Tatsumoto, 1978), Oahu (Stille and others, 1983), Koloa Volcanics, Kauai (Sun, 1980), and Loihi (Staudigel and others, 1984). Data of shield building and caldera-filling rocks from West Maui plot in large area similar to Loihi data but with lower $^{208}Pb/^{204}Pb$, whereas posterosional rocks are less radiogenic and plot close to Hana Volcanics (Haleakala) and Honolulu Volcanics (Oahu). Hawaiian basalt data fall on apparent isochron of ~0.9 Ga, whereas some data plot near 1.8-Ga MORB trend. In upper diagram, reference lines with K ($^{232}Th/^{238}U$) = 3.0 are shown for ages of 0.9 and 1.8 Ga. Uncertainty ellipses apply to data of this study.

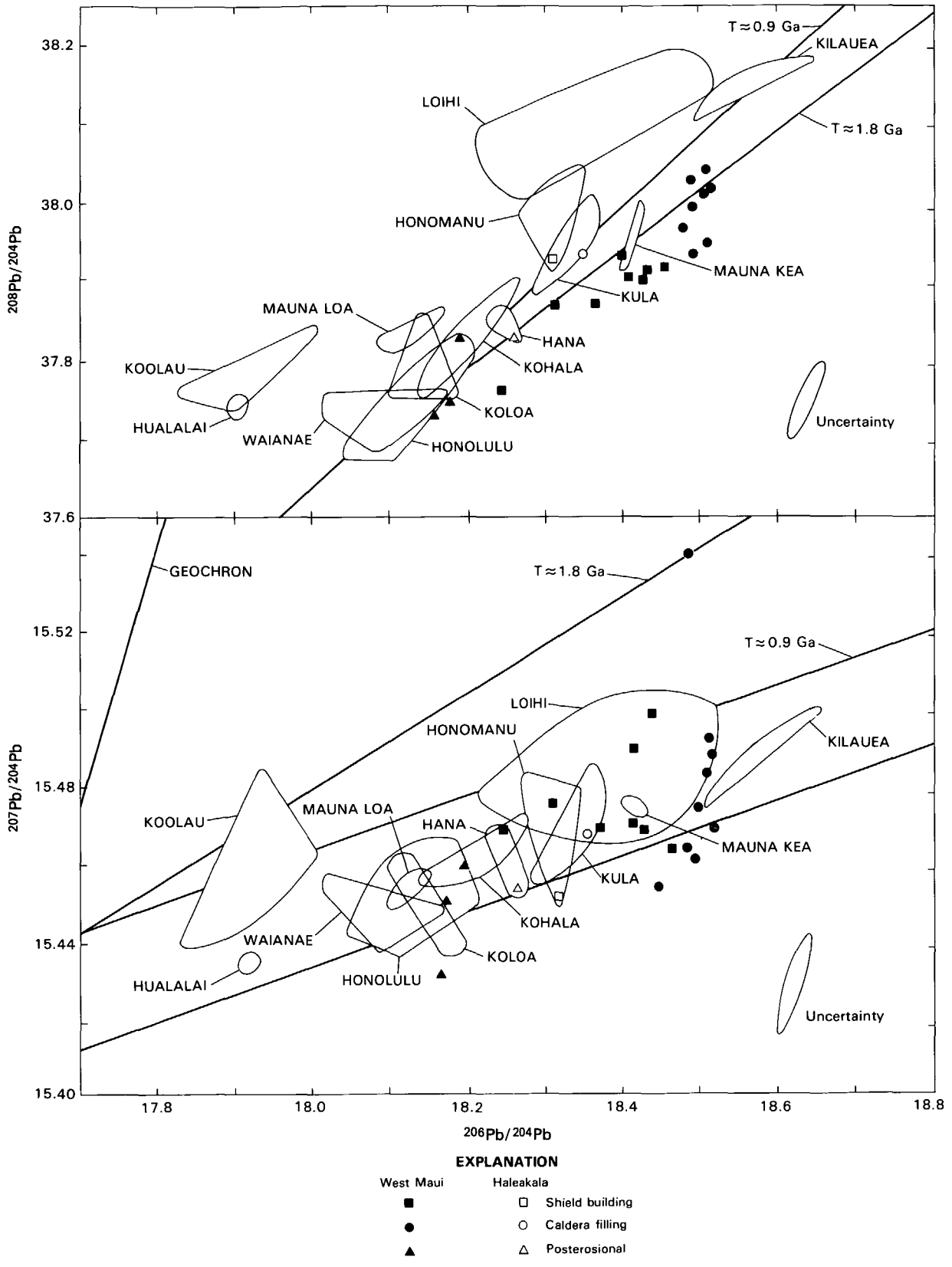
T≈0.9 Ga
KILAUEA
LOIHI
T≈1.8 Ga
HONOMANU
MAUNA KEA
KULA
MAUNA LOA
HANA
KOHALA
KOOLAU
KOLOA
HUALALAI
WAIANAE
HONOLULU
Uncertainty
38.2
38.0
37.8
37.6
208Pb/204Pb
GEOCHRON
T≈1.8 Ga
T≈0.9 Ga
15.52
15.48
15.44
15.40
207Pb/204Pb
17.8
18.0
18.2
18.4
18.6
18.8
206Pb/204Pb
EXPLANATION
West Maui
Haleakala
Shield building
Caldera filling
Posterosional

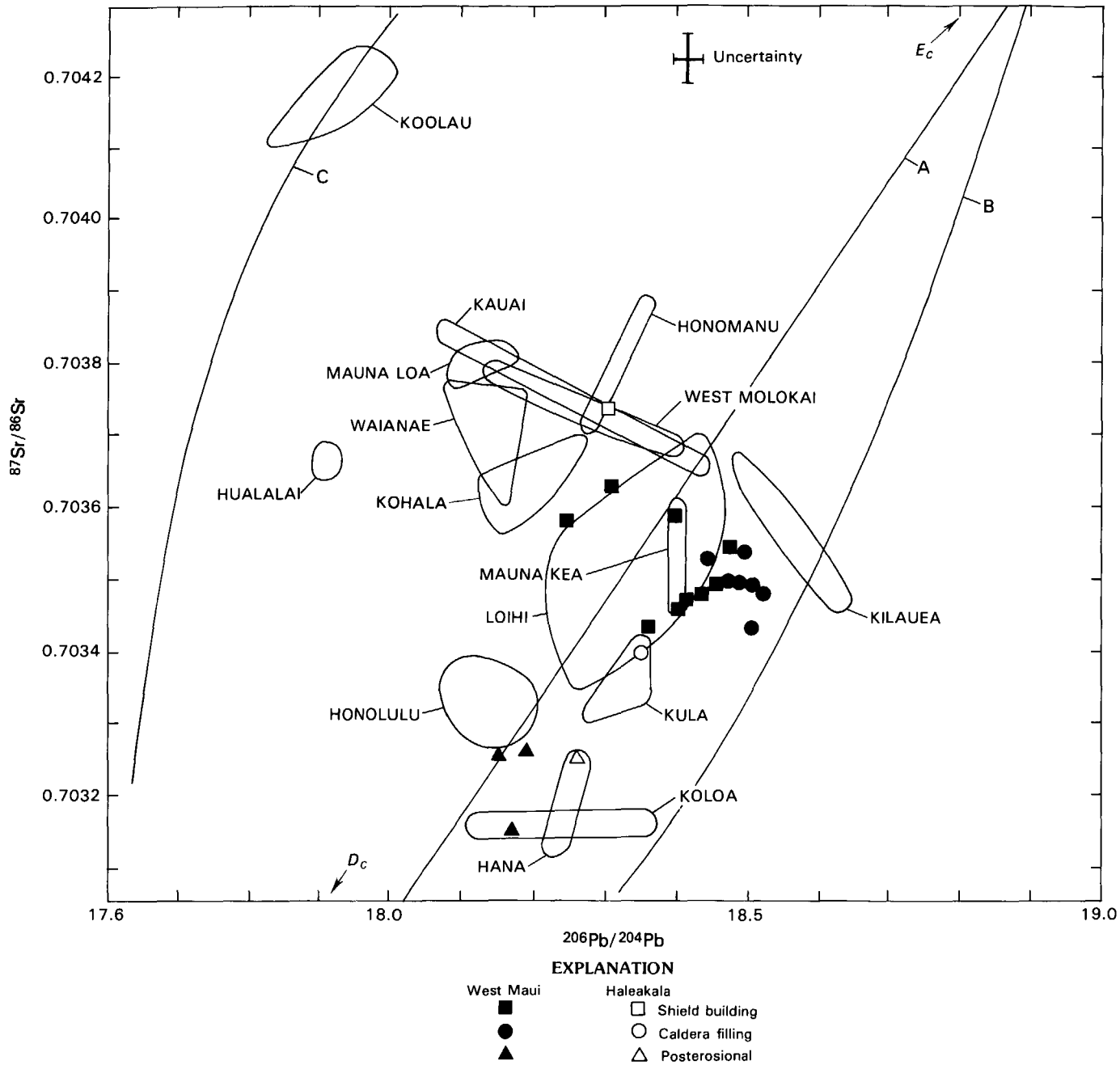

FIGURE 26.6.—Plot of $^{206}Pb/^{204}Pb$ ratio against $^{87}Sr/^{86}Sr$ ratio for Hawaiian rocks. Sources of data as in figures 26.4 and 26.5. Shield-building and caldera-filling rocks from West Maui plot in and near field for Loihi, whereas posterosional rocks plot to less radiogenic side of trend. Also shown are hypothetical mixing curves between depleted and enriched sources: A, $Q_1 = 1$; B, $Q_1 = 0.5$; C, $Q_1 = 10$. See discussion in text. D_c and E_c, inferred depleted and enriched components, respectively.

basalt. Although these peculiar data need confirmation, it is conceivable that the high $^{207}Pb/^{204}Pb$ ratio is the reflection of oceanic lower crust involvement; the basalt locally contains 1-cm gabbroic clots. Basanite of the Lahaina sequence has less radiogenic Pb than Wailuku tholeiite, indicating a different origin from the underlying volcanic rocks.

The Pb, Sr, and Nd data for Hawaiian volcanic rocks are shown in plots of $^{206}Pb/^{204}Pb$ versus $^{87}Sr/^{86}Sr$ and $^{143}Nd/^{144}Nd$ diagrams in figures 26.6 and 26.7. Differences between the posterosional Lahaina Volcanics and the underlying rocks are more evident on the Sr-Pb diagram. The Pb becomes slightly more radiogenic, and the Sr becomes slightly less radiogenic moving from

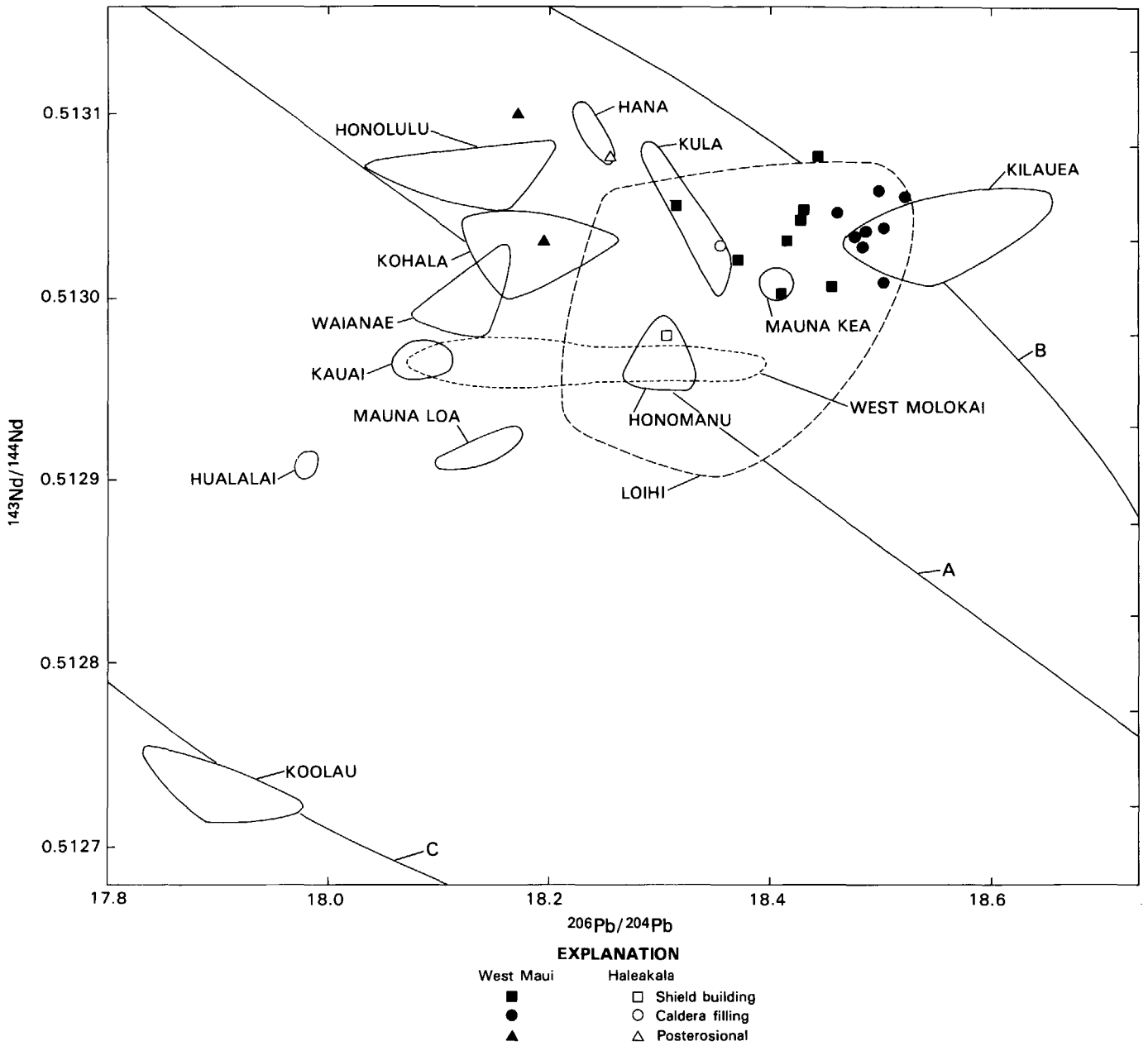

FIGURE 26.7.—Plot of $^{206}Pb/^{204}Pb$ ratio against $^{143}Nd/^{144}Nd$ ratio for Hawaiian rocks. Sources of data as in figures 26.4 and 26.5. Plot can be regarded as upside-down image of figure 26.6. Hypothetical mixing curves calculated as in figure 26.6: A, $Q_2 = 1$; B, $Q_2 = 0.5$; C, $Q_2 = 10$.

tholeiite to caldera-filling basalt, and the data define a crude negative correlation. The negative correlation is similar to the main Hawaiian trend that supports a model in which two-component mixing occurs between a mantle plume and depleted mantle or lithosphere. The mixing with depleted mantle progressively increases as the volcano evolves (Chen and Frey, 1983). However, the data for posterosional basalt do not appear to be related to the main trend and indicate the possible presence of a second depleted source with relatively non-radiogenic Pb and Sr.

DISCUSSION

Results of high-pressure experiments show that alkali olivine basalt can be produced from olivine tholeiite magma by orthopyroxene and olivine fractionation at pressures greater than 1.2 GPa (12 kbar)(see, for example, Kushiro, 1969; Presnall and others, 1979). No significant differences in Pb isotopes between tholeiite and alkali basalt were found for Kohala and Mauna Kea (Tatsumoto, 1978) nor for Pb, Sr, Nd, and Hf isotopic composition between the two

rock types from the Waianae Volcano (Stille and others, 1983). These isotopic similarities between tholeiite and alkali basalt appear to be consistent with results of high-pressure experiments. Distinct differences in $^{87}Sr/^{86}Sr$ ratio between shield-building Koolau tholeiite and nephelinitic Honolulu Volcanics from Oahu have been observed for about two decades (Powell and Delong, 1966). Recent Sr-isotope measurements (Lanphere and Dalrymple, 1980) as well as studies of Pb, Nd, and Hf isotopes in Oahu volcanic rocks (Stille and others, 1983; Roden and others, 1984) have confirmed the isotopic differences between the two rock series. Thus Tatsumoto (1978) and Stille and others (1983) suggested a close genetic relationship exists between tholeiite and late-stage alkali basalt, but that nephelinitic rocks are of independent origin. This suggestion derived from isotopic studies is consistent with Jackson and Wright's (1970) view; from a study of xenoliths they concluded that the Honolulu Volcanics originated from garnet lherzolite at greater depths than the Koolau tholeiite magma.

In contrast, Chen and Frey (1983) found that Sr and Nd isotopic compositions of Honomanu Basalt (shield-building stage), Kula Volcanics (alkalic basalt), and Hana Volcanics from Haleakala are distinctly different among the three sequences and are inversely correlated with Rb/Sr and Sm/Nd ratios. Chen and Frey invoked a two-component melt-mixing model to account for the isotopic and incompatible-element relationships. Present Nd and Sr isotopic data for West Maui volcanics do not show such clear distinctions as Chen and Frey observed for the east. These results may indicate that Haleakala late-stage magma had crustal contamination along differentiation and changed its isotopic signature, while West Maui magma had little assimilation along differentiation.

Staudigel and others (1984) stated that the heterogeneous isotopic character of Loihi Seamount volcanic rocks may attest to Loihi's inability to homogenize lava before eruption, whereas parental magma of more mature and active volcanoes may be well mixed in established magma chambers. Waianae (Stille and others, 1983) and West Maui data seem to support such a hypothesis.

Staudigel and others (1984) argued that Honolulu and Koolau data define two extreme positions in the $^{143}Nd/^{144}Nd$-$^{87}Sr/^{86}Sr$ correlation diagram, with Kilauea data falling in the center, but that the Honolulu and Koolau data fall close to one end of the $^{206}Pb/^{204}Pb$-$^{207}Pb/^{204}Pb$ trend (fig. 26.5). They used this inconsistency to preclude simple mixing of two end members. We observe, as shown in the previous section, that on the plot of $^{87}Sr/^{86}Sr$ versus $^{143}Nd/^{144}Nd$ (fig. 26.4) Kilauea and Koolau are two extremes (Kilauea does not fall in the center) that define the general trend (tholeiite and late-stage samples) of the Hawaiian volcanic rocks. Posterosional volcanic rocks of Honolulu, Hana, and Lahaina deviate to the left of the general trend, implying a three-component system.

On the $^{206}Pb/^{204}Pb$-$^{207}Pb/^{204}Pb$ plot of figure 26.5, Koolau deviates slightly from the general trend of Waianae, Honolulu, and Kilauea. This deviation is even more pronounced in the plot of $^{206}Pb/^{204}Pb$ versus $^{208}Pb/^{204}Pb$. In these Pb-Pb diagrams, the denominator of the ratios on each axis is the same (^{204}Pb); therefore, data representing two-component mixing should

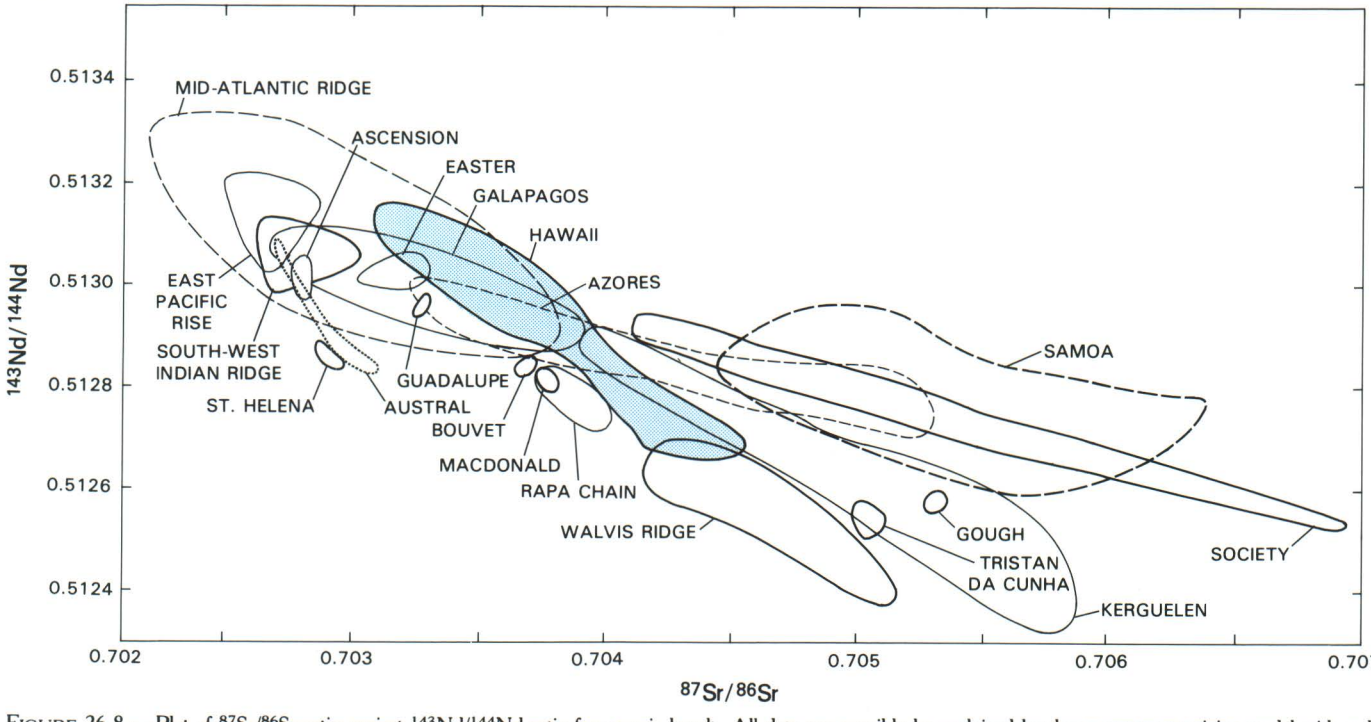

FIGURE 26.8.—Plot of $^{87}Sr/^{86}Sr$ ratio against $^{143}Nd/^{144}Nd$ ratio for oceanic basalt. All data can possibly be explained by three-component mixing model with end-member isotopic compositions close to N-MORB, Austral-St. Helena, and Kerguelen-Society Islands. Data from literature as summarized by Zindler and others (1982), Hart (1984), and White (1985). Data sources for Indian MORB and Rapa-Macdonald chain are from Hamelin and Allègre (1985) and Tatsumoto and others (1984), respectively.

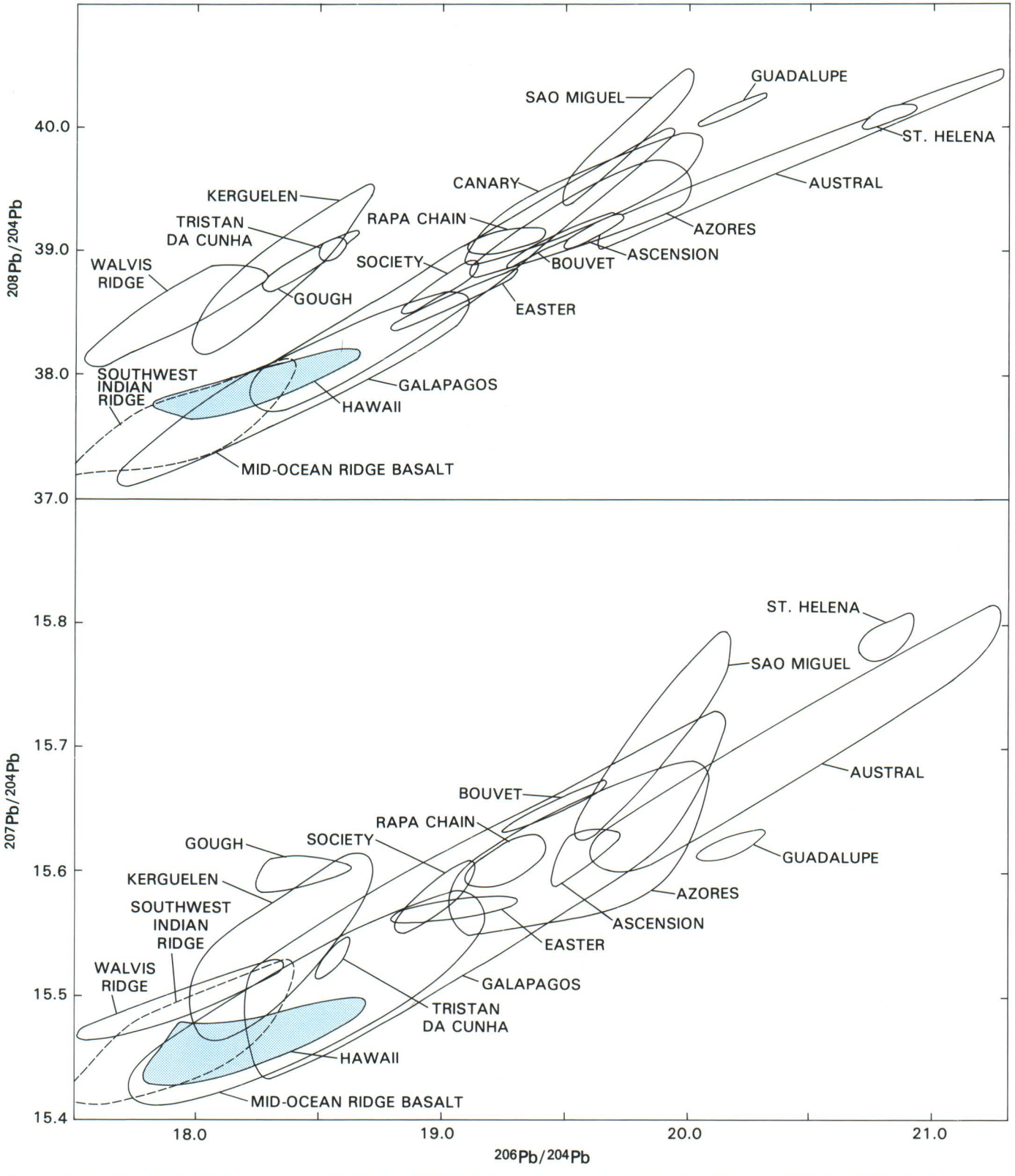

FIGURE 26.9.—Plot of $^{206}Pb/^{204}Pb$ ratio against $^{207}Pb/^{204}Pb$ and $^{208}Pb/^{204}Pb$ ratios for oceanic basalt. Data from Tatsumoto (1978), Sun (1980), Zindler and others (1982), Dupré and Allègre (1983), Stille and others (1983, in press), and Staudigel and others (1984).

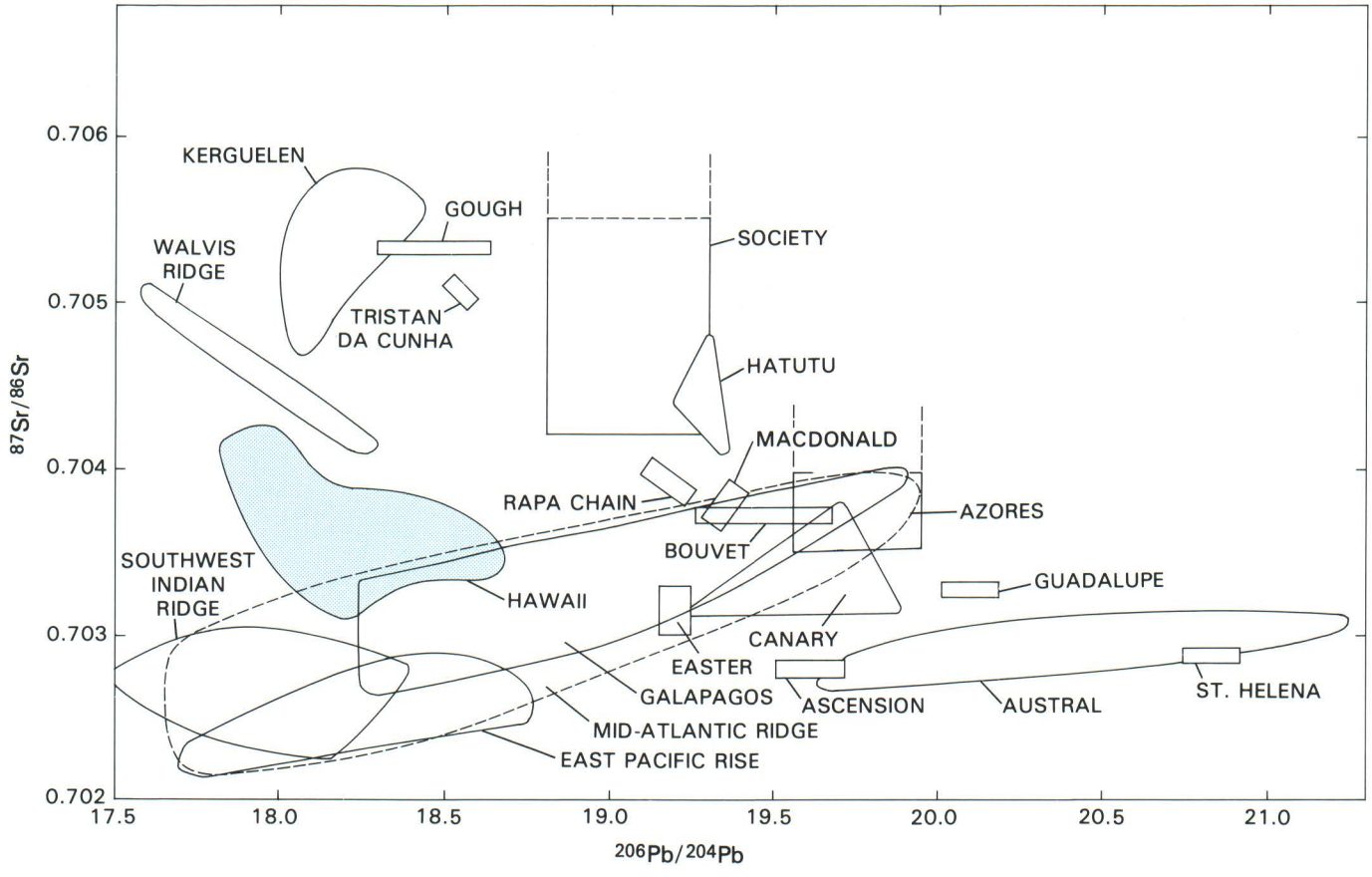

FIGURE 26.10.—Plot of $^{206}Pb/^{204}Pb$ ratio against $^{87}Sr/^{86}Sr$ ratio for oceanic basalt. Data from Tatsumoto (1978), Sun (1980), Zindler and others (1982), Dupré and Allègre (1983), Stille and others (1983, in press), and Staudigel and others (1984).

define a linear correlation. It is evident from the Pb data that Hawaiian volcanics must be described by a model using at least three components.

Evidence for at least three components can also be obtained from the Pb-Sr and Pb-Nd relations among Hawaiian basalt, as shown in figures 26.6 and 26.7. Relative positions of data points for Hawaiian basalt on the $^{206}Pb/^{204}Pb$-$^{87}Sr/^{86}Sr$ diagram (fig. 26.6) are very similar to those on the $^{206}Pb/^{204}Pb$-$^{207}Pb/^{206}Pb$ diagram (fig. 26.5), and the former resembles an expanded (y-axis) plot of the latter. This resemblance is observable not only for Hawaiian rocks but also on a global scale for all oceanic-island basalt (OIB) (see figs. 26.8 and 26.9). The plot $^{206}Pb/^{204}Pb$ versus $^{143}Nd/^{144}Nd$ is an upside-down image of the plot of $^{206}Pb/^{204}Pb$ versus $^{87}Sr/^{86}Sr$ (see figs. 26.10 and 26.11). The shield-building Wailuku Basalt and the late-stage Honolua Volcanics lie close to the Koolau-Kilauea trend, but the posterosional Lahaina Volcanics plots near Hana Volcanics data on both diagrams (figs. 26.6 and 26.7).

In our previous paper (Hegner and others, 1986), in order to test Chen and Frey's two-component mixing model, we followed their premise that the enriched component has isotopic compositions close to those of bulk-earth Sr and Nd (similar to Koolau) and the depleted source has isotopic compositions similar to MORB or to Kilauea. However, the Pb isotopic compositions of the depleted MORB and Kilauea are not similar, and we use the depleted-MORB-like Pb for the present discussion instead of Kilauea-like Pb used in our previous paper. Posterosional alkali basalt of the Lahaina (West Maui), Hana (Haleakala), Honolulu (Oahu), and Koloa (Kauai) sequences all have similar Pb values near $^{206}Pb/^{204}Pb = 18.2$, which is higher than that ($\sim$17.9) of Koolau, and these rocks cannot be one of the end members in the two-component mixing model, even though their Sr-Nd characteristics are closest to MORB among Hawaiian basalt. In figures 26.6 and 26.7, we set the following values of ratios for the two hypothetical end members in order to demonstrate the shortcomings of a two-component mixing model: $^{206}Pb/^{204}Pb = 17.3$, 19; $^{87}Sr/^{86}Sr = 0.702$, 0.7045; $^{143}Nd/^{144}Nd = 0.5134$, 0.51264—for the depleted and enriched components, respectively.

Chen and Frey's (1983) model proposed that a melt produced from the enriched end member (mantle plume) mixes with melt formed by low degrees of melting (<2 percent) of a depleted MORB source. The melting degree of MORB progressively decreases (thereby abundances of incompatible elements increase) but mixing amounts progressively increase from tholeiite through late-stage alkalic rocks to posterosional volcanic rocks. According to this model, elements with stronger incompatibility in mantle minerals

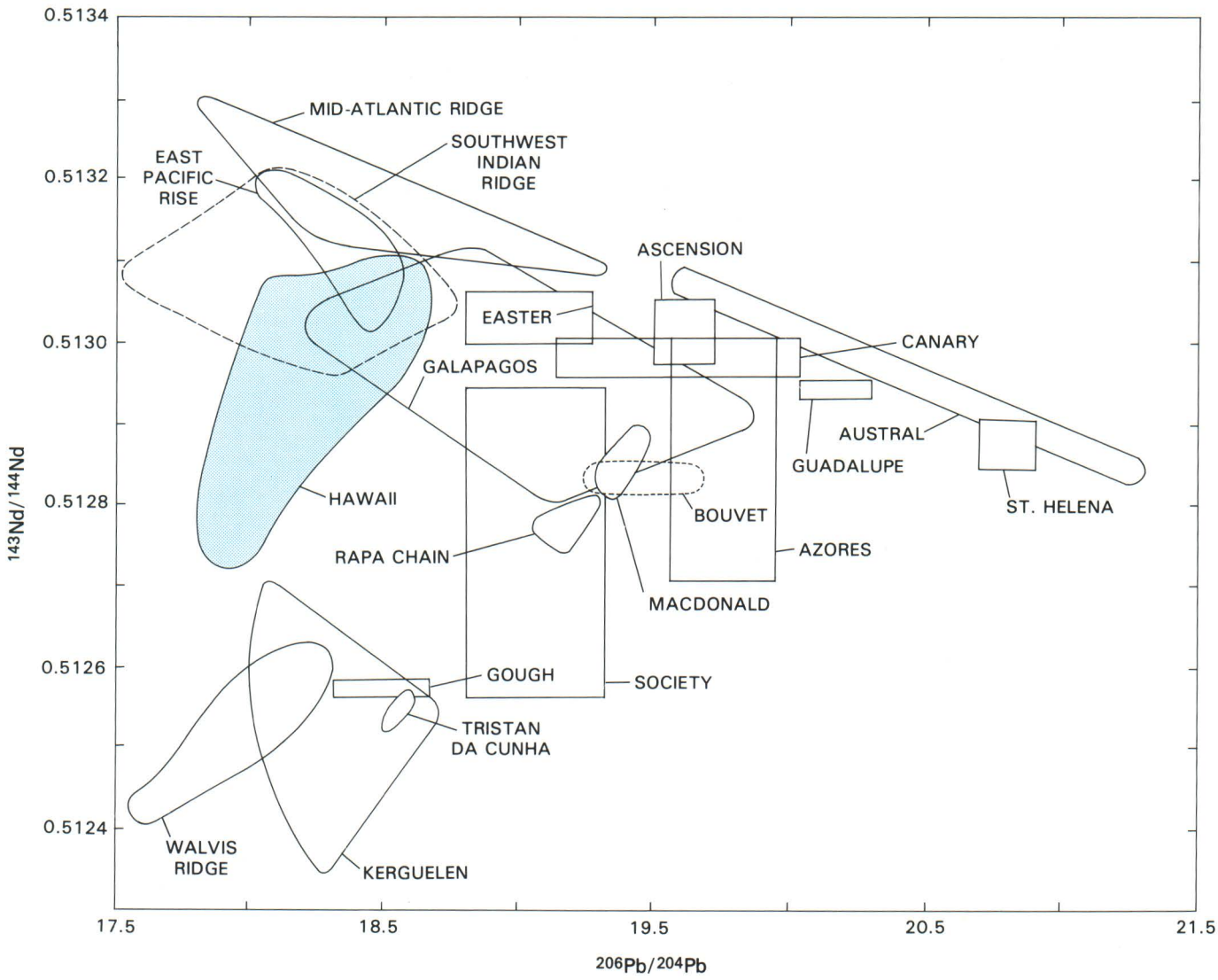

FIGURE 26.11.—Plot of $^{206}Pb/^{204}Pb$ ratio against $^{143}Nd/^{144}Nd$ ratio for oceanic basalt. Data are from Tatsumoto (1978), Sun (1980), Zindler and others (1982), Dupré and Allègre (1983), Stille and others (1983, in press), and Staudigel and others (1984).

are more enriched in later stage volcanic products. Because isotopic compositions of Pb, Sr, and Nd do not change by melting, these elements must have more MORB characteristics in posterosional volcanic rocks than in underlying volcanic rocks. Consequently, parent-daughter elemental abundances and isotopic compositions of Sr and Nd are negatively correlated in Haleakala volcanic rocks.

General equations for two-component mixing have been discussed by Vollmer (1976) and Langmuir and others (1978). Mixing curves of ratio-to-ratio plots of $^{206}Pb/^{207}Pb$ versus $^{87}Sr/^{86}Sr$ (fig. 26.6) and $^{206}Pb/^{204}Pb$ versus $^{143}Nd/^{144}Nd$ (fig. 26.7) are hyperbolae, whose curvature is controlled by the ratio of elemental abundance ratios of the two elements in a MORB melt relative to that in a melt of enriched component (that is, $Q_1 = (Pb/Sr)_{MORB}/(Pb/Sr)_{enriched}$ or $Q_2 = (Pb/Nd)_{MORB}/(Pb/Nd)_{enriched}$. When Q_1 or Q_2 is in unity, the mixing curve will be a straight line. Partition coefficients of common mantle minerals are listed in table 26.4. The values for Rb, Sr, La, Ce, Nd, and Sm are from Chen and Frey (1984) and Clague and Frey (1982). For setting the Th values, those reported by Clague and Frey (1982), Tatsumoto (1978), and Sun (1980) are used. The values for U and Pb are selected rather arbitrarily from the consideration of U/Pb and U/Th ratio changes in basaltic rocks. Incompatibility of Pb is assumed to be less than U, but higher than Sr, considering that the U/Pb ratio in a melt increases from that in the source during partial melting. The actual Pb partition coefficient for mantle silicate minerals may be smaller than the value estimated. However, Pb is one of the chalcophile elements, and the bulk partition coefficient for the mantle may not be much different from the value estimated from

TABLE 26.4.—*Partition coefficients of orthopyroxene (opx), olivine, clinopyroxene (cpx), and garnet for selected elements*

[Coefficients other than for Pb, U, and Th are from Chen and Frey (1983)]

Element	Opx	Olivine	Cpx	Garnet
Rb	0.00010	0.0001	0.0080	0.0010
Sr	.00020	.0005	.0720	.0070
Nd	.00190	.0013	.0900	.0184
Sm	.00280	.0019	.1400	.0823
Pb	.00015	.0002	.0500	.0050
U	.00010	.0001	.0180	.0015
Th	.00010	.0001	.0150	.0010
La	.00050	.0005	.0200	.0010
Ce	.00090	.0008	.0400	.0033

U/Pb ratios in basalt.

The initial concentrations of the relevant elements for MORB and enriched sources are listed in table 26.5. The values, except U, Th, and Pb, are from Chen and Frey (1983). The values for U, Th, and Pb were chosen on the basis of the concentration data reported in this study and previously reported (for example, Tatsumoto, 1978; Sun, 1980) and on the basis of partition coefficients listed in table 26.4.

Modal compositions of the MORB and enriched sources, melt compositions, and partition-coefficient values for Sr and Nd are from Chen and Frey (1983). The bulk solid/liquid partition coefficients of Th, U, Pb, and Sr calculated for a basaltic liquid in equilibrium with a solid composed of 60 percent olivine, 25 percent orthopyroxene, 10 percent clinopyroxene, and 5 percent garnet (Chen and Frey, 1983) are 0.00164, 0.00196, 0.00541, and 0.00790, respectively. We assumed that the melts composed of olivine (10 percent), orthopyroxene (10 percent), clinopyroxene (40 percent), and garnet (40 percent). If these partition coefficients and concentrations in the two end members of table 26.5 are used, Q_1 and Q_2 must both be about 10 in order to cover Koolau data on the hyperbolae. However, if the values in tables 26.4 and 26.5 are used, the maximum calculated Q_1 and Q_2 are only 1.23 and 1.34, respectively, even for an extreme mixing case of 0.001 percent melt of the MORB source with 20 percent melt of the enriched source.

Tests were made using varying D_{Pb} in the range of 0.0025–0.010 and Pb concentrations of the enriched mantle source in the range of 0.08–1.7 ppm. However, we could not obtain Q_1 and Q_2 larger than 4 in any conceivable combination. Therefore, we conclude that the two-component mixing model is not adequate to explain Hawaiian isotope data and that at least three isotopically distinct sources are required to account for the observed data. Stille and others (in press) reached the same conclusion by using depleted and enriched end members similar to those listed above but with the Pb isotopic compositions of the two end members reversed.

Recent isotope studies of Hawaiian volcanic rocks also imply multicomponent hypotheses (for example, Stille and others, 1983, in press; Roden and others, 1984; Staudigel and others, 1984; Hegner and others, 1986), but some differences exist between studies in the assignment of the isotopic components to specific mantle sources. From the preceding discussion on the Pb-Sr-Nd isotopic characteristics, it is essential that Koolau, Kilauea, and the

TABLE 26.5.—*Elemental compositions of the inferred MORB and enriched mantle sources of West Maui volcanic rocks*

Component	MORB	Enriched mantle
Initial concentration (ppm)		
Rb	0.1	0.73
Sr	13.2	23.7
Nd	.86	1.2
Sm	.32	.39
Pb	.08	.17
U	.009	.02
Th	.028	.077
La	.31	.71
Ce	.95	1.9
Isotope ratios		
$^{238}U/^{204}Pb$	7.08	8.12
$^{232}Th/^{238}U$	3.21	3.98

posterosional volcanic rocks (Lahaina, Hana, and Honolulu) are the most extreme in terms of isotopic composition, and all other Hawaiian data fall in a field bounded by these end members. In the following discussion on the origin of Hawaiian basalt, we will refer to these as the Koolau, Kilauea, and PE (posterosional) components (Stille and others, in press), although we recognize that the pure end members are probably more extreme in composition than the Koolau, Kilauea, and PE. A rigorous test using three-dimensional regressions of the Hawaiian data was made in our previous paper (Stille and others, in press) and will not be repeated here.

Staudigel and others (1984) proposed that the Koolau component represents an enriched portion of the oceanic lithosphere, Kilauea the mantle plume, and PE the uppermost lithosphere or crust. We have previously proposed (Tatsumoto, 1978; Stille and others, 1983, in press; Hegner and others, 1986) that the main tholeiite and late-stage alkalic trend is predominantly a plume-lithosphere mixing trend with Koolau having the largest proportion of plume and Kilauea having the largest proportion of oceanic crust or lithosphere. In our previous model, the PE component was derived from the depleted upper mantle (MORB source or material residual from MORB production). The reasoning behind this interpretation is presented below.

The Koolau component has low $^{206}Pb/^{204}Pb$ and $^{143}Nd/^{144}Nd$ ratios, but high $^{207}Pb/^{204}Pb$, $^{208}Pb/^{204}Pb$, and $^{87}Sr/^{86}Sr$ ratios; Koolau data therefore plot distinctly below the mantle plane of Zindler and others (1982). Such isotopic characteristics might be assigned to recycled oceanic lithosphere (Hofmann and White, 1982). However, as will be discussed later (fig. 26.9), Koolau and Walvis Ridge data fall on the left side of the mantle array in a Nd-Sr correlation diagram with Kerguelen as the enriched member, whereas Samoa and Society Island data, which are considered to present the most convincing evidence for having a recycled-crust component (White and Hofmann, 1982), plot on the opposite side of the mantle array.

Staudigel and others (1984) alternatively proposed that the Koolau component may represent an enriched part of the (lower)

oceanic lithosphere, which originated from ancient metasomatized mantle and accreted to the lithosphere at or near the ridge. Such an interpretation may be possible, but the proposed physical process should be tested as more OIB data become available. The process of metasomatism is not well understood, and the chemical composition of the hydrothermal fluids proposed to be involved in metasomatism appear to vary widely depending on the type of process postulated. This obscurity is, we believe, largely caused by a tendency to arbitrarily attribute unexplainable enrichments in incompatible elements to metasomatism.

Wright (1984) postulates, from rigorous comparison of chemical composition between MORB and Hawaiian tholeiite, that the latter originated from depleted mantle that has been metasomatized by a liquid with a composition of nephelinite plus amphibole (plus some minor phases); hence such metasomatism is characterized by H_2O and alkali-rich fluids (Hawkesworth and others, 1979). The metasomatized rocks would have high Rb/Sr ratios and eventually high $^{87}Sr/^{86}Sr$ ratios. Consequently, Nd-Sr data for these rocks would plot on the right-hand side of the mantle array on a Nd-Sr diagram. Most Nd-Sr data of the Hawaiian tholeiite plot is indeed on the right-hand side and support Wright's postulation. However, Koolau data plot on the lower left side of the array. Furthermore, because Koolau Pb-Sr data appear to be unique among all OIB (see next section), we interpret Koolau as a unique end member. If Koolau originated from metasomatized mantle, the proposed metasomatizing fluids would also have to have been unique in their enrichment in alkali and light REE without enrichment in U relative to Pb.

In contrast, we have postulated that ancient metasomatism would slightly decrease the Rb/Sr ratio and increase U/Pb if the metasomatizing fluid is carbonatite-like (Tatsumoto and others, 1984) so that fairly low $^{87}Sr/^{86}Sr$ but high ^{206}Pb and ^{207}Pb values would result from the process. Koolau data plot on the lower left of the mantle array on the Nd-Sr correlation diagram but show very low ^{206}Pb values. Thus, Koolau isotope data are not consistent with a hypothesis of such a metasomatized source. Kilauea tholeiite, however, could be related to metasomatism because those data plot on the right-hand side of the Nd-Sr mantle array and show a high $^{206}Pb/^{204}Pb$ ratio (although in this paper we interpret the Kilauea end member to represent lithosphere contamination instead of metasomatism).

Stille and others (1983, in press) have shown that the isotopic characteristics of Koolau samples are consistent with an origin from primitive lower mantle and that the Koolau component may be unique among oceanic basalt. Alternatively, the Koolau component may represent a less depleted or possibly even enriched upper mantle material that exists as a distinct body (see, for example, Davies, 1984) or is preserved in the center of a concentrically zoned convection cell (see, for example, Tatsumoto. 1978).

The Honolulu, Hana, and Lahaina Volcanics all have $^{206}Pb/^{204}Pb \simeq 18.2$, $^{87}Sr/^{86}Sr \simeq 0.71031$, and $^{143}Nd/^{144}Nd \simeq 0.51315$. In the Nd-Sr correlation diagram (fig. 26.4) it is evident that these PE volcanic rocks are most depleted and are isotopically closest to MORB among Hawaiian rocks. Because basanite may originate, in the presence of garnet, at greater depth than tholeiite (Presnall and others, 1979; Jackson and Wright, 1970), the PE component may represent the depleted upper mantle.

The Kilauea component has moderately radiogenic Pb, but MORB-like isotopic compositions of Sr, Nd, and Hf (Stille and others, in press). The Pb isotopic compositions in volcanics from the Kea trend are generally more radiogenic than those from the Loa trend (Tatsumoto, 1978). The isotopic difference was thought to reflect contamination of the ~80-Ma lithosphere (MORB) under Hawaii, and Kilauea was thought to represent a lithosphere component. The half-life of ^{238}U (4.47×10^9 yr) is short compared to those of ^{87}Rb (4.9×10^{10} yr) and ^{147}Sm (1.06×10^{11} yr), and so an increase in the $^{206}Pb/^{204}Pb$ ratio may be detected in ~100-Ma lithosphere (a $^{207}Pb/^{204}Pb$ increase is not detectable because of the small amount of ^{235}U). Recent detailed studies of Nd, Sr, and Hf isotopes support this view (Stille and others, in press). However, Staudigel and others (1984) assigned the Kilauea component to the plume, and the differences between Loa and Kea isotope trends were considered to have been generated by mixing of plume material with the sublithospheric Koolau component. While such a model may be formally allowed, we maintain that the isotopic differences observed between the presently active Kilauea and Mauna Loa would be extremely difficult to produce if mixing occurs below the lithosphere. Furthermore, the isotopic characteristics of the Kilauea component are not those considered typical for mantle plumes but are actually quite MORB-like. Thus we maintain our earlier conclusions that the Kilauea component represents MORB-related old oceanic lithosphere and that the isotopic differences among volcanoes of the Loa and Kea trends are best explained if mixing occurs within the lithosphere.

COMPARISON OF HAWAIAN DATA WITH THOSE OF OTHER OCEANIC BASALT

In this section we compare isotopic data of Hawaiian basalt with those of other oceanic basalt and discuss the genesis of oceanic basalt.

The Nd-Sr, Pb-Pb, Pb-Sr, and Pb-Nd isotopic correlation diagrams for selected OIB and MORB from the literature are shown in figures 26.8–26.11 and an explanatory combined diagram in figure 26.12. The diagrams contain data for Walvis Ridge basalt that are not corrected for in-place growth of radiogenic isotope during the 70–80 m.y. of their existence (Richardson and others, 1982). However, the isotopic compositions are very similar to those of Koolau Basalt, and in-place growth of radiogenic isotope should not change the overall picture.

Recently, several researchers (for example, Allègre, 1982; Hart, 1984) have argued that the isotopic characteristics of oceanic basalt could be correlated geographically. Allègre (1982) contends that systematic variations occur within each ocean basin and are probably related to convection units in the mantle. Hart (1984) emphasizes that isotopic differences can be observed between the northern and southern hemispheres. However, for the sake of

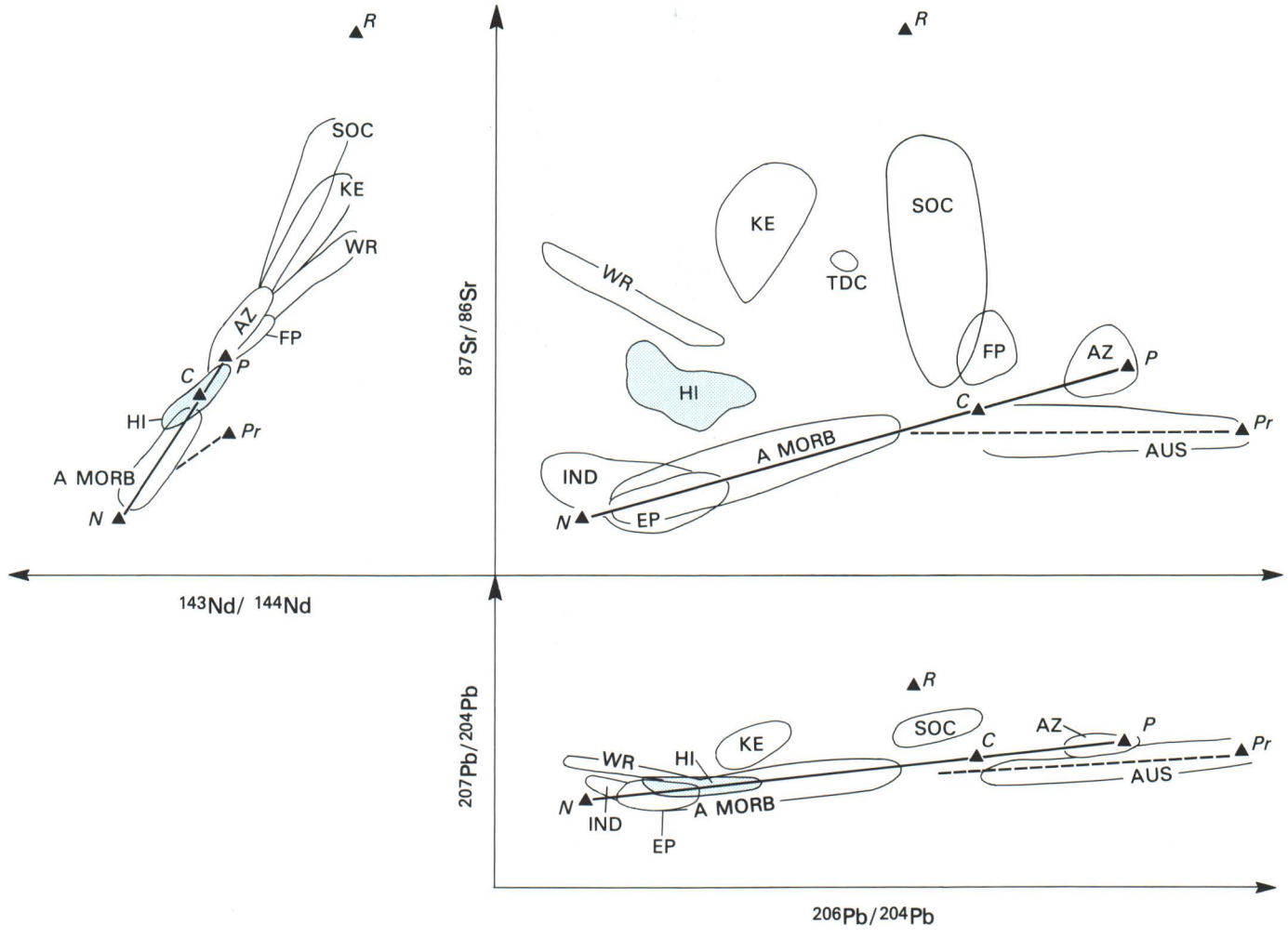

FIGURE 26.12.—Explanatory diagram for oceanic-basalt isotope data. Combined diagram consists of plots of $^{206}Pb/^{204}Pb$ versus $^{207}Pb/^{204}Pb$, $^{206}Pb/^{204}Pb$ versus $^{87}Sr/^{86}Sr$, and $^{87}Sr/^{86}Sr$ versus $^{143}Nd/^{144}Nd$. Triangles, hypothetical parent materials in possible three-component mixing of *N* (depleted MORB), *Pr* (enriched source represented by Austral-St. Helena), and *R* (recycled crust). Data for islands on or near ridges fall on *N*–*P* line (depleted–enriched MORB) or its extension. In alternative multicomponent mixing model, plume (stars labeled C) ascending from lower mantle mixes with heterogeneous upper mantle and oceanic crust. Fields represent Mid-Atlantic Ridge (A MORB), East Pacific Rise (EP), Indian Ocean Ridge (IND), Hawaiian Islands (HI), Walvis Ridge (WR), Kerguelen (KE), Tristan da Cunha (TDC), Society Islands (SOC), French Polynesia islands other than Society and Austral (FP), Azores (AZ), and Austral (AUS). For scales on plots and sources of data, see figures 26.8–26.10.

simplicity, we will proceed with our discussion on the basis of oceanic basalt in general, and later we will demonstrate that the systematic geographic variations that occur are probably caused by upper mantle heterogeneity.

It is widely accepted from isotope data of oceanic basalt that their sources are chemically heterogeneous and that such heterogeniety has existed for a long time (>1 b.y.). The variety of trace-element and isotope signatures in oceanic basalt has often been explained by a layered-mantle model involving mixing of partial melts from a depleted upper mantle and an undepleted lower mantle (see for example, Schilling, 1973; Sun and Hansen, 1975; Allègre and others, 1983). When Nd isotopic data became available (for example, DePaolo and Wasserburg, 1976), the layered-mantle hypothesis appeared to be substantiated. Mass balance, computed with Sm-Nd and Rb-Sr data, indicated that only 30–50 percent of the whole mantle could be involved in continental crust formation (Jacobsen and Wasserburg, 1979: O'Nions and others, 1979; Allègre and others, 1980; DePaolo, 1980). In these computations, the boundary between depleted and enriched mantle was set at a depth of 700 km, which coincides with the seismic discontinuity.

The mantle array observed for MORB and OIB in the Nd-Sr correlation diagram was often interpreted as a mixing line between the depleted mantle and the mantle plumes. However, as more data for oceanic basalt were accumulated, more exceptions that did not plot on a linear mantle array were found (fig. 26.8). In the Nd-Sr diagram, one can easily see that data trends for oceanic basalt do not form a linear mantle array. McCulloch and others (1983) and Anderson (1986) argued that, if some extreme isotopic

values are assigned to depleted and enriched reservoirs, a two-component mixing model may be sufficient to explain all basalt data. However, as discussed above for Hawaiian data, the Pb data plotted in figure 26.9 cannot be explained by a two-component mixing model because the denominator is the same and two-component mixing must therefore define a straight line. The negative correlations of Hawaiian and Walvis Ridge data in the Pb-Sr plot (fig. 26.10) are also difficult to explain by a two-component mixing model.

The diversity of isotope data for oceanic basalt may be adequately explained by a three-component model. The depleted MORB component (N-type) has the least radiogenic Pb and Sr and the most radiogenic Nd and occupies one corner in the Pb-Sr-Nd correlation diagrams (figs. 26.8–26.11). N-MORB and trace-element-rich P-MORB form a single trend that corresponds to a 1.8-Ga isochron on the Pb-Pb diagram. Data for oceanic islands on or near ridges, such as the Iceland-Reykjanes Ridge, Galapagos Islands, Easter Island , and the Azores, also lie on this line (defined as N–P in figure 26.12). This line has been interpreted as a mixing line between a depleted component and mantle plumes instead of a differentiation trend, and the Pb isotopic composition of the plume as defined from Pb-Sr-Nd relations is $^{206}Pb/^{204}Pb = 20.6$, $^{207}Pb/^{204}Pb = 15.75$, $^{208}Pb/^{204}Pb = 40.8$ (Tatsumoto and others, 1984). A similar composition was defined by Dupré and Allègre (1980) as the "Planetary Lead Atlantic" value, although they did not specify that this could represent the plume component. Very radiogenic Pb from St. Helena and Ascension (Sun, 1980) appears to lie on an extension of the N–P trends in the Pb-Pb diagram (fig. 26.9), whereas radiogenic Pb from the Australs plots on a slightly shallower trend (Tatsumoto and others, 1984; Vidal and others, 1984). In the Pb-Sr diagram, however, data from St. Helena, the Australs, and Ascension form a trend that is distinctly shallower than the N–P trend. We define the component that shows extremely radiogenic Pb (but less radiogenic Sr and Nd) as Pr in figure 26.12.

Enrichment of incompatible elements or metasomatism in some part of the depleted mantle may have occurred by mixing or contamination with carbonatite-like fluid (high in CO_2, and U/Pb and Sr/Rb ratios and slightly enriched in light REE), which originated somewhere else in the depleted mantle within the last ~1.8 b.y. Thus, when time passed, this contaminated mantle (*Pr*) source has extremely radiogenic Pb, moderately radiogenic Nd, but less radiogenic Sr. Consequently, the *Pr* component plots on a distinctly lower position from the mantle array (Tatsumoto and others, 1984; White, 1985). The Austral Pb may represent a more recently contaminated mantle source because it plots below the N–P line in the diagram $^{206}Pb/^{204}Pb$ versus $^{207}Pb/^{204}Pb$.

As can be seen in figure 26.12, all oceanic data can be explained by a three-component mixing model with *N*, *Pr*, and another component (R) that has high $^{87}Sr/^{86}Sr$ (>0.706), moderate $^{206}Pb/^{204}Pb$ (~18.2), and very low $^{143}Nd/^{144}Nd$ (<0.5123) ratios. Such a component is most likely recycled crust. If so, then the Koolau and Walvis Ridge data that plot above the N–P line on the Pb-Sr diagram might indicate involvement of a small amount of recycled oceanic crust, and data for Kerguelen and Society Islands indicate involvement of large amounts of this crust component.

According to this interpretation, Koolau may contain the largest proportion of the recycled crust among Hawaiian volcanoes because its Sr is the most radiogenic. Therefore, if the subducted oceanic crust penetrates down to the mantle-core boundary, as proposed by Hofmann and White (1982), then Koolau could represent a recycled crustal plume at Hawaii. If this hypothesis is correct, all OIB that plot above the N–P line in the Pb-Sr diagram contain a component of recycled oceanic crust (R) whose isotope ratios vary regionally. Those OIB that plot on the N–P or N–Pr trends contain little or no R component.

On the Nd-Sr correlation diagram (fig. 26.8), the so-called mantle array (N–P line) extends to Kerguelen. Society Islands data plot above the extension of the N–P line, but Koolau and Walvis Ridge plot below the line. This positioning is not consistent with that observed above on the Pb-Sr diagram.

Dupré and Allègre 983) and Hamelin and Allègre (1985) found that the depleted end member of Indian MORB, which they considered to represent the asthenosphere, is characterized by particularly nonradiogenic $^{206}Pb/^{204}Pb$, but higher $^{207}Pb/^{204}Pb$, $^{208}Pb/^{204}Pb$, and $^{87}Sr/^{86}Sr$ and lower $^{143}Nd/^{144}Nd$ ratios compared to Atlantic and Pacific MORB. This means that the asthenosphere is heterogeneous but there is still a regional similarity that may be related to each convection unit. Thus, in the same manner, the higher $^{207}Pb/^{204}Pb$, $^{208}Pb/^{204}Pb$, and $^{87}Sr/^{86}Sr$ and low $^{143}Nd/^{144}Nd$ ratios of Koolau and Walvis Ridge basalt may be interpreted as due to regional upper mantle heterogeneities instead of a contribution from the recycled oceanic crust.

In any case, Koolau basalt is unique with respect to its relatively primitive isotopic composition (Stille and others, in press). Hawaiian basalt contains the highest $^{3}He/^{4}He$ ratios thus far reported for oceanic basalt (Lupton and Craig, 1975; Kaneoka and Takaoka, 1978; Kurz and others, 1982; Allègre and others, 1983; Rison and Craig, 1983). If our argument is correct, Koolau would have had the highest $^{3}He/^{4}He$ value among Hawaiian basalt (Stille and others, in press). Conversely, the Hawaiian basalt with a high $^{3}He/^{4}He$ and relatively primitive Pb, Nd, and Sr isotopic composition would not support the assumption of radiogenic plume lead proposed by Tatsumoto and others (1984).

White (1985) argued that at least five trends can be observed in Pb-Sr-Nd isotopic systematics: MORB, St. Helena, Kerguelen, Society Islands, Hawaii (see figs. 26.10 and 26.12). Extrapolations of the latter four trends all intersect the central part (C) of the N–P trend, but they do not trend toward *P* or *Pr*. The intersection corresponds to $^{206}Pb/^{204}Pb \simeq 18.5–19.5$, $^{87}Sr/^{86}Sr \simeq 0.7030–0.7035$, and $^{143}Nd/^{144}Nd \simeq 0.5129–0.5130$. It is conceivable that this point represents the plume component instead of *P* in figure 26.12. According to this interpretation, more than five trends are easily observable, because each hot spot creates its own trend by mixing C with upper mantle of variable isotopic composition.

In this context, the Galapagos and Azores trends should be separated from the N–C trend if the radiogenic components do not lie on the N–C trend but on the extension. Walvis Ridge and Rapa-Macdonald may be separated from Hawaii and Society

Islands trends, respectively, because the Walvis Ridge and Hawaii may not plot on the same trends in the Pb-Sr and Pb-Nd diagrams and Rapa Macdonald data plot apart from Society Islands data on the Nd-Sr diagram. This means that as more data become available, more trends will show up as regional variations. The fact that C cannot be defined as a unique point but has a small range in isotopic compositions may indicate that small regional variations also exist for the lower mantle values.

It should be noted that Austral-St. Helena data do not appear to converge to C on the Nd-Sr plot. Their Pb is extremely radiogenic and indicates extremely enriched sources, while their slightly radiogenic Sr indicates a moderately depleted source. We retain our earlier interpretation that these data reflect an old metasomatized component enriched in U and Sr from carbonatite-like fluids derived from a previously depleted (MORB) source (Tatsumoto and others, 1984). Thus the Austral-St. Helena-Ascension trend is predominantly an upper mantle trend.

We previously suggested that Kilauea contains the most MORB component derived from the oceanic crust because of the depleted nature of its Sr and Nd isotopes. Alternatively, Kilauea might be considered to contain the most plume component since Kilauea occupies the position closest to C (Staudigel and others, 1984). However, as previously mentioned, this interpretation does not adequately account for the observed isotopic differences among simultaneously active volcanoes: Kilauea and Mauna Loa.

The important role of subduction of oceanic crust and sediments for isotope evolution of the crust-mantle system was first suggested by Armstrong (1968), and influences of subducted material on Pb isotopes were detected for volcanics from the Japanese Islands (Tatsumoto, 1969) and the Aleutian Island arc (Kay and others, 1978) but not detected for those from the Mariana arc (Maijer, 1976). Extremely low $^{238}U/^{204}Pb$ ratios (as low as 2.1) in Japanese arc volcanics (Tatsumoto, 1960; Tatsumoto and Knight, 1969) indicate that volatile Pb is preferentially extracted from the subducted material by arc volcanism, whereas $^{238}U/^{204}Pb$ ratios of the Mariana arc volcanics are about 7. Thus, plumes generated from the recycled crust are likely to have variations in isotope ratios depending on their storage times and environments; this implies the existence of a heterogeneous lower mantle (see for example, Davies, 1984) providing that the subducted crust penetrates into the lower mantle.

Several seismic studies have presented evidence that subducting slabs penetrate into the lower mantle (Jordan, 1977; Creager and Jordan, 1984). Although some workers suggest that the penetration is only a few hundred kilometers below the seismic boundary at a depth of 670 km (see for example, Christensen and Yuen, 1984), others consider that the subducted slabs reach the core-mantle boundary (Hofmann and White, 1982; Davies, 1984; Loper, 1985). Loper (1985) suggested that numerous narrow axisymmetric plumes rise up into the upper mantle. Thus, it may be possible that numerous plumes with various isotope signatures rise from the lower mantle. However, with the presently available isotopic evidence, we prefer a convective layered mantle model with a chemically heterogeneous upper mantle and a nearly homogeneous (less differentiated) lower mantle because (1) the upper mantle is strongly differentiated by magma extraction and (2) no high $^{87}Sr/^{86}Sr$ signature of subducted material is found for volcanics from Hawaii where the volcanism is most likely related to a mantle plume as evidenced by high $^{3}He/^{4}He$ ratios. Contamination of magmas as they rise through the oceanic lithosphere makes the isotopic signatures more complicated.

CONCLUSIONS

Pb, Sr, and Nd isotope data of Hawaiian basalt provide strong evidence for the involvement of three distinct sources in the production of these rocks. The volcanoes or groups of rocks that most closely approach the three end members are Koolau (representing the mantle plume), Kilauea (the oceanic crust), and the Honolulu-Hana-Lahaina posterosional volcanic rocks (the depleted mantle). Pb, Sr, and Nd relationships are not compatible with a two-component mixing model for Hawaiian basalt genesis.

Pb, Sr, and Nd isotope characteristics of oceanic basalt from other areas are also compatible with a three-component mixing model. The three main sources are the depleted upper mantle, enriched lower or upper mantle, and recycled oceanic crust. However, the oceanic basalt data form several trends that intersect in the middle of the three-component field. These trends may indicate multicomponent mixing between a heterogeneous upper mantle and a nearly homogeneous lower mantle, plus contamination by the lithosphere.

REFERENCES CITED

Allègre, C.J., 1982, Chemical geodynamics: Tectonophysics, v. 81, p. 109–132.

Allègre, C.J., Brevart, O., Dupré, BH., and Minster, J.-F., 1980, Isotopic and chemical effects produced in a continuously differentiating convecting Earth mantle: Philosophical Transactions of the Royal Society of London, Ser. A, v. 297, p. 447–477.

Allègre, C.J., Staudacher, T., Sarda, P., and Kurz, M., 1983, Constraints on the evolution of Earth's mantle from rare gas systematics: Nature, v. 303, p. 762–766.

Anderson, D.L., 1985, Hotspot magmas can form by fractionation and contamination of MORB: Nature, v. 318, p. 145–149.

Armstrong, R.L., 1968, A model for Sr and Pb isotope evolution in a dynamic Earth: Review of Geophysics, v, 6, p. 175–199,

Brooks, C., Hart, S.R., Hofmann, A., and James, D.E., 1976, Rb-Sr mantle isochrons from oceanic regions: Earth and Planetary Science Letters v. 32, p. 51–61.

Chen, C.-Y., and Frey, F.A., 1983, Origin of Hawaii tholeiite and alkalic basalt: Nature, v. 302, p. 785–789.

Christensen, U.R., and Yuen, D.A., 1984, The interaction of a subducting lithospheric slab with a chemical or phase boundary: Geophysical Research, v. 89, p. 4389–4402.

Clague, D.A., Frey, F.A., 1982, Petrology and trace element geochemistry of the Honolulu volcanics, Oahu: Implications for the oceanic mantle below Hawaii: Journal of Petrology, v. 23, p. 447–504.

Cohen, R.S., and O'Nions, R.K., 1982, The lead, neodymium and strontium isotopic structure of ocean ridge basalts: Journal of Petrology, v. 23, p. 299–324.

Creager, K.C., and Jordan, T.H., 1984, Slab penetration into the lower mantle: Journal of Geophysical Research, v. 89, p. 3031–3050.

Dalrymple, G.B., and Clague, D.A., 1976, Age of the Hawaii-Emperor bend: Earth and Planetary Science Letters, v. 31, p. 313–329.

Dalrymple, G.B., Silver, E.A., and Jackson, E.D., 1973, Origin of the Hawaiian Islands: American Scientist, v. 61, p. 294–308.

Davies, G.F., 1984, Geophysical and isotopic constraints on mantle convection: An interim synthesis: Journal of Geophysical Research, v. 89, p. 6017–6040.

DePaolo, D.J., 1980, Crustal growth and mantle evolution: Inferences from models of element transport and Nd and Sr isotopes: Geochimica et Cosmochimica Acta, v. 44, p. 1185–1196.

DePaolo, D.J., and Wasserburg, G.J., 1976, Inferences about magma sources and mantle structure from variations of $^{143}Nd/^{144}Nd$: Geophysical Research Letters, v. 3. p. 743–746.

Dodson, M.H., 1970, Simplified equations for double-spiked isotopic analyses: Geochimica et Cosmochimica Acta, v. 34, p. 1241–1244.

Dupré, B., and Allègre, C.J., 1980, Pb-Sr-Nd isotopic correlation and the chemistry of the North Atlantic mantle: Nature, v. 286, p. 17–22.

———1983, Pb-Sr isotope variation in Indian Ocean basalts and mixing phenomena: Nature, v. 303, p. 142–146.

Feigenson, M.D., Korr, K., and Raczek, I., 1984, Trace element and isotopic evidence for the formation of transitional basalts of West Maui Volcano [abs.]: Eos, v. 65. p. 300.

Frey, F.A., and Clague, D.A., 1983, Geochemistry of diverse basalt types from Loihi Seamount, Hawaii: petrogenetic implications: Earth and Planetary Science Letters, v. 66, p. 337–355.

Hamelin, B., and Allègre, C.J., 1985, Large scale regional units in the depleted upper mantle revealed by an isotope study of the South-West Indian Ridge: Nature, v. 315, p. 196–199.

Hamilton, E.I., 1965. Distribution of some trace elements and the isotopic composition of strontium in Hawaiian lavas: Nature, v. 206, p. 251–253.

Hart, S.R., 1984, A large scale isotope anomaly in the Southern Hemisphere mantle: Nature, v. 309. p. 753–757.

Hawkesworth, C.J., Norry, M.J., Roddick, J.C., and Vollmer, R., 1979, $^{143}Nd/^{144}Nd$ and $^{87}Sr/^{86}Sr$ ratio from Azores and their significance in LIL-element enriched mantle: Nature, v. 280, p. 28–31.

Hegner, E., Unruh, D.M., and Tatsumoto, M., 1986, Sr, Nd, and Pb isotopic evidence for the origin of the West Maui volcanic suite, Hawaii: Nature, v. 319. p.478–480.

Hofmann, A., and White, W., 1982, Mantle plumes from ancient oceanic crust: Earth and Planetary Science Letters, v. 57, p. 421–436.

Jackson, E.D., Silver, E.A., and Dalrymple, G.B., 1972, Hawaiian-Emperor chain and its relation to Cenozoic circum-Pacific tectonics: Geological Society of America Bulletin, v. 83, p. 601–618.

Jackson, E.D., and Wright, T.L., 1970, Xenoliths in the Honolulu volcanic series, Hawaii: Journal of Petrology, v. 11, p. 405–430.

Jacobsen, S.B., and Wasserburg, G.J., 1979, The mean age of mantle and crustal reservoirs: Journal of Geophysical Research, v. 84, p. 7411–7427.

Jordan, T.H., 1977, Lithospheric slab penetration into the lower mantle beneath the Sea of Okhotsk: Journal of Geophysical Research, v. 79, p. 2679–2685.

Kaneoka, I., and Takaoka, N., 1978, Excess ^{129}Xe and high $^{3}He/^{4}He$ ratio in olivine phenocrysts of Kapuho lava and xenolithic dunites from Hawaii: Earth and Planetary Science Letters, v. 39, p. 382–386.

Kay, R.W., Sun, S.-S., and Lee-Hu, C.-N., 1978, Pb and Sr isotopes in volcanics from Aleutian Islands and Pribilof Island, Alaska: Geochimica et Cosmochimica Acta, v. 42, p. 263–274.

Kurz, M.P., Jenkins, W.J., and Hart, S.R., 1982, Helium isotopic systematics of oceanic islands and mantle heterogeneity: Nature, v. 297, p. 43–47.

Kushiro, I., 1969, The system forsterite-diopside-silica with and without water at high pressures: American Journal of Science, v. 267A, p. 269–294.

Langmuir, C.H., Vocke, R.D., Jr., and Hanson, G.N., 1978, A general mixing equation with applications to Iceland basalts: Earth and Planetary Science Letters, v. 37, p. 380–392.

Lanphere, M.A., and Dalrymple, G.B , 1980, Age and strontium isotopic composition of the Honolulu volcanic series, Oahu, Hawaii: American Journal of Science, v. 280A, p. 736–751.

Lanphere, M.A., Dalrymple, G.B., and Clague, D.A., 1980, Rb-Sr systematics of basalts from the Hawaiian-Emperor volcanic chain: Initial Report of the Deep Sea Drilling Project, Volume 55: Washington, U.S. Government Printing Office, p. 695–706.

Lessing, P., and Catanzaro, E.J., 1964, $^{87}Sr/^{86}Sr$ in Hawaiian lavas: Journal of Geophysical Research, v. 69, p. 1599–1601.

Loper, D.E., 1985, A simple model of whole-mantle convection: Journal of Geophysical Research, v. 90, p. 1809–1836.

Lupton, J.E., and Craig, H., 1975, Excess ^{3}He in oceanic basalts: evidence for terrestrial primordial helium: Earth and Planetary Science Letters, v. 26, p. 133–139.

Macdonald, G.A., 1949, Hawaiian petrographic province: Geological Society of America Bulletin, v. 60, p. 1541–1596.

———1968, Composition and origin of Hawaiian lavas: Geological Society of America Memoirs, v. 116, p. 477–522.

Macdonald, G.A., and Katsura, T., 1964, Chemical composition of Hawaiian lavas: Journal of Petrology, v. 5, p. 82–133.

McCulloch, M.T., Jaques, A.L., Nelson, D.R., and Lewis, J.D., 1983, Nd and Sr isotopes in kimberlites and lamproites from western Australia: an enriched mantle origin: Nature, v. 302, p. 400–403.

McDougall, I., 1964, Potassium-argon ages from lavas of the Hawaiian Islands: Geological Society of America Bulletin, v. 75, p. 107–128.

Meijer, A., 1976, Pb and Sr isotopic data bearing on the origin of volcanic rocks from the Mariana island-arc system: Geological Society of America Bulletin, v. 87, p. 1358–1369.

Moore, J.G., Clague, D.A., and Normark, W.R., 1982, Diverse basalt types from Loihi seamount, Hawaii: Geology, v. 10, p. 88–92.

Nakamura, N., Tatsumoto, M., Nunes, P.D., Unruh, D.M., Schwab, A.P., Wildeman, T.R., 1976, 4.4 b.y.-old clast in Boulder 7, Apollo 17: A comprehensive chronological study of U-Pb, Rb-Sr and Sm/Nd methods: Proceedings of the Lunar Scientific Conference, 7th, p. 2309–2333.

O'Nions, R.K., Evensen, N.M., and Hamilton, P.J., 1979, Geochemical modelling of mantle differentiation and crustal growth: Journal of Geophysical Research, v. 84, p. 6091–6101.

O'Nions, R.K., Hamilton, P.J., and Evensen, N.M., 1977, Variations in $^{143}Nd/^{144}Nd$ and $^{87}Sr/^{86}Sr$ ratios in oceanic basalts: Earth and Planetary Science Letters, v. 34, p. 13–22.

Powell, J.L., and DeLong, S.E., 1966, Isotopic composition of strontium in volcanic rocks from Oahu: Science, v. 153, p. 1239–1242.

Presnall, D.C., Dixon, S.A., Dixon, J.R., O'Donnell, T.H., Brenner, N.L., Schrock,, R.L., Dycus, D.W., 1979, Liquidus phase relations on the join diopside-forsterite-anorthite from 1 atm to 20 kbar: Their bearing on the generation and crystallization of basaltic magma: Contributions to Mineralogy and Petrology, v. 66, p. 203–220.

Richardson, S.H., Erlank, A.J., Duncan, A.A., and Reid, D.L., 1982, Correlated Nd, Sr and Pb isotope variation in Walvis Ridge basalts and implications for the evolution of their mantle source: Earth and Planetary Science Letters, v. 59, p. 327–342.

Rison, W., and Craig, H., 1983, Helium isotopes and mantle volatiles in Loihi Seamount and Hawaiian Island basalts and xenolights: Earth and Plantetary Science Letters, v. 66, p. 407–426.

Roden, M.F., Frey, F.A., and Clague, D.A., 1984, Geochemistry of tholeiitic and alkalic lavas from the Koolau Range, Oahu, Hawaii: implications for Hawaiian volcanism: Earth and Planetary Science Letters, v. 69, p. 141–158.

Schilling, J.G., 1973. Iceland mantle plume: Geochemical study of the Reykjanes Ridge: Nature, v. 242, p. 565–571.

Staudigel, H., Zindler, A., Hart, S.R., Leslie, T., Chen, C.-Y., and Clague, D., 1984, The isotope systematics of a juvenile intraplate volcano: Pb, Nd, and Sr isotope ratios of basalts from Loihi Seamount, Hawaii: Earth and Planetary Science Letters, v. 69. p. 13–29.

Stearns, H.T., and Macdonald, G.A., 1942, Geology and ground-water resources of the island of Maui, Hawaii: Hawaii Division of Hydrography Bulletin, v. 7, p. 344.

Stille, P., Unruh, D.M., and Tatsumoto, M., 1983, Pb, Sr, Nd and Hf isotopic evidence of multiple sources for Oahu, Hawaii basalts: Nature, v. 304, p. 25–29.

———in press, Pb, Sr, Nd and Hf isotopic constraints on the origin of Hawaiian basalts and evidence for a unique mantle source: Geochimica et Cosmochimica Acta.

Sun, S.-S., 1980, Lead isotope study of young volcanic rocks from mid-ocean ridges, ocean islands and island arcs: Philosophical Transactions of the Royal Society of London, v. A. 297, p. 409–445.

Sun, S.-S, and Hanson, G., 1975, Evolution of the mantle: Geology, v. 3, p. 297–301.

Tatsumoto, M., 1969, Lead isotopes in volcanic rocks and possible ocean floor thrusting beneath island arcs: Earth and Planetary Science Letters, v. 6, p. 369–376.

———1978, Isotopic composition of lead in oceanic basalt and its implication to mantle evolution: Earth and Planetary Science Letters, v. 38, p. 63–87.

Tatsumoto, M., Hedge, C.E., and Engle, A.E.J., 1965, Potassium, rubidium, strontium, thorium, uranium, and the ratio of strontium-87 to strontium-86 in oceanic tholeiitic basalts: Science, v. 150, p. 886–889.

Tatsumoto, M., and Knight, R.J., 1969, Isotopic composition of lead in volcanic rocks from Central Honshu—with regard to basalt genesis: Geochemical Journal, v. 3, p. 53–86.

Tatsumoto, M., and Unruh, M., 1976, KREEP basalt age: Grain by grain U-Th-Pb systematics study of the quartz monzodiorite clast 15405,88: Proceedings of the 7th Lunar Scientific Conference, Geochimica et Cosmochimica Acta, Supplement 7, v. 2, p. 2107–2129.

Tatsumoto, M., Unruh, D.M., Stille, P., and Fujimaki, H., 1984, Pb, Sr, and Nd isotopes in oceanic island basalts: International Geological Congress, 27th, Proceedings, v. 11, p. 485–501.

Vidal, P., Chauvel, C., and Brousse, R., 1984, Large mantle heterogeneity beneath French Polynesia: Nature, v. 307, p. 536–538.

Vollmer, R., 1976, Rb-Sr and U-Th-Pb systematics of alkaline rocks: the alkaline rocks from Italy: Geochimica et Cosmochimica Acta, v. 40, p. 283–295.

White, W.M., 1985, Sources of oceanic basalts: Radiogenic isotopic evidence: Geology, v. 13. p. 115–118.

White, W.M., and Hofmann, A.W., 1982, Sr and Nd isotope geochemistry of oceanic basalts and mantle evolution: Nature, v. 296, p. 821–825.

Wilson, J.T., 1963, A possible origin of the Hawaiian Islands: Canadian Journal of Physics, v. 41, p. 863–870.

Wright, T.L., 1984, Origin of Hawaiian tholeiite: a metasomatic model: Journal of Geophysical Research, v. 89. p. 3233–3252.

Zindler, A., Jagoutz, E., and Goldstein, S.T., 1982, Nd, Sr and Pb isotopic systematics in a three component mantle: a new perspective: Nature, v. 298, p. 519–523.

Zindler, A., Staudigel, H., and Batiza, R., 1984, Isotope and trace element goechemistry of young Pacific seamounts: implications for the scale of upper mantle heterogeneity: Earth and Planetary Science Letters, v. 70, p. 175–195.

CONSTRAINTS ON THE CHARACTERISTICS OF MAGMA SOURCES FOR HAWAIIAN VOLCANOES BASED ON NOBLE-GAS SYSTEMATICS

By Ichiro Kaneoka[1]

ABSTRACT

The implications of noble-gas-isotope signatures of Hawaiian volcanic rocks and ultramafic nodules for the characteristics of Hawaiian volcanism are discussed. Hawaiian volcanic rocks have higher $^{3}He/^{4}He$ ratios and lower $^{40}Ar/^{36}Ar$ ratios than MORB, strongly indicating that they derived from a source enriched in volatile and primordial components. That source is probably located in the deeper part of the Earth's interior (lower mantle?). These observations are compatible with the hot-spot hypothesis.

The variations in the observed $^{3}He/^{4}He$ and $^{40}Ar/^{36}Ar$ ratios for Hawaiian volcanic rocks and nodules can be explained in terms of varying degrees of mixing among noble-gas components of three types: *P*(plume), *M*(MORB), and *A*(atmosphere). Mixing of *P* and *M* components occurs during ascent of a diapir through the asthenosphere and lithosphere, followed by introduction of the *A* component during eruption.

Systematic variations in the $^{3}He/^{4}He$ ratios with the volume of individual volcanoes, together with other radiogenic-isotope signatures, indicate a possible model for the evolution of Hawaiian volcanism based on the rise of volatile-enriched diapirs from the Earth's deep interior. However, the amount of noble-gas (volatile) components would vary at each stage of a volcano's evolution. The model suggests that the partially melted zone plays an important role during the evolution of Hawaiian volcanism. It is further pointed out that the voluminous outpourings of Hawaiian volcanoes do not always reflect the direct material supply from the hot-spot source but may reflect the combined effects of material transfer and heat supply.

INTRODUCTION

Because the Hawaiian Islands have formed far from any lithospheric plate boundary, they provide a good opportunity to study the characteristics of intraplate volcanism, especially of hot-spot areas as identified by Wilson (1963) and Morgan (1971).

Noble gases are chemically inert and include both radiogenic and stable isotopes. Furthermore, their isotopic ratios are rather insensitive to the physical and chemical processes occurring during magmatic fractionation. Hence, the isotopic ratios of noble gases can give us unique information concerning the characteristics of source materials. In this paper, I summarize the noble-gas data so far obtained for Hawaiian samples and discuss the characteristics of source materials for Hawaiian rocks based on those noble-gas data.

Dalrymple and Moore (1968) identified that recent submarine pillow basalts erupted on the east rift zone of Kilauea showed excess ^{40}Ar. Similar results were obtained for the same kind of samples by Noble and Naughton (1968). It has been realized that magmatic Ar is trapped in glassy rims because of rapid cooling under a high hydrostatic pressure of sea water, which hinders the degassing. Compared to the atmospheric values of 295.5, the $^{40}Ar/^{36}Ar$ ratio in these samples is as high as about 1,200. However, these ratios are not so high as those observed in some glassy pillow samples of midocean ridge basalt (MORB), which reach as high as about 10,000 (Funkhouser and others, 1968).

Funkhouser and Naughton (1968) examined radiogenic He and Ar in ultramafic inclusions from Hualalai Volcano, Hawaii, and Salt Lake Crater, Oahu, and concluded that they include magmatic radiogenic components in fluid and gaseous inclusions in the minerals of the nodules. This confirmed the previous results by Lovering and Richards (1964), who suggested the presence of excess ^{40}Ar in clinopyroxene from a pyroxenite nodule erupted at Salt Lake Crater that showed an apparently very old K-Ar age of 1.4 Ga. The radiogenic components in these ultramafic nodules were further investigated by Gramlich and Naughton (1972), who inferred, on the basis of diffusion experiments of He and Ar, that the $^{4}He/^{40}Ar$ ratio in the environment where the minerals of lherzolite nodules were concentrated at Salt Lake Crater had a value of 1.2 ± 0.2. These investigations demonstrate the occurrence of radiogenic noble gases such as ^{4}He and ^{40}Ar of magmatic origin in pillow glass and ultramafic nodules. At that time, these data were interpreted to show the characteristics of noble-gas isotopes in the Earth's interior in a general sense, and it was premature to discuss the characteristics of noble-gas isotopes that might be unique for Hawaiian samples.

The value of noble-gas isotope studies on Hawaiian samples was illustrated by Hennecke and Manuel (1975) when they found excess ^{129}Xe in ultramafic nodules. Furthermore, Craig and Lupton (1976) found a higher $^{3}He/^{4}He$ ratio in Kilauea fumaroles than in those of MORB, which is known to be relatively uniform on a global scale. Such data are significant because they might characterize the uniqueness of Hawaiian magma sources. The occurrence of high $^{3}He/^{4}He$ ratios and excess ^{129}Xe in Hawaiian samples was confirmed in both lava flows and ultramafic nodules (Kaneoka and

[1]Geophysical Institute, University of Tokyo, Bunkyo-ku, Tokyo 113, Japan.

Takaoka, 1978; Kaneoka and others, 1978). On the basis of systematic differences in $^{3}He/^{4}He$ and $^{40}Ar/^{36}Ar$ ratios, Kaneoka and Takaoka (1980) discussed the difference of magmatic sources between lava flows and ultramafic nodules. Further data on these samples were accumulated, discussed, and compared with similar data from other areas (Kyser and Rison, 1982). Detailed studies on samples from Loihi Volcano have revealed that high $^{3}He/^{4}He$ ratios for Hawaiian magma sources are real but rather variable even between different eruptions of the same volcano (Kaneoka and others, 1983; Kurz and others, 1983; Rison and Craig, 1983). However, no excess ^{129}Xe has been found in samples of Loihi pillow glass (Allègre and others, 1983; Kaneoka and others, 1983). Furthermore, large variation in the $^{3}He/^{4}He$ ratio is found even for different volcanoes on the same island (Kurz and others, 1983). These data could indicate more complexity in magmatic sources for Hawaiian magmatism, which however still remain distinct from those of MORB.

ACKNOWLEDGMENTS

For my experimental work on noble-gas systematics of Hawaiian samples, I have benefited much from using a mass spectrometer developed by N. Takaoka of Yamagata University. R.W. Decker of the U.S. Geological Survey and K. Nakamura of the Earthquake Research Institute, University of Tokyo, have given me the chance to write this review paper and gave encouragement through the work. The constructive reviews by G.B. Dalrymple and T.L. Wright of U.S. Geological Survey were very helpful for improving the manuscript.

This study was financially supported in part by a Grant-in-Aid for Scientific Research from the Ministry of Education, Science and Culture, Japan, under contracts No. 58540220 and No. 59065001.

ABUNDANCES AND TRAPPING SITES OF NOBLE GASES IN HAWAIIAN ROCK SAMPLES

Noble-gas abundances in a sample reflect both the characteristics of the source and the sample's subsequent history (see, for example, Dymond and Hogan, 1978; Kaneoka and Takaoka, 1985). If we can evaluate the latter contribution properly, it is possible to get some information on the characteristics of the sample source, though it is generally not easy to do so. Noble gases in selected samples of different kinds from the Kilauea region are compared in table 27.1. Since these samples can be regarded as almost recent, it is not necessary to consider the effect of radiogenic components formed after extrusion on the surface. Hence, these samples should show similar isotopic ratios and characteristic abundances of noble gases reflecting the processes involved in their magmatic history. Judging from the $^{40}Ar/^{36}Ar$ ratio and relative noble-gas abundance patterns, Kapoho lava seems to have lost most magmatic gas and to have been equilibrated with atmospheric noble gases. The observed amount of ^{40}Ar in this sample (2.0×10^{-7} cm^3/g at standard temperature and pressure) is just the value expected in a molten magma in equilibrium with the Earth's atmosphere as inferred from the solubility data of Ar in melt of tholeiitic basalt (Hayatsu and Waboso, 1982). However, there still remain small amounts of magmatic noble gases in this sample, which is shown by the relative enrichment of ^{4}He and ^{132}Xe compared with Ar (see the data for lava in figure 27.1).

On the other hand, olivine phenocrysts (diameter >1 mm) in this sample contain lesser amounts of noble gases (except for ^{4}He) than lava, but they show definitely higher $^{3}He/^{4}He$ and $^{40}Ar/^{36}Ar$ ratios than the atmosphere. These phenocrysts are considered to have been formed in the magma reservoir at depth without atmospheric contaminations. Hence, these values can be considered to approximate the values for the magmatic noble gases, or at least for their isotopic ratios.

It has been known that the chilled margins of submarine basalt pillows contain magmatic noble gases (see, for example, Dalrymple and Moore, 1968; Funkhouser and others, 1968; Noble and Naughton, 1968). However, the efficiency of trapping of noble gases is dependent on both the cooling rate and the ambient hydrostatic pressure. As shown in table 27.1, tholeiite from the east rift zone reflects such tendencies (Kyser and Rison, 1982). The sample from the derived depth of 2,960 m clearly shows the evidence of magmatic noble gases, but that from the depth of 30 m does not, though the latter seems to retain a small amount of ^{4}He.

In a subaerial sample (glassy spatter), the observed amounts of noble gases are quite large, but the $^{40}Ar/^{36}Ar$ ratio is atmospheric and the noble-gas abundance pattern is similar to that of the atmosphere (fig. 27.1). Hence, it is not likely that these gases truly represent those in the original magma. Many microscopic gas pores are observed in this sample; atmospheric noble gases were probably trapped in such pores when it erupted.

The high $^{3}He/^{4}He$ ratio reported in Kilauea gas samples (Craig and Lupton, 1976) is similar, within their analytical uncertainties, to those observed in phenocrysts and pillow glass from this region. However, we have no guarantee that the observed values for fumarolic gases approximate those of the magmatic gases for heavier noble gases, since they are much more easily contaminated from the atmosphere (see, for example, Ozima and Podosek, 1983; Kaneoka and Takaoka, 1985).

Thus it is essential in noble-gas analyses to select appropriate samples to infer the conditions of magmatic noble gases. For this purpose, pillow glass and large olivine and pyroxene phenocrysts have been regarded as suitable. Ultramafic nodules also contain magmatic noble gases, since they are formed at depth without atmospheric contaminations. For $^{3}He/^{4}He$ analyses, fumarolic gas and even water samples can be used, because the effect of atmospheric contamination is generally quite small for He compared with the abundance of magmatic He in these samples.

Noble-gas abundances in different kinds of samples from the Hawaiian region are compared in figure 27.1. To exclude the ambiguity from the addition of secondary atmospheric components, low-temperature (500–700 °C) and high-temperature (1,700–1,800 °C) fractions were taken for most samples, and the values for the higher temperature fraction are shown in figure 27.1. These samples include some from Loihi Seamount and from Hawaii, Maui, and Oahu Islands. Except for some quite different

TABLE 27.1—*Comparison of noble gases in different kinds of samples from Kilauea Volcano*

[Values for gas contents are at standard temperature and pressure; atmospheric values calculated from total amount in atmosphere divided by mass of the Earth; R/R_A given by $(^3He/^4He)_{sample}/(^3He/^4He)_{air}$; —, not determined]

Sample	Noble-gas content ($cm^3/g \times 10^{-8}$)			Noble-gas content ($cm^3/g \times 10^{-10}$)		Ratios			Reference
	^4He	^{20}Ne	^{36}Ar	^{84}Kr	^{132}Xe	$^3He/^4He$ ($\times 10^{-6}$)	R/R_A	$^{40}Ar/^{36}Ar$	
Kapoho lava	.063	.0111	.0674	.256	.0796	<226	<161	297.0±1.6	1
Olivine phenocrysts in Kapoho lava	4.43	.0100	.0245	.0476	.0058	25.1±3.4	17.9±2.4	732.0±2.2	2
Glassy splatter on Kilauea caldera floor, erupted November29, 1975	2.46	4.25	9.76	26.9	.682	———	———	294.0±1.4	3
Pillow glass									
Tholeiite of east rift zone, depth=30 m	1.9	.0103	.039	.084	.0058	0±14	0±10	296±22	4
Tholeiite of east rift zone, depth=2,960 m	32.6	.129	.213	.473	.0245	17±2	12±1	1175±22	4
Kilauea gas	——	——	——	——	——	20.9±1.1	14.9±0.8	———	5
Atmosphere	.347	1.09	2.08	4.31	.152	1.399	1	295.5	

1. Kaneoka and Takaoka (unpublished data).
2. Kaneoka and Takaoka (1978).
3. Kaneoka and others (1978).
4. Kyser and Rison (1982).
5. Craig and Lupton (1976).

samples (lava and glassy spatter in table 27.1), the samples show generally similar noble-gas abundance patterns, in which high enrichment of He is significant. Among different kinds of samples, lighter noble gases (He, Ne) are generally more enriched in ultramafic nodules and glassy samples than in phenocrysts. Nodule samples include dunite, lherzolite, and pyroxenite; however, their noble-gas abundance patterns are similar.

Noble gases are generally more abundant in dunite nodules than in olivine phenocrysts. Numerous microscopic gas or liquid inclusions (probably CO_2) are observed in such ultramafic nodules, and most noble gases are expected to have been entrapped in such inclusions. This inference has been supported by crushing or decrepitation of samples (see, for example, Funkhouser and Naughton, 1968), which showed that rather large amounts of He and radiogenic ^{40}Ar were released. Furthermore, it has been demonstrated that most He is included in vesicles and not dissolved in the glass itself in pillow-glass samples from Loihi Seamount (Kurz and others, 1983; Rison and Craig, 1983). Hence, the noble-gas abundances in these samples would correspond to those in inclusions or vesicles.

Phenocrysts seem to contain fewer inclusions than nodules and glassy samples, and this probably affects the noble-gas abundances. Olivine phenocrysts from Hawaii contain amounts of noble gases comparable to those in samples from Reunion Island, whereas samples from Iceland contain lesser amounts of the lighter noble gases than those from Hawaii and Reunion (Kaneoka and Takaoka, 1985). This difference may reflect different tectonic environments for extrusion of magma; the samples from Hawaii may be closer to the original abundances of noble gases in the magma reservoir than those from Iceland.

Noble-gas abundances in MORB are also shown in figure 27.1 for comparison (plotted to the right of the Hawaii data). MORB samples are typically enriched in lighter noble gases, especially He. There is no reason to believe that U(+Th) is more abundant in the MORB source than in that of Hawaii, and such enrichment probably reflects secondary processes that occurred during the formation and transportation of MORB magma to the surface.

NOBLE-GAS ISOTOPIC CHARACTERISTICS OF HAWAIIAN SAMPLES

HELIUM ISOTOPES

As noted in the previous section, the concentrations of noble gases in a sample are susceptible to secondary processes and it is therefore useful to evaluate such processes. To infer the characteristics of magma sources, however, isotopic ratios are more useful than elemental concentrations, since they are much less affected by the processes of formation, transportation, and extrusion of a magma, except for the effects of mass fractionation and mixing among different sources. Among the many aspects of noble-gas isotope systematics, the $^3He/^4He$ ratio ($=R$) has been most

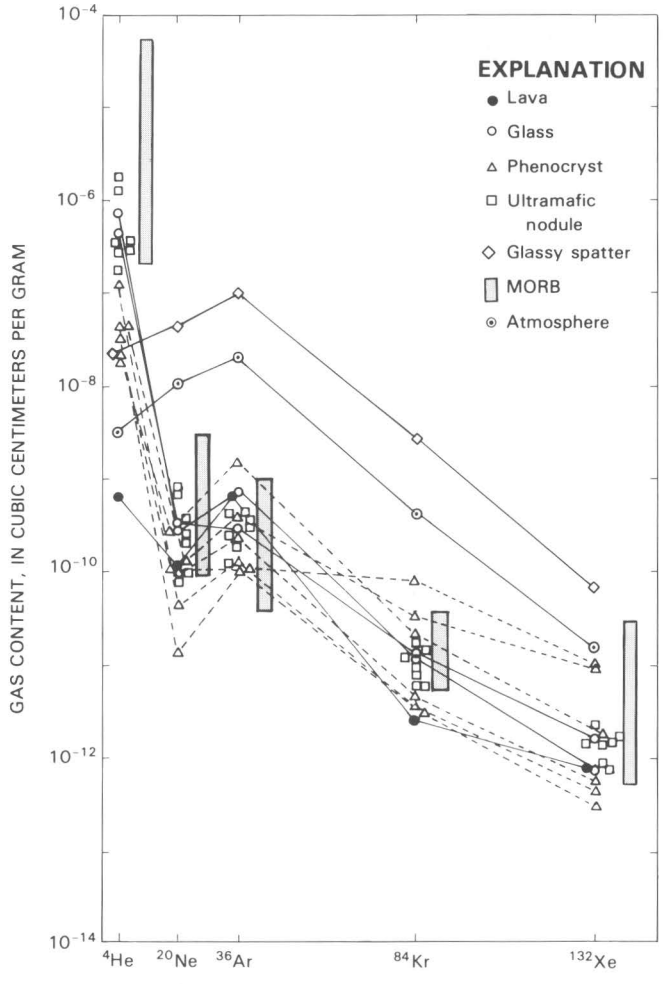

FIGURE 27.1.— Noble-gas abundances in Hawaiian rock samples. Values plotted are total amounts of noble gases in the samples adjusted to standard temperature and pressure. Values for atmosphere derived from total amounts of noble gases in the atmosphere divided by mass of the Earth. Data sources for Hawaiian samples: Hennecke and Manuel (1975); Kaneoka and Takaoka (1978, 1980); Kaneoka and others (1983). Data sources for MORB: Kyser and Rison (1982); Allègre and others (1983); Ozima and Zashu (1983).

successfully used so far because He is least contaminated by the atmosphere.

It has been revealed that MORB shows a rather uniform ^{3}He/^{4}He ratio that varies from 1.1×10^{-5} to 1.4×10^{-5} ($R=8$–$10R_A$, where R_A is the ratio of ^{3}He/^{4}He for air) irrespective of regional differences and elemental fractionation, whereas other samples show more variability and some systematic differences. For example, crustal gases generally show a lower ^{3}He/^{4}He ratio than that of atmospheric He ($R_A=1.4\times10^{-6}$). Examples are shown in figure 27.2, where the ^{3}He/^{4}He ratio is plotted against the ^{4}He/^{20}Ne ratio for each sample. The ^{3}He/^{4}He ratio for MORB is rather uniform, though the ^{4}He/^{20}Ne ratio varies by a factor of more than 10^4. Such uniformity in the ^{3}He/^{4}He ratio for MORB surely reflects a characteristic of the magma source.

Hawaiian samples show rather different characteristics from those of MORB in figure 27.2. Although most ultramafic nodules show similar ^{3}He/^{4}He ratios to that of MORB, which has an ^{4}He/^{20}Ne ratio of 0.5×10^3–5×10^3, phenocryst samples have higher ^{3}He/^{4}He ratios. This indicates that Hawaiian magma sources are isotopically different from that of MORB.

Detailed studies of the ^{3}He/^{4}He ratio have revealed that it varies among different volcanoes on each Hawaiian island and even within the individual volcanoes (Kaneoka and Takaoka, 1980; Kurz and others, 1983; Rison and Craig, 1983). The geographical variation of the ^{3}He/^{4}He ratio for Hawaiian samples is summarized in figure 27.3.

Such variations in the ^{3}He/^{4}He ratio surely reflects the conditions in the magma sources for these volcanoes. Furthermore, the variation in the ^{3}He/^{4}He ratio seems to be related to the rock type and the sequence of volcano formation. For example, tholeiite from Loihi Seamount shows higher ^{3}He/^{4}He ratios than alkali basalt (Kurz and others, 1983; Rison and Craig, 1983). Kurz and others (1983) further reported that the ^{3}He/^{4}He ratio for basalt on the Island of Hawaii seems to decrease with either increase in the volume of a volcano or decrease in the eruption age. Such observations are significant for interpreting Hawaiian volcanism and will be discussed later in more detail.

ARGON ISOTOPES

It has been known that ultramafic nodules from Hawaii, such as those from Hualalai and the Salt Lake Crater region, contain large amounts of excess ^{40}Ar, resulting in high ^{40}Ar/^{36}Ar ratios of more than a few thousand (see, for example, Funkhouser and Naughton, 1968). Since these ultramafic nodules are mantle derived (they are mostly cumulates with minor amounts of mantle materials), such values have sometimes been considered to represent the ^{40}Ar/^{36}Ar value in the mantle. Although submarine glassy pillows from the east rift zone of Kilauea show ^{40}Ar/^{36}Ar ratios as high as about 1,200 (see, for example, Dalrymple and Moore, 1968; Kyser and Rison, 1982), these ^{40}Ar/^{36}Ar ratios are still much lower than those observed in MORB. Furthermore, Kaneoka and Takaoka (1980) have demonstrated that higher ^{3}He/^{4}He ratios that exceed the MORB value seem to be associated with lower ^{40}Ar/^{36}Ar ratios. Hence, there is a possibility that such relatively low ^{40}Ar/^{36}Ar ratios represent the characteristics of the source materials for hot-spot areas.

The most serious problem in the measurement of the ^{40}Ar/^{36}Ar ratio is that the value is easily modified by the addition of atmospheric components, since the atmosphere (and sea water) contains fairly large amount of Ar. For this reason, it is often argued that the observed low ^{40}Ar/^{36}Ar ratios that are closer to the atmospheric value were caused by atmospheric contamination (see for example, Fisher, 1983). Such effects should be properly evaluated to infer the significance of the Ar isotopic ratios. One solution is to make comparison with other isotopic ratios that are not seriously affected by the atmospheric contamination. Another solution is to check the observed data in a plot of ^{40}Ar/^{36}Ar against $1/^{36}$Ar, in which samples contaminated with atmospheric component should be

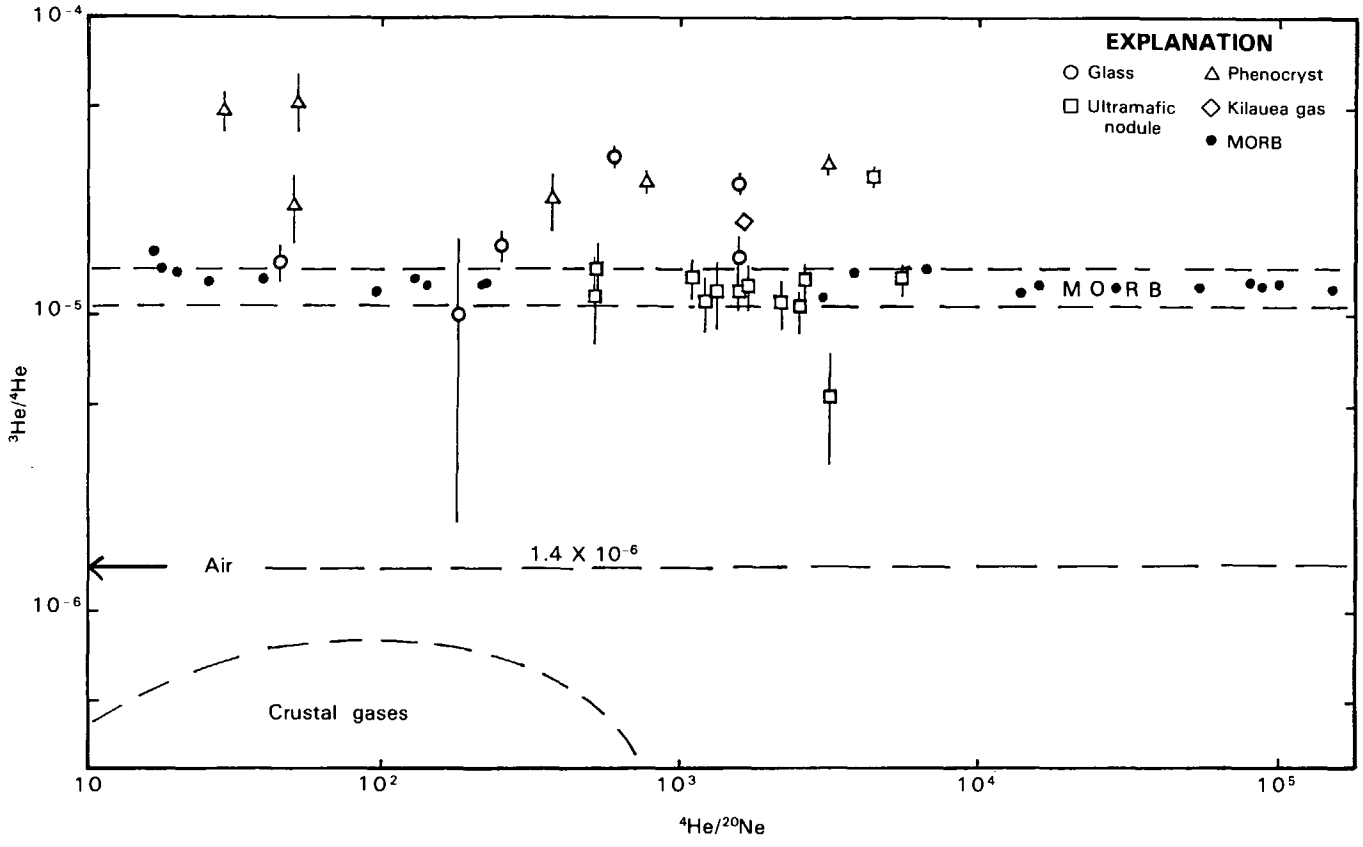

FIGURE 27.2.—Plot of $^3He/^4He$ ratio against $^4He/^{20}Ne$ ratio for Hawaiian samples and MORB. Vertical lines show uncertainty in the $^3He/^4He$ ratio measured. In spite of large variation in $^4He/^{20}Ne$ ratio for MORB, its $^3He/^4He$ ratio is rather uniform (as shown by brochetting dashed lines), but $^3He/^4He$ ratios for Hawaiian samples are generally higher than those of MORB. Data sources: Lupton and Craig (1975); Craig and Lupton (1976); Kaneoka and Takaoka (1978, 1980); Kyser and Rison (1982); Kaneoka and others (1983); Ozima and Zashu (1983).

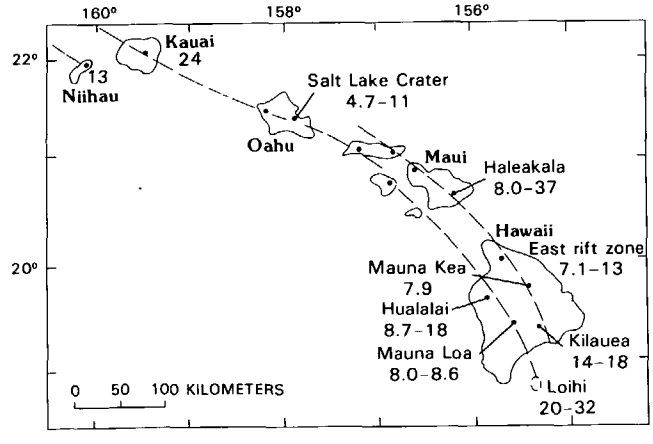

FIGURE 27.3.—Distribution of $^3He/^4He$ ratio for rock and gas samples from the Hawaiian Islands. Each number corresponds to the value or range of values of R/R_A, where R is the $^3He/^4He$ ratio in the sample(s) and R_A indicates the atmospheric value (1.4×10^{-6}). Dashed lines mark the two lines of volcanic centers (dots). Data sources: Craig and Lupton (1976); Kaneoka and Takaoka (1978, 1980); Kyser and Rison (1982); Kaneoka and others (1983); Kurz and others (1983); Lupton (1983); Rison and Craig (1983).

on a line that connects the atmospheric $^{40}Ar/^{36}Ar$ ratios (295.5) on the ordinate and the point for uncontaminated sample, as long as the samples contain the same amount of ^{36}Ar (see, for example, Dymond and Hogan, 1978). The data for Hawaiian samples are plotted on such a diagram in figure 27.4; in this diagram, the data scatter and do not define any single line. However, it is worthwhile to point out that most ultramafic nodules show systematically higher $^{40}Ar/^{36}Ar$ ratios of more than 1,000, whereas glass samples and phenocrysts show mostly values of less than 1,000, irrespective of the amount of ^{36}Ar. These submarine glass samples are not different in their eruptive conditions from MORB. Hence there is no reason why they should be much more contaminated with atmospheric components through sea water than MORB. In effect, these glass samples retain magmatic He. Hence, even if the relatively low $^{40}Ar/^{36}Ar$ ratios observed are affected by the atmospheric contamination for some samples, it does not preclude the possibility of a low $^{40}Ar/^{36}Ar$ ratio for magmatic Ar in Hawaii. This point will be discussed again later in discussing the $^3He/^4He$ - $^{40}Ar/^{36}Ar$ diagram.

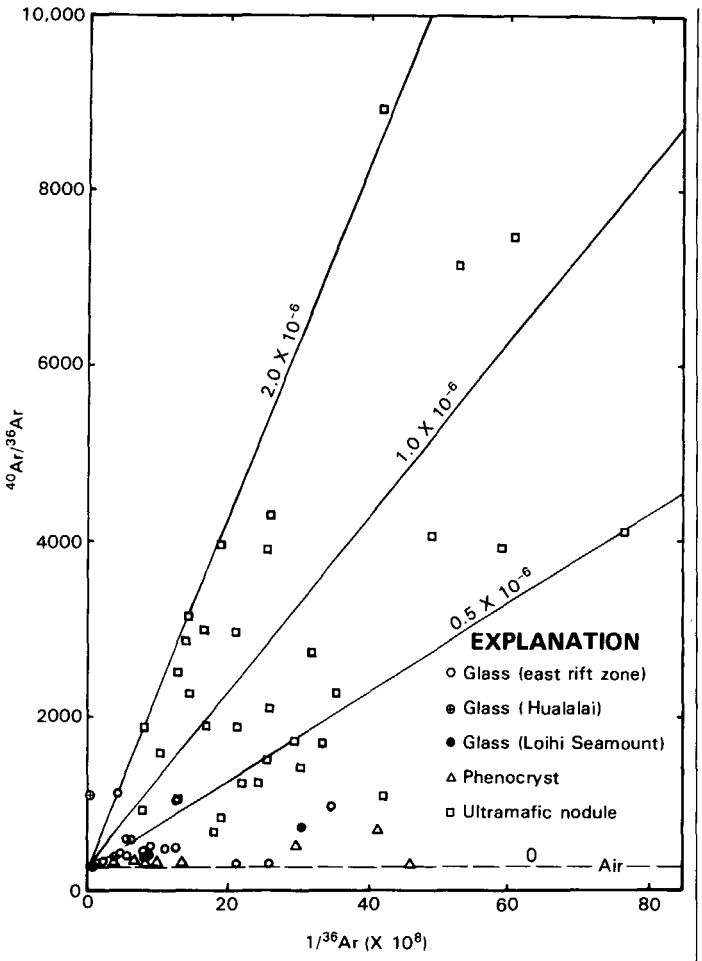

FIGURE 27.4.—Plot of $^{40}Ar/^{36}Ar$ ratio against $1/^{36}Ar$ for Hawaiian rock samples. Value of $^{40}Ar/^{36}Ar$ in air indicated by dashed line. The lines in the figure indicate reference lines which correspond to the mixing line between the original magmatic Ar and the atmospheric Ar, where the concentration of magmatic ^{40}Ar in each sample is assumed as the numerical figures on each line in the unit of cubic centimeters at standard temperature and pressure for one gram sample. Data sources: Dalrymple and Moore (1968); Funkhouser and Naughton (1968); Noble and Naughton (1968); Hennecke and Manuel (1975); Kaneoka and Takaoka (1978, 1980); Kyser and Rison (1982); Allègre and others (1983); Fisher (1983); Kaneoka and others (1983).

OTHER NOBLE GAS ISOTOPES

In Kilauea gas and in MORB, a higher $^{20}Ne/^{22}Ne$ ratio (10.3) than the atmospheric value (9.80) was reported by Craig and Lupton (1976), who considered it as evidence that the primordial Ne component of solar type may be still retained in the Earth's deep interior. However, this value and the corresponding $^{21}Ne/^{22}Me$ ratio can also be explained by mass fractionation from the atmospheric value (Kaneoka, 1980), and the occurrence of primordial Ne component has not yet been confirmed.

On the other hand, the occurrence of higher $^{129}Xe/^{130}Xe$ ratios than the atmospheric value has been confirmed in ultramafic nodules from Hualalai (Hennecke and Manuel, 1975; Kaneoka and others, 1978; Kyser and Rison, 1982). Even olivine phenocrysts of Kapoho lava, Kilauea, seem to contain excess ^{129}Xe (Kaneoka and Takaoka, 1978). However no excess ^{129}Xe has been confirmed in Loihi samples (Allègre and others, 1983; Kaneoka and others, 1983). Since excess ^{129}Xe has been regarded as the decay product of extinct ^{129}I (half-life, 17 m.y.), its occurrence indicates that the magma source was not totally equilibrated with the surrounding part for more than 4 b.y. Allègre and others (1983) reported the occurrence of excess ^{129}Xe in MORB.

The $^{129}Xe/^{130}Xe$ ratio is plotted in figure 27.5 against the $^{40}Ar/^{36}Ar$ ratio for Hawaiian samples and some MORB samples. Although the uncertainty in the $^{129}Xe/^{130}Xe$ ratio is fairly large, the array of samples seems to indicate on a mixing line of $r \geqq 0.5$, where r is defined as the ratio of $^{130}Xe/^{36}Ar$ for air divided by $^{130}Xe/^{36}Ar$ for the MORB source and the value of $^{130}Xe/^{36}Ar$ for air is 1.13×10^{-4}. For $^{130}Xe/^{36}Ar$ of the MORB source, if we adopt the value observed for a pillow glass that showed the highest excess ^{129}Xe in MORB (Allègre and others, 1983), it becomes 11.6×10^{-4}. Hence, mixing between this component and the atmosphere indicates a value of r close to about 0.1. The data array observed in figure 27.5 do not seem to be explained by the addition of an atmospheric component alone. This may imply that the Hawaiian magma source, which may be a typical hot-spot area, shows an atmospheric $^{129}Xe/^{130}Xe$ ratio and a rather low $^{40}Ar/^{36}Ar$ ratio close to the atmospheric value. Large analytical

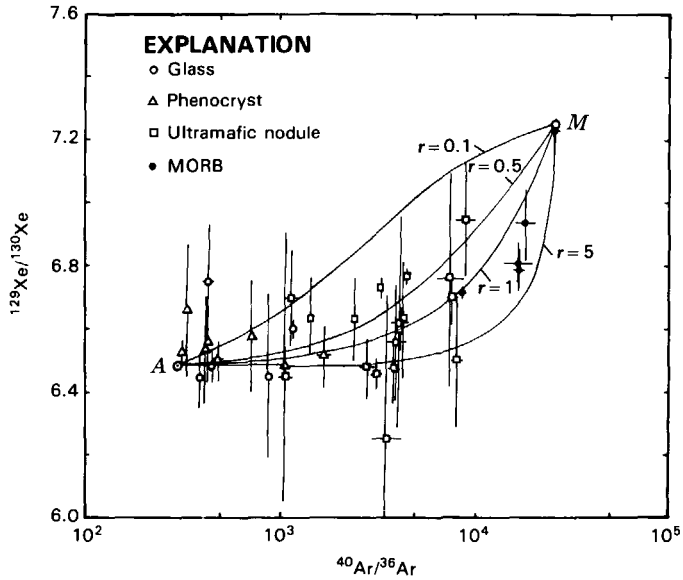

FIGURE 27.5.—Plot of $^{129}Xe/^{130}Xe$ ratio against $^{40}Ar/^{36}Ar$ ratio for Hawaiian rock samples and a few MORB samples. Mixing lines between the atmospheric component (*A*: $^{40}Ar/^{36}Ar = 295.5$; $^{129}Xe/^{130}Xe = 6.48$) and an assumed MORB source component (*M*: $^{40}Ar/^{36}Ar = 25{,}000$; $^{129}Xe/^{130}Xe = 7.25$) are drawn with a function of r, where r is $(^{130}Xe/^{36}Ar)air/(^{130}Xe/^{36}Ar)_{MORB}$ source. Vertical and horizontal lines indicate uncertainty. Data sources: Hennecke and Manuel (1975); Kaneoka and Takaoka (1978, 1980); Kyser and Rison (1982); Allègre and others (1983); Kaneoka and others (1983).

uncertainties remain, however, concerning the $^{129}Xe/^{130}Xe$ ratio for most samples from Hawaii. Hence more precise data are necessary to draw a definite conclusion.

THE $^3He/^4He$-$^{40}Ar/^{36}Ar$ SYSTEM

A magma source would be more clearly characterized by an appropriate combination of isotopic ratios than by a single one. For this purpose, the $^3He/^4He$-$^{40}Ar/^{36}Ar$ system is one of the most effective ones among possible combinations of noble-gas isotopic ratios. The merits of using this system have been discussed in detail elsewhere (Kaneoka and Takaoka, 1985).

All the available data for samples from Hawaiian volcanoes are plotted on the $^3He/^4He$-$^{40}Ar/^{36}Ar$ diagram in figure 27.6. Except for a dunite nodule from Loihi Seamount, higher $^3He/^4He$ ratios seem to be accompanied by lower $^{40}Ar/^{36}Ar$ ratios. Furthermore, ultramafic nodules are located in the region defined by MORB. Such relations for Hawaiian samples were first identified by Kaneoka and Takaoka (1980), who argued for different magma sources for Hawaiian magma and ultramafic nodules. As pointed out previously, the accumulation of data on the $^3He/^4He$ ratio in lava phases has suggested that Hawaiian volcanism is characterized by some complexity of processes in each locality, but this would not change the main scheme fundamentally from that stated above. This point will be discussed later in more detail.

However, the plot in figure 27.6 strongly suggests at least that a magma source enriched in primordial noble-gas components exists under the Island of Hawaii. If we extend such data to other areas, the same tendencies as observed for Hawaiian samples are also identified (fig. 27.7). The most remarkable feature of figure 27.7 is that higher $^3He/^4He$ ratios than the MORB value are always associated with relatively lower $^{40}Ar/^{36}Ar$ ratios, except for a few cases, and such high $^3He/^4He$ ratios are observed in typical hot-spot areas. This does not mean that samples from all hot-spot areas show such a trend. For example, volcanic rocks from the Tristan da Cunha and Gough Islands show lower $^3He/^4He$ ratios than that of MORB, but the ratios are still higher than that of the atmospheric component (Kurz and others, 1982). Such a trend may be explained by the addition of a crustal component to the pure plume-type component that has a high $^3He/^4He$ ratio (see, for example, Kurz and others, 1982; Kaneoka and Takaoka, 1985).

On the basis of the $^3He/^4He$-$^{40}Ar/^{36}Ar$ systematics, we can identify at least four end members as shown in figure 27.7: *P*(plume-type), *M*(MORB-type), *A*(atmosphere-type), and *C*(crust-type) (Kaneoka, 1983; Kaneoka and Takaoka, 1985). *C* components are multi-divided further depending on the local and regional inhomogeneities including time-integrated effects. Although *P* and probably *M* components can be subdivided on a local scale, we need not do so to discuss general trends on rather global scales. The observed noble-gas data can be explained by mixing among these components, including the data observed at subduction zones, which may be mixtures of *M*, *A*, and *C* components.

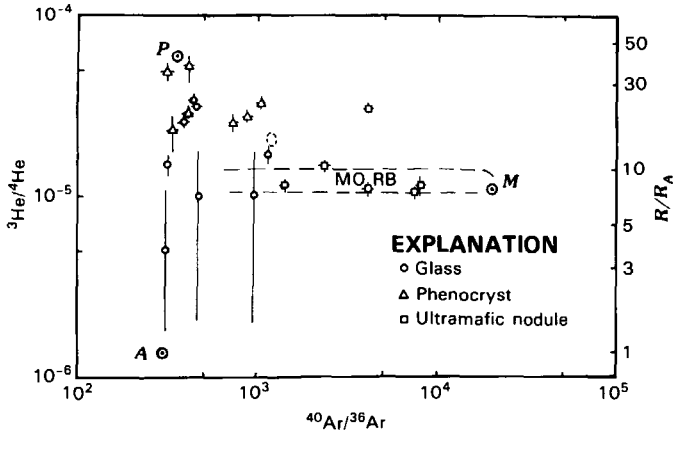

FIGURE 27.6.—Plot of $^3He/^4He$ ratio against $^{40}Ar/^{36}Ar$ ratio for Hawaiian rock samples. For most samples, only the results from high-temperature fractions are shown here. *A*, atmosphere; *P*, plume-type source; *M*, MORB source; dashed lines, approximate range of MORB samples. Vertical and horizontal lines indicate analytical uncertainties for each sample. Dashed circle indicates a combined value for samples for Kilauea, where $^3He/^4He$ ratios were obtained for fumarolic gases and $^{40}Ar/^{36}Ar$ ratios for pillow glasses from east rift zone. Data sources: Kaneoka and Takaoka (1978, 1980); Kyser and Rison (1982); Allègre and others (1983); Kaneoka and others (1983).

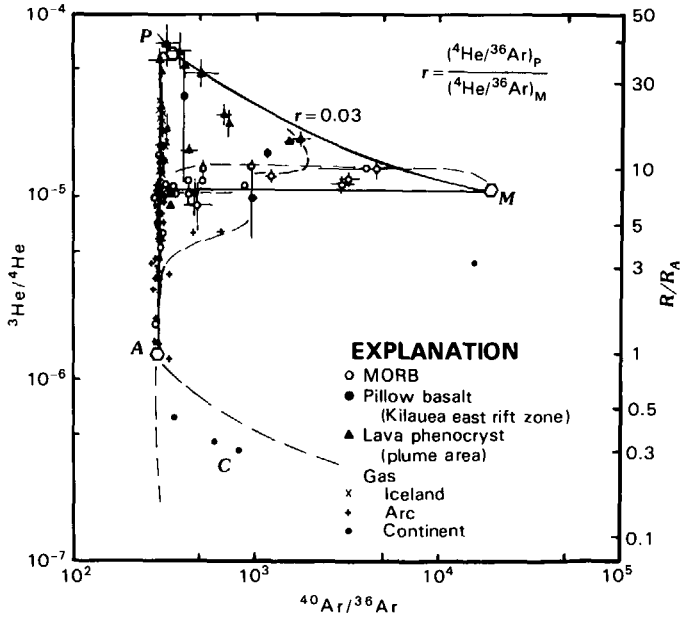

FIGURE 27.7.—Plot of $^3He/^4He$ ratio against $^{40}Ar/^{36}Ar$ ratio for samples that represent the recent state of the Earth's interior. *P*, *M*, *A*, and *C* represent assumed typical values for source materials of plume, MORB, atmosphere and crust types, respectively. Uncertainties are indicated by short vertical and horizontal lines. Solid lines show calculated mixing lines between sources. Dashed lines indicate regions where each component is dominant (though arc-type source material is not discussed in the present study) (after Kaneoka and Takaoka, 1985).

In this context, it is interesting to examine the data for Hawaiian samples in figure 27.7. Most data for Hawaiian samples are located in a region bordered by the three mixing lines, *P–M*, *M–A*, and *P–A*. Since *A* component is composed of atmospheric noble gases from the atmosphere, sea water, and ground water, those data located away from the mixing line *P–M* would have been secondarily contaminated on the surface or at a relatively shallow depth. On the other hand, some Hawaiian samples seem to lie on the *P–M* mixing line. Since the fit for mixing line is fairly good, the variation in the observed data bas been interpreted as showing the mixing between these probably mantle-derived components (Kaneoka and Takaoka, 1980, 1985; Kyser and Rison, 1982; Kaneoka, 1983).

Because this diagram is composed of two kinds of noble-gas isotopic ratios, the variation in it can be explained rather simply as long as He and Ar behave similarly in the main process concerned. On the other hand, if we take a set of elements of different kind, such as He and Sr (see, for example, Kurz and others, 1982), the system is more easily disturbed because of the different transfer of elements caused by the difference in the chemical behavior. Hence, the occurrence of completely different components (*P* and *M*) in the $^{3}He/^{4}He$-$^{40}Ar/^{36}Ar$ systematics is of great significance in inferring chemical characteristics of the Earth's interior. The component *P* would surely represent the source material of less depleted or fertile mantle that lies under the *M*-type (MORB) source, which is considered to have been much depleted in incompatible elements (Kyser and Rison, 1982; Kaneoka, 1983; Kaneoka and Takaoka, 1985). Although some investigators argue for the occurrence of fertile mantle as a result of enrichment process in the asthenosphere (for example, Anderson, 1982), this seems unlikely on the basis of noble-gas systematics (Kaneoka, 1983).

Thus, noble-gas isotopes for Hawaiian samples clearly suggest that the Hawaiian rocks are derived from fertile mantle, which is richer in primitive noble gases and incompatible elements such as K and U than the MORB source. Although similar inferences have been made on the basis of Nd-Sr systematics (see, for example, Jacobsen and Wasserburg, 1979; DePaolo, 1981), the identification of the typical component for the fertile mantle has remained hypothetical and could be interpreted in a different way in the $^{143}Nd/^{144}Nd$-$^{87}Sr/^{86}Sr$ diagram. In the $^{3}He/^{4}He$-$^{40}Ar/^{36}Ar$ diagram, however, we can identify it clearly as the *P* component. This component seems to be found in samples from typical hot-spot areas such as Hawaii, Iceland, and Reunion. Thus, noble-gas data give clear evidence for the inference that Hawaiian volcanism has been caused by a mantle plume or plumes from a hot spot that lies at a relatively deeper level (lower mantle?) in the Earth's interior (see Kaneoka, 1983, for further discussion).

NOBLE GAS ISOTOPES AS CONSTRAINTS TO INFER THE GENETIC RELATIONS FOR HAWAIIAN ROCKS

In attempts to reveal the orgin of Hawaiian volcanic rocks by petrological, mineralogical, and geochemical studies, it has often been assumed that the ultramafic nodules included in Hawaiian volcanic rocks represent either the source materials of these volcanic rocks or cumulates from them (for example, Jackson and Wright, 1970). On the basis of $^{3}He/^{4}He$ and $^{40}Ar/^{36}Ar$ ratios, however, it has been shown that phenocrysts in Hawaiian volcanic rocks (tholeiite and alkalic basalt) and ultramafic nodules would have been derived from different sources (Kaneoka and Takaoka, 1978, 1980). The source for ultramafic nodules seems to be similar to that for MORB. Such results have been supported by subsequent work (Kyser and Rison, 1982). It has been known that $^{87}Sr/^{86}Sr$ ratios for ultramafic nodules (0.7031–0.7032) (Shimizu, 1975) are slightly lower than those of Hawaiian tholeiite (0.7034–0.7038) (see, for example, O'Nions and others, 1977). However, the difference in the $^{3}He/^{4}He$ and $^{40}Ar/^{36}Ar$ ratios is so large between phenocrysts and ultramafic nodules (see fig. 27.6) that we cannot regard them as derived from similar sources. Recent summarized studies on the origin of Hawaiian tholeiite have also suggested that most ultramafic nodules are not directly related to the origin of Hawaiian volcanic rocks (Wright, 1984).

As discussed in the previous section, Hawaiian ultramafic nodules show similar $^{3}He/^{4}He$ and $^{40}Ar/^{36}Ar$ ratios to those of MORB. These analyzed nodules were mostly samples from Hualalai Volcano and Salt Lake Crater, and their rock types include dunite, spinel lherzolite, and garnet pyroxenite. As far as noble-gas data are concerned, these ultramafic nodules include gas components that were derived from the same source or a quite similar source to that of MORB. Hence, these nodules might have been the source rock or cumulates of MORB, or they might represent rocks formed in the asthenosphere to constitute the lower part of the lithosphere. More strictly, if the accompanying volcanic rocks also show *M*-type noble-gas isotopes, we cannot preclude the possibility of a genetic relation between such ultramafic nodules and the volcanic-rock source. However, dredged tholeiite samples from Hualalai show definitely higher $^{3}He/^{4}He$ ratios (14-18 R_A) than those of ultramafic nodules (8.6-9.2 R_A) (Kurz and others, 1983). Hence they have no direct genetic relation between them.

For the samples from Salt Lake Crater, we unfortunately have no noble-gas data on volcanic rocks. Since volcanic rocks of the Honolulu Volcanics are reported to have rather lower $^{87}Sr/^{86}Sr$ ratios (about 0.7033) than those of the Koolau Basalt[2] (about 0.7039) (Lanphere and Dalrymple, 1980), there is a possibility that volcanic rocks of the Honolulu Volcanics may have *M*-type noble-gas isotopes. If this is so, then we can regard those ultramafic nodules as related to some source rocks or cumulates that also were a source for volcanic rocks of the Honolulu Volcanics.

In a detailed study of $^{3}He/^{4}He$ ratios for volcanic rocks from the Island of Hawaii, Kurz and others (1983) have revealed that each volcano shows different $^{3}He/^{4}He$ ratios and that the ratio seems to decrease with increasing volume of a volcano and with decreasing age of the volcano. In their results, it is noteworthy that tholeiite samples from Mauna Loa and an alkali basalt from Mauna Kea show very similar $^{3}He/^{4}He$ ratios (7.9-8.6 R_A) to that of

[2]Stratigraphic nomenclature used in chapter is from Langenheim and Clague (chapter 1, part II).

MORB. Rison and Craig (1983) also report a similar value (8.5 R_A) for one Mauna Loa sample from analyzing olivine phenocrysts. Unfortunately, we have no heavier noble-gas data for these samples. However, even these data give us important information to infer the processes that are occurring underneath the Island of Hawaii.

With reference to He isotopes, the He sources should be similar to that of MORB. Hence in the present frame of ideas the He source should be either in the asthenosphere or in the lithosphere itself, since *P*-type noble gases are assumed to be derived from the deeper part of the Earth's interior.

Samples from Loihi give us a unique chance to study the relations of rock types and nodule gas isotopes. Because Loihi Seamount is regarded as the most recent volcano in the evolution of the Hawaiian-Emperor Chain, from it we can get information on an earlier state of a volcano's evolution along the chain. Furthermore, the dredged rocks from the seamount show diverse basalt types, including tholeiitic, transitional, and alkali basalt and basanite, including dunite nodules (Moore and others, 1982).

The He isotopic measurements have shown very high $^3He/^4He$ ratios (up to 32 R_A) and tholeiite samples show generally higher $^3He/^4He$ ratios than those of alkali rocks (Kurz and others, 1983; Rison and Craig, 1983). Since dunite nodules show $^3He/^4He$ ratios similar to that of alkalic lava that included nodules, Kurz and others (1983) have conjectured that the apparent lower $^3He/^4He$ ratios for alkalic rocks might be due to contamination by He included in xenocrysts of nodules. On the other hand, Kaneoka and others (1983), who examined all noble gases in both tholeiitic and alkalic rocks, found that the $^{40}Ar/^{36}Ar$ ratios for lava are not so high as observed in MORB and are still located in the region defined by the three kinds of mixing lines among *P*, *M*, and A components in the $^3He/^4He$-$^{40}Ar/^{36}Ar$ diagram. Only a dunite nodule from Loihi Seamount seems to be an exception. Although this nodule shows a high $^3He/^4He$ ratio (22 R_A), its $^{40}Ar/^{36}Ar$ ratio is also high (4,200). To explain this, Kaneoka and others (1983) have conjectured that only He was equilibrated with the surrounding magma and the nodule had originally *M*-type noble gases.

In Loihi samples, fairly large variation in the $^3He/^4He$ ratio has been observed. This may be a characteristic of the initial state of a volcano's evolution caused by different degrees of contamination with lithospheric and (or) asthenospheric components that are similar to that of MORB.

On the other hand, apparent uniformity in the observed value of noble gases may simply reflect the sampling problem, because we have data only on lava flows of relatively limited time periods of young active volcanoes such as Mauna Loa and Kilauea. In fact, for Haleakala Volcano, we have observed very high $^3He/^4He$ ratios for olivine and augite phenocrysts of ankaramite (32–36 R_A) from the vent known as White Hill Cone (Kaneoka and Takaoka, 1980; Rison and Craig, 1983), which probably belongs to the Pleistocene Kula Volcanics (hawaiite). However, both pyroxene phenocrysts from the A.D. 1790 ankaramite flow in the post erosional Hana Volcanics and olivine phenocrysts from the tholeiitic shield lava of the Honomanu Basalt show *M*-type $^3He/^4He$ ratios of 8.1 R_A and 8.0 R_A, respectively (Rison and Craig, 1983). Except for the Hana Volcanics, such tendency is at variance with that predicted from some trace-element data and from Sr and Nd isotopic ratios for Haleakala Volcano (Chen and Frey, 1983). This means that noble gases (and probably some volatile elements, too) may not always behave similarly with other nonvolatile elements, even in a mantle plume.

HAWAIIAN VOLCANISM AS INFERRED FROM NOBLE-GAS DATA

As discussed previously, Hawaiian volcanism seems to be strongly related to a mantle plume or plumes of deep origin. Noble-gas data require a source material that still retains more of primitive components than does that of MORB (see, for example, Kyser and Rison, 1982; Kaneoka, 1983). If Hawaiian volcanism was initiated by propagation of a tensional fracture through the lithosphere, the magma source should be located in the uppermost part of the asthenosphere. However, it seems difficult to keep such a source in a relatively shallow part of the Earth's interior for a long time, because the source material is inferred to retain primitive components, including He, which would show one of the largest mobilities in the Earth's interior (Kaneoka, 1983).

The $^3He/^4He$ ratios for each volcano in the Hawaiian Islands are plotted against the volume of each volcano in figure 27.8. If we consider only the Island of Hawaii, volcanoes with small volume show high $^3He/^4He$ ratios, and volcanoes with large volume show $^3He/^4He$ ratios similar to that of MORB (for example, Mauna Kea and Manua Loa). This suggests that the contribution of *P*-type source material is larger in the early stage of a volcano's evolution relative to that of *M*-type source material. Such a relation has been shown by Kurz and others (1983). If we include other volcanoes from different islands, however, such systematics seem to be disturbed, as shown in figure 27.8. Volcanic rocks from Haleakala on Maui Island and those from Kauai Island indicate relatively high $^3He/^4He$ ratios in spite of the large volumes of their volcanoes. From Haleakala Volcano, volcanic rocks with $^3He/^4He$ ratios similar to that of MORB have also been reported (Rison and Craig, 1983). Ultramafic nodules from Salt Lake Crater, Oahu Island, show $^3He/^4He$ ratios fairly similar to that of MORB. Hence, the situation may be not so simple as reported initially for samples from the Island of Hawaii. Relatively high $^3He/^4He$ ratios observed for samples from Haleakala Volcano indicate that the *P*-type component of noble gases could have been added even at a later stage in a volcano's evolution.

On the basis of the systematic changes in elemental ratios and $^{87}Sr/^{86}Sr$ and $^{143}Nd/^{144}Nd$ ratios with eruption age for volcanic rocks of Haleakala Volcano, Chen and Frey (1983) have predicted a systematic decrease over time in the rate of contribution of plume-derived material to the formation of a magma. Basically their model seems to explain well the variations of elemental and isotopic data for Hawaiian volcanism. However, the data in figure 27.8 do not always follow the model. As suggested by Rison and Craig (1983), the Honomanu Basalt (shield-building tholeiite) of Haleakala Volcano shows *M*-type He component, whereas *P*-type He component would be expected in the model. Although higher $^3He/^4He$ ratios seem to be accompanied by higher $^{87}Sr/^{86}Sr$ ratios or lower

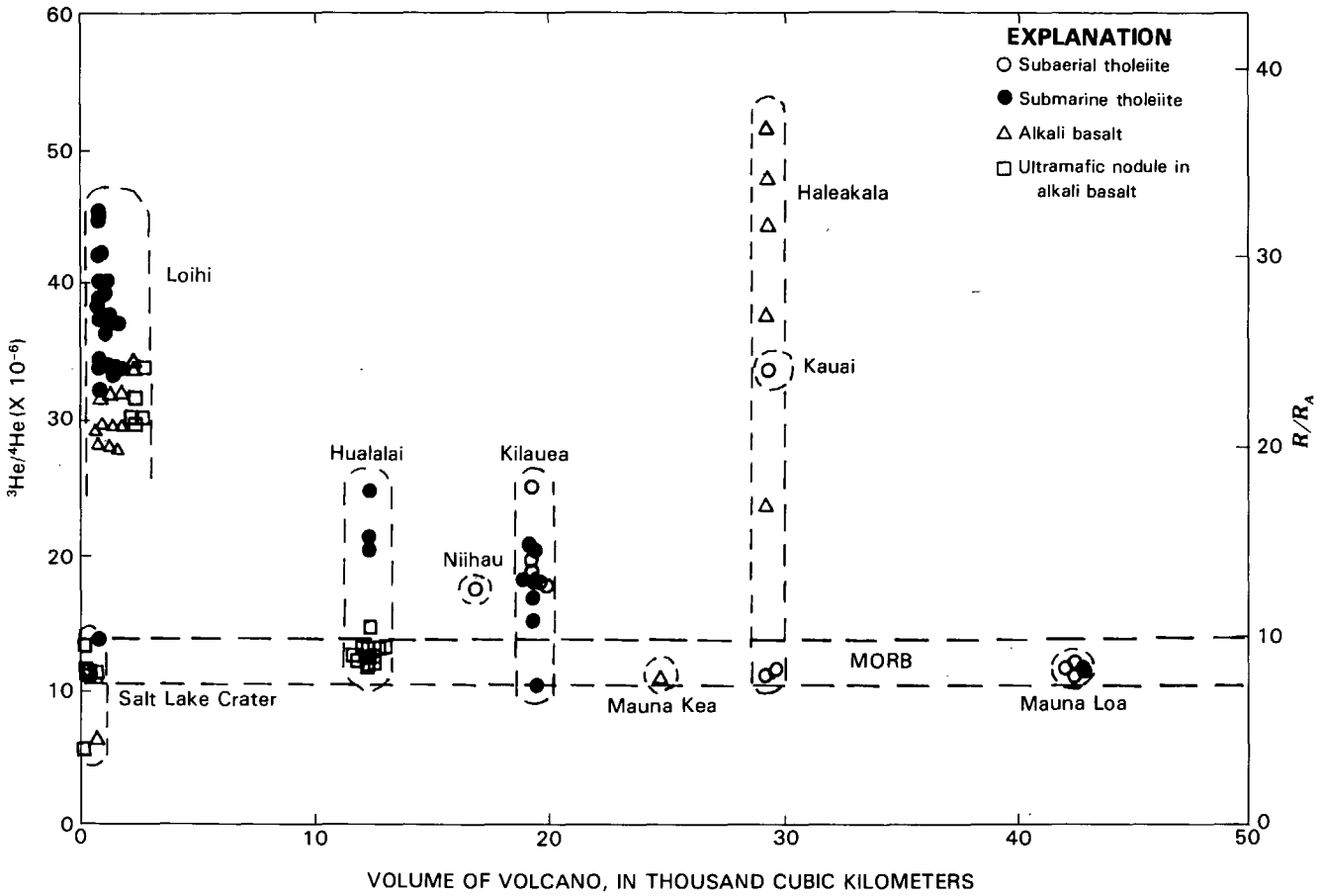

FIGURE 27.8.—Plot of $^3He/^4He$ ratio against volcano volume for Hawaiian volcanoes. Volcano volumes taken from Bargar and Jackson (1974). Typical range of $^3He/^4He$ values for MORB indicated by horizontal dashed lines. Data sources: Craig and Lupton (1976); Kaneoka and Takaoka (1978, 1980); Kyser and Rison (1982); Kurz and others (1982, 1983); Kaneoka and others (1983); Lupton (1983); Rison and Craig (1983).

$^{143}Nd/^{144}Nd$ ratios for Loihi samples (Kurz and others, 1983; Staudigel and others, 1984), such trends are not always retained when the data from other volcanoes are included. Furthermore, although tholeiitic shield lava from the Hawaiian Islands shows generally slightly higher $^{87}Sr/^{86}Sr$ and lower $^{143}Nd/^{144}Nd$ ratios that those of MORB (see, for example, Staudigel and others, 1984), the $^3He/^4He$ ratio is quite similar to the MORB value, at least for Mauna Kea and Mauna Loa. Thus, noble-gas isotopes seem to be not always correlated with the other radiogenic isotopes such as Sr, Nd, and Pb. Such differences probably reflect the different geochemical behavior of noble gases from the other nonvolatile elements. This implies that noble gases would be transported in varying degrees together with other volatile components during the different stages of evolution of Hawaiian volcanoes. Furthermore, the $^3He/^4He$ ratios for Hawaiian rocks have not always varied smoothly. Such noble gases may have been transported in a mantle diapir rather than in a mantle plume.

So far, a number of models for Hawaiian volcanism have been proposed (see, for example, Macdonald, 1968; Chen and Frey, 1983; Sen, 1983; Staudigel and others, 1984). However, those do not take properly into account the noble-gas-isotope signature. As discussed in previous sections, the most significant feature of this signature is the occurrence in Hawaiian lava of much higher $^3He/^4He$ ratios than that of MORB, which strongly suggests the involvement of a source material that contains fairly primordial components and is located in the deeper part of the Earth's interior (lower mantle?). We cannot deny the involvement of oceanic lithosphere during the formation of a magma. As far as the noble gases (and probably volatile components) are concerned, however, the contribution from the oceanic lithosphere would be not so significant as has been suggested for nonvolatile elements (Staudigel and others, 1984). If the age of the oceanic lithosphere is great enough to have increased the $^{87}Sr/^{86}Sr$ ratio, the $^3He/^4He$ ratio would have been lowered by the addition of radiogenic ^4He, resulting in a lower $^3He/^4He$ ratio than that of MORB. When the $^3He/U$ ratio can be postulated to be similar to that of the MORB source, the $^3He/^4He$ ratio would have to be similar also. However, it is very difficult to conjecture that the $^3He/U$ ratio is maintained

higher than that of the MORB source, because He would be easily lost during formation of the lithosphere around the ridge, resulting in lowering the $^3He/U$ ratio. If the lower part of the oceanic lithosphere is formed by the addition of the components of the asthenosphere, its isotopic composition would be similar to that of MORB. At least some Hawaiian ultramafic nodules might have been derived from such lower lithosphere.

Volcanic rocks from Loihi Seamount show definitely higher $^3He/^4He$ ratios than those of Kilauea (fig. 27.8). This implies that the contribution of *P*-type component is larger for Loihi samples than for Kilauea samples as indicated by the He data. Large variations in the observed values can be explained by varying degrees of addition of *M*-type component during the ascent of volatile-enriched mantle diapirs. It is true that magma chemistry as determined by the last depth of equilibration would have little bearing on the initial depth of origin for source diapirs (Staudigel and others, 1984). Even the voluminous outpourings are not always good indicators for characterizing the source material of a plume, because we cannot exclude the possibility of interaction during the ascent of a mantle diapir with *M*-type source materials. The $^3He/^4He$ ratio may be used more efficiently to indicate the plume component for noble-gas (volatiles) components.

From the noble-gas data together with those of other radiogenic isotopes, we can summarize a model for Hawaiian volcanism as shown schematically in figure 27.9.

The initial (infant) stage of Hawaiian volcanism would be exemplified by Loihi Seamount (fig. 27.9*A*). When the relatively cold lithosphere approaches the hot spot, volcanism would be initiated by the rise of volatile-enriched mantle diapirs with *P*-type noble gases derived from the deeper part of the Earth's interior

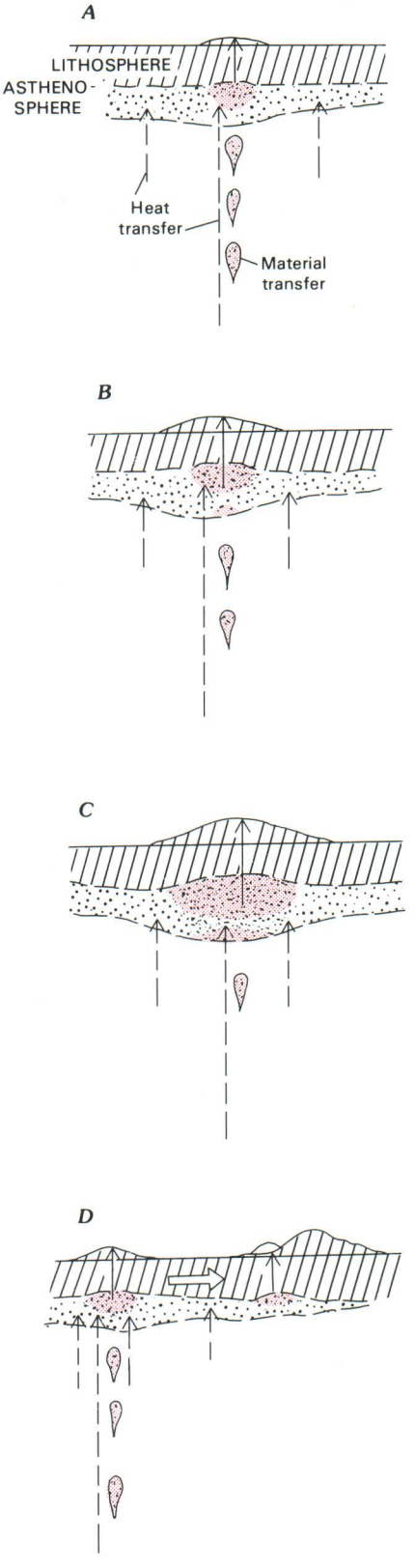

FIGURE 27.9.—Schematic model to show the evolution of Hawaiian volcanism. Red color shows regions of intensive partial melting. ***A,*** Infant stage: volcanism is initiated by rise of diapir(s) from hot-spot source in Earth's deep interior (lower mantle?). Diapir will be enriched in volatile components. Possible example of this stage is Loihi Seamount. ***B,*** Early part of tholeiitic shield-building stage: diapirs still rise through asthenosphere and lithosphere. Partially melted zone will be increased because of accumulation of heat energy through diapirs and conduction, causing downward swelling and thinning of lithosphere over hot spot. Plume-type source material will mix with surrounding MORB-type source material during rise of diapirs(s) through asthenosphere and lithosphere (example, Kilauea Volcano). ***C,*** Later part of tholeiitic shield-building stage: contribution from diapir(s) probably much reduced. Instead, most melt may be derived from partially melted zone in uppermost part of asthenosphere. Most MORB-type He might be supplied from this portion (example, Mauna Loa). Although no example is shown here, in a volcano at the postcaldera stage, no significant contribution from diapirs can be expected. Diminishing heat and material supplies from hot-spot source cause eruption frequency of a volcano to decrease. Degrees of partial melting also decrease, resulting in production of alkalic basalt (example, Kula Volcanics, Haleakala Volcano). ***D,*** Posterosional stage: when a volcano migrates far away from hot-spot area, some melt would still remain at bottom of lithosphere. Addition of conductive heat from initial thermal anomaly and release of latent heat from solidification of melt may form some melt pockets under the volcano and produce alkalic and (or) nephelinitic rocks. Source material for such rocks is quite similar to that of MORB (example, Honolulu Volcanics, Oahu Island).

(lower mantle?). During ascent to the surface, such diapirs will interact with surrounding materials at various depths both in the asthenosphere and the lithosphere. Such interaction would have caused large variation in both isotopic and chemical signatures of magmas. We assume the existence under the lithosphere of a partially melted zone enriched with *M*-type noble gases that is indicated seismically as the low-velocity zone. The occurrence of such a zone may help the interaction between the diapirs and the surrounding materials.

The second stage is that of tholeiitic shield-building (fig. 27.9*B*, *C*). During this stage, melting in the partially melted zone of the asthenosphere would be increased because of the addition of heat from the ascending diapirs and by conduction. This may cause swelling of the partially melted zone and thinning of the lithosphere over the hot-spot area. During such processes, *M*-type noble gases might be enriched in the partially melted zone under the lithosphere. At Kilauea Volcano (fig. 27.9*B*), the contribution from mantle diapirs will still be significant, but the mixing rate of *M*-type noble gas will increase, resulting in lower $^{3}He/^{4}He$ and $^{87}Sr/^{86}Sr$ ratios and higher $^{143}Nd/^{144}Nd$ ratios compared with those of the infant stage.

On the other hand, for Mauna Kea and Mauna Loa Volcanoes (fig. 27.9C), the role of diapirs may be much less than for Kilauea Volcano. As shown in figure 27.8, we observe no difference in the $^{3}He/^{4}He$ ratio between these volcanoes and MORB. This implies that even when voluminous out-pourings occur from these volcanoes, it does not always mean a contribution from mantle diapirs as far as He isotopes are concerned. On the other hand, $^{87}Sr/^{86}Sr$ and $^{143}Nd/^{144}Nd$ ratios are still different for these volcanoes from those of MORB (see, for example, Staudigel and others, 1984). This suggests that most He was derived from the partially melted zone in the uppermost asthenosphere and that the voluminous outpourings of lava were also caused by the expansion of the partially melted zone compared with the infant stage. At this stage, the hot spot may act mainly as a heat source, but not the main source for adding materials, though some small diapirs will still rise. The isotopic ratios for Sr and Nd may be explained by the interaction of melts formed in the asthenosphere with the oceanic lithosphere. The occurrence of mantle metasomatism is possible (Wright, 1984).

Another possibility is that the contribution from diapirs still continues but the diapirs are less enriched in volatile components than those of the infant stage. Hence, even if isotopic ratios for nonvolatile elements are still different from those of MORB, the $^{3}He/^{4}He$ ratio might become similar to that of MORB because of mixing with the volatile-enriched *M*-type source in the partially melted zone. At present, we have no good evidence to select one or the other possibility. In both cases, however, most He would have been derived from the partially melted zone in the uppermost asthenosphere, and the occurrence of such a zone is significant for Hawaiian volcanism at this stage.

When the volcano migrates away from the hot spot, the supply of heat and materials will be diminished. The rate of melting in the partially melted zone also decreases, resulting in the decrease of eruption frequency of a volcano. Total amounts of melt produced would also decrease. Since the degree of partial melting would also decrease, alkalic basalt would be dominant. Isotopic ratios for both nonvolatile elements and noble gases may approach those of MORB. However, relatively primitive ratios may still be observed in some cases, since the addition of diapir components would dominate the isotopic ratios in the melt because of the mass balance between melts from diapirs and the surrounding materials. The very high $^{3}He/^{4}He$ ratios for the Kula Volcanics of Haleakala Volcano (Kaneoka and Takaoka, 1980; Rison and Craig, 1983) might have originated in such a way.

The final stage of Hawaiian volcanism is identified as the posterosional stage, which occurs after a period of volcanic quiescence. In this stage, no contribution from diapirs is expected because the volcano has migrated far away from the hot spot. At the bottom of the oceanic lithosphere, some melt remains after producing alkalic basalt. The addition of conductive heat from the initial thermal anomaly together with the release of some latent heat during solidification of melt may form some melt pockets under a volcano that produce alkalic and or nephelinitic rocks. In this case, the source materials would be mostly the *M*-type material in the uppermost asthenosphere. Thus, it is reasonable to conjecture that such volcanic rocks would show values for isotopic ratios, including $^{3}He/^{4}He$ ratios, very similar to those of MORB. The Honolulu Volcanics on Oahu Island and the Hana Volcanics at Haleakala Volcano, Maui Island, are good examples of such late volcanism (fig. 27.9*D*).

This model is rather qualitative, and the major scheme is not seriously different from those which have been proposed before. Furthermore, the present scheme shows only a general trend; small variations would occur on a local scale. However, it is worth noting that voluminous outpourings of Hawaiian volcanoes do not always reflect direct matieral supply from the hot-spot source but may rather reflect the combined effects of material transfer plus heat supply. The occurrence of a partially melted zone under the lithosphere would play an important role in controlling the activity and characteristics of Hawaiian volcanoes. The occurrence of such a partially melted zone might be related to the conductive transfer of heat from the deeper part of the Earth together with the existence of the overlying, less conductive lithosphere acting as an insulator.

To clarify further and in greater detail the evolutionary scheme for Hawaiian volcanism, more systematic isotopic surveys, both of the noble gases and of other elements are required.

REFERENCES CITED

Allègre, C.J., Staudacher, T., Sarda, P. and Kruz, M., 1983, Constraints on evolution of Earth's mantle from rare gas systematics: Nature, v. 303, no. 5920, p. 762-766.

Anderson, D.L., 1982, Isotopic evolution of the mantle: a model: Earth and Planetary Science Letters, v. 57, no. 1, p. 13-24.

Barger, K.E., and Jackson, E.D., 1974, Calculated volumes of individual shield volcanoes along the Hawaiian-Emperor Chain: Journal of Research of the U.S. Geological Survey, v. 2, p. 545-550.

Chen, C.-Y., and Frey, F.A., 1983, Origin of Hawaiian tholeiite and alkalic basalt: Nature, v. 302, no. 5911, p. 785-789.

Craig, H., and Lupton, J.E., 1976, Primordial neon, helium and hydrogen in oceanic basalts: Earth and Planetary Science Letters, v. 31, no. 3, p. 369-385.

Dalrymple, G.B., and Moore, J.G., 1968, Argon-40: excess in submarine pillow basalts from Kilauea Volcano, Hawaii: Science, v. 161, no. 3846, p. 1132-1135.

DePaolo, D.J., 1981, Nd isotopic studies: some new perspectives on earth structure and evolution: Eos, Transactions, American Geophysical Union, v. 62, no. 14, p. 137-140.

Dymond, J., and Hogan, L., 1978, Factors controlling the noble gas abundance patterns of deep sea basalts: Earth and Planetary Science Letters, v. 38, no. 1, p. 117-128.

Fisher, D.E., 1983, Rare gases from the undepleted mantle?: Nature, v. 305, no. 5932, p. 298-300.

Funkhouser, J.G., Fisher, D.E., and Bonatti, E., 1968, Excess argon in deep-sea rocks: Earth and Planetary Science Letters, v. 5, no. 2, p. 95-100.

Funkhouser, J.G., and Naughton, J.J., 1968, Radiogenic helium and argon in ultramafic inclusions from Hawaii: Journal of Geophysical Research, v. 73, no. 14, p. 4601-4607.

Gramlich, J.W., and Naughton, J.J., 1972, Nature of source material for ultramafic minerals from Salt Lake Crater, Hawaii, from measurement of helium and argon diffusion: Journal of Geophysical Research, v. 77, no. 17, p. 3032-3042.

Hayatsu, A., and Waboso, C.E., 1982, The solubility of rare gases in rock melts: implications for K-Ar dating and Earth degassing: *in* Abstracts for the Fifth International Conference on Geochronology, Cosmochronology and Isotope Geology, p.139.

Hennecke, E.W., and Manuel, O.K., 1975, Noble gases in Hawaiian xenoliths: Nature, v. 257, no. 5529, p. 778-780.

Jackson, E.D., and Wright, T.L., 1970, Xenoliths in the Honolulu Volcanic Series, Hawaii: Journal of Petrology, v. 11, part 2, p. 405-430.

Jacobsen, S.B., and Wasserburg, G.J., 1979, The mean age of mantle and crustal reservoirs: Journal of Geophysical Research, v. 84, no. B13, p. 7411-7427.

Kaneoka, I., 1980, Rare gas isotopes and mass fractionation: an indicator of gas transport into or from a magma: Earth and Planetary Science Letters, v. 48, no. 2, p. 284-292.

———1983, Noble gas constraints on the layered structure of the mantle: Nature, v. 302, no. 5910, p. 689-700.

Kaneoka, I., and Takaoka, N., 1978, Excess ^{129}Xe and high $^{3}He/^{4}He$ ratios in olivine phenocrysts of Kapuho lava and xenolithic dunites from Hawaii: Earth and Planetary Science Letters, v. 39, no. 3, p. 382- 386.

———1980, Rare gas isotopes in the Hawaiian ultramafic nodules and volcanic rocks: constraints on genetic relationships: Science, v. 208, no. 4450, p. 1366-1368.

———1985, Noble-gas state in the Earth's interior—some constraints on the present state: Chemical Geology, v. 52, no. 1, p. 75-95.

Kaneoka, I., and Takaoka, N., and Aoki, K., 1978, Rare gases in mantle-derived rocks and minerals, *in* Alexander, E.C., Jr., and Ozima, M., eds., Terrestrial Rare Gases: Tokyo, Center for Academic Publications, p. 71-84.

Kaneoka, I., and Takaoka, N., and Clague, D.A., 1983, Noble gas systematics for coexisting glass and olivine crystals in basalts and dunite xenoliths from Loihi Seamount: Earth and Planetary Science Letters, v. 66, p. 427-437.

Kurz, M.D., Jenkins, W.J., and Hart, S.R., 1982, Helium isotopic systematics of oceanic islands and mantle heterogeneity: Nature, v. 297, no. 5861, p. 43-47.

Kurz, M.D., Jenkins, W.J., Hart, S.R., and Clague, D., 1983, Helium isotopic variations in volcanic rocks from Loihi Seamount and the Island of Hawaii: Earth and Planetary Science Letters, v. 66, p. 388-406.

Kyser, T.K., and Rison, W., 1982, Systematics of rare gas isotopes in basic lavas and ultramafic xenoliths: Journal of Geophysical Research, v. 87, no. B7, p. 5611-5630.

Lanphere, M.A., and Dalrymple, G.B., 1980, Age and strontium isotopic composition of the Honolulu Volcanic Series, Oahu, Hawaii: American Journal of Science, v. 280-A, part 2, p. 736-751.

Lovering, J.F., and Richards, J.R., 1964, Potassium-argon age study of possible lower-crust and upper-mantle inclusions in deep-seated intrusions: Journal of Geophysical Research, v. 69, no. 22, p. 4895-4901.

Lupton, J.E., 1983, Terrestrial inert gases: isotope tracer studies and clues to primordial components in the mantle: Annual Review of the Earth and Planetary Sciences, v. 11, p. 371-414.

Lupton, J.E., and Craig, H., 1975, Excess ^{3}He in oceanic basalts: evidence for terrestrial primodial helium: Earth and Planetary Science Letters, v. 26, no. 2, p. 133-139.

Macdonald, G.A., 1968, Composition and origin of the Hawaiian lavas: Memoir of the Geological Society of America, no. 116, p. 477-522.

Moore, J.G., Clague, D.A., and Normark, W.R., 1982, Diverse basalt types from Loihi Seamount, Hawaii: Geology, v. 10, no. 2, p. 88-92.

Morgan, W.J., 1971, Convection plumes in the lower mantle: Nature, v. 230, no. 5288, p. 42-43.

Noble, C.S., and Naughton, J.J., 1968, Deep-ocean basalts. Inert gas content and uncertainties in age dating: Science, v. 162, no. 3850, p. 265-269.

O'Nions, R.K., Hamilton, P.J., and Evensen, N.M., 1977, Variations in $^{143}Nd/^{144}Nd$ and $^{87}Sr/^{86}Sr$ ratios in oceanic basalts: Earth and Planetary Science Letters, v. 34, no. 1, p. 13-22.

Ozima, M., and Podosek, F.A., 1983, Noble gas geochemistry: Cambridge University Press, 367 p.

Ozima, M., and Zashu, S., 1983, Noble gases in submarine pillow volcanic glasses: Earth and Planetary Science Letters, v. 62, no. 1, p. 24- 40.

Rison, W., and Craig, H., 1983, Helium isotopes and mantle volatiles in Loihi Seamount and Hawaiian Island basalts and xenoliths: Earth and Planetary Science Letters, v. 66, p. 407-426.

Sen, G., 1983, A petrologic model for the constitution of the upper mantle and crust of the Koolau shield, Oahu, Hawaii, and Hawaiian magmatism: Earth and Planetary Science Letters, v. 62, no. 2, p. 215-228.

Shimizu, N., 1975, Geochemistry of ultramafic inclusions from Salt Lake Crater, Hawaii and from Southern African kimberlites: Physical Chemistry of the Earth, v. 9, p. 655-669.

Staudigel, H., Zindler, A., Hart, S.R., Leslie, T., Chen, C.-Y., and Clague, D.A., 1984, The isotopic systematics of a juvenile intraplate volcano: Pb, Nd, and Sr isotope ratios of basalts from Loihi Seamount, Hawaii: Earth and Planetary Science Letters, v. 69, no. 1, p. 13-19.

Wilson, J.T., 1963, A possible origin of the Hawaiian Islands: Canadian Journal of Physics, v. 41, p. 863-870.

Wright, T.L., 1984, Origin of Hawaiian tholeiite: a metasomatic model: Journal of Geophysical Research, v. 89, no. B5, p. 3233-3252.

HAWAIIAN ERUPTIVE GASES

By L. Paul Greenland

ABSTRACT

Analysis of eruptive gases began at Kilauea Volcano in 1912. After the classic gas collections of 1917–19, there was a lapse of 40 years until sampling of eruptive gases recommenced in 1960. This paper summarizes results of gas analyses from Kilauea for the 1912–19 and 1968 Halemaumau eruptions, two summit eruptions in 1982, the 1960, 1965, 1977, and 1983–84 east-rift eruptions, and a shallow southwest-rift intrusion in 1981. Also included are results from the 1919 and 1984 eruptions of Mauna Loa. These data show the following: (1) Hawaiian eruptive gases predominantly have one of two compositions, defined by an atomic carbon/sulfur ratio (C/S) of ~0.2 for gases exsolving from magma that has had even brief storage in shallow summit reservoirs, and (much less commonly) a C/S ratio of ~2 for gases associated with eruptions of magma directly from the mantle. (2) The major causes of compositional variation in these gases is the introduction of varied amounts of assimilated crustal water and near-surface mixing of meteoric water. (3) The total volatile content of Hawaiian magma stored in summit reservoirs is approximately uniform and amounts to less than 0.5 weight percent.

INTRODUCTION

Studies of eruptive gas at Kilauea Volcano began in 1912 with collections from an active lava lake by Day and Shepherd (1913). Because of the sampling technique, only partial analyses of these gases could be obtained. Improvements in sampling and analytical procedures resulted in the first complete volcanic gas analyses in 1917 (Shepherd, 1919) and the culminating studies of T.A. Jaggar's classic collections of 1918–19 (Shepherd, 1921). Between 1919 and 1980, sporadic collections of volcanic gas associated with eruptive activity at Kilauea were obtained from vents during the 1960 east-rift eruption (Heald and others, 1963), from an actively filling lava lake (Finlayson and others, 1968), and from the 1977 east-rift eruption (Graeber and others, 1979).

Systematic gas studies were reinstituted at the Hawaiian Volcano Observatory with the installation of modern gas-analysis facilities in 1980. Partial analyses were obtained of gases from a near-surface intrusion in 1981 and from two summit eruptions in 1982; both partial and complete analyses have been obtained from the episodic east-rift eruption of 1983-4 and from the 1984 eruption of Mauna Loa. The present paper summarizes previous work on eruptive gases and describes heretofore unpublished results of the 1981–84 partial analyses. Complete gas analyses of the 1983–84 east-rift eruption of Kilauea and of the Mauna Loa eruption are being described concurrently (Greenland, chapter 30) and will not be considered here.

To improve comparability, all analyses cited from the literature have been recalculated to an air-free basis. Furthermore, I have followed Matsuo (1962) in apportioning the S_2 reported in the 1917–19 analyses to H_2S and SO_2, and, where reported, SO_3 to SO_2; for the 1981–84 partial analyses, I have assumed thermodynamic equilibrium in the gases in order to estimate apparent-equilibrium H_2O and H_2S contents. The effects of oxidation and of temperature on the composition of volcanic gas samples have been avoided by considering the analyses on an atomic basis (that is, all hydrogen-bearing species are combined to yield a value for total atomic hydrogen, and so on), and these values form the basis for most of the discussion.

ACKNOWLEDGMENTS

I am grateful to E. Wolfe and T. Wright for thorough and helpful reviews of the manuscript.

RESULTS AND DISCUSSION

GAS COLLECTIONS FROM 1912 TO 1919

Analyses of gases collected from a continuously active lava lake in Kilauea's caldera over this period are fiven in table 28.1, which also includes two samples from the 1919 eruption of Mauna Loa. The equilibrium compositions of the 1918–19 gas collections as estimated by Gerlach (1980) also are included in table 28.1 for reference.

The 1912 gases were collected by a pumping technique, and thus only the concentrations of gases insoluble in the acid aqueous condensate (CO_2, H_2, and CO) could be determined; these provide too little information for interpretation, though it is notable that temperatures (1,150–1,250 °C) inferred from the CO_2/CO ratio (from equations 1 and 5, see below) are reasonable for a protracted summit eruption.

The 1917–19 analyses have been discussed extensively (Shepherd, 1938; Jaggar, 1940; Matsuo, 1962; Nordlie, 1971; Gerlach, 1980); conclusions have ranged from Shepherd's (1921, p. 87) "We are not here dealing with a mixture of gas which is definite in composition and given off steadily by the magma. Each bubble has its own composition, ***" to Gerlach's (1980, p. 303) "***(after making allowance for meteoric water contamination)***(1) the erupted gases initially had compositions closely approaching equilibrium, and (2) the reacting gases were quenched at some temperature near the collection temperature." These views are less far

TABLE 28.1.—*Composition of Hawaiian eruptive gases, 1912–1919*

[n.d., not determined; __, not detected]

Sample	Constituents (mole percent)						Atomic ratios	
	H_2O	H_2	CO_2	CO	SO_2	H_2S	H/S	C/S
1912 Kilauea Summit (Day and Shepherd, 1913)								
D–1 ____	n.d.	7.2	23.8	5.6	n.d.	n.d.	n.d.	n.d.
D–2 ____	n.d.	6.7	58.0	3.9	n.d.	n.d.	n.d.	n.d.
D–8 ____	n.d.	7.5	62.3	3.5	n.d.	n.d.	n.d.	n.d.
D–11 ___	n.d.	7.0	59.2	4.6	n.d.	n.d.	n.d.	n.d.
D–17 ___	n.d.	10.2	73.9	4.0	n.d.	n.d.	n.d.	n.d.
1917 Kilauea Summit (Shepherd, 1919)								
S–1 _____	87.8	5.45	3.42	1.34	.809	1.20	96.7	2.36
S–2 _____	61.4	2.16	28.7	.575	6.13	1.04	18.0	4.08
S–3 _____	20.5	1.78	38.1	1.62	35.3	2.72	1.31	1.04
S–4 _____	69.7	1.28	10.0	3.53	5.16	10.3	10.5	.875
S–5 _____	70.2	1.66	10.3	1.21	12.7	3.93	9.11	.692
S–6 _____	90.6	.212	1.99	.827	2.77	3.63	29.5	.440
S–7 _____	67.8	.803	18.2	.655	11.0	1.50	11.2	1.51
S–8 _____	75.5	.704	15.4	.452	7.35	.657	19.2	1.98
S–9 _____	64.7	1.96	8.98	.885	19.9	3.57	5.98	.420
S–10 ____	90.5	.372	1.55	.433	2.39	4.78	26.7	.277
1918–19 Kilauea Summit (Shepherd, 1921)								
J–2 _____	85.3	__	6.58	__	8.14	__	21.0	0.808
J–3 _____	83.6	.156	6.90	.229	9.10	__	18.4	.783
J–4 _____	87.4	.175	6.99	.144	5.05	.206	33.4	1.36
J–6 _____	98.4	.088	1.09	.200	.175	__	1130.	7.37
J–8 _____	37.1	.493	48.9	1.50	11.9	.055	6.30	4.22
J–10 ____	60.0	.118	19.4	.130	20.2	.079	5.94	.963
J–11 ____	64.2	.334	21.8	.615	12.7	.348	9.95	1.72
J–12 ____	97.8	.081	1.43	.050	.561	.094	299.0	2.26
J–13 ____	69.9	.994	17.6	.601	10.8	.124	13.0	1.67
J–14 ____	79.1	.175	15.2	.484	4.88	.137	31.7	3.13
J–15 ____	79.0	.107	12.3	.139	8.40	.043	18.7	1.47
J–16 ____	68.4	.692	18.6	.578	11.5	.206	11.8	1.64
J–17 ____	80.2	.587	11.7	.374	6.72	.324	23.0	1.71
J–18 ____	64.8	.869	18.4	.775	14.8	.307	8.73	1.27
1918–19 Kilauea Summit: estimated equilibrium composition (Gerlach, 1980)								
J–8 _____	37.1	.490	48.9	1.51	11.8	0.040	6.36	4.26
J–11 ____	40.1	.550	36.7	1.03	21.1	.200	3.84	1.77
J–13 ____	69.3	1.01	17.8	.620	10.9	.080	12.8	1.68
J–14 ____	35.1	.540	47.4	1.52	15.1	.150	4.69	3.21
J–16 ____	60.4	.870	23.2	.740	14.3	.140	8.50	1.66
J–17 ____	66.0	1.02	20.3	.620	11.4	.320	11.5	1.78
J–18 ____	58.1	1.03	21.8	.930	17.5	.170	6.71	1.29
1919 Mauna Loa (Shepherd, 1920)								
ML–1 ___	75.4	__	3.84	0.03	3.30	__	45.7	1.16
ML–2 ___	67.4	.01	6.42	.19	10.07	__	13.5	.66

apart than one might think: Gerlach (1980) recognizes the effects of oxidation and of shallow degassing of CO_2 on these compositions; furthermore, thermodynamic analyses such as Gerlach's are concerned with the relative proportions of oxidized and reduced species rather than the relative proportions of all hydrogen-bearing, carbon-bearing, and sulfur-bearing species. In addition, it may indeed be possible that each bubble has its own composition and yet approaches equilibrium when one considers the possible effects of differential degassing with pressure and of the incorporation of air and water into the vent system by a chimney effect. The highly porous edifice of Kilauea combines with the high-temperature vertical pipes of the fissure system to produce a chimney effect whereby air, water vapor, and other gases are pulled through the edifice into the depths of the fissure, heated, expanded, and expelled to the surface. A similar effect has been observed at Pagan Volcano (see Banks and others, 1984.)

The effects of oxidation and temperature, but not of water contamination, can be avoided by considering the analyses on an atomic basis. Table 28.1 includes the analytical values normalized to atoms of S for ease of comparison, and figure 28.1 is a ternary atomic H-C-S plot of these data. If all of these analyses were related simply by water contamination (with or without oxidation effects), the analyses would plot along a water-control line such as the two shown in figure 28.1; in fact, however, there is a large amount of scatter in figure 28.1, implying considerable variation in carbon/sulfur ratio independent of the obvious water variation. Gerlach (1980) attributed this variation to the preferential degassing of the very insoluble CO_2, and he suggested that the most CO_2-rich samples are most characteristic of undegassed magma. On the other hand, preferential degassing of CO_2 at least raises the possibility of the contamination of eruptive magma with deeper released CO_2. Several observations may be made from the plot in figure 28.1: (1) although the 1917 samples show considerably more scatter than the 1918–19 collections, perhaps because of the poorer sampling conditions of 1917 noted by Shepherd (1921), the compositions of the two groups overall are indistinguishable. (2) As noted by Shepherd (1920), the two Mauna Loa samples are similar in composition to the Kilauea samples. (3) The 1918–19 analyses selected as superior by Gerlach (1980) show much less scatter and much closer adherence to a water-control line than does the original complete set. (4) Nearly all samples have an atomic C/S ratio much higher than do collections made since 1979, which follow the water-control line with C/S = 0.18 in figure 28.1. The third observation

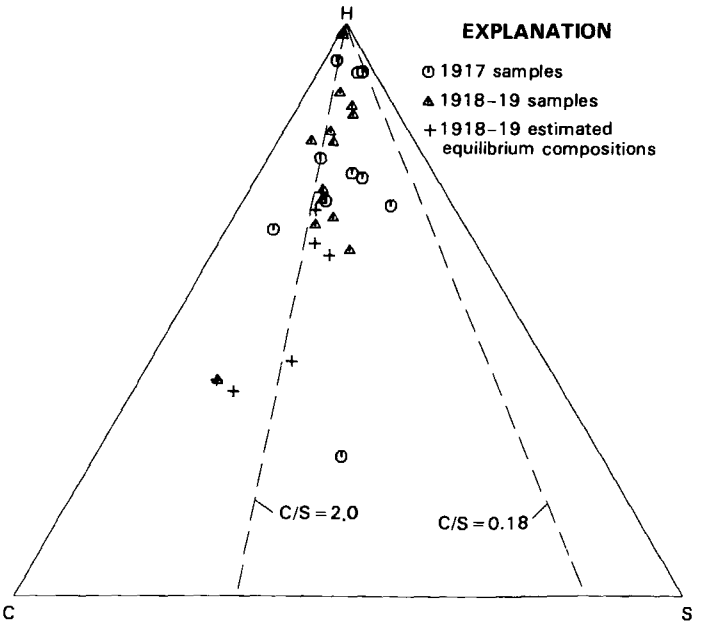

FIGURE 28.1.—Ternary H-C-S plot for 1917–19 Hawaiian eruptive gases. Data from table 28.1. Dashes indicate water-control lines for specific values of the C/S ratio. Atomic hydrogen has been reduced by a factor of 0.5 to increase clarity.

above raises the unanswerable question of how much of the observed scatter in the 1917–19 analyses might be due to analytical error; a modern analyst reading Shepherd's (1925) account of his analytical procedure can only be awed by his skill and meticulous attention to detail, while remaining aware of the inherent limitations imposed by the equipment available to him. The fourth observation above has been attributed to degassing of CO_2 during storage of magma in the summit reservoir of Kilauea, and it forms the basis of recent models (Gerlach and Graeber, 1985; Greenland and others, 1985) of magma-degassing processes at Kilauea.

The two samples from Mauna Loa have been largely neglected in the literature, perhaps because both are highly oxidized and both were collected from a low-temperature (~300 °C) ground crack near advancing lava and about 100 m from the eruptive fissure. However, oxidation does not affect the atomic composition, and it has been my experience that such sampling sites at Kilauea frequently provide excellent gas samples. The significance of these samples is that their C/S ratio is closer to that of the 1917–19 Kilauea collections than to the much lower ratio found for the 1984 Mauna Loa eruption. The distinction between high 1917–19 and low 1983–84 C/S ratios at Kilauea has been attributed to degassing during storage in the summit reservoir (Gerlach and Graeber, 1985; Greenland, and others, 1985; Greenland, in press), and the same mechanism has been invoked to account for the low C/S ratios of the 1984 Mauna Loa gases (Greenland, chapter 30). However, the 1919 Mauna Loa eruption was also a rift eruption and thus the magma would be expected to have passed through, and been degassed in, the summit reservoir; therefore, it is not obvious how the different C/S ratios of the 1919 and 1984 eruptions are to be accounted for. Perhaps the very high content of SO_3 shown in the analysis of 1919 gas (Shepherd, 1920) led to condensation of H_2SO_4 and reaction with wallrock; also, the chemistry of lava erupted on the southwest rift zone differs from that of the northeast rift zone (T.L. Wright, written commun., 1985), indicating a possibility of different storage reservoirs for the two rifts.

KILAUEA GAS COLLECTIONS FROM 1920 TO 1979

Gas collections representing the 1959 Kilauea Iki eruption were made from the degassing cinder cone of Puu Puai and from drill holes in the cooling lava lake (Heald and others, 1963). Both of these sites give information on the degassing of lava after eruption but are only indirectly related to eruptive magmatic gas compositions and will not be considered here.

Three samples were collected from the 1960 east-rift eruption at Kapoho (table 28.2). These samples, collected from a high-temperature fumarole near a lava fountain, are remarkable in showing a significant amount of CH_4 and extremely high water content and C/S ratio. Heald and others (1963) suggest, very reasonably, that these samples have been contaminated by meteoric water and by buried organic matter. In view of the probable high degree of contamination, these analyses shed little light on the nature of magmatic gases.

TABLE 28.2.—*Composition of eruptive gases from Kilauea, 1920–1979*

[n.d., not determined; --, not detected]

Sample	Constituents (mole percent)							Atomic ratios	
	H_2O	H_2	CO_2	CO	SO_2	H_2S	CH_4	H/S	C/S
Kapoho, 1960 East Rift (Heald and others, 1963)									
Ka–1	97.2	0.373	2.34	0.059	0.009	--	0.047	22,000.0	267.0
Ka–2	97.5	.394	1.97	.019	.152	--	.034	1,290.0	13.1
Ka–4	97.2	.432	2.21	.086	.001	.031	.023	6,100.0	71.8
Makaopuhi, 1965 East Rift Lava Lake (Finlayson and others, 1968)									
26–M	67.1	--	8.54	--	24.4	--	--	5.50	0.35
27–M	98.0	.057	1.90	--	--	--	--	n.d.	n.d.
28–M	87.5	.137	1.96	--	6.61	3.79	--	17.6	.19
29–M	97.0	1.125	1.92	--	--	--	--	n.d.	n.d.
38–M	95.8	.011	.597	--	3.60	--	--	26.6	.17
Halemaumau Fountain, 1968 (Naughton and others, 1969)									
HMM–1	95.0	n.d.	4.0	n.d.	1.0	n.d.	n.d.	190.0	4.0
1977 East Rift (Graeber and others, 1979)									
G–5	89.1	--	5.06	--	5.45	--	--	32.7	0.93
G–6	96.9	--	1.99	--	.84	--	--	235.	2.38
G–7	93.6	--	1.87	--	4.42	--	--	42.3	.42

Table 28.2 gives the analyses of five gas samples collected from the filling lava lake at Makaopuhi during the 1965 east-rift eruption. (For further analyses of gas samples from the cooling lava lake, see Finlayson and others, 1968). As shown by the low content of H_2 and the absence of CO, these samples are highly oxidized; the very high water content in four of the samples and the absence of sulfur species in two also raises doubts about the quality of the samples. Nevertheless, on an atomic basis, the three samples that contain detectable sulfur have C/S ratios very similar to the ratios observed in the 1983–84 east-rift eruption (see below) and two of these have H/S ratios in the range of the later analyses. Therefore, although these samples have been subjected to oxidation and, probably, contamination with meteoric water, they are consistent with suggestions (Gerlach and Graeber, 1985; Greenland and others, 1985) that all summit-stored magma at Kilauea has about the same composition of volatiles.

In 1968, Naughton and others (1969) made an interesting direct measurement of the major gases in a lava fountain (Halemaumau eruption of 1967–68, table 28.2) using an infrared technique. Naughton and others (1969) stress the exploratory nature of their study and the tentativeness of the results; nonetheless, fountain-gas measurements obviously are impossible to obtain by conventional sampling procedures, and it is encouraging to note the similarity of this analysis, particularly in C/S ratio, to those of the 1917–19 Halemaumau samples (table 28.1). The high water content in this analysis may be due to uncertainties inherent in the technique (a very large, and not entirely certain, correction was required for atmospheric water in the light path). However, in view of the observation that degassing of melt continues within the fountain (Swanson and Fabbi, 1973), it may be that fountain gas is enriched in water, which, because of its high solubility in the melt, is the last gas to be exsolved. It is unfortunate that this potentially rewarding technique has not been pursued.

Table 28.2 gives analyses of three gas samples from the 1977 east-rift eruption (Graeber and others, 1979). These samples were collected from one of the main vents of the fissure eruption three days after eruption of the sampled vent had ceased; the observation that the samples were almost entirely air and completely oxidized parallels my experience in sampling similar sites during the 1982 summit eruptions, the 1983–84 east-rift eruption, and the 1984 Mauna Loa eruption: sampling gases from major vents after fountaining ceases during fissure eruptions seems unrewarding. A remarkable feature of these analyses is the great variation in C/S ratio, which ranges from 0.4 to 2.4 in the three samples collected within 15 minutes of each other at the same vent. This is a greater range than shown in 14 months of the 1983–84 eruption (see below). Graeber and others (1979) observed reddish flame at this vent during the night, and it may be that the varying C/S ratio reflects pyrolyzing organic matter swept into the vent by the chimney effect, a phenomenon recognized frequently during early stages of the 1983–84 eruption.

KILAUEA GAS COLLECTIONS FROM 1980 TO 1982

During this period, gas samples were collected from a shallow intrusion into the southwest rift zone and from two summit eruptions. Gas samples during these events were collected in flowthrough bottles. The sampling technique and subsequent gas chromatographic analysis have been described previously and the results compared with conventional techniques (Greenland, 1984).

Only partial analyses (H_2, CO_2, CO, and SO_2) could be made of these samples, and, for comparison with other eruptions, it is necessary to make an estimate of the H_2O and H_2S content of the gases. Following the procedure described elsewhere (Greenland, chapter 30), equilibrium constants for the elementary oxidation reactions of the major gases can be expressed as

$$\log K1 = 2\log[CO_2/CO] - \log[O_2] \quad (1)$$

$$\log K2 = 2\log[H_2O/H_2] - \log[O_2] \quad (2)$$

$$\log K3 = 2\log[SO_2/H_2S] + \log[H_2] - \log[O_2] \quad (3)$$

and, over a limited temperature range, the temperature dependence of the equilibrium constant can be approximated by

$$\log K = [A/T] + B, \quad (4)$$

where A and B are thermodynamic constants. Complete gas analyses of both the 1983–84 east-rift eruption (Greenland, in press) and of the 1984 Mauna Loa eruption (Greenland, chapter 30) have shown that the partial pressure of oxygen in these gases was buffered by the magma; therefore, $\log[O_2]$ is a linear function of the reciprocal of temperature. Averaging the results from the cited complete analyses yields

$$\log[O_2] = -[18{,}600/T] + 4.06. \quad (5)$$

Combining equations 1, 4, and 5 makes it possible to estimate an equilibrium temperature for a gas sample from the observed CO_2/CO ratio, and equations 2 and 3 provide estimates of the equilibrium amounts of H_2O and H_2S in the sample.

Table 28.3 provides the estimated equilibrium composition of gas samples collected in the 1980–82 period. These estimates depend on the assumptions that (1) the gases were in thermodynamic equilibrium and (2) there has been no oxidation of CO or H_2. That many eruptive gas samples approximate equilibrium assemblages has been demonstrated widely (Greenland, chapter 30; Gerlach, 1980, 1982; Greenland, in press). Examination of equations 1 and 2 show that oxidation of CO would yield a low estimate of temperature and a high estimate of water, whereas oxidation of H_2 would result in a low estimate of water. There can be no independent check on the oxidation state of these samples, and therefore the water and temperature estimates should not be taken too literally; on the other hand, as shown below, results from this calculation procedure appear to be generally reasonable and are preferable to no estimate at all. Note that this procedure does not alter the observed gas ratios, and thus the original analyses may be recovered directly from table 28.3.

A major intrusion into the southwest rift zone of Kilauea occurred on August 10, 1981, and resulted in ground cracking over a large area. A small segment of the dike reached within 250 m of the surface (estimated from deformation measurements, A. Okamura, oral commun., 1981) and magmatic gases issued from low-temperature ground cracks in this local area. The estimated equilibrium compositions of samples of these gases (table 28.3) show a rapid change with time. The initial sample has a composition similar to some of the east-rift Makaopuhi and 1983–84 east-rift gases (this paper), but subsequent samples are water-rich and show increasing C/S ratios with continued outgassing. A sample collected the following morning (August 11), after the intrusion had ended, had a C/S ratio of >100 and too little CO to attempt an equilibrium estimate. Because CO_2 is much less soluble than S, the increase of C/S ratio with time cannot reflect degassing of the near-surface melt. Perhaps CO_2 that exsolved from the deeper part of the dike percolated through the local, shallow segment as an easy route to the surface; this would account for the observation that CO_2 emissions from these cracks ceased after a few weeks when, presumably, freezing of the shallow segment of the dike blocked egress for the CO_2.

A brief fissure eruption adjoining Halemaumau occurred in April 1982. It was impossible to obtain gas samples from the erupting vents, and samples obtained from these vents after fountaining ceased consisted only of air. Two strongly fuming ground cracks, on strike with the fissure and less than 100 m from fountains, provided the analyses given in table 28.3. The initial sample from crack no. 1 has a composition similar to east-rift samples, but the C/S ratio increases rapidly in the subsequent samples, which also become very water rich. The first sample from crack no. 2 already has a high C/S ratio and high water content, and subsequent samples show increases in both parameters. The probable explanation for the increase in C/S ratio with time at these cracks lies in their location at the edge of Halemaumau: it is likely that these cracks tap into the extensive Halemaumau fumarole system; they have continued to emit CO_2-rich gases typical of these fumaroles through May 1985. The composition of the magmatic gas probably is best

TABLE 28.3.—*Composition of eruptive gases from Kilauea, 1980–1982*
[--, no data]

Collection		Temperature (°C)		Constituents (mole percent)						Atomic ratios	
Date	Hour	Collection	Equilibrium	H_2O	H_2	CO_2	CO	SO_2	H_2S	H/S	C/S
AUGUST 1981 SOUTHWEST-RIFT-ZONE INTRUSION											
8/10/81	0800	84	878	83.222	0.524	3.772	0.029	11.379	1.073	13.623	0.305
	1200	84	810	93.688	.388	1.497	.006	3.906	.515	42.792	.340
	1530	82	919	90.178	.714	3.165	.034	5.421	.487	30.930	.541
	1730	82	823	91.709	.413	3.713	.017	3.692	.456	44.630	.899
APRIL 1982 SUMMIT ERUPTION											
Ground crack No. 1											
4/30/82	1540	94	1,002	79.712	0.962	3.064	0.063	15.228	0.972	10.080	0.193
	1745	85	755	94.943	.268	3.766	.008	.872	.143	187.923	3.719
	1940	80	712	94.487	.192	4.713	.006	.503	.097	315.613	7.859
	2210	79	689	94.143	.159	5.427	.006	.218	.046	713.306	20.537
	2400	--	652	93.509	.115	6.241	.004	.105	.026	1,432.087	47.747
Ground crack No. 2											
	1530	82	909	89.578	0.672	3.333	0.033	5.846	0.538	28.442	0.527
	1735	86	816	92.110	.397	4.211	.018	2.897	.367	56.906	1.296
	1940	85	743	93.566	.242	4.844	.009	1.145	.194	140.410	3.625
	2220	82	698	94.369	.172	5.343	.006	.091	.019	1,732.875	49.017
SEPTEMBER 1982 SUMMIT ERUPTION											
Ground cracks											
9/25/82	1910	22	1,128	87.644	1.813	1.732	0.080	8.297	0.434	20.591	0.208
	1920	40	1,113	88.580	1.726	1.236	.052	7.971	.435	21.589	.153
	2000	85	1,132	87.261	1.833	1.299	.062	9.076	.469	18.766	.143
Active vent											
9/25/82	2300	1,120	1,004	47.068	0.573	6.239	0.129	44.316	1.675	2.145	0.138
	2325	1,070	1,042	72.311	1.048	3.261	.088	22.129	1.164	6.399	.144
9/26/82	0125	--	995	78.632	.914	3.488	.067	15.878	1.020	9.536	.210
	0405	--	958	91.220	.887	.974	.014	6.384	.521	26.830	.143

approximated by the first sample from crack no. 1.

Another brief summit eruption of Kilauea took place in the south caldera in September 1982. Actively fountaining vents were unapproachable, but fuming ground cracks (the leading edge of the progressively opening fissure) yielded three gas samples (table 28.3). One isolated vent erupted very briefly and then continued to emit a continuous blue-green flame with spatter and occasional small lava overflows for the rest of the eruption; this provided the gas samples identified as from an active vent in table 28.3. Unlike those from the preceding eruption and intrusion, these samples maintain an approximately constant C/S ratio throughout; this ratio is the same as that of the samples considered best from the April 1982 eruption and the 1983–84 east-rift eruption. The active-vent samples show an increase in apparent water content with time. Whether this is a real effect or an anomaly caused by the procedure for estimating water is uncertain. An important observation is the similarity of the gas compositions in very low temperature samples from ground cracks and in high-temperature samples at the active vent: apparently, gases are quenched very rapidly by contact with the cold country rock, a significant result to consider when attempting to sample fissure eruptions.

KILAUEA GAS COLLECTIONS FROM 1983

A middle-east-rift eruption of Kilauea began in January 1983 and has continued episodically (through February 1986). Results of complete analyses of gas samples from this eruption are described elsewhere (Greenland, in press) and will not be considered here. More than 400 gas samples were collected for partial analysis (CO_2, CO, H_2, and SO_2); more than half of these contained too much air or organic gases or were too greatly oxidized to be of much significance. Tables 28.4–28.8 present the results for the remainder of the samples, selected with the constraints that (1) CO_2 and SO_2 constitute more than 0.1 percent and CO and H_2 more than 0.001 percent of the original sample to ensure adequate determination and (2) the CO/H_2 ratio be less than 0.3 to exclude samples with organic contamination and some of the oxidized samples. Estimated equilibrium temperatures and H_2O and H_2S contents (see above) are included in tables 28.4–28.8; as noted above, these estimates have large uncertainties and only the general tendency of the results can be regarded as significant.

This eruption began as a fissure eruption that provided an abundance of gas sampling sites along a line of vents several kilometers long through January and part of February 1983; by June 1983, the eruption had become localized at a single vent that has provided far fewer gas-sampling opportunities. With the restriction of sampling sites, samples were increasingly collected for complete analysis rather than the rapid partial analyses described here; therefore most of the results in tables 28.4–28.8 refer to the January–March 1983 interval.

These results are summarized in the ternary atomic H-C-S diagram of figure 28.2. This diagram shows that most of the samples adhere closely to a water-control line with a C/S ratio of 0.18. A few of the samples, particularly at higher water contents,

TABLE 28.4.—*Composition of gases from east rift eruption of Kilauea, 1983: actively erupting vents*

[--, no data]

Sample	Date (mo/d)	Temperature (°C)		Constituents (mole percent)						Atomic ratios	
		Collection	Equilibrium	H_2O	H_2	CO_2	CO	SO_2	H_2S	H/S	C/S
70	1/10	--	823	68.427	0.308	6.503	0.030	22.611	2.121	5.730	0.264
71	1/10	--	811	67.474	.282	6.508	.026	23.450	2.260	5.447	.254
259	3/31	--	827	57.568	.266	9.151	.043	30.584	2.387	3.653	.279
386	8/12	--	830	65.766	.309	6.453	.031	25.217	2.223	4.978	.236
387	8/13	--	920	74.629	.595	3.485	.038	19.772	1.482	7.218	.166
389	8/13	1,048	1,089	87.004	1.538	1.488	.054	9.386	.530	17.965	.156
390	8/13	820	954	56.578	.539	6.660	.095	34.348	1.780	3.260	.187
391	8/13	820	966	78.035	.790	3.413	.053	16.570	1.139	9.031	.196
393	8/14	820	919	64.112	.508	5.227	.056	28.265	1.831	4.416	.176
394	8/14	820	977	83.633	.895	2.629	.045	11.946	.852	13.343	.209
395	8/14	1,120	1,083	84.515	1.457	2.153	.076	11.177	.623	14.677	.189
396	8/14	1,120	1,035	92.098	1.289	2.158	.055	4.121	.279	42.575	.503
404	9/02	1,115	1,039	85.476	1.222	1.692	.045	10.887	.678	15.110	.150
405	9/02	1,115	1,051	80.879	1.216	2.359	.067	14.636	.841	10.717	.157
406	9/02	1,115	1,024	83.432	1.115	1.972	.047	12.635	.798	12.707	.150
407	9/02	1,110	982	79.500	.870	1.976	.035	16.511	1.108	9.249	.114
408	9/02	1,110	863	58.040	.335	4.311	.029	34.849	2.437	3.262	.116
409	9/03	1,113	1,074	90.476	1.502	1.319	.044	6.279	.381	27.735	.205
410	9/04	1,110	1,078	85.853	1.451	1.435	.049	10.605	.606	15.683	.132
411	9/04	1,110	1,076	85.390	1.429	1.514	.051	10.987	.628	15.058	.135
414	10/28	--	658	68.036	.088	4.118	.003	23.398	4.330	5.228	.149

TABLE 28.5.—*Composition of gases from east rift eruption of Kilauea, 1983: presently inactive*

[--, no data]

Sample	Date (mo/d)	Temperature (°C)		Constituents (mole percent)						Atomic ratios	
		Collection	Equilibrium	H_2O	H_2	CO_2	CO	SO_2	H_2S	H/S	C/S
10	1/05	721	1,025	74.674	1.000	4.647	0.111	18.519	1.408	7.842	0.243
11	1/05	721	1,023	71.293	.948	5.543	.131	20.948	1.137	6.645	.257
20	1/05	92	1,025	88.274	1.185	5.412	.130	4.688	.311	35.915	1.109
49	1/07	--	1,116	65.527	1.295	5.373	.233	26.503	1.070	4.925	.203
50	1/07	--	1,108	67.292	1.286	4.934	.203	25.221	1.064	5.299	.195
54	1/09	285	820	48.154	.212	10.515	.046	38.491	2.581	2.481	.257
61	1/09	95	837	56.567	.278	10.208	.053	30.624	2.270	3.594	.312
69	1/09	941	1,071	71.143	1.170	3.295	.108	23.164	1.120	6.048	.140
88	1/13	498	978	50.672	.543	9.150	.156	37.831	1.648	2.678	.236
90	1/14	720	1,083	67.925	1.173	6.170	.217	23.460	1.055	5.723	.261
93	1/14	935	1,082	57.134	.984	6.672	.234	33.697	1.279	3.396	.197
98	1/15	500	963	59.777	.594	4.708	.072	33.079	1.771	3.566	.137
113	1/15	888	1,084	64.240	1.115	6.300	.224	26.976	1.145	4.730	.232
115	1/15	890	1,118	68.469	1.363	5.283	.231	23.660	.993	5.746	.224
116	1/16	888	1,076	71.707	1.202	4.874	.164	21.039	1.014	6.704	.228
118	1/16	888	1,092	71.225	1.277	4.249	.159	22.071	1.019	6.368	.191
119	1/17	887	1,064	75.852	1.209	3.346	.104	18.520	.969	8.008	.177
120	1/17	887	1,048	67.626	1.006	4.054	.114	25.940	1.260	5.139	.153
122	1/18	863	1,052	57.602	.871	5.590	.161	34.364	1.412	3.348	.161
123	1/18	863	1,054	73.850	1.124	3.952	.115	19.918	1.041	7.254	.194
143	2/12	900	990	47.358	.539	5.482	.102	44.752	1.766	2.135	.120
144	2/12	350	1,101	65.042	1.208	4.234	.167	28.181	1.168	4.594	.150
154	2/14	1,008	950	59.720	.557	2.779	.038	34.967	1.938	3.372	.076
155	2/14	1,006	677	58.464	.089	2.734	.002	33.758	4.952	3.281	.071
156	2/14	--	796	33.420	.126	9.531	.033	54.144	2.746	1.276	.168
165	2/15	985	987	67.390	.754	2.113	.039	28.116	1.589	4.695	.072
178	2/17	867	1,023	73.915	.981	3.115	.074	20.746	1.169	6.942	.146
179	2/17	867	1,003	50.070	.607	5.613	.115	41.905	1.690	2.402	.131
187	2/23	975	963	63.474	.631	3.242	.049	30.851	1.752	4.040	.101
188	2/23	975	866	77.200	.452	2.309	.016	18.345	1.678	7.924	.116
194	2/24	930	898	69.084	.487	3.968	.036	24.597	1.828	5.404	.152
195	2/24	930	896	69.048	.480	3.972	.035	24.622	1.843	5.394	.151
250	3/29	230	765	30.731	.093	8.753	.022	57.391	3.010	1.120	.145
275	4/05	900	716	41.175	.086	7.202	.010	47.427	4.099	1.761	.140
279	4/07	--	873	80.300	.492	2.025	.015	15.711	1.457	9.582	.119
281	4/08	832	842	82.835	.421	1.840	.010	13.470	1.424	11.371	.124
285	4/08	862	817	73.319	.317	3.067	.013	21.114	2.170	6.511	.132
311	5/06	810	685	48.394	.079	5.679	.006	41.046	4.797	2.324	.124
315	5/16	795	805	83.659	.334	2.477	.009	12.058	1.462	12.641	.184
317	5/20	765	839	71.198	.354	4.160	.022	22.212	2.053	6.067	.172
322	5/24	750	778	85.187	.284	2.143	.006	10.897	1.483	14.047	.174
323	5/24	750	783	85.164	.294	2.225	.007	10.860	1.450	14.120	.181

TABLE 28.6.—*Composition of gases from east rift eruption of Kilauea, 1983: ground cracks near eruptive center*

[--, no data]

Sample	Date (mo/d)	Temperature (°C)		Constituents (mole percent)						Atomic ratios	
		Collection	Equilibrium	H_2O	H_2	CO_2	CO	SO_2	H_2S	H/S	C/S
2	1/03	140	1,143	63.183	1.388	7.571	0.385	26.498	0.974	4.772	0.290
3	1/03	141	1,296	74.433	2.771	4.913	.557	16.782	.545	8.974	.316
22	1/05	205	1,034	68.096	.952	4.723	.121	24.852	1.256	5.386	.186
23	1/05	88	1,012	71.712	.907	3.752	.082	22.295	1.252	6.274	.163
24	1/06	80	1,023	86.327	1.144	2.894	.068	8.979	.588	18.409	.310
25	1/06	77	970	91.516	.944	2.283	.037	4.838	.383	35.565	.444
26	1/06	78	1,070	80.157	1.312	3.563	.116	14.085	.766	11.075	.248
27	1/06	67	1,045	85.588	1.253	4.105	.113	8.423	.518	19.541	.472
28	1/06	82	1,075	88.020	1.472	3.915	.131	6.103	.359	27.809	.626
29	1/06	78	1,052	86.814	1.315	4.781	.138	6.551	.401	25.469	.708
30	1/06	78	1,047	87.346	1.293	4.826	.135	6.025	.375	27.817	.775
31	1/06	77	1,056	89.185	1.370	4.605	.136	4.429	.276	38.610	1.008
32	1/06	--	1,054	90.351	1.376	4.401	.128	3.521	.223	49.119	1.210
34	1/06	335	1,084	77.589	1.343	3.263	.115	16.829	.861	9.021	.191
46	1/06	48	1,107	83.573	1.589	6.113	.250	8.055	.420	20.196	.751
47	1/07	69	1,091	76.085	1.359	5.081	.188	16.475	.812	9.054	.305
72	1/11	90	919	64.839	.514	5.442	.059	27.354	1.792	4.607	.189
73	1/11	91	830	62.308	.293	6.589	.032	28.402	2.376	4.222	.215
74	1/11	--	860	72.512	.411	5.159	.033	20.122	1.762	6.826	.237
75	1/11	88	888	76.237	.508	4.909	.041	16.884	1.421	8.540	.270
162	2/14	330	941	45.600	.406	8.355	.107	43.638	1.894	2.104	.186
167	2/15	835	1,007	62.530	.771	2.588	.055	32.439	1.617	3.812	.078
168	2/15	835	1,010	60.083	.751	2.693	.058	34.762	1.654	3.432	.076
169	2/15	440	791	69.461	.252	1.661	.005	25.844	2.776	5.066	.058
198	2/27	385	1,031	62.644	.863	4.091	.102	30.850	1.449	4.022	.130
199	2/27	275	1,045	50.472	.740	4.979	.137	42.127	1.544	2.416	.117
205	3/01	270	892	44.853	.305	9.908	.085	42.741	2.108	2.108	.223
211	3/04	83	712	68.129	.139	11.184	.015	17.969	2.563	6.900	.545
212	3/04	244	766	40.682	.125	10.502	.027	45.520	3.143	1.806	.216
244	3/28	210	661	43.642	.058	7.842	.006	43.346	5.106	2.015	.162
249	3/29	125	660	61.175	.081	6.607	.005	27.576	4.556	4.096	.206
251	3/29	--	749	40.860	.111	7.646	.016	47.811	3.556	1.734	.149
329	6/13	67	965	55.816	.561	2.267	.035	39.361	1.961	2.824	.056
330	6/13	85	1,010	87.580	1.094	.517	.011	10.105	.693	16.553	.049
331	6/13	117	999	57.747	.687	2.199	.044	37.559	1.765	3.062	.057

TABLE 28.7.—*Composition of gases from east rift eruption of Kilauea, 1983: ground cracks distant from eruption center*

[--, no data]

Sample	Date (mo/d)	Temperature (°C)		Constituents (mole percent)						Atomic ratios	
		Collection	Equilibrium	H_2O	H_2	CO_2	CO	SO_2	H_2S	H/S	C/S
13	1/05	571	1,079	61.882	1.051	5.253	0.180	30.375	1.258	4.058	0.172
14	1/05	561	1,106	69.929	1.326	4.113	.167	23.434	1.031	5.909	.175
15	1/05	441	1,108	68.678	1.313	5.441	.224	23.339	1.004	5.833	.233
16	1/05	441	1,111	70.619	1.370	4.614	.194	22.228	.975	6.289	.207
17	1/05	420	1,079	65.772	1.117	5.367	.185	26.398	1.160	4.939	.201
18	1/05	--	1,066	64.907	1.041	4.991	.157	27.665	1.239	4.649	.178
51	1/09	72	858	85.494	.478	5.663	.036	7.551	.778	20.831	.684
52	1/09	86	816	66.681	.287	6.933	.030	23.838	2.231	5.309	.267
53	1/09	6	894	77.888	.535	9.650	.084	10.924	.919	13.399	.822
55	1/09	160	803	55.117	.218	10.728	.040	31.350	2.546	3.415	.318
62	1/09	150	923	58.210	.470	5.872	.065	33.432	1.951	3.427	.168
63	1/09	150	921	54.940	.439	6.501	.071	36.051	1.998	3.016	.173
65	1/09	70	802	69.317	.272	7.870	.029	20.426	2.085	6.368	.351
66	1/09	90	807	79.636	.322	4.267	.017	14.134	1.624	10.354	.272
67	1/09	90	768	53.077	.165	5.892	.015	37.484	3.368	2.771	.145
68	1/09	91	847	74.979	.391	9.323	.053	13.940	1.313	10.055	.615
82	1/13	90	838	58.741	.291	11.954	.063	26.896	2.056	4.220	.415
83	1/13	90	812	74.217	.310	8.945	.036	14.922	1.569	9.229	.545
85	1/13	82	835	56.364	.273	12.964	.066	28.235	2.098	3.873	.430
87	1/13	88	923	57.383	.465	10.472	.117	29.854	1.709	3.774	.335
89	1/14	145	859	54.313	.305	10.186	.065	32.950	2.182	3.234	.292
91	1/14	85	815	60.104	.257	8.989	.038	28.217	2.396	4.100	.295
114	1/15	87	843	76.489	.389	15.664	.086	6.721	.650	21.036	2.137
117	1/16	87	830	78.725	.371	12.576	.061	7.489	.778	19.324	1.529
133	1/24	732	745	75.602	.198	3.363	.007	18.292	2.539	7.521	.162
180	2/17	869	633	42.954	.044	5.198	.003	45.656	6.145	1.897	.100
226	3/08	--	830	40.895	.192	9.740	.048	46.564	2.561	1.777	.199

TABLE 28.8.—*Composition of gases from east rift eruption of Kilauea, 1983: January 23 crack*

[--, no data]

Sample	Date (mo/d)	Temperature (°C)		Constituents (mole percent)						Atomic ratios	
		Collection	Equilibrium	H_2O	H_2	CO_2	CO	SO_2	H_2S	H/S	C/S
130	1/24	540	779	65.687	0.220	4.913	0.014	26.369	2.796	4.711	0.169
132	1/24	732	757	70.251	.201	3.780	.009	22.933	2.826	5.690	.147
135	2/04	508	688	63.512	.106	4.915	.005	27.348	4.113	4.306	.156
139	2/10	406	657	63.532	.082	4.512	.003	27.140	4.731	4.289	.142
140	2/12	385	696	44.111	.079	8.844	.010	42.657	4.298	2.065	.189
141	2/12	385	666	55.642	.077	6.624	.005	32.844	4.808	3.215	.176
176	2/17	410	744	45.538	.119	8.866	.018	41.914	3.545	2.165	.195
177	2/17	410	747	49.863	.133	7.814	.016	38.629	3.545	2.539	.186
185	2/23	407	688	33.766	.057	9.415	.010	52.559	4.194	1.340	.166
186	2/23	407	711	48.525	.098	7.338	.010	39.883	4.145	2.397	.167
192	2/24	403	738	41.876	.104	8.466	.016	45.871	3.667	1.843	.171
193	2/24	403	715	39.490	.083	8.788	.012	47.675	3.952	1.686	.170
196	2/27	403	851	37.138	.199	8.283	.049	51.917	2.413	1.463	.153
197	2/28	403	853	42.441	.230	7.798	.047	46.995	2.489	1.825	.159
202	3/01	452	764	37.414	.113	7.651	.019	51.495	3.308	1.490	.140
203	3/01	452	758	38.045	.110	7.649	.018	50.787	3.391	1.534	.142
210	3/04	435	765	45.426	.138	6.660	.017	44.318	3.441	2.052	.140
227	3/08	--	720	52.150	.113	6.601	.010	37.141	3.985	2.735	.161
228	3/08	--	733	51.516	.123	6.543	.011	37.986	3.820	2.653	.157
236	3/22	423	754	49.671	.140	5.898	.013	40.666	3.612	2.413	.133
237	3/22	423	756	47.385	.135	6.237	.014	42.638	3.592	2.211	.135
242	3/22	419	620	39.594	.036	7.780	.003	46.437	6.150	1.741	.148
243	3/28	419	663	45.064	.061	6.403	.005	43.255	5.211	2.077	.132
247	3/29	409	743	53.558	.139	5.317	.011	37.251	3.724	2.803	.130
252	3/30	394	665	54.701	.076	5.088	.004	35.051	5.081	2.983	.127
257	3/31	401	671	54.481	.079	5.058	.004	35.405	4.972	2.949	.125
262	4/01	405	676	65.667	.100	3.824	.003	26.125	4.281	4.608	.126
270	4/04	385	654	55.888	.070	5.035	.003	33.734	5.270	3.140	.129
276	4/05	392	655	54.748	.069	5.014	.003	34.843	5.323	2.995	.125
280	4/08	410	660	56.312	.074	4.820	.003	33.644	5.147	3.173	.124
286	4/08	402	666	57.777	.081	4.800	.004	32.410	4.928	3.363	.129
288	4/11	411	664	57.985	.079	4.731	.004	32.232	4.969	3.389	.127
291	4/13	398	654	59.521	.074	4.457	.003	30.820	5.124	3.601	.124

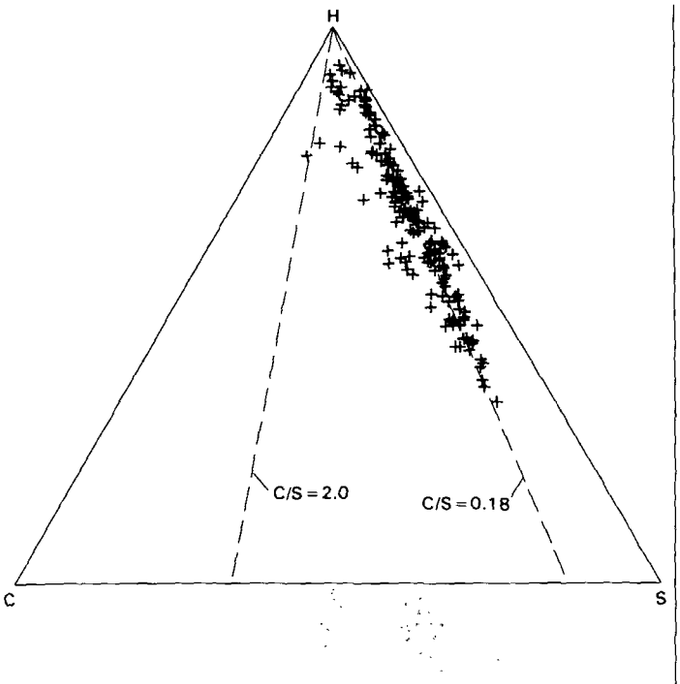

FIGURE 28.2.—Ternary H-C-S plot for gas samples from 1983 Kilauea east-rift-zone eruption. Data from tables 28.4–28.8. Dashes indicate water-control lines for specific values of the C/S ratio. Atomic hydrogen has been reduced by a factor of 0.5 to increase clarity.

deviate considerably from this line, becoming carbon-rich. Examination of the tables shows that almost all of the samples with a C/S ratio >0.3 were collected from ground cracks during January 1983; the eruption began in a heavily vegetated area, and thus contamination of the magmatic gas with organic pyrolysis products is likely. Furthermore, the eruptive area contained numerous preexisting low-temperature fumaroles emitting CO_2-rich steam, and mixing of these vapors with the magmatic gas may account for some of the samples rich in H_2O and CO_2. Samples with a C/S ratio <0.1 are associated with vents at which fountaining had ceased and with ground cracks near eruptive centers, and all were collected after the January activity; remobilization of S from the January lava is a possible explanation for the low C/S ratios of these samples.

The samples from actively erupting vents (table 28.4) were all collected within a few meters, usually a few centimeters, of actively churning, spattering or fountaining melt. All but three of these were collected in the period after July 1983, when eruptive episodes were preceded by the formation of a lava lake in the central vent that persisted for several hours to several days before full-scale eruption. This lava lake frequently became crusted over, with small vents emitting spatter, gas, and occasional overflows of lava through the crust; the August–October samples in table 28.4 were obtained from such vents. The three January–March samples in table 28.4 were collected from small holes in vigorously fountaining spatter cones. Examination of table 28.4 reveals a clear trend for apparent water (that is, the thermodynamic estimate of water content) to

increase and for the C/S ratio to decrease from the pre-April samples through the August samples to the September samples; however, this trend is not apparent in samples collected from other sites (tables 28.5–28.7) and it seems more likely to reflect vagaries in the degassing process rather than a change in the volatile composition of the magma.

The samples of gas from vents no longer active (table 28.5) collected before March 1983 were invariably from very small vents that had erupted only weakly, forming spatter ramparts less than a meter high. Samples collected from vents that had erupted vigorously either consisted solely of air or were thoroughly oxidized, often to the point where not even SO_2 was detectable. The March–April eruptive episodes ended with partial collapse of the crater wall in the central vent cone (the later Puu Oo), which completely blocked the main vent; the samples in table 28.5 from this period were obtained from degassing cracks in the debris pile. The observed variation in the C/S ratio of these samples might well be accounted for by remobilization of sulfur from the edifice and adjoining lava and by incorporation of pyrolyzed organic matter through the chimney effect.

Gas samples collected from fuming ground cracks have been distinguished as "near" (table 28.6), meaning within 200 m of an actively erupting vent, and "distant" (table 28.7), usually meaning more than 1 km from any eruptive site or collected during a noneruptive period of this episodic eruption. Comparison of tables 28.6 and 28.7, however, shows this to be a distinction without a difference; the composition of gas issuing from ground cracks appears to be unrelated to the relative proximity of eruptive centers or to whether an eruption is actually occurring. A notable feature of gas samples from these ground cracks is the high temperature of apparent gas equilibrium in spite of the very low collection temperatures, many less than 100 °C. This result, as with the 1981–82 gas collections (see above), indicates that an abundance of gas samples should be easily obtainable from Hawaiian fissure eruptions. (On the other hand, an abundance of samples is required from such sites: about half of the analyses excluded from tables 28.4–28.8 as being too oxidized or too contaminated were obtained from low-temperature ground cracks.) Comparison of these samples with samples collected in immediate contact with melt (table 28.4) shows a general tendency for the apparent water content of the crack samples to be lower; this distinction may be related to the depth at which gas became separated from the melt (see Greenland, chapter 30) but the possibility of greater oxidation of H_2, leading to low estimates of H_2O, in the low-temperature samples cannot be excluded.

On January 23, 1983, an isolated very small eruption took place at a single vent. Associated with this eruption, a ground crack formed starting at a point about 30 m from the vent and extending for about 100 m. This crack fumed strongly into April, making possible a study of the change of gas composition at a single site with time (table 28.8). These data show a general decrease in observed collection temperature with time and a corresponding, though smaller, decrease of apparent equilibrium temperature. Within this general trend, there was a notable increase in collection temperature on March 1, preceded by an equally notable increase in apparent equilibrium temperature two days earlier; it may be significant that these temperature increases accompany the main episode 2 eruptive activity (February 25 to March 4). Paralleling the overall trend of temperature decrease is a decrease of the C/S ratio in the gas. However, the eruptive activity of episode 2 and episode 3 (March 28 to April 9) produced lava that encroached upon and even overran parts of the crack, and it is possible that significant contributions of remobilized sulfur came from these flows.

MAUNA LOA GAS COLLECTIONS FROM 1984

Complete gas analyses of collections from the recent Mauna Loa eruption are discussed in detail elsewhere in this volume (Greenland, chapter 30) and will not be considered here. Two types of gas-sampling sites were available for this eruption: "active" vents that were emitting spatter interspersed with occasional low fountains or small lava flows or both, and "feeder" vents uprift of the active vents. The feeder vents at 3,350 m elevation produced major fountains and lava flows early in the eruption but ceased activity when the lower vents at 2,930 m elevation became active. Abundant fume produced from the feeder vents after lava emission ceased there originated from magma degassing as it flowed through the conduit to the actively erupting vents. Flowthrough-bottle collections of gases for partial analysis largely overlap the collections for complete analysis, which were mostly being made at the same vent at the same time.

Results of these analyses are given in table 28.9, which includes estimates of the equilibrium temperature and content of H_2O and H_2S made as described above. These data are summarized in a ternary H-C-S plot in figure 28.3, which shows the analyses to lie along a water-control line with a C/S ratio very close to that of the 1983 Kilauea east-rift gases and very much lower than the C/S ratio of the 1919 Mauna Loa eruptive gases (see above). The low C/S ratio in these gases has been attributed, as at Kilauea, to degassing of the magma during storage in the shallow summit storage reservoir (Greenland, chapter 30).

There is no obvious difference in composition or apparent equilibrium temperature between samples collected from actively erupting vents and those from feeder vents (table 28.9). As with Kilauea (see table 28.4), apparent equilibrium temperatures of samples collected at magmatic temperatures (~1,100 °C) are uniformly lower than collection temperatures, whereas samples collected at temperatures below 900 °C almost always have apparent equilibrium temperatures that are higher than the collection temperature. This result indicates that quenching of the high-temperature flowthrough collections is not sufficiently fast to prevent gas reactions down to ~1,000 °C. The similarity of apparent equilibrium water contents of samples from the two kinds of sites contrasts with the observation from the complete analyses (Greenland, chapter 30) that the active vents have a higher total water content than do the feeder vents. However, estimating equilibrated water in the complete analyses yields the same results given here for the partial analyses (Greenland, chapter 30); the distinction between total and equilibrated water was attributed to nonequilibrium degassing of the erupting magma.

TABLE 28.9.—*Composition of gases from Mauna Loa, 1984*

[--, no data]

Date (mo/d)	Temperature (°C)		Constituents (mole percent)						Atomic ratios	
	Collection	Equilibrium	H_2O	H_2	CO_2	CO	SO_2	H_2S	H/S	C/S
Actively erupting vents										
3/25	1,075	969	54.713	0.562	6.754	0.108	36.124	1.739	3.012	0.181
3/26	1,100	1,016	62.186	.800	5.635	.127	29.811	1.442	4.123	.184
3/26	1,100	975	47.237	.499	8.324	.139	42.079	1.723	2.258	.193
3/26	1,120	955	53.429	.510	6.534	.094	37.594	1.839	2.829	.168
3/27	1,100	978	63.592	.683	5.680	.097	28.400	1.548	4.396	.193
3/27	1,130	981	55.892	.608	7.480	.130	34.257	1.632	3.240	.212
3/30	1,100	903	52.966	.385	8.922	.084	35.641	2.003	2.941	.239
3/31	1,100	941	51.902	.461	7.672	.098	37.989	1.877	2.721	.195
4/02	1,100	1,098	57.307	1.055	8.137	.316	32.010	1.175	3.588	.255
4/02	1,100	1,073	58.389	.965	7.668	.253	31.478	1.249	3.704	.242
4/02	--	837	41.372	.204	9.987	.052	45.894	2.491	1.821	.207
4/05	835	944	44.512	.402	8.520	.112	44.582	1.873	2.014	.186
Feeder vents										
4/03	1,100	1,007	51.039	0.631	8.819	0.187	37.790	1.535	2.706	0.229
4/03	--	911	48.799	.369	10.795	.108	38.005	1.924	2.559	.273
4/05	1,010	1,078	71.865	1.214	4.309	.147	21.434	1.031	6.598	.198
4/05	1,100	1,097	58.075	1.063	6.842	.264	32.541	1.215	3.576	.211
4/05	895	983	50.474	.555	7.658	.136	39.487	1.690	2.561	.189
4/07	880	976	51.350	.544	7.412	.124	38.843	1.726	2.643	.186
4/09	875	957	49.212	.474	8.574	.124	39.830	1.785	2.474	.209
4/09	875	972	51.808	.540	8.514	.139	37.312	1.687	2.771	.222
4/11	840	946	49.270	.450	8.109	.108	40.204	1.858	2.452	.195
4/11	840	906	56.669	.417	6.900	.067	33.922	2.025	3.289	.194
4/13	820	939	48.468	.427	8.742	.111	40.381	1.871	2.403	.210

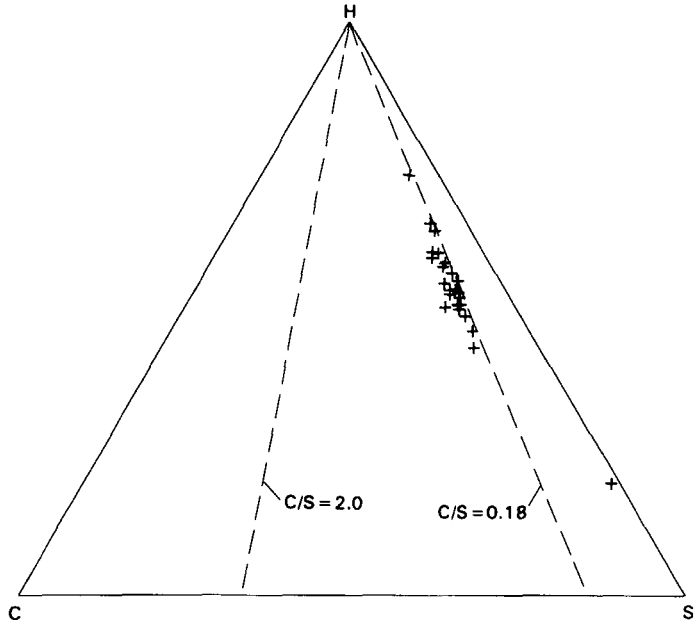

FIGURE 28.3.—Ternary H-C-S plot for gas samples from 1984 Mauna Loa eruption. Data from table 28.9. Dashes indicate water-control lines for specific values of the C/S ratio. Atomic hydrogen has been reduced by a factor of 0.5 to increase clarity.

CONCLUSIONS

Compositions of Hawaian eruptive gas are summarized in figure 28.4. Plotted in a ternary H-C-S diagram are averages for the 1917, 1919, 1965, September 1982, and 1983 eruptions of Kilauea, and the initial (best) compositions of the April 1982 eruption and 1981 intrusion at Kilauea, and averages for the 1919 and 1984 eruptions of Mauna Loa.

It is apparent from figure 28.4 that eruptive gases in Hawaii predominantly have C/S ratios of ~2.0 or ~0.2; exceptions are the 1968 Halemaumau Fountain gas (C/S = 4.0) and the 1919 Mauna Loa eruption (C/S = 0.9), both of which are particularly uncertain determinations. The high (2.0) C/S ratio is associated with protracted summit eruptions of Kilauea and the low (0.2) ratio is associated with rift and brief summit eruptions. Current degassing models of Kilauea (Gerlach and Graeber, 1985; Greenland and others, 1985) and of Mauna Loa (Greenland, chapter 30) indicate that mantle-derived magma arrives in shallow (2–6 km) summit storage reservoirs bearing an immiscible CO_2-rich fluid phase and having an overall C/S ratio of about 2. Degassing of the CO_2-rich fluid phase through summit fumaroles is rapid, at least at Kilauea (days to weeks; see Greenland and others, 1985), leaving the magma with a C/S ratio of about 0.2. A consequence of this view is that eruptive gas in Hawaii will have the low C/S ratio if the magma has resided even briefly in the summit reservoir. The high ratio will be found only when magma passes directly through the reservoir to

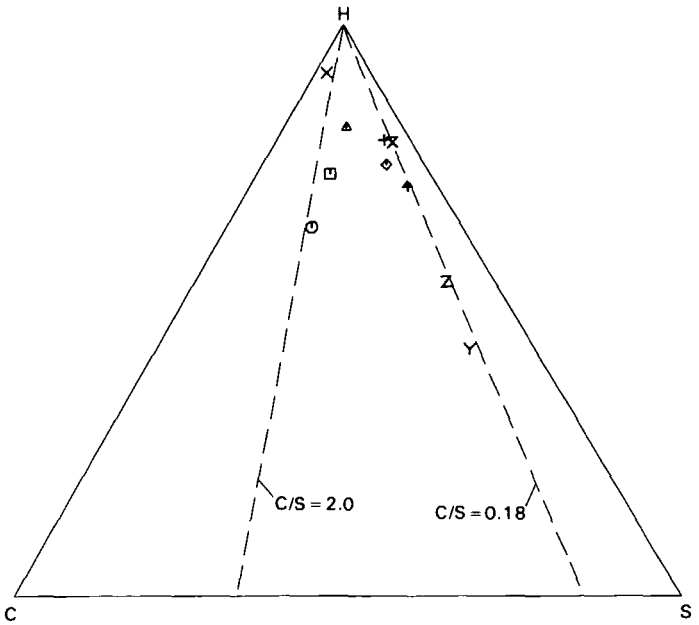

EXPLANATION

- 1917 Kilauea summit eruption
- 1919 Kilauea summit eruption
- 1919 Mauna Loa eruption
- 1965 Kilauea east-rift-zone eruption
- 1968 Halemaumau fountain
- 1981 Kilauea southwest-rift-zone intrusion
- April 1982 Kilauea summit eruption
- September 1982 Kilauea summit eruption
- Z 1983 Kilauea east-rift-zone eruption
- Y 1984 Mauna Loa eruption

FIGURE 28.4.—Summary ternary H-C-S plot of Hawaiian eruptive gas compositions from 1917 through 1984. Dashes indicate water-control lines for specific values of the C/S ratio. Atomic hydrogen has been reduced by a factor of 0.5 to increase clarity.

the eruption center, which in practical terms means only for continuous summit eruptions that are lengthy enough to flush a passageway through the reservoir. An actual suite of gas samples collected from an eruption, however, can be expected to exhibit a considerable range of C/S ratios because of contamination by organic matter and by remobilized sulfur.

The major source of variation in these eruptive gases within a particular eruption is the water content, as is shown by figures 28.1–28.3, and water is also the primary distinguishing variable between eruptions, as indicated by figure 28.4. Hydrogen isotope studies yield convincing evidence that magma absorbs crustal water somewhere between its formation in the mantle and eruption (Kyser and O'Neil, 1984), and studies of submarine basalt (Moore, 1965) show that water is undersaturated in Hawaiian magma at the pressure and temperature conditions of the summit reservoir. It seems probable, then, that much of the water variation in these eruptive gases is due to varying amounts of assimilation of water by magma in transit between mantle and eruption site. A further source of water variation in gas samples is contamination of the magmatic gas with meteoric water both in the vent system and from the atmosphere at the sampling site; this problem is exacerbated because meteoric water in the vent system may be equilibrated with the magmatic gas, and it is possible that the last exsolved magmatic water may be collected before equilibration with previously exsolved gas is complete (Greenland, chapter 30). It may be that variation of water among eruptions is due primarily to variable assimilation and that variation within an eruption largely reflects meteoric contamination, but only hydrogen isotope studies can resolve this problem.

Studies of gas composition as summarized here offer no direct information about the actual content of gas in the magma, which is an important question to those concerned with petrology and eruptive mechanics. If the degassing model described above is correct, however, it can be inferred that the carbon and sulfur content of Hawaiian summit-stored magma is constant and is fixed by the pressure and temperature conditions of the summit reservoir; the equilibrium amounts of carbon and sulfur dissolved in reservoir magma have been estimated (Gerlach and Graeber, 1985; Greenland and others, 1985) as about 0.03 percent CO_2 and 0.1 percent S by weight. The water content of summit-stored magma, which is not fixed by solubility limits, probably varies with the extent of assimilation of crustal water. The water content is difficult to estimate because of uncertainties about meteoric water contamination of gas samples; Greenland and others (1985) and Gerlach and Graeber (1985) independently estimate about 0.3 weight percent H_2O, which, even with the uncertainties, probably is close to correct. Therefore, excluding protracted summit eruptions, the total content of volatiles in Hawaiian eruptive magma probably is less than 0.5 percent by weight and probably varies little from eruption to eruption.

REFERENCES

Banks, N.G., Koyanagi, R.Y., Sinton, J.M., and Honma, K.T., 1984, The eruption of Mount Pagan Volcano, Mariana Islands, 15 May 1981: Journal of Volcanology and Geothermal Research, v. 22, p. 225–269.

Day, A.L., and Shepherd, E.S., 1913, L'eau et les gaz magmatiques: Comptes Rendu Seances de l'Academie des Sciences, v. 157, p. 1–7.

Finlayson, J.B., Barnes, I.L., and Naughton, J.J., 1968, Developments in volcanic gas research in Hawaii, *in* The Upper Crust and Upper Mantle of the Pacific Area: American Geophysical Union, Geophysical Monograph, v. 12, p. 428–438.

Gerlach, T.M., 1980, Evaluation of volcanic gas analyses from Kilauea Volcano: Journal of Volcanology and Geothermal Research, v. 7, p. 295–317.

———1982, The interpretation of volcanic gas data from tholeiitic and alkaline mafic magmas: Bulletin Volcanologique, v. 45-3, p. 235–244.

Gerlach, T.M., and Graeber, E.J., 1985, Volatile budget of Kilauea Volcano: Nature, v. 313, p. 273–277.

Graeber, E.J., Modreski, P.J., and Gerlach, T.M., 1979, Compositions of gases collected during the 1977 east rift eruption, Kilauea, Hawaii: Journal of Volcanology and Geothermal Research, v. 5, p. 337–344.

Greenland, L.P., 1984, Gas composition of the January 1983 eruption of Kilauea Volcano, Hawaii: Geochimica et Cosmochimica Acta, v. 48, p. 193–195.

———in press, Gases from the 1983–84 east-rift eruption of Kilauea Volcano, *in* Wolfe, E.W., ed., The Puu Oo eruption of Kilauea Volcano, Hawaii: the first 1½ years: U.S. Geological Survey Professional Paper.

Greenland, L.P., Rose, W.I., and Stokes, J.B., 1985, An estimate of gas emissions and magmatic gas content from Kilauea Volcano: Geochimica et Cosmochimica Acta, v. 49, p. 125–129.

Heald, E.F., Naughton, J.J., and Barnes, I.L. Jr., 1963, Use of equilibrium calculations in the interpretation of volcanic gas samples: Journal of Geophysical Research, v. 68, p. 545–557.

Jaggar, T.A., 1940, Magmatic gases: American Journal of Science, v. 238, p. 313–353.

Kyser, T.K., and O'Neil, J.R., 1984, Hydrogen isotope systematics of submarine basalts: Geochimica et Cosmochimica Acta, v. 48, p. 2123–2133.

Matsuo, S., 1962, Establishment of chemical equilibrium in the volcanic gas obtained from the lava lake of Kilauea, Hawaii: Bulletin Volcanologique, v. 24, p. 59–71.

Moore, J.G., 1965, Petrology of deep-sea basalt near Hawaii: American Journal of Science, v. 263, p. 40–52.

Naughton, J.J., Derby, J.V., and Glover, R.B., 1969, Infrared measurements on volcanic gas and fume: Kilauea eruption, 1968: Journal of Geophysical Research, v. 74, p. 3273–3277.

Nordlie, B.E., 1971, The composition of the magmatic gas at Kilauea and its behavior in the near surface environment: American Journal of Science, v. 271, p. 417–463.

Shepherd, E.S., 1919, The composition of the gases of Kilauea: Hawaiian Volcano Observatory Bulletin, v. 7, no. 7, p.94–97.

———1920, Two gas collections from Mauna Loa: Hawaiian Volcano Observatory Bulletin, v. 8, no. 5, p. 65–67.

———1921, Kilauea gases, 1919: Hawaiian Volcano Observatory Bulletin, v. 9, no. 5, p. 83–88.

———1925, The analysis of gases obtained from volcanoes and from rocks: Journal of Geology, v. 33, p. 289–370.

———1938, The gases in rocks and some related problems: American Journal of Science, v. 236, p. 311–351.

Swanson, D.A., and Fabbi, B.F., 1973, Loss of volatiles during fountaining and flowage of basaltic lava at Kilauea Volcano, Hawaii: Journal of Research of the U.S. Geolgical Survey, v. 1, p. 649–658.

SO_2 AND CO_2 EMISSION RATES AT KILAUEA VOLCANO, 1979–1984

By Thomas J. Casadevall, J. Barry Stokes, L. Paul Greenland, Lawrence L. Malinconico, John R. Casadevall, *and* Bruce T. Furukawa

ABSTRACT

Quiescent outgassing of the summit region of Kilauea Volcano produces a plume of gas and particles that contains sulfur dioxide and carbon dioxide as principal constituents. The SO_2 and CO_2 are derived from outgassing of magma temporarily stored in the shallow reservoir at a depth of 2–6 km beneath the summit.

Since June 1979 we have made regular measurements of SO_2 emission rates from Kilauea. In 1983 and 1984, measurements of CO_2 emission rates were also made for Kilauea. The average daily SO_2 emission rate from 1979 through 1982 was 170±50 t/d; from 1983–1984, the average daily emission rate had increased to 260±90 t/d. The 1979–1982 rate occurred during a time when no major eruptive activity occurred at Kilauea summit. The increase in 1983 is coincidental with the start of major eruptive activity at the Puu Oo vent on the east rift zone and probably reflects an increase in the rate of magma supply.

The total SO_2 production in 1979–1982 is calculated at approximately 63,000 tonnes annually. In 1983–1984, this annual production is calculated at 95,000 tonnes annually. The SO_2 from quiescent outgassing of Kilauea Volcano contributes less than 1 percent of the total annual global contribution from volcanoes. The 1983–1984 episodes of the Puu Oo eruption produced about 370,000 tonnes of SO_2, or as much as 3 percent of the annual volcanic contribution.

INTRODUCTION

A plume of gas and microscopic particles continuously enters the atmosphere from fumaroles in the southern half of Kilauea caldera. The plume is generally transparent with a light-bluish-gray color due to scattering of light by tiny particles. It contains H_2O, CO_2, and SO_2 as the major gaseous constituents (Cadle and others, 1969, 1971; Darzi, 1981; Darzi and Winchester, 1982c).

In this paper we describe the techniques used to measure SO_2 and CO_2 emission rates at Kilauea, the results from June 1979 through December 1984, and the interpretation of the data. These measurements form a part of the program to monitor Kilauea Volcano from the Hawaiian Volcano Observatory. Their purpose is to determine the long-term emission rates for SO_2 from Kilauea; to evaluate the usefulness of the measurements for forecasting eruptions; and to integrate geochemical observations with geophysical and geologic observations of activity to refine our understanding of how Kilauea Volcano works.

We will show that (1) during periods of relative quiescence, Kilauea emitted a nearly constant flux of SO_2; (2) during the 1983–1984 eruptions at Puu Oo on Kilauea's east rift zone, the rate of SO_2 release at the summit doubled and has remained at an elevated level; and (3) eruption plumes from Kilauea are characterized by increases in SO_2 of about two orders of magnitude over rates of non-eruptive or quiescent degassing.

BACKGROUND AND PREVIOUS STUDIES

The principal gases released from fumaroles at Kilauea are H_2O, CO_2, and SO_2 (Heald and others, 1963; Cadle and others, 1969, 1971; Gerlach, 1980; Greenland, 1984; Gerlach and Graeber, 1985; Greenland and others, 1985). The SO_2 is interpreted to be of magmatic origin (Sakai and others, 1982). The summit fumaroles at Halemaumau Crater and along the 1971 and 1974 eruptive fissures are the most notable sources of SO_2 in the summit region (Casadevall and Hazlett, 1983) and overly a shallow magma reservoir, envisioned as a plexus of sills and dikes, at a depth of 2 to 6 km (Fiske and Kinoshita, 1969; Ryan and others, 1981). Magma is fed into this shallow reservoir from a zone of generation at a minimum depth of 60 km (Eaton and Murata, 1960; Wright, 1984). Pre-eruptive degassing of magma while enroute to and temporarily stored in the shallow reservoir produces a CO_2-rich gas phase (atomic C/S ratio greater than 10); eruptive degassing produces a CO_2-rich gas phase during summit eruptions (atomic C/S is 5 or less) (Gerlach and Graeber, 1985; Greenland and others, 1985). An SO_2-rich gas phase (atomic C/S less than 1) is produced during rift eruptions from a magma which had already lost much of its CO_2 during equilibration at the pressure conditions of the shallow reservoir (Greenland, 1984; Gerlach and Graeber, 1985).

The preeruption content of sulfur in Hawaiian magma has been determined by Harris and Anderson (1983) to be about 1,300 ppm based on examination of melt inclusions in olivine phenocrysts. Basalt erupted on the sea floor under high confining pressure has lost some sulfur, but still contains between 700 and 1,000 ppm (Moore and Fabbi, 1971; Fornari and others, 1979) and surface flows contain from 50 to 200 ppm (Moore and Fabbi, 1971; Swanson and Fabbi, 1973; Sakai and others, 1982).

The continuous loss of sulfur during noneruptive periods to produce the volcanic plume is due largely to distillation of gas from magma as it reequilibrates to the pressure conditions of the shallow summit reservoir (Harris and Anderson, 1983; Greenland and others, 1985). Greenland and others (1985) suggest this mechanism results in about 150 ppm sulfur loss, while Gerlach and Graeber (1985) suggest a loss of between 300 and 600 ppm from the magma prior to eruption. Magma intruded to shallower depths in the

summit or rift zones may lose additional volatiles including SO_2. Further SO_2 loss occurs through effervescence of the basaltic magma (Swanson and Fabbi, 1973; Naughton and others, 1974; Harris and Anderson, 1983) during eruptions, a process which decreases the concentration of sulfur by approximately 600 ppm (Moore and Fabbi, 1971).

ACKNOWLEDGMENTS

Early support and encouragement for this program came from G. Eaton, Scientist-in-Charge at the Hawaiian Volcano Observatory from 1977–1979, and from R. Christiansen, Coordinator for the U.S. Geological Survey Geothermal Program which funded the purchase of the COSPEC. Continued support from the staff of the Hawaiian Volcano Observatory, in particular R. Decker, R. Okamura, and J. Forbes, is appreciated and gratefully acknowledged. Measurements during July and August 1982 were made by J.T. Prosser of Dartmouth College. The airborne measurements of SO_2 emission rates at Kilauea in July 1983 were made with the assistance of R. Symonds. W.I. Rose, Jr. (Michigan Technological University) and T.M. Gerlach (Sandia Laboratory) provided helpful reviews of earlier drafts of this paper. We dedicate this paper to our friend and teacher Richard E. Stoiber.

ACTIVITY OF KILAUEA, 1979–1984

Since June 1979, Kilauea has experienced two short-lived eruptions in the summit caldera (April and September 1982), a brief eruption at Pauahi Crater on the upper east rift zone (November 1979), a long-lived eruption in the middle east rift zone (January 1983–March 1985), and 13 intrusions (table 29.1). Each intrusion was accompanied by ground deformation and intense seismic activity that included discrete earthquakes and harmonic tremor (Dvorak and others, 1986). Five intrusions were also accompanied by the release of heat and (or) gases at the ground surface in the area of the intrusion.

TABLE 29.1.—*Summary of activity, Kilauea Volcano: 1979–1984*

[S, summit: ERZ, east rift zone; SWRZ, southwest rift zone; I, intrusion; E, eruption; *, gas and (or) heat detected at ground surface above intrusion; n.d., not determined. Intruded volume calculated from Uwekahuna summit tilt ($0.33 \times 10^6 m^3 = 1$ microradian). Modified from Dzurisin and others (1984)]

Date	Duration (days)	Location			Erupted volume	Intruded volume
		S	ERZ	SWRZ	(in million cubic meters)	
1979						
May 29	1	I				1.0
Aug 12	1		I			.6
Nov 16	1		E		0.4	
1980						
Mar 2	1		I			0.6–1.0
Mar 10	2–3		I*			5.3
Aug 27	1		I*			2.3
Oct 22	1		I*			.6
Nov 2	1		I			2.0
1981						
Jan 19	2	I				n.d.
Jan 24	16			I		>8.0
Jun 25	1	I				1.6
Aug 10	2			I*		35.0
1982						
Apr 30	1	E			0.5	
Jun 22	3			I*		14.1
Sept 25	2	E			3.0	
Dec 9	1		I			1.0
1983						
Jan 3	800+		E		360+	

METHODS, UNCERTAINTIES, AND ASSUMPTIONS

SO_2 emission rates have been measured at volcanoes since 1972 (Casadevall and others, 1981, 1984; Stoiber and others, 1983) including Kilauea in February 1975 (Stoiber and Malone, 1975) and in October 1978 (Stoiber and others, 1979). Regular ground-based measurements of SO_2 emission rates at Kilauea began in June 1979. Airborne measurements of SO_2 and CO_2 emission rates of the non-eruptive plume at Kilauea caldera and the eruption plume at the Puu Oo began in December 1983.

The emission rates of SO_2 and CO_2 are calculated by multiplying the plume velocity and the gas concentration in a cross-sectional profile of the plume. In this section we describe the methods and uncertainties for the measurements of wind speed, SO_2, and CO_2.

WIND SPEED MEASUREMENTS

On the east side of the Island of Hawaii northeasterly trade-winds travel from 3 to 20 m/s. These winds carry the plume of gas from the fumaroles on the caldera floor out into the southwest rift zone of Kilauea (fig. 29.1). During winter months this wind pattern is frequently reversed as Kona winds blow from the southwest. We usually assume that the wind speed stays constant during the period of measurement.

For ground measurements of SO_2, the plume velocity is measured at Uwekahuna Bluff on the west side of Kilauea caldera (fig. 29.1) using a hand-held anemometer. Five 1-minute measurements of wind velocity are taken before and after the SO_2 measurements. The average of the before and after wind measurements is used to calculate the SO_2 emission rate.

For airborne measurements of SO_2 and CO_2, we rely primarily on wind direction and speed determinations made twice daily at Hilo Airport by the NOAA radiosonde. These are checked during flight. When possible, we compare true air speed of the aircraft determined while flying in the plume with true ground speed measured by flying a fixed distance (usually 10 miles) both with (tailwind) and against (headwind) the wind. The difference between the true ground speed and true air speed gives the wind speed.

The uncertainty in the measurement of wind speed is typically between 10 and 30 percent. This measurement is the largest single source of uncertainty in measuring the rates of SO_2 and CO_2 emission.

SO_2 MEASUREMENTS

The emission rates of SO_2 are measured using the Correlation Spectrometer (COSPEC; Barringer Research Ltd. of Canada) originally designed for use in pollution studies (Millan and others, 1976; Millan and Hoff, 1978) and adapted to the study of volcanoes (Stoiber and others, 1983). Correlation spectrometry is a remote-sensing technique that uses solar ultraviolet light scattered by the Earth's atmosphere as a source. The spectrally tuned instrument measures the amount of uv absorption by SO_2 present along the optical path through the plume in units of concentration-pathlength (ppm·m) at one atmosphere. Calibration is performed using an internal standard with a known concentration-pathlength of SO_2. A cross-section profile of the plume is determined by multiplying the plume width (m) with the concentration-pathlength. The product of this profile (ppm·m^2) and the wind speed (m/s) is the mass flux (ppm·m^3/s) and is usually expressed as tonnes per day (t/d).

Most measurements reported here were made with the COSPEC mounted in an automobile that is driven at a constant velocity of 40 km/h beneath the plume as it passes over a road that encircles Kilauea caldera (fig. 29.1*B*). An SO_2 cross section of the plume is continuously recorded on a chart recorder, and the changes in SO_2 pathlength concentration and geographic position are recorded. Four to six traverses can be made beneath the plume in about one hour. The techniques for airborne measurements are the same as those used at Mount St. Helens (Casadevall and others, 1981).

The large amounts of SO_2 and the enormous size of the eruption plumes at Kilauea presented added problems for airborne measurements. During eruptions in 1979, 1982, 1983, and 1984, the concentrations of SO_2 in the eruption plumes exceeded the measurable capacity using the COSPEC technique and caused saturation of the signal. In April 1984, we installed a high concentration SO_2 disc and calibration cells into the COSPEC to permit measurement of higher concentrations of SO_2. An additional problem is that the large plumes produced during eruptions of Kilauea often remain close to the ground, thereby preventing the aircraft from flying completely beneath the plume. Thus, many of the airborne measurements of SO_2 emission rates of eruption plumes are minimum values.

UNCERTAINTIES

The reported emission rate of SO_2 incorporates uncertainties due to both instrumental factors and variations from natural causes (Casadevall and others, 1981; Stoiber and others, 1983). The latter include real-time variation in gas emission, short-term (minutes to hours) variation in wind speed, and changes in cloud cover. Estimated uncertainties arising from operator and instrumental factors include uncertainty in the instrument calibration (± 5 percent); variation in speed of vehicle used to measure the plume (± 10 percent); uncertainty in data processing (± 5 percent); and uncertainty in the measurement of wind speed (± 10–30 percent). The effect of these uncertainties and variations on the reported SO_2 emission rate can be minimized by averaging the results of from 4 to 20 traverses each day. In practice, the average of these traverses, that is the average daily emission rate, usually has an uncertainty of ± 10 to ± 30 percent of the reported value.

CO_2 MEASUREMENTS

The emission rates of CO_2 have been measured within the noneruptive summit plume and at the Puu Oo eruption site (Greenland and others, 1985) beginning in 1983. The technique uses an infrared spectrometer that is flown through the plume at successively higher altitudes while the concentration of CO_2 is continuously measured (Harris and others, 1981). The concentration of CO_2 in excess of the background atmospheric CO_2 content is inferred to be from the volcano. This excess CO_2 generally ranges from 1 to 15 ppm (by volume), compared to an average atmospheric concentration of approximately 320 ± 20 ppm. The altitude-concentration data are used to make a map of excess CO_2 concentration in a cross section of the plume. The product of the cross section-concentration (ppm·m^2) and the plume velocity (m/s) gives the emission rate of CO_2 (ppm·m^3/s) and is reported as tonnes per day. Each daily value represents a single cross section of the plume requiring between 90 and 120 minutes of continuous in-flight measurement.

The utility of the CO_2 method is limited by the practicality of flying repeatedly through a plume that is usually not visible, as well as by the threshold emission rate. We are aided in tracking the plume by simultaneously using the COSPEC to measure SO_2. Experience at Mount St. Helens (Casadevall and others, 1981; Harris and others, 1981) has shown that SO_2 and CO_2 are usually well mixed in the plume and that maximum CO_2 concentration is typically coincident with maximum SO_2 concentration.

The threshold value for detecting excess CO_2 in the plume depends on the wind speed and dispersion of the plume and the distance from the source at which measurements are made (that is, degree of air dilution). Excess CO_2 of less than 2 ppm is difficult to determine accurately. This concentration effectively becomes our threshold value for detecting excess CO_2 in the plume; in practical terms, emission rates of less than 1,000 t/d are difficult to measure. We estimate a maximum uncertainty in these measurements of ± 40 percent of the reported value.

DATA QUALITY

In addition to real changes in the emission rates of gases, other factors, both natural and operator related, affect the quality of the data. These factors include changes in cloud cover, variation in wind speed and direction, experience of the operators, and instrumentation. Operator experience is important both in making the measurements of SO_2 and wind speed, as well as in reduction of data. Judgment must be used to evaluate the quality of a given day's measurement conditions and in interpreting the chart records. Judgment improves with practice and becomes more uniform with experience. Measurements made daily or at least several times each

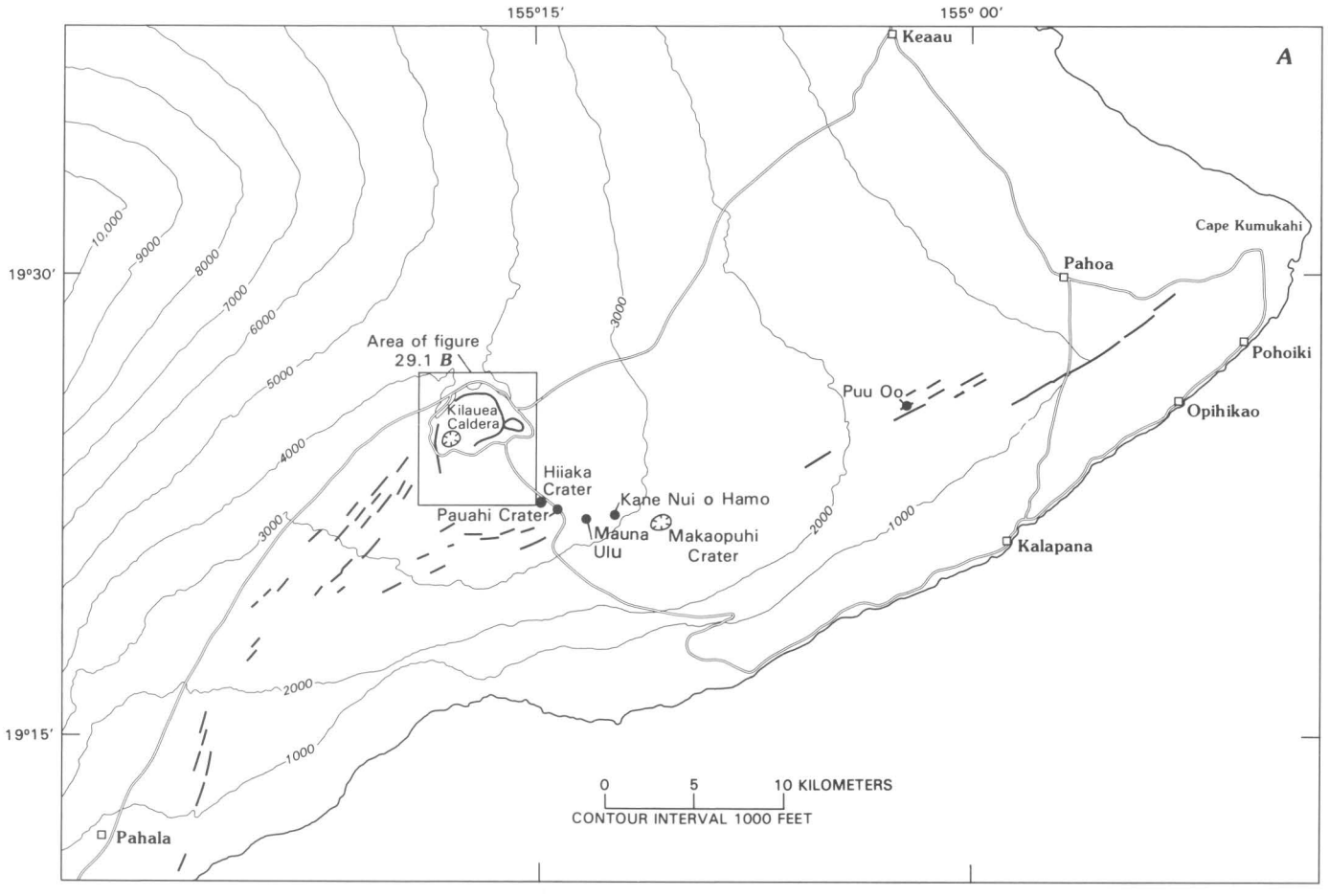

FIGURE 29.1.—Index map of Kilauea Volcano. ***A***, Summit area and rift zones. ***B***, Kilauea caldera area.

week provide a more reliable indication of background values than measurements made only weekly or less frequently. We have designated data quality as good if the frequency of measurement was weekly or better and if the measurements were made by the same experienced operator. Data of good quality include the summit measurements from June 1979 to June 1980, and from November 1981 through December 1984. Data of poor quality are those which have been collected infrequently by one or more inexperienced operators. The data collected from September 1980 through October 1981 are generally considered to be of poor quality. In addition, during many of the airborne measurements, the concentration of SO_2 exceeded that measurable by the COSPEC. These data should be treated with caution since they likely represent minimum rates for SO_2 emission.

REMOVAL OF SO_2 FROM THE PLUME

We have assumed that the SO_2 measured in the plume accurately represents the mass of sulfur released from the summit fumaroles. We recognize that while enroute to the surface, the SO_2-bearing gas mixture may be affected by a variety of conditions and processes that reduce the amount of sulfur reaching the fumaroles (Gerlach and Graeber, 1985). Measurements made during the season of heavy rainfall (December through March) show no significant change in SO_2 emission rate, suggesting that removal of SO_2, at least by the shallow ground-water table, is probably minimal. Eruption plumes do not appear to be affected by subsurface removal of SO_2 as there is little evidence for magma-ground water interaction during eruption (Greenland, 1984).

SO_2 in the plume may be removed through rainout and through dry deposition. Dry deposition occurs onto soil and vegetation as well as onto atmospheric particles such as sea spray and tropospheric dust (Darzi and Winchester, 1982a, 1982b). Direct deposition of SO_2 may damage vegetation (Winner and Mooney, 1980) and acidify rainfall (pH = 3.0–4.0), owing to scavenging of SO_2 by rain droplets (Harding and Miller, 1982; Russell, 1982). Salt and dust particles have been detected at the summit of Kilauea (Woodcock, 1960; Darzi and Winchester, 1982b), but their efficiency as scavengers of SO_2 and other gases is unknown. In eruption plumes, where the concentration of particles is higher than in noneruptive plumes, scavenging of SO_2 by tephra particles may be significant (Naughton and others, 1974; Rose, 1977).

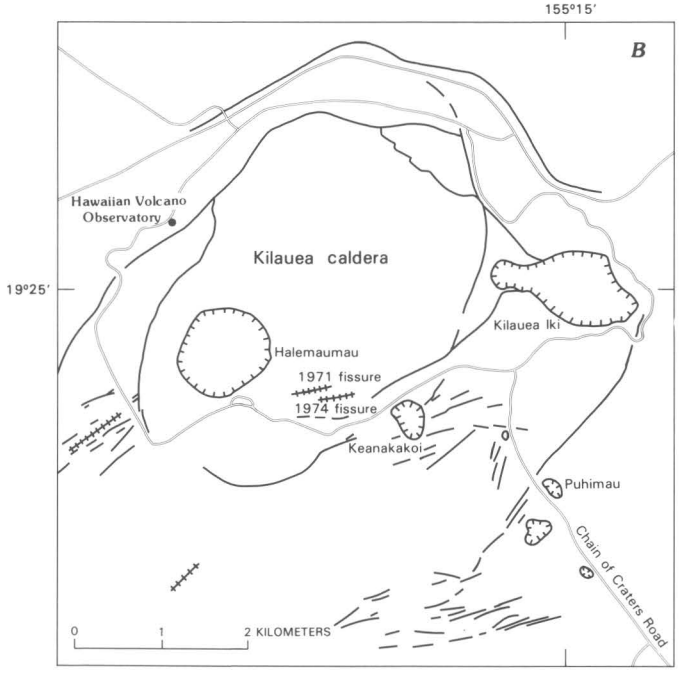

FIGURE 29.1.—Continued.

Some SO_2 in the plume is eventually converted to sulfate; however, studies of Kilauea fume by Cadle and others (1971) indicate that SO_2 dominates over other oxidized forms of sulfur. When the plumes at Kilauea summit and at Puu Oo were measured, they had usually been in the atmosphere for less than a few minutes; some measurements of the larger Puu Oo eruptive plumes require flying farther downwind where plumes may be as much as 1 hour old. This time is short as compared to the removal rates calculated from study of industrial plumes (Roberts and Williams, 1979; Williams and others, 1981) and estimated (Graedel, 1977; Maahs, 1983a; Martin, 1983; Barrie, 1985) as being on the order of less than about 1 percent SO_2 per hour. Removal rates increase only slightly with humidity and with acidity of the water droplets (Maahs, 1983b). The short-lived (usually tens of seconds) condensation cloud at Halemaumau may temporarily absorb some SO_2, but as the condensate evaporates the sulfur is probably released to the atmosphere as SO_2 (Hegg and Hobbs, 1978).

RESULTS

QUIESCENT SUMMIT EMISSIONS OF SO_2

The average daily emission rates of SO_2 from June 1979 through December 1984 are tabulated in table 29.2 and all data are plotted in figure 29.2. To examine these data for trends and changes, we have applied several statistical methods, including analysis of variance, multiple range test (Duncan), and regression analysis with step-wise selection of data to determine the timing and magnitude of changes in SO_2 emission rates. We have applied these tests to address the following questions: (1) Is it possible to identify periods during which SO_2 emission rates remained relatively constant? (2) If yes, what are the mean SO_2 emission rates during those periods and are there statistically significant differences between means for the different periods? (3) Which means are different and by how much? (4) Are there significant variations within periods which might not be apparent from visual inspection of the data? We have not weighted the data for instrument-related uncertainty, owing mainly to the difficulty in distinguishing between variation due to instrumental or operator errors and variation due to natural causes.

TABLE 29.2.—*Summary of SO_2 emission rates for the quiescent plume, Kilauea: 1979–1984*

[Values given in tonnes per day; *b*, the slope coefficent of the model; B estimate of *b*; R^2, percent of the SO_2 emission rate explained by the model; N, number of measurements]

Period	Dates	Daily rate (mean)	95 percent confidence interval for mean	B	$b=0$	R^2
1A	June 1979 to Mar 15, 1980	160 (N=120)	151–169	0	yes	--
1B	Mar 15 to Jun 1980(?)	100 (N=23)	75–120	0	yes	--
2	Sept 1980 to Aug 11, 1981	190 (N=43)	162–210	0	yes	--
3	Aug 11 to Dec 1981	300 (N=13)	265–326	0	yes	--
4	Feb 1982 to Jan 1983	160 (N=34)	100–220	0	yes	--
5	Jan 1983 to Dec 30, 1984	260 (N=172)	250–265	+0.04	no	2.8

To begin, we visually inspected the data of figure 29.2 and selected 5 periods during which emission data appeared to have remained constant and calculated the mean SO_2 emission rate for each period. These periods include: (1) June 1979–June 1980, (2) September 1980–mid-August 1981, (3) mid-August 1981–December 1981, (4) February 1982–January 1983, and (5) late-January 1983–December 1984. Using the analysis of variance, we tested the null hypothesis (H_o) that the means for periods 1, 2, 3, 4, and 5 are the same ($H_o = u_1 = u_2 = u_3 = u_4 = u_5$ versus H_1 such that at least one pair u_i is not equal to u_j) where u_j is the mean SO_2 flux for period j. The test statistic (F-ratio) is highly significant (50.48), and we may conclude that the means are not all identical. Table 29.2 contains a summary of the analysis of variance for the five phases including the means of the data and the 95 percent confidence intervals.

To examine if the data within each period are constant within the 95 percent confidence limits, we performed a regression analysis using the least-squares method to test the regression model:

$$Y_i = a + bx_i$$

where Y_i is the SO_2 flux and x_i is the number of days since December 31, 1978. The coefficient a is of no particular use in this application since the origin is arbitrary. The important test statistics are B (the estimate of b, the slope coefficient of the model) and R^2 (the proportion of the SO_2 flux explained by the model). The analysis of variance (table 29.2) for each period tests the hypothesis that $b=0$, which indicates that the slope of a least-squares line is flat. In the initial test for periods 1 and 5, b was not equal to 0, indicating that there are trends to the data for these periods.

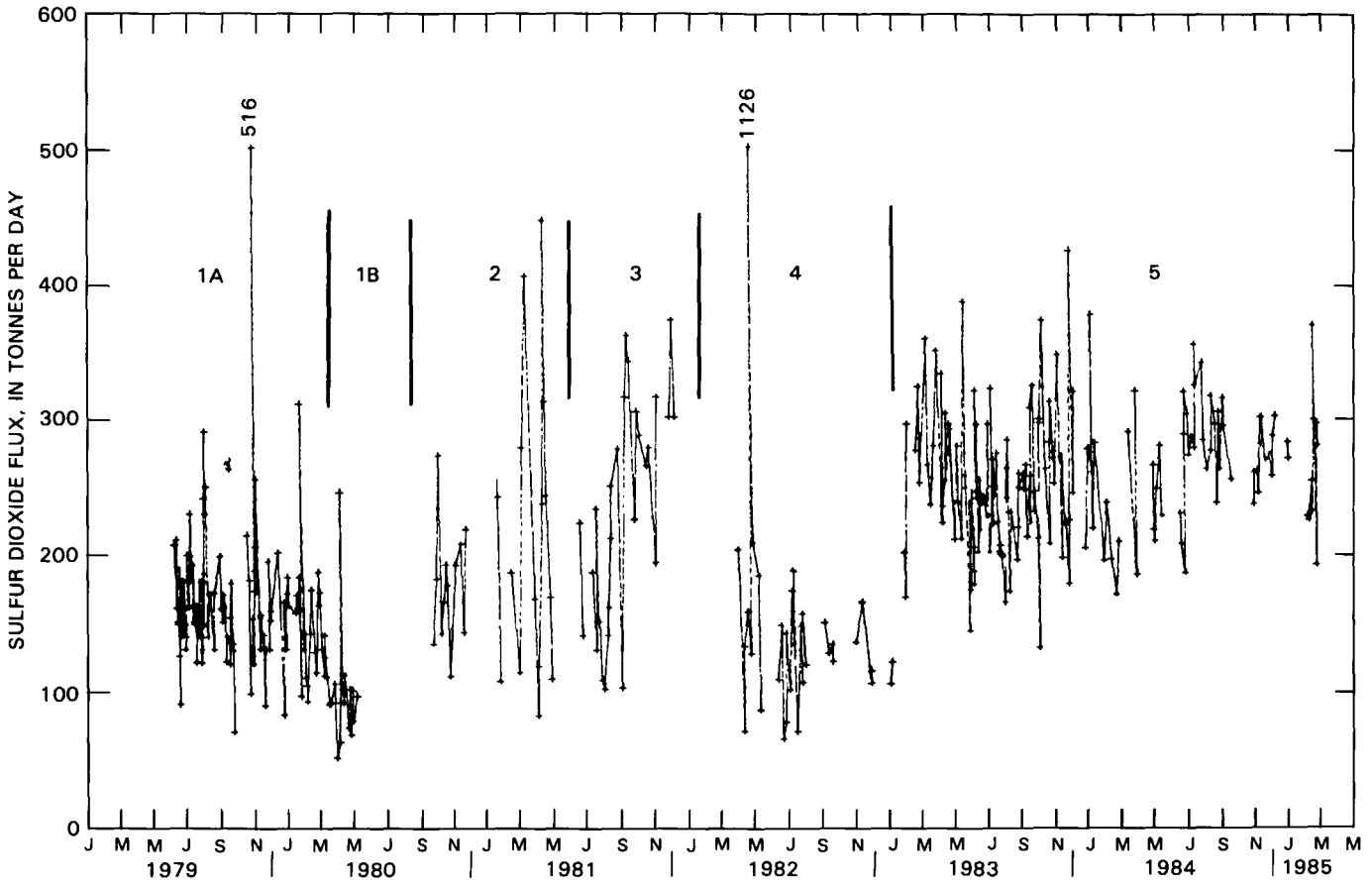

FIGURE 29.2.—SO_2 emission rate data obtained from COSPEC for Kilauea summit area, 1979–1984. Periods 1A–5 separated by heavy black lines.

However, the high R^2 value and negative sign for B (−0.17) for period 1 indicates that the trends in the data for this period are not smooth, but may be due instead to an abrupt decrease in the SO_2 emission rate.

By applying an iterative procedure using step-wise selection of data, we find that a significant decrease in SO_2 emission rates in period 1 occurred in mid-March 1980. On the basis of this test we have subdivided period 1 into 1A and 1B with the break occurring in mid-March 1980. The mean for period 1A (to mid-March 1980) is 160 t/d; the mean for period 1B (after mid-March 1980) is only 100 t/d. Regression analyses show that *b* for periods 1A and 1B equals 0, indicating that the trends for these two subsets of the data are flat.

We used the multiple range test (Duncan) to identify if the mean emission rates are significantly different from one another. Period 1B has the lowest mean and is significantly different from means for all the other periods at the 0.05 level. Periods 1A, 2, and 4 are not significantly different from each other at the 0.05 level. Periods 3 and 5 have the highest means, but are not significantly different from one another at the 0.05 level.

Lack of measurements for part of the second half of 1980 prevent us from determining whether the transition from period 1B to period 2 is abrupt or gradual. For period 5, the slope of the regression equation is slightly positive with a low value of B indicating that the data fit a trend of slight increase in SO_2, equivalent to about 0.05 t/d.

SO_2 EMISSION RATES DURING SUMMIT AND UPPER EAST RIFT ZONE ERUPTIONS

On April 30, 1982, a summit eruption lasted for 19 hours and produced about 0.5×10^6 m^3 of lava from an eruption fissure located northeast of Halemaumau Crater on the floor of Kilauea caldera. A peak emission rate of 1,150 t/d was measured during the middle of the eruption, and rates dropped to pre-eruption values quickly after activity ceased. On September 25, 1982, another summit eruption began at about 1900 (H.s.t.) and was over by the next morning after the eruption of about 3.0×10^6 m^3 of lava. The September eruption took place at night from vents located south of the Crater Rim Road, so COSPEC measurements were not possible. In contrast to the August 1971 and the July 1974 eruption fissures, which host prominent solfataras within the caldera, both 1982 eruptive fissures quickly cooled to ambient temperature and ceased emitting sulfur gases at the end of eruptive activity.

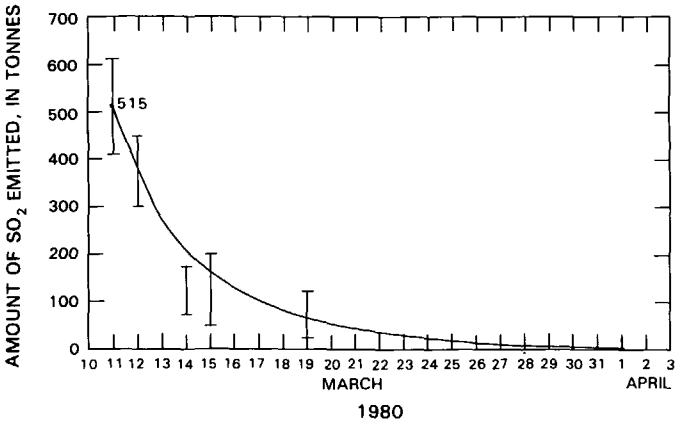

FIGURE 29.3.—SO_2 emission rates following Mauna Ulu intrusion, March–April 1980.

In November 1979, a 22-hour-long eruption occurred from vents east and west of, as well as within Pauahi Crater (fig. 29.1*A*) and approximately 3.5×10^6 m^3 of lava was erupted. COSPEC measurements were possible only during the first several hours of the eruption, before the Chain of Craters Road was closed by a lava flow, and an emission rate of 700 t/d of SO_2 was measured for the vent within Pauahi Crater. The 1979 fissures ceased emitting sulfur gases at the end of eruptive activity.

THE MARCH 10–12, 1980, INTRUSION

On March 2 and 10–12, 1980, two intrusions into the upper east rift zone of Kilauea (fig. 29.1*A*) between Pauahi Crater and Mauna Ulu were followed within minutes by deflation of the summit region. No lava was observed during these events; however, field studies in 1982 discovered a small volume (about 1 m^3) of fresh lava at 770 m elevation along the southeast end of the March 12 fracture (R. Moore, oral commun., 1982).

The March 10–12 intrusion released large amounts of CO_2 and SO_2 from the summit crater of the Mauna Ulu shield and from a 300-m-long N. 60° E. fracture set located between Mauna Ulu and Kane Nui o Hamo (fig. 29.1*A*). The fractures were quickly coated by elemental sulfur and fumed heavily for several days. The maximum temperature of the gas coming from the cracks was 98 °C. SO_2 emission rates from March 11 to 19 decreased from approximately 520 to 100 t/d, and within 30 days emission rates were less than 3 t/d (fig. 29.3). Approximately 3,000 tonnes of SO_2 was produced from March 11 through April.

SO_2 AND CO_2 EMISSIONS: AIRBORNE MEASUREMENTS: 1983–1984

Airborne measurements of SO_2 and CO_2 emission rates were made for eruption and intra-eruptive plumes at Puu Oo and for non-eruptive plumes at Kilauea caldera beginning in 1983 (table 29.3). The plumes from the eruptive episodes of Puu Oo are enormous in terms of SO_2 burden and physical size. The high concentration of SO_2 saturated the COSPEC signal, and plume widths often exceeded 50 km.

TABLE 29.3.—*Emission rates of SO_2 and CO_2 during Puu Oo eruption episodes: 1983–1984*

[--, no data; n.d., not determined]

Phase	Duration (hr)	Date	SO_2 (tonnes/day)	[1]CO_2 (tonnes/day)	Lava volume ($m^3 \times 10^6$)	Rate (m^3/hr)
			1983			
6	73	Jul 24	24,000 ± 4,700	--	9.4	0.13
7	56	Aug 15	15,700 ± 4,200	--	10.2	.18
7	56	Aug 17	17,500 ± 5,500	--	n.d.	n.d.
8	24	Sept 6	6,700 ± 1,800	--	7.0	.29
9	52	Sept 16	17,600 ± 10,300	--	8.7	.17
			1984			
14	19	Jan 31	11,800 ± 4,300	--	5.9	[3]0.31
15	19	Feb 15	[2]27,000	[1]4,700	8.6	.42
16	31	Mar 4	[2]18,000	[1]3,200	11.8	.37
17	22	Mar 30	5,100 ± 3,100	--	9.6	[3] .46
21	8	Jun 30	28,000 ± 6,200	--	5.7	[3] .71
28	15	Dec 4	32,000 ± 10,400	--	n.d.	[3] .85

[1]From Greenland and others (1985).
[2]Calculated values (see Greenland and others, 1985).
[3]Calculated from HVO monthly reports.

The episodes of the Puu Oo eruption have been well documented (Wolfe and others, chapter 17), including accurate measurements of erupted volumes and rates of lava production (table 29.3). Emission rates of SO_2 were measured during 8 eruptive episodes (6, 7, 8, 9, 14, 17, 21, and 28) of Puu Oo in 1983–1984; these rates range from 5,100 to 32,000 t/d (table 29.3). Rates for episodes 15 and 16 have been calculated from CO_2 flux measurements and fumarole gas composition (Greenland and others, 1985). The uncertainty in these measurements ranges from 15 to 40 percent of the reported values.

Between eruptive episodes at Puu Oo, gas is emitted continuously. On December 2, 1983, 24 hours after the end of phase 12, the SO_2 emission rates averaged 260 t/d; a week later the emission rates were 20 t/d. The CO_2 emission rates at Puu Oo were below the level of detection (less than 800–1,000 t/d) on both December 2 and 9. These data are consistent with gas sampling from the Puu Oo vent and with airborne measurements of eruptive plumes that indicate the CO_2/SO_2 ratio has been less than 1 (Greenland, 1984; Greenland and others, 1985).

On December 9, 1983, the emission rate of SO_2 in the summit region was 300 ± 30 t/d; the emission rate for CO_2 was 3,600 t/d. On February 13, 1984 the emission rates for SO_2 and CO_2 were 220 and 1,600 t/d, respectively (Greenland and others, 1985). These airborne measurements indicate a CO_2/SO_2 ratio greater than 5, in general agreement with measurements of fumaroles in the summit region.

DISCUSSION AND INTERPRETATION

RATES OF SO_2 EMISSION: NON-ERUPTIVE PLUME

The statistical analysis of the COSPEC data for 1979–1984 reveals that levels of SO_2 release remain relatively constant for

periods of months to years. Changes in the SO_2 flux generally correlate with other events at Kilauea such as eruptions or intrusions. We suggest that rates of SO_2 emissions, and changes in those rates, closely reflect magmatic processes at Kilauea. The relatively constant rates of SO_2 emission during periods 1A (before mid–March 1980), 3 (from August through December 1981), and 4 (February 1982 through January 1983) reflect the steady supply of magma to the shallow reservoir. The intrusions of magma into the upper east rift zone in March 1980 apparently diverted some magma out of the shallow reservoir and caused a 35 percent decrease in the rate of SO_2 emission from the summit region. In contrast, the southwest rift zone intrusion of August 1981 was followed by an increase in SO_2 emission rates (period 3), reflecting a temporary increase in the rate of magma supply as indicated by rapid reinflation of the summit chamber (Dvorak and others, 1986). Another rapid increase in the emission rate starting in January 1983 (period 5) occurred coincidently with an increase in magma supply rate that began with the Puu Oo eruption (Wolfe and others, chapter 17; Greenland and others, 1985).

For the period 1976–1982, magma was supplied to the shallow reservoir at about 5.6×10^6 m^3/mo (Dzurisin and others, 1984), and at 12×10^6 m^3/mo for the period 1983–1984 (chapter 17). From the mean rate of SO_2 emission from 1979–1982, we calculate that between 150 and 400 ppm sulfur were released by the magma stored in the shallow reservoir. A similar amount of sulfur was released during 1983-1984 using the higher rates of magma supply (Wolfe and others, chapter 17) and higher rates of SO_2 emission. This calculation suggests that about 10 to 30 percent of the 1,300 ppm sulfur (Harris and Anderson, 1983) initially dissolved in the parental melt is released to provide the daily rates of SO_2 measured in the non-eruptive plumes.

We noted earlier that distillation of magma as it re-equilibrates in the shallow reservoir may account for a sulfur loss of between 150 ppm (Greenland and others, 1985) and from 300 to 600 ppm (Gerlach and Graeber, 1985) prior to eruption. Thus, though some overlap exists in the amount of sulfur lost as determined from magma supply rates and SO_2 emission rates (150–400 ppm) as compared to the range of sulfur expected, the quantity of sulfur detected at the surface is apparently less than the amount of sulfur actually released from the magma. Gerlach and Graeber (1985) suggest that some SO_2 may be prevented from reaching the surface due to removal in the hydrothermal alteration of the volcanic pile or reaction with the deep hydrothermal brine, or it may be lost by separation of an immiscible sulfide melt during summit storage.

To discuss this problem more thoroughly, we need (1) to know more about the nature of the hydrothermal system postulated to overly the shallow magma reservoir, (2) more careful study of the volatile contents of intrusive bodies, and (3) additional study of melt inclusions to determine more precisely the primary sulfur content in Hawaiian basaltic magmas.

MAUNA ULU INTRUSION, MARCH 10–12, 1980

The fate of the sulfur remaining in the magma after its partial distillation in the shallow reservoir depends on its subsequent history. For the period 1956–1983, Dzurisin and others (1984) have shown that approximately 65 percent of the magma supplied to the shallow reservoir was stored through intrusion into the summit and rift zones of the volcano; approximately 35 percent was erupted. Only the extruded volume is largely outgassed of sulfur, whereas the intruded magma is less completely outgassed.

If intrusion is sufficiently shallow, further gas loss may be quite efficient. The initially large flux and subsequent rapid decrease in SO_2 emission rates which followed the intrusion near Mauna Ulu in mid-March 1980 is interpreted to reflect the pattern of outgassing of a portion of magma following its intrusion to a shallow depth. The SO_2 emission rates at the summit decreased significantly after this intrusion and remained low for at least three months. The volume of intruded magma estimated from the net summit deflation (16 microradians) during the event is approximately 5.2×10^6 m^3 (that is 0.33 million m^3 per microradian; Dzurisin and others, 1984). Assuming efficient degassing of 2.2 kg/m^3 of sulfur (loss of 800 ppm S; $\rho = 2.8$ g/cm^3), the 3,000 tonnes of SO_2 released during this event require a magma volume of 1.4×10^6 m^3. However, overburden pressures require greater solubility of sulfur in the melt, thus only about 30 percent of the dissolved sulfur in the reservoir-equilibrated magma would have had to escape to produce the SO_2 emissions of this event.

SO_2 FROM KILAUEA—ANNUAL BUDGET AND GLOBAL IMPACT

From the averaged monthly emission rates for SO_2 (table 29.2) we have calculated the average annual emission rates of SO_2 from quiescent outgassing of Kilauea from 1979–1984. These are: 1979, $58,500\pm15,000$ t/yr; 1980, $52,000\pm15,000$ t/yr; 1981, $83,000\pm30,000$ t/yr; 1982, $58,500\pm18,000$ t/yr; 1983, $95,000\pm33,000$ t/yr; and 1984, $95,000\pm33,000$ t/yr. The global anthropogenic contribution of SO_2 to the atmosphere is estimated at between 100×10^6 t/yr (Likens, 1979; Cadle, 1980) and 150×10^6 t/yr (Berresheim and Jaeschke, 1983). The global volcanic contribution is estimated to be 15×10^6 t/yr (Berresheim and Jaeschke, 1983) with the majority coming from a few large eruptive events. The contribution of SO_2 from quiescent outgassing of Kilauea contributes less than 1 percent of the annual global contribution from volcanoes.

The 1983–1984 eruptions of Puu Oo produced about 0.37×10^6 t/yr of SO_2 (calculated from the 1983–1984 total erupted magma of 307×10^6 m^3, corrected to dense rock equivalent, or DRE, using a 20 percent vesicularity correction, and estimated to release 3 kg of SO_2 per cubic meter of DRE lava) and may have contributed as much as 3 percent of the annual volcanic contribution. Though the individual eruptive episodes of Puu Oo contributed large amounts of SO_2 to the atmosphere, these emissions were confined to the lower troposphere, and eruptions seldom continued for longer than 72 hours. The local impact of such emissions on vegetation and rainfall chemistry may be dramatic (Winner and Mooney, 1980); however, their global impact remains small.

ERUPTION PREDICTION USING EMISSION RATE DATA

At Asama Volcano, Japan, Noguchi and Kamiya (1963) demonstrated that the amounts of sulfur gas emitted by the volcano increased prior to explosive eruptions. At Mount Etna, large increases in the rate of SO_2 emission were observed before each of two Strombolian eruptions in 1977 (Malinconico, 1979). At Mount St. Helens, increases in SO_2 emission rates were noted two to four weeks prior to 2 of 12 eruptions between 1981 and 1983 (Casadevall and others, 1983). These studies indicate that increases in SO_2 emission rates precede some, but not necessarily all, types of eruptive activity.

From experience with emission-rate data at Mount St. Helens, Casadevall and others (1983) note that confidence in using the data for prediction of activity increases with the frequency and regularity of measurements. We have scrutinized the present data for Kilauea and find no hindsight indication of pending activity. If such increases happen only days or hours before activity, it is unlikely that we would recognize them using the frequency of measurements made during 1979–1984.

Measurements of SO_2 and CO_2 emission rates require considerable investments of time and effort, and the present techniques simply are not practical for making continuous measurements. Different methods of measurement, as well as more careful integration of geochemical data with other geophysical measurements, are necessary if we hope to use emission rates to improve our abilities to predict impending activity.

REFERENCES

Barrie, L.A., 1985, Scavenging ratios, wet deposition and in-cloud oxidation: an application to the oxides of sulphur and nitrogen: Journal of Geophysical Research, v. 90, p. 5789–5799.

Berresheim, H., and Jaeschke, W., 1983, The contribution of volcanoes to the global atmospheric sulfur budget: Journal of Geophysical Research, v. 88, p. 3732–3740.

Cadle, R.D., 1980, A comparison of volcanic with other fluxes of atmospheric trace gas constituents: Reviews of Geophysics and Space Physics, v. 18, p. 746–752.

Cadle, R.D., Lazrus, A.L., and Shedlovsky, J.P., 1969, Comparison of particles in the fume from eruptions of Kilauea, Mayon, and Arenal volcanoes: Journal of Geophysical Research, v. 74, p. 3372–3378.

Cadle, R.D., Wartburg, A.F., and Grahek, F.E., 1971, The proportion of sulfate to sulfur dioxide in Kilauea Volcano fume: Geochimica et Cosmochimica Acta, v. 35, p. 503–507.

Casadevall, T.J., and Hazlett, R.W., 1983, Thermal area of Kilauea and Mauna Loa: Journal of Volcanology and Geothermal Research, v. 16, p. 173–188.

Casadevall, T.J., Johnston, D.A., Harris, D.M., Rose, W.I., Jr., Malinconico, L.L., Stoiber, R.E., Bornhorst, T.J., Williams, S.N., Woodruff, Laurel, and Thompson, J.M., 1981, SO_2 emission rates at Mount St. Helens from March 29 through December, 1980, *in* Lipman, P.W., and Mullineaux, D.L., eds., The 1980 eruptions of Mount St. Helens, Washington: U.S. Geological Survey Professional Paper 1250, p. 193–200.

Casadevall, T.J., Rose, W.I., Jr., Fuller, W.H., Hunt, W., Hart. M., and Moyers, J.L., 1984, SO_2 and particles in quiescent volcanic plumes from Poas, Arenal, and Colima Volcanos, Costa Rica and Mexico: Journal of Geophysical Research, v. 89. p. 9633–9641.

Casadevall, T.J., Rose, W.I., Jr., Gerlach, T.M., Greenland, L.P., Ewert, J., Wunderman, R., and Symonds, R., 1983. Gas emissions and the eruptions of Mount St. Helens through 1982: Science, v. 221, p. 1383–1385.

Darzi, Michael, 1981, Fumarolic aerosols from Kilauea volcano, Hawaii: Nuclear Instrumentation Methods, v. 181, p. 359–365.

Darzi, Michael, and Winchester, J.W., 1982a, Aerosol characteristics at Mauna Loa observatory, Hawaii, after East Asia dust storm: episodes: Journal of Geophysical Research, v. 87, p. 1251–1258.

——— 1982b, Resolution of basaltic and continental aerosol components during spring and summer within the boundary layer of Hawaii: Journal of Geophysical Research, v. 87, p. 7262–7272.

——— 1982c, Volcanic aerosol phosphorus, chlorine, and sulfur at Kilauea, Hawaii: Journal of Geophysical Research, v. 87, p. 11,095–11,101.

Dvorak, J.J., Okamura, A.T., English, T.T., Koyanagi, R.Y. Nakata, J.S., Sako, M.K., Tanigawa, W.T., and Yamashita, K.M., 1986, Mechanical response of the south flank of Kilauea Volcano, Hawaii, to intrusive events along the rift systems: Tectonophysics, v. 124, p. 193–209.

Dzurisin, Daniel, Koyanagi, R.Y., and English, T.T., 1984, Magma supply and storage at Kilauea Volcano, Hawaii: Journal of Geophysical Research, v. 21, p. 177–206.

Eaton, J.P., and Murata, K.J., 1960, How volcanoes grow: Science, v. 132, p. 925–938.

Fiske, R.S., and Kinoshita, W.T., 1969, Inflation of Kilauea Volcano prior to its 1967–1968 eruption: Science, v. 165, p. 341–349.

Fornari, D.J., Moore, J.G., and Calk, L., 1979. A large submarine sand-rubble flow on Kilauea Volcano, Hawaii: Journal of Volcanology and Geothermal Research, v. 5, p. 239–256.

Gerlach, T.M., 1980, Evaluation of volcanic gas analyses from Kilauea Volcano: Journal of Volcanology and Geothermal Research, v. 7. p. 295–317.

Gerlach, T.M., and Graeber, E.J., 1985, The volatile budget of Kilauea: Nature, v. 313, p. 273–277.

Graedel, T.E., 1977, The homogeneous chemistry of atmospheric sulfur: Reviews of Geophysics and Space Physics, v. 15, p. 421–426.

Greenland, L.P., 1984, Gas composition of the January 1983 eruption of Kilauea Volcano, Hawaii: Geochimica et Cosmochimica Acta, v. 48, p. 193–195.

Greenland, L.P., Rose, W.I., Jr., and Stokes, J.B., 1985, An estimate of gas emissions and magmatic gas content from Kilauea Volcano: Geochimica et Cosmochimica Acta, v. 49. p. 125–129.

Harding, Duane, and Miller, J.M., 1982, The influence of volcanic outgassing on rain chemistry of the Hawaiian volcano Kilauea: Journal of Geophysical Research, v. 87, p. 1225–1230.

Harris, D.M., and Anderson, A.T., Jr., 1983, Concentrations, sources, and losses of H_2O, CO_2, and S in Kilauean basalt: Geochimica et Cosmochimica Acta, v. 47, p. 1139–1150.

Harris, D.M., Sato, Motoaki, Casadevall, T.J., Rose, W.I., Jr., and Bornhorst, T.J., 1981, Emission rates of CO_2 from plume measurements, *in* Lipman, P.W., and Mullineaux, D.L., eds., The 1980 eruptions of Mount St. Helens, Washington: U.S. Geological Survey Professional Paper 1250, p. 201–207.

Heald, E.F., Naughton, J.J., and Barnes, I.L., 1963, The chemistry of volcanic gases. 2. Use of equilibrium calculations in the interpretation of volcanic gas samples: Journal of Geophysical Research, v. 68, p. 545–557.

Hegg, D.A., and Hobbs, P.V., 1978, Oxidation of sulfur dioxide in aqueous systems with particular reference to the atmosphere: Atmospheric Environment, v. 12, p. 241–253.

Likens, G.E., 1979, Acid rain: Scientific American, v. 241, p. 43–51.

Maahs, H.G., 1983a, Measurements of the oxidation rate of sulfur (IV) by ozone in aqueous solution and their relevance to SO_2 conversion in nonurban tropospheric clouds: Atmospheric Environment, v. 17. p. 341–345

——— 1983b, Kinetics and mechanism of the oxidation of S(IV) by ozone in aqueous solution with particular reference to SO_2 conversion in nonurban tropospheric clouds: Journal of Geophysical Research, v. 88, p. 10,721–10,732.

Malinconico, L.L., 1979, Fluctuations in SO_2 emission during recent eruptions of Etna: Nature, v. 278, p. 43–45.

Martin, L.R., 1983, Kinetic studies of sulfite oxidation in aqueous solution, *in*

Calvert, J.G., ed., SO_2, NO, NO_2 oxidation mechanism: atmospheric considerations, v. 3, of Acid precipitation series: Boston, Butterworth, p. 63–100.

Millan, M.M., Gallant, A.J., and Turner, H.E., 1976, The application of correlation spectroscopy to the study of dispersion from tall stacks: Atmospheric Environment, v. 10, p. 499–511.

Millan, M.M., and Hoff, R.M., 1978, Remote sensing of air pollutants by correlation spectroscopy—instrumental response characteristics: Atmospheric Environment, v. 12, p. 853–864.

Moore, J.G., and Fabbi, B.P., 1971. An estimate of the juvenile sulfur content of basalt: Contributions to Mineralogy and Petrology, v. 33, p. 118–127.

Naughton, J.J., Lewis, V.A., Hammond, D., and Nishimoto, D., 1974, The chemistry of sublimates collected directly from lava fountains at Kilauea Volcano, Hawaii: Geochimica et Cosmochimica Acta, v. 38, p. 1679–1690.

Noguchi, K., and Kamiya, H., 1963, Prediction of volcanic eruption by measuring the chemical composition and amounts of gases: Bulletin Volcanologique, v. 26, p. 367–378.

Roberts, D.B., and Williams, D.J., 1979. The kinetics of oxidation of sulphur dioxide within the plume from a sulphide smelter in a remote region: Atmospheric Environment, v. 13, p. 1485–1499.

Rose, W.I., Jr., 1977, Scavenging of volcanic aerosol by ash: atmospheric and volcanic implications: Geology, v. 5, p. 621–624.

Russell, C., 1982, The effects of acid environments on metabolic gas exchange in *Usena australis* Fr.: Honolulu, University of Hawaii, MS thesis, 131 p.

Ryan, M.P., Koyanagi, R.Y., and Fiske, R.S., 1981, Modeling the three-dimensional structure of magma transport systems: Application to Kilauea Volcano, Hawaii: Journal of Geophysical Research, v. 86, p. 7111–7129.

Sakai, H., Casadevall, T.J. and Moore, J.G., 1982, Chemistry and isotope ratios of sulfur in basalts and volcanic gases at Kilauea Volcano, Hawaii: Geochimica et Cosmochimica Acta, v. 46, p. 729–738.

Stoiber R.E., Malinconico, L.L., and Casadevall, T.J., 1979. SO_2 monitoring by remote sensing at Kilauea Volcano, Hawaii [abs.]: Hawaii Symposium on Intraplate Volcanism and Submarine Volcanism, Hilo, HI, Abstract volume, p. 174.

Stoiber R.E., Malinconico, L.L., and Williams, S.N., 1983, Use of the correlation spectrometer at volcanoes, *in* Tazieff, H., and Sabroux, J.C., eds., Forecasting Volcanic Events: Amsterdam, Elsevier, p. 425–444.

Stoiber R.E., and Malone, G.B., 1975, SO_2 emission at the crater of Kilauea, at Mauna Ulu and at Sulfur Banks, HI [abs.]: Eos, v. 56, p. 461.

Swanson, D.A., and Fabbi, B.P., 1973, Loss of volatiles during fountaining and flowage of basaltic lava at Kilauea Volcano, Hawaii; U.S. Geological Survey Journal of Research, v. 1, p. 649–658.

Williams, D.J., Carras, J.N., Milne, J.W., 1981, The oxidation and long-range transport of sulphur dioxide in a remote region: Atmospheric Environment, v. 15, p. 2255–2262.

Winner, W.E., and Mooney, H.A., 1980, Response of Hawaiian plants to volcanic sulfur dioxide: stomatal behavior and foliar injury: Science, v. 210, p. 789–791.

Woodcock, A.H., 1960, The origin of trade-wind orographic shower rains: Tellus, v. 12, p. 315–326.

Wright, T.L., 1984, Origin of Hawaiian tholeiite: a metasomatic model: Journal of Geophysical Research, v. 89. p. 3233–3252.

COMPOSITION OF GASES FROM THE 1984 ERUPTION OF MAUNA LOA VOLCANO

By L. Paul Greenland

ABSTRACT

The March–April 1984 eruption of Mauna Loa Volcano provided an excellent opportunity for sampling eruptive gases. These Mauna Loa gases are similar to those from adjacent Kilauea Volcano, but they have less Sater and halogens relative to sulfur than Kilauea gases. The very low atomic C/S ratio (0.2, as at Kilauea) is attributed to pre-eruption degassing of the magma during storage in Mauna Loa's shallow (3–4 km) summit reservoir. Thermodynamic calculations show that most of these samples contain excess water above that required for equilibrium with other species. It is suggested that the excess water in these analyses is not a meteoric contaminant but is magmatic water which has not equilibrated with the other gases because of the rapid rate of rise of the magma in the vent system.

INTRODUCTION

A flank eruption of Mauna Loa Volcano, Hawaii, began on March 25, 1984, and ended by April 14. The eruption began in the summit caldera and extended about 3 km down the southwest rift zone and about 19 km down the northeast rift zone. By 0930 Hawaiian standard time (H.s.t.) of March 25, fountaining was restricted to a 21-km-long curtain of fire between about 3,400-m and 3,470-m elevation on the northeast rift zone; by 0640 H.s.t. the next day, activity had ceased at these vents except for profuse fume emission, which continued through May 5. As eruptive activity at these vents waned, new vents opened downrift at about 2,800-m elevation; these vents were active along a 500-m segment of the fissure until April 14. A preliminary summary of geologic, deformational, and seismic studies of this eruption may be found in Lockwood (1984).

Many of the vents in the active area of the fissure at 2,800-m elevation were fully productive only intermittently, having long intervals of only low-level spatter activity and occasional small lava flows overflowing the vent. These provided nearly ideal sites for sampling gases. Continued eruptive activity made these sites inaccessible after April 5, and gas sampling was then restricted to the fuming, noneruptive vents above 3,400 m. Gases emitted by the noneruptive vents originated from magma in the feeder dike as it passed through the conduit system to be erupted downrift. This paper reports the results of gas collections made in these two areas.

ACKNOWLEDGMENTS

I am greatly indebted to T.M. Gerlach for a thorough and trenchant review of an earlier draft of this paper. I have also benefited from thoughtful comments by I. Barnes, M. Sato, and A. Truesdell.

EXPERIMENTAL METHODS

SAMPLING SITES

Two classes of sampling sites will be distinguished in this paper: "active" sites are those where gas samples were taken from, or immediately adjacent to, vents actively emitting spatter, fountains, and (or) lava flows; "feeder" sites were at posteruptive vents through which the magma was degassing as it flowed through the conduit to the actively erupting vents. After March 25, the active sites were located at 2,800-m to 3,000-m elevation, while the feeder sites were in the area of 3,400-m elevation. Only active sites were sampled until April 3; these then became generally inaccessible, and subsequently attention was concentrated on the feeder sites.

SAMPLING TECHNIQUE

Gas samples were collected through lead-in tubes using evacuated bottles as described elsewhere (Greenland, 1984). Lead-in tubes used at various times were lengths of titanium, stainless steel, quartz, or mullite tubing 1–2 m long and 1–4 cm in diameter; they were inserted up to two-thirds of their length into the vent and left for several minutes in order for the natural gas flow to flush out air. At the active vents, the entrance of the tube was always within a meter or so of molten magma and often within centimeters. When first used, metal tubes were inserted in a vent for as long as 30 min to develop corrosion; no samples were taken during this conditioning process. Experience in Hawaii has shown that 1–2 min of flushing is adequate, while more than 10–15 min of flushing of stainless steel or titanium at temperatures above 1,000 °C results in samples having increased H_2 content; all samples reported here were collected within 5 minutes of tube insertion when stainless steel or titanium was used. Quartz or mullite tubes are much less reactive than the metal ones, but they are discouragingly fragile under rough field conditions. With the sampling technique used here, there appears to be no difference in sample composition related to composition of lead-in tube.

The evacuated bottles used for gas collection were similar to those described by Giggenbach (1975) but contained a different aqueous solution. Piccardi and Cellini-Legittimo (1983) discussed the advantages of a Cd solution for separating H_2S, and T.M. Gerlach (oral commun., 1983) suggested replacing caustic solutions with NH_4OH. (Subsequently, Gerlach has returned to caustic solutions). The present collections were made with bottles containing 25–45 mL of $3M$ NH_4OH–$0.1M$ $NH_4CH_3CO_2$–$0.04M$ CdO. Gas collections were made by covering the exit of the lead-in tube with a metal washer to reduce air contamination, inserting the stem (2–4 cm) of the inverted bottle, and opening the stopcock allowing the gases to bubble through the ammonia solution; H_2S was immediately precipitated as CdS, the acid gases were absorbed in the aqueous solution, and H_2 and CO passed into the headspace.

Temperatures were measured with a chromel-alumel thermocouple. Because of the difficult conditions, measured temperatures at the active vents may be as much as 25–50 °C lower than actual temperatures.

Extreme precautions to exclude air from the samples were not taken. An abundance of experiments made in Hawaii have shown that gas collections made in this way are stable for 4–6 h even with 95 percent air in the sample; left overnight for analysis, however, such gas samples usually become oxidized. Because of the proximity of laboratory facilities and the availability of helicopter transport, it usually was possible to complete the gas chromatography analyses within 5 h of collection; on the few occasions when this was not possible, the samples were discarded. The aqueous solutions of the acid gases are unaffected by air contamination except for the possible oxidation of SO_3^{2-} to SO_4^{2-}; all S in these solutions was calculated as SO_2, and these analyses could be performed at leisure.

GAS CHROMATOGRAPHY

The H_2 and CO collected in the headspace of the evacuated bottles were determined by gas chromatography. Because of the high temperature of the sampling and because sampling was occasionally interrupted before the bottles were completely full, air was admitted to the bottles just before analysis to adjust the pressure to atmospheric pressure. The H_2 was separated on 4.9 m (16 ft) of 5A molecular sieve with N_2 carrier gas at room temperature and determined by thermal conductivity (helium was sought simultaneously but was not present at >0.001 percent). The gas chromatograph for this determination was assembled locally from a commercially available sampling valve, detector, and integrator. For the determination of CO and CH_4, samples were injected onto 3.6 m (12 ft) chromosorb 102 with He carrier gas in a Hewlett-Packard 5840 gas chromatograph; a valve permitted backflushing of CO_2, H_2O, and SO_2 while the more rapidly eluted gases passed to 2.4 m (8 ft) of 5A molecular sieve. After elution of oxygen from this column, a valve switched the gas stream to enable reaction of CO with H_2 in the presence of a nickel catalyst to form CH_4 (CH_4 originally present in the sample eluted subsequently and passed through this converter unchanged). The CO (converted to CH_4) and CH_4 were then determined with a flame ionization detector. Analytical precision of the gas chromatography analyses was ±3–5 percent.

WET CHEMISTRY

The CO_2, SO_2, H_2S, HCl, and HF were determined in aliquants of the aqueous solution in the evacuated-bottle collections. For CO_2, 0.5 mL was added to 1 mL of $6M$ H_2SO_4 saturated with $K_2Cr_2O_7$ in a closed vial; the CO_2 liberated into the headspace was then determined by gas chromatography. The HF was determined by specific-ion electrode after adjusting the pH of an aliquant to 6 with dilute H_2SO_4. The HCl also was determined by specific-ion electrode after acidification with $6M$ H_2SO_4 and oxidation of SO_3^{2-} with $NaNO_2$. The Cd remaining in the supernatant solution was determined by atomic-absorption spectrometry; the difference from that originally present was attributed to CdS, thus H_2S. The SO_3^{2-} and SO_4^{2-} were determined by conventional ion chromatography with $3mM$ $NaHCO_3$–Na_2CO_3 as eluent; SO_3^{2-} and SO_4^{2-} were combined and calculated as SO_2. The analytical precision of these determinations was ± 10–15 percent.

The evacuated bottles were weighed before and after sample collection. The weight gained, after subtraction of CO_2 and SO_2, was taken as water.

RESULTS

Analyses of the evacuated-bottle collections on an air-free basis are given in table 30.1. The water content of these samples ranges from 55 to 91 percent, and, because of the constant sum condition, this variation induces an apparent variability in the less abundant components. Furthermore, the abundances of H_2, CO, and H_2S are thermodynamic functions of the temperature and partial pressure of oxygen at which they were last in equilibrium, and thus variations in these gases may simply reflect the temperature and oxidation state of the gases. These effects are reduced in table 30.2, which gives the analyses on the basis of atomic ratios (atoms per sulfur atom) and compares their average with the composition of gas from the recent east-rift-zone eruption of adjacent Kilauea Volcano. Even on this basis, the compositional variability remains fairly large, with the range of each component extending over more than a factor of three.

Two samples were collected after the eruption ended on April 15. Table 30.1 shows these samples to be greatly depleted in SO_2 and enriched in H_2O; by April 18, halogen acids also became more abundant.

The abundance of halogen acids is generally very low in these gases, less than 1 percent of the sulfur content, and quite variable, ranging over more than an order of magnitude. It is obvious from table 30.1 that the halogens are highly correlated with each other, but statistical tests show that they vary independently of H, C, or S species. The average atomic Cl/F ratio, 1.1 ± 0.46, is not significantly different from the ratio (0.92) found for the 1983 eruption of Kilauea (table 30.2), although the halogen/S ratios from Kilauea are almost an order of magnitude higher than these Mauna Loa

TABLE 30.1.—*Composition of gas samples from 1984 Mauna Loa eruption*

[Lead-in tube materials: 1, Ti: 2, stainless steel; 3, quartz; 4, mullite]

Sample	Collection date (mo/d)	Constituents (mole percent)								Temperature (°C)	Tube Materials
		H_2O	H_2	CO_2	CO	SO_2	H_2S	HCl	HF		
Active vents											
1	3/25	75.6	0.36	3.22	0.108	19.9	0.58	0.074	0.064	1,080	1
2	3/25	59.2	.66	6.34	.156	32.9	.62	.018	.100	1,075	1
3	3/25	64.9	.55	4.57	.157	28.7	.92	.130	.101	1,080	1
4	3/26	73.0	.64	3.23	.146	22.1	.69	.108	.051	1,100	1
5	3/26	73.4	.48	4.15	.158	21.0	.56	.161	.096	1,100	1
6	3/26	77.6	.49	2.38	.090	18.0	1.05	.194	.118	1,120	4
7	3/26	75.7	.30	4.25	.073	19.0	.51	.066	.072	1,050	4
8	3/27	77.2	.73	2.23	.150	19.0	.56	.077	.036	1,130	1
9	3/27	79.8	.86	3.05	.168	15.3	.74	.094	.098	1,130	1
10	3/27	70.2	.80	3.45	.115	24.5	.79	.059	.103	1,100	1
11	3/27	78.5	.75	2.45	.137	16.9	1.01	.174	.086	1,100	1
12	3/27	69.4	.66	4.57	.164	24.7	.38	.015	.025	1,130	1
13	3/30	73.1	.32	5.34	.117	20.1	.81	.049	.055	825	3
14	3/30	70.7	.27	6.64	.094	21.0	1.11	.089	.110	825	3
15	3/31	64.9	.94	7.79	.346	25.0	.85	.093	.116	1,080	3
16	4/ 1	71.7	1.31	6.61	.322	17.9	2.02	.065	.054	1,100	1
17	4/ 1	78.7	.93	4.69	.238	14.0	1.35	.048	.039	1,100	1
18	4/ 2	82.3	.33	4.36	.143	11.7	1.11	.028	.030	1,050	1
19	4/ 2	79.8	.60	4.54	.102	13.9	.97	.049	.060	1,050	1
24	4/ 5	71.8	.31	2.11	.063	25.1	.47	.063	.073	1,010	1
25	4/ 5	65.6	.90	6.13	.109	24.8	2.45	.040	.029	1,010	1
26	4/ 5	65.8	1.30	6.53	.306	23.3	2.49	.139	.174	1,100	1
Feeder vents											
20	4/ 3	71.1	.17	5.21	.096	22.2	1.02	.082	.102	735	1
21	4/ 3	64.2	.28	4.91	.083	29.2	1.15	.059	.078	870	1
22	4/ 3	71.3	.15	5.11	.072	22.2	1.02	.092	.099	775	1
23	4/ 3	62.0	.30	6.58	.078	29.1	1.41	.208	.265	835	1
27	4/ 5	61.1	.41	6.54	.125	30.4	1.23	.119	.124	875	3
28	4/ 5	55.3	.58	8.72	.157	33.2	1.61	.165	.199	895	1
29	4/ 7	59.8	.57	6.16	.129	31.6	1.63	.035	.019	880	1
30	4/ 9	65.0	.46	5.88	.122	27.5	1.01	.024	.018	875	2
31	4/11	70.2	.29	5.07	.060	23.6	.80	.020	.022	840	1
32	4/11	66.1	.28	5.06	.089	27.2	1.12	.061	.056	840	2
33	4/13	64.9	.25	5.34	.107	27.5	1.64	.097	.136	820	1
34	4/13	64.7	.16	6.01	.046	28.0	1.03	.042	.045	820	2
Posteruption samples											
35	4/16	91.2	.51	1.66	.009	5.1	1.44	.042	.077	760	2
36	4/18	86.8	.07	4.05	.004	6.7	1.72	.193	.469	745	2

ratios. The great difference in halogen/S ratios may reflect a difference in the magma chemistry of Mauna Loa versus that of Kilauea; alternatively, eruptive degassing may have been more efficient for the Kilauea samples than for those from Mauna Loa.

Examination of tables 30.1 and 30.2 suggests a difference in water content between samples taken in the area of actively eruptive vents and samples taken where the feeder dike was degassing through posteruptive vents. Student's t-test (Fisher, 1936) confirms the difference in means (72.6 and 64.6 percent H_2O, respectively) to be significant at the 99-percent confidence level. A ternary plot of atomic H-C-S (fig. 30.1) shows the clear distinction between active vents and feeder vents in their content of water, the major contributor to atomic H. Samples from both types of vent plot closely along the same atomic-H control line, defined by a C/S ratio of ~0.2, indicating that the major source of variability among these samples is a process that has added or subtracted water to or from the gas. Most of the samples from the feeder sites were taken after the lower vents became inaccessible; it is possible, therefore, that the lower water content of these samples reflects a change in the gas composition with time. But, as discussed below, it seems more probable that this difference reflects the greater depth (thus greater solubility of water) of the degassing in the feeder dike compared with the near-surface degassing in the eruption area.

DISCUSSION

EQUILIBRIUM CONSIDERATIONS

A fundamental question concerning the complete analyses given in table 30.1 is the extent to which they represent an equilibrium assemblage. There are several techniques for studying volcanic gas equilibria (Heald and others, 1963; Nordlie, 1971; Gerlach, 1980). A simple, rapid technique that does not require a computer will be described here. The following three oxidation reactions include all of the gas species commonly reported in a volcanic gas analysis:

$$2CO + O_2 = 2CO_2 \quad (1)$$

$$2H_2 + O_2 = 2H_2O \quad (2)$$

$$H_2S + O_2 = SO_2 + H_2 \quad (3)$$

All other reactions of the common volcanic gases can be derived

TABLE 30.2.—*Atomic composition of gas samples from 1984 Mauna Loa eruption*

[Figures are atoms per atom of S; Mauna Loa average excludes posteruption samples; Kilauea average is of east-rift-zone eruption of 1983 (Greenland, 1984)]

Sample	Collection date (mo/d)	Element H	C	O	S	Cl (×10³)	F (×10³)
Active vents							
1	3/25	7.48	0.163	5.96	1.00	3.61	3.15
2	3/25	3.62	.194	4.12	1.00	.53	2.98
3	3/25	4.49	.160	4.44	1.00	4.39	3.41
4	3/26	6.52	.148	5.43	1.00	4.74	2.22
5	3/26	6.92	.200	5.75	1.00	7.47	4.45
6	3/26	8.31	.129	6.21	1.00	10.17	6.18
7	3/26	7.84	.221	6.26	1.00	3.35	3.68
8	3/27	8.03	.122	6.13	1.00	3.92	1.83
9	3/27	10.16	.201	7.27	1.00	5.85	6.13
10	3/27	5.68	.141	4.99	1.00	2.35	4.05
11	3/27	8.99	.145	6.56	1.00	9.71	4.83
12	3/27	5.61	.188	5.10	1.00	.60	.98
13	3/30	7.11	.261	5.94	1.00	2.33	2.65
14	3/30	6.53	.305	5.70	1.00	4.03	4.98
15	3/31	5.17	.315	5.06	1.00	3.61	4.49
16	4/ 1	7.54	.348	6.08	1.00	3.25	2.70
17	4/ 1	10.56	.321	7.58	1.00	3.14	2.53
18	4/ 2	13.08	.352	8.94	1.00	2.17	2.31
19	4/ 2	10.95	.312	7.86	1.00	3.28	4.01
24	4/ 5	5.68	.085	4.94	1.00	2.45	2.85
25	4/ 5	5.06	.229	4.68	1.00	1.48	1.05
26	4/ 5	5.41	.265	4.88	1.00	5.39	6.75
Feeder vents							
20	4/ 3	6.23	.229	5.43	1.00	3.55	4.39
21	4/ 3	4.33	.165	4.37	1.00	1.93	2.57
22	4/ 3	6.25	.223	5.43	1.00	3.98	4.24
23	4/ 3	4.19	.218	4.37	1.00	6.82	8.69
27	4/ 5	3.98	.211	4.27	1.00	3.76	3.92
28	4/ 5	3.31	.255	4.00	1.00	4.74	5.72
29	4/ 7	3.73	.189	4.08	1.00	1.06	.58
30	4/ 9	4.66	.211	4.63	1.00	.85	.64
31	4/11	5.85	.210	5.23	1.00	.84	.89
32	4/11	4.77	.182	4.62	1.00	2.16	1.98
33	4/13	4.59	.187	4.49	1.00	3.33	4.67
34	4/13	4.54	.209	4.57	1.00	1.44	1.54
Posteruption vents							
35	4/16	28.59	.256	16.06	1.00	6.37	11.84
36	4/18	21.22	.484	12.92	1.00	23.03	55.97
Mauna Loa average							
		6.39	.214	5.45	1.00	3.59	3.47
Kilauea average							
		15.5	.260	10.0	1.00	21.6	23.4

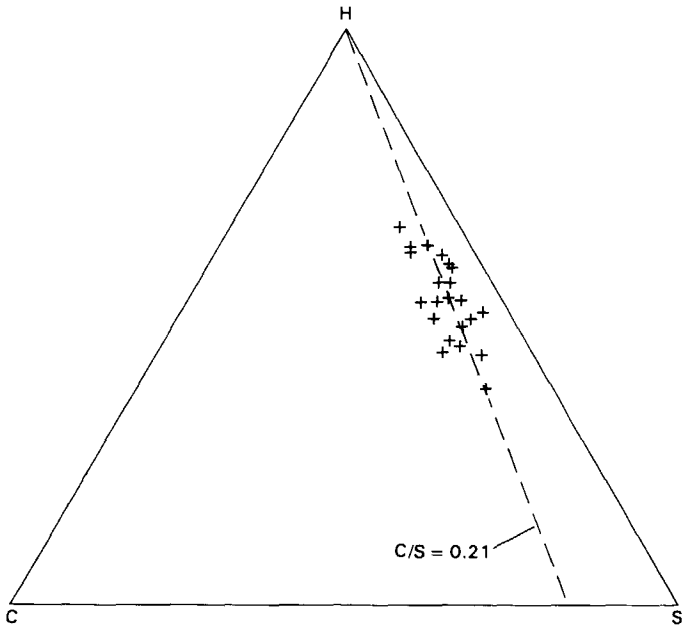

FIGURE 30.1.—Ternary plot of atomic H, C, and S from data in table 30.2. Atomic H has been divided by a factor of 5 for clarity of plotting. Dashes indicate water-control line for a C/S value of 0.21.

from these elementary reactions. Equilibrium constants, K, for these reactions can be expressed in the form

$$\log(O_2) = 2\log(CO_2/CO) - \log\ K_1 \quad (4)$$

$$\log(O_2) = 2\log(H_2O/H_2) - \log\ K_2 \quad (5)$$

$$\log(O_2) = \log(SO_2/H_2S) + \log(H_2) - \log\ K_3 \quad (6)$$

where the individual species have been written to indicate their respective partial pressures.

Because the heat of reaction for gaseous reactions is nearly constant over a limited temperature range, the temperature dependence of the equilibrium constant can be approximated by

$$\log\ K = (A/T) + B \quad (7)$$

where T is the temperature in Kelvin and A and B are thermodynamic constants. From the functional temperature dependence of the equilibrium constant, it is obvious that a plot of $\log(pO_2)$ versus $1/T$ for equations 4–6 will yield three straight lines intersecting at a single point if the analysis represents an equilibrium assemblage; equally, divergence to three distinct intersections implies disequilibrium. The major virtue of such plots is that they can easily be constructed during an analysis from a table giving equilibrium constants at two temperatures, thus serving as an immediate control on analyses.

Alternatively, an analytic solution may be obtained by combining equations 1–3 to eliminate oxygen:

$$CO + H_2O = CO_2 + H_2 \quad (8)$$

$$2CO + SO_2 + H_2 = 2CO_2 + H_2S \quad (9)$$

$$3H_2 + SO_2 = 2H_2O + H_2S \quad (10)$$

Temperatures calculated from equation 7 for these reactions necessarily will be the same if all species are in equilibrium.

Applying this procedure to the samples of table 30.1 shows that some are close to equilibrium, while many others are far from equilibrium. Equilibrium temperatures (table 30.3) were calculated for all the analyses of table 30.1 from equations 8–10 with the partial pressure of oxygen calculated from equation 4 at the temperature given by equation 9. The results demonstrate a consistent pattern of equation 8 yielding temperatures above the measured magma temperature (1,150 °C), temperatures from equation 9 being close to gas-collection temperatures, and temperatures from equation 10 being less than those of collection. Because changes in the H_2O/H_2 ratio change the calculated temperatures of equations 8 and 10 in opposite directions, this ratio is the obvious candidate for

TABLE 30.3.—*Observed temperature, calculated equilibrium temperatures, and calculated oxygen partial pressure for gas samples from 1984 Mauna Loa eruption*

[Oxygen partial pressure (pO_2) calculated from equation 4 at the temperature given by equation 9]

Sample	Observed temperature (°C)	Equilibrium temperature (°C) From equation 8	From equation 9	From equation 10	log pO_2
Active vents					
1	1,080	2,063	1,039	889	−10.461
2	1,075	1,120	1,060	1,044	−9.838
3	1,080	1,494	1,058	968	−10.166
4	1,100	1,703	1,096	982	−9.796
5	1,100	1,829	1,071	942	−10.043
6	1,120	1,861	1,032	898	−10.687
7	1,050	1,547	972	866	−11.084
8	1,130	2,076	1,150	1,002	−9.316
9	1,130	1,695	1,109	998	−9.755
10	1,100	1,271	1,074	1,025	−9.881
11	1,100	1,835	1,092	964	−10.035
12	1,130	1,440	1,111	1,036	−9.363
13	825	1,675	979	859	−11.174
14	825	1,427	923	827	−11.896
15	1,080	1,300	1,110	1,062	−9.559
16	1,100	1,218	1,074	1,036	−10.212
17	1,100	1,540	1,068	973	−10.334
18	1,050	2,286	978	814	−11.540
19	1,050	1,284	985	917	−11.087
24	1,010	2,038	1,042	894	−10.309
25	1,010	903	966	987	−11.228
26	1,100	1,156	1,072	1,049	−10.204
Feeder vents					
20	735	2,192	931	773	−11.954
21	870	1,459	951	854	−11.476
22	775	1,996	904	758	−12.275
23	835	1,173	916	857	−11.878
27	875	1,256	978	914	−11.080
28	895	1,008	980	971	−10.989
29	880	1,118	990	956	−10.934
30	875	1,273	994	930	−10.386
31	840	1,259	929	857	−11.609
32	840	1,513	953	849	−11.481
33	820	1,712	943	819	−11.781
34	820	1,306	869	782	−12.527
Post-eruptive samples					
35	760	810	813	814	−13.541
36	745	883	661	610	−16.499

the source of disequilibrium in these samples. Oxidation of CO, on the other hand, would increase the temperature from equation 8 (which is already too high), whereas oxidation of H_2S would leave this temperature unaffected. Gerlach (1980, 1982) has noted the importance of the addition of meteoric water and of the oxidation of H_2 in volcanic-gas collections. Either excess, unequilibrated, H_2O or a lack of H_2 in the analyses because of oxidation could account for the discrepant temperatures of table 30.3: Subtracting H_2O or adding H_2 to the analytical values decreases the temperature from equation 8 and increases that from equations 9 and 10 (water affects equation 9 because the constant sum of partial pressures requires a change in H_2 opposite to that of H_2O).

Forcing the analyses in table 30.1 to apparent equilibrium by adjusting either H_2O or H_2 yields the results shown in table 30.4. Assuming only oxidation of H_2 as the cause of disequilibrium, apparent equilibrium H_2 was obtained by combining equations 8 and 9 to eliminate H_2:

$$3CO + H_2O + SO_2 = 3CO_2 + H_2S \qquad (11)$$

With an equilibrium temperature from this reaction, oxygen was calculated from equation 1 and apparent equilibrium H_2 from equation 2. Alternatively, assuming disequilibrium to be due solely to H_2O, apparent equilibrium H_2O was obtained by subtracting H_2O incrementally from a starting partial pressure of 1.0 (simultaneously correcting H_2 for the constant sum requirement) until the temperatures calculated from equations 8–10 agreed within 10 °C. The apparent equilibrium temperatures from these two processes (see table 30.4) agree within 20 °C and are close to collection temperatures. Both processes also require very large changes from the observed values (table 30.4): about half of the samples require more than half of the H_2 to have been oxidized, and a fifth of the samples have apparent equilibrium water contents of less than 45 percent. Thus neither process alone seems an entirely plausible explanation for the observed disequilibrium in the samples.

That neither oxidation of H_2 nor excess H_2O is the sole cause of disequilibrium may be seen from the size of deviations from the analytical values required for apparent equilibrium. One can define the magnitude of the correction required to force apparent equilibrium as the positive difference between observed and calculated (table 30.4) values divided by the observed value. If disequilibrium is attributed solely to oxidation of H_2, then the observed H_2O content is the equilibrium amount, and the extent of oxidation of H_2 should be independent of H_2O content. In fact, there is a positive correlation, significant at the 99-percent confidence level, between the required deviation of H_2 and the observed H_2O content in both active-vent and feeder-vent samples. This correlation, indicating a tendency for samples with higher H_2O contents to require greater apparent oxidation corrections of H_2, implies that forcing apparent equilibrium by adding H_2 to the analysis is correcting, at least partially, for excess, unequilibrated, water in the samples rather than solely for oxidation.

Because of the constant sum of partial pressures and because the greatest deviations of H_2O are associated with higher water contents, there is necessarily an inverse correlation between the required correction in H_2O and other components of the sample: the negative correlation of H_2O deviation with CO_2, for example, is significant at the 99-percent confidence level for both active and feeder vents. This problem is eliminated by considering the H_2/CO_2 ratio: the negative correlation of H_2O deviation with this ratio is significant at the 99-percent confidence level for the feeder vents, but not significant (<90 percent) at the active vents. Negative correlations of H_2/CO and H_2/H_2S with water deviation also are significant at the feeder vents but not at the active vents. This result implies that, at least at the feeder vents, forcing equilibrium in the samples by subtracting water is compensating, at least partially, for the oxidation of H_2 in the samples. It seems probable, then, that both addition of unequilibrated water and oxidation processes have contributed significantly to the observed disequilibrium.

Gerlach (1982) noted that magma tends to have an oxygen fugacity in the area bounded by the quartz-magnetite-fayalite (QMF) and nickel-nickel oxide (NNO) buffers and showed that most equilibrated volcanic gases also plot in this area. A similar plot of these Mauna Loa samples (fig. 30.2) shows that they follow an oxygen-temperature curve very close to QMF, regardless of whether the analyses are forced to apparent equilibrium by subtracting H_2O or by adding H_2, and that both processes yield the same relation

TABLE 30.4.—*Apparent equilibrium values of temperature and oxygen partial pressure assuming excess H_2O or oxidation of H_2 for gas samples from 1984 Mauna Loa eruption*

Sample	Observed temperature (°C)	Assuming excess H_2O			Observed H_2O (mole percent)	Assuming oxidation of H_2			Observed H_2 (mole percent)
		Temperature (°C)	log(pO_2)	Estimated H_2O (mole percent)		Temperature (°C)	log(pO_2)	Estimated H_2 (mole percent)	
Active vents									
1	1,080	1,078	−9.813	47.0	75.6	1,101	−9.455	1.196	0.360
2	1,075	1,064	−9.781	56.2	59.2	1,066	−9.740	.741	.660
3	1,080	1,078	−9.832	48.0	64.9	1,092	−9.608	1.070	.550
4	1,100	1,125	−9.351	53.8	73.0	1,140	−9.119	1.435	.640
5	1,100	1,104	−9.522	50.2	73.4	1,122	−9.234	1.260	.480
6	1,120	1,069	−10.069	53.4	77.6	1,086	−9.790	1.428	.490
7	1,050	1,001	−10.561	54.8	75.7	1,014	−10.320	.747	.300
9	1,130	1,141	−9.274	64.0	79.8	----	------	-----	----
10	1,100	1,086	−9.680	62.4	70.2	1,092	−9.595	1.125	.800
11	1,100	1,129	−9.477	58.4	78.5	1,143	−9.257	1.897	.750
12	1,130	1,129	−9.089	57.4	69.4	1,138	−8.945	1.087	.660
13	825	1,008	−10.630	48.2	73.1	1,026	−10.314	.893	.320
14	825	946	−11.427	48.8	70.7	960	−11.149	.658	.270
15	1,080	1,121	−9.388	57.2	64.9	1,127	−9.296	1.287	.940
16	1,100	1,083	−10.056	66.0	71.7	1,087	−9.995	1.696	1.310
17	1,100	1,096	−9.897	64.4	78.7	1,105	−9.750	1.867	.930
18	1,050	1,025	−10.679	50.4	82.3	1,047	−10.309	1.434	.330
19	1,050	1,004	−10.733	69.2	79.8	1,010	−10.626	1.040	.600
24	1,010	1,078	−9.715	42.6	71.8	1,103	−9.322	1.006	.310
25	1,010	962	−11.318	69.2	65.6	960	−11.360	.768	.900
26	1,100	1,077	−10.118	62.0	65.8	1,080	−10.072	1.520	1.300
Feeder vents									
20	735	967	−11.253	33.0	71.1	998	−10.674	.783	.170
21	870	972	−11.075	42.0	64.2	989	−10.754	.662	.280
22	775	938	−11.591	34.6	71.3	965	−11.044	.652	.150
23	835	929	−11.617	48.2	62.0	938	−11.429	.513	.300
27	875	991	−10.828	47.6	61.1	1,001	−10.642	.692	.410
28	895	981	−10.960	53.6	55.3	982	−10.936	.618	.580
29	880	997	−10.806	53.0	59.8	1,002	−10.714	.741	.570
30	875	1,009	−10.571	52.2	65.0	1,018	−10.408	.766	.460
31	840	947	−11.260	54.6	70.2	956	−11.069	.552	.290
32	840	976	−11.042	42.6	66.1	993	−10.711	.702	.280
33	820	969	−11.275	35.6	64.9	994	−10.822	.785	.250
34	820	887	−12.111	42.4	64.7	902	−11.797	.383	.160
Posteruptive samples									
35	760	813	−13.559	91.2	91.2	813	−13.549	.505	.510
36	745	676	−15.977	75.6	86.8	679	−15.877	.147	.070

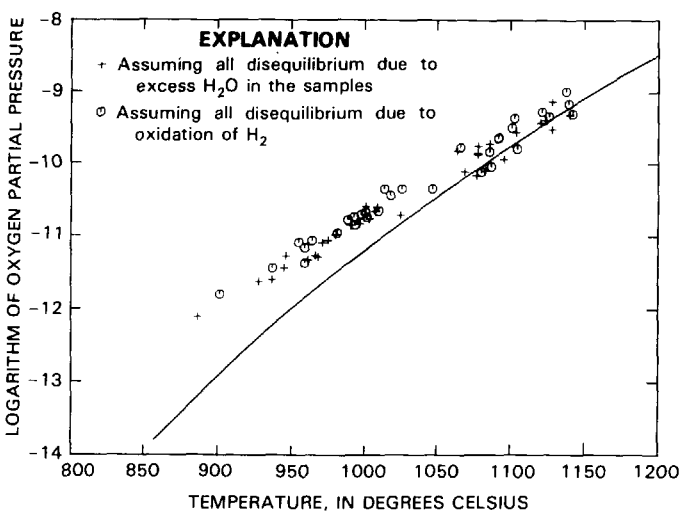

FIGURE 30.2.—Apparent equilibrium partial pressure of oxygen plotted against apparent equilibrium temperature for gas samples from the 1984 Mauna Loa eruption. Line indicates the quartz-magnetite-fayalite buffer.

between temperature and partial pressure of oxygen. This relationship,

$$\log(pO_2) = -19300/T + 4.46 \qquad (12)$$

provides a means of estimating the equilibrium partial pressures of H_2O and H_2 independently of each other. Because the lower temperature of the posteruption samples involves considerable extrapolation of this relation, those samples are excluded from the following.

With equation 12, an equilibrium temperature for an analysis can be estimated from equation 4, the H_2 content from equation 6, and the H_2O content from equation 5, assuming that the CO_2/CO and SO_2/H_2S ratios are equilibrium values. When this procedure is followed, nine of the analyses from table 30.1 yield temperatures above 1,150 °C or partial pressures of H_2O above 1.0 or both, implying that the assumption is not justified for these samples, which are therefore rejected. About half the remaining samples have estimated H_2 contents less than the observed values (after correction for constant sum), indicating either that oxidation is not a major effect or that the either CO_2/CO or SO_2/H_2S or both ratios are not equilibrium values. Examination of equation 6 shows that oxidation

TABLE 30.5.—*Comparison of observed and estimated equilibrium temperature and composition of gas samples from 1984 Mauna Loa eruption*

[Compositional figures in mole percent; observed values of H_2 from table 30.1 corrected for the new sum of partial pressures, (see text)]

Sample	Temperature (°C)		H_2O		H_2		H_2S	
	estimated	observed	estimated	observed	estimated	observed	estimated	observed
Active vents								
1	1,075	1,080	47.127	75.6	0.789	0.780	0.628	0.580
2	1,028	1,075	54.684	59.2	.747	.733	1.342	.620
3	1,079	1,080	48.289	64.9	.821	.810	.920	.920
4	1,123	1,100	53.860	73.0	1.097	1.094	.718	.690
5	1,095	1,100	50.759	73.4	.924	.889	.683	.560
7	978	1,050	54.161	75.7	.584	.566	.871	.510
9	1,157	1,130	85.935	79.8	1.993	.599	.740	.740
10	1,074	1,100	62.176	70.2	1.037	1.015	1.022	.790
12	1,085	1,130	56.242	69.4	.984	.944	.908	.380
13	1,012	825	51.871	73.1	.656	.573	.810	.810
14	953	825	58.400	70.7	.555	.383	1.110	1.110
15	1,120	1,080	57.151	64.9	1.151	1.148	.867	.850
24	1,057	1,010	41.521	71.8	.644	.643	.727	.470
Feeder vents								
20	988	735	55.665	71.1	.629	.261	1.020	1.020
21	976	870	46.298	64.2	.494	.420	1.150	1.150
22	952	775	50.680	71.3	.480	.258	1.020	1.020
23	930	835	50.312	62.0	.425	.392	1.410	1.410
27	993	875	49.651	61.1	.574	.531	1.230	1.230
28	985	895	58.279	55.3	.648	.541	1.610	1.610
29	1,005	880	65.353	59.8	.803	.491	1.630	1.630
30	1,004	875	52.233	65.0	.638	.628	1.137	1.010
31	930	840	54.385	70.2	.459	.444	1.237	.800
32	981	840	49.082	66.1	.538	.421	1.120	1.120
33	999	820	74.401	64.9	.888	.182	1.640	1.640
34	879	820	42.403	64.7	.269	.261	1.332	1.030

of H_2S would lead to underestimating H_2; table 30.5 shows the result of reversing this oxidation by adding H_2S incrementally to the analyses and recalculating H_2 and H_2O until the estimated H_2 content is at least as great as that observed. (Note that the H_2S/SO_2 ratio is used in equation 6, and thus the comparison of observed versus estimated H_2S in table 30.5 is not affected by the new sum of partial pressures; H_2, on the other hand, is estimated in absolute terms from equation 6 and thus comparison requires correction of the observed value for the new sum produced by the change in H_2O.)

An interesting feature of table 30.5 is the distinction between active and feeder vents: oxidation appears to have affected primarily H_2S rather than H_2 at the active vents, whereas at the feeder vents H_2 appears to have been oxidized to a greater extent than H_2S. This is consistent with the observation noted above that simple subtraction of H_2O from the analysis to force apparent equilibrium results in a negative correlation between excess H_2O and H_2/CO_2 at the feeder vents (implying that oxidation of H_2 is actually being "corrected") but not at the active vents. The distinction between oxidation of H_2 and H_2S may be related to the lower temperature, or to the longer time between separation of the gases from magma and their collection at the feeder vents relative to active vents. Regardless of the vent type and of the extent of apparent oxidation, most samples in table 30.5 yield considerably less H_2O in the apparent equilibrium composition than in the observed analysis.

The calculations for table 30.5 depend on the assumptions that the samples follow rigidly an oxygen-temperature buffer relationship and that the CO_2/CO and SO_2/H_2S ratios are equilibrium values, assumptions which table 30.5 makes manifest are not valid for at least half the table 30.1 samples. An alternative set of assumptions, relying on the buffer relationship and the CO_2/CO ratio and water content, fares even less well. Estimating temperature from equation 1, H_2 from equation 2, and H_2S from equation 3 yields less than the observed H_2S content in one-third of the samples and, as previously, a strong correlation between the extent of apparent oxidation and the observed water content, implying that the oxidation "correction" is actually correcting for excess, unequilibrated water in the samples. It is apparent that a multiplicity of effects has been the cause of disequilibrium in these samples, and it is most improbable that all effects have been equally operative in all samples.

WATER CONTENT

The data in table 30.5 demonstrate that these gas samples have been affected by incorporation of unequilibrated water and by oxidation of both H_2 and H_2S. Because H_2S is separated immediately on collection as CdS, and because H_2 is stable in these collections (after quenching) over the 4–6 h period before analysis (see above), oxidation of these gases must occur in the vent or immediately during collection; opportunity exists in both cases. Because this oxidation is a nonequilibrium process (equilibrium oxidation obviously would not produce a disequilibrium assemblage), high-temperature reaction rates must be slow relative to the few seconds between separation of the gas from the melt and quenching in a sample bottle. This is also shown by the observation that even the best gas collections, where near-perfect equilibrium can be demonstrated, actually contain a partial pressure of oxygen orders of magnitude higher than the equilibrium value (0.01 percent air in the sample yields 4–5 orders of magnitude more oxygen than

equilibrium). The slow (seconds) rate of reaction suggests the possibility that un-equilibrated water in the samples is magmatic water that, because its solubility in the melt is much greater than those of CO_2 and S, is exsolved in abundance in the last few seconds of the magma's rise and may be collected before reaction with C and S species is complete.

The observed water contents from table 30.1 are compared in figure 30.3 with the apparent equilibrium water content of those samples from table 30.5 that show no evidence of oxidation of H_2S. Whether one restricts consideration to only the samples in which neither H_2S nor H_2 appears to be oxidized or includes all of the table 30.5 values does not affect the conclusions. A notable feature of figure 30.3 is that the bimodal distribution of water in the original analyses disappears in the apparent equilibrium water values, which show no distinction between active and feeder vents. The mean apparent equilibrium water content of the samples giving no evidence of H_2S oxidation in table 30.5 is 56 percent; in comparison, the observed water content is 65 percent at the feeder vents and 73 percent at the active vents (table 30.1). There is no reason to expect the active vents to be more contaminated with meteoric water than the feeder vents (one would expect the contrary, given the longer passage through country rock before collection at the feeder vents), and thus the lower total water at the feeder vents probably is related to the greater depth of degassing (greater solubility of water) at the feeder vents. A consequence of this is that neither the feeder-vent nor the active-vent samples reflect the gas composition of the magma: degassing a water-poor gas from the magma through the feeder vents prior to eruption results in the gas at the active vents being depleted in CO_2 and SO_2, thus enriched in water.

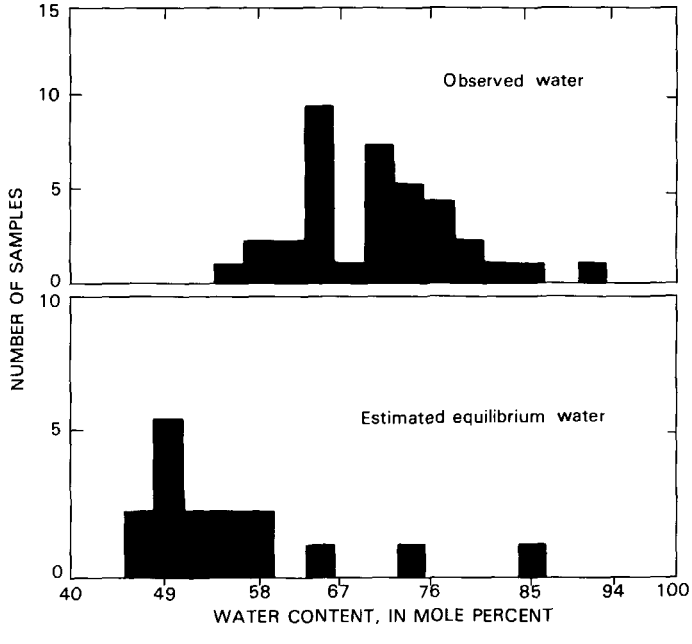

FIGURE 30.3.—Comparison of observed water content (from table 30.1) with apparent equilibrium water content (from table 30.5 data for samples showing no H_2S oxidation) for gas samples from 1984 Mauna Loa eruption.

Both the apparent equilibrium atomic H/S ratio and the observed ratio at the feeder vents is very low (table 30.6) compared with adjacent Kilauea Volcano or other basaltic volcanoes; even basing the ratio on total water at the active vents still leaves Mauna Loa with among the lowest H/S ratios in table 30.6. Comparison of the atomic H/S ratio of undegassed intrusive dike rocks collected from the summit caldera of Mauna Loa with the gas ratios (table 30.6) shows no reason to expect Mauna Loa magma to be unusually deficient in water. The very low atomic H/S ratio of the gas samples can be explained by assuming that (1) this particular batch of Mauna Loa magma had a remarkably low initial water content, (2) eruptive degassing was so inefficient that equilibrium at atmospheric pressure between melt and gas was not even approached, leaving the melt supersaturated in water, or (3) gases were sampled and quenched before they could react completely with the newly exsolved water, implying that total water in these samples represents equilibrated plus unequilibrated magmatic water. I suggest that some combination of the last two alternatives provides a more plausible explanation for the low H/S ratio of these gases than does invoking a special origin for the magma.

Anderson (1975) pointed out that a spectrum of gas compositions may be derived from the same melt with varying pressure and suggested this as a plausible mechanism to account for varying proportions of volcanic gases. About 77 percent of the mean total water at active vents and 86 percent of the mean total at feeder vents is in apparent equilibrium with other gases. Studies of submarine basalt (Moore, 1965) indicate that the saturation pressure for water in the melt is about 8 MPa (80 bars). Given a rock density of 2.3 g/cm^3, this corresponds to a depth of 350 m. If the solubility curve above this point is linear, 25 percent of the total water is exsolved in the final 90 m of magma rise. Thus the final eruptive surge and degassing of the melt might well be too rapid to maintain equilibrium in samples collected in virtual contact with erupting melt.

PRE-ERUPTION DEGASSING

The average atomic C/S ratio in these Mauna Loa gas samples is 0.21 (table 30.2). This value is similar to the ratio (0.25) found for the current east-rift-zone eruption of Kilauea (Greenland, 1984)

TABLE 30.6.—*Atomic H/S ratios of gases from basaltic volcanoes*

Gas source	Atomic H/S ratio	Source of data
Mauna Loa	3.4	Equilibrated H_2O, this paper
Mauna Loa, feeder vents	4.7	Total H_2O, this paper
Mauna Loa, active vents	7.3	Total H_2O, this paper
Mauna Loa, intrusive dikes	11	Easton and Lockwood (1983)
Kilauea, Halemaumau	7.2	Equilibrated H_2O, Gerlach (1980)
Kilauea, Halemaumau	15	Total H_2O, Gerlach (1980)
Kilauea, original magma	13	Greenland and others (1985)
Kilauea, original magma	8.6	Gerlach and Graeber (1985)
Kilauea, east rift	15	Greenland (1984)
Erta Ale, 1971	13	Equilibrated H_2O, Gerlach (1982)
Erta Ale, 1973	21	Equilibrated H_2O, Gerlach (1982)
Erta Ale, 1974	18	Equilibrated H_2O, Gerlach (1982)
Ardoukoba	8.8	Equilibrated H_2O, Gerlach (1982)
Surtsey, 1971	36	Equilibrated H_2O, Gerlach (1982)
Surtsey, 1965	58	Equilibrated H_2O, Gerlach (1982)
Surtsey, 1967	55	Equilibrated H_2O, Gerlach (1982)

but is much lower than most basaltic gases, in which carbon is usually more abundant than sulfur (Gerlach, 1982). Gerlach (1980, 1982) has emphasized the importance of shallow degassing of CO_2-rich gas for controlling the composition of volcanic gases, and Greenland and others (1985) and Gerlach and Graeber (1985) have suggested that the composition of Kilauea gas is controlled by degassing of magma to equilibrium in the shallow summit reservoir of Kilauea. Mauna Loa also has a summit storage chamber (Decker and others, 1983) at about the same depth as at Kilauea (3–4 km); thus the coincidence of Kilauea and Mauna Loa magmas being depleted in CO_2 to the same extent probably reflects their common degassing to equilibrium at the temperature and pressure of the summit storage reservoir. If this is so, then the eruptive gases sampled here reflect the composition of the reservoir rather than the composition of the initial magma formed in the mantle.

Gerlach (1980, 1982) has shown the usefulness of H/C versus S/C diagrams for indicating the effect of early CO_2 degassing on the composition of volcanic gas. Such a diagram yields a vertical trend if H_2O is the only significant source of variation and a diagonal trend if CO_2 variation is important; figure 30.1 has shown that H_2O is the major cause of variation in these gases, but figure 30.4 shows that an independent variation of CO_2 also is an important contributor to the total variance of composition. (In the following, I exclude the anomalous active vent sample with a C/S ratio of 0.085). The trend, shown in figure 30.4, for H/C to increase with increasing S/C is statistically significant at the 95-percent confidence level and implies that pre-eruption degassing of CO_2 has had a significant effect on eruptive gas composition. Examination of figure 30.4 shows, however, that the CO_2-degassing trend in these samples is produced almost entirely by the early samples from the active vents. Student's t-test confirms the higher mean S/C ratio of samples collected in the March 25–27 period relative to both the later active vents and the feeder vents at the 99-percent confidence level; the latter two sample groups also are significantly (99 percent) different from each other in S/C ratio. The daily average S/C ratio, plotted in figure 30.5, shows a high initial value for the gases, a decline after March 28 at the active vents, and a subsequent small increase at the later feeder vents. Removing the pre-March 30 samples from the population removes the CO_2 degassing trend from figure 30.4 (no statistical correlation between H/C and S/C) suggesting that the early eruptive magma was degassed of CO_2 relative to the later, more uniform, eruptive magma.

Equilibrium degassing of magma at pressures less than the solubility limit of CO_2 and S cannot change the S/C ratio of the emitted gas. Assuming a linear pressure dependence of the solubility, the mass M of gas exsolved per cubic meter of magma at any pressure P is:

$$M = aP + M_o \qquad (13)$$

where M_o is the initial mass of gas per cubic meter dissolved in the saturated melt. It is obvious that for two gases, the slopes, a, of equation 13 will be in the same proportion as the initial contents, and thus the exsolved gas will have the same composition regardless of decreasing pressure after both gases have become saturated. Degassing of Kilauea magma during storage in the shallow summit reservoir (Gerlach and Graeber, 1985; Greenland and others, 1985) and, presumably, of this Mauna Loa magma in Mauna Loa's reservoir (see above) leaves the melt saturated in CO_2 and S; therefore changes in S/C ratio must reflect variations in retention of the CO_2-rich fluid phase with which the magma entered the

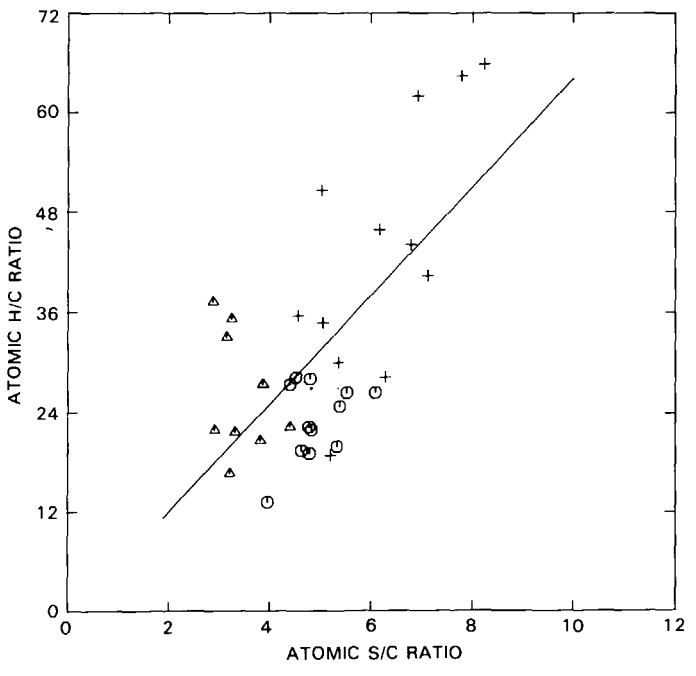

FIGURE 30.4.—Plot of atomic H/C ratio against atomic S/C ratio for gas samples from 1984 Mauna Loa eruption, showing effect of carbon degassing. Crosses, active-vent samples, March 25–27; triangles, active-vent samples, March 30 through April 5; circles, feeder-vent samples, April 3–13. Least-squares line fitted to the data.

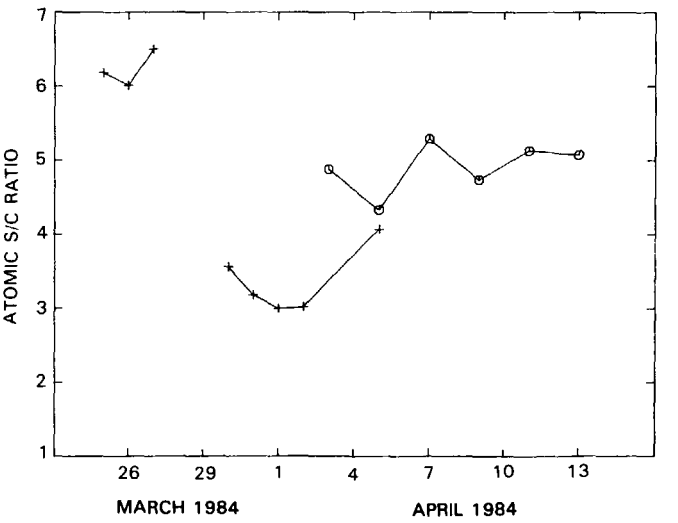

FIGURE 30.5.—Daily average atomic S/C ratio of gas samples from 1984 Mauna Loa eruption plotted against collection date. Crosses, active-vent samples; circles, feeder-vent samples.

reservoir. Seismic evidence suggests (R.Y. Koyanagi, oral commun., 1984) that some of this magma had been injected into the rift at a depth of ~3 km over a period of years prior to eruption. This rift-stored magma would be the first to be erupted, and it may be that storage of a small body of magma in the rift would provide a better opportunity for separation and loss of the original CO_2-rich fluid phase than would storage in the larger summit reservoir system. If this is so, then the change in S/C ratio of the gas suggests that at least three but less than six days of eruption were required to flush the rift conduit. Lipman and Banks (chapter 57) report a ~10-fold decrease in lava-effusion rate beginning about April 6; perhaps the lower flow rate through the conduit permitted a greater loss of the residual fluid phase from the reservoir by degassing during transit to the feeder vents, accounting for the higher S/C ratio at the feeder vents relative to the later active vents. In any case, the change in S/C ratio with time observed in these gases seems to require at least two magma batches having retained different fractions of a CO_2-rich fluid phase exsolved during ascent to the reservoir.

POSTERUPTION DEGASSING

It was noted above that the two posteruption gas samples in table 30.1 are greatly enriched in water. By April 18, halogens also became greatly enriched relative to S (table 30.2). This pattern is consistent with the final degassing of a cooling dike, in which the most soluble components (water and halogens) become enriched relative to less soluble ones (CO_2, SO_2). This pattern has been observed repeatedly at posteruptive vents and cones during the 1983–1984 east-rift-zone eruption of Kilauea (upublished data).

However, CO_2 actually became enriched relative to S by April 18; further samples collected on May 5 had CO_2 as much as five times more abundant than SO_2. The posteruption enrichment of CO_2 relative to SO_2 in the gas cannot be due to degassing of a static dike and implies the existence of another source of CO_2. Tentatively, I suggest a refilling of the shallow summit reservoir from the mantle (see above) and degassing of CO_2 from this new magma through vents created by the eruption.

CONCLUSIONS

Most of the gas samples collected from this eruption of Mauna Loa contain more water than is compatible with an equilibrium assemblage of gases. The apparent equilibrium compositions contain much lower atomic H/S ratios than have been observed for other basaltic gases or in un-degassed dikes from Mauna Loa; basing the H/S ratio on total, rather than equilibrated, water content of the active vents alleviates but does not completely solve the problem posed by these very low H/S ratios. This observation suggests that the latest exsolved water may not have reacted completely with the other gases before being quenched during sampling.

Halogen/sulfur ratios also are very much lower than those in eruptive gases from the adjacent Kilauea Volcano, whereas atomic C/S ratios are almost identical at the two volcanoes. On the basis of evidence for a shallow (3–4 km) magma storage reservoir under Mauna Loa, and by analogy with Kilauea, it can be suggested that this Mauna Loa magma was largely degassed of CO_2 during storage before eruption. Degassing at this depth, however, does not account for the low water and halogen contents of these gases. I suggest that the rate of flow of magma through the eruptive vent was too great for maintenance of equilibrium between magma and exsolved gases; thus variations in the water content of these samples reflect variations in the amount of water exsolved, a rate phenomenon rather than an equilibrium phenomenon. The low abundance of halogens also may be a result of incomplete exsolution, but the possibility of a low initial abundance in the magma cannot be excluded.

This study suggests that Hawaiian magmas degas in stages: CO_2 is primarily degassed from 3–4 km depth long before the start of eruption, SO_2 as the eruptive magma begins its ascent from the reservoir, and H_2O and halogens only as the magma nears the surface. An implication of this hypothesis is that gas samples collected from eruptive vents do not reflect the gas composition of the original magma and may not even reflect the gas composition of the erupting magma. Additionally, if physical rate processes create significant variations in observed gas compositions, then recalculating a gas analysis to an equilibrium assemblage may prove more misleading than enlightening.

REFERENCES CITED

Anderson, A.T., 1975, Some basaltic and andesitic gases: Review of Geophysics and Space Physics: v. 13, p. 37–55.

Decker, R.W., Koyanagi, R.Y., Dvorak, J.J., Lockwood, J.P., Okamura, A.T., Yamashita, K.M., and Tanigawa, W.R., 1983., Seismicity and surface deformation of Mauna Loa Volcano, Hawaii: Eos, v. 64, p. 545–547.

Easton, R.M. and Lockwood, J.P., 1983, Surface-fed dikes—The origin of some unusual dikes along the Hilina fault zone, Kilauea Volcano, Hawaii: Bulletin Volcanologique, v. 46-1, p. 45–53.

Fisher, R.A., 1936, Statistical methods for research workers (6th ed.): Edinburgh, Oliver and Boyd, 360 p.

Gerlach, T.M., 1980, Evaluation of volcanic gas analyses from Kilauea Volcano: Journal of Volcanology and Geothermal Research, v. 7, p. 295–317.

——— 1982, The interpretation of volcanic gas data from tholeiitic and alkaline mafic lavas: Bulletin Volcanologique, v. 45-3, p. 235–244.

Gerlach, T.M., and Graeber, E.J., 1985, Volatile budget of Kilauea Volcano: Nature, v. 313, p. 273–277.

Greenland, L.P., 1984, Gas composition of the January 1983 eruption of Kilauea Volcano, Hawaii: Geochimica et Cosmochimica Acta, v. 48, p. 193–195.

Greenland, L.P., Rose, W.I., and Stokes, J.B., 1985, An estimate of gas emissions and magmatic gas content from Kilauea Volcano: Geochimica et Cosmochimica Acta, v. 49, p. 125–129.

Giggenbach, W.F., 1975, A simple method for the collection and analysis of volcanic gas samples: Bulletin Volcanologique, v. 39, p. 132–145.

Heald, E.F., Naughton, J.J., and Barnes, I.L., Jr., 1963, The chemistry of volcanic gases: Journal of Geophysical Research, v. 68, p. 545–557.

Lockwood, J.P., 1984, Mauna Loa Volcano, Hawaii: SEAN Bulletin 9 (3), p. 1–9.

Moore, J.G., 1965, Petrology of deep-sea basalt near Hawaii: American Journal of Science, v. 263, p. 40–52.

Nordlie, B.F., 1971, The composition of the basaltic gas phase: NASA Technical Report R–348, 81 p.

Piccardi, G., and Cellini-Legittimo, P., 1983, A sampling and chemical analysis procedure for fumarolic gases: Mikrochimica Acta, v. 11, p. 159–167.

SULFUR AND CARBON ABUNDANCES IN HAWAIIAN THOLEIITE LAVAS: 1972–1975 ERUPTIONS OF KILAUEA AND 1975 ERUPTION OF MAUNA LOA

By Karen J. Franczyk, Everett K. Gibson, Jr.[1], *and* Robert I. Tilling

ABSTRACT

Analysis of sulfur and carbon abundances in 135 samples of fresh Hawaiian basalts erupted subaerially during 1972–1975 indicates that the different degassing behavior of sulfur and carbon volatiles and the ease of contamination by atmospheric carbon explain the different relationships observed between the sulfur and carbon contents in the samples and their density, flowage distance, and type of eruptive material. Sulfur abundances range from 37 to over 15,000 μg/g (median value 153 μg/g); these values are lower by a factor of 4 to 6 than those for submarine tholeiitic basalts. Decreases in sulfur abundance away from the vent further document previous findings that sulfur is progressively lost by degassing during lava fountaining and flowage; the greatest loss occurs within about 2 km of the active vent. Sulfur abundance is best preserved in spatter (mean value 177 μg/g) and more depleted in pahoehoe (mean value 152 μg/g) and aa (mean value 96 μg/g) flows, a distribution controlled largely by increasing distance from the vent. A weaker inverse relation was found between sulfur content and relative sample density.

The carbon content measured in this study reflects the combined contribution from the magmatic carbon (CO_2 dissolved in the basaltic glass) and a nonmagmatic surficial component adsorbed after eruption and even after sample collection. Total carbon abundances range from 11 to 1,099 μg/g; the median value (69 μg/g) falls within the range of total carbon abundances reported for submarine basalts, but the value range is considerably greater. This distribution is opposite from that expected from a comparison between submarine (nondegassed) and subaerial (degassed) samples; posteruption contamination by atmospheric carbon is inferred to account for the wide dispersion in our data. In contrast to the sulfur data, the carbon data show no systematic relation of measured abundance to sample type, relative density, or distance from the vent. Such an observation is compatible with recent experimental and volcanic-gas studies that demonstrate extensive and rapid loss of CO_2 from the magma during storage in Kilauea's shallow summit reservoir and at the onset of an eruption. Alternatively, this absence of any recognizable degassing pattern for carbon volatiles during lava fountaining and flowage could mean simply that any variations in magmatic carbon content are obscured by contamination-caused variations in nonmagmatic carbon. Subsequent studies involving stepwise combustion in the analytical procedure are required to determine the carbon budget for subaerial basalts.

INTRODUCTION

The sudden escape of volatiles from magma provides the driving force for volcanic eruptions. Many investigations have been conducted, therefore, of the distribution of volatiles, principally water, sulfur, and carbon, in the gaseous and solid eruptive products of volcanoes. Because of their high eruption frequency and good accessibility, Kilauea and Mauna Loa Volcanoes on the Island of Hawaii (fig. 31.1) have provided abundant materials for such studies.

The staff of the Hawaiian Volcano Observatory (HVO) systematically sampled, in time and space, the eruptive products of the long-lived 1972–74 Mauna Ulu activity (Tilling and others, chapter 16), as well as eruptive products of the following short-lived activity: the July, September, and December 1974 Kilauea eruptions (Lockwood and others, chapter 19); the July 1975 eruption at Mauna Loa summit (Lockwood and others, 1976); and the small eruption at Kilauea summit triggered by the magnitude −7.2 Kalapana earthquake on November 29, 1975 (Tilling and others, 1976).

We have determined the total sulfur and carbon abundances in 135 selected samples from these events (tables 31.1–31.2) in an attempt to describe their variation and to document any patterns of volatile behavior during subaerial eruption. To the best of our knowledge, the data set presented herein is the most comprehensive obtained to date for subaerially erupted tholeiitic basalts. Problems involving initial degassing, collection state of the samples, and ease of sample contamination by atmospheric carbon (Des Marais and Moore, 1984) combine to introduce a large degree of uncertainty in interpretation of the data. Nonetheless, in this paper we note several general systematic relations. The validity of these relations remains to be tested by additional studies specifically designed to eliminate or minimize posteruption carbon contamination by utilizing better controlled field sampling, sample storage and preparation, and modified analytical procedures.

ACKNOWLEDGMENTS

Our thanks go to the staff members of the Hawaiian Volcano Observatory for their diligent and timely efforts in making the systematic collection of eruptive products of Kilauea and Mauna Loa during 1972–1975. Some of the materials, had they not been sampled at, or shortly after, the time of their eruption, would have been unavailable for study because of burial by later flows. Robert L. Engram assisted with sample preparation and some of the analyses. Careful and incisive reviews of earlier versions of this paper by our USGS colleagues L. Paul Greenland (Hawaiian Volcano Observatory) and James G. Moore (Menlo Park) were most helpful and greatly appreciated.

[1]Johnson Space Center, NASA, Houston, Texas.

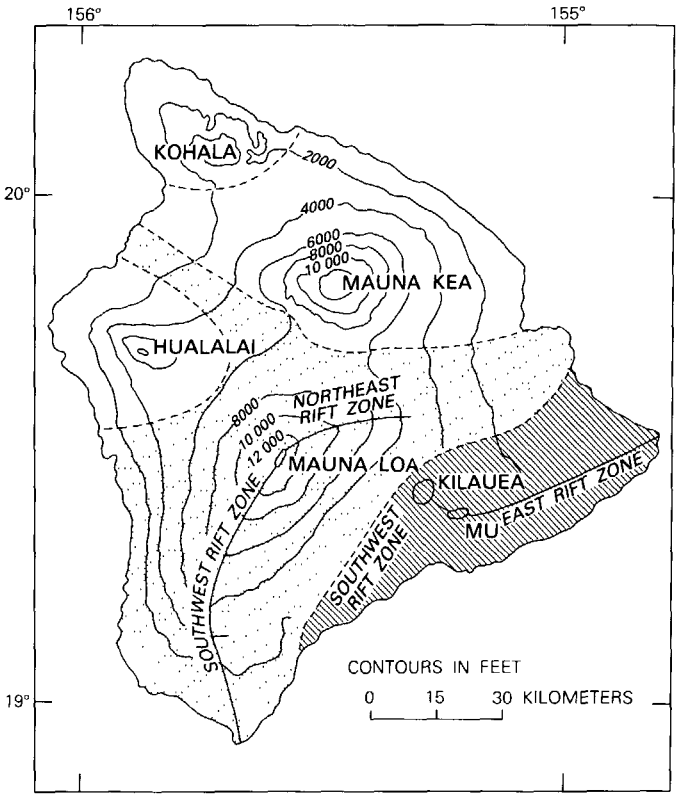

FIGURE 31.1.—Index map of Hawaii from Tilling and others (chapter 24) showing the five volcanoes that make up the island. Elevation contours are in feet. The site of the 1969–74 Mauna Ulu eruptions on Kilauea's upper east rift zone is also shown. (For more details on the Mauna Ulu eruptions, see Tilling and others, chapter 16).

ANALYTICAL METHODS

Sulfur and carbon abundances were determined in 127 samples from the 1972–75 eruptions of Kilauea Volcano and 8 samples from the 1975 Mauna Loa eruption. The analytical data, together with pertinent information on the samples (location, type, relative density, distance from the vent, and collection state), are given in tables 31.1–31.2.

Measurements of total sulfur and carbon were made using a LECO IR–32 sulfur analyzer and a LECO IR–12 carbon analyzer following the procedures of Gibson and Moore (1973). Powdered samples of approximately 300 mg were combusted in oxygen at 1,800 °C, and the resulting SO_2 and CO_2 measured with an infrared Luft-cell detector. Detection limits were 1 μg sulfur or carbon. Each sample was ground and divided into three parts that were individually analyzed and the results averaged to provide the reported sulfur and carbon abundances given in tables 31.1–31.2. The accuracy of the sulfur and carbon analyzers were checked against the National Bureau of Standards reference steel 55e (S: 110±10 μg/g; C: 112±10 μg/g). The analytical uncertainty of the determinations is estimated to be less than 10 percent of the amount of S or C in the samples.

The relative density of each sample was qualitatively assigned after visual examination. Samples with very few or no vesicles were designated as having a high relative density, and those with extremely abundant or large vesicles were designated as having very low relative density. Samples falling between these two extremes were ranked as moderately high, moderate, moderately low, and low.

PREVIOUS WORK

During the past two decades, significant advances have been made in the understanding of the distribution and the isotopic compositions of volatiles in ocean-floor and Hawaiian basalts (Moore and Fabbi, 1971; Moore and Schilling, 1973; Swanson and Fabbi, 1973; Mathez, 1976; Javoy and others, 1978, 1982; Muenow and others, 1979; Harris, 1981; Harris and Anderson, 1983; Des Marais and Moore, 1984; Kyser and O'Neil, 1984; Mattey and others, 1984; Sakai and others, 1984). More recently, complementary studies of the volcanic gases emitted at Hawaiian volcanoes have made possible improved models of the magmatic budgets of carbon and sulfur for the Kilauea and Mauna Loa volcanic systems (Greenland, chapter 28, 1984, in press; Gerlach, 1980, 1982; Gerlach and Graeber 1985; Greenland and others, 1985, in press). Many of these studies have focused on estimations of the juvenile contents of sulfur and carbon and their implications for the abundance and occurrence of these elements in the magma source regions. It is now well known that submarine basalts erupted under conditions of great hydrostatic pressure are the least degassed, and hence the measurements of their sulfur and carbon abundances most closely approximate juvenile concentrations. Subaerially erupted basalts are typically lower in total sulfur abundance than submarine basalts because of the substantial degassing loss to the atmosphere during fountaining at the vent and lava flowage (Moore and Fabbi, 1971; Gibson and Moore, 1974, fig. 5).

Des Marais and Moore (1984) have demonstrated that carbon abundance in submarine basalt decreases with decreasing ocean depth of eruption site. This relation reflects the increased solubility of CO_2 in the melt at high pressure and the attendant greater tendency for volatiles to escape from magma at shallow water depths (that is, at lower confining pressure). Several recent studies (Des Marais and Moore, 1984; Mattey and others, 1984; Sakai and others, 1984) have shown that carbon typically occurs in three forms: (1) posteruption carbon on sample surfaces (adsorbed gases, organic matter, weathering coatings, and other nonmagmatic carbon species acquired by the basaltic glasses); (2) magmatic carbon dioxide trapped in vesicles; and (3) magmatic carbon dissolved in basaltic glasses. For the 12 midocean basalts they analyzed, Des Marais and Moore (1984) found that forms (1) and (3) provide the bulk of the measured total carbon content. Furthermore, they demonstrated that posteruption carbon can be easily acquired by the sample, as evidenced by the 19 μg/g of surficial carbon yielded by reanalysis of a sample exposed to the atmosphere for four days following a previous analysis (maximum combustion temperatures 504 °C).

We designed our study as a broad survey of the carbon and sulfur abundances in Hawaiian tholeiitic basalts in order to build on the earlier studies of Moore and Fabbi (1971), Swanson and Fabbi (1973), and Swanson (1973) with the following general objectives: (1) To obtain a larger data base for fresh subaerially erupted Hawaiian basalts that have not been subjected to weathering; (2) to examine the relation between volatile content and the different materials produced during the course of an eruption; (3) to document better the degassing behavior of sulfur and carbon during lava fountaining and flowage; and (4) to detect changes, if any, in volatile content of magma through time. We did not anticipate the magnitude of the problem of sample contamination by atmospheric carbon recently brought to light and the additional uncertainty in data interpretation created by posteruption contamination effects. Despite the difficulty in data interpretation presented by these factors, we believe that it is useful to report our carbon data because they constitute the best available data set for subaerial basalts obtained to date.

DISTRIBUTION OF SULFUR AND CARBON CONTENT IN DIFFERENT ERUPTIVE PRODUCTS

The gas content and degassing patterns of magma are some of the primary controls on the morphology of lava flows (Swanson, 1973). In our study, spatter (near-vent) and pahoehoe and aa flows were extensively sampled, but we did not differentiate between the varieties of pahoehoe (see, for example, Swanson, 1973) nor the varieties transitional between pahoehoe and aa (see, for example, Peterson and Tilling, 1980). Because these products have undergone different degassing histories and the lavas may have varied in original volatile content, the eruptive products might be expected to differ in measured sulfur and carbon contents.

To facilitate comparison of the data, which show great scatter, we computed mean sulfur and carbon values according to sample type for each of the eruptive episodes of Kilauea, for Kilauea samples as a whole, and for the 1975 Mauna Loa eruption (tables 31.3–31.5). The small sample populations for many of the eruptive episodes allow only a general comparison between the products of the same episode. However, the mean values for aggregated Kilauea data provide a better statistical basis for comparison.

On the basis of the aggregated Kilauea data, the mean sulfur content of 177 μg/g for spatter is the highest, followed by 152 μg/g for pahoehoe, and 96 μg/g for aa. There are deviations from this general pattern when the products of a single eruptive event are compared, but these probably result from the small sample populations for most of the single events, as well as from the lumping of pahoehoe varieties and the disregard of the transitional flow types between pahoehoe and aa. Comparison of the products of the 1975 Mauna Loa eruption is hampered by a small sample population; the one pahoehoe sample exceeds in sulfur content the mean for spatter, but some individual spatter samples contain more sulfur than the pahoehoe sample.

The time of formation and location of deposition of these three eruptive products explain the general decrease in sulfur content from spatter to pahoehoe to aa. Spatter, deposited by lava fountaining in the vicinity of the active vent, commonly represents material ejected early in the eruption or during more vigorous vent activity. Because spatter is an air-quenched product, it undergoes minimal degassing and thus retains a relatively high sulfur content. In contrast, the pahoehoe and aa form lava streams that are continually degassing as they advance from the vent.

Swanson (1973) documented numerous types of pahoehoe and concluded that gas content and mode of flowage of the lava determine the resultant morphology and gross texture. Different types of pahoehoe were not differentiated in our study, but some of the variations we found in sulfur content in the pahoehoe samples no doubt reflect different morphologic types, distances from the vent, and multiple phases of pahoehoe formation. The role of gas loss in the transition from pahoehoe to aa has been debated. Pahoehoe is generally regarded to be richer in gas than aa (see, for example, Williams and McBirney, 1979). Swanson (1973), however, believed that a higher rate of cooling, and not the loss of gases, causes the transition from pahoehoe to aa. Others (Sparks and Pinkerton, 1978) have attributed aa formation to the high yield strength of lava that has lost a significant amount of gas. Peterson and Tilling (1980), though not directly addressing the issue of gas loss, proposed that lava changes from pahoehoe to aa once a certain critical relation (the so-called transition threshold) between viscosity and rate of shear is attained. In general, magma viscosity increases with decreasing gas content, and we interpret the lower mean sulfur values for aa to indicate that it had degassed to a greater extent than the pahoehoe or spatter. This interpretation is consistent with the observation that aa lava is predominantly found at the toe of an advancing flow, hence farther from the vent, and so has had more opportunity to degas than its associated pahoehoe lava.

The carbon values for spatter, pahoehoe, and aa show more variation and, unlike the sulfur values do not exhibit any systematic trend. Swanson and Fabbi (1973) similarly did not observe any demonstrable trends in the behavior of carbon volatiles and suggested that their analytical techniques were not precise enough to detect small but possibly significant changes. However, the low solubility of CO_2 in the melt and its tendency to degas rapidly before or during eruption (see Greenland, chapter 28; Basaltic Volcanism Study Project, 1981; Gerlach and Graeber, 1985; Greenland, in press) may better explain the incoherent variation pattern for carbon abundances. If indeed most of the CO_2 is lost by degassing during storage in the shallow summit reservoir or immediately with the onset of eruption, then products that formed later in the eruption and flowage sequence would not on average contain noticeably less carbon than those formed early in the eruption. Moreover, the great range in carbon content within each category of material analyzed and the slightly higher mean carbon value for pahoehoe than for spatter, contrary to expected degassing behavior, probably also reflect scatter in the data resulting from posteruption contamination by atmospheric carbon. Given these great uncertainties, the difference between the mean carbon values for Kilauea aa (85 μg/g)

TABLE 31.1.—*Sulfur and carbon contents and other characteristics of selected lava samples from Kilauea Volcano*

[For most samples, the date given is both the date of eruption and the date of sample collection; where they differ, the collection date is given in parentheses. Relative density estimated by visual inspection of sample vesicularity before crushing: H, high; MH, moderately high; M, moderate; ML, moderately low; L, low; VL, very low; *, density not estimated. Physical state of sample at time of collection: S, solid; H, hot; W, warm; C, cool; L, liquid. Most spatter samples collected in the immediate vicinity of the vent; approximate distances from vent are given for other samples]

Sample	Date erupted (Date collected)	Material	Relative density	Collection state	S (μg/g)	C (μg/g)	Distance from vent	Remarks
Mauna Ulu eruption (upper east rift zone), February 1972 - May 1973								
MU272-2	2/8/72	Spatter	M	S,H	164	46	0	Still glowing when collected
MU272-3	2/9/72	Pahoehoe	MH	L	153	223	1 km	Toe of active flow
MU272-16	2/27/72	Spatter	M	S,H	182	270	0	
MU372-23	3/18/72 (3/19/72)	Spatter	L	S,W	232	181	0	
MU372-27	3/21/72	Pahoehoe	ML	L	170	245	20 m	
MU472-30	4/11/72	Pahoehoe	L	L	258	350	40 m	Dipped from Alae lava lake
MU472-32	4/14/72	Aa	MH	L	120	68	200 m	Pasty, glowing core of moving flow
MU472-33	3/18/72 (4/14/72)	Spatter	ML	S,C	216	226	0	
MU572-34	5/8/72	Pahoehoe	VL	L	299	561	0	Dipped from Alae lava lake (air-quenched)
MU572-35	5/8/72	Pahoehoe	VL	L	163	114	0	Dipped from Alae lava lake (water-quenched)
MU572-39	5/23/72	Spatter	MH	S,H	189	94	0	Alae lava lake
MU672-41	6/1/72	Pahoehoe	M	S,H	301	112	0	N. rim overflow, Alae lake
MU672-43	6/9/72	Spatter	M	S,W	162	119	0	
MU772-47	7/11/72	Spatter	MH	S,C	201	60	0	
MU772-48	7/11/72	Pahoehoe	M	L	197	123	2 km	Flowing from Alae
MU872-51	8/4/72	Pahoehoe	H	L	105	54	2 km	Makaopuhi Crater floor
MU872-55	8/12/72	Pahoehoe, spinose	M	L	132	68	2 km	Liquid cooled on thermocouple tip
MU972-57	9/3-5/72 (9/5/72)	Spatter	M	S,C	201	56	0	
MU972-61	9/28/72	Pahoehoe	H	L	123	77	10 km	Very viscous flow, lava lake
MU1072-64	9/28/72 10/13/72	Stalactite and wall glaze	M	S,H	15,025	68	1.5 km	Edge of skylight, active tube
MU1072-65	10/16/72 (10/17/72)	Spatter	MH	S,W	227	115	0	
MU1072-66a	10/25/72	Lava	MH	L	133	66	2 km	Quenched; outside of steel bucket; glassy
MU1072-66b	10/25/72	Lava	M	L	157	221	2 km	Inside of bucket; more slowly cooled
MU1172-68	11/7/72	Pahoehoe	H	L	153	36	3 km	
MU1172-69	11/28/72	Pahoehoe	M	L	182	92	250 m	
MU1272-70	11/29-12/1/72 (12/1/72)	Spatter	M	S,C	197	74	0	
MU1272-74	12/14/72	Pahoehoe	ML	L	190	47	1 km	
MU173-76	1/9/73	Pahoehoe	M	L	102	107	2.5 km	Temperature measured
MU173-77	1/9/73	Pahoehoe	M	L	100	84	3 km	
MU173-78a	1/9/73	Aa	H	L	64	36	7.2 km	Pasty, glowing core; air-quenched
MU173-78b	1/9/73	Aa	H	L	57	68	7.2 km	Water-quenched
MU173-79a	1/9/73	Pahoehoe	M	L	105	94	7 km	Air-quenched
MU173-79b	1/9/73	Pahoehoe	M	L	92	83	7 km	Water-quenched
MU173-80	1/9-1/10/73 (1/10/73)	Spatter	L	S,W	166	157	0	
MU173-89	1/31/73	Pahoehoe	MH	L	85	21	8 km	
MU273-95	2/28/73	Pahoehoe	H	L	111	31	1 km	Leaking from tumulus
MU273-97	2/28/73	Pahoehoe	H	S,H	94	23	10 km	5-m depth sea
MU373-98	3/3/73	Pahoehoe	H	S,H	223	66	10 km	Average S and C values for entire sample
MU373-98a					389	67		Glassy rim, 1 cm thick
MU373-98b					157	92		21-cm thick fine-grained interior
MU373-98c					123	39		Glassy lower rim
MU373-99	3/4/73	Pahoehoe	MH	S,H	120	24	10 km	Collected in tide pool
MU373-101	3/6/73	Black sand	*	S,C	121	53	10 km	Newly formed
MU373-103	3/14/73	Spatter	MH	S,C	190	51	0	
MU373-107	3/23/73	Pahoehoe	H	L	107	20	10 km	Temperature measured
MU473-108	4/10/73	Spatter	MH	S,H	133	26	0	
MU473-109	4/10/73	Pahoehoe	M	L	112	11	10 km	Temperature measured
MU573-111	5/1/73	Spatter	M	S,W	217	25	0	
MU573-112	5/1/73	Pahoehoe	M	L	150	48	1.5 km	

TABLE 31.1.—*Sulfur and carbon contents and other characteristics of selected lava samples from Kilauea Volcano—Continued*

[For most samples, the date given is both the date of eruption and the date of sample collection; where they differ, the collection date is given in parentheses. Relative density estimated by visual inspection of sample vesicularity before crushing: H, high; MH, moderately high; M, moderate; ML, moderately low; L, low; VL, very low; *, density not estimated. Physical state of sample at time of collection: S, solid; H, hot; W, warm; C, cool; L, liquid. Most spatter samples collected in the immediate vicinity of the vent; approximate distances from vent are given for other samples]

Sample	Date erupted (Date collected)	Material	Relative density	Collection state	S (μg/g)	C (μg/g)	Distance from vent	Remarks
			Pauahi-Hiiaka eruption (upper east rift zone), May 5, 1973					
PH573-1	5/5/73	Pumice	VL	S,C	213	437	0	Highest fountaining
PH573-2	5/5/73	Pahoehoe	M	L	135	99	1 km	
PH573-3	5/5/73	Spatter	M	S,H	161	110	0	
PH573-4	5/5/73	Spatter	M	S,W	165	85	0	
PH573-5	5/5/73 (5/23/73)	Pahoehoe	MH	S,C	324	123	0	High lava lake, Hiiaka stand
PH573-6	5/5/73 (5/23/73)	Pumice	VL	S,C	210	181	0	Hiiaka Crater
PH973-8	5/5/73 (9/10/73)	Spatter	M	S,C	177	109	0	Pauahi Crater
PH973-10	5/5/73 (9/10/73)	Pahoehoe	ML	S,C	121	119	0	Pauahi, high lava lake stand
PH973-11	prehistoric 9/10/73	Lava	H	S,C	37	106		Prehistoric lava; wall of Pauahi
			Mauna Ulu eruption (upper east rift zone), June 1973 - November 1973					
MU673-115	6/5/73? (6/7/73)	Pahoehoe	L	S,W	413	77	100 m	Glassy rind of shelly pahoehoe, Alae
MU673-116	6/7/73	Pahoehoe	M	L	175	13	0	Dipped from Mauna Ulu lava lake
			(Mauna Ulu not sampled again until October)					
MU1073-117	10/30/73	Spatter	L	S,H	234	114	0	
MU1173-120	11/4/73	Spatter	ML	S,W	229	15	0	
MU1173-122	11/4/73	Pahoehoe	ML	L	253	32	200 m	Lava lake overflow
MU1173-125	11/8/73	Pahoehoe	M	L	140	29	150 m	Dipped lava lake
			Pauhi eruption (upper east rift zone), November - December, 1973					
PH1173-12	11/10/73	Spatter	L	S,C	187	146	50 m	Watch it fall
PH1173-15	11/11/73	Pahoehoe, glassy rind	ML	S,H	197	118	0	Glowing toe
PH1173-16	11/11/73	Spatter	*	S,W	318	135	300 m	Fissure 300 m from Puu Huluhulu
PH1173-21	11/29/73	Spatter	M	S,C	102	135	0	
PH574-25	12/9/73 (5/1/74)	Pahoehoe, glassy skin	M	S,C	86	119	0	Last erupted material in west pit
			Mauna Ulu eruption (upper east rift zone), December 1973 - June 1974					
MU1273-127	12/14/73 (12/27/73)	Pahoehoe	M	S,C	286	62	<100 m	Lava-lake high stand
MU174-131	1/25/74	Pahoehoe	M	L	78	66	<25 m	
MU174-132	1/25/74	Spatter	L	S,W	243	69	0	Collected as it fell
MU174-133	1/25/74	Pahoehoe	M	L	81	46	140 m	
MU174-134	1/25/74	Pahoehoe	M	L	80	69	400 m	Slabby pahoehoe
MU274-142	1/25-26/74 (2/2/74)	Aa	*	S,C	208	91	2 km	Terminus of 1/25/74 flow
MU274-143	1/25-26/74 (2/2/74)	Pahoehoe, spinose	M	S,C	70	81	0.6 km	Edge of 1/25-26/74 flow
MU274-147	2/14/74	Pahoehoe	ML	L	144	58	10 m	
MU274-148	2/14/74	Pahoehoe	ML	L	168	31	50 m	
MU374-154	3/5/74	Spatter	ML	S,C	149	67	0	Vent F
MU374-155	3/17/74 (3/18/74)	Spatter	L	S,W	202	36	0	Vent E
MU374-156	3/23/74	Spatter	L	S,H	229	41	0	Collected as it fell
MU374-157	3/23/74	Pahoehoe	M	L	168	45	24 m	
MU374-158	3/23/74	Pahoehoe	M	L	118	48	0.6 km	
MU474-161	4/3/74	Pahoehoe, interior	MH	S,H	93	67	5 km	Collected 3 minutes after solidification
MU474-161a	4/3/74	Pahoehoe, crust	MH	S,H	119	77	5 km	Collected 3 minutes after solidification
MU474-162	4/5/74	Spatter	ML	S,C-W	141	57	0	
MU474-163	4/8/74	Spatter	MH	S,H	146	53	0	
MU474-168	4/22/74	Pahoehoe	*		162	115	5 m	Vent F
MU574-169a	5/3/74	Pahoehoe	H	S,H	159	62	5 km	Collected a few hours after solidification
MU574-169b	5/3/74	Pahoehoe	MH	S,H	151	143	5 km	Collected a few hours after solidification
MU574-170	5/6/74	Spatter	H	S,W	162	83	0	
MU574-171	5/30/74	Spatter	L	S,H	155	98	0	Watched it fall
MU574-172	5/31/74	Pahoehoe	ML	L	149	127	25 m	
MU674-173	6/3-5/74 (6/8/74)	Spatter	M	S,W	147	82	0	

TABLE 31.1.—*Sulfur and carbon contents and other characteristics of selected lava samples from Kilauea Volcano—Continued*

[For most samples, the date given is both the date of eruption and the date of sample collection; where they differ, the collection date is given in parentheses. Relative density estimated by visual inspection of sample vesicularity before crushing: H, high; MH, moderately high; M, moderate; ML, moderately low; L, low; VL, very low; *, density not estimated. Physical state of sample at time of collection: S, solid; H, hot; W, warm; C, cool; L, liquid. Most spatter samples collected in the immediate vicinity of the vent; approximate distances from vent are given for other samples]

Sample	Date erupted (Date collected)	Material	Relative density	Collection state	S (μg/g)	C (μg/g)	Distance from vent	Remarks
			Summit eruption, July 19-22, 1974					
KIL774-1	7/19/74	Pahoehoe	L	L	149	84	0	
KIL774-2	7/19/74	Spatter	L	S,H	177	81	0	Watched it fall
KIL774-6a	7/20/74	Pahoehoe	M	L	107	67	0	Fissure F
KIL275-10	7/19/74 (2/16/75)	Spatter	ML	S,C	166	70	0	Fissure A
KIL275-11	7/19/74 (2/16/75)	Spatter	M	S,C	154	159	0	
KIL275-12	7/19/74 (2/16/75)	Pahoehoe	M	S,C	110	135	0.5 km	Terminus of flow fed by fissure F
KIL275-13	7/19/74 (2/16/75)	Aa	H	S,C	111	97	2 km	Terminus of flow fed by fissure A
			Summit eruption, September 19, 1974					
KIL974-8	9/19/74	Spatter	MH	S,H	141	64	0	
KIL375-14a	9/19/74 (3/24/75)	Pahoehoe	M	S,C	123	139	0	
KIL375-14b	9/19/74 (3/24/75)	Spatter	ML	S,C	152	114	0	Same location as KIL375-14a
KIL375-15	9/19/74 (3/24/75)	Pahoehoe	M		123	149	1 km	Glassy skin of toe
			Southwest flank eruption, December 31, 1974					
SWR1274-1	12/31/74	Spatter	L	S,H	135	127	0	First material, fissure E
SWR1274-2	12/31/74	Spatter	ML	S,H	122	89	0	Last material, fissure E
SWR1274-3	12/31/74	Spatter	L	S,W-C	192	191	0	Fissure B
SWR1274-4	12/31/74	Spatter	M	S,C	122	35	0	Fissure B
SWR1274-5	12/31/74	Spatter	MH	S,C	125	137	0	Fissure I
SWR1274-6	12/31/74	Spatter	L	S,C	156	147	0	Last material, last fountain, fissure D
SWR175-7	12/31/74 (1/18/75)	Pahoehoe	MH	S,C	65	118	1.5 km	Average S and C content for entire sample
SWR175-7a					79	117		Glassy top rim
SWR175-7b					61	92		Fine-grained interior
SWR175-7c					56	144		Fine-grained bottom rim
SWR175-8	12/31/74 (1/18/75)	Pahoehoe	M	S,C	80	110	2.5 km	
SWR175-9	12/31/74 (1/18/75)	Pahoehoe	M	S,C	78	142	5.5 km	
SWR175-10	12/31/74 (1/18/75)	Aa	H	S,C	48	38	5.5 km	
SWR175-11	12/31/74 (1/18/75)	Pahoehoe	MH	S,C	58	159	9 km	Transitional pahoehoe
SWR175-12	12/31/74 (1/18/75)	Aa	H	S,C	66	200	10.5 km	Weathered - terminus of 12/31/74 flow
			Summit eruption, November 29, 1975					
KIL75-1	11/29/75	Pahoehoe	L	S,H	334	99	400 m	From vent A
KIL75-2	11/29/75 (12/3/75)	Spatter	M	S,C	132	38	10 m	From vent B-1
KIL75-3	11/29/75 (12/3/75)	Spatter	MH	S,C	160	48	0	Irregular, clinkery
KIL75-4	11/29/75 (12/3/75)	Cinder	*	S,C	695	49	0	Irregular
KIL75-5	11/29/75 (12/4/75)	Spatter	L		200	69	0	
KIL75-6	11/29/75 (12/4/75)	Pahoehoe	M		174	443	1 km	Average S and C content for entire sample
KIL75-6a					172	163		Glassy rim
KIL75-6b					179	68		Fine-grain interior; vesicles 1-2 mm
KIL75-6c					173	1099		Fine-grained basal, rim; vesicles <1 mm

TABLE 31.2.—*Sulfur and carbon contents and other characteristics of selected lava samples from the July 5–6, 1975, summit eruption of Mauna Loa Volcano*

[For most samples, the date given is both the date of eruption and the date of sample collection; where they differ, the collection date is given in parentheses. Relative density estimated by visual inspection of sample vesicularity before crushing: H, high; MH, moderately high; M, moderate; ML, moderately low; L, low; VL, very low; *, density not estimated. Physical state of sample at time of collection: S, solid; H, hot; W, warm; C, cool; L, liquid. Most spatter samples collected in the immediate vicinity of the vent; approximate distances from vent are given for other samples.]

Sample	Date erupted (Date collected)	Material	Relative density	Collection state	S (μg/g)	C (μg/g)	Distance from vent	Remarks
ML775-1	7/6/75	Aa	MH	S,H	48	28	5 km	Red hot when collected at active flow front
ML775-17	7/6/75) (7/15/75)	Spatter	ML	S,C	227	199	0	
ML775-21	7/6/75 (7/15/75)	Spatter	H	S,C	108	58	40 m	
ML775-22	7/6/75 (7/15/75)	Spatter	ML	S,C	134	52	0	
ML775-23	7/5/75 (7/21/75)	Spatter	L	S,C	238	205	8 m	
ML775-24	7/5/75 (7/21/75)	Pahoehoe	L	S,C	196	115	0.5 km	
ML775-26	7/6/75) (7/29/75)	Spatter	ML	S,C	184	73	0	
ML775-27	7/5/75 (7/31/75)	Aa	H	S,C	28	41	2.5 km	

TABLE 31.3.—*Distribution of mean sulfur and carbon contents in spatter from Kilauea and Mauna Loa Volcanoes*

Location and month of eruption	Number of samples	Mean S (μg/g)	Mean C (μg/g)
Kilauea Volcano, all samples	45	117	96
Mauna Ulu 2/72-5/73	14	191	99
Pauahi-Hiiaka 5/73	3	168	101
Mauna Ulu 6/73-11/73	2	231	64
Pauahi-Hiiaka 11/73-12/73	3	202	139
Mauna Ulu 12/73-6/74	9	175	65
Summit 7/74	3	166	103
Summit 9/74	2	147	89
Southwest flank 12/74	6	142	121
Summit 11/75	3	164	52
Mauna Loa Volcano 7/75	5	178	117

TABLE 31.4.—*Distribution of mean sulfur and carbon contents in pahoehoe from Kilauea and Mauna Loa Volcanoes*

Location and month of eruption	Number of samples	Mean S (μg/g)	Mean C (μg/g)
Kilauea Volcano, all samples	60	152	103
Mauna Ulu 2/72-5/73	25	153	108
Pauahi-Hiiaka 5/73	3	193	114
Mauna Ulu 6/73-11/73	4	245	38
Pauahi-Hiiaka 11/73-12/73	2	141	119
Mauna Ulu 12/73-6/74	15	130	68
Summit 7/74	3	122	95
Summit 9/74	2	123	144
Southwest flank 12/74	4	70	132
Summit 11/75	2	254	271
Mauna Loa Volcano 7/75	1	196	115

and for spatter (96 μg/g) is probably not significant, even though the difference is compatible with the presumed greater degassing of the aa samples.

Several eruptive products other than the three general types discussed above were sampled and analyzed. The only cinder sample collected (KIL75–4) has the highest sulfur content (695 μg/g) of any of the material (excluding the stalactite) we analyzed but a low carbon content (49 μg/g). The relatively low carbon content is suggestive of little posteruption contamination; therefore, if sulfur has not been adsorbed, then the sulfur content, which is similar to the mean (680 μg/g) for submarine basalts (Moore and Fabbi, 1971), perhaps approaches the original sulfur content of the basaltic magma erupted in November 1975 at Kilauea. Two pumice samples (PH573–1 and PH573–6), collected during the May 1973 Kilauea eruption at Pauahi and Hiiaka craters, also contain high sulfur contents (213 and 210 μg/g, respectively) and high carbon contents (437 and 181 μg/g, respectively). Sample PH573–1 formed during the highest fountaining observed for the Pauahi-Hiiaka eruption. If this sample was not contaminated, then the comparison of this carbon value to a spatter sample (MU1173–120) that contains only 14 μg/g carbon indicates that almost complete degassing of CO_2 is possible during eruption. Alternatively, the wide ranges in sulfur and carbon contents observed for the cinder and pumice samples could simply reflect adsorption trapping of plume gases during high fountaining, as suggested by unpublished data of L. Paul Greenland of the

TABLE 31.5.—*Distribution of mean sulfur and carbon contents in aa from Kilauea and Mauna Loa Volcanoes*

Location and month of eruption	Number of samples	Mean S (μg/g)	Mean C (μg/g)
Kilauea Volcano, all samples	7	96	85
Mauna Ulu 2/72-5/73	3	80	57
Mauna Ulu 12/73-6/74	1	208	91
Summit 7/74	1	111	97
Southwest flank 12/74	2	57	119
Kilauea Volcano totals	7	96	85
Mauna Loa Volcano 7/75	2	38	35

Hawaiian Volcano Observatory (written commun., 1985) from the Puu Oo eruption on Kilauea's east rift zone that began in 1983 (Wolfe and others, chapter 17).

A sample of red, oxidized, hollow-cored stalactite (MU1072–64) taken from the roof of an active lava tube through a skylight has an extremely high sulfur content of 15,025 μg/g but a low carbon content of 68 μg/g. The high sulfur content possibly results from degassed sulfur volatiles that condensed and formed a sulfide-mineral phase near the skylight because of changes in temperature and Eh conditions. The very low carbon content suggests that most of the CO_2 degassed before the lava entered the lava tube or that carbon escaped through the skylight without reacting with the wall material.

A sample of prehistoric lava (PH973–11) from the wall of Pauahi crater has a very low sulfur content of 37 μg/g, which would place it in the range of modern aa samples analyzed in this study. The moderate carbon content of 106 μg/g provides no clues to its origin or its distance from the vent, because carbon abundances vary greatly in all categories of eruptive products. In addition, such a prehistoric (older than A.D. 1750) lava must have a higher probability of being affected by atmospheric carbon contamination than the fresh materials erupted during 1972–75 at Kilauea.

Three samples of pahoehoe were selected for analysis of sulfur and carbon contents in each of several distinct textural zones (glassy upper rind; fine grained, moderately vesicular interior; and glassy or fine-grained, slightly vesicular basal rim) for comparison with results of zoned pillow basalts analyzed by Moore and Fabbi (1971). Two samples (MU373–98 and SWR175–7) have sulfur content highest in the upper glassy rim and lowest in the lower rim. Sample KIL75–6 showed no significant variation in sulfur content among the zones. Thus, the sulfur distribution in our zoned subaerial pahoehoe samples generally follows the trend observed by Moore and Fabbi (1971) for zoned submarine pillow basalts, but the sulfur contents in the pahoehoe are much lower. The carbon distribution for the three zoned pahoehoe samples is irregular, most probably because of posteruption contamination; carbon was not analyzed in the Moore and Fabbi pillow-basalt study.

VARIATIONS IN SULFUR AND CARBON CONTENT WITH DISTANCE FROM VENT

Degassing of lava during fountaining and flow from the vent has been previously observed and documented (Swanson, 1973; Swanson and Fabbi, 1973; Gibson and others, 1975). If the degassing process is efficient and systematic, eruptive products that have travelled greater distances from the vent should show progressively lower sulfur and carbon contents.

In general, sulfur abundance does tend to decrease with increasing distance from the vent, the greatest loss occurring within 2 km of the vent (fig. 31.2). Sulfur abundances in samples collected 2–10 km from the vent do not show a well-defined decreasing trend, indicating that variations caused by differences in sample type,

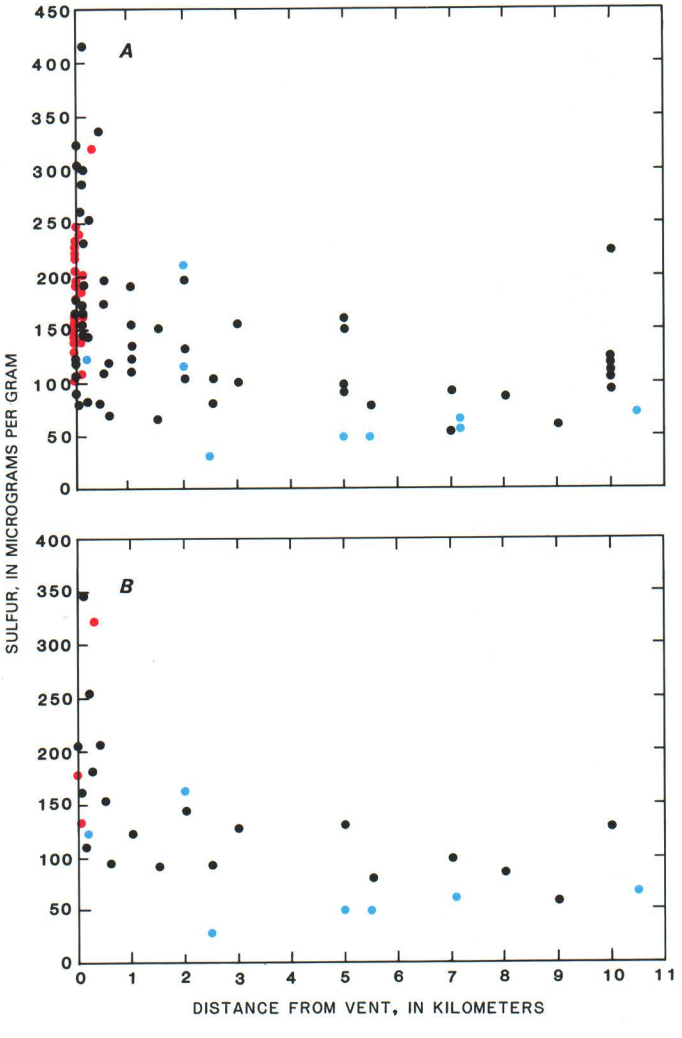

FIGURE 31.2.—Sulfur contents of Kilauea and Mauna Loa lavas plotted against distance from eruptive vent. Red, spatter; black, pahoehoe; blue, aa. ***A***, Sulfur content of individual samples. ***B***, Mean sulfur content of samples grouped by distance from eruptive vent. Samples collected 5–50 m from vent are grouped together and the mean value is plotted at 0.05 km.

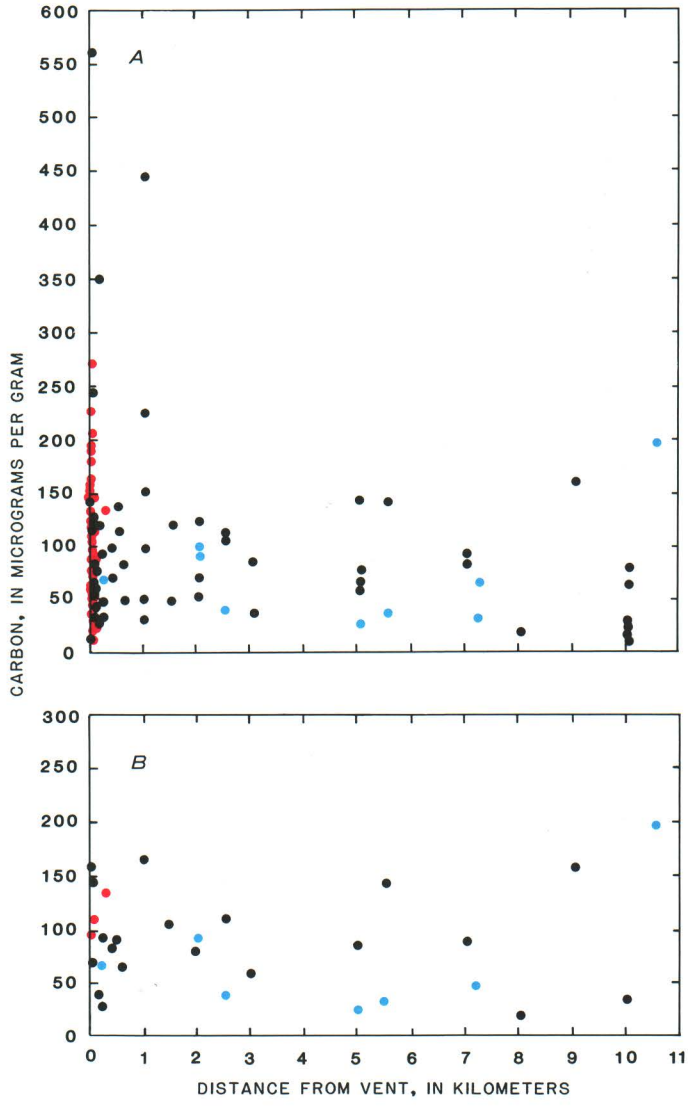

FIGURE 31.3.—Carbon contents of Kilauea and Mauna Loa lavas plotted against distance from eruptive vent. Red, spatter; black, pahoehoe; blue, aa. ***A***, Carbon content of individual samples. ***B***, Mean carbon content of samples grouped by distance from eruptive vent. Samples collected 5–50 m from vent are grouped together and the mean value is plotted at 0.05 km.

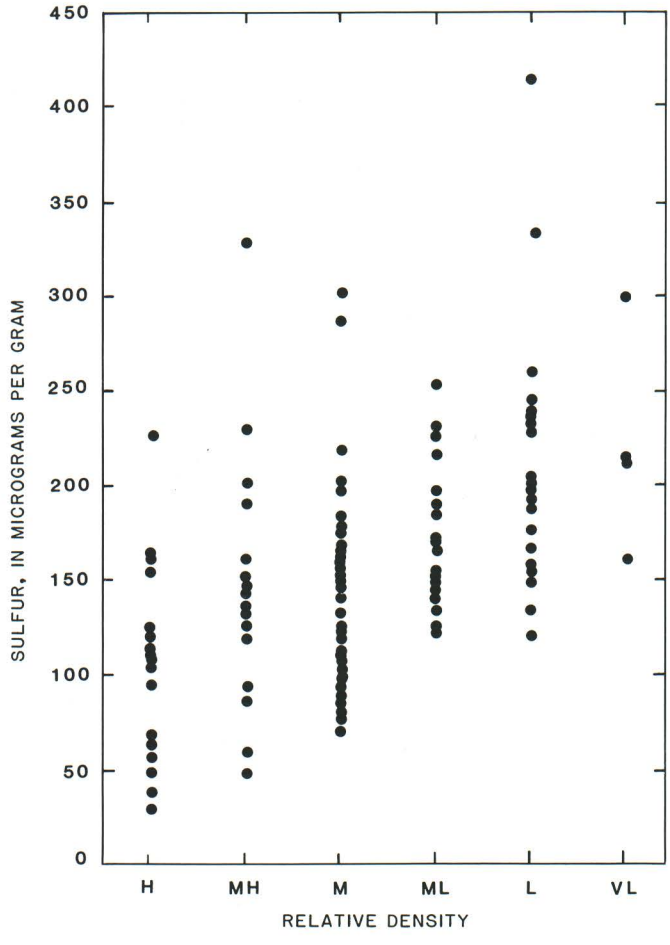

FIGURE 31.4.—Sulfur contents of Kilauea and Mauna Loa lava samples plotted by relative density estimated qualitatively from visible vesicularity. H, high; MH, moderately high; M, moderate; ML, moderately low; L, low; VL, very low.

especially for pahoehoe, are greater in that interval than those related to degassing alone. Although the distance the lava flows from the vent is an important determinant of the type of pahoehoe formed, it is not the sole control. Swanson (1973) has shown that the original volatile content, the rate of flow of the lava, the gradient of the surface over which the lava flows, and the mode of lava extrusion all help control the type of pahoehoe formed. Presumably pahoehoe with different morphologies and volatile contents can occur at the same distance from the vent; the sampling in our study was inadequate to permit such distinctions.

Carbon abundance shows little apparent correlation with distance from the vent (fig. 31.3). Although the highest carbon values do occur closest to the vent, whatever progressive degassing trend may exist is obscured by contamination-caused variations in total carbon content. If immediate, sudden release of most carbon volatiles occurs during the initial phases of the eruption, then the high carbon contents in some samples collected far from the vent are difficult to explain and are almost certainly related to posteruption contamination.

VARIATION IN SULFUR AND CARBON WITH SAMPLE DENSITY

Sulfur and carbon abundances show different general patterns when plotted against relative density (figs. 31.4 and 31.5). Although high sulfur contents may be encountered in most of the arbitrarily defined density classes, sulfur values generally become lower as the density increases. This general trend corresponds to a decrease in lava vesicularity as degassing of volatiles progresses. For

example, Swanson (1973) noted a 10-percent decrease in lava vesicularity that he attributed to gas loss during 4 km of flowage. Without actual measurements of the density, we cannot estimate the average decrease in vesicularity with lava flowage, but our qualitative data affirm the occurrence of generally lower concentrations of sulfur volatiles in denser, more degassed lavas.

A similar plot of carbon content against relative density (fig. 31.5) yields an almost random pattern. The highest carbon contents are not restricted to the samples with lowest density, and the lowest carbon values are distributed almost equally among all density classes. This lack of correlation is compatible with the notion that carbon volatiles may degas rapidly before or during the earliest vent activity rather than systematically during flowage. The wide range and scatter in carbon contents may again reflect the ease of posteruption contamination of the samples.

POSSIBLE VARIATION IN SULFUR AND CARBON CONTENT WITH TIME

Temporal and spatial variations in the chemical composition of Hawaiian basalts, even those formed during a single eruption, have been well documented in many previous studies (see, for example, Tilling and others, chapter 24; Wright, 1971; Wright and others, 1975; Wright and Tilling, 1980; Hoffman and others, 1984). Theoretically, variations in the volatile content of the eruptive products might be expected to correlate with differences in the composition of the magma in equilibrium with the volatiles. Swanson and Fabbi (1973) suggested that the differences in the energy level of vent fountaining might be linked to changes in volatile content of the magma; the most vigorous fountaining indicated the highest volatile content. They did not believe that the original volatile content of a magma could be estimated by analyzing subaerial eruptive products, because more than 80 percent of that content would have been lost. Swanson and Fabbi (1973) concluded, however, that spatter samples would retain the original volatiles better than any other eruptive product.

Although we cannot estimate the original volatile content of the magma associated with each eruptive event, we have plotted the sulfur and carbon content of spatter as a function of time (figs. 31.6, 31.7) in an attempt to ascertain any systematic secular changes in volatile content. Sulfur values (fig. 31.6) for most spatter samples fall in the range 125–250 μg/g, but the distribution appears random and no systematic temporal trend is apparent. Spatter samples collected during the same eruptive suquence may vary by as much as 130 μg/g. The plot of carbon content versus time (fig. 31.7) shows even more variation than that for sulfur. Spatter samples formed during the same eruption may differ in carbon content by as much as 156 μg/g. Such variations indicate that many more analyses of spatter samples, together with modifications in analytical procedure (such as stepwise combustion for carbon analysis), are needed before the possible existence of systematic temporal variations in volatile content of magma can be tested with any confidence. Furthermore, recent studies of volcanic gases from Kilauea rift eruptions indicate remarkable uniformity in the contents and proportions of the carbon and sulfur gases (Greenland, 1984; Gerlach and Graeber, 1985; Greenland and others, 1985). Such uniformity implies that the magma source region in the mantle beneath Hawaii is very homogeneous in volatile contents and, correspondingly, that variation in the volatile content of Hawaiian eruptive magmas may be so slight as to be extremely difficult to demonstrate with presently available sampling and analytical techniques.

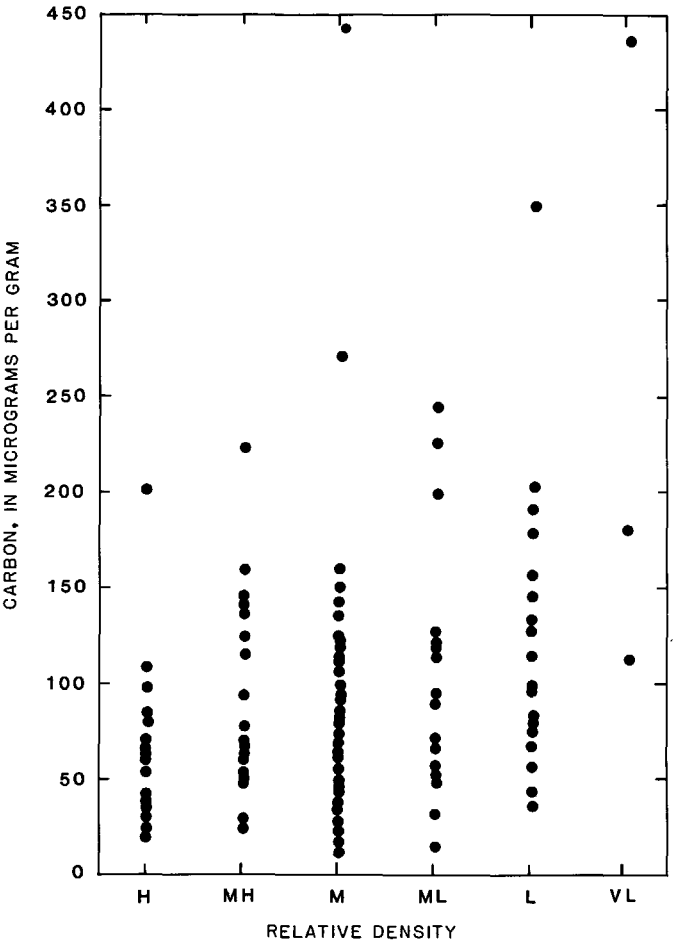

FIGURE 31.5.—Carbon contents of Kilauea and Mauna Loa lava samples plotted by relative density estimated qualitatively from visible vesicularity. H, high; MH, moderately high; M, moderate; ML, moderately low; L, low; VL, very low.

DISCUSSION

In our broad survey of recently erupted subaerial Hawaiian basalts, the total sulfur abundances ranged from 37 to 15,025 μg/g (median value 153 μg/g). The greatest sulfur abundances were found in a stalactite sample and wall glaze from an active lava tube. Presumably the stalactite sample served as a cold surface on which sulfur had condensed and accumulated; evidence of elemental sulfur deposits could be observed on the sample. The sulfur abundances for the subaerial basalts we analyzed are lower by a factor of 4 to 6

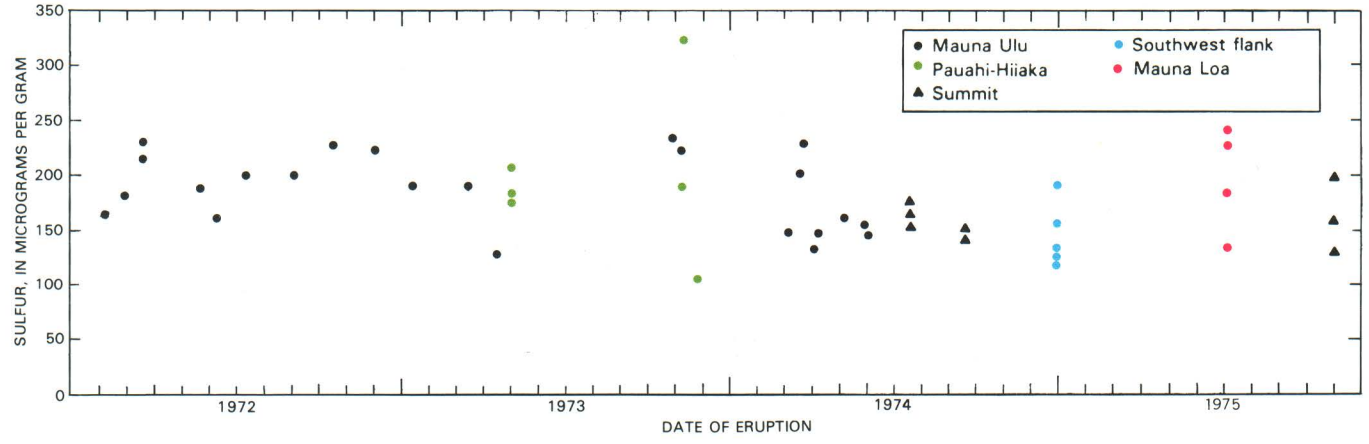

FIGURE 31.6.—Sulfur content of Kilauea and Mauna Loa lava spatter samples plotted by date of eruption.

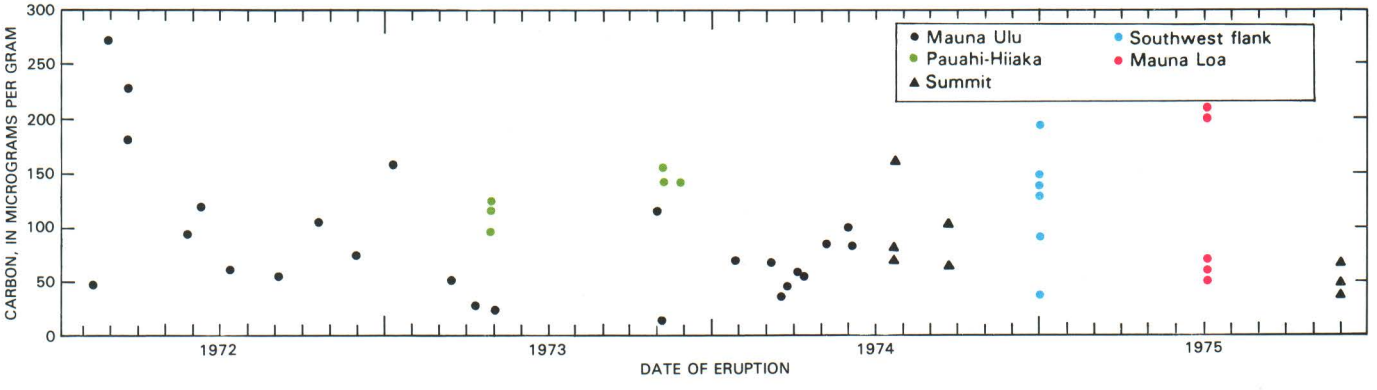

FIGURE 31.7.—Carbon content of Kilauea and Mauna Loa lava spatter samples plotted by date of eruption.

than those reported for submarine basaltic glasses (Des Marais and Moore, 1984; Sakai and others, 1984).

Sulfur abundances for ocean-floor basalts range from 60 to 990 μg/g (Moore and Fabbi, 1971; Moore and Schilling, 1973; Killingley and Muenow, 1975; Delaney and others, 1978; Naldrett and others 1978; Garcia and others, 1979; Des Marais and Moore, 1984; Sakai and others, 1984). The upper value approaches the inferred limit of saturation for lavas dredged at water depths exceeding 200 meters (Moore and Calk, 1971; Mathez, 1976). Swanson and Fabbi (1973) noted that recent subaerially erupted basalts contain 50 to 2,000 μg/g S, with the lower value typical of degassed samples and the upper value characteristic only of glass inclusions in phenocrysts (Anderson, 1974). Naldrett and Goodwin (1977) and Naldrett and others (1978) found that the sulfur contents of Archean basalts range between zero and 8,000 μg/g, with a maximum frequency near 1,000 μg/g. Their interpretation of these S concentrations, which are extraordinarily high compared to those of recent basalts, is that the retention of sulfur, despite extensive redistribution by metamorphism, resulted from the rapid accumulation of the Archean volcanic pile, allowing little interaction with seawater.

Carbon abundances of the basalts we analyzed range from 11 to 1,099 μg/g (median value 69 μg/g). The median value falls within the range of total carbon values reported for submarine basalts (see Des Marais and Moore, 1984; Sakai and others, 1984). However, our range of carbon contents in the subaerial basalts of Kilauea and Mauna Loa is considerably greater (by a factor of 4–5) than that for submarine basalts, contrary to what would be expected from subaerial (degassed) samples. Although additional factors may help account for this anomaly, we suspect that posteruption contamination by atmospheric carbon is most likely the principal cause of the wide dispersion observed in our data.

In terrestrial basalts, carbon is present usually as CO_2, the second most abundant volatile associated with volcanic systems. Most other volcanic gases are far more soluble in basaltic melts than CO_2 (Anderson, 1975), and this carbon gas species should dominate the vapor phase at fairly high pressures (about 400 MPa), in accordance with the experimental data of Kadik and others (1972).

Because the samples analyzed in this study were powders, most or all of the carbon dioxide that might have been present within vesicles in the rock has been lost during sample preparation. The total carbon abundances we measured represent the combined contributions of magmatic carbon (dissolved CO_2 in the glass) and nonmagmatic carbon acquired by the sample after eruption. Some of the samples contained olivine phenocrysts, generally making up less than 2 percent of the sample, and these phenocrysts were not removed from the sample. Any CO_2 inclusions in the phenocrysts therefore also contributed, though probably only a minor amount, to the total carbon abundance. For several submarine basalts from Kilauea's east rift zone, the carbon dissolved in the glass (released at combustion temperatures 1,200 to 1,270 °C) constituted 49 to 85 percent of the total carbon abundance (Des Marais and Moore, 1984, table 1). However, for a subaerial Kilauea basalt they analyzed, the carbon released in the high-temperature combustion represented only 5 percent of the total carbon.

For subaerial basaltic volcanism, Swanson and Fabbi (1973), on the basis of limited data, suggested that carbon dioxide volatilization does not vary appreciably with fountaining activity or with distance of lava flowage. If this is so, it implies that because of its low solubility in basaltic melt, CO_2 escapes very rapidly during the onset of eruptive activity and during the effervescent stage immediately preceding. In addition, recent studies of volcanic gases at Kilauea (Gerlach and Graeber, 1985; Greenland and others, 1985; Greenland, in press) indicate that substantial loss of CO_2 from the magma may occur during storage in the volcano's summit reservoir (at a depth of 2–6 km). In order to obtain a direct estimate of the magmatic carbon in subaerially erupted basalts and of the variations in its abundance induced by degassing, it would require determination of individual abundances for the various forms of carbon that contribute to the total carbon abundance. Such studies would need to use analytical procedures involving stepwise combustion and sample preparation methods similar to those used in the recent detailed studies of submarine basalts (for example, Des Marais and Moore, 1984). We hope that our broad data base of total carbon and sulfur abundances in fresh subaerial basalts from Kilauea and Mauna Loa will provide a starting point for the subsequent, more systematic studies required to evaluate the carbon budget in the subaerial eruption and attendant degassing of basaltic lavas.

REFERENCES CITED

Anderson, A.T., 1974, Chlorine, sulfur, and water in magmas and oceans: Geological Society of America Bulletin, v. 85, no. 9, p. 1485–1492.

——— 1975, Some basaltic and andesitic gases: Review of Geophysics and Space Physics, v. 13, no. 1, p. 37–55.

Basaltic Volcanism Study Project, 1981, Volatiles in planetary basalts: hydrogen, carbon, and sulfur gas species, *in* Basaltic Volcanism on the Terrestrial Planets: New York, Pergamon Press, Inc., p. 385–398.

Delaney, J.R., Muenow, D.W., and Graham, D.G., 1978, Abundance and distribution of water, carbon and sulfur in the glassy rims of submarine pillow basalts: Geochimica et Cosmochimica Acta, v. 42, no. 6B, p. 581–594.

Des Marais, D.J., and Moore, J.G., 1984, Carbon and its isotopes in mid-oceanic basaltic glasses: Earth and Planetary Science Letters, v. 69, p. 43–57.

Garcia, M.O., Liu, N.W., and Muenow, D.W., 1979, Volatiles in submarine volcanic rocks from the Mariana Island arc and trough: Geochimica et Cosmochimica Acta, v. 43, no. 3, p. 305–312.

Gerlach, T.M., 1980, Evaluation of volcanic gas analyses from Kilauea Volcano: Journal of Volcanology and Geothermal Research, v. 7, no. 3–4, p. 295–317.

——— 1982, Interpretation of volcanic gas data from tholeiitic and alkaline mafic lavas: Bulletin Volcanologique, v. 45–3, p. 235–244.

Gerlach, T.M., and Graeber, E.J., in press, The volatile budget of Kilauea Volcano: Nature.

Gibson, E.K., Jr., Chang, S., Lennon, K., Moore, G.W., and Pearce, G.W., 1975, Sulfur abundances and distributions in mare basalts and their source magmas: Proceedings 6th Lunar Science Conference, p. 1287–1301.

Gibson, E.K., Jr., and Moore, G.W., 1973, Carbon and sulfur abundances in lunar fines: Proceedings 4th Lunar Science Conference, p. 1577–1586.

——— 1974, Sulfur abundances and distributions in the valley of Taurus-Littrow, *in* Lunar Science Conference, 5th, Houston, Tex., 1974, Proceedings: Geochimica et Cosmochimica Acta, supp. 5, v. 2, p. 1823–1837.

Greenland, L.P., 1984, Gas composition of the January 1983 eruption of Kilauea Volcano, Hawaii: Geochimica et Cosmochimica Acta, v. 48, p. 193–195.

——— in press, Estimated mantle content of volatiles from basaltic gas composition: Journal Geology.

Greenland, L.P., Casadevall, T.J., and Stokes, J.B., in press, Emission rate of CO_2 and SO_2 from Kilauea Volcano, Hawaii: Nature.

Greenland, L.P., Rose, W.I., and Stokes, J.B., 1985, An estimate of gas emissions and magmatic gas content from Kilauea Volcano: Geochimica et Cosmochimica Acta, v. 49, no. 1, p. 125–130.

Harris, D.M., 1981, The concentration of CO_2 in submarine basalts: Journal of Geology, v. 89, . 689–701.

Harris, D.M., and Anderson, A.T., 1983, Concentrations, sources and losses of H_2O, CO_2, and S in Kilauean basalt: Geochimica et Cosmochimica Acta, v. 47, p. 1139–1150.

Hoffman, A.W., Feigenson, M.D., and Raczek, Ingrid, 1984, Case studies on the origin of basalt: III. Petrogenesis of the Mauna Ulu eruption, Kilauea, 1969–71: Contributions to Mineralogy and Petrology, v. 88, p. 24–35.

Javoy, M., Pineau, F., and Allegre, C., 1982, Carbon geodynamic cycle: Nature, v. 300, p. 171–173.

Javoy, M., Pineau, F., and Iiyama, I., 1978, Experimental determination of the isotopic fractionation between gaseous CO_2 and carbon dissolved in tholeiitic magma: Contributions to Mineralogy and Petrology, v. 67, p. 35–39.

Kadik, A.A., Lukanin, O.A., Lebedev, Y.B., and Korovushkina, E.Y., 1972, Solubility of H_2O and CO_2 in granite and basalt melts at high pressures: Geochemistry International, v. 6, p. 1041–1050.

Killingley, L.S., and Muenow, D.W., 1975, Volatiles from Hawaiian submarine basalts determined by dynamic high temperature mass spectrometry: Geochimica et Cosmochimica Acta, v. 39, p. 1467–1473.

Kyser, T.K., and O'Neil, J.R., 1984, Hydrogen isotope systematics of submarine basalts: Geochimica et Cosmochimica Acta, v. 48, p. 2123–2133.

Lockwood, J.P., Koyanagi, R.Y., Tilling, R.I., Holcomb, R.T., and Peterson, D.W., 1976, Mauna Loa threatening: Geotimes, v. 21, no. 6, p. 12–15.

Mathez, E.A., 1976, Sulfur solubility and magmatic sulfides in submarine basalt glass: Journal of Geophysical Research, v. 81, p. 4269–4276.

Mattey, D.P., Carr, R.H., Wright, I.P., and Pillinger, C.T., 1984, Carbon isotopes in submarine basalts: Earth and Planetary Science Letters, v. 70, p. 196–206.

Moore, J.G., and Calk, L., 1971, Sulfide spherules in vesicles of dredged pillow basalt: American Mineralogist, v. 56, p. 476–488.

Moore, J.G., and Fabbi, B.P., 1971, An estimate of the juvenile sulfur content of basalt: Contributions to Mineralogy and Petrology, v. 33, p. 118–127.

Moore, J.G., and Schilling, J.G., 1973, Vesicles, water, and sulfur in Reykjanes Ridge basalts: Contributions to Mineralogy and Petrology, v. 41, p. 105–118.

Muenow, D.W., Graham, D.G., and Liu, N.W.K., 1979, The abundance of volatiles in Hawaiian tholeiitic submarine basalts: Earth and Planetary Science Letters, v. 42, p. 71–76.

Naldrett, A.J., and Goodwin, A.M., 1977, Volcanic rocks of the Blake River Group, Abitibi Greenstone Belt, Ontario, and their sulfur content: Canadian Journal of Earth Sciences, v. 14, p. 539–550.

Naldrett, A.J., Goodwin, A.M., Fisher, T.L., and Ridler, R.H., 1978, The

sulfur content of Archean volcanic rocks and a comparison with ocean-floor basalts: Canadian Journal of Earth Sciences, v. 15, p. 715–728.

Peterson, D.W., and Tilling, R.I., 1980, Transition of basaltic lava from pahoehoe to aa, Kilauea Volcano, Hawaii: Field observations and key factors: Journal of Volcanology and Geothermal Research, v. 7, p. 271–293.

Sakai, H., Des Marais, D.J., Ueda, A., and Moore, J.G., 1984, Concentrations and isotope ratios of carbon, nitrogen, and sulfur in ocean-floor basalts: Geochimica et Cosmochimica Acta, v. 48, no. 12, p. 2433–2442.

Sparks, R.S.J., and Pinkerton, H., 1978, The effect of degassing on the rheology of basaltic lava: Nature, v. 276, p. 385–386.

Swanson, D.A., 1973, Pahoehoe flows from the 1969–71 Mauna Ulu eruption, Kilauea Volcano: Geological Society of America Bulletin, v. 84, p. 615–626.

Swanson, D.A., and Fabbi, B.P., 1973, Loss of volatiles during fountaining and flowage of basaltic lava at Kilauea Volcano, Hawaii: U.S. Geological Survey Journal of Research, v. 1, p. 649–658.

Tilling, R.I., Koyanagi, R.Y, Lipman, P.W., Lockwood, J.P., Moore, J.G., and Swanson, D. A., 1976, Earthquake and related catastrophic events, Island of Hawaii, November 29, 1975: A preliminary report: U.S. Geological Survey Circular 740, 33 p.

Williams, Howel, and McBirney, A.R., 1979, Volcanology: San Francisco, Freeman, Cooper & Co, 397 p.

Wright, T.L., 1971, Chemistry of Kilauea and Mauna Loa lava in space and time: U.S. Geological Survey Professional Paper 735, 40 p.

Wright, T.L., Swanson, D.A., and Duffield, W.A., 1975, Chemical compositions of Kilauea east-rift lava, 1968–1971: Journal of Petrology, v. 16, p. 110–133.

Wright, T.L., and Tilling, R.I., 1980, Chemical variations in Kilauea eruption 1971–74: American Journal of Science, v. 280-A, p. 777–793.

VARIATION OF $\delta^{13}C$ IN FUMAROLIC GASES FROM KILAUEA VOLCANO

By Irving Friedman, Jim Gleason, *and* Trevor Jackson

ABSTRACT

Values of $\delta^{13}C$ in fumarolic gases from Sulphur Bank, the Puhimau thermal area, and a fumarole at Halemaumau have been determined for samples collected from June 1984 through December 1985. Samples from Sulphur Bank and Halemaumau have a $\delta^{13}C$ of -3.5 ± 0.2 parts per thousand (permil) and show little change during this period. In contrast, the $\delta^{13}C$ of samples from the Puhimau thermal area increased from -3.5 to values of -2.7 permil at the end of the collection period. Applying an equilibrium fractionation factor of 1.004 for the ^{13}C distribution between carbon dissolved in the magma and the CO_2 gas in equilibrium with the magma resulted in a calculated primary $\delta^{13}C$ value of -7.5 permil for carbon dissolved in the Kilauea magma. The change of $\delta^{13}C$ at Puhimau can be the result of cooling of a pod of magma beneath Puhimau caused by the closure of its feeder passage from the main magma body.

INTRODUCTION

The $\delta^{13}C$ values of fumarolic gases are of interest for several reasons. The isotopic composition of mantle carbon is still a matter of conjecture, and the isotopic composition of mantle-derived gases is of importance in understanding the carbon cycle. Fumarolic gases are an important source of CO_2 to the atmosphere, and a knowledge of the $\delta^{13}C$ of such gases will help in understanding the atmospheric CO_2 cycle.

The first analyses of fumarolic gases from Hawaii were made by Naughton and Terada (1954). Conversion of their published atomic ratios to modern δ notation gives the following values in parts per thousand, permil to a precision of about ± 2 permil.

Sulphur Bank fumarolic gas	
1949, Mauna Loa in eruption	0 permil
1952, Kilauea in eruption	0 permil
1953, both volcanoes quiet	0 permil
Gas collected from Mauna Loa lava flow	-24 permil
CO_2 extracted from 1950 Mauna Loa olivine basalt	-19 permil

Those authors commented on the constancy of the Sulphur Bank ratios and on the relative enrichment of Sulphur Bank samples in ^{13}C as compared to the gas extracted from the chilled lava or from above the active lava flow. Thomas (1977) reported data on samples collected at Sulphur Bank as well as at 1971 and 1974 fissures at Halemaumau. His data are given in table 32.1.

EXPERIMENTAL PROCEDURE

In order to determine whether the variations found by Thomas were related to eruptive events, we initiated frequent sample collections at Sulphur Bank, Halemaumau, and at the Puhimau thermal area. Samples were collected by drawing the gases with a hand vacuum pump through a metal sample tube fitted with valves at both ends. The samples have been shipped to our laboratory in Denver where they were drawn through a metal trap cooled with liquid nitrogen. After the water was separated from the CO_2 at dry ice temperature, SO_2 was separated from the CO_2 by distillation at the temperature of melting ethanol. Analysis for $\delta^{13}C$ was carried out in the conventional manner on a 12-inch, triple-collector 90°-sector mass spectrometer.

RESULTS

Our results are given in table 32.2 and plotted in figure 32.1. Analysis of probable errors indicates two standard deviations (2σ) equal 0.1 permil.

There does not appear to be any correlation between $\delta^{13}C$ values of gases collected at any of the three collection sites and the short-term phases of the eruption at Puu Oo.

TABLE 32.1.—*Values of $\delta^{13}C$ obtained by Thomas (1977) for samples of fumarole from Sulphur Bank, Kilauea Volcano, Hawaii*

[Values given in permil (parts per thousand)]

Location	Date	$\delta^{13}C$
Sulphur Bank	5 Aug 75	−3.2
		−2.6
	18 Aug 75	−3.4
		−2.3
	8 Nov 75	−3.2
		3.0
	Dec 75	2.5
	13 Aug 76	−3.4
	17 Aug 76	−3.4
	13 Aug 76	−3.0
	1 Dec 76	−2.7
	28 Dec 76	−3.5
	28 Jan 77	−3.3
1971 fissure	13 Aug 75	−3.4
	19 Aug 75	−3.2
	8 Nov 75	−3.3
		−3.2
	1 Dec 75	−3.3
	9 Aug 76	−3.2
		−3.3
	26 Aug 76	−3.4
		−2.8
	13 Oct 76	−2.8
		−3.5
	1 Dec 76	−3.2
	28 Dec 76	−4.2
	29 Dec 76	−3.6
1974 fissure	29 Jan 77	−3.1
	10 Feb 77	−3.0

TABLE 32.2.—*Values of $\delta^{13}C$ for samples of fumarolic gas from localities on Kilauea Volcano, Hawaii*

[Values given in permil; date is date of collection of sample]

Date	Puhimau	Halemaumau	Sulphur Bank
		1984	
26 June	−3.6	−3.5	------
25 July	−3.2	−3.8	−3.9
6 Aug	−3.1	−3.6	−3.2
24 Aug	−3.0	−3.2	−3.4
11 Sept	−3.3	−3.6	------
19 Sept	−3.2	−3.5	−3.3
26 Sept	−4.0	−3.9	−3.3
2 Oct	−3.0	−3.6	−3.5
12 Oct	−3.2	−3.8	−3.4
29 Oct	−2.7	−3.5	−3.5
31 Oct	−2.8	−3.6	−3.4
13 Nov	−2.5	−3.5	−3.5
27 Nov	−2.7	−3.5	−3.4
4 Dec	−2.7	−3.4	−3.3
		1985	
10 Mar	−2.9	−3.5	−3.3
21 Mar	−2.9	−3.5	−3.4
1 Apr	−2.9	------	−3.1
3 Apr	-------	------	−3.3
12 Apr	−2.6	−3.4	------
19 Apr	−2.6	[1]−1.9	−3.1
1 May	−2.6	−3.0	−3.1
14 May	−2.6	------	−3.0
20 May	−2.7	−3.1	−3.3
31 May	−2.6	−3.5	------
4 June	−2.7	------	−3.4
17 June	−2.7	−3.5	−3.5
24 June	−2.7	−3.5	−3.2
28 June	−2.7	−3.4	−3.6
3 July	−2.8	−3.4	−3.5
19 July	−2.6	−3.3	−3.7
24 July	−2.7	−3.3	−3.4
9 Aug	−2.6	−3.4	−3.4
20 Aug	−2.8	−3.3	−3.5
13 Sept	−2.8	−3.4	−3.5
23 Sept	−2.5	−3.2	−3.3
30 Sept	−2.6	−3.5	−3.2
4 Oct	−2.7	−3.3	−3.3
11 Oct	−2.7	------	------
16 Oct	−2.8	−3.7	−3.6
25 Oct	−2.7	−3.4	------
31 Oct	−2.8	−3.3	−3.5
8 Nov	−2.7	−3.4	−3.4
14 Nov	−2.1	−2.8	−3.5
19 Nov	−1.9	−3.3	−3.4
22 Dec	−3.2	−3.5	−3.5
30 Dec	−3.2	−3.5	−3.4

[1]We have no explanation for this apparent anomalous value.

The $\delta^{13}C$ values of gases from both Halemaumau and Sulphur Bank appear to be fairly constant at -3.5 ± 0.3 permil, in reasonable agreement with the results of Thomas. We plan to continue to research long enough to determine if this constancy of $\delta^{13}C$ will persist during periods of quiescence at Kilauea.

Gases emitted at the Puhimau thermal area show greater variation and indicate an increase in $\delta^{13}C$ from -3.6 permil in late June, 1984, to -2.7 permil in November, followed by a slow decrease to -2.9 permil in March 1985. The $\delta^{13}C$ at Puhimau remained constant until early November, when it increased to -1.9, and then decreased to -3.2 in late December. These changes may have been caused by a temperature decline in the gas source, related to either cooling of an isolated body of magma beneath the thermal area or to withdrawal of magma from under the site, followed in December by reintroduction.

DISCUSSION

Pineau and others (1976) found the $\delta^{13}C$ of CO_2 released from vesicles in tholeiitic basalt from the mid-Atlantic ridge to be -7.6 ± 0.5 permil and postulated that this value represents the $\delta^{13}C$ of primary deep-seated carbon in the ridge area. Mattey and others (1983) postulated that the $\delta^{13}C$ of volcanic carbon is -4.2 to -7.5 for basalt midocean ridges, -2.8 to -6.7 permil in glass from Hawaiian and Explorer Seamounts, and -7.7 to -16.3 permil for glass from basalts in backarc basins.

The $\delta^{13}C$ of dissolved carbon in 11 samples of glass from midocean basalt was determined by Des Marais and Moore (1984) to range from -5.6 to -7.5.

Javoy and others (1978) determined experimentally that CO_2 in equilibrium with carbon dissolved in tholeiitic magma at 1,120–1,280 °C and 7.0–8.4 Kb, is enriched in ^{13}C by 4.0 to 4.6 permil relative to the magma. Therefore, if basaltic magma containing dissolved carbon with a $\delta^{13}C$ of -7.5 permil loses carbon dioxide to the atmosphere, we can expect that the initial fumarolic CO_2 will have a $\delta^{13}C$ of about -3 to -3.5 permil. Our results obtained at Halemaumau and Sulphur Bank agree with these expected values.

If the magma continues to lose CO_2 in an equilibrium distillation (a Rayleigh process), then the $\delta^{13}C$ of the CO_2 will continuously decrease as the amount of carbon in the magma decreases with time because of CO_2 loss.

The fairly constant $\delta^{13}C$ of the gases sampled at Halemaumau and Sulphur Bank indicate that only a small amount of CO_2 is lost from a large amount of magma, or that new magma enters the system in a continuous manner.

The increase of $\delta^{13}C$ with time observed at Puhimau thermal area can be explained by a decrease in the temperature of isotopic equilibration from about 1,250 to 1,100 °C. This could occur by the cooling of a small pod of magma isolated by interruption of its feeder dike from a larger magma body, which has been the source of heat for the thermal area since its formation in 1936 or 1937. If this explanation is correct, the isolation must have occurred just before our initial sampling in late June 1984. The decrease in $\delta^{13}C$ observed in December 1985 may be due to reintroduction of fresh magma beneath the site.

Monitoring the $\delta^{13}C$ of fumarolic CO_2 at Kilauea can yield important insights into magma movement and the opening and closing of feeder dikes.

REFERENCES

Des Marais, D.J., and Moore, J.G., 1984, Carbon and its isotopes in mid-oceanic basaltic glasses: Earth and Planetary Science Letters, v. 69, p. 43–57.

Javoy, M., Pineau,F., and Iiyama, I., 1978, Experimental determination of the isotopic fractionation between gaseous CO_2 and carbon dissolved in tholeiitic magma: Contributions to Mineralogy and Petrology, v. 67, p. 35–39.

Mattey, D.P., Carr, R.H., Wright, I.P., and Pillinger, C.T., 1983, Carbon isotopes in submarine basalts: Earth and Planetary Science Letters, v. 70, p. 196–206.

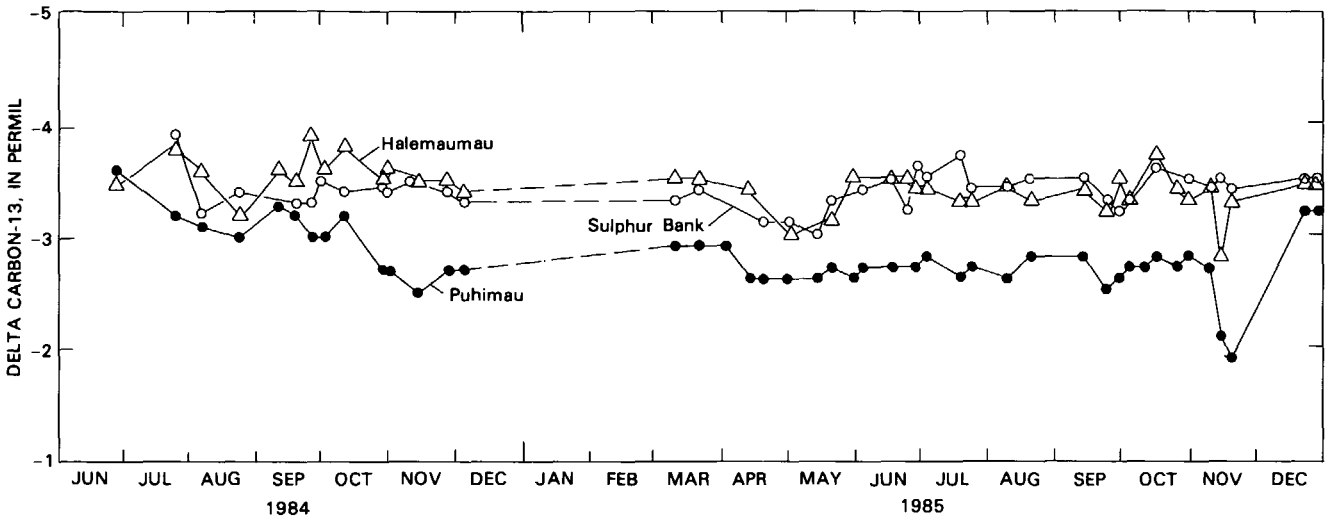

FIGURE 32.1.—Variation of $\delta^{13}C$ in samples of fumarolic gas from three localities on Kilauea Volcano, Hawaii.

Naughton, J.J., and Terada, K., 1954, Effect of eruption of Hawaiian volcanoes on the composition and carbon isotopic composition of associated volcanic and fumarolic gases: Science, v. 120, p. 580–581.

Pineau, F., Javoy, M., and Bottinga, Y., 1976, $^{13}C/^{12}C$ ratios of rocks and inclusions in popping rocks of the Mid-Atlantic Ridge and their bearing on the problem of isotopic composition of deep-seated carbon: Earth and Planetary Science Letters, v. 29, p. 413–421.

Thomas, D.M., 1977, The isotopic profile of gases from the summit and flank of Kilauea Volcano: Honolulu, University of Hawaii, Department of Chemistry, Ph. D. thesis.

HELIUM AT KILAUEA VOLCANO

Part I
Spatial and Temporal Variations at Sulphur Bank

By Irving Friedman *and* G. Michael Reimer

ABSTRACT

A survey of helium in soil gas was conducted at Sulphur Bank, Kilauea Volcano. The resulting helium-isograd map shows the highest helium abundance in an area about 75 m southwest of the experimental well drilled about 50 years ago.

Variation of helium abundance over time was investigated using an automated helium analyzer installed adjacent to Sulphur Bank. The gas effluent from a new well drilled at Sulphur Bank was piped to the instrument. The gas was analyzed every 3 hours and the equipment was operated periodically for 2 years. Helium data from July 1982 to August 1984 show periods of higher helium from August 1982 to January 1983 and again from February to August 1984.

INTRODUCTION

In 1978, a helium sniffer shipped from Denver to the Hawaiian Volcano Observatory was used by Irving Friedman and Ted Denton to conduct a survey of helium in soil gas at Sulphur Bank, on Kilauea Volcano. In order to conduct this survey, sampling was carried out by first pounding a thick-wall steel tube of 6-mm (0.25-in) diameter into the ground to a depth of about 0.5 m. A rubber septum was attached to the top of the tube and a plastic hypodermic syringe was used to withdraw a gas sample. Immediately upon withdrawal of the sidehole hypodermic needle from the septum, the hole in the needle was sealed by placing a piece of close-fitting, soft silicone-rubber tubing over the needle. At the laboratory, the gas sample was injected from the syringe through another rubber septum into the inlet system of the helium mass spectrometer. The spectrometer response was calibrated by frequent injections of gas standards of known helium content. Errors in the sampling and analysis process are estimated to be less than ± 5 percent of the amount of helium present. The data from this survey at Sulphur Bank are given in figure 33.1.

The uranium and thorium contents of soil derived from Hawaiian basalt are very low, and the parent rocks at Kilauea are very young. Thus, these soils contain very little helium derived in place from radioactive decay of uranium and thorium. The content of helium in the soil gas at Sulphur Bank, however, is very high, even compared to that in soils developed on old granitic rocks, in which the concentrations of uranium and thorium are orders of magnitude greater than at Sulphur Bank.

The high helium content of the soil gas at Sulphur Bank reinforced the authors' earlier inference that Sulphur Bank taps a deep magma source, even though it does not appear to be along a major rift zone.

ACKNOWLEDGMENTS

We wish to thank the following: Reggie Okamura and the Hawaiian Volcano Observatory crew for drilling the new well; Don McNair for constructing the original electronics and assembling the unit in Hawaii; Joe Jurceka for constructing the automated inlet system; and Barry Stokes for maintaining the instrument, as well as making many modifications to the wellhead and sampling equipment.

PRESENT SURVEY

Shortly after the completion of the (earlier) survey of Friedman and Denton, Thomas and Naughton (1979) observed changes in the ratio of helium to carbon dioxide at both Sulphur Bank and Halemaumau before inflation and eruptive events at Kilauea.

In 1979 we decided to install at Sulphur Bank an automated helium analyzer similar to that at a site 5 miles north of Gardiner, Montana, near Yellowstone National Park (Friedman and others, in press).

A new well at Sulphur Bank was successfully drilled about 100 m east of the old well (see fig. 33.1). The well was drilled to a depth of about 25 m, and the upper 13 m was cased with heavy-wall stainless steel pipe. The new well is shown in figure 33.2. Although the well casing was not cemented in place, alteration of the surrounding rock by the acid gases emitted along the casing has resulted in self-sealing of the casing. A slight positive gas pressure is observed in the casing.

The helium sniffer was placed in a trailer parked in the Park Service service area above Sulphur Bank Pali (see fig. 33.3). A 12-mm-diameter polyethylene tube inside a protective polyethylene pipe was used to convey the gas sample from well to trailer, a distance of 100 m, including 30 m of vertical rise.

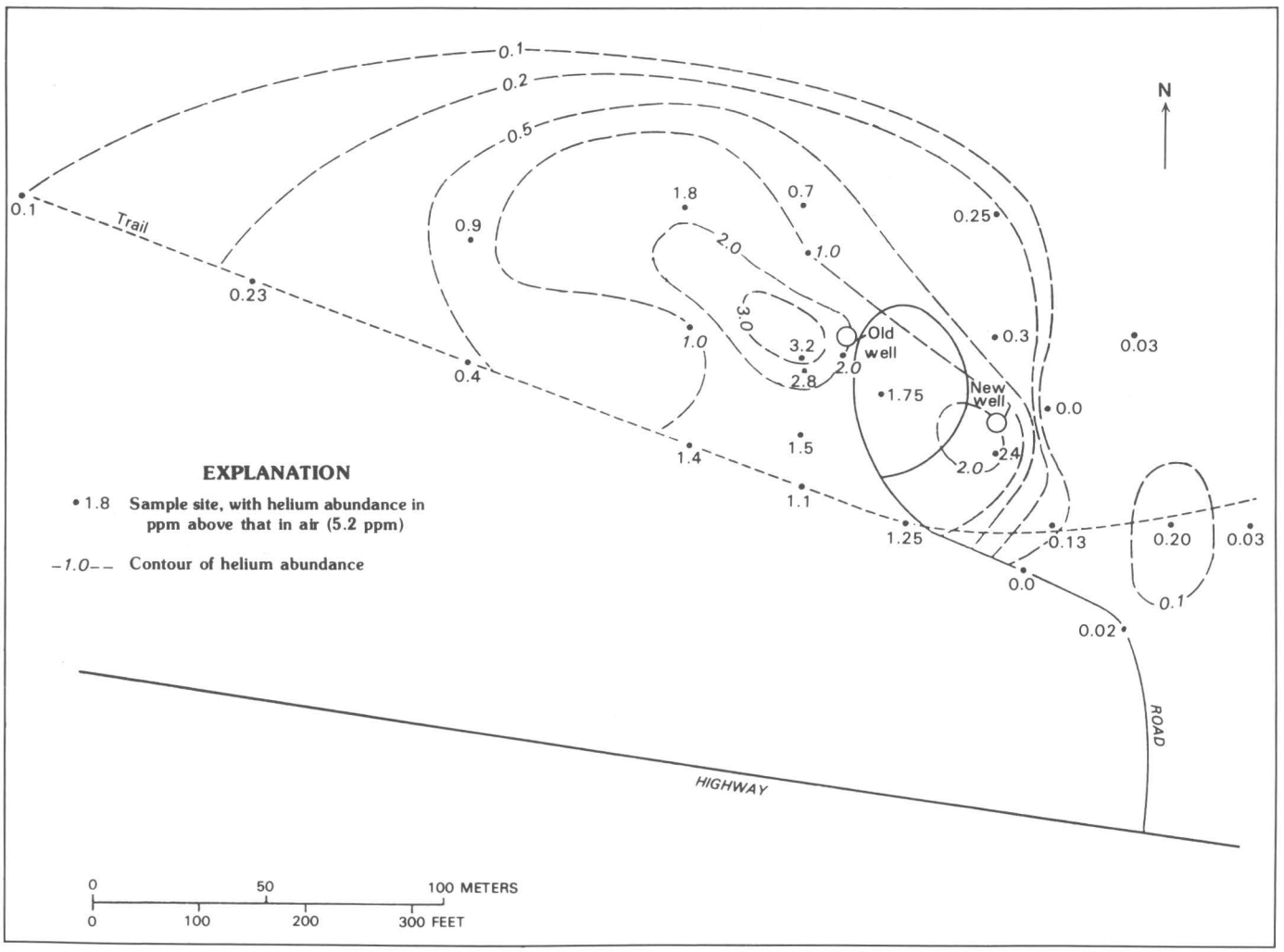

FIGURE 33.1.—Distribution of helium abundance in soil gas in the Sulphur Bank area, Kilauea Volcano, Hawaii. For location of Sulphur Bank, see figure 33.6.

Several attempts were made to condense the steam emitted by the well before it entered the polyethylene tube. Some schemes would work during dry periods when the steam flow was minimal, only to fail during increased steam flow associated with rainy intervals. In addition, metal condenser parts corroded at a very rapid rate, particularly at junctions of dissimilar metals. This problem was eventually solved by making all the wellhead fittings of Kynar plastic. A teflon tube connects these wellhead fittings to the steam condenser, which consists of 13 m of 37-mm-diameter thick wall copper pipe drained through a U-shaped tube. We found that the first few meters of copper pipe would corrode completely through in about 6 months, and it was replaced as needed. All parts, except for the two copper pipes joined with a plastic coupling, are now plastic.

FIGURE 33.2.—Wellhead of new well, completed 1979, for sampling soil gas at Sulphur Bank, Kilauea Volcano. White teflon tube carries gas from actual wellhead (left) to end of dark copper condensing tube. Note U-shaped glass tube (about 15 cm high) that allows condensed water to escape but prevents air from entering.

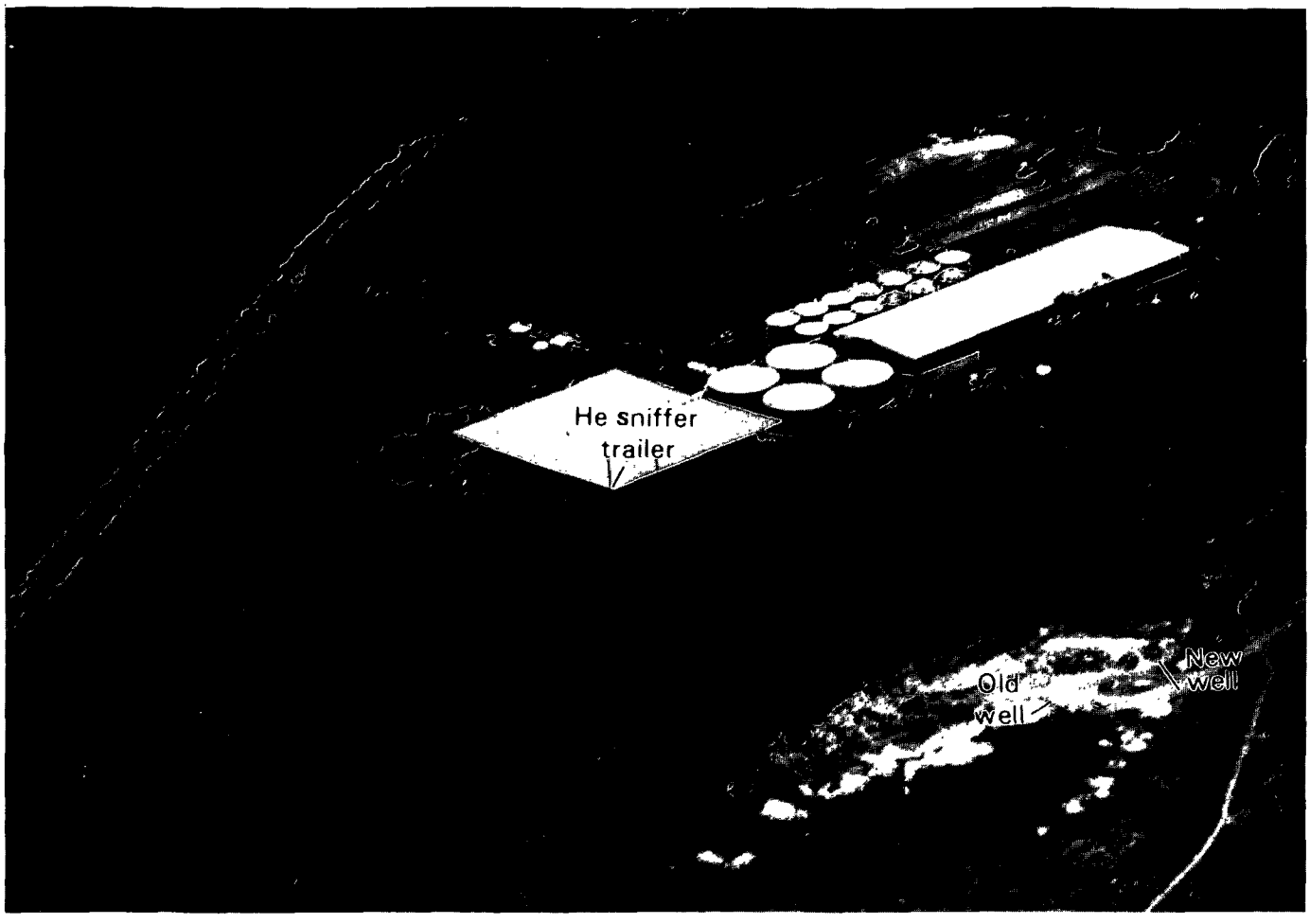

FIGURE 33.3.—Aerial view of Sulphur Bank area, Kilauea Volcano, showing location of old and new gas wells and of trailer containing helium sniffer (under corner of rain shed).

A small vacuum pump continuously pumped the well at about 100 mL/min. In order to remove water vapor that was not removed by the copper condenser pipe at the well site, the gas was passed through a silica-gel trap before entering the mass spectrometer sampling system.

At regular intervals (hourly at first, later changed to every 3 hours) the valve was opened automatically to admit a sample into the helium spectrometer for analysis. Immediately before and after each sample analysis, an aliquot of standard gas was analyzed, and after the second standard, a sample of ambient air was also analyzed. The results of these analyses were recorded on analog charts, an example of which is shown in figure 33.4.

Besides this automated mode of operation, it was possible to manually inject samples and compare the results to those for the standard gas. Approximately once a day, a sample of gas was collected manually at the wellhead by a sidehole hypodermic needle through a rubber septum; it was then analyzed manually on the automated instrument. These manually collected samples were used as a check on the operation of the automated system. In general, results from the two types of samples agreed within experimental error (± 50 ppb).

For a time, until the failure of the western GOES satellite, we were able to telemeter the results of the analysis via satellite to Wallops Island, Virginia and by land-line to Denver.

RESULTS

The helium concentrations in the samples show both short-term and long-term changes, as well as one abrupt change that preceded the January 1983 east-rift-zone eruption (fig. 33.5). From August 1982 through December 1983. the helium content decreased from about 11 ppm to 8 ppm. The helium content then rose again from about 8 ppm in mid-January 1984, to 16 ppm in mid-July 1984 at which time the instrument was decommissioned. An abrupt decrease occurred during December 21–28, 1982, coinciding with a hydrogen-gas increase noted on Kilauea (McGee and others, 1984) and preceding the January 1983 eruption.

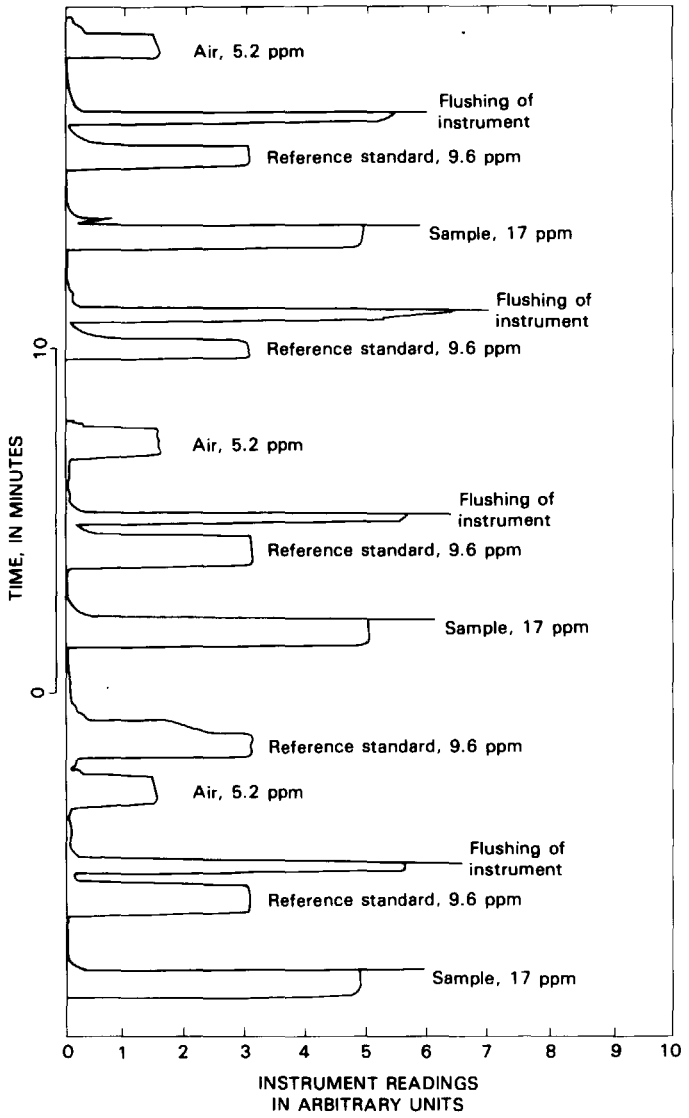

FIGURE 33.4.—Example of segment of instrument chart from the helium sniffer at Sulphur Bank, showing a typical helium analysis.

Other large and abrupt changes in helium abundance have been observed for which there is no obvious correlation with eruptive or meteorological events. If there is a link between the gas events and the east-rift-zone eruptions, we suspect that a change in the pressure regime of the magma source feeding the eruption should have been sufficient to be seen throughout the caldera.

Although the installation was automatic, it required weekly maintenance of the filters and occasional servicing of the mass spectrometer. Because the project investigators resided in Denver and could only visit the field site periodically, suitable personnel were not continuously available near the site, and even the usual teething problems required a long time to solve. These difficulties finally led us to abandon the effort and to substitute daily manual sample collection, the samples being mailed to Denver for analysis.

CONCLUSIONS

The map of helium abundance in soil gas at Sulphur Bank (fig. 33.1) shows a high concentration of helium in the vicinity of the old experimental well drilled in the 1920's.

Although helium abundance in the gases emitted from the newly drilled well vary with time (fig. 33.5), we were not able to correlate these variations conclusively with eruptive events during the two years in which we have collected data. A longer term record would be desirable, and this is now being collected.

REFERENCES

Friedman, I., Jurceka, J., Doering, W., Long, W., and McNair, D., in press, An automated helium analysis station. U.S. Geological Survey Professional Paper.

McGee, K.A., Sutton, A.J., and Sato, M., 1984, Observations of hydrogen gas events prior to volcanic seismicity [abs.]: International Chemical Congress of Pacific Basin Societies, American Chemical Society, Honolulu, December 16–21, 1984.

Thomas, D.M., and Naughton, J.J., 1979, Helium/carbon dioxide ratios as premonitors of volcanic activity: Science, v. 204, p. 1195–1196.

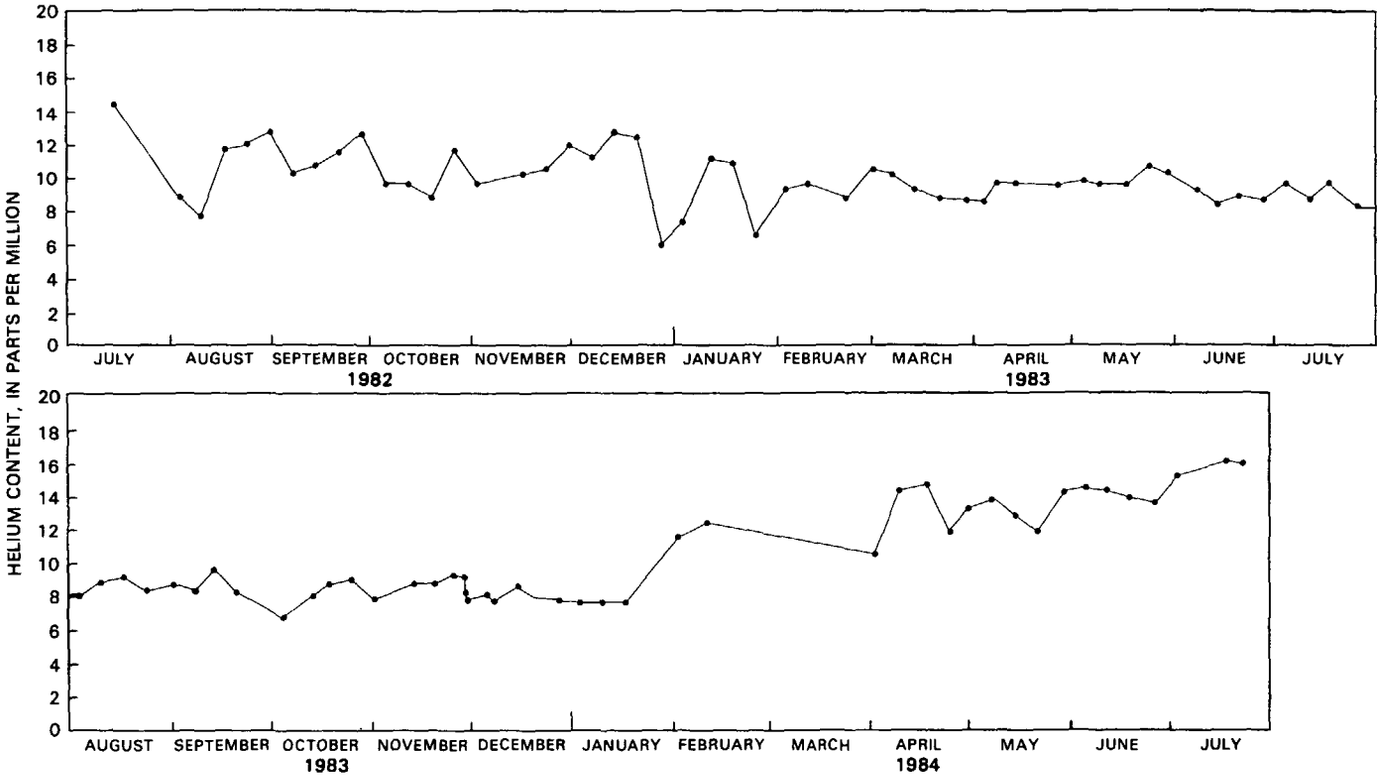

FIGURE 33.5.—Variation of helium abundance in soil gas at Sulphur Bank, Kilauea Volcano, from July 1982 to July 1984. All readings on samples from new gas well.

HELIUM AT KILAUEA VOLCANO

Part II
Distribution in the Summit Region

By G. Michael Reimer

ABSTRACT

A helium soil-gas survey was performed in the summit region of Kilauea Volcano, Hawaii. The average concentration found was about 5,250 parts per billion, only a little in excess of the atmospheric concentration of 5,240 parts per billion. High helium concentrations are not always associated with steaming areas which are most likely responding to meteoric water reacting with hot subsurface rocks. One anomalous area at Sulphur Bank and Steaming Bluff contained over 8,000 parts per billion helium and is interpreted as originating from at least as deep as the Kilauea magma reservoir and possibly from a mantle source. The anomalous Sulphur Bank area and a few higher than average helium concentrations at the village of Volcano occur along strike of the southwest rift zone and may be indicative of a northeast extension of that rift zone across Kilauea caldera. If the areal extent of the helium anomaly and the flux rate could be determined, it would be possible to estimate the mantle helium concentration at Kilauea.

INTRODUCTION

The helium-4 isotope is produced by the natural alpha-particle radioactive decay of uranium and thorium. On a gross scale, its distribution in the earth is controlled by the presence and concentration of the parent generating material, various trapping mechanisms, pathways for migration, and the primordial distribution. Primordial helium is characterized by high concentrations of the helium-3 isotope such that it may be on the order of 10^5 times more abundant (as in chondrites) than in minerals containing mostly radiogenically produced helium. The data in this paper refer only to helium-4 unless otherwise noted.

Helium has unique chemical and physical properties that make it an excellent gas for use in geochemical surveys. It is chemically inert, biogenically neither produced nor consumed, radioactively stable, highly diffusive, and has a low solubility in water. These characteristics provide helium with some advantages over other gases commonly used in surveys such as radon, which has a 3.8 day half-life, or methane and carbon dioxide, which can be involved in biological reactions.

Most helium soil-gas analyses have been performed as a geochemical guide in the search for oil and gas or uranium energy resources (Dyck, 1976; Reimer and others, 1979; Roberts, 1981). Several studies have shown the usefulness of helium in locating, tracing the extent of, or generally characterizing hot-water geothermal occurrences (Roberts and others, 1975; McCarthy and others, 1982; Baldi and others, 1984). An interesting observation from many of the energy-related studies has been that there is frequently unequivocal control of helium concentrations by geologic structure, such as faulting or jointing (Reimer and Adkisson, 1977; Jones and Drozd, 1983). This observation is presently being explored for potential applications in tracing faults or monitoring faults for helium variations that may be precursory to seismic activity (Reimer, 1980).

Very few helium soil-gas studies have been performed in volcanic areas. Hinkle (1978) performed a limited survey at the Puhimau Steaming Area on Kilauea. Friedman (chapter 33, part I) performed a survey at Sulphur Bank on Kilauea in 1978 preparatory to establishing an automated helium analyzer near the site. Hinkle and Kilburn (1980) and Green (1984) performed field surveys at the Long Valley caldera, California. A change in the helium distribution occurred there in the 4 years separating those two surveys, and the change is speculatively thought to be related to subsurface movement of magma and concomitant degassing within the system. Lombardi and others (1984) performed surveys at the Phlegraean Fields near Pozzuoli, Italy, in July and September 1983 and recorded a pronounced change in the helium distribution. The change is thought to be the effect of an increase of earthquakes which released 10 times the strain as in previous months and possibly reopened older fissures and fractures.

This study presents the results of a systematic survey of the helium soil-gas distribution at the Kilauea summit. It will provide a data base for future studies that will be especially important if the dramatic changes observed by Lombardi at Pozzuoli are characteristic precursors of seismic or eruptive events. In addition, this study will augment the data obtained by Cox (1983) on the soil content of radon and mercury at Kilauea. Various volatile species have their own unique chemical and physical properties; when considered collectively, they provide a better insight into the mechanisms controlling surface distribution and concentration of the gases.

ACKNOWLEDGMENTS

I thank Trevor Jackson and Barry Stokes for assistance with the sample collection and Josh Been and Don Murrey for help with the analyses.

STUDY AREA AND SAMPLING METHODS

This helium soil-gas survey was conducted in the vicinity of the summit of Kilauea Volcano on the Island of Hawaii. At the time of the survey in December 1984, eruptive activity on the east rift zone, which commenced in January 1983, was in the post-phase 28 interim. Kilauea has formed primarily from the extrusion of tholeiitic basalts and ash. Subsurface magma intrusion and movement contribute to the formation of the numerous and complex fault zones in the area, and the prominent Kilauea caldera and Halemaumau crater were formed by subsidence. Several of the fracture systems give rise to large steaming areas such as those at the northeast edge of the Kilauea caldera and at Sulphur Banks 0.6 km farther northeast. Numerous other vents from smaller areas of fractures and cracks produce gas, the bulk of which is water but containing varying amounts of other trace gases such as CO_2, SO_2, and He (Gerlach, 1980; Greenland, 1984).

There is a diversity in soil type and ground cover around Kilauea. The areas north and east of the caldera have well-developed soils capable of supporting tropical vegetation; the areas south and west have poorly developed or non-existing soils and are covered by historical lava flows, ash, and cinders.

Soil gas is that gas accumulated within the soil pores and is in quasi-equilibrium with the soil moisture. The gas is mobile to an extent controlled principally by the soil permeability, and represents a time-integrated sample, the period of which is also controlled by mobility. Mobility, in turn, especially in near-surface samples, is strongly influenced by external meteorological factors. Precipitation can provide water that decreases permeability; temperature differences can create convective pumping effects; wind-speed variations can create venturi pumping effects. Soil gases reside in a dynamic environment but the gas concentration variations induced in the environment are not so great that they limit the usefulness of the method (Reimer, 1980).

In this study, soil gases were collected by pounding an 8-mm-diameter hollow steel probe into the soil to a depth of 0.5 m. A septum-containing cap was placed on the probe to create an air-tight seal, and the gas was slowly withdrawn through the system by a hypodermic syringe. The probe nominally contains a dead volume of 2 cm^3 and was first purged by withdrawing and discarding 5 cm^3, of gas. A sample of 15–20 cm^3 was then withdrawn into the syringe and transferred to a pre-evacuated stainless steel container of 6-cm^3 internal volume for shipment to the laboratory for analysis. The container is overpressurized with sample and sealed with a single valve on one end with a septum in series through which the sample was injected. Soil-gas samples collected by the probe method commonly are taken from a depth of 0.75 or 1.0 m. This depth represents a compromise between ease of sampling and reduction of variation from meteorological conditions (Reimer, 1980). However, meteorology is usually a factor when a survey takes several days to perform. Because of the variation in soil depth at the Kilauea summit a sample depth of 0.5 m was chosen to permit uniformity. All samples were collected in a 9-hour daylight period on December 11, and the weather conditions at the summit were extremely consistent throughout the sampling: clear to partly cloudy, trade winds 15–30 km/h, temperature 17–22 °C, and no precipitation. The good fortune of uniform weather minimized site-to-site variation in the samples taken at the 0.5-m depth.

Samples were analyzed using a small leak-detector mass spectrometer tuned specifically for the helium mass-to-charge ratio of 4+. The minor modifications to this type of instrument, commercially used for testing leaks in vacuum systems, to allow it to be used for high precision analytical work are described by Reimer and others (1979). Analytical precision for helium is ±10 parts per billion (10 in 10^9). The atmosphere nominally contains 5,240 parts per billion helium and is a remarkably constant reservoir (Glueckauf, 1949; Oliver and others, 1984). Samples are withdrawn from the stainless steel cylinders by inserting a hypodermic needle through the septum and opening the valve. The syringe rebounds in response to the overpressure in the cylinder. Knowing the amount of sample injected into the cylinder and the amount of rebound during extraction, a gross check on the integrity of the cylinder is obtained. Samples with rebounds not within 1 cm^3 of that anticipated are rejected. The sample is injected into the spectrometer inlet system, where gases other than helium and neon are removed on activated charcoal at liquid-nitrogen temperatures. The sensitivity of the spectrometer is determined every 10 samples by analyzing two reference gases containing different helium concentrations, and each unknown sample is bracketed by two reference analyses. From the calibrated instrument sensitivity and the difference in peak height for the sample-standard combination, the concentration of helium in the sample is determined.

DATA AND DISCUSSION

The area of the survey and location of sample collection points are shown in figure 33.6. This area is roughly equivalent to that sampled by Cox (1983) for radon and mercury, but the exact stations were not reoccupied. A total of 93 soil-gas samples were collected and analyzed. The distribution of the helium concentration was fairly uniform, with only three samples from Sulphur Bank and Steaming Bluff being anomalously high. The average helium concentration, excluding the 3 high values, is 5,248 ± 23 ppb, which is about that of the nominal atmospheric concentration. Table 33.1 presents the helium concentrations of the samples keyed to figure 33.6. The ΔHe is the difference in helium from the atmospheric concentration. Concentrations of soil-gas helium less than the atmospheric content are the result of dilution by other gases such as carbon dioxide or water vapor. Concentrations of helium greater than atmospheric content result when a subsurface source is present. Overall, the helium concentration throughout the Kilauea summit

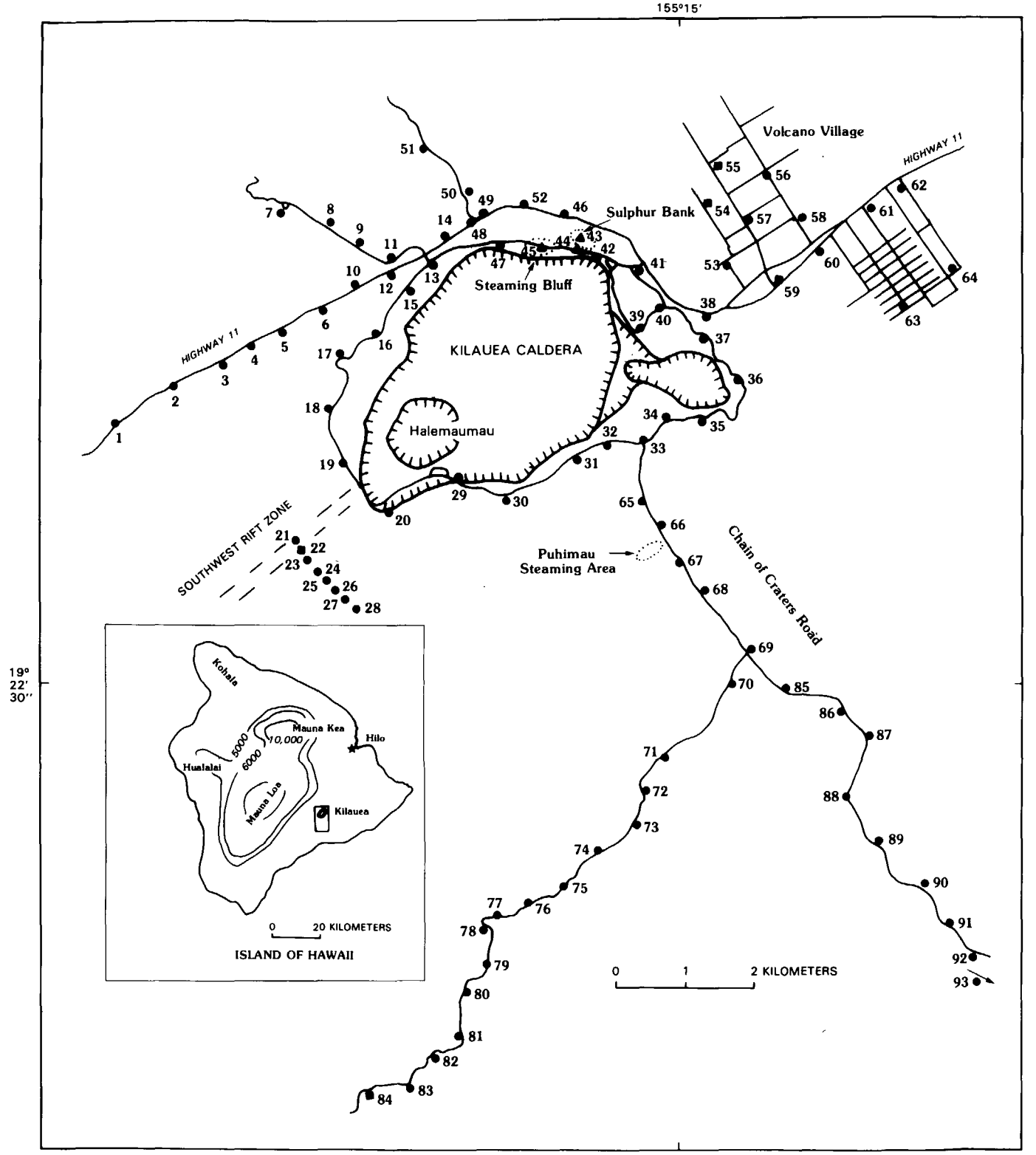

FIGURE 33.6.—Summit region of Kilauea Volcano, Hawaii, showing sampling sites for survey of helium in soil gas. Dots, samples yielding average helium concentrations; squares, slightly higher helium concentrations (greater than two standard deviations from that of air); triangles, the anomalously high concentrations at Sulphur Bank and Steaming Bluff. Sample numbers keyed to table 33.1. Hachures indicate infacing scarps of caldera and craters.

TABLE 33.1.—*Helium concentrations in soil-gas samples from Kilauea Volcano, Hawaii*

[All samples collected December 11, 1984; sample locations shown in figure 33.6. Δ helium is the difference in the helium concentration between the sample and the air reference at 5240 ppb. N.A. for sample 8 means it was not analyzed because of obvious leakage of the sample cylinder. The precision of the analyses was ±10 ppb helium; the reported concentrations are those determined by the signal processing computer and do not imply greater precision]

Sample number	Helium (ppb)	Δ helium (ppb)	Sample number	Helium (ppb)	Δ helium (ppb)	Sample number	Helium (ppb)	Δ helium (ppb)
1	5244	4	32	5261	9	63	5229	−11
2	5239	−1	33	5226	−14	64	5257	17
3	5222	−18	34	5250	10	65	5265	25
4	5240	0	35	5260	20	66	5224	25
5	5254	14	36	5248	8	67	5226	−14
6	5268	28	37	5227	−13	68	5251	11
7	5252	12	38	5200	−40	69	5233	−7
8	N.A.	N.A.	39	5245	5	70	5233	−7
9	5265	25	40	5217	−23	71	5253	13
10	5255	15	41	5261	21	72	5260	20
11	5238	−2	42	5229	−11	73	5259	19
12	5265	25	43	8084	2844	74	5211	−29
13	5250	10	44	8774	3534	75	5215	−25
14	5265	25	45	5712	472	76	5249	9
15	5249	9	46	5252	12	77	5249	9
16	5270	30	47	5227	−13	78	5295	−45
17	5246	6	48	5241	1	79	5277	37
18	5248	8	49	5277	37	80	5265	25
19	5230	−10	50	5262	22	81	5294	54
20	5224	−16	51	5232	−8	82	5263	23
21	5252	12	52	5253	13	83	5284	44
22	5257	67	53	5243	3	84	5295	55
23	5245	5	54	5294	54	85	5248	8
24	5262	22	55	5309	69	86	5228	−12
25	5247	7	56	5270	30	87	5241	1
26	5248	8	57	5263	23	88	5235	−5
27	5227	−13	58	5236	−4	89	5270	30
28	5252	12	59	5296	56	90	5219	−21
29	5223	−17	60	5236	−4	91	5218	−22
30	5241	1	61	5267	27	92	5215	−25
31	5249	9	62	5265	25	93	5277	37

area is similar to that found in other regional surveys such as those in the Powder River Basin of Wyoming (Reimer and others, 1980) and the Basin and Range Province of Utah and Nevada (Reimer and Bowles, 1983). This observation is consistent with the fact that there are no high concentrations of uranium or thorium contributing to a high helium background at Kilauea.

The helium concentration of Sulphur Bank and Steaming Bluff is quite anomalous, in excess of 8,000 ppb for some samples. This is the area in which Cox (1983) reported the highest radon concentrations from his survey. The high helium and radon concentrations are typical of areas where there is a surface manifestation of hot spring activity (Roberts and others, 1975; McCarthy and others, 1982; Baldi and others, 1984). The high concentrations of radiogenic byproducts from hot springs, however, may be the result of local concentrations of uranium daughter isotopes, notably radium in precipitates. Samples collected in the vicinity of the Puhimau Steaming Area did not show similarly anomalous helium or radon concentrations. The steaming activity at Puhimau is attributable to meteoric water contacting the residual heat of the 1938(?) intrusion in that area. In neither area, Puhimau nor Steaming Bluff and Sulphur Bank, is there a known, near-surface concentration of helium-producing daughter isotopes. It is inferred, therefore, that there is a large helium component to the gases venting on the northeast side of the Kilauea caldera. Helium-3/helium-4 ratios have indicated that the helium component is derived in large part from the mantle (Craig and others, 1978). Steaming areas alone do not necessarily imply gas supply from a deep source. If the areal extent of the helium anomaly and the flux rate through the soil could be determined by future studies, the volume of mantle-derived helium could be determined from Kilauea alone and compared to the total Earth values derived by Naughton and others (1973), who used helium/carbon ratios. In contrast to the earlier view of Macdonald and Abbott (1977), these recent helium data support the idea of connection of Sulphur Bank gases to a magma source, most likely that feeding Kilauea.

Another area at the Kilauea summit with slightly higher helium concentrations is within the village of Volcano. The values are not exceptionally high, only 50 to 70 ppb above the atmospheric concentration, but they are interesting because they occur in an area of low radon concentrations (Cox, 1983).

Cox interprets the low radon concentrations to represent either low permeability of strata or downflow of gas in that vicinity. For the helium, the similarity of soils in the area (U.S. Dept. of Agriculture, 1973) tends to rule out permeability differences very near the surface or at the sampling depth, and the positive values are not representative of inhalation. I suggest that this region may be an extension of the area receiving mantle-derived helium because of the proximity to Sulphur Bank, only 2.5 km southwest. Alternatively, these higher concentrations, with those at Steaming Bluff and Sulphur Bank, could be indicative of a northeast extension of the

southwest rift zone. They all occur along the strike of the rift across the caldera. A more detailed survey could indicate if the areas might be linked.

CONCLUSIONS

The reconnaissance helium soil-gas survey at the summit of Kilauea Volcano has indicated only one broad area of high helium concentration. That area, comprising Sulphur Bank and Steaming Bluff on the northeast side of the caldera, had soil-gas helium concentrations greater than 8,000 ppb. Thermally induced concentration and release of helium is typical in areas where the host rock can provide the uranium or thorium alpha-particle-producing daughters that ultimately produce the helium. At Kilauea, the character of the host rock and its young age generally preclude the concentrating of uranium and thorium (Newman and others, 1984). The high bulk helium concentration is thought, therefore, to be the result of a mantle-derived source. It may be possible with future studies to estimate the amount of helium contributed from the mantle at Kilauea, or at least set limits on the amount. In addition, the helium soil-gas technique may be useful in finding areas in which the mantle helium is being degassed at the surface and distinguishing those areas from the ordinary thermal steaming areas. It would be a particularly helpful method to locate areas not marked by surface fracture systems where gases in magma reservoirs have the most permeable pathway to the surface.

REFERENCES CITED

Baldi, P., Ceccarelli, A., Bertrami, R., Friedman, I., and Lombardi, S., 1984, Helium in soil gases in geothermal areas: Seminar on the utilization of geothermal energy for electric power production and space heating, Florence, Italy, May 14–17, 1984, United Nations Economic Commission, EP/SEM.9/R.10, 12 p.

Cox, M.E., 1983, Summit outgassing as indicated by radon, mercury, and pH mapping, Kilauea Volcano, Hawaii: Journal of Volcanology and Geothermal Research, v. 16, p. 131–151.

Craig, H., Lupton, J.E., and Horibe, Y., 1978, A mantle helium component in circum-Pacific volcanic gases: Hakone, the Marianas, and Mt. Lassen, *in* Alexander, E.C., and Ozima, M., eds., Terrestrial Rare Gases: Tokyo, Japan Scientific Societies Press, Advances in Earth and Planetary Sciences, v. 3, p. 3–16.

Dyck, Willy, 1976, The use of helium in mineral exploration: Journal of Geochemical Exploration, v. 5, p. 3–20.

Gerlach, T.M., 1980, Evaluation of volcanic gas analyses from Kilauea Volcano: Journal of Volcanology and Geothermal Research, v. 7. 295–317.

Glueckauf, E., 194 A micro-analysis of the helium and neon contents of air: Proceedings of the Royal Society of London, v. 185, p. 98–119.

Green, K.R., 1984, An algorithm for determining soil and water helium concentrations from headspace analyses: Examples of geochemical applications in Long Valley, California, and the Fiji Islands: Golden, Colorado, Colorado School of Mines, Master's thesis, 197 p.

Greenland, L.P., 1984, Gas composition of the January, 1983, eruption of Kilauea Volcano, Hawaii: Geochimica et Cosmochimica Acta, v. 48, p. 193–196.

Hinkle, M.E., 1978, Helium, mercury, sulphur compounds, and carbon dioxide in soil gases of the Puhimau Thermal Area, Hawaii Volcanoes National Park, Hawaii: U.S. Geological Survey Open-File Report 78–246, 14 p.

Hinkle, M.E., and Kilburn, J.E., 1980, Survey of helium in soil gases of Long Valley, California: U.S. Geological Survey Open-File Report 80–612, 19 p.

Jones, V.T., and Drozd, R.J., 1983, Predictions of oil or gas potential by near-surface geochemistry: American Association of Petroleum Geologists Bulletin, v. 67. p. 932–952.

Lombardi, S., DiFilippo, M., and Zantedeschi, L., 1984, Helium in Phlegraean Fields soil gases: July 20–26, September 19–25. 1983: Bulletin Volcanologique, v. 47-2, p. 259–265.

Macdonald, G.A., and Abbott, A.T., 1977, Volcanoes in the sea: Honolulu, Hawaii, University of Hawaii Press, 441 p.

McCarthy, K.P., Been, J.M., Reimer, G.M., Bowles, C.G., and Murrey, D.G., 1982, Helium and ground temperature surveys at Steamboat Springs, Colorado: Denver, Colorado, Colorado Geological Survey, Special Publication 21, 11 p.

Naughton, J.J., Lee, J.H., Keeling, D., Finlayson, J.B., and Dority, G., 1973, Helium flux from the Earth's mantle as estimated from Hawaiian fumarolic degassing: Science, v. 180, p. 55–57.

Newman, S., Finkel, R.C., Macdougall, J.D., 1984, Comparison of ^{230}Th–^{238}U disequilibrium systematics in lavas from three hot spot regions: Hawaii, Prince Edward and Samoa: Geochimica et Cosmochimica Acta, v. 48, p. 315–324.

Oliver, B.M., Bradley, J.G., and Farrar, Harry, 1984, Helium concentration in the Earth's lower atmosphere: Geochimica et Cosmochimica Acta, v. 48, p. 1759–1768.

Reimer, G.M., 1980, Use of soil-gas helium concentrations for earthquake prediction: limitations imposed by diurnal variations: Journal of Geophysical Research, v. 85, p. 3107–3114.

Reimer, G.M., and Adkisson, C.W., 1977, Reconnaissance survey of the helium content of soil gas in Black Hawk, Eldorado Springs, Evergreen, Golden, Morrison, Ralston Buttes and Squaw Pass quadrangles, Colorado: U.S. Geological Survey Open-File Report 77–464, 10 p.

Reimer, G.M., and Bowles, C.G., 1983. Helium concentration in soil-gas of the Ely and Delta 1° by 2° quadrangles, Basin and Range Province: U.S. Geological Survey Open-File Report 83–589, 26 p.

Reimer, G.M., Denton, E.H., Friedman, Irving, and Otton, J.K., 1979, Recent developments in uranium exploration using the U.S. Geological Survey's mobile helium detector: Journal of Geochemical Exploration, v. 11, p. 1–12.

Reimer, G.M., Murrey, D.G., and Been, J.M., 1980, Helium soil-gas concentrations in the Torrington, Newcastle, Gillette, and Ekalaka 1° x 2° quadrangles: Data from a reconnaissance survey: U.S. Geological Survey Open-File Report 80–452, 14 p.

Roberts, A.A., 1981, Helium emanometry in exploration for hydrocarbons II, *in* Gottlieb, B.M., ed., Unconventional methods for exploration for petroleum and natural gas: Dallas, Texas, Southern Methodist University Press, p. 136–149.

Roberts, A.A., Friedman, I., Donovan, T.J., and Denton, E.H., 1975, Helium survey, a possible technique for locating geothermal reservoirs: Geophysical Research Letters, v. 2, p. 209–210.

U.S. Department of Agriculture, 1973, Soil survey of the Island of Hawaii, State of Hawaii: Washington, D.C., Soil Conservation Service, U.S. Department of Agriculture, 115 p., 195 plates.

USE OF SATELLITE TELEMETRY FOR MONITORING ACTIVE VOLCANOES, WITH A CASE STUDY OF A GAS-EMISSION EVENT AT KILAUEA VOLCANO, DECEMBER 1982

By Kenneth A. McGee, A. Jefferson Sutton, *and* Motoaki Sato

ABSTRACT

A telemetry system using geostationary satellites for data relay has several advantages over ground-based systems that are widely used as a means for relaying geophysical and geochemical data from volcanoes. The National Oceanic and Atmospheric Administration's NESDIS (National Environmental Satellite, Data, and Information Service) maintains two operating Geostationary Operational Environmental Satellites (GOES) to monitor the Earth's weather systems. These satellites are part of a worldwide network of meteorological satellites, and each is equipped to relay data transmissions from networks of data-collection platforms. A degassing event at Kilauea Volcano in December 1982, observed and recorded some 9,000 km away, is cited as an example of how satellite telemetry can be a viable alternative for monitoring potentially active volcanoes.

INTRODUCTION

Radio telemetry is widely used as a means for relaying geophysical and geochemical data from active volcanoes to observatories or other data-collection centers. Most existing telemetry networks are ground based and are constrained by topographic conditions. In order to extend the range of the telemetry, repeater stations may be installed or telephone lines leased. However, the cost of maintaining these systems adds substantially to the total cost of the operation. Moreover, the complexity of the system increases and the flow of data becomes more vulnerable to equipment failure as more links are added to the data-relay chain.

A telemetry system using geostationary satellites for data relay has advantages over ground-based systems (McGee and Sato, 1982). The need for repeaters, multiple telemetry links, and dedicated telephone lines is eliminated. Although the initial cost of the transmitters may be higher, the elimination of repeater stations and leased telephone lines reduces the operational costs and, more importantly, extends the potential useful range to thousands of kilometers. Since the telemetry antennas must be pointed skyward at a high angle (30° to 60° depending on latitude), the elevation and local topography of the monitoring site become less important. Also, because satellite-relayed telemetry systems operate at higher radio frequencies than typical ground-based systems they have shorter antenna element lengths and fewer interference problems. Smaller antenna systems in turn reduce the vulnerability of monitoring sites to damage from wind or ice. Finally, a telemetry system using geostationary satellites for data relay allows more than one observatory or laboratory to collect data from volcanoes scattered across continents or oceans.

DESCRIPTION OF A SATELLITE DATA-COLLECTION SYSTEM

The National Oceanic and Atmospheric Administration's NESDIS (National Environmental Satellite, Data, and Information Service) operates a series of Geostationary Operational Environmental Satellites (GOES) to image and monitor the Earth's cloud cover and weather systems (National Oceanic and Atmospheric Administration, 1983). These satellites, placed in orbits coincident with the Earth's equatorial plane at an altitude of about 35,500 km, rotate at the same speed as the Earth and appear from the Earth to be in a fixed position. Unlike earlier polar-orbiting satellites, these geostationary or geosynchronous satellites, which are part of a worldwide network of meteorological satellites, have nearly a full hemisphere of continuous view (fig. 34.1). NESDIS maintains operational satellites at 75° and 135° west longitudes. One or more older satellites, located about midway between these two operational sites, are used if one of the primary satellites fails. These in-orbit spares can be turned on and moved to the operational location to provide continuity of coverage.

Each of the satellites is equipped to relay data transmissions from networks of data-collection platforms to one or more receiving sites. The onboard instrumentation that performs the relay function is a satellite transponder, which is a combination radio receiver and transmitter that receives data and instantaneously retransmits it back to Earth with no change except for frequency. Each of the two NESDIS satellites can relay environmental data from as many as several thousand individual data-gathering devices located at virtually any point in the Western Hemisphere. Likewise, the large beam width of the satellite transmitter antenna permits reception of the signal from the satellites over the same wide area.

In addition to the spacecraft itself, a satellite data-collection system is made up of four major parts: (1) sensors; (2) data-collection platforms; (3) Earth receiving stations; and (4) a data processing and storage system (fig. 34.2). Because NESDIS operates a central Earth Receiving Station, the user need only

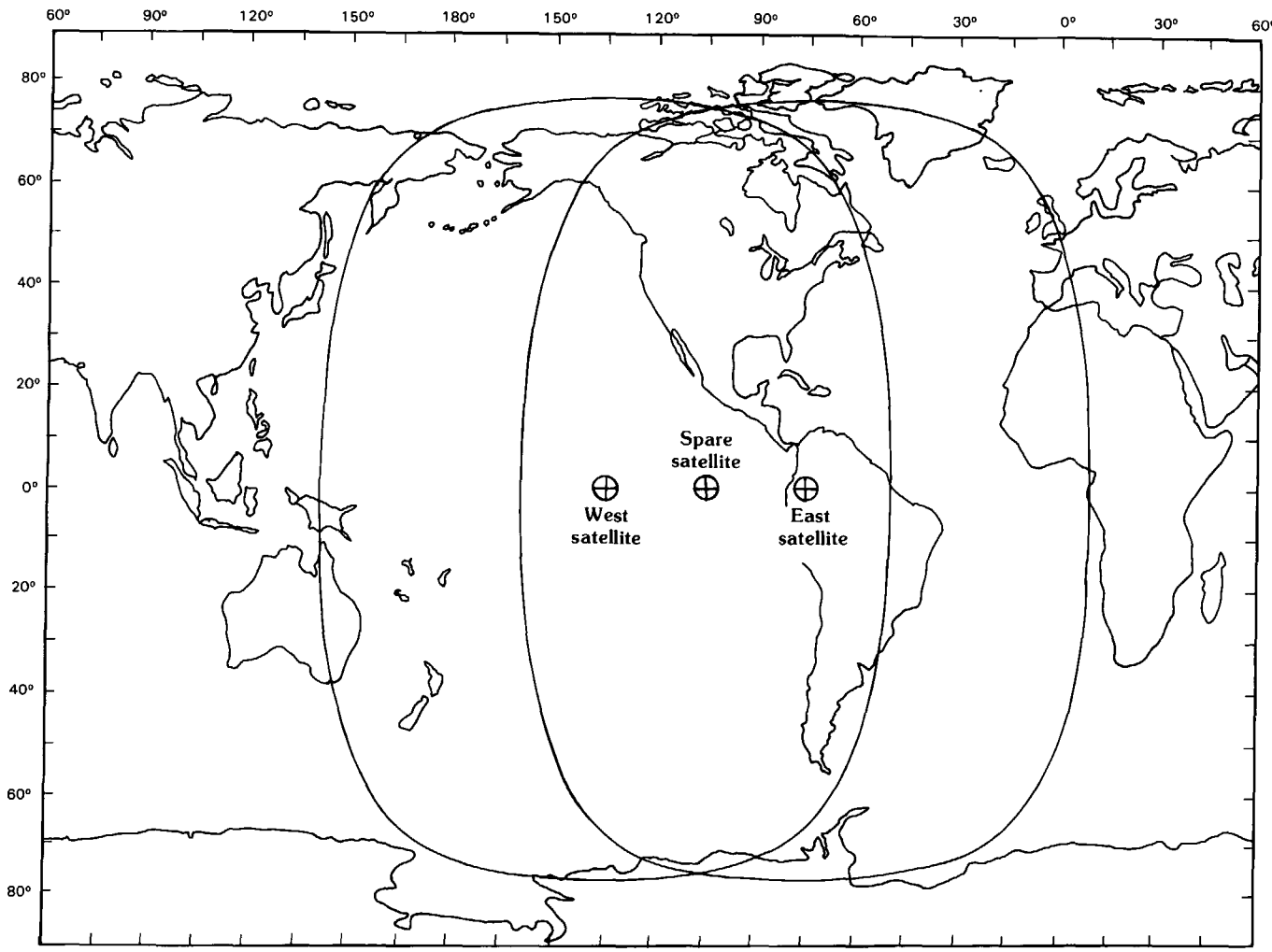

FIGURE 34.1.—Areal coverage of the Earth's surface by geostationary satellites located at long 75° and 135° W. (from National Oceanic and Atmospheric Administration, 1983, fig. 1–2, p. 4).

supply the remaining three parts. In a minimum network configuration (1–20 monitoring sites), the user provides only the sensors, data-collection platforms, and some sort of data processing and storage system. As the number of monitoring sites increases, it may be beneficial to acquire a direct-readout ground receiving station.

The GOES system is particularly suited to monitoring slowly varying parameters. In a volcanic region, parameters of interest may include tilt, magnetic field strength, self-potential, gas emissions, fumarole temperatures, and meteorological data. In some instances, it is possible to transmit higher frequency data through the system if some onsite preprocessing is done. For example, seismicity, in the form of earthquake counts, can easily be accommodated. This might have particular application to remote volcanoes where recording the number of earthquakes may be more pertinent to assessing the level of activity than recording the actual waveforms. GOES data-collection platforms (DCP's) typically require sensors with analog voltage outputs in the range 0–5 V, although other output ranges and certain sensing devices with digital outputs can often be accommodated.

GOES DCP's are small, battery-powered, 402-megahertz radio transmitters that transmit data to the satellite at a rate of 100 bits per second (National Oceanic and Atmospheric Administration, 1984). Higher data rates are possible though not currently used. The major components of a DCP are the sensor interface, programmable microprocessor, memory, radio, clock, and antenna. Many GOES DCP's operate in the self-timed mode, which requires the platform periodically to transmit its data under the command of a precise timer. In this self-timed mode, the platform, under control of the timer and microprocessor, scans its sensor interface. A typical DCP sensor interface can accommodate as many as 16 sensors. Data from each scan may be stored in the memory of the DCP until the prescribed transmission interval. Some DCP's are capable of performing preliminary data manipulation including data conversion, averaging, slope computation, and warning-level assessment, for emergency transmissions. Reliable, environmentally hardened DCP's are commercially available from a number of sources. A complete site installation, exclusive of sensors, can be performed in less than four hours.

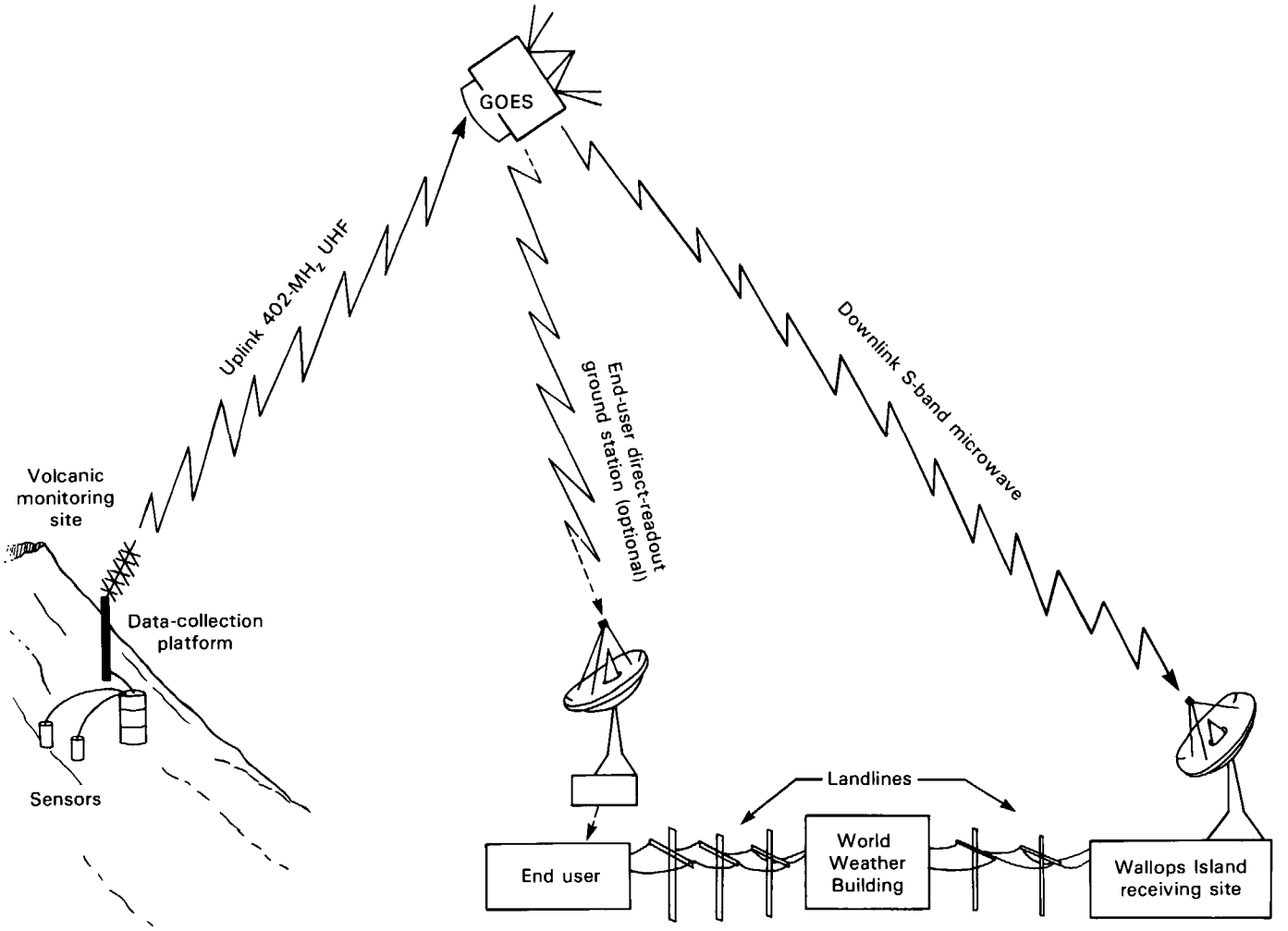

FIGURE 34.2.—Diagram of Geostationary Operational Environmental Satellite (GOES) data-flow path from remote site through satellite to end user.

Each satellite can support more than 250 radio channels, many of which are dedicated to self-timed platforms. The technique for defining the schedule of DCP reporting is called frequency-division multiple access with time-shared channel occupancy. A GOES platform typically uses a 1-min time interval every 3 h on its assigned radio channel for transmission of its data to the satellite. Sensor data can be collected as often as every 10 min and stored in memory until the prescribed transmission interval. Depending on the number of sensors and data points, transmission message lengths average about 30 s. In addition to self-timed transmission, two other modes of DCP transmission initiation are possible in the GOES system: (1) interrogation by the satellite, and (2) emergency transmission because of a predetermined sensor-threshold value being exceeded. The latter capability can be useful in providing warnings of imminent floods or mudflows.

NESDIS operates only one Earth receiving site, located at Wallops Island, Va., for the GOES satellite data-collection system. This receiving site performs a number of functions including command and control of the spacecraft, reception of data, and monitoring of signal quality. From the Wallops Island location, NESDIS forwards data from the satellites to a computer in the World Weather Building at Camp Springs, Md. From there, the data are distributed to users via the telephone system using either dedicated circuits or dial-in lines. Many users of the GOES system, in an effort to reduce system complexity and dependence on land lines, are establishing their own local direct-readout ground station terminals. These terminals are becoming less expensive and can provide a user with immediate access to the data transmitted from the satellite.

Because NESDIS does not store data in its computer for longer than a few days, it is necessary for the user to transfer the data regularly to his own computer system for processing and storage. Collecting data from one sensor at 10-min intervals produces more than 52,000 data points in a year. A network of several DCP's, each with several sensors, can thus produce a large data base. In addition, since the data are in numerical form, a mechanism for converting the data to graphical form for viewing is a must. Frequent visual inspection of the recorded data for significant sensor variations is necessary to take full advantage of the nearly real-time

nature of satellite-relayed telemetry. An optimum computer system for end users of the GOES system would include screen and hard-copy graphics capability and several megabytes of online data-storage capacity.

EXAMPLE OF A WIDE-AREA NETWORK FOR MONITORING VOLCANOES

The current U.S. Geological Survey network of volcanic-gas monitoring stations at several widely scattered volcanoes is an excellent example of a wide-area network using satellite telemetry. In the summer of 1981, satellite-relayed hydrogen-gas monitoring stations were installed at Mount Baker and Mount St. Helens, Wash., and Lassen Peak, Calif. Similar monitoring stations were installed in 1982, at Long Valley Caldera, Calif., and Kilauea, Hawaii, and in 1983 at Mauna Loa, Hawaii, and Coso Hot Springs, Calif. Until mid-1984, data from all of these stations were scrutinized and recorded at the U.S. Geological Survey National Center in Reston, Va. (more than 4,000 km from the nearest monitoring site). In June 1984, the responsibility for collecting data from these stations was transferred to the Cascades Volcano Observatory in Vancouver, Wash. This change of recording facility was completed without the necessity for a single visit to any field site and clearly demonstrates the extreme flexibility of a satellite-relayed telemetry system.

Although some of the field sites in the gas network are located near existing ground-based telemetry systems, many of the monitoring locations are in remote areas where there is no possibility of linking into a ground-based telemetry system or telephone line. That any data can be collected at all from these sites in nearly real-time fashion is a tremendous accomplishment. Clearly, the wide-area gas monitoring network owes its existence to the availability of satellite telemetry.

CASE STUDY—EVIDENCE FOR A WIDESPREAD GAS EVENT AT KILAUEA VOLCANO, DECEMBER 1982

Hydrogen gas sensors were strategically deployed in or near fumaroles at the Kilauea summit caldera ('71 Fissure and Halemaumau West), along the east rift zone (Mauna Ulu and Puu Kiai), and on the southwest rift zone (Kau Desert) in the late 1970's with conventional ground-based telemetry used at each site to transmit the data to the Hawaiian Volcano Observatory for recording (McGee, 1979). In mid-December 1982, a GOES satellite data-collection platform was interfaced with the receivers of the land-based telemetry system to produce an integrated telemetry system. Previous data acquisition involved the mailing of strip-chart recordings to a distant laboratory for analysis (months later). This marriage of ground-based and satellite telemetry allowed a wide area of Kilauea to be monitored using a single central DCP for data relay to the satellite.

On December 23, 1982, a degassing event was recorded at both Kilauea summit stations and at Mauna Ulu in the upper east rift zone (fig. 34.3). Although the distance between the summit monitoring sites and the Mauna Ulu site is about 8 km, the onset time and duration (2 days) of the gas event are essentially concurrent at the three locations. In addition, hydrogen sensors with on-site recording at two nearby locations, Puhimau and a different fumarole at Mauna Ulu, recorded similar peaks. On December 26, a distinct gas event that had rapid onset and lasted only a few hours was recorded at Puu Kiai. This event is noteworthy because it is the only hydrogen gas event ever recorded at that location. Puu Kiai is located about 13 km down the east rift zone from Mauna Ulu.

Other independent evidence also points to a widespread gas release during this time period. Friedman and Reimer (chapter 33, part I) report a distinct helium anomaly at Sulfur Bank in late December 1982. In addition, a substantial radon peak was observed near the western rim of Kilauea's caldera at about the same time (Donald Thomas, oral commun., 1984). It is likely that this widespread gas release was a precursory manifestation of the intrusion of a large body of magma into the Kilauea summit area. Subsequent injection of this magma into the east rift zone resulted, on January 3, 1983, in the first of a long series of east-rift eruptions.

The crucial point to note here is that the degassing event, as detected in satellite-relayed data from the hydrogen-monitoring stations, was identified and recorded 9,000 km away almost instantly, leaving ample opportunity for telephone notification of personnel near the site of the event before the onset of eruptive activity. This episode illustrates the utility of using satellite telemetry for monitoring pertinent parameters of potentially active volcanoes from long distances.

CONCLUSIONS

The potential for utilizing geostationary satellites for monitoring remote and widely scattered volcanoes has not yet been fully realized. The techniques recently developed are directly applicable to many areas of the world where real-time data on natural hazards are required. The availability of low-cost and reliable data-collection platforms and direct-readout ground stations can provide a data-telemetry system free from the usual communications infrastructure (Shope and Paulson, 1981). The United States, the European Space Agency, and the Japanese Meteorological Agency all currently operate geostationary satellites capable of data relay. There are few areas in the world where potential users could not gain access to a geostationary satellite. The example cited earlier clearly demonstrates that satellite telemetry is now a viable alternative to other types of data-collection systems for monitoring potentially active volcanoes.

REFERENCES CITED

McGee, K.A., 1979, An analog data telemetry system for remote monitoring applications, version II: U.S. Geological Survey Open-File Report No. 79–946, 11 p.

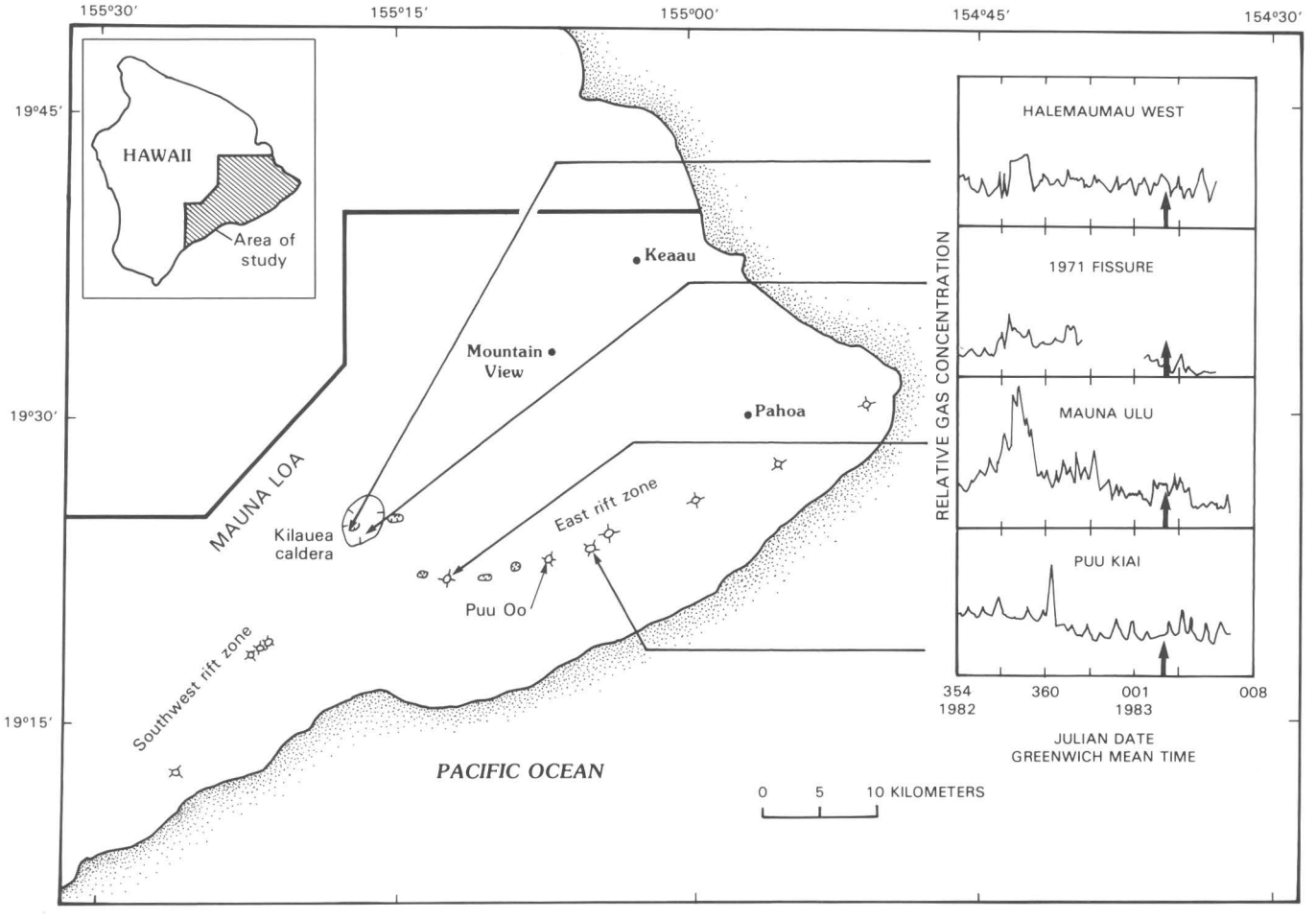

FIGURE 34.3.—Results from satellite-telemetered gas monitoring stations at Kilauea for late December 1982 to early January 1983. Occurrence of gas-emission event is essentially simultaneous at the two caldera stations and Mauna Ulu. Vertical arrow marks onset of eruptive activity at Puu Oo.

McGee, K.A. and Sato, Motoaki, 1982, The use of satellite telemetry for monitoring active volcanoes [abs.]: International Association of Volcanology and Chemistry of the Earth's Interior, Symposium on the Generation of Major Basalt Types, Reykjavik, Iceland, 1982, Proceedings, p. 109.

National Oceanic and Atmospheric Administration, 1983, The geostationary operational environmental satellite data collection system: Washington, D.C., National Oceanic and Atmospheric Administration Technical Memorandum National Environmental Satellite Data and Information System 2.

———1984, GOES data collection system and data processing system: Washington, D.C., National Environmental Satellite Data and Information System User Interface Manual, 132 p.

Shope, W.G., and Paulson, R.W., 1981, Data collection via satellite for water management: Transportation Engineering Journal, American Society of Civil Engineers, 107, no. TE4, p. 445–455.

HAWAIIAN VOLCANOES AND THE BIOGEOLOGY OF MERCURY

By Barbara Z. Siegel[1] *and* Sanford M. Siegel[1]

ABSTRACT

The global importance of volcanoes as a source of mercury appears to have been underestimated. The highly active Kilauea Volcano in Hawaii lies in the middle of one of the world's most productive forest ecosystems; hence it provides an ideal situation for the study of biological-geological-chemical interactions and interrelationships.

Mercury-rich emissions from Hawaiian volcanoes were discovered in 1971. Since then, the local sources of mercury in Hawaii, its chemical species, accompanying gases, release during lava weathering, dispersal, and vertical distribution have been studied. Parallel investigations have been made of bioaccumulation, biotransformation, and biovolatilization of mercury.

The most significant results during the period covered in this report, 1970–84, are:

1. Mercury emission data have been obtained from the Mauna Loa and Kilauea summit calderas, the Kilauea east rift and nearby fumaroles.

2. A provocative drop in mercury output was observed during the recent (1983–84) Puu Oo eruption compared to the 1977 Kalalua event.

3. The first measurements of mercury over a vertical range (rift level to 2,500-m elevation) were made during the 1977 Kalalua eruption.

4. The relation between Hg^0 and HgX_2 have been studied with respect to site, time, and distance, and a specific Hg-CO_2 correlation has been derived.

5. The regulatory role of vegetation in mercury distribution as a sink and secondary source through facile conversion of the ion to Hg^0 and its continuous release has been established.

6. It has been found that seedlings have a 300-fold greater sensitivity to Hg^0 than mature plants, which respond by premature senescence.

INTRODUCTION

Mercury is produced by Hawaii's active volcanoes, Kilauea and Mauna Loa, and by many other volcanoes the world over, including Hekla, Erebus, and St. Helens, irrespective of their chemical description (basaltic or andesitic) or location (midplate or plate margin). In spite of the element's global scarcity, mercury appears to be a ubiquitous constituent of volcanic gases, lavas, and pyroclastic deposits.

Recent flux measurements indicate that the amount of mercury attributable to volcanic activity has been underestimated in the past. Output figures from Mount St. Helens and several Central American volcanoes are remarkably similar to those reported from Halemaumau, the main vent of Kilauea, which produces approximately 270 tons annually (Varekamp and Buseck, 1981; Siegel and Siegel, 1984a). If, in fact, 200–300 tons of mercury were released annually by each of the 50–60 terrestrial volcanoes considered active (1975–80 annual average from Simkin and others, 1981), then the volcanic contribution to the global total would equal or exceed the commonly cited value of 10×10^9–20×10^9 g/yr for all mercury transfer to the atmosphere (U.S. National Academy of Sciences, 1977; Andren and Nriagu, 1979).

In 1970 we identified Kilauea as the major source of mercury in air over Oahu, 320 km away. Our work since that time has attempted to develop a comprehensive picture of the primary and secondary sources of the mercury, its sites of temporary storage, transfer modes, and sinks.

The cool upland forest in and around Hawaii Volcanoes National Park on the Island of Hawaii is one of the most productive ecosystems on this planet. Few volcanoes are situated in environments so heavily covered with vegetation as is Kilauea. Since the biosphere exerts a remarkable degree of control over the chemistry of the air, water, and soil, the location of Kilauea on Hawaii offers an exceptional opportunity to examine the transformation and distribution of volcanic mercury in a geobotanical and biogeochemical framework. On the other hand, few volcanoes are situated in locations so barren that their activity can be studied and their behavior interpreted without reference to geobiology; Mount Erebus in Antarctica may be one of those few (Siegel and others, 1980b) and therefore allow for interesting comparisons.

We have worked more than 15 years on this problem in Hawaii and elsewhere; much information has also been contributed by many others. Nevertheless, a great deal still remains unknown about the cycling of mercury on Earth, and this paper is only a progress report.

ACKNOWLEDGMENTS

Our research was made possible by the generous research funds, travel support, and facilities provided by many organizations and institutions. We thank the National Aeronautics and Space Administration; National Geographic Society; National Science Foundation, Division of Polar Programs; National Institutes of Health, Division of Research Resources; Department of Energy,

[1]University of Hawaii, Honolulu, Hawaii.

Lawrence-Livermore Laboratory (Institutional Grants Program); North Atlantic Treaty Organization; the Cottrell Foundation; the Environmental Center, the Hawaii Natural Energy Institute, and the Office of Research Administration of the University of Hawaii at Manoa; the University of British Columbia; and the British Columbia Science Council.

Thanks are also due Professor Gudmunder Sigvaldasson, Nordic Institute of Volcanology, University of Iceland; Professors Neil Towers and Harry Warren, Department of Botany and Geology, respectively, University of British Columbia; Gordon Eaton and Robert Decker, past Scientists-in-Charge, Hawaii Volcano Observatory (HVO), U.S. Geological Survey; and to Hawaii Volcanoes National Park Superintendents Bryan Harry, Robert Barbee, and David Ames.

Individuals who have generously shared data or field time include Paul Greenland, Thomas Casadevall, John P. Lockwood, Reginald Okamura, and many other members of the HVO staff, and also Thomas Speitel and Gary McMurtry, University of Hawaii at Manoa; Alan Eshleman, Berkeley, CA; Conrad Bachmann, University of Heidelberg; David Penny, Massey University, and Pauline Penny, Ministry of Works, New Zealand.

Finally, we dedicate this paper to the late Gordon A. Macdonald, Professor of Geology and Geophysics, University of Hawaii at Manoa, and the late Irving Breger, United States Geological Survey, who actively encouraged us in the exciting interdisciplinary maze that is biogeochemistry.

MINERALOGY, GEOCHEMISTRY, AND CHEMISTRY

For a more comprehensive review of mercury's physical parameters, the reader is referred to several excellent texts (King, 1951; Goldschmidt, 1954; Rankama and Sahama, 1950; Hem, 1970; Aylett, 1973).

The mineralogy of mercury is comparatively simple. Cinnabar is the only common mineral; it can be primary or found as an alteration product of more complicated base-metal sulfides containing mercury. Native mercury is frequently an oxidation product of cinnabar. The other known mercury minerals are curiosities; among them the oxysalts are indicators of arid climatic conditions. Traces of mercury may occur in some minerals, including tetrahedrite and tennantite (they are then called schwazite and hermesite), penroseite, argyrodite, clausthalite, altaite, and sphalerite.

Mercury has a high ionization potential (I.P.) and tends strongly to remain in the elemental state. Its first I.P. is 10.39 eV (gold's is 9.20 eV and silver 7.53 eV), and its second I.P. is 18.65 eV.

Mercury has a uniquely low melting point (-39 °C) and high vapor pressure (1.9×10^{-3} mmHg at 25 °C), indicative of its very low interatomic forces. Its viscosity, similar to that of water, is also low.

Mercury vapor is almost all monatomic, even at room temperature; apart from the noble gases, mercury is the only element to show this behavior at such low temperatures. Viscosity measurements suggest that the closest interatomic approach in the vapor phase is about 3.25 A at 850 K, little greater than in the liquid state. Both absorption and emission spectra of mercury vapor yield data that indicate the presence of a very small proportion of weakly bonded Hg_2 molecules.

The solubility (6×10^{-6} g/100 g water at 25 °C) of Hg^0 in air-free water is exceptional, being much higher than that of most other metals. Addition of air increases the solubility 700 times, up to a value almost identical with the solubility of HgO in water. Mercury is also appreciably soluble in n-hexane (2.7×10^{-7} g/100 g at 40 °C), benzene (2.0×10^{-7} g/100 g at 20 °C), methanol (3.6×10^{-7} g/100 g at 63 °C) and dioxane (7.0×10^{-7} g/100 g at 25 °C).

Oxygen and dry air do not react with mercury appreciably at room temperature, but the reaction may be greatly promoted by ultraviolet radiation. Ozone rapidly attacks mercury at room temperature to give Hg^{2+}.

All the halogens react directly with mercury at room temperature: mercurous halides seem to be formed first, followed by mercuric halides if halogen is in excess.

Air-free water below about 200 °C does not react chemically with mercury. Other elements that react directly with mercury, especially on heating, include sulphur, selenium, and tellurium; on the other hand, nitrogen, phosphorus, arsenic, carbon, silicon, and germanium do not seem to combine with it. Dry halides such as HX(X = F,Cl), H_2S, NH_3, PH_3, and AsH_3 do not react with mercury below about 200 °C. Some reaction with HBr, HI, and H_2Se occurs even at room temperature. Various nonmetallic halides react readily with mercury. Among oxides, SO_2, SO_3, N_2O, CO, and CO_2 are without effect at room temperature, but NO_2 reacts very rapidly to give mixtures of mercury (I) nitrite and nitrate as initial products.

Dilute hydrochloric and sulphuric acids do not react with mercury, but moderately concentrated solutions ($>6N$) attack it superficially to give a little mercurous salt. Concentrated hot H_2SO_4 dissolves mercury to yield Hg_2SO_4, $HgSO_4$, and SO_2, and nitric acid gives a range of products depending on conditions that include $Hg_2(NO_2)_2$, $Hg(NO_2)$, $Hg(NO_3)_2$, NO, and NO_3. Phosphoric acid does not react appreciably.

Mercury is not attacked by alkali, but ammonia solutions in air rapidly lead to the production of Millon's base, Hg_2NOH.

Under natural conditions of temperature and pressure that occur in river and lake water and water-saturated sediment, mercury can be present in one or more of its three different oxidation states. The most reduced, in a chemical sense, of these forms is the metal, which has a distinct tendency to vaporize because it is a liquid at ordinary temperatures. The other two forms are ionic: where the average valence of mercury is $+1$, the more reduced of the two ions is the mercurous ion Hg_2^{2+}; in oxidizing conditions, especially at low pH, the stable form is the mercuric ion, Hg^{2+} (Hem, 1970).

Although chemical oxidation reactions do not require the presence of oxygen, it is the most common oxidizing agent. Systems in contact with air tend to be oxidized, and in its absence reducing conditions readily become established. In moderately oxidizing conditions of pH above 5 the predominant mercury species in

solution is undissociated mercury. Its solubility, constant over the whole range of temperature where the liquid metal is stable, is fairly low (25 ppb), and the mercury exists as Hg^0. This solubility value represents the likely upper equilibrium limit of mercury in low-chloride surface streams and lakes.

Mildly reducing conditions, which are likely to occur in many lake and streambed sediments, can cause the mercury to be precipitated as cinnabar, which has an extremely low solubility. In the field at neutral pH, $Hg(HS)_2^0$ aq and HgS_2^{2-} have an equilibrium solubility lower than 0.002 ppb. Very strongly reducing conditions, however, may increase the solubility somewhat by converting the mercuric ion to free metal.

In solutions high in chloride the solubility of mercury in oxygenated water may be greatly increased by the formation of the uncharged $HgCl_2$ complex, or anionic complexes such as $HgCl_4^{2-}$ (Wagman, 1969).

The frequent departure of natural systems from equilibrium is well known and must be kept in mind when using equilibrium calculations. There are two aspects of mercury chemistry that are particularly important sources of departure from what is predicted theoretically. One of these is the formation of organic complexes and participation of mercury in biochemical processes, especially in the production of methyl mercury by sedimentary bacteria (Jensen and Jernelov, 1969). A secondary property of importance is the tendency for mercury to participate in dismutation reactions—that is, in reactions of the type $Hg_2^{2+} \rightleftharpoons Hg^0 + Hg^{+2}$ that provide a means whereby mercury can be first converted to the liquid form and then escape as vapor.

Although there is some understanding of the aqueous chemistry of mercury, a considerable amount of basic research is still needed, especially on rates and mechanisms of reaction and on the behavior of organic mercury complexes.

TOXICOLOGY

The onset of symptoms from mercury poisoning in humans is insidious, and the symptoms, with the exception of tremor, may often be ignored or attributed to other causes (Bidstrup, 1964). This is especially true of a peculiar emotional instability called erethism, which is defined by irritability, irrational outbursts of temper, excitability, shyness, and sometimes depression; such symptoms are often just attributed to an anxiety state.

The classic signs of poisoning by mercury in the inorganic form are gingivitis and stomatitis accompanied by excessive salivation or a metallic taste, burning, swelling and ashy discoloration of the mouth followed by intense thirst and abdominal pain; erethism; and tremor (Goldwater, 1951). Vomiting may occur, and in some cases circulatory collapse with a fatal outcome appears suddenly and at an early stage. Delayed effects on the kidneys or large intestine are generally the cause of death (Sollman, 1957). There is no clear difference between the acute, subacute, and chronic forms except that the symptoms develop more quickly and are of greater intensity, and generally the oral and gastrointestinal symptoms are more obvious in acute and subacute poisoning (Bidstrup, 1964). Mercuric chloride especially is irritating to the skin and mucous membranes, causing irritation, vesication, and corrosion. Absorption through the skin and mucous membranes may cause systemic poisoning.

Acrodynia (so-called pink disease) occurs in infants and young children; it is characterized by mental disturbances, insomnia, sweating, disordered sensation of the extremities, and peripheral vascular phenomena and is often fatal. Strong evidence exists that the absorption of mercury is the most important cause of this disease, although there is confusing etiology (Warkany and Hubbard, 1953).

When cinnabar, HgS, has been used for the red color in tattooing, mercury dermatitis has been reported, and occasionally an eczematous rash has spread to involve the entire body.

Acute poisoning from metallic mercury or its vapor rarely occurs now and is usually the result of an accidental exposure (Matthes and others, 1958), but historically it was a common occurrence among men exposed to mercury in certain occupations. Hunter (1955, p. 256) quotes from Ramazzini concerning miners and goldsmiths:

> It is from mercury mines that there issues the most cruel bane of all that deals death and destruction to miners.
>
> * * * * *
>
> We all know what terrible maladies are contracted from mercury by goldsmiths, especially those employed in gilding silver and copper objects. Hence craftsmen of this sort very soon become subject to vertigo, asthma and paralysis. Very few of them reach old age, and even when they die young their health is so terribly undermined that they pray for death.

and also mirror makers:

> you may see these workmen gazing with reluctance and scowling at the reflection of their own sufferings in their mirrors and cursing the trade they have adopted.

Acute and subacute poisoning among persons engaged in the mining and refining of mercury have been reported, but improvements in ventilation of mines, refinery processes, and the use of personal protective measures have reduced the numbers and severity of poisoning. Vouk and others (1950), reporting on environmental conditions in the Idria (Yugoslavia) mercury mines, stated that there were 93 cases in 1949 and 53 reported in the first half of 1950. In Idria mercury occurs both as cinnabar and in the free form, and the mining of Hg^0 is particularly hazardous.

Concentrations of mercury in the air in pits where cinnabar, alone or with free mercury, is mined are 50–59 $\mu g/m^3$. Dizon and others (1960) investigated a mercury mine in the Philippines, where it is a relatively new industry and the processes are highly mechanized. The highest atmospheric concentrations reported were 100–400 $\mu g/m^3$ in the vicinity of the ore crushers, and 6 of the 11 men employed at the crushers had symptoms of mercury poisoning. In Peru, Carlin and others (1960) reported that 16 out of 18 refinery workers were found to have high mercury excretion in the urine (average 224 $\mu g/L$), and 13 had definite evidence of mercury poisoning.

More general problems of animal toxicity have been discussed in detail in the compilations of Buhler (1973) and Nriagu (1979). Included are behavioral effects, cell and organ degeneration, and developmental abnormalities in birds, terrestrial vertebrates, and aquatic marine forms from mammals to fish.

In spite of the obvious role of plants in primary life support, the effect of mercury on vegetation has received little more than token attention until recently. From the first account of mercury intoxication of plants (Deiman and others, 1797), the only reports up to 1930 were those of Boussingault (1867a,b), Harrington (1917), and Le Van (1930). Zimmermann and Crocker (1933, 1934) and Ratsek (1933) revived the experimental study of mercury toxicity in conjunction with seed and greenhouse problems, but they did not recognize major developmental features of mercury toxicity and its dependency on the chemical species used.

Typically, plant-cell damage takes place with aqueous solutions containing as little as 10 μg/L of Hg ion (Siegel, 1977).

In contrast, when 18 species and varieties of seeds were germinated in air containing 14 μg/L of Hg^0 vapor (Siegel and Siegel, 1979a; Siegel and others, 1984a), root growth was stimulated in 4 species, inhibited by 25 percent or less in 6, and did not exceed 50 percent inhibition in the 8 remaining species. Shoot growth was even less adversely affected; only 4 species were inhibited by more than 25 percent.

Of castor bean seedlings 20 days old in air containing 0.05 μg/L of Hg^0, only 14 percent lost their leaves, and none showed zones of discoloration or morbidity after seven days. Coleus seedlings of the same age were even less affected. However, mature plants of both species after seven days in air containing 0.05 μg/L of Hg^0, lose 50–90 percent of their leaves. In terms of toxic thresholds, mature plants are approximately 300 times more sensitive to mercury than seedlings.

At the concentration of 0.05 μg/L $HgCl_2$ vapor has essentially no toxic effect on seedlings or mature plants.

The principal toxic effect of Hg^0 seems to be an acceleration of the aging process mediated by induction of the plant stress hormone ethylene (Siegel and others, 1973b; Goren and Siegel, 1976).

MERCURY IN HAWAII

DISCOVERY

Mercury in Hawaii was first found in stream sediments on the Island of Oahu and later in the air (Siegel and others, 1973b). To determine the source of this mercury, widespread monitoring, sampling, and analyses were carried out. Air mercury levels on Oahu were found to be highest in the southeastern part of the island and lowest at sites facing the northeast tradewinds; this indicated that the primary source was the thermally active Island of Hawaii (Eshleman and others, 1971). The verification of volcanic-fumarolic mercury sources in 1970–71 led in turn to a program of study that has continued to the present. The main focus has been the active volcanic areas of Hawaii, but the studies have also included Iceland, Alaska, New Zealand, and Antarctica.

The sources of mercury on Oahu, with its long-dormant (or extinct) volcanoes Kaala and Waianae (Macdonald and Abbott, 1970), have provided us with opportunities for research involving residual mercury, mercury transport, and biological compartments. These subjects will be discussed later.

PRIMARY SOURCES AND SPECIATION

There are two active centers of gas emission on the Island of Hawaii—the volcanoes Kilauea and Mauna Loa. Kilauea and the thermal features of the east rift zone have been studied extensively; the Mauna Loa summit caldera, Mokuaweoweo, has also been sampled, but emissions during flank eruption have only been measured for mercury during March 1984. The most commonly studied sites on Kilauea have been Halemaumau (the main vent) and the Sulphur Bank fumaroles, first sampled in 1970 (Siegel and Siegel, 1980, 1984a).

In our ongoing studies, air samples have been regularly collected in nitric acid/pyrex-fiberglass impingers at flow rates of 1–2 L/min for periods of 4–7 h, thus assuring a gas volume of at least 240 L (0.24 m^3). Samples have been analyzed by flameless atomic absorption (Eshleman and others, 1971; Siegel and Siegel, 1978, 1979; Siegel and others, 1985). Parallel sampling was also carried out by drawing air through gold-foil traps, which were subsequently stripped of mercury in nitric acid. Millipore filters were used to trap particles with diameters larger than 0.22 μm. The nitric acid traps collect total mercury; the gold foil collects Hg^0 only and millipore filters insoluble HgS (cinnabar). Cinnabar was verified by solubility in aqua regia and insolubility in cold nitric acid. Any difference observed between total mercury and particulate mercury plus Hg^0 is considered to be HgX_2, presumably a mixed halide (Cadle, 1975), but mainly the chloride.

Another approach to air sampling is fallout measurement or deposition (Siegel and Siegel, 1977). Here copper foil, which reduces Hg^{2+}, and gold foil, which amalgamates Hg^0, are used to distinguish the mercury species.

We assume that copper foil collects both Hg^0 and Hg^{2+}, hence the amount of mercury trapped on gold foil subtracted from the amount of mercury on copper foil yields a value for Hg^{2+}. This calculation is valid only if the HgS particulate fraction is negligible.

The average total mercury concentration in the open air 2 m above the ground (at right angles to the slope) at Sulphur Bank ranged from 2,700 to 40,600 ng/m^3 through 1977, but in subsequent years exceeded 1,000 ng/m^3 only during January–February 1982, at the start of the current Puu Oo eruption series (fig. 35.1; table 35.1). The Halemaumau vent of Kilauea (fig. 35.1, table 35.2) has also been highly productive, behaving similarly to Sulphur Bank in eruptive and quiescent periods. Overall, it would appear that the normal value for mercury in air in the Kilauea summit area ranges from 400 to 1,000 ng/m^3. Similar values are seen along the approach to Kilauea caldera from the northeast (as seen in the 500- to 1,000-m transects along the volcano highway; fig. 35.2). For the period 1971–78, the average mercury value in the immediate vicinity of the caldera lies between 400 and 1,400 ng/m^3, but it falls off dramatically to the northeast into the tradewinds.

Air samples taken at Royal Gardens during the Kalalua rift eruption of 1977 show the mercury level rising suddenly from a putative baseline (June–July) of about 300 ng/m^3 to 200,000 ng/m^3 (200 μg/m^3) or more by September 15, then dropping precipitously after the fountaining and tremor ended in October (Siegel and Siegel, 1978).

TABLE 35.1.—*Mercury concentration in air at the Sulphur Bank fumaroles Kilauea Volcano, 1971–1980*

[s.d., standard deviation; part., particulates]

Year	Number of samples	Total mercury (ng/m^3) (± s.d.)	Mercury species (percent)		
			Hg^0	Hg (part.)	HgX_2
1971	26	28,400±11,000	69	1	30
1972	27	3,700± 520	24	13	63
1973	10	4,900± 640	62	2	36
1974	9	4,500± 660	71	<1	29
1975	17	2,700± 390	44	<1	56
1976	24	8,600± 1,200	32	<1	68
1977	38	40,600± 4,680	28	<1	72
1978	26	500± 70	10	5	85
1979	29	880± 95	60	1	39
1980	29	500± 85	59	<1	41
	241 (total)	9,528± 1,464 (avg)	45.9 (avg)	2.2 (avg)	51.9 (avg)

In all the measurements of mercury concentration in air, there appears a consistent downward trend by as much as 95 percent after about 1978. This trend downward may even apply to Mauna Loa mercury output, although the sample data are limited.

It is clear from the record, however, that Kilauea's mercury output since 1977 has not approached that of the Kalalua rift emissions, in spite of the far greater output of fluids and gases since January 1983. This leads to the provocative question of whether the mercury output of Hawaiian volcanoes is really declining. If so, is this phenomenon a long-term downtrend or merely the downward limb of a cyclical process? Either alternative poses interesting challenges for interpretation.

With few exceptions, particulate mercury has not been found in samples of the air around Kilauea, even during periods of eruptive activity (table 35.1). The 10-year average of particulate mercury is 2.2 percent of the total, but commonly less than 1 percent of the total mercury was found on the filters.

The wide variation in Hg^0 and HgX_2 content of air samples was unexpected—Hg^0 ranged from 10–71 percent of the total at Sulphur Bank (Siegel and Siegel, 1979b). This was also seen in fallout data from the same location (Siegel and Siegel, 1977):

Date	Hg^0 (ng/m^3)	HgX_2 (ng/m^3)	Hg^0/HgX_2
1972 January	80±9	377±44	0.21
April	300±31	1,220±369	.25
1975 May	250±31	540±60	.46
December	438±48	42±7	10.43
1976 May	575±66	250±27	2.30
June	119±22	612±12	.20

On the other hand, concurrent fallout samples taken on Oahu, about 400 km northwest of Kilauea, always yielded far less total mercury (about 10 percent of that detected near Kilauea) and mostly as Hg^0. At Halemaumau, Hg^0 accounted for 15–21 percent of the total mercury released, but on the floor of Kilauea, at the very active

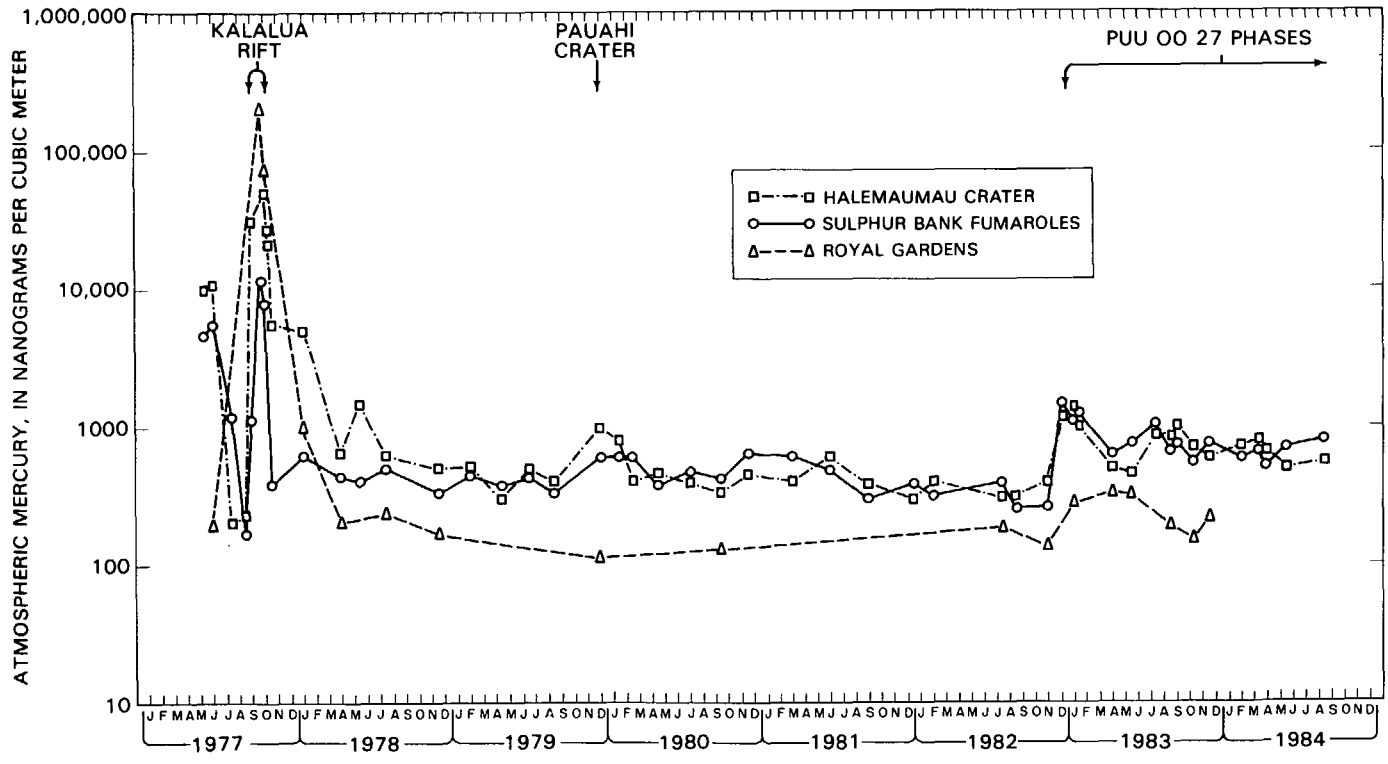

FIGURE 35.1.—Mercury emission record for Kilauea at Halemaumau main vent, the nearby Sulphur Bank fumaroles,and south of east rift at Royal Gardens, 1977–1984. Three events noted: major Kalalua rift eruption lasting nearly one month; one-day Pauahi Crater eruption of 1979; and exceptionally prolonged rift eruption at Puu Oo, beginning January 1983, through its 27th episode. Note that the ordinate scale is logarithmic.

TABLE 35.2.—*Measurements of mercury in air at various locations on Kilauea and Mauna Loa Volcanoes*

[See also Conners, 1979]

Site	Sampling period	Total mercury (ng/m^3)	Hg^0 (percent)
Kilauea Volcano			
Halemaumau	1971 August	40,500	16
	1977 August	48,100	21
	1978 August	1,400	15
Caldera floor			
1971 fissure	1978 August	79,900	1
	1981 August	3,600	2
1974 fissure	1978 August	29,800	2
	1981 August	1,900	5
Kalalua rift	1977 August	1,200	22
	1977 September	>200,000	50
	1977 October	18,500	58
	1977 November	500	80
Puhimau thermal area	1978 January	5,800	72
	1978 August	12,200	49
	1981 January	930	56
Mauna Loa Volcano			
Mokuaweoweo caldera	1978 July	24,600	35
Upper rift	1984 March	4,850	—

1971 and 1974 fissure the Hg^0 fraction fell to only 1–5 percent of the total emitted. During the 1977 eruption, the Hg^0 fraction rose from its minimum of 22 percent to a peak at 80 percent after the active phase ended.

Mercury is, of course, a minor constituent of volcanic and fumarolic gas emissions, wet or dry. It is accompanied by H_2S, SO_2, and CO_2 (Siegel and Siegel, 1979b, 1980). An exception is the Puhimau thermal dieback area, where sulfur in any form has only been detected in the parts per billion range (Phelps and others, 1979). This area formed in 1938–9 after an earthquake and magma shifting brought heat near the surface, causing several acres of forest to die; the ground temperature 5 cm below the surface here averages 97 °C.

At Halemaumau, measurements during 1971–78 gave mole ratios of 590 for H_2S, 6,300 for SO_2, and 2.10×10^6 for CO_2 (table 35.3). Obviously, sulfur-mercury relations are highly varied, even within a single volcanic system, and are highly site dependent. It is, therefore, of special interest to note that the ratio CO_2/Hg is nearly constant at Kilauea; individual measurements do differ somewhat, however, and data from other locations such as Mount St. Helens are distinctly different.

Lava flows constitute another source of mercury. Weathering brings about the slow release of soluble or solubilized constituents as the igneous materials degrade into soil minerals. Lava samples were analyzed by digestion of 100-mesh powder with 0.1*N* HCl to remove soluble and loosely bound mercury. This was followed by hot 2*N* HNO_3 digestion to remove any mercury complex with organic ligands, and then concentrated HF to destroy the silicate matrix

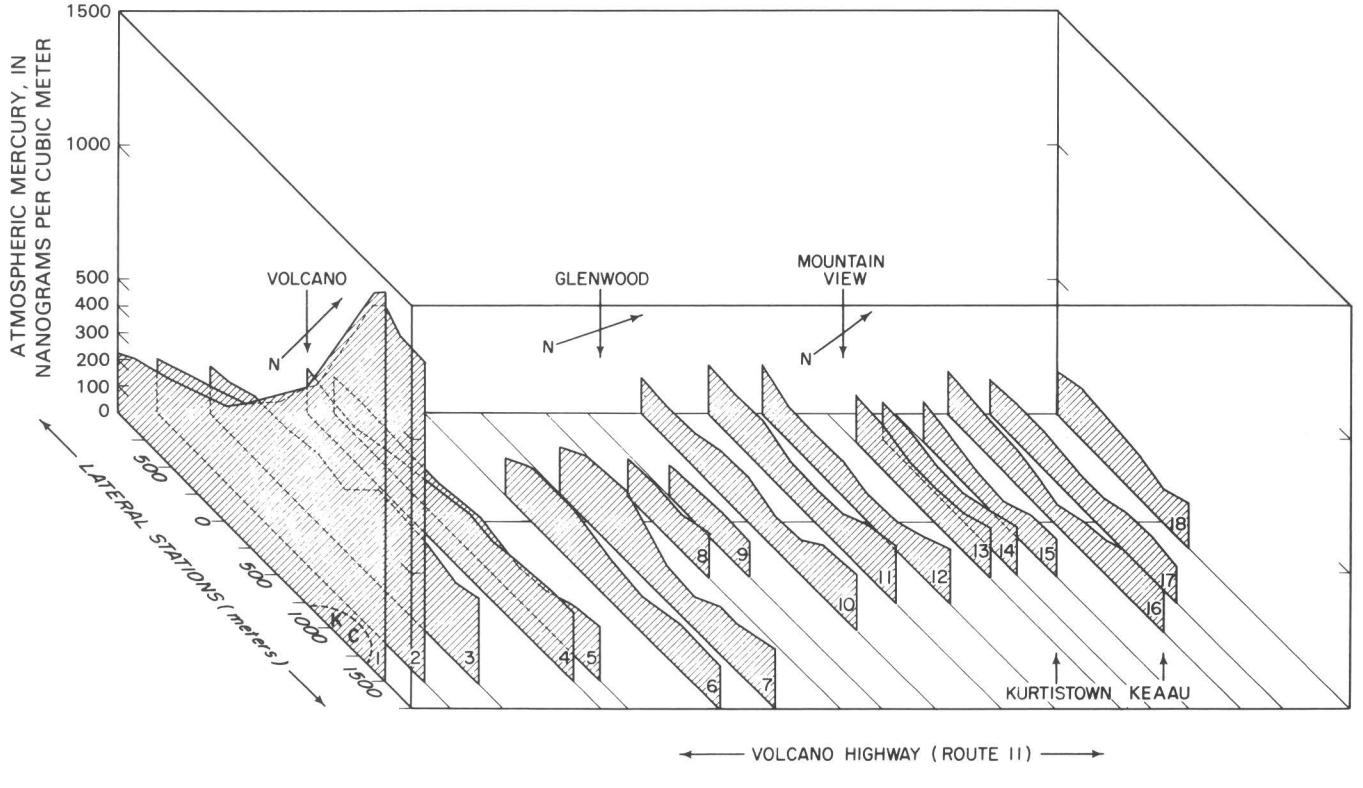

FIGURE 35.2.—Average atmospheric mercury concentration along volcano highway from Kilauea caldera (KC) northeast to the Village of Keaau. North is indicated at three villages. Highway is plotted as straight line perpendicular to transects 1–18.

TABLE 35.3.—*Relations between mercury and other gaseous omissions at thermal sites*

[s.d., standard deviation; n.d., not determined]

Thermal site	Number of samples	Sampling date	Flux (tons/yr)	Plume (μmol/m^3)	Mole ratios		
					H_2S/Hg	SO_2/Hg	$(CO_2/Hg)10^{-6}$
Kilauea Volcano							
Halemaumau	86	1971–80	260	0.054±0.014	590	6,300	2.10
Sulphur Bank	18	1976–78	—	.012±0.083	3,700	3,050	2.75
1971 Fissure	8	1977–78	—	.396±0.055	0	239	2.75
1974 Fissure	8	1977–78	—	.146±0.016	0	96	2.19
Puhimau Thermal	10	1976–78	—	.026±0.005	0	0	3.66
Mount St. Helens	5	1980	365	.005±0.002	—	2,750	.013
Costa Rica							
Fumarole Poas		1980–82	52	—	—	1,030,000	—
Volcan Arenas		1980–82	32	—	—	5,000	—

(Siegel and others, 1975). Samples from flows of 1840, 1923, and 1955 were obtained with the assistance of the late Gordon Macdonald; fresh Pauahi samples were collected in 1979. The results (below) suggest a 50 percent release in about 50 years and a gradual infiltration of oxidizable, presumably humic, complexing substrates.

Year of flow	HG concentration μ/kg in lava		
	HCl soluble	HNO_3 soluble	HF digest
1840	5	81	45
1923	16	66	310
1955	10	59	970
1979	0	15	1,290

If Kilauea lava typically cools with about 1,000 μg/kg of mercury and proceeds to release 90 percent, then this still constitutes only a minor source of the element. The 1840 eruption produced about 400×10^6 m^3 of lava weighing perhaps 16×10^9 kg. Thus, this lava contained a total of 16×10^6 g (16 tons) of mercury, of which about 14 tons was released in about a century. In contrast, Halemaumau yields 260 tons annually when it is not erupting (Siegel and Siegel, 1984a).

Of course, the impact of a small though continuous and localized release of mercury cannot be discounted as a possible selection factor for mercury tolerance in the endemic vegetation of Hawaii. It is clear, as we show below, that plants in volcanic areas can become well adapted to life in mercuric environments. Also, Hg^0 slowly released by lava at ground level will, like any heavy gas, tend to accumulate in enclosed pockets and depressions and form areas of local concentration.

At the end of the weathering process, some mercury remains in the clays and derivative soils. In areas of heavy precipitation, such as the Sulphur Bank, acid red clays are common and contain no readily soluble mercury, but when they are heated in closed vessels, their mercury output can be collected on gold foil and measured.

The following data on mercury release from Sulphur Bank soil were obtained in this way:

T(°C)	Rate (ng/kg·h)
25	0.254
70	5.67
120	68.1

Using this kind of data and the Arrhenius equation, we have calculated an apparent heat of activation of 13.81 kcal/mole (Siegel and Siegel, 1983). This value compares well with the molar heat of vaporization calculated similarly from CRC Handbook vapor-pressure data. Thus atmospheric mercury released from soils directly may have been held entirely as Hg^0.

DISPERSAL

The northeast tradewinds with velocity of 20–40 km/h constitute a major and well-known determinant of climate in Hawaii. However, the assumption that these winds continually cleanse the atmosphere of pollutants, conveniently displacing them to the southwest, is not borne out by experience. During the 1977 eruption, with tradewinds normal, measurements were made on samples of air from 30 m above ground level at a station on Oahu about 400 km northwest of Kilauea. The mercury content rose from 40 ng/m^3 to 160 ng/m^3 in only 30 hours after the first fountaining at Kalalua (Siegel and Siegel, 1978). The mercury released along the rift and at Halemaumau traveled no less than 13 km/h in a direction about 90° to the tradewind vector. Increases in atmospheric turbidity 1–3 days after the onset of fountaining in a volcanic eruption have often been observed, not only in Honolulu, but also on the west side of the Island of Kauai.

The tradewind air masses move southwestward across the North Pacific and then encounter the high relief and rough terrain of the Island of Hawaii, where they become turbulent. Furthermore, the major sources of emission extend from the tradewind zone upward into air masses moving in other directions. During the final stages of the 1977 eruption, mercury in the air showed a rapid dropoff above the Kalalua rift to an asymptotic value of about 1,000 ng/m^3 at elevations of 1,200–2,500 m (fig. 35.3). Mercury at these higher elevations was over 90 percent Hg^0. This observation agrees with the fallout data discussed above that showed the proportion of Hg^0 in total mercury was higher on Oahu (sea level) than at the Sulphur Bank when samples collected at the same time were compared (Siegel and Siegel, 1977). The comparison of the Hg^0/HgX_2 ratio at the two locations is as follows:

	January 1972	May 1975	June 1976
Hawaii	0.212	0.463	0.195
Oahu	2.86	3.16	3.31

It must also be recalled that the Mauna Loa caldera continually fumes at an elevation of about 4,500 m, and numerous fissures are always injecting hot mercuriferous gas into an often turbulent atmosphere. The gas column is subject in its dispersal to a variety of wind vectors, including some that carry the mercury northward and downward as it cools. These may account largely for the distribution of mercury on Oahu (fig. 35.4; see also, Siegel and Siegel, 1980), where higher values occur to the south and west. The same is true of the Island of Kauai. Residual thermal activity on Maui, however, tends to obscure the direct impact that the Island of Hawaii's volcanic activity may have on its mercury distribution, and anomalies are often related to anthropogenic pollution.

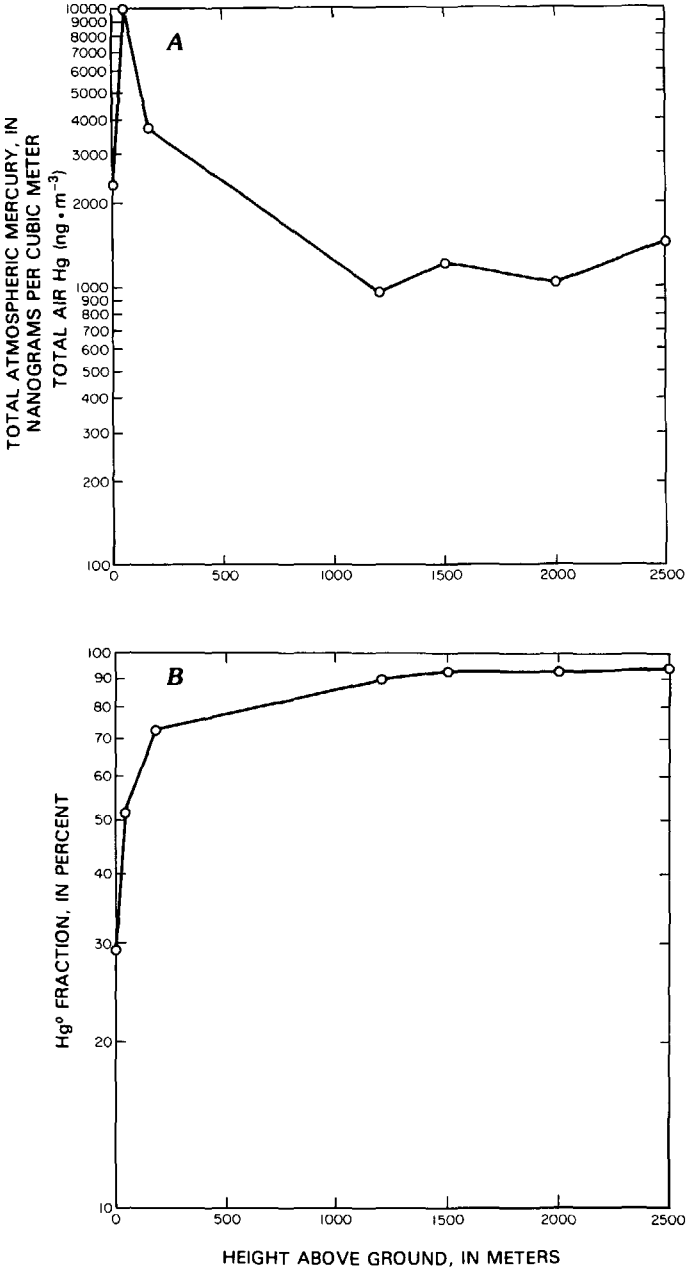

FIGURE 35.3.—Vertical distribution of atmospheric mercury over the Kalalau fissures during the 1977 eruption. Data obtained using dual-trap method: nitric-acid impinger and gold foil. ***A***, Concentration from ground level to height of 2,500 m. ***B***, Percentage of Hg^0 in total mercury.

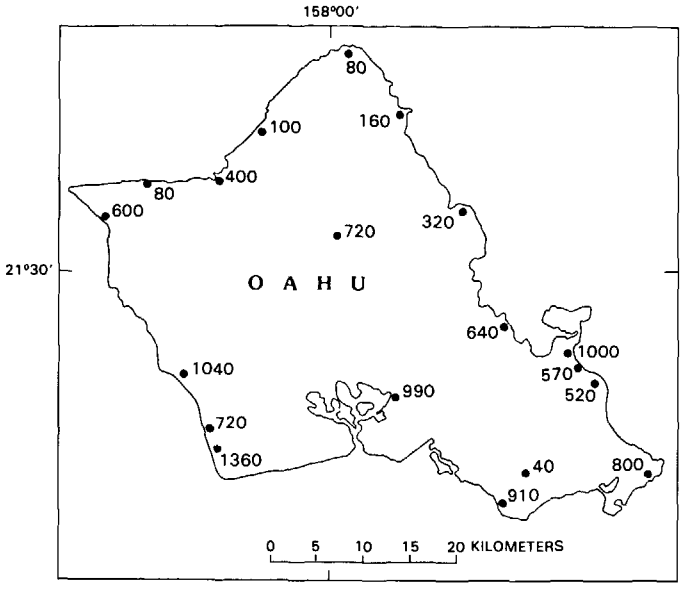

FIGURE 35.4.—Distribution of atmospheric mercury (in ng/m³) around Oahu at 2 m above ground. Figures are means of samples taken 1971–78.

GEOBOTANY AND BIOGEOCHEMISTRY

One factor relating to dispersal of mercury in Hawaii remains to be considered, however, and that is the role of vegetation in its cycling and dispersal. For example, toward the back of the Palolo Valley (Honolulu) the old, weathered soils contain little mercury, only 15×3 μg/kg (Siegel and others, 1975), yet the two grass species growing in that soil (*Digitaria and Andropogon*) contain much more (68 ± 8 and 79 ± 11 μg/kg, respectively). When these grasses die, their decaying residues retain most of the mercury (56 ± 6 μg/kg), which is then taken in by soil invertebrates, the earthworm *Lumbricus* (388 ± 21 μg/kg) and the millipedes *Trigonialis* (467 ± 21) and *Oxydus* (382 ± 12). In this simple example, the earthworm to soil mercury ratio is about 31.

All of the aquatic plants that we have encountered accumulate mercury (Siegel and others, 1973b, 1975, 1984b, 1985; Siegel and Siegel, 1982, 1984b), usually with sizeable enrichment (table 35.4). The same is true for marine animals including fish, but not limited to vertebrates. High ratios are in part a consequence of the low mercury concentrations found in natural (nonindustrial) waters. Near black sand (basaltic) beaches in Hawaii, the highest mercury levels yet found reach 2–3 μg/L.

Many terrestrial plants also accumulate mercury, but nearly 300 samples from four widely separated areas (table 35.5) show a clear bimodality in the concentration ratio. Overall, 55–77 percent

TABLE 35.4.—*Mercury accumulation in marine organisms*

Sample	Content in organism (μg/kg)	Concentration ratio (organism/water)
Algae		
Hawaii		
Ulva	40–200	25–145
Padina	140–185	65–88
Sargassum	26–46	12–23
Iceland		
Ulva	106	1,060
Mastigocladus	380	3,800
Antarctica		
Ulva	1.5–3.1	8–16
Fish		
Hawaii		
Marlin	>500	>250
Tuna	220–1,370	110–685
Iceland		
Tuna	287	2,870
Antarctica		
Cod	36	200

TABLE 35.5.—*Distribution of mercury concentration ratios in vascular plants at various localities*

[Figures in percent of species; number of species sampled given beneath each locality name; after Siegel and others, 1975]

Mercury concentration ratio (plant/soil)	Iceland (79)	Hawaii (105)	New England (38)	Alaska (66)
<0.1	13	14	32	30
.1 –0.67	10	22	10	0
.67–1.33	0	8	0	5
1.33–2.0	14	4	18	10
>2	63	54	40	55

of all the plants studied contained at least 1.33 times as much mercury as the soil around their roots, but 23–42 percent of the plants from the four locations contained less mercury than the soil in which they were growing.

Although it may seem reasonable to hypothesize a mechanism whereby plants exclude mercury, there are too many essential nutrient cations similar in charge and size to Hg^{2+}, among them, Ca^{2+} and Fe^{2+}, that could not be biologically distinguished. It is difficult to construct an energetically and structurally sound model that can include Hg^{2+} with virtually absolute selectivity. An alternate mechanism, however, was suggested when we found that mercury concentrations in air at Sulphur Bank were not determined by inorganic processes alone. Thus, an Arrhenius plot based on air samples taken at one meter over the vegetation on the flats, about 100 m from the fumaroles, shows that there are two slopes (fig. 35.5), implying two limiting processes or mechanisms. The higher temperature process (>20 °C) has a slope parallel to the vapor-pressure line, but at lower temperatures mercury in air is limited by a process other than evaporation, possibly biological in nature.

This surmise has been verified experimentally in more than 50 species of plants (Kama and Siegel, 1980; Siegel and others, 1980a; Siegel and Siegel, 1983). Examples of terrestrial Hg^0 producers include leaves of pineapple, sugar cane, ferns, mosses, lichens, and mushrooms (table 35.6).

This process that may be called biovolatilization is not unique to land species; the unicellular green alga *Chlorella* has been shown to possess a photosynthetic reduction system that generates Hg^0 vapor (Ben-Bassat and Meyer, 1975, 1977).

TABLE 35.6.—*Rates of elemental mercury release from various vascular plants*

[Uncertainty figures are one standard deviation; after Kama and Siegel, 1980; Siegel and others, 1980; Siegel and Siegel, 1983]

Vascular plant	Rate (ng/kg·m)	Plant	Rate (ng/kg·m)
Aloe	850±50	Lichens	
Pineapple	820±30	*Usnea*	660±190
Coconut	240±90	*Cladonia*	120±30
Nutgrass	340±45	*Stereocaulon*	840±91
Staghorn fern	730±45	Mosses	
Hibiscus	490±45	*Leucobryum*	50±215
Leucanea	3,050±300	*Bryum*	400±50
Pandanus	1,590±390	*Polytrichum*	400±160
Avocado	4,130±220	Fungi	
Mangrove	100±40	*Polyporus*	1,200±105
Sugarcane	650±40	*Fomes*	2,430±1200
Papyrus	700±49	*Trametes*	950±480

Most of these studies on release of Hg^0 from plants have emphasized Hawaiian species and the Hawaiian environment. However, the New Zealand manuka, *Leptospermum scoparium*, also appears to release mercury adaptively, keeping levels in tissue down and delaying or preventing toxic buildup (fig. 35.6). As soil

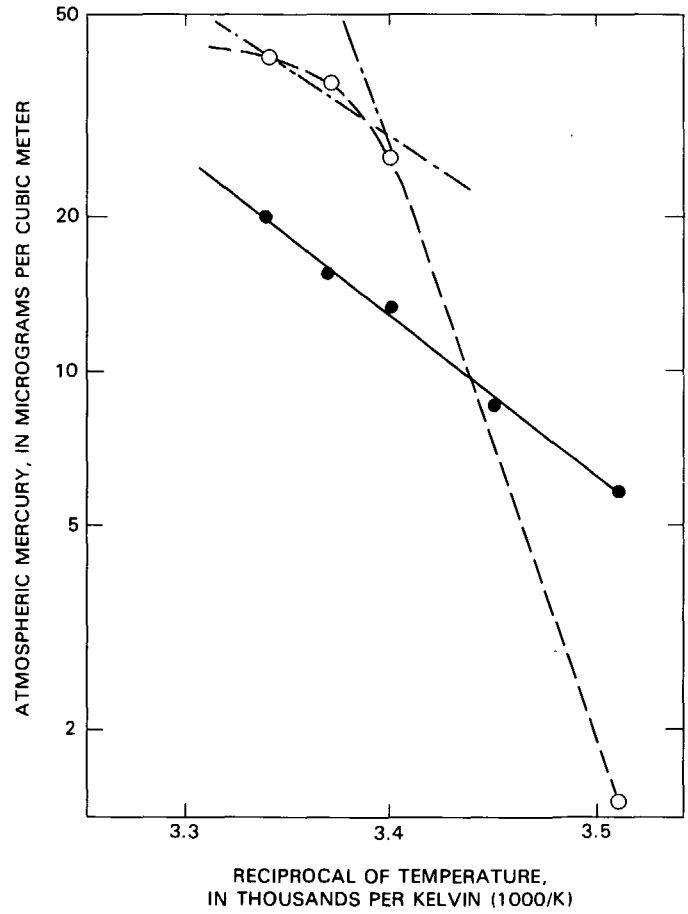

FIGURE 35.5.—Variation of atmospheric mercury concentration with air temperature over the vegetation near Sulphur Bank fumaroles. Data are presented as Arrhenius plot. Dashed curve, field data; dots and solid line, vapor pressure data. See text for discussion.

mercury rises approximately 30-fold from nonthermal Wellington to the Hell Gate thermal area, manuka shoots increase in mercury less than 5-fold. The detoxification mechanism, however, has increased the Hg^0 release rate by a factor of 9.

Presumably, Hg^{2+} is taken up from soil and ground water and translocated rapidly into the leaves, where reduction is followed by evaporative release. In a number of leguminous species growing in Hawaiian soils, it has been shown that mercury in seeds is selectively eliminated during the ripening process, thereby reducing the concentration below that at which cytological damage to the embryo may take place (Ramel, 1969; Siegel and Siegel, 1985).

Re-emission of Hg^0 may be followed by its direct uptake by nearby plants with or without toxic consequences according to species and concentration (Siegel and others, 1973a; Siegel and Siegel, 1979a). Accordingly, mercury as Hg^{2+} or its complexes may be taken up from soil or ground water and converted to Hg^0 for subsequent release and, perhaps, re-uptake.

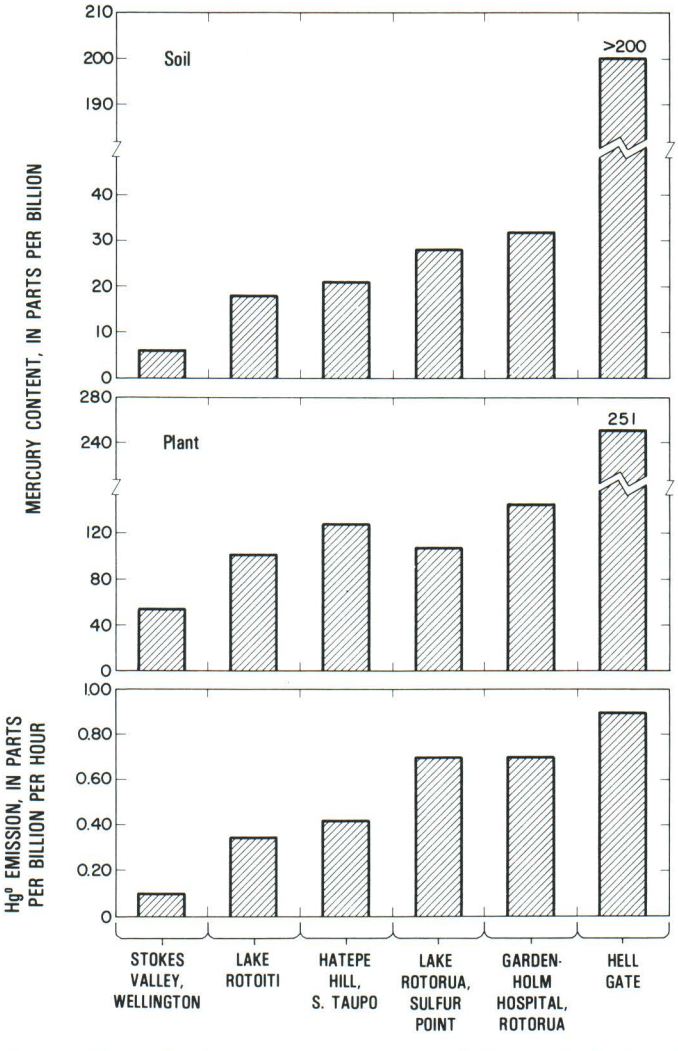

FIGURE 35.6.—Relation between mercury content of New Zealand soils and plants and rates of Hg^0 emission by *Leptospermum scoparium*.

Such recycling processes in local areas may well lead to diffuse patterns of mercury distribution. This has been noted in the lower Puna district, the eastern portion of the Island of Hawaii, site of the Kilauea east rift zone. Mercury levels in the leaves of the native forest tree ohia, *Metrosideros collina* var. *polymorpha*, follow approximately the mercury levels along the east rift zone, as does the mercury content of the soil in which the trees grow (figs. 35.7, 35.8). In contrast, the distribution of mercury in air (fig. 35.9) shows far more sharply defined areas of concentration than the mercury content of either plant or soil. This seems to imply the direct degassing process along the rift zone proceeds substantially faster than the release from soils and plants.

Biological release of Hg^0 is obviously a regulated process and it differs mechanistically from simple vaporization. Our data show that simple vaporization does occur in the soil; however, soil does not begin to release mercury until a concentration of about 25 μg/kg (ppb) is attained (fig. 35.10). It is, in any case, clear that the impact of the ecosystem on mercury cycling is as great as the impact of natural mercury emission on vegetation and the ecosystem, though they are of a different character.

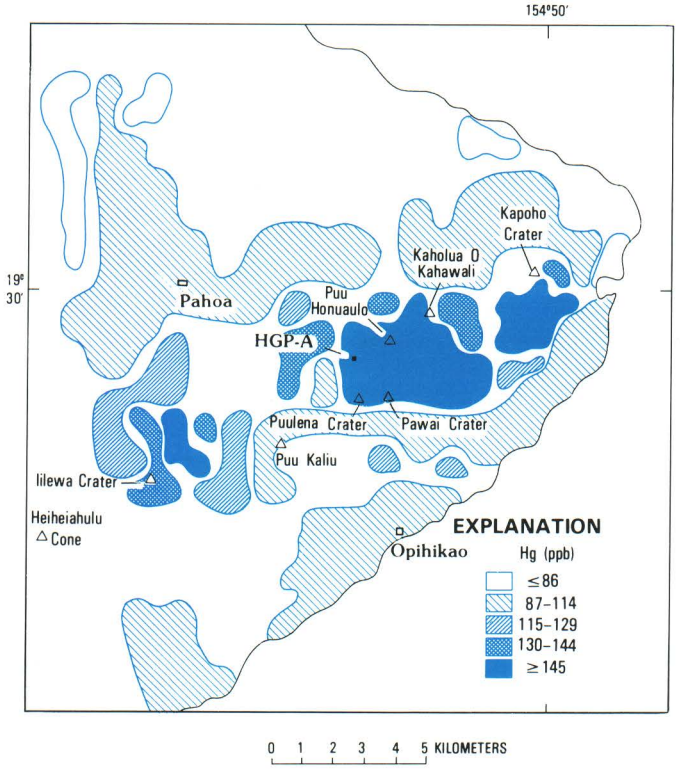

FIGURE 35.7.—Mercury content of ohia leaves (*Metrosideros*) East Puna District, Hawaii. Sampled areas delimited by closed lines; other areas not sampled because of poor access or other limitations. Samples collected between 1975 and 1982, excluding periods of heavy rains, strong winds, and volcanic eruptions. Midrange values of 87–114 ppb represent one standard error on either side of the mean for entire Puna collection.

REFERENCES CITED

Andren, W., and Nriagu, J., 1979, Global mercury, *in* Biochemistry of mercury in the environment: Amsterdam, Elsevier, p. 173–130.

Aylett, B.J., 1973, The chemistry of zinc, cadmium and mercury: New York, Pergamon Press, volume 18.

Ben-Bassat, D., and Mayer, A., 1975, Volatilization of mercury by algae: Physiologia Plantarum, v. 38, p. 128–132.

———1977, Reduction of mercury chloride by Chlorella: Physiologia Plantarum, v. 40, p. 157–162.

Bidstrup, P.L., 1964, Toxicity of mercury and its compounds: Amsterdam, Elsevier.

Boussingault, M., 1867a, Sur l'action deletere que la vapeur emanant du mercure exerce sur les plantes (premiere partie): Paris, Academie des Sciences Compte Rendu, v. 64, p. 924–928

———1867b, Sur l'action deletere que la vapeur emanant du mercure exerce sur les plantes (deuxieme partie): Paris, Academie des Sciences Compte Rendu, v. 64, p. 983–989.

Buhler, D.R. ed., 1973, Mercury in the western environment: Continuing Education Publication, Corvallis Oregon, Proceedings of a Workshop, Portland Oregon, February 25–26, 1971.

Cadle, R.D., 1975, Volcanic emissions of halides and sulfur compounds to the troposphere and stratosphere: Journal of Geophysical Research, v. 80, p. 1650–1652.

Carlin, C.E., Corigliana, P.J., Gastanaga, C.A., and Ochoa, L.R., 1960, Occupational risk in a mercury plant: Salud Ocupationale, v. 5, p. 3 (Abstract Bulletin of Hygeine, 1961, v. 36, p. 440).

Connor, J.J., 1979, Geochemistry of Vegetation, Puhimau Thermal Area, Hawaii: Science of Total Environment, v. 12, p. 241–250

Deiman, Paats, Van-Troostwyck, and Lauwerenburgh, 1979, Experiences sur l'action du mercure sur la vie vegetale: Annales de Chimie, Paris, v. 21, p. 122–127.

Dizon, G.D., Anselmo, J.E., and Villanueva, J., 1960, Examination of the risk in mercury mine in the Philippines: Medicale Seguridad Trabido, v. 8, p. 29. (Abstract Bulletin of Hygeine, 1961, v. 36, p. 745).

Eshleman, A., Siegel, S.M., and Siegel, B.Z., 1971, Is mercury from Hawaiian volcanoes a natural source of pollution?: Nature, v. 233, p. 471–472.

Goldschmidt, V., 1954, Geochemistry: Oxford, Clarendon Press, p. 287.

Goldwater, L.J., 1951, The toxicology of inorganic mercury: New York Academy of Sciences Annals, v. 65, p. 498–503.

Goren, R., and Siegel, S.M., 1976, Mercury-induced ethylene formation and abscission in citrus and coleus explants: Plant Physiology, v. 57, p. 628–631.

Harrington, 1917, Further studies of the germination of Johnson grass seeds: Proceedings of the Association of the Official Seed Analysts of North America 1916–1917, p. 71–70

Hem, J.D., 1970, Chemical behavior of mercury in aqueous media, *in* Mercury in the Environment: U.S. Geological Survey Professional Paper 713, p. 19–24.

Hunter, D., 1955, The Disease of Occupations: London, English Universities Press, p. 256.

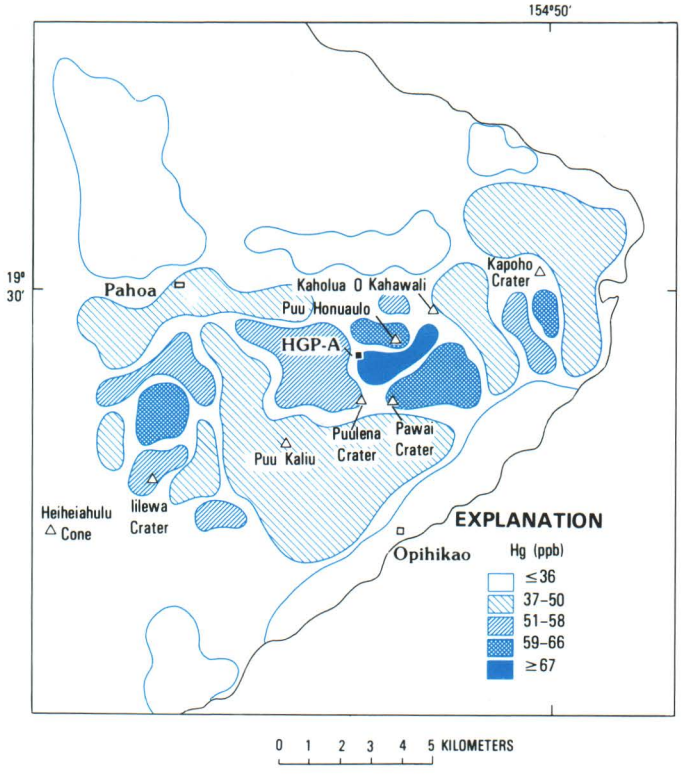

FIGURE 35.8.—Soil mercury content in East Puna District, Hawaii. Samples areas delimited by closed lines; other areas not sampled because of poor access or other limitations. Samples collected between 1975 and 1982, excluding periods of heavy rains, strong winds, and volcanic eruptions. Midrange values of 37–50 ppb represent one standard error on either side of the mean for entire Puna collection. Symbols same as in figure 35.7.

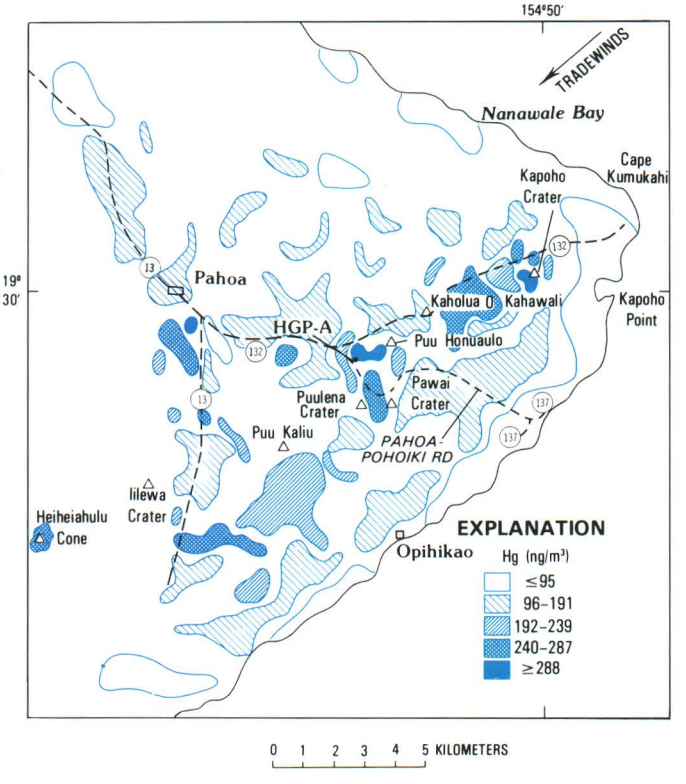

FIGURE 35.9.—Atmospheric mercury content in East Puna District, Hawaii. Sample areas delimited by closed lines; other areas not sampled because of poor access or other limitations. Midrange values of 96–191 ng/m³ represent one standard error on either side of the mean for entire East Puna collection. Samples collected between 1975 and 1982, excluding periods of heavy rains, strong winds, and volcanic eruptions. Triangles, volcanic cones and vents; squares and rectangles, villages; dashed lines, roads; numbers in circles identify highways; HGP–A, Hawaii Geothermal Project—Abbott.

Jensen, S., and Jernelov, A., 1969, Biological methylation of mercury in aquatic organisms: Nature, v. 223, p. 753–754.

Kama, W., and Siegel, S.M., 1980, Volatile mercury release from vascular plants: Organic Geochemistry, v. 2, p. 99–101.

King, C.V., 1951, Mercury: Its scientific history and its role in physical chemistry and electrochemistry: New York Academy of Sciences Annals, v. 65, p. 360–368.

Le Van, W.C., 1930, The effects of metals on the respiration of *Lupine albus*: American Journal of Botany, v. 17, p. 381–395.

Macdonald, G.A., and Abbott, A. T., 1970, Volcanoes in the Sea, The Geology of Hawaii: Honolulu, Hawaii, The University Press of Hawaii, 441 p.

Matthes, R.T., Kirschner, R., Yow, M.D., and Brenna, J.C., 1958, Acute poisoning associated with inhalation of mercury vapor: Pediatrics, v. 22, p. 675.

Nriagu, J., ed., 1979, Biogeochemistry of Mercury in the Environment: Amsterdam, Elsevier North-Holland Biomedical Press, 696 p.

Phelps, D., Siegel, B., Siegel, S., Buseck, P.R., Copp, J., Hinkle, M., and Casadevall, T., 1979, The distribution of Hg in the Puhimau Area, Hawaii Volcanoes National Park: [abs.] American Geophysical Society Meeting, San Francisco, Dec. 3–7, 1979.

Piotrowski, J.K., and Coleman, D.O., 1980, Environmental hazards of heavy metals: Summary evaluation of lead, cadmium and mercury: Global Environmental Monitoring System Programme Activity, London.

Ramel, C., 1969, Genetic effects of organic mercury compounds. I. Cytological investigations on *Allium* roots: Hereditas, v. 61, p. 208–230.

Rankama, K., and Sahama, T.G., 1950, Geochemistry: Chicago, University of Chicago Press, p. 334.

Ratsek, J.C., 1933, Injury to roses from mercuric chloride used in soil for pests: Floral Review, v. 72, p. 11–12.

Siegel, B.Z., Lasconia, M., Yaeger, E. and Siegel, S.M., 1984a, The phytotoxicity of mercury vapor: Water, Air and Soil Pollution, v. 23, p. 15–24.

Siegel, B.Z., and Siegel, S.M., 1978, The Hawaii geothermal project: An aerometric study of the Kalalua eruption of 1977: Environmental Science and Technology, v. 12, p. 1036–1039.

———1979a, Biological indicators of atmospheric mercury, *in* Nriagu, J., ed., The biochemistry of mercury in the environment: Amsterdam, Elesevier/North-Holland Biomedical Press, p. 131–159

———1979b, Mercury and other toxic emissions from Kilauea: Site and time patterns: Division of Environmental Chemistry, ACS/CSJ Chemical Congress, Honolulu, Hawaii, April 1979, Abstracts, part 1, No. 30.

———1982, Mercury content of *Equisetum* plants around Mount St. Helens one year after the major eruption: Science, v. 216, p. 292–293.

Siegel, B.Z., Siegel, S.M., and Horsky, S., 1984, *Equisetum* plants and the cycling of mercury at Mount St. Helens: Environmental Science and Technology, v. 18, p. 174–181.

Siegel, S.M., 1977, The cytotoxic response of *Nicotiana* protoplasts to metal ions: A survey of the chemical elements: Water, Air, and Soil Pollution, v. 8, p. 293–304.

Siegel, S.M., Eshleman, A., Umeno, I., Puerner, N., and Smith, C.W., 1973a, The general and comparative biology of toxic metals and their derivatives: Mercury and Lead: Mercury in the western environment: Oregon, Continuing Education Publishing Company.

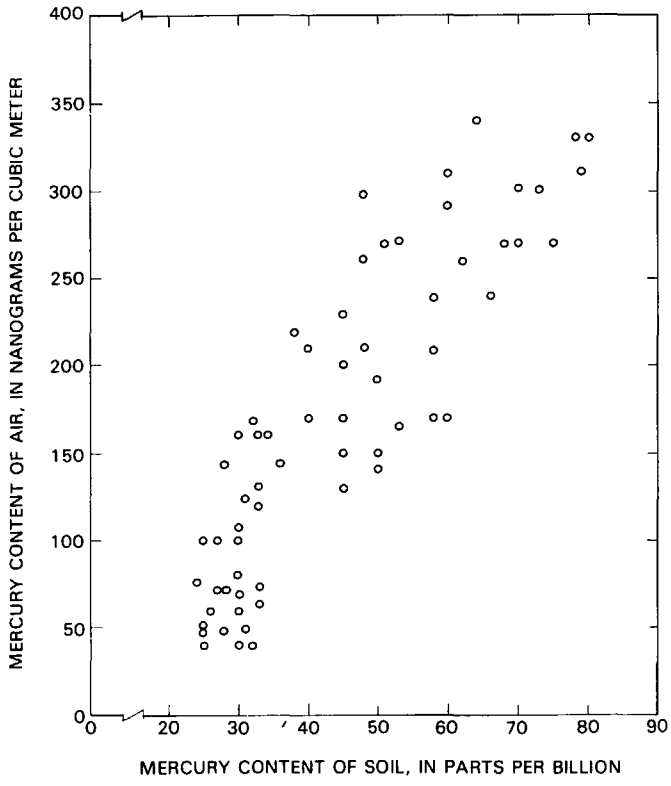

FIGURE 35.10.—Relation between atmospheric and soil mercury in East Puna District, Hawaii. Data represent replicated analyses of air and soil at same locations for 63 sample sites.

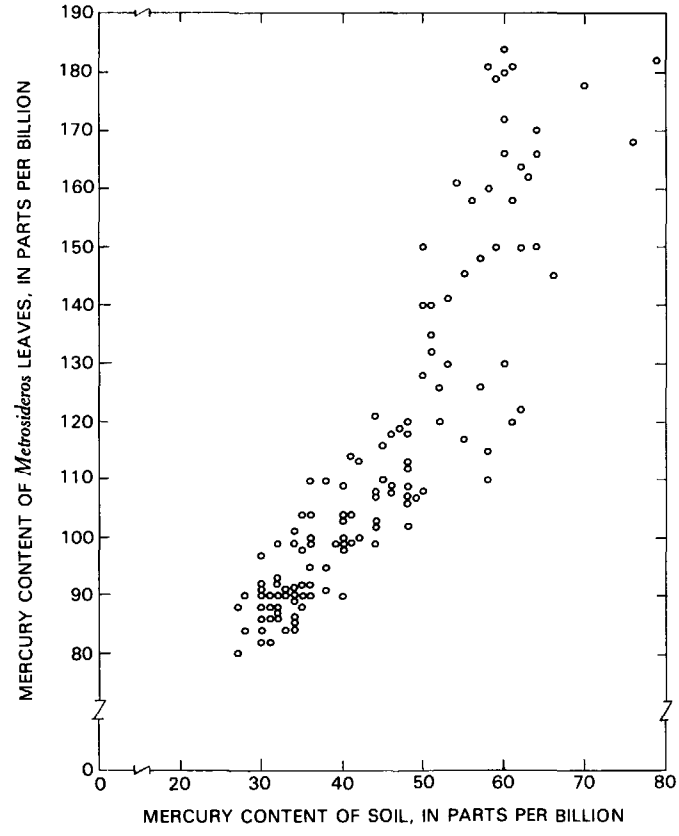

FIGURE 35.11.—Relation between mercury content of ohia leaves and soil in East Puna District, Hawaii. Data represent replicated analyses of leaves and soil at the same location for 121 sample sites.

Siegel, S.M., Okasako, J., Kaalakea, P., and Siegel, B.Z., 1980a, Release of volatile mercury from soils and non-vascular plants: Organic Geochemistry, v. 2, p. 139–140.

Siegel, S.M., and Siegel, B.Z., 1977, Mercury fallout in Hawaii: Water, Air, and Soil Pollution, v. 9, p. 113–118.

———1980, Hawaii Energy Resource Overview: Geothermal, Siegel, B., ed., The Environmental Impact, UCRL–1552. Vol. 4. National Technical Information Service (NTIS), DE830–12947. p. 7–14, 99–127, 138–146.

———1983, Vegetation and the atmospheric cycling of mercury: Advanced Space Research, v. 3, p. 135–139.

———1984a, First estimate of annual mercury flux at the Kilauea main vent: Nature, v. 309, no. 5964, p. 146–147.

———1984b, Regional differences in plant-soil mercury relations in *Equisetum*, *Plantago* and *Taraxacum*: Organic Geochemistry, v. 5, no. 4, p. 255–257.

———1985, Differential elimination of mercury during maturation of leguminous seeds: Phytochemistry, v. 24, p. 235–236.

Siegel, S.M., Siegel, B.Z., Eshleman, A.M., and Bachman, K., 1973b, Geothermal sources and distribution of mercury in Hawaii: Environmental Biology and Medicine, v. 2, p. 81–89.

Siegel, S.M., Siegel, B.Z., Lipp, C., Kruckeberg, A., Towers, G.H.N., and Warren, H., 1985, Indicator plant-soil mercury patterns in a mercury-rich mining area of British Columbia: Water, Air, and Soil Pollution, v. 27, p. 73–85.

Siegel, S.M., Siegel, B.Z., and McMurtry, G., 1980b, Atmosphere-soil mercury distribution: The biotic factor: Water, Air, and Soil Pollution, v. 13, p. 109–112.

Siegel, S.M., Siegel, B.Z., Puerner, N., and Speitel, T., 1975. Water and soil biotic relations in mercury distribution: Water, Air, and Soil Pollution, v. 4, p. 9–18.

Simkin, T., Siebert, L., McClelland, L., Bridge, D., Newhall, C., and Latter, J., Jr., 1981, Volcanoes of the World: Stroudsburg, Penn., Smithsonian Institute, Hutchinson Ross Publishing Co.

Sollman, T., 1957, Manual of Pharmacology 8th ed.: Philadelphia, Sauders, p. 1310.

United States National Academy of Sciences, 1977, An assessment of mercury in the environment: Washington, D.C.

Varekamp, J.C., and Buseck, P.R., 1981, Mercury emissions from Mount St. Helens during September 1980: Nature, v. 293, p. 555–556.

Vouk, V.B., Fugas, M., and Topolnik, Z., 1950, Environmental conditions in the mercury mine of Idria: British Journal of Industrial Medicine, v. 7, p. 168.

Wagman, D.C., Evans, W.H., Parker, V.B., Harlow, I., Bailey, S.M., and Schum, R.H., 1968, Selected values of chemical thermodynamic properties: National Bureau of Standards (US) Technical Note 270-3, p. 1–264.

Warkany, J., and Hubbard, D.M., 1953, Acrodynia and mercury: Journal of Pediatrics, v. 42, p. 365.

Zimmerman, P.W., and Crocker, W., 1933, The injurious effect of mercury vapor from biochloride of mercury in soil of rose houses: Florists Exchange, v. 81, p. 13

———1934, Plant injury caused by vapors of mercury and compounds of mercury: Contributions of the Boyce Thompson Institute, v. 6, p. 167–187.

Volcanism in Hawaii

Edited by Robert W. Decker, Thomas L. Wright, *and* Peter H. Stauffer

Volume 2

- Structure
- Dynamics
- History of Investigations of Hawaiian Volcanism

U.S. GEOLOGICAL SURVEY PROFESSIONAL PAPER 1350

UNITED STATES GOVERNMENT PRINTING OFFICE, WASHINGTON : 1987

DEPARTMENT OF THE INTERIOR

DONALD PAUL HODEL, *Secretary*

U.S. GEOLOGICAL SURVEY

Dallas L. Peck, *Director*

Library of Congress Cataloging-in-Publication Data

Volcanism in Hawaii.

(U.S. Geological Survey Professional Paper 1350)
Contents: v.1. Physiography, tectonics, and submarine geology; Geology of the Island of Hawaii; Petrogenesis and volcanic gases. v.2. Structure; Dynamics; History of investigations of Hawaiian volcanism.
Supt. of Docs. no.: I 19.16:1350
1. Volcanism—Hawaii. 2. Volcanic ash, tuff, etc.—Hawaii. I. Decker, Robert Wayne, 1927–. II. Wright, Thomas Llewellyn, 1935–. III. Stauffer, Peter Herman, 1935–. IV. Series: United States. Geological Survey. Professional Paper 1350.
QE524.V65 1987 551.2'2'09969 86–600292

**For sale by the Books and Open-File Reports Section,
U.S. Geological Survey, Federal Center, Box 25425, Denver, CO 80225**

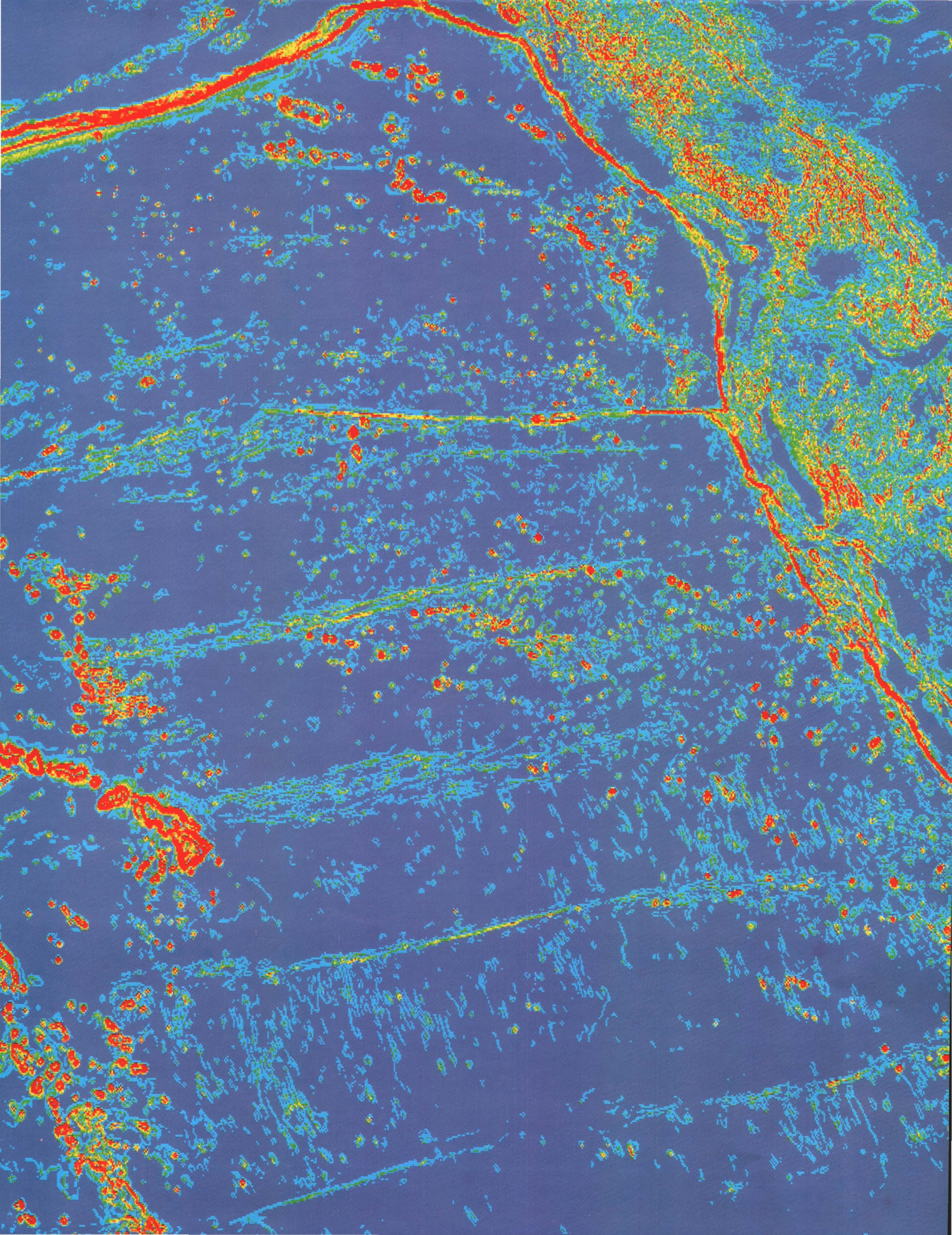

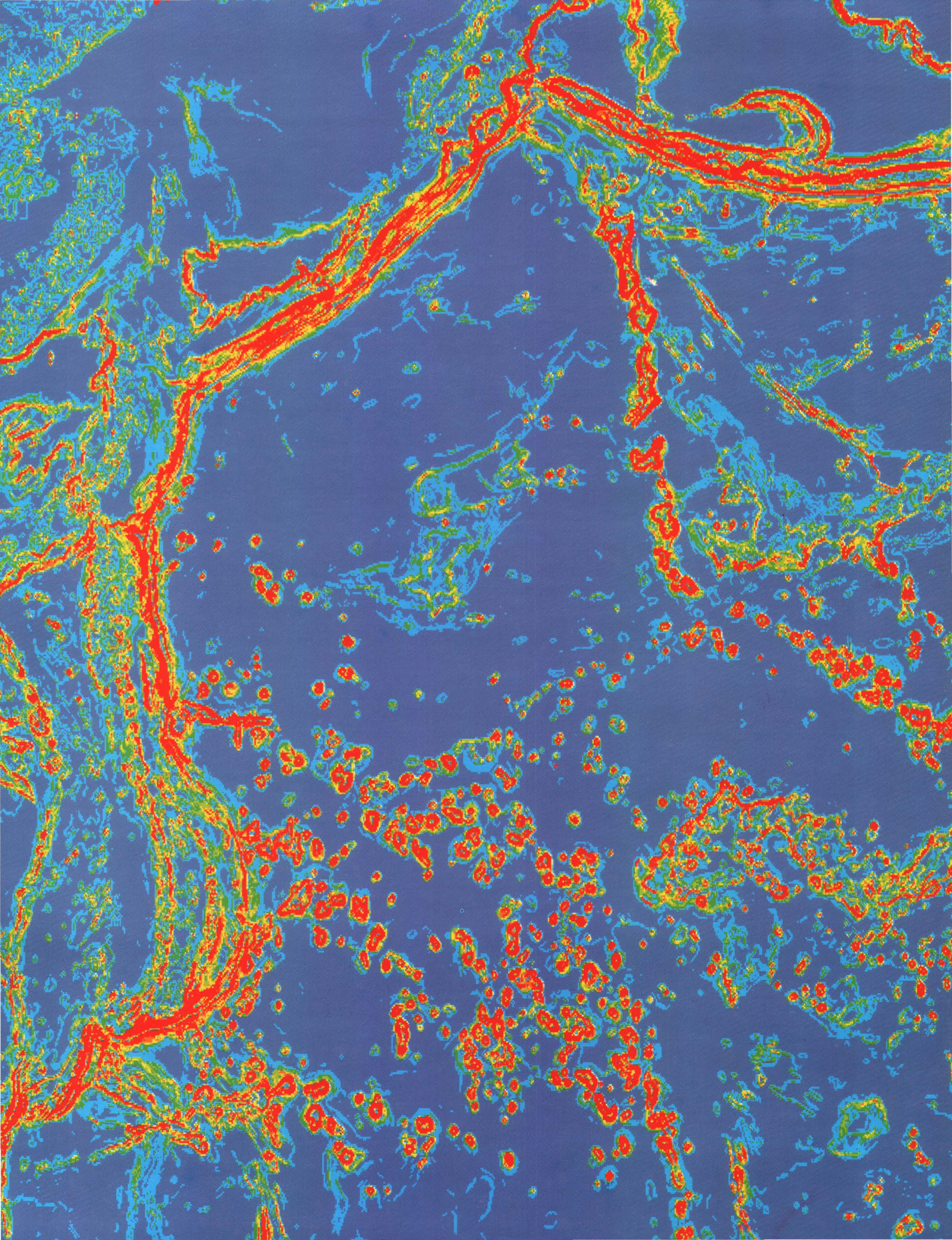

DIAMOND JUBILEE
(1912–1987)

HAWAIIAN VOLCANO OBSERVATORY

Volcanism in Hawaii

Papers to commemorate the 75th anniversary of the founding of the Hawaiian Volcano Observatory

Overleaf: Slope map of the northern Pacific Ocean, showing prominence of Hawaiian-Emperor volcanic chain (compare with ocean-floor map in front of volume 1). From world slope map by James G. Moore and Robert K. Mark, based on data from National Geophysical Data Tape ETOPO–5, digital relief of the surface of the Earth. Steepness of slope indicated by colors: deep red, >3.4°; red, 2.9°–3.4°; orange, 2.3°–2.9°; yellow, 1.7°–2.3°; green, 1.1°–1.7°; blue, 0.57°–1.1°; purple, <0.57°.

CONTENTS

VOLUME 1

PHYSIOGRAPHY, TECTONICS, AND SUBMARINE GEOLOGY

GEOLOGY OF THE ISLAND OF HAWAII

PETROGENESIS AND VOLCANIC GASES

VOLUME 2

STRUCTURE

Chapter 36. Hawaiian volcanic features: A photoglossary *845*
Taeko Jane Takahashi and Jim D. Griggs

37. Geophysical constraints on the structure of Kilauea and Mauna Loa Volcanoes and some implications for seismomagmatic processes *903*
David P. Hill and John J. Zucca

38. Seismic structure and tectonics of Kilauea Volcano *919*
Clifford H. Thurber

39. Aeromagnetic and near-surface electrical expression of the Kilauea and Mauna Loa volcanic rift systems *935*
Vincent J. Flanigan and Carl L. Long

40. Regional self-potential anomalies at Kilauea Volcano *947*
Dallas B. Jackson and James Kauahikaua

41. The dike complex of Koolau Volcano, Oahu: Internal structure of a Hawaiian rift zone *961*
George P.L. Walker

DYNAMICS

Chapter 42. Dynamics of Hawaiian volcanoes: An overview *997*
Robert W. Decker

43. The seismicity of Kilauea's magma system *1019*
Fred W. Klein, Robert Y. Koyanagi, Jennifer S. Nakata, and Wilfred R. Tanigawa

44. Structural damage and ground failures from the November 16, 1983, Kaoiki earthquake, Island of Hawaii *1187*
Jane M. Buchanan-Banks

Chapter 45. Origin of volcanic tremor in Hawaii
Part I. Data from the Hawaiian Volcano Observatory 1969–1985 *1221*
Robert Y. Koyanagi, Bernard Chouet, and Keiiti Aki
Part II. Theory and discussion *1259*
Bernard Chouet, Robert Y. Koyanagi, and Keiiti Aki

46. A hydraulic model to explain variations in summit tilt rate at Kilauea and Mauna Loa Volcanoes *1281*
John J. Dvorak and Arnold T. Okamura

47. Elastic and inelastic magma storage at Kilauea Volcano *1297*
Daniel J. Johnson

48. Cycling of magma between the summit reservoir and Kilauea Iki lava lake during the 1959 eruption of Kilauea Volcano *1307*
Jerry P. Eaton, Donald H. Richter, and Harold L. Krivoy

49. Tidal effects on Hawaiian volcanism *1337*
Daisuke Shimozuru

50. Geoelectric character of Kilauea Iki lava lake crust *1345*
Lennart A. Anderson

51. Uniqueness of volcanic systems *1357*
Herbert R. Shaw

52. Elasticity and contractancy of Hawaiian olivine tholeiite and its role in the stability and structural evolution of subcaldera magma reservoirs and rift systems *1395*
Michael P. Ryan

53. Origins of blade-like dikes in volcanic rift zones *1449*
Allan M. Rubin and David D. Pollard

54. Heat and mass transport in the east-rift-zone magma conduit of Kilauea Volcano *1471*
Harry C. Hardee

55. Conceptual models of brine evolution in magmatic-hydrothermal systems *1487*
Robert O. Fournier

56. A geochemical model of the Kilauea east rift zone *1507*
Donald Thomas

57. Aa flow dynamics, Mauna Loa 1984 *1527*
Peter W. Lipman and Norman G. Banks

58. Preliminary estimates of the rheological properties of 1984 Mauna Loa lava *1569*
Henry J. Moore

Chapter 59. The role of lava tubes in Hawaiian volcanoes *1589*
Ronald Greeley

HISTORY OF INVESTIGATIONS OF HAWAIIAN VOLCANISM

Chapter 60. James D. Dana and the origins of Hawaiian volcanology: The U.S. Exploring Expedition in Hawaii, 1840–41 *1607*
Daniel E. Appleman

61. Thomas A. Jaggar, Jr., and the Hawaiian Volcano Observatory *1619*
Russell A. Apple

62. Staff of the Hawaiian Volcano Observatory, 1912–present *1645*
Compiled by Taeko Jane Takahashi and Thomas L. Wright

Guide to pronunciation of Hawaiian words *1663*
Compiled by Taeko Jane Takahashi

Any use of trade names and trademarks in this publication is for descriptive purposes only and does not constitute endorsement by the U.S. Geological Survey.

Oblique aerial photograph of Kilauea caldera, looking north. USGS photograph taken November 1, 1954.

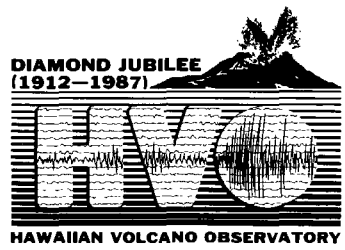
DIAMOND JUBILEE
(1912—1987)
HVO
HAWAIIAN VOLCANO OBSERVATORY

Volume 2

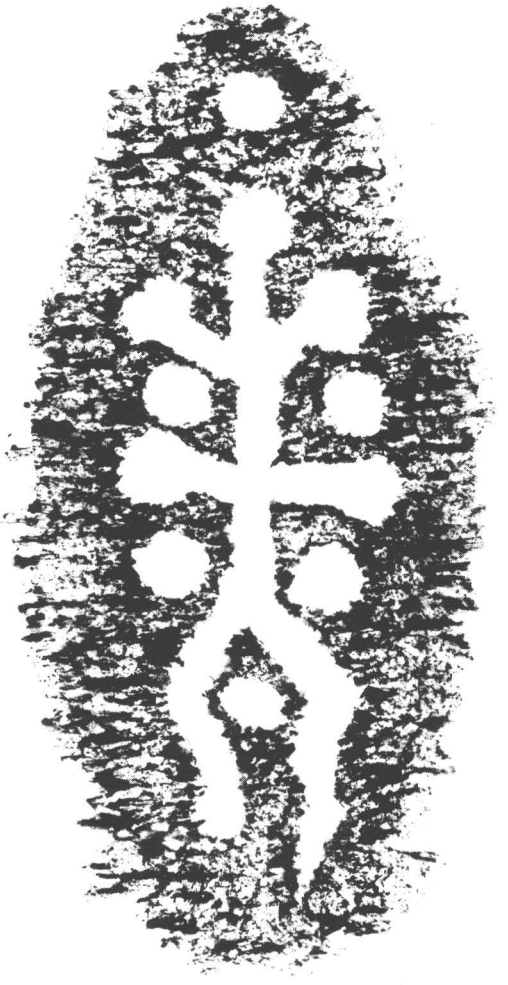

Man and His Family
Hawaiian Petroglyph
Puuloa, Hawaii

STRUCTURE

Guided by geological, geophysical, and geochemical observations, the mind's eye attempts to see beneath the Earth's surface. Conceptual models are proposed, tested against the data, and adjusted to fit.

Surface features on the Island of Hawaii are mostly formed by volcanic processes and often buried by subsequent eruptions. Calderas and pit craters collapse and reveal the structures in their walls. Erosion, roadcuts, and quarries expose dike swarms on ancient rift zones. These features and exposures are geologists' windows to the Earth's interior.

Earthquake waves and magnetic and electric fields are shaped by the rocks, pore fluids, and magma bodies through which they pass. When the variations of these geophysical data are inverted, inferred subsurface features emerge.

Using these approaches, the six chapters in this section describe and interpret some of the surface features and subsurface structures of the Islands of Hawaii and Oahu.

HAWAIIAN VOLCANIC FEATURES: A PHOTOGLOSSARY

By Taeko Jane Takahashi *and* Jim D. Griggs

ABSTRACT

Selected Hawaiian volcanic features, ranging from shield volcanoes to strands of volcanic glass, are illustrated in 62 photographs. Each feature is defined in a glossary, with a description as to its location, scale, photographer, and date photographed.

INTRODUCTION

Type examples of volcanic structures, forms, and textures are represented in this glossary through photographs, arranged alphabetically by the name of the feature shown, that were selected from the archives of the Hawaiian Volcano Observatory. Selections were based on the accessibility of the features' locations and the clarity of the illustrations. The features range in scale from large structures, such as volcanic shields, to textures, such as Pele's hair and tears. For some features (for example, lava flows), photographs taken during and after eruptions give a sense of the changing volcanic landscape.

The descriptions and definitions in this glossary include the location and scale of the feature, the date photographed, and the name of the photographer. Most definitions are from the Glossary of Geology (Bates and Jackson, 1980), and permission to use them has been kindly granted by the American Geological Institute. All photographs were taken by members of the U.S. Geological Survey unless otherwise noted.

More extensive discussions of these and other volcanic features in Hawaii have been published by Stearns and Macdonald (1946), Wentworth and Macdonald (1953), Greeley (1974), Carr and Greeley (1980), and Macdonald and others (1983). A photographic atlas and glossary of volcanic features on a global scale has been published by Green and Short (1971). The photoglossary in this volume provides new illustrations of many features described in the works cited above.

ACKNOWLEDGMENTS

The authors wish to thank J.P. Lockwood and R.B. Moore for reviewing the photographs and text for this paper. We also thank G.E. Ulrich for his invaluable assistance with definitions of selected features, A.T. Okamura for directing the authors to many of the features, and other staff members of the Hawaiian Volcano Observatory for contributing photographs to this glossary.

GLOSSARY

The photographs that illustrate this glossary are U.S. Geological Survey photographs unless otherwise indicated. Photographer and date photographed are noted in parentheses. Quoted definitions of features are from Bates and Jackson (1980), except where another source is cited.

REFERENCES CITED

Bates, R.L., and Jackson, J.A., 1980, Glossary of geology, 2nd ed.: Falls Church, Va., American Geological Institute, 751 p.

Carr, M.H., and Greeley, R., 1980, Volcanic features of Hawaii: a basis for comparison with Mars: Washington, D.C., National Aeronautics and Space Administration, Scientific and Technical Information Branch, 363 p.

Greeley, R., ed., 1974, Guidebook to the Hawaiian Planetology Conference: National Aeronautics and Space Administration, Ames Research Center, University of Santa Clara, and U.S. Geological Survey, 184 p.

Green, J., and Short, N.M., eds., 1971, Volcanic landforms and surface features: a photographic atlas and glossary: New York, Springer-Verlag, 519 p.

Lockwood, J.P., and Williams, I.S., 1978, Lava trees and tree moulds as indicators of lava flow direction: Geological Magazine, v. 115, no. 1, p. 69–74.

Macdonald, G.A., 1972, Volcanoes: Englewood Cliffs, New Jersey, Prentice-Hall, 510 p.

Macdonald, G.A., and Abbott, A.T., 1977, Volcanoes in the sea: The geology of Hawaii: Honolulu, University Press of Hawaii, 441 p.

Macdonald, G.A., Abbott, A.T., and Peterson, F.L., 1983, Volcanoes in the sea: the geology of Hawaii, 2nd ed.: Honolulu, Hawaii, The University of Hawaii Press, 517 p.

Neal, C.A., and Decker, R.W., 1983, Surging of lava flows at Kilauea Volcano, Hawaii: Eos, American Geophysical Union Transactions, v. 64, no. 45, p. 904.

Peck, D.L., 1966, Lava coils of some recent historic flows, Hawaii: U.S. Geological Survey Professional Paper 550–B, p. B148–B151.

Stearns, H.T., and Macdonald, G.A., 1946, Geology and ground-water resources of the Island of Hawaii (Bulletin 9): Honolulu, Hawaii, Hawaii Division of Hydrography and U.S. Geological Survey, 363 p.

Wentworth, C.K., Macdonald, G.A., 1953, Structures and forms of basaltic rocks in Hawaii: a description of the physical features of basaltic rocks and their origin: U.S. Geological Survey Bulletin 994, 98 p.

Aa

"A Hawaiian term for lava flows typified by a rough, jagged, spinose, clinkery surface." Compare with **pahoehoe.**

Aa flow in Royal Gardens, Kalapana, east rift zone of Kilauea Volcano. The height of the flow front is approximately 2.5 m (April 9, 1983, J.B. Stokes).

Aa

Detail of aa from Mauna Ulu flow, east rift zone of Kilauea Volcano. The diameter of the coin is 24 mm (June 10, 1985, J.D. Griggs).

Accretionary lapilli

"More or less spherical masses, mostly between 1 mm and 1 cm in diameter, of cemented ash; the cementation is often weak. Formed by accretion of particles around wet nuclei, e.g., raindrops falling through a cloud of ash" (Macdonald, 1972, p. 133).

Accretionary lapilli from the 1790 eruption, Kau Desert (October 29, 1984, J.P. Lockwood).

Accretionary lava ball

"A rounded mass, ranging in diameter from a few centimeters to several meters, [carried] on the surface of a lava flow such as aa, or on cinder-cone slopes, [and formed] by the molding of viscous lava around a core of already solidified lava."

Incandescent accretionary lava ball (top) approximately 0.75 m long, Royal Gardens, Kalapana, east rift zone of Kilauea Volcano (July 2, 1983, J.D. Griggs). Accretionary lava ball (bottom) approximately 2.5 m high, formed during the eruption of the prehistoric Keamoku flow from Mauna Loa Volcano, Footprints Trail, Kau Desert (November 24, 1984, T.J. Takahashi).

Arching fountain

For definition, see **lava fountain**.

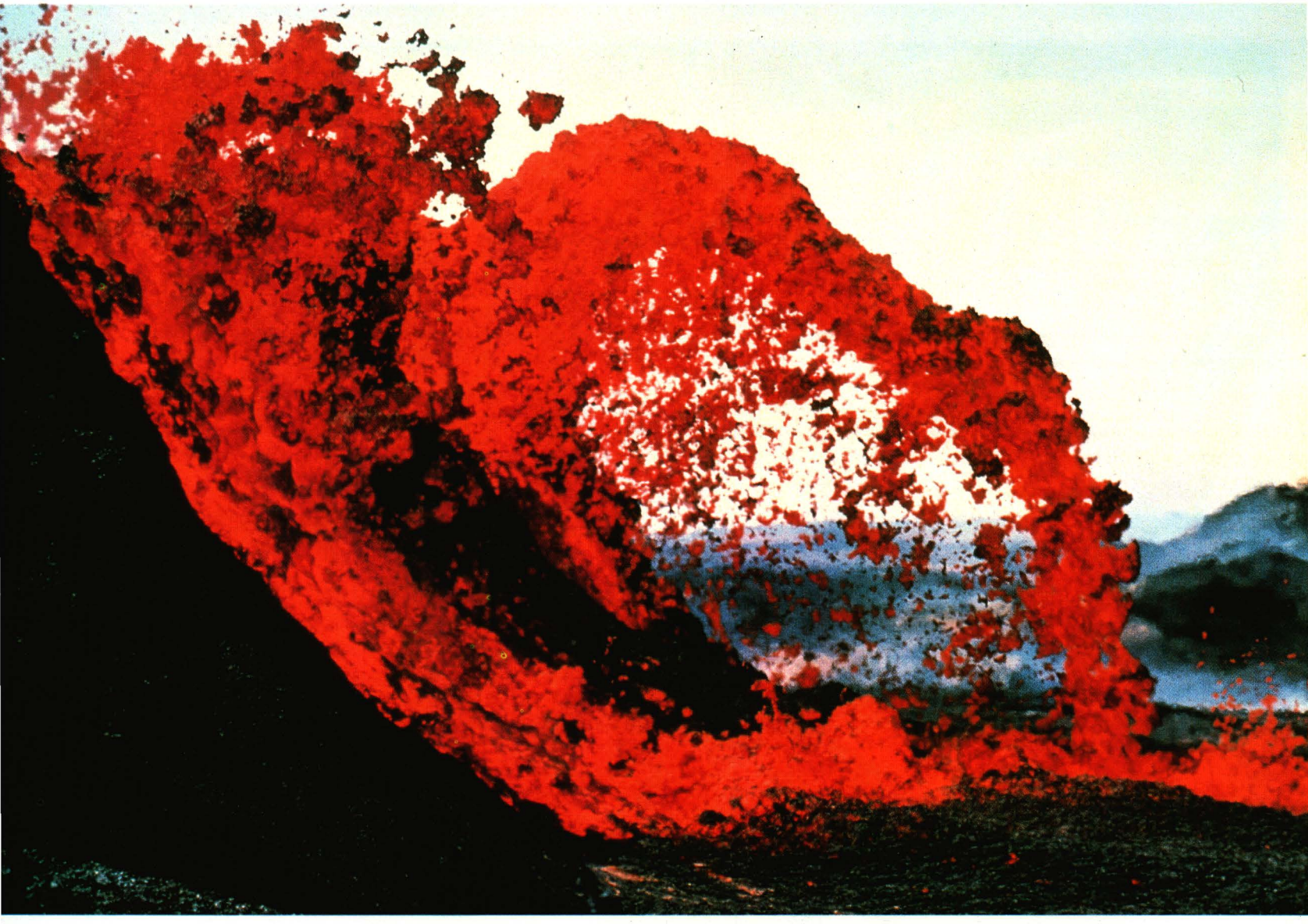

Fountains of the so-called 0740 vents, east rift zone of Kilauea Volcano; the view is to the west-southwest. The approximate height of the fountains is 10–15 m (February 25, 1983, J.D. Griggs).

Bedded pyroclastic deposits

"*** nonsedimentary material that exhibits depositional layering, such as the 'bedded deposits' of volcanic tuff alternating with lava in the mantle of a stratovolcano."

Bedded pyroclastic deposits (1790 eruption) visible in the southwest rift zone of Kilauea Volcano. The depth of the exposed area in the photograph is approximately 1.5 m (October 28, 1984, T.J. Takahashi).

Breach

A break or opening in the rim of a crater. "Breached" is used to describe "a volcanic cone or crater, the rim of which has been broken through by the outpouring lava."

Aerial view of Puu Oo cinder-spatter cone, with breach on the right, east rift zone of Kilauea Volcano; the view is to the northeast (May 12, 1983, E.W. Wolfe).

Caldera

"A large, basin-shaped volcanic depression, more or less circular *** the diameter of which is many times greater than that of the included vent or vents***."

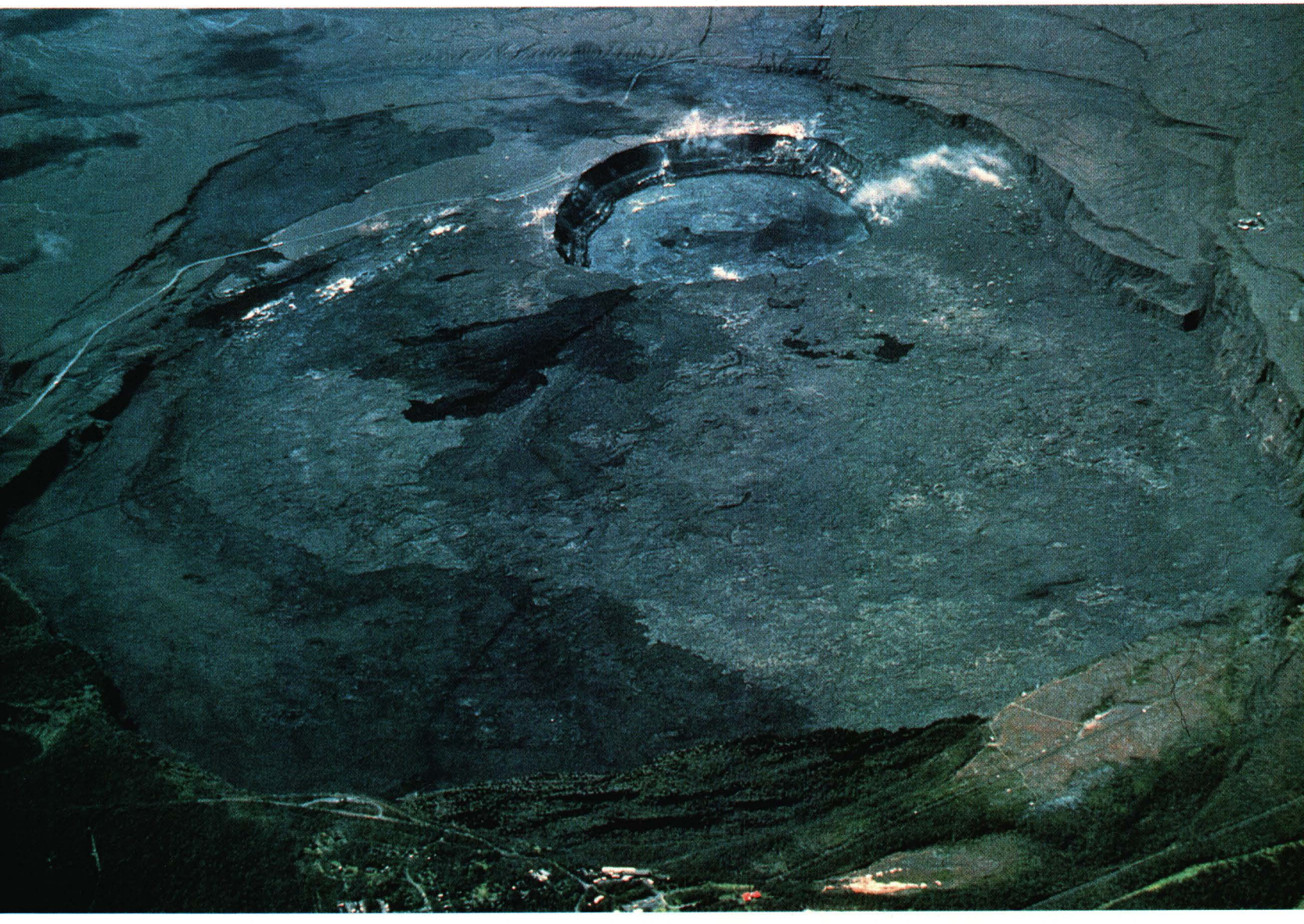

Aerial view of Kilauea Volcano summit caldera; the view is to the southwest. The caldera is 4.5 km by 3 km, and Halemaumau Crater, in the upper center, is 1 km in diameter (January 10, 1985, J.D. Griggs).

Channel

"A narrow, sinuous flow channel, commonly formed in lava flows."

Aerial view of a flow in a lava channel (top), northeast rift zone of Mauna Loa Volcano; the view is to the south. The direction of the flow is from left to right, and the channel width is approximately 6 m (April 4, 1984, J.D. Griggs). Lava channel wall (bottom), July 1974 flow, Kilauea caldera. The height of the wall is approximately 1.5 m (November 11, 1984, T.J. Takahashi).

Channel

Lava channel at a low flow level, northeast rift zone of Mauna Loa Volcano. The channel is approximately 1 m wide at the top, widening to more than 2 m below the overhang, and is 2.5 m deep to the flow level (April 4, 1984, M.L. Summers).

Cinder cone

"A conical hill formed by the accumulation of cinders and other pyroclasts, normally of basaltic or andesitic composition."

Puu ka Pele cinder cone, Humuula Saddle; the view is to the west. This Mauna Kea cone is 95 m in height, and the diameter of the bowl-like depression is 400 m. Hualalai Volcano is in the background (December 1, 1975, J.P. Lockwood).

Curtain of fire

"A row of coalescing lava fountains along a fissure; a typical feature of a Hawaiian-type eruption" (Macdonald, 1972, p. 214).

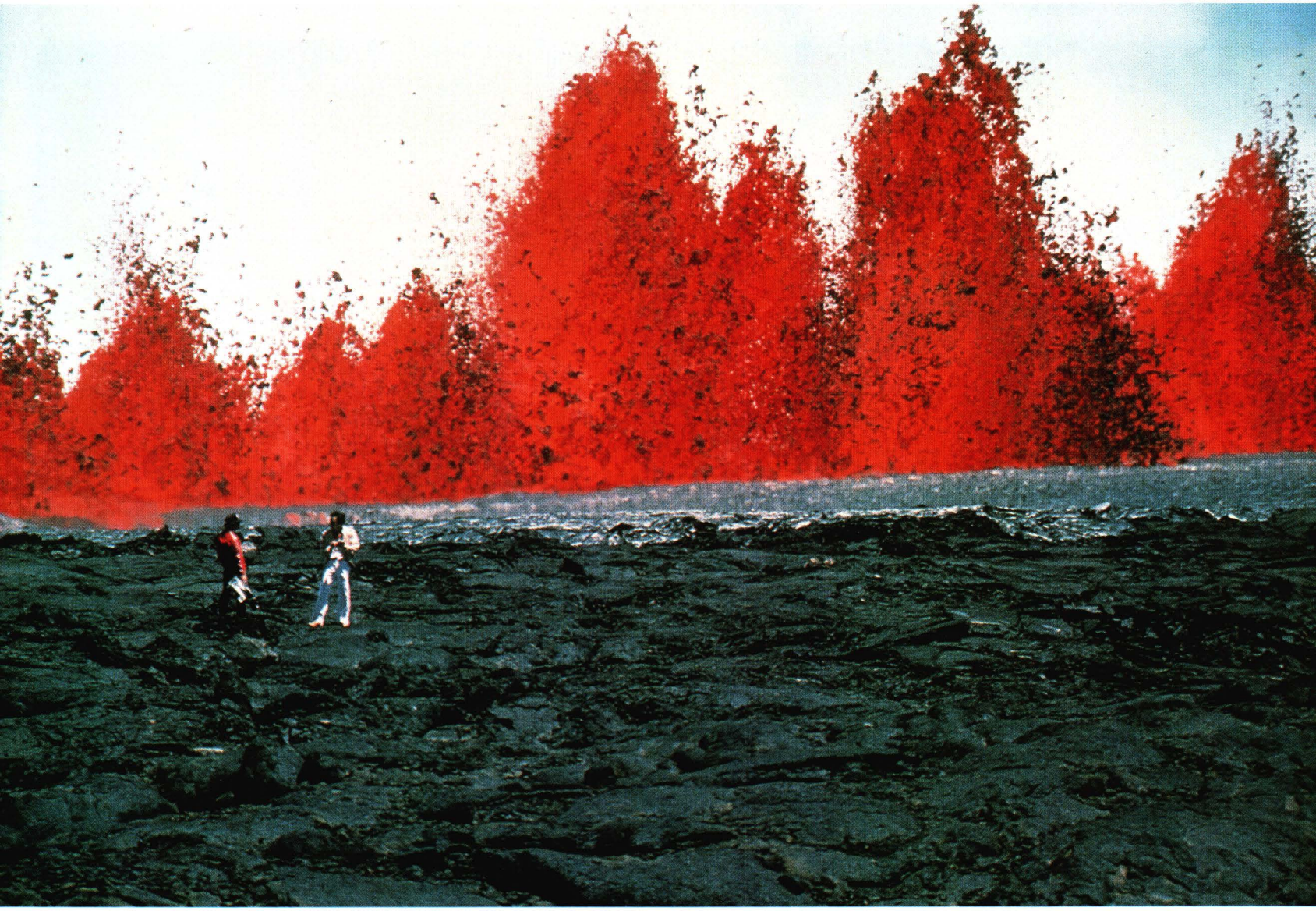

Curtain of fire along the northeast rift zone of Mauna Loa Volcano; the view is to the south. The height of the fountain is approximately 25 m (March 25, 1984, R.B. Moore).

Dike

"A tabular igneous intrusion that cuts across the bedding or foliation of the country rock."

Dike (1.5 m wide), now mostly covered by 1984 lava drapery, cutting the northeast wall of Lua Poholo, Mauna Loa Volcano (March 1983, J.P. Lockwood).

Dome fountain

Hemispherically shaped lava fountain that is approximately in equilibrium between the upward pressure of magma from the conduit below and the mass of ponded lava through which the fountain rises. It normally occurs in a low-energy and gas-poor eruptive state and may be several tens of meters high.

Dome fountain formed during the eruption of Mauna Ulu, east rift zone of Kilauea Volcano. The height of the dome is 20 m (October 11, 1969, J.B. Judd).

Drainback

Lava that returns to the subsurface by flowing into an open fissure, especially lava that, in the late phases of an eruption, reverses its normal direction of movement and flows back into the eruptive fissure that was its vent. It commonly forms dripstone features on the walls of the fissure, showing its downward flow direction.

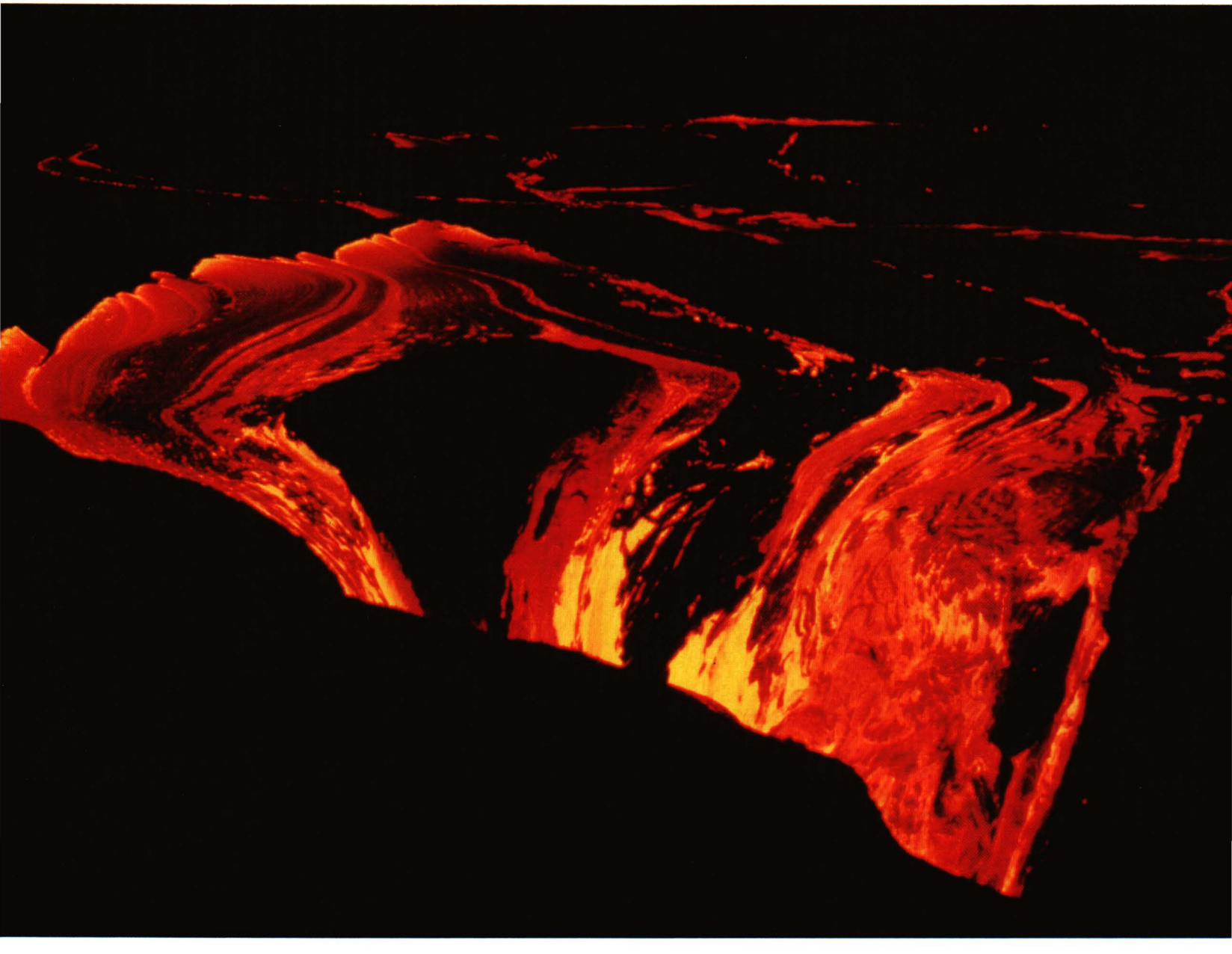

Drainback into a fissure near the west lip of Aloi Crater, east rift zone of Kilauea Volcano (June 29, 1970, D.A. Swanson).

Drainback

Congealed drainback into 1971 fissure, Kilauea caldera (October 1964, T.J. Takahashi).

Echelon

"Said of geologic features that are in an overlapping or staggered arrangement, e.g. faults. Each is relatively short but collectively they form a linear zone, in which the strike of the individual features is oblique to that of the zone as a whole."

Aerial view of fountains along echelon fissures on the northeast rift zone of Mauna Loa Volcano. Pohaku Hanalei cinder-spatter cone is at the upper left (March 25, 1984, J.D. Griggs).

Fault scarp

"A steep slope or cliff formed directly by movement along a fault and representing the exposed surface of the fault before modification by erosion and weathering."

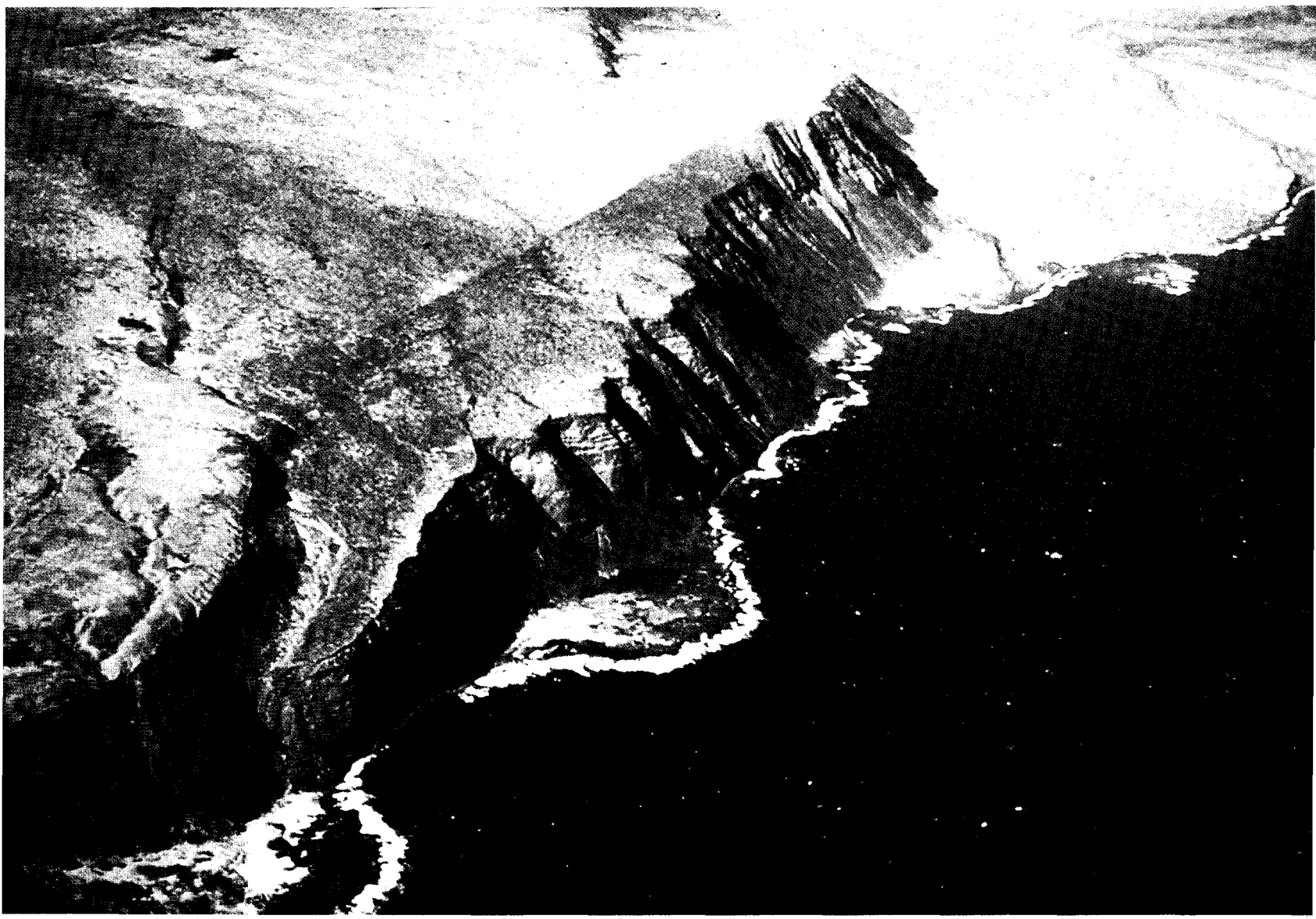

Aerial view of Puu Kapukapu, south flank of Kilauea Volcano; the view is to the northeast. Maximum height of the scarp is 320 m (June 24, 1971, D.A. Swanson).

Fumarole

"A vent, usually volcanic, from which gases and vapors are emitted; it is characteristic of a late stage of volcanic activity ***. Fumaroles may occur along a fissure or in apparently chaotic clusters or fields."

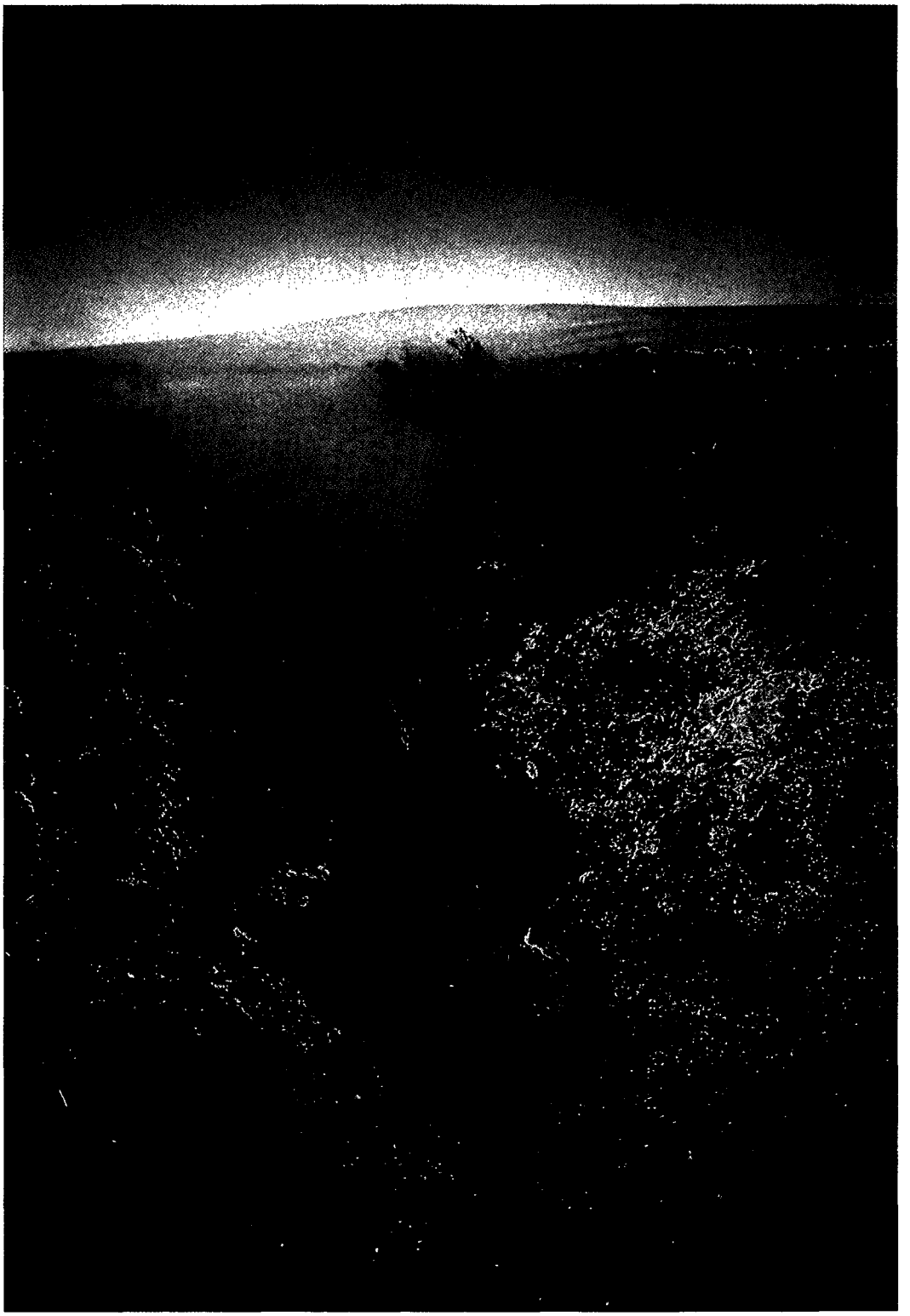

Fumarole near Steaming Bluff, summit of Kilauea Volcano; the view is to the west. The vent is approximately 1.5 m wide. Mauna Loa shield is in the background (October 1984, J.D. Griggs, personal collection).

Fume cloud

"A vaporous cloud of volcanic gases from a body of molten lava."

Fume cloud from the northeast rift zone of Mauna Loa; the view is to the southwest (April 2, 1984, J.D. Griggs).

Kipuka

"An area surrounded by a lava flow."

Aerial view of kipuka in 1955 flow, east rift zone of Kilauea Volcano. Whitish cast is lichen growing on lava (1977, R.B. Moore).

Laccolith

"A concordant igneous intrusion with a known or assumed flat floor and a postulated dikelike feeder commonly thought to be beneath its thickest point. It is generally planoconvex in form and roughly circular in plan***."

Aerial view of Uwekahuna Bluff on the north caldera wall (150 m high) at the summit of Kilauea Volcano. The laccolith is the light-colored lenticular area at the base of the caldera wall, along the middle left side of the photograph (September 1977, R.B. Moore).

Lava bomb

"A pyroclast that was ejected while viscous and received its rounded shape while in flight. It is larger than 64 mm in size, and may be vesicular to hollow inside."

Lava bombs collected from above Hale Pohaku, Mauna Kea Volcano (July 10, 1982, J.P. Lockwood).

Lava cascade

"A cascade of fluid, incandescent lava, formed when a lava river passes over a cliff or steep part of its course."

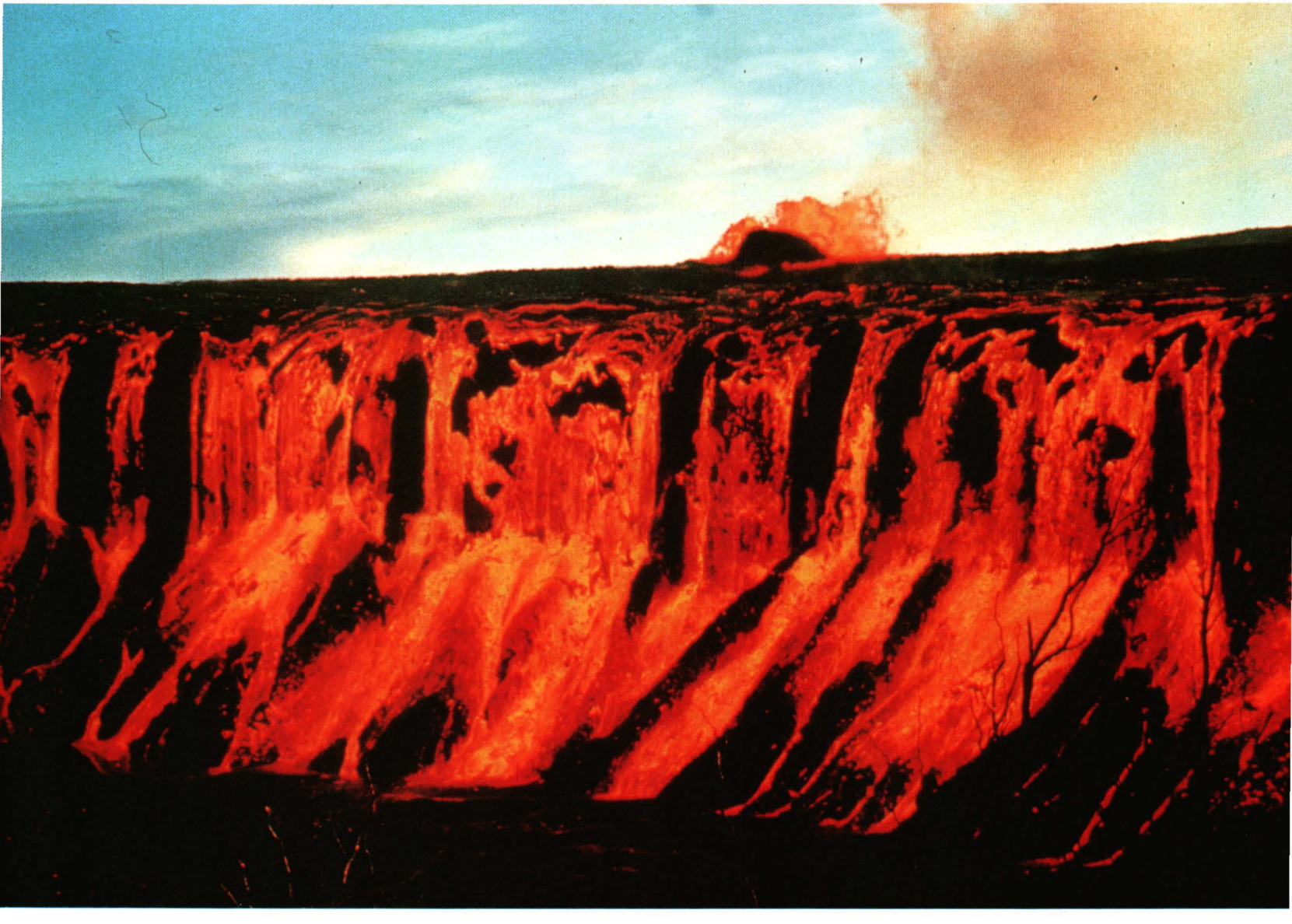

Cascade into Aloi Crater, east rift zone of Kilauea Volcano. The approximate height of the cascade is 25 m, and the height of fountain in the background is 30 m (December 30, 1969, D.A. Swanson).

Lava coils

"Voluted [spiral or scroll-shaped] strips of lava" along a shear zone (Peck, 1966, p. B148).

Lava coils formed during the eruption of Puu Kiai, east rift zone of Kilauea Volcano. Lens cap used for scale is 55 mm in diameter (May 13, 1978, R.B. Moore).

Lava drapery

A congealed lava cascade (see also **lava cascade**).

Lava drapery over the September 1971 fissures from the eruption in Kilauea caldera. The drapery from the top of the fissure to the fern (center right of photograph) is approximately 1 m (November 11, 1984, T.J. Takahashi).

Lava fountain

"A jet of incandescent lava, shot into the air as the magma reaches the surface by the hydrostatic pressure on the liquid and the expansion of gas bubbles forming in it. Fountains usually range from about 10 to 100 m in height, but occasionally reach 300 m. They are characteristic of Hawaiian-type eruptions."

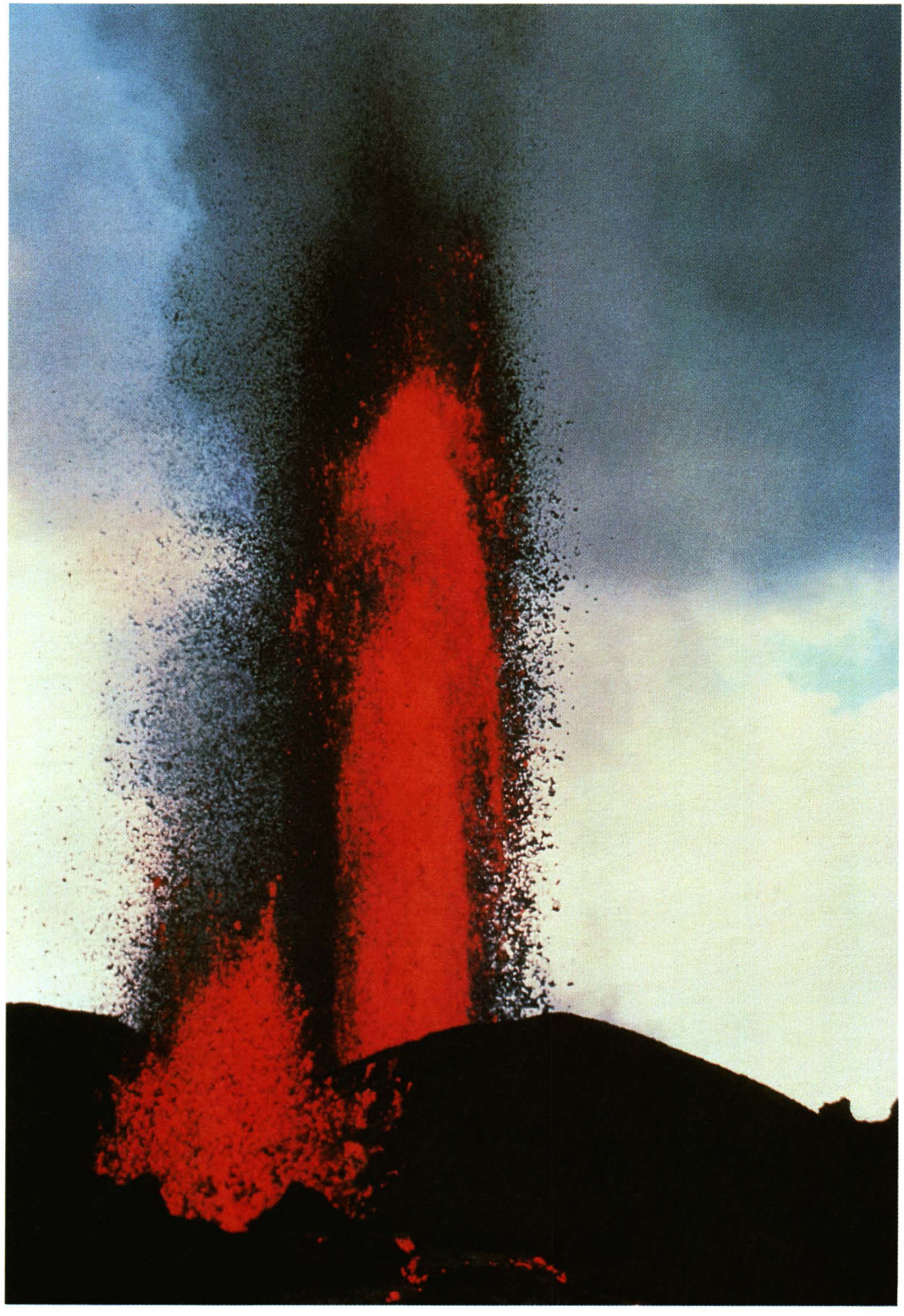

Lava fountains of Puu Halulu (formerly known as "1123 vent"), east rift zone of Kilauea Volcano; the view is to the northeast. The approximate height of the fountains is 350 m (April 4, 1983, J.D. Griggs).

Lava lake

"A lake of molten lava, usually basaltic, in a volcanic crater or depression. The term refers to solidified and partly solidified stages as well as to the molten, active lava lake."

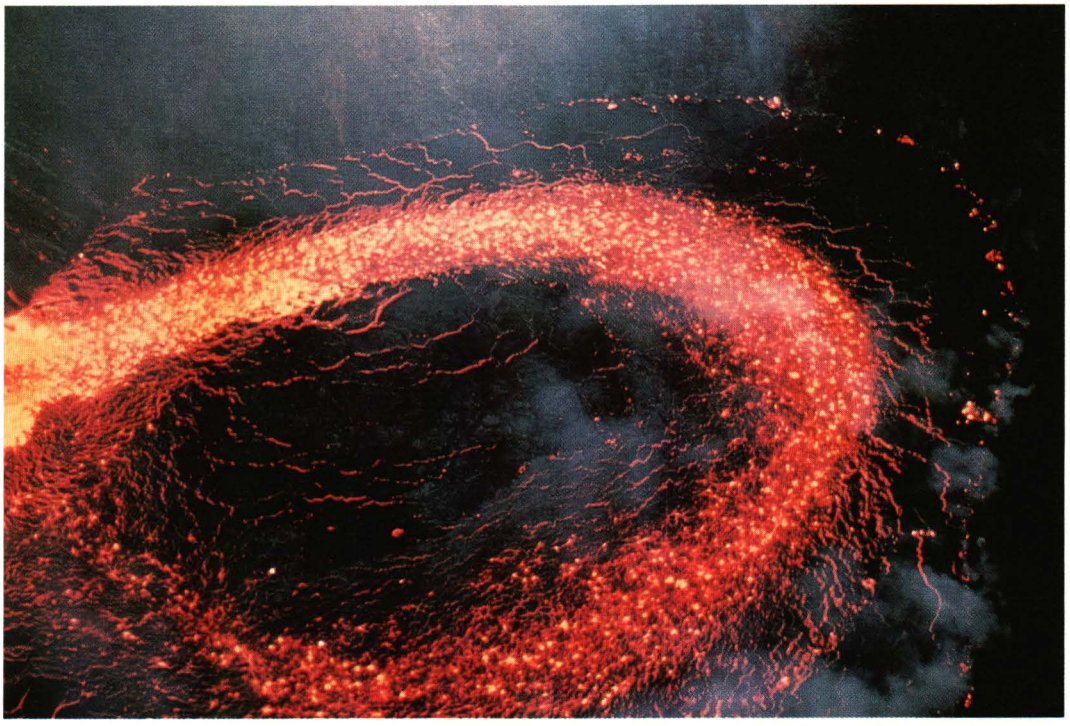

View at night of the west pit of Makaopuhi Crater, east rift zone of Kilauea Volcano. The depth of the crater before the eruption was approximately 310 m, and the depth of the lake during this phase was 42 m (March 3, 1965, D.P. Hill).

View in daylight of the lava lake in the west pit of Makaopuhi Crater, east rift zone of Kilauea Volcano (March 11, 1965, D.L. Peck).

Lava tree

A sheath of solidified lava, roughly cylindrical in shape, formed when fluid pahoehoe quickly surrounds a living tree and chills against it; when the molten lava drains away, the lava that congealed against the tree stands in relief above the flow surface (Lockwood and Williams, 1978; Wentworth and Macdonald, 1953).

Lava trees formed during the eruption of Puu Kiai, November 1977, east rift zone of Kilauea Volcano. The height of the lava tree in the foreground is approximately 3 m (May 13, 1978, R.B. Moore).

Lava-tree mold

"A cylindrical hollow in a lava flow formed by the envelopment of a tree by the flow, solidification of the lava in contact with the tree, and disappearance of the tree by burning and subsequent removal of the charcoal and ash. The inside of the mold preserves the surficial features of the tree."

Lava-tree mold (diameter 23 cm, depth 40 cm) formed during the eruption of Kilauea Iki, located along the Devastation Trail, Kilauea Volcano (October 1984, T.J. Takahashi).

Lava tube

"A hollow space beneath the surface of a solidified lava flow, formed by the withdrawal of molten lava after the formation of the surficial crust."

Thurston Lava Tube, Kilauea Volcano. The height of the tube near the entrance is approximately 4 m (September 7, 1984, T.J. Takahashi).

Pahoehoe

"A Hawaiian term for a type of basaltic lava flow typified by a smooth, billowy, or ropy surface. Varieties include corded, elephant-hide, entrail, festooned, filamented, sharkskin, shelly, and slab pahoehoe." Compare with **aa**.

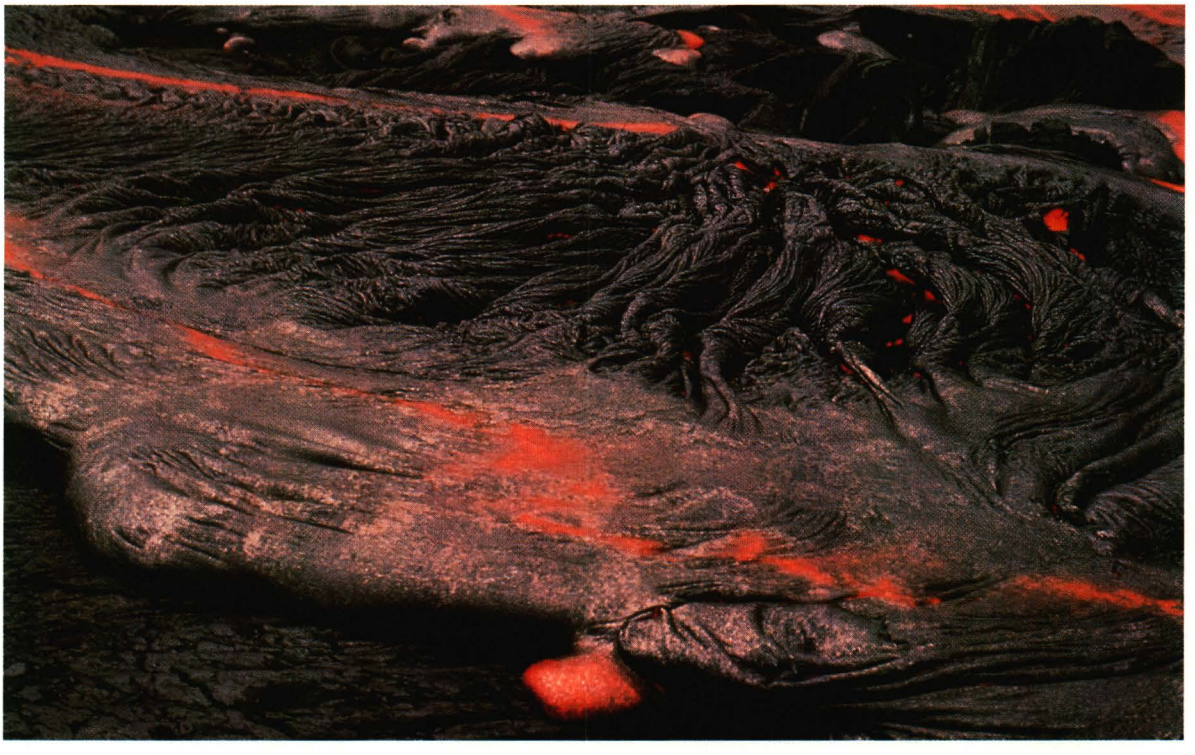

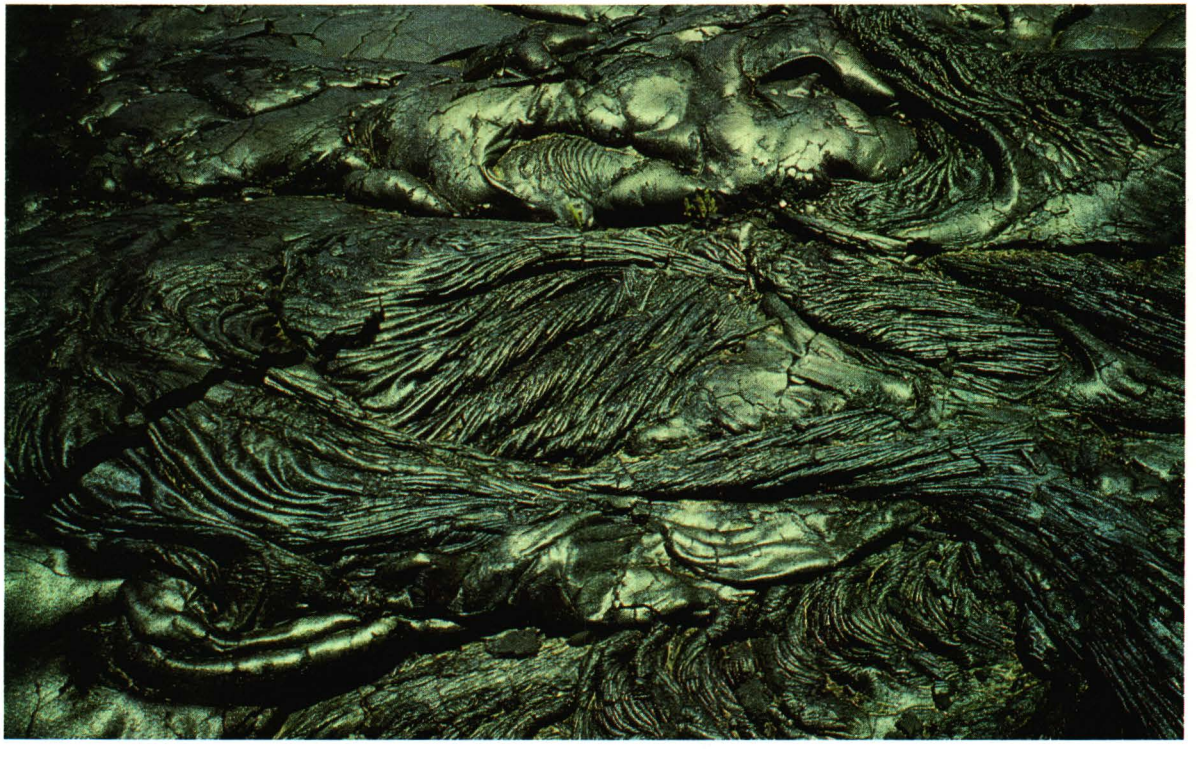

Fluid pahoehoe flow (top) on the south-southwest flank of Alae Crater, east rift zone of Kilauea Volcano (December 14, 1972, D.W. Peterson). Detail (bottom) of pahoehoe from Mauna Ulu flow, east rift zone of Kilauea Volcano (October 1984, J.D. Griggs, personal collection).

Pele's hair

"A natural spun glass formed by blowing-out during quiet fountaining of fluid lava, cascading lava falls, or turbulent flows, sometimes in association with **Pele's tears**. A single strand, with a diameter of less than half a millimeter, may be as long as two meters."

Pele's hair from the eruption of Mauna Ulu, east rift zone of Kilauea Volcano (March 27, 1984, D.W. Peterson).

Pele's tears

"Small, solidified drops of volcanic glass behind which trail pendants of Pele's hair. They may be tear-shaped, spherical, or nearly cylindrical."

Pele's tears collected from Hilina Pali Road, south flank of Kilauea Volcano, carried westward by wind during the eruption of Mauna Ulu, 1969–74 (November 1984, J.D. Griggs).

Perched lava pond

An impounded body of pahoehoe lava whose margins consist of chilled lava-flow fronts or spatter ramparts formed earlier in the same or in a previous eruption. The surface of the pond is thus retained at a higher (perched) level one or more meters above the surrounding surface.

Aerial view of the perched lava pond on the north flank of Mauna Ulu satellite shield, east rift zone of Kilauea Volcano; the view is to the south. The diameter of the pond is 130 m (September 1984, T.J. Takahashi).

Pillow lava

"A general term for those lavas displaying pillow structure and considered to have formed in a subaqueous environment; such lava is usually basaltic or andesitic."

Pillow lava formed where a 3,500-year-old flow poured into the lower Wailuku River, Hilo. Note river conglomerate at the base of the pillows (pick used for scale is 30 cm long) (June 14, 1982, J.P. Lockwood).

Pit crater

"A crater formed by sinking in of the surface; not primarily a vent for lava" (Macdonald and Abbott, 1977, p. 419).

Aerial view of Makaopuhi Crater on the east rift zone of Kilauea Volcano; the view is to the south. The crater is 1.5 km by 1 km, with a maximum depth of 150 m at the north wall. Flows from the eruption of Mauna Ulu (1969–74) are at the upper right (January 10, 1985, J.D. Griggs).

Pressure ridge

"An elongate uplift of the congealing crust of a lava flow, probably due to the pressure of underlying still-flowing lava."

Pressure ridge along the western margin of the September 1982 flow, Kilauea caldera. The approximate height of the ridge is 1.5 m (November 1984, T.J. Takahashi).

Reticulite

"Basaltic pumice; also called 'thread-lace scoria'" (Macdonald and Abbott, 1977, p. 419).

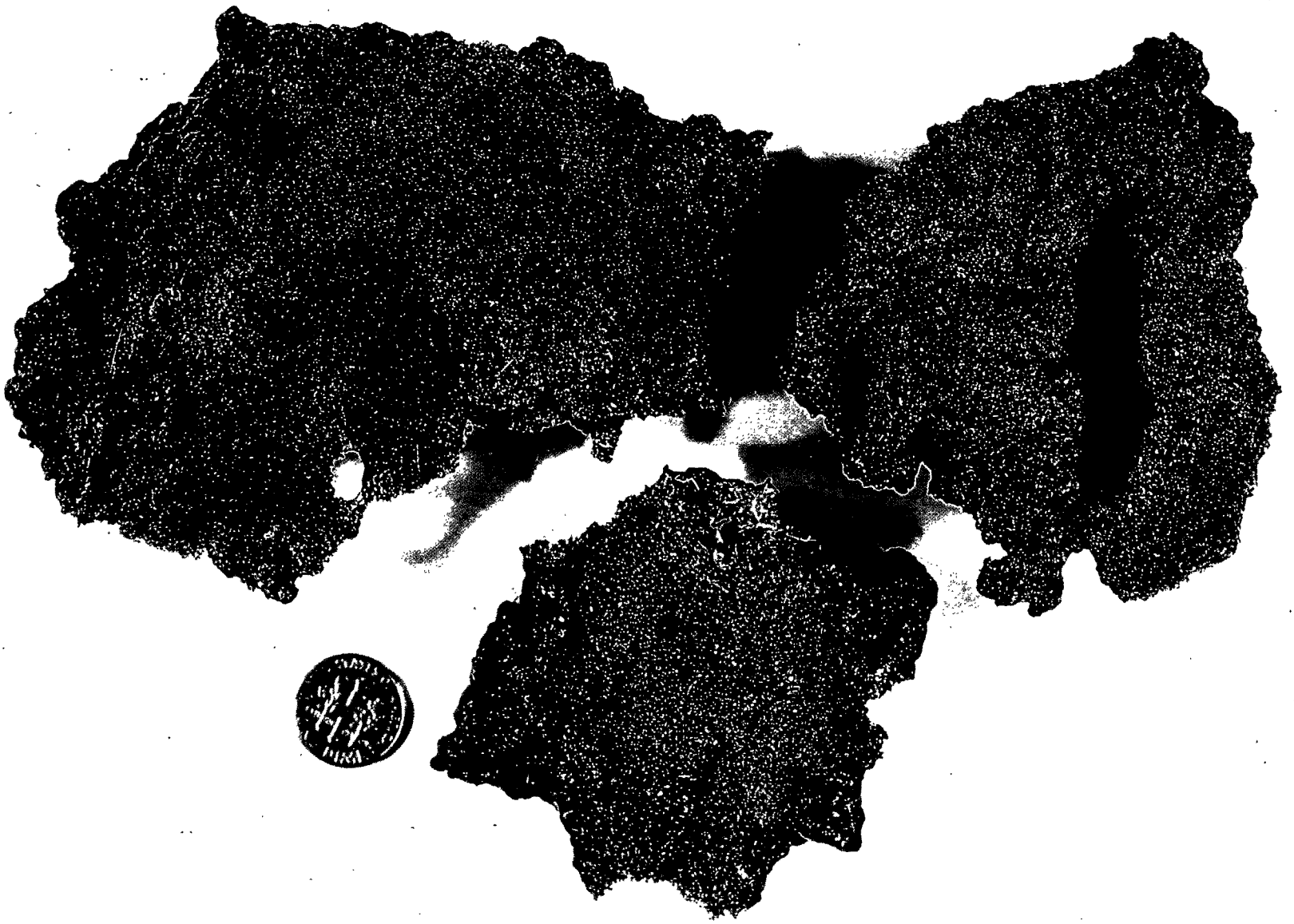

Reticulite collected from Hilina Pali Road, south flank of Kilauea Volcano, blown westward by wind during the eruption of Mauna Ulu, 1969–74 (October 1984, J.D. Griggs).

Rift zone

"In Hawaii, a zone of volcanic features associated with underlying dike complexes."

Aerial view of the upper southwest rift zone of Kilauea Volcano; the view is to the east. Crater Rim Drive and Halemaumau Crater are seen across the top of the photo. Darker flows are from the 1971 eruption (March 4, 1985, J.D. Griggs).

Shield volcano

"A volcano in the shape of a flattened dome, broad and low, built by flows of very fluid basaltic lava***."

Aerial view of Kilauea Volcano from the summit to the east rift zone, with Puu Oo fuming in the background and Hawaiian Volcano Observatory in the center foreground (January 10, 1985, J.D. Griggs).

Shield volcano

Aerial view of the summit and the northeast rift zone of Mauna Loa Volcano; the view is to the west-northwest. Darker areas are younger flows; the summit of Hualalai Volcano is in the upper right background (January 10, 1985, J.D. Griggs).

Skylight

An opening, formed by collapse, in the roof of a lava tube.

Skylight at Mauna Ulu, east rift zone of Kilauea Volcano (May 2, 1983, R.L. Christiansen).

Solfatara

"A type of fumarole, the gases of which are characteristically sulfurous."

Solfatara on the east rift zone of Kilauea Volcano (May 6, 1983, J.D. Griggs, personal collection).

Spatter

"An accumulation of very fluid pyroclasts, coating the surface around a vent."

Spatter caught in a tree, west of Hilina Pali, south flank of Kilauea Volcano (May 5, 1973, D.W. Peterson).

Spatter cone

"A low, steep-sided cone of spatter built up on a fissure or vent; it is usually of basaltic material."

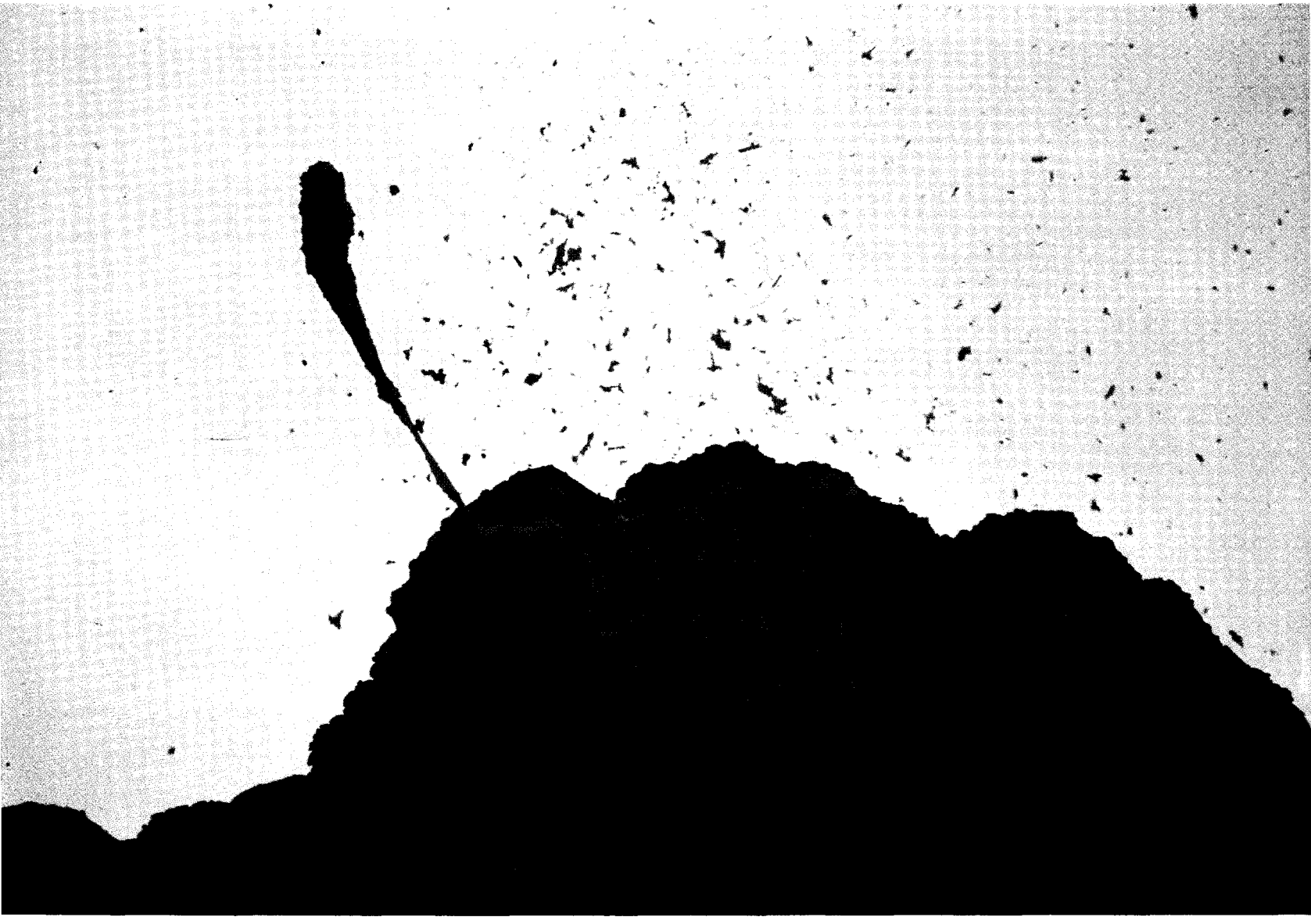

Spatter cone formed during the April 30, 1982, eruption in Kilauea caldera. The approximate diameter of the vent is 2 m (April 30, 1982, T.T. English).

Spatter rampart

A ridge of congealed pyroclastic material, usually basaltic, built up on a fissure or vent.

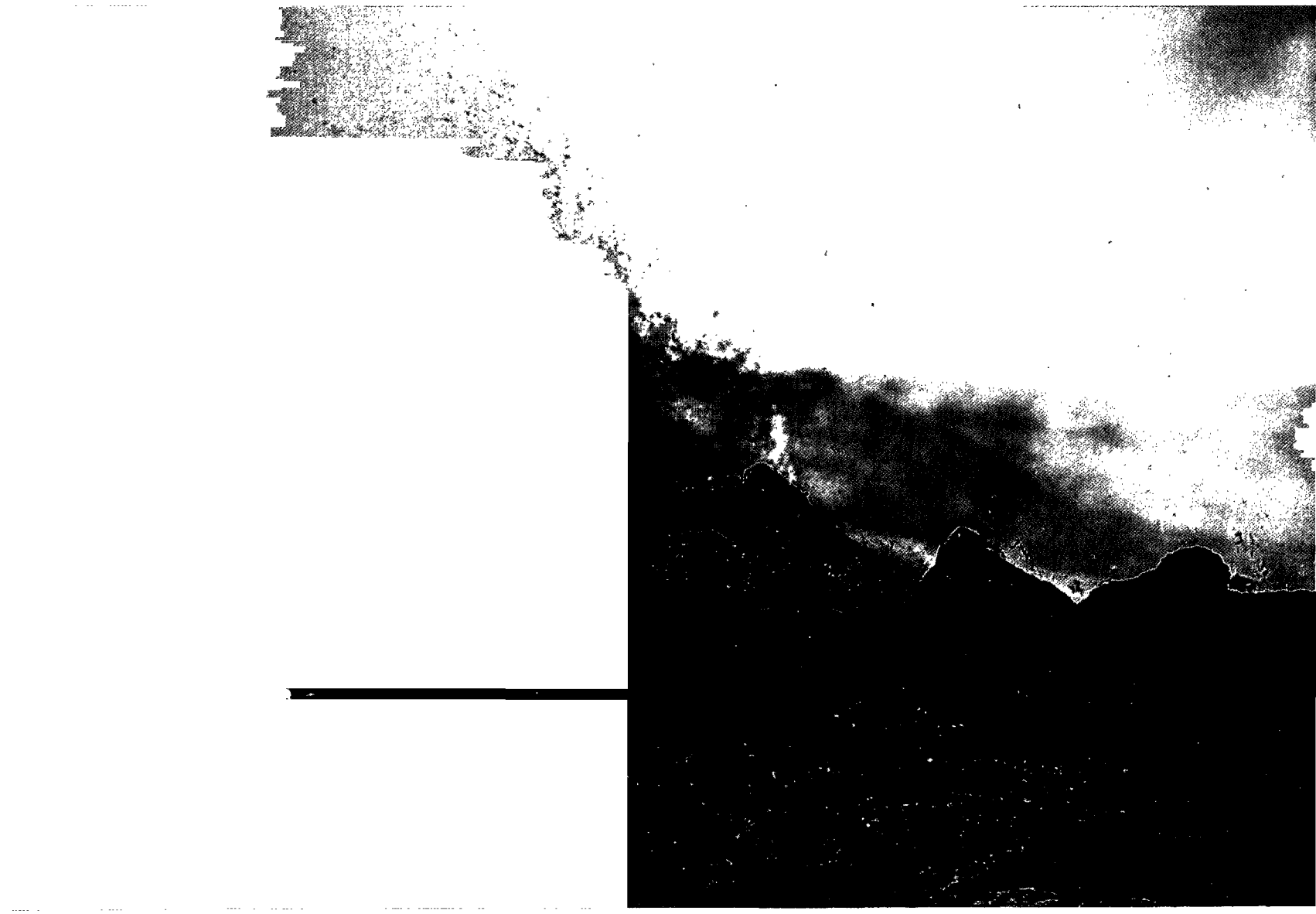

View of fountains along a spatter rampart, the principal vents of the 1984 eruption on Mauna Loa Volcano's northeast rift zone, looking northwest (March 26, 1984, J.D. Griggs).

Spillway

"Overflow channel."

Spillway of Puu Oo cinder-spatter cone on the east rift zone of Kilauea Volcano (spillway is on the northeast side). The height of the cone during this episode was 20–30 m (June 16, 1983, E.W. Wolfe).

Squeeze-up

"A small extrusion of viscous lava, or toothpaste lava, from a fracture or opening on the solidified surface of a flow, caused by pressure."

Squeeze-up (length 64 cm; width 18 cm) from September 1982 flow, Kilauea caldera (November 25, 1984, T.J. Takahashi).

Standing wave

"A *** wave, the wave form of which oscillates vertically between two points or nodes, without progressive movement."

Standing waves in lava channel, east rift zone of Kilauea Volcano. The height of the wave is approximately 2–3 m (November 6, 1983, C.A. Neal).

Step fault

"One of a set of parallel, closely spaced faults over which the total displacement is distributed***."

Aerial view of step faults on the northwest caldera wall at the summit of Kilauea Volcano. Hawaiian Volcano Observatory is at the upper right (January 10, 1985, J.D. Griggs).

Surge

"A transient increase, of variable duration and magnitude, in the volume flux of a lava flow. Some surges are caused by the sudden release of lava ponded upstream. Surges usually result in the acceleration of the flow front and may produce thin, short-lived breakouts of fluid lava" (Neal and Decker, 1983).

Aa surge, Royal Gardens, Kalapana, east rift zone of Kilauea Volcano. The direction of the flow is from right to left. The height of the glowing area of the surge is approximately 6 m (June 16, 1984, R.W. Decker).

Tension crack

"A fracture caused by tensile stress" (**Tensile stress**: "A normal stress that tends to cause separation across the plane on which it acts").

The magnitude 6.6 earthquake on November 16, 1983, caused a landslide of sections of the north rim into Kilauea caldera. Tension cracks are at the top of the landslide; the view is to the east from the northeast rim of Kilauea caldera (November 16, 1983, J.D. Griggs).

Tephra

"A general term for all pyroclastics of a volcano."

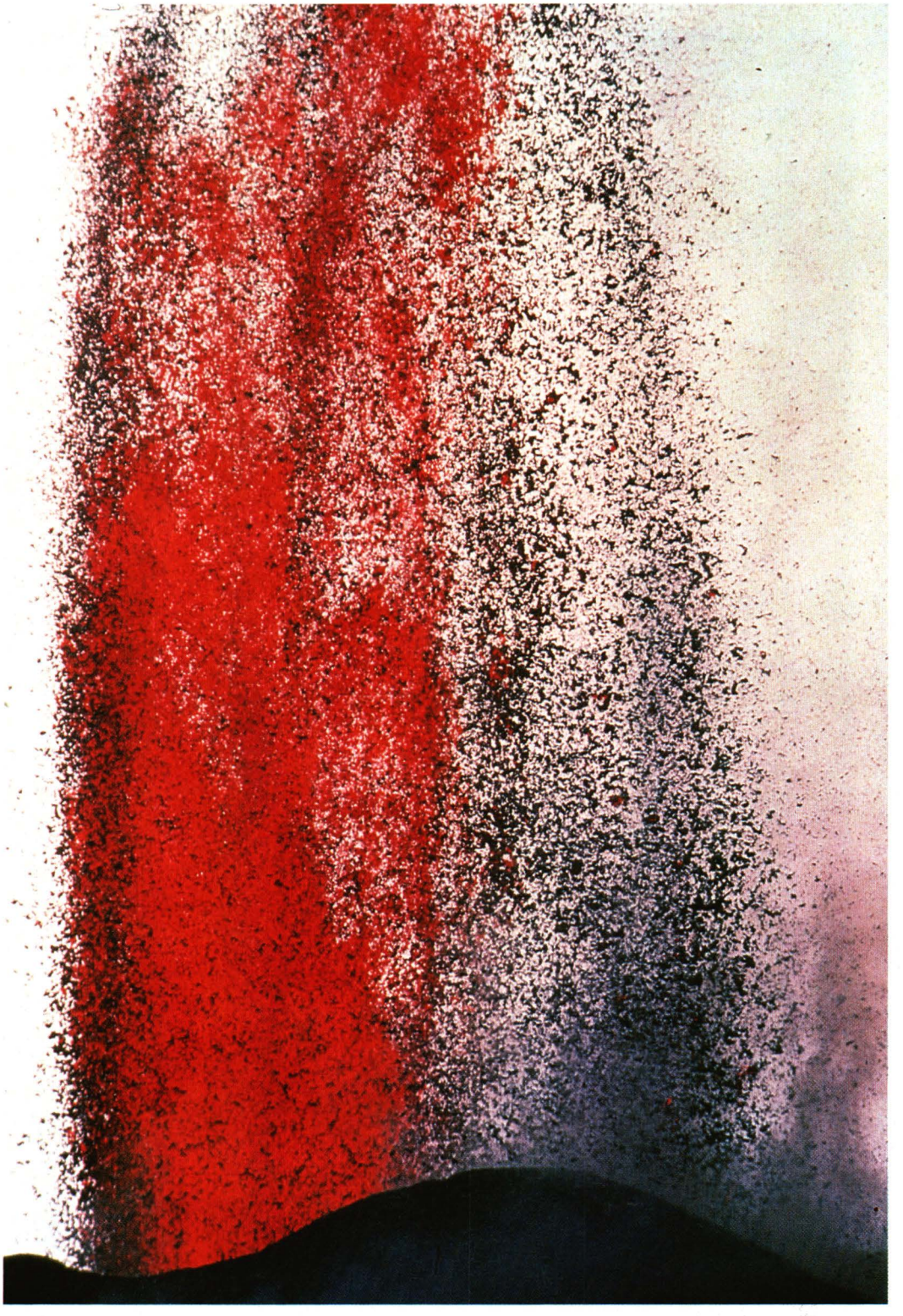

Tephra fall (dark material) from Puu Oo, east rift zone of Kilauea Volcano; the view to the east from Puu Kamoamoa (October 5, 1983, J.D. Griggs).

Tumulus

"A doming or small mound on the crust of a lava flow, caused by pressure due to the difference in rate of flow between the cooler crust and the more fluid lava below. Unlike a *blister* *** it is a solid structure."

Tumulus on Hilina Pali Road, south flank of Kilauea Volcano. The approximate diameter of the base of the tumulus is 10 m (September 23, 1984, J.D. Griggs, personal collection).

Vent

"The opening at the Earth's surface through which volcanic materials are extruded***."

Aerial view of Puu Oo vent (left) during the period between eruptive episodes, east rift zone of Kilauea Volcano; the view is to the southwest. Note scientists at the edge of the vent, which is 20–25 m wide and approximately 10 m deep to the incandescent area (January 24, 1985, J.D. Griggs). Aerial view of Puu Oo vent (right) at the end of an eruptive episode, east rift zone of Kilauea Volcano; the view is from the north side of the cone (April 22, 1985, J.D. Griggs).

Xenolith

"A foreign inclusion in an igneous rock."

Lava-encrusted xenoliths collected from Hualalai Volcano. The sample on the left is 14 cm long and that on the right, 10 cm across (November 1984, J.D. Griggs).

GEOPHYSICAL CONSTRAINTS ON THE STRUCTURE OF KILAUEA AND MAUNA LOA VOLCANOES AND SOME IMPLICATIONS FOR SEISMOMAGMATIC PROCESSES

By David P. Hill *and* John J. Zucca[1]

ABSTRACT

Seismic-refraction and gravity data on and adjacent to Kilauea and Mauna Loa Volcanoes show that the Cretaceous oceanic crust bends downward beneath the load of the volcanic edifice. Dip on the base of the crust (*M*-discontinuity) increases from 3° under the submarine flanks of the volcanoes to 6°–10° under the subaerial flanks; depth to the *M*-discontinuity increases from about 10 km beneath the open ocean to roughly 13 km and 18 km beneath the high, subaerial flanks of Kilauea and Mauna Loa, respectively. This profile of the oceanic crust is consistent with flexural-lithosphere models for flexural response to the load of the volcanoes. *P*-wave velocity structure of the volcano flanks supports the Moore-Fiske model for the volcanic pile, in which an inner wedge of submarine pillow basalt is covered by a mantle of halyoclastics and subaerial basalt flows. Fast *P*-wave traveltimes and positive gravity anomalies over rift zones and summit vent indicate that dense, intrusive cores to these structures form a significant mass-fraction of the volcanic edifice. The triangular shape of these intrusive cores supports the view that the volcanoes grow in part by the spreading of unbuttressed flanks along subhorizontal decoupling surfaces near the base of the volcanic pile in respones to forceful magma intrusion into the rift zones.

INTRODUCTION

The internal structure of the Hawaiian volcanoes and the underlying oceanic lithosphere hold important clues to processes governing the growth and contemporary seismomagmatic activity of these massive, midoceanic, basaltic shield volcanoes. Kilauea and Mauna Loa on the Island of Hawaii are of special interest in this regard because, together with Loihi Seamount 55 km south of Kilauea's summit, they are the youngest and most active volcanoes in the Hawaiian-Emperor volcanic chain, and they mark the present position of the Hawaiian hot spot beneath the Pacific plate (see Clague and Dalrymple, chapter 1).

Eaton (1962) first developed a model for the crustal structure of the Island of Hawaii using the traveltimes of *P*-waves recorded on seven seismic stations located at distances of 18–390 km from two magnitude 5 earthquakes that occurred beneath the southeast flank of Kilauea in 1955. His resulting one-dimensional model (velocity varying with depth only) for the average crustal structure of the Island of Hawaii indicated that the volcanoes forming the island rest on a slightly thickened oceanic crust, with the Mohorovicic (*M*) discontinuity at a depth of 14–15 km and with the upper most mantle having a *P*-wave velocity of 8.25 km/s. More recent efforts by Ward and Gregersen (1973), Crosson and Koyanagi (1979), and Klein (1981) to define an average velocity structure for Hawaii in terms of one-dimensional models are based on *P*-waves from a large number of local earthquakes recorded on an increasingly dense seismograph network. These models all place the *M*-discontinuity at depths between 13 and 16 km and indicate an upper mantle velocity of 8.2–8.3 km/s, in general agreement with Eaton's initial model. In these more recent models, however, the average depth to intermediate *P*-wave velocities (6.5–6.8 km/s) is significantly shallower (5–6 km) than the 11 km in Eaton's (1962) model.

An image of the three-dimensional structure of the Hawaiian volcanoes began to come into focus with the gravity survey of Hawaii by Kinoshita and others (1963), the series of seismic-refraction measurements around the island by Ryall and Bennett (1968), Hill (1969), Zucca and Hill (1980), and Zucca and others (1982), and the study of teleseismic *P*-wave delays by Ellsworth and Koyanagi (1977). Results from these experiments indicate that the central vents and rift zones of Kilauea and Mauna Loa are underlain by dense cores of intrusive rocks having high *P*-wave velocities (6.5–7.4 km/s) and reaching to within a few km of the surface; they further indicate that these intrusive cores represent a significant fraction of the volume of the volcanic pile forming the Island of Hawaii.

In this paper we reexamime some of the evidence from seismic-refraction experiments and gravity measurements on the structure of Kilauea and Mauna Loa Volcanoes. We will focus in particular on evidence concerning (1) the relation of the volcanic pile formed by the volcanoes to the underlying Cretaceous oceanic crust (upper lithosphere) and (2) the geometry of the dense intrusive masses forming cores beneath the summit vents and rift zones. We conclude

[1]Lawrence Livermore National Laboratory, Livermore, CA 94550.

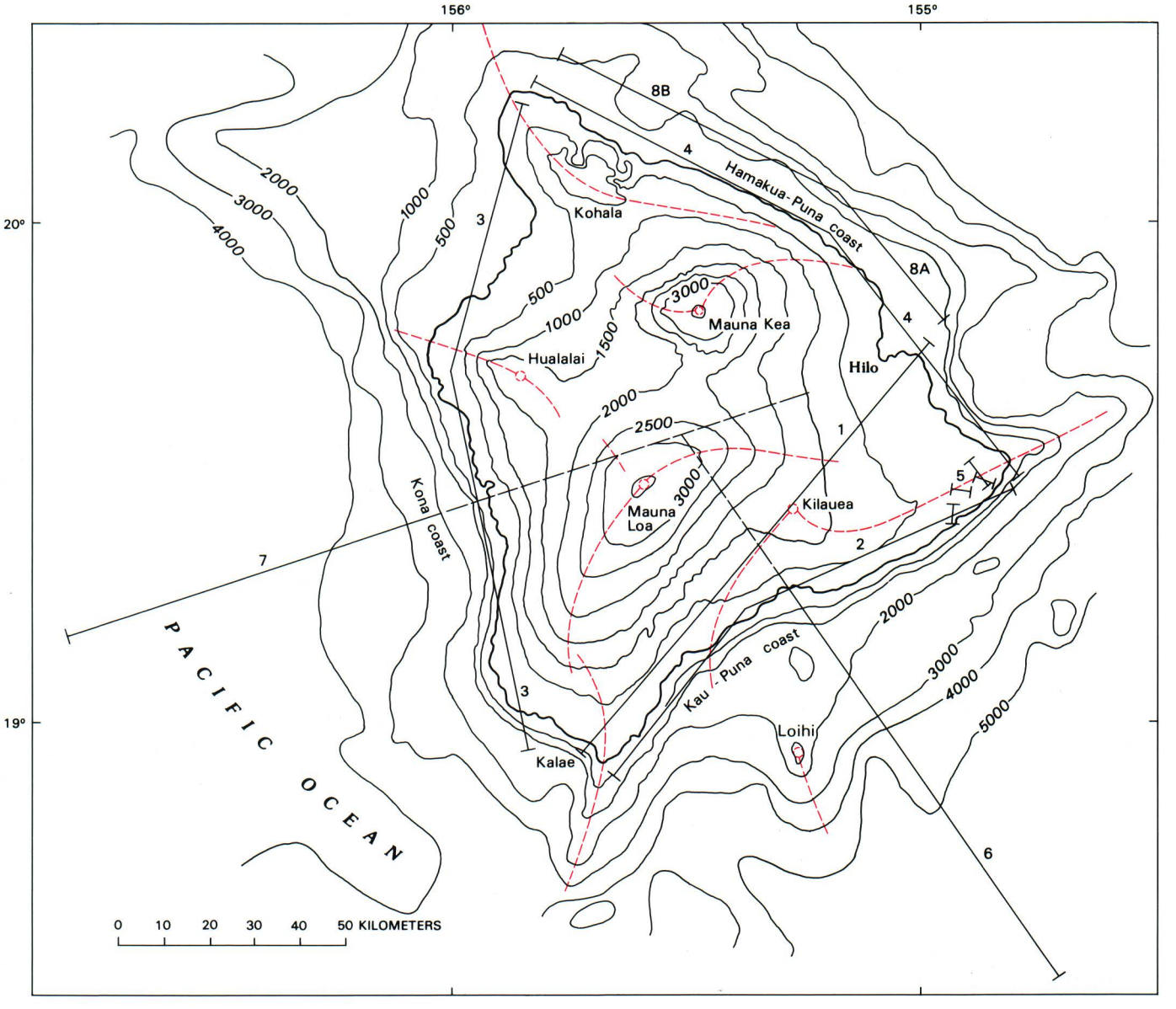

FIGURE 37.1.—The Island of Hawaii showing location of seismic-refraction profiles identified by number: 1, Ryall and Bennett (1968); 2–4, Hill (1969); 5, Broyles and others (1979); 6, Zucca and Hill (1980); 7, Zucca and others (1982); 8A–8B, Pollard and Eaton (1964). Dashed red lines, major rift zones. Elevation and depth contours in meters; contour interval 500 m on land, 1,000 m offshore.

with some thoughts on the significance of these structures for the processes governing the growth of Kilauea and Mauna Loa.

ACKNOWLEDGMENT

We are grateful to Alan Ryall for providing the traveltime data from the Hilo and Kaloe shot points.

SEISMIC-REFRACTION PROFILES

The locations of seismic-refraction profiles on and adjacent to the Island of Hawaii are shown in figure 37.1. With the exception of some of the short profiles across Kilauea's east rift zone done by the University of Hawaii (Broyles and others, 1979), all of the profiles were established using offshore shot points and onshore recording arrays. The permanent stations of the Hawaiian Volcano Observatory (HVO) seismic network form a common recording array for all of the profiles, although the number of stations in this array increased for successively later experiments as the HVO network grew with time (see Klein and Koyanagi, 1980). Additional portable stations were used to record the shots at either end of the profile across the summit of Kilauea (Ryall and Bennett, 1968), the series of shots forming the three coastal profiles (Hill, 1969), and the

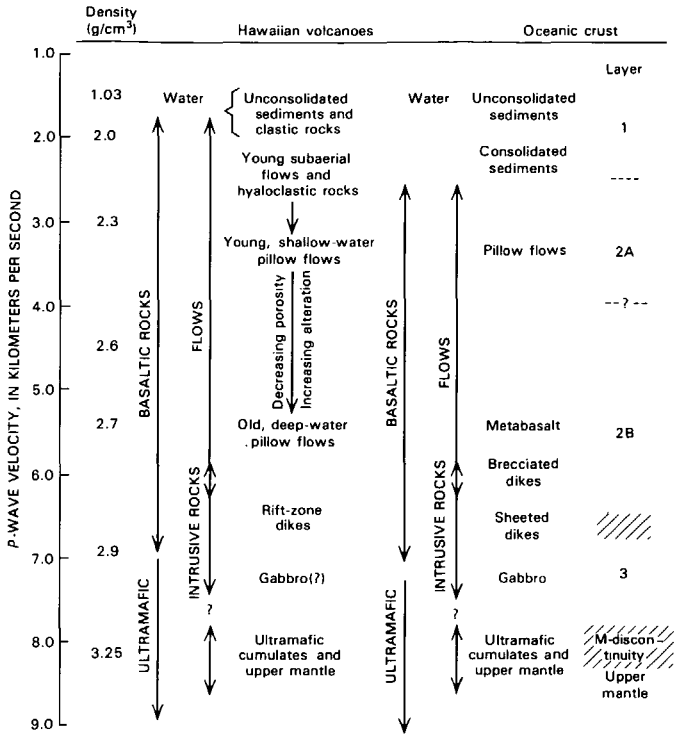

FIGURE 37.2.—Relation between *P*-wave velocity, rock density, and rock type for Hawaiian volcanoes and for oceanic crust. Density is used to compute gravity profiles in figures 37.7 and 37.8 (see Zucca and others, 1982). Moho is the M-discontinuity.

Mauna Loa offshore profile (Zucca and others, 1982). The series of shots perpendicular to the Kau-Puna coast (fig. 37.1, profile 6) were also recorded by two ocean-bottom seismographs deployed along the profile by the University of Hawaii (see Zucca and others, 1979).

These approximately linear seismic-refraction profiles are intrinsically two-dimensional. The internal structure of the volcanoes, however, is dominated by a roughly conical symmetry about the central vents. Profiles that cut obliquely across this dominant structure will be complicated by lateral (out-of-plane) reflections and refractions. Distortion in the interpretation from such out-of-plane ray paths will be more of a problem for coastal profiles than for profiles oriented radial to the central vents.

P-wave velocity structure serves as an important guide to subsurface rock types and geologic structure. The association of *P*-wave velocities with the rock types that we used in this paper for Kilauea and Mauna Loa Volcanoes and for the adjacent Cretaceous oceanic crust is illustrated in figure 37.2. This association is based on (1) published values of seismic velocities for rocks compiled by Christensen (1982), (2) petrographic models of the oceanic crust as described by Salisbury and Christensen (1978), and (3) recognition that the Hawaiian volcanoes consist almost entirely of basaltic rocks. Note in particular that *P*-wave velocities ranging from less than 2.0 km/s to more than 6.5 km/s on the Hawaiian volcanoes primarily reflect the wide variation in bulk porosity (bulk density) in rocks having essentially the same basaltic composition. The high bulk porosity in young, subaerial lava flows is produced by clinkery flow tops and bottoms, extensive sets of open fractures, large gas bubbles, and lava tubes; in older, deep-water pillow flows the porosity is reduced by alteration products that largely fill vesicles and cracks, and in basaltic dikes it is limited to small vesicles and intercrystalline cracks with dimensions of micrometers or less.

VOLCANIC FLANKS AND THE OCEANIC CRUST

The two offshore profiles that extend radially away from the volcanic centers (fig. 37.1, profiles 6, 7) define the base of the oceanic crust (the *M*-discontinuity) from the open ocean to the subaerial flanks of Kilauea and Mauna Loa. Interpretations of these profiles by Zucca and Hill (1980) and Zucca and others (1982), illustrated in figures 37.3 and 37.4, indicate that, beginning 50–60 km from shore, the oceanic crust dips at about 3° beneath the submarine flanks of the volcanoes. The depth to the *M*-discontinuity increases from 10–11 km beneath the unperturbed oceanic crust at distances greater than 50 km from the island to about 13 km under the southeast coast of Kilauea on the Island of Hawaii and 14–15 km under the west coast of Mauna Loa. Zucca and others (1982) inferred that the dip on the base of the crust increases toward the center of the island and is nearly 9° under the west (Kona) coast of Mauna Loa.

Structural details of the unperturbed oceanic crust beyond the submarine flank of Hawaii remain poorly resolved. The Mauna Loa radial profile does not have reversed seismic-refraction coverage, nor does the seaward half of the Kilauea radial profile. The structure for the oceanic crust shown in figures 37.3 and 37.4 is simply a seaward horizontal extension of the structure found for the oceanic crust beneath the distal end of the volcanic wedge in each case. For the Kilauea profile, this structure is based on reversed and overlapping

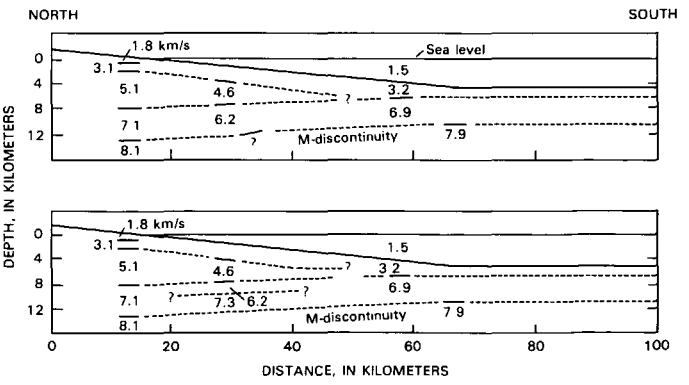

FIGURE 37.3.—*P*-wave velocity structure for the offshore profile perpendicular to the Kau-Puna coast of Kilauea (profile 6 in fig. 37.1). Numbers on profiles indicate *P*-wave velocity in kilometers per second. Upper and lower profiles show alternate interpretations of the traveltime data. Heavy lines and velocities at left (beneath the shoreline) indicate structure along the Kau-Puna coast from Hill (1969). Adopted from Zucca and Hill (1980).

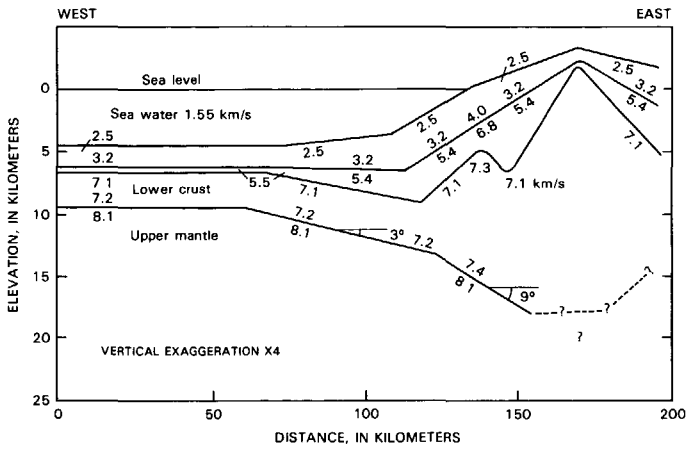

FIGURE 37.4.—*P*-wave velocity structure for the offshore profile perpendicular to the Kona coast of Mauna Loa (profile 7 in fig. 37.1). Inferred dip angle for base of crust shown for two parts of profile; other numbers on profile indicate *P*-wave velocity in kilometers per second. Adopted from Zucca and others (1982).

refraction coverage over the landward half of the profile (Zucca and Hill, 1982); for the Mauna Loa profile, however, it is based only on the overlapping (but unreversed) coverage provided by the array of onshore stations (Zucca and others, 1982). On the basis of the data from these profiles, we can say little more than the following: (1) The oceanic crust south and west of Hawaii is 5–6 km thick, with that west of Mauna Loa being slightly thinner than that southeast of Kilauea; (2) the *P*-wave velocity at the top of layer 2 is approximately 3.0 km/s, and layer 2 appears to be somewhat thicker west of Mauna Loa than it is southeast of Kilauea; and (3) the *P*-wave velocity in layer 3 (the deepest and thickest layer) is approximately 7.0 km/s. These data provide no direct information on the relatively thin sedimentary layer (layer 1) that covers the oceanic crust in the vicinity of the Hawaiian Islands (see Watts and others, 1985).

Our estimate of total thickness for the oceanic crust illustrated in figures 37.3 and 37.4 may be slightly low because the first arrival *P*-wave data did not sample the lower parts of layer 2. In most sections of the oceanic crust, the *P*-wave velocity in layer 2 increases rapidly with depth and averages about 5.6 km/s (see figure 37.2). If the average *P*-wave velocity in layer 2 in the vicinity of Hawaii is closer to 5.6 km/s than the 3.0–3.2 km/s value indicated by our first arrival data, we have underestimated the total crustal thickness by 1.0–1.4 km. In this case, the thickness of the oceanic crust off Hawaii is comparable to the 6.5-km thickness off of Oahu reported by Watts and others (1985).

The 7.9-km/s *P*-wave velocity for the uppermost mantle (P_n velocity) derived from the offshore Kilauea profile (fig. 37.3) is slightly lower than the 8.0- to 8.4-km/s values determined elsewhere beneath the Island of Hawaii and along the Hawaii-Emperor chain (Furumoto and others, 1968; Watts and others, 1985). Because the 7.9-km/s value is based both on reversed traveltime branches over the submarine flank of Kilauea and on clear P_n arrivals over the presumably flat oceanic crust beyond, we feel it is probably reliable. It is also consistent with evidence for anomalously low (by 1–2 percent) *P*-wave velocity in the top 35 km of the upper mantle off the southeast coast of Hawaii found by Ellsworth and Koyanagi (1977) in their three-dimensional inversion of teleseismic *P*-wave residuals recorded on Hawaii.

The wedge of volcanic products that forms the submarine flank of the volcanoes consists of an inner wedge having a *P*-wave velocity ranging from 4.6–5.4 km/s, which rests directly on the Cretaceous oceanic crust. Overlying this inner wedge is a blanket of material 1–3 km thick having a *P*-wave velocity of 3.0–3.2 km/s (see figs. 37.3, 37.4). This *P*-wave velocity structure is consistent with the model proposed by Moore and Fiske (1969) for the substructure of the volcano flanks from their study of dredge samples and ocean-bottom photographs. From the relation between *P*-wave velocities and rock types suggested in figure 37.2 and from the Moore-Fiske model, we infer that the inner wedge consists dominantly of deep-water pillow basalt and the overlying blanket consists dominantly of hyaloclastic rocks (vitric explosion debris, littoral-cone ash, and flow breccia). The shallower part of the 2.8–3.2-km/s layer probably also include young pillow flows and subaerial flows that have been submerged as the crust subsided in response to the growing load of the volcanoes.

Because we cannot distinguish the pillow flows and metabasalt forming layer 2 of the Cretaceous oceanic crust from the pillow flows and clastic rock that form the submarine flanks of the volcanoes on the basis of *P*-wave velocity (fig. 37.2), the position of the distal edge of volcanic debris from Kilauea and Mauna Loa remains ambiguous. The same is true for the position of the boundary between the bottom of the inner wedge of pillow lava and the top of layer 2. Moore (1964) has demonstrated that downslope movement in the form of massive submarine landslides is an important process on the steep submarine flanks of the Hawaiian volcanoes. This raises the possibility that the exceptional thickness of the 3.0-km/s layer in the oceanic crust off the coast of Mauna Loa (fig. 37.4) is due to accumulations of landslide debris extending well beyond the obvious break in slope at the distal end of the volcanic wedge.

The sections of the coastal seismic-refraction profiles interpreted by Hill (1969) that are not adjacent to major rift zones generally support the structural model for the flanks of the volcanoes based on the radial profiles just described (see fig. 37.5). Differences in structure between the coastal and radial profiles near their junction along the central section of the Kau-Puna coast are minor (figs. 37.3, 37.5).

Agreement between layer depths and *P*-wave velocities is not as close, however, for the coastal and radial profiles near their junction along the Kona coast on the west flank of Mauna Loa (see figs. 37.4, 37.5). The problem here probably lies with out-of-plane propagation paths complicating the two-dimensional interpretation of the coastal profile. This profile runs sub-parallel to a pronounced elongate gravity high located just inland of the Kona coast (see fig. 37.5), and it is likely that high *P*-wave velocity in the shallow crust associated with this gravity high provides a lateral, least-time path for seismic waves propagating between sources and receivers along the coast. Accordingly, we are inclined to place more confidence in the structure beneath the coast based on data from the radial profile

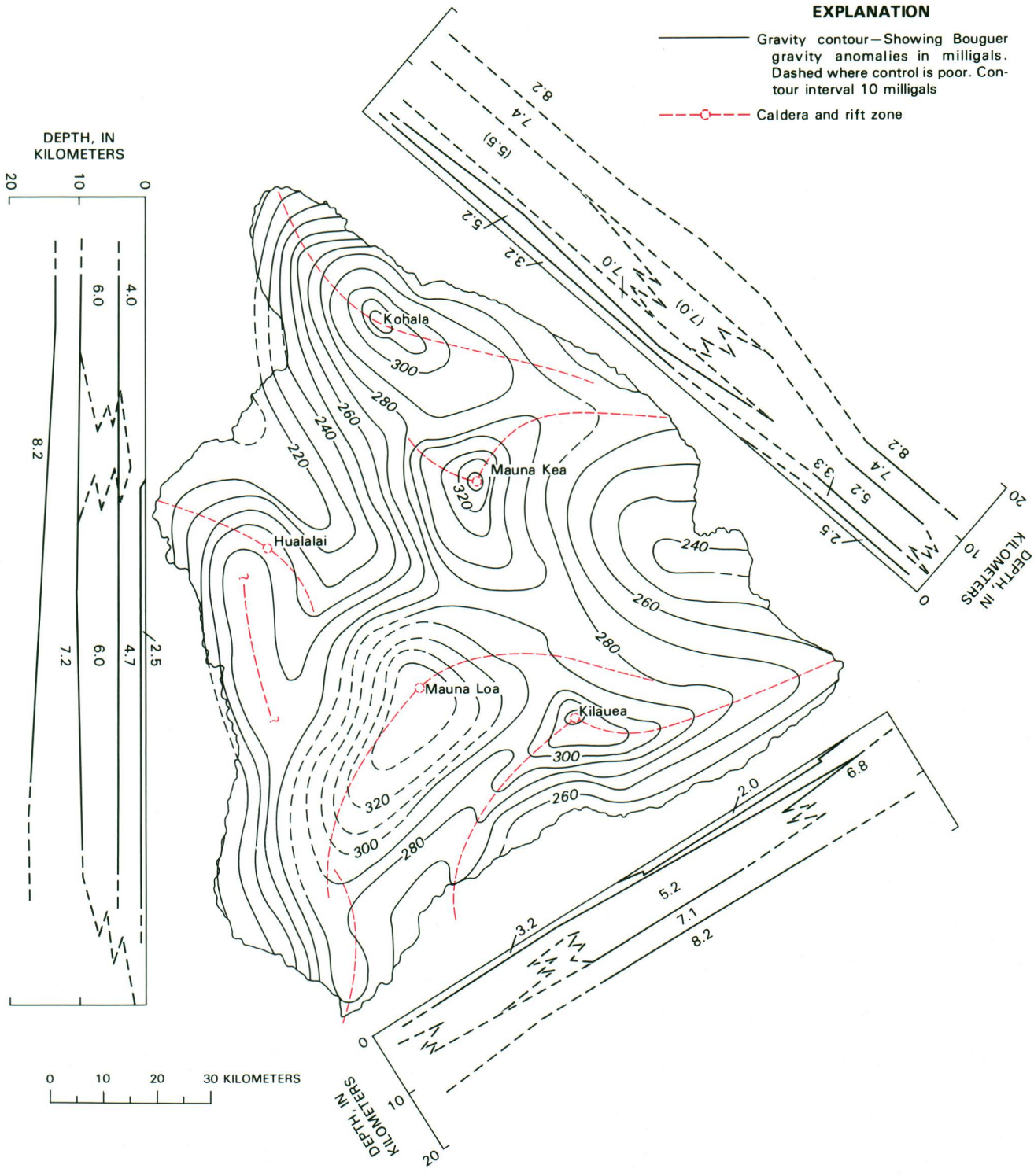

FIGURE 37.5.—Bouguer gravity map of Island of Hawaii (from Kinoshita and others, 1965) and *P*-wave velocity structure for the three coastal profiles (profiles 2–4 in fig. 37.1) around the island (adopted from Hill, 1969). Gravity contours dashed where control is poor; contour interval 10 milligals. Dashed red lines, major rift zones of the volcanoes.

(fig. 37.4) than in that based on the profile along the southern section of the Kona coast (fig. 37.5). In particular, we feel that the crustal thickness directly beneath the Kona coast west of Mauna Loa is closer to the 14 km indicated in figure 37.4 than to the 18 km indicated in figure 37.5 and that the layer depths and P-wave velocities for the southern section of the Kona profile in figure 37.5 give a poor image of the structure beneath the coast.

Results from profiles along the Hamakua-Puna coast (Hill, 1969) and from the Hilo-Kalae profile (Ryall and Bennett, 1968) indicate that the base of the crust deepens from about 13 km beneath Hilo to more than 15 km midway between Hilo and Kilauea and then appears to shallow again toward the summit region of Kilauea (figs. 37.1, 37.6). More than 10 km of effusive rocks with an average P-wave velocity of 5.3 km/s fill the resulting basin-like depression of the oceanic crust. This thick accumulation of rather porous flows is associated with a distinct gravity low centered just south of Hilo (fig. 37.5). Some of the deeper lava flows in this basin may be from Mauna Kea, but the bulk of the flows were probably fed by vents on Mauna Loa and, to a lesser degree, vents along the east rift zone of Kilauea. The increase in P-wave velocity from 3.3 to 5.2 km/s at about 2 km beneath the subaerial surface probably reflects reduced porosity due to alteration and compression; it is not necessarily the boundary between subaerial and pillow flows. Near intrusive cores, in particular, low-grade metamorphism between widely spaced dikes may markedly reduce the bulk porosity (and increase the P-wave velocity) in a mass dominated by hyaloclastic rocks and subaerial flows.

RIFT ZONES

The major rift zones of Kilauea and Mauna Loa are marked by elongate ridges sloping away from the respective summits and by strong, elongate gravity highs closely coincident with the topographic ridges (see figs. 37.1, 37.5). Topographic expression of the rift zones on the older volcanoes of the Island of Hawaii (Mauna Kea, Hualalai, and Kohala) tends to be masked by lava flows from scattered vents that developed in the later evolutionary stages of the volcanoes, but the expression of these older rift zones in the gravity field remains clear. The strong, elongate gravity high extending southward from Hualalai subparallel to the Kona coast, for example, probably defines the location of an ancient rift zone (from Hualalai?) now buried by lava flows from Mauna Loa's actively growing west flank.

As is evident from figures 37.1 and 37.5, seismic-refraction data on the substructure of the rift zones are limited to profiles that either terminate in the vicinity of a rift zone or run subparallel to the axial trend of a rift zone. Taken together, these data provide a patchwork image for the rift-zone substructure. That the rift zones are underlain by rocks with high P-wave velocities is indicated by the uniformly early arrival times for P-waves propagating along ray paths that penetrate the rift zones. Apparent velocities for first-arrival traveltime curves on profiles that closely parallel rift zones, such as those along the eastern section of the Kau-Puna coast or the northern half of the Hamakua coast (fig. 37.1), are typically 6.5–7.3 km/s (see Hill, 1969, figs. 3, 5, 10). The waves propagating with these high apparent velocities have almost certainly followed laterally refracted ray paths. Nevertheless, reversed traveltime branches limit depths to the high-velocity rocks to no more than 2–5 km. Because of lateral refraction, the apparent depth to the high-velocity rift-zone rocks plotted in the cross sections in figure 37.5 should be regarded as a perpendicular distance (slant depth) between the average surface trace of the seismic-refraction profile and the subsurface flank of the adjacent rift zone. The series of short seismic-refraction profiles across Kilauea's lower east rift zone established by Broyles and others (1979) provides clear evidence that rocks with high P-wave velocities beneath the rift zones are at shallow depths. Their results indicate that, along the axis of the rift zone, rocks with P-wave velocites of 7.0 km/s lie at depths of only 2.1–2.3 km beneath recent lava flows with P-wave velocities averaging about 3.0 km/s.

Available seismic-refraction data provide only loose constraints on the deeper structure of rift zones. In general, it appears that the mass of intrusive rocks forming the high-velocity core of a rift zone broadens with both depth and proximity to the central vent of the volcano. Zucca and Hill (1980), for example, have used the pattern of P_n delays recorded on selected stations of the HVO seismic network from the line of offshore shots southeast of Kilauea, together with average teleseismic residuals at the same stations reported by Ellsworth (1977), in an effort to put constraints on the deeper structure of the rift zones beneath Kilauea. The pattern of P_n and teleseismic delays along a line of stations crossing the central section of the east rift zone indicates that the high-velocity core increases in breadth from about 2 km near the surface to perhaps 13–14 km at depths of 8–9 km, where it merges with the oceanic crust. Based on these sparse data, the sides of the high-velocity rift-zone core have an effective slope of 45°–50° (see Zucca and Hill, 1980, fig. 8). Results from a similar profile crossing the southwest rift zone and extending to the summit of Mauna Loa indicate that there the breadth of the high-velocity core increases more rapidly with depth (effective slope 30°–40°) and the rift-zone core merges with the massive high-velocity core associated with the central vent of Mauna Loa at a depth of 5 km or less (see Zucca and Hill, 1980, fig. 9).

The Bouguer gravity data for the Island of Hawaii (fig. 37.5) also suggest that the dense cores beneath the rift zones broaden with depth (Kinoshita and others, 1963; Broyles and others, 1979). Dense, closely spaced gravity measurements, however, currently stop at the shoreline, where both the topographic and gravity gradients are still quite steep. Until the gravity field is better defined offshore, beyond the steep gradients and the submarine flank of the volcanoes, it is hardly worth attempting to model the gravity field in terms of detailed three-dimensional density structure of the intrusive cores of the volcanoes.

SUMMIT REGIONS AND CENTRAL CORES

The summits of both Mauna Loa and Kilauea contain large calderas, within which most summit eruptions occur. An elongate conduit system connects the summit vents and subjacent magma chamber located within the edifice of each volcano to magma sources in the upper mantle at depths of 40–60 km (Eaton and Murata,

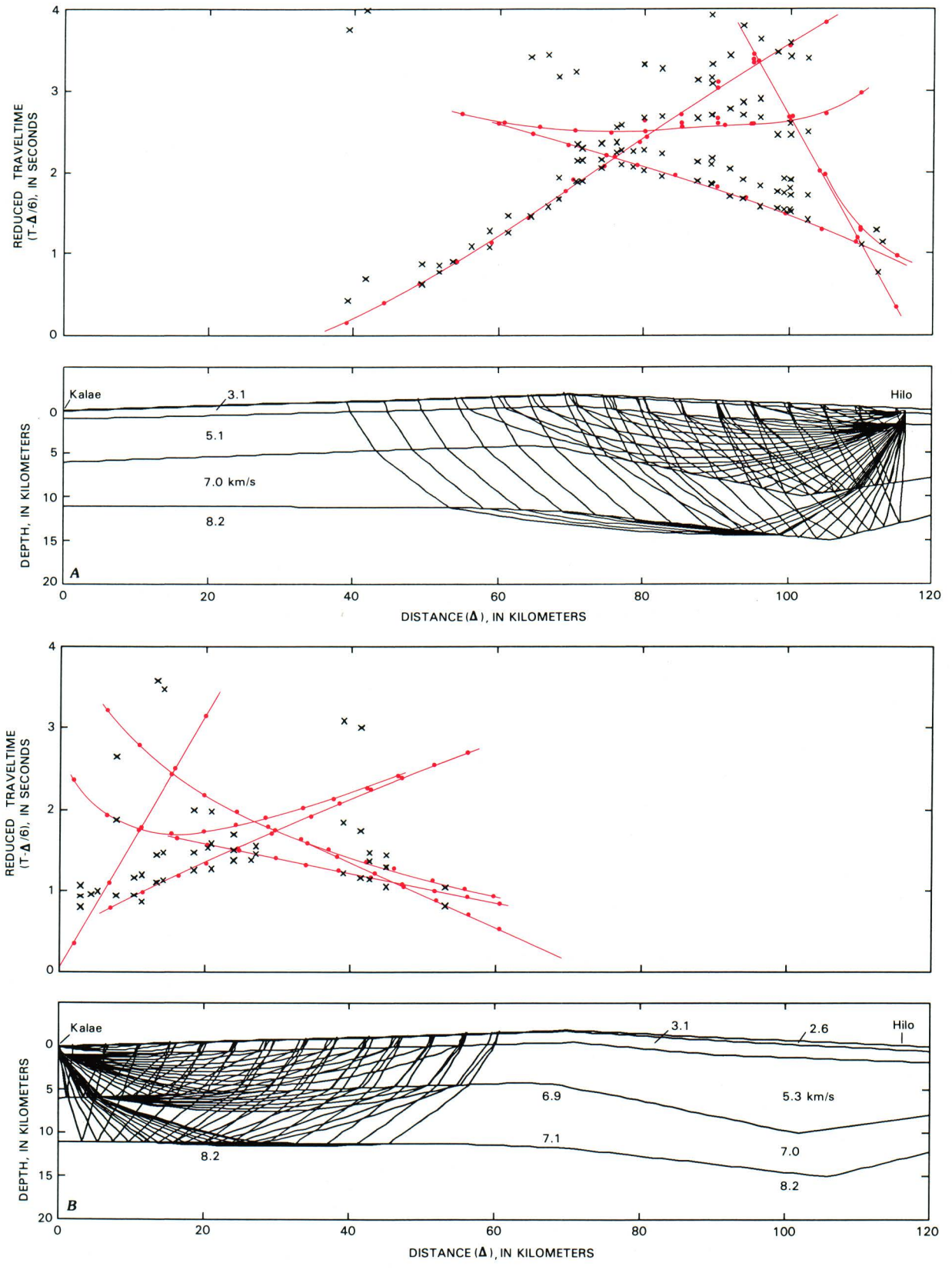

FIGURE 37.6.—Alternate interpretations of the traveltime data for the Hilo-Kalae profile of Ryall and Bennett (1968) across the summit of Kilauea (profile 1 in fig. 37.1). Interpretations done for shot point at Hilo (***A***) and shot point at Kalae (***B***). Upper diagram in each shows reduced traveltime data (crosses) and the computed traveltime curves (dots and red lines); traveltimes (T) are reduced by distance (Δ) divided by 6 km/s. Lower diagram in each shows *P*-wave velocity model and ray paths.

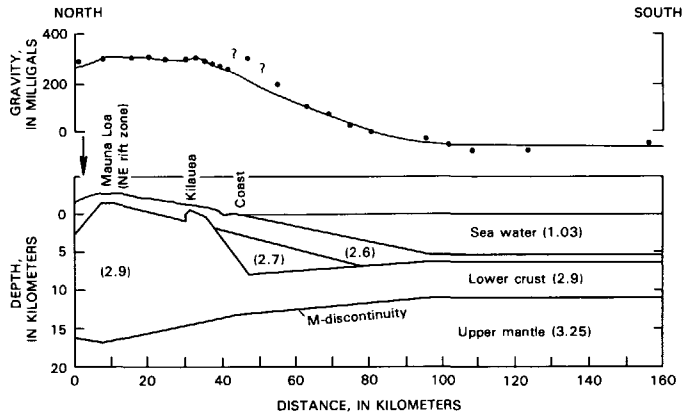

FIGURE 37.7.—Gravity profile and density structure along the offshore Kilauea profile (profile 6 in fig. 37.1) Dots, measured gravity values; gravity curve is that computed from the density model. Figures indicate density of layers in model, in grams per cubic centimeter. Arrow indicates intersection with the profile in figure 37.8. Adapted from Zucca and others (1982).

1960; Ryan and others, 1983). This conduit system forms a vertical axis about which the principal mass of each volcano has accumulated. A core of dense intrusive rock surrounds the conduit system and magma chamber within the summit edifice, producing the positive gravity anomalies over the summit area of each of the volcanoes (compare the topography and gravity fields in figs. 37.1 and 37.5).

The profile established by Ryall and Bennett (1968) between Kalae and Hilo passes immediately northwest of the summit of Kilauea Volcano (fig. 37.1). Although the opposing traveltime curves from the two shotpoints are not reversed (see fig. 37.6), they provide important clues on the deep crustal structure beneath the summit region of Kilauea.

Ryall and Bennett (1968) interpreted the Hilo-Kalae profile in terms of a major northwest-striking, northeast-dipping normal fault beneath the summit of Kilauea that offsets the oceanic crust by nearly 7.5 km and brings the base of the crust to within 10.3 km of the surface beneath the summit (Ryall and Bennett, 1968, fig. 7). We find that the traveltime data can also be fit rather well by a more continuous velocity structure that does not involve offset across a major crustal fault (fig. 37.6). In this structure, we interpret the thickening of a layer of velocity 6.9–7.1 km/s toward the summit region as due to intrusive cores of the southwest rift zone and the central conduit of Kilauea that lie just southeast of the profile where it crosses the summit. An intrusive core associated with the buried end of the Mauna Loa east rift zone may also contribute to the increased thickness of this layer northeast of Kilauea (see figs. 37.1, 37.5).

The profile extending northwest from Kalae runs subparallel to and about 5 km inland from the southeastern half of the Kau-Puna coastal profile (fig. 37.1). Both profiles show a similar structure for the 11 to 13-km-thick crust beneath the coastal flank of Mauna Loa between Kalae and the point where Kilauea's southwest rift zone intersects the coast (figs. 37.5, 37.6). The unreversed traveltime data from the Kalae profile, however, give no indication that the crust thickens significantly toward the summit of Kilauea, a result seemingly at odds with the evidence from the perpendicular profile (fig. 37.3) that the base of the crust dips at about 3° beneath the flank of Kilauea toward the summit region. Whether this apparent discrepancy means that the dip on the base of the crust flattens under the subaerial flank of Kilauea, or, as seems more likely, it reflects the level of uncertainty associated with the interpretation of these unreversed traveltime curves remains to be seen. In any case, the opposing traveltime data along the Hilo-Kalae profile indicate upper mantle *P*-wave velocities at fairly shallow depths (10–11 km below sea level) beneath the summit region of Kilauea. Thurber (chapter 38) finds independent evidence for unusually shallow depths of rocks with 8.0-km/s velocity beneath the summit of Kilauea in his inversion of local earthquake arrival-time data.

Constraints on the structure of the intrusive core beneath Mauna Loa derive from the onshore extensions of the two offshore radial seismic-refraction profiles (figs. 37.1, 37.3, 37.4). The *P*-wave velocity structure in figure 37.4 summarizes results obtained by Zucca and others (1982) from their inversion of the overlapping record sections from each of the nine stations forming the onshore section of the Mauna Loa profile passing just north of the summit. These results indicate that the mass of rocks with *P*-wave velocities of 7.0–7.3 km/s thickens dramatically toward the summit of Mauna Loa, beginning about 10 km west of the present coastline. The thickening occurs as a combination of an increased dip of the *M*-discontinuity and a decreasing depth to rocks with 7.0-km/s velocity toward the summit.

The fairly narrow zone of elevated *P*-wave velocity beneath the coast is consistent with but not required by the seismic-refraction data. A comparable zone of elevated density is required, however, by the elongate gravity high that extends southward along the coast from Hualalai (see fig. 37.5; Zucca and others, 1982). As mentioned in the previous section, this elongate zone of density and velocity probably corresponds to an ancient rift zone buried by the actively growing flank of Mauna Loa.

Unfortunately, none of the record sections on the Mauna Loa profile include waves that bottomed in the lower crust under the summit of Mauna Loa, and we are left with no information on the structure of the lower crust beneath the summit from these seismic-refraction data.

Further constraints on structural models for the Mauna Loa and Kilauea seismic-refraction profiles come from coincident gravity profiles, which Zucca and others (1982) constructed by joining the onshore (complete) Bouguer gravity data of Kinoshita and others (1963) with offshore free-air gravity data compiled by Watts and Talwani (1975). These profiles and their interpretation in terms of the density structure are reproduced in figures 37.7 and 37.8. Zucca and others (1982) modeled the density structure by assuming the relations between velocity and density summarized in figure 37.2 and modifying the layer configurations in the *P*-wave velocity models (figs. 37.3, 37.4) to obtain an acceptable fit between the computed and observed gravity profiles. They used a two-dimensional algorithm for computing the gravity field modified to approximate

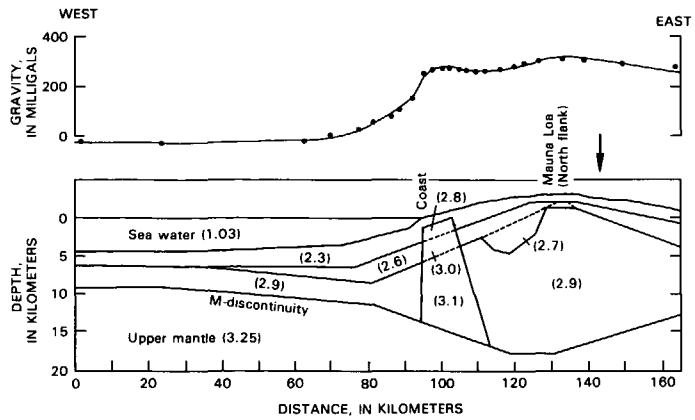

FIGURE 37.8.—Gravity profile and density structure along the offshore Mauna Loa profile (profile 7 in fig. 37.1). Dots, measured gravity values; gravity curve is that computed from the density model. Figures indicate density of layers in model, in grams per cubic centimeter. Arrow indicates intersection with profile in figure 37.7. Adapted from Zucca and others (1982).

the three-dimensional structure of the volcanoes by incorporating an approximate end correction developed by Cady (1977).

The density models in both profiles (figs. 37.7, 37.8) fit the gravity reasonably well, and the boundaries in the density models correspond closely to those in the *P*-wave velocity models of figures 37.3 and 37.4. Taken together, these velocity and density models indicate that the crust beneath Mauna Loa thickens to about 18 km toward the summit region and that the core of dense, high-velocity (intrusive) rocks is the dominant mass (and volume) forming Mauna Loa's central edifice.

DISCUSSION

GEOLOGIC SECTIONS

The cross sections in figures 37.9, 37.10, and 37.11 summarize our interpretation of the *P*-wave velocity structure and density structure of Mauna Loa and Kilauea in terms of geologic structures. Two possible geologic interpretations of the velocity structure along the profile crossing the summit of Kilauea from Kalae to Hilo are illustrated in figure 37.9*A*, *B*; a third possibility was shown in Ryall and Bennett (1968, fig. 7). These cross sections are drawn without vertical exaggeration, and the rock types illustrated are keyed to the *P*-wave velocity structure along corresponding seismic-refraction profiles by means of the relations indicated in figure 37.2.

The volcanoes are draped with a surficial blanket as much as 3 km thick that consists of young, subaerial basalt flows, shallow submarine flows, and clastic debris. As described by Moore and Fiske (1969), the submarine portions of this blanket (away from the submarine extensions of rift zones along which pillow flows predominate) consist mostly of clastic debris produced near sea level by the shattering of rapidly quenched lava flows and eruption of ash at littoral cones. Downslope movement in the form of massive submarine landslides carries this clastic debris to the distal ends of the submarine flank and onto the adjacent sections of the Cretaceous oceanic crust (Moore, 1964).

Older submarine pillow flows constitute the dominant effusive product of the volcanoes. These flows were erupted at depths of 100–500 m or more (Moore and Fiske, 1969) and have further submerged with the deflection of the lithosphere in response to the growing load of the volcanoes. Pillow flows probably make up the dominant fraction of the exceptionally thick sequence of effusive rocks in the basin-like depression between the east rift zones of Mauna Loa and Kilauea to the south and the east rift zone of Mauna Kea to the north (fig. 37.9).

The cores of the rift zones and summits of the volcanoes consist of a sequence of densely packed dikes analogous to the sheeted-dike complex forming the uppermost part of layer 3 in the oceanic crust (Salisbury and Christensen, 1978). These intrusive cores, which reach to within 2 km of the surface beneath the summit calderas and rift-zone axes, broaden with depth in a shape that is an exaggerated mimic of the overlying surface topography. The outer boundaries of the intrusive cores are no doubt transitional between altered effusive rocks with widely spaced dikes to a nearly solid mass of intrusive rocks. Walker (chapter 41) finds that, where the dense Koolau dike swarm is exposed on Oahu, most of this transition occurs within a distance of about 1 km. The wave lengths of the *P*-waves refracted by the intrusive rift-zone cores are 0.5–1.0 km for most of our data, and a 1-km-thick transition zone would appear as a relatively sharp boundary to these waves. At the other extreme, a poorly developed intrusive core such as that beneath Kilauea's southwest rift zone may be transitional across its entire width. In any case, though our sampling of the subsurface structure of these intrusive cores is still incomplete, it seems clear that they form an important fraction of the volume of Mauna Loa and Kilauea Volcanoes.

The orientation of the dikes within the intrusive cores reflects the direction of greatest horizontal principal stress at the time of their intrusion (Nakamura, 1977). Within the rift-zone cores, this direction is parallel or subparallel to the rift-zone axis (Fiske and Jackson, 1972). One might expect a more complex configuration of dikes within the summit cores. In the case of Kilauea, it appears as though the complexity in the orientation of more recently emplaced dikes is limited to a relatively small volume surrounding the current position of the central magma chamber beneath the southern margin of the summit caldera. Data from earthquake focal mechanisms (Endo, 1977; Thurber, chapter 38) and the orientation of fissures from recent eruptions (Holcomb, chapter 12) indicate that the stress field of the east rift zone (characterized by an east- to east-northeast-trending greatest horizontal principal stress axis) dominates both the northwest-trending upper east rift zone (see Hill, 1977) and much of the summit caldera. These same data indicate that the stress field of the southwest rift zone (characterized by a northwest trending greatest horizontal principal stress axis) extends only a short distance into the southern part of the summit caldera. The rather abrupt 30°–40° change in the orientation of the greatest horizontal principal stress where the stress fields from the two rift zones intersect coincides closely with the center of inflation for recent eruptive cycles and the current position of the central magma chamber (see Johnson,

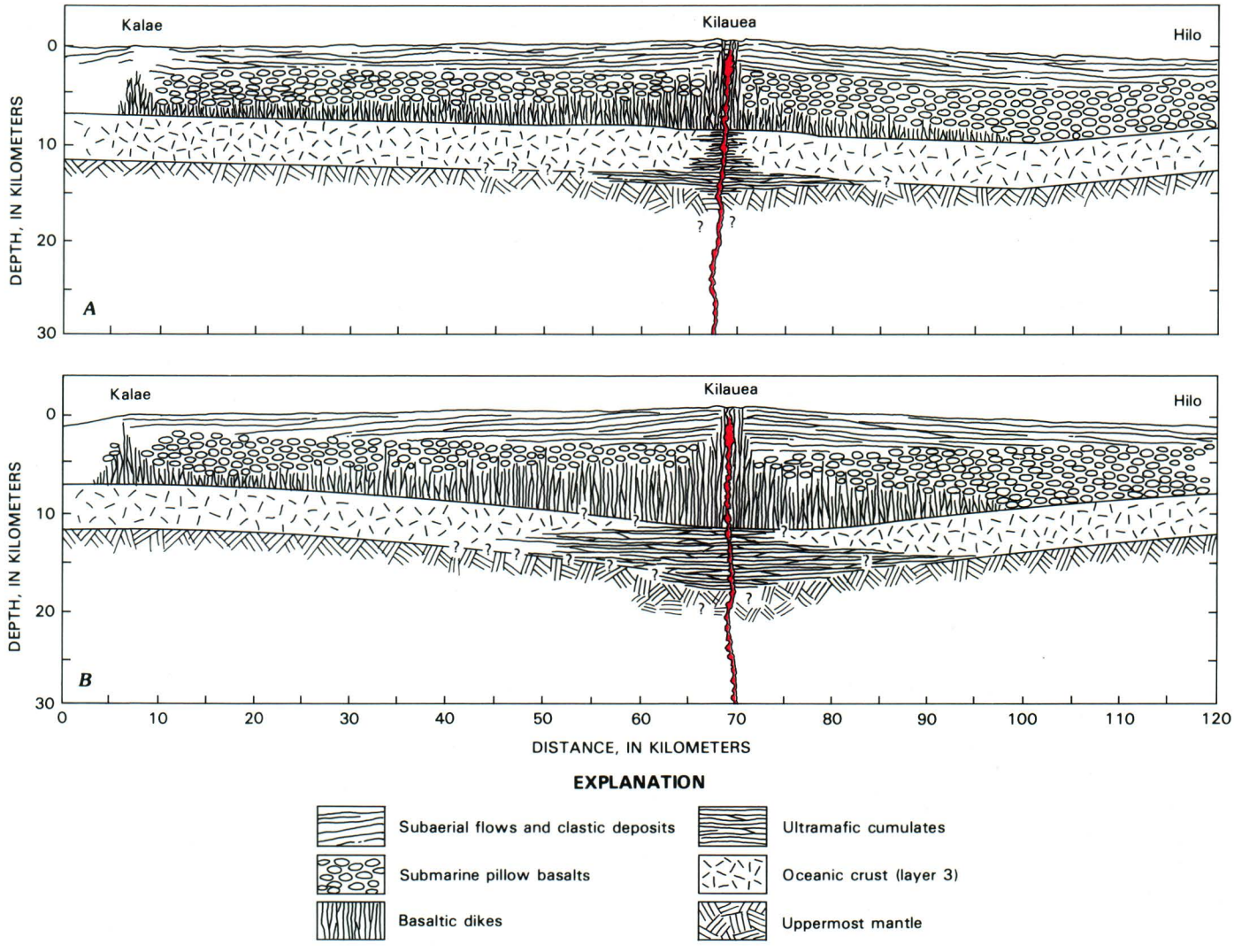

FIGURE 37.9.—Schematic cross sections showing two interpretations of the geologic structure along the Hilo-Kalae profile (profile 1 in fig. 37.1) based on *P*-wave velocity structure (see figs. 37.3, 37.6, 37.7). Main magma conduit and summit magma chamber indicated in red. The seismic profiles do not pass directly over the summit, and they provide no evidence for the small intrusive cupola included beneath the summit in these sections. ***A***, Interpretation involving little crustal depression and taking high-velocity material at depth beneath Kilauea to be the upper mantle. ***B***, Interpretation involving greater crustal depression and taking high-velocity material at depth beneath Kilauea to be ultramafic cumulate.

chapter 47). The stress field in the summit region may, of course, have had different orientations during earlier stages in the growth of the volcano, and the orientation of older (and deeper) dikes may therefore differ from that of dikes intruded under the influence of the present stress field.

Though dikes appear to be the dominant intrusive form in at least the outer portions of the intrusive cores, sills and somewhat larger, tabular bodies of gabbro are probably also locally important (see, for example, Ryan and others, 1983, p. 1452). Indeed, *P*-wave velocities near 7 km/s strongly suggest the presence of somewhat more mafic rocks such as pyroxene gabbro or olivine gabbro in the intrusive cores; *P*-wave velocities in basaltic (tholeiitic) dikes or sills seldom exceed 6.5 km/s under confining pressures lower than 200–300 MPa (Christensen, 1982). That isolated pockets of magma would be left in the rift zones to form gabbroic bodies seems plausible. The active intrusion of sills is limited to shallow depths in the volcanic edifice, where the overburden pressure forms a vertical least principal stress. It seems likely, for example, that the base of the intrusive cores may consist of a sequence of sills that were intruded below a fairly thin veneer of early pillow basalt on the oceanic crust.

The ultramafic cumulate forming a high-density, high-velocity inner core to the intrusive core of the volcanoes is the most speculative aspect of the structure suggested in figures 37.9 and 37.11. Its existence is consistent with but not required by the seismic-refraction data. Evidence from ultramafic inclusions in erupted basalt, however, indicates that early magma chambers must

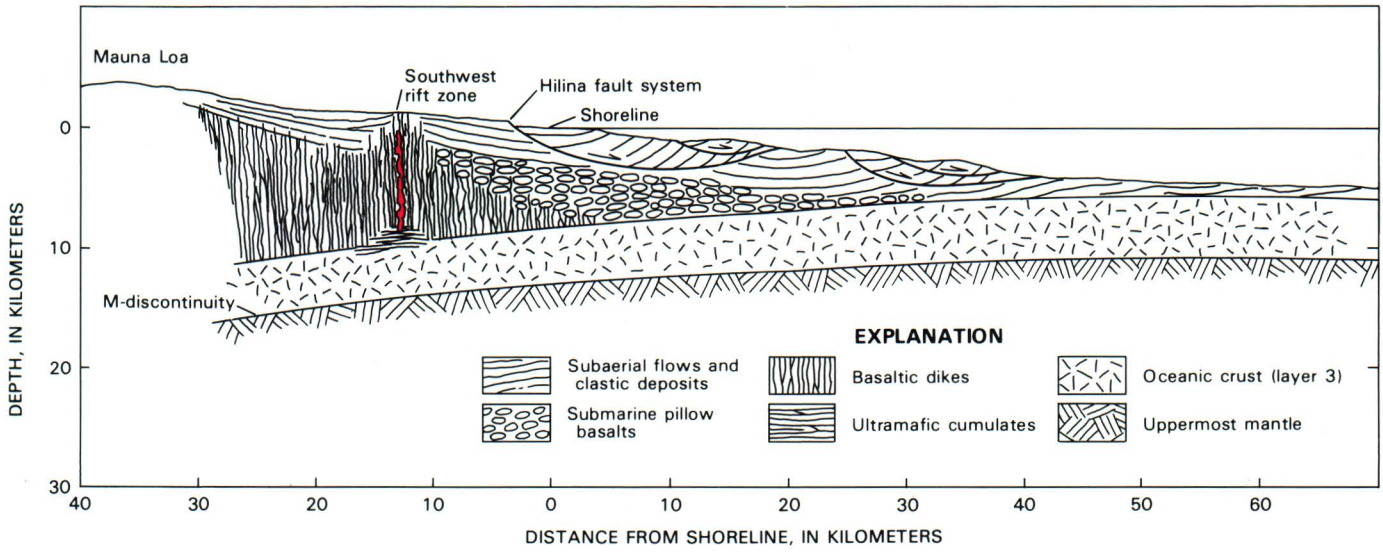

FIGURE 37.10.—Schematic cross section showing inferred geologic structure along the offshore Kilauea profile (profile 6 in fig. 37.1) based on *P*-wave velocity and density models in figures 37.3 and 37.7, respectively. Main magma conduit indicated in red.

have left a trail of residual ultramafic deposits as they migrated upward through the oceanic crust and volcanic pile during the construction of the submarine volcanic edifice (Jackson, 1968). The ultramafic cumulates shown in figure 37.9*A* are limited to a small volume around the central conduit. In this case, the base of the oceanic crust is only about 13 km below sea level under the summit of Kilauea, implying minimal deflection of the lithosphere under the load of Kilauea. In figure 37.9*B*, the ultramafic cumulate forms an extensive mass of sill-like bodies that have disrupted the depressed part of the oceanic crust beneath the summit region of Kilauea. The ultramafic cumulate has mantle-like *P*-wave velocity and its upper surface masquerades as the *M*-discontinuity beneath the summit region. Although we prefer this interpretation (fig. 37.9*B*) because it fits current ideas on the response of the oceanic lithosphere to the loads of the volcanoes, we cannot ignore the simpler interpretation (fig. 37.9*A*) of the Hilo-Kalae velocity structure (fig. 37.6*B*).

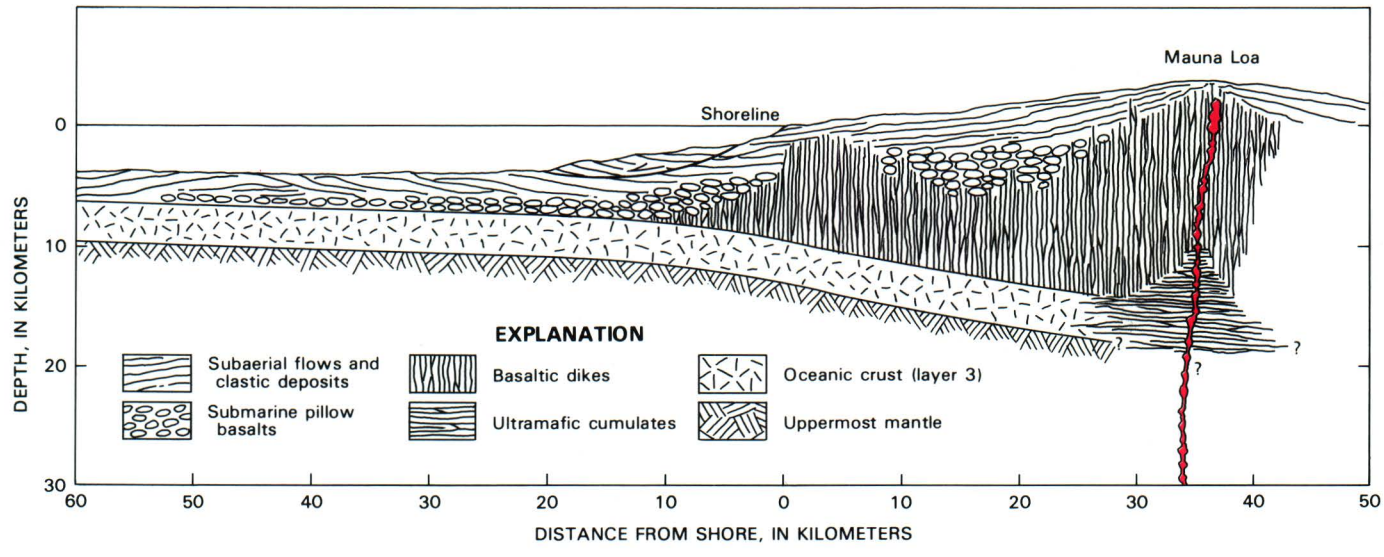

FIGURE 37.11.—Schematic cross section showing inferred geologic structure along the offshore Mauna Loa profile (profile 7 in fig. 37.1) based on *P*-wave velocity and density models in figures 37.4 and 37.8, respectively. Central magma conduit of Mauna Loa Volcano and its summit magma chamber shown in red.

It remains uncertain whether an inner core of ultramafic cumulate extending up to shallow depths under the central vents is an integral part of the Hawaiian volcanoes. The evidence described by Furumoto and others (1968) indicating protrusions of upper mantle *P*-wave velocity (7.7 km/s and above) to shallow depths beneath the center of the eroded core of Koolau Volcano on Oahu and beneath Penguin Banks (a submarine volcanic structure east of Molokai) is consistent with this possibility. Watts and others (1985) describe a body with *P*-wave velocity of 7.4–7.8 km/s as thick as 4 km that underlies the oceanic crust where their multichannel transect crosses the axis of the Hawaii-Emperor chain between Oahu and Molokai. They see no evidence in their data that this subcrustal body extends upward into the axis of the volcanic chain, but their transect does not cross the central vent of a major volcanic edifice.

The evidence for concave-downward curvature on the *M*-discontinuity and the oceanic crust under the subaerial flanks of Mauna Loa supports Walcott's (1970) model for the flexural response of the lithosphere to the load of the volcanoes. Watts and others (1985) find a similar result along the transect between Oahu and Molokai. The evidence for this model at Kilauea, however, is equivocal.

The 8.2-km/s *P*-wave velocity found from the P_n waves propagating in the uppermost mantle under the Island of Hawaii is typical of uppermost mantle elsewhere within the Pacific plate, implying that at least the upper section of the lithosphere beneath Hawaii has undergone little heating from either the Hawaiian hot spot or the narrow conduits that supply magma to the summit reservoirs of Mauna Loa or Kilauea. Immediately southeast of Kilauea, however, and directly over the current position of the hot spot, the P_n velocity is 7.9 km/s (Zucca and Hill, 1980) and the *P*-wave velocity is 8.0–8.1 km/s (1–2 percent low compared to 8.2 km/s) to depths of at least 35 km (Ellsworth and Koyanagi, 1977). Possible explanations for the anomalously low P_n velocity measured on the profile southeast of Hawaii include the following: (1) Anisotropic *P*-wave propagation in uppermost mantle (Zucca and Hill, 1980) similar to that reported by Shor and others (1970) for an area northeast of Oahu; and (2) the presence of a small velocity gradient at the top of the mantle such that P_n apparent velocity recorded at short distances (less than 100 km) would be somewhat lower than that recorded at greater distances (Zucca and others, 1982).

A third possiblility is that the low, lithospheric mantle *P*-wave velocity is related to the hot spot within the underlying asthenosphere. For this to be true, however, the effect must involve mechanical disruption of the upper lithosphere. Thermal conduction alone cannot supply measurable heat to the shallow parts of the lithosphere directly above the hot spot when the relative motion between the lithosphere and the hot spot is on the order of 10 cm/yr as is the case for Hawaii. Mechanical disruption of the lithosphere might be related to the southeastward progression of the flexural front associated with the growing loads of Kilauea and Loihi on the oceanic crust (see Moore, chapter 2). In principle, mechanical disruption of the lithosphere would also allow the rapid transfer of heat into the upper lithosphere by the upward migration of hot fluids from the asthenosphere. Conceivably, the low *P*-wave velocity off the southeast coast of Kilauea represents an early stage in the development of the subcrustal body with velocity of 7.4–7.8 km/s described by Watts and others (1985). Their subcrustal body, however, extends at least 100 km on either side of the ridge axis, and we see no evidence for reduced subcrustal velocity under the flanks of Mauna Loa. At this stage, we do not have adequate data to clearly discriminate between these several possibilities.

GROWTH OF THE VOLCANIC PILE AND INTRUSIVE CORES

Moore and Fiske (1969) have outlined clearly the events in the growth of the effusive portion of a Hawaiian volcanic edifice: (1) progressive accumulation of pillow basalt flows fed by submarine vents; (2) mantling of the pile of pillow flows by hyaloclastic rocks produced when the vents reach within a few hundred meters of sea level; (3) progressive accumulation of subaerial flows as the central vents emerge above sea level, accompanied by continued production of hyaloclastic rocks where subaerial flows reach the sea; and (4) large-scale submarine slumping that transports the hyaloclastic rocks to the base of the volcanic pile and beyond.

The triangular cross section of the intrusive cores is most readily explained if the rift zones and central vents behave as spreading centers. Indeed, accumulating evidence indicates that spreading plays a central role in the growth of Hawaiian volcanoes. Swanson and others (1976) present a convincing case that the entire south flank of Kilauea Volcano has moved progressively upward and southward over the underlying oceanic crust in response to repeated episodes of forceful magma intrusion into both the summit region and east rift zone. The displacements associated with the magnitude 7.1 Kalapana earthquake of November 29, 1975, which indicate that the south flank of Kilauea moved 2–3 m southward on a low-angle plane at a depth of 8–10 km, add considerable support to this concept (Ando, 1979; Furumoto and Kovach, 1979; Nakamura, 1980).

A series of idealized structural cross sections (fig. 37.12) incorporate the concept suggested by Swanson and others (1976) together with the internal structure of rift zones summarized in figures 37.9–37.11 to illustrate sucessive stages in the growth of a rift zone. In this case the active core of the rift zone (the spreading center) moves away from the buttressed flank and pushes the unbuttressed (mobile) flank ahead of it over the oceanic crust. This process produces an intrusive core that broadens with depth as the progressively older dikes, which were injected into a progressively older and lower edifice, become further displaced from the zone of active intrusion (spreading).

If spreading within the rift-zone core were symmetric (that is, new dikes were nearly always injected midway between the next most recent series of intrusions). the mobile flank would move away from the buttressed flank at twice the rate of the active rift zone (twice the one-sided spreading rate). In the case of Kilauea, at least, it appears that active intrusion preferentially occurs on the side of the mobile flank, producing an asymmetric profile for both the rift-zone core (reflected in the gravity field) and the rift-zone topography (Swanson and others, 1976). In the absence of buttressing, the rift-zone axis would presumably remain stationary with respect to the under-

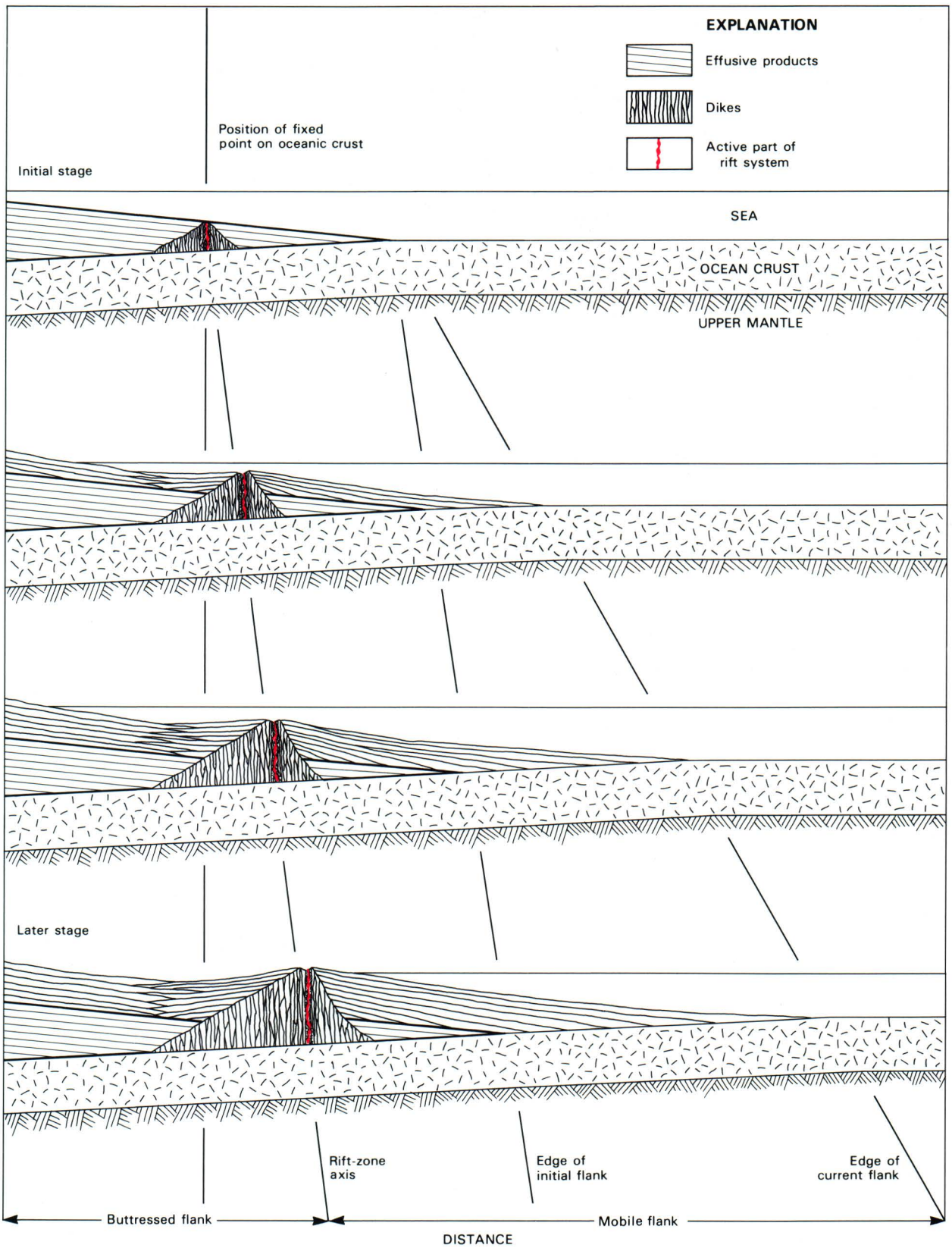

FIGURE 37.12.—Space-time diagram illustrating successive stages in the growth of a rift zone on a volcano's flank. Corresponds approximately to the east rift zone of Kilauea, buttressed on the north (here left) side by the still-growing flank of Mauna Loa. Heavy lines show successive configurations of the initial flank. Decoupling surface assumed to be at top of oceanic crust.

lying oceanic crust and both flanks would move away from the rift-zone spreading center at equal rates, resulting in symmetric topographic and core profiles.

One consequence of this process is that the axis of a rift zone with one buttressed flank will migrate with respect to the more stable position of a summit vent or the axis of a rift zone with two unbuttressed flanks. Indeed, the northward bend in Kilauea's upper east rift zone (see fig. 37.1) probably reflects the southward migration of the east rift zone with respect to the summit vent (Swanson and others, 1976). Similarly, the left-stepping offset in Mauna Loa's southwest rift zone probably reflects the westward migration of the upper part of the rift zone, which is buttressed on the east by Kilauea, with respect to the lower part, which has two unbuttressed flanks (Lipman, 1980).

The location and nature of the decoupling surface (or surfaces) along which the mobile flanks of the rift zones move under this process remains a matter of discussion. We feel that the most likely candidate for this surface is the sedimentary layer of the oceanic crust, as was suggested by Ando (1979), Furomoto and Kovach (1979), Nakamura (1980), and Zucca and Hill (1980). If this layer of abyssal ooze and clay were left more or less intact as the initial flows of pillow basalt were erupted onto the ocean floor, it would form a preexisting weak surface for later displacement between the oceanic crust and the overlying volcanic pile. Swanson and others (1976), however, suggest that decoupling occurs over a zone within the lower section of pillow basalt somewhere near the base of the volcanic pile. Fault plane solutions for the 1975 Kalapana earthquake show slip on a low-angle plane at about the proper depth for the sedimentary layer at the top of the oceanic crust beneath the southeast flank of Kilauea. Furumoto and Kovach (1979) conclude that the fault plane dips about 4° toward the island consistent with the local dip on the top of the oceanic crust. Ando (1979), however, concludes that the fault plane dips about 20° away from the island. Ando's solution is constant with a decoupling surface within the pillow basalt along the lines proposed by Swanson and others (1976). The differences between these two solutions to a large degree reflects the uncertainties involved in determining the dip on the fault plane of a large, shallow earthquake in a region with strong lateral variations in both velocity structure and topography.

We envision that the intrusive core beneath a central vent grows in much the same manner as suggested for the intrusive core within a rift zone. The principal differences are presumably that growth of the summit core would tend to develop with conical symmetry about the central conduit (in contrast to planar symmetry across the rift-zone axis) and the position of the central vent would be anchored by the deep-seated central conduit system. The angles with which rift zones intersect the summit region would no doubt strongly influence the growth pattern within the central core.

Many of the processes occurring at an actively spreading rift zone must be analogous with those occurring at the spreading center of a midocean ridge. In particular, it seems likely that the deeper parts of a rift zone might resemble a small-scale ophiolite sequence complete with pillow basalt, sheeted dikes, gabbroic bodies, and perhaps even layered ultramafic cumulate near the base of the complex. Spreading associated with the Hawaiian volcanoes, however, is a superficial process limited to the volcanic pile on top of the oceanic crust and underlying lithosphere.

CONCLUSIONS

The seismic-refraction and gravity data reviewed in this paper provide some important clues to the structure of Kilauea and Mauna Loa Volcanoes, but critical details remain blurred. These data make clear that the intrusive cores to the summit regions and rift zones form a significant mass fraction of the volcanic edifice. Reliable estimates of this fraction, however, will require better definition of intrusive core morphology by seismic techniques and by densely spaced gravity measurements over the submarine flanks of the volcanoes. The wedge shape of the intrusive cores supports the idea that spreading plays an important role in the growth of the volcanic edifice. This spreading involves the lateral displacement of unbuttressed flanks over the oceanic crust in response to forceful magma intrusion in rift zones. Understanding the details of this process, however, demands a sharper image of the intrusive-core structure and better constraints on the nature of the decoupling zone between the mobile flanks and the oceanic crust. The profile of the oceanic crust beneath the volcanic pile appears to be consistent with the bending of a fractured lithosphere in response to the load of the pile. Clear delineation of the strongly three-dimensional structure of the deep crust beneath the volcano summits, however, presents a special challenge to high-resolution seismic and gravity techniques.

REFERENCES CITED

Ando, M., 1979, The Hawaii earthquake of November 29, 1975: low dip angle faulting due to forceful injection of magma: Journal of Geophysical Research, v. 84, p. 7616–7626.

Broyles, M.L., Suyenaga, W., and Furumoto, A.S., 1979, Structure of the lower east rift zone of Kilauea Volcano, Hawaii, from seismic and gravity data: Journal of Volcanology and Geothermal Research, v. 5, p. 317–336.

Cady, J.W., 1977, Calculation of gravity and magnetic anomalies along profiles with end corrections and inverse solutions for density and magnetization: U.S. Geological Survey Open File Report 77–463, 110 p.

Christensen, N.I., 1982, Seismic velocities; *in* Carmichael, R.S. ed., Handbook of physical properties of rocks, v. II: Boca Raton, CRC Press p. 2–228.

Crosson, R.S., and Endo, E.T., 1982, Focal mechanisms and locations of earthquakes in the vicinity of the 1975 Kalapana earthquake aftershock zone 1970–1979: implications for tectonics of the south flank of Kilauea Volcano, Island of Hawaii: Tectonics, v.l, p. 495–542.

Crosson, R.S., and Koyanagi, R.Y., 1979, Seismic velocity structure below the Island of Hawaii from earthquake data: Journal of Geophysical Research, v. 84, p. 2331–2342.

Eaton, J.P., 1962, Crustal structure and volcanism in Hawaii, *in* The Crust of the Pacific Basin: American Geophysical Union Monograph, v. 6, p. 13–29.

Eaton, J.P., and Murata, K.J., 1960, How volcanoes grow: Science, v. 132, p. 925–936.

Ellsworth, W.L., and Koyanagi, R.Y., 1977, Three-dimensional crust and mantle structure of Kilauea Volcano, Hawaii: Journal of Geophysical Research, v. 82, p. 5379–5394.

Endo, E.T., 1971, Focal mechanisms for the May 15–18, 1979, shallow Kilauea earthquake swarm: San Jose, Calif., San Jose State University, M.S. thesis, 165 p.

Fiske, R.S., and Jackson, E.D., 1972, Orientation and growth of Hawaiian volcanic rifts: the effect of regional structure and gravitational stress: Proceedings of the Royal Society of London, Series A, v. 329, p. 299–326.

Furumoto, A.S., and Kovach, R.L., 1979, The Kalapana earthquake of November 29, 1975: an intraplate earthquake and its relation to geothermal processes: Physics of the Earth and Planetary Interiors, v. 18, p. 197–208.

Furumoto, A.S., Wollard, G.P., Campbell, J.F., and Hussong, D.M., 1968, Variations in the thickness of the crust in the Hawaiian Archipelago, *in* Knopoff, L., Drake, C.L., and Hart, P.J., eds., Crust and upper mantle of the Pacific area: Washington D.C., American Geophysical Union, Geophysical Monograph 12, p. 94–111.

Hill, D.P., 1969, Crustal structure of the Island of Hawaii from seismic-refraction measurements: Bulletin of the Seismological Society of America, v. 59, p. 101–130.

——— 1977, A model for earthquake swarms: Journal of Geophysical Research, v. 82, p. 1347–1352.

Jackson, E.D., 1968, The character of the lower crust and upper mantle beneath the Hawaiian Islands: International Geological Congress, v.I, p. 135–150.

Kinoshita, W.K., Krivoy, H.L., Mabey, D.R., and MacDonald, R.R., 1963, Gravity survey of the Island of Hawaii: U.S. Geological Survey Professional Paper 475–C, p. C114–C116.

Klein, F.W., 1981, A linear gradient crustal model for south Hawaii: Bulletin of the Seismological Society of America, v. 71, p. 1503–1510.

Klein, F.W., and Koyanagi, R.Y. 1980, Hawaiian Volcano Observatory seismic network history 1950–1979: U.S. Geological Survey Open File Report 80–302, 84 p.

Lipman, P.W., 1980, The southwest rift zone of Mauna Loa: implications for structural evolution of Hawaiian volcanoes: American Journal of Science, v. 280–A, p. 752–776.

Moore, J.G., 1964, Giant submarine landslides on the Hawaiian ridge: U.S. Geological Survey Professional Paper 501–D, p. D95–D98.

Moore, J.G., and Fiske, R.S., 1969, Volcanic substructure inferred from dredge samples and ocean-bottom photographs, Hawaii: Geological Society of America Bulletin, v. 80, p. 1191–1202.

Nakamura, K., 1977, Volcanoes as possible indicators of tectonic stress orientation—principal and proposal: Journal of Volcanology and Geothermal Research, v. 2, p. 1–16.

——— 1980, Why do long rift zones develop in Hawaiian volcanoes— a possible role of thick oceanic sediments (in Japanese): Bulletin of the Volcanological Society of Japan, v. 25, p. 255–267.

Pollard, D.D., and Eaton, J.P., 1964, Crustal structure of the Island of Hawaii [abs.]: Geological Society of America Special Paper 76, p. 218.

Ryall, A.S., and Bennett, D.L., 1968, Crustal structure of southern Hawaii related to volcanic processes in the upper mantle: Journal Geophysical Research, v. 73, p. 4561–4582.

Ryan, M.P., Blevins, J.Y.K., Okimura, A.T., and Koyanagi, R.Y., 1983, Magma reservoir subsidence mechanics: theoretical summary and application to Kilauea Volcano, Hawaii: Journal of Geophysical Research, v. 88, p. 4147–4181.

Ryan, M.P., Koyanagi, R.Y., and Fiske, R.S., 1981, Modeling the three-dimensional structure of macroscopic magma transport systems: Application to Kilauea Volcano, Hawaii: Journal of Geophysical Research, v. 86, p. 7111, 7129.

Salisbury, M.H., and Christensen, N.I., 1978, The seismic velocity of a traverse through the Bay of Islands ophiolite complex, Newfoundland, an exposure of oceanic crust and upper mantle: Journal of Geophysical Research, v. 83, p. 805–817.

Shor, G.G., Menard, H.W., and Raitt, R.W., 1970, Structure of the Pacific Basin, *in* Maxwell, A.E., ed., The sea; ideas and observations on progress of the seas: Interscience, New York, v. 4, part II, p. 3–27.

Swanson, D.A., Duffield, W.A., and Fiske, R.S., 1976, Displacement of the south flank of the Kilauea Volcano: the result of forceful intrusion of magma into the rift zones: U.S. Geological Survey Professional Paper 963, 39 p.

Walcott, R.I., 1970, Flexure of the lithosphere at Hawaii: Tectonophysics, v. 9, p. 435–446.

Ward, P.L., and Gregersen, S., 1973, Comparison of earthquake locations determined with data from a network of stations and small tripartite arrays on Kilauea Volcano, Hawaii: Bulletin of the Seismological Society of America, v. 63, p. 679–711.

Watts, A.B., and Talwani, M., 1975, Gravity field of the northwest Pacific Ocean basin and its margin, Hawaii and vicinity: Geological Soceity of America MC–9, 6 p.

Watts, A.B., ten Brink, U.S., Buhl, P., and Brocher, T.M., 1985, A multichannel seismic study of lithospheric flecture across the Hawaii Emperor seamount chain: Nature, v. 315, p. 105–111.

Zucca, J.J., and Hill, D.P., 1980, Crustal structure of the southeast flank of Kilauea Volcano, Hawaii, from seismic refraction measurements: Bulletin of the Seismological Society of America, v. 70, p. 1149–1159.

Zucca, J.J., Hill, D.P., and Duennebier, F.K., 1979, A compilation of the data from the 1976 Hawaii seismic refraction experiment: U.S. Geological Survey Open-File Report 79–711, 30 p.

Zucca, J.J, Hill, D.P., and Kovach, R.L., 1982, Crustal structure of Mauna Loa Volcano, Hawaii, from seismic refraction and gravity data: Bulletin of the Seismological Society of America, v. 72, p. 1535–1550.

SEISMIC STRUCTURE AND TECTONICS OF KILAUEA VOLCANO

By Clifford H. Thurber [1]

ABSTRACT

Local earthquake data have been used to study the internal structure and tectonics of Kilauea Volcano. A three-dimensional model of Kilauea's seismic velocity structure, determined using simultaneous inversion techniques, reveals features on a scale of one to a few kilometers. The core and rift zones of the volcano are marked by relatively high seismic velocity; a small, shallow, aseismic low-velocity zone beneath the summit coincides with the inferred locus of the summit magma reservoir. High-quality fault plane solutions have been derived for a suite of local earthquakes using this three-dimensional model. The spatial variations in focal mechanisms provide information on the complex tectonics of the volcano; the temporal variations in mechanisms observed for summit-area events may provide clues to help us understand and perhaps predict Kilauea's eruptive behavior.

INTRODUCTION

Kilauea Volcano is an excellent natural laboratory for investigating the relations among stress state, seismicity, and magma migration within an active volcano. Seismicity patterns have been used to outline the structure of Kilauea's magma-transport system (Ryan and others, 1981). Earthquake focal mechanisms from the upper east rift zone (UERZ) have been interpreted in terms of a model for magma transport (Hill, 1977). However, magma migration itself is a poorly understood process. Shaw (1980) suggests that seismic data, coordinated with eruption and deformation data, may provide critical tests of hypotheses related to magma transport. It is in this context that a detailed seismotectonic study of Kilauea Volcano has been initiated.

Routinely available local earthquake data, particularly body-wave arrival times and first-motion polarities, can be used as powerful probes of the structure and stress state of the Earth's interior on a local scale. Focal mechanisms derived from first-motion polarities are indicative of the principal stress directions. However the local Earth structure must be known to determine accurately both the source location (the hypocenter) and the direction from which seismic rays leave the source (focal azimuth and takeoff angles). Fortunately, the method of three-dimensional simultaneous inversion of body-wave arrival times is an effective method for determining a detailed model of earth structure on a scale appropriate for the investigation of focal mechanisms (Thurber, 1981). Obviously the velocity model itself also has important bearing on the understanding of the volcano's structure.

Thousands of instrumentally locatable earthquakes occur each year on the Island of Hawaii. These events are thought to be related primarily to the ascent of magma from the mantle, the injection of magma into crustal rift zones, the eruption of lava at the surface, and the mechanical failure of the crust due to volcanic loading. There are two key factors that permit the application of simultaneous inversion and related techniques to the study of volcanic/tectonic processes and of the volcano's internal structure. Firstly, the earthquake activity is broadly distributed laterally and with depth, and the earthquake focal mechanisms vary with location (and perhaps time) according to the nature of the volcanic and tectonic processes causing them. Secondly, the Hawaiian Volcano Observatory (HVO) has been continuously monitoring Kilauea's seismic and magmatic activity for many years, accumulating a substantial catalog of arrival-time data and allowing the possibility of observing temporal variations.

The Island of Hawaii has been the subject of a large number of investigations of crustal and upper-mantle structure (Eaton, 1962; Ryall and Bennett, 1968; Hill, 1969; Ellsworth and Koyanagi, 1977; Broyles and others, 1979; Crosson and Koyanagi, 1979; Zucca and Hill, 1980; Klein, 1981; Zucca and others, 1982) and earthquake focal mechanisms (Endo, 1971; Ando, 1979; Estill, 1979; Furumoto and Kovach, 1979; Unger and Ward, 1979; Crosson and Endo, 1981, 1982; Klein, 1981; Bosher and Duennebier, 1985). Few structure studies modeled laterally heterogeneous Earth structure, and all the focal-mechanism studies adopted simple one-dimensional velocity models for their analyses. Given the strong evidence for laterally varying structure and the somewhat ambiguous results of some of the focal-mechanism studies, a systematic investigation of three-dimensional crustal structure and earthquake source mechanisms is warranted.

ACKNOWLEDGMENTS

The seismic data used for this study were collected and processed by staff members of the Hawaiian Volcano Observatory. I would especially like to thank Bob Koyanagi, Tom English, Jennifer Nakata, and Will Tanigawa: without their continuing efforts, this study would not have been possible. Reviews by Fred

[1]Department of Earth and Space Sciences, State University of New York, Stony Brook, N.Y. 11794.

Klein and Dave Oppenheimer led to significant improvements in the manuscript. I would like to acknowledge the contributions of Tim Karpin and Sagarika Das to the focal-mechanism study. Thanks are also due to Kei Aki, Bill Ellsworth, Elliot Endo, Bill Prothero, and Donna Eberhart-Phillips for advice and assistance. This paper is based on research supported by National Science Foundation grant EAR 82-06266.

METHODOLOGY

I use a method for simultaneously determining both the velocity structure of the Earth beneath a seismic network and the hypocenters of a set of local earthquakes. This simultaneous inversion method can be thought of as a generalization of the standard earthquake location procedure (Geiger's method) to include parameters describing the Earth model as unknowns along with the hypocentral parameters. The details of the method have been described in earlier papers (Thurber, 1983, 1984).

Two recent developments have made iterative three-dimensional simultaneous inversion practical. One is parameter separation, introduced independently by Pavlis and Booker (1980), Spencer and Gubbins (1980), and Rodi and others (1980). This is a mathematical device for maintaining a tractable computational problem size even when large numbers of earthquakes are included in the inversion. The second is approximate ray tracing (ART), originally introduced by Thurber and Ellsworth (1980), with variants developed by Thurber (1983) and Thurber and others (1984). These ART methods exploit Fermat's principle of stationarity to derive approximate ray paths and traveltimes in arbitrary velocity structures. The method of Thurber and others (1984) comes closest to being a true ray-tracing method.

One of the most important facets of the crustal-modeling approach is the manner in which the velocity structure is represented or parameterized. The ideal would be to specify the seismic velocity at any point within the volcano, but in practice this is not attainable. As a compromise, a reasonably dense three-dimensional grid of points is defined at which the velocity is to be estimated by the inversion. A simple interpolation function is used for intervening points. In each iteration, the inversion algorithm solves for the fractional change in velocity, using damped least squares. The F-test (De Groot, 1975) is used to terminate the iterations. The final velocity values derived by the inversion should represent an average velocity for the volume surrounding each grid point.

Once a three-dimensional model of crustal structure is available, it can be used in a straightforward way for the determination of focal mechanisms. The equivalent of Geiger's method and an appropriate ray-tracing method are used to locate the earthquake in the three-dimensional model, and the focal angles are obtained from the ray paths for the final hypocenter location. This study finds that fault-plane solutions are better constrained and contain fewer inconsistent polarities when a realistic three-dimensional crustal structure is employed.

In order to take best advantage of the distribution of the HVO seismic-network stations and the distribution of seismic activity, an area 20 km by 30 km encompassing Kilauea Volcano was chosen for study (fig. 38.1). The coordinate origin for the study area is at latitude 19° 13.5′ N., longitude 155° 14.0′ W., with the Y axis rotated 28° clockwise from north. The seismic-velocity model of Klein (1981), developed for Kilauea's south flank, was adopted as a reasonable starting model for the inversion. Grid-point spacings of 3–4 km in the X direction and 2–3 km in the Y and Z directions were adopted, reflecting the station density and dispersion of seismicity (figs. 38.1, 38.2). A set of 85 earthquakes from 1980 and 1981 (the years of data originally made available by HVO for this study) was selected for the inversions, on the basis of their having well-constrained epicenters, a large number of observing stations, and (most importantly) at least one station within a focal depth of the epicenter, so that the earthquake depths were well constrained. Arrival times from two man-made explosions near the summit in 1976 were also included.

A composite model for the P-wave velocity structure of Kilauea was constructed by averaging the results of a series of inversions for which the grid spacing was kept fixed but the grid as a whole was shifted systematically 1–2 km in the X, Y, and Z directions. The resulting velocity values varied smoothly among the set of inversion models. Typically, the inversions achieved an 80-percent reduction in the data variance after three or four iterations. Unweighted (RMS) residuals for individual events generally were reduced from about 0.11 to 0.04–0.05 s, close to the estimated reading error for P-wave arrival times. Estimated standard errors and model resolution (diagonal elements) for velocity parameters averaged 3 percent (fractional error) and 0.7, respectively. Resolution was poorest for grid points in the deepest layer, on the fringe of the model, and in the near-surface layer not close to a seismic station.

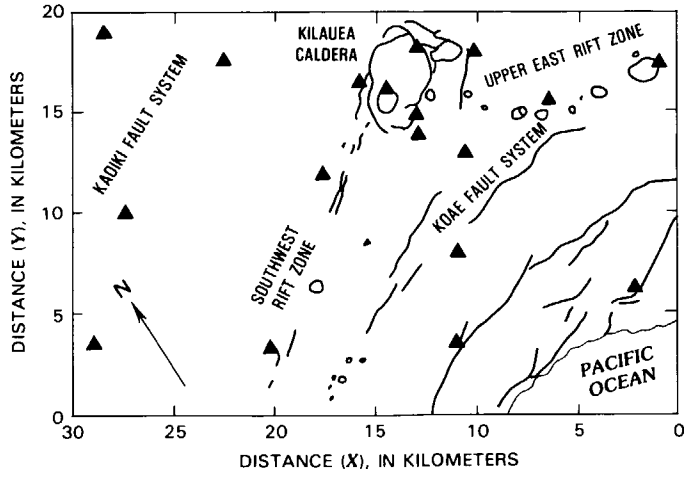

FIGURE 38.1.—Study area on Island of Hawaii, showing principal geologic features and HVO seismic stations (triangles). See figure 38.2 for regional location map. Modified from Thurber (1984, fig. 1), copyright 1984 by American Association for the Advancement of Science.

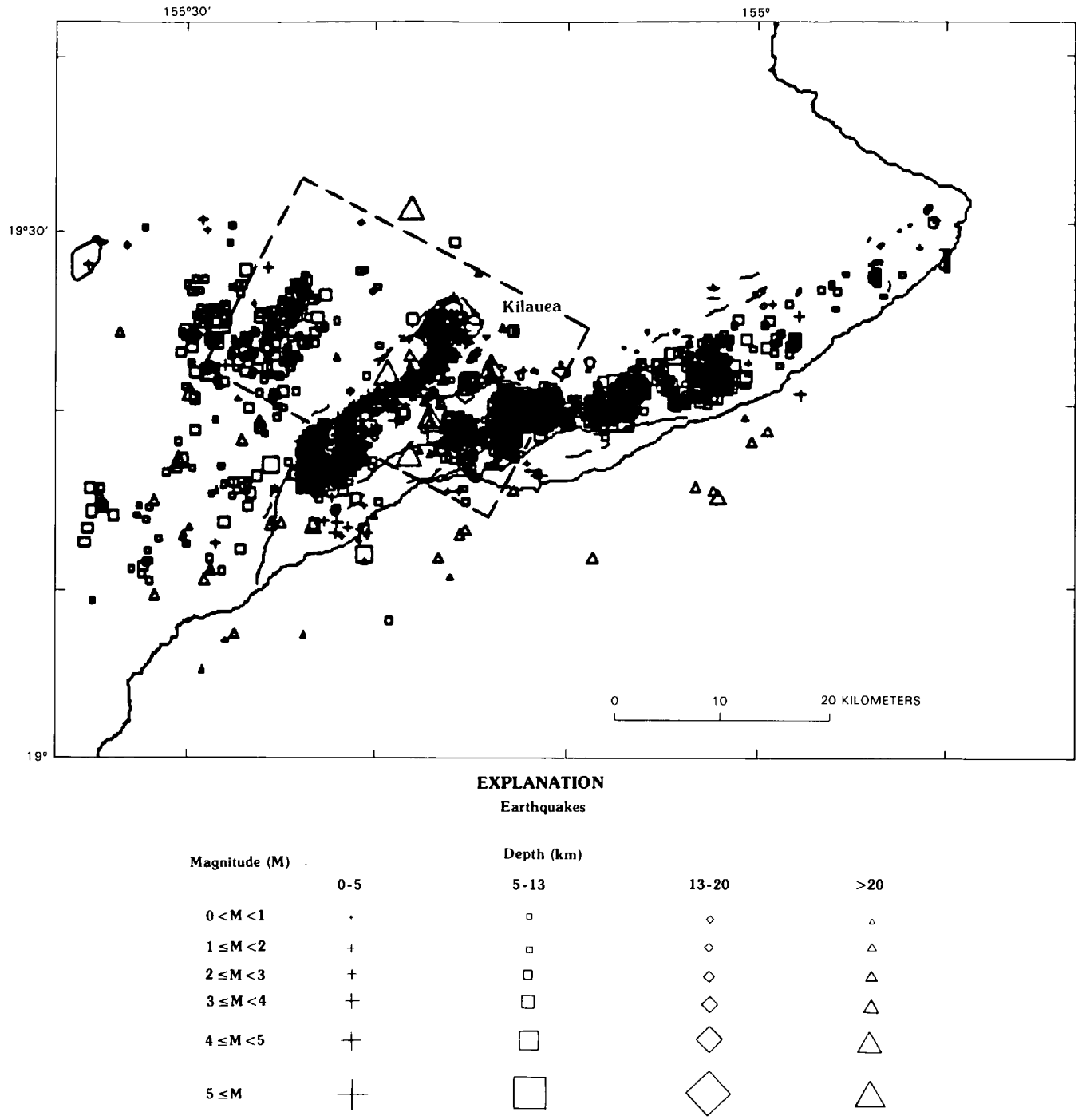

FIGURE 38.2.—Seismicity of southeastern Hawaii for 1981 (Nakata and others, 1982). Dashed lines indicate study area.

CRUSTAL STRUCTURE

Four grid layers of the composite *P*-wave velocity model are shown in map view in figure 38.3. They are positioned at 1 km above and 2, 5, and 8 km below sea level. In the top layer (fig. 38.3) a velocity high directly beneath the caldera corresponds to the roof of the summit magma complex, and velocity highs also are present along the upper east and southwest rift zones (fig. 38.1). A deeper look into the crust (fig. 38.3), shows a continuation of the velocity highs along the two rift zones to 2 km below sea level. The nonrift areas, particularly the Kaoiki region, have significantly lower seismic velocities.

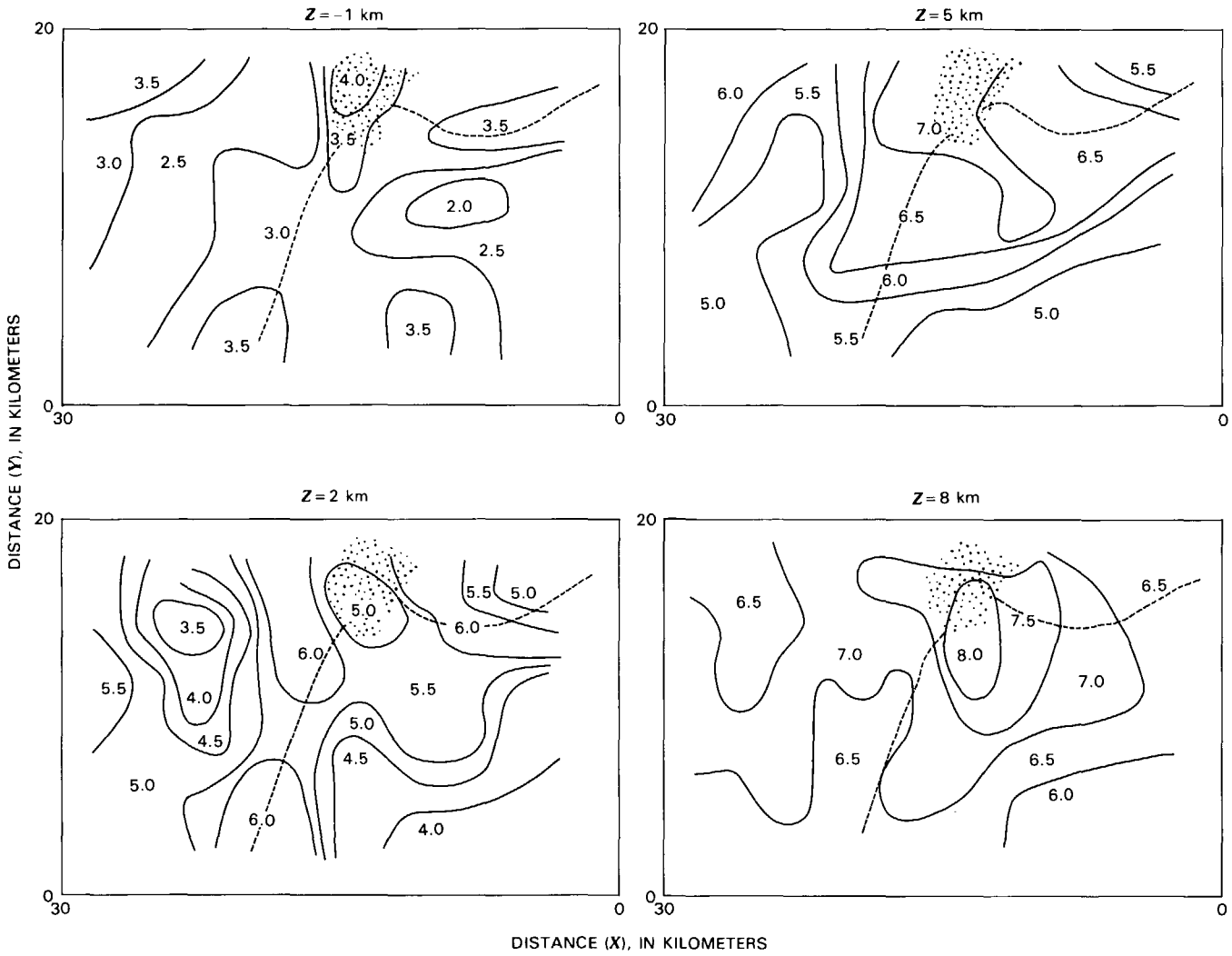

FIGURE 38.3.—Four horizontal slices through composite seismic-velocity model for Kilauea Volcano, positioned at 1 km above and 2, 5, and 8 km below sea level. Velocity is contoured at intervals of 0.5 km/s. Stippling and dotted lines indicate position of caldera and its rift zones, respectively. From Thurber (1984, fig. 2), copyright 1984 by American Association for the Advancement of Science.

Two other important features are apparent at this depth. A high-velocity area along the Koae fault zone indicates the presence of dense, probably competent rock. Recent episodes of intrusive activity in this area have been documented (Swanson and others, 1976), particularly at the northeastern and southwestern boundaries of the fault system, where it intersects the major rift zones. A distinct velocity low is found beneath the caldera, coinciding with the inferred location of Kilauea's summit magma reservoir. Tests with synthetic arrival-time data indicate that the data set is adequate to resolve a small (diameter 2–3 km) low-velocity zone at this point, increasing confidence in the validity of the model results. The actual low-velocity zone could be somewhat smaller, of course, as some degree of smoothing is inherent in the velocity inversion.

At a depth of 5 km (fig. 38.3), the high-velocity core of Kilauea is clearly evident, extending along the UERZ and the southwest rift zone (SWRZ) and intruding into the Koae area. Kaoiki and other nonrift areas continue to exhibit rather low velocities. At 8 km depth (fig. 38.3) the model resolution has become somewhat poor, but the high velocities of the volcano core are still evident, apparently with a slight southward shift from the shallower levels. A similar southward shift with increasing depth is apparent in the estimation of inflation and deflation centers from surface deformation data (Dvorak and others, 1983). Unfortunately, our model does not extend to a sufficient depth to detect the low-velocity layer reported by Crosson and Koyanagi (1979).

These dramatic lateral variations in seismic velocity can be explained in terms of the difference in properties between magma intruded at depth and lava extruded at the surface. As magma nears the surface, the reduction in ambient pressure permits the exsolution of volatiles, creating gas bubbles within the magma. As a result, the

extruded lava is vesicular and has high porosity, low density, and, hence, low seismic velocity. Since the flank areas of Kilauea are constructed predominantly from extruded lava, the low seismic velocities from the inversion are to be expected. In contrast, the rift zones at depth are formed principally from numerous dikes. Except for the very near surface portion of each dike, the intruded magma will not have undergone significant vesiculation. Thus the dikes are probably composed of fairly dense rock with lower porosity and therefore higher seismic velocity.

It is interesting to compare the inversion results with models derived by other seismological techniques. For example, the very high velocity (>8 km/s) at about 8 km depth directly beneath the caldera is consistent with the results of the refraction study of Hill (1969). Rift-zone velocities exceeding 6 km/s at shallow depth have been documented in several refraction studies, and flank velocities on the order of 5 km/s or less are also confirmed (Broyles and others, 1979; Zucca and Hill, 1980; Zucca and others, 1982). Perhaps the most significant comparison is with the teleseismic results of Ellsworth and Koyanagi (1977). The uppermost layer of their model spans the entire depth range of my model, but the correspondence between the results from the two disparate methods is surprisingly strong. The Ellsworth and Koyanagi model displays significantly high seismic velocities beneath Kilauea caldera and its rift zones and also indicates high velocity beneath the Koae area. The Kaoiki and south flank areas are marked by quite low velocities. This agreement strengthens the confidence in both studies.

A rather different comparison can be made between my velocity model and the pattern of seismicity beneath Kilauea caldera. Koyanagi and others (1976) inferred the location of Kilauea's magma chamber from the position of an aseismic zone directly beneath the caldera that spanned a depth range of 2–6 km. However, most evidence favors a smaller, shallow magma reservoir (interconnected sills?) rather than such a large zone of partial melt (Ryan and others, 1983). A nearly east-west cross-section (fig. 38.4) through Kilauea caldera (at $Y = 16$ km in figure 38.1) illustrates the association between my model of the velocity structure and the seismicity in the immediate vicinity of the caldera. Earthquakes cluster around the low-velocity zone at shallow depth directly beneath the caldera. An aseismic zone coincides precisely with the zone of low P-wave velocity. Thus, the summit magma complex is clearly detectable in the seismic velocity structure of the volcano. The low velocity is most likely due to a combination of elevated temperature and the presence of partial melt and (or) pockets of magma.

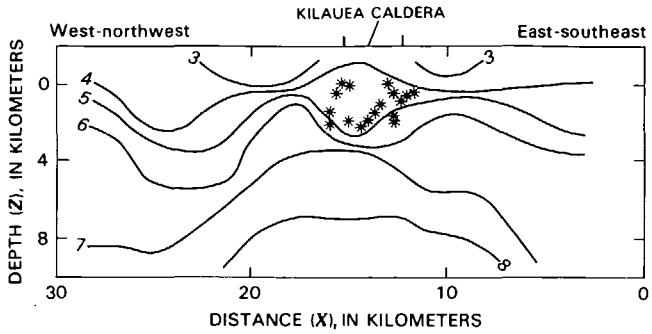

FIGURE 38.4.—Vertical cross section of seismic-velocity model through Kilauea caldera. Section is oriented west-northwest–east-southeast along line $Y = 16$ km in figure 38.1. Contours of seismic velocity in kilometers per second. Note association of aseismic region (outlined by earthquake hypocenters indicated by asterisks) with zone of low seismic velocity. For clarity, only shallow earthquakes in immediate vicinity (within 2 km) of caldera are shown. From Thurber (1984, fig. 3), copyright 1984 by American Association for the Advancement of Science.

EARTHQUAKE RELOCATIONS

Use of a three-dimensional model of the structure of Kilauea has a significant effect on the estimation of earthquake hypocenters (fig. 38.5*A*, *B*). I compare the computed location using the three-dimensional crustal model (3-D) with the HVO catalog location (Tanigawa and others, 1981; Nakata and others, 1982) and also with the location using the one-dimensional starting model (1-D). The 1-D crustal model is essentially the same as the HVO model (Klein, 1981) but does not include the ad-hoc station corrections used in the HVO solutions. One systematic difference is the general shallowing of all hypocenters in the one- and three-dimensional cases relative to the HVO solutions, because of the latter's referral of depths to the ground surface rather than sea level; an additional bias arises from HVO's neglect of station-elevation differences. I also suspect that the relative locations of events are more accurate from my results, as I use a uniform set of stations to locate the entire set of events. In contrast, HVO solutions for a given area are likely to incorporate additional observations from varying sets of stations in the surrounding region, introducing slightly different location biases for each event.

The epicentral shifts of figure 38.5*A* (1-D versus 3-D) indicate the general effect on hypocenters caused by lateral velocity variations, while in figure 38.5*B* (HVO versus 3D) they are indicative of possible location bias in the HVO catalog. The HVO and 3-D locations agree quite well in the UERZ and Kaoiki areas, although there appears to be a slight bias in the northeast Kaoiki region, with the HVO locations displaced 1–2 km southward. The 1-D locations are 1–2 km north of the 3-D locations in both the UERZ and northeast Kaoiki, but they are displaced 2 km eastward in southwest Kaoiki. In comparing the 1-D and 3-D solutions, it appears that accounting for the strong velocity low along the northeast Kaoiki area acts to pull epicenters in that area closer towards Kilauea, whereas the southwest Kaoiki events are pushed away because of the high velocity of the SWRZ. Similarly, the UERZ events are displaced southwards as a result of modeling the high UERZ and summit area velocities.

The comparisons for the summit and upper SWRZ are rather different. Here the 1-D and 3-D locations agree well, but the HVO solutions are displaced 1–2 km southward, most notably for the deeper summit events. This seems to indicate a significant bias in the HVO catalog for this area. Such a bias could have important implications for relating seismicity patterns beneath the summit, and the inferred magma conduit structure, to features visible at the surface (Ryan and others, 1981).

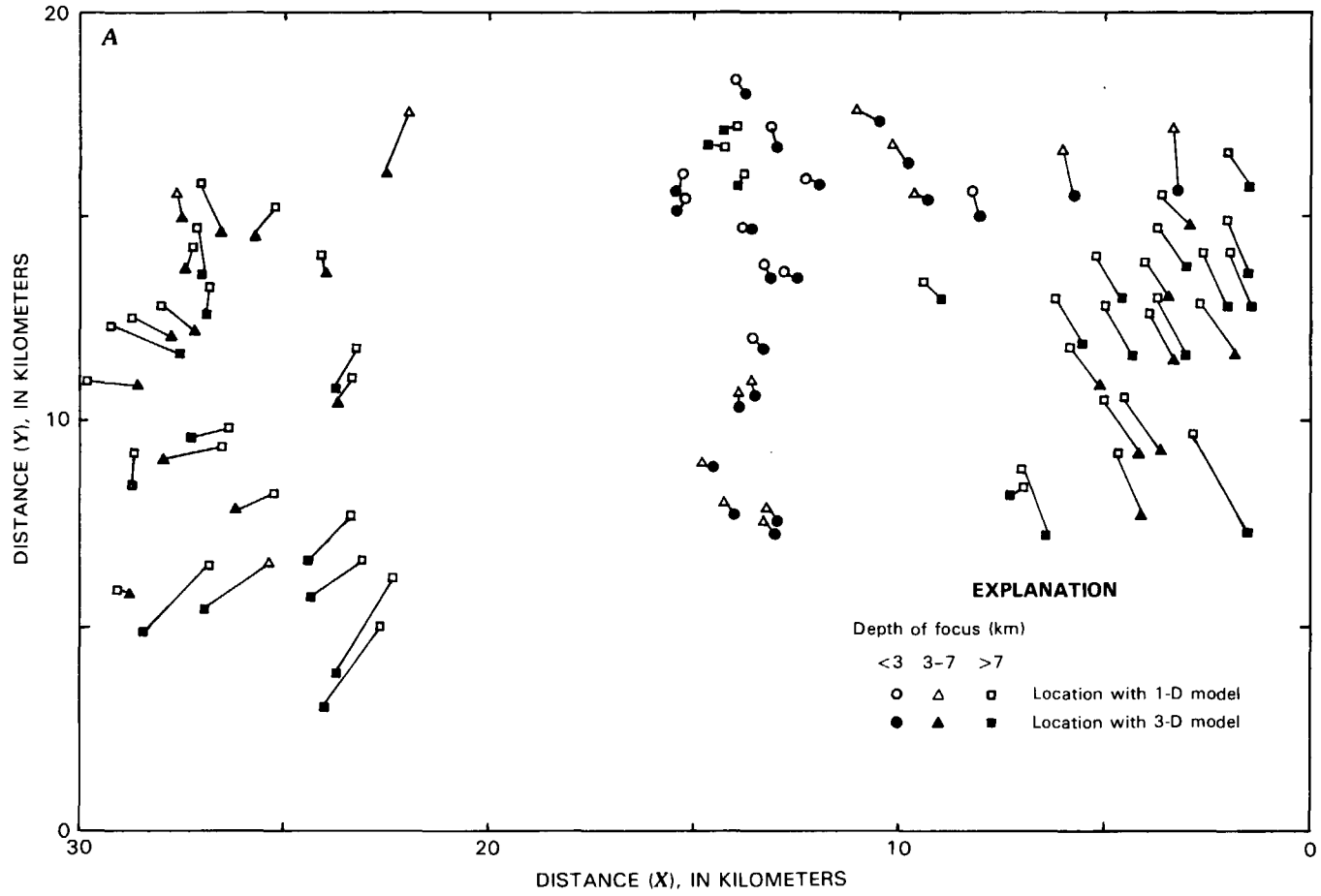

FIGURE 38.5.—Earthquake epicenters in study area relocated using 3-D model in figure 38.3. ***A***, Compared with locations using a 1-D model with no station corrections. ***B***, Compared with HVO catalog locations.

FINE-SCALE STRUCTURE

To derive a crustal model with significantly better spatial resolution (about 1 km) in a small zone directly beneath Kilauea caldera, I take as a starting point the fairly coarse three-dimensional model for Kilauea's velocity structure described above (which I shall call the regional model). A finer scale velocity grid is imbedded within this regional model, and an inversion is carried out to solve for perturbations to the velocity values on the fine grid only, keeping the values fixed on the coarse grid outside of the imbedded grid. Data from a large number of earthquakes within the imbedded region are included to aid in resolving the detailed structure, in addition to events distributed throughout the regional model.

Such a fine velocity grid, with five nodes by five nodes horizontally by three vertically and a uniform spacing of 1 km, was set up to model the shallow structure of the south caldera area of Kilauea (fig. 38.6). The quality of the fine-scale inversion model was limited by the tight clustering of the available events (from 1980 and 1981), as is clear in figure 38.7*A*. Many events in the south caldera fall within about 100 m of a planar surface 2 km in length and 500 m high dipping 60° to the east; presumably this is either a dike or a normal fault overlying a deflating sill. As a result of this clustering, the resolution of the model is only fair (diagonal elements average 0.4 for the 75 nodes, central nodes closer to 0.7). Nevertheless, consistent results were obtained from a set of inversions, typically achieving an additional 25 to 30 percent variance reduction compared to the regional 3-D model.

Slices through the model from one inversion at depths of 0, 1, and 2 km with respect to sea level are shown in figure 38.7*B–D*. Lateral velocity variations of roughly 1 km/s are present in the model at any given depth. There appear to be two separate zones of low *P*-wave velocity: one lies directly beneath Halemaumau Crater, and the other underlies the Ahua Kamokukolau area. The summit zone corresponds well with the location of the summit reservoir. The velocity low beneath Ahua is at the corner of the grid and therefore is less well resolved, but it may correspond to Ryan and others' (1981) UERZ pipe, which appears to lie about 1 km north of the velocity low. Additional earthquake data from more recent years may allow construction of a more definitive model for the fine-scale structure in this region.

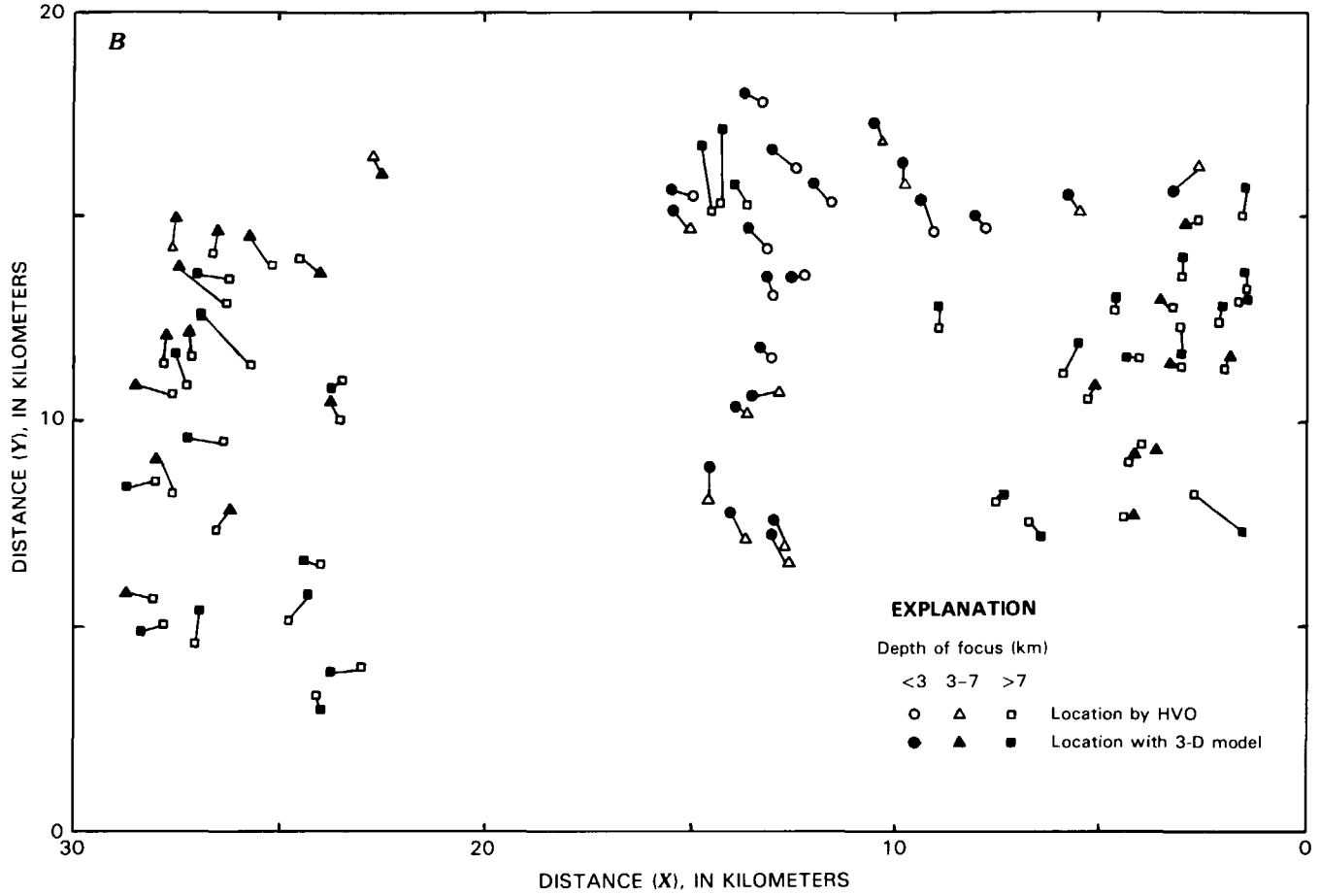

FIGURE 38.5.—Continued.

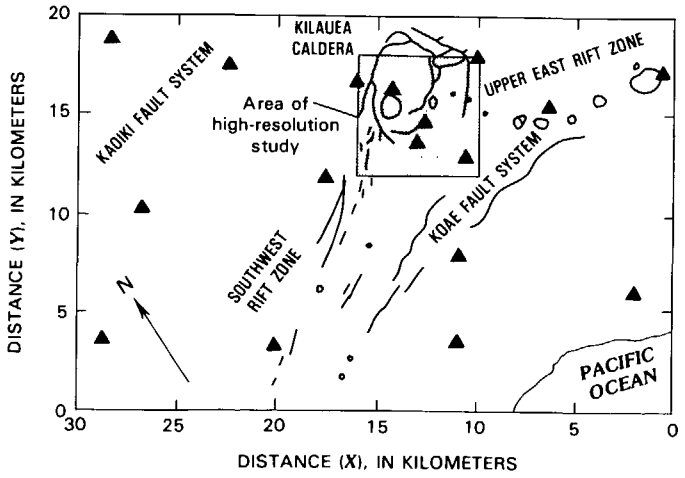

FIGURE 38.6.—Study area near Kilauea caldera (shaded) selected for high-resolution seismic imaging study.

FOCAL MECHANISMS

The state of stress within Kilauea Volcano arises from a complex interplay among crustal density variations, magma pressure, surface loading, and failure along zones of weakness. Fault-plane solutions of earthquakes are generally indicative of the deviatoric stresses in the earth, so they can be used to explore spatial and temporal variations in stress. Care must be taken in interpreting fault-plane orientations directly in terms of stress, however (Ellsworth, 1982; Gephart and Forsyth, 1984; Michael, 1984).

Using a realistic three-dimensional model for the seismic structure of Kilauea, a detailed study of the source mechanisms of earthquakes in the area has been initiated. The earthquake locations are computed using ray tracing in the three-dimensional model, and the focal angles of the rays for the final locations are taken to construct the fault-plane solutions. In general, markedly improved constraint and increased consistency are found in the 3-D solutions compared to the results obtained for the same events using a one-dimensional crustal model. Some of the more dramatic examples are shown in figure 38.8, but these are not atypical.

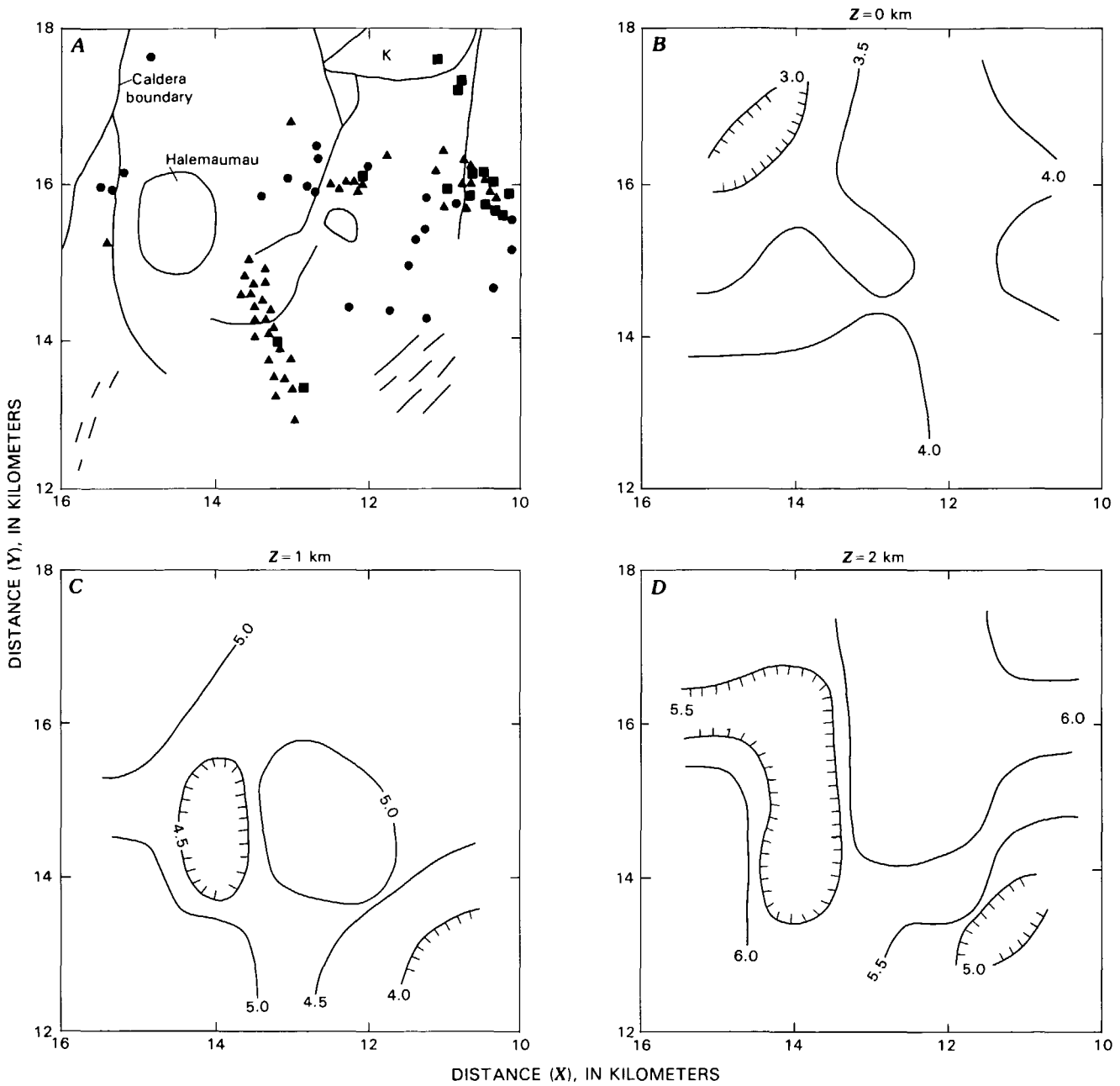

FIGURE 38.7.—Earthquake epicenters and seismic-velocity contours at three levels in high-resolution study area. ***A***, Surface geology and epicenters. Outlines of Kilauea caldera and Halemaumau and Kilauea Iki (K) shown for reference. Faults in lower right are in Ahua area. Focal depths: dots, <1 km; triangles, 1–2 km; squares, 2–3 km. ***B***, Seismic velocities along horizontal slice at sea level. ***C***, Velocities at depth of 1 km below sea level. ***D***, Velocities at depth of 2 km below sea level. Velocity contours in kilometers per second. Hachures indicate closed velocity lows. Two distinct low-velocity zones are evident, although model resolution is only fair.

SPATIAL VARIATIONS

Sets of earthquake focal mechanisms are first used to explore the tectonics of the major geologic areas surrounding Kilauea caldera: the Kaoiki fault system, the SWRZ, the UERZ, and the Koae fault system. A brief survey of source mechanisms from these regions clearly shows a general relation between the faulting in microearthquakes and the surface expression of the tectonics.

The Kaoiki fault system is thought to be a tectonic boundary between the shields of Kilauea and Mauna Loa. Mechanisms for three small events (magnitudes 2.5–3) are shown in figure 38.9*A*; the earthquake depths ranged from 5 km to 8 km. All three events are almost purely strike slip, presumably right lateral. The microearthquake data suggest east-west compressive stress, in agreement with the mechanism of the November 1983 Kaoiki earthquake of magnitude 6.7 (U.S. Geological Survey, 1983). These observations

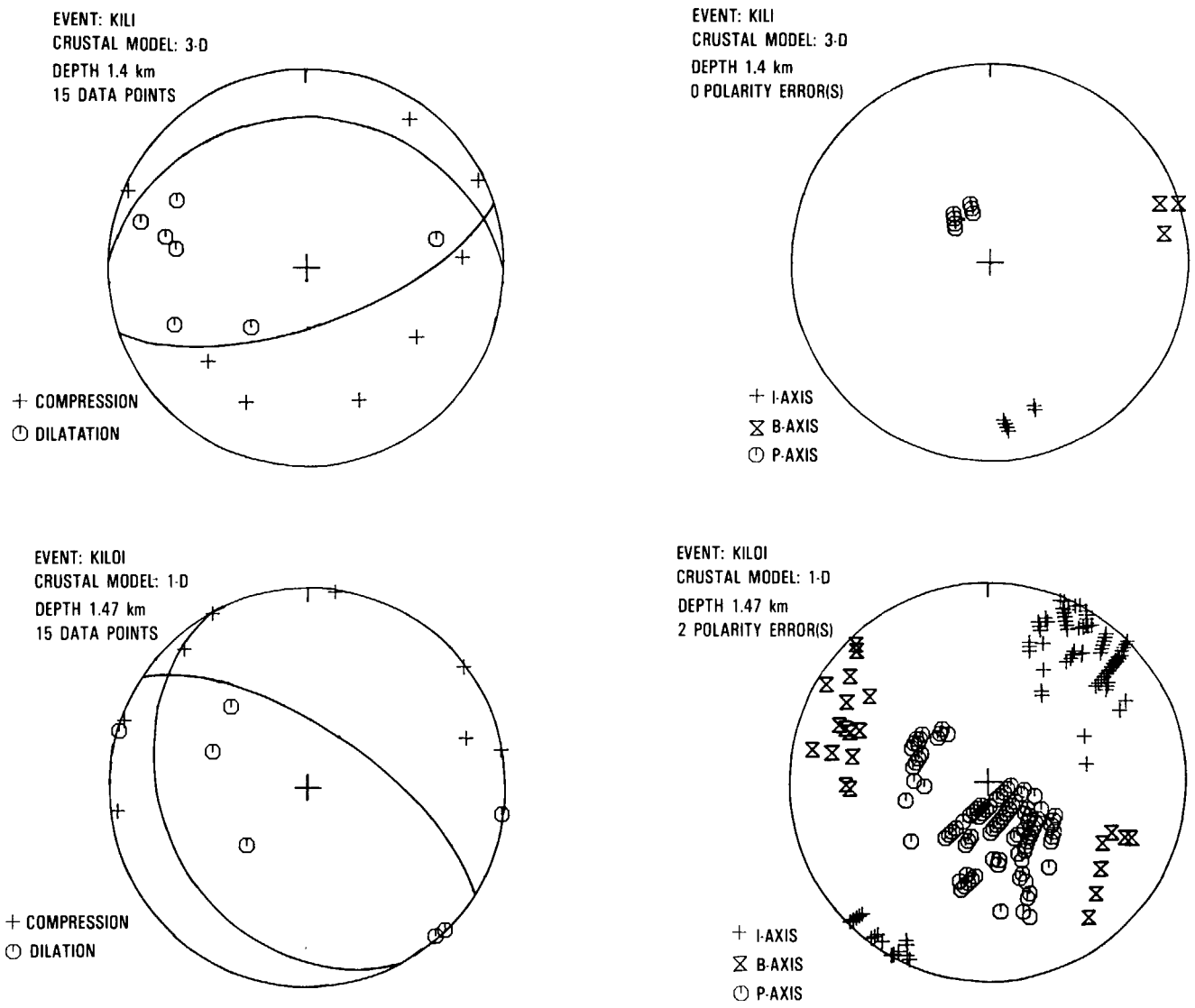

FIGURE 38.8.—Examples of fault plane solutions comparing results using 3-D model (above) to 1-D model (below). Diagrams at left display first motions and reasonable fault-plane solutions; those at right show orientations of permissible maximum, minimum, and intermediate compressive stress axes.

are generally consistent with the notion of stress caused by the nearby growing shields (Endo and others, 1986). Alternatively, it could be thought of as resulting from lateral density variations within Kilauea and Mauna Loa, arising from their dense central cores and in turn producing horizontal stresses oriented radially to their summits. Finally, note that the Kaoiki main shock was located slightly to the northwest and deeper than our events, just off the left side of figure 38.9*A*; if the small events are right lateral, then their northwest-dipping fault plane would dip toward the Kaoiki main shock.

Turning to the SWRZ (fig. 38.9*B*), mechanisms for five 1981 earthquakes of magnitudes 2–3 and depths of 1–3 km are shown. The year 1981 was atypical in that the SWRZ was active and the east rift zone (ERZ) was quiet. With one exception, the mechanisms are clearly consistent with northwest-southeast tension, favorable for intrusive activity on this northeast-southwest rift zone. The discrepant event, number 65, occurred on August 10, 1981, as part of a major intrusive episode, and it may perhaps reflect breaking of an asperity at a bend along the SWRZ.

Along the UERZ (fig. 38.9C) is a very clear pattern consistent with east-west compression, permitting intrusion on this east-west rift zone. Five events of magnitude 2–3 and depths of 1–3 km occurred in 1980, when the ERZ was active and the SWRZ was quiet. Except for number 21, all are strike-slip events, but in most cases neither possible fault plane parallels the rift-zone trend, indicating predominance of echelon faulting as suggested by Hill (1977). A similar relation was found by Smith (1984) for a shallow earthquake swarm in Long Valley Caldera, California.

Finally, in the area of the Koae fault system (fig. 38.9*D*) the pattern is as complicated as the surface geology. Five events from

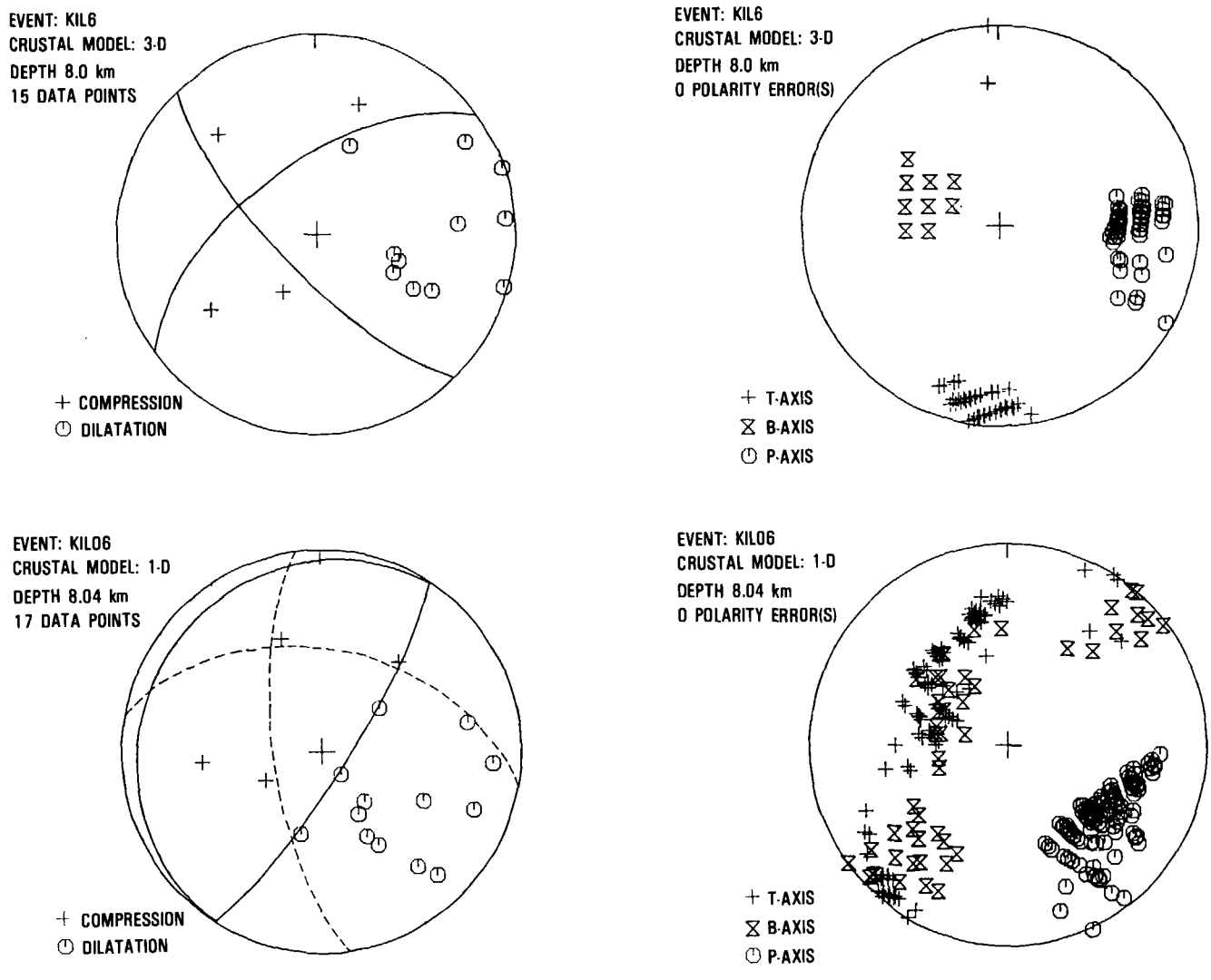

FIGURE 38.8.—Continued.

1980 and 1981 are shown, with magnitudes of 2.5–3 and depths of 4–8 km. Along the eastern section of this area, the earthquakes indicate north-south tension, but those in the western part indicate north-south compression. The eastern events are possibly related more closely to the magma conduit system of the UERZ than to the Koae faults. The western events occurred in 1981, when the SWRZ was experiencing major intrusive activity; the apparent compressive stress south of the SWRZ may be related to this intrusive activity. Mechanisms of events from other years need to be investigated to seek possible temporal variations.

Taken together, these results clearly demonstrate the spatial variability of the stress field surrounding Kilauea Volcano. We suspect these stresses are due in large part to the dramatic lateral density variations present inside the shield, as well as to uneven localized stresses introduced by dike formation. Combining gravity measurements with our model for the seismic velocity structure may enable the direct modeling of these forces.

TEMPORAL VARIATIONS

For a number of years preceding 1981, Kilauea's eruptive and intrusive activity took place exclusively along the ERZ or at the summit. In 1981, activity shifted abruptly to the SWRZ; subsequently, it has returned to the ERZ. I chose to investigate whether focal mechanisms of summit-area earthquakes might show a shift in fault-plane orientation because of a change in stress orientation related to this shift in direction of magmatic activity. For the ERZ to be active, the hypothesis would predict northwest-southeast compression at the summit, whereas a 90° shift to northeast-southwest compression would be required for the SWRZ to be active. It should be noted, however, that direct inferences of stress orientations cannot be made from earthquake focal mechanisms (MacKenzie, 1969), although efforts have been made recently to formally invert focal-mechanism data for the stress tensor (for

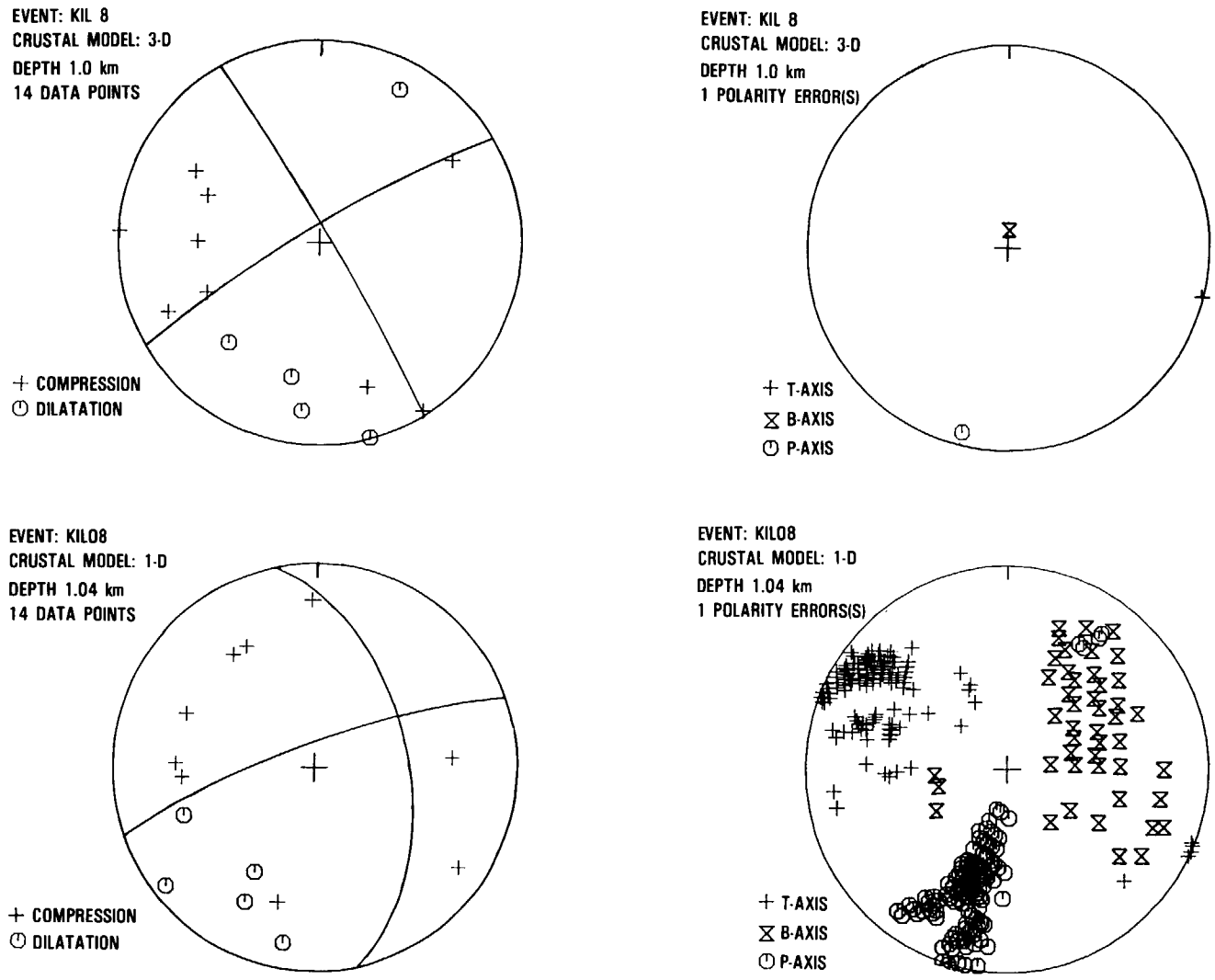

FIGURE 38.8.—Continued.

example, Ellsworth, 1982; Gephart and Forsyth, 1984; Michael, 1984).

Initially, four shallow summit-area earthquakes of magnitude 3 and above were examined (fig. 38.10), one pair from 1980 and a second pair from 1981. These events were the largest and best recorded from the area during this time period. As expected, the 1981 events indicate northeast-southwest compression, and the 1980 events are consistent with northwest-southeast compression. The second 1980 event occurred on December 24, less than one month before the beginning of SWRZ activity. A suite of events encompassing the largest summit earthquakes from January 1981 was therefore selected to seek possible precursory evidence for the impending change in the pattern of magmatic activity.

In order to minimize any confounding effect of spatial variations in stress, only shallow summit earthquakes were examined from two small areas of the caldera (fig. 38.11), all with magnitudes between 2 and 2.5. The range of focal depths was also kept quite small to further reduce the possibility of spatial effects. This series of predominantly strike-slip events, seven along the caldera's southeast rim and four from its west side, indicate a cyclic variation in P-axis orientation during January 1–18, with a very sharp change apparent from east-southeast to east-northeast over the last 6 days of the period (fig. 38.12). Unfortunately, no other earthquakes occurred in the vicinity during this time period that were large enough to yield a reliable mechanism.

What are possible causes of this apparent stress reorientation? One possibility would be a rapid change in the rate of magma flow into the summit storage complex. However, the records from tiltmeters around the caldera (fig. 38.13; A.T. Okamura, written commun., 1981) show only minor deviations from a smooth pattern of inflation. The beginning of a major tilt change is evident on January 19, well after the reorientation of the fault-plane solutions is apparent, but before the first SWRZ intrusive episode beginning January 20. Thus this reorientation could have provided early

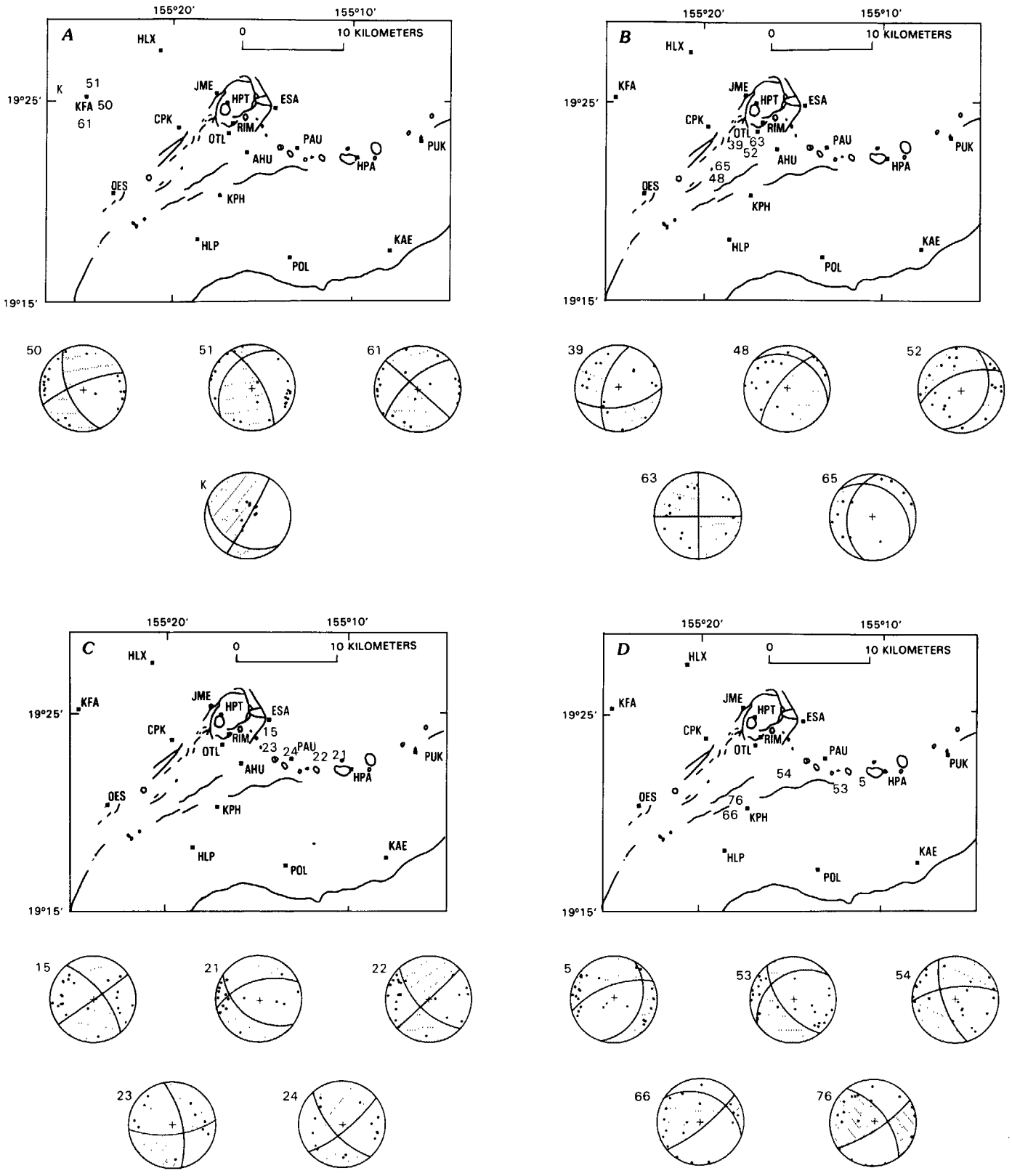

FIGURE 38.9.—Fault-plane solutions for microearthquakes from different sections of study area. Letters refer to HVO seismic stations. ***A***, Kaoiki fault system (including mechanism of 1983 Kaoiki earthquake; U.S. Geological Survey, 1983). ***B***, Southwest rift zone. ***C***, Upper east rift zone. ***D***, Koae fault system.

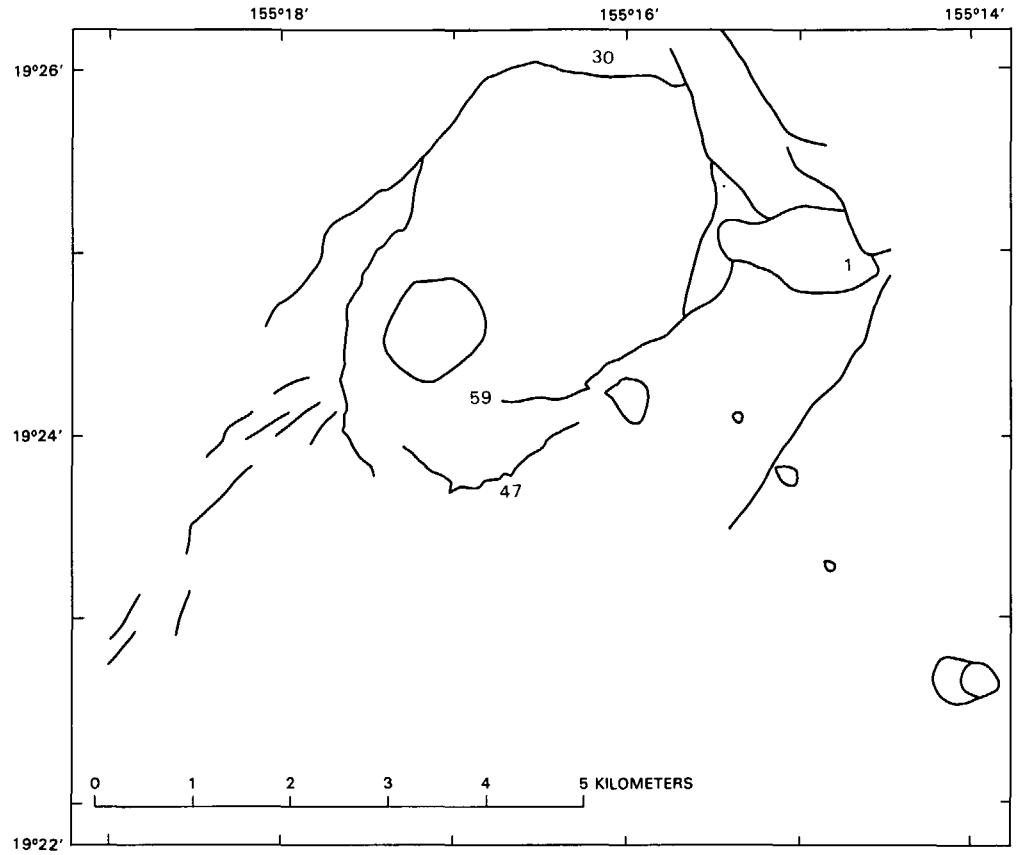

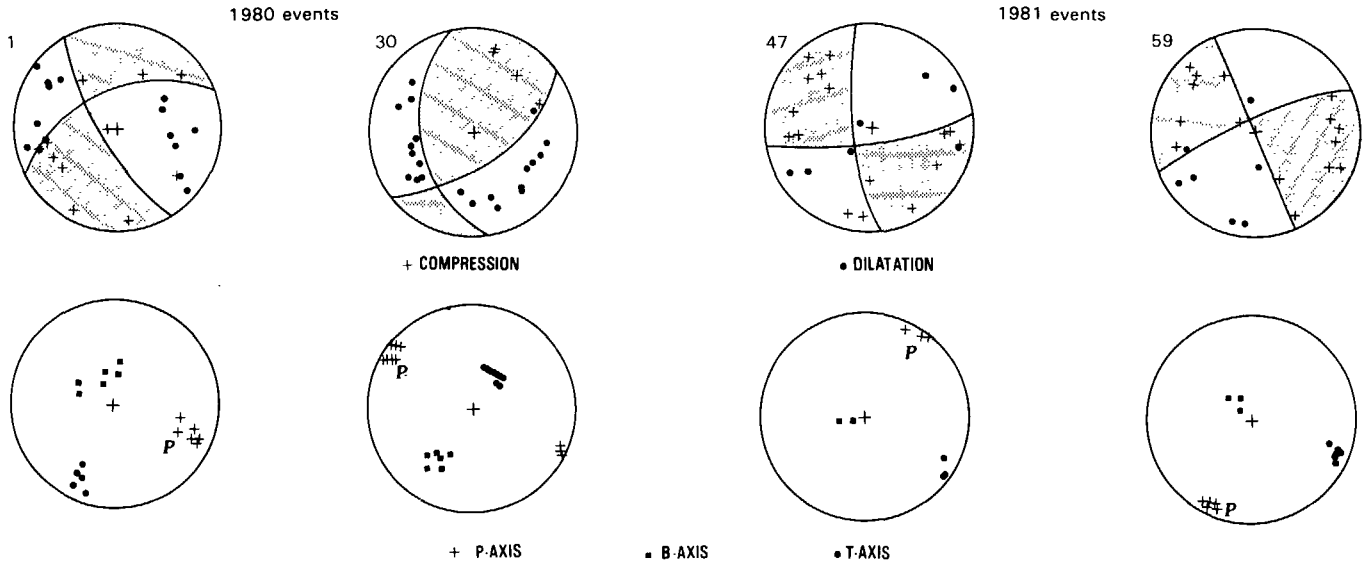

FIGURE 38.10.—Comparison of fault-plane solutions from two caldera-area events in 1980 and two in 1981; differences indicate area-wide change in P-axis orientation.

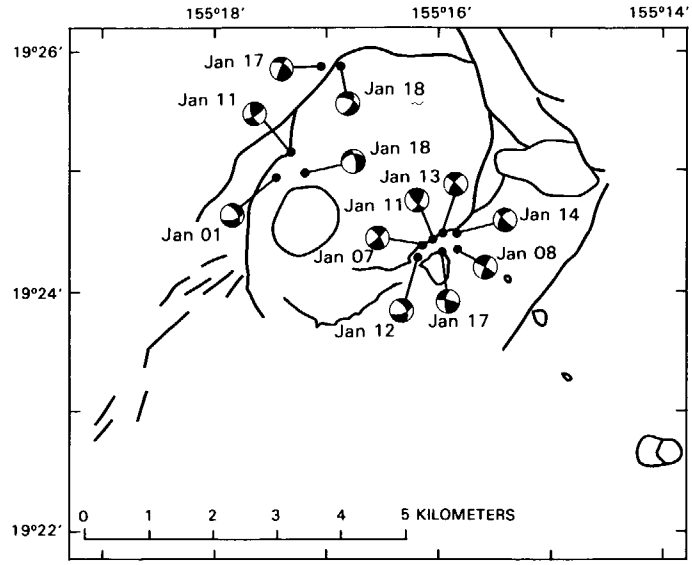

FIGURE 38.11.—Sequence of fault-plane solutions for Kilauea summit earthquakes in two small areas during January 1981 that demonstrates significant temporal variation in faulting orientation (see fig. 38.12).

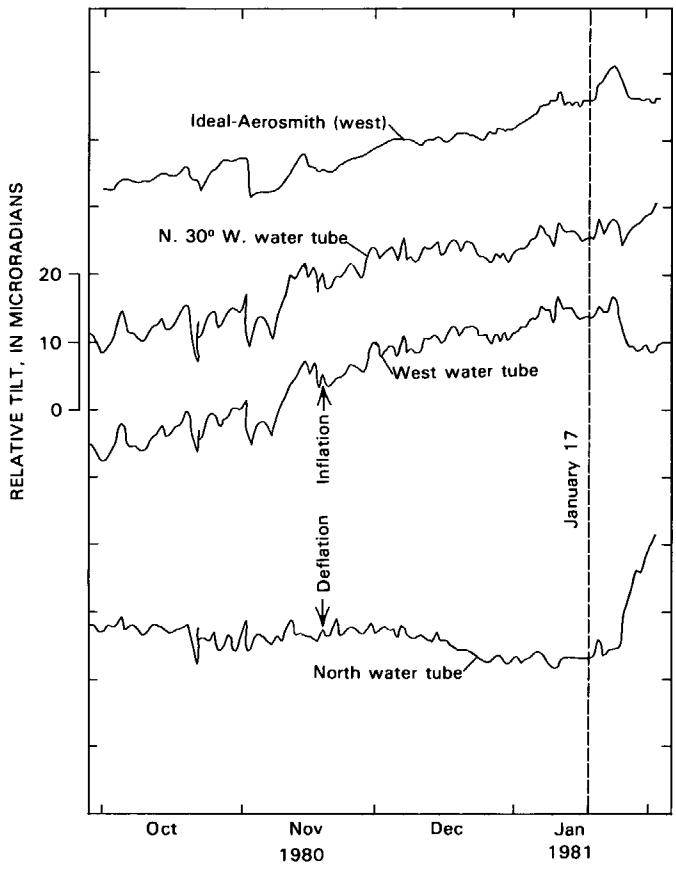

FIGURE 38.13.—Summit tiltmeter records preceding January 1981 southwest rift zone intrusion (A.T. Okamura, unpub. data, 1981), showing no anomalous features before January 17, when earthquake fault-plane solutions had already clearly shown an orientation change.

warning of the impending activity along the SWRZ. This also may be evidence that external forces control the pattern of magma intrusion, rather than the excess pressure of the magma itself.

An extension of this study is necessary to determine the trend of *P*-axis orientation before and after the time period considered. Some questions that need to be addressed include the following: Is this cyclic variation typical or unusual at Kilauea's summit? Are most major intrusions and eruptions preceded by a rapid change in apparent stress reorientation? If so, can this observation be used to help predict eruptions? Planned studies of summit earthquakes for the time period leading up to the 1983 ERZ eruption will seek confirmational evidence.

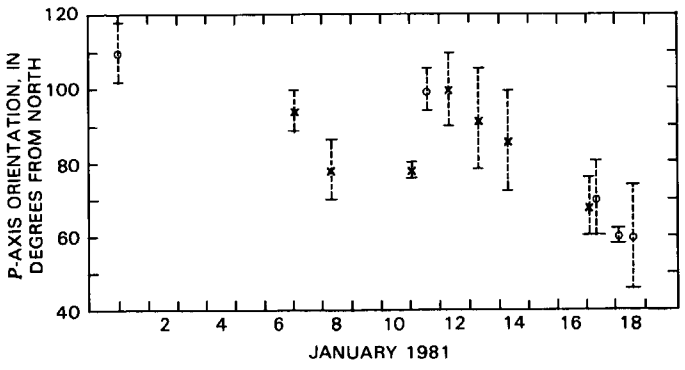

FIGURE 38.12.—Time history of *P*-axis direction (with estimated uncertainties) for focal mechanisms from figure 38.11, showing apparent cyclic variation in faulting orientation from January 1 to January 18, 1981. Crosses and circles indicate events in eastern and western parts of caldera, respectively.

CONCLUSION AND FUTURE RESEARCH DIRECTIONS

Seismological data clearly are valuable for exploring the structure and dynamics of an active volcano. The vast resource of local earthquake data for Kilauea is just beginning to be tapped; these investigations of volcano structure should be continued and extended both to larger and finer scales. Three-dimensional inversion techniques are perhaps the most promising tool for geophysical imaging of the interior of Kilauea. Fine-scale studies of seismically active areas could be achieved through the deployment of a large network of portable seismographs (for example, PASSCAL), or such an array could be used simultaneously for a larger scale local earthquake and for teleseismic investigation. Detailed focal-mechanism studies should constitute an integral part of the latter type of study.

It seems clear, though, that digital seismic data will hold the key to the analysis of the dynamics of magma transport within the volcano. Earthquake source parameters (moment, dislocation, stress drop, fault area) have already proven useful for the study of Usu Volcano, Japan (Takeo, 1983). Where practical, moment tensor analysis (Wu and Ioannidou, 1985) would provide a means to

explore the relative degrees of shear versus tensile failure (that is, faulting versus magma injection) in local earthquakes associated with magmatic activity. Simply demonstrating the existence of significantly non double-couple events would be of considerable value. A detailed study of an earthquake swarm apparently related to dike formation, like that of 1981, might shed light on the mechanics of magma intrusion. Furthermore, shear-wave attenuation could be used to map the magma conduit system and to search for possible temporal variability. These tasks are difficult but realistic: accomplishing them would make a major contribution toward our understanding of how a volcano works.

REFERENCES

Ando, M. 1979, The Hawaii earthquake of November 29, 1975: low dip angle faulting due to forceful injection of magma: Journal of Geophysical Research, v. 84, p. 7616–7626.

Bosher, R., and Duennebier, F.K., 1985, Seismicity associated with the Christmas 1965 event at Kilauea Volcano: Journal of Geophysical Research, v. 90, p. 4529–4536.

Broyles, M.L., Suyenaga, W., and Furumoto, A.S., 1979, Structure of the lower east rift zone of Kilauea Volcano, Hawaii, from seismic and gravity data: Journal of Volcanology and Geothermal Research, v. 5, p. 317–336.

Crosson, R.S., and Endo, E.T., 1981, Focal mechanisms of earthquakes related to the 29 November 1975 Kalapana, Hawaii earthquake: the effect of structure models: Bulletin of the Seismological Society of America, v. 71, p. 713–729.

——— 1982, Focal mechanisms and locations of earthquakes in the vicinity of the 1975 Kalapana earthquake aftershock zone 1970–1979: implications for tectonics of the south flank of Kilauea Volcano: Tectonics, v. 1, p. 495–542.

Crosson, R.S., and Koyanagi, R.Y., 1979, Seismic velocity structure below the Island of Hawaii from local earthquake data: Journal of Geophysical Research, v. 84, p. 2331–2342.

DeGroot, M.H, 1975, Probability and statistics: Reading, Mass., Addison-Wesley.

Dvorak, J., Okamura, A., and Dieterich, J.H., 1983, Analysis of surface deformation data, Kilauea Volcano, Hawaii: October 1966 to September 1970: Journal of Geophysical Research, v. 88, p. 9295–9304.

Eaton, J.P., 1962, Crustal structure and volcanism in Hawaii: American Geophysical Union, Geophysical Monograph, v. 6, p. 13–29.

Ellsworth, W.L., 1982, A general theory for determining state of stress in the earth from fault slip measurements: Terra Cognita, v. 2, p. 170–171.

Ellsworth, W.L., and Koyanagi, R.Y, 1977, Three-dimensional crust and mantle structure of Kilauea Volcano, Hawaii: Journal of Geophysical Research, v. 82, p. 5379–5394.

Endo, E.T., 1971, Focal mechanisms for the May 15–18, 1970, shallow Kilauea earthquake swarm: San Jose, Calif., San Jose State University, M.S. thesis.

Endo, E.T., Crosson, R.S., Koyanagi, R.Y., and Nakata, J., (in press), A catalog of earthquake focal mechanisms for the southeast flank of Mauna Loa, 1959–1982: U.S. Geological Survey Open-File Report.

Estill, R.E., 1979, Seismotectonics and velocity structure of the southeastern Hawaiian ridge: Honolulu, University of Hawaii, Ph.D. thesis.

Furumoto, A.S., and Kovach, R.L., 1979, The Kalapana earthquake of November 29, 1975: an intraplate earthquake and its relation to geothermal processes: Physics of the Earth and Planetary Interiors, v. 18, p. 197–208.

Gephart, J.W., and Forsyth, D.W., 1984, An improved method for determining the regional stress tensor using earthquake focal mechanism data: application to the San Fernando earthquake sequence: Journal of Geophysical Research, v. 89, p. 9305–9320.

Hill, D.P., 1969, Crustal structure of the Island of Hawaii from seismic refraction measurements: Bulletin of the Seismological Society of America, v. 59, p. 101–130.

——— 1977, A model for earthquake swarms: Journal of Geophysical Research, v. 82, p. 1347–1352.

Klein, F.W., 1981, A linear gradient crustal model for south Hawaii: Bulletin of the Seismological Society of America, v. 71, p. 1503–1510.

Koyanagi, R.Y., Unger, J.D., Endo, E.T., and Okamura, A.T., 1976, Shallow earthquakes associated with inflation episodes at the summit of Kilauea Volcano, Hawaii: Bulletin Volcanologique, v. 39, p. 621–631.

McKenzie, D.P., 1969, The relation between fault plane solutions for earthquakes and the directions of the principal stresses: Bulletin of the Seismological Society of America, v. 59. p. 591–601.

Michael, A.J., 1984, Determination of stress from slip data: faults and folds: Journal of Geophysical Research, v. 89, p. 11517–11526.

Nakata, J.S., Tanigawa, W.R., and Klein, F.W., 1982, Hawaiian Volcano Observatory Summary 81, part 1, seismic data, January to December 1981: U.S. Geological Survey unpublished report.

Pavlis, G.L., and Booker, J.R., 1980, The mixed discrete-continuous inverse problem: application to the simultaneous determination of earthquake hypocenters and velocity structure: Journal of Geophysical Research, v. 85, p. 4801–4810.

Rodi, W.L., Jordan, T.H., Masso, J.F., and Savino, J.M., 1980, Determination of the three-dimensional structure of eastern Washington from the joint inversion of gravity and earthquake travel-time data: Systems, Science and Software Report SSS-R-80-4516.

Ryall, A., and Bennett, D.L., 1968, Crustal structure of southern Hawaii related to volcanic processes in the upper mantle: Journal of Geophysical Research, v. 73, p. 4561–4582.

Ryan, M.P., Blevins, J.Y.K., Okamura, A.T., and Koyanagi, R.Y., 1983, Magma reservoir subsidence mechanics: theoretical summary and application to Kilauea Volcano, Hawaii: Journal of Geophysical Research, v. 88, p. 4147–4181.

Ryan, M.P., Koyanagi, R.Y., and Fiske, R.S., 1981, Modeling the three-dimensional structure of macroscopic magma transport systems: application to Kilauea Volcano, Hawaii: Journal of Geophysical Research, v. 86, p. 7111–7129.

Shaw, H.R., 1980, The fracture mechanisms of magma transport from the mantle to the surface, *in* Hargraves, R.B., ed., Physics of Magmatic Processes: Princeton, NJ, Princeton University Press.

Smith, A.T., 1984, High-resolution microseismicity study of possible magmatic intrusion in the Long Valley Caldera: U.S. Geological Survey Open-File Report 84–939, p. 527–535.

Spencer, C., and Gubbins, D., 1980, Travel time inversion for simultaneous earthquake location and velocity structure determination in laterally varying media: Geophysical Journal of the Royal Astronomical Society, v. 63, p. 95–116.

Swanson, D.A., Duffield, W.A., and Fiske, R.S., 1976, Displacement of the south flank of Kilauea Volcano: the result of forceful intrusion of magma into the rift zones: U.S. Geological Survey Professional Paper 963.

Takeo, M., 1983, Source mechanisms of Usu Volcano, Japan, earthquakes and their tectonic implications: Physics of the Earth and Planetary Interiors, v. 32, p. 241–264.

Tanigawa, W.R., Nakata, J.S., and Klein, F.W., 1981, Hawaiian Volcano Observatory Summary 80, part 1, seismic data, January to December 1980: U.S. Geological Survey unpublished report.

Thurber, C.H., 1981, Earth structure and earthquake locations in the Coyote Lake area, central California: Cambridge, Massachusetts Institute of Technology, Ph. D. thesis.

——— 1983, Earthquake locations and three-dimensional crustal structure in the Coyote Lake area, central California: Journal of Geophysical Research, v. 78, p. 8226–8236.

——— 1984, Seismic detection of the summit magma complex of Kilauea Volcano, Hawaii: Science, v. 223, p. 165–167.

Thurber, C.H., and Ellsworth, W.L., 1980, Rapid solution of ray tracing problems in heterogeneous media: Bulletin of the Seismological Society of America, v. 70, p. 1137–1148.

Thurber, C.H., Karpin, T., and Um, J.H., 1984, Focal mechanisms of earthquakes at Kilauea Volcano: a detailed study [abs.]: Eos, Transactions of the American Geophysical Union, v. 65, p. 1001.

Unger, J.D., and Ward, P.L., 1979, A large deep Hawaiian earthquake—the

Honomu, Hawaii event of April 26, 1973: Bulletin of the Seismological Society of America, v. 69, p. 1771–1781.

U.S. Geological Survey, 1983, Preliminary determination of epicenters, Nov. 1983.

Wu, F.T., and Ioannidou, E., 1985, Linearized source moment tensor inversion of near-source seismograms [abs.]: Eos, Transactions of the American Geophysical Union, v. 66, p. 315.

Zucca, J.J., and Hill, D.P., 1980, Crustal structure of the southeast flank of Kilauea Volcano, Hawaii, from seismic refraction measurements: Bulletin of the Seismological Society of America, v. 70, p. 1149–1159.

Zucca, J.J., Hill, D.P., and Kovach, R.L., 1982, Crustal structure of Mauna Loa Volcano, Hawaii, from seismic refraction and gravity data: Bulletin of the Seismological Society of America, v. 72, p. 1535–1550.

AEROMAGNETIC AND NEAR-SURFACE ELECTRICAL EXPRESSION OF THE KILAUEA AND MAUNA LOA VOLCANIC RIFT SYSTEMS

By Vincent J. Flanigan *and* Carl L. Long

ABSTRACT

Aeromagnetic and electromagnetic data from a draped (90-m terrain clearance) survey of the rift systems extending east and southwest from the summits of Kilauea and Mauna Loa Volcanoes are interpreted to reflect near-surface magnetic and electrical resistivity characteristics of the rift zones. Shallow dike complexes of more intense magnetism than their extrusive equivalents are the main source rocks for the observed magnetic anomalies along the rift zones. Conductive rocks are reflected in the electromagnetic data as apparent resistivity lows. Sharp lateral changes of conductivity are detected as VLF magnetic anomalies and are interpreted to represent relatively narrow, conductive zones over feeder dikes along active parts of the rift zones.

The spatial relations of the interpreted magnetic source rocks to observed apparent resistivity and VLF magnetic anomalies are generally consistent with geologic and structural observations. The active part of the east rift zone of Kilauea lies south of the magnetic source rocks in the upper one-third of the east rift zone, reflecting southward movement of Kilauea's south flank. Farther east, beyond Napau Crater, the active part of the east rift zone of Kilauea, as interpreted from VLF magnetic anomalies, lies in the central to northern part of the interpreted magnetic source rocks. This change of spatial relation of the geophysical anomalies is interpreted to reflect structures transverse to the rift zone that are associated with large-scale block slumping of the south flank of Kilauea. Similarly, large-scale block slumping on the west flank of Mauna Loa is reflected by magnetic anomalies east of the active part of the rift zone. A major apparent resistivity and magnetic low transverse to the southwest rift zone of Mauna Loa may reflect the southern boundary of the subaerial Alika slide, which extends 80 km offshore from Mauna Loa's west coast.

The buttressing of Mauna Loa by Mauna Kea on the north and Kilauea on the south, as recognized by geophysical data, contributes to the complexity of the Mauna Loa northeast rift zone. The VLF magnetic anomalies defining the active northeast rift zone of Mauna Loa are present only in the upper 10–12 km of the rift, thus indicating that the action of buttress forces limits recent volcanic activity farther east along the rift zone.

Two interpretations of an apparent reversely polarized magnetic dipole anomaly over Kapoho Crater are modeled. One model assumes an intrusive body in which the direction of remanent magnetism is nearly opposite to the present magnetic field of the Earth. The other model assumes a nonmagnetic body separating two magnetic dike systems—the northern system related to development of Mauna Loa's northeast rift zone and the southern one related to Kilauea's east rift zone.

INTRODUCTION

Mauna Loa and its smaller neighbor, Kilauea, have been studied, and volcanic activity extensively documented for only the relatively brief historical period extending back to the late 19th century. Accumulated evidence from observations of earth scientists has allowed a better understanding of growth, structural complexity, and volcanic activity of these two shield volcanoes. The purpose of this paper is to examine some of the more obvious aeromagnetic and electromagnetic features and show how they complement or augment observations of other earth scientists.

In early 1978 the U.S. Geological Survey (USGS) conducted several airborne surveys that covered large areas of the Island of Hawaii. An aeromagnetic survey of the entire island was flown at a mean terrain clearance of 300 m (Godson and others, 1981). In addition, a low-level (90-m mean terrain clearance) total-field magnetic and very low frequency (VLF) electromagnetic survey was flown over the rift zones extending east and southwest from the summits of Kilauea and Mauna Loa Volcanoes (fig. 39.1; Flanigan and others, 1986a, b). Data from the low-level survey form the basis of this paper.

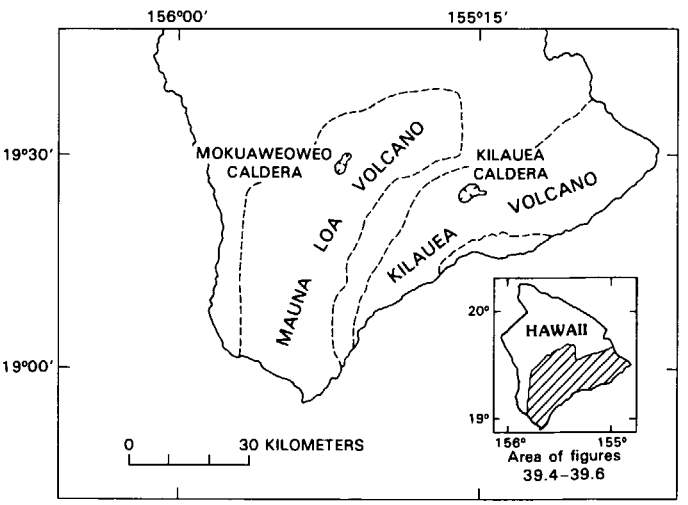

FIGURE 39.1.—Index map of Island of Hawaii, showing boundary (dashed) of airborne electromagnetic-magnetic surveys over Kilauea and Mauna Loa Volcanoes.

Extensive airborne and shipborne magnetic surveys were made over the Hawaiian Ridge in the mid-1960's by Malahoff and Wollard (1966) and Malahoff and McCoy (1967). Most of the data from these earlier magnetic surveys were used with the 1978 data to compile a composite aeromagnetic map of the Hawaiian Islands as part of a cooperative ongoing effort by the Society of Exploration Geophysicists and the USGS to produce gravity and magnetic maps of the United States (Godson and others, 1984).

The low-level airborne survey made by the USGS, primarily designed to record VLF responses, was the first and perhaps only such airborne survey on the Island of Hawaii. The airborne VLF method has proven practical in engineering and geologic applications on the contiguous continental United States and Alaska (Frischknecht, 1971; Hoekstra and others, 1975; Arcone, 1978, 1979).

Extensive ground VLF surveys, along with other electromagnetic methods, have been utilized in geophysical studies mainly in the Kilauea Volcano summit area and parts of the rift zones extending east and southwest from the summit (Zablocki, 1978).

METHODS

Problems related to aeromagnetic surveying, and in particular over magnetic Hawaiian terrain, are addressed by Malahoff and Wollard (1966). Topographic aeromagnetic anomalies are expected in those areas where the survey aircraft cannot maintain constant terrain clearance. Studies are currently being done in an effort to evaluate and remove terrain effects from aeromagnetic maps (Blakely and Grauch, 1983). Aeromagnetic surveys flown at constant altitude (barometric) or constant terrain clearance (draped) are both subject to some degree of erroneously induced magnetic anomalies due to rugged topography. In fact, terrain effects may be enhanced in magnetic terrane in drape-flown surveys over that of traditional barometric-flown magnetic surveys (Grauch and Campbell, 1984). In the low-level aeromagnetic survey described here the fixed-wing aircraft was successful in maintaining ± 30 m of the nominal survey height, except when the aircraft passed over pit craters and cinder cones.

Theoretical terrain-induced magnetic anomalies were computed for two-dimensional models approximating volcanic cones, craters, and calderas to qualitatively evaluate the observed magnetic anomalies (not shown here). Terrain anomalies, using magnetic susceptibilities of approximately 1.0×10^{-2} cgs units, were not over 400 nanoteslas (nT). The most distinguishing feature about the theoretical terrain anomalies is the short wavelength of the anomaly, usually much shorter than the wavelength of many of the observed anomalies. Thus, in an area of abrupt terrain variation, the observed anomaly is a composite magnetic response of the terrain and the magnetic geologic sources.

Hawaiian intrusive rocks, primarily in the form of dikes, have an intensity of remanent magnetization more than 10 times that of the induced magnetization (Decker, 1963; Malahoff and Strange, 1965). It is evident from aeromagnetic data and confirmed by theoretical modeling (Flanigan and others, 1986a) that about the same apparent order of magnitude difference exists between the magnetic properties of intrusive dike systems and lava flows. The reason for this apparent difference of bulk magnetic properties is not clear because the dike rocks are a composite (over time) of the same extrusive rocks comprising the lava flows. The direction of remanent magnetization of lava flows on the Island of Hawaii is essentially the same as the Earth's present field direction. However, remanent magnetization directions on samples of massive basalt flows may not be representative of the overall section. Sequences of exposed Hawaiian lavas (in fault scarps and sea cliffs) are highly porous. L.A. Anderson (oral commun., 1984) says drill core recovery from drill holes in the Kilauea area is about 20 percent, suggesting that the bulk of the section is composed of porous rocks not easily recovered during drilling. We assume that postcooling movement of the lava flows either by tumbling of blocks in breccia envelopes in flows or by postcooling compaction of pahoehoe flows has caused a jumbled assemblage of remanent magnetization directions. The net result would be an apparent lower bulk magnetization of the flow rocks than the intrusive rocks. Induced magnetization would remain unaffected.

Sources of magnetic anomalies are based upon a qualitative interpretation, consistent with the magnetic anomaly shape and approximate orientation of the body with respect to the Earth's magnetic field direction. To illustrate the relative amplitude and anomaly shape that might be expected, an assumed two-dimensional dike representing intrusive rocks of bulk magnetism 10 times greater than the extruded basalt flows was rotated in the Earth's magnetic field, and the theoretical magnetic response calculated (fig. 39.2) at several positions. The magnetic anomaly varies from a symmetrical magnetic high of about 400-nT amplitude, when the dike is oriented parallel to the direction of the Earth's magnetic field (solid line on fig. 39.2), to a dipole anomaly of over 3,000-nT amplitude for a dike oriented about normal to the direction of the Earth's magnetic field (azimuth 90° or 120° on fig. 39.2). Note: for rocks normally polarized—that is, the direction of the remanent magnetism is the same as the Earth's present field direction—the dipole magnetic high is on the south and the low is on the north. For magnetic features oriented normal to the Earth's magnetic field direction, the edges of the magnetic body lie under the apex of the dipole high and low. For magnetic sources oriented parallel to the Earth's magnetic field, the edges of the causative body lie under the point of steepest gradient of the magnetic anomaly. Of course there are any number of cases in between the two extremes mentioned above. Thus, locations for magnetic source rocks based on these qualitative considerations have greater uncertainty in those areas where the strike of the magnetic source rocks is not parallel or normal to the direction of the Earth's present magnetic field.

The theory of radio wave propagation and the measurement of electric and electromagnetic properties of the Earth's near surface has been extensively discussed elsewhere (Wait; 1962; Paal, 1965, 1968; Barringer and McNeil, 1969; Patterson and Ronka, 1971; and Frischknecht, 1973). Details of the electrical and electromagnetic parameters measured by the USGS airborne VLF equipment used to acquire data presented in this paper are given in Flanigan and others (1986b).

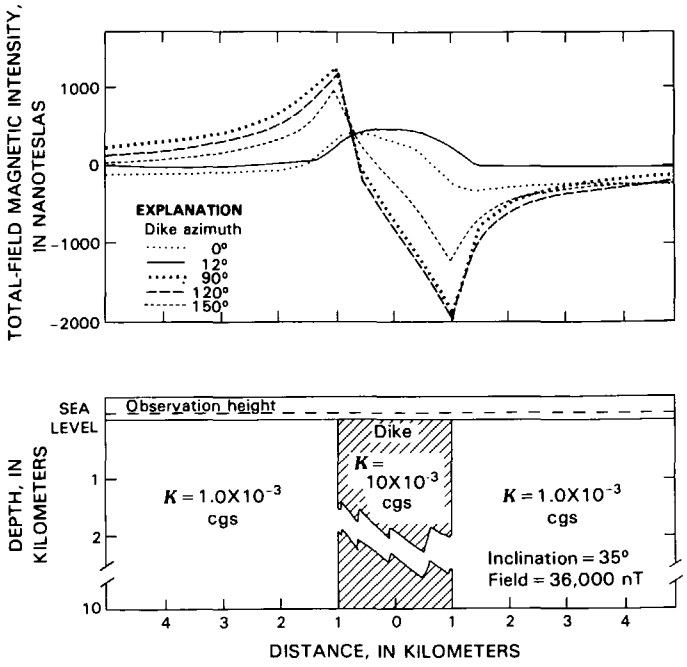

FIGURE 39.2.—Theoretical models of magnetic dike rocks rotated in Earth's magnetic field showing relative amplitude and anomaly shape. Remanent magnetism is considered to be parallel to direction of Earth's present magnetic field. Susceptibilities (K) are shown in cgs units.

Briefly, the VLF technique measures the local electric and magnetic characteristics of a vertically polarized groundwave transmitted by one of many VLF communication transmitters located worldwide. The local amplitude of the electric and magnetic fields of the transmitted radiowave is dependent on several factors, such as: transmitted power output, distance between transmitter and receiver site, propagation events in the ionosphere, local topography, and resistivity of the Earth between the transmitter and receiver.

Earth resistivity values are computed from the amplitude ratio of the horizontal electric field to the vertical electric field (wave tilt; Hoekstra and others, 1975). Inasmuch as the Earth resistivities determined by the wave tilt usually are a combined response over a layered earth composed of differing resistivities, they are called apparent resistivities. Wave-tilt apparent resistivities may vary significantly from those determined by ground VLF methods mainly because the airborne and ground methods use different magnetic and electric field components of the transmitted radiowave which are affected differently by the conductivity (inverse of resistivity) and thicknesses of the layered Earth.

The thickness of the upper surface of the Earth that influences the VLF electromagnetic responses, called the skin depth, is related to the surface apparent resistivity and the frequency of the electromagnetic field. The skin depth for rocks of 100 Ω-m apparent resistivity is about 36 m, and for 10,000 Ω-m is about 360 m.

VLF magnetic measurements discussed in this paper are the responses of the measured magnetic field to geologic sources of differing conductivities. The VLF magnetic responses are particularly sensitive to sharp lateral changes of conductivity. In addition, the vertical and horizontal VLF magnetic field components have diagnostic responses to geologic sources, particularly those of high conductivity contrast. To illustrate these diagnostic responses, the real part of the VLF magnetic responses for the horizontal and vertical field components are shown in figure 39.3 over conductive bodies of different widths. The distinctive shape of the VLF magnetic responses over narrow and wide conductive bodies is readily apparent.

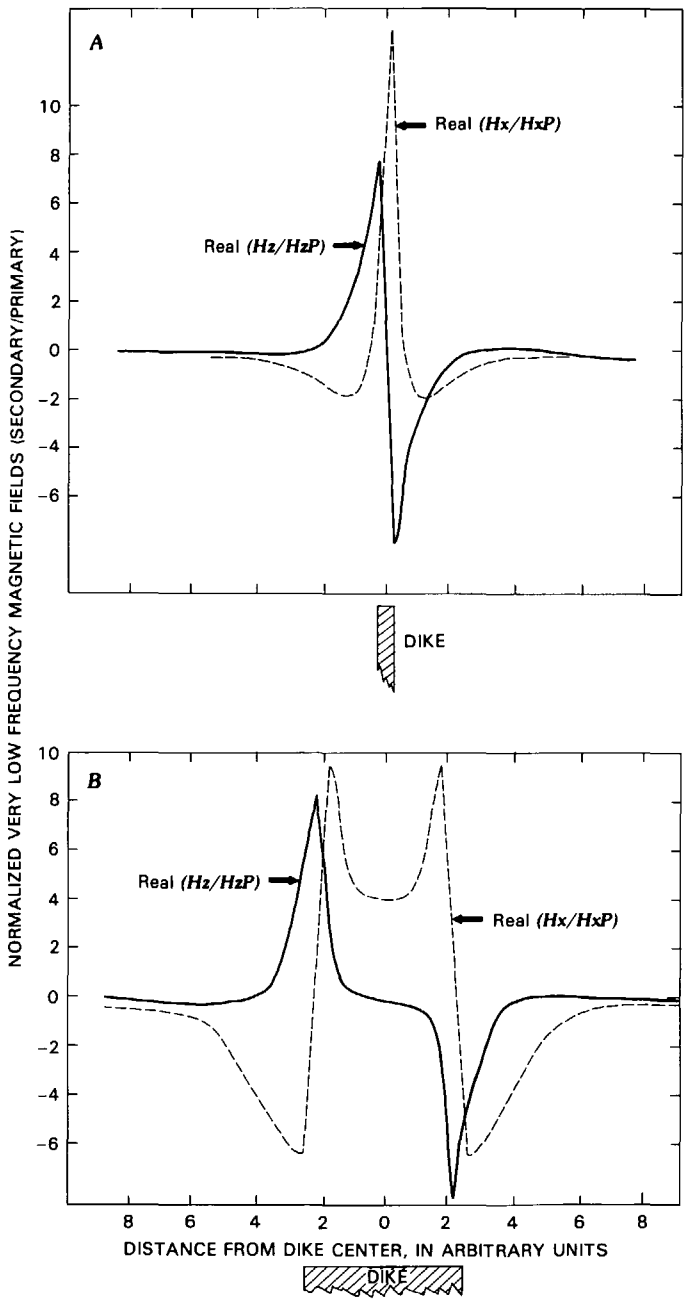

FIGURE 39.3.—VLF magnetic field component response over conductive dikes of 30-m (***A***) and 500-m (***B***) width. Conductivity contrast is 10, that is, a conductive dike of 0.01 mho/m in host of 0.001 mho/m. Horizontal (Hx) and vertical (Hz) magnetic fields have been normalized to primary (P) field components.

Factors affecting the resistivity of basalt over the rift systems of Kilauea and Mauna Loa Volcanoes are important in understanding the VLF data presented in this paper. In nonthermal areas, resistivities of basalt lava flows are $3-20 \times 10^3$ Ω-m (Keller and Rapolla, 1974; Zablocki, 1976). Zablocki (1978) suggests several possible causes for these high resistivities: (1) high permeability of the lava flows resulting in very little water in the zone of aeration above the local water table; (2) resistive pore water in the vadose zone, probably resulting from previous leaching of exchangeable ions from the rock by heavy rainfall; (3) negligible chemical alteration of the flows and surficial ash deposits, thereby maintaining to a minimum the amount of clays in the rock which can contribute to double-layer conductivity in the rock pores (Keller and Frischknecht, 1966).

In contrast to nonthermal areas, areas of recent volcanic activity along the rift systems are often associated with low resistivity (high conductivity) values. Conductive zones associated with magma injected from the summit reservoirs of Kilauea and Mauna Loa are generally relatively narrow, probably because of low thermal conductivity of the basalt, which impedes heat transfer from the injecting magma to the surrounding rocks (Zablocki, 1978). Basalt flows directly over eruptive fissures and related ground cracks become conductive by ascending hot mineralized water or vapor derived from the interaction of ground water with high-temperature magma in the injecting dikes. Large zones of conductive basalt are expected to be developed over magma reservoirs where thermal convection cells have been operative for long periods of time.

Factors other than thermal may also reduce ground resistivities. Thick soils are expected to contribute to lower apparent resistivity values than in areas where overburden is thin or absent. Such soils are widely present in the northwest and northern edges of the Kilauea survey area.

Some apparent resistivity lows along the edges of the survey areas may be an artifact of the automatic gridding program (Webring, 1981), which projects data 2 km beyond the end of real data. Thus, caution should be used when viewing automatically contoured data, particularly near the boundary of the survey area.

ACKNOWLEDGMENTS

The authors owe much to and acknowledge the contributions of many associates in the U.S. Geological Survey who were instrumental in the original concept of the airborne survey, in particular C.J. Zablocki, John Lockwood, and other scientists of the Hawaiian Volcano Observatory who conceived the project and assisted in the logistics during the actual survey. To the aircraft flight crew, Donald Rohret, electronic technician, and pilot M.G. Steward we extend thanks. To Frank Frischknecht who has led the research and development of the airborne VLF method and provided the authors with many helpful hints and suggestions during the compilation and interpretation of the data we extend a special thanks. Last but not least, we acknowledge the assistance of technicians Mark Sherrard and Pam Mohr who were extremely helpful in the actual compilation of the data. Obviously, responsibility for the validity of the interpretations presented here are the authors' alone.

MAGNETIC AND ELECTROMAGNETIC FEATURES

KILAUEA VOLCANO

Numerous magnetic features were delineated over the east and southwest rift zones of Kilauea Volcano. The most prominent magnetic feature on figure 39.4 is associated with the east rift of Kilauea Volcano and consists of linear dipole anomalies, of nearly 2,000-nT amplitude, extending eastward from the summit of Kilauea to within 7 km of the coast, where the dipole anomaly abruptly terminates as a linear feature. East of this termination point, several individual magnetic highs and lows characterize the magnetic expression of the rift zone.

An east-trending series of linear magnetic dipoles, having about one-half the amplitude of the east rift magnetic anomaly, are present 10–12 km farther north. The wavelength of this northernmost linear magnetic anomaly is 6 km, as compared to the east rift magnetic anomaly of about 2 km.

The southwest rift of Kilauea Volcano is characterized by a series of magnetic highs, generally aligned with the eruptive fissures, ground cracks, and scarps of the southwest rift zone, but mostly southeast of the surficial volcanic features.

A north- to northeast-trending belt of magnetic highs, only partially delineated by the low-level survey, is evident along the northwest to north edges of the Kilauea survey area in the more extensive aeromagnetic survey of Godson and others (1981).

The apparent resistivities of near surface (less than 100 m depth) lava flows in the central part of the Kilauea survey area range from under 100 to over 2,500 Ω-m (fig. 39.5). Steep apparent resistivity gradients along the northern edge of the Kilauea survey area are related to powerline interference (see Flanigan and others, 1986b). The steep apparent resistivity gradient along the southern part of the Kilauea survey area, where the survey aircraft flew over the ocean, is the response to the high resistivity contrast between rock and sea water. Several small (less than 1-km diameter) conductive zones are associated with Kilauea caldera and along the active parts of the east rift zone. Three conductive zones (40–250 Ω-m) trend north-northwest from near the seacoast to the east rift of Kilauea. Apparent resistivities of less than 400 Ω-m cover a large area south of Kilauea caldera.

VLF magnetic anomalies associated with zones of comparatively sharp lateral changes of conductivity are also shown on the apparent resistivity map (fig. 39.5). Where the VLF magnetic anomalies were detected by adjacent flightlines, they have been connected to indicate the general trend of the conductor axis. Trends of VLF magnetic anomalies follow volcanic features along the east and southwest rifts of Kilauea, along the southern part of Kilauea caldera, and along east-west conductors in the area south of Kilauea caldera.

Geophysical features discussed above have been combined in a single illustration for ease of discussion (fig. 39.6).

DISCUSSION OF RESULTS

The spatial relations of the magnetic source rocks to the VLF electromagnetic anomalies along the east rift of Kilauea Volcano is

particularly interesting. The interpreted boundaries of the magnetic source rocks encompass most of the surficial expression of the east rift zone (cones, craters, and cracks) as shown by Stearns and Macdonald (1946). Assuming that the VLF magnetic anomalies are associated with narrow, shallow, abrupt changes of conductivity related to feeder dikes along the east rift, then the currently active zone extends south to at least Napau Crater (fig. 39.6), and generally along the southwest and south edges of the interpreted composite dike system built by earlier injections along the east rift zone (Swanson and others, 1976). East of Napau Crater, the active dike system as defined by the VLF magnetic anomalies (fig. 39.6) changes direction to the northeast and continues eastward along the central and northern part of the interpreted magnetic dike system. The reason for the shift to the central part of the interpreted composite dike system is not readily apparent.

Several indirect lines of evidence suggest a structure zone trending about normal to the east rift that may intersect the rift just east of Napau Crater. A north-northwest zone of conductive lava flows (marked R_1, fig. 39.6) intersects the east rift of Kilauea in the area just east of Napau Crater. Rocks are an order of magnitude more conductive than outside of the zone. Assuming the upper 50–60 m of basalt has been altered or contains higher amounts of conductive waters than outside of the zone, then a break in the impervious dikes constraining fluid flow on the southeast side of the rift similar to the reasoning hypothesized by Zablocki (1977, p. 9; Zablocki and Koyanagi, 1979) might be invoked.

Although no surface transverse structure is associated with this conductivity anomaly, several geologic features support this conclusion. Topographic contours within the conductive zone change in direction to the northeast. Fault scarps of the Hilina fault system have an apparent left-lateral offset in this area. Block movement to the southeast on the south flank of Kilauea Volcano, suggested by Fiske and Kinoshita (1969) and well documented by Swanson and others (1976), would allow for such transverse structures, particularly if the south flank is not being forced southward as a contiguous block.

The distribution of 1968–71 earthquakes (Koyanagi and others, 1972) in the south flank of Kilauea has a density pattern that delineates two aseismic zones parallel but offset from the shallow resistivity anomalies R_1 and R_2 (fig. 39.6). The seismicity is caused

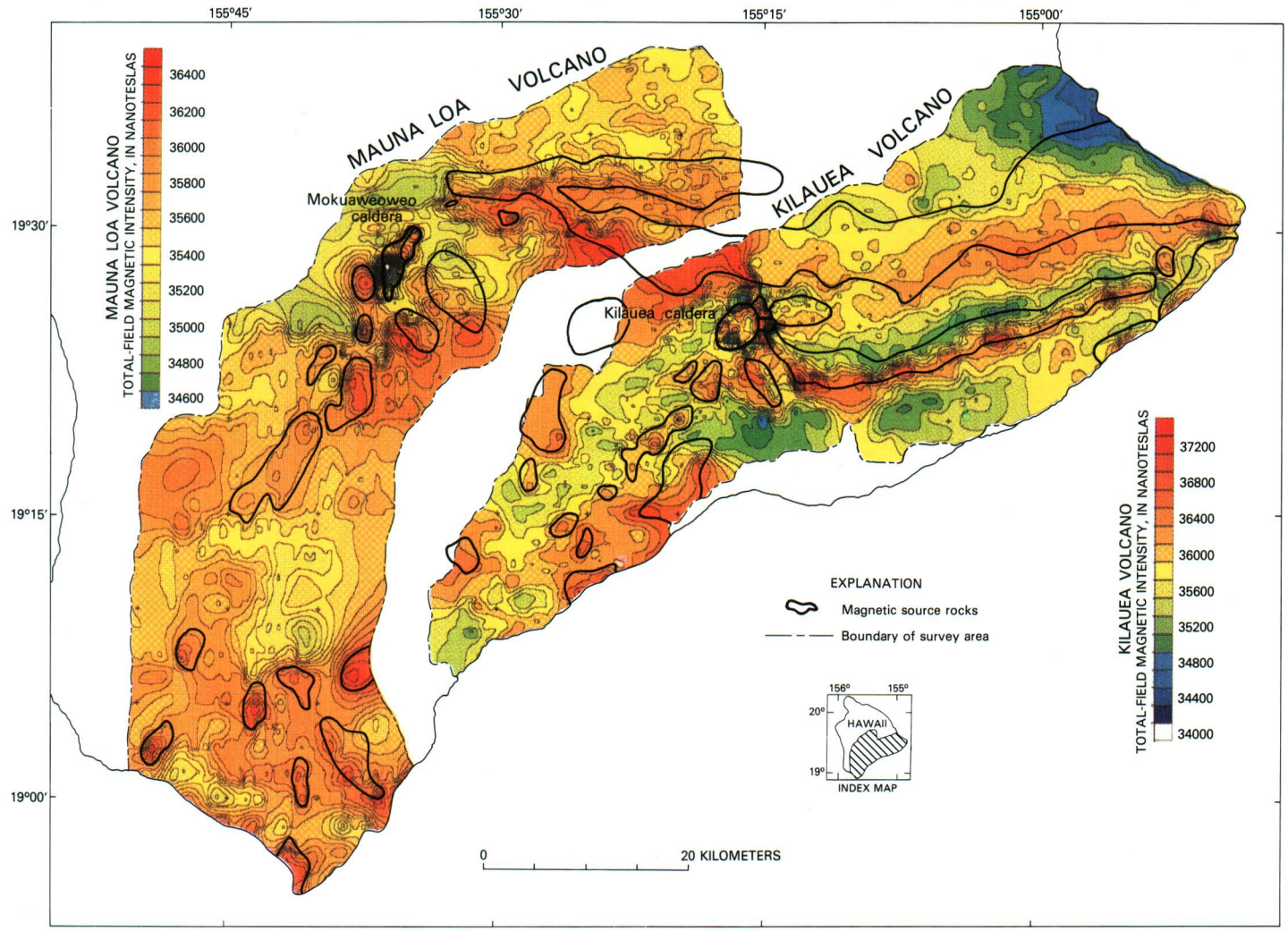

FIGURE 39.4.—Aeromagnetic map of total intensity of Earth's magnetic field over Kilauea and Mauna Loa rift systems.

by volcanic activity in the summit and the rift zones and the subsequent adjustment of the south flank to these stresses (Koyanagi, and others, 1972). If there is differential movement within the south flank, then transverse structures are likely along the edges of the blocks moving seaward from the rift zones. The Kealakakua and Kahuku faults are thought to represent the landward boundaries of sizable terrain subject to large-scale submarine block faulting on Mauna Loa's west flank (Lipman, 1980, fig. 2) analogous to movement of Kilauea's south flank.

Two other zones of conductive rocks, roughly transverse to the east rift were delineated farther east (R_2 and R_3, fig. 39.6). Conductive zone R_2 is situated at another apparent offset (left-lateral) in the currently active part of the rift zone. Here again rocks are considerably more conductive (<160 Ω-m) than the surrounding basalt flows. Though conductive zones R_1 and R_2 have not been confirmed by ground measurements, independent geophysical work generally confirms the existence of the third transverse conductive zone (Zablocki, 1977). A significant self-potential (SP) anomaly, aligned northwest, was attributed by Zablocki and Koyanagi (1979) to permeable fractures that maintain fluid continuity with a heat source. Numerous warm springs along the downslope beaches and the occurrence of hot (55 °C) brackish water in wells in the conductive area (Macdonald, 1973) support the conclusion that the zone is related to a transverse structure that has offset the rift zone in a left-lateral sense. The linear dipole magnetic anomaly also has a left-lateral offset at this point. A small (300 nT) magnetic low, correlative with a resistivity low, is centered over the Puulenna Crater area, suggesting that Zablocki and Koyanagi's (1979) heat source may still be above the Curie temperature.

An apparent reversely polarized magnetic anomaly is present over the Kapoho Crater area (figs. 39.4, 39.6). The detailed data (fig. 39.7*A*) show a dipole anomaly with a 900-nT low south of a 700-nT high. The apex of the high-low is oriented about 30° counterclockwise to the Earth's present magnetic field direction. If the direction of the remanent magnetic field were exactly opposite the Earth's present magnetic field, the alignment of the dipole anomaly would be in the same direction as the Earth's present magnetic field and the sign of the dipole anomaly would be opposite, that is, with a magnetic high north of the magnetic low. A three-dimensional magnetic anomaly was computed over a cube-shaped body 2.5 km

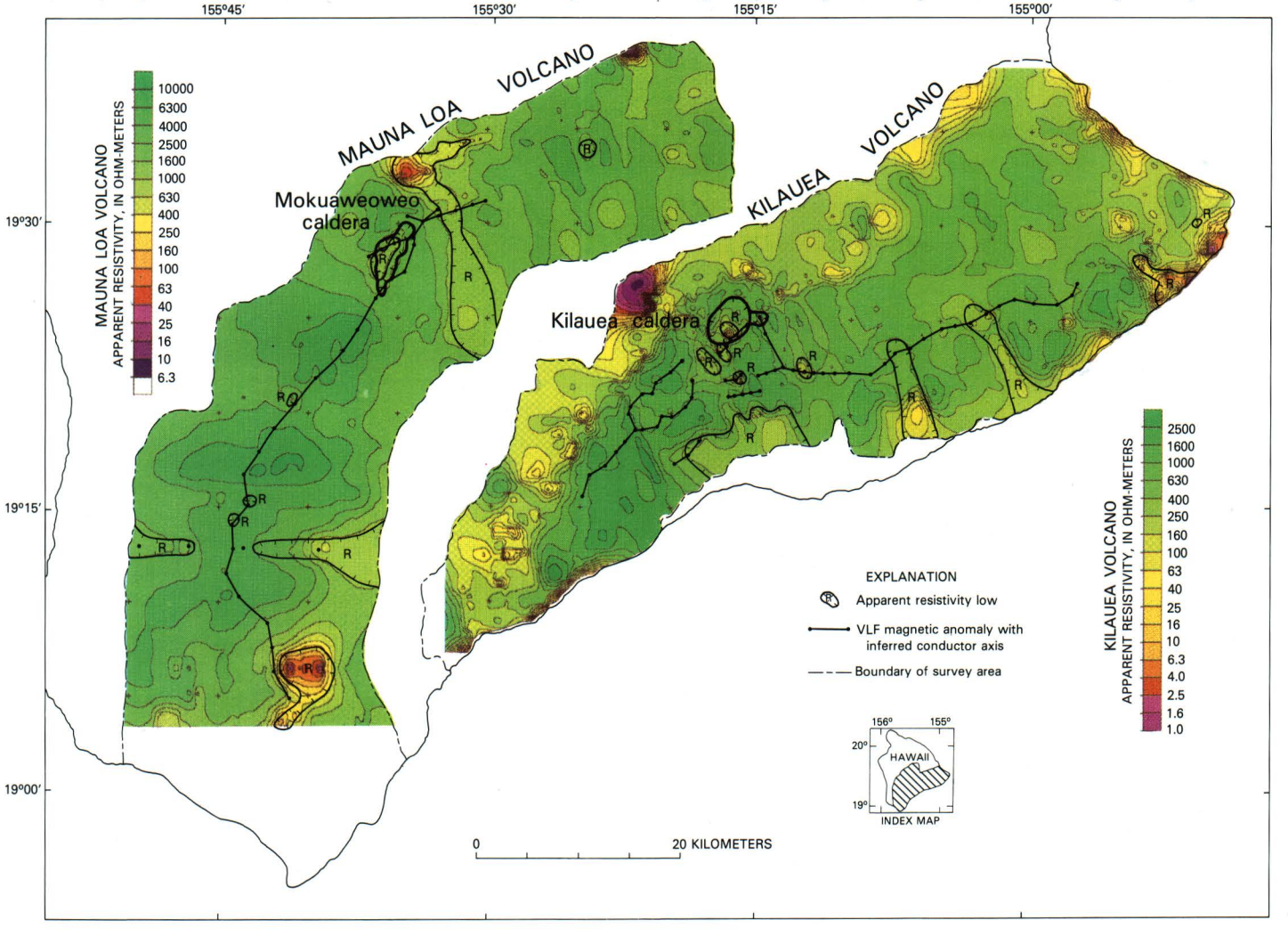

FIGURE 39.5.—Apparent resistivity map and location of VLF magnetic anomalies relative to Kilauea and Mauna Loa rift systems.

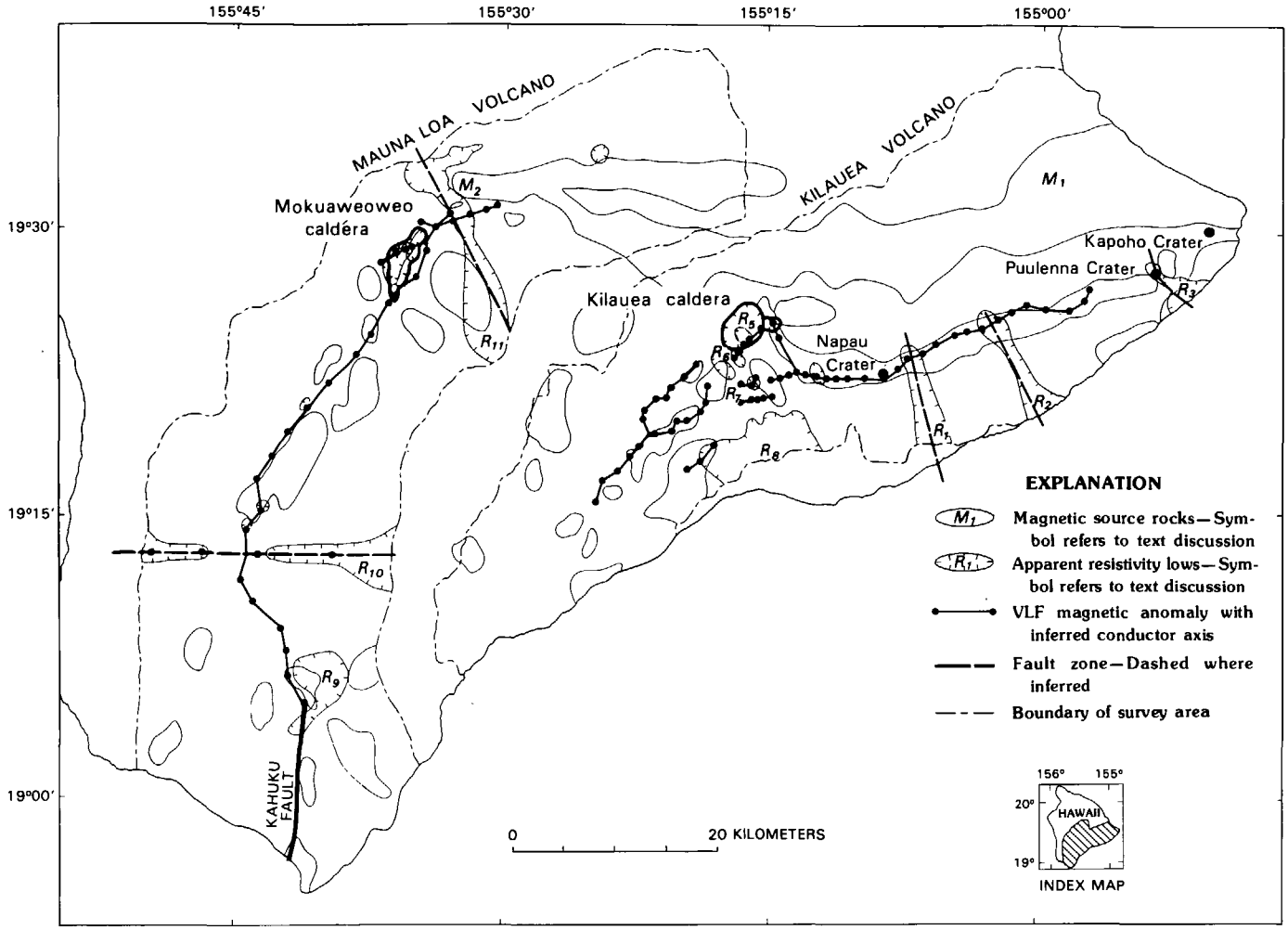

FIGURE 39.6.—Interpretive map of Kilauea and Mauna Loa rift systems, showing magnetic source rock, apparent resistivity anomalies, and VLF magnetic anomalies.

on each side (fig. 39.7*B*; from T.G. Hildenbrand, written commun., 1984). In order to produce a magnetic anomaly that matches the observed data (fig. 39.7*A*) it was necessary to rotate the remanent magnetic direction 30° counterclockwise from the exact opposite of the Earth's present field direction. Thus, one possible explanation to the Kapoho Crater apparently reversed dipole magnetic anomaly is that a body of rock of about 15.6 km^3 cooled when the Earth's magnetic field was in a period of reversal. An alternate explanation when considering the magnetic setting of the dipole anomaly is that the magnetic high is part of a broad magnetic high extending eastward from the summit of Mauna Loa (M_1, fig. 39.6) and the magnetic low is the magnetic expression of a magma chamber still above the Curie temperature and thus nonmagnetic. Norris (1976), commenting on data from a ground magnetic survey, observed a magnetic high over Kapoho Crater and suggested "that if subsequent measurements were to show a proportionate magnetic low near the south rim, then it could be concluded that there is an anomalously nonmagnetic body beneath Kapoho Crater." To test this theory, a configuration of magnetic bodies was assembled and the magnetic response calculated (M.W. Webring, written commun., 1984). Susceptibilities and vertices describing the body location were allowed to vary in order for the theoretical calculations to best-fit the observed data in a least-squares sense (fig. 39.8). Considering the oversimplification of the theoretical model the calculated data fit the observed data reasonably well. The model represents intrusive dike rocks associated with the east rifts of Mauna Loa and Kilauea separated by a magma chamber all of which have been buried by flows from Kilauea's east rift zone.

Additional geologic and geophysical evidence is necessary to determine which of the two (if either) above possible explanations for the apparent reversed dipole anomaly over Kapoho Crater is the most geologically reasonable. Reversely polarized rocks have not been reported for the Island of Hawaii where they are considered to be younger than the last period of magnetic field reversal, thus suggesting that the first model is unreasonable. We would expect low apparent resistivities caused by alteration of flow rocks lying directly

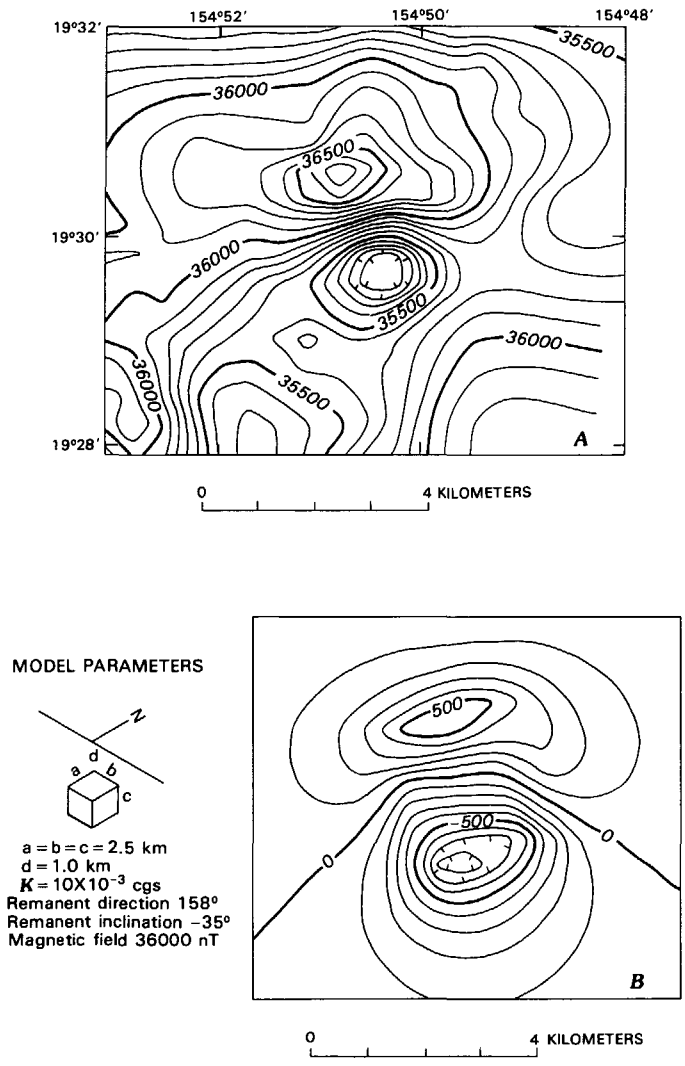

FIGURE 39.7.—Magnetic contour maps of Kapoho Crater. Contour interval is 100 nT. Hachures indicate closed low. ***A***, Observed magnetic anomaly. ***B***, Theoretical magnetic anomaly over assumed magnetic body (from T.G. Hildenbrand, written commun., 1984). Remanent magnetization direction assumed nearly reversed to direction of Earth's present magnetic field.

over the magma chamber as assumed in the second model, and apparent resistivity lows were not observed. However, recent volcanic activity in the Kapoho Crater area may have masked any near-surface apparent resistivity anomalies associated with the inferred underlying magma chamber. Dipole resistivity data presented by Skokan (1974, fig. 29b) indicates that a deep conductivity anomaly may be present in the Kapoho Crater area. This conductivity anomaly may be related to intrusion of sea water or possibly to a very conductive magma body.

Numerous aeromagnetic anomalies are present in the Kilauea Volcano summit area. Terrain-induced magnetic anomalies occur over the abrupt edges of the caldera (Decker, 1963) and are particularly noticeably over Halemaumau and Kilauea Iki Craters. Models (not shown) computed at 90 m above terrain features in the Kilauea summit area have an amplitude of about 150 nT, less than 20 percent of the observed anomalies, suggesting the observed anomaly is a combined aeromagnetic response of topography and geologic magnetic sources. Magnetic source rocks trending north-northwest intersect northeast- east-trending magnetic sources in the summit area.

A simple theoretical model over an assumed 1-km diameter, 4-km deep nonmagnetic magma chamber south of Halemaumau, as suggested by Eaton (1962), would produce an aeromagnetic anomaly of about 100 nT. It is doubtful that one could positively identify the Kilauea summit magma chamber by magnetic modeling because of the presence of magnetic source rocks of unknown configuration

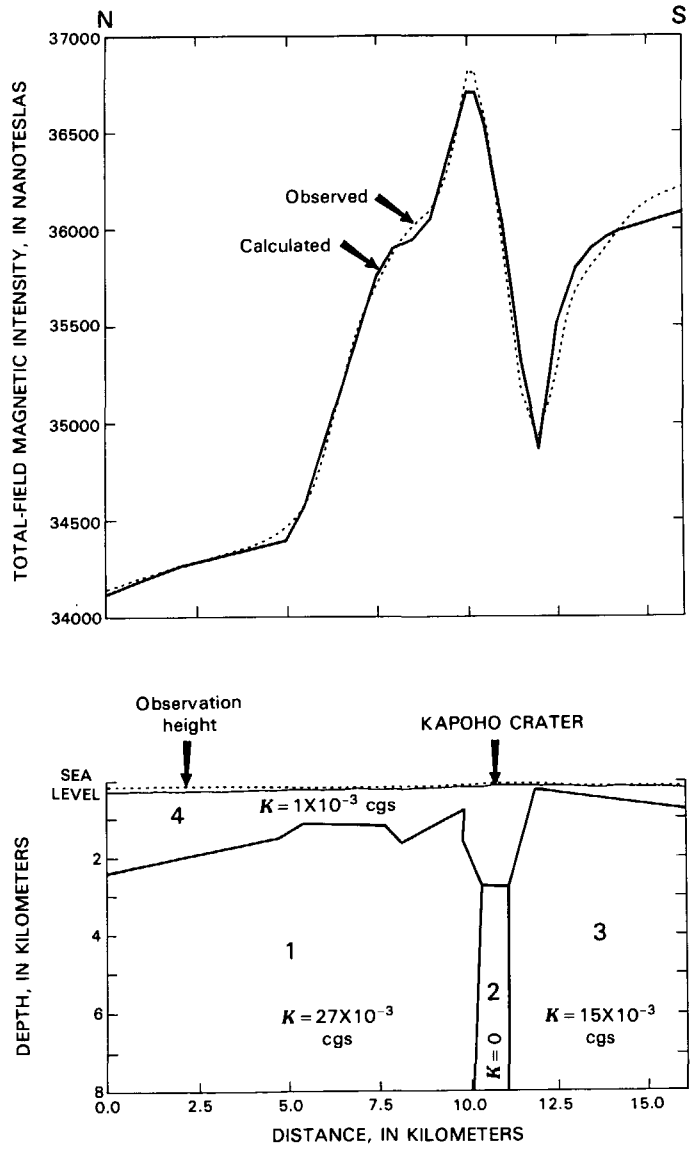

FIGURE 39.8.—Theoretical 2½-dimensional model over Kapoho Crater area assuming intrusive dike rocks to north (body 1) and south (body 3) of Kapoho Crater and nonmagnetic magma chamber (body 2) about 2 km deep beneath flow rocks (body 4). Susceptibilities (K) are shown in cgs units.

which are the apparent sources of the bulk of the observed aeromagnetic anomaly.

Apparent resistivity anomalies in the Kilauea summit area are thought to be caused by conductive rocks related to eruptive volcanic features similar to those outlined by Zablocki (1978, fig. 24) in the Sand Spit horst area. The airborne VLF data indicate an apparent resistivity low (R_5, fig. 39.6) just southeast of Halemaumau Crater. The airborne VLF magnetic-anomaly locations correspond very closely to Zablocki's VLF tilt and ellipticity measurement across Sand Spit horst. Apparent resistivity low R_5 lies north of the VLF magnetic anomaly, suggesting surface rocks are more conductive than to the south. Eaton (1962), by use of tilt measurements, indicates that the pre- and post-eruptive swelling and subsidence of Kilauea point to a magma reservoir just south of Halemaumau Crater. The VLF apparent resistivity data do not reflect directly the magma reservoir, but indirectly indicate increased alteration and (or) conductive hot circulating fluids associated with rock overlying the reservoir.

Other apparent resistivity lows have been delineated in the area southwest of Kilauea caldera (R_6, fig. 6). These conductive zones were also detected by surface VLF measurements by Zablocki (1978), who attributed them to conductive anomalies associated to cracks and hot steaming fissures. Apparent resistivity low R_7 (fig. 39.6) is thought to be associated with conductive features caused by intrusion into the Koae fault system at its junction with the east rift zone as described by Duffield (1975), and generally confirms ground geophysical observations of Jackson and Sako (1979). A broad apparent resistivity low (R_8, fig. 39.6) covers a significant area just north of the Hilina fault scarps south of Kilauea caldera. Gravity subsidence of large blocks of the unbuttressed south flank of Kilauea is largely responsible for the Hilina fault system (Swanson and others, 1976, p. 33). In places the surface of the fault blocks are nearly level or dip gently inland. These gentle slopes suggest the possibility of soils, which would contribute to low apparent resistivities. However, only a thin layer of ash is present in the near-surface rocks that could contribute to low VLF apparent resistivities (D.B. Jackson, written commun., 1985).

VLF magnetic anomalies are associated with many of the apparent resistivity anomalies in the Kilauea summit area (fig. 39.6). Most notable are VLF magnetic anomalies related to the conductive anomalies in the southern part of Kilauea caldera and to the southwest and an east-trending conductive zone parallel to the Koae fault system. Abrupt lateral changes in resistivity contrast are the causes for the VLF magnetic anomalies, and inasmuch as only one anomaly was detected at the edge of the feature they are considered to be narrow features. One would expect to see two VLF magnetic anomalies, one at each edge, of a broad conductive feature that had a sharp lateral resistivity contrast at each edge.

Several VLF magnetic anomalies extend southwest from Kilauea caldera. One of these was briefly ground-checked and thought to be related to a seismic cable extending from the Hawaiian Volcano Observatory. This anomaly was not included on figures 39.5 and 39.6. However, the other long VLF magnetic anomalies shown may have similar sources (J.P. Kauahikaua, written commun., 1984).

MAUNA LOA VOLCANO

Magnetic data (fig. 39.4) in the Mauna Loa survey area are similar to that recorded over Kilauea Volcano in several ways. The northeast rift of Mauna Loa, like the east rift of Kilauea, is characterized by linear magnetic dipoles (M_2, fig. 39.6) extending eastward from several kilometers northeast of Mokuaweoweo caldera; however, the amplitude of the magnetic dipoles is about one-half that of the Kilauea east rift. A southeast-trending linear magnetic dipole intersects the Mauna Loa east rift about 15 km east of the summit and appears to be contiguous with the east-west long-wavelength (6 km) linear magnetic dipole (M_1, fig. 39.6) crossing the northern part of the Kilauea survey area. Steep magnetic gradients outline Mokuaweoweo caldera.

The magnetic expression of the Mauna Loa southwest rift, like the Kilauea southwest rift, is composed of discontinuous linear magnetic highs of a few hundred nanoteslas extending southwest from the summit to beyond the southern tip of the island. The magnetic data accurately reflect the prominent westward bulge in the rift zone coincident with the topographic ridge of Mauna Loa's southwest rift zone (Lipman, 1979).

Two conspicuous breaks in the linear magnetic anomalies occur in the Mauna Loa magnetic data: (1) a northwest-trending magnetic low crosses the northeast rift zone at the northeast end of Mokuaweoweo caldera and (2) an east-west magnetic low crosses the southwest rift zone near the apex of the bulge.

Qualitative interpretive lines (fig. 39.4) show the approximate location of intrusive rock considered to be the source of the magnetic anomalies mentioned above.

Apparent resistivities of near-surface rocks in the Mauna Loa survey area range from 16 to over 10^4 Ω-m (fig. 39.5). Lava flows of highest apparent resistivity are present mainly in the upper one-third of the southwest rift zone. Apparent resistivity lows (<1,000 Ω-m) occur over Mokuaweoweo caldera and in the southern part of the survey area; these lows coincide with the two transverse magnetic breaks mentioned above. VLF magnetic anomalies (fig. 39.5) were detected along the entire length of the southwest rift zone except near the southern tip of the island where powerline interference and an equipment malfunction rendered the VLF data unuseable. Conductive zones produce VLF magnetic anomalies in Mokuaweoweo caldera and along its southeast edge that extends northeast for 10 km or more, beyond which no other VLF magnetic anomalies were seen. Northeast of the caldera, pairs of VLF magnetic anomalies, spaced 1 km or more apart along the flightline, were detected on several flightlines.

DISCUSSION OF RESULTS

Injection of magma into Hawaiian shield volcanoes, surface eruptions, and subsequent gravitational slumping of the flanks of the volcanoes are important mechanisms for volcano growth (Swanson and others, 1976; Lipman, 1979; Normark, 1979).

The structural complexities and growth of Mauna Loa, like Kilauea Volcano, reflect the interaction of concurrent and past volcanic activity in adjacent volcanoes (Fiske and Jackson, 1972; Lipman, 1980). For example, Mauna Kea Volcano interferes with the unrestricted growth of Mauna Loa by forming a northern buttress. The same is true of Kilauea Volcano, which is buttressed on the northwest by Mauna Loa. Lipman (1979, 1980) postulates that the buttressing effect of Mauna Kea and the growing Kilauea Volcano has affected the recent growth of Mauna Loa: (1) recent volcanic activity along the Mauna Loa northeast rift zone has been limited to the first 20 km from the summit; (2) buttressing of the south flank of Mauna Loa by the growing Kilauea Volcano has limited southeast gravitational slumping of that flank, with the net result that the active part of the Mauna Loa southwest rift zone has migrated to the west; (3) westward migration of the active part of the rift zone accompanied by block slumping to the west accounts for the west bulge in the zone.

The spatial relation of the interpreted magnetic source rocks (dike and dike swarms) and the VLF magnetic data (narrow conductive zones) add weight to Lipman's observations. For instance, VLF magnetic anomalies (fig. 39.6), probably associated with the active part of the Mauna Loa southwest rift zone, follow the fissure vents, spatter cones, and pit craters that are thought to be less than 5,000 yr old. Magnetic source rocks generally lie to the east of the VLF magnetic anomalies, suggesting westward migration of the active part of the rift zone similar to the postulated south to southeast migration of the active rift zone on the upper one-third of Kilauea's east rift zone (Swanson and others, 1976). The eastward offset of the magnetic anomalies in relation to the VLF magnetic anomalies also confirms Lipman's (1980) gravity observations, which generally indicate dense rocks are present east of the surface evidence of recent volcanic activity. The dense rocks are interpreted to be dikes and dike swarms of greater density than the adjacent rocks.

Several small, circular, apparent resistivity lows with associated VLF magnetic anomalies along the active part of the Mauna Loa southwest rift zone are thought to reflect conductive rocks associated with volcanic vents.

Another subcircular apparent resistivity low (R_9, fig. 39.6) covers a significantly larger area (30 km^2) than the small conductive zones mentioned above. The long axis of apparent resistivity low R_9 is aligned roughly north-south and lies just east of Kahuku fault (Lipman, 1980, fig. 1). Aeromagnetic anomalies southeast of apparent resistivity low R_9 are aligned northwest-southeast and appear to be a continuation of the southeast structural trend of the rift zone at the lower end of the bulge (fig. 39.6). Apparent resistivity low R_9 is thought to be related to the high conductivity of near-surface rocks at the intersection of Kahuku fault and an inferred northwest- to southeast-trending fault zone, possibly the northwest extension of Waiohinu fault (Malahoff and Wollard, 1966). The characteristics of the conductive rock in the inferred fault intersection area are unknown; however, the salinity of intrapore fluids and clay content in the zone may contribute to the low apparent resistivity of the zone. The anomaly also appears to coincide with the 1868 eruption vent. The 1868 eruption was accompanied by movement along the Waiohinu fault, all of which suggest a possible thermal anomaly as the source of the observed resistivity anomaly.

An east-west apparent resistivity low (R_{10}, fig. 39.6) cuts across the southwest rift zone a few kilometers north of the apex of the bulge in the rift zone. The east-west trend is along the aircraft flightline direction so the possibility of an equipment-base shift that would contribute to such an apparent resistivity low was considered. The anomaly is considered valid for three reasons: (1) it was detected on three successive flightlines, thus its width (north-south) is at least 3.2 km; (2) the east-west apparent resistivity anomaly is coincident with an east-west aeromagnetic low, as seen on, not only the aeromagnetic data presented here, but also the 300-m flight-height aeromagnetic survey of Godson and others (1981); (3) the high-level (12,000-ft barometric) aeromagnetic data of Malahoff and Wollard (1966) also show a similar break in the magnetic data in this area. Malahoff and Wollard (1966, p. 289) interpret the east-west to southeast magnetic feature to be related to a now-buried ancient volcanic complex lying along an east-west rift zone crossing the Hawaiian Ridge.

Assuming that a deep-seated crustal fracture zone crosses the Mauna Loa southwest rift zone at the apex of the bulge, it has affected the conductivity of the near-surface rocks. The most obvious reason is near-surface water held in by rift-related dikes flows out and downslope along the transverse structure, analogous to transverse structures on Kilauea's east rift zone. Several VLF magnetic anomalies were detected on one flightline crossing the area, indicating that in some places there are rather sharp boundaries of rock of differing resistivity. Though the Malahoff and Wollard aeromagnetic survey was better suited to detect deep magnetic sources, there is apparently some shallow geophysical expression of the same features reflected in the low-level aeromagnetic-electromagnetic data presented here.

The aeromagnetic and electromagnetic data follow an asymmetric bulge in the topographic and geologic expression of the Mauna Loa southwest rift zone, and it seems plausible that the east-west zone just discussed has played some part in the development of this asymmetry. Of course it is obvious that the buttressing effect of Kilauea on the east-southeast flank of Mauna Loa prevents growth of Mauna Loa in the southeast direction, which adequately accounts for the westward migration of the active part of the southwest rift zone, but it does not address the asymmetry seen in the geophysical data. The subaerial Alika slide, a result of oversteeping of Mauna Loa's west flank, (Normark, 1979) extends 80 km off the west coast and may have been controlled on the south by the transverse zone inferred from the geophysical data.

Another zone transverse to the northeast rift of Mauna Loa has a similar geophysical relation to that just discussed; that is, it is a northwest-trending apparent resistivity low (R_{11}, fig. 39.6) coincident with an aeromagnetic low and occurs just north of Mokuaweoweo caldera. Here, once again, the high-level aeromagnetic data of Malahoff and Wollard (1966, fig. 13) indicate a northwest-trending magnetic low that crosses Mauna Loa's northeast rift zone in the same area. Many eruptive fissures cut the north flank of Mauna Loa at high angles (Lockwood, 1979) and may be indicative of stresses active during the evolution of Mauna Loa that are also responsible for the aeromagnetic and electromagnetic fea-

tures seen in the near-surface rocks. Here, once again, northeast-trending rift dikes ruptured by a transverse structure may allow near-surface water to flow downslope and are, thus, the cause of the conductive anomaly.

A VLF magnetic anomaly, thought to be associated with eruptive volcanic features, extends about 10 km northeast of Mauna Loa summit (fig. 39.6). The VLF magnetic anomaly defines a conductor axis cutting the northwest-trending apparent resistivity low and generally lies south of magnetic source rocks (M_2, fig. 39.6). These relations imply that in the first 10 km northeast from the summit the presently active part of the rift zone has moved south relative to presumably older complex dikes (the source of the aeromagnetic anomalies). Farther to the east no VLF magnetic anomalies were detected, although volcanic cones extend for 25 km or more east of the summit. Perhaps buttressing of the lower part of Mauna Loa's northeast rift zone by Mauna Kea Volcano on the north and Kilauea Volcano on the south has restricted volcanic activity. Or perhaps conductive zones associated with feeder dikes are deeper, having been covered by lava flows occurring at higher elevations, hence are at a depth greater than can be detected by the VLF method. Alternatively, the presence of VLF magnetic anomalies only along the upper (10 km) part of Mauna Loa's northeast rift zone may be more closely related to the presence of greater amounts of conductive electrolytes than occur farther east along the rift zone.

The middle to lower Mauna Loa northeast rift zone is implied to be complex by the distribution of dike swarms interpreted as the aeromagnetic source rocks in area M_1 (fig. 39.6). The aeromagnetic expression of the northeast rift zone divides about 15 km from the summit, one fork continuing east, the other, southeast—toward Kilauea Volcano. Whether this southeast fork represents a one-time interconnection between the volcanoes is not known. It is almost certainly an early evolutionary feature of Mauna Loa development because: (1) prehistoric volcanic centers, if they ever existed, are absent along this zone, having been covered by flows from the summit area and (2) the long wavelength of the magnetic anomaly suggests deeper source rocks than associated with the Kilauea east rift zone.

SUMMARY AND CONCLUSIONS

Linear magnetic dipoles reflect intrusive dikes along the rift zones of Kilauea and Mauna Loa Volcanoes. The linear magnetic anomalies, normally polarized, vary in shape and amplitude according to the orientation of the source rocks with respect to the Earth's present field direction. At least 2 km of southward displacement of Kilauea's south flank is necessary to accommodate the intrusive dike system associated with the Kilauea east rift. The linear magnetic dipole anomaly along the Kilauea east rift zone is terminated on the eastern end of the island by an interpreted structure transverse to the rift zone. The magnetic data suggest a left-lateral offset of about 1.5 km in the rift zone beyond the termination point.

VLF magnetic anomalies are interpreted to reflect zones of conductive rocks of limited horizontal extent, but having relatively sharp lateral boundaries with large conductivity contrasts, and are interpreted as defining the currently active part of the rift zones. Most of the VLF magnetic anomalies are present along eruptive and intrusive volcanic features, thus confirming earlier ground electrical geophysical surveys.

The spatial relation of interpreted magnetic source rocks to the active part of the rift zones are important indicators of the recent evolutionary development of Kilauea and Mauna Loa Volcanoes. In the upper one-third of the Kilauea east rift zone the active part of the rift zone lies along the southern edge of interpreted magnetic source rocks, correlating with independent observations that the south flank of Kilauea is being forceably moved to the south by repeated magma injection from the summit reservoir. Just east of Napau Crater the active part of the Kilauea east rift zone is over the central and northern part of the interpreted intrusive dike system, suggesting controlling factors such as transverse fault zones caused by differential movement of Kilauea's south flank. Large-scale block slumping with accompanying transverse boundary faults of Kilauea's south flank are proposed as a possible explanation for the spatial relation of the active rift zone to early magnetic dike rocks. Rupture of impervious dikes bounding the east rift zone allowing downslope movement of conductive hot-water electrolytes may produce apparent resistivity lows along the postulated transverse boundary faults.

Two explanations for an apparently reversely magnetized magnetic dipole over the Kapoho Crater area are suggested from theoretical magnetic models. One model assumes a 2.5-km cube-shaped body of rock in which the remanent magnetic direction is nearly opposite the Earth's present magnetic field direction. This model has two drawbacks: (1) reversely polarized magnetic rocks have not been reported on the Island of Hawaii; (2) in order to compute a magnetic response of this theoretical model that closely resembles the observed data, the remanent magnetic direction must be rotated about 30° counterclockwise. This rotation infers that either there has been postcooling rotation of that part of the island or that the remanent magnetic field direction was not exactly opposite to the Earth's present magnetic field direction, a condition seldom seen or recognized in magnetic data interpretation. The second model assumes magnetic dike rocks north and south of Kapoho Crater are separated by a nonmagnetic shallow magma chamber. Absence of a resistivity anomaly over the proposed shallow magma chamber may be due to covering by young resistive lava flows.

The effects of concurrent growth of Kilauea and Mauna Loa Volcanoes are reflected in the magnetic and electromagnetic data, most clearly in evidence along Mauna Loa's southwest rift zone. Interpreted source rocks for aeromagnetic anomalies along the upper part of Mauna Loa's southwest rift zone lie east of the active rift zone as defined by VLF magnetic anomalies and are consistent with gravity data and geologic observations indicative of westward migration of the rift zone. An east-west aeromagnetic and apparent resistivity low near the apex of the bulge in the Mauna Loa southwest rift zone is interpreted as offset of water-constraining dikes along the southwest rift by a transverse structure, allowing conductive ground water to flow downslope. The Alika landslide which incorporates a large part of the west flank of Mauna Loa, may have been controlled on the southern boundary by this inferred transverse structure.

A northwest-trending zone just north of Mokuaweoweo caldera, reflected as apparent resistivity and aeromagnetic lows in the airborne data, is interpreted as another transverse structure that has allowed impounded near-surface water to flow downslope.

Many of the conclusions and observations presented here have a reasonable correlation with the observations of other earth scientists, others are highly speculative and hopefully will stimulate future research in understanding the evolutionary development of these two very interesting Hawaiian volcanoes.

REFERENCES CITED

Arcone, S.A., 1978, Investigation of a VLF airborne resistivity survey conducted in northern Maine: Geophysics, v. 43, p. 1399–1417.

——— 1979, Resolution studies in airborne resistivity surveying at VLF: Geophysics, v. 44, p. 937–946.

Barringer, A.R., and McNeill, J.D., 1969, The radio-phase technique of airborne resistivity mapping: Geophysics, v. 36, p. 1014.

Blakely, R.J., and Grauch, V.J.S., 1983, Magnetic model of crystalline terrane: Geophysics, v. 48, p. 1551–1557.

Decker, R.W., 1963, Magnetic studies on Kilauea Iki lava lake, Hawaii: Bulletin Volcano, v. 26, p. 23–35.

Duffield, W.A., 1975, Structure and origin of the Koae fault system: U.S. Geological Survey Professional Paper 856, 12 p.

Eaton, J.P., 1962, Crustal structure and volcanism in Hawaii: Crust of the Pacific Basin: American Geophysical Union Geophysical Monograph Series, no. 6, p. 13–29.

Fiske, R.S, and Jackson, E.D., 1972, Orientation and growth of Hawaiian volcanic rifts: The effect of regional structure and gravitational stresses: Proceedings, Royal Society of London, Ser. A, v. 329, p. 299–326.

Fiske, R.S., and Kinoshita, W.T., 1969, Rift dilation and seaward displacement of the south flank of Kilauea Volcano, Hawaii, *in* Symposium on volcanoes and their roots, Oxford, England: International Association of Volcanology and Chemistry of the Earth's Interior, p. 53–54.

Flanigan, V.J., Long, C.L., Rohret, D.H., and Mohr, P.J., 1986a, Aeromagnetic map of the rift systems of Kilauea and Mauna Loa Volcanoes, Island of Hawaii, Hawaii: U.S. Geological Survey Miscellaneous Field Investigations Map MF–1845A.

——— 1986b, Apparent resistivity map of the rift systems of Kilauea and Mauna Loa Volcanoes, Island of Hawaii, Hawaii: U.S. Geological Survey Miscellaneous Field Investigations Map MF–1845B.

Frischknecht, F.C., 1971, Results of some airborne VLF surveys in northern Wisconsin: U.S. Geological Survey Open-File Report, 28 p.

——— 1973, Electromagnetic scale model studies of geophysical methods using a plane wave source: Golden, Colo., University of Colorado, Ph.D. thesis.

Godson, R.H., 1984, Composite magnetic anomaly map of the United States, Part B, Alaska and Hawaii: U.S. Geological Survey Geophysical Investigations Map GP–954B, scale 1:2,500,000.

Godson, R.H., Zablocki, C.Z., Pierce, H.A., Frayser, J.B., Mitchell, C.M., and Sneddon, R.A., 1981, Aeromagnetic map of the Island of Hawaii: U.S. Geological Survey Geophysical Investigations Map GP–946, scale 1:250,000.

Grauch, V.J.S., and Campbell, D.L., 1984, Does draping aeromagnetic data reduce terrain induced effects: Geophysics, v. 49, pp. 75–80.

Hoekstra, P., Sellmann, P.V., and Delaney, A., 1975, Ground and airborne resistivity surveys of permafrost near Fairbanks, Alaska: Geophysics, v. 40, p. 641–656.

Jackson, D.B., and Sako, Maurice, 1979, Self-potential mapping on the southwest rift zone of Kilauea Volcano [abs.]: Hawaii Symposium on Intraplate Volcanism and Submarine Volcanism, abstract volume, p 165.

Keller, G.V., and Frischknecht, F.C., 1966, Electrical methods in geophysical prospecting: New York, Pergamon Press, 519 p.

Keller, G.V., and Rapolla, A., 1974, Geoelectric surveys of thermal areas, *in* Civetta, L., Gasparini, P., Luongo, G., and Rapolla, A., eds., Physical Volcanology: Amsterdam, Elsevier, p. 133–166.

Koyanagi, R.Y., Swanson, D.A., and Endo, E.T., 1972, Distribution of earthquakes related to mobility of the south flank of Kilauea Volcano, Hawaii: U.S. Geological Survey Professional Paper 800–D, p. D89–D97.

Lipman, P.W., 1979, The southwest rift zone of Mauna Loa; implications for structural evolution of Hawaiian volcanoes [abs.]: Hawaii Symposium on Intraplate Volcanism and Submarine Volcanism, abstract volume, p. 169.

——— 1980, The southwest rift zone of Mauna Loa; implications for structural evolution of Hawaiian volcanoes: American Journal of Science, v. 280–A, p. 752–776.

Lockwood, J.P., 1979, Asymmetry of the northwest rift zone of Mauna Loa Volcano, Hawaii, evidence for a mobile south flank [abs.]: Hawaii Symposium on Intraplate Volcanism and Submarine Volcanism, abstract volume, p. 170.

Macdonald, G.A., 1973, Geological prospects for development of geothermal energy in Hawaii: Pacific Science, v. 29, no. 9, p. 209–219.

Malahoff, Alexander, and McCoy, Floyd, 1967, The geologic structure of the Puna submarine ridge, Hawaii: Journal of Geophysical Research, v. 72, no. 2, p. 541–548.

Malahoff, Alexander, and Strange, W.E., 1965, The paleomagnetic significance of aeromagnetic surveys of the Hawaiian Islands: Pacific Science, v. 19, no. 3, p. 390–392.

Malahoff, Alexander, and Wollard, G.P., 1966, Magnetic surveys on the Hawaiian Islands and their geologic implications: Pacific Science, v. 20, p. 265–311.

Normark, W.R., 1979, Regional slump structures on the west flank of Mauna Loa Volcano, Hawaii [abs.]: Hawaii Symposium on Intraplate Volcanism and Submarine Volcanism, abstract volume, p. 172.

Norris, R., 1976, Puna magnetics, *in* The Hawaiian geothermal project initial phase II progress report: University of Hawaii, p. 32–33.

Paal, G., 1965, Ore prospecting based on VLF-radio signals: Geoexploration, v. 3, p. 139–147.

——— 1968, Very low frequency measurements in northern Sweden: Geoexploration, v. 6, p. 141–149.

Patterson, N.R., and Ronka, V., 1971, Five years of surveying with the very low frequency-electromagnetic method: Geoexploration, v. 9, p. 7–26.

Skokan, C.K., 1974, A time-domain electromagnetic survey of the east rift zone, Kilauea Volcano, Hawaii: Golden, Colo., Colorado School of Mines Ph.D. thesis, no. T–1700, 152 p.

Stearns, H.T., and Macdonald, G.A., 1946, Geology and groundwater resources of the Island of Hawaii, territory of Hawaii: Division of Hydrology Bulletin, no. 9, 363 p.

Swanson, D.A., Duffield, W.A., Fiske, R.S., 1976, Displacement of the south flank of Kilauea Volcano; the results of forceful intrusion of magma into the rift zones: U.S. Geological Survey Professional Paper 963, 39 p.

Wait, J.R., 1962, Electromagnetic waves in stratified media: New York, Pergamon Press.

Webring, M.W., 1981, MINC; a gridding program based on minimum curvature: U.S. Geological Survey Open-File Report 81–1224, 12 p.

Zablocki, C.J., 1976, Mapping thermal anomalies on an active volcano by the self-potential method, Kilauea, Hawaii: Proceedings of the 2d United Nations symposium on the Development and Use of Geothermal Resources, San Francisco, California, May 1975, v. 2, p. 1299–1309.

——— 1977, Self-potential studies in east Puna, Hawaii, *in* Geoelectric studies on the east rift, Kilauea Volcano, Hawaii Island: Geothermal Resources Exploration in Hawaii, v. 3, University of Hawaii, HIG–77-15, p. 175–193.

——— 1978, Applications of the VLF induction method for studying some volcanic processes of Kilauea Volcano, Hawaii: Journal of Volcanology and Geothermal Research, p. 155–195.

Zablocki, C.J., and Koyanagi, R.Y., 1979, An anomalous structure in the lower east rift zone of Kilauea Volcano [abs.]: Hawaii Symposium on Intraplate Volcanism and Submarine Volcanism, abstract volume, p. 127.

REGIONAL SELF-POTENTIAL ANOMALIES AT KILAUEA VOLCANO

By Dallas B. Jackson *and* James Kauahikaua

ABSTRACT

Self-potentials (SP) at Kilauea Volcano, when referenced to the potential at sea level, appear as a broad, negative bowl-shaped anomaly with smaller wavelength anomalies that are positive-tending, but not necessarily of positive amplitude, superimposed over thermal volcanic features. To a first approximation, the broad-wavelength negative anomaly is inversely correlated with topography. Plots of SP versus topography and (or) vadose-zone thickness determined from vertical electrical soundings show linear, sometimes segmented, correlations along four lengthy SP profiles on Kilauea. The slopes of the correlation lines are used to calculate an apparent water-table elevation along the entire profile. When compared with surface geology and nearby well data, the apparent water table is reasonable. The ground water table is near sea level for most areas south of the middle and lower east rift zone and at the boundary between the southwest rift zone of Kilauea and the southeast flank of Mauna Loa near the coast. By contrast the profiles show that water may be impounded to high elevations within the east rift zone, both east and west of the upper east rift zone, and beneath the summit region. The water table is also elevated beneath the southwest flank of Kilauea.

INTRODUCTION

The self-potential or spontaneous-potential (SP) method measures naturally occurring electric-field potentials that exist at the Earth's surface. Extensive potential-field mapping on Kilauea shows there is a direct relation between volcanic structure and SP field distribution at the summit of Kilauea Volcano (Zablocki, 1976). An SP map of the intersection of the lower east rift zone of Kilauea with the coast (Zablocki, 1977) and two new profiles, each referenced to the potential at sea level, show that the regional (that is, the long-wavelength) portion of SP appears strongly correlated with topography. Zablocki suggested that a more meaningful correlation is between SP and vadose-zone thickness. In this paper we will first discuss SP-measurement techniques and possible measurement errors in order to demonstrate that our field measurements genuinely reflect natural Earth potentials. Then we will quantify the relation of SP magnitude to topography and (or) thickness of the vadose zone in an attempt to isolate a cause of regional SP.

MEASUREMENT TECHNIQUES

The measurement of self-potential is quite simple, requiring only a high-impedance millivoltmeter, nonpolarizing electrodes, and approximately 2 km of insulated single-conductor wire. It is desirable to space reference points as far apart as practical to keep cumulative errors to a minimum, but to make measurements also at smaller intervals between reference points. For example, we commonly make measurements at 100-m intervals, but only move reference points every 1.5 km.

A typical nonpolarizing electrode consists of a bare copper strip immersed in a supersaturated copper-sulfate solution in a porous ceramic cup. The cup has sides wrapped in fiberglass for added strength and can be fabricated with a large bottom surface area to improve electrical contact with the ground.

At Kilauea, it is essential that a very high impedance millivoltmeter be used. The electrical resistance between the electrodes and the earth can easily vary between a few tens of ohms for deeply weathered or altered ash and lava flows to megaohms for dry sand and ash or unweathered lava flows. A millivoltmeter input impedance several orders of magnitude larger than the largest expected electrode resistance insures that errors due to electrode resistance are kept small. We use a very simple system designed by Zablocki (1976) that incorporates an electrometer amplifier (10^{14} ohms impedance) with a filtered input to reject AC signals and a digital display of 1 to 999 mV. The amplifier has an input bias current of only 10^{-14} A, an important consideration because large bias currents will polarize the measuring electrodes.

In the field, a reference electrode is established and a second electrode is moved successively to each measurement site. The electrode is positioned by simply placing it on the ground and rotating it to make contact with the soil-moisture layer that is usually present just a few millimeters beneath the surface. Only in rare cases is it necessary to disturb the ground surface by digging to make adequate contact. If a reading is not repeatable to within 1–2 mV or is unstable, we assume that contact resistance is probably very high, and readings are discontinued at that location. In areas where soil texture varies from very coarse ash (commonly well drained and dry) to finer grained ash, the electrical contact may improve at the next reading position and readings are continued. The most common cause of high contact resistance is usually a long period of drought, in which rainfall has been too low to maintain fluid continuity between the ground surface and the film of water that is always present in the vadose zone (unsaturated zone between the ground surface and the water table).

Water is almost never added to the ground surface to improve electrical contact because watering of electrodes can produce extraneous potentials and a complex voltage drift (one exception to this is

described later). A good example of such behavior is shown in Corwin and Hooever (1979). The same considerations do not apply to the surfaces of fresh lava flows. There a moist rag or a sponge pushed into cracks in the flow surface is usually sufficient to lower contact resistance enough to give readings repeatable to within 1–2 mV.

The only exception we have made to the rule of not watering electrodes is on a monitored profile on Mauna Loa Volcano at the 3,400-meter elevation (Lockwood and others, 1985), where rainfall is very low most of the year. Even with a high impedance millivoltmeter, stable readings are normally not possible in this environment. As an experiment, water was added at each position that a reading was to be made, and then the SP drift was observed. After about 2 hours, the initial rapid potential drift (that began at about 10 mV/min) stopped; readings thereafter appeared stable and the profile was measured. A repeat of the profile 24 hours later gave readings that differed by less than 10 mV from the first measurements. Although very time-consuming, watering of electrodes appears to be permissible under these circumstances and may be the only way data can be collected in extremely dry areas.

POSSIBLE MEASUREMENT ERRORS

Measurement errors related to mapping can be caused by (1) poor electrical contact with the ground surface in extremely dry areas, as discussed above; (2) failure to reoccupy electrode positions exactly when changing references on a traverse; (3) use of electrodes that are polarized; and (4) telluric currents.

INEXACT REFERENCE ELECTRODE POSITIONING

The failure to reoccupy exact reference-electrode positions can produce measurement errors in areas of anomalous gradients (for example, on the flanks of short-wavelength high-amplitude anomalies). This is a simple error to correct because high gradient areas are easily recognized during data collection and can be avoided as reference locations. Typical closures calculated for a wide variety of grounding conditions have always been less than 10 mV/km. Such errors are insignificant in mapping large potential changes; we are convinced that serious reference-electrode positioning errors can generally be avoided with a bit of care.

ELECTRODE BIAS

Copper sulfate nonpolarizing electrodes can sometimes drift from a balanced state (zero difference between electrodes) as they age or if they are contaminated. Such offsets can range from common values of 1–10 mV to more than 50 mV in extreme cases. To correct this, readings may be numerically compensated for the polarization by linearly distributing potential differences along a traverse, or matched pairs of electrodes with minimal bias can be selected from a large set of electrodes maintained for mapping.

TELLURIC CURRENTS

Temporal variations of the Earth's magnetic field induce current flow in the Earth (telluric currents). The fluctuations of the electric field range in duration from milliseconds to centuries and can produce electric-field gradients of several hundred millivolts per kilometer over highly resistive terrain (Keller and Frischknecht, 1966), as is common in the continental interior. However, in an island setting such as Hawaii, where the rocks may also be highly resistive, the telluric currents tend to flow around the island in the conductive ocean water (Klein and Larson, 1978). At Kilauea, tellurics are generally too small (less than 1 mV/km) to be seen while SP readings are being made. Longer term and higher amplitude variations could conceivably introduce errors in SP traverse readings if their rate of change is such that measurable electric-field changes are produced during the time required for successive profile readings (about 4–8 minutes). The magnitude of potentials related to telluric currents is approximately proportional to the length of line on which they are recorded; therefore, the greater the distance between the reference and measuring electrodes the larger will be the error.

There is no way to quantitatively correct for changes related to telluric currents. However, one can attempt to estimate the perturbations and then dismiss them as sources of error if they are small. We estimate that a 1.5-km profile segment should take no longer than 2 hours to sample at 100-m intervals. The best set of published telluric measurements at Kilauea are those by Zablocki (1980) for potentials continuously recorded over 5 months in 1974 on two stationary orthogonal lines near the upper-east-rift-zone (UERZ) profile in figure 40.1. During that study, the largest excursions recorded over a 2-hour period were 25 mV/km. The great majority of such excursions were of about 10 mV/km or less. Therefore, for the worst case, it might be possible to have an error of about 40 mV over the 1.5 km segment. When mapping anomalies with amplitudes of several hundred millivolts, even this worst case would not seriously affect the results.

GEOLOGIC SP SOURCES

Two source mechanisms seem to be capable of generating large self-potentials. The first mechanism, electrokinetic coupling or streaming potentials, is related to the circulation of fluids through porous rock (Sill, 1983). The second mechanism, thermoelectric coupling, can generate anomalous potentials at the ground surface from thermal gradients near dike-like heat sources (Fitterman, 1983).

THERMOELECTRIC COUPLING

Rocks are capable of producing an electric potential gradient in response to a thermal gradient. Fitterman (1984) has shown that the necessary conditions for the generation of a thermoelectric SP anomaly are a heat source and a change in the thermoelectric coupling property (ratio of voltage change to temperature change) in the vicinity of the heat source within the earth. Examples of theoretical SP anomalies produced by various heat sources and

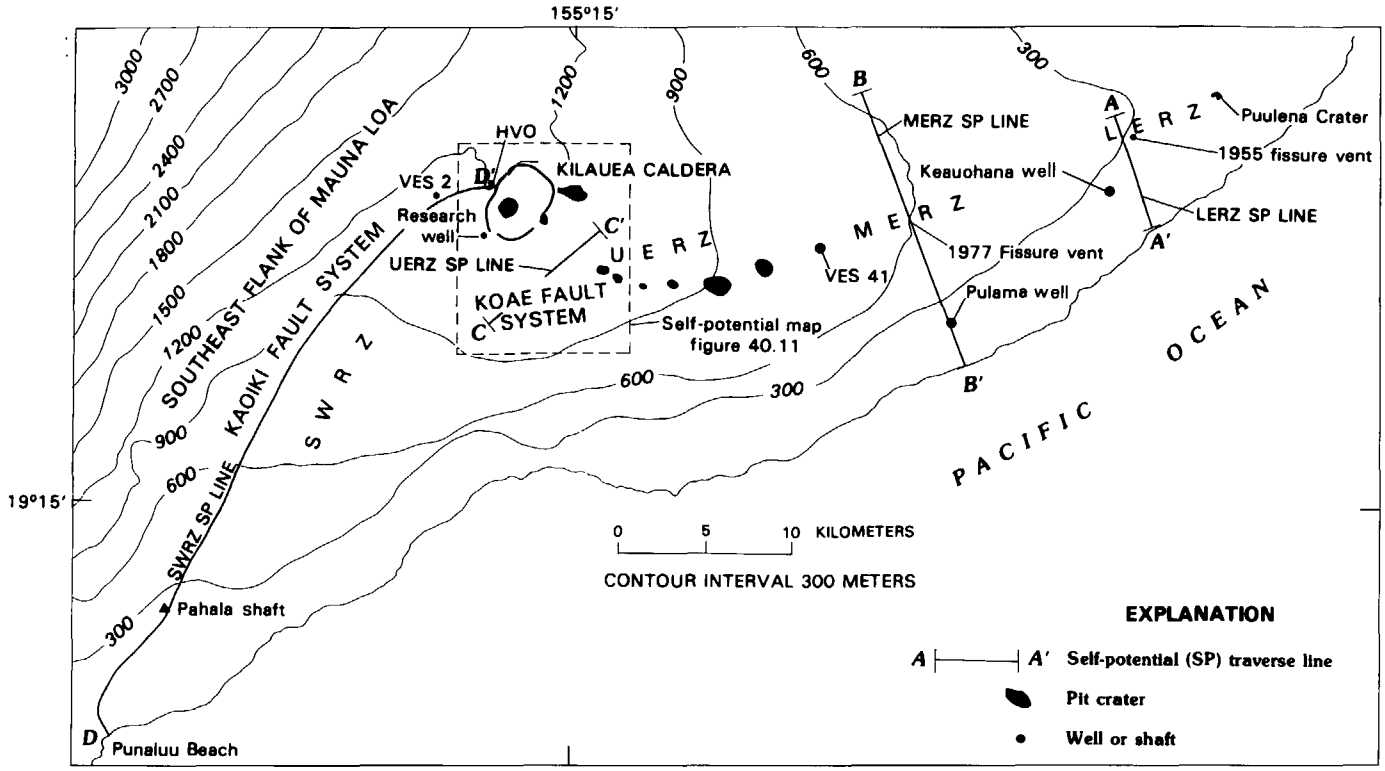

FIGURE 40.1.—Self-potential (SP) lines and major geologic features on Kilauea Volcano. SWRZ, southwest rift zone; UERZ, upper east rift zone; MERZ, middle east rift zone; LERZ, lower east rift zone.

various distributions of thermoelectric coupling property are shown in Fitterman (1978, 1979, 1983, 1984). Typical Earth heat sources in a volcanic terrain are buried magma bodies.

ELECTROKINETIC COUPLING

Rocks can also be a source of electric potential gradients if subjected to fluid flow within the rock pores. Necessary conditions for production of an electrokinetic SP anomaly are a fluid pressure gradient and a change in the electrokinetic coupling property (ratio of voltage change to pressure change) in the vicinity of the pressure gradient. Sill (1983) models various geometries for point pressure sources (abstract representations of pumping wells or springs) and for fluid which is convecting (Sill, 1982). As a rule, electric potentials become more positive in the direction of flow. In a uniform halfspace with nonzero electrokinetic coupling properties, positive anomalies are produced over a convection cell which is flowing vertically upward at the center and over a point source (such as a pumping well) in which fluid is flowing toward the point source. Electrokinetic causes have been hypothesized for SP anomalies observed in Yellowstone National Park (Zohdy and others, 1973) and Long Valley caldera, California (Anderson and Johnson, 1976).

SP CORRELATIONS WITH TOPOGRAPHY

A negative correlation between ground elevation (topography) and self-potential has been recognized for many years (Poldini, 1939; Yungul, 1950). Such correlations have been observed in many places, including Adagdak Volcano, Adak Island, Alaska (Corwin and Hoover, 1979), Hualalai Volcano, Hawaii (Jackson and Sako, 1982), and Kilauea Volcano (Zablocki, 1977).

The correlation with topography was initially thought to be due to the flow of nonthermal subsurface water (Poldini, 1939; Yungul, 1950) presumably through an electrokinetic mechanism. More recently, Zablocki (1978) proposed that the vertical descent of meteoric water through the vadose zone to the water table is the source mechanism, implying that SP intensities should actually be correlated to the underlying vadose-zone thickness, not to topography.

SP is clearly correlated with topography where the water table is horizontal near the coast. When both topography (meters) and SP (millivolts) are referenced to sea level and are plotted against one another, linear trends are commonly found which can be described by an equation of the form

$$\text{SP} = \text{ground elevation} \times C_e + A,$$

where C_e is the coefficient relating SP and ground elevation and A is the Y-axis intercept. For coastal areas where the water table is horizontal and at sea level, the constant (A) is zero. However, more than one value of the coefficient is found even for single SP profiles, indicating that SP is not primarily related to ground elevation but possibly instead to vadose zone thickness.

SP should also be plotted against vadose-zone thickness where data are available, such as vertical electrical (Schlumberger) soundings or drilled wells. Linear trends of the form

$$\text{SP} = \text{vadose zone thickness} \times C_v + A$$

should be sought, where C_v is the constant of proportionality between SP and vadose-zone thickness. The constant, A, should be zero in this case. Unfortunately, measurements of vadose-zone thickness are not as common as ground elevation measurements. Only one of the four profiles (UERZ) presented in this paper has enough measurements of vadose-zone thickness available to determine a value for C_v. The other profiles have only one or two vadose-zone thickness determinations. For those, the SP correlation with topography was determined at the coast where the water table is almost certainly horizontal and at sea level. Using the value of C_e so derived, which in this case is equivalent to C_v, we calculated apparent water-table elevations for the entire profile by means of the equation

$$\text{water-table elevation} = \text{ground elevation} - \text{SP}/C_v.$$

These calculated values were then compared with the few known water-table elevations to test the supposition that regional scale SP is related more directly to vadose-zone thickness than to topography.

Many shorter wavelength SP anomalies may also be related to local vadose-zone thickness variations. For the most part, these anomalies are positive, monopolar, and located over thermal areas. Zablocki (1978, p. 747) proposes that these anomalies "may simply reflect the shallow depths to which cool meteoric water may descend before encountering higher temperature fluids rising above a deeper heat source. Enhancement of the anomalies may result from the ascending water vapor over the thermal area and from a large flux of liquid-phase water diverted laterally downward along the immediate flanks of the thermal zone." These short-wavelength anomalies may also be produced by thermoelectric sources (heat produced by intrusive magma) or electrokinetic sources other than the descent of meteoric water (such as thermal convection of water below the water table).

SP PROFILES MEASURED ON KILAUEA VOLCANO

The following section describes four SP profiles measured on long traverses over large changes either in elevation and (or) in thickness of the vadose zone.

MIDDLE EAST RIFT ZONE (MERZ)

A 17-km traverse was run from the ocean up the south flank and across the MERZ to the north flank of the rift (fig. 40.2; see also fig. 40.1). This SP profile has the form of a broad potential low, becoming increasingly more negative relative to sea level as the rift zone is approached. A positive-tending, high-amplitude (about 1,000 mV relative to adjacent levels) SP anomaly about 3–4 km wide is present over the active rift zone. Prominent but narrow positive-tending inflections on the SP profile also mark a fissure associated with a 1977 eruption (10.2 km from the SW. end of the profile at the coast), a 1963 eruptive fissure (10.7 km), and a 1968 fissure (11.5 km) that erupted lava from vents about 1.5 km on either side of the profile.

A zone with a good correlation ($C_e = -1.7$ mV/m) between topography and SP (circles on fig. 40.3) extends approximately 8.2 km from the coast to the northwest beyond the large fault scarps of the steep south flank. We infer from well data (Pulama well) at about the 2.8-km position on the profile that the water table is nearly horizontal and at sea level in this portion of the profile (State of Hawaii Department of Land and Natural Resources, 1970). The linear gradient of -1.7 mV/m ends at 8.2 km where the large positive-tending SP anomaly over the active rift begins (fig. 40.2).

At 10.2 km, the potentials rise above the zero reference by about 200 mV for a short distance across the 1977 fissure vent. Similar short-wavelength (<1 km) monopolar features (fig. 40.2) are also associated with the 1963 vent and the 1968 fissure. A fourth short-wavelength anomaly, similar in appearance to those at the 1963 vent and 1968 fissure, occurs on the SP profile between 13 km and 14 km. This feature is not directly associated with any surface feature but is only about 0.5 km beyond the northern limit of a horst-and-graben structure that is probably related to shallow intrusions of prehistoric (before the first recorded MERZ eruption in 1790) age but less than 300 years old (Holcomb, 1980).

Northwest of the rift zone (beyond any surface expression of eruptive features), the SP gradually increases (fig. 40.2). The slope of SP plotted against elevation for this section of the profile is about -4.4 mV/m (fig. 40.3), steeper than that measured southeast of the rift zone. Calculations of apparent water-table elevations using the coefficient of -1.7 mV/m are shown in figure 40.2.

LOWER EAST RIFT ZONE (LERZ)

The LERZ SP mapped by Zablocki (1977, fig. 2), has basically the same pattern of potential distribution as the MERZ. All areas not associated with obvious thermal features are more negative than potentials at sea level. Only two areas, one associated with a 1955 fissure vent (fig. 40.4) and the other associated with a prehistoric pit crater, Puulena (located on fig. 40.1; data not shown), are positive relative to sea level (about 50 mV). The one data set that Zablocki (1977, fig. 4) examined for a topographic-SP correlation runs from the ocean to a 1955 fissure vent and has a correlation coefficient (C_e) of -1.8 mV/m (fig. 40.5). This is comparable to the correlations we have found for other parts of the volcanic edifice where we believe the water table to be nearly horizontal. Using the SP and topographic data from Zablocki's figure 4, we have calculated and plotted the apparent water table along the profile (fig. 40.4).

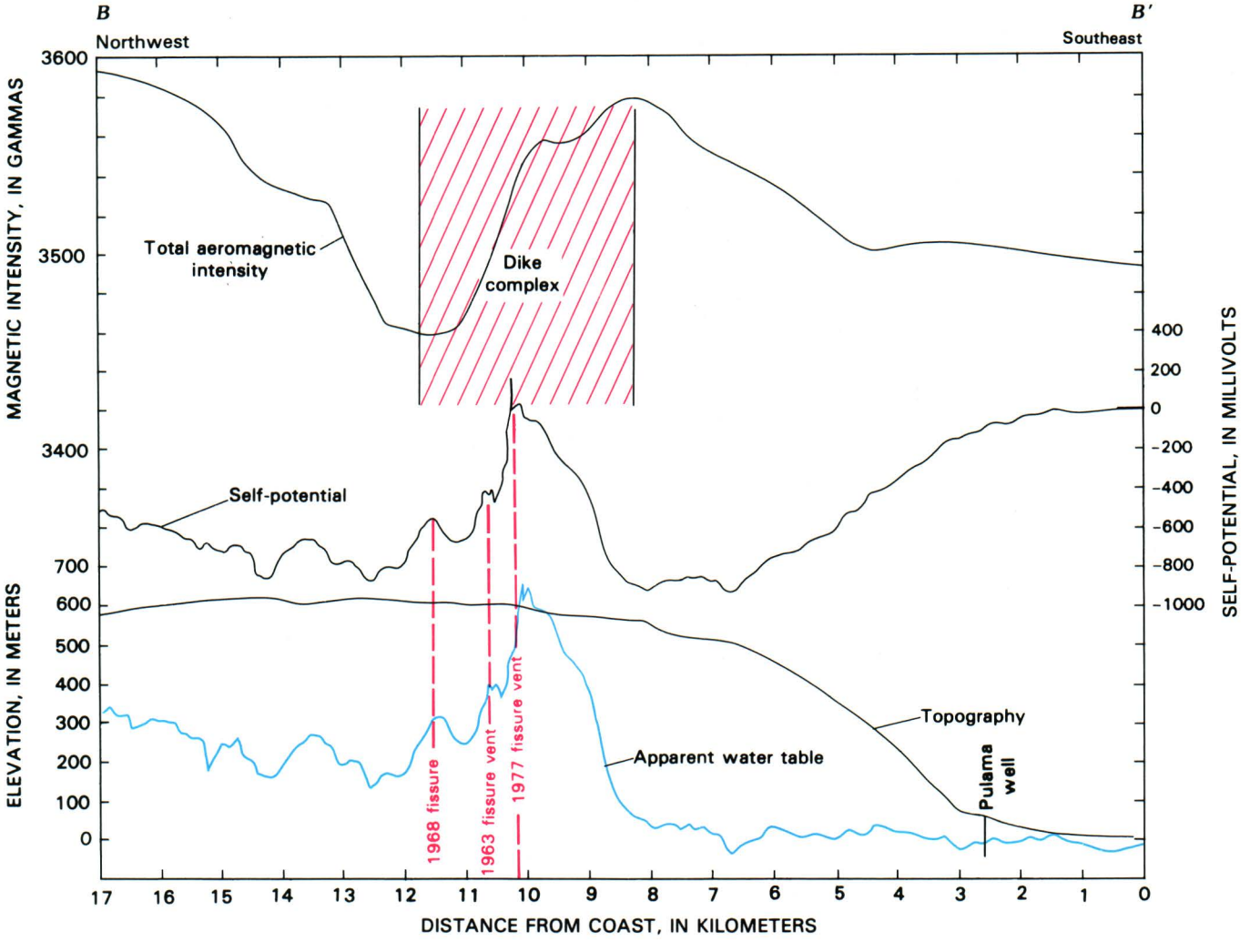

FIGURE 40.2.—Topography, self-potential, apparent water table, and total magnetic intensity (aeromagnetic) for profile B–B′ across the middle east rift zone of Kilauea Volcano. See figure 40.1 for profile location.

UPPER EAST RIFT ZONE (UERZ)

The SP anomaly over the UERZ (fig. 40.6) has much the same form in cross section as the SP profile across the MERZ in figure 40.2, that is, a major positive anomaly (relative to nearby potentials) flanked by adjacent major potential lows. The UERZ anomalies are correlated with pit craters as far downrift as Pauahi and with fissure vents (not visible at the figure scale) northeast of Pauahi as far east as the right edge of the figure.

A plot of elevation against SP for the UERZ profile (fig. 40.7) shows no clear correlation. Lacking more direct measures of vadose-zone thickness for this profile, we choose to use interpretations from nearby vertical electrical soundings (VES). VES 1, 3, and 17 (fig. 40.8; locations shown in fig. 40.11) show the vadose zone to be 480, 230, and 690 m thick, respectively. These values are plotted with the corresponding SP values in figure 40.7 along with a line showing the determined value of C_v, the correlation coefficient of vadose vent thickness to SP, of -3.6 mV/m. An apparent water table calculated using this value is shown in figure 40.6.

SOUTHWEST RIFT ZONE (SWRZ)

An SP profile from ocean to the summit of Kilauea (fig. 40.1, left side) is shown in figure 40.9. This profile is 43 km long and extends from Punaluu Beach on the southwest flank of Kilauea to the Hawaiian Volcano Observatory (HVO) on the northern rim of the caldera at 1,246-m elevation. As in the MERZ profile, potentials become increasingly more negative as elevation increases. The SP at the end point of the profile (HVO) is $-1{,}430$ mV relative to sea level.

The Punaluu-summit profile parallels the SWRZ of Kilauea and the Kaoiki fault zone and runs for its entire length over a

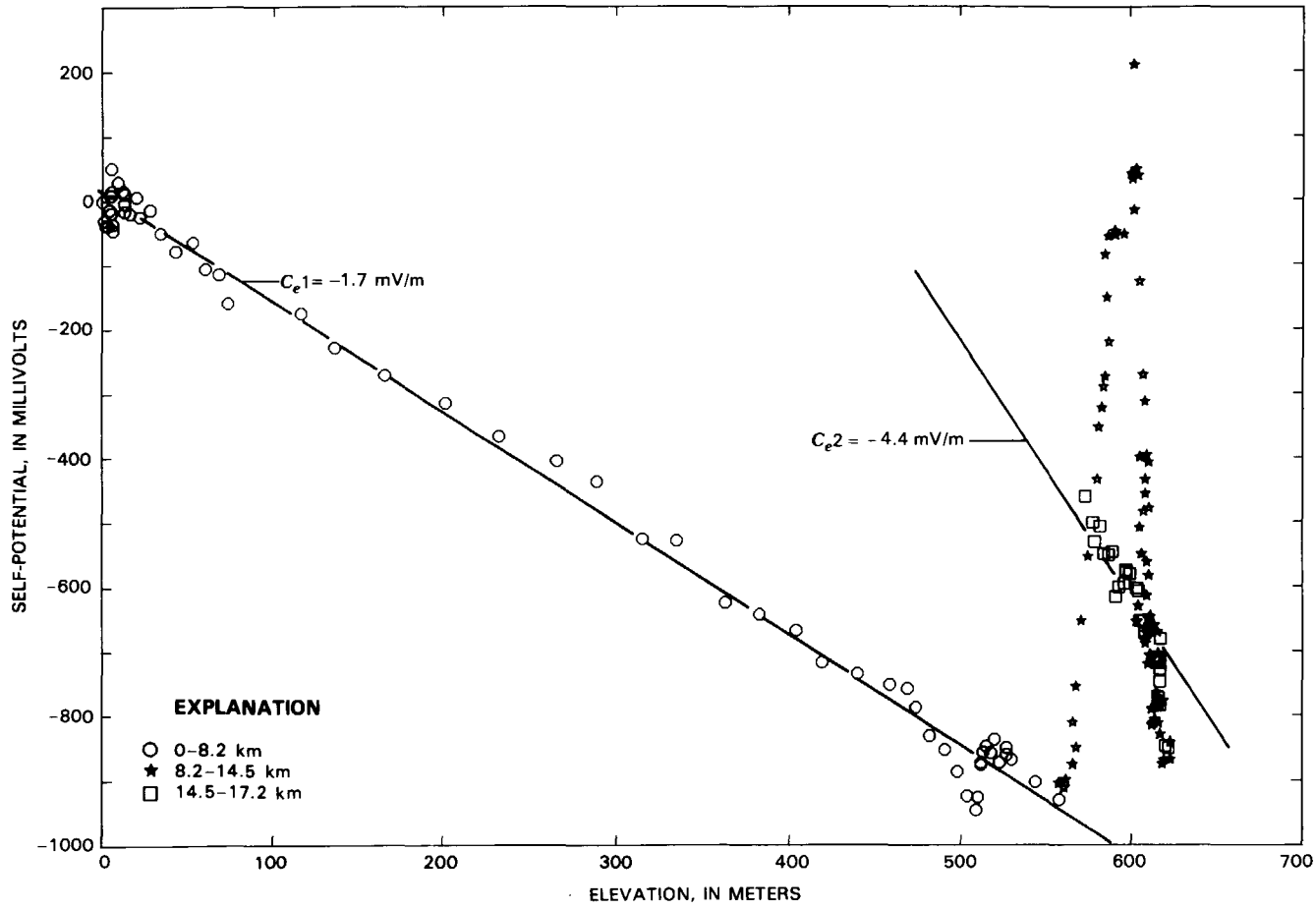

FIGURE 40.3.—Plot of elevation versus self-potential for the 17-km MERZ profile shown in figure 40.2. The lines show linear correlations (graphically determined) between self-potential and elevation with coefficients (C_e) of -1.7 mV/m and -4.4m V/m.

section in which flows from Kilauea and Mauna Loa interfinger. The Kaoiki fault zone extends from just north of Kilauea summit nearly to Pahala, and in places seems to act as a hydrologic barrier between Kilauea and the south flank of Mauna Loa (HVO unpublished electrical sounding data, 1980).

A plot of topography against self potential (fig. 40.10) shows three distinct values of C_e (labeled C_e1, C_e2, and C_e3) increasing in value from the coast toward the summit:

(1) C_e1, from the coast to 500-m elevation, about 6 km above the town of Pahala, has a value -0.6 mV/m.

(2) C_e2, from 500-m elevation to 1,100-m elevation, about 2 km from the summit caldera, has a value of -1.6 mV/m; this is approximately the same as observed on both the south flanks of the MERZ (-1.7 mV/m) and the LERZ (-1.8 mV/m).

(3) C_e3, from the 1,100-m elevation to the caldera rim at HVO, has a value of -3.2 mV/m.

Apparent water-table values along this profile were calculated three times, once for each of the C_e values determined above. Only those calculated for C_e2 and C_e3 were hydrologically reasonable (that is, they did not go below sea level); both these apparent water-table plots are shown in figure 40.9.

DISCUSSION

Three of the four self-potential profiles at Kilauea, one from the summit down the SWRZ, another from the MERZ down the south flank, and a third covering most of the LERZ (Zablocki, 1977), all referenced to sea level, clearly show that the edifice of Kilauea sits within a broad potential low. Within this low, and coinciding with the active elements of the volcano (rift zones, intrusions, pit craters, and fissure vents) are large self-potential highs that, with few exceptions, are nonetheless still negative with respect to sea level.

In each of these three areas, at places where it is reasonable to expect a nearly horizontal water table, ground elevation shows an excellent correlation to self-potential with a coefficient of approximately -1.7 mV/m. Along the UERZ profile, a good correlation was found between vadose-zone thickness and SP with a coefficient of -3.6 mV/m.

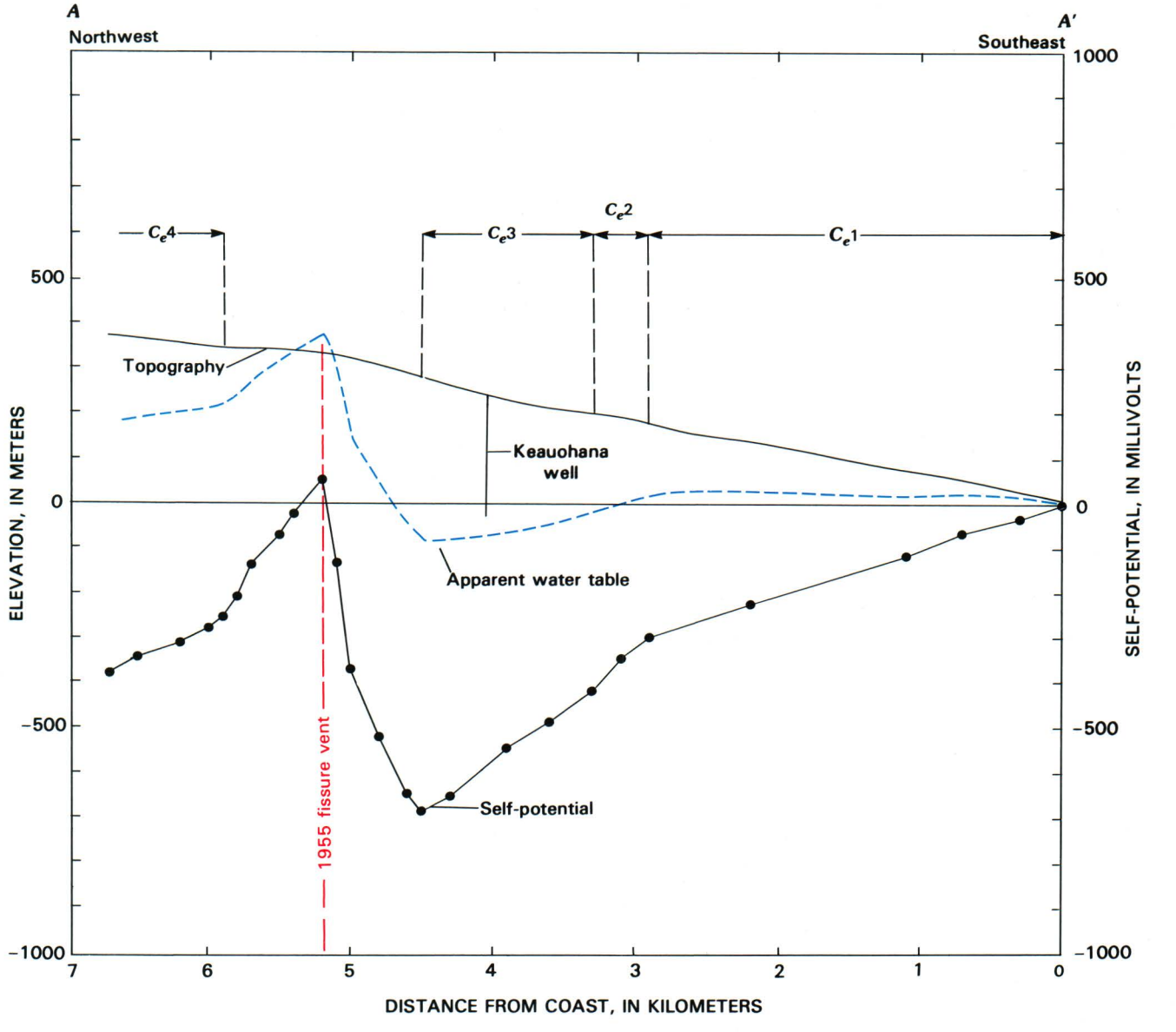

FIGURE 40.4.—Topography, apparent water table, and self-potential for profile A–A′ on the lower east rift zone of Kilauea Volcano. Self-potential and topography digitized from Zablocki (1977, fig. 2). Segments of the profile that correspond to different linear correlations (C_e1 through C_e4 on fig. 40.5) are shown. See figure 40.1 for profile location.

We believe, along with Zablocki (1978), that the regional pattern of SP is more directly related to the distance to which water can percolate vertically through the vadose zone before reaching the water table than it is to topography. We recognize that our anlaysis is not definitive but only indicative. Inconsistencies can be shown in the correlation of SP to topography, and those inconsistencies indicate a relationship of SP to vadose-zone thickness. The exact mechanism by which the negative potentials are generated is not known, but it is probably related to streaming potentials generated within the vadose zone by water moving downward.

If we suppose a valid relationship between vadose-zone thickness and self-potential, then self-potentials referenced to sea level at known elevations may be converted to apparent water-table depths. Circumstantial evidence that such a conversion is valid would come from any agreement of these apparent water-table elevations with actual determinations (well data and electrical resistivity soundings) at the same sites.

MIDDLE-EAST-RIFT-ZONE PROFILE

The apparent water-table elevations remain near sea level from the shore inland to the edge of the dike complex and then increase rapidly toward the 1977 eruptive fissure (fig. 40.2). Northwest of the 1977 fissure, apparent water-table elevations decrease to a point

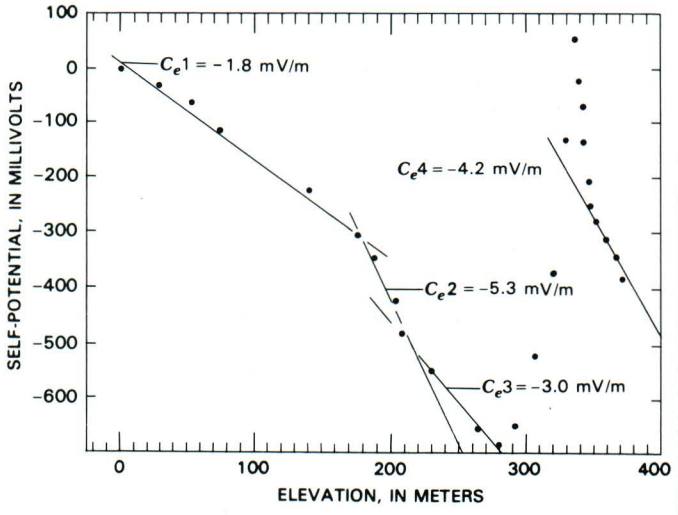

FIGURE 40.5.—Plot of elevation versus self-potential for the LERZ profile shown in figure 40.4. Four linear segments and the values of their correlation coefficients (C_e1–C_e4) are shown. Correlation lines are graphically determined.

about 14 km from the coast, from where they rise slowly to the end of the profile.

The apparent water-table elevations rise dramatically along the MERZ profile over the portion of the rift underlain by a dike complex. The long-wavelength (about 3 km) high in SP over the dike complex and the shallow apparent water table derived from the SP within this high are best explained as a thinning of the vadose zone caused by impoundment of ground water by dikes within the rift zone. An elevated water table within the rift is confirmed by VES 41 approximately 5 km uprift from the MERZ profile. For VES 41, at 740-m elevation (figs. 40.1 and 40.8), the water table is interpreted to be at 390 m above sea level. Although VES 41 is evidence of elevated water within this structure, its location is too far uprift to allow direct comparison with the MERZ profile.

At 8.2 km from the shore on the profile is the southern boundary of the active rift as indicated by the southernmost occurrence of pyroclastic cones in this area (Holcomb, 1980, p. 167). A low-level total-intensity aeromagnetic profile of the east rift zone (fig. 40.2; see also Flanigan and Long, chapter 39) also shows that the southern margin of the dike complex is about 8.2 km from the coast,

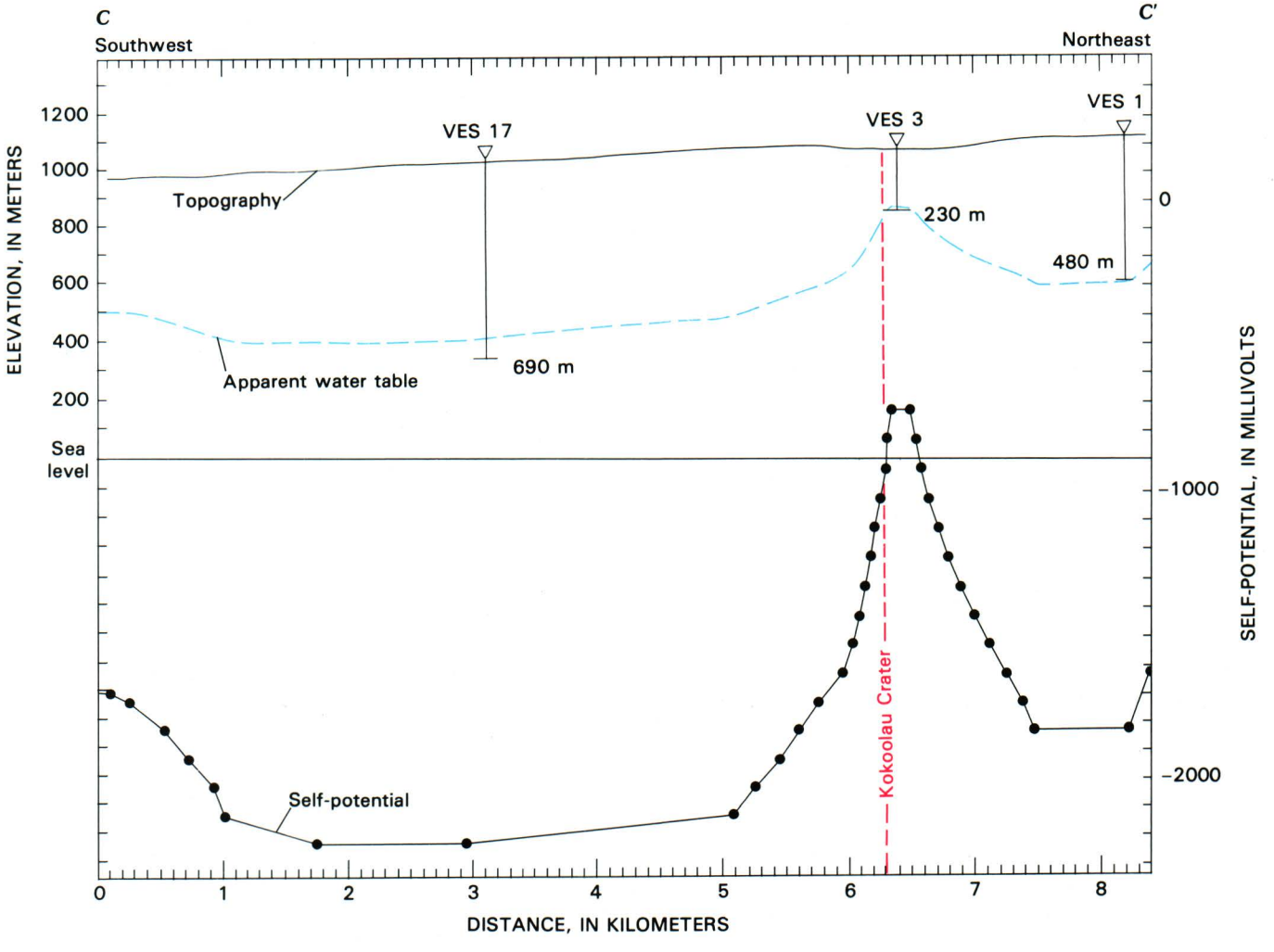

FIGURE 40.6.—Topography, apparent water table, and self-potential for profile C–C′ on the upper east rift zone of Kilauea Volcano. See figures 40.1 and 40.11 for profile location and figure 40.8 for VES interpretations.

and the complex extends to at least the 11.5-km position on the profile. The interpreted dike-complex margins on the aeromagnetic profile correspond to the crest of the aeromagnetic high to the southeast and the trough of the aeromagnetic low to the northwest (fig. 40.2).

The point at which the apparent water table rises above the ground surface (fig. 40.2) coincides with a short-wavelength (<1.5 km) anomaly that is positive relative to sea level and thus cannot be attributed to vadose-zone thinning. Because the short-wavelength anomaly coincides with a fissure vent, it must be caused by a thermoelectric or electrokinetic mechanism (or a combination of both) associated with the subsurface heat source responsible for the fissure. The other short-wavelength anomalies along the profile that are associated with fissure vents may also not be related directly to the vadose zone.

The more gradual decrease of apparent water-table elevation northwest of the 1977 fissure may be the result of a leaky dike system that cannot support the same hydraulic head that is maintained southeast of the fissure. The gradual rise of the apparent water table at the northwest end of the profile may be evidence for high-level impoundment of ground water by an older ERZ dike system or possibly by older dikes related to an aeromagnetic lineation that branches off from the Mauna Loa northeast rift zone 15 km from the summit and parallels the north side of the Kilauea ERZ (Flanigan and Long, chapter 39).

LOWER-EAST-RIFT-ZONE PROFILE

The apparent water table calculated for the LERZ profile (fig. 40.4) begins at zero elevation at the coast then dips as much as 100 m below sea level (4.5 km inland) in the area immediately southeast of a 1955 fissure vent (at 5.2 km). The Keauohana well located to the south of the rift just off the profile at the 4-km position shows that the water table is about 1 m above sea level (State of Hawaii Department of Land and Natural Resources, 1970), though the apparent water table is about 100 m below sea level. The discrepancy implies that this portion of the profile either is affected by SP mechanisms associated with the 1955 vent more than by vadose-zone variations or that it has a different coefficient for the correlation of vadose-zone thickness and SP.

Northwest of the fissure vent and within the rift, the apparent water table is elevated nearly 200 m above sea level; this is consistent with interpretations of elevated water tables in the middle and upper east rift. Self-potentials associated with the 1955 fissure vent and (or) a changing coefficient, C_v, may also bias the apparent water-table depths northwest of the vents, but we do not know how much. A discrepancy is obvious at the position of the fissure vent, where the apparent water table is about 30 m above the ground surface. Here again we believe that these eruptive-vent anomalies, which are generally short wavelength, are due to thermoelectric or electrokinetic phenomena associated with subsurface heat sources.

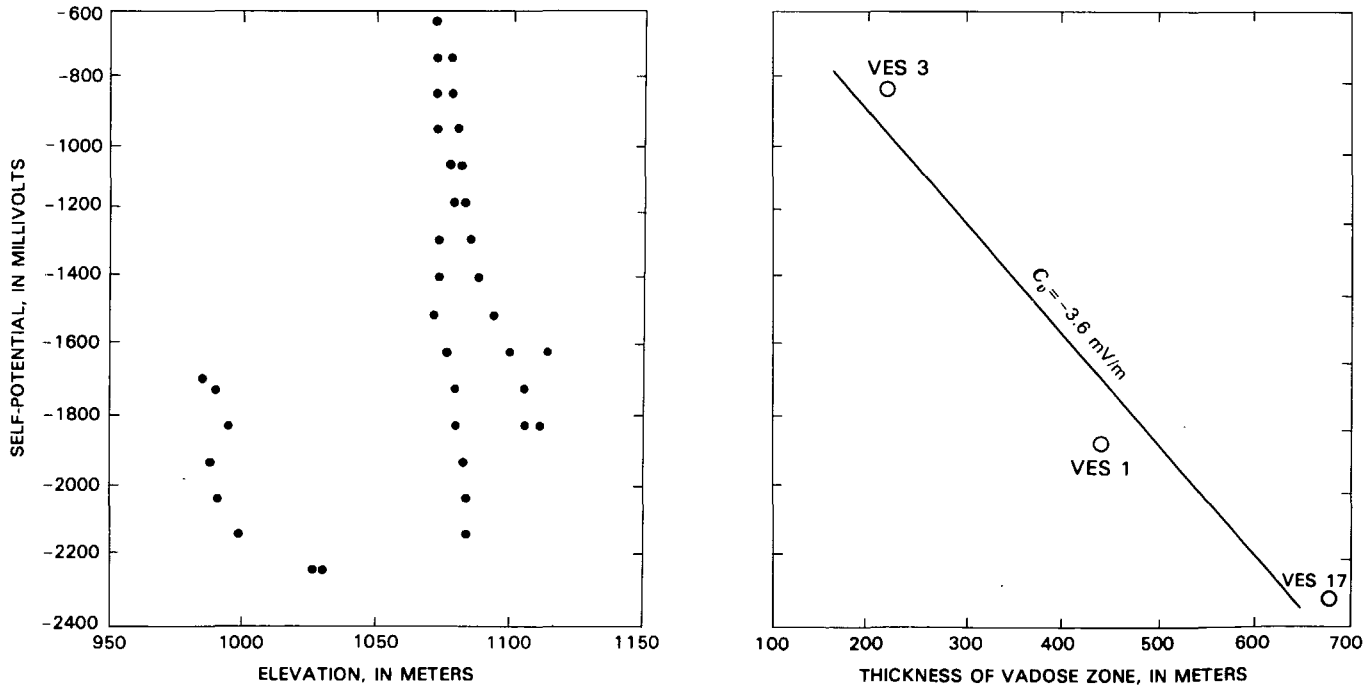

FIGURE 40.7.—Plots of self-potential versus elevation and versus vadose-zone thickness for the UERZ profile shown in figure 40.6. In the latter plot, the correlation of self-potential and vadose zone thickness is derived from VES interpretations discussed in the text. Correlation line is graphically determined.

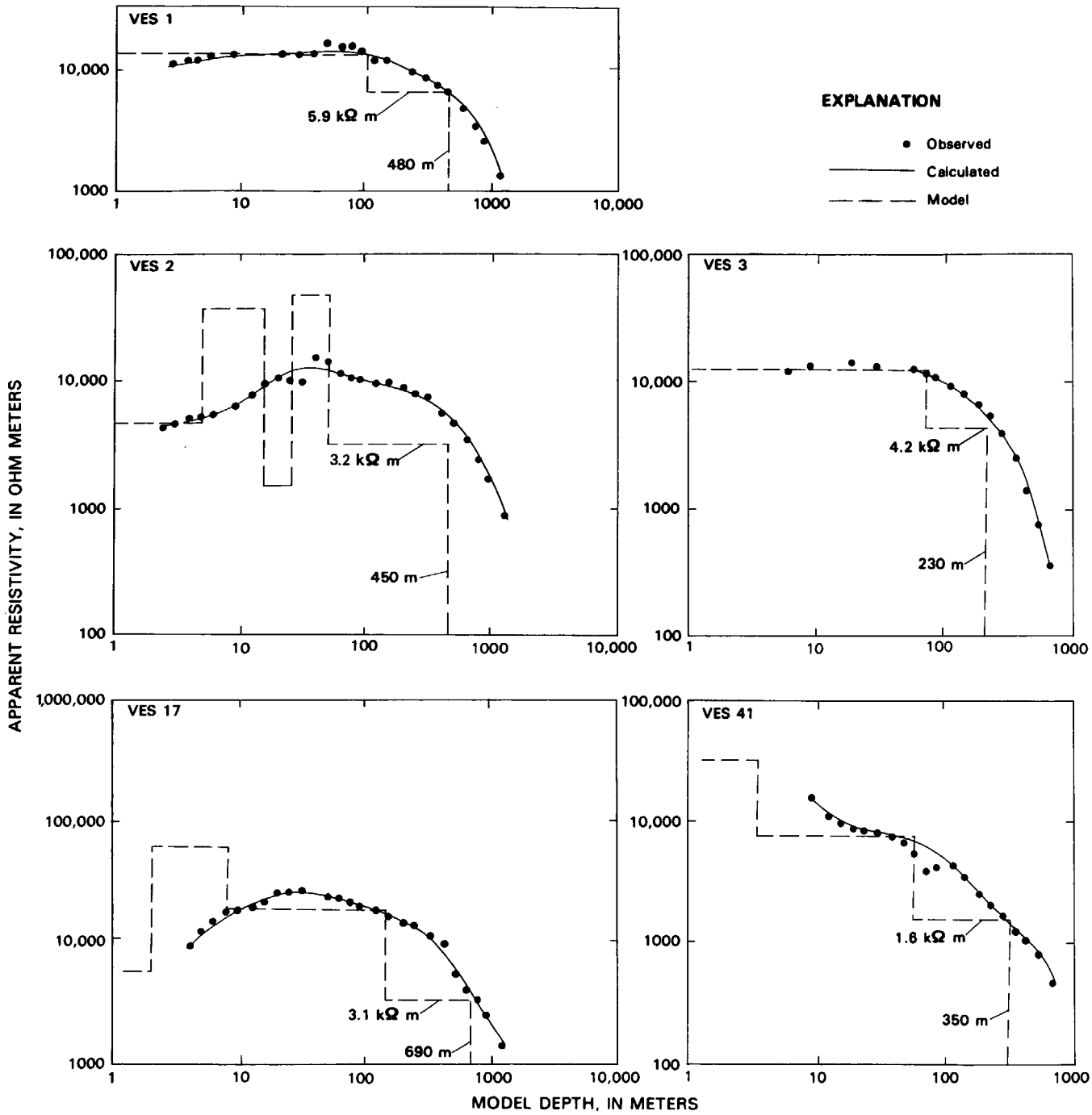

FIGURE 40.8.—Data plots and interpretations for vertical electrical soundings (VES) 1, 2, 3, 17, and 41. See figures 40.1 and 40.11 for locations of soundings. Data for VES 1, 2, and 3 provided by C.J. Zablocki (written commun., 1985).

UPPER-EAST-RIFT-ZONE PROFILE

The calculations of apparent water table beneath the UERZ profile (fig. 40.6) shows a generally elevated water table, locally even higher beneath the zone of pit craters. This seems reasonable; the water table is elevated about 610 m above sea level in a research well (location shown in fig. 40.1) about 3.5 km north of the profile (Zablocki and others, 1974). These water-table elevations are far too high to represent the basal water-table conditions that one expects to find in Hawaii within permeable volcanic rocks where no lateral barriers such as dikes or fault gouge exist (Stearns, 1966). Therefore, the elevated water table must be impounded by high-angle, water-impermeable structures such as dikes. The presence of high-level water outside of the visible surface expression of the rift

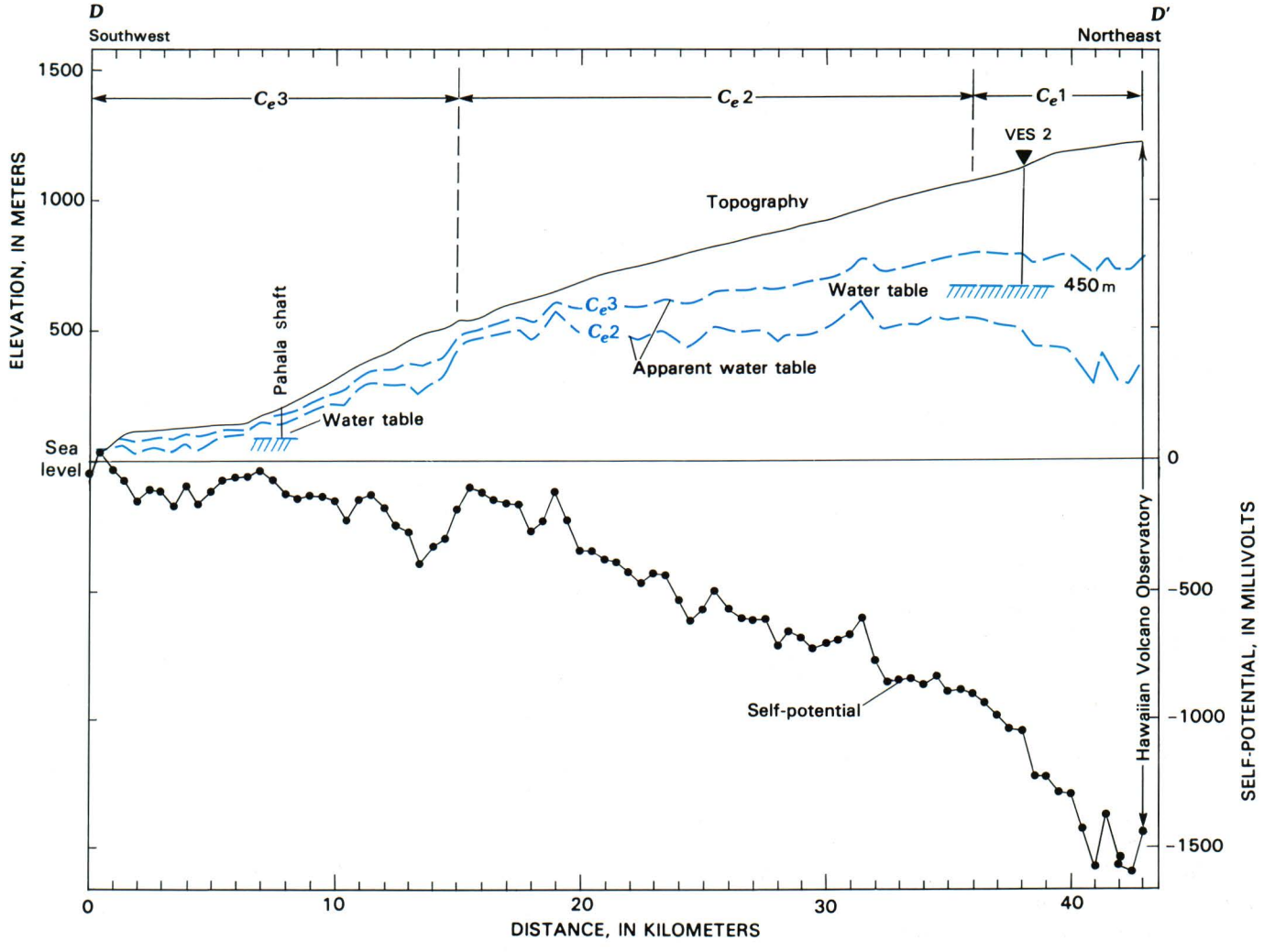

FIGURE 40.9.—Topography, apparent water-table elevations, and self-potential for profile D–D′ from Punaluu to the summit (HVO) of Kilauea. An interpretation for VES 2 and the water table in the Pahala shaft are shown for comparison. Segments of the profile that correspond to different linear correlations (C_e1 through C_e3 in fig. 40.10) are indicated. See figure 40.1 for profile location.

zone indicates either that the rift is broader than its surface expression or that faults exist that may be impeding the lateral flow of water.

VES 1 (fig. 40.8, see fig. 40.11 for location) is just within the aeromagnetic anomaly that delineates the northeast boundary of the dike complex (Flanigan and Long, chapter 39). The fact that no short-wavelength SP anomalies (fig. 40.6) occur northeast of the rift suggests that only the southwest side of the rift (coincident with the UERZ line of pit craters) is still active. The elevated water table on the northeast side of the rift can be satisfactorily explained as caused by impoundment by dikes that are now buried and without surface expression. The position at which the elevated water table becomes basal should be the boundary on the northeast side of the rift-zone anomaly. It follows that the northeast boundary of the rift zone is beyond the SP data that we see in figures 40.6 and 40.11. If so, the wavelength of the SP anomaly should be much broader than indicated in either figure 40.6 or 40.11.

VES 17, southwest of the rift, lies outside of the aeromagnetic expression of the dike complex (Flanigan and Long, chapter 39). However, numerous large normal faults of the Koae fault system (figs. 40.1 and 40.11) probably act as the hydrologic barrier that elevates the water table beneath VES 17. Either gouge on the Koae faults or dikes intruded into the fault planes (in May 1969 for example; see Swanson and others, 1979) from either the SWRZ or the UERZ probably form the actual impermeable part of the hydrologic barrier.

SOUTHWEST-RIFT-ZONE PROFILE

The plots of apparent water table (fig. 40.9) indicate that an elevated (nonbasal) water table, which dips to the southwest, underlies the profile between the 28-km and 43-km positions. This inference is supported by ground-water studies near the town of Pahala. Ground water beneath the town stands at approximately 72

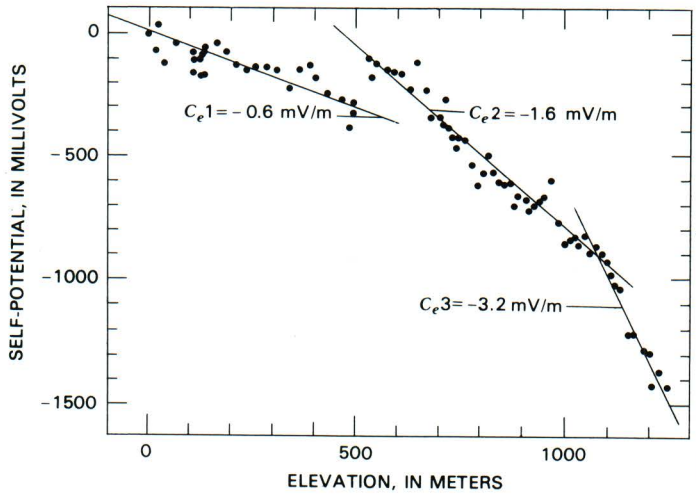

FIGURE 40.10.—Plot of elevation versus self-potential for the 43-km profile shown in figure 40.9. Three gradients, C_e1, C_e2, and C_e3, show the linear correlations between self-potential and elevation for 3 segments of the profile. Correlation lines are graphically determined.

m above sea level (fig. 40.9) in a Maui-type well (Stearns and Macdonald, 1946) and is probably impounded by older dikes of the SWRZ. Evidence from an electrical sounding survey (Hussong and Cox, 1967) in the immediate area around Pahala indicates that the anomalously high water-table elevation extends to at least 1 km northeast of Pahala (the edge of the study area) and along the highway towards Punaluu. This explains the shallow C_e gradient (C_e1) for this part of the profile in figure 40.10.

The portion of the profile between 7-km and 28-km positions appears underlain by a nearly horizontal water table that is at an even higher level than that under the seaward part of the profile. A low-resistivity zone beneath VES 2 (figs. 40.8–40.9) at the 5-km position is interpreted to be the top of the water table; it lies at 450-m depth or about midway between the two plotted apparent water tables. The estimation of water table from SP is only approximate, but the qualitative agreement between the apparent water table and data from the Pahala shaft and VES 2 seems meaningful. Additional determinations of actual water-table elevation would allow a more accurate value of the correlation coefficient of SP and vadose-zone thickness (C_v) to be chosen.

CONCLUSIONS

The edifice of Kilauea sits in a broad self-potential low that appears to be related to negative potentials generated by the percolation of ground water through the vadose zone to the underlying water table. Plots of SP against elevation often have more than one linear segment, which indicates that SP is correlated to something other than elevation. Examination of SP plotted against elevation for profiles where water-table elevation is known indicate the SP correlation is really with vadose-zone thickness rather than with elevation. An empirical gradient of about −1.7 mV per meter of elevation above sea level seems to best fit the vadose-zone-related potentials along the MERZ and LERZ profiles. A value of −3.6 mV/m appears better for the UERZ profile. A gradient of either −1.6 or −3.2 mV/m may best fit the SWRZ profile; a choice cannot be made without additional data. The observation that the correlation between vadose-zone thickness and SP is not always constant, even when the water table is at a constant elevation, implies the possible addition of potentials related to deep or broad heat sources or possible variation of the parameters of the presumably electrokinetic generating mechanism.

The self-potential profiles, referenced to sea level, have been used to calculate an apparent water-table configuration. Electrical soundings have confirmed the water-table depth directly at critical places and shown places where potentials unrelated to the thickness of the vadose zone must be taken into account.

At only a few locations on the volcano, related to obvious thermal features, do self-potentials become more positive than potential at sea level. On the basis of that observation we are in partial agreement with Zablocki (1978), who conjectured that all

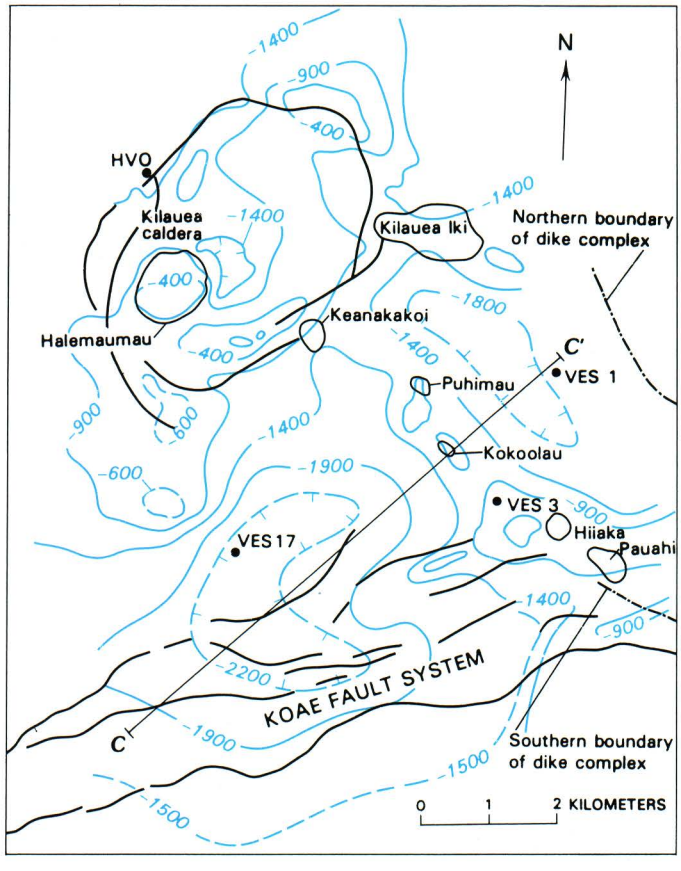

FIGURE 40.11.—Self-potential map of the summit region of Kilauea Volcano (after Zablocki, 1976). Selected contours (blue) show values in millivolts. The potentials are referenced to sea level via the SWRZ profile in figure 40.9. Also shown are the location of profile C–C′ and VES 1, 3, and 17 and main geologic features. The northern and southern boundaries of the dike complex defining the east rift zone derived from aeromagnetic studies (Flanigan and Long, chapter 39).

anomalies on Kilauea reflect the distance that water in the vadose zone descends before encountering higher temperature fluids rising above a deeper heat source. Over the rising fluids the more positive potentials (which might still be negative in relation to sea level) reflect (1) a thinner vadose zone and (2) electrokinetic potentials contributed by the rising fluids. We infer, however, that the primary means by which the vadose zone is thinned is high-level impoundment of ground water by dikes in areas known to be loci of intrusions and eruptions on the volcano. The impoundment results in broad anomalies (>3 km) associated with Kilauea's summit and rift zones. The long-wavelength anomalies are not restricted to currently active thermal features but also appear to reflect older dike systems left behind as the rift systems shifted in position to the south. Shorter wavelength anomalies, superimposed on the longer wavelength anomalies, are probably caused by a combination of thermoelectric and electrokinetic effects associated either with specific, recently active fissure vents or with known areas of recent intrusions.

Use of a variety of geophysical techniques combined with observation of recent volcanic activity can contribute to understanding the geologic history of a volcano. An example of this is the UERZ, which is defined by (1) a zone of pit craters on the currently active rift, (2) a broad SP anomaly that extends about 2 km farther to the northeast, and (3) an aeromagnetic anomaly, which is nearly coincident with the SP anomaly. The lack of any high-amplitude narrow-wavelength features in the zone of broad SP and aeromagnetic anomalies northeast of the active rift is consistent with the lack of volcanic activity in that area. The fact that the water table is elevated in this zone indicates that water is impounded northeast of the line of UERZ pit craters by older dikes of the rift system. A second example can be found in the MERZ profile: a rising apparent water table north of the MERZ can best be explained as dike impoundment of ground water by an older dike system of the ERZ or by a postulated inactive branch of the northeast rift zone of Mauna Loa Volcano.

REFERENCES CITED

Anderson, L.A., and Johnson, G.R., 1976, Application of the self-potential method to geothermal exploration in Long Valley, California: Journal of Geophysical Research, v. 81, no. 8, p. 1527–1532.

Corwin, R.F., and Hoover, D.B., 1979, The self-potential method in geothermal exploration: Geophysics, v. 44, no. 2, p. 226–245.

Fitterman, D.V., 1978, Electrokinetic and magnetic anomalies associated with dilatant regions in a layered earth: Journal of Geophysical Research, v. 83, p. 5923–5928.

——— 1979, Calculations of self-potential anomalies near vertical contacts: Geophysics, v. 44, p. 195–205.

——— 1983, Modelling of self-potential anomalies near vertical dikes: Geophysics, v. 48, no. 2, p. 171–180.

——— 1984, Thermoelectrical self-potential anomalies and their relationship to the solid angle subtended by the source region: Geophysics, v. 49, p. 165–170.

Holcomb, R.T., 1980, Preliminary geologic map of Kilauea Volcano, Hawaii: U.S. Geological Survey Open-File Report 80–796, 2 sheets, scale 1:50,000.

Hussong, D.M., and Cox, D.C., 1967, Estimation of ground-water configuration near Pahala, Hawaii, using electrical resistivity techniques: Water Resources Research Center, University of Hawaii, Technical Report 17, 35 p.

Jackson, D.B., and Sako, M., 1982, Self potential surveys related to probable geothermal anomalies, Hualalai Volcano, Hawaii: U.S. Geological Survey Open-File Report 82–127, 10 p.

Keller, G.V., and Frischknecht, F.C., 1966, Electrical methods in geophysical prospecting: New York, Pergamon Press, 517 p.

Klein, D.P., and Larson, J.C., 1978, Magnetic induction fields (2–30 cpd) on Hawaii Island and their implications regarding electrical conductivity in the oceanic mantle: Royal Astronomical Society Geophysical Journal, v. 58, no. 53, p. 61–77.

Lockwood, J.P., Banks, N.G., English, T.T., Greenland, P., Jackson, D.B., Johnson, D.J., Koyanagi, R.Y., McGee, K.A., Okamura, A.T., and Rhodes, M.J., 1985, The 1984 eruption of Mauna Loa Volcano, Hawaii: Eos, Transactions of the Americal Geophysical Union, v. 66, no. 16, p. 169–171.

Poldini, E., 1939, Geophysical exploration by spontaneous polarization methods: Mining magazine, v. 60, p. 22–27.

Sill, W.R., 1982, Self-potential effects due to hydrothermal convection-velocity crosscoupling: Earth Sciences Laboratory, University of Utah Research Institute, no. DOE/ID/12079–68, 23 p.

——— 1983, Self potential modeling from primary flow: Geophysics, v. 48, p. 76–86.

State of Hawaii Department of Land and Natural Resources, 1970, An inventory of basic water resources data—Island of Hawaii: Report R34, 188 p.

Stearns, H.T., 1966, Geology of the State of Hawaii: Palo Alto, California, Pacific Books, 266 p.

Stearns H.T., and Macdonald, G.A., 1946, Geology and ground water resources of the Island of Hawaii: Hawaii Division of Hydrography Bulletin 9, 363 p.

Sawnson, D.A., Duffield, W.A., Jackson, D.B., and Peterson, D.W., 1979, Chronological narrative of the 1969–71 Mauna Ulu eruption of Kilauea Volcano, Hawaii: U.S. Geological Survey Professional Paper 1056, 55 p.

Yungul, Sulhi, 1950, Interpretation of spontaneous polarization anomalies caused by spheroidal ore bodies: Geophysics, v. 15, no. 2, p. 237–246.

Zablocki, C.J., 1976, Mapping thermal anomalies on an active volcano by the self-potential method, Kilauea, Hawaii, *in* Proceedings, 2nd United Nations Symposium on the Development and Use of Geothermal Resources, San Francisco, Calif., May 1975, v. 2, p. 1299–1309.

——— 1977, Self-potential studies in East Puna, *in* Geoelectric studies on the east rift, Kilauea Volcano, Hawaii Island: Honolulu, Hawaii Institute of Geophysics, University of Hawaii Technical Report HIG–77–15, p. 175–195.

——— 1978, Streaming potentials resulting from the descent of meteoric water—a possible source mechanism for Kilauean self-potential anomalies: Geothermal Resources Council, Transactions, v. 2, sec. 2, p. 747–748.

——— 1980, Observations from self-potential monitoring studies on Kilauea Volcano, Hawaii (1973–1975): U.S. Geological Survey Open–File Report 80–99, 15 p.

Zablocki, C.J., Tilling, R.I., Peterson, D.W., Christiansen, R.L., Keller, G.V., and Murray, J.C., 1974, A deep research drill hole at the summit of an active volcano, Kilauea, Hawaii: Geophysical Research Letters, v. 1, no. 7, p. 23.

Zohdy, A.A.R., Anderson, L.A., and Muffler, L.J.P., 1973, Resistivity, self-potential and induced polarization surveys of a vapor dominated geothermal system: Geophysics v. 38, no. 6, p. 1130–1144.

THE DIKE COMPLEX OF KOOLAU VOLCANO, OAHU: INTERNAL STRUCTURE OF A HAWAIIAN RIFT ZONE

By George P.L. Walker[1]

ABSTRACT

The Koolau dike complex in the deeply eroded lava shield of Koolau Volcano on Oahu is extraordinarily intense and where widest contains an estimated 7,400 subparallel dikes totaling 3–5 km in width. Quantitative study involving measurement of 3,550 dikes reveals that the complex has a non-Gaussian intensity distribution. Dikes generally constitute 50–70 percent of the total rock and form an intensity plateau across the complex, decreasing very rapidly to <5 percent at the edges. A proposed model for formation of the complex envisages the highly mobile tholeiitic magma as being tightly constrained by the zonation of bulk-rock density in the volcanic edifice. This model, applied to the active Hawaiian volcanoes, explains well the marked propensity of magma to stay underground in what is evidently a gravitationally very stable situation. Flow lineations on Koolau dike margins indicate that the magma generally rose obliquely, from two distinct magma supply centers situated 5 km apart and 2–3 km deep. The dikes are systematically nonvertical and form two complementary sets dipping at 65° to 85° in opposite directions, like normal faults in an extensional setting. Predominance of one dip direction over a wide area may indicate an early tendency to seaward creep of the volcano in that area. Stages in the buildup of the complex are marked by increasing proportions of dikes entering multiple clusters, these clusters having the characteristics of a sheeted dike complex. The Koolau Volcano has a wide caldera of downsag type, with probable conventional calderas in the middle. The strong inward decrease in dike concentration is interpreted to mean a general inward increase in subsidence rate, subsidence in the central area exceeding the rate of upward growth of the dike complex. This leads to the concept that subsidence of Hawaiian calderas is caused by the weight of intrusions in an area of lithospheric weakness above a hot spot.

INTRODUCTION

Many dikes are exposed where denudation has cut deeply into the older basaltic shield volcanoes of the Hawaiian Islands, and in some volcanoes they are concentrated into well-defined dike complexes. These complexes have long been regarded as the subsurface expression of rift zones such as those in which eruptions on Kilauea and Mauna Loa Volcanoes are concentrated.

A full understanding of active rift zones requires a knowledge of dike complexes, just as surely as understanding the dike complexes depends on knowing how active rift zones develop. The general distribution patterns and characteristics of the dike complexes are well established, but very little detailed information about them is available, and the present study is aimed at documenting one complex more fully than has been attempted before.

Another reason for documenting one of these complexes is that they are very similar to the sheeted dike complexes of the ophiolite suite. This suite is interpreted to form by oceanic crustal spreading along globally extensive spreading zones, whereas the dike complexes of denuded Hawaiian lava shields occur in an intraplate tectonic setting and extend high into the individual volcanic edifices. It is important to have a basis by which they can be compared with sheeted complexes.

One of the most intense and accessible of the Hawaiian dike complexes is that exposed in the core of the Koolau shield volcano on Oahu. Lava of this shield gives K-Ar ages of 2.67–1.83 Ma (McDougall and Aziz-ur-Rahman, 1972; Doell and Dalrymple, 1973). The Koolau Volcano is strongly elongate on a northwest-southeast axis and has a subaerial length of 57 km. The shield surface is well preserved on the lower parts of the interfluves along the southwestern or leeward side, and the shield form may be reconstructed (fig. 41.1) by drawing generalized contours that neglect all the lesser topographic features.

The position of the long axis of the Koolau shield is apparent from curvature of the generalized contours around the northwestern end, and this coincides with the antiform on the two sides of which the lava dips outward in opposite directions. The position is less clear at the southeast end, but the antiform lies between the Mokulua Islands and Makapuu Head, and its approximate position is shown in figure 41.1.

Erosion of the Koolau shield has been concentrated on the northeastern or windward side; between Waikane and Waimanalo, deep embayments cut right across the long axis, and more than half of the original shield has there disappeared. I agree with Moore (1964) in regarding much of the loss as having been accomplished by great landslides. An impressive cliff (the pali), which faces northeast and is as high as 900 m (3,000 ft), marks the headwall of the series of landslide scars.

A strip of low-lying ground 4–8 km wide extends from Waikane to Waimanalo and between the pali and the coast consists mostly of alluvium and reef deposits, but it is transected by

[1]Hawaii Institute of Geophysics, Honolulu, HI 96822.

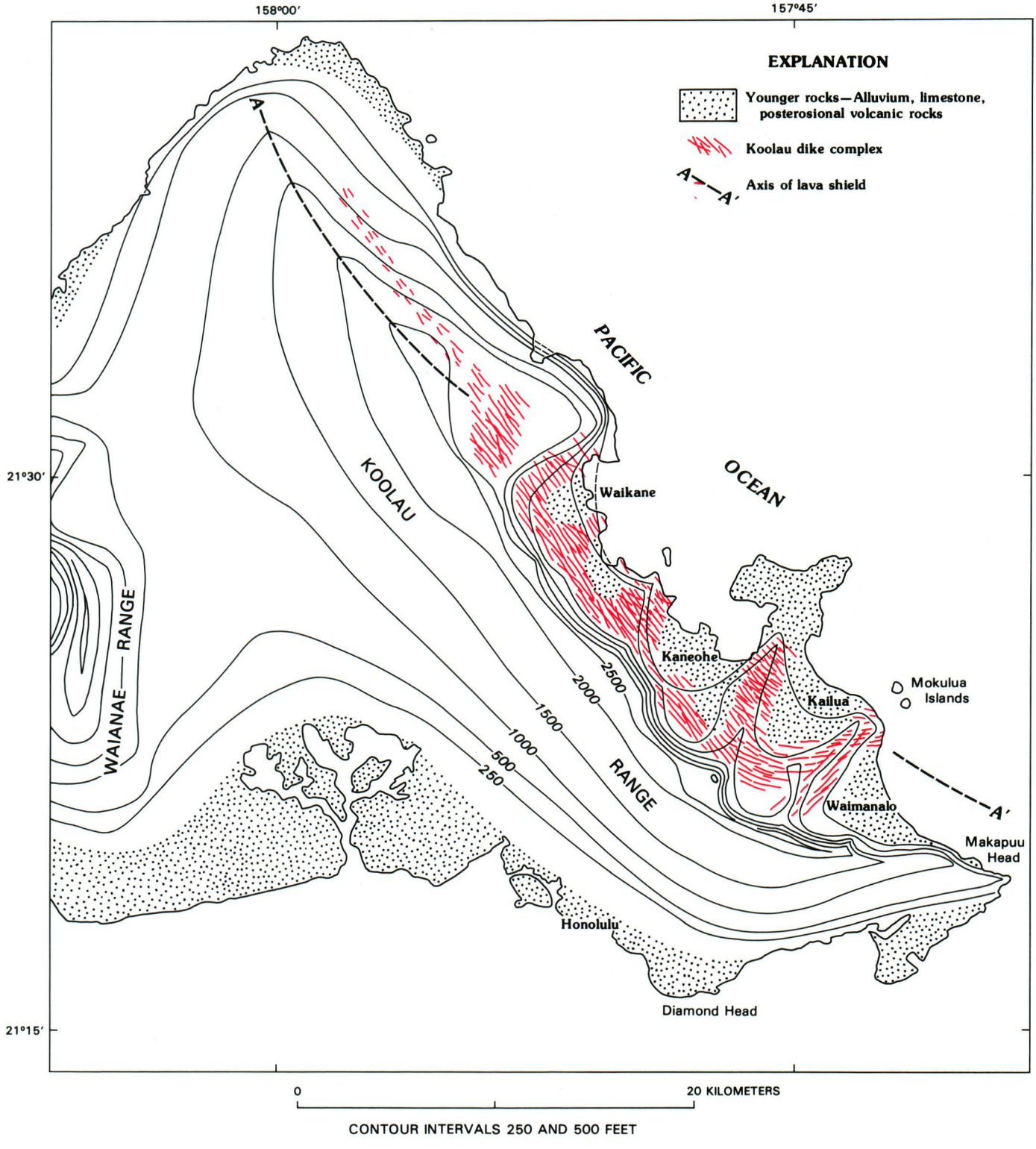

FIGURE 41.1.—Setting of Koolau dike complex on Island of Oahu. Distribution of complex (modified from Stearns, 1939) shown in relation to Koolau lava-shield volcano, form of which is portrayed by generalized topographic contours. Volcano is very strongly elongate northwest-southeast and position of axis is based on generalized contours and opposing dip directions of shield lava.

northeast-trending ridges—possibly these are septa between the landslide scars—where most exposures of the Koolau dike complex are found. Natural exposures tend to be difficult of access and unfavorable for quantitative studies. A notable exception is the two small Mokulua Islands, on which are found the finest known outcrops.

The present study has relied much on artificial exposures. Noteworthy among these are roadcuts in the unfinished H3 Highway, the two large Kapaa quarries, and cuts in new housing subdivisions in the Keolu Hills. The available artificial and natural exposures are thought to be just adequate to reveal the principal features of the Koolau dike complex.

ACKNOWLEDGMENTS

This research was not funded and was undertaken as a part-time activity to satisfy scientific curiosity, contribute to the geological understanding of Hawaii's volcanism, and complement the fine research done on active volcanoes of Hawaii by personnel of the Hawaiian Volcano Observatory. It was made possible by my employment at the University of Hawaii. I thank Kevin Kennedy for introducing me to the Mokulua Islands, the Manager of Kapaa Quarry for permission to visit, and the U.S. Air Force for permission to visit Bellows Air Force Base. I also acknowledge useful comments by reviewers Paul Delaney, Mary M. Donata and Tom L. Wright, and my wife for her help and forebearance. This paper is Hawaii Institute of Geophysics contribution number 1706.

PREVIOUS WORK

The distribution of the dike complex and the positions and trends of isolated dikes elsewhere, were clearly shown on the 1:63,360-scale map of Stearns (1939) and described by Stearns and Vaksvik (1935). They distinguished two dike complexes lying alongside one another and having a parallel trend. The former cuts volcanic rocks of the Kailua Volcanic Series (now Kailua Member of the Koolau Basalt) which they interpreted to have accumulated under or close by the caldera of the Koolau shield volcano, whereas the latter cuts shield-building lava of the Koolau Volcanic Series (now Koolau Basalt). Takasaki and others (1969, 1982) accepted the distinction between caldera infill and shield-building lava but regarded the complex as one, and I follow this usage.

Wentworth (1951) applied the term "dike complex" to areas where there are 100 or more dikes per mile, and Takasaki and others (1969) applied it to areas where dikes constitute more than 5 percent of the rock. The latter authors called the zone adjacent to the dike complex, characterized by scattered dikes that constitute less than 1 percent of the rock, the marginal dike swarm, and pointed out (p. 14) that "although the strike of dikes is generally the same in both zones, the dike complex and the marginal dike zone are distinct, and no transition zone intervenes." Dike complex is a useful term for an intense swarm in which the dikes are so narrow, numerous and intertwined that it is not feasible to map individual members.

The important influence of the Koolau dikes on ground-water storage in the Koolau Range led to studies of them by Takasaki and others (1969), Takasaki (1981), and Takasaki and Mink (1982). These authors mapped the dike complex and marginal zone and measured the dike trend and intensity in six water-supply tunnels west of Waikane.

The maps of Stearns (1939), Takasaki and others (1969), and Takasaki and Mink (1982) show clearly the predominant northwest-southeast trend of the dikes, parallel with the longitudinal axis of the Koolau shield. They also show dikes trending in a southwesterly direction from Kailua into the leeward side of the Koolau Range towards Diamond Head; these have been identified as a secondary swarm (the Kaau or southwest rift zone) analogous with the minor rift zones that occur on some active Hawaiian volcanoes.

Few studies have hitherto been made of the dike structures, apart from that by Wentworth and Jones (1940) on jointing and the distribution of amygdules. Among recent workers, Ryan and others (1983) most clearly recognized how important it is to study the dike swarms when seeking to understand rift zones. Walker and Kennedy (in preparation) describe aspects of the dike complex exposed on the Mokulua Islands, and Walker (1986) discussed the origin of the complex in an earlier report on the present study.

DIKE DISTRIBUTION

The present quantitative study of the Koolau dike complex is based on measurements made at 55 localities in windward Oahu, distributed as shown in figure 41.2 and listed in table 41.1. At each locality the width, trend, and dip of each dike was measured; the dike widths in a measured traverse were also totaled so as to yield the dike intensity, expressed as the percentage of rock composed of dikes, as shown in figure 41.3. Intensity is alternatively expressed as the calculated number of dikes per 100 m of traverse in a direction at right angles to the predominant dike trend, as shown in figure 41.4. The measured traverses totaled 7.4 km in length and contained 3,550 dikes aggregating to 2.6 km in width. Data from these 55 localities are supplemented by data from six water-supply tunnels (Takasaki and others, 1969; Takasaki, 1981).

The dikes very commonly occur in multiple clusters as wide as about 20 m, in which successive subparallel members were injected either along the margins of, or inside, preceding dikes; dikes constitute 100 percent of the width of such a cluster. Screens of country rock occur between clusters. A valid value for the dike intensity is obtained only if the measured traverse includes at least several dike clusters and their intervening screens.

The highest intensity (80–85 percent) occurs on the coast at Heeia (locality 41) and on the Mokulua Islands (localities 19 and 20); a measured 185-m traverse most of the way across the northwestern island recorded 240 dikes totaling 145 m thick. The dike intensity is high, exceeding 40 percent, in a belt of country 3–6 km wide extending northwest from Kailua, but it is not uniformly high over the entire length or width of this belt; in particular it drops to 2 percent in the Kailua caldera, which interrupts the continuity of the complex. The calculated number of dikes per 100 m (fig. 41.4)

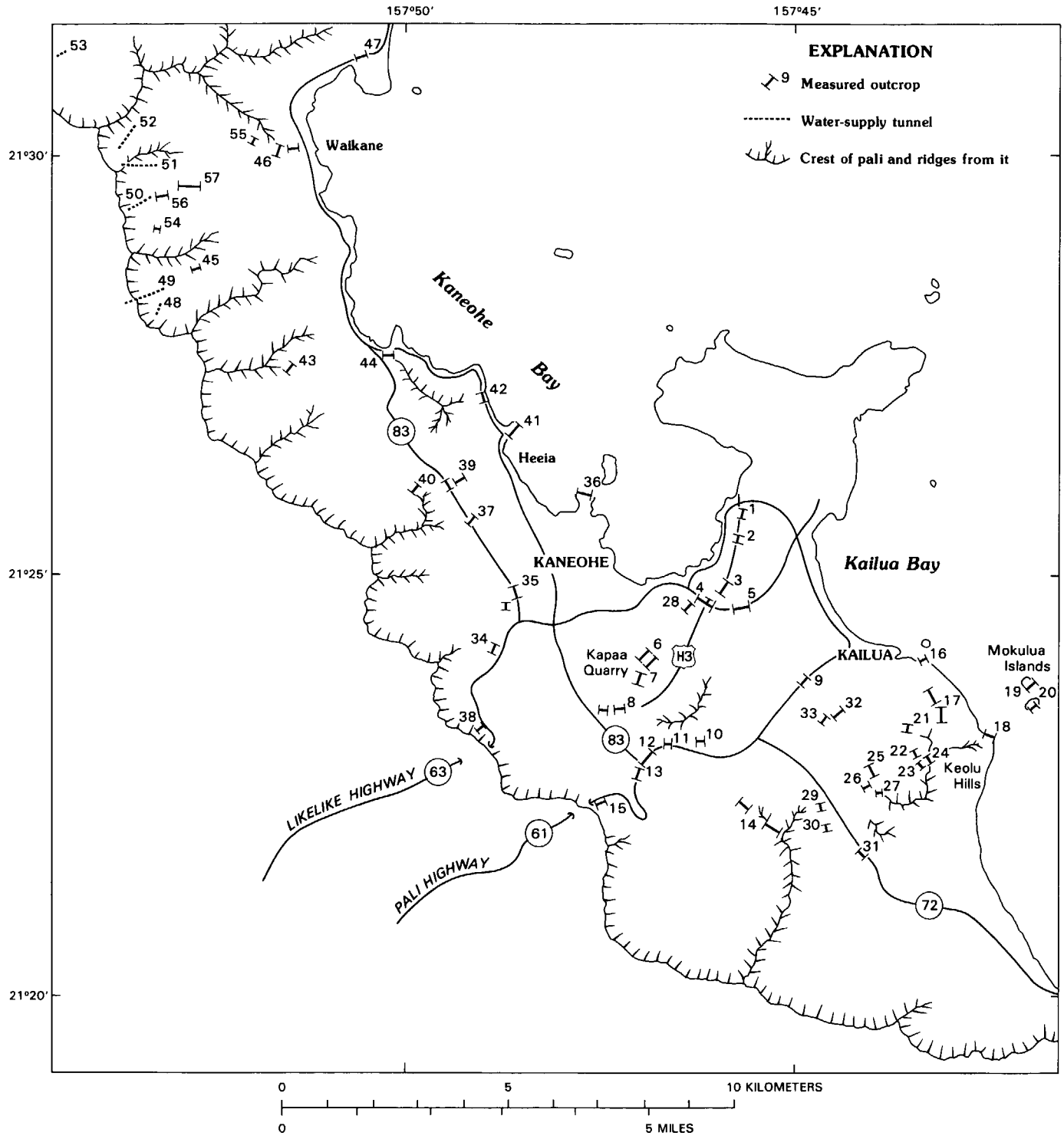

FIGURE 41.2.—Windward side of Oahu showing location of outcrops at which dike complex was studied. Numbers identify outcrops listed in table 41.1. All but outcrops 14, 15, and 38 are less than 240 m (800 ft) above sea level, and most are less than 120 m (400 ft) above sea level.

TABLE 41.1.—*Localities in the Koolau dike complex used for the present study*

[W, deeply weathered outcrop]

Number	Location and description
1.	Northernmost deep cut in Highway H3.
2.	Middle cuts beside viewpoint on Highway H3.
3.	Southernmost deep cut in the Highway H3 north of the join with Mokapu Saddle Road.
4.	Cuts in Mokapu Saddle Road near the Highway H3 overpass and adjacent cuts.
5.	Cut in Mokapu Saddle Road near Kalaheo High School.
6.	Kapaa Quarry, northeastern of two.
7.	Kapaa Quarry, southwestern of two.
8.	Cuts in Highway H3 between Kapaa Quarry and Kamehameha Highway (W).
9.	Cut in Kailua Road south of its join with Kaelepulu Street.
10.	Cut behind Kailua Drive-in Theatre (W).
11.	Cut in Kalanianaole Road 0.8 km (0.5 mi) northeast of join with Kamehameha Highway (W).
12.	Cut in Kalanianaole Road just northeast from join with Kamehameha Highway (Castle Junction) (W).
13.	Cut in Kalanianaole Road just southwest from join with Kamehameha Highway.
14.	Northwest ridge of Olomana Peak.
15.	Cuts in Old Pali Highway, northeast from pass.
16.	Coast exposures and nearby road cuts, Alala Point.
17.	Northern part of Kaiwa Ridge.
18.	Coast exposures at Wailea Point.
19.	Coast exposures on northwestern Mokulua Island, northwestern of two.
20.	Coast exposures on Mokulua Islands.
21.	Hillside west of Kaiwa Ridge, above Kamahele Place.
22.	Cuts behind subdivision alongside Kuuna Place.
23.	Cuts at north end of Apokula Street.
24.	Cuts on hilltop east of Apokula Street.
25.	Cuts behind subdivision alongside Auwaiku Street.
26.	Cuts west of Auauki Street.
27.	Cuts near hilltop south of Aunauma Street.
28.	Cut in track off Kahinani Way.
29.	Northern section of Old Kalanianaole Road.
30.	Middle section of Old Kalanianaole Road.
31.	Southern end of Old Kalanianaole Road.
32.	Cuts north of Akiohala Place.
33.	Cuts north of Akiohala Street.
34.	Cut on southwest Kahekile Highway 0.8 km (0.5 mi) of join with Likelike Highway (W).
35.	Cuts in and near Kahekile Highway 0.8 km (0.5 mi) north of join with Likelike Highway (W).
36.	Coast exposures and nearby road cuts at Pohakea Point.
37.	Cut in Kahekile Highway 1 km (0.6 mi) northwest of join with Haiku Road (W) and behind subdivision east of Highway (W).
38.	Stream section at foot of Pali just north of Wilson Tunnel.
39.	Cut in Kahekile Highway just southeast of Temple Valley Shopping Center and in fields to east (W).
40.	Cuts in Valley of the Temples Memorial Garden (W).
41.	Coast exposures at Kealohi Point (Heeia State Park) (W in part).
42.	Coast exposures 0.8 km (0.5 mi) northwest of Kealohi Point.
43.	Pit at foot of southeastern spur of Kalahaku Ridge (W).
44.	Cuts in Lulani Street and at join of Kamahameha Highway with Kahekile Highway.
45.	Roadcuts west of Waiahole Camp (W).
46.	Badland and ridge exposures on southeastern side of Puu Pueo Ridge (W).
47.	Cuts in Kamahameha Highway west of Kualoa Park turnoff.
[1]48.	Intake tunnel A.
[1]49.	Main transmission tunnel R.
[1]50.	Uwau tunnel.
[1]51.	Waikane 2 tunnel.
[1]52.	Waikane 1 tunnel.
[1]53.	Kahana tunnel.
54.	Path cuts at head of Waianu Valley.
55.	Badland exposures at southwestern foot of Puu Pueo (W).
56.	Path cuts east of Uwau tunnel.
57.	Path cuts on southern side of interfluve between Waikeekee and Uwau Valleys.

[1]From Takasaki and others (1969).

is between 50 and 100 over most parts of the complex where the intensity exceeds 40 percent, and reaches 130 in the Mokulua Islands; it drops to less than 10 in the Kailua caldera.

The Koolau dike complex was shown by Stearns (1939) to extend at least 35 km from Kailua in a northwest direction. It is assumed to extend also southeast beyond Waimanalo; exposures deep in the volcano are absent there, however, and all that is seen is a few southwest-trending dikes cutting lavas near the original shield surface on and near Makapuu Head.

The dikes predominantly have a northwest-southeast strike parallel with the longitudinal axis of the Koolau shield (fig. 41.5) and show a high degree of parallelism. Dike swarms elsewhere tend to have a fascicular (that is, cornsheaf-like) or radial arrangement, with at least some degree of divergence away from the volcanic center to which the dikes are related; the Koolau complex is noteworthy for the lack of divergence.

A subsidiary dike complex, well defined but narrower and less intense, trends southwest across the Keolu Hills in the general direction of Diamond Head, and the generalized contours of figure 41.1 show that the volcano bulges out slightly in this direction. This subsidiary complex attains a maximum intensity of about 15 percent at locality 31. Southwest-trending dikes on its extension to the leeward side of the Koolau Range were mapped by Stearns (1939) and Wentworth and Jones (1940).

The center of the Koolau Volcano is considered to be situated in the general area of Kailua, and the two complexes are regarded as the subsurface expression of two rift zones, a main northwest one and a minor southwest one. Note, however, that the pattern is not a simple one of two intersecting orthogonal dike complexes: the western part of the main complex seen in localities 12 and 13 curves around toward the Keolu Hills, where it converges on the minor southwest one. The dike swarm intensity of 80 percent at locality 23 in the Keolu Hills is therefore not simply that of the southwest rift zone.

At localities 23 and 24, where both northwest- and southwest-trending dikes occur, crosscutting relationships indicate that the injection of northwest dikes alternated with that of southwest dikes (fig. 41.6*A*), and similar relationships are seen at locality 4 (fig. 41.6*B*) and elsewhere. This shows that the periods of injection in the two directions overlapped.

This time relationship was not expected: in the model of Fiske and Jackson (1972), dike orientation is controlled by the overall geometry of a Hawaiian volcano and tends to run parallel with the long axis of the edifice. It is difficult to see how the edifice effect by itself could generate dikes alternating in trend along two orthogonal axes.

DESCRIPTION OF THE DIKES

WIDTH

Widths were measured on 3,550 dikes of the Koolau complex and are recorded by the histogram, figure 41.7*A*. Dikes range in width from less than 5 cm to 670 cm, and the median width is 53 cm. The arithmetic average width is 73 cm; this is greater than the median because of the contribution made to the total width by the small number of very broad dikes. The dike widths can also be portrayed in a different way, as the percentage of total dike width contributed by each width class (fig. 41.7*B*); 50 percent of the dikes are 60 cm or less wide, but these narrow dikes account for only 20 percent of the total width, and the 20 percent of dikes that are more

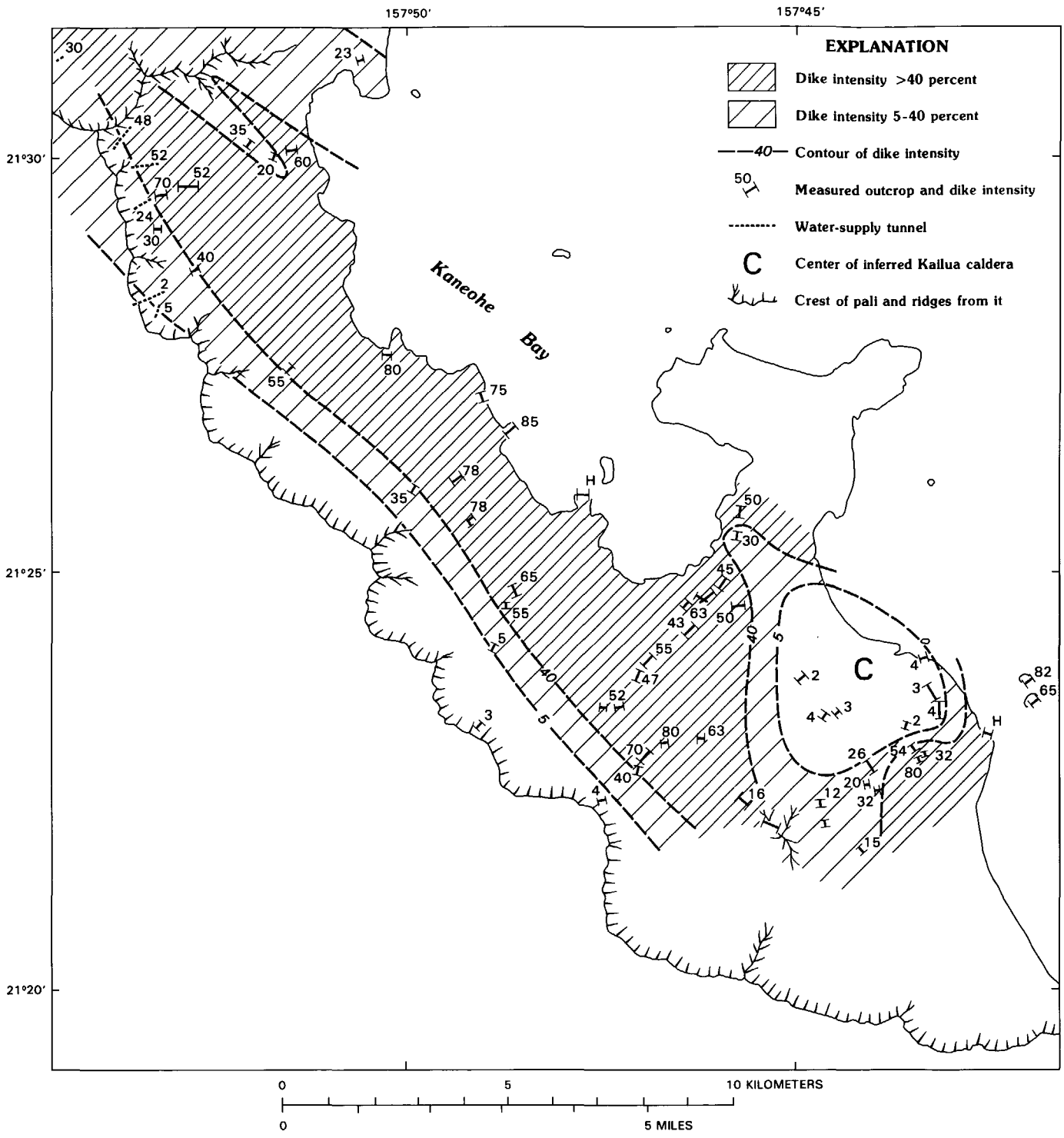

FIGURE 41.3.—Intensity of Koolau dike complex, expressed as percentage of outcrop width occupied by dikes. Close-shaded area is that in which dikes constitute 40 percent or more. Complex attains its maximum width of about 7 km in Kailua area, and narrows significantly toward northwest. The dike intensity is anomalously low in a large area centered on Kailua, interpreted to mark a caldera or caldera cluster. The intensity values at localities 3, 5, and 10 include 30 percent added for early brecciated dikes. H denotes a high intensity, but no measurement obtained.

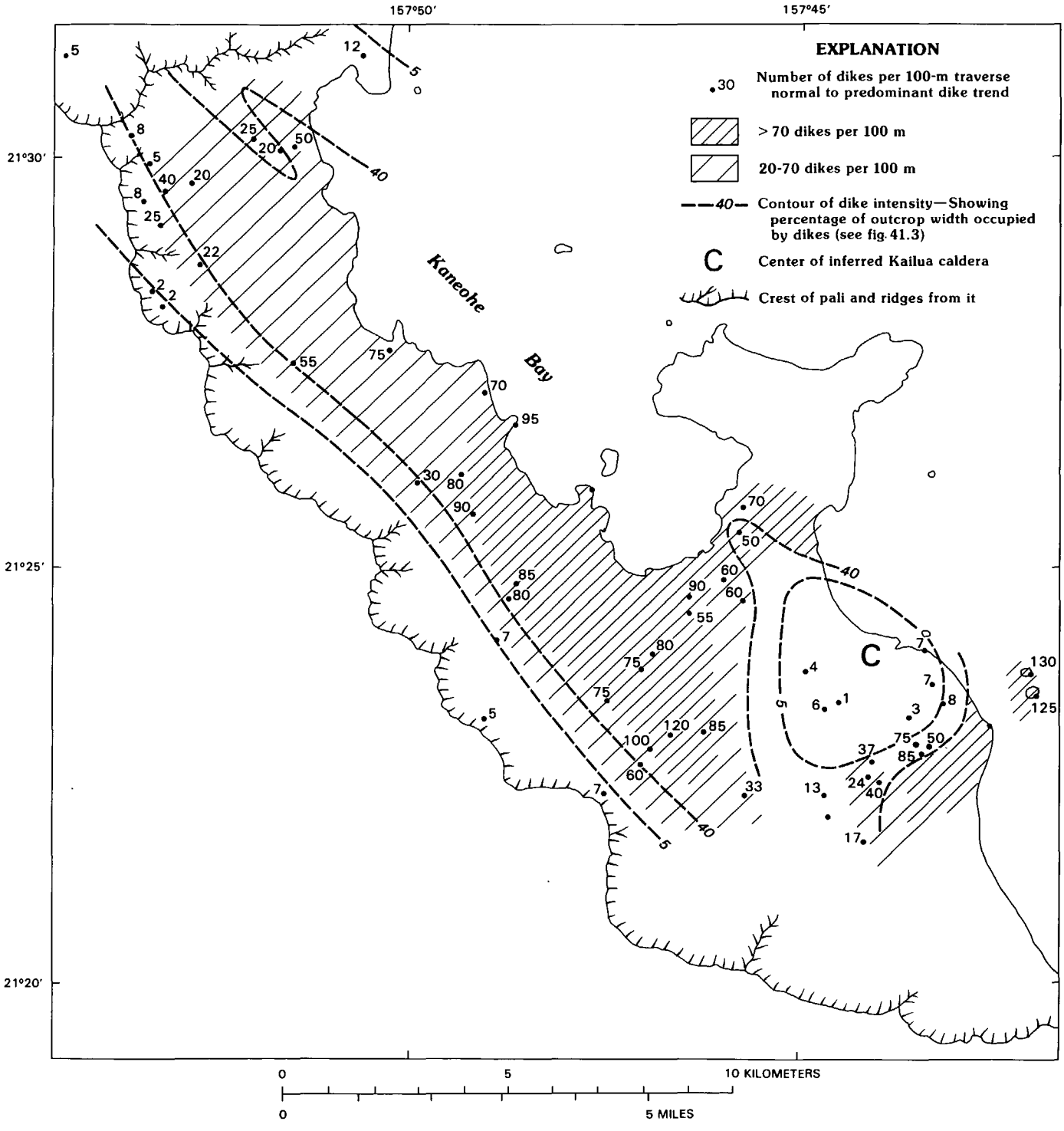

FIGURE 41.4.—Intensity of Koolau dike complex, expressed as number of dikes per 100-m traverse at right angles to predominant dike trend. Intensity contours from figure 41.3 also shown. Highest numbers of dikes (>100) occur where dikes form a high percentage of outcrop and also are narrow.

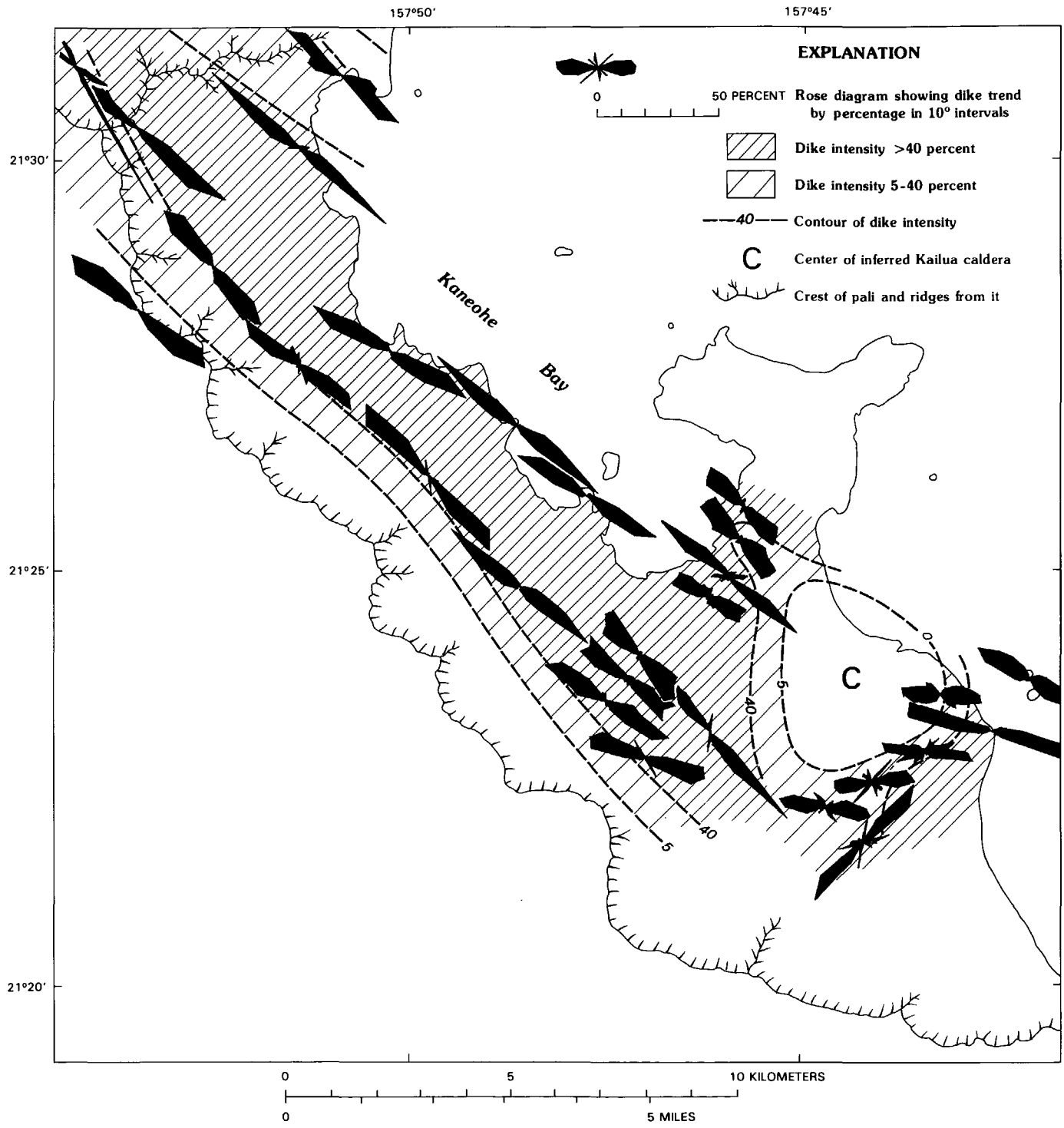

FIGURE 41.5.—Dike trends in Koolau dike complex. Rose diagrams constructed using 10° interval. Pattern is dominated by northwesterly trend: 70 percent of all measured dikes have a trend within 22.5° of N. 50° W. Subordinate but distinct southwest-trending complex occurs in south of area.

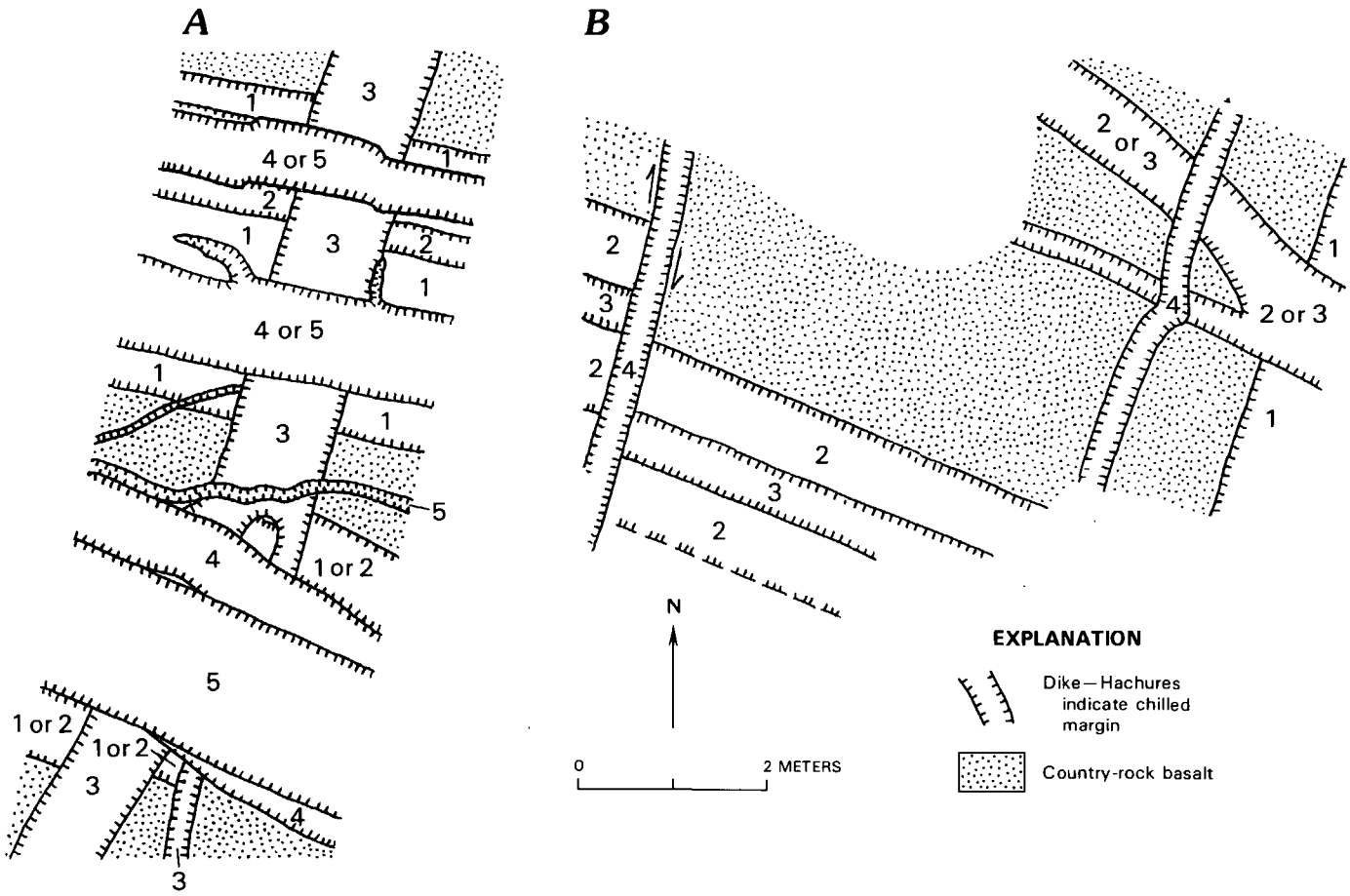

FIGURE 41.6.—Examples of age relationships at outcrops in Koolau dike complex where orthogonal dike intersections occur, shown somewhat schematically. ***A***, At locality 24. West-northwest-trending dikes (1 and 2) are cut by north-northeast-trending dike (3) that is cut by west-northwest-trending dikes (4 and 5). ***B***, Locality 4. North-northeast-trending dike (1) is cut by west-northwest-trending dikes 2 and 3, which are in turn cut by north-northeast trending dike (4). Note that significant fault movement occurred on one of the dikes (4).

than 110 cm wide account for 50 percent of the total width. The distribution in figure 41.7*B* closely approximates a lognormal distribution.

The dike widths of the Koolau complex are compared in figure 41.8 with those of Tertiary basaltic dike swarms in Iceland (Walker, 1959; Gudmundsson, 1984), which occur in the tectonic setting of an oceanic spreading center. The Koolau dikes are on the whole much narrower. This may reflect a generally lower viscosity of the Koolau magma but is at least partly attributable to the close proximity of most of the measured Koolau dikes to their volcanic center. Most of the measured Koolau sections lie within 15 km of the Kailua center, whereas the Icelandic dikes were mostly measured farther than 15 km from the respective volcanic centers to which they are related.

The width of dikes varies in different parts of the Koolau complex; it trebles from the Kailua volcanic center to the Waikane area (figs. 41.9, 41.10). The most obvious reason for this increase in width is that the lateral distance a dike travels from its source is related to its width: broader dikes are more far-ranging, and therefore far from the source the dikes tend all to be wide ones. As discussed in a later section, the trebling of average dike width is accompanied by a decrease to less than one third of the number of dikes present in transects across the complex.

LITHOLOGY

The Koolau dikes are basalts and diabases and are generally aphyric or have only a small content of phenocrysts. Phenocrysts are of olivine, augite, and plagioclase and are mostly less than 4 mm in size. Some dikes are highly porphyritic; the most common type, several examples of which are seen at localities 1 and 3, has aphyric margins and a central part containing abundant olivine phenocrysts. The abrupt juxtaposition of aphyric and porphyritic rocks is suggestive of the injection of two successive magma fractions. One porphyritic dike at locality 4 contains about 50 percent of platy plagioclase crystals, many exceeding 1 cm in size, decreasing in abundance toward the margins.

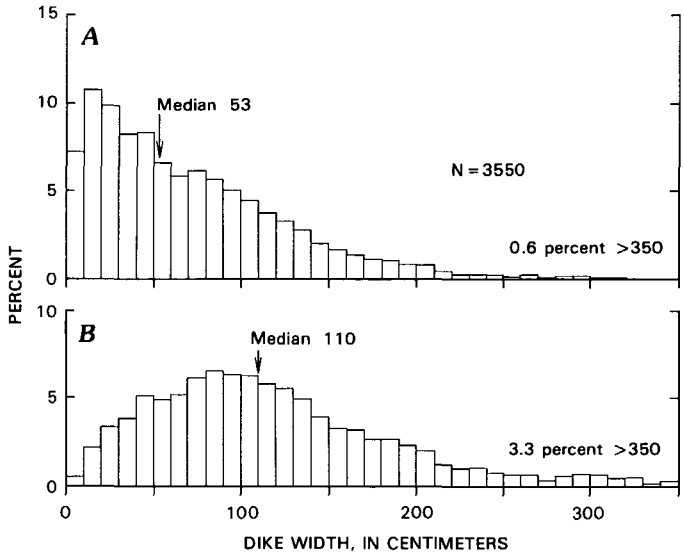

FIGURE 41.7.—Distribution of dike width in Koolau dike complex. N, total number of dikes. ***A***, Histogram of dike widths. Median width is 53 cm, arithmetic average 73 cm. About 90 percent of the dikes are less than 150 cm wide. ***B***, Percentage of total dike width contributed by each width category.

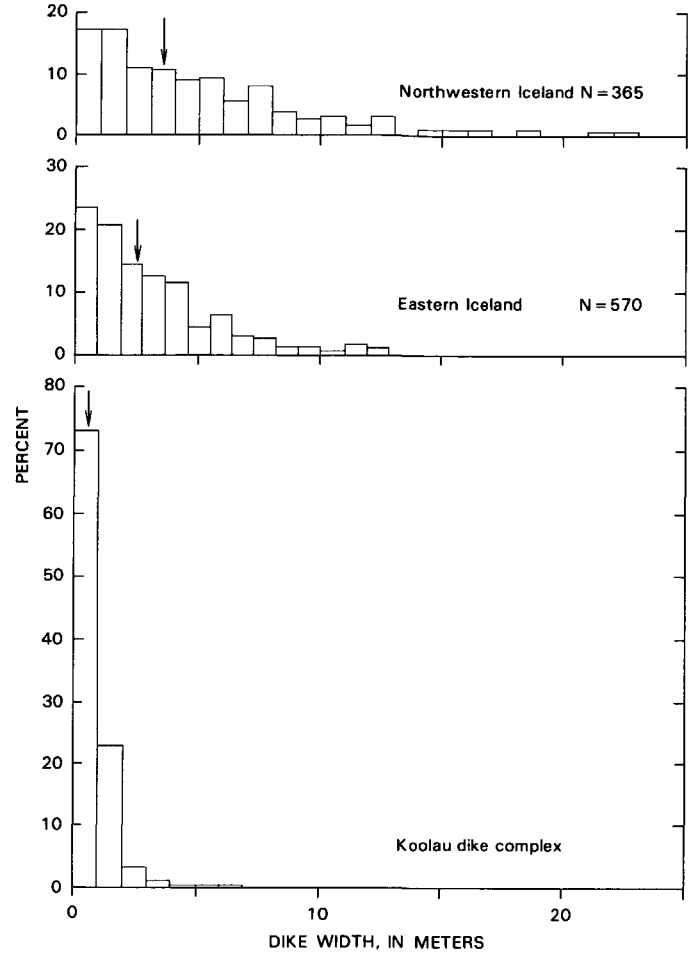

FIGURE 41.8.—Dike widths in Koolau complex compared with Tertiary basaltic dike swarms in eastern Iceland (Walker, 1959) and northwestern Iceland (Gudmundsson, 1984). Arrows indicate median width. Dikes in the Icelandic swarms are significantly wider than those in Koolau complex (median width 5–6 times greater). N, total number of dikes.

The dikes typically have glassy chilled margins and show a gradual steady increase in grain size inward from rim to center. The inner part of the glassy selvage is generally altered to orange palagonite, and this makes the dike margins easy to see. The width of the layer of glassy rock averages about 1 cm but varies from less than 1 cm to about 5 cm. One dike on the shore at locality 41 has glassy margins about 10 cm wide; the glass has varioles scattered through it or concentrated in narrow bands, and the banding is locally folded.

The three main roadcuts in the completed section of Highway H3 (localities 1–3 in figure 41.2 and table 41.1) provide fine exposures of the Koolau dike complex, and close examination of localities 1 and 3 reveals that the complex actually consists of two complexes, as follows: (1) An older complex consisting of highly irregular sheetlike intrusions, many of them amygdaloidal, which lack their own individual sets of cooling joints and have been affected at locality 3 by a pervasive propylitic alteration; and (2) a younger complex consisting of nearly planar dikes, which mostly have a low content of amygdules, possess their own individual sets of prismatic or sheetlike cooling joints normal to their margins, and are less altered.

An outstanding feature of the older dikes is that they are highly irregular, often curved and with outwardly convex protuberances, suggesting that they were intruded into a loose and yielding environment. The best explanation is that these dikes were injected into thin and strongly disjointed lava flows near the land surface of their day and sent off many sheetlike and irregular apophyses into these flows.

Near-surface lava in Hawaii is typically transected by a great many cooling joints, vesicle partings, flow-unit boundaries, rubble layers and other planes of weakness, and dikes cutting them are highly irregular. Good examples are seen in the walls of Kilauea caldera and in roadcuts near Makapuu Head in Oahu.

The older dikes are amygdaloidal, often conspicuously so, and this is consistent with their intrusion near the surface. Amygdules tend to increase in size toward the dike center (fig. 41.11C), and attain a greater size (commonly exceeding 1 cm) in the wider dikes than in the narrower ones (fig. 41.11*A*). They tend to be concentrated in layers parallel with the dike margins. The amygdules contain zeolites (notably laumontite) and other secondary minerals.

A few older dikes contain pipe amygdules in a zone near the margin. The pipes on either side of a dike form parallel sets, the orientations of which combine growth of the pipes inward from the dike margin and their alignment in the magma flow direction.

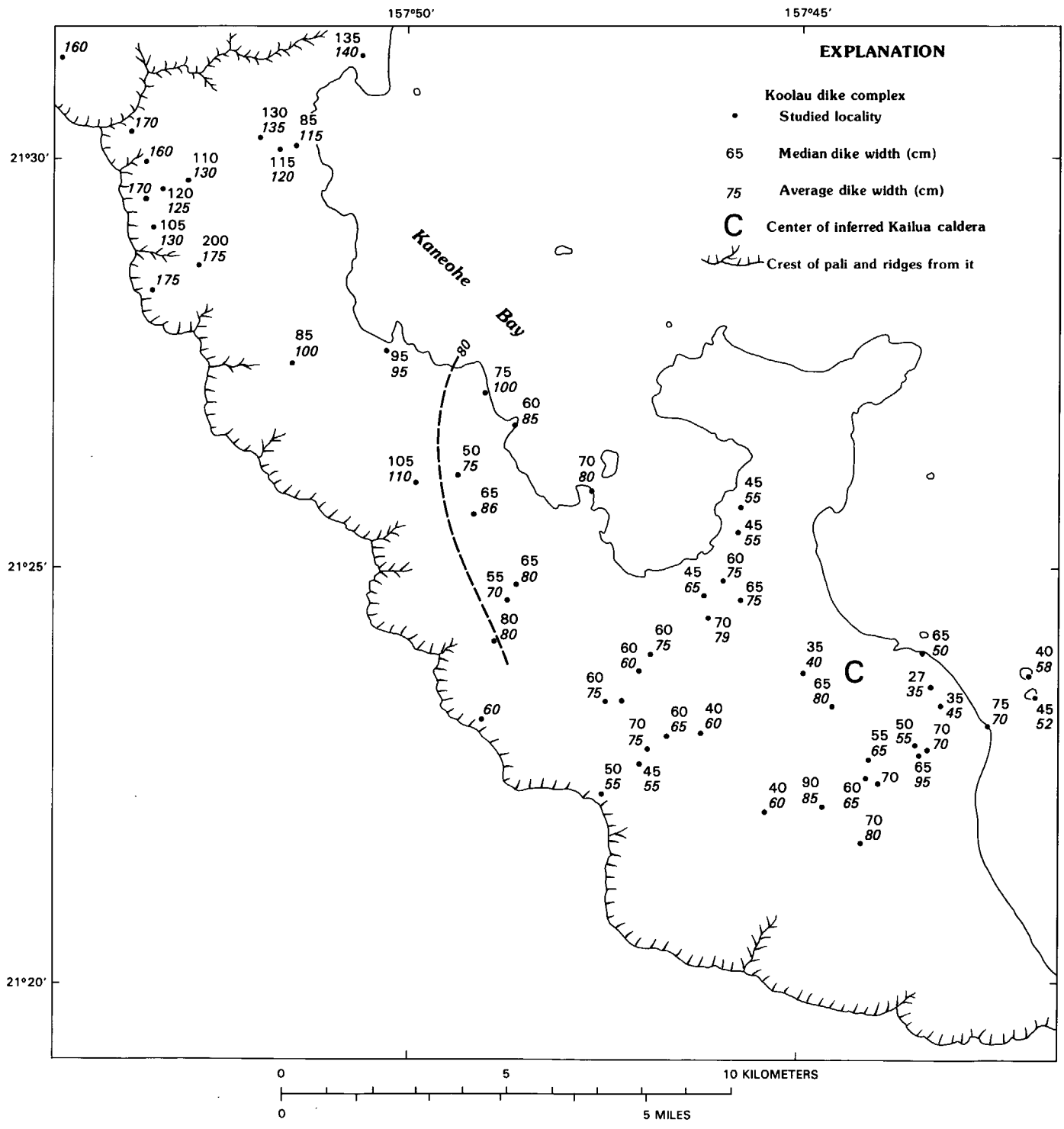

FIGURE 41.9.—Geographic variation of dike width in Koolau complex. Figures give width in centimeters. Arithmetic average width is generally larger than median. Note that lowest values occur in Kailua area, where center of Koolau Volcano was situated, and values tend to increase with increasing distance from center.

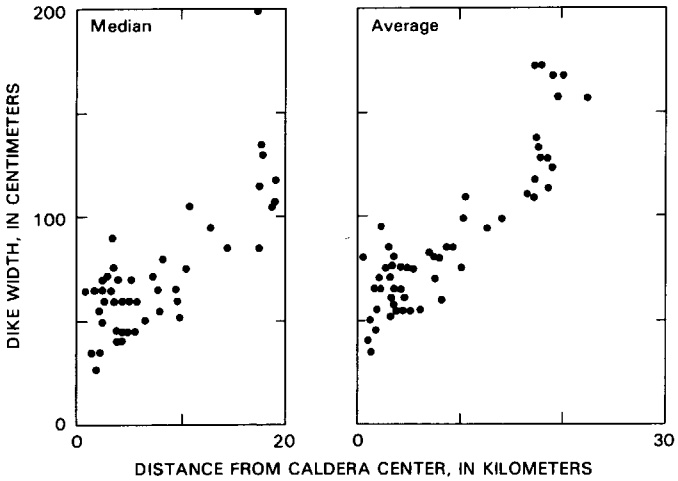

FIGURE 41.10.—Variation in median and average dike widths in Koolau complex with distance from presumed center of Kailua caldera (see figure 41.9 for location). Both median and average widths show a clear tendency to increase with increasing distance.

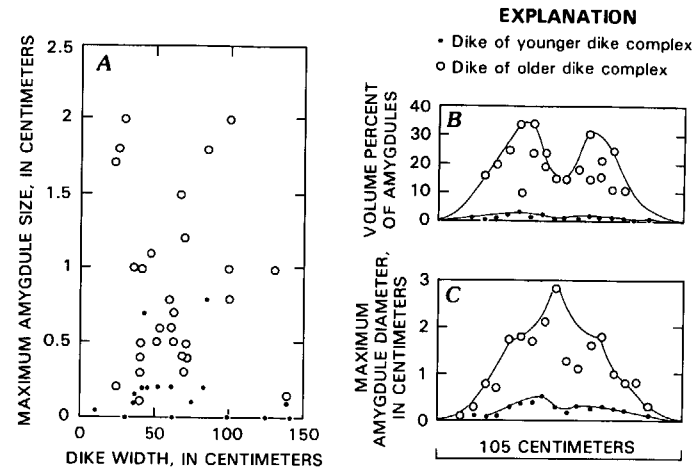

FIGURE 41.11.—Variation of amygdule size and content in dikes of Koolau dike complex. ***A***, Maximum amygdule size versus dike widths for 49 dikes at localities 2, 3, and 4, showing tendency for amygdule size to increase with dike width. ***B***, Profiles showing amygdule content across two dikes at locality 3, a typical member from each of older and younger complexes; each dike is 105 cm wide. ***C***, Profiles showing maximum amygdule size across same two dikes as in *B*.

Another important feature of the older dikes is the presence on them of conspicuous pale green rims 1–2 cm and occasionally as much as 5 cm wide, interpreted to consist of altered glass of a thickness suggestive of quenching in water. The loose and yielding lava pile into which they are interpreted to have been intruded may have contained abundant ground water.

The younger dikes in the roadcuts on Highway H3 tend to possess their own joint sets instead of imposed joint systems such as cut the older dikes. Close-spaced cooling joints normal to the margins are particularly well developed in marginal parts of many dikes. The nearly planar form of the dikes indicates that they were intruded into rigid rocks. The general scarcity and small size of amygdules indicates that the younger dikes were probably intruded under a thick cover.

The observed relations among the dikes in localities 1 and 3 are consistent with the view that the earlier members were intruded in a very shallow setting, near the land surface of their time, into an assemblage of thin and mechanically very weak lava flows with a high water table; the younger members on the other hand were intruded at a much deeper level after a considerable thickness of lava had been added to the Koolau shield volcano. The differences are similar to those that Wentworth and Jones (1940) inferred to be related to different depths of intrusion; at localities 1 and 3, however, dikes intruded thus at different depths are now found side by side at the same level, instead of (as Wentworth and Jones found) at different levels in the shield.

FLOW LINEATIONS

The chilled edges of many dikes carry a lineation that appears to have been produced by magma flowage through the dike fissure. The flow lines of this lineation generally consist of millimeter-high wrinkles projecting out from the glassy surface of the dike or from planes within the glass selvage. Streaky coloration often also occurs in the outermost few millimeters of glass. Slickensidelike grooves are occasionally seen on a sheet joint a few centimeters inside the dike margin. Pipe vesicles in marginal parts of a few dikes have a parallel orientation neither vertical nor normal to the dike margins but in the flow direction. Spindle-shaped vesicles are also rarely found in the dike margins elongate in the flow direction.

The attitude of the flow lineation has been systematically measured to investigate its utility. Such mapping has rarely been attempted since attention to its potential was drawn by Harker (1904). Flow lineations are common on the Koolau dikes but have been measured on fewer than 10 percent of the dikes examined because they are seen only where a sufficiently broad dike surface is bared and is not so weathered that the outermost few millimeters have been stripped off.

The lineation plunges at an angle that, within a few meters, typically varies over a range of about 50°, as illustrated by figure 41.12. Some of this variation is clearly related to local irregularities in the dike surface as where the flow lines curve around surface bulges.

Wherever possible, measurements of the plunge were made at different points on the same dike, avoiding places where the lineation was strongly curved. The median plunge angle was then determined. In all, measurements were made and the median angle determined on more than 100 dikes.

At some localities, the lineations in most dikes plunge in the same direction, though the angle varies from dike to dike over about 50°, as illustrated by figure 41.13*A*. At such localities the median plunge angle was determined and is plotted on figure 41.14. At other localities the dikes fall into two groups having opposing plunge

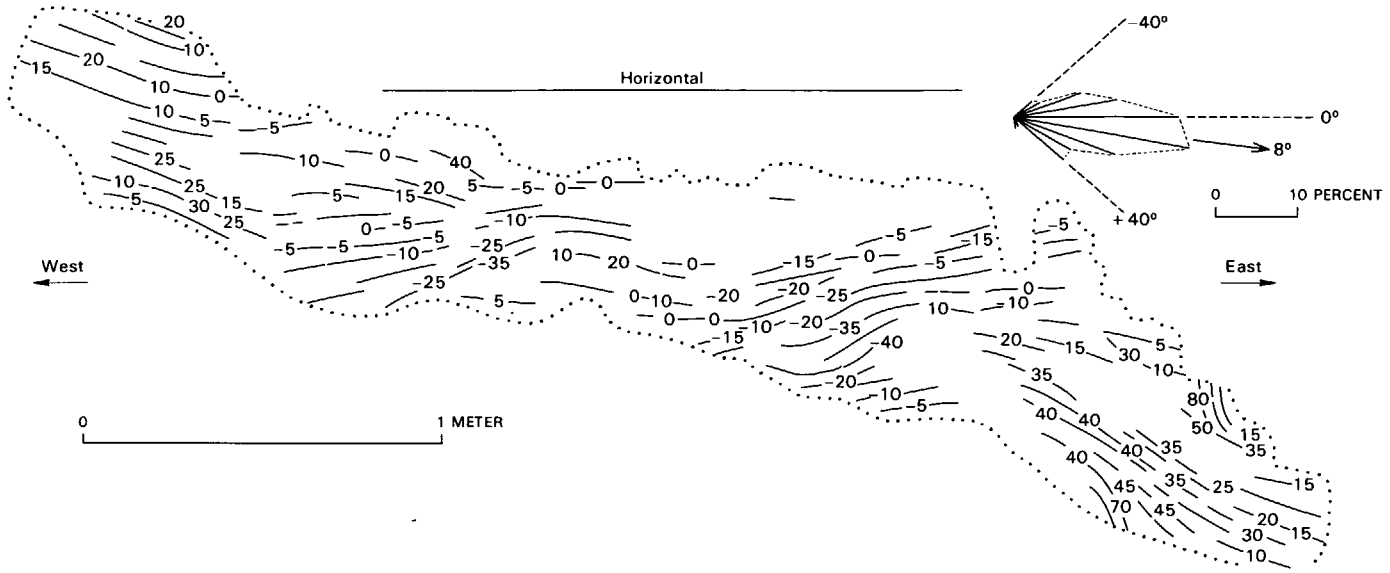

FIGURE 41.12.—Flow lineations on steeply dipping dike surface (area 1.8 m²) in Koolau dike complex (loc. 4). Numbers give measured plunge in degrees measured from horizontal. Inset at upper right: rose diagram showing variation in plunge angle, based on 89 measured values. Median plunge angle is 8° to east; 75 percent of measured values are within about 25° of this angle.

directions, as illustrated by figure 41.13*B*; at these localities the median plunge angle for each group was determined, and both angles were plotted on figure 41.14.

The arrows on figure 41.14 record the predominant directions of the flow lineation at each locality, and the numbers give the median plunge angle. Most of the arrows point toward Kailua or to an area southwest of Kailua, but many point toward Kaneohe Bay.

In interpreting these data it is assumed that the magma rose through each dike fissure, and the arrows that record the predominant plunge directions on figure 41.14 thus point back towards the source regions from which the dike magma came. At least two source regions are indicated, one below Kailua caldera and the other below Kaneohe Bay. The depth at which the plunge lines would intersect is about 2–3 km below sea level.

DIKE SIDESTEPS

Dike sidesteps are commonly observed in which a dike tapers out and then resumes on a parallel course as much as several meters to one side. In some examples the two sidestep segments are joined by a narrow stringer; in others a connection is presumed to have existed above or to exist below the present erosion surface. Sidesteps are observed on both vertical and horizontal surfaces, but outcrops in the Koolau complex are less favorable for studying the latter. Attention is therefore concentrated on the features of sidesteps seen in vertical sections.

At a sidestep in a dike having the dominant northwesterly trend, the upper segment may step either to the southwest or the northeast side; these are referred to as southwest and northeast sidesteps, respectively. A study was made at several sites to determine if one sidestep direction is particularly favored and whether dike sidesteps have utility in structural studies. Curry and Ferguson (1970) considered the origin of offsets, and Pollard and others (1975) and Delaney and Pollard (1981) investigated the position of offset segments in sheet intrusions relative to the propagation direction. Few studies, however, have attempted to relate dike sidesteps to the overall structure of a rift zone (see Duffield and Nakamura, 1973).

Eight good examples of sidesteps were identified among the younger dikes in locality 3 (fig. 41.15), and it is seen that southwest and northeast sidesteps are roughly equal in number. This is also true at other localities, and thus the sense of sidesteps is probably not determined by any regional pattern.

Closer examination of the dike sidesteps at locality 3 reveals that about half occur where the sidestep dike cuts across an earlier dike and steps across from one to another plane of structural weakness.

I conclude that the dike sidesteps form mostly where the course of a dike trends obliquely across the preexisting grain (the trend of earlier intruded dikes) of a dike complex.

DIKE INCLINATION

The dikes of the Koolau complex are predominantly steeply dipping (generally 65°–85°) but not vertical. The measured dips are plotted on the histograms of figure 41.16. The reason for this departure from verticality is one of the most intriguing of the problems posed by the complex.

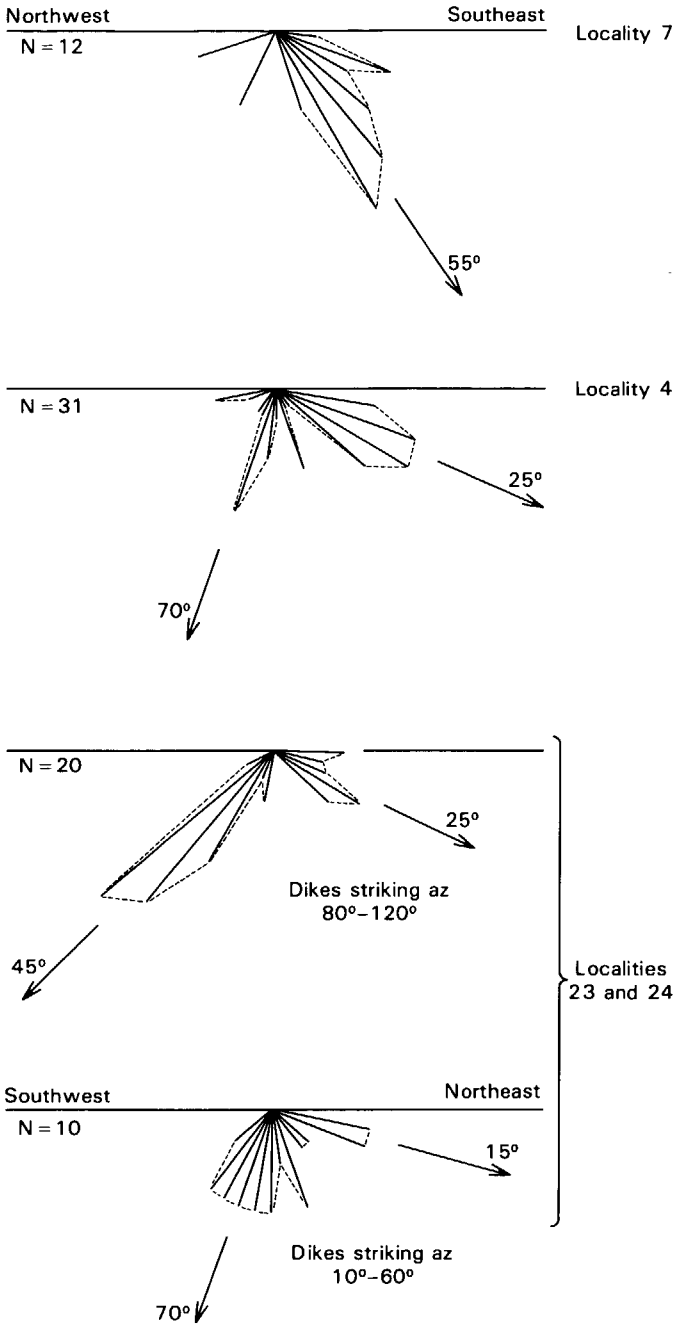

FIGURE 41.13.—Rose diagrams of average plunge of flow lineation measured on dikes at localities 4, 7, 23, and 24. At least one source is deduced for locality 7 and two sources for locality 4; arrows give predominant plunge. N, number of measured dikes.

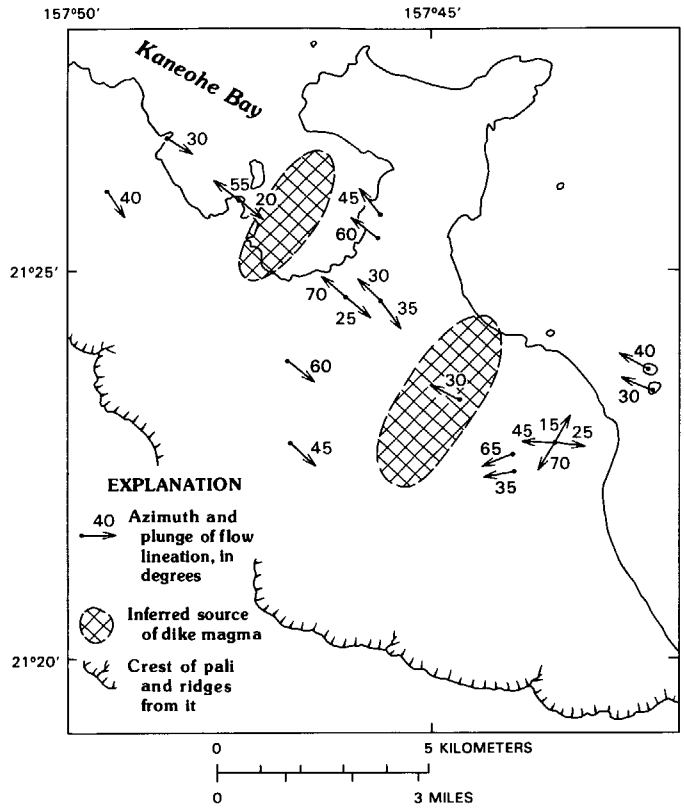

FIGURE 41.14.—Predominant plunge of flow lineation on dikes in Koolau complex. On the assumption that arrows point back to sources from which dike magma came, two sources are inferred, one near Kailua and the other under Kaneohe Bay.

The most common relationship is that the dikes in part of an exposure mostly dip in the same direction and at about the same angle, whereas farther along in the same exposure the dikes mostly dip in the opposite direction. This is clearly shown at locality 12, where the predominant dip direction changes from southwest to northeast several times along the 350-m length of the outcrop. The frequent change in the dip direction is well shown on the Mokulua Islands (localities 19 and 20): there the same cluster of dikes that in one place dips predominantly in one direction may be found to swing over and dip in the opposite direction a short distance along strike or higher up on the same cliff section. There are also many places at locality 12 and on the Mokulua Islands where, though the dikes predominantly dip in one direction, a significant number dip in the opposite direction and intersect to produce a braided pattern.

Individual dikes commonly vary in dip over several tens of degrees in the same outcrop, and it is often difficult to know what to measure. An attempt was generally made to measure the dip of a plane joining the points on each dike at top and bottom of the outcrop. This value for the dip obviously has a different validity depending on whether the outcrop is 1 m or 10 m high. Although the individual dip readings are of varied validity, the collective readings from many dikes at the same locality should define significant trends.

On the whole the dikes dip predominantly outward on either side of the Koolau Volcano (fig. 41.17). This would be in accord with the anticipated dip of normal or listric faults on either side of a high-standing edifice. The axis separating mainly southwest-dipping from mainly northeast-dipping dikes, however, coincides with the axis of the volcano only near Waikane; elsewhere it is strongly

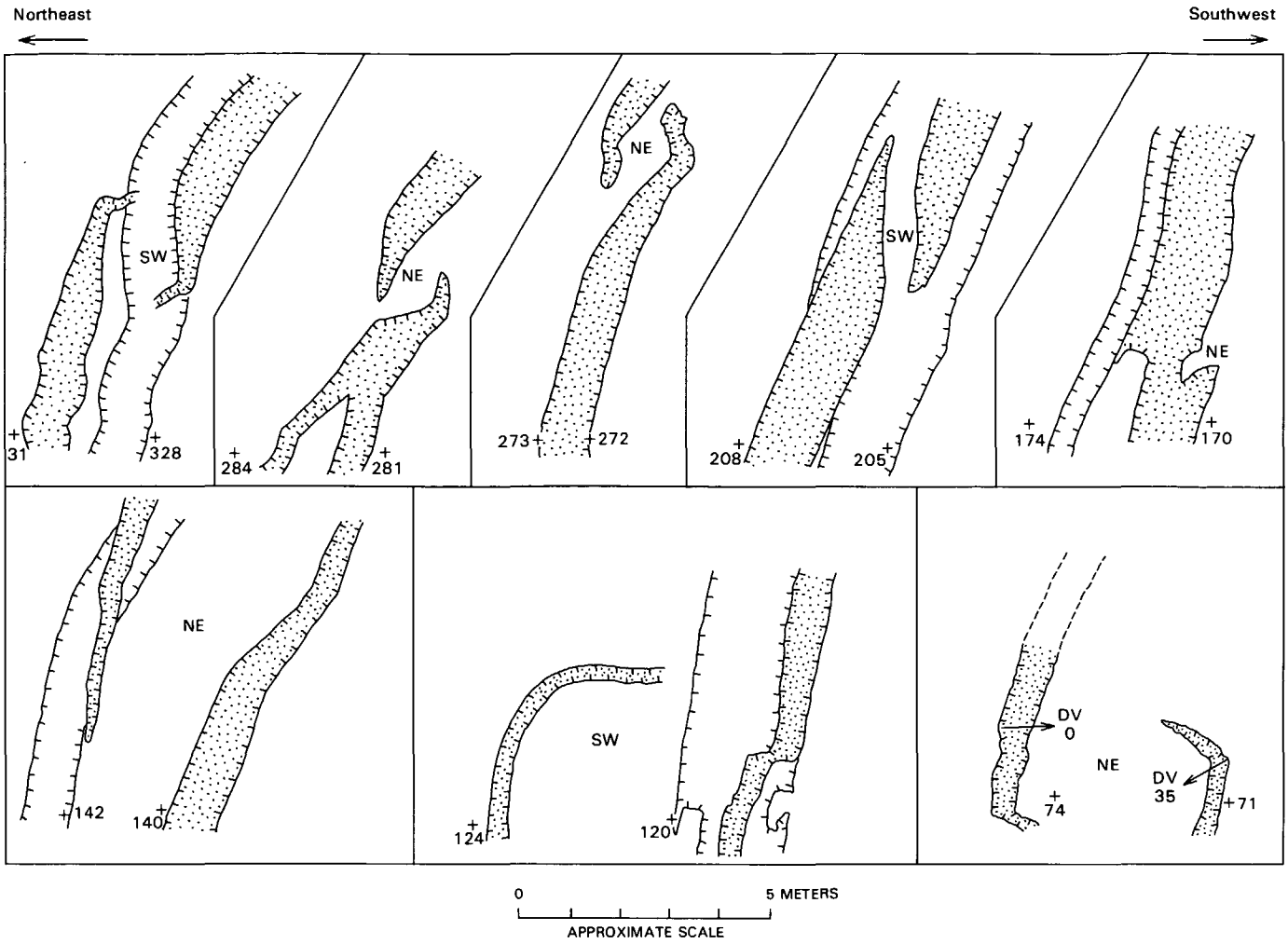

FIGURE 41.15.—Eight examples of dike sidesteps in Koolau complex of roadcut on Highway H3, locality 3. Where dike cuts dike, younger one is stippled. NE, SW, examples in which dike sidesteps upward to northeast and southwest, respectively. Numbers give distance in meters from south end of roadcut. DV, orientation and plunge angle of dilation vector, where known. Hachures indicate chilled margins.

displaced toward the southwest. In the area of locality 15 the part with northeast-dipping dikes embraces the entire width of the complex. This anomalous dip could indicate a weakness of the volcano and a tendency for it to creep northeastward toward the deep ocean in this area.

An older dike complex may be distinguished from a younger one at localities 1–7 as described earlier, and both dip predominantly in the same direction, showing that this weakness of the volcano was manifested early.

A late-manifested consequence of the weakness of the northeastern side of Koolau Volcano was the collapse by landsliding of much of that side (Moore, 1964). It is interesting to note that landsliding extended farthest across the volcano in the same area in which predominantly northeast-dipping dikes extend farthest. This may mean that both are manifestations of the same weakness. Alternatively, the predominance of northeast-dipping dikes in this area may have facilitated the landsliding.

The dip directions and angles of the dikes are apparently unrelated to the dip of the country rock lava; they are instead strikingly similar to those of normal faults developed in a tensional setting, which form complementary sets having opposing dips. The dikes of the Koolau complex may likewise form complementary sets oriented by a stress pattern similar to that which generates normal faults.

In many dike swarms elsewhere in the world the dikes are vertical or approximately so, as documented in Iceland by Gudmundsson (1983, 1984; fig. 41.16*D*). The problem is why the dikes of the Koolau complex systematically depart from verticality.

Dikes are conventionally interpreted to lie in the plane containing the maximum and intermediate principal stress axes and thus at right angles to the minimum principal stress axis (fig. 41.18). On the other hand, in an extensional tectonic setting in which horsts and grabens form, sets of normal faults form on planes oriented at about 20° on either side of the vertical plane that contains the maximum

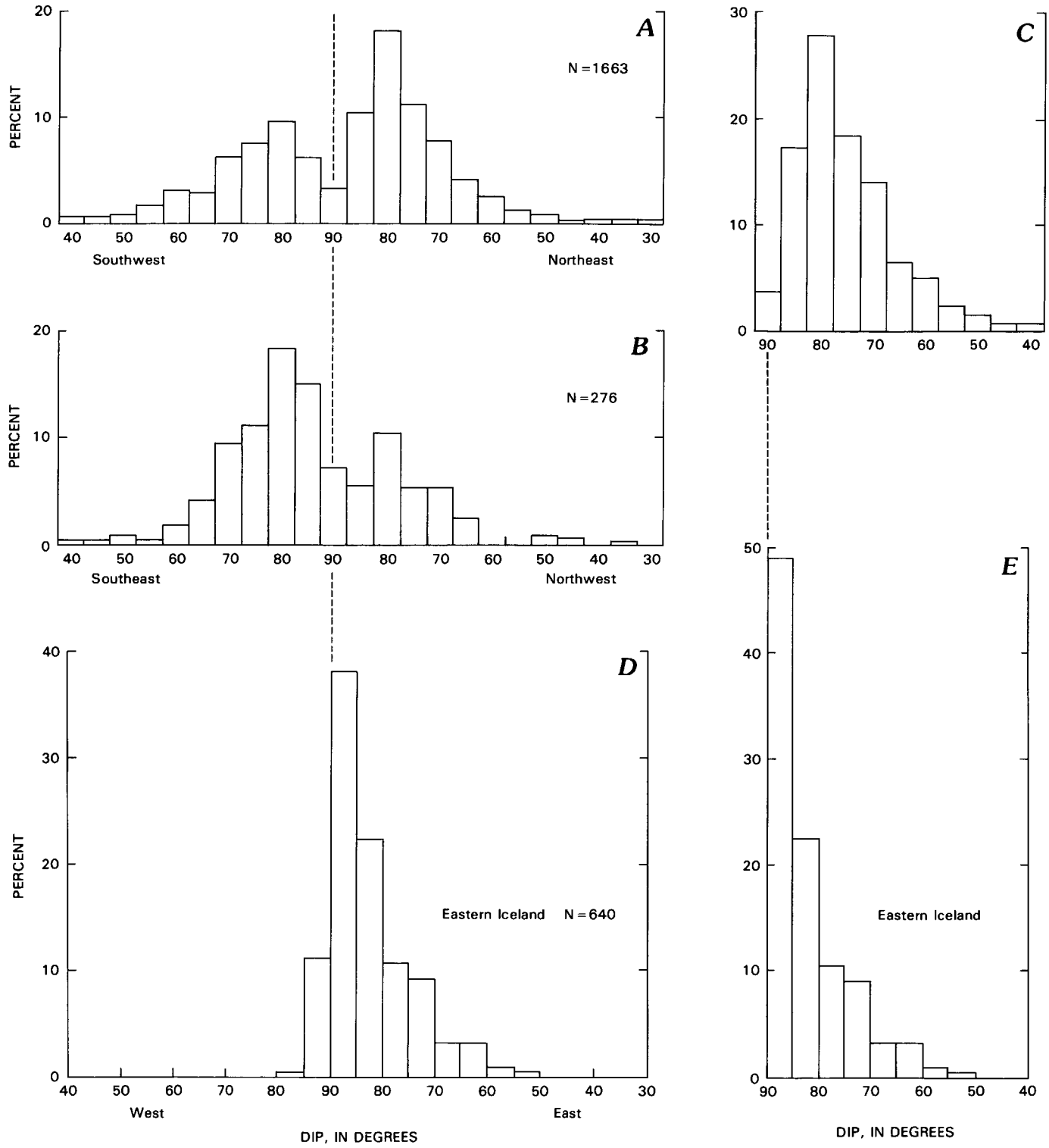

FIGURE 41.16.—Dip angles of dikes in Koolau dike complex and Tertiary dike swarm of eastern Iceland. N, number of dikes in each set. ***A***, Dips of northwest-trending dikes in Koolau dike complex. Note two peaks at 10°–20° on either side of vertical. ***B***, Dips of northeast-trending dikes in Koolau dike complex. Note similar peaks as for northwest-trending dikes. ***C***, Numerical values of dike dips in Koolau dike complex, disregarding both strike direction and dip direction. ***D***, Dips of dikes in Tertiary dike swarm of eastern Iceland (Gudmundsson, 1983); 73 percent are within 10° of vertical (this remains true even after compensation for 5° of later westward tilt). These dips were measured to nearest degree, whereas Koolau dikes are so irregular that their dips were measured to nearest 5°. ***E***, Numerical values of dike dips in Tertiary dike swarm of eastern Iceland, disregarding dip direction.

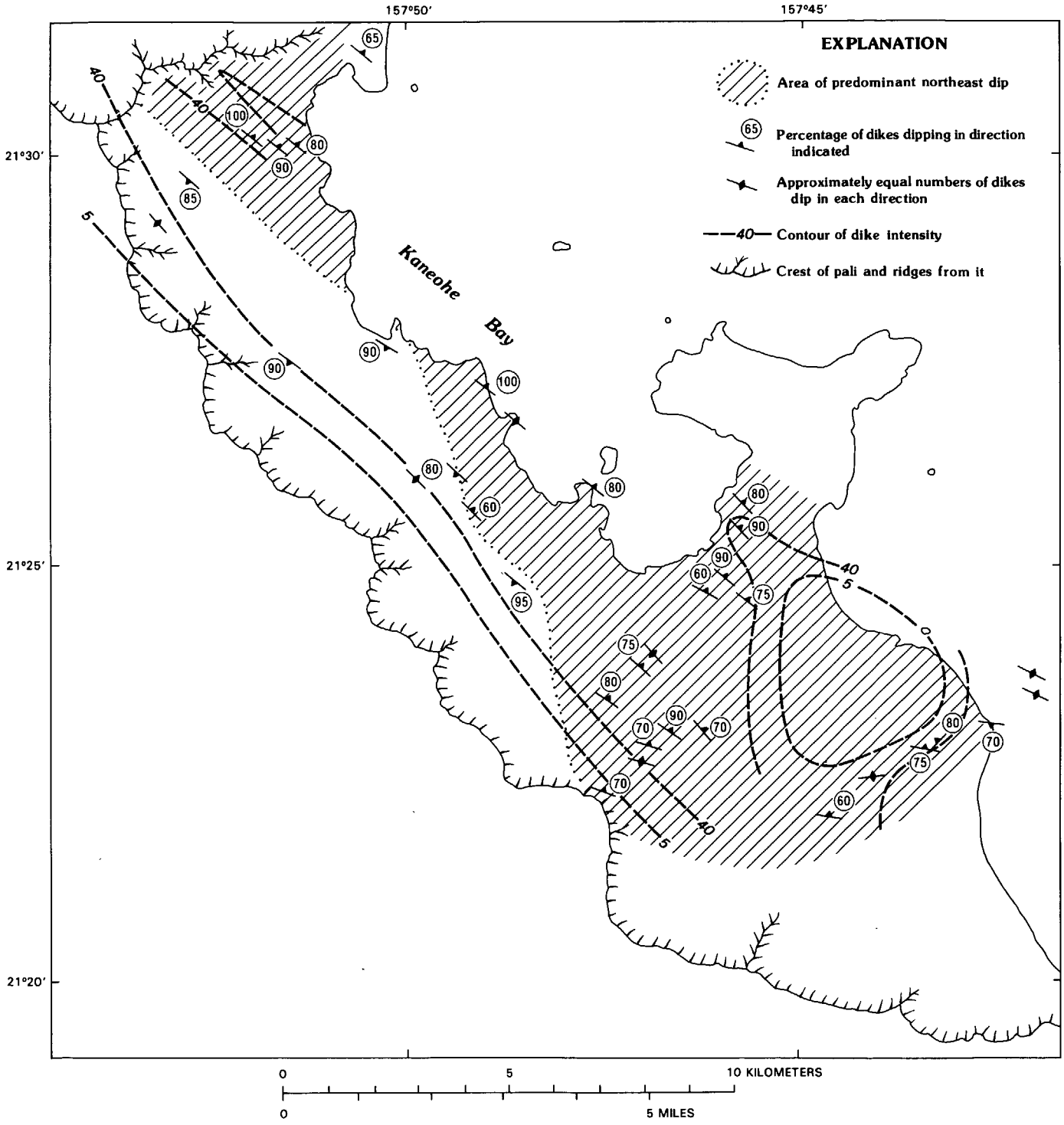

FIGURE 41.17.—Predominant dip directions of dikes in Koolau dike complex. Generally dip is outward on either side of axis of Koolau Volcano. In a large anomalous area, however, predominant northeast dip extends across entire width of complex. Intensity contours from figure 41.3.

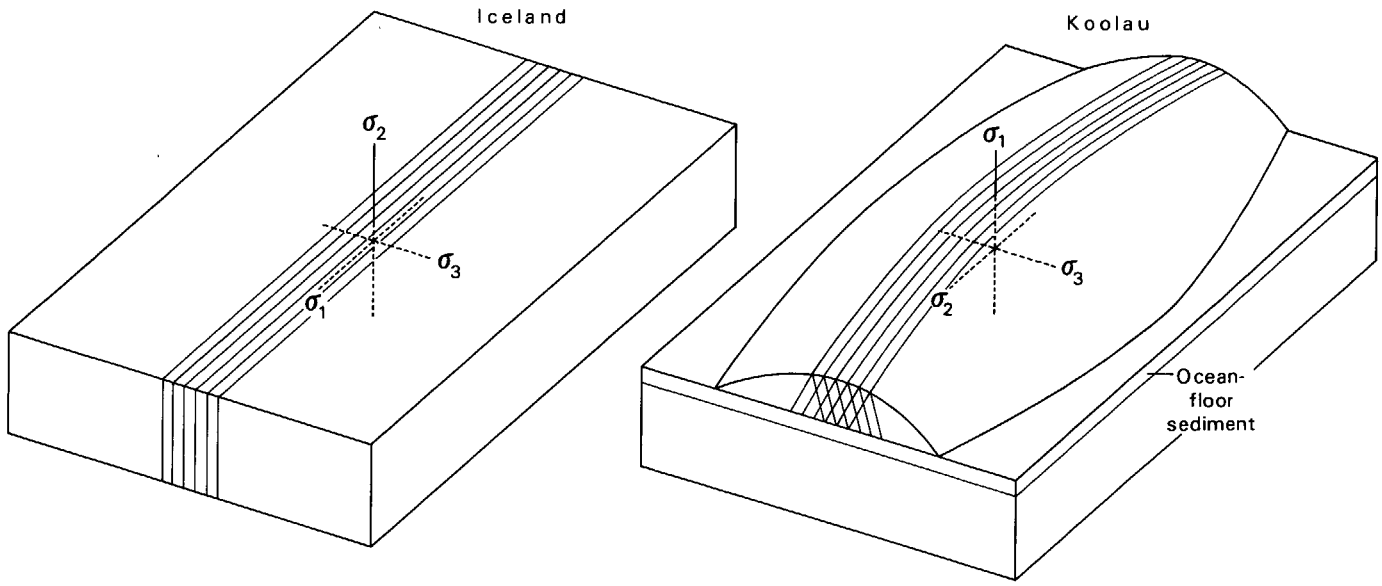

FIGURE 41.18.—Comparison of rift zones in two tectonic settings showing postulated positions of maximum (σ_1), intermediate (σ_2), and minimum (σ_3) stress axes. An oceanic spreading ridge is exemplified by Iceland (see Keith, 1981), which rises 3 km above deep ocean floor in 300–400 km. An intraplate volcanic edifice is exemplified by Koolau Volcano on Oahu, which rises 5 km above deep ocean floor in 60 km. Icelandic rift zone can be regarded as being confined at both ends, and formation of vertical dike fissures is favored. Hawaiian edifice is not confined at sides or ends and is free to move on its underlying layer of ocean-floor sediment (Nakamura, 1980); hence σ_1 is much greater than σ_2 and σ_3 and formation of inclined dike fissures forming two complementary sets is favored.

and intermediate stress axes. Vertical dikes like those in Iceland and complementary sets of faults both form in an extensional setting. How may the vertical orientation of most dikes be reconciled with the nonvertical orientation of normal faults and Koolau dikes?

I propose that the explanation for this is that Hawaiian volcanoes, being high-standing and comparatively steep structures (the Koolau Volcano rises 5 km above the deep ocean floor in 60 km), have a strong tendency to spread laterally (Fiske and Jackson, 1972) and have axes of minimum and intermediate stress both lying in the horizontal plane. The maximum stress axis is vertical and greatly exceeds the other two. In contrast, fissure eruptions in Iceland occur in a setting in which the tendency for gravitationally induced lateral spreading is small (Iceland rises only 3 km above the deep ocean floor in 300–400 km), and under these conditions the maximum stress axis may be horizontally oriented in this direction and if vertical will not be much greater in magnitude than the other two (compare with Keith, 1981). It is postulated that dikes in this situation tend to be vertical.

A possible alternative explanation for the nonverticality of the Koolau dikes is the mechanical anisotropy of a Hawaiian volcanic pile. Ryan and others (1983) pointed out that, though the pile behaves as a mechanical continuum, an elastic solid, the rock is so disjointed in the vertical direction that it lacks mechanical continuity in the horizontal plane. When, for example, horizontal displacement magnitudes are made up of reversible and irreversible components, the restoring forces for the former tend to be either weak or nonexistent. Lateral extension then tends to generate nonvertical fractures. Thus, where a vertical fissure passes up into poorly consolidated ash or sediment, a graben between nonvertical normal faults develops in that deposit; good examples are seen where fissures of Kilauea's southwest rift zone, just outside the caldera rim, transect thick pyroclastic deposits of the 1790 explosive eruption.

Though mechanical anistropy is capable of accounting for the extreme irregularity and nonverticality of the older dikes, it does not readily explain the nonverticality of younger dikes such as are seen cutting well-lithified breccias in locality 3. I conclude therefore that the nonverticality is mainly attributable to the edifice effect—the tendency for lateral spreading in a very high volcanic edifice.

CONE SHEETS AND SILLS

A small proportion (about 1 percent) of the dikes have a dip of less than 50°, and the possibility that they might be cone sheets (as was suggested by Macdonald and Abbott, 1970) must be considered. The essential attribute of cone sheets is that they dip toward a common focus. When the low-angle sheet intrusions found in the present study are plotted on a map (fig. 41.19), no tendency toward a centripetal dip can be discerned, which lends no support to the idea that they are cone sheets. These dikes are therefore regarded as constituting simply the low-angle tail of a Gaussian distribution.

Only one sill was noted; it is highly irregular, is about 1 m thick, and can be traced for a few tens of meters in a roadcut where the highway climbs the pali at Makapuu Head.

VERTICAL DISPLACEMENTS CAUSED BY DIKE INJECTION

The injection of vertical dikes does not cause any uplift or subsidence of the country rock apart from that which may result by

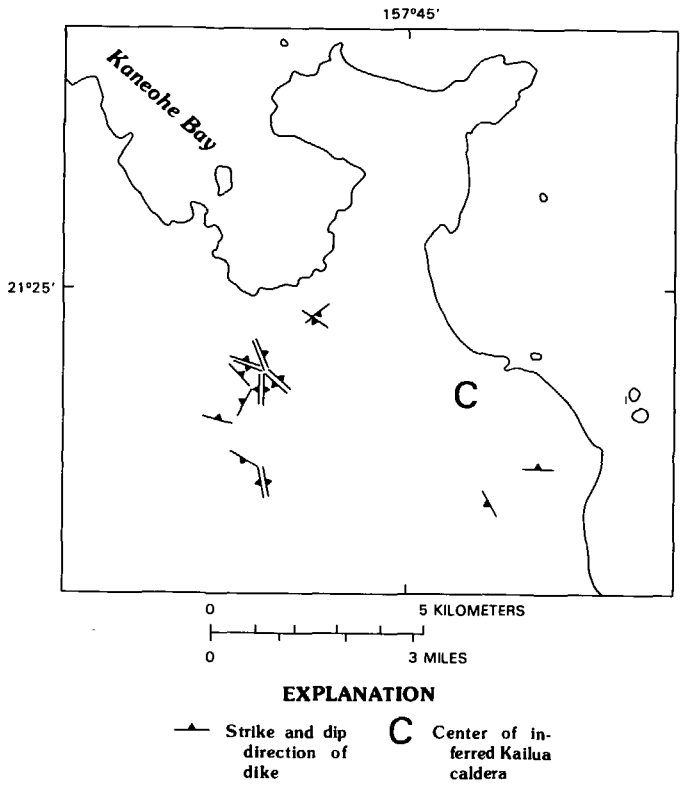

FIGURE 41.19.—Strike and dip direction of 1 percent of dikes in Koolau complex that dip less than 50°. Attitudes show no tendency toward centripetal pattern and thus lend no support to idea that these intrusions are cone sheets.

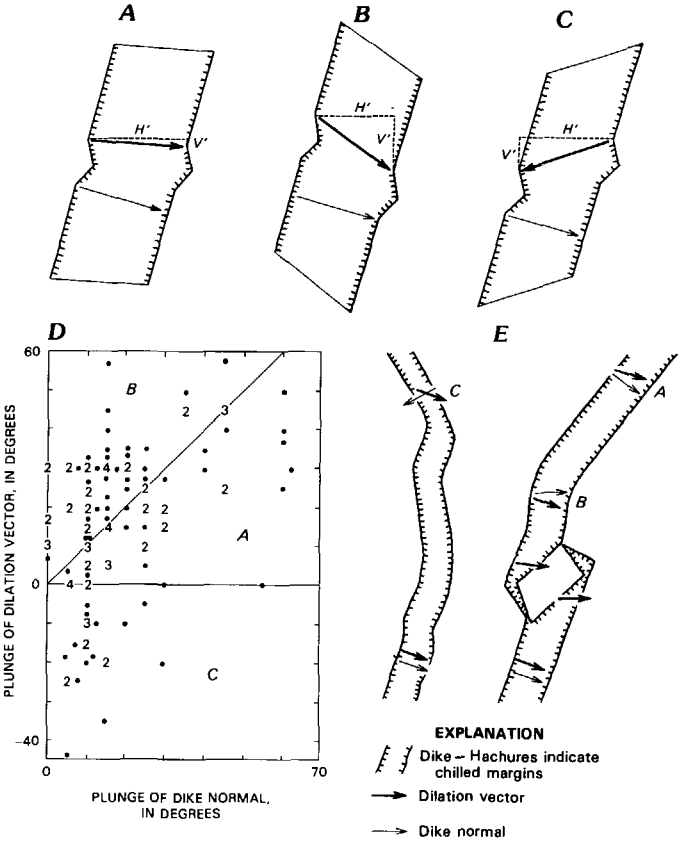

FIGURE 41.20.—Dilation relationships in vertical cross sections of dikes in Koolau dike complex. ***A***, Example of dike in which dilation vector plunges less steeply than dike normal. ***B***, Example of dike in which dilation vector plunges more steeply than dike normal. ***C***, Example of dike in which dilation vector plunges in the opposite direction to dike normal. ***D***, Plunge of dilation vector plotted against plunge of dike normal in sample of 126 dikes from localities 1, 3, 6, 7, and 23. For some dikes dilation vector (given a negative value on the plot) plunges in opposite direction from dike normal, giving a negative value of V'. Letters indicate regions exemplified by dikes in *A*, *B*, and C. Duplicate values from different measurememts shown by numbers. ***E***, Schematic profiles across two irregular dikes showing how departures of dilation vector from dike normal can be explained by variations in dip of dike. Note variation in plunge of dilation vector at dike sidestep where rotation of block has occurred.

eventual isostatic adjustment: it simply causes a lateral displacement of the country rock. Pollard and others (1983) have shown that injection of a vertical dike that fails to reach the surface does cause uplift, but the amount is very small.

Because the Koolau dikes are, in general, not vertical, their intrusion by simple dilational opening resulted not only in a horizontal dilation but also in a vertical displacement that uplifted the hanging wall relative to the footwall. The component of dilation in the horizontal plane (H) exceeds that in the vertical direction (V) in dikes dipping at more than 45°, but V approaches H as the dip approaches 45°.

It is generally tacitly assumed that dilational opening of a dike is along the direction normal to the dike. On many of the Koolau dikes it is possible to determine the direction of opening (called here the dilation vector, figure 41.20) by matching features on the two walls of the dike, and it is found that in general this direction does not coincide with the normal to the dike. The components of dilation in the horizontal and vertical directions, referred to as H' and V', respectively, are therefore different from H and V. Few studies have hitherto been made on this aspect of dikes; measurements were therefore made to investigate its significance. Outcrops in the Koolau complex are generally not favorable for determining the attitude of the dilation vector in three-dimensional space; measurements were therefore mostly made where dikes are exposed in vertical section. The data are summarized in figure 41.20*D*.

For about half of the measured dikes the dilation vector plunges more steeply than the dike normal, thereby increasing V' (fig. 41.20*B*). For a small proportion of dikes it plunges in the opposite direction from the dike normal (fig. 41.20C); V' is then negative, because intrusion of the dike resulted in a subsidence of the hanging wall relative to the footwall.

For each of the measured dikes, H' and V' were calculated, and their average values together with the two values of dike width (measured along the dike normal and along the dilation vector) are summarized in table 41.2.

TABLE 41.2.—*Widths and dilation components of dikes in the Koolau dike complex*

[All measurements in meters; H, H', horizontal components; V, V', vertical components. H, H', V, V' in per meter of dike width, N]

	Locality							
	1	3	6	7	24	30	Total	Average
Number of dikes	21	28	18	37	16	6	126	--
Measurements along dike normal								
Total dike width, N	8.08	19.76	11.27	23.20	11.58	4.90	78.79	0.625
Average dike width	.385	.706	.626	.627	.724	.817		
H	.891	.944	.899	.911	.941	.990	--	.925
V	.277	.277	.314	.335	.275	.134	--	.290
Measurements along dilation vector								
Total dike width	8.06	21.13	12.02	24.61	12.14	5.08	83.04	.659
Average dike width	.384	.755	.668	.665	.759	.847		
H'	.914	.970	.997	.921	.958	1.009	--	.954
V'	.208	.278	.226	.424	.274	.159	--	.298

It is seen that the average values of H' and V' differ only very slightly from the average values of H and V, and the small difference is probably not significant. This, together with the apparently random scatter of points seen in figure 41.20*D*, suggests that the dilation vector varies randomly about the dike normal. An explanation which appears adequately to explain this randomness is illustrated in figure 41.20*E* and is based on the observed irregularity of most dikes in the complex. It is postulated that on average the dilation vector of each dike coincides with the dike normal, but where a dike trend departs from its average trend the dike normal will depart from its dilation-vector direction.

The average values for H' and V' per meter of dike-normal width are 95.4 cm and 29.8 cm respectively. If the measured dikes are representative, injection of the dike complex having a total H of 3.3–4.8 km would involve a total relative uplift or subsidence (V) of 1–1.5 km, which is comparable to the height above sea level of the Koolau Volcano and is thus not insignificant. Note that axial uplift has accompanied some recent activity in the east rift zone of Kilauea Volcano (Swanson and others, 1976).

The question then arises whether intrusion of the dike complex has caused any significant net uplift or subsidence. The obvious test is by mapping a distinctive stratigraphic horizon right across the complex, but this does not seem feasible because of generally unfavorable topography in the Koolau Range combined with the relatively uniform lithology of the shield lava; the existence of a large collapse caldera in the area where exposures would otherwise be the most favorable is a further hindrance.

In many older, eroded volcanoes, the floor has been strongly updomed; a good example is the Carlingford Tertiary volcanic center in Ireland. Le Bas (1971) attributed the updoming at Carlingford to the intrusion of a swarm of cone-sheets that, like the Koolau dikes, have a significant V' vector. The evidence is, however, ambiguous, because it is also possible that the updoming was caused by an underlying granophyre pluton.

THE CALDERA OF THE KOOLAU VOLCANO

Hawaiian active volcanoes have a central caldera from which rift zones radiate like spokes, and the fact that the northwest and southwest dike complexes of the Koolau Volcano radiate from the Kailua area implies that the center of the volcano was located there. There is good evidence for the existence of a caldera in this general area.

Stearns and Vaksvik (1935) distinguished a Kailua Volcanic Series, occupying a circular area 5 km (3 mi) across centered on Kailua, which they interpreted to consist of lava infilling the caldera of the Koolau Volcano. Woollard (1951) and Strange and others (1965) found a major positive gravity anomaly centered on this caldera, and they attributed it to a concealed high-density intrusive pipe underlying the caldera. The postulated intrusion is not exposed. Adams and Furumoto (1965) and Furumoto and others (1965) explored the gravity high by seismic profiling and found high velocity (v_P=7.7 km/s) rocks at a depth of less than 2 km beneath the caldera.

Certain coarse breccias on the ridge between Kaneohe and Kailua Bays were interpreted by Stearns and Vaksvik (1935, p. 97) as a caldera infilling "a throat breccia such as exists in the bottom of Halemaumau built up chiefly as talus within a crater or caldera, and [which] appears to mark the main vent of the Koolau volcano." They found that the breccia crops out over nearly 2.5 km^2 (1 mi^2), reaches 160 m (520 ft) thick, and consists of angular to subangular fragments mostly under 50 cm in size of amygdaloidal basalt of diverse lithologies set in a fine green matrix. Macdonald and Abbott (1970), however, interpreted the breccia to consist probably of mudflows.

New evidence is now available, and in presenting it the distinction is made between evidence for the existence of a caldera, and evidence on the origin of the breccia.

EVIDENCE FOR A CALDERA

New evidence for the existence of a caldera comes from three roadcuts in Highway H3, in two of which (localities 1 and 3) older, amygdaloidal and altered dikes can be distinguished from younger, massive and fresh dikes. In the third (locality 2), which lies at about the same elevation, no older dikes can be identified, and the dike complex is similar in character and intensity to the younger complex at localities 1 and 3. The country rock at locality 2, moreover, consists of more massive lava.

The most plausible explanation for the differences is that the basalt of locality 2 is younger than the older dike swarm of localities 1 and 3; this is consistent with its being the infilling of a caldera postdating the older complex. A schematic view of these relationships is given in figure 41.21. The massive flows of locality 2 are suggestive of ponding in a depression. The lower dike intensity in locality 2 most likely indicates that the lava flows are younger than those exposed in contiguous areas, and less time was thus available for dikes to cut them. An alternative mechanism, namely downfaulting of these thick lava flows, can explain the lower dike intensity but not the absence of strongly amygdaloidal dikes.

Caldera infill can, thus, be identified here by three criteria:

1. It consists mainly of thick massive lava flows unlike the thin pahoehoe flow units that characterize most of the Koolau lava shield.
2. It has a significantly lower dike intensity than contiguous areas.
3. It may lack strongly amygdaloidal dikes like those of the earlier complex found in sites 1 and 3. This lack presumably indicates rapid infilling of the caldera.

Within a large area centered on Kailua the lava flows have dip directions and amounts that are anomalous and quite different from those of the shield lava; the dip, though variable, is on the whole centripetal and varies in amount from 15° to 30° or rarely as much as 60°, whereas the shield lavas dip at 5° to 15° outward from the shield axis. This large area of centripetal dip is interpreted to be a caldera of the downsagged type (Walker, 1984). No comparable feature has been recognized on the active Hawaiian volcanoes, but it could be concealed beneath young lava.

Important evidence bearing on the downsag caldera comes from the Kapaa Quarry, where the country rock consists of thin pahoehoe lava flows that resemble shield building lava. These flows dip in the contrary direction to the shield lava and at an angle (30° to 60°) that is excessive for shield lava. Some flows moreover contain pipe amygdules, which, it has recently been demonstrated, are good paleoslope indicators. Their presence show that the lava was deposited on a slope of less than 4°. The Kapaa quarry lava must therefore have been tilted at least 30°–60° after being deposited. The amount of subsidence by down-sagging can be estimated to have been about 1 km.

The dike complex that cuts the lava of Kapaa Quarry consists of the usual two complementary sets having opposed dips of 65°–85° (fig. 41.23), and this implies that these dikes were injected after the lava had been more or less fully tilted. The dike complex here built up to its full intensity of more than 50 percent after a major episode of subsidence had occurred. Note that where the country rock has the steepest dip, at the northeast end of the northeast quarry, several intrusions follow the stratification of the lavas. Technically these intrusions are sills, but in relation to the volcanic edifice they are dikes.

The approximate extent of the downsag caldera as determined from dip measurements is shown on figure 41.22; it is greater than that given by the other criteria and is similar to that mapped by Stearns and Vaksvik (1935) as constituting the caldera fill of their Kailua Volcanic Series.

The Kailua caldera as delineated by these several criteria varies greatly in intensity of dike injection, from 1 percent to 50 percent or more. Some variation would of course be anticipated in different parts of the same caldera transected by one or more rift zones, but a more plausible explanation is that two or more calderas of different ages occur, the older being cut by more numerous dikes than the younger. This multiple origin is evidenced by the dike relationships in the Highway H3 roadcuts and is consistent with the fact that the Kailua caldera measures at least 13 by 10 km, which is far greater than the diameter of calderas on Kilauea and Mauna Loa (2.5–4.5 km).

The very low intensity of the dike complex in the inner part of Kailua caldera implies that subsidence there was a very fast or late event relative to formation of the dike complex and considerably exceeded 1 km. Most likely this area of low dike intensity is a conventional caldera nested within a much broader area dominated by downsagging.

NATURE AND ORIGIN OF THE BRECCIAS

The coarse breccias that make up much of the ridge between Kaneohoe and Kailua Bays and that are well exposed at localities 1, 3, 4, 5, and 10 have long been enigmatic. Important evidence relating to their origin is that much of the breccia consists of dike fragments (fig. 41.24). This leads to a new interpretation, namely that the breccias consist of the older part of the dike complex (together with country-rock basalt screens), which has suffered an extensive and pervasive brecciation.

The evidence for brecciation of a dike complex seems unequivocal because all stages in disruption of dikes are seen:

1. The dike rock is pervasively brecciated but little relative movement of the fragments has occurred: sufficient to generate angular spaces (infilled with secondary minerals) between fragments but not sufficient to break the continuity of the dike, which is contained by chilled margins.
2. The dike as a whole is still continuous, but it is thoroughly brecciated, and relative movement of fragments has caused it to have a jagged shape.
3. The dike is thoroughly brecciated, and relative movement and intermixture of dike fragments with country rock basalt has occurred, but dike fragments remain concentrated in a relatively narrow zone within the breccia, showing that in-place brecciation of a dike has occurred.
4. The dike is totally disrupted, and all continuity is lost; abundant breccia fragments that possess a chilled edge on one side are all that attest to the derivation of much of the breccia from dikes.

All indications are that the breccia formed by a pervasive fragmentation in place of country-rock lava cut by dikes. The degree of brecciation varied apparently in a rather haphazard way, leaving areas, several meters to tens of meters across, of intact lava and dikes enveloped in breccia. These areas pass upwards and laterally into breccia and generally lack any discrete boundaries.

The measured length of chilled dike margin exposed at locality

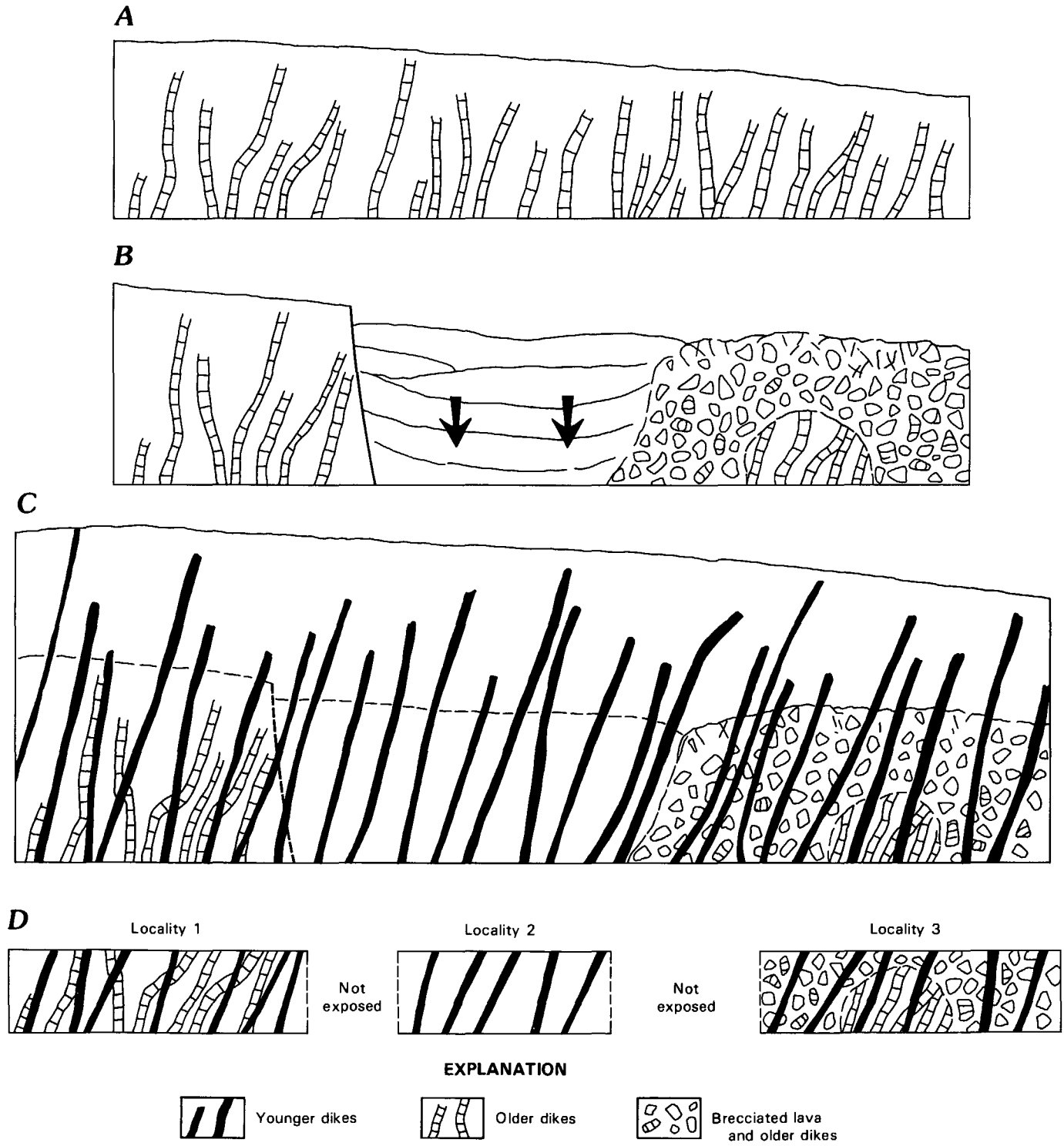

FIGURE 41.21.—Inferred origin of dike relations at localities 1–3. ***A***, Inital intrusion of older dikes. ***B***, Subsequent caldera subsidence (arrows), pervasive brecciation of part of lava and older dikes, and infilling of caldera by thick massive flows. ***C***, Later intrusion of younger dikes. ***D***, Dike relations as presently seen at localities 1–3.

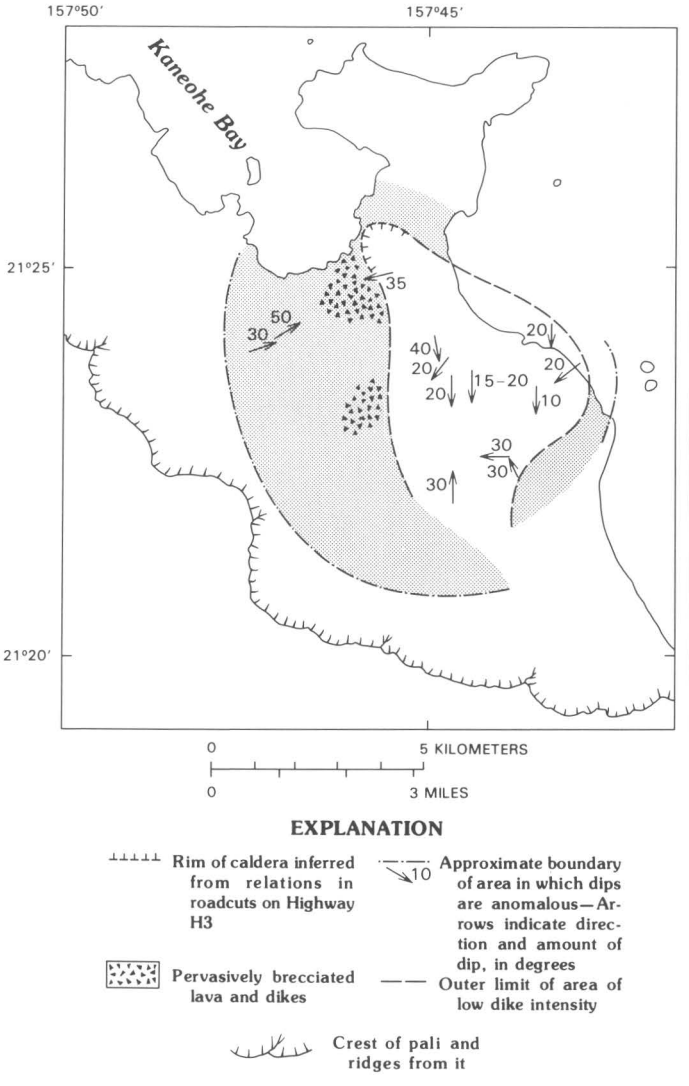

FIGURE 41.22.—Evidence indicating position and extent of caldera complex (shaded) in Kailua area. Area of low dike intensity shown in more detail in figure 41.3; relations in roadcuts on Highway H3 shown in figure 41.21.

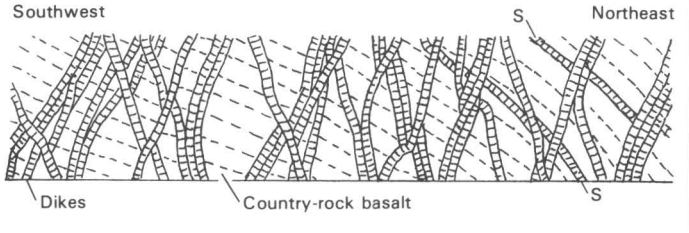

FIGURE 41.23.—Schematic relations at Kapaa Quarry. Strongly tilted lava flows are cut by dike complex in which dikes form two sets; opposing dips of sets are equal in amount, indicating that complex was intruded after lava had been fully tilted. Some dikes (S) cutting steeply inclined lava are conformable and technically sills, but they are better identified as inclined dikes.

3 varies from 0–2.6 m per square meter of rock surface, and the average of 20 measurements is 1.2 m. Where the older dike complex is intact at the same locality and has a local intensity of 100 percent in dike clusters, the measured total length of chilled margin per square meter averages 2.9 m. This is consistent with derivation of the breccia from a moderately intense (about 40 percent) older dike complex cutting lava.

The abundance of dike fragments would be opposed to the idea that the breccia is a kind of talus that accumulated in a crater or caldera: exposures at a level sufficiently high to generate talus on a Hawaiian volcano contain very few dikes. Casadevall and Dzurisin (chapter 14) counted only 18 dikes on the 6.5-km-long western and northern wall of Kilauea caldera, for example. The absence of stratification in the breccia and the way in which dikes show various degrees of in-place brecciation are opposed to an epigene formation for the breccia.

An alternative breccia-forming mechanism is hyaloclastic brecciation of dikes injected into rocks saturated by ground water. There are many places at localities 3–7 and 28 where green rims, presumed to be propylitized glass, are unusually conspicuous and thick, and some hyaloclastic fragmentation has almost certainly occurred. It seems, however, to have been on a small scale. Another alternative mechanism is auto-brecciation of dike injected into dike. What seem to be unequivocal examples of this are found among earlier dikes on the Mokulua Islands and in outcrops west of Waikane, but the brecciation is very localized.

The best explanation is that the bulk of the breccia is of tectonic origin and developed in place at or near the margin of a caldera, where the strain, instead of being confined to discrete fault planes, was distributed over a broad zone. As here envisaged, the stress acted on a pile of lava with a great many planes of weakness of various kinds, cut by a swarm of highly irregular dikes that had been injected into water-saturated rocks and hence were strongly jointed. The stress therefore caused a pervasive brecciation.

Formation of the breccia at localities 3–5 was followed by a metamorphic event that produced a widespread propylitic alteration accompanied by the deposition of laumontite, epidote, calcite and other secondary minerals (Fujishima and Fan, 1977). This event effectively lithified the breccia so that to the younger dikes it behaved as a rigid rock.

ORIGIN OF CALDERAS OF BASALTIC VOLCANOES

Many large basaltic shield volcanoes possess a caldera. Fine examples occur on oceanic islands such as Grand Comore, the Galapagos, Hawaii, Mauritius, and Reunion; other examples occur in continental-margin settings and include Masaya (Nicaragua) and Osima (Japan). The calderas of basaltic volcanoes differ in six important respects from calderas of volcanoes that have significant amounts of felsic or silicic products:

1. They tend to develop by incremental subsidence events and not consequent on a single major eruption (whether explosive or effusive).
2. Subsidence events are sometimes but not always correlated with eruptive activity.

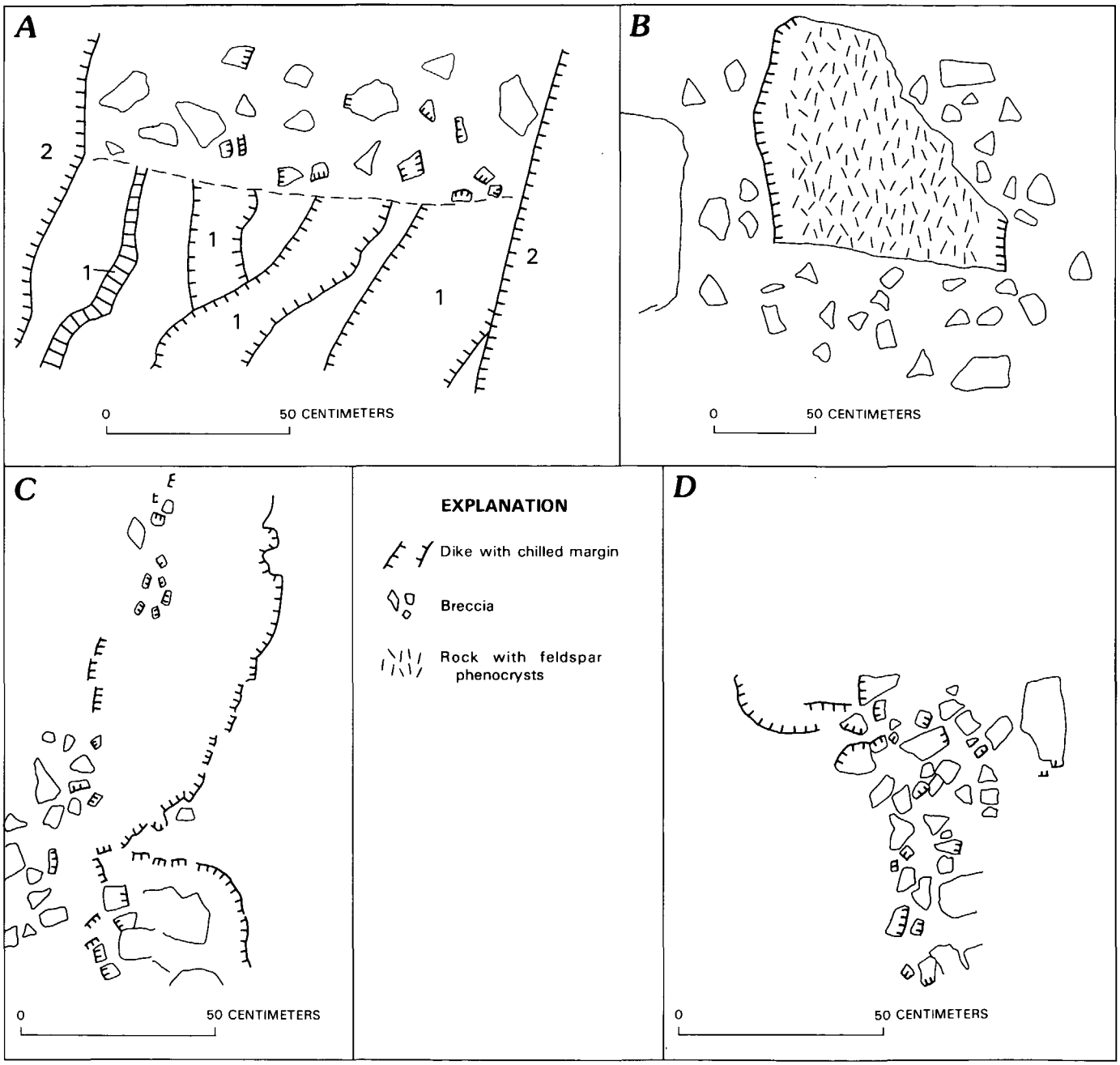

FIGURE 41.24.—Relations shown by breccia at locality 3. ***A***, Group of older dikes (1) terminates abruptly against breccia. Some fragments in breccia originate from dikes and have chilled margin on one side. Younger dikes (2) intruded after breccia had been lithified. ***B***, Intact but isolated fragment of richly feldspar-porphyritic dike. ***C***, Dike with one margin fairly complete but other brecciated and the fragments somewhat dispersed. ***D***, Breccia containing dispersed dike fragments characterized by chilled margins on one side.

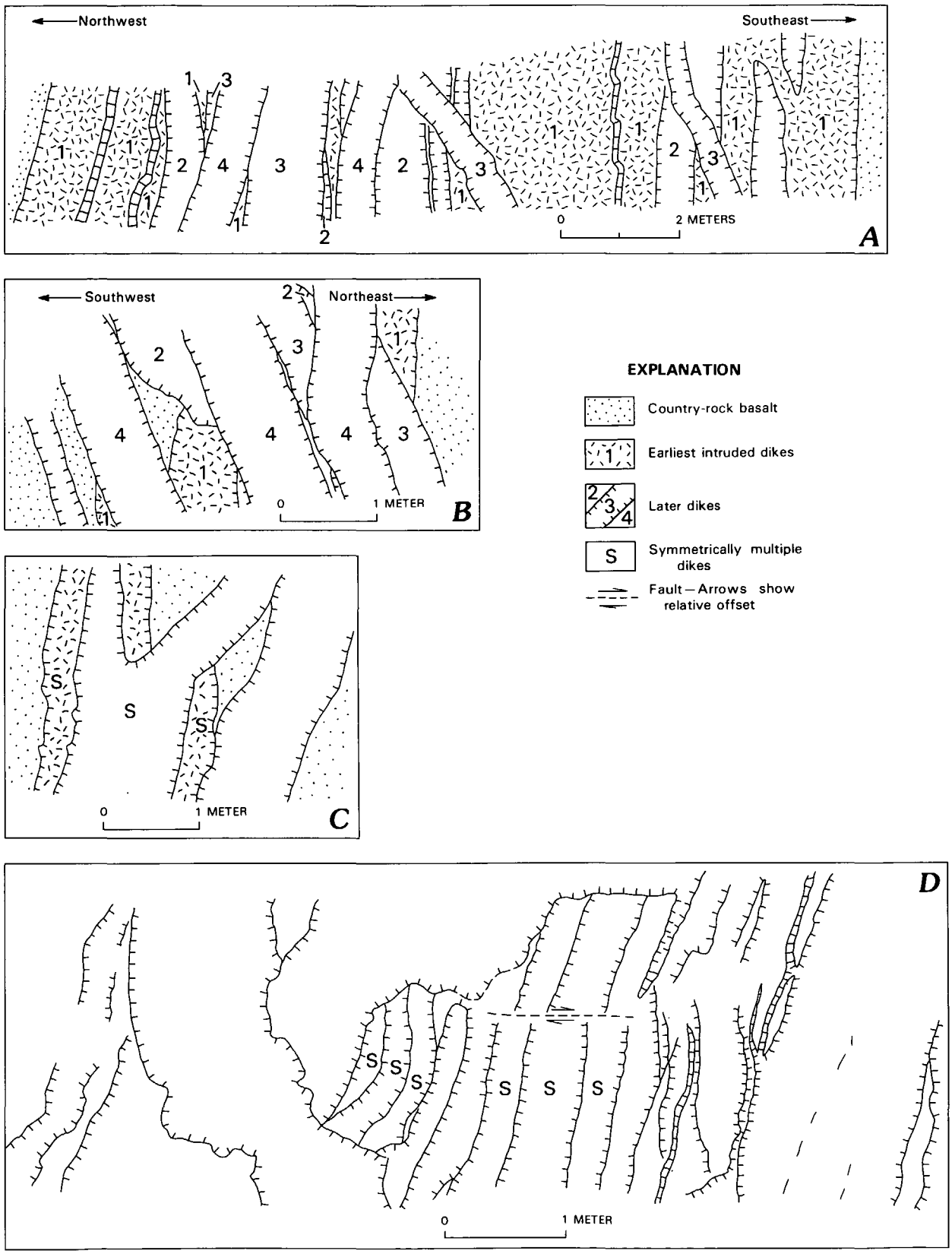

FIGURE 41.25.—Examples of multiple dike clusters. ***A***, Cluster of 14 dikes totaling 13.6 m thick at locality 23. Oldest dike is unusually wide (about 6.4 m) and is split into many screens. Country-rock screen at northwest end of cluster is 16 cm wide; that at southeast end is 330 cm wide. ***B***, Dikes intersecting at acute angle forming braided pattern (locality 5). ***C***, Symmetrically multiple dike (locality 3). ***D***, Part of a cluster of more than 14 dikes (locality 1). Four of the dikes are symmetrically multiple pairs.

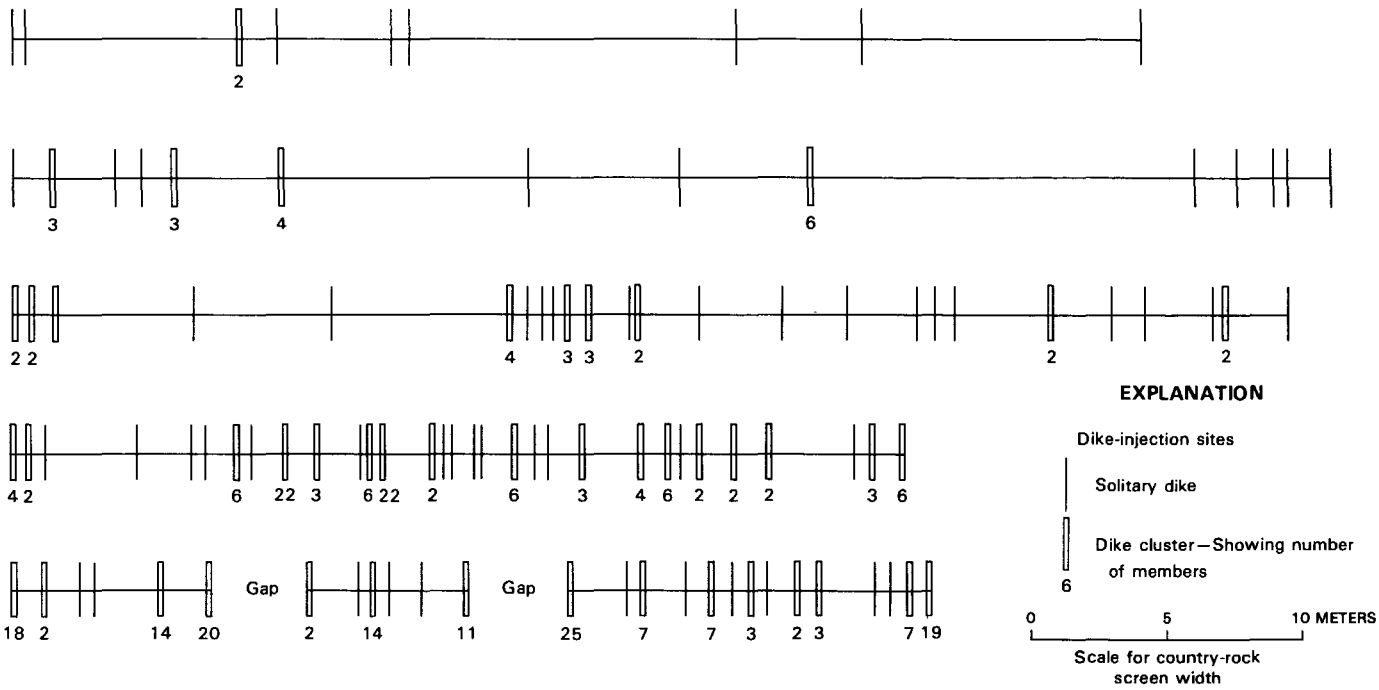

FIGURE 41.26.—Distribution pattern of dikes in representative exposures of Koolau complex (localities 47, 5, 2, 20, and 41, from top down), showing how number of dike-injection sites and multiple dikes vary. As intensity of dike complex increases, so dike spacing decreases and number of dikes in multiple clusters increases. Widths refer only to country-rock screens; dike widths are ignored.

3. They tend to have a complex history of alternating subsidence and partial infilling by lava flows, and significant changes in topography may occur on the more active volcanoes in a period as short as a century. These changes are well documented for Kilauea and Mauna Loa by Macdonald and Abbott (1970).
4. They tend to have a number of more or less concentric fractures on which downdropping has occurred instead of a single bounding fault, and the displacement on these faults tends to increase inwards; Kilauea is a good example. They also are often associated with or contain pit craters.
5. They coincide approximately with positive Bouguer gravity anomalies, in contrast with the negative anomalies shown by calderas associated with felsic and silicic volcanism.
6. They are transected by one or more rift zones along which activity is concentrated; in deeply dissected examples they are seen to be in line with, or are cut by, intense swarms or complexes of dikes and associated intrusions.

I now propose a new concept for the origin of basaltic calderas: that their subsidence is a consequence of the high density of the intrusive complex combined with the reduced strength of the lithosphere above a hot spot, which makes localized downward creep possible. Macdonald (1965) considered but rejected the idea that the calderas were caused by the weight of intrusions because he did not consider the possibility of creep occurring.

The pile of basaltic lava that constitutes much of the edifice of a Hawaiian volcano is estimated to have an overall density of about 2.35 g/cm^3 (Kinoshita and others, 1963), whereas a dike complex having >50 percent intensity is likely to be at least 0.35 g/cm^3 denser. Large gabbroic and ultramafic intrusions are likely to underlie the caldera and may be as much as 1.0 g/cm^3 denser than the lavas. A complex of dikes and associated large intrusions therefore represents a great localized and unevenly distributed load, the cause of the large Bouguer anomalies of the Koolau Volcano (Strange and others, 1965) and the active volcanoes on Hawaii (Kinoshita and others, 1963).

The very low dike intensity in the central part of the Kailua caldera is interpreted to indicate that the subsidence rate there exceeded the buildup rate of the dike complex, whereas in marginal parts of the caldera the reverse applied. This is important evidence in support of the postulated caldera-forming mechanism, in which the subsidence rate should be greatest at the locus of magmatic activity.

GROWTH MECHANISMS OF THE KOOLAU DIKE COMPLEX

PREFERENTIAL DIKE PATHWAYS

A large proportion of dikes in the Koolau complex are multiple and occur in parallel clusters, in which most commonly the members lie alongside and in chilled contact with one another without any intervening country-rock screen (fig. 41.25).

These dike clusters indicate that dike margins were structural planes of weakness that offered very favorable pathways guiding later intrusions. This is underscored by the fact that when an intrusion trends obliquely to an earlier dike it commonly changes course and follows the margin of the earlier dike for a space before resuming its oblique trend. The ease with which a dike breaks apart

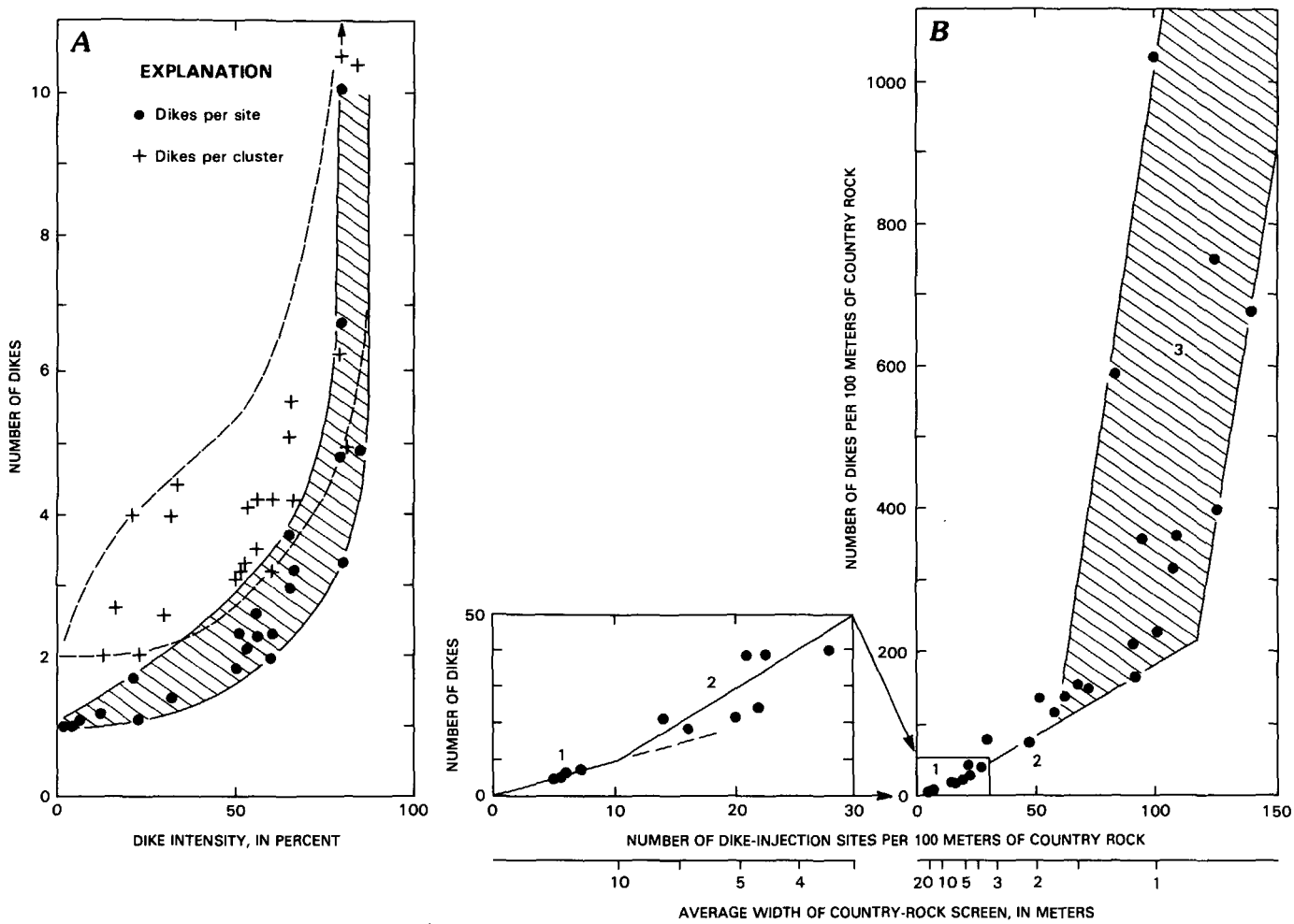

FIGURE 41.27.—Diagrams illustrating build-up of dike complex. ***A***, Plot of number of dikes per site and per cluster against dike intensity of complex. As intensity increases, average numbers of dikes per site and per cluster increase. ***B***, Plot of number of dikes and dike-injection sites per 100 m of country rock. In segment 1, the numbers are comparable. In segment 2, number of dikes increases twice as fast as number of sites, showing that half the dikes are forming multiple clusters. In segment 3, number of dikes increases much faster than number of sites because most of dikes are entering multiple clusters.

from the country rock or from an adjacent dike is clearly evident in any roadcut.

Data on dike spacings from a number of localities covering a wide range of dike intensities (fig. 41.26) form a basis from which to assess the manner in which the dike complex developed. It is assumed that these outcrops record stages in a progressive process, halted at each location by the cessation there of further dike injections. A dike-injection site is defined as a site in which either a solitary dike or a multiple dike cluster occurs.

Two features of the relationships shown in figure 41.26 are portrayed in figure 41.27: the average number of dikes per intrusion site, and per multiple cluster, increases at an increasing rate as the dike intensity increases (fig. 41.27*A*); and the number of dikes rises increasingly rapidly as the number of dike-injection sites per 100 m of country rock increases (or the average country-rock screen width decreases) (fig. 41.27*B*).

The dike-injection pattern has been reconstructed from figure 41.27*B* as follows. The first dikes to be injected all followed independent pathways through the country-rock basalt and subdivided the basalt into screens. In this early stage the number of dikes per unit width of country rock equaled the number of dike-intrusion sites (segment 1 on figure 41.27*B*).

When the average screen width decreased to less than 10 m, a proportion of the dikes began to follow the margins of previously intruded dikes instead of new pathways through the country rock, and the first dike clusters were thus formed.

As the dike-swarm intensity increased, and the average screen width decreased from 10 m to less than 2 m, roughly the same number of dikes followed margins of previously intruded dikes as followed new pathways in the basalt; the total number of dikes then

increased at about twice the rate that the number of dike-injection sites increased (segment 2 of figure 41.27*B*). Because of the strong tendency for dikes to intrude into existing clusters, where planes of weakness were concentrated, the average number of dikes per cluster increased faster than the proportion of clusters to solitary dikes.

With further dike injection, the proportion of dikes following margins of preexisting dikes became very much greater than that following new pathways through the lava (segment 3 of figure 41.27*B*). It is thought that at this stage the average country-rock screen width tended to become stabilized at about 1 m. The screens were pushed farther and farther apart as more dikes were injected into the clusters between them until, in the most intense parts of the complex, narrow screens occur at intervals of tens of meters.

SYMMETRICALLY MULTIPLE DIKES

A proportion of the dikes in multiple clusters were intruded inside earlier dikes; an example is shown in figure 41.25*A* in which a broad dike is cut by 13 subparallel dikes situated at various distances from its margins. This particular example is unusual because the first dike fused the country rock, to which it is firmly welded, and later dikes hence showed no tendency to follow these margins.

A few dikes are symmetrically multiple, with the youngest intrusion in the middle and the halves of earlier narrow intrusions that have been split up the middle symmetrically disposed on either side (fig. 41.25*C*, *D*). The best examples are seen on the Mokulua Islands, where as many as four successively injected members occur in the same narrow multiple dike. Each member has chilled against the earlier member.

Solitary dikes of the Koolau complex in general lack any visible median parting or plane of weakness such as could direct a later intruded dike. This raises the possibility that the middle of a dike may be a preferred pathway for thermal reasons. The center of a cooling dike remains fluid longest and after solidification remains hot longest. Even if solid, the still-hot center remains mechanically weak. Thus Ryan and Sammis (1981) demonstrated that the value of Young's modulus at 700 °C is 10 percent less than it is at 25 °C.

HOW MANY DIKES?

An interesting question is the total number of dikes in the Koolau complex. Exposures are too incomplete to permit this to be determined by counting, but they are adequate for a good estimate to be made.

In a transect of the complex just south of Kaneohe Bay the exposed intense part is 6 km wide (fig. 41.3), and the intensity over this width varies from 30 to 63 percent. If the average intensity is 50 percent, dikes would total 3.0 km. In marginal zones on the southwest side and presumably also on the northeast side of the complex, the dike intensity drops from 40 percent to 5 percent in about 1 km. At an average intensity of 15 percent, these two strips would contribute 0.3 km, bringing the total dike width to 3.3 km.

The average width of dikes at different localities in this transect varies from 55 to 75 cm (fig. 41.9). If we take 65 cm as an overall average, this yields a total of about 5,100 dikes in 3.3 km of dike width. This estimate is probably a minimum: if the complex possesses bilateral symmetry about the Koolau lava-shield axis shown on figure 41.1, the full width of the intense part of the complex would have been about 9 km, increasing the total width of dikes to 4.8 km and the number of dikes to 7,400.

Consider now the number of dikes in a transect of the complex at or near Waikane. The intense part of the complex there is 3.5 km wide and has an average intensity of about 45 percent, giving 1.6 km total width of dikes. To this may be added 0.8 km for the low-intensity strips 2 km wide on either side, giving a total dike width of 2.4 km. The average width of dikes at different localities in this transect varies from 115 to 175 cm. If we take 150 cm as an overall average, this yields a total of 1,600 dikes.

The number of dikes in any given transect cannot be equated with the total number of dikes in the complex; estimation of the latter requires a knowledge of the length-width ratio of the dikes, on which no direct information is available. Gudmundsson (1983) assumed a length-width ratio of 10^2–10^3 in eastern Iceland. If we apply this on Oahu, dikes 50 cm wide would have a length of 50–500 m. This is unrealistically short; it is more than an order of magnitude less than the known length of eruptive fissures on Kilauea and Mauna Loa, and seems incompatible with the origin of the dikes by lateral movement outwards from the volcano center.

If it is assumed that the number of dikes decreases linearly from 7,400 in a transect along the south of Kaneohe Bay to 1,600 at Waikane and to zero at the northwest tip of the Koolau Volcano, and that the average dike length is 5 km, then the dikes would number about 30,000.

DIKES IN THE BUILDUP OF KOOLAU VOLCANO

Koolau Volcano is deeply dissected; the highest point on the Koolau Range is 960 m (3,150 ft) above sea level, and the original shield crest, extrapolated from the generalized contours of figure 41.1 would have been about 1,100 m above present sea level (actual elevation must have been higher, because the edifice has subsided since then) without allowing for the Kailua caldera. Characteristics of the older dikes such as at locality 3 indicate intrusion at a shallow depth, possibly 100 m or less, at an early stage of shield growth; the younger dikes seen in the same outcrop could have been intruded at a depth of 1,000 m or more.

No information exists on what proportion of dikes fed lava flows. No example is known on Oahu of a lava connected with its feeder dike. Recent experience on Kilauea indicates that dike-injection events without lava eruption are more frequent than fissure eruptions (Dzurisin and others, 1984), and even among the latter some (for example, the two caldera eruptions in 1982) erupt only a negligibly small amount of lava. Most of the Koolau dikes are very narrow, and it is likely that few erupted much lava.

The volume ratio of dikes to lava in subaerial parts of the Koolau Volcano is readily estimated after making two assumptions, namely, that the original volcano possessed a bilateral symmetry about its axis (fig. 41.1) and that the intensity of the dike complex decreases linearly upwards. This second assumption was docu-

mented for eastern Iceland by Walker (1974), but has not been demonstrated in the Koolau Range because of the unfavorable topography. All that is known is that the dike intensity in Kapaa Quarry does not measurably decrease through 95 m of elevation increase.

The reconstructed form of the Koolau Volcano and the distribution of dikes in it are shown in a transverse section in figure 41.28. The maximum total width of dikes in a transect is 4.8 km; the derived total dike cross-sectional area is thus about 2.4 km^2. The subaerial part of the volcano on the same transect has a cross-sectional area of 13 km^2; dikes therefore compose 15–20 percent of the subaerial volume. Intrusions are likely to constitute an increasing proportion at deeper levels.

Mention was made earlier of several localities where dikes of different ages intersect orthogonally; this is not readily explained if dike trends are determined primarily by the overall form of the volcanic edifice. The dike complex has a total dike width of 4.8 km near the caldera, decreasing to zero very rapidly toward the southeast and less rapidly in the opposite direction. These variations in width caused local stresses concentrated near the caldera, where the rate of change was greatest. Such local stresses may have been sufficient to cause the injection of the transverse dikes.

COMPARISON OF KOOLAU VOLCANO WITH KILAUEA

The active Hawaiian volcano that is most closely similar to Koolau appears to be Kilauea. Both are very strongly elongate structures having a single dominant rift zone intersecting the caldera, and they are comparable in size. The subaerial part of Kilauea is 30 percent higher and 43 percent longer. The bathymetric chart of Oahu shows a marked increase in slope at 500 m off the north tip of Koolau; if this marks the earlier shoreline then Koolau would have been 77 km long and 1,600 m high before subsidence to its present level. These dimensions are almost identical to those of subaerial Kilauea.

Both volcanoes are buttressed on one side by an older volcanic structure, though the Waianae buttress of Koolau is much smaller than the Mauna Loa buttress of Kilauea. Kilauea shows strong seaward creep on the unbuttressed side. Much of the unbuttressed side of the Koolau Volcano has already collapsed, and the predominantly northeast dip of dikes in part of the Koolau complex may be an early manifestation of this process.

The similarity between Koolau and Kilauea extends also to some of the less immediately obvious features, notably the asymmetry of each volcano along its length (fig. 41.29); their calderas do not occupy a central position, because one rift zone is longer and has been built up higher and wider than the other.

The caldera is assumed to mark the effective center of the volcano, below which magma rises from its deep source and then moves to intrusive or eruptive sites. The plunge of flow lineation on the dikes, however, appears to point to two main magma sources in the Koolau Volcano, one below Kailua caldera and the other below Kaneohe Bay. Possibly the bay is occupied by another caldera or by an extension of the Kailua caldera. Alternatively, the position of Kaneohe Bay is analogous with the setting of Mauna Ulu (site of the 1969–74 eruption) on Kilauea. Some of the Mauna Ulu magma may have come up a separate pathway, which branched off from the main Kilauea one (Ryan and others, 1981), and the Kaneohe Bay center may be a similar branch.

The curvature of the Koolau dike complex west of Kailua is reminiscent of the curvature of the Chain of Craters segment of Kilauea's east rift zone. Surface ground fissures along the Chain of Craters form an echelon group in which the individual fissures preserve the main trend of the east rift zone, and it can only be surmised whether these ground fissures overlie a swarm of dikes paralleling the Chain of Craters (as was proposed by Duffield, 1975; some kind of conduit by which lateral magma movement occurs must unquestionably be present along the chain).

In summary, there are such close similarities between Koolau and Kilauea Volcanoes that the main dike complex in the one may be accepted as a close and valid analog to the subsurface region of the east rift zone in the other.

A MODEL FOR THE FORMATION OF THE KOOLAU DIKE COMPLEX

In a number of respects the Koolau dike complex is unique among described examples of the dike swarms associated with volcanic centers. The nondivergence of the dikes northwestward from the Kailua center shown on figure 41.5 contrasts with the radial or fascicular structure usually found, in which there is at least some degree of divergence away from the volcanic center. The Koolau complex is unusually coherent and the intensity rises inward from less than 5 percent to 50 percent or more in a remarkably short distance and then tends to be fairly uniform at 50–65 percent across its width, unlike the Gaussian intensity distribution found across most described dike swarms. The Koolau complex also reaches a far higher intensity (maximum 85 percent) than most swarms, which peak at 25 percent or less.

A model for the formation of the Koolau complex that explains these unique features and takes account also of the implications of recent magmatic activity on Kilauea Volcano (Walker, 1986) considers that three effects constrain the intrusion of dikes in the complex. One is the edifice effect, which tends to localize dike injection parallel with the long axis of the volcano. A second is the existence of plentiful pathways along margins of existing dikes in the complex. The third is a hydrostatic effect by which magma is able to reach a high crustal level in the relatively high-density environment of the dike complex.

Consider the third effect more closely. The generally high fluidity of Hawaiian tholeiitic magma gives it great freedom to move through the disjointed lava shields, and in these free conditions it comes to move into and become localized in those regions of the volcano in which it is gravitationally most stable. These regions are the marginal zones of the dike complexes, in which the average density of the rocks—a mix of lava flows and 5–50 percent of dikes—is closely comparable with that of weakly vesicular tholeiitic magma (fig. 41.28*B*).

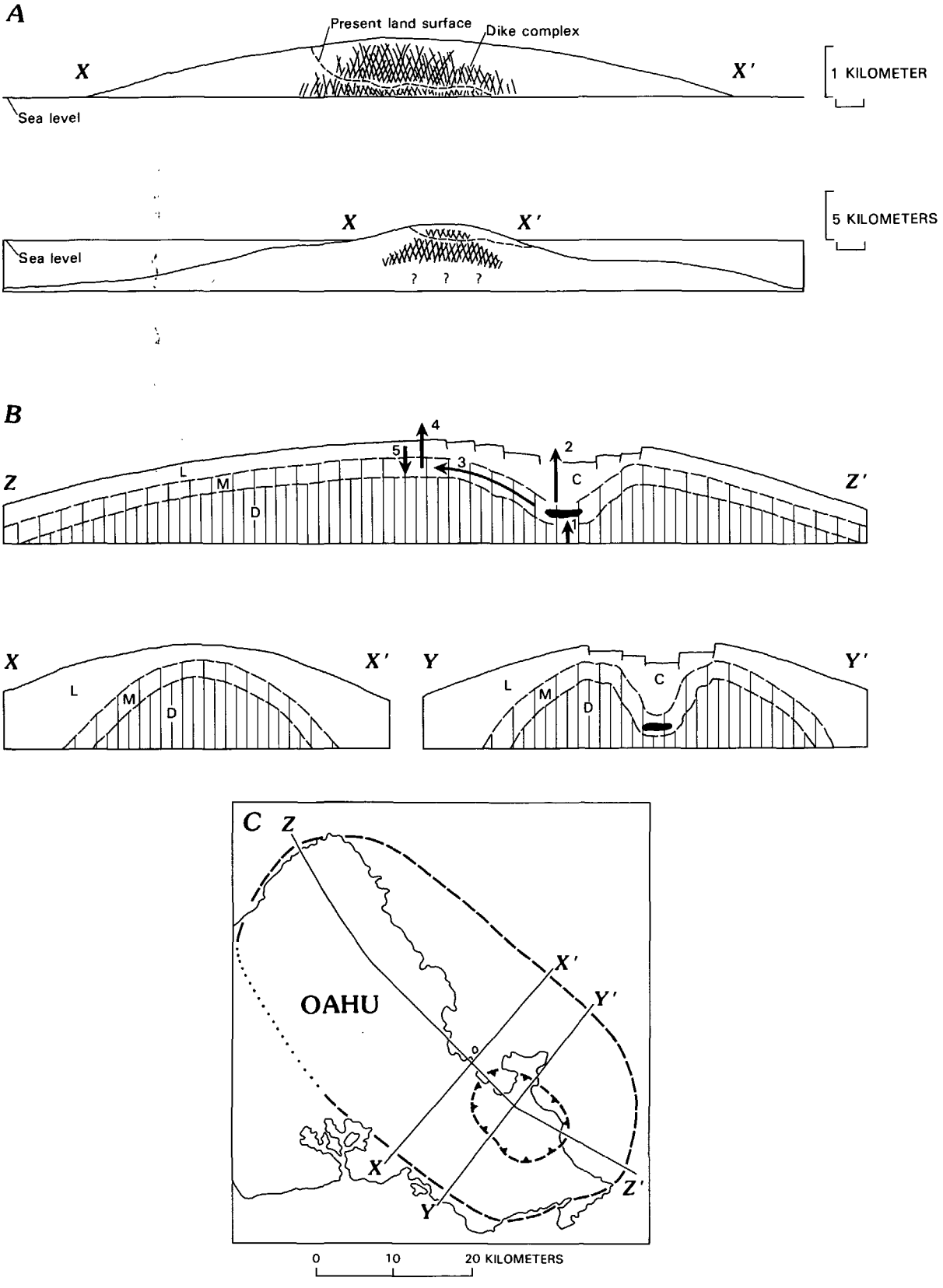
A
Present land surface
Dike complex
X
X'
Sea level
1 KILOMETER
X
X'
Sea level
? ? ?
5 KILOMETERS
B
Z
Z'
L
M
D
C
1
2
3
4
5
X
X'
L
M
D
Y
Y'
L
M
D
C
C
Z
X'
Y'
OAHU
X
Y
Z'
0
10
20 KILOMETERS

It can be surmised that when part of a dike complex has built up to 50–65 percent intensity it becomes denser on average than tholeiitic magma so that magma tends to avoid it; hence an intensity of significantly more than 65 percent is attained only locally.

Because of increased vesiculation, the magma density may then decrease so as to fall below that of the lava, and when this happens the magma rises to the surface. This concept explains well the activity of Kilauea Volcano in recent years, in which dike injection events into the rift zone without lava effusion have occurred repeatedly and the eruptions have been mostly short events characterized by vigorous fire-fountaining. The geyserlike regularity of eruptive phases 4–46 in the 1983–6 activity of Kilauea is also strongly suggestive of a gas-accumulation control. Moreover it has often been observed that after magma has reached the surface and degassed, much of the degassed lava flows back down into fissures and presumably returns to the gravitationally stable zone.

SUMMARY AND CONCLUSIONS

When I began to study the Koolau dike complex I did not anticipate that it would prove to be in any way unusual, yet a wide range of unexpected features has emerged. Earlier workers were handicapped by a general paucity of good exposures, and the present study was feasible because of many new outcrops generated in the past 10 years. Some unexpected features were revealed only because of the quantitative nature of the present study, made possible by these new outcrops.

The Koolau dike complex is much more intense, and contains five to ten times more dikes, than was previously realized. Indeed, it is the most intense documented example of a dike swarm of volcanic-edifice type, and its 4.8 km of total dike width compares with the 1–2 km of total dike width for Tertiary dike swarms in eastern Iceland (Walker, 1974; Gibson and others, 1966), Scotland (Speight and others, 1982), and the Columbia River basalts (Taubeneck, 1970). If cone sheets are included, then some of the intrusive complexes in Scotland (for example, Mull; Bailey and others, 1924) will have an intensity closely comparable with Koolau.

One of the most intriguing features of the Koolau complex is the nonverticality of the dikes, which form two sets having opposing dips of 65° to 85°. These are interpreted to be complementary sets, closely analogous with normal faults in an extensional environment, and are thought to have resulted when the maximum principal stress direction acted vertically and was much greater in magnitude than the principal stresses acting in the horizontal plane. The nonverticality is a consequence of dike injection into a high-standing volcanic edifice. The dikes tend to dip out from the axis of the Koolau Volcano, but there is a large anomalous area in which the dikes predominantly dip in a contrary direction, toward the northeast. This seems to reflect a tendency, manifested very early in the history of the complex, toward seaward creep in that area; this creep later culminated in the major collapse of that same part of the volcano.

The Koolau complex displays many of the features of a sheeted dike complex, although it occurs in an intraplate setting unlike the sheeted complexes of the ophiolite suite. The sheeted structure resulted because the Koolau dikes showed a pronounced tendency to intrude along the margins of earlier dikes. As the dike-complex intensity increased, so an ever-increasing proportion of dikes utilized such planes, leading to the development of multiple dike clusters tens of meters wide containing tens of members. Some dikes followed a pathway along the middle of an earlier dike, which, when still hot, was a favored site for thermal reasons.

Many dikes possess a flow lineation on their margins, and the measured attitudes point to two main centers, about 5 km apart and situated at 2–3 km below present sea level, from which the dikes are presumed to have risen obliquely into higher parts of the edifice.

Because of their nonverticality, injection of the Koolau dikes involved a significant vertical component of dilation totaling more than 1,000 m. The contribution of this vertical component to the buildup of the Koolau shield is not known; we cannot distinguish absolute uplift of a dike hanging wall from subsidence of a dike footwall.

The Koolau dike complex is much denser than the lava pile and is so intense and concentrated as to represent a great localized load, reflected in the high positive Bouguer anomaly. The unequal bulk-density distribution in the volcano is considered to have had two consequences: one was to channel magma batches into a zone, in marginal parts of the dike complex, in which the magma was gravitationally most stable; the other was to tend to cause differential subsidence where the dike complex was widest and heaviest.

The preferential channeling of magma into a zone at the margins of the dike complex, where the magma density matches the bulk-rock density, is the key mechanism of a proposed model which explains buildup of the dike complex into a remarkably coherent structure having an intensity plateau at a level of 50–65 percent. This mechanism also explains the strong propensity of Hawaiian tholeiitic magma to remain underground, evidenced clearly by the record of the most recent magmatic activity; even when, because of vesiculation, magma does reach the surface, it may then promptly plunge underground again when it loses its gas bubbles.

The tendency for differential subsidence can account for the calderas of Hawaiian volcanoes: I propose that their subsidence is

FIGURE 41.28.—Relation of dike complex to bulk-density zonation and magma pathways of Hawaiian volcanoes. ***A***, Profiles across Koolau lava-shield volcano on two different scales, showing setting of dike complex. ***B***, Schematic profiles across a Hawaiian volcano such as Koolau, showing bulk-density zonation and typical magma pathways. L, lava shield cut by only a few scattered dikes, less dense than nonvesicular tholeiitic magma; M, marginal zone of dike complex, intensity 5–50 percent, into which nonvesicular or weakly vesicular tholeiitic magma tends to be channeled because of matching densities; D, dike complex, intensity >50 percent, denser than nonvesicular or weakly vesicular tholeiitic magma; C, caldera complex; calderas of varying sizes and ages where density zones are strongly depressed; 1, magma residing in a chamber in zone M where it is lowest (in caldera complex). This is gravitationally most stable situation for nonvesicular magma in entire edifice; 2, rapid vesiculation carries a magma batch to the surface, producing caldera (summit) eruption; 3, slow vesiculation carries a magma batch into a rift zone channeled along zone M; 4, vesiculation carries a magma batch to the surface, producing rift-zone eruption; 5, degassed lava returns to zone M. ***C***, Map of Koolau Volcano showing location of profiles in *A* and *B*.

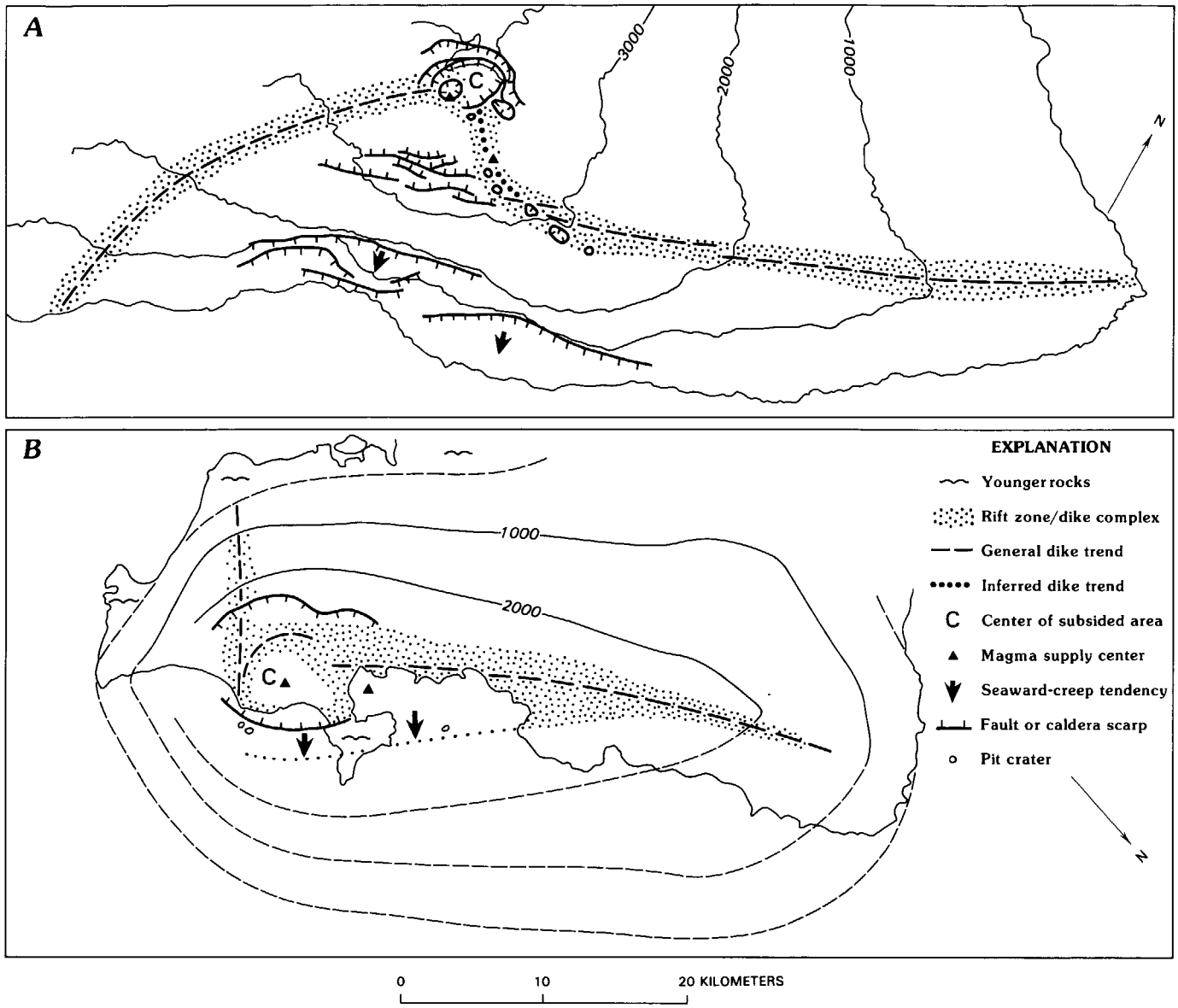

FIGURE 41.29.—Maps of Kilauea and Koolau Volcanoes at same scale. ***A***, Kilauea on the Island of Hawaii. Volcano contour interval 1,000 ft; heights in feet above sea level. ***B***, Koolau Volcano on Island of Oahu. Contours, in feet above present sea level, are generalized from present topography to show original form of volcano; dashed where very uncertain because of deep erosion.

caused by the load of intrusions and is possible because the hot lithosphere above a hot spot is sufficiently weak to permit downward creep of a prism of the dike complex.

The Koolau Volcano has a broad subsidence area that measures at least 10 km by 12 km. In part this is an area of general downsagging, and in part it may consist of discrete down-faulted cauldrons. The Kailua caldera is now exposed at an erosion level 1 km beneath the final top surface of the Koolau Volcano, and variations in the makeup of the caldera rocks can be explained by an imbalance between two processes that operated at different rates. One process was subsidence, which caused high-level rocks having few or no dikes to appear at today's erosion level. The other process was the injection of dikes seeking to rebuild the dike complex to the 50 percent to 65 percent intensity at the same level. In some outer parts of the Kailua caldera where subsidence was caused by downsagging, the rebuilding of the complex was completed. In the middle part of the Kailua caldera, subsidence greatly exceeded the capacity of dike injection to rebuild the complex. It is thought that Kilauea caldera is a good present-day analog, and the magma chamber which is postulated to be situated in the marginal zone of its dike

complex is now 3–5 km deep, maintained at that depth by rapid subsidence.

This mechanism is consistent with features of Hawaiian calderas such as their highly dynamic nature—great changes in caldera geometry can occur within a century—and the fact that the calderas are the locus of dike injections.

REFERENCES CITED

Adams, W.M., and Furumoto, A.S., 1965, A seismic refraction study of the Koolau volcanic plug: Pacific Science, v. 19, p. 296–305.

Bailey, E.B., Clough, C.T., Wright, W.B., Richey, J.E., and Wilson, G.V., 1924, Tertiary and post-Tertiary geology of Mull, Loch Aline, and Oban: Memoir of the Geological Survey of Scotland.

Currie, K.L., and Ferguson, J., 1970, The mechanism of intrusion of lamprophyre dikes indicated by "offsetting" of dikes: Tectonophysics, v. 9, p. 525–535.

Delaney, P.T., and Pollard, D.D., 1981, Deformation of host rocks and flow of magma during growth of minette dikes and breccia-bearing intrusions near Ship Rock, New Mexico: U.S. Geological Survey Professional Paper 1202, 61 p.

Doell, R.R., and Dalrymple, G.B., 1973, Potassium-argon ages and paleomagnetism of the Waianae and Koolau Volcanic Series: Geological Society of America Bulletin, v. 84, p. 1217–1242.

Duffield, W.A., 1975, Structure and origin of the Koae fault system, Kilauea Volcano, Hawaii: U.S. Geological Survey Professional Paper 856, 12 p.

Duffield, W.A., and Nakamura, K., 1973, A photogeologic method for determining the direction of horizontal dilation from patterns of en echelon fracturing: U.S. Geological Survey Journal of Research, v. 1, p. 283–287.

Dzurisin, D., Koyanagi, R.Y., and English, T.T., 1984, Magma supply and storage at Kilauea Volcano, Hawaii, 1956–1983: Journal of Volcanology and Geothermal Research, v. 21, p. 177–206.

Fiske, R.S., and Jackson, E.D., 1972, Orientation and growth of Hawaiian volcanic rifts: the effect of regional structure and gravitational stress: Proceedings of the Royal Society of London, Series A, v. 329, p. 299–326.

Fujishima, K.Y., and P-F. Fan, 1977, Hydrothermal mineralogy of the Keolu Hills, Oahu, Hawaii: American Mineralogist, v. 62, p. 574–582.

Furumoto, A.S., Thompson, N.J., and Woollard, G.P., 1965, The structure of Koolau Volcano from seismic refraction studies: Pacific Science, v. 19, p. 306–314.

Gibson, I.L., Kinsman, D.J.J., and Walker, G.P.L., 1966, Geology of the Faskrudsfjordur area, eastern Iceland: Visindafelag Islendinga, Reykjavik, Greinar, v. 4, no. 2, 52 p.

Gudmundsson, A., 1983, Form and dimensions of dykes in eastern Iceland: Tectonophysics, v. 95, p. 295–307.

——— 1984, Tectonic aspect of dykes in northwestern Iceland: Jokull, v. 34, p. 81–96.

Harker, A., 1904, Tertiary igneous rocks of Skye: Memoir of the Geological Survey of Scotland.

Keith, M.L., 1981, Regional mid-ocean stress and a proposed focal mechanism of 'stress-discordant' earthquakes: Geophysical Journal of the Royal Astronomical Society, v. 65, p. 627–644.

Kinoshita, W.T., Krivoy, H.L., Mabey, D.R., and Macdonald, R.R., 1963, Gravity survey of the island of Hawaii: U.S. Geological Survey Professional Paper 475-C, p. 114–116.

Le Bas, M.J., 1971, Cone-sheets as a mechanism of uplift: Geological Magazine, v. 108, p. 373–376.

Macdonald, G.A., 1965, Hawaiian calderas: Pacific Science, v. 19, p. 320–334.

Macdonald, G.A., and Abbott, A.T., 1970, Volcanoes in the sea: Honolulu, University of Hawaii Press, 441 p.

McDougall, I., and Aziz-ur-Rahman, 1972, Age of the Gauss-Matuyama boundary and the Kaena and Mammoth events: Earth and Planetary Science Letters, v. 14, p. 367–380.

Moore, J.G., 1964, Giant submarine landslides on the Hawaiian Ridge: U.S. Geological Survey Professional Paper 501-D, p. 95–98.

Nakamura, K., 1980, Why do long rift zones develop in Hawaiian volcanoes—a possible role of thick oceanic sediments: Bulletin of the Volcanological Society of Japan, v. 25, p. 255–269.

Pollard, D.D., Delaney, P.T., Duffield, W.A., Endo, E.T., and Okamura, A.T., 1983, Surface deformation in volcanic rift zones: Tectonophysics, v. 94, p. 541–584.

Pollard, D.D., Muller, O.H., and Dockstader, D.R., 1975, The form and growth of fingered sheet intrusions: Geological Society of America Bulletin, v. 86, p. 351–363.

Ryan, M.P., Blevins, J.Y.K., Okamura, A.T., and Koyanagi, R.Y., 1983, Magma reservoir subsidence mechanics: theoretical summary and application to Kilauea Volcano, Hawaii: Journal of Geophysical Research, v. 88, p. 4147–4181.

Ryan, M.P., Koyanagi, R.Y., and Fiske, R.S., 1981, Modeling the three-dimensional structure of macroscopic magma transport systems: application to Kilauea Volcano, Hawaii: Journal of Geophysical Research, v. 86, p. 7111-7129.

Ryan, M.P., and Sammis, C.G., 1981, The glass transition in basalt: Journal of Geophysical Research, v. 86, p. 9519–9535.

Speight, J.M., Skelhorn, R.R., Sloan, T., and Knapp, R.J., 1982, The dyke swarms of Scotland, *in* Sutherland, D.S., ed., Igneous rocks of the British Isles: New York, Wiley, p. 449–459.

Stearns, H.T., 1939, Geologic map and guide to the island of Oahu, Hawaii: Territory of Hawaii Division of Hydrography Bulletin 2, 75 p.

Stearns, H.T., and Macdonald, G.A., 1946, Geology and ground-water resources of the Island of Hawaii: Honolulu, Hawaii Division Hydrography Bulletin 9.

Stearns, H.T., and Vaksvik, K.N., 1935, Geology and ground-water resources of the Island of Oahu, Hawaii: Territory of Hawaii Division of Hydrography, Bulletin 1, 479 p.

Strange, W.E., Machesky, L.F., and Woollard, G.P., 1965, A gravity survey of the Island of Oahu, Hawaii: Pacific Science, v. 19, p. 350–353.

Swanson, D.A., Duffield, W.A., and Fiske, R.S., 1976, Displacement of the south flank of Kilauea Volcano: the result of forceful intrusion of magma into the rift zones: U.S. Geological Survey Professional Paper 963, 39 p.

Takasaki, K.J., 1981, Evaluation of major dike-impounded ground-water reservoirs, Island of Oahu: U.S. Geological Survey Open-File Report 81–1119, 146 p.

Takasaki, K.J., Hirashima, G.T., and Lubke, E.R., 1969, Water resources of windward Oahu, Hawaii: U.S. Geological Survey Water-Supply Paper 1894, 119 p.

Takasaki, K.J., and Mink, J.F., 1982, Water resources of southeastern Oahu, Hawaii: U.S. Geological Survey Water Resources Investigations 82–628, 97 p.

Taubeneck, W.H., 1970, Dikes of Columbia River Basalt in northeastern Oregon, western Idaho, and southeastern Washington: Proceedings of the Second Columbia River Basalt Symposium, p. 73–96.

Walker, G.P.L., 1959, Geology of the Reydarfjordur area, eastern Iceland: The Geological Society of London, Quarterly Journal, v. 114, p. 367–393.

———1974, The structure of eastern Iceland, *in* Kristjansson, L., ed., Geodynamics of Iceland and the North Atlantic area: Reidal, Dordrecht, p. 177–188.

———1984, Downsag calderas, ring faults, caldera sizes, and incremental caldera growth: Journal of Geophysical Research, v. 89, p. 8407–8416.

———1986, Koolau dike complex, Oahu: Intensity and origin of a sheeted-dike complex developed high in a Hawaiian volcanic edifice: Geology, v. 14, p. 310–313.

Wentworth, C.K., 1951, Geology and groundwater resources of the Honolulu—Pearl Harbor area, Oahu, Hawaii: Board of Water Supply, Honolulu, Hawaii, 111 p.

Wentworth, C.K., and Jones, A.E., 1940, Intrusive rocks of the Leeward slope of the Koolau Range, Oahu: Journal of Geology, v. 48, p. 975–1006.

Wentworth, C.K., and Winchell, H., 1947, Koolau basalt series, Oahu, Hawaii: Geological Society of America Bulletin, v. 58, p. 49–78.

Woollard, G.P., 1951, A gravity reconnaissance of the Island of Oahu: American Geophysical Union Transactions, v. 32, p. 358–368.

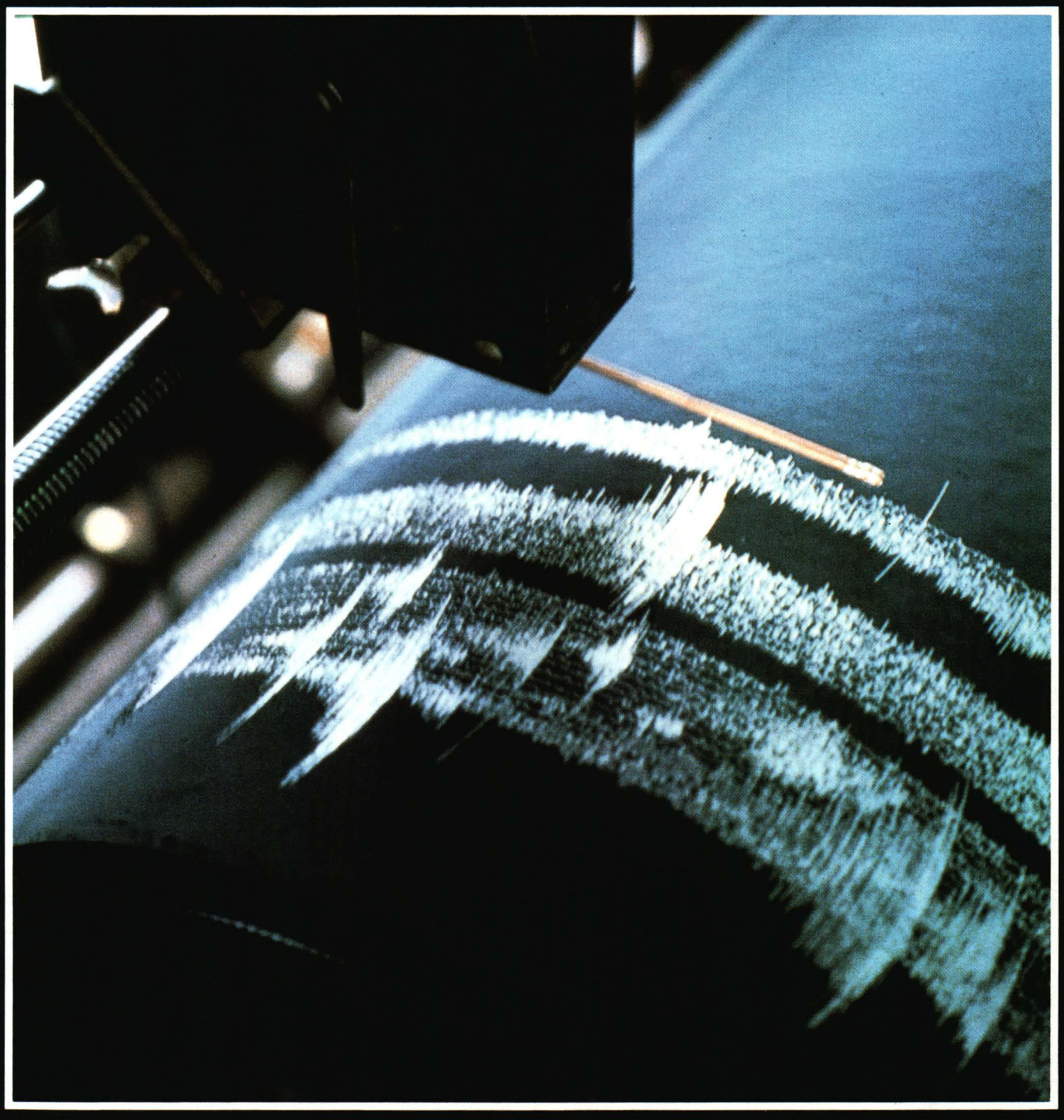

Earthquake swarm and volcanic tremor being recorded on seismograph at Hawaiian Volcano Observatory, November 16, 1979. Photograph by R.W. Decker.

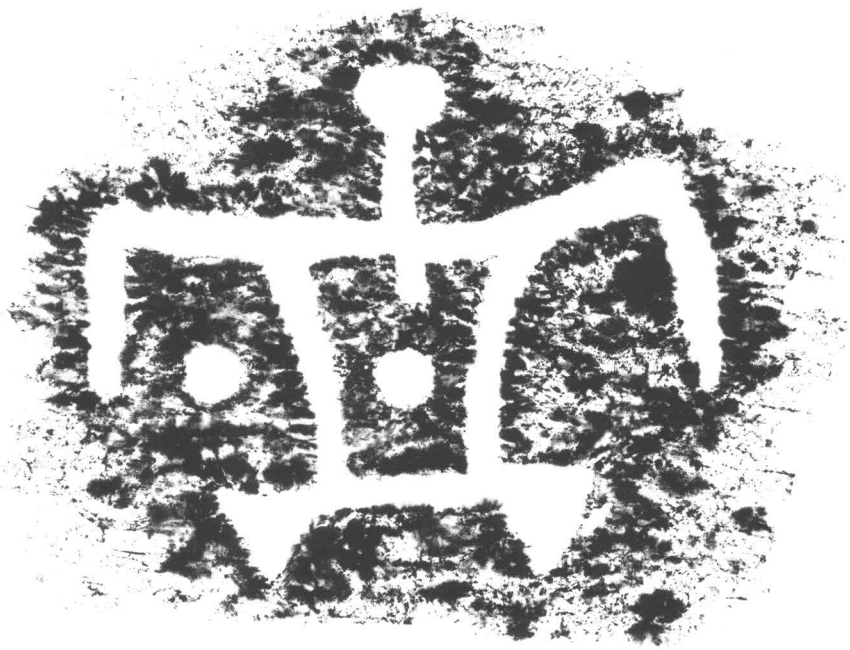

Turtle
Hawaiian Petroglyph
Puuloa, Hawaii

DYNAMICS

Much of the present research on Hawaiian volcanoes is directed towards understanding how they work. It is appropriate, therefore, that this section on dynamics is the longest in the two volumes on Volcanism in Hawaii.

The eighteen chapters in this section address questions about the physical and chemical dynamics of magma formation, accumulation, ascent, storage, intrusion, and eruption. These questions cannot be investigated in isolation, and many of the papers in the section on petrogenesis and volcanic gases and in that on structure are closely related.

An overview chapter is followed by three chapters on earthquakes and volcanic tremor, four chapters on ground-surface deformation related to magma movements, and one on the geoelectric contrast between the crust and molten core of a lava lake. Chapter 51 points out the resemblance of the cyclical behavior of Hawaiian volcanoes to patterns predicted by attractor dynamics, a new conceptual approach to understanding the interactions in complex systems. The next two chapters delve into the rock mechanics that constrain the physical dynamics of Hawaiian volcanoes, and chapters 54 through 56 consider the thermodynamics and geochemistry of the magmatic-geothermal systems formed on active Hawaiian volcanoes. The last three chapters in this section discuss the flow dynamics of Hawaiian lava.

DYNAMICS OF HAWAIIAN VOLCANOES: AN OVERVIEW

By Robert W. Decker

ABSTRACT

Eaton and Murata's cross section of Kilauea Volcano, published in 1960 (Science,v. 132), remains the basic model of how Hawaiian volcanoes work. Magma forms by partial melting of mantle rock at depths between 60 and 170 km in a specific area of mantle known as the Hawaiian hot spot. The melt accumulates by migrating through small fractures, or by shear coalescense, into volumes large enough to ascend. The ascensive pressure is caused by the greater density of the rocks surrounding and overlying the magma. Ascent through the lithosphere occurs in discontinuous conduits that are generated by magmafracting. Apparently there are enough of these ascensive conduits so that magma is supplied to a shallow reservoir system 3–7 km beneath the summit caldera at rates that vary by less than an order of magnitude over time scales of months to decades. When the shallow magma reservoir fills to about lithostatic pressure, magmafracting emplaces dikes upward or laterally into the rift zones; those dikes that reach the surface erupt. Eruptions at high-volume rates rapidly reduce the pressure in the shallow magma reservoir and are of brief duration. Long-lived eruptions occur at low-volume rates and are sustained by the resupply of magma from depth. Lava fountains are produced by the rapid expansion of magmatic gases—H_2O, CO_2, and SO_2—at near-surface pressures. Major caldera collapses, sometimes associated with explosive eruptions, occur repeatedly at intervals of a few thousand years. One probable cause of these collapses is intrusion or eruption on the submarine rifts which produce major draindown of the shallow reservoir system. The newly formed volcanic islands subside at exponentially decreasing rates as the Pacific plate moves slowly northwestward past the Hawaiian hot spot.

INTRODUCTION

The literature on Hawaiian volcanism contains many descriptions of eruptions, but fewer interpretations of the dynamic processes that form magma and that cause it to ascend and erupt at the surface. Present studies, however, are concentrating on obtaining the necessary surface and subsurface data to compare with inferences from dynamic models of how Hawaiian volcanoes work. Those models, constrained by geological, geophysical, and geochemical data, are beginning to give a glimpse of the complex, hidden processes that occur beneath Kilauea and Mauna Loa Volcanoes. The purpose of this chapter is to synthesize these studies into a comprehensive model of the dynamics of Hawaiian volcanoes, particularly during their stage of vigorous growth.

The earliest recorded speculations on the subsurface structure and dynamics of Hawaiian volcanoes appear in the journal of William Ellis, a Christian missionary from England, who walked around the Island of Hawaii in 1823. While visiting Kilauea caldera, Ellis (1827, p. 171) noted that his Hawaiian guides told him about many eruptions on the flanks of Kilauea "on which occasions they supposed Pele went by a road under ground from her house in the crater to the shore." Present-day interpretations of rift-zone eruptions on the flanks of Kilauea are considerably more detailed, but in essence are the same as this "road under ground" of the native Hawaiians.

Ellis goes on to speculate about the dynamic processes beneath the active lava lakes that he saw in Kilauea caldera (p. 181): "Perforated with innumerable apertures in the shape of craters, the island forms a hollow cone over one vast furnace." This concept has not survived as well as Pele's road.

J.D. Dana (1890, p. 174–175), geologist with the U.S. Exploring Expedition to Hawaii in 1840, was the first to distinguish clearly the more or less steady ascensive force of magma at depth from the rapid fountaining of erupting lava that is caused by the sudden boiling off of gases at near-surface pressures. Dana (1895, p. 303) attributed the ascensive force in the volcano to "1) the expansive action of moisture from the deep-seated source of the lavas; and 2) the gravitational pressure of the contracting crust of the globe, forcing up the lavas* * *." He noted that the top of the Kilauea magma column had risen 360 feet in 6 years. Both of Dana's interpretations are close to, but not quite the same as, present interpretations. These two causes of ascensive force could now be reworded as follows: (1) The expansive action of fluids, particularly CO_2, from the deep-seated source of the lava, forming separate phases; and (2) the gravitational pressure of the overlying, heavier crust and upper mantle of the globe, forcing up the lighter lava.

Eaton and Murata (1960) were the first to draw a dynamic cross section of a typical Hawaiian volcano (fig. 42.1). In their model, magma moves upward by density contrast, more or less continuously, through conduits from the top of a source region at 60 km depth to a storage reservoir at a depth of 3–7 km. Intermittent eruptions from the shallow magma reservoir to the surface occur through newly formed fractures breaking upward to the caldera or laterally into the rift zones. The eruption rates from the shallow magma reservoir to the surface are often much higher than the rate of resupply from depth, and thus the eruptions tend to be self-limiting and intermittent. Sometimes low-volume-rate eruptions form active lava lakes in the caldera, presumably sustained by the resupply rate. Such more or less steady-state eruptions can last for months or years. This overall model fits well with the seismic data and observed ground-surface deformation on Kilauea Volcano, and it is still the

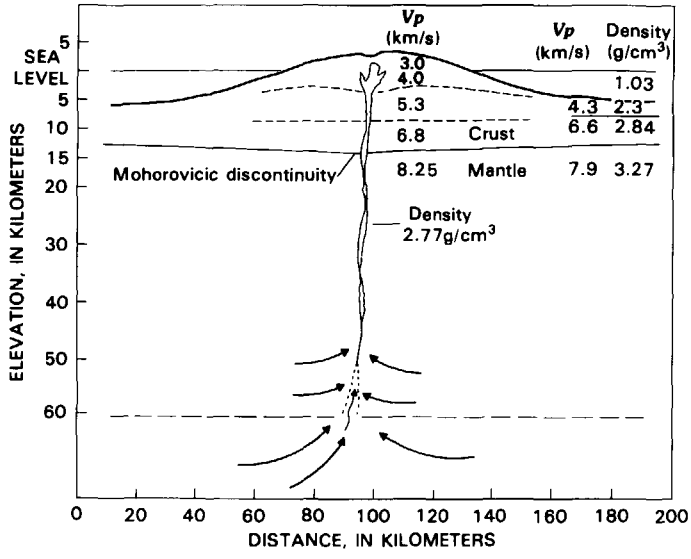

FIGURE 42.1.—Schematic cross section through idealized Hawaiian volcano. Magma from a source about 60 km deep streams up through conduits and collects in shallow reservoir beneath caldera. Occasional discharge of lava from shallow reservoir through dikes that split to surface constitute eruptions. Note slight depression of Mohorovicic discontinuity beneath volcano. V_p is the velocity of seismic *P*-waves. Modified from Eaton and Murata (1960).

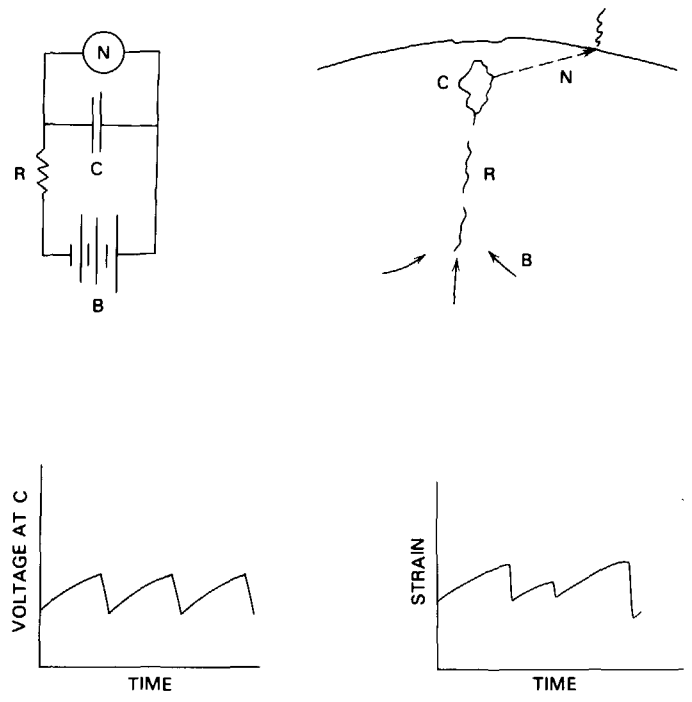

FIGURE 42.2.—Electrical analog of dynamics of Kilauea Volcano. Electrical circuit is a battery (B) charging a condenser (C) through a resistor (R). When voltage across condenser reaches firing voltage of neon bulb (N), bulb winks on until voltage drops below sustaining level. In Kilauea deep ascensive force of magma represents battery, conduits from deep source to shallow magma reservoir form resistor, and shallow magma reservoir is condenser. Dike breaking to surface or intruding a rift zone reduces magma pressure (voltage) and is equivalent to neon bulb. Variation of strain in volcanic edifice is similar to variation of voltage in circuit, but less regular in its cycles.

basic concept of how Hawaiian volcanoes work.

Building on Eaton and Murata's model, Decker (1968) and Shimozuru (1981) have noted that the fluid and fracture dynamics of this model are analogous to the storage and discharge of electricity in a resistance-capacitance (RC) circuit (fig. 42.2). The ascensive pressure is analogous to a battery, the resistance to fluid flow through the system is analogous to a network of electrical resistors—within the battery, between the battery and the condenser, and between the condenser and the surface—and the shallow magma reservoir is analogous to a condenser. If the resistance between the condenser and the surface operates in two modes—almost infinite resistance or very low resistance, as in a neon bulb—then intermittent discharges of the condenser in the electrical model will be analogous to eruptions.

Although this electrical analog model is greatly oversimplified, it has the advantage of allowing thought experiments about what happens when changes occur in the ascensive pressure, the resistance to flow, or the volume of the shallow magma reservoir, either separately or in combination. For example, if the ascensive pressure were doubled, the repose time between eruptions would be halved and long-term lava output would double, but the individual eruptions would have the same volume as before. Increasing the capacity of the shallow magma reservoir would increase the repose time between eruptions, but the eruptions would be of proportionately greater volume. Changing the breakdown strength of the rocks between the shallow magma chamber and the surface—analogous to changing neon bulbs—could change both the repose time between eruptions and the volume of the eruptions. If the values of the various components are computed or assumed, then their quantitative interrelation can be calculated using well-established electrical or hydraulic equations.

Realistic models of the structure and dynamics of Hawaiian volcanoes are strongly dependent on the physical properties of magma and its host rocks. Some of these properties vary greatly, and the numerical values of others are only poorly known. Refined models are therefore dependent on improved knowledge of these physical properties.

Attempting to understand the hidden dynamics of an active volcano calls upon the most eclectic abilities of volcanologists. A valid dynamic model must explain the geologic and eruptive history of the volcano, as well as the seismic, deformational, and electromagnetic changes that occur before, during, and after eruptions. In addition it must explain the composition and changes in composition of the solid, liquid, and gaseous products emitted from the volcano. Besides all this, the model must be consistent with the laws of physics and chemistry and, if possible, satisfy the philosophy of Ockham's Razor—that is, not to be unnecessarily complicated. Such a task clearly requires a team effort. This article is therefore a selected synthesis of the data and interpretations of many students of Hawaiian volcanism.

ACKNOWLEDGMENTS

Jerry Eaton, Howard Powers, and Gordon Eaton were my kind hosts and patient teachers while I was a guest investigator at the Hawaiian Volcano Observatory (HVO) in the 1960's and 1970's. Robert Tilling offered me the opportunity of returning to HVO as Scientist in Charge, and my fine colleagues at HVO continued my education during my tenure there from 1979 to 1984. Jerry Eaton, Dan Dzurisin, and Barbara Decker gently but thoroughly reviewed earlier versions of this chapter. My warmest thanks to all these fellow students of volcanoes.

MAGMA FORMATION

When, where, and how does magma form? There are no clear answers to these questions, but there is no lack of hypotheses. Since volcanism has been a persistent geologic process for billions of years, it seems reasonable to assume that magma has continued to form during most of the Earth's history. A counter argument could be that magma only formed in the early history of the Earth, has always been present within the Earth, and has been released slowly enough to stretch out volcanism for billions of years. This alternative has not been proven wrong, but since most geologic processes work at levels close to equilibrium, it is difficult to accept a process that could be restrained for such enormous periods of time. For this reason it is assumed that magma is forming within the Earth at the present time.

There is reasonably good agreement about where basaltic magma is formed. Yoder (1976) carefully reviewed the geophysical and geochemical evidence and concluded that basaltic magma may be generated in broad regions generally at depths of 50–170 km; in more restricted environments the source of basaltic magma may be as deep as 300–400 km. Eaton and Murata (1960) concluded on the basis of depths of earthquake sources that the magma source region beneath Hawaii has its top at a depth of 60 km, but they were not able to infer how far the source region may extend below this level. Wright's model (1984) for the origin of Hawaiian tholeiite proposes a depth of formation ranging from 60 to 90 km. Recent studies by Anderson and Dziewonski (1984) using seismic tomography indicate an anomalously slow (hot) zone in the Earth's mantle at a depth of 350 km over a broad area south of Hawaii. Mantle flow in this area is apparently upward. At shallower depths in the upper mantle, the anisotropy of Rayleigh wave velocity suggests horizontal flow in a southeastward direction beneath Hawaii. As a working hypothesis, it is assumed that magma is currently being formed beneath Hawaii at some depth interval between 60 and 170 km.

The question of how magma forms is even more complex than when or where it forms. From what rock material is it melted, and what is the source of heat? Yoder (1976) thinks that the best candidate for the parent rock of basaltic liquids is garnet peridotite, a crystalline aggregate of olivine, orthopyroxene, clinopyroxene, and garnet. He accepts this source—tentatively—and lists the following features of garnet peridotite as supportive evidence (Yoder, 1976, p. 42):

(1) Its occurrences are appropriate to deep-seated environments of origin.

(2) Its close compositional relation to meteorites supports a derivation from material accumulated in the primordial Earth.

(3) Partial melts of natural samples at high pressure have basaltic compositions.

(4) The mineral asmblage was found experimentally to be stable at high pressure and temperature.

(5) It has appropriate density and seismic velocity.

Wright (1984) prefers a source rock for Hawaiian tholeiite magma composed of lherzolite, a crystalline aggregate of olivine, orthopyroxene, and clinopyroxene, with some other constituents (amphibole, nephelinite, ilmenite, apatite, and ferrous iron oxide) added from depth.

The source of heat to melt a basaltic liquid from a crystalline rock aggregate must be either internal or external to the rock being melted. If it is external, some thermal process such as conduction, convection, or radiation must transport heat into the source region. If it is internal, the heat must be generated by some process such as radioactive decay or mechanical friction, unless it is heat that is already present in the rock. In the latter case, some other process must be called upon to lower the melting temperature of the basaltic liquids, such as lowering the confining pressure or introducing fluxing elements or compounds into the source region.

The problem is not a lack of possibilities, but too many permutations and combinations to choose among. Yoder (1976, p. 60–61) lists 21 proposed mechanisms to melt rock into magma. Several of these are not tenable for Hawaii; for example, those mechanisms that require subsidence of continental crustal layers of the Earth by 5 km or more (Hess, 1960). Among the more reasonable mechanisms for generating Hawaiian magmas are the following (in alphabetical order by author):

(1) Melting caused by the friction of shear strain released from stored elastic strain energy along a propagating crack (Griggs and Baker, 1969).

(2) Internal radioactive heat production (Joly, 1909).

(3) Conductive heat trapping caused by changes in thermal conductivity with temperature and pressure (McBirney, 1963).

(4) Rise of the source material as a buoyant diapir, thus reducing confining pressure and melting temperature (Ramberg, 1972).

(5) Melting caused by the friction of viscous strain. In this thermal feedback or runaway model, constant shear stress on a crystalline rock at its melting temperature causes small viscous strains that increase the temperature. This temperature increase lowers the viscosity, increases the strain rate, and thus further increases the temperature (Shaw, 1973).

(6) Melting caused by the friction of shear strains associated with tidal energy dissipated in the solid Earth (Shaw, 1970).

(7) Rise of the source region by solid-state convection, thus reducing the confining pressure and melting temperature (Verhoogen, 1954).

(8) Reduction in melting temperature of the basaltic liquids by addition of volatiles (H_2O, CO_2) to the parent-rock source region (Yoder and Tilley, 1962).

Radioactive uranium, potassium, and thorium isotopes are

apparently ubiquitous in upper-mantle rocks but low in amount. Hawaiian lava exhibits no abnormal content of these radioactive isotopes, so radioactive heating (mechanism 2) does not seem to be a principal cause of the high rate of Hawaiian magma production. However, on a global basis and over tens to hundreds of millions of years, radioactive heat production probably contributes significantly to heating the rocks of the upper mantle to near melting temperatures.

Choosing among the 7 remaining mechanisms to explain Hawaiian magma generation depends in part on tectonic prejudices. Those who favor the hot-spot hypothesis (chapter 1, part I) will probably favor the diapiric rise (4) and (or) volatile transfer (8) mechanisms, while those who favor a propagating fracture may prefer the stored elastic energy release (1) and (or) the conductive heat trap (3) mechanisms. Wright's model (1984) combines a thermal plume to drive up the added chemical elements from depth and thermal feedback to provide the principal heat of melting. It is probably best to say that the melting problem is not resolved at this time. Detailed seismic tomography studies may soon provide more definite evidence on this important but difficult subject of the heat source of Hawaiian magma.

In all the proposed mechanisms for melting crystalline rock to form magma, the enthalpy of melting is about $4.2–5.2 \times 10^5$ J/kg (100–125 cal/g). This heat of fusion has a major buffering effect on the temperature and rate of melting or freezing in the source region, implying that basaltic magmas of similar composition at similar depths of formation are nearly isothermal. At 60-km depth, Hawaiian tholeiite magma has a calculated formation temperature of 1,350–1,400 °C (T.L. Wright, oral commun., 1985). Measured temperatures of erupting Hawaiian lava are in the range of 1,100–1,200 °C.

MAGMA ACCUMULATION AND ASCENT

Melting a garnet peridotite or lherzolite mantle involves a 10–15 percent volume increase from the crystal aggregate to the basaltic fluid. A change from solid to 30 percent partial melt would thus bring about a 3–5 percent increase in the bulk volume of the rock-liquid mixture.

In experimental studies on crystalline silicate aggregates, the first melt forms films between mineral grains that then unite into a liquid-bonded aggregate—a network of melt coating the mineral grains with a thin film of fluid (Yoder, 1976, p. 164-165). The volume of these molten films can reach 10 percent of the mineral-liquid mixture. As the volume of melt increases, deformation from internal volume expansion and (or) interaction with external stresses takes on an increasingly important role.

Extension fractures perpendicular to the direction of the least compressive stress can form even at mantle depths if the pore-fluid pressure exceeds the tensile strength of the rock. Shaw (1980) found that these conditions are probable in the thermal and stress domains estimated to occur in the asthenosphere beneath Hawaii. His model of melt accumulation and ascent is shown in figure 42.3; in it the accumulation fractures are subhorizontal (sills) if the least compressive stress is vertical, or they are nearly vertical fractures (dikes) if the intermediate compressive stress is vertical. Because of small transient changes in the shear stresses, pore pressures, or gravitational load on this deep region where the three major compressive stresses are nearly but not quite equal, Shaw thinks both of the above conditions will occur and will generate a set of planar melt lenses oriented at 50°–90° to one another, with intersections parallel to the general direction of maximum compressive stress. These intersections are shown schematically in figure 42.3 by the broken horizontal line segments within the asthenosphere. The inferred lenses of melt accumulation would tend to lie both (vertically) in the plane of the cross section and (horizontally) perpendicular to it. Since there is no seismic evidence for major brittle fracturing in the asthenosphere beneath Hawaii, these proposed cracks would have to be small or form slowly.

An alternative way of expressing the fracture-accumulation hypothesis is shearing of the films of melt into progressively larger pockets of molten rock. Shaw (1969, p. 533) refers to the melt fraction as being "kneaded from the crystalline source"; Weertman (1972), on the basis of observed bubble coalescense in deforming glacial ice, believes a similar process may occur during shear creep in partially melted rock. Spera (1980) points out that the rate of melt segregation is governed by the rheology of the rock-liquid mush and by the balance among buoyancy, pressure, and viscous forces. He also notes that he can estimate buoyancy reasonably well and stress gradients to within an order of magnitude, but viscous forces and permeabilities only poorly. Nevertheless, Spera, on the basis of correlation to rigid porous-media systems, estimates that the segregation rate is highly dependent on the melt fraction; in dimensionless terms it would be 6,500 times larger for a 30-percent partial melt than for a 2-percent partial melt.

Whatever the mechanism of melt segregation is beneath Hawaii, it must be rapid enough throughout the source volume to provide about 0.1 km^3/yr of magma to Kilauea Volcano for time periods longer than a few decades (Swanson, 1972; Dzurisin and others, 1984) and a roughly similar but less well known amount to Mauna Loa Volcano. Assuming that the source region is approximately cylindrical, as wide as the island (100 km), and 30 km thick, the source volume would be approximately 2.5×10^5 km^3. Using a partial melt of 30–40 percent (Wright and others, 1979; Wright, 1984), the calculated average fraction of the total melt delivered to shallow levels in Hawaii on a yearly basis is only $2–3 \times 10^{-6}$. About 2.5×10^{17} J (6×10^{16} cal) of heat of fusion are needed by this slowly evolving source region on a yearly basis to maintain a steady-state supply rate of 0.2 km^3/yr. Under the above assumptions, this translates into about 3.2×10^{-5} J/m^3/s (7.7×10^{-12} cal/cm^3/s), an amount of heat nearly 10^3 times greater than the heat production from radioactivity in an average garnet peridotite. These numbers assume that the melting and segregation processes are spread evenly throughout the source region; it is likely that these processes in fact become more concentrated near the apex of the source region.

The mechanism of the ascent of magma through the more rigid rocks of the lithosphere must be both qualitatively and quantitatively

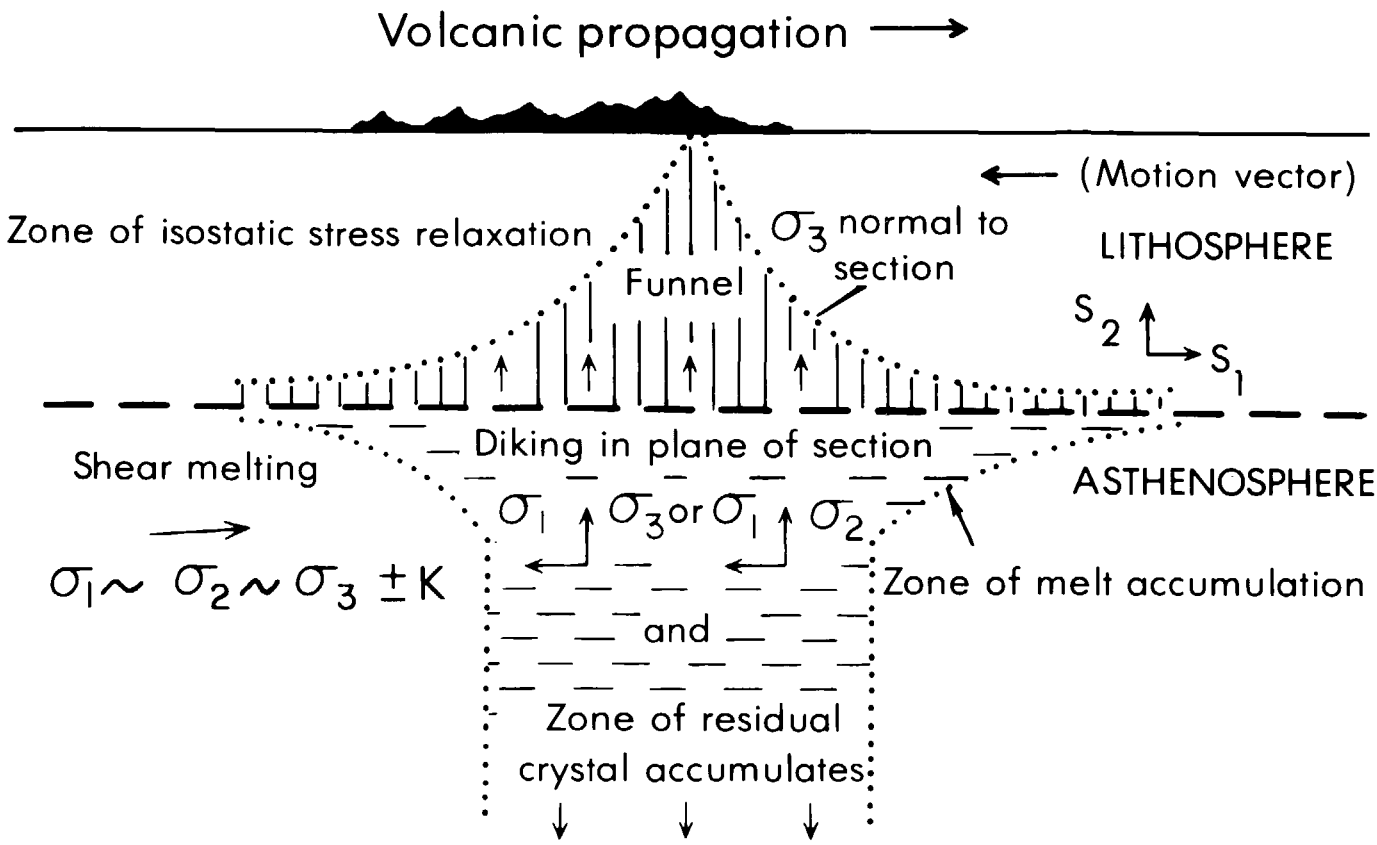

FIGURE 42.3.—Schematic longitudinal section showing stress domains beneath active Hawaiian volcanoes. S, total normal stress acting at a point in rock; σ, effective normal stress acting in rock containing an interconnected fluid phase. Subscripts 1, 2, and 3 refer to maximum, intermediate, and minimum principal stresses, respectively. K, tensile strength. In zone of melt accumulation, fractures would be either nearly vertical in plane of section, or nearly horizontal in plane perpendicular to section. In ascent funnel, fractures would be nearly vertical in plane of section. Modified from Shaw (1980).

different from that of its segregation and ascent in the source region. The tensile strength of the lithospheric host rocks is greater than that in the asthenosphere, although it may become weakened by heating from ascending magma. Deviatoric stresses in the lithosphere may be much greater than in the asthenosphere, and beneath Hawaii the lithosphere is seismically active whereas the asthenosphere is apparently not.

Magma is pushed upward into and through the lithosphere by the pressure gradient caused by gravity acting on the density difference between lighter magma and heavier host rocks. This explanation of the ascensive force was first clearly proposed by Daly (1914, p. 183) who suggested "that magmatic eruption is, in the first instance, a hydrostatic phenomenon." Daly later became even more convinced. His second edition (1933, p. 247) states "The leading cause for the ascent of primary magma, assumed to move up abyssal fissures, is naturally found in the weight of the adjacent crust." Almost no one would now disagree with this explanation of the ascensive force; the origin of the abyssal fissures, however, is much more debatable.

Does Hawaiian magma passively rise through conduits in the lithosphere generated by external stresses, or does it actively generate or help to generate these conduits? Turcotte and Oxburgh (1978) propose that deformation of the Pacific plate in adjustment to thermal and Earth-curvature changes may cause a major propagating intraplate fracture. They suggest that magma leaking up this propagating fracture has progressively formed the Hawaiian volcanic chain. Since Wilson (1963) proposed the hot-spot origin for the Hawaiian Islands, most other researchers believe the melting anomaly is fixed in position and that plate motion over the hot spot causes the age progression of the Hawaiian chain (Dalrymple and others, 1973; McDougall, 1979). Implicit in the hot-spot hypothesis is the idea that magma in sufficient quantities can somehow force itself upwards through the lithosphere. Possibly the stresses proposed by Turcotte and Oxburgh (1978) may assist in this magmafracting process.

The concept that magma can actively fracture its way upward is strengthened by the distribution of earthquake hypocenters beneath Kilauea Volcano (see chapter 43). Over periods of years this earthquake distribution outlines a zone of active fracturing in the lithosphere that is shaped like a steeply dipping inverted funnel reaching generally to a depth of 45 km and occasionally to nearly 60 km (Eaton, 1962). Close association of the earthquakes with the inferred conduit path of the rising magma, rather than with the site of

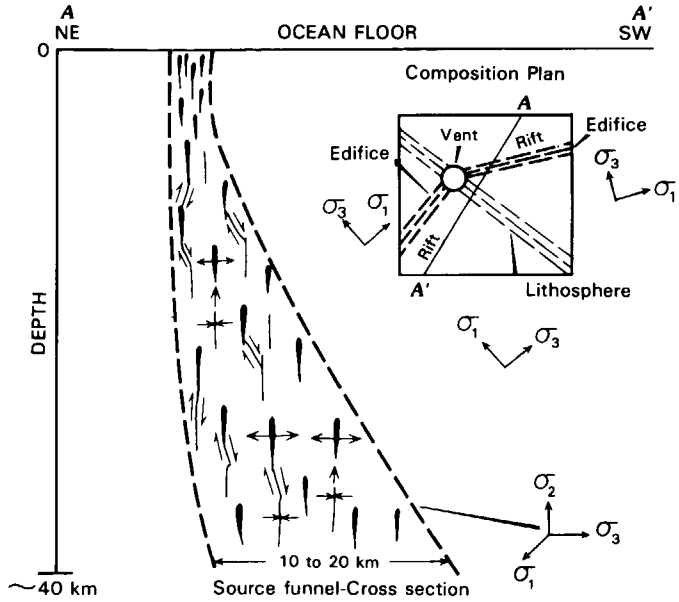

FIGURE 42.4.—Schematic cross section of lithosphere beneath Kilauea Volcano showing magma ascent funnel as region of extensional fractures and magma batches migrating upward from asthenosphere. Inset shows simplified plan of rift zones. Stress orientations and dike orientations have different directions in lithosphere and in edifice of volcano. Symbols have same meaning as in figure 42.3. Modified from Shaw (1980).

the postulated intraplate fracture, indicates that the magma plays an active role in the formation of the conduits.

Shaw (1980) proposes that magma is injected into the lithosphere by a process analogous to hydraulic fracturing of the wall rocks in a borehole by increasing fluid pressure. The normal compressive stresses in the buried host rock can be balanced or exceeded by the magma pressure to produce zero or even negative effective stresses. When these effective stresses equal or exceed the tensile strength of the rock, extensional fractures form perpendicular to the direction of least compressive stress (figure 42.4). Yoder (1976, p. 179) has called this process magmafracting. In this view most of the earthquakes beneath Hawaii are the effect, not the cause, of the transport of magma.

As the vertical dikes of magma shown in figure 42.4 intermittently force their way upward by brittle fracture, they must be resupplied with more magma from the source region, or the trailing edge of the rising dike will close off because of the recovering compressive stresses (Pollard, 1976). Hill (1977) shows that shear stresses will cause the active dike system to become a complicated network of dike-like lenses connected by faults. Movement of magma within one of the dikes will change the local pattern of deviatoric and effective stresses, and this may trigger new fractures or movements on the existing fracture network. Hill uses this model to explain earthquake swarms in Hawaii, and Shaw calls such resulting swarms failure cascades.

Shaw (1980) then inverts the seismic data from Hawaii in order to estimate the volume and magma fraction of the active intrusion zone in the lithosphere located between the deep source region in the asthenosphere and the shallow magma-reservoir system beneath Kilauea Volcano. His calculations suggest that this zone has a volume of about 10^3 km^3 and a melt fraction between 10^{-5} and 10^{-4} (that is, 0.01–0.1 km^3 of magma). For continuity, the 0.1-km^3 yearly magma supply to Kilauea would thereby have an average residence time of only a month to a year while rising through this zone. Magma ascent may appear relatively continuous over time spans of months to years, but can be quite variable at time scales of minutes to days. Several batches of lava may be moving upward in independent spurts. Some batches may rise 30 km in a few weeks, while other batches may never reach shallow levels. The varying rate of inflation of the summit region of Kilauea, as measured by continuously recording tiltmeters, supports this model of semicontinuous rise of magma into the shallow reservoir system.

MAGMA STORAGE

Batches of Hawaiian magma rising through the lithosphere apparently take various paths and various amounts of time in their ascent, but most of the magma supplying Kilauea Volcano during the past several decades has paused in a shallow magma storage system before erupting to the surface.

Mogi (1958), using data from Wilson (1935), first identified the presence and depth of this shallow magma reservoir by analysis of surface uplift and subsidence of the summit and upper flanks of Kilauea. Using elastic-deformation theory he identified two major sites of pressure and (or) volume change in the region beneath Kilauea caldera: one well-defined site at 4 km depth and another less well defined site at 25 km depth. Eaton (1962) rejected the deeper site as an apparent artifact of leveling-rod error in the long survey traverse from Hilo to the summit of Kilauea. Using additional level and tilt data, Eaton confirmed the shallow reservoir system and showed it on his schematic cross section (fig. 42.1) as an irregular vertical cylinder about 4 km wide and at 3–7 km depth beneath the summit of Kilauea.

Patterns of continuously recorded summit tilt over the past two decades (fig. 42.5) indicate that this shallow magma-reservoir system slowly inflates over periods of months to years during the intervals between eruptions and then rapidly deflates over periods of days to weeks during flank eruptions or lateral intrusions into the rift zones. Expansions and contractions of the caldera diameter by as much as a few meters accompany these inflations and deflations.

On many of the inflation cycles shown in figure 42.5, the rise of the summit shows a high rate of inflation immediately after a deflation event. This is followed by an exponentially decreasing rate of inflation, probably caused by the decreasing pressure gradient between the shallow magma-reservoir system and the sources of magma at greater depths and (or) by the increased leakage of magma into parts of the shallow magma reservoir away from the summit as the pressure in the shallow reservior system increases.

Considerable research has been done to attempt to define the depth, shape, and dynamic nature of the shallow magma-reservoir

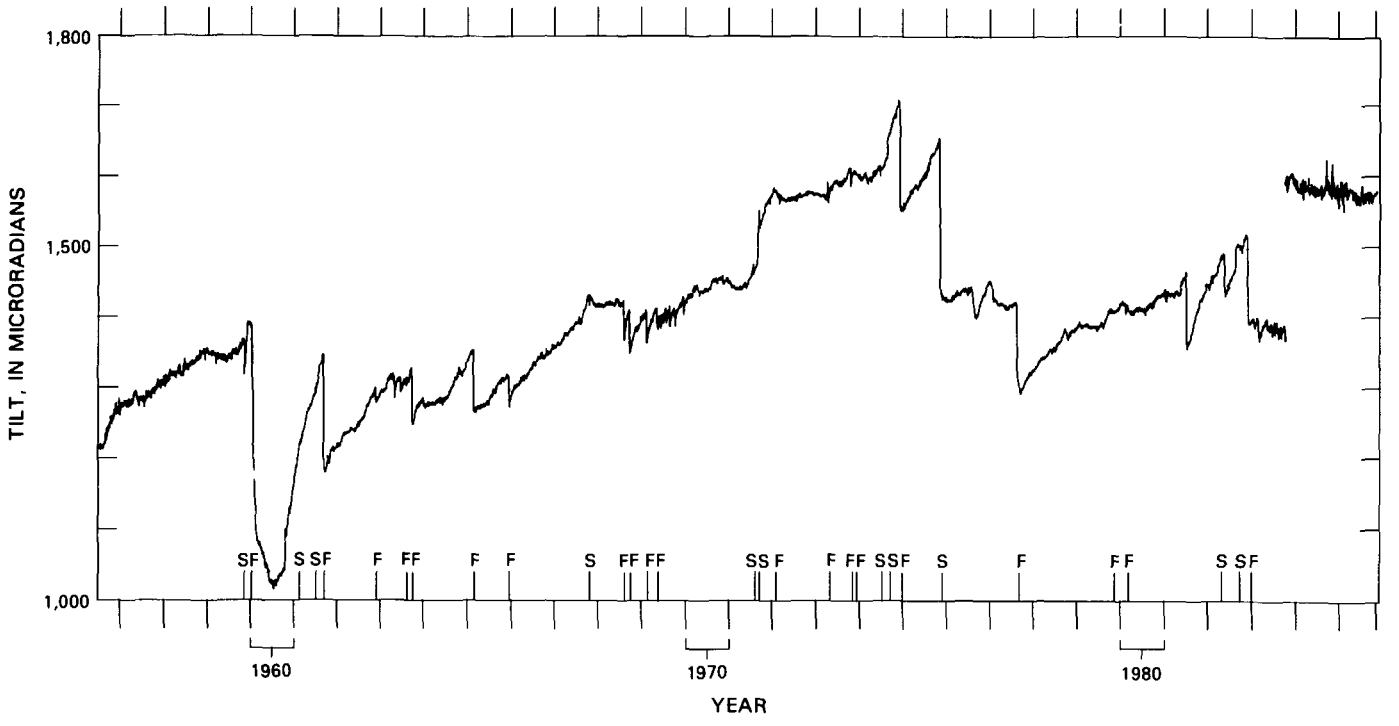

FIGURE 42.5.—Radial tilt at Hawaiian Volcano Observatory (HVO) on northwest rim of Kilauea caldera. Increasing tilt (radially outward) indicates inflation of summit region; decreasing tilt indicates deflation. One hundred microradians (μrad) of tilt at HVO indicates uplift of apex of summit bulge by about 50 cm. Rapid deflation marked by sharp drops in tilt represent volume change of bulge of about 3.3×10^5/μrad and pressure drop in shallow magma reservoir system of about 90 kPa/μrad. Magma is added slowly to shallow reservoir system from depth between eruptions and is rapidly removed during flank eruptions. Vertical lines indicate eruptions; S, summit eruptions; F, flank eruptions. Offset in tilt record in November 1983 was caused by M=6.6 earthquake (see Buchanan-Banks, chapter 44).

system. Geologic evidence from the location and form of Kilauea caldera and the pit craters along the upper east rift zone gives some indication of the subsurface location and lateral extent of the reservoir system. The caldera and pit craters have formed by collapse and thus identify the subsurface regions from which magma has been removed in such large quantities that the deflation cannot be accommodated by elastic or plastic surface deformation. Presumably these large removals occur during major eruptions from the distant submarine portions of the east rift zone. Interpretation of this morphological evidence indicates that the main magma reservoir beneath Kilauea caldera is (or was) roughly elliptical in plan—4 km NE.-SW. by 3 km NW.-SE.—and that about 3 km^3 of magma had been removed from the shallow subsurface reservoir to accommodate the volume of the caldera as it appeared in 1823.

The location of the pit craters is evidence that the magma storage system extends (or extended) southeast and then northeast beneath the upper east rift zone at least as far as Napau Crater, 15 km east of the summit caldera. The pit craters range in diameter and volume from 1 km and 77×10^6 m^3 (Makaopuhi before 1965) to 25 m and 90×10^3 m^3 (Devil's Throat); these figures put some limits on the width and volume of previous magma-storage regions beneath the east rift zone. There are only two small but deep pit craters along the southwest rift zone, indicating its subordinate role as a magma-storage region. Duffield and others (1982) conclude that the southwest rift zone breaks primarily because of accumulated movements of the east rift zone and to a lesser degree because of magmatic pressure from the summit reservoir system.

Geodetic data on the changing elevations and displacements of the deforming ground surface above the shallow magma-reservoir system have provided the best evidence on the dynamic nature of these magma storage chambers (Ryan and others, 1983). Detailed leveling of the summit area of Kilauea during an inflation period by Fiske and Kinoshita (1969) shows that the apex of inflation migrates over distances of 1–3 km within or near the caldera (figure 42.6). This shift of the center of inflation indicates that the summit reservoir is a plexus of interconnected storage zones. It can be compared to a Mickey Mouse balloon whose head inflates separately from the ears. Recording tiltmeters near HVO show that this migration of the apex of inflation or deflation during the larger cycles of magma influx and discharge has a repetitive pattern. After a major summit deflation, reinflation begins beneath the northern part of the caldera and then moves southward; during the next major deflation, the northern part of the caldera also subsides first and is quickly followed by the south end subsiding. This implies that the main input and withdrawal conduits for the summit reservoir plexus are on the north side of the general storage zone, which lies mainly beneath the south end of the caldera.

Dvorak and others (1983) analyzed the surface deformation

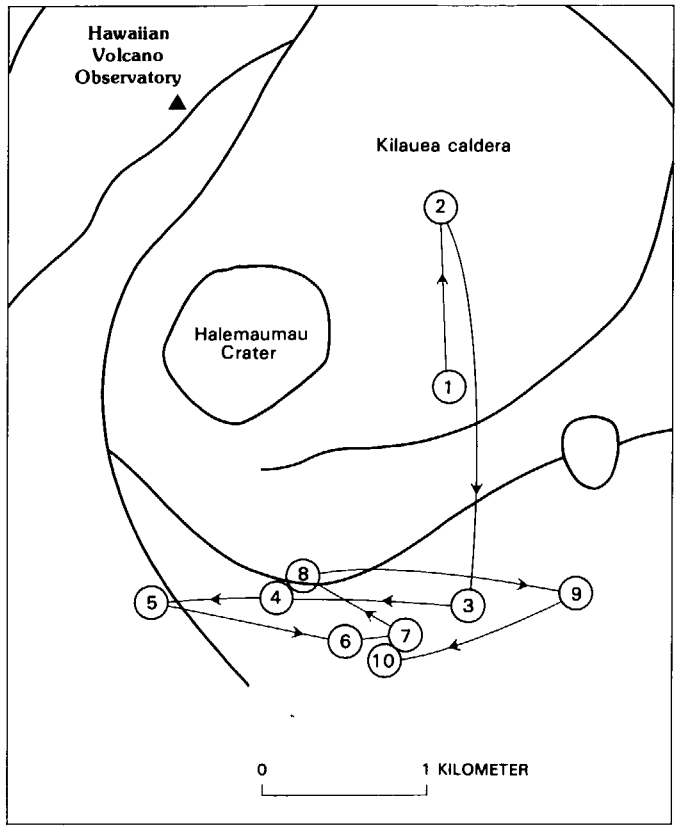

FIGURE 42.6.—Lateral shift of apex of uplift of inflating bulge at summit of Kilauea Volcano, modified from Fiske and Kinoshita (1969). Level surveys demonstrate shifting center of uplift: (1) January–July 1966; (2) July–October 1966; (3) October 1966–January 1967; (4) January–February 1967; (5) during February 1967; (6) February–May 1967; (7) May–June 1967; (8) June–July 1967; (9) July–September 1967; (10) September–October 1967. Position of Hawaiian Volcano Observatory and caldera and crater walls (heavy lines) shown for reference. Total uplift of the 10-km-wide bulge at its apex from January 1966 to October 1967 was approximately 70 cm; summit eruption of Kilauea began in November 1967.

data on Kilauea for the period 1966–1970 by simultaneous inversion of the level, tilt, and horizontal-distance measurements. They determined 32 centers of inflation and deflation, which clustered into two groups, one at the south end of Kilauea caldera at depths from 2–7 km and the other near Makaopuhi Crater on the east rift zone at depths of 3–8 km. Their results show that although the general deformation pattern is apparently elastic, there are departures from ideal elastic behavior. The differences between measured and calculated horizontal displacements indicates that a gradual north-south extension across the summit caldera occurred during 1966–1970.

Changes in gravity as much as a few tenths of a milligal accompany the inflation and deflation of the summit area of Kilauea (Johnson, chapter 47; Dzurisin and others, 1980; Jachens and Eaton, 1980). These changes are more complex than those expected from simple changes in elevation, and they indicate that mass that is not proportional to the volume changes can be both added to and removed from the summit region.

The volume of the shallow magma-reservoir system beneath Kilauea can be estimated by assuming that it is roughly spherical with a diameter similar to the 3.5-km diameter of the caldera. Because the magma-reservoir system is probably a network of magma bodies separated by screens of solid rock, only part of this 22-km^3 volume is estimated to be molten rock. A net volume of 11 km^3 would be the same as the estimate of magma-reservoir volume made by Wright (1984, p. 3238) on the basis of his summary analysis of the geodetic data.

Earthquake hypocenters also provide important and independent evidence on the shallow magma-reservoir system. Koyanagi and others (1976), on the basis of an aseismic zone largely surrounded by an envelope of seismic sources beneath Kilauea caldera, estimated that the zone of primary summit magma storage has a mean diameter of 3 km and extends from a depth of 3 km to 6 km beneath the surface. Their interpretation is based on the concept that the magma reservoir is too ductile to produce earthquake-generating fractures, whereas the rocks above and around the magma storage zone respond to inflation and deflation of the magma reservoir by brittle fracturing.

Ryan and others (1981) expanded this approach and produced a detailed model of Kilauea's magma-reservoir system from the surface to a depth of 15 km (fig. 42.7). Their model has a primary conduit extending vertically beneath the south end of the caldera, an upper-east-rift-zone pipe extending vertically through depths of 2–6 km beneath the Koae fault zone 1 km southwest of Kokoolau Crater, two horizontal ducts connecting the primary conduit and the pipe at depths of about 2 km and 6 km, and an extension of the upper horizontal duct beneath the east rift zone to the Mauna Ulu eruption site.

The main shallow magma-storage reservoir beneath Kilauea is apparently not completely aseismic. During times of rapid summit collapse and initial reinflation, swarms of peculiar microearthquakes have their apparent source within or very near the margins of the summit magma reservoir. These earthquakes generally have magnitudes less than 1 and have a low-frequency, emergent signal. They are difficult to locate because they are only recorded on a few seismographs near the summit of Kilauea and their onset signals are not clear enough to establish accurate arrival times. These swarms of long-period earthquakes are thought to be related to rapid readjustments among magma pockets within the plexus of the main magma reservoir.

The question of a deeper storage reservoir about 25 km beneath Kilauea remains unresolved. At present, deformation data are not accurate enough to detect small inflations and deflations of a zone that deep. The region at that depth is relatively aseismic, but no envelope of earthquake hypocenters surrounds it. Wright (1971) proposed a region of temporary accumulation of magma at a depth of 20–30 km beneath Kilauea to allow for removal of olivine and pyroxene (fig. 42.8) He called this region the intermediate staging area.

The dynamic nature of the well-established shallow magma-reservoir system beneath Kilauea is currently being investigated from several directions. Epp and others (1983) have shown that there is a

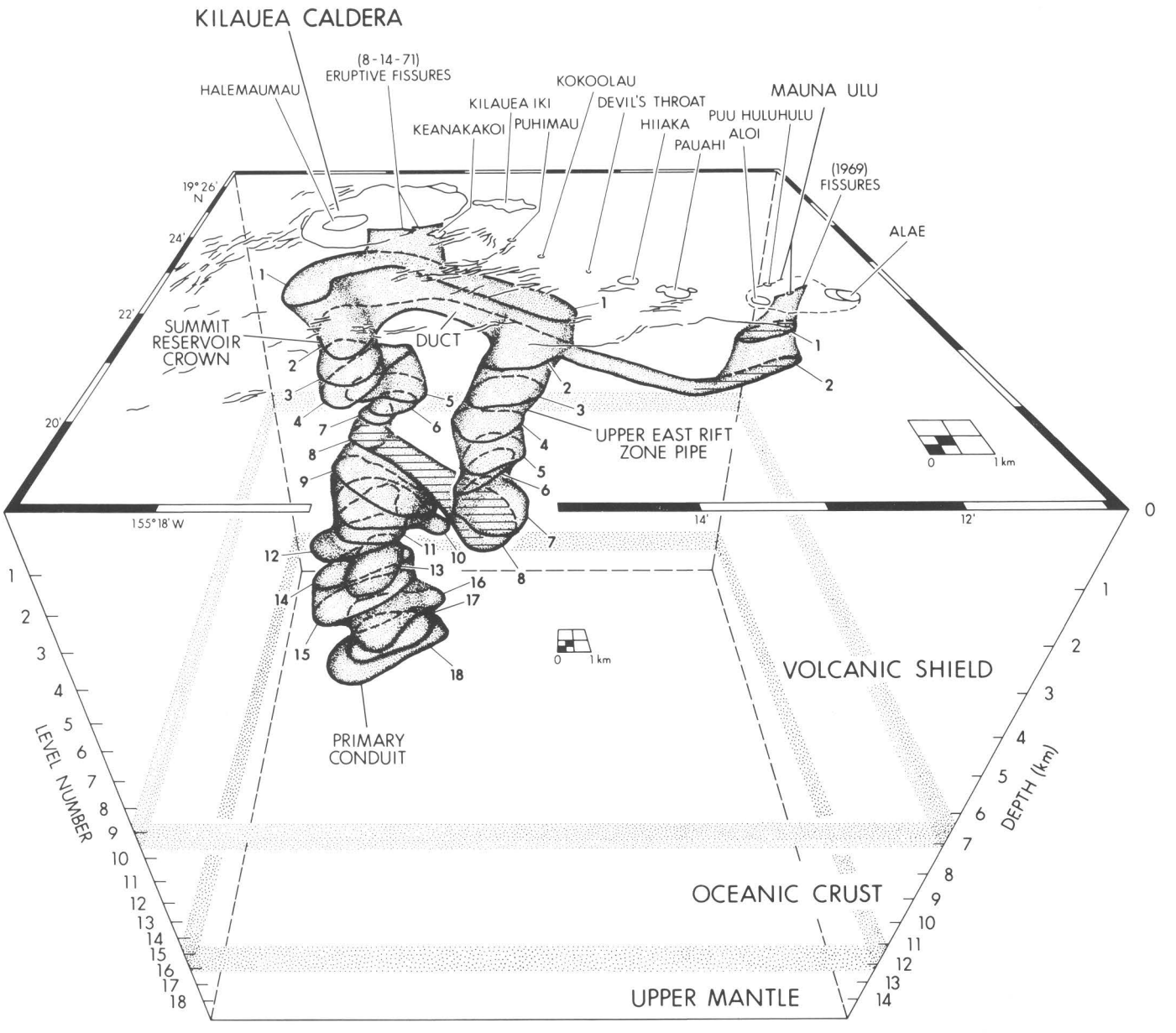

FIGURE 42.7.—Perspective view northward and downward into interior of Kilauea Volcano, from Ryan and others (1981). Magma conduits are defined by zones of earthquake hypocenters that surround them over periods of several years. Numbers on magma conduits represent horizontal sections at depths corresponding to level-number scale on left side.

strong linear correlation between the amount of summit deflation and the elevation of a flank eruption of short duration (fig. 42.9). Summit eruptions involve little or no deflation, whereas low-elevation flank eruptions are accompanied by large deflations. A simple explanation of this relation is that the magma pressure in the reservoir drops until it is balanced by the back pressure from the column of magma in the conduit from the reservoir to the surface. If this is the case, the magma pressure in the reservoir at the end of an eruption is simply the product of the average density of the magma column multiplied by the elevation difference and the gravitational constant. For example, assuming the average density of the magma column is 2.7 g/cm^3, the pressure in the magma reservoir 3 km below sea level beneath Kilauea following the eruption at Kapoho (30-m elevation) in 1960 would have been 83 MPa (830 bars); the lowest pressure in the magma reservoir during the past few decades. Since there are no major deflations associated with summit eruptions, there must be little or no pressure drop in the magma reservoir during these eruptions. The pressure of a magma column from the present floor of Kilauea caldera to a depth of 3 km below sea level would be 109 MPa. This difference of 26 MPa (109 minus 83) is the approxi-

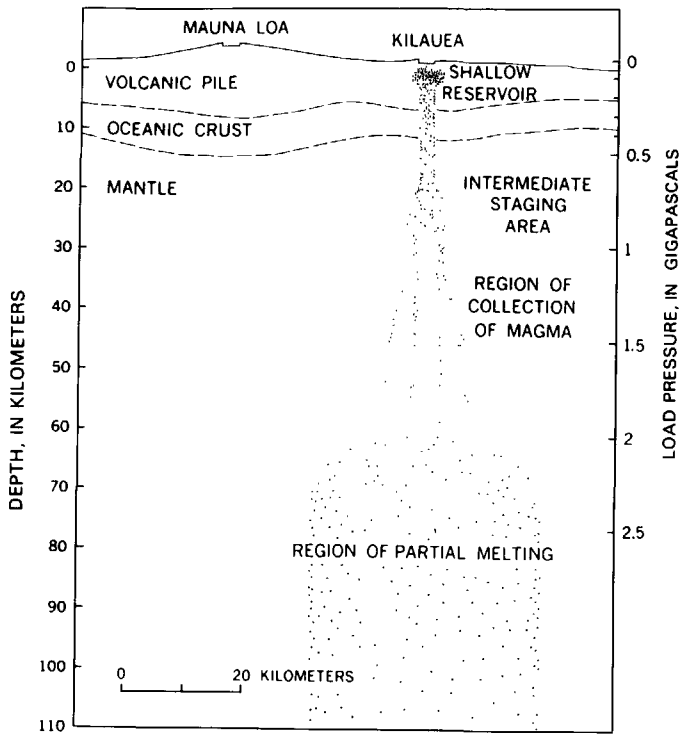

FIGURE 42.8.—Schematic cross section of Kilauea Volcano by Wright (1971) outlining regions of melting, transport, and storage of magma. Fractionation of magma occurs mainly in intermediate staging area and shallow reservoir, but also during its ascent from 60 to 30 km.

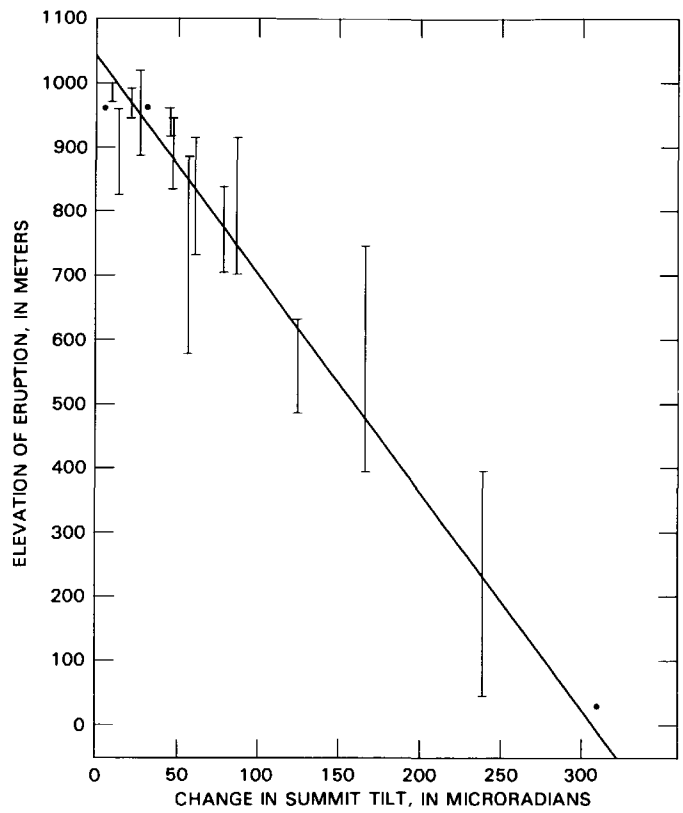

FIGURE 42.9.—Deflation measured by change in radial summit tilt at Kilauea Volcano versus elevation of associated vents during eruptions from 1955–1979. Bars indicate that eruptions occurred from fissures with considerable range in elevation. Linear relation of deflation and vent elevation indicates that pressure drop in summit magma reservoir is closely related to hydraulic head of magma at erupting vent. Modified from Epp and others (1983).

mate maximum range of pressure change in the shallow magma-reservoir system beneath Kilauea during the past few decades. In addition, the pressure change related to the amount of rapid deflation can be estimated from the data of Epp and others as 0.17 MPa (1.7 bars) per centimeter of summit deflation. Davis and others (1973, 1974, 1979) concluded from the absence of any marked piezomagnetic effects related to tilt changes at the summit of Kilauea that the volcano can support no large-scale pattern of shear stresses. They suggested that the rocks surrounding the shallow magma reservoir are of low shear strength and may behave in a plastic manner. Because the summit region of Kilauea probably does not behave in a perfectly elastic manner, particularly over time periods of months to years, slow inflations may represent volume changes more closely than pressure changes in the magma reservoir.

Magmafracting of the host rocks surrounding the magma reservoir appears to take place when the magma pressure reaches or slightly exceeds lithostatic pressure. This indicates low bulk tensile strength in the surrounding rocks.

The residence time for magma storage in the shallow reservoir system beneath Kilauea is easily estimated from the annual supply rate (0.11 km^3/yr, Swanson 1972; 0.086 km^3/yr, Dzurisin and others, 1984) and the volume of the reservoir system (11 km^3, Wright, 1984). The result, 100–120 yr, should be regarded as an average residence time. Some magma may crystallize in remote niches in the reservoir system and never erupt, while other magma batches, such as some of that which supplied the Kilauea Iki eruption in 1959, may spend only a small fraction of the average residence time in the magma reservoir system.

Another dynamic quality of shallow Hawaiian magma-reservoir systems on a vastly different time scale is their apparent ability to migrate upward as the volcano they supply grows in height. The submarine volcano Loihi is assumed to be in a youthful stage of growth, yet already a caldera and rift zones have apparently developed upon it (Klein, 1982a; Malahoff and others, 1982). This implies that it has probably developed a shallow magma-reservoir system. The depth to Loihi's magma reservoir is not known, but the summit area of Loihi is about 1 km below sea level. Mauna Loa Volcano, at the other extreme, has reached a height of 4,169 m, and recent studies by Decker and others (1983) indicate that it has a shallow magma-reservoir system similar to that beneath Kilauea. The source of inflation shown by deformation measurements before the 1984 eruption of Mauna Loa was at a depth of only 3 km beneath the summit. Thus, the top of the magma-reservoir system beneath Mauna Loa is at nearly the same elevation as the ground

surface at the summit of Kilauea. The long-term evolution of Hawaiian volcanoes apparently involves progressive upward remelting, stoping, and (or) shoving aside of the rocks overlying the shallow magma-reservoir systems.

SHALLOW INTRUSIONS

As the shallow magma-reservoir system slowly inflates with magma added from depth, the increasing pressure and volume puts new stresses on the surrounding rocks. Sometimes the summit deflates slowly or remains level as magma moves almost aseismically into the open magma conduit of the upper and middle east rift zone of Kilauea. These slow intrusions or readjustments of the existing shallow magma-reservoir system involve volume flow rates of 1–10 m^3/s. When stresses reach the breaking strength of the host rocks surrounding the magma- reservoir system, fractures occur and a dike or sill is intruded upward or laterally into the shallow, brittle rocks of the volcanic edifice. These rapid intrusions are common at the summit and along the rift zones of Hawaiian volcanoes, and they occur at volume flow rates of 10^2–10^3 m^3/s. During 1959–1980, 21 rapid intrusions without eruptions occurred at Kilauea Volcano and 25 other rapid intrusions led to eruptions (Klein, 1982b).

The orientation of rapid, shallow intrusions is controlled by the strength of the rocks and by ambient stresses generated by both internal magma pressure and external gravitational forces. Fiske and Jackson (1972) have shown that the topography of the earlier volcanoes in Hawaii affects the orientation of the rift zones of later forming, adjacent volcanoes (see Peterson and Moore, chapter 7, fig. 7.7). Rift zones form perpendicular to the direction of least compressive stress; once a topographic ridge has formed from numerous dike-fed eruptions along a rift zone, the gravitational slumping of this ridge reinforces the least compressive stress in a direction perpendicular to the ridge. The name Mauna Loa means long mountain, and this great shield volcano is markedly elongated by the gently-sloping ridges along its northeast and southwest rift zones. Kilauea Volcano is younger than Mauna Loa Volcano and inherited the gravitational stress system on the southeast flank of Mauna Loa. Kilauea thus developed a principal east rift zone and subsidiary southwest rift zone.

A typical rapid intrusion into a rift zone of Kilauea Volcano is characterized by a swarm of small earthquakes occurring at rates of 2–4 events per minute that lasts for a few hours to a few days. The sources of these earthquakes are concentrated at 2- to 4-km depths beneath a segment of the rift zone several kilometers long. The hypocenters of the swarm outline a tabular shape a few kilometers high and about 1 km wide. The hypocenters also migrate progressively in time and space, both vertically and along the rift zone, indicating that the intruding fracture is propagating at a velocity of a few hundred to a few thousand meters per hour. The linear trace of intrusions that reach the surface as eruptions, and the eroded rift zones of older Hawaiian volcanoes, indicate that the rapid intrusions are steeply dipping dikes that parallel the rift zones. However, the shapes of the rapidly intruded bodies and the more open magma conduit along the upper and middle east rift zone of Kilauea below a few kilometers depth have not been established. The concentration of earthquake hypocenters at depths of 2–4 km in the seismic swarms associated with rapid intrusions suggests that the intrusion has some sort of axis at that depth.

In addition to their associated earthquakes, rapid intrusions are generally characterized by rapid deformation of the summit area and ground deformation above the intruded region. Volcanic tremor, new gas emissions and electromagnetic field changes also accompany some intrusions.

Rapid intrusions into the summit region of Kilauea Volcano are accompanied by rapid summit inflations, whereas rapid flank intrusions into the rift zones remove magma from the summit region and are accompanied by rapid subsidence of the summit area. Rapid intrusions into the rift zones of Kilauea have typical magma volumes of 10^6–10^7 m^3 and they occur at volume rates of 10^2–10^3 m^3/s. These typical volumes are associated with subsidence of the summit by 1–15 cm and pressure drops of 0.3–3 MPa in the shallow magma reservoir. An approximate rate of magma supply to a dike intruding the rift zones can be estimated from the tilt record. The radial tilt at HVO on the northwest side of Kilauea caldera has been calibrated as representing about 3.3×10^5 m^3 of subsided volume for each microradian (μrad) of inward tilt (Dzurisin and others, 1984). This is a minimum value for the amount of magma removed because of the unknown values of strength in the rocks surrounding the summit magma reservior and of the bulk compressibility of the reservoir. In addition, one microradian of inward radial tilt at HVO also indicates an approximate vertical subsidence of 5 mm at the apex of the deformation bulge and an approximate pressure drop in the summit magma reservoir of 90 kPa (0.9 bars).

Ground deformation in the area above a rapid intrusion causes rapid excursions and sometimes reversals of tilt vectors on nearby recording tiltmeters. Ground cracking is also common with the larger and shallower intrusions, and new or renewed volcanic-gas fumaroles are sometimes formed along these surface fractures.

When the volume rate of magma intrusion exceeds about 0.5 μrad of summit subsidence per hour (about 50 m^3/s), shallow volcanic tremor begins to appear as a background vibration between individual events in the earthquake swarm. Shallow volcanic tremor is a continuous ground vibration with a predominant frequency of 2–5 Hz, and it is associated with shallow subsurface movement and eruption of magma.

Increases in the electrical self-potential anomalies associated with active rift zones and changes in the electrical conductivity of the summit region of Kilauea also occur in association with the larger intrusions. The absence of observable magnetic anomalies associated with rapid subsidence of the summit area of Kilauea has led Davis and others (1974) to postulate a plastic envelope of low-rigidity rock material surrounding the summit magma reservoir.

During 1980 there were five rapid intrusions without eruptions into the east rift zone of Kilauea Volcano (table 42.1). During 1981 the intrusions shifted into Kilauea's southwest rift zone and on August 10–12 a large intrusion affected an 18-km-long segment of that rift. Excellent observations were made on this rapid intrusion, and they are summarized as follows:

TABLE 42.1.—*Rapid intrusions without eruptions into the east rift zone of Kilauea Volcano during 1980*

[*, possible eruption of a few cubic meters of lava; EM, electromagnetic; n.d., not determined]

Date	Location	Length (km)	Height (km)	Minimum depth (km)	Volume ($m^3 \times 10^6$)	Propagation rate (m/h)	Gases	EM anomalies
March 2	Hiiaka	2	2	1	.6	n.d.	no	no
March 10–12*	Mauna Ulu	5	3	.5	5.3	200–500	yes	no
August 27–28	Puhimau	4	3	.5	2.3	1,000	yes	yes
October 22	Mauna Ulu	2	2	2	.6	n.d.	yes	yes
November 2	Kokoolau	2	2	1	2.0	700	no	no

The August 10–12, 1981, event involved at least 4×10^7 m^3 of magma and was the largest rapid intrusion without an eruption of Kilauea Volcano since increased seismic and deformation monitoring began in the late 1950's.

Thousands of small earthquakes occurred in a swarm at rates as high as 3–4 per minute and although most were microearthquakes, a few reached magnitudes of 3.5–3.9. The hypocenters of the earthquakes in the region of the intrusion formed a zone 18 km long, 1–2 km wide, and extending from the surface to 5-km depth beneath the southwest rift zone (see Klein, chapter 43, fig. 43.90). Downrift migration of the earthquake locations indicates an intrusion propagation rate of 2 km/h slowing to 0.5 km/h (fig. 43.90).

Shallow volcanic tremor and rapid summit subsidence at about 10 μrad/h indicate a high-volume rate of intrusion, as much as 10^3 m^3/s. The tilt at HVO totaled 107 μrad of deflation, and an elastic model of the summit level changes indicates 4×10^7 m^3 of subsidence volume. The ratio of the volume rate to the downrift migration rate gives an estimate of the cross sectional area of the intrusion. This area is 2×10^3 m^2, and if the intrusion is a dike 3 km high, then its width is about 0.7 m.

Large horizontal and vertical displacements occurred along the southwest rift zone, indicating major extension across the rift on the order of 1 meter; and a horst-and-graben pattern developed that indicates a shallow dike intrusion parallel to the rift and dipping steeply southeast. New surface cracks parallel to the rift follow the trend of the 1974 eruption vents and continue southwest for several kilometers (fig. 42.10). Much of the new surface cracking involves reactivation of 1974 or older fractures.

Renewed gas emissions and increased temperatures were measured at a fumarole on a newly activated surface crack. Self-potential anomaly changes were measured in the Koae fault system 5 km east of the trend of the seismic swarm; except near the renewed gas vent, no significant self-potential changes occurred over the seismic zone.

During 1982, rapid intrusions causing eruptions occurred twice in the summit area of Kilauea, in April and September. In June 1982 there was another large rapid intrusion without eruption into the southwest rift zone. Activity then switched back to the east rift zone and a major rapid intrusion and eruption occurred there during January 2–3, 1983. That event formed the magma conduit that has erupted through 47 episodes so far (as of June 1986) during the long-lasting 1983–1986 (and continuing) eruption of Kilauea Volcano.

The dike swarms formed by many rapid intrusions over the years tend to wedge apart the volcanic edifice and lead to long-term dynamic evolution of the rift zones.

RIFT ZONES

The rift zones of Hawaiian volcanoes are "Pele's under ground roads" referred to by Ellis' Hawaiian guides in 1823 (Ellis, 1827). They are persistent zones of weakness in the volcanoes' flanks, resulting from thousands of rapid lateral intrusions. Many of these rapid intrusions also cause eruptions.

The rift zones are not primary conduits that penetrate to magmatic source depths; rather they are secondary features that form from radial pressures generated in the summit reservoirs at depths of

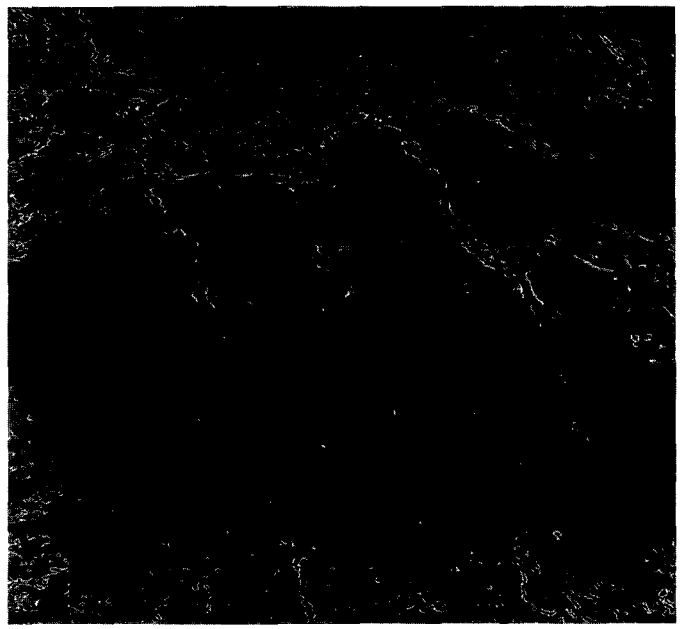

FIGURE 42.10.—Aerial photograph of ground cracks formed during August 10, 1981, intrusion beneath southwest rift zone of Kilauea Volcano. Area here covered by barren lava flows and by reworked volcanic ash from 1790 eruption. Cracks are as much as 1 m wide, and a shallow graben about 20 m wide has formed between principal fractures. Some of these cracks existed before the August 10, 1981 intrusion and were reactivated by the event. U.S. Geological Survey photograph by Norman Banks.

a few kilometers. Earthquake locations along the rifts of Kilauea Volcano indicate that the main dynamic axes of the rifts are about 3 km beneath the surface and that the overall rift zones extend from the surface to a depth of about 8 km below sea level. Because of isostatic subsidence of the Island of Hawaii, 8 km is about the depth of the old Cretaceous sea floor on which the Hawaiian volcanoes formed. It appears that the rift zones penetrate virtually the entire volcanic pile but do not extend down into the underlying oceanic crust.

Fiske and Jackson's (1972) analysis of the evolution and orientation of Hawaiian rift zones is also consistent with the concept that the rift zones are fairly shallow and secondary features compared to the deep magma conduits that supply the summit magma reservoirs. In their view, the rifts are fed by lateral intrusions from the summit magma reservoirs, and their orientations are controlled by the gravitational stresses of the surface topography.

The north-south elongation of the submarine topography and seismicity of Loihi Seamount (Klein, 1982a) indicates that rift zones are generated in the early stages of life of Hawaiian volcanoes, and the major rift systems still active on Hualalai and Haleakala Volcanoes indicate that rift zones persist into the waning stages. Thus, although the rifts are secondary features, they play a major and long-lived role in the structure and dynamics of Hawaiian volcanism.

The rift zones of Kilauea Volcano have been very active during the past few decades, and their dynamic behavior is therefore fairly well known. From 1959 through 1984 there were 20 rapid intrusions into the east rift zone without eruptions and 19 rapid intrusions that resulted in eruptions. During the same period there were 8 rapid intrusions into the southwest rift zone without eruptions and 2 rapid intrusions that resulted in eruptions. Summit activity over this same period consisted of 4 rapid intrusions without eruptions and 12 with eruptions. Eleven of these intrusions beneath the summit area were emplaced between 1966 and 1984.

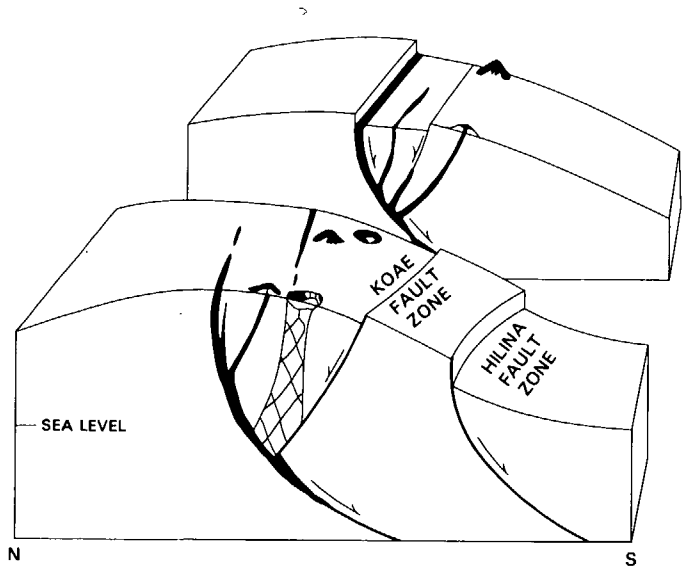

FIGURE 42.11.—Schematic block diagrams of the east rift zone of Kilauea Volcano looking downrift, from Moore and Krivoy (1964). In this interpretation stresses causing rift are largely gravitational, and rift zone dips seaward at depth. Pit craters (cross-hatched example) form by collapse into voids within rift if magma is drained far downrift.

Since each rapid intrusion and eruption involves a dike being injected into the carapace or flank of the volcano, the volcano must widen to accommodate these multiple intrusions. Using an estimate of 0.5 m for an average dike width, we can infer that the summit and upper rift zones of Kilauea Volcano should have widened by 5.5 m over this 19-year period. The actual measured widening of Kilauea caldera, between HVO on the northwest rim and Ahua on the southeast is 4.2 m from 1966 to 1984. There are various possible reasons why the estimate and the corrected measurement differ: the average dike width may be less than 0.5 m; each dike probably extends only part way across the summit area; and there probably is some elastic compression stored in the rocks adjacent to the intruded dikes. Even allowing for these considerations, it is clear that major widening of the summit of Kilauea Volcano perpendicular to its rift zones has occurred in the past few decades.

The widening of the rift zones becomes less downrift because fewer dikes reach long distances from the summit. The fact that some summit eruptions are followed by progressive downrift migration of rapid intrusions and flank eruptions can be explained by this progressive summit wedging effect extending down the rift zones.

Eaton and Murata (1960) suggested that a core of magma in the east rift zone of Kilauea remains molten between some eruptions, and Swanson and others (1976b) discussed this concept more thoroughly on the basis of seismic evidence from 1968 and 1969 eruptions on the east rift zone. Hardee (1982) has shown by theoretical heat-flow calculations that if a sufficient number and volume of intrusions are injected into a region, part of these intrusions will remain molten. He calculated (written commun., 1983) that the recorded intrusions into the east rift zone of Kilauea Volcano should result in a molten conduit from the summit to about 30–40 km downrift. The number and volume of intrusions into the southwest rift zone, however, have not been sufficient to maintain a molten conduit. The evidence for slow intrusions into the east rift zone provided by slow aseismic deflations of the summit and measurable inflation along the east rift zone as far as 32 km from the summit (Dieterich and Decker, 1975; Swanson and others, 1976a) give strong support to Hardee's conclusion.

Moore and Krivoy (1964) were among the first to consider the dynamics of the east rift zone of Kilauea Volcano. They suggested that gravitational slumping was the major factor causing the rift to widen and that magma moved rather passively into the fractures formed in the head of the slumping block (fig. 42.11). Swanson and others (1976a) took the opposite position that magmatic pressure pushed the rift apart and that slumping was the result rather than the cause of the rifting process (fig. 42.12). In a sense they are all correct; the gravitational and magmatic stresses are additive, and together they control the evolution of the rift zone.

Swanson and others (1976a) measured the progressive shortening of survey lines across the Hilina fault system on the south flank of Kilauea Volcano south of the east rift zone. They recognized that

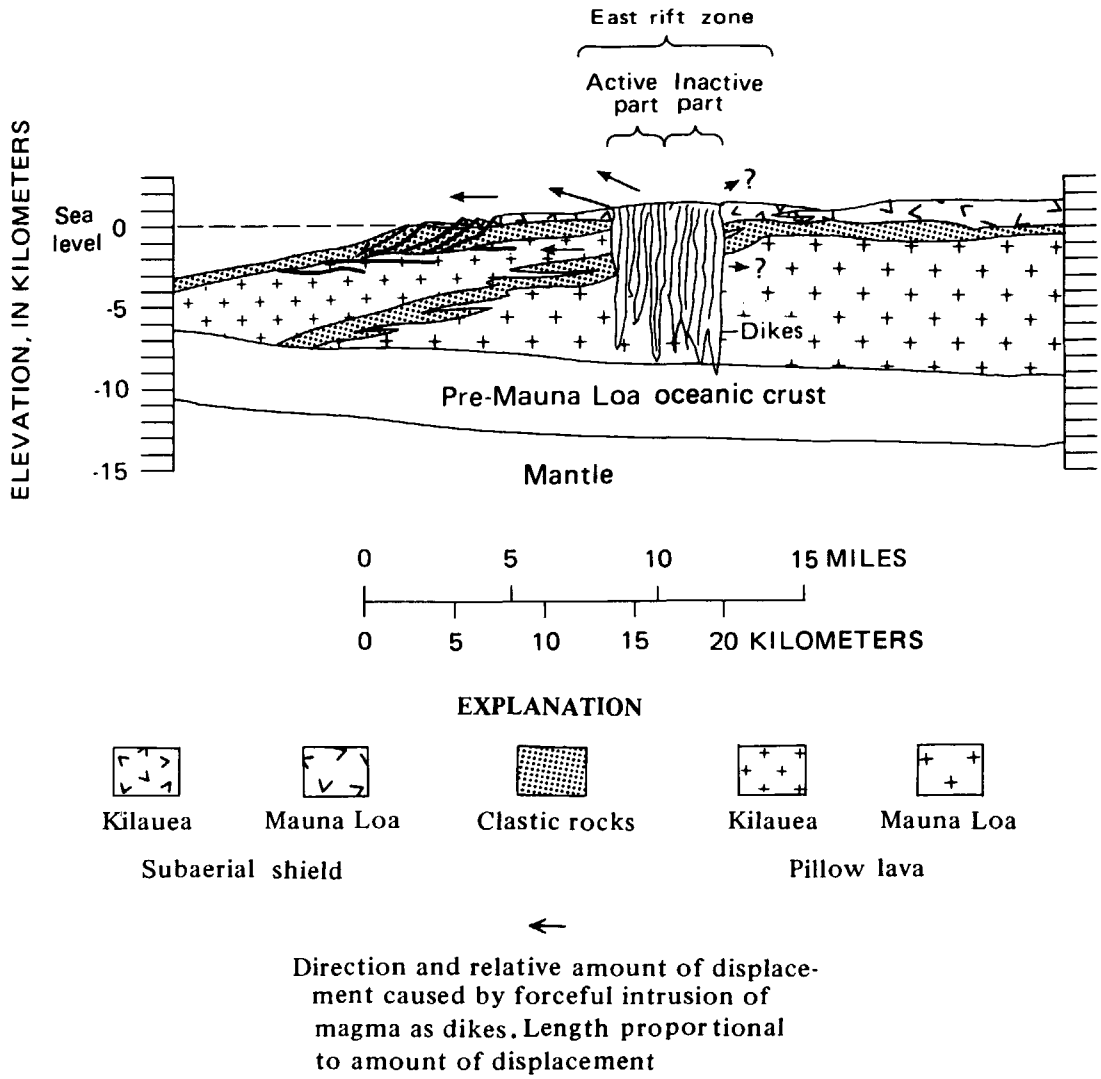

FIGURE 42.12.—Schematic cross section at true scale of east rift zone of Kilauea Volcano looking uprift, from Swanson and others (1976). In this interpretation stresses causing rift arise from forceful injection of magma, and dikes are nearly vertical.

the intrusions and eruptions occurring on the east rift zone in the late 1960's and early 1970's were wedging the rift apart but that much of the widening was being accommodated by compression and uplift of the flanks of the rift zone. They realized that this accumulating strain might be released by sudden failure of the Hilina fault system, and they wrote in 1974 (Swanson and others, 1976a, p. 35): "Some of the data suggest that the Hilina fault system is poised for another episode of subsidence, with only minor additional ground displacement needed to trigger it. Most of the strain acquired since 1965 remains, however, and we anticipate a subsidence (strain-release) event of unknown magnitude in the not too distant future."

Fifteen months later, but before their work was formally published, a magnitude-7.2 earthquake released the pent-up compressive strain in the south flank of Kilauea. Portions of the south coast moved seaward several meters and subsided as much as 3.5 m (Tilling and others, 1976; Lipman and others, 1985). Swanson and others (1976a) had clearly forecast the nature and imminence of that major earthquake.

Analysis of the source mechanism and aftershock pattern for this earthquake (Ando, 1979; Furumoto and Kovach, 1979) indicates that the strain was released by rupture on a nearly horizontal fault about 8–10 km beneath the south flank of Kilauea along 50 km of the coastline and across a region 10–20 km wide, bounded on the north by the east and the southwest rift zones. The slip on the fault was several meters in a seaward direction away from the rift zones (fig. 42.13). The net long-term result of dikes wedging into a rift zone therefore appears to be widening of the rift zone down to a depth of about 8 km, and this widening is accommodated by intermittent movement of the seaward flank of the volcano along a nearly horizontal slip surface close to the old sea floor on which the volcano grew.

More than 3 m of extension occurred on survey lines on the

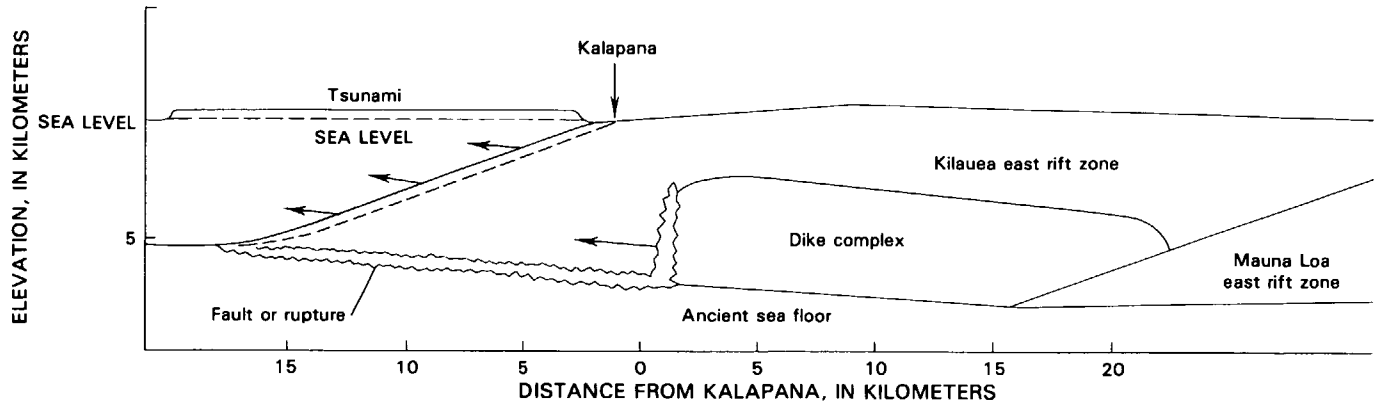

FIGURE 42.13.—Schematic cross section of east rift zone of Kilauea Volcano looking uprift and showing inferred mechanism of 1975 earthquake (M=7.2) and tsunami. Dike intrusions (at left side of dike complex) compress adjacent rocks over time. When stress reaches breaking point, unbuttressed flank of rift zone suddenly fails. Modified from Furumoto and Kovach (1979).

south flank of Kilauea Volcano during the period of the major earthquake; figure 42.14 shows changes from 1970 to 1984 in the 8.6-km-long line that extends from the north side of the Hilina fault system to the south coast.

It appears that Hawaiian volcanoes do not only grow upward from successive lava flows piled one upon another, but they also grow sideways by successive intrusions into the summits and rift zones and by intermittent failure of the seaward flanks of the rift zones to accommodate these intrusions. The east rift zone of Kilauea Volcano slopes down gently for 50 km from the summit at 1,200 m to sea level. It continues for another 70 km eastward as a slightly steeper submarine ridge to depths of nearly 5,000 m below sea level (Moore, 1971). Since Epp and others (1983) have shown that eruptions at lower elevations on the rift tend to be more voluminous than single short-lived eruptions high on the rift, it is clear that eruptions must become progressively much rarer at large distances from the summit. This decrease is probably caused by at least two factors: the widening of the rift zone and its wedging effect apparently decrease with distance from the summit; and the molten core in the rift zone also apparently decreases in size and finally disappears with distance from the summit. The very even slope of the ridge along the axis of the east rift zone indicates that the frequency and volumes of eruptions maintain a steady equilibrium over long time spans.

ERUPTIONS

Most volcanic eruptions in Hawaii are outpourings of incandescent lava from linear or point-source vents. Lava fountains from linear vents are called curtains of fire and reach heights up to about 200 m. Lava fountains from point-source vents reach heights up to about 600 m.

A reduction in the volume rate of eruption or in the gas content reduces the vigor of lava fountaining until incandescent lava simply pours out from the linear or point-source vent. Vents in the bottoms or sides of craters feed active lava lakes that, at low-volume rates of eruption, can remain in eruption for years.

Lava flows fed by the erupting vents move down the slopes of the volcano or pond in topographic depressions. The formation of various lava textures and structures such as aa, pahoehoe, and lava tubes depends upon the complex interaction of the rheological properties of the lava, the volume rate and continuity of the eruption, and the environment and topography over which the flows are moving (Swanson, 1973; Holcomb and others, 1974; Peterson and Swanson, 1974; Peterson and Tilling, 1980). Lava commonly drains back down old surface cracks or even down the active fissures as the eruption wanes.

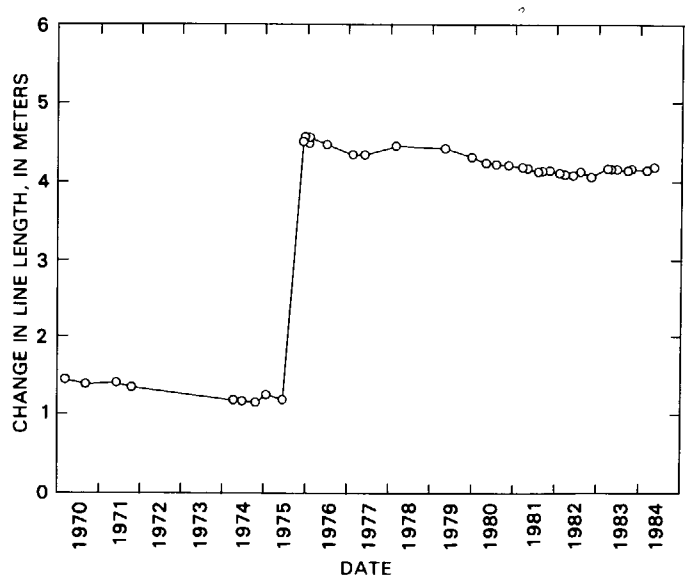

FIGURE 42.14.—Multiple surveys (small circles) of 8.6-km-long line on south flank of upper east rift zone of Kilauea Volcano indicate gradual contraction from 1970 to 1975, sudden extension related to the M=7.2 earthquake of November 1975; and renewed gradual contraction since 1975. Surveyed line runs from Goat to Apua Point.

Data on the eruptions of Kilauea and Mauna Loa Volcanoes since 1823 are compiled in Peterson and Moore (chapter 7, tables 7.3, 7.4). The long-lived, low-volume-rate eruptions of active lava lakes in the caldera of Kilauea Volcano that continued with a few interruptions from their first-recorded observation in 1823 until 1924 are not included in table 7.4.

The quality of these data on eruptions becomes, in general, better for more recent times. Continuous scientific observation began in 1912, and aerial observation and helicopter access to remote eruption sites has increased progressively during the past few decades.

Several major changes in the character of eruptions of Kilauea are evident in table 7.3. Between 1823 and 1919, during the century of active lava lakes and slow filling of Kilauea caldera, there was only one confirmed east-rift-zone eruption (in 1840) and one southwest-rift-zone eruption (1868). Beginning in 1919 and culminating with a probable east-rift submarine eruption in 1924, three rift eruptions marked the end of a long period of predominance of summit activity. The 1924 summit eruption, associated with subsidence of more than 400 m in the magma column feeding the active lava lake in Halemaumau Crater, has been the only explosive eruption in Hawaii since written records began in 1823.

From 1924 to 1934, seven small eruptions filled the bottom of the deep Halemaumau Crater formed by subsidence in 1924; from 1934 until 1952 there were no eruptions of Kilauea. This hiatus was ended by two eruptions in Halemaumau Crater in 1952 and 1954, and then a major eruption on the lower east rift zone in 1955 began a still-continuing period (1955–1986) of major eruptive activity on the east rift zone (18 eruptions), the summit (12 eruptions), and the southwest rift zone (2 eruptions).

What constitutes a separate eruption of Kilauea is not always clear. The breakout of an eruption in an entirely new location—not just an extension of a fracture associated with an ongoing rapid intrusion—is one criterion. Another criterion is the occurrence of a seismic swarm at the beginning of an eruption in a familiar location, like Halemaumau Crater. This indicates that a new subsurface fracture has been opened to feed the surface eruption. In long-lived eruptions such as the Mauna Ulu eruption on the upper east rift zone from 1969 to 1974 and the current Puu Oo eruption on the middle east rift zone from 1983 to 1986 (and still continuing), there have been periods of repose between episodes of high lava fountaining or other changes in the character of the eruption phases. However, the same general conduit system appears to be involved throughout these continuing eruptions, and on this basis these distinct episodes or phases are not considered separate eruptions.

Under these limits of definition, the eruption statistics for Kilauea from 1918 through 1984 are as follows: The average time from the beginning of one eruption to the next is 494 days (range is 2 to 6,504 days). The average duration of an eruption is 86 days (range is less than 1 to 1,884 days). The average volume of an eruption is 2.7×10^7 m^3 (range is less than 10^5 to over 4×10^8 m^3). The average area coverered by an eruption is 4.4 km^2 (range is 0.1 to 55.7 km^2).

Dzurisin (1980) has compared tidal stresses to the onset times of eruptions of Kilauea and concludes that more eruptions begin near maximum fortnightly tidal stress (new moon and full moon) than would be expected by random chance at the 90-percent confidence level. He ascribes this to the triggering effect of tidal stresses on a system that has almost reached the point of eruption.

Klein (1982b) has investigated the statistical pattern of the eruptions of Kilauea since 1918 and concludes that the overall pattern is largely random, but that some non-random features appear. He finds that summit eruptions tend to cluster, that large-volume eruptions are usually followed by repose times that are longer than average, and that long periods of increased activity of Kilauea—for example during 1960–1979, when the average repose period was only 261 days—are associated with periods of less vigorous activity of Mauna Loa Volcano.

A complete list of known historical Mauna Loa eruptions is presented in table 7.4. Mauna Loa has not had any sustained lava-lake activity during this time period. There is less apparent variation in the pattern of Mauna Loa eruptions than in that of Kilauea eruptions, but the eight summit eruptions of Mauna Loa that occurred between 1870 and 1876 show an unusual clustering of locations and shorter-than-average repose times. In addition, the complete lack of eruptions between 1950 and 1975 was an unusually long repose period for Mauna Loa.

Statistics for Mauna Loa eruptions are as follows: The average time period from the beginning of one eruption to the next is 1,459 days (range is 104 to 9,165 days). The average duration of an eruption is 69 days (range is less than 1 to 547 days). The average volume of an eruption is 1.88×10^8 m^3 (range is 2.7×10^7 to 6.88×10^8 m^3). The average area covered above sea level by an eruption is 34 km^2 (range is 5 to 91 km^2).

All historical eruptions of Kilauea and Mauna Loa Volcanoes appear to have started with a rapid intrusion injecting a dike upwards or sideways from some part of the shallow magma reservoir into the summit or flank of the volcano. These rapid intrusions precede the eruptions by minutes to days, and provide important warnings of both the probable imminent occurrence and the probable location of an eruption.

The character of an eruption depends on several factors and is best explained by examples:

The long-lived eruptions of active lava lakes in Kilauea caldera begin with a dike injection into the summit area. Pressure in the shallow magma reservoir is high enough to push magma to the surface, and the resupply rate from depth is sufficient to match the low-volume rate of eruption, which is typically about 3 m^3/s. The rift zones are strong enough to withstand magmafracting. These eruptions have become less common as Kilauea caldera has refilled because the higher the magma column, the more pressure there is to fracture the rift zones and thereby lower the magma column. The latest long-lived eruption of an active lava lake occurred in Halemaumau Crater in 1967 and lasted 251 days (Kinoshita and others, 1969).

Short-lived eruptions at the summits and along the rift zones of Kilauea and Mauna Loa Volcanoes are the most numerous. The volume rates of these eruptions are typically 10–200 m^3/s; since this

exceeds the resupply rate from depth, pressure rapidly drops in the shallow magma reservoirs. The eruptions stop when the reservoir pressure can no longer push magma to the surface. The latest eruption of this type on Kilauea Volcano occurred in the caldera in September 1982 and lasted 16 hours (Scientific Event Alert Network, 1982). The latest one of this type on Mauna Loa Volcano occurred along the northeast rift zone in March–April 1984 and lasted 21 days (Lockwood and others, chapter 19).

Although long-lived flank eruptions are more unusual, two have occurred on Kilauea Volcano since 1969: the Mauna Ulu eruption on the upper east rift zone from 1969 to 1974 (Tilling and others, chapter 16; Peterson and others, 1976; Swanson and others, 1979), and the Puu Oo eruption on the middle east rift zone from 1983 to 1986 and still continuing (Wolfe and others, chapter 17). These eruptions consist of many episodes from essentially the same vent area. The subsurface magma conduits apparently remain open between eruptive events because the onsets of new episodes are not preceded or accompanied by earthquake swarms. Individual episodes of lava fountaining involve volume flow rates of 50–400 m^3/s, but they generally last only about 10–20 hours and produce lava volumes of about 5×10^6–15×10^6 m^3. The longer term volume flow rates through several fountaining episodes or during sustained low-volume-rate phases average about 3 m^3/s, which is approximately the resupply rate of Kilauea Volcano for the past two decades.

The spectacular lava fountains and curtains of fire that characterize many Hawaiian eruptions are caused almost entirely by the rapid effervescense of gases boiling out of the magma at near-surface pressures and by the geometry of the vents. High-volume-rate eruptions of gas-rich magma in constricted vents produce the highest fountains. Gerlach and Graeber (1985), and Gerlach (written commun., 1985) have determined that magmatic gases of the volume and composition normally occurring in flank eruptions of Kilauea Volcano begin to boil rapidly out of magma at pressures equivalent to depths of only 40–100 m. In addition, as Paul Greenland has noted (written commun., 1984), near-surface pressures will move downward into an open magma column as rapid lava fountaining progressively unloads the upper part of the column, and the actual depth at which sustained effervescense is formed will be deeper than 40–100 m below the surface.

Most Hawaiian eruptions begin with linear vents (curtains of fire). After a few hours or days the fountaining becomes restricted to one or a few principal point-source vents. Apparently zones along the erupting fissure that were wider than average at the start of the eruption become enlarged by melting and erosion, while the narrower zones along the original fissure tend to freeze shut (Delaney and Pollard, 1982).

Once the magma flow supplying a fountaining vent is no longer replenished from depth, the fountaining will cease, and degassed surface lavas ponded near the vent will drain back into the conduit. Drainback in an active lava lake may also occur if the feeder dike is extended or some newly formed dike is generated in the subsurface. Magma in hydraulic communication will move toward the lowest pressure region in the system.

CALDERA COLLAPSE AND EXPLOSIVE ERUPTIONS

Hawaiian volcanoes have a reputation for producing numerous but relatively harmless eruptions of fluid lava. Explosive eruptions, similar to those at Surtsey Volcano in Iceland in 1963 (Thorarinsson, 1965), were probably common during the transition from submarine to subaerial eruptions in the Hawaiian Islands, but these usually cease after the summit of a volcano grows above sea level. Less than 1 percent of Hawaiian volcanic products above sea level are pyroclastic (Macdonald, 1972, p. 355), and most of these are tephra from high lava fountains. Nevertheless, major explosive eruptions of hydromagmatic and hydrothermal character have occurred in Hawaii. Their occurrence appears to be closely related to episodes of major caldera collapse.

The last major collapse and explosive eruption of Kilauea caldera occurred in 1790 (Swanson and Christiansen, 1973; Christiansen, 1979; Decker and Christiansen, 1984). The caldera was more than twice its present depth when visited by Ellis in 1823 (Ellis, 1827), but its depth and configuration prior to 1790 are not known.

Holcomb's paleomagnetic data (1980) indicate that lava overflows were occurring from the summit region of Kilauea during the period of about 1–0.3 ka, and Ellis' Hawaiian guides told him that "in earlier ages it used to boil up, overflow its banks, and inundate the adjacent country" (Ellis, 1827, p. 171).

A much smaller collapse accompanied by small explosive eruptions occurred at Kilauea in 1924 (Jaggar and Finch, 1924). A nearly full lava lake in Halemaumau Crater drained down more than 400 m as a major intrusion was injected into the lower east rift zone of Kilauea near Kapoho. This intrusion possibly fed an eruption on the submarine extension of the east rift zone, but there was no direct evidence of this.

As the magma column in Halemaumau Crater drained below zones of subsurface water beneath the summit of Kilauea Volcano, the equilibrium between the magma column and subsurface water was destroyed and steam explosions of hydromagmatic and hydrothermal origin issued from the crater (fig. 42.15).

The subsidence in 1924 occurred during February through April, and the multiple steam explosions occurred for 18 days in May. Since magma moves out of the summit reservoir through conduits in the rift zones, the volume rate of magma removal is limited and the process of caldera collapse occurs over periods of weeks to months rather than minutes to hours. In theory there should be time for people to evacuate the summit region of Kilauea in case of future caldera collapses.

Overflows of lava that were erupted from the summit region of Mauna Loa Volcano as recently as 590 years ago as determined by radiocarbon dating (J.P. Lockwood, oral commun., 1985) are beheaded by Mauna Loa caldera. When first mapped in 1841 (Wilkes, 1845), the caldera was 50–100 m deeper than the present surface of ponded lavas. Thus it appears that the present caldera on Mauna Loa is similar in many ways to Kilauea caldera; it formed only a few hundred years ago and has been rapidly refilled with

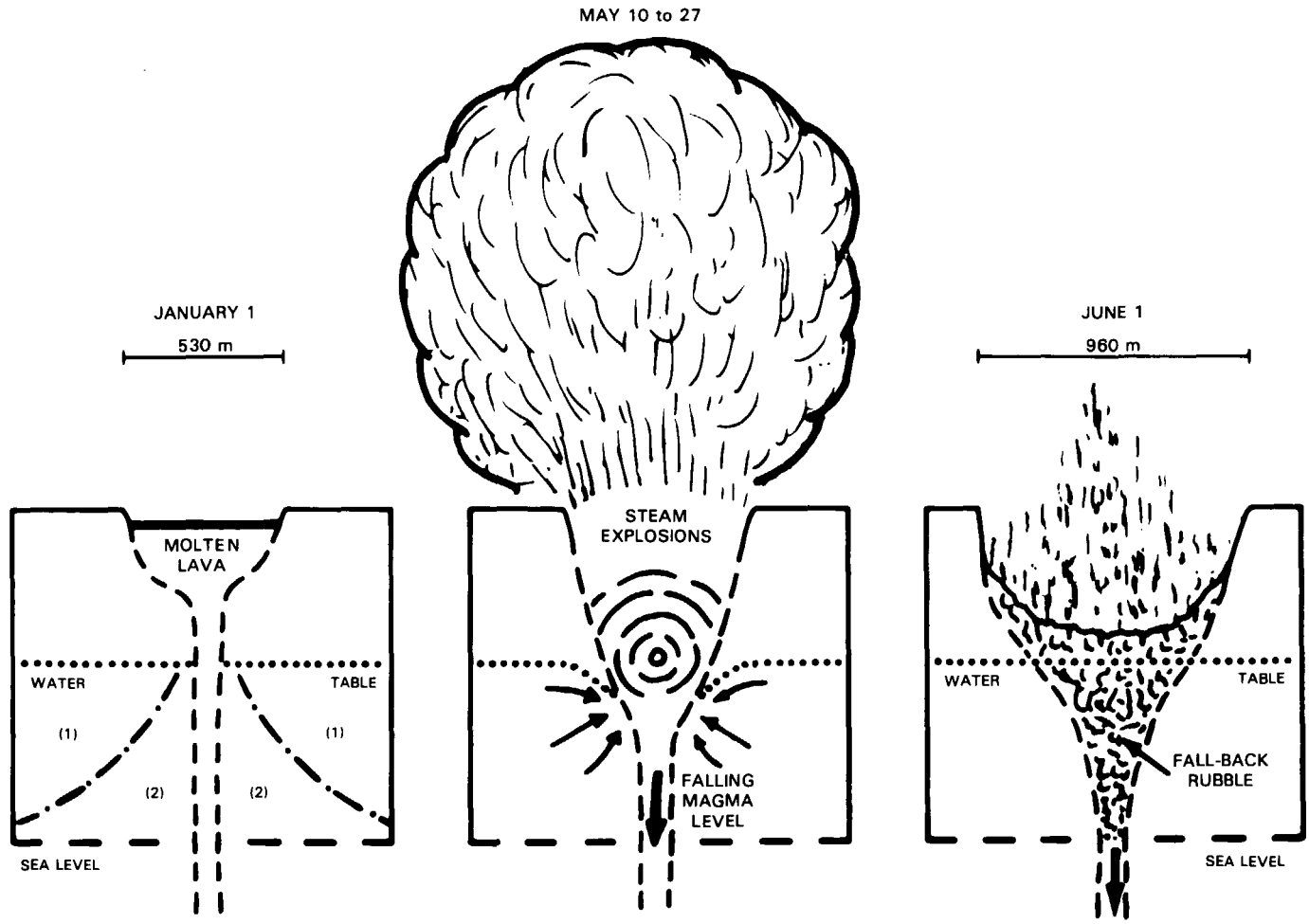

FIGURE 42.15.—Schematic cross sections showing conditions at Halemaumau Crater before, during, and after 1924 explosive eruption. On January 1, one zone of subsurface water (1) is cooler than boiling temperature, and other zone (2) is at boiling temperature for that depth; dash-dot line marks approximate boundary. During May 10–27, as magma column subsides below water table, equilibrium between subsurface water and magma is destroyed, and water from zone 1, rushes into broken hot rocks surrounding subsiding magma column and flashes into steam. Water from zone 2 also flashes into steam as hydrostatic pressures are suddenly reduced. Explosions are multiple because of progressive lowering of the magma column; they stop in late May with exhaustion of thermal energy above the subsided magma column, leaving a collapsed crater. From Decker and Christiansen (1984).

ponded lavas. There are scattered blocks of explosive ejecta on the rim of Mauna Loa caldera, but any explosive eruptions that may have accompanied the caldera collapse were minor compared to the 1790 eruption of Kilauea. This difference in explosive habits of Kilauea and Mauna Loa Volcanoes is probably related to the greater depth from the surface to zones of subsurface water beneath Mauna Loa.

Major caldera collapses of Kilauea Volcano have occurred repeatedly, with an average recurrence time of about 2,000 years (Decker and Christiansen, 1984; Dzurisin and Casadevall, 1986). Refilling the caldera with ponded lavas apparently takes several hundred years. Since both the young submarine volcano Loihi and Kilauea's older neighbor volcano Mauna Loa have calderas, this repeated process of caldera collapse and refilling apparently occurs during most of a Hawaiian volcano's active life span—roughly 0.5–1 m.y. If the caldera recurrence interval of 2,000 years at Kilauea is typical, this indicates that 200–500 generations of major caldera collapse and refilling occur during the evolution of a Hawaiian volcano.

This concept of repeated caldera collapse and refilling, combined with the evidence of progressively upward migration of the shallow magma reservoir systems of Hawaiian volcanoes (fig. 42.16), suggests that some lavas ponded in early calderas may be partly reassimilated into the summit magma-reservoir systems.

SUBSIDENCE OF THE ISLANDS

Hawaiian volcanoes form a massive load on the lithosphere of the Pacific plate. The great positive gravity anomalies of young Hawaiian volcanoes—as much as 330 mGal Bouguer (Kinoshita, 1965)—indicate that they are not compensated by local roots of less dense rock. As Hawaiian volcanoes form, therefore, they also begin

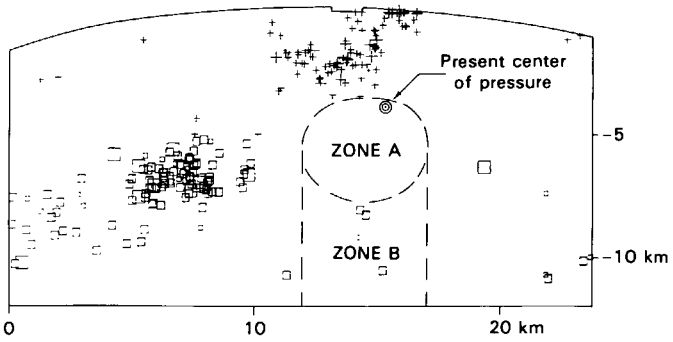

FIGURE 42.16.—Schematic cross section at true scale of inferred magma-reservoir system beneath summit of Mauna Loa Volcano. Zone A is more active region of magma addition and removal. Zone B is more passive; it contains magma and allows magma to move through it, but does not increase or decrease in volume as does zone A. Zone A migrates upward as the volcano grows in height. Pluses and squares represent well-located hypocenters of earthquakes (M=2 or greater) that occurred from January 1962 through May 1983 within 2.5 km of the cross-section plane. From Decker and others (1983).

to sink, and this process has been largely completed when the volcano becomes extinct.

Moore (chapter 2) and Moore and Fornari (1984) have determined from tide-gauge and drowned-reef data that the average rate of subsidence of the west shore of the Island of Hawaii is about 2 mm/yr over the past 150,000 yr and that the rate of subsidence has been generally increasing during this time period. The subsidence is apparently more rapid near the center of the island than at the shoreline. Eustatic sea-level changes are superimposed on this general subsidence and complicate the actual change of sea level. For example, the worldwide rise in sea level over the past century added to the subsidence of the Island of Hawaii has caused a rise in sea level at Hilo of about 4 mm/yr during the past few decades. Tide-gauge data at Honolulu reflect a eustatic rise in sea level but do not indicate any measurable subsidence of the Island of Oahu.

Very high sea-level stands reported by Stearns (1978), which imply periods of major uplift following the subsidence of some Hawaiian islands, have recently been interpreted by Moore and Moore (1984) as deposits from giant waves. Present opinion favors general subsidence of the Hawaiian islands rather than some complex oscillating tectonic movements.

Tectonic subsidence probably results from at least four factors: (1) removal of magma from beneath the active volcanoes; (2) elastic compression of the lithosphere nearly as fast as load is added; (3) plastic flow in the lower lithosphere and upper mantle as a result of volcanic load over periods of 10^5–10^6 yr; and (4) the slow thickening of the oceanic lithosphere and its subsidence as it loses heat over periods of 10^7 to 10^8 yr (Yoshii and others, 1976). Liu and Kosloff (1978) calculated factors (2) and (3) using an elastic/plastic plate-bending model with laboratory data on rock deformation.

This concept of general subsidence of the Hawaiian Islands has some interesting geologic implications. If any mineral deposits were ever formed by interaction of magma and subsurface water, these deposits would probably not be exposed above sea level by later erosion. In addition, subaerial erosion would in general not expose any Hawaiian volcanic rocks or structures formed below sea level.

FUTURE RESEARCH DIRECTIONS

As in most geologic problems, our understanding of how Hawaiian volcanoes work decreases with depth below the surface. Nevertheless, there are some research paths that look promising over the next decade or two for providing new insights into the structure and dynamics of Hawaiian volcanoes.

More detailed information on the variations in temperature and kinetics of the Earth's mantle should be forthcoming from worldwide seismic tomography. The deep anomalies beneath the central Pacific, emerging in the present work of Anderson and Dziewonski (1984), should become clearer if a worldwide net of digital seismometers is deployed, particularly at sites on the ocean floor.

Deployment of a few ocean-bottom seismometers around the Island of Hawaii would also greatly improve the capability of the present seismometer network of the Hawaiian Volcano Observatory. Potential specific benefits from this type of research effort include better location of earthquake sources beneath Loihi Seamount, the ability to determine the source functions of deeper earthquakes beneath Hawaii, and the ability to gain more depth and detail for the seismic velocity structure beneath Hawaii.

Volcanic tremor speaks in a language we do not yet clearly understand, but the technology probably exists to translate this babble into meaningful words and sentences. Arrays of portable digital broad-band seismometers are needed to record volcanic tremor in sufficient detail to interpret its source functions. With such data in hand, we may be able to resolve some of the ambiguity in present models of how volcanic tremor is generated.

Recent developments in satellite geodesy suggest that a revolution in the technology of measuring the surface deformation on active and potentially active volcanoes is only a few years away. The ability to measure distance changes between points that are not intervisible, and the potentially great consequent improvements in the quality of far-field data, would make observations possible that cannot now be made with conventional surveying devices. These new observations are essential for testing more complex theoretical models of the size, shape, and depth of subsurface magma bodies. Add to this the great potential savings in surveying time and manpower, and the attractiveness of satellite global positioning systems becomes clear.

The recent successes in observing detailed gravity changes related to activity of Kilauea and Mauna Loa Volcanoes (Johnson, chapter 47; Dzurisin and others, 1980; Jachens and Eaton, 1980), and the fact that these new data indicate important mass changes in the shallow magma-storage systems not quantitatively shown by surface deformation measurements, clearly demonstrate the importance of long-term measurement of gravity changes on the summits and rift zones of Kilauea and Mauna Loa Volcanoes. Recording gravity meters in conjunction with recording tiltmeters would provide the most definitive data on the mass and volume changes in the shallow magma reservoir systems.

Significant changes in the electrical, magnetic, and electromagnetic fields associated with the activity of Kilauea Volcano (Davis and others, 1973; Zablocki, 1976; Dzurisin and others, 1980; Jackson, 1983) indicate that these methods of geophysical research should continue to be pursued vigorously at HVO. Needed most in this research are a comprehensive analysis of the available data and the generation of theoretical models to try to explain the data. This type of effort would define more clearly what types of field observations are most important.

Great progress has been made in the past few years in determining the composition of gases in Hawaiian magma, and in understanding the complex manner in which some of these gases exsolve from the melt and escape to the atmosphere (chapters 27–36; Gerlach and Graeber, 1985) These studies have set the stage for determining the role of volcanic gases in the dynamics of the ascent, the shallow storage and intrusion, and the eruption of magma. Carbon dioxide apparently forms a separate but dense fluid phase at depths as great as 40 km beneath the summits of Hawaiian volcanoes. Studies of the thermodynamic and mechanical behavior of oxygen, carbon, hydrogen, and sulfur in the generation, ascent, shallow storage and intrusion, and eruption of Hawaiian magmas is a research opportunity of great importance.

The destruction of homes and property in the 1983–1985 eruption of Kilauea Volcano, and the threat to Hilo from flows of the 1984 Mauna Loa eruption, make it clear that we need to know more about the mechanical processes of Hawaiian lava flows in order to predict their behavior better. The complex interaction of the volume rate of eruption, the rheological properties of lava, and the topography over which the flows are moving combine to make a challenging research area that needs more study. Careful plans must be made for future experiments. When an eruption begins it is usually too late to start planning.

As a parting note, one area of the dynamics of Hawaiian volcanism that has been almost entirely overlooked is the study of the interaction of magma with subsurface water beneath the summits and rift zones of the active volcanoes. Few direct data are available: only one 1,260-m drill hole into the summit of Kilauea (Keller and others, 1979), and a few geothermal wells on the east rift zone of Kilauea whose data are still largely proprietary. Some resistivity data on the depth to the water table at various places are available. The potential for important new insights into the interaction of magma and ground water awaits a creative hydrogeologist who wants to venture into volcanology.

REFERENCES CITED

Anderson, D.L., and Dziewonski, A.M., 1984, Seismic tomography: Scientific American, v. 251, no. 4, p. 60–68.

Ando, M., 1979, The Hawaii earthquake of November 29, 1975: Low angle faulting due to forceful injection of magma: Journal of Geophysical Research, v. 84, p. 7616–7626.

Christiansen, R.L., 1979, Explosive eruption of Kilauea Volcano in 1790 [abs.]: Hawaii Symposium on Intraplate Volcanism and Submarine Volcanism, Hilo, Hawaii, Abstract Volume, p. 158.

Dalrymple, G.B., Silver, E.A., and Jackson, E.D., 1973, Origin of the Hawaiian Islands: American Scientist, v. 61, p. 294–308.

Daly, R.A., 1914, Igneous rocks and their origin: New York, McGraw-Hill, 563 p.

——— 1933, Igneous rocks and the depths of the Earth (2nd ed.): New York, McGraw-Hill, 598 p.

Dana, J.D., 1890, Characteristics of volcanoes: New York, Dodd Mead and Co., 399 p.

——— 1895, Manual of geology (4th ed.): New York, American Book Company, 1088 p.

Davis, P.M., Hastie, L.M., and Stacey, F.D., 1974, Stresses within an active volcano—with particular reference to Kilauea: Tectonophysics, v. 22, p. 355–362.

Davis, P.M., Jackson, D.B., Field, J., and Stacey, F.D., 1973, Kilauea Volcano, Hawaii: A search for the volcanomagnetic effect: Science, v. 180, p. 73–74.

Davis, P.M., Stacey, F.D., Zablocki, C.J., and Olson, J.V., 1979, Improved signal discrimination in tectonomagnetism: Discovery of a volcanomagnetic effect at Kilauea, Hawaii: Physics of the Earth and Planetary Interiors, v. 19, p. 331–336.

Decker, R.W., 1968, Kilauea volcanic activity: an electrical analog model [abs.]: Eos, Transactions American Geophysical Union, v. 49, p. 352–353.

Decker, R.W., and Christiansen, R.L., 1984, Explosive eruptions of Kilauea Volcano, Hawaii, *in* Explosive volcanism: Inception, evolution, and hazards: Washington, D.C., National Academy of Science, p. 122–132.

Decker, R.W., Koyanagi, R.Y., Dvorak, J.J., Lockwood, J.P., Okamura, A.T., Yamashita, K.M., and Tanigawa, W.R., 1983, Seismicity and surface deformation of Mauna Loa Volcano, Hawaii: Eos, Transactions of the American Geophysical Union, v. 64, p. 545–547.

Delaney, P.T., and Pollard, D.D., 1982, Solidification of basaltic magma during flow in a dike: American Journal of Science, v. 282, p. 856–885.

Dieterich, J.H., and Decker, R.W., 1975, Finite element modeling of surface deformation associated with volcanism: Journal of Geophysical Research, v. 80, p. 4094–4102.

Duffield, W.A., Christiansen, R.L., Koyanagi, R.Y., and Peterson, D.W., 1982, Storage, migration and eruption of magma at Kilauea Volcano, Hawaii, 1971–1972: Journal of Volcanology and Geothermal Research, v. 13, p. 273–307.

Dvorak, J.J., Okamura, A.T., and Dieterich, J.H., 1983, Analysis of surface deformation data, Kilauea Volcano, Hawaii: October 1966 to September 1970: Journal of Geophysical Research, v. 88, p. 9295–9304.

Dzurisin, D., 1980, Influence of fortnightly earth tides at Kilauea Volcano, Hawaii: Geophysical Research Letters, v. 7, p. 925–928.

Dzurisin, D., Anderson, L.A., Eaton, G.P., Koyanagi, R.Y., Lipman, P.W., Lockwood, J.P., Okamura, R.T., Puniwai, G.S., Sako, M.K., and Yamashita, K.M., 1980, Geophysical observations of Kilauea Volcano, Hawaii, 2. Constraints on the magma supply during November 1975–September 1977: Journal of Volcanology and Geothermal Research, v. 7, p. 241–269.

Dzurisin, D., and Casadevall, T.J., 1986, Stratigraphy and chemistry of Uwekahuna Ash: Product of prehistoric phreatomagmatic eruption at Kilauea Volcano, Hawaii [abs.]: Auckland, N.Z., Abstracts volume, International Volcanological Congress, p. 100.

Dzurisin, D., Koyanagi, R.Y., and English, T.T., 1984, Magma supply and storage at Kilauea Volcano, Hawaii, 1956–1983: Journal of Volcanology and Geothermal Research, v. 21, p. 177–206.

Eaton, J.P., 1962, Crustal structure and volcanism in Hawaii: American Geophysical Union, Geophysical Monograph 6, p. 13–29.

Eaton, J.P., and Murata, K.J., 1960, How volcanoes grow: Science, v. 132, p. 925–938.

Ellis, W., 1827, Journal of William Ellis: London, reprinted 1963 by Advertiser Publishing Co., Honolulu, Hawaii, 342 p.

Epp, D., Decker, R.W., and Okamura, R.T. 1983, Relation of summit deformation to east rift zone eruptions on Kilauea Volcano, Hawaii: Geophysical Research Letters, v. 10, p. 493–496.

Fiske, R.S., and Jackson, E.D., 1972, Orientation and growth of Hawaiian

volcanic rifts: The effect of regional structure and gravitational stresses: Proceedings of the Royal Society of London, Ser. A, v. 329, p. 299–326.

Fiske, R.S., and Kinoshita, W.T., 1969, Inflation of Kilauea Volcano prior to its 1967–1968 eruption: Science, v. 165, p. 341–349.

Furumoto, A.S., and Kovach, R.L., 1979, The Kalapana earthquake of November 29, 1975: An intra-plate earthquake and its relation to geothermal processes: Physics of the Earth and Planetary Interiors, v. 18, p. 197–208.

Gerlach, T.M., and Graeber, E.J., 1985, Volatile budget of Kilauea Volcano: Nature, v. 313, p. 273–277.

Griggs, D.T., and Baker, D.W., 1969, The origin of deep-focus earthquakes, *in* Mark, H., and Fernback, S., eds., Properties of matter under unusual conditions: New York, Interscience Publishers, p. 23–42.

Hardee, H.C., 1982, Incipient magma chamber formation as a result of repetitive intrusions: Bulletin Volcanologique v. 45, p. 41–49.

Hess, H.H., 1960, Stillwater igneous complex, Montana: Geological Society of America Memoir 80, 230 p.

Hill, D.P., 1977, A model for earthquake swarms: Journal of Geophysical Research, v. 82, p. 1347–1352.

Holcomb, R.T., 1980, Preliminary geologic map of Kilauea Volcano, Hawaii: U.S. Geological Survey Open-File Report 80–796, 2 sheets, scale 1:50,000.

Holcomb, R.T., Peterson, D.W., and Tilling, R.I., 1974, Recent landforms at Kilauea Volcano, a selected photographic compilation, *in* Greeley, R., ed., Hawaiian Planetology Conference, NASA TMX 62362, p. 49–86.

Jachens R.C., and Eaton, G.P., 1980, Geophysical observations of Kilauea Volcano, Hawaii, 1. Temporal gravity variations related to the 29 November, 1975, M=7.2 earthquake and associated summit collapse: Journal of Volcanology and Geothermal Research, v. 7, p. 225–240.

Jackson, D.B., Kauahikaua, J., and Zablocki, C.J., 1983, Resistivity monitoring of an active volcano: Application of the controlled-source electromagnetic technique at Kilauea Volcano, Hawaii [abs.]: Eos, Transactions of the American Geophysical Union, v. 64, p. 1072.

Jaggar, T.A., and Finch, R.H., 1924, The explosive eruption of Kilauea in Hawaii: American Journal of Science, Ser. 5, v. 8, p. 353–374.

Joly, J., 1909, Radioactivity and geology: London, Archibald Constable and Co., 287 p.

Keller, G.V., Grose, L.T., Murray, J.C., and Skokan, C.K., 1979, Results of an experimental drill hole at the summit of Kilauea Volcano, Hawaii: Journal of Volcanology and Geothermal Research, v. 5, p. 345–385.

Kinoshita, W.T., 1965, A gravity survey of the Island of Hawaii: Pacific Science, v. 19, p. 339–340.

Kinoshita, W.T., Koyanagi, R.Y., Wright, T.L., and Fiske, R.S., 1969, Kilauea Volcano: The 1967–68 summit eruption: Science, v. 166, p. 459–468.

Klein, F.W., 1982a, Earthquakes at Loihi submarine volcano and the Hawaiian hot spot: Journal of Geophysical Research, v. 87, p. 7719–7726.

——— 1982b, Patterns of historical eruptions at Hawaiian volcanoes: Journal of Volcanology and Geothermal Research, v. 12, p. 1–35.

Koyanagi, R.Y., Unger, J.D., Endo, E.T., and Okamura, A.T., 1976, Shallow earthquakes associated with inflation episodes at the summit of Kilauea Volcano, Hawaii: Bulletin Volcanologique, v. 39, p. 621–631.

Lipman, P.W., Lockwood, J.P., Okamura, R.T., Swanson, D.A., and Yamashita, K. M., 1985, Ground deformation associated with the 1975 magnitude-7.2 earthquake and resulting changes in activity of Kilauea Volcano, Hawaii: U.S. Geological Survey Professional Paper 1276, 45 p.

Liu, H., and Kosloff, D. 1978, Elastic-plastic bending of the lithosphere incorporating rock deformation data, with application to the structure of the Hawaiian Archipelago: Tectonophysics, v. 50, p. 249–274.

Macdonald, G.A., 1972, Volcanoes: Englewood Cliffs, N. J., Prentice-Hall, 510 p.

Malahoff, A., McMurtry, G.M., Wiltshire, J.M., and Yeh, H., 1982, Geology and chemistry of hydrothermal deposits from Loihi, the latest active submarine volcano of the Hawaiian hot spot: Nature, v. 298, p. 234–239.

McBirney, A.R., 1963, Conductivity variations and terrestrial heat-flow distribution: Journal of Geophysical Research, v. 68, p. 6323–6329.

McDougall, I., 1979, Age of shield-building volcanism of Kauai and linear migration of volcanism in the Hawaiian Island chain: Earth and Planetary Science Letters, v. 46, p. 31–42.

Mogi, K., 1958, Relation between the eruptions of various volcanoes and the deformation of the ground surface around them: Tokyo, Bulletin of the Earthquake Research Institute, v. 36, p. 99–134.

Moore, J.G., 1970, Relationship between subsidence and volcanic load, Hawaii: Bulletin Volcanologique, v. 34, p. 562–576.

——— 1971, Bathymetry and geology—East Cape of the Island of Hawaii: U.S. Geological Survey Miscellaneous Geological Investigations Map I–677, Scale 1:62,500.

Moore, J.G., and Fornari, D.J., 1984, Drowned reefs as indicators of the rate of subsidence of the Island of Hawaii: Journal of Geology, v. 92, p. 752–759.

Moore, J.G., and Krivoy, H.L., 1964, The 1962 flank eruption of Kilauea Volcano and structure of the east rift zone: Journal of Geophysical Research, v. 69, p. 2033–2045.

Moore, J.G., and Moore, G.W., 1984, Deposit from a giant wave on the Island of Lanai, Hawaii: Science, v. 226, p. 1312–1315.

Peterson, D.W., Christiansen, R.L., Duffield, W.A., Holcomb, R.T., and Tilling, R.I., 1976, Recent activity of Kilauea Volcano, Hawaii, *in* International Association for Volcanology and Chemistry of Earth's Interior, Symposium on Andean and Antarctic Volcanology Problems, Santiago, Chile, Proceedings, p. 646–656.

Peterson, D.W., and Swanson, D.A., 1974, Observed formation of lava tubes during 1970–71 at Kilauea Volcano, Hawaii: Studies in Speleology, v. 2, p. 209–233.

Peterson, D.W., and Tilling, R.I., 1980, Transition of basaltic lava from pahoehoe to aa, Kilauea Volcano, Hawaii: Field observations and key factors: Journal of Volcanology and Geothermal Research, v. 7, p. 271–293.

Pollard, D.D., 1976, On the form and stability of open fractures in the Earth's crust: Geophysical Research Letters, v. 3, p. 513–516.

Ramberg, H., 1972, Mantle diapirism and its tectonic and magmagenetic consequences: Physics of Earth and Planetary Interiors, v. 5, p. 45–60.

Ryan, M.P., Blevins, J.Y.K., Okamura, A.T., and Koyanagi, R.Y., 1983, Magma reservoir subsidence mechanics: Theoretical summary and application to Kilauea Volcano, Hawaii: Journal of Geophysical Research, v. 88, p. 4147–4181.

Ryan, M.P., Koyanagi, R.Y., and Fiske, R.S., 1981, Modeling the three-dimensional structure of macroscopic magma transport systems: Application to Kilauea Volcano, Hawaii: Journal of Geophysical Research, v. 86, p. 7111–7129.

Scientific Event Alert Network, 1982–1985, Monthly accounts of the activity of Kilauea and Mauna Loa Volcanoes, Hawaii: SEAN Bulletin v. 8-10, no. 1-12, Washington, D.C., Smithsonian Institution.

Shaw, H.R., 1969, Rheology of basalt in the melting range: Journal of Petrology, v. 10, p. 510–535.

——— 1970, Earth tides, global heat flow, and tectonics: Science, v. 168, p. 1084–1087.

——— 1973, Mantle convection and volcanic periodicity in the Pacific; evidence for Hawaii: Geological Society of America Bulletin, v. 84, p. 1505–1526.

——— 1980, The fracture mechanisms of magma transport from the mantle to the surface, *in* Hargraves, R.B., ed., Physics of Magmatic Processes: Princeton, New Jersey, Princeton University Press, p. 201–264.

Shimozuru, D., 1981, Magma reservoir systems inferred from tilt patterns: Bulletin Volcanologique, v. 44-3, p. 499–504.

Spera, F.J., 1980, Aspects of magma transport, *in* Hargraves, R.B., ed., Physics of Magmatic Processes: Princeton, New Jersey, Princeton University Press, p. 265–323.

Stearns, H.T., 1978, Quaternary shorelines in the Hawaiian Islands: Bernice P. Bishop Museum, Bulletin 237, Honolulu, 57 p.

Swanson, D.A., 1972, Magma supply rate at Kilauea Volcano, 1951–1972: Science, v. 175, p. 169–170.

——— 1973, Pahoehoe flows from the 1969–1971 Mauna Ulu eruption, Kilauea Volcano, Hawaii: Geological Society of America Bulletin, v. 84, p. 615–626.

Swanson, D.A., and Christiansen, R.L., 1973, Tragic base surge in 1790 at

Kilauea Volcano: Geology, v. 1, p. 83–86.

Swanson, D.A., Duffield, W.A., and Fiske, R.S., 1976a, Displacement of the south flank of Kilauea Volcano: The result of forceful intrusion of magma into rift zones: U.S. Geological Survey Professional Paper 963, 39 p.

Swanson, D.A., Duffield, W.A., Jackson, D.B., and Peterson, D.W., 1979, Chronological narrative of the 1969–71 Mauna Ulu eruption of Kilauea Volcano, Hawaii: U.S. Geological Survey Professional Paper 1056, 55 p.

Swanson, D.A., Jackson, D.B., Koyanagi, R.Y., and Wright, T.L., 1976b, The February 1969 east rift eruption of Kilauea Volcano, Hawaii: U.S. Geological Survey Professional Paper 891, 30 p.

Thorarinsson, S., 1965, Surtsey: Island born of fire: National Geographic Magazine, v. 127, p. 713–726.

Tilling, R.I., Koyanagi, R.Y., Lipman, P.W., Lockwood, J.P., Moore, J.G., and Swanson, D.A., 1976, Earthquake and related catastrophic events, Island of Hawaii, November 29, 1975: A preliminary report: U.S. Geological Survey Circular 740, 33 p.

Turcotte, D.L., and Oxburgh, E.R., 1978, Intraplate volcanism: Philosophical Transactions Royal Society of London, Ser. A., v. 288, p. 561–579.

Verhoogen, J., 1954, Petrological evidence on temperature distribution in the mantle of the earth: Eos, Transactions of the American Geophysical Union, v. 35, p. 85–92.

Weertman, J., 1972, Coalescence of magma pockets into large pools in the upper mantle: Geological Society of America Bulletin, v. 83, p. 3531–3632.

Wilkes, C., 1845, Narrative of the United States exploring expedition during the years 1838–1842: Philadelphia, v. 4, p. 87–231.

Wilson, J.T., 1963, Continental drift: Scientific American, v. 208, p. 86–100.

Wilson, R.M., 1935, Ground surface movement at Kilauea Volcano, Hawaii: University of Hawaii, Honolulu, Research Publication 10, 56 p.

Wright, T.L., 1971, Chemistry of Kilauea and Mauna Loa lava in space and time: U.S. Geological Survey Professional Paper 735, 40 p.

——— 1984, Origin of Hawaiian tholeiite: a metasomatic model: Journal of Geophysical Research, v. 89, p. 3233–3252.

Wright, T.L., Shaw, H.R., Tilling, R.I., and Fiske, R.S., 1979, Origin of Hawaiian tholeiitic basalt: a quantitative model [abs.]: International Association for Volcanology and Chemistry of the Earth's Interior, Symposium on intraplate volcanism and submarine volcanism, Hilo, Hawaii, July 16–22, 1979, Abstracts Volume, p.

Yoder, H.S., 1976, Generation of basaltic magma: Washington, D.C., National Academy of Sciences, 265 p.

Yoder, H.S., and Tilley, C.E., 1962, Origin of basalt magmas: an experimental study of natural and synthetic rock systems: Journal of Petrology, v. 3, p. 342–532.

Yoshii, T., Kono, T., and Ito, K., 1976, Thickening of the oceanic lithosphere: American Geophysical Union, Monograph 19, p. 423–430.

Zablocki, C.J., 1976, Mapping thermal anomalies on an active volcano by the self-potential method, Kilauea, Hawaii: United Nations Symposium on the development and use of geothermal resources, 2nd San Francisco, Proceedings, v. 2, p. 1299–1309.

THE SEISMICITY OF KILAUEA'S MAGMA SYSTEM

By Fred W. Klein, Robert Y. Koyanagi, Jennifer S. Nakata, *and* Wilfred R. Tanigawa

ABSTRACT

Earthquake-hypocenter data collected by the Hawaiian Volcano Observatory during 1960–83 provide a wealth of information on the active processes of Kilauea's magma system. The magma conduits produce volcanic earthquakes that occur in episodic swarms often accompanied by tilt changes or eruptions. Tectonic earthquakes in Kilauea's flanks and some parts of the upper mantle occur more continually and are punctuated with mainshock-aftershock sequences. Volcanic earthquakes also have smaller magnitudes, a greater proportion of small events, and frequent association with tremor. Three-dimensional earthquake patterns and separation of volcanic and tectonic seismicity can be visualized in a series of hypocenter depth slices and cross sections. Earthquakes reveal a magma system consisting of a vertical conduit from Kilauea caldera to about 60 km depth, two shallow rift zones radial to the caldera, and a shallow magma reservoir joining these three conduits.

The shallow magma reservoir is an aseismic zone beneath the south edge of Kilauea caldera. The reservoir is surrounded on two sides by intensely active rift conduits centered near 3 km depth, above by a seismically active cap in the caldera mostly between 1 and 2 km depth, and below by the vertical magma conduit having earthquakes as shallow as 7 km. The deformation centers are mostly between 2 and 4 km depth, near the top of the aseismic zone that is between 3 and 7 km depth. Inflation of the reservoir produces earthquakes above and in the adjacent rift conduits by extension in the summit region and slow magma intrusion into the rifts.

The vertical magma conduit, as defined by earthquakes, consists of two parts: a narrow and nearly vertical pipe between 7 and 20 km depth mostly having swarms of volcanic earthquakes, and a zone that widens into a diffuse and south-dipping region between 20 and 60 km depth. Earthquakes in the deeper conduit are larger in magnitude and more continuous in time, as if tectonic in origin. Earthquakes below 40 km depth merge with the Hawaiian hot spot below Kilauea, Loihi and Mauna Loa Volcanoes. Kilauea's deep earthquakes also join a band of seismicity along the island's south coast, which is probably caused by shear stress applied from Kilauea's mobile south flank and by the growing and asymmetrical weight of the Kilauea shield. The number of earthquakes in the vertical conduit dropped dramatically at the time of the $M=7.2$ Kalapana earthquake in 1975. This decrease indicates that conduit earthquakes are partly driven by regional stresses derived from the seaward push of the south flank.

The vertical distribution of conduit earthquakes shows pronounced gaps near depths of 5, 13 and 20 km. The first gap results from the magma reservoir between 3 and 7 km depth, and the 13-km-depth gap is probably bounded by the Moho and the prevolcanic oceanic sediments. The depth of 20 km is also a gap for earthquakes in the surrounding lithosphere, marks the change from volcanic-style earthquakes above to tectonic below, and is probably the zone of the neutral stress axis in the lithosphere bending under the island's weight. The vertical magma conduit thus is similar to a passive, weak zone in the lithosphere that triggers earthquakes mainly driven by regional stresses.

Kilauea's rift zones produce shallow swarms of varied intensity and complexity arising from periods of summit inflation, slow intrusions, and rapid intrusions that may also result in eruptions. Slow intrusions may feed the rifts adjacent to the caldera during inflation, send slow pulses of magma (and hence earthquakes) down the rifts, or be aseismic except at the terminus of the intrusion where magma collects. Much of this paper documents earthquakes from swarms during 1962–84. To examine the dynamics of intrusion and dike formation, computer plots for each swarm are designed to show the position, depth, size and shape of the seismic zone, deflation and seismicity with time, and migration of earthquakes along the rift or vertically.

Rapid intrusions generally begin with earthquakes in a small volume near the main rift conduits at 3 km depth and may spread along the rift and upward. Migration and growth speeds are about 0.1 to 6 km/h. An intrusion often loses upward speed as it approaches the surface, or downrift speed as it nears its terminus. Earthquakes occur at and behind the front of the dike as the conduit widens and the walls compress. Barriers within the rifts, where the conduit is pinched shut or stress is concentrated, often generate clusters of earthquakes and act as places where intrusions start and stop. The most prominent barriers are adjacent to the summit magma reservoir and in the east rift zone below Pauahi Crater and Mauna Ulu, but many are present along both rifts. The Pauahi-Mauna Ulu barrier is important because many intrusions start there and move uprift and downrift, and it also marks a bend in the rift, where it intersects the Koae fault zone. A possible small magma reservoir below Pauahi Crater is recognized by the absence of earthquakes; this reservoir is dammed uprift of the Pauahi-Mauna Ulu barrier.

The most common earthquake migration direction at Kilauea is downrift and is presumably driven by gravity and a pressure gradient along the magma conduit. Upward earthquake migration is visible in many intrusions and reflects ascending magma presumably driven by buoyancy forces. The east rift zone between Kilauea caldera and Mauna Ulu is an anomalous zone of earthquake migration; uprift, downrift and bilateral migration of earthquakes are equally likely. This zone is also unusual in its high degree of activity, its northwest trend oblique to the regional stress, its shallowness of earthquakes, its ability to feed two intrusions simultaneously, and its short 2- to 3-hour interval from the beginning of an intense earthquake

swarm to the start of an eruption. The upper east rift zone thus seems to be a multitiered and complex honeycomb of conduits. The various directions of earthquake migration in this area may result from a complex pattern of stresses and pressure gradients, or from an uprift-traveling pressure pulse within magma flowing downrift. The latter may have caused the reflection of a downrift earthquake migration off a rift barrier back uprift, as observed in many intrusions.

Intrusions occur in larger cycles that alternate between rifts. Intrusions are often grouped in pairs or triplicates within a few weeks of each other—they may retrace the same path or occur adjacent to their predecessors. In addition, four complete cycles of east-rift-zone to southwest-rift-zone shifts, each lasting 3–4 years, occurred during 1968–83. A basic cycle consists of several east-rift-zone intrusions (beginning near Mauna Ulu), a period of inflationary swarms at the summit, a major intrusion usually in the southwest rift, and about one year of no new intrusions before beginning the cycle again. This cycle may be an oscillatory tectonic process involving the south flank. A series of intrusions in one rift apparently helps trigger other intrusions and also compresses the adjacent flank. This compression inhibits additional intrusions and hinges open the other rift until a switch occurs. The Kalapana earthquake in 1975 may have disrupted the basic pattern set by the first two cycles: periods of inflationary swarms did not occur in 1977 and 1980–81, no southwest-rift intrusions occurred in 1977–78, and the switch from the southwest rift zone to the east rift zone in 1982–83 occurred without a pause.

INTRODUCTION

Few volcanoes in the world are as seismically active and as extensively monitored as Kilauea has been since 1960. The Hawaiian Volcano Observatory (HVO) has steadily expanded its seismic network and data-processing effort, and routinely analyzes several thousand earthquakes each year. This paper draws heavily on a catalog of about 70,000 earthquakes of all types carefully gathered by the past and present staff of HVO during 1962 through 1983.

Kilauea is a tholeiitic shield volcano, and eruptions occur in the summit caldera or from either the east rift zone (ERZ) or southwest rift zone (SWRZ) (fig. 43.1). The basic model of Kilauea has been refined by HVO through the years, but is not fundamentally changed from that stated by Eaton and Murata (1960) and Eaton (1962). The key feature of the Kilauea model is a magma reservoir beneath the caldera. The basic eruption cycle begins with gradual inflation of the magma reservoir as it fills via feeder conduits from below. The inflation is revealed by a bulge of the ground surface and by an increase of small earthquakes within the caldera. The summit becomes unstable when the barriers holding back the magma give way and magma rapidly intrudes the caldera or the rifts. Formation of vertical dikes appears to be the dominant process in rift-zone intrusion (for example, see Macdonald, 1956; Fiske and Jackson, 1972; Swanson and others, 1976a; Pollard and others, 1983). The intrusion may take a few hours or days and is revealed by a rapid deflation of the summit, inflation or extension above the new dike, an intense earthquake swarm caused by stress surrounding the new dike, harmonic tremor, and an eruption if the dike reaches the surface.

THE SUMMIT MAGMA RESERVOIR

Deformation data provide the best evidence for the location and depth of the magma reservoir beneath Kilauea caldera. Using tilt data from 1960, Eaton (1962) determined a center of deflation 3–4 km beneath the southern part of the caldera. Fiske and Kinoshita (1969) obtained similar depths and a migrating pattern of uplift deformation centers using leveling data from 1966 and 1967. Dieterich and Decker (1975) used level and trilateration data from 1967 to infer a vertically elongate zone of inflation extending from about 1 to 3 km depth. Ryan and others (1983) modeled several subsidence events as magma withdrawal from a sill-like body. Careful inversions of tilt, level and trilateration data from several inflation and deflation episodes during 1966–70 produced a set of about 26 deformation centers within and just outside of the southern part of the caldera (Dvorak and others, 1983). The deformation centers scattered within a radius of about 2 km from a point 2 km south-southeast of Halemaumau Crater. Depths were mostly between 2 and 4 km, but occasional deformation centers may have been as deep as 7 km. The buried centers of deformation coincide with the seismically defined magma reservoir.

The above papers inferred that the magma reservoir is in fact a honeycomb of interconnected fluid pockets from the many different deformation centers. The top of the reservoir complex is about 2 km beneath the southern part of the caldera, and it extends at least to 4 km depth. The nature of magma storage below 4 km is difficult to determine from deformation measurements, because surface displacements are dominated by the shallowest active parts of the reservoir and because parts of the reservoir below 4 km may be too weak to partake in large elastic changes.

The magma reservoir was delineated seismically and was spatially related to the dynamics of intrusions and earthquake swarms (Koyanagi and others, 1976a, 1976b). Using selected summit earthquakes during 1971–73, they identified several regions: (1) a vertical conduit below about 7 km depth delineated by mostly long-period earthquakes, (2) a region of relatively low seismicity between about 3 and 6 km depth that they interpreted as the magma reservoir, (3) a seismically active cap above the magma reservoir, and (4) two seismic zones that form the uppermost parts of the rift zones adjacent to the reservoir. Their study also related the temporal activity of these regions to the eruption cycle. The cap above the magma reservoir is mainly active during periods of inflation and prior to eruptions and intrusions. The rift zones adjacent to the reservoir are mainly active when magma intrudes the rift zones and deflates the reservoir.

The three-dimensional distribution of hypocenters beneath Kilauea's summit and upper ERZ was clarified by a transparent model and series of perspective figures by Ryan and others (1981). Using the same 1971–73 data as Koyanagi and others (1976a), Ryan and others expanded the discussion of magma storage and transport and identified the same seismic and aseismic regions. In addition, the latter paper identified a vertical pipe below the upper ERZ and inferred a feeder conduit connecting its base with Kilauea's main conduit. The pipe was about 3 km downrift of Kilauea caldera (1 km southwest of Kokoolau) and was defined by

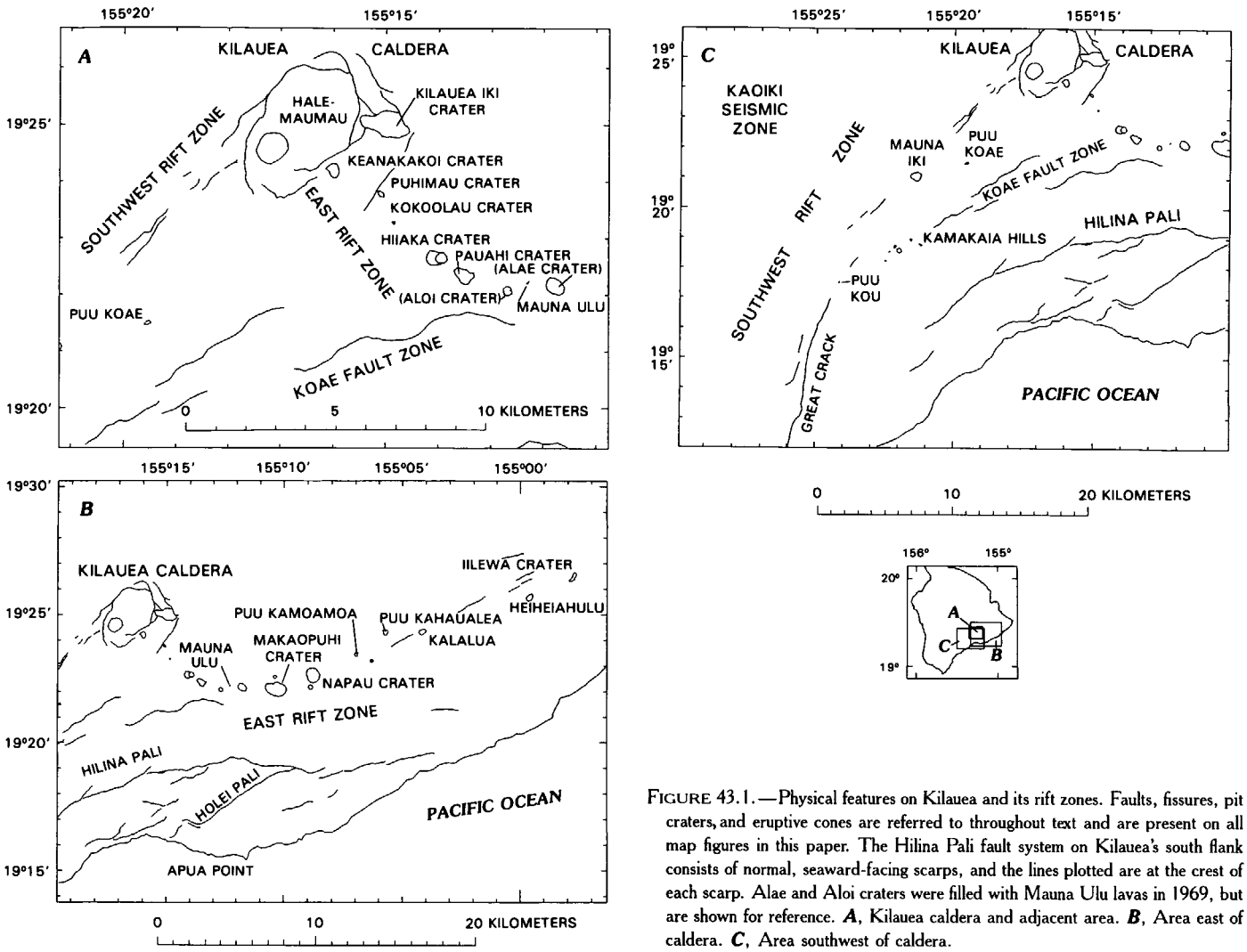

FIGURE 43.1.—Physical features on Kilauea and its rift zones. Faults, fissures, pit craters, and eruptive cones are referred to throughout text and are present on all map figures in this paper. The Hilina Pali fault system on Kilauea's south flank consists of normal, seaward-facing scarps, and the lines plotted are at the crest of each scarp. Alae and Aloi craters were filled with Mauna Ulu lavas in 1969, but are shown for reference. ***A***, Kilauea caldera and adjacent area. ***B***, Area east of caldera. ***C***, Area southwest of caldera.

hypocenters between 1.9 and 5.7 km depth. This ERZ pipe is not visible in the present study, which uses a much expanded and revised data set.

In addition to seismicity, the newer technique of three-dimensional seismic-velocity inversion reveals the presence and location of Kilauea's magma reservoir (Thurber, chapter 38; 1984). The reservoir is recognized as a zone at least 0.5 km/s slower than the surrounding rock, and its position coincides with that obtained from other methods within the resolution of the technique.

INFERRING MAGMA FROM EARTHQUAKES

Ideally Hawaiian earthquakes could be used to infer the positions and dynamics of magma conduits and storage reservoirs, but several precautions must be heeded when doing this. Most importantly, earthquake generation requires rock that is both stressed and brittle. In addition, rock that already contains fractures or faults is far more likely to be seismically active than an equivalent perfectly homogeneous region. Aseismic regions, however, may be either unstressed, unfractured or hot and ductile. Direct associations, therefore, cannot always be made between seismicity and magma. In addition, pressured magma as a source of stress can generate earthquakes in brittle rock that is adjacent to or intermixed with the magma conduit. Earthquakes may occur on systems of fault planes between echelon tips of active dikes (Hill, 1977). Thus, two possible lines of thought could lead one to infer that magmatic zones are either seismic or aseismic. Thus, other factors such as earthquake time behavior, their relation to deformation measurements and geology must be considered. Relating seismicity to magma is not a simple process, but requires a fabric of related observations and assumptions.

We generally interpret regions of swarm seismicity to be zones of dike intrusion or magma conduits (the rift zones or vertical feeder conduit). An aseismic region adjacent to volcanically related seismicity is either an inferred zone of primary magma storage (the

summit magma reservoir) or a stable block (such as Kilauea's north flank).

Earthquake locations have both systematic and random errors, and give a somewhat blurred view of the magma system. Largely because of a finite number of stations and an inability to perfectly model the true three-dimensional velocity structure, the earthquake location error and hence resolution in the summmit region is typically several hundred meters and sometimes more. Therefore, resolving structures of meters to tens of meters in size is hopeless, although determining and using a three-dimensional velocity model offers some improvement locally (Thurber, chapter 38; Thurber and others, 1984).

All earthquakes in Hawaii are ultimately attributable to volcanism, but several characteristics of seismicity can be used to infer the closeness of its relation to magma. We use the term "volcanic" earthquake for those that are in or immediately adjacent to magma conduits. By "tectonic" earthquake, however, we mean those that are at least one step removed from a magma conduit: although deriving their driving stress from dike intrusion or volcano growth, they may be several kilometers from any magma. Kilauea's volcanic earthquakes occur beneath its mappable rift zones and summit caldera, where they are less than 5 km deep. Volcanic seismicity is also typical of the vertical conduit below the reservoir, which extends to 55–60 km depth. Tectonic seismicity occurs on Kilauea's active flanks, such as south of the rift zones (for example, Koyanagi and others, 1972; Crosson and Endo, 1982), and in the Kaoiki seismic zone between Mauna Loa and Kilauea's SWRZ (for example, Endo and others, 1978; Koyanagi and others, 1984; Endo, 1985). These flank earthquakes typically occur between about 5 and 13 km depth. Location and depth are thus good discriminants of volcanic and tectonic earthquakes.

The time behavior of a sequence, seismic *b*-value, maximum magnitude and association with tremor also are significantly different in volcanic and tectonic earthquake source areas. Volcanic earthquakes at Kilauea typically occur in swarms (a sequence more or less isolated in time and without a single dominating mainshock). The swarm may last for hours or days if it accompanies rapid dike intrusion in the summit or rift zones, or it may be days or weeks long if driven by the gradually inflating magma reservoir. Tectonic earthquakes, however, occur both continuously and in mainshock-aftershock sequences. Mogi (1963) interpreted earthquake swarms as characteristic of concentrated sources of stress and heterogeneous material properties (such as magma conduits and dike swarms), and mainshock-aftershock sequences as typical of more homogeneous regions (such as volcano flanks). Swarms are also typical of geothermal regions. Because intrusions and eruptions generally produce both earthquake swarms and tremor, their frequent association implies that moving magma is a direct cause for both.

In addition to swarm character, volcanic earthquakes on Hawaii have other distinguishing characteristics. As will be discussed later, volcanic events generally show higher seismic *b*-values, which is the slope of the statistical frequency-magnitude distribution. The maximum magnitudes of tectonic events are larger because these regions can sustain higher stress over a larger volume and because the faults or other stressed structures that can slip in a single event are larger than in volcanic earthquake regions. The $M=7.2$ Kalapana earthquake in 1975 (for example, Ando, 1979) ruptured nearly the entire length of Kilauea's south flank. The Kaoiki seismic zone broke with a $M=6.6$ event in 1983 (Koyanagi and others, 1984). By contrast, the largest volcanic events located near Kilauea's magma system are about magnitude 4.

The differing behavior of earthquake sequences in time, the *b*-values and maximum magnitudes of volcanic and tectonic earthquakes are all expressions of the differing regimes in which they occur: the magmatic zones are heterogeneous and highly fractured, and have concentrated sources of stress; the tectonic flanks are more homogeneous in stress and material properties. Kilauea's earthquakes are somewhat analogous to those on plate boundaries on a larger scale around the world: the characteristics of volcanic earthquakes are typical of spreading ridges, and tectonic events bear resemblance to those at transcurrent faults and subduction zones.

Note that many of the differences we infer between volcanic and tectonic earthquakes are statistical or based on a property of a group of events. These methods will of course not work for a single earthquake. No difference may be apparent in individual seismograms between the two event types, but discrimination occurs only after it is located and assigned to a region known to be volcanic or tectonic. One may thus use either location or group behavior to determine the type of a group of events, and only one type of information may be available at a sparsely monitored volcano or one whose magma system has a poor surface expression.

Earthquakes elsewhere in Hawaii are analogous to those at Kilauea. The submarine volcano Loihi generates earthquakes of both types, indicating that it is an active volcano with mobile flanks (Klein, 1982a). Mauna Loa's summit and rifts produce volcanic seismicity (for example, Decker and others, 1983), and tectonic earthquakes are characteristic of its southeast flank to the west of Kilauea. Earthquakes scattered elsewhere around the island appear to be mostly tectonic and may often be generated by deformation of the lithosphere and subsidence of the island under its own weight. Seismicity of Kilauea's vertical conduit below about 25 km depth displays some characteristics of both volcanic and tectonic regimes. At this depth the seismic zone is much wider than those above and may represent a distributed network of magma channels. The broad conduit complex may then experience more uniform stresses associated with lithospheric flexure.

The remainder of this paper will explore some aspects of Kilauea's volcanic earthquakes in space and time. We will begin with a description of the earthquake data and how it is processed. Then we examine the three-dimensional seismicity structure of Kilauea through a series of earthquake depth slices. The physical relations and time histories of the seismic zones seen in the depth slices provides a basis for their classification as volcanic or tectonic. The following sections explore the size and shape of Kilauea's shallow reservoir and vertical magma conduit using maps and cross sections of earthquakes. We then examine the chronology of shallow earthquake swarms in Kilauea's rift zones as one expression of magma flow and storage. This section does contain interpretations of

individual swarms, but casual readers may wish to skip it owing to its length and chronological format. The paper concludes with a summary and discussion of various types of rift swarms and what they reveal of the intrusion process, the structure of the rifts, and large-scale interactions of intrusions with each other.

ACKNOWLEDGMENTS

The vast amount of earthquake data summarized here is the work of many of the past and present staff of the Hawaiian Volcano Observatory. People whose persistence in the face of boredom contributed to the completeness and continuity of this data set include Karen Meagher, Pat Stevenson, Irene Takayesu, Alvin Tomori and many others. George Kojima's dedication to maintaining and recording the seismic network over the years made it all possible. We are grateful to Elliot Endo and Michael Ryan for their thoughtful reviews, and to Bob Decker for his editorship and determined coaxing to get the manuscript ready for this volume.

EARTHQUAKE DATA GATHERED BY THE HAWAIIAN VOLCANO OBSERVATORY

A network of high-gain seismometers has operated on Kilauea since the 1950's, and its steady improvement brought an explosion in both quantity and quality of earthquake data. The number and sensitivity of stations, their recording and timing accuracy, and the effort devoted to reading records and locating earthquakes have all greatly improved. The growth of the seismic network operated by HVO is clear from figure 43.2, which shows the station sites operating in 1963, 1973 and 1983. The greater number and improved accuracy of located earthquakes means that small swarms during the 1980's often can be studied in greater detail than larger sequences in the 1960's. The characteristics and growth of the network are documented by Klein and Koyanagi (1980), but we briefly summarize a few milestones here:

1958–60 Network of six Kilauea summit stations centrally recorded at HVO on smoked paper with telemetry by overland wire. Five distant stations independently timed and recorded.

1962–63 Increase in seismic staff (R.Y. Koyanagi) resulted in daily analysis and more earthquakes systematically timed and analyzed. Addition of 3 smoked-paper recorders.

1968–71 Rapid increase in number and sensitivity of stations. Introduction of telemetry by radio and recording on a Develocorder permit a reading precision of 0.10–0.05 s. Additional staff increase.

1974–75 Growth in number of stations, especially on Mauna Loa.

1978–79 Arrival of Eclipse computer at HVO for all seismic processing. Timing precision now 0.01–0.02 s.

1985 Network consists of 50 station sites on the Island of Hawaii. Increased numbers of 3-component stations.

The improvements in the seismic network resulted directly in increases in numbers of Kilauea earthquakes (a smaller magnitude

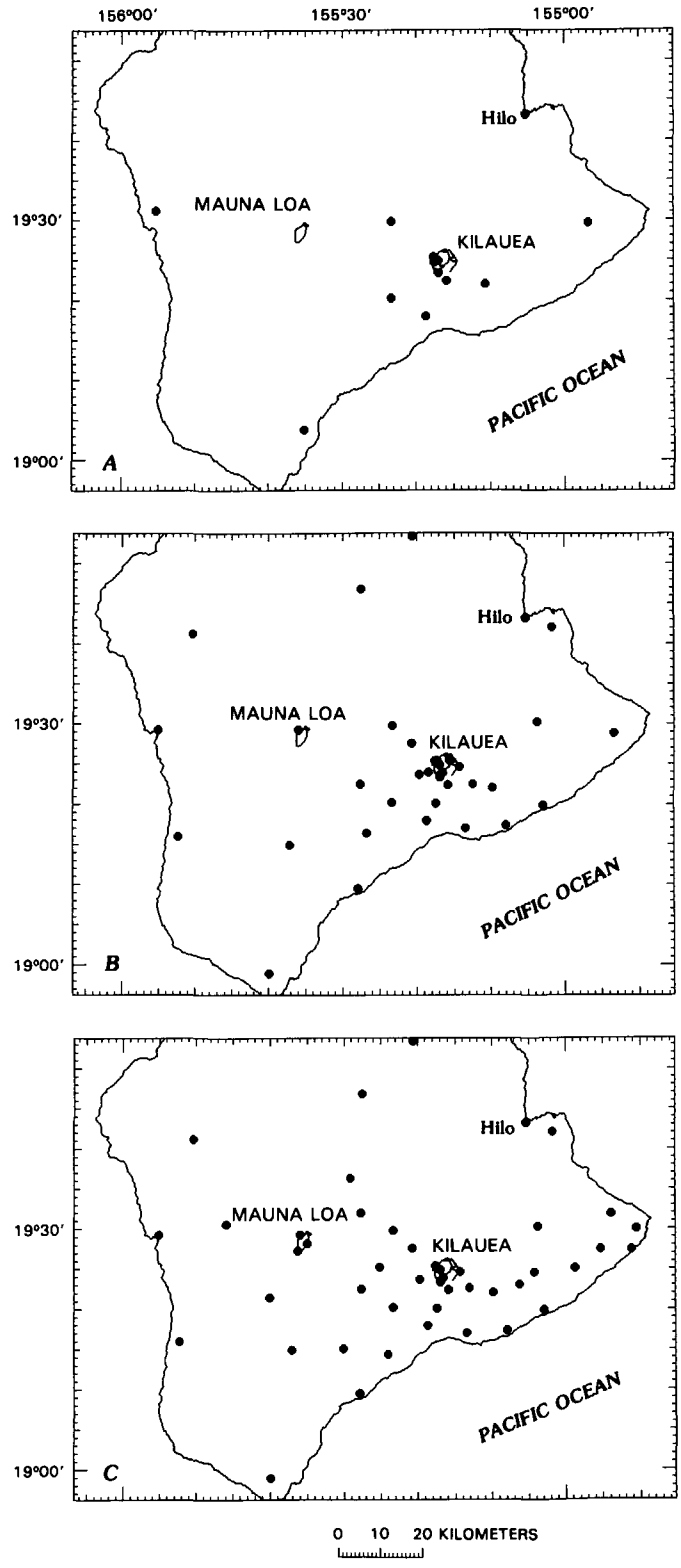

FIGURE 43.2.—Growth and coverage of network of seismic stations operated by the Hawaiian Volcano Observatory. ***A***, December 1963, 13 station sites. ***B***, December 1973, 34 station sites. ***C***, December 1983, 47 station sites. Faults, fissures, and pit craters are as shown in figure 43.1.

above which events are complete) and in the precision of locations. Shallow Kilauea earthquakes in the early 1960's were often only located if larger than about magnitude 2, but the level of completeness in the early 1980's is now about 1. This means roughly a tenfold increase in the number of events with which to study swarms and other features, and smaller magma intrusions can now be identified. The number of seismic stations used for earthquake location by computer was often less than 10 in the 1960's, but was usually more than 20 in the 1980's. The level of completeness of Kilauea events deeper than about 13 km and flank earthquakes more than about 10 km from the caldera has been about magnitude 2 in the 1970's and 1980's. Structures such as magma conduits revealed by earthquakes can now be resolved and associated reasonably well with geologic features. In the early 1960's location and depth errors of 2–5 km meant swarms looked like formless clouds, but errors of 0.5–1 km in the 1980's give swarm clusters internal detail.

All earthquake data presented in this paper have been reprocessed using the same procedures currently used to locate earthquakes at HVO. Thus no bias occurs to the earlier hypocenters other than larger errors resulting from sparser station coverage and poorer timing precision. The earthquake data presented in this paper are more systematically located and slightly more accurate than those used in previous papers (for example, Koyanagi and others, 1976; Ryan and others, 1981). Annual seismic summaries (for example, Nakata and others, 1982) list earthquake hypocenters and other seismic data together with a description of the analysis procedure. The computer program HYPOINVERSE (Klein, 1978) locates all events. A crustal velocity model incorporating linear gradients within velocity layers (Klein, 1981) was used. Earthquake depths determined by this method are referred to the land surface above the hypocenter. In the Kilauea summit region the depth datum is about 1 km above sea level. Both the velocity model and two sets of station corrections were designed to minimize the residuals between observed and calculated arrival times and were derived using numerous earthquakes under south Hawaii. The stations which operated during the year, and their locations and timing corrections are listed in the annual seismic summaries. The space, time and magnitude coordinates of earthquakes are plotted for this paper using the program QPLOT (Klein, 1983).

A THREE-DIMENSIONAL OVERVIEW OF KILAUEA SEISMICITY

Representing the three-dimensional distribution of earthquakes is difficult on any two-dimensional plot. Klein and Koyanagi (1985) produced a seismicity map of the south side of Hawaii, but depths are only indicated by one of four symbol colors. One of the easiest ways to visualize earthquakes is by depth slices using only a narrow, horizontal layer of events plotted on each map. Depth slices suit Kilauea very well because patterns change with depth and an earthquake's depth is often useful in discriminating it as volcanic or tectonic. The intent of this section is to present an overview; later sections of this paper will explore the magma system in more detail.

A series of depth slices for Kilauea from the surface to 40 km depth is shown in figure 43.3. Because the vertical magma conduit broadens with depth, deeper slices should cover a broader area. Figure 43.4 thus includes the entire south side of Hawaii and covers depths from 20 to 60 km. Figures 43.3 and 43.4 include data from 1970 through 1983. Figure 43.5 duplicates the slices of figure 43.4, but covers the 1960–69 period. The earlier data is plotted separately because it differs somewhat in pattern and is poorer in quality. The layers plotted thicken from 1 km at the surface to 4 km at depth, thus compensating for both spatial patterns that change less rapidly at depth and the slightly larger location errors associated with deeper events. Typical location errors for each depth range are about one-half the cutoffs chosen, which only eliminate the poorest events. Thus, an error in depth could possibly place a given event in an adjacent layer from where it actually occurred. Descriptions of the main features in different depth ranges follow.

THE SHALLOW CRUST BETWEEN 0 AND 5 KILOMETERS DEPTH

Events in the depth range 0–5 km are mostly volcanic earthquakes at Kilauea's caldera, rift zones and the Koae fault zone. Caldera seismicity extends mainly from 0 to 4 km depth. The aseismic magma reservoir beneath the southern part of the caldera is indistinguishable at this scale. Earthquakes in the northern and central parts of the caldera are most intense between 1 and 3 km depth and thus are mainly in the rocks of the caldera floor capping the summit reservoir. Southern caldera seismicity occurs both above and to the side of the reservoir and thus is active during periods of inflation and during rapid intrusions of dikes connected to the reservoir.

The most active part of the ERZ is between 2 and 4 km depth, at which nearly all of the 25 km of rift just east of the caldera has experienced some seismicity during 1970–83. Most of these earthquakes were produced during rapid intrusions or eruptions. The main ERZ magma conduit is most active at about 3 km depth. Unlike the SWRZ and the rest of the ERZ, the 6 km of ERZ adjacent to the caldera is seismically active nearly to the surface (fig. 43.3*A*). This shallow part of the ERZ may form a secondary conduit system that is intruded repeatedly and is a region brittle and stressed enough to generate earthquakes. This shallow earthquake zone could also be the result of tensile deformation when the main conduit below is intruded.

The SWRZ seismicity also forms a narrow and nearly continuous band. It does not exactly follow the course of the rift at the surface, but heads south from the caldera for about 3 km before bending to the southwest. The center of the ERZ earthquake band is displaced about 0.5 km south of the surface axis of the rift (defined by pit craters and eruptive centers), whereas the SWRZ seismic axis is displaced as much as 2 km south of the surface rift. The buried SWRZ magma conduit active during the last decade thus has no obvious surface expression. The SWRZ probably consists of a 3-km-wide zone of parallel dike systems that are active

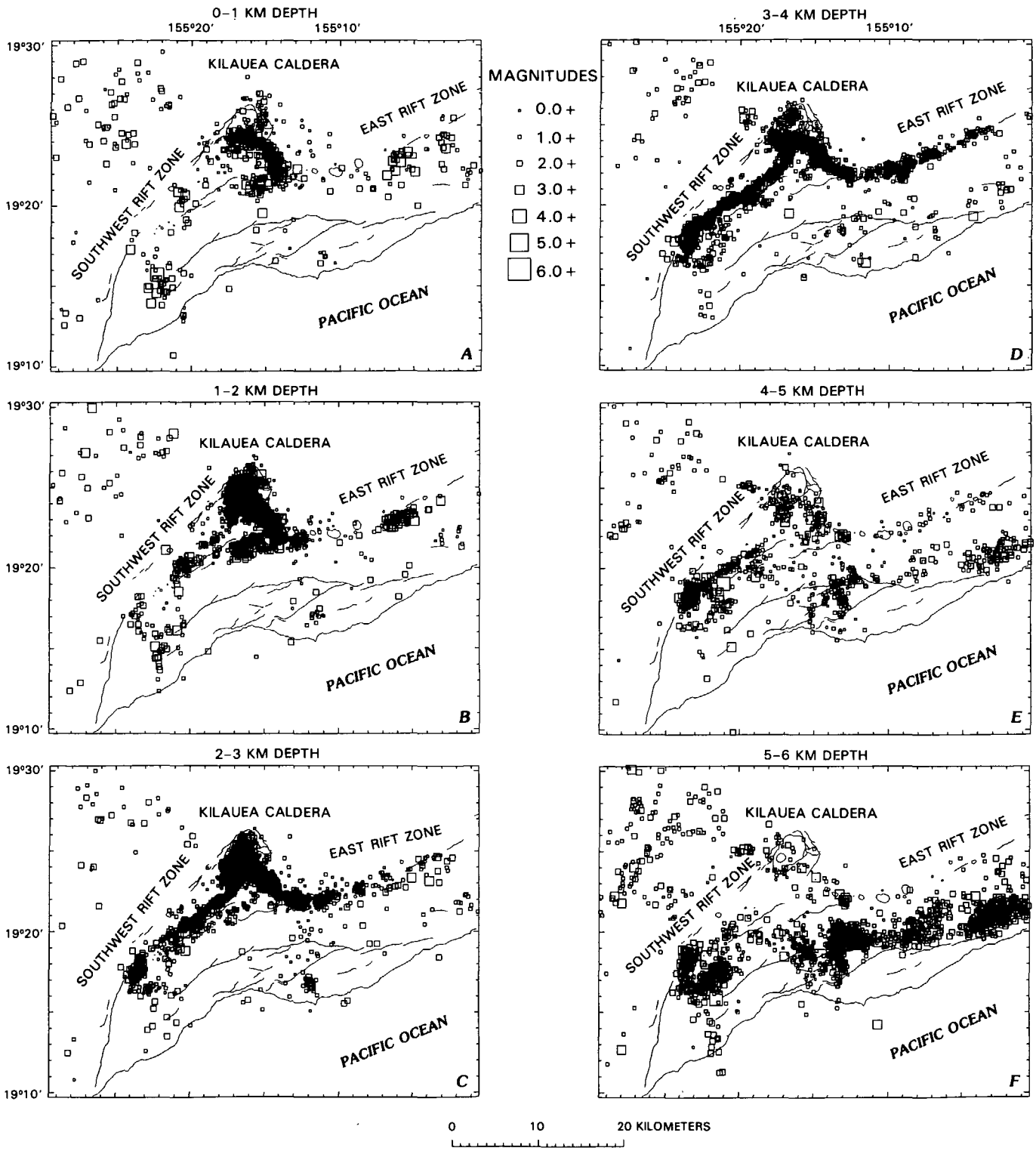

FIGURE 43.3.—Depth slices from 0 to 40 km showing hypocenters of Kilauea earthquakes, 1970–83. Earthquake symbols are squares whose size depends on magnitude. Maximum horizontal error of plotted hypocenters is: ***A–O***, 2 km; ***P–T***, 4 km. Maximum vertical error is: ***A–J***, 2 km; ***K–O***, 3 km; ***P–T***, 5 km. Faults, fissures, and pit craters are as shown in figure 43.1.

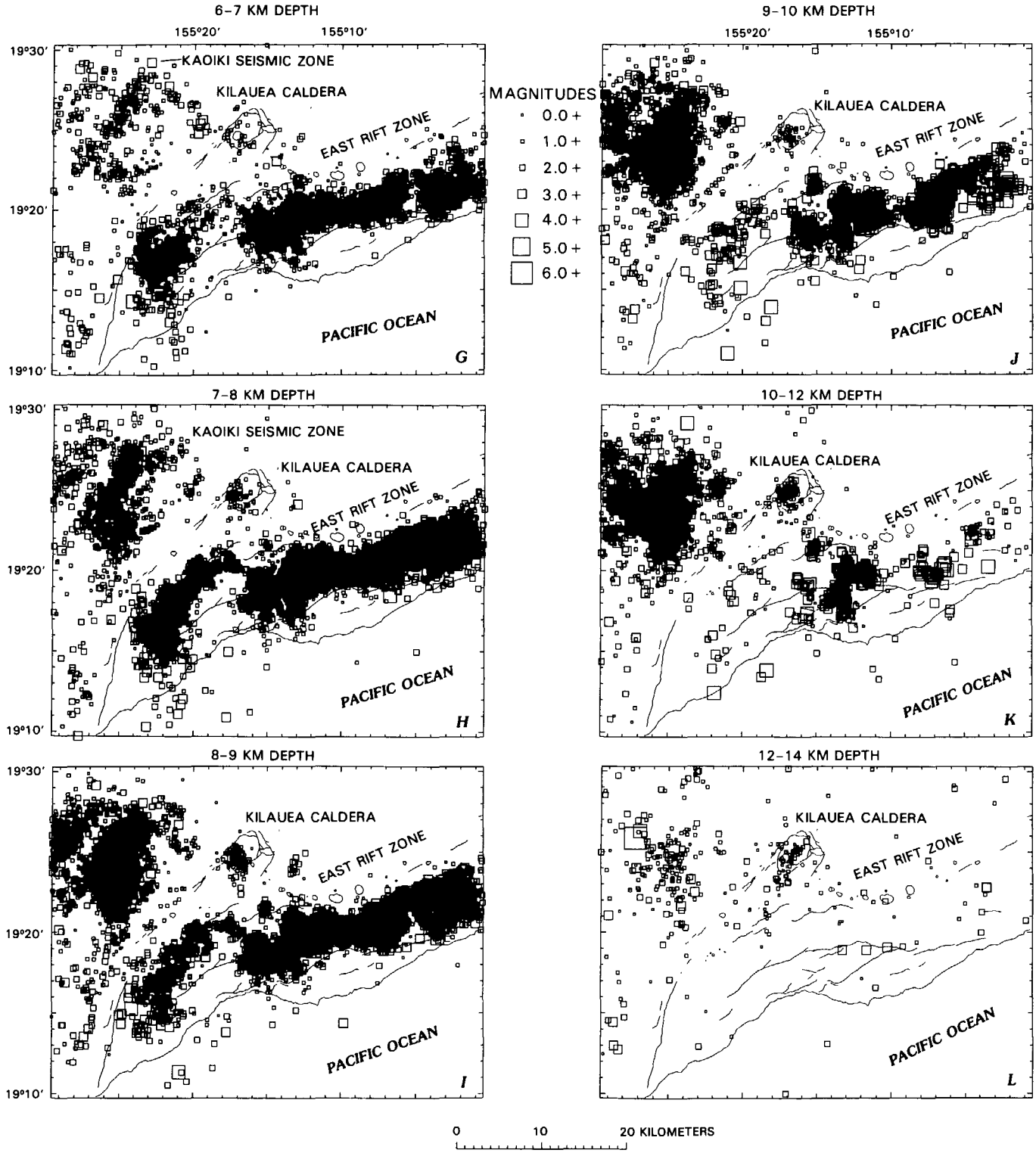

FIGURE 43.3.—Continued.

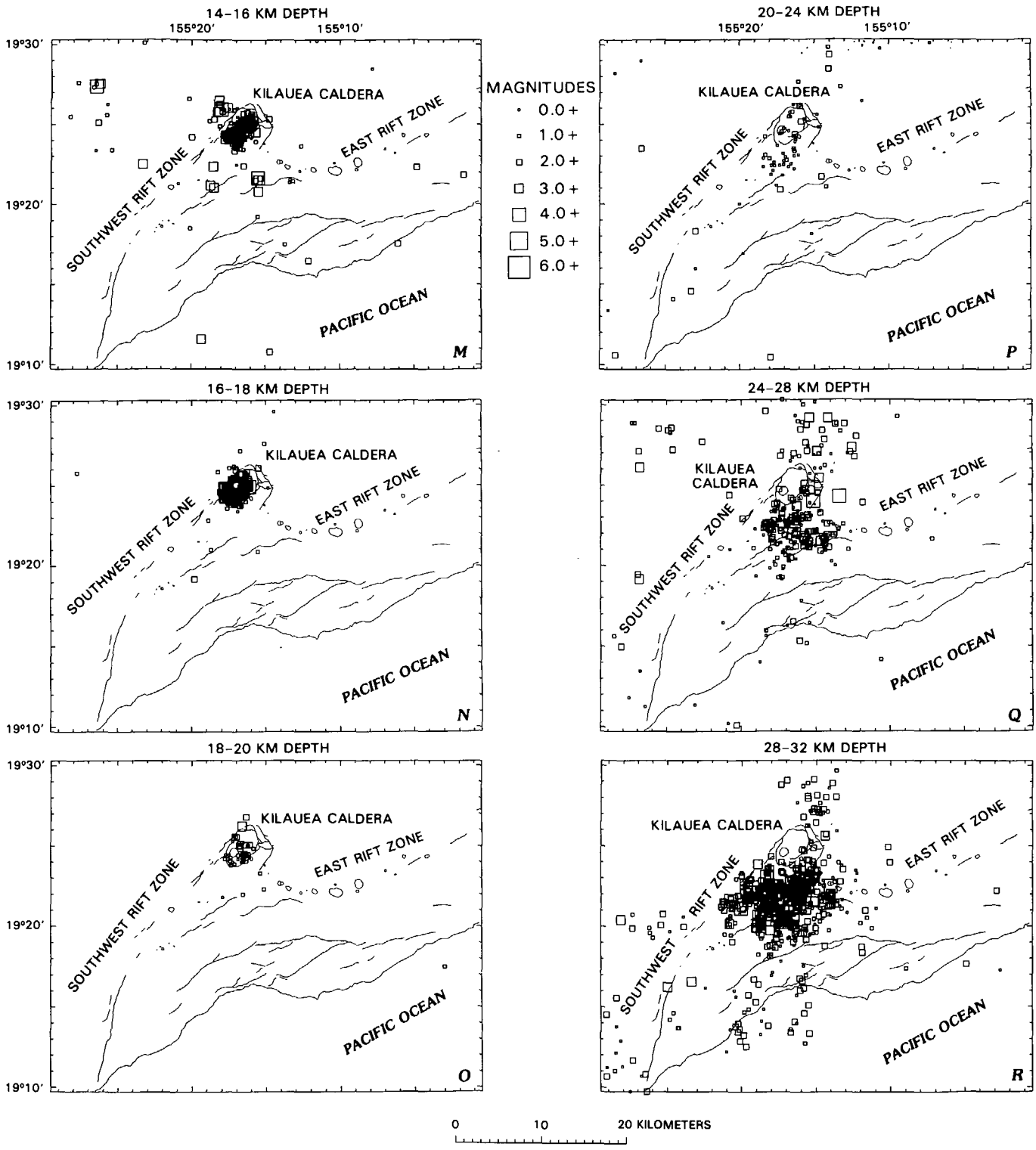

FIGURE 43.3.—Continued.

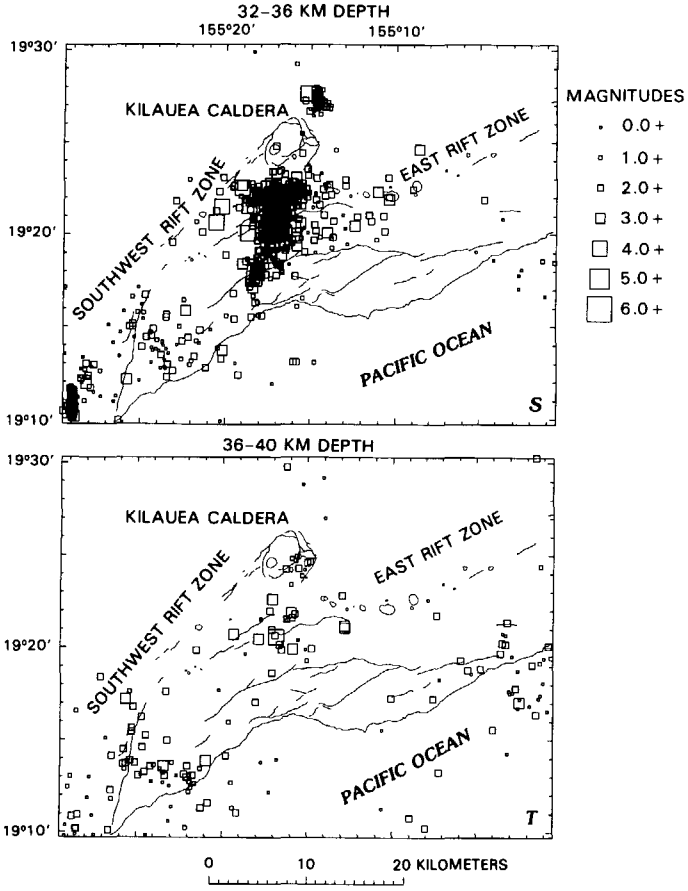

FIGURE 43.3.—Continued.

at various times and that evolve with time. Because the contemporary magma conduits of both the ERZ and SWRZ are south of the established surface features, the vertical dike trajectories must dip southward. The offset of earthquakes and surface geology could be a consequence of southward migration of the rifts with time (Swanson and others, 1976a).

Like the ERZ, the primary conduit of the SWRZ is at about 3 km depth, with seismicity extending for about 1 km above and below. A notable exception is the shallow clump just downrift of Puu Koae (19°20′ N., 155°20.5′ W.; fig. 43.3*A*, *B*). Surface cracks appeared in this area during the August 1981 SWRZ intrusion and were probably caused by a dike branching upward from the main conduit. A similar shallow extension occurs above the ERZ conduit near Mauna Ulu (19°22′ N., 155°12.5′ W.; fig. 43.3*B*). Much of the shallow seismicity near Puu Kamoamoa and Puu Kahaualea (19°23′ N., 155°06′ W.; fig. 43.3*A*, *B*), however, occurred in a series of extended swarms that coincided with inflation of the rift near the earthquake epicenters. The very shallow seismicity thus appears to be over a part of the rift conduit that was accumulating magma and is analogous to the seismic cap over the summit magma reservoir. The rift inflation occurred cyclically and coincided with times of slow summit deflation.

The linear part of the SWRZ active during 1970–83 extends only to the north end of the Great Crack (19°17′ N., 155°25′ W.; figs. 43.1*C*, 43.3*A–E*), where the rift bends to a more southerly trend. The seismicity in this lower southwest rift (LSWR) region is somewhat complex and diffuse. Earthquakes scatter south of the rift over a wide range of depths. Between 0 and 3 km depth this area is active most of the way to the coast, and below 2 km the seismically active rift branches into parallel segments just south of the main rift axis. Unlike the rest of the SWRZ, the LSWR can be intensely active below 4 km depth, and seismicity merges with the region of tectonic earthquakes in Kilauea's south flank. In addition, LSWR earthquakes accompany both the larger SWRZ intrusions and major tectonic events on the south flank, such as the November 1975 Kalapana earthquake. The LSWR thus seems to be a weak but brittle zone extending from 0 to 10 km depth in which activity can be triggered either by intrusions in the SWRZ to the north or by tectonic events to the east.

Other scattered events at 0–4 km depth occur away from the volcanic conduits. The events distributed broadly through the upper part of Kilauea's south flank occurred both as aftershocks of the $M=7.2$ Kalapana earthquake and as induced events associated with larger ERZ intrusions (Dvorak and others, 1985). This area thus responds both to large scale slip in the lower crust (tectonic events) and to compressional stress generated by dike intrusion to the north (volcanic events). The Kaoiki seismic zone also produces some shallow tectonic earthquakes even though most activity lies below 5 km depth. Small isolated clusters of tectonic earthquakes also occur near Apua Point (0–4 km depth) and 4 km west of Kilauea caldera (3–8 km depth).

TECTONIC EARTHQUAKES BETWEEN 5 AND 14 KILOMETERS DEPTH

The vast majority of Kilauea earthquakes at 5–14 km depth are tectonic events on the south flank and in the Kaoiki seismic zone. The tectonic events plotted in figure 43.3*F–L* are composed of both continuous seismicity and aftershocks of larger earthquakes. The majority of earthquakes on the portion of the Kaoiki seismic zone included in figure 43.3 show right-lateral slip on northeast striking planes (Endo and others, 1978). Lineations of earthquakes also follow this trend. The typical focal mechanism of south-flank events is low-angle faulting with the upper block slipping seaward (Crosson and Endo, 1982). Unlike the Kaoiki seismic zone, no clear alignment of hypocenters on fault planes is apparent, and many slip planes are active.

THE MAGMA CONDUIT BETWEEN 5 AND 20 KILOMETERS DEPTH

The vertical magma conduit below Kilauea caldera is clearly defined by hypocenters below about 6 km depth. In the depth slices of figure 43.3*G–O*, the seismic conduit is centered below Halemaumau and Kilauea's summit magma reservoir. The shape and size of the seismic conduit varies only slightly with depth, and typically is about 3 km in diameter. The earthquake location errors from both random and systematic sources means that small variations in cross-sectional shape and a precise diameter probably are not significant within about 1 km. It is tempting to interpret the ring of seismicity in figure 43.3*N* surrounding an aseismic magma conduit, but the precision of hypocenter position does not justify the interpretation. The earthquakes represent a zone of deformation in brittle rock surrounding the conduit itself, which is probably much smaller than the seismic zone and may even be multiple. An upper limit to the diameter of the seismically active conduit complex is thus about 3 km. Magnitudes of these events are small and seldom exceed 3.0.

THE MAGMA CONDUIT BETWEEN 20 AND 40 KILOMETERS DEPTH

The seismicity of the magma conduit changes character in several ways below 20 km: (1) the earthquake zone broadens to about 13 km in diameter (fig. 43.3*R–S*) (2) the seismic pipe plunges southward, unlike its vertical direction above 20 km; (3) the activity is more intense, with more events as large as magnitude 4.5; and (4) events are more continuous in time and generally not in swarms like the seismicity above. Earthquakes in the upper conduit are thus typically volcanic, whereas those between 20 and 40 km are mostly tectonic. The broadening with depth and southward plunge of the seismic conduit were plotted but not interpreted by Koyanagi and Endo (1971).

Inversion of teleseismic *P*-times for lateral velocity variations (Ellsworth and Koyanagi, 1977) showed another change in the conduit that occurs near 20–30 km depth. Although the resolution was limited by the 8-km wavelength, the average velocity is a few percent low directly below and to the south of Kilauea caldera at 28–58 km depth, suggesting a laterally extensive conduit system. Conduit velocities above that depth, however, are several percent higher than their surroundings (Ellsworth and Koyanagi, 1977; Thurber, 1984). These inversion studies also demonstrate high seismic velocities in the upper crust below the rifts, suggesting that a narrow conduit lies within a high-velocity intrusive complex in both the rifts and upper vertical conduit.

The narrow finger of earthquake hypocenters between 5 and 20 km depth is adjacent to the magma conduit and is thus seismically somewhat analogous to the shallow rift zones. The stress causing earthquakes in the upper pipe is thus partly derived from magma pressure within the conduit. The stress driving the earthquakes centered near 30 km depth, however, seems to be more than just that from magma pressure within the conduit complex. The magma conduit apparently passes through the 30-km-deep seismic zone and may have triggered its formation initially. But the size and intensity of the 30-km-deep seismic zone indicate a more regional stress source. Possibilities include flexure of the lithosphere under the gravitational load of the island or response to tractional stress applied from the volcanic edifice. Depletion of mass near this depth could also cause intense local seismicity. The behavior of these earthquakes in time (see next section) provides additional evidence bearing on the cause of these earthquakes.

Kilauea's magma conduit seismicity below 20 km must be examined in the context of a wider seismic region. Figure 43.4 plots depth slices below 20 km and includes deeper earthquakes from Mauna Loa and Loihi Volcanoes. The main seismic root of Kilauea is the prominent feature between 20 and 40 km, but a smaller funnel-shaped zone between 24 and 34 km is recognized just north of the caldera (figs. 43.3*Q–S*, 43.4*B-D*).

THE MAGMA CONDUIT AND HOT SPOT BELOW 40 KILOMETERS DEPTH

Earthquakes below about 30 km depth mostly occur in a wide band roughly coincident with the south coast of Hawaii (fig. 43.4*C–J*). The deep seismic zone consists partly of dense earthquake clusters (fig. 43.4*F–H*). The small clusters do not extend vertically more than about 8 km, so they cannot clearly be identified with long magma conduits. The clusters may occur at places weakened by past and present magma flow, or simply at points having a high density of fractures. Seismicity concentrates in the triangle with corners at Kilauea, Mauna Loa and Loihi, but also extends to the northeast and southwest. Kilauea loses its narrow seismic root at about 40 km depth in this diffuse cloud. Earthquakes become sparse below about 50 km (fig. 43.4*I–J*) and none are located reliably below 60 km depth.

Earthquakes mark an isolated, narrow conduit beneath Mauna Loa that can be traced between about 28 and 48 km depth (fig. 43.4*C–G*). The earthquakes north of Hilo around 40 km depth are mostly aftershocks of the April 1973 Honomu earthquake (Unger and Ward, 1979).

Most deep earthquakes occur continually, which suggests a relatively uniform stress by analogy with crustal events. A few deep earthquakes are in swarms, which may be associated with pulses of ascending magma. The part of the seismic zone equidistant from Kilauea, Mauna Loa and Loihi is a frequent source of deep harmonic tremor, and magma certainly is present there. Tremor originating in this region can be quantitatively related to Kilauea's magma supply and transport to the shallow reservoir (Aki and Koyanagi, 1981). The coincidence of tremor, of the center of the deep seismic zone, and of the major earthquake cluster shown in figure 43.4*E–G* suggests that the contemporary Hawaiian hot spot is centered there (Klein, 1982a).

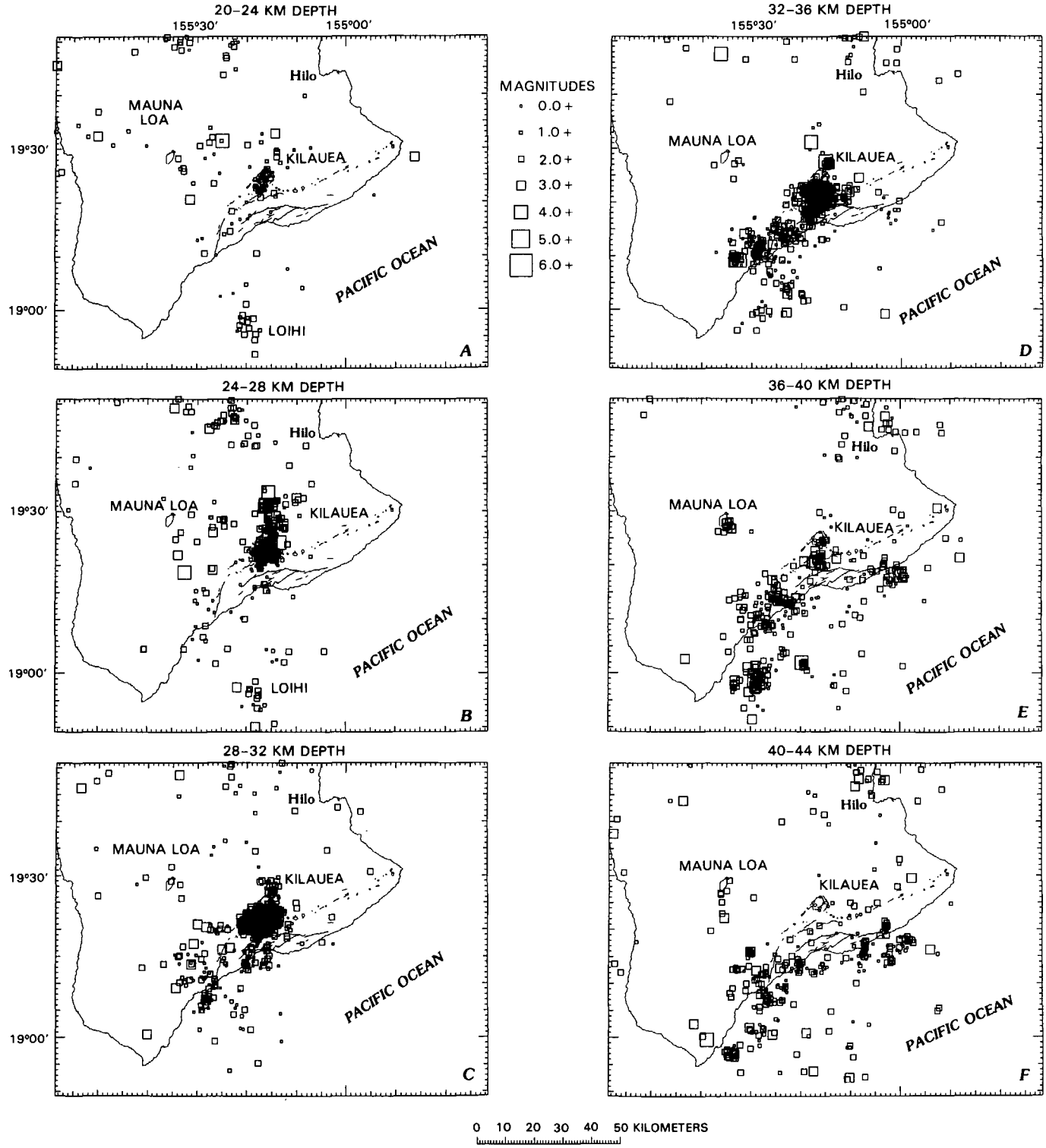

FIGURE 43.4.—Depth slices from 20 to 60 km showing hypocenters of south island earthquakes, 1970–83. Earthquake symbols are squares whose size depends on magnitude. Maximum horizontal and vertical errors for *A–J* are 5 and 7 km, respectively. Note that *J* includes hypocenters to 99 km depth, but those below 60 km are not reliably located. Faults, fissures, and pit craters are as shown in figure 43.1.

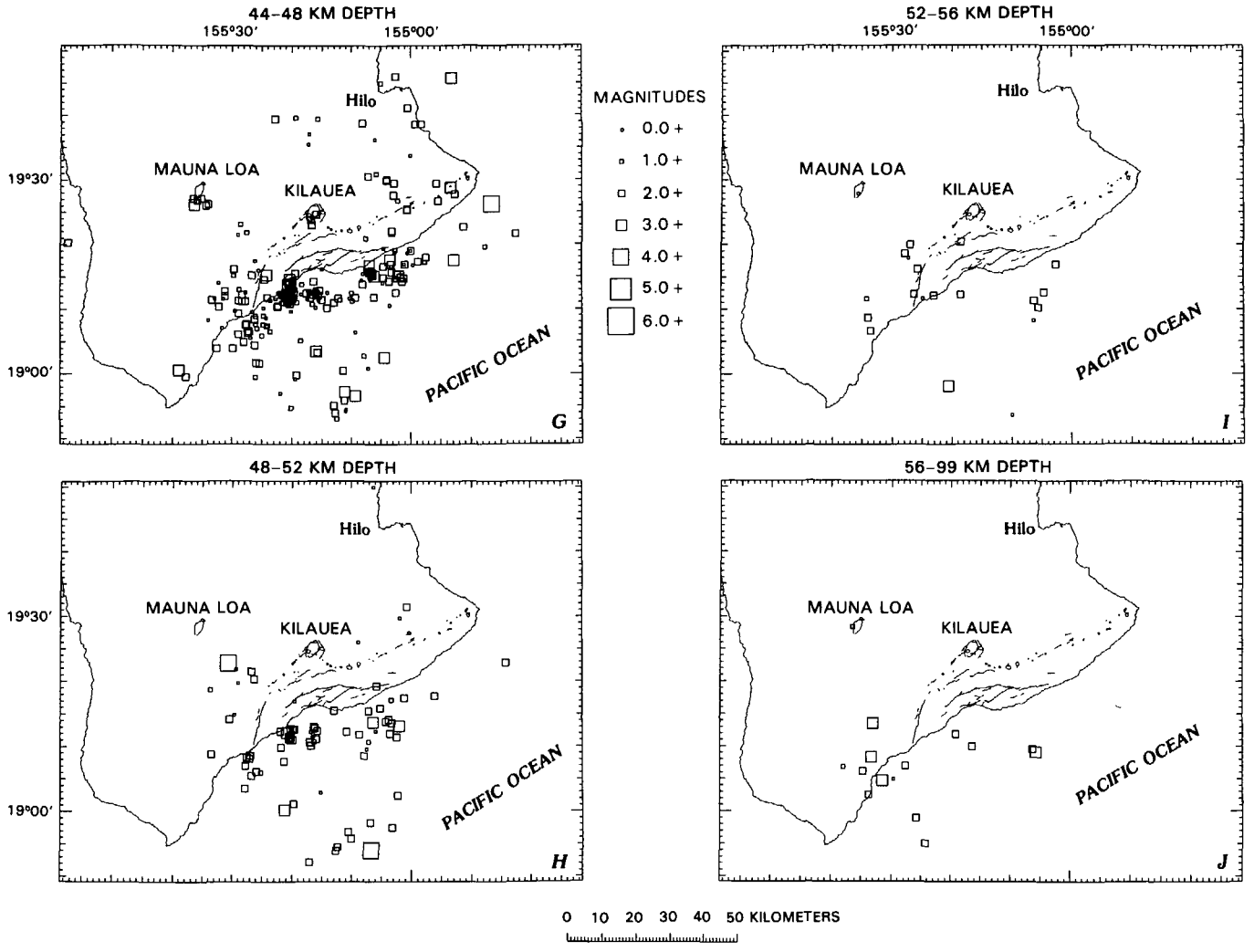

FIGURE 43.4.—Continued.

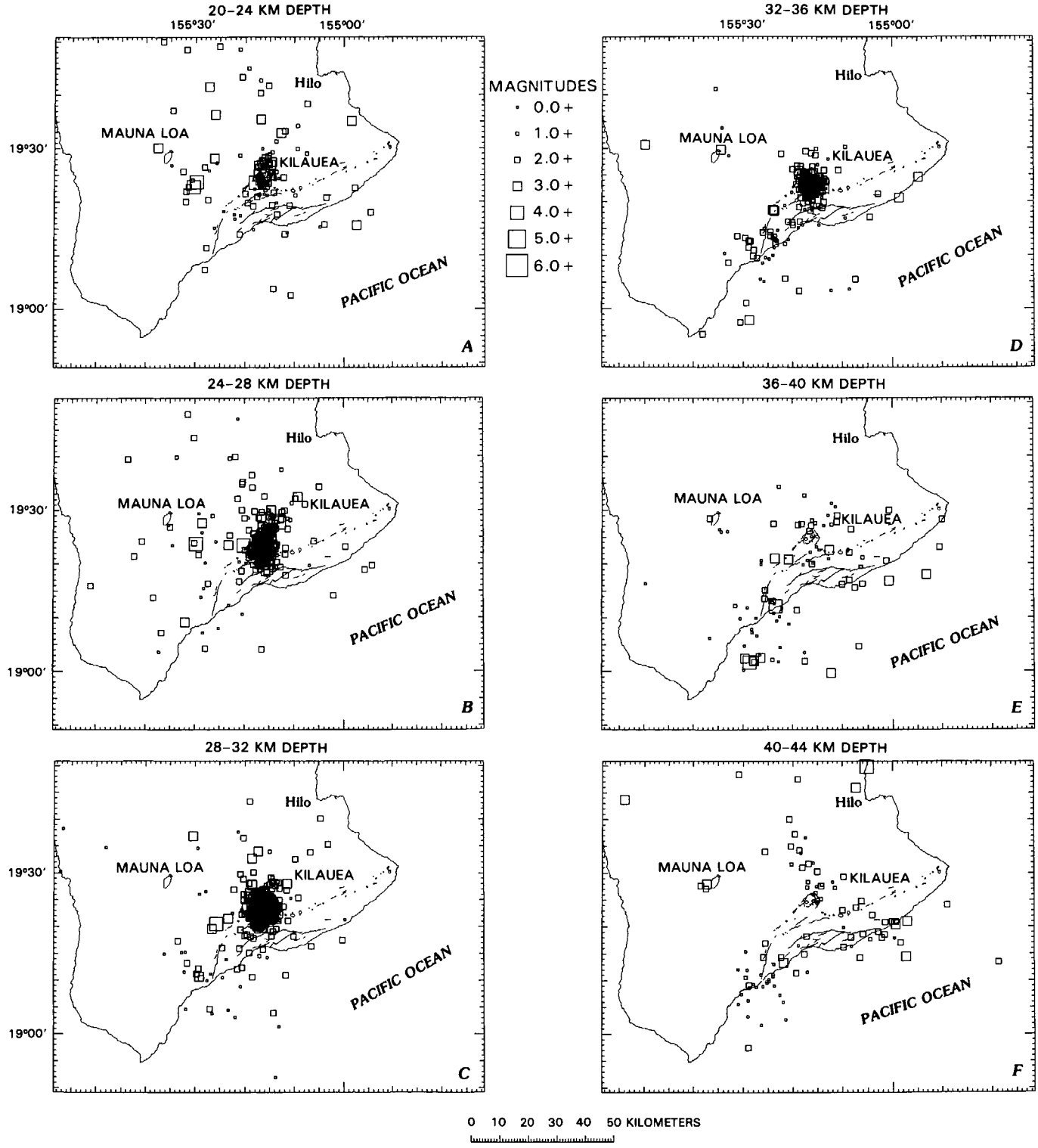

FIGURE 43.5.—Depth slices from 20 to 60 km showing hypocenters of south island earthquakes, 1960–69. Earthquake symbols are squares whose size depends on magnitude. Maximum horizontal and vertical errors for ***A–J*** are 10 and 15 km, respectively. Note that *J* includes hypocenters to 99 km depths, but those below 60 km are not reliably located. Faults, fissures, and pit craters are as shown in figure 43.1.

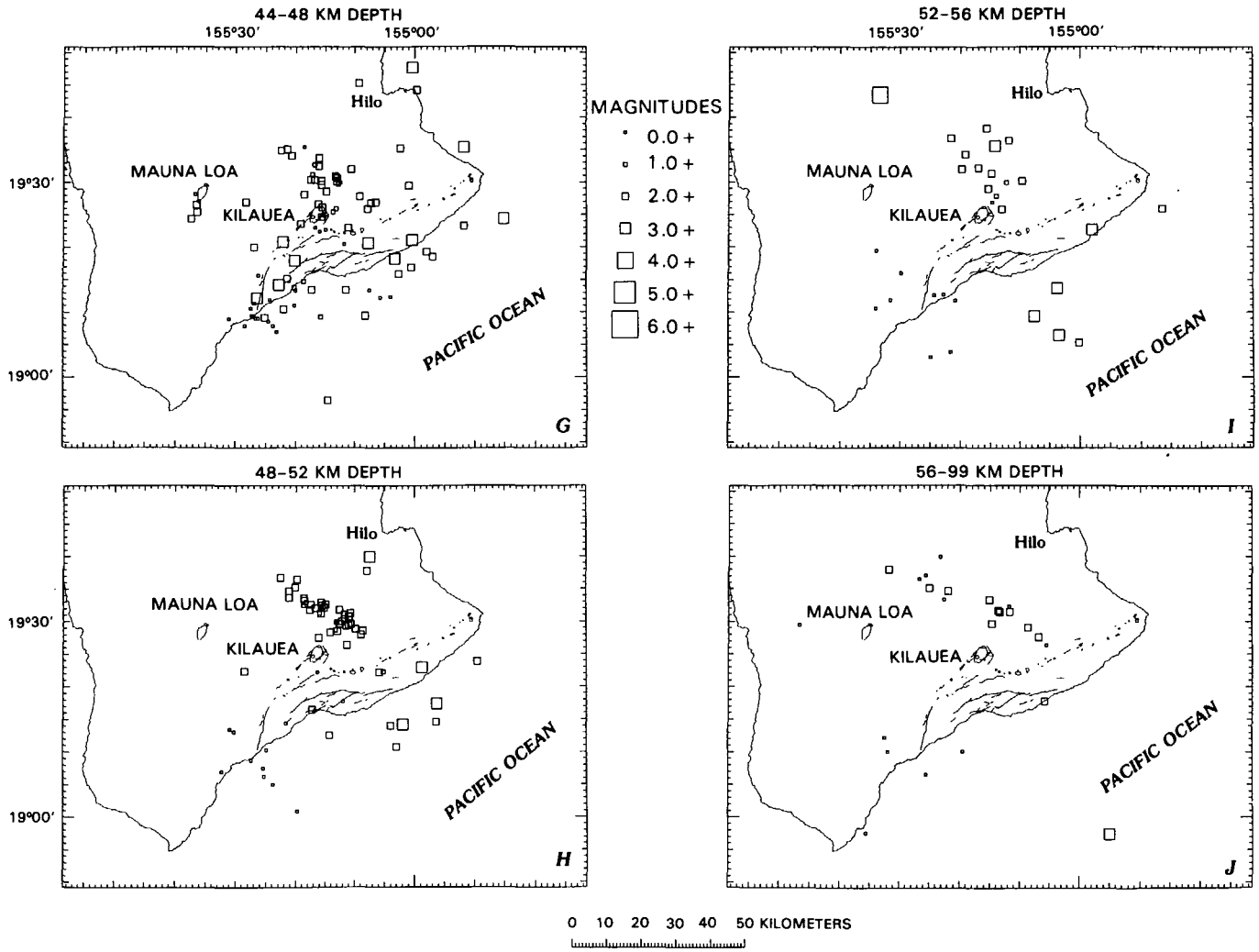

FIGURE 43.5.—Continued.

THE MECHANISM OF DEEP EARTHQUAKES

The deep seismic band roughly coincides with the mobile and growing south flank of the island. This coincidence suggests that the stress causing the earthquakes is related to the dynamics of the volcanic pile above. In recent decades, the south side of the island has been most active volcanically, seismically and tectonically, and the three phenomena are related. Stress at depth could arise in three main forms: (1) the unbuttressed and mobile south flanks of Kilauea and Mauna Loa exert a lateral shear on the lithosphere as they are pushed seaward by their growing rift zones and gravitational slumping; (2) the added weight of new lava and dikes continually increases the normal gravitational stress on the lithosphere, and its nonuniformity causes earthquakes near the additional load; and (3) the mantle beneath the seismicity is being melted and depleted, and mass from above slumps down along active faults to replenish the lost volume.

The circumstantial evidence favors some combination of shear and normal stress applied from the volcanic pile above as a driving mechanism of Kilauea earthquakes below 13 km. First, the fact that most deep earthquakes do not occur in swarms argues against the close association of earthquakes and partial melting. If widely distributed pockets and conduits of magma were present, then local stress concentrations would result in swarms, as it does in the shallow rift and conduit systems. Seismicity resulting from settling to compensate for much deeper melt depletion would produce continuous seismicity essentially similar to the effects of applying stress from above. The stress and geometry of magma distribution at 20-40 km depth may change with time, as suggested by the absence of earthquakes at this depth prior to 1961, and the fact that some swarms did occur in the early 1960's (Eaton and others, chapter 48).

Second, the time behavior of Kilauea's deep earthquakes (13–60 km) is linked to the stress state of Kilauea's south flank. The rate of Kilauea's deep seismicity dropped markedly at the time of the 1975 Kalapana earthquake (see next section). The effect of the $M=7.2$ earthquake was to relieve compressional stress stored in the mobile south flank by slipping seaward, thus also releasing shear stress that had been applied to the mantle below. The sudden drop of applied stress could have caused the drop in rate of Kilauea's deep earthquakes. The occurrence of the Kalapana earthquake suppressed the seismicity of Kilauea's vertical magma conduit from 6 to 60 km, and its effect on earthquake rates diminished with depth. The Kalapana earthquake, however, had little influence on the deep and broad band of earthquakes along Hawaii's south coast. Apparently the effects of relieving stress in 1975 did not extend beyond Kilauea's immediate vicinity.

Third, the position of the band of earthquakes below 36 km along Hawaii's south coast argues that stress applied from volcanic and tectonic activity is a causative mechanism. Growth of the island's volcanic pile is on the south half of the island, but was primarily under Kilauea during recent decades. Addition of mass is far greater on land north of the band of deep earthquakes than to the south offshore. This differential loading produces a stress gradient under the coastline. The unbuttressed seaward coasts of both Kilauea (Ando, 1979; Crosson and Endo, 1982) and Mauna Loa (for example, the $M=5.6$ and $M=5.4$ Ninole Hills earthquakes of January 21, 1982) are mobile and experience large tectonic earthquakes in which the upper block slips seaward. The stress build-up which causes these earthquakes also exerts a shear on the lithosphere that is greatest along the south flank of the island.

Lithospheric flexure also appears to play a part in the distribution and cause of deep earthquakes. It is a complex problem, with varying shear and normal stresses applied to the top of a rigid lithosphere containing weaker magma conduits. Kilauea's deep seismicity thus seems to result from a combination of tectonic and gravitational stress applied from above, perturbation from its magma conduit, flexure of the lithosphere, and interaction with the Hawaiian hot spot.

EARTHQUAKES AT 20–60 KILOMETERS DEPTH DURING 1960–69

Earthquakes during 1970–83 are more accurately located and more complete than those before, but earlier events are important because some changes of spatial pattern occur with time. The seismic coverage during 1960–69 was not good for resolving fine details in shallow seismicity, but was adequate for larger patterns of deeper earthquakes. Figure 43.5 plots the same depth slices and map area as figure 43.4, but contains only 1960–69 data.

Kilauea's seismic root above 36 km depth appears the same during both periods (compare fig. 43.4*A–D* with fig. 43.5*A–D*), but differences are obvious in other areas. The band of earthquakes that coincides with the island's south coast was better developed during 1970–83 (fig. 43.4*C–H*). Although the many small earthquake clusters cannot be resolved by the sparser network during 1960–69, the band itself had roughly the same size and shape (fig. 43.5*C–H*). Most Loihi earthquakes occurred during swarms in 1971-72 and 1975 (fig. 43.4*A*, *B*; Klein, 1982a). The absence of Loihi events during 1960–69 is a combination of its inactivity and reduced network sensitivity to distant earthquakes.

The greatest seismicity differences are deeper than 40 km (compare fig. 43.4*F–J* and fig. 43.5*F–J*). The area about 20 km north of Kilauea caldera was very active in 1960, but during 1961–83 the southwest corner of Kilauea was most active. This shift is not a result of changing seismic network geometry, but stems from deep swarms in July and October 1960 that did not recur in the subsequent 23 years. Earthquakes in 1959 similar to those in 1960 were interpreted by Eaton and Murata (1960) as originating from Kilauea's magma conduit. The apparent northwest trend of epicenters in this deep 1960 zone (fig. 43.5*H–J*) is partly real and partly an artifact of the station geometry: this is the direction of poorest control by the stations to the southwest. By looking at only 1960 data one might conclude that Kilauea's main seismic root plunged north rather than southwest as current evidence suggests. No seismic pattern should be considered permanent, and our view of the vertical magma conduit will surely be modified in subsequent decades.

THE *b*-VALUES OF SHALLOW EARTHQUAKES

The earthquake regions discussed in this "Three-dimensional overview" section differ in their time history, maximum magnitude and a statistical parameter called earthquake *b*-value. The log-number of events is generally a linear function of magnitude when the sample of earthquakes is complete. The constant of proportionality is the *b*-value and usually ranges from about 0.5 to 1.5 (Richter, 1958). Higher *b*-values are often characteristic of volcanic areas and should be typical of regions with lower and heterogenous stress (Mogi, 1962; Wyss, 1973). A detailed survey of *b*-values is beyond the scope of this paper, but preliminary results suggest that *b*-values are higher in Kilauea's volcanic earthquake regions. Earthquake *b*-values were computed for each region shown in figure 43.6 using events shallower than 20 km depth during 1970–79. Major swarms and aftershock sequences were removed, but their inclusion would not significantly change the results. The regions with *b*-values larger than 1.1 include Kilauea's rift zones and parts of the immediately adjacent south flank, Mauna Loa and Loihi: these are volcanic areas where magma presumably produces concentrated stress and larger *b*-values. Lower *b*-values are characteristic of Kilauea's flanks more distant from rift zones. These flank areas apparently can sustain higher and more uniform stresses.

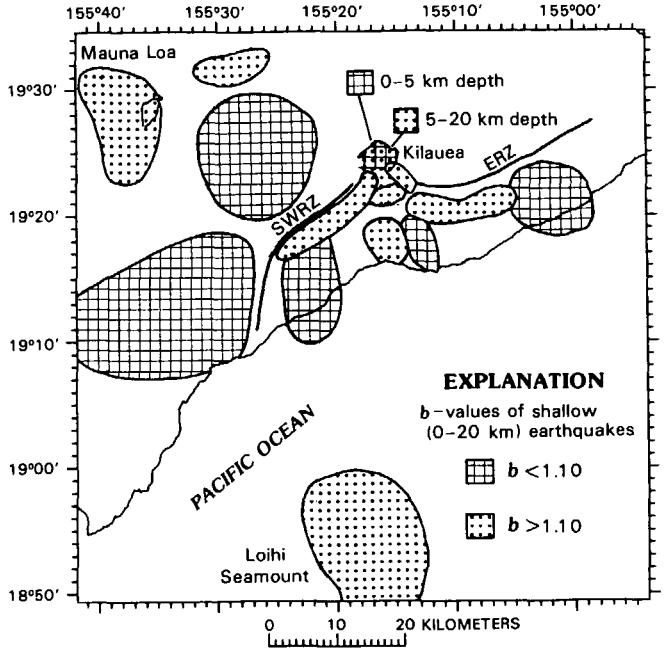

FIGURE 43.6.—Kilauea and part of Mauna Loa, differentiating areas of higher *b*-values (>1.1, dot pattern) from areas of lower *b*-values (<1.1, grid pattern). The *b*-values were only calculated for the regions shown. Earthquake data from 1970 to 1979 were used, but swarms and aftershock sequences were excluded.

GENERALIZED HISTORY OF KILAUEA EARTHQUAKES

A key discriminant between volcanic and tectonic earthquake regions is whether seismicity occurs in episodic volcanic swarms or combines continual activity with mainshock-aftershock sequences as in tectonic regions. Changes in the rate of earthquake occurrence also indicate times when stress is changing. We divided Kilauea into several regions (fig. 43.7) and plotted the cumulative number of earthquakes versus time for each (fig. 43.8). Only events larger than a particular cutoff magnitude were chosen so that the detection would be complete or at least consistent. For shallow earthquakes at Kilauea, coverage is reasonably complete to magnitude 1 except during the most intense swarm periods. Kilauea's deep and flank events are mostly complete to about magnitude 2, except during times of exceptionally high seismicity, such as aftershocks of the 1975 Kalapana earthquake. For present purposes, it is better to choose a cutoff magnitude low enough to provide sufficient events to characterize an area's behavior, than to choose it high to be sure of an absolutely complete sample above the cutoff magnitude.

SHALLOW VOLCANIC EARTHQUAKES

The cumulative plots of shallow earthquakes in volcanic areas have a characteristic sawtooth pattern resulting from episodic swarms. For shallow caldera earthquakes (fig. 43.8*A*), the curve for a typical eruption cycle begins as a plateau with few earthquakes following an intrusion and deflation. During reinflation seismicity gradually increases, resulting in an upward curving line. The cycle ends with an upward jump in the graph whose length is the number of events in the swarm larger than magnitude 1. Because figure 43.8*A* includes both caldera and some adjacent rift zone events, we see both the gradually building earthquakes related to inflation (in the caldera and upper rifts) and the rapid swarms (usually in the rift zones). The prominent increase in the rate of seismicity beginning in 1979 appears not to be just an artifact. The lower rate prior to 1979 is not a simple result of incomplete reporting of events larger than magnitude 1 because cumulative curves with magnitude cutoffs larger than 1 show the same increase. The beginning of a new procedure based on computer processing at HVO occurred in 1979, so the apparent increase arises from a combination of changes in event selection and magnitude calculation.

Seismicity of the upper ERZ and middle ERZ (fig. 43.8*B*, C) also shows a sawtooth pattern. The background rate is typically low, but is punctuated by short swarms that cause the curve offsets. Many of the larger swarms contributed earthquakes to both ERZ regions and hence to both curves of figure 43.8*B* and C. Some immediate aftershocks of the $M=7.2$ Kalapana earthquake contribute to figure 43.8C, but this is the only earthquake large enough to have caused aftershocks in this region. During 1979 and 1980, the middle ERZ experienced several cyclic intrusions that occurred too slowly to produce an intense swarm or eruption. Drops in summit tilt and seismicity were coupled with periods of inflation and intermittent earthquakes at shallow depth below the rift.

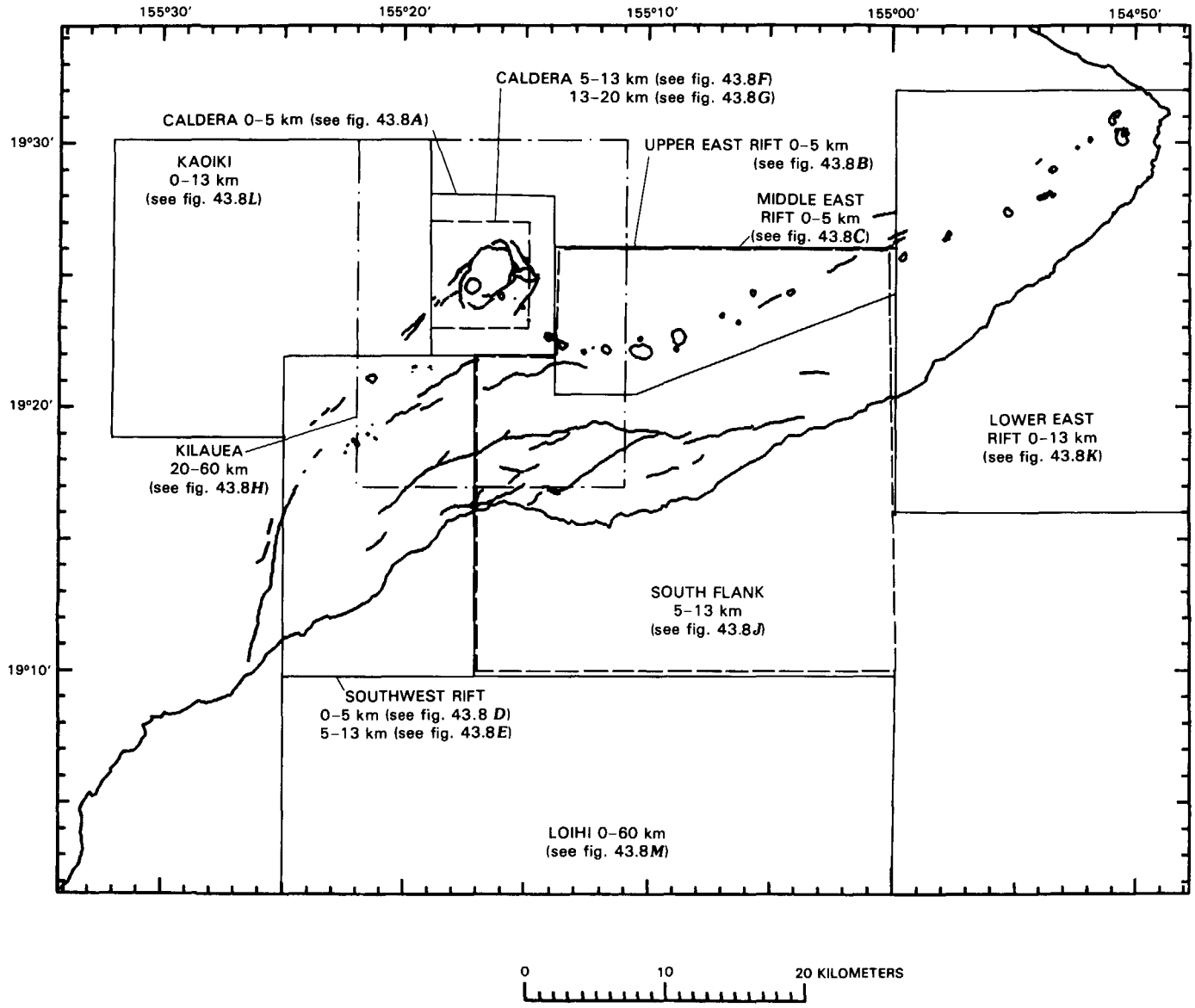

FIGURE 43.7.—Locator map of regions used to select earthquakes for cumulative seismicity curves shown in figure 43.8. Boundaries were chosen to enclose approximately homogeneous seismic regions, but seismicity is certainly not distributed uniformly in each region. Solid lines are used for boundaries that extend up to the surface, dashed lines for regions between 6 and 20 km depth, and a dash-dot line for Kilauea's root below 20 km. The Loihi region between 155° 00′ and 155° 25′ W. longitude extends south (beneath the figure) to 18° 40′ N. latitude.

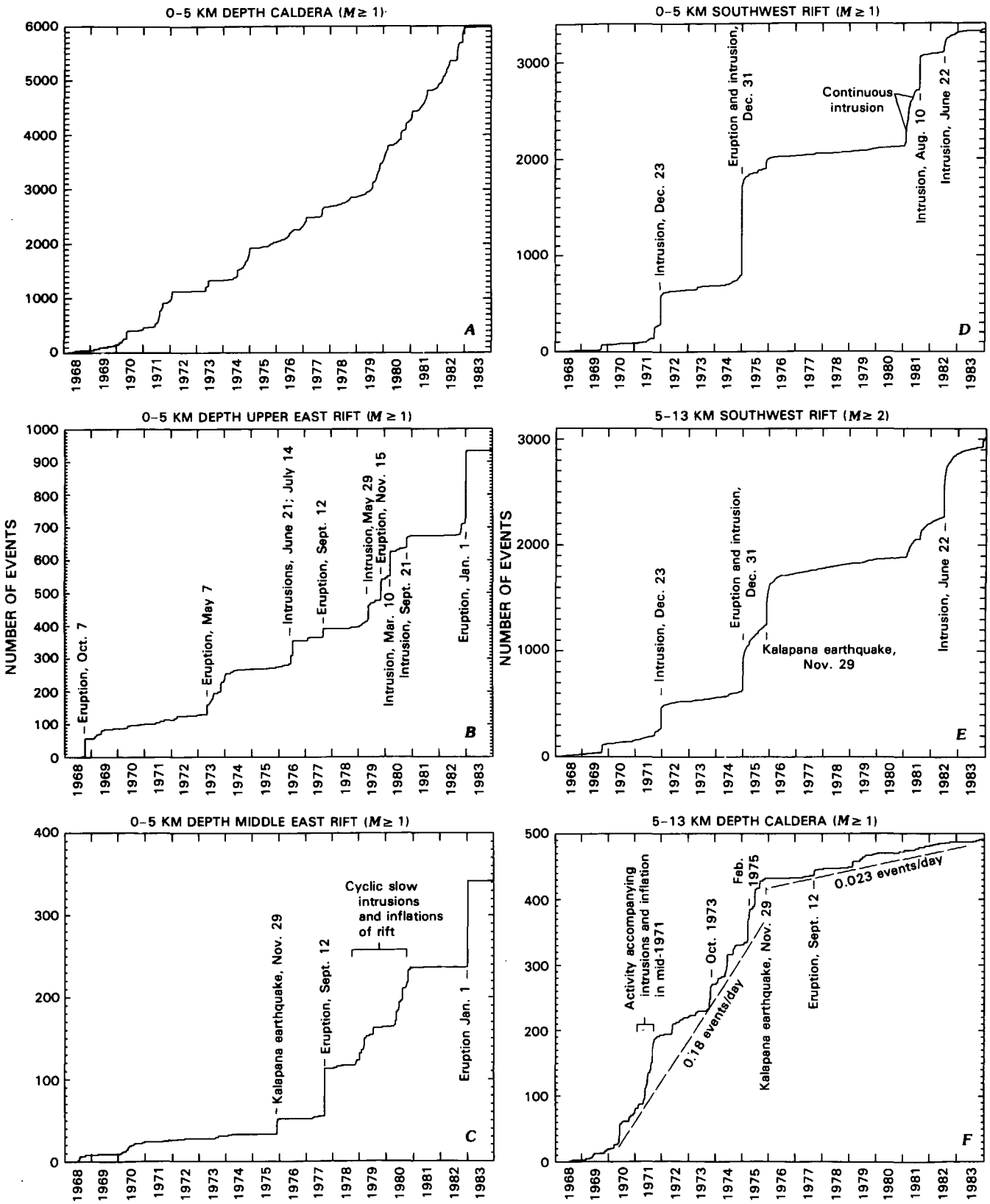

FIGURE 43.8.—Cumulative numbers of earthquakes plotted versus time. ***A–M***, Regions outlined in figure 43.7. The "south island" region of figure 43.8*I* includes the entire area of figure 43.7. Curve shape indicates how episodic or continuous seismicity is. Only events larger than indicated magnitude are included in count, in an attempt to maintain uniform completeness. Apparent increase in activity after 1969 in some areas may be an artifact of network improvements at about that time. Some large earthquakes, eruptions and intrusions are noted. Dashed lines are labeled with their slopes in events per day.

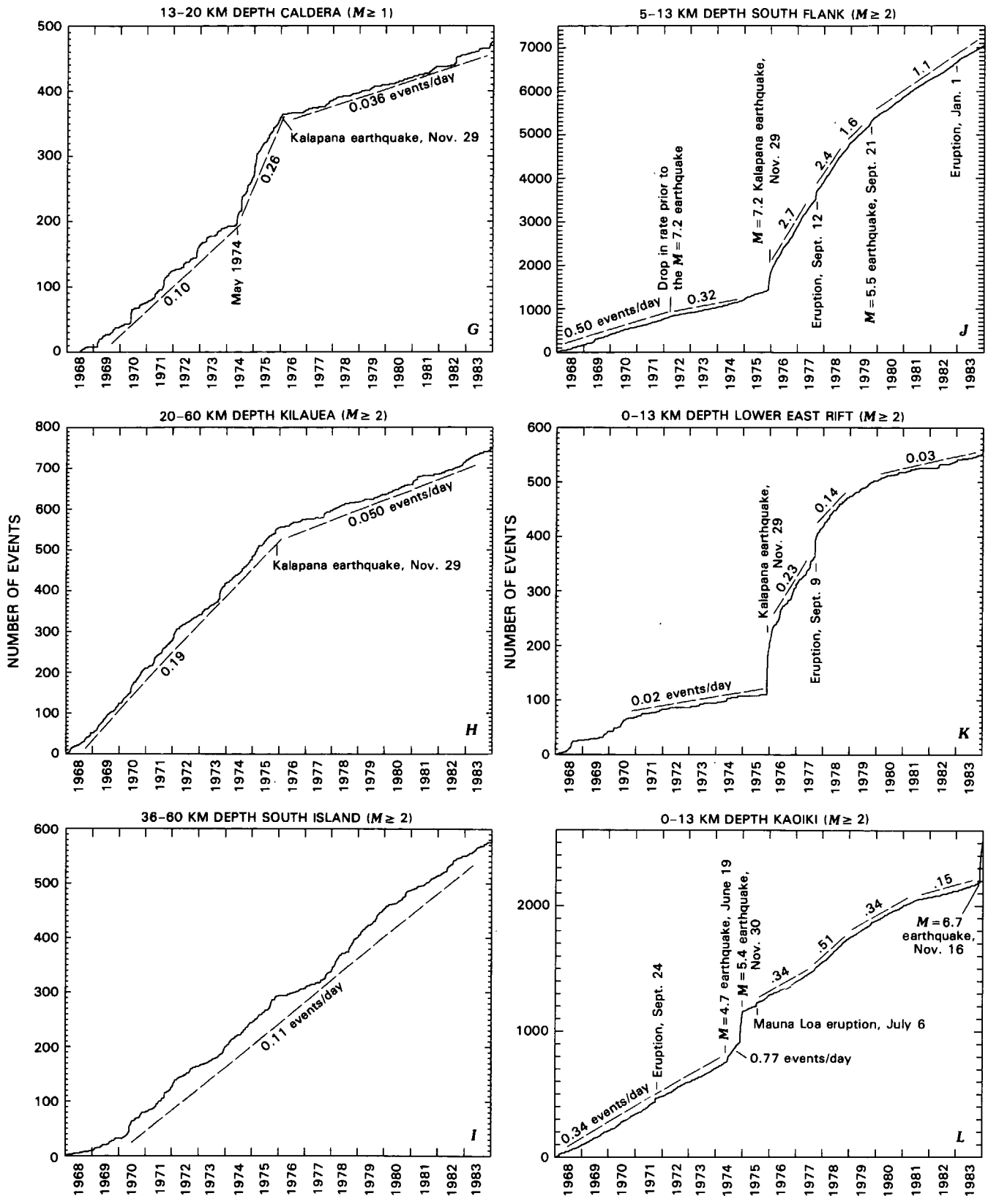

FIGURE 43.8.—Continued.

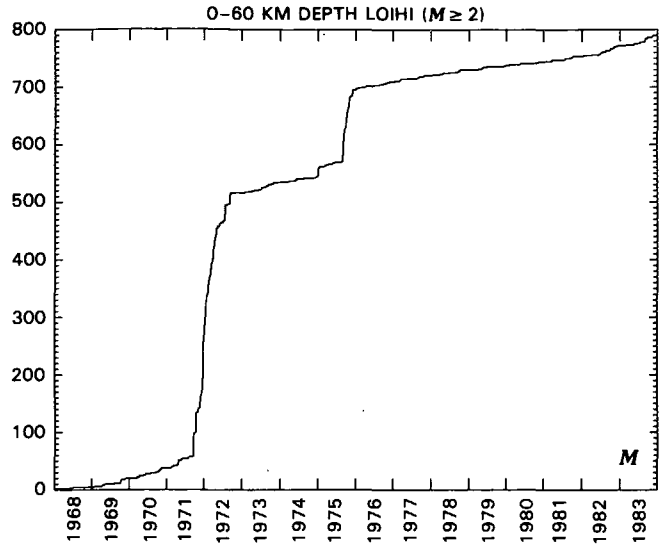

FIGURE 43.8.—Continued.

Shallow SWRZ seismicity (fig. 43.8*D*) is composed mostly of major intrusions in 1971, 1974 and 1981. The pattern is similar to that of the ERZ but with fewer and more seismogenic intrusions. Similar to the ERZ in 1979 and 1980, the SWRZ experienced a prolonged and continuous intrusion in the first half of 1981. This intrusion was marked by continuous but low-level seismicity of 5–10 events of magnitude 1 or larger per day. Summit tilt was nearly constant, suggesting that Kilauea's magma supply was being diverted into the rift without accumulating in the summit reservoir. At 5–13 km depth beneath the same region (fig. 43.8*E*), most earthquakes were in swarms and were south of the rift axis. Note that seismicity following the intrusions of 1974 and 1982 wanes gradually, as expected for tectonic earthquakes within the south flank produced indirectly by stress generated at the rift zone. The region of figure 43.8*E* also includes part of the Kalapana aftershock zone, so both south flank (tectonic) and rift (volcanic) events induce earthquakes here. The seismicity between intrusions in figure 43.8*D* and *E* comes mostly from the region's inclusion of small portions of the constantly active south flank and Kaoiki seismic zones.

KILAUEA'S MAGMA CONDUIT BELOW 5 KILOMETERS DEPTH

Seismicity rate curves for Kilauea's vertical magma conduit below 5 km depth are shown in figure 43.8*F–H*. Most of the events in the upper region (fig. 43.8*F*) occurred in swarms, but deeper activity becomes more continuous in time (fig. 43.8*H*). This change apparently is caused by a shift from volcanic earthquakes and concentrated stress in the shallow system to more uniform stress in the deeper conduit.

Earthquake data prior to 1968 is incomplete, but was not as continuous in time as the 1968–83 period of figure 43.8*G–H*. The 30-km-depth source was relatively inactive in the years prior to January 1961 (Eaton and others, chapter 48). In addition, several major swarms from 40–60 km depth occurred in late 1959 and 1960 (Eaton and others, chapter 48). The change from swarms to continuous seismicity may have been associated with the major subsidence of the summit of Kilauea during the 1960 Kapoho eruption, which was twice as large as any subsidence since.

Many swarms at 5–13 km depth (fig. 43.8*F*) occur in the days or weeks following major subsidence of the summit during large intrusions or eruptions. Examples include January–February 1975 and September 1977. The post subsidence swarms often consist of events having a long period seismic. signature and are probably related to rapid refilling of the magma reservoir from below. This intermediate-depth seismicity was also high accompanying a series of swarms at the summit during 1971 (Koyanagi and others, 1976a). The summit seismicity was associated with both slow and rapid intrusions into the upper parts of both rifts. Other swarms in figure 43.8*F*, such as October 1973, are not obviously related to shallow volcanic or seismic activity.

The most prominent characteristic of the vertical conduit seismicity (fig. 43.8*F–H*) is the sharp drop in rate following the November 1975 Kalapana earthquake. The long-term drop in rate is not the result of masking by Kalapana aftershocks. The aftershocks interfered with the analysis of other earthquakes in two ways: (1) the intense seismicity for several days after the Kalapana earthquake masked most everything on the seismograms; and (2) the magnitude threshold for reading all events was raised to 2.6 for most of 1976 owing to the intense activity.

The drop in earthquake rate after the Kalapana earthquake was most pronounced between 5 and 13 km depth where it dropped by a factor of 8. The earthquake rate fell less for deeper events: there was a factor of 5 decrease between 13 and 20 km, and a factor of 4 below 20 km depth. Because the slip plane of the earthquake was at 10 km depth and displaced the entire block above, its effect on conduit seismicity was greatest in the crust.

As discussed above in the section "The Mechanism of Deep Earthquakes," the Kalapana earthquake relieved stress on both the magma conduit and upper mantle as the south flank moved seaward and expanded. The south flank had been compressed by numerous dike intrusions into the rifts during the century preceding the magnitude-7.2 earthquake (Swanson and others, 1976a). The sudden decompression and slip of the south flank caused the immediate intrusion of about 100 million cubic meters of magma into the ERZ (Dzurisin and others, 1980). The earthquake also triggered a shift in volcanic behavior from mostly eruptions to mostly intrusions, because the reduced stress near the rift accommodated magma below the surface without sufficient pressure to come to the surface and erupt (Klein, 1982b). The 1975 earthquake, however, apparently did not cause a drop in Kilauea's magma supply rate (Dzurisin and others, 1984). The Kalapana earthquake thus relieved stress on Kilauea's shallow magma system, and the rate drop of vertical conduit earthquakes indicates stress relief on the deeper

system as well. A future study of fault-plane solutions and history of vertical conduit earthquakes is planned to help constrain the space and time changes in stress.

The effects of the Kalapana earthquake on volcanic seismicity suggest that the stresses driving rift and vertical conduit earthquakes are slightly different. At depths below 5 km, the earthquake both relieved elastic stress and reduced seismicity in distributions that diminish with depth, thus suggesting that vertical conduit seismicity and tectonic earthquakes on the flanks are driven by interacting regional stresses. The conduit seismicity occurs because this stress is geometrically concentrated around the zone weakened by the presence of magma. In contrast, the Kalapana earthquake had no obvious effect on either the earthquake occurrence rate or intensity of individual swarms in the shallow summit and adjacent ERZ where swarms are frequent (fig. 43.8*A*, *B*). Seismicity was unchanged even though the shallow conduit system should have experienced stress and displacement changes larger than in the deeper conduits. Earthquakes in the shallow conduit system must therefore result more directly from very local stress generated by magma pressure than by regional or tectonic stress. This difference in the local versus regional scale of driving stress is in perfect agreement with the contrast in magnitude, time and space characteristics of shallow and deeper earthquakes.

The magnitude-2 or larger earthquakes below 36 km depth and under the entire south side of the island occur at a nearly constant rate of about 0.11 per day (fig. 43.8*I*). A few of the deepest events directly below Kilauea are plotted in both figure 43.8*H*, *I*, but they are a small percentage and do not dictate the behavior of either plot. The Kalapana earthquake appears to have caused a temporary drop in rate that is probably not real; for much of 1976, aftershocks were so numerous that processing of all smaller events was not completed. The recovery of rate indicates that the Kalapana earthquake had no lasting effect (either real or artificial) on the deepest seismicity. Earthquakes below about 36 km thus depend on the long-term mantle processes discussed earlier, and not on stress or volcanic changes in the crust.

TECTONIC EARTHQUAKES ON KILAUEA'S SOUTH FLANK

Kilauea's south flank seismicity is nearly continuous (fig. 43.8*J*), unlike the swarms that characterize the adjacent ERZ. Earthquake rates vary as the mechanical state of the flank changes. The 1968–71 period probably represents the most normal time in figure 43.8*J* and has a background rate of 0.50 events per day. The rate for the entire south flank dropped to about 60 percent of its prior value in early 1972. The change was localized to a few areas of the south flank and was interpreted by Wyss and others (1981) as premonitory to the 1975 Kalapana earthquake. The drop in rate presumably resulted from partial stress release adjacent to areas that remained locked and seismically active, but that showed different precursory anomalies.

The November 29, 1975 earthquake caused both immediate aftershocks and a massive seismic excitation of the south flank that persists a decade later. The upward step in figure 43.8*J* is from immediate aftershocks. The step should be larger than plotted because data during December 1975 and most of 1976 is incomplete between magnitudes 2.0 and 2.6. The bending over of the seismicity curve to a constant rate of about 2.7 events per day (which is a reliable value in 1977) signified the end of immediate aftershocks. This immediate aftershock sequence diminished with a time constant of weeks to months, but the value is difficult to determine with the presently incomplete data. For seismicity to continue at a rate about 5 times above background level more than a year following the earthquake is unusual for a magnitude 7.2 event. South-flank seismicity in this extended aftershock sequence is diminishing very slowly, as shown in figure 43.8*J*. The rate of decrease is approximately exponential with a time constant of about 6 years. One possibility for the high south-flank seismicity is simply relaxation of localized stress changes caused by the earthquake, but at an unusually low rate. In addition, the south-flank seismicity is above the nearly horizontal slip plane of the Kalapana earthquake. These aftershocks are thus not simple in the sense of being confined to the mainshock fault plane, and may thus have a more complex history.

Earthquakes in the south flank are ultimately driven by stress applied from repeated intrusions into the ERZ to the north. The largest events, such as September 1977 and January 1983 (fig. 43.8*J*), induce south-flank earthquakes that decrease after a few days or weeks (Dvorak and others, 1985). It is difficult to reconcile the rate of decrease of intrusions (days to weeks) and immediate Kalapana aftershocks (weeks to months) with the prolonged decrease of the extended aftershocks. Additional magma intrudes the rift steadily and between the rapid intrusions at rates difficult to estimate (Dzurisin and others, 1984). Stress was therefore applied incrementally but often to the south flank, at least during the period plotted in figure 43.8*J*. The cause of the extended aftershocks may therefore lie not in response to incremental stress from the Kalapana earthquake, but in a fundamental change in the mechanical behavior of the flank as it responds to stresses applied more or less steadily. For example, the creation of many new fractures by the Kalapana earthquake may shift the flank's response from elastic compression and aseismic creep to seismic slip on new faults. The new faults could then heal or become locked on a several-year time scale and eventually shift the balance back to aseismic deformation. This difficult problem needs more detailed work.

Kilauea's lower ERZ experienced a similar dramatic increase in seismicity at the time of the Kalapana earthquake (fig. 43.8*K*). From a pre-1975 rate of 0.02 events per day for magnitude-2 and larger earthquakes, the rate jumped by an order of magnitude even after the immediate aftershocks decreased. The rate diminished steadily and in the early 1980's was close to the pre-earthquake value. The decay time constant is roughly one-half that of the central south flank to the west. Earthquake swarms related to volcanic processes also occur in this section of rift (Koyanagi and others, 1981), such as in 1970, 1977 and 1982 (fig. 43.8*K*). The earthquakes determining the basic shape of the cumulative event curve, however, are primarily tectonic.

TECTONIC EARTHQUAKES IN THE KAOIKI SEISMIC ZONE

The Kaoiki seismic zone is the second most active region of tectonic flank earthquakes in Hawaii, and the cumulative curve shows continuous activity punctuated by aftershock sequences (fig. 43.8*L*). A background rate of 0.34 events per day is characteristic of 1968–73 and appears to be typical for the years following the two aftershock sequences of 1974. Between the aftershock sequences of June and November 1974 the rate is nearly constant at 0.77 events per day.

The Kaoiki seismic zone, however, cannot be considered in isolation from Kilauea and Mauna Loa. Mauna Loa's seismic reawakening in 1974 was in preparation for its July 1975 eruption (Koyanagi and others, 1975), and its accompanying inflation added stress to the Kaoiki seismic zone and may have helped trigger the $M=4.7$ (June 19, 1974), $M=5.4$ (Nov. 30, 1974) and $M=4.7$ (Dec. 15, 1974) earthquakes. The November Kaoiki earthquake was followed one month later by a large intrusion into Kilauea's SWRZ. The earthquake probably did not cause the intrusion, but may have caused Kilauea to shift its attention away from the ERZ, where eruptions and intrusions occurred during the previous three years. The strike-slip mechanism of the November 1974 earthquake (Endo and others, 1978) would have relieved confining stress on the SWRZ permitting an easier intrusion path than before. Seismic shaking of Kilauea's magma system may also have changed the magma conduit of least resistance and led to the shift from the ERZ to the SWRZ.

The variations in seismic rate of the Kaoiki seismic zone after 1974 are also significant. The drop in rate in mid-1981 to one-half its former value is readily identifiable and can be interpreted as the onset of seismic quiescence precursory to the November 1983 earthquake (M. Wyss, written commun., 1985). The variations in rate during 1975–80 are real, but it is harder to identify breaks in slope and the three periods of varying seismicity whose rates are indicated in figure 43.8*L*. The origin of the high seismicity of 1977–78 has not been identified.

SEISMICITY NEAR KILAUEA'S SHALLOW MAGMA RESERVOIR AND RIFT ZONES

Kilauea's summit region produces its most intense seismicity, which is detailed in a series of depth slices only 0.5 km thick in figure 43.9. Several earthquakes per minute can be generated within volumes smaller than a few cubic kilometers during rapid intrusions. Most active are the short sections of the two rifts within about 4 km of the summit caldera (fig. 43.9*E–G*). Events are highly concentrated both in time and space, indicating that the source of stress producing them is nearby, produces large gradients and can change rapidly. The most intense and linearly continuous seismicity is between 2.5 and 3.5 km depth (fig. 43.9*F, G*), and the main magma conduits are presumably centered at about 3 km depth.

Most seismicity between intrusions is caused by inflation of the magma reservoir. The reservoir is capped by brittle rock within the caldera, which produces earthquakes when the reservoir inflates. As stated in the previous section, a gradual buildup of caldera earthquakes lasting several days to months often precedes an intense swarm and intrusion. The pre-intrusion activity is not only within the caldera and reservoir cap, but may include slow intrusions of the sections of rift adjacent to the reservoir. Portions of the rifts thus appear at times to be magma-filled and directly connected to the inflating summit reservoir.

THE SUMMIT MAGMA RESERVOIR

The summit magma reservoir, as defined by a gap in seismicity, is at the intersection of the active conduits of the two rifts. The seismic gap coincides with the geodetic deformation center and is part of a zone of low rigidity (fig. 43.9*F, G*). The rift conduits constrain the reservoir's position on its south and east sides near 3 km depth. The clusters of earthquakes in the north-central caldera and just southwest of Halemaumau apparently form other parts of an incomplete ring of brittle deformation surrounding the magma reservoir. Some earthquakes do plot within this region identified with the magma reservoir, however: these may either be slightly mislocated owing to the large lateral and unmodeled velocity gradients, or actually inside brittle slivers within a magma storage complex. All of the limitations of location precision discussed earlier apply here and mean that we cannot resolve detail within this 1- to 2-km-diameter void.

These relations can be seen from a different perspective by examining vertical cross sections taken through the summit magma reservoir. Figure 43.10*A* is a map showing the rectangular areas included in the four sections of figure 43.10*B–E*. The cross sections intersect at summit magma reservoir. Only earthquakes with both horizontal and vertical errors less than 1 km are plotted in figure 43.10, so structures of about this size should be resolvable. This also means that proportionally more earthquakes below about 4 km than above this depth are eliminated from the plots, because errors increase somewhat with depth.

A zone with few or no earthquakes below the caldera contains the magma reservoir complex. The dashed oval in figure 43.10*B–E* is not meant to portray its exact size or shape, but only to sketch the outer limits of sparse seismicity. Its position is constrained by four zones of seismicity: a cap of earthquakes mostly between 1 and 2 km depth directly above the reservoir, the intensely active segments of the ERZ and SWRZ adjacent to the reservoir's upper part near 3 km, and the top of the vertical conduit at a depth of about 7 km.

The reservoir's seismic cap is centered and most intense beneath Halemaumau, but extends across most of Kilauea caldera (fig. 43.10). The greater intensity of seismicity between 1 and 2 km compared to just above is probably a result of its proximity to the source of stress below. The reduced activity above 1 km may also be a result of lessened confining stress on the shallowest fault planes or a concentration of seismicity in very small-magnitude events that are detected but are not locatable with the seismic network. The northern half of the caldera produces events most intensely near 2 km

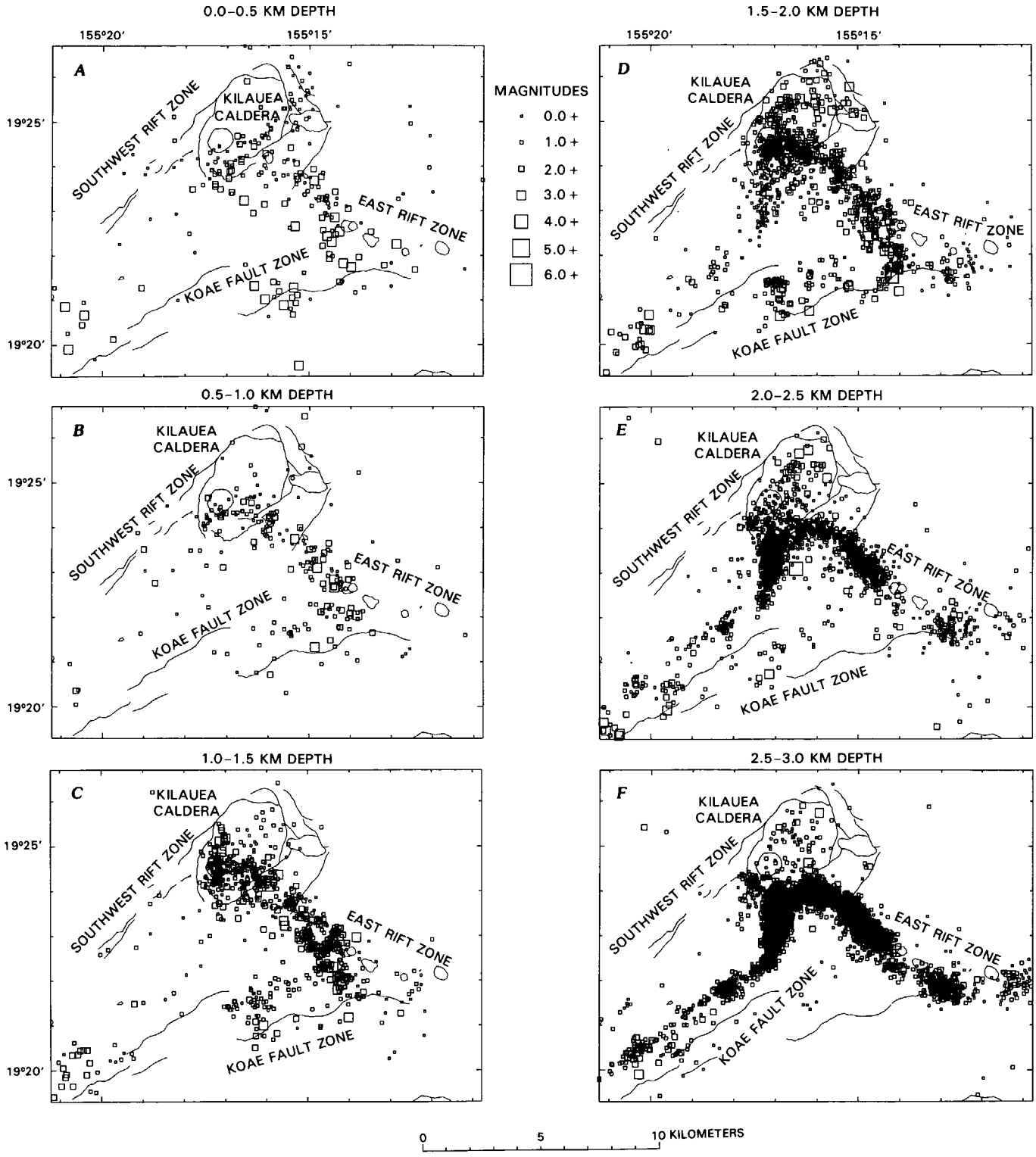

FIGURE 43.9.—Depth slices, 0.5 km thick, of 1970–83 earthquakes near Kilauea caldera between 0 and 5 km depth. Maximum location error of plotted events is 3 km horizontally or vertically. Earthquake symbol size scales with magnitude. Faults, fissures, and pit craters are as shown in figure 43.1.

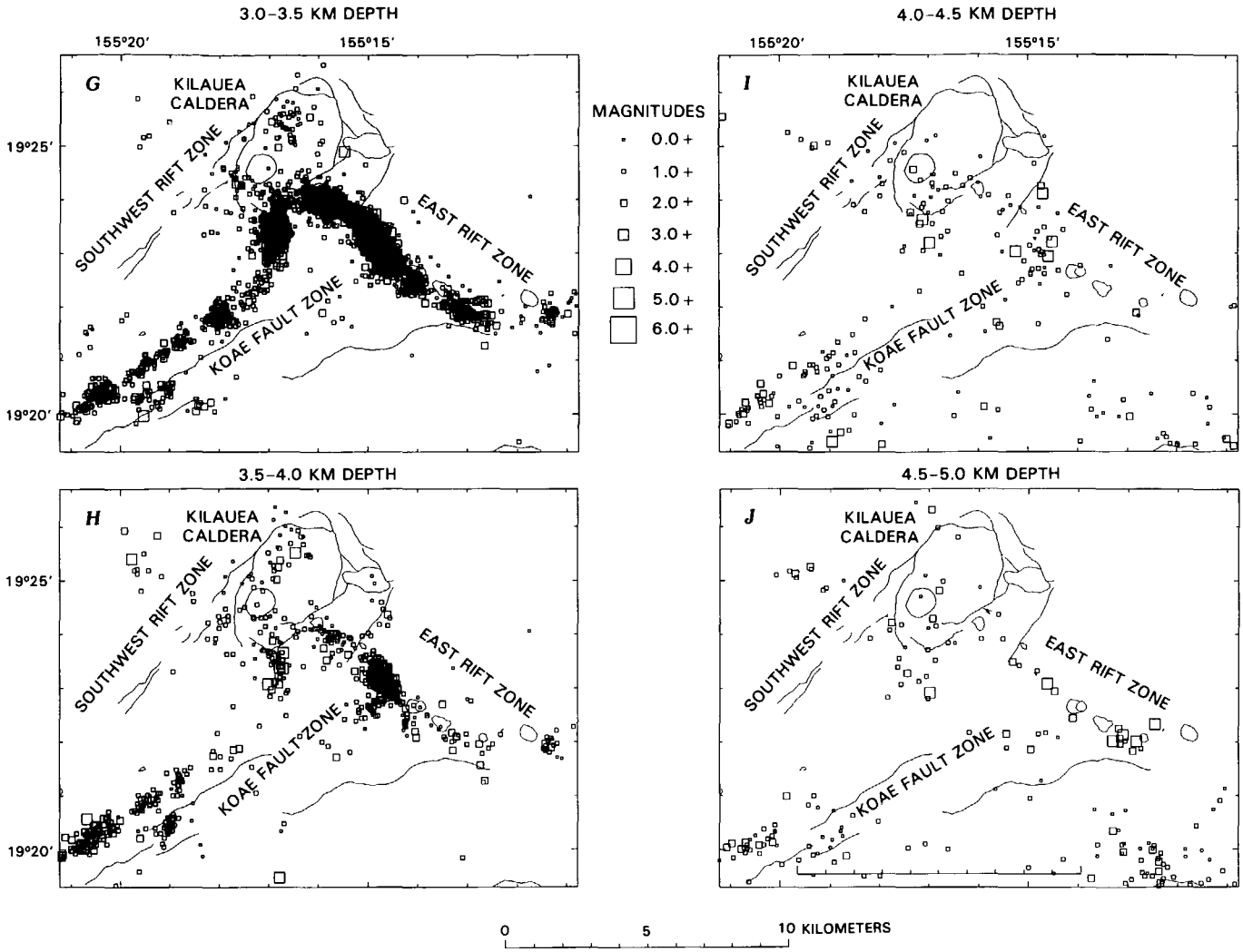

FIGURE 43.9.—Continued.

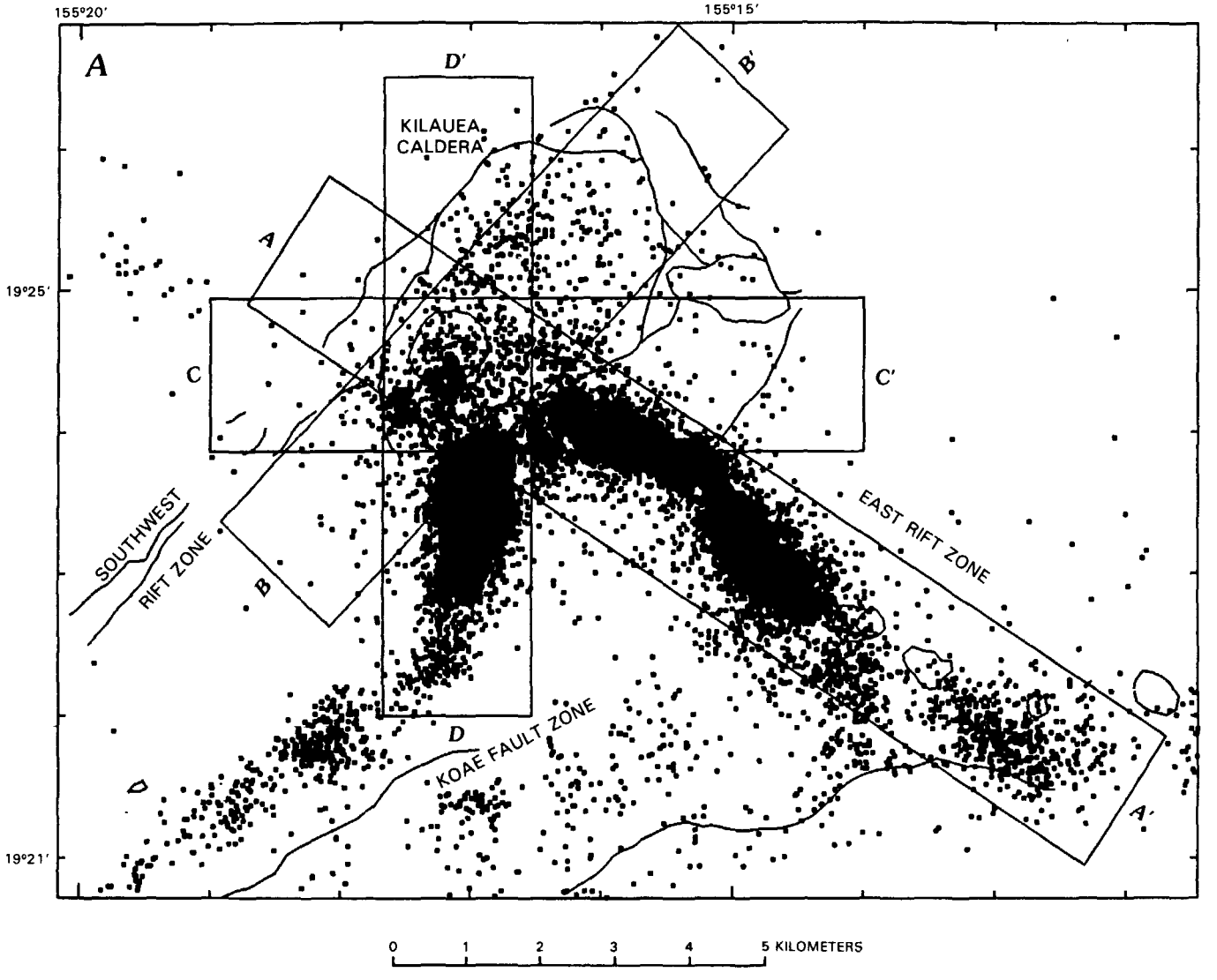

FIGURE 43.10.—Epicenters and hypocenters of shallow 1970–83 earthquakes near Kilauea caldera. ***A***, Epicenter map showing positions of cross sections. Sections cross over buried magma reservoir. Endpoints of sections are labeled with letters keyed to the distance axes of figure 43.10*B–E*. Only earthquakes inside the 2-km-wide rectangular areas of figure 43.10*A* are plotted on figure 43.10*B–E*. ***B–E***, Cross sections of 1970–83 hypocenters. Position of magma reservoir is approximated by dashed oval. Horizontal and vertical errors of all hypocenters plotted is 1 km or less. Datum for sections is ground surface. When comparing earthquake patterns in map and sections note that sections extend to 12 km depth, but map only plots events in upper 5 km for clarity. Faults, fissures, and pit craters are as shown in figure 43.1.

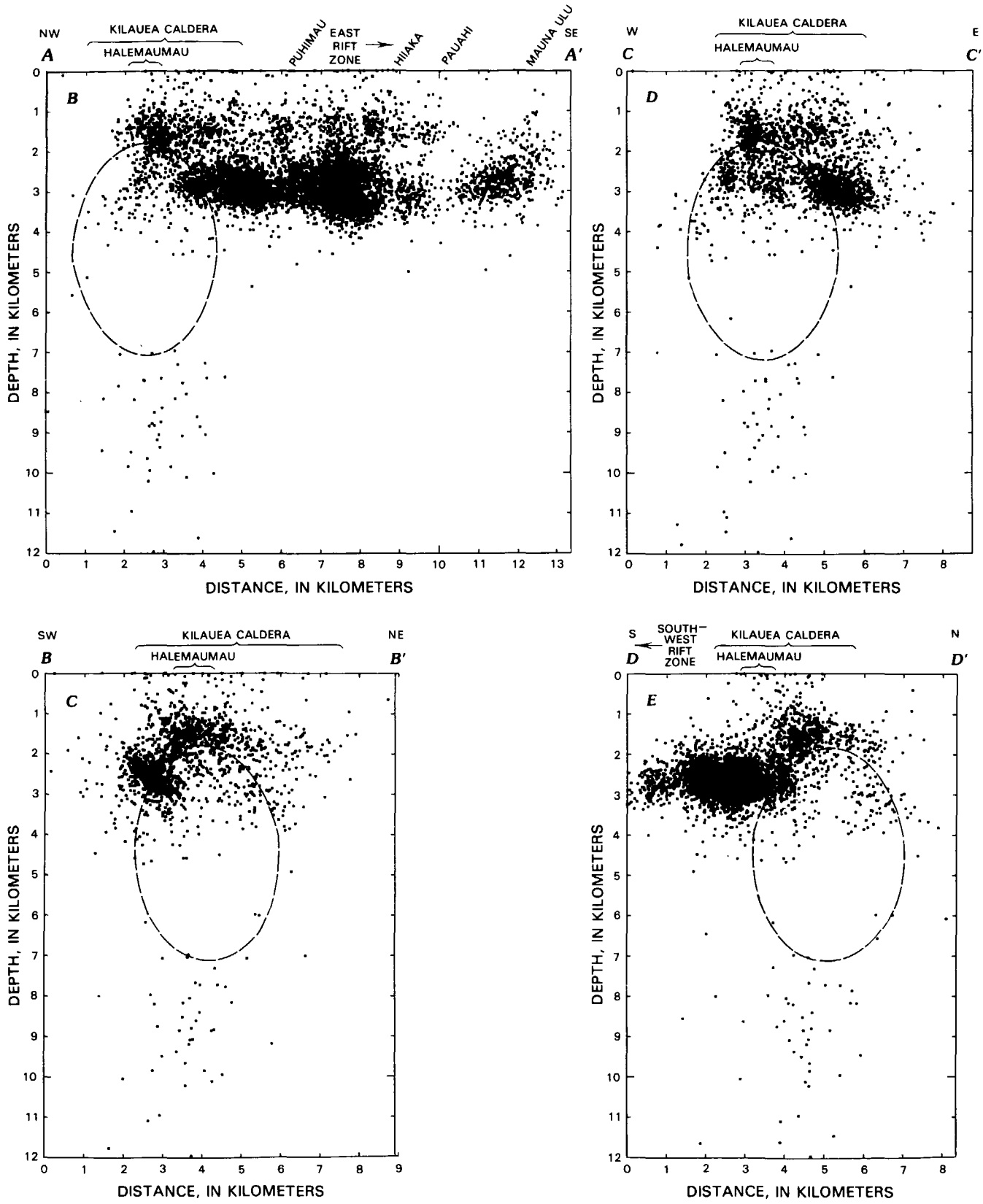

FIGURE 43.10.—Continued.

depth (fig. 43.9*D*, *E*). Most of these earthquakes occur at times of rapid inflation and probably are triggered by lifting and extension of the brittle cap over the magma reservoir. Seismicity above the reservoir also accompanies major and rapid deflations such as in September 1977, August 1981 and January 1983. The band of very shallow events north of Kilauea Iki (fig. 43.9*A*) parallels the caldera rim and appears to be caused by movement on rim faults during periods of inflation.

The upper and lower parts of the magma reservoir behave differently. The buried centers of inflation and deflation of Dvorak and others (1983) are mostly in the upper half of the dashed oval shown in figure 43.10*B–E*. These deformation centers are below the base of the seismic cap at 2 km, but above the completely aseismic region between 4.5 and 7 km depth. The upper section of the magma storage complex is thus the active portion: it produces some seismicity, the changes in magma volume near the deformation centers occur there, and it is surrounded by the zones in which seismicity and intrusions occur. The lower section of the reservoir is passive and has low rigidity, however: it is aseismic and seldom supports centers of elastic deformation. Any deformation of the lower half of the reservoir would probably be masked by that in the upper half, to which surface measurements are most sensitive. The reservoir can also be viewed as the upper part of a fluid column whose top level fluctuates with changes in stored magma volume. Variations in level then change the pressure on the confining cap where the seismicity and uplift occur. The magma reservoir is apparently a connected network of liquid and solid segments, as indicated by the limited seismicity and the fact that different centers of deformation are active at different times (Fiske and Kinoshita, 1969; Ryan and others, 1983; Dvorak and others, 1983).

THE SUMMIT SECTION OF THE EAST RIFT ZONE

Unlike the SWRZ, the ERZ between Halemaumau and Pauahi (fig. 43.1) generates seismicity above its main conduit and essentially to the surface (fig. 43.9*A–D*). During the last few decades the ERZ has been more active magmatically than the rest of the rift system. This high magmatic activity may extend the ERZ dike network vertically and stress the upper 2 km to such a degree that it deforms seismically. The shallow seismicity usually occurs at the same times and places as the earthquake swarms in the more intense zone centered at 3 km. There is thus a close seismic and probably magmatic coupling to the main conduit. We interpret the shallow seismicity and patterns of shallow intrusions as evidence of a multitiered and complex honeycomb of magma conduits in the upper ERZ.

Internal structures in the ERZ appear to control seismically active and inactive regions. There is a major cluster of earthquakes about 1 km uprift of Mauna Ulu (fig. 43.10*B*, *C*). The earthquakes that plot below this cluster at 5 to 8 km depth (fig. 43.10*B*) mostly occur just after intrusions and are immediately adjacent to tectonic earthquakes in the south flank. The ERZ bends eastward and the Koae fault zone meets the rift there. This area is thus structurally complex. Migrating swarms (and by inference also propagating dikes) often begin between Pauahi and Mauna Ulu. We interpret this cluster as a barrier or pinched zone that sometimes blocks downrift magma flow at this point. Earthquakes are then generated by the formation or rejuvenation of dikes that break through the barrier.

Just uprift of the Mauna Ulu cluster is a seismically inactive zone beneath Pauahi (fig. 43.10*A*, *B*). A break in continuity of earthquakes is at 3 km depth, and the 1- to 2-km-deep seismicity essentially ends there. This apparently is a low stress or low rigidity zone of relatively unobstructed magma passage. The magma conduit here is possibly very similar to the rest of the ERZ, but for some structural reason such as proximity to the Koae fault zone, it does not accumulate stress to be released seismically. We favor an alternative interpretation of this seismic gap as a small magma storage reservoir within the rift. Magma stored there would be held in place by the barrier just downrift. In addition to times of intrusion, this Pauahi reservoir could easily receive magma during periods of summit inflation when the rift between it and the summit reservoir is seismically active and is slowly being fed magma. This possible magma reservoir will be treated below in the section "Discussion of Rift Zone Intrusions." The total volume of magma stored below Pauahi may be small, but if it is consistently kept hot and low in rigidity, seismic stresses will never accumulate to be released in earthquakes.

EARTHQUAKE HYPOCENTERS IN THE SOUTHWEST RIFT AND CENTRAL EAST RIFT ZONES

The SWRZ and the ERZ downrift of Mauna Ulu (fig. 43.11) are in some ways simpler than the uprift section of the ERZ: they are less frequently active and have simpler earthquake patterns. Longitudinal cross sections of earthquakes during 1970–83 from both rifts are plotted in figure 43.12. The main magma conduit at about 3 km depth is prominent in each section. The conduits of both rifts plunge from about 2.5 km depth below the surface at their uprift end to about 3.5 km downrift. The apparent 3.7-degree plunge of the ERZ conduit must be added to the 1.3-degree surface slope to give a plunge of about 5 degrees. The SWRZ is somewhat steeper, with apparent and surface slopes of about 5.0 and 1.7 degrees respectively for a total of about 7 degrees. The apparent plunges are probably real, although unmodeled seismic velocity variations are a source of error in the apparent slopes.

The quantity of ERZ earthquakes diminishes with distance from the caldera owing to the reduced frequency and intensity of intrusions. The ERZ conduit cannot be defined seismically farther than 30 km from the caldera. Major intrusions of the SWRZ, however, produce earthquakes in most of the 20 km of rift between the caldera and Puu Kou in a way that does not diminish with distance along the rift.

Considerable rift-zone structure is visible in the sections of figure 43.12. We associate the prominent and persistent clusters of events along both rifts with barriers or blockages of the magma conduit that resist penetration by dikes and produce high stresses during intrusions. The major SWRZ barrier near Puu Kou, for example, has produced an intense cluster of earthquakes and prevented any intrusion from continuing downrift during the period

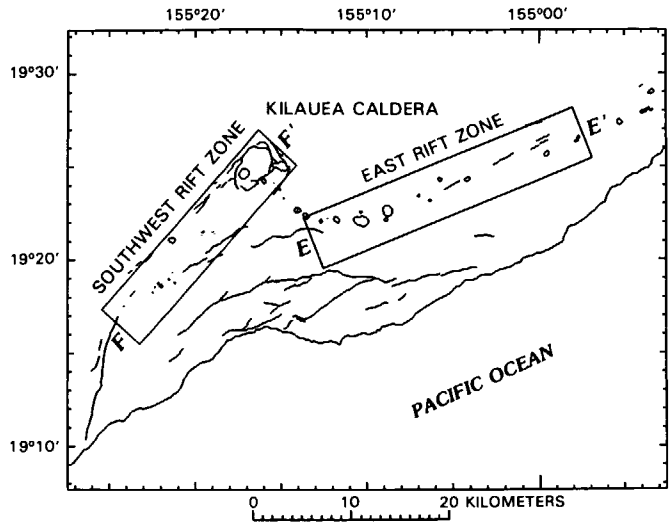

FIGURE 43.11.—Areas included in longitudinal cross sections of rift zones. Only earthquakes within rectangles are plotted in sections. Section *E-E'* is shown in figure 43.12*A* and *F-F'* in figure 43.12*B*. Faults, fissures, and pit craters are as shown in figure 43.1.

of historical observation. This barrier also coincides with a bend in the rift (fig. 43.1*A*). The earthquake gaps between clusters are apparently places of unstressed magma passage, and some may be secondary magma storage pockets. The most prominent gap just northeast of Puu Kamoamoa is such a storage reservoir. This section of rift was geodetically observed to inflate during the slow intrusions of 1978–80. In addition, the earthquakes above the main conduit (0–2 km depth in figure 43.12*A* occurred during these intrusive pulses, much as shallow caldera earthquakes occur above the summit magma reservoir when it inflates.

Earthquakes in Kilauea's flanks are separated from the rift magma conduits in both map position and depth. Most of the events shown deeper than 5 km in figure 43.12 are tectonic earthquakes from the south flank that fall within the cross-section regions. The base of the zone of tectonic earthquakes is near 10 km and is the approximate depth of the prevolcanic layer of ocean sediments on which the mobile south flank slips seaward (for example, Crosson and Endo, 1982). A series of transverse sections, whose positions are shown in figure 43.13, will make this clear. Figures 43.14*A–D* are sections successively downrift along the ERZ. The main magma conduit at 3 km depth and north of the deeper south-flank seismicity is visible in each section. The detailed cross-sectional shape of the magma conduit cannot be determined owing to errors in earthquake hypocenters. The sections uprift of Mauna Ulu (fig. 43.14*A*, *B*) and near Puu Kamoamoa (fig. 43.14*D*) include seismicity above the main conduit. Shallow events plotted at the south end of figure 43.14*A* are in the Koae fault zone. Only the section including Pauahi and Mauna Ulu (fig. 43.14*B*) reveals significant activity beneath the main magma conduit.

The relation between rift and flank seismicity is very similar in the SWRZ. Figures 43.14*E–G* are transverse cross sections successively downrift along the SWRZ (fig. 43.13). The main magma conduit is visible at about 3 km depth in each section, defined largely by the major intrusions of December 1974 and August 1981. The scattered earthquakes northwest of the main conduit near the caldera (fig. 43.14*E*) are partly from the September 1971 intrusion into the northern portion of the SWRZ. The shallow earthquakes southeast of the conduit in the same section are from the west end of the Koae fault zone. The conduit near Mauna Iki (fig. 43.14*F*) splits into two strands. The shallow (0–2 km depth) earthquakes in this area were generated by an apparent upward branch of the dike formed in the August 1981 intrusion, which also produced surface cracks in this area. Considerable seismicity also occurs southeast of the rift near Puu Kou in Kilauea's mobile south flank (fig. 43.14*G*).

The rift and adjacent flank earthquakes are spatially better separated at the ERZ than at the SWRZ (compare fig. 43.14*B–D* with fig. 43.14*F*, *G*). The greater distance of flank events from the ERZ correlates with their greater independence from the times of rift intrusions. Earthquakes adjacent to the SWRZ, however, are more closely coupled to the rift in both time and space. The greater separation of rift and flank earthquakes in the ERZ may also result from the narrowness of the surface expression of the ERZ: the wider SWRZ at the surface may be related to the multiple seismic strands and closely coupled flank earthquakes at depth.

The rift zones below about 5 km depth are mostly aseismic. Rifting must extend to about 10 km depth where the volcanic pile is decoupled from the prevolcanic oceanic crust. The lack of seismicity then means the deep rifts are too hot and too ductile to support earthquakes, and the timing of deep rifting relative to the episodic shallow intrusions is unknown. There are, however, some deep rift earthquakes. The main SWRZ magma conduit downrift of Mauna Iki directly overlies a deeper but somewhat diffuse seismic zone (figs. 43.12*B*, 43.14*F*, *G*). This deep zone was active in the intrusion of June 1982, in which rifting apparently extended downward through the crust. A few hypocenters 5 to 10 km beneath Mauna Ulu in the ERZ (fig. 43.10*B*) are also produced by rifting. These deep ERZ events occurred during and immediately after several shallower swarms and apparently represent a locally brittle zone that responds to intrusions above.

THE KOAE FAULT ZONE

The Koae fault zone is seismically active, though far less so than either rift zone. The Koae consists of noneruptive fissures and north-facing normal fault scarps and is interpreted as a tear-apart zone linking the ERZ and SWRZ (Duffield, 1975; Unger and Koyanagi, 1979). Nearly all Koae earthquakes occurred during a few short swarms apparently caused by magma intrusions from the ERZ into an otherwise dry fault zone. No recent eruption from the Koae is known, however, and confining stress is probably so low that magma can be accommodated underground without building enough

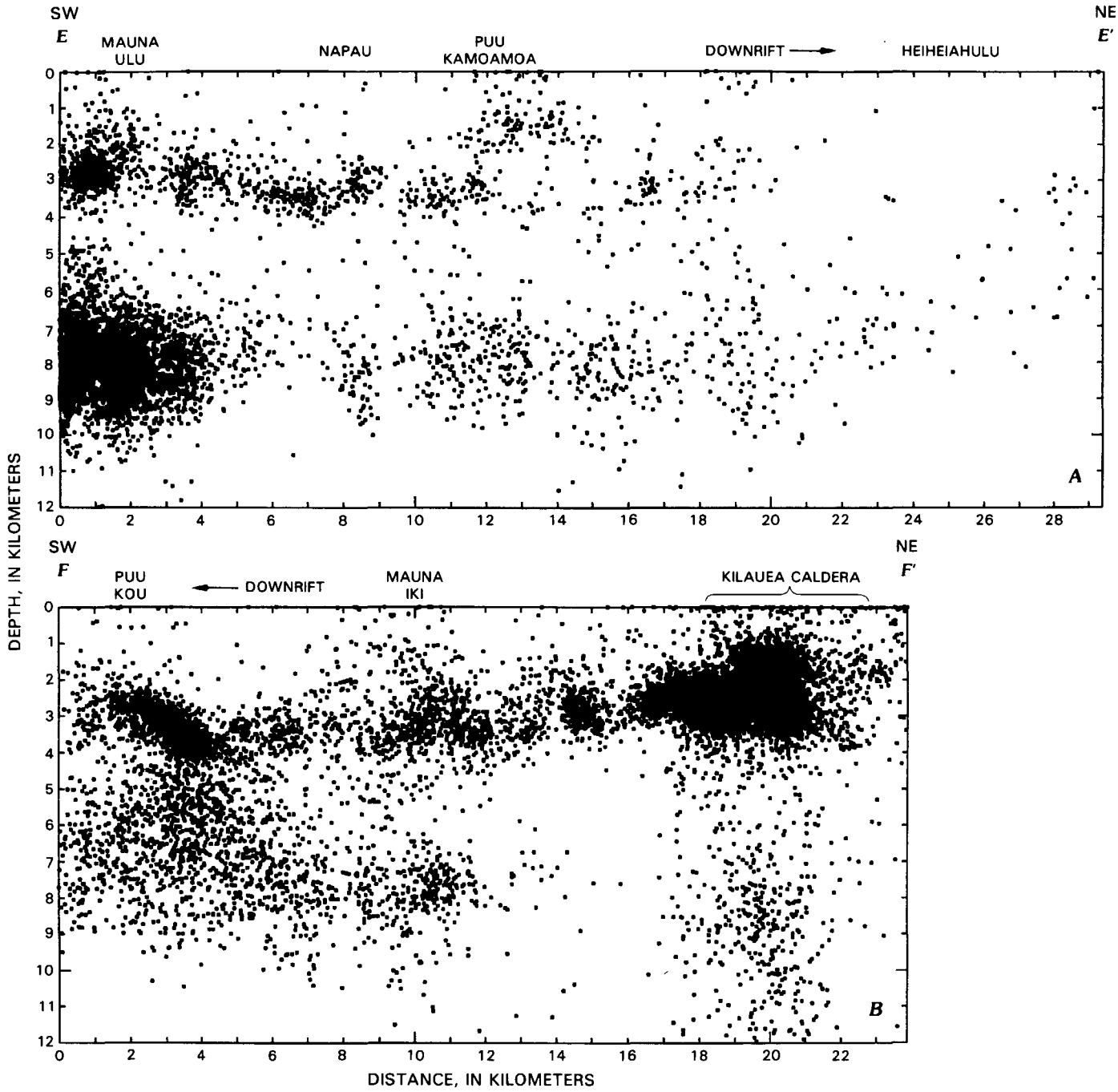

FIGURE 43.12.—Longitudinal cross sections of earthquakes below east rift zone (*A*) and southwest rift zone (*B*). Positions and areas of sections are shown in figure 43.11. Main magma conduits are at about 3 km depth.

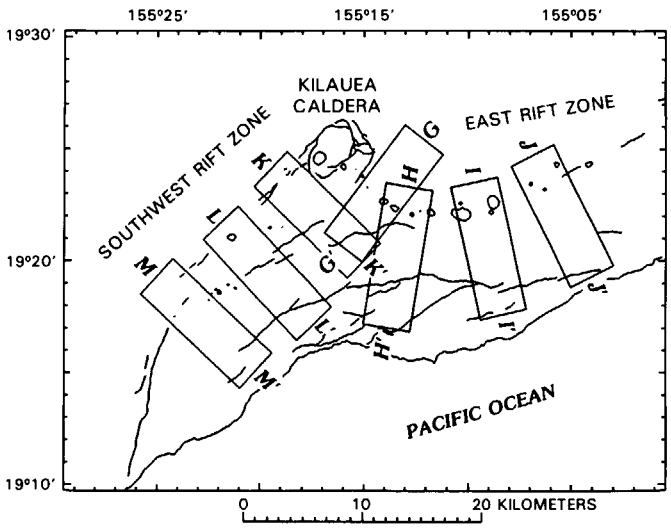

FIGURE 43.13.—Areas included in transverse cross sections of rift zones. Only 1970–83 earthquakes within rectangles are plotted in sections. Sections *G-G'* through *J-J'* are plotted in figure 43.14*A–D*, *K-K'* through *M-M'* in figure 43.14*E–G*. Faults, fissures, and pit craters are as shown in figure 43.1.

hydrostatic pressure to erupt. Earthquakes generally migrate rapidly from east to west as intrusions penetrate the Koae. The immediate source of magma might be the suspected magma reservoir in the adjacent ERZ below Pauahi.

Figure 43.15 shows a map and cross section of shallow Koae earthquakes. The seismicity extends about 6 km from the ERZ in a linear band that underlies the zone of faults and fissures. Earthquake depths are mainly between 1 and 2 km, the same as the shallow seismic conduit system in the uprift part of the ERZ (figs. 43.10*B*, 43.15*B*). The Koae intrusions may thus be related to the shallow ERZ conduit system. The main ERZ conduit at 3 km depth, however, is not seismically expressed in the Koae. The earthquakes below 6 km depth in figure 43.15*B* (not plotted in figure 43.15*A*) are part of the tectonic seismicity in Kilauea's south flank. Very shallow earthquakes are seen in a small area of the SWRZ (fig. 43.9C, *D*, lower left corner). These earthquakes apparently result from an upward-branching dike within the rift zone, which may be influenced by the intersection of the SWRZ magma conduit with the Koae.

KILAUEA'S VERTICAL MAGMA CONDUIT AND THE PATTERN OF DEEP EARTHQUAKES

Kilauea's magma conduit is clearly recognized in the earthquake depth slices discussed earlier. Although depth slices show the size and position of the conduit at a particular depth very well, variations in seismicity with depth are more easily seen in a vertical cross section. The map positions of three sections are shown in figure 43.16, along with epicenters of earthquakes below 13 km depth. The three sections (fig. 43.17) extend from the surface to 60 km depth and all include the seismically defined magma conduit. Enlargements of the central parts of each section restricted to 0–25 km depth (fig. 43.18) clarify the dense seismicity in the upper part of the conduit. Most plotted earthquakes between 0 and 5 km depth are related to Kilauea's summit and rifts, and those between 5 and 13 km occur mostly under the south flank and Kaoiki seismic zones. The magma conduit earthquakes are most clearly separated from shallow seismicity when viewed from the east (figs. 43.17*A*, 43.18*A*).

An important geometrical feature of the seismicity associated with the conduit is its unevenness with depth. Earthquakes tend to cluster near depths of 9, 16 and 30 km with reduced activity centered near 5, 13 and 20 km (figs. 43.17*A*, 43.18A). Several possible reasons exist for the seismic gaps based on either low rigidity, low stress or a low fracture density relative to the conduit above or below. As has been inferred, the gap at 4–7 km results from the low rigidity of the summit magma reservoir. The possibility of magma storage near 13 or 20 km is much more difficult to determine, however: (1) a deeper reservoir may not accumulate enough magma to swell elastically and deform the surface, but merely transmit magma passively; and (2) it would be difficult to detect because of its greater distance from the surface and because of the much larger deformation from the shallow reservoir. The present gradation from volcanic seismicity in the shallow parts of the conduit to more tectonic earthquakes at depth argues against a deep magma reservoir large enough to influence seismicity.

The gaps in seismicity near 13 and 20 km probably result from differences in lithology or stress within the lithosphere, and not necessarily magma reservoirs. The base of the south flank zone of tectonic earthquakes at about 10 km depth (fig. 43.18*A*) and the basal slip during the 1975 Kalapana earthquake may coincide with the layer of ocean sediments at the base of the Hawaiian volcanic pile (Furumoto and Kovach, 1979; Crosson and Endo, 1982). The depth and landward dip of the oceanic Moho beneath the island's south coast (Hill and Zucca, chapter 37; Zucca and Hill, 1980) if projected, should intersect the vertical magma conduit around 15 km near the base of the seismic gap. The gap in seismicity near 13 km would then roughly coincide with the old oceanic crust and be bounded by the old Moho and sediment layers. The low-rigidity sediment layer could be viewed as a low-stress zone that partially decouples the stresses above and below.

One must consider the interaction between the lithosphere and the whole volcanic system to determine the cause of the very clear absence of earthquakes in the volcanic conduit near 20 km depth. Note that very few events occur at this depth anywhere beneath Kilauea (figs. 43.3*O*, *P*, 43.17). This observation suggests that stresses are low at this depth in the lithosphere beneath Kilauea. The lithosphere beneath Hawaii can be modeled as an elastic plate flexing downward under the weight of the volcanic pile (for example, Watts and Cochran, 1974; Watts and others, 1985). More detailed modeling of the lithosphere as an elastic-plastic plate suggests that its neutral stress axis (relative extension above and compression below) may lie at a depth of about 23 km (Liu and Kosloff, 1978). The

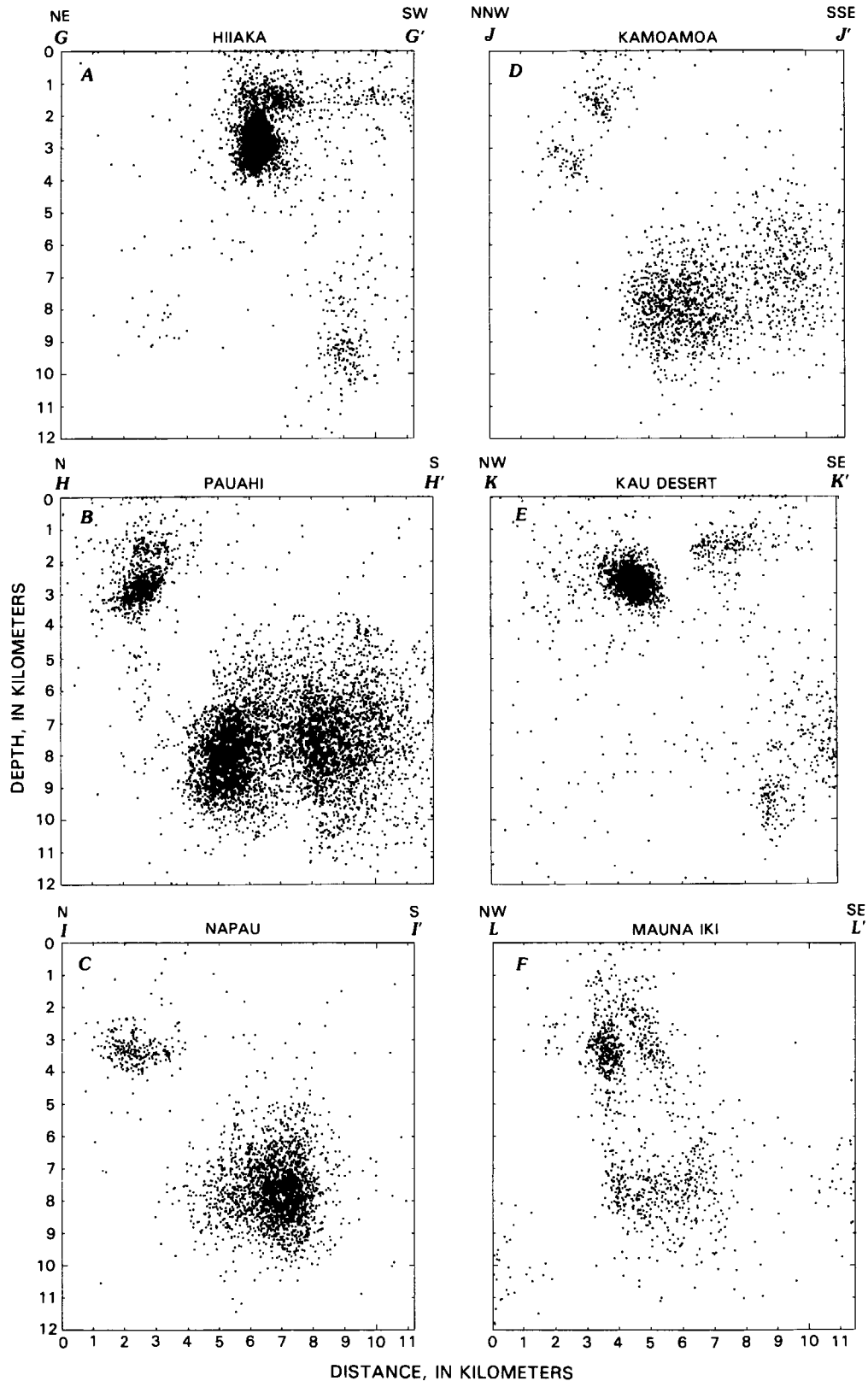

FIGURE 43.14.—Transverse cross sections of earthquakes beneath east rift zone (***A–D***) and southwest rift zone (***E–G***). Positions and areas of sections are shown in figure 43.13. Main magma conduits are at about 3 km depth.

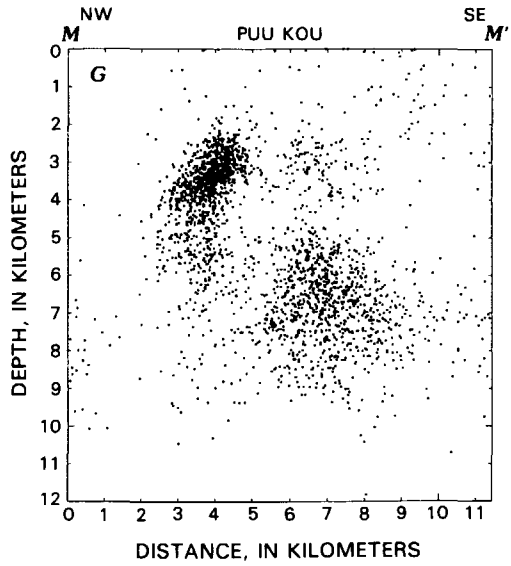

FIGURE 43.14.—Continued.

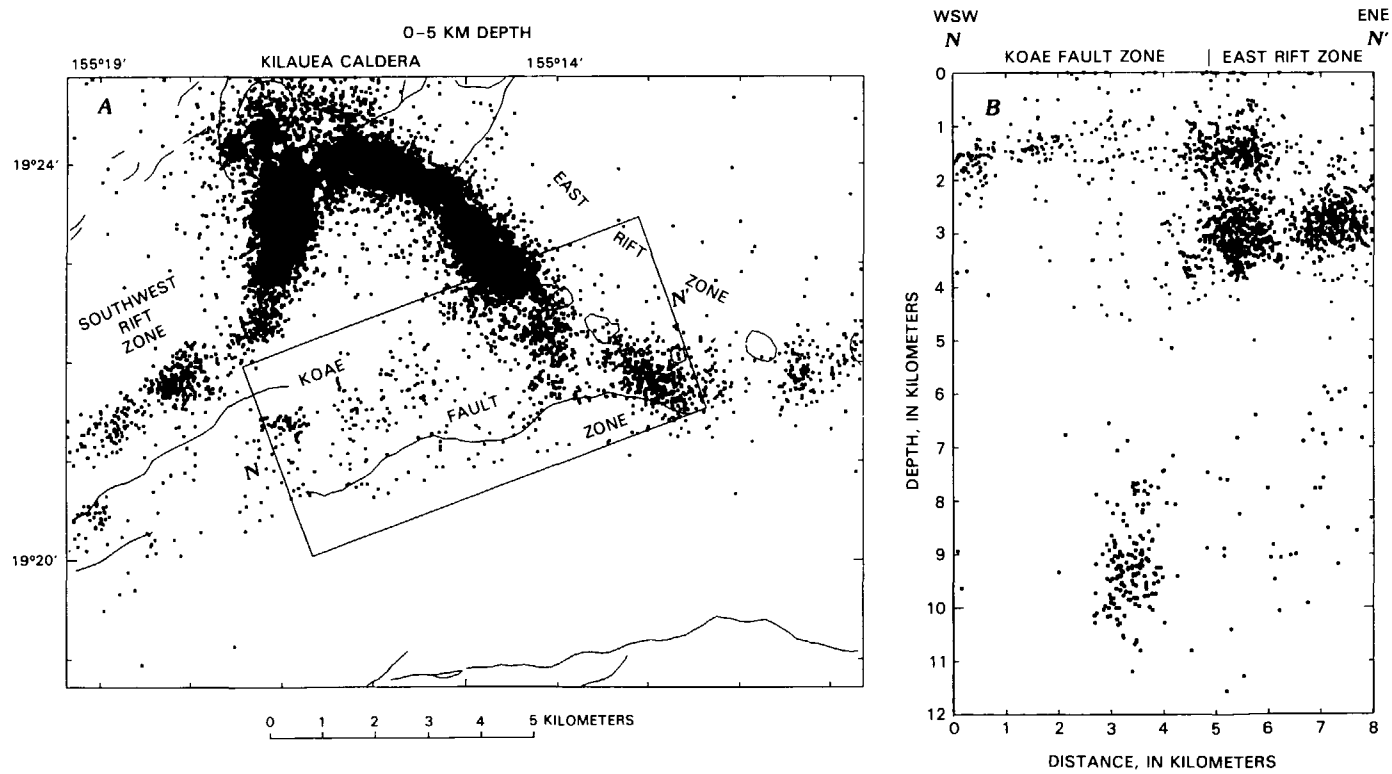

FIGURE 43.15.—Locations of shallow 1970–83 earthquakes south of Kilauea caldera in Koae fault zone. ***A***, Map view showing rectangular area of seismicity plotted in cross section *N-N'*. Faults, fissures, and pit craters are as shown in figure 43.1. ***B***, Cross section *N-N'* showing earthquakes to 12 km depth, but *A* only plots earthquakes to 5 km depth for clarity.

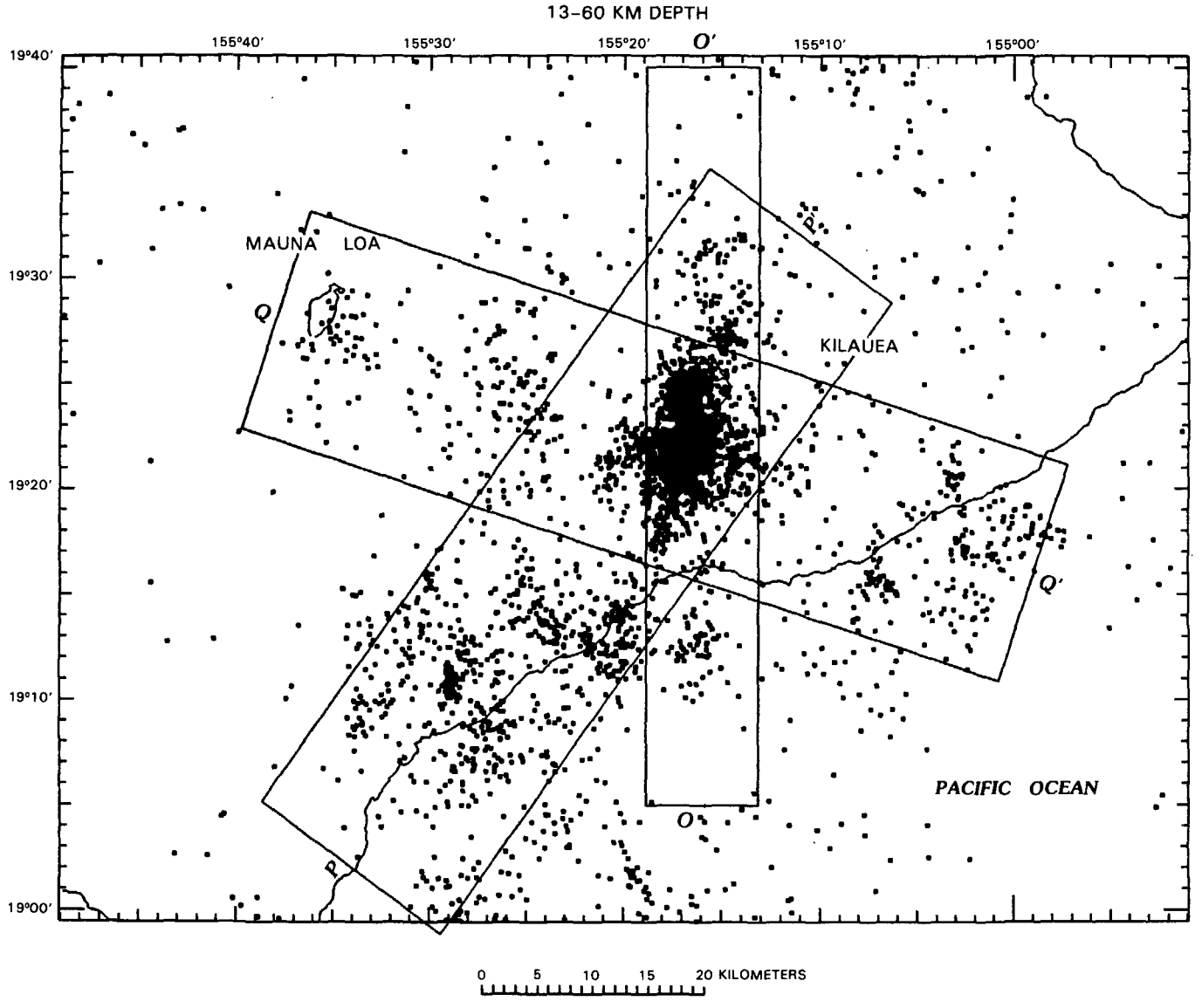

FIGURE 43.16.—Locations of 1970–83 earthquakes from 13–60 km depth beneath south side of Hawaii. Cross sections O-O′ through Q-Q′ are shown at different scales in figures 43.17*A*–*C* and 43.18*A*–*C*. Only earthquakes within rectangular areas are plotted on sections. Although events above 13 km are plotted on sections, they are omitted from map for clarity. All three sections include Kilauea's vertical magma conduit. Faults, fissures, and pit craters are as shown in figure 43.1.

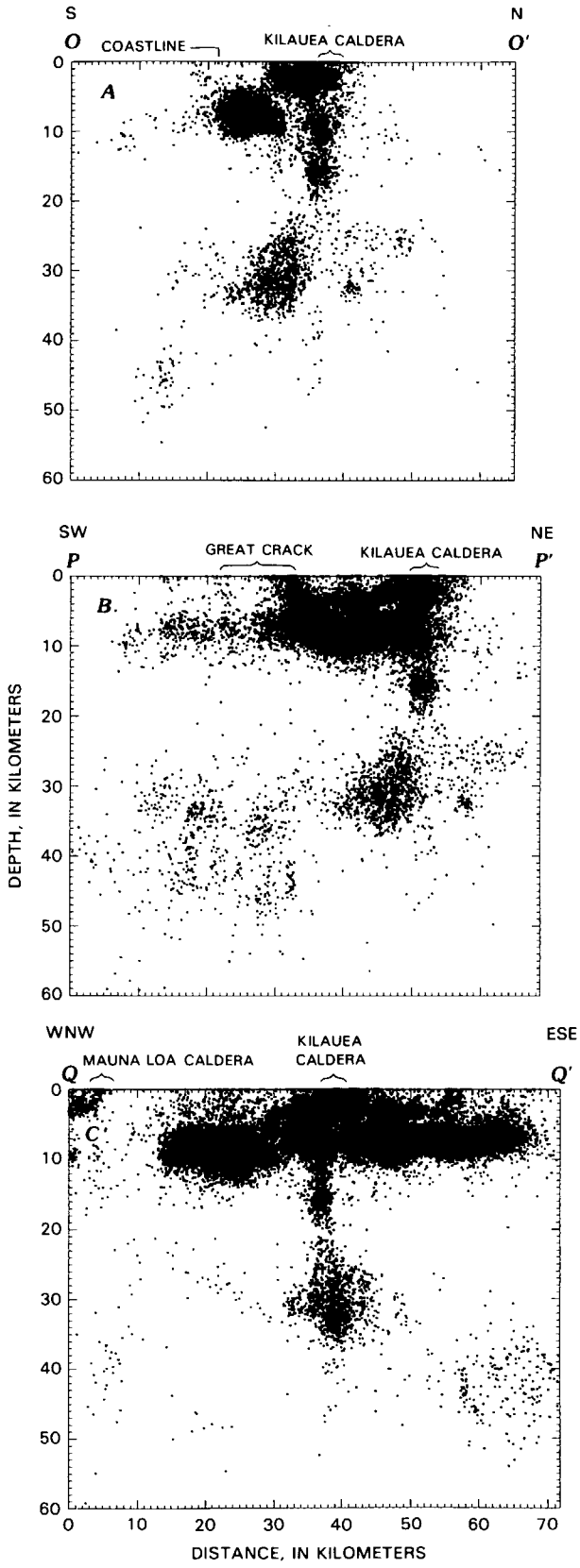

relative absence of earthquakes near 20 km depth thus may mark the lithosphere's neutral stress axis and locally help constrain flexure models. The earthquake gap also means that it is lithospheric stress, and not the magma pressure at this depth, that is the driving stress for these earthquakes. The fault plane solutions of a large set of Kilauea earthquakes deeper than 27 km have compressional axes radial to a point below Hawaii and thus may be oriented by flexure stress below the neutral axis (Elliot Endo, written commun., 1977). The seismic gap at 20 km depth and focal mechanisms of events below that thus suggest that regional stresses arising from lithospheric flexure play a dominant part in Kilauea's deeper seismicity.

The 20-km-depth point not only is a seismic gap, but also marks other differences in earthquake patterns: (1) a change occurs at 20 km from a conduit that is narrow and vertical above and broad and south-plunging below; (2) few events other than near the magma conduit are seen between 13 and 20 km, but earthquakes scatter widely under the south side of Hawaii below 20 km depth; and (3) earthquakes between 13 and 20 km are small and seldom exceed magnitude 2, but those below often exceed magnitude 4. These differences suggest that different lithospheric stresses prevail above and below 20 km. If the neutral stress depth is at 20 km, then the compressive regime below appears to favor earthquake production whereas the relatively extensional conditions above do not generate seismicity except where stresses are perturbed by the magma conduit or active rifts and flanks.

As discussed earlier, the seismically defined magma conduit merges with a diffuse cloud of hypocenters southwest of Kilauea that apparently marks the Hawaiian hot spot at 40–50 km depth. This cloud also lies centrally between Kilauea, Mauna Loa and Loihi, and is commonly a source of volcanic tremor and long-period earthquakes. Kilauea's deepest seismicity and conduit system thus become involved with the diffuse hot spot itself and become difficult to trace.

Not all deep seismicity is as readily interpreted as the major cloud southwest of Kilauea caldera. A smaller but similar cluster is southeast of Kilauea near 40–50 km depth (figs. 43.4*E–H*, 43.17C). These earthquakes are tectonic and do not appear to be related to tremor or to another volcano. This earthquake cluster can also be considered a part of the band of seismicity that underlies Hawaii's active south coast. The south coast is where the greatest amount of mass has been added to the island as lava flows and intrusives in recent decades and where seaward slip of the south flank occurs. Shear stress in the deep seismic zone is produced both from asymmetric loading by Kilauea growth to the north and southward motion of the flank driven by intrusive growth of the ERZ. Thus,

FIGURE 43.17—Cross sections through Kilauea taken from the surface to deepest seismicity at 60 km. Events from 1970–83 within areas of rectangles shown on figure 43.16 are projected onto sections. ***A***, Section *O-O'*. ***B***, Section *P-P'*. ***C***, Section *Q-Q'*.

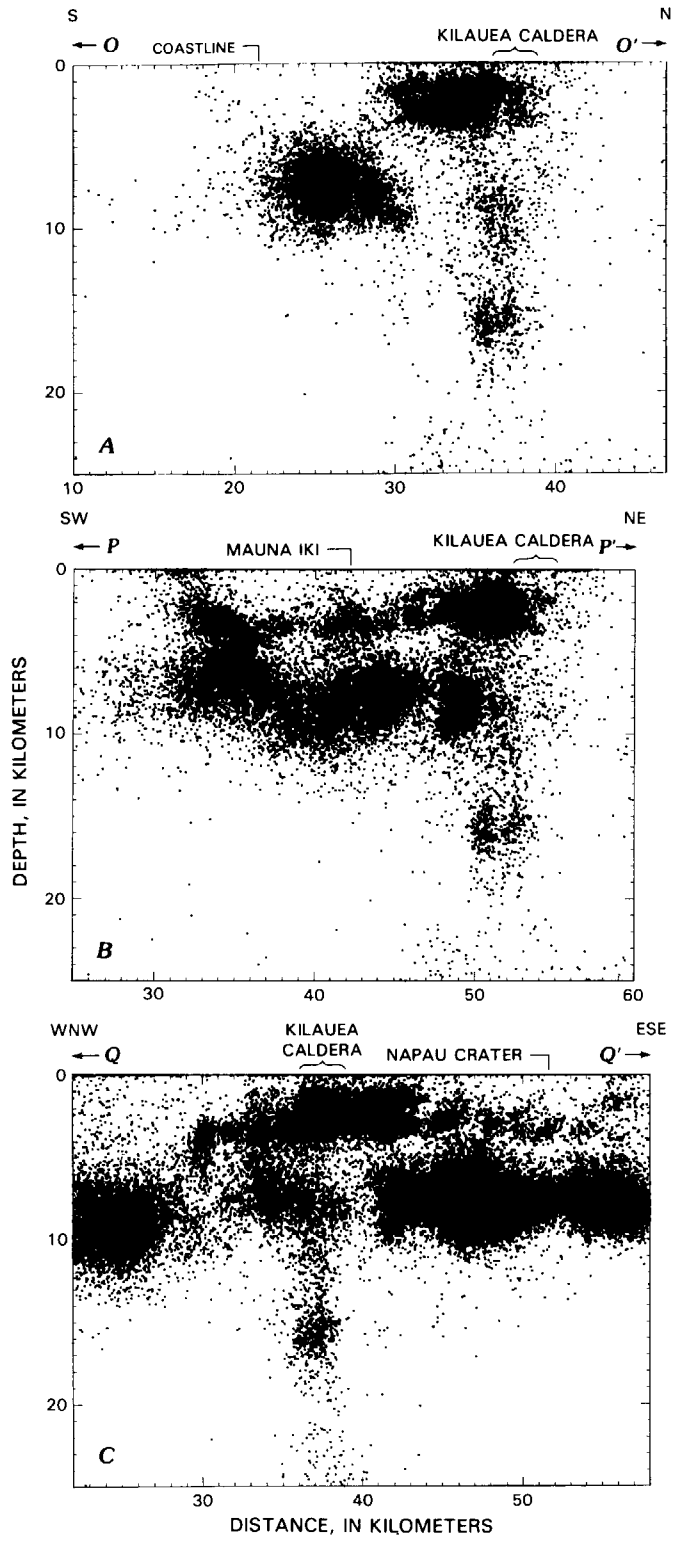

FIGURE 43.18—Enlargements of central portions of cross sections of figure 43.17*A*–*C* showing finer detail in upper part of Kilauea's vertical conduit system. ***A***, Section *O*-*O*'. ***B***, Section *P*-*P*'. ***C***, Section *Q*-*Q*'.

rapid loading and stress on the lithosphere possibly produces this concentration of events. The fact that earthquakes do not diminish smoothly with depth in the mantle means that the distribution of stress and material properties is more complex than for a simple halfspace.

Other noteworthy concentrations of seismicity are: (1) the northward extension of the major cluster at 25 to 35 km beneath Kilauea (fig. 43.17*A*, *B*); (2) a deep seismic root of Mauna Loa Volcano (fig. 43.17C)—although far less active than Kilauea's, the Mauna Loa conduit is nearly vertical to a depth of almost 50 km; and (3) a diffuse thread of earthquakes linking Kilauea's conduit at 35 km with Mauna Loa's near 20 km depth (fig. 43.17C). Whether this thread represents a magmatic connection between the two volcanoes is not known, but it emphasizes the complex and multizoned web of upper mantle seismicity. Also note that the tectonic events under the south flank (right side of fig. 43.18C) extend to about 10 km, but the Kaoiki zone is active to 12–13 km (left side of fig. 43.18C). If these boundaries are both controlled by the layer of prevolcanic sediments below the volcanic pile, then it deepens toward the interior of the island as expected from the observed dip of the Moho (Zucca and Hill, 1980).

To make some of the major seismic zones easier to see, we present in figure 43.19 some paired hypocenter plots to view with a pocket stereoscope. The earthquakes plotted were selected to represent each major seismic zone with enough events to define it, but not so many as to obscure other features. Figure 43.19*A* shows most of the island and includes Loihi Submarine Volcano south of the island. Figure 43.19*B*, *C* show boxes including nearly all of Kilauea, the summit of Mauna Loa and part of Loihi. The vertical magma conduit with its southward plunge into the zone of deepest earthquakes is clearly visible. Note the prominent cloud centered near 30 km depth. The shallow earthquakes below the ERZ and their distinct separation from the south flank zone at 6–10 km depth can also be seen. Figure 43.19*D* zooms in for a closer look at the central part of Kilauea and includes earthquakes to a depth of 35 km. Figure 43.19*E* is a close-up of the shallow magma system beneath the caldera to a depth of 18 km. The very active sections of both rift zones are adjacent to the summit magma reservoir. The earthquakes in the foreground between 6 and 10 km depth are tectonic events in the south flank.

We have examined the depth distribution of Kilauea's vertical magma conduit and found three zones of low or no seismicity: the summit magma reservoir causes an absence of earthquakes between 3 and 7 km; the reduced activity near 13 km may be an effect of the buried oceanic crust and sediment layer; and the absence of earthquakes near 20 km depth under all of Kilauea might be associated with the neutral stress level within a lithosphere flexing under the load of the volcanic pile. The vertical conduit thus looks like a passive intruder in the lithosphere: it is a zone weakened by magma in which earthquakes seem to be ultimately driven by regional lithospheric stresses. The low-rigidity conduit both concentrates regional stress and fails more easily than its surroundings. The conduit thus does not need to produce enough magmatic stress to cause earthquakes by itself. If the conduit produced magma pressures much higher than

stress in the adjacent mantle, one would probably see major swarms of volcanic earthquakes and a depth distribution different from its surroundings. The reduction in deep seismicity caused by the stress change during the 1975 Kalapana earthquake also argues for regional rather than magmatic stress as driving the deep earthquakes. A planned examination of earthquake statistics, depth and time history, and earthquake focal solutions will better address the interaction of magma ascent and lithospheric stress.

THE HISTORY OF KILAUEA'S SHALLOW EARTHQUAKE SWARMS, 1963–83

This section presents a summary of the basic data on two decades of Kilauea's summit and rift-zone earthquake swarms. The emphasis here is on a consistent treatment of basic earthquake patterns, not detailed chronologies. Particular attention will be paid to migration of earthquakes with time as an indicator of magma flow or dike propagation. We will be looking for characteristics common to many swarms and what they reveal of rift-zone dynamics. This section is thus complementary to the traditional treatment of a few well-studied examples. We feel the benefits of this survey approach outweigh the necessary omissions in dealing with so much data.

One benefit of treating two decades of swarms at once is the ability to classify swarms into similar groups, make comparisons and look for simple evolutionary trends. Shallow Kilauea swarms can be loosely divided into fast, intense swarms lasting for a few hours to a couple of days and slow swarms lasting several days to a few weeks. The fast swarms accompany rapid intrusions, which are presumably either the opening of an older magma conduit or the emplacement of a new dike. An eruption occurs if the dike reaches the surface, so nearly all eruptions are accompanied by intrusions and fast swarms. Except for harmonic tremor generated near an erupting vent, intrusions and eruptions are seismically indistinguishable. Summit tilt generally falls rapidly during fast swarms because of the high rate of magma flow. If the eruption or intrusion is within the caldera, however, the superposition of the deformation fields of the deflating reservoir and the nearby dike may cause rapid tilt changes in any direction.

Slow swarms occur between eruptions and intrusions, and are generally related to resupply of magma from depth. The most common slow swarms are within the caldera or immediately adjacent rift zones and result from gradual extension of the caldera during inflation or pressure increase of the magma reservoir. Summit tilt will usually be high and slowly rising during inflationary swarms. Seismicity and tilt levels are often closely correlated, as many examples will show. During some of the intereruption periods, the new magma supply partly or completely flows into a rift zone as a slow intrusion. These slow intrusions are generally accompanied by little or no gain in summit tilt and by a long-lived but low-intensity earthquake swarm in the part of the rift where magma accumulates. These four types of swarms will be referred to as eruptions, intrusions (fast), inflationary swarms and slow intrusions.

Most of the information in this section is contained in a series of figures, one set per swarm. The basic characteristics of all but the smallest swarms will be presented in four types of earthquake plots: map, cross section, hourly number of earthquakes versus time and downrift position versus time. Because most of the larger swarms form linear seismic zones, the distance axis for both cross sections and position versus time plots will be the same and along the appropriate section of rift zone. When different rift segments are active during the same swarm, more than one set of cross section and position versus time plots may be presented. For a particular swarm, all of the distance and depth scales will be the same on the maps and distance axes. The time scales, however, will vary as appropriate to the swarm.

Time on the position versus time plots proceeds from top to bottom. Significant migrations of earthquakes are noted by lines whose slope is the inverse of the migration speed. Solid lines are used where the migration and speed are clearest, dashed lines where the continuity and speed are uncertain, and a small arrow where a general migration is only suggested. Formal errors of the migration speeds cannot be given, but can be judged qualitatively from the scatter of earthquakes in the distance versus time plots used to determine speeds. For eruptions, the eruptive vents are shown for comparison by red lines on maps, cross sections and distance versus time plots. Vent positions are approximate and not plotted accurately. The position versus time history of vents refers only to the eruption start time of the earliest episode. The time histories of vents are particularly approximate and are usually sketched from limited observations like the beginning times of lava emission at only a few places.

The basic data for all swarms are listed in table 43.1, including the time period for each figure. Each of the several cross sections are identified with a set of letters (T–T' for the upper ERZ, for example). The endpoints and halfwidths of all sections are listed in table 43.2.

INTRUSIONS AND ERUPTIONS OF 1963

The seismic network and recording during the early and mid-1960's were not adequate to resolve fine spatial details in the swarms. The 1963 sequences are good examples of swarms whose approximate positions are known, but with no resolvable internal structure. Depth control may also not be adequate for some of the early swarms. Therefore, we cannot assume that events with calculated depths below 5 km are tectonic earthquakes, as is reasonable for most sequences after the late 1960's. Open squares are used in some swarm figures for events between 5 and 13 km depth and may include both tectonic and mislocated swarm earthquakes.

The first swarm for which adequate seismic data exists began on May 9, 1963 (fig. 43.20). This swarm was apparently a SWRZ intrusion, because the shallow swarm cloud is centered at a part of the SWRZ seismically active in later, better located intrusions. Earthquakes began at the time of summit deflation (fig. 43.20*B*), which is typical for earthquakes caused by rapid magma flow. The swarm's location may have been controlled by the intersection of the SWRZ magma conduit and the west end of the Koae fault zone. Ground cracking and inflation were observed in the

TABLE 43.1.—*Data for individual Kilauea swarms during 1963–83*

[The date the main part of the swarm started is not necessarily same date as an accompanying eruption. Event type is classified: Inf, swarm accompanying inflation; SI, slow intrusion; I, intrusion; E, eruption; Defl, caldera swarm accompanying major deflation. Main swarm locations are Cald, caldera; UERZ upper east rift zone; ERZ, east rift zone; USWR, upper southwest rift zone; SWRZ, southwest rift zone; LSWR, lower southwest rift zone; Koae, Koae fault zone. Swarm location may not coincide with eruptive vents. Seismic zone size refers to map view, parentheses imply epicenters are diffuse and poorly located. Query (?) for earthquake migration speed indicates migration appears to have occurred but with a speed too uncertain to measure. Map and cross-section plots include earthquakes from number of days listed. Delay times are between start of swarm beneath a vent and eruption at vent. Tilt changes are at Uwekahuna and are negative for deflation and positive for inflation. Tilt rates are computed at same time(s) as earthquake migration speed(s). Conduit area is obtained by dividing tilt rate by earthquake migration speed (for example see section "Southwest Rift Zone Intrusions and Caldera Eruption, January through August 1981")]

Figure number	Swarm start date	Swarm type	Swarm location	Swarm duration	Seismic zone size (km)	Downrift speed (km/h)	Uprift speed (km/h)	Upward speed 1-3 km (km/h)	Upward speed 0-1 km (km/h)	Plot duration (days)	Swarm-eruption delay (hours)	Tilt change (mrad)	Tilt rate (mrad/h)	Conduit area (m)
43.20	May 9 63	I	SWR	3 d	(9 by 5)	--	--	--	--	8	--	-32	--	--
43.21	Jul 2 63	I	Koae	3 d	(6 by 4)	east?	--	--	--	6	--	-20	--	--
43.22	Aug 21 63	E	UERZ	1 h?	--	--	--	--	--	2	--	-11	--	--
43.23	Oct 5 63	E	ERZ	3 d	(8 by 3)	--	--	--	--	8	--	-79	--	--
			Koae		(2 by 2)									
43.24	Mar 5 65	E	ERZ	3 d	(8 by 4)	--	--	--	--	5	--	-84	--	--
43.25	Aug 24 65	I	ERZ	1.5 d	(15 by 5)	--	--	--	--	8	--	-3	--	--
43.26	Dec 28 65	E	Koae	2 d	(5 by 5)	--	--	--	--	5	--	-45	--	--
43.27	Nov 5 67	E	Cald	1 h?	--	--	--	--	--	3	--	-11	--	--
43.28	Aug 22 68	E	Koae	4 h	2 by 2	west	--	--	--	3	3	-54	--	--
43.29	Oct 7 68	E	ERZ	2.5 d	11 by 2	3.4	--	--	--	5	3	-60	--	--
43.30	Feb 18 69	Inf	Cald	2.5 d	1 by 1	--	--	--	--	6	--	+11	--	--
43.31	Feb 22 69	E	ERZ	10 h	(11 by 3)	--	?	--	--	5	5	-46	--	--
43.32	Mar 21 69	I?	UERZ	2 h	2 by 2	--	14	--	--	3	--	<3	--	--
43.33	May 20 69	Inf?	ERZ	2.5 d	(8 by 4)	--	--	--	--	4	--	<3	--	--
43.34	May 24 69	E	ERZ	13 h	6 by 6	--	4.4	--	--	6	1	-24	--	--
43.35	Jul 3 69	I	UERZ	18 h	7 by 3	1.3	1.4	--	--	4	--	<3	--	--
43.36	Oct 7 69	SI	LSWR	4 d	7 by 4	--	--	--	--	6	--	+5	--	--
43.37	Nov 3 69	I	ERZ	1 h	1 by 1	6	--	--	--	3	--	-6		
43.38	Dec 22 69	Inf	USWR	7 d	1 by 1	--	--	--	--	8	--	+5,-23	--	--
43.39	Jan 22 70	I	Cald	4 h	2 by 2	--	2.2	--	--	3	--	<3	--	--
43.40	Feb 3 70	Inf	UERZ	8 d	5 by 1	.13,.02	--	--	--	9	--	+3	--	--
			USWR		2 by 1	.017								
43.41	Mar 17 70	Inf	USWR	6 d	2 by 1	?	--	--	--	7	--	+5	--	--
43.42	Apr 2 70	Inf	UERZ	7 d	2 by 2	--	--	--	--	8	--	+6,-10	--	--
			USWR		2 by 2									
43.43	May 15 70	I	UERZ	3 d	5 by 2	4.2	.13	--	--	8	--	-8	--	--
43.44	Dec 12 70	Inf	Cald	2 d	5 by 3	--	--	--	--	3	--	<3	--	--
43.45	Dec 22 70	Inf	Cald	19 d	11 by 3	.02	(1.3)	--	--	20	--	+4	--	--
43.48	Jun 6 71	Inf	Cald	9 d	3 by 3	--	--	--	--	10	--	+2	--	--
43.49	Jun 11 71	Inf	USWR	5 d	3 by 1	.35,.05	--	--	--	5	--	-2	.01	70
43.50	Jul 19 71	Inf	UERZ	12 d	2 by 2	.17,.008	--	--	--	12	--	+3	--	--
			USWR		3 by 1	?								
43.51	Aug 8 71	Inf	UERZ	7 d	6 by 1	.22	--	--	--	8	--	+12	--	--
			USWR		4 by 1	.02								
43.52	Aug 14 71	E	Cald	12 h	1 by 1	--	--	--	--	1	--	-16	--	--
43.53	Sep 6 71	Inf	UERZ	8 d	6 by 1	--	--	--	--	8	--	+3	--	--
			USWR		4 by 1									
43.54	Sep 17 71	Inf	UERZ	6 d	3 by 1	--	--	--	--	7	--	+5	--	--
			USWR		4 by 1	?								
43.55	Sep 24 71	E	SWRZ	7 d	13 by 3	.53,.31	--	--	--	7	4-18	+12,-23	.44	280
43.56	Dec 23 71	SI	LSWR	7 d	8 by 6	.29	--	--	--	8	--	<3	--	--
			UERZ		4 by 1		?							
43.57	Jan 19 72	Inf	UERZ	9 d	4 by 1	.08	.15,.15	--	--	10	--	+5	--	--
43.58	Feb 1 72	E	UERZ	5 d	2 by 1	--	--	--	--	7	.5-2 d	<3	--	--
43.59	May 5 73	E	Koae	25 h	8 by 2	.36 west	--	3	1	2	6	-23	1.7	1500
			ERZ				3.6							
43.60	Jun 9 73	I	Koae	23 h	3 by 1	1.0 west	--	--	--	1	--	-7	2.2	700
43.61	Nov 10 73	E	UERZ	16 h	3 by 1	?	--	1.6	?	2	5	-25	--	--
43.62	Mar 24 74	I	UERZ	3 h	1 by 1	?	--	--	--	1	--	-2	--	--
43.63	Jul 19 74	E	UERZ	10 h	3 by 1	--	.16	.55	.18	1	2	-18	--	--
43.64	Sep 16 74	Inf,E	USWR	3 d	7 by 1	?	--	--	--	4	--	+12	--	--
43.66	Dec 24 74	Inf	UERZ	7 d	4 by 1	.06	--	--	--	7	--	+4	--	--
			USWR		3 by 1	.03								
43.67	Dec 31 74	E	SWRZ	>14 d	20 by 2	1.3,.67	?	--	--	14	--	-128	5.3	1400
			USWR		3 by 1	.08	.17	5	.3		2			
43.68	Jun 21 76	I	UERZ	19 h	5 by 1	?	1.3	.5	--	2	--	-7	--	--
43.69	Jul 14 76	I	UERZ	17 h	6 by 1	?	?	.7	--	2	--	-13	--	--
43.70	Jan 22 77	Inf	UERZ	26 h	4 by 1	.7	--	--	--	2	--	+2	--	--
43.71	Feb 8 77	I	UERZ	7 h	4 by 2	.37	?	--	--	2	--	-6	--	--
43.72	Sep 12 77	E	ERZ	5.5 d	17 by 3	1.23,.23	--	--	--	8	11	-91	3.2	870
			Koae		4 by 2	.09 east								
			Cald		4 by 4									
43.73	Sep 27 77	Defl	Cald	5 d	2 by 1	.01	--	--	--	16	--	-7	--	--
43.75	May 29 79	I	ERZ	8 h	5 by 2	.65	.67	6	--	2	--	-3	--	--
43.76	Aug 12 79	I	UER	5 h	5 by 1	1.6	--	--	--	5	--	-2	--	--
43.77	Sep 22 79	Inf	Cald	3 h	2 by 2	--	--	--	--	1	--	<2	--	--
43.78	Nov 15 79	E	UERZ	21 h	5 by 2	3.8	4.0	1.2	.09	7	11	-8	0.5	44
43.79	Mar 2 80	I	UERZ	4 h	3 by 2	--	?	--	--	3	--	-2	--	--
43.80	Mar 10 80	E	ERZ	30 h	6 by 2	?	1.8	4.3	--	3	--	-16	--	--
			Koae			.22 west								
43.81	Jul 30 80	I	UERZ	1 h	2 by 1	30	--	--	--	1	--	<2	--	--
43.82	Aug 27 80	I	UERZ	12 h	5 by 1	1.6	.75	3	3	2	--	-9	2.6	860
43.83	Oct 21 80	I	ERZ	27 h	6 by 2	--	--	--	--	3	--	<1	--	--
43.83	Oct 22 80	I	UERZ	3 h	2 by 2	2.7	--	2.1	--	3	--	-3	--	--
43.84	Nov 2 80	I	UERZ	4 h	2 by 2	.7	?	?	?	3	--	-6	2.2	740
43.86	Jan 20 81	SI	USWR	1.2 d	2 by 1	--	.04	--	--	3	--	<3	--	--
43.87	Jan 24 81	SI	USWR	5 d	4 by 1	--	--	--	--	5	--	-5	--	--
43.88	Feb 9 81	SI	LSWR	8 d	4 by 1	?	--	?	--	8	--	-12	--	--
43.89	Aug 2 81	SI	USWR	8 d	5 by 1	?	--	--	--	8	--	-2	--	--
43.90	Aug 10 81	I	SWRZ	3.5 d	22 by 2	2.6,.28	.14	.46	--	9	--	-107	11	1500
			USWR		4 by 1	2.6	3.5							
43.91	Mar 23 82	I	USWR	1 h	2 by 1	--	?	--	--	1	--	<2	--	--
43.92	Apr 30 82	E	Cald	4 h	2 by 2	--	14	--	--	2	--	+5	--	--
43.93	Jun 22 82	I	SWRZ	5 d	12 by 2	.2	--	?	--	3	--	-45	.83	1400
43.94	Sep 25 82	E	UERZ	1.6 d	5 by 1	1.4	--	1	1	7	2	+18	--	--
			USWR		2 by 1	1.4								
43.96	Dec 9 82	I	UERZ	2 d	5 by 1	6.4	--	.8	--	3	--	-3	--	--
43.97	Jan 1 83	E	ERZ	6 d	16 by 2	.62	.06	?	?	9	21	-120	1	540
			ERZ			.025,.61								

TABLE 43.2.—*Endpoints and widths of cross sections*

[Half-width of each cross section is distance from cross-section plane within which earthquakes are included on plot. Latitude and longitude are given in degrees and minutes]

Cross Section	Left endpoint		Right endpoint		Half-width (km)
	Latitude	Longitude	Latitude	Longitude	
A-A'	19 25.35	155 18.4	19 21.4	155 12.0	0.8
B-B'	19 23.0	155 18.5	19 26.5	155 15.0	0.8
C-C'	19 24.4	155 19.0	19 24.4	155 14.0	0.8
D-D'	19 22.0	155 17.1	19 26.5	155 17.1	0.8
E-E'	19 20.9	155 13.1	19 26.8	154 57.5	2.7
F-F'	19 16.4	155 24.3	19 26.0	155 15.2	2.6
G-G'	19 25.4	155 12.1	19 20.6	155 16.0	2.0
H-H'	19 23.3	155 12.8	19 17.0	155 13.9	2.0
I-I'	19 23.5	155 9.7	19 17.6	155 8.3	2.0
J-J'	19 24.7	155 6.9	19 19.3	155 4.0	2.0
K-K'	19 24.1	155 19.5	19 20.0	155 15.0	2.0
L-L'	19 21.7	155 21.9	19 17.2	155 17.4	2.0
M-M'	19 19.3	155 25.0	19 15.1	155 20.2	2.0
N-N'	19 20.9	155 17.0	19 22.4	155 12.7	1.7, 2.1
O-O'	19 5.0	155 16.0	19 40.0	155 16.0	5.0
P-P'	19 2.0	155 34.0	19 32.0	155 11.0	10.0
Q-Q'	19 28.0	155 38.0	19 16.0	154 59.0	10.0
R-R'	19 21.0	155 18.8	19 26.0	155 15.9	1.6
S-S'	19 20.9	155 17.9	19 22.4	155 12.7	1.7, 2.1
T-T'	19 24.8	155 17.5	19 21.3	155 12.0	1.3
U-U'	19 23.5	155 18.5	19 23.5	155 2.5	4.3
V-V'	19 21.8	155 15.2	19 22.4	155 9.5	1.3
W-W'	19 21.3	155 16.0	19 21.3	155 5.8	3.8
X-X'	19 22.3	155 20.3	19 26.6	155 14.6	1.6

Koae, and magma may also have intruded the fault zone (Kinoshita, 1967). Some downrift earthquake migration appears to have occurred (fig. 43.20*D*), but location accuracy is not sufficient to be sure. All subsequent large SWRZ intrusions have shown clear downrift migration of earthquakes.

Another intrusion involving the Koae occurred two months later on July 2, 1963. Earthquakes occurred east of the previous swarm in the central and eastern Koae (fig. 43.21*A*). Many earthquakes were sharply felt and heard as cracking and booming sounds by observers in the epicentral area on July 1 and 2. Ground cracking was also noticed in the epicentral area and was confined to the eastern Koae fault zone. These observations suggest that many hypocenters were shallow and above about 2 km depth. The deflation indicates that magma left the summit reservoir, though the relative amounts of magma emplaced in the ERZ, SWRZ and Koae are uncertain. Two more accurately located and more clearly paired Koae intrusions occurred in May and June 1973. Earthquake migration (and presumably magma flow), however, was westward from the ERZ in the latter intrusions.

Relatively few earthquakes were located during the August and October 1963 ERZ eruptions (figs. 43.22*A*, 43.23*A*). This decrease is more an effect of inadequate instrumentation than failure of the volcano to produce earthquakes. No seismic stations were in this area of the ERZ (fig. 43.2*A*), and the masking of earthquakes by harmonic tremor is a more serious problem on the smoked-paper records then used to measure earthquakes. The recently active Koae experienced earthquakes during the October event (fig. 43.23*A*). Geologic and seismic descriptions are given by Moore and Koyanagi (1969).

THE ERUPTIONS AND INTRUSION OF 1965 AND 1967

The ERZ eruption of March 5, 1965 (fig. 43.24; Wright and Kinoshita, 1968) and the August 24, 1965 intrusion (fig. 43.25) were both accompanied by swarms with many earthquakes exceeding magnitude 2. As before, seismic-station geometry did not permit accurate locations. Inaccuracy may account for the scattering of earthquakes away from the rift and into the south flank. Shallow south-flank earthquakes are seen accompanying more recent, better recorded ERZ intrusions and eruptions, but only as events clearly secondary to the main swarm beneath the rift. These 1965 earthquakes must be considered poorly located. Earthquakes during the August event apparently migrated eastward at a speed of 12 km/h, but concluding anything more than the possibility of a migration is ruled out by the location inaccuracies.

Seismic data from the ERZ eruption of December 1965 (fig. 43.26) and the caldera eruption that began on November 5, 1967 (fig. 43.27) are incomplete. None of the events in the first 3 days of the December 1965 eruption (and intrusion) were initially timed and located owing to their quantity and intensity. Although the eruption was on the ERZ, earthquakes were generated by an intrusion into the Koae (fig. 43.26*A*). Boscher and Duennebier (1985) timed many small events not plotted here and concluded that the Koae hinged apart in response to stresses in the volcano. The eruption, seismicity and ground cracking in the Koae are described by Fiske and Koyanagi (1968). The migration direction of major ground cracking and earthquakes was westward, as it was for earthquakes in later events combining ERZ eruptions with Koae intrusions. Only two earthquakes accompanying the November 1967 summit eruption were located, owing to the brevity of the swarm prior to the eruption and the intensity of harmonic tremor. The location of the two earthquakes suggests that an intrusion of the adjacent SWRZ initially accompanied the eruption (fig. 43.27*A*). The eruption that episodically continued until July 1968 is documented in detail by Kinoshita and others (1969).

THE EAST RIFT ERUPTIONS OF 1968 TO MARCH 1969

The period from August 1968 to March 1969 was active for the central ERZ between Hiiaka and Puu Kamoamoa, which experienced three eruptions and one intrusion. The ability to adequately record and locate earthquakes improved markedly during this period. The eruptions of August 22 and October 7, 1968, are fully described by Jackson and others (1975). No earthquakes in the immediate vicinity of the August 1968 eruptive vents were large enough to time and locate, but events did occur to the southwest in the adjacent section of the Koae fault zone (fig. 43.28*A*). The Koae earthquakes anticipated the onset of eruption by about 3 hours and also apparently began an eastward migration of vent opening (fig. 43.28*D*). This eruption was seismically complex, because it began with small and unlocatable earthquakes near Makaopuhi (Jackson and others, 1975) and involved a Koae intrusion at the opposite end of the eruptive zone.

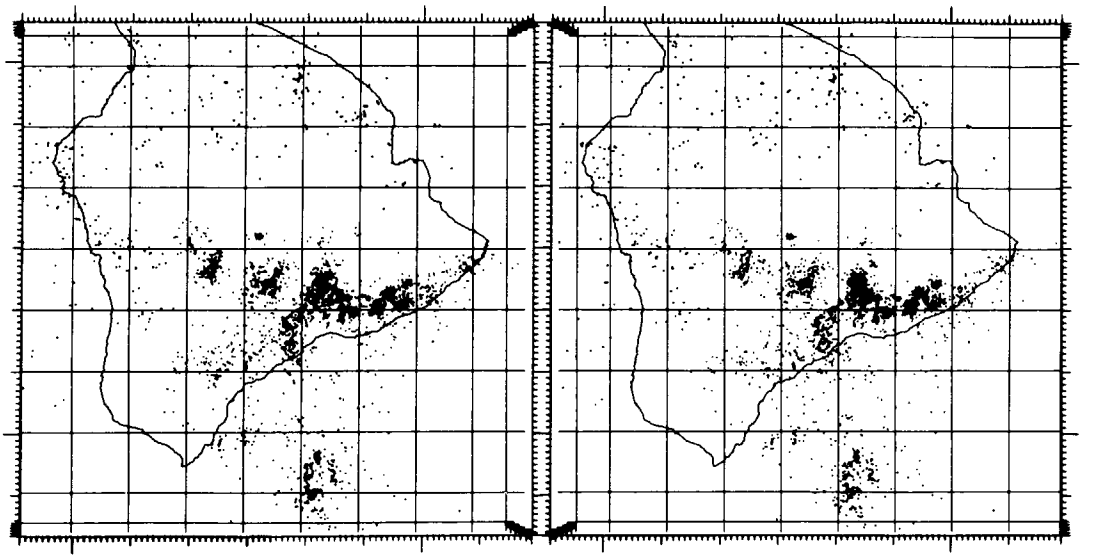

A

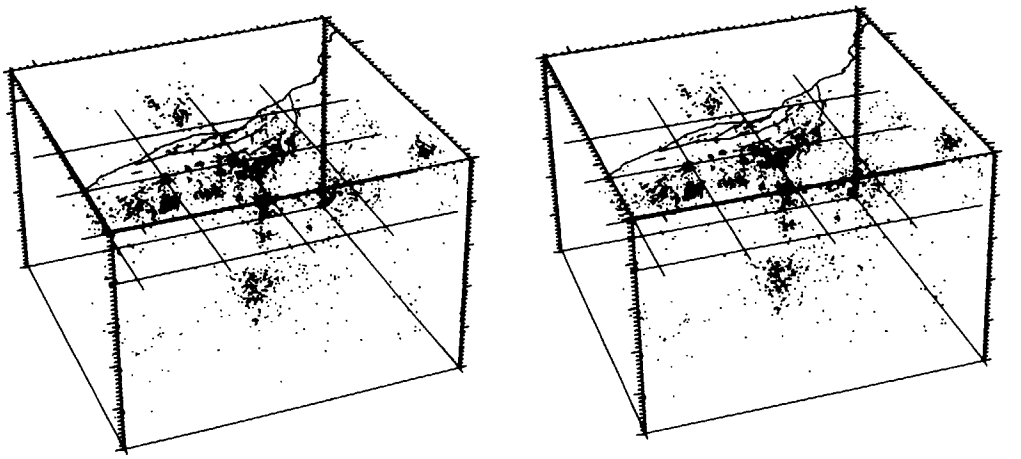

B

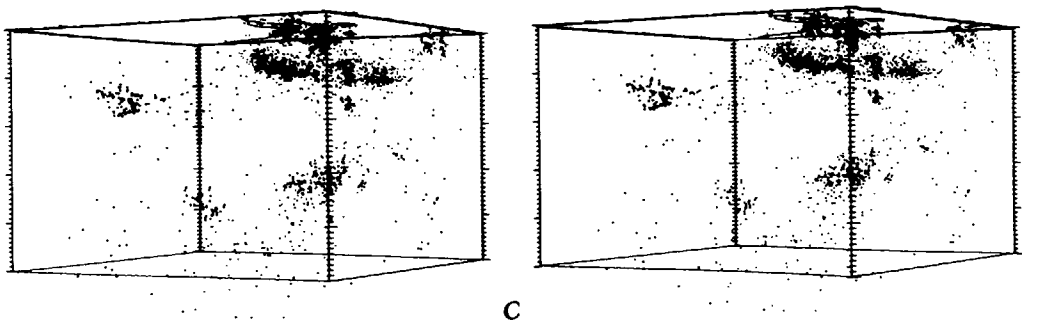

C

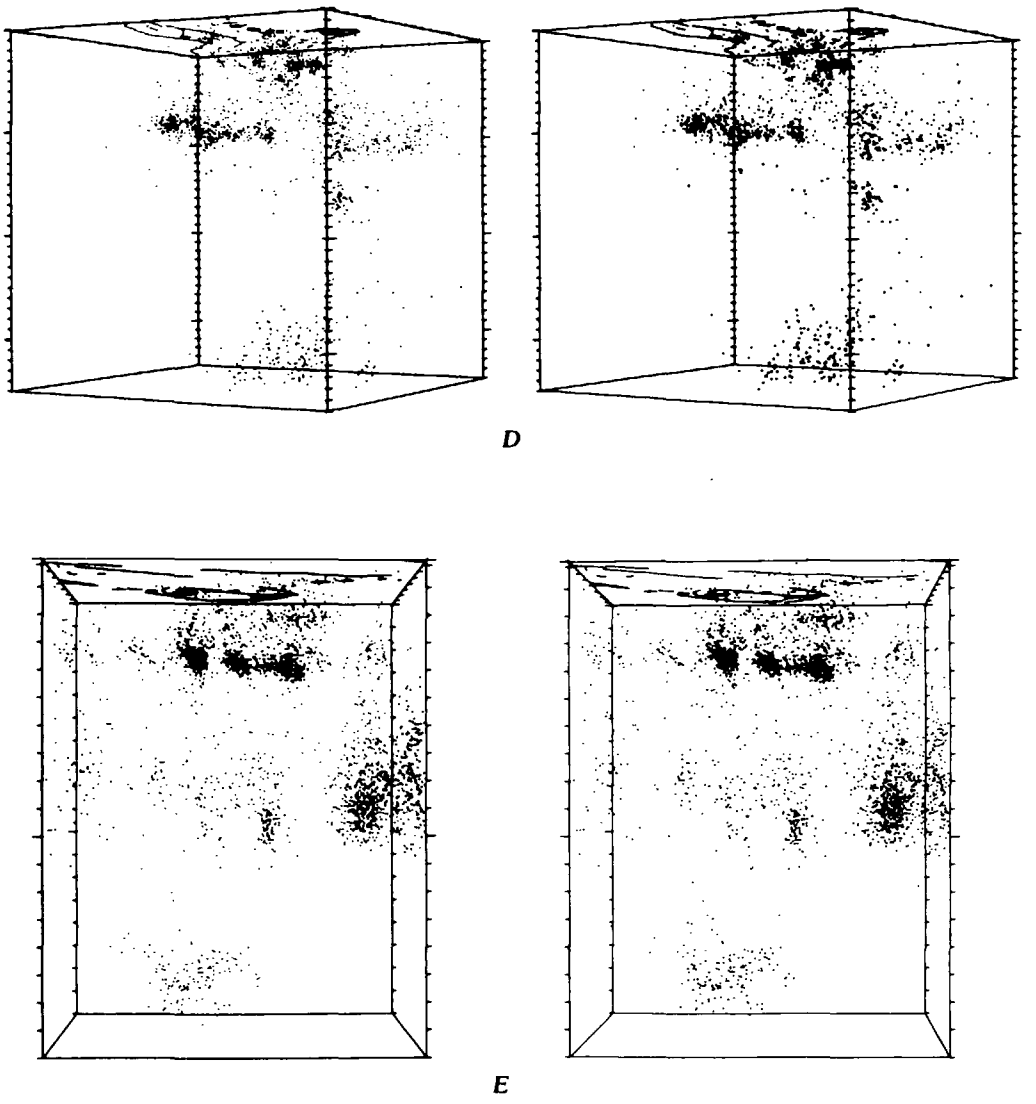

FIGURE 43.19—Stereopair views of 1970–81 Kilauea earthquakes showing major seismic zones. Tick marks on horizontal axes are plotted every minute of latitude and longitude, and those on depth axes are every kilometer. ***A,*** View from above Hawaii. Loihi Volcano is to south. Coastline is at surface, and grid of lines is at 13 km depth and approximates Moho. ***B,*** Closer view of Kilauea from north. Grid is plotted at 13 km depth near Moho, and box is 50 km high. Most of shallowest seismicity is below rift zones. Tectonic earthquakes below Kilauea's south flank are mostly between 6 and 10 km depth. Vertical magma conduit and major cluster near 30 km are clearly visible. ***C,*** Same box as in *B* viewed from northeast at depth of 25 km. Magma conduit merges with diffuse cloud of seismicity in far lower corner, which marks present Hawaiian hot spot. Earthquakes from Loihi are to left and from Mauna Loa in upper right corner. ***D,*** Closer view of Kilauea from northeast at depth of 17 km. Box is 35 km high. Low seismicity associated with summit magma reservoir is below caldera between about 3 and 7 km. ***E,*** Close-up view of Kilauea summit region from south at a depth of 9 km. Unlike other stereopairs, essentially all available earthquakes are plotted in *E*. Intense seismic zones at 3 km depth are rift conduits that abut magma reservoir behind and beneath them. Foreground events between about 6 and 10 km depth are tectonic earthquakes in south flank.

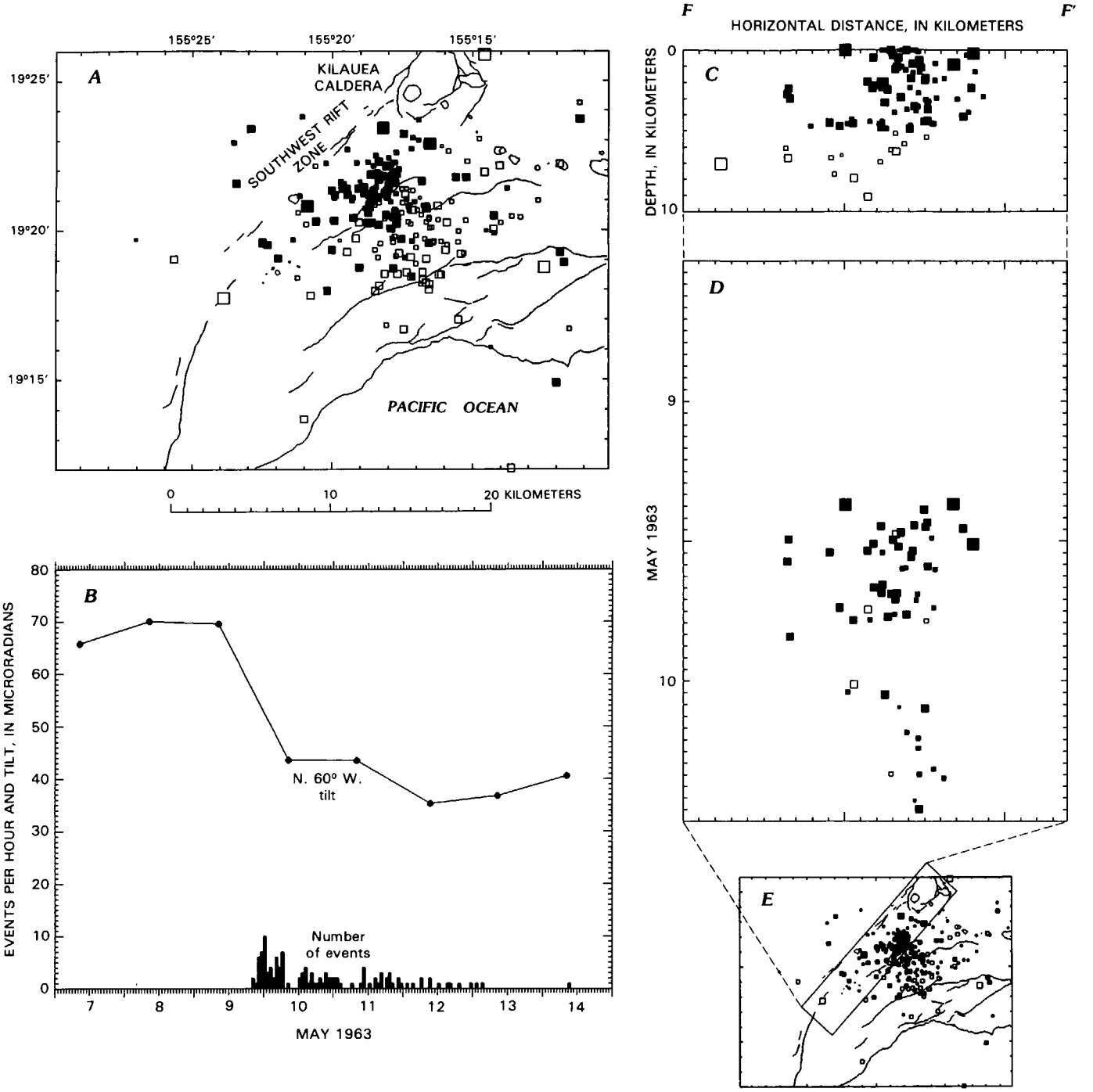

FIGURE 43.20.—Earthquake swarm (and presumed magma intrusion) beginning on May 9, 1963. Only earthquakes that were timed and located are plotted. ***A,*** Map of earthquake epicenters. Solid squares, earthquakes in depth range 0–5 km; open squares, 5–13 km below surface. Faults, fissures,and pit craters are as shown in figure 43.1. ***B,*** Plot of tilt at Uwekahuna and hourly number of earthquakes on same time base. Decreasing tilt values correspond to tilt down to east and south and generally to deflation of summit magma reservoir. Connected points are readings from two-component water-tube tiltmeter rotated to N. 60° W., approximately in line with deformation center. Continuous line, beginning with figure 43.49, is from east-west Ideal Aerosmith tiltmeter. ***C,*** Cross section of hypocenters. End points of cross section and half-width distance from cross section plane are presented in table 43.2. Ticks on horizontal axis at 1-km intervals. Beginning date of earthquakes included in *A* and C is the starting swarm date unless otherwise noted. The number of days included in *A* and C is given as plot duration in table 43.1 and is not necessarily the same as time axis of tilt and seismicity graph. ***D,*** Horizontal position of earthquakes versus time; time increases downward, ticks at hourly intervals. Lateral migration of epicenters is recognized as diagonal bands of points. ***E,*** Rectangular area within which earthquakes are plotted on C and *D*.

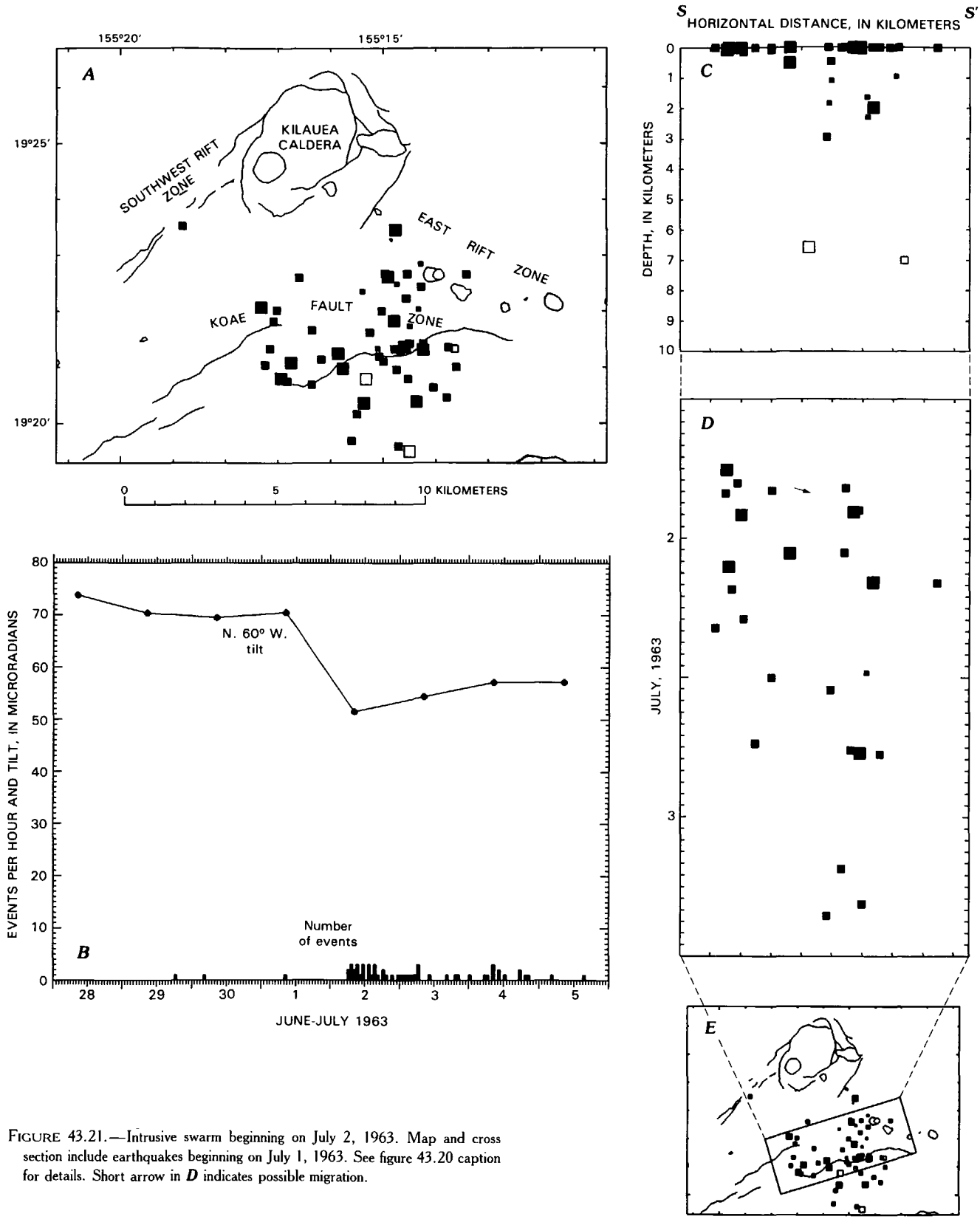

FIGURE 43.21.—Intrusive swarm beginning on July 2, 1963. Map and cross section include earthquakes beginning on July 1, 1963. See figure 43.20 caption for details. Short arrow in *D* indicates possible migration.

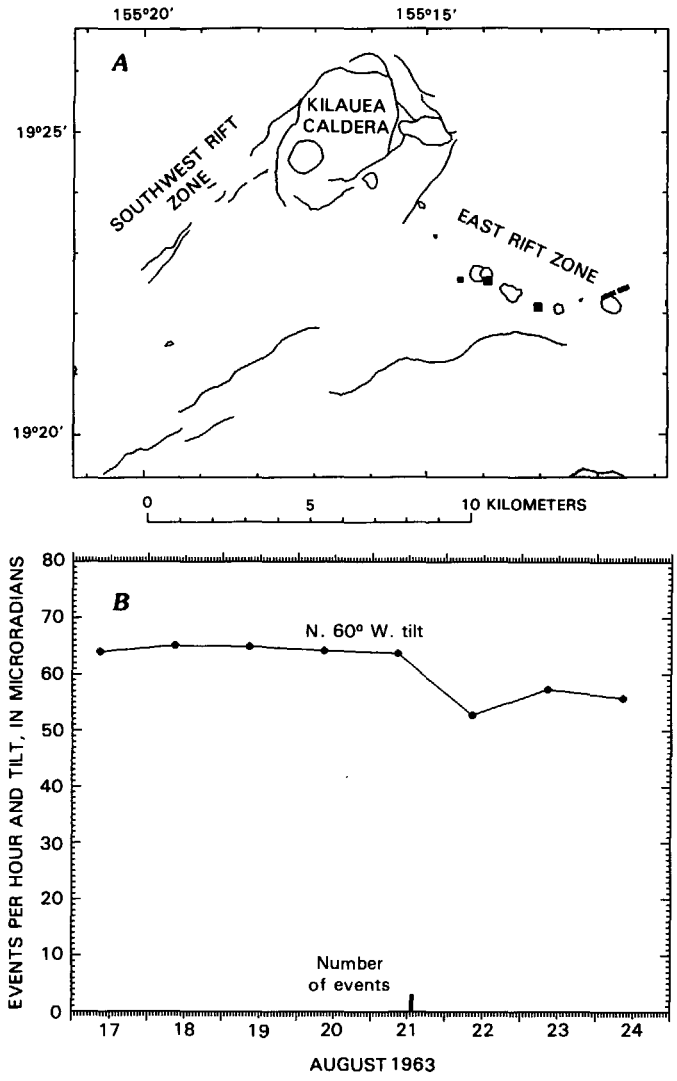

FIGURE 43.22.—Eruptive swarm beginning on August 21, 1963. See figure 43.20 caption for details. Red, eruptive vents.

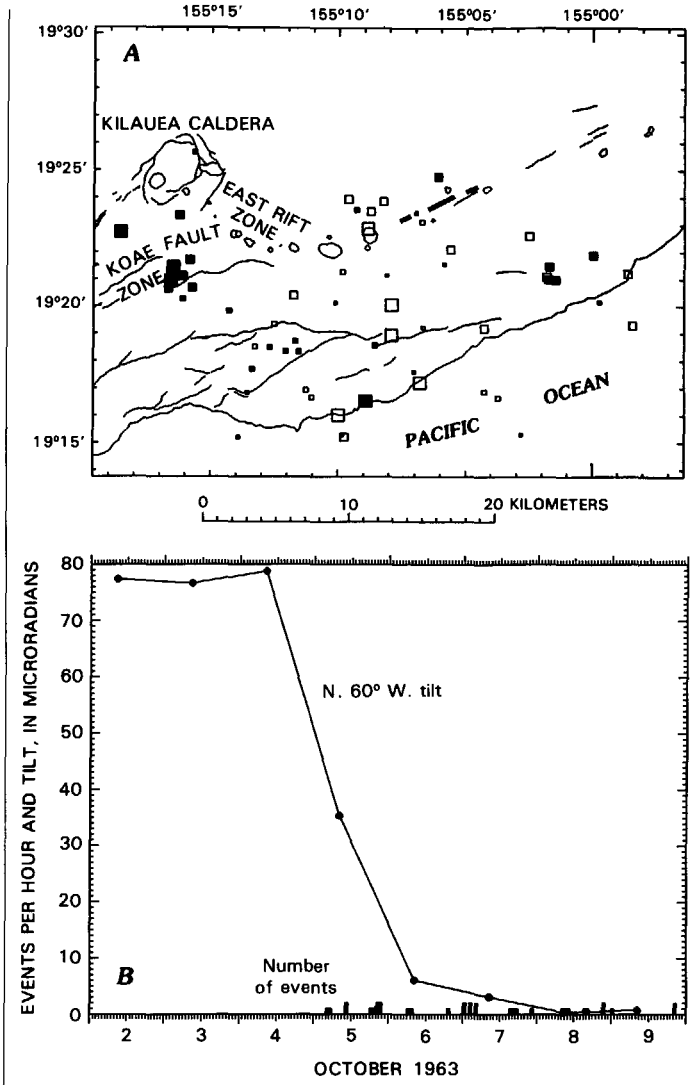

FIGURE 43.23.—Eruptive swarm beginning on October 5, 1963. See figure 43.20 caption for details. Red, eruptive vents.

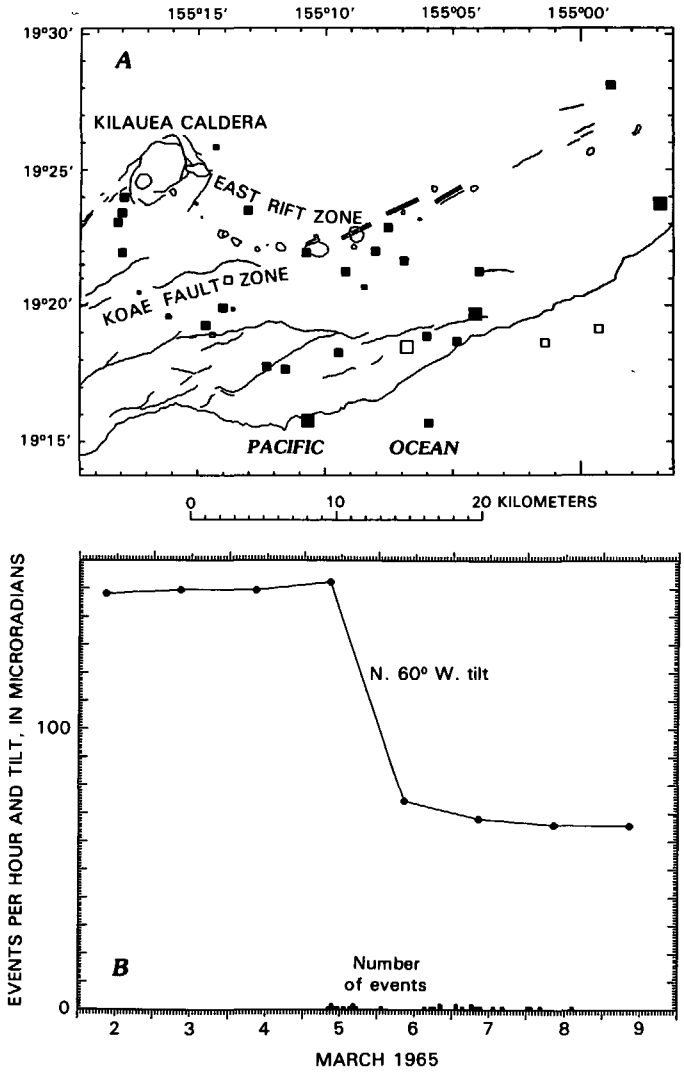

FIGURE 43.24.—Eruptive swarm beginning on March 5, 1965. See figure 43.20 caption for details. Red, eruptive vents.

Earthquakes and volcanism were much more clearly related during the October 1968 eruption. The length and position of the eruptive vents and seismic zone coincide very closely (fig. 43.29*A*). The displacement of the seismic zone slightly south of surface rift and eruptive vents is typical of later ERZ swarms, but may partly be a result of a biased distribution of seismic stations. A clear downrift migration of earthquakes at about 3-4 km/h occurred uprift of Puu Kamoamoa (fig. 43.29*D*). The speed then slowed to about 1 km/h. Eruptive vents opened in the same direction and at comparable speed, and followed the earthquakes in a given place by about 3 hours. The dike thus grew downrift at 1–3 km/h and upward at about 0.6 km/h simultaneously. Passage of magma upward from the main conduit at 3 km depth was essentially aseismic, as seen by the absence of earthquakes within 2 km below the vents (fig. 43.29*C*).

The ERZ eruption of February 22, 1969, is associated with two swarms. The first preceded the eruption by several days and was in the southern part of the caldera (fig. 43.30*A*). It occurred gradually over several days and was concurrent with a premonitory rise in Uwekahuna tilt (fig. 43.30*B*). The earlier swarm was thus caused by summit inflation. This pulse of inflation may have also triggered the eruption by incrementing magma pressure just above a critical level. The eruption itself was immediately preceded by a swarm located mostly south of the ERZ eruptive vents (fig. 43.31*A*). Most of these earthquakes are probably mislocated too far south of the rift zone and vents. The first vents to erupt were near Alae crater, and vents opened rapidly to the east and slowly to the west (Swanson and others, 1976b). In each part of the vent system, earthquakes essentially ceased when the vent began erupting (fig. 43.31*C*). This cessation could result from masking of smaller earthquakes by strong vent-related tremor, by stress and pressure release when the dike reached the surface, or both.

A small swarm lasting less than three hours occurred on March 21, 1969. It was concentrated in a small cluster 1–2 km uprift of the future site of Mauna Ulu and preceded the Mauna Ulu eruption by two months. The March swarm may have been associated with small-scale magma movement in some sense preliminary to the later eruption. Any summit deflation associated with this small intrusion was below the tilt noise level (fig. 43.32*B*). An apparent and very rapid westward migration of epicenters (fig. 43.32*D*) is not well seen since the swarm is so small.

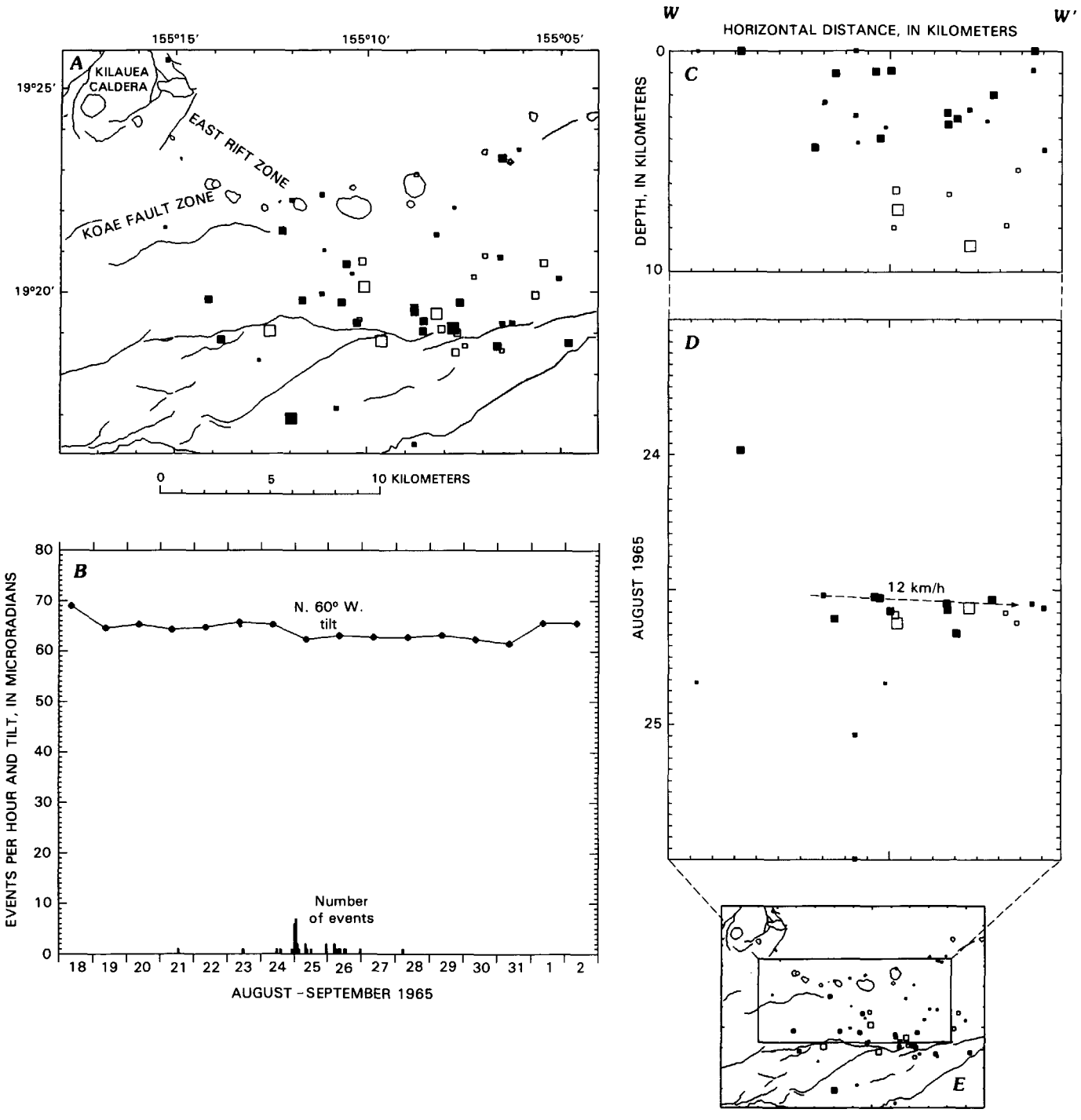

FIGURE 43.25.—Intrusive swarm beginning on August 24, 1965. Map and cross section include earthquakes beginning on August 21, 1965. See figure 43.20 caption for details. Dashed line in ***D***, poorly resolved shift in seismicity.

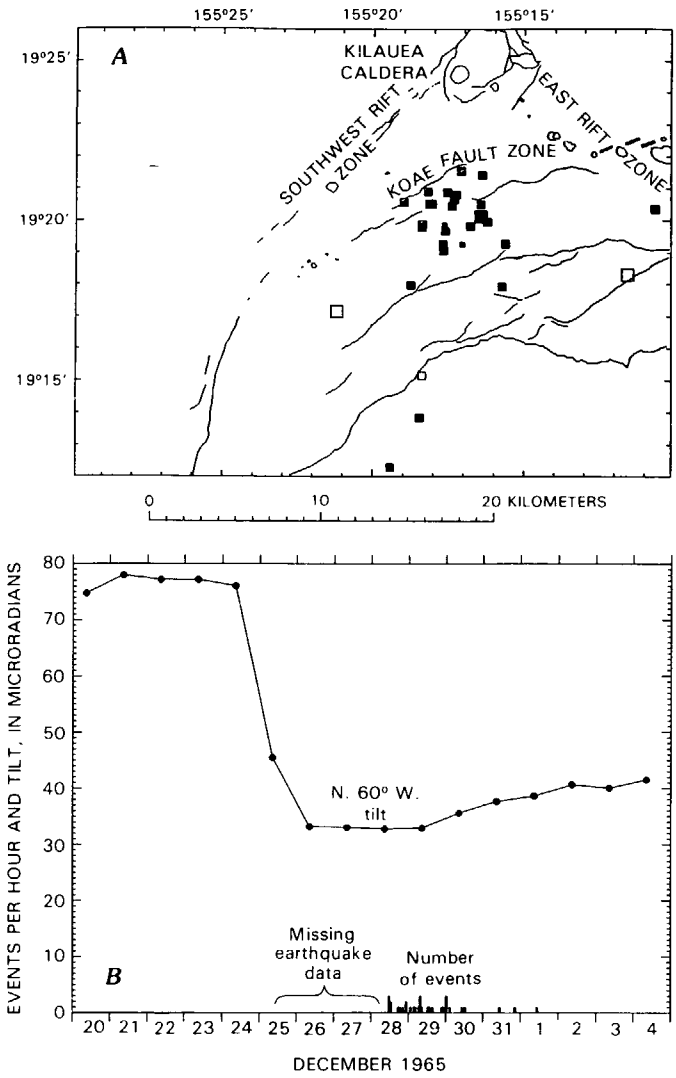

FIGURE 43.26.—Eruptive swarm beginning on December 28, 1965. Map and plot include earthquakes beginning on December 27, 1965. See figure 43.20 caption for details. Red, eruptive vents.

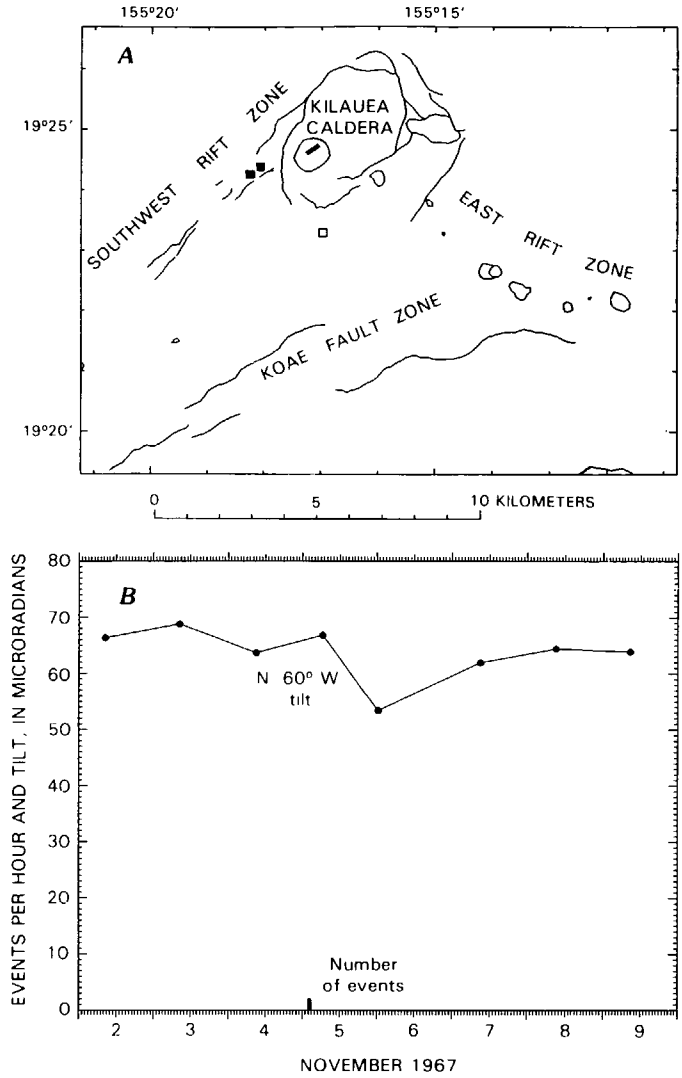

FIGURE 43.27.—Eruptive swarm beginning on November 5, 1967. Map and plot include earthquakes beginning on November 4, 1967. See figure 43.20 caption for details. Red, eruptive vent.

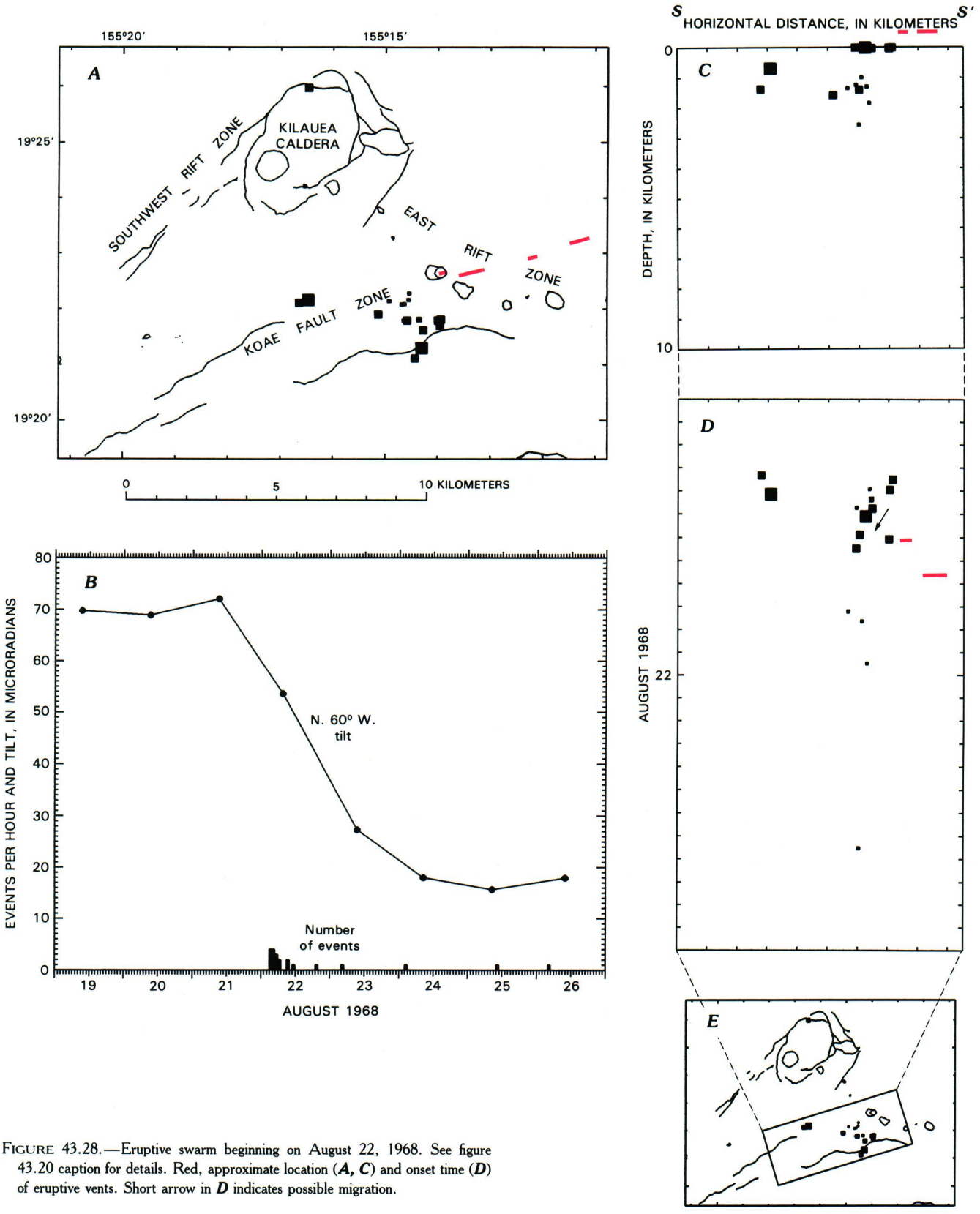

FIGURE 43.28.—Eruptive swarm beginning on August 22, 1968. See figure 43.20 caption for details. Red, approximate location (***A, C***) and onset time (***D***) of eruptive vents. Short arrow in ***D*** indicates possible migration.

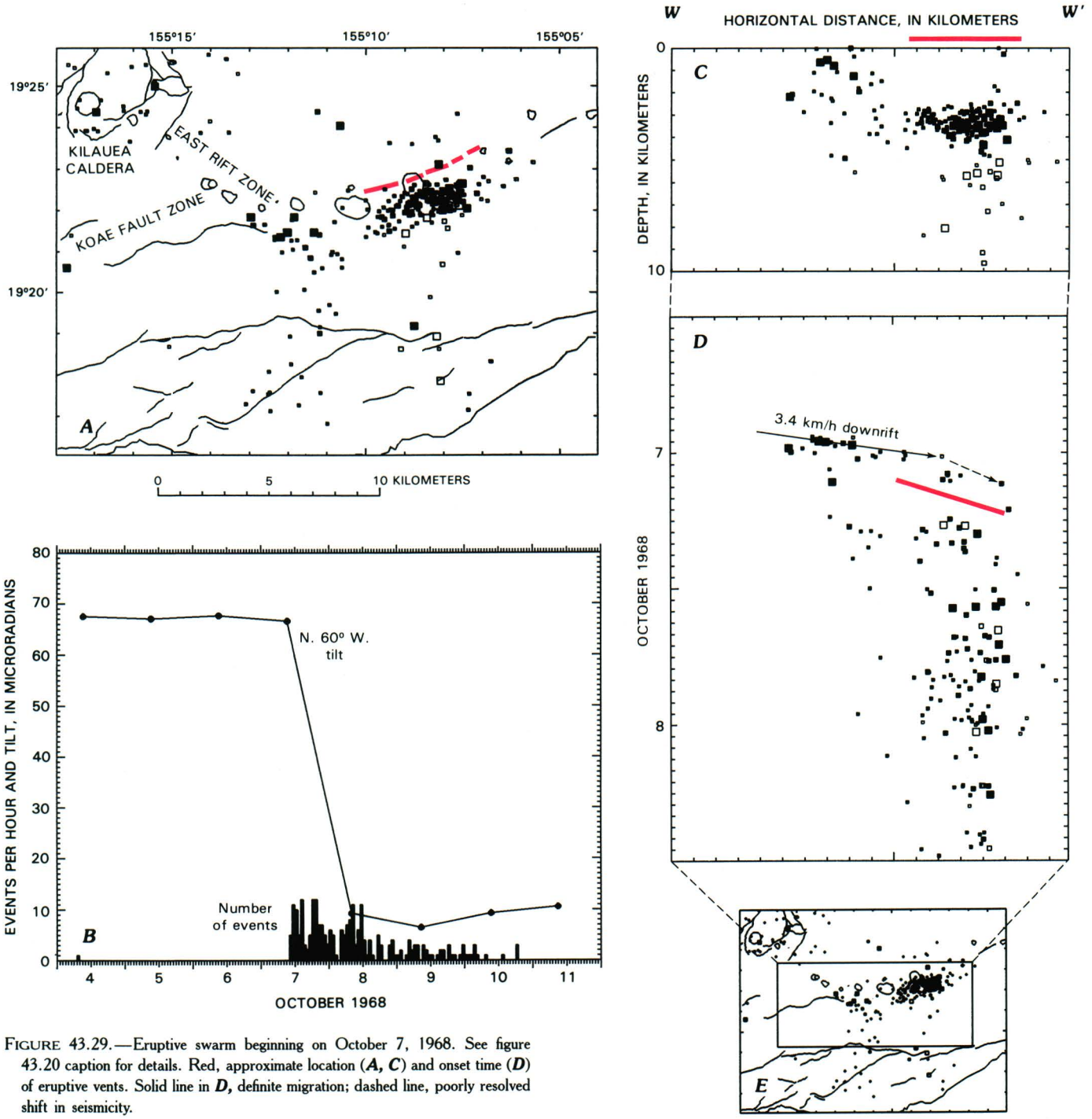

FIGURE 43.29.—Eruptive swarm beginning on October 7, 1968. See figure 43.20 caption for details. Red, approximate location (***A, C***) and onset time (***D***) of eruptive vents. Solid line in ***D***, definite migration; dashed line, poorly resolved shift in seismicity.

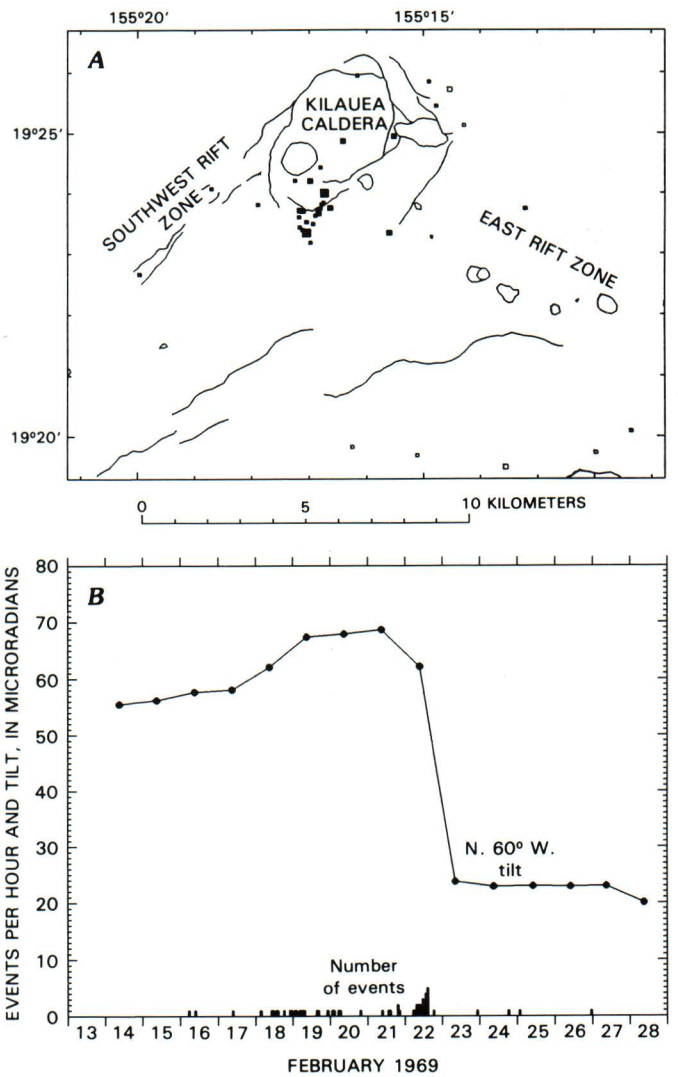

FIGURE 43.30.—Inflationary swarm beginning on February 18, 1969, immediately preceding eruption of February 22. Map and plot include earthquakes beginning on Fegruary 16, 1969. See figure 43.20 caption for details.

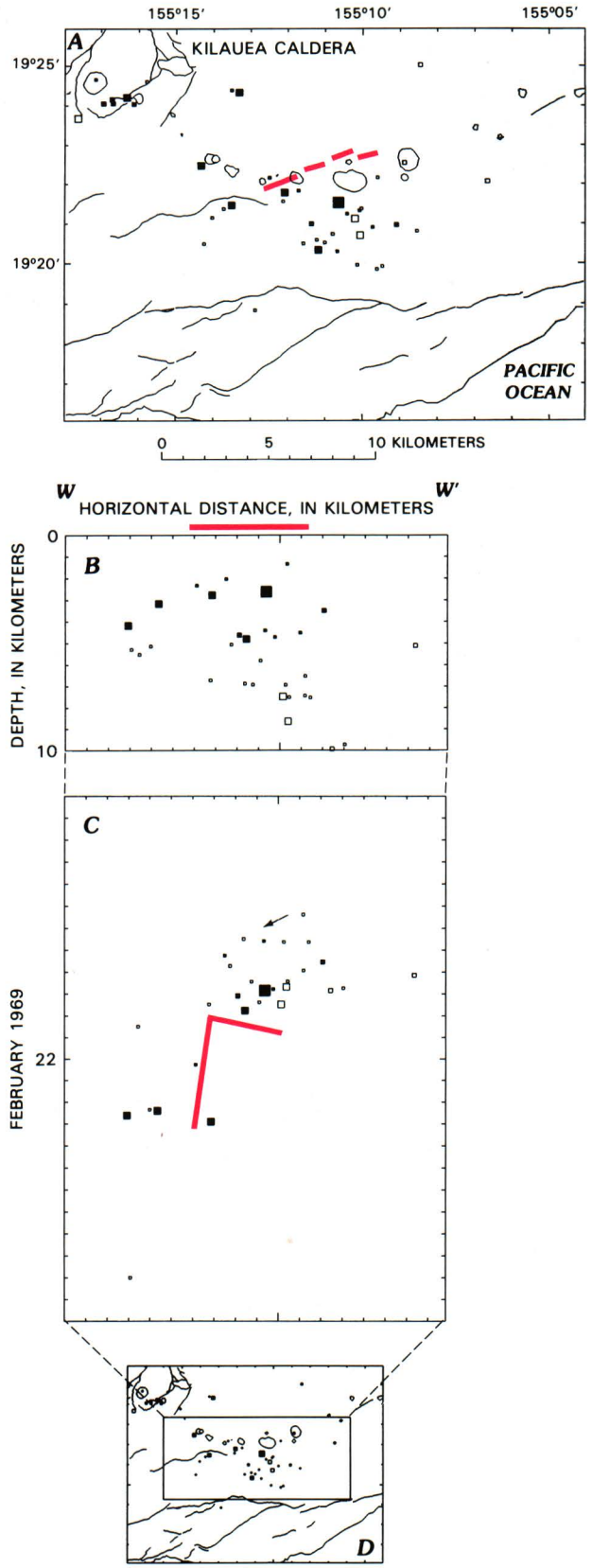

FIGURE 43.31.—Eruptive swarm beginning on February 22, 1969. See figure 43.20 caption for details and figure 43.30*B* for tilt and hourly earthquake rate. Red, approximate location (***A, B***) and onset time (***C***) of eruptive vents. Short arrow in ***C*** indicates possible migration.

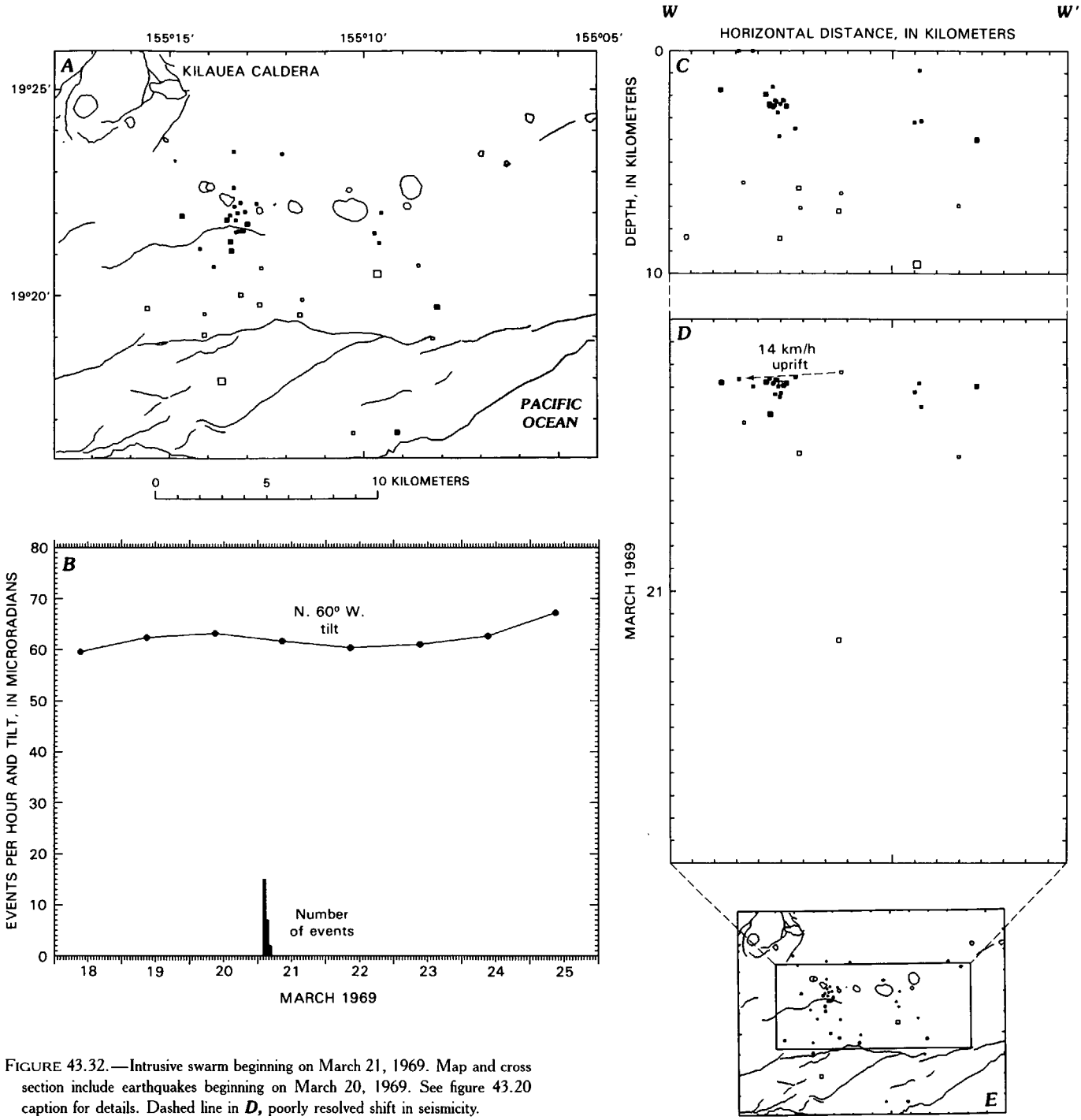

FIGURE 43.32.—Intrusive swarm beginning on March 21, 1969. Map and cross section include earthquakes beginning on March 20, 1969. See figure 43.20 caption for details. Dashed line in ***D***, poorly resolved shift in seismicity.

THE MAY 1969 MAUNA ULU ERUPTION AND INTRUSIONS THROUGH NOVEMBER 1969

Like the February 1969 eruption, the Mauna Ulu eruption commencing on May 24, 1969, was preceded by about three days of low-level seismicity. The pre-Mauna Ulu seismicity, however, appears to emanate from Kilauea's flank south of Makaopuhi and Napau (fig. 43.33*A*). This swarm was very unusual in that it was not in or near the summit caldera and thus not clearly related to inflation prior to the eruption. The shallow earthquakes were in the south flank near the areas active during the March and August 1965 and February 1969 swarms. This precursory swarm was possibly caused by some sort of south-flank instability that triggered the Mauna Ulu eruption. Because later volcanic swarms seen with an improved seismic network have all been located much closer to the ERZ, the May 20–23, 1969 swarm is probably mislocated too far south.

The swarm accompanying the onset of the Mauna Ulu eruption scatters within about 3 km of the eruptive vent (fig. 43.34*A*). These earthquakes are shallower than 4 km and locate very close to the surface in the vent area (fig. 43.34*B*). The intense seismicity began soon after 0300 H.s.t. on May 24 and rapidly migrated westward at an apparent speed of about 4 km/h (fig. 43.34C). This event was apparently a minor intrusion into the east end of the Koae fault zone about one hour before magma reached the surface. This intense seismicity ended about the time the eruption began. The vents opened nearly simultaneously in the eastern half of the fissure, but opened gradually westward (Swanson and others, 1979). This westward vent progression can be extrapolated to a later burst of earthquakes southwest of Mauna Ulu (fig. 43.34C). A dike or pulse of magma possibly moved westward at about 0.3 km/h into the Koae, extending the initial vent and causing earthquakes before it stopped. During the next several hours, scattered earthquakes occurred at depths between about 6 and 9 km to the southeast of Mauna Ulu (figs. 43.33*D*, 43.34). These events apparently were tectonic and were induced by rifting during the onset of the eruption. They also occurred directly beneath the zone of premonitory earthquakes (compare figs. 43.33*C* and 43.34*B*). The relations between pre-eruption and posteruption south-flank earthquakes and the eruption itself are unclear.

While Mauna Ulu continued with a series of its own eruptive episodes, a sequence of intrusions took place in July, October and November 1969. None coincided with Mauna Ulu eruptive episodes, and Kilauea apparently went about the business of generating intrusions between episodes of supplying Mauna Ulu with magma. The shunting of magma to Mauna Ulu during 1969–71 was the apparent cause of the increased frequency of intrusions relative to eruptions at Kilauea (Klein, 1982b). The ongoing Mauna Ulu eruption may have robbed the other intrusions of the magma supply and pressure they needed to erupt themselves.

The July 3, 1969 intrusion was near Hiiaka on the upper ERZ (fig. 43.35*A*). Earthquakes clearly define an east-west lineation about 7 km long that is oblique to the rift axis. The seismic trend is aligned with the local direction (N. 75° E.) of eruptive vents and fissures, and hence the axis of greatest compressive stress. In this unusual case the shallow stress orientation typical where vents form was also dominant at the 2- to 4-km earthquake depth. The swarm began at the intersection of the seismic lineation and the rift magma conduit. Earthquakes rapidly progressed bilaterally east and west at nearly the same speed of about 1.8 km/h, when projected along the lineation (fig. 43.35*D*). We interpret this event as the intrusion of a new dike whose direction is controlled by regional stress rather than the pre-existing ERZ magma conduit. Only a small volume of magma was intruded, because no detectable summit deflation was recognized (fig. 43.35*B*). The intruded magma had likely all been stored within the ERZ near Hiiaka. The observed earthquake migration speed is very typical of other intrusions that propagate along the axes of the rift zones. The processes of intrusion either parallel or oblique to the rift axis must therefore be fairly similar, although dikes off the rift axis may be thinner and not accommodate or store much magma.

Two other small intrusions also occurred between eruptive phases at Mauna Ulu in October and November 1969. The swarm that began on October 7 lasted for about 4 days and was accompanied by slow inflation then deflation (fig. 43.36*B*). All earthquakes were in the south flank 5 to 8 km southeast of Puu Kou (fig. 43.36*A*). This swarm is thus puzzling because there was no seismicity beneath the SWRZ. As discussed earlier, the October earthquakes were in a region frequently activated by large SWRZ intrusions. The October swarm may thus have resulted from a slow and aseismic SWRZ intrusion or some sort of rifting episode that stressed the south flank and triggered the swarm. The earthquakes are not a tectonic aftershock sequence: their time history is like a volcanic swarm with no mainshock. The swarm is similar to that of February 1981 (see below), which is more obviously a slow intrusion, owing to its location directly beneath the rift, to the larger deflation and to other associated SWRZ intrusions in 1981. We tentatively interpret the October 1969 swarm as resulting from a slow SWRZ intrusion or a related south flank adjustment.

The November 3, 1969 ERZ intrusion was small and lasted less than one hour (fig. 43.37). It was accompanied by a small summit deflation (fig. 43.37*B*) and is thus clearly an intrusion. It occurred beneath Mauna Ulu (fig. 43.37*A*), but did not coincide with a major eruptive episode there (see Swanson and others, 1979). The sparse earthquakes rapidly moved downrift at about 6 km/h (fig. 43.37*D*), though the speed is not well defined. This swarm appears to have accompanied the emplacement of a small dike below Mauna Ulu, rather than a new pulse of magma to Mauna Ulu itself. No significant earthquake swarms or new seismic intrusions accompanied any of the later Mauna Ulu eruptive episodes. The independence of Mauna Ulu eruptions and the many other intrusions emphasizes the fact that the upper ERZ is really a network of distinct magma conduits, different segments of which can be active simultaneously.

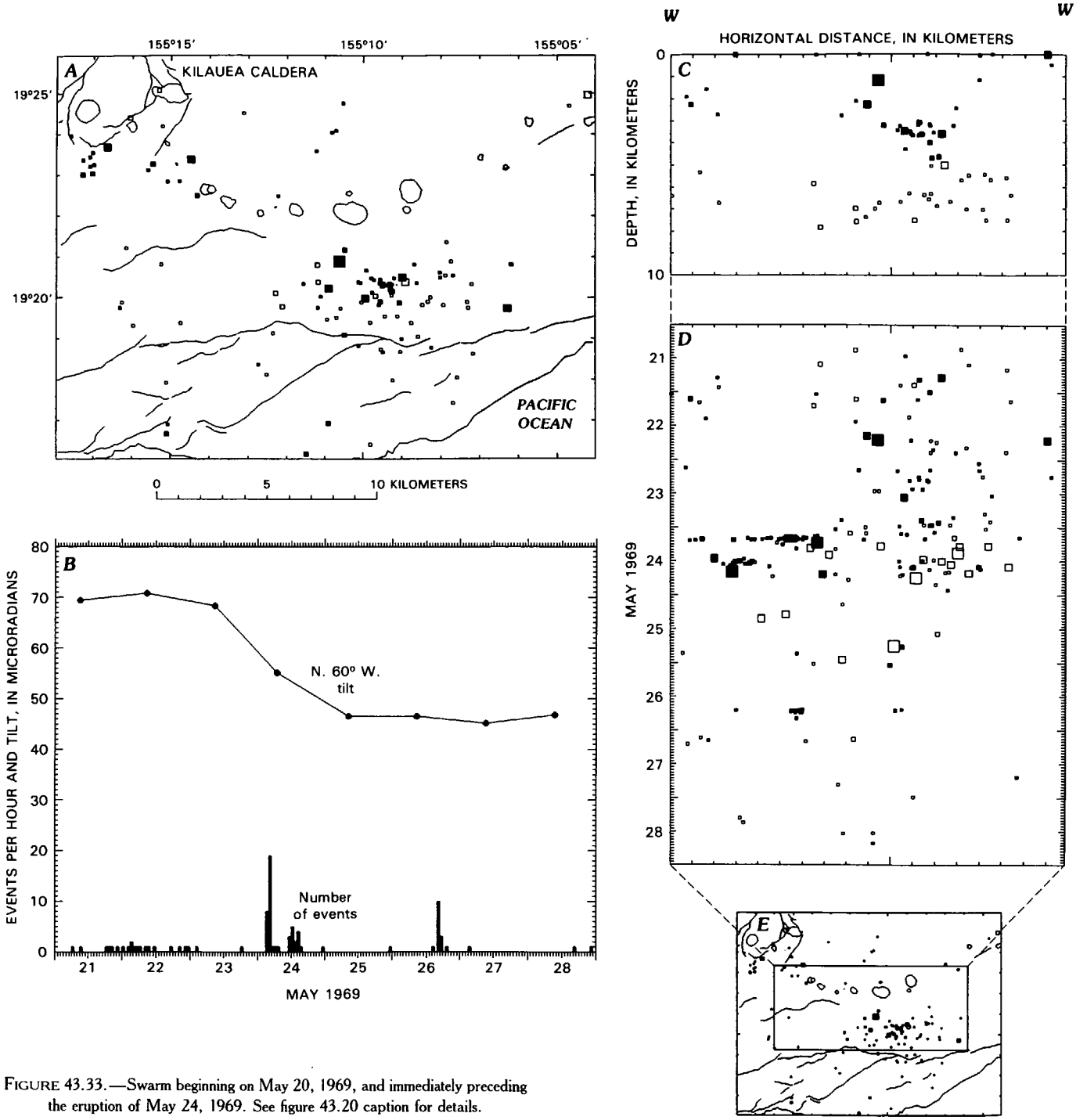

FIGURE 43.33.—Swarm beginning on May 20, 1969, and immediately preceding the eruption of May 24, 1969. See figure 43.20 caption for details.

FIGURE 43.34.—Eruptive swarm beginning on May 24, 1969. See figure 43.20 caption for details, and figure 43.33*B* for tilt and hourly earthquake rate. Red, approximate location (***A, B***) and onset time (***C***) of eruptive vents. Dashed line in ***C***, poorly resolved shift in seismicity.

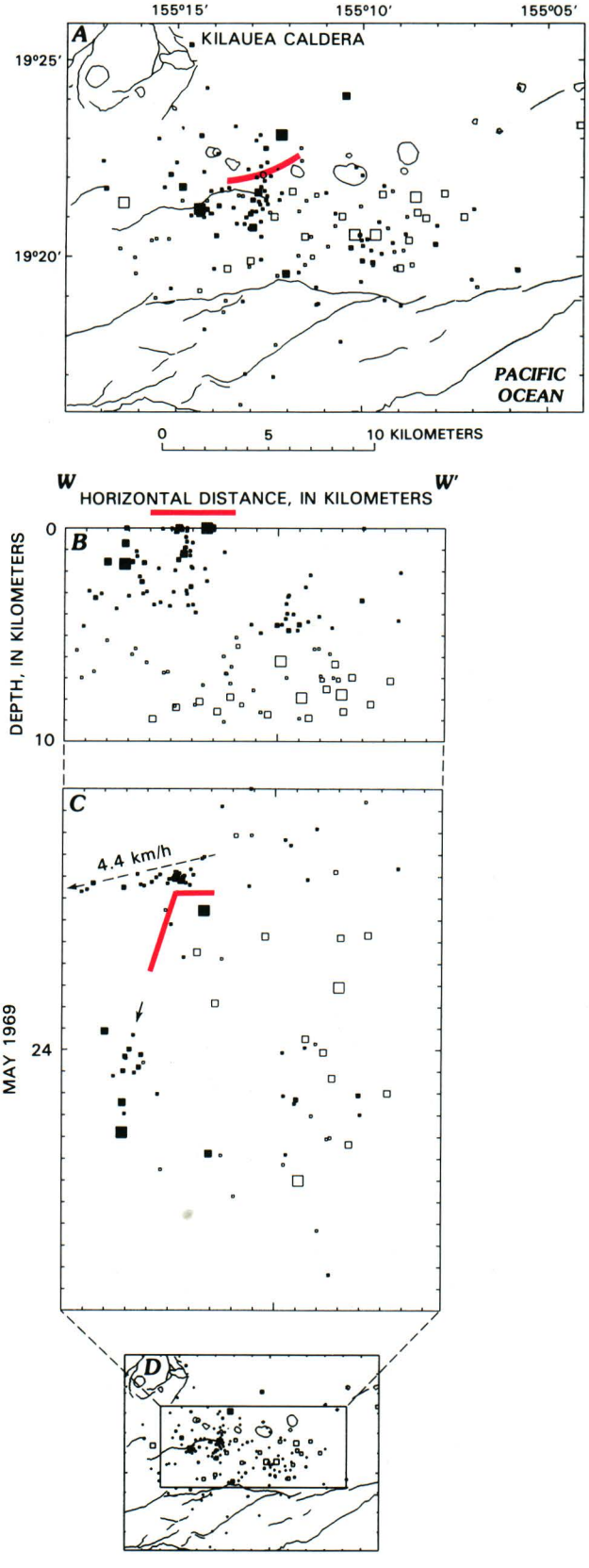

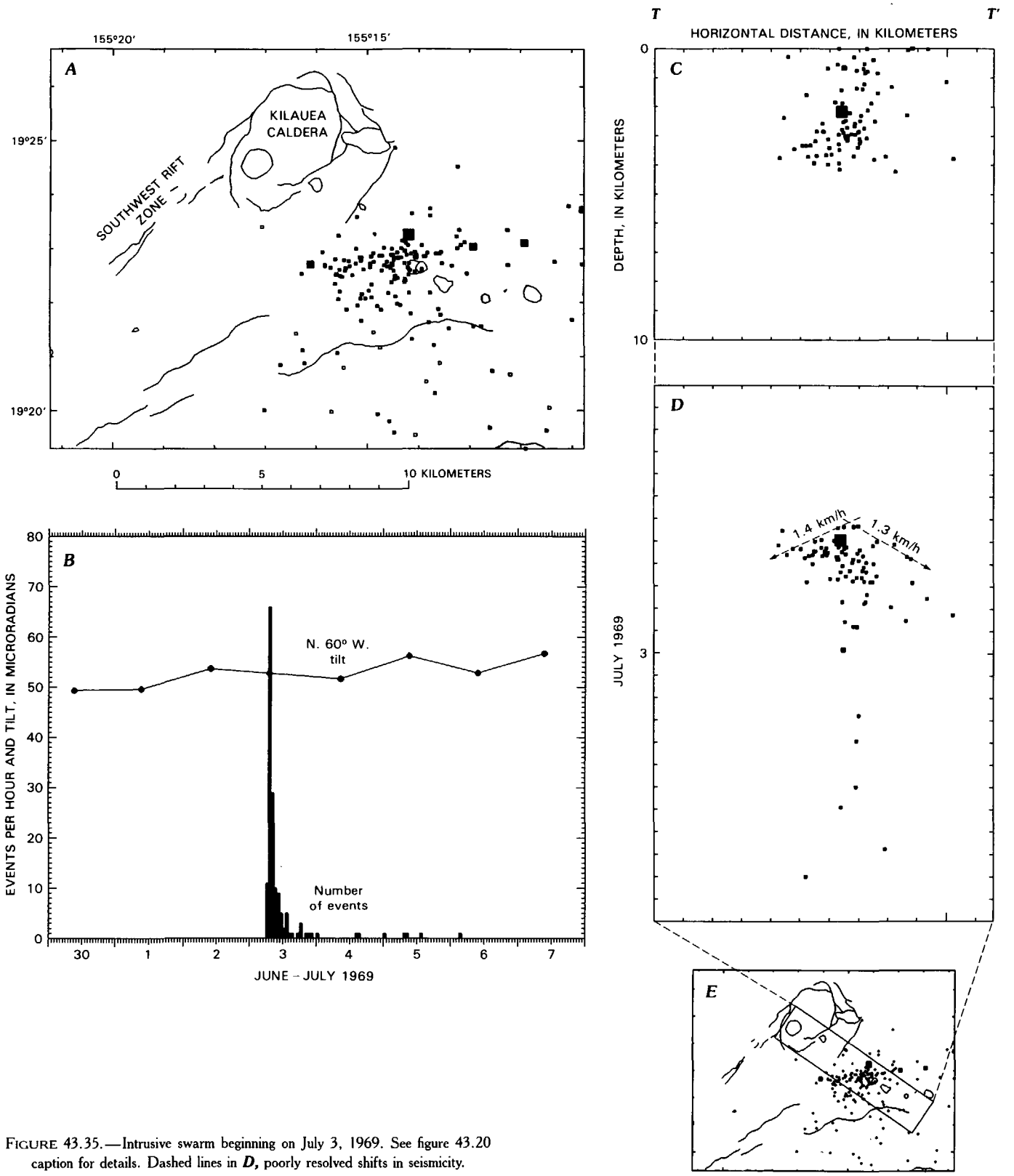

FIGURE 43.35.—Intrusive swarm beginning on July 3, 1969. See figure 43.20 caption for details. Dashed lines in ***D***, poorly resolved shifts in seismicity.

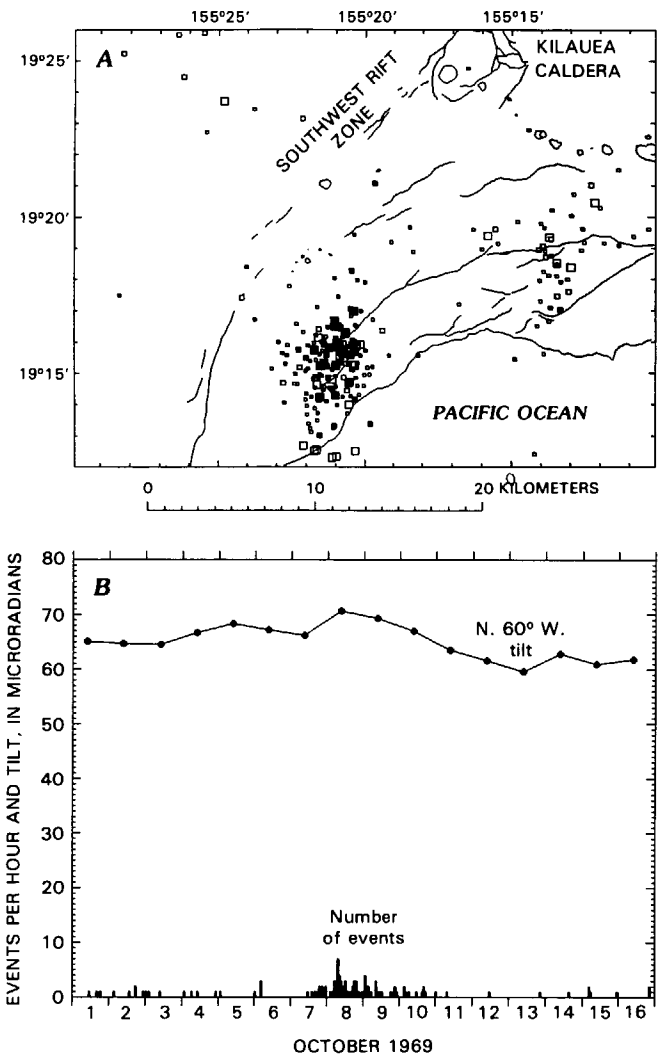

FIGURE 43.36.—Intrusive swarm beginning on October 7, 1969. Map and plot include earthquakes beginning on October 6, 1969. See figure 43.20 caption for details.

INFLATION-RELATED SWARMS AND INTRUSIONS, DECEMBER 1969 TO DECEMBER 1970

Uwekahuna tilt rose steadily during 1970 and most of 1971 as magma accumulated in the summit reservoir. Mauna Ulu's eruption was waning, so that more magma was available for summit storage. An additional consequence of the summit inflation during this period was a series of slow swarms within and adjacent to the caldera. The fluctuating tilt and seismicity were often well correlated, since both are consequences of inflation. The division of these inflation earthquakes into swarms is somewhat arbitrary, because summit seismicity fluctuated between a few and a few dozen locatable earthquakes per day for long periods. We have identified the most active intervals and called them slow swarms. The period from December 1969 through September 1971 contains 11 such slow swarms that last several days each, but only 4 rapid swarms accompanying intrusions or eruptions.

Many of the inflation-related swarms appear to also involve intrusion of magma into the rifts. As with the rapid swarms, earthquakes during inflation often penetrate into the uppermost sections of rift in addition to the caldera. As discussed earlier, the inflation earthquakes and hence the accumulating magma appear to stop at blockages within the rifts. Earthquakes sometimes migrate along the rift conduits. The migration speed of earthquakes and hence the rate of intrusion is generally much slower than during the intrusions that generate intense swarms. The summit tilt changes slowly during these slow intrusions and may either rise, fall or remain unchanged. The 1970–71 period of inflationary seismicity and slow intrusions occurred when tilt values were much higher than average. Inflation swarms generally begin and end gradually, unlike the sharp onset of most swarms accompanying eruptions and rapid intrusions. These contrasts leave the impression that magma leaks or spills over into the rifts during slow intrusions, but pours through a ruptured barrier during rapid intrusions.

Inflationary swarms began on December 22, 1969 (fig. 43.38), February 3, 1970 (fig. 43.40), March 17 (fig. 43.41), and April 2 (fig. 43.42). In each case, tilt and seismicity were correlatable. Each swarm was limited to 2 or 3 km of the ERZ and SWRZ just outside the caldera. The seismicity apparently reached barriers within the rift conduits that could not be overcome by the slow pace of intruding magma. The Mauna Ulu eruptive episode on December 30 and its rapid deflation abruptly ended all earthquakes (fig. 43.38*B*). The eruption phase itself was aseismic, as were all Mauna Ulu episodes except the first. After the initial swarm, the conduit to Mauna Ulu was mostly open, and no new dike growth or rupture of rock was required. Of these inflationary swarms, only the one on February 3 showed a clear migration of earthquakes. Earthquakes penetrated the SWRZ first (fig. 43.40*C*). The ERZ soon followed with a more rapid migration that soon slowed (fig. 43.40*D*). The final downrift speed was only about 0.02 km/h into both rifts. The slow earthquake migration demonstrated that an intrusion occured even while magma accumulated in the summit reservoir.

Rapid intrusions occurred on January 22 (fig. 43.39) and May 15, 1970 (fig. 43.43). The first was near Keanakakoi, only lasted for three hours, and produced no recognizable deflation (fig. 43.39*B*). Apparently the volume of magma was small, or it merely shifted position such that no tilt change at Uwekahuna resulted. The swarm moved rapidly toward the caldera (fig. 43.39*D*). The May swarm was clearly an ERZ intrusion accompanied by about 9 microradians of deflation (fig. 43.43*A*, *B*; Duffield and others, 1976). Pollard and others (1983) used a profile of surface displacements to constrain an elastic model of deformation surrounding a new dike. They inferred a dike dipping 86° NW., extending between 0.4 and 0.8 km depth, and 80 cm thick. The numerous earthquakes close to the surface (fig. 43.43*C*) emphasize the shallow nature of this event. The initial burst of earthquakes may have moved rapidly downrift from Puhimau at about 4.2 km/h (fig. 43.43*D*). Activity

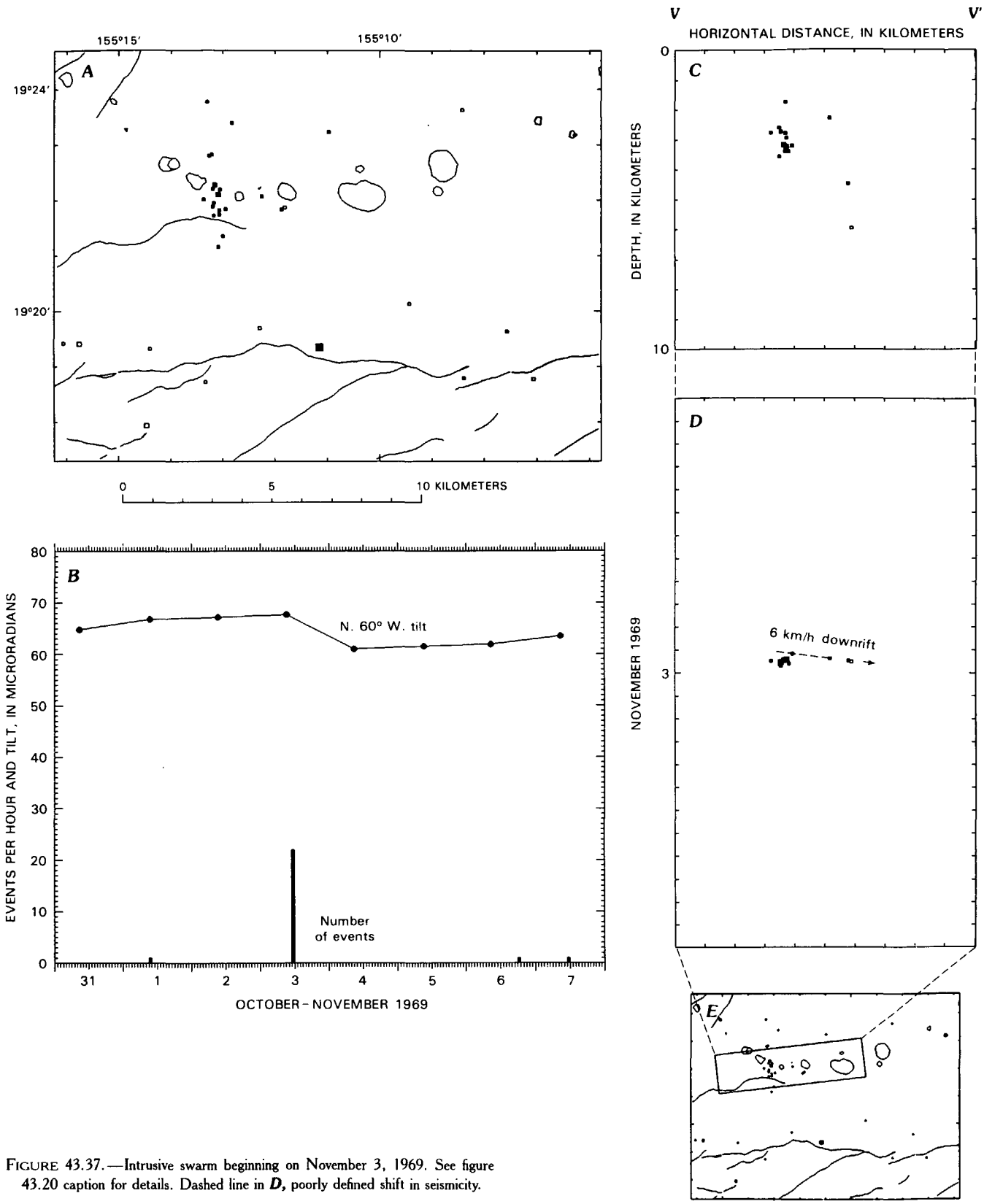

FIGURE 43.37.—Intrusive swarm beginning on November 3, 1969. See figure 43.20 caption for details. Dashed line in ***D***, poorly defined shift in seismicity.

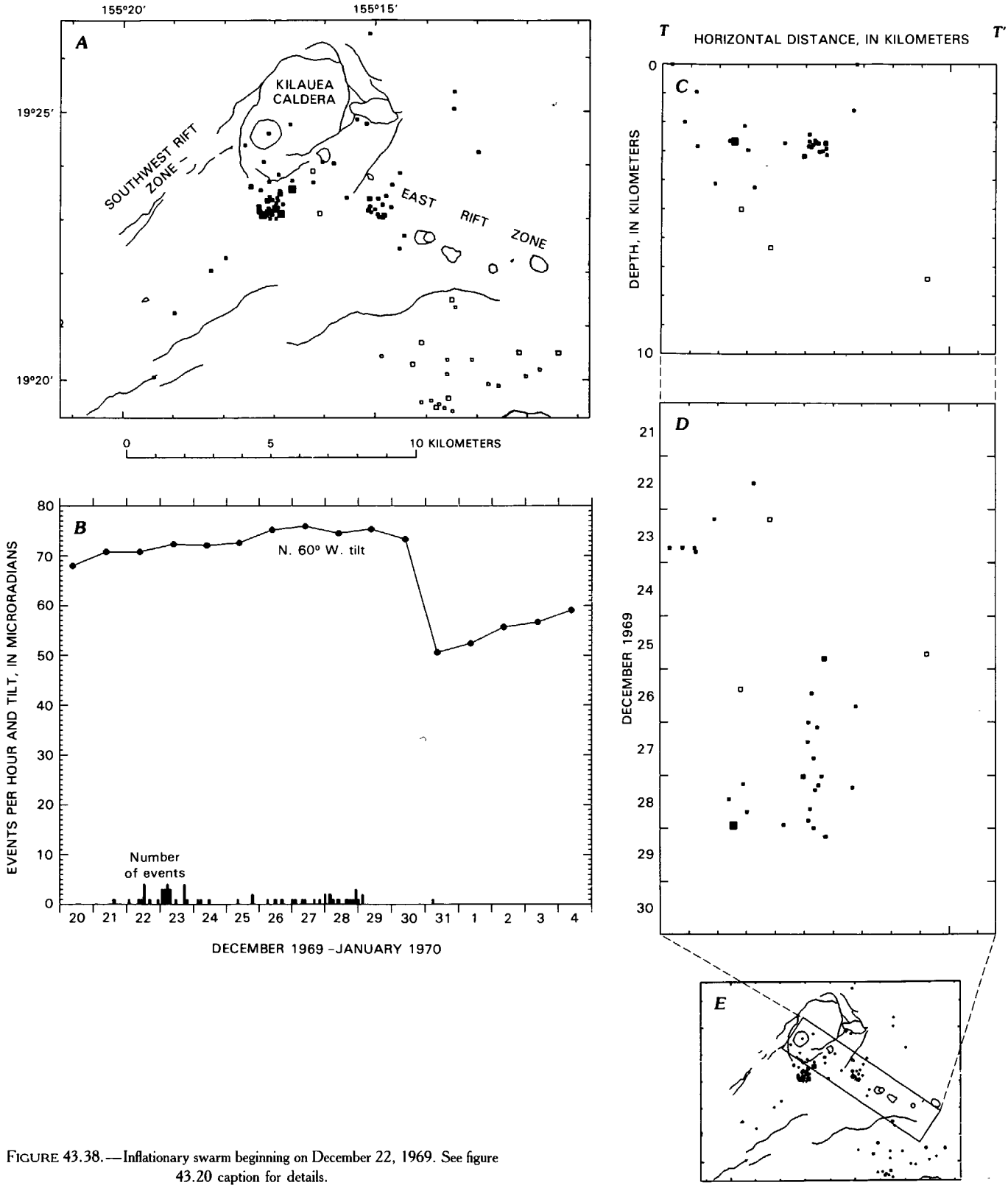

FIGURE 43.38.—Inflationary swarm beginning on December 22, 1969. See figure 43.20 caption for details.

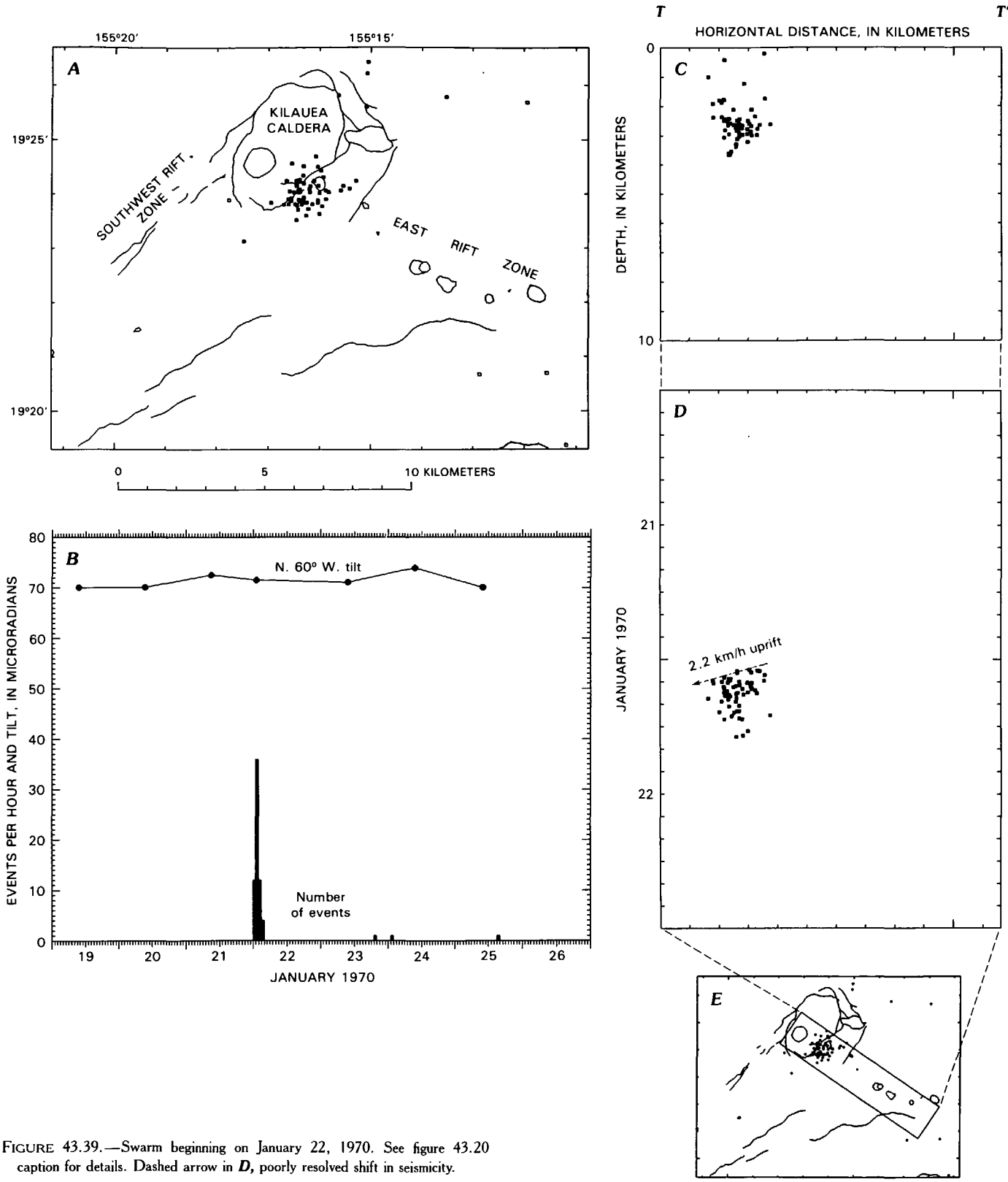

FIGURE 43.39.—Swarm beginning on January 22, 1970. See figure 43.20 caption for details. Dashed arrow in ***D***, poorly resolved shift in seismicity.

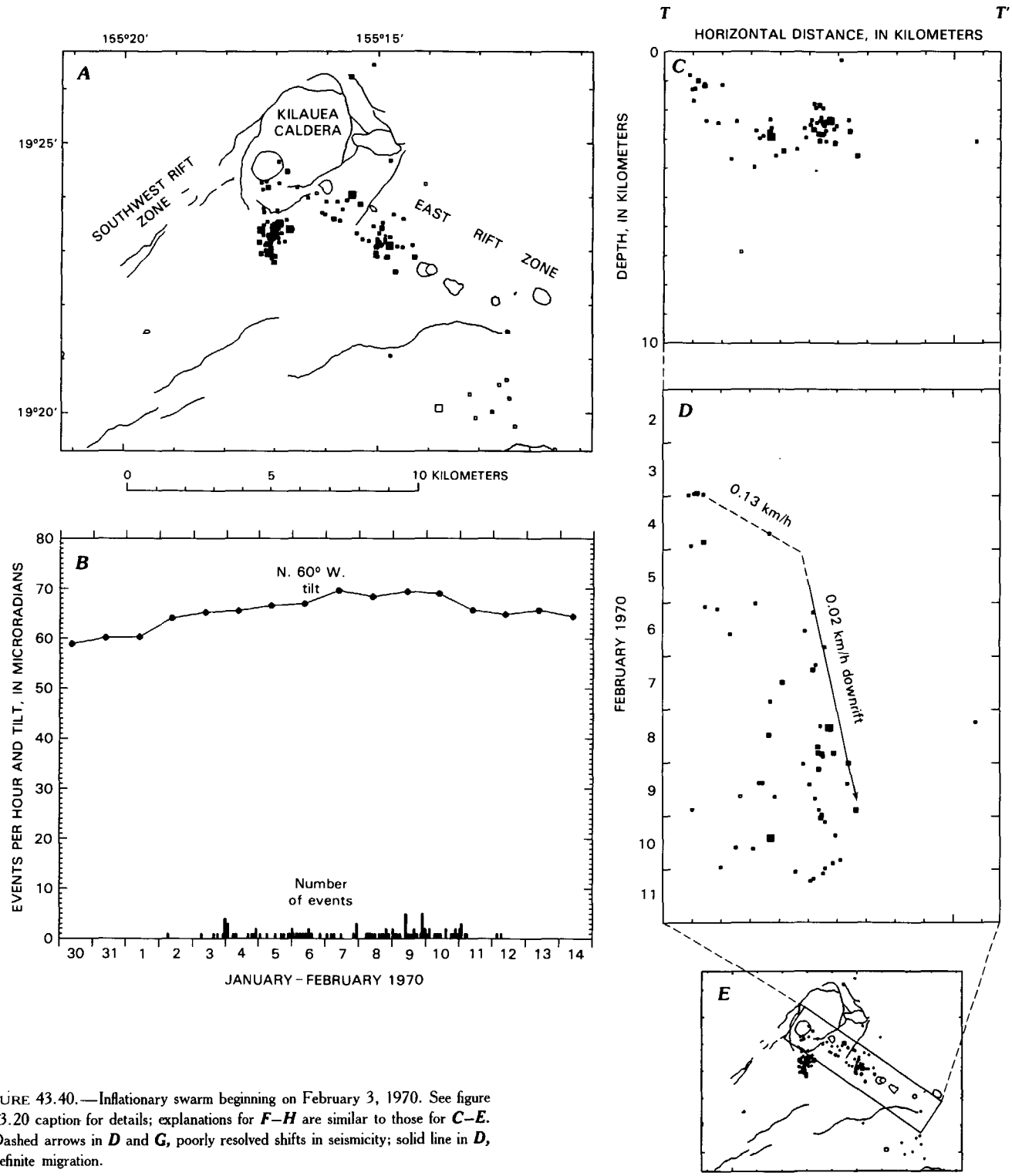

FIGURE 43.40.—Inflationary swarm beginning on February 3, 1970. See figure 43.20 caption for details; explanations for ***F–H*** are similar to those for ***C–E***. Dashed arrows in ***D*** and ***G***, poorly resolved shifts in seismicity; solid line in ***D***, definite migration.

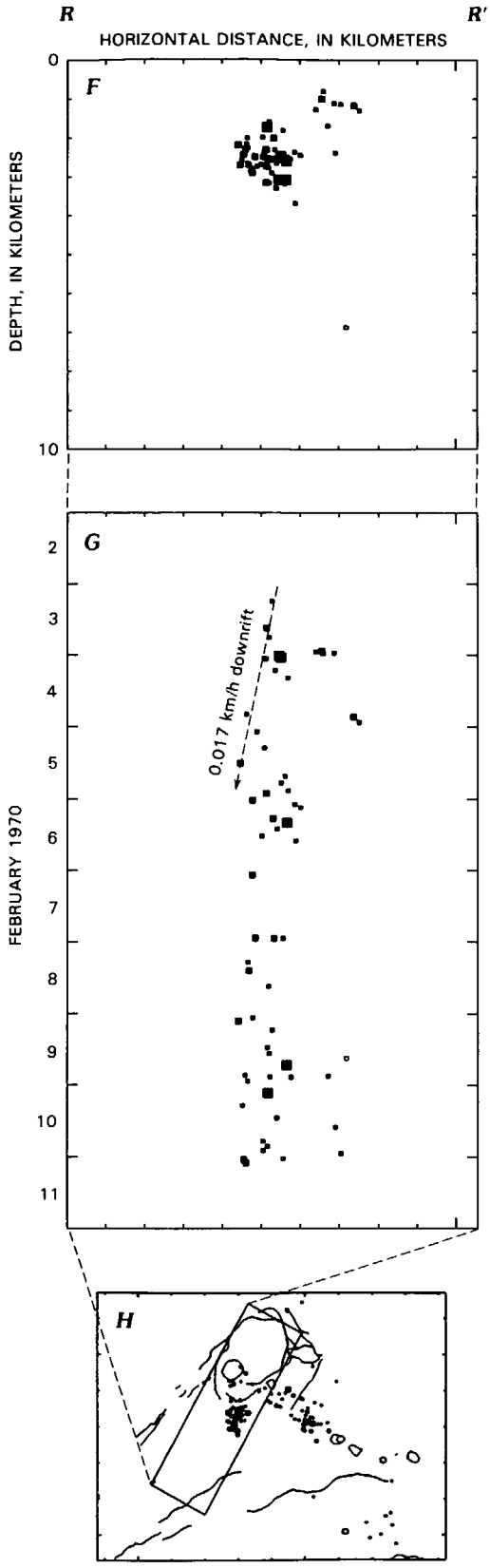

FIGURE 43.40.—Continued.

also moved uprift at about 0.13 km/h and culminated in the second burst about one day later. A few scattered earthquakes near the ERZ between Puu Kamoamoa and Heiheiahulu (fig. 43.43*F*) may have been coincidental.

The inflationary swarms during December 1970 were unlike their predecessors, in that earthquakes occurred throughout the caldera and in particular at its northeast end (figs. 43.44*A* and 43.45*A*). The first swarm began on December 12 as tilt slowly rose and fell synchronously with the earthquakes (fig. 43.44*B*). As tilt rose steadily, the second phase became noticeable on December 22 (fig. 43.45*B*), began in the southwest caldera, and spread rapidly northward into the entire caldera (fig. 43.45*D*). Also note the slow migration and intrusion into the SWRZ at the same 0.2 km/h speed as the February 1970 swarm. The path taken by the December 1970 earthquakes on the northern branch of the SWRZ (fig. 43.45*A*) anticipated the location of the September 24, 1971 eruption.

Another view of these swarms is given by figure 43.46, which superimposes summit tilt and position of earthquakes along the upper ERZ versus time. Figure 43.46*A* plots the entire November 1969 through February 1972 time interval. Figure 43.46*B–D* expands the time scale for this period. Moderate inflation and several swarms (3 intrusions and 4 inflationary swarms) with relative seismic quiet between them characterize the period of figure 43.46*B*. As noted above, the slow swarms are generally at the times of the most rapid inflation. The July 1970 to April 1971 period (fig. 43.46C) saw no net inflation and relatively low summit seismicity. A nearly continuous eruption at Mauna Ulu tapped most of Kilauea's magma supply during this period. By contrast, the next 10 months (fig. 43.46*D*) saw rapid inflation and considerable caldera and rift seismicity, including 2 eruptions, 2 rapid intrusions, 6 inflationary swarms and a high background of seismicity. This graph illustrates the close correlation between inflation and summit seismicity, and the difficulty of identifying discrete inflationary swarms during such active periods.

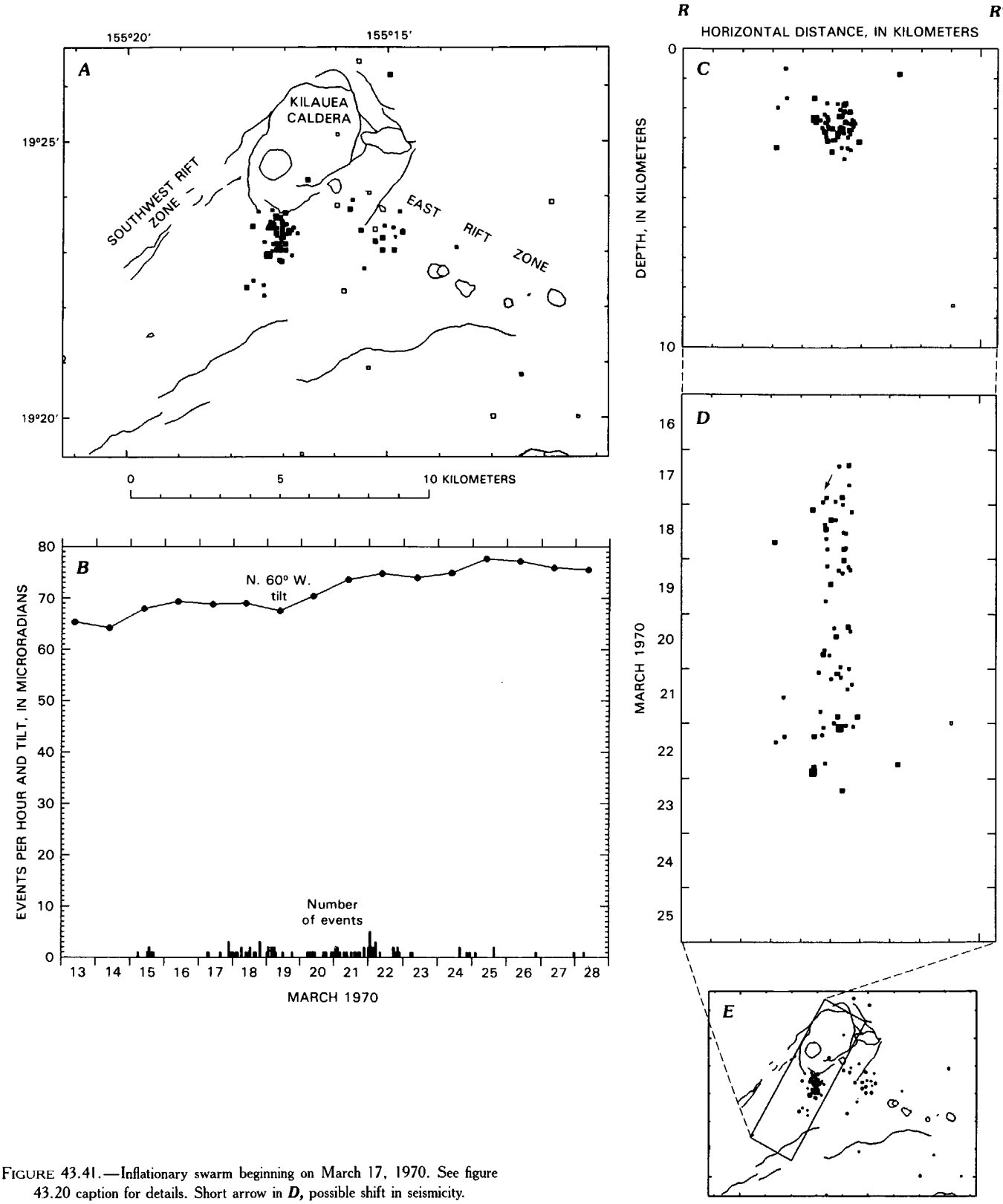

FIGURE 43.41.—Inflationary swarm beginning on March 17, 1970. See figure 43.20 caption for details. Short arrow in ***D***, possible shift in seismicity.

INFLATIONARY SWARMS AND ERUPTIONS, JUNE 1971 THROUGH JANUARY 1972

Rapid inflation and high seismicity returned in the June–September 1971 period (figs. 43.46*D*, 43.47). Earthquakes were primarily close to the caldera, but to a lesser extent within the rift zones. Eight individual swarms from this interval will be discussed below, but there was also a high background of activity.

The activity of early June 1971 continued at a relatively low but continuous level throughout the south caldera and was accompanied by slowly rising tilt (figs. 43.48, 43.49*B*). The June 1–10 seismicity was thus caused by steady inflation. On June 11 the seismicity intensified and concentrated into a small finger that extended south of the caldera (fig. 43.49*A*). Earthquakes migrated southward at a rate that slowed when seismicity crossed the caldera boundary (fig. 43.49*D*). Following the most intense seismicity, continuing but sparse activity began near Mauna Iki (fig. 43.47). The gradual deflation, slow migration, and later downrift seismicity indicate this was a slow intrusion.

Another episode of elevated summit seismicity commenced in July 1971. It was preceded by about one month of increasing activity in the caldera (figs. 43.46*D*, 43.47). The south caldera activity continued, but on July 19 the ERZ near Kokoolau came alive (fig. 43.50*A*). The swarm moved into the ERZ at about 0.17 km/h, but its rate of advance soon slowed considerably to only 8 m/h (0.2 km/d, fig. 43.50*D*). There was also a hint of migration into the SWRZ (fig. 43.50*G*). The HVO staff expected an eruption very soon because of the high tilt and summit seismicity, but with magma apparently leaking into both rift zones, there was no strong indication of where the eruption would be.

The tilt and rate of seismicity were very high prior to the eruption of August 14, 1971 (fig. 43.51*B*). Earthquakes continued in the south caldera and adjacent 3 km of both rifts (fig. 43.51*A*). The summit inflated as simultaneous slow intrusions penetrated into both rifts (fig. 43.51*D*, *G*). What appeared to be moving trends of earthquakes into the ERZ may have been caused by pulses of magma leaking into the rift. The eruption occurred in the southern part of the caldera on August 14 (Duffield and others, 1982). The lack of earthquakes in the hours following the onset of the eruption (fig. 43.51*D*, *G*) was a result of saturation of the seismic network by high tremor. Both tilt and seismicity dropped rapidly, however, indicating that some of the pressure built up during inflation had been relieved. The few earthquakes that could be timed and located after the eruption began were very close to the eruptive vent in the southern part of the caldera (fig. 43.52).

Another prominent episode of inflation and summit seismicity preceded the SWRZ eruption of September 24, 1971. We divided it into two periods beginning on September 6 (fig. 43.53) and on September 17 (fig. 43.54). The distribution of epicenters matched that of the previous inflationary swarms. Thus the August eruption in the caldera did not change the pattern of magma accumulation. Premonitory seismicity did not seem to favor either rift zone for the impending eruption, although there was a suggestion of earthquake migration into the SWRZ (fig. 43.54*G*).

The earthquakes accompanying the September 24 SWRZ eruption did not follow a continuous linear trend below the eruptive fissure (fig. 43.55*A*). Instead, four main clusters of earthquakes occurred along the rift. The first three roughly coincided with the three main zones of eruptive vents, and the fourth was in the south flank adjacent to the intrusion terminus near Puu Kou. We interpret each cluster as a blockage of the rift conduit, which magma forcefully broke through to continue downrift. Earthquakes were triggered as the dike penetrated and wedged apart each barrier. Earthquake clusters and vents would then coincide because the blockages that produced seismicity also diverted the dike upward before the barrier rifted open. Note also that one barrier is directly beneath Mauna Iki (fig. 43.55*A*), which may have been responsible for its formation in 1919–20. This barrier is probably a major one, as it appears to be responsible for much of the seismicity induced adjacent to it on both sides of the rift, including as much as 12 km into the Kaoiki seismic zone (fig. 43.55*A*).

The earthquakes clearly do not form a linear trend that coincides with the main seismic conduit active during 1970–83 (fig. 43.3*C*, *D*). The September 1971 eruption chose a more northwesterly path. Note also that the eruption earthquakes in the south caldera are displaced west of the inflationary swarms prior to the eruption. Thus, two main SWRZ conduits were active during recent decades: the northerly one which was seismically active during the December 1970 inflationary swarm, the September 1971 eruption, and perhaps the November 1967 eruption; and the southerly one, active during the intrusions of December 1974 and August 1981, as well as most periods of inflation. Using deformation data, Duffield and others (1982) concluded that the September 1971 eruption was fed by shallow parts of the summit reservoir, and the observed range of earthquake depths is consistent with this interpenetration (fig. 43.55*B*). The main rift zone conduits, however, tap the summit reservoir at about 3 km depth.

The September 1971 eruptive vents and earthquakes both progressed downrift (fig. 43.55*C*), indicating that both were caused by the same propagating dike. The times of first eruption from the various vent segments and approximate rates of opening of individual fissures from Duffield and others (1982) are plotted with earthquakes in figure 43.55*C*. The apparent downrift movement of vents is about 0.31 km/h. This speed is a little slower than the initial earthquake migration speed of about 0.53 km/h, but a second wave of earthquakes accompanies the progression of migrating vents. Another way to view the slower speed of the vents relative to the initial earthquake wave is that the time delay between passage of earthquakes and the start of eruption at a given place increased with distance down the rift. The delay ranged from 4 hours in the caldera to about 18 hours at the most distant vent. If the first earthquakes at a given spot mark the initial penetration of magma within the main conduit, the time delay of the eruption occurs while magma moves upward from the conduit to the surface. The increase of these delay times may then be a result of the plunge of the conduit to greater depths away from the caldera and the greater upward distance magma had to travel. The pattern of delay times could also be a

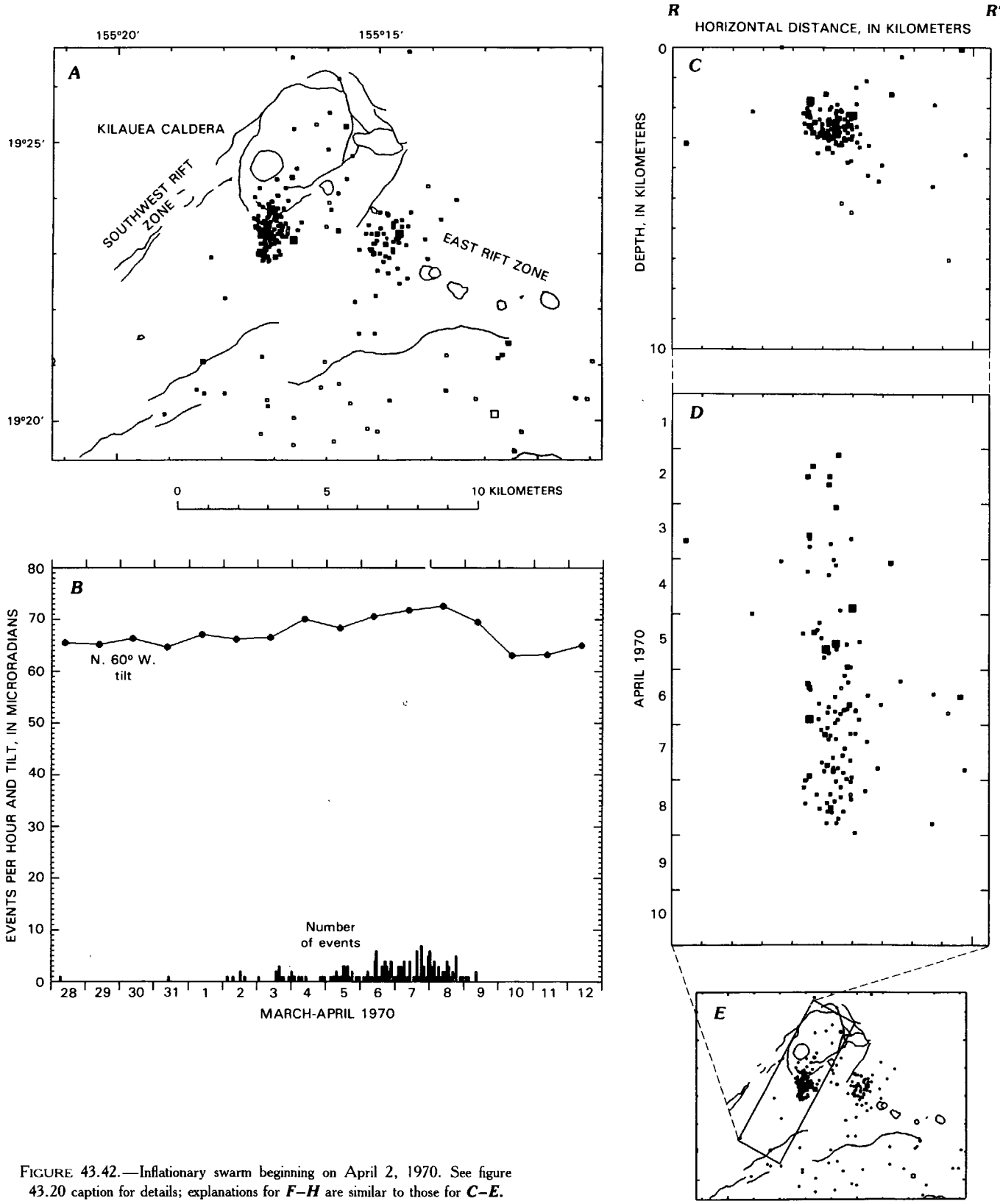

FIGURE 43.42.—Inflationary swarm beginning on April 2, 1970. See figure 43.20 caption for details; explanations for ***F–H*** are similar to those for ***C–E***.

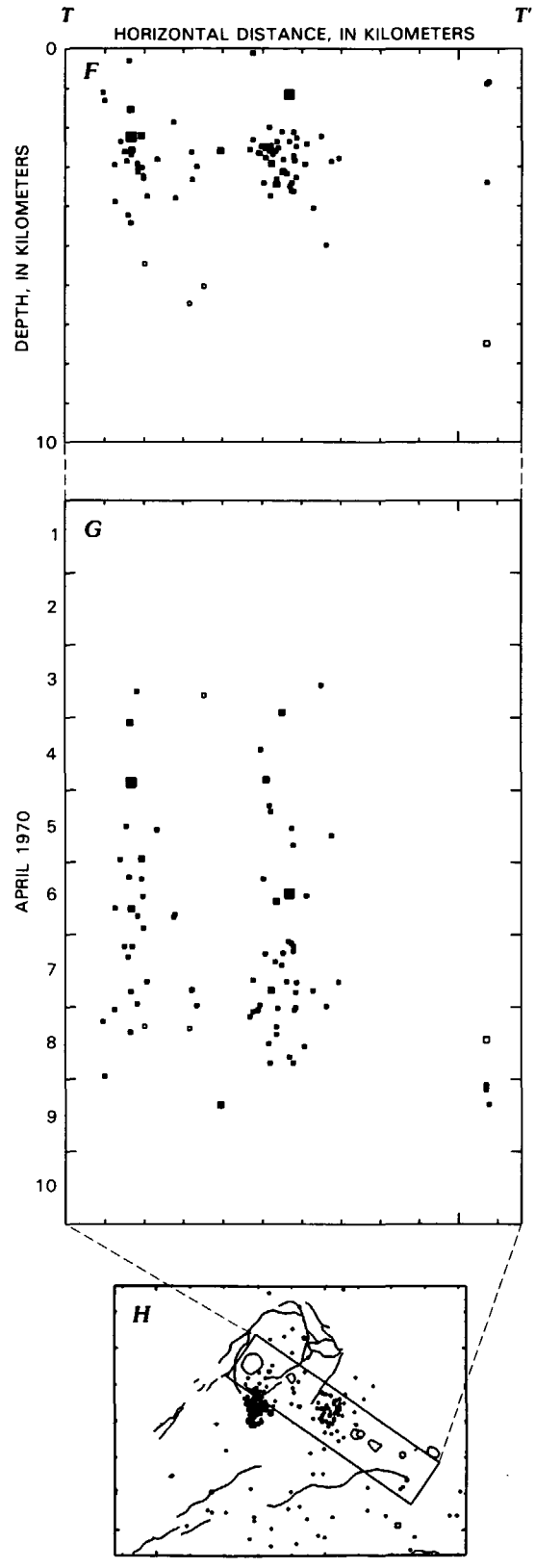

FIGURE 43.42.—Continued.

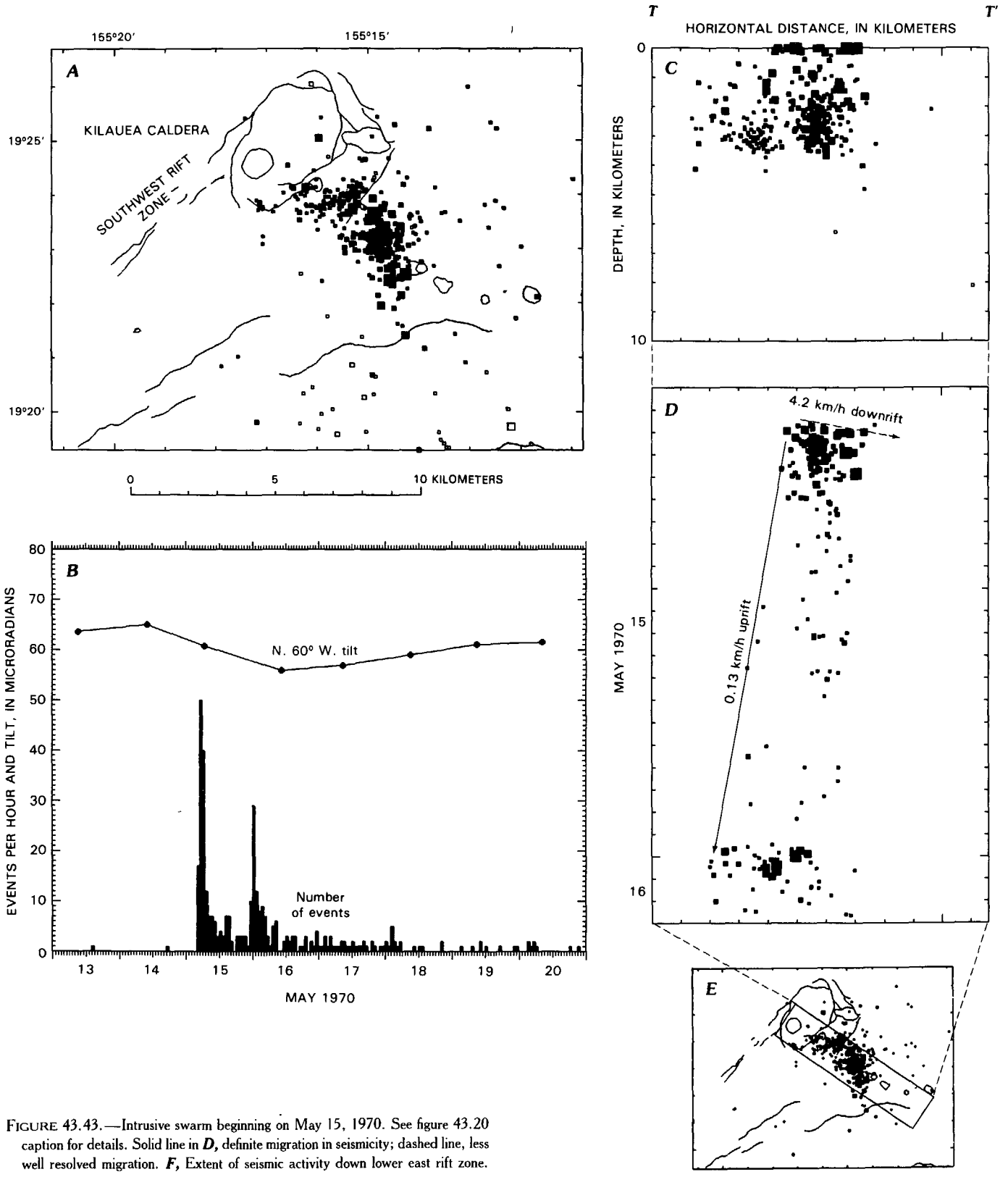

FIGURE 43.43.—Intrusive swarm beginning on May 15, 1970. See figure 43.20 caption for details. Solid line in ***D***, definite migration in seismicity; dashed line, less well resolved migration. ***F***, Extent of seismic activity down lower east rift zone.

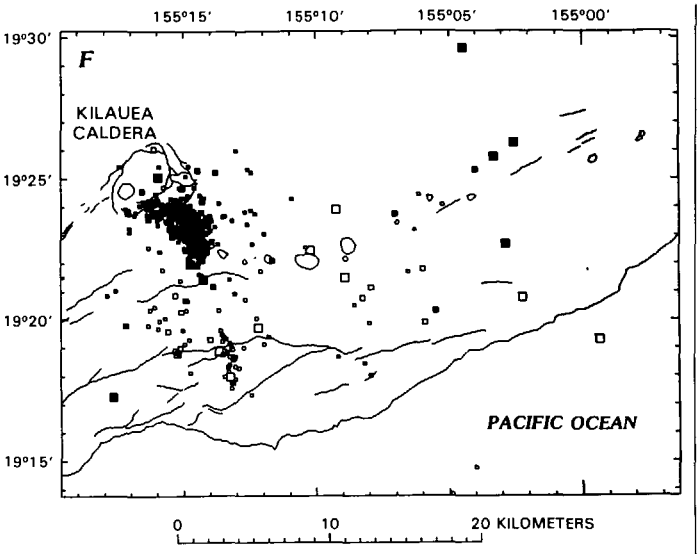

FIGURE 43.43.—Continued.

result of reduced magma pressure and slower upward speed farther down the rift, or a combination of both factors.

The September 1971 eruption is a good example of equating earthquake migration with magma movement and dike propagation. Irregularities in speed do occur, but the leading edge can move at a constant average speed for long segments of the rift. A few scattered earthquakes occur before the magma front passes their location (such as events above the solid line in fig. 43.55C). These events are apparently triggered by small stress increases that move ahead of the growing dike at the much faster speed of elastic waves.

Seismicity declined dramatically following the September eruption (figs. 43.46*D*, 43.47). The rift widened by perhaps 1–2 m (Duffield and others, 1982), so a significant volume of magma was intruded from the summit reservoir in addition to that erupted. Tilt and survey line changes around the caldera were dominated by the effects of the dike. Subsidence of the magma reservoir was difficult to document geodetically, although part of the floor of Halemaumau did fall 45 m (Duffield and others, 1982). The drop in seismicity indicates that a drop in magma pressure took place, however, similar to that during caldera subsidence of other eruptions. Kilauea reinflated rapidly after the eruption, and earthquakes increased and gradually penetrated farther into the ERZ (fig. 43.46*D*).

Another SWRZ swarm three months after the September eruption was probably related to it. The swarm began on December 23, 1971, and lasted about 7 days (fig. 43.56B). Most activity was in the south flank adjacent to the terminus of the September intrusion (fig. 43.56*E*). The flank probably received an increment of stress from the recently intruded SWRZ. Some earthquakes did occur uprift (fig. 43.56*A*, *F*) and they preceded the main part of the swarm in a way suggestive of downrift migration (fig. 43.56*H*). Little or no change occurred in summit tilt, however, so apparently magma (or stress) was redistributed within the rift complex without much new magma from the summit. As noted above, considerable newly intruded magma was available within the SWRZ conduit. Seismicity in the ERZ was concurrent with the central SWRZ earthquakes and generally progressed uprift (fig. 43.56*A*, *D*). The seismicity pattern and lack of a tilt change thus do not suggest a replay of the September event, but rather a readjustment of the two rifts and perhaps the south flank.

Kilauea refocused her attention to the ERZ with an inflation-related swarm there in January 1972. As with similar swarms of the previous two years, seismicity and magma only accumulated above the rift blockage near Pauahi (fig. 43.57*A*). The swarm was accompanied by rising tilt (fig. 43.57*B*). The first swarm episode saw events slowly penetrate the rift (fig. 43.57*D* but two periods of uprift migration appeared to characterize the second episode (fig. 43.57*F*). The possible causes of uprift earthquake migration will be discussed in more detail later, but the phenomenon is probably related to the complex system of multiple conduits in the ERZ above Mauna Ulu and their close magmatic communication with the summit reservoir. If the entire uprift part of the ERZ slowly receives and stores magma from the summit supply, then a propagating episode of rifting and accompanying seismicity could go in either direction, because the magma to drive it is present along the whole rift segment. The January swarm was followed by a major eruptive phase at Mauna Ulu on February 4, 1972 (Tilling and others, chapter 16). The eruption was marked by only minor earthquake activity in the Pauahai to Mauna Ulu area and by a halt to the slow inflation (fig. 43.58). The few earthquakes occurred both before and after the eruption, whose onset time was only approximately known due to lack of direct observations (fig. 43.58*D*).

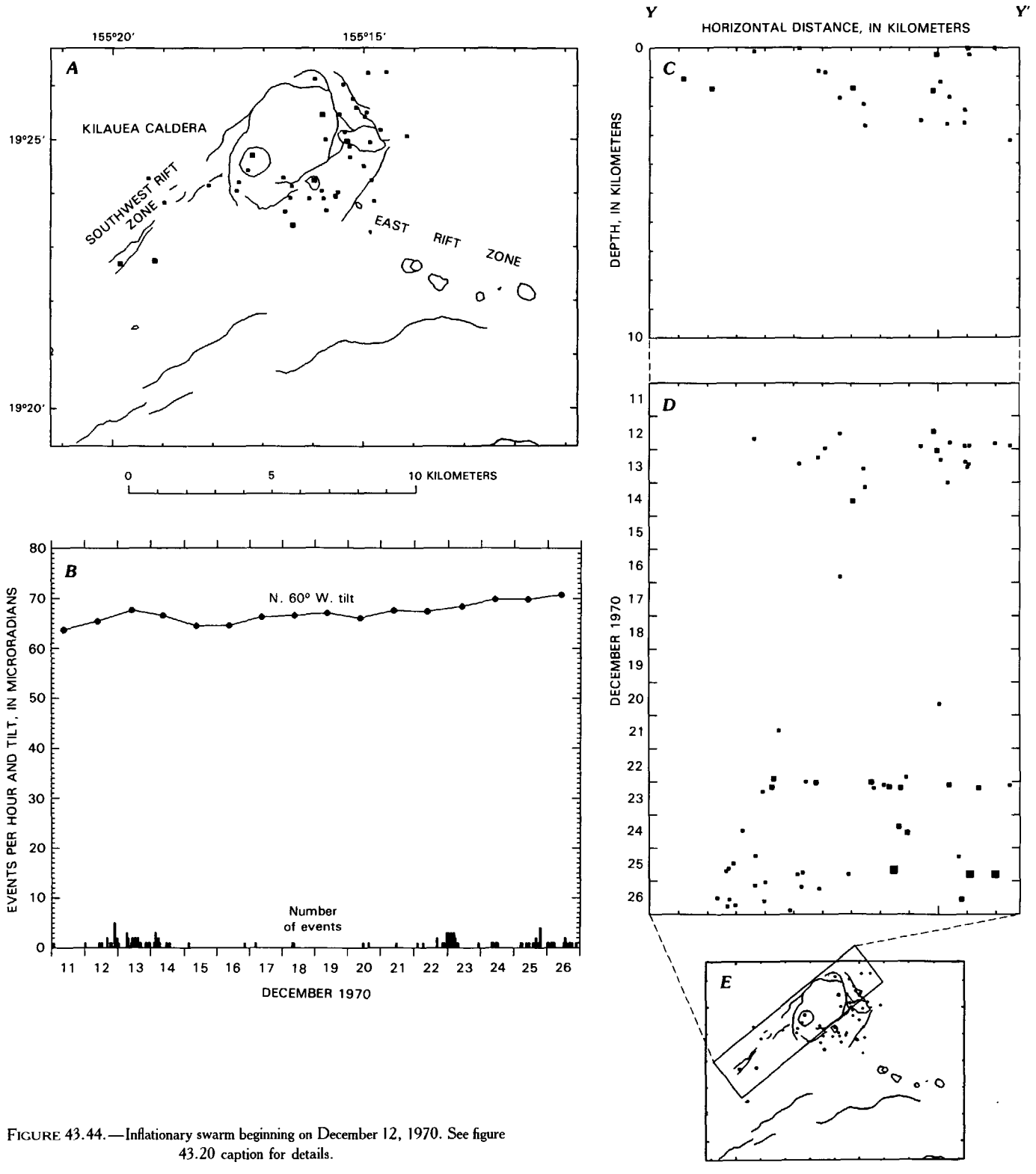

FIGURE 43.44.—Inflationary swarm beginning on December 12, 1970. See figure 43.20 caption for details.

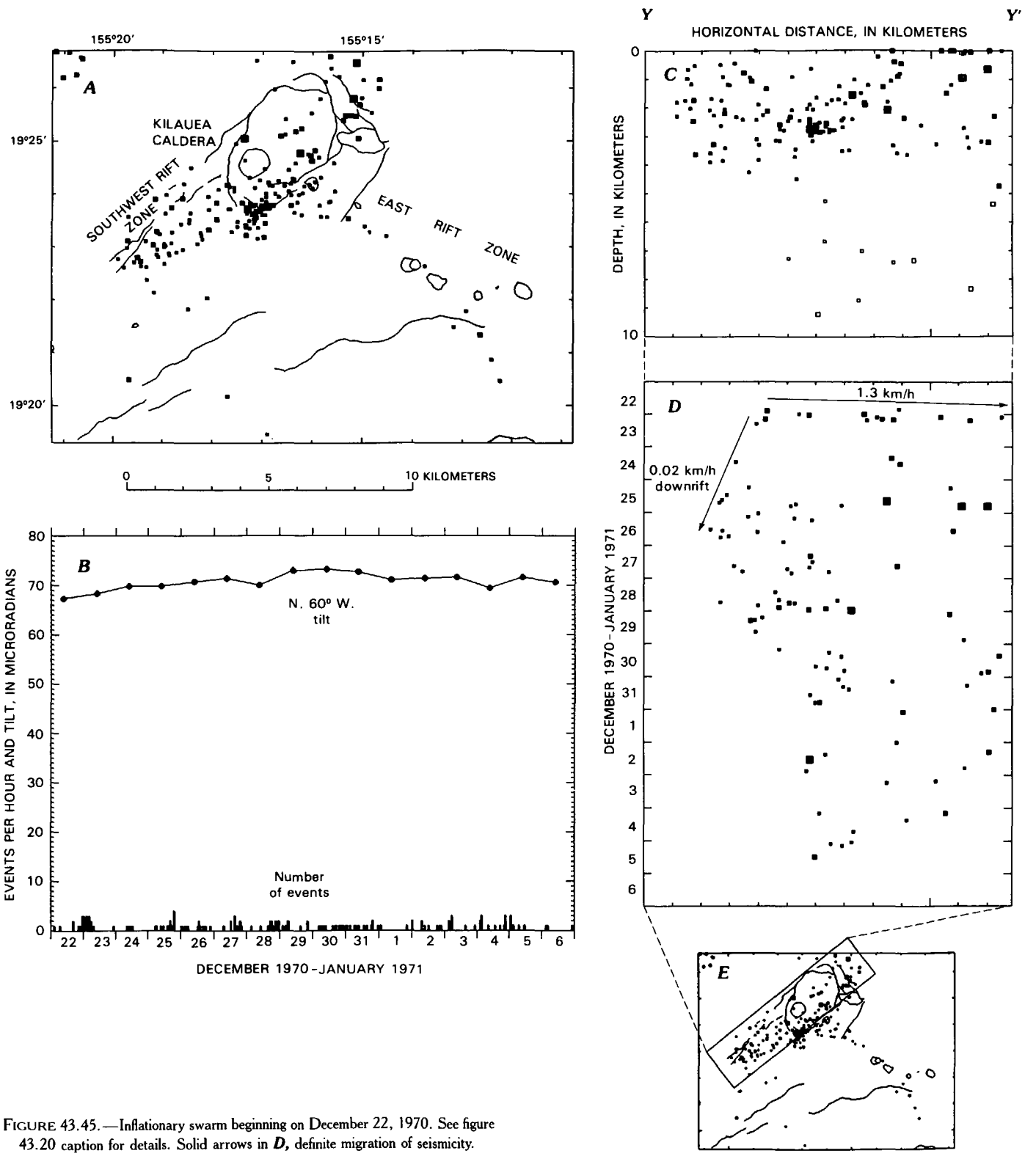

FIGURE 43.45.—Inflationary swarm beginning on December 22, 1970. See figure 43.20 caption for details. Solid arrows in ***D***, definite migration of seismicity.

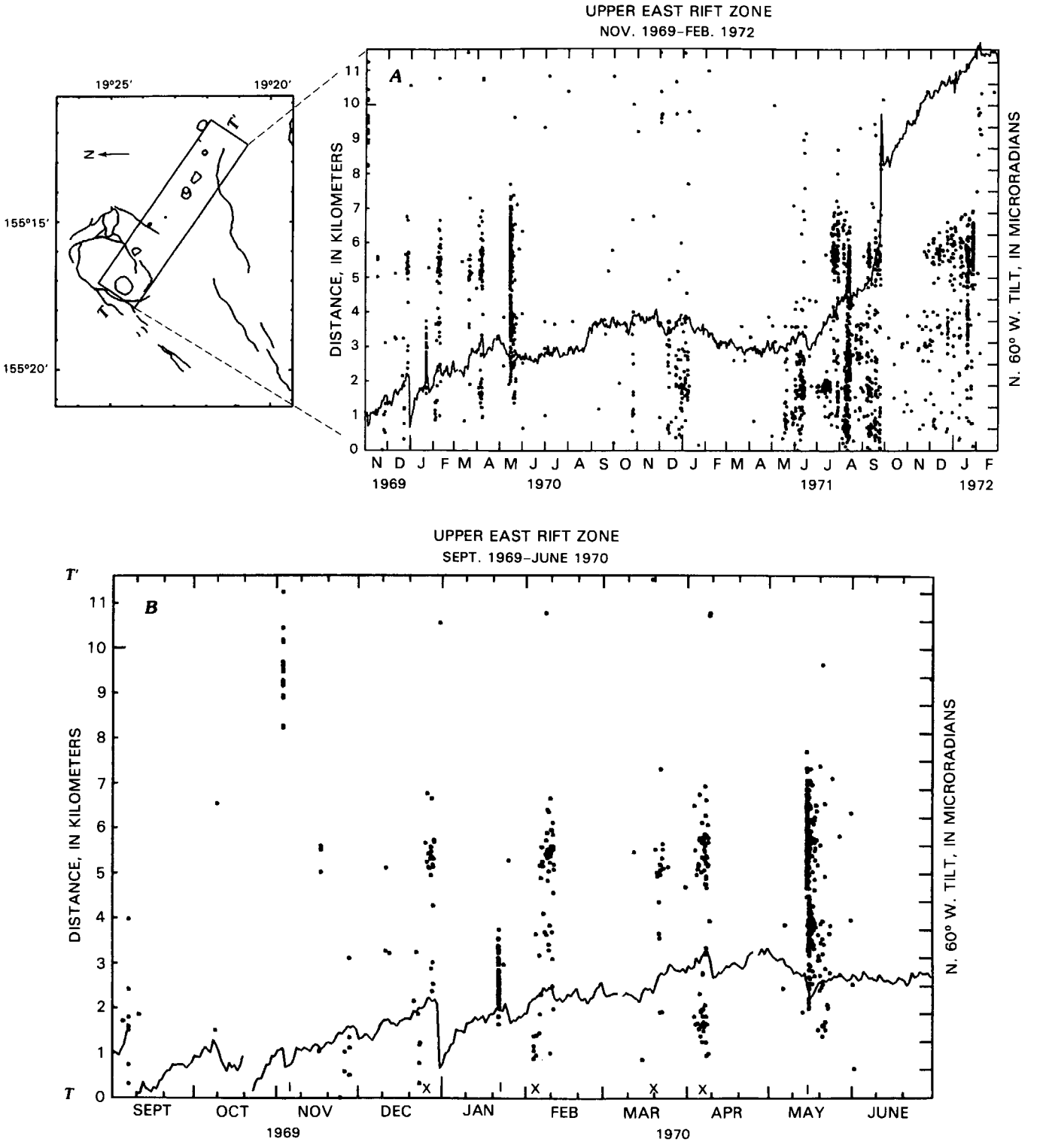

FIGURE 43.46.—Plot of earthquakes along upper east rift zone and N. 60° W. water-tube tilt at Uwekahuna versus time. Tilt axes marked in 10-μrad divisions. All earthquakes shallower than 5 km and within geographic box shown are plotted. Endpoints for T–T' are given in table 43.2. ***A***, Plot for entire 28-month period. ***B–D***, Same plot as in *A*, but on an expanded time scale. Halemaumau is near endpoint T and Alae crater is near T'. Notations along time axis refer to specific swarms detailed in other figures: E, eruption; I, intrusion; X, swarm accompanying inflation.

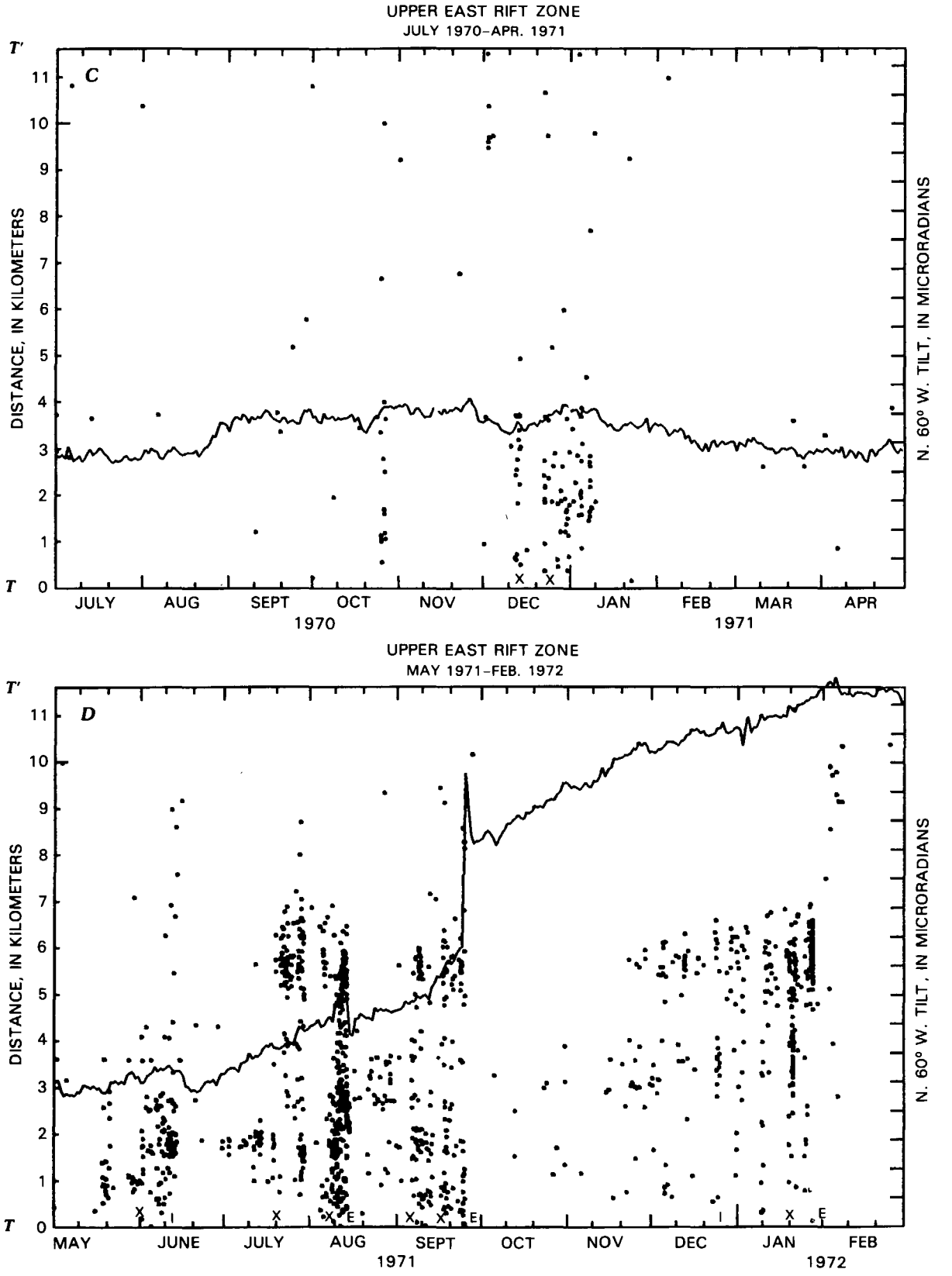

FIGURE 43.46.—Continued.

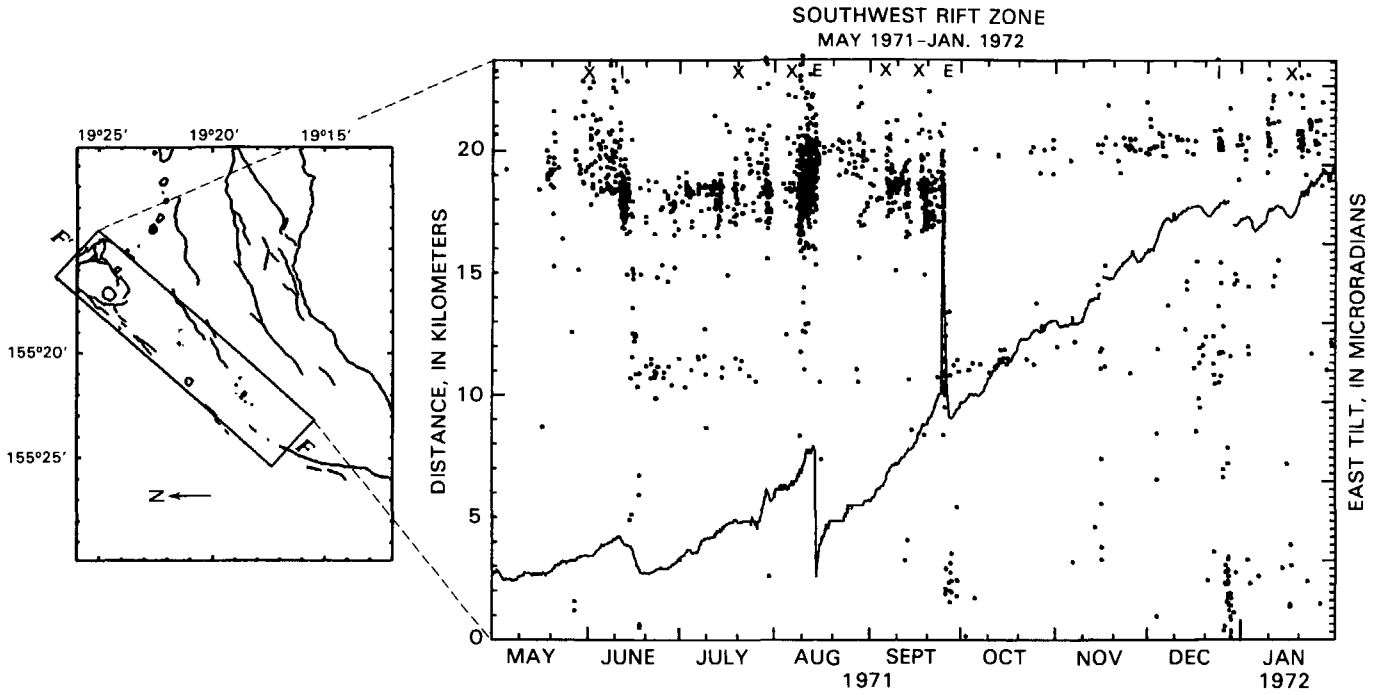

FIGURE 43.47.—Plot of earthquakes along the southwest rift zone and east tilt at Uwekahuna versus time. Endpoints for distance axis F–F' are given in table 43.2. Tilt is from east-west Ideal Aerosmith tiltmeter, where east-down tilt is down on plot and generally indicates deflation of summit caldera. Large divisions on tilt scale are 10 μrad. Notations along time axis refer to specific swarms detailed in other figures: E, eruption; I, intrusion; X, swarm accompanying inflation.

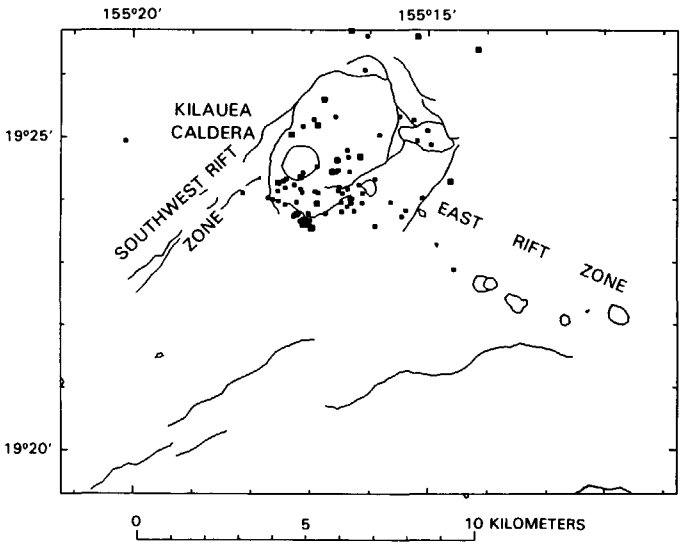

FIGURE 43.48.—Inflationary swarm beginning on June 6, 1971. See figure 43.20 caption for details and figure 43.49*B* for tilt and hourly earthquake rate.

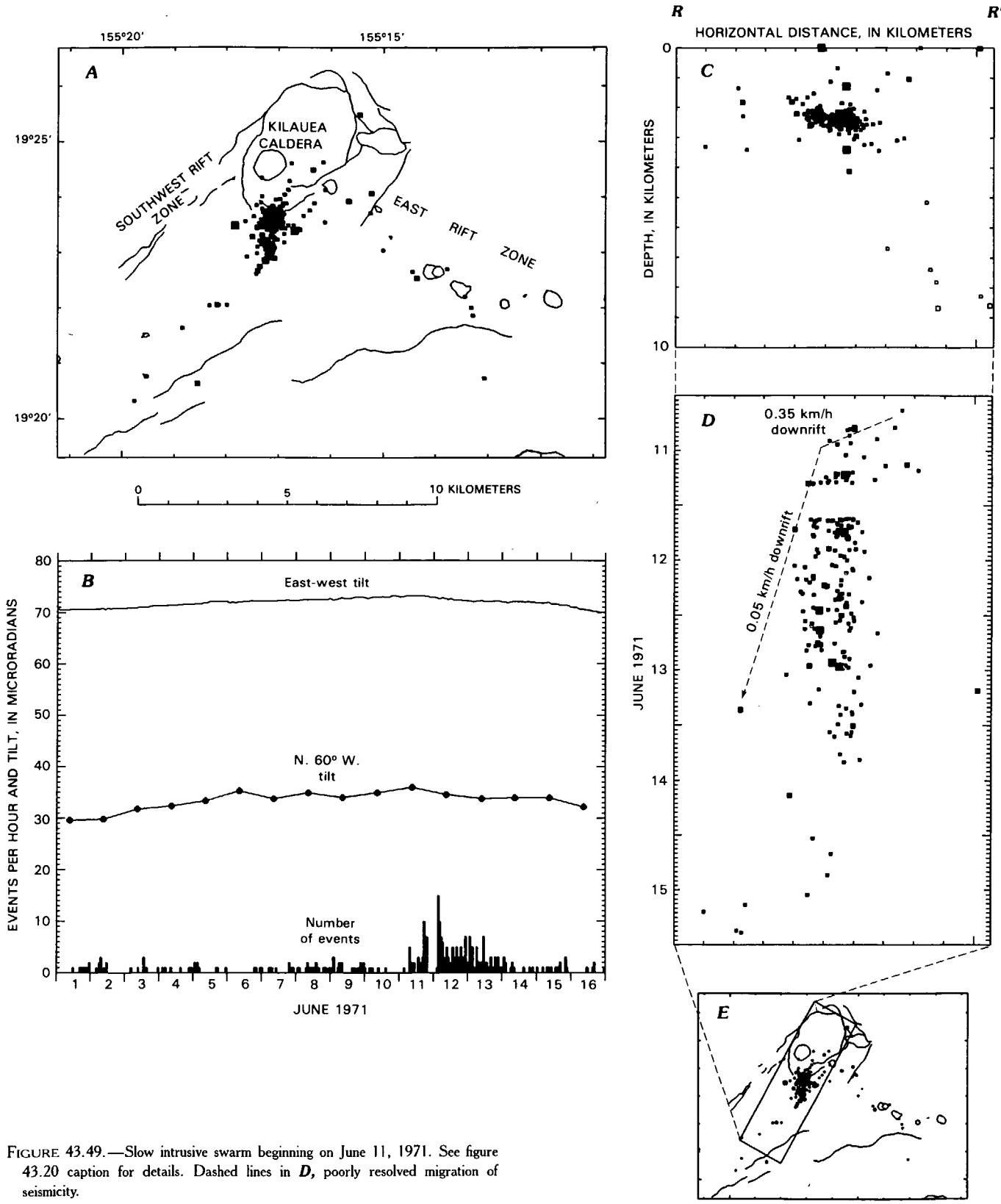

FIGURE 43.49.—Slow intrusive swarm beginning on June 11, 1971. See figure 43.20 caption for details. Dashed lines in ***D***, poorly resolved migration of seismicity.

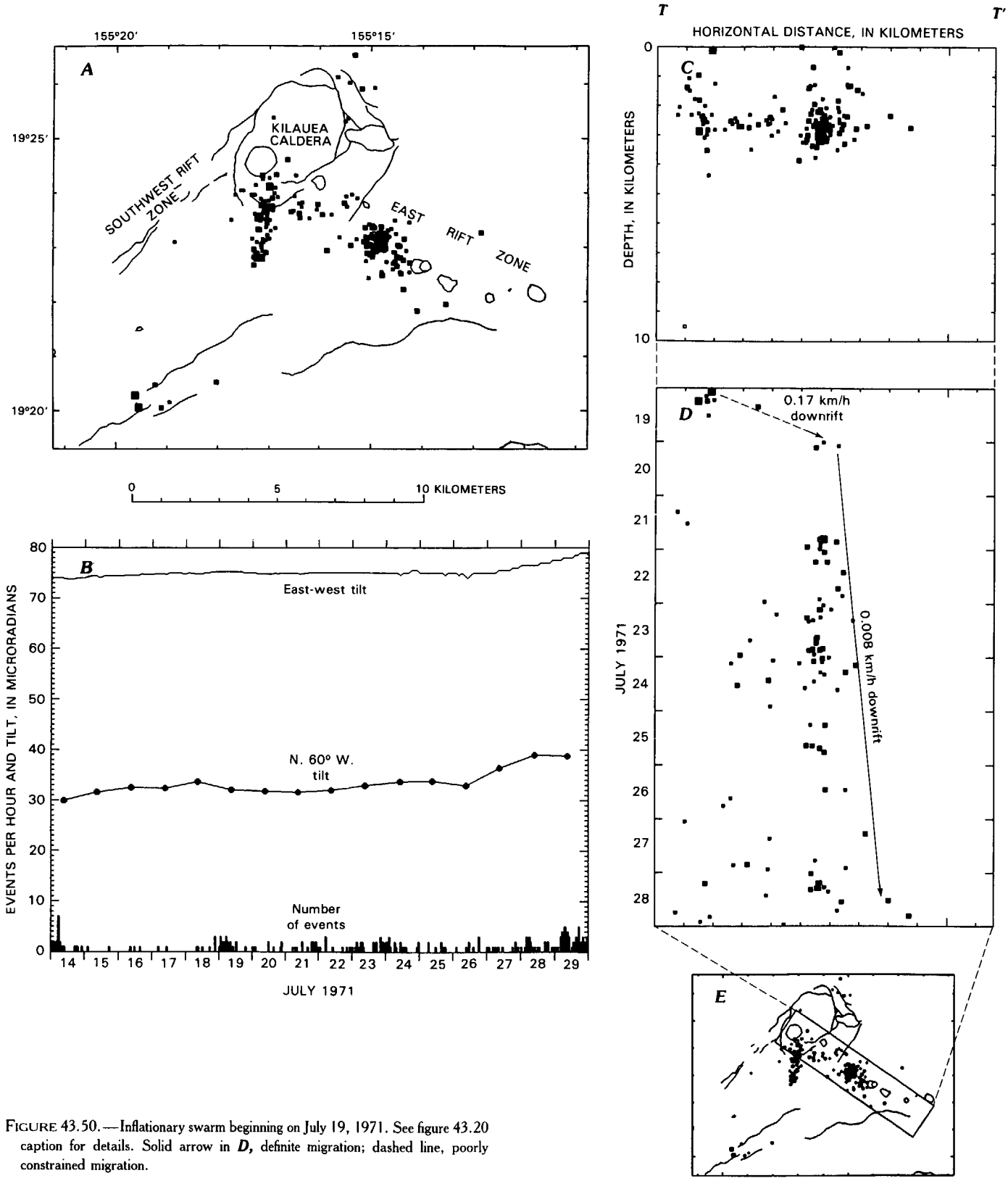

FIGURE 43.50.—Inflationary swarm beginning on July 19, 1971. See figure 43.20 caption for details. Solid arrow in ***D***, definite migration; dashed line, poorly constrained migration.

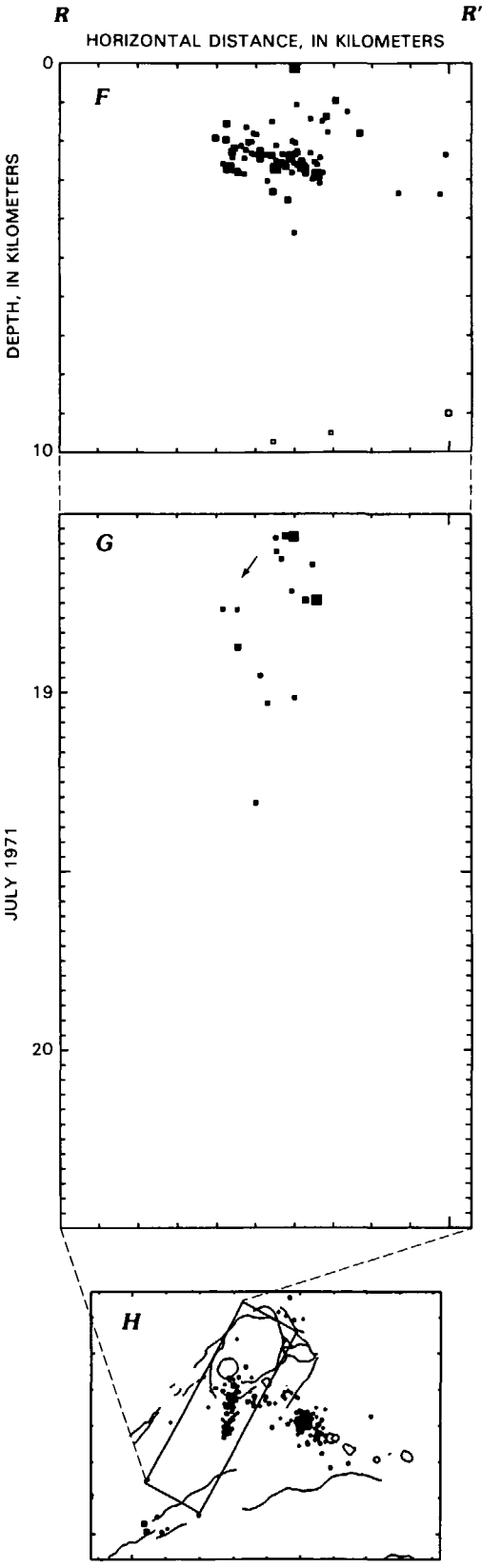

FIGURE 43.50.—Continued.

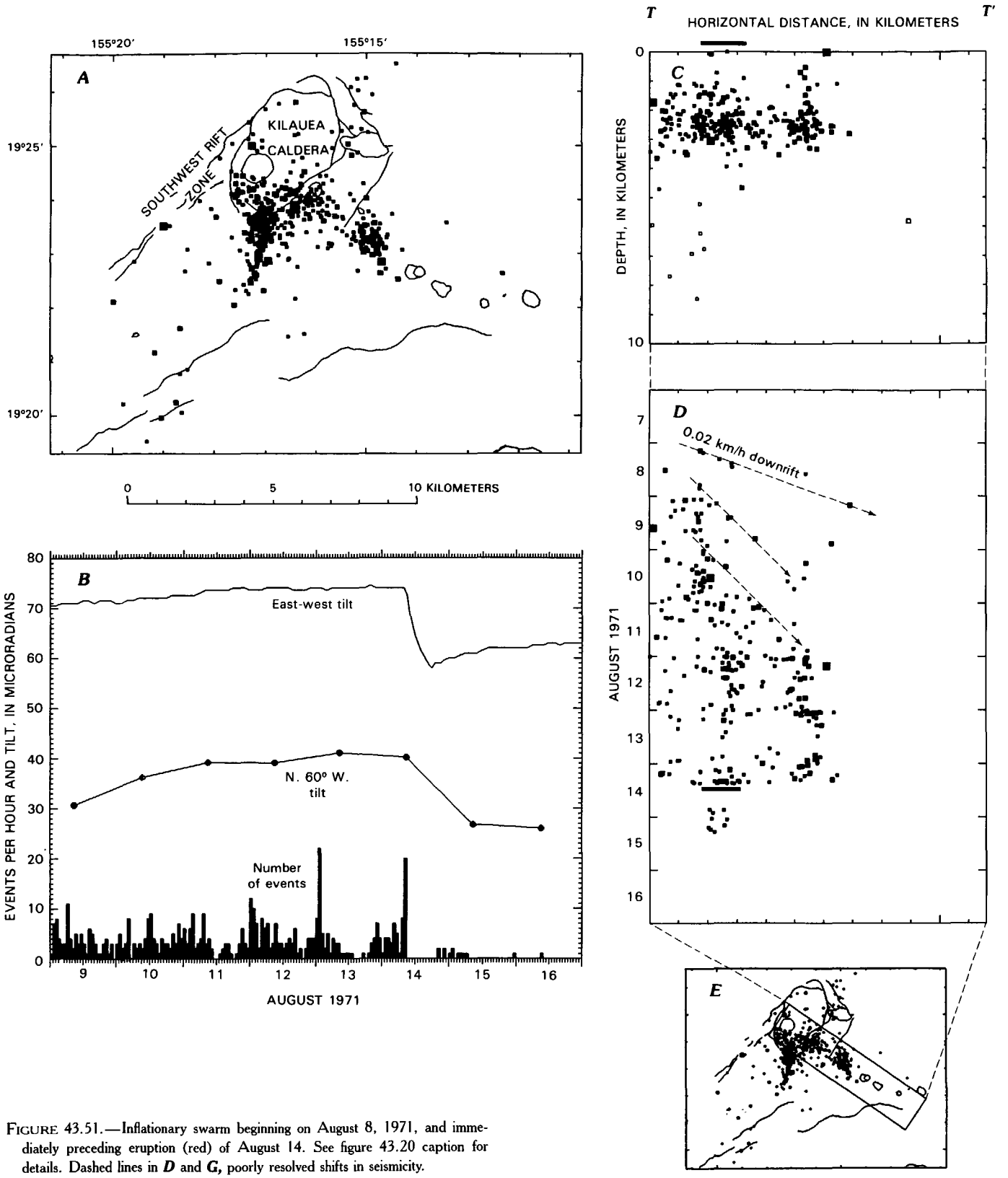

FIGURE 43.51.—Inflationary swarm beginning on August 8, 1971, and immediately preceding eruption (red) of August 14. See figure 43.20 caption for details. Dashed lines in ***D*** and ***G***, poorly resolved shifts in seismicity.

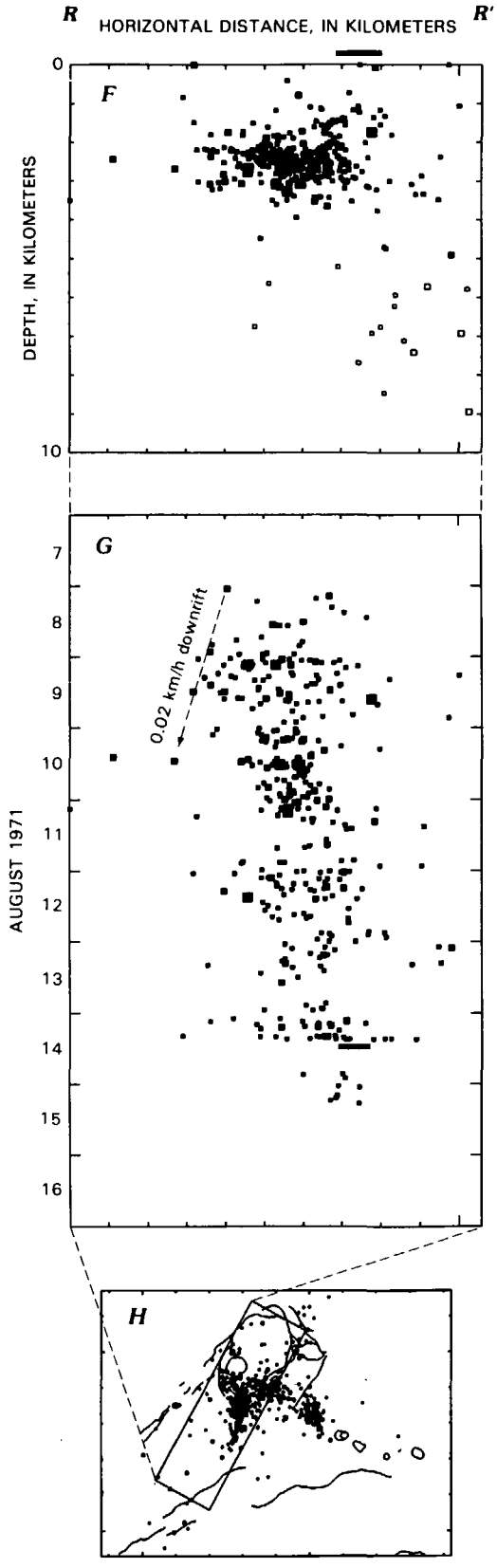

FIGURE 43.51.—Continued.

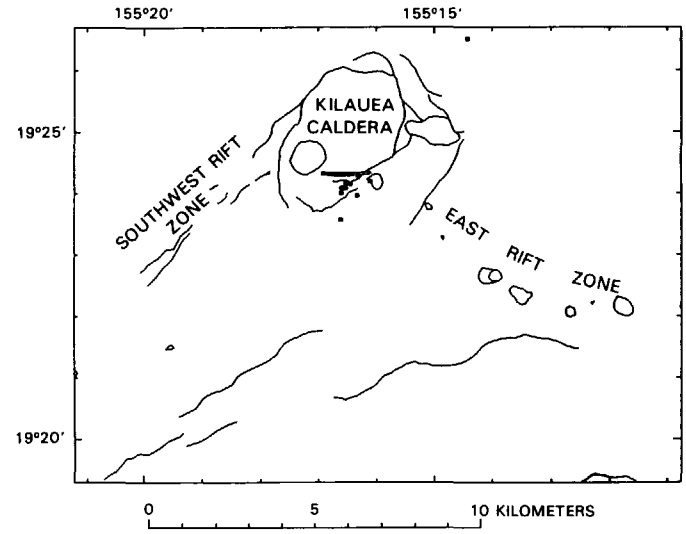

FIGURE 43.52.—Eruptive swarm beginning on August 14, 1971. See figure 43.20 caption for details. Red, location of eruptive vent. See figure 43.51*B* for tilt and earthquake counts, and figure 43.51*D* for relation of eruptive swarm to prior seismicity and onset time of eruptive vent (red).

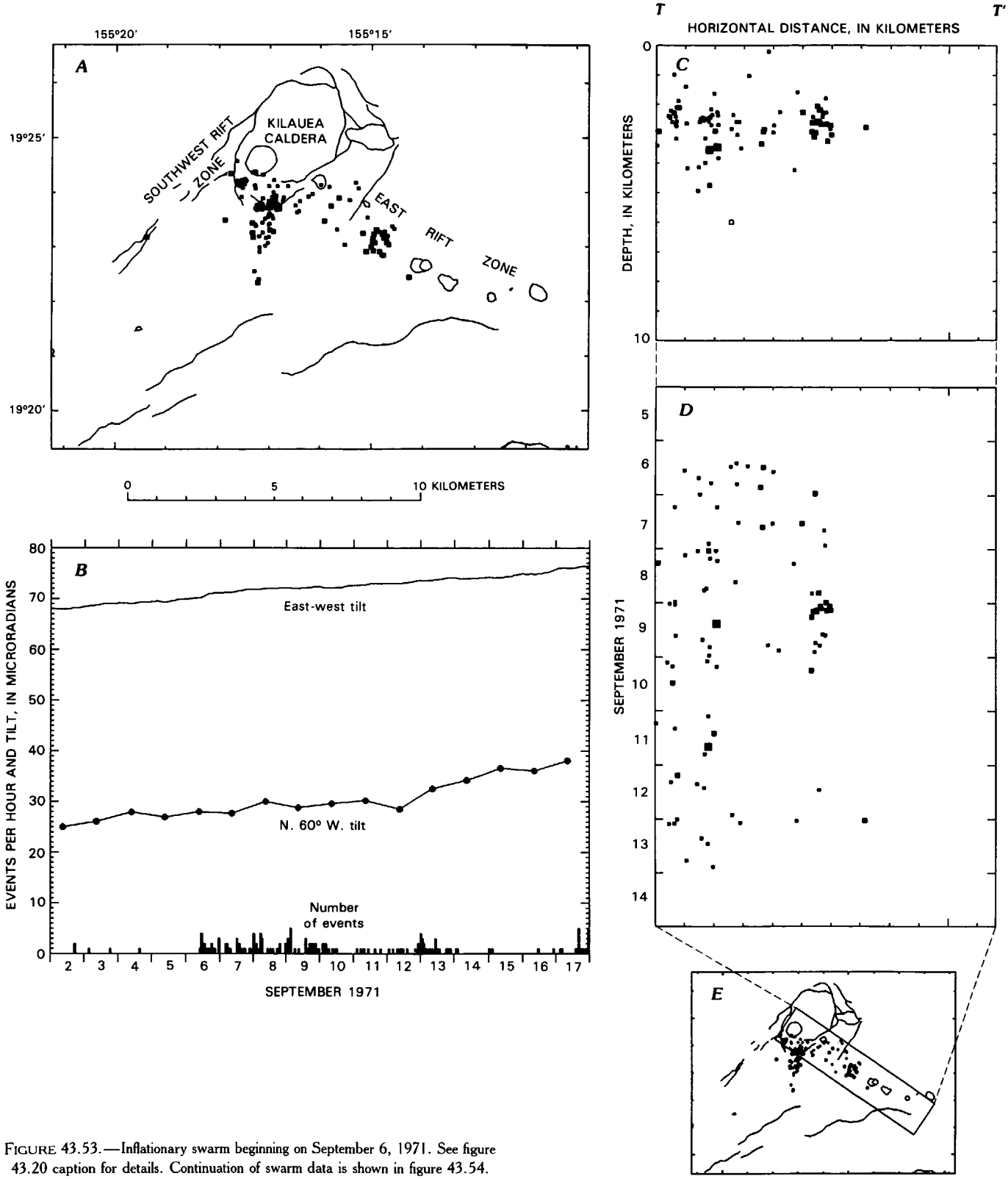

FIGURE 43.53.—Inflationary swarm beginning on September 6, 1971. See figure 43.20 caption for details. Continuation of swarm data is shown in figure 43.54.

THE MAY AND JUNE 1973 INTRUSIONS OF THE KOAE FAULT ZONE

More than one year after the resumption of Mauna Ulu volcanism, activity shifted briefly to an eruption at Pauahi on May 5, 1973. The eruption was accompanied by an intense swarm in the adjacent Koae fault zone (fig. 43.59*A*; Unger and Koyanagi, 1979). The earthquake swarm formed a linear zone extending westward into the Koae from Pauahi (fig. 43.59*A*), lasted for almost 24 hours, produced may surface cracks and saw rapid deflation of the summit caldera (fig. 43.59*B*). The shift of eruptive activity from Mauna Ulu to Pauahi was possibly related to the magnitude-6.2 Honomu earthquake north of Hilo on April 26, 1973. This earthquake did disturb Kilauea caldera enough to trigger rockfalls and small earthquakes. The May 5, 1973, eruption was immediately preceded by draining of the Mauna Ulu and Alae lava lakes. Therefore, the eruption was likely fed by Mauna Ulu lava or at least diverted its magma supply from under the Pauahi-Mauna Ulu region. The time history of earthquakes supports this inference.

The May 5 swarm began under Mauna Ulu, and seismicity rapidly spread up the ERZ to Hiiaka. The lateral speed of this initial migration was 3.6 km/h (fig. 43.59*G*), which reduces to an apparent 3.2 km/h when foreshortened by looking from the south-southeast (fig. 43.59*D*). This initial migration was also from 2–4 km depth below Mauna Ulu to 0–2 km depth below Hiiaka, as seen on the cross sections (fig. 43.59*C*, *F*). An upward movement of earthquakes thus took place, as is evident on a depth versus time plot (fig. 43.59*I*). The initial vertical rate of 3 km/h slowed to 1 km/h within 1.5 km of the surface. These speeds should be regarded as very approximate, because both lateral and vertical migration occurred simultaneously and because they are defined by only a few earthquakes. The observed eruption time requires that vertical migration slowed near the surface, as might be expected for a dike that of 0.36 km/h westward into the Koae for the next 16 hours (fig. 43.59*D*). Note that earthquakes ceased about 2 km or 6 hours behind their point of inception, so that the point at which earthquakes stopped also migrated into the Koae.

We interpret this swarm as the result of a dike propagating from below Mauna Ulu to Pauahi and then into the Koae fault zone. The dike spread from the active pocket of magma presumably feeding Mauna Ulu. The dike initially found an easy and fast path in the ERZ, probably because of the frequency of intrusions and consequent high temperatures there. The advance of the dike slowed in the noneruptive Koae, however, perhaps because of more rapid cooling of the dike. Cooling could slow the dike either by increasing magma viscosity or by chilling dike margins and constricting flow to a narrower space. The constant speed of advance and continuous earthquake migration without halting or jerky movement are suggestive of viscous flow under relatively uniform stress conditions.

The initial activity at the eruptive vents migrated from east to west at about the same 0.3 km/h speed as the earthquakes (fig. 43.59*D*). As noted with other intrusions, vents opened about 3–6 hours after the initial seismic front passed their location. At a particular vent, the time of eruption coincides with the cessation of earthquakes. Thus the earthquakes are not simply being masked by tremor, because events continued to the west. The start of eruption thus relieves some of the stress that caused the earthquakes, probably at the time the dike reaches its maximum width. We then associate the seismicity with the time and place where the dike is growing in width and under increasing pressure, and the moving point at which earthquakes cease is where the dike has reached its maximum width and magma flow is stable.

With the association of earthquakes and dike growth in mind, a very low confining stress in the Koae explains two observations: (1) the dike widens easily, accommodating all the magma it is given without building enough hydrostatic head to reach the surface and erupt, and (2) the dike encounters little resistance from compressive stress normal to itself, and once opened to a width permitting stable and sustained flow, the dike exerts little stress on its walls so that earthquakes cease. The migration speed and width of the earthquake zone during Koae intrusions would then be determined by the mechanical and thermal properties of magma in a cold, dry crack under relatively little stress.

About one month after the May 5 eruption, a second Koae intrusion occurred (fig. 43.60). The June 9, 1973 intrusion was parallel to and about 1 km north of the prior intrusion, but was only about 3 km long (fig. 43.60*A*). It was also smaller than the May event in the sense of a shorter swarm and smaller deflation (fig. 43.60*B*). This intrusion apparently did not involve Mauna Ulu directly, because it began from a point just uprift of Hiiaka on the ERZ. The migration speed was about 1 km/h (fig. 43.58*D*), three times faster than in May. The pairing of these two Koae intrusions is probably not coincidental, and they probably interacted in some way.

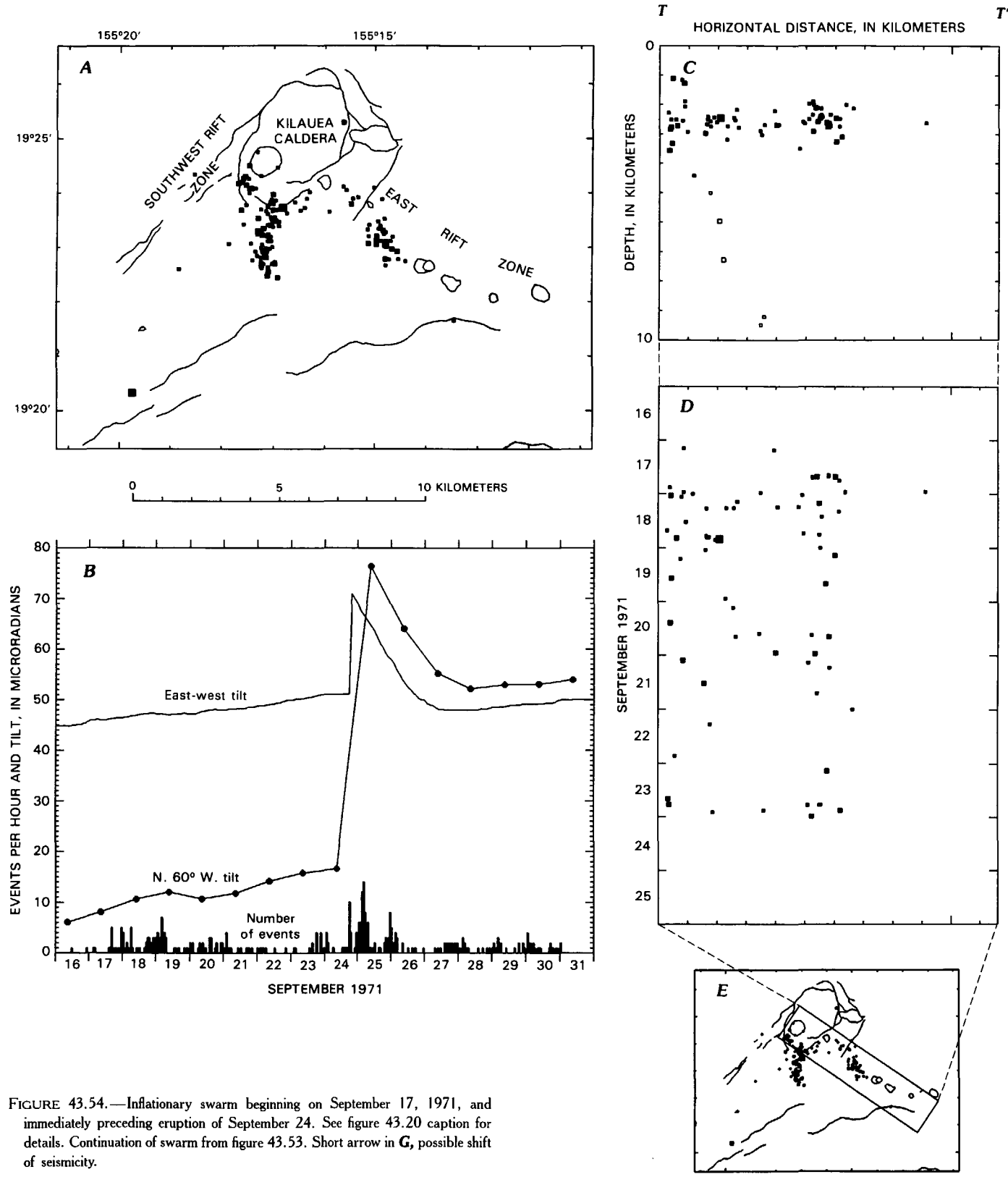

FIGURE 43.54.—Inflationary swarm beginning on September 17, 1971, and immediately preceding eruption of September 24. See figure 43.20 caption for details. Continuation of swarm from figure 43.53. Short arrow in ***G***, possible shift of seismicity.

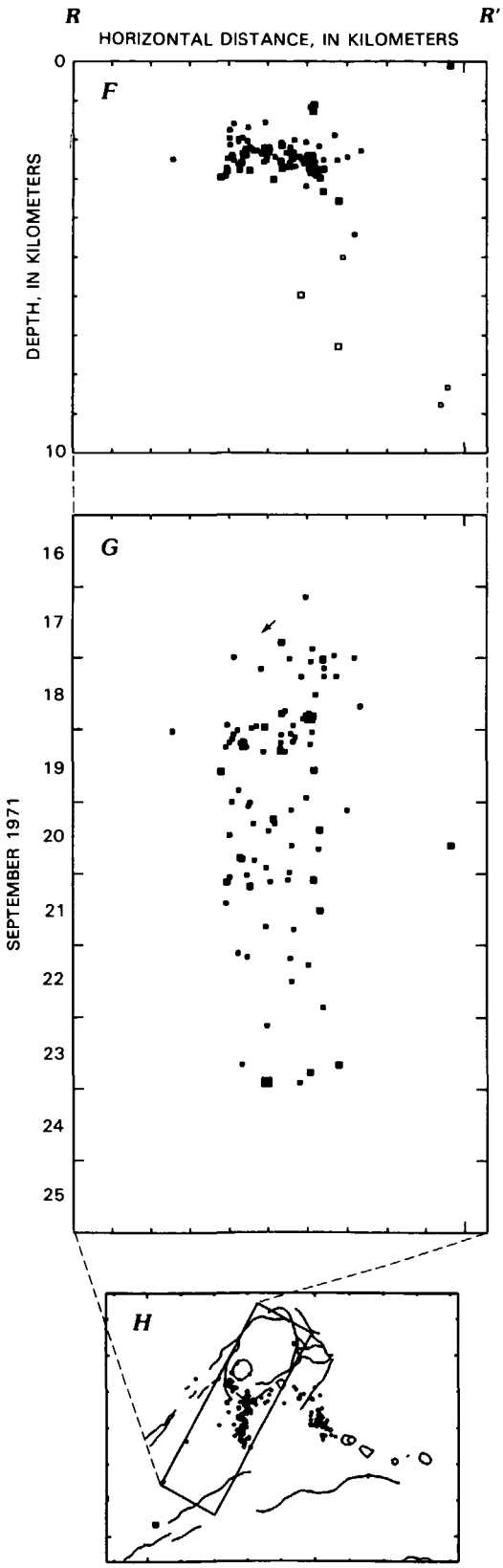

FIGURE 43.54.—Continued.

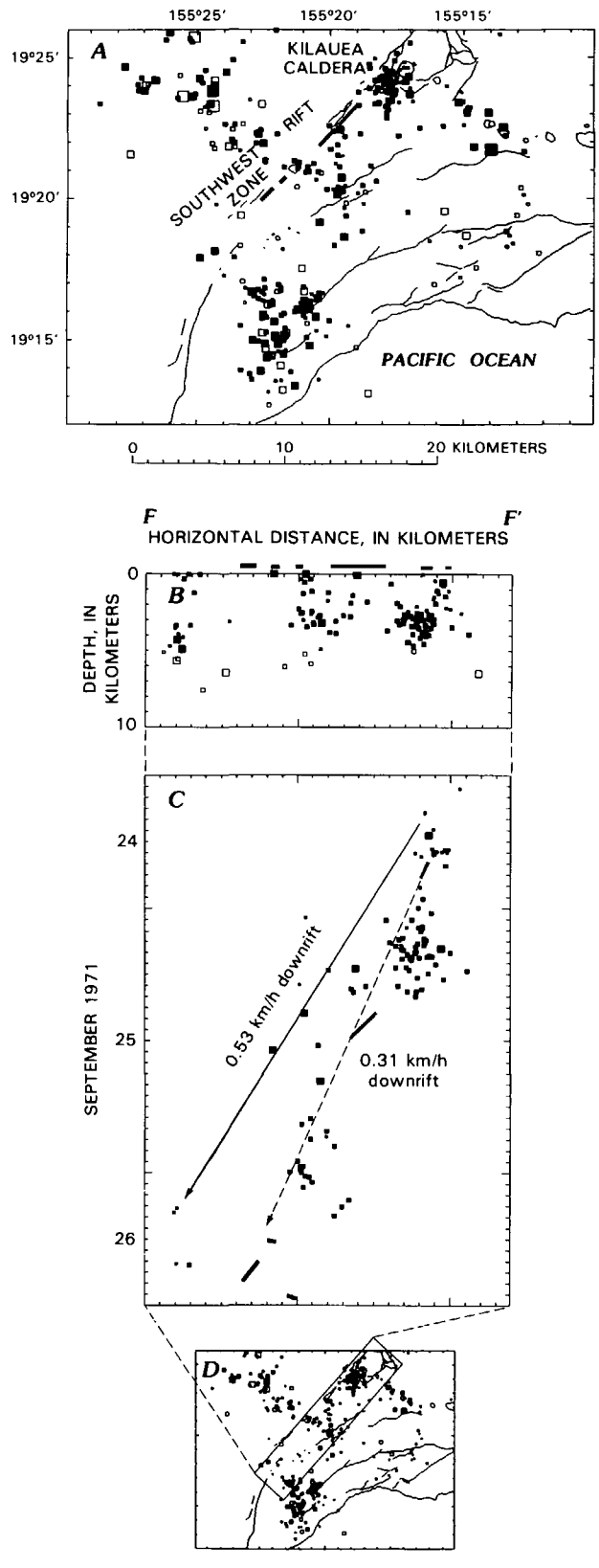

FIGURE 43.55.—Eruptive swarm beginning on September 24, 1971. See figure 43.20 caption for details and figure 43.54 for tilt and earthquake rate. Red, approximate location (***A, B***) and onset time (***C***) of eruptive vents; solid arrow in ***C***, definite migration; dashed arrow, poorly resolved migration of seismicity.

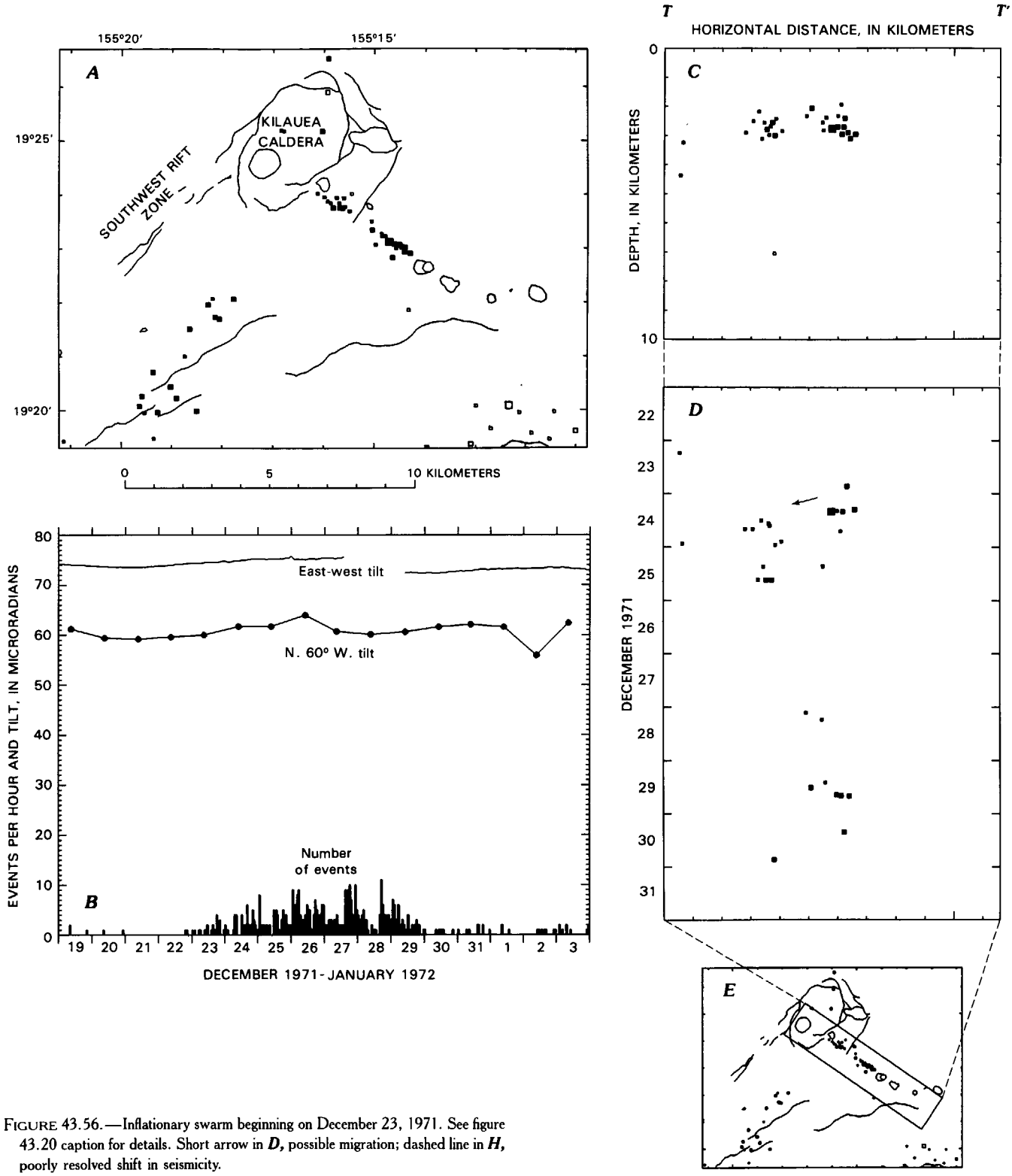

FIGURE 43.56.—Inflationary swarm beginning on December 23, 1971. See figure 43.20 caption for details. Short arrow in ***D***, possible migration; dashed line in ***H***, poorly resolved shift in seismicity.

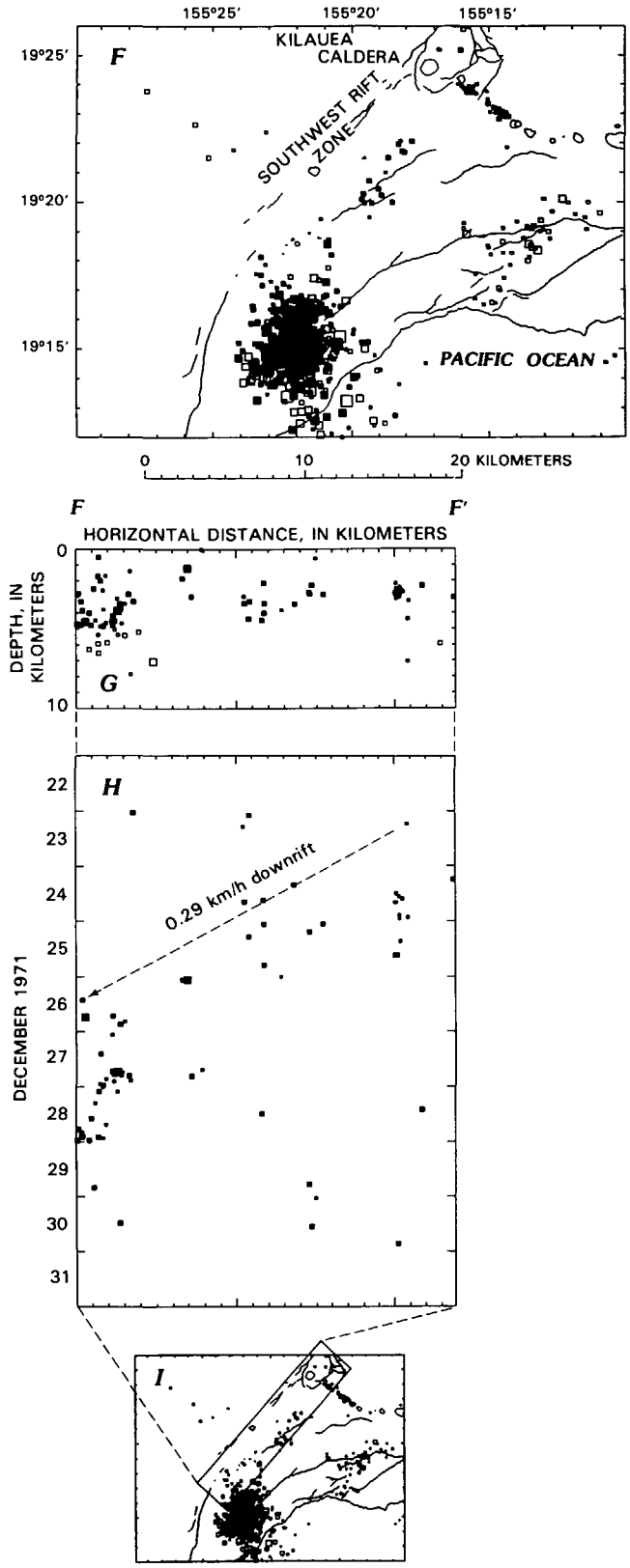

FIGURE 43.56.—Continued.

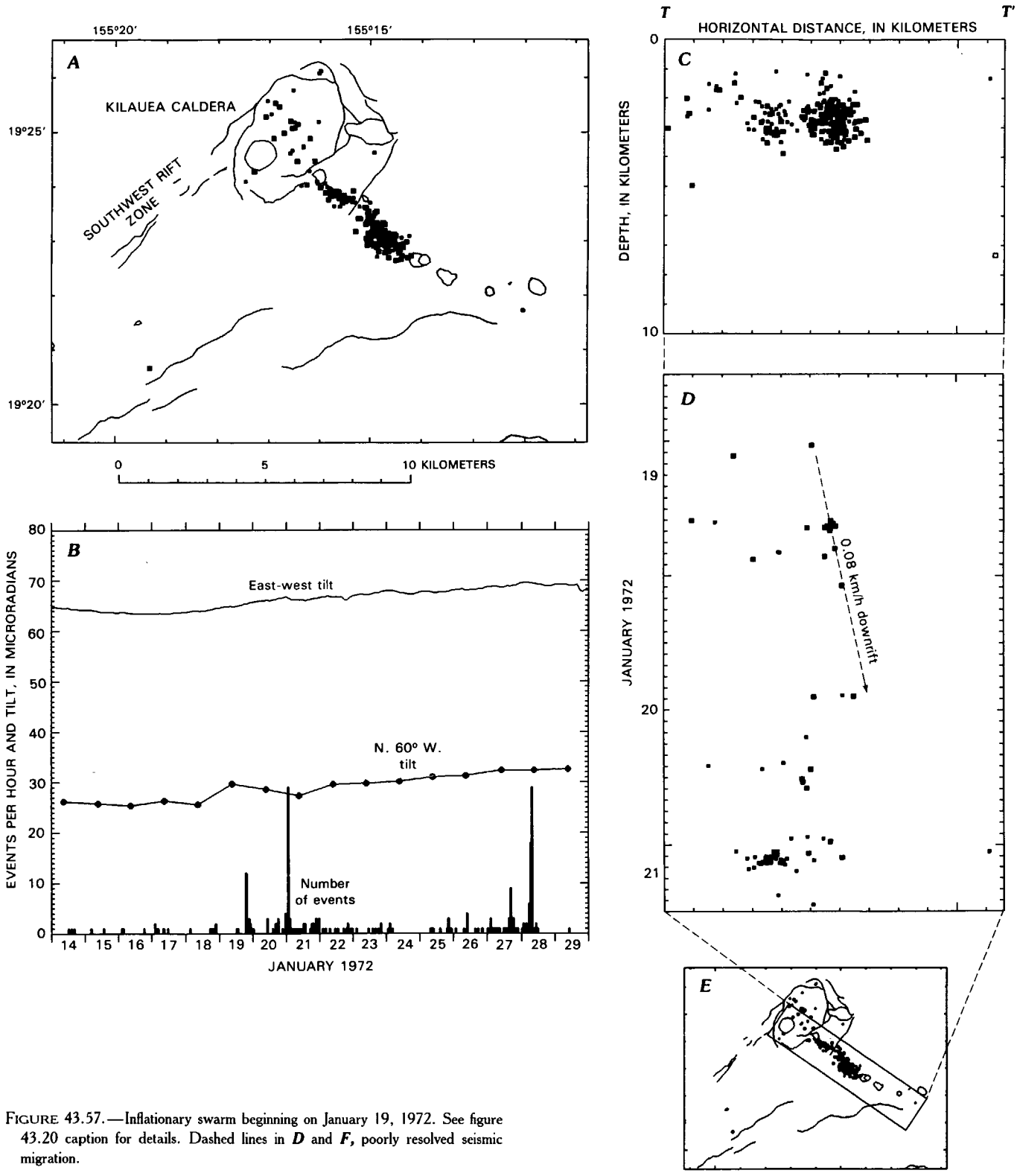

FIGURE 43.57.—Inflationary swarm beginning on January 19, 1972. See figure 43.20 caption for details. Dashed lines in ***D*** and ***F***, poorly resolved seismic migration.

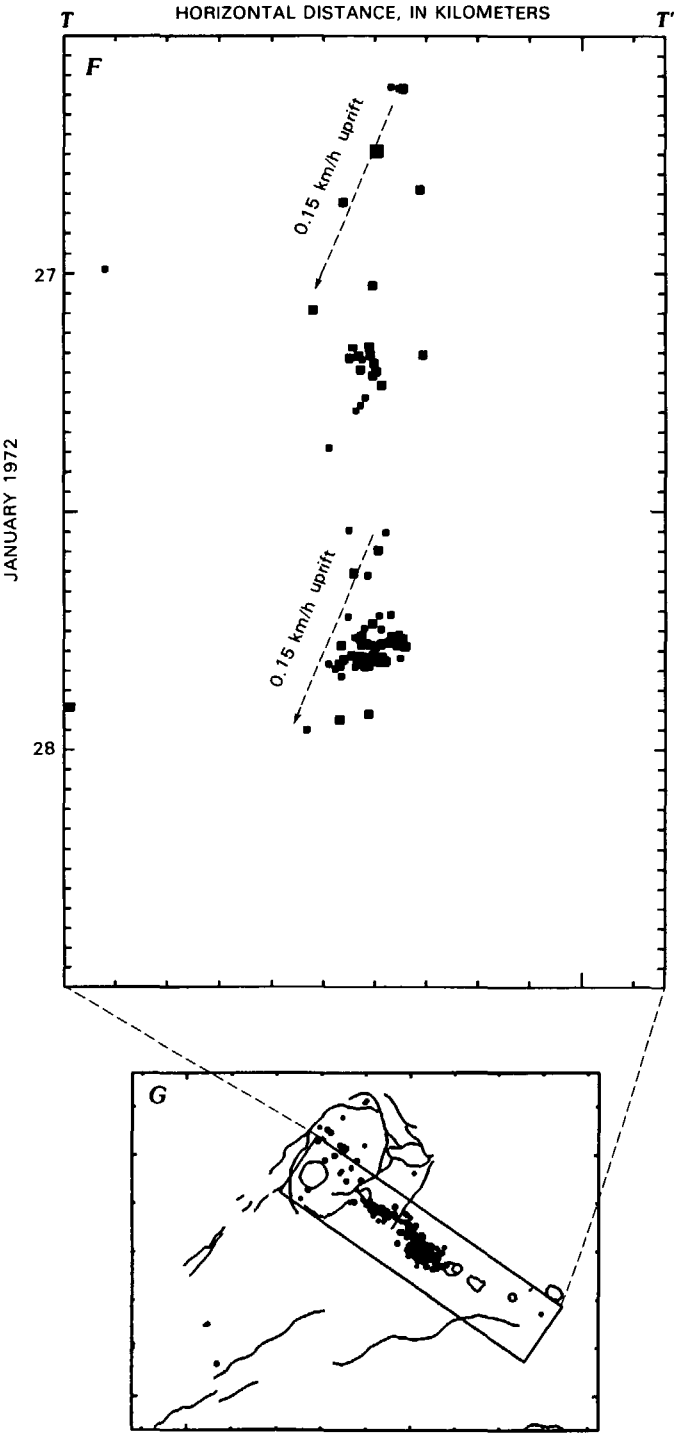

FIGURE 43.57.—Continued.

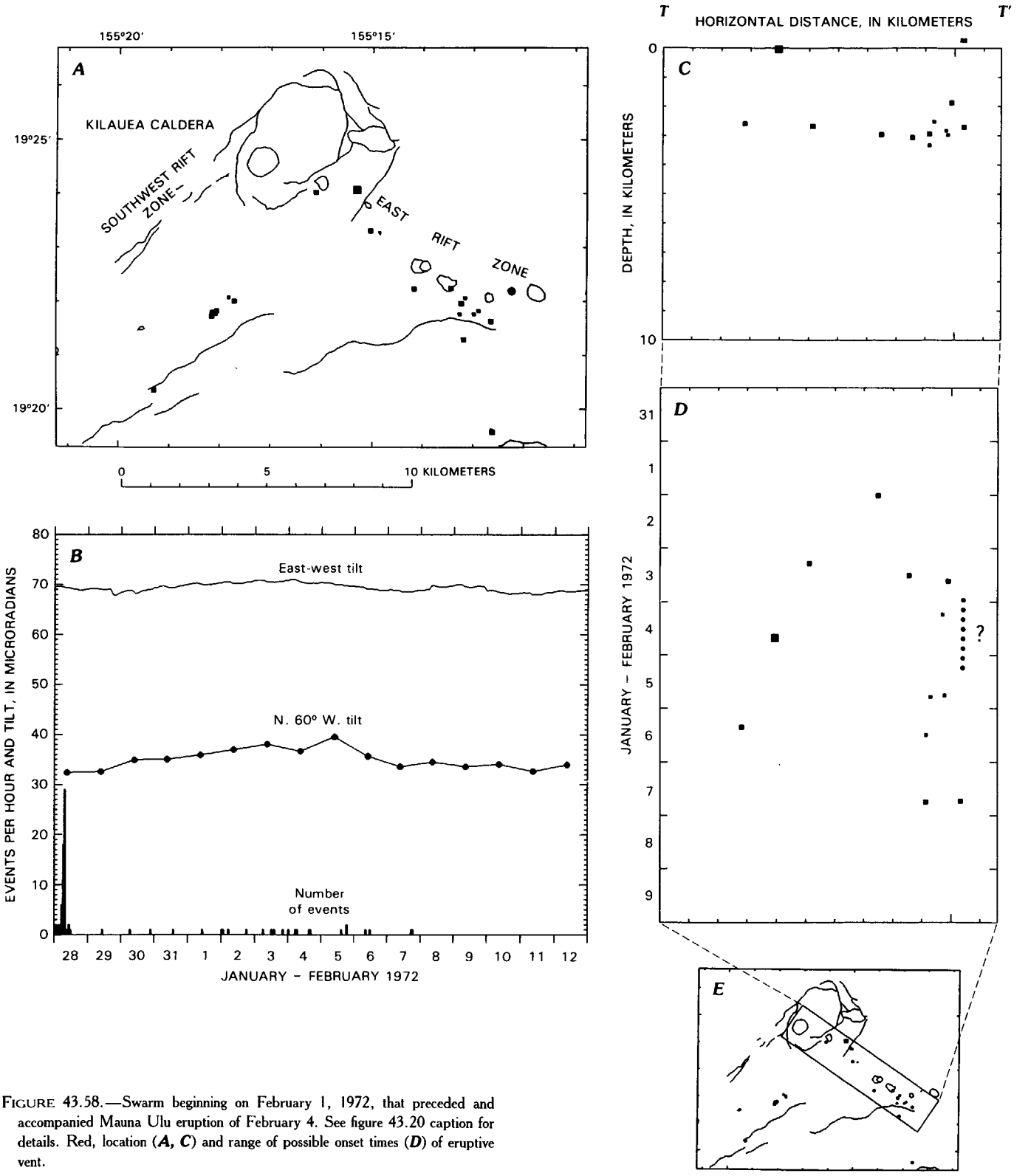

FIGURE 43.58.—Swarm beginning on February 1, 1972, that preceded and accompanied Mauna Ulu eruption of February 4. See figure 43.20 caption for details. Red, location (***A, C***) and range of possible onset times (***D***) of eruptive vent.

ERUPTIONS AND INTRUSIONS, NOVEMBER 1973 THROUGH SEPTEMBER 1974

The next three swarms took place in the ERZ within 8 km of the caldera. The swarm of November 10–11, 1973, preceded and accompanied an eruption near Pauahi. In addition to the main seismic zone parallel to the rift, a few small events extended to the northeast beneath the eruptive vents (fig. 43.61*A*). The absence of earthquakes in the middle of the swarm (fig. 43.61*B*, *D*) is a result of masking of earthquakes by intense tremor. Uprift earthquake migration is suggested, and fountaining spread both east and west along the vent (fig. 43.61*D*). A definite shallowing of earthquakes, however, preceded the eruption (fig. 43.61*F*). The apparent vertical speed was about 1.6 km/h interrupted by a break of about 3 hours, but this pattern is based only on a few earthquakes. Figure 43.61*E* also shows that the depths of events after the start of the eruption averaged about 2 km shallower than those before.

An earthquake swarm lasting less than three hours occurred on March 24 in the Pauahi-Mauna Ulu section of the ERZ (fig. 43.62*A*). This section is a common place for earthquake swarms to begin, as did 3 of the 4 previous swarms. Three microradians of summit deflation accompanied the swarm, as seen on the Uwekahuna tiltmeter (fig. 43.62*B*). The event was accompanied by harmonic tremor and a short-lived increase of lava and gas production in the ongoing Mauna Ulu eruptive activity. We therefore interpret this event as a minor intrusion in which some sort of localized magma adjustment occurred, thus feeding the Mauna Ulu system. The episode caused a small volume of magma to drain from the summit complex through the aseismic section of rift above Pauahi.

The earthquake swarm immediately preceding the July 19, 1974 eruption was very intense and lasted only 9 hours (fig. 43.63*B*). It was in the same Keanakakoi-Kokoolau region active during the preceding 3 months of inflationary seismicity. The summit deflated about 3 microradians, after which tilt nearly leveled off. A larger and more rapid summit deflation followed at 1030 H.s.t., high amplitude tremor began, and the number of earthquakes that could be timed and located sharply diminished. Magma reached the surface about 2 hours later.

The seismic zone is slightly elongate and extends from about 3.5 km beneath Kokoolau to within 1 km or less of the surface near Puhimau (fig. 43.63*C*). The active zone thus plunges steeply to the southeast. The absence of events between 0 and 1 km depth may result from the poor depth control of the very shallowest earthquakes or from the fact that the low-rigidity and low-stress surface layer may be too weak to generate earthquakes of locatable magnitude.

Earthquakes migrated uprift at a well-determined rate of about 0.16 km/h (fig. 43.63*D*). Earthquakes also moved upward at roughly 0.55 km/h (fig. 43.63*F*), which slowed to about 0.18 km/h within 1 km of the surface, assuming the dike moved at constant speed to the surface. A slowing near the surface is typical of most dikes for which upward movement can be seen. The observed migration patterns and vent location are explained by a plunging zone growing first at about 0.6 km/h then 0.24 km/h. This event was apparently a forceful intrusion of a dike leading from the ERZ conduit below Kokoolau up to the surface. The intense seismicity and tilt rate patterns show that rock was initially breaking under high magma pressure and relatively low volume flow. When the dike reached the surface, pressure and seismicity decreased, and flow volume, tremor and tilt rate increased.

The caldera eruption of September 19, 1974, was seismically unlike the others during the year and did not generate an intense earthquake swarm. It was instead preceded by three days of slightly elevated seismicity just south of the caldera under the SWRZ (fig. 43.64*A*) and a slowly inflating caldera (fig. 43.64*B*). The activity of September 16–19 is not distinguishable from other inflationary seismicity during the rest of 1974, although the probability of an eruption is measurably higher when such summit seismicity increases (Klein, 1984).

The pre-eruption earthquakes may have accompanied a slow and low-volume intrusion into the SWRZ. Although the swarm was a weak one, there is a hint of a downrift earthquake migration (fig. 43.64*D*). The absence of an intense swarm indicates that magma came to the surface without having to create a new dike in a high stress environment. When the eruption began, earthquakes abruptly ceased. This relation is expected if magma pressure induces the earthquakes and suddenly drops when flow and pressure are redirected to an active vent.

A pattern of increasing seismicity in the SWRZ during 1974 suggests that the rift participated in Kilauea's continuing inflation and slowly received magma. The seismic and tilt changes can be seen in figure 43.65, which plots earthquake positions and tilt from May 1974 through February 1975. In May and June most earthquakes were confined to the inflating summit area, but the July–December period saw increasing seismicity as far downrift as Mauna Iki. The rapid inflation of September through December produced the highest tilt values yet recorded. Kilauea appeared to be preparing for a SWRZ event, which came in December and dramatically shifted the active area from the upper to the lower SWRZ.

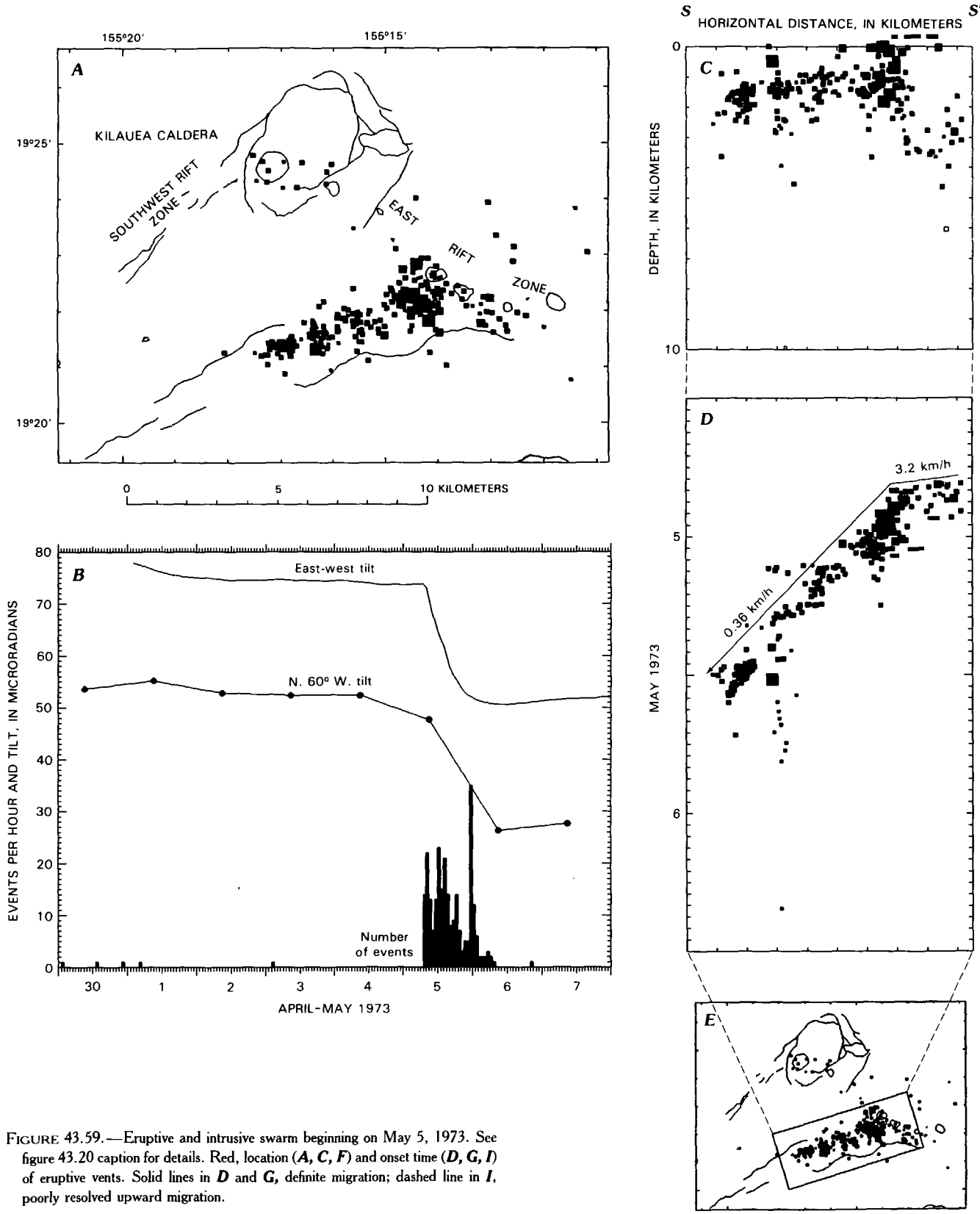

FIGURE 43.59.—Eruptive and intrusive swarm beginning on May 5, 1973. See figure 43.20 caption for details. Red, location (*A, C, F*) and onset time (*D, G, I*) of eruptive vents. Solid lines in *D* and *G*, definite migration; dashed line in *I*, poorly resolved upward migration.

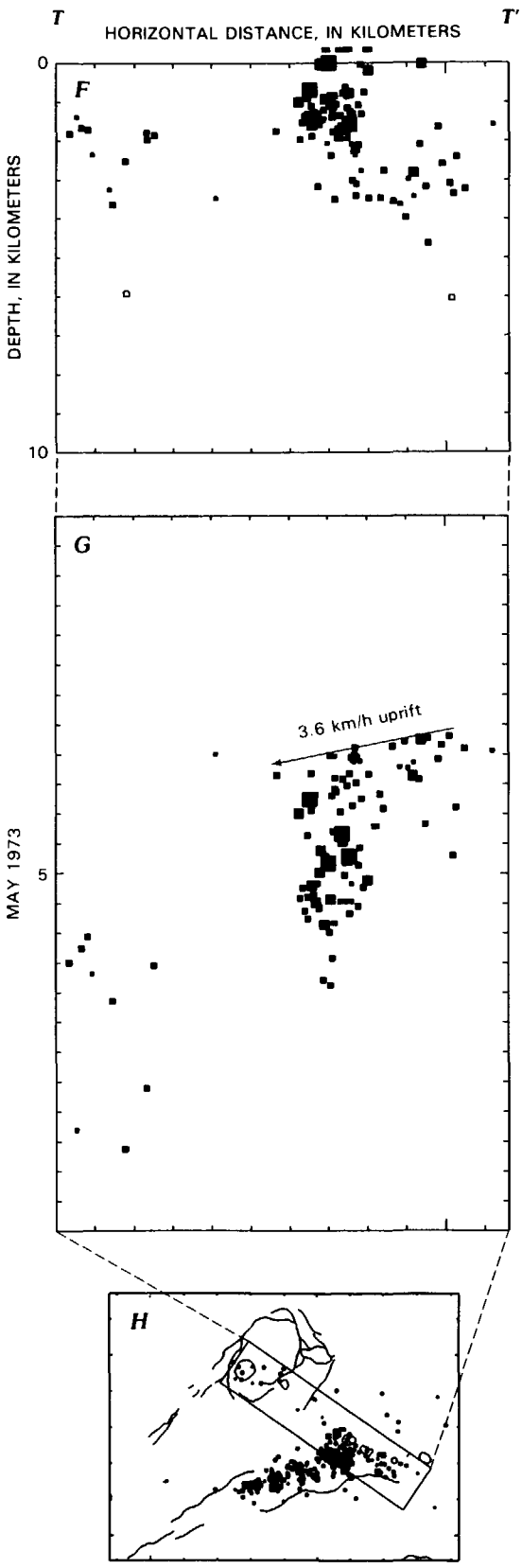

FIGURE 43.59.—Continued.

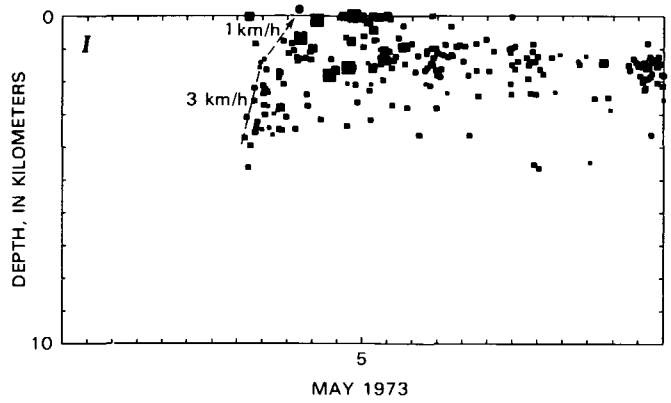

FIGURE 43.59.—Continued.

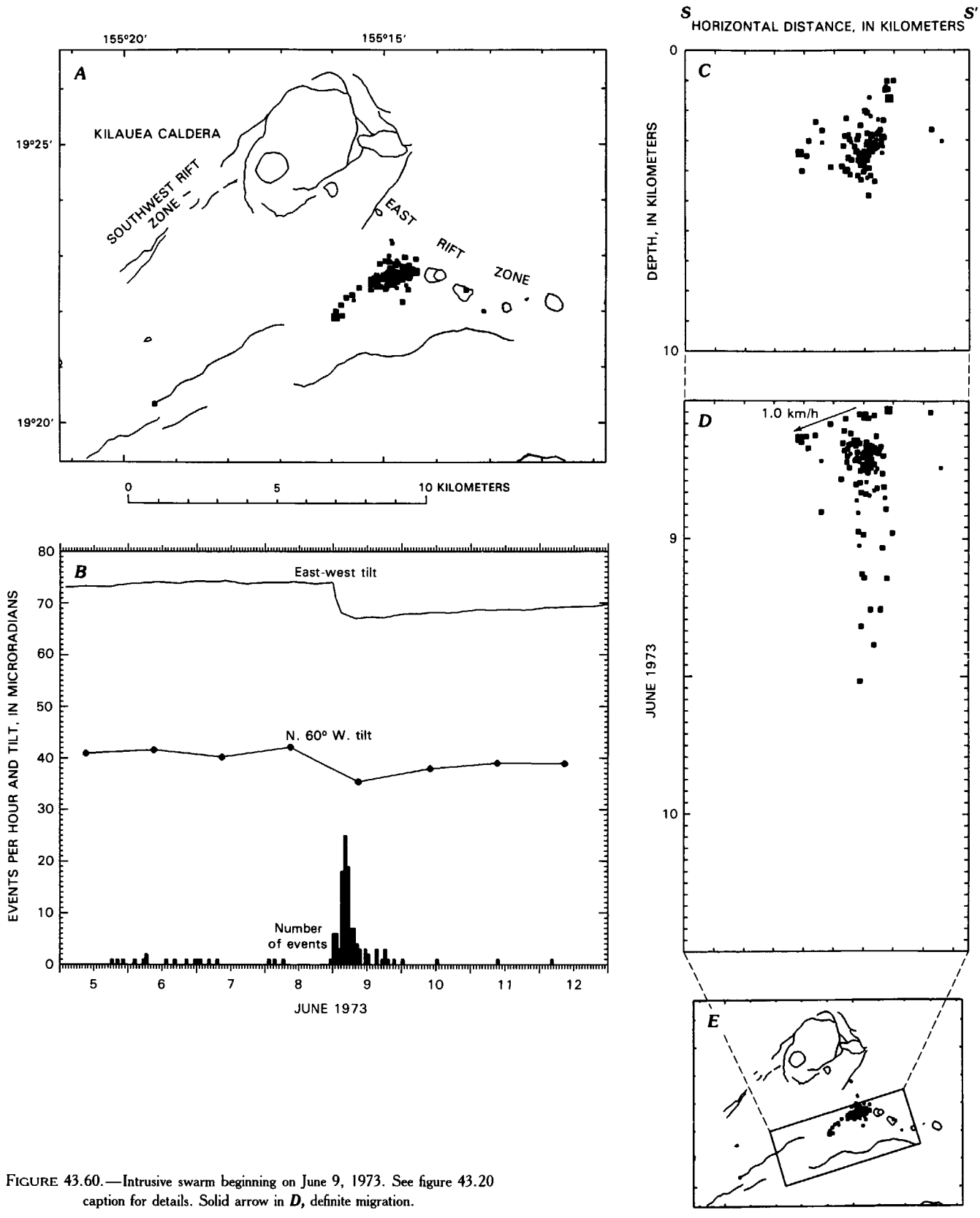

FIGURE 43.60.—Intrusive swarm beginning on June 9, 1973. See figure 43.20 caption for details. Solid arrow in ***D***, definite migration.

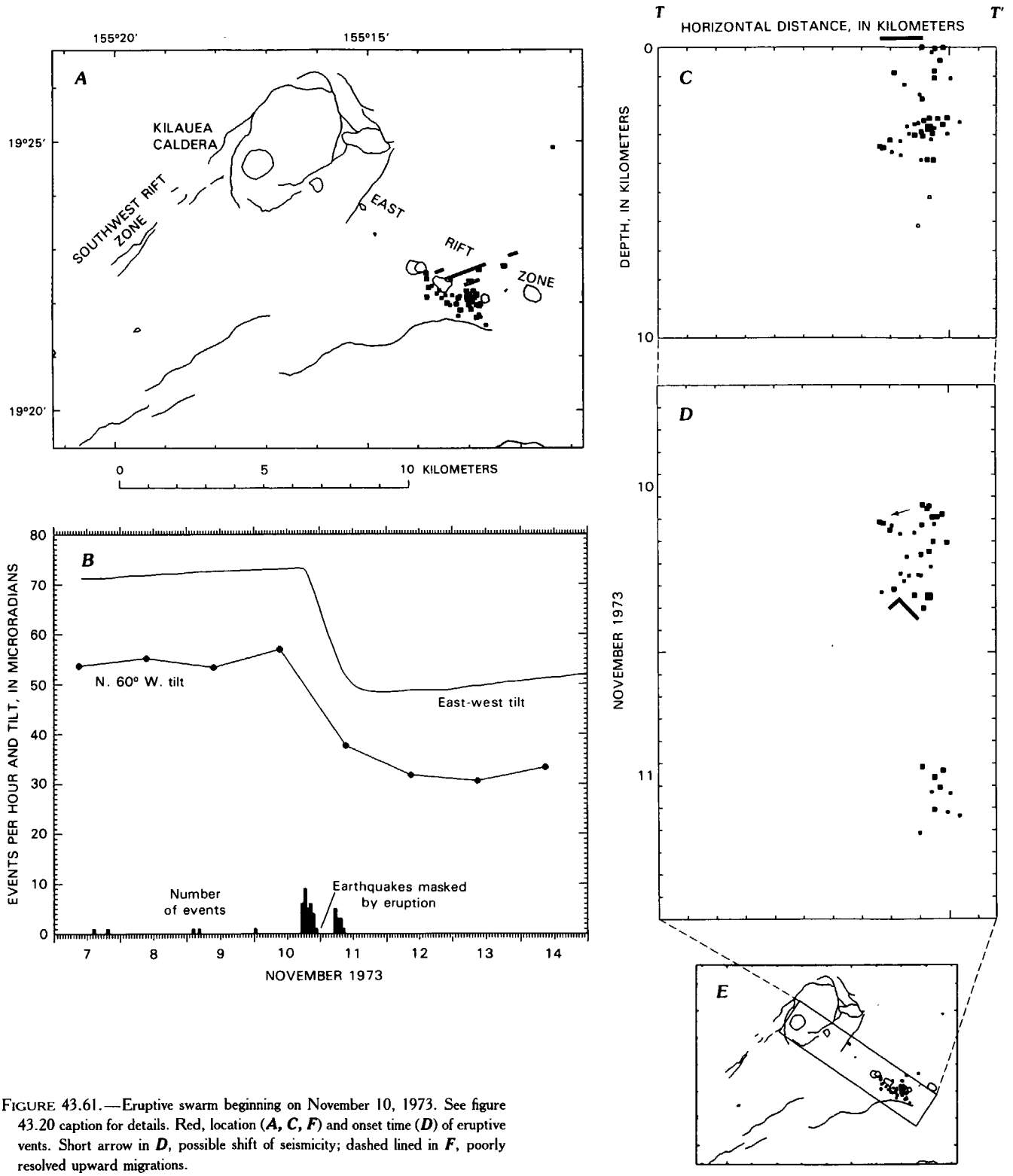

FIGURE 43.61.—Eruptive swarm beginning on November 10, 1973. See figure 43.20 caption for details. Red, location (***A, C, F***) and onset time (***D***) of eruptive vents. Short arrow in ***D***, possible shift of seismicity; dashed lined in ***F***, poorly resolved upward migrations.

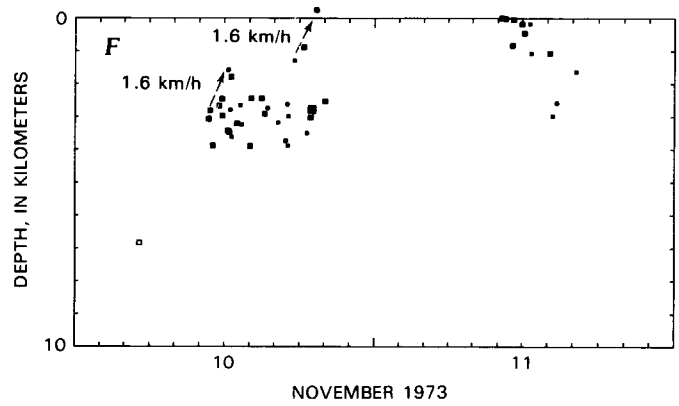

FIGURE 43.61.—Continued.

THE DECEMBER 1974 SOUTHWEST RIFT ZONE ERUPTION

Summit seismicity in the parts of both rift zones adjacent to the caldera intensified during the week prior to the December 31 eruption (fig. 43.66). Beginning on December 24, this heightened activity apparently migrated very slowly into both rifts at roughly one kilometer per day (fig. 43.66*D*, *G*). These slow intrusions of magma into both rifts simultaneously were another indication of abundant supply in the summit reservoir.

Seismic patterns divide the eruption into two different phases: an intense but short swarm just south of the caldera related to the dike that fed the eruption, and a subsequent intrusion into an additional 18 km of the SWRZ.

The small cluster of earthquakes about 3 km south of Halemaumau occurred beneath the eruptive vent (fig. 43.67*A*). Earthquakes began in the middle of this cloud around 1600 H.s.t. on December 30 (fig. 43.67*D*), and were about 2.5 km deep. The seismic zone slowly grew in size until 0100 H.s.t. on December 31, when it was about 2 km in diameter and the swarm reached maximum intensity. The events then ranged between 1 and 4 km depth. Earthquakes migrated upward at about 5 km/h during this intense period, but the dike grew aseismically upward at about 0.3 km/h during the last 3 hours of its journey to the surface (fig. 43.67*K*). Earthquakes then diminished and tremor intensity grew prior to lava breakout shortly before 0300 H.s.t. As in July, an intense swarm accompanied the lateral and vertical growth of the dike that fed the eruption.

About the time this first swarm reached maximum intensity, additional earthquakes began migrating downrift. The seismically active dike grew about 1.3 km/h for about 14 km, then slowed to one-half that speed as it grew an additional 4 km (fig. 43.67*G*). Earthquakes not only occurred near the shallow rift conduit at 3 km depth, but also well southeast of the rift near the terminus of the new dike (fig. 43.67*B*). The events within Kilauea's mobile south flank are typical of those induced by other large SWRZ intrusions and large tectonic earthquakes. The effects of the intrusion (though probably not magma itself) thus reached at least 10 km from the rift axis.

Compressional stress generated by the new dike acting on a weak zone already close to seismic failure apparently caused the south flank earthquakes, including one of magnitude 5.5. Both rift and flank seismicity lasted for several days after the eruption and deflation ceased (figs. 43.66*B*, 43.67*I*). Thus either magma continued draining down the rift after its source at the summit was cut off, or the whole system displays a relaxation time of several days, or both. The seismic response of the section of rift adjacent to the caldera was rapid, and earthquakes diminished when the dike reached the surface and the pressure dropped. The lower rift, however, accommodates magma pressure by seismic slip and deformation in the mobile south flank, a process that takes several days because of its mechanical lag time (Dvorak and others, 1985).

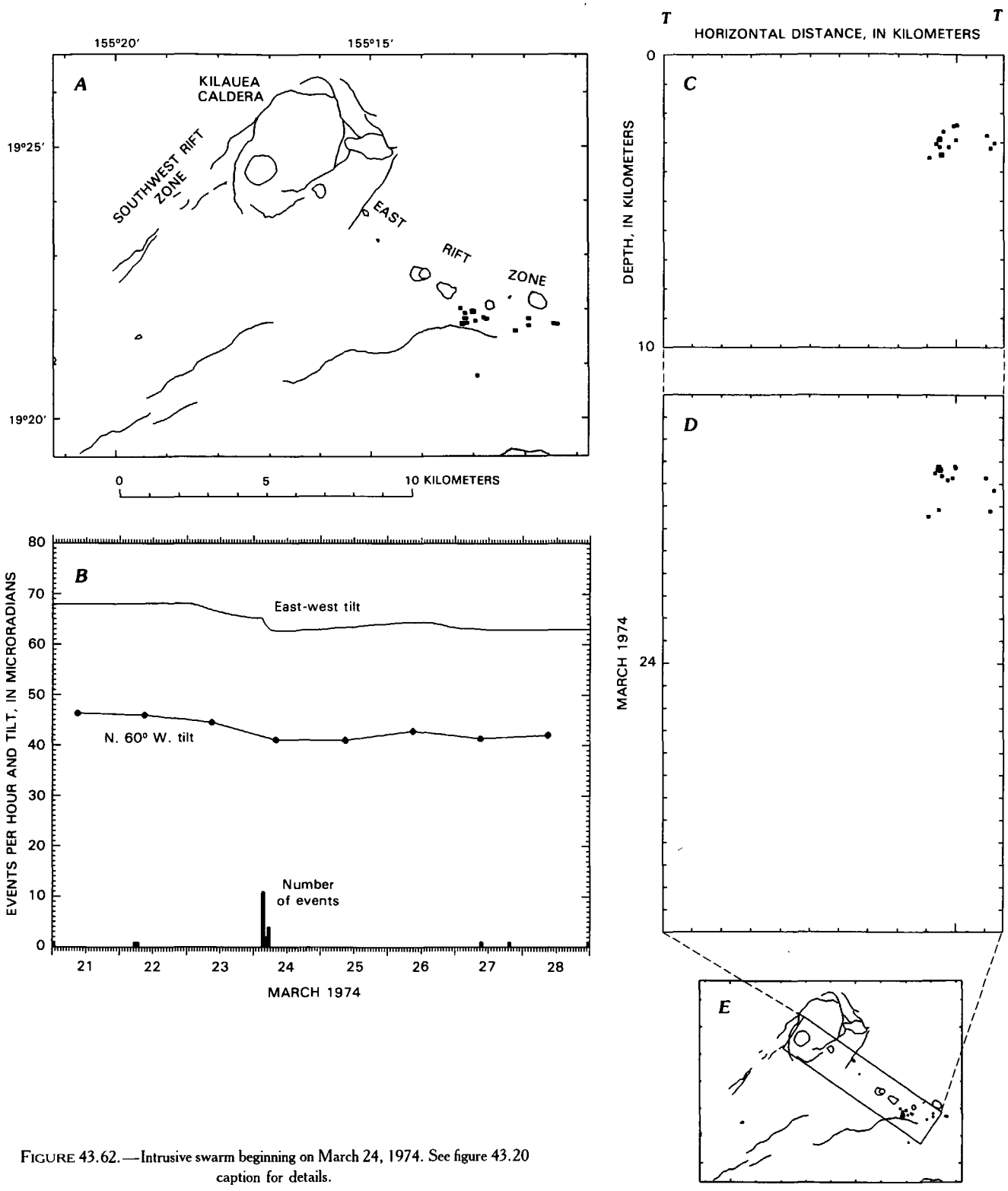

FIGURE 43.62.—Intrusive swarm beginning on March 24, 1974. See figure 43.20 caption for details.

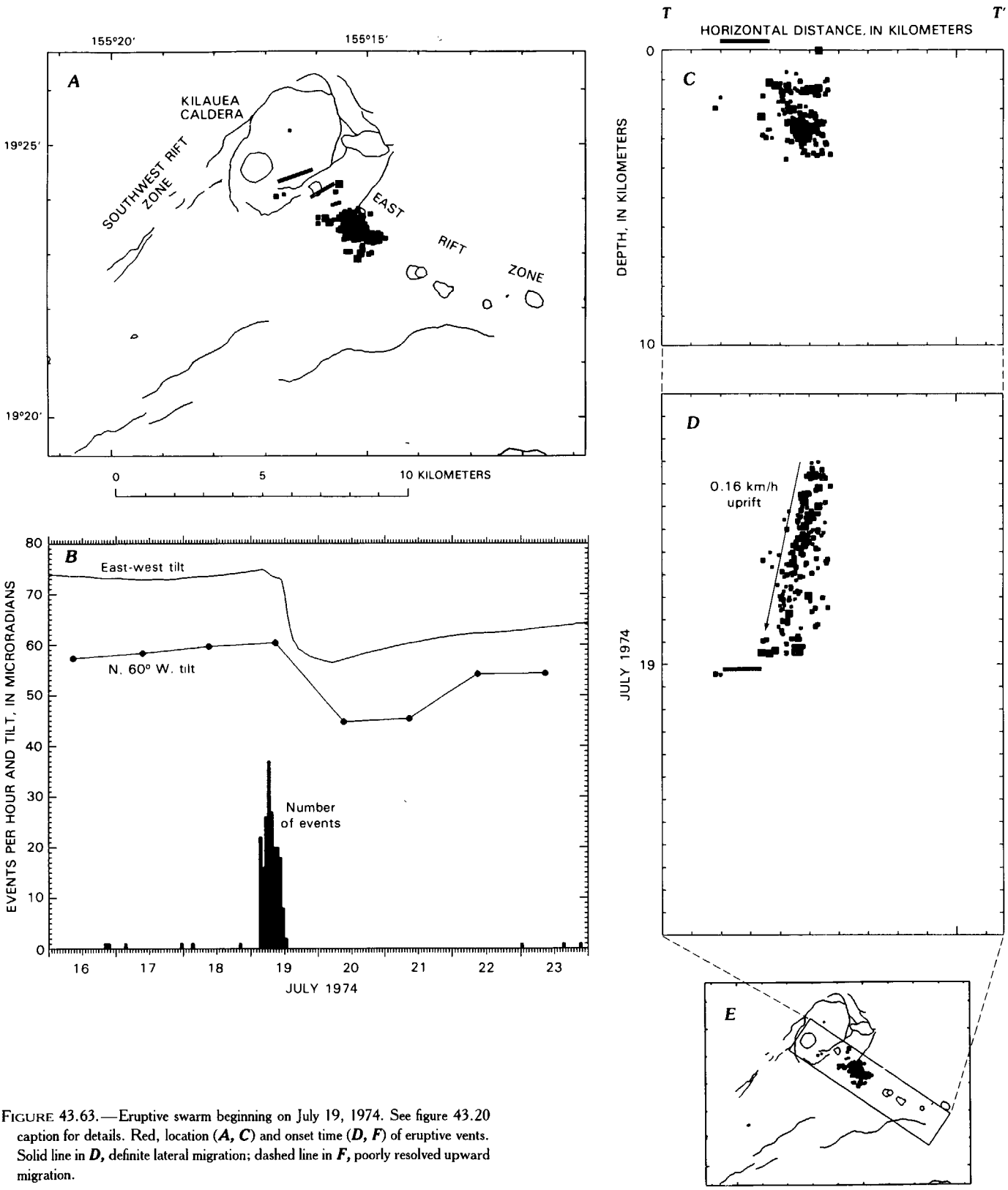

FIGURE 43.63.—Eruptive swarm beginning on July 19, 1974. See figure 43.20 caption for details. Red, location (***A, C***) and onset time (***D, F***) of eruptive vents. Solid line in ***D,*** definite lateral migration; dashed line in ***F,*** poorly resolved upward migration.

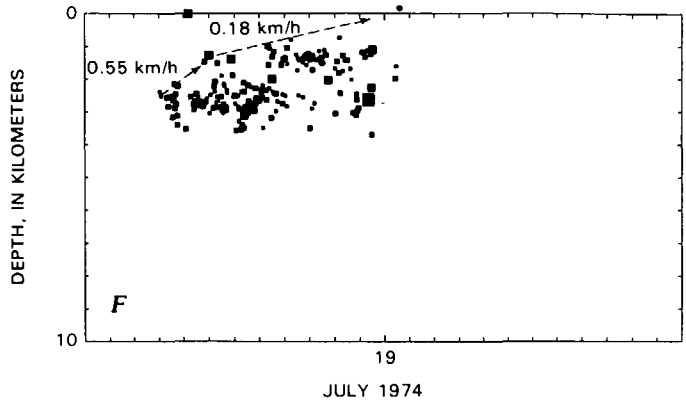

FIGURE 43.63.—Continued.

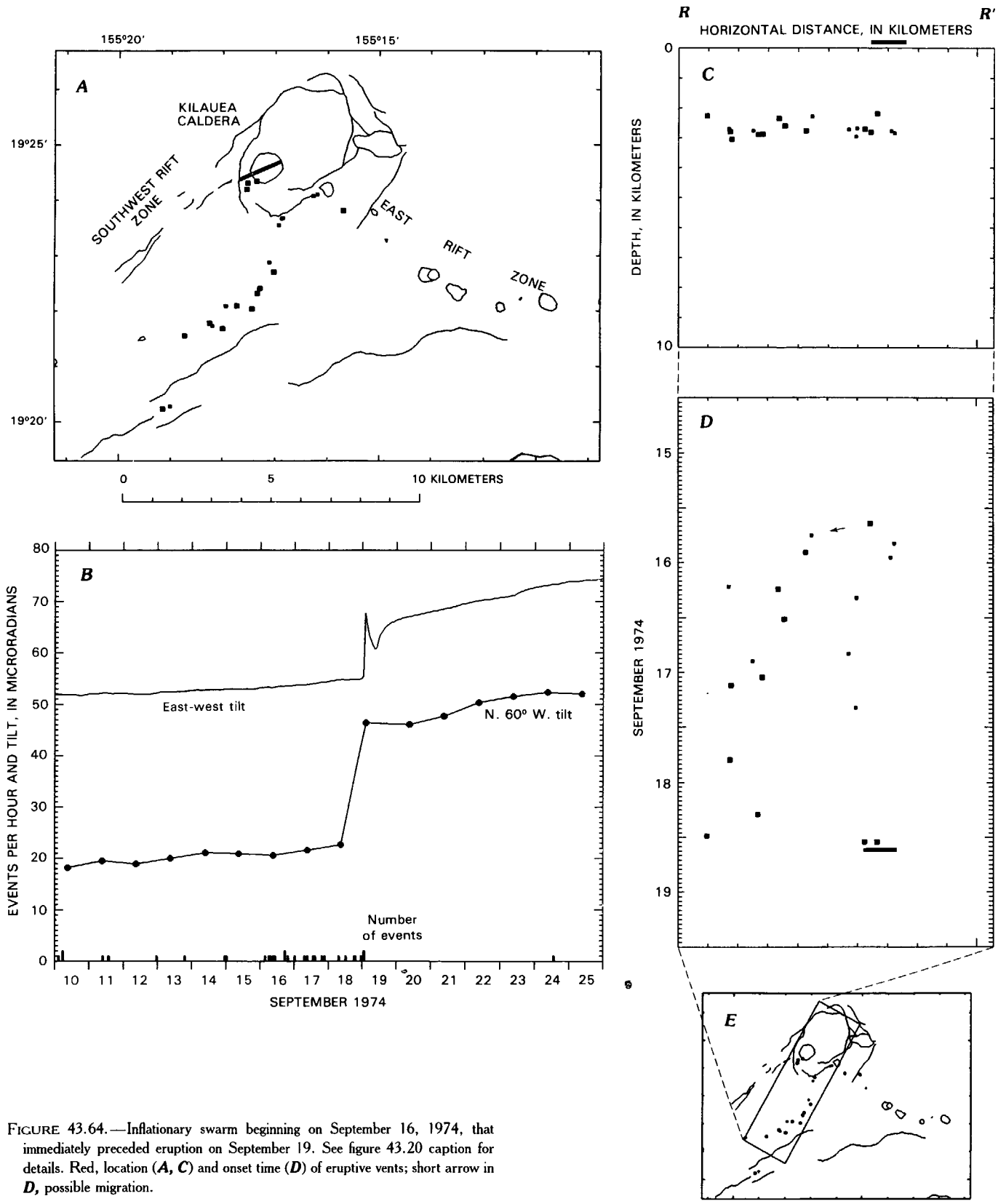

FIGURE 43.64.—Inflationary swarm beginning on September 16, 1974, that immediately preceded eruption on September 19. See figure 43.20 caption for details. Red, location (***A, C***) and onset time (***D***) of eruptive vents; short arrow in ***D,*** possible migration.

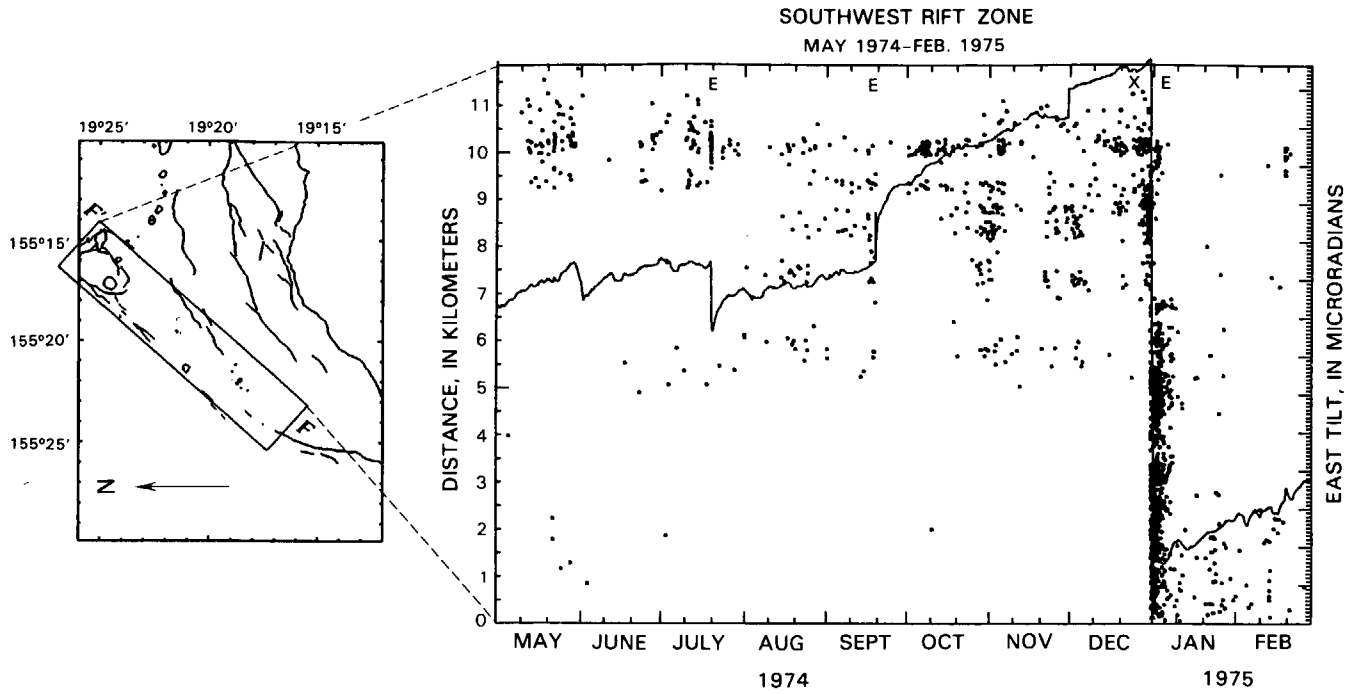

FIGURE 43.65.—Plot of earthquakes along southwest rift zone and east tilt at Uwekahuna versus time. Endpoints for distance axis *F-F'* are given in table 43.2. Tilt is from east-west Ideal Aerosmith tiltmeter, where east-down tilt is down on plot and generally indicates deflation of summit caldera. Notations along time axis refer to specific swarms detailed in other figures: E, eruption; X, swarm accompanying inflation. Small tick marks on tilt scale are 1 μrad.

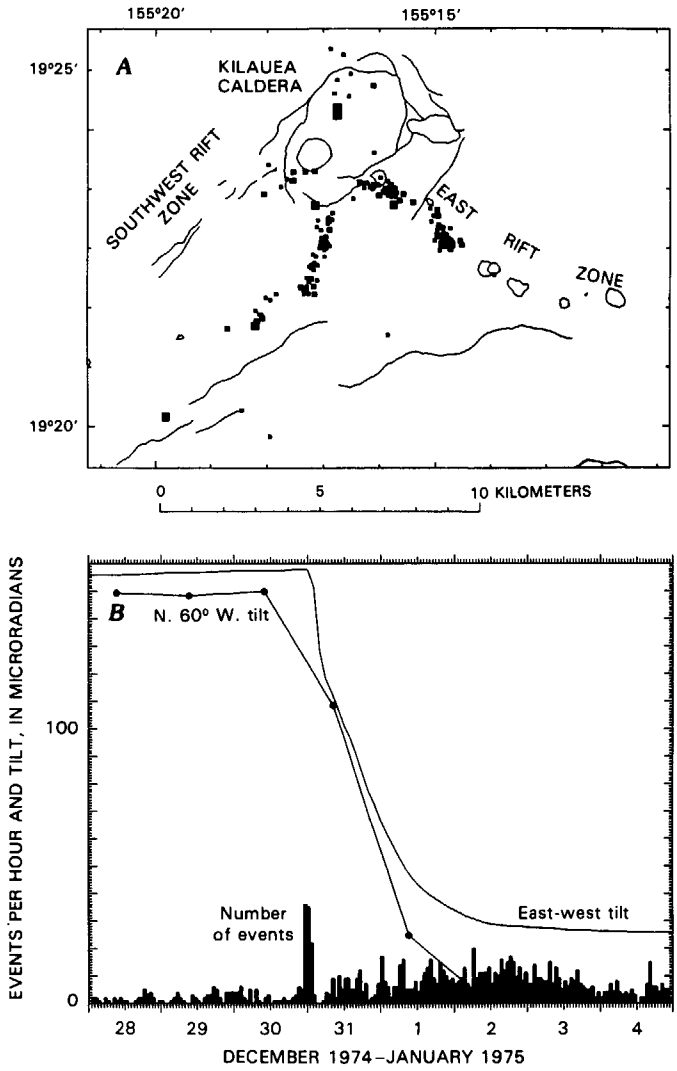

FIGURE 43.66.—Inflationary swarm beginning on December 24, 1974, that immediately preceded the eruption on December 31. See figure 43.20 caption for details. Dashed lines in ***D*** and ***G***, poorly defined migration of seismicity.

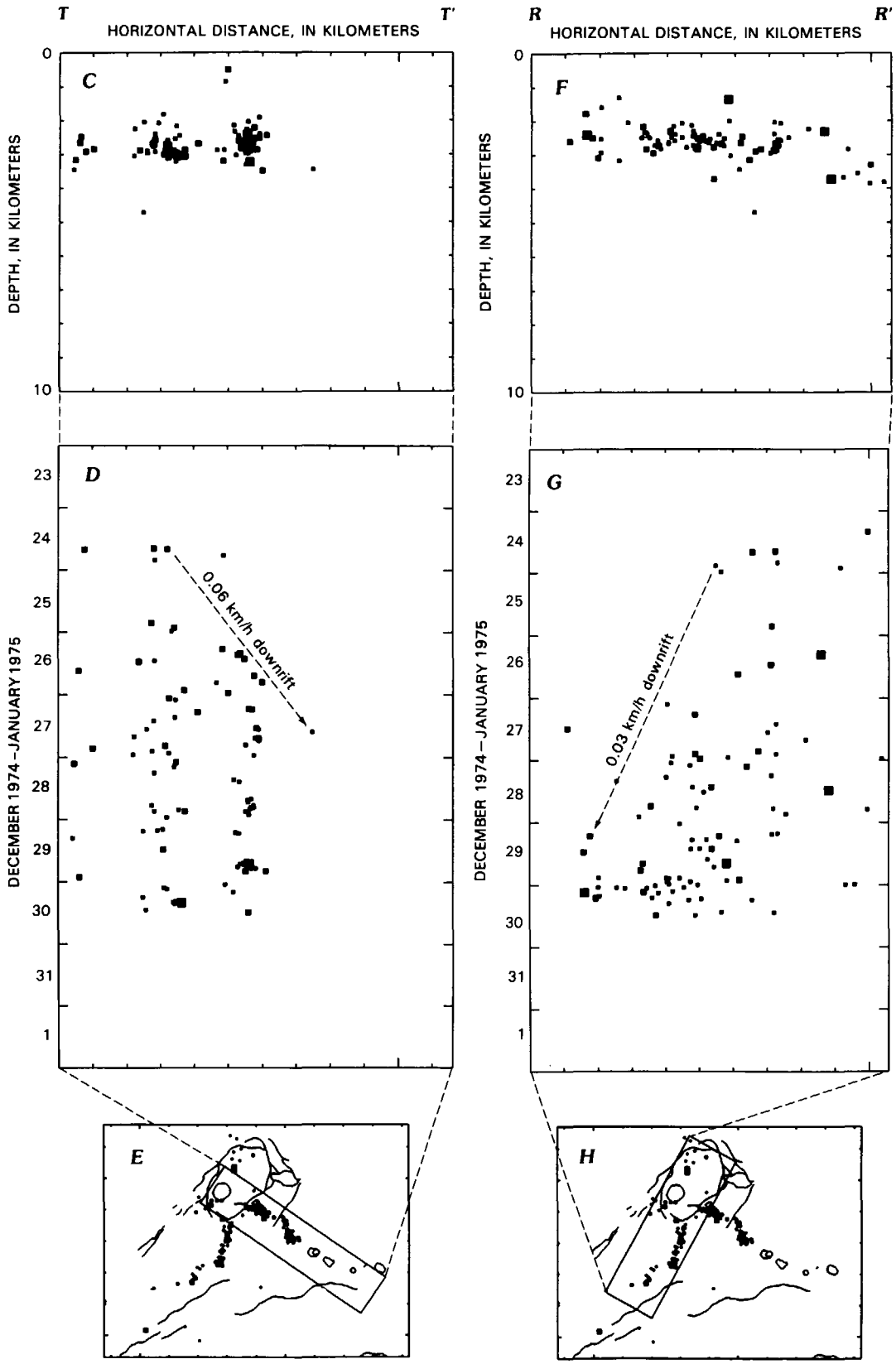

FIGURE 43.66.—Continued.

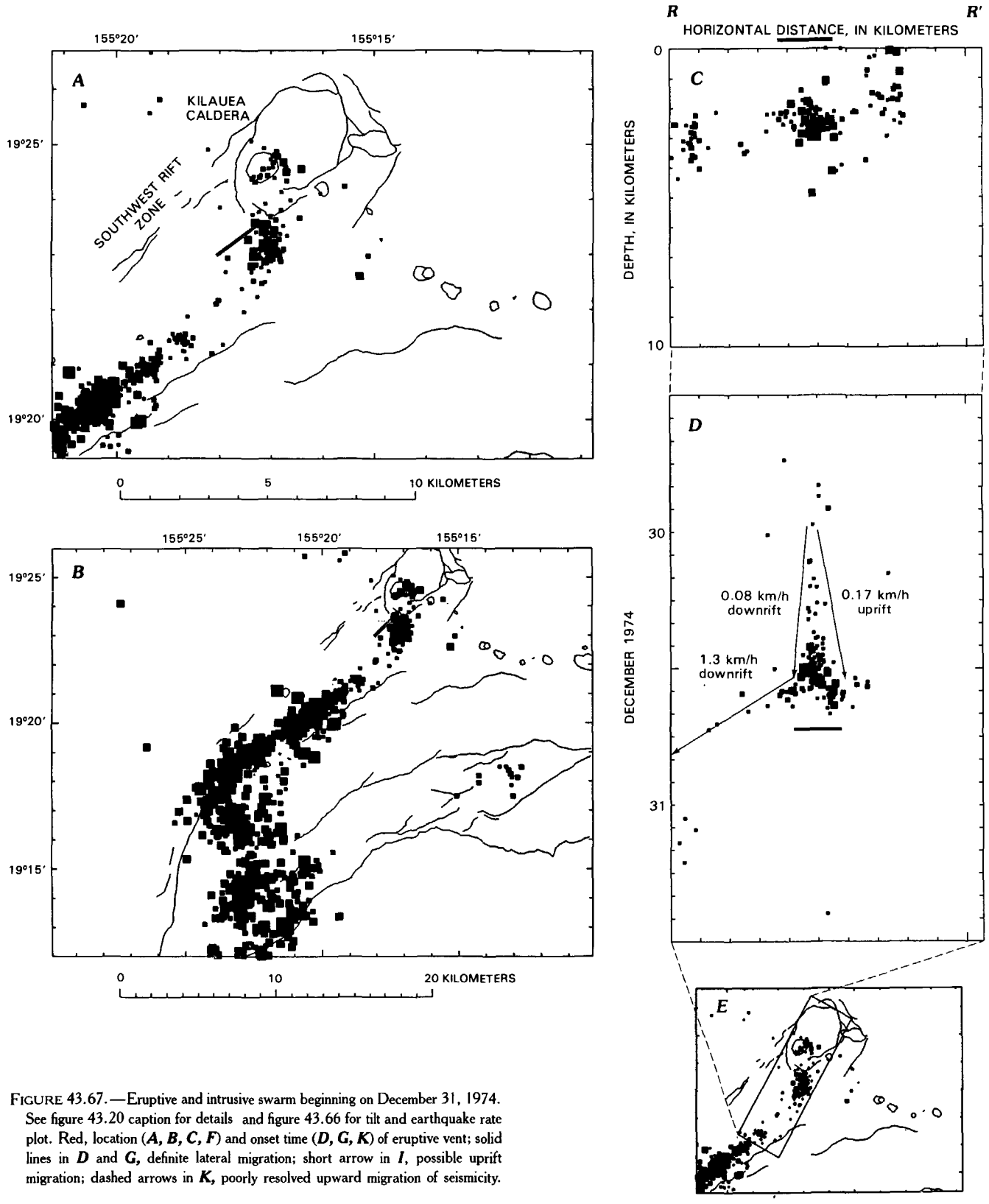

FIGURE 43.67.—Eruptive and intrusive swarm beginning on December 31, 1974. See figure 43.20 caption for details and figure 43.66 for tilt and earthquake rate plot. Red, location (***A, B, C, F***) and onset time (***D, G, K***) of eruptive vent; solid lines in ***D*** and ***G***, definite lateral migration; short arrow in ***I***, possible uprift migration; dashed arrows in ***K***, poorly resolved upward migration of seismicity.

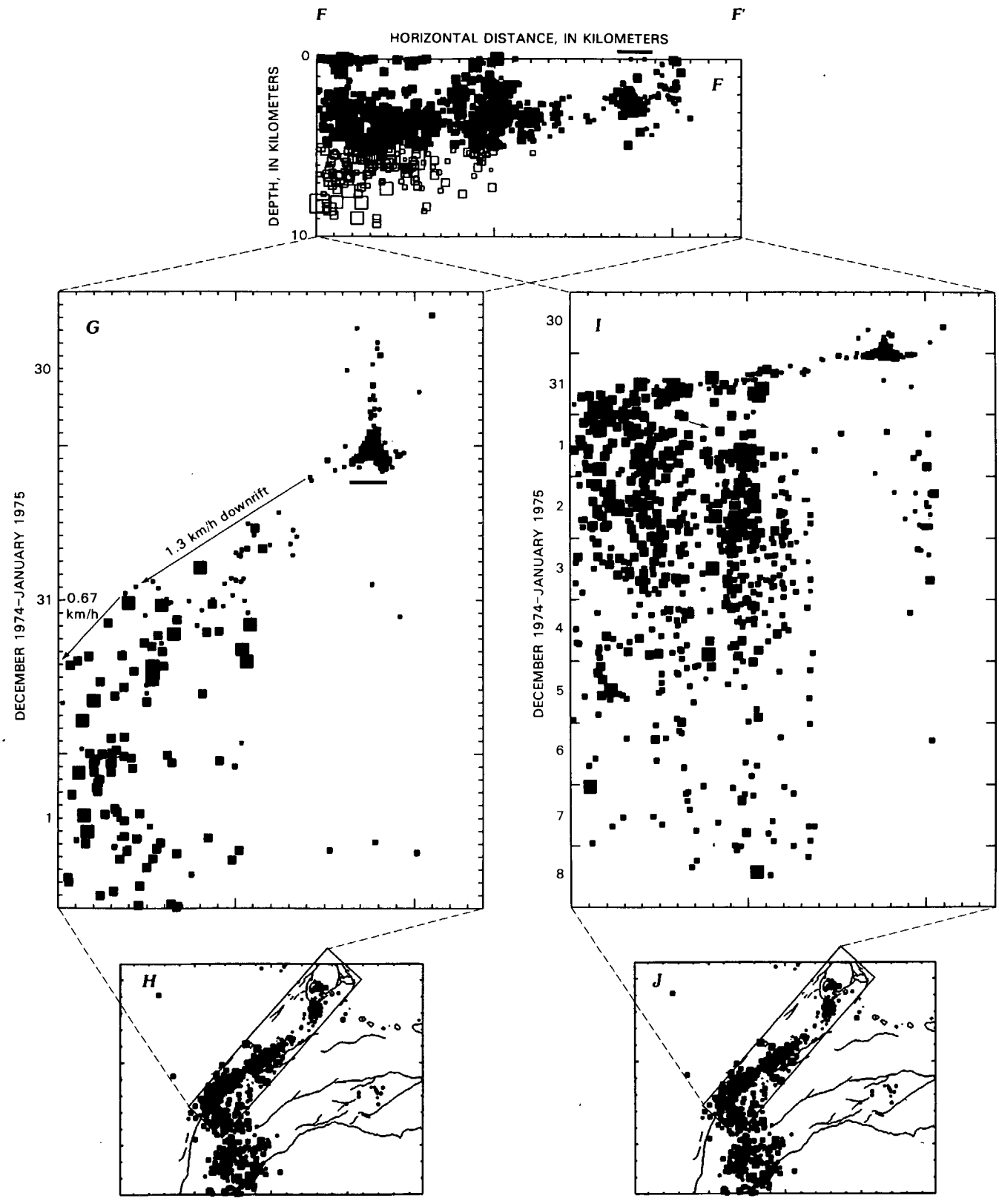

FIGURE 43.67.—Continued.

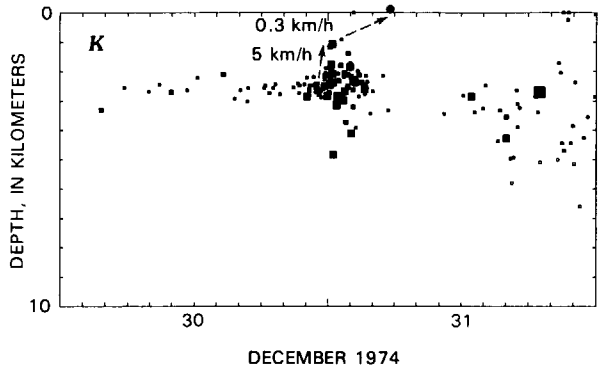

FIGURE 43.67.—Continued.

1976-77 EAST RIFT ZONE INTRUSIONS AND ERUPTION

The next major event at Kilauea was the magnitude-7.2 Kalapana earthquake on November 29, 1975. The south flank's accumulated elastic compression was partly released, and it slipped seaward as much as 8 m (Lipman and others, 1985). The ERZ dilated and accommodated roughly 100 million cubic meters of magma as the summit deflated (Dzurisin and others, 1980). A small summit eruption was triggered by the earthquake, but no ERZ eruption occurred and its magma remained below the surface. We do not consider the November 29, 1975 eruption here because of its atypical origin and because any intrusion seismicity was completely masked by the large earthquake and its aftershocks.

A major change in the short-term volcanic behavior of Kilauea resulted from the Kalapana earthquake. Whereas most swarms immediately prior to the earthquake culminated in eruptions, intrusions outnumbered eruptions during 1976–81. This change in behavior is statistically significant and can be attributed to lowered confining stress on the ERZ and its ease of rifting to accommodate new magma without sustaining pressures necessary for it to reach the surface (Ando, 1979: Klein, 1982b). A second change associated with the Kalapana earthquake was a shift of activity from the SWRZ to the ERZ. Following the December 1974 eruption, the SWRZ did not experience another intrusion until 1981.

The ERZ intrusions of June 21 and July 14, 1976, occurred while aftershocks of the Kalapana earthquake continued. The swarms were very similar. Both extended from Kokoolau to Mauna Ulu (figs. 43.68*A*, 43.69*A*). Each swarm lasted less than 24 hours and experienced 10–15 microradians of deflation coincident with the swarm (figs. 43.68*B*, 43.69*B*). Both swarms began between Pauahi and Mauna Ulu and migrated uprift. Migration was more recognizable during the June 21 swarm where the speed was about 1.3 km/h (fig. 43.68*D*). About the time the June earthquakes ceased moving uprift they veered upward to within 1 km of the surface (fig. 43.68*F*). The upward speed was about 0.5 km/h. The July earthquakes also displayed an upward migration (at 0.7 km/h, fig. 43.69*F*). The upward movement in June was between Kokoolau and Hiiaka, but that in July was near the former Aloi Crater.

Both of the 1976 intrusions originated from a point 3 km beneath the surface and just downrift of Pauahi. We interpret the immediate source of these intrusions as a secondary magma pocket below Pauahi. This Pauahi magma reservoir was suggested in an earlier section as the cause of the gap in seismicity below Pauahi, also seen in the 1976 swarms. A barrier containing this reservoir and just downrift of it is then a possible place for magma pressure to initiate earthquake swarms and intrusions. Whatever its cause, a concentration of stress beneath the Pauahi-Mauna Ulu region apparently initiates earthquake swarms that can move along the rift and upward. The magma supplying these intrusions is ultimately from the summit reservoir, but may have been stored within the rift. The summit reservoir must be in close hydraulic communication with the propagating dike, as evidenced by the simultaneity of rift swarm and summit deflation. Intrusions such as these are not simple downrift growth of dikes, and the possible relations of uprift earthquake migration and magma pockets within the rift will be discussed in more detail in the next section.

The ERZ between the caldera and Hiiaka was the site of two brief swarms on January 22 and February 8, 1977. The January swarm began at Keanakakoi, but soon moved to Kokoolau (fig. 43.70*A*, *D*). The fact that the summit did not rapidly deflate, but instead experienced slowly rising tilt (fig. 43.70*B*), and that the swarm's occurrence adjacent to the caldera might lead one to relate this sequence to summit inflation. The brevity of the intense part of the swarm (1 day) and relatively rapid though not precisely determined downrift migration rate (0.7 km/h) were more indicative of a rapid intrusion. This small swarm falls somewhere between the typical event types we have called slow, inflationary swarms and rapid, intrusive swarms.

The January swarm terminated near Kokoolau, where a more intense intrusion began 17 days later on February 8 (fig. 43.71*A*). The February intrusion lasted for about 11 hours and produced a rapid deflation (fig. 43.71*B*). The disturbance spread both uprift and downrift, though the continuity of migration is not well developed (fig. 43.71*D*). The initial 5 earthquakes were followed by an aseismic period, then a more intense episode that coincided with rapid summit deflation. The significant growth in dike volume

thus coincided with the most intense seismicity. At the beginning of the intense part of the swarm, an area of about 3 km by 3 km was active simultaneously (fig. 43.71*A*, *D*), and it did not grow in area. The disturbed zone thus seems to have aseismically enlarged in surface area before it seismically grew in thickness and volume. We therefore generally associate earthquakes primarily with growth of dike thickness and the compression of adjacent brittle rock. The enlargement of the disturbed zone alone does not then generate intense seismicity in these intrusions unless the dike also grows significantly in width.

The early 1977 swarms suggest that an initial low-volume intrusion propagated from the caldera to Kokoolau on January 22, where it encountered a blockage in the magma conduit. The blockage broke on February 8 when a greater magma volume became involved.

The September 1977 swarm and eruption penetrated farther along the ERZ than any other during 1962–83. A detailed eruption chronology is given by Moore and others, (1980). Four disconnected seismic zones were active during the eruption: the southern part of the caldera and central Koae fault zone (fig. 43.72*A*), and the ERZ at Makaopuhi and near Kalalua (fig. 43.72*F*). The deflation of Kilauea summit exceeded 90 microradians and continued for about four days (fig. 43.72*B*). The start of the rapid deflation, the beginning of the swarm in the southern part of the caldera, and four earthquakes south of the former Aloi Crater were all nearly simultaneous (fig. 43.72*D*). Seismicity at Makaopuhi and later at Kalalua shows that the part of the intrusion downrift of Mauna Ulu propagated at 1.2 km/h, then slowed to about 0.23 km/h downrift of Kalalua (fig. 43.72*H*). The absence of earthquakes between the caldera and Aloi and the simultaneity of seismicity at each place indicate that the intrusions of the previous two years left much of the magma conduit open and fluid, and no new dike intrusion or earthquakes were required to transport magma through this area.

The shallow conduit between Makaopuhi and Puu Kamoamoa was aseismic, but deeper earthquakes were induced in the south flank immediately adjacent to the gap in shallow earthquakes (fig. 43.72*F*). This pattern indicates that rifting did occur here, but was probably deeper than elsewhere on the rift. The eruption induced considerable seismicity in the south flank 5–13 km from the vents (fig. 43.69*F*; Dvorak and others, 1985). Considerably more and larger flank earthquakes were induced as a result of the September 1977 eruption than the somewhat similar January 1983 eruption. The induced seismicity is testimony both to the stress caused by the large intrusion and to the sensitivity of the south flank; these earthquakes can be partly considered aftershocks of the Kalapana earthquake less than two years earlier. The south flank was left with residual but local stresses, and these caused both aftershocks and the abundance of seismicity triggered by the 1977 intrusion.

The eruptive vents spanned a length of rift equal to that of the Kalalua seismic zone, but were displaced about 2–3 km downrift from the earthquakes (fig. 43.72*F*). This seismic pattern suggests that the dike intruded at 2–3 km depth and fed the eruption through feeders angled upward and downrift. The vents near Kalalua began erupting 5–10 h after the conduit 2–3 km beneath them became seismically active (fig. 43.72*H*). The time of opening of the easternmost vent was not observed directly, but the end of the uncertain period seems more likely: vent opening would then follow earthquakes as it does elsewhere. The last vent to open (uprift of Kalalua) does not follow the progression, but seems to accompany a new episode of seismic activity.

The earthquakes in the caldera and Koae are related to the large subsidence and deformation in the summit area. Earthquakes in the central Koae began about 12 hours after the intrusion and slowly progressed eastward at about 0.09 km/h (fig. 43.72*K*). This earthquake migration was also upward, owing to the dip of the seismic zone (fig. 43.72*J*). The migration of earthquakes is much slower and of opposite direction to that seen during intrusions of the Koae in 1973, and the seismic zone does not abut either rift. Tectonic movement on Koae faults is thus more likely than an intrusion, because summit subsidence would produce the correct sense of offset on the north-facing fault scarps. The caldera earthquakes began as soon as the intrusion started and slowly diminished during the next 6 days.

Caldera and Koae seismicity resumed on September 27 (fig. 43.73*A*) and accompanied the major eruptive phase that built the Puu Kiai spatter cone. The ERZ was nearly aseismic during this episode. The earthquakes below Halemaumau spread to the south very slowly at about 10 m/h (fig. 43.73*D*) and were apparently caused by the slow deflation. The caldera seismicity during the whole eruption thus generally correlates with deflation rate and is probably caused by compressive stresses in the summit area produced as the caldera contracted. These deflation earthquakes are in a similar location but appear to be the reverse of the slow swarms accompanying summit inflation and extension. The September 1977 eruption, the first following the $M=7.2$ Kalapana earthquake, was thus seismically complex. This complexity arose not only from the length of rift and volume of magma involved, but also from the probable disequilibrium of stresses following the Kalapana earthquake.

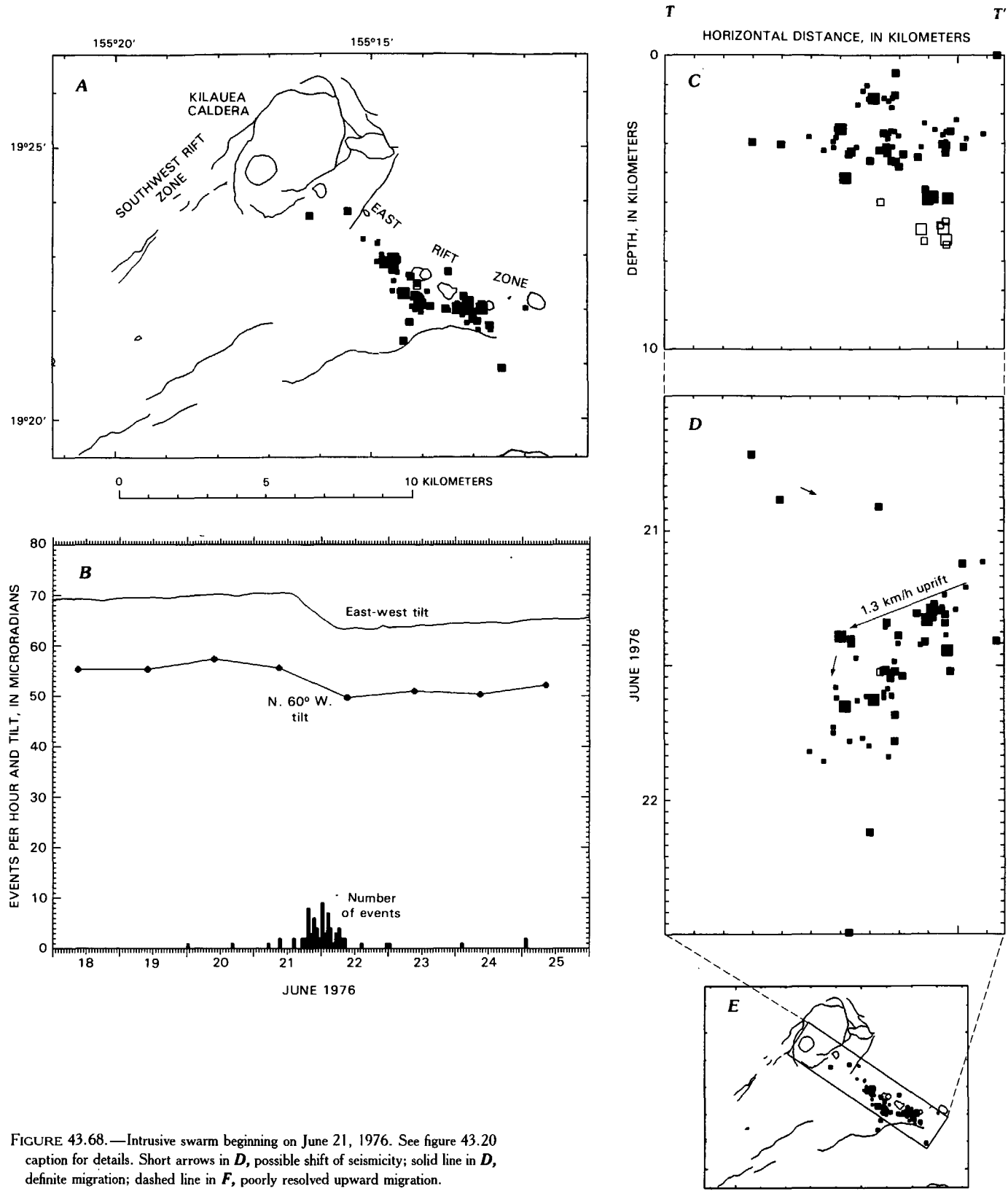

FIGURE 43.68.—Intrusive swarm beginning on June 21, 1976. See figure 43.20 caption for details. Short arrows in ***D***, possible shift of seismicity; solid line in ***D***, definite migration; dashed line in ***F***, poorly resolved upward migration.

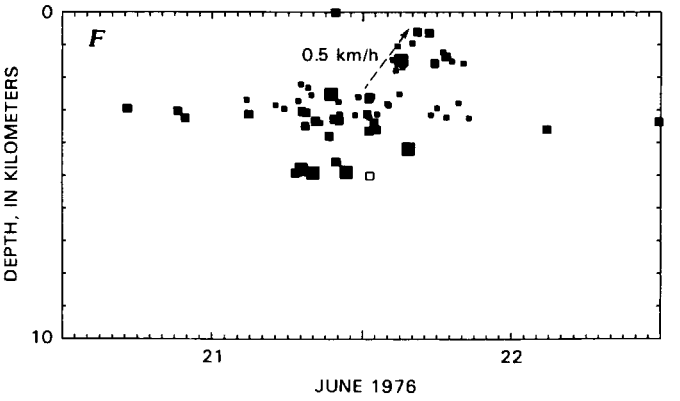

FIGURE 43.68.—Continued.

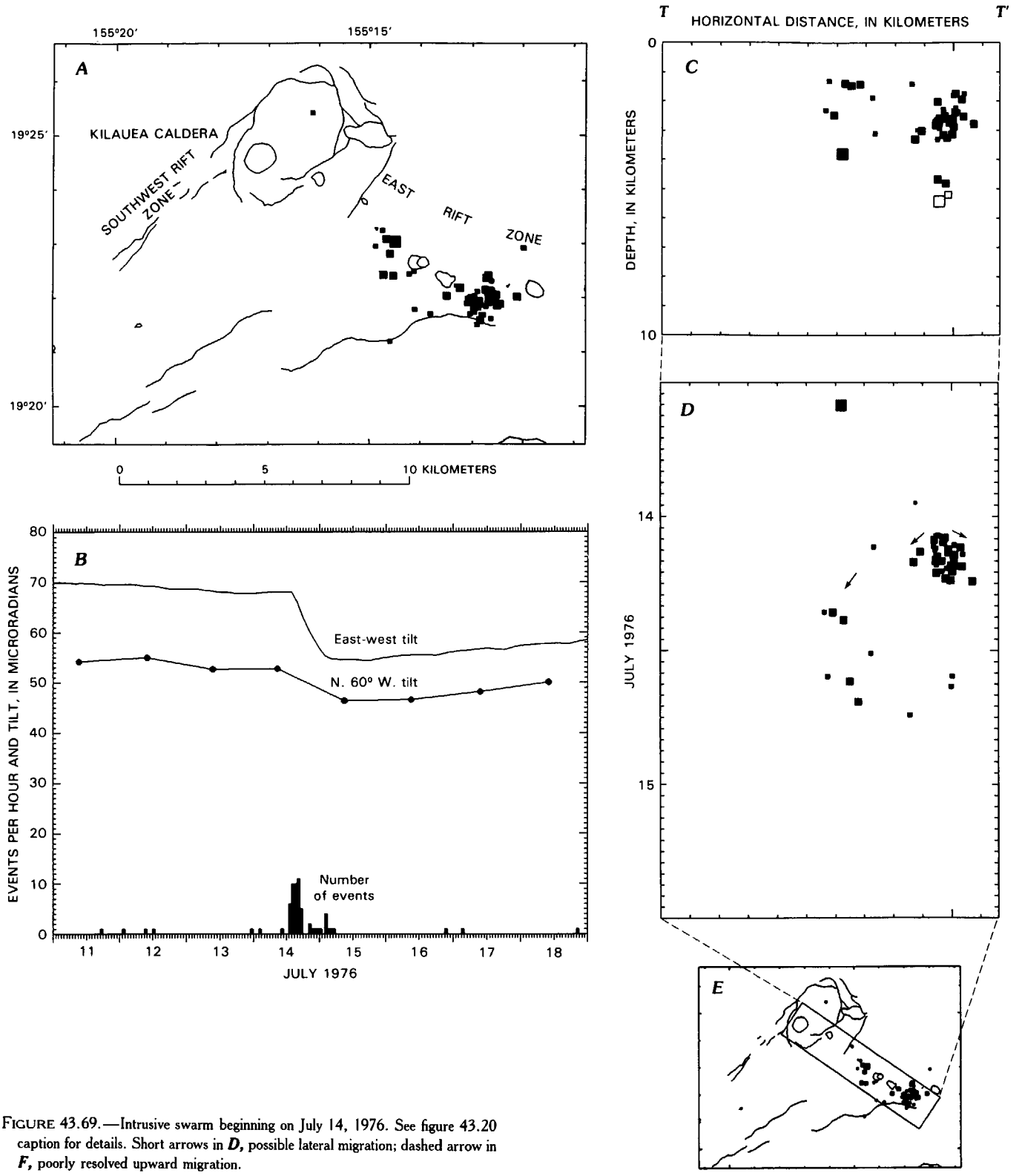

FIGURE 43.69.—Intrusive swarm beginning on July 14, 1976. See figure 43.20 caption for details. Short arrows in ***D***, possible lateral migration; dashed arrow in ***F***, poorly resolved upward migration.

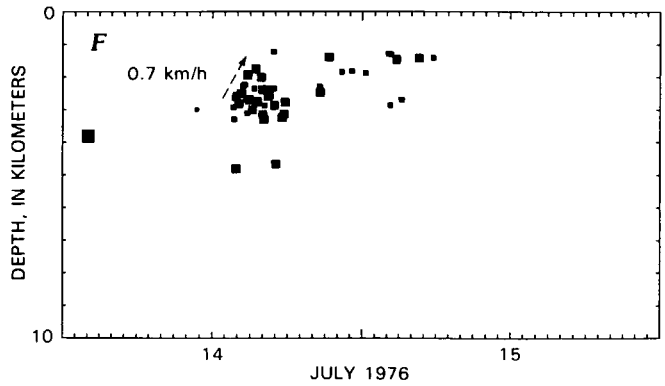

FIGURE 43.69.—Continued.

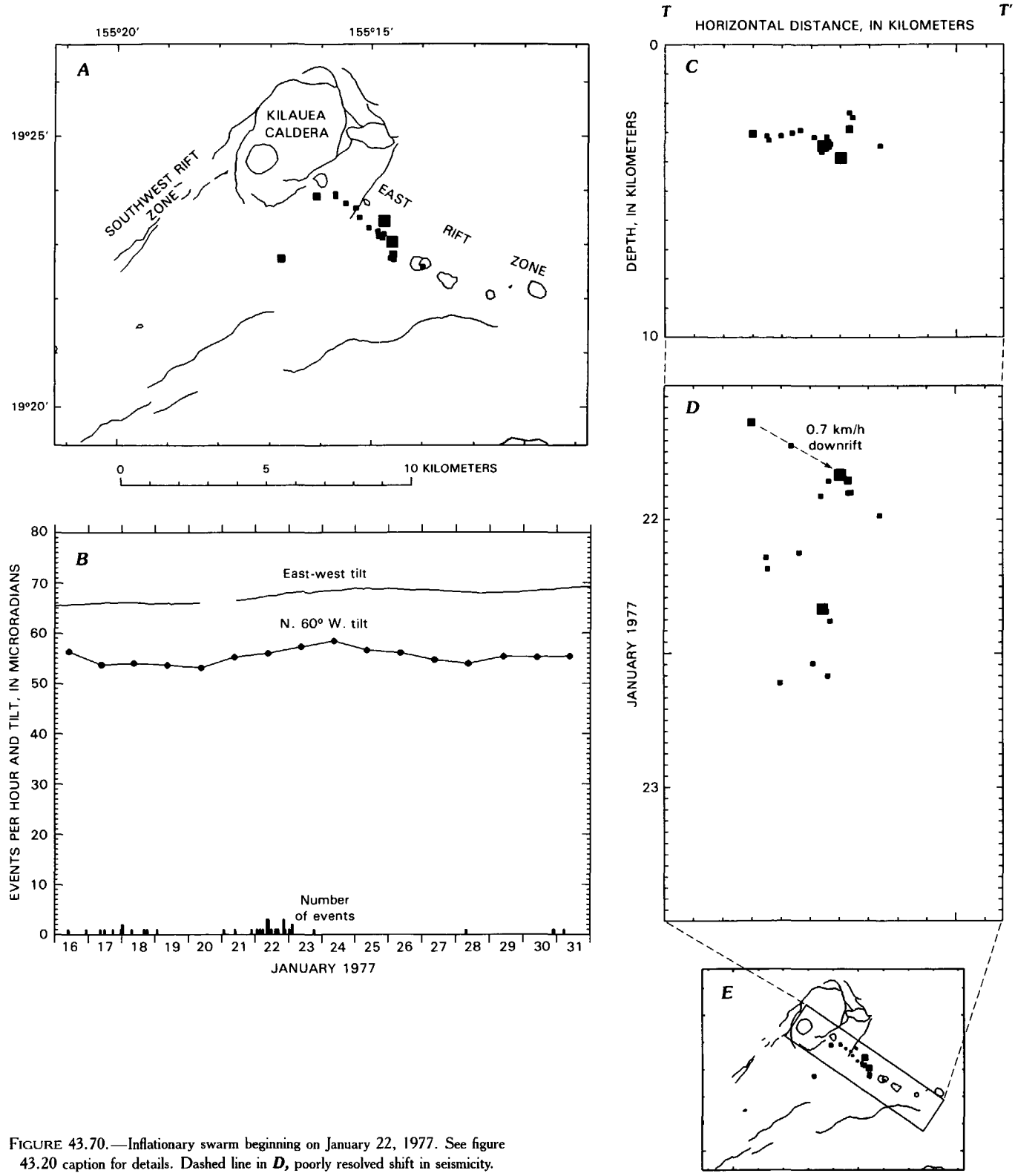

FIGURE 43.70.—Inflationary swarm beginning on January 22, 1977. See figure 43.20 caption for details. Dashed line in ***D***, poorly resolved shift in seismicity.

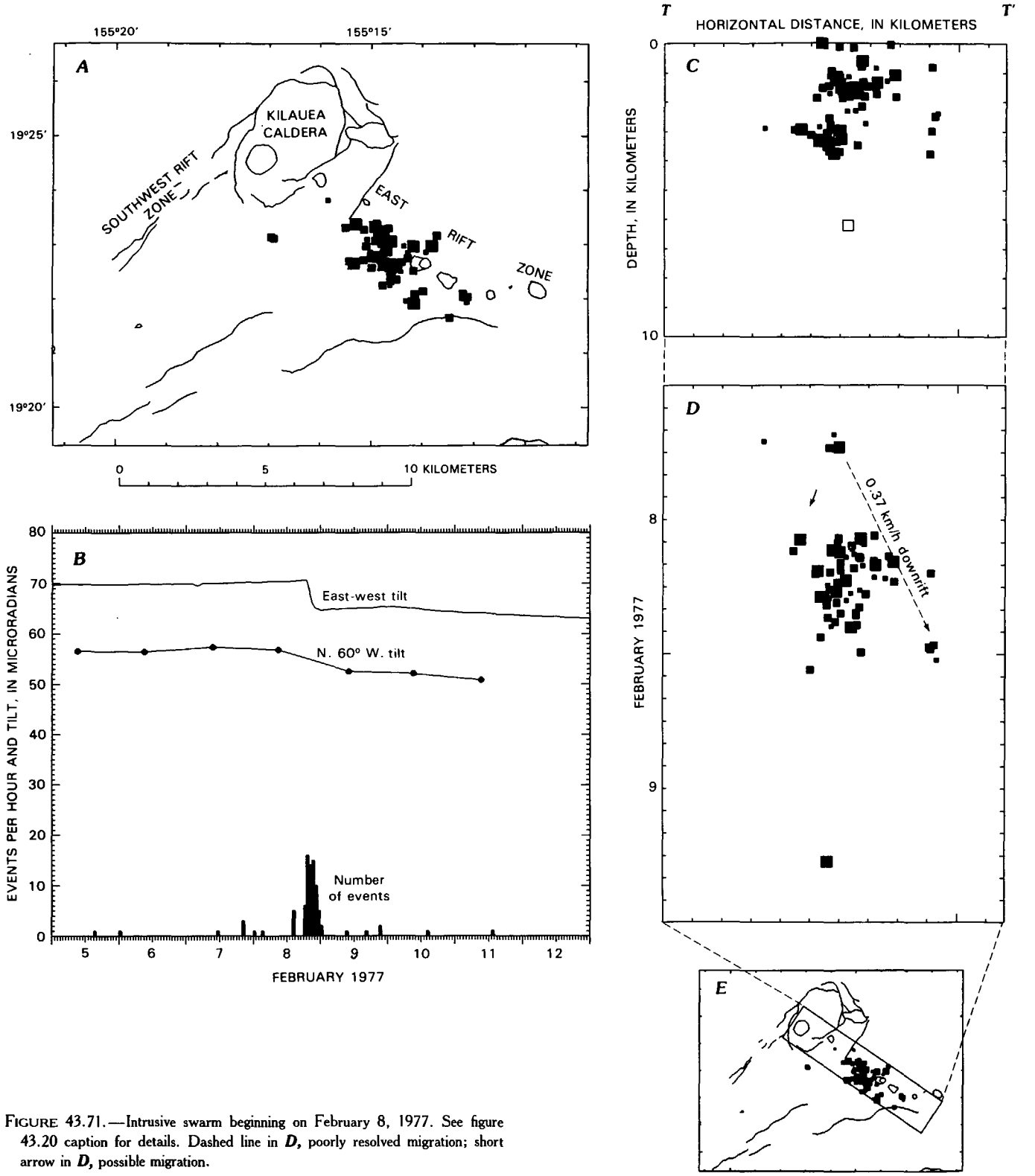

FIGURE 43.71.—Intrusive swarm beginning on February 8, 1977. See figure 43.20 caption for details. Dashed line in ***D***, poorly resolved migration; short arrow in ***D***, possible migration.

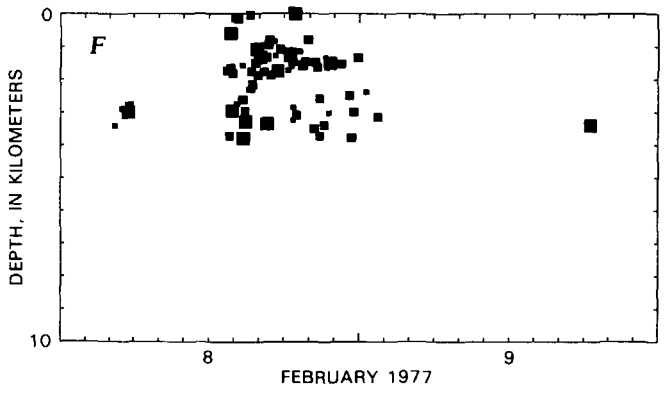

FIGURE 43.71.—Continued.

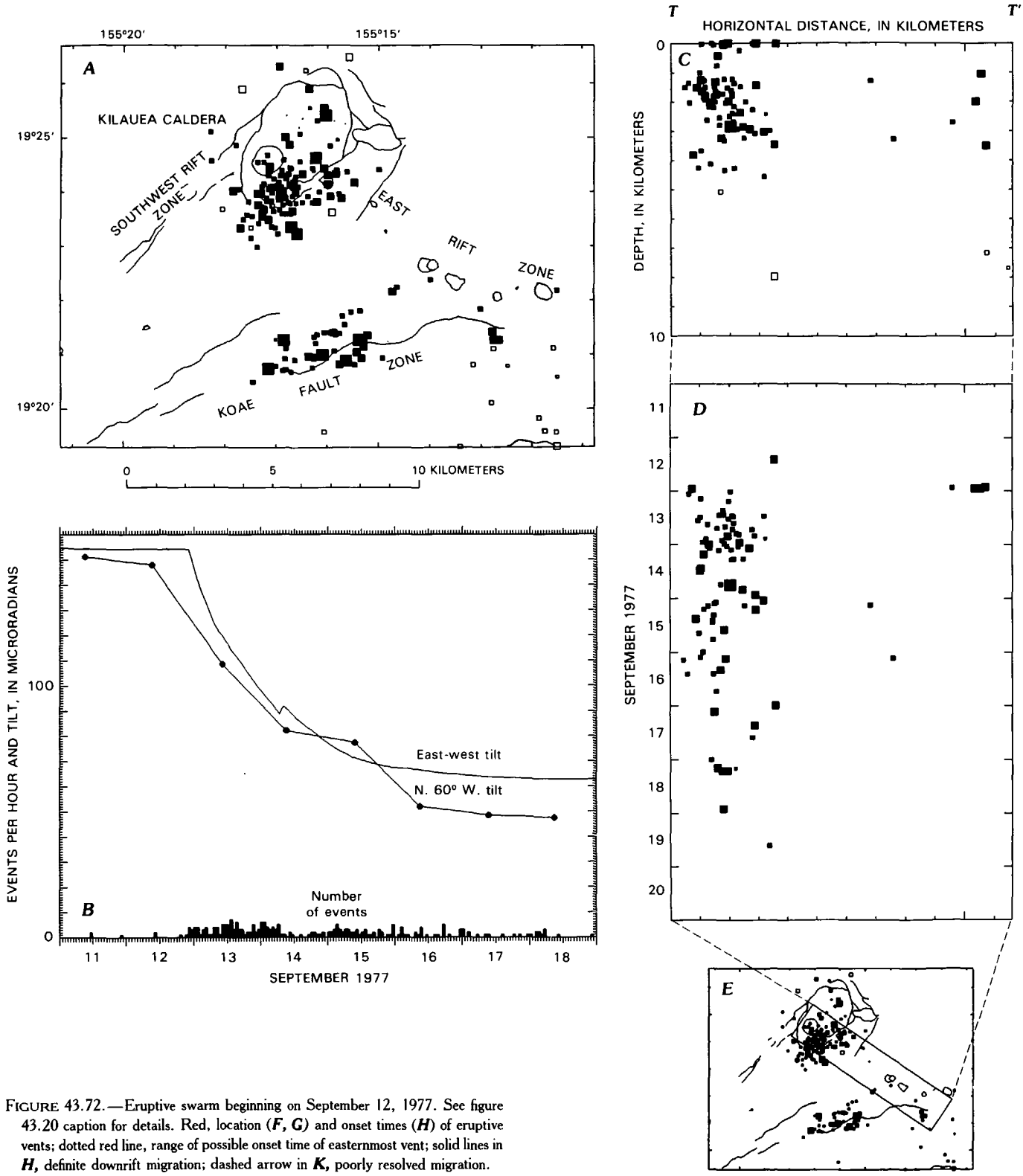

FIGURE 43.72.—Eruptive swarm beginning on September 12, 1977. See figure 43.20 caption for details. Red, location (***F, G***) and onset times (***H***) of eruptive vents; dotted red line, range of possible onset time of easternmost vent; solid lines in ***H***, definite downrift migration; dashed arrow in ***K***, poorly resolved migration.

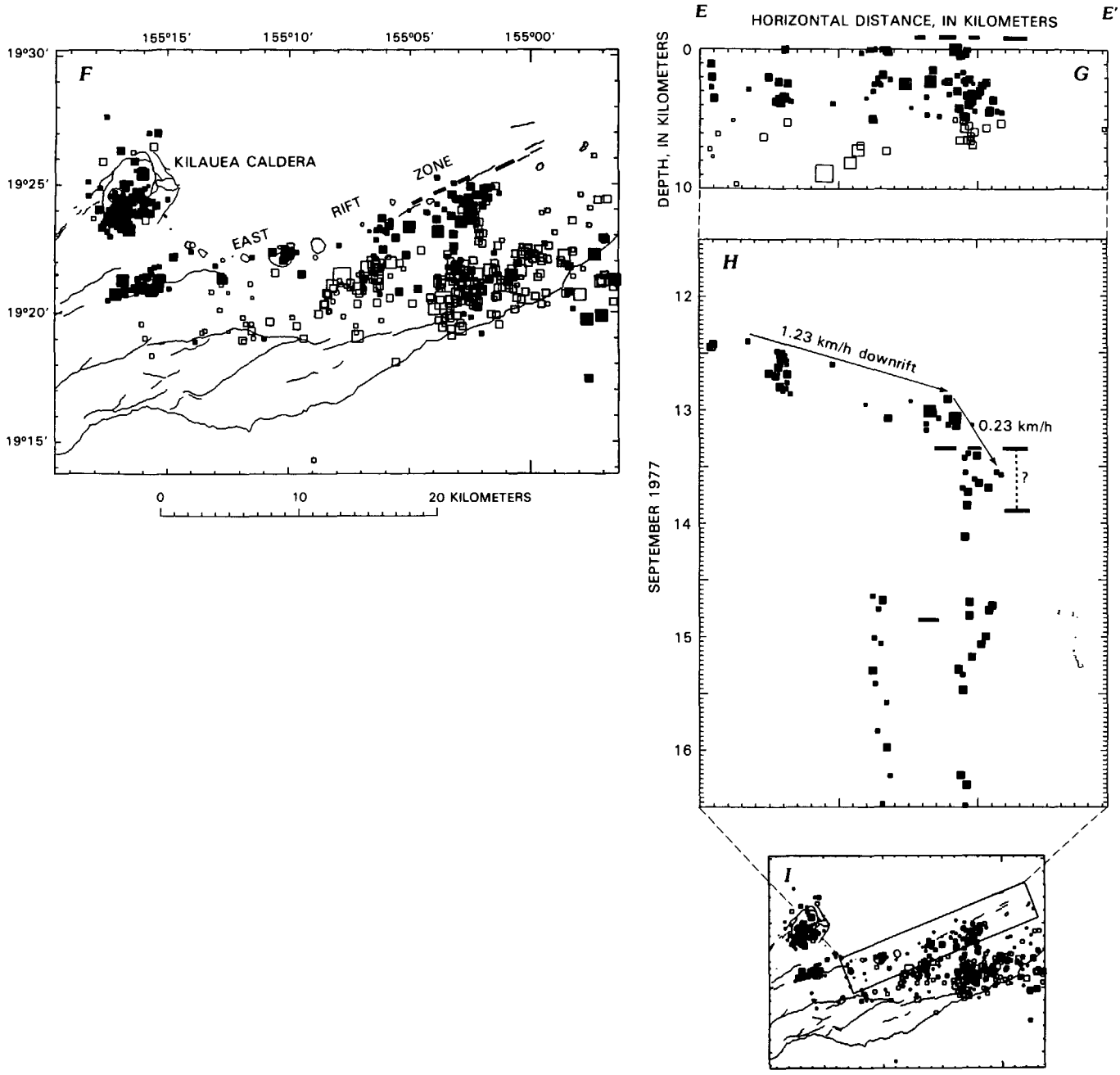

FIGURE 43.72.—Continued.

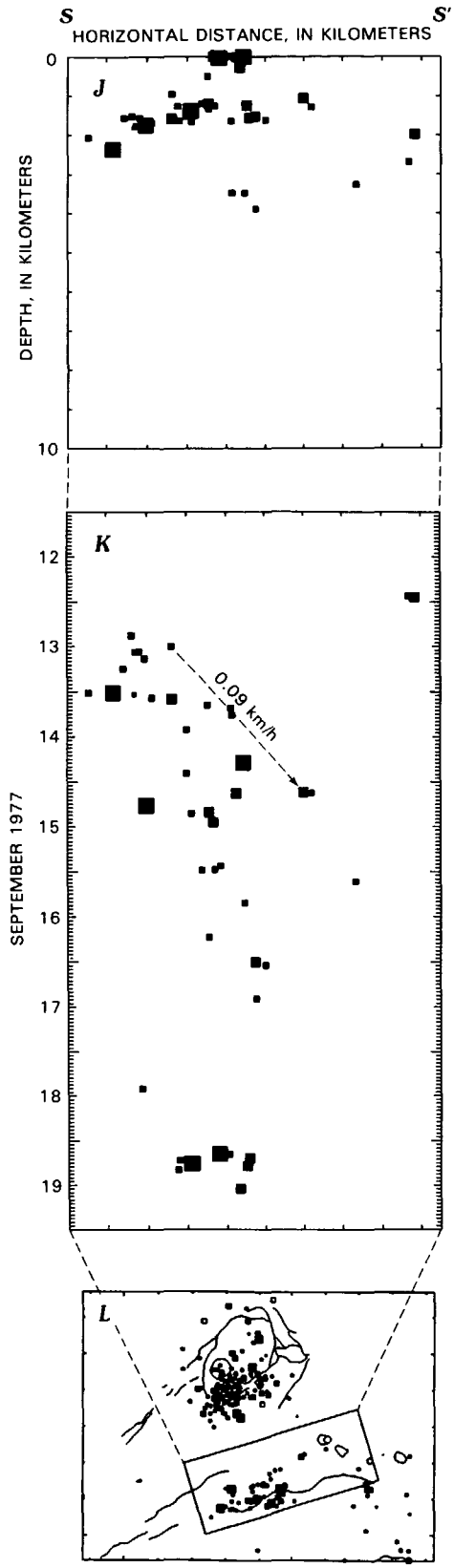

FIGURE 43.72.—Continued.

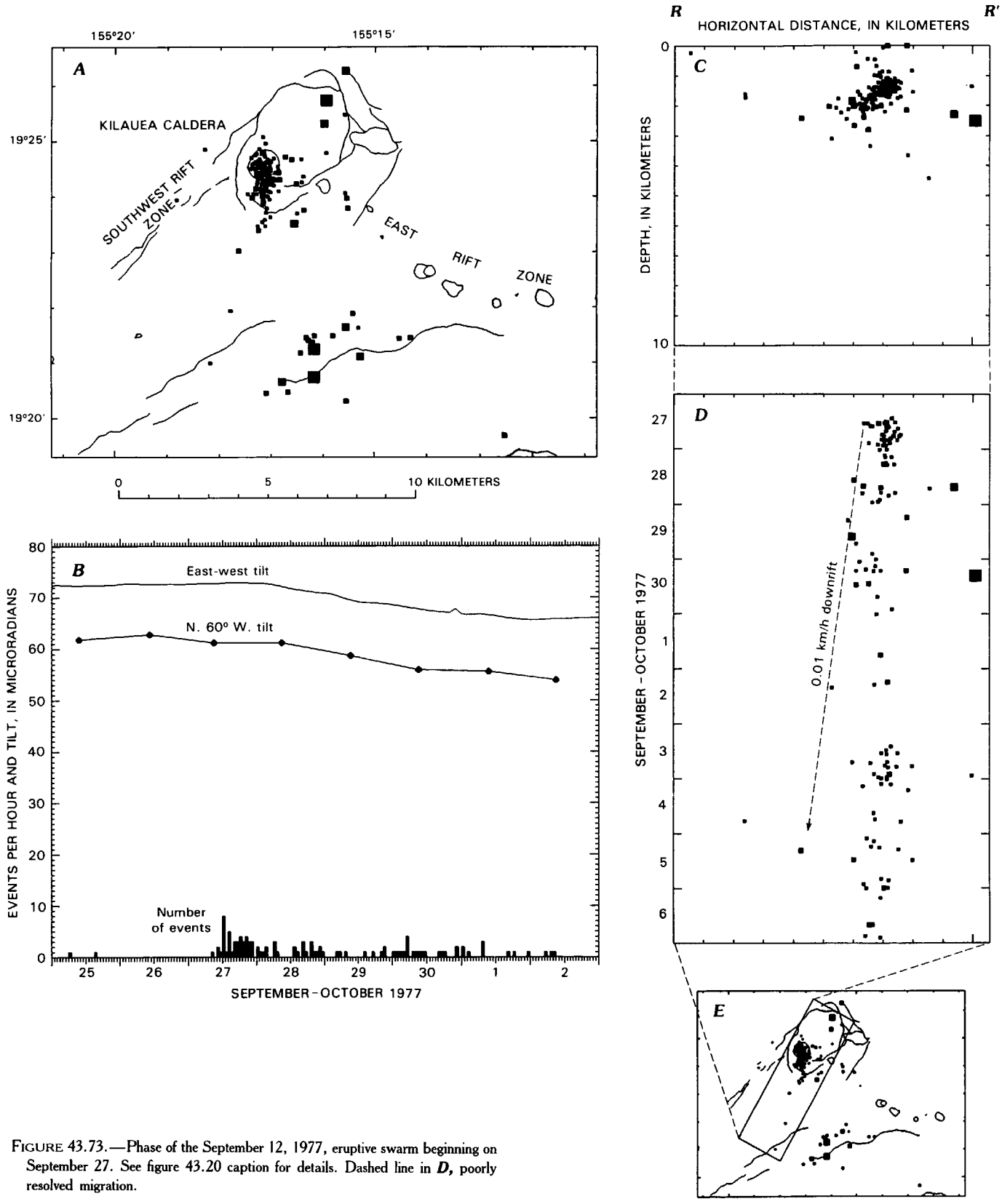

FIGURE 43.73.—Phase of the September 12, 1977, eruptive swarm beginning on September 27. See figure 43.20 caption for details. Dashed line in ***D***, poorly resolved migration.

EAST RIFT INTRUSIONS AND ERUPTION, NOVEMBER 1978 TO NOVEMBER 1979

The ERZ continued to overshadow the SWRZ during 1978–80 with a variety of eruptions and intrusions. An overview of the summit tilt and position of caldera and ERZ seismicity for the November 1978 through November 1980 interval is shown in figure 43.74. Prior to the first intense swarm on May 29, 1979, both tilt and caldera seismicity increased gradually as the summit inflated slowly (fig. 43.74*A*). Episodes of shallow earthquakes in the ERZ near Puu Kamoamoa also appeared during this period. These events were generally in slow swarms lasting several days and coincided with episodes of gradual summit deflation. The Puu Kamoamoa swarms were therefore slow intrusions. Because this activity was most prominent in mid-1980, it will be discussed in more detail below, following the March 1980 intrusions.

The ERZ generated two short but intense intrusive swarms on May 29 and August 12, 1979. Both seismic zones were about 4.5 km long (figs. 43.75*A*, 43.76*A*), but the May swarm was a little larger in terms of maximum magnitudes, swarm duration, and amount of deflation (figs. 43.75*B*, 43.76*B*). The May swarm began under Mauna Ulu and spread simultaneously both uprift to Pauahi and downrift to Makaopuhi (fig. 43.75*D*). It also started at about 3 km depth but spread rapidly both upward and downward (fig. 43.75*F*). The vertical migration speeds of 4–6 km/h were an order of magnitude faster than the lateral speeds of 0.6–0.7 km/h. Since the vertical propagation was much faster than for other intrusions, it may have been by a mechanism other than formation of a new dike, such as transmission of a pressure increase in a still-fluid dike.

A vertical column of earthquakes below 5 km depth was observed after 1200 H.s.t. on May 30, more than 12 hours after the intrusion (fig. 43.75*C*, *D*). The deeper events thus were induced by the intrusion and probably caused by continuation of rifting to depth or a downward moving dike. Growth of the rifts by intrusion must continue to about 10 km depth where the mobile south flank decouples from the pre-Hawaiian sea floor (Crosson and Endo, 1982). The rifting between 5 and 10 km depths is normally aseismic, and its timing is unknown. Only under Mauna Ulu and in the central section of the SWRZ (see the section "The Southwest Rift Zone Intrusions and Caldera Eruption of March through June 1982") are significant numbers of earthquakes below 5 km depth seen during intrusions.

The August 12 intrusion originated near Keanakakoi adjacent to the caldera and moved rapidly downrift at 1.6 km/h (fig. 43.76*D*). The intrusion was centered at 3 km depth and was less than 1 km in vertical extent (fig. 43.76C). The swarm continued for a few days in the downrift portion of the intrusion and extended at a very reduced rate (fig. 43.76*F*). This intrusion is one of the clearest examples of a fairly simple but rapid intrusion originating directly from the summit magma reservoir.

Kilauea continued to inflate and seismicity was nearly continuous in the portions of the SWRZ and ERZ immediately adjacent to the caldera (fig. 43.74*B*). A short swarm confined to the southern portion of the caldera (fig. 43.77*A*) punctuated a 30-day period of rapid and nearly continuous inflation. Inflationary swarms are generally not so short and intense. This one may have been associated with some form of dike intrusion caused by the increasing magma pressure, such as the breaking of rock to bridge two chambers of the magma reservoir.

The Pauahi eruption of November 16, 1979, began with a swarm starting abruptly on November 15. Earthquakes eventually engulfed the ERZ from Puhimau to the former Aloi Crater and partly into the Koae fault zone (fig. 43.78*A*). Both the main magma conduit at 3 km depth and the shallow 1- to 2-km depth zone were active (fig. 43.78C). The cross section also shows that the shallowest ERZ earthquakes mark a branch of the dike extending upward to Pauahi near the eruptive vents.

The temporal pattern of earthquakes in the November swarm is somewhat complex but shows characteristics common to many intrusions in this part of the ERZ. Earthquakes again underscored the key role played by the hypothesized magma blockage just downrift of Pauahi. The first two earthquakes were uprift of Pauahi. They lie along a front moving at about 3.8 km/h which became seismically intense when it reached Pauahi, and continued for another 1–2 km to the southeast (fig. 43.78*D*). When projected along the Koae fault zone, the same migration appears with a foreshortened speed of 1.5 km/h (fig. 43.78*G*). Earthquakes then moved slowly into the Koae at a decreasing speed. Summit deflation did not coincide with the first earthquakes, but commenced just minutes after the initial seismic front reached Pauahi and the intense seismicity began. This relation shows that the initial downrift migration did not draw much magma from the summit reservoir, but that the coincidence of intense seismicity and deflation implies a close hydraulic communication between the summit reservoir and Pauahi. Earthquakes then migrated back uprift at about the same speed, almost as if some sort of disturbance was reflected from a barrier just downrift of Pauahi.

After the intense seismicity began, the sense of migration was generally uprift: (1) the western boundaries of the seismic zone moved uprift and into the Koae, (2) the eastern boundary of the seismic zone moved uprift at about 0.08 km/h, and (3) the eruptive vents opened westward (fig. 43.78*D*). The possible mechanisms of this uprift migration will be discussed in the section "Discussion of Rift Zone Intrusions." Coincident with the initial uprift movement was an upward migration from 3 km depth that slows and becomes nearly aseismic at a depth of 1 km (fig. 43.78*I*). These patterns reinforce the earlier suggestion of a secondary magma reservoir about 3 km beneath Pauahi and a blockage of the magma conduit just downrift of Pauahi. The initial downrift migration was not strong enough to penetrate the barrier, where a stress concentration triggered a rifting episode fed by summit magma. Even though possibly triggered by a pulse from the summit, the sequence of events culminating in the eruption at Pauahi were initiated at Pauahi.

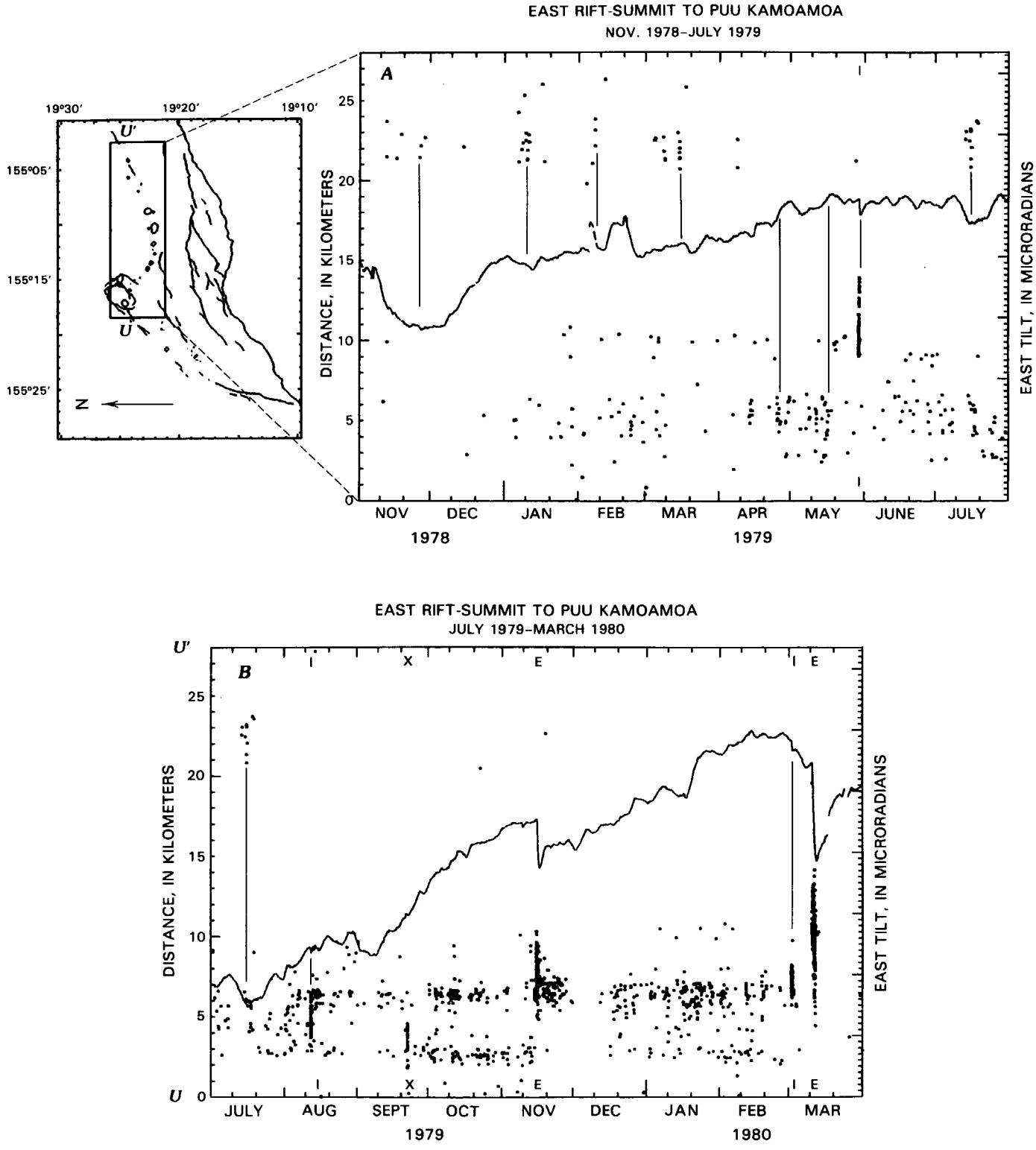

FIGURE 43.74.—Plot of earthquakes along east rift zone and east tilt at Uwekahuna versus time. ***A,*** November 1978 through July 1979. ***B,*** July 1979 through March 1980. ***C,*** March through November 1980. Plot shows changes of position of seismicity with time. Endpoints for distance axis *U-U'* are given in table 43.2. Tilt is from east-west Ideal Aerosmith tiltmeter, where east-down tilt is down on plot and generally indicates deflation of summit caldera. Large divisions on tilt scale are 10 μrad. Notations along time axis refer to specific swarms detailed in other figures: E, eruption; I, intrusion; X, swarm accompanying inflation. Vertical lines connect swarms or concentrations of earthquakes with corresponding changes in tilt. Mid-1980 was a period of oscillating tilt and alternating locations of seismicity corresponding to cyclic slow intrusions of the east rift zone.

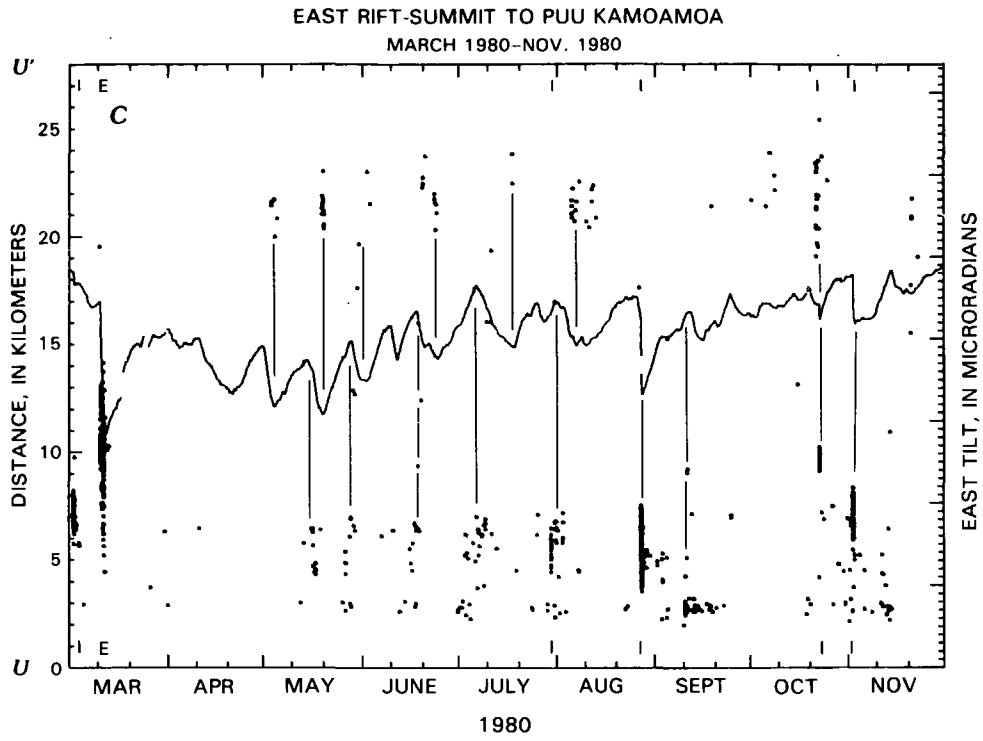

FIGURE 43.74.—Continued.

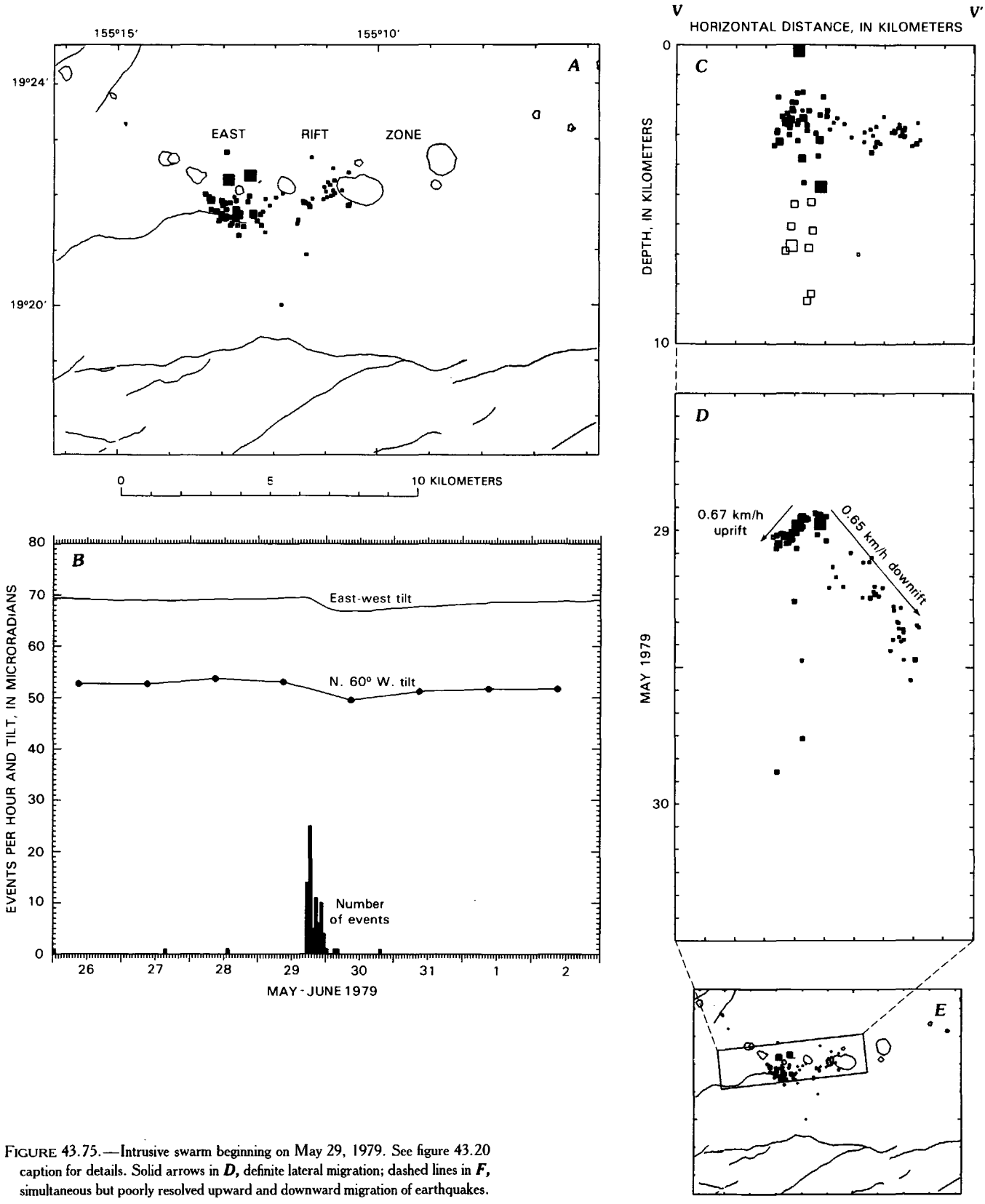

FIGURE 43.75.—Intrusive swarm beginning on May 29, 1979. See figure 43.20 caption for details. Solid arrows in ***D***, definite lateral migration; dashed lines in ***F***, simultaneous but poorly resolved upward and downward migration of earthquakes.

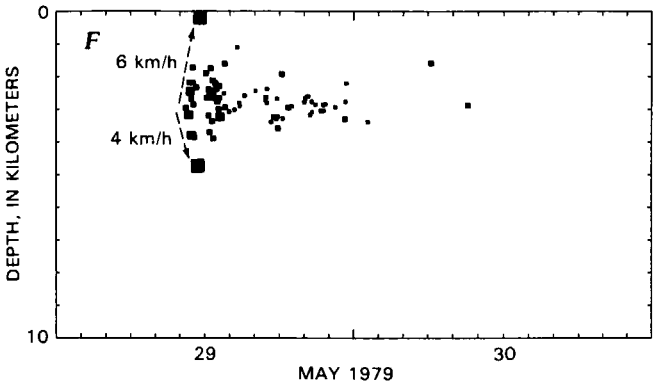

FIGURE 43.75.–Continued.

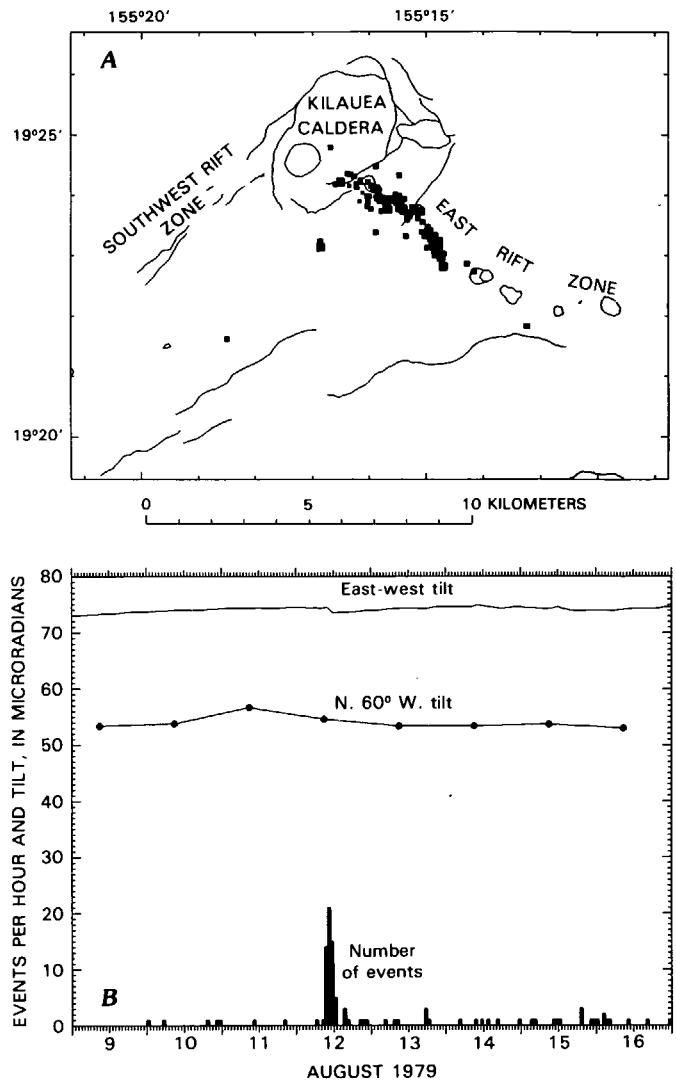

FIGURE 43.76.—Intrusive swarm beginning on August 12, 1979. See figure 43.20 caption for details. Solid line in ***D***, definite migration; short arrows in ***F***, possible additional downrift migration.

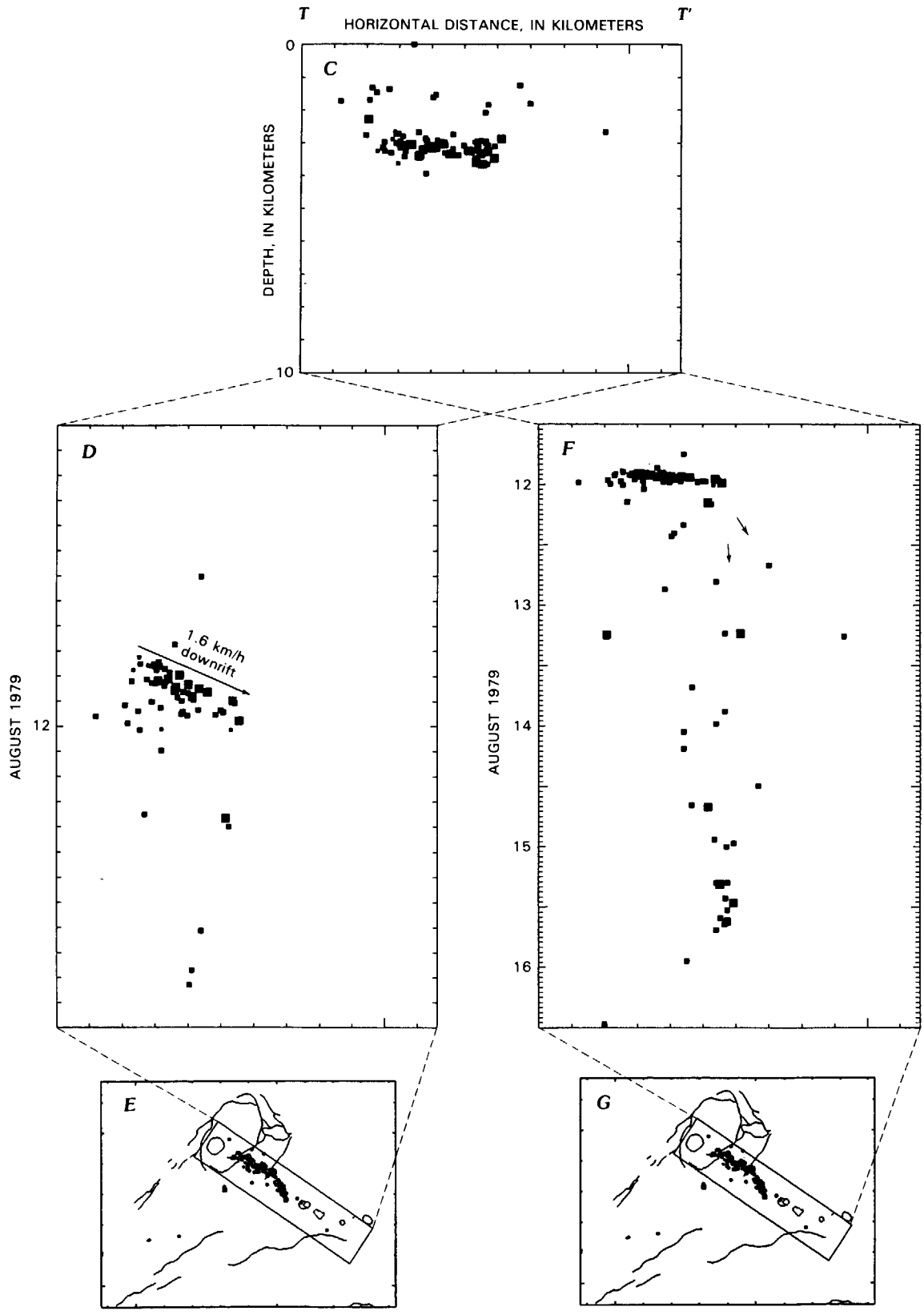

FIGURE 43.76.—Continued.

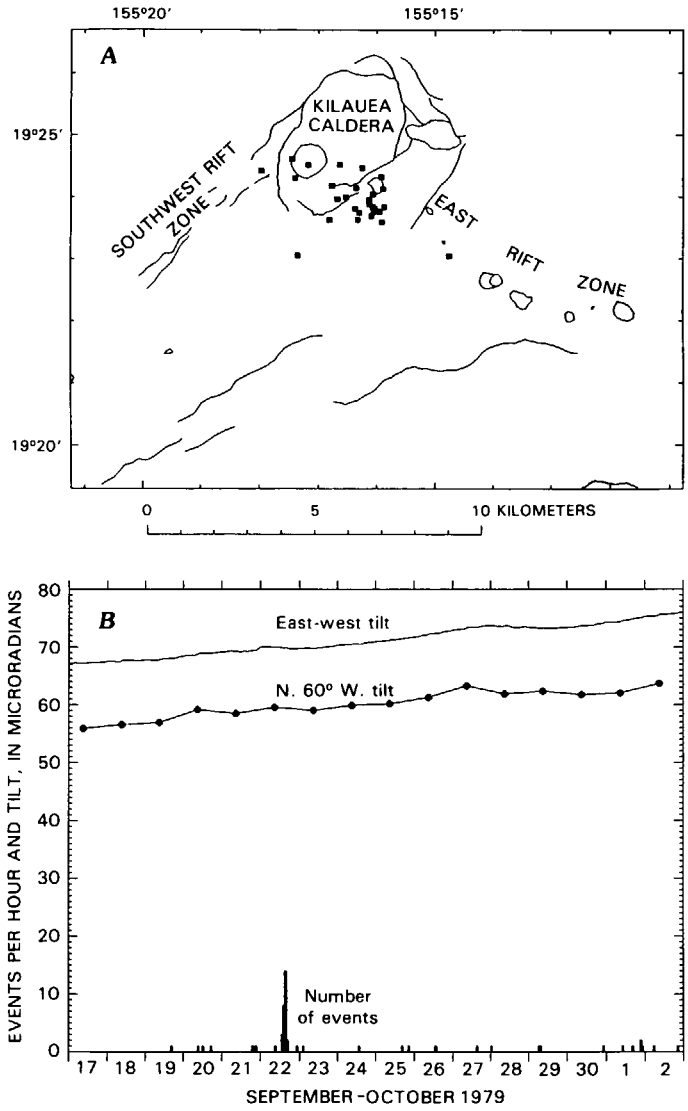

FIGURE 43.77.—Inflationary swarm beginning on September 22, 1979. See figure 43.20 caption for details.

EAST RIFT ZONE INTRUSIONS OF MARCH 1980

The ERZ was very busy during 1980 and produced six rapid intrusions, one of which was apparently also a very small eruption. A condensed position versus time summary of the summit and ERZ seismicity is plotted in figure 43.74*C*. The first two intrusions in March and the last four in the last half of 1980 are readily identified by their intense swarms and sudden deflations in the summit tilt record. The other swarms during May through August were cyclic slow intrusions and will be discussed separately below.

The intrusions of March 1980 were only 8 days apart and successively activated adjacent sections of the ERZ. They appear to be causally related. The March 2 earthquakes were from Kokoolau to Pauahi (fig. 43.79*A*), and the March 10 swarm continued downrift from Pauahi nearly to Makaopuhi (fig. 43.80*A*). The March 2 intrusion was shorter in time, less in deflation, more compact spatially, smaller in earthquake magnitude, and less complex than the March 10 event. The March 2 swarm began about 1 km west of Pauahi where it was most active, but earthquakes soon moved uprift (fig. 43.79*D*).

The March 10 intrusion produced a complex earthquake pattern and apparently also erupted a few cubic meters of lava that was not noticed until after the event (Norman Banks, written commun., 1981). The intrusion began under Mauna Ulu, and earthquakes rapidly moved uprift at 1.8 km/h for about 2 km (fig. 43.80*D*) and upward at roughly 4 km/h (fig. 43.80*I*). The next earthquakes were between the former Alae crater and Makaopuhi, and they probably accompanied the tiny eruption. Next, a relatively slow movement of small earthquakes at 0.2 km/h westward along the rift and into the Koae occurred (fig. 43.80*D*, *G*). The halo of small earthquakes in the north and south flanks adjacent to the intrusion also diffused outward at this time. Before the swarm ended, a burst of earthquakes just south of the former Aloi crater moved downrift at 3 km/h in the same place as the first part of the swarm.

Clearly, a complex system of dikes and conduits were magmatically active in March 1980. We favor a scenario similar to the following, though many variations and possibilities may exist. During January and February 1980, Kilauea inflated and the accumulating magma produced earthquakes in the ERZ uprift of Pauahi (fig. 43.74*B*). Magma collected behind a blockage of the conduit, which also forms the uprift side of the magma pocket below Pauahi. The slowly rising magma pressure on the barrier eventually ruptured it, producing the March 2 swarm. This intrusion also drained a small volume of magma from the summit reservoir, which passed through the uppermost section of the ERZ conduit triggering a few earthquakes there.

The summit then deflated slowly and aseismically, sending magma to accumulate behind the next barrier in the conduit near Aloi crater. This second barrier was intruded by a dike on March 10, that moved upward and uprift from a point 3 km beneath Mauna Ulu. The resulting episode of rifting then moved both up and down the ERZ and was fed by summit magma for the 1.5-day duration of the swarm. The rifting and a possible small intrusion also penetrated the Koae fault zone. Magma collected on the uprift side of the Aloi blockage faster than it could pass through and thus triggered a second rupture through it, this time in the downrift direction. The amount of dike widening was significant over much of the length of the intrusion and induced small earthquakes as much as 3 km from the rift. The fact that earthquakes migrated in several directions and at different speeds requires rifting by various processes involving shifting stress and moving magma. This complexity also requires more than a single linear magma conduit, a conclusion reinforced by the range of earthquake depths in cross sections of this area.

The ERZ intrusions and eruptions of August and November 1979 and March 1980 each penetrated farther along the rift (fig. 43.74*B*). They may each have thus opened new sections of the rift conduit and prepared the rift for the passive intrusions of mid-1980.

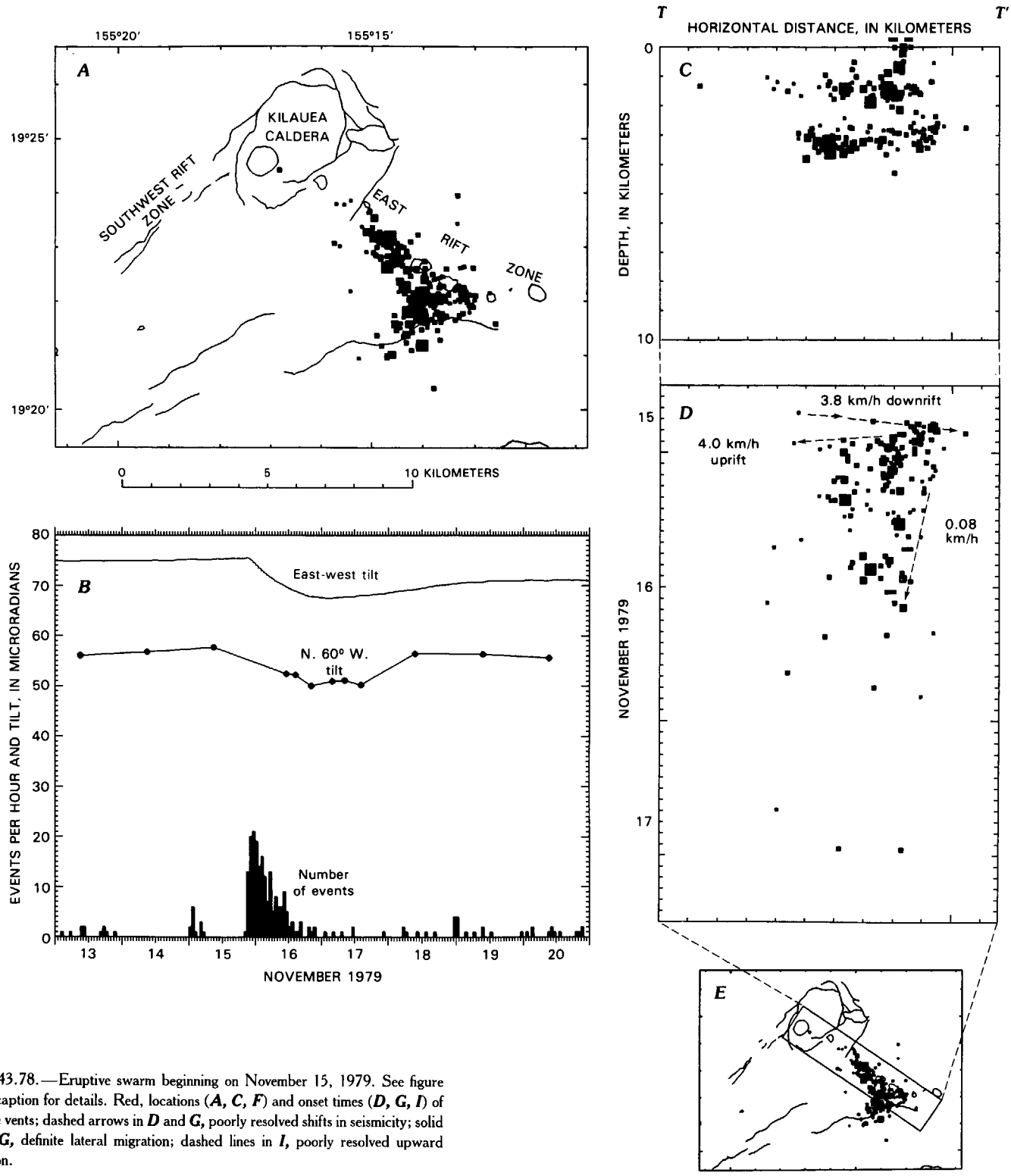

FIGURE 43.78.—Eruptive swarm beginning on November 15, 1979. See figure 43.20 caption for details. Red, locations (***A, C, F***) and onset times (***D, G, I***) of eruptive vents; dashed arrows in ***D*** and ***G,*** poorly resolved shifts in seismicity; solid line in ***G,*** definite lateral migration; dashed lines in ***I,*** poorly resolved upward migration.

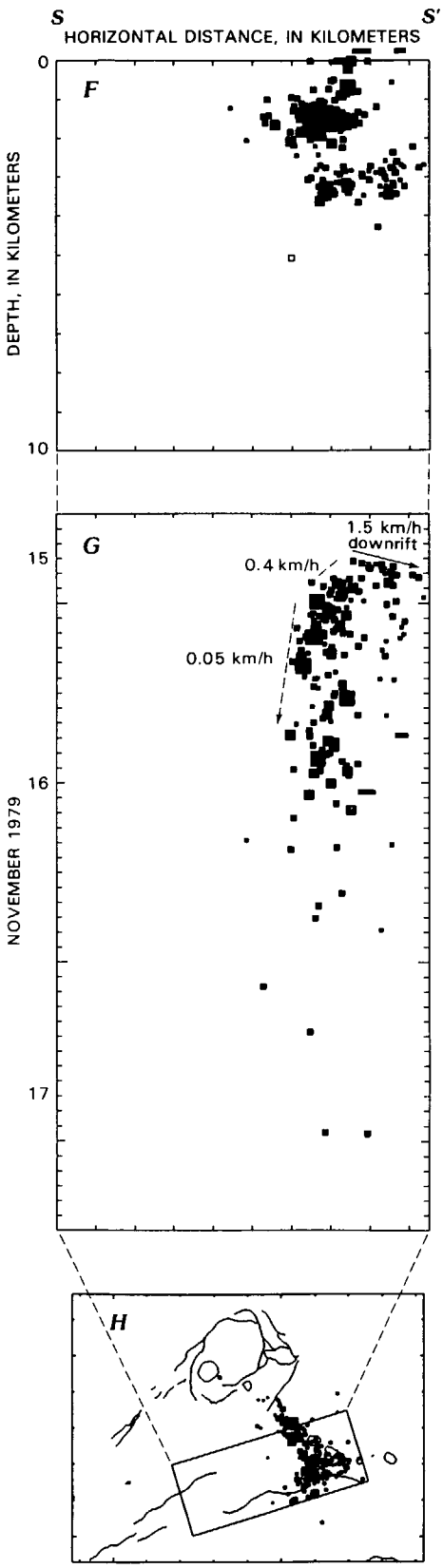

FIGURE 43.78.—Continued.

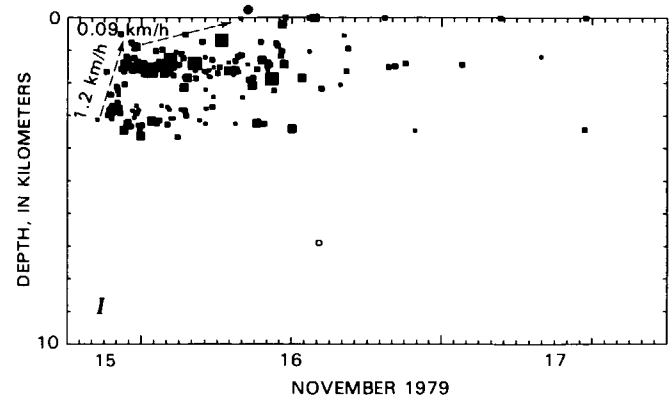

FIGURE 43.78.—Continued.

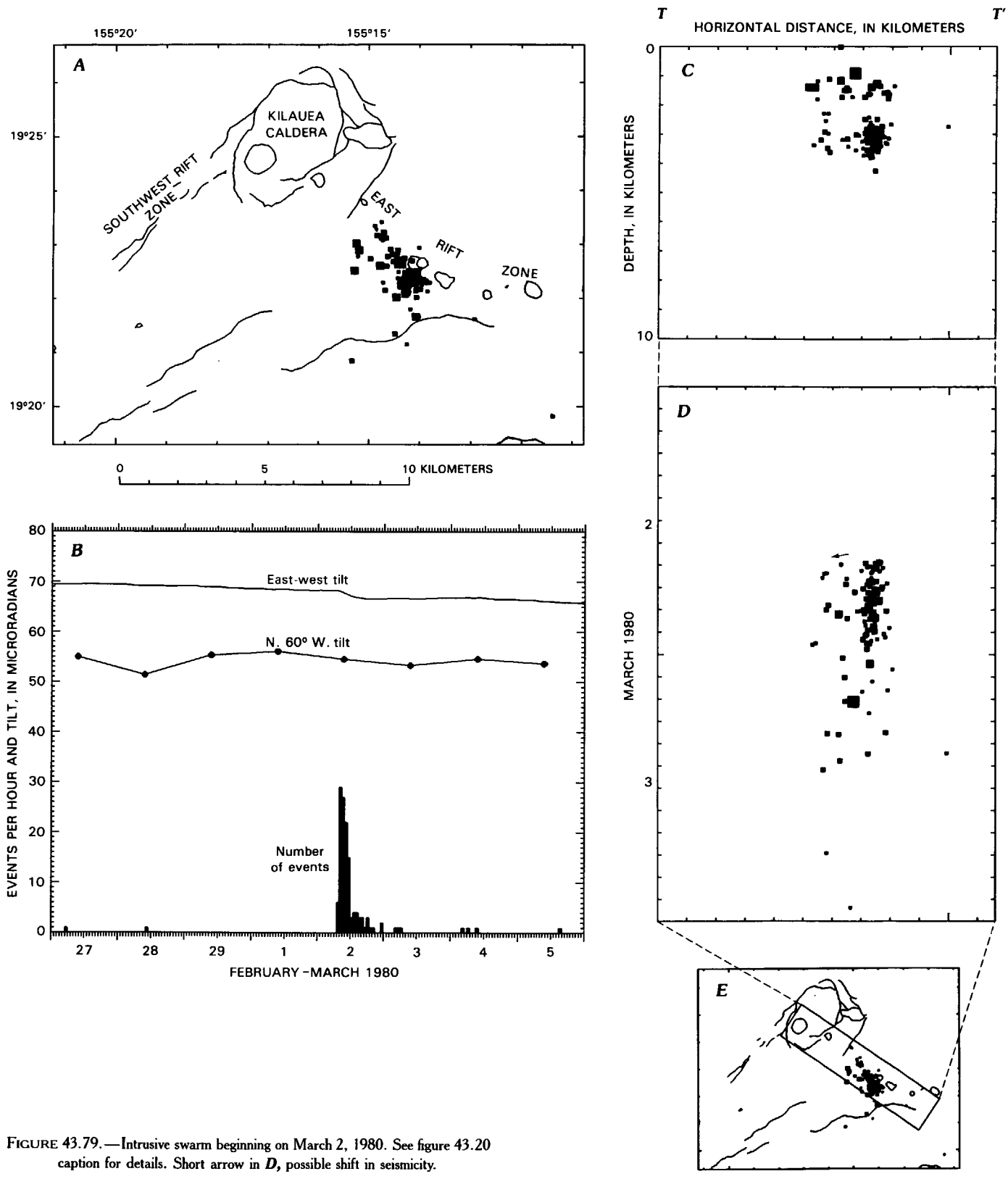

FIGURE 43.79.—Intrusive swarm beginning on March 2, 1980. See figure 43.20 caption for details. Short arrow in *D*, possible shift in seismicity.

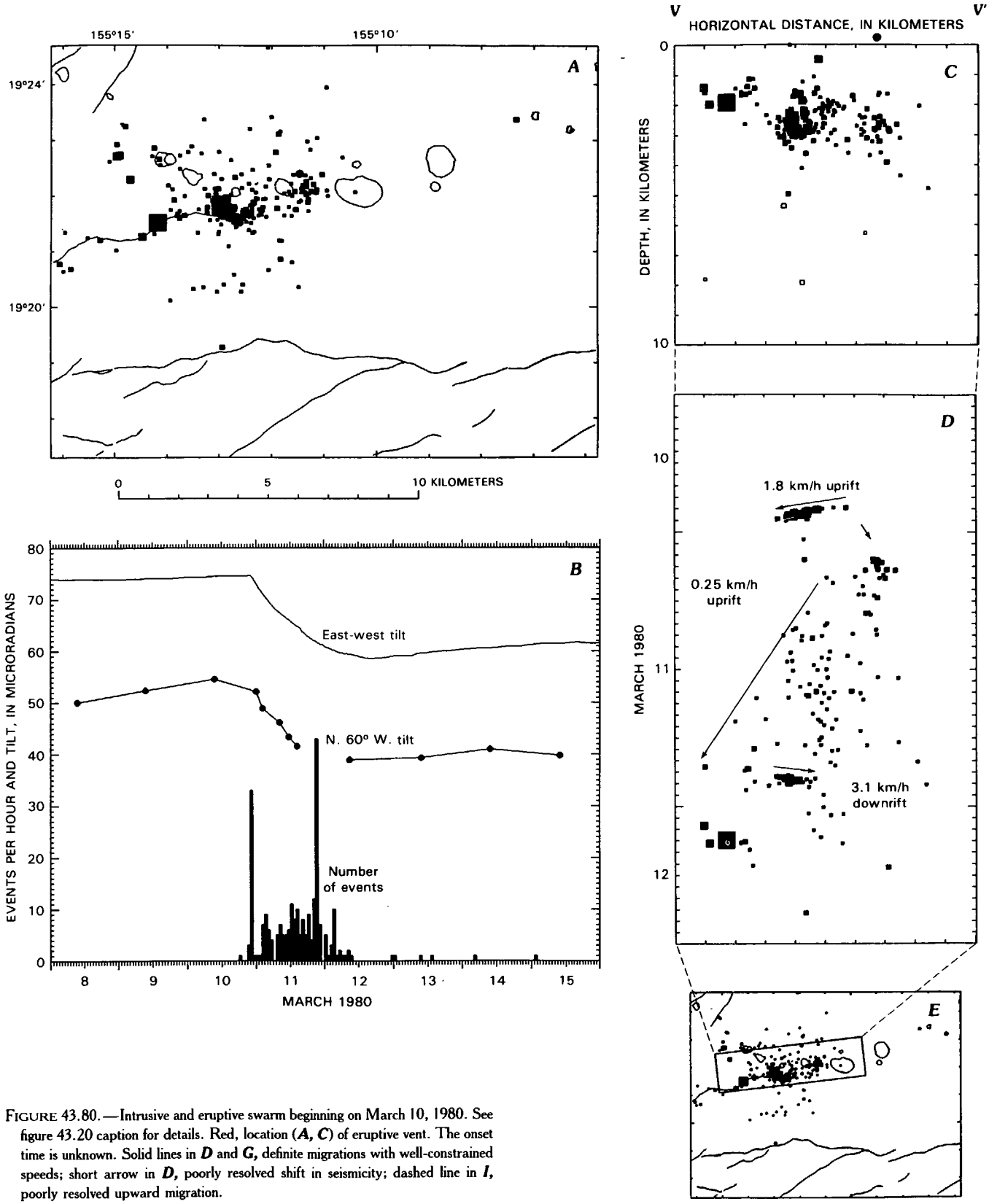

FIGURE 43.80.—Intrusive and eruptive swarm beginning on March 10, 1980. See figure 43.20 caption for details. Red, location (*A, C*) of eruptive vent. The onset time is unknown. Solid lines in *D* and *G*, definite migrations with well-constrained speeds; short arrow in *D*, poorly resolved shift in seismicity; dashed line in *I*, poorly resolved upward migration.

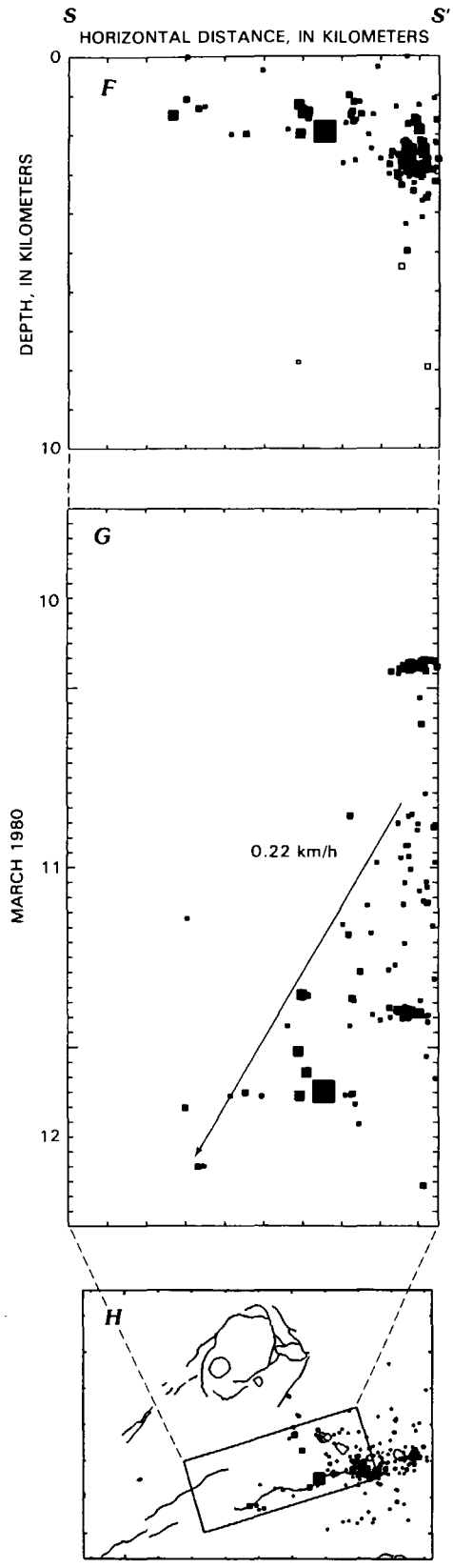

FIGURE 43.80.—Continued.

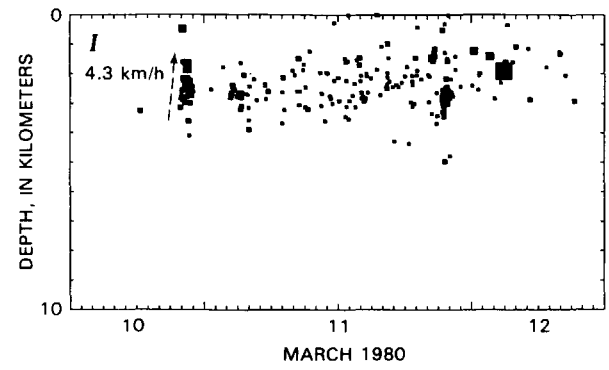

FIGURE 43.80.—Continued.

CYCLIC EAST RIFT ZONE INTRUSIONS OF MAY–AUGUST 1980

After the March 1980 intrusions, Kilauea began an unusual mode of transferring magma from the summit reservoir to storage in a section of rift near Puu Kamoamoa. The intrusions were cyclic and at intervals more regular than other intrusive swarms. Kilauea inflated gradually for 5–10 days, then deflated at a similar rate for 5–10 days. The accumulating magma in the ERZ during mid-1980 and a similar episode in 1978–79 was measured by outward tilt from a linear zone of inflation (Dzurisin and others, 1984). The largest tilts were near Puu Kamoamoa and Kalalua, close to the shallow earthquakes. Dzurisin and others (1984) attributed the rift and summit tilt patterns to a passive and steady transfer of magma from summit to rift. We add the view that earthquake swarms at both summit and rift are variants of the inflationary swarms cataloged in this paper.

A cyclic pattern of magma transfer and oscillatory tilt may also be characteristic of successive episodes of eruption from the same vent, as during the early phases of the Mauna Ulu eruption in 1969–70 or the episodes of the Puu Oo eruption starting in January 1983. Unlike the symmetrical oscillations of tilt during the 1980 cyclic intrusions, the shape of the tilt curve for eruption phases is one of gradual inflation and sudden deflation. Both phenomena accompany a regular delivery of magma to the ERZ.

The cyclic intrusive pattern can easily be seen from the oscillatory tilt in figure 43.74C. The net gain in tilt during this period was very small. A slow swarm of caldera earthquakes generally coincided with peaks in the tilt, and similar swarms near

Puu Kamoamoa were at tilt minima. These swarms are very similar to but smaller than those accompanying inflation and slow intrusions. Caldera earthquakes signaled an inflated summit and ceased as magma drained downrift. Rift earthquakes were caused by local inflation of the rift and occurred while or just after magma was transferred there from the summit. The epicenters of events at the inflating rift can be seen in figure 43.3*B* as an elongate zone above the main magma conduit. One Puu Kamoamoa swarm (fig. 43.83*A*) occurred one day before another ERZ intrusion.

Similar episodes of shallow ERZ earthquakes near Puu Kamoamoa were observed from November 1978 to July 1979 (fig. 43.74*A*). These slow swarms also were generally at or just before minima in summit tilt. Episodes of summit earthquakes similar to those in 1980 were not apparent during this period, except possibly for earthquakes in April and May 1979 that coincided with brief intervals of rapid inflation (fig. 43.74*A*). The oscillations of tilt and an alternating pattern of earthquake locations did not develop as during the otherwise similar rift inflation of 1980. The rift dilation caused by the 1975 Kalapana earthquake and the ERZ eruption of September 1977 apparently opened most of the ERZ conduit and encouraged the passive magma transfer of 1978–79. Opening of the rift continued with the intrusions and eruptions of August and November 1979 and March 1980. Four additional but rapid ERZ intrusions in the latter half of 1980 apparently disrupted the delicate equilibrium of the magma conduit that permitted the regular cycles of slow intrusion in mid-1980.

EAST RIFT ZONE INTRUSIONS OF JULY-NOVEMBER 1980

The ERZ intrusions of July, August and October 1980 successively penetrated farther along the rift, as did the intrusions of August and November 1979 and March 1980. The July 30, 1980 swarm lasted only for about one hour and activated only the 2-km section of rift between Keanakakoi and Puhimau (fig. 43.81). No deflation was detected, apparently because only a small volume of magma was transferred. Earthquakes began nearly instantaneously along the zone. The high speed of swarm growth is probably a result of the presumed high temperatures and lower magma viscosity where the rift conduit adjoins the summit reservoir.

The intrusion of August 27, 1980, reached an additional 3 km downrift to Hiiaka (fig. 43.82*A*). The swarm began 3 km below Puhimau where the July intrusion terminated. The initial intense seismicity moved downrift at 1.6 km/h and remained at 3 km depth (fig. 43.82*D*, *F*). As the main dike moved downrift, earthquakes also moved upward and uprift (fig. 43.82*D*). The dike had two horizontal lobes end-to-end at 3 km depth and a connecting vertical lobe (fig. 43.82*C*). Earthquakes propagated outward along each lobe from the initial center of activity. Summit reservoir deflation and the enlargement of all three seismic lobes were simultaneous. The uprift lobe may have fed magma to the dike system in the downrift direction, with earthquake migration opposite to magma flow. The process by which earthquakes can migrate uprift while magma flows downrift may be complex, but not impossible; for example, widening of an already open dike and the consequent earthquakes may begin from the end toward which magma is flowing and move against the flow direction as the dike fills.

The next intrusion on October 21–22, 1980, may actually have been two unrelated but nearly simultaneous events. The swarm beginning on October 21 near Puu Kamoamoa is apparently one of the last of the slow intrusions recurring from 1978 through 1980. The second intrusion occurred one day later and 14 km uprift of Puu Kamoamoa below the former Alae crater (fig. 43.83*A*, *E*). The Puu Kamoamoa swarm happened at a broad minimum in summit tilt typical for these slow intrusions (fig. 43.74*C*). The rapid deflation and more intense seismicity of the Alae swarm were on a much shorter time scale (fig. 43.83*B*, *D*). The second swarm was very compact (1.5-km diameter) and short (3 hours), but movement with time could be resolved. The downrift speed of 2.7 km/h (fig. 43.83*H*) and upward speed of about 2 km/h (fig. 43.83*J*) are consistent with the dip of the main finger of earthquakes seen in cross section (fig. 43.83*G*). The October 22 event appears to be a dike intruded into the rift blockage just downrift of the Pauahi magma pocket. Magma feeding the Puu Kamoamoa inflation probably traveled through a different rift conduit several days earlier, although a local increase in magma pressure could have triggered the second intrusion.

The October intrusion was followed in 11 days by another on November 2, 1980, just 2–3 km uprift (fig. 43.84*A*). The swarm was very intense but lasted only 4 hours. It began just uprift of Hiiaka and expanded downrift at 0.7 km/h (fig. 43.84*D*). Earthquakes also moved uprift, but only for about 1 km. No consistent depth migration can be seen, but earthquakes did spread up and down from 3 km depth (fig. 43.84*F*). Apparently a dike grew outward from a point near the main ERZ magma conduit. This intrusion was the last of a series of ERZ intrusions before Kilauea shifted its magma supply to the SWRZ.

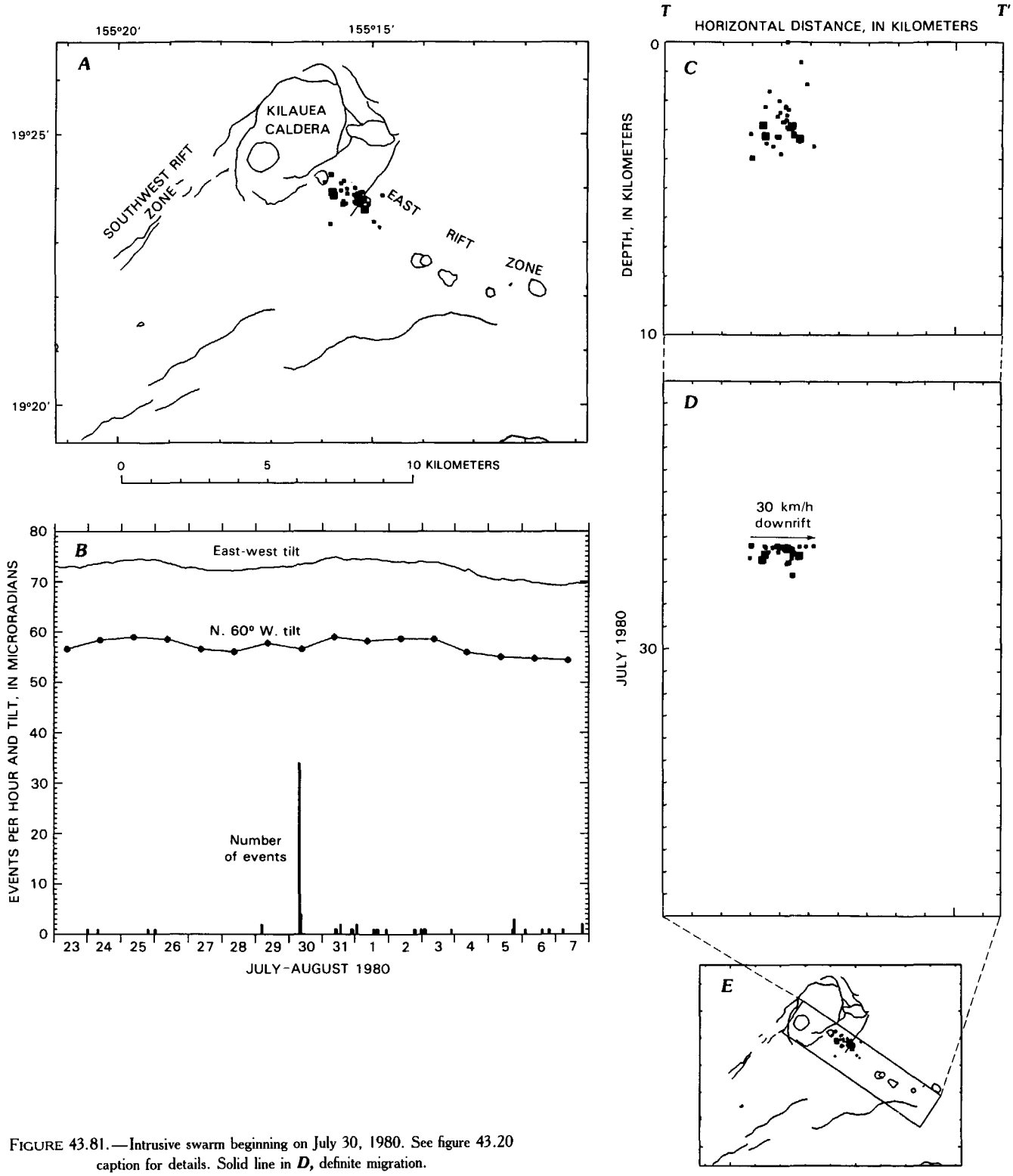

FIGURE 43.81.—Intrusive swarm beginning on July 30, 1980. See figure 43.20 caption for details. Solid line in ***D***, definite migration.

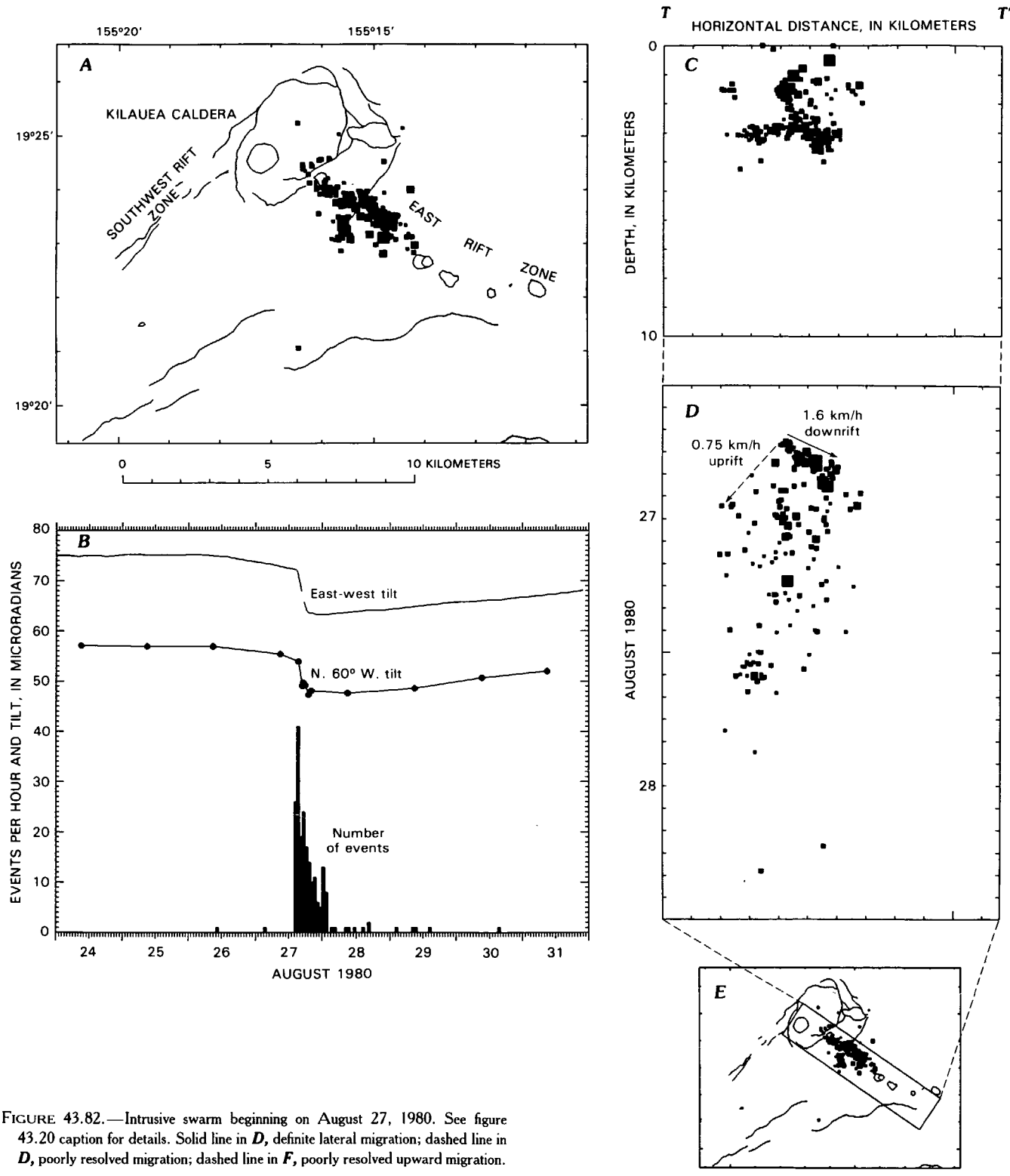

FIGURE 43.82.—Intrusive swarm beginning on August 27, 1980. See figure 43.20 caption for details. Solid line in ***D***, definite lateral migration; dashed line in ***D***, poorly resolved migration; dashed line in ***F***, poorly resolved upward migration.

FIGURE 43.82.—Continued.

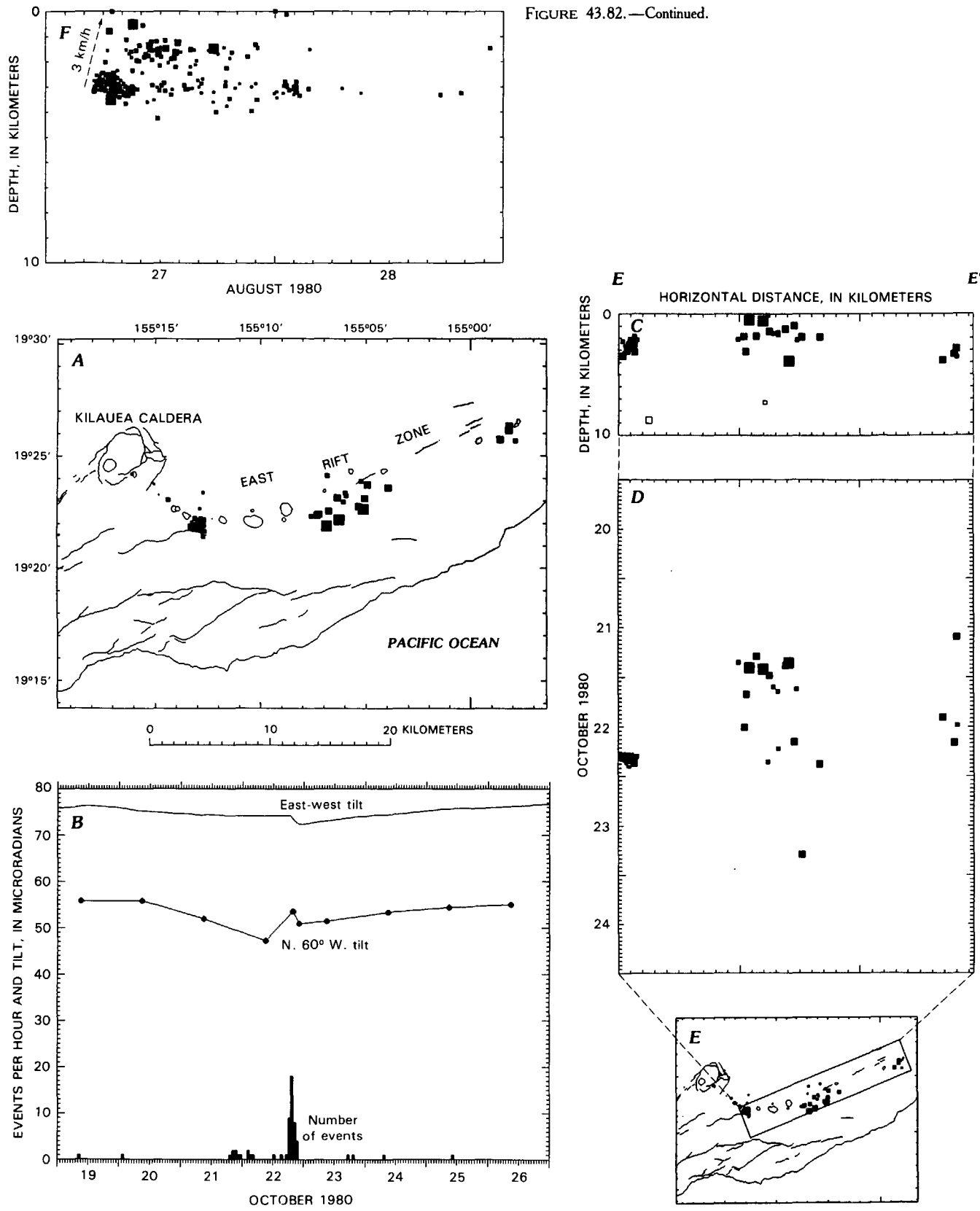

FIGURE 43.83.—Intrusive swarm beginning on October 21, 1980. See figure 43.20 caption for details. Solid line in ***H***, definite lateral migration; dashed line in ***J***, poorly resolved upward migration.

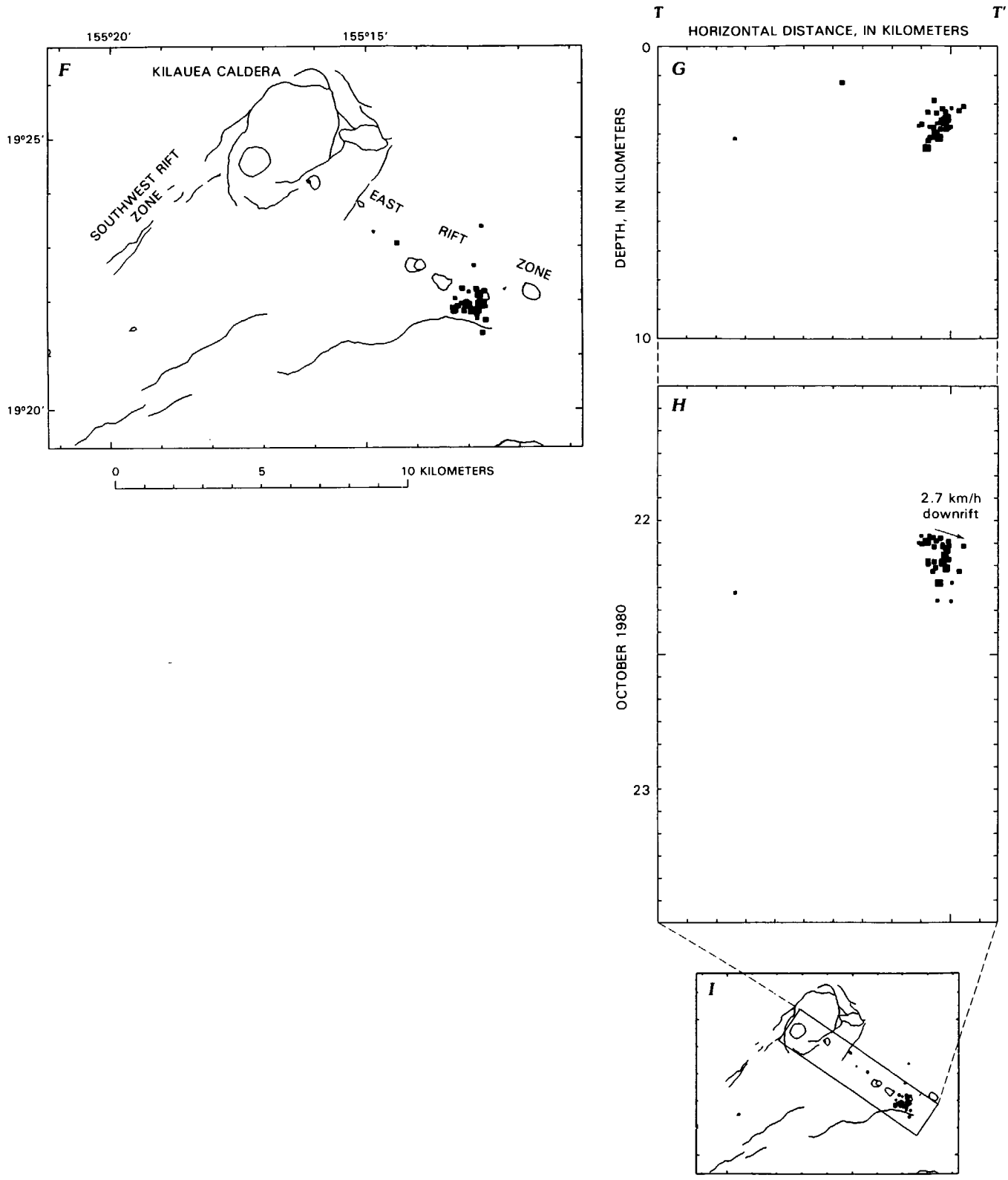

FIGURE 43.83.—Continued.

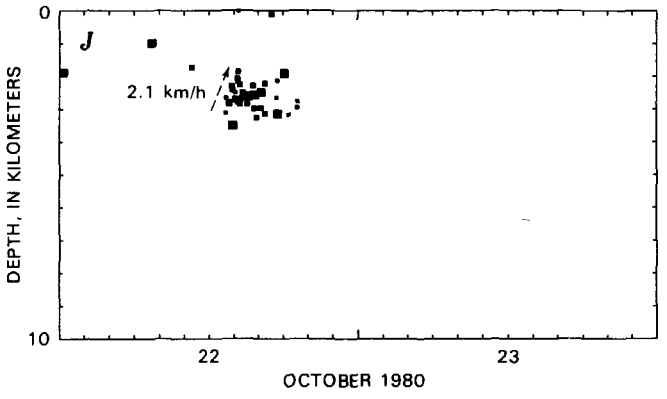

FIGURE 43.83.—Continued.

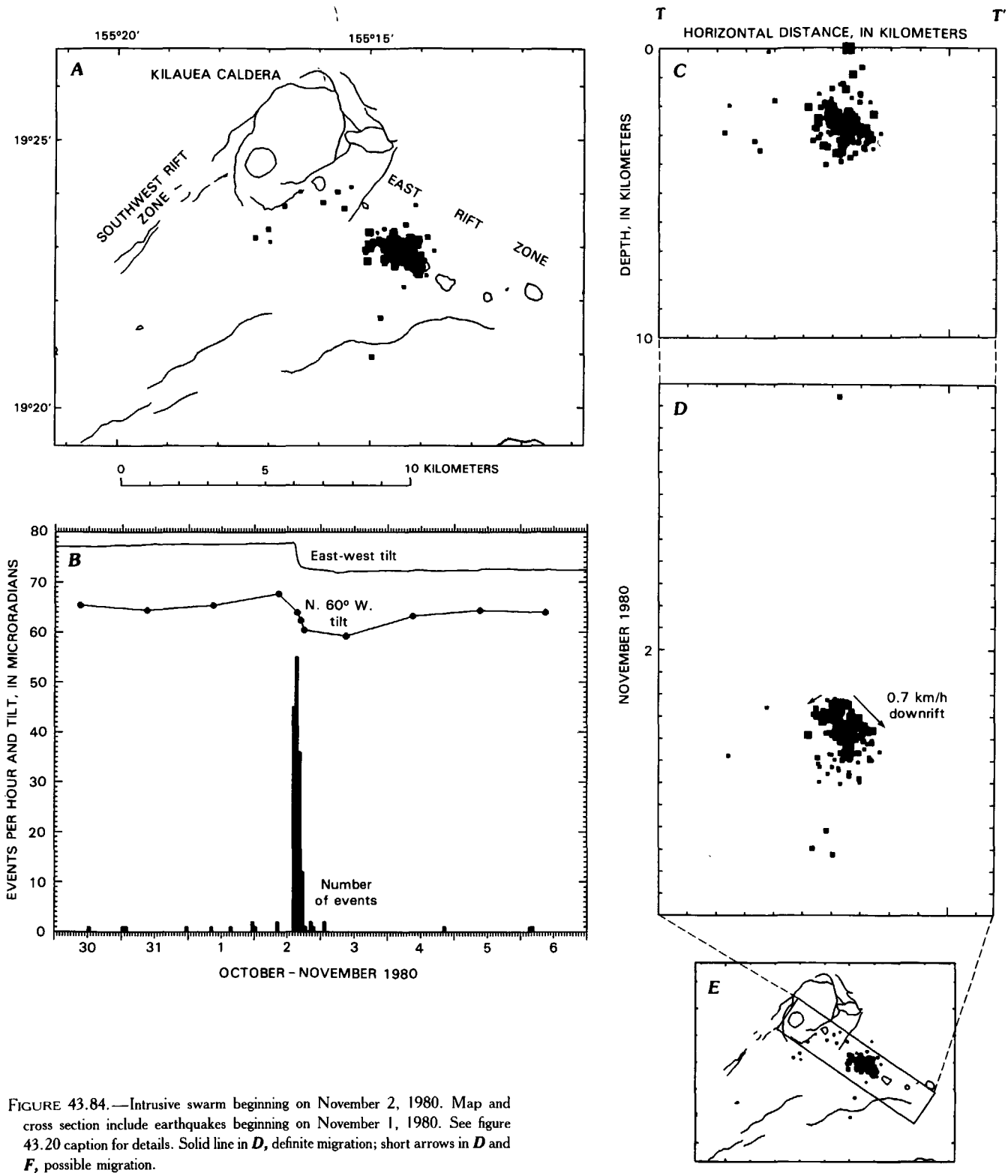

FIGURE 43.84.—Intrusive swarm beginning on November 2, 1980. Map and cross section include earthquakes beginning on November 1, 1980. See figure 43.20 caption for details. Solid line in ***D***, definite migration; short arrows in ***D*** and ***F***, possible migration.

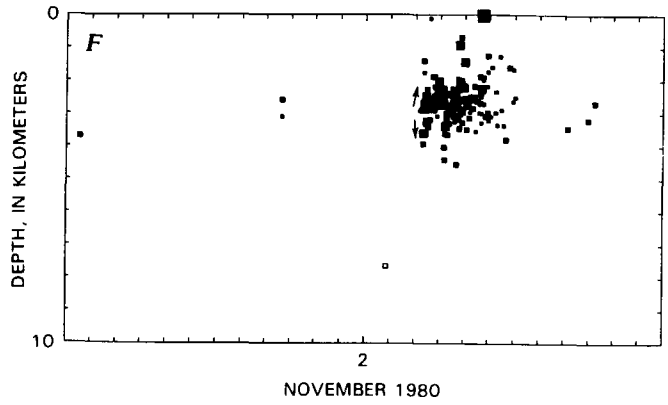

FIGURE 43.84.—Continued.

SOUTHWEST RIFT ZONE INTRUSIONS AND CALDERA ERUPTION OF JANUARY–AUGUST 1981

From January 1981 to mid-1982, Kilauea focused most of its magmatic activity on the SWRZ. Figure 43.85 summarizes the positions of shallow SWRZ earthquakes and summit tilt during this 18-month period. Three major intrusions occurred; the first penetrated the SWRZ in three progressive steps in January and February 1981, and continued to slowly pass magma into the SWRZ through June. The prolonged nature of this first intrusion did not require a major summit deflation. The other two intrusions in August 1981 and June 1982 followed a more conventional pattern of rapid summit deflation during a brief earthquake swarm, followed by reinflation of the summit reservoir.

The first phase of the January–February intrusion began on January 20, 1981, with a compact swarm in the main SWRZ magma conduit just south of the caldera (fig. 43.86*A*). No measurable deflation accompanied this first phase, and in fact Kilauea was inflating at this time (figs. 43.85*A*, 43.86*B*). Earthquakes did not migrate downrift, but did spread slowly north into the caldera as the seismic zone enlarged (fig. 43.86*D*). This phase was apparently the breaking open of a part of the magma passageway in response to inflation of the summit reservoir, but very little magma volume was actually intruded. Had it not been associated with the subsequent SWRZ intrusion and also produced so many earthquakes in a short period of time, this event may have been mistaken for a typical inflationary swarm.

The intrusion's second phase began on January 24 and demonstrated that a slow intrusion was in progress. Earthquakes now extended an additional 3 km along the rift in a zone including the bend in the magma conduit (fig. 43.87*A*). The deflation and earthquake rates were several times slower than in typical rapid intrusions (fig. 43.86*B*). Earthquakes began almost simultaneously along the seismic zone, which remained uniformly active for 3–4 days (fig. 43.87*C*). This time behavior suggests that a section of the magma conduit filled slowly enough that its expansion was very uniform and without a fast-moving stress concentration such as the tip of a new dike. This pattern is consistent with earlier observations that the sections of rift adjacent to the caldera are often in direct magmatic communication and inflate with the summit reservoir. The January 20 swarm thus accompanied the breaking of a barrier and slow intrusion of the uppermost 5 km of the SWRZ during January 24–27.

The next phase of the intrusion began when magma moved almost aseismically down the SWRZ and generated a swarm near Puu Kou (fig. 43.88*A*). The sparse seismicity between the caldera and terminus of the intrusion seems to result from the low deflation rate (fig. 43.88*B*) and probable accommodation of magma flow through an existing conduit without additional rifting. The intrusion apparently stopped at a blockage of the conduit where the rift axis bends just north of the Great Crack. The main seismic zone tilts upward (fig. 43.88*C*), suggesting that the magma conduit began rising up and over the barrier until it lacked sufficient pressure to overcome it. The slowing expansion of the seismic zone upward and downrift (fig. 43.88*D*, *F*) would also be expected if the dike encountered a dipping barrier.

The unusual nature of the January SWRZ intrusion is underscored by the continuing seismicity along the rift through the first half of 1981. After the initial intrusion in January and February, earthquakes persisted in the Puu Koae, Mauna Iki and Puu Kou areas through June (fig. 43.85*A*). The positions of earthquakes can be related to summit tilt to infer where magma accumulated during this period. The initial major deflation in February caused caldera earthquakes to stop for about two months, but they returned during the very slow reinflation in April. Their numbers increased as tilt rate accelerated in July. The seismicity of the rift was complementary to that in the caldera, and the pattern paints the following picture. In February and March, all of Kilauea's magma supply was directed into the SWRZ: the summit did not inflate and all earthquakes were downrift and caused by the intruded magma. In April, May and June very slight inflation occurred, a partial shift of seismicity back to the caldera was evident, and a fraction of the magma supply remained in the summit reservoir. The intrusion stopped in July, and typical inflation and earthquakes returned to the summit. This period illustrates the coincidence of falling or level tilt and rift seismicity during intrusions, and rising tilt and caldera earthquakes during inflation.

The passage of magma down the SWRZ was somewhat episodic: migrating pulses of earthquakes and hence magma may be discernable (dashed lines in fig. 43.85*A*). The speeds of these pulses ranged from about 0.12 km/hr (3 km/d) to 0.024 km/h (0.6

km/d), which are comparable to the speeds of other slow intrusions discussed in this paper. Kilauea's reinflation during July, combined with the opening and heating of the SWRZ magma conduit during the previous six months, apparently combined to permit the rapid intrusion in August 1981.

Just as before the January 1981 intrusion, earthquakes and magma leaked into the rift as a prelude to the August intrusion. Earthquakes slowly expanded into the SWRZ during July as the summit inflated (fig. 43.85*A*). A pre-intrusion also extended 5 km from the caldera on August 2 (fig. 43.89*A*). This pre-intrusion was scarcely noticed because no increase in earthquake activity or significant deflation was recognized (fig. 43.89*B*), only a shift in epicenters down the SWRZ (fig. 43.89*D*). The slight deflation suggests that some magma did move into the rift, but when this pre-intrusion reached the blockage in the magma conduit 5 km from the caldera, magma backed up and rapid inflation began, triggering the main intrusion on August 10. This pattern is very similar to that in January.

The intrusion on August 10 began with earthquakes just south of the caldera, which rapidly spread both into the caldera and downrift (fig. 43.90*D*). Some of the initial seismicity moved from the rift conduit at 3 km depth back and up over the magma reservoir (fig. 43.90*C*, *D*, *F*). The swarm soon engulfed the SWRZ from Halemaumau to Puu Kou (fig. 43.90*G*). The rapid downrift speed of 2.6 km/h slowed near the Kamakaia Hills by a factor of 10 to only 0.28 km/h (fig. 43.90*I*). The tilt rate slowed dramatically when the dike front reached Puu Kou on August 11 (fig. 43.90*B*). Earthquakes persisted mainly in the Puu Kou and Mauna Iki areas for about 5 days (fig. 43.90*K*). The seismicity near Mauna Iki actually spread back uprift. This uprift migration may have resulted from a wave of back pressure in the conduit produced when the downrift migration stopped. Earthquakes also continued in the caldera for about 5 days and were mostly long-period events associated with the subsidence and adjustment of the reservoir and its feeder conduit.

Many earthquakes were in dense clusters along the rift (fig. 43.90*G*, *H*). We associate these clusters with constrictions and barriers in the magma conduit. The passage of magma at these places thus required either formation of a new dike or the widening of an existing conduit too narrow to accommodate the magma flow. Either process causes earthquakes. Note that the terminus of the pre-intrusion on August 2 about 3 km east of Puu Koae was very active then, but nearly aseismic during the August 10 intrusion (compare fig. 43.89*A* and 43.90*A*). Apparently this area had already rifted open, allowing the main intrusion to pass through aseismically.

Although the intrusion deepened with distance from the caldera, a cluster of earthquakes at only 1 km depth were seen just southwest of Puu Koae (fig. 43.90*H*). These shallow earthquakes were below the surface cracks produced by the intrusion. Both phenomena were apparently the result of an upward-branching dike from the main conduit that did not quite reach the surface. A plane joining the area of surface cracks and the main seismic conduit dips about 80° SE. This dip matches the shape of the seismic conduit in this area seen in cross section (fig. 43.19*E*, *F*) and the dip of the intruded dike deduced from leveling lines crossing the rift (Dvorak and others, 1983).

Comparing the August 1981 intrusion with others in the SWRZ is informative. The August intrusion was much faster and more energetic than the one in January–June, perhaps because the earlier intrusion opened and heated the magma conduit making subsequent intrusions easier. The migration rate in August was double that of the December 1974 intrusion, probably again because of the prior intrusive activity in 1981. Both the 1974 and 1981 intrusions activated the same section of rift, and both produced an apparent reflection from the intrusion terminus of earthquakes migrating back uprift. The 1974 intrusion was about 50 percent larger in magma volume and produced more earthquakes, especially in the flank south of the rift. The reduced flank seismicity in 1981 may have resulted from the intrusion's smaller size, a different distribution of emplaced magma, or release of compressive stress in the flank in 1975 during the intervening Kalapana earthquake.

The geometry of the August 1981 dike can be estimated from the observed rates of deflation and earthquake migration. Using a deflation rate of 11 μrad/h at the time of the 2.6-km/h migration yields a cross-sectional area of $(11/3)/2.6 \times 1000 = 1{,}500$ m^2. A dike averaging 1.5 km by 1 m is consistent with earthquake migration speed and depth range and with deflation and geodetic observations. Pollard and others (1983) used a profile of surface displacements to constrain an elastic model of deformation surrounding a new dike. They inferred a dike dipping 82° SE., which is consistent with the dip of the seismically defined conduit of figure 43.14*F*. Their solution of a 1-m-thick dike extending from 0.25 to 2.75 km depth fits the surface profile everywhere except the central 3 km over the dike, where inelastic deformation occurred. Their cross-sectional area of 2,500 m^2 may include a shallow portion of the rift that grew aseismically and inelastically and that did not participate in the magma flow reflected in our 1,500-m^2 area.

The volume of intruded magma in August 1981 was about 35 million cubic meters, using the observed deflation and the value of 0.3 million cubic meters per microradian of Uwekahuna tilt from Dzurisin and others (1984). The August 1981 volume is comparable to that of the January-June intrusion. The tilt was nearly flat for the earlier period, so Kilauea's magma supply rate of about 9 million cubic meters per month (Swanson, 1972; Dzurisin and others, 1980) was mostly supplied to the SWRZ. Thus about 45 million cubic meters was supplied to the rift during the 5 months of the intrusion, but at a rate 100 times slower than in August.

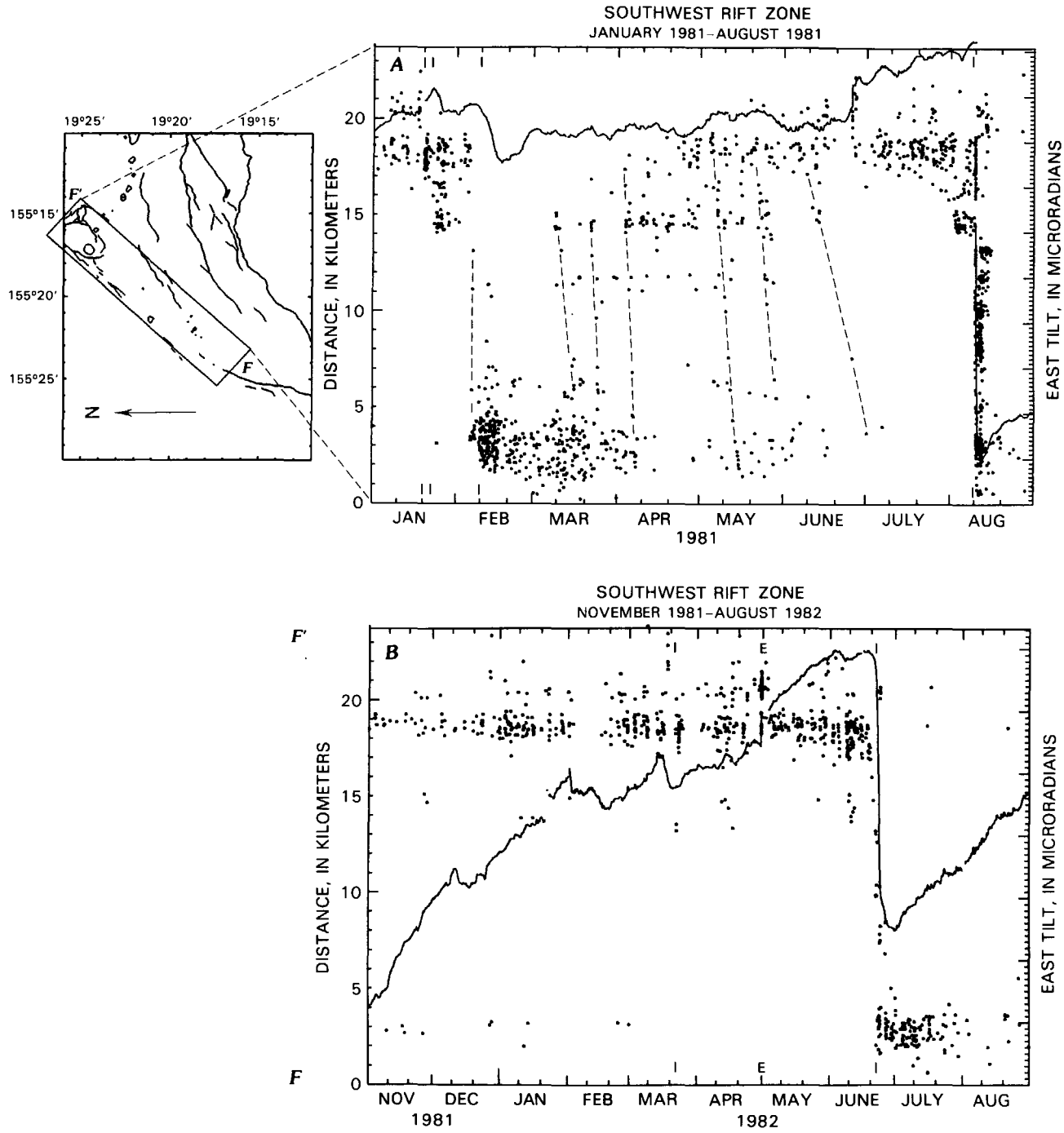

FIGURE 43.85.—Plot of earthquakes along the southwest rift zone and east tilt at Uwekahuna versus time. ***A***, January through August 1981. ***B***, November 1981 through August 1982. September and October 1981 are omitted and were a seismically quiet time of reinflation. All earthquakes shallower than 5 km and within geographic box shown are plotted. Kilauea caldera is at top and Puu Kou is near bottom. Tilt is from Ideal-Aerosmith instrument and down on plot generally indicates deflation of summit caldera. Notations along time axis refer to specific swarms detailed in other figures: E, eruption; I, rapid intrusion. Dashed lines in *A* suggest individual intrusive pulses.

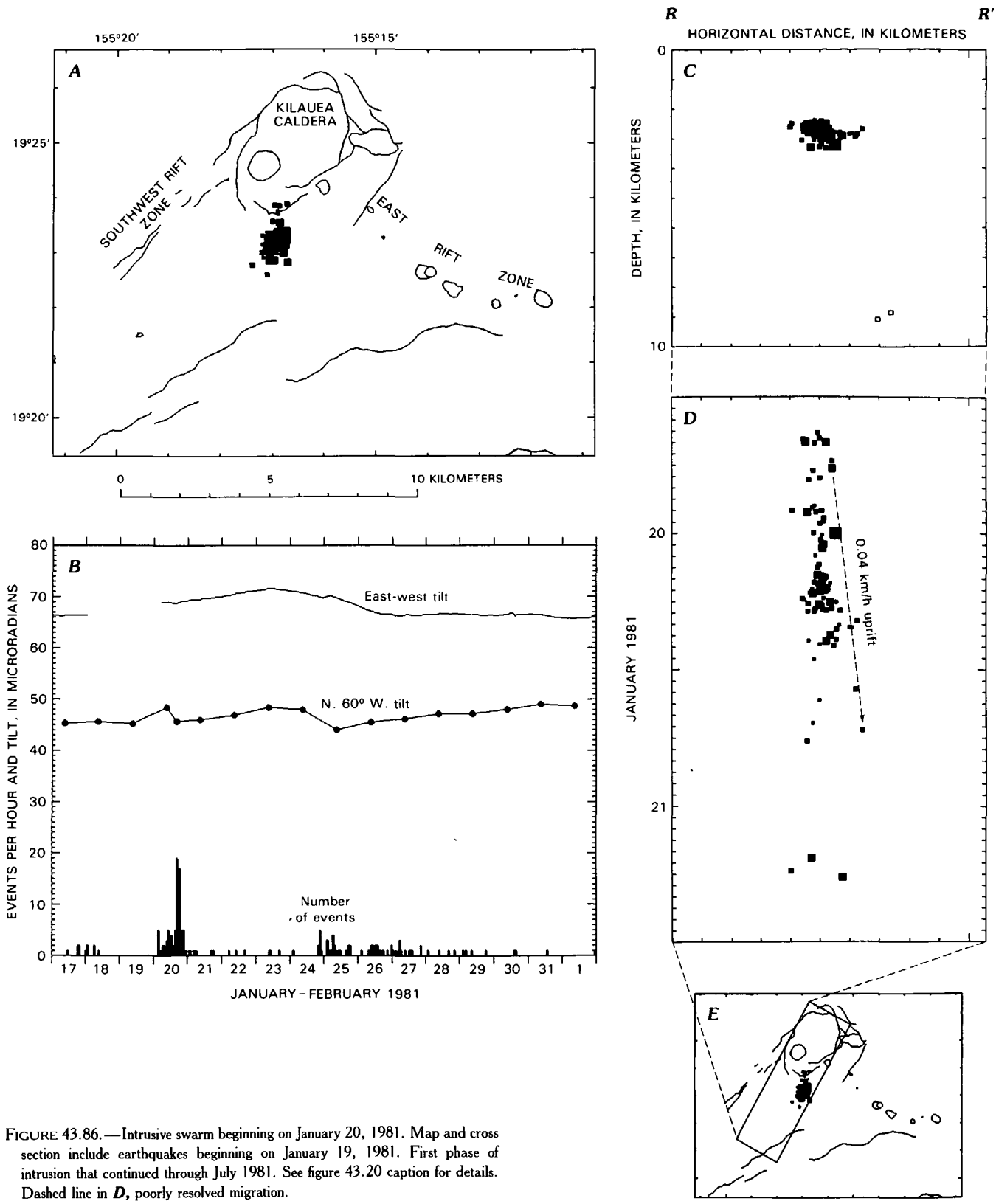

FIGURE 43.86.—Intrusive swarm beginning on January 20, 1981. Map and cross section include earthquakes beginning on January 19, 1981. First phase of intrusion that continued through July 1981. See figure 43.20 caption for details. Dashed line in ***D***, poorly resolved migration.

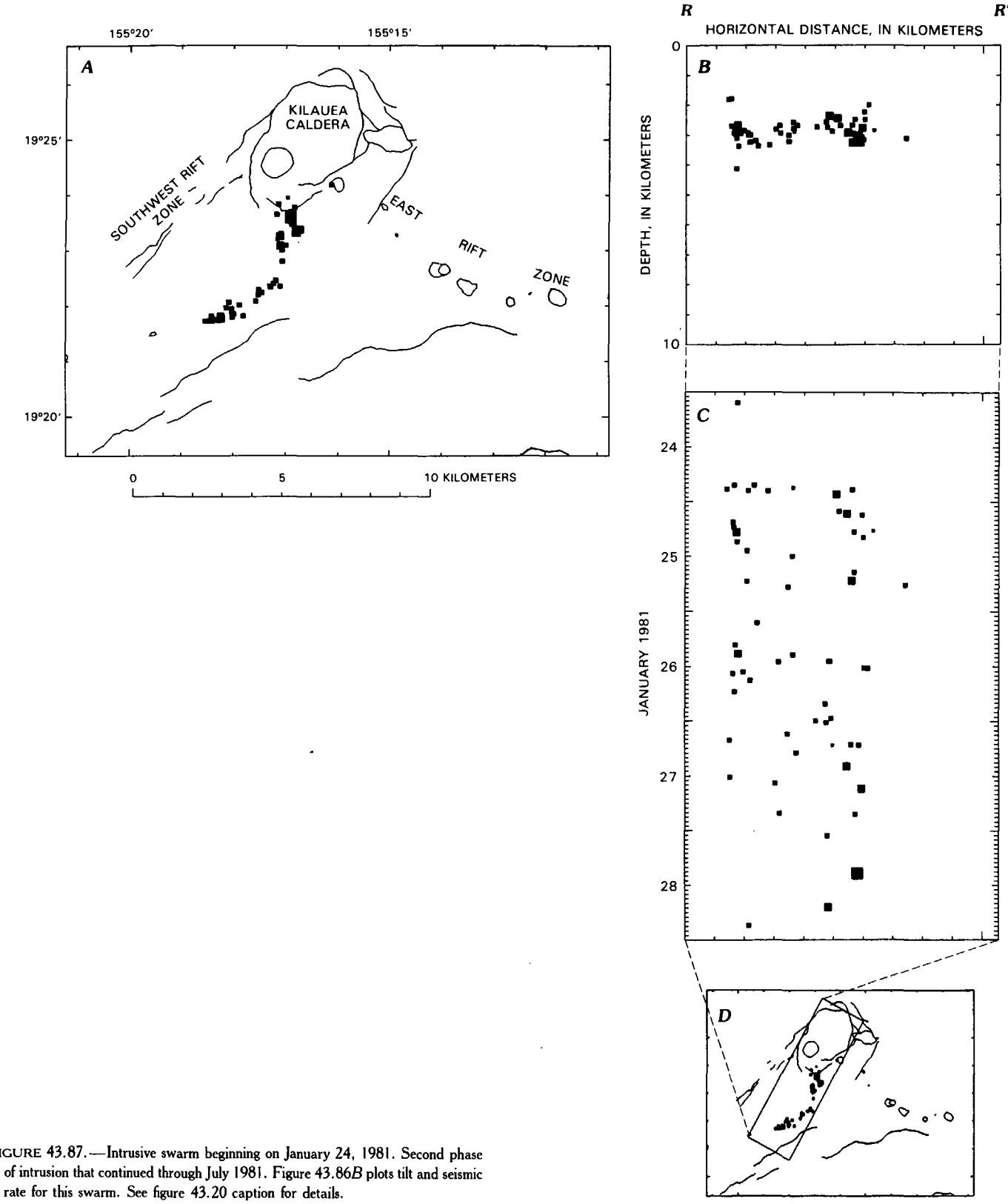

FIGURE 43.87.—Intrusive swarm beginning on January 24, 1981. Second phase of intrusion that continued through July 1981. Figure 43.86*B* plots tilt and seismic rate for this swarm. See figure 43.20 caption for details.

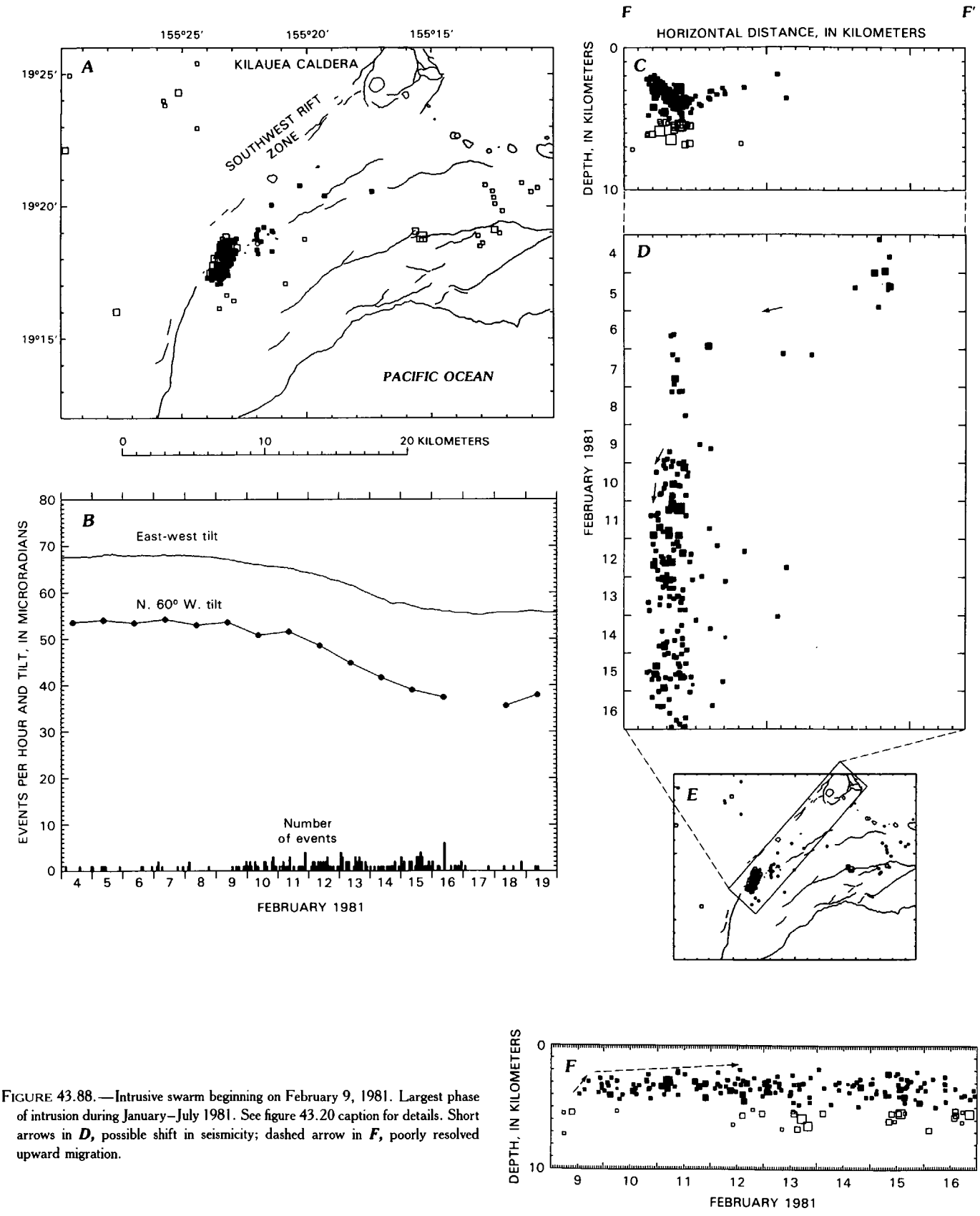

FIGURE 43.88.—Intrusive swarm beginning on February 9, 1981. Largest phase of intrusion during January–July 1981. See figure 43.20 caption for details. Short arrows in ***D***, possible shift in seismicity; dashed arrow in ***F***, poorly resolved upward migration.

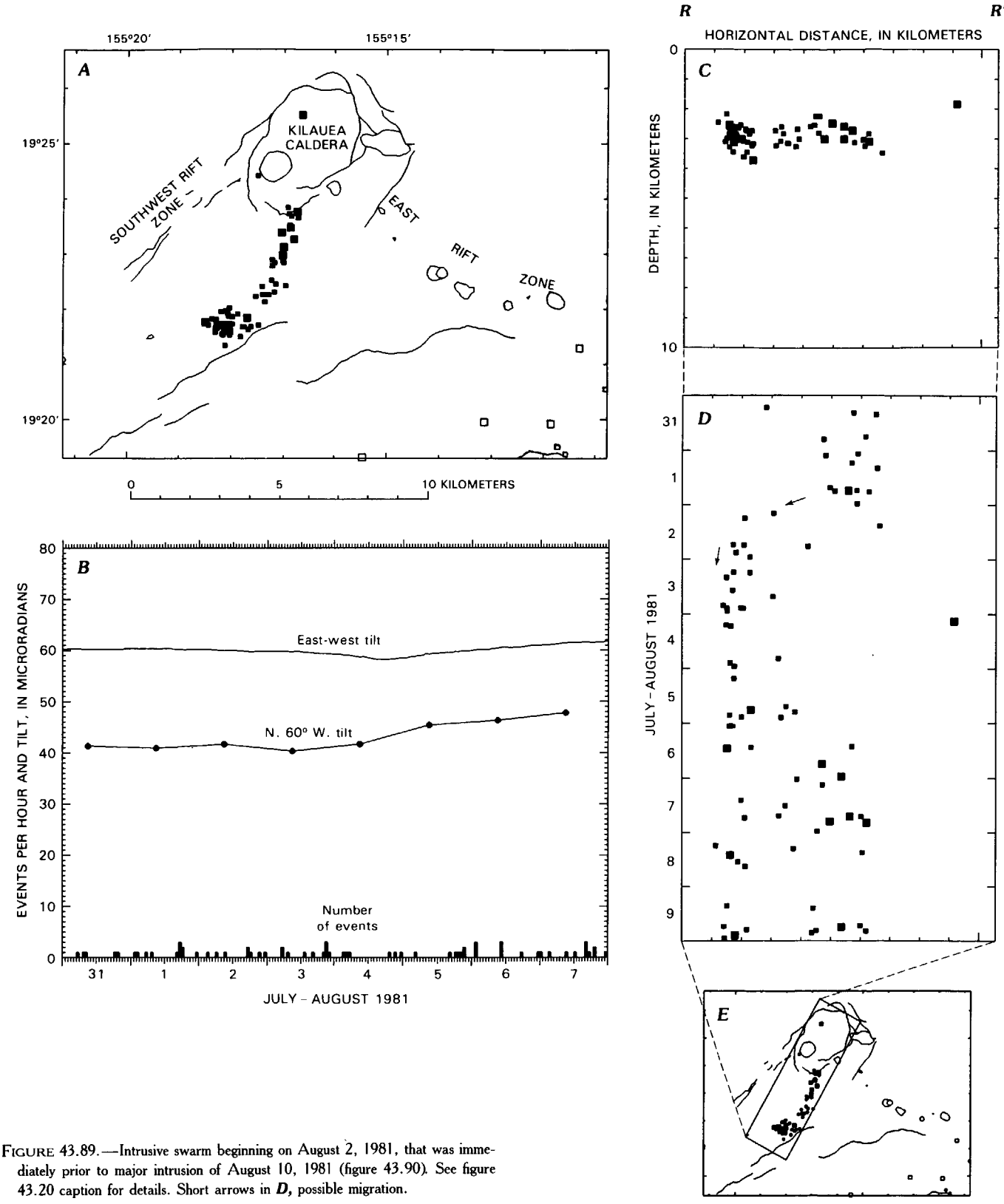

FIGURE 43.89.—Intrusive swarm beginning on August 2, 1981, that was immediately prior to major intrusion of August 10, 1981 (figure 43.90). See figure 43.20 caption for details. Short arrows in ***D***, possible migration.

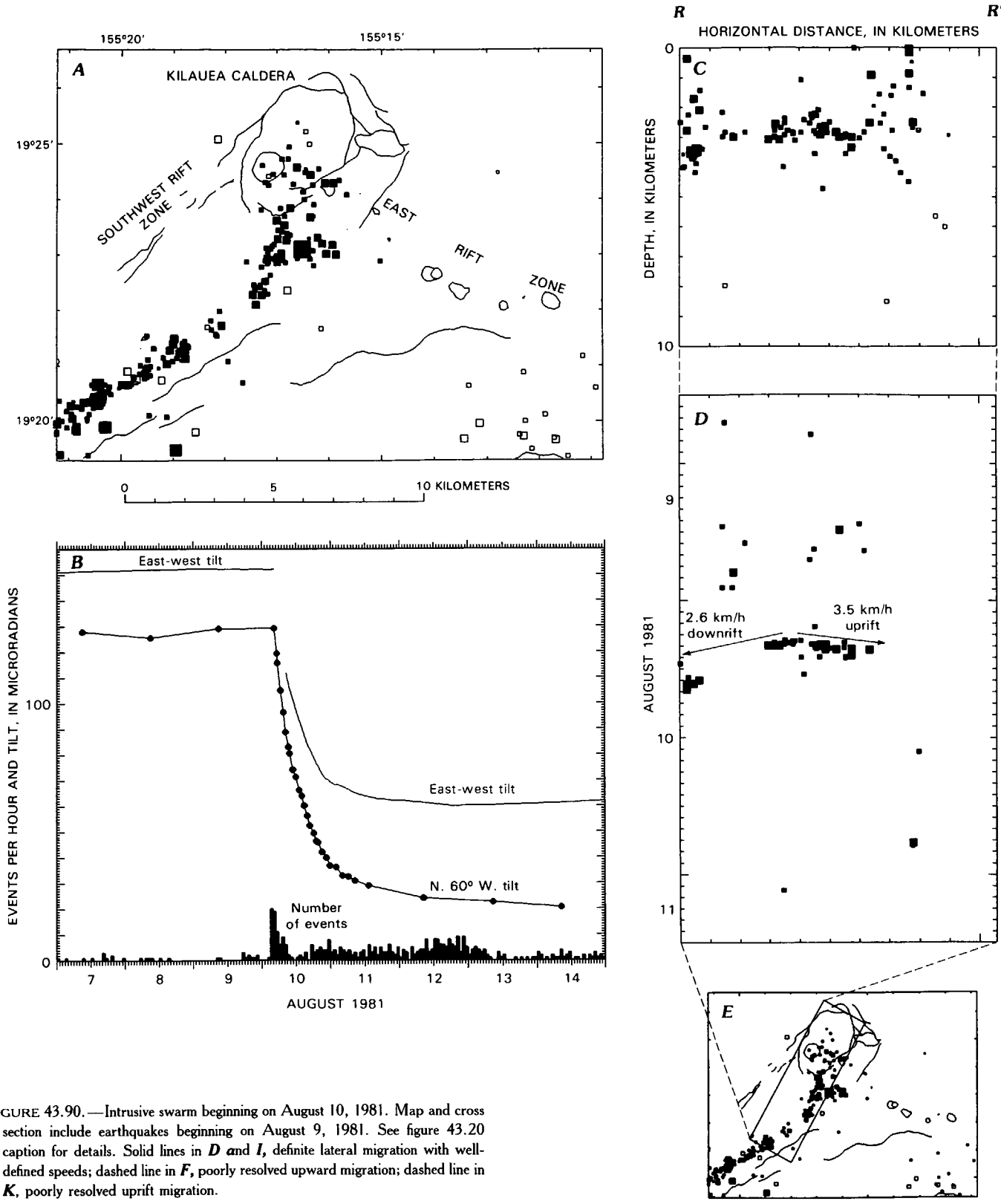

FIGURE 43.90.—Intrusive swarm beginning on August 10, 1981. Map and cross section include earthquakes beginning on August 9, 1981. See figure 43.20 caption for details. Solid lines in ***D*** and ***I***, definite lateral migration with well-defined speeds; dashed line in ***F***, poorly resolved upward migration; dashed line in ***K***, poorly resolved uprift migration.

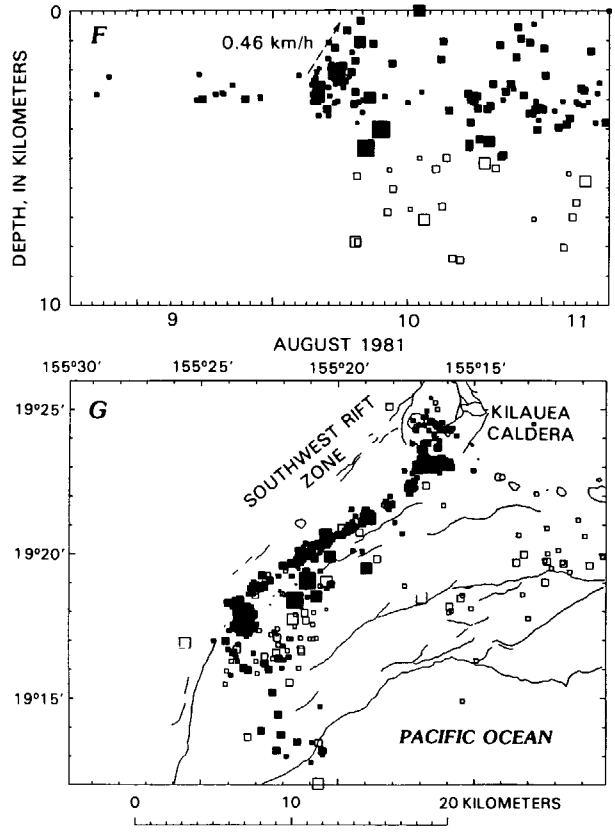

FIGURE 43.90.—Continued.

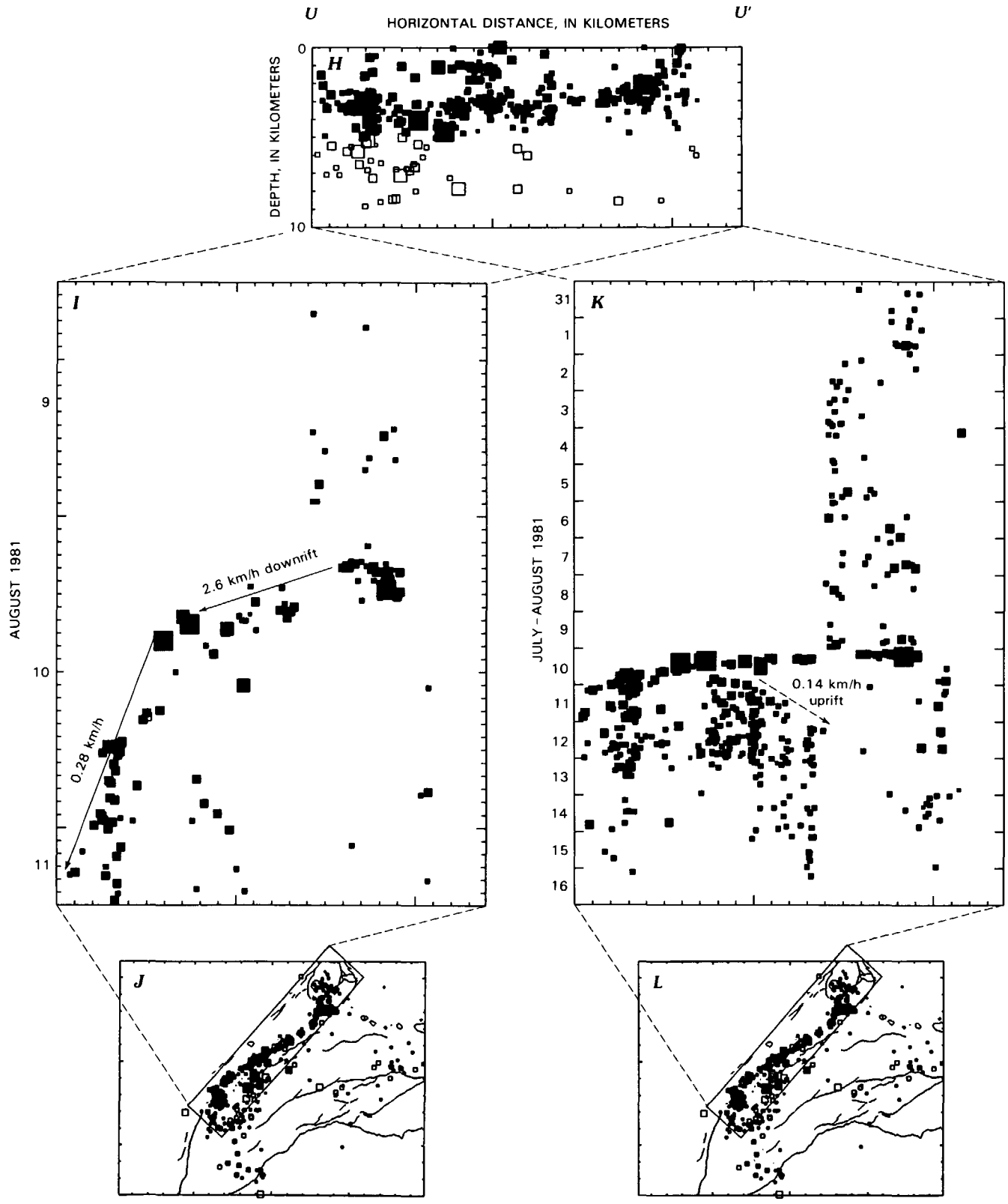

FIGURE 43.90.—Continued.

THE SOUTHWEST RIFT ZONE INTRUSIONS AND CALDERA ERUPTIONS OF MARCH–JUNE 1982

In the 10 months following the August 1981 intrusion, Kilauea reinflated rapidly and earthquakes in the south and central caldera steadily increased (fig. 43.85). Very little magma appears to have been intruded into the SWRZ, except possibly for three brief periods of slow deflation. The second deflation in February 1982 temporarily halted the caldera seismicity. The third deflation nearly did the same except for a one-hour swarm on March 23. The swarm may have marked a small intrusion just south of the caldera (fig. 43.91*A*), but if so the quantity of magma intruded during the swarm itself was so small it was nearly invisible on the tilt record (fig. 43.91*B*).

Kilauea's reinflation was also punctuated by a brief caldera eruption on April 30, 1982. Earthquakes were located in the central caldera between Keanakakoi and the eruptive vent (fig. 43.92*A*). Earthquake depths primarily 1–2 km beneath the caldera were shallower than the main magma conduit of the adjacent ERZ (fig. 43.92*C*). The seismic zone was therefore above and to the side of the magma reservoir and did not align with the April vents. The earthquakes may thus have surrounded a set of dikes branching upward from the magma reservoir to the ERZ conduit. The redistribution of magma within the summit complex caused a brief tilt step at Uwekahuna (fig. 43.92*B*). The onset of the swarm was nearly instantaneous, but appeared to move very rapidly to the northwest (fig. 43.92*D*). The swarm preceded the eruption by about 2.5 hours, slightly shorter than for typical rift eruptions.

An intrusion in late June 1982 continued the SWRZ activity, but in a pattern very different from the other SWRZ intrusions of the previous 18 months. The June intrusion saw seismicity shift from the summit to the lower SWRZ, as had occurred after the August 1981 intrusion (fig. 43.85). Earthquakes only extended from Puu Koae to Puu Kou, however, and most of the activity was below 6 km depth (fig. 43.93*A*, *C*). The main magma conduit at 3 km depth scarcely produced any earthquakes, in marked contrast to all other SWRZ intrusions. The pattern of summit deflation was also unusual, having begun very gradually and without reaching the high tilt rates typical of the other SWRZ intrusions (fig. 43.93*B*). In addition, earthquakes lagged deflation by 1–2 days. Intrusive earthquakes generally begin at the onset of deflation and correlate closely in time with deflation rate, making this an unusual event.

The rates of deflation and earthquake migration suggest that the same uprift section of the magma conduit was involved in the December 1974, August 1981 and June 1982 intrusions. The observed downrift rate of earthquake migration in 1982 was about 0.2 km/h (fig. 43.93*D*). If the magma front proceeded at the same speed through the aseismic upper 6 km of rift, about 30 hours would have been required, which is close to the observed time delay between the onset of deflation and the first earthquakes seen downrift. We can also repeat the calculation of rift cross-sectional area done for the August intrusion using 0.2 km/h and a deflation rate of 0.83 μrad/h. The result is an area of 1,400 m^2 involved in magma flow, which matches the values of 1,500 (1981) and 1,400 (1974) remarkably well.

We interpret the June 1982 intrusion as a relatively passive one into a magma conduit already rifted open by two major intrusions in the previous 1.5 years. The energetic seismicity and rapid deflation characteristic of new dike formation or a highly pressured intrusion were absent. The dike at 3 km depth was aseismic because it was filled with still-liquid magma from the recent intrusions. This older magma could be quietly pushed through the conduit without the wedging apart of wall rock that creates earthquakes. Downrift of Puu Koae, rifting did extend below the shallow conduit to 10 km, which is the approximate depth of the pre-Hawaiian ocean floor. The intrusion probably represents a downward flow of magma within the SWRZ. The event then completed the cycle of SWRZ intrusions by separating the two flanks down to the base of the volcanic pile at which the south flank is decoupled from the lower crust.

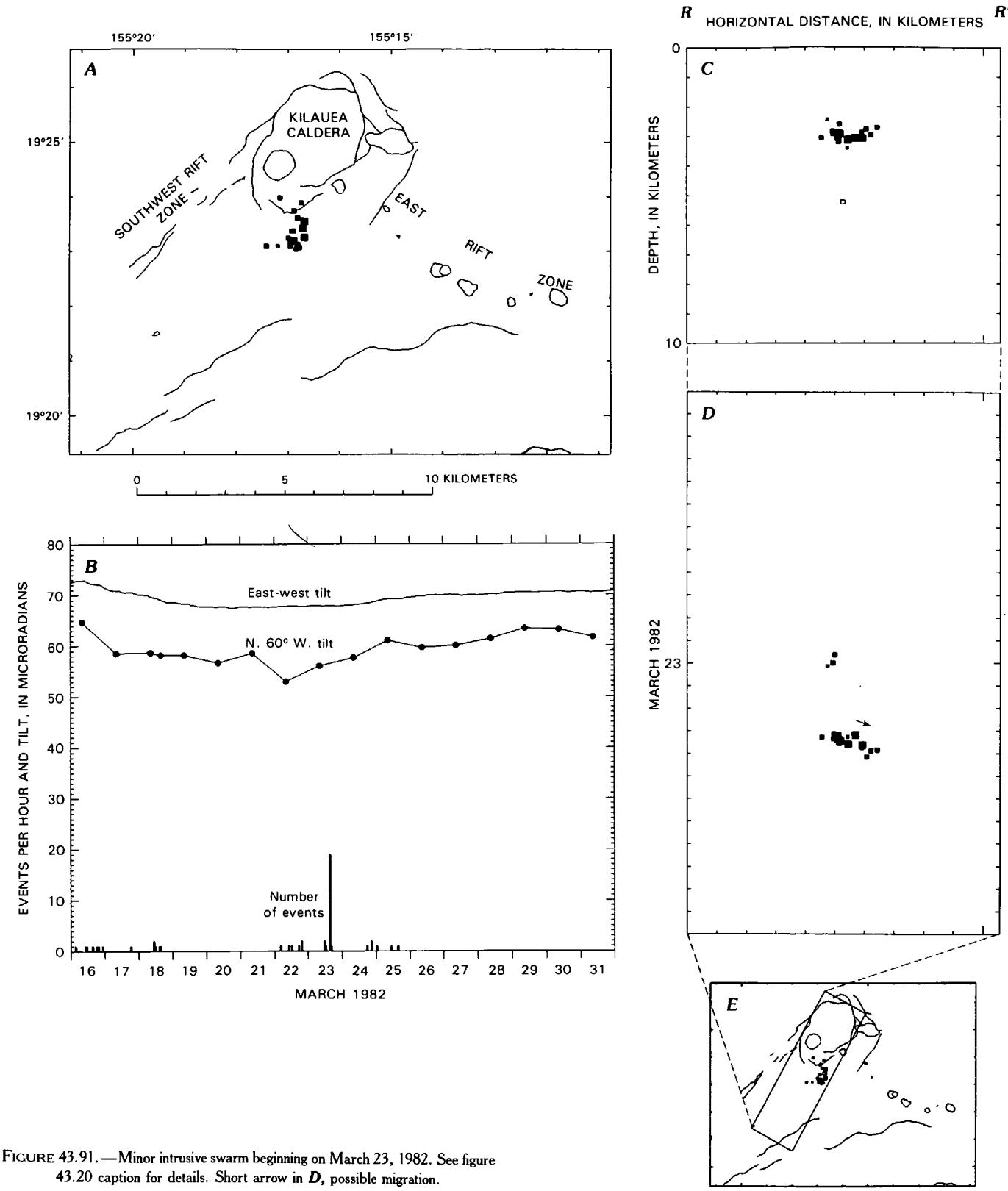

FIGURE 43.91.—Minor intrusive swarm beginning on March 23, 1982. See figure 43.20 caption for details. Short arrow in ***D***, possible migration.

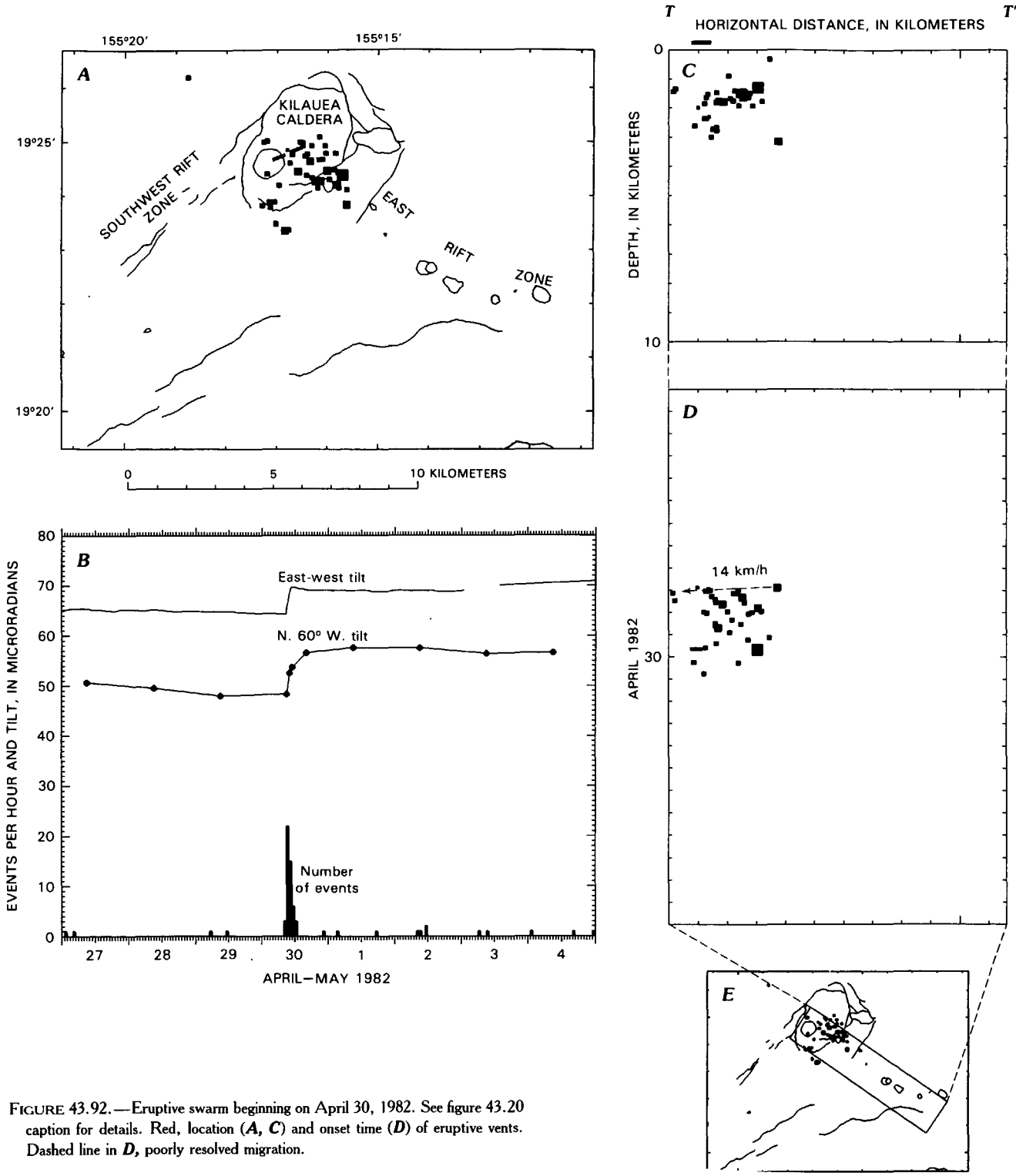

FIGURE 43.92.—Eruptive swarm beginning on April 30, 1982. See figure 43.20 caption for details. Red, location (*A, C*) and onset time (*D*) of eruptive vents. Dashed line in *D*, poorly resolved migration.

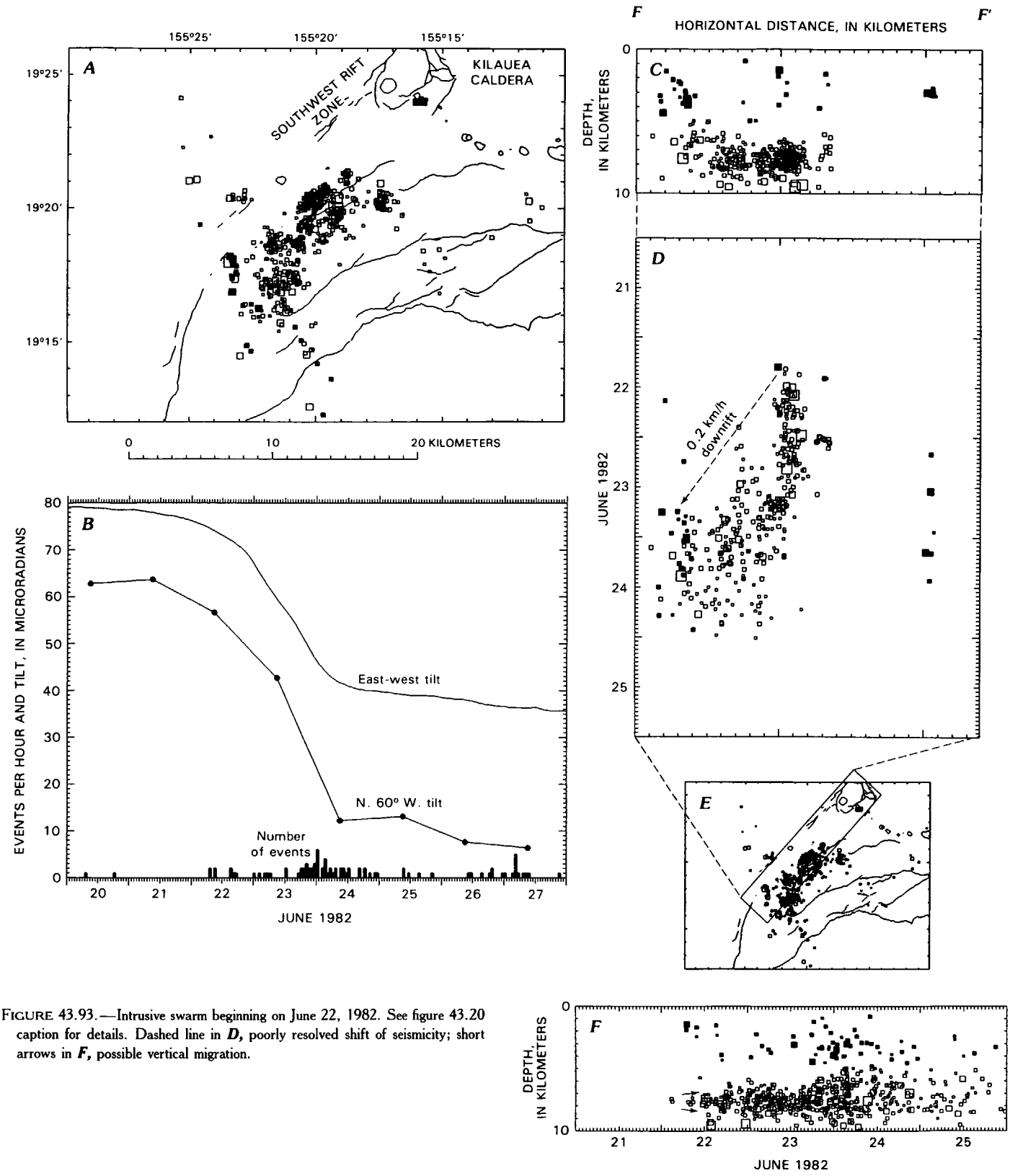

FIGURE 43.93.—Intrusive swarm beginning on June 22, 1982. See figure 43.20 caption for details. Dashed line in ***D***, poorly resolved shift of seismicity; short arrows in ***F***, possible vertical migration.

CALDERA AND EAST RIFT ERUPTIONS OF SEPTEMBER 1982 THROUGH JANUARY 1983

After several SWRZ intrusions, Kilauea began turning her attention back to the ERZ with a caldera eruption on September 25, 1982. The swarm began abruptly and coincided with a rapid step in summit tilt (fig. 43.94*B*). The intrusion affected portions of both the SWRZ and the ERZ adjacent to the caldera (fig. 43.94*A*). Earthquakes began under the area of the eventual vent in the south caldera. Seismicity soon spread to the ERZ and moved into both rifts at a speed of roughly 1.4 km/h for a short time (fig. 43.94*D*, *G*). A larger but slower wave of earthquakes moved into the ERZ about one hour later, presumably triggered by a major pulse of magma. As the intrusion progressed into the rifts, a dike also moved upward at about 1 km/h producing an eruption only about 2 h after the swarm began (fig. 43.94*I*).

When the dike reached the surface, earthquakes in the south caldera abruptly ceased (fig. 43.94*G*). This relation shows that the eruptive and intrusive dikes were hydraulically connected and the erupting dike dropped the magma pressure below the point needed to generate earthquakes. Earthquakes continued in the ERZ, however, which presumably was not as closely connected and did not feel the pressure drop at the time of eruption (fig. 43.94*D*). The sharp decline in seismicity early in the morning of September 26 is partly a result of masking of the seismograms by high tremor and partly of the real cessation of seismicity caused by magmatic pressure release accompanying the eruption. Conversely, the burst of ERZ seismicity following the eruption at about 0900 H.s.t. on September 26 is a result of timing more earthquakes and the apparent diversion of magma from the eruption to intrusion in the ERZ.

The September 1982 caldera eruption appears to have reactivated the ERZ following its quiescence during the series of SWRZ intrusions. This ERZ activity is partly demonstrated by the multiple pulses of magma intruded at the time of the eruption (fig. 43.94*D*). The ERZ also appears to have received magma during a slow and continuous intrusion during the month following the eruption. This slow intrusion is revealed by the flat summit tilt, the continuing seismicity in the Kokoolau area and the general tendency of earthquakes to migrate slowly downrift (fig. 43.95). The migration speed was a very slow 6 m/h (0.14 km/d). It was thus not surprising that the next two magmatic events were in the ERZ.

A rapid intrusion of the ERZ on December 9, 1982, extended from the caldera almost to Hiiaka (fig. 43.96*A*). Earthquakes thus reactivated the same area which was intruded during September and October (fig. 43.95), and the same conduit or dike was likely active at both times. Earthquakes migrated downrift at a rapid 6.4 km/h (fig. 43.96*D*), one thousand times faster than in October. The earlier slow intrusion, as with the SWRZ in 1981, may have prepared and heated the magma conduit and thus enabled the succeeding intrusion to move very rapidly. The high speed of intrusion may also have been aided by its proximity to the magma reservoir and the frequency of intrusion in this section of the ERZ. Coincident with the most intense seismicity, earthquakes migrated upward at about 0.8 km/h (fig. 43.96*F*). The upward movement thus followed the downrift migration by 1–2 hours. Magma apparently was deflected upward by the same blockage in the main conduit that halted both this and the October intrusion between Kokoolau and Hiiaka. The three weeks following the December 9 intrusion saw continuing seismicity in the Kokoolau area (fig. 43.95). After December 19, earthquakes began downrift of Pauahi, suggesting that the ERZ was transferring magma downrift in possible preparation for another event.

The ERZ swarm that began on January 1, 1983, was to lead to a major and long-lived eruption. Earthquakes only accompanied the first few eruption phases in early January, however. All succeeding major eruptive episodes were localized to the Puu Oo vent area, a continuous ERZ magma conduit was kept open by the eruption, and essentially no additional volcanic seismicity and probably no new dikes were created. Because this eruption captured most of Kilauea's magma supply, none was left to produce an eruption or intrusion elsewhere. The January 1983 sequence is thus the last

volcanic swarm in this chronology, which is complete through mid-1985.

The earthquake swarm and other studies of the first part of the eruption are treated in detail by Koyanagi and others (in press) and Wolfe and others (in press). The seismic zone extended 17 km from Makaopuhi to just east of Kalalua (fig. 43.97*A*). Eruptive vents were confined to an 8-km segment from Napau to Puu Kahaualea, so the zone of intrusion was about twice the length of the ERZ experiencing extrusion. Earthquakes were concentrated along the ERZ magma conduit centered at about 2.5 km depth near Makaopuhi, but deepening to 3.5 km beneath Kalalua (fig. 43.97*C*). Most earthquakes are clustered and are probably at highly stressed areas where magma flow is constricted.

Magma was supplied from the summit reservoir for the 7 days of the swarm, but at a slower average rate than during other intrusions of comparable size. The summit tilt curve (fig. 43.97*B*) does not show the typical initially rapid subsidence followed by a gradual leveling off: the deflation rate was instead relatively constant except for pauses on January 3, 4 and 6. Seismicity was roughly correlated with deflation rate, both being higher on January 2, 5 and 7.

Both earthquakes and eruptive vents moved successively downrift and in a complex and protracted pattern, eventually localizing near what was to become Puu Oo. The initial seismicity just uprift of Makaopuhi on January 1 broke downrift at 0.6 km/h on January 2 (fig. 43.97*D*). This first intense seismicity stopped when it reached Napau. The first emission of lava was at Napau about 24 hours after the first earthquakes reached that point. Earthquakes also shallowed with time on January 2 just prior to the first eruption (fig. 43.97*F*). The vent then opened progressively downrift at the same speed as the downrift earthquake migration, stopping near Puu Kamoamoa. The progress of the vent coincided with the cessation of earthquakes at the same point, which thus apparently released the magma pressure that caused the earthquakes. In fact the first phase of the swarm consisted of a zone of earthquakes whose leading and trailing edges both moved downrift at 0.6 km/h (fig. 43.97*D*). The last part of the trailing edge of earthquakes coincided with the start of eruption. Earthquakes at any one point lasted for about 24 hours, which probably represents the time for stress to be released either by the growth of the dike to its full width and height or for magma to reach the surface and relieve pressure.

The next phase of the swarm from noon on January 3 through January 6 was marked by somewhat reduced seismicity that expanded slowly both uprift and downrift from near Puu Kamoamoa (fig. 43.97*D*). Both deflation and the eruption had stopped during the first 2 days of this period. A shallowing of earthquakes preceded the resumption of lava emission at noon on January 5 to the east of Puu Kamoamoa (fig. 43.97*F*). For the last phase of the swarm, earthquakes shifted from uprift of the vents (fig. 43.97*D*). The intrusion then extended an additional 4 km downrift, moving at the same 0.6 km/h speed as the initial intrusion from Makaopuhi to Napau. The intrusion and most earthquakes stopped when the next eruption phase began on the morning of January 7.

The complexity of the swarm in space and time indicates that it was really several successive intrusions that opened the magma conduit from Makaopuhi to the eventual site of the Puu Oo vent. The conduit opened rapidly from Makaopuhi to Puu Kamoamoa, then at about 1/25 the initial speed to the lowermost vent, which was established at about the same time as another rapid but short extension of the dike downrift. When the swarm was less than half over at about 1530 H.s.t. on January 3, the eruption stopped, the number of earthquakes diminished and they began moving back uprift, and the summit tilt had leveled off. Apparently the major downrift flow from summit reservoir to vent was momentarily stopped or blocked, and increasing magma pressure and dike growth moved back uprift. This uprift growth originated at the same hypothesized barrier in the magma conduit that initially prevented the vent from opening farther downrift. A variety of these space and time relations are common to many intrusions and will be summarized and discussed in the next section.

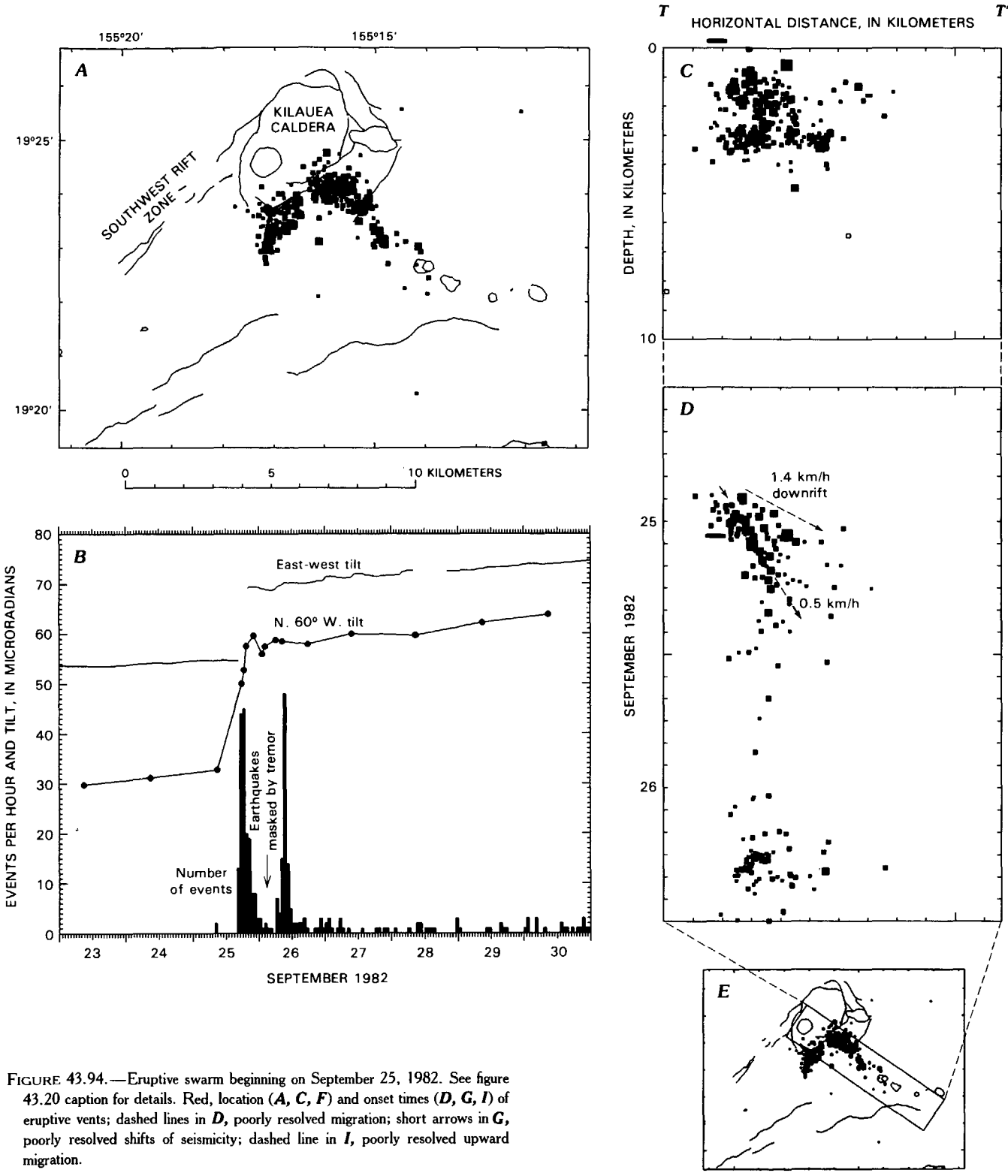

FIGURE 43.94.—Eruptive swarm beginning on September 25, 1982. See figure 43.20 caption for details. Red, location (***A, C, F***) and onset times (***D, G, I***) of eruptive vents; dashed lines in ***D***, poorly resolved migration; short arrows in ***G***, poorly resolved shifts of seismicity; dashed line in ***I***, poorly resolved upward migration.

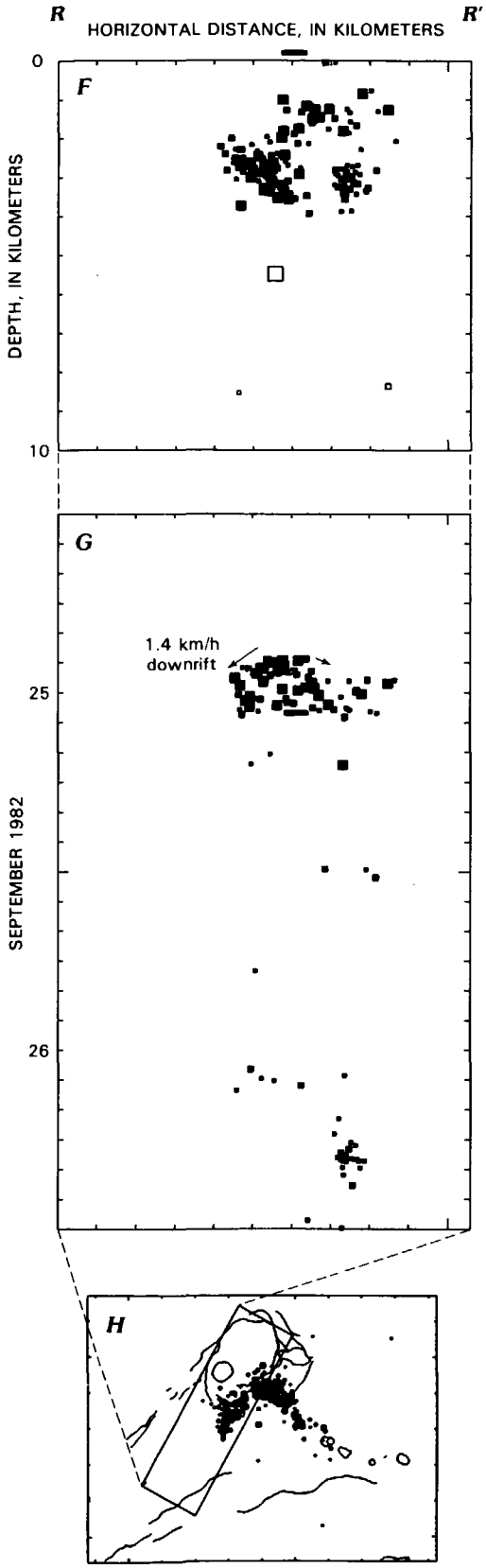

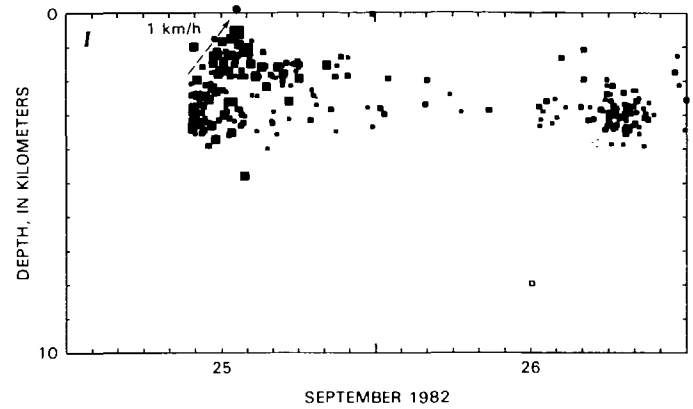

FIGURE 43.94.—Continued.

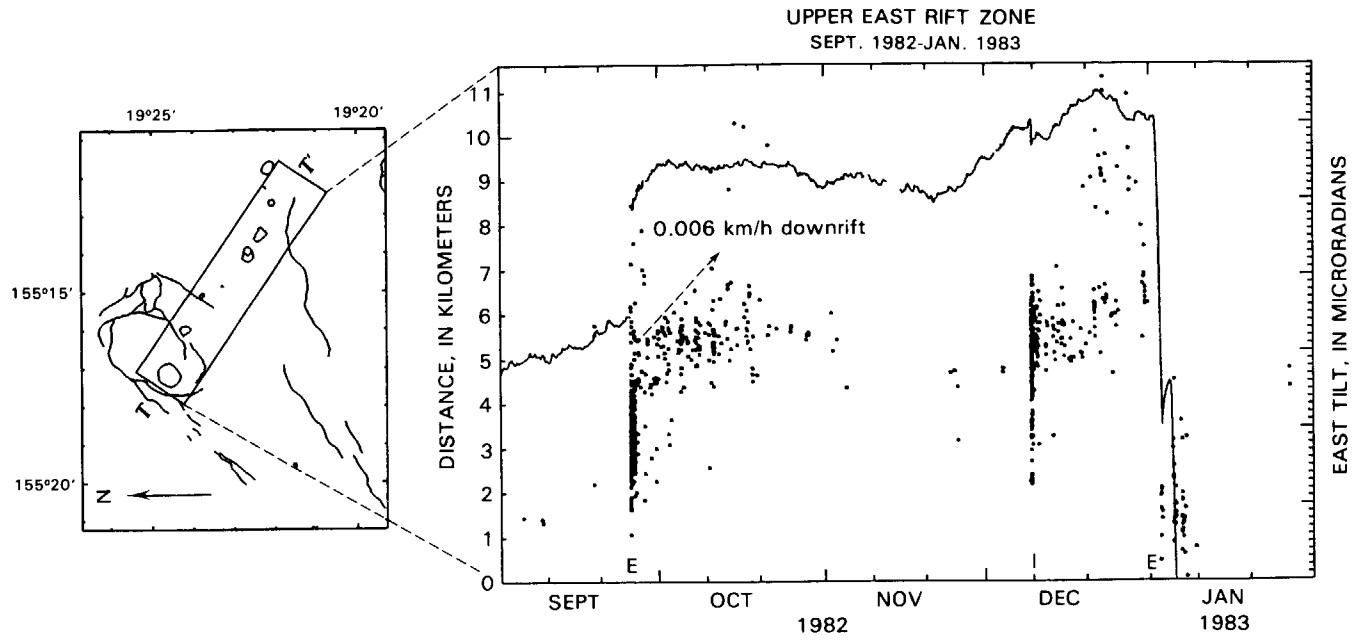

FIGURE 43.95.—Plot of earthquakes along east rift and east tilt at Uwekahuna versus time. All earthquakes shallower than 5 km and within geographic box shown are plotted. Halemaumau is at bottom and Mauna Ulu is near top. Tilt is from Ideal-Aerosmith instrument and down on plot generally indicates deflation of summit caldera. Large divisions on tilt scale are 10 μrad. Notations along time axis refer to specific swarms detailed in other figures: E, eruption; I, rapid intrusion. Dashed line, poorly resolved but very slow migration.

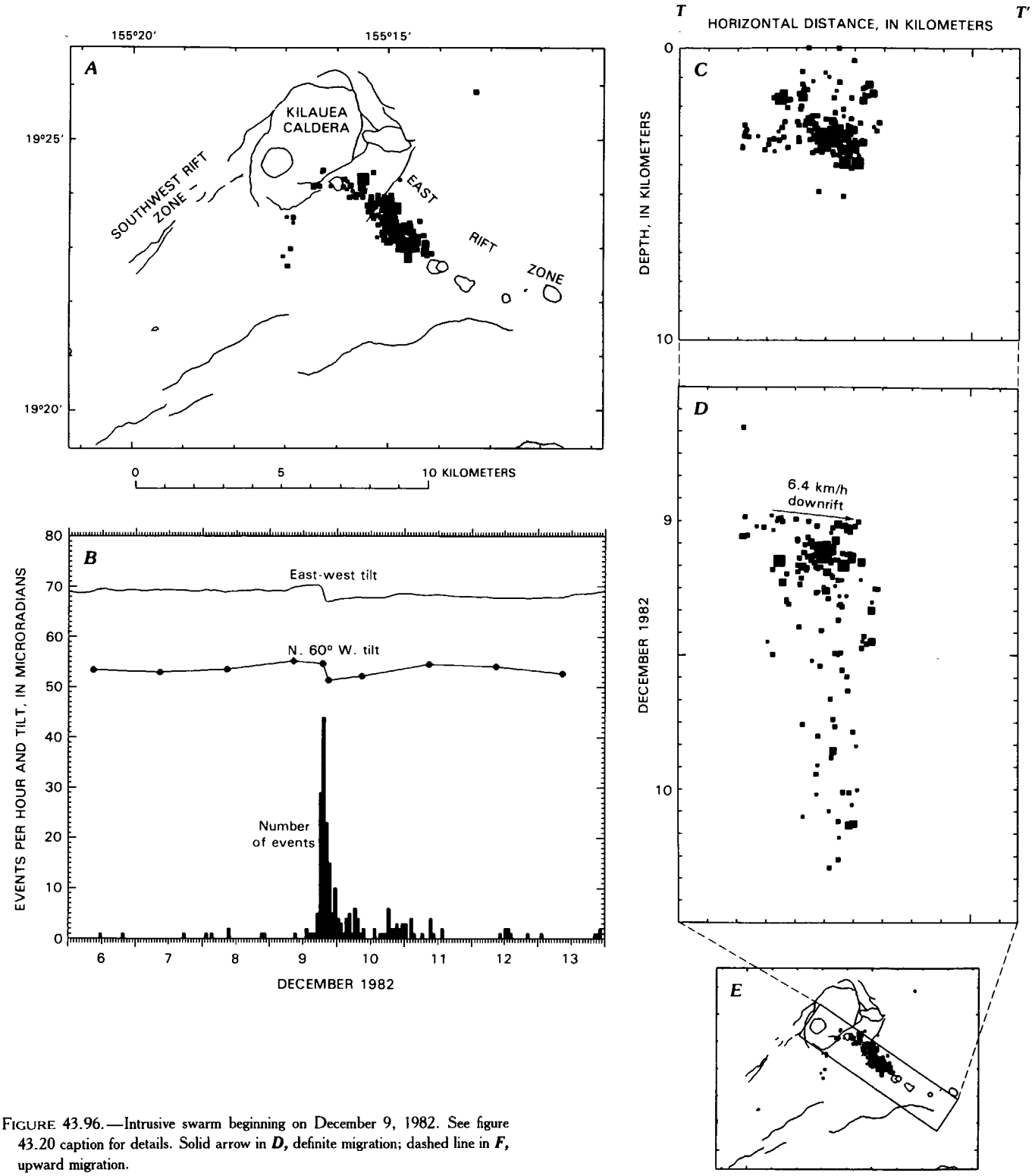

FIGURE 43.96.—Intrusive swarm beginning on December 9, 1982. See figure 43.20 caption for details. Solid arrow in ***D***, definite migration; dashed line in ***F***, upward migration.

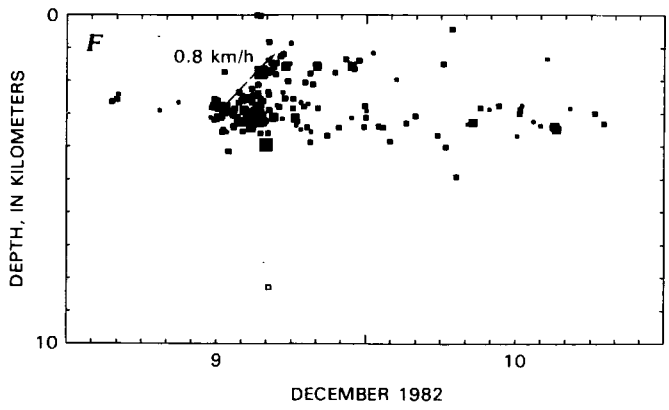

FIGURE 43.96.—Continued.

DISCUSSION OF RIFT-ZONE INTRUSIONS

This section summarizes and discusses many of the basic seismic patterns seen during intrusions. We will mention processes common to many intrusions and eruptions and discuss their implications for the structure and dynamics of the rifts. We will also point out some relations between different intrusions and how one might affect a later one. Many of these patterns were mentioned in the previous section, but could not be developed in a comparative way because of its chronological format. For detailed descriptions and interpretations of individual swarms, the reader is referred to the previous section. Table 43.1 summarizes the basic data of the individual swarms enumerated in this paper.

Nearly all shallow volcanic earthquakes at Kilauea can be attributed to magma intrusion in some form. We have given different names to different types of swarms based essentially on their location and intensity, but they all result from magma transfer. Swarms accompanying inflation of the summit reservoir are generally of low intensity, in or near the caldera, and are caused by intrusion of the reservoir with magma from below. Slow intrusions may produce a low level of seismicity lasting several days or weeks along the rift zones. Rapid intrusions generally produce an intense, short swarm in the caldera or rift zones and transport magma much faster than Kilauea's magma supply rate. Rapid intrusions either create or enlarge dikes, which produce an eruption if one reaches the surface.

The mechanics of rift intrusions in Hawaii have been treated in many previous studies. Fiske and Jackson (1972) emphasized the large-scale effects of gravitational and edifice stresses on rift-zone development. Dieterich and Decker (1975) and Pollard and others (1983) calculated the deformation and stress field surrounding a dike interacting with the Earth's surface. Duffield and others (1976, 1982) discussed and interpreted deformation measurements for several Kilauea intrusions in terms of forceful magma transport and dike emplacement. Swanson and others (1976a) and Dvorak and others (1985) discussed ERZ intrusions and their effect on deformation of the adjacent south flank. Shaw (1980) treated magma transport and ascent in terms of fracture mechanics in an applied stress field. Nakamura (1980, 1981) discussed the role of decoupling of the volcanic pile at the buried sediment layer in the formation of long rift zones.

INFLATIONARY SWARMS AND SLOW INTRUSIONS

Most rapid intrusions are preceded by a period of inflation and consequent slowly increasing seismicity at the summit. A period of inflation lasting several weeks may produce intermittent swarms during that period. The level of swarm seismicity may only be a few times that of the background level and is often accompanied by a brief increase in the rate of rising summit tilt. Seismicity and tilt are highly correlated during inflation, and the caldera seismicity generally ends abruptly if rapid deflation feeds an intrusion downrift. Inflationary swarms are thus caused by increasing magma pressure, uplift and extension in the summit region. The rift zones adjacent to the caldera become active in many inflationary swarms and may receive magma in pulses and slow intrusions. Inflationary swarms were most numerous from December 1969 to January 1972 and during 1974 when tilt and caldera inflation reached the highest values sustained in recent years.

Some inflationary swarms occur immediately before rapid intrusions and are precursory in some sense. Notable examples include February 1969 and September 1974. Other inflationary swarms, such as those of January 22, 1977, and January 20, 1981, may be distinct but precede a rapid intrusion by a few days. These paired inflationary and intrusive swarms are not coincidences, because they are typically adjacent in both space and time. Many inflationary swarms represent periods of accelerated inflation, during which the barriers containing the accumulating magma are more likely to break. Many intrusions may thus be triggered by episodes of rapid inflation.

Some seismic precursors to intrusions are not as obvious as inflationary swarms at the summit. A swarm of shallow ERZ and south flank earthquakes preceded the first Mauna Ulu eruption in May 1969. Although the quality of epicenter locations is poor, the precursory swarm was definitely not at the summit. The Mauna Ulu eruption may have thus been triggered by some south flank instability or downrift magma movement. Some rapid intrusions are immediately preceded by an adjacent intrusion that may also be a precursor or trigger. This pattern will be discussed below in the section "Sequential Relations Between Intrusions Along the Rift Zones."

Slow intrusions have been observed along the active segments of both rifts within 20 km of the caldera, and all share several features in common. Summit tilt may slowly rise, fall or stay level, but the rate is never more than a few microradians per day. Typical rapid intrusions, in contrast, deflate the summit at rates of several microradians per hour. The slow intrusion may be aseismic or weakly seismic, or may produce earthquakes only near the terminus of the intrusion where magma accumulates. As with all intrusions,

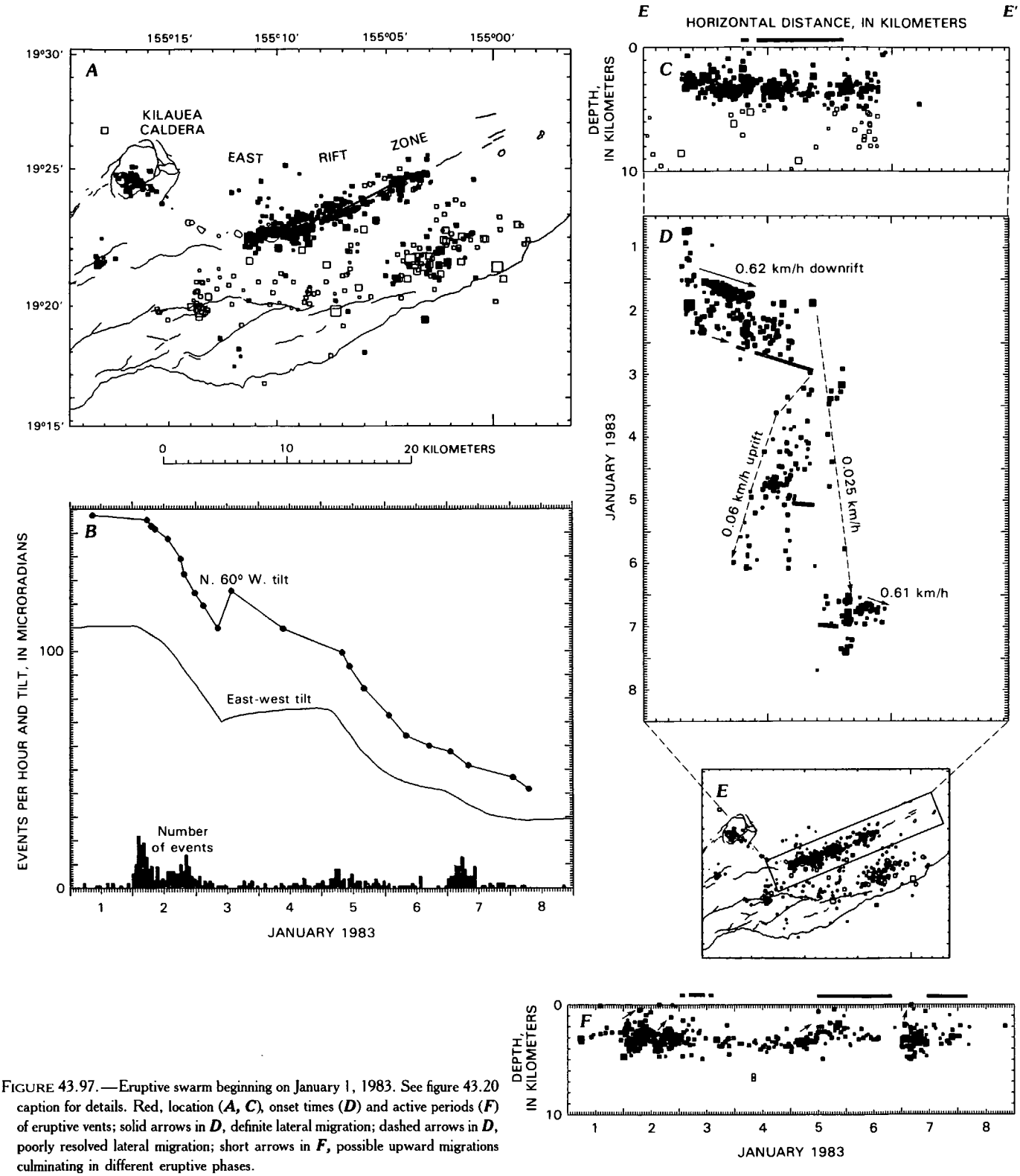

FIGURE 43.97.—Eruptive swarm beginning on January 1, 1983. See figure 43.20 caption for details. Red, location (***A, C***), onset times (***D***) and active periods (***F***) of eruptive vents; solid arrows in ***D***, definite lateral migration; dashed arrows in ***D***, poorly resolved lateral migration; short arrows in ***F***, possible upward migrations culminating in different eruptive phases.

aseismic magma passage is presumed to indicate that the rift conduit is unstressed and in equilibrium, and need not widen to accommodate the magma flow. Completely aseismic intrusions are not considered in this paper, but Dzurisin and others (1984) used downward steps in tilt to account for magma transfer into the rifts. We infer that slow intrusions reveal magma leaking passively into the rifts at a rate comparable to that of its accumulation at the summit.

The most common slow intrusions occur from the summit reservoir during periods of inflation. The distinction between steady accumulation and pulsed flow of magma can often only be made if migrations of earthquakes are visible. Pulses of slowly intruding magma are seen in the intrusions of February and December 1970, June and July 1971, January 1972 and December 1974. Migration speeds are typically 0.01–0.05 km/h, which is 1 to 2 orders of magnitude slower than during rapid intrusions. At these speeds, several days are required for magma to traverse a few kilometers of rift. Some intrusions do not fall neatly into a category: the January 1977 event accompanied a short episode of inflation (as might a slow intrusion), but showed a rapid 0.7 km/h speed typical of a rapid intrusion.

Slow intrusions more than 5 km from the caldera have different characteristics on each rift zone. The SWRZ intrusions of October 1969 and February 1981 each generated earthquakes only near Puu Kou, lasted several days, and were accompanied by gradual deflation. Magma thus moved aseismically down 20 km of rift conduit. Pulses of slowly moving magma similar to ones near the summit triggered seismicity along the SWRZ following the June 1971 intrusion, in the 6 months prior to the December 1974 eruption, and during February–June 1981. The ERZ experienced a series of cyclic slow intrusions during November 1978–July 1979 and May–October 1980. The summit tilt oscillated as discrete pulses of magma were dispatched downrift. Episodes of summit seismicity coincided with peaks in tilt, and very shallow swarms near Puu Kamoamoa close to minima in tilt were caused by accumulating magma downrift. The rift between the caldera and Puu Kamoamoa did not produce migrating earthquakes as magma passed through. The intrusion thus was slow, magma transfer was passive, and seismicity was produced only at places of local inflation.

SEQUENCE OF EVENTS WITHIN A RAPID INTRUSION

Most intrusions occur in stages, only some of which may be evident during any one event. Larger and longer intrusions often display the most complexity, such as multiple phases and a variety of earthquake migration patterns.

The seismic zone formed by a rapid intrusion nearly always grows in size or shifts location as magma flows through conduits or fills a dike. In the first tens of minutes an intrusion often produces earthquakes in a small volume 1 km^3 or less in size. Most intrusive swarms begin from the rift-zone magma conduits (and sometimes the summit reservoir itself) near 3 km depth. When shifts in epicenter locations can be resolved, downrift migration of earthquakes and magma is typical of the SWRZ and the ERZ downrift of Mauna Ulu. The caldera and the ERZ between the caldera and Mauna Ulu are more complex, and swarms may migrate either uprift or downrift with comparable likelihood. A shallowing of earthquakes with time is often observed in swarms where a range of depths can be resolved.

Major intrusions that also produce an eruption often divide into two types of processes, which can be illustrated by the July 1974 eruption. The first phase produced intense seismicity and a moderate deflation rate. Earthquakes migrated laterally (in this case uprift) and also upward from the ERZ magma conduit in a linear fashion toward the vent. We infer a high magma pressure and a growing dike from the intense seismicity, but a relatively low-volume flow from the deflation rate. When the dike reached the surface and the eruption began, tremor and the deflation rate increased dramatically. Earthquakes then ceased, partly because of masking by high tremor on the seismograms and partly because the dike stopped growing. Magma flow through an open-ended dike presumably dropped the magma pressure and did not require a lengthening or widening of the dike. Intense seismicity is therefore associated with a dike that is growing and compressing its walls.

Larger and more complex eruptions may display these seismic dike growth and aseismic magma flow modes simultaneously. If a dike is many kilometers long, eruption from a vertical feeder may start while the dike continues to intrude downrift, as seen in the September 1977 and January 1983 eruptions. Earthquakes at a given place will generally cease when the dike there reaches the surface and magma pressure drops, but seismicity will continue where the dike is still growing. The time between the first earthquakes and eruption at a given location is a measure of the time required for magma to migrate from the conduit at 3 km depth to the surface. This time may be 2–24 hours but is typically 3–6 hours. The deflation rate (and hence the magma volume rate) generally correlates either with the extrusion rate or the intensity of seismicity, depending on the importance of additional dike growth. This correlation of tilt rate and seismicity is easiest to see during large multiphase eruptions such as September 1977 and January 1983.

THE GEOMETRY AND DYNAMICS OF INTRUSIVE SWARMS

An intrusion may occur either by the fracturing of rock and emplacement of a new dike or by the opening of an older magma conduit. In either case the pressurized expansion of dike width apparently produces earthquakes in the rock near the dike. How much seismicity if any is produced by tensile fracture at the tip of a dike expanding into fresh rock is presently difficult to say. The recurrence of intrusive swarms in the same rift zone suggests that most intrusions propagate along planes of weakness that are the molten cores or boundaries of older dikes. Thus tensile failure at the crack tip is seismically a minor process compared to shear failure in the compressed rock near the dike. This view is consistent with Hill's (1977) earthquake swarm model, in which earthquakes occur on shear planes joining echelon dike segments.

The mechanics of rapid and slow intrusions determine whether a given event is forceful or passive. The compression and seaward displacement of Kilauea's south flank is a result of forceful intrusions

in the rift zones (Swanson and others, 1976a). We believe that the amount of seismicity and to some degree the speed of migration provide the distinction: rapid and seismically intense intrusions are forceful, and slow intrusions with weak seismicity result from a more passive flow of magma.

Patterns of seismic and aseismic migration of intrusions support the concept of earthquake generation adjacent to an expanding dike. Most Kilauea intrusions produce earthquakes for some distance behind its leading edge, not just at its foreward tip. This presumably is the region in which the dike continues to widen after its initial opening. Seismicity then stops at a given place when the dike reaches its full width. Magma-filled conduits are clearly present in the ERZ much of the time, otherwise each intrusion would produce earthquakes along the entire rift between the summit and the intrusion terminus.

Intrusions may alternately migrate both seismically and aseismically. The aseismic migration occurs where the dike is already open and fluid, the adjacent rock is easily and aseismically compressed, or the dike widens only enough to supply magma to its leading tip. One example of aseismic migration through a previously rifted area was seen in the SWRZ intrusions of August 1981. The pre-intrusion of August 2 produced earthquakes out to only 5 km from the caldera before stopping. The main intrusion on August 10 produced no earthquakes where the earlier intrusion stopped because that section was already rifted open. Another type of aseismic dike growth is illustrated by the February 1977 intrusion. An initial and small burst of earthquakes was followed by about 3 hours of seismic quiescence and no deflation. The intense swarm then began simultaneously throughout the seismic zone and was rapidly fed by magma from the deflating summit. We interpret the aseismic period as growth of the dike to its eventual area but only to a small thickness. The dike was then filled at a high volume rate and generated earthquakes as it grew in thickness simultaneously over most of its area.

Earthquakes alone are not adequate to resolve the cross-sectional shape of the conduit, but do constrain its area through which magma flows. The ratio of magma supply rate (deflation rate converted from microradians of summit tilt to magma volume using the value of 0.3 million cubic meters per microradian from Dzurisin and others, 1984) to the earthquake migration rate is equal to the cross-sectional area of the dike. The SWRZ intrusions of December 1974, August 1981 and June 1982 all yield about 1,500 m^2 as the effective area of the main SWRZ conduit (table 43.1). Modeling the August 1981 dike as about 1,500 m by 1 m matches an observed leveling profile (Pollard and others, 1983), so these dimensions are consistent with all seismic and deformation data. The cross-sectional area of the northern SWRZ dike active in September 1971, however, is only about 280 m^2. The ERZ conduits are also smaller than the main SWRZ conduit and do not exceed 900 m^2 (table 43.1).

Intrusions are most efficient at producing earthquakes between 2 and 4 km depth in most of the rift system, which is apparently the depth of the main magma conduits. The uppermost 2 km of the rifts probably lack sufficient confining stress, and slip occurs aseismically. Unseen intrusion probably occurs below 4 km, which may be too hot and ductile to deform seismically. Intrusion in some form extends from the surface to at least 10 km depth where the volcanic pile rests on the pre-Hawaiian sea floor. Intrusive volume is ultimately accommodated by seaward slip of the unbuttressed south flank on its base at about 10 km depth.

When intrusive earthquakes do occur above 2 km depth, they often migrate up from the main conduit and follow an upward-branching dike. Many recent examples of upward earthquake migration are apparent, especially in the ERZ from the caldera to Mauna Ulu. Examples of intrusions whose earthquakes display both an upward branching finger and clear shallowing of hypocenters with time are November 1979 and July, August and October 1980. The SWRZ intrusion of August 1981 also contained a vertical branch that produced shallow earthquakes and a zone of surface cracking.

Earthquakes directly beneath the main conduit are less common, but have been recognized under both rifts. The central SWRZ swarm in June 1982 followed 1.5 years of shallow SWRZ intrusions. The swarm appeared to accompany a downward draining of magma to complete the rifting process to the base of the volcanic pile. The most common place that deeper volcanic earthquakes are seen below the ERZ is in a rootless cluster at 5–7 km depth below Mauna Ulu. Activity there (see fig. 43.3*F*, *G*) was recognized during the intrusions of June 1976, September 1977, May 1979, and to a lesser extent during many others. Earthquakes during the May 1979 intrusion spread both upward and downward and reached 7 km depth the day after the main swarm. Most of the rifting process below 4 km depth is aseismic, and the study of earthquakes cannot determine the degree to which magma is supplied from the main rift conduit above or through a deeper and lateral system directly from Kilauea's vertical magma conduit.

THE MECHANICS OF EARTHQUAKE MIGRATION

As we have seen many times, migrating earthquakes reveal moving magma and the growth of dikes within the rift zones. Earthquakes mostly originate at or just behind the leading edge of the dike, where it is growing in width. Some earthquakes occur ahead of a smoothly advancing front of seismicity. These may be from (1) irregular or jerky dike motion, (2) a stress increase in front of the dike, or (3) triggering by elastic waves radiated by earlier earthquakes.

The direction of migration is generally downrift, except within the caldera and in the ERZ between the caldera and Mauna Ulu. Magma is supplied at the summit, and both its pressure gradient and downslope gravitational flow transport it primarily in the downrift direction. Note that upward movement by bouyancy requires that magma have at least lithostatic pressure. The observed combinations of upward and downrift magma movement thus require the rift to be in a mixture of lithostatic and sublithostatic stress conditions. Sublithostatic pressure might thus prevail in places where downrift magma movement is rapid, continuous or aseismic. Lithostatic pressure probably prevails near blockages of the rift conduit and places where dikes branch upward to form eruptive vents.

The intrusive patterns for the SWRZ are simpler than for the ERZ. The positions, starting points, migration directions and migration speeds for the earthquake swarms discussed in this paper are summarized in figure 43.98. This distance versus time plot shows what happened where and when. For example, most SWRZ intrusions begin near or just south of the caldera. Within 3 km of Halemaumau, intrusions are about equally likely to migrate into or out of the caldera. The region close to the summit magma reservoir is presumably a complex of conduits that grow as an interconnected network. All intrusions in the SWRZ more than 3 km from the caldera migrate in the downrift direction. The six best observed SWRZ intrusions all reached Puu Kou. Thus, no major barriers capable of stopping an intrusion are present between the south caldera and Puu Kou. The migration speed slowed significantly near the terminus of the major 1974 and 1981 intrusions. This speed decrease could be caused by a drop in temperature or pressure near the end of the intrusion, or the observed upward bend of the seismic conduit over a barrier near Puu Kou.

Intrusions downrift of Mauna Ulu in the ERZ are also relatively simple. For the present discussion we exclude the intrusions of 1963, 1965 and February and May 1969 owing to their diffuse earthquake distributions within the south flank. Each of the seven events that penetrated downrift of Mauna Ulu started within 1 km of that point, and each intruded in the downrift direction. The major September 1977 and January 1983 intrusions slowed with distance from the summit, as did the two largest SWRZ intrusions. Long intrusions apparently cannot sustain a high speed for the entire length of the dike. Unlike the SWRZ, the three ERZ intrusions that passed Makaopuhi each stopped at different places, implying that many barriers capable of stopping intrusions exist in the ERZ. The simplicity of a single, linear magma conduit at 3 km depth appears to exclude complexities such as uprift earthquake migration in the SWRZ and central ERZ.

BEHAVIOR OF THE EAST RIFT ZONE FROM THE CALDERA TO MAUNA ULU

Intrusions between the caldera and Mauna Ulu in the ERZ are varied and often complex. This section of rift is distinctly different from the rest of the rift system in several ways: (1) intrusions in recent years were much more frequent than elsewhere; (2) the area often partakes in inflation of the summit magma reservoir and may continuously produce earthquakes during these times; (3) it is the only section of Kilauea's rift system that trends north of west and is therefore most oblique to the greatest principal stress, which controls the strikes of individual vents and the majority of the rift system; (4) the Koae fault zone meets the ERZ near Mauna Ulu, tectonically separating this section from the simpler ERZ downrift; (5) the only major intrusion to trend oblique to the rift axis was here in July 1969, and some eruptive vents also obliquely extend several kilometers from the rift; (6) earthquakes near 1–2 km depth are numerous—though the main magma conduit at 3 km depth is typical of the whole rift system; (7) magma may supply two events

FIGURE 43.98.—Diagram of position of swarms and intrusions versus time as documented in this paper. Horizontal scale in ***A*** is in kilometers from center of Halemaumau along the SWRZ (left) and ERZ (right). Solid lines show time and lateral extent of rapid intrusions. Dashed lines, intrusions with diffuse hypocenters; F, swarms in flanks off rift axis; dotted lines, inflationary swarms and slow intrusions; each swarm is labeled with its month and year; solid circles, initiation point of each swarm where earthquakes started; arrowheads and numbers in parentheses, direction, extent, and speed (in kilometers per hour) of earthquake migration. Swarms with a starting point but no arrowhead or speed have speeds that are difficult to measure. ***B***, Similar diagram as *A* for the Koae fault zone.

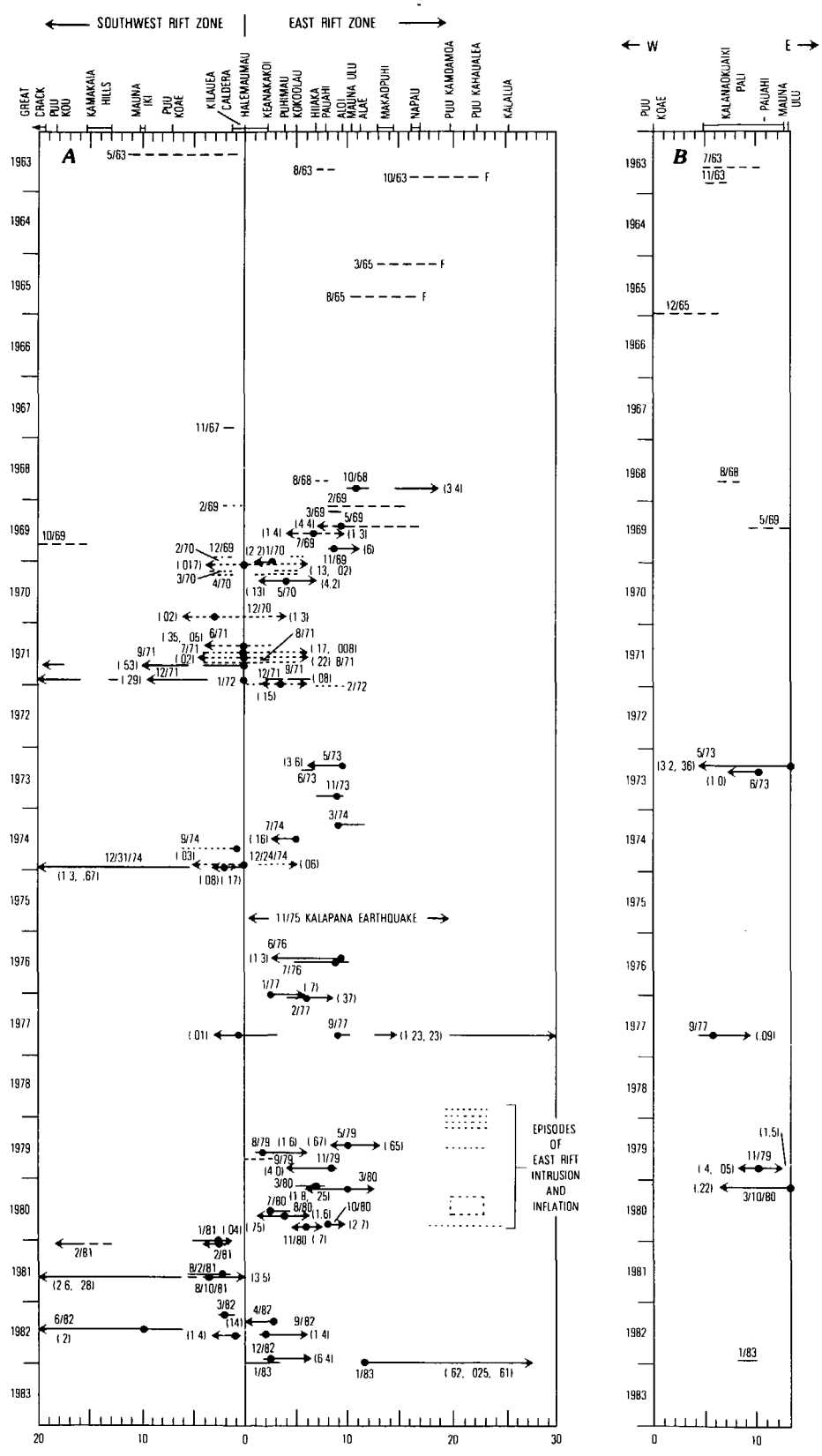
SOUTHWEST RIFT ZONE
EAST RIFT ZONE
GREAT CRACK
PUU KOU
KAMAKAIA HILLS
MAUNA IKI
PUU KOAE
KILAUEA CALDERA
HALEMAUMAU
KEANAKAKOI
PUHIMAU
KOKOOLAU
HIIAKA
PAUAHI
ALOI
MAUNA ULU
ALAE
MAKAOPUHI
NAPAU
PUU KAMOAMOA
PUU KAHAUALEA
KALALUA
A
B
W
E
KALANAOKUAIKI
PALI
PAUAHI
MAUNA ULU
11/75 KALAPANA EARTHQUAKE
EPISODES OF EAST RIFT INTRUSION AND INFLATION

simultaneously, as with the series of eruptions and intrusions during the 1969–74 Mauna Ulu activity or the two intrusions during October 21–22, 1980; (8) intrusions are equally likely to migrate uprift or downrift and sometimes move outward in both directions from their starting points; (9) intrusions may begin and end at several different places, implying a population of significant blockages within the conduit system; (10) the suspected magma reservoir beneath Pauahi is in this section of rift; and (11) the time between the first seismicity and later eruption at the same point is typically 2–3 h, but is at least 5–6 h elsewhere in the rift system. Though many of these differences are probably interrelated and are consequences of the evolution of the ERZ, we will only discuss a few of them in detail. We interpret differences in the seismicity of the ERZ from the caldera to Mauna Ulu as a result of a complex honeycomb of magma conduits, a high frequency of intrusions and the local trend oblique to the rest of the rift system.

The ERZ as a whole has been seismically and volcanically more active than the SWRZ, both historically and prehistorically. This greater activity is recognized by eruption frequency, higher topography, and larger gravity and magnetic anomalies (Duffield and others, 1982). Of the intrusions and eruptions during 1962–83, about 75 percent have been in the ERZ, and about 75 percent of those primarily involved the section uprift of Mauna Ulu.

The extensive seismicity above 2 km depth uprift of Mauna Ulu probably derives from a complex honeycomb of magma conduits and from a response to frequent slow and fast intrusions of the main magma conduit at 3 km depth. Shallow earthquakes may thus be produced in two ways: (1) The direct intrusion of magma into the shallow parts of the interconnected conduit system produces earthquakes near fingers of dikes that branch upward. These vertical intrusions produce upward earthquake migration and may feed an eruption if they reach the surface. (2) The region above the main magma conduit responds mechanically to intrusions below. A fast intrusion produces earthquakes by frequently extending and uplifting a zone that is highly fractured. A slow intrusion generates the same seismic and deformation patterns as a fast intrusion, but is analogous to the shallow seismicity in the caldera above the main magma reservoir. The occurrence of 0- to 2-km seismicity both above the magma reservoir and within the section of rift that can inflate during slow intrusions suggests that extensional stresses applied for long periods play a part in generating the shallow earthquakes.

The misalignment of the rift axis and greatest principal stress may contribute to the complex seismicity of the ERZ between the caldera and Mauna Ulu. Locally, the shallow stress orientation is defined by eruptive fissures in the rifts and faults in the Koae fault zone, which trend east-northeast. Evidence of a similar trend at 3 km depth comes from the intrusion of July 1969, which trended east-northeast and crossed the rift near Hiiaka. Earthquakes migrated east and west from the dike's intersection with the main ERZ magma conduit, which thus fed the intrusion. Regionally, the greatest principal stress is also defined as east-northeast by the remainder of Kilauea's rift system. Most intrusions of the ERZ between the caldera and Mauna Ulu, however, follow the southeast trend of the main magma conduit. The magma conduit is self-sustaining and may have twisted southward with the apparent southward migration of the ERZ (Swanson and others, 1976a). We believe that the rift conduit is now oblique to the greatest principal stress, and this stress direction complicates many of the observed seismic patterns. Stress orientation possibly changes with depth, or the intersecting Koae fault zone perturbs stresses locally. Additional work including focal mechanisms will be required before stress patterns can be adequately discussed.

UPRIFT EARTHQUAKE MIGRATION

A unique characteristic of the ERZ between the caldera and Mauna Ulu is uprift migration of earthquakes during intrusions. Figures 43.98 and 43.99*B* show that roughly one-half of the migrating intrusions in this section of rift do so in the uprift direction. This observation underscores the fact that intrusions are complex redistributions of magma and stress. Three complicating factors bear on the mechanism of uprift earthquake migration: (1) We interpret the greater vertical extent of earthquakes and the simultaneity of two intrusions or eruptions as indicators of a multitiered honeycomb of magma conduits in the uprift section of the ERZ. (2) Earthquakes appear to be generated by expansion of dike walls under magma pressure. Earthquakes may thus be produced either by rock fracturing near the leading edge of an advancing dike or by a pressure pulse moving within an existing dike. (3) Magma will only flow downward by gravity if confined below hydrostatic pressures, but will flow upward by bouyancy if confined at or above the higher lithostatic pressure. Various intrusion paths are thus possible.

Consider a few examples of how uprift earthquake migration might occur: (1) Over a distance of many kilometers, the magma conduit slopes downward in the downrift direction. Downrift flow might then accompany low stress conditions, and later uprift or bouyant flow might result from high stress conditions. The opening and closing of the connections between conduits in the honeycomb only complicates the possible flow directions. (2) While magma flows downrift, a pulse of pressure causing dike widening and earthquakes might travel uprift. This pulse could occur, for example, after a downrift-moving intrusion reaches a barrier that stops it and creates a back wave of pressure against the flow of magma. Such reversals from downrift to uprift migration accompanied the intrusions of January 1972, December 1974, June 1976, November 1979 and January 1983. (3) The entire intrusion and rifting process may begin at one of the conduit blockages, which serves as a point of stress concentration within the rift. The intrusion may then grow outward from this point in several directions, as did the August 1980 event. The fact that summit deflation begins within minutes of the first intense seismicity argues that a magma storage pocket within the rift, such as suspected at Pauahi, acts only as an initiating stress concentration rather than a major source of magma feeding nearby intrusions. We conclude that the variety of earthquake migration directions in the upper ERZ indicates a complex interaction of varying stresses and pressure gradients on a multiplicity of magma conduits.

THE STARTING POINTS OF INTRUSIONS

An examination of the places where intrusions begin producing earthquakes reveals likely blockages within the rift conduit where magmatic stresses are concentrated. These blockages probably occur where dikes are squeezed shut or have completely solidified. Magma then accumulates at these barriers, which are the first to break under rising magma pressure. Figure 43.99*A* shows where well-resolved swarms have begun. Five inferred blockages are near the southern part of the caldera, Keanakakoi, Puhimau, Hiiaka and Pauahi-Mauna Ulu. The Keanakakoi zone is adjacent to the summit magma reservoir. The southern part of the caldera initiates nearly all SWRZ intrusions and also surrounds the summit reservoir. These two barriers are the most intuitive, because they regulate inflating magma and are stressed directly by the inflating reservoir. The barriers identified here in seismicity patterns are larger scale versions of the barriers linking dike segments proposed as a source of harmonic tremor (Aki and others, 1977; Aki and Koyanagi, 1981).

The Pauahi-Mauna Ulu barrier, however, initiates more intrusions than any other. The ERZ bends there and meets the Koae fault zone. Structural stresses thus can concentrate in the Pauahi-Mauna Ulu area, where the conduit appears to be frequently pinched closed. Most central ERZ intrusions begin here, and only the January 1983 swarm was observed to begin downrift of this point. Inflationary earthquakes are not recognized downrift of this point, which is the final barrier containing this process. Swanson and others (1976b) proposed a barrier there to account for the pattern of eruption locations during 1965–69 and the absence of any ERZ activity between the August 1965 and August 1968 events. The Pauahi-Mauna Ulu zone was also a major barrier during the June 1976 and November 1979 intrusions: downrift migration of a few earthquakes were immediately followed by a reflected pulse of intense seismicity moving uprift. A wave of magma pressure may have been reflected from this major barrier, which also prevented the intrusion from penetrating farther downrift.

Other barriers within the rifts are recognized by earthquake clusters and by places where intrusive swarms end. Earthquake clusters apparently are caused by barriers having a high stress concentration. The high density and distribution of earthquakes at Puu Kou in the SWRZ implicate it as a major barrier, and it has stopped every intrusion that reached it since at least 1962. Shallow earthquake clusters beneath Mauna Iki (September 1971) and just southwest of Puu Koae (August 1981) also mark significant SWRZ blockages. Another barrier 5 km south of the caldera held the small intrusion of August 2, 1981, before it broke on August 10. Places where the intrusions of September 1977, May 1979, March 1980 and January 1983 started, stopped or paused also suggest five additional barriers in the ERZ. All of these major or suspected barriers are plotted in figure 43.100. The lifetime of these barriers beyond the period of seismic observation is not known.

We summarize the starting points and directions of intrusions in figure 43.99*B*. Triangles point in the approximate directions taken by intrusions, and thin diamonds are used for swarms that spread in both directions from that point. Swarms in the ERZ uprift of Mauna Ulu are about equally likely to spread downrift, uprift, or in both directions. Two such intrusions moved primarily into the Koae. All moving SWRZ intrusions went downrift except for three that started 1.5 km south of the caldera.

The gap between the Hiiaka and Pauahi-Mauna Ulu blockages is a suspected pocket of magma storage within the ERZ conduit. Magma apparently collects behind the major Pauahi-Mauna Ulu barrier. Like the summit magma reservoir, the Pauahi zone is aseismic and is bordered by barriers that initiate intrusions. This magma pocket apparently fed the November 1979 Pauahi eruption with degassed lava (Norm Banks, written commun., 1979), and its existence and proximity are supported by the short 2-hour interval between the first earthquakes and the start of the eruption. Another rift magma reservoir beneath Puu Kamoamoa inflated during the cyclic and slow intrusions of 1978–80. The two ERZ reservoirs and the main summit reservoir are plotted in figure 43.100. A magma reservoir was proposed beneath Makaopuhi by Swanson and others (1976b) and Jackson and others (1975) that may account for the deformation centers reported by Dvorak and others (1983). Seismicity beneath Makaopuhi, however, is not sufficient to resolve a magma reservoir. Other reservoirs are likely present but are not obvious from seismicity patterns. Parts of the rift system between the barriers plotted in figure 43.100 are probably good places to look for reservoirs.

UPWARD MIGRATION OF EARTHQUAKES

The vertical extent of earthquakes in the ERZ uprift of Mauna Ulu makes upward earthquake migration recognizable and reveals a shallow conduit system. The vertical speed of a dike is generally not as accurate as its lateral speed owing to the greater depth error and narrower depth range of hypocenters, but are observed between 0.1 and 5 km/h (see table 43.1). The retarding effect of gravity may explain why vertical speeds are typically less than lateral speeds. Upward migration is best determined between 3 km depth, where it typically starts, and about 1 km, where the production of earthquakes diminishes as the dike moves upward. The times of eruptions demonstrate that dikes generally slow to a fraction of their initial speed during the last kilometer of their trip to the surface. The persistence of earthquakes below the upward-moving top of a dike shows that typical growth is like a wedge with expansion continuing after the leading edge passes a given point. Clear vertical migration with a slowing near the surface is seen, for example, in the intrusions and eruptions of May and November 1973, July 1974 and November 1979.

Another view of upward movement is provided by the delay time between a dike first reaching a point below an eventual vent (the first earthquakes) and the moment of eruption. This approach is most useful for intrusions where simultaneous migration in several places masks a simple trend on a plot of earthquake depth versus time. Typical delay times are 2–3 h near the caldera and uprift of Mauna Ulu. Short times of dike migration to the surface are reasonable here owing to the vertical extent and shallowness of the conduit system, and the high frequency of intrusive activity. Longer

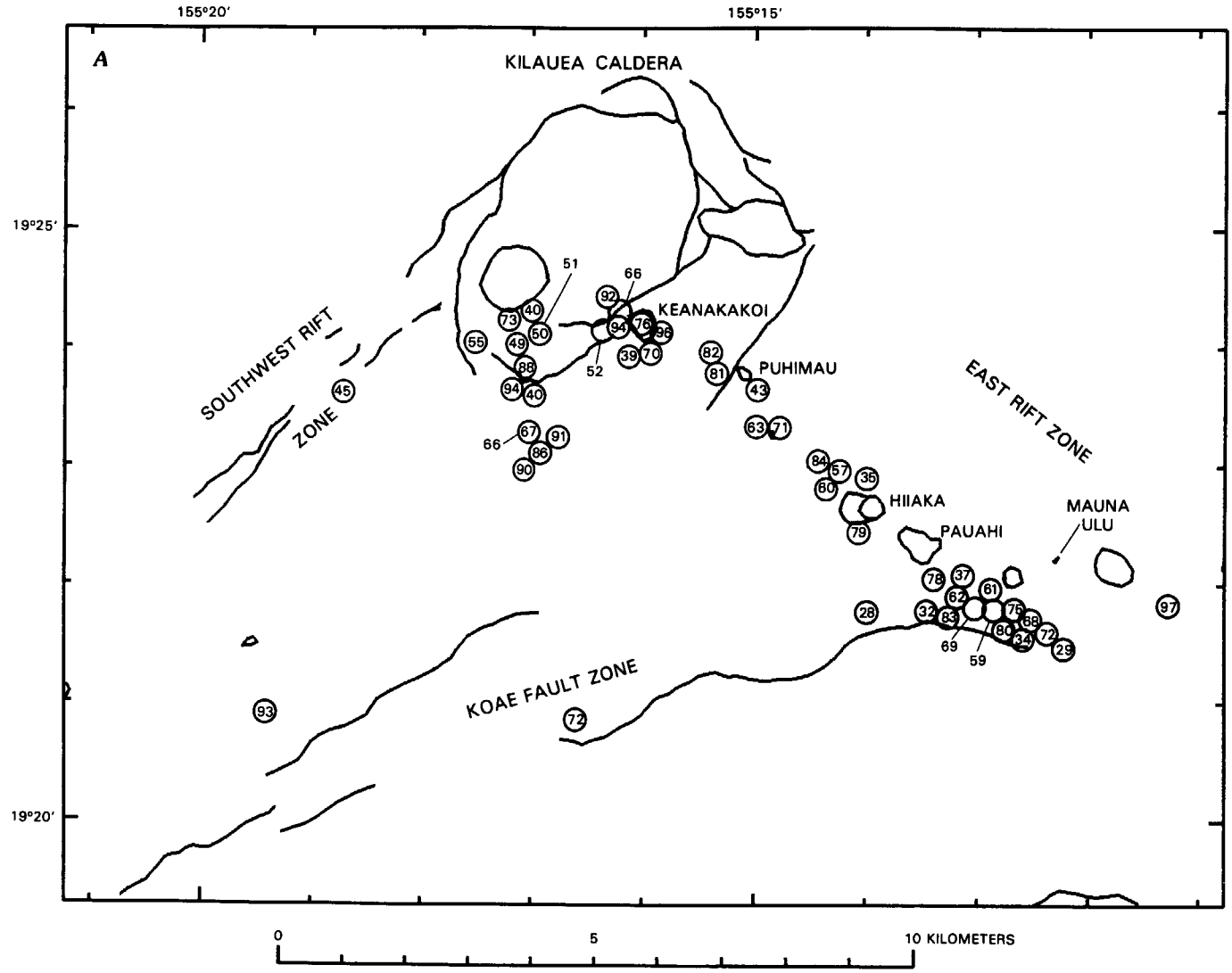

FIGURE 43.99.—Locations of starting points of intrusions. ***A***, Those that can be determined from locations of first earthquakes. Circled numbers are figure numbers and are listed in table 43.1. Starting points cluster into five stress points or rift zone barriers. ***B***, Locations of starting points and directions of intrusions. Thin triangles show general direction of migration (uprift, downrift, or into the Koae fault zone). Thin diamonds indicate earthquakes moved out in both directions.

10- to 12-h delay times are occasionally observed in the caldera-Mauna Ulu area, namely from the December 1974 and November 1979 eruptions, but may be as short as the 1-h delay of the May 1969 Mauna Ulu eruption. The times required for magma to reach the surface characteristically increase with distance from the caldera. A good example is the September 1971 SWRZ eruption, where the delay ranged from about 4 h near the caldera to about 18 h downrift of Mauna Iki. Delays observed in the ERZ are 5 h near Makaopuhi (February 1969), 21 h at Napau (January 1983) and 11 h near Kalalua (September 1977). The infrequency of intrusion, the increased distance from magma conduit to the surface and the reduced magma pressure and temperature downrift presumably all contribute to lengthened transit times of magma to the surface.

SEQUENTIAL RELATIONS BETWEEN INTRUSIONS ALONG THE RIFT ZONES

Intrusions clearly tend to occur near their predecessors (fig. 43.98), and activity shifts between the ERZ and the SWRZ. For the moment we exclude the 1963–67 period from discussion because of the reduced sensitivity and resolution of the seismic network.

Many intrusions occur in groups of two or three, and may retrace nearly the same path, as in September and December 1971, May and June 1973, June and July 1976, and February and August 1981. In these cases the first intrusion may weaken and heat a conduit for the second. The second intrusion finds an open conduit and may easily push out magma from the previous event rather than

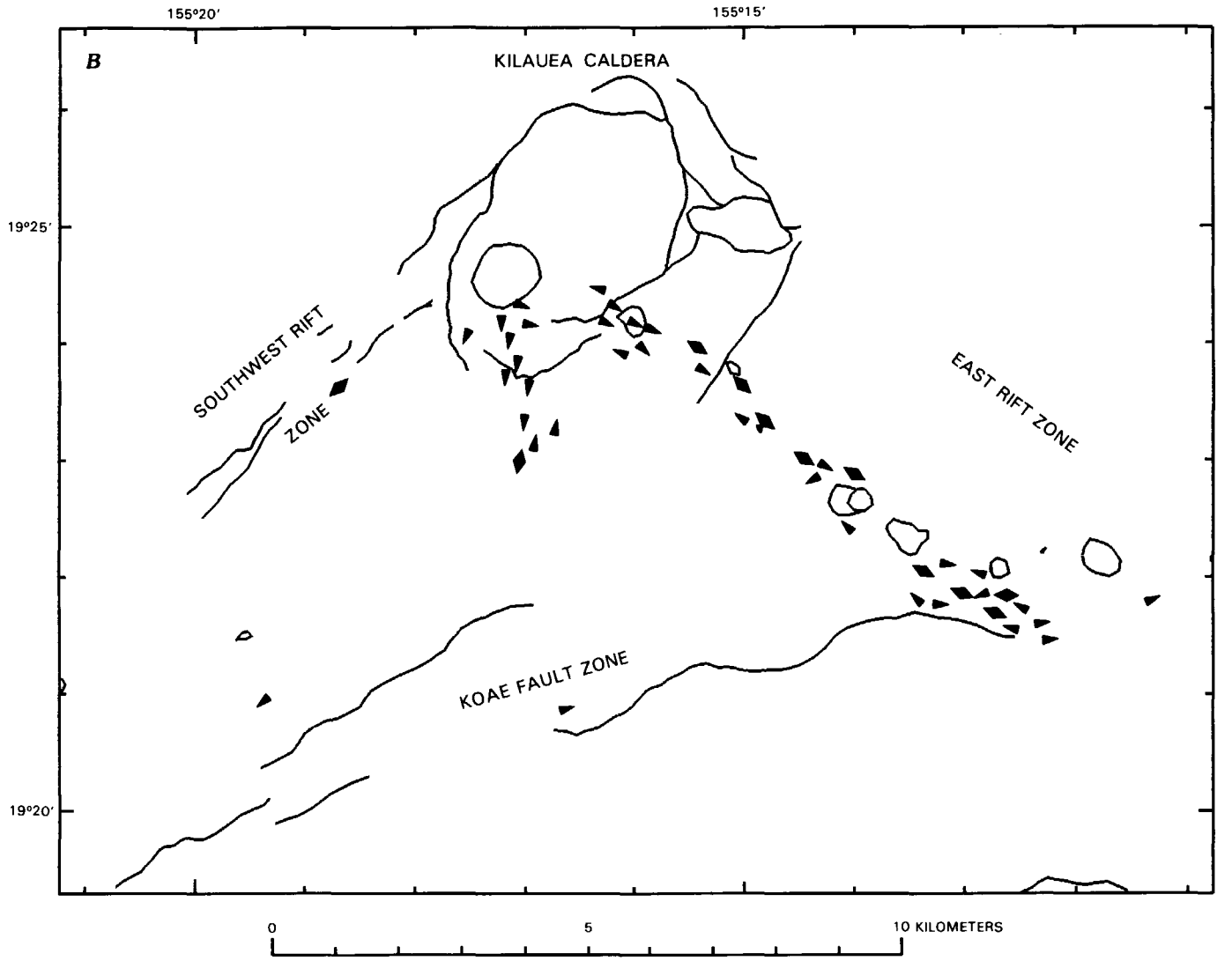

FIGURE 43.99.—Continued.

starting a new one elsewhere. Intrusions may also trigger an adjacent one, as in May, July and November 1969, January and February 1977, May, August and November 1979, March 2 and 10, 1980, July through November 1980, December 1982 and January 1983. These intrusions apparently stressed an adjacent section of rift, which was in turn intruded when magma supply and pressure became sufficient to do so. Alternatively, one intrusion may inhibit a later one if a dike solidifies and increases the compressional stress near it, or locally makes the rift more competent. We prefer the interpretation that a barrier in the magma conduit stops the first intrusion, and this newly stressed barrier becomes the initiation point for the next intrusion.

A shifting pattern of intrusions from the ERZ to the SWRZ and back is also apparent from figure 43.98. Four cycles of activity occurred during the 1968–83 period, each lasting 3–4 yr. The cycle begins in the ERZ with intrusions originating in the general region of Mauna Ulu, noted above as a major stress point of the rift. Subsequent intrusions in the first part of the cycle are mostly in the Kilauea caldera-Mauna Ulu section of the ERZ. As a whole they may migrate uprift, as during 1968–70. In two of the four cycles, this ERZ activity was followed by a period of inflationary swarms and high summit tilt (1970–71 and 1974). The westward progression of activity continued into the SWRZ for three of the four cycles. Kilauea did not activate the SWRZ in 1977–78. The last stage in the cycle is 1–2 years of quiescence. The quiescent stage was omitted in 1982, when intrusions immediately migrated from the SWRZ back to the ERZ. A distorted and probably incomplete fifth cycle may have occurred during 1963–67. A shift from the

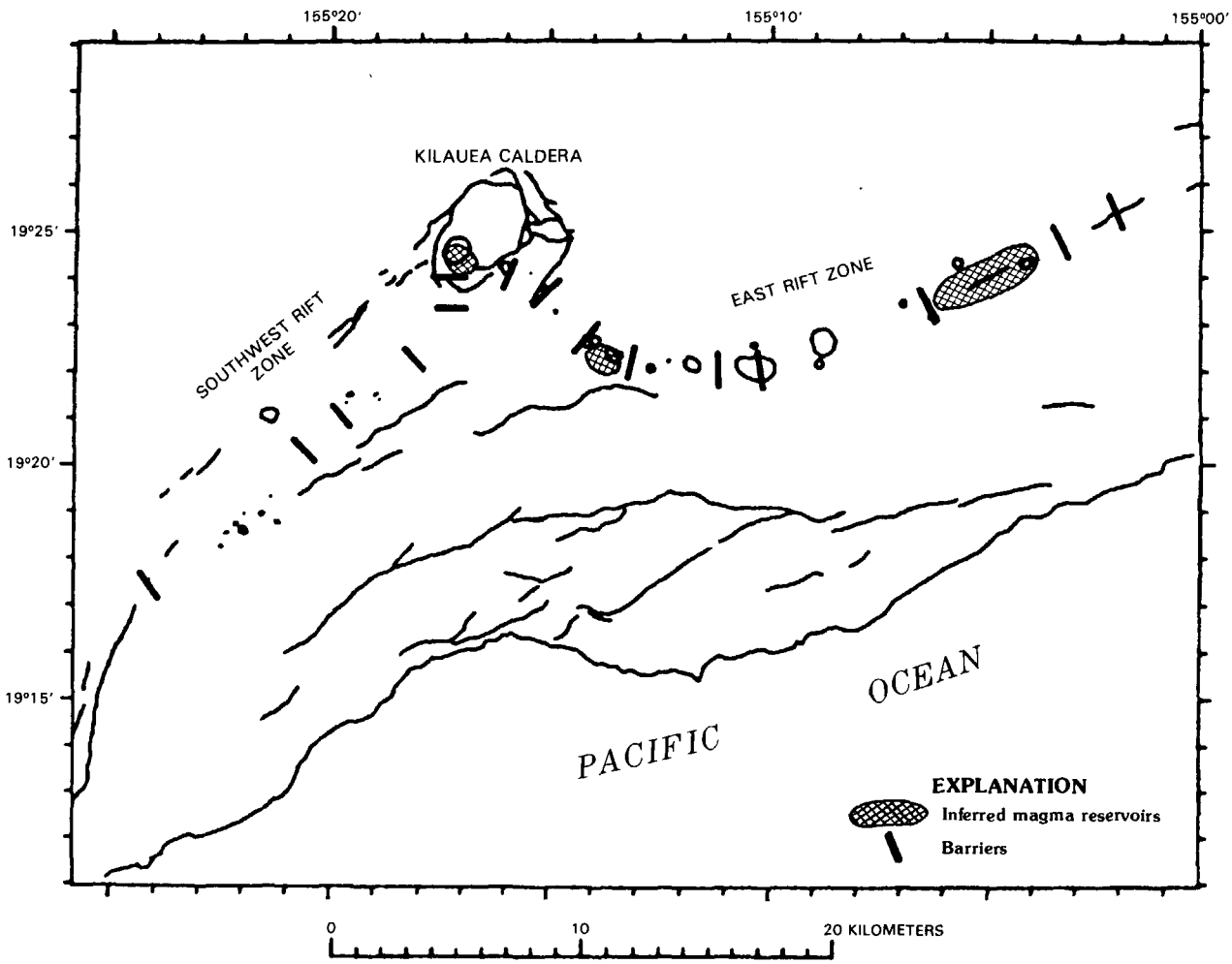

FIGURE 43.100.—Magma reservoirs and barriers within Kilauea caldera and its rift zones. Thick lines transverse to rifts, locations of stress points or barriers within rift zone conduits. Barriers are derived from points at which intrusions frequently start and stop. Three shaded zones mark main magma reservoir beneath caldera and secondary reservoirs in east rift zone inferred from seismicity.

SWRZ to the ERZ occurred in 1963, but without a long pause. Activity moved up the ERZ to the caldera in 1967 but did not then produce a SWRZ intrusion. The overall pattern is then one of intrusions progressing up the ERZ through the summit to the SWRZ, followed by a rest before the cycle starts again.

These large-scale shifts of intrusion location may be aided by the tendency of one intrusion to trigger an adjacent one, but this tendency alone cannot produce such systematic shifts. Some regional and oscillatory tectonic process seems also to be at work. The accumulated compression in the south flank adjacent to one rift may hinge the other rift open, making intrusions there more probable. Once a series of intrusions begins in one rift zone, they tend to trigger each other until compression of the south flank retards intrusion in that rift and favors the other one. Using similar reasoning, Duffield and others (1982) suggested that a combination of south-flank displacement and a deflated Mauna Loa foster SWRZ intrusions by a reduction of compressional stress there.

Completion of rifting downward to the 10-km depth at which the volcanic pile is decoupled from the prevolcanic sea floor may play a part in the cycle. We interpret the 5- to 10-km depth swarm and intrusion of the SWRZ in June 1982 as extension of rifting to depth following the series of shallow 1981 intrusions. A similar but aseismic process may occur after each cycle or half-cycle, possibly during the seismically quiescent interval between cycles.

If changes in regional stress play a part in the intrusion cycle, then large earthquakes within Kilauea's flanks must also interact with the cycle. The $M=7.2$ Kalapana earthquake in November 1975 was by far the largest during this period and caused Kilauea's south

flank to slip seaward as much as 8 m. Surprisingly, the earthquake did not disrupt the cycle in a major way: the SWRZ intrusion of December 1974 was followed in 18 months by resumption of intrusions in the ERZ, as if no earthquake had occurred. The Kalapana earthquake, however, may have caused some significant changes. (1) Intrusions outnumbered eruptions in the six years following the earthquake, but the reverse was true prior to the earthquake (Klein, 1982b). This switch may have resulted from a drop in confining stress on the rifts and the inability of magma to develop sufficient pressure to reach the surface. (2) The cycle following the earthquake was disrupted to the extent that no SWRZ intrusion occurred. The greatest coseismic displacements were in the flank south of the ERZ, which may have favored it as the site of intrusions until the end of the following cycle. (3) The two cycles following the earthquake had no period of inflationary swarms. (4) Two major ERZ eruptions penetrated downrift of Kalalua, but no others had since the 1960 eruption. (5) The cyclic slow intrusions and magma accumulation near Puu Kamoamoa may have been made possible by reduced stress across the ERZ. (6) The shift of intrusions from the SWRZ back to the ERZ in 1982 without a quiescent period shows that the ERZ was in some sense favored for intrusion, as in (2) above. (7) The Puu Oo eruption that started in January 1983 captured all of Kilauea's magma supply and prevented any other eruptions or intrusions. The long-lived Mauna Ulu eruption, however, coexisted with other intrusions. The intervening Kalapana earthquake may have permitted the establishment of a major magma path to the exclusion of others.

Another tectonic change may have been coupled with the shift of intrusive activity from the ERZ to the SWRZ during 1974. Significant earthquakes occurred in the Kaoiki seismic zone on June 19, 1974 ($M=4.8$), November 30, 1974 ($M=5.5$) and December 15, 1974 ($M=4.8$). The mechanism of the events was strike-slip (Endo and others, 1978; Endo, 1985), which acted to relieve compressive stress across the SWRZ and permit an easier intrusion path than before. Shaking from the larger earthquake may also have disturbed the delicately balanced equilibrium of the magma system. The Kaoiki earthquakes may have been triggered by the inflation accompanying the seismic reawakening of Mauna Loa (Koyanagi and others, 1975), which would have acted to increase the shear stress on the ultimate fault plane. Thus, shifts in rift activity could be accomplished through mechanical coupling with Kilauea's flanks. Large earthquakes in the flanks apparently play a part, but aseismic deformation and even Mauna Loa may contribute as well. Seismicity and magma movement at Kilauea are clearly linked in a variety of ways, and earthquakes provide many insights into the dynamics of Kilauea Volcano.

REFERENCES

Aki, K., Fehler, M., and Das, S., 1977, Source mechanism of volcanic tremor: fluid-driven crack models and their application to the 1963 Kilauea eruption: Journal of Volcanology and Geothermal Research, v. 2, 259-287.

Aki, K., and Koyangi, R.Y., 1981, Deep volcanic tremor and magma ascent mechanism under Kilauea, Hawaii: Journal of Geophysical Research, v. 86, p. 7095-7109.

Ando, M., 1979, The Hawaii earthquake of November 29, 1975: low dip angle faulting due to forceful injection of magma: Journal of Geophysical Research, v. 84, p. 7616-7626.

Bosher, R., and Duennebier, F.K., 1985, Seismicity associated with the Christmas 1965 event at Kilauea Volcano: Journal of Geophysical Research, v. 90, p. 4529-4536.

Crosson, R.S., and Endo, E.T., 1982, Focal mechanisms and locations of earthquakes in the vicinity of the 1975 Kalapana earthquake aftershock zone 1970–1979: implications for tectonics of the south flank of Kilauea Volcano, Island of Hawaii: Tectonics, v. 1, p. 495-542.

Decker, R.W., Koyanagi, R.Y., Dvorak, J.J., Lockwood, J.P., Okamura, A.T., Yamashita, K.M., and Tanigawa, W.R., 1983, Seismicity and surface deformation of Mauna Loa Volcano, Hawaii: Eos, Transactions, American Geophysical Union, v. 64, p. 545-547.

Dieterich, J.H., and Decker, R.W., 1975, Finite element modelling of surface deformation associated with volcanism: Journal of Geophysical Research, v. 80, p. 4094-4102.

Duffield, W.A., 1975, Structure and origin of the Koae fault system, Kilauea Volcano, Hawaii: U.S. Geological Survey Professional Paper 856, 12 p.

Duffield, W.A., Christiansen, R.L., Koyanagi, R.Y., and Peterson, D.W., 1982, Storage, migration and eruption of magma at Kilauea Volcano, Hawaii, 1971–1972: Journal of Volcanology and Geothermal Research, v. 13, p. 273-307.

Duffield, W.A., Jackson, D.B., and Swanson, D.A., 1976, The shallow, forceful intrusion of magma and related ground deformation at Kilauea Volcano, May 15–16, 1970: Bulletin Volcanologique, v. 39, p. 577-597.

Dvorak, J., Okamura, A.T., and Dieterich, J.H., 1983, Analysis of surface deformation data, Kilauea Volcano, Hawaii, October 1966 to September 1970: Journal of Geophysical Research, v. 88, p. 9295-9304.

Dvorak, J.J., Okamura, A.T., English, T.T., Koyanagi, R.Y., Nakata, J.S., Sako, M.K., Tanigawa, W.R., and Yamashita, K.M., 1986, Mechanical response of the south flank of Kilanea Volcano, Hawaii to intrusive events along the rift zones, Tectonophysics, v. 124, p. 193-209.

Dzurisin, D., Anderson, L.A., Eaton, G.P., Koyanagi, R.Y., Lipman, P.W., Lockwood, J.P., Okamura, R.T., Puniwai, G.S., Sako, M.K., and Yamashita, K.M., 1980, Temporal variations in gravity on Kilauea Volcano, Hawaii: implications for the magma budget, November 1975–September 1977: Journal of Volcanology and Geothermal Research, v. 7, p. 241-270.

Dzurisin, D., Koyanagi, R.Y., and English, T.T., 1984, Magma supply and storage at Kilauea Volcano, Hawaii, 1956–1983: Journal of Volcanology and Geothermal Research, v. 21, p. 177-206.

Eaton, J.P., 1962, Crustal structure and volcanism in Hawaii, *in* Crust of the Pacific Basin: American Geophysical Union Monograph no. 6, p. 13-29.

Eaton, J.P., and Murata, K.J., 1960, How volcanoes grow: Science, 132, p. 925.

Ellsworth, W.L., and Koyanagi, R.Y., 1977, Three dimensional crust and mantle structure of Kilauea Volcano, Hawaii: Journal of Geophysical Research, v. 82, p. 5379-5394.

Endo, E.T., 1985, Seismotectonic framework for the southeast flank of Mauna Loa Volcano, Hawaii: Seattle, University of Washington, PhD dissertation, 350 p.

Endo, E.T., Koyanagi, R.Y., and Klein, F.W., 1978, Geologic and seismic evidence for strike-slip faulting between Kilauea and Mauna Loa Volcanoes, Hawaii [abs.]: Seismological Society of America, annual meeting, Sparks, Nevada.

Fiske, R.S., and Jackson, E.D., 1972, Orientation and growth of Hawaiian volcanic rifts: the effect of regional structure and gravitational stresses: Proceedings of Royal Society of London, series A, v. 329, p. 299-326.

Fiske, R.S., Kinoshita, W.T., 1969, Inflation of Kilauea Volcano prior to its 1967–68 eruption: Science, v. 165, p. 341-349.

Fiske, R.S., and Koyanagi, R.Y., 1968, The December 1965 eruption of Kilauea Volcano, Hawaii: U.S. Geological Survey Professional Paper, 607, 21 p.

Furumoto, A.S., and Kovach, R.L., 1979, The Kalapana earthquake of November 29, 1975: an intraplate earthquake and its relation to geothermal processes: Physics of the Earth and Planet Interiors, v. 18, p. 197-208.

Hill, D.P., 1977, A model for earthquake swarms: Journal of Geophysical Research, v. 82, p. 1347-1352.

Jackson, D.B., Swanson, D.A., Koyanagi, R.Y., and Wright, T.L., 1975, The August and October 1968 east rift eruptions of Kilauea Volcano, Hawaii: U.S. Geological Survey Professional Paper 890, 33 p.

Kinoshita, W.T., 1967, May 1963 earthquakes and deformation in the Koae fault zone, Kilauea Volcano, Hawaii: U.S. Geological Survey Professional Paper 575–C, p. C173-C176.

Kinoshita, W.T., Koyanagi, R.Y., Wright, T.L., and Fiske, R.S., 1969, Kilauea Volcano: the 1967–1968 summit eruption: Science, v. 166, p. 459-468.

Klein, F.W., 1978, Hypocenter location program HYPOINVERSE: U.S. Geological Survey Open-File Report 78–694, 113 p.

——— 1981, A linear gradient crustal model for south Hawaii: Bulletin of the Seismological Society of America, v. 71, p. 1503-1510.

——— 1982a, Earthquakes at Loihi submarine volcano, and the Hawaiian hot spot: Journal of Geophysical Research, v. 87, p. 7719-7726.

——— 1982b, Patterns of historical eruptions at Hawaiian volcanoes: Journal of Volcanology and Geothermal Research, v. 12, p. 1-35.

——— 1983, Users guide to QPLOT, an interactive computer plotting program for earthquake and geophysical data: U.S. Geological Survey Open-File Report 83-621, 40 p.

——— 1984, Eruption forecasting at Kilauea Volcano, Hawaii: Journal of Geophysical Research, v. 89, p. 3059-3073.

Klein, F.W., and Koyanagi, R.Y., 1980, Hawaiian volcano observatory seismic network history 1950–79: U.S. Geological Survey Open-File Report 80-302, 84 p.

——— 1985, Earthquake map of south Hawaii 1968–1981: U.S. Geological Survey Miscellaneous Field Investigations Map I–1611, scale, 1:100,000.

Koyanagi, R.Y., and Endo, E.T,, 1971, Hawaiian seismic events during 1969: U.S. Geological Survey Professional Paper 750–C, p. C158-C164.

Koyanagi, R.Y., Endo, E.T., and Ebisu, J.S., 1975, Reawakening of Mauna Loa Volcano, Hawaii: a preliminary evaluation of seismic evidence: Geophysical Research Letters, v. 2, p. 405-408.

Koyanagi, R.Y., Endo, E.T., Tanigawa, W.R., Nakata, J.S., Tomori, A.H., and Tamura, P.N., 1984, Kaoiki, Hawaii earthquake of November 16, 1983: a preliminary compilation of seismographic data at the Hawaiian Volcano Observatory: U.S. Geological Survey Open-File Report 84–798, 6 p.

Koyanagi, R.Y., Endo, E.T., and Ward, P.L., 1976b, Seismic activity on the Island of Hawaii, 1970–1973, *in* The geophysics of the Pacific Ocean basin and its margin: American Geophysical Union Monograph 19, p. 169-173.

Koyanagi, R.Y., Nakata, J.S., and Tanigawa, W.R., 1981, Seismicity of the lower east rift zone of Kilauea Volcano, Hawaii, 1960–1980: U.S. Geological Survey Open-File Report 81–984, 15 p.

Koyanagi, R.Y., Swanson, D.A., and Endo, E.T., 1972, Distribution of earthquakes related to mobility of the south flank of Kilauea Volcano, Hawaii: U.S. Geological Survey Professional Paper 800–D, p. D89-D97.

Koyanagi, R.Y., Tanigawa, W.R., and Nakata, J.S., in press, Seismicity associated with the eruption of Kilauea Volcano from January 1983 to July 1984, *in* Wolfe, E.W., ed., The Puu Oo eruption of Kilauea Volcano, Hawaii: the first 1½ years: U.S. Geological Survey Professional Paper.

Koyanagi, R.Y., Unger, J.D., Endo, E.T., and Okamura, A.T., 1976a, Shallow earthquakes associated with inflation episodes at the summit of Kilauea Volcano, Hawaii: Bulletin Volcanologique, v. 39, p. 621-631.

Liu, H-P., and Kosloff, D., 1978, Elastic-plastic bending of the lithosphere incorporating rock deformation data, with application to the structure of the Hawaiian Archipelago: Tectonophysics, v. 50, p. 249-274.

Lipman, P.W., Lockwood, J.P., Okamura, R.T., Swanson, D.A., and Yamashita, K.M., 1985, Ground deformation associated with the 1975 magnitude-7.2 earthquake and resulting changes in activity of Kilauea Volcano, Hawaii: U.S. Geological Survey Professional Paper 1276, 45 p.

Macdonald, G.A., 1956, The structure of Hawaiian volcanoes, Koninklijk Nederlandsch Geologisch Mijnbouwkundig Gehootschap, v. 16, p. 274-295.

Mogi, K., 1962, Study of the elastic shocks caused by the fracture of heterogeneous materials and its relation to earthquake phenomena: Bulletin of the Earthquake Research Institute of Tokyo University, v. 40, p. 125-173.

——— 1963, Some discussions on aftershocks, foreshocks, and earthquake swarms—the fracture of a semi-infinite body caused by an inner stress origin and its relation to the earthquake phenomena, 3: Bulletin of the Earthquake Research Institute of Tokyo University, v. 41, p. 615-658.

Moore, J.G., and Koyanagi, R.Y., 1969, The October 1963 eruption of Kilauea Volcano, Hawaii: U.S. Geological Survey Professional Paper 614–C, p. C1-C14.

Moore, R.B., Helz, R.T., Dzurisin, D., Eaton, G.P., Koyanagi, R.Y., Lipman, P.W., Lockwood, J.P., and Puniwai, G.S., 1980, The 1977 eruption of Kilauea Volcano, Hawaii: Journal of Volcanology and Geothermal Research, v. 7, p. 189-210.

Nakamura, K., 1980, Why do long rift zones develop in Hawaiian volcanoes: a possible role of thick oceanic sediments (in Japanese with English abstract): Bulletin of the Volcanological Society of Japan, v. 25, no. 4, p. 255-269.

——— 1981, Why do long rift zones develop better in Hawaiian volcanoes: a possible role of thick oceanic sediments: Symposium on Oceanic Volcanism, International Association of Volcanology and Chemistry of the Earth's Interior, Azores University, 1980, Proceedings.

Nakata, J.S., Tanigawa, W.R., Klein, F.W., and Decker, R.W., 1982, Hawaiian Volcano Observatory Summary 81, Seismic data, January to December 1981: U.S. Geological Survey Hawaiian Volcano Observatory, Hawaii National Park.

Pollard, D.D., Delaney, P.T., Duffield, W.A., Endo, E.T., and Okamura, A.T., 1983, Surface deformation in volcanic rift zones: Tectonophysics, v. 94, p. 541-584.

Richter, C.F., 1958, Elementary seismology: W.H. Freeman, San Francisco, 768 p.

Ryan, M.P., Blevins, J.Y.K., Okamura, A.T., and Koyanagi, R.Y., 1983, Magma reservoir subsidence mechanics: theoretical summary and application to Kilauea Volcano, Hawaii: Journal of Geophysical Research, v. 88, p. 4147-4181.

Ryan, M.P., Koyanagi, R.Y., and Fiske, R.S., 1981, Modelling the three-dimensional structure of macroscopic magma transport systems: application to Kilauea Volcano, Hawaii: Journal of Geophysical Research, v. 86, p. 7111-7129.

Shaw, H.R., 1980, The fracture mechanisms of magma transport from the mantle to the surface, *in* Hargraves, R.B., ed., Physics of magmatic processes: Princeton, Princeton University Press, p. 201-264.

Swanson, D.A., 1972, Magma supply rate at Kilauea Volcano, 1952–1971: Science, v. 175, pp. 169-170.

Swanson, D.A., Duffield, W.A., and Fiske, R.S., 1976a, Displacement of the south flank of Kilauea Volcano: the result of forceful intrusion of magma into the rift zones: U.S. Geological Survey Professional Paper 963, 39 p.

Swanson, D.A., Duffield, W.A., Jackson, D.B., and Peterson, D.W., 1979, Chronological narrative of the 1969–71 Mauna Ulu eruption of Kilauea Volcano, Hawaii: U.S. Geological Survey Professional Paper 1056, 55p.

Swanson, D.A., Jackson, D.B., Koyanagi, R.Y., and Wright, T.L., 1976b, The February 1969 east rift eruption of Kilauea Volcano, Hawaii: U.S. Geological Survey Professional Paper 891, 30 p.

Thurber, C.H., Um, J.H., and Das, S., 1983, New ideas in seismic ray tracing and velocity inversion: applications to Kilauea Volcano, Hawaii [abs.]: Eos, Transactions, American Geophysical Union, v. 64, p. 901.

Thurber, C.H., Karpin, T., and Um, J.H., 1984, Focal mechanisms of earthquakes at Kilauea Volcano: a detailed study [abs.]: Eos, Transactions, American Geophysical Union, v. 65, p. 1001.

Thurber, C.H., 1984, Seismic detection of the summit magma complex of Kilauea Volcano, Hawaii: Science, v. 223, p. 165-167.

Unger, J. D., and Koyanagi, R.Y., 1979, Evidence of the effects of shallow magma intrusion on Kilauea Volcano [abs.]: Hawaii Symposium on Intraplate Volcanism and Submarine Volcanism, Hilo, Hawaii, July 1979.

Unger, J.D., and Ward, P.L., 1979, A large, deep Hawaiian earthquake—the Honomu, Hawaii event of April 26, 1973: Bulletin of the Seismological Society of America, v. 69, p. 1771-1781.

Watts, A.B., and Cochran, J.R., 1974, Gravity anomalies and flexure of the lithosphere along the Hawaiian-Emperor Seamount Chain: Geophysical Journal of the Royal Astronomical Society, v. 38, pp. 119-141.

Watts, A.B., ten Brink, U.S., Buhl, P., and Brocher, T.M., 1985, A multichannel seismic study of lithospheric flexure across the Hawaiian-Emperor Seamount Chain: Nature, v. 315, pp. 105-111.

Wolfe, E.W., Neal, C.A., Banks, N.O., Duggan, T., and Ulrich, G., in press. Geologic observations and chronology of the first 20 episodes of the Puu Oo eruption, January 3, 1983 through June 8, 1984, *in* Wolfe, E. W., ed., The Puu Oo eruption of Kilauea Volcano, Hawaii: the first 1½ years: U.S. Geological Survey Professional Paper.

Wright, T.L., and Kinoshita, W.T., 1968, March 1965 eruption of Kilauea Volcano and the formation of Makaopuhi lava lake: Journal of Geophysical Research, v. 73, p. 3181-3205.

Wyss, M., 1973, Towards a physical understanding of the earthquake frequency distribution: Geophysical Journal of the Royal Astronomical Society, v. 31, p. 341.

Wyss, M., Klein, F.W., and Johnston, A.C., 1981, Precursors to the Kalapana $M=7.2$ earthquake: Journal of Geophysical Research, v. 86, p. 3881-3900.

Zucca, J.J., and Hill, D.P., 1980, Crustal structure of the southeast flank of Kilauea volcano, Hawaii, from seismic refraction measurements: Bulletin of the Seismological Society of America, v. 70, p. 1149-1159.

STRUCTURAL DAMAGE AND GROUND FAILURES FROM THE NOVEMBER 16, 1983, KAOIKI EARTHQUAKE, ISLAND OF HAWAII

By Jane M. Buchanan-Banks

ABSTRACT

On November 16, 1983, at 0613 (H.s.t.), a magnitude 6.6 earthquake occurred on the Island of Hawaii at a depth of 12 km midway between the active volcanoes of Mauna Loa and Kilauea. The right-lateral strike-slip faulting was probably generated by compressional stresses caused by inflation of the crustal magma reservoirs of both volcanoes. The earthquake shaking was felt for nearly one minute and caused substantial damage to structures in the southeastern part of the island. Landslides occurred on steep slopes throughout the island and, together with cracking of the ground and vibrational settling of subsurface materials, caused temporary closure of some roads. Fortunately, only a few people received minor injuries as a result of the earthquake; this was most likely because it struck at an early hour, when most people were still in bed.

INTRODUCTION

At 0613 Hawaii standard time (H.s.t.) on Wednesday, November 16, 1983, most residents of the Island of Hawaii were awakened by a magnitude 6.6 earthquake. The shaking from this earthquake was felt for nearly one minute and caused substantial damage in the southeastern part of the island, throwing houses from foundations, toppling water tanks, and causing electrical power and telephone outages in the epicentral area. Instruments at the U.S. Geological Survey's Hawaiian Volcano Observatory (HVO) were rendered temporarily inoperative. Landslides occurred on the steep caldera and crater walls in Hawaii Volcanoes National Park and on steep slopes elsewhere on the island. These landslides together with ground cracking and failure of subsurface materials made some roads impassable.

Only four or five people were injured in the earthquake and their injuries were slight. This was probably because it occurred at an early hour, when most residents were still in bed. However, financial losses from the earthquake were estimated at $7 million (Harry Kim, Hawaii Civil Defense Director, oral commun., 1983).

ACKNOWLEDGMENTS

The author gratefully acknowledges the cooperation of the residents of the Volcano Golf and Country Club Subdivision and of Upper Wright Road, Volcano, who, at a time of great personal stress and loss, assisted in the accumulation of damage information, and of J. Barclay Stokes, U.S. Geological Survey (USGS), who took many of the photographs in those communities. Information on the location of the fault trace and on damage in the towns of Pahala, Wood Valley, Kapapala Ranch and parts of Volcano were supplied by Elliot T. Endo, USGS, Vancouver, Washington, who was also kind enough to review the manuscript. Harry Kim, Hawaii Civil Defense Director, Hilo, supplied much of the information on locations of road and structural damage, both public and private, in the Hilo area. I thank David K. Keefer for thorough and thoughtful review of the manuscript. Discussions with Robert Y. Koyanagi and Norman G. Banks provided many helpful insights that contributed to this research.

THE EARTHQUAKE

The earthquake was located in the Kaoiki region between the centers of Hawaii's most active volcanoes, Mauna Loa and Kilauea, at a depth of nearly 12 km (fig. 44.1). Inflation of the summit regions of both Mauna Loa and Kilauea apparently caused sufficient horizontal compressional stress between the two crustal magma reservoirs to generate the faulting. A *P*-wave first-motion analysis from local seismic data indicates a strike-slip mechanism with a northeast-trending nodal plane (see fig. 44.1, inset); right-lateral motion is preferred on the basis of the pattern of ground cracking from this and previous seismic events in the Kaoiki region (Koyanagi and others, 1984, p. 1). Ground cracking indicating right-lateral faulting included a system of left-stepping echelon extension fractures found at about the 1,900-m elevation on Mauna Loa Road. The fractures were traced 4.5 km to either side of the road. Extension of 20–30 cm was common across the longer fractures (Endo, 1985, p. 67).

Detailed analysis of the mainshock and aftershock sequence, however, did not substantiate a simple strike-slip mechanism. There were several discrepancies: (1) The distribution of aftershocks did not define a fault plane that substantiated the mechanism derived from the mainshock. (2) Most aftershocks occurred at shallower depths than the mainshock. (3) Teleseismic fault-plane solutions from other locations were slightly, but significantly, different (Endo, 1985, p. 186-187, 211-213). To explain these discrepancies Endo suggests that the initial right-lateral strike-slip movement was immediately followed by southeastward low-angle slip of part of the southeast flank of Mauna Loa (Endo, 1985, p. 213-215). Such slip would relieve the compressional stresses in the epicentral area, thereby altering the pattern and depth of the aftershocks, and would account for the differences in teleseismic solutions.

KAOIKI EARTHQUAKES

Seismic events called Kaoiki earthquakes occur in a region midway between the summits of Mauna Loa and Kilauea Volcanoes. Although the region takes its name from the Kaoiki fault system, a prominant geologic feature on the southeast flank of Mauna Loa, the seismically active area lies more than 5 km northwest of the Kaoiki system. The Kaoiki fault system probably developed as a result of gravitational stresses induced by forceful intrusions of magma along the southwest rift zone of Mauna Loa before Kilauea was large enough to provide a buttress (Swanson and others, 1976, p. 32). Radiocarbon dating of lava flows and stratigraphic relationships along the fault system, however, indicate that the normal faults of the Kaoiki system have been inactive for tens of thousands of years (Lipman and Swenson, 1984).

The Kaoiki region, on the other hand, is an area of constantly high seismicity with hundreds to thousands of earthquakes recorded by nearby seismographs each year. During the past 25 years, three earthquakes of magnitude greater than 5 have occurred in the Kaoiki region (table 44.1); these events were aligned within the seismic zone in a northeast-southwest direction and were separated from each other by about 3 km (Koyanagi and others, 1984, p. 3). This pattern of seismicity could not be related to any known geologic structure until 1976, when surface fissures probably related to the November 1974 Kaoiki earthquake were discovered (Endo, 1985, p. 42). First-motion data compiled by Endo (1985) for crustal earthquakes from 1959 to 1982 at depths less than 16 km beneath the southeast flank of Mauna Loa and nearby areas of Kilauea confirm a fault system trending predominantly northeast-southwest between Mauna Loa and Kilauea. However, the combination of strike-slip and dip-slip solutions from this compilation also imply a complex tectonic region having both compressional and extensional local stresses (Koyanagi and others, 1984, p. 4).

SEISMIC INTENSITY

The greatest structural damage and abundance of landslides occurred in the epicentral area. Maximum intensity was estimated at VIII to IX (modified Mercalli scale) in parts of Kau and Puna Districts (fig. 44.2). Especially hard hit were the summit area of Kilauea and parts of Hilo. A table of relative intensities for the island was compiled from residents' reports received at the HVO, from information provided by the Hawaii Civil Defense Agency, and from fieldwork (table 44.2; for locations see fig. 44.1).

DESCRIPTION OF DAMAGE

The fault rupture in the epicentral area occurred in an uninhabited part of the island (fig. 44.1) and therefore caused no direct damage to structures. However, the earthquake shaking damaged more than 350 homes and 35 businesses in the southeastern part of the island (Hawaii Tribune-Herald, 1983). A preliminary survey of public buildings conducted by governmental agencies found minor to moderate damage to two health facilities (one in Hilo, one in south Kona), seven schools (five in Hilo, two in Kau), two libraries (one in Hilo, one in Laupahoehoe), and one church in North Kohala (Hawaii County Civil Defense, written commun., 1983). In addition, there was structural damage to Hilo Hospital, resulting in a reduction in available beds in some units. The new Hilo Hospital under construction at the time of the earthquake was almost undamaged.

In the epicentral area, telephone service, electricity and water supplies were affected (Chiu and others, 1984). Most telephone and electrical services were restored within a few hours. However, residents of the area obtain water from rain-catchment systems; hence the destruction of, and damage to, water tanks and connecting pipes caused great inconvenience and disruption to many people.

STRUCTURAL DAMAGE

Most houses on the island are single-story wood-frame structures with either post-and-pier (fig. 44.3) or concrete slab foundations. In this earthquake, houses with post-and-pier construction sustained greater structural damage, primarily because of lateral displacement of the piers and consequent decoupling of the piers from the houses. The piers often moved with respect to each other as well as to the ground. Most structures with concrete slab foundations, on the other hand, had little damage, generally limited to hairline cracks through the slabs. However, the degree of shaking damage to loose objects inside houses seemed to have little or no relation to the type of foundation.

KAU DISTRICT

KA LAE, WAIOHINU, NAALEHU, PUNALUU AND PAHALA

There was little structural damage reported from these towns. One house about one mile south of the highway on the Ka Lae Road moved 1.2–1.5 m northward off its foundation (fig. 44.1, locality 1; Vicki and Robert Taylor, oral commun., 1983). The house was supported on cylindrical concrete piers almost 1 m high and about 0.4 m in diameter with a 2.5-cm length of reinforcing steel bar (rebar) protruding through the piers into beams in the subfloor of the house. The rebars penetrated the subflooring when the house landed on them during the ground movement.

WOOD VALLEY

Wood Valley is a sparsely populated agricultural community built mostly on an ash deposit and on deposits of landslides induced by the magnitude 7.5–8 1868 earthquake and earlier earthquakes (Brigham, 1869, p. 574-576; Tilling and others, 1976, p. 29-30; fig. 44.1, locality 2; fig. 44.4). Several houses of post-and-pier construction (two built on ash and (or) landslide deposit) moved more than 0.5 m off their foundations toward the southeast at azimuths 105°–155° (fig. 44.4, vectors a, b, c). The 8-cm by 8-cm posts of one house were connected to the foundation piers with 0.5-cm-thick steel plates. The plates were not always on the same side of the posts, and therefore some posts were snapped at the anchor bolts connecting the post to the plate; other posts were relatively

undamaged, but the steel plate was bent at an angle of about 45° (fig. 44.5*A*, *B*). Nearby houses with concrete slab foundations on ash or with post-and-pier foundations on a pahoehoe flow sustained little movement (fig. 44.4, vectors d, e). Greenhouses were moved as much as 0.15 m in a complex pattern toward azimuths anywhere from 67° through 340° (fig. 44.4, vector e). These structures had few central supports or walls, hence the various structural elements may have failed at different times during the shaking, which could account for the range in direction of failure.

The Wood Valley Buddhist Temple had only a few centimeters of displacement with respect to its piers, but the two-story frame dormitory structure situated in the front yard of the temple shifted 0.26 m northeastward (fig. 44.4, vector f). Nearly every headstone in the cemetery was overturned, according to a spokesperson. The pattern of movement was complex: One headstone that had been mortared to a larger base was displaced 0.28 m to the northwest (az 290°), but a similarly constructed headstone fell in a southeasterly direction (az 140°). This divergence in direction of fall may be due to the headstones breaking loose from their mortar at different times during the earthquake shaking. Restoration work was nearly completed when the site was visited eight days after the mainshock, hence no other observations were possible (E.T. Endo, written commun., 1984).

Kapapala Ranch

The main house shifted 0.18 m downhill toward the south-southeast (fig. 44.1, locality 3; fig. 44.4, vector g) whereas a ranch house (locality 4 on figs. 44.1, 44.6) located 19 km (12 mi) to the northeast, nearer the epicenter, was displaced about 0.8 m northeastward (az 55°) off its foundation piers (fig. 44.7). A water tank about 100 m uphill from the ranch house had a length of PVC pipe, which was originally connected to the body of the tank, trapped underneath it (fig. 44.8). It seems likely that the pipe was severed early in the shaking, fell to the ground, and then rolled beneath the tank as the tank swayed back and forth. Several wooden water tanks located elsewhere on the ranch, one with a 378,500-L (100,000-gal) capacity and nearly full, were leaning precariously and leaking profusely; they were eventually dismantled.

Volcano Golf and Country Club Subdivision

Most houses in this subdivision were built on a thin pahoehoe flow that overlies an ash deposit at least 0.5 m thick (locality 5 on figs. 44.1, 44.6). At the time of the earthquake, 48 houses had been built or were under construction in the subdivision. Of these, 18 houses with post-and-pier construction were displaced 0.2–1.2 m southwest from their foundations. Only one of the houses had 2.5 cm of reinforcing rebar protruding through the foundation piers into the posts (fig. 44.9). After the earthquake, this house was southwest of its piers, but the posts were not sheared by the rebar nor were most of the rebars bent, suggesting that the house rocked laterally and slid up along the rebars during the earthquake shaking.

Some houses with post-and-pier foundations had attached garages with concrete-slab foundations. In most such cases, the house moved farther than the garage, causing a tearing of the shared wall (figs. 44.10*A*, *B*). In one case, however, the garage was situated on the southwest side of the house (the general direction of movement) and because of its greater rigidity, may have kept the house on its foundation.

Of the 30 other houses in the subdivision, 9 moved on their post-and-pier foundations and suffered minor damage, and the remaining 21 houses, most of which were on concrete slabs, showed no evidence of movement. However, large metal water tanks adjacent to some of these houses showed 5–9 cm of movement north-northeastward. A few fiberglass water tanks had vertical ruptures in their sides wide enough to allow loss of all the water.

There were reports of extensive breakage inside many houses, regardless of foundation type, and of heavier applicances and furniture displaced more than lighter pieces.

Hawaii Volcanoes National Park

Although no buildings within the national park moved off their foundations, there was extensive interior damage in some buildings (locality 6 on figs. 44.1, 44.6). At the HVO, a concrete foundation slab was cracked in two places but not offset, and work areas were chaotic with toppled equipment and books (fig. 44.11). Some seismic stations were disabled because of damage to the sensors or recorders, while the operating stations were saturated for several hours with signals from ground oscillations. Tiltmeters could not be reset until there was a substantial reduction in the oscillation of the ground. Within the park residential area just south of park headquarters, damage to houses was minor and seemingly arbitrary. Similarly constructed and situated houses differed greatly in the amount of dishevelment of the interiors. There was no damage nor dishevelment to the park headquarters' buildings. Damage to leaking water pipes and valves in the park amounted to $16,000.

At Kilauea Military Camp within the national park boundary, buildings moved but stayed on their foundations. In the Short Stop, a grocery store, bottled foods and beverages were broken and the concrete slab floor, supported on piers about 1 m high, was cracked and vertically offset about 1 cm. The Post Exchange also had breakage of glass items. Concrete slabs and walkways were cracked, and some concrete steps were buckled compressively where they abutted buildings. Service pipes from the water storage tanks to the camp were damaged and had to be replaced (Glenn Higa, Foreman, Engineers' Section, oral commun., 1985). Stone chimneys were cracked but could be repaired.

PUNA DISTRICT

Upper Wright Road, Volcano

Damage was severe and affected nearly every structure in this part of Volcano, which is underlain by an ash deposit locally as much as 4.7 m thick (locality 7 on figs. 44.1, 44.6). Patterns of movement were complex and are difficult to interpret; many houses in this part of Volcano are older and have combined post-and-pier and slab construction. Houses were displaced off their post-and-pier

foundations as much as 0.7 m, generally in either a southwesterly or northeasterly direction. One three-story-high wood frame house had recently had its original piers replaced with steel-reinforced concrete piers poured as a single unit (fig. 44.12*A*, *B*). This house was displaced about 0.3 m northeastward (az 35°) of the piers, and the steel rebar had sheared most of the posts that supported the upper story of the house. The use of rebar alone to connect the posts to the foundation proved inadequate. The superstructure of the house appeared to be undamaged.

More water tanks collapsed or were damaged in this community than elsewhere in the epicentral area; others, though undamaged, were moved as much as 0.8 m southeastward (E.T. Endo, written commun., 1984; fig. 44.13). Wooden water tanks were more severely damaged than those made of fiberglass or metal, probably because the former were less rigid. Many of the collapsed tanks were observed by residents to sway back and forth during the period of shaking before their failure. Evidence of a few centimeters of movement of heavier metal tanks could be seen in the soft ground. Connecting pipes were often severed or damaged.

In this largely argicultural community, financial losses resulted from crop damage when the earthquake shaking caused greenhouses to collapse, shook vegetables off plants (fig. 44.14), and caused vibrational settling of loose earth into adjacent furrows, thereby uncovering seeds and seedlings.

SOUTH HILO DISTRICT

Hilo

Major structural damage in Hilo occurred in two main areas, shown in figure 44.15 as areas A and B. There was also structural damage at Hilo Hospital, located near a cliff overlooking the Wailuku River (see table 44.2 for details). Minor structural damage, ranging from collapsed rock stairways to cracked rock walls, was common throughout the Hilo area.

Most of the damaged residences in Hilo were built on a thick ash deposit or near the edges of lava flows overlying an ash deposit (fig. 44.1, locality 8; fig. 44.15, area A). Several houses were damaged when they moved downslope off their post-and-pier foundations in response to the earthquake shaking. Others were severely damaged because of the steeper slopes on which they were built (fig. 44.16*A*) or their location alongside unbuttressed slopes such as stream channels. A few houses built across steep slopes were structurally damaged by the shaking (fig. 44.16*B*), although there was no evidence of ground failure. Houses with concrete slab foundations fared better, with only minor hairline cracks in some slabs.

The old part of Hilo, built on an ash deposit locally as thick as 4.7 m (fig. 44.15, area B), was also severely shaken; major structural damage resulted to two buildings (figs. 44.17, 44.18), but most losses were due to breakage of plate-glass windows and damage to goods. A heavy canopy that recently had been installed on a commercial structure fell off during the shaking. It probably had been inadequately connected to the structural elements of the building. A gas station reported the severing of connecting pipes to an underground gasoline-storage tank, causing the loss of some 11,355 L (3,000 gal) of fuel.

ANALYSIS OF STRUCTURAL DAMAGE

Structural damage was influenced by three main factors: (1) shaking of the ground, (2) lithology of the substrate, and (3) construction practices.

SHAKING OF THE GROUND

Damage to structures in the epicentral area may have been caused by the prolonged, strong ground shaking of greater than one-tenth the acceleration of gravity (0.1 g) for 8.5 seconds (table 44.3). One exception to this may have been the ranch house at location 4 (fig. 44.1). Because of its nearness to the epicenter, it is likely that the *P* and *S* waves arrived there nearly simultaneously, thus causing greatly enhanced first motion at this locality. The block south of the fault on which the ranch house was located, moved laterally to the southwest, decoupling the piers from the house and leaving the house northeast of its foundation.

In Hilo, the shaking damage in the Kaumana area (fig. 44.15, area A) may have been enhanced by the decoupling effect of a thin lava flow from Mauna Loa Volcano overlying a 3- to 6-m-thick ash deposit and deeply-weathered lava flows from Mauna Kea Volcano. That this type of enhancement could be expected was anticipated by Nielsen and others (1977), Wieczorek and others (1982), and Buchanan-Banks (1983).

LITHOLOGY OF THE SUBSTRATE

Structural damage appeared to be worse in areas where buildings were constructed on ash deposits 0.5 m or more thick; however, not every area underlain by ash had structural damage to buildings.

The volcanic ash was originally composed of particles of volcanic glass and crystal fragments, but severe weathering resulting from high average annual temperatures and abundant rainfall has altered most of the original constituents (Bates, 1960; Wieczorek and others, 1982; Buchanan-Banks, 1983). The ash has a large amount of clay-size material and a water content as high as 392 percent (weight of water as a percentage of weight of dry sample). Undisturbed deposits are fairly well indurated and resistant to erosion, forming road cuts at angles often steeper than 60°, even greater than the high angle of internal friction of the material (40°–43°). However, the ash has been found to become plastic after repeated passes of heavy equipment but to subsequently harden again after cessation of the vibrational stress (Hirashima, 1948, p. 485). Although the ash deposits were found to have a sensitivity to slope failure classed as medium to very sensitive (Wieczorek and others, 1982, p. 5), no evidence of large-scale slope failures were

found in the Hilo area. The shear wave velocity of the ash was calculated by Nielsen and others (1977, p. 34) to be between 67 to 142 m/s (219 to 467 ft/s) at strain percents of 10^{-1}–10^{-3} and an undrained shear strength of 136 kg/m^2 (300 lb/ft^2).

Data on the response of the ground to strong motion from this earthquake was collected and analyzed by the USGS from strong-motion accelerographs scattered throughout the island (Acosta and Maley, unpub. data, 1984; see fig. 44.1 for location of accelerographs and thickness of ash deposits at some recording sites). The amplification of the earthquake waves because of ash deposits is apparent when data from the U.S. Fish and Wildlife accelerograph, located on ash deposits about 3 m thick, and the University of Hawaii, Hilo, accelerograph, located on lava flows, are compared (table 44.3); these two accelerographs are essentially equidistant from the epicenter. The records from the accelerograph situated on ash show peak accelerations that are 5 to 6 times greater than the accelerations recorded on the lava flow, indicating that the amplitude of the earthquake waves was increased in the ash deposits.

In the 1973 Honomu earthquake (for data on this earthquake see table 44.1), similar results were found after analysis of a pseudovelocity response spectrum derived from seismic data from a selected aftershock. A simple response peak was obtained from the spectrum from a seismometer sited on lava about 17 km (11 mi) south of the epicenter, whereas a spectrum from a seismometer on ash (located about 14 km (9 mi) south of the epicenter near the U.S. Fish and Wildlife accelerograph that recorded the 1983 earthquake) showed a complex pattern with at least three periods of high response indicating greater wave amplitude on the ash (Nielson and others, 1977, p. 11-12). Nielsen and others (1977) estimate that the velocity response of the volcanic ash was 5–10 times greater than the response measured on the lava flows. Although the difference in response in 1973 between the ash and lava might be attributed to the closer location of the seismometer on ash deposits to the epicenter, the data are consistent with the 1983 damage pattern.

On the other hand, during the 1975 Kalapana earthquake (for data about this earthquake see table 44.1), data from two seismoscopes at the same locations as the seismometers that recorded the 1973 earthquake do not indicate an increase in velocity response in the ash; the maximum motion of the seismoscope pen was 3.4 cm on the University of Hawaii, Hilo, seismoscope, 43 km (29 mi) from the epicenter, and the seismoscope on ash, 45 km (31 mi) from the epicenter, recorded 3.1 cm displacement (Rojahn and Morrill, 1977, p. 499). It seems likely that the 1975 earthquake did not produce enough energy in a frequency band to cause the ash to respond.

CONSTRUCTION PRACTICES

Few houses with post-and-pier construction had structural ties between the house, the piers, and the ground, and each element was therefore left free to move with respect to the others. In the few cases where structural ties such as rebar and bracing were used between the house and the piers, they appear to have been too few, flimsy, or poorly connected. Neither rebar nor bracing was adequate when used alone. Houses built across steep breaks in slope or near the edges of unsupported slopes generally sustained structural damage.

GROUND FAILURES

For several hours after the earthquake, the air at Kilauea's summit was brown with dust from the initial and continuing landslides off the caldera walls and within Halemaumau Crater (fig. 44.19). Hundreds of landslides, of volume generally less than 3,000 m^3, occurred within the epicentral area; rock slides, falls, and topples were the dominant types of failure. These failures caused extensive road and trail damage in Hawaii Volcanoes National Park and temporarily closed the major highway around the island. For many kilometers southwest and northeast of the epicentral area, small rock falls, extensional cracks in the ground, and collapsed lava tubes were evident. Slope failures also occurred at Kealakekua Bay, about 50 km from the epicenter, and along the Hamakua Coast, nearly 60 km from the epicenter. The generation of landslides at such distances from an epicenter is in good agreement with the findings of Keefer (1984, fig. 2*A*, *B*) for worldwide data on earthquake-induced landslides. Only small failures occurred in the thick and seismically sensitive ash deposits near Hilo and Pahala.

No fatalities or damage to dwellings resulted from the landslides, but two people were injured in rock falls onto the highway along the Hamakua coast about 25 km north of Hilo.

KAU DISTRICT

Hawaii Volcanoes National Park

Most landslides from the earthquake occurred within Hawaii Volcanoes National Park, where the lava flows of Kilauea Volcano form cliffs as much as 120 m high (locality 6 on figs. 44.1, 44.6). These nearly flat-lying lava flows are a few tens of centimeters to a few meters thick, and thin ash beds occur between some of them. The flows are well indurated and fairly young (0.2–1.5 ka), but are extensively cracked and jointed because of rapid cooling and initial deformation (fig. 44.20). Locally the flows are overlain by about 2 m of loosely consolidated tephra deposits from phreatomagmatic eruptions of Kilauea Volcano.

Hiking trails along the northern edge of the caldera between Kilauea Iki Crater and Uwekahuna Bluff were extensively damaged where perhaps as many as 200 rock slides and rock falls removed sections of trails and covered those at lower elevations with landslide debris (fig. 44.20). A few had volumes greater than 3,000 m^3. Some vertical cliff faces failed by toppling, when outward-rocking slabs of coherent material failed at the top because of imbalance; the upper parts of such landslides traveled farthest from the slope.

A reconnaissance survey of damage along Crater Rim Drive was conducted immediately after the earthquake. Although the road pavement was extensively cracked throughout its length, only the zones of greatest damage are shown in figure 44.6. Most of the road cracks depicted in this figure were caused by cracking of the ground beneath the road. The road damage included small apparent offsets in both right- and left-lateral senses, major to minor failures of subsurface material, and extensive compressional and extensional cracking, with the most severe damage where the road crosses

fracture systems related to Kilauea caldera (fig. 44.6, sites *a*, *b*, *c*; St. Ours, 1982). All the damage was attributable to the shaking effects of the earthquake.

At the eastern roadway into Kilauea Military Camp (fig. 44.6, site *a*) vibrational compaction of fill caused the road to collapse where a system of earth cracks lies under the road (fig. 44.21). Earlier failures of this type had occurred periodically along the verge of the road at this location, though on a smaller scale and usually induced by drenching rains removing supporting material. Tilling and others (1976, p. 26) describe compressional damage to a roadway near this locale in the 1975 earthquake.

Highway 11 near the northwestern roadway into Kilauea Military Camp (fig. 44.6, site *b*) was closed for several hours because of failure of subsurface material at a circum-caldera fault.

The southwest rift zone of Kilauea lies parallel to the Kaoiki fault system and is characterized by gaping cracks and fissures. Where Crater Rim Drive crosses the 0.5-km-wide zone (fig. 44.6, site *c*), there was both extensional and compressional damage throughout the zone, with an overall extension of about 4 cm (fig. 44.22*A*, *B*).

The roadway cracks at Keanakakoi Crater are subparallel to the west wall of the crater and probably reflect a subsurface zone of fractured rock related to the collapse of the pit crater. The cracks show only small right-lateral offsets and slight upward movement of the northeast side. The viewing overlook had extension cracks approximately 1 cm wide through it, and the rock wall slumped downward and outward toward the crater.

From Keanakakoi Crater, Crater Rim Drive was extensively cracked for 2 km. This earthquake-induced cracking is most likely related to preexisting crack systems in the area (St. Ours, 1982) as well as to settling of uncompacted tephra deposits from the 1959 Kilauea Iki eruption upon which the road was built.

Crater Rim Drive, which is adjacent to Crater Rim Trail between Waldron Ledge and Volcano House, was permanently closed to traffic, and the hiking trail rerouted, because of landslide damage and cracking of the road from vibrational settling of tephra deposits and fill (fig. 44.6, site *d*). This section of road also was badly damaged in the 1975 Kalapana earthquake, when cracks as much as 1 m wide formed parallel to the caldera rim (Tilling and others, 1976, p. 24). The cracks were subsequently filled in and the road repaired; many of the repaired areas failed again in the November 1983 earthquake.

Of the several large landslides that formed on the cliffs, 60–120 m high, along Waldron Ledge, the largest failure was a rock slide with a volume of about 4,600 m^3 that occurred at a site that had been identified as an incipient landslide and had been monitored since April 1980 by the USGS (compare fig. 44.23*A*, *B*). Details of this monitoring program are included at the end of this section. At the time of the earthquake, a resident of the park housing area, who ran outside after the severe shaking had ceased, heard a whooshing sound that lasted 15–20 seconds and came from the direction of the caldera. This sound was probably generated by the rapid failure of this slide and others along this section of cliff. Judging from the shape of the headwall scarp, the slide probably began as a block slide and disintegrated as it fell down the cliff face (fig. 44.24*A*, *B*). The debris did not travel far from the base of the cliff.

Major to minor arcuate cracking reflecting subsurface movement of material toward a free face also occurred at several locations along the road, from the park residential area to park headquarters and between the headquarters and Sulphur Banks.

South of Kilauea caldera, the Chain of Craters and Ainahou Ranch Roads (fig. 44.1) were extensively cracked by the shaking, and the road cracks in the Hilina Pali Road originally caused by a large intrusion in March 1980 were reactivated by the earthquake shaking. North of the caldera, damage to Mauna Loa Road was particularly severe and increased toward the epicenter and the zone of surface faulting. Some cracks in the epicentral area showed extension of as much as 5 cm, while others showed evidence of the pavement on either side having been repeatedly compressed (fig. 44.25).

Monitoring Program at Incipient Waldron Ledge Landslide

Soon after torrential rainstorms in early 1979, a series of cracks appeared in a section of Crater Rim Drive along Waldron Ledge (fig. 44.6, site *d*). These cracks widened in the heavy rains of March 1980. In order to watch for changes that might forecast the failure by landsliding of this part of Crater Rim Drive and Trail, a monitoring program was established by the USGS in April 1980.

Monitor 1 consisted of five nails set out as a quadrilateral centered over the road cracks (fig. 44.26). The distance between the nails was measured with steel tape once a week for the first month, then once a month for the next few months, and thereafter with lessened frequency (table 44.4). Within the first few months, nearly all the lines began showing measurable and cumulative extension, particularly those normal to the cracks (figs. 44.26, lines AE, BC, BD, 44.27*A*). In addition, the cracks had lengthened at both ends, and vertical offsets had become apparent.

To assess the rate of vertical change, a leveling line was added to monitor 1 in November 1980; it consisted of two lengths of rebar driven into bedrock, rebar 1 and Base, in a line northeast of, and off, the landslide (fig. 44.26). The level gun was placed at point 0 between the rebars to check their respective stabilities (fig. 44.26, right center); the gun was then moved to rebar 1 and the rod to each nail of the quadrilateral to measure its elevation.

Monitor 2 was added to the program in April 1981 to measure horizontal movement on cracks not crossed by the quadrilateral (fig. 44.26). Line X′-X was established northwest of the quadrilateral beyond the zone of visible cracking; it extended 23.7 m from X′, a nail in a tree at the caldera edge to X, a nail in the centerline of the road. A second line was established across the quadrilateral and comprised two segments; one segment, line Y′–Z (24.1 m) was measured from Y′, a nail in a tree at the caldera's edge to Z, another nail in a tree northeast of the road, and the second segment, line Y′ to Y.

The monitors were measured frequently until mid- to late

1982. Measurements were discontinued in January 1983 because of the onset of the prolonged east rift eruption of Kilauea Volcano.

RESULTS OF THE MONITORING PROGRAM

During the period of measurement, all of the monitors normal to the cracks showed lengthening of lines and small vertical offsets indicating that the incipient landslide block was moving slowly outward and downward toward the caldera.

The lines of the quadrilateral were measured 14 times between April 1980 and October 1982 (table 44.4). Cumulative extensions above background level on the lines normal to the cracks (for background level see data for line ED, parallel to the cracks) was detected within a few months of the establishment of monitor 1 (fig. 44.27*A*). Continued documented movement of the incipient landslide block toward the caldera led to a decision by the Superintendent, Hawaii Volcanoes National Park, to close this section of road to traffic in April 1981 (fig. 44.6, site *d*). Although monitoring frequency decreased after the closing of the road, accelerated movement both laterally and vertically can be seen in the data after July 1981. The largest changes in line lengths within the quadrilateral occurred between July 1981 and July 1982 on lines AC, AD, AE, BC and BD, crossing the cracks (table 44.4, fig. 44.27*A*). The largest vertical changes also occurred during the same period when nails C, D, and E (the three on the caldera side of the cracks), moved downward with respect to rebar 1 (table 44.4, fig. 44.27*B*).

Line Y′–Z, which also crossed the cracks curving away from the caldera (see fig. 44.23*A*, *B*, location B) as well as the cracks monitored by the quadrilateral, extended about 7 mm more than the shorter quadrilateral lines, AE and BD, over the period June 1981 to July 1982 (table 44.4, fig. 44.27*C*), suggesting that incipient failure was also developing on the cracks curving away from the caldera.

The monitors were destroyed by landslides caused by ground shaking associated with the November 1983 earthquake. Nails A, B and E of the quadrilateral survived the earthquake but E was on a separated block and could not be reached for measurement. The distance between A and B shortened 0.3 m. Lines X′–X, Y′–Y and Y′–Z, could not be remeasured because the trees on the caldera rim holding the nails, and the section of road where nail Y was located, were gone.

SOUTH AND NORTH HILO DISTRICTS

Dozens of soil falls and slides of volume about 15 m^3 occurred in the ash deposits near Hilo, and at one location along Kaumana Drive there was evidence of minor subsidence (fig. 44.28). Narrow cracks in asphalt were common.

Small (volume <20 m^3) rock falls and soil slumps were observed along the highway from Hilo northward to Ookala, where Mauna Kea ash deposits blanket lava flows of the Hamakua Volcanic Series, also from Mauna Kea Volcano (Stearns and Macdonald, 1946, pl. 1). These flows are deeply weathered and have locally produced saprolite consisting of well-rounded to subangular rock remnants in a clayey matrix. The rocks are in large part soft and frequently slide during periods of heavy rain. Six landslides with volumes less than 500 m^3 deposited debris on the highway between Maulua Bay and Kaawalii Gulch causing temporary closure of the road (fig. 44.1, locality 9; fig. 44.29). The debris was removed by midday of November 16 and the highway was reopened (Harry Kim, oral commun., 1983).

In mid-January, when fieldwork was conducted north of Hilo, only four of the six landslides could be located. All the observed failures were rock slides from the steep roadcuts and all appeared to have shallow head scarps, 1–2 m deep. Close examination of the landslides was limited because of the busy, narrow road and the steep slopes. Rock slides could be seen in the roadcuts in each of the highway's large horseshoe bends, with the largest slide occurring in Laupahoehoe Gulch (estimated volume 420 m^3) from the near-vertical cliff west of the road. During the next heavy rainstorm, material loosened by the earthquake shaking west of the earthquake-induced slope failure in Laupahoehoe Gulch caused another large landslide in this gulch (fig. 44.30). For several months after the earthquake, similar landslides occurred in this location during rainy periods.

The earthquake-induced rock slide in Maulua Gulch (volume about 6 m^3) was the one that caused injury to two people travelling in autos. Another rock slide (volume about 36 m^3) covered both lanes of the narrow secondary road to Laupahoehoe Point (fig. 44.31) making it impassable for a short time.

Similar ground failures occurred at these locales as a result of the 1975 earthquake (Tilling and others, 1976, table 1) and the 1973 earthquake (Nielsen and others, 1977, p. 15). Rock and soil falls also occurred on the steep wave-cut cliffs just north of Hilo, about 17 km south of the 1973 earthquake epicenter (Nielsen and others, 1977, p. 14).

KONA DISTRICT

Kealakekua Bay

Shortly after the earthquake occurred, a large dust cloud over Kealakekua Bay was reported to the USGS as possible volcanic venting from beneath the bay (fig. 44.1, locality 10). Aerial reconnaissance determined the cause of the cloud as dust from several rock slides off the steep slopes around the bay. Currents of brown, cloudy water were observed from the air to extend about one kilometer from the shore (J.P. Lockwood, written commun., 1983).

Several rock slides at Kealakekua Bay occurred from about the 120-m elevation on the face of a nearly vertical cliff of weathered Mauna Loa lava flows with intercalated thin ash beds (fig. 44.32; Stearns and Macdonald, 1946, pl. 1). This cliff section has been dated as spanning the interval 2–30 ka by charcoal samples collected from beneath lava flows near the top and at the base of the cliff, respectively (J.P. Lockwood, oral commun., 1985). The largest of these rock slides had a volume of about 5,500 m^3. The slides could not be examined closely because of the steep slopes, but the head scarps appeared to be fairly shallow (volume <3 m). Several smaller rock falls also occurred from the steeper lower slopes.

ANALYSIS OF GROUND FAILURES

Ground failures appeared to be influenced by three main factors: (1) proximity to the epicenter, (2) lithology of the substrate, and (3) slope steepness.

PROXIMITY TO THE EPICENTER

The greatest ground cracking occurred in the epicentral area; most landslides also occurred there, the size and abundance of failures decreasing with distance from the epicenter (fig. 44.33). This localization of ground failures is most probably due to the shallow depth of the earthquake and to the generating mechanism. The strike-slip faulting occurred on a near-vertical fault plane that ruptured the ground surface; the seismic energy released along the fault was thereby transferred to the surface as earthquake waves, and the resulting strong ground shaking in the epicentral area caused abundant ground failures.

LITHOLOGY OF THE SUBSTRATE

The lava flows from Hawaii's five volcanoes are typically flat lying, forming broad, shield-shaped volcanic edifices. These gentle slopes are locally modified by faulting, collapse features, and erosional processes, each of which can form steep cliffs. The lava flows, extensively cracked and jointed as a result of cooling and initial deformation, vary in their degree of weathering with the age of the deposit, the density of the rock, and the amount of rainfall to which they have been subjected. The thickness of the flows also varies from a few centimeters to several meters, and they are sometimes interbedded with volcanic ash deposits that are locally as much as 9 m thick (Hirashima, 1948, p. 484; Buchanan-Banks, 1983). In some areas the ash units are the surficial deposits. Landslides and small soil slips frequently occur in the ash and, locally, in the underlying materials following heavy rains. The deeply weathered Mauna Kea lava flows are particularly susceptible to failure induced both by saturating rains and by earthquake shaking.

SLOPE STEEPNESS

Topography was a factor in controlling the location of landslides, and, to a lesser degree, areas of structural damage in the November 1983 earthquake. The largest landslides invariably occurred from the near-vertical cliffs in the epicentral area and from steep slopes elsewhere on the island. Numerous rock falls could be observed along highways where roads were cut through lava flows regardless of the height of the cut. Small soil slumps in ash deposits also occurred where the slope had been steeply cut.

CONCLUSIONS

The 1983 Kaoiki earthquake provided a unique opportunity to examine earthquake-induced structural damage and ground failures in Hawaii. Although the 1975 Kalapana earthquake had a higher magnitude (M 7.2) and hence more seismic energy, its location near the coast allowed some of this energy to be propagated seaward away from the main cultural centers of the island. The inland location of the Kaoiki earthquake, therefore, resulted in greater structural damage (Koyanagi and others, 1984, p. 4).

Damage to structures was greatest in the epicentral area, where the foundations under some houses moved as much as 1.2 m away from the house. Structures with post-and-pier foundations were more severely damaged in this earthquake than those with concrete slab foundations. In some cases, the posts and piers were joined together with steel plates or rebar reinforcement; these houses nonetheless came off their foundations.

Lithology and topography also seemed to affect the location and degree of structural damage. Houses in Wood Valley, Volcano Golf and Country Club Subdivision, Volcano, and Hilo were damaged where ash deposits at or near the surface were at least 0.5 m thick. Houses built across breaks in slope, on uneven terrain, on sloping ground, or near the edges of unsupported embankments sustained greater damage than those on flat ground.

The regional distribution of landslides resembles the overall pattern of seismic intensity, most failures occurring in the epicentral area. The threshold intensity for triggering small rock falls and soil slumps was IV to V (modified Mercalli scale).

The predominant types of landslide generated by this earthquake were shallow rock slides and falls. They most commonly occurred on the steep slopes and were induced by the earthquake shaking.

Virtually all large landslides occurred in extensively cracked and jointed lava flows. Small soil failures and extensional cracks also occurred in the thick ash deposits in the epicentral area and in Hilo.

Because of the relatively sparse population in the epicentral area and the early hour at which the earthquake occurred, there were few injuries from the landslides. However, landslides along the Hamakua coast slightly injured two people and caused closure of the circum-island highway for a few hours until debris was removed. Compactional failure of road fill also closed the circum-island highway in the epicentral area for a few hours.

REFERENCES

Bates, T.F., 1960, Rock weathering and clay formation in Hawaii: College Station, Pennsylvania State University, Bulletin, College of Mineral Resources, v. 29, no. 8, 4 p.

Brigham, W.T., 1869, The eruption of the Hawaiian Volcanoes, 1868: Boston Society of Natural History, Memoirs, v. 1., p. 564-587.

Buchanan-Banks, J.M., 1983, Reconnaissance map showing thicknesses of volcanic ash deposits in the greater Hilo area, Hawaii: U.S. Geological Survey Miscellaneous Field Studies Map MF–1499, scale 1:24,000.

Buchanan-Banks, J.M., and Lockwood, J.P., 1982, Geological map of the Alenaio-Waipahoehoe Stream area, South Hilo District, Hawaii: U.S. Geological Survey Open-File Report 82–655, map scale 1:24,000.

Chiu, A.N.L., Lum, W.B., Nielsen, N.N., and Koyanagi, R., 1984, Damage survey of the Kaoiki, Hawaii earthquake of November 16, 1983: Earthquake Spectra, v. 1, no. 1, p. 173-182.

Endo, E.T., 1985, Seismotectonic framework for the southeast flank of Mauna Loa: Seattle, University of Washington, PhD. thesis, 253 p.

Hawaii Tribune-Herald, 1983, Quake toll: 350 houses, 35 businesses: Hawaii Tribune-Herald, Friday, December 9, 1983, no. 287, p. 1.

Hirashima, K.B., 1948, Highway experience with thixotropic volcanic clay: Proceedings of the Highway Research Board, v. 28, p. 481- 494.

Keefer, D.K., 1984, Landslides caused by earthquakes: Geological Society of America Bulletin, v. 95, no. 4, p. 406-421.

Koyanagi, R.Y., Endo, E.T., Tanigawa, W.R., Nakata, J.S., Tomori, A.H., and Tamura, P.N., 1984, Kaoiki, Hawaii, earthquake of November 16, 1983: A preliminary compilation of seismographic data at the Hawaiian Volcano Observatory: U.S. Geological Survey Open-File Report 84–798, 6 p.

Lipman, P.W., and Swenson, Alan, 1984, Generalized geologic map of the southwest rift zone of Mauna Loa Volcano, Hawaii: U.S. Geological Survey Miscellaneous Investigations Series Map I–1323, scale 1:100,000.

Nielson, N.N., Furumoto, A.S., Lum, Walter, and Morrill, B.J., 1977, The Honomu, Hawaii, earthquake: report of inspection: Washington, D.C., National Academy of Science, 79 p.

Peterson, D.W., 1967, Geologic map of the Kilauea Crater quadrangle, Hawaii: U.S. Geological Survey Geologic Quadrangle Map GQ–667, scale 1:24,000.

Rojahn, Christopher, and Morrill, B.J., 1977, The island of Hawaii earthquakes of November 29, 1975: Strong-motion data and damage reconnaissance report: Seismological Society America Bulletin v. 67, no. 2, p. 493-515.

St. Ours, Patrice, de, 1982, Structural map of the summit area of Kilauea Volcano, Hawaii: U.S. Geological Survey Miscellaneous Field Studies Map MF–1368, scale 1:24,000.

Stearns, H.T., and Clark W.O., 1930, Geology and water resources of the Kau district, Hawaii: U.S. Geological Survey Water Supply Paper 616, 194 p.

Stearns, H.T., and Macdonald, G.A., 1946, Geology and groundwater resources of the Island of Hawaii: Hawaii Division Hydrography Bulletin 9, 363 p.

Swanson, D.A., Duffield, W.A., and Fiske, R.S., 1976, Displacement of the south flank of Kilauea Volcano: The result of forceful intrusion of magma into the rift zones: U.S. Geological Survey Professional Paper 963, 39 p.

Tilling, R.I., Koyanagi, R.Y., Lipman, P.W., Lockwood, J.P., Moore, J.G., and Swanson, D.A., 1976, Earthquake and related catastrophic events, Island of Hawaii, November 29, 1975: A preliminary report: U.S. Geological Survey Circular 740, 33 p.

Wieczorek, G.F., Jibson, R.W., Wilson, R.C., and Buchanan-Banks, J.M., 1982, Geotechnical properties of ash deposits near Hilo, Hawaii:, U.S. Geological Survey Open-File Report 82–279, 20 p.

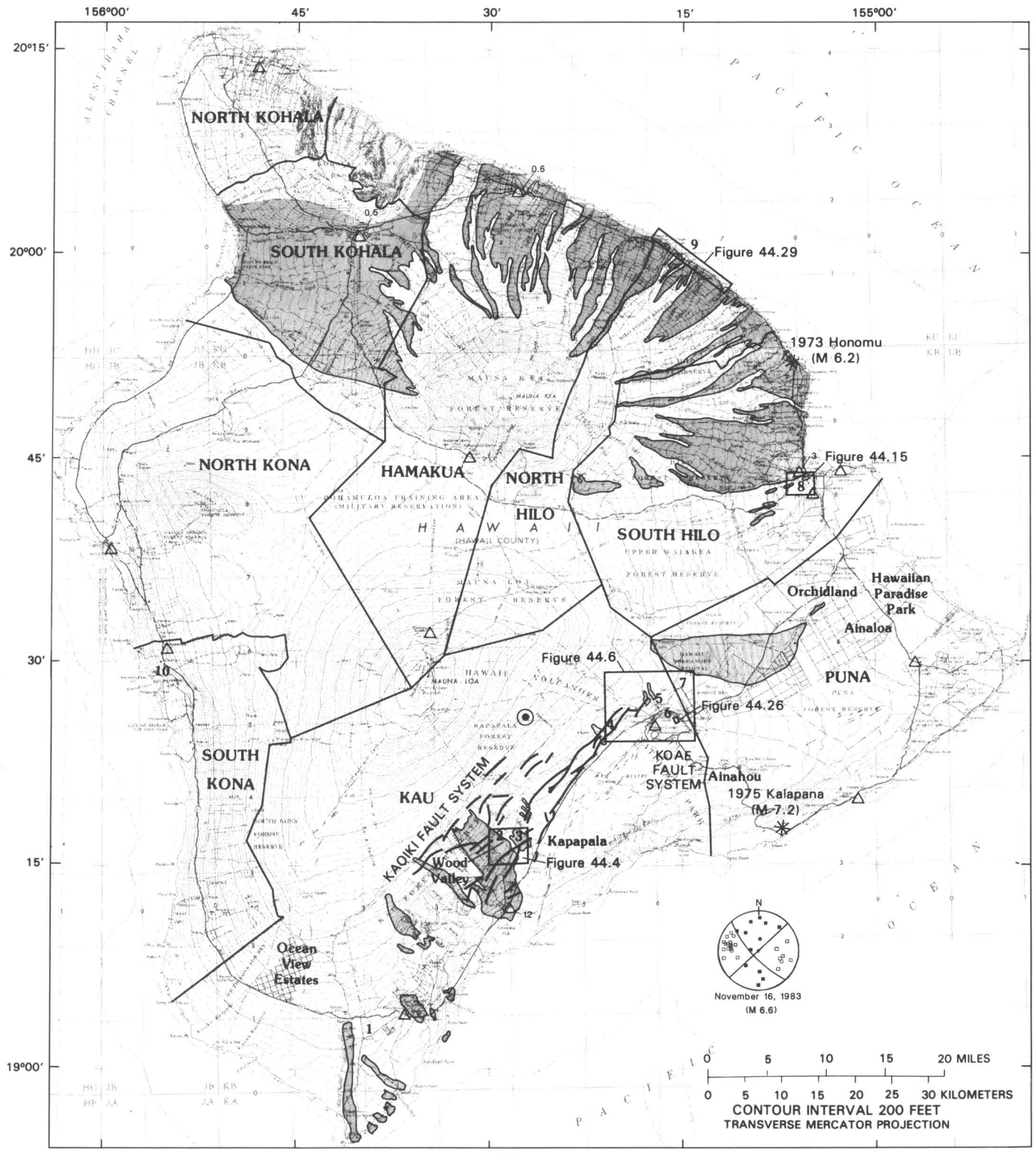

FIGURE 44.1.—The Island of Hawaii showing epicenters of November 16, 1983, Kaoiki earthquake and two earlier damaging earthquakes; also shown are areas of 1983 structural damage and earthquake-related ground failures discussed in text. Additional text figures cited where applicable. Inset shows focal-mechanism solution for 1983 earthquake from Endo (1985, p. 186): *P*-wave first motions plotted on lower hemisphere equal-angle stereograph; open squares, down first motions; solid squares, up first motions. Topography from U.S. Geological Survey Hawaii Island series W532, 1975, 1:250,000.

EXPLANATION

Earthquake epicenters

Kaoiki earthquake, November 16, 1983

1973 and 1975 earthquakes

1 Areas of structural damage or ground failure during 1983 earthquake: 1, Ka Lae Road; 2, Wood Valley; 3, Kapapala Ranch house; 4, Ranch house at east end of Kapapala Ranch; 5, Volcano Golf and Country Club Subdivision and Keauhou Ranch house; 6, Hawaii Volcanoes National Park; 7, Upper Wright Road; 8, Hilo; 9, North Hilo District; 10, Kealekekua Bay

Ash deposits

3 Accelerograph location and ash thickness, in meters

Fault trace, from Stearns and Macdonald (1946, pl. 1) and Lipman and Swenson (1984)

District boundary

FIGURE 44.1.—Continued.

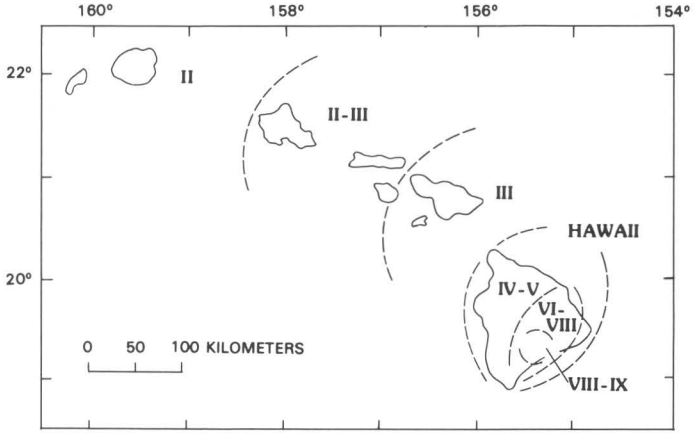

FIGURE 44.2.—Isoseismal map for November 16, 1983, earthquake prepared from observations of damage and felt reports from residents compiled by Hawaii County Civil Defense Agency. Numbers indicate intensity on modified Mercalli scale (from Koyanagi and others, 1984, fig. 3).

FIGURE 44.3.—Post-and-pier house support displaced in November 16, 1983, earthquake. In this type of construction, two concrete blocks form pier and a vertical wooden 10-cm by 10-cm post supports house. Larger block is resting on ground; smaller is placed on top of this and usually not connected to it. Between upper block and post is a termite shield of thin metal. At this locality, both post and upper foundation block have moved several centimeters to right on their respective supports. Dashed line indicates original position of post; arrow shows direction of movement.

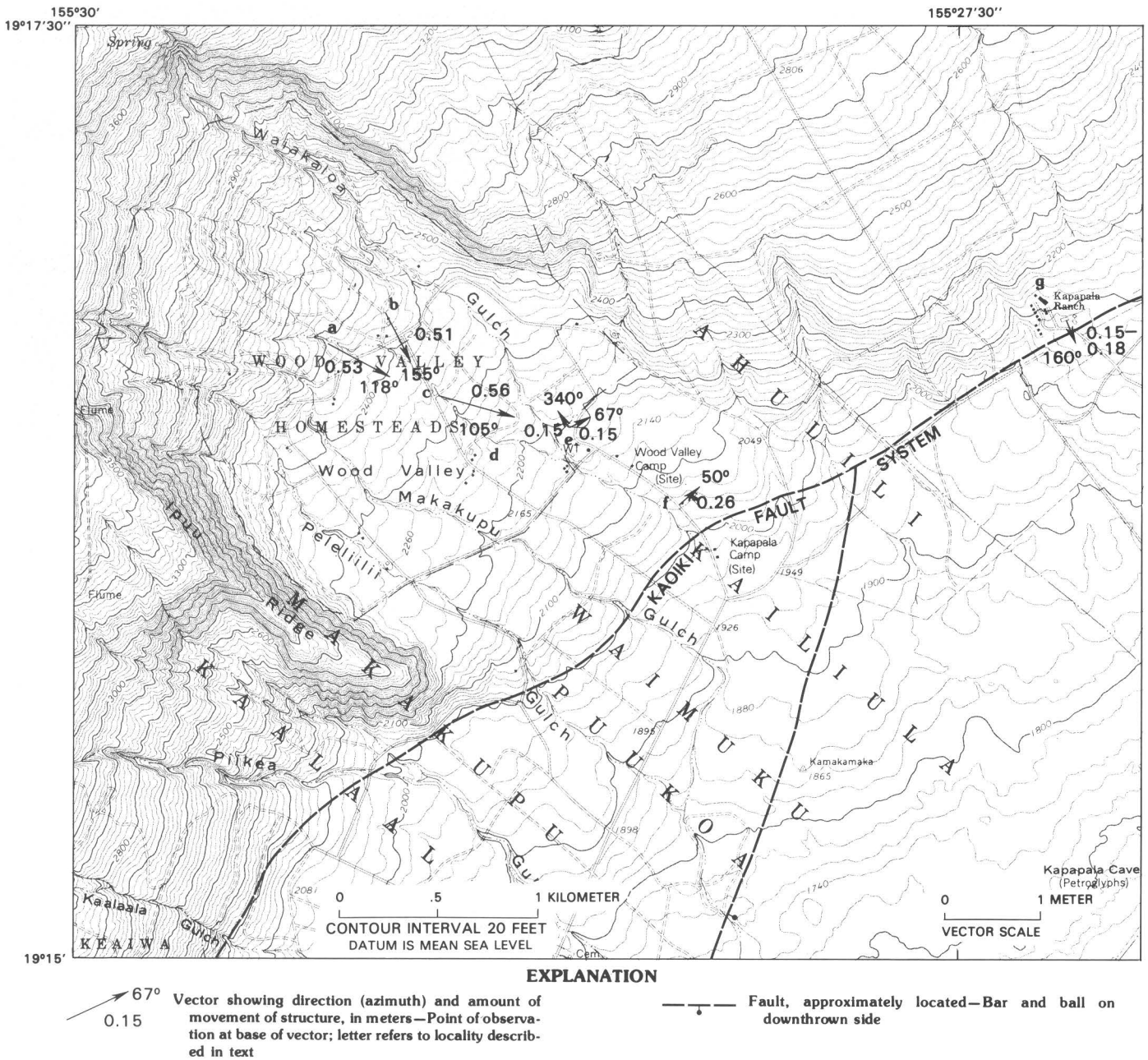

FIGURE 44.4.—Earthquake-related movement of structures in Wood Valley and western Kapapala Ranch, November 1983 (fig. 44.1, localities 2, 3). Topography from U.S. Geological Survey Wood Valley 7.5-minute quadrangle, 1981, scale 1:24,000. Location of faults from Stearns and Clark (1930, pl. 1) and Lipman and Swenson (1984).

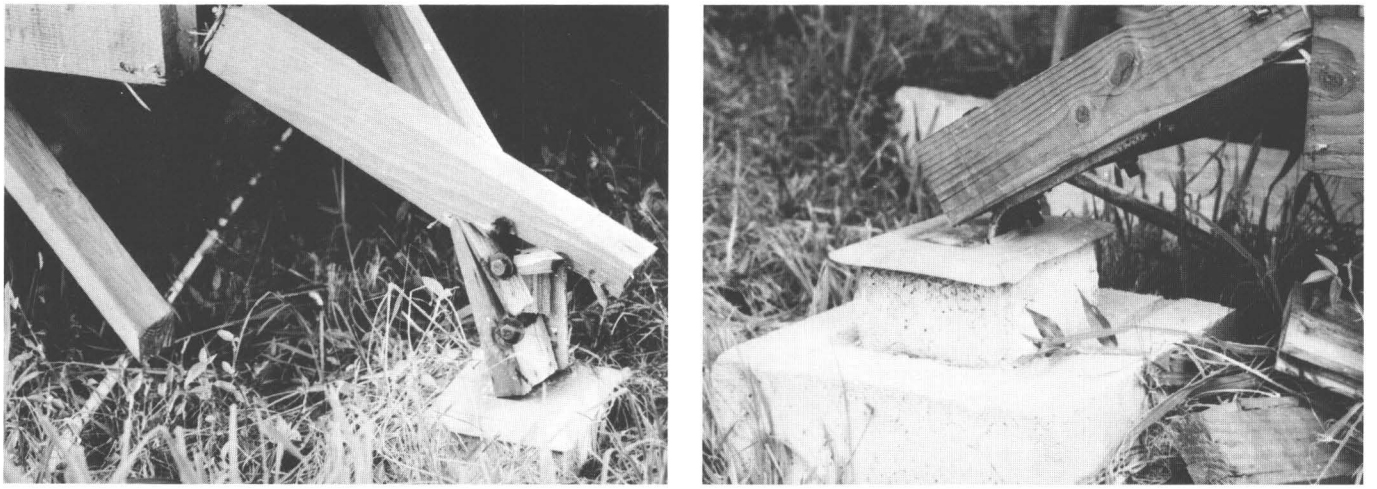

A ***B***

FIGURE 44.5.— Damage to a wood-frame house with post-and-pier construction in Wood Valley (fig. 44.4, locality b). ***A***, Northeast corner post fractured where anchor bolts connected it to 0.5-cm-thick steel plate positioned on southwest side of post (away from the viewer). Concrete foundation block appears to have been poured as single unit around the steel plate. Post also was torn loose from house and from diagonal bracing when ground, pier, and post moved southeastward. ***B***, Northwest corner post with steel plate on south side of post. The 0.5-cm-thick steel plate is bent at 45° angle. Photographs by E.T. Endo.

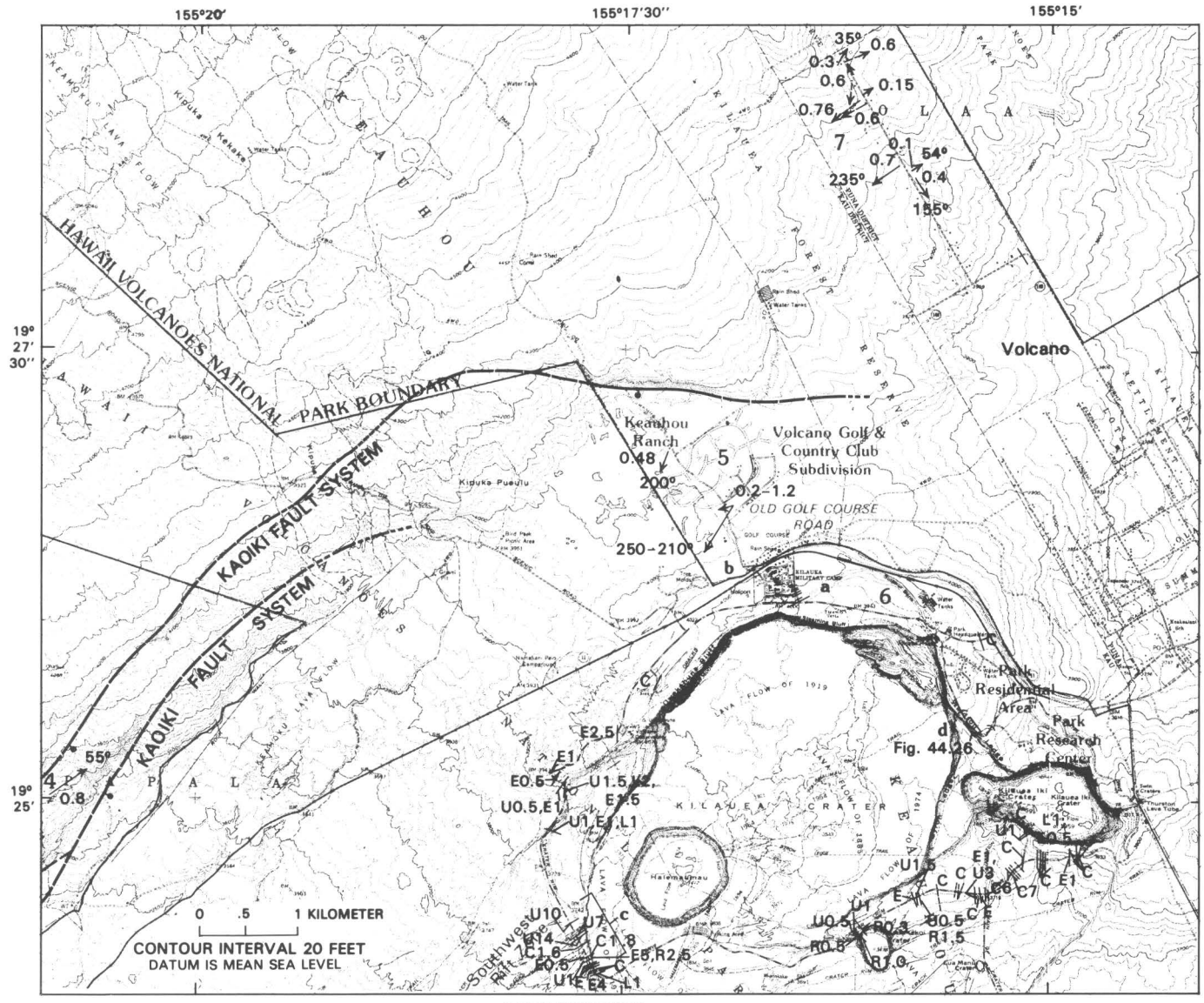

FIGURE 44.6.—Earthquake damage in epicentral region near Kilauea summit (localities 4–7, fig. 44.1). Some of the worst structural damage occurred in this area. Topography from U.S. Geological Survey Kilauea Crater and Volcano 7.5-minute quadrangles, 1981, scale 1:24,000.

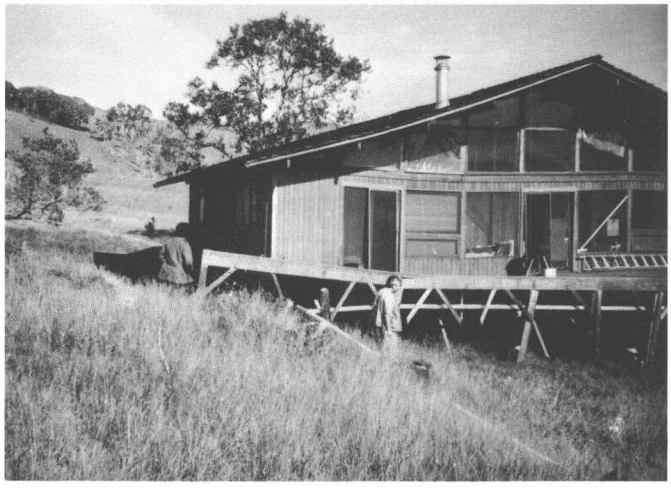

FIGURE 44.7.—House on Kapapala Ranch about 12 km east of epicenter was displaced 0.8 m northeastward during earthquake. Most supporting posts remained vertical, but those used to frame a basement room were tilted. Concrete foundation piers, partly obscured by grass, behind figure in dark jacket. Windows broken during earthquake are covered with plastic. Near clump of trees on hill behind house, small soil slips can be seen and broken branches strew the ground.

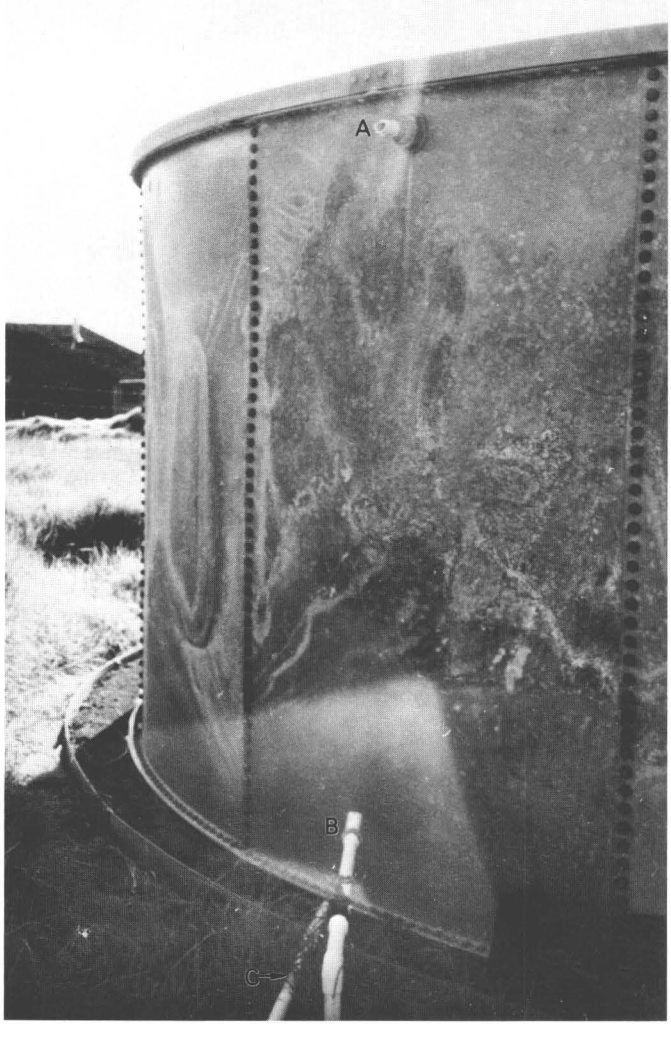

FIGURE 44.8.—Water tank that may have moved as much as 0.12 m southward (to right in photograph) during November 1983 earthquake. The 1.8-m length of pipe that originally extended from A to B now lies under tank at C. First motion apparently snapped pipe, which rolled under tank as tank tilted back and forth.

FIGURE 44.9.—North corner pier of damaged two-story frame house in Volcano Golf and Country Club Subdivision. Although house is now 1.2 m southwest of its foundation, rebar protruding through piers is still straight. Termite shield from atop pier can be seen on ground. House subfloor was originally 1 m above ground, but most supporting posts collapsed.

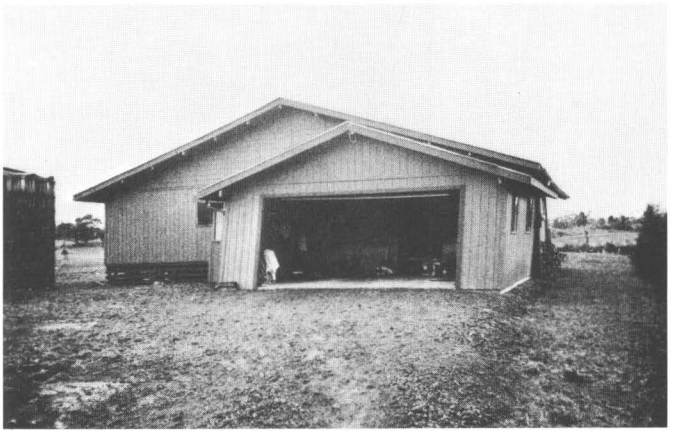

A

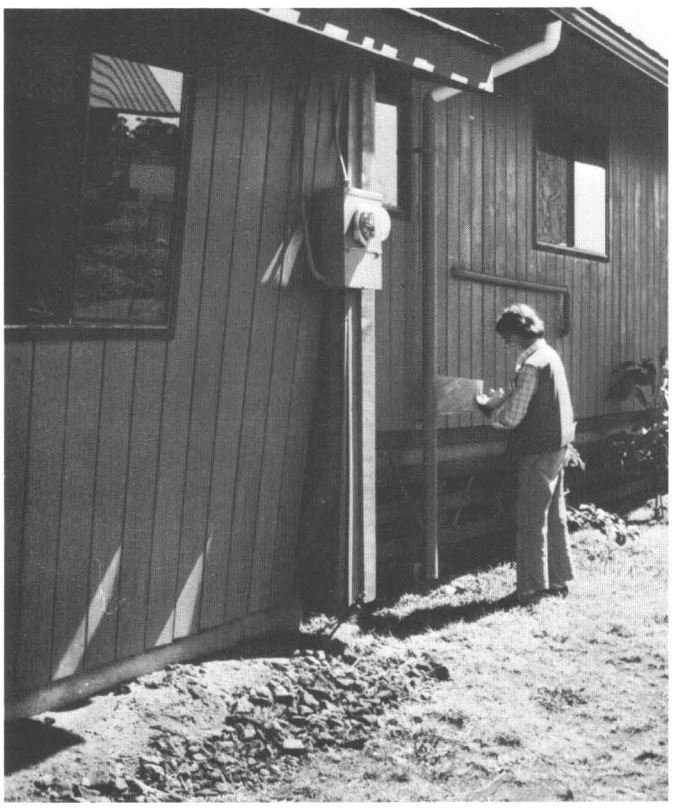

B

FIGURE 44.10.—Damaged frame house in Volcano Golf and Country Club Subdivision. ***A***, View of attached garage (with concrete foundation) and house (post-and-pier foundation). House moved farther than garage, breaking a 10-cm by 10-cm upright and causing a tear in southwest wall at electric meter. Photograph by R.Y. Hanatani. ***B***, Detailed view of right side of house; to right of drainpipe, a supporting post can be seen resting on ground southwest of pier on which it originally stood. Photograph by J.B. Stokes.

FIGURE 44.11.—Main meeting room and library at Hawaiian Volcano Observatory after 1983 earthquake. Bookcases were torn from back wall and fell onto table; storage cabinets were moved as much as 0.5 m. Preearthquake location of cabinets is documented by dust marks on floor behind and to right of plastic waste bin. Smoked-drum seismographs (obscured by easel) located under windows to right were temporarily out of order because their drive mechanisms jammed. Photograph by J.D. Griggs.

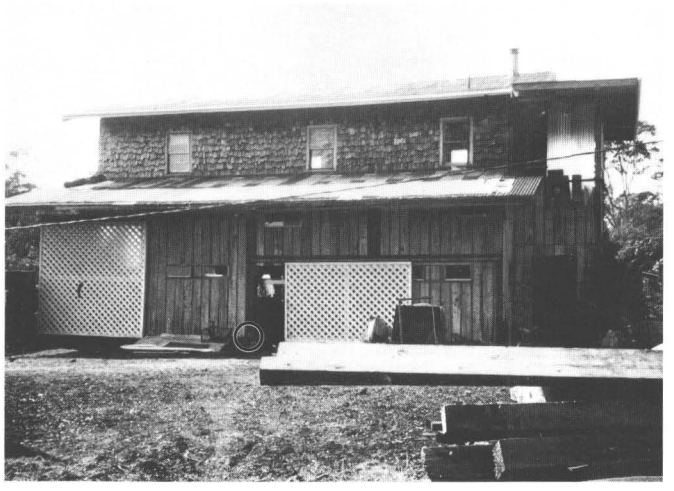

A

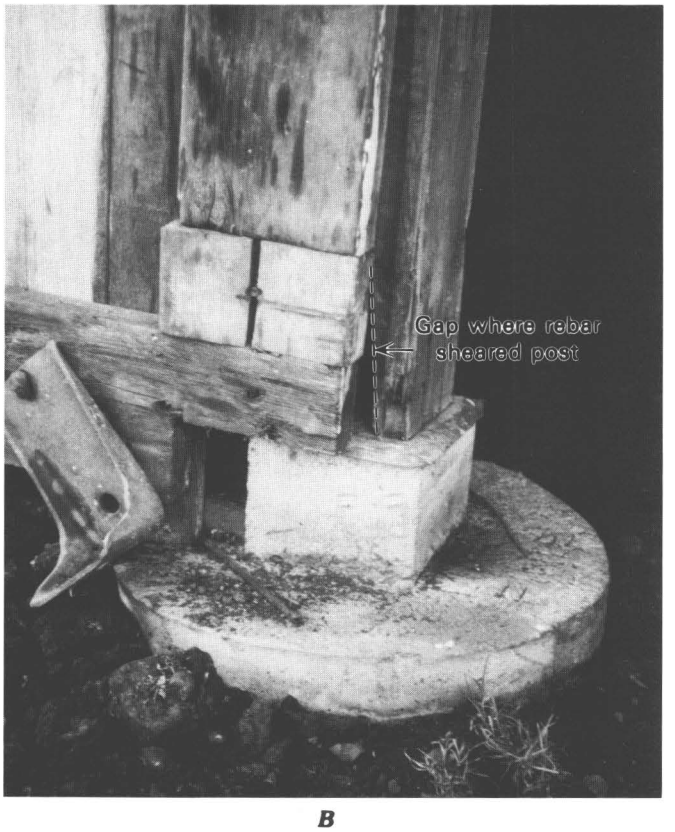

B

FIGURE 44.12.—Barnlike three-story-high frame house in Puna District that was moved off its foundation about 0.3 m toward northeast in 1983 earthquake. ***A***, View of house showing position of one of sheared support posts (circled). ***B***, Close-up of footing circled in *A*. The 14-cm by 14-cm wooden post was sheared by rebar that extended from base of footing upward into post as much as 11 cm; most other posts supporting upper story were similarly sheared. House has been replaced on piers.

FIGURE 44.13.—Water tanks in Volcano affected by 1983 earthquake. Most water tanks here were constructed like one standing at right rear. Tank in foreground has collapsed, while other appears little damaged although displaced southwestward 0.7 m. This difference in response to earthquake may be because of a difference in water level in tanks at time of earthquake, or because of a difference in age or condition of tanks. Photograph by E.T. Endo.

FIGURE 44.14.—Greenhouse on Upper Wright Road leaning to southwest after earthquake; view to southeast. Crop loss in this area was severe because of collapse of some greenhouses and uncovering of planted furrows. Crop shown here is tomatoes. Photograph by E.T. Endo.

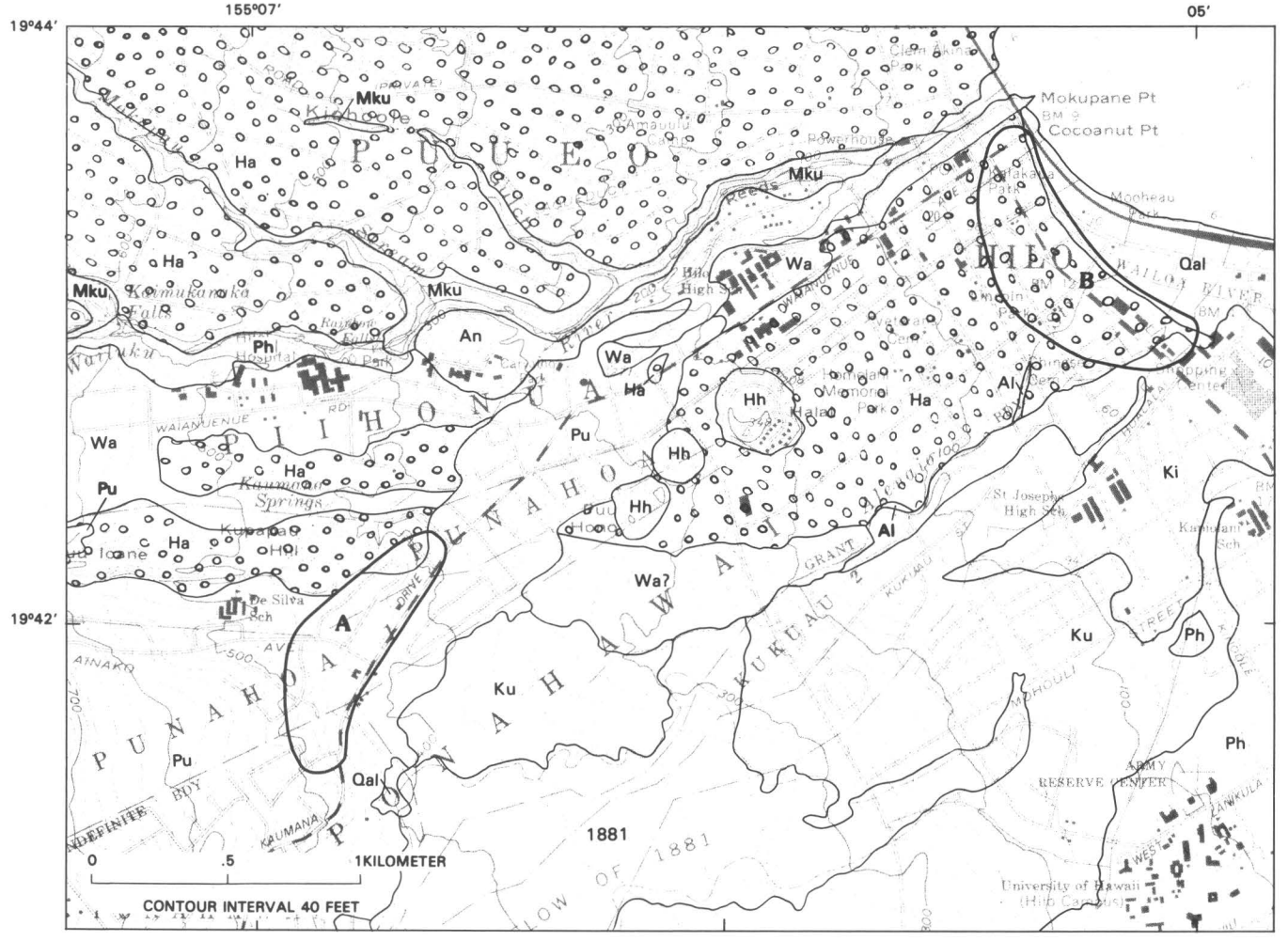

EXPLANATION

A — Area of earthquake damage— Letters refer to discussion in text

CORRELATION OF MAP UNITS

Surficial deposits

- Qal — Quaternary alluvium

Mauna Loa Volcano

- 1881 — 1881 pahoehoe
- Ku — Kukuau pahoehoe, Age —1.35 ka
- Pu — Punahoa pahoehoe, Age —3.5 ka
- Ki — Kinoole aa, Age <8.0 ka
- Ph — Malaai picrite, Age —9.7 ka
- An — Anuenue aa, Age —10.6 ka
- Wa — Waianuenue pahoehoe, Age —14.2 ka

Mauna Kea Volcano

- Ha — Homelani ash, Age >14.2 ka
- Al — Alenaio Stream picrite, Age >14.2 ka
- Hh — Halai Hills spatter, Age >14.2 ka
- Mku — Lavas of Mauna Kea, undivided

FIGURE 44.15.—Geologic map of Hilo and vicinity showing areas of structural damage from November 1983 earthquake (fig. 44.1, locality 8). Adapted from Buchanan-Banks and Lockwood (1982). Topography from U.S. Geological Survey Hilo 7.5-minute quadrangle, 1981, scale 1:24,000.

A

B

FIGURE 44.16.—Damage to houses in South Hilo District. ***A***, Wood braces have been emplaced to prevent second story of this house from moving farther downslope. Broken and twisted drain pipe gives an indication of amount of distortion this house has undergone. ***B***, Living area of this wood-frame house extends across break in slope from street level, marked by vegetation on left, to above four-car garage. Concrete blocks of garage level are broken both through and between blocks. Upper story is warped and has moved toward back of house (toward viewer) and to right. New uprights and cross bracing behind garage doors (not visible in this photograph) have been added to support weight of upper story. Drainpipe has been reattached at street level with rope. A decorative rock wall has collapsed and rocks rolled downhill.

FIGURE 44.17.—Damaged commercial building in old part of Hilo. Side wall separated from main structure, leaving a gap at roof level of about 21 cm.

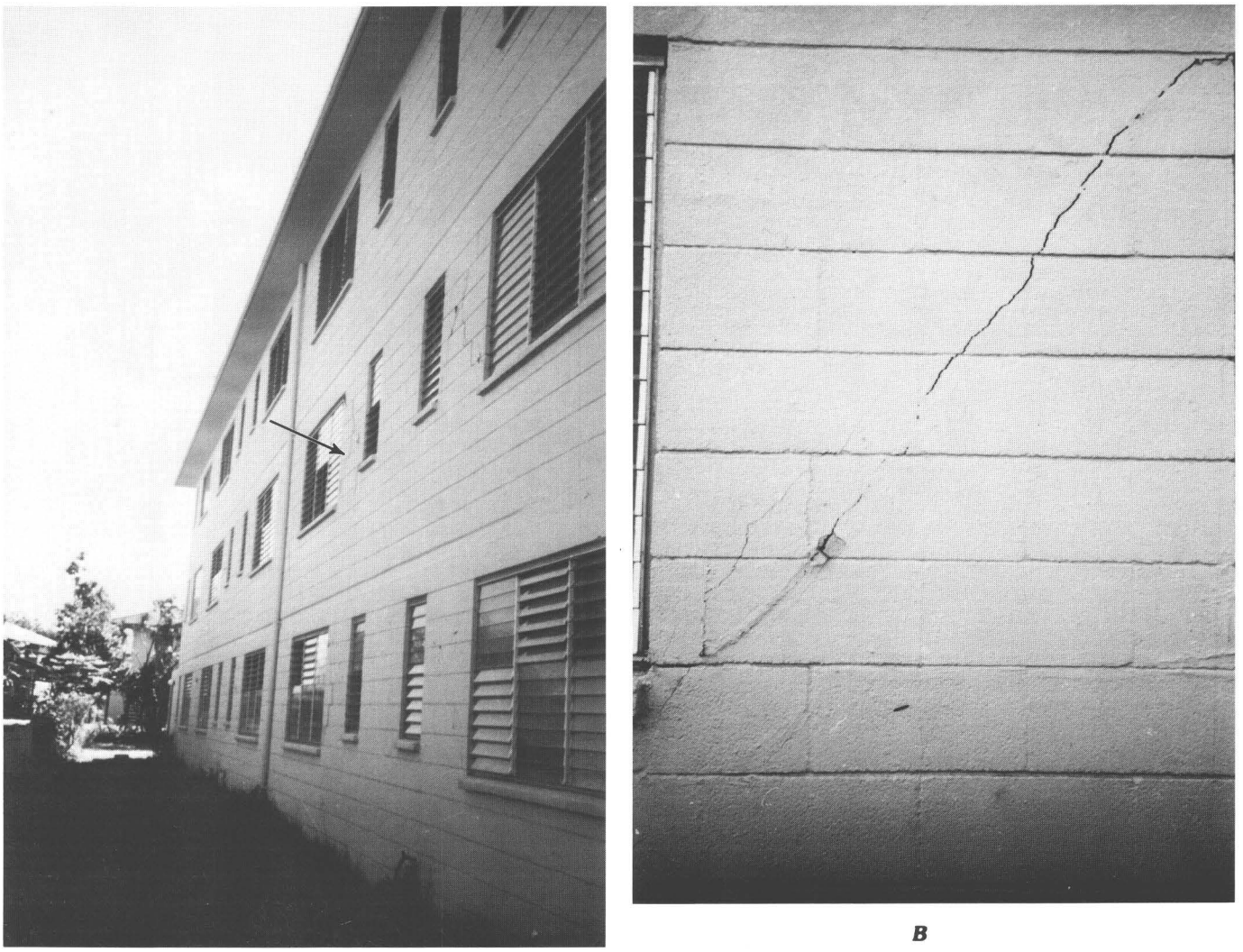

FIGURE 44.18.—Apartment building in Hilo damaged in November 1983 earthquake. ***A***, View along two-thirds of length of building, which was difficult to photograph because of steep slope down to left. Cracked cinder block can be seen between most of windows of first and second floors; less structural damage was apparent at third floor. Arrow indicates area shown in detail in C. ***B***, Detail of damage to a part of first floor not shown in *A*. Along longest and widest crack, smeared texture and flaking paint indicate an old crack that had been repaired and repainted. As a result of earthquake, there is renewed cracking along this feature as well as some new cracks through cinder blocks. This building probably was damaged originally by the 1973 Honomu earthquake and (or) by 1975 Kalapana earthquake. ***C***, Detail of damage indicated by arrow in *A*. Some blocks were broken in such a way that pieces of them protruded from block or spalled off.

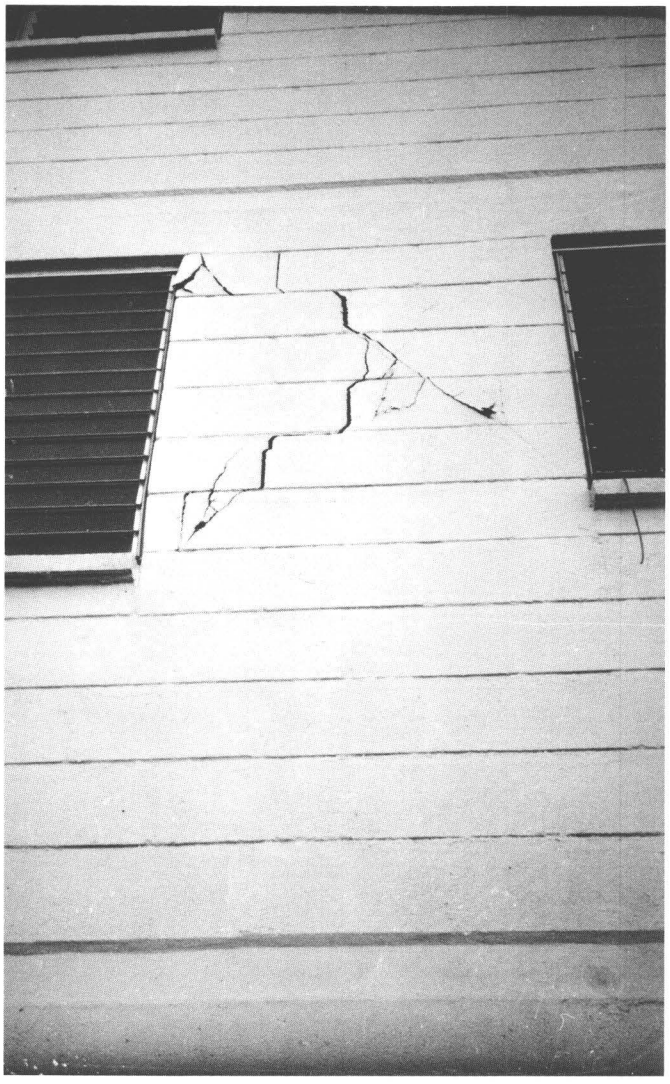

C

FIGURE 44.18.—Continued.

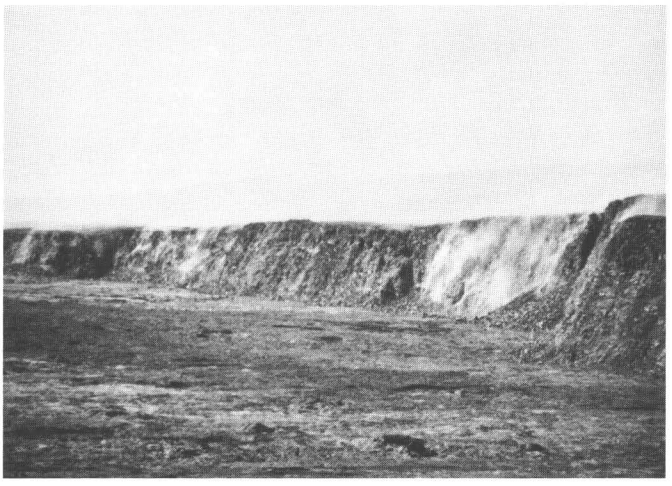

FIGURE 44.19.—View of Uwekahuna Bluff in Kilauea caldera, taken from Crater Rim Trail a few hours after November 1983 earthquake. Dust plumes mark rock falls that were still occurring along this section of caldera wall. Hawaiian Volcano Observatory is just out of photograph to right. Photography by J.D. Griggs.

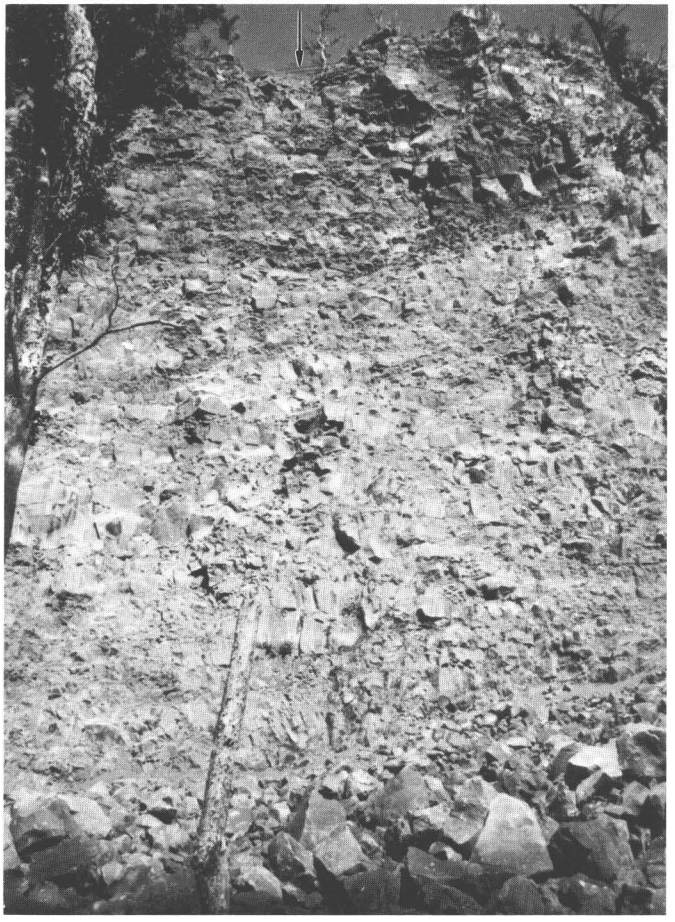

FIGURE 44.20.—Typical section of cliff in Kilauea caldera composed of flows from Kilauea Volcano. View looking up from Halemaumau Trail below Volcano House toward Crater Rim Trail; guardrail (arrow) can be seen suspended over 60-m-high cliff where a rock slide has removed part of trail.

FIGURE 44.21.—Section of Crater Rim Drive at eastern entrance to Kilauea Military Camp that collapsed in November 1983 earthquake along a system of cracks trending at az 60°. Earthquake shaking caused subsurface material to settle, thus undermining road. Note pavement patch from repair of earlier failure at same place.

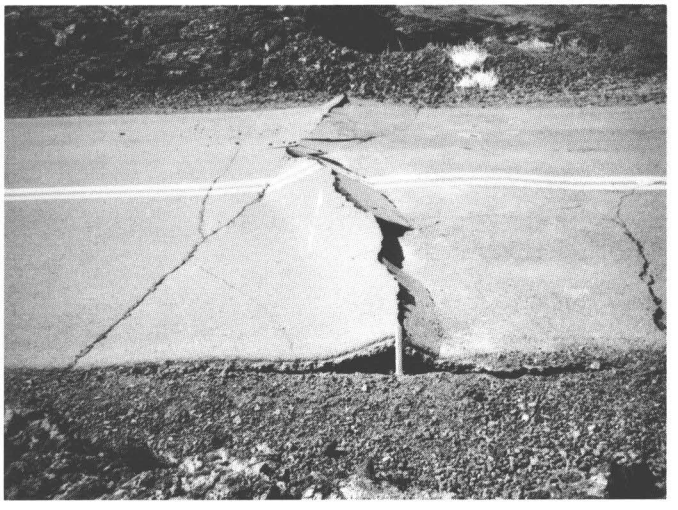

A

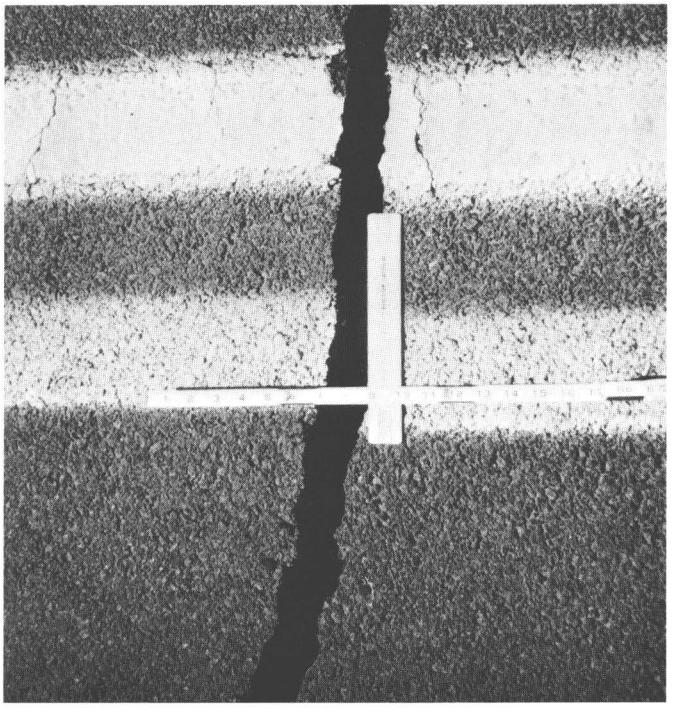

B

FIGURE 44.22.—Compressional and extensional features produced by November 1983 earthquake where Crater Rim Drive crosses southwest rift zone of Kilauea Volcano. ***A***, A compressional fold 12 cm high; far end of fold has been collapsed by passage of vehicle. ***B***, An open extension crack 5 cm wide, which shows apparent right-lateral offset of about 2 cm, and vertical offset up to north (left) of about 1 cm.

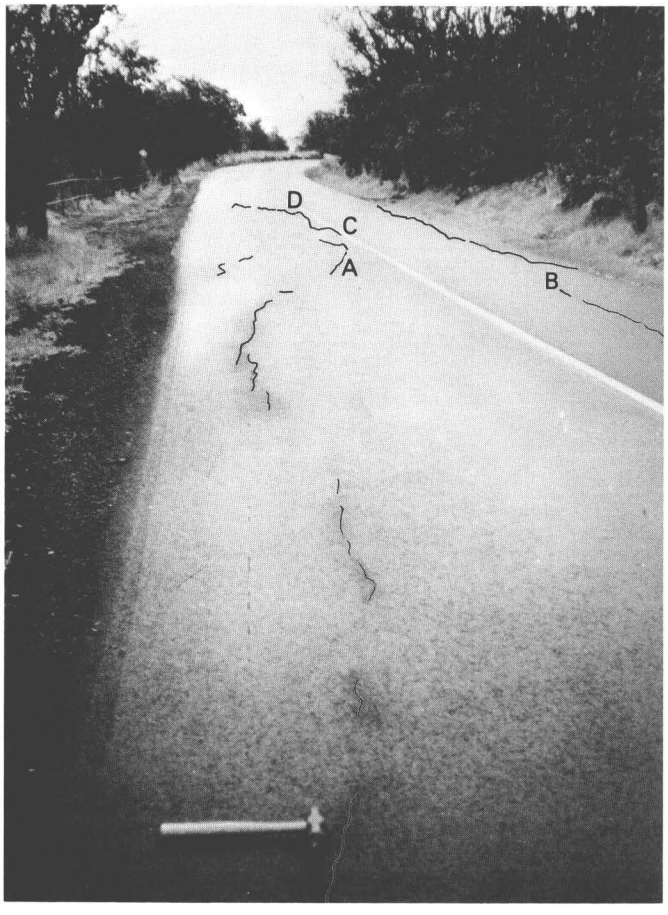

A

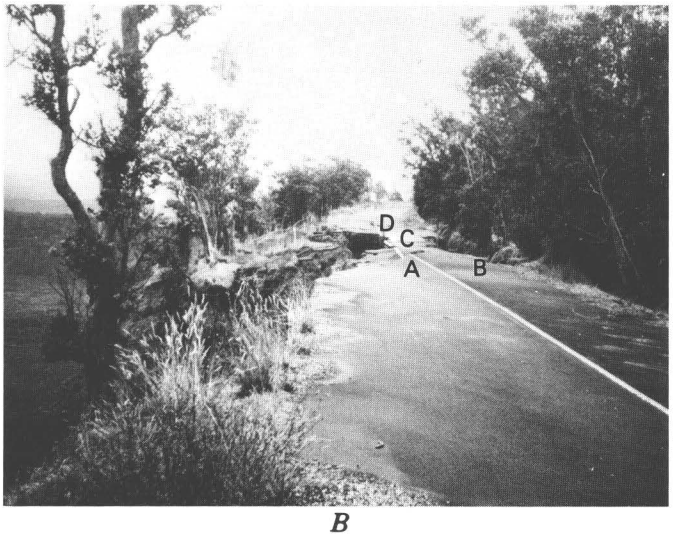

B

FIGURE 44.23.—Ground failure in November 1983 earthquake along Crater Rim Drive between Waldron Ledge Overlook and Research Center turnoff. ***A***, Photograph taken in March 1980, looking northwest, showing road cracks curving toward caldera (left) and outlining incipient landslide (A, C, D). Along the right edge of pavement, additional cracks curving away from caldera (B) mark west side of graben-like depression that runs parallel to roadway for nearly same length as incipient landslide cracks. ***B***, Photograph of same section of road taken in October 1984. Slope failed along preexisting cracks (A, C, D) during earthquake shaking. A graben about 2 m deep by 1–2 m wide has formed along cracks at right side of road (B) and caused trees to tilt.

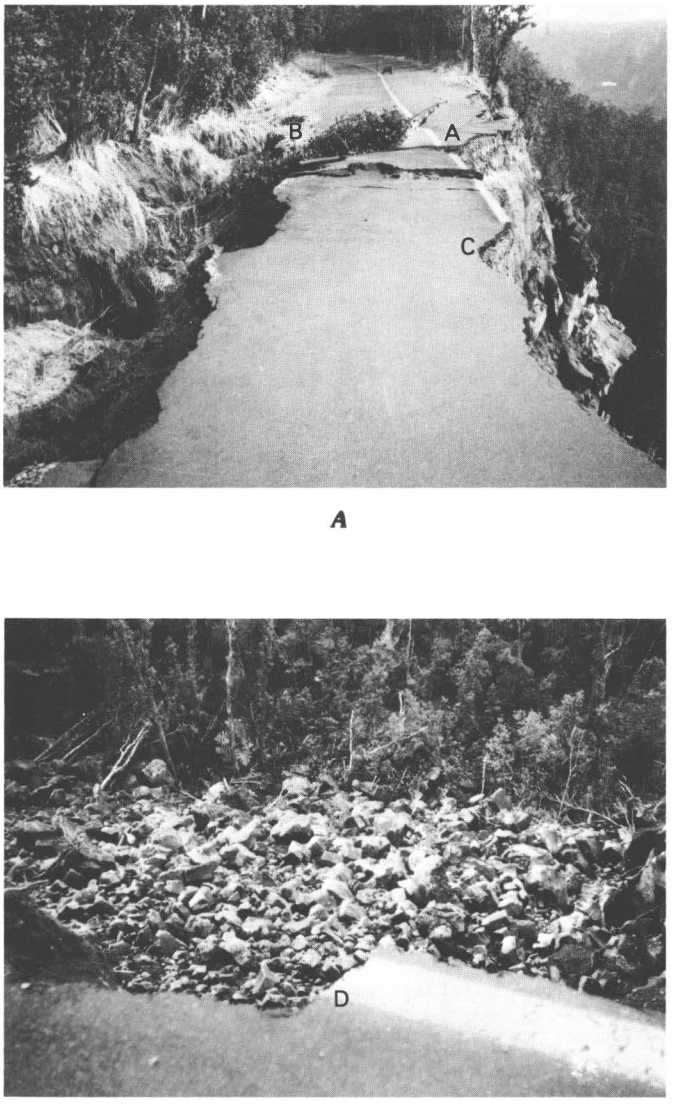

A

B

FIGURE 44.24.—Details of failure of Waldron Ledge landslide. Labelled points (A, B, C, D) are same as in figure 44.23. ***A***, View southeast at head scarp of landslide and of parallel graben on other side of road. Headwall scarp was approximately 14 m high and 30 m long; landslide removed 11-m-wide section of road and trail. ***B***, View downward from road of jumbled mass of rock resulting from disintegration of slide block; mass did not travel far from base of cliff.

FIGURE 44.25.—Earthquake-produced crack across road at northwest entrance to Waldron Ledge Overlook. Chips of broken pavement indicate sides of crack were bashed together repeatedly. Photograph by J.B. Stokes.

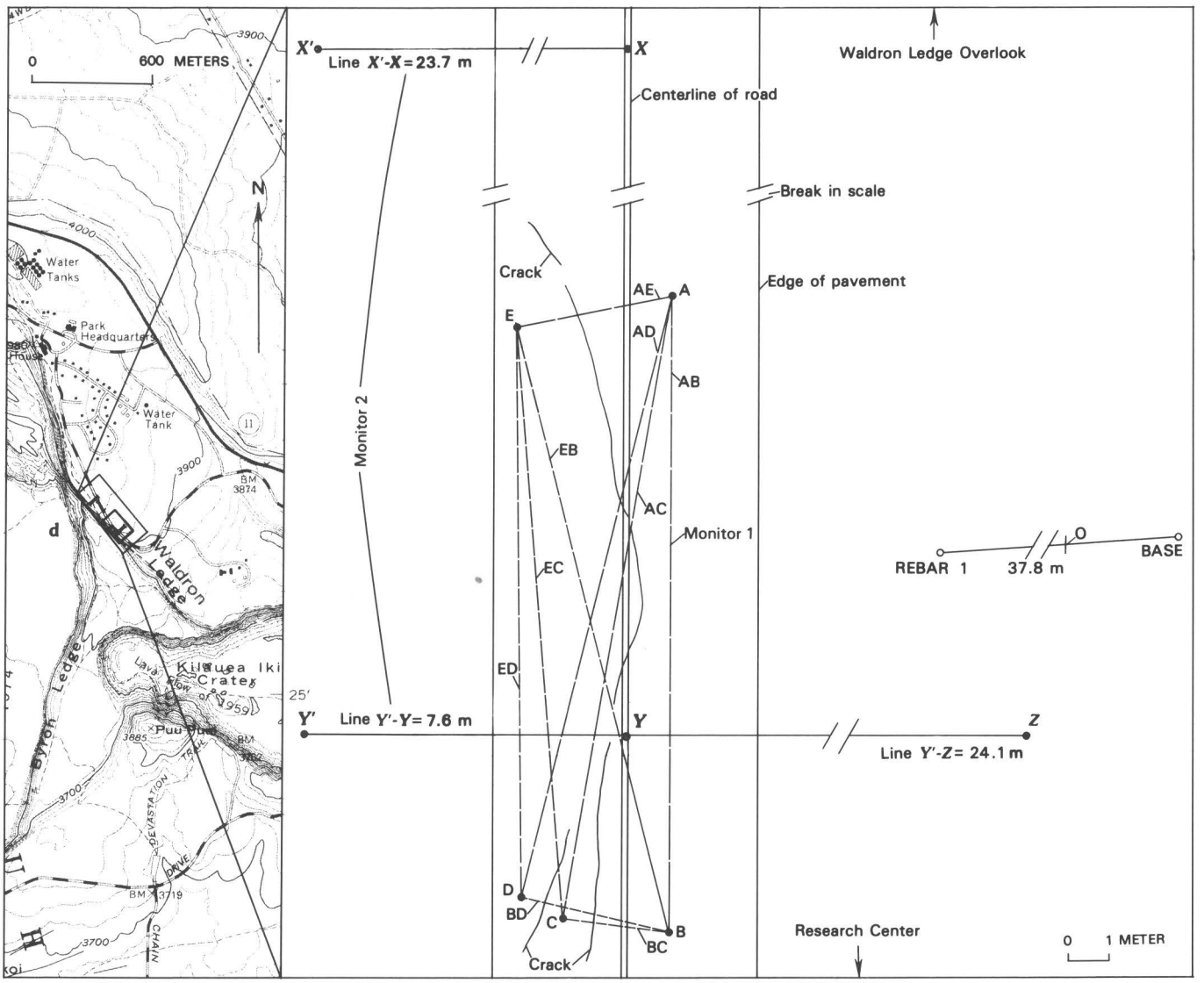

FIGURE 44.26.—Location map and plan of monitors established by USGS across series of cracks in Crater Rim Drive near Waldron Ledge. Topography from USGS Kilauea Crater 7.5-minute quadrangle, 1981, scale 1:24,000.

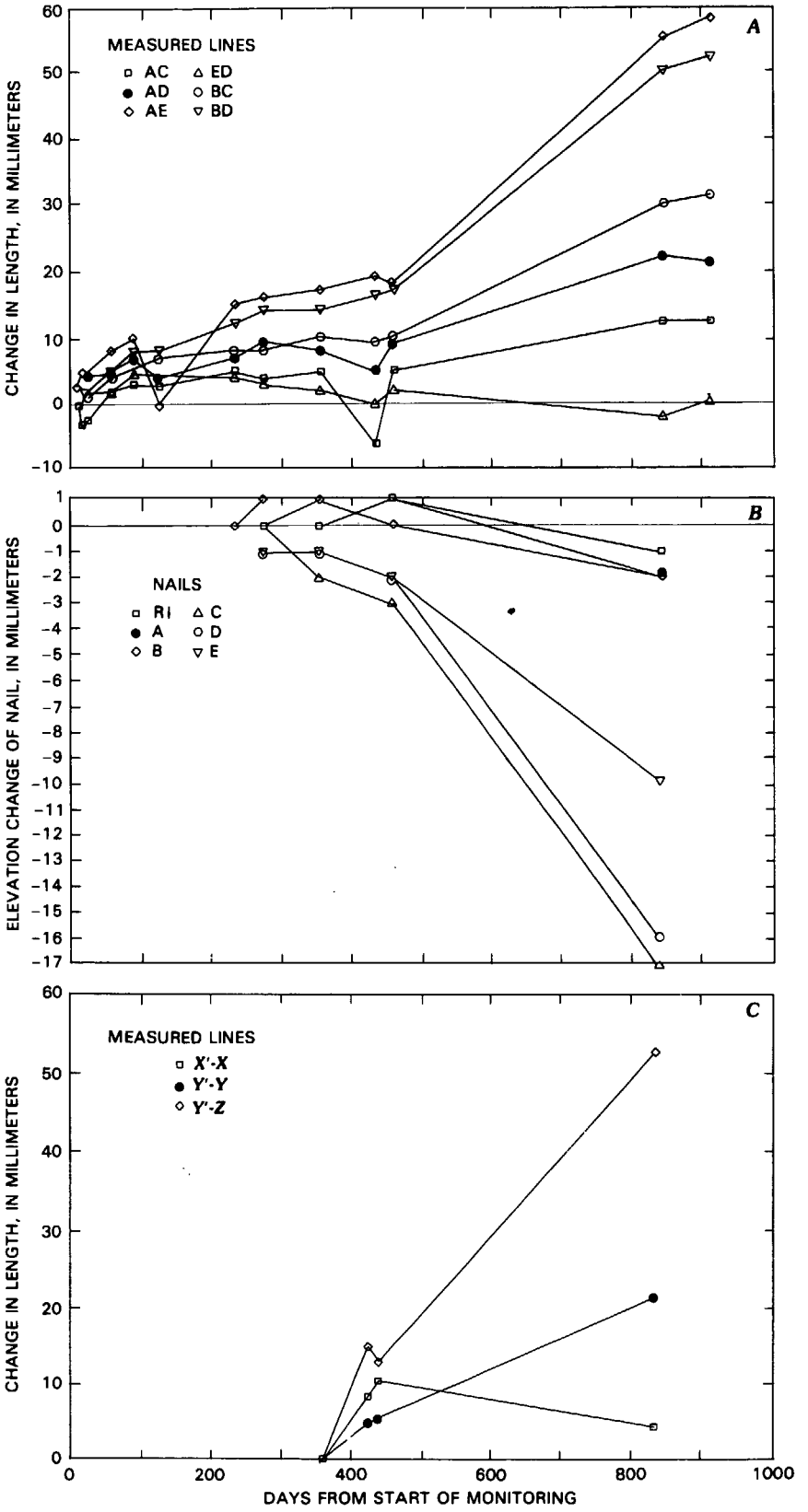

FIGURE 44.27.—Results from monitors established across incipient landslide on Waldron Ledge. ***A***, Changes in line lengths recorded by monitor 1, the quadrilateral. ***B***, Vertical changes recorded by monitor 1 between nails of quadrilateral and rebar 1 (R1). ***C***, Changes in line length recorded by monitor 2, lines measured with steel tape.

FIGURE 44.28.—Arcuate road crack along Kaumana Drive (fig. 44.15, area A) formed in November 1983 earthquake. Ground slopes downward to right. Houses were structurally damaged and water main was broken in area just out of photograph to left.

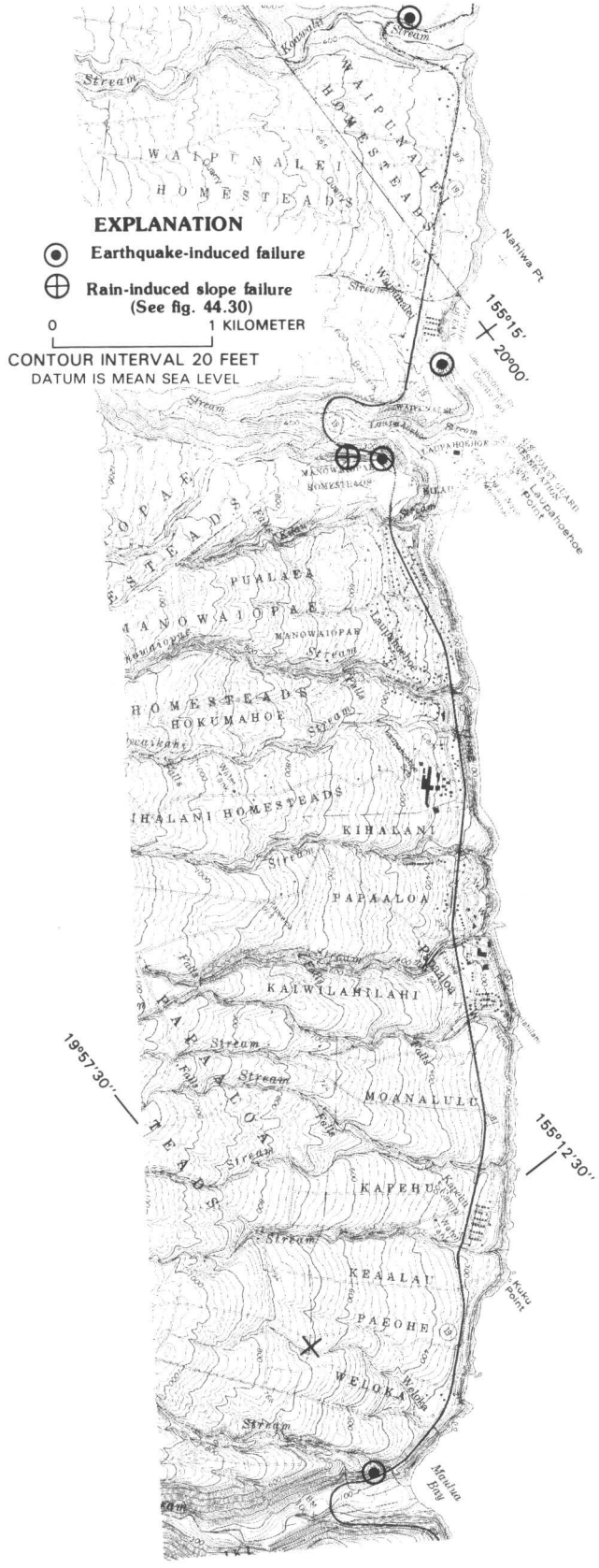

FIGURE 44.29.—Locations of earthquake-induced and subsequent rain-induced slope failures that occurred in North Hilo District between Maulua Bay and Kaawalii Gulch as a result of November 16, 1983, earthquake. Topography from U.S. Geological Survey Keanakolu, Kukaiau, and Papaaloa 7.5-minute quadrangles, 1981, scale 1:24,000.

FIGURE 44.30.—Rain-induced slope failure in Laupahoehoe Gulch a few months after November 1983 earthquake. Heavy rains caused earthquake-loosened material to slide. Material below road was pushed over by bulldozer. Light-colored grassy area above road to right of new slide lacks vegetation and indicates that area has been site of landslides in past. At time of earthquake, a smaller rock slide occurred from the nearly vertical cliff just below the power poles (left), and blocked highway for a few hours. Photograph by N.G. Banks.

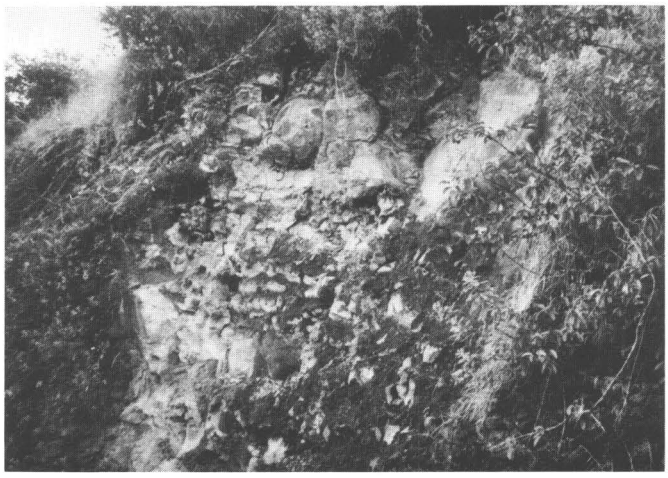

FIGURE 44.31.—Headwall scarp of earthquake-induced rock slide that briefly blocked secondary road to Laupahoehoe Point. It was not possible to picture entire slide in one photograph because of steep cliff bounding road and fact that slide occurred between two curves in road. Lower part of rock slide cannot be seen here; slide was about 1 m deep, 9 m high, and 4 m across (volume about 36 m^3). In-place formation of spheroidal boulders of weathering in Mauna Kea lava flows attests to severity of disintegration of these rocks.

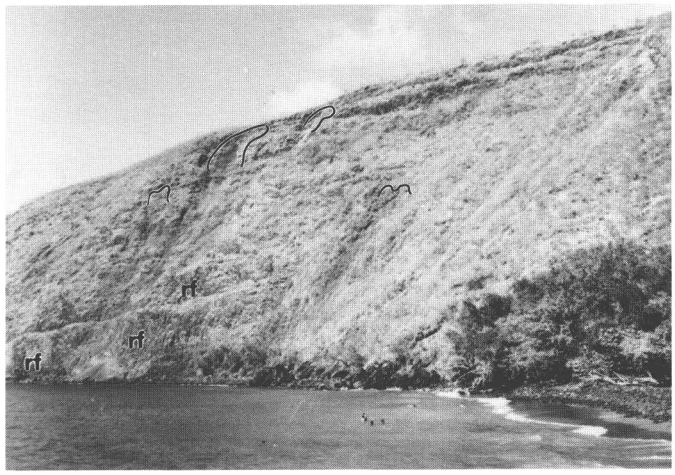

FIGURE 44.32.—Narrow chutes (outlined) formed at time of November 1983 earthquake by landslides from steep slopes surrounding Kealakekua Bay, west coast, Island of Hawaii. Rock falls (rf) occurred on lower, steeper slopes. View northwestward.

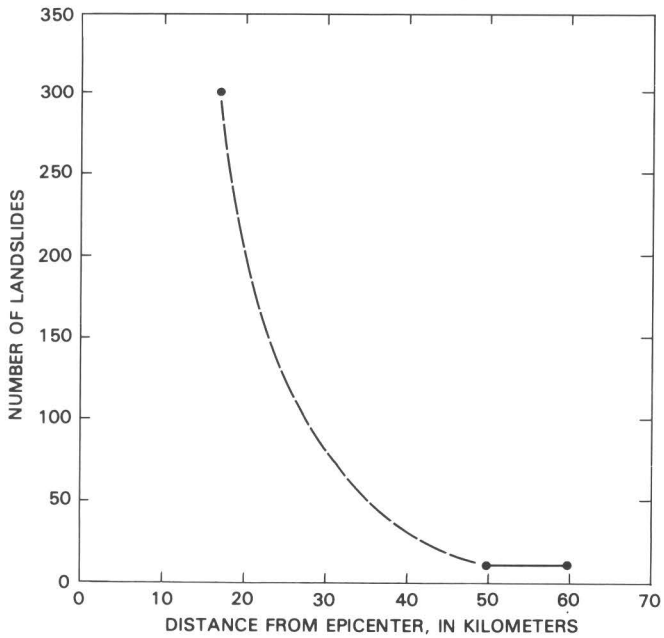

FIGURE 44.33.—Number of landslides caused by November 1983 earthquake in relation to distance from epicenter. Dashed line is estimated interpolation.

TABLE 44.1.—*Selected parameters of damaging earthquakes in Hawaii, 1962–1983*

[Modified from Koyanagi and others, 1984, table 1]

Date	Location	Magnitude	Energy release (10^{12} J)	Maximum intensity (modified Mercalli)	(location)	Damage (millions)	Depth (km)	Focal mechanism
June 27, 1962	Kaoiki	6.1	40	VI	Volcano	$1.0(?)	8	Strike slip
April 26, 1973	Honomu	6.2	60	VII	Hilo, Hamakua	5.6	48	Strike slip
November 30, 1974	Kaoiki	5.5	4	V	Kapapala, Volcano, Hilo	<1	6	Strike slip
November 29, 1975	Kalapana	7.1	2170	VIII	Hilo, Puna, Volcano	4.1	8	Low-angle thrust?
November 16, 1983	Kaoiki	6.6	260	VIII-IX	Volcano, Kapapala, Hilo	7.0(?)	12	Strike slip

TABLE 44.2.—*Intensity and description of damage at various localities on the Island of Hawaii, November 16, 1983, Kaoiki earthquake (magnitude 6.6)*

City, town, village	Intensity (modified Mercalli)	Description of damage
		South Hilo District
Hilo	V-VIII	Extensive damage in downtown area. Minor cracks in roads and water pipes, concrete walls and floors, and plaster. Connecting pipes to an underground gasoline storage tank were ruptured. Most public buildings sustained damage to architectural plaster and acoustic-tile ceilings, and had spalling concrete. The public library also had plate glass windows broken. Hilo Hospital suffered structural damage, roofing, and architectural-plaster damage estimated at $250,000. Apartments and business buildings suffered structural and equipment damage. Numerous plate glass windows broke. Shelved items in markets fell or tumbled over. Homeowners reported losses because of houses and garages shifting from foundations; cracked windows, retaining walls, driveways, and concrete house pads; broken windows; water pipes, and water heater fittings; collapse of rock walls and fences; steps torn away from houses; plumbing damage and septic tank cave-ins; doorways, window frames and cupboard doors distorted; chimneys separated from walls; lightweight furniture and table lamps fell over; loose and hanging objects fell and broke. Several people experienced difficulty standing. A driver described his car trying to wander as if it had a flat tire. Another observer described undulating ground waves with crests and troughs approximately 0.3 m high and 0.5 m across.
Papaikou	VI	Septic tank caved in; shelves fell from framing; objects fell from high shelves; books and mirrors fell; dishes broke; minor cracks to interior walls. One householder reported damage to interior walls, as well as structural damage to house and cracking of concrete slab in carport.
Pepeekeo	VI	Water splashed out of sink.
Honomu	VI	Loose objects fell off shelves and broke; dishes and bottles broke; stone walls opened up.
		Puna District
Hawaiian Paradise Park	V-VII	A few knickknacks tipped or fell; 5 percent of the water in a 75,500-L (20,000-gal) pool was lost through sloshing. There was one report of a destroyed water tank.
Orchidland	IV	Many objects on shelves fell. Nothing broke.
Ainaloa		Cupboard doors opened and dishes toppled out; book shelves fell; two support beams for a deck moved 10 cm off blocks.
Keaau	VI	House rocked; objects on shelves and in cupboards fell over but few broke. Water sloshed out of catchment tank.
Kurtistown	VI	Television, lamp, and statue fell off shelves. Dishes broke and pictures fell off wall.
Mountain View	VI-VIII	One house shifted 2 cm on its foundation piers, pulling away from back wall. A resident reported water pipe to toilet broke and fittings to water heater were damaged and leaking; water sloshed in water tank; cupboard doors opened and contents fell out; dishes and lamps broke; bookcases overturned and books were scattered; furniture was moved; loose objects tumbled off shelves. Hand-stacked rock wall collapsed in some places. A driver traveling at about 50 mph uphill on Highway 11 between Mountain View and Glenwood found it impossible to maintain control of the car. It felt as though the car had several flat tires, and he was forced to stop. He observed two other cars coming downhill whose drivers also stopped and got out to examine their cars.
Glenwood	VII-VIII	Loose objects fell off shelves; items fell from cupboards and freezer; contents of closets spilled; television overturned and books were dumped off bookshelves; large appliances moved, drywall was cracked in some places; stacked lumber was unstacked; full doughboy water tank moved about 5 cm.

Volcano	VI-VIII	Houses and garages were moved off foundations as much as 1 m. Masonry was broken and house frames cracked. Carports were leaning and a few collapsed. Many water tanks were damaged and some collapsed; others were moved as much as 0.5 m and pipes were broken. Three fireplace chimneys at residential homes collapsed. Ground cracks opened about 2 cm; pavement cracks occurred and small soil slips were observed on steep road cuts. Doors of cabinets and refrigerators opened and contents spilled out; dishes broke; objects fell off shelves; cabinets overturned. Chest drawers opened. Books fell from shelves, and furniture moved. A driver travelling northeast on Wright Road felt as if car had flat tire, then it turned at right angle to the road. He saw the ground undulating.
Kau District		
Hawaii Volcanoes National Park	VIII	Substantial ground cracking and ground failures resulted in extensive road damage. On Crater Rim Drive damage was severe at Waldron Ledge, Kilauea Military Camp, the Southwest Rift Zone, Keanakakoi Overlook, and Puu Puai. The main highway was damaged at the entrance to Kilauea Military Camp. Ground cracking also occurred on the Chain of Craters, Ainaho, Hilina Pali, and Mauna Loa Roads. Many hiking trails were damaged by slope failures that removed parts of trails and buried other trails. Some instruments at the Hawaiian Volcano Observatory were temporarily out of order and others were damaged; books were tossed from shelves and bookcases fell over; file cabinets shifted. There was some cracking and minor offsetting of concrete foundation slabs. Dishes and loose objects on shelves fell and broke.
Volcano Golf and Country Club Subdiv.	IX	Many houses and garages were moved off their foundations towards the southwest. Hairline cracks occurred in concrete slabs. People reported difficulty in standing or walking. Water tanks moved across their gravel beds as much as 5 cm, and some of their roofs were knocked off or damaged; water sloshed out of many tanks; water heaters were moved and the PVC lines to the water tanks were snapped. Refrigerator and cupboard contents were dumped on floors; cabinet drawers opened; books and tools were thrown off shelves; televisions were overturned, and bookcases toppled. Lamps and canned goods fell to the floor. Heavier furniture moved.
Old Golf Course Road	VIII	Dishes broke and scattered; books fell off shelves; bookcases overturned; file cases moved; objects thrown out of closet and medicine chest with velocity. An 18,500-L (5,000-gal) water tank that was two-thirds full moved 2.5 cm.
Kapapala Ranch	VII-VIII	Main house moved nearly 17 cm off its foundation toward the southest. Hot water tank torn from pipes and thrown over; partially collapsed rock walls.
Wood Valley	VII-VIII	A few wood-frame houses moved off their foundations; PVC pipes broken and minor cracks in stucco facing; nearly every headstone in the cemetery overturned.
Pahala	VI	In Kau Hospital, bookshelves fell over, ceiling panels dislodged, patients' beds moved as much as 1.5 m, wall clocks dangled by wires and contents of cabinets were displaced. Dishes fell from cupboards and loose objects fell from shelves; pictures and mirrors fell from walls; bookcases, books and shelving fell; tables and floor lamps were broken as well as dishes and an aquarium. Cabinet, refrigerator and freezer doors opened and contents fell out. Appliances and furniture moved as much as 10 cm from original locations and small applicances fell from stands. A few water heaters were knocked over and one was moved about 0.3 m, breaking and connecting pipes. At a store, 75 percent of the merchandise fell from the shelves and was damaged.
Naalehu	V	Table lamps, bookshelves, and knickknacks tipped over and dishes broke; television and microwave oven were moved; water splashed out of fish tank; slight leak in water pipe.

TABLE 44.2.—*Intensity and description of damage at various localities on the Island of Hawaii, November 16, 1983, Kaoiki earthquake (magnitude 6.6)*—Continued

City, town, village	Intensity (modified Mercalli)	Description of damage
		Kau District (continued)
Ka Lae	V	Part of cliff fell into ocean; a large sand hill subsided; rock walls in north-south direction were damaged. One house was moved about 1.5 m off its foundation. North of the highway, a few water pipes were broken; refrigerator doors opened and contents fell out; loose objects on shelves fell; damage to bookshelves, table lamps, and glassware; stone walls were severely damaged.
Ocean View Estates	IV	Cabinets and drawers opened; objects on shelves fell to floor; rocks fell into driveway.
		South Kona District
Honaunau	V	Rocks tumbled from stone walls; houses shook vigorously; loose objects tumbled from shelves and cupboards, and some broke; bookshelves fell over; filing cabinets moved; a few water pipes were broken. Wave action was observed in a pond and a concrete water tank. Water spilled out of toilet tank.
Kealakekua Bay	IV	Landslides from cliff into bay discolored water and caused substantial dust cloud over bay. Rock falls also occurred off slopes into some driveways. Loose objects tumbled from shelves but there was little breakage.
Captain Cook	IV	Lamp, vases, bottles and books fell from shelves.
		South and North Kohala
Hawi, Kapaau, Kamuela	V	Buildings shook, rattling dishes; pictures fell; loose objects fell from shelves; hanging plants swayed.
		Hamakua
Kukuihaele	V	Houses shook and dishes rattled; a few dishes and loose objects fell from shelves; a stone wall cracked. There was one report of house siding splitting and clocks being damaged.
Honokaa	V	Wood-frame buildings shook severely. A few objects fell from shelves; rocks fell from roadcuts.
Paauhau	V	Minor damage to objects on shelves.
Paauilo	V-VI	Some objects fell off shelves, houses shook. Driver on main highway did not feel quake while driving his truck, but noted rock debris on highway.
		North Hilo
Laupahoehoe	VI	Landslides from slopes along the circum-island highway and on the road down to the coastal village blocked roads. Buildings swayed, cupboard doors opened and items fell out; loose objects fell from shelves and broke; items inside cabinets fell over. At the school library, ceiling tiles fell, books fell off shelves and scattered, bookcases were loosened from walls.
Ninole	VI	Report spoke of wierd rumbling noise accompanied by vigorous rolling and shaking; bottles and pictures fell.

TABLE 44.3.—*Data from strong-motion accelerographs for November 16, 1983, Kaoiki earthquake*

[Distance is distance of station from epicenter. Components are: L, longitudinal with instrument; V, vertical; T, transverse to instrument; figures by horizontal components are azimuth directions. Slightly modified from Arnold V. Acosta and Richard P. Maley, USGS, Branch of Engineering Seismology and Geology, unpublished table, 1984]

Station	Latitude, Longitude	Distance (km)	Component	Peak acceleration of gravity	Comments
Volcano Observatory, Hawaii Volcanoes National Park	19.423°N. 155.291°W.	17	360°L up V 270°T	[1]0.67 .21 .39	Greater than 0.1 acceleration of gravity for 8.5 seconds.
Wahaula Maintenance Center, Hawaii Volcanoes National Park	19.329° 155.031°	45	145°L up V 055°T	.12 .07	Long period record. 18 Hz superimposed near beginning.
Fire Station, Pahoa	19.498° 154.951°	53	087°L up V 357°T	.18 .07 .11	
Sewage Plant, Hilo	19.734° 155.050°	54	333°L up V 243°T	.10 .02 .07	
University of Hawaii, Hilo	19.707° 155.083°	49	085°L up V 355°T	.07 .04 .11	Dominant sinusoidal response, about 2.8 Hz horizontal.
U.S. Fish and Wildlife Office, Hilo	19.731° 155.100°	49	360°L up V 270°T	.40 .15 .50	
Fire Station, Honokaa	20.080° 155.465°	72	021°L up V 291°T	.25 .10 .37	Dominant sinusoidal response, about 8 Hz horizontal.
Kahala Police Station, Kapaau	20.230° 155.801°	95	102°L up V 012°T	.07 .05 .09	
Fire Station, Kamuela	20.03° 155.66°	70	155°L up V 065°T	.13 .07 .08	Dominant sinusoidal response, about 7 Hz horizontal.
Mauna Kea State Park, Saddle Road	19.752° 155.530°	36	050°L up V 320°T	.17 .21 .26	
Mauna Loa Observatory, 3,350-m (11,000-ft) elevation, Mauna Loa	19.539° 155.580°	18	030°L up V 300°T	.34 .46 .58	V and T peaks were single simultaneous spikes.
Fire Station, Kailua-Kona	19.649° 155.996°	62	312°L up V 222°T	.04 .01 .03	
Kona Hospital, Kealakekua	19.523° 155.879°	46	346°L up V 256°T	.10 .07 .10	
Kau Baseyard, Waiohinu	19.070° 155.615°	43	065°L up V 335°T	.19 .09 .17	
Kau Hospital, Pahala	19.20° 155.47°	26	188°L up V 098°T	.59 .16 .31	

[1]A high-frequency peak (raw scaling 0.87 acceleration of gravity) was superimposed on the main pulse. This is believed to be other than ground motion.

TABLE 44.4.—*Length and elevation changes recorded by monitoring programs at head of incipient Waldron Ledge landslide, April 1980 to October 1982*

[Positive length changes represent extension, negative ones, shortening; positive elevation changes represent uplift, negative ones subsidence; --, not measured]

Measured item	Original measurement (m)	Measured change (mm)														
		1980							1981					1982		
		[1]Apr. 14	[1]Apr. 21	[3]Apr. 28	[3]Jun. 2	[2]Jul. 3	[2]Aug. 8	[2]Nov. 25	[2]Jan. 5	[2]Mar. 26	Jun. 13	[3]Jun. 27	[2]Jul. 9	[3]Jul. 23	[2]Jul. 26	[2]Oct. 1
Length changes in lines of monitor 1 originally measured April 7, 1980																
Line AB	14.905	0	0	0	0	4	3	3	2	3	[2]14	--	0	--	6	-2
Line AC	15.712	0	-3	-2	2	3	3	5	4	5	[2]-6	--	5	--	12	12
Line AD	15.444	3	0	2	5	7	4	7	9	8	[2]5	--	9	--	22	21
Line AE	3.726	3	5	5	8	10	0	15	16	17	[2]19	--	18	--	55	58
Line EC	14.102	3	-2	2	3	5	3	5	-9	2	[2]-2	--	3	--	-3	-5
Line ED	13.558	3	0	2	2	5	4	4	3	2	[2]0	--	2	--	-2	0
Line EB	13.885	2	-2	2	5	8	3	3	3	2	[2]-1	--	3	--	2	2
Line BC	2.525	2	1	1	4	5	7	8	8	10	[2]9	--	10	--	30	31
Line BD	3.651	2	2	4	5	8	8	12	14	14	[2]16	--	17	--	50	52
Elevation changes, relative to rebar 1, at monitor 1 originally measured November 25, 1980																
Base	0.234	--	--	--	--	--	--	--	0	0	--	--	1	--	-1	--
Nail A	1.854	--	--	--	--	--	--	--	0	1	--	--	1	--	-2	--
Nail B	2.461	--	--	--	--	--	--	--	1	1	--	--	0	--	-2	--
Nail C	2.487	--	--	--	--	--	--	--	0	-2	--	--	-3	--	-17	--
Nail D	2.477	--	--	--	--	--	--	--	-1	-1	--	--	-2	--	-16	--
Nail E	1.949	--	--	--	--	--	--	--	-1	-1	--	--	-2	--	-10	--
Length changes in lines of monitor 2 originally measured April 10, 1981																
Line X'-X																
Hard pull	23.764	--	--	--	--	--	--	--	--	--	[3]6	10	--	6	--	--
Soft pull	23.771	--	--	--	--	--	--	--	--	--	[3]11	11	--	3	--	--
Line Y'-Y																
Hard pull	7.620	--	--	--	--	--	--	--	--	--	[3]5	0	--	11	--	--
Soft pull	7.623	--	--	--	--	--	--	--	--	--	[3]5	11	--	32	--	--
Line Y'-Z																
Hard pull	24.098	--	--	--	--	--	--	--	--	--	[3]14	12	--	52	--	--
Soft pull	24.101	--	--	--	--	--	--	--	--	--	[3]16	14	--	54	--	--

[1]Measurement by J.M. Buchanan-Banks and R.B. Moore.
[2]Measurement by K.M. Yamashita and M.K. Sako.
[3]Measurement by J.M. Buchanan-Banks and N.G. Banks.

ORIGIN OF VOLCANIC TREMOR IN HAWAII

PART I
Data from the Hawaiian Volcano Observatory 1969–1985

By Robert Y. Koyanagi, Bernard Chouet, *and* Keiiti Aki[1]

ABSTRACT

Harmonic tremor characterized by an almost constant frequency pattern throughout the duration of its seismic signal is associated with eruptive activity and magma movement in Hawaii. The signal frequency is believed to vary inversely to the length of the generating source, and amplitude varies according to rate of magma movement under confining pressure. The eruption related tremor reflects high-frequency seismic and acoustic disturbance from lava-fountain activity. The amplitude of eruption tremor oscillates at intervals of a few seconds in a temporal pattern resembling that of intense lava fountaining, in which high bursts repeatedly occur seconds apart. This characteristic pattern may be related to pulsating magma movement driven by continual pressure fluctuations. Added to the eruption zone activity, tremor and long-period events that are localized at the summit vary in intensity according to the magnitude and rate of the associated inflation-deflation episodes. Long-period events and tremor are inferred to share a common origin, and selected long-period events with identifiable onset times are locatable using standard earthquake locating techniques. The locations of long-period events may, in turn, be used to identify the source region of tremor beneath Hawaii and to further define depth-time classifications of tremor.

The clustered hypocentral distribution of long-period events defines a magma transport system originating from a broad 30-km-wide central complex at depths of 30–60 km. This central complex separates laterally and connects discontinuously to smaller cylindrical conduit zones that rise steeply to the summit regions of Kilauea, Mauna Loa, and Loihi. Gaps occur in tremor activity in some regions expected to be passageways for magma along the lateral rift conduit and at depths of 15–30 km in the vertical plumbing system. These gaps may be low-stress regions that allow quasi-steady flow accompanied by pressure pertubations too small to generate measurable tremor in the normally recorded frequencies of 1–10 Hz.

INTRODUCTION

Harmonic tremor, a seismic indicator of magma movement and eruptive activity, has been instrumentally documented at the Hawaiian Volcano Observatory (HVO) since 1912. It is identified on seismograms by a sustained signal that varies within a limited range of frequencies. Its duration is determined by the duration of volcanic eruption or of accelerated magmatic activity within the transport system. At HVO, tremor is classified into three categories of inferred depth on the basis of relative amplitude and areal extent of detection in the seismic network. Tremor is logged in terms of minutes per hour for short episodes and hours per day for longer events. Most of our tremor data is related to activity at Kilauea, since that is where most activity has occurred in the past 20 years and where our network of seismometers is densest. Seismic data collected from such prolonged Kilauea eruptions as the Mauna Ulu sequence in 1969–1974 and the Puu Oo sequence in 1983–1985, and from a significant southwest rift intrusion in August 1981 have provided a comprehensive record of shallow tremor associated with eruptions and intrusions, as well as, tremor associated with the aftermath of eruptive-intrusive activity or during periods of increased magmatic activity within the magma transport system at depth. Tremor near eruptive vents varies in amplitude according to the vigor of eruption. Abrupt changes in tremor amplitude occur simultaneously with changes in lava extrusion rate and fountain intensity, indicating that shallow tremor is dominantly produced at the eruption site. The seismic signal associated with eruption attenuates rapidly with increasing distance from the eruptive vent. Even low-level tremor between major outbreaks often varies in amplitude according to the intensity of lava movement in the vent.

Harmonic tremor that occurred in places or times unrelated to eruptions is presumed to be associated with magma movement at depth. It is commonly localized beneath the Kilauea summit region at crustal depths but spreads to cover a large area beneath the active volcanoes in the south Hawaii region at mantle depths. Episodes of such tremor are often accompanied by increased numbers of long-period events, which have measurable onsets and travel times across the seismic network that fit *P*-wave velocities expected for normal earthquakes. The amplitude and signal duration of the long-period events vary like those of earthquakes, but otherwise their spectra resemble those of tremor in having consistently peaked frequencies

[1]Department of Geological Sciences, University of Southern California, Los Angeles, California 90089-0741.

throughout the coda. Similarity of the distance-attenuation rates for the long-period events and for tremor further implies a common source or origin. If we accept a common origin for long-period events and tremor, then the precise determination of hypocenters for a sufficient number of long-period events accurately constrains the source region for tremor beneath Hawaii. The depth distribution of located long-period events as a function of time provides insight into the dynamic processes involved in the ascent of magma from the mantle through temporary storage and transport in the shallow magma plumbing system to eruptions of lava on the surface.

Koyanagi and others (1976) have shown how swarms of short-period earthquakes outline the upper boundary of the shallow storage system beneath the summit of Kilauea and how a persistent source of long-period events defines the magmatic feeding system below. A region in which few earthquakes occur, located at a depth of 3–6 km, is interpreted to be the storage zone of magma having an expected low rigidity. Since that earlier compilation, expansion of the seismic network and added records of intrusive and eruptive activities have provided more locatable short-period earthquakes and long-period events in the lower magnitude range that occurred episodically during rapid changes in ground tilt at the summit. Thurber (chapter 38), from a study of seismic velocity anomolies using seismic data collected by HVO in recent years, infers a smaller and shallower aseismic zone about 2 km in diameter and located 2–4 km beneath the summit caldera. This zone is surrounded by earthquakes that were relocated using a ray-tracing method in his three-dimensional velocity model. In our recent compilation of data, very small long-period events sometimes accompanied short-period earthquakes during critical stages of inflation before intrusive or eruptive events. More common, however, were those long-period events that followed a significant deflation event; these were shallow events concentrated near the center of deflation.

Swarms of shallow earthquakes and rapid changes in ground tilt during vigorous intrusions of magma are often accompanied by a background of low-amplitude tremor. Upon eruption of lava, the tremor amplitude increases and the frequency of earthquakes decreases. During the eruption, the amplitude of tremor is influenced by lava movement and fountaining at the eruption site and by magma movement within the conduit system near the summit.

Bursts of tremor at intermediate depths beneath Kilauea are occasionally recorded during eruptions, but these usually accompany gradual inflation of the summit. Persistent deep tremor in the mantle beneath south Hawaii has individual episodes that last one-half hour to several hours, and their cumulative reduced displacement as a function of time yields a rate of magma ascent from the mantle (Aki and Koyanagi, 1981). Reduced displacement refers to the source intensity of tremor calculated from seismographically measured ground amplitudes. In our search for the origin of volcanic tremor in Hawaii, we describe its seismic signature in terms of spectral content and amplitude of the ground motion. We consider the spatial and time distribution of tremor in relation to volcanic processes at Kilauea. The source region of tremor and the inferred magma-transport system is outlined from hypocenters of long-period events; the time sequence of these events describes the pattern of magma movement in the transport system. These collections of field observations and instrumental records complement Chouet and others (chapter 45, part II), who discuss the origin of volcanic tremor and outline the evolution of theoretical models. We draw upon those current concepts in organizing our presentation of the data collected at HVO over the past 16 years.

ACKNOWLEDGMENTS

The authors appreciate the helpful reviews of this paper by Thomas Wright and Elliot Endo. Technical support and corroborating scientific information provided by the staff of HVO are gratefully acknowledged. Wil Tanigawa, Jennifer Nakata, and Sandra Zane assisted in the preparation of essential data plots for our figures. Pauline Tamura and Dorothy Footer prepared type drafts of the manuscript. Jim Griggs made photographic reproductions of seismograms used in our figures.

SEISMIC INSTRUMENTATION

The U.S. Geological Survey's Hawaiian Volcano Observatory (HVO) maintains a continuously operating network of 50 seismometer stations on the Island of Hawaii (figure 45.1; table 45.1). The system, designed for microearthquake detection, consists primarily of vertical-component stations with a peak magnification of 10^5 at about 15 Hz (figure 45.2, type 1, based on the Develocorder format). Thirteen are three-component stations with horizontal seismometers of type 1 response, operated at about −12 dB in relation to the vertical component for preferential detection of *S*-waves of local events, or a modified Wood-Anderson response that is flat over a relatively wide range of frequencies for amplitude measurements. With the exception of two stations, signals are continually telemetered to the observatory and recorded on rotating-drum recorders, Develocorder film, and magnetic tape. One station on Maui and one on Oahu provide additional coverage of regional seismicity in the Hawaiian Islands.

The history of HVO seismograph operation was presented in detail by Klein and Koyanagi (1980), and an updated description of station parameters is given by Nakata and others (1984). Information pertaining to the capability and limitations of the HVO seismic net and to the routine processing of data is included in Koyanagi and others (in press).

DATA PROCESSING

In the day-to-day processing of data, seismic events are classified according to their signatures by comparison with an assemblage of seismograms obtained on rotating drum recorders and two 20-channel Develocorders. The variations from station to station of recorded arrival times, amplitudes, and spectral features provide the basic criteria to classify seismic events into different categories. The procedure for routine processing of the standard seismograms obtained at HVO and the characteristic differences in signature used as the basis for general classification were outlined in a preliminary report (Koyanagi, 1982). Computer processing of seismic data and determination of earthquake hypocenters are based

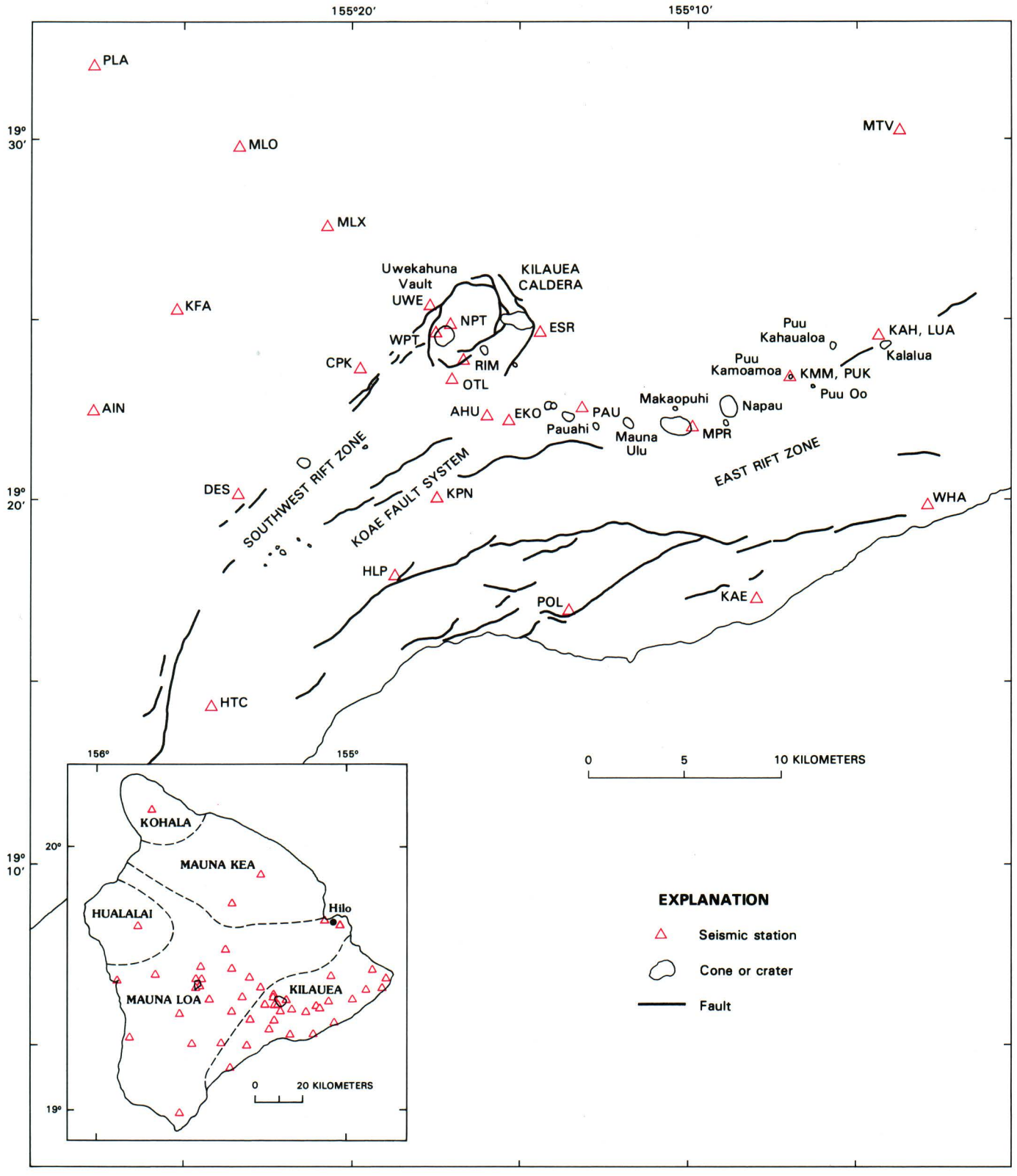

FIGURE 45.1.—Geologic features and seismometer stations in the region around the summit of Kilauea, southeast Hawaii. The seismometer stations are identified by their three-letter codes (see table 45.1). Inset shows all seismometer stations (triangles) operated in 1983 on the Island of Hawaii (Nakata and others, 1984) and the boundaries of the island's five volcanoes.

TABLE 45.1.—*Seismometer stations in Hawaii operated by the U.S. Geological Survey*

[Vertical components are designated by 3-letter codes and horizontal components by 4-letter codes, the last letter of which indicates their orientations, east-west (E) or north-south (N). Operation of stations EKO and WPT was discontinued by 1972. Following minor relocations made due to new lava flows in 1983, station Puu Kamoamoa (PUK) was replaced by Kamoamoa (KMM) and station Kalalua (LUA) was replaced by Kahaualea (KAH)]

Name	Code	Number of Components	North latitude (deg)	(min)	West longitude (deg)	(min)	Elevation (m)
Ahua	AHU,AHUE,AHUN	3	19	22.40	155	15.90	1,070
Ainapo	AIN,AINE,AINN	3	19	22.50	155	27.62	1,524
Captain Cook	CAC	1	19	29.29	155	55.09	323
Cone Peak	CPK	1	19	23.70	155	19.70	1,038
Dandelion	DAN	1	19	21.42	155	40.04	3,003
Desert	DES	1	19	20.20	155	23.30	815
East Koae	[1]EKO	1	19	22.17	155	14.99	1,009
Escape Road	ESR	1	19	24.68	155	14.33	1,177
Hawaiian Beaches	HAB	1	19	31.89	155	53.89	92
Hilo	HIL,HIE,HIN	3	19	43.20	155	5.30	20
Hilina Pali	HLP	1	19	17.96	155	18.63	707
Hale Pohaku	HPU	1	19	46.85	155	27.50	3,396
Humuula Sheep Station	HSS	1	19	36.31	155	29.13	2,445
Hot Caves	HTC	1	19	14.33	155	24.02	361
Hualalai	HUA	1	19	41.25	155	50.32	2,189
Heiheiahulu	HUL,HULE,HULN	3	19	25.13	154	58.72	369
Kaapuna	KAA	1	19	15.98	155	52.28	524
Kaena Point	KAE	1	19	17.35	155	7.95	37
Kahaualea	KAH	1	19	24.58	155	4.36	625
Kaoiki Faults A	KFA	1	19	25.26	155	25.14	1,579
Kaoiki Faults B	KFB	1	19	25.26	155	25.14	1,579
Kahuku	KHU	1	19	14.9	155	37.10	1,939
Kanekii	KII	1	19	30.56	155	45.90	1,841
Keanakolu	KKU	1	19	53.39	155	20.58	1,863
Puu Kaliu	KLU	1	19	27.48	154	55.26	271
Kamoamoa	KMM,KMME,KMMN	3	19	23.47	155	6.98	750
Kohala	KOH,KOHE,KOHN	3	20	7.69	155	46.77	1,166
Kipuka Nene	KPN	1	19	20.10	155	17.40	924
Kapoho	KPO	1	19	30.02	154	50.51	134
Kalalua	[1]LUA	1	19	24.55	155	4.25	622
Mauna Loa	MLO,MLOE,MLON	3	19	29.80	155	23.30	2,010
Mauna Loa X	MLX	1	19	27.60	155	20.70	1,475
Mokuaweoweo	MOK	1	19	29.28	155	35.98	4,104
Makaopuhi	MPR	1	19	22.07	155	9.85	881
Mountain View	MTV	1	19	30.25	155	3.75	409
National Guard	NAG	1	19	42.12	155	1.72	18
North Pit	NPT,NPTE,NPTN	3	19	24.90	155	17.00	1,115
Outlet	OTL	1	19	23.38	155	16.94	1,038
Pauahi	PAU,PAUE,PAUN	3	19	22.62	155	13.10	994
Puu Ulaula	PLA	1	19	32.00	155	27.67	2,992
Pohoiki	POI	1	19	27.42	155	51.22	16
Poliokeawe Pali	POL	1	19	17.02	155	13.47	169
Puu Pili	PPL	1	19	9.50	155	27.87	35
Puu Kamoamoa	PUK	1	19	23.00	155	6.25	704
Rim	RIM	1	19	23.90	155	16.60	1,128
South Point	SPT,SPTE,SPTN	3	18	58.91	155	39.92	244
Southwest Rift	SWR	1	19	27.26	155	36.30	4,048
Trail	TRA	1	19	24.91	155	32.96	3,207
Uwekahuna	UEEE,UENN,UEZ,USEE, USZ	5	19	25.40	155	17.60	1,240
Wahaula	WHA	1	19	19.90	155	2.92	29
Weather Observatory	WOB	1	19	32.31	155	35.01	3,396
West Pit	[1]WPT	1	19	24.70	155	17.50	1,115
Wilkes Camp	WIL	1	19	28.15	155	35.02	4,037
Wood Valley	WOO	1	19	15.08	155	30.12	909

[1]Not currently in operation.

on the program HYPOINVERSE (Klein, 1978). Graphical representations of the seismic data for this manuscript were mainly prepared on the format prescribed in the plotting program QPLOT (Klein, 1983).

Tremor is identified by its continuous signal of sustained amplitude at frequencies within a limited range. Long-period events are discrete signals having an amplitude envelope like that of normal earthquakes but spectral feature like those of tremor. Frequency content and pattern remain relatively unchanged from start to end of their signals. The frequent occurrence of long-period events together with tremor indicates they share a common source. Distinguishable arrival times of long-period events fit the *P*-wave travel pattern of normal earthquakes and so allow their source to be located. The normal earthquakes termed short-period earthquakes to distinguish

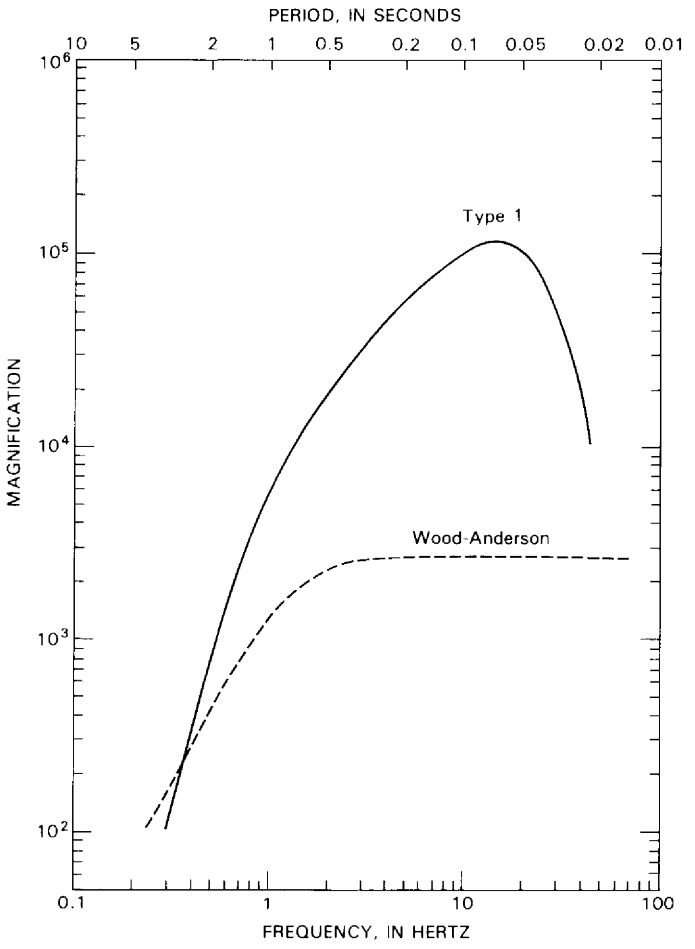

FIGURE 45.2.—Principal system-response curves for short-period seismographs operated by the U.S. Geological Survey in Hawaii. Type 1 curve applies to standard HVO high-gain vertical components on the FM system; Wood-Anderson response applies to the lower-sensitivity horizontal seismometers on 3-component stations. See Nakata and others (1984) for further description of seismic instrumentation and their system-response curves used at HVO.

them from long-period events and tremor have characteristic features, including sharp *P*-wave and *S*-wave onsets and recorded initial frequencies of about 10 Hz that change systematically in time to lower frequencies of less than 1 Hz. Seismograms of the various types of seismic events associated with volcanic activity beneath Kilauea are shown in figure 45.3.

CASE HISTORY 1: THE MAUNA ULU ERUPTION IN 1969

Background information for activity at Mauna Ulu is from Swanson and others (1979), who provide a narrative account of eruptive activity and cursory summaries of seismic activity and ground deformation.

The Mauna Ulu eruption series was preceded by increased frequency of shallow earthquakes in the summit region several weeks before and a subsequent increase in the number of east-rift earthquakes a week before the pre-eruption seismic swarm. The initial outbreak on May 24, 1969, started within hours of earthquake swarms and weak tremor in the east rift and deflation of the summit. Increased harmonic tremor occurred just before the lava outbreak on the east rift. After a two-week repose, activity renewed with high lava output accompanied by high fountains. A pattern of activity featuring short intervals of intense lava emission alternating with long periods of quiescence persisted until the end of the year, producing 12 pronounced episodes of strong eruption. The intense fountaining episodes accompanied by high-amplitude tremor generally lasted less than a day; they were spaced at intervals varying from several days to more than two months. Between the major episodes, low-amplitude tremor was continuous in the area of the active vents. The repeated pattern of eruption and accompanying sequence of tilt and seismic events is summarized in figure 45.4. The nearness of the eruptive vent to the summit made it difficult to distinguish tremor possibly generated from separate sources along the conduit system during major episodes of eruption. Strong eruption tremor dominated at stations near the eruptive vents, as well as at those in the summit region.

Gradual inflation and an increase in shallow earthquakes at the summit preceded the eruptive outbreaks. Shallow tremor at the eruption vent increased in amplitude simultaneously with the increase in lava output and fountaining. Abrupt onsets and endings of these eruptive episodes were accompanied by equally rapid changes in tremor amplitude. Sustained high rates of summit deflation associated with the major eruptive outbreaks were followed by an increase in very small long-period events and harmonic tremor at the summit.

Harmonic tremor sometimes developed into a fluctuating pattern, in which bursts of higher amplitude lasting 5–10 seconds occurred repeatedly and as frequently as several times per minute (figure 45.5). The activity sometimes decayed to a barely detectable level of continuous tremor, and long-period events with higher amplitude and more definable onset times occurred at wide intervals of many minutes (compare with the samples shown in figure 45.14*E–F*).

The areal variation of tremor amplitude is shown in figure 45.6 by 1-min samples of seismograms from temporary stations occupied with a jeep-mounted mobile seismic unit. This survey was made a few hours after a major eruptive episode in order to avoid seismic and acoustic noise from high fountaining and during a time interval when tremor amplitude remained fairly stable so that time difference had minimal effect on station-to-station comparisons. However, the sampling was intended to be soon enough after the eruptive episode to capture the expected stabilizing movement of magma within the conduit system following a major outbreak. The survey was repeated several times after major episodes of lava fountaining. For comparability, the tremor was recorded at the same instrumental gain at each station. Amplitudes read from continuously recording stations near the eruptive vent and in the summit area were used for reference. The comparisons of amplitudes in figures 45.6*A* and 45.6*B* (immediately following and one day after eruptive episode 4, respectively) generally indicate a persistent source at the active vent, and a secondary source at the summit caldera region, which decayed to background after about a day of activity.

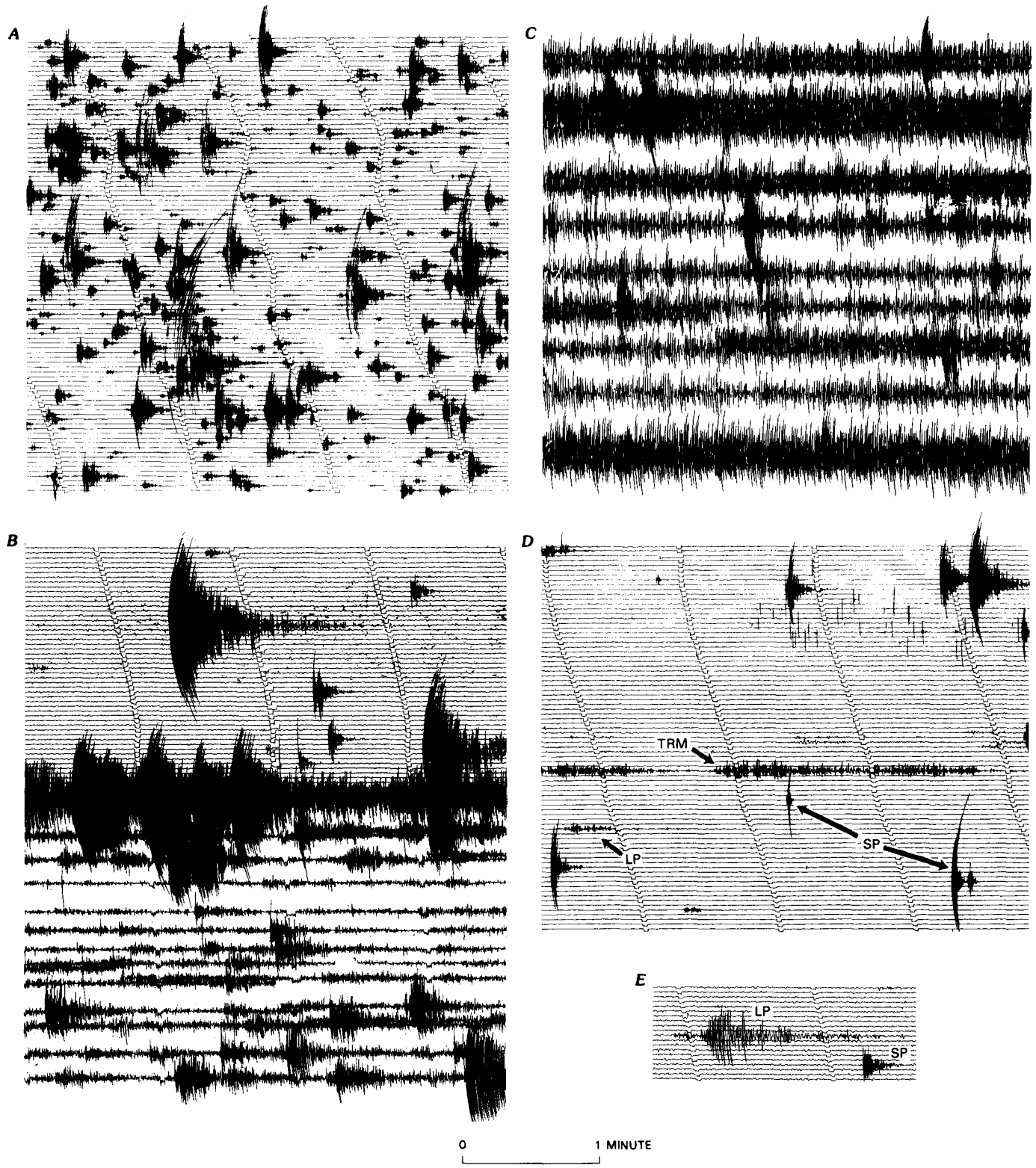

FIGURE 45.3.—Smoked-drum seismograms showing records of earthquakes and volcanic tremor in south Hawaii. ***A***, Swarms of short-period earthquakes. ***B***, Intrusion-related swarms of short-period earthquakes followed by eruption tremor (lower part). ***C***, Continuous harmonic tremor during sustained eruption. ***D***, Short-period earthquakes (SP), long-period event (LP), and intermediate-depth tremor burst (TRM). ***E***, Signatures of a long-period event (LP) and a smaller short-period earthquake (SP).

Between major episodes of lava fountaining, when eruptive activity was limited to varying rates of visible lava movement in the vent (Swanson and others, 1979), the amplitude of harmonic tremor recorded on seismographs within a few km of the vent changed according to the rate of lava movement. An example of time variation in tremor amplitude that correlated with a pattern of lava oscillation in the Mauna Ulu vent is shown in figure 45.7. High and low activity alternated at intervals of a few to many hours.

During other intervals between major outbreaks of lava, low tremor activity showed fairly constant amplitude sustained for many days, or erratic fluctuations with peak amplitudes lasting from less than a minute to many minutes, or cyclic patterns with regular time intervals of amplitude changes. One variety of cyclic oscillation, described as gas piston activity (Swanson, 1971), was defined by tremor of low amplitude for 5–15 minutes during gradual rise of the lava column in the vent, alternating with about one minute of higher amplitude associated with a dramatic collapse of the column and spattering within the vent. The increased seismic signal during collapse of the lava column characteristically has a symmetrical cigar-shaped envelope: amplitude increases gradually, reaches a peak at least several times above the initial background, and finally decreases at a rate comparable to the rate of increase during onset. Signal frequencies at peak amplitudes are 2–5 Hz at a recording distance of about one kilometer from the eruptive vent. The tremor signal is generally local and decreases below background noise a few kilometers from the source vent.

This oscillating pattern of lava and tremor activity, sometimes lasting for many days, was observed again during the Puu Oo eruption. It will be further described in the next section (see figure 45.8*A*).

CASE HISTORY 2: THE PUU OO ERUPTION IN 1983-1985

The pattern of seismicity from mid-1982 to 1985 and continuing reflects the mechanical process within Kilauea Volcano that developed into a major eruptive sequence in the east rift zone (Koyanagi and others, in press). The geologic and geophysical data pertaining to the sequence of rift intrusions, fissure outbreaks, and eruptive episodes from a centralized vent system for this eruption from 1983 to mid-1984 are summarized by Wolfe and others (chapter 17). From September to December 1982, increase of shallow earthquakes in the summit region during periods of inflationary ground tilt, alternating with downrift-migrating swarms of earthquakes in the east rift zone during deflationary periods, indicated that episodic surges of magma were supplying the conduit system in the rift zone. This episodic activity led to a major intrusive event on January 2, 1983: rapid summit deflation and vigorous downrift migration of shallow earthquakes were sustained for 24 hours and finally resulted in a fissure outbreak in the east rift zone. High-frequency tremor accompanied the pre-eruption swarm of earthquakes in the east rift. The sustained deflation at the summit was accompanied by short-period earthquakes, presumably due to fracturing of the host rocks in response to the withdrawal of magma, and harmonic tremor and long-period events associated with the accelerated magmatic activity.

The onset of eruption was accompanied by a marked increase in east-rift tremor, followed by five days of incremental intrusion earthquakes and outbreak of lava farther downrift. The subsequent history of eruptive activity is given in detail by Wolfe and others (in press).

The early weeks of the Puu Oo eruption were characterized by strong tremor with erratic high-frequency signals from a wide source area. As the pattern of eruption changed from fissure outbreaks to multiple-vent eruption and eventually to repeated lava emissions from a single vent system at Puu Oo, weaker and more continuous harmonic tremor originated near the eruptive vent and corresponded in amplitude to the vigor of eruptive activity. Episodes of high lava fountains accompanied by high-amplitude tremor that usually lasted from less than a day to more than a week occurred at intervals of about one to nine weeks. Between major episodes of eruption, the amplitude of the local tremor varied according to the level of the limited lava activity, which was sometimes visible, at depths of 0–50 m in the vent. The patterns of tremor recorded near the active Puu Oo vent between eruptive episodes are illustrated in figure 45.8. As in the Mauna Ulu eruption, bursts of moderate-amplitude tremor lasting about one minute occurred repeatedly during periods of low-amplitude background tremor lasting 5–15 minutes that characterized gas piston activity (figure 45.8*A*). More sustained episodes consisting of increased amplitude lasting about one-half to nearly one hour alternating with low amplitude lasting about three hours were observed during a repose period in February 1985 (figure 45.8*B*). Seismicity associated with microfracturing caused by structurally and thermally induced adjustments at the vent and under new lava flows is also recorded in figure 45.8. Major episodes of high fountains and lava output were accompanied by increased tremor, whose amplitude exceeded by more than an order of magnitude the continuous background tremor during intervals of subdued eruptive activity. The rapid response of seismic amplitude to changes in lava fountaining and output rate imply that the principal source of tremor is shallow and localized at the eruption site.

Convincing evidence of a deeper tremor source beneath the summit of Kilauea, separated from activity in the eruption region, was the tremor recorded at the North Pit (NPT) station (see table 45.1 for list of stations) following sustained high rates of deflationary tilt at the summit. This relationship of tremor that varied in amplitude and duration according to the rate and magnitude of the deflationary tilt was observed fairly consistently for the successive episodes of the Puu Oo eruption from 1983 to mid-1984, and a reduction of the data indicating this relation is documented by Koyanagi and others (in press). These episodes of summit tremor that accompanied major episodes of the eruption were frequently preceded by increasing rates and amplitudes of discrete long-period events, which peaked into continuous tremor and then decayed gradually back to background, with bursts of long-period events at progressively lower amplitude and wider intervals of time (figure 45.9).

In contrast to both the summit storage zone and the east-rift eruption site, the rift conduit connecting them remained virtually free of detectable harmonic tremor during the repeated major episodes of

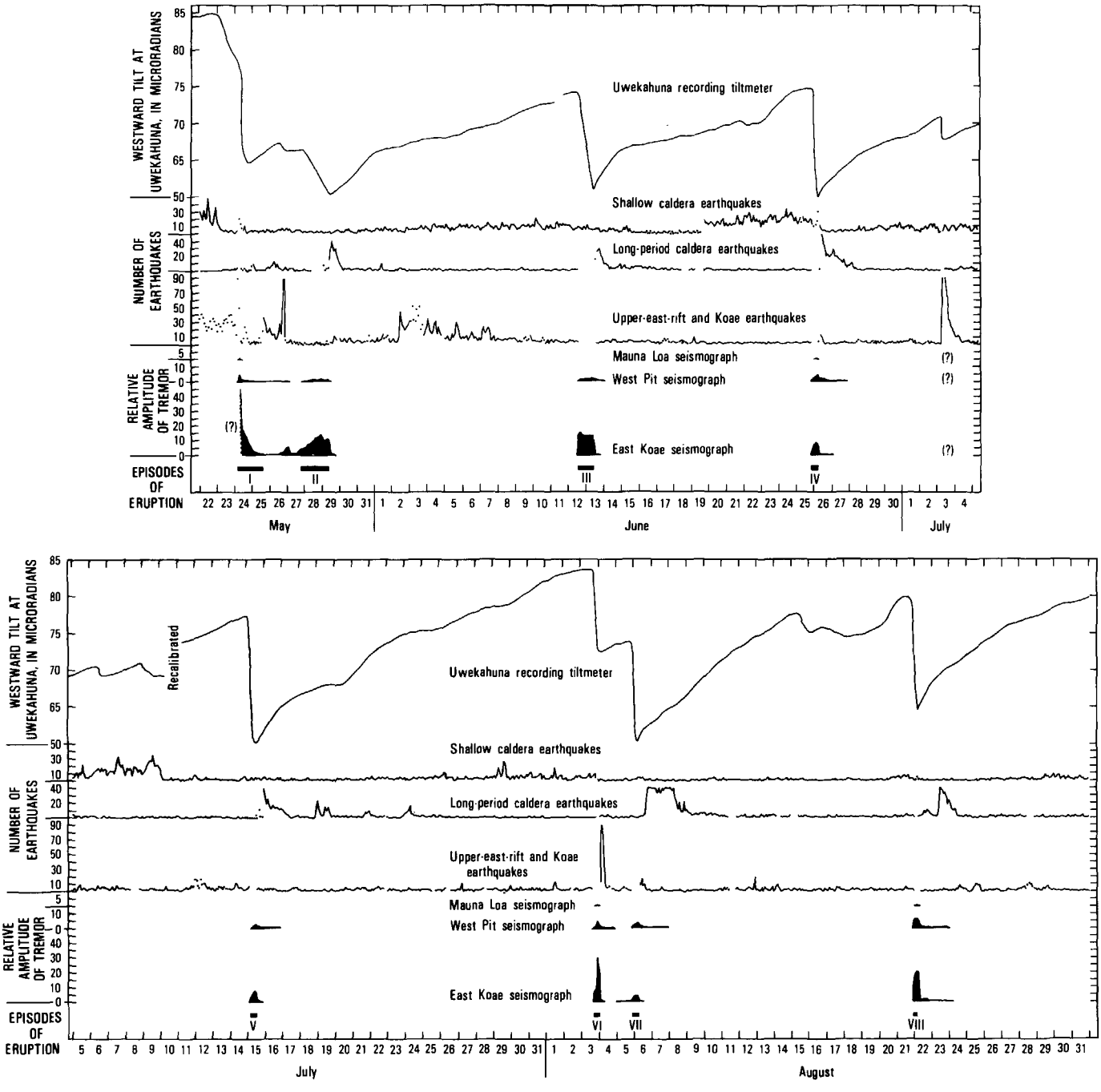

FIGURE 45.4.—Plot of summit tilt, numbers of shallow earthquakes, relative amplitude of tremor, and episodes of eruption for the Mauna Ulu eruption of Kilauea Volcano, May–October 1969. Tilt measurements at 2-hour intervals from the Uwekahuna east-west component tiltmeter near the northwest rim of Kilauea caldera. Earthquake counts at 2-hour intervals from selected local stations, detection threshold estimated at about magnitude 0.1. Amplitude of tremor taken from adjusted hourly readings of smoked-paper records and plotted in relative units above background noise at three stations: Mauna Loa (MLO), 25 km from the eruption site; West Pit (WPT), 11 km from the eruption site; and East Koae (EKO), 5 km from the eruption site. Times of major eruptive episodes indicated by horizontal bars and labeled with their sequence numbers. Data beyond October incomplete and therefore omitted.

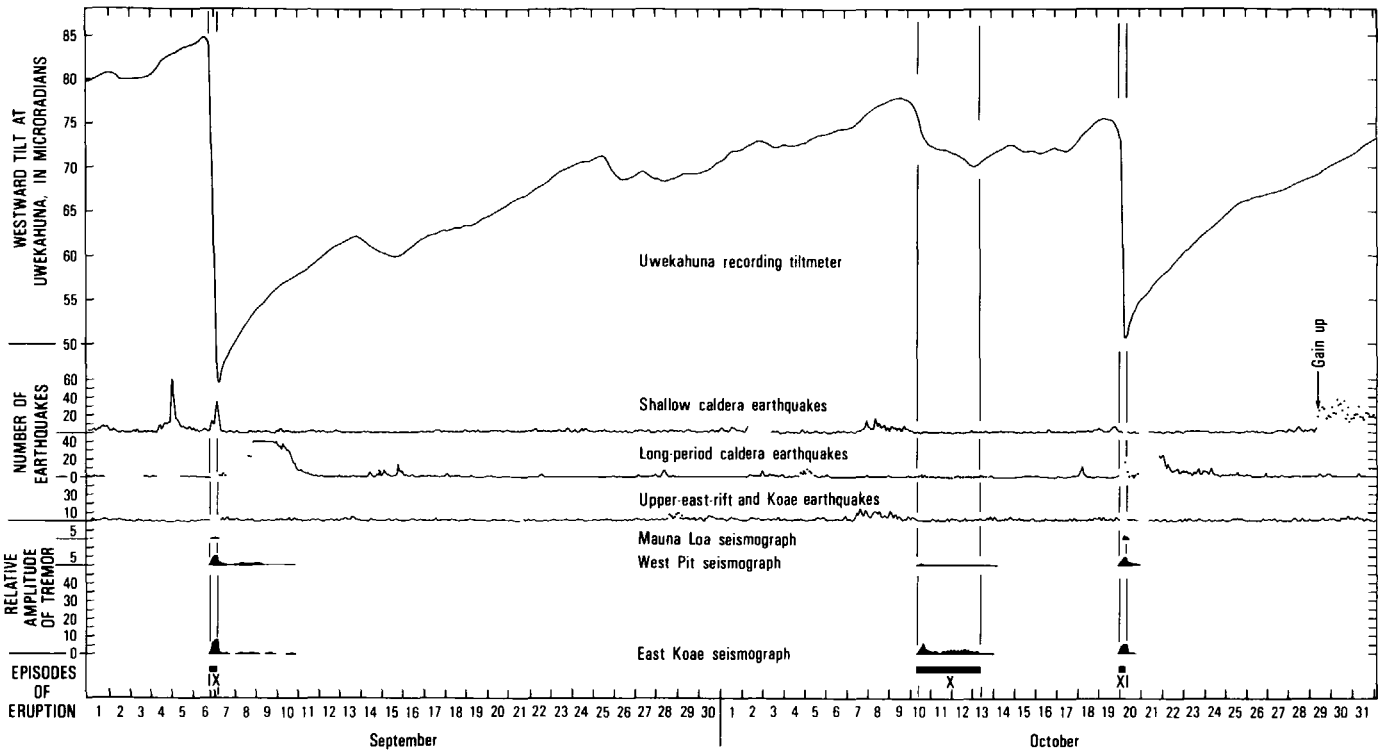

FIGURE 45.4.—Continued.

eruption. From this we infer an absence of barriers in the central part of the lateral conduit system, allowing quasi-steady flow of magma with minimal pressure fluctuations.

A chronological sequence of lava production, increased harmonic tremor in the east rift zone and summit, and ground tilting is outlined in figure 45.10 for one of the vigorous eruptive episodes in the prolonged east rift eruption.

Ground tilt showing rapid deflation during the twenty-fifth eruptive episode in September 1984 (figure 45.10) was measured as the east-west component on a continuously recording tiltmeter located at Uwekahuna vault northwest of the summit deformation center. Deflationary tilt started gradually at about 1400 (H.s.t.) on September 19 and accelerated in rate at 1700. It continued at a high rate until 0600 on September 20 and then gradually declined, ending by about 0900. The deflationary tilt during these 19 hours totaled 15 microradians, and it reached a maximum rate of 1.35 μrad per hour at about 2000 on September 19 (R. Hanatani, written commun.)

Peak-to-peak amplitude of harmonic tremor was measured on Develocorder seismograms from station MPR for east-rift tremor and from station NPT for summit tremor. Ground oscillation in micrometers was reduced from the amplitude measurements averaged for about one minute at each hour and adjusted for instrumental magnification at the recorded frequency and for station corrections. The average period of the east-rift tremor signal recorded at MPR was about 0.5 s, and that of the summit tremor recorded at NPT was about 0.3 s. Station MPR, situated about 6 km west of the eruptive vent, recorded rapid increase and decrease of east-rift tremor at the onset and end of the eruptive episode, with a temporary decrease in the middle. The hourly sampling rate used in figure 45.10 omitted a strong burst of tremor between 1622 and 1633 during the early activity, as well as the exact times of rapid changes at the onset and end of the vigorous fountaining episode. Continuous-record seismograms indicate that east-rift tremor started to increase in amplitude at about 1530 on September 19. The amplitude increased rapidly from about 1600, reached peaks of 0.4 ± 0.2 micrometers at about 2300 and 0400 (September 20), and remained variably high until 0532. A rapid decrease accompanied the end of sustained high fountaining at 0532. As is typical of later episodes in prolonged eruptions, there were no precursory swarms of intrusion-related microearthquakes. This may be because the repeated outbreaks created a hydraulically connected magma conduit system free of barriers and affected only by episodic adjustments in the fluid pressure.

Summit tremor and the accompanying long-period events started to increase rapidly at about 2100 on September 19, peaked to about 0.3 micrometers of ground amplitude at 0700 on September 20, and gradually decreased with increasing numbers of distinctive long-period events. Summit tremor decreased to nearly background level by the end of September 21. Summit tremor and summit tilt, both of which are assumed to be measures of magma movement, did not always correlate in their pattern of amplitude

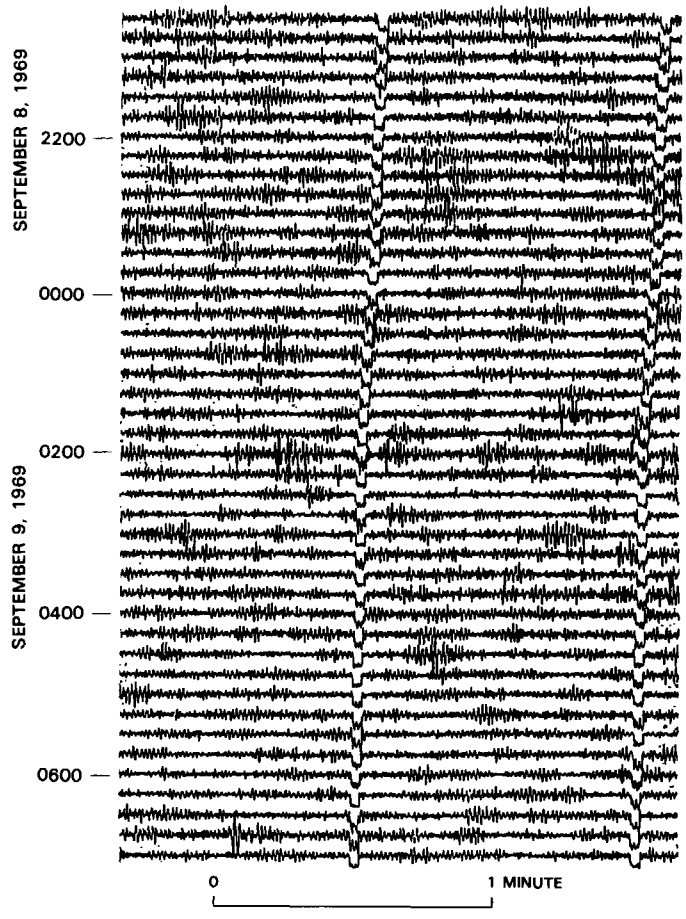

FIGURE 45.5.—Portion of a smoked-drum seismogram from the West Pit station (WPT) in the summit caldera of Kilauea showing local long-period events and weak harmonic tremor. These events were recorded about 1.5 days after episode XI of the Mauna Ulu eruption during a post-deflation period of rapid reinflation of the summit.

changes; the increase, peak, and decay patterns of tremor amplitude generally lagged behind changes in tilt rate by several hours to many hours.

Field observations and time-lapse photographs documented the increased eruption activity that started at about 1604 on September 19. The activity peaked with a fountain height of nearly 500 m and lava extrusion rates estimated at 8×10^5 m^3/h, and ended at about 0532 on September 20. Subsequent measurements of the area and thicknesses of the flows produced indicate an approximate total volume of 11×10^6 m^3 of lava was extruded from, this eruptive episode that lasted 13.5 hours (G. Ulrich, oral commun.).

Tremor associated with high fountaining during vigorous eruption on September 19–20 was high in amplitude near the eruptive vent; its amplitude and dominant frequencies varied at intervals of several seconds. The short-term pattern of amplitude repeatedly changing by nearly half an order of magnitude and frequencies varying from about 2 to 5 Hz was partly influenced by the peaked response of the instrumental system, which increasingly amplified the high frequencies. Otherwise, however, the tremor pattern resembles the oscillating pattern of lava fountaining, in which bursts of high fountain repeatedly occur seconds apart. Summit tremor that accompanies sustained deflation produces a signature with comparable amplitude and spectral features.

Normalized power spectra of tremor recorded during a major episode of the Puu Oo eruption on August 20, 1984, are shown in figure 45.11*A–C* for a station located 1.25 km from the active vent. These spectra were derived from seismograms recorded with a three-component digital seismograph using 1.0-Hz geophones. The results were obtained by computing the spectra for 20-second windows of data and averaging the results of all windows. The spectra are characterized by a series of dominant and subdominant frequencies that vary among the three components of ground motion. As these data were obtained during heavy fountaining activity, they represent the contribution of fountain noise in addition to the excitation of the magmatic conduit.

CASE HISTORY 3: THE AUGUST 1981 SOUTHWEST-RIFT INTRUSION

On August 10–12, 1981, an intrusion occurred on the southwest rift of Kilauea (Klein and others, chapter 43; Nakata and others, 1982). It was identified by summit-to-rift migration of shallow earthquakes, summit deflation, and rift dilation (A.T. Okamura, oral commun.); increased CO_2 gas emission (L.P. Greenland, oral commun.); and geo-electrical anomalies (D.B. Jackson, oral commun.). The intrusion is a significant one in terms of the volume of magma transferred from the summit to the southwest rift, as inferred from the 107 μrad of deflationary ground tilt measured at Uwekahuna station on the northwest rim of the summit caldera.

The progression of seismic events, initiated by an increased number of short-period earthquakes in the summit region, developed into an earthquake swarm and tremor that migrated into the southwest rift zone, followed by long-period events that culminated in continuous harmonic tremor at the summit. This sequence is

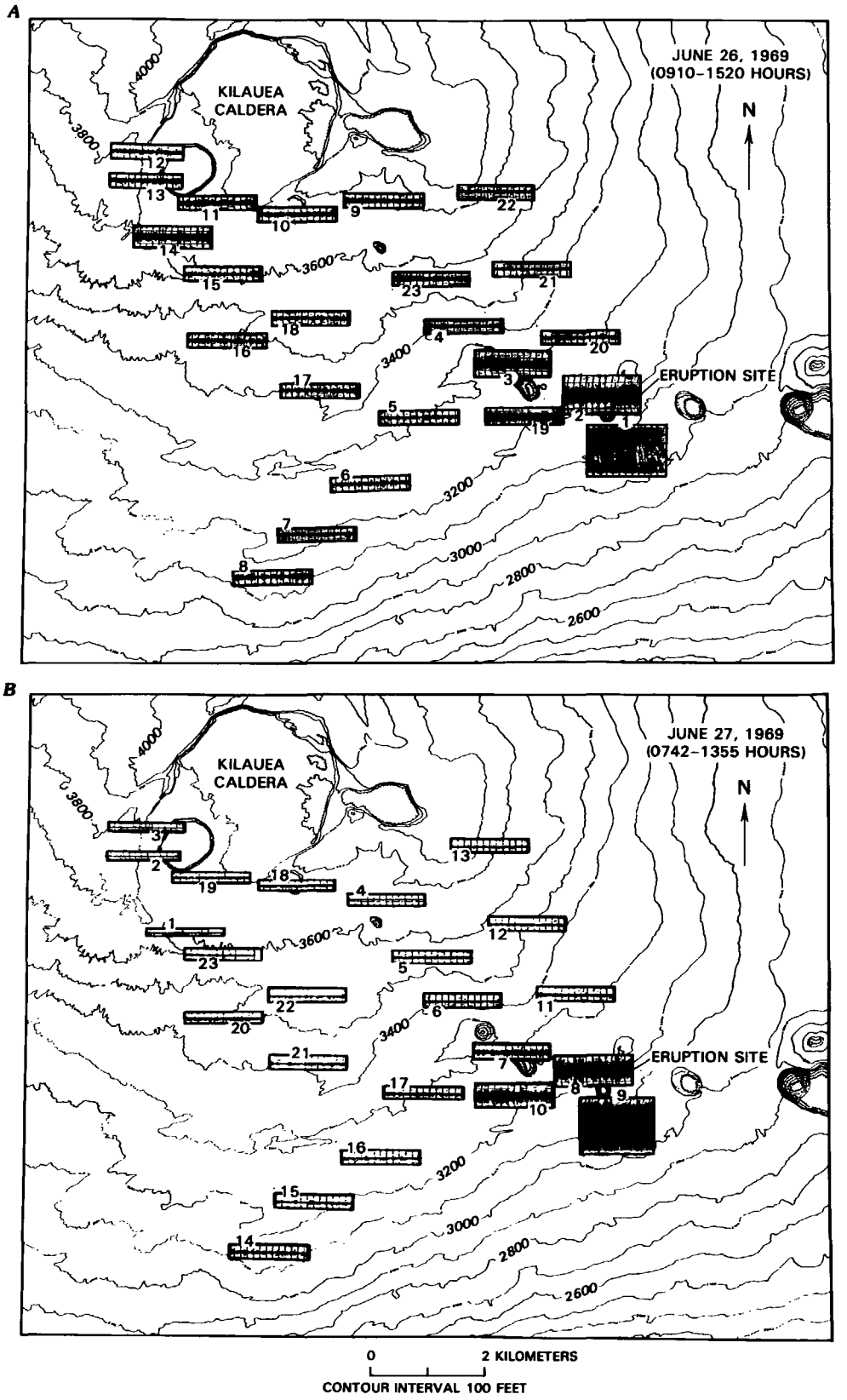

FIGURE 45.6.—Harmonic tremor recorded by portable seismograph following eruptive episode IV of the Mauna Ulu eruption. The numbers indicate the order in which each site was monitored. All seismogram segments are one minute long. ***A***, Immediately after the eruptive episode. Note the moderate-amplitude tremor at the summit stations 11 and 14. ***B***, One day after the eruption. Note that tremor in the summit area (stations 1 and 19 here) has decreased to background noise.

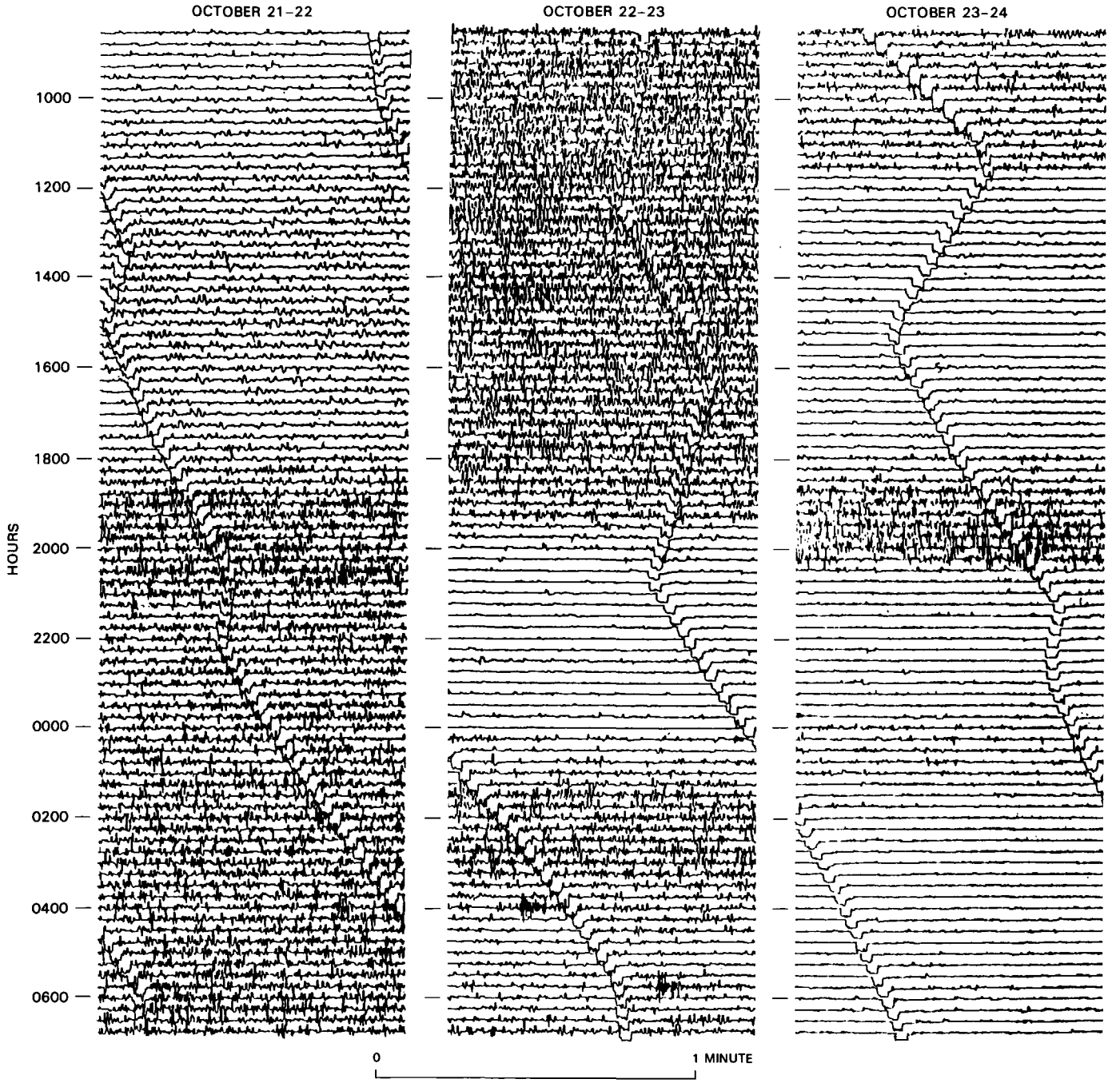

FIGURE 45.7.—Portions of a smoked-paper seismogram from a station (EKO) on the upper east rift zone of Kilauea, 4.5 km from the eruptive vent, that monitored varying amplitudes of low tremor associated with confined lava movement following a major episode of the Mauna Ulu eruption in October 1969. Recording speed and instrumental magnification were kept constant over the entire interval of time.

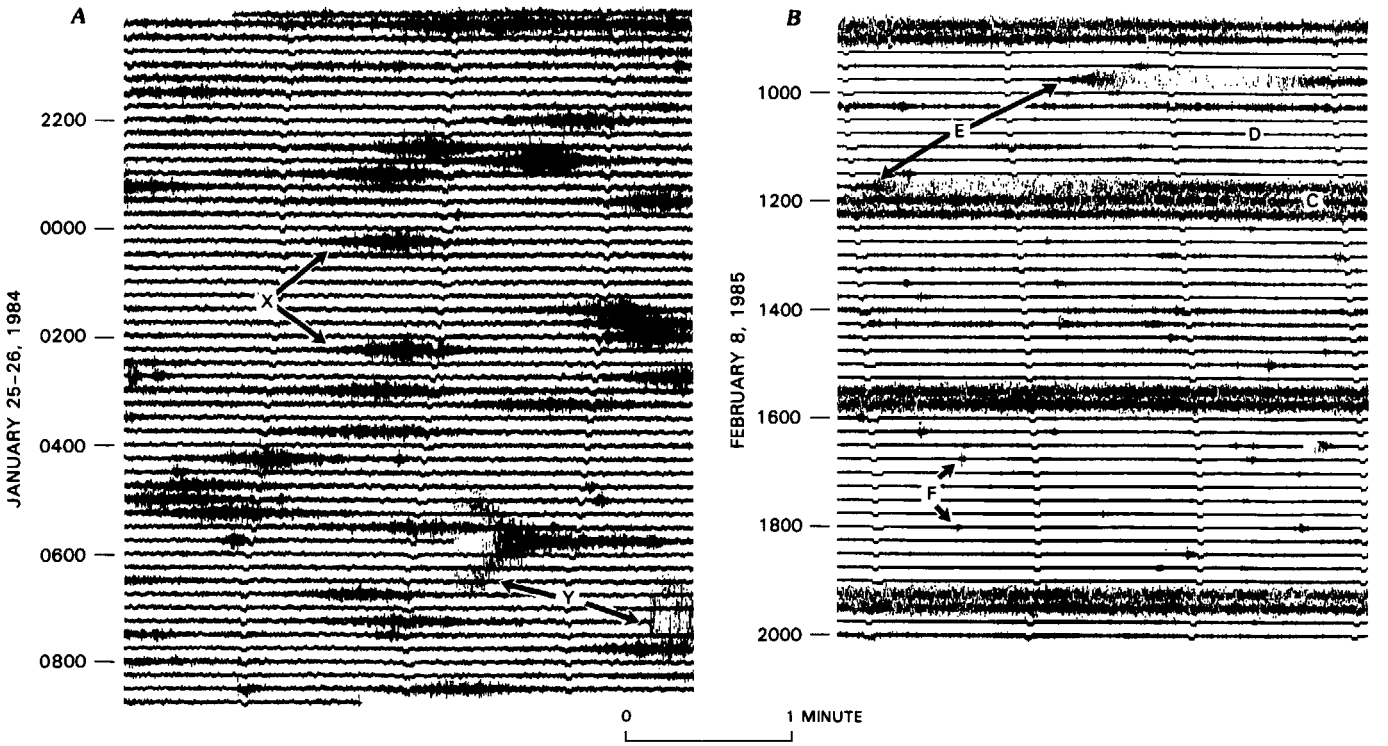

FIGURE 45.8.—Portions of seismograms from revolving-drum recorders at stations on Kilauea Volcano showing various seismic events. ***A***, Record from station PUK, about 1 km west of the eruptive vent Puu Oo showing gas-piston events (X) and south flank earthquakes (Y). ***B***, Record from station KMM showing a cyclic pattern of low tremor at the eruptive vent between the major episodes on February 4 and March 13, 1985, of the Kilauea east-rift eruption. Episodes of high tremor (C) less than an hour in duration repeatedly alternated with several hours of lower amplitude (D) during February 7–11, 1985. Two cigar-shaped events (E) recorded at 0946 and 1145 were signals characteristic of cyclic lava movement, termed gas-piston activity, in the vent. Numerous microshocks (F) associated with thermal contraction cracking on the adjacent new lava flows, degassing explosions, and continual structural adjustments at the vent were conspicuous during times of low-background tremor. Other varieties of repose tremor during the prolonged eruption at Puu Oo are described by Wolfe and others (in press).

clearly seen in the series of smoked-paper seismograms that recorded the changes in seismicity (see figure 45.12).

The high rate of inflationary tilt and frequency of summit earthquakes were interrupted on August 10 by a rapid collapse and simultaneous increase of earthquakes and tremor that propagated into the southwest rift zone. With the onset of deflation and the apparent relaxation of the summit, the number of inflation-related caldera earthquakes decreased. A pattern of southwest-rift inflation complemented the summit deflation and migrating swarm of shallow earthquakes to further indicate summit-to-rift transfer of magmatic pressure. Near the end of the two days of summit collapse and during the early reinflation period starting August 12, a swarm of long-period events was recorded at the summit stations (figure 45.13). These events increased in size until August 14 and then became smaller again. As the number of long-period events decreased, continuous tremor gradually increased and peaked in amplitude on August 15. Subsequently, from August 16 to about August 20, the amplitude of tremor gradually decayed below detection level.

A variety of seismic events were identified on seismograms according to arrival-time patterns, wave frequencies, and amplitude envelopes during the August intrusion (figure 45.14*A–F*). Shallow rift tremor was locally recorded with a broadly variable range of high frequencies, in contrast to intermediate-depth summit tremor, which retained a narrower band of lower frequencies. Rockfalls along the crater walls resulting from the increased instability caused by summit collapse generated strong local high-frequency seismic signals, which rapidly decreased with increasing epicentral distance; at distant stations these events had signatures dominated by low-frequency surface waves. Long-period events had signatures varying from nearly monochromatic, with sharp peaks in frequencies and very gradual beginnings comparable to tremor (figure 45.14*D*), to a wider band of frequencies that sometimes showed sharper onsets (figure 45.14*E–F*). The patterns of amplitude attenuation with distance for long-period events and for the concurrent tremor were similar, indicating a common source region (figure 45.15). Long-period events recorded by arrival times that could be matched for about ten or more stations were read and processed by the same location procedure used for normal earthquakes, from which reasonably accurate locations were obtained. Such long-period events are used in a later section of this chapter to determine the spatial distribution of harmonic tremor sources in Hawaii.

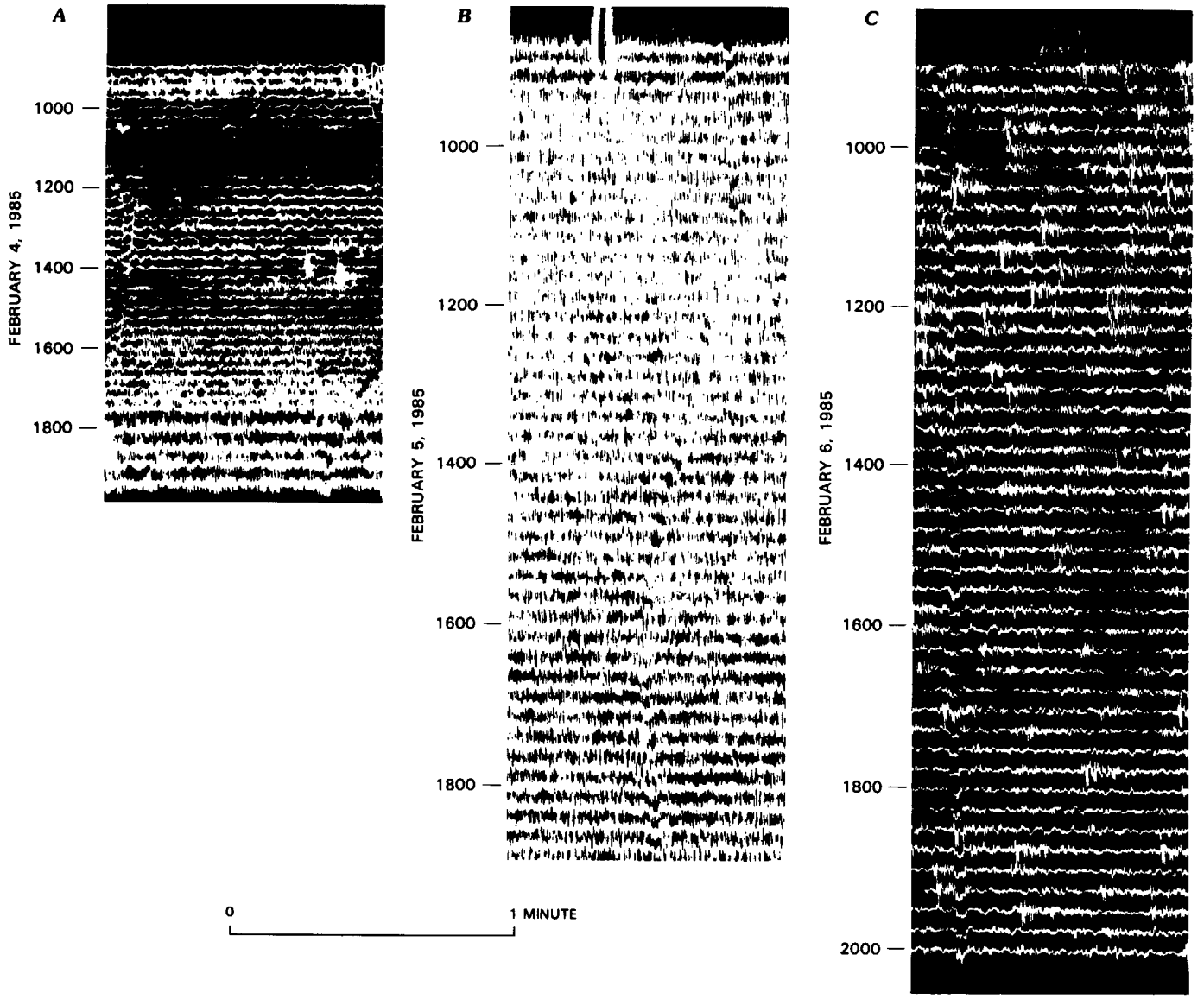

FIGURE 45.9.—Sections of smoked-paper seismograms from station NPT showing the sequence of harmonic tremor and long-period events at the summit following episode 30 of the east-rift eruption on February 4–6, 1985. Recording speed and instrumental magnification were kept constant over the entire time interval. ***A***, Period from 0900 to 1800 on February 4, 1985, shows increasing level of summit tremor from about 1600; the drum rotation interval was subsequently doubled to increase the spacing between seismic traces. ***B***, Period from 0900 to 1900 on February 5, near the peak of activity, shows continuous high tremor. ***C***, The final stage of the activity from 0900 to 2000 on February 6 shows an increased number of discrete long-period events in a decreasing background of continuous tremor. Occasionally, stronger long-period events were recorded widely on the summit network of stations.

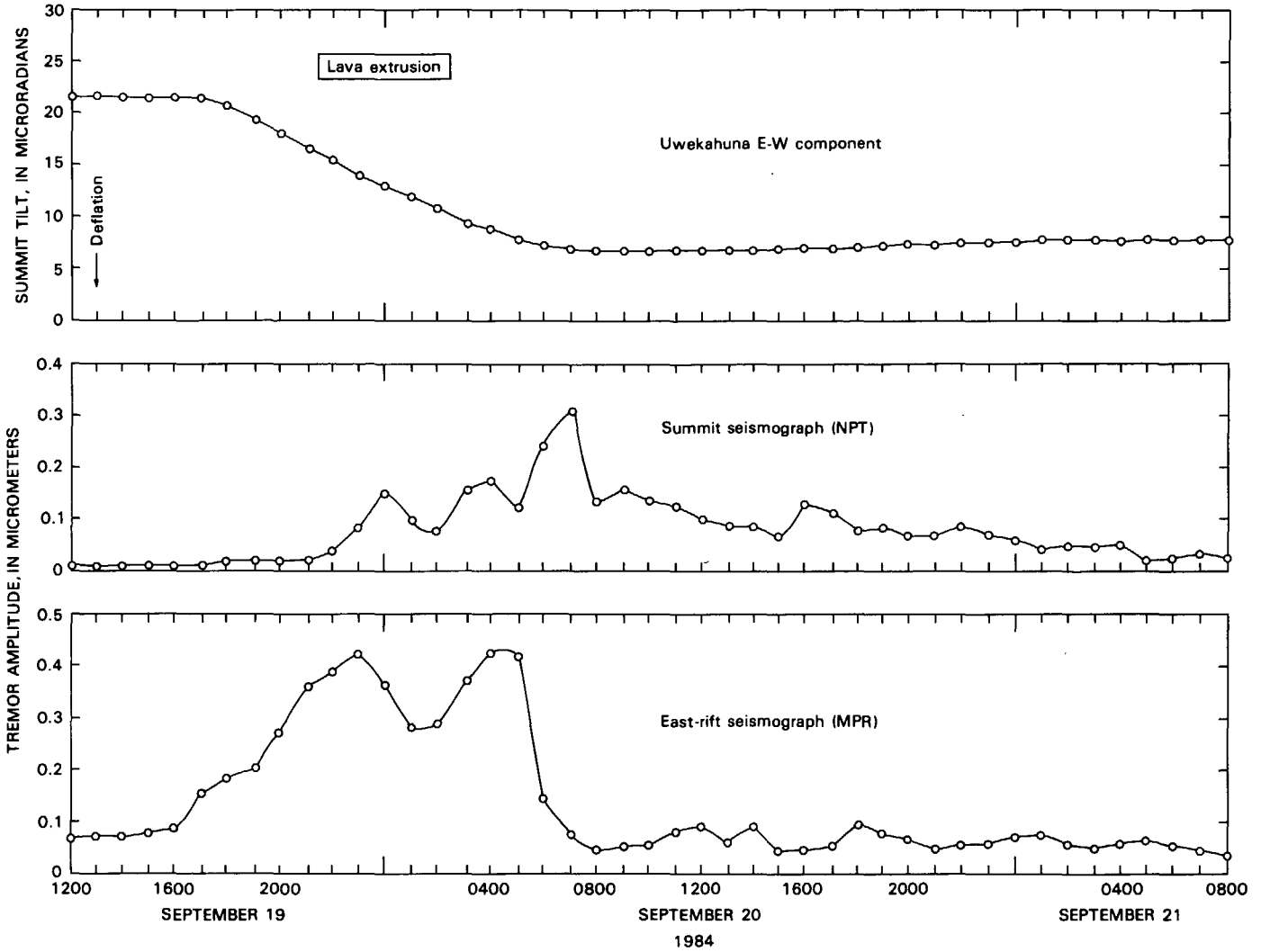

FIGURE 45.10.—Changes in tilt and tremor amplitude during and after episode 25 of the prolonged Kilauea east-rift eruption characterized by high lava production and fountaining. Tremor amplitudes are approximate averages, ±0.2 micrometers. Curves between hourly readings were interpolated.

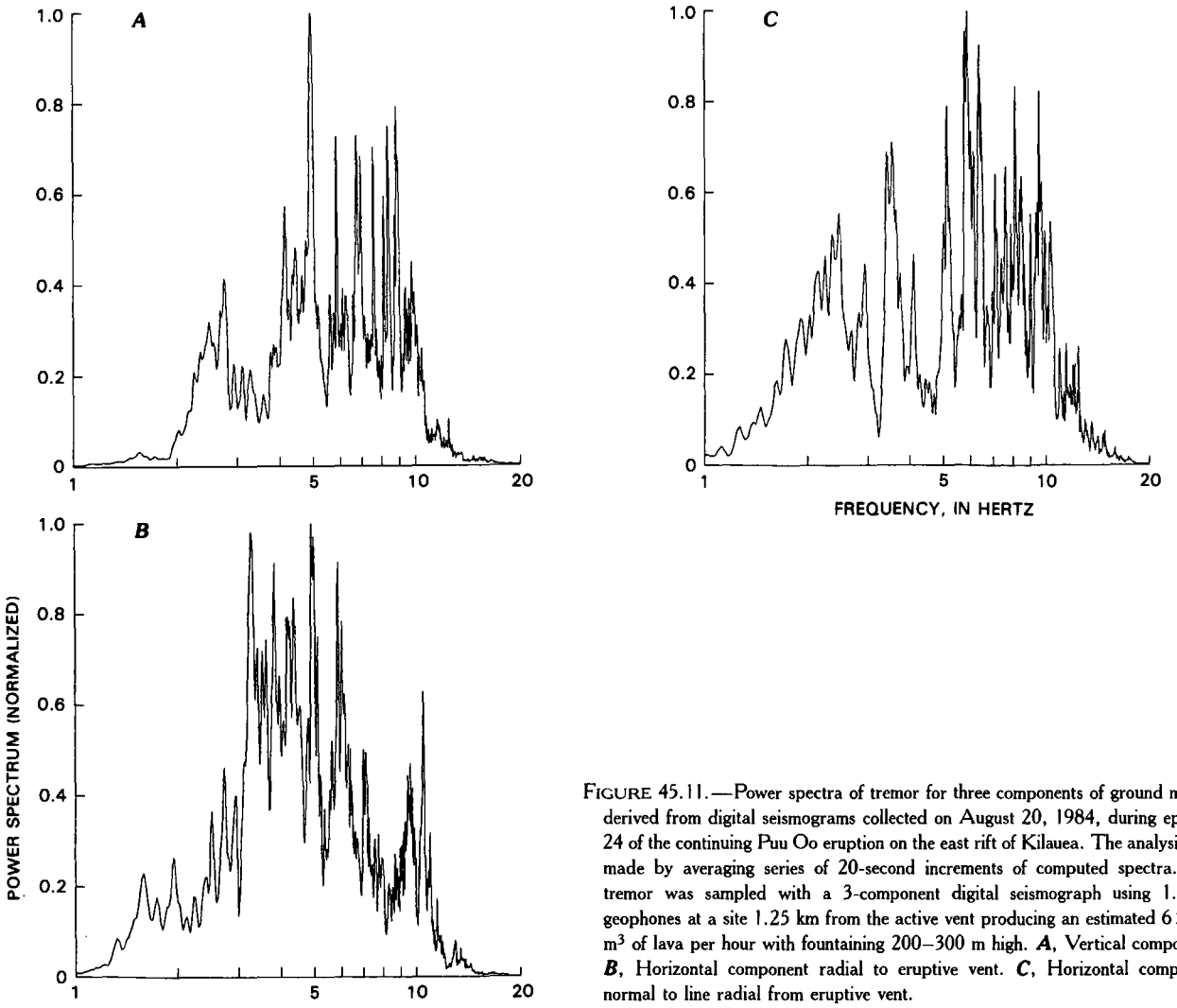

FIGURE 45.11.—Power spectra of tremor for three components of ground motion derived from digital seismograms collected on August 20, 1984, during episode 24 of the continuing Puu Oo eruption on the east rift of Kilauea. The analysis was made by averaging series of 20-second increments of computed spectra. The tremor was sampled with a 3-component digital seismograph using 1.0-Hz geophones at a site 1.25 km from the active vent producing an estimated 6×10^5 m^3 of lava per hour with fountaining 200–300 m high. ***A***, Vertical component. ***B***, Horizontal component radial to eruptive vent. ***C***, Horizontal component normal to line radial from eruptive vent.

FIGURE 45.12.—Seismograms from smoked-drum seismographs showing the sequence of seismic events accompanying the August 1981 magma intrusion in the southwest rift zone of Kilauea. Unless otherwise indicated, recording speed and instrumental magnification were constant over this interval of time. Time advances right and down in all seismograms. ***A***, August 9–10. Left seismogram shows the background of high microearthquake activity preceding the seismic swarm at the onset of magmatic activity as recorded from station AHU in the south summit area. Right seismogram shows the continuing harmonic tremor and microearthquakes recorded at a lowered sensitivity during the peak of the intrusive event at the summit caldera station NPT. ***B***, August 13–14. Left seismogram shows a flurry of long-period earthquakes that followed the moderate collapse of the summit in the late stage of the intrusion as recorded at station NPT. Right seismogram shows the decreasing level of continuing microearthquake activity in the intruded part of the southwest rift zone as recorded by the nearby station DES. ***C***, August 15–19. Left seismogram shows harmonic tremor presumably due to magmatic movement during the adjustment process in the summit storage complex, following a major deflation as recorded locally at the summit station NPT on August 15–16. Right seismogram shows the gradual decay of harmonic tremor as the vigor of magmatic activity subsides at the summit, August 18–19, and occasional tectonic earthquakes as the volcano's south flank responds to the rift dilation.

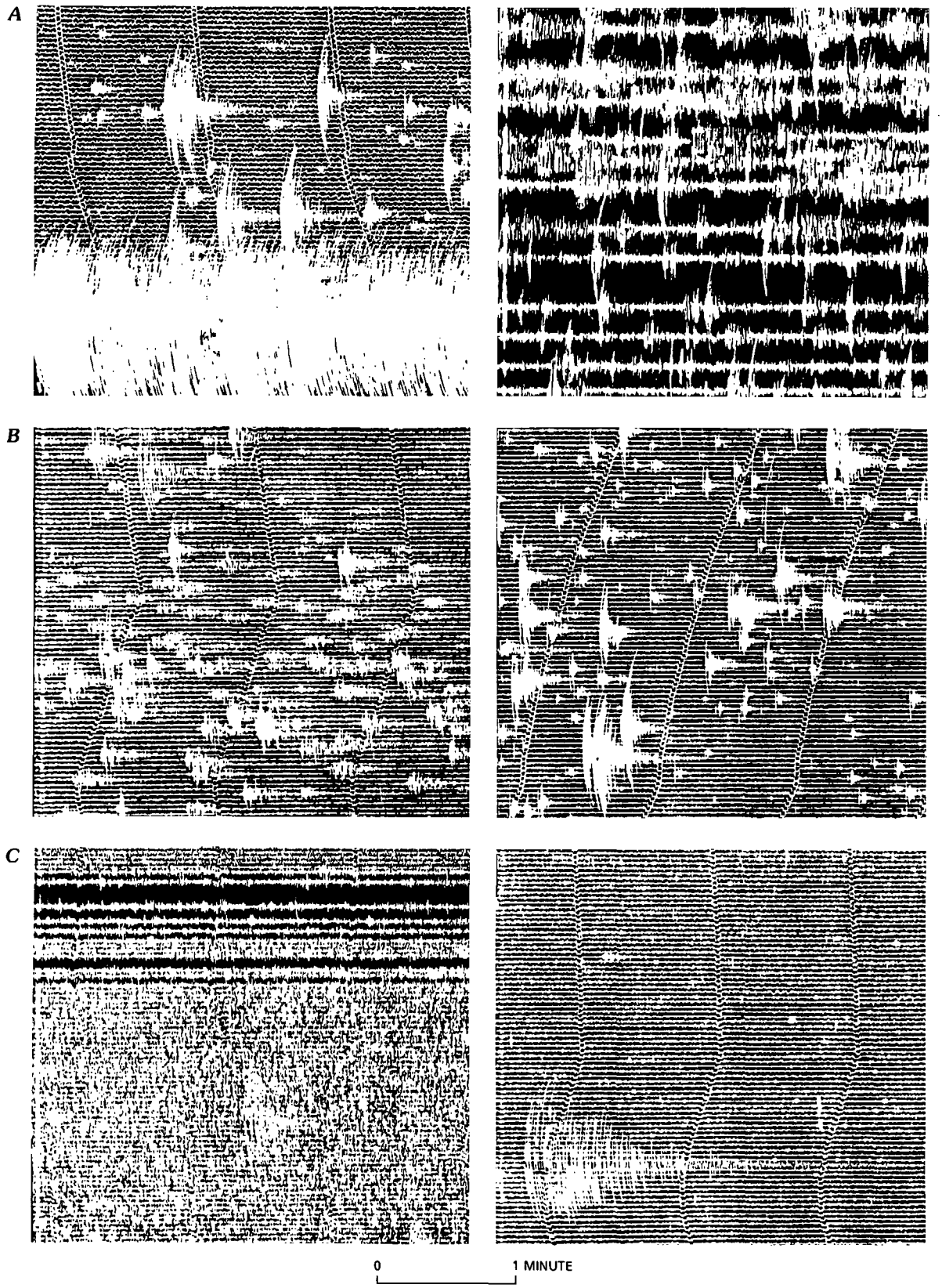
A
B
C
0
1 MINUTE

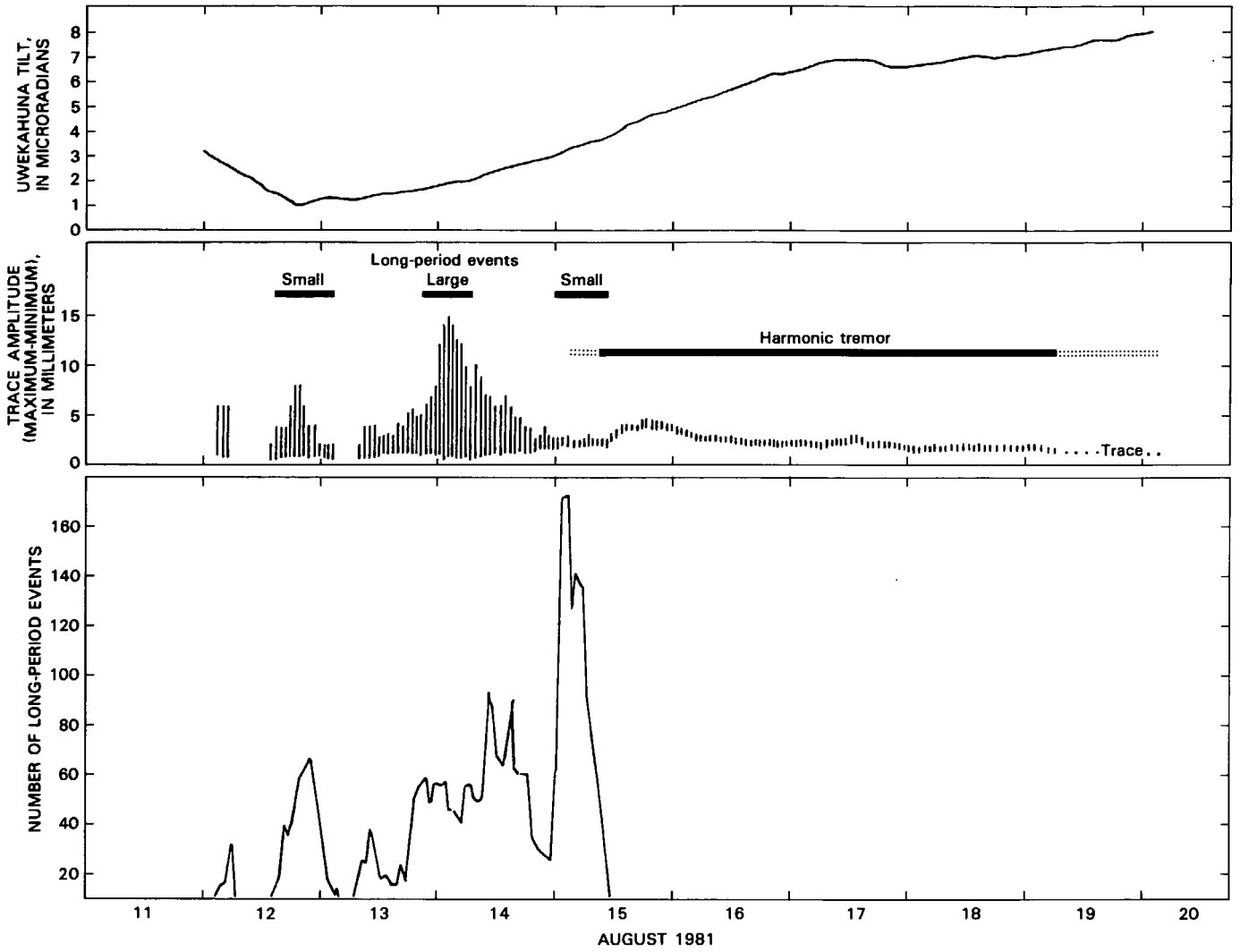

FIGURE 45.13.—Ground tilt, long-period earthquakes, and tremor plotted hourly following and during the later part of the August 1981 intrusion in the east rift zone of Kilauea. In the upper plot, the east-west component of tilt at Uwekahuna indicates reversal and reinflation of the summit following a major collapse. In the middle plot, vertical lines represent the hourly maximum-to-minimum amplitude range from tremor and long-period events read on station NPT at standard gain using Develocorder seismograms magnified 20 times. A wide maximum-minimum range implies large long-period events in a low background of tremor, whereas a narrow range and high minimum amplitude indicate high harmonic tremor with no discernible long-period events. The lower plot shows the hourly number of long-period events (>10 events per hour) recorded at station NPT.

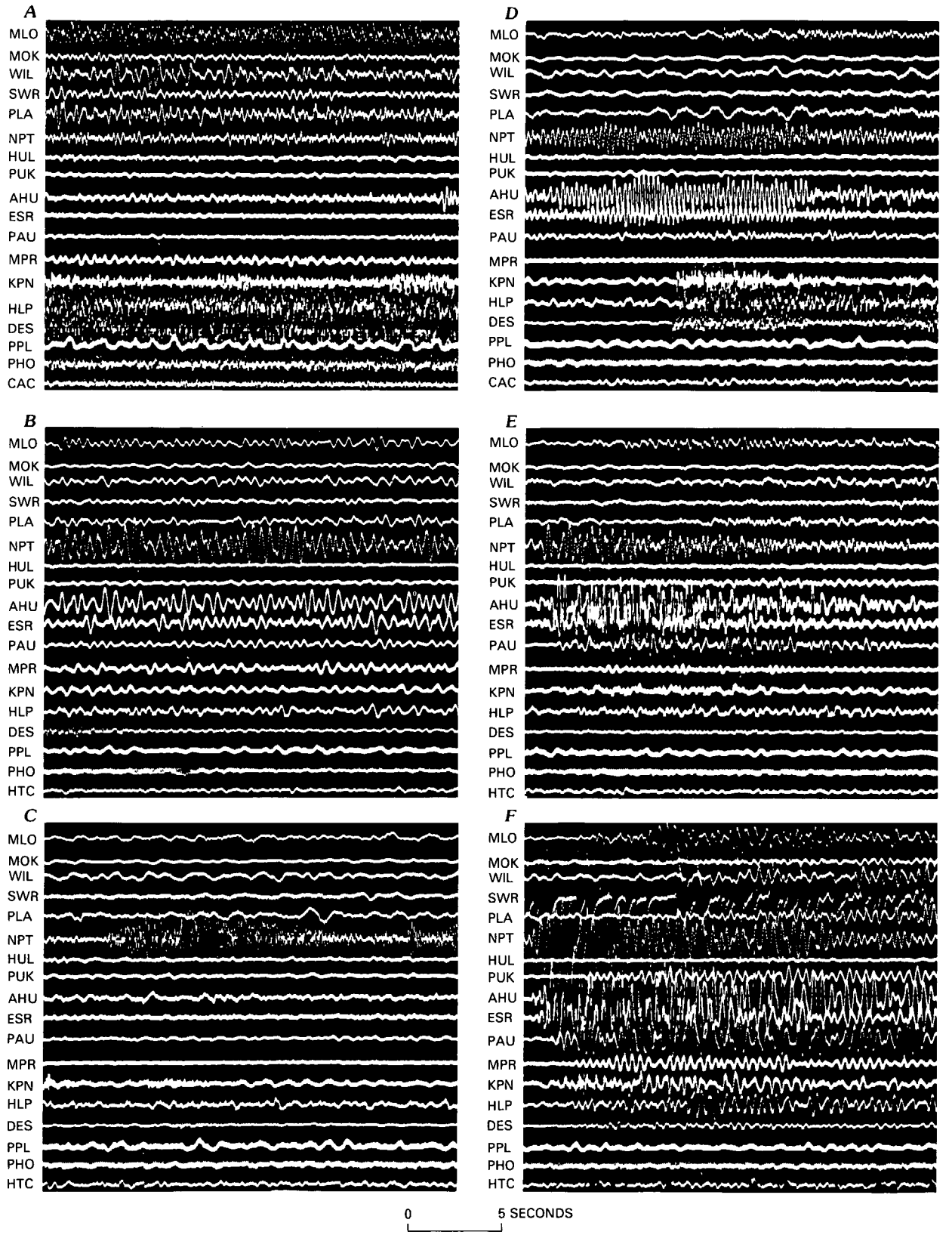

FIGURE 45.14.—Seismograms showing signatures of common events recorded during the August 1981 intrusion on Kilauea's southwest rift zone. ***A***, High-frequency tremor on stations DES and HLP, August 10. ***B***, Intermediate-depth tremor, strong on station NPT and weak on stations AHU, MLO, and ESR, August 15. ***C***, Rockfall on station NPT, August 13. ***D***, Uniform-frequency long-period event on stations NPT, AHU, and ESR and deeper short-period southwest-rift earthquake on stations KPN, HLP, and DES, August 12. ***E***, Long-period event on stations NPT, AHU, ESR, and PAU, August 13. ***F***, Long-period event strong on stations NPT, AHU, ESR, and PAU, August 13.

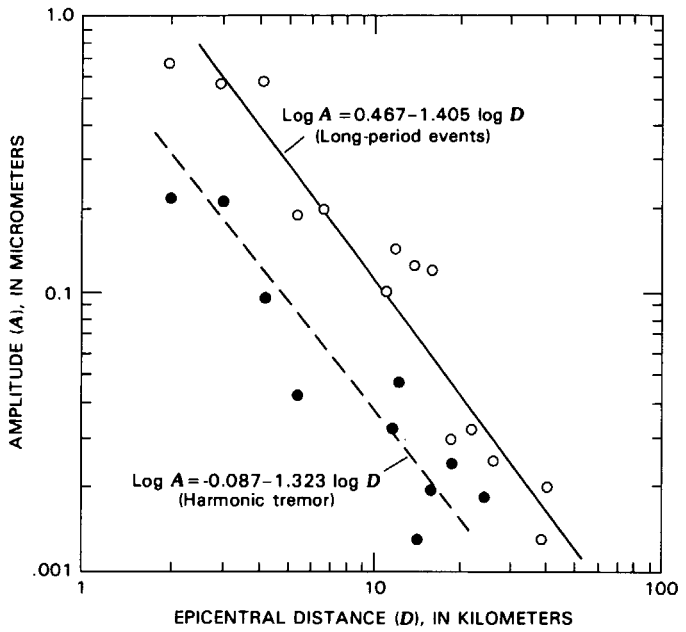

FIGURE 45.15.—Log-log plot of amplitude against epicentral distance for harmonic tremor (dots) and a 4-km-deep long-period earthquake (circles) on Kilauea. Trace amplitudes read at corresponding times at various stations from the summit to 40 km away were reduced to actual ground movement compensated for instrumental magnification at the dominant frequency of the seismic waves. Equations and straight lines are from linear least-squares regression.

The locatable long-period events were concentrated beneath the summit deflation epicenter for the August 1981 event (figure 45.16). This region is notably free of normal short-period earthquakes and has been interpreted to be a shallow storage zone for magma (Koyanagi and others, 1976).

The proportionality of amplitude and signal duration that exists for normal short-period earthquakes also applies generally to long-period events. This provides a means to estimate energy radiation from the long-period events on the basis of their magnitude. Magnitude is calculated for each event by signal duration and amplitude measurements applied in the earthquake-location program HYPOINVERSE (Klein, 1978), and temporal and spatial variation of the size of long-period events may then be examined. Because of the normally elongate signals for long-period events, magnitude determined by duration appear to be generally higher than magnitude determined by amplitude, when calibrated to normal earthquake magnitudes. The narrow range of magnitude and the relative lack of linearity in the magnitude-frequency distribution, to be further discussed later, suggest their source parameters differ from those of normal earthquakes. The long-period events of the August activity processed for locations were limited to a narrow range of magnitude (0.6–1.7), with the largest ones generally occurring during the peak of activity on August 13–14 (figure 45.17).

In a depth-time graph, focal depths of long-period events were persistent at 2–6 km for most of the duration of high activity on August 12–13 (figure 45.18). Depths expanded to a wider range of approximately 1–8 km during the peak of activity in the late hours of August 12 and early hours of August 13.

CASE HISTORY 4: INTERMITTENT BURSTS OF INTERMEDIATE-DEPTH TREMOR

Intermediate-depth tremor at Kilauea usually occurred in series of short bursts, each a few minutes long, that lasted for a few days to several weeks. It was generally dominated by long-period events, sometimes with measurable onsets, whose signals were best registered on stations within a few tens of kilometers of the summit (figure 45.19). These events sometimes accompanied shallow tremor following deflation at the summit, but more commonly they occurred during periods of inflation not associated with intrusion or eruption.

Locatable long-period events at intermediate depths (7–12 km) beneath the summit region of Kilauea increased in February and

FIGURE 45.16.—Long-period events of August 13–15, 1981, at the summit caldera of Kilauea following the August 1981 intrusion. Crosses designate hypocenters at depths of 0–4.9 km; squares designate those at depths of 5.0 km or deeper. ***A***, Map showing epicenters. The summit caldera, pit craters, and faults are also shown. W–E and N–S are reference centerlines for the following vertical sections *B* and *C*. ***B***, Hypocenters projected onto a vertical west-east section within 3 km on either side of line W–E. ***C***, Hypocenters projected onto a vertical north-south section within 3 km on either side of line N–S.

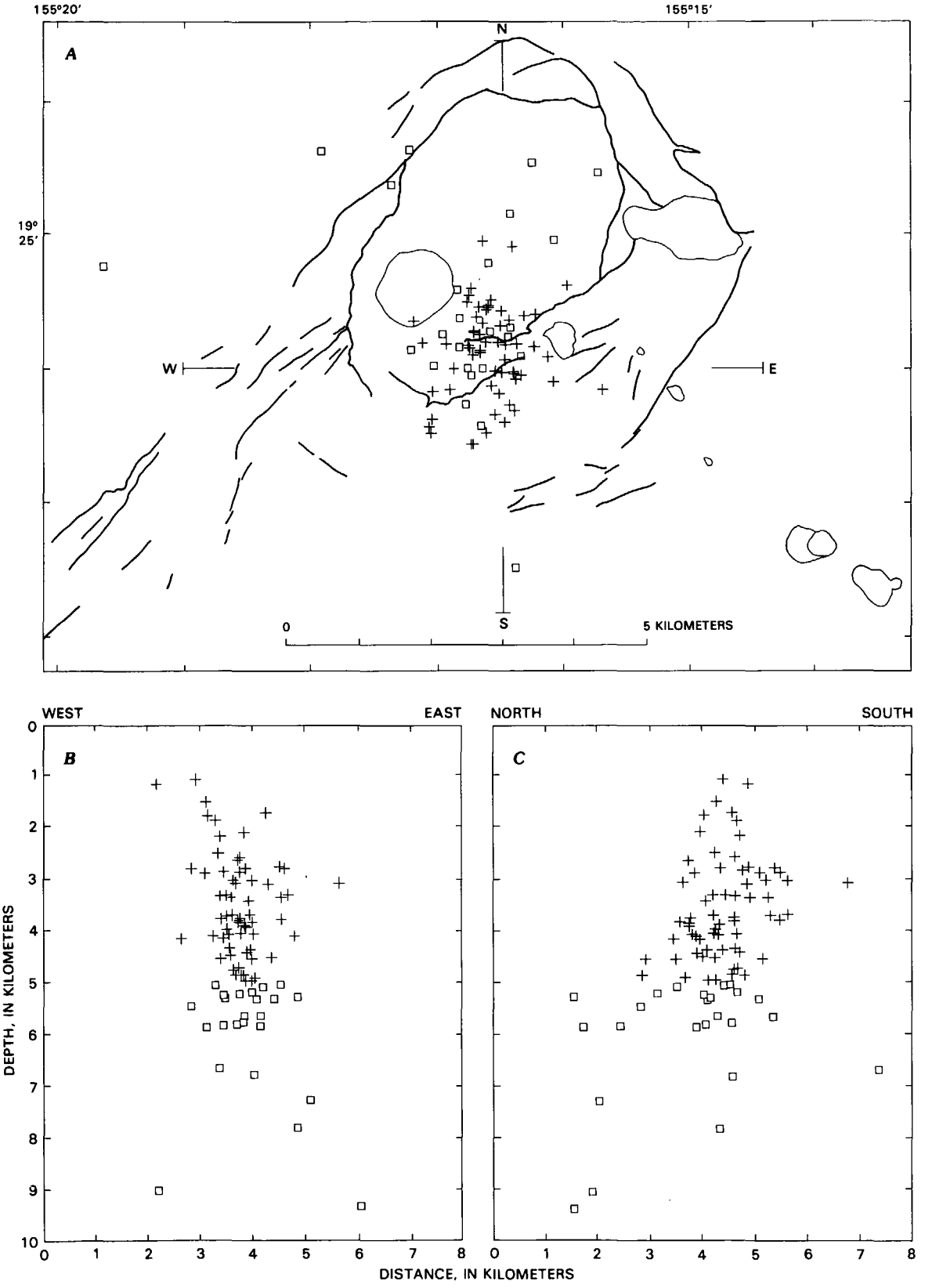
155°20'
155°15'
A
N
19° 25'
W
E
S
0
5 KILOMETERS
WEST
EAST
B
NORTH
SOUTH
C
DEPTH, IN KILOMETERS
DISTANCE, IN KILOMETERS

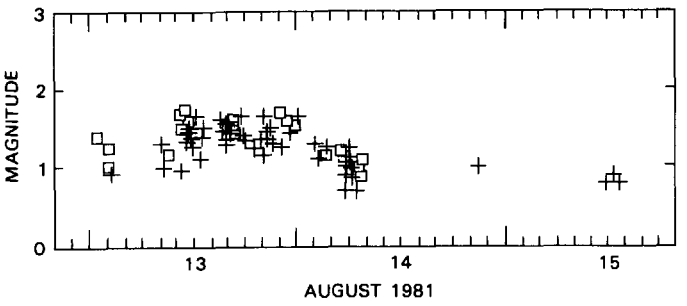

FIGURE 45.17.—Magnitudes of long-period events at the summit caldera of Kilauea (see figure 45.16) following the August 1981 intrusion, plotted against time. Symbols indicate hypocentral depths: crosses, 0–4.9 km; squares, 5.0 km or deeper.

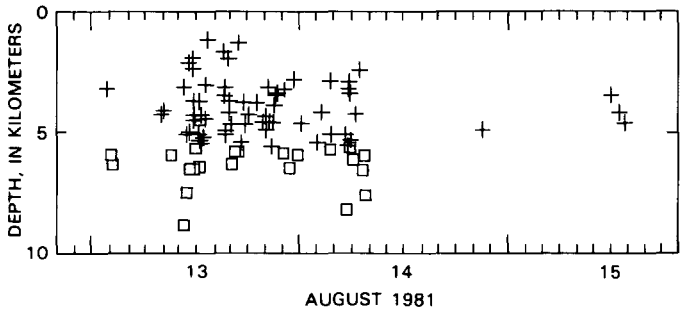

FIGURE 45.18.—Depths of long-period events at the summit caldera of Kilauea (see figure 45.16) following the August 1981 intrusion, plotted against time. Symbols indicate hypocentral depths: crosses, 0–4.9 km; squares, 5.0 km or deeper.

March 1985. They persisted over the following months at intermittently high rates, especially in periods of sustained inflation during the continuing eruption on the middle east rift. Differences in the amplitude envelope and spectral features on seismograms distinguish these long-period events from short-period earthquakes in the shallow summit region and intermediate-depth zone in the south flank (see figure 45.19). The smoked-paper seismogram from the summit station NPT on June 26–27, 1985 (figure 45.19*A*), shows the characteristics of shallow summit earthquakes, intermediate-depth south flank earthquakes, and intermediate-depth long-period events. The signatures of these seismic events are also illustrated on record from station PAU, located on the upper east rift zone about 8 km southeast of station NPT (figure 45.19*A*). The initially sharp onset and the high amplitude that attenuates rapidly with distance for short-period earthquakes contrasts with the uniform spectral features and gradually changing pattern of amplitude for long-period events. Digitized records from an array of stations at various epicentral distances emphasize the differences in the arrival pattern, amplitude envelope, and spectral features between the short-period earthquakes and long-period events (figure 45.19*B–E*).

Over the years, a variety of amplitude patterns and dominant periods have been recorded for different flurries of the intermediate-depth events. The amplitude patterns vary from isolated single bursts to series of multiple bursts. Recorded frequencies vary from monochromatic to fairly erratic. Dominant periods of 0.3–1.0 s are common. Some events possess longer periods of 1.0 s or more. On some occasions, energetic long-period events at intermediate depth beneath the summit were weakly recorded by the nearby recording tiltmeter which normally responds to long-period signals of about 20 s or more. The similarity in the envelope at various frequencies in figure 45.19 indicates a stationary spectral shape throughout the coda, which is characteristic of long-period events and tremor.

Short-period earthquakes and long-period events are routinely separated according to pattern of seismic-wave frequencies read on rotating-drum or Develocorder seismograms. The short-period earthquakes are initiated by sharp beginnings of high frequencies at about 10 Hz, followed by progressively lower frequencies. In contrast, long-period events persist within a limited band throughout the coda.

CASE HISTORY 5: INTERMITTENT BURSTS OF DEEP TREMOR

Deep tremor and its associated long-period events were described by Aki and Koyanagi (1981). A common source region for the long-period events and tremor is inferred on the basis of the coincidence in their time of occurrence and the similarity in the distance attenuation of their amplitudes across the seismic network; therefore, the hypocenter determinations for the long-period events were used to define the source region for the concurrent tremor. Widely recorded signals for deep long-period events with the earliest arrivals at stations southwest of Kilauea were commonly observed on seismograms (figure 45.20). These events frequently occurred in deep-tremor episodes of variable amplitude that were consistently limited in duration to about one-half to several hours (figure 45.21). Deep tremor contained frequency components up to 10 Hz, which is

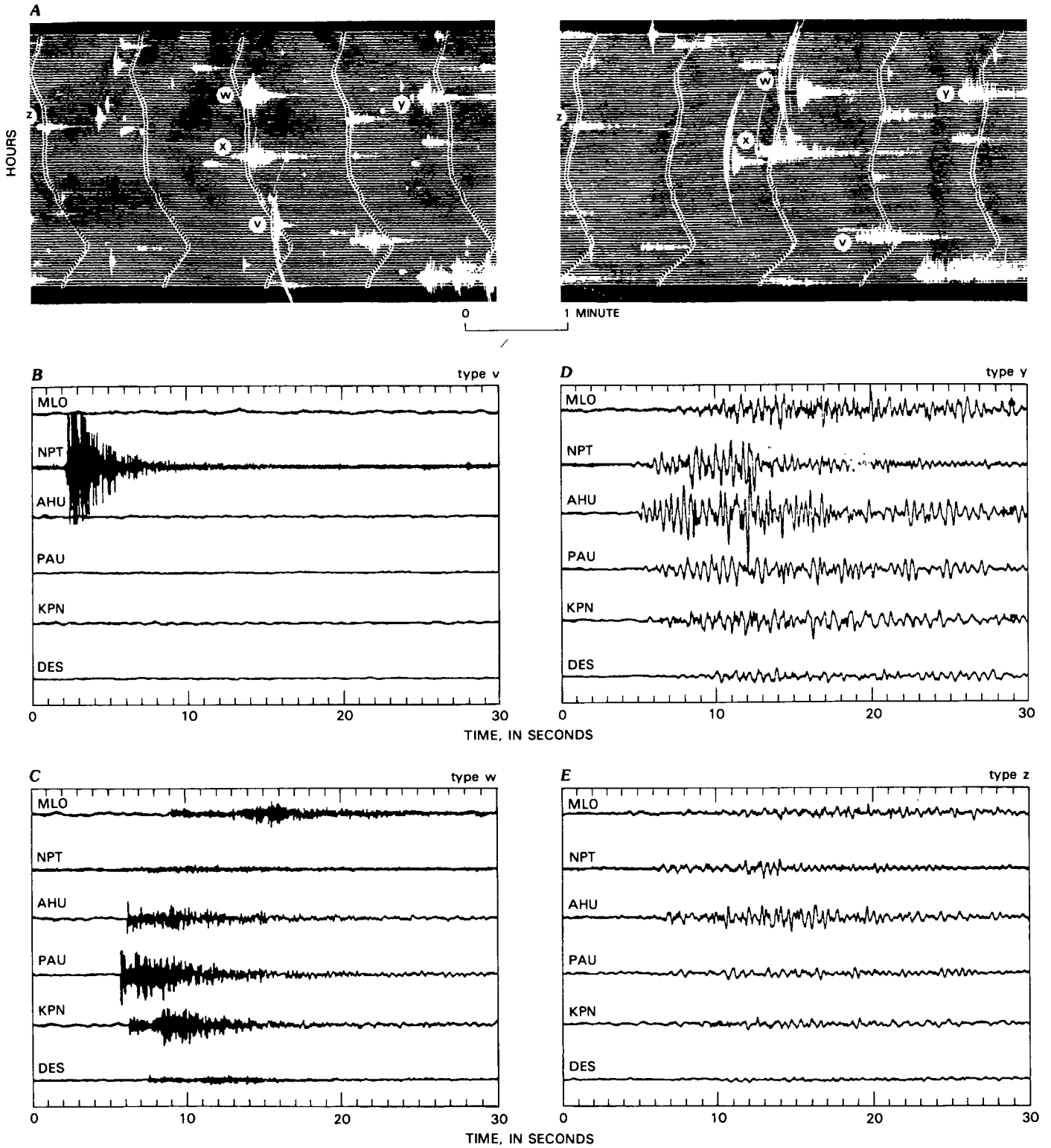

FIGURE 45.19.—Records showing high seismicity during an inflationary trend of the summit about two weeks following eruptive episode 33 in the continuing eruption of the middle east rift zone of Kilauea. The variety of seismic events in the crustal region of Kilauea in the magnitude range of about 0.1 to 1.5 included a shallow summit earthquake less than 5 km in depth (v), a south-flank earthquake at 9 km in depth (w), and long-period events 8–10 km beneath the summit region of Kilauea (x,y,z). ***A***, Portions of smoked-paper seismograms for (left) June 26–27, 1984, from station NPT at the summit of Kilauea and (right) June 26–27, 1984, same time section, from station PAU in the east rift zone 8 km southeast of NPT. Instrumental sensitivity to ground motion between NPT and PAU stations are not identical, but restrictively compatible; relative differences of up to 20 percent should be expected. ***B***, The shallow summit earthquake (v) shown on seismograms from digitized magnetic tape records for an array of six stations. For locations of stations see figure 45.1. Instrumental sensitivity for individual stations was kept constant but differences in magnification from station to station of as much as 20 percent may be present. ***C***, The south-flank earthquake (w). ***D***, The long-period event at 10 km in depth (y). ***E***, The small long-period event at 8 km in depth (z).

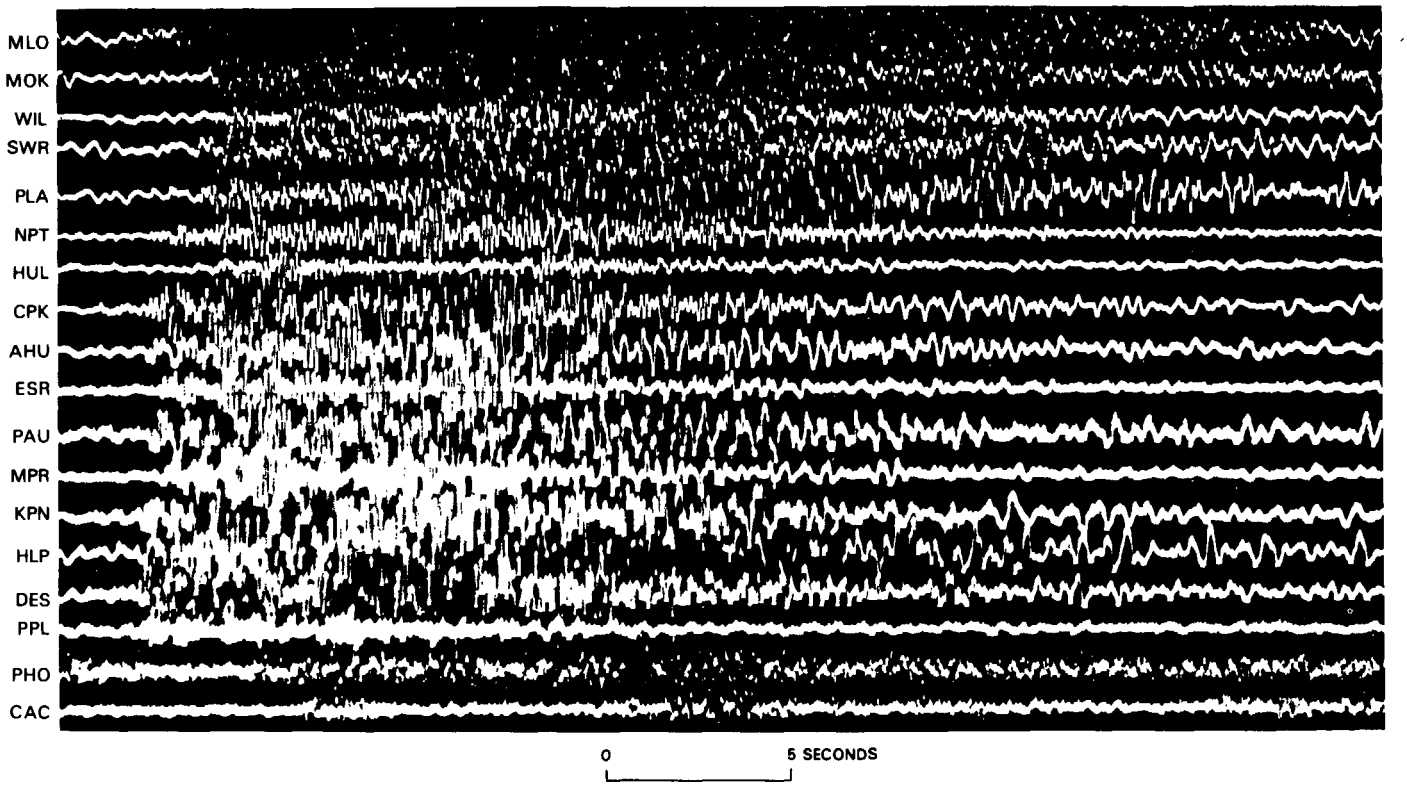

FIGURE 45.20.—Develocorder seismogram of a uniform-frequency long-period event 50 km deep southwest of Kilauea recorded at 0017 (H.s.t.), January 14, 1978. Three-letter codes indicate seismograph stations (see figure 45.1).

slightly higher than those in tremor from shallower sources other than the tremor near eruptions.

DEPTH CLASSIFICATION OF TREMOR AND COMPARISON WITH LONG-PERIOD EVENTS

In the routine processing of seismic records at HVO, tremor is classified into three depth categories on the basis of the distance-attenuation pattern of amplitude. Episodes of tremor not related in time or space to eruptions and presumed to be caused by magmatic activity vary in their amplitude-attenuation pattern across the network of stations. This variation was used to classify the tremor as shallow, intermediate-depth, and deep tremor. If tremor was related to an eruptive event and its amplitude varied according to the intensity of lava movement, fountaining, and extrusion rate, it was considered to be shallow.

The tremor in the various depth categories was frequently accompanied by short bursts of long-period events with envelopes that resembled those of tectonic earthquakes and spectral features similar to those of the concurrent tremor. These long-period earthquakes often had onset times or identifiable bursts that were measurable to within 0.1 s at a significant number of stations. The arrival times of their onsets are consistent with P-wave travel times for local earthquakes in Hawaii, thus permitting standard earthquake-location procedure to be used for hypocenter determination. The compilation of well-located long-period events from 1972–1984 was used to outline the source region of tremor beneath Hawaii.

Normalized amplitudes of clearly recorded and located long-period events, corrected for instrumental magnification and station noise, generally showed an exponential pattern of spatial attenuation rates that decreased with increasing focal depth. Attenuation patterns averaged from several long-period events at approximate mean depths representing our three general depth categories of Kilauea tremor (shallow: less than 5 km; intermediate: 5–15 km; and deep: 30–60 km) were compared with those of the concurrent background of tremor (figure 45.22).

Using the epicentral distances for the long-period events and replacing the normalized amplitude measurements with those of the concurrent harmonic tremor, we found a similar pattern of amplitude attenuation with distance, indicating a common source region. In the attenuation of amplitude with distance, the linear relation between log amplitude and log distance is represented by

$$\log A = x - y \log D,$$

where A is the relative amplitude, D is the epicentral distance in kilometers, and x and y are constants. Values of y, the measure of amplitude attenuation, determined for Kilauea tremor decrease with increasing focal depth; they are 1.3–1.4 for shallow tremor, 0.9–1.0 for intermediate-depth tremor, and 0.4–0.5 for deep

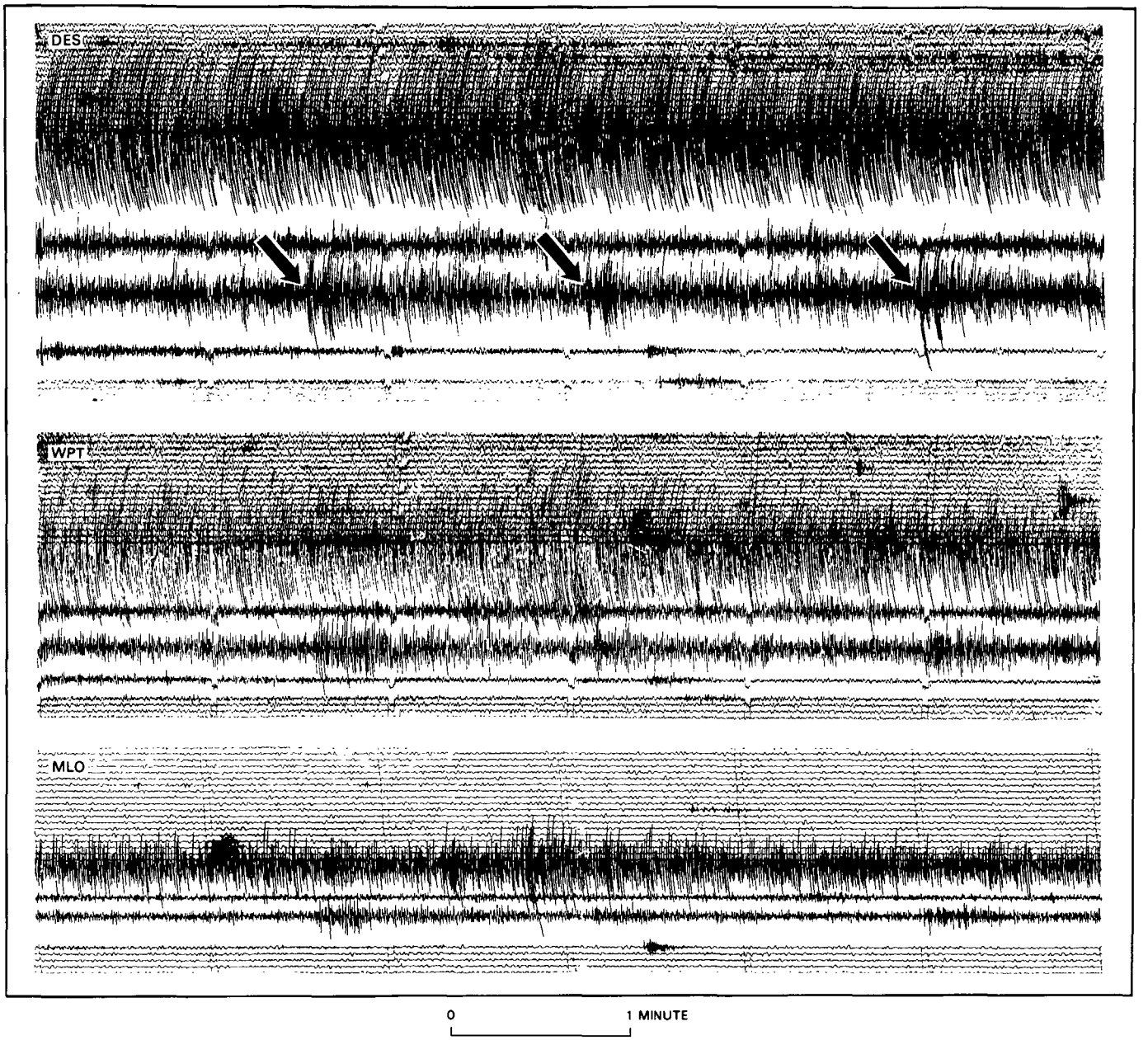

FIGURE 45.21.—Part of a 50-minute burst of tremor and intermittent deep earthquakes on July 22, 1969, recorded on smoke-drum seismograms at the Desert (DES), West Pit (WPT) and Mauna Loa (MLO) stations. The long-period events, defined by abrupt increase in amplitude and higher frequency, are marked by arrows on the Desert seismogram. Average distances from earthquake focus to seismometer are: Desert, 45 km; West Pit, 52 km; and Mauna Loa, 57 km.

tremor. The characteristics and associated volcanic events for the various categories of tremor are summarized in table 45.2.

HYPOCENTER DETERMINATION OF LONG-PERIOD EVENTS USING STANDARD EARTHQUAKE LOCATION PROCEDURE

Long-period events with reasonably sharp onset times or identifiable episodes that could be matched at 10 or more stations around the epicentral region were selected and read from Develocorder or digitized magnetic-tape seismograms. The arrival times based on *P*-wave velocities were used to process locations using the earthquake-location program HYPOINVERSE (Klein, 1978).

These events were located within the bounds of accuracy expected for earthquakes. The accuracy in terms of horizontal and vertical standard error was reasonably good: most events were located with a precision better than ± 5.0 km and many within ± 2.0 km (figure 45.23). Events located with standard errors less than ± 2.0 km amounted to 96 percent of events shallower than 5

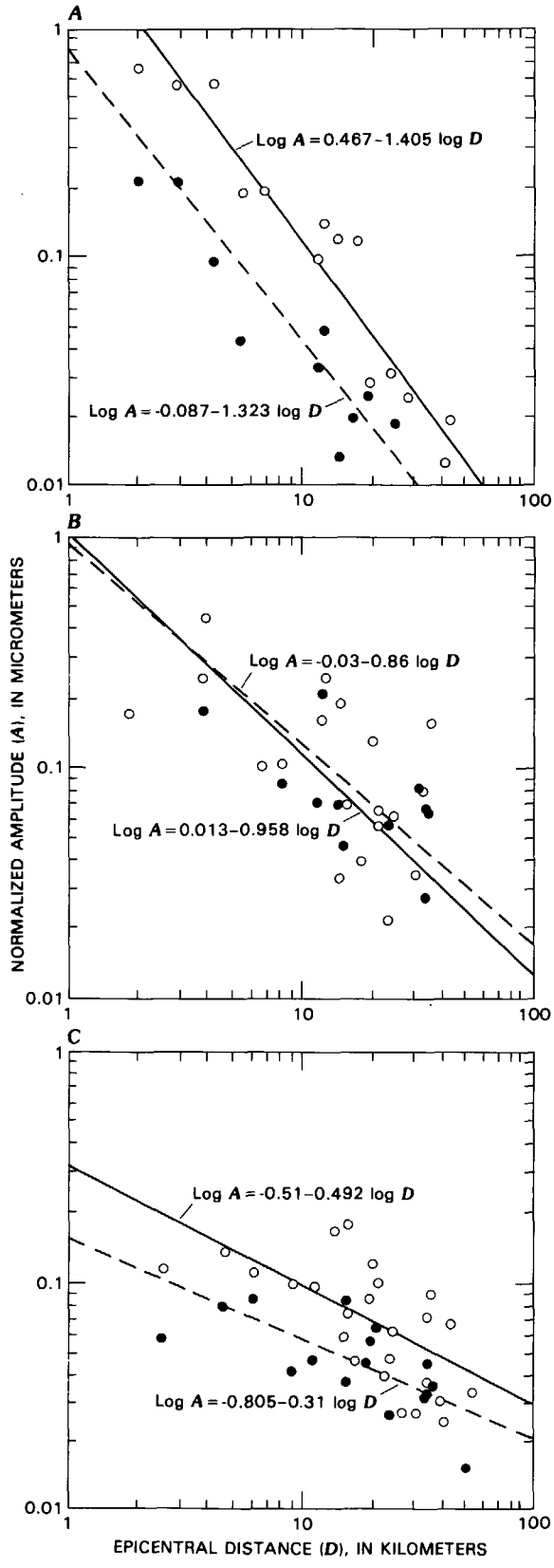

km, 62 percent of intermediate-depth events in the depth range of 5–15 km, and 26 percent of deep events at depths of 15–60 km.

Amplitude and signal-duration patterns for long-period events were roughly consistent with those of short-period earthquakes. A comparison of magnitudes derived from signal amplitude (M_a) and from signal duration (M_d) for shallow, intermediate-depth, and deep long-period events indicates an approximately linear relation (figure 45.24). There is some deviation from linearity toward higher magnitudes, with a tendency for duration magnitude (M_d) to be progressively overestimated in the higher magnitude range. This may reflect some inherent differences between long-period events and short-period earthquakes. Source duration differences are expected between short- and long-period events (see Chouet and others, chapter 45, part II). Attenuation rate for long-period events may be lower and the same calibration curve may not apply to both. Controlled by the seismometric coverage and signal clarity, the magnitude thresholds of the located long-period events were generally, less than 0.5 for shallow events, about 1.0 for intermediate-depth events and nearly 1.5 for the deep events.

TREMOR SOURCE REGION BENEATH HAWAII INFERRED FROM LOCATIONS OF LONG-PERIOD EVENTS FROM 1972 TO 1984

The normal short-period earthquakes between January 1981 and December 1982 were widely spread beneath Kilauea, outlining the regions of rock fracturing caused by intrusive events at the summit and rift zones and the seaward displacement of the south flank (figure 45.25*A*). A view of these events projected onto an east-west profile (figure 45.25*B*) indicates that most of the events were confined in the crust at depths of less than 10 km.

In contrast to the broadly distributed short-period earthquakes defining the tectonic environment beneath Kilauea, long-period events located beneath Kilauea during 1972–1984 with horizontal and vertical standard errors of less than ±2.0 km were concentrated in the summit region (figure 45.26*A*). These hypocenters were projected onto cross sections in an east-west plane (figure 45.26*B*) and in a north-south plane (figure 45.26*C*); they outline a columnar source region separated into two depth concentrations in the crust. The shallow concentration beneath the caldera was centered at depths of about 2–4 km and the deeper one at 6–12 km, leaving a zone of low activity at 4–6 km depth.

On an islandwide scale the long-period events located for 1972–1984 with less than ±5.0-km horizontal and vertical standard errors were concentrated at the summits of Kilauea, Mauna Loa, and Loihi and in a broad region at depth about equal distances

FIGURE 45.22.—Amplitude plotted against epicentral distance for located Kilauea long-period events (circles) at various depths and the tremor (dots) associated with each. The derived linear regression equation is given for each plot; solid lines for long-period events and dashed lines for tremor. Amplitude normalized to remove effects of instrument differences. ***A***, Shallow events (4 km). ***B***, Intermediate-depth events (10 km). ***C***, Deep events (37 km).

TABLE 45.2.—*Classification of tremor types beneath Kilauea Volcano by depth and area of origin*

[Dominant frequencies are those commonly recorded on HVO network stations, recorded distance is the maximum distance at which tremor type recorded on typical HVO type I station]

Type	Origin		Associated events	Duration	Amplitude at nearest station (μm)	Dominant frequencies (Hz)	Recorded distance (km)
	Depth (km)	Area					
Shallow 1 (strong)	<5	Rift and summit	Earthquake swarm, summit deflation, high lava fountains, high rate of lava extrusions, degassing during strong intrusions and eruptions	Few to many days	More than 5 at distance about 1 km	2–10	About 40
Shallow 2 (weak)	<5	Rift	Low lava movement, lava spattering, degassing between episodes in prolonged eruptions	Few days to many weeks	Less than 1 at distance of about 1 km	2–10	Less than 5
Shallow 3 (weak)	<5	Summit	Sustained rate of summit deflation, long-period events	Few to many days	Less than 1 at distance of about 1 km	2–5	Less than 5
Intermediate	5–15	Kilauea	Summit inflation, long-period events	Several minutes to hours in sequences that may last for days	Less than 5 at distance of about 1 km	1–3	About 50
Deep	30–60	South Hawaii	Long-period events	Less than one to several hours	Less than 1 at distance of about 15 km	2– 10	About 100

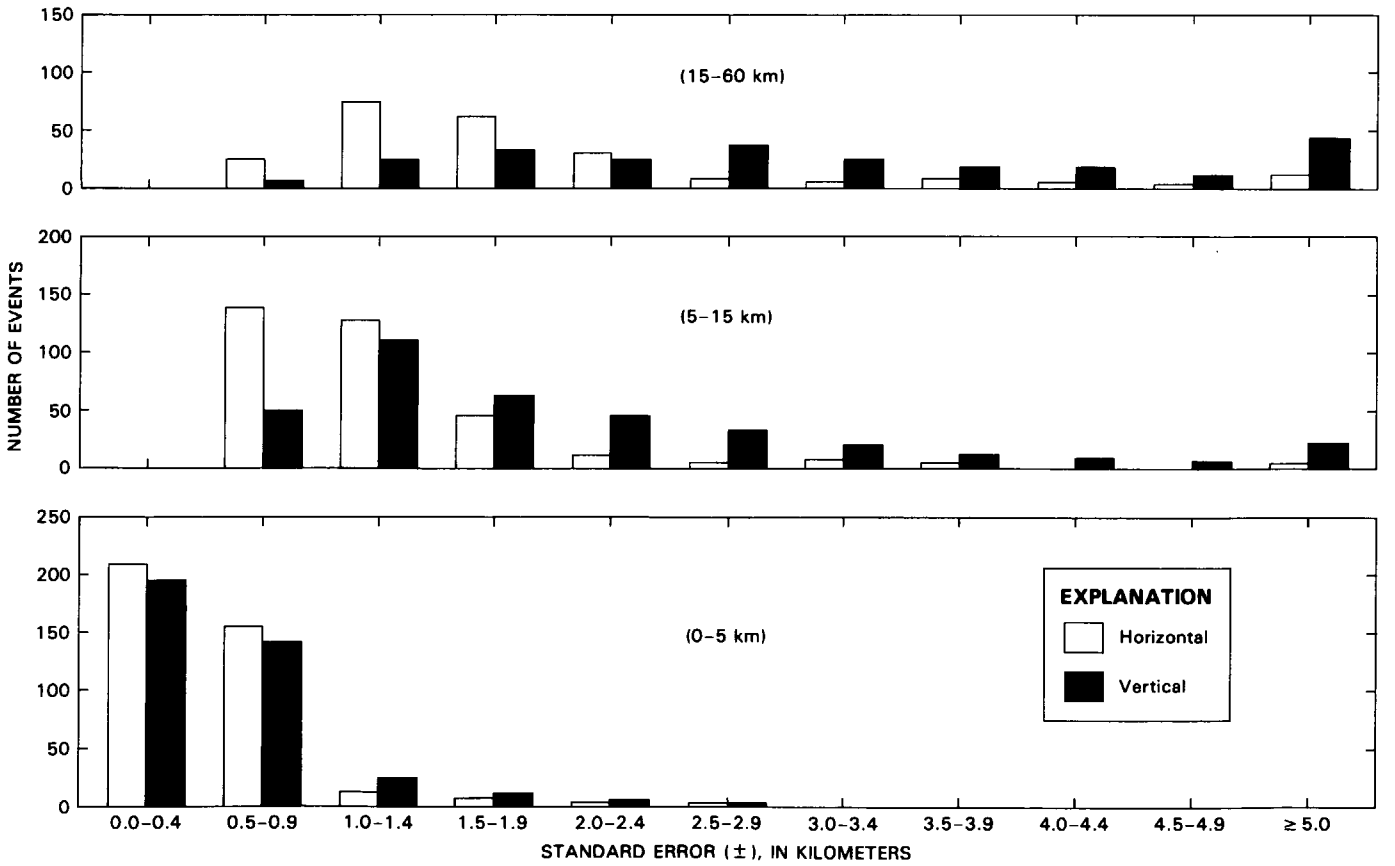

FIGURE 45.23.—Standard errors in the horizontal (white bars) and vertical (black bars) location of long-period events within three depth intervals beneath Hawaii from 1974 to 1984.

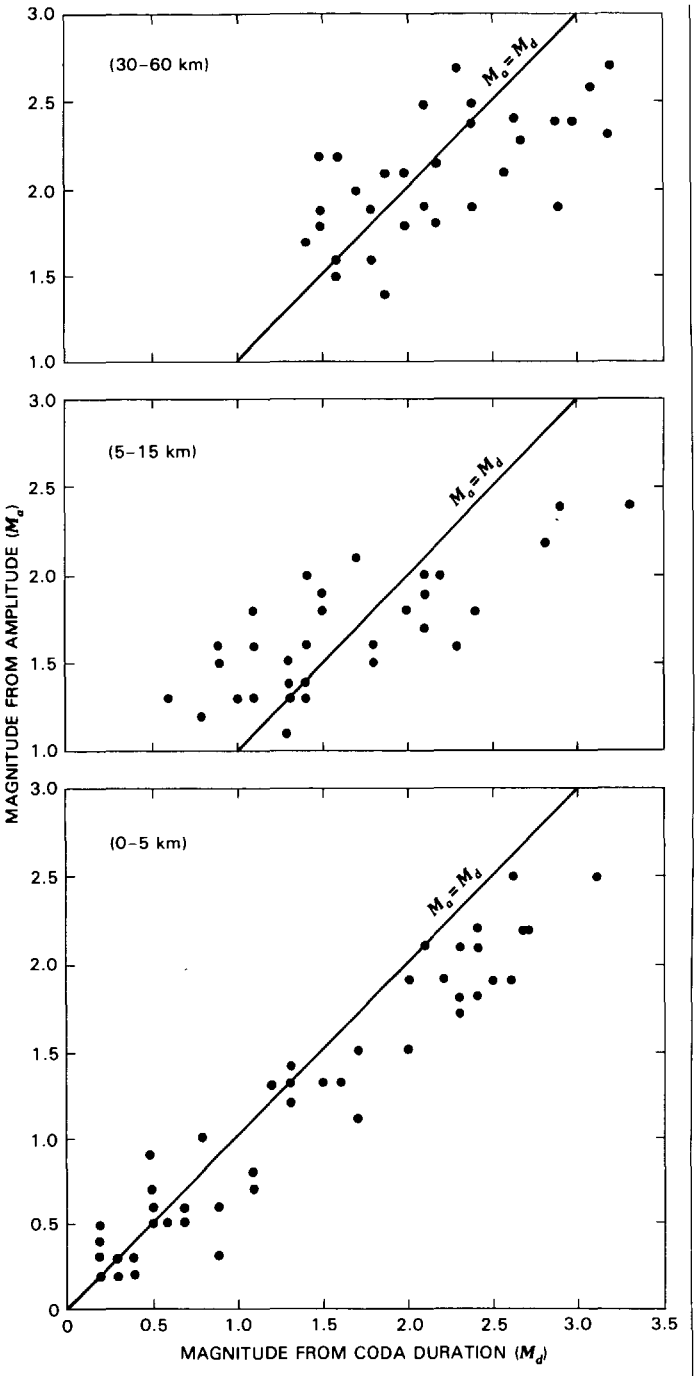

FIGURE 45.24.—Plot of magnitude determined from amplitude (M_a) against magnitude determined from coda duration (M_d) for long-period events on Kilauea at three depth intervals.

from these three summit localities. The map distributions for various depth intervals of these events beneath the Island of Hawaii are shown in figure 45.27*A–D*. Hypocenters are also shown projected onto the southwest-northeast line w–x from 40 km on either side of it, effectively including the entire seismic zone (figure 45.27*E*) projected onto the same line from a narrower zone 10 km on either side, selectively defining the plumbing system for Kilauea (figure 45.27*F*); and projected onto the northwest-southeast line y–z from a region 40 km on either side of it, showing the alignment of the three dynamic volcanic centers with the deep central system in the mantle.

Circular source regions of nearly equal size, about 5 km in diameter, define the summit of each of the volcanoes. The seismic zone centrally located between the three summit clusters is broader and has width of about 30 km. Cross-sectional profiles outline a columnar distribution from shallow summit regions that discontinuously connect with the deeper central source.

HISTORY OF TREMOR AND LONG-PERIOD EVENTS FROM 1972 TO 1984

An index to the history of tremor in Hawaii is provided by the daily seismic records at HVO, on which harmonic tremor is routinely identified, separated into three general depth categories, and logged as minutes of tremor per hour (Nakata and others, 1984). Shallow tremor has characterized times of major intrusions and eruptions in addition to sporadic internal activity. Significant bursts of intermediate-depth tremor have generally decreased in recent years, with a background level that typically fluctuates from month to month. Duration of deep tremor was fairly steady throughout 1972–1984, with repeated bursts of activity.

Because the selection of long-period events for the determination of hypocenters was dependent largely on the quality of their onset times, our compilation may be incomplete in terms of sizes and numbers of events located. Gaps in our file of located long-period events, and inconsistencies between the number of located long-period events and the actual number of events detected are normal discrepancies to be expected. Allowing for such discrepancies, however, our data are sufficiently complete to provide an approximate quantitative base from which to evaluate long-period events according to their spatial distribution over many years and their temporal relation to major volcanic events. By considering the total number of long-period events detected and classified generally according to time and region, temporal gaps in our collection of accurately located long-period events can be filled by estimation.

A compilation of locatable long-period events provides a means to quantify the spatial distribution and magnitude parameters of the tremor-related activity. Depth-time plots of long-period events, with symbol sizes designating magnitudes, show the sporadic nature of shallow activity related to eruptions and to shallow magmatic events and the more dispersed but persistent pattern of deep events (figure 45.28). The magnitudes for the located events were confined to less than about 3.5, with deep events showing a tendency toward larger magnitude. There also appears to be a tendency for activity of deeper events to increase following accelerated shallow activity.

Locatable shallow (depth less than about 5 km) long-period events correlated with major eruptive or intrusive events such as those in December 1974, September 1977, and August 1981 (figure 45.29). The depth-time plots in general indicate that episodic shallow activity is related to significant volcanic events and that deeper events increase over a longer timespan.

The time-relation of long-period events to the inflation-deflation pattern of the summit is plotted on a longer time base in figure 45.30. A marked increase in long-period events, which are usually shallow, followed major collapses. Deeper crustal events appear dispersed during general periods of inflation.

The rates of deep-tremor generation, magma movement in the shallow summit storage system at Kilauea, lava extrusion at Kilauea, and times of significant volcanic events and earthquakes from 1972 to 1984 are compared in figure 45.31.

The time plot of reduced displacement of deep tremor was expanded from Aki and Koyanagi (1981, figure 10), who interpreted reduced displacement in terms of magma flow rate. Tremor readings were made from standard optical-drum seismograms and checked with smoked-drum records. Peak-to-peak amplitudes were measured in 5-min increments and reduced to micrometers of ground movement according to the instrumental response (basically types 3 and 4, see Nakata and others, 1982) for the averaged frequency of the deep tremor. Variations in system response for the predominant range of frequencies of the deep tremor may introduce discrepancies as large as a factor of two in the reduction of absolute amplitude, but they should not affect the relative continuity over the entire period. The instrumental response and analysis procedure emphasized signals in the range of frequencies from about 2 to 10 Hz.

The volume of magma movement in the shallow summit storage system at Kilauea could be estimated from tilt changes on the east-west component continuously monitored from Uwekahuna on the northwest side of Kilauea caldera. An average magma volume to tilt ratio of 0.63×10^6 m^3/ μrad was derived from the volumes of lava extruded as extrapolated from field surveys compared with the east-west tilt changes during episodes 2–20 of the Puu Oo eruption in 1983–1984, ratios for individual episodes range in variation by $\pm 0.21 \times 10^6$ m^3/ μrad (Wolfe and others, chapter 17). The volume of erupted lava was adjusted for 25 percent porosity. In view of the relatively wide variation in volume to tilt ratios observed for the individual eruptive episodes that may be caused by lateral migration of the summit tilt center or magma drainage within the conduit system, as well as the difficulties in measuring extruded lava, we chose a slightly high conversion value of 0.8×10^6 m^3 to use in our calculation in figure 45.31.

Steady long-term trends of deep-tremor production are occasionally interrupted following sustained high rates of lava emission, such as during the Mauna Ulu eruption at Kilauea in 1969–1974 and the continuing Puu Oo eruption in 1983–1984. The increasing rate of deep tremor from late 1983 subsequent to the onset of the Kilauea eruption in January 1983, and then again in 1984 following the start of the major eruption of Mauna Loa in March, indicate that a pressure reduction in the upper conduit system may induce increased buoyancy of the magma along the interconnecting plumbing system, propagating downward to accelerate the feeding rate from the mantle source. The possibility of such a mechanism was recently suggested by Dzurisin and others (1984) and is also consistent with evaluations based on geochemical data (Wright, 1984).

CONCLUSIONS

Data from study of volcanic tremor in Hawaii justify the following generalizations and inferences.

(1) Harmonic tremor, a seismic signal with relatively constant frequency content and pattern from start to end, is generated and sustained by eruptive activity and magma movement, and its amplitude varies according to its intensity.

(2) Shallow tremor at an eruption site is strongly influenced by flow impact and acoustical noise from high fountains, as well as by the rate of lava extrusion. Eruption tremor is characterized by a peaked spectrum and amplitude variations that alternate at intervals of a few seconds. This pattern generally reflects the activity of intense fountaining in which recurring lava bursts occur at intervals of about 5 s. The continuously fluctuating tremor signal produces a multipeaked spectrum at 1–10 Hz.

(3) Repose periods between major episodes of lava production in prolonged eruptive series, such as the Mauna Ulu and Puu Oo eruptions of Kilauea, are characterized by a nearly continuous background of tremor local to the active vents. The relatively weak tremor varies in amplitude according to the rate and intensity of lava movement and degassing activity within the eruptive vents.

(4) Long-period events are a unique form of seismic event closely associated with harmonic tremor and magmatic activity. A common source for tremor and long-period events is implied by their similarity in spectral features, time of occurrence, and spatial attenuation of amplitude. Long-period events sometimes increase progressively and culminate in continuous tremor, and tremor sometimes decays into episodic bursts evolving into long-period events; tremor may therefore be a collective aggregate of long-period events.

(5) Some long-period events with identifiable onset times are locatable within the accuracy constraints of normal earthquakes. The locations of these events thus outline the source regions of tremor beneath Hawaii. Shallow events are concentrated in epicentral areas about 5 km in diameter centered at the summits of Mauna Loa, Kilauea, and Loihi Volcanoes in expected locations of magma storage. The three centers appear to be connected, though not continuously, to a broader and deeper common source region; together they are inferred to outline the plumbing system beneath Hawaii that supplies magma from a common mantle source to the separate volcanoes. The broad mantle source may be compartmental to explain the chemical differences in the erupted lavas of Kilauea, Mauna Loa, and Loihi, which are believed to have formed within the mantle (Wright, 1984).

(6) The located long-period events provide a quantitative means to classify tremor according to depth and associated volcanic events into (i) shallow rift and summit tremor less than 5 km beneath the eruptive vent; (ii) shallow summit tremor less than 5 km deep associated with deflation episodes at the summit; (iii) intermediate-depth tremor at 5–15 km beneath Kilauea and generally associ-

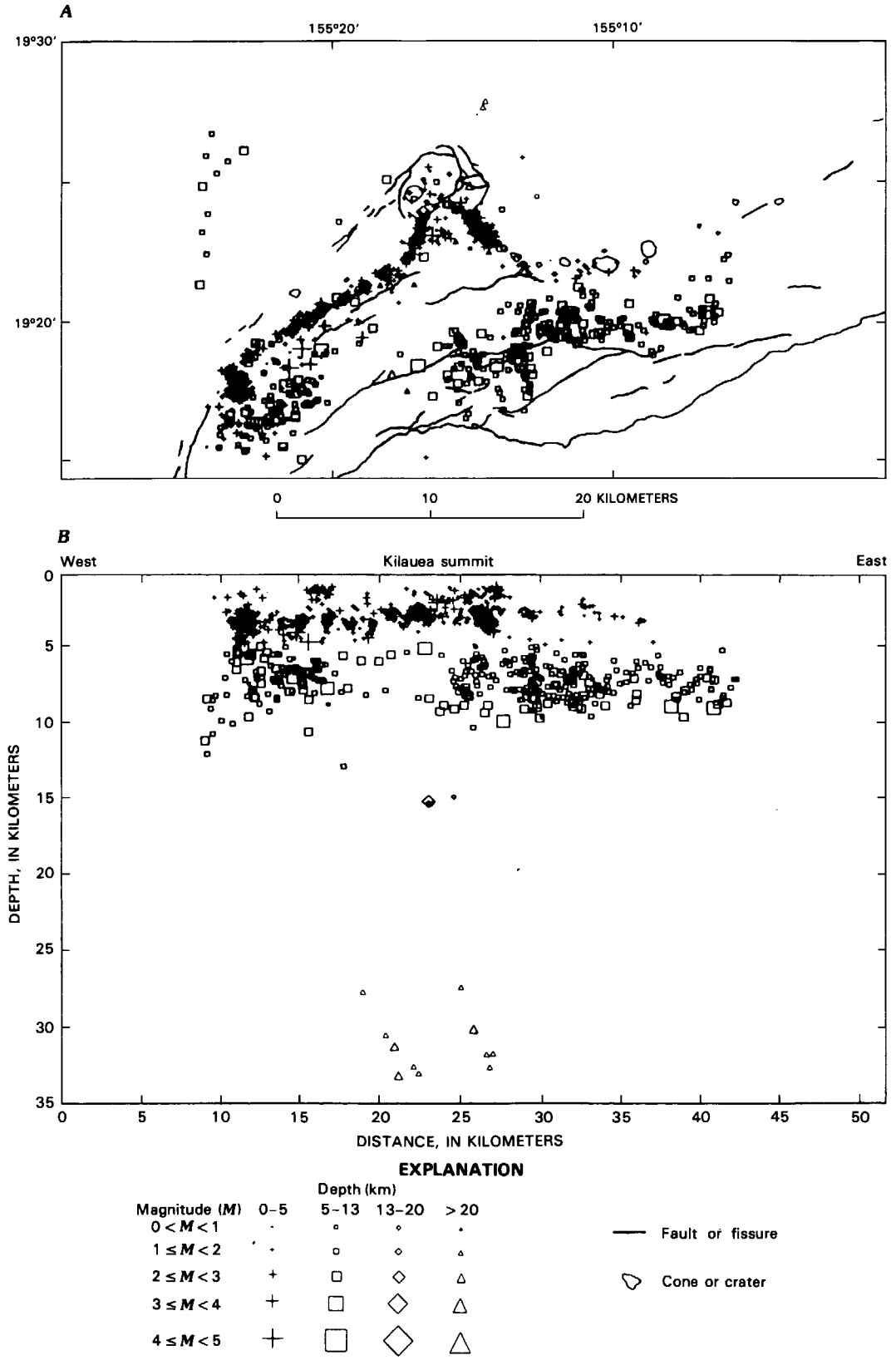

FIGURE 45.25.—Short-period earthquakes in the region of Kilauea caldera, January 1981 to December 1982. Horizontal and vertical standard errors for these events were less than ±2 km. ***A***, Epicentral locations. ***B***, Depth profile of the earthquakes projected onto an east-west plane.

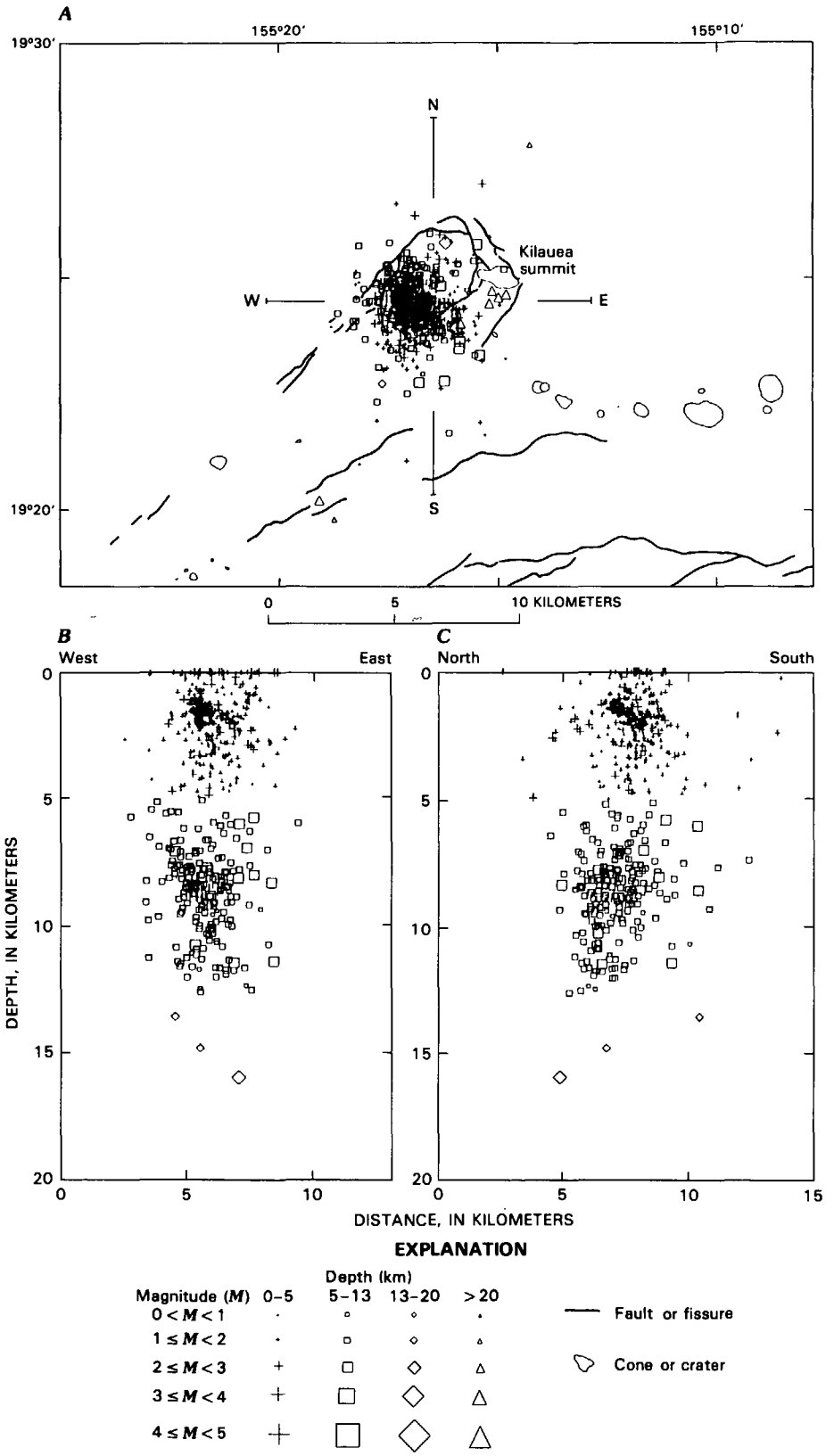

FIGURE 45.26.—Long-period earthquakes 0–20 km beneath Kilauea region from 1972 to 1984. Only events with horizontal and vertical standard errors less than ±2.0 km were plotted. ***A***, Locations of epicenters, and lines of two depth sections W–E and N–S. ***B***, West-east depth section with events projected onto line W–E. ***C***, North-south depth section with events projected onto line N–S.

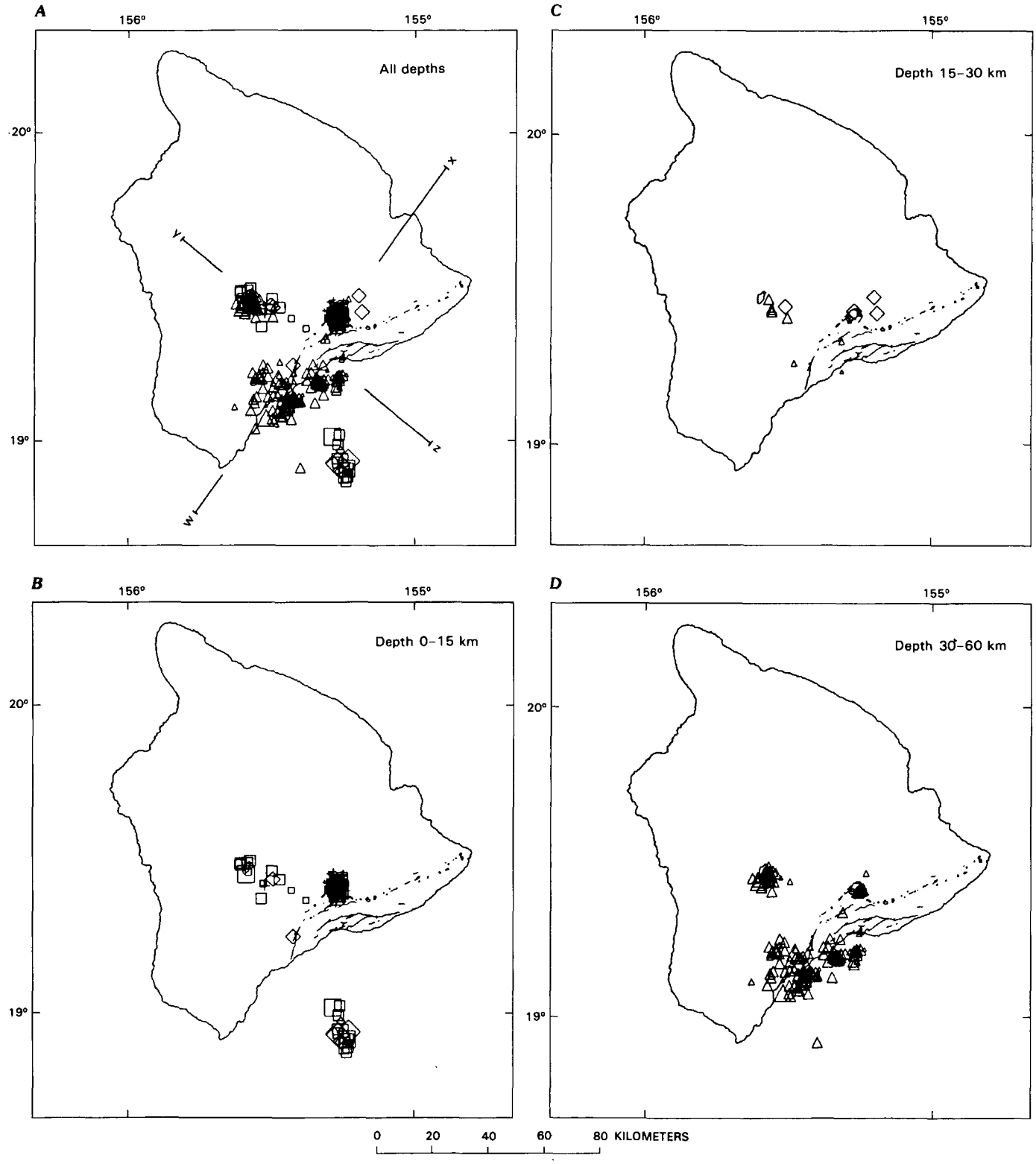

FIGURE 45.27.—Long-period earthquakes beneath the Island of Hawaii region from 1972 to 1984. Only events with horizontal and vertical standard errors less than ±5.0 km were plotted. ***A***, Locations of all epicenters and reference lines for depth sections. ***B***, Locations of epicenters for events at depths 0–15 km. ***C***, Locations of epicenters for events at depths 15–30 km. ***D***, Locations of epicenters for events at depths 30–60 km. ***E***, Southwest-northeast depth section with events projected from a zone 80 km wide onto line w–x. Projected positions of Mauna Loa and Kilauea summit areas are indicated. ***F***, Southwest-northeast depth section with events projected from a zone 20 km wide onto line w–x. Approximate position of Kilauea summit is indicated. ***G***, Northwest-southeast depth section with events projected from a zone 80 km wide onto line y–z. Projected positions of Mauna Loa, Kilauea, and Loihi summit regions are indicated.

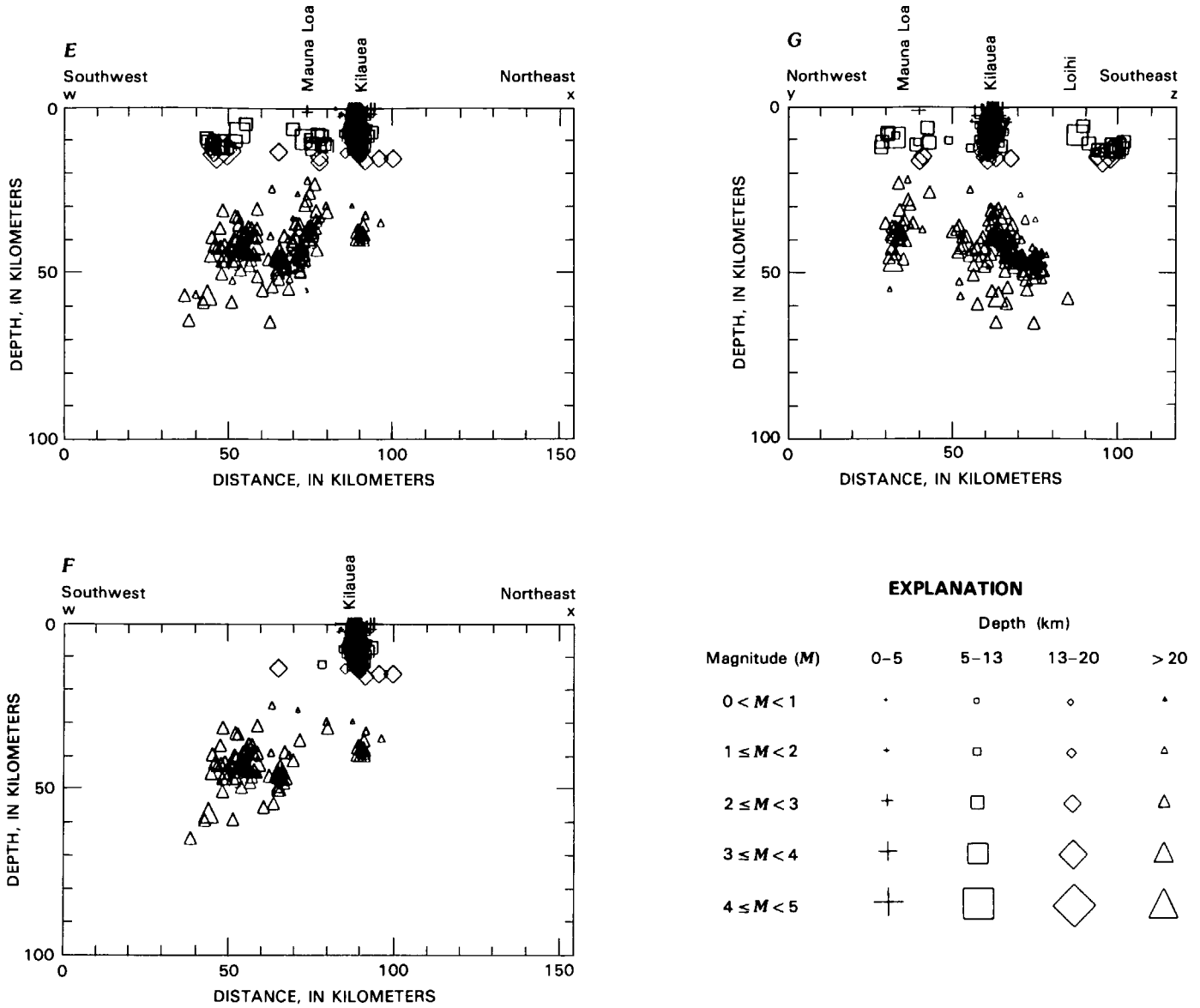

FIGURE 45.27.—Continued.

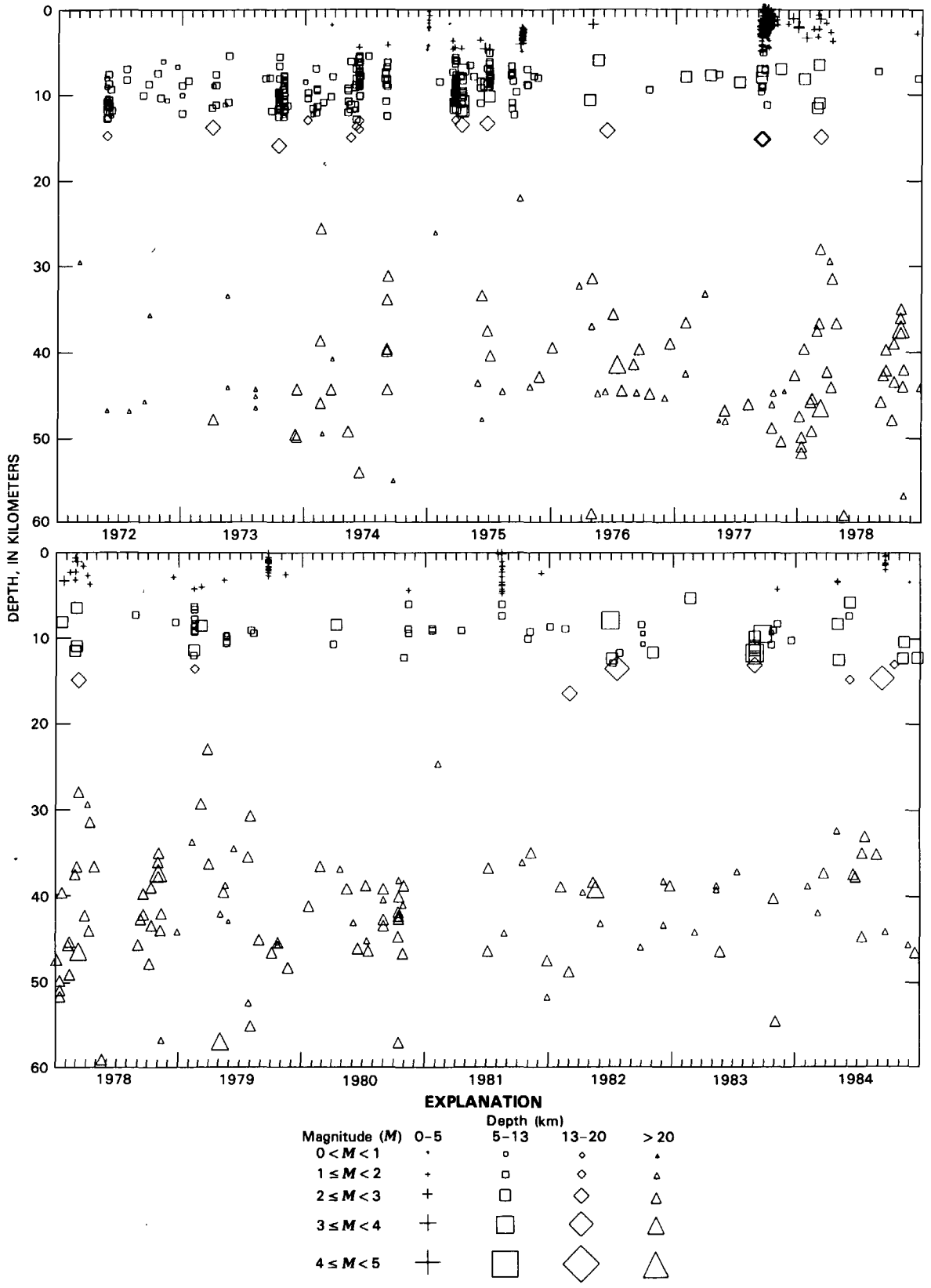

FIGURE 45.28.—Depth-time plot of long-period events 0–60 km beneath Hawaii between north latitudes 18°45′ and 20°20′ and west longitudes 154°40′ and 156°20′ from January 1972 to December 1984. Magnitude ranges are designated by symbol sizes. The selected events were those with horizontal and vertical standard errors of ±5.0 km or less. Data for 1978 repeated where plot is broken.

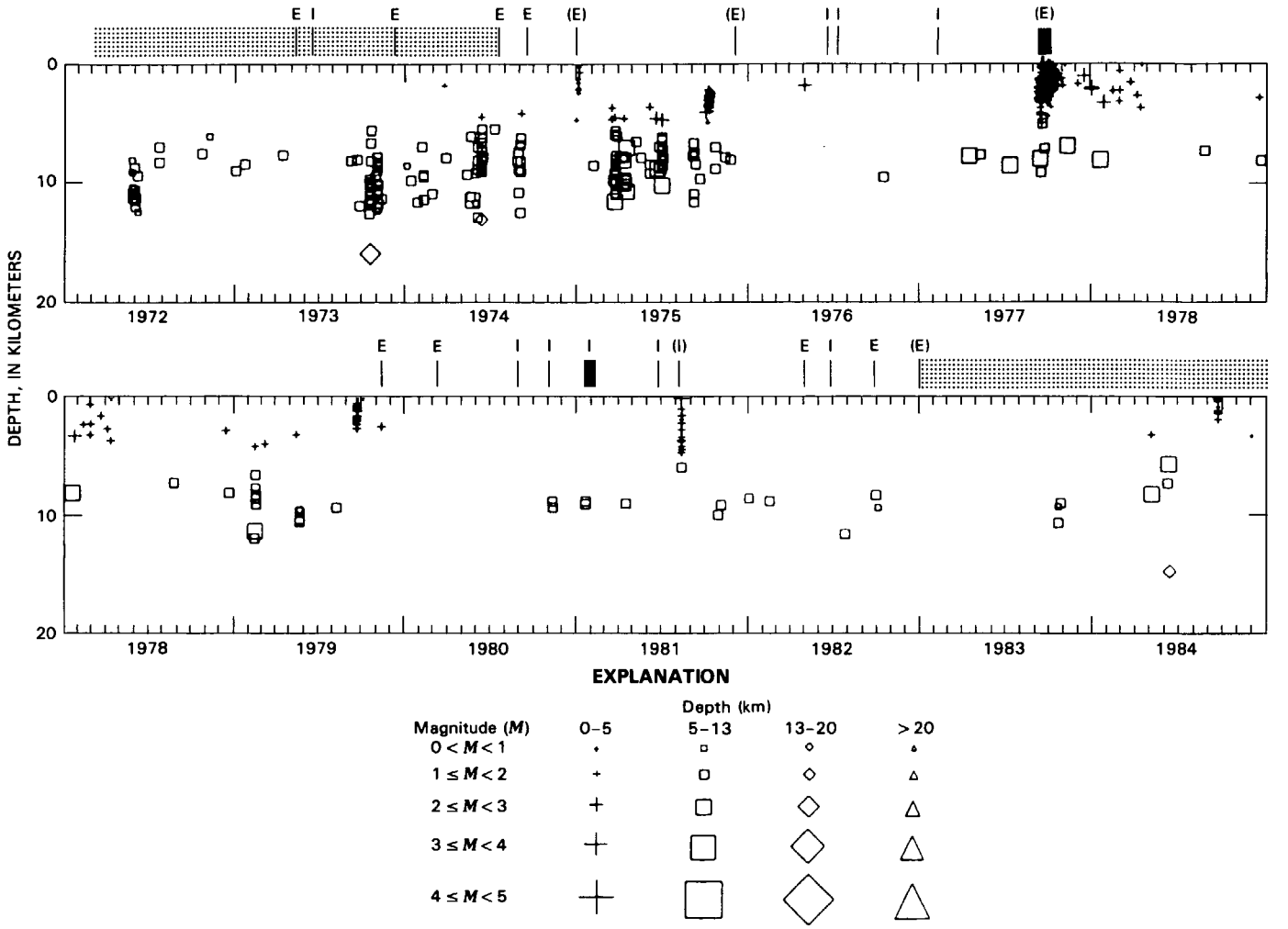

FIGURE 45.29.—Depth-time plot of long-period events 0–20 km beneath the summit region of Kilauea between north latitudes 19°23′ and 19°26′ and west longitudes 155°15′ and 155°18′. Only events with horizontal and vertical standard errors ±2.0 km or less were plotted; therefore the number of events selected is comparably less than in figure 45.28 for the region considered here. Solid bars above plot indicate: (I), magmatic intrusions accompanied by major deflation of the summit, as indicated by more than 100 microradians of east-west tilt measured at Uwekahuna station near the northwest edge of Kilauea caldera; (E), intrusions with subsequent eruptions accompanied by major deflation of the summit; I, intrusions without major deflation but with at least 5 microradians of east-west tilt; E, intrusions with eruption and at least 5 microradians of east-west tilt but without major deflation. Dotted bars above plot indicate prolonged eruptions of repeated episodes at Mauna Ulu (renewed, 1972–1974) and Puu Oo (1983–1984, continuing).

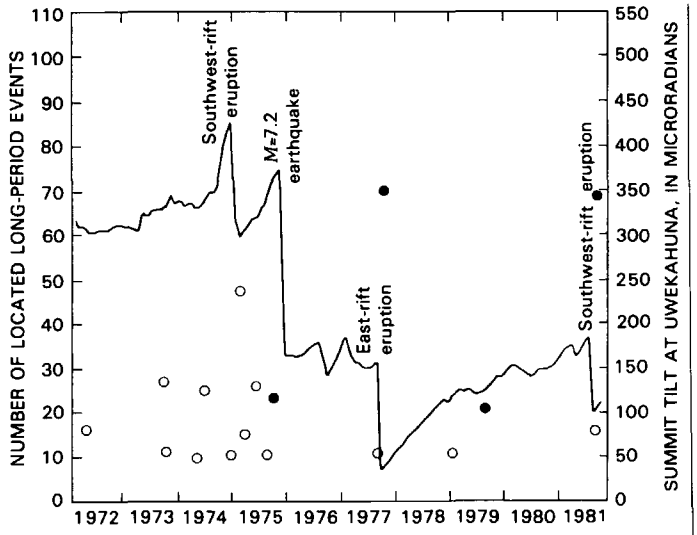

FIGURE 45.30.—Time plot of summit tilt and number of located long-period events of 10 or more per day on Kilauea, 1972–1981. Dots, shallow events (depth less than 5 km), circles, deep crustal events (depth 5–15 km).

ated with inflation at the summit; and (iv) deep tremor at 30–60 km beneath south Hawaii that occurs at a fairly constant rate of reduced displacement, with a subtle increase sometimes following major volcanic events near the surface.

(7) The time-depth distribution of long-period events outlines the dynamic process in the magma transport system. Shallow events are closely associated with observed volcanic events. The activity of progressively deeper events becomes more diffuse but also more persistent over long time intervals. After sustained high rates of shallow intrusions, deep long-period events tend to persist and the rate of reduced displacement of deep harmonic tremor tends to increase. This may be explained by a hydraulically linked system in which a decrease in pressure at shallow depths is propagated to the deeper source and increases the buoyancy of the rising magma.

(8) The source regions of harmonic tremor inferred from the locations of long-period events have a clustered distribution, with gaps along the intermediate and deep parts of the plumbing system. These aseismic regions connecting the seismic sources along the expected magma transport paths may be relatively open, low-stress passages in which magma can maintain a state of quasi-steady flow that does not generate measurable seismic signals.

(9) In the Kilauea region, large numbers of short-period earthquakes reflect the tectonic response to magmatic pressure, and their distribution only broadly encompasses the interconnecting regions of magmatic activity. The spatial distribution of long-period events, on the other hand, outlines a more confined region that presumably represents the actual magma transport system beneath Hawaii.

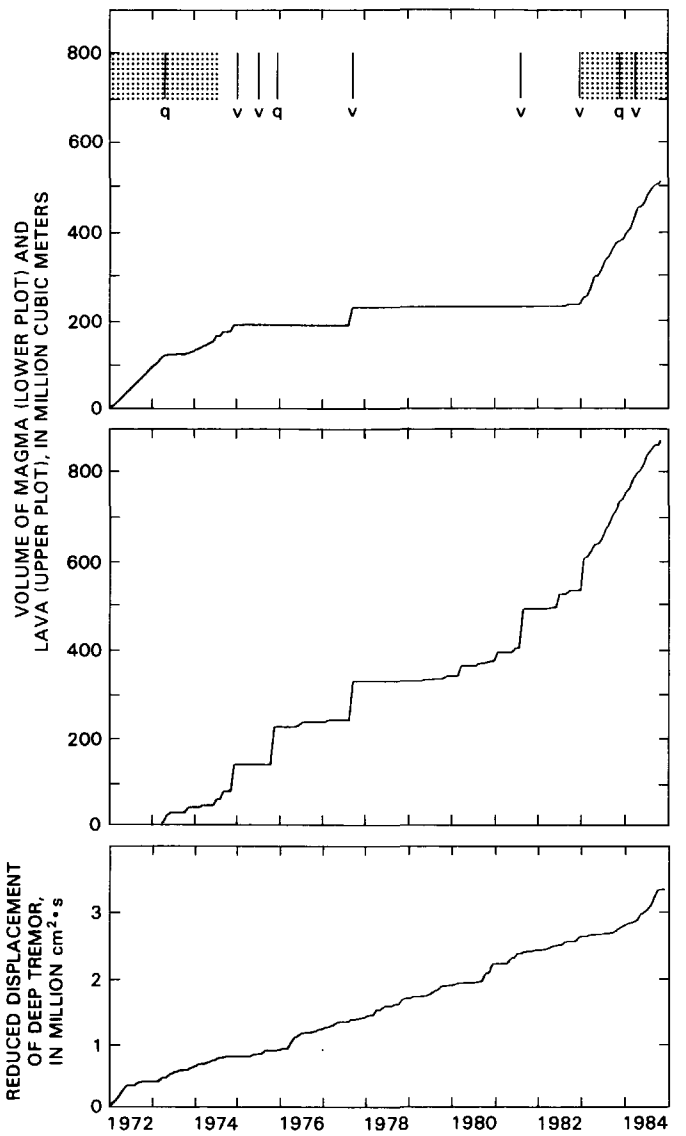

FIGURE 45.31.—Cumulative plots, for period 1972-1984, of reduced displacement of deep tremor, volume of magma removed from the summit storage system of Kilauea (estimated from tilt changes at Uwekahuna), and volume of lava extruded in eruptions on Kilauea Volcano. The plots are derived from monthly totals. Solid vertical bars mark onset times of significant volcanic events with more than an estimated ten million cubic meters of magma withdrawal from the summit storage system at Kilauea and Mauna Loa (v) and times of strong earthquakes of magnitude greater than 6.0 in Hawaii (q). Dotted vertical bars mark prolonged eruptions with frequently repeating episodes of lava output at Kilauea's Mauna Ulu (1972–1974) and Puu Oo (1983–1984).

(10) The temporal and spatial distribution of long-period events usually infer their immediate relation to harmonic tremor and magma movement. In some instances, however, shallow long-period events that develop above the summit reservoir during sustained ground deformation and continued swarms of short-period earthquakes may be the result of attenuation of high frequency signals transmitted through a path of increasingly fractured cap rocks. These are very shallow events within a few km of the surface that often do not lead to eruptions, and because they are typically small and recorded on a limited number of nearby stations, the possibility for a tectonic origin attributed to structural adjustments above the magma body cannot be conclusively excluded.

REFERENCES

Aki, K., and Koyanagi, R.Y., 1981, Deep volcanic tremor and magma ascent mechanism under Kilauea, Hawaii: Journal of Geophysical Research, v. 86, no. B8, p. 7095–7109.

Dzurisin, D., Koyanagi, R.Y., and English, T.T., 1984, Magma supply and storage at Kilauea Volcano, Hawaii, 1956–1983: Journal of Volcanology and Geothermal Research, v. 21, p. 177–206.

Klein, F.W., 1978, Hypocenter location program HYPOINVERSE, U.S. Geological Survey Open-File Report 78–694, 113 p.

———1983, Users guide to QPLOT, an interactive computer plotting program for earthquake and geophysical data, U.S. Geological Survey Open-File Report 83–621, 45 p.

Klein, F.W., and Koyanagi, R.Y., 1980, Hawaiian Volcano Observatory seismic network history 1950–79: U.S. Geological Survey Open-File Report 80–302, 84 p.

Koyanagi, R.Y., 1982, Procedure for routine analyses and classification of seismic events at the Hawaiian Volcano Observatory, part I: U.S. Geological Survey Open-File Report 82–1036, 77 p.

Koyanagi, R.Y., Tanigawa, W.R., and Nakata, J.S., in press, Seismicity associated with the eruption of Kilauea Volcano from January 1983 to July 1984, *in* Wolfe, E.W., ed., The Puu Oo eruption of Kilaeua Volcano, Hawaii: the first 1½ years: U.S. Geological Survey Professional Paper.

Koyanagi, R.Y., Unger, J.D., Endo, E.T., and Okamura, A.T., 1976, Shallow earthquakes associated with inflation episodes at the summit of Kilauea Volcano, Hawaii: Proceedings of the Symposium on Andean and Antarctic Volcanology and Chemistry of the Earth's Interior, special series, 11 p.

Nakata, J.S., Tanigawa, W.R., and Klein, F.W., 1982, Hawaiian Volcano Observatory summary 81, part I: U.S. Geological Survey Preliminary Report, 77 p.

Nakata, J.S., Tomori, A.H., Koyanagi, R.Y., and Tanigawa, W.R., 1984, Hawaiian Volcano Observatory summary 83, seismic data January to December, 1983: U.S. Geological Survey Preliminary Report, 86 p.

Swanson, D.A., Duffield, W.A., Jackson, D.B., and Peterson, D.W., 1979, Chronological narrative of the 1969–71 Mauna Ulu eruption, Kilauea Volcano, Hawaii: U.S. Geological Survey Professional Paper 1056, 55 p.

Swanson, D.A., Jackson, D.B., Duffield, W.A., and Peterson, D.W., 1971, Mauna Ulu eruption, Kilauea Volcano: Geotimes, v. 16, no. 5, p. 12–16.

Wright, T.L., 1984, Origin of Hawaiian tholeiite: a metasomatic model: Journal of Geophysical Research, v. 89, no. B5, p. 3233–3252.

Wolfe, E.W., Neal, C.A., Banks, N.G., and Duggan, T.J., in press, Geologic observations and chronology of eruptive events during the first 20 episodes of the Puu Oo eruption, January 3, 1983, through June 8, 1984, *in* Wolfe, E.W., ed., The Puu Oo eruption of Kilaeua Volcano, Hawaii: the first 1½ years: U.S. Geological Survey Professional Paper.

ORIGIN OF VOLCANIC TREMOR IN HAWAII

Part II
Theory and Discussion

By Bernard Chouet, Robert Y. Koyanagi, *and* Keiiti Aki[1]

ABSTRACT

Seismic events at Kilauea and other volcanoes suggest that harmonic tremor results from the sustained random occurrence of so-called long-period events. The long-period event can be viewed as the elementary process of tremor and interpreted as the impulse response of the tremor-generating system. Kinematic and dynamic source models are discussed, in which the tremor is generated by the excitation of a fluid-filled conduit triggered by an impulsive pressure transient. In one model, applicable to shallow tremor, a fluid-filled crack is excited into resonance by the brittle failure of rock caused by excess fluid pressure. The crack expands by the incremental extension of its tip or by the opening of a channel allowing the migration of fluid between neighboring cracks. Two types of sources are considered; in the first, the fluid behaves passively as a cushion and there is no acoustic source within the crack. In the second, the crack contains a viscous fluid that supports acoustic wave propagation. The crack behavior depends critically on a parameter called the crack stiffness, $C=(k/\mu)(L/d)$, where k is the bulk modulus of the fluid, μ the rigidity of the solid, L the crack length, and d the crack thickness. This dimensionless factor characterizes the ability of the crack to vibrate passively; oscillation of the wall is most pronounced when C is zero. For a passive fluid in a crack of stiffness $C=5$, simulating a shallow dike filled with molten basalt, the source duration never exceeds a few cycles. The resulting ground-motion spectrum displays broadband peaks whose dominant frequencies are markedly dependent on location and the component of motion considered.

Two time scales characterize the dynamics of the crack when the fluid participates actively in the motion of the source: the duration of brittle failure and the period of acoustic resonance of the fluid-filled crack. The failure of the crack tip has a duration proportional to the distance that the crack propagates. The resonant period is proportional to the length of the crack and varies inversely with the acoustic velocity in the fluid; it is generally much greater than the duration of brittle failure. Source duration depends strongly on fluid viscosity and associated viscous damping at the crack wall. When the fluid viscosity is low, the main mechanism of dissipation of energy is elastic radiation. The radiation loss only weakly affects the long-period motions of the crack, with the result that the fundamental mode of oscillation of the source can be maintained over a considerable length of time, the crack acting then as a high-Q oscillator.

Another model, in which the motion of a magmatic pipe is excited by the sudden flashing of ground water to steam as magma intrudes into the phreatic layer, displays similar characteristics. The motion of the source is represented by the excitation of the organ-pipe modes, whose bandwidths are determined from the combined losses due to viscous attenuation in the fluid and elastic radiation in the solid. In a cylindrical magma column, the radiation loss and the loss related to viscous damping are proportional and inversely proportional, respectively, to the square of the pipe radius, indicating that their relative importance depends critically on the geometry of the magma reservoir.

A kinematic model of fluid transport to explain deep tremor under Kilauea involves a constant total volume of magma and periodic magmatic injection, the period being proportional to the source length and inversely proportional to the velocity of the magma front. The predicted tremor spectrum is independent of the radiation direction, in agreement with observations. This model yields a simple relationship between the radiated elastic field and magmatic transport: the volume flow rate of magma ($\dot{q}$) is about 20 times the product of the velocity of the compressional wave in the solid (α) and the reduced displacement (the RMS displacement corrected for geometrical spreading and instrument magnification).

Seismic estimates of the volume of magma transported under Kilauea are consistently and significantly lower than estimates from deformation measurements for both deep and shallow tremor, suggesting that some magma flow occurs without significant pressure fluctuations in zones of undisturbed transport.

INTRODUCTION

A successful model for the source of volcanic tremor must account for the mass balance from magmatic transport in addition to the observed seismic wave field. The constraints on the flow, obtained mainly from deformation studies (that is, tilt and geodetic measurements) and surface observations of eruption products, must be compatible with the seismic amplitudes recorded. The model must also be consistent with the eruptive sequence, the spatial distribution of tremor amplitude, and the spectral characteristics and duration of the observed signal. Since harmonic tremor can last for a long time, it is not easy to perform a deterministic analysis of the entire signal. So efforts have been directed toward regarding tremor as a random sequence of shorter individual events that are more

[1] Department of Geological Sciences, University of Southern California, Los Angeles, California 90089-0741.

easily tractable. Recent observations point to the common characteristics shared by volcanic tremor and so-called long-period or low-frequency events. For example, at Ruapehu and Ngauruhoe Volcanoes in New Zealand, Latter (1979) distinguished volcano-tectonic earthquakes occurring in competent rock from low-frequency events associated with weak, low-impedance materials such as gas, magma, or fractured rock; he viewed volcanic tremor as a train of low-frequency events. At Mount Etna, Seidl and others (1981) identified transient seismic events that they termed wave packets. The spectral characteristics of these wave packets are similar to those of tremor and they are probably also low-frequency events. At Mount St. Helens, Fehler (1983) noted a strong similarity between the spectra of long-period events and of volcanic tremor and proposed that a tremor episode is nothing but a sustained sequence of long-period events. A similar conclusion was reached by Malone (1983), who studied a larger set of earthquakes at the same volcano. At Kilauea in Hawaii, long-period events and harmonic tremor show similar spatial distributions of observed amplitudes, share common spectral characteristics, and occur concurrently, implying a common source region (see Koyanagi and others, chapter 45, part I). Other studies pointing out the similarities in the frequency content of tremor and long-period events include Schick and Riuscetti (1973), Dibble (1974), Guerra and others (1976), Riuscetti and others (1977), Capaldi and others (1978) and McNutt (1986).

The evidence thus seems to suggest that volcanic tremor is simply a swarm of long-period events. Although this inference appears similar to the old notion that volcanic tremor is a swarm of Minakami's *b*-type events (see, for example, Minakami, 1974), there is a fundamental difference between these two concepts. In the earlier idea, the spectral characteristic of tremor is attributed to a path effect, while in the other it is viewed as a source effect. The *b*-type events' lack of clear shear arrivals and their spindle-shaped envelope of signal amplitude were attributed by Minakami to the extreme shallowness of the source. A similar idea is shared by many seismologists, who know that seismograms with signatures similar to that of *b*-type earthquakes are often observed for nonvolcanic sources such as explosions or tectonic earthquakes when the wave path is extremely heterogeneous and absorptive, as might be expected in volcanic areas. If volcanic tremor is nothing but a swarm of *b*-type earthquakes, it is logical to conclude that the spectral signature of tremor is also due to the path effect.

This conclusion, however, fails to explain some of the most spectacular observations made on volcanic tremor. Aki and Koyanagi (1981) presented conclusive evidence for the existence of sources of volcanic tremor at depths around 40 km below Kilauea and showed that their spectral characteristics and the temporal change of these characteristics cannot be explained by a path effect. The tremor frequency became lower as the volcanic activity increased, suggesting an increase in the source region and a larger volume of magma involved in the vibration. Temporal changes in the spectra of shallow tremor, which also cannot be explained by path effects, have been reported for various volcanoes including Mount Aso (Kubotera, 1974), Kilauea (Shimozuru and others, 1966), Mount St. Helens (Fehler, 1983), Etna (Schick and others, 1982), and Sakurajima (Kamo and others, 1977). Among these observations, that of *c*-type tremor at Sakurajima by Kamo and others (1977) offers the most convincing evidence. The Fourier spectra of the tremor they studied show many peaks spaced at regular frequency intervals; these can be attributed to the fundamental mode and higher harmonics of a one-dimensional oscillator. A typical one of their tremor episodes starts with the occurrence of shallow earthquakes and ends with a summit eruption. During the episode the frequency of the fundamental mode increases gradually and continuously from 0.5 to 1.3 Hz, and there is a corresponding increase in the frequencies of the higher modes. These observations can be explained by the vibration of magma and gas in a pipe, in which a rise of the magmatic column decreases the volume occupied by the gas and increases the eigenfrequency of vibration.

A shift of the tremor spectrum to higher frequencies during increased volcanic activity was also observed by Schick and others (1982) at Mount Etna, although the shift was probably not continuous in that case, because the various peaks were attributed to different segments of the feeder pipe.

These considerations appear convincing enough for us to reject Minakami's idea and to adopt the working hypothesis that the peaked spectra of volcanic tremor and long-period events are due to source effects. Furthermore, we can consider the long-period event as the basic element of the tremor signal, which means that we can view this event as the impulse response of the tremor-generating system. The standard tools of earthquake seismology can then be used for a quantitative description of this volcanic process. We will review the seismic-source models that have been proposed to account for the observations of tremor and discuss their implications.

ACKNOWLEDGMENTS

We are grateful to Bruce Julian and Elliot Endo for their careful reviews of this paper. This work was partially supported by the Department of Energy under contract DE–FG03–85ER13336 (Keiiti Aki).

A DYNAMIC MODEL FOR SHALLOW TREMOR

The first attempt to tie the seismic signature of tremor to the process of magma transport in a quantitative way was made by Aki and others (1977) for shallow tremor. They proposed three models of a fluid-filled crack driven by excess fluid pressure, in which they related the observed signal to physical parameters of the source while at the same time offering a geometry adequate for mass transport. In these models, magma intrusion can occur either by the incremental extension of a crack tip or by the opening of a channel allowing the migration of magma between neighboring cracks. The sudden extension of the tip or opening of the channel triggers the vibration of the crack wall, from which elastic waves are radiated into the solid. Sustained tremor is obtained by the superposition of many such events occurring randomly in time and depending in their spatial location on the actual path of magma.

To model this process, Aki and others (1977) considered two-dimensional cracks filled with fluid in an unbounded elastic medium

and assumed that the crack thickness was much smaller than the seismic wavelengths of interest. When the crack expands or a channel breaks open, an excess pressure is applied to the newly created crack surface. To calculate the motion of the crack resulting from this sudden local application of pressure, Aki and others (1977) used the finite-difference method with the boundary condition that the normal stress at the crack surface is equal to the pressure of the fluid. In this model, the fluid behaves passively as a cushion, and there is no acoustic pressure source within the fluid. A further simplifying assumption is that the fluid viscosity can be neglected; the fluid then does not support shear waves, and the shear stress vanishes at the crack surface.

An example of the solutions obtained by Aki and others (1977) for the opening of a channel between two cracks of length $L/2$ is given in figure 45.32. These plots show the normal component of particle velocities and displacements obtained at five positions on the surface of the double crack and expressed in dimensionless form in terms of the excess pressure (fluid pressure minus overburden pressure) ΔP, lengths L and Δl of the double crack and channel, respectively, as well as of the compressional velocity α and rigidity μ of the solid. Since the solution is symmetrical about the channel, the opening is depicted for one half of the source only. These results were calculated assuming a Poisson's ratio of 0.25 in the rock matrix and depend critically on a dimensionless parameter, C, called the crack stiffness factor and given by

$$C = \frac{k}{\mu}\frac{L}{d} \qquad (1)$$

where k is the bulk modulus of the fluid and d is the crack thickness. This important parameter characterizes the ability of the crack to vibrate passively. The oscillation of the wall is most pronounced when C is zero.

The value $C=0$ represents a dry (empty) crack, whereas the value $C=5$ is assumed to portray the minimum stiffness for a shallow crack filled with molten basalt. Since the rigidity of rock is practically constant and both L and d are more or less fixed from observations (the first by the predominant period of tremor, the second by the measurements made on rift zones or exposed sections of dikes), the critical assumption underlying the choice of C concerns the bulk modulus of the fluid. The observed ratio L/d being on the order of 10^3 for Hawaiian dikes, the low stiffness value $C=5$ chosen by Aki and others (1977) implies that the bulk modulus of the liquid is roughly a thousand times lower than the rigidity of the surrounding rock. This can only be achieved through the presence of bubbles within the fluid, and it is postulated that the source of these bubbles may be the drop of pressure induced in the liquid by the sudden opening of the crack faces.

Aki and others (1977) calculated the far-field body waves radiated by a variety of expanding wet and dry cracks and showed that in all cases the resulting seismic motion has a peaked spectrum because of the finite preexisting crack, in contrast to that of earthquake faulting, in which the crack nucleates at a point and expands continuously to its final size (Aki, 1967; Brune, 1970). Several strong peaks are present in the theoretical frequency-wavenumber spectra obtained by Aki and others (1977), but most of the high-frequency peaks are outside the range of seismic radiation, suggesting that high-frequency oscillations may be trapped in the near field of the source. Aki and others (1977) pointed out that these features for a crack vibrating by jerky extension correspond well to observed characteristics of volcanic tremor, such as the existence of spectral peaks, the strong high-frequency oscillations in the immediate vicinity of the eruption site, and the temporal change of peak frequency, which is naturally expected if the crack size changes with time. The idea that the high-frequency vibrations commonly observed near eruptive sites are due to inhomogeneous waves is attractive, but in view of the approximations involved in the calculations of Aki and others (1977), this idea needs further testing. An improved model that includes the details of the viscoelastic field within the fluid is also required to provide further insight into the effects of crack geometry and fluid properties on the characteristics of tremor observed near the source.

The model depicted in figure 45.32 was applied by Aki and others (1977) to the shallow tremor recorded by Shimozuru and others (1966) during the October 5–6, 1963, eruption of Kilauea. This eruption occurred along a 10-km fissure segment in the central part of the east rift zone between Napau Crater and Kalalua. According to Moore and Koyanagi (1969), the episode began at 0306 Hawaiian standard time (H.s.t.) on October 5 with a rapid deflation of the Kilauea summit, followed 10 min later by strong continuous harmonic tremor near the summit and in the upper east rift. The outbreak of lava presumably started at 0525 in Napau Crater (see fig. 45.33*A*), some 15 km east of the summit, when an acoustic shock was heard by local residents. By 0930 the line of vents had extended 5–6 km east-northeast of Napau Crater; beginning slightly before 1400, new outbreaks of lava occurred 5–10 km east of this crater. The eruptive activity ceased shortly before 0630 on October 6, but harmonic tremor continued for many hours thereafter. The total volume of extruded lava was estimated as 8.3×10^6 m^3, while the subsidence of the Kilauea summit is consistent with the withdrawal of nearly four times that amount of magma (about 30×10^6 m^3) and its injection into the east rift.

The data of Shimozuru and others (1966) clearly outline the source region of tremor, delineating a zone of maximum intensity centered near Halemaumau early on October 5 and showing a gradual elongation of this zone into a narrow belt extending into the east rift as the eruption progressed. The sequence of summit subsidence followed by onset of tremor, as well as the geodetic data and the relative amplitude of seismic motion at different stations, strongly suggest that the tremor was caused by a forceful injection of magma migrating progressively eastward into the rift zone. The simultaneous occurrence of tremor near the Kilauea summit and at Makaopuhi Crater, however, does not support the idea that the migration of magma occurred on a single well-defined front. Another argument against the idea of a single crack growing through the 25 km between the Kilauea summit and Kalalua is the lack of shift in the observed tremor frequency. For example, the dominant frequency decreased only slightly from 1.27 Hz to 1.08 Hz between 0600 and 1800 on October 5 at the Kaoiki station, while it increased from 1.19 Hz to 1.37 Hz at Ohale during the same period

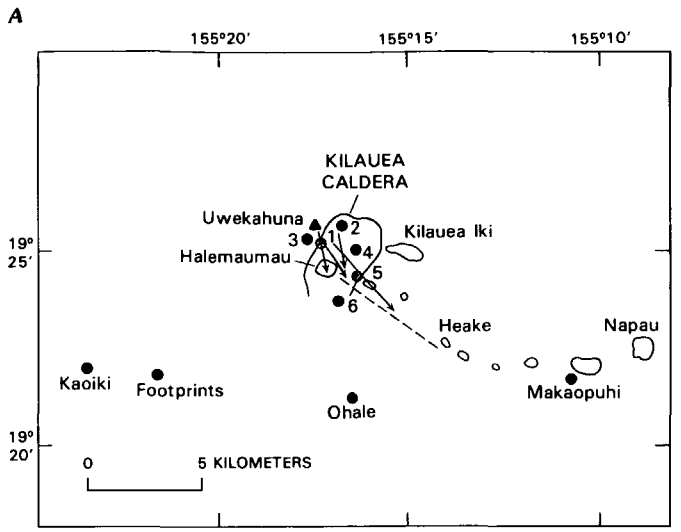

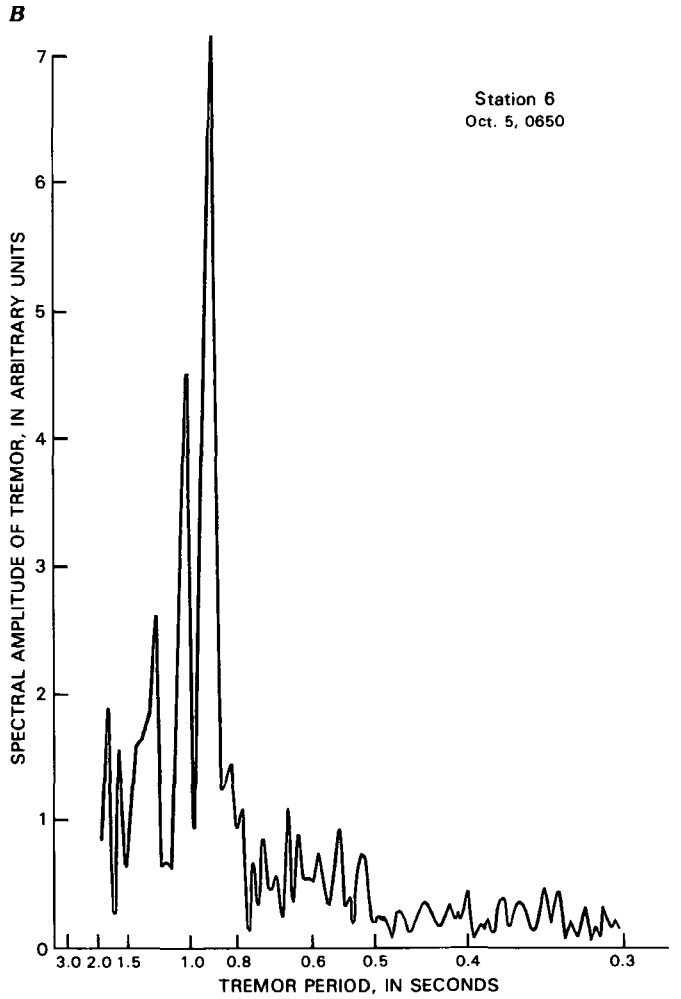

(see figure 45.33*A* for the location of the stations). The decreases of frequency shown by other stations are also too small to be significant. These observations can be explained if one assumes that the rift was still charged with melt from previous episodes of non-eruptive summit collapses and that magma started to move en masse into the rift as the eruption began.

To fit these observations, Aki and others (1977) proposed a transport model that consists of a chain of cracks connected by narrow channels and extending from the summit caldera to the eruption site. In this scheme, the motion of each pair of cracks excited by the opening of the channel linking them constitutes a seismic source and represents an individual long-period event. The tremor signal is then visualized as the sum of the contributions from the ensemble of these sources triggered independently of each other. Using the data of figure 45.32, Aki and others (1977) calculated the elastic radiation at a large distance from the source region, assuming that the channel openings occur randomly at a rate of n events per unit time. For shallow sources with focal depths in the range of 0.1–1 km and for epicentral distances exceeding a few wavelengths from the source, Rayleigh waves dominate the signal on the vertical component of motion. The root-mean-square (RMS) amplitude of Rayleigh waves radiated by an ensemble of shallow tremor sources embedded in a homogeneous half-space is given by

$$\mathrm{RMS}(u^R) = \frac{1}{\beta\mu}\sqrt{\frac{1}{\lambda r}}\,(p + q\sin^2\psi)cL\Delta P\Delta S\sqrt{2n\Delta f} \qquad (2)$$

where β is the shear wave velocity, p and q are constants depending on focal depth, r is the epicentral distance, ψ the azimuthal angle, c a constant approximately equal to 0.2 fixed by the source model, λ the wavelength, ΔS the area of the channel, and Δf the bandwidth of the dominant spectral peak of tremor. Assuming $\beta \simeq 2$ km/s, $\mu \simeq 3\times 10^{11}$ dyne/cm^2, and $(p + q\sin^2\psi) \simeq 0.1$, this equation becomes

$$L\Delta P\Delta S\sqrt{2n\Delta f} \simeq 3\times 10^{18}\cdot(\text{reduced displacement}), \qquad (3)$$

where the reduced displacement is the RMS displacement corrected for geometrical spreading and instrument magnification. This is given by Fehler (1983):

$$\text{reduced displacement} = \mathrm{RMS}(u^R)\sqrt{\lambda r} = \frac{A}{2\sqrt{2}}\,\frac{\sqrt{\lambda r}}{M}, \qquad (4)$$

FIGURE 45.33.—Some characteristics of tremor recorded at Kilauea Volcano in October 1963. ***A***, Map showing seismic stations (red dots) and pit craters in region of Kilauea caldera and upper east rift zone. Dashed line marks trend of maximum ground amplitude of volcanic tremor developed during the first 14 hours of activity on October 5, 1963. Arrows show azimuth of approach of tremor obtained for individual spectral components recorded with two tripartite arrays of seismographs, one near Uwekahuna (red triangle), the other inside the caldera (stations 1, 2, and 4). ***B***, Sample of tremor spectrum obtained at station 6 at 0650 on October 5. The spectrum shown is for the vertical component of motion and has been corrected for instrument response (from Shimozuru and others, 1966).

where A is the peak-to-peak amplitude of tremor and M is the magnification of the seismograph at the tremor frequency.

Using the vertical displacements observed at Ohale, Foot Prints, and Kaoiki (fig. 45.33*A*), Aki and others (1977) obtained an average reduced displacement of 4 cm^2, from which they estimated

$$L\Delta P\Delta S\sqrt{2n\Delta f} \simeq 10^{19} \text{ dyne·cm/s.} \quad (5)$$

This quantity is termed the seismic moment rate and expresses the intensity of volcanic tremor at its source. The seismic moment for the October eruption, obtained by integration of the moment rate over the entire episode of tremor activity, is about 0.5×10^{24} dyne·cm, which is roughly equivalent to a single magnitude 5 earthquake.

The length of the double crack constituting an individual source can easily be derived by comparing the dominant frequency on the synthetic seismograms of figure 45.32 with that observed in the records, yielding $L \simeq 1.2$–2.6 km. The continuity of tremor at frequencies near 1 Hz (see, for example, fig. 45.33*B*) further suggests that n (the event occurrence rate) cannot be very different from 1 per second, or else either the signal would become spasmodic or its frequency would be too high. Using the bandwidth $\Delta f \simeq 0.1$ Hz observed by Shimozuru and others (1966), one can easily derive from equation (5) the force F applied by the fluid to open the channel,

$$F = \Delta P\Delta S \simeq 10^{14} \text{ dyne.} \quad (6)$$

The excess magmatic pressure and area over which this pressure is applied cannot be uniquely determined from the seismic data alone in this simple two-dimensional model. To obtain additional constraints on these parameters it is necessary to construct a three-dimensional model of mass transport between the two cracks. Such a model was considered by Chouet (1981), who made a detailed analysis of the motion of the ground in the near field of the tremor source postulated by Aki and others (1977).

GROUND RESPONSE IN THE NEAR FIELD OF A FLUID-DRIVEN CRACK

Using the discrete wave number method (Bouchon, 1979), Chouet (1981) obtained the ground response in the near field of the opening crack whose source space-time dependence is depicted in figure 45.32. His model, tailored to fit the parameters derived earlier by Aki and others (1977), consists of two vertical cracks with dimensions of 1 km by 1 km separated by a channel as shown by the rectangle in figure 45.34. The space-time history of crack opening depends on the horizontal dimension of the double crack only; the opening is taken to be independent of the vertical coordinate. Thus, the situation considered is that of the opening of a vertical strip bisecting the source; however, as Chouet's model uses the source function obtained for a two-dimensional crack by Aki and others (1977), the effect of the finite vertical dimension of the crack is neglected.

Chouet (1981) calculated the ground motion for a variety of earth structures compatible with the medium under Kilauea as determined by Ryall and Bennett (1968). He considered the motion

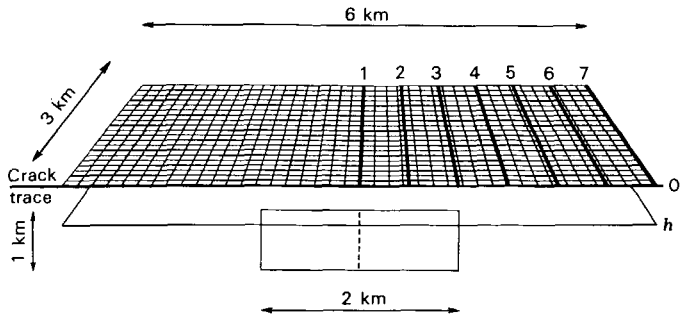

FIGURE 45.34.—Configuration of source, medium, and receivers used in computing ground motion produced by the jerky opening of a channel between two cracks. Source is represented by vertical rectangular plane, 2 km by 1 km; channel is marked by dashed vertical line bisecting the source plane. Ground displacements are computed at 861 locations over an area 3 km by 6 km adjacent to the crack trace. Separation between stations is 0.15 km in both the transverse and longitudinal directions. Heavy lines give positions of seven transverse profiles, spaced 0.5 km apart (see text). Plane at depth h represents bottom of surficial layer used in three of Chouet's case studies.

in an area of 3 km by 6 km adjacent to the crack trace, calculating the displacements at 861 locations spaced every 0.15 km in the directions normal and parallel to the crack plane. The configuration of the source, medium, and receivers is shown in figure 45.34, where each node represents a station and the plane at depth h represents the bottom of a surficial layer used in some of the calculations. In addition, Chouet (1981) made a detailed analysis of the synthetic seismograms obtained at selected stations along seven profiles marked by the heavy lines in the figure. These profiles, spaced 0.5 km apart, are set such that profile 1 bisects the source, and profile 7 is 2 km away from the crack tip.

The basic features of the ground response are displayed in a series of snapshots (fig. 45.35) obtained for the simple case of a fluid-filled crack with stiffness $C = 5$, buried at a depth of 0.5 km in a homogeneous half space with compressional velocity $\alpha = 3$ km/s, shear velocity $\beta = \alpha/\sqrt{3}$ and density $\rho = 2.7$ g/cm^3. The snapshots are taken at intervals of 0.25 s, starting 0.25 s after the failure and covering the entire duration of motion for this event. The three components u, v, and w correspond to the horizontal axis along the crack plane (positive to the right in fig. 45.34), the horizontal axis normal to the crack plane (positive away from the source in fig. 45.34), and the vertical axis (positive upward).

The sequence displayed in figure 45.35 clearly shows the onset of the disturbance and the propagation of the various wave fronts over the area, leaving a pattern close to the static displacements after 3 s. Note that the first motion is compressive everywhere but the static longitudinal and vertical displacements are inward and downward immediately above the source. Note also the behavior of the peak dynamic motion in the time interval 0.5–1.5 s, which shows a pattern similar to the static deformation rather than to the first motion; that is, the maximum displacement of w is negative (downward) immediately above the source, and u is negative to the right of the epicenter and positive to the left of the epicenter. The crack trace

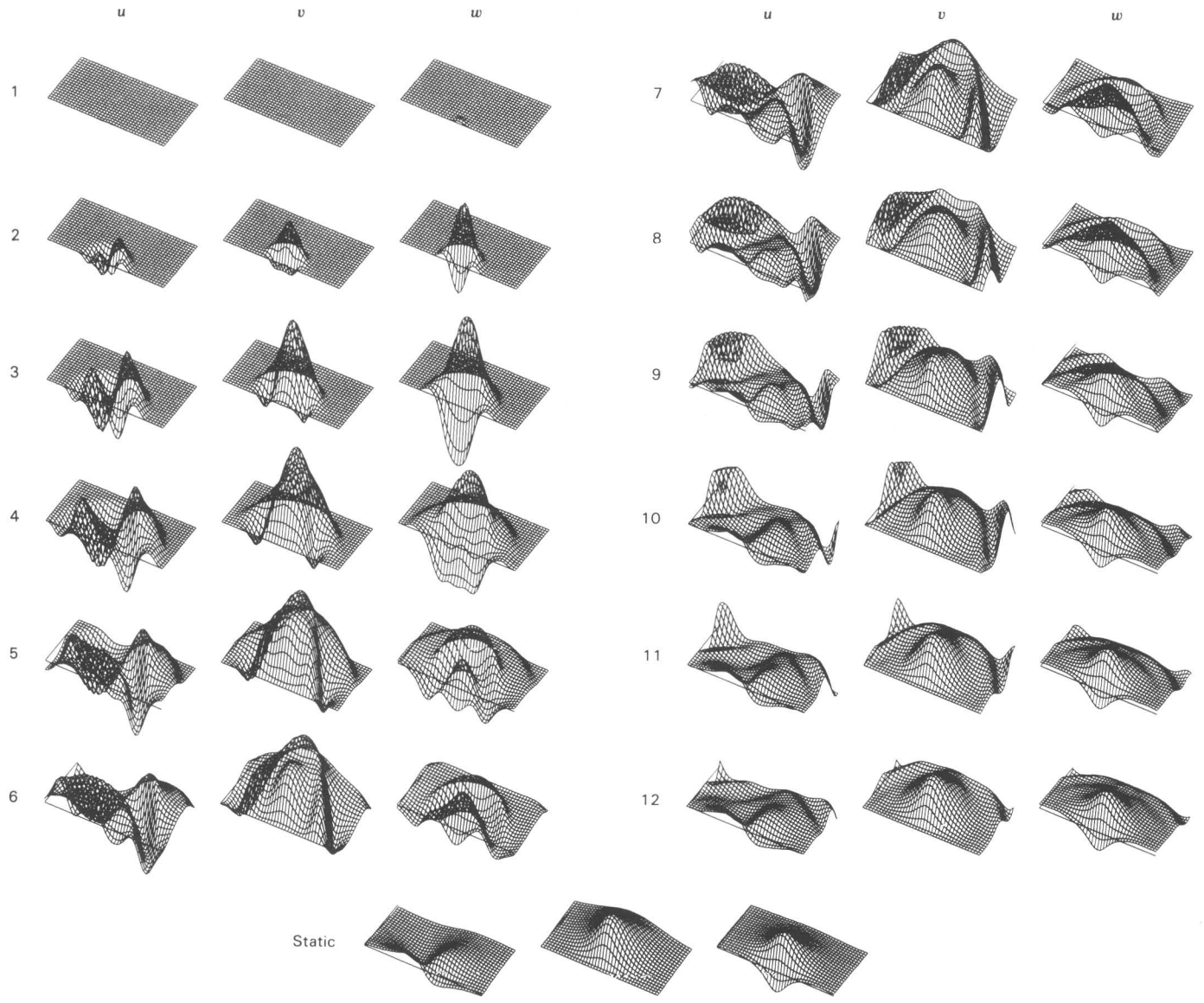

FIGURE 45.35.—Computer-generated snapshots of surface displacements produced by the jerky opening of a double crack in a homogeneous half-space. Depth to the top of the source is 0.5 km. Three components of displacement shown at top: *u*, longitudinal; *v*, transverse; and *w*, vertical. Snapshots are taken every 0.25 s, starting 0.25 s after rupture and covering the first 3 s of the event history. Final static displacement shown at bottom.

and the direction of profile 1 are both nodes for horizontally polarized shear (*SH*) motion because of the antisymmetry of the horizontal displacements about these two lines.

A useful tool in the study of tremor is the representation of the ground response in the frequency domain. This is done in figure 45.36, which displays the spectral amplitude of the ground velocity as a function of frequency and distance along individual profiles. These three-dimensional plots are obtained by sampling the entire record of motion depicted in figure 45.35 over the band of 0–3 Hz. The spectra have a characteristic structure marked by dominant and subdominant peaks at frequencies that depend on the receiver location and on the component of motion being considered. The shift of the dominant spectral peak as a function of receiver location is most pronounced on the horizontal component of velocity normal to the crack plane: the strong peak observed at low frequency eventually vanishes completely, giving place to another peak roughly one octave higher as we move along a line parallel to the crack trace. By comparison, the other two components of motion are much more stable, showing shifts of only 20–30 percent at several locations close to the source. The remarkable variation of the dominant peak observed on the transverse horizontal component reflects the rapid evolution in the composition of the wave field from compressional and shear motions that are purely vertically polarized (*P–SV* motions) along profile 1 to motions that are dominantly *SH* along profile 7. There is no strong evidence in these plots or in other models analyzed by Chouet (1981) that high-frequency energy is predominant near

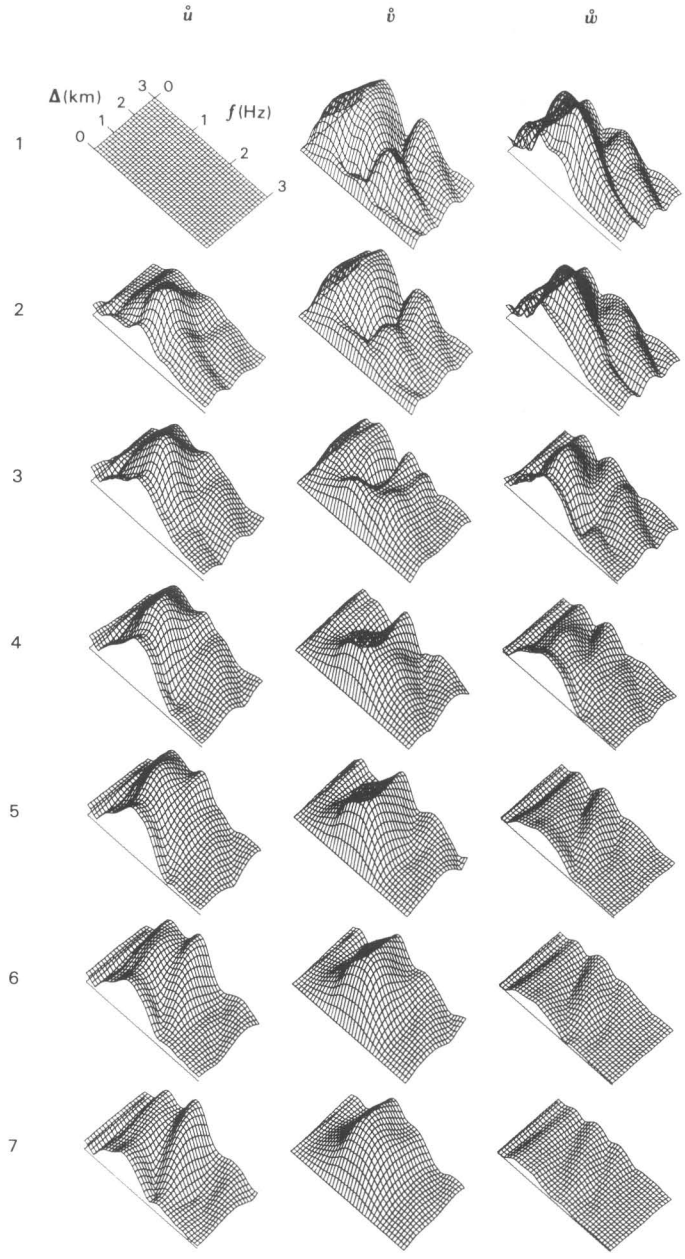

FIGURE 45.36.—Spectra of the three components of ground velocity at 21 stations along 7 profiles of figure 45.34 for a wet crack with stiffness $C=5$ opening in a homogeneous half-space. Profiles are numbered at left; components are indicated at top: $\dot{u}$, longitudinal; $\dot{v}$, transverse; and $\dot{w}$, vertical. Disposition of the plots is given at upper left: Δ, distance along the profile from the crack trace; f, frequency. The spectra are representative of the entire 3-s record of motion.

the source. These models, however, do not extend far enough from the crack to allow a meaningful comparison of near- and far-field spectral characteristics in the ground motion; hence they cannot fully resolve the question of the partitioning of elastic energy between radiating and nonradiating fields. The main factor contributing to the complexity of the ground-response spectra in Chouet's models is the structure of the medium. For example, the presence of a layer in the medium can affect the dominant frequency of the signal by two octaves or more on any component of motion.

Synthetic seismograms of the ground displacements are shown in figure 45.37 for the more complex response obtained in a structure that consists of a single surficial layer underlain by a half space. The layer is 0.25 km thick and has the density and compressional and shear velocities ($\rho=2.3$ g/cm^3, $\alpha=1.7$ km/s, and $\beta=\alpha/\sqrt{3}$, respectively), appropriate for the unconsolidated volcanic deposits found along the east rift (Ryall and Bennett, 1968; Aki and others, 1977). The parameters of the half space and depth of the source are the same as in the previous model. The displacements are shown for 56 stations located along the 7 profiles given in figure 45.34. There are 8 stations per profile, set at distances from 0 km to 3 km from the crack trace. The synthetics have been normalized by the product $\Delta P \Delta l$, the excess pressure applied in the channel times the length of the channel.

The pattern of radiation is similar to that seen earlier and depicts the evolution of the signal from a rather simple signature close to the source to a complex train of Love and Rayleigh waves, as well as multiply reflected *SH* and *SV* waves at larger ranges. Vertical motion attenuates more rapidly than horizontal motion, with the result that *SH* motion dominates at distances greater than a few source depths. The maximum radiation for this type of motion is in the azimuth bisecting the two nodal lines represented by the crack trace and profile 1. These nodal lines also correspond to maxima in the Rayleigh-wave radiation, the maximum Rayleigh motion being found in the direction of profile 1. Indeed, well-developed Rayleigh waves are conspicuous in the later part of the signal on the vertical component at distances beyond 2 km along this profile. The calculations made by Chouet (1981) indicate that these surface waves dominate the dynamic response at a distance of roughly 9 km, in agreement with the assumption made by Aki and others (1977) in computing the far-field radiation from the source. As observed earlier, the first motion is always a compression. Notice the very small amplitude of this first arrival close to the crack trace, where it is followed by a strong dilatation corresponding to the peak signal amplitude on the vertical and longitudinal components. This dilatational response is predominantly a near-field effect, and its amplitude decreases quickly at larger ranges from the source.

IMPLICATION OF THE DYNAMIC MODEL FOR MAGMA TRANSPORT

The results depicted in figure 45.37 were applied by Chouet (1981) to the data obtained by Shimozuru and others (1966) at stations 5 and 6 in the near field of the tremor source (see fig. 45.33*A*). From these observations, and assuming the rate of channel opening to be one event per second as considered earlier by Aki and others (1977), he derived the magnitude of the force applied by the fluid $F \simeq 4\text{–}12 \times 10^{13}$ dyne, in close agreement with the result derived from the analysis of the data from the Ohale, Foot Prints, and Kaoiki stations. Using the data from figure 45.32, Chouet

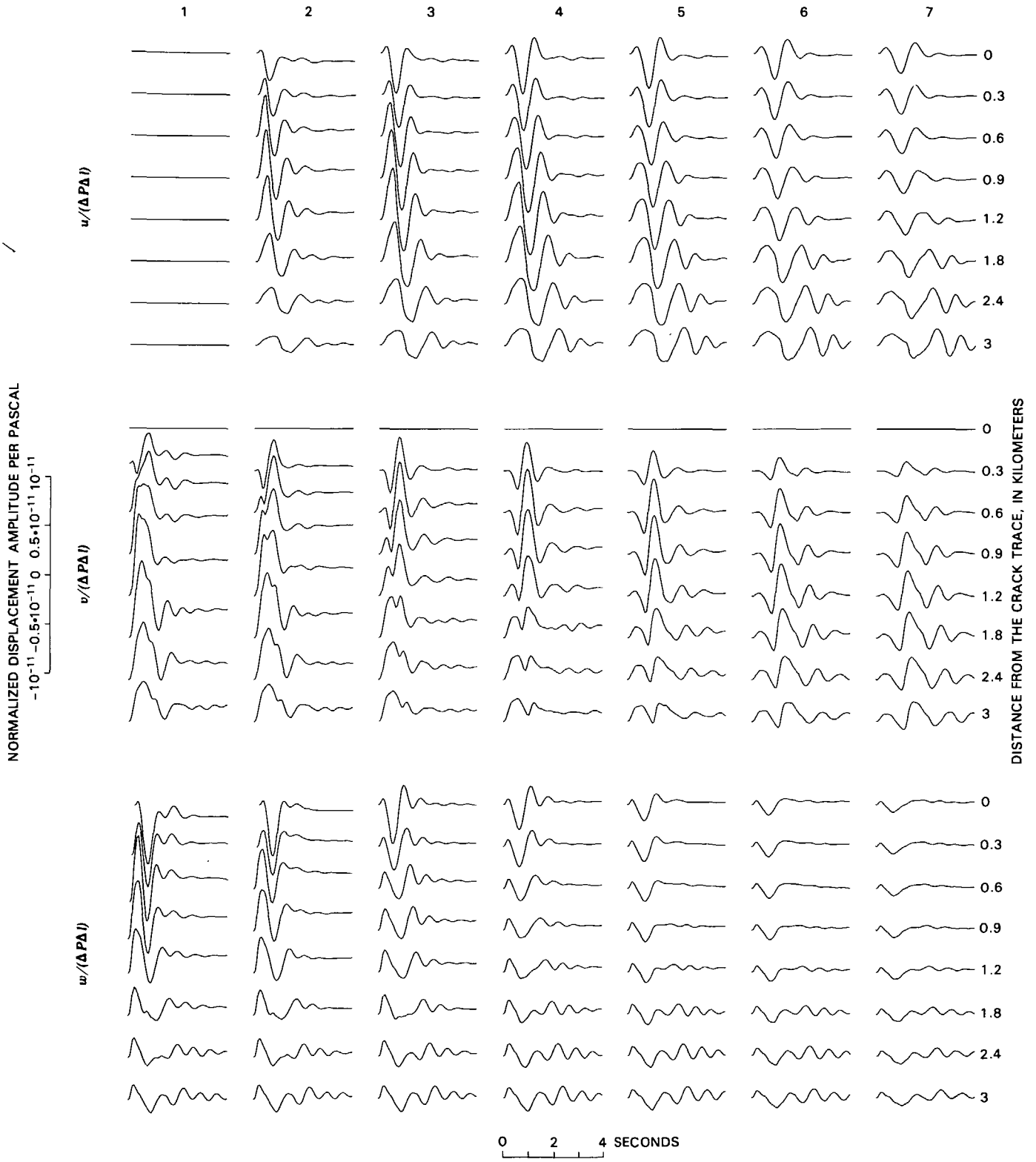

FIGURE 45.37.—Synthetic seismograms of three components of normalized ground displacement at eight stations along each of the seven profiles of figure 45.34 for the case of an opening crack in a half space with a surface layer. The source depth is 0.5 km, and the layer thickness is 0.25 km. For each component of motion marked at the left and for each profile indicated at the top of the figure, records are shown for distances of 0 (top), 0.3, 0.6, 0.9, 1.2, 1.8, 2.4, and 3 km (bottom) from the crack trace. Each record starts with the arrival of the *P* wave and is approximately 4 s long.

(1981) then determined the static channel opening, Δv, to be about 0.1 mm and the incremental volume of the source, ΔV, to be about 40 m^3. From equation 1 he found that the assumed value $C = 5$, together with the values $L = 2$ km and $\mu = 8.1 \times 10^{10}$ dyne/cm^2 that are compatible with the medium parameters, gives the ratio $k/d = 2 \times 10^6$ dyne/cm^3. For a crack 0.5 m thick, representative of the average Hawaiian dike (Swanson and others, 1976), this requires a bulk modulus for the fluid of 10^8 dyne/cm^2.

A critical result obtained by Chouet (1981) is the width of the channel opening compatible with the seismic data, which is too small to account for significant mass transfer between the two cracks. This suggests that numerous incremental openings are necessary for fluid flow to take place, and since the total area of the double crack is fixed by the observed frequency of tremor, the only way to accommodate this idea is to assume that the channel does not open over the entire height of the source at once. The assumption that the source space-time function is independent of the vertical crack dimension, which stems from the two-dimensional model of Aki and others (1977), is violated in that case, but the seismic moment estimate itself will not change, because it represents the integral of the opening over the area of the crack, a figure independent of the details of the rupture history. Therefore, the seismic estimate of ΔV derived above will not change, and the area of the channel cross section will remain the same, although the actual shape of this cross section may be different from the simple model that Chouet (1981) assumed. This, of course, is important from the standpoint of the transport problem, because the amount of fluid migrating between the two cracks is a function of this cross section.

To model the magma-transport process, Chouet (1981) assumed that the excess pressure in the magma-supplying crack is constant and that there is no outflow from the magma-receiving crack. He further assumed that the channel opens at a steady rate of one event per second and used the results from the seismic data to define the rate of increase of its cross-sectional area. Considering a Poiseuille flow, he obtained a model in which the fluid flow increases with the cumulative jerky openings, reaches a peak, and then decreases with the decrease in pressure difference between the two cracks. His result is depicted in figure 45.38 for an assumed excess pressure in the magma-supplying crack of $\Delta P = 4$ MPa, a channel length of $\Delta l = 0.5$ m, and fluid viscosity of $\eta = 10^2$ poise. The loading time in this model is 617 s, or approximately 10 min, and the final opening of the channel is 6.17 cm; the peak volume flow rate through the channel is 929 m^3/s, reached 307 s after the onset of loading; the peak flow velocity is 31.5 m/s, reached 278 s into loading; and the total volume of fluid accumulated in the receiving crack during this process is about 0.2×10^6 m^3.

The subsidence of the Kilauea summit indicates that approximately 2.2×10^7 m^3 of magma was injected and remained in the east rift during the October eruption. Since the distance between the summit reservoir and Kalalua is about 25 km, a chain of about 25 1-km cracks is required to provide a continuous fluid connection to the erupting fissures. This suggests that the total amount of magma accumulated in the rift by the above process is roughly 25 times 0.2×10^6 m^3 or 5×10^6 m^3. Thus there is a significant discrepancy between the seismic estimate of the magmatic intrusion and the

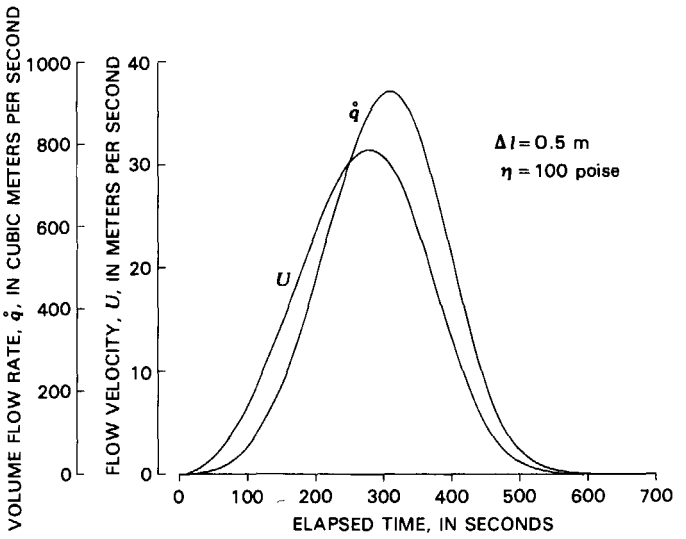

FIGURE 45.38.—Loading characteristics of dike, showing the volume flow rate and flow velocity in the channel separating the two cracks as functions of the time elapsed since onset of channel opening. Channel length (Δl) and viscosity η are indicated.

estimate from summit deformation. Another difficulty with the above model is the apparent disparity between the observed total duration of the tremor episode, which amounts to about 35 hours, and the duration expected for the model process. For the channel-opening rate of one event per second and loading time of approximately 10 min per crack, the model can satisfactorily explain the 150 min delay observed between the onset of subsidence at the Kilauea summit and the presumed breakout of lava in Napau Crater. The additional distance to Kalalua can perhaps account for another two or three hours of activity, but then one would expect the tremor to stop. Thus, while the postulated failure process may play a significant role in the magmatic transport, it does not easily account for the total balance of fluid transport or the duration of a tremor episode. We shall come back to this problem later.

A KINEMATIC MODEL FOR DEEP TREMOR

We have seen from the previous model that the basic requirement for a fluid-filled crack to vibrate is for it to have a low stiffness (C) on the order of 1, a condition which can only be satisfied by assigning a value as low as 10^8 dyne/cm^2 to the bulk modulus of magma; this low figure implies that there is a large amount of bubbles in the fluid. Although this requirement may seem reasonable for shallow tremor, it is unlikely to be met at depths of 30–50 km, where the confining pressure exceeds 1 GPa. Furthermore, both near-field spectra calculated by Chouet (1981) and far-field spectra calculated by Aki and others (1977) show a dependence on the radiation direction, at odds with observations made on deep tremor, which show the same period at every station.

In view of these limitations, the dynamic model of Aki and others (1977) cannot be applied to the source of deep tremor under

Kilauea. For such tremor Aki and Koyanagi (1981) proposed a new kinematic model that offers a direct relation between magmatic transport and tremor amplitude and also provides an identical period at every station. Because the high ambient pressure in the source region should prevent the formation of a cavity during any mode of crack vibration, they considered a model of transport in which the total volume of magma remains constant. Their two-dimensional source, depicted at the top of figure 45.39*A*, consists of a pair of cracks of lengths $L/2$ linked by a narrow channel, a situation reminiscent of the earlier model. The channel opens in response to excess pressure buildup in the left crack, allowing magma to migrate rapidly into the crack at the right. The successive snapshots of the source shown in the figure graphically depict the deformation of the two cracks during magma transport. To simulate this process, Aki and Koyanagi (1981) assumed a uniform-displacement model, in which the magma migrates with a constant velocity a and the tensile displacement of the crack walls $\pm\Delta v$ associated with this migration is steplike in character. The far-field radial displacement produced by this kinematic source has a Fourier transform given by

$$u^r(\vec{R},\omega)=\frac{\lambda+2\mu\sin^2\theta}{4\pi\rho\alpha^3R}W\Delta v\frac{1}{i\omega}\cdot\left[\left(1-\exp\left[-i\omega\frac{L}{2}\left(\frac{1}{a}-\frac{\cos\theta}{\alpha}\right)\right]\right)\left(\frac{1}{a}-\frac{\cos\theta}{\alpha}\right)^{-1}-\left(1-\exp\left[-i\omega\frac{L}{2}\left(\frac{1}{a}+\frac{\cos\theta}{\alpha}\right)\right]\right)\left(\frac{1}{a}+\frac{\cos\theta}{\alpha}\right)^{-1}\right],\quad(7)$$

where $\vec{R}$ is the observation point, $R=|\vec{R}|$, θ is the angle between the direction of magma movement and the direction of the observation point, W the crack width (in the direction perpendicular to the plane of figure 45.39*A*), ω the frequency, ρ the density, and λ the first Lamé elastic modulus.

The pulse shape corresponding to the large bracketed term premultiplied by $1/(i\omega)$ in equation 7 is shown in figure 45.39*B*. The total duration of the signal is $\Delta t=(L/2)[(1/a)+(\cos\theta/\alpha)]$, and the seismic moment of the source is zero because there is no net change of volume. To account for tremor sustained over many cycles, Aki and Koyanagi (1981) arbitrarily assumed that the magmatic injection is a periodic process with a period $T\simeq L/a$. The signal during $T-\Delta t$ was assumed to be zero.

This model offers the following simple relation between the volume flow rate of magma and the observed seismic displacement:

$$\dot{q}=WL\Delta v/(2T)\simeq aW\Delta v/2.\quad(8)$$

For an order-of-magnitude estimate of the magma transport associated with the source of deep tremor, Aki and Koyanagi (1981) assumed that the observed free-surface displacement is composed mainly of P waves. Neglecting anelastic attenuation, they defined the reduced displacement for body waves as

$$\text{reduced displacement}=RMS(u^r)\cdot R=\frac{A}{2\sqrt{2}}\frac{R}{M},\quad(9)$$

where the root-mean-square amplitude of P waves obtained from equation 7 is

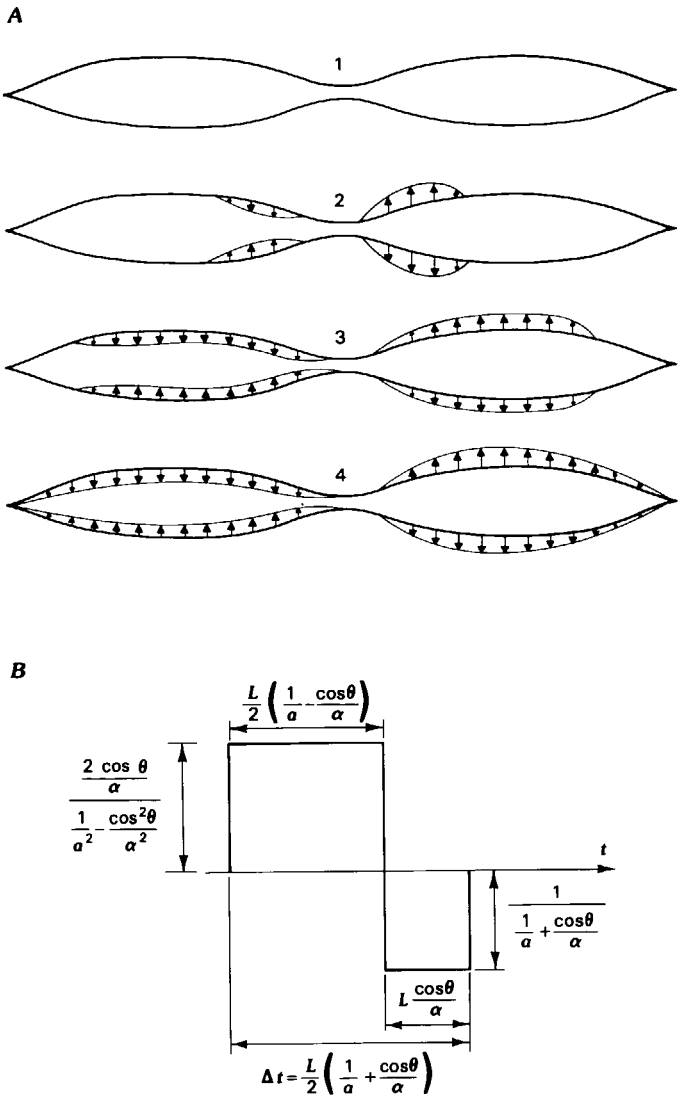

FIGURE 45.39.—Magma transport between two cracks connected by a channel. ***A***, Schematic view of magma transport from the crack on the left to the crack on the right. Arrows indicate change of crack shape as magma movement spreads over whole crack area. ***B***, Far-field waveform of P waves radiated from the source represented by this double crack (see text for explanation).

$$\mathrm{RMS}(u^r)=\frac{\lambda+2\mu\sin^2\theta}{4\pi\rho\alpha^3R}W\Delta v\cdot\left(\frac{2\cos\theta}{\alpha}-\frac{L}{T}\right)^{1/2}\left(\frac{1}{a^2}-\frac{\cos^2\theta}{\alpha^2}\right)^{-1/2},\quad(10)$$

which corresponds to equation 5 of Aki and Koyanagi (1981), corrected for a missing exponent of ½. Assuming $\lambda=\mu$, $\theta=45°$ and $\alpha/a=4$, we obtain from equations 8, 9, and 10

$$\dot{q}\simeq 20\alpha\cdot(\text{reduced displacement}),\quad(11)$$

which, for $\alpha=8$ km/s, gives a flow rate in cm^3/s of 1.6×10^7 times the reduced displacement. The reduced displacement is plotted

against the dominant frequency of deep tremor in figure 45.40, which yields the relation that reduced displacement is about $(1/T)^2$, from which one can obtain a quantitative estimate of the flow. For example, tremor with a period around 0.5 s has a reduced displacement of 30 cm^2, which corresponds to a flow of 0.5×10^9 cm^3/s or 5×10^2 m^3/s. The slope of $-1/2$ depicted in this figure can be explained if strong and weak tremor are dynamically similar, or, in other words, if the nondimensional products made of physical parameters are the same for strong and weak tremor. While the observed similarity between large and small earthquakes (Aki, 1972; Kanamori and Anderson, 1975) implies a constant stress drop, independent of earthquake size, the similarity for deep tremor implies a constant excess pressure, independent of crack size. This similarity, however, breaks down for shallow tremor, which is clearly nonfractal (Mandelbrot, 1977), because the period appears fixed, independent of signal amplitude, for a given episode (Shimozuru and others, 1966; Fehler and Chouet, 1982; Fehler, 1983). It is interesting to note that dike widths have a fixed average value for a given area. For example, the average width is 4 m in Iceland, 1.8 m in Scotland, 6 m at the Columbia River (Williams and McBirney, 1979), and 0.5 m at Kilauea (Swanson and others, 1976). Thus, dikes near the surface appear to be nonfractal. The data of figure 45.40, therefore, provide an exceptional observation in support of a trend toward self-similarity for deeper magmatic processes.

Aki and Koyanagi (1981) made a systematic search for deep tremor episodes during the period 1962–1979 using data from stations around Kilauea. These data consist of narrow-band smoked-paper records that predominantly sample the longer-period tremor. Selecting records with duration longer than about 10 min and peak-to-peak ground motion larger than a few hundredths of a micrometer, they tabulated the starting and ending time of each episode, as well as the period and average peak-to-peak amplitude of tremor for every 5-min interval of the seismic trace. From these data they derived the reduced displacement assuming an average distance of 52 km obtained from sources of tremor episodes with known locations. Their results are summarized in table 45.3, and the average yearly duration of tremor with calculated reduced displacement larger than a specified value is shown in figure 45.41. The duration decreases exponentially with increasing displacement, reflecting the predominant length scale sampled by the narrow-band records. These long-period tremors represent the dominant contribution to the observed surface displacements.

To determine the cumulative reduced displacement over the 18-year period, Aki and Koyanagi (1981) took the reduced displacement for each interval, multiplied it by the duration of the interval, and summed over successive episodes cumulatively with time. The result, shown in figure 45.42, indicates a steady accumulation of reduced displacement with time. This plot can easily be converted to cumulative magma flow as a function of time, in which case the left-hand vertical coordinate becomes cumulative magma flow in units of 1.6×10^{13} cm^3, indicating a total magma flow of 10^{14} cm^3, or 0.1 km^3 in 18 years. This is about 1/20 of the 1.8 km^3 expected from Swanson's (1972) estimate of 0.1 km^3 per year, and about 1/5 of the erupted lavas as shown on the right hand side of the figure.

The low estimate of magma ascent obtained by Aki and Koyanagi seems to suggest that a significant volume of magma is transported through Kilauea without generating measurable tremor. Although one cannot discount the possibility that part of the magma may be transported in a steady flow that would not generate any tremor at all, a more plausible explanation may be that the pressure fluctuations associated with the unsteadiness of the flow are too small to be observable. To see the implication of this result in terms of the excess magmatic pressure involved at the source, we have to deal with the energetics of the process of tremor generation.

According to Aki (1984), from simple energy conservation we can derive the following relation between the reduced displacement for body waves and the root-mean-square pressure fluctuation, RMS(ΔP), applied over the volume V of the source:

$$\mathrm{RMS}(u^r)R = \frac{1}{2\pi}\left(\frac{1}{Q_s}\right)^{1/2}\left(\frac{V}{2f\alpha\rho k}\right)^{1/2}\mathrm{RMS}(\Delta P), \qquad (12)$$

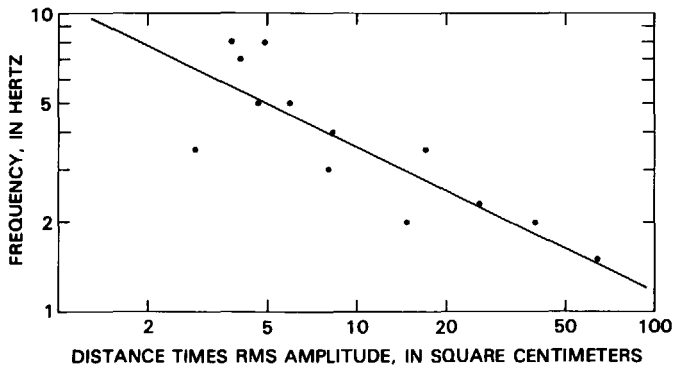

FIGURE 45.40.—Relation between tremor period and reduced displacement for body waves. The slope of $-1/2$ can be explained by the similarity between large and small cracks, implying a constant excess pressure independent of crack size.

TABLE 45.3.—*Duration of tremor at Kilauea per year, 1969–1979*

[After Aki and Koyanagi, 1981; RD, reduced displacement, in cm^2]

Year	Duration of tremor (min)			
	RD≥5	RD≥10	RD≥15	RD≥20
1962	316	164	90	35
1963	250	83	43	0
1964	516	213	127	85
1965	234	93	63	25
1966	152	72	27	17
1967	312	108	35	25
1968	425	241	117	69
1969	401	218	126	76
1970	438	241	109	61
1971	358	189	136	46
1972	505	310	141	70
1973	305	142	50	25
1974	214	80	39	19
1975	153	50	7	7
1976	352	160	93	62
1977	231	77	30	15
1978	314	206	137	83
1979	267	121	81	36
	319	154	81	42

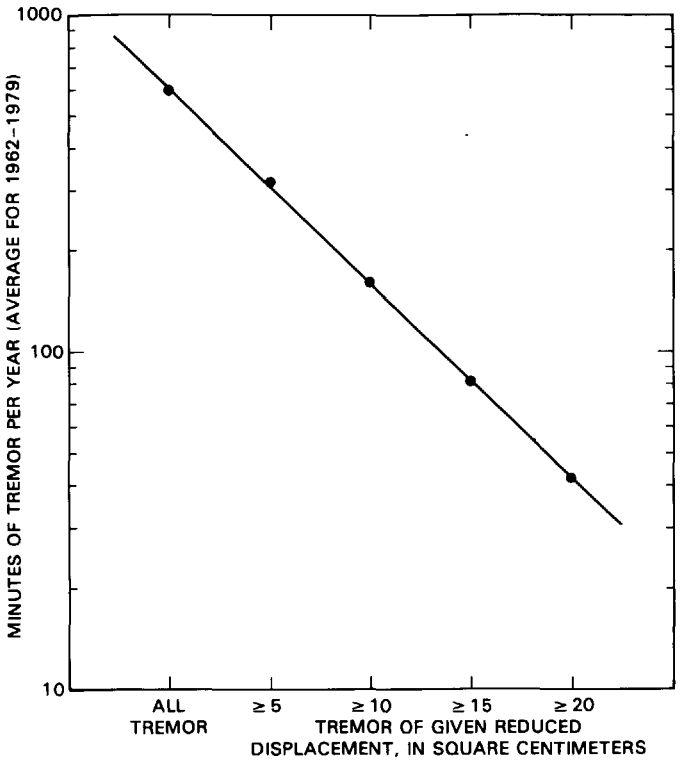

FIGURE 45.41.—Duration of tremor recorded per year with reduced displacements greater than specified values.

where f is the dominant frequency of tremor and Q_s is the quality factor corresponding to the radiation loss. This factor is given by

$$\frac{1}{Q_s} = \frac{1}{Q} - \frac{1}{Q_\eta}, \tag{13}$$

where Q is the apparent quality factor and Q_η is the quality factor due to magma viscosity. The apparent quality factor can be measured directly from the observed spectra of tremor as $Q \simeq f/\Delta f$. For Hawaiian tremor, Q is about 10 and the quantity $(1/Q_s)^{1/2}$ is on the order of 0.1. The observed reduced displacements (fig. 45.40) themselves range from 1 to 10^2 cm^2 in the frequency interval 1–10 Hz. Since $f = a/L$ in the above kinematic model, one can obtain L once the velocity of the magma front is known. Assuming $a = 2$ km/s (Aki and Koyanagi, 1981), the observed frequencies correspond to single crack lengths in the range of 0.1–1 km. For a rough order-of-magnitude estimate of the volume of fluid involved at the source, we further assume that the crack is circular and has a thickness on the order of 1 m, from which we obtain V in the range of 10^{10}–10^{12} cm^3. Other parameters in equation 12 that are easily estimated are $\rho \simeq 3$ g/cm^3, $\alpha \simeq 8$ km/s and $k \simeq 10^{11}$ dyne/cm^2 (assuming no bubbles in magma). This yields RMS$(\Delta P) = 8 \times 10^4$–$2.5 \times 10^5$ Pa, indicating that the minimum root-mean-square pressure fluctuation required at the source to generate observable tremor is on the order of 10^5 Pa for the case of deep tremor in Hawaii.

The above kinematic model implies an actively participating fluid in the tremor-generation process, and in that sense it is a precursor to the more elaborate models unifying the fluid dynamics and elastodynamics that we discuss in the next section.

KINEMATIC AND DYNAMIC MODELS WITH ACTIVE FLUID PARTICIPATION

Although the injection model of Aki and others (1977) is in general agreement with various seismic observations, it does not provide a ready explanation for the sharply peaked nature of the tremor spectrum. The observed spectral peaks are, in fact, much narrower than the theoretical peak derived from the model (compare, for example, the bandwidth of the dominant peak of tremor shown in figure 45.33*B* with the synthetic data of figure 45.36). A similar characteristic is displayed by the long-period events of Mount St. Helens (Fehler and Chouet, 1982), which last much longer than the vibrations triggered by the opening channel, a difference that cannot be ascribed to path or station-site effects. In addition, figure 45.36 shows a marked dependence of the spectral characteristics of the tremor model on radiation direction, in contrast to observations, which consistently indicate that the tremor spectrum is only weakly dependent on azimuth. The negligible attenuation with distance displayed in figure 45.37 does not easily fit the observations either.

To resolve these discrepancies, it is necessary to include the fluid as an active element in the vibration of the source. The idea that the excitation of fluid motion plays an important role in the origin of tremor is not new; it actually has been advocated by volcanologists for many years, and several models have recently been proposed (Kamo and others, 1977; St. Lawrence and Qamar, 1979; Wada, 1980, 1981; Ferrick and others, 1982; Ferrick and St. Lawrence, 1984). In these models , however, analysis of the coupling of the fluid motion to the elastic medium surrounding the fluid body has not been sufficiently quantitative for comparison with seismic observations.

Aki and Koyanagi (1981) proposed a kinematic model that includes a simple relationship between the radiated elastic field and magmatic transport, as discussed in the previous section. Recently, Crosson and Bame (1985) considered a purely elastic model, in which a spherical magma chamber buried in a homogeneous isotropic elastic full-space is excited by excess pressure applied over the wall of a small spherical cavity at the center of the chamber. This model is an extension of the cavity model of Blake (1952) and the liquid sphere model of Shima (1958), and it simulates a sudden gas expansion in the magma. The magmatic fluid is treated as an elastic solid with very low rigidity and with damping introduced by adding a complex part to the shear modulus. The simplicity of the model allows a closed-form analytical solution for the radial displacement, which depicts a peaked spectrum and an oscillating decaying seismogram. The fundamental mode is a pure radial mode in which the fluid and solid participate in the motion with phase synchronization. The fundamental frequency becomes insensitive to the size of the magma chamber when both inner and outer radii are greater than a specified value, but depends significantly on the shear velocity of the magma. Thus, the fundamental resonant radial-oscillation mode of this source is dependent on the existence of a compliant gas or

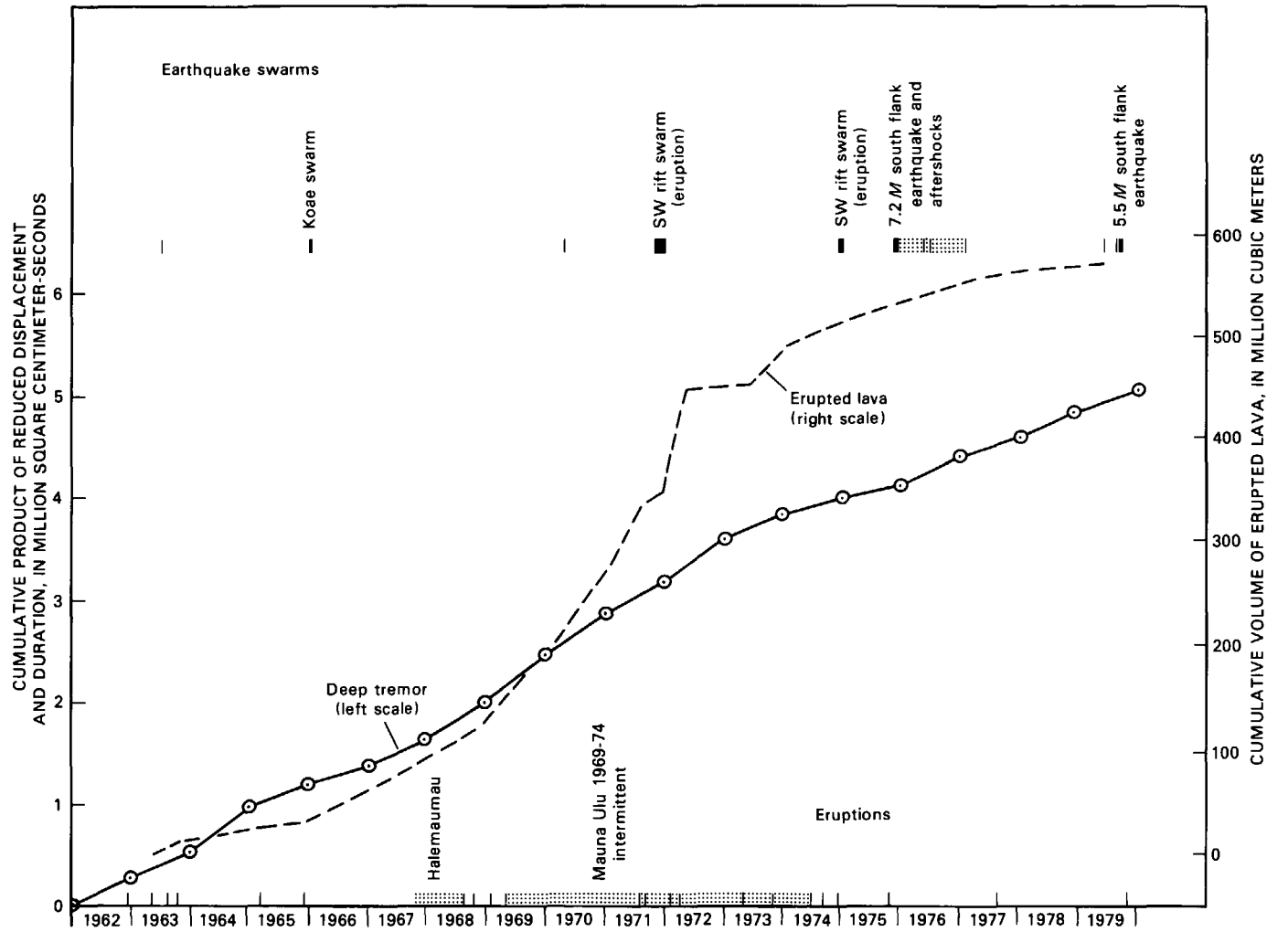

FIGURE 45.42.—Cumulative reduced displacement of deep tremor and cumulative volume of erupted lava at Kilauea, 1962–1979. According to the kinematic model of Aki and Koyanagi (1981), each unit of the vertical coordinate of reduced displacement corresponds to cumulative magma flow of about 16×10^6 m^3. Major earthquake swarms and eruptive activities also shown for comparison. Dotted line at the bottom marks periods of prolonged eruptive activity with frequent episodes of lava output during the Halemaumau and Mauna Ulu eruptions. Dotted pattern at the top marks aftershocks of M=7.2 south flank earthquake.

froth region of significant extent inside the magma chamber. This dependence of the excitation on the source stiffness is similar to the results obtained by Aki and others (1977) and Chouet (1981). However, the extreme simplicity of this model's geometry does not allow a realistic approach to the magmatic transport problem. Furthermore, the model does not allow fluid flow, because the equations for the transfer of mass and momentum in the fluid are not specifically considered. The physical nature of effective cavity formation for a gas phase over dimensions of meters, which is required to produce the frequencies observed for long-period events and tremor, also remains an elusive question. Finally, the model does not explain the driving force of tremor and requires a source of pulsation in the gas that is difficult to realize by simple physical means.

An initial attempt at unifying the fluid vibration and seismic radiation in the tremor source was made by Chouet (1985), who considered the motion of a magmatic pipe excited by the sudden flashing of ground water to steam as magma intrudes the phreatic layer. This model, displayed in figure 45.43, consists of a vertical pipe shut at the bottom by a horizontal disk and terminated at the top by a gas-filled hemispherical cavity acting as an explosive trigger. The source of tremor is the acoustic resonance of the fluid-filled conduit triggered by the excess gas pressure; the motion of the source is expressed in terms of the excitation of the well-known organ-pipe modes, while the bandwidth of these modes is determined from the combined losses due to viscous attenuation in the fluid and elastic radiation in the solid. Two assumptions are implicit in this model: first, that the volume of gas is large enough to sustain a pressure

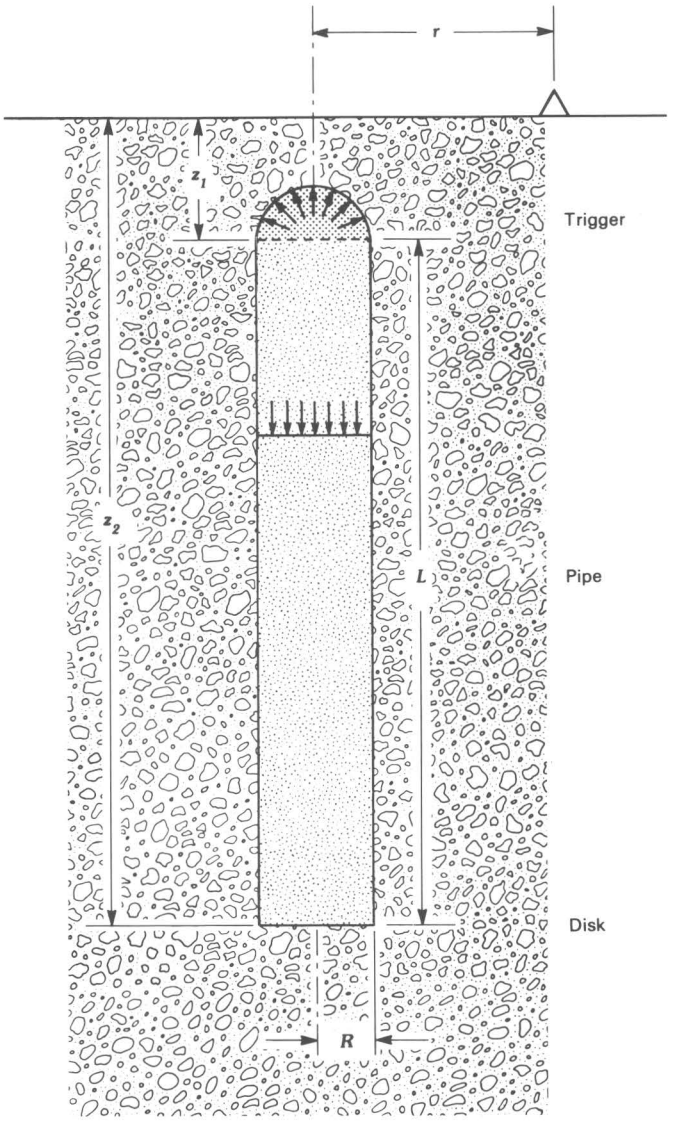

FIGURE 45.43.—Configuration of source, medium, and receiver used in computing ground motion produced by the excitation of a fluid-filled pipe. The composite source consists of a vertical conduit of radius R and length L capped by a hemisphere and shut at the bottom by a horizontal disk at depth z_2. Pipe is filled with liquid; hemispherical cap contains gas. Depth to pipe inlet is z_1, and receiver is located at epicentral distance r.

pulse of sufficient magnitude to generate the observed excitation; second, that the volume of magma is large enough to allow a high-Q vibration. In relation to the magmatic transport problem, this seismic model represents the characteristic scale length of a magmatic conduit between changes in its cross section or direction. The model is thus applicable to long-period events or tremor with a stable dominant frequency. It bears some similarities to the model of Crosson and Bame (1985) in that it incorporates a gas-filled chamber; however, this is done only for the source excitation and does not affect in a fundamental manner the determination of the oscillating frequency as in Crosson and Bame's model.

By restricting his analysis to seismic wavelengths that are large compared to the pipe diameter and demonstrating that the damping of the fluid system due to elastic radiation is trivial at low frequencies, Chouet was able to treat the problem of seismic radiation separately from that of the fluid dynamics, thus considerably simplifying the analysis of tremor generation. The space-time histories of the flow pressure and velocity, derived from the solution of the equations for the conservation of mass and momentum in the fluid, are given in figure 45.44, which also shows the triggering event, a pressure transient of the form $P_0 = \Delta P \exp[\ln(t) - (t/T)]/\exp[\ln(T) - 1]$ applied at the pipe inlet (fig. 45.44*A*). The pertinent source parameters, listed in table 45.4, are taken to be representative of a dacitic magma such as is involved in the current activity at Mount St. Helens.

Examples of the ground response to the excitation of the magmatic pipe, calculated by the discrete-wave-number synthetic method, are shown in figure 45.45 for 18 stations at epicentral distances of 0–10 km. The situation considered is that of a pipe buried at a depth of 50 m in a homogeneous half-space with the compressional velocity $\alpha = 4$ km/s and shear velocity $\beta = \alpha/\sqrt{3}$. The records start with the *P*-arrival from the trigger and cover most of the duration of the ground motion at each location.

The four traces displayed for each station represent, from left to right, the contributions from the trigger source, the pipe source, and the disk source, and the composite source from the superposition of these three elements; the two components of the displacement are identified at the top. No *SH* waves are present in the signal because of the isotropic distribution of the equivalent body forces representing the source in the horizontal plane. Furthermore, no clear shear-wave arrival can be recognized in the ground response, because the contributions of the *SV* waves are completely buried in the complex signature generated by the source.

The first motion due to the trigger and pipe elements is always a compression. That due to the disk, on the other hand, shows up as a dilatation everywhere, as can be expected from the downward orientation of the force applied by the fluid at the bottom of the conduit. As this arrival is delayed with respect to the others by an amount equal to the travel time of the tube wave over the length of the pipe, the onset of the signal from the composite source is always a compression. The trigger and pipe elements dominate the ground response in the immediate vicinity of the source, producing a pulse-like waveform characteristic of the disturbance exciting the source (see fig. 45.44*A*). The contributions of these sources, however, diminishes rapidly with increasing epicentral distance, so that at distances exceeding 250 m the free-surface response effectively reflects the repeated hammering of the fluid at the bottom of the conduit. The resulting motion then evolves into a well-developed harmonic wavetrain dominated by Rayleigh waves at distances greater than 3 km.

The spectral characteristics of the ground response are given in figure 45.46, which displays contour maps of the displacement spectral amplitude versus frequency and epicentral distance. Both components of motion display a maximum amplitude at 0 Hz within

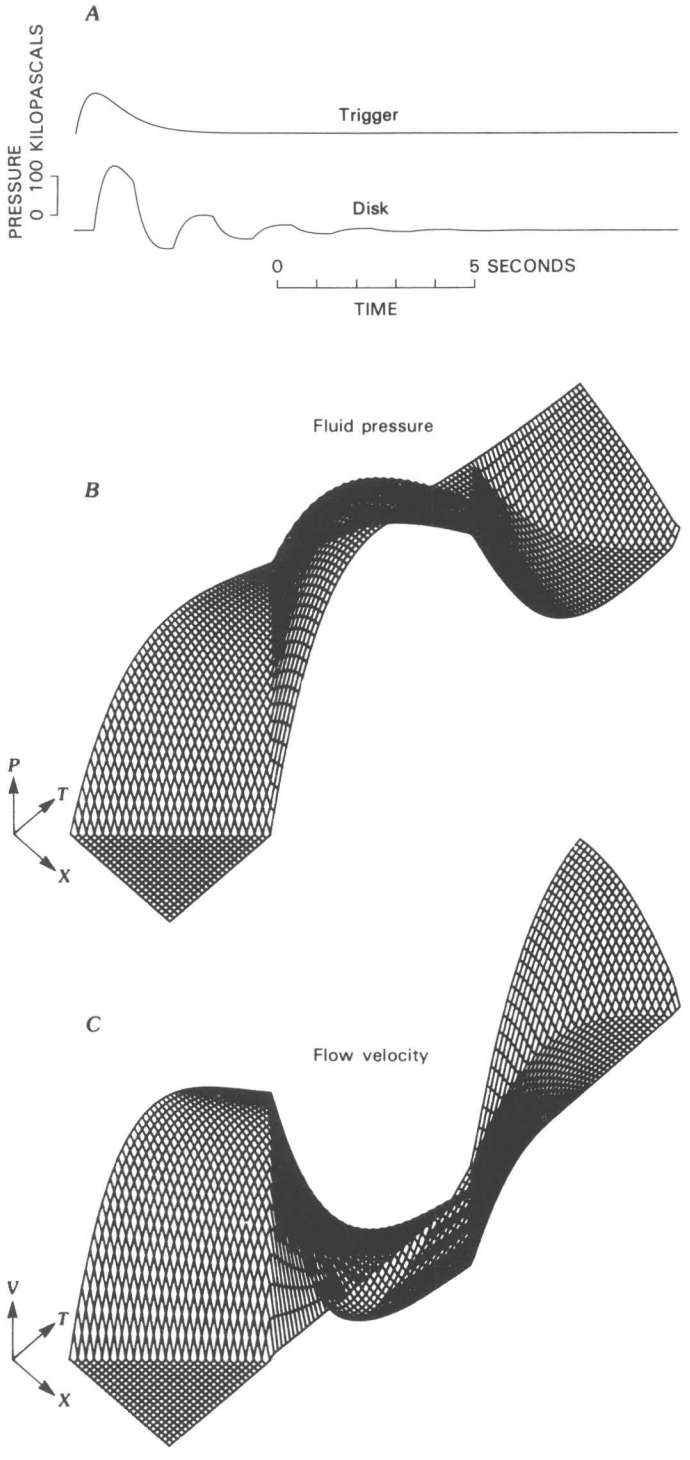

FIGURE 45.44.—Time variation of pressure and flow velocity for the elements of the composite tremor source. ***A,*** Pressure-time functions for the trigger and disk sources. ***B,*** Space-time dependence of the fluid pressure for the pipe source. Peak pressure is 160 kilopascals. ***C,*** Space-time dependence of the flow velocity for the pipe source. Peak velocity is 2.4 cm/s.

TABLE 45.4.—*Source parameters for the pipe model of tremor*

Fluid properties	
Viscosity	$\eta = 2 \times 10^5$ N·s/m^2 ($= 2 \times 10^6$ poise)
Density	$\rho = 2.7$ g/cm^3
Tube wave velocity	$a = 1.6$ km/s
Dimensions of pipe	
Radius	$R = 25$ m
Length	$L = 800$ m
Excess pressure	$\Delta P = 10^5$ Pa ($= 10^6$ dyne/cm^2)
Rise time of trigger pulse	$T = 0.5$ s

100 m of the epicenter. Dominant and subdominant peaks are observed at frequencies near 0.5, 1.5, 2.5, and 3.5 Hz, corresponding to the organ-pipe modes of the conduit. As noted in figure 45.45, the fundamental mode of the source is indistinct in the spectra obtained at short distances; in fact, it is not until the range exceeds a few hundred meters that this mode becomes a dominant feature. As for the dominant mode, the higher harmonics are not strongly developed in the epicentral area. The dominant frequency is slightly lower on the vertical component than on the horizontal one, and the vertical spectrum has more variability at higher frequencies than its horizontal counterpart. The spectral peaks are much narrower than those produced by the model of Aki and others (1977). The importance of the fluid viscosity in the shaping of the spectral response in Chouet's model is well demonstrated in figure 45.47 for a station located at a range of 200 m. A lower viscosity produces a more peaked spectrum and amplifies the dominant and subdominant peaks on both components of motion.

The analysis made by Chouet has interesting implications for the radiation and viscous damping losses of the fluid system. For the cylindrical magma column considered, the radiation loss is proportional to the square of the pipe radius, while the loss related to viscous damping is inversely proportional to the same factor. Thus, the relative importance of the two loss mechanisms (see equation 13) is critically dependent on the geometry of the magma reservoir. The relative importance of the pipe and disk elements of the source in shaping the ground response is likewise a function of the conduit cross section. Since the observed Q represents the sum of these losses, a unique measurement of Q from the amplitude decay of long-period events cannot separate the two mechanisms. The radiation loss, however, may be estimated from seismic measurements made in the far field, while the total energy of vibration in the fluid can be determined by the measurement of near-field motion trapped in the vicinity of the oscillating fluid. In fact, the synthetic seismograms of figure 45.45 show that the displacement attributed to the pipe is of the nature of near-field motion, while that due to the disk is of the nature of far-field motion. Changes in the conduit cross section would change the relative contributions of the pipe and disk elements, thus suggesting the possibility of determining the geometry of the source, as well as the radiation loss and in-situ magma viscosity from a comparison of near- and far-field observations.

A further step toward understanding the interaction of the fluid and solid in the tremor source was taken by Chouet and Julian (1985), who extended the original finite-difference crack model of Aki and others (1977) by improving the boundary conditions

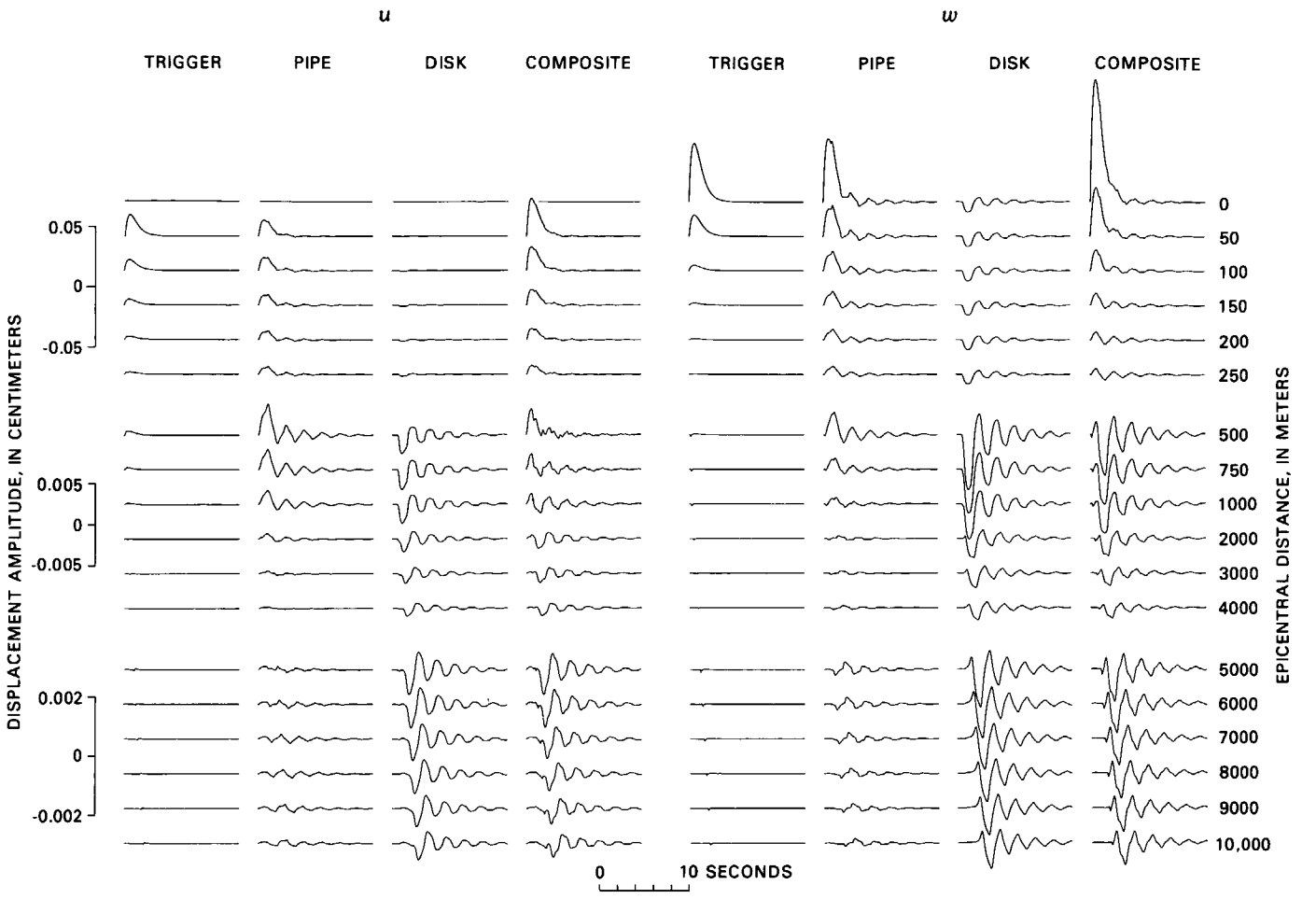

FIGURE 45.45.—Synthetic seismograms of the two components (u, horizontal; w, vertical) of ground displacement resulting from excitation of a fluid-filled pipe buried in a homogeneous half-space. Depth to pipe inlet is 50 m, and records are shown for 18 stations at increasing epicentral distances. Four sources are represented: the hemispherical cap that triggers the motion of the fluid column; the pipe; the disk shutting off the bottom of the conduit; and the composite source resulting from superposition of these three. Each record starts at a time corresponding to arrival of the P-wave from the trigger and lasts 13 s.

applied in the plane of the crack and by coupling the equations for mass and momentum transfer in the fluid to the elastodynamic equations in the solid. As in Aki and others (1977), the model of Chouet and Julian consists of a two-dimensional crack with thickness much smaller than the seismic wavelengths of interest and containing a fluid whose bulk modulus is low because of bubbles. They follow Aki and others (1977) in formulating the initial conditions and assume that the crack tip suddenly propagates by a small increment in response to excess fluid pressure. The area of the crack thus suddenly increases by ΔS and the dynamic motion of the crack surface triggered by the rupture is considered as the response of the crack to a pressure step of amplitude ΔP applied over this incremental area. Although the magma has a finite viscosity in this model, the rate of fluid flow into the expanding crack tip is considered to be instantaneously equal to the rate of increase of the crack-tip volume, and the rupture of the crack tip over the area ΔS is also assumed to be instantaneous. Thus, the rate-limiting effect of the viscosity in the propagation of the fracture is not taken into account, and the details of the coupling between the acoustic and elastic processes at the expanding crack tip are greatly simplified.

The basic features of the solutions obtained by Chouet and Julian (1985) are displayed in figures 45.48–45.50. These examples are given for a Poisson ratio of 0.25 in the solid and for a ratio k/μ of 0.1. The behavior of the fluid is characterized by three dimensionless parameters, namely the crack stiffness $C=(k/\mu)(L/d)$, seen previously, the viscous damping loss $F=6(\eta/k)(a/d)$, and the velocity ratio $G=\alpha/a$, where η is the viscosity and a the acoustic velocity of the fluid.

The normal displacement of the crack surface is shown in figure 45.48 for an increment of the crack tip $\Delta l=L/20$. As in figure 45.32, the variable plotted is a dimensionless combination of the applied pressure step, the crack length, and the rigidity and compressional velocity of the solid. Of particular interest is the direction of the dominant motion following the initial response of the wall at various locations on the crack surface; the initial motion at the expanding tip is an opening, but at other locations the main

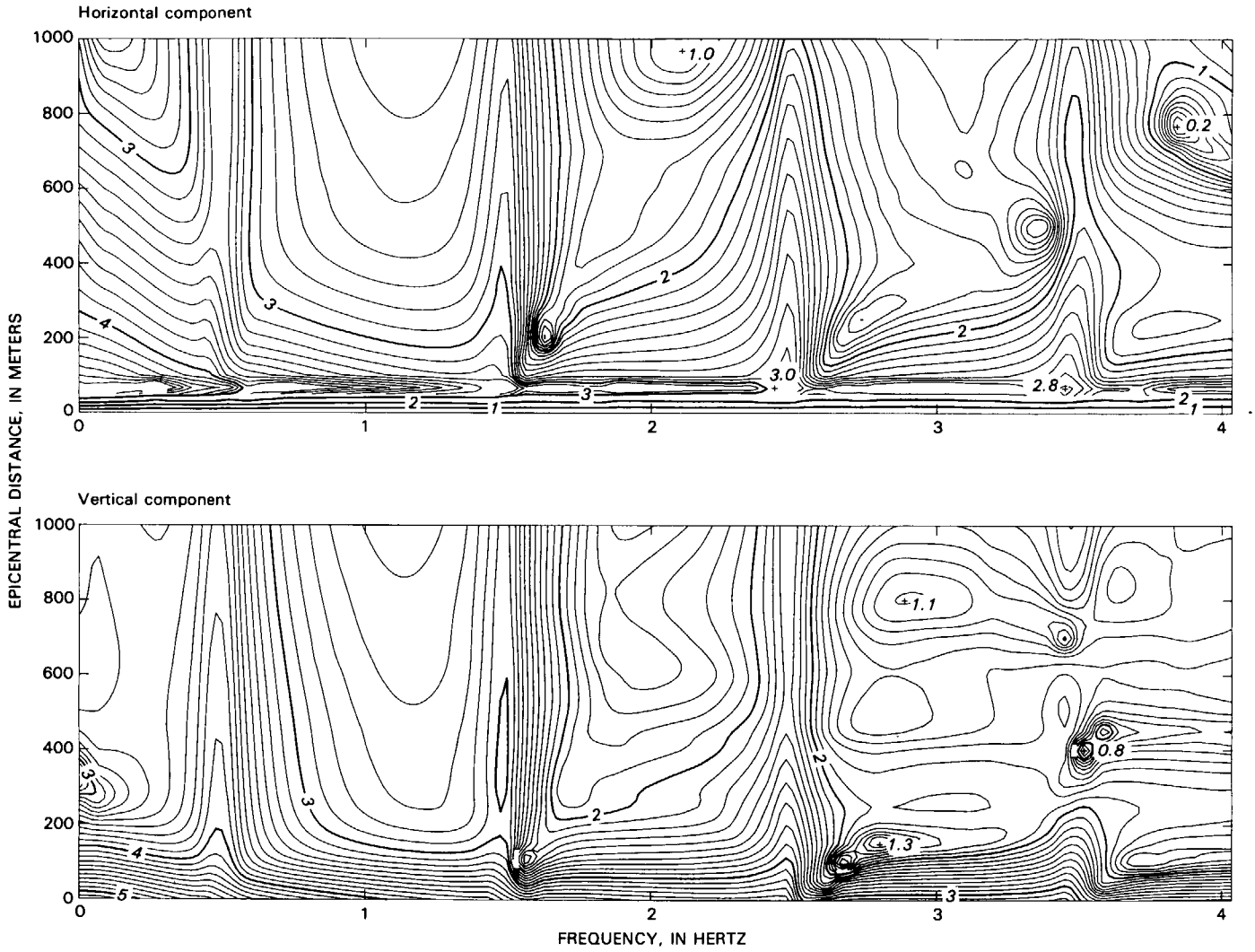

FIGURE 45.46.—Contour maps of the spectral amplitudes of the horizontal and vertical components of ground displacement obtained in the band 0–4 Hz and epicentral range 0–1,000 m for the source model defined in table 45.4. The plots show the logarithm in base 10 of the displacement spectral amplitudes (in cm·s) magnified by a factor of 10^6. Every tenth contour is labeled.

component of motion clearly shows a partial collapse of the crack walls. This closure occurs because the opening of the crack tip causes a drop in the fluid pressure, which propagates across the crack with a velocity slightly lower than the acoustic velocity because of elastic yielding of the crack faces. This large low-frequency wave has the characteristics of the Stoneley wave observed in fluid-filled boreholes (Biot, 1952; Cheng and Toksöz, 1981) and corresponds to the so-called water-hammer wave in pipes (Wylie and Streeter, 1978).

For a crack containing an inviscid fluid, the only mechanism of energy loss is the radiative loss into the solid. This process is well illustrated in figure 45.48, which shows that the higher frequency components of the wall vibration are quickly damped over the first cycle of flow oscillation. This behavior is at odds with the earlier suggestion of Aki and others (1977) that high-frequency motions are trapped near the source. The problem of high-frequency radiation was not treated in detail by Chouet and Julian and is clearly of a complex nature that depends on the physical parameters of the fluid (see fig. 45.50 and comments below); this question is presently the subject of further investigation. The lower frequencies, on the other hand, are only weakly affected by radiation losses, suggesting that the elastic energy is a trivial part of the available acoustic energy of the fluid at these frequencies and confirming the assumption made earlier by Chouet (1985). The effect of viscosity is shown in figure 45.49 for a fluid characterized by the parameter $F = 0.01$ (note that this particular choice for the value of F implies viscosities in the range of 10^4–10^6 poise if we assume $\mu \simeq 10^{11}$ dyne/cm^2, $k = 0.1\mu$, $a \simeq 10^1$–10^3 m/s, and $d \simeq 10^{-1}$–10^1m). The factors C and G and the extension Δl are the same as in the previous figure, so this plot offers a direct comparison with the result obtained for a

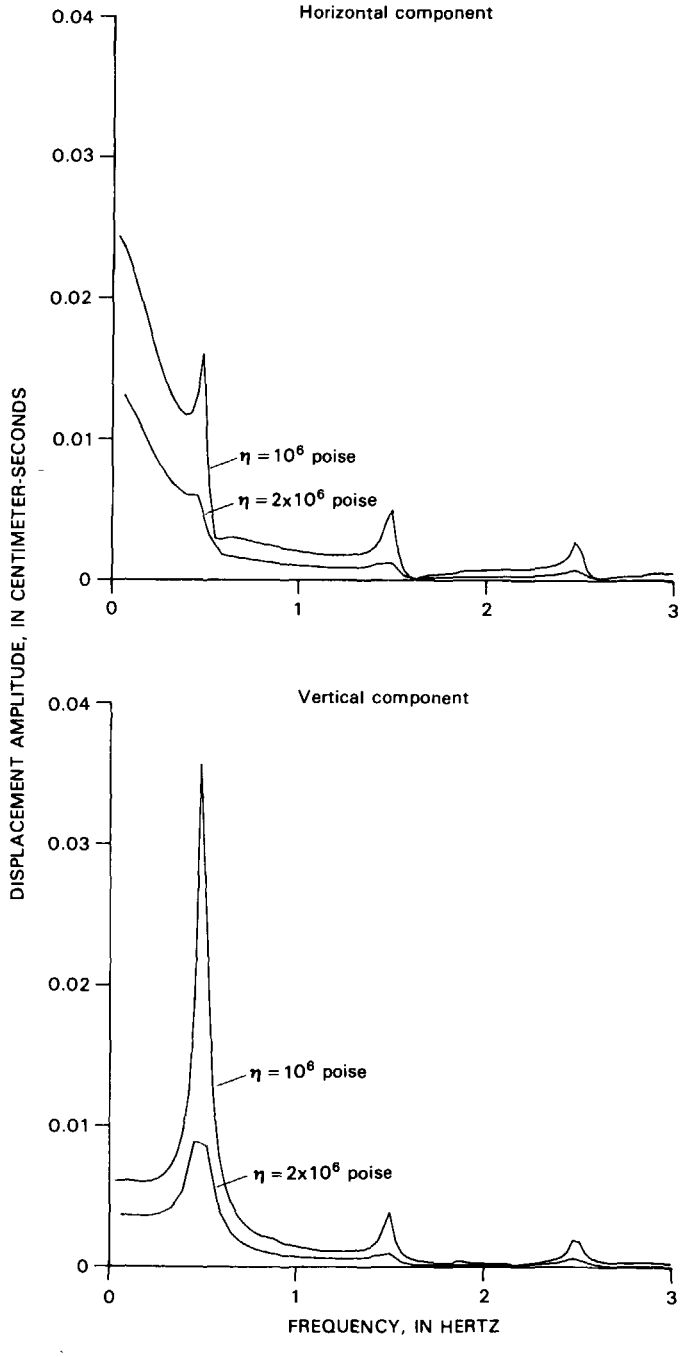

FIGURE 45.47.—Effect of the fluid viscosity on the displacement spectra observed in the band 0–3 Hz at an epicentral range of 200 m. Two values of viscosity are considered; other source parameters are listed in table 45.4.

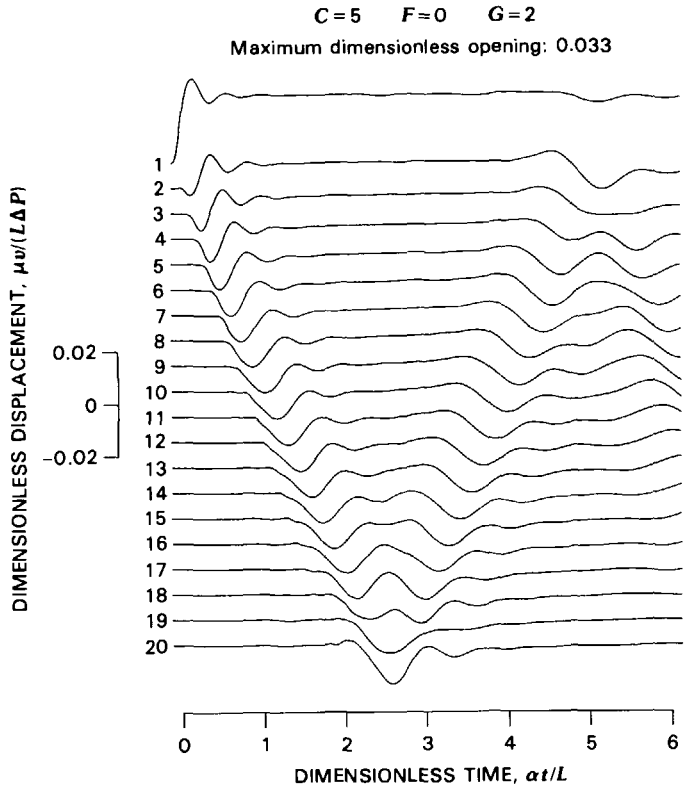

FIGURE 45.48.—Transverse displacement of the crack surface in dimensionless units for a crack 20 grid-intervals long that contains an inviscid fluid and that expands by $\Delta l = L/20$. Crack parameters are listed (see text for details). Traces 1–20 are spaced at 1 grid interval along the crack length.

nonviscous fluid. Viscous dissipation at the crack wall strongly affects the duration of dynamic motion but does not markedly change the shape or period of the signal over the first few cycles of flow oscillation.

The motion of the crack has two time scales: the duration of brittle failure, which is proportional to the length Δl that the crack extends, and the period of acoustic resonance of the fluid, which is a function of the length of the crack and the acoustic velocity of the fluid. This is obvious in figures 45.48 and 45.49, when one compares the period of the high-frequency response of the wall associated with the incremental extension to the period of the acoustic cycle; the latter period is usually much longer than the duration of brittle failure.

Finally, the effect of a lower acoustic velocity in the fluid is illustrated in figure 45.50, which displays the normal particle velocity at 160 locations on the surface of a crack extending by $\Delta l = L/160$. The parameter G is set equal to 4, that is, the acoustic velocity in the fluid is one-fourth of the compressional velocity in the solid; the other crack parameters are identical to those used in figure 45.48. The plot depicts the motion of the crack over roughly a quarter of the acoustic cycle, showing three wave fronts propagating over the wall. The first of these wave fronts is a weak P wave which rapidly attenuates away from the expanding tip. Following the P wave, another stronger wavetrain propagates across the crack with a velocity lower than the shear velocity in the solid. These guided waves are similar in nature to the pseudo-Rayleigh waves observed at the solid-fluid interface in a fluid-filled borehole (see, for example, Cheng and Toksöz, 1981). They are highly dispersive, having phase velocities bounded by the shear velocity of the rock at low frequencies and approaching the acoustic velocity of the fluid at higher frequencies. The final front corresponds to the acoustic arrival.

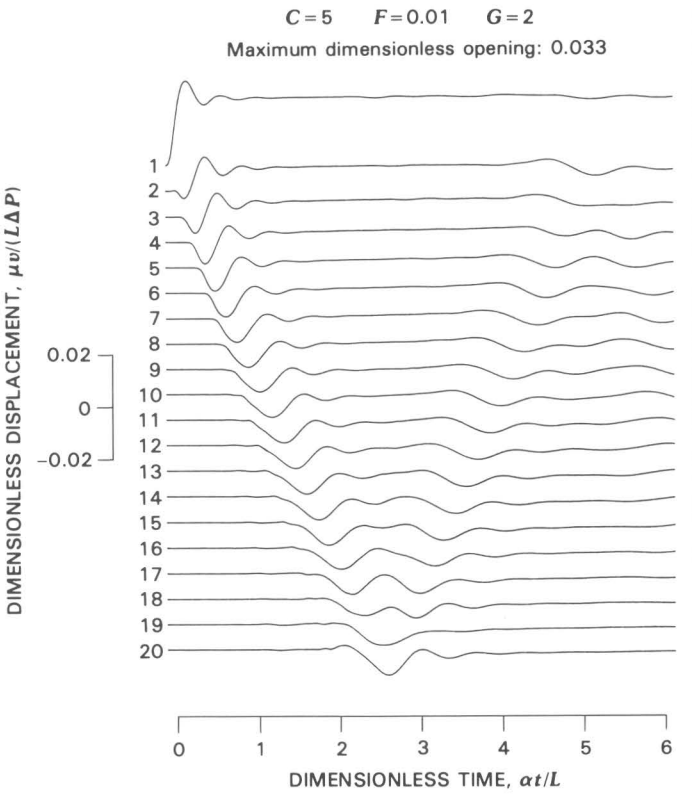

FIGURE 45.49.—Transverse displacement of the crack surface in dimensionless units for a crack 20 grid-intervals long that contains a viscous fluid and that expands by $\Delta l = L/20$. Other than the changed fluid viscosity, the source is the same as that in figure 45.48. Traces 1–20 are spaced at 1 grid interval along the crack length.

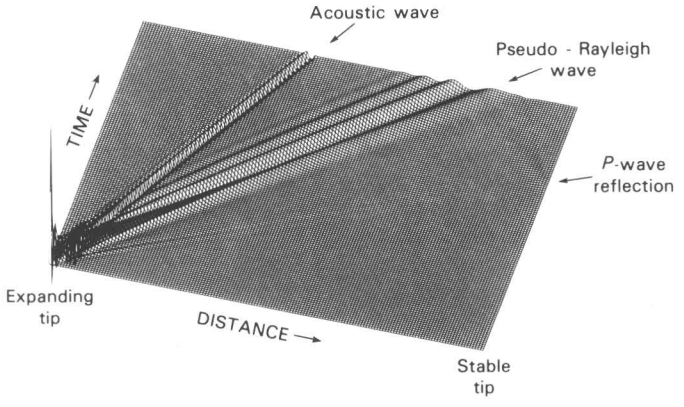

FIGURE 45.50.—Normal component of the particle velocity plotted at 160 locations on the surface of a crack expanding by $\Delta l = L/160$. Crack contains an inviscid fluid and has a stiffness $C = 5$. Acoustic velocity in the fluid is ¼ the compressional velocity in the solid. Note the individual wavefronts labeled and marked by arrows.

In the same configuration of source, medium, and receivers, the ground displacements produced by the expanding crack show a pattern similar to that depicted in figures 45.35 and 45.37 for the opening of a channel. In the present model, however, the duration of motion is essentially controlled by the fluid viscosity and the associated damping at the crack wall. In particular, when the fluid viscosity is low, the vibration of the source at the fundamental mode can persist for a considerable time, with the crack acting then as a high-Q oscillator. The inhomogeneous waves trapped near the liquid-solid interface (see fig. 45.50) produce high-frequency motions that are observed only in the immediate vicinity of the source.

IMPLICATIONS OF THE MODELS FOR TRANSPORT MECHANISMS

By including the fluid as an active element in our seismic-source model of tremor, we have now established the premise for a unified theory that not only accounts for the driving force in the fluid and the elastic radiation in the solid, but also explains the observed frequency, bandwidth, amplitude, and duration of tremor. When the fluid viscosity is low and the viscous damping is small, the main mechanism of dissipation of energy is through elastic radiation. This radiation loss only weakly affects the low-frequency motion of the source, with the result that the fundamental mode of oscillation of the source can be maintained over a considerable period of time, the source acting then as a high-Q oscillator. This low-frequency signal represents the so-called long-period event, which may be viewed as the impulse response of the tremor generating system. According to this view, sustained harmonic tremor simply results from the superposition of the responses of a volcanic conduit to many individual pressure impulses occurring randomly in time. Various mechanisms can trigger the oscillation of the fluid in the source. Fluid flow in an open vent during active fountaining, rock failure, and thermal and chemical mechanisms are probably all equally plausible triggers. In that sense, the opening of a channel or jerky extension of a crack, as well as the thermal interaction of magma with ground water that we have considered in our models remain highly speculative. Clearly, the identification of the elusive trigger associated with the postulated sequence of long-period events is one of the major challenges facing us in our modeling attempts.

An interesting result stemming from our analysis is the apparent discrepancy between the volume estimates of magma transport obtained from the seismic data and those derived from deformation studies. The seismic estimates were found to be consistently and significantly lower than those obtained from deformation measurements for both deep and shallow tremor, suggesting that magma transport in the lithosphere may be largely aseismic. Although this conclusion is somewhat unfortunate for the seismologist who wants to determine magma flow solely from seismic measurements, it is supported by field observations of shallow tremor made during prolonged eruptions such as those at Halemaumau in 1967 and at Mauna Ulu during 1969–1974, as well as the current activity at Puu Oo. The initial phase of an eruption usually is accompanied by stronger tremor than the later phases, when larger volumes of lavas

are erupted, and some eruptions even occur without measurable tremor. Furthermore, the size of the tremor source region at Kilauea decreases during repeated eruptions at the same location; that is, the tremor becomes restricted to the vent area while the summit area remains active at a lower level. A conspicuous gap in tremor activity appears to develop in the rift zone between the erupting vent and the summit reservoir during a sustained eruption in the east rift. A gap also exists at depths of 15–30 km along the conduit system beneath the summit region. The lack of measurable tremor activity in these regions suggests that there are undisturbed zones of transport where magma flow may occur without significant pressure fluctuations. Indeed, if tremor is generated by unsteady fluid flow, as the evidence gathered so far seems to indicate, then it is easy to relate the absence of tremor to episodes of steady flow. It is possible that strong barriers may become weakened by continued or repeated magma flow, accounting for the disappearence of tremor during an eruption and the absence of tremor at some depths below Kilauea.

Further data are needed on tremor. The deployment of an array of broadband three-component instruments in the active east rift of Kilauea could provide the high-quality data essential for resolution of the basic questions remaining on tremor.

REFERENCES CITED

Aki, Keiiti, 1967, Scaling law of seismic spectrum: Journal of Geophysical Research, v. 72, p. 1217-1231.

———1972, Earthquake mechanism: Tectonophysics, v. 13, p. 423-446.

———1984, Evidence for magma intrusion during the Mammoth Lakes earthquakes of May 1980 and implications of the absence of volcanic (harmonic) tremor: Journal of Geophysical Research, v. 89, p. 7689-7696.

Aki, Keiiti, Fehler, Michael, and Das, Shamita, 1977, Source mechanism of volcanic tremor: fluid-driven crack models and their application to the 1963 Kilauea eruption: Journal of Volcanology and Geothermal Research, v. 2, p. 259-287.

Aki, Keiiti, and Koyanagi, R.Y., 1981, Deep volcanic tremor and magma ascent mechanism under Kilauea, Hawaii: Journal of Geophysical Research, v. 86, p. 7095-7109.

Biot, M.A., 1952, Propagation of elastic waves in a cylindrical bore containing a fluid: Journal of Applied Physics, v. 23, p. 997-1005.

Blake, F.G., 1952, Spherical wave propagation in solid media: Journal of the Acoustical Society of America, v. 24, p. 211-215.

Bouchon, Michel, 1979, Discrete wave number representation of elastic wave fields in three-space dimensions: Journal of Geophysical Research, v. 84, p. 3609-3614.

———1981, A simple method to calculate Green's functions for elastic layered media: Bulletin of the Seismological Society of America, v. 71, p. 959-971.

Brune, J.N., 1970, Tectonic stress and the spectra of seismic shear waves from earthquakes: Journal of Geophysical Research, v. 75, p. 4997-5009.

Capaldi, G., Guerra, I., Lo Bascio, A., Luongo, G., Pece, R., Rapolla, A., Del Pezzo, E., Martini, M., Ghiara, M.R., Lirer, L., Munno, R., and La Volpe, L., 1978, Stromboli and its 1975 eruption: Bulletin Volcanologique, v. 41, p. 259-285.

Cheng, H.C., and Toksöz, M.N., 1981, Elastic wave propagation in a fluid-filled borehole and synthetic acoustic logs: Geophysics, v. 46, p. 1042-1053.

Chouet, Bernard, 1981, Ground motion in the near field of a fluid-driven crack and its interpretation in the study of shallow volcanic tremor: Journal of Geophysical Research, v. 86, p. 5985-6016.

———1985, Excitation of a buried magmatic pipe: a seismic source model for volcanic tremor: Journal of Geophysical Research, v. 90, p. 1881-1893.

Chouet, Bernard, and Julian, B. R., 1985, Dynamics of an expanding fluid filled crack: Journal of Geophysical Research, v. 90, p. 11187-11198.

Crosson, R.S., and Bame, D.A., 1985, A spherical source model for low frequency volcanic earthquakes: Journal of Geophysical Research, v. 90, p. 10237-10247.

Dibble, R.R., 1974, Volcanic seismology and accompanying activity of Ruapehu Volcano, New Zealand, in Civetta, L., Gasparini, P. Luongo, G., and Rapolla, A., eds., Physical Volcanology: Amsterdam, Elsevier, p. 49-85.

Fehler, Michael, 1983, Observations of volcanic tremor at Mount St. Helens volcano: Journal of Geophysical Research, v. 88, p. 3476-3484.

Fehler, Michael, and Chouet, Bernard, 1982, Operation of a digital seismic network on Mount St. Helens volcano and observations of long-period seismic events that originate under the volcano: Geophysical Research Letters, v. 9, p. 1017-1020.

Ferrick, M.G., Qamar, Anthony, and St. Lawrence, W.F., 1982, Source mechanism of volcanic tremor: Journal of Geophysical Research, v. 87, p. 8675-8683.

Ferrick, M.G., and St.Lawrence, W.F., 1984, Comment on "Observations of volcanic tremor at Mount St. Helens volcano" by Michael Fehler: Journal of Geophysical Research, v. 89, p. 6349-6350.

Guerra, I., Lo Bascio, A., Luongo, G., and Scarpa, Roberto, 1976, Seismic activity accompanying the 1974 eruption of Mt. Etna: Journal of Volcanological and Geothermal Research, v. 1, p. 347-362.

Kamo, K., Furuzawa, T., and Akamatsu, J., 1977, Some natures of volcanic micro-tremors at the Sakurajima Volcano: Bulletin of the Volcanological Society of Japan, v. 22, p. 41-58.

Kanamori, Hiroo, and Anderson, D.L., 1975, Theoretical basis for some empirical relations in seismology: Bulletin of the Seismological Society of America, v. 65, p. 1073-1095.

Kubotera, A., 1974, Volcanic tremors at Aso Volcano, in Civetta, L., Gasparini, P., Luongo, G., and Rapolla, A., eds., Physical Volcanology : Amsterdam, Elsevier, p. 29-47.

Latter, J.H., 1979, Volcanological observations at Tongariro National Park, 2 types and classification of volcanic earthquakes, 1976-1978: New Zealand Department of Science and Industrial Research, Geophysics Division, Wellington Report 150, 60 p.

Malone, S.D., 1983, Volcanic earthquakes: Examples from Mount St. Helens, in Kanamori, H., and Boschi, E., eds., Earthquakes: Observations, Theory and Interpretation ; Amsterdam, Elsevier/North Holland Publishing Co., p. 436-455.

Mandelbrot, B.B., 1977, Fractals, form, chance, and dimension : San Francisco, W.H. Freeman and Co., 365 p.

McNutt, S.R., 1986, Observations and analysis of B-type earthquakes, explosions, and volcanic tremor at Pavlov Volcano, Alaska: Bulletin of the Seismological Society of America, v. 76, p. 153–175.

Minakami, T., 1974, Seismology of volcanoes in Japan, *in* Civetta, L., Gasparini, P., Luongo, G., and Rapolla, A., eds., Physical Volcanology: Amsterdam, Elsevier, p. 1-27.

Moore, J.G., and Koyanagi, R.Y., 1969, The October 1963 eruption of Kilauea Volcano, Hawaii: U.S. Geological Survey Professional Paper 614–C, 13 p.

Riuscetti, M., Schick, R., and Seidl, S., 1977, Spectral parameters of volcanic tremors at Etna: Journal of Volcanological and Geothermal Research, v. 2, p. 289-298.

Ryall, A., and Bennett, D.L., 1968, Crustal structure of southern Hawaii related to volcanic processes in the upper mantle: Journal of Geophysical Research, v. 73, p. 4561-4582.

Sassa, K., 1935, Volcanic micro-tremors and eruption earthquakes: Memoirs of the College of Science, Kyoto Imperial University Series A, v. 18, p. 255-293.

Schick, R., Lombardo, G., and Patane, G., 1982, Volcanic tremors and shocks associated with the eruptions at Etna (Sicily), September 1980: Journal of Volcanology and Geothermal Research, v. 14, p. 261-279.

Schick, R., and Riuscetti, M., 1973, An analysis of volcanic tremors at south Italien volcanoes: Zeitschrift fur Geophysics, v. 39, p. 247-262.

Seidl, D., Schick, R., and Riuscetti, M., 1981, Volcanic tremors at Etna: a model for hydraulic origin: Bulletin Volcanologique , v. 44, p. 43-56.

Shima, M., 1958, On the second volcanic micro-tremor at volcano Aso: Bulletin of the Disaster Prevention Institute of Kyoto University, v. 22, p. 1-6.

Shimozuru, D., Kamo, K., and Kinoshita, W.T., 1966, Volcanic tremor at Kilauea Volcano, Hawaii, during July-December 1963: Bulletin of the Earthquake Research Institute of the University of Tokyo, v. 44, p. 1093-1133.

St. Lawrence, William, and Qamar, Anthony, 1979, Hydraulic transients: a seismic source in volcanoes and glaciers: Science, v. 203, p. 654-656.

Swanson, D.A., 1972, Magma supply rate at Kilauea Volcano, 1952-1971: Science, v. 1975, p. 169-170.

Swanson, D.A., Duffield, W.A., and Fiske, R.S., 1976, Displacement of the south flank of Kilauea Volcano: the result of forceful intrusion of magma into the rift zones: U.S. Geological Survey Professional Paper 963, 39 p.

Wada, T., 1980, Mechanism generating volcanic tremor, I: Bulletin of the Volcanological Society of Japan, v. 25, p. 211-278.

———1981, Mechanism generating volcanic tremor, II: Bulletin of the Volcanological Society of Japan, v. 26, p. 1-8.

Williams, H., and McBirney, A.R., 1979, Volcanology: San Francisco, Freeman, Cooper and Co., 397 p.

Wylie, E.B., and Streeter, V.L., 1978, Fluid transients : New York, McGraw

A HYDRAULIC MODEL TO EXPLAIN VARIATIONS IN SUMMIT TILT RATE AT KILAUEA AND MAUNA LOA VOLCANOES

By John J. Dvorak *and* Arnold T. Okamura

ABSTRACT

For a period of several months to a few years preceding eruptive activity, magma accumulates in shallow reservoirs centered 3 to 5 km beneath the summits of Kilauea and Mauna Loa Volcanoes. During flank eruptions, magma movement from the summit reservoir to the rift system is indicated by subsidence of the summit. Progress of the subsidence is monitored by telemetered tiltmeters, by 3-m-long watertube tiltmeters, and by releveling 40-m-long triangles.

During large summit-subsidence events at Kilauea, the tilt pattern indicates that the subsidence center may initially migrate 1 to 2 km to the south. Following the initial southward migration, the tilt direction remains constant for the remainder of the subsidence event, suggesting no further horizontal migration of the subsidence center during this period. No variation in tilt direction was measured in the Mauna Loa summit region during the March 25–April 15, 1984, northeast-rift eruption of this volcano.

The amount of vertical migration of the subsidence center is estimated from relative tilt rates recorded at different horizontal distances from the subsidence center. During the January 18–May 10, 1960, event at Kilauea, the subsidence center migrated upward 1 km in mid-February 1960. Vertical migration of the March 25–April 15, 1984, summit subsidence at Mauna Loa was less than 0.7 km.

During most subsidence events at both Kilauea and Mauna Loa, the tilt curve follows an exponential decay rate. Since 1955, the time constants for the exponential decay in tilt rate at Kilauea have varied from 0.25 days to 21 days; longer time constants are associated with eruptions that occur at greater distances from the summit. An exception to the exponential decay was the January 2–8, 1983, summit subsidence at Kilauea, which consisted of three separate subsidence episodes.

We propose a hydraulic model to explain the observed variation in tilt rate recorded during summit-subsidence events. Magma flow rate is assumed proportional to the pressure difference between the summit reservoir and a separate reservoir within the rift system. We further assume that magmatic pressure is linearly related to volumetric strain. On the basis of these assumptions, the magma flow rate and, hence, the summit tilt curve will follow the exponential decay observed during summit subsidences.

INTRODUCTION

Frequent periods of eruptive activity at two Hawaiian volcanoes, Kilauea and Mauna Loa (fig. 46.1), make these volcanoes especially well suited for studying the accumulation and movement of magma within the crust. Processes that control the volume and rate of flow of magma within Hawaiian volcanoes may also influence magma migration from the mantle to the surface; so, results derived from monitoring near-surface magma movement at Hawaiian volcanoes should be applicable to magma movement deeper in the crust and upper mantle, at depths too remote for current studies.

Several months to a few years preceding eruptive activity, magma accumulates in shallow reservoirs beneath the summits of both Kilauea and Mauna Loa (Fiske and Kinoshita, 1969; Decker and others, 1983). The accumulation and withdrawal of magma from the summit region produce a pattern of surface displacement that is recorded as change in ground tilt (fig. 46.2). The intersection of tilt vectors locates the average center of uplift or subsidence for the time interval between surveys.

The variation in tilt magnitude as a function of distance from the uplift or subsidence center can be modeled by a single point source embedded in an elastic half-space. The tilt magnitude, Φ, is given by (Eaton, 1962)

$$\Phi = \frac{3V}{2\pi} \frac{dh}{(d^2+h^2)^{5/2}}, \qquad (1)$$

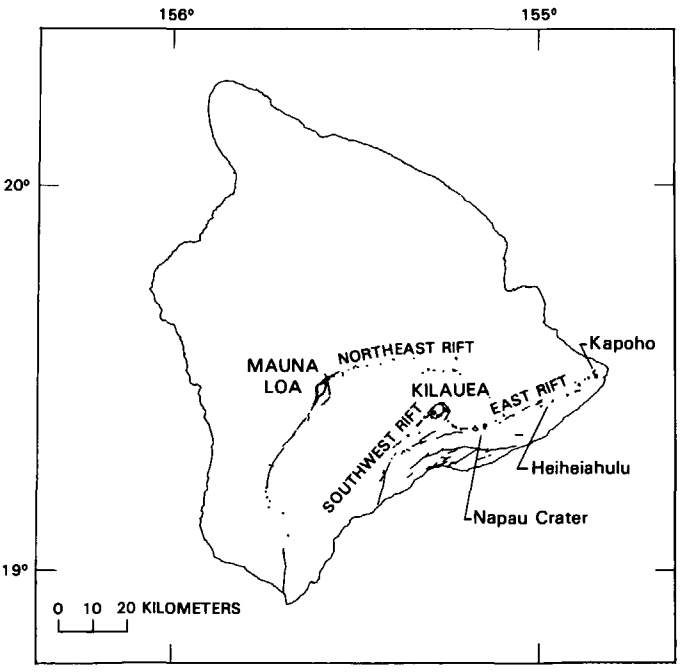

FIGURE 46.1.—Structural features associated with summit regions and rift systems of Mauna Loa and Kilauea on Island of Hawaii. Places along east rift of Kilauea mentioned in text are identified.

where h is the horizontal distance, d is the depth to the source, and V is the volume of elastic uplift. No tilt change is recorded directly above ($h=0$) or at large distances from the point source; the maximum tilt change occurs at $h=d/2$ (fig. 46.3). Comparison of theoretical curves and measured tilt changes show that the summit reservoirs at Kilauea and Mauna Loa are centered 3 to 5 km beneath the summits of both volcanoes (fig. 46.4; table 46.1). A similar depth range to the summit reservoirs has been estimated from level data, using a point-source elastic model, by many earlier investigators (Mogi, 1958; Fiske and Kinoshita, 1969; Decker and others, 1983; Dvorak and others, 1983).

During periods of magma accumulation in the Kilauea summit region, the uplift center usually begins in the central caldera region 1 km northeast of Halemaumau and migrates as much as 2 km south (Fiske and Kinoshita, 1969). A similar migration of the uplift center has not been recognized for Mauna Loa. Magma that accumulates in the summit reservoir may erupt in the summit region or move laterally into either rift system, where it may eventually be erupted. During periods of magma withdrawal from the summit reservoir, the subsidence center may also migrate a few kilometers within the caldera region (Jackson and others, 1975; Swanson and others, 1976).

The accumulation and withdrawal of magma in the Kilauea summit region is easily recorded by making frequent tilt measurements (fig. 46.5*A*). Higher tilt values in figure 46.5 correspond to uplift of the summit region caused by increased magmatic pressure and accumulation of additional magma within the summit reservoir. Prolonged periods of summit uplift are interrupted by much shorter

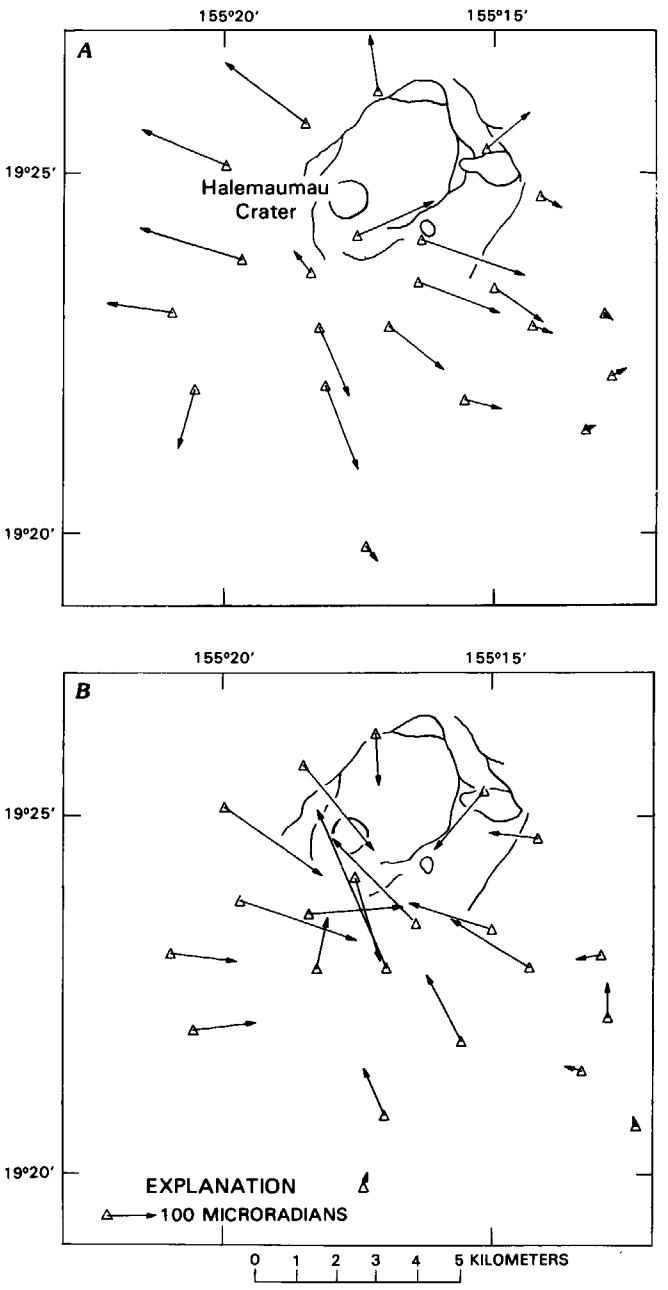

FIGURE 46.2.—Tilt vectors measured in Kilauea summit region. ***A***, Uplift of August 12–14, 1981, to March 3–April 5, 1982. ***B***, Subsidence of September 27–October 14, 1982, to February 2–11, 1983. Vectors were determined by measuring changes in relative elevation along 40-m-long triangles. Station locations, triangles. Tilt vectors point in direction of downward deflection of surface. General radial pattern of tilt vectors indicates that most active part of summit magma reservoir lies beneath southern part of caldera.

TABLE 46.1.—*Point source solutions to Kilauea summit tilt data*

	August 12–14, 1981 to March 29–April 5, 1982	September 27–October 14, 1982 to February 7–11, 1983
Longitude	155°17.7′ (±0.36 km)	155°17.0′ (±0.30 km)
Latitude	19°23.7′ (±0.34 km)	19°23.8′ (±0.28 km)
Depth	4.31 km (±0.84 km)	4.38 km (±0.58 km)
Volume of elastic uplift or subsidence	53×10^6 m^3($\pm26\times10^6$ m^3)	-72×10^6 m^3($\pm26\times10^6$ m^3)

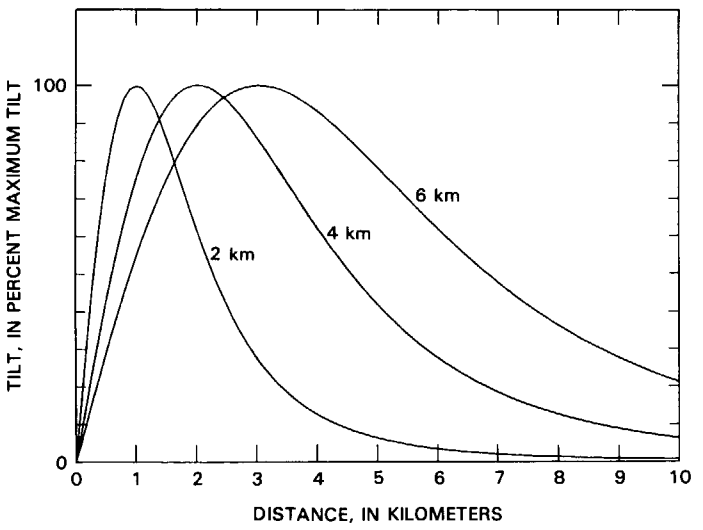

FIGURE 46.3.—Theoretical tilt changes as a function of horizontal distance from a point source embedded in an elastic half-space. Curves, normalized to maximum tilt change, are parametrized by depth to source.

periods of summit subsidence, indicated by sudden decreases in tilt value. These summit-subsidence events are caused by the movement of magma from the summit reservoir to either rift system and are usually associated with eruptive activity along the rift (Eaton and Murata, 1960; Jackson and others, 1975; Swanson and others, 1976). A similar pattern of slow accumulation and rapid withdrawal of magma from the summit reservoir at Mauna Loa is also indicated by summit tilt measurements (fig. 46.5*B*).

We have selected data from 14 subsidence events at Kilauea, indicated by vertical dashed lines in figure 46.5*A*, to determine what factors may control variations in summit tilt rate. Data from the summit subsidence associated with the 1984 Mauna Loa eruption are also included. Based on these data, a simple hydraulic model is proposed to explain magma flow rate in the conduit systems within Kilauea and Mauna Loa.

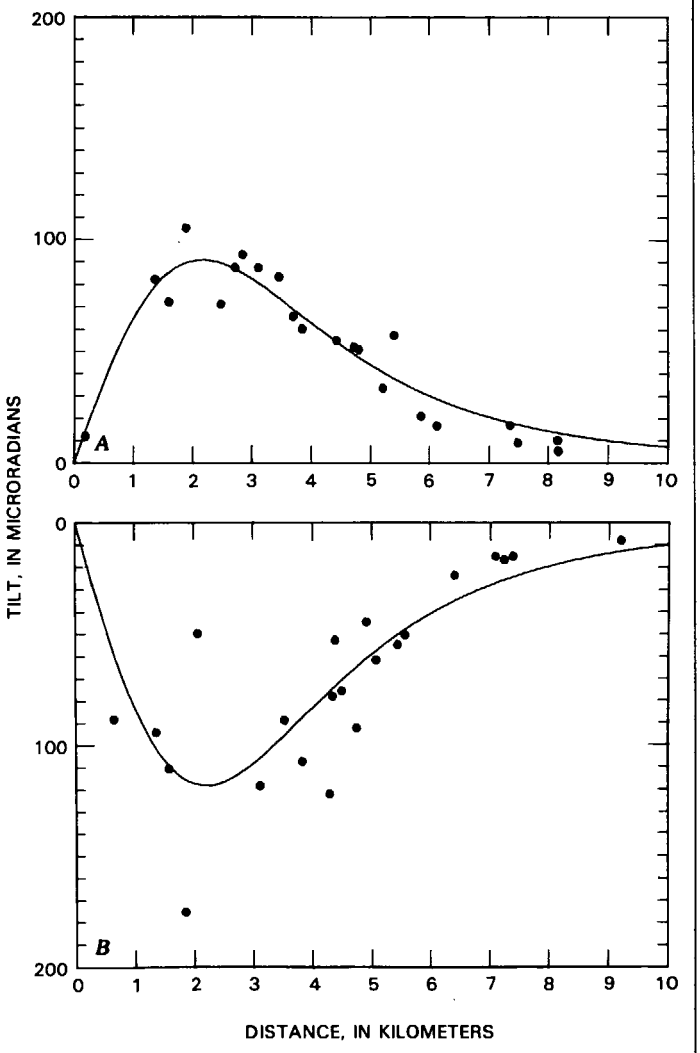

FIGURE 46.4.—Measured changes in radial tilt component and theoretical curves based on a point source embedded in an elastic half-space. ***A***, Uplift. ***B***, Subsidence. Data are same as shown in figure 46.2*A*, *B*. Model parameters are listed in table 46.1.

ACKNOWLEDGMENTS

This research has built upon measurements made over the past 30 years by the staff of the Hawaiian Volcano Observatory. R. Decker, J. Dieterich, D. Dzurisin, and T. Wright provided useful comments and suggestions to this manuscript.

MEASUREMENTS

Tilt measurements were begun in the summit region of Kilauea a few years after the establishment of the Hawaiian Volcano Observatory (HVO) in 1912; however, instruments specifically designed to record tilt changes were not in use until the 1950's. Tilt measurements in the summit region of Mauna Loa were begun 5 months after the July 1975 summit eruption.

Kilauea summit tilt measurements have been made at Uwekahuna since at least 1950 and at Outlet since October 1955 (fig. 46.6*A*). Between 1950 and June 1956, tilt changes at Uwekahuna were recorded by measuring the trace offset from a horizontal-pendulum seismograph. This technique could probably record tilt changes of 10–20 microradians (μrad). In 1955 and 1956, 3-m-long watertube tiltmeters, capable of resolving tilt changes of 2 μrad, were installed at Uwekahuna and Outlet (Eaton, 1959).

Since 1966, a continuously recording, one-component tiltmeter has operated in the Uwekahuna vault. This instrument is a mercury capacitance instrument that records tilt changes along the east-west direction to a sensitivity of 0.1 μrad. In recent years, additional electronic tiltmeters installed in the Kilauea summit region transmit readings at approximately 10-min intervals to a recording system located at HVO.

Tilt measurements in the Mauna Loa summit region (fig. 46.6*B*) are made by the dry-tilt method, which consists of releveling 40-m-long triangles (Yamashita, 1981). The use of 3-m-long wooden rods with permanently installed Invar strips allows tilt changes at MOK (tilt station at Mokuaweoweo) to be measured to 3–4 μrad. At other tilt sites, an accuracy of 8–12 μrad is achieved by the use of 1.5-m-long stainless-steel rods with removable Invar strips.

Repeated tilt measurements at Uwekahuna were made during 14 summit-subsidence events at Kilauea (fig. 46.5*A*) and during the 1984 northeast-rift eruption of Mauna Loa. The beginning dates of summit subsidence and the locations of the related rift intrusion or eruption are given in table 46.2. Parts of the east rift from the summit to Napau Crater, to Heiheiahulu, and to Kapoho are referred to as the upper, middle, and lower east rift, respectively (fig. 46.1). The distance from the summit-subsidence center to the rift eruption is measured along the rift axis to the major lava-producing eruptive vent. For the two events not accompanied by eruptive activity, in August 1981 and June 1982, the distance to the rift intrusion was assumed to correspond to the central region of shallow rift earthquakes. The beginning times and the durations of rift eruptions associated with each subsidence event are also listed in table 46.2. The occurrence of later eruptive phases, which may follow a large summit subsidence and initial eruptive phase, such as

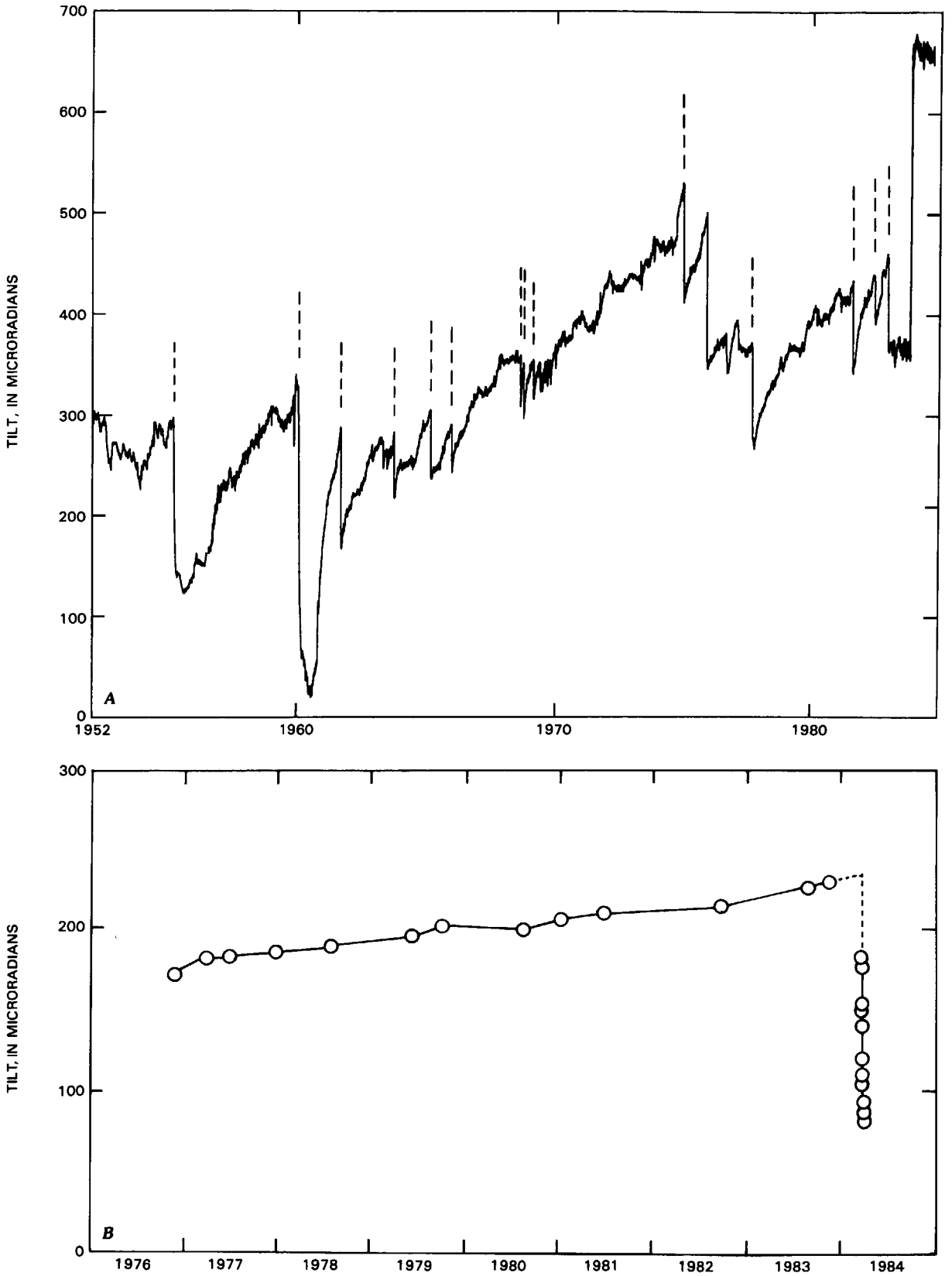

FIGURE 46.5.—Long-term tilt patterns recorded in summit regions of Kilauea and Mauna Loa. A greater tilt value generally corresponds to summit uplift and magma accumulation. ***A***, West-east component of daily tilt recorded in Kilauea summit region at Uwekahuna (see figure 46.6*A* for location). The 300-μrad tilt increase on November 16, 1983, is related to a magnitude 6.5 earthquake located 13 km west-northwest of Uwekahuna. Sudden tilt change probably did not involve magma movement in summit region. Summit subsidences examined in this paper (see table 46.2) are identified by vertical dashed-line segments. ***B***, North-south tilt component recorded in Mauna Loa summit region at MOK (see figure 46.6*B* for location). Sudden tilt decrease in March 1984 corresponds to recent Mauna Loa northeast-rift eruption.

in March–April 1955, September 20–25, 1977, and the succession of eruptive phases that began in February 1983, are not considered in determining eruption duration because these events are associated with smaller, individual summit subsidences.

HORIZONTAL AND VERTICAL MIGRATION OF SUBSIDENCE CENTERS

Jackson and others (1975) and Swanson and others (1976) noted a horizontal migration of the subsidence center associated with some subsidence events. We show in this section that, though there is a systematic migration, most of the tilt change occurs while the subsidence center is stationary.

Horizontal migration of the subsidence center is indicated by variations in tilt direction, which is determined by examining the amount of north-south and west-east tilt. A constant direction is indicated by a linear relation between north-south and west-east tilt values.

The variation in tilt direction recorded by the Uwekahuna watertube instrument during the December 31, 1974–January 3, 1975, summit subsidence is typical of most events at Kilauea (fig. 46.7). The subsidence center was initially located directly east of Uwekahuna. As the subsidence proceeded, the center migrated southward, indicated by a change in tilt direction at Uwekahuna from east to southeast. The dominant southeastern tilt recorded at Uwekahuna suggests that the subsidence center remained in the same horizontal position throughout most of the subsidence. A second, relatively minor migration of the subsidence center to a position south of Uwekahuna may have occurred near the end of the event.

The net tilt change recorded at Uwekahuna for each subsidence event is listed in table 46.2. Tilt directions listed in this table are for the period following the initial southward migration of the subsidence center. Since 1977, this direction from Uwekahuna has been remarkably constant. The only subsidence that did not display a dominant tilt direction was the February 21–23, 1969, event, which consisted of two different directions equal in tilt change, initially to the southeast and then to the south of Uwekahuna.

The tilt directions at Uwekahuna associated with the August 1981 southwest-rift intrusion and the January 1983 east-rift eruption

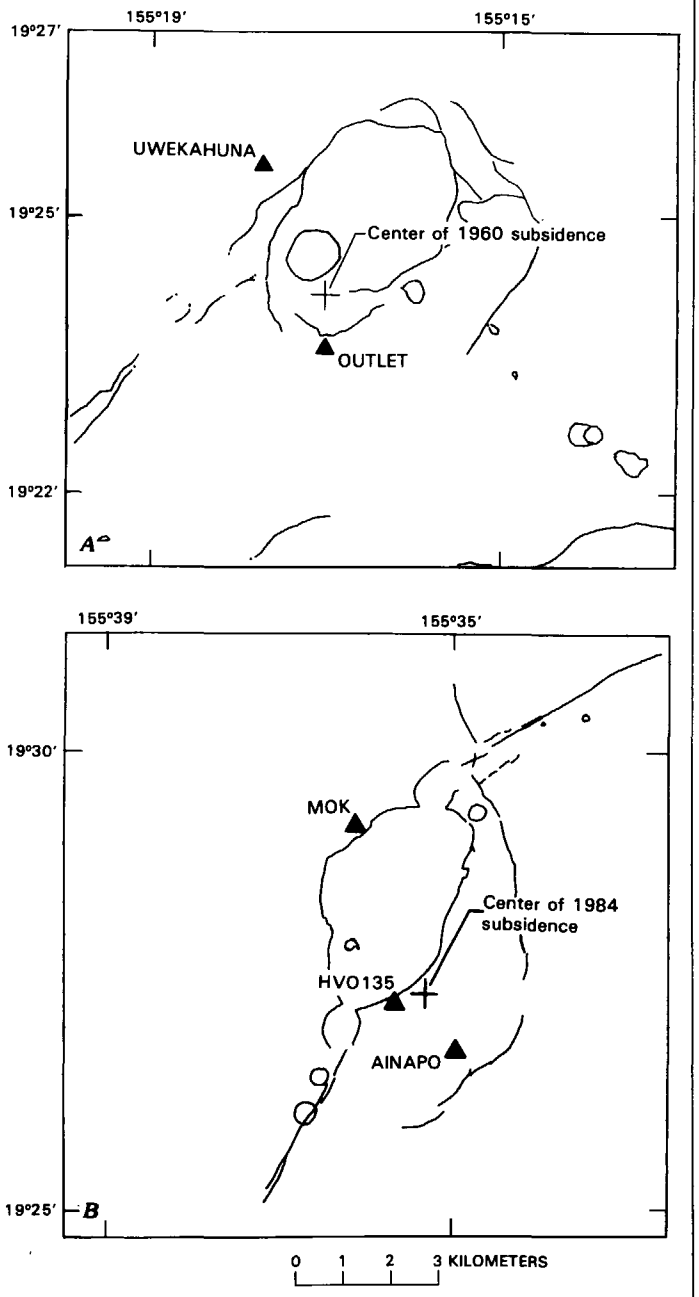

FIGURE 46.6.—Tilt sites (triangles) and subsidence centers. *A*, Kilauea summit region. *B*, Mauna Loa summit region. MOK, tilt station at Mokuaweoweo Crater.

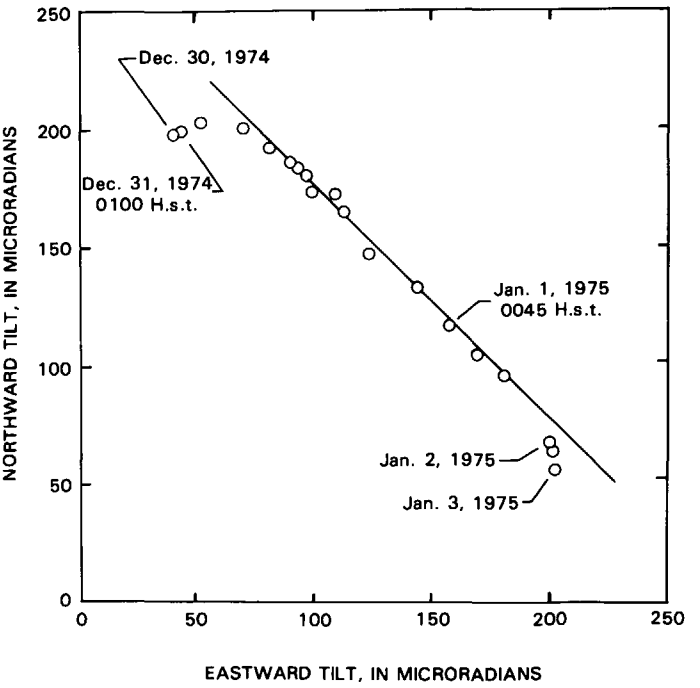

FIGURE 46.7.—Tilt directions measured at Uwekahuna during December 1974 southwest-rift eruption. Linear trend indicates constant tilt direction.

TABLE 46.2.—*Summit subsidence of Hawaiian volcanoes*

[UER, upper east rift; MER, middle east rift; LER, lower east rift; SWR, southwest rift; NER, northeast rift]

Beginning of summit subsidence	Distance from summit subsidence to rift intrusion (km)	Location of rift intrusion	Eruption		Tilt change (μrad)	Tilt direction	Time constant (days)	References
			Beginning (Date, hour)	Duration (days)				
Kilauea								
3/7/55	37	LER	2/28/55 0800	[1]38	192	S. 57° E.	16	Macdonald and Eaton (1964)
1/8/60	47	LER	1/13/60 1935	36	345	S. 60° E.	21	Richter and others (1970)
9/21/61	32	UER	9/22/61 0430	3	174	S. 35° E.	1	Richter and others (1964)
10/5/63	20	UER	10/5/63 0306	1	104	S. 55° E.	.5	Moore and Koyanagi (1969)
3/5/65	16	UER	3/5/65 0921	10	108	S. 45° E.	.25	Wright and others (1968)
12/24/65	10	UER	12/24/65 2130	.25	60	S. 85° E.	.25	Fiske and Koyanagi (1968)
8/22/68	6	UER	8/22/68 0615	5	58	S. 68° E.	.25	Jackson and others (1975)
10/7/68	16	UER	10/7/68 1435	15	78	S. 65° E.	.25	Jackson and others (1975)
2/22/69	10	UER	2/22/69 0950	6	58	([2])	.25	Swanson and others (1976)
12/31/74	4	SWR	12/31/74 0255	1	219	S. 44° E.	.75	([3])
9/13/77	25	MER	9/13/77 1910	[1]3	104	S. 47° E.	1.5	Moore and others (1981)
8/10/81	6	SWR	([4])	([4])	103	S. 47° E.	.5	([3])
6/21/82	11	SWR	([4])	([4])	50	S. 47° E.	1	([3])
1/2/83	25	MER	1/3/83 0030	[1]4	149	S. 47° E.	([5])	Dvorak and others (1985)
Mauna Loa								
3/25/84	18	NER	3/25/84 0130	20	--	--	5	Lockwood and others (1985)

[1]Duration of initial eruptive phase, later eruptive phases had relatively small tilt changes (all <30 μrad; most <15 μrad) recorded at Uwekahuna.
[2]No dominant tilt direction during the major summit subsidence.
[3]Hawaiian Volcano Observatory, unpublished data.
[4]No eruptive activity associated with these events.
[5]Multiple subsidence event.

were almost identical. Both events began with an eastward-directed tilt and rotated to the southeast (fig. 46.8), similar to the beginning of the 1974 summit subsidence. The tilt directions measured at Uwekahuna during the August 1981 and January 1983 events were identical, suggesting the same subsidence center, even though magma moved into different rift systems. No clear relation exists between location of subsidence center, measured by tilt at Uwekahuna, and movement of magma into either rift system (table 46.2).

A constant tilt direction recorded at a single station does not eliminate the possibility that the subsidence center may migrate radially to that station. Tilt measurements made at two different sites during the January–May 1960 summit subsidence show that at least

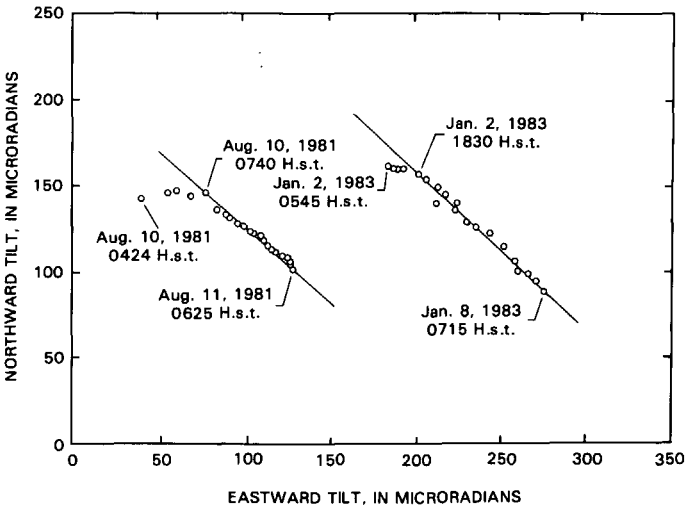

FIGURE 46.8.—Tilt directions measured at Uwekahuna during August 1981 southwest-rift intrusion and January 1983 east-rift eruption.

for this event the subsidence center remained in approximately the same horizontal position (fig. 46.9).

Tilt measurements made at three sites in the Mauna Loa summit region during the March 25–April 15, 1984, northeast-rift eruption showed no horizontal migration of the subsidence center (fig. 46.10). The subsidence center associated with the 1984 Mauna Loa northeast-rift eruption was located 1 km southeast of the rim of the summit caldera Mokuaweoweo (fig. 46.6*B*), a position identical to the uplift center determined from repeated geodetic surveys conducted since 1977 (Decker and others, 1983).

The amount of vertical migration of the subsidence center can be estimated when simultaneous tilt measurements are made at different distances from the subsidence center. The surface displacements produced by magma withdrawal from the summit reservoir are assumed to be adequately represented by a point source embedded in an elastic half-space (Dvorak and others, 1983). The ratio of the magnitude of tilt change (Φ_1 and Φ_2) at different horizontal distances from the subsidence center (h_1 and h_2) is given by

$$\Phi_1/\Phi_2 = \frac{h_1}{h_2}\,\frac{(d^2+h_2^2)^{5/2}}{d^2+h_1^2}. \qquad (2)$$

If the subsidence center does not migrate horizontally, then changes in the ratio of the magnitude of tilt change are a result of vertical migration. The amount that a small change in depth to the source, Δd, will change the ratio $\Delta(\Phi_1/\Phi_2)$ is determined by differentiating equation 2:

$$\Delta(\Phi_1/\Phi_2) = 5d\,\frac{\Phi_1}{\Phi_2}\left(\frac{1}{d^2+h_2^2}-\frac{1}{d^2+h_1^2}\right)\Delta d. \qquad (3)$$

For Kilauea, simultaneous tilt measurements were made during the January 18–May 11, 1960, event at Outlet and Uwekahuna

located 1 and 3 km, respectively, from the subsidence center. The ratio of tilt rates between Outlet and Uwekahuna in mid-February is not related to a change in tilt direction (fig. 46.11). The increase in ratio of tilt rates from 0.5 to 0.9 between Outlet and Uwekahuna is consistent with an upward migration of the subsidence center from 4 to 3 km that occurred in mid-February.

Simultaneous tilt measurements made at three different stations in the Mauna Loa summit region during the 1984 northeast-rift eruption showed no apparent change in the ratios of tilt rate (fig. 46.12). The MOK, HVO135, and AINAPO tilt sites are located at horizontal distances of 3.5, 0.5, and 1.5 km, respectively, from the subsidence center (fig. 46.6*B*). Using a value of 4 km for the depth to the source in (3) and noting that the slopes in figure 46.12 do not vary by more than 0.3, data in figure 46.12 indicate that the subsidence center related to the 1984 Mauna Loa eruption did not migrate vertically more the 0.7 km.

EXPONENTIAL DECAY IN SUMMIT TILT RATE

The summit tilt rate measured during subsidence events usually decreases with time (figs. 46.13–46.15). We have fitted exponential curves to both tilt components recorded during the first 13 Kilauea subsidences listed in table 46.2 and the 1984 Mauna Loa subsidence. For each subsidence event we estimate the magnitude of the north-south and the west-east tilt change, the time constant related to the decay rate, τ, and the beginning time of subsidence.

The time dependence of the summit tilt curves recorded during subsidences of both Kilauea and Mauna Loa is adequately matched by exponential curves, especially when tilt measurements are made by the 3-m-long watertube instrument (fig. 46.13) and by the dry-tilt technique (fig. 46.15). The poorer agreement between measured tilt changes and exponential curves for the March 1955 Kilauea subsidence is probably caused by less precise tilt measurements obtained from the horizontal-pendulum seismograph (fig. 46.14).

The only summit subsidence listed in table 46.2 that significantly departs from an exponential decay is the January 1983 Kilauea subsidence. This subsidence was a multiple event; the summit subsided in three stages over a period of 7 days (fig. 46.16). These three stages correspond to three episodes of downrift earthquake migration, crack opening, and eruption.

The exponential decay in summit tilt rate is reminiscent of a rheological response observed in the laboratory when crustal material is subjected to sudden stress changes, such as may result from the sudden movement of magma. For example, transient creep of crustal material will exhibit an exponential decay in strain rate (Jaeger and Cook, 1969). The time constants for summit subsidences at Kilauea

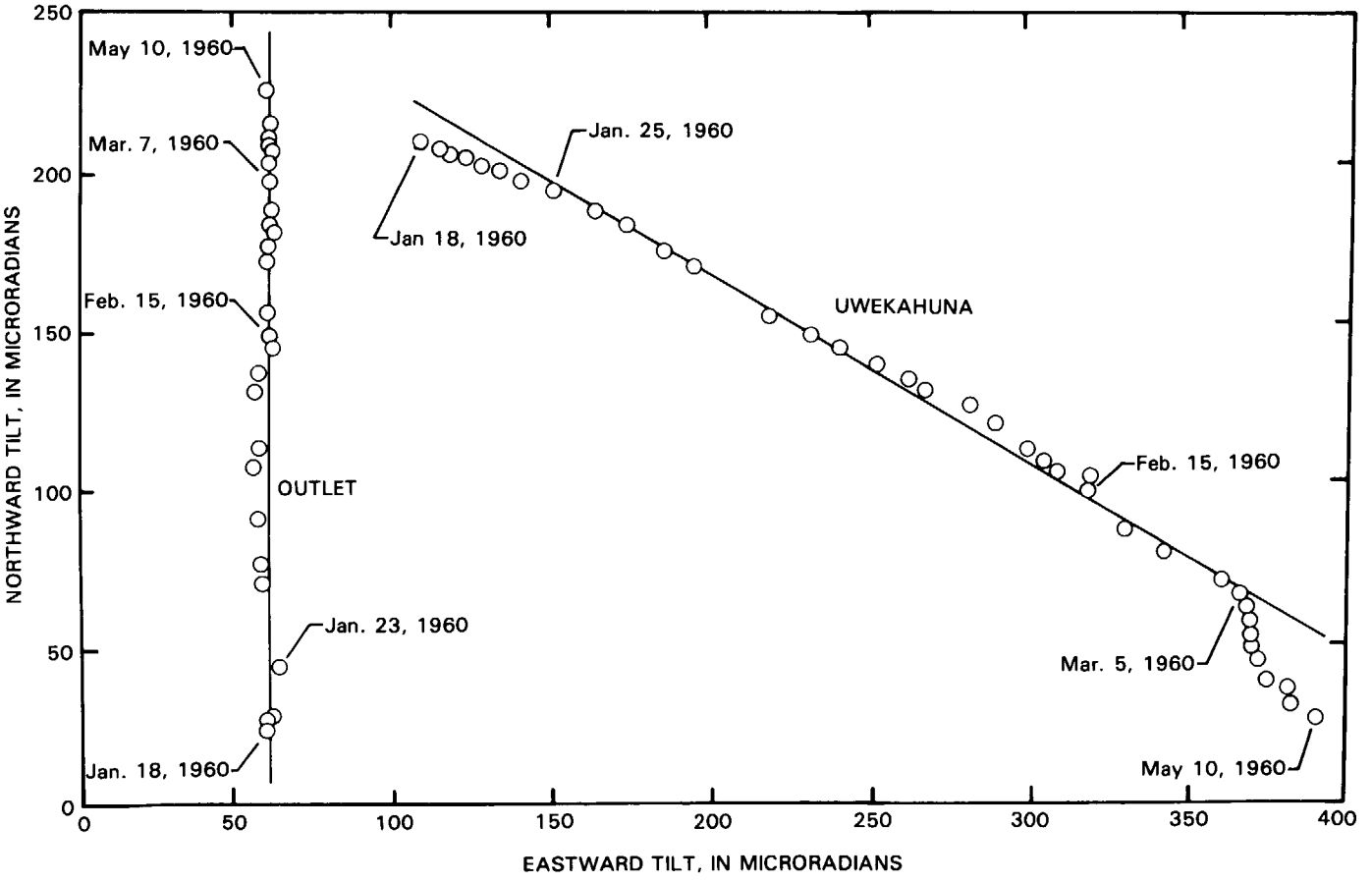

FIGURE 46.9.—Tilt directions measured at Outlet and Uwekahuna during January–May 1960 summit subsidence of Kilauea.

vary by a factor of more than 80. It seems unlikely that transient creep could control summit tilt rates, because rheological properties of the Kilauea summit would also have to vary by a factor of 80.

Along the east rift of Kilauea, the time constant appears to be related to the distance from the summit-subsidence center to the affected part of the rift (fig. 46.17). Longer time constants are associated with eruptions located farther downrift, suggesting that conduit length from the summit reservoir to the eruptive site controls, in part, the summit tilt rate. Time constants related to eruptions along the southwest rift of Kilauea and the northeast rift of Mauna Loa are longer than at comparable distances along the east rift of Kilauea.

Tilt rates recorded during periods of magma accumulation in the summit reservoir from a deeper source may also display an exponential decay. The west-east tilt component at Uwekahuna measured by a continuously recording tiltmeter revealed a cyclic pattern during a recent series of eruptive phases along the middle east rift (fig. 46.18). Beginning in February 1983 and lasting at least two years, the Kilauea summit went through several cycles of gradual uplift and more rapid subsidence. Periods of subsidence were associated with eruptive activity along the middle east rift. The summit tilt curve during noneruptive periods approximately followed an exponential decay curve with a maximum tilt change of 32 μrad. The time constant for summit uplift from February to September 1983 was 40 days, a time constant a factor of 2 greater than the maximum value determined for periods of summit subsidence and rift eruption.

We have argued that migration of the subsidence center and rheology of the volcano are unimportant in explaining summit-subsidence tilt curves. Moreover, an exponential time dependence of tilt rate observed during periods of both magma accumulation and withdrawal suggests that factors that control magma flow rate may be responsible for observed tilt rates.

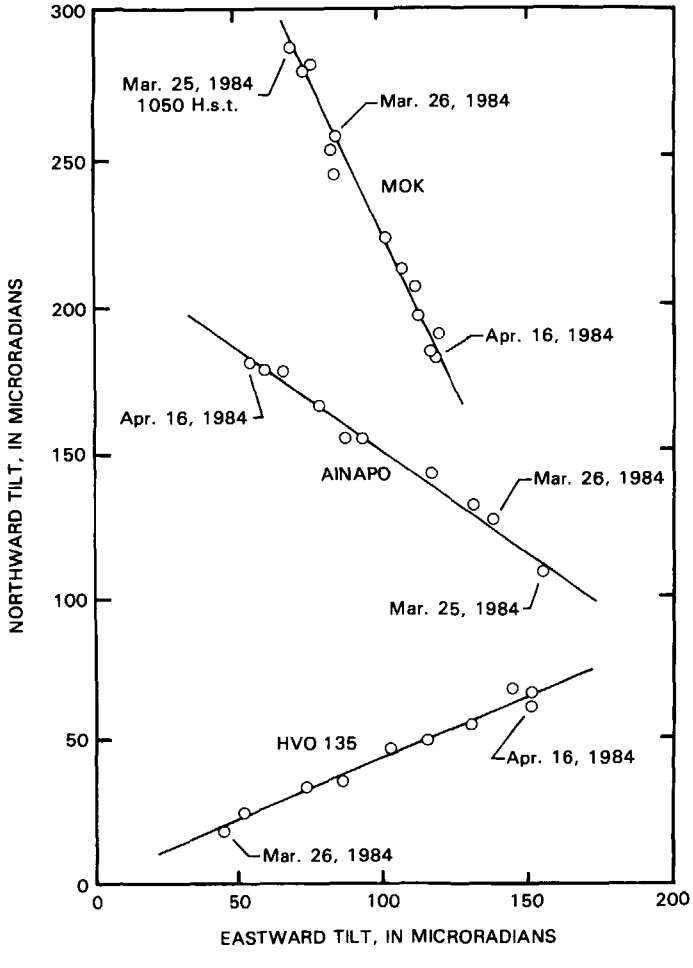

FIGURE 46.10.—Tilt directions measured at MOK, AINAPO, and HVO 135 during March 25–April 15, 1984 summit subsidence of Mauna Loa.

HYDRAULIC MODEL

We adopt a hydraulic model for magma movement that was originally applied by Machado (1974) to explain decreasing extrusive rates observed at some volcanoes. Magma is stored in reservoirs between the upper mantle and the summit and along the rift systems. Magma moves within a conduit system that connects reservoirs that are under different confining pressures.

The magma flow rate, Q, is assumed to be proportional to the pressure change, ΔP, between reservoirs

$$Q = \alpha \Delta P, \tag{4}$$

where the constant of proportionality, α, depends on type of fluid flow.

We further assume that magma pressure is linearly related to volumetric strain, $\Delta V/V$,

$$\Delta P = -E\frac{\Delta V}{V}, \tag{5}$$

where E is a constant of proportionality, the bulk modulus of the system. A pressure decrease results in a volume increase. When flow starts, pressure will change according to the equation (Machado, 1974, equation 48)

$$\Delta P = -\frac{E}{V}\left(\Delta V + \int_0^t Q\,dt\right). \tag{6}$$

Substitution of (4) into (6) yields

$$Q = Q_0 - \frac{1}{\tau}\int_0^t Q\,dt, \tag{7}$$

where

$$\frac{1}{\tau} = \alpha\frac{E}{V} \tag{8}$$

and

$$Q_0 = -\frac{\Delta V}{\tau}. \tag{9}$$

Differentiating (7) gives a simple differential equation for the magma flow rate:

$$\frac{dQ}{dt} + \frac{1}{\tau}Q = 0. \tag{10}$$

The solution to the above equation is

$$Q = Q_0 e^{-t/\tau}. \tag{11}$$

Several types of fluid flow are based on flow rate proportional to the pressure difference (4). In particular, for laminar fluid flow through a circular pipe of radius r, Poiseuille's law gives the constant of proportionality relating flow rate to pressure difference as:

$$\alpha = \frac{\pi}{8\eta} f r^4 \left(\frac{\Delta P}{l}\right) \tag{12}$$

where η is magma viscosity, f is the frictional-loss factor, and l is the conduit length. The quantity $\Delta P/l$ is the pressure gradient between the two reservoirs. The time constant is given by

$$\tau = \frac{8\eta}{\pi} \frac{\Delta V}{f r^4} \left(\frac{l}{\Delta P}\right). \tag{13}$$

The change in volume, ΔV, is related to the subsidence volume. The time constant increases with conduit length in (13), a relation observed along the east rift of Kilauea (fig. 46.17), though not linearly along the entire rift, as would be expected if r, f, and ΔP remained constant.

Equation 13 emphasizes the importance of conduit width on magma flow rate. A 50-percent decrease in conduit width will decrease the flow rate by a factor of 16. Because conduit width probably does not remain constant along the rift system, a time constant derived from the summit tilt curve relates to the minimum constriction along the active part of the conduit.

INITIAL EARTHQUAKE LOCATIONS AND SHAPE OF THE SUMMIT TILT CURVE

Earthquakes located in the summit region and along the rift zones of Kilauea are probably directly related to the magma conduit system within the volcano (Ryan and others, 1983). The location of the initial earthquake swarm associated with a summit subsidence may indicate where magma movement was initiated. We might expect that earthquake swarms initiated at different locations within the volcano will influence the initial shape of the summit tilt curve.

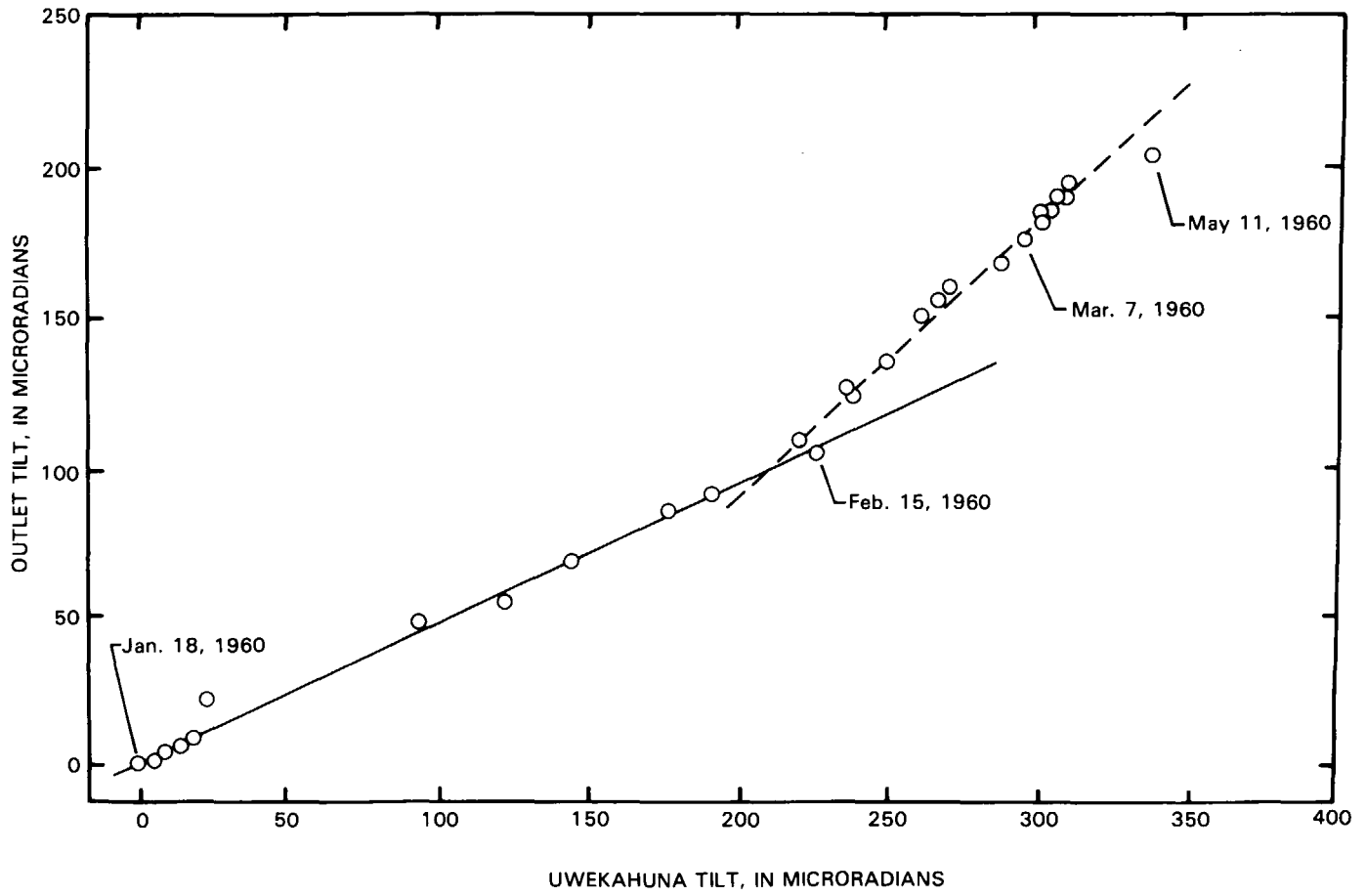

FIGURE 46.11.—Tilt magnitudes recorded at Outlet as a function of tilt magnitudes recorded at Uwekahuna during January–May 1960 summit subsidence of Kilauea.

Increased coverage of the seismic network and advances in seismic processing at HVO have improved hypocenter determinations on the Island of Hawaii (Klein and Koyanagi, 1980). In particular, earthquake swarms occurring at Kilauea over the past decade can be located to within a few kilometers on any part of the volcano with greater resolution in the summit region and along the upper rift systems.

Earthquake hypocenters associated with the onset of summit subsidence and southwest-rift intrusion frequently begin in the south caldera area of Kilauea. For example, earthquake swarms associated with the December 1974 eruption (fig. 46.19*A*) and the August 1981 intrusion (fig. 46.19*B*) began in the south caldera area and migrated along the southwest rift for several hours (Klein and others, chapter 43). The beginning of these two earthquake swarms coincided with an abrupt change in slope of the summit tilt curves (fig. 46.20). On the basis of the location of the initial earthquake swarm and the initial, rapid summit tilt change, we infer that magma movement on December 31, 1974, and on August 10, 1981, was initiated in the summit reservoir.

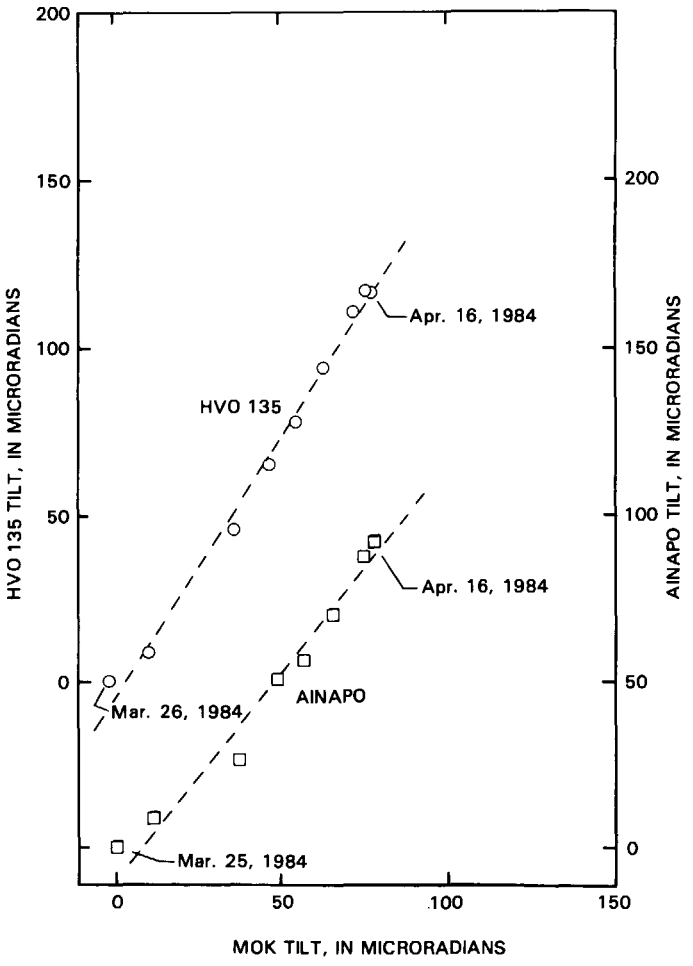

FIGURE 46.12.—Tilt magnitudes recorded at HVO 135 and AINAPO as a function of tilt magnitudes recorded at MOK during March 25–April 14, 1984 summit subsidence of Mauna Loa.

During the two most recent Kilauea subsidences listed in table 46.2, in June 1982 and January 1983, initial earthquake swarms were located along the rift and not in the south caldera area (fig. 46.21). The summit tilt responded gradually for several hours to these two events (fig. 46.22). Along the east rift near the site of the initial earthquake swarm in January 1983, a tiltmeter did record an abrupt change in slope (fig. 46.23). Presumably, initial magma movement was from a reservoir within the southwest rift in June 1982 and within the east rift in January 1983 and not from the summit reservoir. Initial magma flow from the summit reservoir was slower as pressure along the conduit system from the summit to the rift was gradually reduced as magma moved within the rift system.

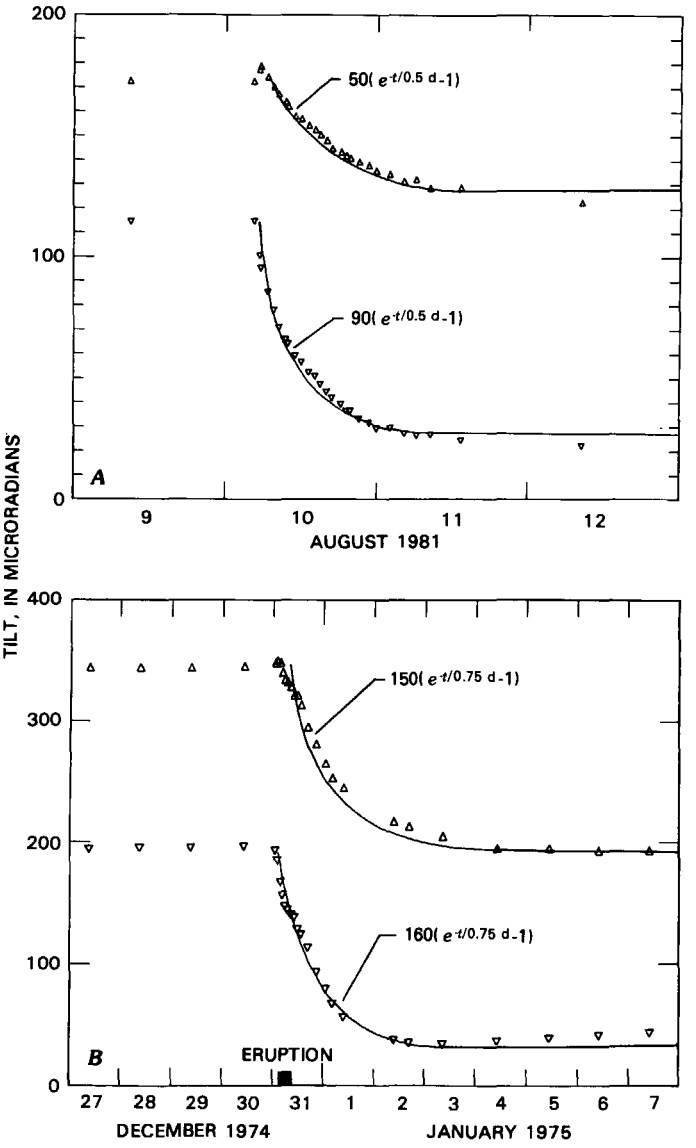

FIGURE 46.13.—Tilt changes recorded by 3-m-long watertube instrument at Uwekahuna. North-south tilt changes, upper curve; west-east tilt changes, lower curve; solid lines, exponential functions empirically fitted to tilt data; numerical constant in each equation is value of total tilt change in microradians. ***A***, August 1981 southwest-rift intrusion. ***B***, December 1974 southwest-rift eruption of Kilauea.

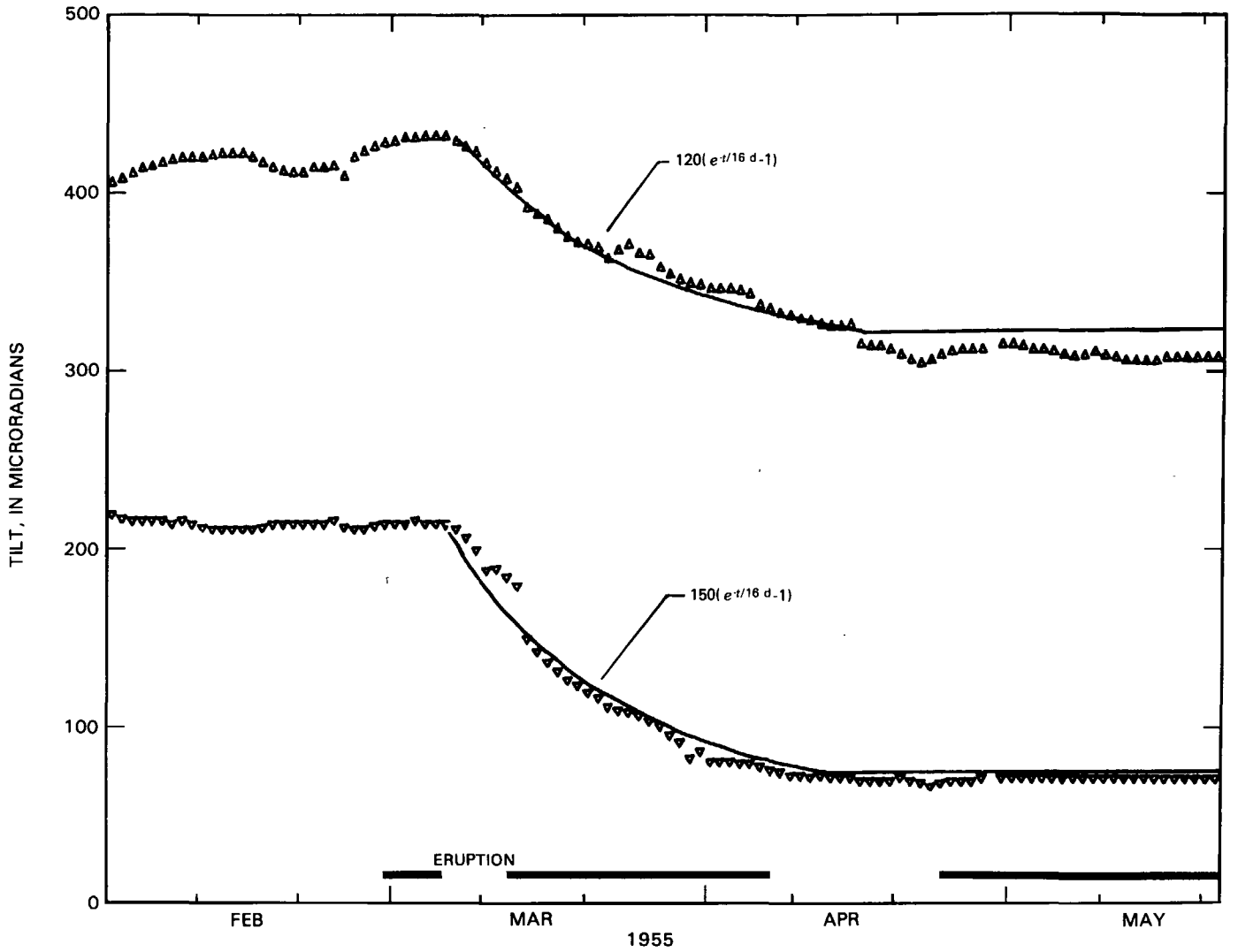

FIGURE 46.14.—Tilt changes recorded by horizontal pendulum seismograph at Uwekahuna during March 1955 lower-east-rift eruption of Kilauea. North-south tilt changes, upper curve; west-east tilt changes, lower curve; solid lines, exponential functions empirically fitted to tilt data; numerical constant in each equation is value of total tilt change in microradians.

A gradual response of summit tilt for 1 to 3 days was also observed after the onset of eruptive activity along the lower east rift in March 1955 and January 1960. Initial earthquake swarms and ground cracking in these two cases began along the rift.

DISCUSSION

The well-establish relation between summit-subsidence events and rift intrusions and eruptions at Hawaiian volcanoes can be exploited to characterize magma movement within a long conduit system. In particular, we have examined the relation between rate of magma withdrawal from the summit reservoir and the rate and location of rift eruptions. Magma movement from the Kilauea summit reservoir to the east-rift system may be an analog to vertical magma ascent through the upper mantle and crust beneath Hawaiian volcanoes. Therefore, our results may also contribute to understanding how deeper magmatic sources influence eruptive activity at other volcanoes.

Summit tilt measurements at Kilauea and Mauna Loa record magma accumulation and withdrawal from a shallow reservoir. Magma originating in the mantle migrates through the upper mantle and crust and accumulates in the summit reservoir prior to eruption. Horizontal migration of the uplift center at Kilauea suggests that the summit reservoir consists of a plexus of dikes and sills (Fiske and Kinoshita, 1969).

Several lines of evidence indicate that magma also resides in shallow reservoirs along the east rift of Kilauea. The 4- to 5-day delay between the onset of eruptive activity along the lower east rift

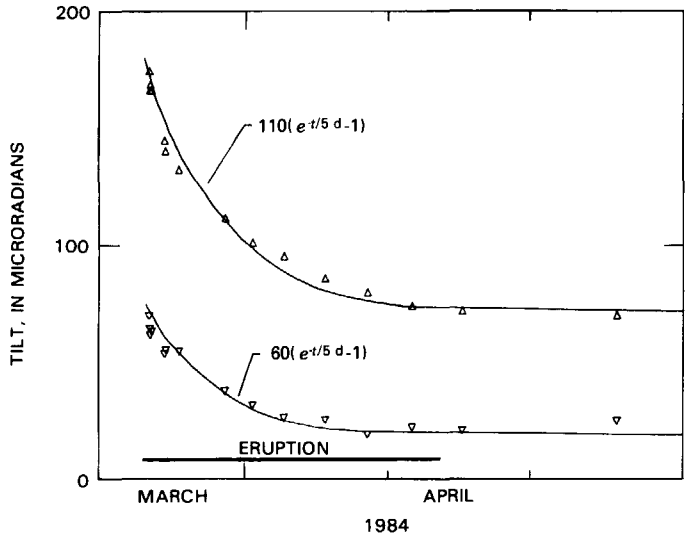

FIGURE 46.15.—Tilt changes recorded by dry-tilt method at MOK during March 25–April 15, 1984, northeast-rift eruption of Mauna Loa. North-south tilt changes, upper curve; west-east tilt changes, lower curve; solid lines, exponential functions empirically fitted to tilt data; numerical constant in each equation is value of total tilt change in microradians.

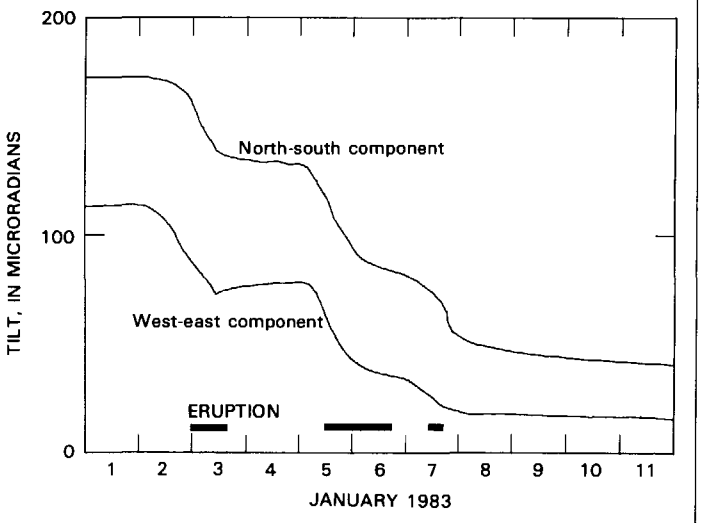

FIGURE 46.16.—Tilt changes recorded by automatic tiltmeter located at Uwekahuna during January 1983 middle-east-rift eruption of Kilauea.

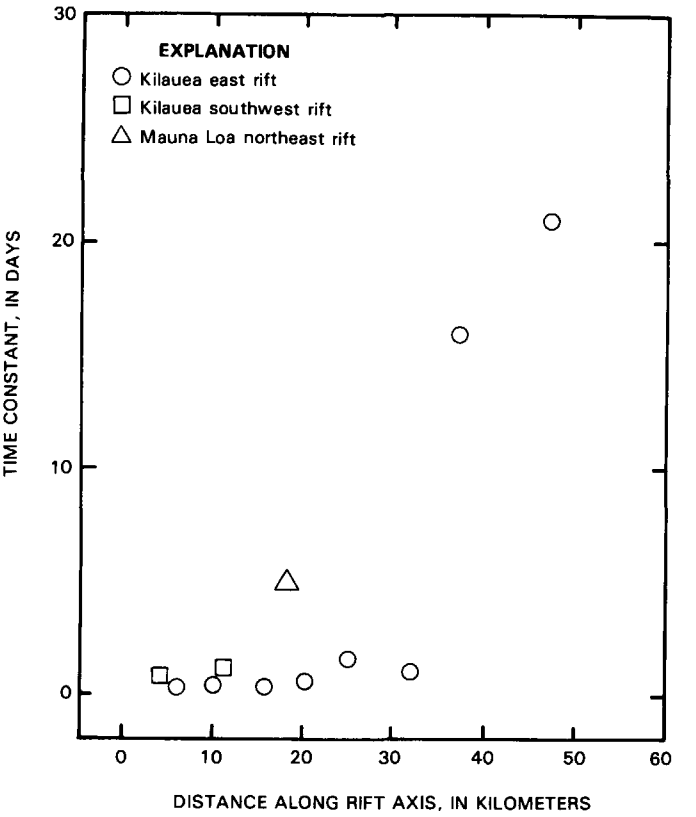

FIGURE 46.17.—Time constants for summit subsidences plotted as a function of distance from subsidence center to rift intrusion or eruption.

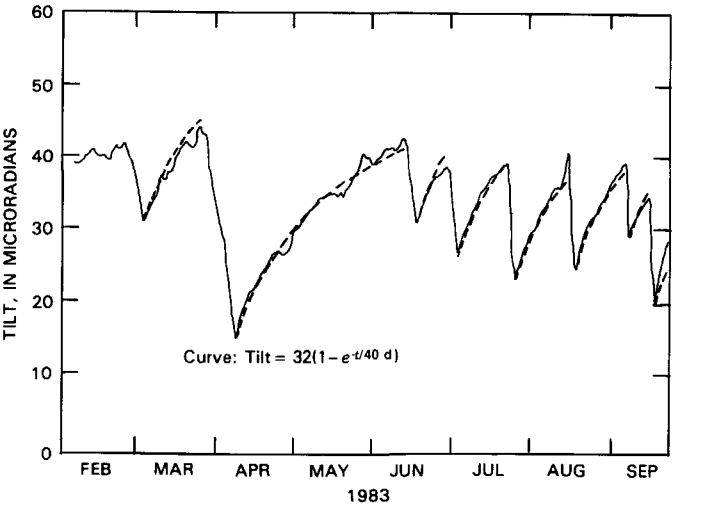

FIGURE 46.18.—West-east tilt changes recorded from February to September 1983 by tiltmeter located at Uwekahuna. Periods of generally increasing tilt values correspond to summit uplift and magma accumulation in Kilauea summit region; periods of rapid decrease in tilt values correspond to magma withdrawal from Kilauea summit region and eruptive activity along middle east rift. Same exponential curve (dashed lines) has been empirically fitted to periods of summit uplift. Exponential curve is for a maximum tilt change of 32 μrad and a time constant of 40 days.

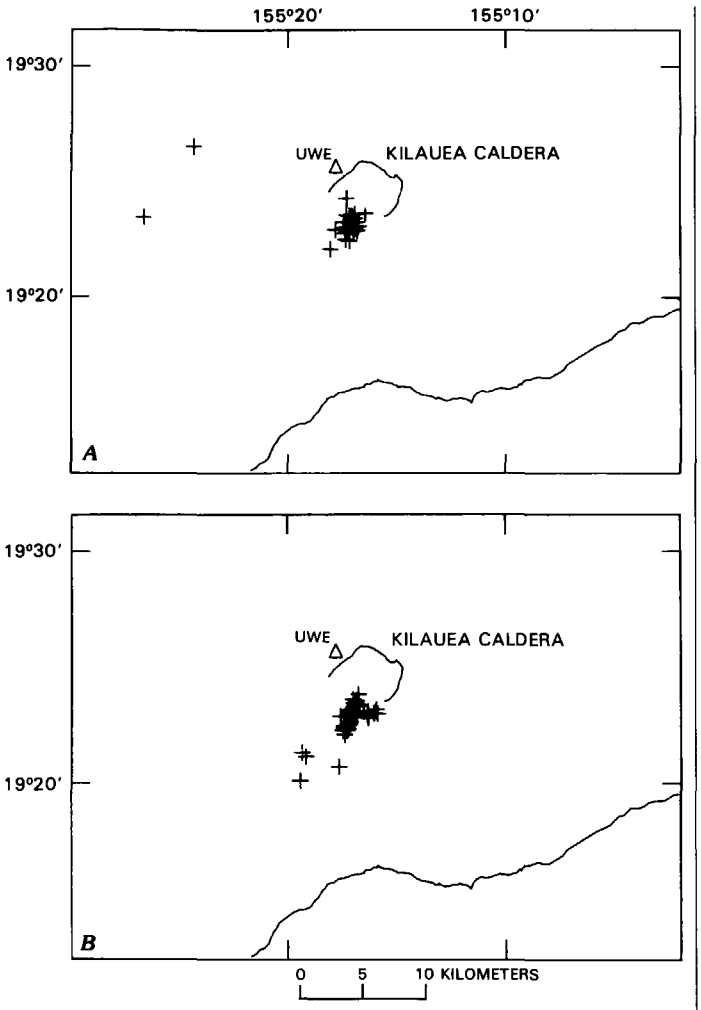

FIGURE 46.19.—Initial earthquake epicenters. UWE, Uwekahuna seismometer station. ***A***, December 31, 1974 (0000–0600 H.s.t.), southwest-rift eruption. ***B***, August 10, 1981 (0300–0600 H.s.t.), southwest-rift intrusion.

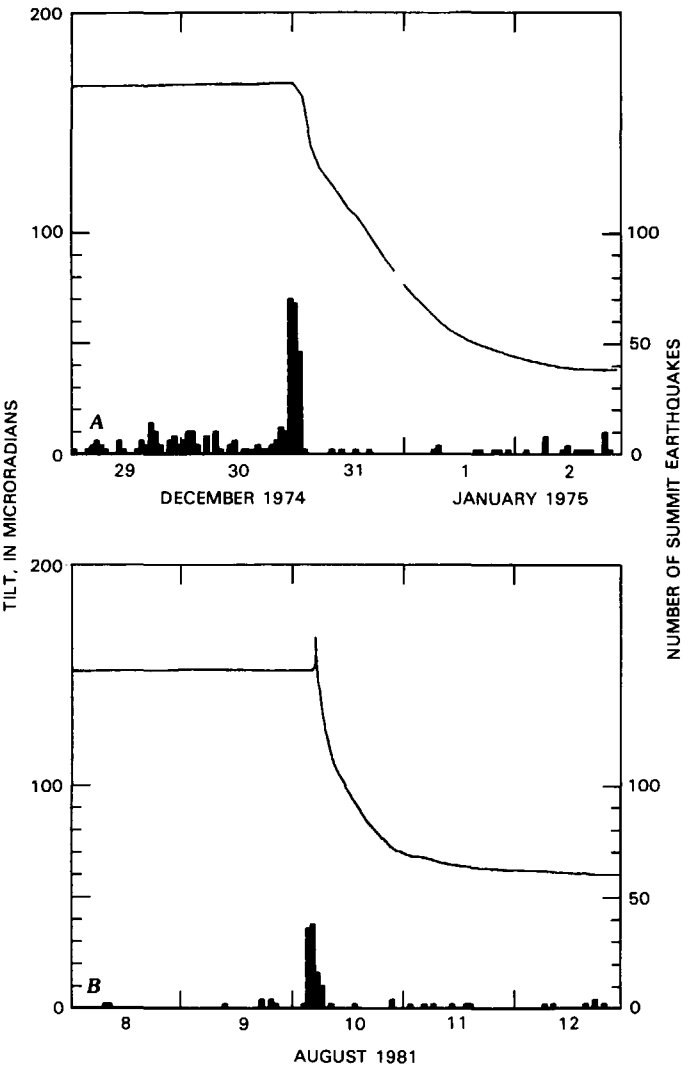

FIGURE 46.20.—West-east tilt curve recorded at Uwekahuna. ***A***, December 1974 southwest-rift eruption. ***B***, August 1981 southwest-rift intrusion. Hourly rate of locatable summit earthquakes is shown by bar graph.

and the onset of summit subsidence in March 1955 and January 1960 led Eaton (1962) to suggest that magma was stored within the rift system. Jackson and others (1975) noted that the volume of summit subsidence at Kilauea exceeds the volume of lava erupted along the rift: some magma withdrawn from the summit remains in the rift system. Differentiated lava initially erupted from the east rift during a new eruptive sequence suggests that rift eruptions are initially fed by magma that has resided for longer periods at shallow levels in the crust than magma erupted in the summit (Wright and others, 1968; Moore, 1983). Finally, geodetic surveys conducted along the east rift of Kilauea have identified centers of uplift presumed to be regions of magma accumulation (Jackson and others, 1975; Swanson and others, 1976; Dzurisin and others, 1984), one persistent center along the upper east rift is centered 2 to 4 km beneath the surface (Dvorak and others, 1983).

Along the east rift of Kilauea, the volume of summit subsidence increases with distance to the rift eruption (Epp and others, 1983). The subsidence rate also increases with distance, though not linearly, along the entire east rift (fig. 46.17). Time constants for summit subsidence range from 0.25 to 1.5 days for southwest- and east-rift eruptions that occur within 35 km of the summit; time constants for lower-east-rift eruptions were considerably longer, from 16 to 21 days. The abrupt increase in time constant for rift eruptions downrift of Heiheiahulu (fig. 46.1) may be caused by constriction of the magma conduit between the middle and the lower parts of the east rift.

The time constant for the 1984 Mauna Loa summit subsidence and northeast-rift eruption is close to the linear trend extrapolated from time constants for the Kilauea lower-east-rift eruptions. This similarity may be related to the several-year interval between rift

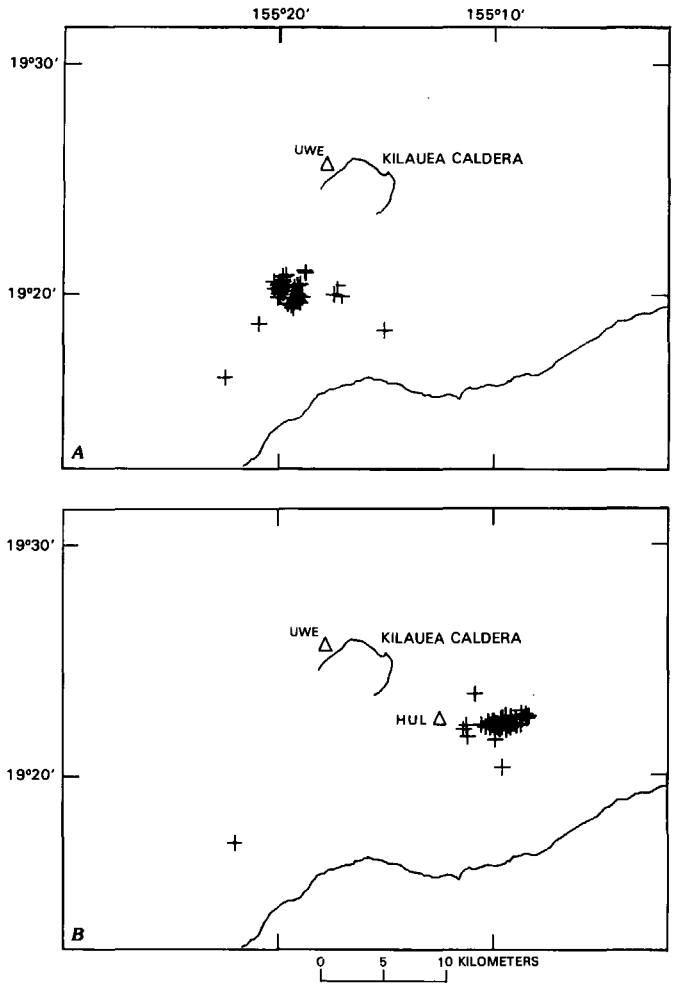

FIGURE 46.21.—Initial earthquake epicenters. Seismometer stations: UWE, Uwekahuna; HUL, Heiheiahulu. ***A***, June 22, 1982 (1200–2300 H.s.t.), southwest-rift intrusion. ***B***, January 2, 1983 (0000–0600 H.s.t.), east-rift eruption.

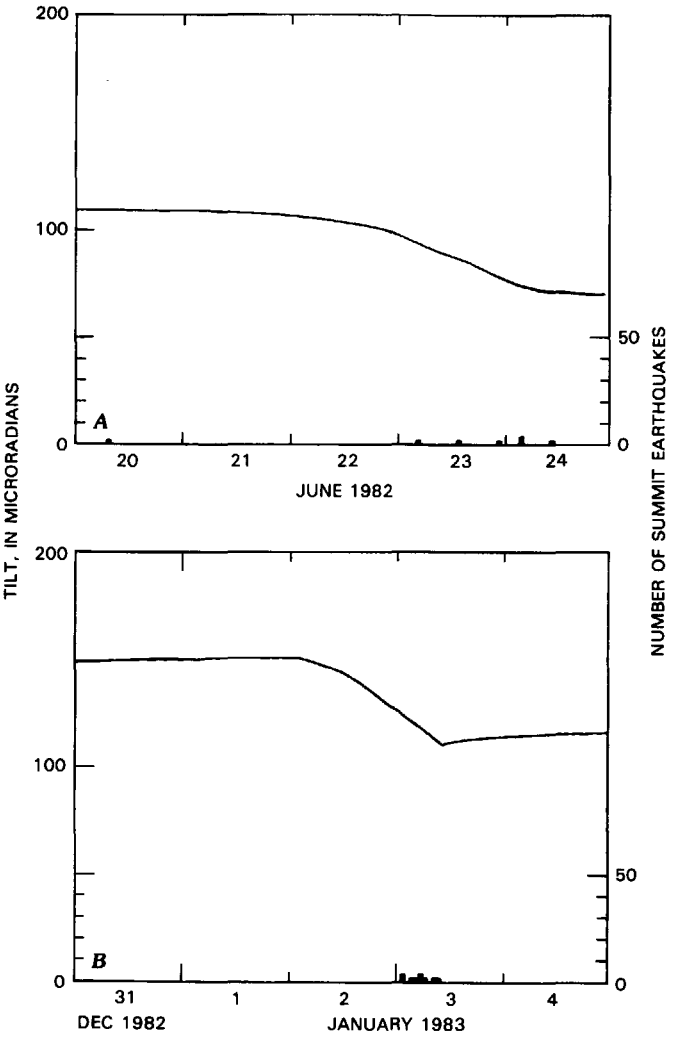

FIGURE 46.22.—West-east tilt curve recorded at Uwekahuna. ***A***, June 1982 southwest-rift intrusion. ***B***, January 1983 middle-east-rift eruption. Hourly rate of locatable summit earthquakes is shown by bar graph.

intrusions into the lower east rift of Kilauea and the northeast rift of Mauna Loa. By comparison, more frequent episodes of magma movement in the upper east rift result in less flow resistance and, hence, much shorter time constants (Dvorak and Okamura, 1985).

Changes in summit tilt rate recorded during subsidence events usually follow an exponential decay. Periods of magma accumulation in the summit reservoir may also follow an exponential decay in tilt rate, a result previously recognized by Shimozuru (1981), who proposed an electrical analog for the summit magma reservoir.

If we assume that summit tilt changes are related to summit magma accumulation or withdrawal, then the rate of magma accumulation in the summit reservoirs of Kilauea and Mauna Loa may be as much as a factor of 100 less than the rate of magma withdrawal (figs. 46.5, 46.17, 46.18). The different rates of magma accumulation and withdrawal for an eruptive cycle may reflect a basic difference between the vertical conduit feeding the summit reservoir and the horizontal conduit along the rift system. In the context of our model, an increase by a factor of 100 in magma flow rate could correspond to an increase by a factor of 10 in cross-sectional area or of 100 in pressure gradient (equation 13).

If the east rift of Kilauea is an appropriate analog for the vertical conduit beneath Hawaiian volcanoes, then we may have a better understanding of the possible role the upper mantle has on magma supply rate. The 40- to 60-km length of the vertical conduit from the mantle source to the summit, based on maximum earthquake depths beneath Hawaiian volcanoes and on a hydraulic model (Eaton and Murata, 1960), is comparable to the distance from the Kilauea summit to the 1960 lower-east-rift eruption. Because individual magma reservoirs exist along the east rift, magma reservoirs may also be expected to exist along the vertical conduit. Conduit width probably varies with length along both the vertical conduit and the rift system; the conduit width in equation 13 is the width at a constriction that limits the flow rate in the remainder of the conduit.

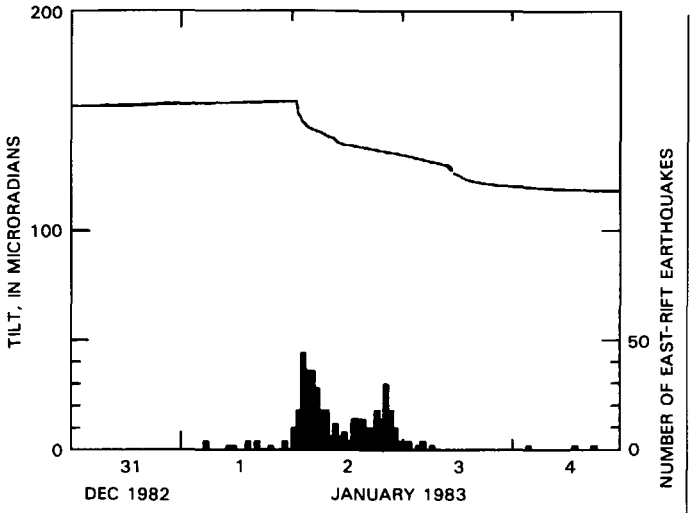

FIGURE 46.23.—West-east tilt curve recorded during early January 1983 along upper east rift (HUL in fig. 46.21*B*). Lower tilt value corresponds to downward deflection to east.

Magma flow may be initiated in a reservoir that lies along the rift system; however, the summit reservoir strongly influences the total volume of magma moved, as evidenced by continued summit subsidence several weeks after the end of eruptive activity in 1955 and 1960. Similarly, magma flow may be initiated in a reservoir within the vertical conduit, although the mantle source region may control the magma flow rate and total volume of magma involved. Recently, Dzurisin and others (1984) have suggested a close link between bursts of deep harmonic tremor, an indicator of magma movement, and magma supply rate to the Kilauea summit. Recognition of a relation between magma volume and flow rate from the Kilauea summit reservoir to east-rift eruptions supports their suggestion.

SUMMARY

Summit magma reservoirs exist within a few kilometers of the surface at both Kilauea and Mauna Loa. The accumulation and withdrawal of magma in the reservoir is monitored by tilt measurements that can easily be made over periods of a few minutes to several weeks.

Summit tilt curves recorded during subsidence events frequently begin with an abrupt change in slope. The tilt rate is usually greatest at the beginning of the event and steadily decreases with time.

Horizontal or vertical migration of the subsidence center are unimportant in explaining variations in summit tilt rate at Kilauea and Mauna Loa. The summit-subsidence pattern at Kilauea is independent of the rift system involved in magma movement.

Most summit tilt curves associated with subsidence events follow an exponential decay. At Kilauea, the decay time constant has varied by more than a factor of 80, which suggests that rheological properties of the volcano do not control subsidence rate. The rate of magma accumulation in the summit reservoir may also follow an exponential decay.

A simple hydraulic model may explain the observed exponential decay in summit subsidence rate. The model assumes that magma flow rate is proportional to the pressure difference along the magma conduit from the summit reservoir to a second reservoir or eruptive site located along the rift system. Furthermore, magmatic pressure is assumed to be linearly proportional to volumetric strain. One type of fluid flow consistent with these assumptions is laminar flow through a circular pipe.

REFERENCES

Decker, R.W., Koyanagi, R.Y., Dvorak, J.J., Lockwood, J.P., Okamura, A.T., Yamashita, K.M., and Tanigawa, W.R., 1983, Seismicity and surface deformation of Mauna Loa Volcano, Hawaii: Eos, Transactions of the American Geophysical Union, v. 37, p. 545–547.

Dvorak, J.J., and Okamura, A.T., 1985, Variations in tilt rate and harmonic tremor amplitude during the January–August 1983 east rift eruptions of Kilauea Volcano, Hawaii: Journal of Volcanology and Geothermal Research, v. 25, p. 249–258.

Dvorak, J.J., Okamura, A.T., and Dieterich, J.H., 1983, Analysis of surface deformation data, Kilauea Volcano, Hawaii: October 1966 to September 1970: Journal of Geophysical Research, v. 88, p. 3295–3304.

Dzurisin, D., Koyanagi, R.Y., and English, T.T., 1984, Magma supply and storage at Kilauea Volcano, Hawaii: 1956–1983: Journal of Volcanology and Geothermal Research, v. 21, p. 177–206.

Eaton, J.P., 1959, A portable water-tube tiltmeter: Bulletin of the Seismological Society of America, v. 49, p. 301–316.

———1962, Crustal structure and volcanism in Hawaii, *in* Macdonald, G.A., and Kuno, H., eds., The crust of the Pacific Basin: American Geophysical Union, Geophysical Monograph Series, v. 6, p. 13–29.

Eaton, J.P., and Murata, K.J., 1960, How volcanoes grow: Science, v. 132, p. 925–938.

Epp, D., Decker, R.W., and Okamura, A.T., 1983, Relation of summit deformation to east rift zone eruptions of Kilauea Volcano, Hawaii: Geophysical Research Letters, v. 10, p. 493–496.

Fiske, R.S., and Koyanagi, R.Y., 1968, The December 1965 eruption of Kilauea Volcano, Hawaii: U.S. Geological Survey Professional Paper 607, 21 p.

Fiske, R.S., and Kinoshita, W.R., 1969, Inflation of Kilauea Volcano prior to its 1967–68 eruption: Science, v. 165, p. 341–349.

Jackson, D.B., Swanson, D.A., Koyanagi, R.Y., and Wright, T.L., 1975, The August and October 1968 east rift eruptions of Kilauea Volcano, Hawaii: U.S. Geological Survey Professional Paper 890, 33 p.

Jaeger, J.C., and Cook, N.G.W., 1969, Fundamentals of rock mechanics: London, John Wiley and Sons, Inc.

Klein, F.W., and Koyanagi, R.Y., 1980, Hawaiian Volcano Observatory seismic network history 1950–1979: U.S. Geological Survey Open-File Report 80–302, 84 p.

Lockwood, J.P., Banks, N., English, T.T., Greenland, P., Jackson, D., Johnson, D., Koyanagi, R.Y., Okamura, A.T., and Rhodes, M., 1985, The 1984 eruption of Mauna Loa Volcano, Hawaii: Eos, Transactions of the American Geophysical Union, v. 66, p. 169–171.

Macdonald, G.A., and Eaton, J.P., 1964, Hawaiian volcanoes during 1955: U.S. Geological Survey Bulletin 1171, 170 p.

Machado, F., 1974, The search for magmatic reservoirs, *in* Civetta, L., Gasparini, P., Luongo, G., and Rapolla, A., eds., Physical volcanology, developments in solid earth geophysics, v. 6: Amsterdam, Elsevier, p. 255–273.

Mogi, K., 1958, Relations between the eruptions of various volcanoes and the deformation of the ground surface around them: Bulletin of the Earthquake Research Institute, University of Tokyo, v. 36, p. 99–134.

Moore, J.G., and Koyanagi, R.Y., 1969, The October 1963 eruption of Kilauea Volcano, Hawaii: U.S. Geological Survey Professional Paper 614–C, 13 p.

Moore, R.B., 1983, Distribution of differentiated tholeiitic basalts on the lower east rift zone of Kilauea Volcano, Hawaii: A possible guide to geothermal exploration: Geology, v. 11, p. 136–140.

Moore, R.B., Helz, T.R., Dzurisin, D., and Eaton, G.P., 1981, The 1977 eruption of Kilauea Volcano, Hawaii: Journal of Volcanology and Geothermal Research, v. 7, p. 189–210.

Richter, D.H., Ault, W.U., Eaton, J.P., and Moore, J.G., 1964, The 1961 eruption of Kilauea Volcano, Hawaii: U.S. Geological Survey Professional Paper 474–D, 34 p.

Richter, D.H., Eaton, J.P., Murata, K.J., Ault, W.U., and Krivoy, H.L., 1970, Chronological narrative of the 1959–60 eruption of Kilauea Volcano, Hawaii: U.S. Geological Survey Professional Paper 537–E, 73 p.

Ryan, M.P., Blevins, J.Y.K., Okamura, A.T., and Koyanagi, R.Y., 1983, Magma reservoir subsidence mechanics: theoretical summary and application to Kilauea Volcano, Hawaii: Journal of Geophysical Research, v. 88, p. 4147–4181.

Shimozuru, D., 1981, Magma reservoir system inferred from tilt patterns: Bulletin Volcanologique, v. 44, p. 499–504.

Swanson, D.A., Jackson, D.B., Koyanagi, R.Y., and Wright, T.L., 1976, The February 1969 east rift eruption of Kilauea Volcano, Hawaii: U.S. Geological Survey Professional Paper 891, 30 p.

Wright, T.L., and Fiske, R.S., 1969, Origin of the differentiated and hybrid lavas of Kilauea Volcano, Hawaii: Journal of Petrology, v. 12, p. 1–65.

Wright, T.L., Kinoshita, W.T., and Peck, D.L., 1968, March 1965 eruption of Kilauea Volcano and the formation of Makaopuhi lava lake: Journal of Geophysical Research, v. 73, p. 3181–3205.

Yamashita, K.M., 1981, Dry tilt: a ground deformation monitor as applied to active volcanoes of Hawaii: U.S. Geological Survey Open-File Report 81–523, 21 p.

ELASTIC AND INELASTIC MAGMA STORAGE AT KILAUEA VOLCANO

By Daniel J. Johnson

ABSTRACT

Gravity, leveling, and trilateration data recently obtained at Kilauea Volcano indicate that magma is accommodated within the summit reservoir by a combination of elastic magma compression, elastic chamber expansion, and gradual inelastic edifice widening in a south-southeast direction.

Elastic (reversible) magma storage is modeled using data from 15 brief summit-deflation episodes in 1984–85 and assuming a spherical geometry for the magma reservoir. Changes in pressure in the reservoir produce the deformation; changes in mass in the reservoir produce the gravity changes. The ratio of residual gravity change (corrected for the free-air effect) to elevation change, measured near the apex of maximum subsidence, averaged 0.28 ± 0.025 μGal/mm. If magma density is assumed to be 2.75 g/cm^3, the volume of magma withdrawn from the reservoir averaged 2.4 ± 0.21 times the associated volume of subsidence. This volume difference is dependent on both the magma bulk modulus (which constrains bulk compression of the reservoir contents) and the edifice shear modulus (which constrains distortion of the surrounding edifice). If deformation is assumed to be from a point dilatational source in an elastic half-space, the observed volume difference implies that the shear modulus of the edifice is 2.0 ± 0.24 times the bulk modulus of the magma.

Trilateration data show that Kilauea's edifice widens inelastically in time intervals of months to years, primarily in a northwest direction. Over these long time periods, gravity and elevation changes indicate both surface subsidence and mass addition. These observations imply that horizontal extension of Kilauea's edifice decreases lateral support of the fluid magma reservoir, thus lowering the pressure in the reservoir and allowing more magma to be injected without vertical uplift.

Increased summit collapse occurred during the November 1975 earthquake, when new reservoir space created by inelastic seaward displacement of the volcano's south flank was not immediately filled by new magma from depth. For 16 months after the earthquake, additional reservoir capacity created by continued edifice dilation was filled with new magma. From January 1984 to July 1985, Kilauea's edifice subsided by 200 mm and widened by as much as 250 mm. No net subsurface mass changes were measured during this period, implying that the subsidence was entirely the result of horizontal extension.

A complete magma-budget estimate for Kilauea must therefore consider both elastic and inelastic magma storage. This requires a synthesis of leveling, trilateration, and gravity data.

INTRODUCTION

Kilauea Volcano grows by the accumulation of mantle-derived magma that is initially stored in a shallow summit magma reservoir (Eaton and Murata, 1960). The location of this storage region, indicated by an aseismic zone (Koyanagi and others, 1976) and by the inversion of measured surface displacements (Fiske and Kinoshita, 1969; Dvorak and others, 1983), is in a zone below the south rim of the caldera about 3 km in diameter and from 2 to 6 km below the surface. Slow uplift of the volcano's summit over several weeks to a few months is caused by the gradual addition of new magma from a deep source region. Occasional rapid surface subsidence, over periods of hours to days, occurs as magma is withdrawn from the reservoir, either migrating upward or laterally through a conduit system into one of two rift zones (Ryan and others, 1981). Though a part of the mantle-derived magma supply may eventually reach the surface, some magma remains in the summit reservoir and rift systems (Dzurisin and others, 1984).

Previous estimates of magma-volume changes in the subsurface reservoir have been based on geodetic measurements (Duffield and others, 1982; Dvorak and others, 1983; Dzurisin and others, 1984). Because the elastic properties of both magma and volcanic edifice are poorly known, subsurface volume changes cannot be determined from geodetic data alone. Rather, the volume change of the edifice, as determined by integrating vertical displacements measured at the surface, is typically used to approximate the subsurface volume change.

Subsurface volume changes can be estimated more accurately if measurements of changes in both gravity and elevation are available. Gravity and elevation measurements obtained at Kilauea by Jachens and Eaton (1980) and Dzurisin and others (1980) demonstrated that between November 1975 and September 1977 changes in the volume of magma in the reservoir exceeded changes in the volume of the edifice. This was attributed to the effect of void spaces created during periods of magma withdrawal (Jachens and Eaton, 1980), later refilled during periods of magma accumulation (Dzurisin and others, 1980). Gravity studies by Johnsen and others (1980) at Krafla, Iceland, by Sanderson and others (1983) at Mount Etna, Italy, and by Eggers (1983) at Pacaya Volcano, Guatemala, also indicate differences between edifice and subsurface volume changes. Sanderson and others (1983) explained the differences by bulk compression of the magmatic fluid and changes in volume of exsolved gas enabling subsurface magma accumulation to exceed the volume of edifice expansion. Eggers (1983) proposed density changes of about 0.4 g/cm^3 in shallow magma bodies caused by changes in the magmatic water content and vesicularity.

A series of gravity observations made in the Kilauea summit region between January 6, 1984, and July 8, 1985, have been

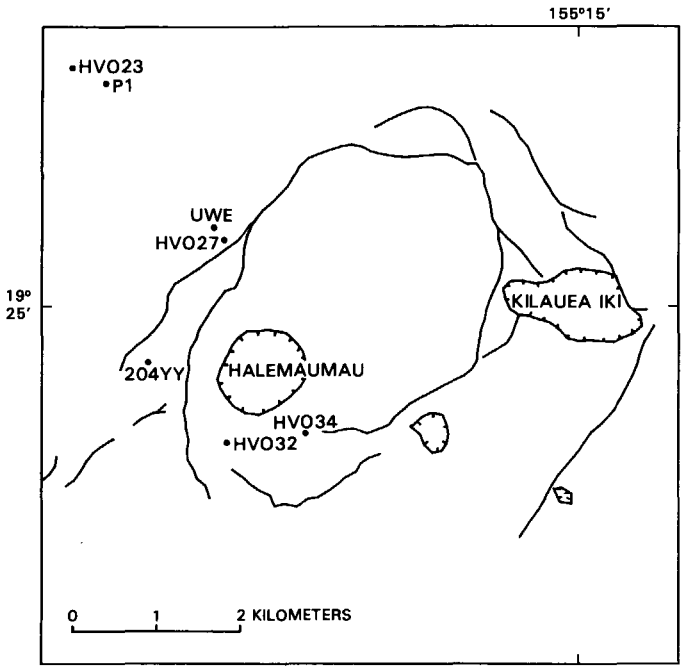

FIGURE 47.1.—Location map of Kilauea summit region showing principal fault scarps and craters, gravity monitoring sites HVO23, P1, HVO27, 204YY, HVO32, and HVO34, and east-west component electronic tiltmeter at Uwekahuna (UWE). Hachures mark inner side of crater walls.

analyzed to determine the empirical relation between magma-volume changes in the summit reservoir and edifice-volume changes as evidenced by surface uplift or subsidence. The short-term relation observed during brief episodes of elastic deflation corresponding to eruptions at the Puu Oo vent along Kilauea's middle east rift zone (Wolfe and others, chapter 17) has been used to estimate the relative elastic properties of the magma reservoir region and the surrounding volcanic edifice. The long-term relation has been used to evaluate the effect of inelastic summit widening on volume changes of the edifice and magma content of the summit reservoir. Results of this study will help improve estimates of the rate of magma supply to Kilauea.

ACKNOWLEDGMENTS

This study is part of a doctoral dissertation in progress at the Department of Geology and Geophysics of the University of Hawaii. The Hawaiian Volcano Observatory of the U.S. Geological Survey provided logistical support and funds for field expenses. I thank Eduard Berg, Robert Decker, Roger Denlinger, John Dvorak, Daniel Dzurisin, Albert Eggers, Robert Jachens, and Thomas Wright for helpful ideas, suggestions, and assistance given during all phases of this study. I am indebted to Thomas Wright for his continued interest and kind support. He showed this in an exceptional manner by personally doing most of the gravity surveys made after July 1984. This manuscript has benefited from reviews by Edward Brown, John Dvorak, Daniel Dzurisin, Harry Glicken, Robert Jachens, and Michael Ryan.

DATA

A total of 141 gravity surveys were conducted in the Kilauea summit region between January 6, 1984, and July 16, 1985. Initially, measurements were made at five monitoring sites referenced to a base station (P1) 5 km northwest of the point of maximum vertical movement (from earlier leveling surveys). The monitoring network was reduced to two sites after February 16, 1984, and to one site, HVO34, after July 12, 1984, because data from this site were found to be representative of the others. Only gravity data for HVO34, referenced to P1, are presented in this paper; locations of all measured stations are shown in figure 47.1.

Two LaCoste and Romberg model-G gravimeters, each equipped with galvanometer-assisted readout, were used throughout the study. Measurements were made over two (109 surveys) or three (32 surveys) closed loops between P1 and the network stations. The time to complete each loop, initally 4 h shortened to 1 h as the number of sites was reduced. Gravity readings were corrected for tidal effects (Longman, 1959) using a compliance factor of 1.16. The effects of instrumental drift and residual tide variations were removed by a least-squares solution of a second-order polynomial approximating time-dependent changes in the reading level of each gravimeter. Linear and sinusoidal gravimeter calibration functions were determined from standard calibration loops and applied to all the Kilauea data (table 47.1).

No attempt was made to correct the gravity data for water-table changes. As P1 and HVO34 are only 5 km apart, gravity variations caused by water-table changes are probably similar at both sites and do not affect the relative gravity differences.

Because data from each gravimeter were analyzed separately, agreement between the two gravimeters is a measure of the precision of the observations. A plot of the measurement discrepancy of the two gravimeters at HVO34 versus time is shown in figure 47.2 for surveys done with three loops (triangles) and with two loops (circles). The standard deviation of the intermeter difference for triple-looped surveys is 9.7 μGal and for double-looped surveys is 11.9 μGal. These figures correspond to standard errors of the mean of 3.4 μGal and 4.2 μGal, respectively.

Elevation changes were determined by optical leveling of a line from P1 to HVO34. The surveys were made in only one direction to third-order standards. East-west tilt variations, measured by a continuously recording, 1-m-base, mercury-capacitance tiltmeter at

TABLE 47.1.—*Linear and sine-form calibration functions for LaCoste and Romberg gravimeters G-615 and G-721 as a function of dial reading*

[Linear factor determined by resurveying 6 stations of calibration line established by Jachens and Eaton (1980) on Mauna Kea Volcano. Sine-form calibration functions determined in June 1984 by measuring 25 stations near Palm Desert, California, and comparing results to values obtained by Robert Jachens (written commun., 1984) with LaCoste and Romberg model-D gravimeters. Sine functions were checked and adjusted slightly by comparing values for G-615 and G-721 obtained at Ocean View Estates, Hawaii, in December 1984. c.u., dial reading in counter units; n.d., not detected]

	Wavelength = 73.33 c.u.		Wavelength = 36.67 c.u.		
Gravimeter	1/2 amp (μGal)	Phase zero (c.u.)	1/2 amp (μGal)	Phase zero (c.u.)	Linear factor
G-615 -----	0.01739	2,924.54	n.d.	n.d.	1.000573
G-721 -----	.01415	2,996.05	.02817	2,928.51	1.000296

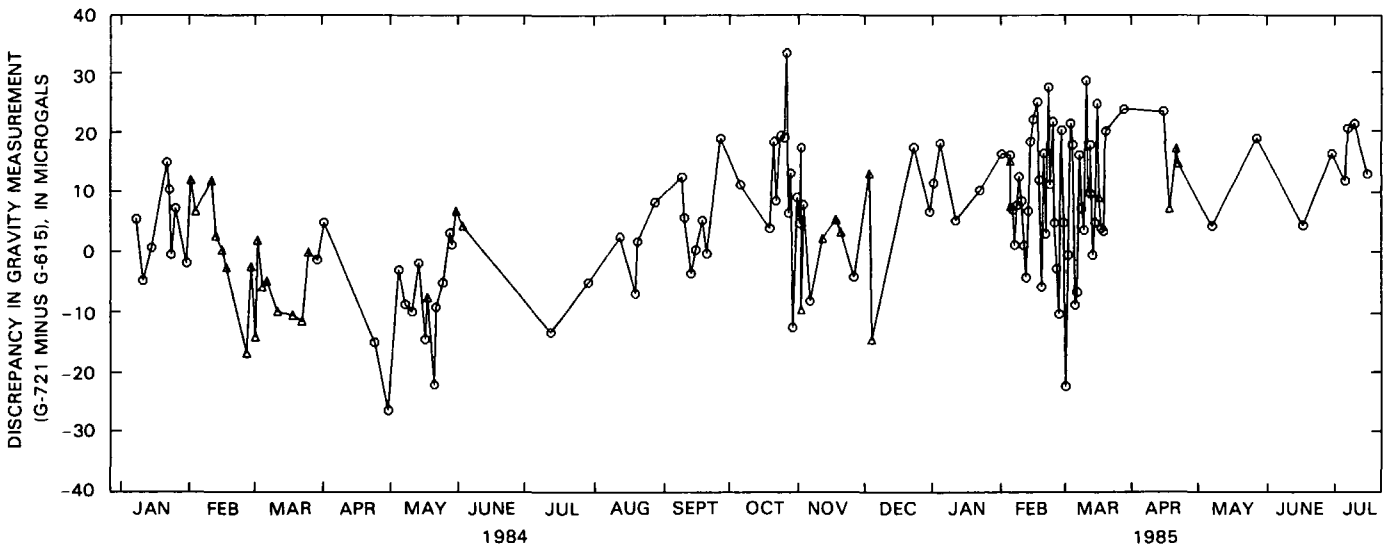

FIGURE 47.2.—Discrepancy between gravity measurements made by gravimeters G–615 and G–721 at site HVO34 plotted as a function of time. Triangles, surveys done with three loops; circles, surveys with two loops.

Uwekahuna (fig. 47.1, UWE), were used to interpolate elevation and edifice-volume changes to values corresponding in time with the gravity surveys. Resurveys of an extensive trilateration network in the summit area of Kilauea in January 1984 and July 1985 provided information on horizontal displacement.

RESULTS

Observed gravity differences (fig. 47.3C) and elevation differences (fig. 47.3*A*) between HVO34 and P1 and changes in east-west tilt (fig. 47.3*B*) at Uwekahuna have been plotted as a function of time. Episodes of the eruption at Puu Oo are sequentially numbered (fig. 47*B*). Increasing tilt values correspond to inflation of the volcano. Tilt data indicate that activity was characterized by cycles of gradual inflation followed by brief deflation episodes during eruptive pulses at the Puu Oo vent (Wolfe and others, chapter 17). Considering the uncertainty of the gravity observations (3–4 μGal), no systematic short-term gravity changes can be inferred. Apparently the free-air gravity changes caused by cycles of elevation variations are compensated by gravity changes caused by fluctuations in the mass of magma in the reservoir. Superimposed on these eruptive cycles is a net deflation of the summit indicated by a tilt change of −42 μrad and an elevation change of −200 mm. During the same period, the gravity at HVO34 gradually increased by about 65 μGal. These long-term variations follow a free-air relation, implying that there was no net subsurface mass change.

INTERPRETATION

The gravity data for HVO34 presented in figure 47.3C are corrected for earth tides. The effects of anomalous earth tides, ocean tides, and variations in atmospheric pressure are at least partly removed by the drift correction. The remaining processes that affect the gravity values include (1) accumulation or loss of magma from the reservoir, (2) vertical movement of the observation point in the Earth's gravity field (the free-air effect), and (3) density distribution change in the edifice as a result of deformation. These processes are usually coupled at Kilauea. For example, an intrusion of magma will increase gravity because of its mass, but it will decrease gravity because of the surface uplift that it causes. The gravity effect of (3) for a spherically symmetric source of dilatation is zero, as shown by a numerical analysis (Rundle, 1978) and by an analytical treatment (Walsh and Rice, 1979). The gravity effect of (3) for other source geometries, such as vertical and horizontal cracks, are not zero (Savage, 1984). While other geometries (consistent with the geologic structures seen in ancient volcanoes) have been suggested by Dieterich and Decker (1975) and Ryan and others (1983), the point source approach has been used in this report because of its computational convenience. In considering the gravity data presented here, the assumption was made that the gravity effect of (3) was indeed zero.

Because changes in the magma content of the subsurface reservoir are partly accommodated by slight elastic compression of the total volume of reservoir magma, the density of the reservoir magma can change slightly through time. In this analysis, the phrase magma-volume change indicates a change in the magma content of the reservoir and is expressed using units of volume calculated at a constant, arbitrary density of 2.75 g/cm^3. Although the parameter that is actually being measured by gravity is the mass change, conversion to volume change is done here to enable comparison with dense-rock equivalent volumes of lava flows and intrusions reported elsewhere. Another type of subsurface volume change discussed here is changes in the capacity of the reservoir, which refers to changes in the physical dimensions of the reservoir.

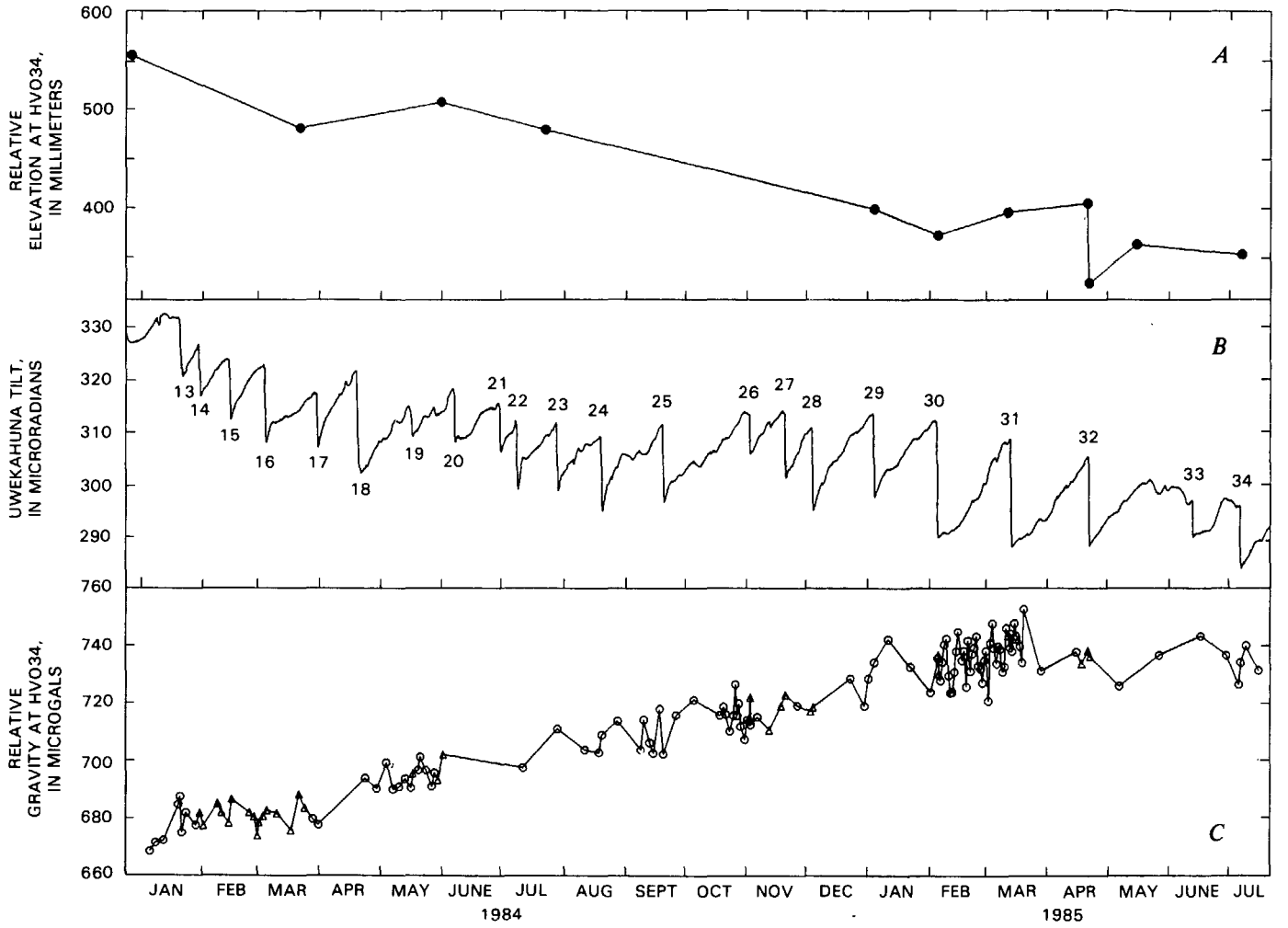

FIGURE 47.3.—Time plots of relative elevation and gravity at HVO34, and east-west tilt at Uwekahuna. ***A***, Relative elevation of site HVO34. ***B***, East-west tilt at Uwekahuna; eruptive episodes at Puu Oo vent indicated by numbers. ***C***, Relative gravity at site HVO34, uncorrected for vertical uplift. Triangles, gravity surveys done with three loops; circles, surveys done with two loops.

RELATION BETWEEN EDIFICE AND SUBSURFACE VOLUME CHANGES

The ratio of the change in magma volume of the reservoir, ΔV_m, to change in volume of the edifice, ΔV_e, may be estimated from gravity changes, $\Delta g'$, derived from the observed gravity differences, Δg, by correcting for vertical displacement with a free-air gradient of -0.3086 μGal/mm, and from elevation differences, Δh. The analysis is based on a point dilatational source in an elastic half-space (see, for example Mogi, 1958). The volume change of the edifice was determined by integrating vertical surface displacement. Uplift at the surface is given (Mogi, 1958) by:

$$\Delta h = \frac{3a^3\Delta P}{4\mu_e} \cdot \frac{Z}{(X^2+Z^2)^{3/2}}, \qquad (1)$$

where a is the radius of the source, ΔP is the pressure change, μ_e is Lame's constant for the edifice, Z is depth to the source, and X is horizontal distance to the chamber. Integration of equation 1 over the Earth's surface gives an expression for the volume increase of the edifice, ΔV_e:

$$\Delta V_e = \frac{3\pi a^3\Delta P}{2\mu_e}. \qquad (2)$$

Division of equation 2 by equation 1 and rearrangement yields:

$$\Delta V_e = \frac{2\pi(X^2+Z^2)^{3/2}\Delta h}{Z}. \qquad (3)$$

The mass change of the reservoir was determined next. So that it may be compared with volumes of subsidence and of eruptive products, mass change is expressed in terms of an effective magma-volume change, ΔV_m, using a constant density ρ for the magma.

The graviational attraction of the new magma, approximated by a point mass, is given by:

$$\Delta g = \Delta V_m \gamma \rho \frac{Z}{(X^2+Z^2)^{3/2}}, \quad (4)$$

where γ is the universal gravitational constant (6.67×10^{-11} nm^2/kg^2) and ρ is the standard magma density. If the location of the dilational source in equation 3 is assumed to be the same as the new magma in equation 4, a combination of equations 3 and 4 yields an expression relating the observed gravity and elevation change to volume changes of the edifice and magma within the reservoir:

$$\frac{\Delta V_m}{\Delta V_e} = \frac{\Delta g'}{\Delta h 2\pi\gamma\rho}. \quad (5)$$

Jachens and Eaton (1980) and Dzurisin and others (1980) found a good spatial correlation between gravity changes and elevation changes at Kilauea; their results are consistent with coincident sources for the gravity changes and the dilatation. This correlation of gravity and elevation changes indicates that in equation 5 the ratio of relative changes at two or more points showing differential changes can be used as validly as the ratio of absolute changes. The present analysis uses relative changes between two points.

Notice that when $\Delta V_m = \Delta V_e$ (that is, when there is no subsurface density change), equation 5 is equivalent to the Bouguer gradient. Furthermore, when $\Delta V_e = 1.5\Delta V_m$ (that is, no magma compression but dilation of the edifice as predicted by the Mogi model with a Poisson's ratio of 0.25), equation 5 plus the free-air gradient is equivalent to theoretical gravity gradients proposed by Dzurisin and others (1980, equation A-11) and Hagiwara (1977, equation 19). In this analysis, the ratio of magma accumulation in the reservoir to surface uplift is considered to be an independent variable. Equation 5 shows that the gravity-change gradient $\Delta g'/\Delta h$ is near 0.08 μGal/mm for an incompressible magma with a density of 2.75 g/cm^3 accommodated by edifice expansion. The gradient approaches infinity for magma compressed into an unyielding edifice.

Gravity measurements were made near the beginning and end of 15 summit-deflation events corresponding to eruptive episodes 13–17, 24–32, and 34 at Puu Oo. Because of the brevity of each deflation, these gravity changes should not be influenced by long-term changes (for example, south-flank movement or magma migration unrelated to eruption), but should reflect mass and elevation changes related to simple elastic deflation. The changes in relative gravity at HVO34 and in east-west tilt at Uwekahuna during the monitored deflations are summarized in table 47.2. No real gravity changes (Δg) significantly larger than the data uncertainty were measured during these events because the gravity data reflect a composite of free-air gravity increases owing to subsidence and gravity decreases, $\Delta g'$, owing to removal of magma.

Elevation changes of HVO34 between gravity surveys were estimated for the period from December 28, 1983, to July 16, 1985, from the calculated relation between elevation of HVO34 and tilt at Uwekahuna. A factor of 5.19 mm/μrad was derived by a least-squares fit to tilt and elevation data (fig. 47.4). Elevation changes during eruptive episode 32 were measured directly by leveling surveys conducted on April 21 and 22, 1985. Table 47.3 summarizes the estimates of $\Delta g'$ (corrected for vertical displacement with a free-air gradient of -0.3086 μGal/mm), Δh, and the ratio $\Delta V_m/\Delta V_e$ calculated using equation 5. Because virtually no real gravity changes (Δg) were measured, most of the $\Delta g'$ values shown in table 47.3 result from the free-air correction. These calculations show that the volume of magma lost from the reservoir is 1.2 to 4.5 times (average 2.4 ± 0.21, 1 standard error) greater than the volume of subsidence at the surface during the periods of rapid deflation.

SUBSURFACE VOLUME CHANGES DURING DEFLATION EVENTS

The empirical relation between volume changes of magma within the summit reservoir and volume changes of the volcanic edifice can be used to estimate the former from measurements of the latter. This means of estimating magma-volume changes at depth is

TABLE 47.2.—*Nominal relative gravity change at HVO34 and tilt changes at Uwekahuna for deflation intervals corresponding to 15 eruptions at Puu Oo, 1984–85*

[Times given are Hawaii standard time; figures for loops give number of closed loops between HVO34 and P1 for each gravity survey. s.e., standard error]

Eruptive episode	First survey				Second survey				Δg (±1 s.e.) (μGal)	Δ tilt (μrad)
	Date	Start time	Duration (h)	Loops	Date	Start time	Duration (h)	Loops		
13	Jan. 20, 1984	1445	4.00	2	Jan. 22, 1984[2]	0900	4.75	2	−4 (5.8)	−10.4
14	Jan. 29, 1984	1200	5.00	2	Jan. 31, 1984[2]	0800	7.50	3	4 (5.1)	−7.3
15	Feb. 14, 1984[1]	2145	4.25	3	Feb. 16, 1984	0845	6.25	3	8 (4.4)	−8.9
16	Mar. 3, 1984	0815	6.00	3	Mar. 5, 1984	0745	6.50	3	2 (4.4)	−14.1
17	Mar. 28, 1984	1230	3.75	2	Mar. 31, 1984	1245	3.75	2	−2 (5.8)	−9.5
24	Aug. 19, 1984	1130	2.00	2	Aug. 20, 1984	1845	2.00	2	6 (5.8)	−14.1
25	Sept. 18, 1984	1000	1.50	2	Sept. 20, 1984	0645	1.75	2	−16 (5.8)	−14.4
26	Nov. 2, 1984	0845	1.75	2	Nov. 3, 1984	0500	2.00	2	−1 (5.8)	−7.5
27	Nov. 18, 1984	1045	3.00	3	Nov. 20, 1984	1415	2.00	3	4 (4.4)	−12.5
28	Dec. 3, 1984	0815	2.75	3	Dec. 4, 1984	1315	3.00	3	2 (4.4)	−15.6
29	Jan. 1, 1985	0645	1.50	2	Jan. 4, 1985	0730	1.50	2	6 (5.8)	−15.2
30	Feb. 2, 1985	0645	1.75	2	Feb. 5, 1985	0400	2.00	2	12 (5.8)	−21.5
31	Mar. 12, 1985	0930	2.00	3	Mar. 14, 1985	0615	1.50	2	6 (5.1)	−19.9
32	Apr. 21, 1985	1515	2.25	3	Apr. 22, 1985	1445	4.25	6	−2 (3.8)	−16.9
34	July 6, 1985	1130	1.25	2	July 7, 1985	1245	1.25	2	8 (5.8)	−12.2

[1]First gravity survey done shortly after onset of deflation.
[2]Second gravity survey done shortly before deflation was complete.

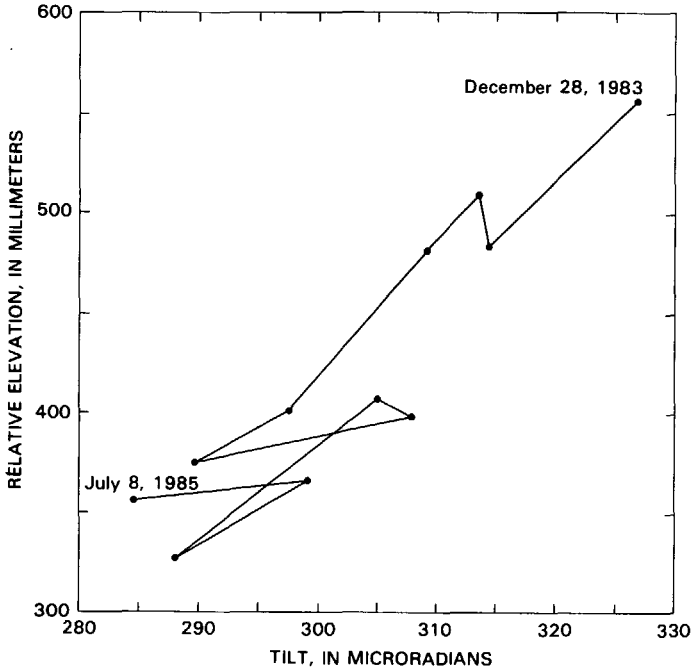

FIGURE 47.4.—Relative elevation of site HVO34 plotted against east-west tilt measured at Uwekahuna between December 28, 1983, and July 8, 1985.

particularly useful for studying intrusions, in which no lava reaches the surface.

The change in volume of the edifice (ΔV_e) was computed by fitting a point-source model (Dvorak and others, 1983) to measured elevation changes for periods when sufficient elevation change and a uniform pattern of surface displacement enabled a stable solution. These periods were: December 28, 1983, to March 22, 1984; July 23, 1984, to January 4, 1985; and April 21 to 22, 1985. The solutions obtained are listed in table 47.4.

Edifice-volume changes (table 47.4) were interpolated to the time of the gravity surveys by means of the continuous record of tilt change at Uwekahuna. From the estimated volume changes of the edifice and the calculated ratios of subsurface-magma to edifice volume change given in table 47.3, the changes of magma volume in the reservoir were calculated. These volume changes are listed in table 47.5, together with estimated lava-flow volumes from the Puu Oo vent for comparison (Wolfe and others, chapter 17; George Ulrich, written commun., 1985).

Absence of significant geodetic change along the rift zones during 1984 and early 1985 indicates that the cumulative volume of lava erupted was equal to the volume of magma drained from the summit reservoir. This inference is supported by the gravity and surface-displacement data. A total of 125×10^6 m^3 of lava was extruded during the monitored eruptive episodes (table 47.5). Corrected for 20 percent (Swanson, 1972) to 25 percent (Wolfe and others, chapter 17) vesicularity, the total volume of lava flows is 94×10^6–100×10^6 m^3. For comparison, the cumulative volume of reservoir magma lost during the deflations, based on gravity and geodetic measurements, is an estimated 120×10^6 m^3 (table 47.4).

Gravity and elevation data for eruptive episode 32 were obtained over a timespan of 24 h bracketing the deflation. Because independent calculations of the volume change of the edifice and of the subsurface magma were made from these data, without requiring tiltmeter interpolation, the results for this period provide a good check of the more general procedure. While the edifice subsided by about 6×10^6 m^3 during eruptive episode 32, nearly 18×10^6 m^3 (calculated to 2.75 g/cm^3) of magma was removed from the reservoir (table 47.5). This agrees well with the estimated 12×10^6–13×10^6 m^3 (table 47.5, corrected for 20–25 percent vesicularity) of lava erupted at Puu Oo.

The general agreement between reservoir magma-volume change and lava output supports the idea of a volume-for-volume link between the summit reservoir and Puu Oo, with magma transfer from summit to rift zone taking place principally during episodes of summit deflation. In other words, during eruptions at Puu Oo, summit magma enters the rift-zone conduit system and forces out an equal volume of rift-zone magma at the Puu Oo vent.

ELASTIC PROPERTIES OF VOLCANO AND MELT

Data for the ratio of edifice-volume to subsurface magma-volume changes for summit deflations accompanying eruptions of Puu Oo may be used to model the relative strength of the volcanic edifice and the magma-reservoir region. For this purpose, I have derived an expression that relates the ratio of subsurface-magma and edifice-volume changes to the ratio of the rigidity of the edifice, μ_e, and the compressibility of the reservoir melt, K_m. Assumptions are that Poisson's ratio for the edifice is 0.25, that the source region can be approximated by a spherical volume of fluid, that the injected magma has a density of 2.75 g/cm^3, and that the response of the volcanic edifice and contained fluid to subsurface pressure changes is elastic. Although the source region most likely contains subsolidus rock in addition to a melt phase, the aggregate bulk modulus of the

TABLE 47.3.—*Changes in residual gravity ($\Delta g'$) and elevation (Δh), ratio between them, and ratio of subsurface (ΔV_m) to edifice volume (ΔV_e) changes for 15 Kilauea deflation episodes, 1984–85*

[Elevation changes interpolated from tilt changes using factor of 5.19 mm/μrad. Subsidence during eruptive episode 32 was determined by leveling surveys before and after period of deflation]

Eruptive episode	$\Delta g'$ (μGal)	Δh (mm)	$\Delta g'/\Delta h$ (μGal/mm)	$\Delta V_m/\Delta V_e$
13	−21	−54	0.38	3.3
14	−8	−38	.20	1.8
15	−6	−46	.13	1.2
16	−20	−73	.28	2.4
17	−17	−49	.35	3.0
24	−16	−73	.23	2.0
25	−39	−75	.52	4.5
26	−13	−39	.33	2.9
27	−16	−65	.25	2.1
28	−23	−81	.28	2.5
29	−18	−79	.23	2.0
30	−22	−111	.20	1.7
31	−26	−103	.25	2.2
32	−27	−80	.33	2.9
34	−11	−63	.18	1.6
Average				2.4

TABLE 47.4.—*Point-source solutions to level data for selected time intervals in Kilauea summit-area deflation events*

[Uncertainties given are 1 standard error]

Time interval	Longitude (W.)	Latitude (N.)	Depth (km)	Edifice volume change (10^6 m^3)	Vertical movement of HVO23 (mm)
Dec. 28, 1983–Mar. 22, 1984	155.2848°(±0.06 km)	19.4003°(±0.13 km)	2.92(±0.19)	−4.42(±0.70)	−9(±2)
July 23, 1984–Jan. 4, 1985	155.2801°(±0.58 km)	19.4014°(±0.62 km)	2.46(±0.78)	−3.26(±0.13)	−0.5(±2)
Apr. 21, 1985–Apr. 22, 1985	155.2753°(±0.30 km)	19.4101°(±0.11 km)	2.87(±0.37)	−6.09(±2.04)	−15(±7)
Dec. 28, 1983–July 8, 1985	155.2822°(±0.13 km)	19.3960°(±0.26 km)	3.06(±0.26)	−13.68(±3.38)	−24(±6)

source region is assumed equal to the bulk modulus of the melt phase. This assumption is valid because the effect of the melt phase is to reduce the aggregate bulk modulus to close to that of melt (Ryan, 1980). First, the change in capacity of the spherical source region was determined. A pressure change within the reservoir displaces the reservoir boundary radially outward. The change in radius, Δa, of a spherical source region of radius a is given by (Hagiwara, 1977):

$$\Delta a = \frac{a\Delta P}{4\mu_e}. \tag{6}$$

If the radius of the source is large relative to the change in radius, the volume of the the newly added shell, ΔV_r, is approximately:

$$\Delta V_r = \frac{\pi a^3 \Delta P}{\mu_e}. \tag{7}$$

The volume of magma, ΔV_c, accommodated by compression of the fluid within the spherical reservoir region of volume $4\pi a^3/3$ and within the newly added shell of magma, ΔV_r, is dependent on the bulk modulus of the magma, K_m:

$$\Delta V_c = \frac{\Delta P}{K_m}\left(\frac{4\pi a^3}{3} + \Delta V_r\right). \tag{8}$$

For simplicity, the relatively small term ΔV_r in equation 8 can be ignored. The total amount of magma injected is the sum of magma accommodated by enlargement of the reservoir (equation 7) and by compression of the material in the reservoir (equation 8):

$$\Delta V_m = \frac{4}{3}\pi a^3 \Delta P\left(\frac{1}{K_m} + \frac{3}{4\mu_e}\right). \tag{9}$$

The combination of equations 9 and 2 gives:

$$\frac{\Delta V_m}{\Delta V_e} = \frac{8}{9}\cdot\frac{\mu_e}{K_m} + \frac{2}{3}, \tag{10}$$

which can be related directly to the gravity gradient by equation 5.

Some edifice deformation and magma compression are expected during magma injection. Equation 10 shows that, for a given value of $\Delta V_m/\Delta V_e$, a relatively strong edifice implies more magma compression. Conversely, a relatively strong magma implies more edifice deformation. Solution of equation 10, incorporating the average $\Delta V_m/\Delta V_e$ factor of 2.4±0.21 (1 standard error) from the 15 deflations listed in table 47.3, yields $\mu_e = 2.0 \pm 0.24\ K_m$. Additional error stems from uncertainty of the magma density, here assumed to be 2.75 g/cm^3.

The effective shear modulus of Kilauea's edifice, μ_e, is difficult to determine independently because Kilauea is built of many vesicular, commonly rubbly lava flows with abundant void space (Ryan and others, 1983). The intrinsic shear modulus of Hawaiian basalt was found by pulse transmission to average 25 GPa (Manghnani and Wollard, 1968) with a range of 4.7–40.5 GPa. Samples with greater porosity had a lower shear modulus. Presence of voids in the volcanic pile results in an effective shear modulus of the volcano that is less than the intrinsic shear modulus of hand samples.

Seismic velocities, and hence rigidity, determined from P-wave arrival data from earthquakes and explosions increase with depth and vary laterally (Thurber, chapter 38; Hill and Zucca, chapter 37). This reflects partly the compressive reduction of porosity with increasing depth, and the solidified intrusive zones surrounding the cores of the summit reservoir and rift zones. Any estimate of μ_e from seismic velocities would be strongly dependent on the depth and horizontal position of the source, and size of the region chosen to represent the edifice.

The bulk modulus of magma, K_m, in Kilauea's reservoir should be uniform because the size of the summit magma reservoir is perhaps 1,000 times the yearly magma supply rate (Swanson, 1972), so short-term fluctuations in the gas content and chemical composition of the supplied magma are distributed over a large volume and do not affect the overall bulk modulus. Laboratory

TABLE 47.5.—*Edifice volume change (ΔV_e), subsurface volume change (ΔV_m), and lava flow volume for 12 Kilauea eruptive episodes, 1984–85*

[All figures in millions of cubic meters. Edifice volume changes, from level data inversion, interpolated to time of gravity surveys by tilt variations. Subsurface mass changes, expressed as volume change at standard density of 2.75 g/cm^3, estimated using equation 5 and changes of edifice volume, relative gravity, and relative elevation. Measured lava-flow volumes (Wolfe and others, chaper 17; George Ulrich, written commun., 1985) not adjusted for flow porosity]

Eruptive episode	ΔV_e	ΔV_m	*Lava volume*
13	−3.7	−12.3	10
14	−2.6	−4.7	6
15	−3.2	−3.7	8
16	−5.1	−12.3	12
17	−3.4	−10.2	10
24	−4.0	−7.9	12
25	−4.0	−18.2	11
26	−2.1	−6.1	7
27	−3.5	−7.3	8
28	−4.4	−11.0	12
29	−4.3	−8.6	13
32	−6.1	−17.7	16
Total	−46.4	−120.0	125

determinations of the bulk modulus made from lava erupted from Kilauea, therefore, should be representative of the bulk modulus of magma in the reservoir. The value of 11.5 GPa determined for K_m of molten Kilauea 1921 olivine tholeiite by Murase and others (1977) was used to calculate the shear modulus of Kilauea's edifice from the relation $\mu_e = (2.0 \pm 0.24) \cdot K_m$ determined above. The value for μ_e so determined, 23 ± 3 GPa, is close to the value for the average shear modulus of Hawaiian basalt given above. Note that this value does not apply to Kilauea's edifice as a whole, but only to the region surrounding the magma reservoir. This is because it was determined by modeling in-place melt-volume changes in the reservoir and resulting surface displacements.

Presence of a CO_2 gas phase in the magma would lower the aggregate bulk modulus of the magma. This may not be important for Kilauea, because, as Greenland and others (1985) assert, as CO_2 is lost from the magma as soon as it reaches the shallow magma reservoir. However, if some CO_2 is retained in the reservoir, then both the magma bulk modulus and the predicted edifice shear modulus would be reduced.

RELATION BETWEEN LONG-TERM INELASTIC EDIFICE WIDENING AND SUBSURFACE VOLUME CHANGES

The ratio of the long-term change of magma volume within Kilauea's summit reservoir to the edifice volume change between January 6, 1984, and July 16, 1985, may be determined from equation 5 and from the long-term elevation and gravity changes. A gradient of $\Delta g/\Delta h = -0.29$ μGal/mm was determined for the interval by a least-squares fit to the tilt and gravity data, adjusted by the elevation/tilt correlation of 5.19 mm/μrad given above. This is essentially the free-air gradient, so $\Delta g'$ is zero and equation 5 shows that the ratio of $\Delta V_m/\Delta V_e$ is zero. That is, there was no net change in magma storage in the summit reservoir during this interval.

The long-term ratio of volume changes in edifice and subsurface magma is different from that in short-term deflations accompanying Puu Oo eruptions (table 47.3). This implies that different processes affect the volume changes over longer time intervals. Earlier, the short-term deflations of Kilauea were explained using an elastic model, with inflow and outflow of magma accompanied by compression and decompression of the melt. Because short-term and long-term processes occurred concurrently, variations in the physical properties of the magma cannot explain differences in the volume-change ratios. The differences between the long-term and short-term volume changes must then be due to some superimposed long-term process that affects Kilauea's edifice. That process produces subsidence at the surface without a change in the magma content of the reservoir. One possibility is that horizontal spreading of the volcano's summit removes lateral support of the fluid magma reservoir, thereby decreasing the pressure in the reservoir and causing the summit to subside. Horizontal distance measurements at Kilauea have shown that the summit region is prone to widening in a south-southeast direction (Dvorak and others, 1983). This widening was particularly notable during the 1975 magnitude 7.2 earthquake along the south flank and for several months afterward (Lipman and others, 1985).

To investigate the possibility of summit extension during 1984–85, horizontal displacements measured by trilateration surveys conducted on January 16, 1984, and July 16, 1985, were analysed. In order to isolate the pattern of regional displacements in the vicinity of Kilauea's summit from the effects of observed deflation, the contribution of changes in the inflation level of the reservoir (approximated by use of a point source of dilatation determined from leveling data) was subtracted from the observed horizontal displacements. Residual line lengths were then used to compute horizontal displacement vectors (fig. 47.5). South-southeastward movement as great as 250 mm of points located on the south side of Kilauea caldera relative to points to the north show that the caldera widened slightly.

A $\Delta g'/\Delta h$ gradient of 0.138 μGal/mm was measured by Jachens and Eaton (1980) during the subsidence accompanying the November 29, 1975, earthquake and eruption. A value for the $\Delta V_m/V_e$ ratio of 1.2 was calculated from the gravity gradient and equation 5 using an assumed magma density of 2.75 g/cm^3. This ratio indicates a greater component of surface collapse following the 1975 eruption, compared to the 1984–85 deflations (table 47.3). This difference results from 1.8 m of south-southeast crosscaldera extension during the November 1975 event (Lipman and others, 1985), in contrast to no measurable extension during the periods of very brief (1–3 d) deflation associated with eruptions in 1984 and 1985. The increased collapse in November 1975 is consistent with horizontal dilation of the edifice and surface subsidence because of the resultant drop in reservoir pressure.

Horizontal extension of Kilauea's edifice lowers the pressure in the magma reservoir; additional magma can be injected without uplifting the surface. In this way the reservoir volume increases by lateral growth. Growth by horizontal spreading and magma intrusion occurs during rift-zone development (Swanson and others, 1976), and it might also apply to the growth of the summit reservoir. Swanson and others (1976) attributed horizontal dilation of the rift zone to forceful injection of magma into dikes. However, at Kilauea's summit area, observation of subsidence concurrent with extension indicates that magma accumulation there is a passive response to dilation. Perhaps the extension of Kilauea's summit that increases the capacity of the reservoir is an indirect response to the forceful dilation of the rift zones that bound the caldera on both the east and west sides.

Net gravity and elevation changes for the 16-mo period following the November 1975 deflation imply mass filling of the reservoir concurrent with subsidence. Dzurisin and others (1980) reported a $\Delta g'/\Delta h$ gradient of -0.294 μGal/mm for December 1975 to April 1977, which corresponds to a $\Delta V_m/\Delta V_e$ ratio of -2.5 from equation 5, using a magma density of 2.75 g/cm^3. This, combined with observed subsidence of the summit area of as much as 180 mm, indicates that the volume of magma in the reservoir actually increased despite the subsidence. The summit region widened by about 0.5 m in a south-southeast direction (Lipman and others, 1985) during this period; that extension created more reservoir space in which additional magma accumulated.

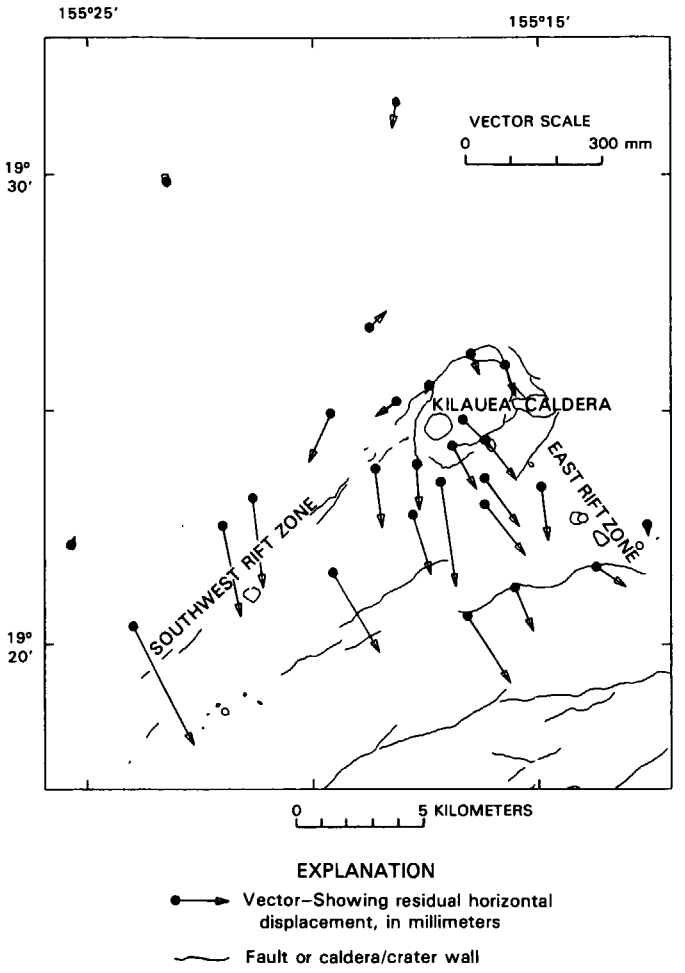

FIGURE 47.5.—Horizontal displacements in the Kilauea summit region determined from line-length changes (January 16, 1984, to July 16, 1985). To remove effects of summit subsidence, computed horizontal displacements based on inversion of level data obtained on December 28, 1983, and July 8, 1985 (table 47.4), were subtracted from measured changes in line lengths between January 16, 1984, and July 16, 1985. Computed residual displacements indicate south-southeastward widening of Kilauea summit area.

CONCLUSIONS

Gravity and surface-displacement data demonstrate that volume changes of Kilauea's edifice, as determined by integrating vertical displacements, are dependent, not only on the balance between volume of magma supplied from the mantle and volume of magma lost from the reservoir by eruption but also on the volume of summit collapse owing to horizontal extension of the summit region. During times of elastic inflow or outflow of magma from the reservoir, the ratio of subsurface-magma volume change to edifice volume change is 2.4 ± 0.21 (1 standard error). This is consistent with expected changes, calculated using a ratio of shear strength of edifice to bulk modulus of magma of 2.0 ± 0.24 (1 standard error). On the basis of a laboratory-determined magma bulk modulus of $K_m = 11.5$ GPa, the shear modulus of the edifice is $\mu_e = 23$ GPa. Inelastic horizontal dilation of the edifice in a south-southeast direction increases the capacity of the summit reservoir to accept magma without surface uplift. For the 16-mo period following the November 1975 deflation, additional magma was accommodated by this process. When insufficient magma is supplied to fill space created by summit widening, the pressure in the reservoir drops and the surface subsides as it did during and after the November 1975 earthquake and between January 1984 and February 1985.

REFERENCES CITED

Dieterich, J.H., and Decker, R.W., 1975, Finite element modeling of surface deformation associated with volcanism: Journal of Geophysical Research, v. 80, p. 4094–4102.

Duffield, W.A., Christiansen, R.L., Koyanagi, R.Y., and Peterson, D.W., 1982, Storage, migration, and eruption of magma at Kilauea Volcano, Hawaii, 1971–1972: Journal of Volcanology and Geothermal Research, v. 13, p. 273–307.

Dvorak, J., Okamura, A., and Dieterich, J.H., 1983, Analysis of surface deformation data, Kilauea Volcano, Hawaii, October 1966 to September 1970: Journal of Geophysical Research, v. 88, p. 9295–9304.

Dzurisin, D., Anderson, L.A., Eaton, G.P., Koyanagi, R.Y., Lipman, P.W., Lockwood, J.P., Okamura, R.T., Puniwai, G.S., Sako, M.K., and Yamashita, K.E., 1980, Geophysical observations of Kilauea Volcano, Hawaii, 2, Constraints on the magma supply during November 1975–September 1977: Journal of Volcanology and Geothermal Research, v. 7, p. 241–269.

Dzurisin, D., Koyanagi, R.Y., and English, T.T., 1984, Magma supply and storage at Kilauea Volcano, Hawaii, 1956–1983: Journal of Volcanology and Geothermal Research, v. 21, p. 177–206.

Eaton, J.P., and Murata, K.J., 1960, How volcanoes grow: Science, v. 132, p. 925–938.

Eggers, A.A., 1983, Temporal gravity and elevation changes at Pacaya Volcano, Guatemala: Journal of Volcanology and Geothermal Research, v. 19, p. 223–237.

Fiske, R.S., and Kinoshita, W.T., 1969, Inflation of Kilauea Volcano prior to its 1967–1968 eruption: Science, v. 165, p. 341–349.

Greenland, L.P., Rose, W.I., and Stokes, J.B., 1985, An estimate of gas emissions and magmatic gas content from Kilauea Volcano: Geochimica et Cosmochimica Acta, v. 49, p. 125–129.

Hagiwara, Y., 1977, The Mogi model as a possible cause of the crustal uplift in the eastern part of Izu Peninsula and the related gravity change: Bulletin of the Earthquake Research Institute, University of Tokyo, v. 52, p. 301–309 (in Japanese).

Jachens, R.C., and Eaton, G.P., 1980, Geophysical observations of Kilauea Volcano, Hawaii, 1, Temporal gravity variations related to the 29 November 1975, $M = 7.2$ earthquake and associated summit collapse: Journal of Volcanology and Geothermal Research, v. 7, p. 225–240.

Johnsen, G.V., Bjornsson, A., and Sigurdsson, S., 1980, Gravity and elevation changes caused by magma movement beneath the Krafla caldera, northeast Iceland: Journal of Geophysics, v. 47, p. 132–140.

Kinoshita, W.T., Krivoy, H.L., Mabey, D.R., and MacDonald, R.R., 1963, Gravity survey of the Island of Hawaii: U.S. Geological Survey Professional Paper 475-C, p. C114–C116.

Koyanagi, R.Y., Unger, J.D., Endo, E.T., and Okamura, A.T., 1976, Shallow earthquakes associated with inflation episodes at the summit of Kilauea Volcano, Hawaii: Bulletin Volcanologique, v. 39, p. 621–631.

Lipman, P.W., Lockwood, J.P., Okamura, R.T., Swanson, D.A., and Yamashita, K.M., 1985, Ground deformation associated with the 1975 magnitude-7.2 earthquake and resulting changes in activity of Kilauea Volcano 1975–1977: U.S. Geological Survey Professional Paper 1276, 45 p.

Longman, I.M., 1959, Formulas for the tidal acceleration of gravity: Journal of Geophysical Research, v. 64, p. 2351–2355.

Manghnani, M.H., and Woollard, G.P., 1968, Elastic wave velocities in Hawaiian rocks at pressures to ten kilobars: American Geophysical Union Geophysical Monograph 12, p. 501–516.

Mogi, K., 1958, Relations of eruptions of various volcanoes and the deformation of the ground surfaces around them: Earthquake Research Institute Journal, Tokyo University, v. 39, p. 99–134.

Murase, T., Kushiro, I., and Fujii, T., 1977, Compressional wave velocity in partially molten peridotite: Annual Report of the Director, Geophysical Laboratory, Carnegie Institution, 1976–1977, p. 414–416.

Rundle, J.B., 1978, Gravity changes and the Palmdale uplift: Geophysical Research Letters, v. 5, p. 41–44.

Ryan, M.P., 1980, Mechanical behavior of magma reservoir envelopes: elasticity of the olivine tholeiite solidus: Bulletin Volcanologique, v. 43-4, p. 743–772.

Ryan, M.P., Blevins, J.Y.K., Okamura, A.T., and Koyanagi, R.Y., 1983, Magma reservoir subsidence mechanics: Theoretical summary and application to Kilauea Volcano, Hawaii: Journal of Geophysical Research, v. 88, p. 4147–4181.

Ryan, M.P., Koyanagi, R.Y., and Fiske, R.S., 1981, Modeling the three-dimensional structure of macroscopic magma transport systems: application to Kilauea Volcano, Hawaii: Journal of Geophysical Research, v. 86, p. 7111–7129.

Sanderson, T.J.O., Berrino, G., Corrado, G., and Grimaldi, M., 1983, Ground deformation and gravity changes accompanying the March 1981 eruption of Mount Etna: Journal of Volcanology and Geothermal Research, v. 16, p. 299–315.

Savage, J.C., 1984, Local gravity anomalies produced by dislocation sources: Journal of Geophysical Research, v. 89, p. 1945–1952.

Swanson, D.A., 1972, Magma supply rate at Kilauea Volcano, 1952–1971: Science, v. 175, p. 169–170.

Swanson, D.A., Duffield, W.A., and Fiske, R.S., 1976, Displacement of the south flank of Kilauea Volcano: The result of forceful intrusion of magma into the rift zones: U.S. Geological Survey Professional Paper 963, 39 p.

Walsh, J.B., and Rice, J.R., 1979, Local changes in gravity resulting from deformation: Journal of Geophysical Research, v. 84, p. 165–170.

CYCLING OF MAGMA BETWEEN THE SUMMIT RESERVOIR AND KILAUEA IKI LAVA LAKE DURING THE 1959 ERUPTION OF KILAUEA VOLCANO

By Jerry P. Eaton, Donald H. Richter, *and* Harold L. Krivoy

ABSTRACT

The fortunate combination of observations of deformation of the summit of Kilauea Volcano during the 1959 Kilauea Iki eruption and an accurate log of the eruption of lava into Kilauea Iki lava lake and its subsequent partial withdrawal provides a record of movement of magma into and through the summit reservoir during that eruption. The initial eruption of 30×10^6 m^3 of lava into Kilauea Iki, with an accompanying 50 μrad of eastward tilt at Uwekahuna, established a scaling factor relating the change in volume of the summit reservoir to tilting at Uwekahuna. A record of the initial deflation and subsequent reinflation of the summit reservoir was obtained by the liquid-level tiltmeter at Uwekahuna. A good record of episodic eastward tilting during the eruptive stage and westward tilting during the backflow stage of the later phases of the eruption was obtained by analysis of the zero-line deflections of the east-west-component Press-Ewing seismograph. Converted to volumes of deflation and inflation, the tilting associated with eruption of lava into and withdrawal of lava from the lava lake offers a means of determining the net gain or loss of lava in the lake-reservoir system during each phase. Analysis of the interplay between volcanic tremor and the details of the reinflation tilt records permits estimation of the volume of lava that escaped from the summit reservoir during individual backflow episodes.

The 30×10^6 m^3 of lava originally withdrawn from the reservoir was eventually more than replaced by about 60×10^6 m^3 of lava rising from depth. Of this 60×10^6 m^3, 40×10^6 m^3 finally was retained in the reservoir, 8×10^6 m^3 was added to the lava lake, and about 12×10^6 m^3 was driven out of the summit reservoir during the late-phase backflow episodes. Lava that erupted into Kilauea Iki from phase 2 onward was material from the reservoir, which was being refilled with new lava from below; this lava was repeatedly erupted from the reservoir and then withdrawn back into it. Overfilling of the reservoir, combined with sharp reinflation pulses during later backflow episodes, drove an estimated 12×10^6 m^3 of lava out of the reservoir, possibly into the upper end of the east rift zone.

The recycling process was made possible by a lava conduit, which remained open after phase 1, that connected a supply of lava in the lake with one in the reservoir. Large-scale vesiculation of lava in the conduit effectively pumped lava from the reservoir up into the lake. Flooding of the vent by devesiculated lake lava quenched the fountain and permitted lake lava to flow back into the reservoir. The process was rekindled repeatedly, after backflow stopped, by the introduction of fresh gas-charged reservoir lava into the conduit, which permitted the vesiculation pump to operate again.

INTRODUCTION

The 1959 eruption in Kilauea Iki Crater at the summit of Kilauea Volcano consisted of 16 separate principal phases that poured lava into the bowl-shaped crater from a main vent on the south wall about 90 m above its original floor (Richter and others, 1970). The first phase died out abruptly after the lake surface rose above the level of the vent, leaving a lake 102 m deep and containing 30×10^6 m^3 of lava ponded in Kilauea Iki. Except for basaltic pumice blown downwind (southwest) from the vent, much of which accumulated on the crater rim above the vent to form a cinder cone, all of the lava erupted was caught in the crater, where its volume could be determined from a simple measurement of the height of the lava lake surface. After each phase, a substantial volume of lava escaped back underground into the main vent or into another somewhat lower vent hidden by the lake nearby. Backflow of lava after cessation of fountaining is not uncommon at Kilauea (for example, the 1954 eruption in Halemaumau; see Macdonald and Eaton, 1957), but the 1959 eruption is the only one for which we have such complete measurements of ground deformation and volumes of eruption and backflow. Except for their smaller volumes of erupted lava and shorter durations, the 15 subsequent principal phases were much like the first. Lava that erupted from the vent collected in the lake, increasing its depth until ponded lava rose above the vent and caused the fountain to die out abruptly. As the lake flooded the base of the fountain, the height of the fountain often oscillated wildly before it was quenched. At the ends of several phases, notably phases 4 and 16, lowering of the lake surface and strong backflow toward the base of the still-active fountain showed that withdrawal of lava from the lake need not await cessation of fountaining. The drainback point appeared to be at or just below the base of the fountain.

Total volumes of lava erupted into and withdrawn from Kilauea Iki during its 16 principal eruptive phases between November 14 and December 19 were 102×10^6 m^3 and 63×10^6 m^3, respectively, leaving 38×10^6 m^3 of lava in the lake at the end of the eruption. Of the 71×10^6 m^3 of lava poured into the lake after the end of phase 1 fountaining, only 8×10^6 m^3 remained at the end of the eruption.

What was the fate of the 63×10^6 m^3 of lava that drained back underground from the lava lake? If it returned to its immediate source to be erupted again in later phases, then only about 8×10^6 m^3 of drainback lava must be accounted for (maximum lake volume at end of phase 8 minus final lake volume at end of eruption). The other 56×10^6 m^3 represents the same lava that was erupted many times in small batches and then withdrawn. An important question for this apparently closed lake-reservoir system is: What provided the driving force to erupt the same limited volume of lava over and over again? If the drainback lava escaped from an open lake-reservoir system into another storage zone beneath the summit or into the fluid core of the east rift zone (in preparation for the impending 1960 east-rift eruption), however, then the entire 63×10^6 m^3 must be found.

In addition to the unusual features of the eruption itself, some of which have been outlined above, the 1959 Kilauea Iki eruption was unusual in the range and abundance of geologic and geophysical observations on its progress and effects. There were reasons for this fortunate situation: a new geochemical laboratory had recently been added to the Hawaiian Volcano Observatory (HVO), with an appropriate augmentation of the observatory staff, and the networks of seismometers and tiltmeters around the summit of Kilauea were in the process of being upgraded and expanded in response to lessons learned during the 1954–55 summit and flank eruptions.

Specific measurements that were important for tracking magma as it rose into the volcano from depth, as it was stored temporarily in a shallow summit reservoir, and as it was subsequently erupted into Kilauea Iki Crater and then partially withdrawn include the following:

(1) Seismic network records for (a) locating individual earthquakes and earthquake swarms associated with the eruption and with the expansion of the reservoir before, and its deflation after, the eruption, and (b) the detection and approximate location of the source of volcanic tremor associated with underground movement and eruption of lava;

(2) Measurements of tilting of the Earth's surface around the summit of the volcano as magma moved into or out of the summit reservoir, including: (a) periodic releveling of a network of tilt bases around the summit of the volcano to map the slowly changing pattern of deformation of the entire summit, (b) daily measurement of level changes (tilting) at the Uwekahuna vault (west of Kilauea caldera) and at the Whitney vault (northeast of the caldera), and (c) minute-by-minute monitoring of the rate of tilting and short-term accumulation of tilting at the Uwekahuna vault by analysis of the zero-line drift of the horizontal-component long-period Press-Ewing seismograph;

(3) Systematic observation of the progress of the eruption and periodic measurement of parameters related to the eruption of lava into, and its withdrawal from, the lava lake, including: (a) accurate timing of the beginning and end of eruptive phases, frequent measurement of fountain height, and physical description of the fountain and any unusual phenomena associated with it, (b) periodic measurement of the height of the lava-lake surface, particularly at the end of fountaining and after cessation of drainback, (c) frequent sampling of basaltic pumice thrown out by the fountain and sampling of recently erupted lava from the lake, and (d) measurements of lava fountain temperatures (by optical pyrometer) when conditions at the fountain permitted.

Part of the data covered by item 3 above is from Richter and others (1970), where methods as well as results are described. Data on the volumetric progress of the Kilauea Iki eruption, which form the basis for Richter and others' (1970) figure 2, are presented in table 48.1. The seismic and tilt networks and results have not been treated comprehensively elsewhere, so we shall treat them in detail.

The main purpose of this paper is to present the record of ground-surface deformation at and around the summit of Kilauea that traces the movement of lava within the summit region of the volcano before, during, and after the 1959 eruption and to correlate that record with other measurements and observations carried out during the eruption to answer the question posed above: What was the fate of the 63×10^6 m^3 of lava that drained back underground from the lava lake? A second objective is to analyze the data on tremor amplitude, rate of eruption, fountain height, and recharge of the summit reservoir to discover what they might reveal about the process that caused the repeated eruptions in Kilauea Iki.

We shall begin with explanations of the methods used to measure long-, intermediate-, and short-term tilting at Kilauea and with a brief summary of the seismic network and some of the results obtained from it. Next, we shall trace the course of the eruption to examine the pattern of deformation associated with individual phases and with longer episodes of activity during the eruption. We shall then make a kinematic reconstruction that traces lava into the summit reservoir and through the phases of the Kilauea Iki eruption and that conforms with the observations presented. Finally, we shall examine the relationships among tremor, eruption rate, fountain height, and reservoir recharge quantitatively to develop a better understanding of the mechanics of the eruption.

ACKNOWLEDGMENTS

The manuscript was reviewed by David P. Hill and Fred Klein, whose many helpful suggestions help to clarify and augment the paper.

TILT MEASUREMENTS

TILT BASES

At the time of the 1959 eruption the primary system for measuring deformation of the summit region of Kilauea was a network of 9 permanent tilt bases encircling Kilauea caldera (fig. 48.1) and extending about 10 km south of the caldera. A typical tilt base consists of three concrete piers planted firmly in the ground (on rock if possible) at the vertices of an equilateral triangle about 50 m on a side. Each pier is capped by a brass hub that provides a reference surface and a clamp-down for a precise liquid-level system for measuring height differences between adjacent pairs of piers (Eaton, 1959). The tilt bases are releveled at intervals of 3–6 mo, and changes in the relative heights of the piers reveal any tilting of the base during the interval between measurements. Tilting as small as a few tenths of a microradian (<0.3 μrad) can be detected. The

TABLE 48.1.—*Volumetric progress of the 1959 Kilauea Iki eruption*

[H.s.t., Hawaii standard time; duration is time since last measurement or onset of new eruptive phases; bottom of crater before November 14 at elevation 954 m (3,130 ft) defines zero depth of lava lake; ΔV, change in lake volume since last depth measurement; V, volume of lava lake; rate, average rate of lava outpouring since last depth measurement or onset of new eruptive phase]

Date	Time (H.s.t.)	Duration (h)	Lava lake Depth (m)	Lava lake Area (acres)	Volume of lava ΔV (10^6 m^3)	Volume of lava V (10^6 m^3)	Volume of lava Rate (10^3 m^3/h)
Phase 1							
Nov. 14	2008	0	0(elev. 954.0)	37.0	0	0	0
Nov. 15	0300	7.0	1.5	37.0	.2	.2	33
	1800	15.0	4.6	39.0	.7	.5	31
Nov. 16	1215	18.25	7.6	41.0	.5	1.1	25
	1400	1.75	8.2	41.5	.1	1.2	44
Nov. 17	1045	20.75	16.8	47	1.4	2.7	70
	1400	3.25	18.3	48.5	.3	3.0	94
	2030	6.5	22.0	51	.7	3.7	106
Nov. 18	1200	15.5	34.1	59	2.5	6.2	163
	2315	11.25	45.7	68	2.8	9.0	252
Nov. 19	1150	12.5	57.9	79	3.5	12.5	281
	2115	9.5	68.6	88	3.6	16.1	378
Nov. 20	1210	15.	82.3	106	5.4	21.5	357
Nov. 21	0930	21.25	97.5	120	7.0	28.4	327
	1925	10.0	102.1	125	2.2	30.7	222
Nov. 23	1000	[1]38.5	100.0	123	−1.1	29.6	−28
Phase 2							
Nov. 26	0100	0					
	1000	9.0	102.4	125	1.1	30.7	128
	1635	6.6	107.0	130	2.4	33.2	371
	1940	3.0	103.9	127	−1.5	31.7	−510
Nov. 27	1230	16.75	[2]97.8	121	−3.0	28.7	−178
Phase 3							
Nov. 28	1645	0					
Nov. 29	1500	22.25	100.9	124	1.5	30.2	69
	2147	6.75	103.9	126	1.5	31.7	226
Dec. 1	1500	41.25	[3]100.3	123	−1.8	29.9	−44
Phase 4							
Dec. 4	[4]0100	0					
	2325	[4]22.5	114.3	138	7.4	37.3	368
Dec. 5	0330	4.0	117.3	142	1.7	39.0	420
	0630	3.0	120.4	145	1.8	40.7	586
	0730	1.0	[5]118.0	142	−1.5	39.3	−1453
	0927	2.0	120.1	145	1.2	40.5	612
	1155	2.5	115.5	140	[6]−2.5	38.0	−1009
	1230	0.5	114.0	137	−.8	37.2	−1682
Dec. 6	1448	26.25	110.0	134	−2.1	35.1	−79
Phase 5							
Dec. 6	1448	0					
	2300	8.25	121.9	147	6.6	41.7	797
Dec. 7	0023	1.4	122.8	148	.5	42.2	382
	1530	15.1	114.3	138	−4.7	37.5	−314
Phase 6							
Dec. 7	1530	0					
Dec. 8	0245	11.25	125.9	152	6.6	44.0	584
	0300	0.25	125.3	151	−.4	43.7	−1529
	1200	9.0	118.6	143	−3.7	39.9	−416
Phase 7							
Dec. 8	[7]1300	0					[7](881)
	2012	7.25	125.3	151	3.7	43.7	518
Dec. 9	1045	14.5	118.9	143	−3.6	40.1	−248
Dec. 10	1515	28.5	115.2	139	−2.0	38.1	−70
Phase 8							
Dec. 10	[8]1515	0					[8](746)
Dec. 11	1048	[8]19.5	126.2	153	6.2	44.3	317
	1130	0.75	124.7	150	−.9	43.3	−1223
	1200	0.5	124.1	150	−.4	43.0	−765
Dec. 12	1000	22.0	116.4	141	−4.2	38.8	−191
Dec. 13	0720	21.3	115.5	140	−.5	38.3	−21
Phase 9							
Dec. 13	[9]0508	0					[9](765)
	1340	8.5	125.9	152	5.7	44.0	674
	1545	2.1	120.4	145	−3.1	40.9	−1492
Dec. 14	1000	18.25	112.5	136	−3.8	37.1	−209
Phase 10							
Dec. 14	[10]0705	0.					[10](1269)
	1536	8.5	124.7	150	6.3	43.4	746
	1605	0.5	123.8	149	[11].5	43.0	917
Dec. 15	0800	15.9	115.5	140	−4.4	38.5	−279
Phase 11							
Dec. 15	0611	0.					
	0800	1.8	118.3	143	1.3	39.8	722
	1025	2.4	123.4	149	2.7	42.5	1115
	1115	0.8	121.9	147	−.8	41.7	−1051
	2030	9.25	116.4	141	−2.6	39.4	−281
Phase 12							
Dec. 15	1930	0					
	2030	1.0	118.0	142	.8	39.8	765
	2130	1.0	120.7	146	1.4	41.3	1453
Dec. 16	1015	12.75	114.6	138	−3.1	38.1	−246
Phase 13							
Dec. 16	1335	0					
	1625	2.8	119.5	144	2.5	40.7	901
	1650	0.4	120.1	143	.4	41.1	956
	1719	0.5	120.7	146	.3	41.4	612
Dec. 17	0245	9.4	116.1	140	−2.4	38.9	−260
Phase 14							
Dec. 17	0215	0					
	0402	1.75	[12]119.8	144	1.8	40.7	1048
	1100	7.0	118.0	142	−1.0	39.8	−142
Phase 15							
Dec. 17	[13]1110	0					[13](989)
	1532	4.4	121.3	146	1.7	41.4	382
	1800	2.5	120.4	145	−.5	41.0	−183
Dec. 18	1500	21.0	115.2	139	−2.8	38.2	−131
Phase 16							
Dec. 19	[14]0240	0					[14](1271)
	0616	3.6	122.8	148	4.1	42.4	1147
	1115	5.0	119.5	144	−1.7	40.7	−336
Dec. 20	1300	25.75	114.3	138	−2.7	38.0	−104
Phase 17							
Dec. 19	2045 to						
Dec. 20	0800	11.25: Slight fountaining activity; no significant output of lava					

[1]This subsidence probably occurred during the first few hours of the period.
[2]These figures are approximate. Subsidence of the east pond was 25–30 ft; the smaller west pond subsided 35–45 ft.
[3]These figures are approximate. Subsidence of the east pond was about 7 ft; the smaller west pond subsided irregularly between 15–30 ft.
[4]Strong lava extrusion only during last half of this period. Continuous fountain and tremor after 0320 H.s.t.
[5]Visual estimate of subsidence in pond during eruption.
[6]Volume figures from end of phase 4 through phase 16 take into consideration the volume of the "black ledge."
[7]No appreciable lava output until 1515 on Dec. 8, 1959.
[8]No appreciable lava output until 0230 on Dec. 11, 1959.
[9]No appreciable lava output until 0615 on Dec. 13, 1959.
[10]No appreciable lava output until 1040 on Dec. 14, 1959.
[11]From phase 10 to phase 16 no appreciable volume of lava flowed into the small west pond.
[12]Estimated. Lava level never rose above the "black ledge."
[13]No appreciable lava output until 1350 on Dec. 17, 1959.
[14]No appreciable lava output until 1301 on Dec. 19, 1959.

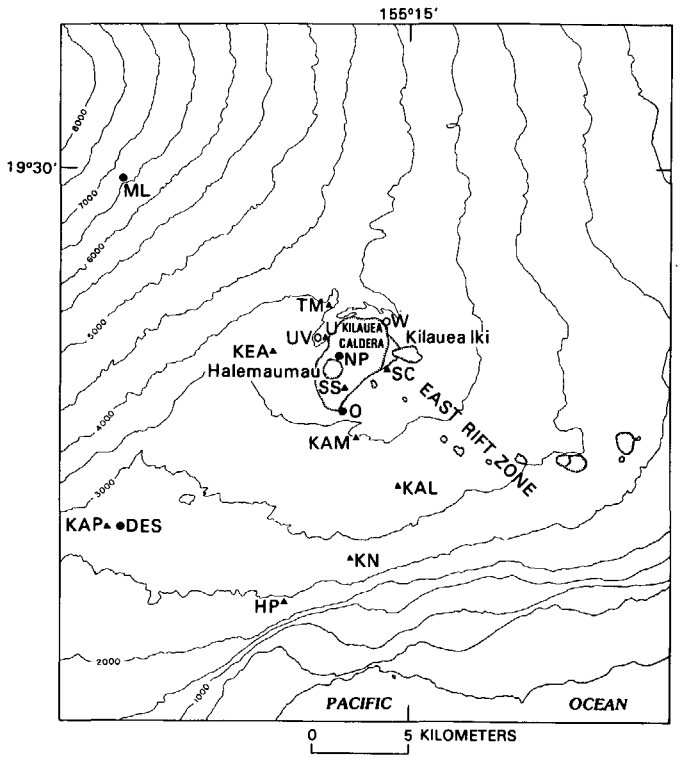

FIGURE 48.1.—Summit of Kilauea Volcano, showing tilt bases as triangles (TM, SC, SS, KEA, KAP, KAM, KAL, KN, HP), tiltmeter vaults as circles (UV and W), telemetered seismographs as dots (ML, DES, NP, O), and geographic localities mentioned in the text. Pit craters are indicated by hachures. Elevation contours in feet.

results are displayed as a map of vectors scaled according to the magnitude of tilt and pointing in the direction of maximum relative subsidence of the ground. Tilt maps for 12 intervals spanning the period February 1959 to November 1960 are shown in figures 48.2 and 48.3.

WHITNEY VAULT: BOSCH OMORI SEISMOGRAPH

The longest record of tilt measurements on Kilauea Volcano is from the Bosch-Omori horizontal pendulum seismograph at the Whitney vault on the northeast rim of Kilauea caldera. This mechanical seismograph responds to a tilt perpendicular to the seismometer boom by a deflection of the recording point. Systematic tracking of the position of the recording point relative to some standard reference provides a record of ground tilting. Such a measurement was made once a day from 1912 through 1961 (Jaggar and Finch, 1929). This measurement is a relative one and the reference must be reset whenever the instrument is adjusted. Moreover, the Whitney vault has proved to have a very large annual tilt cycle that must be removed before tilting caused by the volcano can be detected (Powers, 1946, 1947). For very large tilts like those associated with the 1959–1960 eruption, however, the signals from this instrument (north-south and east-west components) are much larger than the uncertainties due to the foregoing problems.

UWEKAHUNA VAULT: LIQUID-LEVEL TILTMETER

The Uwekahuna vault on the west rim of the caldera has proved to be much more stable than the Whitney vault. A liquid-level tiltmeter mounted on the walls of this vault has provided daily readings of tilt since 1956. The daily readings scatter through a range of several microradians, so the measurements are normally reported as weekly averages (Eaton and Fraser, 1958). During periods of strong tilting, such as during the 1959–1960 eruption, the daily scatter in readings is modest compared to the real tilt changes. The daily tilt readings at Uwekahuna and Whitney provide a somewhat noisy time history of tilting at Kilauea caldera that fills in details of tilting between the infrequent resurveys of the tilt bases. Tilt records for these two stations for the interval October 15, 1959, to April 1, 1960, are shown in figure 48.4.

UWEKAHUNA VAULT: PRESS-EWING SEISMOGRAPH

The most unusual record of tilting at the summit of Kilauea during the 1959 eruption was obtained from the long-period Press-Ewing seismograph in Uwekahuna vault. Part of the tilt response of the instrument is expected and can be calibrated in terms of the operating parameters of the seismograph. Another part of the response was unexpected: it resulted from faulty attachment of the suspension fibers in the galvanometers, which permitted them to detect tilting in the same way as a horizontal pendulum seismograph. This part of the Press-Ewing response is accidental, but it can be calibrated by reference to the liquid-level tiltmeter that was operating in the same vault.

The layout of the Press-Ewing seismometer pendulums and their recording galvanometers, as well as the two components of the Uwekahuna liquid-level tiltmeter, is shown in figure 48.5. The velocity transducer of the Press-Ewing horizontal component seismograph (a coil attached to the mass and moving in the field of a magnet fixed to the frame) produces a signal (output voltage) proportional to the rate at which the coil is moving relative to the fixed magnet. Thus, one obtains a constant output for a constant tilt rate. For tilt rates that change slowly (compared to the 90-s period of the Press-Ewing galvanometer), the displacement of the galvanometer is directly proportional to the output voltage from the seismometer and, hence, to the rate of tilting.

The response of the Press-Ewing seismograph to slow tilting of the ground is thus a displacement of the zero-line trace about which normal shorter period ground movements are recorded. A given seismograph responds to the same component of tilting as it does to displacement. A sharp northward or eastward displacement of the ground produces an upward displacement of the trace on the seismogram (as the HVO instruments are connected), but tilting downward toward the north or east produces a downward displacement of the seismogram trace. From the manufacturer's specifications for the seismometers and galvanometers and for the manner in which

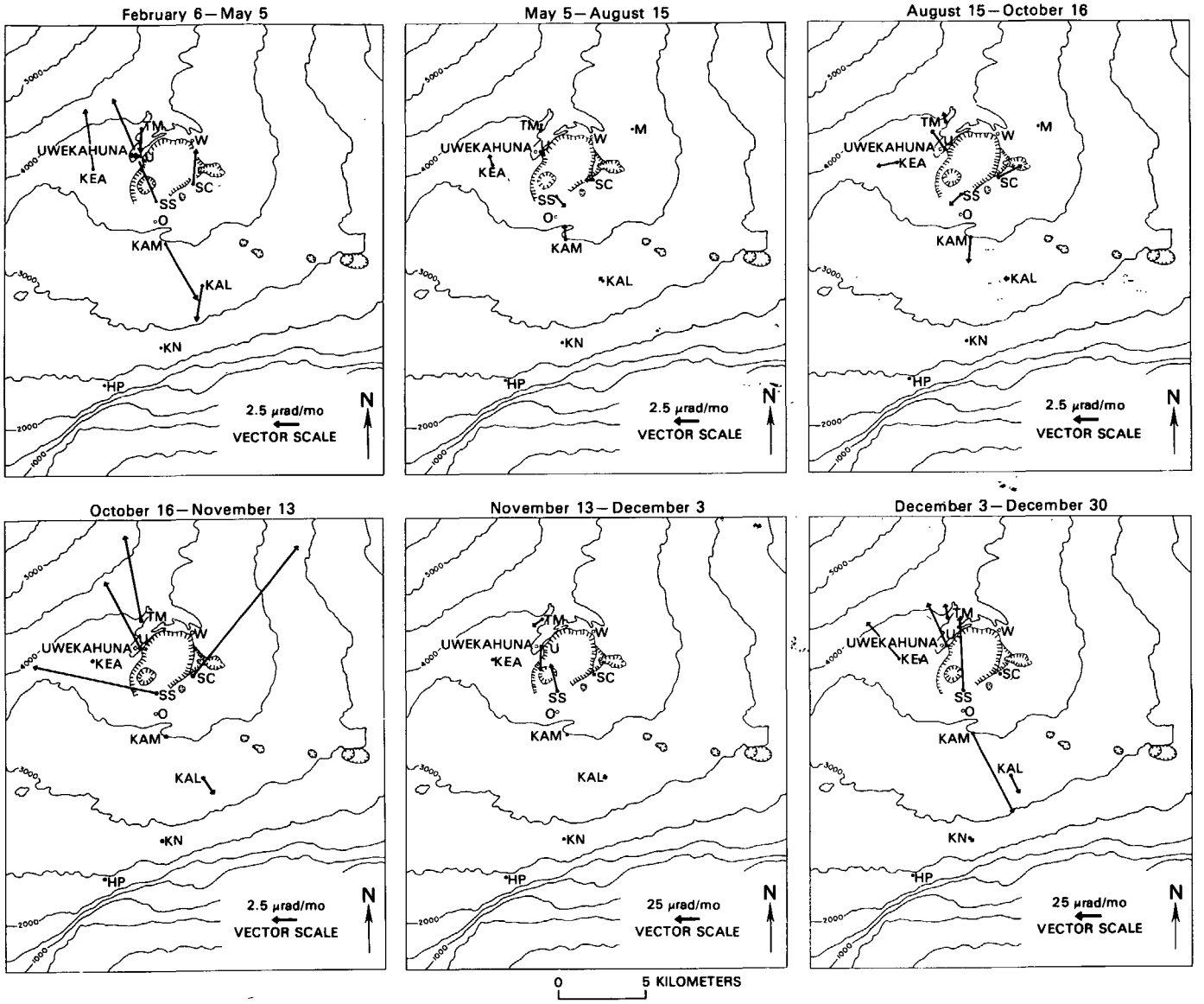

FIGURE 48.2.—Tilt diagrams for summit region for six intervals from February 6, 1959, to December 30, 1959. Tilt vectors point in direction of maximum subsidence of the ground. Note different vector scales used, depending on rate of tilt. For identity of data stations and geographic features, see figure 48.1.

they are set up at Uwekahuna, the theoretical rate-of-tilt sensitivity of both the north-south and east-west Press-Ewing seismographs (neglecting the direct tilt response of the galvanometers) is approximately 0.374 μrad/h per millimeter deflection of the trace.

The principal challenge in using the Press-Ewing seismograms to measure rate of tilt is in establishing an acceptable normal position of the trace from which deflections are to be measured. Surprisingly, however, measuring the position of the ambient zero line to within a fraction of a millimeter even in the presence of 5-mm microseisms is not too difficult. In the plotted results, features that repeat at intervals of 1 h or 1 d (corresponding to one rotation of the drum and to the daily record change, respectively) probably result from errors in the reference base. The east-west Press-Ewing seismogram for December 16–17, 1959, is shown in figure 48.6. Each line across the record is 1 h long. Zero-line excursions associated with the beginning and end of phases 13 and 14 are labeled.

An analysis of the Press-Ewing zero-line deflections from November 8 to December 1 (rapid collapse and recovery associated with the first phase of the eruption) revealed the imperfection in the galvanometers noted above: their coils are suspended in such a manner that the galvanometers, by themselves, act like simple tiltmeters for tilt at right angles to the normals to the galvanometer

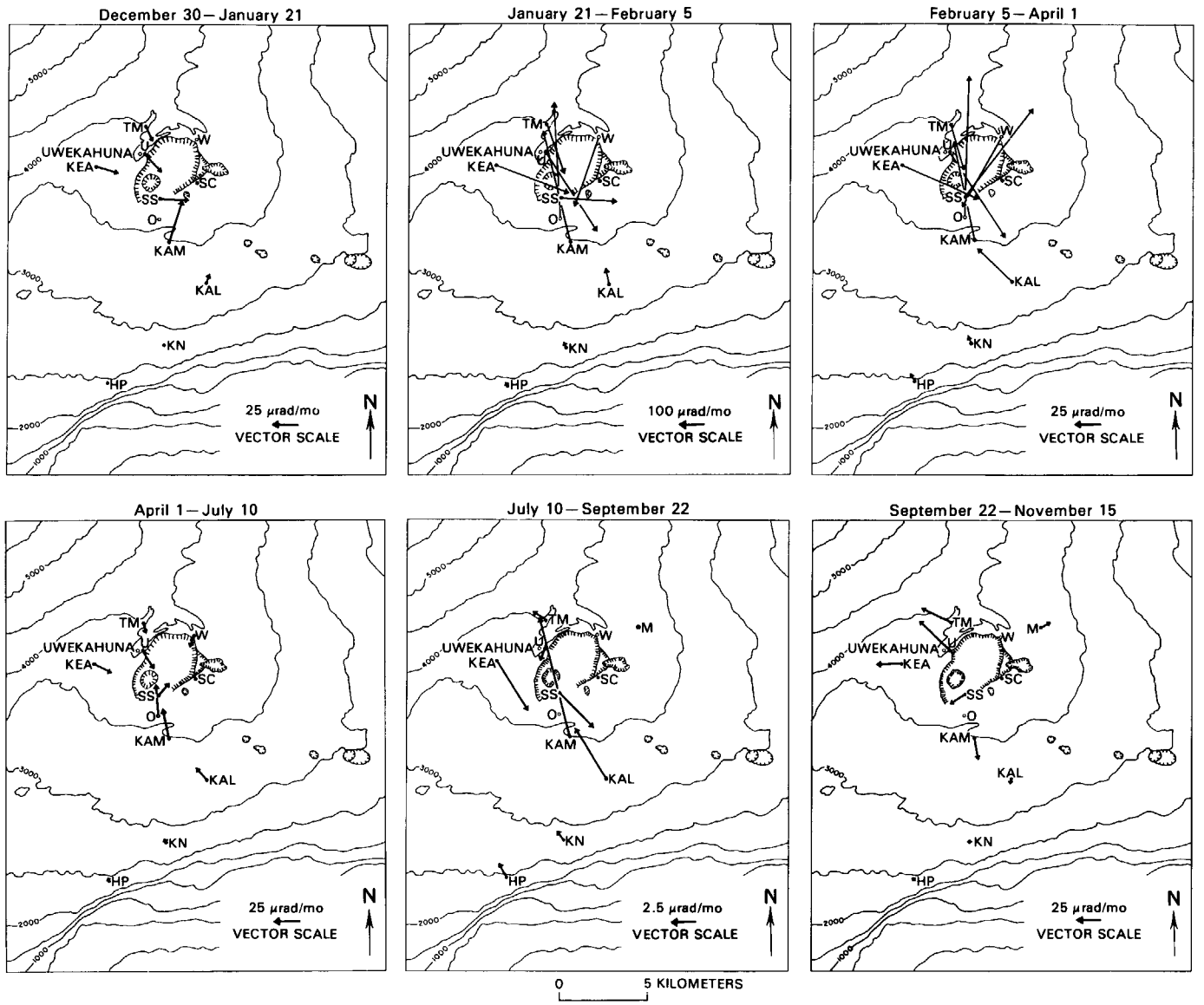

FIGURE 48.3.—Tilt diagrams for summit region for six intervals from December 30, 1959, to November 15, 1960. Tilt vectors point in direction of maximum subsidence of the ground. Note different vector scales used, depending on rate of tilt. For identity of data stations and geographic features see figure 48.1.

mirrors, in our case for tilt in an east-west direction. This effect is small for the east-west galvanometer, so the total seismometer-galvanometer response is dominated by the rate-of-tilt signal from the seismometer. The north-south galvanometer, on the other hand, is quite sensitive to the east-west state of tilt. As seen from Uwekahuna (on the liquid-level tiltmeter, for example) the center of swelling and collapse associated with Kilauea Iki eruptive phases lies almost due east. Thus, the north-south-component seismometer-galvanometer system response is dominated by the galvanometer (which records the east-west state of tilt with moderate sensitivity), the north-south component of tilt and its rate of change being small because of the azimuth to the active region. Large north-south rate-of-tilt deflections detected by the north-south Press-Ewing seismometer were recorded during the preoutbreak swarm on November 14 and during a large tilt transient between phases 4 and 5; moderate ones were recorded as transients when most of the phases stopped abruptly. In these cases the active center appears to have been south of that associated with the eruptions in Kilauea Iki.

In summary, during episodes of tilting associated with the Kilauea Iki eruption, the east-west Press-Ewing instrument measured east-west rate of tilt, and the north-south Press-Ewing instrument measured principally the east-west cumulative tilt at Uwekahuna. This point may be confusing, so it should be noted carefully.

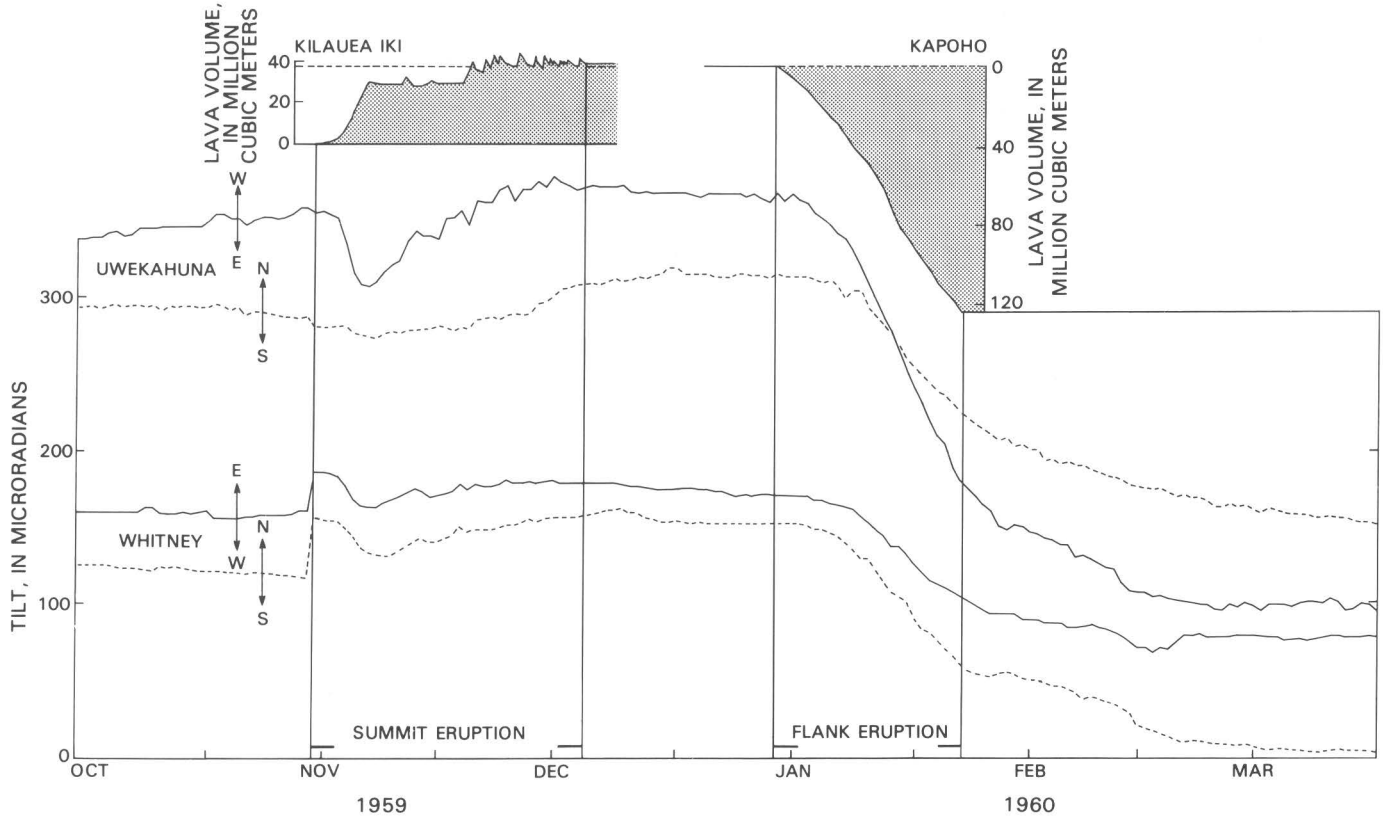

FIGURE 48.4.—Tilt at Uwekahuna and Whitney on Kilauea summit (UV and W of figure 48.1) from October 15, 1959, to April 1, 1960, and volumes of lava in Kilauea Iki Crater erupted during the 1960 eruption from the east rift zone near Kapoho.

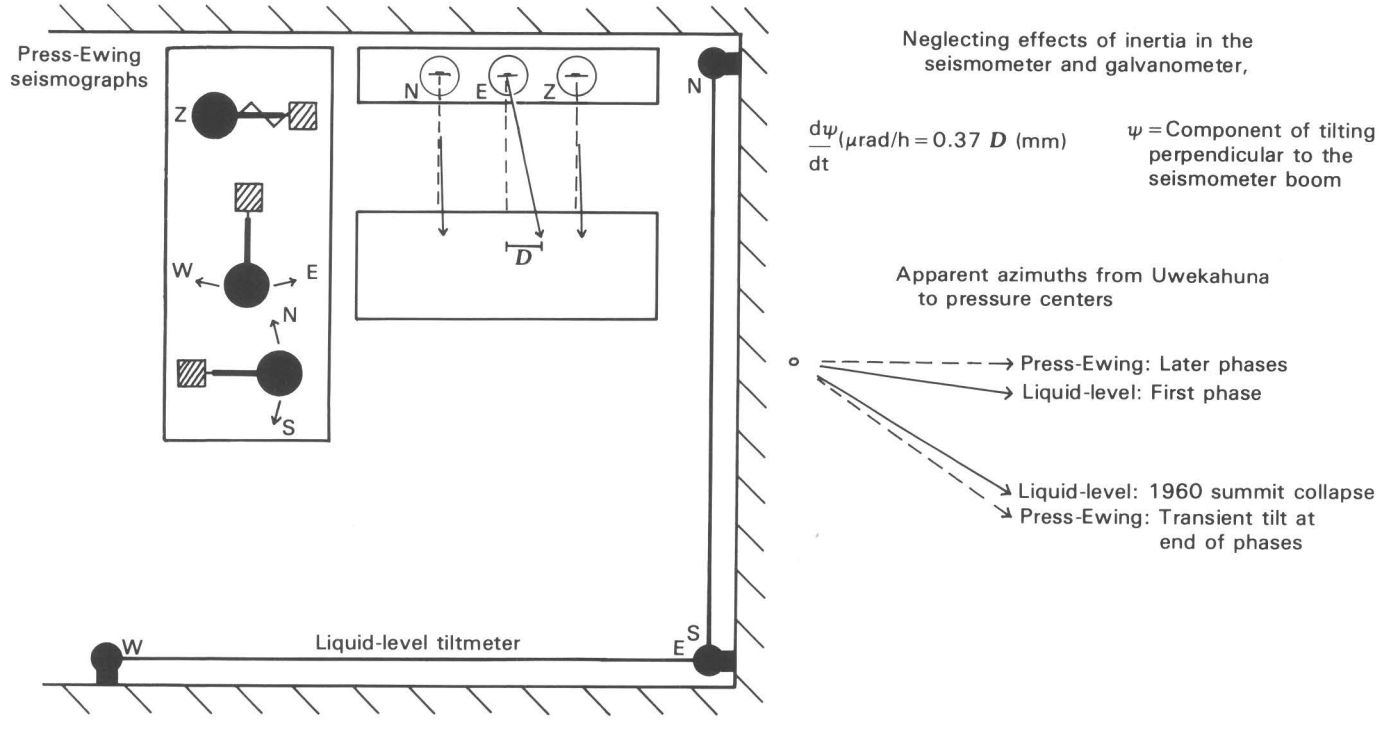

FIGURE 48.5.—Layout of liquid-level tiltmeter and long period Press-Ewing seismographs in Uwekahuna vault. Press-Ewing seismometers are shown at left, and their galvanometers are shown at top of figure. Letters Z, N, and E denote parts of instruments and the components of tilting they record: Z, vertical; N, north-south (N, S); E, east-west (E, W). D, deflection of seismogram trace from normal; dψ/dt, rate of tilting.

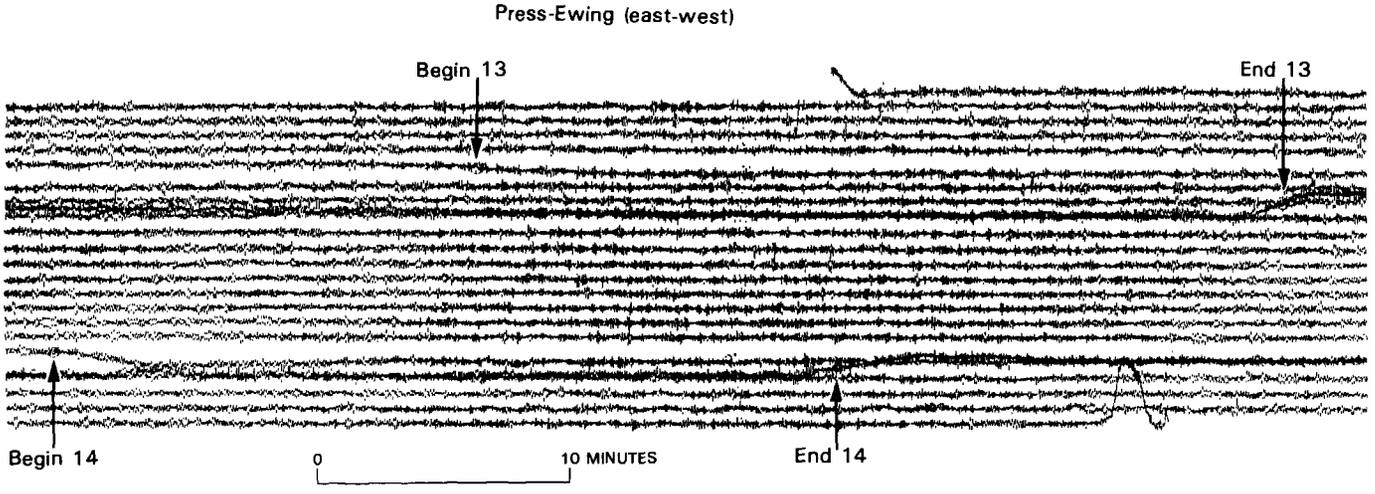

FIGURE 48.6.—Seismogram from east-west Press-Ewing seismograph for December 15–16, 1959, showing shifts in zero line associated with phases 13 and 14 (arrows).

SEISMIC NETWORK

Before the 1959 eruption a network of sensitive, telemetered, short-period seismographs had been installed around the summit of Kilauea and on the adjacent flank of Mauna Loa to facilitate study of the many earthquakes occurring regularly in that region. The telemetered network was augmented by optically recording seismographs with similar response characteristics that were deployed in a ring around the Island of Hawaii. The combined network provided the means for detecting and locating a variety of seismic manifestations associated with the volcano, including the following:

(1) Individual earthquakes throughout the volcano;

(2) Occasional swarms of small earthquakes marking the opening of dikes around the summit reservoir and in the rift zones;

(3) Volcanic tremor generated by rapid movement of magma within the volcano, particularly during eruptions; and

(4) Swarms of tiny deep earthquakes and associated irregular tremor thought to mark the region from which magma is collected to feed the volcano.

Activity of the last 3 types figure prominently in our analysis of the 1959 eruption.

OVERVIEW OF THE REGIONAL DEFORMATION OF THE KILAUEA SUMMIT AND DEEP EARTHQUAKE SWARMS ASSOCIATED WITH THE 1959 ERUPTION

DEFORMATION

The patterns of regional deformation of the Kilauea summit area during the 6 intervals from February 6, 1959, to December 30, 1959, that are shown in figure 48.2 indicate the location and intensity of inflation and deflation in this area before and during the 1959 eruption. The next 6 intervals (fig. 48.3), from December 30, 1959, to November 15, 1960, show the patterns of regional deformation of the summit area during the 1960 Kapoho eruption, the rapid deflation of the summit reservoir accompanying and following the Kapoho eruption, and the onset of rapid reinflation of the summit reservoir in the fall of 1960. The vectors depicting rate of tilting point outward away from centers of inflation and inward toward centers of deflation (fig. 48.3). The lengths of the vectors are scaled according to the rate of tilting. Note the large variation in scale factor from one interval to the next. These plots are shown together for easy comparison, but we shall return to consider them one at a time as the need arises.

A more continuous, but spatially limited, picture of inflation and deflation of the Kilauea summit region is shown in figure 48.4, where the north-south and east-west components of daily tilt measurements at Uwekahuna vault and Whitney vault are compared with the volume of lava ponded in Kilauea Iki and the volume of lava later erupted on the east rift zone near Kapoho in the 1960 eruption. Tilting in response to eruption of lava into Kilauea Iki during phase 1, and its removal from the summit reservoir, is most marked on the Uwekahuna east-west record, where the curve of eastward tilting very closely matches the lava-volume curve. After an initial sharp northeast offset in tilt at Whitney, the curves of both westward and southward tilting also closely match the lava-volume curve. Vectors representing tilting at these two stations during the phase 1 eruption both point into Kilauea caldera; they cross near the center of the caldera, indicating that the lava erupted into Kilauea Iki was removed from beneath Kilauea caldera. Rapid refilling of the depleted reservoir appears to have begun by the time phase 1 ended. Both the east-west and north-south curves at Uwekahuna had recovered approximately to their levels at the start of the phase 1 eruption by the time phase 4 began. As the east-west tilt curve rose still further during the next two weeks, the volume of lava retained in the lake after subsequent eruptive phases (and the height of the lake surface) also increased beyond the 30×10^6 m^3 left by phase 1 in

about the same proportion that the east-west curve rose above its pre-phase 1 level. The movement of the east-west Uwekahuna curve during the later eruptive phases, such as phase 4, suggests eastward tilting while the eruptions were in progress followed by rapid westward tilting when they stopped. However, the once-per-day interval for tilt samples is too large to track individual phases, some of which lasted only a few hours.

A still simpler picture of the swelling and collapse of the Kilauea summit region is shown by a plot of the radial component of tilting at Uwekahuna tilt base relative to the center of collapse near the south rim of Kilauea caldera during and after the 1960 east-rift eruption near Kapoho. Figure 48.7 (adapted from Eaton, 1962) shows this curve for the period 1957–62. The approximate scale for ΔV, volume of the collapse, is based on fitting the tilt changes between January 21–April 1, 1960 (intervals January 21–February 5, 1960, and February 5–April 1, 1960, in fig. 3), to a curve based on Mogi's (1958) theoretical results for change in elevation versus distance for a small spherical source embedded in an elastic half-space (Eaton, 1962, fig. 12).

DEEP EARTHQUAKE SWARMS

From the early 1950's until the fall of 1960 occasional swarms of small earthquakes, accompanied by a continuous background agitation resembling tremor that waxed and waned during the swarms, were recorded from a source 45–65 km deep beneath the summit of Kilauea and the adjacent flank of Mauna Loa to the north. Until the introduction of the sensitive telemetered seismic net around the summit of Kilauea in 1958, these earthquakes were recorded most clearly on a mechanical horizontal-component seismograph, about 10 km northwest of Kilauea caldera (station ML, figure 48.1, with magnification of about 200). Typically, several hundred events were counted during a swarm, and the location of the swarm, including its depth, was poorly determined. From 1958 onward the detection threshold was lower and the locations were much improved, though still poor by modern standards. The sharpest recordings were obtained at stations 10 km northwest (station ML) or 10 km southwest (station DES) of the caldera (fig. 48.1), which were equipped with high-gain short-period vertical seismographs whose signals were telemetered to Uwekahuna for recording; but the earliest P-wave onsets clearly were at Uwekahuna. Swarms recorded by the improved network contained from less than 100 to several thousand individual events, plus many hours of background tremor during the larger swarms. The times of occurrence of nine of these swarms are indicated by arrows along the time axis in figure 48.7, and samples of two swarms are shown in figures 48.8 and 48.9. Between September 1953 and June 1956 (not shown on fig. 48.7) there were 10 additional swarms, but there were none between June 1956 and April 1958.

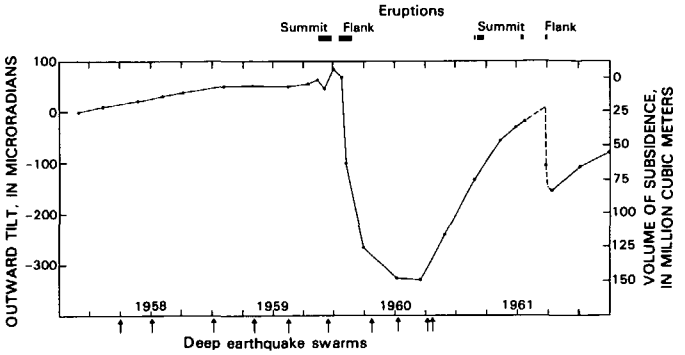

FIGURE 48.7.—Radial component of tilting at Uwekahuna tilt base for 1957–62, relative to 1960 center of subsidence at south edge of Kilauea caldera, showing swelling and subsequent collapse of Kilauea summit. Occurrence times of deep swarms of earthquakes beneath summit of Kilauea and of summit and flank eruptions also indicated.

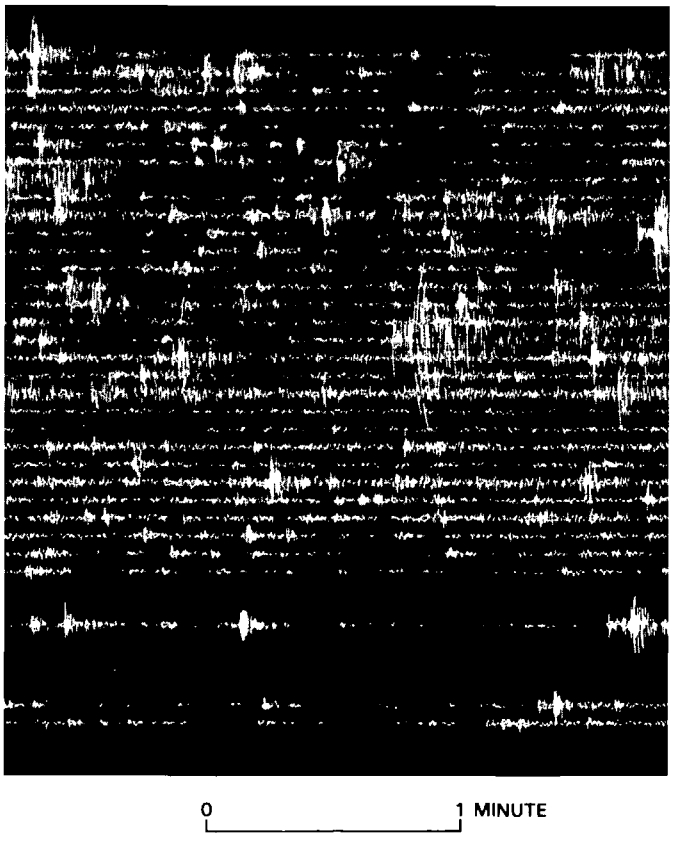

FIGURE 48.8.—Sample of Desert seismogram from August 16, 1959, illustrating swarm of deep earthquakes beneath the summit of Kilauea. Several thousand small earthquakes were accompanied by intervals of continuous tremor.

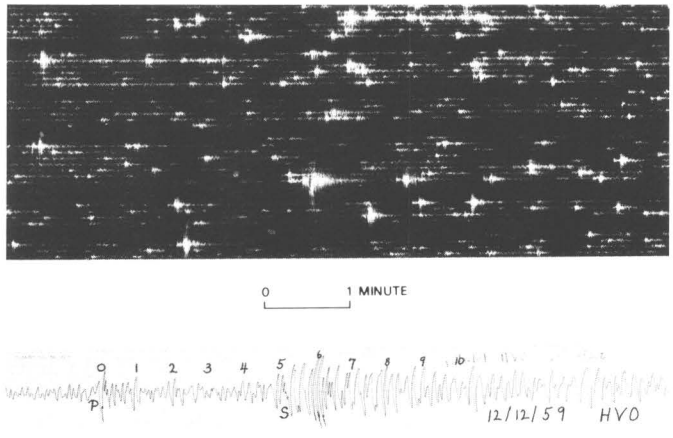

FIGURE 48.9.—Sample of Mauna Loa seismogram of swarm of deep earthquakes on December 11–12, 1959, beneath summit of Kilauea. Large-scale record of a member of this swarm recorded at Uwekahuna is shown at bottom (*P* and *S* arrivals and time in seconds after *P* are indicated).

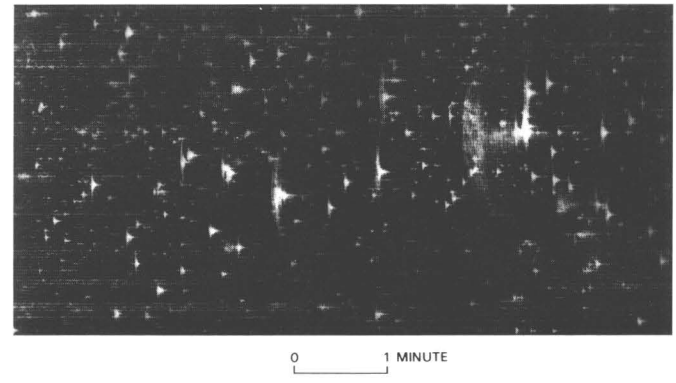

FIGURE 48.10.—North Pit seismogram from November 9–10, 1959, illustrating intense swarm of very small earthquakes that emanated from Kilauea caldera for several months before the 1959 eruption.

CHRONOLOGY OF TILTING AND EARTHQUAKE SWARMS LEADING UP TO THE 1959 ERUPTION

From November 1957 to May 5, 1959, the summit of Kilauea swelled slowly but steadily (fig. 48.2, 48.7). Deep swarms occurred on April 1, 1958 (weak), July 3–6, 1958 (strong), January 5–6, 1959 (moderate), and May 5, 1959 (very weak). From May 5 to August 15, 1959, the summit subsided very slowly. During August 14–20, 1959, there was a very strong swarm of earthquakes a few kilometers north of Kilauea caldera at a depth of 50–55 km (fig. 48.8). From August 15 to October 16, 1959, swelling of the summit resumed at about the same rate as during 1958.

In mid-September a swarm of tiny very shallow earthquakes began recording on the north Pit seismograph (NP, fig. 48.1) from a source in Kilauea caldera very near the northeast rim of Halemaumau. Initially about 50 per day, the frequency of quakes increased to about 100 per day by the end of September and to about 500 per day during the first week of October. By the first of November earthquakes of this swarm exceeded 1,000 per day, but they were so feeble that they were barely recorded on other seismographs less than 2 km away (fig. 48.10).

Remeasurement of tilting at bases around the caldera in the second week of November revealed that dramatic changes were in progress. The summit was swelling at least three times faster than in previous months (fig. 48.2, interval October 16–November 13, 1959). In midafternoon on November 14, earthquakes emanating from the caldera increased sharply in number and intensity. At frequent intervals during the next 5 h the entire summit region shuddered as earthquakes marked the rending of the crust by the eruptive fissure splitting toward the surface (fig. 48.11). At 2008 (this and all times given in this paper are Hawaii standard time) the lava broke through to the surface in a 900-m-long series of fissures

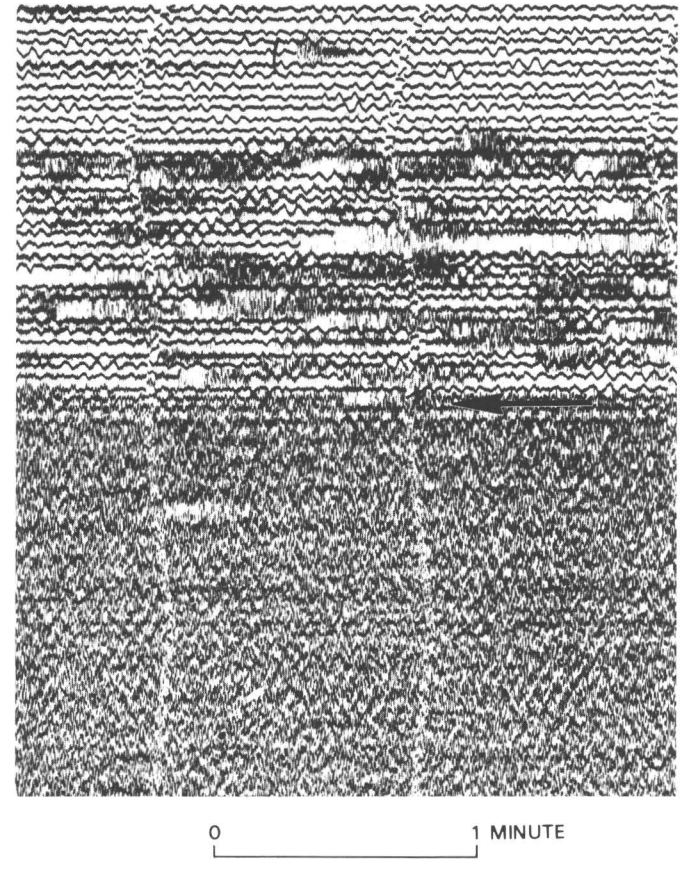

FIGURE 48.11.—Uwekahuna (short-period) seismogram from November 14, 1959, illustrating (upper part) 5-hour-long swarm of earthquakes that preceded the 1959 outbreak. The swarm gave way to strong harmonic tremor when fountaining began (arrow).

about halfway up the 180-m-high south wall of Kilauea Iki Crater, just east of Kilauea caldera. Abruptly the earthquakes stopped, and seismographs around the caldera began to record the strong harmonic tremor characteristic of lava outpouring from Hawaiian volcanoes (fig. 48.11).

Both horizontal components of the Press-Ewing seismograph recorded large excursions of the zero line during the five-hour-long swarm of caldera earthquakes preceding the outbreak of the eruption. Closer examination of the records revealed that the zero lines appeared to be erratic also for the preceding five days. This erratic signal was much stronger, and could be seen earlier, on the east-west than on the north-south component. The deflections of the zero lines from their expected positions were measured from the seismograms for the period 0600 November 6 through 0600 November 15 and the results are plotted in figure 48.12. The activity on the east-west graph before November 9 shows the level of noise (including error of measurement) before the erratic movement of the trace began. On November 9, long-period zero-line shifts began to appear on the east-west component. The disturbance was a distorted sinusoidal oscillation with a period just short of 1 h and a slightly asymmetric appearance: upward peaks (west tilt) were slightly broader than downward peaks (east tilt), and it appeared that the broad upward peaks constituted the zero line away from which the trace moved in brief downward excursions. The amplitude of the disturbance increased and its period decreased (to about 35 min) for several days. From November 12 onward this disturbance, which may be called a tilt storm, was also visible on the north-south component, though its amplitude there was only about one-fourth that of the east-west component. The amplitude of the tilt storm diminished gradually for about one day before the eruption began.

When the caldera swarm suddenly intensified at about 1420 on November 14, both of the Press-Ewing traces deflected abruptly from zero. The southward component of tilting rose rapidly to about 4 μrad/h. It then declined steadily, first to about 0.8 μrad/h by 1700 and then to about 0.2 μrad/h by 2000. The eastward component of tilting was more complex. A strong initial tilting toward the east was replaced after only a few minutes by an equally strong tilting toward the west, which declined rapidly to about 0.5 μrad/h. At 1630 the direction of tilting reversed again, and easterly tilting attained a rate of about 0.9 μrad/h at 1730; after that it decreased steadily to about 0.2 μrad/h by 2000. The complex transient tilting during the outbreak swarm of earthquakes was probably compounded from several effects, including fracturing and propping open of the eruptive fissure and subsidence of the summit owing to escape of lava from the reservoir into the fissure. The tilt storm preceding the outbreak earthquake swarm may have resulted from intermittent escape of lava from the reservoir as it continued to expand before the outbreak.

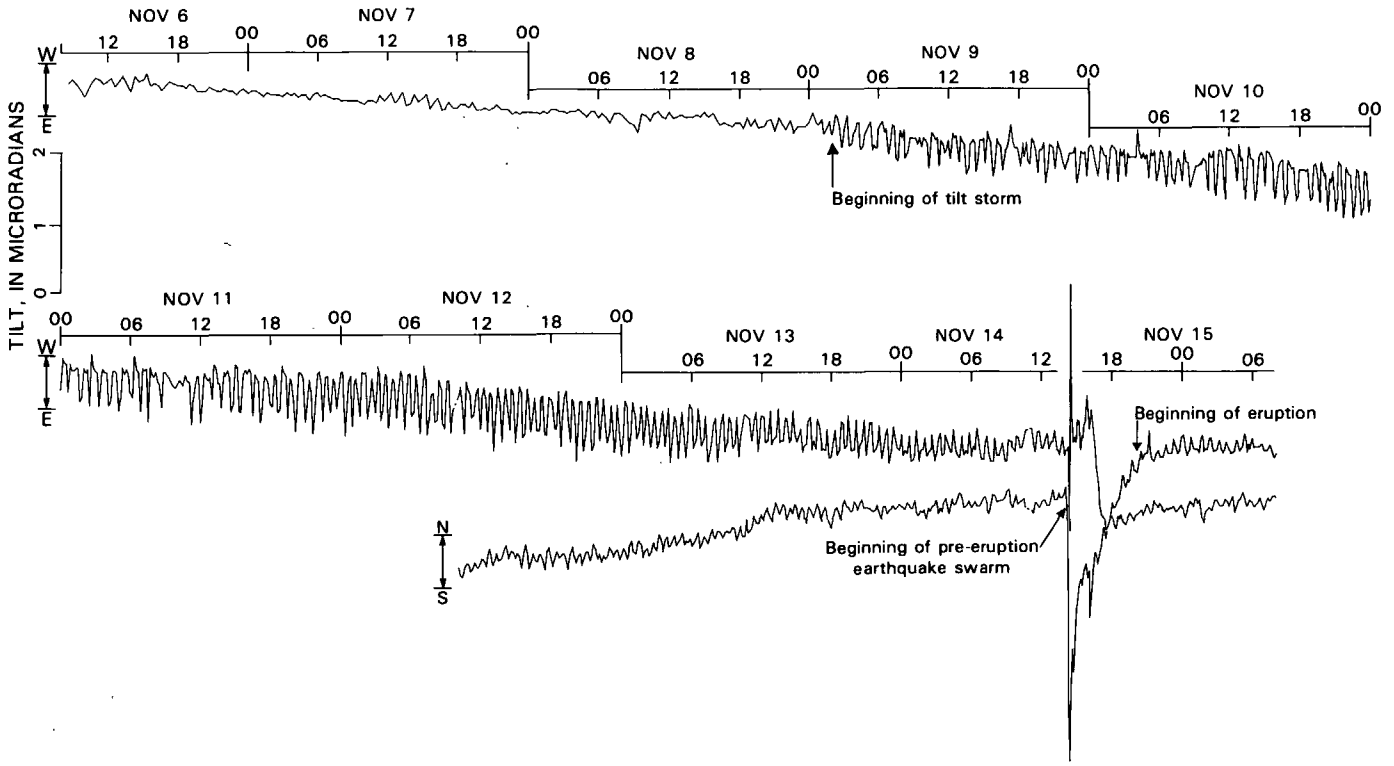

FIGURE 48.12.—Five-day tilt storm and large five-hour tilt excursion recorded by Press-Ewing seismograph before outbreak of 1959 eruption.

SUMMARY OF SELECTED FEATURES OF THE 1959 ERUPTION

The course of the 1959–60 eruption has been described in detail by Richter and others (1970), and we shall borrow several pictures from that report to illustrate features of the eruption that are related closely to the pattern of summit deformation and the amplitude of tremor that accompanied the eruption. The locations of Kilauea Iki Crater and the 1959 eruption vents relative to Kilauea caldera and other features at the summit of Kilauea are shown in figure 48.13 (Richter and others, 1970, fig. 3). The initial outbreak was in a short line of fountains, about half-way up the south wall of Kilauea Iki, which extended rapidly toward the east and slowly toward the west to form a 900-m-long "curtain of fire" during the first 80 min of the eruption (fig. 48.13, vents A through K). The line of fountains is seen in figure 48.14 at its maximum development from Byron Ledge overlook at 2130 on November 14. Fountaining at the ends of the fissure died out slowly, and fountaining near vent A (fig. 48.14, second group from the right) gradually increased in the following hours. By nightfall on November 15 activity was confined to a single fountain 30–45 m high near the site (vent A) that became the main vent for the rest of the 1959 eruption. The fountain grew slowly in height and lava output until it approached its maximum level late on November 18, when the fountain first exceeded 300 m and the depth of the lake reached 45 m. The fountain and lake are shown in figure 48.15 from Byron Ledge overlook when the fountain was 200 m high and the lake was 52 m deep. Spectacular fountaining and rapid filling of the lake continued unabated until the morning of November 20, when the lake, by then 98 m deep, rose above the level of the vent and began to interfere with the fountain. At 1925 on November 21 the fountain ceased abruptly, leaving a 102-m-deep lake containing 30×10^6 m^3 of lava.

Subsequent phases were similar to the last part of the first phase: large fountains with voluminous outpouring of lava filled the lake until it rose above the vent, and then the fountain died abruptly. The large fountains were accompanied by strong volcanic tremor throughout the summit region (fig. 48.16). When the lake rose above the vent, there was strong interaction between the fountain and the lake (fig. 48.17). Large waves generated at the fountain rolled out over the surface of the fluid lake and played against the north shore, alternately revealing and obscuring an incandescent band at the foot of the wall. Unlike the inconspicuous drainback from the first phase, which was not apparent for many hours after the fountain died, drainback from the later phases began almost immediately and was spectacular (fig. 48.18). The rate of withdrawal of lava during the early part of the drainback stage commonly exceeded the rate of eruption of lava during the previous eruptive stage. The very rapid backflow after cessation of fountaining was generally not accompanied by volcanic tremor, although there was a resurgence of tremor after an initial interval of quiet in many cases, particularly in the latest phases (fig. 48.19). At the end of the summit eruption the lake was 111 m deep and contained about 38×10^6 m^3 of lava (fig. 48.20). The level central part of the lake was surrounded by a black ledge about 15 m high and 15–60 m wide that marked the highest level of the lake at the end of phase 8.

The longest and most productive eruptive period, except for phase 1, was phase 4. It was characterized by unusually quiet outpouring of very hot lava and only moderate fountaining. The mouth of the vent had jumped about 12 m upslope between phases 3 and 4, and the level to which drainback could lower the lake appears to have moved upward a somewhat smaller amount.

During December 12–14, a strong swarm of small earthquakes was recorded from a source 15 km north-northeast of Uwekahuna and 40–45 km deep (fig. 48.9).

ANALYSIS OF LAVA MOVEMENT DURING INDIVIDUAL PHASES OF THE 1959 ERUPTION

The parameters of tilting, tremor, fountain height, and lava-lake volume measured during the eruption are closely interrelated. Properly understood, these relations should help clarify three important processes underlying the major facets of the eruption: (1) the accumulation of lava in the summit reservoir, (2) the eruption of lava into Kilauea Iki crater and its subsequent partial withdrawal, and (3) the escape of lava from the summit reservoir into a region other than Kilauea Iki.

The character of the phases changed during the eruption. The first phase differed most from the others, and the subsequent phases evolved generally toward more rapid outpouring and withdrawal of lava and toward more complex relationships among backflow into the vent, postfountaining (resurgent) tremor, and reinflation of the summit reservoir. The first phase offers the best opportunity to study the relations between lava-lake volume and cumulative tilting at Uwekahuna (and Whitney). The later phases are more suited to studies of the relation between the rate of east-west tilting, cumulative amount of east-west tilting, eruption rate, fountain height, and tremor amplitude.

The volume of lava in Kilauea Iki, the east-west component of liquid-level tilting at Uwekahuna, the north-south Press-Ewing zero-line drift (east-west cumulative tilting), the east-west Press-Ewing zero-line drift (east-west rate of tilting), fountain height, and tremor amplitude at Outlet (fig. 48.1) have been plotted against time for the first three phases, November 13–30 (fig. 48.21). The shapes of the first three curves (lava-lake volume, daily readings of east-west tilt from the liquid-level tilt meter, and a continuous record of east-west tilt determined from the north-south Press-Ewing zero-line drift) are so similar from start to finish of the first phase (November 14–21) that suitable scaling brings them into very close correspondence. The continuous east-west tilt curve recorded by the north-south Press-Ewing instrument corresponds almost exactly to the daily liquid-level tilt readings, but it gives far more detail of tilt excursions lasting less than one day. The east-west liquid-level tilt curve also corresponds closely to the lava-lake volume curve from the onset of phase 1 until its end. Eruption of 30×10^6 m^3 of lava into the crater was accompanied by about 50 μrad of eastward tilting.

After an episode of strong tremor with only small fountains during the first day of phase 1, the tremor amplitude diminished markedly. Thereafter, the curves of tremor amplitude and of fountain height are very similar. The rate of lava extrusion built up slowly during phase 1, and any offset of the east-west Press-Ewing zero

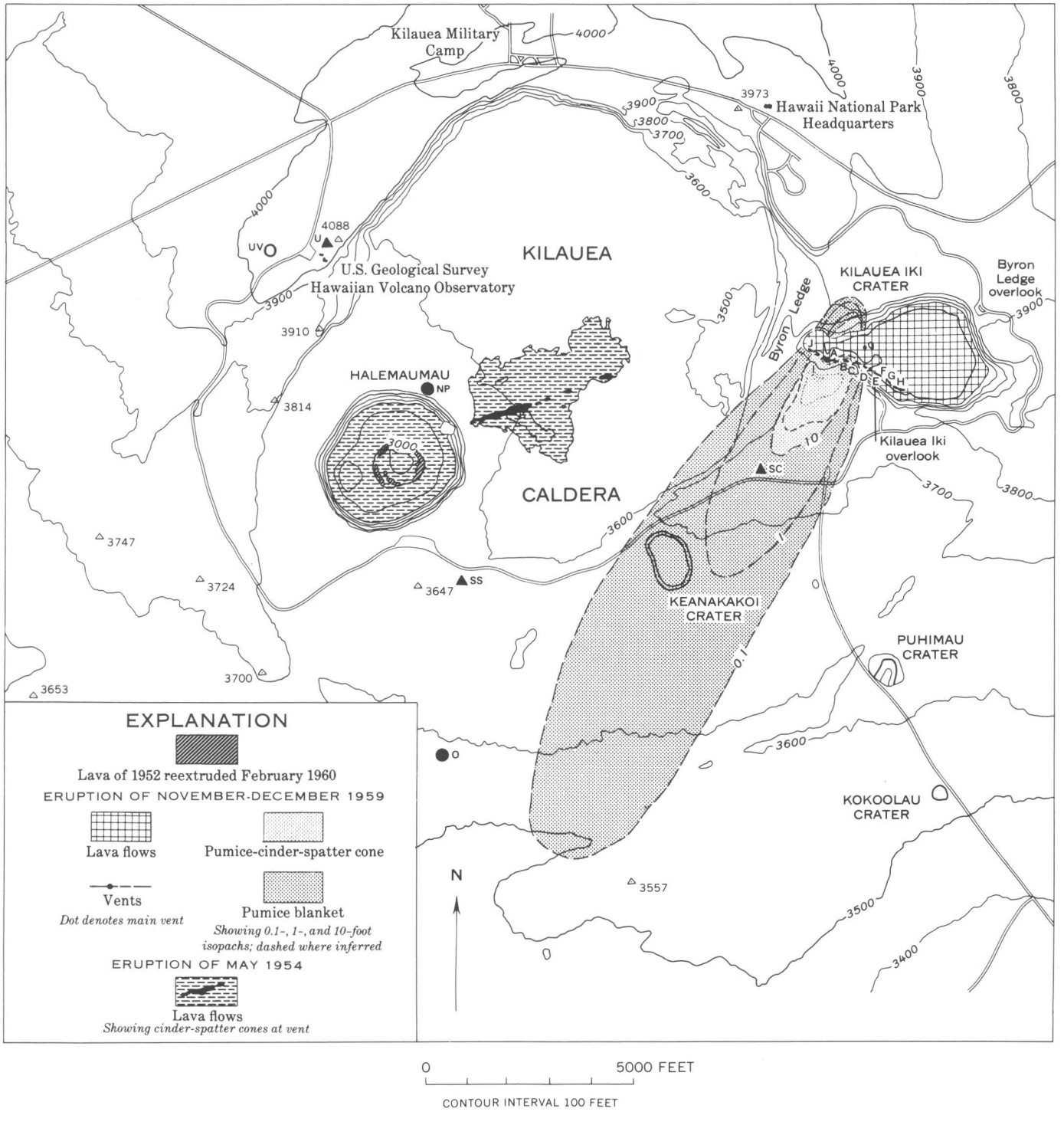

FIGURE 48.13.—Kilauea caldera region, showing relation of 1959 eruption in Kilauea Iki to Kilauea caldera, Halemaumau, east rift zone, and other localities mentioned in text. Modified from Richter and others (1970).

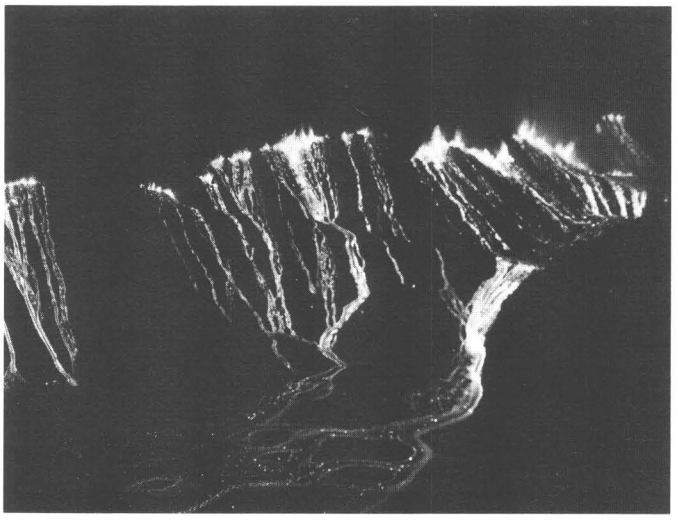

FIGURE 48.14.—Curtain of fire in Kilauea Iki at 2130 on November 14, 1959, 80 min after eruption began, showing maximum development of line of fountains 100 m above floor of crater. View from Byron Ledge overlook.

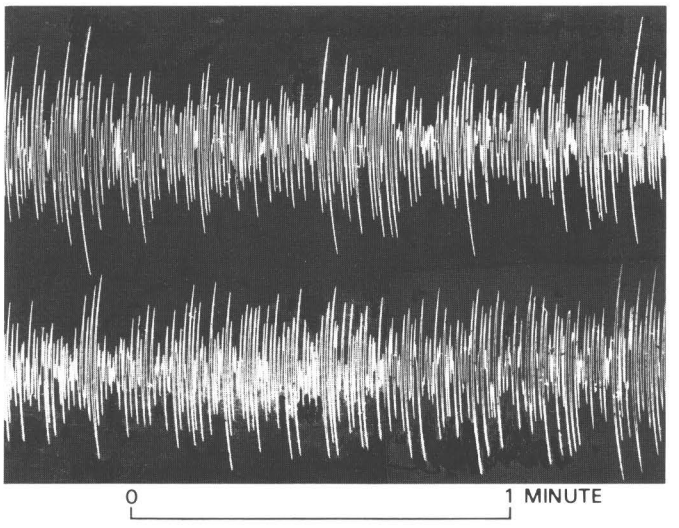

FIGURE 48.16.—Strong harmonic tremor recorded on Outlet seismograph during third phase of the 1959 eruption on November 29.

FIGURE 48.15.—Lava fountain 240 m high at main vent in Kilauea Iki at 0500 on November 19, 1959. Incandescent lava river from fountain is pouring into 50-m-deep lava lake. View from Byron Ledge overlook.

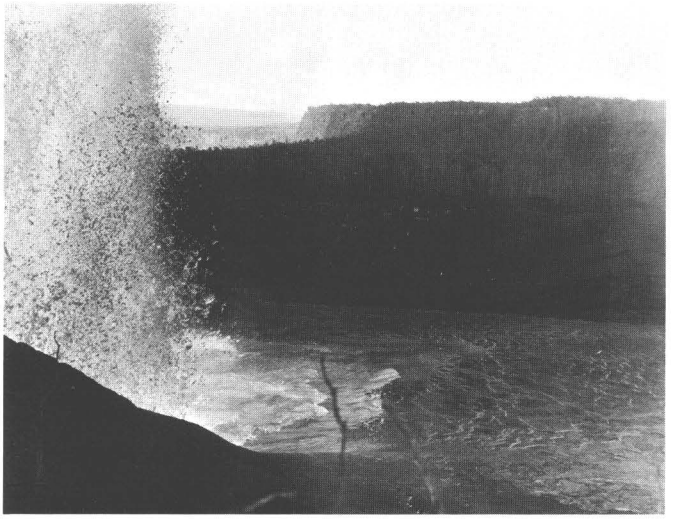

FIGURE 48.17.—Large fountain of phase 10 spurting through edge of lava lake, which has risen above the vent, at 1500 on December 14. Note waves on surface of lake. View from west end of Kilauea Iki overlook.

line resulting from the onset of the eruption would have been masked by the large tilt excursions that immediately preceded the outbreak. Cessation of fountaining was abrupt, however, and a zero-line offset marked the abrupt end of eastward tilting. Withdrawal of lava from the lake was first noticed about 20 h after the fountain died, and the volume of lava that drained back was small. No sharp rebound from eastward to westward tilting was noted at the end of the first phase.

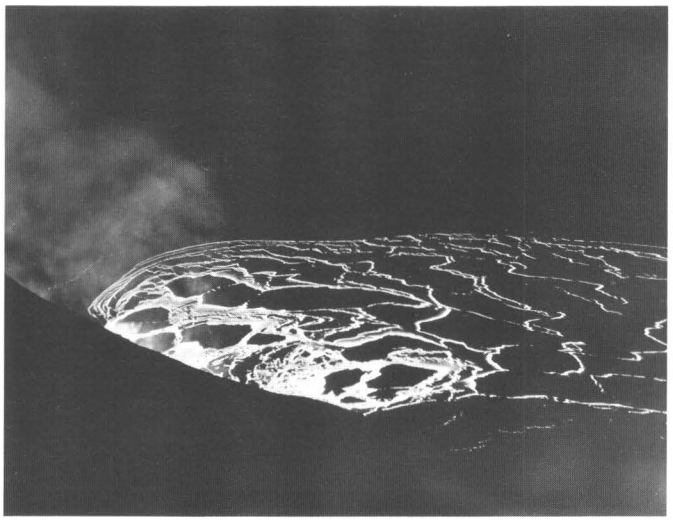

FIGURE 48.18.—Wide stream of lava pouring back into vent at 2200 on December 15, one-half hour after end of phase 12. Huge rafts of solid lake crust, disrupted as backflow stream converges near event, are mixed and swallowed by returning lava. View from top of cone almost directly above vent.

FIGURE 48.20.—Kilauea Iki lava lake on December 20, 1959, after all activity had ceased. The black ledge, 15–60 m wide and about 15 m high, surrounds entire lake surface. View from Byron Ledge overlook. Photograph by R.T. Haugen, National Park Service.

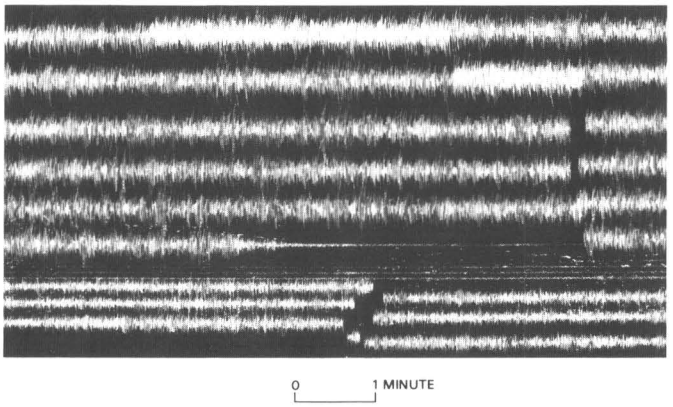

FIGURE 48.19.—Section of Outlet seismogram of December 8, 1959, showing harmonic tremor accompanying phase 7, abrupt dying out of tremor when fountain stopped, and resurgence of tremor during backflow after 50 min of quiet.

For phases 2 and 3, also shown in figure 48.21, the lava-volume changes are small and the east-west tilt changes (both liquid-level and north-south Press-Ewing) are difficult to pick out of the noise. The curves for tremor, fountain height, and rate of east-west tilting (east-west Press-Ewing zero-line offset) are clearly related. At the sharp onset of fountaining, the amplitude of tremor increased suddenly; its amplitude generally followed fountain height throughout each phase. With the onset of fountaining, also, clear eastward tilting began on the east-west rate-of-tilting curve. The shape of the rate-of-tilting curve is similar to those for fountain height and tremor. When the fountain stopped abruptly, tremor amplitude dropped to zero, and the tilt curve reversed rapidly from moderate eastward tilting to strong westward tilting. The reversal in direction of tilting corresponds closely in time to cessation of fountaining and the immediate onset of strong backflow into the vent. The rate of westward tilting was initially several times greater than the rate of eastward tilting just before the fountain died, but it diminished rapidly during the first few minutes of backflow and then more gradually for several hours until it fell below noise level.

With some variations, the remaining phases were similar to phases 2 and 3. Plots of east-west tilt (north-south Press-Ewing) and east-west rate of tilting (east-west Press-Ewing) for phases 4–16 are shown in fig. 48.22. This figure gives a useful overview of tilting for the rest of the 1959 eruption, but the phases were so short that the relationships discussed for the first three phases are not easily seen. From phase 4 onward, east-west rate of tilting and east-west cumulative tilt at Uwekahuna, fountain height, and tremor amplitude at Outlet are plotted against an expanded time scale in figure 48.23 (phase 4), 48.24, (phases 5–7), 48.25 (phases 8 and 9), 48.26 (phases 10–14), and 48.27 (phases 15 and 16). Isolated episodes of tilting and tremor that were unaccompanied by an eruptive phase occurred between phases 4 and 5 (fig. 48.23) and between phases 15 and 16 (fig. 48.27).

To follow the movement of lava from the summit reservoir to the lake and back again to the reservoir, we need good estimates of the total eastward tilting at Uwekahuna during the eruptive stage and of the total westward tilting during the backflow stage. These tilt totals can then be converted to volumes of lava removed or returned to the reservoir by comparison with the ratio of lava-lake volume to eastward tilting at Uwekahuna recorded during the first phase. Such a conversion assumes that all of the phase 1 lava was mined from the

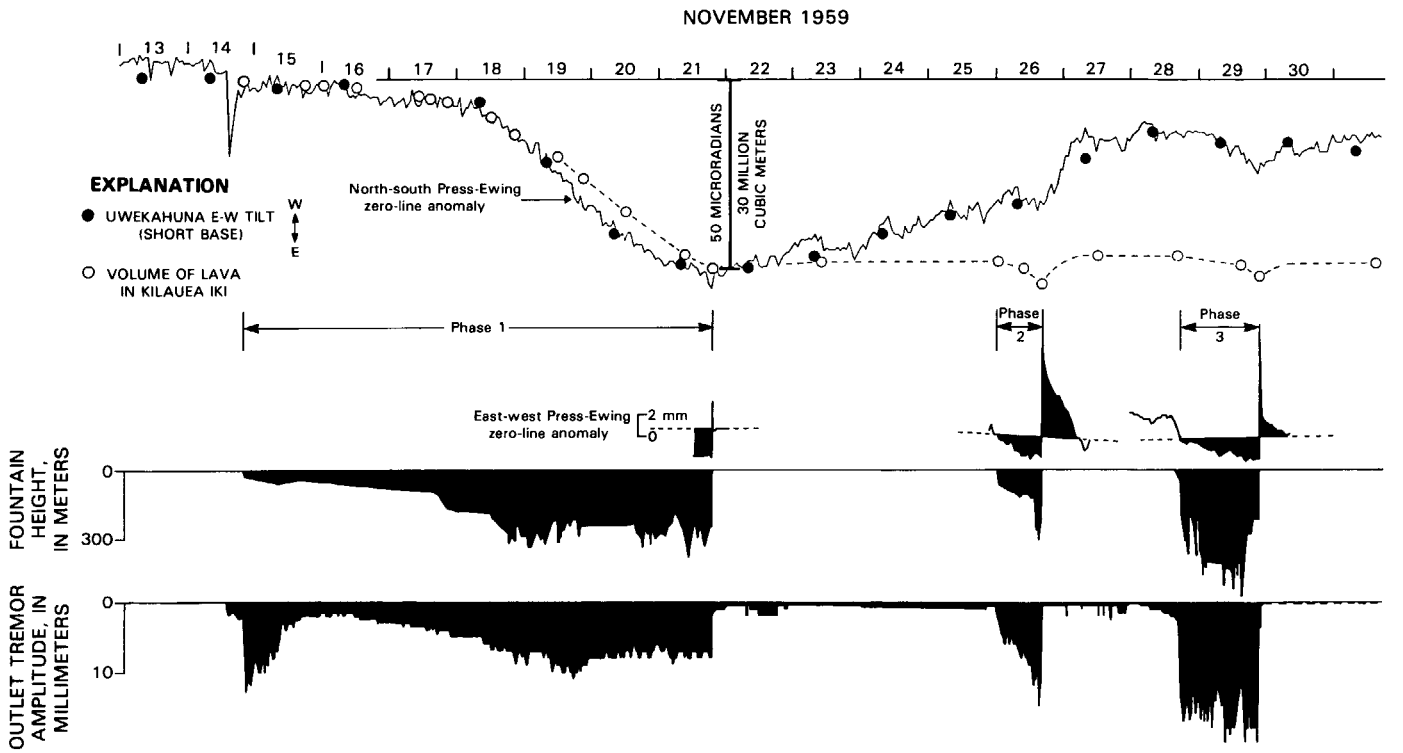

FIGURE 48.21.—Eruption and deformation parameters during first three eruptive phases of 1959 eruption. Volume of lava in Kilauea Iki, east-west component of Uwekahuna liquid-level tiltmeter, and north-south Press-Ewing zero-line anomaly are superposed in upper half of figure; fountain height and tremor amplitude at Outlet station are plotted in lower half. Duration of individual phases indicated.

summit reservoir and that replenishment of the reservoir from the deep source of magma during phase 1 was small compared to the volume of lava erupted. Replenishment during the eruption would lead to the calculated ratio (lava/tilt) being too large. Replenishment would be a less significant factor during very short but voluminous phases, but the estimation of the volume of lava poured into the lake during the later (smaller) phases is relatively less accurate than for the first (larger) phase. The ratio of lava volume to cumulative tilt for phase 1 so calculated is 0.6×10^6 m^3 per microradian of eastward tilting at Uwekahuna.

An independent estimate of the ratio of the volume of lava removed from the summit reservoir to the change in tilt on the east-west liquid-level tiltmeter at Uwekahuna can be obtained from the summit collapse that accompanied the 1960 flank eruption at Kapoho (fig. 48.4). During the actual outpouring of the estimated 0.12×10^9 m^3 of lava near Kapoho between January 13 and February 6, the east-west liquid level tiltmeter measured an eastward tilt of 188 μrad, yielding a ratio of 0.65×10^6 m^3/μrad. The eastward tilting at Uwekahuna did not stop abruptly when the eruption ended but continued until March 10, when the total eastward tilt since January 13 reached 268 μrad, yielding a ratio of 0.45×10^6 m^3/μrad. Considering the possibility of adding lava to, or withdrawing lava from, storage in the east rift zone itself, the range of values 0.45×10^6–0.65×10^6 m^3/μrad for the 1960 eruption is in good agreement with the value 0.6×10^6 m^3/μrad determined from phase 1 of the Kilauea Iki eruption.

To determine the cumulative tilt at Uwekahuna for the eruption and backflow stages of the short later phases, we must depend on the Press-Ewing records. The background noise levels on the north-south and east-west traces are comparable, but the east-west rate-of-tilt signal on the east-west component is much larger than the signal for cumulative east-west tilt on the north-south component; and it appears that the best estimates of cumulative tilting can be obtained by integration of the rate-of-tilt curves. These curves were initially plotted on millimeter cross-section paper, so the integration was performed simply by determining the areas (counting squares) under the rate-of-tilt curves. In some cases uncertainty in the choice of a zero line for the rate-of-tilt curves was a problem. Coupled with the zero-line problem is the fact that rates of backflow less than 0.1×10^6 m^3/h would probably not be above noise level on the rate of tilt curve.

The two principal means of measuring east-west tilt changes at Uwekahuna, the liquid-level tiltmeter and the integrated east-west Press-Ewing zero-line anomaly, are complementary. With only one measurement per day the liquid-level tiltmeter cannot follow the details of short tilting episodes, but it maintains an absolute record of daily changes. The east-west Press-Ewing zero-line anomaly is measured as a deviation from a zero-line reference that is keyed to

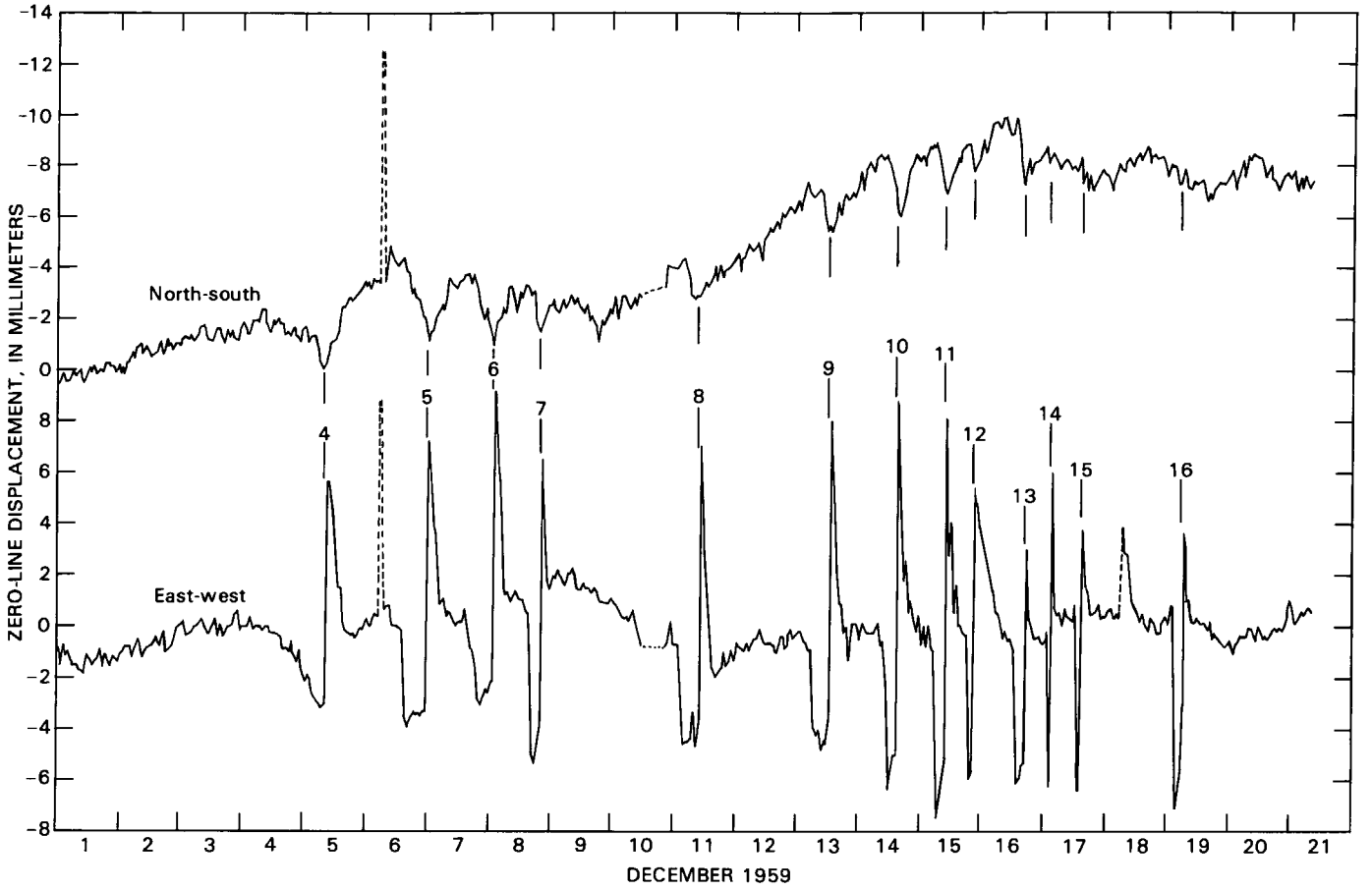

FIGURE 48.22.—Zero-line anomalies from north-south and east-west Press-Ewing seismographs accompanying phases 4–16. Numbers identify ends of individual eruptive phases as shown by abrupt reversals in the east-west zero-line anomaly curve.

what is considered the normal record before and after relatively short anomalous episodes. Thus, it maintains a sensitive record of changes during short episodes of tilting but is blind to slower, underlying, persistent changes like those that can be detected by the liquid-level tiltmeter.

The estimated volumes of lava removed from the summit reservoir during eruptive stages and returned during ensuing backflow stages are compared (table 48.2) with, respectively, the volumes of lava poured into Kilauea Iki and then withdrawn during the principal phases of the eruption. The volume estimates for the summit reservoir were obtained by multiplying the integrated east-west rate of tilt by 0.6×10^6 m^3/μrad.

Use of this ratio of 0.6×10^6 m^3/μrad (volume of lava erupted during phase 1 divided by tilt change measured on the east-west liquid-level tiltmeter) to convert tilt changes determined from the east-west Press-Ewing zero-line anomaly to equivalent volumes of reservoir lava requires some justification. This justification proceeds in two steps. First, the east-west tilt changes detected by the north-south component Press-Ewing were scaled directly to the east-west tilt changes recorded by the liquid-level tiltmeter during phase 1. Second, the sum of eastward tilt during the fountaining stages of phases 4–16 measured by the north-south Press-Ewing (94.6 μrad) is almost exactly the same as that determined by integration of the east-west Press-Ewing zero-line anomaly (95.1 μrad). The comparison was made on the summed response to phases 4–16 because the Press-Ewing tilt measurements are much more certain for these phases than for phases 1–3.

The curves for fountain height, tremor amplitude at Outlet, and rate of eastward tilting at Uwekahuna were similar in shape during actual outpouring of lava (figs. 48.23–48.27). When fountaining ceased, tremor amplitude abruptly diminished nearly to zero, and eastward tilting abruptly reversed to westward tilting. Cumulative eastward tilt increased steadily during outpouring of lava. When fountaining ceased, brief sharp transients were recorded on both the north-south and east-west Press-Ewings instruments. On the east-west component this transient was a westward pulse of tilting superposed on the crest of the newly reversed tilt curve. On the north-south component it was a sharp northward pulse of tilt (detected by the seismometer, not the galvanometer). After the fountain died in phases 4, 5, and 9, tremor amplitude remained very

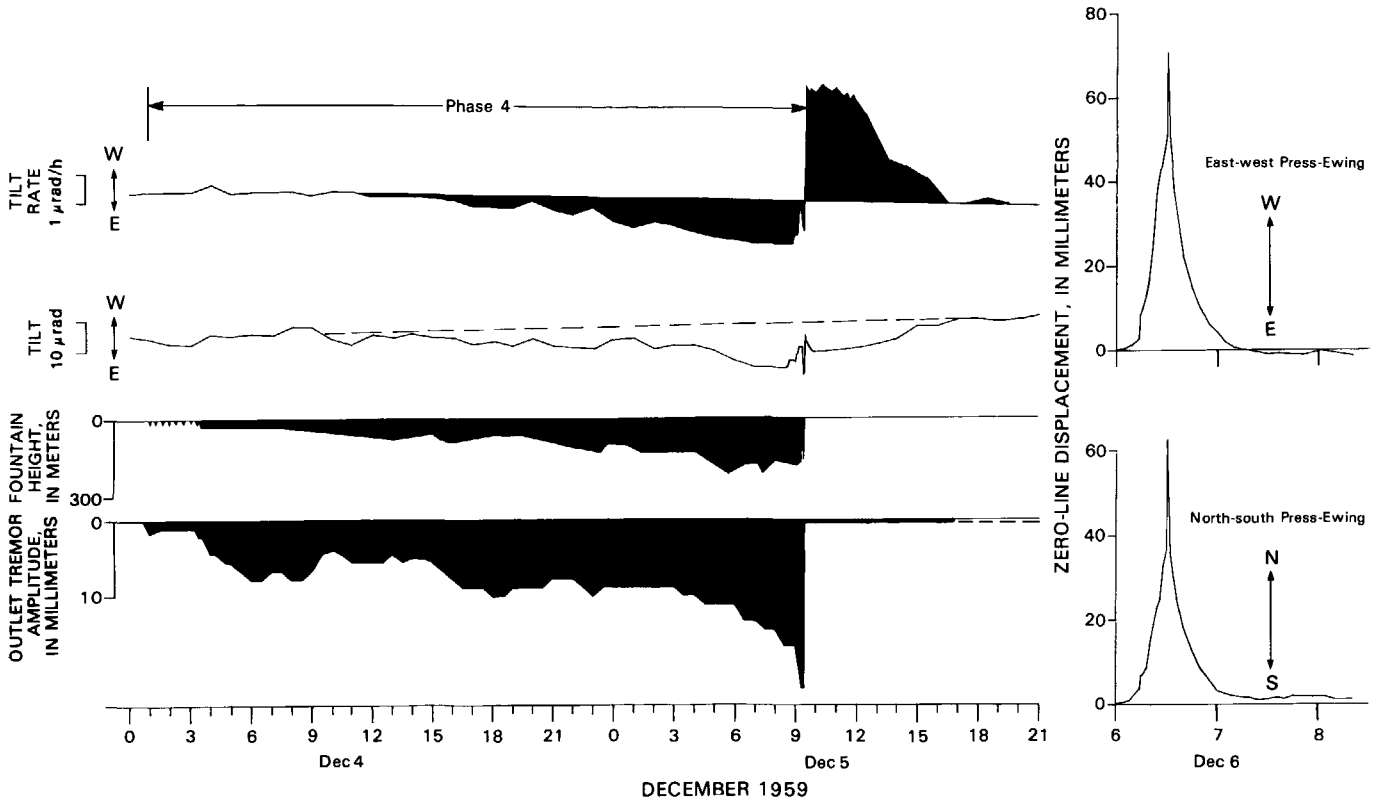

FIGURE 48.23.—East-west rate of tilting, east-west cumulative tilt, fountain height, and Outlet tremor amplitude for phase 4 and for the short but strong tilt excursion between phases 4 and 5.

low for many hours, and the westward tilting accompanying backflow declined steadily from its maximum to the noise level without large offsets or oscillations. Lava backflow rates were large, particularly at the beginning of the backflow stages, when they commonly exceeded the maximum rate of extrusion of lava during the eruptive stage they followed. Yet this rapid backflow was not accompanied by significant tremor. For phases 6–16 (omitting 9) the relationship between westward tilting and tremor was more complex, and it changed with time. After the fountain died and the amplitude of tremor at Outlet decreased abruptly, the tremor revived again after an interval of time that varied from phase to phase: phase 6, 2.5 h; phase 7, 50 min; phase 8, 35 min; phase 10, 1.5 h; phase 11, 50 min; phase 13, 20 min; phases 12, 14, 15, and 16, almost immediately. The renewed onset of tremor (resurgent tremor) was accompanied by a sharp drop in the rate of westward tilting and, presumably, the rate of reinflation of the summit reservoir.

The tremor and east-west rate-of-tilt curves for phases 10 and 11 were unusually complex. After the first resurgence of tremor, the tremor again died out and returned several times, accompanied by matching oscillations in the east-west rate-of-tilt curve. For phase 10, the first three episodes of tremor following cessation of fountaining were accompanied by sharp decreases in the reinflation of the reservoir (westward tilting). but later ones correlated with small increases in the rate of westward tilting. For phase 11 only the first interval of resurgent tremor was accompanied by a sharp drop in reinflation of the summit. Two prominent later episodes of tremor accompanied sharp increases in the rate of westward tilting.

The episode of tremor and tilting unaccompanied by an eruption (phase 15+, table 42.2) between phases 15 and 16 reveals another aspect of the relationship between tremor and tilting. Moderate fluctuating tremor that began abruptly at about 0600 on December 18 was accompanied by matching changes in the east-west rate-of-tilt curve (peaks in the tremor curve correlating with peaks of westward tilting). This behavior lasted for about 3 h. A large increase in tremor amplitude at about 0900 was accompanied by a large increase in rate of westward tilting. Tremor amplitude and westward tilting returned slowly to normal during the next 9 hours. The relationship between tremor and tilting during this episode is the same as that during the later parts of the phases 10 and 11 drainback, but it is opposite to that for the first interval of resurgent tremor for the 10 phases with significant resurgent tremor.

Another episode of very rapid tilting unaccompanied by an eruption took place on December 6 after phase 4. A rapid northwestward excursion began at about 0600. It peaked at 0631 with maximum rates of 26 μrad/h west and 24 μrad/h north, and it had died out by 0715. The net tilting toward the north and west was

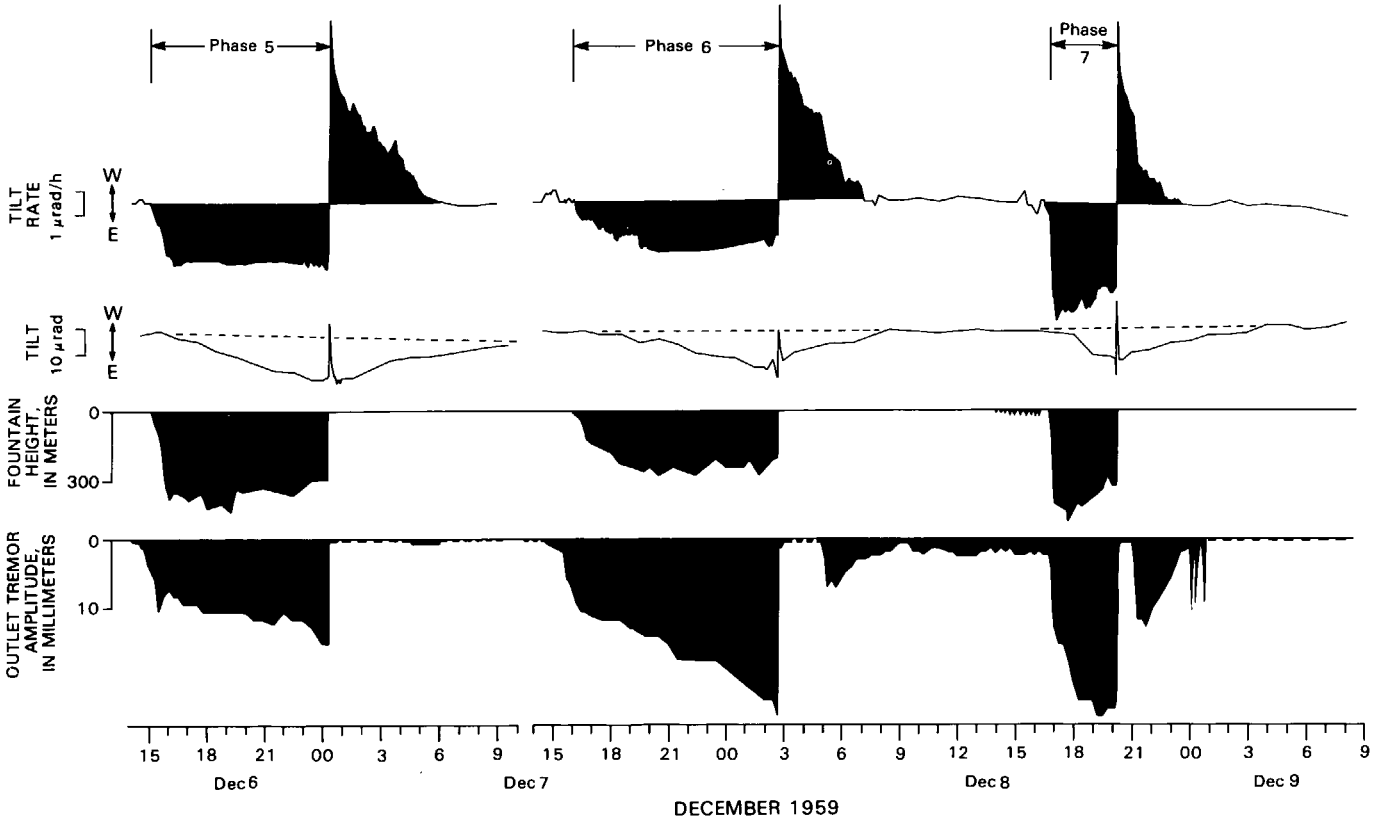

FIGURE 48.24.—East-west rate of tilting, east-west cumulative tilt, fountain height, and Outlet tremor amplitude for phases 5–7.

about 6.6 μrad and 4.8 μrad, respectively. The direction to the center of inflation from Uwekahuna was about az 126°. This azimuth is the same as that for the transient pulses that followed cessation of fountaining in the later phases. Tremor at Outlet remained low during this tilting episode, which was accompanied by a sequence of small earthquakes. At North Pit, inside Kilauea caldera, tremor was strong, and the earthquakes were more numerous and much larger (5–10 times larger amplitude) than at Outlet.

To provide a quantitative basis for discussing the movement of lava at the summit of Kilauea during the 1959 eruption, we have reduced the observations on tilting at Uwekahuna and the corresponding eruption and backflow of lava at Kilauea to tabular form (table 48.2). The state of tilt at the beginning of each eruptive phase (from the Uwekahuna east-west liquid-level tiltmeter) and changes in the east-west component of tilt measured from the Press-Ewing zero-line drift during the deflation and inflation of the summit reservoir that accompanied the eruptive and backflow stages of each phase are shown in columns 2–5. These tilt data are converted to reservoir volume changes and listed in columns 6–8 for comparison with the volumes of lava erupted into Kilauea Iki lava lake (column 9) and then withdrawn from it (column 10).

The best overall summary of the lava budget in the summit reservoir is shown in column 6 of table 48.2, where the volume of lava in the reservoir at the beginning of each phase is compared with that at the end of phase 1 fountaining. At the outbreak of phase 1 the reservoir contained the 30×10^6 m^3 that was poured into the lake during phase 1. Refilling of the reservoir began promptly at the end of phase 1, and it had regained 10.4×10^6 m^3 and 22×10^6 m^3 by the beginning of phases 2 and 3, respectively. At the beginning of phase 4, the entire 30×10^6 m^3 withdrawn during phase 1 had been replenished, presumably by new lava entering the system from below. The reservoir continued to fill steadily, but at a slower rate, until the beginning of phase 8, when at 40.4×10^6 m^3 it had exceeded the phase 1 outbreak level by 9.8×10^6 m^3. The volume of lava in the reservoir at the beginning of subsequent phases fluctuated from a low of 38.5×10^6 m^3 (phases 9 and 15) to a high of 42.8×10^6 m^3 (phases 12 and 14), and at the end of the summit eruption it stood at 40×10^6 m^3.

Net changes in the reservoir volume during deflation (table 48.2, column 7) and inflation (column 8) can be compared with the corresponding volumes of lava erupted into the lake (column 9) and withdrawn from it (column 10). Net changes in the volume of lava in

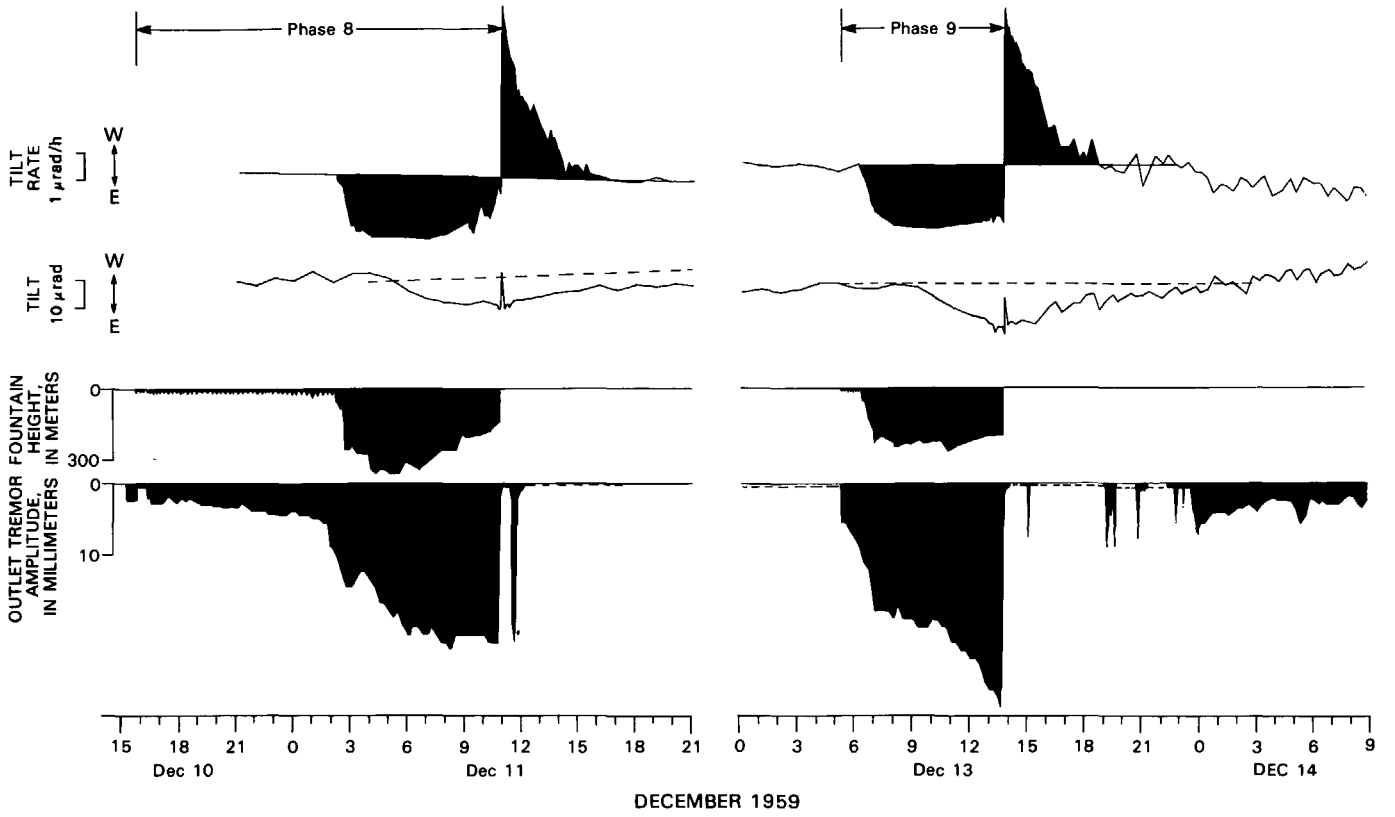

FIGURE 48.25.—East-west rate of tilting, east-west cumulative tilt, fountain height, and Outlet tremor for phases 8 and 9.

the lake-reservoir system during the eruptive stage, during the backflow stage, and during the entirety of each phase can be compared in columns 11, 12, and 13 of table 48.2, respectively. The changes measured during phases 2 and 3 are only poorly determined because of difficulties in establishing appropriate zero-line references for the east-west Press-Ewing instrument. There was a substantial increase in system volume during the first stage of phase 4 and significant increases also during phases 6, 10, and 12. There were substantial losses from the system during phases 7, 8, 9, and 15, principally during the backflow stage. There was a significant loss from the system during phase 13. During phases 5, 11, 14, and 16 the volume of the system showed little change. Phases with large system losses correlate with an overfilled summit reservoir (from phase 7 on), as do the most marked occurrences of resurgent tremor and associated irregularities in the curves of reservoir reinflation during backflow.

PROPOSED MODEL FOR THE 1959 ERUPTION

On the basis of the data on deformation at the summit of Kilauea and on lava eruption and withdrawal at Kilauea Iki during the 1959 eruption, we have constructed a model to explain the principal mechanical features of the eruption. The model is similar to one proposed by Helz (chapter 25) to explain the characteristics of olivine observed in samples collected at various stages of the eruption and in the lava lake. It is broadly based on the model of the Kilauea plumbing system deduced by Eaton and Murata (1960) and Eaton (1962) from the deformation of the Kilauea summit before, during, and after the 1959–60 eruption of Kilauea.

Following the summit collapse associated with the 1955 east-rift eruption, the Kilauea summit reservoir was slowly refilled by magma moving upward from the source zone 40–60 km deep beneath Kilauea. By early November 1959 the reservoir was sufficiently overpressured that a dike from the reservoir split upward through the enclosing rock and reached the surface inside Kilauea Iki Crater. All of the lava (except cinder and pumice blown away by the wind) accumulated inside the crater.

The initial overpressure required to open the dike to the surface sustained the early part of the first phase of the eruption, when lava flowed upward through the dikelike vent propped open by pressure of the lava. Rapid flow of lava through a section of the dike that was locally wider than average enlarged that section of the dike, forming the stable conduit leading to the main fountain and permitting the rest of the dike to close, either by freezing or because of a drop in the pressure of the lava in the dike. Less constricted passage of lava through the enlarging main-vent conduit relieved the confining pres-

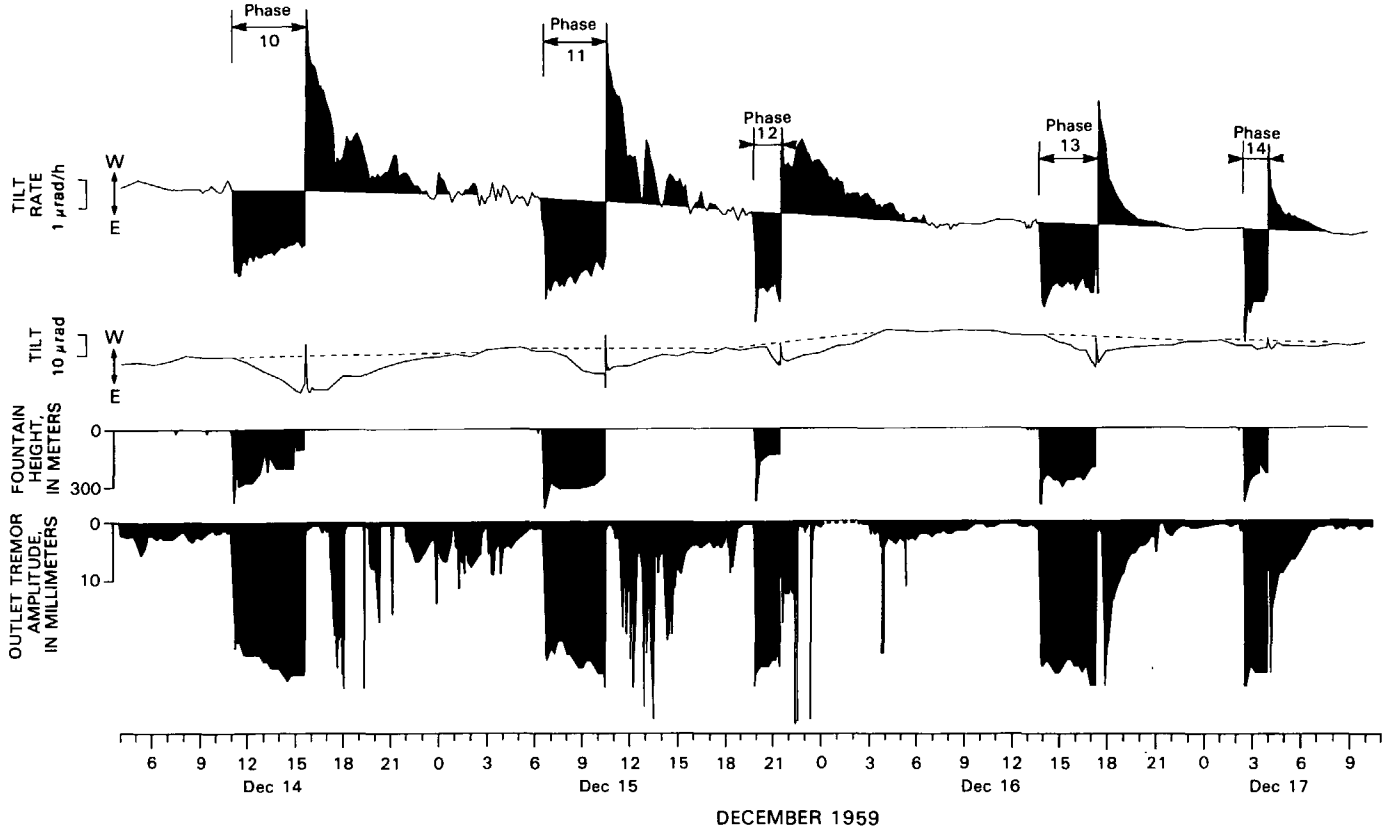

FIGURE 48.26.—East-west rate of tilting, east-west cumulative tilt, fountain height, and Outlet tremor amplitude for phases 10–14.

sure on the rising lava to increasingly greater depths in the conduit, permitting vesiculation and the consequent reduction in the density and viscosity of the lava-gas mixture in the conduit to penetrate to greater depths. This process reduced the average density of the column of lava in the conduit between the reservoir and the vent sufficiently that lava continued to be pumped from the reservoir to the lake even after the reservoir pressure had dropped below the level required to sustain outflow in an unvesiculated conduit. By this process a large volume of lava stored in the reservoir was pumped rapidly to the surface, where it accumulated in Kilauea Iki Crater. When the lava in Kilauea Iki rose significantly above the vent, heavy, degassed lake lava found entry to the conduit, possibly through another opening beside or below the fountaining vent. This inert, heavier lava sufficiently moderated the pumping action of vesiculation in the conduit to cut off the flow of ascending lava entirely, and fountaining stopped abruptly.

During most of phase 1, the rate of inflow of magma to the reservoir remained low. The large drop in reservoir pressure resulting from the rapid transfer of lava from the reservoir to the lake during the last few days of phase 1 led to a substantial increase in the hydraulic potential between the deep supply system and the reservoir, and the rate of inflow from depth therefore increased sharply late in phase 1.

The reservoir began to refill rapidly, and soon the reservoir pressure was again sufficient to raise the lava column, now partially degassed, to the vent in Kilauea Iki. This time overpressure such as required to drive a new dike to the surface was not needed. The flood of new hot magma entering the reservoir from below not only reinflated it but also introduced a supply of gas-rich lava that could help to sustain the vesiculation pump for lifting lava to the lake. The cycle of overfilling the lake, leading to a reversal of the density pump in the conduit, was repeated during phase 2. At the end of phase 2, either because the lake was sufficiently above the vent or because access of lake lava to the conduit was sufficiently less restricted (or both), a substantial volume of degassed lake lava flowed back down the conduit to further reinflate the reservoir. The same pattern was repeated during the subsequent phases of the eruption.

Refilling of the reservoir continued at a rate that was proportional to the hydraulic potential difference between the source at depth and the summit reservoir. As the reservoir was reinflated this potential difference decreased, and so did the rate of lava rising into the reservoir. When the reservoir was refilled to and beyond its state at the outbreak of phase 1, the enclosing rocks were again stressed to near their limits. During the rapid backflow following the later phases, the sudden sharp increase in reservoir pressure induced by the returning lava appears to have opened a temporary passageway,

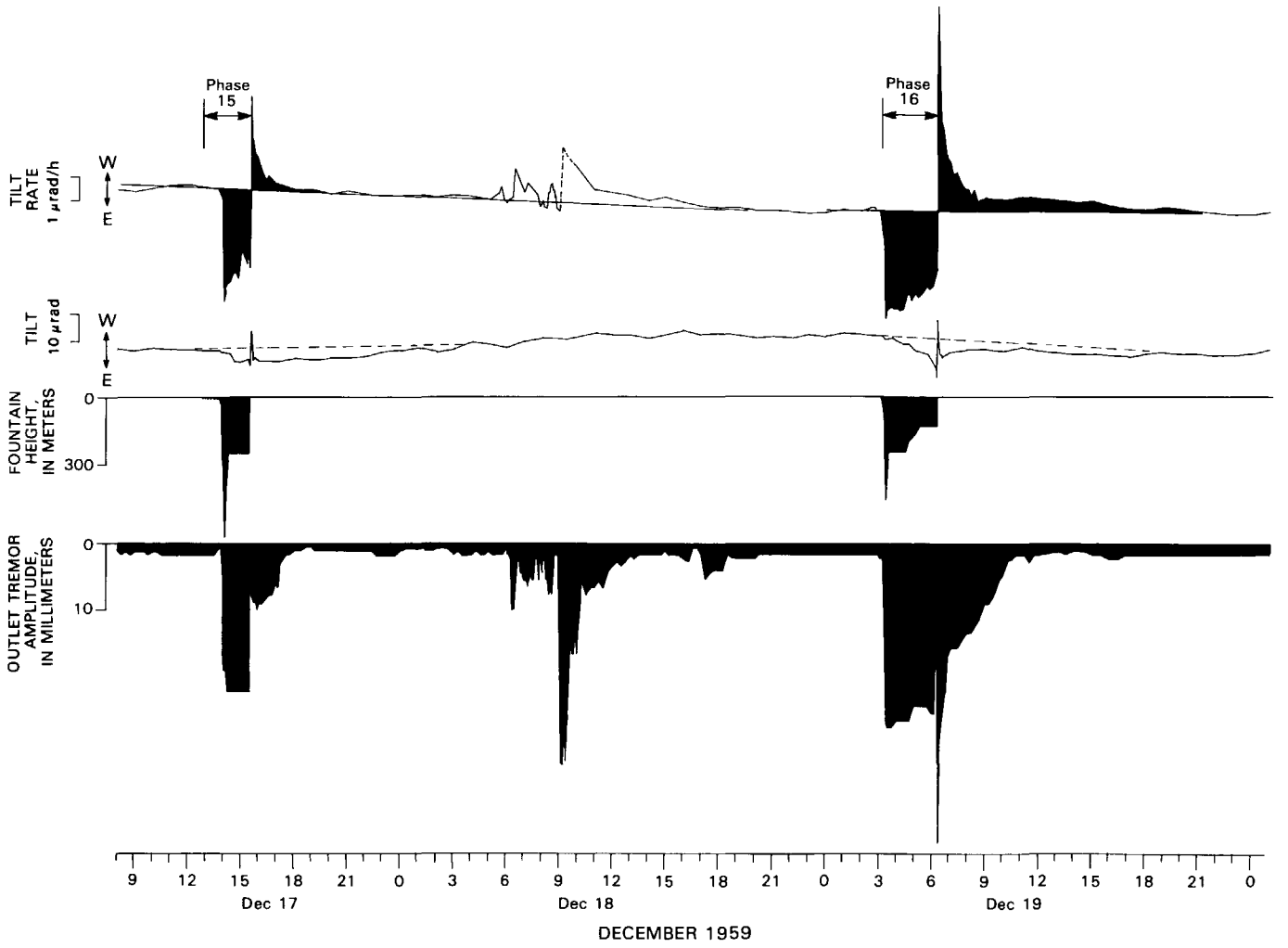

FIGURE 48.27.—East-west rate of tilting, east-west cumulative tilt, fountain height, and Outlet tremor amplitudes for phases 15 and 16 and for episode of tilting and tremor between them.

probably a dikelike zone propped open by excess reservoir pressure, and to have driven some reservoir lava into a nearby zone with lower hydraulic potential, possibly the fluid core of the upper end of the east rift zone.

A summary of the movement of lava into the summit reservoir from depth and out of the summit reservoir into Kilauea Iki lava lake and the east rift zone(?) is given in figure 48.28. The primary withdrawal of lava from the summit reservoir was the 30×10^6 m^3 erupted during the first phase. The outbreak of the eruption depended on the reservoir being overpressured by new lava entering from below. This new, more primitive material may have been included in the initial outbreak, only to be swamped later in phase 1 by larger volumes of lava withdrawn from reservoir storage, as suggested by Helz (chapter 25). The principal system response to the initial deflation of the reservoir was a (somewhat delayed) massive influx of new lava from depth to refill the reservoir, where it presumably was available to mix with lava still retained by the reservoir. Ongoing recharge of the reservoir repeatedly brought the summit reservoir-lava lake system back to a condition that essentially led to a restaging of the last part of the phase 1 eruption: the original conduit and the same vesiculation-pump mechanism that operated during the later part of the phase 1 eruption were utilized over and over again.

Lava draining back from the lake during the early phases was recaptured entirely by the reservoir. During the later phases, however, the reservoir was so full that it could not retain both the new lava that had entered it from below since the last phase and the batch of lava suddenly returned from the lake. Some fraction of the

TABLE 48.2.—*Record of ground tilt at Uwekahuna and volumes of lava erupted into and withdrawn from Kilauea Iki lava lake during the 16 principal phases of the 1959 eruption*

[Data in column 2 from liquid-level tiltmeter; data in column 3 from north-south Press-Ewing instrument; data in columns 4–5 and 7–8 from integrated east-west Press-Ewing instrument; data in column 6 derived from east-west liquid-level tilmeter data; data in columns 2 and 6 are relative to end of phase 1 fountaining]

	Tilt (μrad)				Lava volume (10^6 m^3)					Volume gain or loss (10^6 m^3)		
Phase	E-W at start of phase	Deflation episode (eastward)		Inflation episode (westward)	Reservoir storage relative end phase 1	Deflation episode	Inflation episode	Erupted into lake	Drainback from lake	First stage of phases (9–7)	Second stage of phases (8–10)	Entire phase
1	2	3	4	5	6	7	8	9	10	11	12	13
1	50	50	--	--	30.6	--	--	30.6	1.1	--	--	(−1.1)
2	17	5.5	4.5	21.5	10.4	2.8	13.1	3.6	4.5	+0.8	+8.6	+9.5
3	36	8.1	14.0	4.7	22.0	8.6	2.8	3.2	2.0	−5.4	+.8	−4.5
4	50	9.6	10.2	10.2	30.6	6.3	6.3	11.5	6.3	+5.2	.0	+5.2
5	55	10.0	9.7	7.6	33.6	6.0	4.7	6.5	4.7	+.5	.0	+.5
6	55	8.5	9.4	7.5	33.6	5.7	4.6	6.6	3.8	+.8	+.8	+1.6
7	59	6.7	7.3	3.4	36.1	4.4	2.1	3.7	5.6	−.7	−3.5	−4.2
8	66	7.0	10.2	6.0	40.4	6.2	3.7	6.7	6.0	.0	−2.3	−2.3
9	63	10.4	9.3	6.5	38.5	5.7	4.0	5.7	6.9	.0	−2.9	−2.9
10	67	9.6	8.2	9.9	41.0	5.0	6.0	6.3	4.9	+1.3	+1.1	+2.4
11	65	7.0	8.5	6.8	39.8	5.2	4.1	4.7	4.1	−.5	.0	−.5
12	70	4.8	3.4	7.8	42.8	2.1	4.7	2.2	3.1	+.1	+1.6	+1.8
13	70	8.1	6.4	3.0	42.8	3.9	1.8	3.2	2.4	−.7	−.6	−1.3
14	68	2.2	3.0	1.6	41.6	1.8	1.0	1.8	1.0	.0	.0	.0
15	63	3.3	3.1	1.1	38.5	1.9	.7	1.7	3.2	−.2	−2.5	−2.8
16	64	7.4	6.4	5.6	39.1	3.9	3.4	4.1	4.1	+.2	−.7	−.5
End	65											
[1]15+	63	--	--	3.9	38.5	--	2.4	--	--	--	2.4	+2.4

[1]Episode of reservoir inflation without eruption between phases 15 and 16.

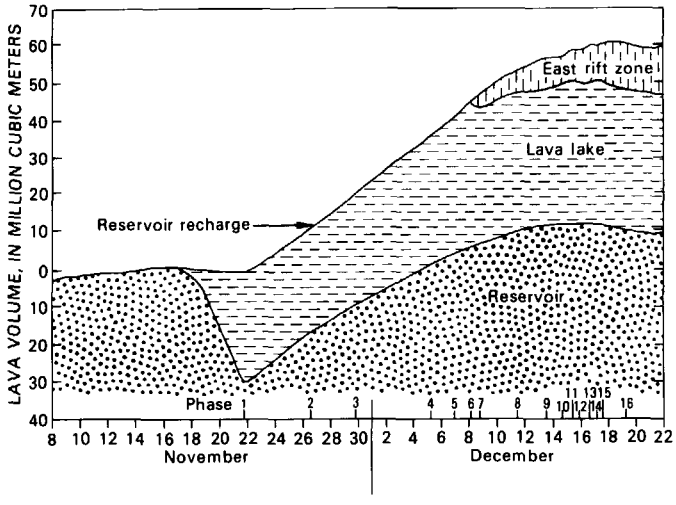

FIGURE 48.28.—Partitioning of lava that was in summit reservoir on November 14 and lava that subsequently recharged it from below between summit reservoir, lava lake, and loss from the reservoir-lake system (to east rift zone?).

returning lava, or a corresponding volume of lava already in the reservoir, was then expelled into the east rift zone (during an episode of resurgent tremor) from the reservoir.

The total volume of lava added to and retained within the summit reservoir after the end of phase 1 fountaining was 40×10^6 m^3. From the gain-loss figures for the individual phases in table 48.1 it appears that some 12×10^6 m^3 of additional lava was added to the reservoir from depth but was then expelled from it during late-phase backflow episodes. An additional 8×10^6 m^3 from the reservoir was added to the lake after phase 1. In summary, it appears that the volume of new lava entering the reservoir after the end of phase 1 was about 60×10^6 m^3, of which 40×10^6 m^3 remained in the reservoir, 8×10^6 m^3 had been transferred to the lava lake, and 12×10^6 m^3 had been driven out of the reservoir, possibly into the east rift zone, by the end of the eruption. Repeated cycling of lava between the reservoir and the lake, with the accompanying turbulence in the upper part of the lava conduit and the fountain, should have been a very effective means of homogenizing the contents of the reservoir. Such cycling of lava also explains the fate of the 63×10^6 m^3 total volume of lava that drained out of the lava lake during the entire eruption.

RATE OF ERUPTION, FOUNTAIN HEIGHT, AND TREMOR AMPLITUDE

Observations of harmonic tremor generated during various stages of lava outbreak, fountaining, and backflow from the lava lake provide a basis for an analysis of tremor amplitude as a possible function of fountain height, rate of eruption, state of recharge of the summit reservoir, and temperature of the erupting lava (the latter determined by Helz, chapter 25, from glass composition near olivine phenocrysts in air-quenched pumice samples collected during the eruption). The relations among the foregoing parameters are not simple, and they appear to have evolved during the eruption as a whole as well as during the first phase itself. Outlet tremor amplitude, rate of eruption, fountain height, and lava temperature are plotted in figure 48.29*A* versus time for phase 1. In figure 48.29*B*, summit reservoir recharge, Outlet tremor amplitude, rate of eruption, fountain height, and lava temperature are plotted versus eruption phase number. The intensity of eruption changed with time

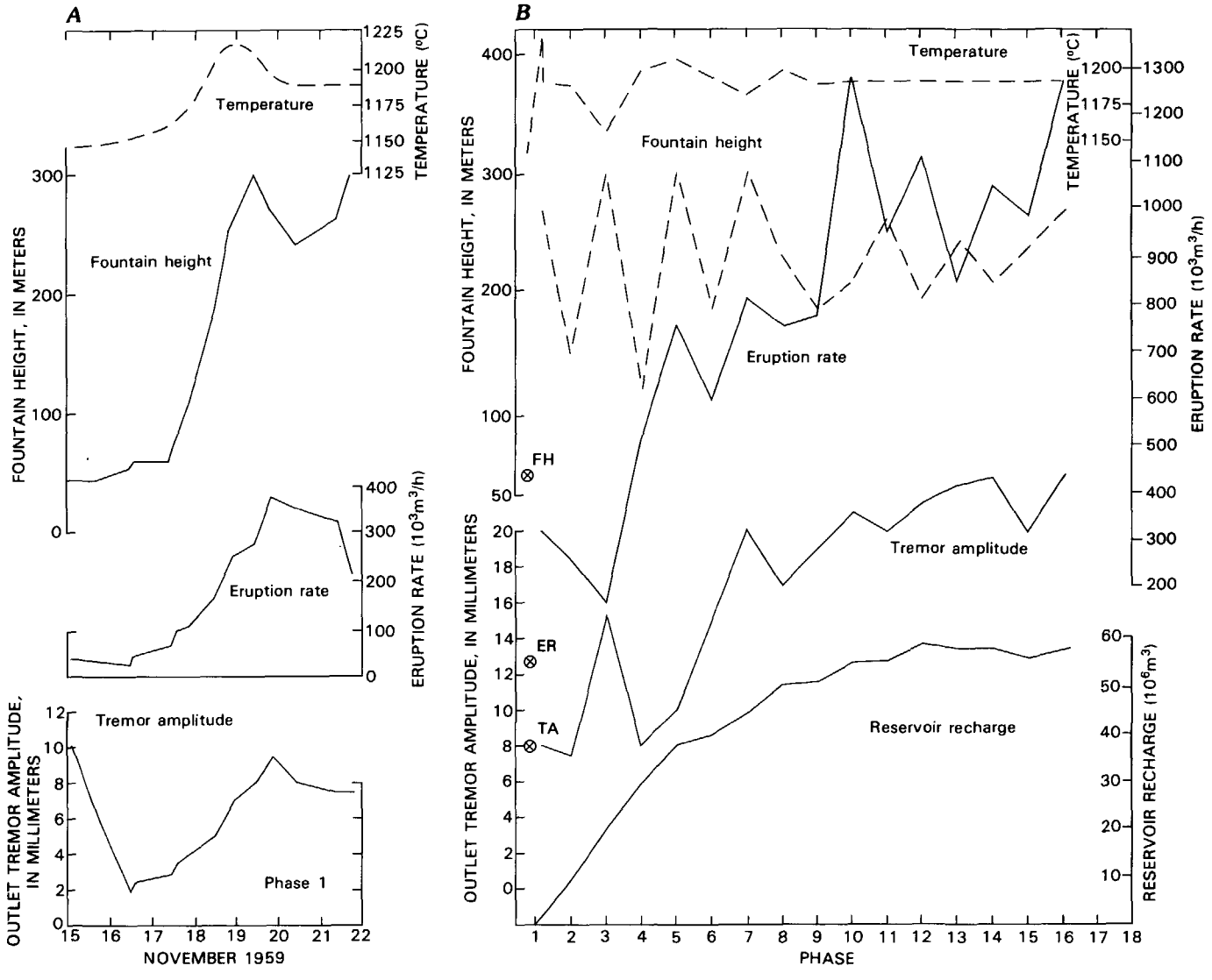

FIGURE 48.29.—Variation of eruption parameters during course of the 1959 Kilauea eruption. ***A***, Tremor amplitude, eruption rate, fountain height, and lava temperature plotted against time for phase 1. ***B***, Reservoir recharge, tremor amplitude, rate of eruption, fountain height, and lava temperature plotted against phase number for phases 1–16. Points for fountain height, eruption rate, and tremor amplitude for the first day of phase 1 are labeled FH, ER, and TA, respectively.

during several phases in addition to phase 1. In order to prepare the simplified plot of parameters versus phase number, values were selected from the parts of phases that seemed best to characterize the phase as a whole. The data plotted in figures 48.29 and 48.30 are also shown in tables 48.3 and 48.4, respectively.

The first few days of phase 1 were very different from the rest of that phase, so two sets of values are plotted. The first set represents the first day; the second set represents the last three days of the fully developed phase 1 eruption. Although tremor amplitude was similar (6–10 mm in the first, 8.5 mm in the second), the contrast between the two sets in other parameters is extreme: 34×10^3 m^3/h eruption rate, 45-m-high fountain, and 1,145 °C lava temperature for the first versus 340×10^3 m^3/h eruption rate, 300-m-high fountain, and 1,185–1,215 °C lava temperature for the second. The tremor amplitude remained virtually unchanged despite 7-fold and 10-fold increases in fountain height and rate of eruption, respectively.

During the first few hours of the eruption, lava streamed to the surface through the long thin dike, probably held open by the pressure of the lava, that was opened in response to overfilling the reservoir. Pressure variations in the moving lava interacted with the elastic walls and with lava velocity in the dike and rhythmically distended and contracted the dike as lava moved unsteadily through it. Such a structure is very efficient for generating tremor because of

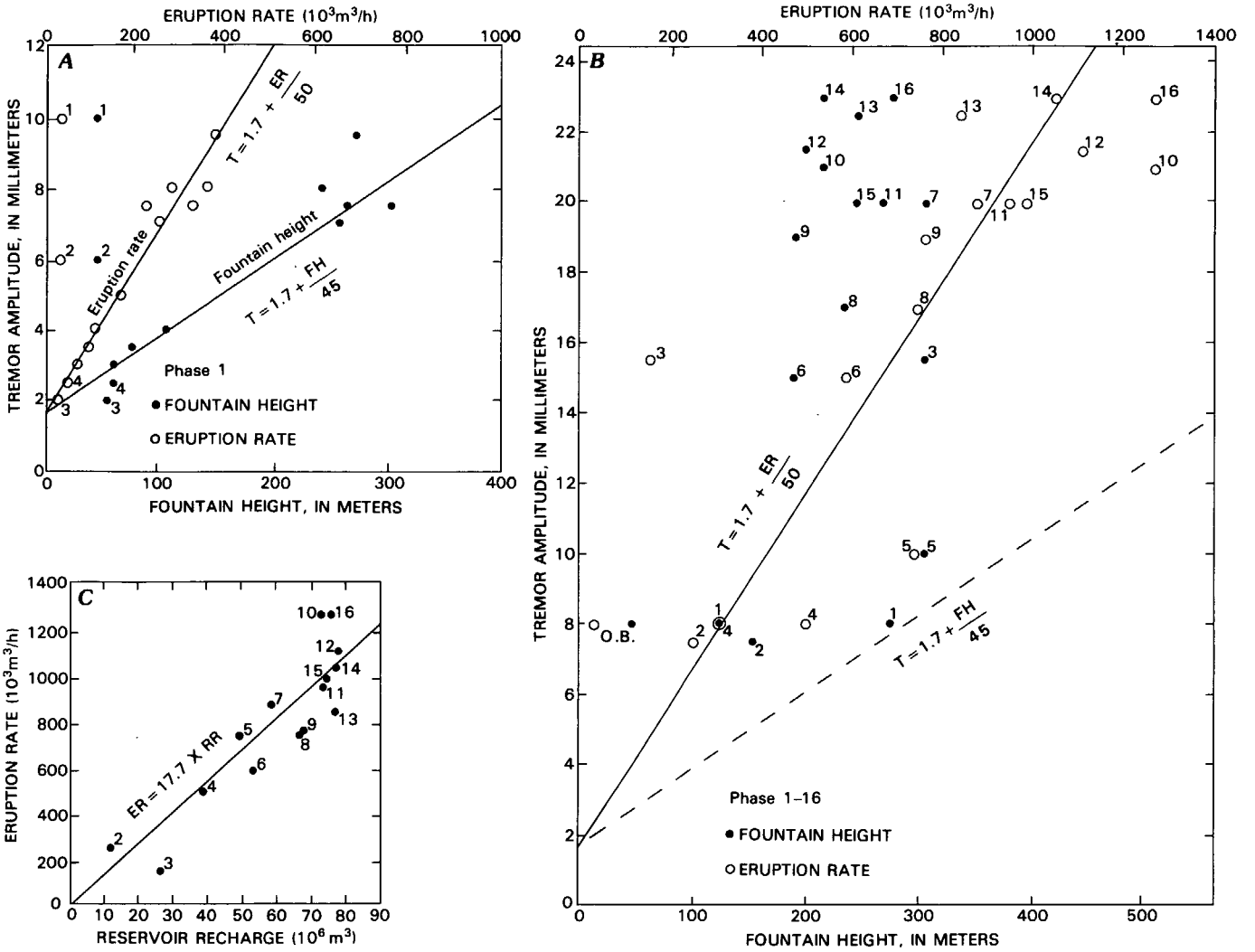

FIGURE 48.30.—Cross plots of eruption parameters for the 1959 Kilauea eruption. Numbers on plot *A* indicate sequence of readings during phase 1 on November 15–16. Numbers on plots *B* and C indicate phases. On plot *B*, the earliest data for phase 1 are plotted separately and labeled O.B. ***A***, Tremor amplitude plotted against eruption rate and fountain height for phase 1. ***B***, Tremor amplitude plotted against eruption rate and fountain height for phases 1–16. ***C***, Eruption rate plotted against reservoir recharge for phases 2–16.

its shape: the large surface-area-to-volume ratio of the dike permits good translation of pressure variations in the lava to movement of the walls of the dike.

In the course of the first day, fountaining died out along all of the original fissure except for one small section, where the main fountain gradually grew in height and volume as it took over the function of the dying fountains. The rate of eruption declined only slightly, but the Outlet tremor amplitude dropped from 10 mm to 2 mm (fig. 48.29*A*). After about 36 h, rate of eruption and tremor amplitude both began to rise steadily; and after about 60 h the height of the fountain began a rapid increase, accompanied by further increases in the growth of eruption rate and of tremor amplitude. Plots of tremor amplitude versus fountain height and tremor amplitude versus eruption rate for the first phase of the eruption are shown in figure 48.30*A*. Excluding the first day (points labeled 1 and 2), tremor amplitude is simply related to both eruption rate and fountain height: $T = 1.7 + ER/50$ and $T = 1.7 + FH/45$, where T is amplitude of Outlet tremor in millimeters, ER is eruption rate in thousand cubic meters per hour, and FH is fountain height in meters. Points 1 and 2, for the initial stage of phase 1, clearly do not fit with the rest of the data. During the first 36 hours of the eruption it appears that the tremor-generating system evolved from an initial stage dominated by the dike conduit, which produced strong tremor, to a later stage dominated by an open central conduit which was

TABLE 48.3.—*Detailed eruption parameters for phase 1 of the 1959 Kilauea Iki eruption*

[Dates and times are lava-lake depth measurements, from table 48.1; volume rate is average rate of eruption since last measurement of lake depth or onset of new eruptive phase; tremor measured at Outlet; temperatures are quench temperatures of pumice samples collected during the time intervals, from Helz (chapter 25)]

Date	Time (H.s.t.)	Volume rate (10^3 m^3/h)	Fountain height (m)	Tremor amplitude (mm)	Temperature (°C)
Nov. 14	2008	--	--	--	--
Nov. 15	0300	33	46	10.0	1,144
	1800	31	46	6.0	--
Nov. 16	1215	25	55	2.0	--
	1400	44	61	2.5	--
Nov. 17	1045	70	61	3.0	--
	1400	94	76	3.5	--
	2030	106	107	4.0	--
Nov. 18	1200	163	185	5.0	--
	2315	252	259	7.0	1,216
Nov. 19	1150	281	305	8.0	--
	2115	378	274	9.5	--
Nov. 20	1210	357	244	8.0	1,187
Nov. 21	0930	327	267	7.5	--
	1925	222	305	7.5	1,188

TABLE 48.4.—*Eruptive parameters characterizing the 16 principal eruptive phases of the 1959 Kilauea Iki eruption*

[Figures for volume rate of eruption, fountain height, and tremor amplitude (measured at Outlet) are averages for the particular phase; temperature is quench temperature of pumice sample collected during phase, from Helz (chapter 25); recharge is volume of lava that entered summit reservoir from depth from end of phase 1 fountaining to onset of current phase]

Phase	Volume rate (10^3 m^3/h)	Fountain height (m)	Tremor amplitude (mm)	Temperature (°C)	Recharge (10^6 m^3)
1a	32	46	8.0	1,142–1,144	--
1b	306	274	8.0	1,187–1,216	--
2	248	152	7.5	1,185	9.4
3	153	305	15.5	1,154	20.1
4	497	122	8.0	1,196	29.9
5	742	305	10.0	1,205	38.1
6	585	189	15.0	--	40.5
7	879	305	20.0	1,181	45.4
8	745	232	17.0	1,197	51.4
9	765	189	19.0	1,188	52.1
10	1,269	213	21.0	1,189	56.2
11	948	265	20.0	--	56.4
12	1,109	198	21.5	--	60.0
13	841	244	22.5	--	59.1
14	1,047	213	23.0	--	59.2
15	986	244	20.0	1,191	57.0
16	1,269	274	23.0	1,190	58.6
End	--	--	--	--	59.7

much less efficient in producing tremor. Thereafter, the eruption increased in intensity, and tremor, rate of eruption, and fountain height all increased proportionally.

The role of lava temperature appears to be important, because the large increases in tremor, rate of eruption, and fountain height appear to coincide with an increase in lava temperature from about 1,145 °C to 1,185–1,215 °C between November 15 and November 18. The exact role of temperature is not clear, however. Higher temperatures certainly are associated with greater fluidity of the lava, but they also mark the lava as being more primitive and less depleted of dissolved gases than cooler lava. The latter attribute may be more important than the former in its effect on the style of eruption.

The evolution of the eruption from phase to phase took a different course from the evolution of phase 1. As the reservoir was recharged with fresh lava after phase 1, tremor amplitude and rate of eruption generally increased from phase to phase, but fountain height was very erratic (fig. 48.29*B*). In an almost regular alternation from one phase to the next, it oscillated between 120–180 m and 270–300 m during the first seven phases. The alternation was slower (2 eruptive phases per half-cycle) and between narrower limits (180–270 m) thereafter. Tremor amplitude is plotted versus eruption rate and fountain height for all 16 phases, in figure 48.30*B*, as it was for phase 1 only in figure 48.30*A*. The lines relating tremor amplitude to rate of eruption and fountain height in the phase 1 plot are repeated in figure 48.30*B*. Although the scatter is somewhat greater here, the data for tremor amplitude versus eruption rate for the 16 phases fit the phase 1 curve very well. The data for tremor amplitude versus fountain height, however, depart widely and systematically from the phase 1 curve. After phase 4, fountain height is restricted to the range 180–300 m, and it appears not to be related to tremor amplitude. The extremely low value for rate of eruption in phase 3 (fig. 48.30*B*) may be explained, at least in part, by the large loss of material blown downwind and away from the lake from the high, very gassy fountain that characterized this phase.

Eruption rate appears to be simply related to reservoir recharge (fig. 48.30C) by the relationship $ER = 17.7 \times RR$, where ER is eruption rate in thousand cubic meters per hour and RR is reservoir recharge in million cubic meters. The error in the eruption rate predicted by this relationship for phases 4–16 is less than 25 percent of the measured value in all 13 cases and less than 10 percent in 7 cases. The predicted eruption rates for phases 2 and 3 are 34 percent too small and 133 percent too large, respectively. The discrepancy for phase 3 would be reduced if the volume of lava represented by the pumice blown away from the very gassy fountain (and the lake) during this phase were included.

A change in fountain behavior between the later phases and the earlier phases that is apparent in figure 48.21 and figures 48.23–48.27 deserves special mention. During the early phases the fountain grew steadily in height until it reached a high level that was maintained until the end of the phase. Exceptions to this rule were phase 2, in which the fountain height increased considerably just before it died, and phase 9, in which the fountain declined steadily from a maximum attained early in the phase. Before phase 10, no phase began with a sharp, high pulse of fountaining that declined rapidly to a lower level that then characterized the rest of the phase. From phase 10 through phase 16, however, all phases began with such an initial outburst. This phenomenon was most pronounced in phase 15, in which the outbreak fountain rose briefly to a height of 580 m, about twice the height of fountaining during the rest of the phase.

This change in behavior may reflect a change in composition or amount of gas in the lava of the summit reservoir. Gerlach and Graeber (1985) calculate very different compositions for the gas in the parental magma at depth and in lava stored in the summit

reservoir equilibrated at 2-km depth. They find the concentrations, in weight percent, of the three principal gas components as follows:

	H_2O	CO_2	SO_2
Parental magma	0.30	0.65	0.13
Stored reservoir lava	0.27	0.034	0.070

At reservoir depths CO_2 would have already exsolved from the lava and collected as a separate phase in fluid inclusions, while H_2O would still be dissolved in the lava. At depths of 2–4 km, such low-density CO_2 inclusions would constitute 5–10 percent, by volume, of the lava and would reduce its density in approximately the same proportion. In the interval between eruptive phases, gravitative separation of lighter lava rich in CO_2 inclusions may have positioned such material near the top of the reservoir for early eruption during the next phase. The CO_2 may also be more effective than H_2O in producing rapid vesiculation because it is already exsolved from the lava, whereas H_2O must first diffuse out of the lava into bubbles before those bubbles can expand in response to a drop in confining pressure. After an episode of abnormally vigorous initial fountaining, the eruption would return to normal when the gas-enriched cap of lava in the reservoir was depleted.

The large phase-to-phase variation in fountain height, particularly during the early phases, that is shown in figure 48.30*B* may also result from variations in the composition and abundance of gas from place to place in the mixture in the reservoir of old stored lava and new lava from depth.

FURTHER DEVELOPMENT OF THE PROPOSED MODEL OF THE 1959 ERUPTION

During the first phase the conduit evolved from a long, thin dike held open by pressure in the lava to a much more stable conduit with a more equidimensional cross section. It remained sufficiently open at the end of phase 1 to admit 1.0×10^6 m^3 backflow from the lake. Descriptions of the onset of all subsequent phases, except the very short phase 14, whose onset is not described (Richter and others 1970), show that the conduit had remained open after the end of the last phase and that a fluid lava column, with large bubbles of gas rising through it and throwing up spatter when they burst, rose slowly to the mouth of the conduit. At the end of these phases lava flowed copiously back into the vent and disappeared underground. These observations strongly suggest that the conduit was an open pipe from the reservoir to the lake, and that the pressure of lava in the reservoir at the base of the conduit was in approximate balance with the weight of lava in the conduit. A slight change in this balance could cause lava to flow out of the reservoir through the pipe to the surface or the reverse.

Following phase 1, which poured about 30×10^6 m^3 of lava into the lake, where it was trapped, new lava from depth streamed up into the reservoir and mixed with the current contents of the reservoir. During subsequent phases some mixture of the older and newer reservoir lava was spewed out into the lake, undergoing intense local mixing in the conduit. Some fraction of the contents of the lake then drained back to the reservoir, with further mixing. As the eruption progressed and more and more lava moved up from depth to recharge the reservoir, its contents gradually took on more of the characteristics of the new lava, including its temperature and charge of dissolved (and exsolved) gases. Reinflation of the reservoir, at least through phase 8 or phase 10, raised the piezometric surface of lava in the reservoir, making onset of the next eruption easier and increasing the pressure drive that would help to sustain it.

As backflow from the last phase ceased, the heavy lake lava occupying the conduit would tend to flow back into the reservoir and be replaced by hotter, lighter lava from the reservoir (if the conduit were not too narrow). This process would be aided by any exsolved CO_2 that had come into the chamber with the recharge from depth. When the combination of lighter lava in the conduit and increased reservoir pressure (from further recharge) raised the top of the column sufficiently that it overflowed into the lake, the conditions for starting the next eruption had been met.

Next, consider the factors that might control rate of eruption and fountain height during an eruptive phase once it has started. In the system we have described the rate of eruption should be determined by the balance between the pressure difference driving the eruption and the pressure drop in the conduit resulting from the flow of lava through it. The pressure difference that drives the eruption is primarily a result of vesiculation of lava in the upper part of the conduit, which reduces its density substantially as it flows to the surface. The resulting decrease in weight of lava in the upper part of the conduit is available as a pressure difference to drive lava upward through the conduit. The efficiency of this vesiculation pump will depend on the gas content of the lava, the speed with which it can accumulate in bubbles, and the rate at which the bubbles can escape from the lava. These factors are related to lava temperature to the degree that temperature controls viscosity and is a measure of the proportion of new material from depth in the erupting lava.

The pressure drop owing to movement of lava through the conduit depends primarily on velocity and viscosity (and hence temperature) of the lava and the geometry of the conduit. In the course of the eruption, constrictions in the conduit would have been eroded (melted) away, progressively decreasing the resistance to flow; as the erupting lava was increasingly enriched in new hotter material from depth, its viscosity would have decreased, further reducing resistance to flow.

During an eruption of fairly viscous lava, we should expect a low rate of flow from the reservoir. For a fairly slow ascent of lava in the conduit, the exsolution and separation of gas should be nearly complete and should yield an abundance of gas deep in the conduit to drive the gas-lava mixture above it out of the conduit rapidly, producing a high fountain. During an eruption of less viscous lava, we should expect a high rate of flow from the reservoir. For a rapid ascent of lava in the conduit we may speculate that the short time that lava would spend in the upper, low-pressure part of the conduit would limit the amount of exsolution and, particularly, separation of gas from the lava and would result in a low, voluminous fountain in which the bubbles of gas would still be retained in the lava as it was thrown out of the vent. In the scheme outlined above, low eruption rates and high fountains would correlate with lower than average lava temperatures, and high eruption rates and low fountains would correlate with higher than average lava temperatures. This tendency would be superposed on one of increasingly larger eruption rates

from phase to phase as the conduit was enlarged by continued use and the summit reservoir was refilled by hot, gas-rich lava from depth.

The first part of this pattern appears to have been observed during phase 3 (with its low lava temperature of about 1,155 °C, high fountain, and very low eruption rate) and the ensuing phase 4 (with its high lava temperature of about 1,200 °C, low fountain, and high eruption rate). The second part of the pattern is demonstrated by the relationship between eruption rate and reservoir recharge shown in figure 48.30C.

The apparent linear relation between tremor amplitude and eruption rate in figures 48.29*A* and 48.29*B* supports the view that tremor is generated primarily in the eruption conduit and that its amplitude is proportional to the rate of flow of lava through the conduit. However, tremor accompanying the initial rapid backflow of lava through the conduit when the fountain died was insignificant compared to tremor during fountaining. Thus, the existence of lava fountaining is strongly correlated with strong tremor, but fountain height (the most obvious measure of intensity of fountaining) does not correlate with tremor amplitude during the later phases of the eruption, which produced the strongest tremor. These observations, taken together, suggest that the source of the tremor accompanying the large fountains of the Kilauea Iki eruption was the vesiculation pump mechanism that operated in the upper part of the eruption conduit to lift lava out of the reservoir. Moreover, the amplitude of the tremor is proportional to the volume rate of lava moving through the conduit or, equivalently, to the power consumed in the pumping mechanism to lift the lava.

This tremor-generating mechanism, which operates in a stable open conduit but with rather low efficiency, does not explain the tremor generated during the initial stages of phase 1 nor during episodes of resurgent tremor accompanying backflow from the lake. In both of these cases, it appears that the movement of lava through a dikelike conduit that is being held open by pressure in the moving lava is a more likely mechanism. An important requirement of such a mechanism is that it produce strong tremor as a consequence of the movement of a fairly small volume of lava.

SUMMARY AND CONCLUSIONS

1. The 30×10^6 m^3 of lava erupted into Kilauea Iki Crater during the first phase of the 1959 eruption was drawn primarily from storage in the summit reservoir. After the outbreak and initial episode of eruption, which were driven by reservoir overpressure, vesiculation in the upper part of the conduit effectively pumped lava from the reservoir up into the lake. During this process the reservoir pressure dropped below that required to hold an unvesiculated column of lava in the conduit up to the level of the vent.

2. When the surface of the lake rose above the level of the vent, heavy degassed lake lava flooded the base of the fountain and poured back into the vent, where it sufficiently inhibited vesiculation in the lava emerging from below that it disabled the vesiculation pump and shut off the eruption. With degassed lake lava in the conduit, the pressure at the base of the conduit exceeded the pressure in the reservoir, and lake lava flowed back into the reservoir. When the lake surface fell below the vent, backflow ceased.

3. The sharp drawdown in reservoir pressure during the final stages of phase 1 led to a sharp increase in the flux of lava into the reservoir from the deep source beneath the volcano. The reservoir inflation rate increased from about 0.3×10^6 m^3/d for the month before the eruption, to about 3×10^6 m^3/d immediately after phase 1. Between the end of phase 1 and the end of the 1959 eruption, about 60×10^6 m^3 of fresh lava entered the reservoir from below.

4. The conduit remained open from the end of phase 1 until the end of the eruption. Increase of pressure in the reinflating reservoir and, possibly, replacement of heavy drainback lava in the conduit by lighter, gas-charged lava from the reservoir raised the lava in the conduit until it rose above the lip of the vent. Vesiculation of the fresh reservoir lava rising in the conduit further reduced the density of lava in the conduit and revitalized the vesiculation pump, turning on the next eruptive phase. When the erupting lava again raised the lake surface sufficiently above the level of the vent, degassed lava from the lake again poured back into the conduit and disabled the vesiculation pump. Cessation of fountaining was again followed by draining of the lake back down to the level of the vent.

5. The process described above was repeated 15 times after phase 1, until the supply to the summit reservoir of fresh lava from below abated. An additional 8×10^6 m^3 of lava was added to the lake, primarily during phase 4, when the mouth of the conduit broke out higher on the south wall of Kilauea Iki about 12 m above the original vent. An estimated 12×10^6 m^3 lava was driven out of the reservoir, probably into the core of the east rift zone, during backflow from the later phases of the eruption. At the end of the eruption the summit reservoir had been refilled with about 40×10^6 m^3 lava to replace the 30×10^6 m^3 that was withdrawn during phase 1. The lava budget of the entire eruption is shown in figure 48.28.

6. Tremor appears to have been generated under two different regimes with very different efficiency. Eruption of lava at even low rates through a long narrow fissure propped open by pressure in the lava produced strong tremor early in phase 1 and, perhaps, during episodes of resurgent tremor accompanying backflow. In the stable conduit that remained open between phases (and was, therefore, not propped open by excess reservoir pressure), tremor was generated with much lower efficiency. In this case, the amplitude of tremor was a linear function of eruption rate during fountaining, but it was much smaller during comparable rates of backflow. Tremor amplitude appears to be independent of fountain height, except during phase 1 when the conduit was being shaped by the flow of lava through it. These observations suggest that tremor in the open conduit was associated with the action of the vesiculation pump that lifted lava from the reservoir to the lake.

7. After the first 3 phases, rate of eruption was proportional to the volume of lava from below that had recharged the summit reservoir. This relation may be a result of the decrease in the work required of the vesiculation pump to move lava from the reservoir to the lake as reservoir pressure increased. It may also be caused by a

progressive change in the ratio in the reservoir of stored reservoir lava to fresh lava from depth.

8. From phase 10 onward, the eruptive phases began with an episode of high fountaining. Fountaining then diminished rapidly to a lower level that was sustained through the rest of the phase. Such behavior might be explained by the accumulation of a light, particularly gas rich batch of lava at the top of the reservoir between phases, which was expelled first during the next phase but was soon depleted. Because H_2O should be completely dissolved in the lava at reservoir depths, it is unlikely that it is the agent for such a process. A far better candidate is CO_2. If present in the amount deduced by Gerlach and Graeber (1985), light fluid inclusions of CO_2 would constitute 5–10 percent by volume of the parental magma when raised to reservoir depths. The large variation in fountain height, which appears to depend on lava temperature to some extent, might also be explained by a mixture of CO_2-depleted stored lava and CO_2-rich fresh lava in the reservoir. In the course of the eruption, as the proportion of fresh lava and the mixing of the reservoir contents increased, the range of variation in fountain height and temperature of erupted lava decreased.

REFERENCES CITED

Eaton, J.P., 1959, A portable water-tube tiltmeter: Bulletin of the Seismological Society of America, v. 39, p. 301–316.

———1962, Crustal structure and volcanism in Hawaii, *in* Macdonald, G.A., and Kuno, Hisashi, eds., The crust of the Pacific Basin: American Geophysical Union Monograph 6, p. 13–29.

Eaton, J.P., and Fraser, G.D., 1958, Hawaiian Volcano Observatory Summary 9, January-March, 1958: U.S. Geological Survey, 8 p.

Eaton, J.P., and Murata, K.J., 1960, How volcanoes grow: Science, v. 132, p. 925–938.

Gerlach, T.M., and Graeber, E.S. 1985, The volatile budget of Kilauea volcano: Nature, v. 313, p. 273–277.

Jaggar, T.A., and Finch, R.H., 1929, Tilt records for thirteen years at the Hawaiian Volcano Observatory: Bulletin of the Seismological Society of America, v. 19, p. 38–50.

Macdonald, G.A., and Eaton, J.P., 1957, Hawaiian Volcanoes during 1954: U.S. Geological Survey Bulletin 1061-B, p. 1–72.

Mogi, K., 1958, Relations between the eruptions of various volcanoes and the deformations of the ground surfaces around them: Bulletin of the Earthquake Research Institute, Tokyo University, v. 36, p. 99–134.

Powers, H.A., 1946, Reanalyzing tilt records at the Hawaiian Volcano Observatory: Volcano Letter 492, p. 1–3.

———1947, Annual tilt pattern at the Hawaiian Volcano Observatory: Volcano Letter 495, p. 1–5.

Richter, D.H., Eaton, J.P., Murata, K.J., Ault, W.U., and Krivoy, H.L., 1970, Chronological narrative of the 1959–60 eruption of Kilauea Volcano, Hawaii: U.S. Geological Survey Professional Paper 537-E, p. E1–E73.

TIDAL EFFECTS ON HAWAIIAN VOLCANISM

By Daisuke Shimozuru[1]

ABSTRACT

This paper summarizes earlier work on possible tidal effects at Kilauea Volcano. From a significant test on 52 historical eruptions of Kilauea, Dzurisin inferred that the likelihood of a fortnightly tidal influence is approximately 90 percent. Reanalysis of early work by Jaggar on the fluctuations of the lava-lake level at Halemaumau shows that semidiurnal oscillations during the highest level of the lava-lake activity are well correlated with solid-Earth tides. This tidal fluctuation of the lake level is attributed to cyclic volume change of the magma reservoir caused by tidal strain. Effective volume of the magma reservoir is estimated to be roughly 800 cubic kilometers from the computed cubical dilatation. The effective magma reservoir beneath Kilauea is suspected to be an assemblage of chambers filled with magma rather than a single large chamber.

INTRODUCTION

Intracrustal stresses caused by lunisolar attraction, though they are small, have been considered by many workers to influence the occurrence of earthquakes and volcanic eruptions. Many attempts have been made to correlate solid-Earth tides with earthquakes (Hoffmann, 1961; Knopoff, 1964; Simpson, 1967; Ryall and others, 1968; Shlien, 1972; Kayano, 1973; Mauk and Kienle, 1973; Klein, 1976).

Some earthquakes or earthquake swarms show significant correlation with tides. For example, earthquakes on several parts of the world rift system are significantly correlated with the semidiurnal tide. This implies an enhancement of stress on parts of tensional spreading axes. From a global viewpoint, however, significant correlations are not found, and this indicates that most earthquakes are not triggered by specific amplitudes of acceleration of Earth-tide components.

As for volcanic eruptions, it seems also intuitively possible that crustal tidal strain could act as a trigger, provided that the volcano is in a nearly critical state. Chamberlin (1918, p. 231) stated that "Pronounced tidal movement might be expected in the necks of volcanoes if they are connected with large reservoirs of lava below, but if there is any response to tidal strains at all, it is scarcely detectable."

Johnston and Mauk (1972) tested for effects of Earth tides on the major eruptions of Stromboli and found a correlation between eruption times and the modulation envelope of the fortnightly tide. However, there was not a good correlation between eruptions and the phase of diurnal tide. Mauk and Johnston (1973) found similar results for the major eruptions of the world's submarine volcanoes since 1900. Hamilton (1973) demonstrated correlations between worldwide volcanic activity and tidal periods, not only for fortnightly periods, but also for periods as long as 18.6 years. Eggers and Decker (1969) made statistical time-series analyses of worldwide volcanic eruptions and suggested a possible relation with the annual component of Earth-tide cycles.

For Hawaiian volcanoes, the pioneering study of tidal effect was by Jaggar (1924), who observed semidiurnal movement of the level of the liquid lava pool at Halemaumau pit crater. Brown (1925) made Fourier analyses of Jaggar's data and found some evidence of tides with periods of 24 h and 12 h 25 min. More recently, Dzurisin (1980) tested the relation between the well-recorded historical eruptions of Kilauea and the phase of fortnightly tidal cycles. From the point of view of forecasting volcanic eruptions of Kilauea, Klein (1984) concluded, on the basis of Dzurisin's analysis, that the fortnightly tidal modulation is a significant eruption predictor, especially for rift-zone eruptions. Shimozuru (1975) made a detailed analysis of Jaggar's (1924) data on fluctuation of the level of Halemaumau lava lake and found a semidiurnal oscillation correlated with Earth tides when the lake was at its highest levels.

In this article I review the previous investigations of tidal effects on the activity of Kilauea Volcano and attempt to use these data to interpret the character of the magma reservoir system beneath the volcano.

EARTH TIDES AND VOLCANIC SYSTEMS

For simplicity, volcanoes are here considered to consist of a major magma reservoir and conduits surrounded by solid rock. A volcanic system's response to solid-Earth tides may be different depending on whether the magma reservoir or conduits are filled with magma or not. Furthermore, tidal strain is a function of latitude, as shown in figure 49.1, and so any tidal effects on volcanic activity should be smaller at high latitudes than low latitudes. These two conditions are principal criteria for the evidence for tidal effects on volcanic activity.

Volcanic activities can be categorized into two types. One type is more or less continuous, such as seismic activity including volcanic tremor, lava-lake activity, and long-lasting eruptive events. The other type is discontinuous, such as sporadic eruptions and short-

[1]Physics Department, Tokyo University of Agriculture.

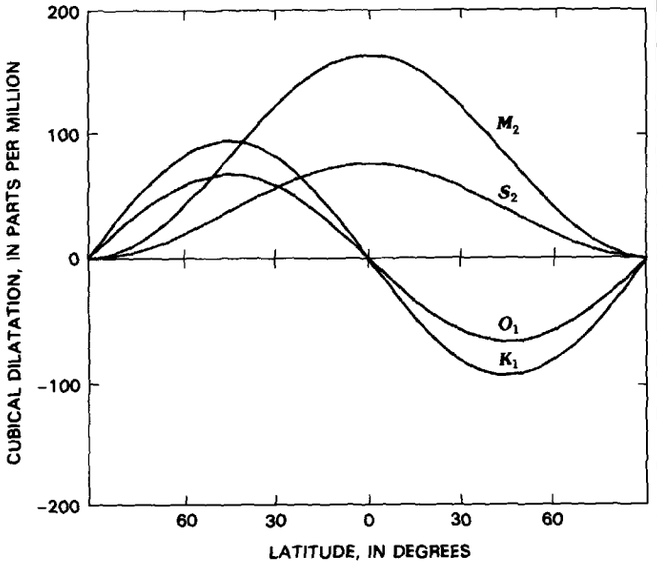

FIGURE 49.1.—Varition of cubical dilatation with latitude due to principal semidiurnal sectorial waves (M_2, S_2) and principal diurnal tesseral waves (K_1, O_1).

term seismic swarms. For the latter type, increasing and decreasing pore pressure caused by the movement of lava and gas resulting from tidal strain may act, together with tidal stress, as the triggering mechanism of volcanic earthquakes. These various modes of activity combined with the above mentioned relations make the problem complex. Most investigations to date have been statistical calculations of the possible relation between solid-Earth tides and volcanic activity.

For a more quantitative approach to this problem, we can learn from the tidal fluctuations of water level in deep wells documented by Pekeris (1940) and Richardson (1956). These investigators observed a high tide in the well at the time when the acceleration from the lunisolar attraction was minimal. Pekeris (1940) estimated that a change of water level of 1 cm in a well of 1-m radius could be brought about by cubical dilatation in a water-bearing hemisphere of only 100-m radius. Replacing water with liquid lava, we can apply this to volcanic episodes.

ROLE OF EARTH TIDES ON ERUPTIONS OF KILAUEA AND MAUNA LOA VOLCANOES—FORTNIGHTLY TIDAL EFFECT

In the light of growing evidence for tidal triggering of volcanic eruptions, Dzurisin (1980) made a statistical study of the onset times of individual eruptions of Kilauea and Mauna Loa in relation to solid-Earth tides. Incorporated in his study were 52 historical eruptions of Kilauea, from 1832 to 1979, and 37 of Mauna Loa, from 1832 to 1972. The beginning of surface lava extrusion was taken as the starting time of each eruption. In light of the results of previous investigations, he concentrated on the influence of the fortnightly tide. Tidal acceleration was computed for the 2-week period centered on each eruption. Examples of the correlation of vertical acceleration of solid-Earth tides and eruptions of Kilauea are shown in figure 49.2. Dzurisin confirmed that eruptions at Kilauea clearly occur preferentially near the fortnightly tidal maxima, with approximately 90 percent likelihood. For Mauna Loa, however, he found that the 37 historical eruptions have been distributed randomly with respect to the fortnightly tide. He inferred that differences in structure or internal plumbing may limit the effectiveness of tidal influences on Mauna Loa. In contrast to the tidal-phase correlation of Kilauea eruptions, Johnston and Mauk (1972) found that eruptions of Stromboli clustered conspicuously about the time of fortnightly tidal minima. This difference in behavior between Kilauea and Stromboli, though they are both basaltic volcanoes, is not understood. Possibly it is related to the difference in tectonic setting.

TIDAL OSCILLATION OF HALEMAUMAU LAVA LAKE IN 1919—SEMIDIURNAL TIDAL EFFECT

Jaggar (1947, p. 7) stated that the routine of the Hawaiian Volcano Observatory "had been determined by the necessity for

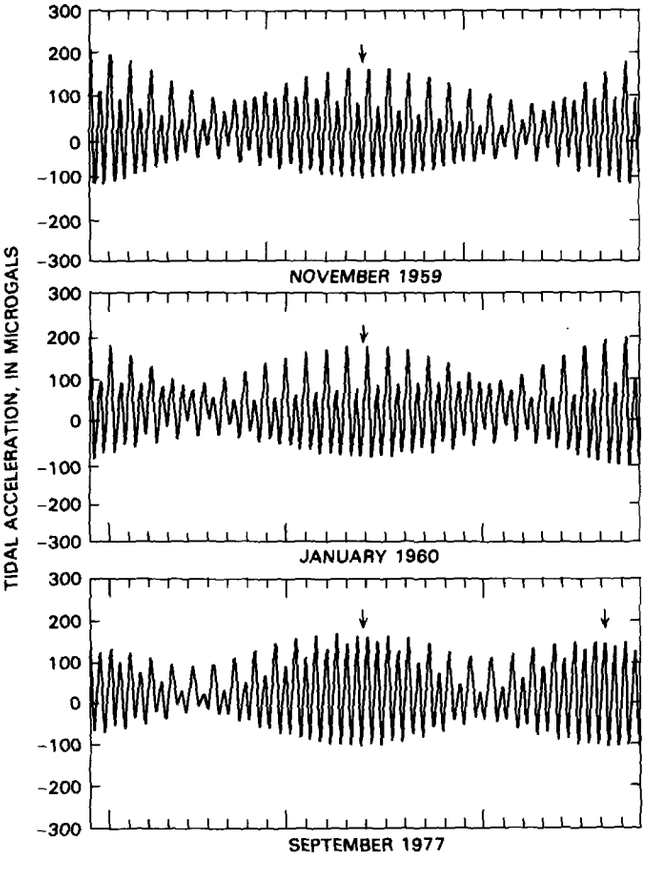

FIGURE 49.2.—Variation of tidal acceleration at Kilauea during time periods in which eruptions occurred. Beginnings of eruptions marked by arrows. After Dzurisin (1980).

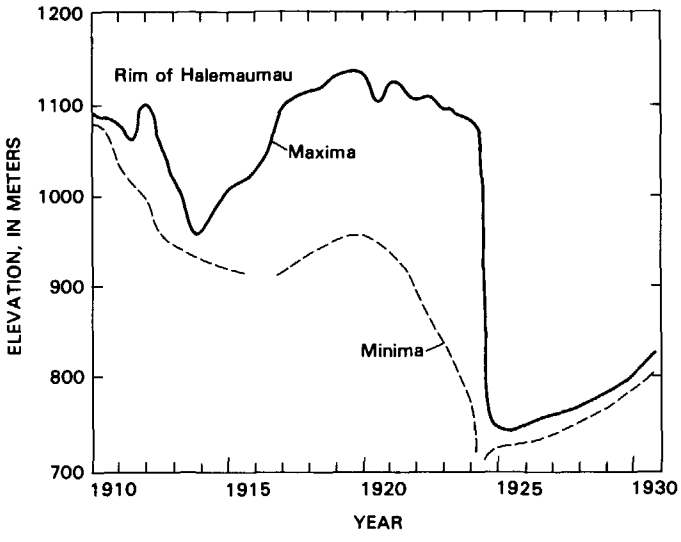

FIGURE 49.3.—Long-term changes in level of Halemaumau lava lake from 1910 to 1930. After Jaggar (1947).

continuous measurement with surveying instruments of the lava pool in Halemaumau pit." The elevation of the surface of the lava lake was measured from 1909 until 1930. Timing of the measurements was arbitrary except during July–August 1919, when the level was highest. A smoothed curve of the level of the lava lake is shown in figure 49.3. The dramatic drop of the level in 1924 was related to magma injection into the east rift zone of Kilauea Volcano and the explosive eruption at Halemaumau.

During the interval of 28 days from July 21 to August 16, 1919, transit measurements of the level of the Halemaumau lava lake were made by Jaggar and his coworkers every 20 minutes. Two points on the edge of the liquid lava lake and two points on the pit floor outside the lava lake were repeatedly measured with reference to a datum station located at the western rim of the crater. The height of the datum station was occasionally checked from the observatory. Brown (1925) made a Fourier analysis of Jaggar's data and found some evidence of tides with periods of the lunar day and lunar half-day, with double amplitudes of about 1 in. His analysis covered the entire measurement interval. However, for a few days near the end of the interval, the liquid lava showed marked oscillations of amplitude 30–60 cm with a period of about 12 h.

While at the Hawaiian Volcano Observatory in 1963 as a member of the Japan-U.S. Cooperative Science Program, I examined Jaggar's data on the level of the Halemaumau lava lake and was very impressed by the detailed measurements. Stimulated by his work, I made an extensive analysis of his data and found that the semidiurnal oscillations during the time of the highest general lake level were in good correlation with the tidal phase (Shimozuru, 1975). This correlation was attributed to squeezing out and drain-back of magma from and to the magma reservoir caused by tidal strain. However, in my previous study there were some uncertain points and a miscalculation. I am therefore revising my analysis of Jaggar's data in order to enhance their scientific value.

DATA

Assuming they approximately reflect the level change of the entire lava lake, I have adopted the hourly mean values of elevation at the edge of the lava lake from the table in Brown (1925, p. 109). For a 7-h period in the middle of the observation interval, no measurements were made; values were interpolated for this missing time. These data are plotted in figure 49.4 together with the variation of gravitational acceleration caused by tidal forces during the corresponding period. The geographical location was taken as latitude 19.42° N., longitude 155.29° W., and elevation 1,800 m above sea level. Though the level of the lava lake shows in detail a ragged rise and fall, there is a general gradual rise until it reaches its highest level about August 15, 1919.

METHOD OF ANALYSIS

The data were treated first by a moving-window analysis as shown in figure 49.5. The starting time was taken as 0300 (Hawaiian standard time) on July 23. A significant semidiurnal spectral component at the later stage of the observation period is seen in figure 49.5. This evidence is more clearly shown by the fast Fourier analysis shown in figure 49.6. Over the whole period, there is no significant peak (fig. 49.6, uppermost curve), however, in the later part (August 10–16), a strong peak appears near to the period of the semidiurnal tidal components M_2, S_2, N_2, and K_2. The period of the dominant peak is slightly longer than that of the semidiurnal tides; this discrepancy may be partly because the analysis covers such a short period. Considering the difficulties of observation and the limitations resulting from the complex dynamics of the lava lake, particularly the horizontal movement of the liquid lava, I conclude that in the later part of the observation period, a semidiurnal period was evident in the lava lake oscillation.

CORRELATION WITH SEMIDIURNAL TIDE

Encouraged by this evidence of correlation, I tried to interpret quantitatively the relation of the semidiurnal fluctuation of the lava-lake level to Earth tides. Using the concept of tidal strain causing magma to squeeze out and drain back from and to the magma reservoir, the cubical dilatation was computed for the period from July 20 to August 19, 1919. The cubical dilatation (Δ) at the surface is, if Lame's constants λ is equal to μ,

$$\Delta = F(r)\frac{W}{rg} = \frac{2}{3}(2h-6l)\frac{W}{rg},$$

where W is the potential due to tide-generating forces, r is the distance from the point under consideration to the center of the Earth, g is the acceleration of gravity, and h and l are Love's numbers (Melchior, 1966). The world-wide means of h and l are 0.610 and 0.085, respectively. When these values are used in the

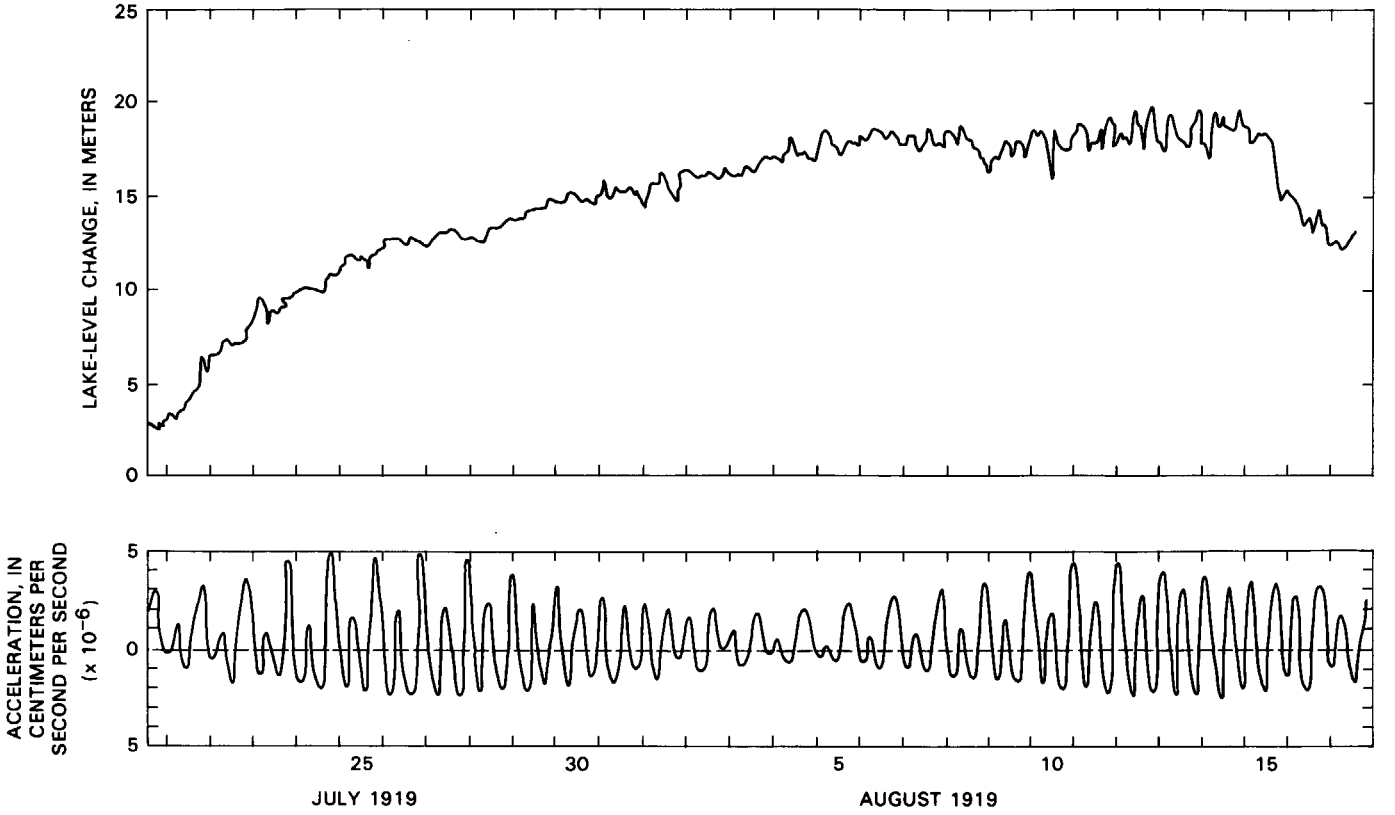

FIGURE 49.4.—Hourly means of level of Halemaumau lava lake and gravitational acceleration due to tide-generating forces during part of 1919. Lake-level data from Brown (1925).

equation, $F(r)$ is 0.47. However, the value of $F(r)$ may be different from the world-wide mean at a hot spot. Cubical dilatation divided by $F(r)$ was computed for the period from August 10–16, 1919, when semidiurnal oscillation of the lava-lake level was dominant. Results are plotted in figure 49.7.

The long-period variation in the original lake-level data was eliminated by Pertzev's method (Pertzev, 1957). The semidiurnal fluctuation of the lake level built up gradually and was mostly pronounced during August 12–14; when the lava lake was at its highest general level. It is interesting to find that the high tide of the lava lake occurs during the time when lunisolar attraction is at a minimum and the low tide occurs when it is at a maximum. A similar relation was also shown by tiltmeter records during the 1968 Halemaumau lava-lake activity (Kinoshita and others, 1969). That eruption started in 1967, and semidiurnal oscillations began to appear in the tilt records during February–March, 1968 (phase 28).

This evidence indicates that magma is transported between the magma reservoir and the lava lake because of semidiurnal dilatational strain. The phase lag of magma transport between the magma reservoir and the lava lake was estimated at 7 minutes, a quantity of time negligible for the present study (Shimozuru, 1975). Phase lag of the oceanic tide is approximately 7 hours at the Island of Hawaii; hence ocean loading had no apparent correlation with the lava-lake fluctuation.

EFFECTIVE VOLUME OF MAGMA RESERVOIR BENEATH KILAUEA INFERRED FROM TIDAL EFFECT

Using the concepts developed above, we can estimate the effective volume of the magma reservoir during Jaggar's observation period from the following formula:

$$V = dh \cdot A/\Delta,$$

where dh is the change of the lake level, A is the area of the lava lake during the measuring interval, and Δ is the cubical dilatation. Difficulties arise in estimating the area of the lava lake. Jaggar's sketch map for July 10, 1919 (Jaggar, 1947), is shown in figure 49.8. The lava lake consisted of the main pool in the east and two other pools at the north and southwest. The total area of the lake was estimated at 21.13×10^3 m^2 by tracing the shoreline of the white and lined areas in Jaggar's map (see fig. 49.8). From the difference between the minima and maxima of the lake level (dh) during the period August 12–14, we can calculate the volume of magma that

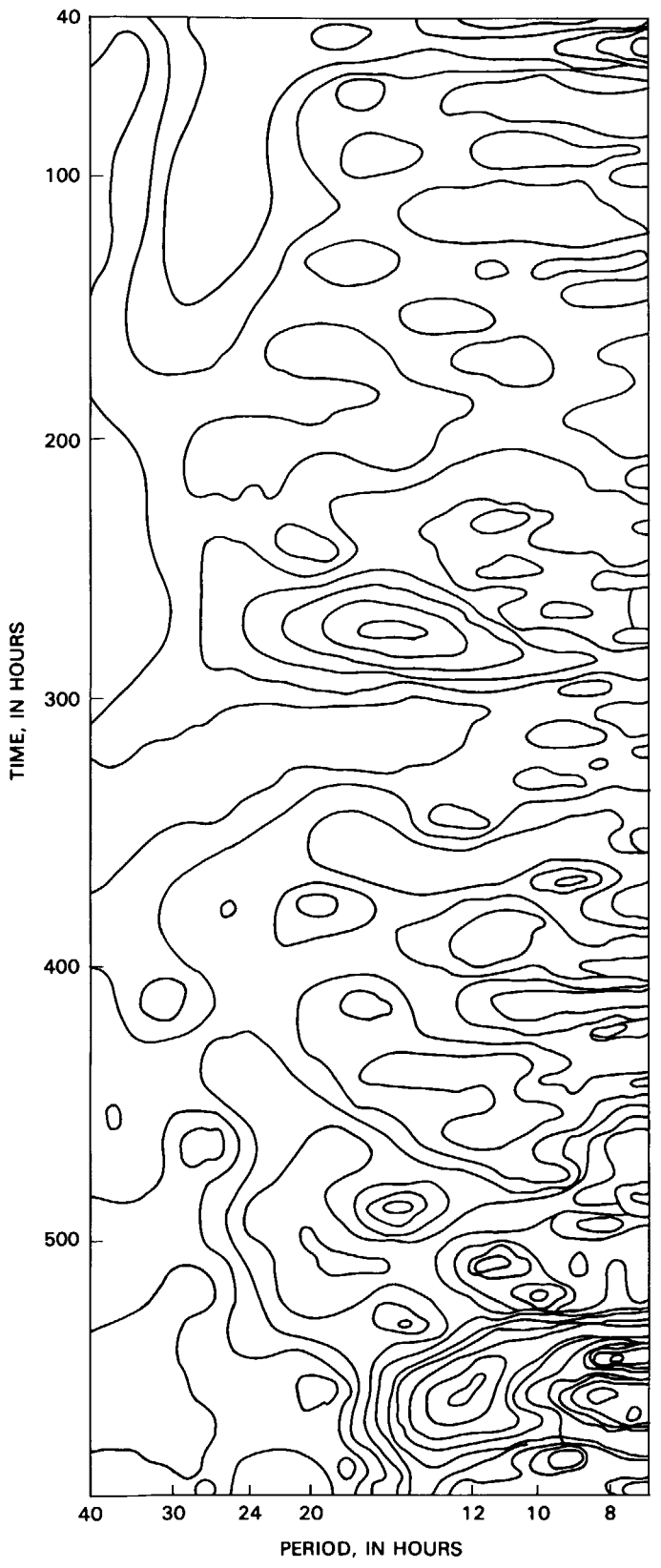

FIGURE 49.5.—Running spectra of fluctuation of height of Halemaumau lava lake during the period from July 21 to August 16, 1919, based on Jaggar's data (Brown, 1925).

squeezed out from the magma reservoir and drained back into it because of semidiurnal tidal strain. If we use the value 0.5 for $F(r)$, then the effective volume of the magma reservoir is roughly 800 km^3. On the other hand, Wright (1984, p. 3238) estimated a volume of 11 km^3 for Kilauea's shallow magma reservoir on the basis of geodetic data. The effective volume of magma reservoir estimated here is two orders of magnitude larger than that estimated from geodetic data. The reason for this large discrepancy is not clear, however, the calculated volume based on tidal strain may involve not only the shallow magma reservoir, but also involve the entire volume including conduits and plumbing system at the rift zone.

The shape of the magma reservoir beneath Kilauea Volcano is probably complex. Using tilt patterns associated with eruptions, Decker (1968) and Shimozuru (1981) prepared an electric-analog model, a kind of relaxation oscillator. I interpreted the complicated inflation pattern of Kilauea to result from an assembly of a main magma reservoir and several surrounding small reservoirs. The equivalent electric analog is the composite parallel and serial connection of components in a single oscillator. This proposed model of the magma reservoir system is reasonable for interpreting tidal fluctuation of the lava-lake level that appears at the highest general level of the lake and also for explaining the wandering of the uplift center at the summit region of Kilauea (Decker and Kinoshita, 1971, p. 58).

CONCLUSION

Dzurisin (1980) confirmed that the beginning of surface lava extrusion during 52 historical eruptions of Kilauea occurred preferentially near the fortnightly tidal maxima with approximately 90

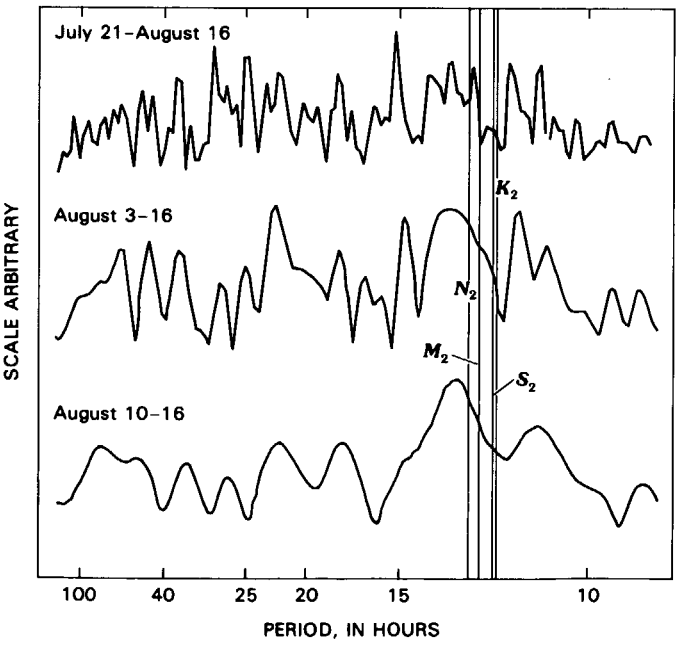

FIGURE 49.6.—Fast Fourier analysis of observed fluctuation in height of Halemaumau lava lake based on Jaggar's (1947) data. Spectra are shown for three different intervals in July–August 1919. Semidiurnal tidal components: M_2, S_2, N_2, K_2.

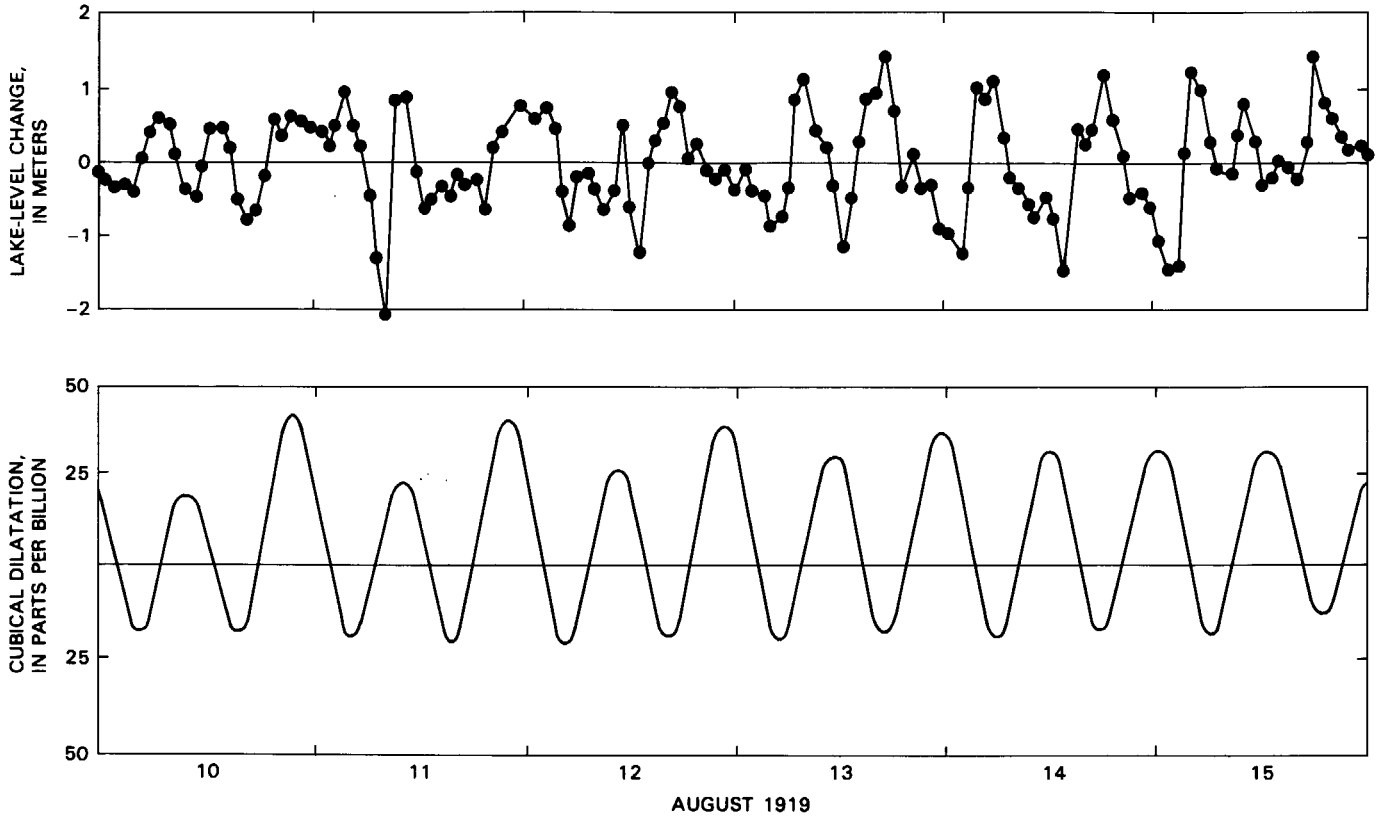

FIGURE 49.7.—Plot of hourly mean of level of Halemaumau lava lake, after filtration of long-term variation, during period August 10–15, 1919, and cubical dilatation ($\Delta/F(r)$) for corresponding interval. Lake-level data from Brown (1925).

percent likelihood. For Mauna Loa, however, he found that 37 historical eruptions began randomly with respect to the fortnightly Earth tide. In earlier work, I analyzed Jaggar's data on the fluctuation of the lava-lake level at Halemaumau in 1919 and found that semidiurnal tidal fluctuations during the highest general lake level correlate well with solid-Earth tides. Using the concept of squeezing out and draining back of magma from and to the magma reservoir caused by tidal strain, I have calculated the concerned volume of magma bodies at roughly 800 km^3 in August 1919. The magma reservoir system at Kilauea is suspected to be an assembly of a main magma reservoir and surrounding smaller reservoirs.

REFERENCES

Brown, E.W., 1925, Tidal oscillations in Halemaumau, the lava pit of Kilauea: American Journal of Science, 5th ser., v. 9, no. 2. p. 95–112.

Chamberlin, T.C., 1918, The Origin of the Earth: Chicago, University of Chicago Press, 231 p.

Decker, R.W., 1968, Kilauea volcanic activity: An electrical analog model: Eos (Transactions of the American Geophysical Union), v. 49, p. 352–353.

Decker, R.W., and Kinoshita. W.T., 1971, Geodetic measurements, *in* The Surveillance and Prediction of Volcanic Activity: Earth Sciences, 8. Unesco, Paris, p. 47–74.

Dzurisin, D., 1980, Influence of fortnightly Earth tides at Kilauea Volcano, Hawaii: Geophysical Research Letters, v. 7, no. 11, p. 925–928.

Eggers, A.A., and Decker, R.W., 1969, Frequency of historic volcanic eruptions [abs.]: Eos (Transactions of the American Geophysical Union), v. 50, p. 343.

Hamilton, W.L., 1973, Tidal cycles of volcanic eruptions: Fortnightly to 19 yearly periods: Journal of Geophysical Research, v. 78, no. 17, p. 3363–3375.

Hoffmann, R.B., 1961, Aftershock-energy release versus tidal effects, Hebgen Lake earthquake, Montana: U.S. Geological Survey Professional Paper 424–C, p. C267–C270.

Jaggar, T.A.. 1924, The lava tide, seasonal tilt, and the volcanic cycle: Pan-Pacific Science Congress, Australia, 1923, Proceedings, v. 2, p. 1369–1375.

———1947, Origin and developments of craters: Geological Society of America Memoir 21, 508 .

Johnston, M.J.S., and Mauk, F.J., 1972, Earth tides and triggering of eruptions from Mt. Stromboli, Italy: Nature, v. 239, p. 266–267.

Kayano, I., 1973, Microearthquake activity in Hiroshima and Shimane Prefectures and surrounding areas, Western Japan: Bulletin of the Earthquake Research Institute, University of Tokyo. v. 26, p. 178–203.

Kinoshita, W.T., and Koyanagi, R.Y., 1969, Kilauea Volcano: The 1967–1968 summit eruption: Science, v. 166, p. 459–468.

Klein, F.W., 1976, Earthquake swarms and semidiurnal solid Earth tide: Geophysical Journal of the Royal Astronomical Society, v. 45, p. 245–295.

———1984, Eruption forecasting at Kilauea Volcano, Hawaii: Journal of Geophysical Research, v. 89, p. 3059–3073.

Knopoff, L., 1964, Earth tides as a triggering mechanism for earthquakes: Bulletin of the Seismological Society of America, v. 54, p. 1865–1870.

Mauk, F.J., and Johnston, M.J.S., 1973, On the triggering of volcanic eruptions by Earth tides: Journal of Geophysical Research. v. 78, p. 3356–3362.

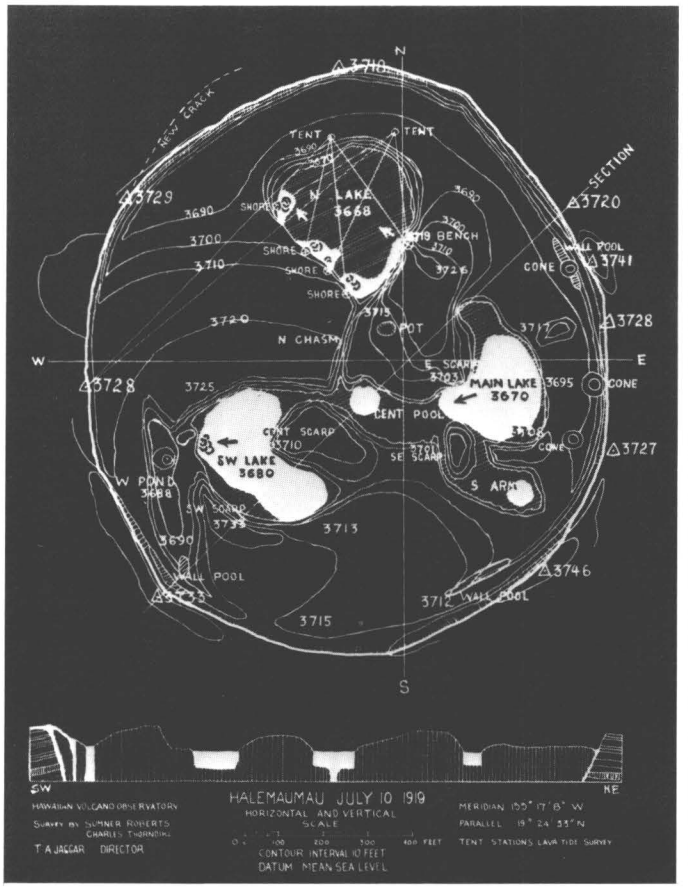

FIGURE 49.8.—Topography and lava pools in Halemaumau pit crater on July 10, 1919. Map originally published in Geological Society of America Memoir 21, (Jaggar, 1947, pl. 79a).

Mauk, F.J., and Kienle, J., 1973, Microearthquakes at St. Augustine Volcano, Alaska, triggered by Earth tides: Science, v. 182, p. 386–389.

Melchior. P., 1966 The Earth Tides: Oxford, Pergamon Press, 609 p.

Pekeris, C.L., 1940, Note on tides in wells: Eos (Transactions of the American Geophysical Union), v. 21, p. 212–213.

Pertzev, B.P., 1957, On the calculation of the drift curve in observation of bodily tides: Marees Terrestres, Bulletin d'Informations, 5. p. 71–72.

Richardson, H.R.M., 1956, Tidal fluctuations of water level observed in wells in East Tennessee: Eos (Transactions of the American Geophysical Union), v. 37, p. 461–462.

Ryall, Alan, VanWormer, J.D., and Jones. A.E., 1968, Triggering of microearthquakes by Earth tides, and other features of the Truckee, California, earthquake sequence of September, 1966: Bulletin of the Seismological Society of America, v. 58, no. 1, p. 215–248.

Shimozuru, Daisuke, 1975, Lava lake oscillations and the magma reservoir beneath a volcano: Bulletin Volcanologique, v. 39, no. 4, p. 570–580.

———1981, Magma reservoir systems inferred from tilt patterns: Bulletin Volcanologique, v. 44, no. 3, p. 499–504.

Shlien, S., 1972, Earthquake-tide correlation: Geophysical Journal of the Royal Astronomical Society, v. 28, p. 27–34.

Simpson, J.F., 1967, Earth tides as a triggering mechanism for earthquakes: Earth and Planetary Science Letters. v. 2, p. 473.

Wright, T.L.. 1984, Origin of Hawaiian tholeiite: A metasomatic model: Journal of Geophysical Research, v. 89, p. 3233–3252.

GEOELECTRIC CHARACTER OF KILAUEA IKI LAVA LAKE CRUST

By Lennart A. Anderson

ABSTRACT

Two orthogonal Schlumberger soundings were made in the Kilauea Iki pit crater on the Island of Hawaii to determine the vertical resistivity of the crust overlying a molten lava lens. The data indicate a relatively good conductor in the 6- to 12-m depth interval interposed between two high-resistivity layers. Subsequent borehole resistivity logging disclosed the existence of a second conductive section in the 29- to 34-m depth interval. The upper conductive zone results primarily from the deposition of wet salt precipitates within the vesicles and pore spaces of the basalt, whereas the lower conductive zone results from a sufficient quantity of meteoric water in the liquid phase to reduce the resistivity of the rock. A dry, highly resistive layer separates the lower conductive zone from the melt. Rock-property measurements on borehole core samples indicate that the in-place resistivity of the rock is controlled by environmental factors rather than by compositional or textural variations. Only in those samples from the 6.1- to 6.7-m depth interval are the laboratory resistivity measurements equal to the resistivities measured in the borehole. A scanning electron micrograph of minerals found within the vesicles of the rock sample from the 6.7-m depth revealed evidence of zeolite and clay development in quantities sufficient to reduce the resistivity of the rock by means of surface conduction.

INTRODUCTION

In the mid-1970's, the Sandia Corporation, under a Department of Energy grant, began a study of shallow magma reservoirs, with the ultimate objective of determining the feasibility of withdrawing heat from a molten lava body for direct conversion into a useful form of energy (Hermance and Colp, 1982). Kilauea Iki lava lake, on the Island of Hawaii, formed during the summit eruption of November–December 1959, was chosen as the site of the initial study, which consisted of first identifying and subsequently delineating an area of near-surface molten lava through the use of various geophysical methods. Staff members of the U.S. Geological Survey's Hawaiian Volcano Observatory (HVO) on Kilauea were invited to participate in the exploration phase, particularly in the application of electrical measurements to a study of the electrical character of the crust of the lava lake and to the mapping of the lateral configuration of the molten lava lens.

Kilauea Iki is a pit crater, approximately 1.6 km long and 0.8 km wide, situated immediately east of Kilauea caldera (fig. 50.1). Before the November 1959 eruption, the pit crater was 213 m deep at its lowest point and, following termination of volcanic activity, a lava lake 111.3 m deep covered the old floor of the crater (Richter and Moore, 1966). In the ensuing years, cooling and subsequent solidification, which is not as yet complete, has caused the lake surface to subside to a level perhaps as much as 10 m below the initial level.

The first geophysical mapping in Kilauea Iki occurred in April 1961, when electromagnetic profiling and sounding methods were used to identify the boundaries of the molten lava and to determine the thickness of the overlying crust. At that time the 100 °C isotherm was at a depth of less than 1 m below the lake surface, and, despite rainfall in excess of 2.5 m/yr, the meteoric water was rapidly vaporized and none remained in the rock. The resulting resistivity contrast between the dry, solidified lava, about 9 m thick at the time (Richter and Moore, 1966), and the conductive molten lava made interpretation of the field data relatively simple. In 1976, the 100 °C isotherm had descended to a depth of approximately 34 meters below the lake surface, and a perennial cycling of water in the liquid-vapor state had been established in the upper part of the lake crust. As a consequence, the added moisture has altered the upper basalt layers, adding to the complexity of an interpretation involving electromagnetic sensing of the molten lava at depth (Smith and others, 1977).

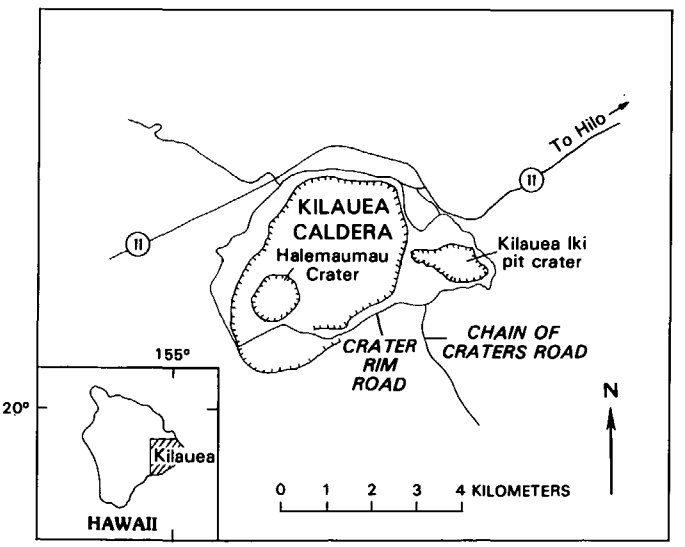

FIGURE 50.1.—Kilauea Volcano showing location of Kilauea Iki pit crater.

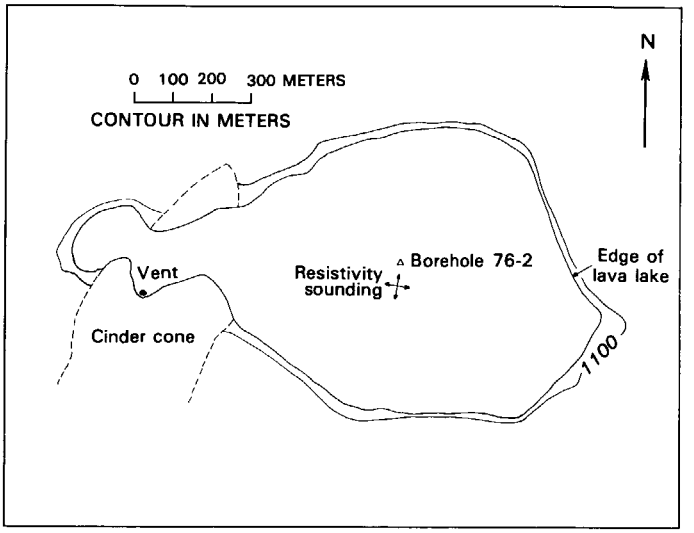

FIGURE 50.2.—Kilauea Iki lava lake showing resistivity sounding and borehole locations.

ACKNOWLEDGMENTS

I wish to express my gratitude to Neil Fishman, Jim Gude, and Richard Sheppard of the U.S. Geological Survey, Denver, for their contributions to the recognition of the unusual occurrence of zeolites within the crust of the Kilauea Iki lava lake. I am also grateful to John Forbes of the Hawaii Volcano Observatory for his help in constructing the borehole probes used in this investigation.

SCHLUMBERGER ELECTRICAL SOUNDINGS

To obtain information on the gross distribution of resistivity of the lake crust with increasing depth, two mutually perpendicular Schlumberger electrical soundings were made near the center of the lava lake in April 1976 (fig. 50.2). The sounding curves and their interpretations in the form of geoelectric sections obtained by means of a computer program developed by Zohdy (1974) of the U.S. Geological Survey are presented in figure 50.3. The east-west sounding shown in figure 50.3*A* was expanded along the major axis of the lake. The interpreted geoelectric section indicates the presence of a relative conductor within the 6- to 12-m depth interval interposed between two layers of much higher resistivity. The near-surface layer is essentially dry and hence, resistive, and as the temperature of the lower layer is increased, ground water is excluded from the rock, causing that section to become increasingly resistive with depth.

The effect of lateral variations in resistivity is evident on the sounding curve shown in figure 50.3*B*. The vertical offset in the field data observed at current electrode spacings within the 12- to 16-m depth interval, resulting from repeated measurements at two different potential electrode spacings while maintaining a fixed current

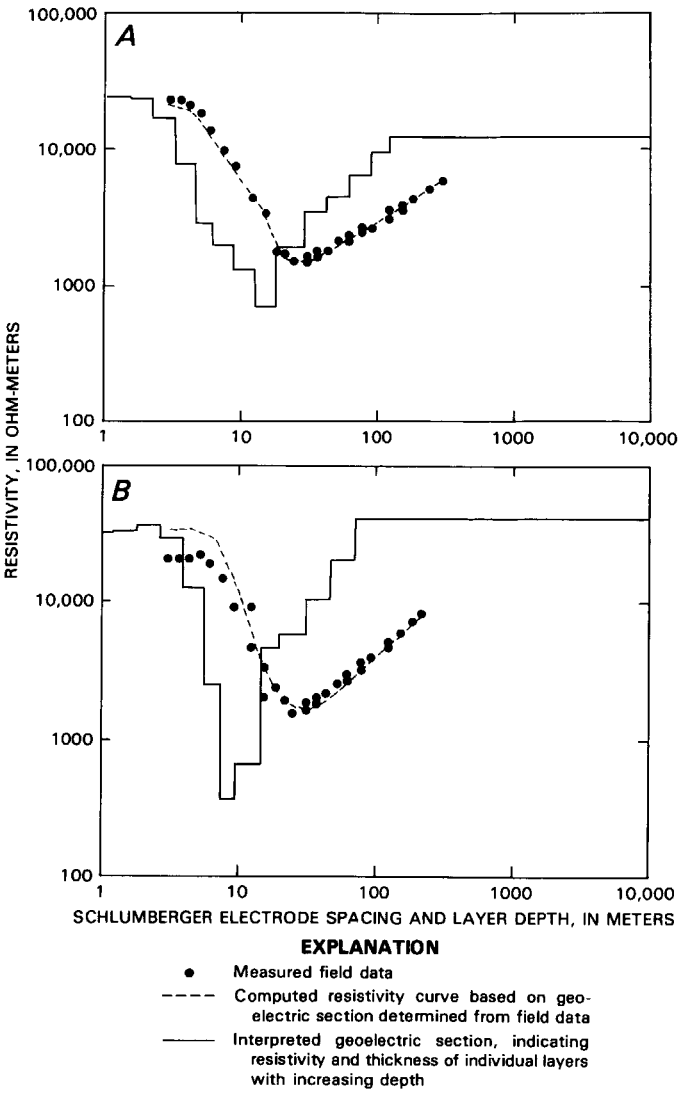

FIGURE 50.3.—Vertical electrical soundings (direct-current resistivity) made by expanding electrode array in (*A*) east-west-direction and (*B*) north-south direction.

electrode spacing, is an indication that the rock resistivity is higher sidewise to the center of the sounding array than at the center of the sounding itself. In Kilauea Iki, the blocklike crustal configuration has produced a network of vertical fractures, some of them visibly open, which tend to interfere with current flow. Following a procedure initiated by Zohdy and others (1973) the curve segment measured at the longest electrode spacings is held fixed in position while the other segments representing shorter electrode spacings are shifted upward or downward to form a continuous curve that can be interpreted in terms of laterally homogeneous media. As the result of an upward shift of the left-hand segment, the surface layer as interpreted from the north-south sounding is appreciably higher than that interpreted from the east-west sounding.

The north-south sounding curve (fig. 50.3*B*) is similar to the

east-west sounding curve in the sense that a shallow conductor is situated between two resistive layers. A fundamental difference exists in that the right-hand branch of the north-south sounding curve rises at a slope of 1, indicating that the resistivity of the lower layer increases abruptly relative to the overlying layer, whereas, the corresponding branch of the east-west curve rises at a slope of less than 1, as if sensing on a zone of gradually increasing resistivity. Neither sounding indicates the presence of an underlying conductive zone.

A problem in interpreting the soundings is to reconcile the nature of the lateral changes in resistivity that produce the slope differences between the right-hand branches of the east-west and north-south sounding curves. Efforts to develop a three-dimensional model representative of the horizontal and vertical resistivity section that may reasonably exist within the lava crust, sufficient to simulate the sounding curves, failed to produce the desired results. The resistivity variations within the lava lake and surrounding environs are highly complex and difficult to reconstruct on the basis of existing data.

BOREHOLE RESISTIVITY LOGGING

Two boreholes located 61 m north of the direct-current resistivity sounding site were drilled 41 cm apart during August 1976; they penetrated the solid-melt interface at 45.52 m (Colp and Okamura, 1978). When a borehole became available for in-hole resistivity measurements, several design schemes and materials were tested until a suitable probe was eventually assembled made of four sections of quarter-round wood moulding and wiper-type electrodes constructed of welding rod. Although the probe charred badly as the temperature increased in the lower part of the hole, its structural integrity was maintained, allowing measurements to be made until the welding rod lost its resilience and slumped to the extent that mechanical contact with the borehole wall was no longer possible. Resistivity measurements were made as with the normal array using current-potential electrode spacings of 1 and 2 m read at 0.5-m intervals.

The first successful resistivity log was obtained by early December 1976 (fig. 50.4). Resistivities are shown plotted as a function of the depth to the midpoint between the potential and current electrodes. In a general sense, each data set portrays a more complicated geoelectric section than that indicated by the vertical electrical soundings. Instead of two layers of varying resistivity overlying the hot, dry, resistive zone above the molten lava, at least four layers exist. The lowermost, relatively conductive section in the 29- to 34-m depth interval identifies the zone of highest water content where the liquid phase of a two-phase system predominates. Above the wet zone, the moisture is primarily in the vapor phase, resulting in higher resistivities. A second conductive layer exists in the 4- to 12-m depth interval; it has resistivities lower than those measured in the lower conductive zone. Obviously no standing water exists in this upper layer nor is there any reason to suspect a difference in mineralogy sufficient to cause the interval to be less resistive than the main body of solidified lava. The cause of the increased conductivity is believed to be primarily the result of wet salt precipitates forming within the vesicles and pore spaces of the rock as some condensation of the upward-moving wet steam takes place because of a subtle drop in temperature. Temperature measurements made at the time of the December logging survey (fig. 50.4) indicated values slightly less than 100 °C above the 16-m depth, thus verifying that the near-surface zone undergoes some degree of cooling as the result of intermixing with downward-moving rain water. The source of the brine is believed to be a dissolution of magmatic gases within the lower water-saturated layer, portions of which are eventually carried upward within the wet steam. Helz and others (1980) have identified the presence of thenardite—a sodium sulfate salt (Na_2SO_4)—within certain intervals of the recovered core. The high-salinity surficial waters coating the rock provide a continuous flow path for electrical current such that the bulk resistivity of the rock is greatly reduced.

In-hole resistivity measurements were repeated in April 1977 with a similar probe at the same electrode spacings as before, the only difference being that the material used for the electrodes was stainless steel rather than welding rod. The character of the resulting data profile is essentially unchanged; however, appreciable changes occurred during the 4-month time period. Among these changes is an overall decrease in the level of resistivity within the entire borehole (fig. 50.5). Apparently the borehole provides an easy escape route for steam, causing an increase in the concentration of salt and possibly the development of clay minerals in the surrounding rock owing to hydrothermal alteration, thereby reducing its bulk resistivity. Another change from the earlier log is an increase in the depth to the lower conductive zone of about 3–4 m during the elapsed 4-month time period. This change is well in excess of the 2.11-m annual solidification rate calculated by Hardee (1980). Possibly the borehole allowed an anomalous quantity of heat to escape, thereby creating a localized deepening of the 100 °C isotherm. In the December 1976 resistivity log (fig. 50.4) the hot, dry zone overlying the molten lava was highly resistive at the depth to which measurement was possible. The April 1977 log (fig. 50.5) indicates this zone to be somewhat less resistive with lower resistivities appearing at greater depth. However, the April log shows an inconsistency in the resistivity correspondence between the 1- and 2-m measurements in the 37- to 39.5-m depth interval. A breakdown in cable insulation may have occurred in the extremely high temperature environment, causing leakage that would produce erroneous resistivity values. Upon removal from the borehole, the probe was checked and found to be intact; however, the probe had cooled considerably once on the surface, so any problem with cable faults relating to thermal expansion may have gone undetected. As with the welding rod, the stainless steel electrodes lost their resilience, making continued contact with the borehole walls impossible. If the contact resistance was high because of the deteriorating condition of the potential electrodes, the measurement may have produced an anomalously low resistivity. Pockets of molten lava could conceivably exist in sufficient quantities in the near-hole environment to produce the low resistivities observed in the dry zone. If the molten lava is nonuniformly distributed, then the bulk

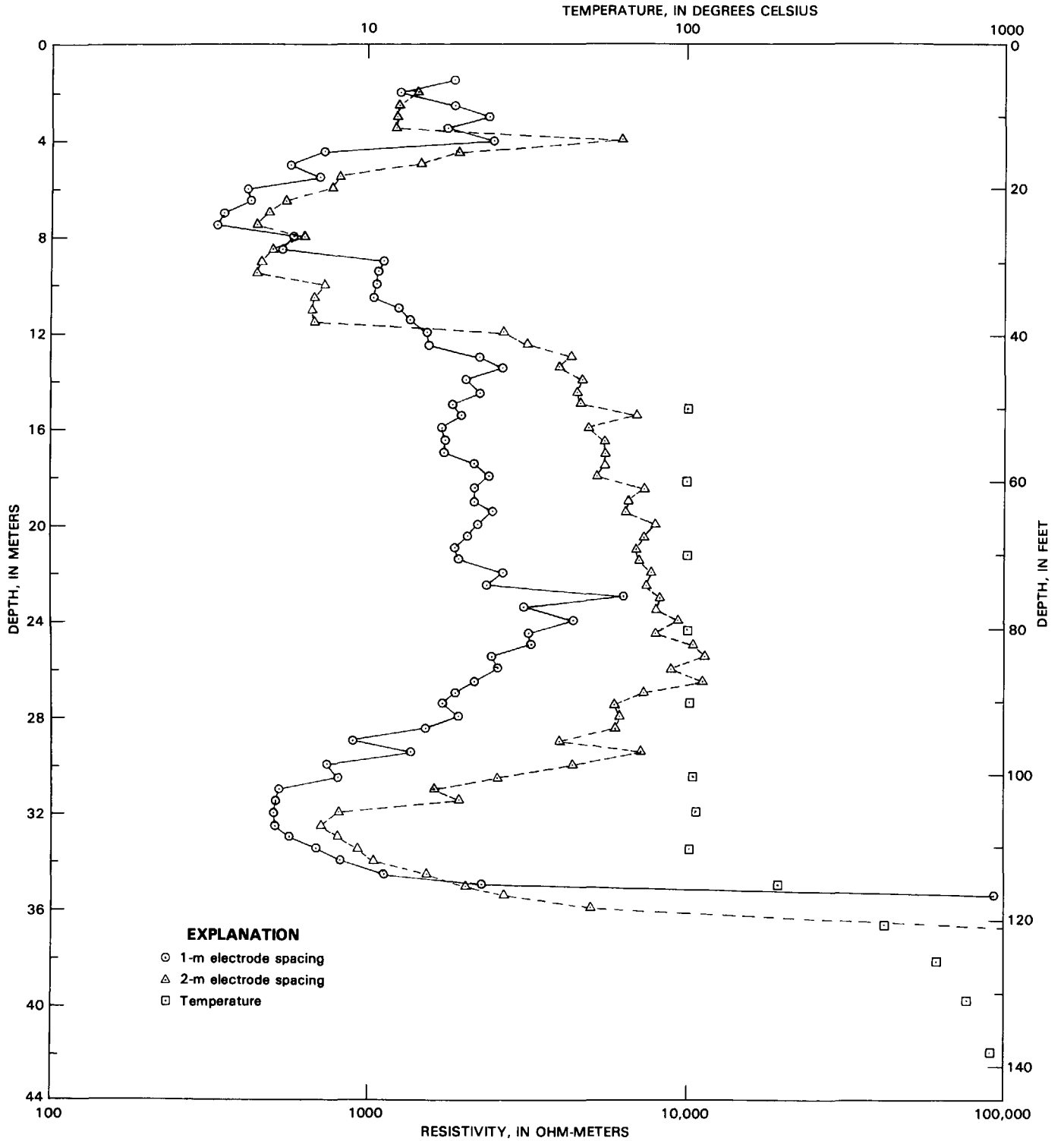

FIGURE 50.4.—Direct-current resistivity and temperature data obtained in Kilauea Iki borehole 76-2 in December 1976.

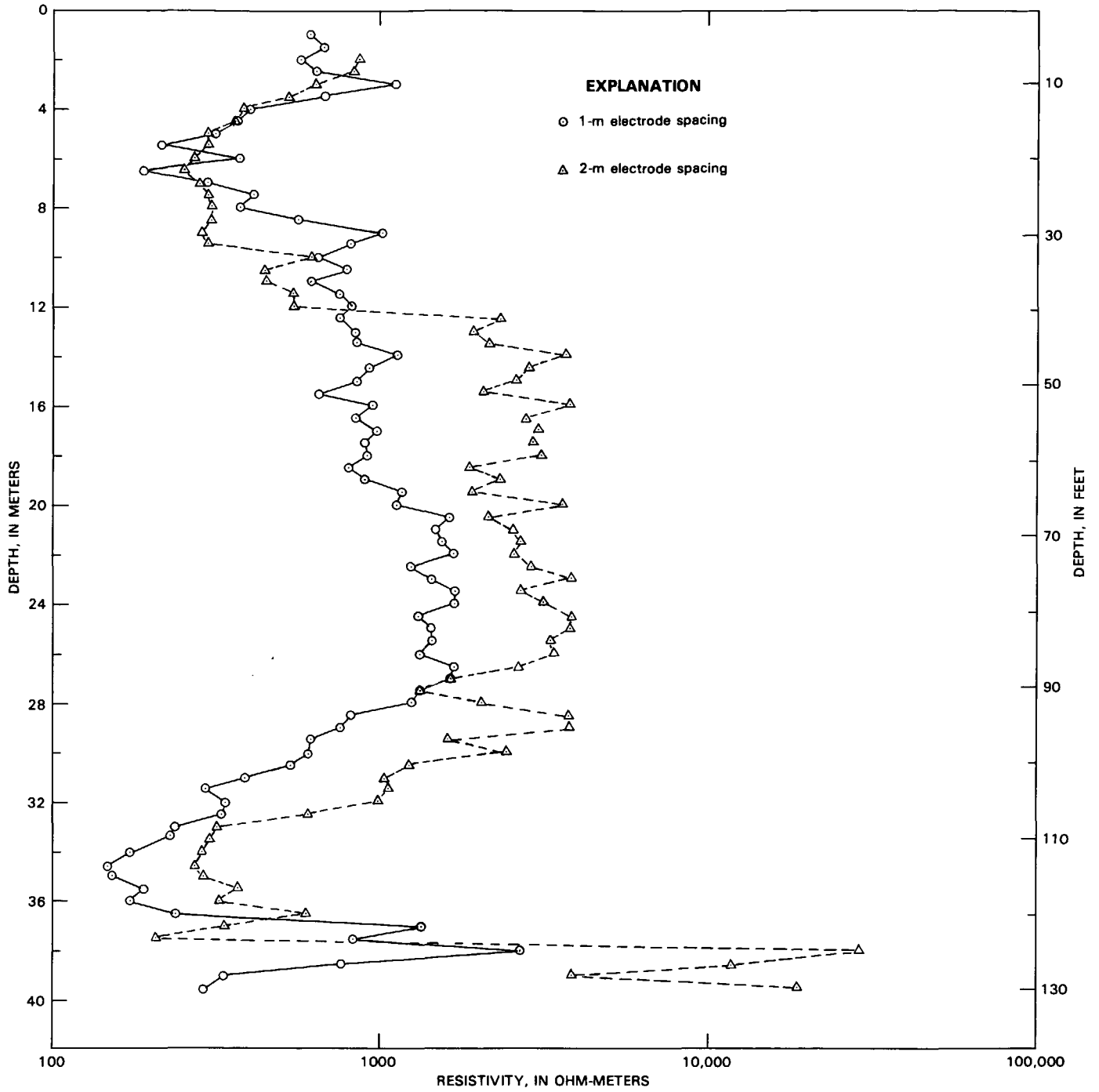

FIGURE 50.5.—Direct-current resistivity data obtained in Kilauea Iki borehole 76-2 in April 1977.

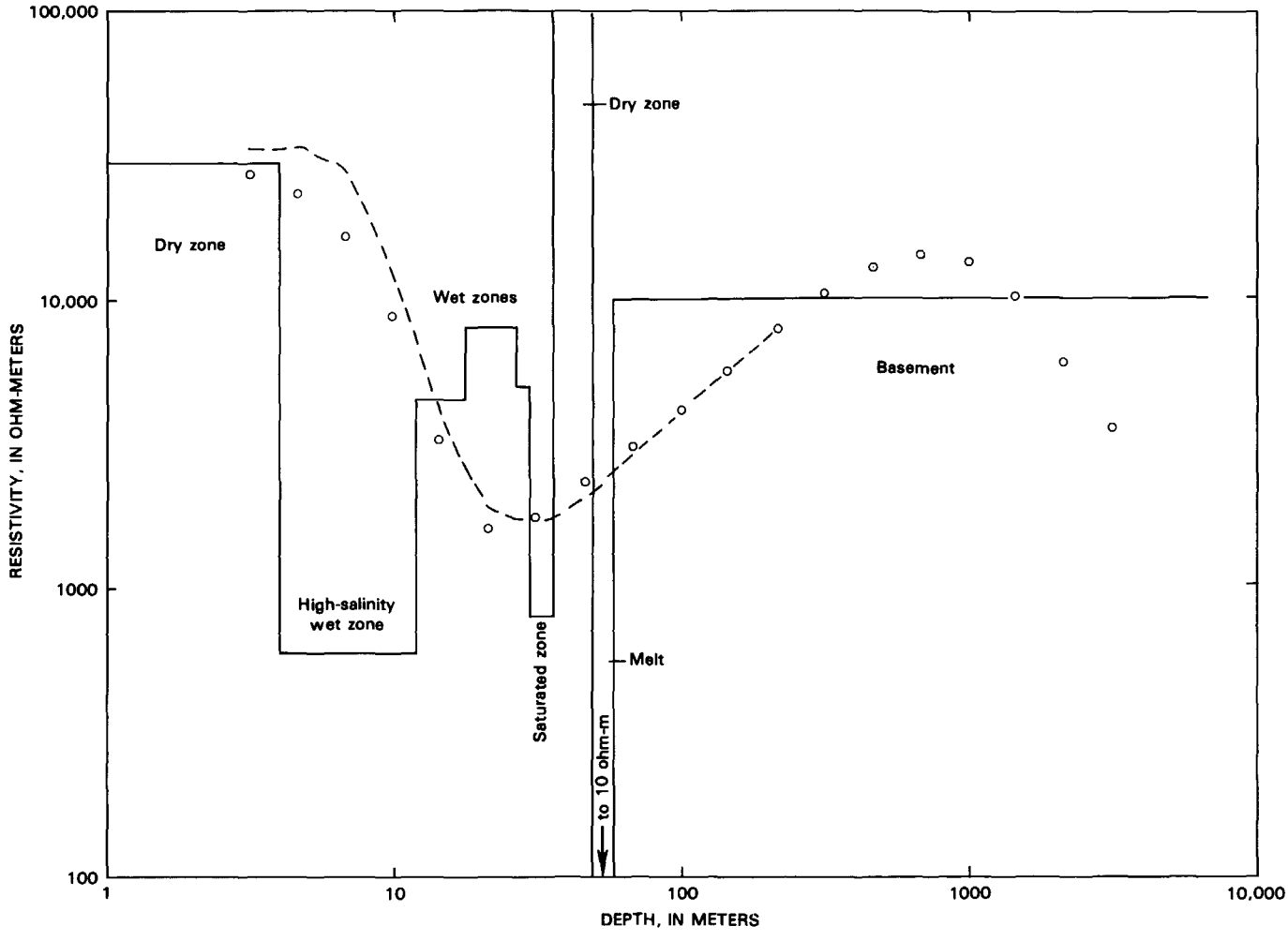

FIGURE 50.6.—Geoelectric section compiled from December 1976 borehole resistivity log obtained at 2-m spacing. Thickness of 100,000 ohm-m section and resistivity of molten lava is inferred from other data. Dashed line, adjusted field curve for north-south resistivity sounding; circles, Schlumberger resistivity values.

resistivity, which is a volume measurement, will differ as a function of electrode spacing. However, intuition suggests that the molten lava would exist in greater abundance with increasing distance from the borehole. The data do not support this notion inasmuch as the resistivities are appreciably higher at the 2-m spacing. A third explanation for the low resistivities near the bottom of the hole may be that the basalt is at a high enough temperature to become ionically conductive. If this were the case the resistivities measured at both electrode spacings would vary in a systematic and uniform manner. Despite the arguments that can be made in support of the validity of the data, the uncertainties are sufficient to judge the resistivity measurements below the 37-m depth to be questionable.

In considering the overall decrease in resistivity of the rock in near proximity to the borehole during the 4-month period between December 1976 and April 1977, it seems likely that the December log may not necessarily be typical of the resistivities of the rock at the time of drilling. As a check on how critical local alteration may have been, a theoretical Schlumberger curve was computed based on layer resistivities and thicknesses derived from the December 1976 2-m log. Because the first resistivity measurement was made at a depth of 2 m, the dry, uppermost part of the surface layer is not represented on the downhole log. Instead, a value of 30,000 ohm-m was selected for the upper 4-m layer.

The computed curve superimposed upon the north-south sounding and the columnar graph showing resistivities and thicknesses selected from the borehole data are shown in figure 50.6. Despite the generalizations made in constructing the model, the fit to the field curve is considered to be satisfactory. To a spacing of 213 m, which is the largest spacing used in the field measurement on the north-south sounding, nine resistivity layers are represented, but from the shape of the sounding curve recognizing more than three is difficult. The existence of the water-bearing conductive zone is obscured by the presence of the underlying hot, dry section arbitrarily assigned a resistivity value of 100,000 ohm-m.

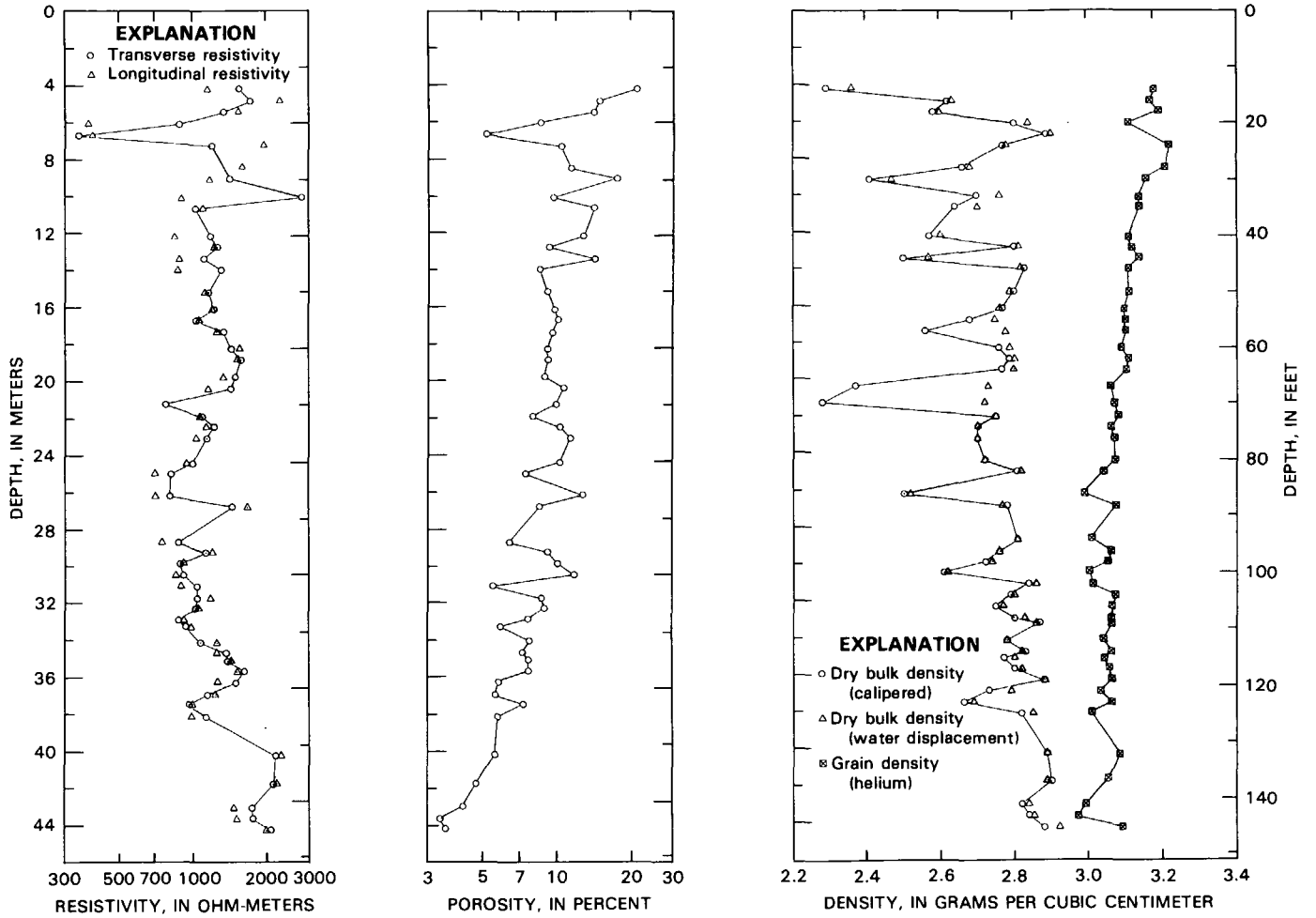

FIGURE 50.7.—Resistivity, porosity, and density values obtained on core samples from Kilauea Iki borehole 76-2.

To determine the half-spacing required to sense on the conductive magma beneath the dry zone the plot was continued by setting constraints on the thicknesses of the layers at depth. According to Hardee (1980) the hot, dry zone has, in recent years, maintained a constant thickness of 12 m. Beyond that knowledge, only estimates can be made of the parameters involving the resistivity and thickness of the molten lava. An indirect measurement of the melt resistivity was made in 1961 (Frischknecht, 1967) and, through curve matching, determined to be precisely 2.09 ohm-m. However, the molten lava was in the early stages of cooling, and subsequent degassing of the lava may have resulted in an increased resistivity requiring that a minimum resistivity of 10 ohm-m be used in order to match the north-south sounding curve. The thickness of the molten section was chosen to be 10 m, underlain by an infinitely thick section of 10,000 ohm-m resistivity. It is apparent from figure 50.6 that a Schlumberger half-spacing in excess of 400 m would be required before the effect of the molten lava becomes evident, and a half-spacing of about 1,000 m is necessary before an actual downturn in apparent resistivity is noted.

LABORATORY CORE ANALYSIS

To evaluate the causes of the resistivity variations observed in the borehole measurements, 51 core samples were obtained from the 4.27- to 44.21-m depth interval of the 76-2 borehole for laboratory rock-property analysis. Core samples were selected at spacings of 0.61 m, where available, and shaped to an approximate size of 3.33 cm diameter and 3.8 cm length. Samples oriented axially parallel (vertical) to the borehole were used for resistivity, density, and porosity measurements, whereas core samples oriented axially perpendicular (horizontal) to the borehole were only measured for resistivity. Sample resistivities were measured in a four-terminal holder (Parkhomenko, 1967) following core saturation with local tap water. Resistance measurements, made at a frequency of 100 Hz using a high-precision digital resistance meter, were converted to resistivity (in units of ohm-m) from caliper measurements of sample length and diameter.

Procedures for obtaining density and porosity data are those described by Johnson (1979a). Samples in the saturated state were

weighed both in air and suspended in water and reweighed when totally dry. Rock volume was obtained using a water displacement technique discussed in Chleborad and others (1975). From the collective data, dry bulk density, saturated bulk density, and porosity were calculated. A helium pycnometer was used to determine grain density. All measured rock-property values are plotted as a function of depth in figure 50.7.

Resistivities were measured on mutually perpendicular cores cut from the same sample to examine the effect of vesicle alignment on current flow through the sample. Normally, a lava block would be expected to possess uniform electrical properties in that no distinct bedding planes are formed in the cooling process. Examination of the core samples, however, often revealed a distinct alignment of gas bubbles, particularly in the horizontal plane. Should hydrated minerals form within these vesicles their physical continuity would certainly cause an appreciably lower resistivity in one direction than in the other. In virtually all rock types, the transverse resistivity exceeds that of the longitudinal resistivity such that the anisotropy coefficient, defined as the square root of the ratio of transverse to longitudinal resistivity, is greater than 1.0 (Keller and Frischknecht, 1966). With few exceptions, the anisotropy coefficient of the Kilauea Iki basalts is very nearly equal to 1.0, and where it is slightly less than 1.0, the discrepancy may be caused by the fact that the material measured in each sample pair is not quite the same. The plot in figure 50.7 shows the transverse resistivity to be generally greater or equal to the longitudinal resistivity, although obvious exceptions do exist, particularly within the upper conductive zone as defined by the borehole resistivity log.

The environmental conditions in which the borehole and sample measurements were made are obviously so different that the character of the sample resistivity log is totally unlike that of the borehole resistivity logs. The most notable change on the sample plot is in the virtual loss of the conductive zones defined in the borehole log. Dissimilarities in measuring conditions involving factors such as temperature, pore-water levels, and water salinity are considered to be the principal cause of the resistivity differences. Samples from the 6.1- and 6.7-m depths are exceptions producing resistivities equal to those measured in the borehole.

It was anticipated that much of the contained thenardite, identified by Helz and others (1980), would be leached from the rock following the resaturation process. The sample measurements would then be expected to produce resistivities that vary as a function of porosity and mineral content. Grain densities vary only slightly, suggesting a relatively uniform mineral content. Grain densities, however, decrease with depth as a result of higher olivine and pyroxene contents in the upper part of the lava crust. According to Johnson (1979b), high density minerals having high separation temperatures are trapped in the rapidly cooling groundmass, whereas, at depth, where cooling has progressed at a much lower rate, the heavy minerals have had time to settle to the lower levels of the molten lava pool. The grain density values in figure 50.7 indicate the transition to be gradual. Large phenocrysts of olivine can be found in the near-surface lavas, but no evidence of olivine exists in the core taken from the lower lava section. The variation of the heavy mineral content of the basalt, however, would do little to alter the resistivity in the manner shown in figure 50.7.

In the absence of conductive minerals as part of the rock composition, the resistivity of a rock is controlled by porosity, the amount of water within the pore structure, and the salinity of the contained water as predicted by Archie's equation, assuming that electrical conduction is by means of the contained pore waters (Keller and Frischknecht, 1966). An attempt to statistically relate the observed resistivities of the core samples to porosity proved unsuccessful; a least-squares fit to a logarithmic model produced a correlation coefficient of -0.17, indicating that other factors also influence the resistivity of the rock.

In an experiment on a Kilauea Iki basalt sample by Olhoeft (1977), a resistivity dependence apart from volume conductance through the pore water was recognized. For resistivity enhancement to occur, alteration products, either in the form of clays or zeolites, must exist within the pore spaces of the rock. Evidence of sparse mineral content was detected within the few vesicles exposed at the surface of the 6.7-m sample. On the premise that the mineral was other than thenardite, a scanning electron micrograph (SEM) was obtained of the mineral (fig. 50.8). That figure shows the wall of the vesicle and tabular crystals of what is thought to be a zeolite. An energy-dispersive X-ray analysis, focusing on the large crystal in the upper left-hand corner of figure 50.8, indicates the mineral to be an aluminosilicate, possibly clinoptilolite or phillipsite based on comparisons of the morphology of zeolite crystals presented in Mumpton and Ormsby (1978).

Further examination of the mineral content of the vesicle revealed what is believed to be clay (montmorillonite?) coating the suspected zeolite (fig. 50.9). The quantity of vug-filling minerals

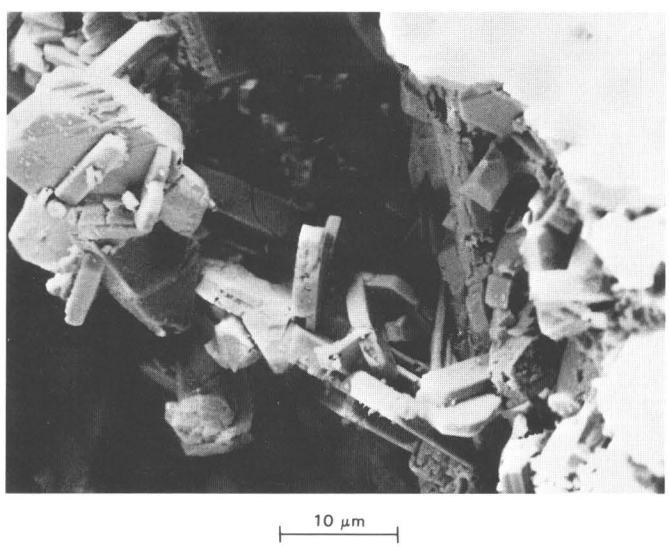

FIGURE 50.8.—Scanning electron micrograph of suspected zeolite mineral found within vesicle of basalt sample from 6.7-m depth of Kilauea Iki lava lake crust.

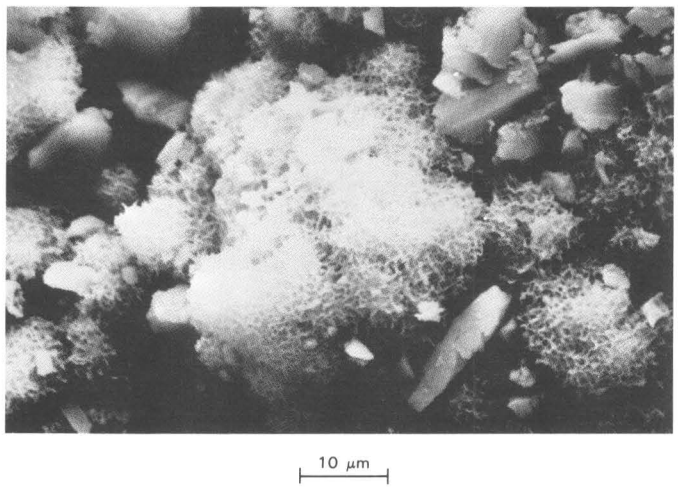

FIGURE 50.9.—Scanning electron micrograph of clay coating on suspected zeolite minerals found within vesicle of basalt sample from 6.7-m depth of Kilauea Iki lava lake crust.

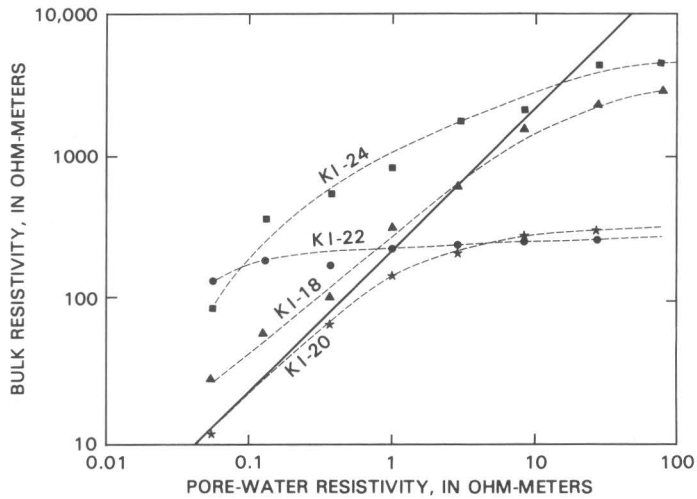

FIGURE 50.11.—Bulk resistivity variation with increasing pore-water resistivity in basalt samples KI-18, KI-20, KI-22, and KI-24, taken from Kilauea Iki lava lake crust at depths of 5.5, 6.1, 6.7, and 7.3 m, respectively. Heavy black line is plot of increasing resistivity as a function of decreasing pore-water conductivity based on Archie's equation.

was, however, insufficient to obtain a positive identification by means of X-ray diffraction.

An SEM of vug-filling minerals, found within the rock covering the surface of the lava lake, is shown in figure 50.10. Although the mineral quantity was adequate for X-ray analysis, the material proved to be an amorphorous mass containing principally silica, aluminum, and potassium. The mineral lining the vug was determined to be opal (R. Sheppard, oral commun., 1984).

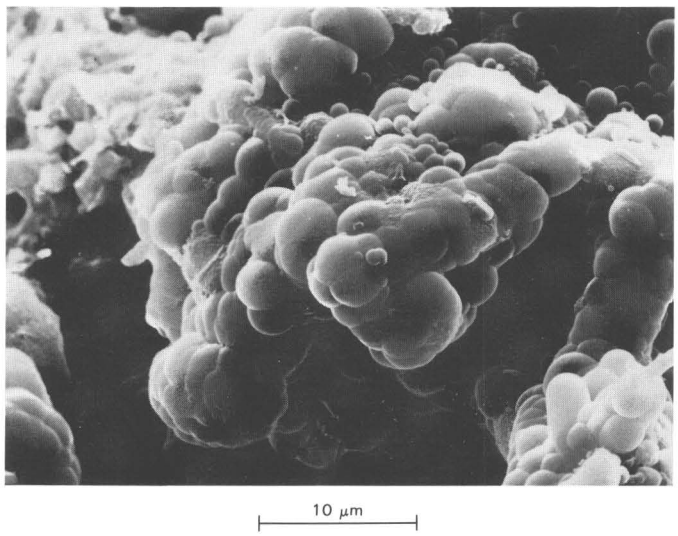

FIGURE 50.10.—Scanning electron micrograph of amorphous mass of silicon, aluminum, and potassium found within vesicles of surface sample of Kilauea Iki basalt. Lining of cavity was determined to be opal (R. Sheppard, oral commun., 1984).

Clays, zeolites, and opal are hydrated minerals and, as such, are capable, by means of surface conduction, of altering the resistivity of the basalt if the minerals exist in sufficient quantities to provide a continuous flow path for electrical current. Surface conduction occurs in certain minerals as the result of an excess ion population within the diffuse layer located on the outer bounds of the electrolyte-solid interface (Keller and Frischknecht, 1966). A thenardite coating on the pore walls of the rock undoubtedly exerts the greatest influence on the in-place resistivity. To determine the extent to which the hydrated minerals contribute to total conduction, resistivities were measured on four samples after progressive saturation with eight KCl solutions of increasing salinity. The core samples are from the 5.49- to 7.32-m depth interval but are labeled in figure 50.11 in units of feet. Figure 50.11 shows the results plotted against increasing pore-water resistivity. Samples KI-20 and KI-22 have similar resistivities when saturated with high-resistivity pore water. As the pore-water resistivity is increased, the resultant decrease in bulk resistivity of the KI-20 sample is dramatic when compared to the relatively small change in the bulk resistivity of the KI-22 sample. The difference in the character of the two resistivity curves is believed to be the result of incomplete invasion of the sequential introduction of the increasingly saline pore water because of the much lower porosity of the KI-22 sample.

The straight line drawn asymptotic to the left hand segment of the curve labeled KI-20 on figure 50.11 is a graph of rock resistivity calculated from Archie's equation using measured values of pore-water resistivity and rock porosity (Keller and Frischknecht, 1966). The departure of the rock resistivity curve from the Archie plot indicates that current flow occurs within the structure of the hydrated

minerals lining the vesicles of the rock as well as through the saturating solution. Although not shown, each sample has an equivalent Archie curve that can be drawn as straight-line projections, illustrating the relative importance of surface conduction in controlling the resistivity of each sample. Surface conduction is most apparent at the higher pore-water resistivities.

Samples KI-20 and KI-22 indicate resistivities most influenced by surface conduction as compared to the bordering samples from the 18- and 24-ft levels. Apparently the conditions for zeolite and clay development are most ideal within a very narrow horizon at the indicated depth interval of the lava crust. From the poor correlation between resistivity and porosity, however, some degree of surface conduction evidently takes place within most samples. Another reason for the lack of correlation is that the original salt content may not have been totally leached from the samples during the resaturation process, thereby causing resistivity variations as a function of differences in pore-water salinity.

SUMMARY

The geoelectric sections interpreted from Schlumberger soundings made at the center of the lava lake are basically the same, differing only in the thickness of the conductive zone and the value of the bottom-layer resistivity. The difference in the shape of the sounding curves results from lateral resistivity variations whose complexities have not been resolved. Each sounding, however, clearly indicates the presence of a conductive zone at a depth of about 7 m with a thickness of at least 3 m. No evidence of a highly conductive zone at depth representing either the water lens or the molten lava can be seen in the sounding data.

The resistivity logs obtained in the 76-2 borehole verify the existence of a conductive layer within the 4- to 12-m depth interval. In addition, an equally conductive layer was detected below the 28-m depth in a zone overlying the very hot, but dry, layer covering the molten lava at the 45.7-m depth as determined from drilling. The 28- to 35-m depth conductive zone is believed to correspond to a gas-charged hot-water lens that increases gradually in resistivity with decreasing depth as the water vapor/liquid ratios increase. In the central zone the pore spaces of the rock are thought to be filled with wet steam containing ionized molecular particles dissolved from magmatic gases mixing with meteoric waters in the lower conductive zone. Temperatures fall slightly below 100 °C in the upper zone and, coupled with possible pressure release, conditions may be ideally suited for the formation of condensation products within the cavities and pore structure of the rock. Even in substantially undersaturated rock, a wet salt coating, such as made possible by the confirmed presence of thenardite within the lake crust, is sufficient to produce an appreciable decrease in rock resistivity.

The borehole-resistivity log was repeated in April 1977. The notable changes occurring in the 4-month intervening period are the overall decrease in resistivities for the entire penetrated section and a substantial increase in the depth to the lower conductive layer identified as a zone containing hot water. According to Hardee (1980) the established rate of cooling now in progress adds 2.11 m/yr to the thickness of the crust; however, according to the resistivity log, the crust had increased almost 4 m in only a 4-month period. Possibly the two boreholes at this site allow for an anomalously high rate of heat energy release, thereby accelerating crustal development.

It is uncertain as to why the overall resistivity of the rock surrounding the borehole has decreased. The resistivity decrease, however, is believed to be related to the upward migration of the steam phase of meteoric water following a preferential path made possible by the two adjacent drillholes. Perhaps the escaping steam has produced a conductive lining on the borehole walls as a result of alteration in the form of clays and zeolites, thereby causing a decrease in the apparent bulk resistivity measured for the surrounding rock. Based on the fact that thenardite is easily recognized within the cored section, it seems more likely that concentrations of the sodium sulfate salt have been deposited within the vesicles of the basalt in near proximity of the borehole, well in excess of that which is normally formed in the rock, thereby enhancing its conductivity.

Although a borehole may alter the electrical character of the rock in the immediate vicinity of the hole, the geoelectric layering is considered to be representative of that which persists laterally within the lake crust. The fact that the December in-hole resistivity log made at the 2-m spacing could be converted to a sounding curve very similar to that measured at a site 61 m displaced from the borehole provides evidence of the continuity of the geoelectric layering. Some variation in the resistivity of the upper conductive zone may occur as rainfall increases and a certain amount of leaching takes place. However, the salt would be expected to ultimately be redeposited in the 4- to 12-m depth interval where temperature and pressure favor concentration of salts carried upward in the liquid-vapor water system.

Rock-resistivity measurements on core obtained from the 76-2 borehole produce a substantially different pattern from that observed on the in-hole resistivity logs. This difference is not surprising considering the dissimilar environments in which each set of data was taken. However, it was hoped that a sufficient quantity of salt would be retained within the samples in order to verify introduced salt as the principal cause of the anomalously low resistivity measured in the 4- to 12-m depth interval. Apparently the high porosity of most samples allowed the salt to leach out during the resaturation process. The sample from the 6.71-m depth is an exception inasmuch as its laboratory resistivity is very nearly the same as that measured in the drillhole during December 1976 at the 1-m spacing. A scanning electron micrograph of the mineral content within a single vesicle of the 6.71-m sample shows evidence of both zeolite and clay development. Resistivity measurements on samples from the 5.49-, 6.10-, 5.71-, and 7.32-m depths, made while saturated with KCl solutions of increasing salinity, show the effects of surface conduction, apparently as a result of the alteration products lining the pore spaces and vesicles of the samples. Surface conduction is most apparent in the 6.10- and 6.71-m samples, indicating that clays and zeolites are most abundant within a very narrow horizontal interval of the lava crust.

A pictorial representation of the geoelectric layering of the Kilauea Iki lava lake to a depth including the molten lava as it existed

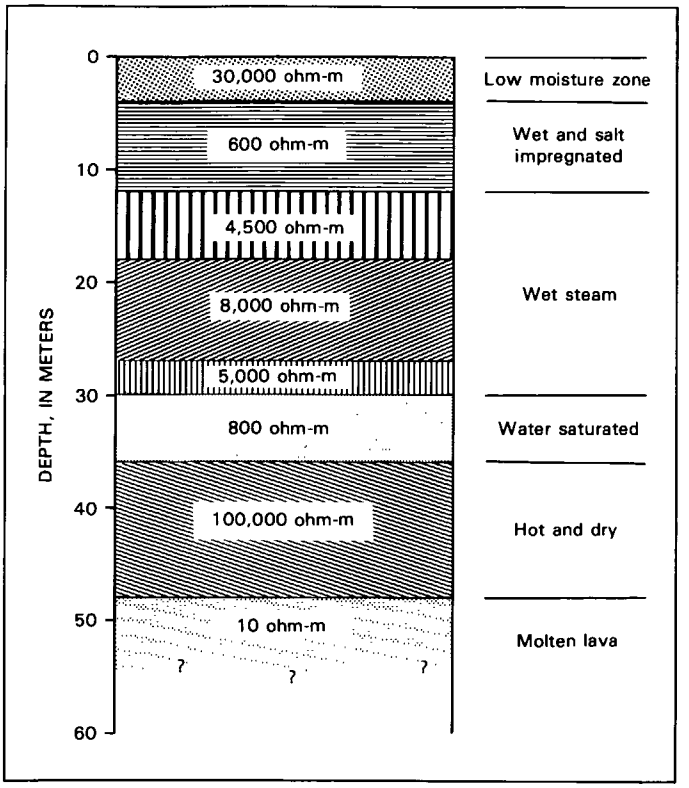

FIGURE 50.12.—Geoelectric layering of Kilauea Iki lava lake crust as determined from December 1976 borehole resistivity log made at 2-m electrode spacing.

in 1977 is shown in figure 50.12. An appreciable thickening of the crust has occurred since that time, most likely adding to the growth of the intermediate zone between the conductive crustal layers and reducing the thickness of the molten lava. From an exploration standpoint the resistivity of both conductive layers within the upper crust is sufficiently low, relative to the surrounding rock, to generate a substantial electromagnetic anomaly. However, if a 600 ohm-m resistivity value is assumed for the entire section overlying the molten lava, at very low frequencies on the order of 20 kHz, the penetrating depth of the primary signal would be more than adequate to sense on the melt. The fact that the resistivity contrast between the solidified and molten lava is at least 60:1 and typically much higher assures that the secondary fields generated by induced eddy currents stem primarily from the molten basalt layer.

REFERENCES

Chleborad, A.F., Powers, R.S., and Farrow, R.A., 1975, A technique for measuring bulk volume of rock material: Association of Engineering Geologists Bulletin, v. 12, no. 4, p. 307–312.

Colp, J.L., and Okamura, R.T., 1978, Drilling into molten rock at Kilauea Iki: Geothermal Resources Council, Transactions, v. 2, p. 105–108.

Frischknecht, F.C., 1967, Fields about an oscillating magnetic dipole over a two-layer earth, and application to ground and airborne electromagnetic surveys: Quarterly Report of the Colorado School of Mines, v. 62, 326 p.

Hardee, H.C., 1980, Solidification in Kilauea Iki lava lake: Journal of Volcanology and Geothermal Research, v. 7, no. 3/4, p. 211–225.

Helz, R.T., Banks, N.G., Casadevall, T.J., Fiske, R.S., and Moore, R.B., 1980, A catalogue of drill core recovered from Kilauea Iki lava lake from 1967 to 1979: U.S. Geological Survey Open-File Report 80–504.

Hermance, J.F., and Colp, J.L.,. 1982, Kilauea Iki lava lake: Geophysical constraints on its present (1980) physical state: Journal of Volcanology and Geothermal Research, v. 13, p. 31–61.

Johnson, G.R., 1979a, Textural properties, *in* Hunt, G.R., Johnson, G.R., Olhoeft, G.R., Watson, D.E., and Watson, K., Initial report of the petrophysics laboratory: U.S. Geological Survey Circular 789, p. 67–74.

———1979b, Porosity and density of Kilauea Volcano basalts: U.S. Geological Survey Professional Paper 1123 A–D, p. B1–B6.

Keller, G.V., and Frischknecht, F.C., 1966, Electrical methods in geophysical prospecting: New York, Pergamon Press, 517 p.

Mumpton, F.A., and Ormsby, W.C., 1978, Morphology of zeolites in sedimentary rocks by scanning electron microscopy, *in* Sand, L.B., and Mumpton, F.A., eds., Natural zeolites, occurrences, properties, use: New York, Pergamon Press, p. 113–132.

Olhoeft, G.R., 1977, Electrical properties of water saturated basalt. Preliminary results to 506 K (233 °C): U.S. Geological Survey Open-File Report D–77–688.

Parkhomenko, E.I., 1967, Electrical properties of rocks: New York, Plenum Press, 314 p.

Richter, D.H., and Moore, J.G., 1966, Petrology of the Kilauea Iki lava lake, Hawaii: U.S. Geological Survey Professional Paper 537–B, p. B1–B26.

Smith, B.D., Zablocki, C.J., Frischknecht. F.C., and Flanigan, V.J., 1977, Summary of results from electromagnetic and galvanic soundings on Kilauea Iki lava lake, Hawaii: U.S. Geological Survey Open-File Report 77–59.

Zohdy, A.A.R., 1974, A computer program for the automatic interpretation of Schlumberger sounding curves over horizontally layered media: Springfield, Va., NTIS (National Technical Information Service) PB-232 703/AS, 25 p.

Zohdy, A.A.R., Anderson, L.A., and Muffler, L.J.P., 1973, Resistivity, self-potential, and induced polarization surveys of a vapor-dominated geothermal system: Geophysics, v. 38, no. 6, p. 1130–1144.

UNIQUENESS OF VOLCANIC SYSTEMS

By Herbert R. Shaw

ABSTRACT

The cyclical behavior of Hawaiian volcanoes resembles patterns predicted on the basis of graphical or numerical attractor dynamics. This is because the recognizable styles of volcanic behavior are outgrowths of contrasts in positive and negative rates of magma transport that control the volumetric states of a growing volcanic edifice. Attractor patterns are likewise the resultants of some specified set of positive-negative rate balances. The distributions of volcanic states (intrusive and extrusive) in space and time constitute sets of complex patterns. Attractor dynamics simulates this complexity. The specification of how unique a given subset of a growth history may be relative to other subsets, or the whole relative to other histories (volcanoes or attractors), involves questions concerning pattern recognition. A totally unique event, pattern, or style of volcanism is one that has never happened before, hence is not recognizable. Volcanism, because it recurs, must represent a hierarchy of simultaneously unique-nonunique patterns. Even though no two growth histories, nor even any two eruptive events, are identical, there are strong resemblances between various volcanic styles that can be classified. Numerical and graphical attractor patterns add insight to such classifications. The problems of discrimination between like and unlike patterns of evolution in volcanic processes are examined on a fourfold basis involving (1) volumes and rates of magma supply and eruption during the evolution of the Hawaiian-Emperor volcanic chain, (2) factors influencing thermomechanical feedback that imply oscillatory changes in conditions of magma generation, storage, and transport, (3) theoretical examples of positive-negative feedback that illustrate methods of constructing attractor diagrams which imply oscillatory and potentially periodic behavior, and (4) comparisons with the observed patterns of Kilauea's volume and rate balances of intrusion and eruption expressed in the same form as the attractor diagrams.

These four aspects of volcanic description are mutually consistent. The rate history is dimensionally consistent with thermomechanical feedback processes, and feedback processes imply attractor-like dynamics in which conditions tend to repeat in the neighborhoods of characteristic patterns. Kilauea's eruptions are associated with intrusive inflation-deflation cycles that occur as closed loops in diagrams where present states are plotted against future states of magma supply and supply rates. Large earthquakes like the 1975 Kalapana event seem to occur during characteristic intervals of such loops, at states involving both high intrusive inflation and high inflation rates of both summit and rift storage systems.

Volcanic eruptions, intrusive events, and earthquakes are individually unique, but volcanism as a whole is a nonunique process in which repeated combinations of rate balances give rise to categorically similar patterns worldwide. Involutions and convolutions of these common pattern-generating mechanisms are the sources of unpredictable uniqueness. Prediction, therefore, involves locating one sort of cyclical loop, temporally periodic or not, within both larger and smaller contexts of recurring loops. Thus, recognition is the act of predicting several different scales of temporal and spatial action simultaneously. Given sufficiently redundant information, pattern recognition becomes automatic, as in everyday experience, rather than analytic. On this basis, specific attractor-like styles are potentially recognizable on local to global scales of volcanism. Expansion of these ideas to include chemically evolved systems (including silicic cratonic systems) implies that the criteria of pattern recognition also involve information describing chemical rates of change.

INTRODUCTION

The purpose of this paper is to examine the general problem of predictability in volcanic processes in terms of the sources of possible periodic and nonperiodic influences. Recurring themes are the issue of scale ratios of relevant properties and processes and the question of self-similarity. As has been my emphasis in other papers, I rely on the documentary history of Hawaiian volcanism to test ideas. In that context, there are two simple tests of self-similarity: first is the extent to which the differing time-scale patterns of day-to-day, historical, and prehistoric activity of the active volcanoes Kilauea and Mauna Loa are distinguishable in regard to the durations and amplitudes of episodic oscillations (whether periodic or nonperiodic). A second test is the degree to which these specific signatures differ from those at the larger scales of the Hawaiian Archipelago, the Hawaiian Ridge, and the Hawaiian-Emperor system as a whole. This paper considers the historical and secular Hawaiian scales quantitatively, explores physical mechanisms that influence the timing of volcanic processes, and points out some conceptual parallels between volcanic phenomena and patterns found in numerical computer experiments in nonlinear dynamics.

The term "nonlinear" is here used loosely to include systems described by equations that are of high order and (or) transcendental, sometimes with nonconstant coefficients, and which involve feedback coupling with other systems, functions, or coefficients. Such a definition is tantamount to saying that the mathematical discussion emphasizes comparisons of patterns without attempting to model sets of descriptive parameters in the form of analytic equations. Undeniably, many basic mechanisms can be described in terms of equations. They are therefore useful in predicting the kinds of mechanisms that may be aspects of a complex system. Such studies are clearly important, even in the absence of any direct applications in forecasting behavior. This is the rationale for including a section on mechanisms of rheological feedback as an important adjunct to studies of pattern recognition (see also Hardee, chapter 54).

The paper consists of five main parts: (1) the remainder of the introduction, which considers some generally relevant concepts from an interdisciplinary perspective; (2) concepts of self-similarity examined in terms of volumetric time-series data for Hawaiian volcanism; (3) rheological concepts of feedback processes; (4) concepts of stationary states expressed from the point of view of mass balance; and (5) Kilauea as a natural example of attractor patterns. Although (5) refers to concepts introduced in (4), the patterns illustrated there do not depend on any theoretical considerations; they are simply plots of the data on Kilauean rate histories recast in a form compatible with attractor patterns and concepts of autocatalytic systems (systems that contain rate-determining steps that catalyze, as well as take part in, subsequent steps in a generally cyclic process; the summit chamber of Kilauea is shown to represent such a controlling step).

I have attempted to make each section of the paper more or less self-contained, so readers who are interested only in specific aspects of the discussion can skip the other parts (if so, however, it may still be helpful to read the introductory and concluding paragraphs in each section). The rheological discussion in (3) is included as an important step in my personal recognition that there is a need for generalized methods of quantitative description of complex processes, as introduced in (4) and (5); otherwise, it can stand alone as an updated commentary on the thermal-feedback processes discussed by Shaw (1969) and as a connection between the present paper and the paper by Hardee (chapter 54).

PREDICTION AND SELF-SIMILARITY

Concepts of predictability in natural processes are currently undergoing what eventually may be recognized as a revolutionary change or paradigm shift. Traditionally, there have been two major approaches to scientific prediction, based on (1) documentation of a clear dependence on a precisely known and inexorably persistent forcing function and (2) documentation of statistical correlations among complex sets of parameters in the absence of any dominating influence by known forcing functions. The former is often called deterministic forecasting, and the latter probabilistic or stochastic forecasting. Most discussions of natural processes involve some mixture of these methods, because even the most deterministic results involve probabilistic estimates of uncertainties, and probabilistic results usually assume that some aspects of an analysis can be expressed deterministically (for example, patterns of seismicity and ground deformation at an active volcano, even though they may be expressed in terms of probabilistic models, may be determined by known volume changes accompanying the transport of magma; in other instances deformation may be expressed in terms of constant rates of motion determined by the data of plate tectonics).

An example of deterministic forecasting is given by the problem of ocean tides, where the forcing frequency and disturbing potentials are known with high precision and accuracy relative to many other kinds of Earth processes. Examples of probabilistic predictions are given by actuarial tables and some forms of weather forecasting, where results are based on analyses of trends in average behaviors involving numerous complicated, unknown, and (or) chance events. Klein (1982) discusses problems of eruption forecasting at Kilauea with emphasis on probabilistic methods. What is called "chance" often reflects ignorance concerning relevant processes, even though at some level there may be processes that are unknowable by instrumental methods of measurement (for example, the Heisenberg uncertainty). Unless there are such sources of random noise dominating our perceptions of a process, however, the process is potentially knowable from the standpoint of predictable recognition, whether or not it can be described in any specific analytical format.

Numerical forecasting represents the implementation of a scheme to quantify the criteria of recognition, which may simply be a statement of the number of times a given "effect" follows a given "cause." For example, I might get a rash one out of every hundred times I recognize poison ivy, and occasionally I may get a rash when I wasn't aware that I was in its proximity. Obviously, if my criteria of recognition are improved (not only of the leaf itself, but of all the many and subtle ecological indications of its presence), the incidence of rash could be reduced nearly to zero, but I can never be sure I'm infallible. So, if the consequences are bad enough, I am continually motivated to improve my powers of observation.

This example is more complex than it might seem. Its complexity could be demonstrated by attempting a quantitative statistical analysis. The analysis and its forecast of effects might be expressed in terms of numerous and complicated statistical cross-correlations of the factors influencing visibility, individual prowess at classifying plants, numbers of vines per unit area, leaf density and toxicity, humidity, wind direction, allergenic predispositions, and so on, resulting in a statement of numerical probability that I will break out in a rash within varying windows of space and time, expressed in terms of calculated significances within stipulated confidence limits. At least in the case of rashes caused by poison oak, subjective experience in pattern recognition is probably the better method of forecasting risk.

Some of the above distinctions between deterministic and probabilistic methods of prediction can be matters of the relative degrees of resolution in comparing patterns of repetitive processes and their interactions, and this is the aspect with which this paper will be primarily concerned. Hence, the scale dimensions in time and space of those processes responsible for significant effects are an important concern. For example, weather becomes deterministically predictable if we are mainly concerned with seasonal behavior. On the other hand, tidal fluctuations become less and less obviously deterministic the more closely they are examined, to the extent that they may appear essentially probabilistic when they are examined at the level of microsecond variations in the length of day. (This problem is particularly instructive because it involves the interactions of numerous and subtle cyclic phenomena, as do patterns of volcanic cyclicity. In this tidal example, influences involve the dynamics of the solid Earth, oceans, atmosphere, ionosphere, magnetosphere, and solar processes responsible for the solar wind. Clearly, the problem of pattern recognition in such a case is highly interdisciplinary. This paper supports the same conclusion with regard to future advances in the recognition of volcanic patterns that may be describable in deterministic as well as in probabilistic terms.) Basically, then, we

are attempting to evaluate the quantitative relations among natural processes over many different scales of size and time.

One approach to the search for characteristic patterns that may have systematic correlations with other patterns of deterministic origins is to examine similarities in behavior at different scales of observation. If a general process, such as global ocean and atmosphere circulations or global volcanism, shows internally consistent patterns that are indistinguishable at different dimensional scales of behavior, the process is said to have elements of self-similarity. The simplest test for self-similarity is to examine any set of data (such as a map of a geometric pattern or a time series of a varying quantity like wind velocity) over domains of different size and (or) over different durations. If the unlabeled graphs are indistinguishable at different scales, the data are self-similar. In an absolute sense, all variations (such as length, velocity, and energy) would retain the same proportionalities with regard to relative amplitudes, waveforms, and periodicities. A less stringent criterion of self-similarity is that the general ranges of these parameters are statistically indistinguishable, even if there are no point-for-point correspondences of the reduced data. In the latter case the pattern is self-similar from the standpoint of having the same complexity of information content at all scales.

THE CONCEPT OF FRACTAL GEOMETRY

The idea of self-similarity is sometimes considered to be essentially synonymous with the newly emerging research tool called fractal geometry. Self-similarity is a separate idea, and its documentation depends on the system of measurement by which it is described. A fractal structure, as described below, may or may not be self-similar, as in any other system of measurement. The way in which a fractal measurement is made, however, automatically involves consideration of those conditions that give rise to geometric self-similarity, particularly of the statistical variety, and departures from it (see Mandelbrot, 1982). It is therefore worth considering the general implications of fractal geometry, although the data described in this paper have not been formulated in these terms (the attractor diagrams described later produce structures that are fractal in character, but there I have restricted the discussion to the terminology of attractor theory).

A measure called the fractal dimension represents the relation of pattern lengths to an independent and unchanging (nonmagnified) unit of length as the pattern as a whole is progressively magnified without limit. Mandelbrot (1982, p. 25) calls such a length "the yardstick length," and I think of it as any ruler chosen as the standard of a particular measurement. Equivalently, the fractal dimension is determined by the ratio of the logarithms of the pattern lengths and standard lengths as the latter are changed. Any pattern, whether continuous or discontinuous, can be measured in such a way that it can be described in terms of fractal dimensions. Such patterns can therefore be referred to as fractal structures. If a pattern can be described by a single fractal dimension, it is said to be a self-similar fractal structure.

Evidently many familiar objects (trees, for example) are fractal structures. The idea extends directly to any ramifying patterns, including lava flows and paths of intrusive magma transport. It remains to be demonstrated whether any one or several such objects, or any subset thereof, are self-similar. The idea of a fractal dimension may seem strange because it describes forms that are not limited to the usual topological constructions based on lines, planes, and "solid" geometrical objects like cubes or spheres. That is to say, fractal structures can have fractional dimensions between those of the integers describing Euclidean topologies. Therefore, fractal geometry is very useful as a measure that allows us to expand our abilities to quantitatively classify complex structures showing dendritic, feathery, dusty, and other seemingly irregular forms. In this respect, it sometimes turns out that what is considered very irregular in the traditional geometric sense is actually quite regular and simple from the fractal perspective. This possibility applies to seemingly noisy time-series data as well as to complex spatial patterns. The study of coastline lengths, tracks of Brownian motion, stream-drainage networks, morphologies of fracture sets, and temporal patterns of economic trends are some common applications. Applications to geology are too numerous to mention and have only just begun.

Although fractal geometry is closely related to issues of self-similarity examined in this paper, my principal concern is with the patterns of magma-transport processes in time as they may relate to attractor diagrams. This implies a number of complex dynamic effects not explicitly measured (the distributions of magma transport in both space and time are not adequately sampled to permit a complete discussion of their fractal properties). The fractal concept is, however, implicit to generalizations of the temporal patterns illustrated later and, in principle, can be applied in dimensional contexts that include time and energy as the quantities of measurement.

APPLICABILITY OF EVOLUTIONARY CONCEPTS TO PATTERNS OF VOLCANISM

A new approach to the study of periodic patterns and complexity in physical processes is arising out of computer studies of the numerical patterns produced by various kinds of recursive algorithms. Numerical recursion refers to some computational scheme (an algorithm)—whether done by hand, graphically, or by computer—wherein repetitive calculations are performed in which the current result, or state, is used to compute the next state, and so on. Except for the initial state, and a set of rules of repetitive computation (which may, for instance, be in the form of a reference equation or a set of "if this, do that" statements), the computation is allowed to guide itself indefinitely. Such programs are sometimes called computational automata, cellular automata, evolutionary strategies, or other names that emphasize the open-ended, self-guiding principle of computation. John von Neumann, famous in the development of computers, influenced terminology and modern computer studies in this area by laying out (in lectures during December 1949 at the University of Illinois) a set of logical criteria by which a machine could reproduce a copy of itself, including a copy of the instructions (these lectures were later completed and published by A.W. Burks; see von Neumann, 1966; Burks, 1970). Resem-

blances to the biological genetic code, which was being discovered almost simultaneously, were noticed later (Judson, 1979, p. 244).

An alternative approach to the development of a system that can reconstruct itself in all details is a computational scheme that is permitted to wander wherever it will without any preconceived goals, subject to a simple set of rules. Such a scheme, invented by John Conway in 1970 (see Poundstone, 1985), is known by the evocative name "Life." Popularized by Martin Gardner in *Scientific American* (his column titled "Mathematical Games"; particularly see issues during the 1970's, or Gardner, 1983), it became the subject of extensive exploration by amateur and professional researchers (and by players of computer games). An extensive description of Life behaviors is given by Poundstone (1985), and a technical note concerning cosmological implications is given by Gosper (1984). A logical extension of computer schemes that would come closer to natural systems is an algorithm that not only reconstructs itself but also invents the rules of evolution, which it subsequently copies, reconstructs, and modifies repeatedly and indefinitely. Because the study of such systems has the potential complexity of natural evolution, a simplifying approach is clearly needed.

The approach taken in this paper is to treat pattern evolution found by means of numerical algorithms in a manner similar to that used in the study of natural systems. I search for resemblances among the results of computer experiments using particular types of recursion algorithms suggested by natural processes, and I look for those properties that have some degree of universality of behavior with natural systems. The recursion strategy I use is derived from concepts of attractor theory, in which a specific governing equation involving aspects of both positive and negative feedback guides the repetitive computation (see May, 1976). Sample computations are discussed later. An important discovery of this approach is that whatever recursive algorithm is used, the resulting numerical patterns generated have some simple properties in common. Among these properties is the observation that numerical patterns (trajectories of plotted points in space and time) often reproduce according to regular geometric progressions in self-similar sets (smaller subsets have the same relative spacings of plotted points as larger subsets; see previous comments on self-similarity). Such patterns are sensitive to the rates of change of a controlling parameter in several different ways: the result may produce one or more stable fixed points (as in the approach to a set of stable thermodynamic equilibrium points, or thermometer readings in a system of steady-state heat flow), or it may produce quasi-periodic, aperiodic, and seemingly chaotic patterns. All of these complex patterns can also be shown to be fractal structures. Some of them are of the fractally self-similar type (sometimes called strange attractors), and these may grow or appear surprisingly out of highly dissipative, random-looking structures (in nature we would describe analogous macroscopic structures as representing states far from equilibrium). In this regard, they are numerical analogs of living systems and of physical devices that do in fact operate far from thermodynamic equilibrium (examples are found in such diverse phenomena as turbulent convection, socioeconomic structures, landform evolution, electronics, laser operation, and many others).

The surprise in the above studies is caused by the complexity of patterns and an inability to follow or to visualize all steps in the evolution, which often takes on an overall form bearing little resemblance to intuition or predictions. In this regard, patterns of numerical evolution have some of the characteristics of natural systems that involve so many different deterministic influences that the resulting behavior looks highly complex and even chaotic. In the numerical context, however, this chaotic behavior is found to contain regions ("windows") of structural simplicity or order. Such substructures are also associated with characteristic temporal periodicities.

Thus, periodicities are produced not only by the deterministic governing algorithm, but also by the evolving autocatalytic properties of repetitive recursion (examples are shown later). Therefore, if natural periodicities are viewed in the same way, there are sources of periodic influences that may be deterministically imposed from outside the system of interest (exogenous forcing functions), and there are others that are generated by the repetitive operation of the system itself (endogenous convergences toward restricted sets of repetitive states). In systems where there are numerous possible forcing functions, it may be difficult to distinguish endogenous from exogenous periodicities, and there may be resonances between some endogenous effects and certain of the exogenous influences (a volcanic example mentioned later is the possible correspondence of self-induced response cycles and tidal cycles). Alternatively, the dynamical context within which the system is described may be expanded so that, in effect, all periodic behavior becomes endogenous. Later I suggest how and why volcanic phenomena show dynamical parallels with patterns generated by numerical algorithms.

I have intentionally avoided using the terms "random" and "nonrandom" in describing patterns in space and (or) in time. The distinction between these terms, as commonly employed, is related to concepts of uniqueness. In my opinion, use of "random" as a descriptor of natural data is unsatisfactory on at least two counts: (1) if a pattern can be recognized, it contains information that already exists in some reproducible form (otherwise, like the unique pattern, it has never been seen before), hence it is nonrandom, and (2) the random state cannot be proven mathematically (a large literature on complexity theory, not cited, concerns the fundamental question of how to quantify departures from this undefinable limit). Statistical tests of randomness really represent comparisons with standardized, hence artificial, concepts of complexity. As such, they are useful ways to classify categories of numerical data. In the process, however, many of the potentially recognizable characteristics of a complex pattern may be lost or overlooked. I contend that natural patterns contain much more usable information than is acknowledged in the application of standard statistical tests as a measure of randomness or nonrandomness.

ACKNOWLEDGMENTS

I thank Dan Dzurisin for discussions of the magma-supply budget at Kilauea, and for numerous constructive suggestions in the manuscript. I also thank Harry Hardee (Sandia National Laboratories) and Patrick Muffler for constructive reviews, Roy Bailey for discussion of the volcanic patterns at Long Valley, Calif., and Tom

Wright for numerous discussions over the years of Hawaiian volcanism.

SELF-SIMILARITY IN HAWAIIAN VOLCANISM

Cumulative volumes of volcanic products versus time are shown in figure 51.1 for the Hawaiian-Emperor Chain as a whole and also for the individual volcanic loci during the chain's 74-m.y. history (data from Shaw and others, 1980, table 2). Rates of volcanism from the same data base presented in figure 51.2 include a composite volume rate, rates along loci, and moving-window averages for the overall rate. Notably, the complexity of time series representing volume rates is similar on different spatial and temporal scales; rate episodes look much the same from time to time, and the ranges of rate amplitudes are similar within short as well as within longer intervals of time. If there were no labels on the graphs, therefore, it would be hard to say what general period of time, or what duration in time, a given graph represents; this satisfies the qualitative definition of self-similarity mentioned earlier.

Statistical periodicities at about 12, 6, 3.6, 2.7, and 2 m.y. (fig. 51.3) were found by fast Fourier transform analysis of average volumes per time taken at equal 1-m.y. intervals of time. Similar, but not identical, periodicities are shown by the same sort of analyses for volumes per length along loci, instantaneous volume rates, linear propagation rates, and variations of the azimuths of loci with time, each set of data read at equal 1-m.y. intervals of time. Such periodicities represent averages of a variety of temporal and spatial variations among many different physical processes at the scale of plate tectonics affecting the Hawaiian-Emperor Chain. I do not imply, nor do I believe, that the above periodicities are coherent, and therefore no numerical estimates of statistical significance are assigned. Any statement of confidence limits would be misleading because the global dynamic context indicates that these apparent periodicities involve many different fundamental periods of shorter duration that can combine in numerous complicated ways. The fact that more localized sampling in space and time, to be discussed, also reveals signatures of similar proportional variability is evidence for the composite nature of such time series as those in figures 51.2 and 51.3. Existing data at the scales of observation illustrated are not sufficient to determine the values and possible varieties of fundamental periods.

The shortest resolvable variations in the above records are at time scales of the order 10^5–10^6 years. The next level of extensive information is given by the historical record (<200 years), with variations resolvable at about yearly intervals. At yet finer scales is the three-decade record of modern geophysical measurements at the Hawaiian Volcano Observatory (HVO), with resolution of months to days. Finally, the east rift zone of Kilauea has had almost continuous activity since January 3, 1983, with episodes of fountaining at or near the vicinity of Puu Oo at intervals of about 1–9 weeks (George Ulrich, written commun., 1984).

Unfortunately, there are large jumps in time and size scales between the current local, historical, and Pacific-plate records. Detailed data on rate variations within the time scales of an individual edifice (~10^5–10^6 yr in duration) or of an individual

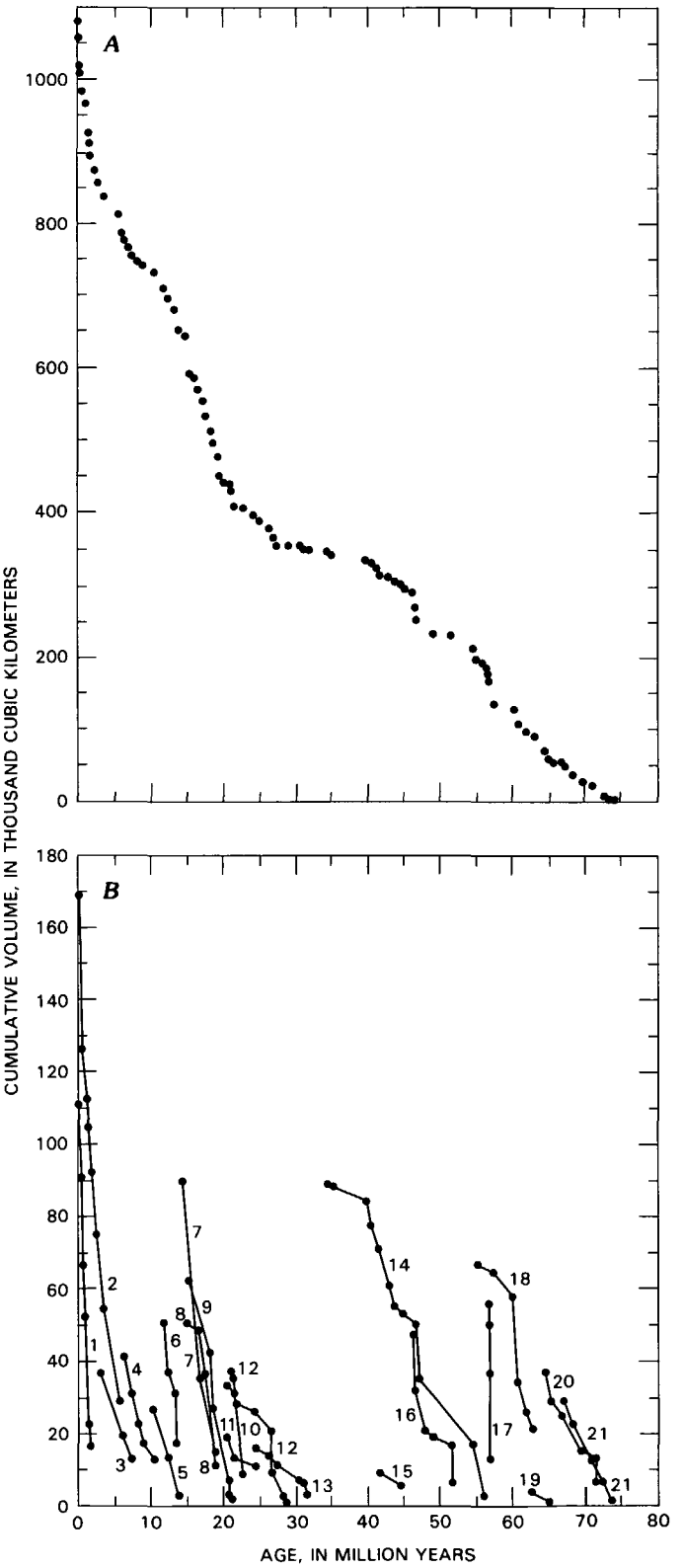

FIGURE 51.1.—Cumulative edifice volume plotted against age for Hawaiian-Emperor Chain. Data from Shaw and others (1980). *A*, Total volume for all volcanic loci. *B*, Cumulative volume for each locus; loci identified by number, see Shaw and others (1980, table 2). Loci numbers 1 and 2 are, respectively, "Kea" and "Loa" trends of Dana (1849).

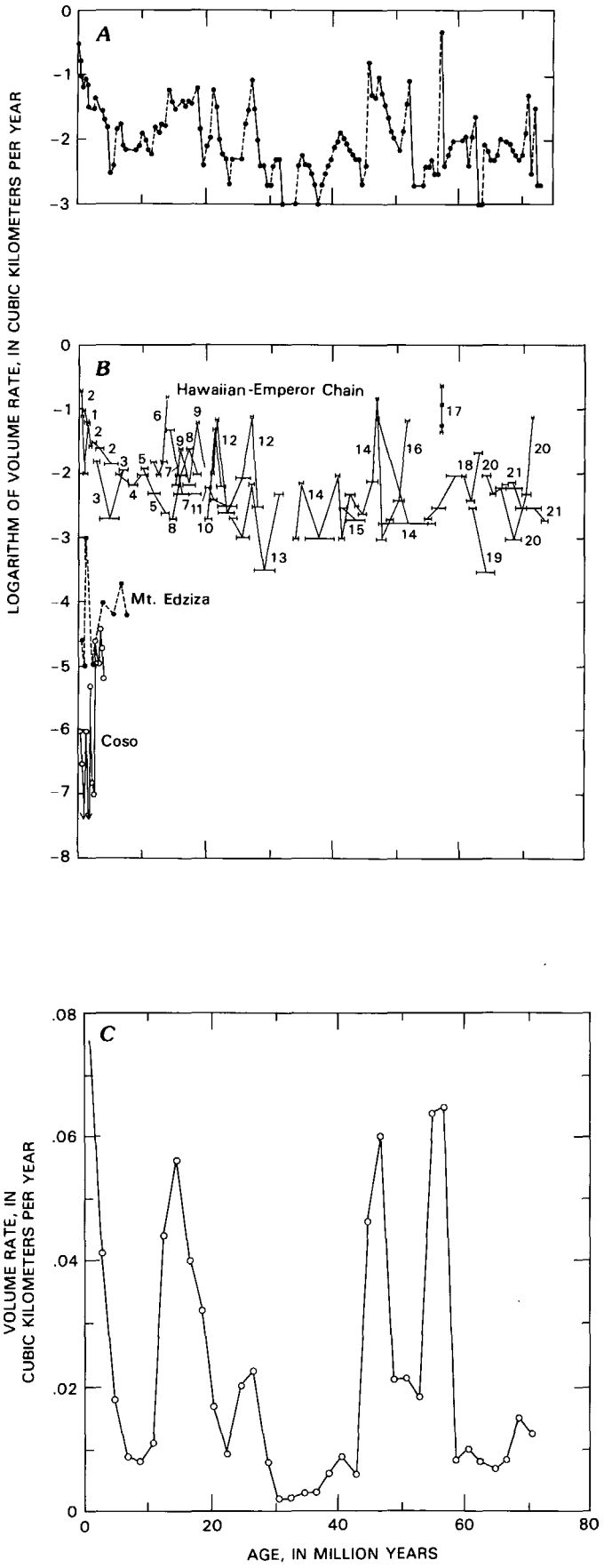

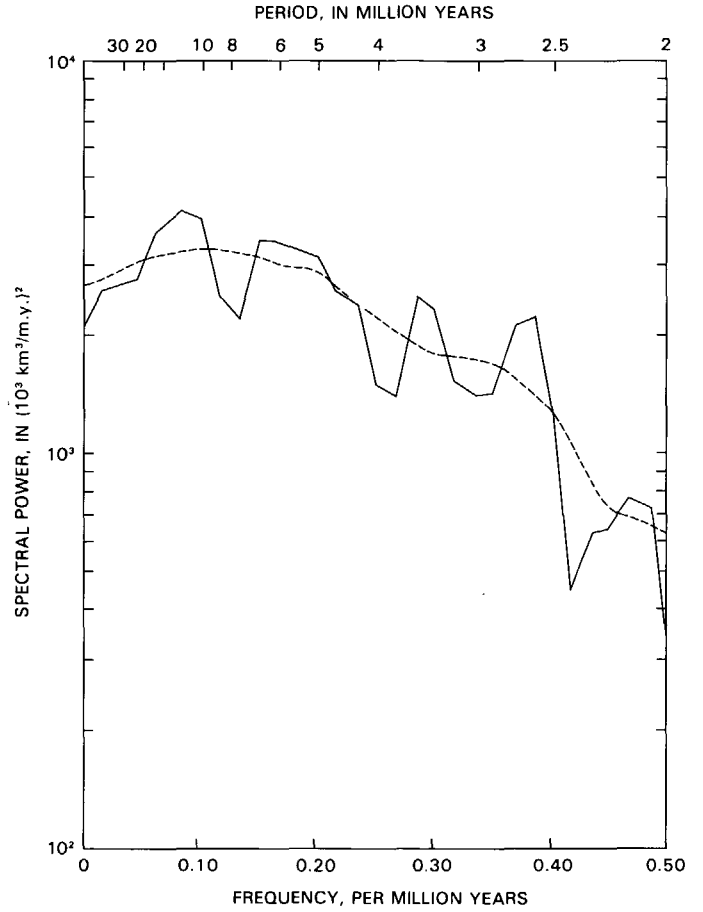

FIGURE 51.3.—Fast Fourier transform analysis of power spectrum for interpolated volumes of volcanic edifices per million years (sampling interval) for Hawaiian-Emperor Chain (Shaw and others, 1980, table 2). Dashed line gives average trend, on which are superimposed localized power maxima (power expressed as square of unit of rate samples). Analysis suggests that maxima may exist near calculated periods 2, 2.7, 3.6, 6, and 12 m.y. with generally increasing power at longer periods, but record is inadequate to demonstrate coherence. Such a trend resembles so-called $1/f$ frequency-dependent spectra that characterize many other kinds of complex time series in nature; see Verveen and Derksen (1968), van der Ziel (1970), and Voss and Clarke (1975).

FIGURE 51.2.—Volume rates of volcanic edifice growth for Hawaiian-Emperor Chain. ***A***, Net rates for all loci. ***B***, Rate along each locus (identified by number; see Shaw and others, 1980) and comparative rates for two cratonic silicic systems; Hawaiian-Emperor data are from Shaw and others (1980, table 2); data for Mt. Edziza, British Columbia, from Souther and Hickson (1984); data for Coso Range, California, from Duffield and others (1980). ***C***, Smoothed values of net rates in *A* using a moving average window of 4 m.y. with 2-m.y. shifts. For comparisons of Hawaiian-Emperor and cratonic systems, see Shaw (1985) and discussions of relations among rate, size, and repose time in text (data for Long Valley, California, during latest 2 m.y., from Bailey, written commun., 1984, somewhat exceed rates for Mt. Edziza). For reference, average eruption rate for ash-flow systems is about 10^{-3} km³/yr (Smith, 1979), and their intrusive supply rate is about 10^{-2} km³/yr (Shaw, 1985).

island (~10^6 yr in duration) are unavailable because of the masking effects of younger lava in undissected edifices. Thus, we are dealing with several discontinuous and widely different scale ratios when comparisons are made between data sets describing Hawaiian volcanism in a context that includes both the historical and Pacific-plate records.

Cumulative volumes of lava extruded from Kilauea and Mauna Loa are shown in figure 51.4, together with inferred volumes of the largest deflation episodes of Kilauea (those associated with earthquake activity), as compiled by Klein (1982) from HVO records. The latest data points terminating the records represent estimates for the cumulative eruptive volumes of the 1983–85 east-rift activity and the 1984 Mauna Loa eruption. The approximate mean trends are indicated by dashed lines of slope 0.025 km^3/yr drawn subjectively through the data; reference slopes of 0.1 and 0.01 km^3/yr are shown for comparison.

The following points of interest are noted in the historical rate behavior of Kilauea and Mauna Loa, as shown in figure 51.4. (1) There is an episodic variation between rates (slopes) of about 0.01 and 0.1 km^3/yr for both Kilauea and Mauna Loa. (2) These rate episodes tend to be steplike at intervals of about 10–40 yr rather than scattered uniformly about the mean trend. (3) The mean extrusion rate on the 100-yr scale is near 0.025 km^3/yr at both volcanoes (the overall magma-supply rates will be discussed later). (4) The eruption frequency is higher for Kilauea than for Mauna Loa despite similar average rates, underscoring the typically larger eruptions and longer repose times at Mauna Loa (see Klein, 1982). (5) The steplike episodicity of rates resembles the variations in Hawaiian-Emperor rates in figure 51.1*A*, and the similarity in mean eruptive rates for Kilauea and Mauna Loa parallels the long-term similarity of slopes between loci 1 and 2 in figure 51.1*B* (the "Kea" and "Loa" lines of Dana, 1849; see Jackson and others, 1972; Jackson and Shaw, 1975). (6) The intrusive volumes, which are based on the larger deflation episodes listed by Klein (1982, table 1), have episodic trends similar to the eruptive trends, and they have about the same mean slope near 0.025 km^3/yr. (7) The slope of the major cumulative intrusive-volume events since about 1960 is less than the slope of eruptive volumes over that time interval, so that eruptive rates intermittently exceed rates of major intrusive volumes; hence, (8) there are decade-long delays in renewed intrusive storage compensating eruptions, and (or) there are components of magma supply that are not recorded by the major intrusive events (evidence described below suggests that the latter factor, acting somewhat like a continually leaking valve, is exceedingly important in the 100-yr scale balances of intrusive and extrusive episodes).

Volumetric variations for Kilauea between 1956 and 1983 are shown in figure 51.5 in more detail, as compiled and interpreted by Dzurisin and others (1984) in terms of magma-supply rates. I intentionally show these data in their units and format to facilitate comparisons of the two discussions and to avoid errors of transcription of the complicated history. This introduces an unavoidable difference in the convention for the orientation of the time axes compared with earlier figures, which were drawn to be compatible with the discussions of time-distance relations given by Shaw and others (1980). Their best estimate of average supply rate during this time (adjusted for vesicle porosity) is about 0.086 km^3/yr (7.2×10^6 m^3/mo), with episodic deviations over an approximate order of magnitude (uppermost curve in fig. 51.5*A*). They also concluded that, during 1956–83, only 35 percent of the magma supply was extruded and 65 percent was stored in Kilauea's rift zones: 55

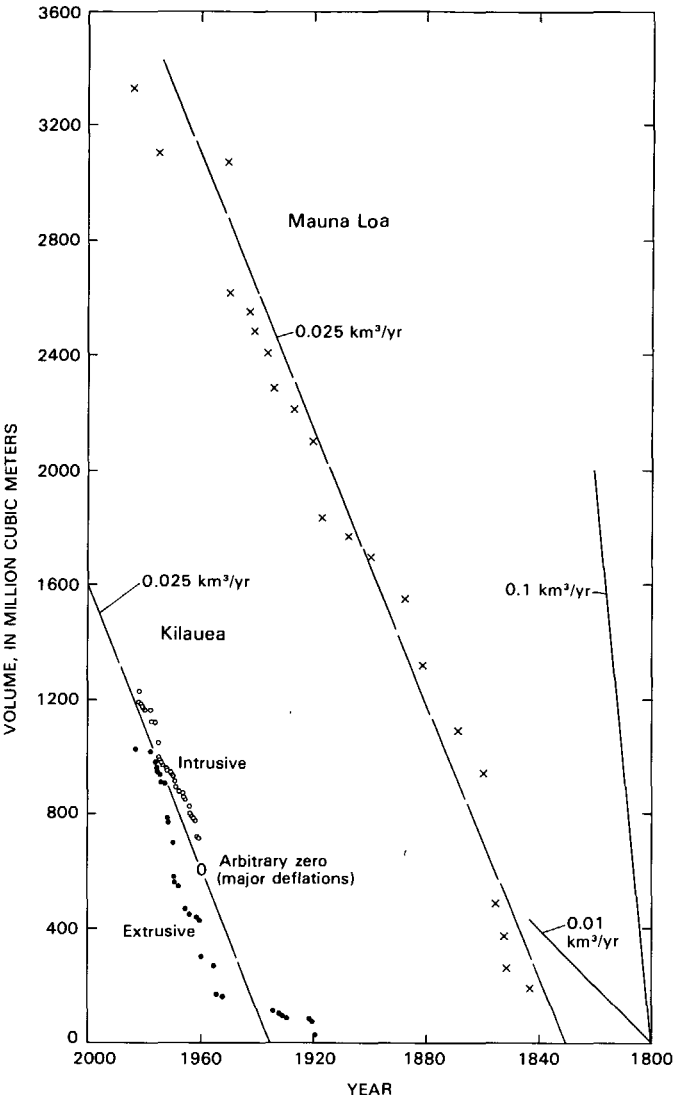

FIGURE 51.4.—Cumulative volumes of erupted lava for Kilauea and Mauna Loa and volumes of major Kilauea intrusive events from Klein (1982, tables 1 and 2); data for Kilauea also given in Dzurisin and others (1984). Intrusive volumes plotted relative to arbitrary initial point on mean trend beginning about 1960. Trend lines (dashed) with slope of 0.025 km^3/yr are drawn to indicate rough parallel between average Kilauea and Mauna Loa eruption rates; reference slopes (light solid lines) of 0.1 and 0.01 km^3/yr also shown. Although average slopes are not rigorously defined; trends suggest that both Kilauea and Mauna Loa may be expected to continue high eruptive activity (see Wadge, 1982, for comparison of steady-state volcanism in other systems). Mean supply rate for Kilauea is about three times larger than mean eruption rate (Dzurisin and others, 1984); similarity of trends suggests that same relation may also hold for Mauna Loa. Data after 1981 supplied from HVO records: Kilauea (George Ulrich, written commun., 1984); Mauna Loa (Robert Decker, written commun., 1984).

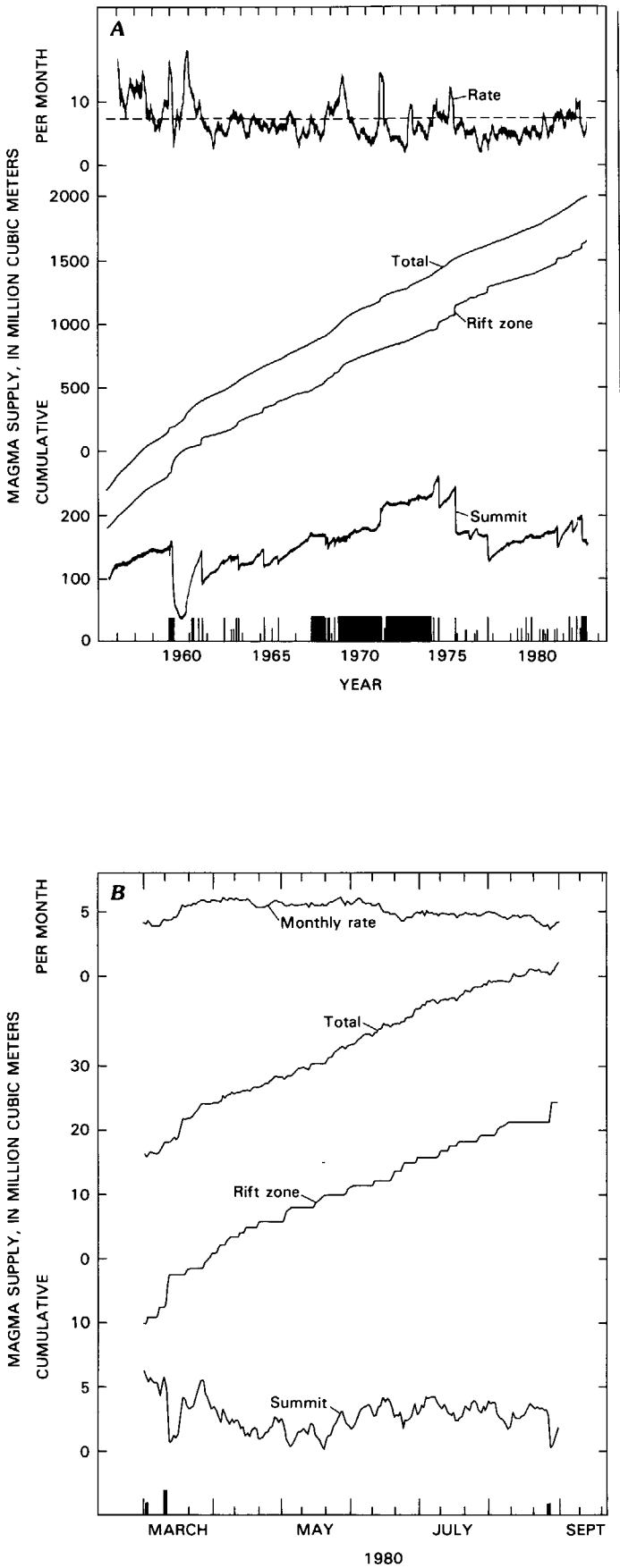

percent in the east rift zone and 10 percent in the southwest rift zone. Thus, their mean extrusive rate for the 1956–83 interval, calculated either from the above percentage of the total or directly from the erupted volume divided by the duration, is about 0.03 km^3/yr, in agreement with the average trends in figure 51.4 for the total historical record.

During an approximate 6-month interval of time (fig. 51.5*B*) there was a quasi-steady balance between total rates of magma supply and rates of transport between the summit and rift zones in the absence of eruptions or large intrusive episodes. The average intrusive rate during this time was about 5.0×10^6 m^3/mo, or 0.06 km^3/yr. Hence, this period seems to be representative of the 28-year intrusive average (that is, roughly two-thirds of the yearly total of 0.086 km^3/yr). Such increments can supply local zones of rift inflation that will become sites of eruption, or they may solidify in situ; the distinction depends on interpretations of deformation data for the east rift zone not considered here.

The fact that Kilauea's extrusive episodes indicated by the volume record of figure 51.4 also transiently equal or exceed the mean supply rate derived by Dzurisin and others (1984) reinforces inference (8) above that either intrusive or extrusive rates may transiently exceed the other for periods of a few years, although overall the average eruption rate is significantly less than the average supply rate. That is to say, the cumulative erupted volume falls far short of the cumulative intrusive volume, at least on the 100-yr scale. This means that intrusion dominates over extrusion in the growth of the volcanic edifice. The overall volumetric rate of growth of the volcanic edifice on the 100-yr scale is about 0.1 km^3/yr, which is about three times the average volumetric rate of lava accumulation (about 0.03 km^3/yr) and about equal to the long-term rates of edifice growth over the latest 10^6 years shown by the data in figures 51.1 and 51.2 (also about 0.1 km^3/yr).

The cumulative volume of eruption of Kilauea since the beginning of 1983 is shown in figure 51.6. The mean slope of 0.15 km^3/yr (12.7×10^6 m^3/mo), uncorrected for porosity (see below), is consistent with the above inferences concerning discrepancies between intrusive and extrusive rate histories. Even allowing for a reasonable porosity correction (for example, a 15-percent correction, as used by Swanson, 1972, gives 0.13 km^3/yr, or 10.8×10^6 m^3/mo), the extrusion rate since the beginning of 1983 (as of this writing, June 1985) is larger than any previous estimates of supply rates and resembles the long-term edifice growth rates for locus 1 in figures 51.1 and 51.2. (Note that the higher rates indicated in fig. 51.2*A* represent the combined growth rates of loci 1 and 2 and of any

FIGURE 51.5.—Record of magma supply for Kilauea, 1957–83 (from Dzurisin and others, 1984), based on continuous records of tilt measurements at Kilauea summit. Vertical bars at bottom of diagrams indicate specific magmatic events: short bars for intrusive events, long bars for eruptions. Estimates of magma supply are independent of measurements of erupted volumes, except as they were used in making tilt calibrations; see Dzurisin and others (1984) for discussion. ***A***, Overall record. ***B***, Record for a six-month period in 1980.

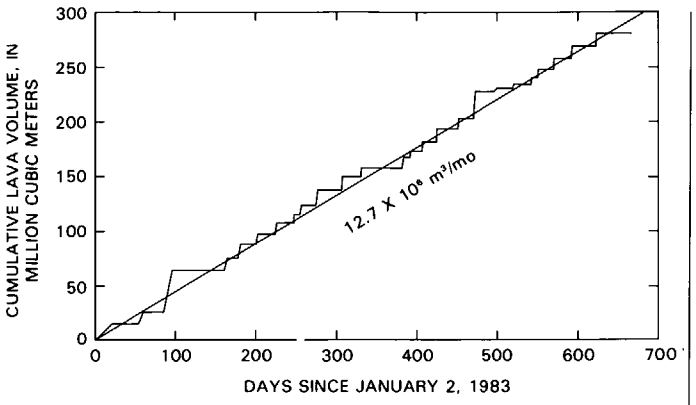

FIGURE 51.6.—Cumulative volume of erupted lava during quasi-continuous east-rift-zone activity of Kilauea (mainly at Puu Oo vent) since January 2, 1983 (George Ulrich, written commun., 1984). Average rate based on gross lava volumes not corrected for porosity. During this time, eruption and supply rates are approximately balanced and roughly equal to long-term Hawaiian-Emperor rates of edifice growth (see fig. 51.7 and discussions in text).

unrecognized loci of new activity. Locus 2, which includes the Hualalai-Mauna Loa-Loihi trend, appears to represent a slightly higher rate history than the Kohala-Mauna Kea-Kilauea trend over the past 10^5 yr, and this could also be true at the 100-yr scale, judging from the respective slopes in fig. 51.4.)

An interpretation of quasi-steady balances between eruption and supply rates during May–December 1969 was the basis for Swanson's (1972) estimate for the Kilauea magma-supply rate. His estimate of mean extrusion rate, including porosity, was 9.9×10^6 m^3/mo, compared with 12.7×10^6 m^3/mo in figure 51.6. He adjusted this rate downward by 15 percent to account for vesicularity, giving 8.4×10^6 m^3/mo (0.10 km^3/yr). This compares with the comparably adjusted value of 10.8×10^6 m^3/mo in figure 51.6 mentioned above (0.13 km^3/yr for the 1983–85 period). Although a mantle-derived magma-supply rate of either 0.10 or 0.13 km^3/yr is larger than the 30-yr average of about 0.09 km^3/yr calculated by Dzurisin and others (1984), each of these values is consistent with the rate magnitudes of figures 51.1*B* and 51.2*B* in the latest 10^5 yr or so (see averages in fig. 51.7). If the 30-yr supply rate is typical of longer term averages for Kilauea, then we might expect to see a return to conditions where eruption rates are again lower than intrusive storage rates within future decade-length variations when the current episode of high activity wanes. By this interpretation, the longer the currently high eruption and (or) intrusion rates continue, the longer will be the next interval of subdued activity at Kilauea on the basis of existing patterns. However, if the long-term "Kea" average at Kilauea resembles the "Loa" average (see Shaw and others, 1980), then the 30-yr as well as the 100-yr averages for Kilauean supply rates are less than the potential rates for deep-seated magma generation, and the currently high values of eruption could represent a supply rate that will continue indefinitely. It is important to distinguish between intrusion and extrusion here. Subdued activity, as judged from eruptions, does not necessarily imply a low magma-supply rate, particularly if the intrusion rate is increased relative to the 30-year average because of tectonic adjustments in the structure of the volcanic edifice.

Notice that the mean rate for the large intrusive events in figure 51.4 is approximately in balance with the average extrusive rate (similar slopes). This suggests to me that eruptive events may be associated with preferred sites and paths of storage in the rift systems relative to the more pervasive and seismically quiet intrusive leakage modes (for example, as represented by fig. 51.5*B*). That is, there is a strong correlation between seismicity, the large intrusive pulses, and eruptive pulses. These events, then, seem to be logical candidates for transport rates in which the rate-determining step may be extensional and (or) extensional-shear fracture, according to the mechanisms discussed by Shaw (1980). This, in turn, suggests the possibility that there may be different modes of stress adjustment associated with different intrusive styles, one more localized and directly keyed to eruptions and another more distributed and keyed to the overall changes in edifice growth related to distributed intrusion. The distinction is partly one of time frame, because the overall changes in longer term edifice stresses also must govern the preferred routes of magma transport, according to the principles discussed by Shaw (1980); compare later discussions of figures 51.22 and 51.23. The coseismically more passive (as contrasted with potential for major delayed seismicity) aspects of overall edifice growth must be compensated by the smaller scale intrusive events which are not accounted for in the eruptive volumes (at least on the 100-yr scale), implying that such volumes solidify in place. Otherwise, eventually a very large magma chamber should evolve with comparably larger eruptive events. However, even if the more passive intrusive fractions do not erupt, they contribute to the high-level mass accumulations that affect the larger scale and longer term edifice stresses that, in turn, contribute to the larger and more regional earthquake events, such as the magnitude 7.2 Kalapana earthquake of 1975 (Shaw, 1980). Sites of intrusive magma accumulation and solidification, then, also contribute to edifice stresses, and therefore to frequencies of eruptions and earthquakes, and possibly to catastrophic landslide events that have occurred in the past along the Hawaiian Archipelago.

The various average rates discussed above are summarized in figure 51.7, which also shows the superimposed historical variability of Kilauea and Mauna Loa eruption rates. Although the average of the historical eruption rates for the two volcanoes have been about the same (see fig. 51.4), the minimum rates for Mauna Loa hover near the overall Hawaiian-Emperor average, on the order of 0.01 km^3/yr, while the highest rates only occasionally reach the overall 0.3-m.y. rate of 0.18 km^3/yr (the value for the "Kea" locus could be lower, depending on how the total volume for Kilauea is reckoned in the 0.3-m.y. average; the 0.3-m.y. average for locus 1 excluding Kilauea is closer to the 1-m.y. average of about 0.08 km^3/yr). This suggests that, as with Kilauea, the average edifice growth rates for Mauna Loa (that is, rates indicated by the longer term overall volume rates) are several times the average historical eruptive rates and that large components of undetected magma storage and solidification are also taking place on a large scale in the Mauna Loa

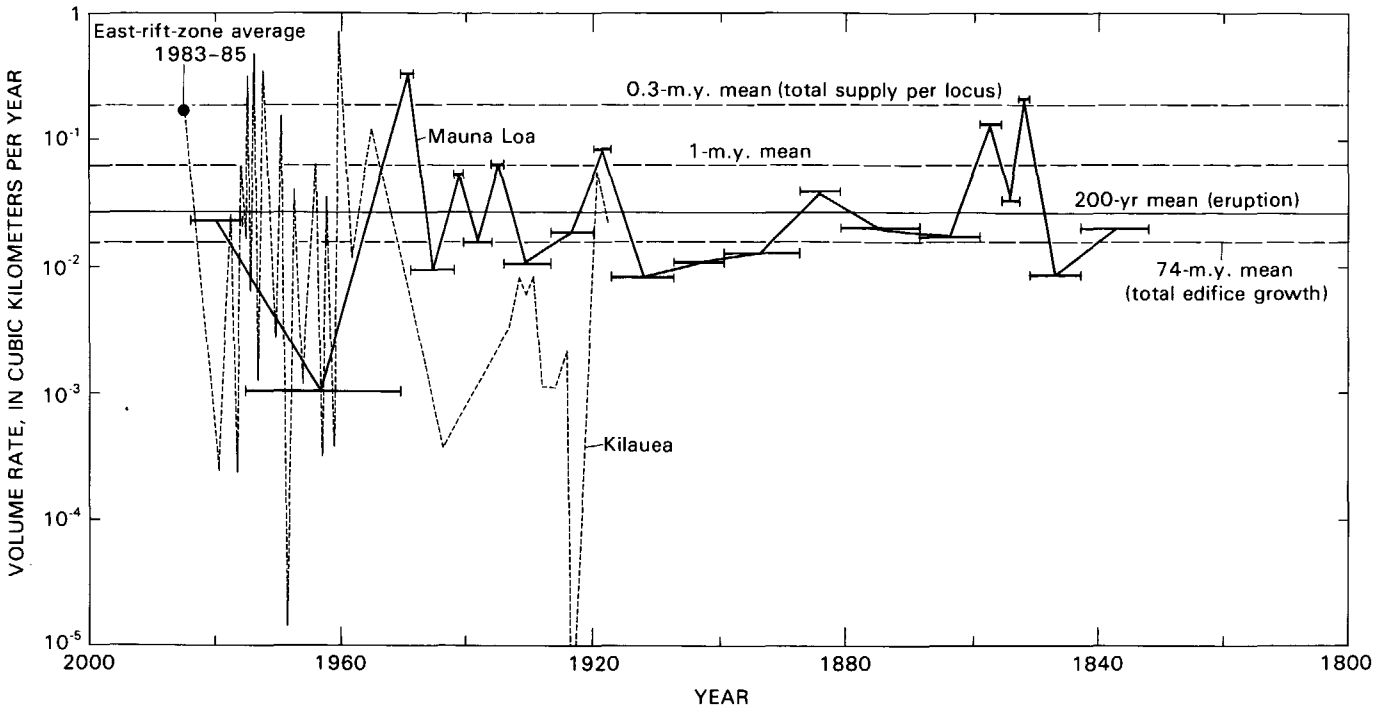

FIGURE 51.7.—Time variation of eruptive activity of Kilauea and Mauna Loa; mean trend from figure 51.4 identified as line labeled "200-yr mean." Average values over different longer term time intervals for Hawaiian-Emperor Chain given by dashed lines, based on data used for figure 51.2*B*. Note that Mauna Loa has oscillated between values near overall average and peak growth rates of Hawaiian-Emperor Chain (about 1 order of magnitude in rate), whereas Kilauea has had much higher frequency oscillations over several orders of magnitude in rate variations (see discussion of relations among rate, size, and repose time in text).

structure. This graph (fig. 51.7) also shows that, despite the same average eruption rates (see fig. 51.4), the fluctuations at Kilauea are of much higher frequencies (since about 1956 the average interval between maxima is about 2 yr for Kilauea compared with an overall average interval of about 20 yr for Mauna Loa) and oscillate over wider ranges of rate amplitudes within the time frame of Mauna Loa repose intervals.

Thus, the temporal variability of events (eruptive and intrusive) seems to relate to their size variability, because the volumes of the higher frequency Kilauea events are typically smaller than the Mauna Loa events (I infer this for the Mauna Loa intrusive events as well, based on the resemblances of extrusive trends in fig. 51.4, but they have not been documented in detail). Present knowledge of the Mauna Loa edifice structure does not allow any rigorous correlation between the periodicity and size/repose-time ratios of Kilauea and Mauna Loa. If repose times were directly proportional to size (that is, the larger the overall edifice volume, the longer the repose times between larger intrusive and extrusive events), Kilauea would be about one-tenth the volume of Mauna Loa (average repose times in fig. 51.7 for Kilauea are about one-tenth those of Mauna Loa). This has some validity on the basis that the overall edifice volume controls the potential magma-storage volume, other factors being equal (neglecting the details of edifice heights and gravitational stress distributions). But according to Shaw and others (1980, table 2) the ratio of the Kilauea to Mauna Loa edifice volume inferred from topography and bathymetry is about one-half, unless much of the volume attributed to Kilauea represents hidden fractions of the Mauna Loa edifice (this possibility is allowed by current knowledge of lava-flow stratigraphy in the region of overlap between Kilauea and Mauna Loa; T. Casadevall, oral commun., 1985; D. Dzurisin, written commun., 1985). The same discrepancy is indicated by a consideration of the relative ages of the Kilauea and Mauna Loa edifices. For example, the estimated age of Mauna Loa given by Shaw and others (1980, table 2) is about 10^5 yr. Therefore, according to the approximate constancy of both the historical and the 0.3-m.y. average growth rates discussed above, Kilauea's age would be about half that of Mauna Loa, or 50,000 yr, if its volume is also half. So Kilauea's age would be reduced to 10,000 yr and its volume to about a tenth that of Mauna Loa if the argument based on frequency ratios were used.

Another way of looking at the proportionalities between edifice sizes and event frequencies is to consider the possibility that repose times are controlled by the ratio of summit-chamber volumes. The periodicity ratio of 10 to 1 (fig. 51.7) would then suggest that the diameter of the summit chamber of Mauna Loa is a little more than twice the diameter of the Kilauea summit chamber (compare Klein, 1982). Assuming that this ratio of chamber diameters is roughly correct, all the data favor the smaller volume and younger age limits

for Kilauea. There is then a reasonably consistent set of constant ratios of the above parameters between Kilauea and Mauna Loa, respectively, as follows: the ratio of average edifice growth rates is about 1 to 1; the ratios of overall edifice volumes and of summit magma-chamber volumes are both about 1 to 10; the ratio of ages since inception is about 1 to 10; the ratio of repose times between distinguishable eruptive and intrusive events is about 1 to 10; and the volumes per event (both intrusive and extrusive) are in the approximate ratio 1 to 10.

If this interpretation is correct, it suggests an interesting property of volcanic evolution: volcanic systems typically evolve from smaller sizes characterized by higher frequency events to larger sizes characterized by lower frequency events at the same overall average growth rate. A similar inference has been drawn by Smith (1979) and by Shaw (1985) concerning cratonic volcanic systems. In fact, the ratio between the periods of repetitive eruptive events per order of magnitude increase in eruptive volume shown by Smith (1979, fig. 12) is also a factor of 10, as was found above for the ratio of repose times between Mauna Loa and Kilauea eruptions (fig. 51.7). Shaw (1985) demonstrates that this proportionality exists for a roughly constant average rate of intrusive magma supply which, for high-level cratonic systems, is about 0.01 km^3/yr; Wadge (1982) discusses other implications of approximately steady-state magma supply in a variety of volcanic systems.

The above proportionalities represent a form of dynamic self-similarity that has some resemblance to fractal self-similarity. That is, if the ratios of event frequencies to average supply rates are decreasing with time as the system as a whole evolves to larger and larger sizes, then there is a great deal more "length" to the time record (more oscillations for the same measure of time) in the smaller systems relative to larger systems (see earlier discussion of fractal length relations). The fact that this tends to occur while the overall rate of magma supply is roughly constant means that the source of the higher frequency oscillations is perpetually present even if it is manifested in eruptive processes having long repose times. This means that on a graph of magma energy fluctuations (as contrasted with a record of erupted volumes of lava) a sufficiently long term record would be very dense with lines (consider the Kilauea record of figure 51.7 extended one thousand years and plotted at the same page size). The analogous map of a coastline length would be so irregular that, somewhat like an ammonite's sutures carried to the extreme, the lines would be essentially area-filling. The area-filling limit for a plane has the fractal dimensional limit of two (it can't be higher unless the map is plotted within a three-dimensional volume); less dense packing gives fractal dimensions between one and two for the coastline problem. By this kind of analogy the simplistic periodicity relation above resembles the fractal limit of two. Such ideas are very important to concepts of what constitutes "live," "dormant," and "extinct" volcanoes, and to the evaluation of possibilities for sudden changes in style (compare Shaw, 1985). The fractal viewpoint considers all such systems equally active but manifesting that activity according to differing "metabolisms" (the suggestive parallel with the relation between sizes and metabolic rates in animals would require a careful assessment of the respective energy budgets in a detail not presently possible).

There is some suggestion of antipathetic alternations of periodic phase between Kilauea and Mauna Loa eruptive activity, as shown in figure 51.7, in that over about 30-yr intervals, when one is at relatively high average rates, the other is at relatively low rates (compare 1920–50 and 1950–80). If this is true, then we might expect increasing eruptive activity at Mauna Loa and decreasing activity at Kilauea within the next few decades (see Klein, 1982). The uncertainty in the ratio of eruptive and intrusive volumes for Mauna Loa, however, precludes rigorous comparisons; we do not have information on the Mauna Loa supply budget that is comparable to the data of Dzurisin and others (1984) for Kilauea. On the time scale of figure 51.1*B*, there are also vague indications of alternating variations between adjacent loci, but during other time intervals adjacent loci appear to be essentially synchronous.

The overall Hawaiian-Emperor curve of cumulative volumes is shown in figure 51.8, scaled down by a factor of 10^6 in both time and volume and superimposed on the 100-yr scale of Kilauea's eruptive volumes. This comparison demonstrates that a crude scale invariance exists between the growth of lava volume at Kilauea and

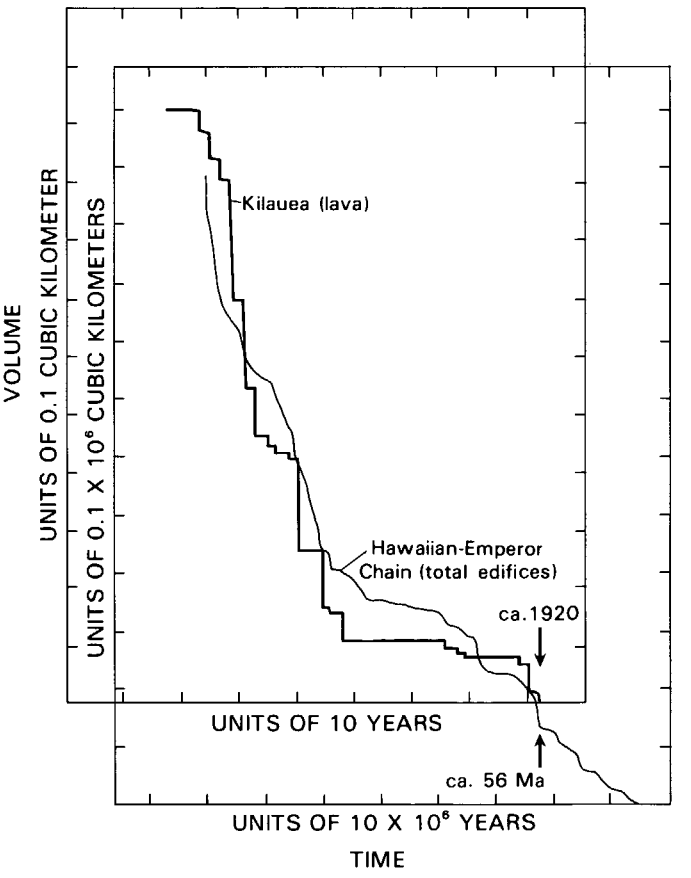

FIGURE 51.8.—Cumulative volumes of Kilauea (lava) and Hawaiian-Emperor Chain (edifice) compared. Composite graph compiled from figures 51.1*A* and 51.4 illustrating crude self-similarity of curves; scale ratio is 10^6. Origin times for comparison taken at 1920 for Kilauea and about 56 Ma for Hawaiian-Emperor Chain (see text for discussion).

the long-term growth of overall edifice volumes for the chain as a whole. This is interesting because the long-term growth history must include the intrusive volumes within the edifice, which have grown at approximately twice the extrusive growth rate during historical activity (see fig. 51.4 and earlier discussion). Thus, the overall rate of edifice growth on the 100-yr scale (intrusive plus extrusive) should be about three times the extrusive rate if the present pattern existed at all times in the past. That is, if this ratio showed up in the comparative record of figure 51.8, the average slope of the long-term record would be about three times the slope of the cumulative curve of lava volume for Kilauea. Therefore, although the youngest part of the long-term record must at present equal the total supply of both Kilauea and Mauna Loa, the fact that the cumulative curve of edifice growth as a whole over about 56 m.y. essentially parallels the 100-yr extrusive curve suggests that Kilauea's extrusive record may faithfully mimic variations in growth rates of the Hawaiian Ridge. If so, the higher intrusive-rate variations indicated by the 30-yr record of figure 51.5*A* might suggest that similarly large relative rate variations also apply to yet deeper components of intrusive magma-supply rates. This would imply the existence of an intrusive magmatic keel at depths greater than the ocean floor with a volume approximately twice the edifice volume. An alternative is offered by the possibility of a compensating rate of loss of volume related to subsidence; Shaw (1973, p. 1523) shows that possible subsidence rates related to the moving front of volcanic loading could be equivalent to a substantial fraction of the observed magma-supply rate. The distinction is largely one concerning the depth range of intrusive storage in the volcanic edifice and its substructure (compare Shaw, 1980).

In either case, the 3-to-1 proportionality of total supply to extrusive volume, when applied to the edifice as a whole, implies an isostatically hidden root system representing the passively intruded magma in the crust-mantle section underlying the ridge system. By this circumstantial inference the average overall magma-supply rates over long times could be as high as 0.3 km^3/yr beneath individual loci, also implying transient fluctuations of edifice supply rates of comparable magnitudes over short periods of time. Such an interpretation may explain the abrupt terminations of the volumetric records along loci in figure 51.1*B*; that is, the volume records sometimes end while the slopes are still very steep, suggesting that unless magmatic volumes and (or) generation rates in the asthenosphere are suddenly turned off or switched to another locus, the terminations may reflect an increased rate of deep over shallow intrusive storage.

Shaw and others (1980) argued that the total volume of magma supply from the asthenosphere could be about a factor of 2 larger than their tabulated values; the above inference suggests that they may be even larger. J.G. Moore (oral commun., 1985) has also emphasized the need to account for larger isostatically hidden volumes on the basis of studies of the chronological histories of drowned terraces along the Hawaiian Archipelago; volumetric corrections suggested by his data are similar to the above estimates. Also, Watts and others (1985) have performed new seismic profiling studies across the ridge system in the vicinity of Oahu, which suggest the possible existence of a substantial intrusive keel with volumes comparable to the above inferences.

The next section explores the relativity of rate episodes and self-similarity in terms of possible physical mechanisms of feedback, and the subsequent section discusses possibilities for self-induced periodicities. Questions concerning correlations with external forcing functions and issues of possible determinism as contrasted with self-guiding processes in volcanic evolution are considered in a closing section.

DISSIPATIVE FEEDBACK AS A SOURCE OF PERIODIC RATE VARIATIONS

This section tries to map out in an approximate way some of the factors that influence the variability of magma production and transport. As mentioned in the introduction, the rationale for discussing dynamic and thermomechanical feedback processes is to identify the basis, and the need, for treating magmatic processes as systems of interacting and self-influencing mechanisms of transport that evolve in space and time. This section describes some of the interactions that tend to focus activity within certain ranges of a general dynamical hierarchy that is characterized by the variety of rate signatures discussed in the preceding section. In the subsequent sections, ideas of rate-controlled feedback are explored in a format that attempts to connect physical ideas of feedback with mathematical ideas of feedback according to concepts of attractors and evolutionary strategies previously outlined. The reason for such approaches is to begin to build toward concepts of cyclical magmatectonic processes that have as their natural outcome the patterns of plutonic and volcanic behavior seen in the worldwide record of igneous provinces interacting with analogous cyclical processes of plate tectonics (and possibly also more exogenous influences; see comments at end of introduction).

The approach in this section is based on the thermomechanical relations discussed in Shaw (1969); for consistency, the same sets of physical properties are used here. Since that paper was written, however, several discussions of so-called "thermal feedback," "thermal runaways," and of the effects of variable viscosity, variable rheologies, and other dissipative phenomena in magma transport have appeared in the literature. Hardee (chapter 54) cites some of these studies that are relevant to volcanism and gives calculations demonstrating applications to concepts of magma transport in Kilauea's rift systems.

The present section focuses on comparisons between characteristic times associated with dissipative heating, cooling by thermal conduction, and variations in viscous and elastic states of stress, and on their possible implications for timing of magma transport. The aim is to delineate regimes of behavior without analyzing specific events. It is found that dynamic parameters tend to group naturally around values characteristic of the time and size scales of the observed ranges of volcanic behavior. From the viewpoint of feedback systems, such dimensional correspondences exist because they are produced by a common process of evolution. The association of characteristic dike or conduit dimensions with characteristic variabilities of flow rates is not externally imposed, but occurs as a product of the tendency for balances between competitive thermal, dynamic, and mass-transport phenomena.

The balances between viscous heating and conductive cooling of basaltic magma subjected to a system of shear can be expressed in a nomogram (fig. 51.9). It applies strictly to plane shear with constant forcing, but it also semiquantitatively identifies regimes appropriate to forced flow in tabular conduits. The lines on the nomogram identify half-thicknesses representing approximately equal times for heating by viscous dissipation and cooling by conduction. Higher stresses or lower initial viscosities relative to a given line lead to positive thermal feedback (conditions of thermal "runaway") in the manner illustrated by Gruntfest (1963) and by Shaw (1969, figs. 6–9) and as discussed by Hardee (chapter 54). The lines represent the balance $t_c = t_\infty$, where t_c is a characteristic time for conductive cooling and t_∞ represents the time during which viscous heating would achieve very high temperatures in the absence of heat losses or decreases in shear stress. Table 51.1 summarizes the physical parameters used in the thermomechanical calculations, and

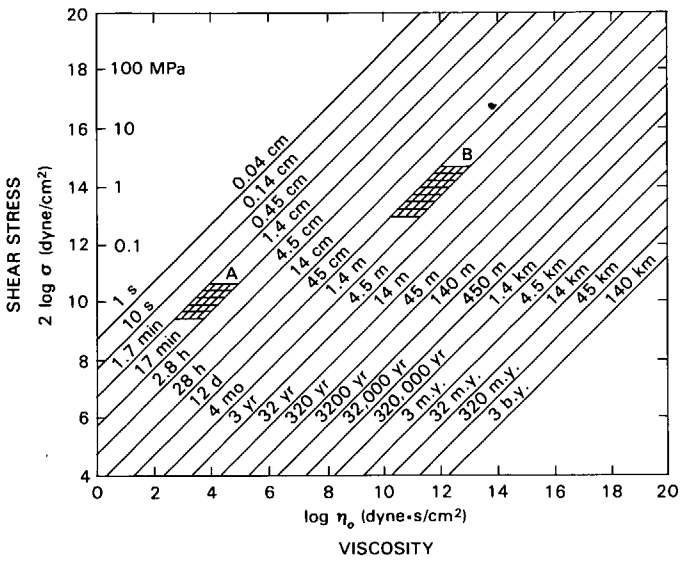

FIGURE 51.9.—Dynamic range of parameters characterizing steady-unsteady thermal-feedback transition defined in terms of equal values of adiabatic viscous-heating time (t_∞) and thermal-diffusion time (t_c) for planar shear layers of the indicated half-thicknesses (see tables 51.1 and 51.2 for definitions); diagonal lines represent values of shear stress and initial viscosity for a given slab thickness (and time) that satisfy equality $t_c = t_\infty$, or $t_c/t_\infty = 1$. If $t_c > t_\infty$ thermomechanical instability (or "thermal runaway") is likely; this occurs for values of shear stress and viscosity above and to left of each line for a given half-thickness of shear flow. Because t_c depends only on thickness, each line is associated with a characteristic time, as shown. Two areas identified by crosshatching represent examples of reasonably well delineated conditions for, respectively, (A) laboratory viscometry (Shaw, 1969) and (B) viscous conduit flow on east rift zone of Kilauea (Hardee, chapter 54; Decker, chapter 42); east-rift-zone behavior was plotted on basis of a shear-layer half-thickness on the order of 1 m and an effective shear stress on the order of 10^7 dyne/cm² (1 MPa). This, in turn, implies an initial viscosity at onset of intermittent shear flow on the order of 10^{11}–10^{12} dyne·s/cm² (10^{10}–10^{11} Pa·s); a compatible crystallinity might be in the neighborhood of 30–40 percent (Shaw, 1969). For additional discussions of thermal feedback, see Shaw (1969) and Hardee (chapter 54).

TABLE 51.1.—*Physical parameters used in analyses*

Symbol	Name	Unit	Reference values
$\underline{a}$	Temperature coefficient of viscosity	K^{-1}	1×10^{-2} (1-phase) 2×10^{-1} (2-phase)
$\underline{c}$	Heat capacity (volumetric)	$erg\cdot cm^{-3}\cdot K^{-1}$	3×10^{7}
$\underline{c}^*$	Effective $\underline{c}$ for crystal + liquid	$erg\cdot cm^{-3}\cdot K^{-1}$	1×10^{8}
$\underline{G}$	Shear modulus[1]	$dyne\cdot cm^{-2}$	$\sim10^{11}$
$\underline{k}$	Thermal conductivity	$erg\cdot sec^{-1}\cdot cm^{-1}\cdot K^{-1}$	2×10^{5}
$\underline{k}^*$	Permeability	cm^2	10^{-11} (1 mdarcy)
$\underline{\ell}$	Half-thickness	cm	Variable
$\underline{R}$	Displacement rate	$cm\cdot sec^{-1}$	Variable
α_p	Diffusivity of pressure ($= \underline{k}^*/c\eta^*\beta$)	$cm^2\cdot sec^{-1}$	2×10^{3} (water) 2×10^{-2} (melt)
β	Compressibility	$cm^2\cdot dyne^{-1}$	5×10^{-11}
η_o	Initial viscosity	$dyne\cdot sec\cdot cm^{-2}$	Assigned (or derived from self-consistent combinations)
η^*	Pore fluid viscosity	$dyne\cdot sec\cdot cm^{-2}$	10^{-3} (water) 10^{2} (melt)
ϵ	Porosity[2]	fraction	0.1
$\dot{\epsilon}$	Shear rate	sec^{-1}	Variable (or assigned, or derived)
γ	Thermal expansion coefficient of pore fluid	K^{-1}	$\sim10^{-3}$
μ	Coefficient dynamic friction	--	~0.5
ρ	Density	$gm\cdot cm^{-3}$	Variable
σ	Shear stress	$dyne\cdot cm^{-2}$	Assigned or derived

1 The shear modulus is not a constant in mixed media such as magma and partial melt systems. In cases where variable G is possible the symbol G* is used; a range of possibilities for magma is indicated in figure 51.11.

2 The porosity ϵ appears only in the definition of α_p and is not to be confused with shear rate $\dot{\epsilon}$ which appears in the time-scale ratios of tables 51.2 and 51.3.

table 51.2 identifies the groups of these parameters that define the intrinsic time scales of thermomechanical processes.

The vicinities of the crosshatched areas in figure 51.9 identify conditions resembling those of laboratory viscometry (Shaw, 1969; crosshatched area *A* in fig. 51.9) and the conditions for eruptions along the east rift zone of Kilauea during the 1983–84 activity as analyzed by Hardee (chapter 54; crosshatched area *B* in fig. 51.9). Periodic instabilities are possible at recurrence times of the indicated magnitudes. That is, in the laboratory viscometer, if shear energy were continuously supplied at approximately 10^5 dyne/cm^2 (10 kPa) at a mean viscosity varying from 10^3 to 10^4 poise (dyne·s/cm^2, or 10^2–10^3 Pa·s), the local values of shear rates and shear stresses would oscillate with an irregular periodicity of about 1–20 min. Similarly, at about 10^7 dyne/cm^2 (1 MPa), the average oscillatory periodicity would be from about one week to a few months for a system of dikelike forced shear flow (rectangular slot or pipe flow) with half-thicknesses on the order of 1 m and an initial static viscosity of 10^{11} or 10^{12} poise (1–10 GPa·s; roughly one-third crystallized). Such a range suggests one kind of contribution to characteristic recurrence times for repetitive eruptions.

Hardee (chapter 54) shows that equivalent arguments can be expressed in terms of either dissipative heating or nonlinear magma rheology (see Shaw, 1969). The important point for the present discussion is that there are intrinsic properties and dynamical conditions that promote crudely periodic phenomena and under some sets of conditions possibly even regular periodic phenomena.

The relations of figure 51.9 are summarized in figure 51.10 over a range of conditions that span most of those possible in terrestrial shear flows (excluding instantaneous fault-slip, explosive, or impact phenomena). The shaded fields represent broad classes of categorically similar behavior; for example, the shaded field labeled "order of 1 m" corresponds in an order-of-magnitude sense to the approximate monthly variations of the 1983–84 east-rift-zone activity, and the field labeled "5–50 m" corresponds to the historical variability of Kilauea and Mauna Loa with an event frequency in the range 3–300 yr. The large field at the highest viscosities and stress magnitudes spans the ranges of variable activity from the scale of individual volcanic systems (less than one to several million years) to the global scale of propagating volcanic systems and igneous cycles seen throughout Earth's history.

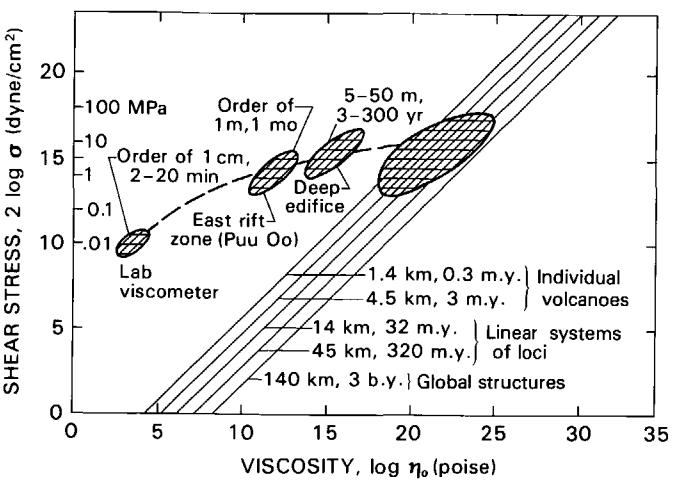

FIGURE 51.10.—Dynamical fields of anticipated oscillatory behavior for self-consistent combinations of shear-layer half-thickness and time according to thermal-feedback relations of figure 51.9 (see tables 51.1 and 51.2). Note that magmatectonic regimes showing intermittent shear-melting instabilities at local to global scales of time and size are characterized by viscosities within liquid-solid range for silicate systems (about 20 orders of magnitude) over a very narrow range of shear stresses (<3 orders of magnitude). Time-thickness pairs selected arbitrarily from geologically reasonable ranges of possibilities. Maximum half-thickness of 140 km would correspond to present-day intermittent shear instabilities in a globally averaged asthenosphere that has evolved over the age of the Earth.

TABLE 51.2.—*Time scales based on parameters of table 51.1 for thermomechanical processes*

Process	Time scale
Thermal diffusion[1]	$t_c = \frac{c\ell^2}{k}$
Stress response	$t_s = \frac{2\ell\sigma}{GR}$ or $t_s = \frac{\sigma}{G\dot{\varepsilon}} = \frac{\eta}{G}$
Viscous heating[1] (thermal feedback)	$t_\infty = \frac{2c\ell}{a\sigma R}$ or $t_\infty = \frac{c}{a\sigma\dot{\varepsilon}} = \frac{c\eta_0}{a\sigma^2}$
Pressure "diffusion"	$t_p = \frac{\ell^2}{\alpha_p}$
Thermal pore pressure[1] (Darcian feedback)	$t_d = \frac{c\beta}{\mu\gamma\dot{\varepsilon}_0}$ or $t_d = \frac{2c\beta\ell}{\mu\gamma R_0}$

1 The effective heat capacity c^* (and assigning $a = 2\times10^{-1}K^{-1}$) is to be used in evaluating equations for magmatic systems in which there are melting reactions (see Shaw, 1969). A subscript o refers to an assigned constant value of the variable.

The above scale relations refer only to thermal balances for a given level of continuous forcing, as reflected in the shear-stress magnitude. Therefore, an important measure of variability of the thermal balance, in addition to the time scale of heat transfer, is the time scale of loss and recovery of stress magnitude associated with a given rate of motion. Table 51.1 indicates that a scaling factor for shear stress is given by the ratio of dynamic viscosity (η) to elastic shear modulus (G), or equivalently by the ratio of the shear stress (σ) to the product of shear rate ($\dot{\varepsilon}$) and elastic shear modulus. This latter ratio is sometimes called the Maxwell or viscoelastic relaxation time.

The physical meaning of stress relaxation can be visualized in terms of the shear rate, which is the ratio of shear displacement per unit time (R, in cm/s) to the thickness of the shear layer ($2l$). Thus, the reciprocal $1/\dot{\varepsilon}$ represents the time associated with a 100-percent

shear strain, and the product $(\sigma/G)(1/\dot{\varepsilon})$ is that time normalized by the ratio of viscous to elastic stress components. The smaller the viscous shear stress relative to the elastic modulus, the shorter is the time for either the loss or recovery of stress equilibration across the sheared layer. A very high shear stress at a given displacement rate, hence a given apparent viscosity of the layer, implies a relatively longer time for a large shear disturbance on one side to permeate or diffuse across the layer. For the conditions illustrated in figures 51.9 and 51.10, however, the ratio σ/G is less than 1, meaning that the rate of stress equilibration is rapid relative to the time required to achieve unit shear strain in viscous flow. Nevertheless, the ratio must be taken into account because of the potentially unlimited shear strains of viscous flow.

The effect of incorporating the stress response time with the thermal relations of figures 51.9 and 51.10 is illustrated in figure 51.11; the circled points represent the formal identities $t_c = t_s = t_\infty$ (for $t_\infty = t_s$, stress is constant). This means that for conditions that are both above the hachured band (symbolizing elastic responses typical of rocks) and above the 45° lines (where conductive cooling is slow relative to dissipative heating), profound melting instabilities ("runaways") can persist over times longer than those indicated on the diagram or in figures 51.9 and 51.10. For conditions of smaller elastic moduli that may apply to magma (media with a liquid fraction, above an unspecified minimum threshold, have greater compliance in shear), the stress level of this regime would be lowered in proportion to the scale of the effective modulus, $G^\star$, as shown at the right in figure 51.11 (see footnote 1, table 51.1); values of $G^\star$ vary with melt fraction, so numerical values are equivocal. Within regions below the hachured band but still above the 45° lines, thermal instabilities can begin at the indicated stress levels (for example, above about 10^7 dyne/cm^2 or 1 MPa for meter-scale shear couples), but they do not persist over the indicated timespans. That is, within these regions the melting instabilities are intermittent and oscillate according to the stress-recovery times; these relations are generally in accord with stress magnitudes associated with the variations described earlier.

Although the labeling of fluid and solid states on such a diagram is relative and simplistic, oscillatory fluid phenomena, possibly such as cavitating flow and tremor, are associated with low apparent viscosities, whereas shear melting of nearly solid aggregates will occur at the highest viscosities; these observations are also consistent with the great span of time scales of the respective processes (the order of a second or less in cavitating flows, the age of the Earth in mantle-wide shear flows).

The above approach to dynamic regimes can be generalized even more in terms of conditions describing fluid migration, either by percolation as a pore fluid or by percolation as injection pulses associated with extensional fracture events (Lachenbruch, 1980; Shaw, 1980). The analysis parallels that of the thermomechanical balances discussed in Shaw (1969), except that fluid pressure, effective stresses (Shaw, 1980), and fluid mobility are coupled with the thermal responses. An analysis for water as the pore fluid is given in more detail by Lachenbruch (1980) in connection with interpretations of heat-flow and stress variations associated with fault motions. A synopsis of analogous effects is repeated here in terms of ratios of response times, using an approach similar to that of figures 51.9–51.11.

Table 51.3 lists the 10 possible ratios of the time scales given in table 51.2 and gives for each of these ratios (where possible) the relation between the logarithm of shear stress (σ) and the logarithm of the product Rl of displacement rate (R) times half-thickness (l) of the shear layer. Equations are written for the condition $t_i/t_j = 1$ ($t_i = t_j$). The quantity Rl is a convenient way to represent deformation rate in viscous systems because it explicitly identifies the roles of both the size of the shear layer and the displacement speed. The coined term "diffusivity of action" is used here for Rl because the product of displacement rate and thickness has the dimensions centimeters squared per second, as in thermal, chemical, or momentum diffusivities (its interpretation, of course, depends on the context considered, for example, faulting or magmatic flow, and the chosen

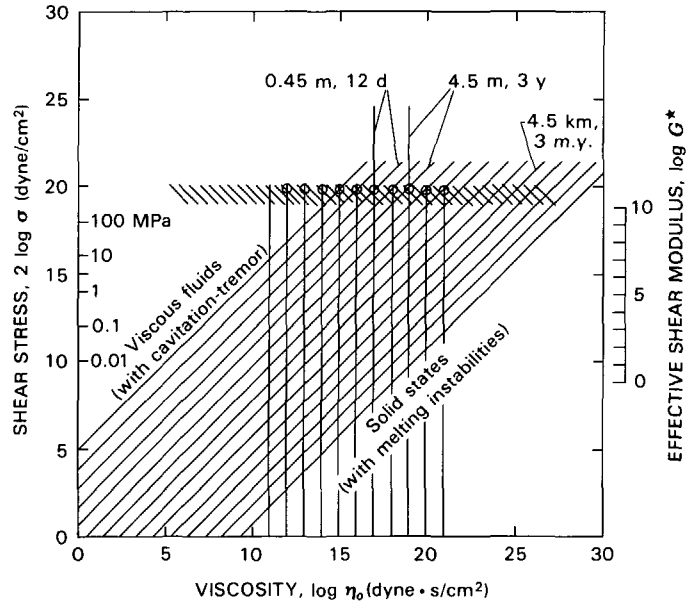

FIGURE 51.11.—Nomogram constructed as in figure 51.9, including stress response times (see table 51.2). Vertical lines represent values of $t_s = \eta/G$; circles represent locus of identities $t_c = t_\infty = t_s$. Also, $t_s > t_\infty$ only above horizontal interval (hachured) for value of shear modulus, G, in table 51.1. Hence, stress responses (both relaxation and recovery) of melt-free rocks are rapid relative to thermal-feedback responses at stress levels appropriate to all conditions shown in figures 51.9 and 51.10. Consequently, intermittent thermal instabilities automatically imply, and (or) are implied by, oscillating stress regimes, unless shear modulus is decreased significantly in the molten state (see table 51.1, footnote 1, and text for explanation of effective shear modulus $G^\star$). When that happens, upper stress limit of combined intermittent stress and thermal-feedback regime is lowered and is indicated by scale of log $G^\star$ at right; consequently, thermal instabilities related to melting may occur at effectively constant shear stress under same conditions that permitted intermittent instabilities in solid state (see Shaw, 1969). However, conditions above horizontal limits $t_s = t_\infty$ are artificial in that thermal feedback at constant stress is necessarily transient; thermal-feedback instabilities inevitably alter material states, so that intermittent stress regimes eventually result. Shear melting events may nevertheless be of large magnitude when $t_s > t_\infty$.

TABLE 51.3.—*Reference equations based on possible equalities of pairs of time scales in table 51.2 using values of constants in table 51.1*

[There are 10 possible combinations of the time scales defined in table 51.2; see text for discussion]

Time-scale ratios	Reference equations[1]	
	Nonmagmatic (solid + aqueous fluid)	Magmatic (melt + solid)
1. t_c/t_s	$\log \sigma = 12.9 + \log(R\ell)$	$\log \sigma = 13.4 + \log(R\ell)$
2. t_c/t_∞	$\log \sigma = 7.6 - \log(R\ell)$	$\log \sigma = 6.3 - \log(R\ell)$
3. t_c/t_p	3×10^5 (constant; $t_c \neq t_p$)	10 (constant; $t_c \neq t_p$)
4. t_c/t_d	$\log (R_o\ell) = -1.4$ (for all σ)	$\log (R_o\ell) = -1.4$ (for all σ)
5. t_s/t_∞	$\log \sigma = 10.2$ (for all $R\ell$)	$\log \sigma = 9.8$ (for all $R\ell$)
6. t_s/t_p	$\log \sigma = 7.4 + \log(R\ell)$	$\log \sigma = 12.4 + \log(R\ell)$
7. t_s/t_d	$\log \sigma = 11.5$ (for all $R\ell$)	$\log \sigma = 12.0$ (for all $R\ell$)
8. t_∞/t_p	$\log \sigma = 13.1 - \log(R\ell)$	$\log \sigma = 7.3 - \log(R\ell)$
9. t_∞/t_d	$\log \sigma = 9.0$ (for all $R\ell$)	$\log \sigma = 7.7$ (for all $R\ell$)
10. t_p/t_d	$\log (R_o\ell) = 3.5$ (for all σ)	$\log (R_o\ell) = -0.4$ (for all σ)

[1] Equations are based on solving for either $\log \sigma$ or $\log (R\ell)$ under conditions where $t_i = t_j$ is possible (that is, when $t_i/t_j = 1$); this is not possible for t_c/t_p with physical constants of table 51.1.

values of physical parameters in table 51.1, or values considered appropriate to other specific applications).

Among the 10 possible ratios, t_c/t_p is unique in being a constant for the parameters of table 51.1; it represents the comparative decay of a thermal pulse by conduction relative to that of a pressure pulse by pore-fluid flow, neglecting the heat-transfer effect of the flow. In this respect, then, it is a measure of the ease of permeation of fluids away from a thermal disturbance; hence, it also indicates conditions under which advective heat transfer should be important. Clearly, pressure decay is very fast for aqueous pore fluids relative to thermal conduction, but for silicate melt the two are more comparable (depending on melt viscosity, latent heat, and other factors).

Except for t_c/t_p, all the other ratios in table 51.3 involve one or both of the quantities $\log \sigma$ and $\log (Rl)$. The equations that involve both terms show that, logarithmically, they are directly proportional, so that their graphs are straight lines with slopes of either $+1$ or -1. Equations for which shear stress (σ) and (or) diffusivity of action (Rl) are constants plot as straight lines parallel to either an axis representing $\log \sigma$ or one representing $\log (Rl)$.

Numerical values of these independent variables calculated from the equations of table 51.2, based on the reference parameters of table 51.1, are plotted in figures 51.12 and 51.13. These figures attempt to show how instabilities characterized by the range of time scales in figures 51.9–51.11 can also be expressed as functions of stress and displacement histories. This is not the place to attempt a complete description of the ramifications of such diagrams; their implications address aspects of rock deformation in a manner somewhat similar to the use of thermodynamic-facies concepts in metamorphic petrology. Instead, I focus on the regions of likely periodic variations important to volcanic phenomena, following the approach already discussed in reference to simplified thermal feedback.

The dots in figure 51.12 and the open circles in figure 51.13 mark the invariant intersections of common sets of equations in table 51.3, as listed in figure 51.12. The heavy lines in these figures represent functions based on the variables t_c, t_s, and t_∞, as in figure 51.11, except for the different choices of independent coordinates. Invariant points c (figure 51.12) and c' (figure 51.13) have the same implications as the circled points in figure 51.11. The hachured triangular regions to the right of c and c' represent conditions of oscillating instabilities limited by the stress-response times, as illustrated in figure 51.11. Figure 51.12 shows the response of a melt-free solid in which the instabilities would take the form of shear fractures rather than melting. If shear melting is allowed, however, the difference between c and c' in figure 51.13 indicates the likely effects of differences in physical properties arising from the inclusion of latent heat and different temperature dependence of viscous activation (see Shaw, 1969).

Points d (fig. 51.12) and d' (fig. 51.13) and the respective regions to their right are related to coupled effects of shear heating, consequent fluid-pressure responses, and tendencies for flow accord-

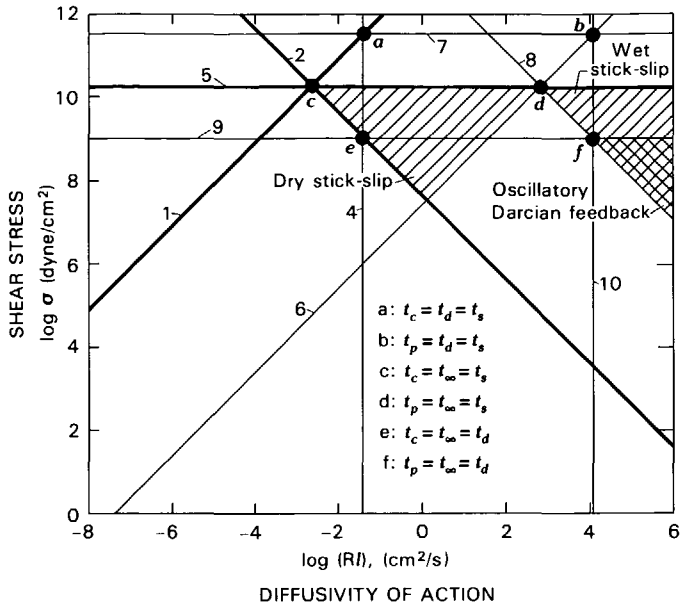

FIGURE 51.12.—All possible dynamic regimes involving thermal feedback, stress oscillations, and aqueous pore-fluid transport according to ratios in table 51.3 based on combining thermomechanical analyses from Shaw (1969) and Lachenbruch (1980). Nodal points labeled *a–f* represent possible invariant identities for variables shear stress, σ, and what I call "diffusivity of action," *Rl*, where *R* represents displacement rate of one side of a shear layer relative to other, and *l* is half-thickness normal to layer. Heavy lines indicate fields delineated by thermal feedback in absence of either melting or pore-fluid transport. Acute angle defined by points *d*, *c*, and *e* represents conditions where thermal feedback results in endothermic processes of fracture rather than pervasive melting; because such fracture would be activated intermittently, it is labeled the region of "dry stick-slip." Analogous region involving pore-fluid weakening to right of line 8, below line 5, and above line 9 is labeled "wet stick-slip"; it occurs because thermal response is faster than both pore-pressure decay and time for weakening due to pore-pressure response to heating (termed "Darcian feedback"). Below line 9 and to right of line 8, however, Darcian response is faster than both dry thermal response and decay of pore-fluid pressure, hence that region is labeled "oscillatory Darcian feedback"; see Lachenbruch (1980) for a detailed analysis of Darcian regimes appropriate to displacements within fault zones.

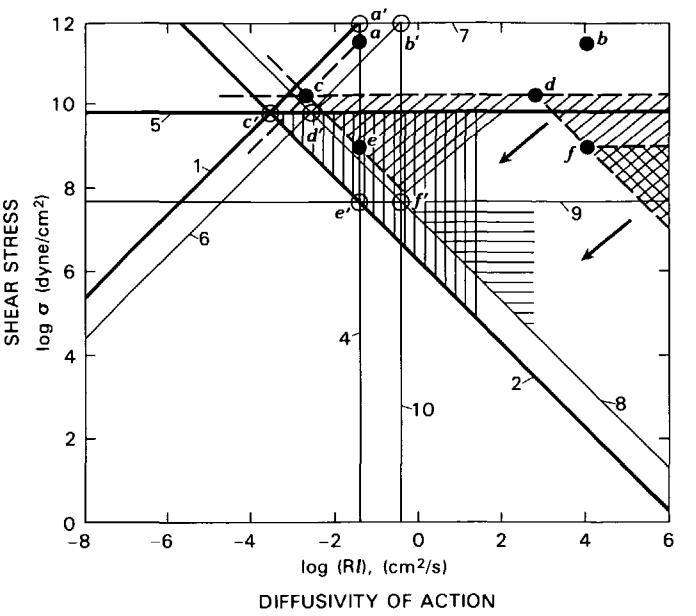

FIGURE 51.13.—Dynamic regimes as shown in figure 51.12 but also including conditions of transport where silicate melt is pore fluid. Dashed lines, unprimed letters, and related shading from figure 51.12; arrows indicate direction in which Darcian regimes shifted when melt is pore fluid. Analogous invariant intersections reflecting properties of solid-melt interactions are indicated by primes (see parameters in table 51.1). In general, fields described in figure 51.12 are telescoped together when melt is pore fluid, and oscillatory Darcian feedback occurs at much lower shear stresses and displacement rates.

ing to Darcy's law in response to the pressure gradient (for details, see Lachenbruch, 1980). Points *f* (fig. 51.12) and *f'* (fig. 51.13) demark the limits of regimes which I will refer to as conditions of "Darcian feedback." This phrase is used in the same context as thermal feedback, in the sense that a tendency for runaway (and eventual changes of state or decreases in effective stress) is countered by a transport rate. The components of negative feedback can be characterized by a thermally coupled pressure diffusivity in the case of Darcian feedback, and a simple thermal diffusivity (which may be an effective value that includes mass transport) in the case of thermal feedback.

In the above terms, the time scale t_d in tables 51.2 and 51.3 represents the time for reduction of frictional resistance owing to Darcian feedback. As such, it represents the relaxation or recovery times for effective stress, hence it also represents conditions of shear failure according to some failure law. A constant value of the coefficient of friction, μ (see table 51.1), is equivalent to a Coulomb failure law, meaning that there is a constant angle of the failure envelope on a Mohr diagram (see Shaw, 1980, figs. 6 and 7). This point is raised because magmatic extensional fracture, as discussed by Shaw (1980), employs a modified Griffith-Coulomb failure law, implying variable and potentially large values of the ratio of frictional resistance to effective normal stresses, and also implying nonconstant values of increasing dynamic friction (μ) as conditions approach those for pure extensional failure. This point will be reiterated in discussing the shifts of points *c*, *d*, and *f* to points *c'*, *d'*, and *f'* from the conditions for nonmagmatic regimes (fig. 51.12) to those representing magmatic regimes (fig. 51.13).

I attempt to focus the meaning of "dynamic regime" by discussing only the regions in the vicinities of points *c*, *d*, and *f*, or *c'*, *d'*, and *f'* in figures 51.12 and 51.13. In figure 51.12, the region near *c* to the right of line 2 and below line 5 has already been mentioned as identifying oscillatory, thermally coupled shear-failure events (there is no involvement of pore fluid as part of the onset conditions, although melt or pseudotachylite could be a product of failure; if so, the validity of the regime boundaries is modified at the instant of failure). Repetitive failures could be described as episodes of reduced and accelerated displacement rates resembling laboratory

stick-slip. To the right of d, below line 5 and above lines 8 and 9 (fig. 51.12), a similar situation occurs, in the sense that the thermal transient (t_∞) is short relative to both the loss of induced pressure (t_p) and the Darcian response time (t_d), meaning that analogous shear failures would occur in wet rocks for conditions of sufficiently low permeability, high stress (greater than about 10^9 dyne/cm^2 or 100 MPa), and high enough displacement rates (for example, about 1 cm/s for a shear zone 1 m in half-thickness). This regime is labeled "wet stick-slip" in figure 51.12. In figure 51.13, an analogous region to the right of d' is implied with magma as the pore fluid; in this case, the magma-wetted stick-slip regime is nearly superimposed on the dry stick-slip regime, because of the changes in physical properties appropriate to magmatic environments.

Persistence of yet higher displacement rates, however, eventually creates a condition where the pressure-response time is longer than the Darcian response time. At that point, f, oscillatory Darcian feedback becomes a possibility; that is, to the right of line 10, but above line 8 and below line 9. This represents the region where Darcian thermal coupling is faster than the loss of induced pressure by flow and also where the Darcian coupling is faster than simple shear heating in the absence of pore fluids. Thus, this region is labeled "oscillatory Darcian feedback" (see labeled area in fig. 51.12; in fig. 51.13 the same area is shown, and an arrow indicates the direction in which this region of oscillatory Darcian feedback is shifted when magma is the pore fluid).

The interpretation of points c', d', and f' in figure 51.13 is parallel to that of c, d, and f with some qualifications. In particular, if a curved failure envelope, such as that implied by a modified Griffith-Coulomb failure law (Shaw, 1960, fig. 7) applies, the constancy of dynamic friction, μ, does not hold. In the limit of pure extensional failure, the ratio t_p/t_d defining line 10 becomes indeterminate because of this fact; also, the effective permeability is governed by transport related to extensional fracture propagation. The combined effect, however, tends to reduce both the pressure-response time (related to greater ease of flow along dikelike fractures rather than through tortuous pore space) and the modified Darcian response time (because of the increasing dynamic friction associated with an increasing failure angle implied by a Griffith envelope). As a consequence of these offsetting tendencies, the more channelized flow of modified oscillatory Darcian feedback may not differ greatly from that implied by flow in porous media.

The general effect for pore fluids with magmatic properties appears to be to telescope the respective oscillatory fields of figure 51.12 to conditions near point f' in figure 51.13; that is, ordinary thermal feedback in magmatic systems implies the existence of a melt fraction. Hence, the general effect of increased transport brings the oscillatory field to lower stresses and higher diffusivities of action (higher displacement rates for the same values of half-thickness).

Values of shear stress implied by the field limited by point f' and lines 8 and 9 in figure 51.13 are within the range 10^6–10^8 dyne/cm^2 (0.1–10 MPa), which is reasonable based on other considerations for natural regimes showing oscillatory behavior (see Decker, chapter 42; Hardee, chapter 54; Shaw, 1980). If we take values of half-thickness ranging from the order of 1 m to 100 km, as in figure 51.10, values of compatible displacement rates, R, can be estimated corresponding to log $(Rl)\simeq 0$ in figure 51.13. These are, respectively, 10^{-2} cm/s (~3 km/yr) and 10^{-7} cm/s (3 cm/yr). The former would be associated with mean effective propagation rates of dikelike injections through the lithosphere, and the latter with rates of mantle flow (the actual propagation rates for Hawaiian-Emperor loci, however, vary as much as an order of magnitude relative to mean plate velocity, implying that the local half-thickness of associated asthenospheric flow may vary between about 10 and 100 km; see Shaw, 1973, and Shaw and others, 1980).

An analysis of magma-driven propagation of cracks by Spence and Turcotte (1985) gives a fracture-propagation velocity of 0.5 m/s for a half-thickness of 0.25 m and a fluid pressure of 6.3×10^8 dyne/cm^2 (63 MPa); this corresponds to a value of log $(Rl)\simeq 3$. Although their analysis does not refer to shear-induced extensional fracture, the energy-rate balances resemble those in the field of modified oscillatory Darcian feedback. The examples plotted in figure 51.9 also plot in this general vicinity when they are converted to the independent variables of figure 51.13.

The main conclusion relevant to this paper from the considerations of dynamical time scaling is that repetitive feedback processes involving melting and magma transport as identified in figures 51.12 and 51.13 are likely to occur over a range of self-determined periodicities indicated by the estimates of time in figure 51.10. Feedback interactions of complex processes tend to be self-focusing in that the likely effects converge toward limited ranges of dynamical parameters. Over a long enough time, therefore, the temporal variability and size scales of geometric structures associated with such systems of interactive feedback are not simply imposed by external constraints on geometric states and forcing functions, as in some laboratory experiments, but become artifacts of the dynamical history. Thus, temporal, spatial, and dynamical variability interact repetitively over all the magnitude scales considered. The crude and repetitive self-similarity shown by the volcanic record as portrayed in figures 51.1–51.8 evidently records elements of dynamical similarity that have evolved according to feedback processes. Many different mechanisms exist at each scale of the general feedback process, and much can be learned through inverse reasoning about these mechanisms (and the need for more information concerning them) by considering their conceptual interactions (for example, the mechanisms and properties of magmatic percolation can be viewed in a manner parallel to the hydraulics of pore fluids as described by Lachenbruch, 1980). This generalization does not preclude interactions with external forcing functions, such as extraterrestrial energy influences mentioned later. In the next section I consider a logistical approach to the description of self-induced periodicity.

STATIONARY STATES AND ENDOGENOUS PERIODICITIES OF ATTRACTION IN THEIR NEIGHBORHOOD

This section, like the previous one, contributes to the idea that there are logical reasons for magmatic systems, and volcanic systems in particular, to be considered as feedback systems subject to the general mathematical principles of recursion outlined in the introduction. In the preceding section, it was found that the repetition of

magmatic processes acts to modify both the dynamic and geometric conditions of localized behavior in a way that leads to focusing of those conditions within limited and characteristic regimes that form a part of a hierarchy of such regimes from the local to global scales. In the present section, the feedback process is viewed as a recursion of characteristic quantities in a way that generates repetitive structures in space and time. The quantities discussed in this section are totally hypothetical, but they can be viewed as sets of data representing imaginary intrusive and (or) volcanic magmatic cycles described in terms of relations between mass, volume, and their rates of change. The purpose is to provide a description in which ideas of dynamic feedback and what may be called "logistical" feedback lead into considerations of the numerical properties of recursion that are treated elsewhere by the theory of attractors (with their implicit relations to fractal self-similarity mentioned earlier).

Whereas the previous section considered conditions consistent with feedback among physical mechanisms, this section considers aspects of logistical processes that are consequences of repetitions involving combinations of net positive-negative feedback rates. That is to say, this section examines the logistics of what I call folded feedback. First, I give working definitions of what I mean by "logistic" and "folded," because both terms are used in a variety of contexts in different disciplines. The usage here is descriptive and does not necessarily correspond to formal definitions found in the literature of economics, biology, mathematics, topology (and catastrophe theory), physics, or other fields.

I use "logistic" to indicate that the method of analysis originates in the logic of numerical sequences (as in the construction of a computer algorithm) and also in the sense of military logistics, where the responsibility entails management of processes affecting aspects of material distributions which support the strategy of operation with or without any absolute knowledge concerning the plan of action. In other words, logistical analysis is the mathematically logical manipulation of quantities, whether they are real or abstract. The quantities can be anything measurable in the sense that there is some kind of unit that can be counted. Depending on the quantities manipulated, the logistical approach in this way resembles the logic of chemical mass balances, physical kinematics, dynamics, and number theory.

"Folded feedback" is shorthand for the net effects of feedback (and feedforward) processes operating in a complex system that contains aspects of both positive (accelerative or regenerative) and negative (decelerative or degenerative) responses. These are the composite processes of the previous section considered to be characteristic of a complex system even in the absence of an ability to dissect, analyze, and describe all mechanisms. The term "feedforward" is sometimes used to describe an input designed to exercise some guiding influence (perhaps via indirect or ancillary information loops) on a following stage of an operation (examples are given by aspects of industrial plant operation or by a satellite-guidance system). It is contrasted with feedback control, which loops output information directly back into the guidance mechanism. Feedforward is subsumed within my meaning of folded feedback and is not subsequently used herein. Thermal and Darcian feedback offer examples of both types of control, depending on the nature of coupling with other processes. Strict thermal feedback in an adiabatic system represents a direct control loop of dissipative output back into the system as an input via the temperature dependence of the stress and shear-rate relations (apparent viscosity). It may be either positive (constant source of shear stress) or negative (constant displacement rate). Thermal feedback also offers a clear demonstration that negative feedback is not necessarily synonymous with stabilizing feedback (see Gruntfest, 1963; Shaw, 1969, p. 531).

The positive and negative aspects of thermal feedback demonstrate some of the general aspects of folded feedback. Folded feedback can be thought of as the combined effects of coupled operations involving a net increase in a quantity followed by a net decrease, for example, an up followed by a down or an in followed by an out. The key idea is that the repetitive action of both kinds of effects as a net consequence of all operative mechanisms, however numerous and complicated they may be, is folded in as an essential aspect of feedback-system operation.

Logistical analyses of biological populations represent examples of folded feedback where there are numerous and complex sets of specific feedback mechanisms. Simpler illustrations are provided by laboratory deformation of elastic solids and viscous liquids. For an elastic solid, it is easy to maintain a constant stress (below the failure stress), whereas the attempt to maintain a constant shearing rate leads eventually to a rising shear stress and failure. Continued shear may then lead to alternating conditions of sticking and slipping along the plane of fracture, with stress oscillations governed by the normal stresses and coefficients of sliding friction (thus conforming to a specific kind of folded feedback). For a liquid, on the other hand, it is usually possible to maintain a constant shearing rate, at least below a critical speed; when one attempts to maintain a constant shearing stress, however, thermal feedback leads to an increasing shear rate. If the layer thickness is large enough, the adiabatic condition is approximated, and the shearing rate is limited only by stress relaxation or by the maximum shearing rate attainable with the instrument, according to the relations already discussed. Because magmatic systems involve both types of behavior and because natural deformation may involve potentially large values of both shear stress and shear rate, conditions tend to oscillate between those approximating constant stress and those approximating constant shear rate, thus implying folded feedback.

These tendencies are schematically summarized in figure 51.14, a type of diagram designed to distinguish between present and future states. The diagonal line at 45° represents those conditions in which the future state of melt concentration is the same as the present state. That is, thermal or mechanical energy is supplied in amounts just sufficient to maintain the status quo. Above the 45° line, each state represents an increase of melt fraction relative to the immediately preceding state; below the line, each state is diminished relative to the immediately preceding state by the combined effects of thermal loss associated with decreased rate of energy dissipation, conduction loss, and melt transport from the region of shear.

The dashed line in figure 51.14 signifies typical paths involving states of increasing melt fraction during episodes of shear melting or intrusive melt transport followed by states of decreasing melt fraction owing to combined effects of stress drop, limitations on shearing rate,

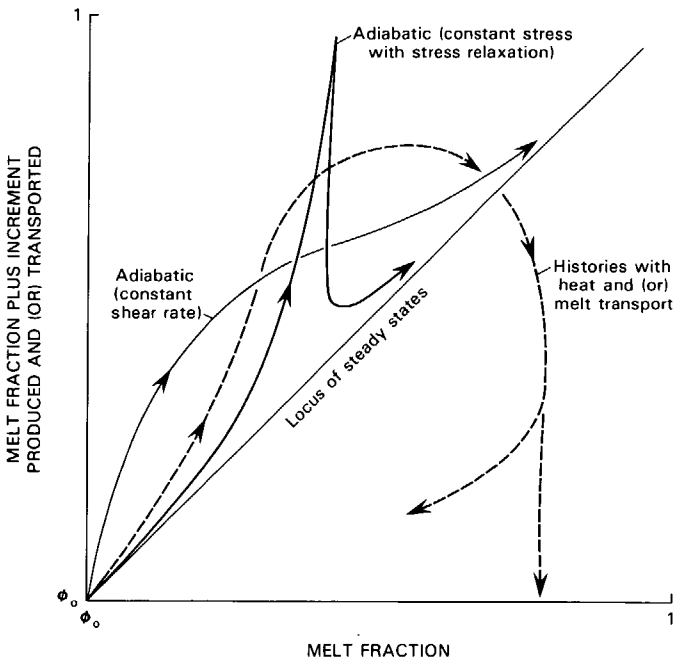

FIGURE 51.14.—Schematic diagram expressing feedback regimes of figures 51.9–51.13 in terms of "future" states plotted against "present" states: ordinate shows values of melt fraction relative to some arbitrary initial value (Φ_0) representing sum of immediately preceding value and amount created or destroyed (for example, by transport loss from system) during specified time increment (Φ_0 not necessarily zero). Each curve is unique, depending on process and on rate and change of rate of that process. Thus, magnitude on ordinate is governed by melting and (or) transport rate. Adiabatic melting without transport is indicated by solid lines, and melting with heat loss and (or) melt transport is indicated by paths resembling dashed lines; if wholesale migration occurs above some critical melt fraction, overall melt concentration may decrease. Steady states, representing thermal balance between melting and solidification and (or) transport, are limited to vicinity of 45° diagonal line. Coupled positive-negative feedback represented by paths like dashed curves is termed in this paper "folded feedback."

melt injection into neighboring domains, and crystallization due to cooling. The foldlike trajectories involving the net effects of positive and negative feedback in figure 51.14 (dashed lines) provide a framework for subsequent diagrams describing the evolution of volcanic volume states. Henceforth, however, the discussion is shifted from dynamics to a logistical description of transport rate.

The strategy of logistical analysis is sketched in figures 51.15–51.18 in terms of the variety of descriptive histories that may be associated with time variation of any general quantity symbolized by the variable x. Subsequent diagrams consider the volumetric histories of Hawaiian volcanism expressed in the same way, replacing the symbol x by V, using the documentation of transport rates by Dzurisin and others (1984).

Consistent with the approach to magma-supply balances taken by Dzurisin and others (1984), figure 51.15 is based on the idea that any net transport rate of a quantity x can be decomposed into apparent rates of gain and loss, or input and output, both expressed as positive numbers. The net rate, then, apparently is given by the positive (input) rate minus the positive value of the negative (output) rate; the qualifier "apparently" is used because this convention is not free of ambiguities, as will be discussed (possibilities of ambiguity exist in any measurement made up of integrated positive and negative increments, where both are taken as positive numbers, because unless there is absolute knowledge of the exact amount and sign of every relative change, a net increase could result if there is either a greater increase in the positive than the negative term, or a greater decrease in the negative than the positive term; the balance between biologic originations and extinctions over time is a notorious example). Symbols designating positive components of the net rate can be thought of as the rates and amounts of addition or input to some general reservoir of quantity, and symbols designating negative components as the rates and amounts of the output or depletion of that reservoir (also written as a positive number).

An example illustrates that the above convention is a common one. Imagine a fuel tank with an input valve and an output valve, each equipped with a flow gauge calibrated the same way. Each gauge registers a positive reading when input and output flow are occurring simultaneously. Their differences integrated over time give the net change of fuel in the tank. An idealized magma chamber can be thought of in the same way if there is the recognition that the reservoir is of unspecified boundaries and size, and there are no predetermined values for initial and final states; also, input and output paths may be numerous, and flow rates are based on less direct evidence than a fuel gauge. This means that the volumetric states of magma chambers are relative to an arbitrary zero at some defined location and time, as is the case in figures 51.1–51.8.

To assist interpretation of the numerous stages in the construction of figure 51.15, as well as subsequent figures, it should be recognized that not only are the figures drawn approximately (don't look for numerical values to check to better than a few percent), but seemingly contradictory numerical states may be noticed (an example is the quantity "x_+" in fig. 51.15*D*; see stepwise description below). An example of materials inventories in commerce indicates how contradictory values can occur in a series of measurements. Consider a wholesale center to be a reservoir of material that is added to by shipments from a factory and subtracted from by shipments to retail outlets. This is the same balance as the fuel tank. Now, however, there are additional degrees of freedom represented by possible returns of items from the wholesaler to the factory and from the retailer to the wholesaler. The count of items received from the factory is a positive number and is either constant or increasing (the running record of items received). But, ignoring the retail transactions for the moment, the input to the reservoir of quantity (the wholesale warehouse) can decrease if more items are returned than received over some interval of time. Obviously the inclusion of this possibility as well as possible returns fom the retailers makes the accounting of inventories a tricky business even in the idealized case. Such transactions, however, are the crux of the logistic diagrams that follow. Ambiguities may be real if records of exchanges are not complete, or they may be apparent ones related to uncertainties in the relative timings of transactions.

The problem of accounting is also a central one from the standpoint that it focuses on the precision of the units of measurement

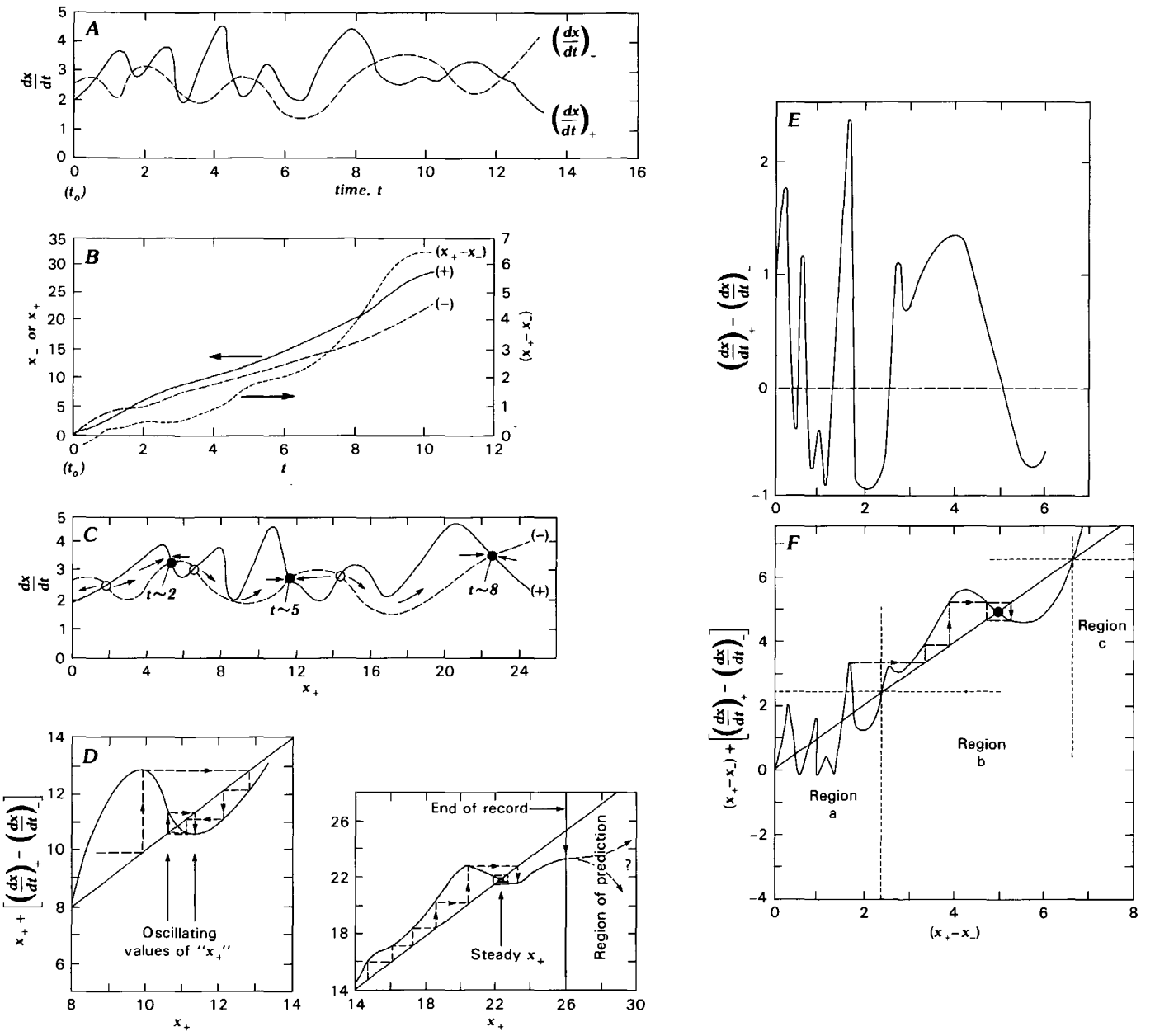

FIGURE 51.15.—Schematic diagrams showing time-variation and x-variation of positive and negative rates of change in any extensive quantity x. ***A***, Hypothetical information concerning positive and negative rate components of the rate dx/dt; used to construct other diagrams. ***B***, Respective integrated positive and negative contributions and net change in x. ***C***, Respective values $(dx/dt)_+$ and $(dx/dt)_-$ versus the positive cumulative values of x_+ read from B at same values of time in A (x_- or net x could be used on abscissa instead of x_+). Dots, values of x_+ that tend toward stationary values (convergent arrows), identifying values where there is relatively slow net increase in x; circles, points of divergence identifying intervals of relatively rapid net increase in x. ***D***, Adjusted future values ("x_+") versus present values referred to x_+ (x_- or net x could be used as reference; see F) calculated from net rates of change $(dx/dt)_+ - (dx/dt)_-$ over a specified unit of time; these two graphs and that in F are analogous to intervals of folded feedback in figure 51.14 (see text for discussion of apparent contradiction between dictated trajectories in D and monotonic curve of x_+ in B). Dashed trajectories with arrows (D, F) show arbitrary constructs where projections indicate that future states are defined by present states. That is, among possibilities limited by rate history, if next value is dictated equal to present value, then next value of x_+ in graph D, or $(x_+ - x_-)$ in graph F, is given by horizontal projections from master curve (solid curve representing trend of available states) to diagonal line as locus of intersections of dashed trajectories; along diagonal, next value on abscissa equals immediately preceding ordinate value. Area labeled "region of prediction" in D represents uncertainties associated with possible trends beyond limit of record. ***E***, Net rate plotted versus net values of $x = (x_+ - x_-)$. ***F***, Corresponding loci of available present-future states and corresponding idealized limits of episodic feedback limited by net x and net x plus net rates relative to diagonal line of steady-state net balances (construction as in D for net x). Regions refer to different regimes of possible episodic feedback (see figure 51.16 and discussions in text). Prescriptions of future values determined by present values based on logistics of population-dependent biological reproduction (see May, 1976) and concentration-dependent feedback melting. Dashed trajectories in D and F represent idealized histories that may: (1) converge to a fixed value, (2) oscillate over some set of regular intervals around a fixed value, (3) oscillate chaotically in vicinity of fixed value, or (4) diverge to totally different neighborhoods of higher or lower x-values.

Types of regions of attraction

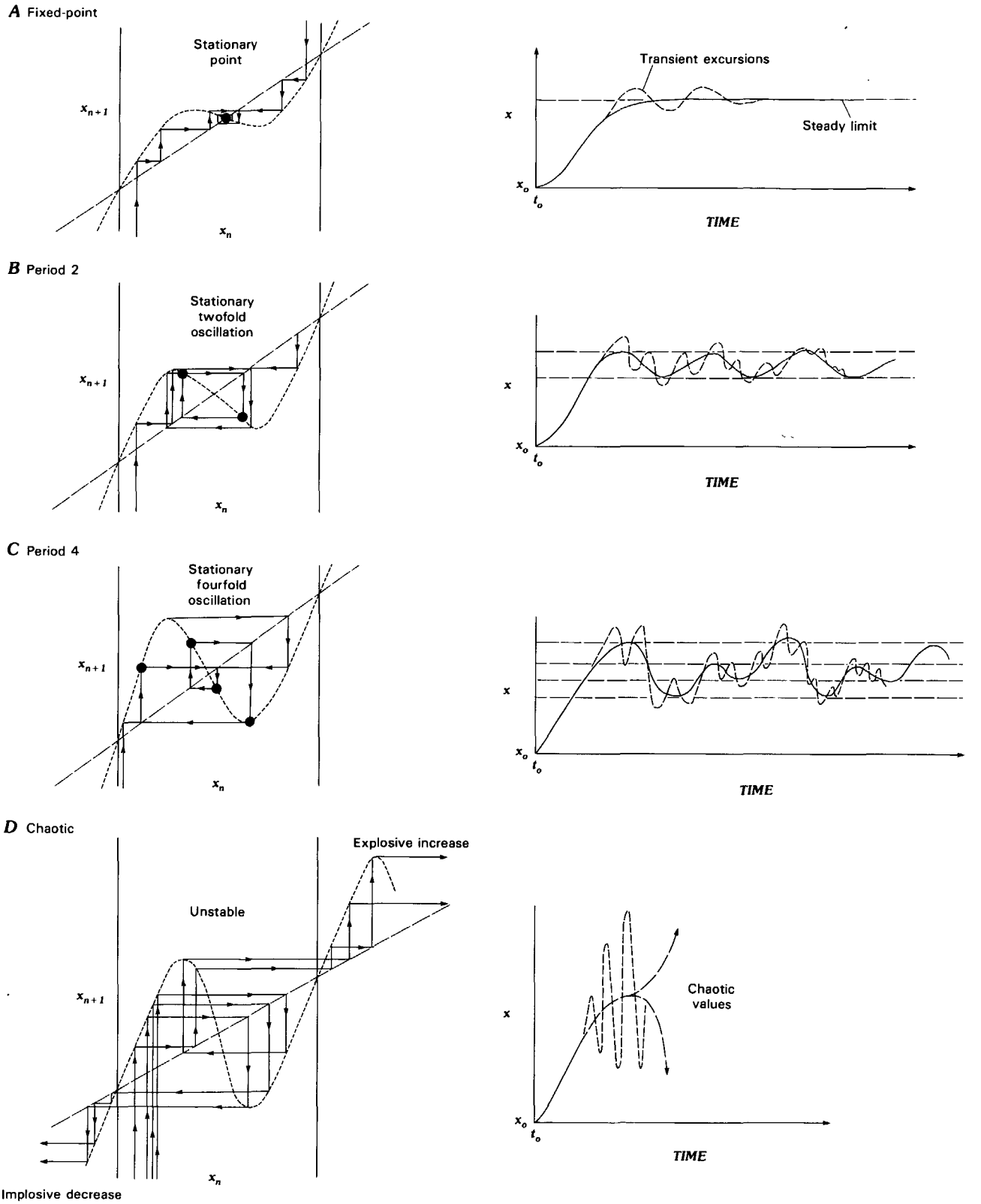

of rate. That is, an input or output record always represents some finite relation between the counts of quantity and time. Notice that the graph in figure 51.15*A* does not specify the units of time. Whatever the choice, there is always a smaller or larger unit possible. Thus, any such curves really represent trends of average readings at an appropriate time scale. The materials inventory above might be taken per day, per week, and so on. At any smaller scale of time the possible measures of rates might be much larger numbers if short-term averages were linearly extrapolated to longer times (for example, if all items are received during one day while the inventory is taken weekly, an extrapolation of the one-day rate overestimates the weekly rate). Inversely, knowledge of longer term averages does not identify the ranges of rates taken over short intervals of time. Examples of this have already been seen in the record of Kilauea's eruption rates (figure 51.7) and in the discussion of fractal self-similarity.

The above kinds of uncertainties are encountered in the later illustrations of magma-supply balances at Kilauea. The budget described by Dzurisin and others (1984) makes the necessary assumption (without it no quantitative inventory could be made) that the inflation of Kilauea's summit documents magma input from deep sources to a near-surface reservoir ("summit reservoir"), and summit deflation documents magma supply to the rift systems from the summit reservoir. In a manner analogous to the uncertainties between the wholesaler-factory and wholesaler-retailer exchanges, this inventory does not explicitly document the possibility of exchanges having more continuous or higher frequency characteristics. For example,

FIGURE 51.16.—Schematic patterns of idealized oscillation relative to possible stationary points (dots) either on or controlled by intersections of locus of steady states (dashed diagonal lines at left) with present-future control curves (dotted lines of present x_n versus future x_{n+1}) of available states in an interval of x (vertical light lines). Trajectories of oscillations in present-future values of quantity x shown by solid lines with arrows in left-hand column; corresponding oscillations of x-values in time shown in right-hand column (solid lines indicate time-independent limits of stabilized oscillations, dashed lines represent transient or unstable short-term and long-term deviations from time-independent limits). Several regimes of behavior represented, at least two of which are implicit. ***A***, Small positive and negative deviations (folded feedback) occur relative to diagonal locus of steady-state limits, so that trajectories (solid lines with arrows) of feedback events involving neighboring values of x within interval (vertical lines) converge toward point of intersection (dot); this regime implies divergence toward lower values of x if dotted curve is totally below dashed diagonal but crosses it at right-hand vertical limit. ***B***, Curves showing larger excursions in x_{n+1} relative to x_n eventually split away from point of intersection in *A*, which can be thought of as bifurcating or fissioning, creating two continuously or stably repetitive alternations of x on opposite sides of steady-state locus; that is, stationary point in *A* becomes stationary zone or region that contains two stationary points counterbalanced across diagonal locus. Note that angles and slopes not exact, hence scale of x_{n+1} not proportional to x_n. If scales 1:1, twofold bifurcation sequence begins when dotted curve exactly perpendicular to dashed diagonal line. ***C***, As folded feedback amplitudes increase, stationary region grows in size and bifurcates or fissions into doubling sequence of counterbalancing stationary points; that is, there is a 4-fold bifurcation that will split to 8-fold, 16-fold, and so on at slightly higher feedback amplitudes. ***D***, At sufficiently high feedback amplitudes, doubling sequence 2^n gives way to complex fissioning events that include possibly regular odd-period repeats and irregular or chaotic trajectories, depending on exact amplitudes and curve forms; if this regime occurs totally within vertical lines, stationary region persists (even though it is "fuzzy" and may contain no stationary points); but if amplitude permits excursions of x_{n+1} to exceed vertical limits in x_n, eventually all trajectories escape to either larger or smaller values of x (called "sensitive dependence on initial conditions"). Values of x initially very close together (for example, magma concentrations within adjacent sites of a volcanic edifice) may rapidly diverge in opposite directions (that is, one set of trajectories escapes to higher concentrations, the other to lower concentrations). Regions of stationary behavior called "basins of attraction"; term "attractor" stems from patterns of regular to chaotic oscillations within basins.

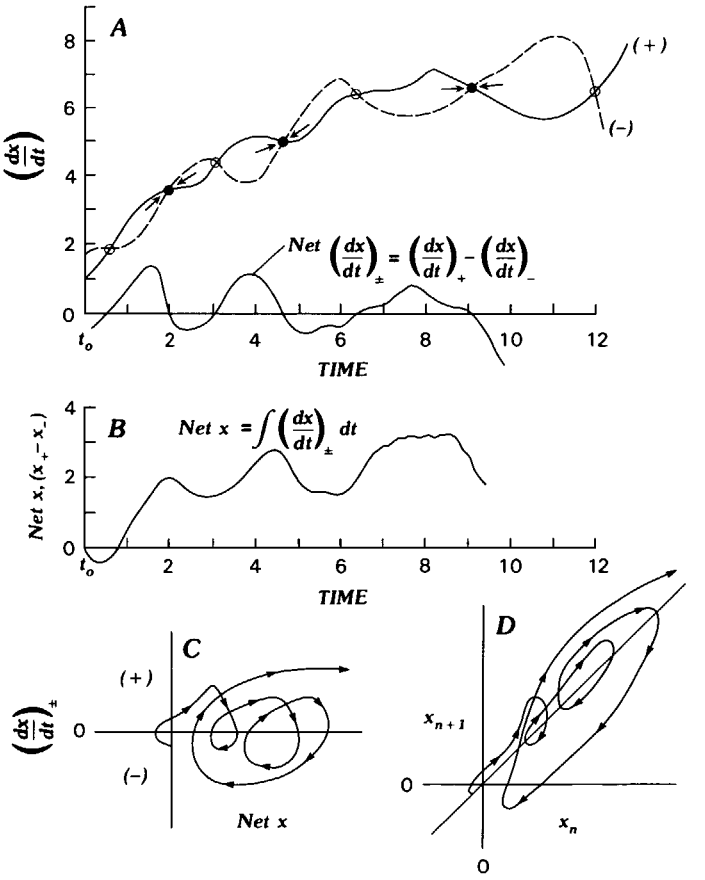

FIGURE 51.17.—Schematic rate histories and derived curves for situation in which net value of x both increases and decreases with time. ***A***, Schematic curves of rate against time. ***B***, Plot of net x against time, showing both increase and decrease rather than monotonic increase as in figure 51.15*B*. ***C***, Rate plotted against net x; note that rate history repeats itself over intervals of x reversals. ***D***, Present states plotted against future states of x. Resulting loops of folded feedback here and in figure 51.17*C* repeat themselves in various patterns of tangled and potentially closed loops. Thus, intervals of closure automatically define regions of stationary states that occur within more inclusive intervals of stationary states in a potentially unlimited series of involutions and convolutions. Trajectories describing stepwise feedback, as in figures 51.15 and 51.16, accordingly imply even more localized sets of potential stationary points and regions within a web of available states. In a sense, control curves in *D* resemble cyclical trajectories of stepwise feedback in more monotonic histories, such as those in figures 51.15*D*, *F* and 51.16 (see discussion of rate uncertainties and time scales in text); compare figure 51.18.

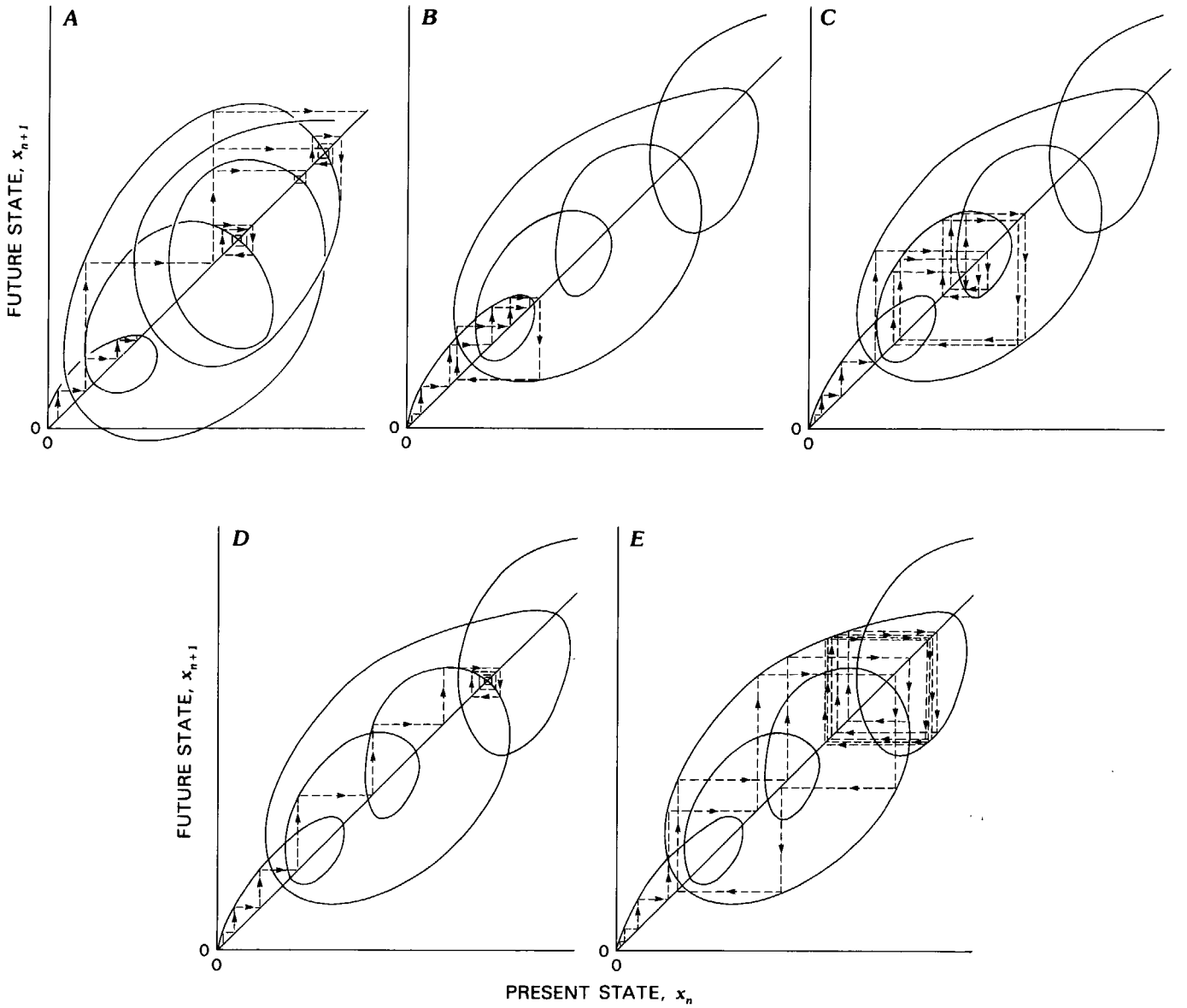

FIGURE 51.18.—Schematic trajectories of feedback steps (dashed lines with arrows) on sets of master control loops (solid curves) conforming to availability of rate histories and x-values analogous to figure 51.17. ***A***, Quasi-circular loops with mainly stable attractor intersections along diagonal locus of steady states except at upper right, which is a divergent and possibly chaotic escape trajectory depending on path of master curve beyond interval shown. ***B***, ***C***, ***D***, ***E***, Quasi-elliptical loops elongate in direction of increasing x (because of aspect ratio, feedback events jump across loops and create complex sets of attractor basins of both quasi-steady and chaotic types). No unique solutions for functional relations between x_{n+1} and x_n exist (behavior is both deterministic and probabilistic); feedback trajectories are multivalued and simple or complex over special time intervals (that is, feedback may both circulate near one or several stable states as well as jump about over many different states). A composite of simultaneous trajectories will circulate within central region if master curve closes back to origin from right-hand termination.

any magma that is continually leaking through the summit chamber into a rift system may not show up as an event in the inflation-deflation record (analogous to a blackmarket operation not recorded in a wholesaler's inventory). Also, no explicit accounting is made of any magma increments that may be analogous to material returns. While errors caused by this possibility can be discounted in the intrusive magma balances on physical grounds, they are possible in principle. A magmatic example where they are explicitly included in the budget is given by the data of Eaton and others (chapter 48, tables 48.1–48.3) describing the history of filling of Kilauea Iki lava lake during the 1959 eruption of Kilauea. There, returns from the ponded lava reservoir to the subsurface reservoir were significant, and there were also losses of pyroclastic components during fountaining.

As a consequence of considerations of these kinds, any rate curves such as those in figure 51.15*A* (and especially any that document a natural process) are really very fuzzy lines if viewed at finer scales of resolution. For example, compare figures 51.5, 51.7, and 51.2, in that order, with attention to the relative changes of time and amplitude scales. That is, the time scales increase greatly while the amplitude scales remain similar (see averages over different durations in fig. 51.7; compare fig. 51.8). I will return to a discussion of how such uncertainties relate to an interpretation of hypothetical trajectories of changing quantities in diagrams like figure 51.15.

The schematic rate curves in figure 51.15*A* are drawn arbitrarily to represent the kind of irregular variations seen in the earlier illustrations of volcanic rates (for example, the derived curve of net rate in fig. 51.15*E* qualitatively resembles the Hawaii-Emperor rate curve in fig. 51.2*C*). Figure 51.15*B* shows the approximate values of graphical integrations of areas under the (+) and (−) rate curves in figure 51.15*A*, as well as the integral defined by their difference (the net rate is not shown in fig. 51.15*A*). The input (+) and output (−) rates are plotted against the integrated input (x_+) in figure 51.15*C*. This plot is analogous to one showing total magma supply rates and depletion rates (either by eruption or other losses from a chamber) versus total magma supply (fig. 51.5 shows these quantities plotted against time; it is also used subsequently to examine volcanic volumes in a manner like that of fig. 51.15).

Plots of future states against present states for positive or negative net rate increments relative to the total input quantity x_+ are shown in figure 51.15*D*; again, the net rate is simply the difference given by the positive (+) curve less the positive (−) curve of figure 51.15*A*. This graph is included to illustrate the implications of applying net rates to the different choices of x-values. One might wish to plot the sum of x_+ and the net rate against x_+ for at least two reasons. (1) It might be desired to see where in the record of input rates there is a tendency for strong depletion effects. (2) The record of output rates might be intermittent and inadequate to permit an integration of x_-; hence, the net value of x that ordinarily would be the abscissa of choice is unavailable (that is, it might not be possible to plot fig. 51.15*F*). When the dashed trajectories of present-future states in figure 51.15*D* are constructed, however, a contradiction is encountered. This is shown by the reversal in the directions of trajectories and the implied oscillation in "x_+."

According to figure 51.15*B*, x_+ is a monotonically increasing function of time; there is no indication that x_+ might decrease anywhere. While it is correct that the literal reading of figures 51.15*B* and *C* indicates that such trajectories of recursion imposed artificially in figure 51.15*D* are impossible, the previous discussion of uncertainty indicates that the master rate curves in figure 51.15*A* are average trends of data that have unidentified fluctuations at smaller scales of time. If we were to also allow the possibility that x_+ stands for an input quantity that could have components of reversals (analogous to the merchandise returns), then actual reversals in x_+ would be possible. Such an effect is equivalent to saying that there are high-frequency fluctuations in at least the (+) rate curve of figure 51.15*C* that extend below zero on the ordinate (that is, the integral must be capable of changing sign locally). The hypothetical trajectories in figure 51.15*D* indicate the magnitudes and locations of where such effects might be looked for in terms of the input record, x_+. These results can then be compared with the same vicinities of figure 51.15*C* (dots indicate tendencies for net convergences, or stationary states if plotted against net x) to see if there are in fact possibilities for stronger fluctuations. These considerations also explain how a seemingly closed repetition, shown on the left of figure 51.15*D*, can escape to higher values of x_+ or net x (see later discussion of basins of attraction and the regions in fig. 51.15*F*). The interval of high variability in Kilauea's eruption record (fig. 51.7) is an example where the record of supply and depletion of the summit chamber is expected to have a highly variable rate history as well. We might suspect complex reversals of flow in such intervals (analogous to drainback; see Eaton and others, chapter 48), although they are also possible in the absence of eruptive phenomena.

The trajectories of recursion in figures 51.15*D* and 51.15*F* symbolize endogenous folded feedback; "endogenous" here refers to the net effects of mechanisms of self-regulation that are dominantly influenced by the way the system has internally evolved, rather than by being dependent on some external system. The crosshatched regions of figures 51.9, 51.10, 51.12, and 51.13 are examples of conditions controlled endogenously, in that the delineated regimes are products of the net effects of several kinds of dynamical feedback intrinsic to the system at different characteristic scales of time and size.

The central idea in figures 51.15*D* and 51.15*F*, and in possible parallels between the logic of repetitive physical processes and the logic of repetitive numerical processes performed graphically or by computer, is the extent to which the quantity portrayed is a product of endogenous folded feedback. That is, if the system states at a given time or quantity (x_+, x_-, and their differences) are products of preceding states and in turn will in some sense dictate the nature of following states, no matter how intricate the paths may be, then the form and amplitude relations of plots such as figures 51.15*D* and 51.15*F* provide logistical information on how stable or unstable that evolution has been and might become relative to variations in the quantity and in time.

Examples such as the factory-wholesaler-retailer system are instructive in illustrating how oscillations can occur out of attempts to stabilize the inventory and maximize profits. For example, if x_+ in figure 51.15*D* represented items from the factory less those returned, then the oscillating behavior of "x_+" could be real. The trajectories of recursion might have been designed to provide negative feedback, perhaps because there is limited storage space in the warehouse. The strategy is revealed as a self-defeating one in the particular example at the left in figure 51.15*D*, because until x_+ eventually increases, no lasting sale of goods is being made (they are just being carried back and forth between the factory and the wholesale warehouse; implicitly, in this case, returns between the consumer and retailer and the retailer and wholesaler also would have to balance). This kind of oscillation applied to the behavior of a magma chamber would correspond to a condition where magma is pumped in and out through the same source conduit without any evidence of lasting outputs in the form of eruptions or intrusive leaks

(if this kind of behavior existed conspicuously in Kilauea's budget, summit inflation-deflation cycles would occur without eruptions or evidence of magma moving into rift systems). It may also be noted that the transport budget of a geyser basin resembles several aspects of the above kinds of oscillatory transactions.

These and other forms of oscillating material inventories essentially reflect imbalances related to time delays of incremental transport which are intrinsic to nonlinear systems (for example, a large sale of goods triggers a large order from the factory, which may be followed by a large return to the factory if subsequent sales are poorer, and so forth). Although we cannot rule out chance or systematic external influences as a part of the record (for example, thefts of merchandise), we can describe the system in terms of endogenous influences represented by patterns such as those shown in figure 51.15C (as another example, if x in fig. 51.15 represented water in an open reservoir, the variations would describe the main features of the material balances, taking into account scale effects as discussed, even if they included the vagaries of rainfall as an input and the chance of external objects falling in).

The relation between positive values of input and output rates versus quantity identifies tendencies for convergence or divergence in the neighborhood of specific values of the quantity. If the positive input is greater than the positive output in some vicinity of the value x, the quantity in question is increasing in that vicinity (and implicitly at a given time, or at a given set of times if the pattern is repetitive). Conversely, if the positive output is greater than the input, the quantity is decreasing in that vicinity. Thus, where the rate curves cross, there is either a convergence or a divergence with respect to that value of x. Loci of convergence in figure 51.15C are identified by the dots with inward-directed arrows, whereas loci of divergence are identified by circles and outward-directed arrows. In a tangible sense, any material states symbolized by the quantity x tend toward the vicinities of the dots relative to any other nearby states. The loci of the circles are avoided, so to speak. In this respect, values of x are "attracted" to the vicinities of convergent rate balances. The circles, therefore, are analogously loci of relative "repulsion" from the standpoint that values of x persist longer in the vicinity of convergent rather than divergent states. Neither type of locus, however, is necessarily an absolute or global center of logistical attraction or repulsion if the net variation of x (as in fig. 51.15*B*, dotted curve) eventually increases beyond the recorded interval. Thus, the set of diagrams in figure 51.15 represents an array of transient states in which are imbedded several quasi-stationary (less transient) attracting states within a set of generally divergent (more transient) states. It may be noted that any system of merchandising that transports goods efficiently and has high sales will have both kinds of states in some optimum balance (barring a factory-outlet system in which goods are made precisely in balance with their consumption at all times).

In computer studies of numerical folded feedback, the incremental paths of convergent circulation just described are often called attractor trajectories. The word "attractor" refers descriptively to the resulting patterns of stable, quasi-stable, or unstable trajectories, much as the terms "cell," "vortex," and others are used in describing fluid motion. The usage stems literally from the circulation of trajectories in the vicinities of stationary loci within a field of numerical possibilities governed by folded feedback. The literature of attractor mathematics is now very extensive, and space does not permit rigorous development. The best introduction I know is given by May (1976); the background of his study is in the biological sciences.

In the present discussion I use the term "attractor" as a shorthand for any patterns represented by the trajectories of present and future states. This is done to distinguish the pattern of trajectories based on numerical recursion from more complete logistical descriptions of all potentially available states represented by loci such as the dots and circles in figure 51.15C. In a parallel context, every attractor pattern also implies its converse as a repellor pattern of divergent circulations; generally, these are not shown.

A brief summary of the types of attractor patterns that can be expected in the vicinities of convergent states is given in figure 51.16. The four types of behavior shown are abstracted from an array of classifiable regimes that have been studied numerically by many other workers of diverse backgrounds (assisted by P. Doherty, USGS Computer Division, I have duplicated many of the published results; we have also written algorithms for attractors of higher dimensions, as well as variants of recursive strategies that contain options for evolutionary choices by the program itself along the lines of evolutionary strategies outlined in the introduction). May (1976) gives a concise summary of the possible numerically generated attractor regimes found relative to standard models of folded feedback (feedback curves of analytically explicit forms involving parabolic and exponential functions). The analytic type of feedback equation, however, is less crucial to the attractor pattern than is the range of slope variations in the vicinities of crossing points of the master curve and the reference line, as shown in figure 51.16. The present research has confirmed to my satisfaction that the general concepts of pattern generation by means of computer experiments can be a powerful tool for the exploration of evolutionary strategies in nature.

In figure 51.16 the parallel vertical lines represent the interval of x to be investigated in terms of trajectories of attraction (solid lines with arrows) in the vicinity of a general trend of present-future states (dotted master curves) relative to a line of equal balance of positive and negative feedback (dashed diagonal lines). The large dots again represent stationary or quasi-stationary states, but in this instance such states are those implied by the convergence or divergence of the attractor trajectories themselves, which are generated from the dotted master curve that describes the average trends of states. Stationary states, as fixed points in the graphical context, represent either the intersection of the dotted curve with the diagonal (fig. 51.16*A*) or the intersections of a stable circulation of attractor trajectories as a limit of exactly repetitive paths (fig. 51.16*B*, *C*). Such circulations in dynamics are often called "limit cycles."

One of the major discoveries of computer experiments with numerical feedback is that there is a systematic diversity of limit cycles and other forms of repetitive or nearly repetitive attractor patterns (see, for example, May, 1976). As shown by figure 51.16C, the repetitive loop may involve cyclical multiplicities that increase in numbers of stationary states as powers of 2 and that can multiply in that fashion theoretically without limit until a critical

amplitude is exceeded. Actually, it is the combinations of amplitudes and slopes of the dotted curve that determine how many stable states are possible.

One example of divergent paths, shown in figure 51.16*D*, is found when the amplitude and slope attain values that imply both (1) the generation of chaotic (unstable, nonrepetitive) trajectories and (2) the likelihood that at least some trajectories will transcend the boundaries of the x-interval. In this diagram there are no stationary states, and two trajectories may begin at almost identical values of x and after one or more circulations spin off, as it were, in totally opposite directions. This is sometimes described as "sensitive dependence on initial conditions."

The statements concerning figure 51.16*D* are qualified in two important respects. (1) Chaotic trajectories lacking any quasi-stationary values can exist between figures 51.16*C* and 51.16*D* for values limited to the interval between the vertical boundary lines; these limits define the region within which a stationary or quasi-stationary attractor pattern can evolve as a distinct, though possibly chaotic, spatial analog of a stationary or quasi-stationary point (within this pattern, discrete odd-period stable attractors are also possible at special values of amplitudes and slopes; they are often called "windows"). (2) If the extrema of the dotted master curve exceed the limits of the intersection with the vertical interval boundaries, and the slope of the master curve at the crossing point with the diagonal is in the neighborhood of -1 (perpendicular for equal units on the ordinate and abscissa), some trajectories of stable fixed point and period-doubling sets of attractors may also escape the interval toward either higher or lower values.

The circulatory regions in figure 51.16 are sometimes called "basins of attraction," and the limits just described indicate the tendencies toward either quasi-stationary or unstable behavior of potential attractor patterns relative to these basins. Because the master curve represents a locus of average feedback balances, however, statistical fluctuations around the overall growth trend, as in figure 51.15, imply a net drift toward higher values and what may be termed "leakage" from any particular basin of attraction.

Such leakages of attractor trajectories refer to the numerical persistence of any particular attractor pattern (including fixed points, period-doubling and odd-period stable sets of points, and chaotic regions) and are not to be confused with physical leakage from an actual physical reservoir. Some deliberation of rate balances should show that the concepts of physical leakage relative to attractor leakage are determined by the definitions of positive-negative transport rates relative to some physical locus. That is to say, a leaky basin of attraction could refer to either a progressively filling or emptying mode of an actual physical reservoir. These considerations are the basis for subdividing figure 51.15*F* into three regions: In region *a*, subintervals like those of figure 51.16 might exist even where the overall trend is below the diagonal line; that is, the attractor leakage might be in a negative direction there, whereas it is in the positive direction at the transition to region *b*, and so forth.

The time variations shown at the right in figure 51.16 mimic the above discussion of attractor trajectories. The solid curves show the tendencies toward stable waveforms identified by circulations between stationary or quasi-stationary states. The dashed lines indicate transient trajectories related to deviations from the master curve of average feedback balances. If there is a one-to-one correspondence or a constant proportionality between x-values and the timing of the attractor oscillations, then the numerical repetitions of x-values are associated with regular time periods of comparable multiplicities; for example, the twofold attractor would have one frequency of oscillation, the fourfold attractor would have a different and phase-shifted frequency of two different amplitudes, and so on.

Because the potential time variations of figure 51.16 are produced by other time variations like those of figure 51.15 that govern the feedback relations of the master curve, it is evident that the overall oscillatory behavior may take place at more than one scale of description in space and time. That is, regular oscillations like those of figure 51.16 may exist at smaller time scales within the irregular oscillations of figure 51.15. By the same token, however, the patterns of figure 51.15 may relate to other scales of variation, which are also describable by relations like those of figure 51.16. Such uncertainties of scale are intrinsic to the behavior of natural open systems and underscore the need to examine rate relations of the sorts just discussed at as many scales of time and size as possible. They are also possible sources of the fractal characteristics and self-similarity in time discussed earlier relative to figures 51.5, 51.7, and 51.8.

These uncertainties of scale are emphasized by figure 51.17, which also draws attention to issues of implicit versus explicit master control curves. This figure is drawn arbitrarily, much like figure 51.15, except that the net rate dips below zero more persistently, rather than being generally positive. As a consequence, the net values of x alternately increase and decrease in magnitudes rather than increasing almost monotonically. Therefore, when the net rate is plotted versus the net quantity, the overall trend loops back on itself over oscillating intervals of x. Thus, the stationarity of patterns in certain vicinities of net x is automatically constrained by this alternation, without consideration of possible attractor trajectories of subsidiary oscillations.

It may be asked, however, what happens if figure 51.17*D* is also considered to represent the average path of a master curve that governs more localized tendencies for folded feedback. Each point on the curve implies a feedback influence on a future value, just as before, except that such values are now potentially multivalued; that is to say, there is a considerable redundancy concerning the overall effects on future states. A graphical or computer algorithm derived for single-valued recursions, such as those shown by the trajectories in figure 51.16, could not distinguish between curves except in a specific temporal sequence along the path of the arrows in figure 51.17. Since this path is the average locus of complex variations and may repeat itself again beyond the range of values shown, no unique trajectories of attraction can be specified. Instead, several kinds of attractor patterns may grow and disappear episodically within the time frame of several overall circulations, as rate values oscillate over the repetitive net values of x.

Simultaneously evolving trajectories of recurring attractor patterns on a redundantly looping master curve are shown schematically in figure 51.18. Each attractor locus represents one possible unique path of graphical recursions (computer-like repetitions of present-

future value decisions). In figure 51.18*A* most of the loops intersect the diagonal line at slopes permitting fixed-point attractors, except at the upper right, where the trajectories progressively diverge from the crossing point. This may mean that the looping system represents a transient stage of growth toward larger values or that the control loop closes back on the origin. In the latter case, the divergent locus will continually feed attractor trajectories back toward lower values of rates and quantities that will endlessly tend toward the vicinities of the stable attractors.

In figure 51.18*B–E*, however, the slopes of the loops at crossing points are less stabilizing (steeper, or more negative than −1). Fixed-point attractors do not exist, and most trajectories generate twofold or higher order circulations. Because these circulations can interact in many combinations, particular trajectories are sensitive to the starting values and to the parts of the loop that exercise dominant control during any particular history. Thus, if the overall control loop is in any way repetitive (for example, by an intermittent repeat of the same general rate relations or by closure of the outermost loop back to the origin without termination), then many possible combinations may recur for twofold to chaotic attractor patterns that will grow and shift in timing and ranges of x as different parts of the curve exercise their influence.

If the control functions alone were rigorously precise and repetitive, eventually a steady distribution of attractor circulations would evolve. Such a pattern is deterministically predictable in the sense that the structure is generated by combinations of many possible trajectories that lead to the same final states. However, the master curves are fuzzy, as already discussed, or have finite widths because they represent averaging of processes at smaller scales of time and size (for example, a thermal-feedback melting event in polycrystalline aggregate is a composite of many localized events that relate to more localized energy balances). Therefore, there is a continual shifting of trajectories relative to any theoretically exact stable-limit cycles. An expectable consequence of such uncertainties within the context of an overall loop that closes on the origin in figure 51.18 is that attractor patterns will themselves migrate back and forth over an unspecifiably large number of possible configurations. In detail, such a pattern is unpredictable, in that there are intervals of chaotic behavior of individual trajectories. At the same time, however, characteristic regimes of transient twofold and higher order attractors repetitively come and go within the same general ranges of x. Thus, even though the overall pattern is unpredictable, there are recurring intervals of subpatterns that show regular temporal periodicities from time to time in a manner like that illustrated in figure 51.16. Unpredictability only refers to the fact that the regularities aren't determined once and for all on the basis of the knowledge symbolized by a master curve that has a finite line width (representing a range of uncertainty in feedback control).

KILAUEA AS A NATURAL SYSTEM OF RECURRING ATTRACTOR PATTERNS

In this section I attempt to show that many of the generalized styles of attractor circulations discussed in the preceding section actually exist in the circulatory patterns of behavior of Kilauea Volcano. In fact, Kilauea and volcanic systems in general appear to be remarkably good analog computers in terms of demonstrating the effects of repetitive recursions in the vicinities of characteristic basins of attraction. These patterns, however, involve multiple trajectories analogous to the schematic trajectories of figure 51.18. Attractor patterns generated by folded feedback evidently are chaotic if rate amplitudes exceed a critical value (figure 51.16). Furthermore, even the generalized basins of attraction, stable or chaotic, are unpredictable if there is a significant imprecision of rate control in the vicinities of potential stationary states of cyclical control loops (figs. 51.17, 51.18). Nonetheless, the circulatory pattern itself may be predictable, in that it retains a characteristic overall form. Before attempting to summarize the implications concerning general patterns of volcanic evolution, I compare the rate histories of Kilauea's activity with the above schematic examples.

The model of magma supply proposed and documented by Dzurisin and others (1984) provides for the first time a quantitative reference frame for these comparisons. It considers the balances of an overall history of supply between about 1957 and 1983 relative to a distribution between generalized summit and rift loci of storage. Although the erupted volumes are also tabulated in their study, they are not specifically included in the magma-supply budget that refers to intrusive gains to and losses from the summit chamber. In the present discussion of positive-negative rate balances, however, several different combinations among the possible types of data exist; these data include the following categories: (1) Total magma-supply rates, (2) total integrated volumes of magma supply, (3) localized rates of summit supply, (4) localized summit volumes, (5) nonsummit supply rates and volumes (representing rates and volumes of supply to rift systems), and (6) net rates and volumes of stored magma at summit and rift localities, taking into account eruptive losses.

From the previous logistical discussion of positive and negative rate contributions to the history of any net quantity, it is evident that in volcanic systems there are many ambiguities as to relations between the algebraic signs of rates and appropriate loci of accumulation. To simplify the discussion, therefore, the balances will be referred to a generalized summit reservoir and a generalized rift reservoir. A similar approach was used by Dzurisin and others (1980) to estimate the magma-supply rate to Kilauea from November 1975 to September 1977; the longer term budget discussed by Dzurisin and others (1984) is based on analogous considerations. Erupted volumes can be considered to represent possible losses from either reservoir or from their combination. Ignoring the eruptive loss, supply to the generalized rift reservoir can also be considered to represent loss from the potential volumetric states of the generalized summit reservoir. Thus, in figure 51.5 (from Dzurisin and others, 1984) the total supply minus the summit supply (volume or rate) defines the positive supply to the generalized rift reservoir or the loss (negative supply) relative to the hypothetical growth of the generalized summit reservoir.

The above relations are summarized in the form of rate diagrams as in the preceding section; figure 51.19 shows the total supply and eruption rates versus the total volume of supply (fig. 51.19*A*), and also the balances of summit and rift supply, ignoring

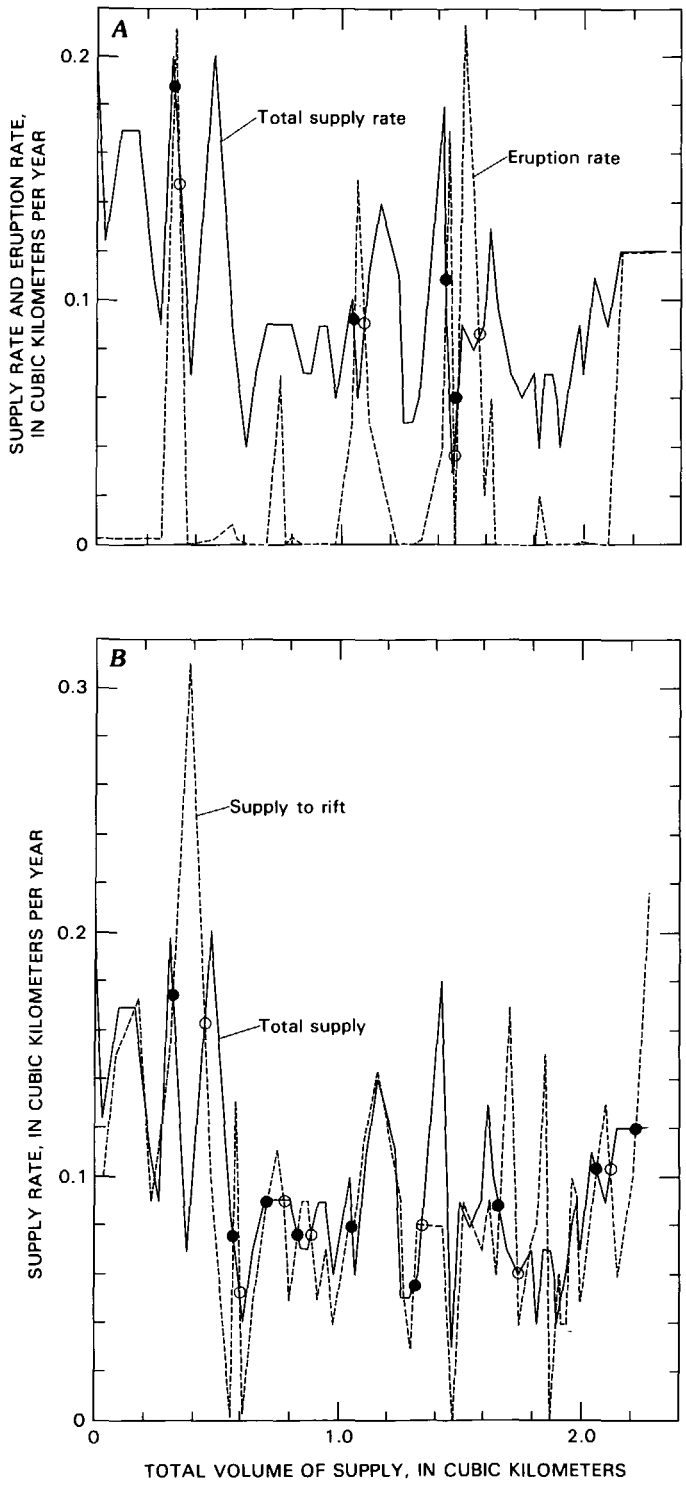

FIGURE 51.19.—Examples of rate histories for behavior of Kilauea since about 1957, based on data in figures 51.4 and 51.5 from Dzurisin and others (1984). Convergent intervals (tendencies toward stationary values) are indicated by dots, and divergent intervals by circles, as in figures 51.15C and 51.17A. ***A***, Total supply rate, corresponding to $(dV/dt)_+$, and eruption rate, corresponding to $(dV/dt)_-$, plotted against total volume of supply with arbitrary zero at beginning of record. ***B***, Total supply rate $(dV/dt)_+$, and supply rate to rift zones (total rate minus summit rate) as $(dV/dt)_-$ plotted against total volume of supply.

eruptions (fig. 51.19*B*). The positions of convergent and divergent tendencies are indicated by dots and circles, as in figures 51.15. Various combinations of rate balances are shown in figures 51.20–51.23, as identified in the captions.

Although the patterns are complicated, there are resemblances in all these diagrams to the hypothetical examples discussed above, as follows. (1) The total and rift supply balances in figure 51.20, and the net-supply-minus-eruption balances of figure 51.21, resemble the patterns in figure 51.15; there is a general history of increasing quantities, with localized circulations related to intervals of large negative rates (eruptive losses). (2) The total and net rates of gain and loss from the summit reservoir, as portrayed in figures 51.22 and 51.23, resemble the cyclical behaviors of figures 51.17 and 51.18, whether or not eruptive losses are taken into account.

These patterns suggest that the generalized rift reservoir behaves as a system of almost monotonically increasing magma storage, with intervals of quasi-stationary states and attractor-like circulations. Eruptive episodes accentuate the stationary states, but they do not control the pattern except over intervals near their occurrences, as in the circulations associated with the negative excursions in figure 51.21. The pattern of overall balances in figure 51.20 is not conspicuously different over times of eruption or noneruption, as shown by the fact that maxima that might be expected to correlate with attractor-like periodicities of gain and loss are not coincident with times of eruption.

The most conspicuous attractor-like behavior is shown by the circulatory states of the generalized summit reservoir. The patterns of repetitive control loops shown in figure 51.22 and 51.23 are analogous to those of figures 51.17 and 51.18, regardless of the way in which the present-future balances are plotted. That is, the patterns seem to oscillate relative to two (or possibly three) general volumetric states, whether they are viewed in terms of total supply rates, net total-minus-rift supply rates, or net total-minus-eruption supply rates.

Perhaps the most informative plots from a pattern-predictive viewpoint are figures 51.22*A* and 51.23, which do not depend on information concerning eruptive volumes; they are determined solely by the volumetric states deduced from summit-tilt data (see Dzurisin and others, 1984). Figure 51.22*A* is hypothetical in the sense that the future states, V_{n+1}, are those that would be implied if each increment of total supply actually inflated the chamber by that amount before the next state is encountered (that is, volumes are predicted by extrapolating rates based on short intervals of time). Figure 51.23, on the other hand, more nearly represents the rate increments associated with the actual changes in net volume of the generalized summit chamber as the remaining magma is entering the generalized rift reservoir. The fact that the two patterns are similar suggests that the oscillatory states of the summit reservoir are "controlling" in the logistical sense of figures 51.17 and 51.18.

The summit-reservoir control loop may operate physically somewhat as follows: When the volume of the generalized summit reservoir exceeds some fairly high value, it returns to the vicinity of the stationary state because of higher-than-average rates of loss to the generalized rift reservoir; conversely, when it is at low volumetric states, it returns to higher volumetric levels because of lower-than-

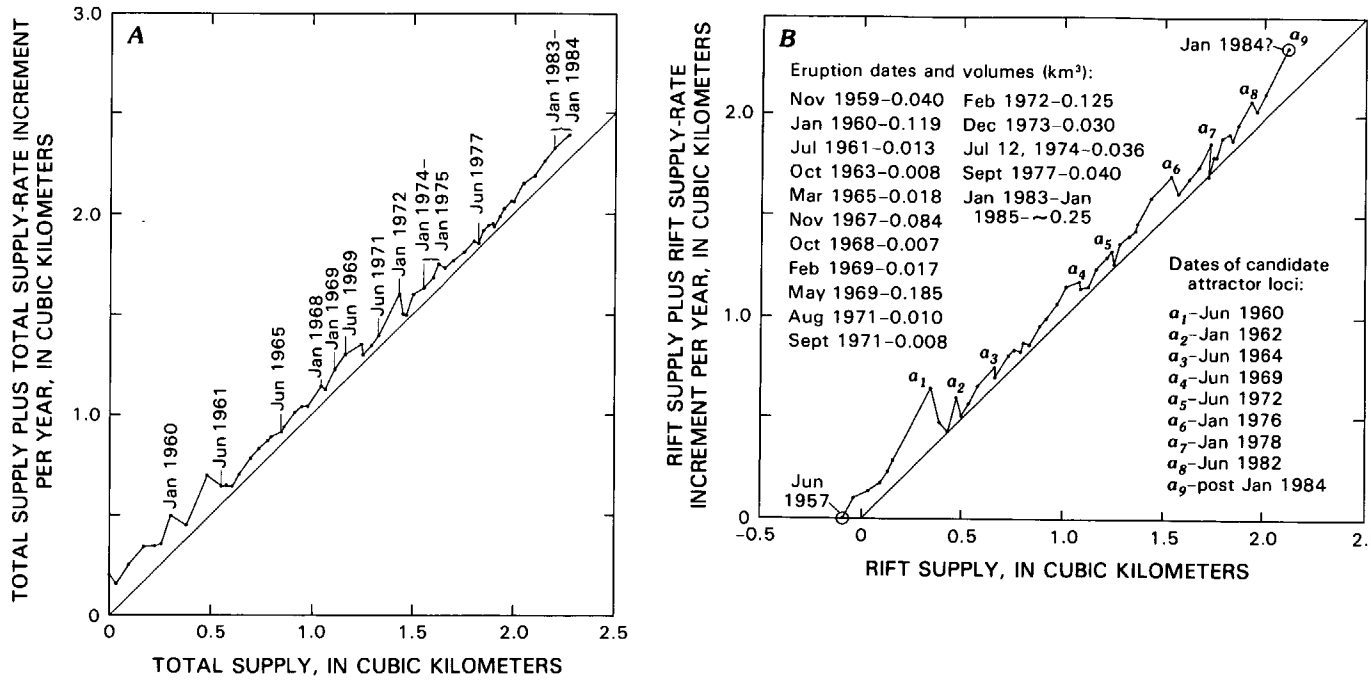

FIGURE 51.20.—Future state, V_{n+1}, plotted against present state, V_n, for Kilauea magma supply: ***A***, Total supply versus total supply plus total supply-rate increment per year. ***B***, Rift supply versus rift supply plus rift supply-rate increment per year. Data from Dzurisin and others (1984). Rift supply represents total volume of supply minus volume stored in summit chamber, and rift supply rate represents total supply rate minus summit supply rate. Points plotted at 6-month intervals, as indicated in figure 51.20*A*. Potential loci of attraction are suggested with corresponding dates (compare with discussion of fig. 51.15*D* and *F* in text); significant eruptive events are indicated in *B* by date and volume (note progressive intrusive increases despite depletions at indicated times of eruption; see fig. 51.5, and compare fig. 51.21).

average rates of loss to the rift reservoir. These rate excursions do not seem to be dominantly eruption controlled; eruptions occur at times of either higher- or lower-than-average rates of return to the stationary states. That is, if eruptions represented the only rate control, presumably they would occur predominately at times of higher-than-average volumetric states.

Another way of describing the pattern is paraphrased from Dzurisin (written commun., 1985); the statement resembles balances described earlier for the factory-wholesaler-retailer system: An important point is that the summit reservoir tends to buffer the rate of shallow magma supply by adding to the inertia of the magma system. Fluctuations in the rate of magma supply from depth are damped at the surface by the effect of the summit reservoir. When the rate of magma supply from depth is low, eruptions can still be fed by magma stored in the reservoir. When the magma-supply rate is high, eruptions can be avoided by increased subsurface storage.

An addition to this concise summary by Dzurisin is implied by figure 51.23. Whereas eruptions evidently can occur at almost any volumetric stage of the summit chamber, large eruptions occur at times near the locus of stationary states. This fact indicates that the eruption mechanisms themselves may be controlled by the summit-rift reservoir balances. A high net inflation state of the summit reservoir seems to require adjustments by increased net transfer to the rift reservoir from the summit reservoir before optimal conditions for eruption can recur. That is, if the values of magma-supply volume and rate are both too high, the resistance to eruption also seems to increase until summit storage returns toward the stationary states by increased rift storage. If both reservoirs increase together, rift earthquakes may be a more likely outcome than eruption, as suggested by the volumetric excursions during 1974–75 (compare figs. 51.20*B* and 51.22*A*). Conversely, if the summit reservoir is operating at much lower volumes than the stationary states, the eruptive head may be too low to overcome the net viscous dissipation associated with inflation. Consequently, eruptions seem to be most likely at values near those of the stationary states, and perhaps at slightly higher volumes, regardless of the net transport rates. Thus, intrusion is the favored mode of growth of Hawaiian volcanoes. Eruptions are special events that occur when certain preconditions are satisfied—that is, near the stationary states. Such balances also seem to be consistent with the earlier observations on the existence of self-similar relations between system size, chamber size, and repose time (see earlier discussion of fig. 51.7 and the relations between Kilauea and Mauna Loa compared with cratonic eruptive periodicities discussed by Smith, 1979, and Shaw, 1985).

There are many interesting analogies to the above patterns from studies of mechanical systems of forced vibrations with damping. Such systems have been studied extensively, in the form of both physical and numerical experiments. In both types of study, damped

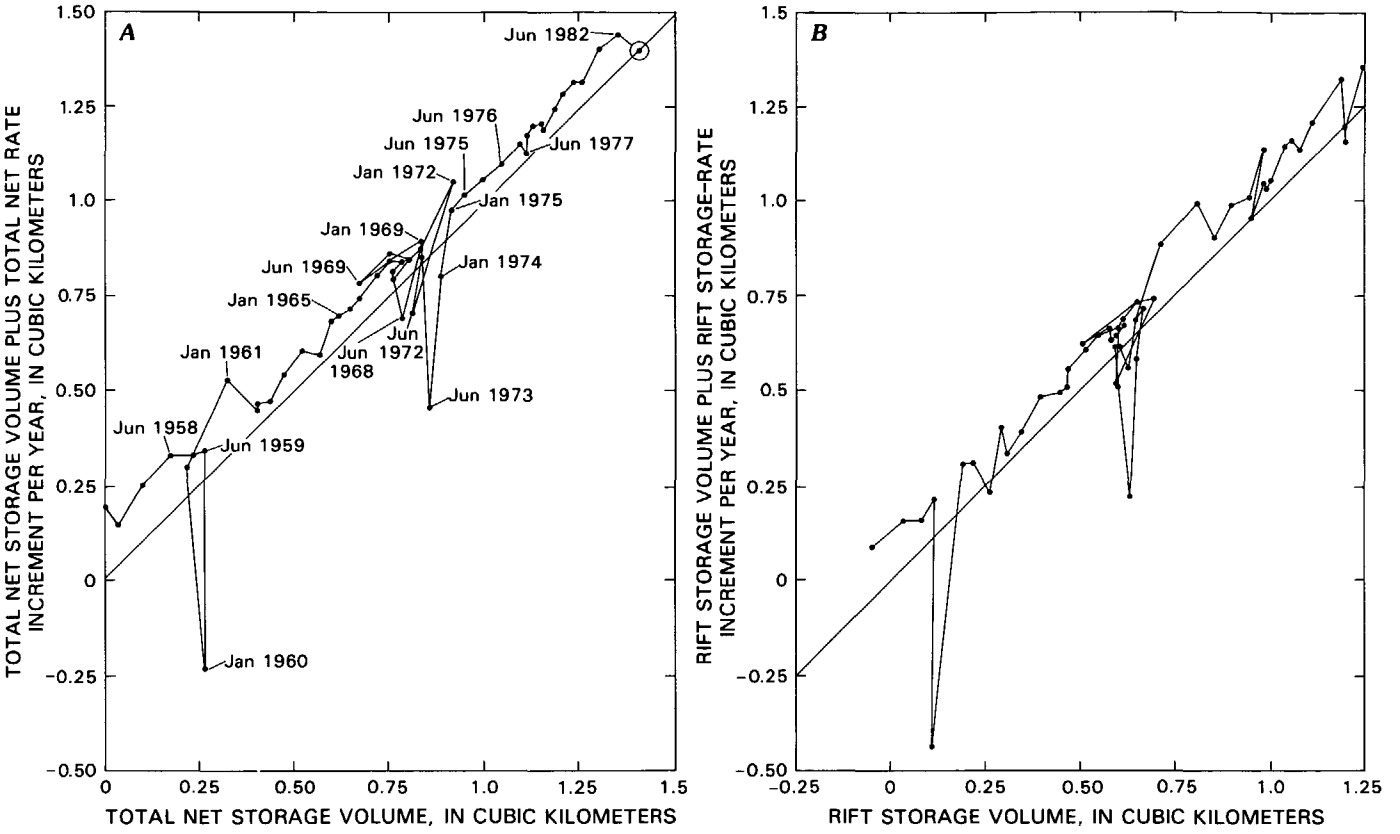

FIGURE 51.21.—Diagrams of future state plotted against present state as in figure 51.20, but taking into account volumes and volume rates of eruption. Eruptions are lumped as representing rift events without regard to location. Points are plotted at 6-month intervals. Strong negative feedback and attractor-like circulations are clearly associated with eruptive events, but these are abrupt excursions that do not control in the sense of forming master control loops. That is, pattern resembles figure 51.20 except for localized circulations. ***A***, Net storage volume (total volume minus erupted volume) versus net volume plus net storage-rate increment per year (total rate minus eruption rate). ***B***, Rift storage volume (rift supply as in fig. 51.20 minus total erupted volume) versus rift storage plus rift storage-rate increment per year (rift supply rate minus eruption rate).

oscillations have been shown to be highly nonlinear and to conform generally to regimes described by mathematical attractors (see Campbell and others, 1985; Shaw, 1984). The physical and numerical forms of behavior of leaky faucets studied by Shaw (1984) show strong resemblances to the descriptions of volcanic behavior. The events of drop formation are analogous to eruptions, and the regimes of overall flow rates supplied at the faucet are analogous to magma supply (except that magma leakage is complicated by many other factors than the setting of a single calibrated valve).

Circulatory patterns and stationary states illustrated in the present paper are analogous to factors influencing oscillations in total rates of leakage in the water-faucet model. At high rates of leakage, drops do not form because flow is continuous; at very low rates of leakage, they do not form because evaporation can keep pace with supply (in the magmatic mode, the analogous process is solidification). The behavior described numerically by Shaw (1984) refers only to the periodicity regimes of drop distributions. These show all the attractor structures mentioned earlier (see fig. 51.16), including stable to chaotic patterns, as documented in terms of the timing between drop-forming events. Eruptions could be illustrated similarly by plotting times between extrusive events. It is evident, from the wide range of extrusive repose intervals, that the eruptive attractor analogous to the faucet attractor is typically much more chaotic. In both cases, however, special regimes of precisely tuned flow can result in stable periodic repetitions. In the faucet model, these regimes can be easily isolated for study. In the volcanic case there is additional feedback among all the other processes mentioned earlier. Therefore, these other systems of oscillation (for example, the oscillation of stress states in the edifice) vitiate any obviously simple interpretation of the possible tuning effects of the faucet model, possibly excepting special intervals of flow (for example, fountaining episodes could represent a subregime in which valvelike control might be sufficiently coordinated that an independent analysis may reveal attractor patterns characteristic of the local process; in this respect there may also be a resemblance to patterns of geyser eruptions described as attractors).

This qualitative explanation of the logistical circulations seems to be in general accord with the earlier discussion of dynamical feedback. That is, the optimal conditions of magma accumulation represent some compromise, between melting and transport, that

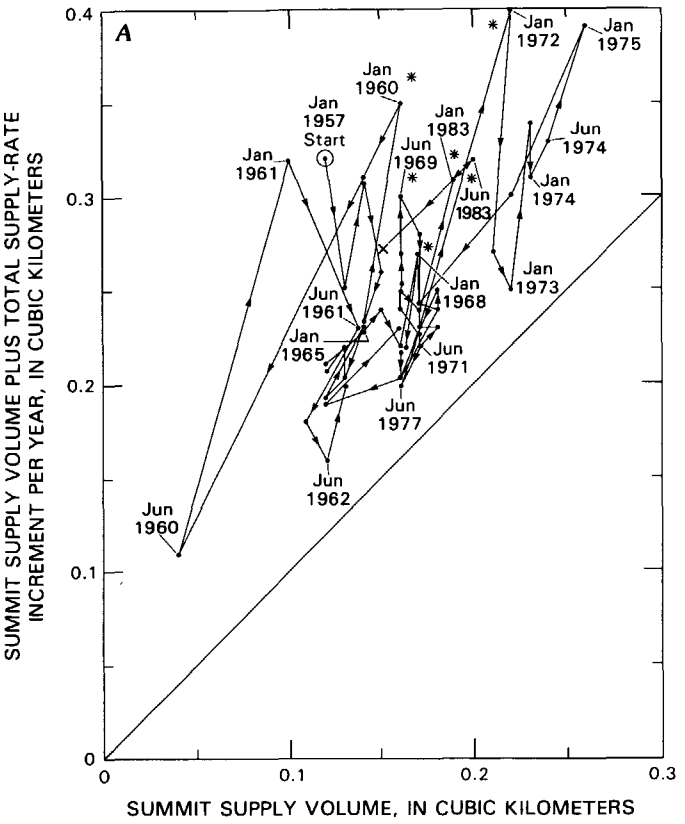

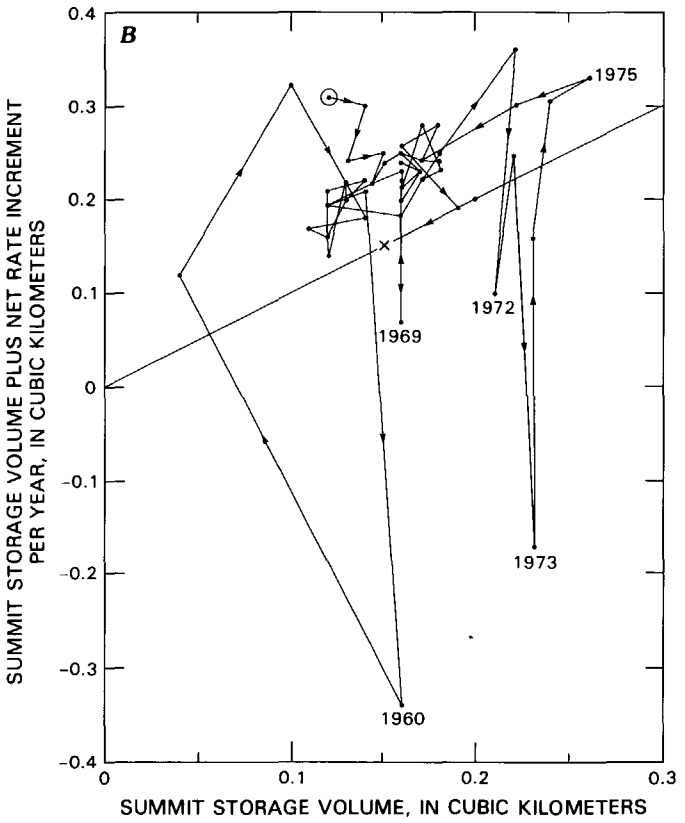

compensates oscillations of stress related to flow rates, rates of solidification, and so on (see Hardee, chapter 54). A logistical interpretation of such balances leads to the analogous inference that there are characteristic regimes of oscillatory behavior that may be products of the path of evolution without the intervention of any externally applied forcing frequency. The inclusion of external influences, however, may also be subsumed by the pattern in a way that is then indistinguishable from the endogenous periodicities. Correlations with characteristic frequencies of external signals may be observable only during times when there are reinforcements of the endogenous periodicities or when the external influence is so large that it overrides the previous patterns.

UNIQUENESS IN PATTERNS OF VOLCANIC EVOLUTION

The words "unique," "pattern," and "evolution" used together raise issues fundamental to prediction as a goal of the natural sciences. I will attempt to summarize a viewpoint concerning their application to volcanology, suggested by the foregoing analysis, as the basis for my concluding comments.

First, I realize after some deliberation, that any rigorous statement concerning this topic is likely to contradict itself before it proceeds very far. Therefore, I limit conclusions to some questioning remarks concerning ways in which the present results may differ from or resemble other viewpoints concerning natural processes. If there is an accepted theory or body of knowledge concerning volcanic evolution (or the meaning of "natural evolution" in general), I do not know where it is stated, so I cannot say that I am commenting on any particular form of conventional wisdom.

Unique means literally "being without a like or equal." That much seems easy, until such questions are asked: How does one know there is no like or equal? Just how much alike do things have to be to be called "like"? What numerical tolerance is applied to

FIGURE 51.22.—Diagrams of future state plotted against present state as in figures 51.20 and 51.21 but based only on volume of supply or storage in summit chamber as defined by Dzurisin and others (1984). Here again, effect of eruption is to superpose large negative feedback events on more general pattern, based on intrusive balances, which circulates in vicinities of two characteristic stationary regions of summit volume, even though future states are expressed in terms of total supply rates (see similar patterns in fig. 51.23 restricted to summit rates). Dates are given for chronological perspective. Major eruptions (of the order 0.1 km^3) are indicated by asterisks; they apparently have occurred within a fairly narrow interval of attractor-like circulation, implying that eruption may reflect an intrusive feedback circulation within a characteristic bandwidth of rate-volume relations (see discussion of fig. 51.18). Note that Kalapana earthquake of 1975 occurred during a time of extreme positive divergence from localized circulations, while eruptions occurred in vicinities of median states; both correlate with summit-rift intrusive balances. ***A***, Summit supply volume versus summit supply volume plus total supply-rate increment per year (extrapolated 6-mo rate); this diagram, like figure 51.23, is generated totally on the basis of summit tilt data (see discussion in Dzurisin and others, 1984). ***B***, Summit storage volume versus summit storage volume plus net rate increment (supply minus eruption) per year. Circled point, beginning of record; x, end of record.

quantitative measures of likeness? What does "equal" mean in any natural context? What are the tolerance limits of numerical equality? (Numerical dynamics makes the latter problem vivid. In some regimes, changes by several digits in the first decimal place of a normalized unit quantity do not change the likeness or equality of a pattern, expressed in terms of periodicity. However, near conditions of critical change between periodicity regimes, such as from period-doubling to chaotic, the likeness of patterns can change drastically with numerical changes at the limit of computer precision. That is to say, in this respect, one part in 10^6 is a large change, in that periodic equality and likeness are drastically changed. This point is illustrated qualitatively in figure 51.16; see May, 1976, for some numerical examples.)

The word "pattern" can be applied to a crystal structure or to a bomb blast. Can one or the other be said to be either unique or nonunique? "Evolution," at least to some protagonists, implies uniqueness in the sense of a path-dependent process involving so many variables that it seems inconceivable that any given structural stage will ever repeat itself exactly. By this view, natural evolution never has nor ever will construct two identical volcanoes. That is, no complex form, including life, ever evolves in exactly the same way twice in the natural record. Yet, ideas of model building, fabrication, cloning, and even the genetic engineering of arbitrarily designed living forms are now almost commonplace and raise questions such as those mentioned above concerning what is meant by the words "unique," "pattern," and "evolution." Although no fundamental discussion of predictability and forecasting can really avoid such conundrums of science, I will attempt to restrict my conclusions to issues of necessarily rather vague criteria of pattern recognition.

If one were to digitize the coordinates of every piece of shrapnel and debris from every bomb blast in the history of explosives technology, it is highly unlikely that any two lists of numbers would be identical, except for individual or short sequences of numbers which may be similar because of the limits of resolution. Yet people who study such patterns, or patterns of shotgun blasts, can classify different types of shells and explosive materials simply in terms of learned recognitions of pattern morphologies.

Uniqueness in any applied sense of recognition is apparently judged in terms of some, usually unspecified, classification of relative complexity. In that context, the question of forecasting complex behavior is partly one of recognizing a class of complexity as distinct from any other class of complexity (implicitly, this also means that there exists some matrix or background system of states that is simple to some recognizable degree relative to what is called complex). If the recognition of distinguishable complexity is accurate, however, it subsumes the issue of forecasting, because the behavior it is desired to forecast is not separable from the criteria of recognition. One can test this idea by contemplating the recognition of any dangerous animal or of poison ivy. Their recognition and the forecasting of consequences are based on a complex system of evolved information; it is a rare person who would choose to attempt prediction solely on the basis of statistical study of the behavior of the particular specimen or situation confronting him. Yet, that is the way some investigations seem to approach volcano and earthquake hazards. Similar processes are operative even when the species is unknown; behavioral forecasting operates within a context of what is presumed will be a recognizable complexity. That recognition, however, obviously must include its own evolution (the reading of the complexity, the learning of the behavior, and the formulation of the forecast).

These comments may sound familiar to anyone who has spent some time studying the eruptions of Kilauea Volcano, or anyone who has studied the patterns of ocean breakers over a period of variable tides and weather on a particular stretch of beach. The behavior of breaking waves offers a particularly apt comparison to issues of volcanic prediction in the light of patterns studied in this paper.

A breaking wave represents a locus of familiar form and generally predictable action which is constructed in detail by the operation of progressive folded feedback from a more general state of chaotic motion. The trajectories of individual water molecules are statistically turbulent; no individual particle trajectory can be predicted in detail, except in the sense of a generalized involvement in a wave cycle. Yet, at stages of growth just prior to and during the course, say, of a surfer's ride, the waveform is highly familiar and even predictable. From the viewpoint of particle trajectories, no two ocean waves are demonstrably identical, hence each is unique. From the standpoint of recognition and regimes of behavior they are familiar and predictable, hence nonunique, except for the unexpected event (for example, a tsunami).

For ocean breakers, the demarcation between the familiar and the unfamiliar and (or) unexpected event (from a fisherman's or surfer's viewpoint) represents a practical criterion for distinguishing between endogenous and exogenous processes in the sense used earlier in this paper. Yet, on a global basis the general states of ocean circulation are net effects of all such processes. Therefore, the terms endogenous and exogenous, too, are relative to the goals of pattern recognition.

If length permitted, it would be possible to derive a series of logistical diagrams that would describe the relation between, say, water level and time along a stretch of coast during a period of variable barometric pressure (for, example, during the passage of a storm front). Expressed as maps of present versus future heights, such diagrams (as I have drawn them from published storm-wave data) resemble the cyclical control loops outlined in figures 51.17 and 51.18. In this case, however, the meaning of the feedback loops is fairly obvious in terms of the incidence, amplitudes, and repetitive frequency ranges of rising storm waves.

From the logistical viewpoint, figures 51.20–51.23 indicate that the recognizable behaviors of Kilauea Volcano may operate in a fashion somewhat parallel to that of storm fronts and breaking waves. The circulatory excursions of volumetric states relative to quasi-stationary states (for example, figs. 51.22 and 51.23) are analogous to frontogenesis associated with an interval of wave evolution. The implications for long-range forecasting are also parallel. A forecast of wave heights on a given stretch of beach depends critically on a knowledge of frontogenesis on at least a regional scale, as well as on such background information as what are considered normal tidal heights. The familiarity of the resulting local pattern is therefore contingent on a familiarity with other contributing patterns on both smaller and larger scales of time and size. Thus, a forecast on a given scale is ultimately conditioned by

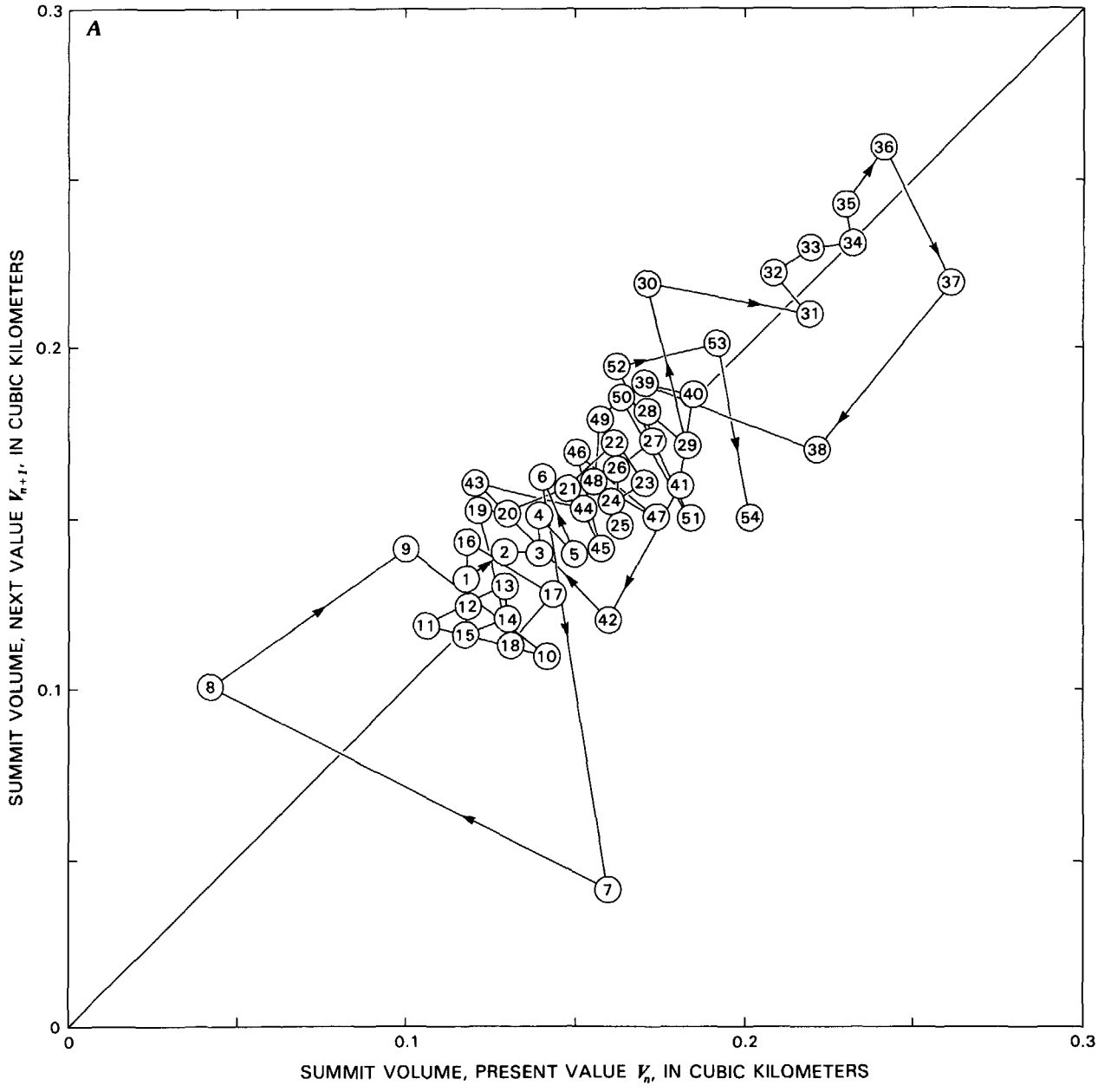

FIGURE 51.23.—Present-future volume states of summit reservoir of Kilauea. Numbers are chronological at half-year intervals beginning with (1) in January 1957. These plots resemble figure 51.22*A*, except that they reflect only summit rate variations rather than total rate variations (that is, they reflect inflation input minus deflation output of summit chamber based on interpretation of tilt data by Dzurisin and others, 1984). Asterisks again mark vicinities of major eruptions, and location of trajectory during time of 1975 earthquake is also indicated. These diagrams and figure 51.22*A* offer an exceedingly simple technique of logistic mapping of future eruption and earthquake patterns based on existing measurements of summit tilt without requiring other information. ***A***, Plot of present value versus next value, based on figure 51.5*A*, in which rate variations are implicit. ***B***, Plot of summit volume versus summit volume plus summit supply-rate increment per year (yearly extrapolation of 6-mo rate shown at each 6-mo interval). This graph amplifies effects of rate amplitudes but illustrates same pattern as in figure 51.23*A*.

both an even more local and a more global forecast; that is to say, the confidence in our recognition of familiarity is conditioned by our confidence in recognizing some more universal pattern of familiarity.

A probabilistic weather forecast evidently represents the measure of nonrecognition of what is, at least potentially, quite familiar. In order to be as candid as possible in the forecast, therefore, it would

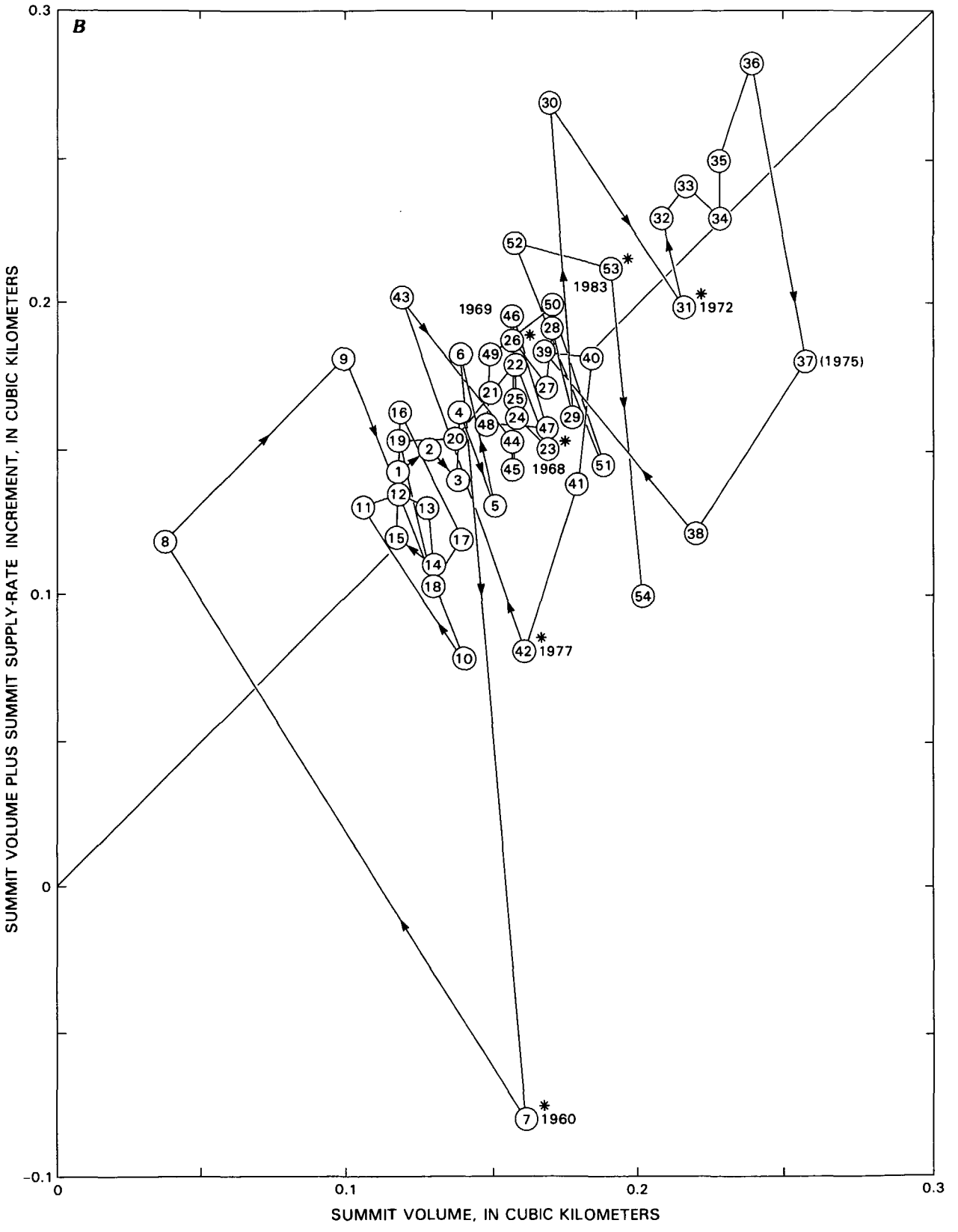

FIGURE 51.23—Continued

have to be concatenated some way according to the possible arrays of logistical folded feedback encompassing the consequences of recognition of all potentially active control loops. The potential diversity and complexity in predicting reasonable variants of diagrams like figures 51.17, 51.18, 51.22, and 51.23 obviously is large. Nevertheless, these alternative histories are integral aspects of the complexity that must be learned if we are to improve the quality of prediction.

The problems of weather forecasting and eruption forecasting are basically little different from everyday processes of pattern recognition. The long timeframe involved in geologic processes and the possibility that there may be future events of unprecedented and hence unrecognizable form, however, are not encompassed by our usual scales of automatic recognition (an example was the May 18, 1980, eruption of Mount St. Helens, Washington; on the other hand, at least several individuals clearly did recognize the potential for that eruption on the basis of familiarity with multiple lines of long-term evidence). The utility of logistical analysis for volcano-hazards forecasting stems from an ability to construct descriptions of folded feedback representing a variety of different scales of volcanic processes. Indications of self-similarity, such as those pointed out earlier in this paper, are important clues to the validity of this approach.

For example, examination of logistical feedback on the scale of monthly variations during the one-year record of figure 51.5*B* also reveals a pattern that shows scaled-down circulations resembling the 28-year pattern of figure 51.23. Another diagram (not shown) is based on the timing of the secular evolution of the Hawaii-Emperor Chain scaled down by a factor of 10^6. The resulting synthetic record also resembles figure 51.23, suggesting self-similarity in the form of circulations about characteristic stationary states at the larger scale. A literal interpretation of this construction would be that the asthenosphere-lithosphere section has relative properties resembling the interactions of the generalized summit and rift reservoirs. The compatible volume scale of magma in the region of storage, relative to the summit reservoir (that is, 10^6 times larger), would be on the order of 10^5 km^3, which is appropriate to the size scale of individual islands (closely coordinated groups of volcanic edifices) along the chain.

The logistical approach can be applied as well to positive-negative rate balances during the growth of fractionated magma reservoirs. Preliminary graphical and numerical experiments along these lines suggest that the structures and periodicity scales in time and size of caldera-forming silicic ash-flow systems may behave in principle much like the diagrammatic processes of folded feedback described in this paper. Obviously, the problem is more intricate because of the multiplicity and scale ranges of control loops. In principle, however, conditions of storage, states of fractionation, and eruption represent circulations about nested sets of stationary basins of attraction much like those described in figures 51.15–51.18. The parallels between conditions of charge and discharge (and eruptibility) of a magma chamber with those describing the conditions of the breaking wave apply as well to nested systems of volcanoes. The only differences are in the varieties of timing and size scales of processes analogous to frontogenesis. In silicic cratonic systems, this aspect of the problem also involves variations of supply rate of primitive magma much like the variations shown by the Hawaiian systems (Shaw, 1985). Therefore, in this sense, there are important elements of self-similarity between patterns of oceanic and continental volcanism (also, compare earlier discussions of fig. 51.7 concerning size and repose time relations).

In the global context, logistical methods may be useful in studying correlations of volcanic periodicities with those of external forcing frequencies such as the earth tides. It seems evident from the earlier discussion that endogenous attractor-like periodicities having some regularity are possible in volcanic systems; basaltic systems apparently involve significant variability at the daily to yearly scale as well as at the more secular scales of variations. Analyses by Klein (1976) and by Dzurisin (1980) have confirmed the existence of significant fortnightly tidal correlations with volcanic behavior during certain intervals of time and location. If a crude endogenous periodicity exists in the vicinity of a more regular external (or exogenous) forcing frequency, entrainment of that frequency is likely. By implication, however, this could apply to any of a variety of sources of similar periodic effects (for example, there may be a 27-day solar geomagnetic signal that, according to numerous recent discussions, conceivably becomes involved even in mantle processes by way of momentum coupling between the atmosphere and the solid Earth affecting microsecond fluctuations in the Earth's rotation).

Forecasting terrestrial events evidently implies eventual familiarity with periodic behavior involving a very broad spectrum of cosmological phenomena. Our (at present) low probabilities of accurate geologic forecasting, aside from issues of humanly unknowable hidden variables, can be viewed either as a measure of the uniqueness of terrestrial evolution or as a measure of our reluctance to seek familiarity with a broader context (including major cosmological processes) that will make Earth processes more familiar. If familiarity with processes of change in the Earth is the aim of volcanological research, it will necessarily involve increased familiarity with methods for documenting the evolution and recognition of complex patterns along lines at least analogous to those proposed in this paper. Obviously, these broader goals will require increased emphasis on analysis of interdisciplinary sets of data with an aim toward discovery of common factors in their evolution.

I conclude with some suggestions concerning what might be done within the existing research efforts at the Hawaiian Volcano Observatory to test and (or) to implement the ideas outlined here. There is no doubt in my mind that the methods of documentation and analysis already in progress are of the highest quality and utility for purposes of day-to-day monitoring of hazards potentials. I recommend, however, that these day-to-day records also be plotted in terms of logistic diagrams such as those constructed in this paper. The same approach can be applied to a variety of different scales, ranging from the records of individual episodes of fountaining behavior to long-term studies of the timing patterns in lava-flow stratigraphy. Similar remarks concern the analysis of seismicity and deformation patterns as data accrue. For example, seismic moments can be summed within specified domains, from scales of time and size associated with Kilauea to scales associated with the Hawaiian Archipelago, and their variations plotted in exactly the same format

as the variations in magma supply (see Shaw, 1980). In an analogous way, times between earthquake events and eruptive events (either separately, or in combination) can be plotted at different scales of resolution to create what can be called attractor maps of possible repetitive patterns and trajectories of change. Such an approach is analogous to the method used by Shaw (1984) to document and classify dynamical regimes of nonlinear drop formation in the leaky-faucet experiments mentioned earlier. Also, volume-time data for deformations of the east rift zone of Kilauea could be plotted in much the same way as the summit-tilt data. Trajectories of circulation could be updated incrementally, as are the present plots of summit tilt versus time.

All these additional maps of the dynamical states of the volcano will provide an additional pictorial image and a greater feeling of confidence in describing patterns of waxing and waning activity. In the process, it may become more evident why eruptions, earthquakes, and other events (for example, large-scale landslides), occur where they do in the cycles of repetitive states such as those illustrated in this paper. Needless to say, we are sorely in need of the same sets of data for parallel analyses of Mauna Loa. In view of the current signs of a waxing period of activity there (see figs. 51.4, 51.7), this goal would appear to be of high priority.

Even though the patterns illustrated here would be formally classed in the chaotic regime of attractor dynamics, this does not mean that they have no predictive value. There are clear indications of characteristic patterns of repetition, even if they are not periodically exact. That is to say, prediction, in this sense, stems from an ability to identify multiple sequences of indications of trajectorial trends toward conditions of imminent instability (that is, toward conditions typical of various types of intrusive episodes, eruption, changing edifice-deformation states, or earthquakes). In the chaotic mode, individual sets of trajectories do not repeat themselves exactly, but some composite set of multiple aperiodic trajectories may be diagnostic (that is, a chaotic attractor is very much a recognizable entity, even though any subset of points may be totally unique and mystifying when examined out of context). In principle, the same criteria are automatically activated when we recognize and predict the behavior of any human individual. Prediction is far from infallible, but if I know a person's habits well, it is often obvious what the behavior will be in sufficiently familiar circumstances. The same could be said of predictive abilities concerning traffic flow in a large metropolitan area. Although no individual trajectories of motion are likely to repeat exactly in daily, weekly, monthly, and yearly cycles, most of us who live in such environments can say, even during a nonperiodic episode (that is, patterns within those that clearly correlate with time of day), what will happen next. At that level of familiarity, statistical probabilities are very useful ways to document that what we sense happening is, in truth, likely.

REFERENCES CITED

Burks, A.W., ed., 1970, Essays on cellular automata: Urbana, Ill., University of Illinois Press.

Campbell, David, Crutchfield, J., Farmer, D., and Jen, E., 1985, Experimental mathematics: The role of computation in nonlinear science: Communications of the ACM (Association for Computing Machinery), v. 28, p. 374–384.

Dana, J.D., 1849, United States Exploring Expedition, during the years 1838, 1839, 1840, 1841, 1842: Geology: Philadelphia, v. 10.

Duffield, W.A., Bacon, C.R., and Dalrymple, G.B., 1980, Late Cenozoic volcanism, geochronology, and structure of the Coso Range, Inyo County, California: Journal of Geophysical Research, v. 85, p. 2381–2404.

Dzurisin, Daniel, 1980, Influence of fortnightly tides at Kilauea Volcano, Hawaii: Geophysical Research Letters, v. 7, p. 925–928.

Dzurisin, Daniel, Anderson, L.A., Eaton, G.P., Koyanagi, R.Y., Lipman, P.W., Lockwood, J.P., Okamura, R.T., Puniwai, G.S., Sako, M.K., and Yamashita, K.M., 1980, Geophysical observations of Kilauea Volcano, Hawaii, 2: Constraints on the magma supply during November 1975–September 1977: Journal of Volcanic and Geothermal Research, v. 7, p. 241–269.

Dzurisin, Daniel, Koyanagi, R.Y., and English, T.T., 1984, Magma supply and storage at Kilauea Volcano, Hawaii, 1956–1983: Journal of Volcanology and Geothermal Research, v. 21, p. 177–206.

Gardner, Martin, 1983, Wheels, life, and other mathematical amusements: San Francisco, W. H. Freeman.

Gosper, R.W., 1984, Exploiting regularities in large cellular spaces, *in* Farmer, D., Toffoli, T., and Wolfram, S., eds., Cellular automata: New York, North-Holland Physics Publishing, p. 75–80.

Gruntfest, I.J., 1963, Thermal feedback in liquid flow; plane shear at constant stress: Transactions of the Society of Rheology, v. 7, p. 195–207.

Jackson, E.D., Silver, E.A., and Dalrymple, G.B., 1972, Hawaiian-Emperor Chain and its relation to Cenozoic circumpacific tectonics: Geological Society of America Bulletin, v. 83, p. 601–617.

Jackson, E.D., and Shaw, H.R., 1975, Stress fields in central portions of the Pacific plate: Delineated in time by linear volcanic chains: Journal of Geophysical Research, v. 180, p. 1861–1874.

Judson, H.F., 1979, The eighth day of creation: New York, Simon and Schuster.

Klein, F.W., 1976, Earthquake swarms and the semidiurnal solid earth tide: Royal Astronomical Society Geophysical Journal, v. 45, p. 245–295.

———1982, Patterns of historical eruptions at Hawaiian volcanoes: Journal of Volcanology and Geothermal Research, v. 12, p. 1–35.

Lachenbruch, A.H., 1980, Frictional heating, fluid pressure, and the resistance to fault motion: Journal of Geophysical Research, v. 85, p. 6097–6112.

Mandelbrot, B.B., 1982, The fractal geometry of nature: San Francisco, W.H. Freeman.

May, R.M., 1976, Simple mathematical models with very complicated dynamics: Nature, v. 261, p. 459–467.

Poundstone, William, 1985, The recursive universe: New York, William Morrow and Co., Inc.

Shaw, H.R., 1969, Rheology of basalt in the melting range: Journal of Petrology, v. 10, p. 510–535.

———1973, Mantle convection and volcanic periodicity in the Pacific: Evidence from Hawaii: Geological Society of America Bulletin, v. 84, p. 1505–1526.

———1980, The fracture mechanisms of magma rise from the mantle to the surface, *in* Hargraves, R.B., ed., Physics of magmatic processes: Princeton, N.J., Princeton University Press, p. 201–264.

———1985, Links between magma-tectonic rate balances, plutonism and volcanism: Journal of Geophysical Research, v. 90, p. 11275–11288.

Shaw, H.R., Jackson, E.D., and Bargar, K.E., 1980, Volcanic periodicity along the Hawaiian-Emperor Chain: American Journal of Science, v. 280–A, p. 667–708.

Shaw, Robert, 1984, The dripping faucet as a model chaotic system: Santa Cruz, Calif., Aerial Press.

Smith, R.L., 1979, Ash-flow magmatism, *in* Chapin, C.E., and Elston, W.E., eds., Ash-flow tuffs: Geological Society of America Special Paper 180, p. 5–27.

Souther, J.G., and Hickson, C.J., 1984, Crustal fractionation of the basalt comendite series of the Mount Edziza volcanic complex, British Columbia: major and trace elements: Journal of Volcanic and Geothermal Research, v. 21, p. 79–106.

Spence, D.A., and Turcotte, D.L., Magma-driven propagation of cracks: Journal of Geophysical Research, v. 90, p. 575–580.

Swanson, D.A., 1972, Magma supply rate at Kilauea Volcano, 1952–1971: Science, v. 175, p. 169–170.

van der Ziel, A., 1970, Noise: Sources, characterization, measurement: Englewood Cliffs, N.J.

Verveen, A.A., and Derksen, H.E., 1968, Fluctuation phenomena in nerve membrane: Institute of Electrical and Electronics Engineering, Proceedings, v. 56, p. 906–916.

von Neumann, John, 1966, Theory of self-reproducing automata (edited and completed by Arthur W. Burks): Urbana, Ill., University of Illinois Press.

Voss, R.F., and Clarke, J., 1975, '1/f noise' in music and speech: Nature, v. 258, p. 317–318.

Wadge, G., 1982, Steady state volcanism: Evidence from eruption histories of polygenetic volcanoes: Journal of Geophysical Research, v. 87, p. 4035–4049.

Watts, A.B., ten Brink, U.S., Buhl, P., and Brocher, T.M., 1985, A multichannel seismic study of lithospheric flexure across the Hawaiian-Emperor seamount chain: Nature, v. 315, p. 105–111.

ELASTICITY AND CONTRACTANCY OF HAWAIIAN OLIVINE THOLEIITE AND ITS ROLE IN THE STABILITY AND STRUCTURAL EVOLUTION OF SUBCALDERA MAGMA RESERVOIRS AND RIFT SYSTEMS

By Michael P. Ryan

ABSTRACT

Experimental data for the high-temperature elasticity of Hawaiian olivine tholeiite have been evaluated to 1133 K. Young's modulus and the modulus of rigidity demonstrate a linear decrease with increasing temperature. Regression equations developed for replicate runs during flexural resonance have yielded the following relation for the high-temperature Young's modulus: $E(T)=(6.054-0.00083T)\times 10$ GPa. For the rigidity, replicate runs conducted in torsional resonance have yielded the following regression relation: $\mu(T)=(2.615-0.00038T)\times 10$ GPa. Parallel experiments conducted to 973 K have yielded evaluations of the high-temperature expansivity of Hawaiian olivine tholeiite. The linear thermal-expansion coefficients range from $\alpha_L=4.58\times 10^{-6}\ ^{\circ}C^{-1}$ at 373 K to $\alpha_L=7.93\times 10^{-6}\ ^{\circ}C^{-1}$ at 973 K. Conducted on the same samples used for the elasticity studies, they have provided a set of internally consistent correction factors for the final evaluations of $E(T)$ and $\mu(T)$. Comparisons of the measured moduli and their temperature derivatives with theoretically predicted values are in good overall agreement. Comparisons of the measured high-temperature thermal expansivities with predictions based on mixing-model computations for basaltic blends of forsterite, augite, and labradorite compare favorably.

A model developed for the high-temperature elasticity of basalt uses the Voigt-Reuss-Hill averaging procedures to provide upper and lower bounds on the aggregate elasticity of basic and ultrabasic rocks. General in nature, it has herein been specialized for basalt. In the general treatment, the composition is variable, ranging from monomineralic aggregates to assemblages with multiple components. The resulting compositional model works directly with the single-crystal properties for each component: molar volumes, adiabatic elastic stiffness and compliance coefficients, and the Voigt and Reuss temperature derivatives for the bulk modulus and rigidity of each mineral phase. The Hill averaging procedure provides a set of median estimates for aggregate elasticity. The parametric contributions of spherical voids (vesicles) and elongate voids (microcracks) that weaken the otherwise pristine solid are incorporated by the self-consistent averaging procedure.

The pressure dependence of elastic-wave velocities for tholeiitic and alkalic basalt, gabbro, periodotite, dunite, and harzburgite is controlled by the progressive closure of microfractures with increasing depth in volcanic systems. For basalt and gabbro, pore-fluid-accessible fracture space is continuously squeezed out as the confining pressures increase within volcanic shields, thus providing a physical background and certain key elements in developing the concept of contractancy in magmatic systems. Combined with geologic observations that bear on the nature of macroscopic fracture networks near the surface of shield volcanoes, the role of contractancy rationalizes: (1) the highly nonlinear confining pressure dependence of compressional and shear wave velocities in intact basaltic rocks; (2) the systematics of $\partial V_p/\partial Z$ for the seismic-velocity profiles for Hawaii, including the low-velocity residuals that characterize the near-surface environment; and (3) the observed in-situ density systematics that characterize the stratigraphy of shield volcanoes, including the frequent observation of their low values at shallow depths. A corollary of the contractant behavior of shield volcanoes is the crossover in the in-situ densities of tholeiitic melt near its liquidus and that of its country-rock environment. This crossover occurs in the nonlinear region of the contractancy curves. In the heart of the crossover is a subregion of neutral buoyancy, where $\rho_{country\ rock}-\rho_{melt}\approx 0$. This behavior rationalizes the long-term stability of tholeiitic magma reservoirs and the frequently observed resting place of intrusives (for example, dikes in rift zones) that lie just beneath the surface of active volcanoes. As Hawaiian volcanoes evolve, they carry their contractancy curves with them. The concept of a contraction profile that has an evolutionary track paralleling the upward growth of the volcanic shield provides the mechanical rationale for the upward climb of subcaldera magma reservoirs as the shield progresses from youth to maturity.

THE HIGH-TEMPERATURE ELASTICITY OF HAWAIIAN BASALT

INTRODUCTION

Elastic moduli are essential to the computation of the displacements, strains, and stress distributions that occur in volcanic systems. Provided the level of the applied loading is below the elastic limit, the strains describing the resulting shape changes are recoverable, and load removal returns the body to its original condition. Imposing the idealization that the load application and strain response is independent of direction allows relating the moduli within a generalization of Hooke's law:

$$T_{ij}=\lambda\epsilon_{kk}\delta_{ij}+2\mu\epsilon_{ij}, \qquad (1)$$

where T_{ij} is a symmetric second-order stress tensor, ϵ_{kk} is a tensor relating volumetric or dilatational strains to the applied loading (T_{ij}), ϵ_{ij} is a second-order tensor that describes the distortional strains that have been generated, δ_{ij} is the Kronecker delta, and λ and μ are the Lamé elastic constants. The Lamé constants are in turn related to the Young's modulus E, the shear modulus G, and Poisson's ratio ν by:

$$\mu = G = \frac{E}{2(1+\nu)} \tag{2}$$

and

$$\lambda = \frac{\nu E}{(1+\nu)(1-2\nu)}; \tag{3}$$

the bulk modulus K, relating mean pressure and volumetric strain, is

$$K = \lambda + \tfrac{2}{3}G = \frac{E}{3(1-2\nu)}. \tag{4}$$

Two of these moduli are of particular use in volcanology. They are the Young's modulus and the modulus of rigidity, or the shear modulus. These moduli are the familiar connecting links between uniaxial stress and strain and shear stress and strain. They are indispensable in continuum analyses of the displacement, stress, and strain fields that accompany magmatic intrusion, the subsidence produced by magmatic withdrawal, and numerous related problems concerned with the mechanics and dynamics of active volcanoes. The experimental program has grown out of the author's interest in the fracture mechanics of intact basaltic rocks near their melting point, in low-pressure environments. Accordingly, a series of experiments was undertaken to provide data on the mechanical parameters required for computations related to crack growth near the solidus.

Prior studies of the temperature dependence of the elastic moduli of basalt have been of two types. The first approach focused on the evaluation of compressional- and shear-wave velocities primarily as a function of confining pressure, but taken over a moderate range in temperature. An example of this approach was provided by Hughes and Cross (1951) and Hughes and Maurette (1957), who evaluated compressional-wave velocities (V_p) and shear-wave velocities (V_s) (from which moduli may be derived) to 600 MPa (6 kbar) and 300 °C. The second approach seeks to determine the temperature dependence in high-temperature environments that cover a significant fraction of the interval from ambient to solidus temperatures. Here, the elastic moduli were of primary interest. Existing work on basalt is limited to the studies of Volarovich and Gurvich (1957), Iida and Kumazawa (1960), and Wingquist (1971). Kern and Richter (1979) extended the earlier temperature limits to 700 °C, in a series of V_p and V_s determinations on altered basalt from the Faroe Islands, with confining pressures to 600 MPa.

The objective of this section is evaluation of the elasticity and expansivity of Hawaiian olivine tholeiite. The primary focus is the evaluation of Young's modulus and the modulus of rigidity, to 1,133 K. Linear thermal-expansion coefficients have been measured in a parallel set of experiments to 973 K.

With respect to the evaluations of the elastic moduli, the present work complements the earlier studies—and is distinct from them—in: (1) combining a theoretical approach for moduli prediction with a parallel experimental program, and using the results of the model predictions to rationalize the compositional and microstructural dependence of elasticity at high temperatures; (2) extending the temperature range from ambient to 1,133 K; (3) focusing on basalt from the Hawaiian province; (4) working with pristine samples that have been unaffected by alteration processes; and (5) refining the resonance approach to incorporate a series of correction factors that properly account for the effects of thermal expansivity.

For the purposes of this report, all rock-unit names are used informally, although some are formal names.

ACKNOWLEDGMENTS

The collaborative support of Robert Koyanagi is gratefully acknowledged. Fred Klein prepared large-format seismic hypocenter maps. David Popish assisted with the early phases of protracted machine-shop activities. Logistical support by the staff of the Hawaiian Volcano Observatory has contributed in several ways. Particularly helpful have been Thomas Wright, Reginald Okamura, Arnold Okamura, and James Griggs. William F. Brace kindly provided samples of diabase. Ruthie Robertson prepared the typescript with characteristic accuracy and grace. Figures have been prepared with the assistance of Jewel Dixon, Lindel Keaton, Marcia Prins, and Betty Shallcross. Tom Chase kindly loaned marine bathymetry negatives. Thoughtful review comments by Richard C. Bradt, Earl K. Graham, Robert Y. Koyanagi, Manuel Nathenson, Eugene C. Robertson, Roger M. Stewart, and Robert I. Tilling have led to improvements in the manuscript. Portions of the work have been carried out with the support of a Grove Karl Gilbert Fellowship under the auspices of the Geologic Division of the U.S. Geological Survey. Additional support has been provided by the U.S. Department of Energy, Office of Basic Science, under interagency agreement No. DE-AI-1-79RA50294.

MEASUREMENTS OF THE ELASTIC MODULI OF BASALT

An early consideration in the experimental program dealt with preparing appropriate samples. Sample-selection criteria included (1) an intact lithology that would be representative of volumetrically large portions of Hawaiian shields; (2) individual samples that are pristine; and (3) a sample site that provides for good cross-sectional exposures within the interior of lava flows. These criteria are well satisfied by the Boiling Pots flow units that crop out west of Hilo (fig. 52.1). Details of the sample sites and flow structures in cross section are provided by Ryan and Sammis (1978).

THE BASALT OF BOILING POTS

Mineralogy and Petrography

Petrographically, the basalt of Boiling Pots is characterized by phenocrysts and microphenocrysts of olivine, scattered microphenocrysts of hypersthene (almost invariably jacketed with augite), plagioclase, and some augite, set in a very fine grained groundmass of subcalcic augite, pigeonite, magnetite, plagioclase microlites, and dark-amber glass. Textural relations are shown in figure 52.2. Modal analyses (table 52.1) are representative of samples in the experimental evaluations of moduli and expansivity.

Electron-microprobe analyses of the crystalline silicates in the basalt of Boiling Pots were performed with an ETAC Autoprobe. The microprobe was operated at 15-kV accelerating voltage and 0.04-μA current and used a 2.0-μm-diameter focused electron beam. Polished petrographic thin sections were prepared from samples from positions in the basalt blocks adjacent to sample locations for high-temperature elastic moduli and expansivity measurements.

TABLE 52.1.—*Modal mineral abundance in the basalt of Boiling Pots*

[Totals for mineral groups are given in last column; values are in modal percent]

Olivine (phenocrysts)	9.3	12.42
Olivine (microphenocrysts)	3.1	
Hypersthene (augite-jacketed)	2.8	
Augite (microphenocrysts)	.1	32.91
Subcalcic augite + pigeonite (groundmass)	29.9	
Plagioclase (microphenocrysts)	1.8	37.37
Plagioclase (microlites)	35.4	
Magnetite (euhedral, groundmass)	4.3	
Glass (with opaque dustings)	12.9	

Olivine.—Olivine is present as subhedral phenocrysts ranging in mean diameter from 2 to 5 mm and as subhedral to anhedral microphenocrysts ranging from 2,000 by 1,300 μm to 520 by 130 μm. Opaque inclusions (chrome-spinel?) are common, while inclusions of amber glass are less common and are in the more poikilitic olivine. Inferred reaction with the melt has corroded crystal faces, and augite rims are present as continuous jackets and as closely spaced neighboring crystals. Transgranular fracture is nearly always present in the larger phenocrysts.

The forsterite content of olivine phenocrysts from the Boiling Pots samples was determined using the X-ray determinative curve of Yoder and Sahama (1957):

$$\text{Fo (in mole percent)} = 4{,}233.91 - 1{,}494.59\ d_{130}$$

where d_{130} refers to the interplanar spacing (in Å) from the (130) reflection. The average of the determinations yielded a composition of $Fo_{90.1}$. The error associated with the determinative curve is 3 to 4 mol percent (Yoder and Sahama, 1957, p. 486). Zoning in olivine microphenocrysts was studied by use of the electron microprobe. Radial microprobe traverses from the center to edge of crystals show relatively magnesian cores and more fayalitic margins. The compositional range covered is $(Mg_{0.86}Fe_{0.14})_2SiO_4$ in the core to $(Mg_{0.78}Fe_{0.22})_2SiO_4$ near the margin. Errors attached to the determination of Mg and Fe are ±1.5 percent and ±2.0 percent, respectively. The combined X-ray analysis and microprobe analyses suggest that the forsterite content of Boiling Pots olivine ranges from $Fo_{90.1}$ in early phenocrysts to $Fo_{78.5}$ as the late olivine crystallized during microphenocryst formation.

Pyroxenes.—Augite is present as reaction rims on olivine and hypersthene microphenocrysts and as discrete euhedral to subhedral crystals ranging from about 200 to 100 μm in diameter. Individual microphenocrysts generally are optically homogeneous but may contain minute inclusions of glass. Microprobe analyses of augite microphenocrysts indicate compositions close to $Wo_{36}En_{50}Fs_{14}$.

Hypersthene microphenocrysts are elongate (1,000 by 100 μm) to stubby (75 by 75 μm) and are invariably mottled medium gray under crossed nicols. Euhedral prismatic (100), (010) faces are typically jacketed with augite reaction rims that range in thickness from 10 to 20 μm. Euhedral terminations, however, are rare, and the hypersthene laths have no augitic jacket on the terminations, suggesting breakage during postreaction fluid movement. Crystallographically aligned blebs, stringers, and lamellae of augite commonly are present within the hypersthene host and have the same optical orientation as the external jackets. Approximately aligned poikilitic zones frequently contain opaque-rich glass inclusions. Hypersthene laths that have grown into contiguity with a neighboring olivine microphenocryst may have jackets of augite that not only rim the hypersthene but enclose the olivine as well. In this role, augite has acted as the welding agent in the formation of occasional glomerocrysts.

Electron-microprobe studies of hypersthene microphenocrysts and their jackets of augite were performed using the ETEC Autoprobe. Hypersthene laths are relatively homogeneous with respect to Ca, Mg, and Fe and have internal compositional ranges near $Wo_{3.8-4.1}$, $En_{81.6-82.1}$, and $Fs_{13.9-14.2}$. The composition of the augitic jackets on the prismatic faces is $Wo_{32.8}En_{47.5}Fs_{19.5}$, suggesting that relative to the melt that produced most augite microphenocrysts, depletion in Ca and Mg and enrichment in Fe had taken place by the time augite jacketing occurred.

Pigeonite is present as irregular groundmass crystals that are invariably anhedral. Mean diameters range from 40 to 20 μm, and their diminutive size lets them occupy vacant positions between adjoining plagioclase microlites in the groundmass topology, thus giving the rock fabric an intergranular character.

Plagioclase.—Plagioclase is present both as sparse microphenocrysts measuring 400 by 60 μm and as tiny groundmass microlites in the 70- to 40-μm length range, with widths of approximately 20 μm. Twinning follows both the Carlsbad law and albite law, and most microlites have 3 to 8 albite-twin individuals. Plagioclase compositions were determined using the ETEC Autoprobe, where the 2-μm beam diameter permitted analyses to be performed in microlite interiors without including surrounding glass or groundmass clinopyroxene within the excitation volume. The results of microlite analyses span the compositional range $Ab_{27.3-39.0}$, $An_{72.2-60.0}$, $Or_{0.5-0.9}$.

Magnetite is present as discrete euhedral crystals whose equant dimensions are approximately 10 μm. These crystals form a minor groundmass component (4.3 modal percent), and they occupy interstitial positions between adjoining plagioclase microlites in the crystalline groundmass network. Glass is medium to dark amber and is generally heavily dusted with opaque particles. Glass is present as thin films separating subparallel plagioclase microlites and as scattered equant pools and triangular patches. No evidence for devitrification has been found and, with the exception of the associated opaques, the glass is optically homogeneous at all levels of magnification.

Plots of weight percent $K_2O + Na_2O$ versus weight percent SiO_2 for the Boiling Pots basalt fall well within the tholeiitic field on an alkali-silica diagram (see, for example, Tilley, 1950; Macdonald and Katsura, 1964). Consistent with a tholeiitic nature, suggested by relations between these oxides, is the common reaction relation between magnesian olivine and their rims of augite.

Microstructure.—The three-dimensional microstructure of several Boiling Pots olivine tholeiite samples was examined using a scanning-electron microscope (SEM). This method provided a means of examining: (1) crystal-glass relations between olivine, pyroxene, plagioclase, and the 13-modal-percent interstitial glass; (2) differences in the behavior of glass above and below the glass-transformation temperature, T_g; (3) intragranular and intergranular

microfractures and the appropriateness of the assumption of a needle-shape geometry for voids representing microfractures in the elastic microstructural model; and (4) vesicles and vesicle shapes to assess the assumption of spherical voids in the approximation used in the elastic microstructural model.

The study employed a Cambridge Stereoscan (600) scanning-electron microscope with a peak accelerating voltage of 25 kV and a maximum resolution of 250 Å. The electron source was a tungsten-wire filament operated at 10^7 electrons s^{-1} and was maintained under a vacuum of 10^{-5} mm Hg.

The results of the SEM study are as follows:

(1) The glass phase covers practically all matrix crystals with a coat of varying thickness. The only general exceptions to this phase are crystals that are immediately adjacent to vesicles.

(2) Spherical geometry is a fair to good approximation for the shape of most observed vesicles, thus suggesting that the assumption of spherical voids in the elastic microstructural model is appropriate (see section "Modeling the High-Temperature Elasticity of Basalt").

(3) Needle-shaped geometry may be a fair approximation for the shape of many observed microcracks. (This is not always the case, however, as many microcracks have irregular geometries that resemble complexly warped planes.)

Porosity.—Most of the porosity in basalt samples may be attributed to spherical or nearly spherical vesicles that, in general, are not interconnected. Another type of porosity occurs in the form of microcracks that are produced as a result of microscopic contraction anisotropy in the fabric of the cooling rock. These microcracks take the form of intracrystalline fractures (especially in olivine microphenocrysts) and intercrystalline fractures along the margins of microlites and surrounding glass.

Because much of the total porosity is of an isolated form, measurement of the absolute porosity was the appropriate approach to assess the overall level of porosity.

The absolute porosity (in percent) may be expressed as

$$\Phi_A = \left(\frac{V_v + V_{mc}}{V_v + V_{mc} + V_{xtl+gl}} \right) \times 100, \qquad (5)$$

where V_v is the volume of vesicles, V_{mc} is the volume of microcracks, and V_{xtl+gl} is the volume of the matrix of crystals and glass.

To measure absolute porosity, the bulk (total) volume of a 5.25-cm by 1.25-cm by 0.75-cm sample was measured with a mercury pycnometer. The sample was crushed to 100 mesh with a percussion mortar and pestle. This method effectively released the contribution of the noncommunicating pores and microcracks in the interior of the sample, so that their volume would be added to the total void volume. The volume of the crushed sample was measured using a Russell volumeter, employing kerosene as the working fluid. The difference between the pycnometer and the volumeter measurements is the contribution of vesicle and microcrack volumes to the total (bulk) volume. The measured values are believed to be accurate to ±0.1 percent. Measured absolute porosities ranged from 21.4 to 14.3 percent for combined samples.

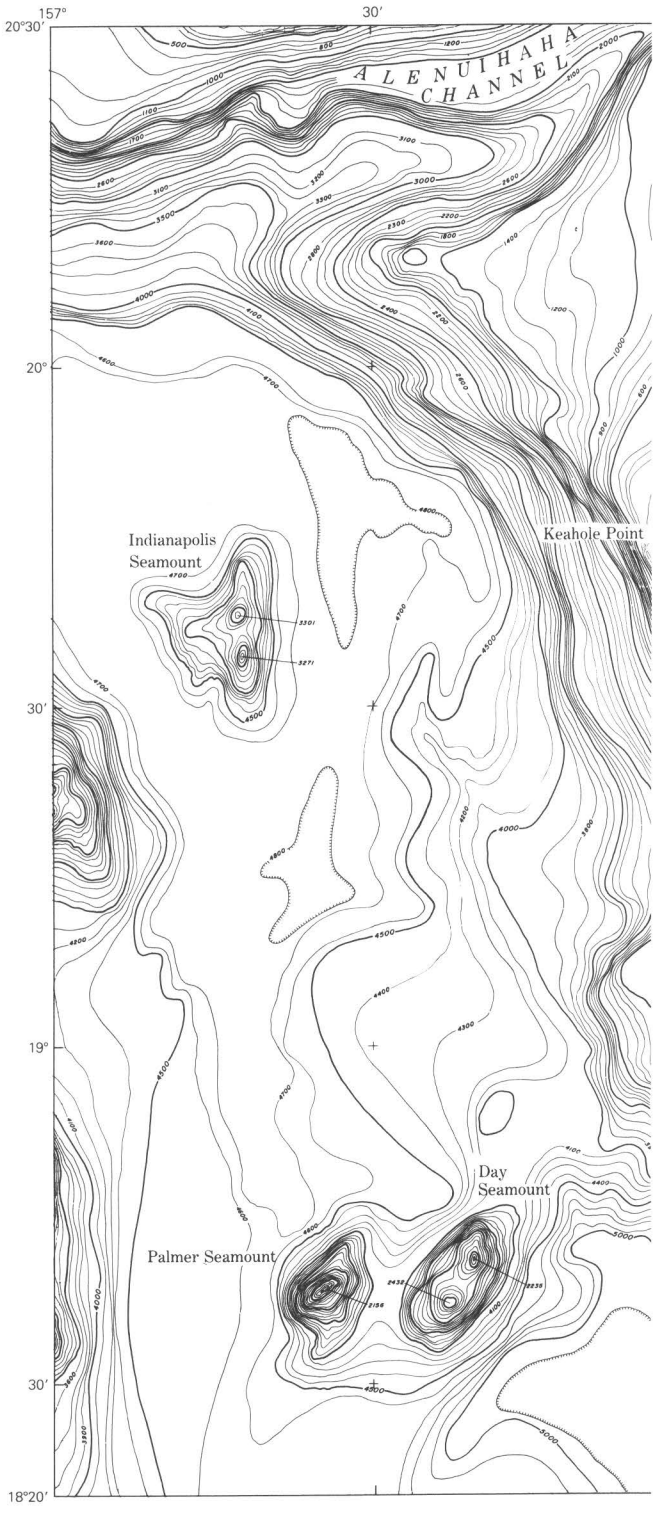

FIGURE 52.1.—Topography of Island of Hawaii, showing summits of principal volcanic shields, Loihi Seamount, and major seamounts of south Hawaii. Surmounting subcaldera magma reservoirs and rift zones of active volcanoes Mauna Loa, Kilauea, and Loihi Seamount is a heavily fractured veneer of country rock characterized by exceptionally low in-situ values of compressional-wave velocity

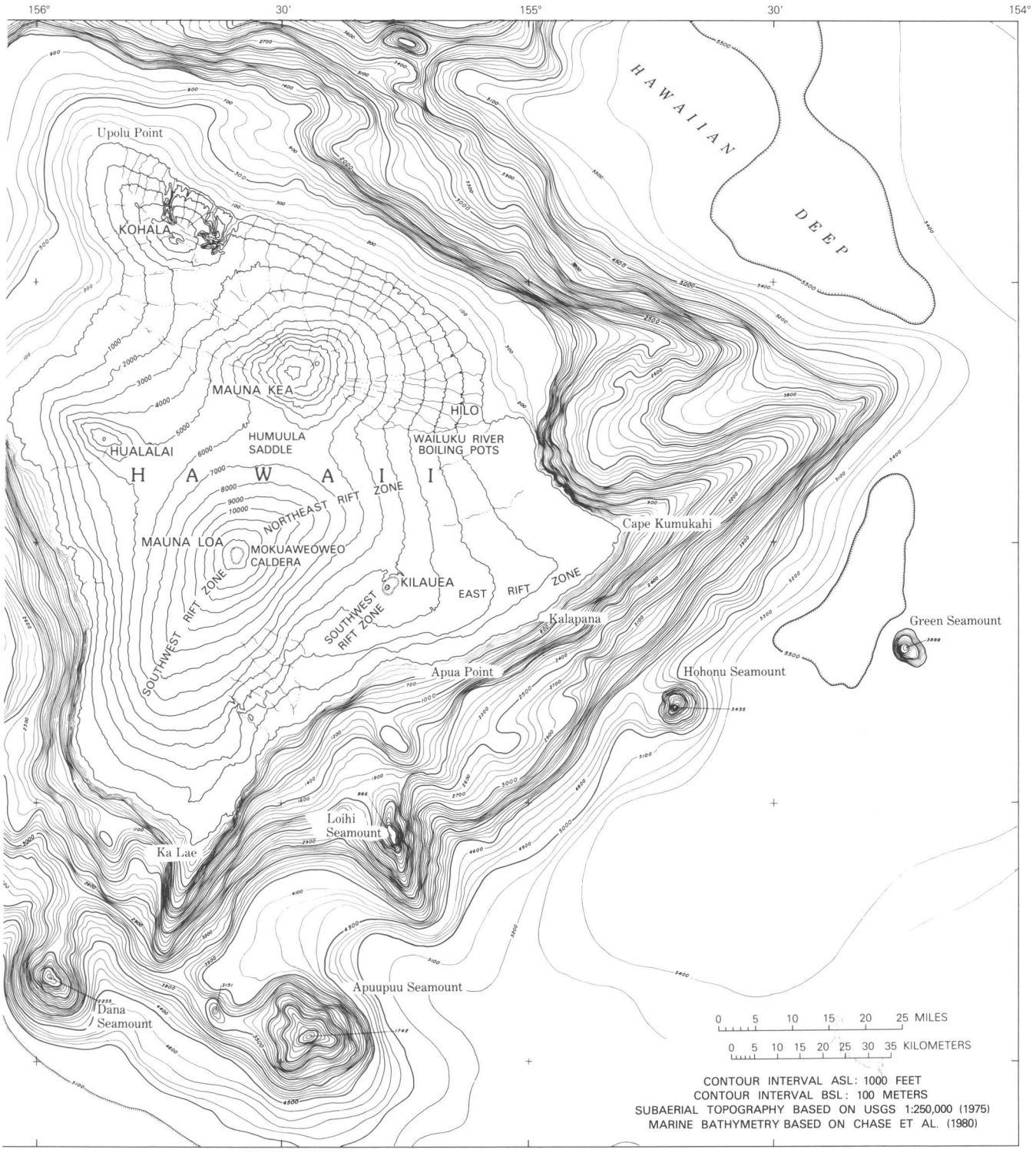

and density. Supersolidus intrusives within magma reservoirs and rift zones of these growing shields are stabilized by crossovers in in-situ density of tholeiitic melt near its liquidus and that of surrounding—and surmounting—country rock. As volcanic centers evolve, they carry their surficial veneer of low-density country rock with them, continuously providing a region of neutral buoyancy for magma within the shield. This, in turn, provides mechanical rationale for upward climb of subcaldera magma reservoirs, as evolving volcano progresses from submarine infancy through subaerial maturity to old age.

EXPERIMENTAL PROGRAM

The experimental program for the evaluation of elastic moduli employs the dynamic resonance technique developed by Spinner and Tefft (1961) and is based on earlier approaches of Ide (1936) and Förster (1937), who first recognized that controlled mechanical resonance provided a means of measuring the elastic moduli of solids. The computational approach used in evaluating the Young's modulus and shear modulus from the respective flexural and torsional resonant frequencies is based on the presentation in Hasselman (1961).

A Nametre (model 12) acoustic spectrometer was used to induce and record the resonant vibrational frequencies. A schematic diagram of the spectrometer and supporting equipment is shown in figure 52.3. The spectrometer consists of a Hewlett-Packard (3310A) function generator, which produces a sinusoidal output waveform ranging from 0.01 Hz to 100 kHz. Mechanical vibrations were transmitted to the sample by an Astatic commercial cutting head. A second Astatic (x-26) cutting head acted as a pickup transducer. The transducers are composed of quartz crystals, which provide the piezoelectric transmission and reception. Output from the pickup-transducer power amplifier was displayed on a Hewlett-Packard (122A) cathode-ray-tube oscilloscope, which provided a

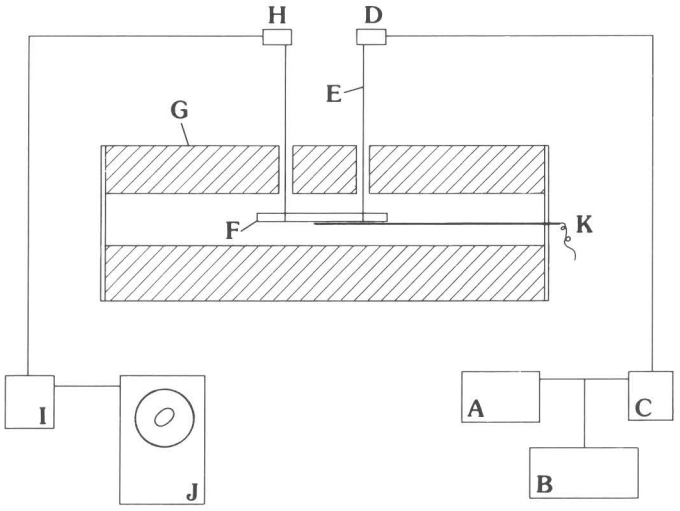

FIGURE 52.3—Schematic diagram of components of assembly for dynamic flexural and torsional resonance measurements at high temperatures: (A) variable-frequency signal generator; (B) digital frequency counter; (C) power amplifier; (D) driving transducer; (E) sample suspension system; (F) sample; (G) Kanthal-wound resistance furnace; (H) pickup transducer; (I) pickup power amplifier; (J) oscilloscope; and (K) platinum-platinum·10 percent rhodium thermocouple.

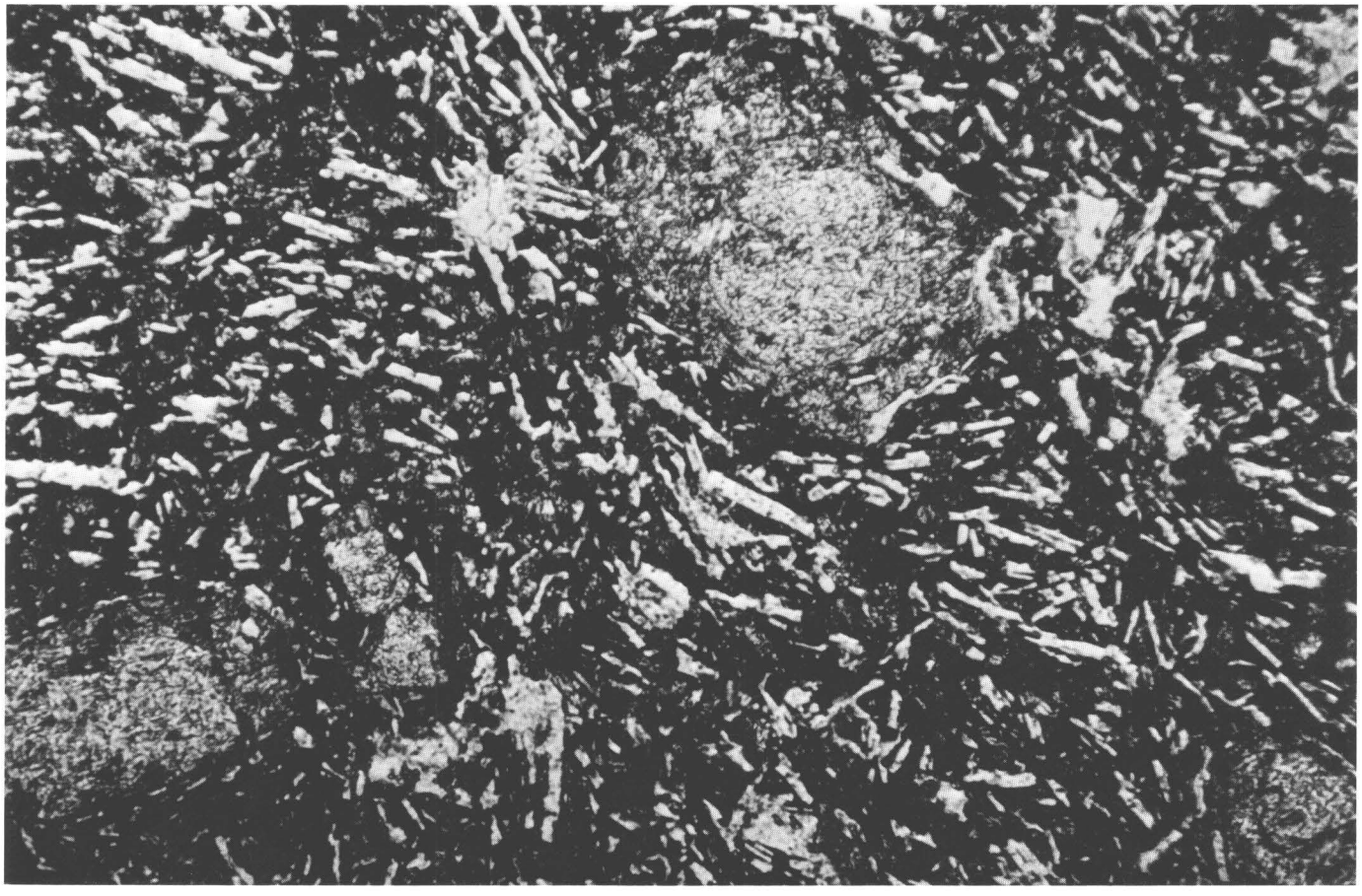

FIGURE 52.2—Photomicrograph of olivine tholeiite from Boiling Pots. Olivine phenocrysts are surrounded by plagioclase microlites set in a finer grained groundmass of pyroxene microcrysts and intercrystalline glass (heavily dusted with opaques). Under crossed nicols. Field of view is 400 μm by 600 μm.

graphical presentation of vertical-displacement amplitudes in the resonating sample. An associated voltmeter provided the means of maximizing the sample resonance via maximizing the pickup-transducer power-amplifier voltage. Digital readout of the resonant frequency was provided by a Hewlett-Packard (5325B) frequency counter with a range of 5 Hz to 10 MHz and a lower resolution of 0.01 Hz.

Ambient temperature measurements for both the Young's modulus and shear modulus evaluations employed electromagnetic noncontact transducers that induced and picked up vibration in the sample via metal tabs epoxyed to the sample ends.

High-temperature measurements employed an Alumel-wire suspension system connected from the transducers to the sample nodal points. A Satec Systems (Se-17p) Kanthal-wound, horizontally mounted furnace provided the high-temperature environment. Temperatures were maintained with a Thermoelectric (400 series) proportional controller, and a platinum-platinum·10 percent rhodium (Pt-Pt·10Rh) thermocouple.

Dynamic Young's Modulus at Ambient Temperatures

The Young's modulus (E) is evaluated at ambient pressure and temperature by applying equations relating the resonant frequency of the first mode of flexural vibration of an isotropic, homogeneous, elastic prism with a rectangular cross section to the sample mass and shape. Thus,

$$E=\left(\frac{0.94645Cmf^2}{B}\right)\times 10^2 \text{ MPa}, \tag{6}$$

where E is the Young's modulus evaluated at 25 °C, m is the mass (in grams) of the sample, f is the resonant frequency (in hertz) for the first mode of flexural vibration, B is the vertical dimension (in centimeters) of the cross section perpendicular to the direction of vibration, and C is a shape factor given by Hasselman (1961):

$$C=\left(\frac{D}{L}\right)-3\left[1+6.585(1+0.0752\nu+0.8109\nu^2)\left(\frac{D}{L}\right)^2-\frac{100.083(1+0.2023\nu+2.173\nu^2)\left(\frac{D}{L}\right)^4}{12+76.06(1+0.14081\nu+1.536\nu^2)\left(\frac{D}{L}\right)^2}-0.86806\left(\frac{D}{L}\right)^4\right], \tag{7}$$

where D is the thickness (in centimeters) of the sample cross section parallel to the direction of vibration, L is the sample length (in centimeters), and ν is Poisson's ratio.

Samples were prepared by machining 5.00- by 1.25- by 0.65-cm prisms from blocks of basalt that were judged to be homogeneous with respect to the distribution of vesicles and olivine phenocrysts. These rectangular bars were then resin-bonded to steel blocks, and the upper (free) surface ground parallel to the base in an automatic grinding machine. Rotation of the sample and subsequent regrinding assured that the upper and lower surfaces were parallel.

Sample dimensions were measured with a Mitutoyo micrometer, with a stated accuracy of ±0.002 cm. Sample masses were measured using a Mettler electronic balance, with an accuracy of ±0.001 g. Sources of error reside primarily in the measurements of sample geometry (length, width, and height) and sample mass. An additional source of error may result from slight deviations in rectilinearity of the overall geometry. Maximum resolution of resonant frequency on the Hewlett-Packard digital counter was 0.01 Hz; however, resonant frequencies were read to the nearest cycle per second. Table 52.2 summarizes the dynamic Young's modulus at 23 °C in selected samples.

Calibration of the acoustic spectrometer was performed by measurements of the dynamic Young's modulus of fused-silica frequency standards and established a precision of ±0.01 Hz for the fundamental bending mode of resonant vibration.

Single Crystals and Basaltic Rocks

A preliminary estimate of the modulus defect ($\Delta E/E_o$) produced by the included voids in basalt may be made by combining single-crystal elastic moduli on a weighted-average basis (see fig. 52.4). The Hill-averaged Young's moduli have been computed for each mineral by application of the standard relation of Birch (1960):

$$E_{\mathrm{VRH}}^{\mathrm{XTL}}=\frac{9(K_{\mathrm{VRH}}^{\mathrm{XTL}}\,\mu_{\mathrm{VRH}}^{\mathrm{XTL}})}{3K_{\mathrm{VRH}}^{\mathrm{XTL}}+\mu_{\mathrm{VRH}}^{\mathrm{XTL}}}, \tag{8}$$

where the subscript VRH denotes a Hill-averaged value and the superscript XTL denotes a single-crystal quantity.

Applying the mixing relations for K_{VRH} and μ_{VRH} for a polyphase mixture (see section "Modeling the High-Temperature Elasticity of Basalt"), the Young's modulus for a model basalt composition, $Fo_{100}=0.10$, augite $=0.45$, $An_{56}=0.45$, may be calculated by a second application of the standard relation, where $K_{\mathrm{VRH}}^{\mathrm{MIX}}$ and $\mu_{\mathrm{VRH}}^{\mathrm{MIX}}$ are evaluated at 25 °C and denote the bulk modulus and rigidity for the aggregate:

$$E_{\mathrm{VRH}}^{\mathrm{MIX}}=\frac{9(K_{\mathrm{VRH}}^{\mathrm{MIX}}\,\mu_{\mathrm{VRH}}^{\mathrm{MIX}})}{3K_{\mathrm{VRH}}^{\mathrm{MIX}}+\mu_{\mathrm{VRH}}^{\mathrm{MIX}}}. \tag{9}$$

Employing the bulk modulus (K) and rigidity (μ) values $K_{\mathrm{VRH}}=129$ GPa and $\mu_{\mathrm{VRH}}=81.6$ GPa for Fo_{100} (Graham and Barsch, 1969), $K_{\mathrm{VRH}}=95.6$ GPa and $\mu_{\mathrm{VRH}}=57.9$ GPa for augite (Aleksandrov and others, 1964), and $K_{\mathrm{VRH}}=72.0$

TABLE 52.2.—*Ambient-temperature dynamic Young's modulus for basalt of Boiling Pots*

[Young's modulus (E) evaluated at 23 °C]

Sample	E (GPa)	Porosity (percent)
BP-75-R7	74.70	14.3
BP-75-R2	62.78	15.1
BP-75-R4	62.60	15.6
BP-75-R6	60.52	15.8
BP-75-R1	60.39	15.8
BP-75-R5	60.06	16.8
BP-75-R3	55.90	17.8

GPa and $\mu_{VRH} = 34.3$ GPa for An_{56} (Ryzhova, 1964) yield a value of 110.39 GPa.

A comparison between the Young's modulus of this basaltic mixture of single crystals and that of the Boiling Pots olivine tholeiite reveals an appreciable gap of 47 GPa.

This difference in predicted and observed elasticity results from voids (vesicles and microcracks) in the basalt matrix, and so the hachured band in figure 52.4 has accordingly been labeled "defects." It probably, however, represents the maximum effect of microstructure, because the contributions of glass and opaque minerals have not been incorporated.

Dynamic Elastic Moduli at High Temperatures

Measurements made at high temperatures employed the following additional procedures:

(1) From 25 °C, the set point on the proportional temperature controller was moved up in 25-°C increments. At each increment, a measurement of the flexural or torsional resonant frequency was made.

(2) As the temperature of a sample increases, the flexural (or torsional) frequency at which it absorbs mechanical energy and resonates is continuously lowered.

(3) A uniform sample temperature was provided by blanketing the entire Kanthal resistance furnace with Kaowool spunglass insulation. Care was taken so that filaments of spunglass made no physical contact with the suspension system.

(4) Thermal equilibrium after a 25-°C increment generally required about 1 hour to achieve after the temperature from the thermocouple had matched the set point on the proportional controller. The test of equilibrium was a stationary resonant frequency for a 10- to 15-minute time interval. The overall heating rate from 25 °C to the maximum temperature (T_{max}) was 1.1 °C min^{-1}.

(5) As temperatures were increased to high levels (in excess of 700 °C), measurements were made until the aperture of the Lissajous figure was no longer a reliable indicator that resonance had been achieved.

(6) Corrections for the effect of thermal expansion were made, using the temperature-dependent linear thermal-expansion coefficients, $\alpha_L(T)$, evaluated at 100 °C increments.

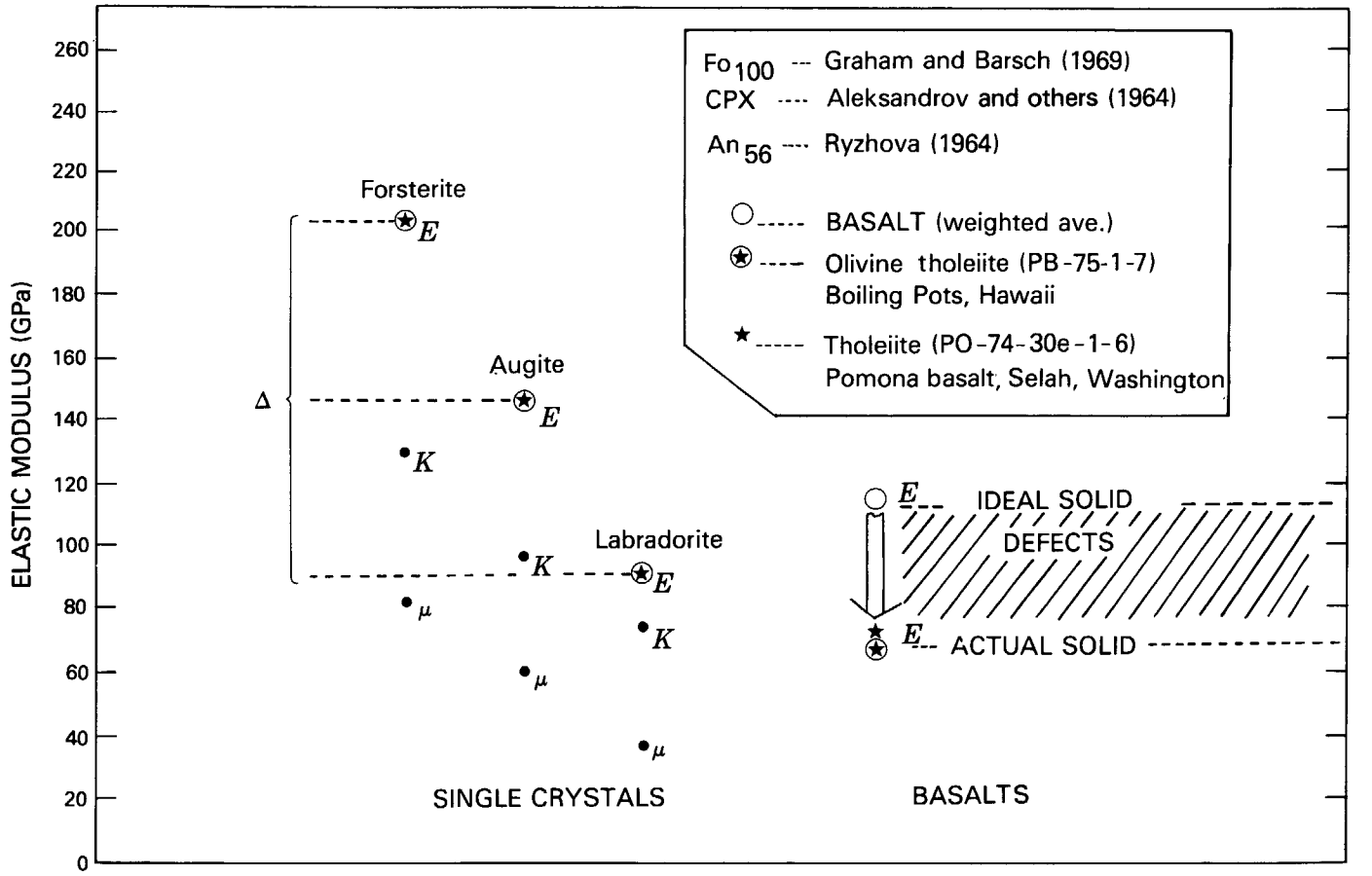

FIGURE 52.4.—Elastic moduli of single-crystal candidates of basalt mineralogy. Young's modulus (E) for ideal solid is weighted average of E values for forsterite, augite, and labradorite. Bulk modulus, K, rigidity, μ, and Young's modulus, E, for forsterite, augite, and labradorite have been included for comparison. Hachured area represents difference between computed composite and measured values for rock and is interpreted as being contribution of defects (vesicles and microcracks) present in rock but not represented in compositional estimate.

(7) Resonant frequencies obtained with the high-temperature Alumel suspension wires at ambient temperature were compared with frequencies obtained with the electromagnetic drive and pickup system.

Shear modulus.—Ambient-temperature evaluations of the shear modulus have followed a procedure that is similar to the Young's modulus evaluations. The essential difference requires the transverse excitation of the sample to induce torsional resonant vibrations instead of flexural vibrations.

Evaluations of the high-temperature shear modulus, μ, were made by relating the temperature-dependent torsional resonant frequency to the shear modulus and torsional resonant frequency determined at 25 °C (Hasselman, 1961):

$$\mu(T)=\mu(25)\,\frac{f_T^2}{f_{25}^2}\left[\frac{1}{1+\alpha_l(\Delta T)}\right], \qquad (10)$$

where $\mu(25)$ is the ambient-pressure, 25-°C shear modulus or rigidity, f_{25}^2 is the 25 °C torsional resonant frequency, f_T^2 is the high-temperature torsional resonant frequency, and $\alpha_L(\Delta T)$ is the temperature-dependent linear thermal-expansion coefficient for basalt, which enters as a correction factor.

Figure 52.5 presents the replicate rigidities and provides a comparison with available data for the high-temperature rigidity of basalt. The values from Wingquist (1971) are for the Dresser basalt, and those from Iida and Kumazawa (1960) are for the 1950 lava of Mihara Volcano (Izu, Oo-Shima, Japan). Table 52.3 lists the rigidity as a function of temperature to 800 °C. The linear-regression relation for $\mu(T)$ from 25 to 700 °C for sample BP-75-R2 is

$$\mu(T)=(2.611-0.00035T)\times 10 \text{ Gpa}, \qquad (11)$$

for sample BP-75-R4

$$\mu(T)=(2.618-0.00042T)\times 10 \text{ GPa}, \qquad (12)$$

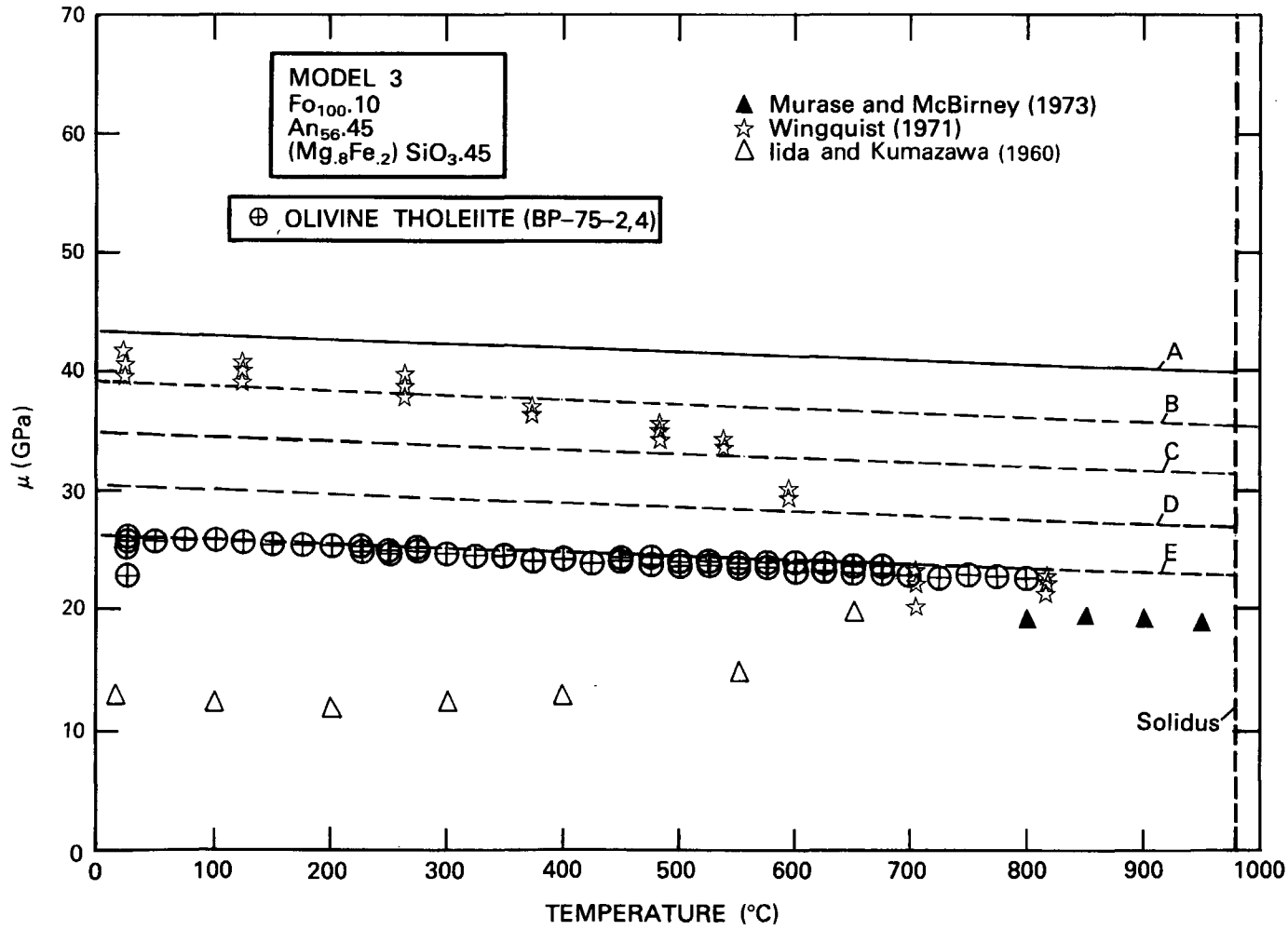

FIGURE 52.5.—High-temperature, ambient-pressure rigidity of Hawaiian olivine tholeiite. Solid line (A) has been computed using V-R-H averaging procedure and a compositional submodel 3 mixture of forsterite, plagioclase, and pyroxene. Computed high-temperature rigidities B, C, D, and E have incorporated progressively higher fractions (5, 10, 15, and 20 percent, respectively) of spherical voids—representing mechanical weakening effects of vesicles. Computed and measured temperature derivatives of μ, $d\mu/dT$, compare favorably.

TABLE 52.3.—*Shear modulus as a function of temperature*
[Sample BP-75-R4(G)]

$$\mu(T)=\mu(25)\underbrace{\left(\frac{F_T^2}{F_{25}^2}\right)}_{A}\underbrace{\left(\frac{1}{1+\alpha_l(\Delta T)}\right)}_{B}$$

Temperature (T) (°C)	A (GPa)	B	$\mu(T)$ (GPa)	$\frac{\mu(T)}{\mu(25)}$
25	26.1	1.0000	26.1	1.00
50	25.9	.9998	25.9	.99
75	25.8	.9997	25.8	.99
100	25.7	.9996	25.7	.98
125	25.6	.9995	25.6	.98
150	25.6	.9993	25.5	.98
175	25.5	.9992	25.4	.97
200	25.4	.9991	25.4	.97
225	25.3	.9989	25.2	.96
250	25.2	.9987	25.1	.96
275	25.1	.9986	25.0	.96
300	25.0	.9984	24.9	.95
325	24.8	.9983	24.8	.95
350	24.7	.9980	24.7	.94
375	24.6	.9979	24.6	.94
400	24.5	.9977	24.4	.93
425	24.3	.9974	24.3	.93
450	24.3	.9972	24.2	.92
475	24.2	.9970	24.1	.92
500	24.0	.9969	24.0	.91
525	23.9	.9962	23.8	.91
550	23.8	.9960	23.7	.90
575	23.7	.9958	23.6	.90
600	23.6	.9957	23.5	.90
625	23.6	.9952	23.4	.90
650	23.5	.9950	23.4	.89
675	23.5	.9948	23.4	.89
700	23.4	.9946	23.3	.89
725	23.3	.9937	23.2	.89
750	23.2	.9935	23.1	.88
775	23.1	.9932	23.0	.88
800	23.0	.9930	22.9	.87

and for the average of samples BP-75-R2 and BP-75-R4

$$\mu(T)=(2.615-0.00038T)\times 10\ \text{GPa}. \tag{13}$$

Rigidities obtained from the resonant-frequency values and their corresponding predicted values from the linear regression treatment have been compared to 700 °C. The value of the differences between measured and predicted values are the regression residuals. Comparisons of the magnitude of these residuals suggest that a linear temperature dependence for rigidity is appropriate over the interval 25–700 °C. An examination of the sign of the residuals with changes in temperature shows no systematics, either within the data of a single sample or between the pooled data of both samples. The evident linearity in the data is consistent with the behavior expected for a solid that is continuously increasing its volume, and concurs with the behavior in single-crystal studies of forsterite (Graham, 1969; Graham and Barsch, 1969) and bronzite (Frisillo, 1972), as well as in studies of nonsilicates (Jones, 1977) and the formalism of lattice dynamics (Leibfried and Ludwig, 1961).

Young's Modulus.—Evaluations of the Young's modulus, E, were made by relating the temperature-dependent flexural resonant frequency to the Young's modulus and the flexural resonant frequency determined at 25 °C (Hasselman, 1961):

$$E(T)=E(25)\frac{f_T^2}{f_{25}^2}\left[\frac{1}{1+\alpha_l(\Delta T)}\right], \tag{14}$$

where $E(25)$ is the ambient-pressure, 25 °C Young's modulus, f_{25}^2 is the 25 °C flexural resonant frequency, f_T^2 is the high-temperature flexural resonant frequency, and $\alpha_l(\Delta T)$ is the temperature-dependent linear thermal-expansion coefficient for basalt.

The thermal-expansion coefficient $\alpha_l(T)$ that was used to correct the shear moduli is the same one employed here. The Young's modulus of 54.0 GPa and an $E(T)/E(25)$ value of 0.894 for one sample may be compared with values of 54.6 GPa and 0.915 for the replicate, evaluated at their common high-temperature point of 725 °C.

Plots of E versus temperature are presented in figure 52.6 for both samples, and comparisons may be made with the available data for basalt, gabbro, and peridotite. Table 52.4 lists the values of $E(T)$ to 865 °C.

The regression equations for the temperature dependence of the Young's modulus in the Boiling Pots basalt for sample BP-75-R6 is

$$E(T)=(6.059-0.00085T)\times 10\ \text{GPa}, \tag{15}$$

for sample BP-75-R1

$$E(T)=(6.049-0.00081T)\times 10\ \text{GPa}, \tag{16}$$

and for the average of samples BP-75-R6 and BP-75-R1

$$E(T)=(6.054-0.00083T)\times 10\ \text{GPa}. \tag{17}$$

TABLE 52.4.—*Young's modulus as a function of temperature*
[Sample BP-75-R1]

$$E(T)=E(25)\underbrace{\left(\frac{F_T^2}{F_{25}^2}\right)}_{A}\underbrace{\left(\frac{1}{1+\alpha_l(\Delta T)}\right)}_{B}$$

Temperature (T) (°C)	A (GPa)	B	$E(T)$ (GPa)	$\frac{E(T)}{E(25)}$
25	60.4	1.0000	60.4	1.00
50	60.2	.9998	60.2	.99
75	60.0	.9997	60.0	.99
100	59.8	.9996	59.7	.98
125	59.6	.9995	59.5	.98
150	59.4	.9993	59.3	.98
175	59.1	.9992	59.0	.97
200	58.9	.9991	58.8	.97
225	58.7	.9989	58.6	.97
250	58.5	.9987	58.4	.96
275	58.4	.9986	58.3	.96
300	58.1	.9984	58.1	.96
325	58.0	.9983	57.9	.95
350	57.8	.9980	57.7	.95
375	57.6	.9979	57.5	.95
400	57.4	.9977	57.3	.94
425	57.3	.9974	57.2	.94
450	56.9	.9972	56.7	.93
475	56.7	.9970	56.6	.93
500	56.6	.9969	56.4	.93
525	56.3	.9962	56.1	.92
550	56.2	.9960	56.0	.92
575	56.0	.9958	55.8	.92
600	55.8	.9957	55.5	.91
625	55.6	.9952	55.3	.91
650	55.4	.9950	55.1	.91
675	55.1	.9948	54.8	.90
700	54.8	.9946	54.5	.90
725	54.3	.9937	54.0	.89
750	53.9	.9935	53.6	.88
775	53.2	.9932	52.8	.87
800	52.8	.9930	52.4	.86
825	52.3	.9928	51.9	.85
865	51.6	.9924	51.2	.84

Inspection of these values reveals that the temperature dependence of the Young's modulus for Hawaiian olivine tholeiite is very nearly linear over the interval 25–700 °C and accords with expectations based on the single-crystal $d(C_{ij})/dT$ for forsterite (Graham, 1969) or bronzite (Frisillo, 1972), or the predictions of lattice dynamics (Leibfried and Ludwig, 1961). Departures in linearity in $E(T)$ have been detected above 700 °C. Examination of the source of this change in slope suggests the presence of the glass transition.

MEASUREMENTS OF THE THERMAL EXPANSIVITY OF BASALT

An accurate evaluation of the temperature-dependent dynamic Young's modulus and dynamic rigidity requires a correction for the effects of thermal expansion within the resonating sample. Thermal expansivity is itself, however, a function of temperature, as the anharmonic vibrations within crystal lattices and within SiO_4 and

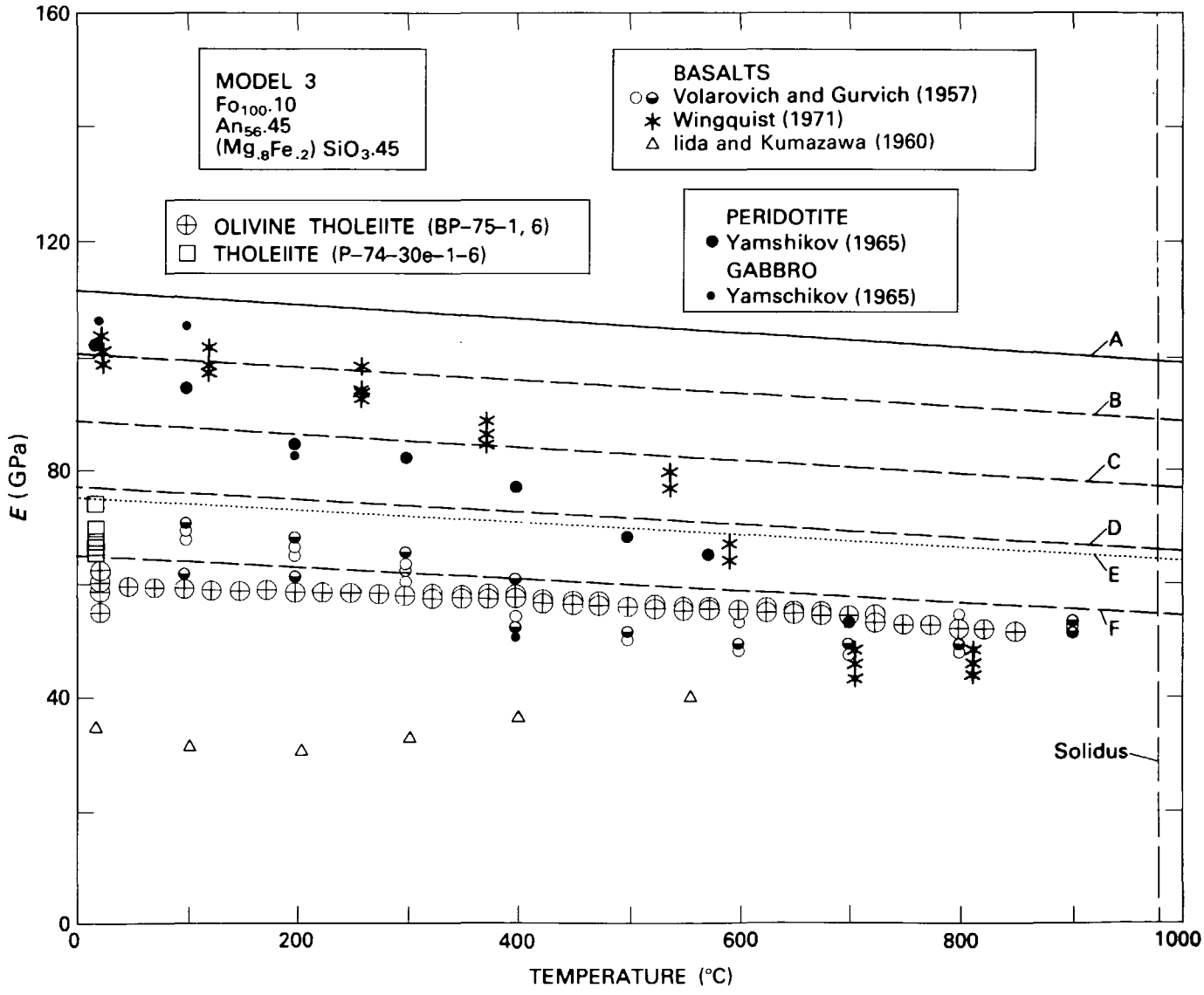

FIGURE 52.6.—High-temperature, ambient-pressure Young's modulus of Hawaiian olivine tholeiite. Available literature data have been included. Squares at 22 °C are data for moduli of Pomona basalt, Selah, Washington. Solid line (A) represents nonflawed computed modulus, without weakening effects of spherical voids (vesicles). Lines B, C, D and F represent progressive increments of 5, 10, 15, and 20 percent voids, respectively. Separation between curves D and E represents addition of 1 volume percent needle-shaped voids, simulating a class of microcracks that occur along crystal junctions. Computed and measured temperature derivatives of E, dE/dT, compare favorably.

AlO_4 tetrahedra in the glass progressively increase in amplitude with temperature.

The objective of this section is to discuss the measurement of linear thermal strain in basalt that will permit the evaluation of linear thermal-expansion coefficients. At the same time, they provide temperature-dependent correction factors that may be applied in the evaluation of the shear modulus and Young's modulus in the same basalt.

Thermal-expansion correction factors were generated by measuring the linear thermal strain by dilatometric methods and by relating incremental changes in longitudinal strain to the change in temperature that produced them. This set of thermal-expansion correction factors covers the temperature range 25–900 °C. The linear expansion coefficients embody within them several expansion components, which involve crystalline and glassy phases in the rock matrix as well as planar voids that heal as temperatures rise (that is, a microstructural component that is temperature dependent).

EXPERIMENTAL PROCEDURE

High-temperature measurements of thermal expansivity were obtained using an Orton Automatic Recording Dilatometer. A schematic diagram of the dilatometer is shown in figure 52.7; it consists of a 25-cm-diameter by 50-cm-long stainless-steel-clad furnace. An alumina sample holder and pushrod house the sample and transmit sample-length changes to a Daytronic (02B600) linearly variable differential transformer (LVDT). A Daytronic (201B) transducer exciter-demodulator produced a dc millivoltage for a Houston Omnigraphic (HR-100) x-y recorder. The x-y recorder automatically plotted sample macroscopic strain and temperature during heating (and cooling) cycles.

Samples were prepared by diamond-barrel coring with a 0.40-in.-inner-diameter core barrel. The sample diameter was 1.01 cm, and the sample lengths were 5.08 ± 0.002 cm. Sample ends were cut square and then ground flat, using an abrasive wheel and lapping grit normally used in preparing standard petrographic thin sections. One end of the sample was slightly beveled to ensure a single contact point against the alumina pushrod of the LVDT.

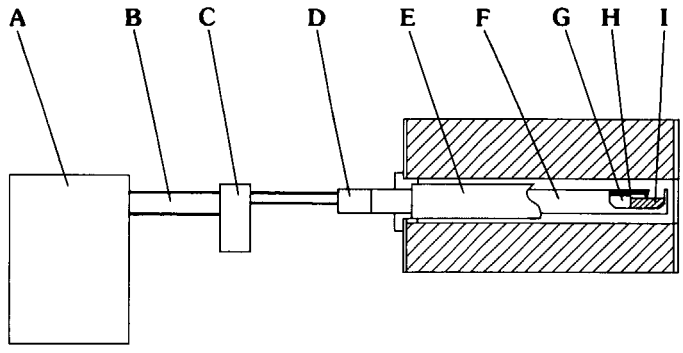

FIGURE 52.7.—Schematic diagram of components in dilatometer assembly used for measurements of linear strain at high temperatures. (A) x-y recording unit; (B) thermocouple leads and LVDT leads; (C) transducer exciter-demodulator; (D) linearly variable differential transformer (LVDT); (E) silicon-carbide resistance heating element; (F) alumina sheath; (G) alumina pushrod assembly; (H) platinum-platinum·10 percent rhodium (Pt-Pt·10Rh) thermocouple; (I) sample.

Dilatometer calibration was done using single crystals of α-quartz as comparators.

Linear thermal-expansion coefficients were evaluated from the defining relation

$$\alpha_l = \frac{1}{l_0}\left(\frac{\Delta l}{\Delta T}\right), \tag{18}$$

and volume coefficients taken as

$$\alpha_V \cong 3\alpha_l. \tag{19}$$

Operation of the dilatometer consisted of placing the machined sample in a split-cylinder alumina cradle whose inside diameter was slightly larger than the sample diameter, thus providing horizontal support while minimizing contact friction during expansion. The flat-cut sample end was placed square against the stop block (stationary end of cradle), and the slightly beveled end contacted the center of the pushrod. Temperature measurements were made with a platinum-platinum·10 percent rhodium (Pt-Pt·10Rh) thermocouple. A slight flexure in the thermocouple shank maintained a constant contact between the thermocouple bead and the upper surface of the sample. The millivoltage outputs of the LVDT and the thermocouple were supplied to an x-y plotter that provided a continuous record of sample-length changes with changing temperature.

LINEAR-STRAIN AND THERMAL-EXPANSION COEFFICIENTS

In contrast with the expansivity of samples of basalt from Kilauea Iki lava lake—where α_v values reached 55×10^{-6} °C^{-1} above 850 °C—expansion above 700 °C does not have a marked component ascribed to the configurational mobility within the glass. This contrast is attributed to the relatively small volume of glass (13 percent) in the Boiling Pots rocks. Ryan and Sammis (1981) discuss the glass transition in basalt and its mechanical significance in regulating the evolution of the fracture front during thermal-stress-induced cracking.

Table 52.5 contains the mean linear coefficients, α_l, for eight replicates and their standard deviation values to 700 °C. Note that variation is highest at low temperatures, lowest at moderate temperatures, and rises again at the 700-°C level. This variation suggests that the progressive closure of randomly oriented microcracks is an important contribution to the aggregate thermal-expansion coefficient below 300 °C and that the minimum variation above 300 °C (but below 700 °C) is reflective of the intrinsic variation in the Boiling Pots basalt expansivity. The larger variation at higher temperatures is interpreted as differences brought about by random differences in the number of olivine phenocrysts from sample to sample. Figure 52.8 illustrates the linear strain produced in basalt samples by controlled heating programs to 925 °C. Figure 52.9 presents the linear and volume thermal-expansion coefficients.

Data on the expansivity of forsterite, augite, and labradorite at 20, 400, and 800 °C (Skinner, 1966) have been employed to form

TABLE 52.5.—*Mean linear thermal-expansion coefficients ($\bar{\alpha}_l$) for basalt of Boiling Pots*

[Mean values determined from samples BP-75-2, BP-75-3, BP-75-4, BP-75-8, BP-75-10, BP-75-11, BP-75-12, BP-75-13]

Temperature (T) (°C)	$\bar{\alpha}_l$($\times 10^{-6}$) °C^{-1}	Standard deviation
100	4.58	1.05
200	5.60	1.06
300	4.90	.65
400	6.52	.75
500	7.01	.58
600	7.43	.32
700	7.93	.821

aggregate volume thermal-expansion coefficients for model aggregates by making use of relations for the expansivity of a mixture:

$$\alpha_V = \frac{1}{V}\sum_{i=1}^{n} x_i v_i \alpha_i, \tag{20}$$

where x_i is the volume fraction of mineral i, v_i is the molar volume of mineral i, α_i is the expansion coefficent of mineral i, and V is the aggregate volume, given by

$$V = \sum_{i=1}^{n} x_i v_i.$$

Molar volumes are available in Robie and Waldbaum (1968) and Robie and others (1978). For a model composition of $Fo_{75} = 0.10$, augite $= 0.45$, $An_{64} = 0.45$, $\alpha^l_{20} = 5.07 \times 10^{-6}$ °C^{-1}, $\alpha^l_{400} = 6.53 \times 10^{-6}$ °C^{-1}, and $\alpha^l_{800} = 8.49 \times 10^{-6}$ °C^{-1}, where the subscripts refer to degrees Celsius. Comparison of these

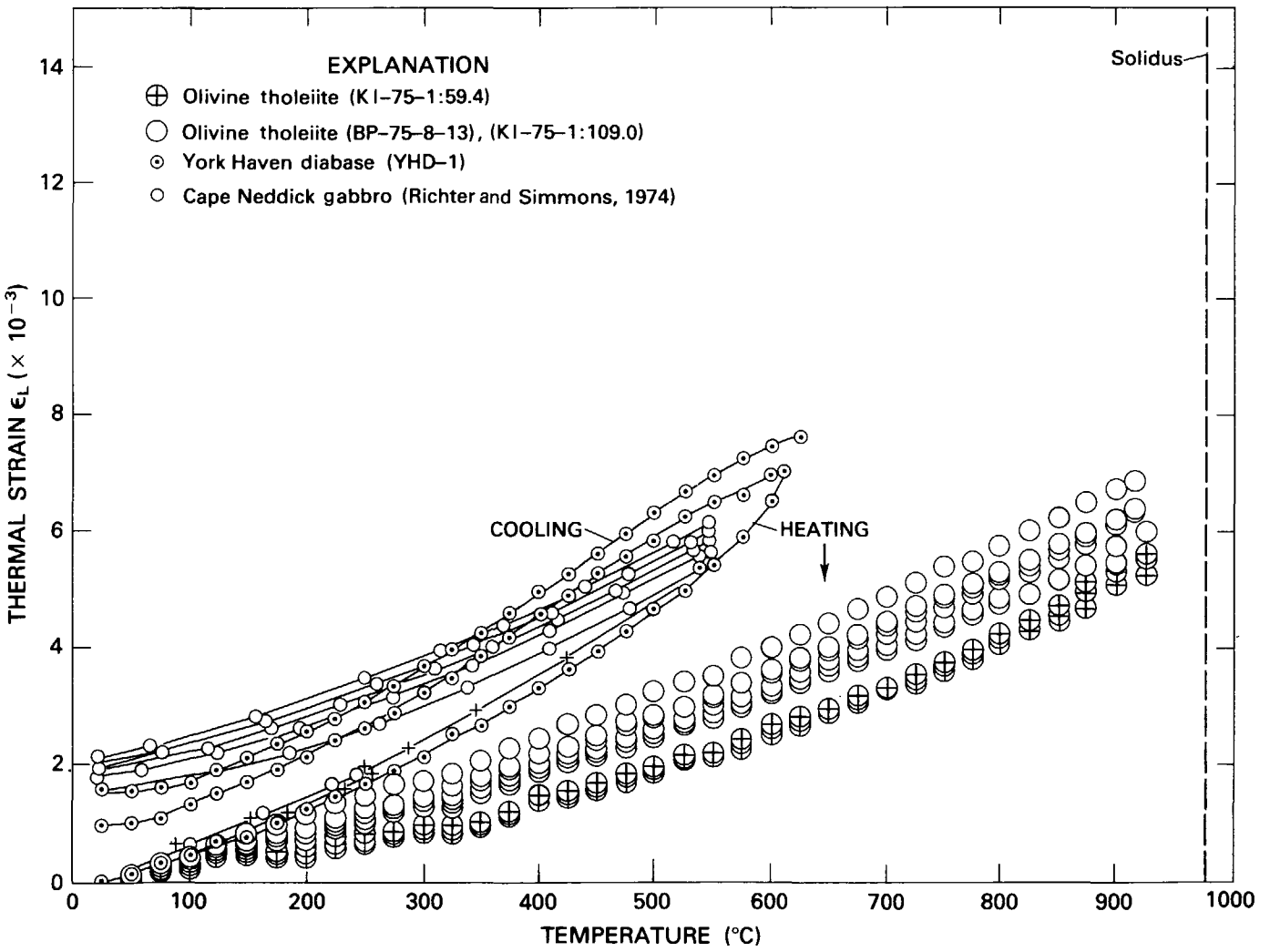

FIGURE 52.8.—Linear strain in olivine tholeiite from Boiling Pots and Kilauea Iki lava lake, Hawaii (open circles from 109-ft level of drill hole KI-75-1 and crossed circles from 59.4-ft level of drill hole KI-75-1). Expansivity has been evaluated from dilatometer measurements made during heating portion of experiment, to minimize contribution of microfractures to α_l. Cyclic runs on York Haven diabase have induced a nonrecoverable strain due to microcracking; this data is superposed on results of Richter and Simmons (1974) for comparison. Each successive cooling cycle has opened a new generation of microfractures, as suggested by progressive temperature-thermal strain hysteresis in heating and cooling curves.

values with the α_l values in table 52.5 shows that the expansivity of Boiling Pots rocks climbs in asymptotic fashion to meet the trend of the model composition. For both the rock and model, expansions from 325 to 700 °C are similar, suggesting that a 300-°C temperature excursion is required for preexisting microcracks to close and the full intrinsic expansivity to become dominant. Above 300 °C, the comparison between the predicted and experimental results is excellent.

CYCLIC EXPANSIVITY AND IRREVERSIBLE THERMAL STRAIN

Experiments have been conducted using cyclic heating and cooling programs, during which the instantaneous sample length has been continuously monitored. These experiments have used the Orton Automatic Recording Dilatometer as configured in the discussion above. In the broadest sense, the experiments have been motivated to develop a qualitative feeling for the ways in which cyclic heating by intrusive bodies (in the near-surface environment) might generate microfractures—of considerable relevance to the discussions in the section "Pressure Dependence of Elasticity in Hawaiian Basalt: Contractancy and Magmatism."

The experiments have been designed to test the following propositions:

(1) For Hawaiian basalt, what are the expansivity effects of cyclic thermal histories?

(2) What proportions of the expansions and contractions are reversible, and how much is irreversible?

(3) What are the mechanical differences in repetitive cycling to the same maximum temperature and in cycling to successively higher temperatures?

(4) Are there essential differences between the cyclic expansivity of porous and nonporous igneous rocks, as exemplified by samples of basalt and diabase?

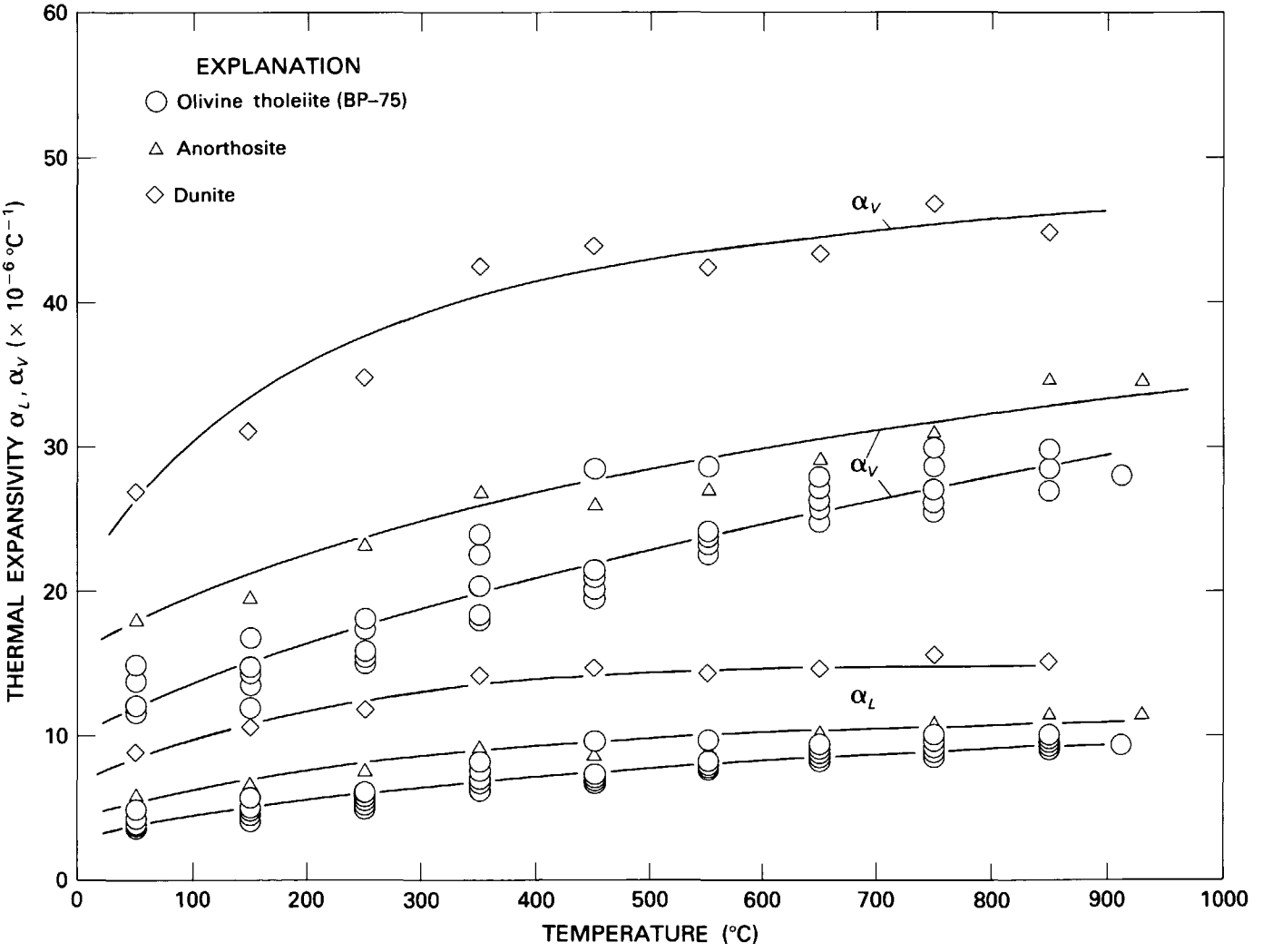

FIGURE 52.9—Linear (α_L) and volume (α_V) thermal-expansion coefficients for olivine tholeiite from Boiling Pots. Dunite and anorthosite expansivities provide comparisons.

Figure 52.10 illustrates the behavior of basalt during a series of heating and cooling cycles to 950 °C. The experiments were performed on olivine tholeiite from the Boiling Pots with a modal mineralogy as shown in table 52.1 and a porosity level of 15 percent. The heating rate was 3 °C min^{-1}, and the cooling rate was determined by the thermal inertia of the furnace at its natural cooling rate. The expansivity-temperature plot has been subdivided into a field of volume increase (as inferred by the sample-length change, in percent) and a field of volume decrease. The line dividing these two fields is the ambient-temperature initial-reference length, l_0. The curves show the following features. (1) The cooling portion of a cycle does not retrace the heating portion but lies beneath it, producing a loop that indicates hysteresis in sample volume and irreversible thermal strain. The separation of the curves at ambient temperature is a measure of the nonrecoverable strain induced within a cycle and between cycles. At the conclusion of cycle 1, the irreversible length change is approximately 0.4 percent, for example. (2) Successive cycles to the same maximum temperature (950 °C) accumulate successive increments of irreversible thermal strain. These increments move continuously in the direction of a net contraction in length. The hysteresis in thermal strain produced by temperature increases and the contraction in sample dimensions that accompanies cooling to ambient temperatures suggest thermally induced changes in the microstructure. Compatible with this behavior is the inferred production of microcracks during heating and the densification induced by the rupture of micropore and vesicle-vesicle bridges (microcrack-induced) during cooling and contraction. The experiments suggest that measurements of elastic moduli taken during heating-cooling cycles would similarly display a hysteresis in behavior—producing, for example, values of K, μ, and E that would not retrack upon

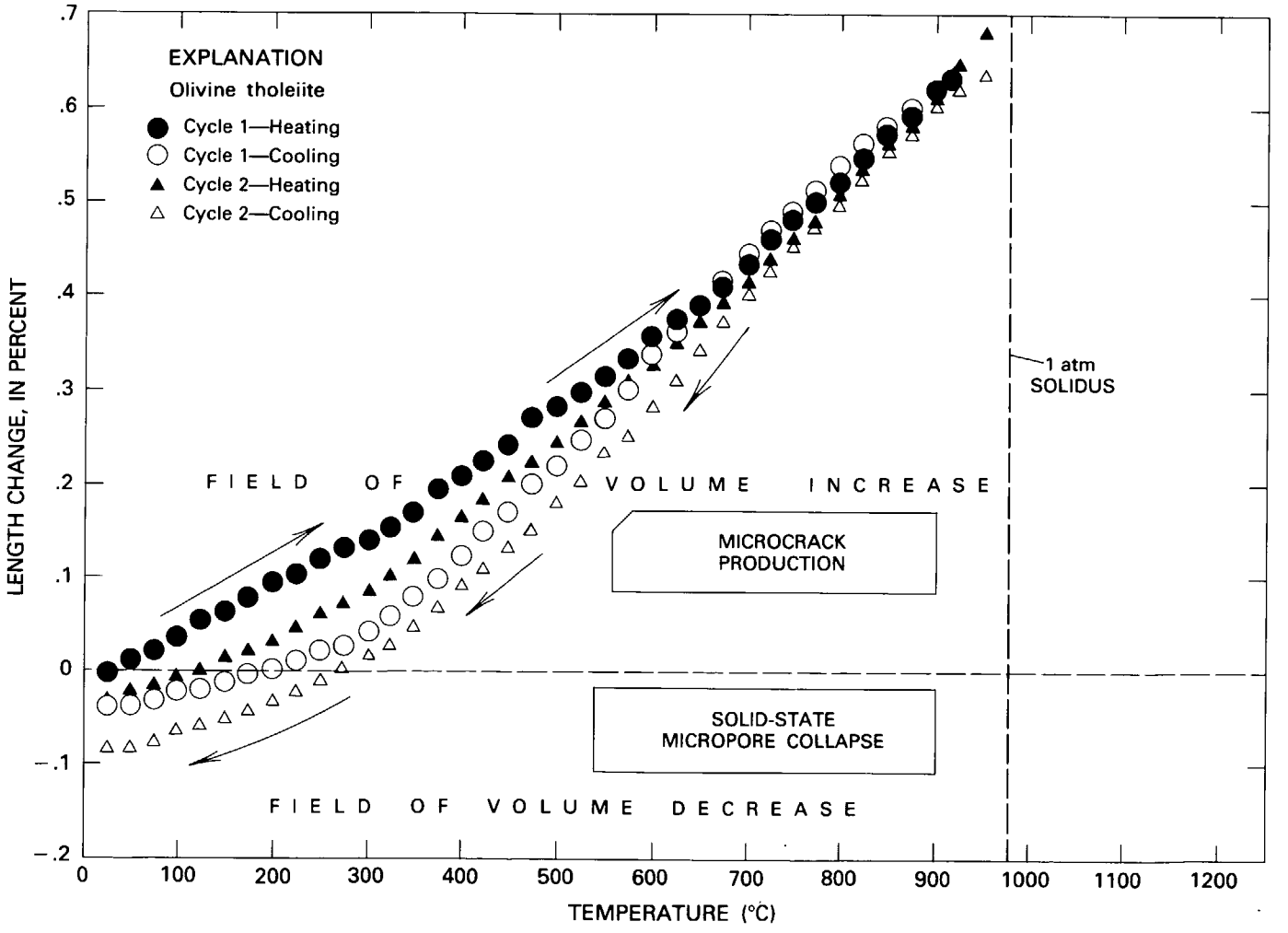

FIGURE 52.10.—Expansivity of Hawaiian olivine tholeiite during cyclic heating and cooling. Solid symbols track change in sample dimensions (length) accompanying heating, whereas open symbols record cooling path within a given cycle. For porous basalt, net effect of cycles to 950 °C, is a reduction in sample length, thus suggesting that microfractures induced during heating have bridged crystal + glass matrix between vesicles, thereby allowing incremental micropore collapse during contraction produced by subsequent cooling portion of a cycle. Contrasting behavior is demonstrated by irreversible length changes produced by microcracking in completely crystalline and nonporous intrusive rocks, as exemplified by diabase in figure 52.11.

cooling those determined during heating. This behavior would qualitatively accord with the results of Ide (1937), who found reductions in the velocity of sound in samples of diabase and norite heated to 700 °C in experiments in which the maximum temperature was raised in successive cycles. Such a program of cyclic elastic-moduli measurements with cooling as well as heating experiments has not been undertaken in this study, and it remains to be determined what, for example, the variance in the Young's modulus or the rigidity induced by, for example, the 0.4-percent change in sample length produced by heating to 950 °C would be after returning the sample to ambient temperature. Note, however, the difference between the net irreversible effects produced in the Ide (1937) samples and those in the olivine tholeiite: the former increasing their dimensions via inferred microcrack production only, and the latter undergoing a decrease in dimension attributed to solid-state densification during micropore collapse. Under confining pressure, we would therefore expect a slight increase in basalt moduli reflecting the sample-volume reduction.

Contrasting with the mechanical behavior exhibited by olivine tholeiite in the heating-cooling cycles is that of diabase, as suggested above. Further evidence of this contrast is provided in figure 52.11, which shows the expansivity of diabase cycled between ambient temperature and 625 °C at a heating rate of 3 °C min^{-1}. As before, thermal-strain/temperature hysteresis loops have been induced by the inferred production of microcracks in the sample during heating. But note the very different signature of this hysteresis: the opening of the loops is produced by an irreversible length increase (consistent with inferred lower elastic moduli), as contrasted with a loop opening

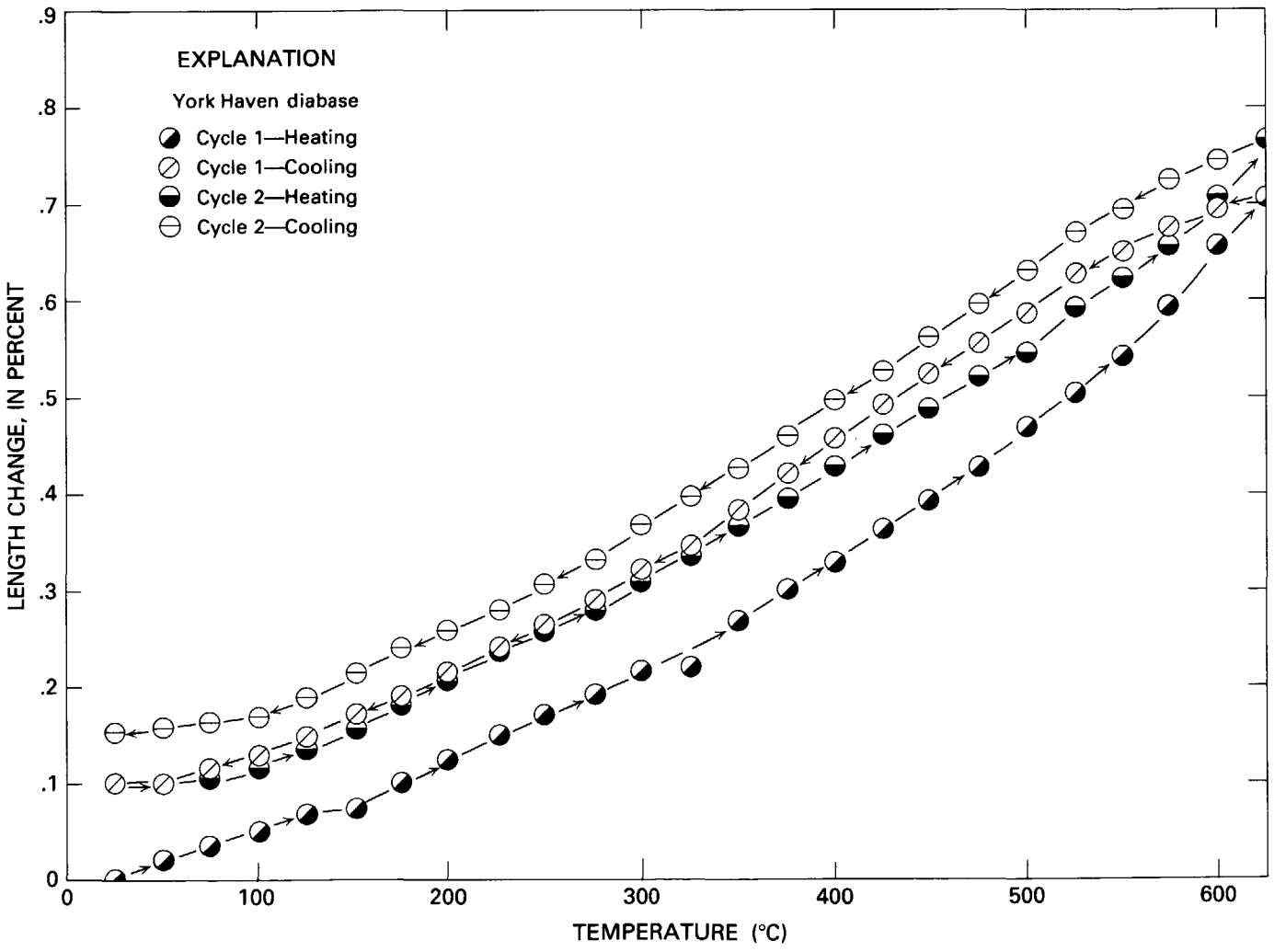

FIGURE 52.11.—Expansivity of diabase during cyclic heating and cooling. Half-filled symbols track change in sample dimensions (length) accompanying heating, whereas open symbols record cooling path within a given cycle. Arrows between data points indicate movement to higher or lower temperatures. For nonporous and holocrystalline intrusives such as diabase, excursions to 625 °C induce microfractures that do not close reversibly upon cooling. Each excursion to high temperatures induces a new generation of microcracks and an additional increment of irreversible dimension change. All cycling is associated with increased sample volume, contrasting with behavior of porous olivine tholeiite (figure 52.10).

induced by length decreases (suggesting higher elastic moduli). Other aspects of the effects of heating-cooling cycles remain qualitatively similar, although the direction in which they move again contrasts with the basalt: successive excursions to high temperature induce progressive increments of irreversible (positive) thermal strain. Thus, sample volumes progressively increase in response to the microstructural changes induced by internal cracking.

Finally, how do the effects of (1) repetitive cycling to the same maximum temperature (T_{max}) and (2) cycling to successively higher values of T_{max} differ? Figure 52.12 draws heavily on the work of Richter and Simmons (1974) and adds to that the results of experiments of type (1) and type (2). For the York Haven diabase, raising the T_{max} to 800 °C (from 610 °C) in three successive increments produces three successive generations of new microcracks and, in turn, three distinctly new levels of thermal strain. On the fifth cycle, the T_{max} is maintained at the same level (800 °C), and, by inference, relatively few new microcracks have been generated, producing only a modest increment of irreversible strain. In an experiment of type (1), the same T_{max} is maintained throughout, producing successive generations of new microcracks with progressively smaller populations. This result accords with the results of Richter and Simmons (1974), who found limiting levels of microstructural damage with large numbers of cycles to the same maximum temperature. In turn, this result suggests that a damage threshold exists that is capable of accommodating successive thermal-deformation cycles through internal shock absorbers made up of assemblages of preexisting microcracks. Accommodating higher levels of thermal strain requires the excursion to significantly higher temperatures, initiating a new round of microcrack production. Simply revisiting the same old T_{max} is insufficient to significantly increase this microcrack population.

MODELING THE HIGH-TEMPERATURE ELASTICITY OF BASALT

In this section, a model for estimating the elastic moduli of basalt is developed. It has been motivated by the desire to construct and apply an approach for computing the ambient and high-temperature moduli, thus providing theoretical guidance for the temperature dependence of the Young's modulus and the rigidity evaluated in the experiments. This modeling therefore forms a complementary companion to the experimental work and has been motivated by the measurements themselves. The primary focus of the modeling is in developing tools for evaluating the temperature dependence of the rigidity ($\mu(T)$) and the Young's modulus ($E(T)$).

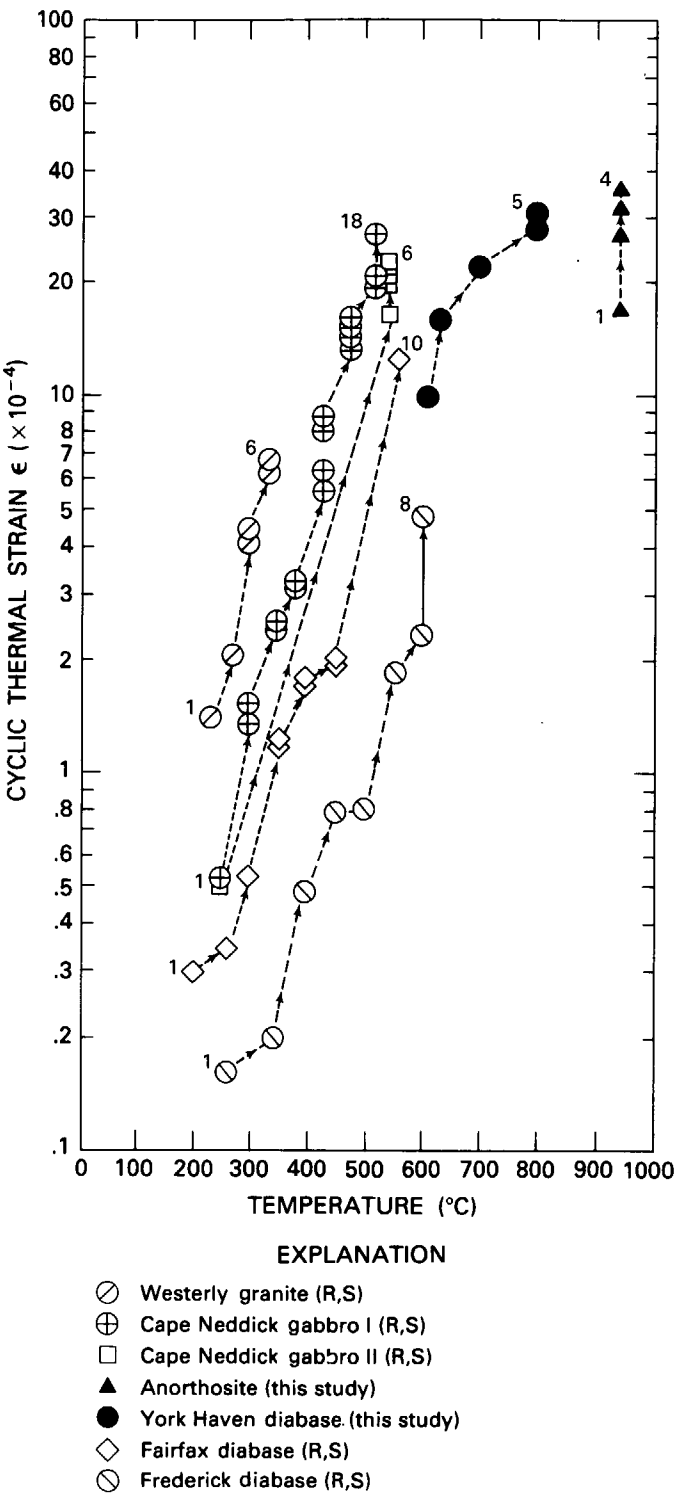

FIGURE 52.12.—Thermal strain-temperature plot of holocrystalline rocks having cyclic heating-cooling thermal histories. Numbers at side of lithologic symbols indicate cycle number within an experimental series; first and last cycle numbers have been labeled. Arrowed pathways indicate temperature (maximum) and correlative thermal strain, through a succession of excursions to high temperatures. For successive cycles to same maximum temperature (symbols line up vertically) relatively small amounts of additional irreversible strain are produced, suggesting diminished production of internal microfractures. Successive excursions to higher levels of temperature (diagonal pathways) induce additional irreversible strain and, by inference, a new generation of thermal microfractures. Samples (Richter and Simmons, 1974) run to maximum temperatures of 600 °C. Experimental comparative runs from the study of Richter and Simmons (1974) are designated (R, S) in the figure explanation.

In the modeling, the temperature range of concern is 25 °C to the solidus for Hawaiian tholeiite (980 ± 5 °C). The rock is assumed to be unconfined, and pressure is not, at this point, a variable. The role of pressure will be discussed in the section "Pressure Dependence of Elasticity in Hawaiian Basalt: Contractancy and Magmatism," with reference to in-situ contractancy.

The model has been divided into two submodels, the first treating compositional effects, and the second one dealing with microstructure. Solids that contain no weakening flaws have elastic properties that are dictated by their composition and their temperature. A compositional model is developed to account for these two contributions to aggregate elasticity. The presence of weakening flaws reduces the moduli that would otherwise result in a pristine solid. A microstructural model has been coupled to the compositional model to account for these effects. Roman numerals have been suffixed to each model to help distinguish one from the other. The compositional model (I) and the microstructural model (II) are shown in figure 52.13.

COMPOSITIONAL MODEL (I)

VOIGT, REUSS, AND HILL AVERAGING SCHEMES AND EFFECTIVE ELASTIC MODULI OF A POLYCRYSTALLINE AGGREGATE

The elastic properties of single crystals of olivine (orthorhombic), augite (monoclinic), and plagioclase (triclinic) are functions of direction within the lattice. To construct a compositional model of basalt elasticity by combining single-crystal elastic data, we need a means of averaging the directional moduli over all orientations and thereby producing a solid that is elastically isotropic in a macroscopic sense. Two averaging methods have been used to effect polycrystalline elasticity from single-crystal data, and they provide, through their assumptions, an upper (Voigt, 1928) and a lower (Reuss, 1929) bound to the aggregate elastic moduli.

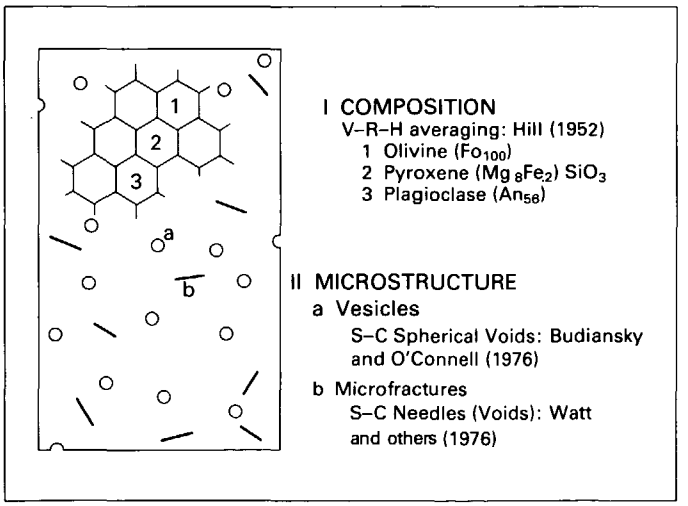

FIGURE 52.13.—Model for high-temperature elasticity of basalt. Compositional submodel I combines contribution of mineral phases (1, 2, 3) to aggregate K, μ, and E by combining single-crystal elastic constants in a Voigt-Reuss-Hill averaging scheme for mixtures. Compositional submodel generates magnitude of modulus and predicts overall temperature dependence by combining temperature derivatives for all component phases. Microstructural submodel II incorporates effects of weakening flaws on moduli. Vesicles (a) formed during posteruption degassing of melt are simulated by spherical voids; microfractures (b) formed between crystals during subsolidus cooling are simulated by needle-shaped voids.

Assuming that the strain distribution in a polycrystalline aggregate was uniform and constant, Voigt (1928) derived an effectively isotropic bulk and shear modulus by averaging the single-crystal stiffnesses over all orientations. This approximation, which requires that the microscopic strain in component grains be equal throughout the matrix and equal to the macroscopic strain of the aggregate, results in a disequilibrium of forces between individual crystals. The bulk modulus (K_V) of Voigt (1928) is expressed in terms of the single-crystal elastic-stiffness coefficients, C_{ij},

$$K_V = 1/9[(C_{11}+C_{22}+C_{33})+2(C_{12}+C_{23}+C_{13})], \quad (24)$$

whereas the rigidity (μ_V) is given by

$$\mu_V = 1/15[(C_{11}+C_{22}+C_{33})-(C_{12}+C_{23}+C_{13}) + 3(C_{44}+C_{55}+C_{66})]. \quad (25)$$

Assuming that the stress distribution in the aggregate was uniform and constant, Reuss (1929) derived an effectively isotropic bulk and shear modulus by averaging single-crystal compliances over all orientations. This approximation, which requires that the microscopic stresses between component crystals be equal throughout the matrix and equal to the macroscopic stress, produces distorted grains that no longer fit together (that is, compatibility is violated).

The bulk modulus (K_R) derived by Reuss (1929) is in turn expressed in terms of the single-crystal elastic-compliance coefficients, S_{ij},

$$\frac{1}{K_R} = [(S_{11}+S_{22}+S_{33})+2(S_{12}+S_{13}+S_{23})], \quad (26)$$

and the rigidity (μ_R) by

$$\frac{1}{\mu_R} = 4/15[(S_{11}+S_{22}+S_{33})-(S_{13}+S_{12}+S_{23}) + 3/4(S_{44}+S_{55}+S_{66})+S_{33}]. \quad (27)$$

Hill (1952) has demonstrated that the Voigt and Reuss moduli are, in fact, upper and lower bounds on K and μ—a result of the assumptive extremes of constant strain and stress, respectively. Hill suggested that a more appropriate measure of aggregate elasticity would lie between these extremes and proposed using an average of the Voigt and Reuss schemes. This intermediate measure is known as the V-R-H average (or simply the Hill average) and is given by

$$K_{VRH} = 1/2(K_V + K_R) \quad (28)$$

and

$$\mu_{VRH} = 1/2(\mu_V + \mu_R). \quad (29)$$

The separation between the Voigt and Reuss bounds for an aggregate is thus a measure of the crystal anisotropy within the aggregate, and $K_V = K_R = K$ for an elastic isotropic substance.

STRUCTURE OF THE COMPOSITIONAL MODEL

The high-temperature bulk modulus and shear modulus for the polyphase mixture, given by Graham and Dobrzykowski (1976), are

$$K(T) = K(25) + \left(\frac{\partial K}{\partial T}\right)\Delta T, \tag{30}$$

and

$$\mu(T) = \mu(25) + \left(\frac{\partial \mu}{\partial T}\right)\Delta T, \tag{31}$$

where $\Delta T = (T - 25)$ in degrees Celsius.

To compute the upper and lower bounds on (30) and (31), the Voigt-averaged and Reuss-averaged moduli for a polyphase mixture are applied.

The upper and lower bounds on the temperature derivatives of the bulk modulus and the shear modulus are computed by applying the appropriate relations for a polyphase mixture.

The Hill-averaged moduli are then evaluated from the averages of the upper and lower bounds for the mixture:

$$K(T)^{\mathrm{MIX}}_{\mathrm{VRH}} = \tfrac{1}{2}[K(T)_V + K(T)_R], \tag{32}$$

and

$$\mu(T)^{\mathrm{MIX}}_{\mathrm{VRH}} = \tfrac{1}{2}[\mu(T)_V + \mu(T)_R]. \tag{33}$$

For an evaluation of the Young's modulus (E) at high temperatures, the standard relation (for example, Birch, 1960) is used:

$$E(T)^{\mathrm{MIX}}_{\mathrm{VRH}} = \frac{9K(T)^{\mathrm{MIX}}_{\mathrm{VRH}} \cdot \mu(T)^{\mathrm{MIX}}_{\mathrm{VRH}}}{3K(T)^{\mathrm{MIX}}_{\mathrm{VRH}} + \mu(T)^{\mathrm{MIX}}_{\mathrm{VRH}}}. \tag{34}$$

For high-temperature upper and lower bounds on the Young's modulus, $K(T)_{\mathrm{VRH}}$ and $\mu(T)_{\mathrm{VRH}}$ in (34) are replaced by $(K(T)_V, \mu(T)_V)$ and $(K(T)_R, \mu(T)_R)$, respectively.

COMPOSITIONAL SUBMODELS

The compositional model employs olivine, clinopyroxene, and plagioclase as matrix components. Three compositional submodels have been formed by varying the volume fractions of component minerals. These submodels are referred to as submodel 1, submodel 2 and submodel 3, and their volume fractions are listed in table 52.6.

Submodel 3 was intended to represent an average basalt, whereas submodels 1 and 2 were intended to represent compositional bounds on basalt elasticity by employing relatively pyroxene-rich (hard matrix) and plagioclase rich (soft matrix) mineralogies. It is expected that submodels 1 and 2 would provide upper and lower bounds on aggregate elastic moduli. They enclose the elastic behavior of a submodel 3 aggregate.

TABLE 52.6.—*Compositional submodels for basalt elasticity*

[Values represent volume fractions]

Component	Submodel 1	Submodel 2	Submodel 3
Olivine Fo_{100}	0.10	0.10	0.10
Pyroxene $(Mg_{0.8}Fe_{0.2})SiO_3$	.60	.20	.45
Plagioclase An_{56}	.30	.70	.45

OLIVINE

Olivine has been incorporated in the model by using the zero pressure, 298 K elastic stiffness and compliance coefficients of forsterite and the temperature derivatives of the bulk modulus and rigidity as reported by Graham and Barsch (1969) and presented by Graham (1969).

PYROXENES

The contribution of pyroxene employs the zero-pressure, 298 K data of Ryzhova (1964) for augite. These data permit pyroxene to be included in aggregate moduli calculations for ambient temperature. Temperature derivatives of the elastic coefficients for augite are not available. For high-temperature calculations, the temperature derivatives for the orthopyroxene bronzite, $(Mg_{0.8}Fe_{0.2})SiO_3$, have been used (Frisillo, 1972).

PLAGIOCLASE

The role of plagioclase in basalt elasticity has been incorporated by employing the results of Aleksandrov and others (1964) as reported for the zero pressure moduli of An_{56} evaluated at 298 K. Data on the temperature dependence of the elastic constants for the plagioclase feldspars is virtually nonexistant. An approximation of this dependence is therefore required. The relatively open structure of α-quartz suggests that the temperature derivatives of the elastic moduli of its framework may approximate the temperature induced changes in the open framework of plagioclase (E.K. Graham, oral commun.). This substitution has been adopted.

The Voigt- and Reuss-averaged bulk and shear moduli for An_{56} based on the Aleksandrov and others (1964) data and reported in Simmons and Wang (1971) are listed in table 52.7.

MICROSTRUCTURAL MODEL (II)

The primary modulus-reducing agents in a basalt microstructure are vesicles and thermally induced microcracks. Though expressions are provided for incorporating both vesicles and microfractures (where needle shaped), the primary objective has been to simulate the effect of vesicles in weakening the otherwise pristine solid. Thin-section petrography and scanning-electron microscopy has demonstrated that vesicles account for most of the porosity in basalt. Including the mechanical effects of vesicles and microcracks in basalt elasticity has been accomplished by incorporating approximations for the elastic contributions of spherical voids and needle-shaped voids by making use of the self-consistent approximation of Hill (1965) and Budiansky and O'Connell (1976), as presented by Watt and others (1976).

TABLE 52.7.—*Compositional-model input properties and derived interim Voigt and Reuss bulk moduli and rigidities*

[Reference in parentheses]

Parameter	Fo_{100}		Augite		An_{56}		Units
V_i	43.79	(2)	66.09	(4)	100.52	(2)	$cm^3\ mol^{-1}$
ρ_i	3.221	(1)	3.320	(5)	2.69	(7)	$g \cdot cm^{-3}$
M_i	140.708	(2)	216.56	(4)	272.44	(2)	$g \cdot mol^{-1}$
K_i^V	1,311.9	(1)	1,048.0	(5)	753	(7)	kbar
K_i^r	1,268.8	(1)	1,021.0	(5)	688	(7)	kbar
μ_i^v	831.8	(1)	754.8	(5)	370	(7)	kbar
μ_i^r	801.9	(1)	738.9	(5)	317	(7)	kbar
α_i^p	24.65×10^{-6}	(1)	47.7×10^{-6}	(6)	12×10^{-6}	(8)	$°C^{-1}$
$(dK/dT)_V^s$	−0.173	(1)	−0.275	(3)	−0.10	(9)	kbar $°C^{-1}$
$(dK/dT)_R^s$	−0.178	(1)	−0.261	(3)	−0.10	(9)	kbar $°C^{-1}$
$(d\mu/dT)_V$	−0.134	(1)	−0.120	(3)	−0.015	(9)	kbar $°C^{-1}$
$(d\mu/dT)_R$	−0.138	(1)	−0.119	(3)	−0.015	(9)	kbar $°C^{-1}$

(1) Graham (1969); Graham and Barsch (1969).
(2) Robie and Waldbaum (1968).
(3) Frisillo (1972) values for bronzite.
(4) Robie and Waldbaum (1968) values for diopside.
(5) Aleksandrov and others (1964) data for augite.
(6) Frisillo and Buljan (1972) data for bronzite.
(7) Ryzhova (1964) data for labradorite.
(8) Skinner (1966) data for An_{95} at 20 °C.
(9) V-R-H averaged values for α-quartz from Anderson and others (1968).

SELF-CONSISTENT TREATMENT

Kröner (1958, 1967) expressed the aggregate moduli of an elastic, isotropic polyphase solid in terms of the individual moduli and individual strains of each component, summed over all included phases and added to the moduli of the matrix. Approximating the strain occurring in an isolated inclusion of the ith material embedded in an infinite (and otherwise homogeneous) elastic matrix subject to pure loading (compressive or shear) at infinity and having the as-yet-to-be-determined elastic constants of the total aggregate led to the first self-consistent approximation.

Budiansky (1965) has combined the Kröner (1958, 1967) approach with the exact results of Eshelby (1957), who demonstrated that the strain state of an inclusion in a matrix sheared at infinity is uniform, to derive coupled, implicit expressions for the effective elastic constants of heterogeneous solids. In the Budiansky approach, the exact Eshelby results are used as estimators of the average shear strain in each phase, which, when coupled to the Kröner aggregate moduli expressions, leads to simultaneous equations for the effective shear and bulk moduli in terms of constituent moduli.

STRUCTURE OF THE MICROSTRUCTURAL MODEL

For a two-phase aggregate, the self-consistent approximation for the effective modulus Watt and others, 1976) may be expressed as

$$\frac{M^*-M_1}{M_2-M_1}=V_2\left[1+\frac{V_1(M_2-M_1)}{M_1+f}\right]^{-1}, \qquad (35)$$

where M^* is the effective modulus of the total aggregate (K^* or μ^*), M_1 is the modulus (K_1, μ_1) of the included phase, M_2 is the modulus of the matrix (K_2, μ_2), V_1 is the volume fraction of the included phase, V_2 is the volume fraction of the matrix, and f is a function that is dependent on the moduli of the included phase as well as on the effective aggregate moduli (though not necessarily at the same time). The two phases are (1) voids and (2) matrix. Note that the matrix itself is actually polycomponent and polycrystalline.

The approximation for spherical inclusions of the minor phase is given by (35), such that for effective bulk modulus

$$K^*: \quad f=\tfrac{4}{3}\mu^*, \qquad (36)$$

and for effective rigidity

$$\mu^*: \quad f=\frac{\mu^*(9K^*+8\mu^*)}{6(K^*+2\mu^*)}. \qquad (37)$$

In this treatment, the included phase is the vapor phase that occupies spherical vesicles and is described by $K_1=0$; $\mu_1=0$. The finite bulk modulus and rigidity of the matrix is solely a function of the modal percentage of the component mineralogy (that is, submodel 1, 2, or 3).

The expressions for aggregate moduli are coupled (nonseparable) and are solved by an iterative computational procedure. In general, four to five iterations were satisfactory for convergence, and in no case has more than ten iterations been required.

The approximation for needle-shaped inclusions of the minor phase is given by (35), such that for the effective bulk modulus

$$K^*: \quad f=\tfrac{1}{3}\mu_1+\mu^*. \qquad (38)$$

and for the effective rigidity

$$\mu^*: \quad f=\frac{5}{\dfrac{1}{3(K_1+\frac{1}{3}\mu_1+\mu^*)}+\dfrac{2(2\mu_1+\mu^*+G)}{(\mu_1+\mu^*)(\mu_1+G)}}-\mu_1, \qquad (39)$$

where

$$G=\frac{\mu^*(K^*+\frac{1}{3}\mu^*)}{K^*+\frac{7}{3}\mu^*} \qquad (40)$$

and μ_1, μ^*, K_1, and K^* have been defined above.

The approximation employs air as the included minor phase that occupies the microcracks that open during cooling, and accordingly, $K_1=0$; $\mu_1=0$.

As in the case for spherical inclusions, the microcrack approximations (needles) are solved iteratively for K^* and μ^*. Convergence rates are comparable to the vesicle approximations.

Flat microcracks have not been explicitly considered, but their incorporation is straightforward (see O'Connell and Budiansky, 1974; Watt and others, 1976).

The results of the combined predictions of the compositional model (I) and microstructural model (II) are presented and discussed below, in light of measured $E(T)$, $\mu(T)$, levels of absolute porosity, and compositional details for Hawaiian basalt.

ELASTIC MODELS AND ELASTIC MEASUREMENTS

The $\mu(T)_{VRH}$ for compositional submodels 1, 2, and 3 are presented and compared in figure 52.14. Compositional submodel 3 has the mineralogy that most closely resembles an average basalt composition, as contrasted with submodels 1 and 2, and thus

submodel 3 should be compared with the data. The nonporous moduli are given by solid lines of different weight that correspond to the dashed (porous) moduli for the appropriate model. For a given composition, all five curves ($\phi = 0$, 0.05, 0.10, 0.15, and 0.20) are parallel, indicating no computed porosity-temperature interaction. This relation accords with what one would expect, because porosity has been shown to have a negligible effect on thermal expansivity in solids (Coble and Kingery, 1956). The rapid inflexion of the E(T) curves for the data of Wingquist (1971) suggests that dehydration was occurring in the alteration minerals of their samples over the range 500–700 °C. The samples of Murase and McBirney (1973) and Iida and Kumazawa (1960) did not have a reported characterization that permits an evaluation of the reason(s) they do not exhibit a linear temperature dependence.

The $\mu(T)_{VRH}$ for compositional submodel 3 is shown in figure 52.15, and the evaluated rigidities of the Boiling Pots replicates are indicated by the crossed circles. Using an average value of ϕ for the entire range of measured porosities gives $\phi = 0.166$. This average is a difference of approximately 3.4 percent porosity based on the magnitude of the predicted and measured ambient-temperature rigidity and the corresponding porosity levels.

The distance between the Voigt- and Reuss-averaged bounds for a nonflawed solid (K_1, μ_1, K_2, and μ_2 are finite) is a measure of the differences in moduli for the single-crystal components. The

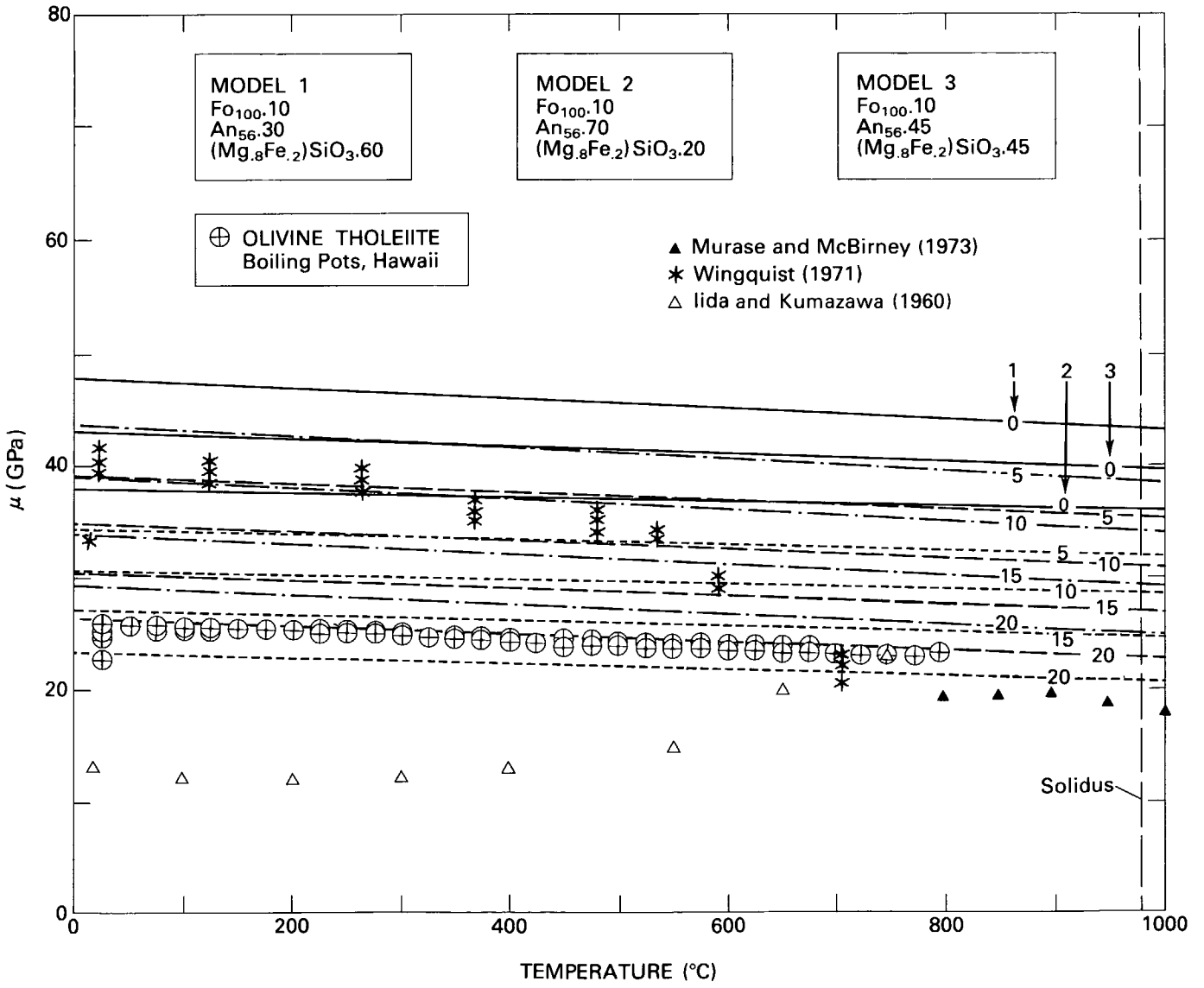

FIGURE 52.14.—Predicted high-temperature, ambient-pressure rigidity for three model basalts (see table 52.6) and rigidity of olivine tholeiite from Boiling Pots. Trends of compositional models without porosity ($\phi = 0$; labeled with 0) are represented by solid lines. Trends of compositional models with varying levels of porosity (labeled 5, 10, 15, 20) are represented by dashed lines for $\phi = 0.05$, $\phi = 0.10$, $\phi = 0.15$, and $\phi = 0.20$ volume fractions of spherical voids, respectively. Bronzite simulates temperature dependence of pyroxenes. Available literature data are included.

V-R-H bounds for the matrix,evaluated at a level of zero porosity, are shown in figure 52.5. This figure illustrates the mineralogical contributions to the model aggregate elasticity.

The Hill-averaged Young's moduli for compositional submodel 3 are presented in figure 52.6 for porosity levels (spherical voids) to $\phi = 0.20$. In addition, the effect of microcracks at dilute concentration are shown (needle-shaped voids) for $\phi = 0.01$. The separation between lines D and E was produced by microcrack additions to an aggregate that already contained 15 percent spherical pores. This addition of microcrack effects produced an additional 1.8-GPa (18-kbar) decrement.

For the temperature-dependent Young's modulus ($E(T)$) replicates evaluated from flexural-frequency measurements of Boiling Pots basalt, the average volume-fraction absolute porosity is $\phi = 0.15$. This value is approximately a 5-percent difference between the porosity value expected, assuming a submodel 3 composition with purely spherical voids, and the determined value.

The temperature dependence of the Hill-averaged bulk modulus, shear modulus, and Young's modulus is presented in table 52.8 for submodel compositions 1, 2, and 3. The highest temperature dependence (largest absolute value) of the moduli on a collective basis is for the pyroxene-rich submodel 1 and is reflective of the relatively large adiabatic temperature derivative of the bulk modulus ($(\partial K/\partial T)^{S}_{VRH}$) value for bronzite ($-26.8$ MPa/ °C) and, in turn, the relatively high volume thermal expansivity of augite (47.7×10^{-6} °C^{-1}). Plagioclase-rich submodel 2 shows the lowest

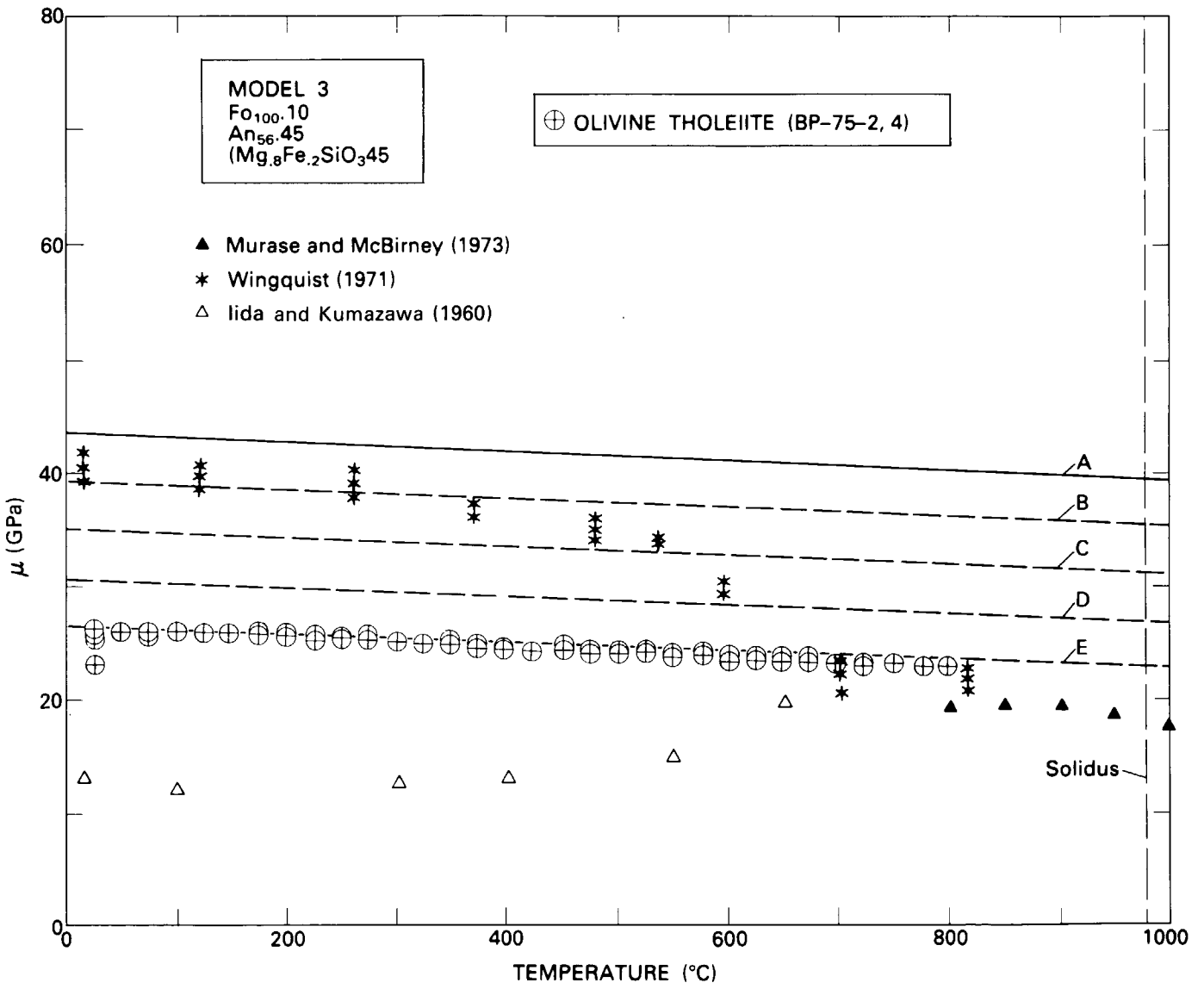

FIGURE 52.15.—Predicted high-temperature, ambient-pressure V-R-H rigidities and matrix Voigt and Reuss bounds on rigidity for compositional submodel 3. Measured rigidity of Boiling Pots olivine tholeiite, crossed circles. Differences between measured and predicted rigidities probably result from iron oxide minerals and intercrystalline glass that have not been incorporated in submodel.

TABLE 52.8.—*Comparison of the temperature dependence of the elastic moduli from the compositional model (1) at $\Phi = 0$ and the measured dynamic rigidity and Young's modulus for olivine tholeiite of Boiling Pots*

	$(\partial K/\partial T)_{VRH}$ (MPa/°C)	$(\partial \mu/\partial T)_{VRH}$ (MPa/°C)	$(\partial E/\partial T)_{VRH}$ (MPa/°C)
Compositional submodel:			
1	−15.31	−4.47	−13.13
2	−11.28	−2.34	−7.32
3	−13.30	−3.39	−10.23
Boiling Pots olivine tholeiite measurements		−3.5[1] −4.2[2] −3.8[3]	−8.5[4] −8.1[5] −8.3[6]

Sample designation:
(1) BP-75-R2(G)
(2) BP-75-R4(G)
(3) BP-75-R2(G)+R4(G)
(4) BP-75-R6 ..... $\Phi = 0.15$
(5) BP-75-R1 ..... $\Phi = 0.15$
(6) BP-75-R6+R1 ..... $\Phi = 0.15$

temperature dependence of K, μ, and E, and the average basalt (submodel 3) lies between 1 and 2 in temperature dependence.

The temperature derivatives for the rigidity and Young's modulus of Hawaiian olivine tholeiite have been generated by the least-squares regression procedure. These derivatives are presented in the lower portion of table 52.8 and may be compared with the model derivatives. In the table, the entries for both $\partial\mu/\partial T$ and $\partial E/\partial T$ of samples BP-75-R2(G), -R4(G), -R6, and -R1 are replicates, whereas the other sample entries are derivatives that were formed via least-squares regression on the averaged-value data set.

Comparison of the model and measured rigidity values in table 52.8 shows that submodel 3 with plagioclase contents of 45–50 percent provides a close approximation to the modulus reduction with temperature of the Boiling Pots olivine tholeiite.

Differences between moduli magnitudes predicted using compositional submodels plus microstructural modeling and those magnitudes evaluated by resonant-frequency measurements are believed to arise from the following sources:

(1) Opaque and glass-filled minor inclusions in olivine, hypersthene, augite, and plagioclase phenocrysts and microphenocrysts;

(2) Groundmass magnetite and opaque-rich groundmass glass pockets that have not been incorporated in the model; and

(3) Subtle differences in the elastic properties of matrix crystals versus model crystals that may arise from (a) compositional zoning and defects in olivine and (or) defects in pyroxene and in labradorite, or (b) unrelieved thermal strains in crystal lattices, induced by posteruption chilling.

For all moduli, the measured values lie between the pyroxene-rich and plagioclase-rich upper and lower values. That is,

$$(\partial\mu/\partial T)_{VRH}^{\text{model 1}} > (\partial\mu/\partial T)_{\text{measured}} > (\partial\mu/\partial T)_{VRH}^{\text{model 2}}$$

and

$$(\partial E/\partial T)_{VRH}^{\text{model 1}} > (\partial E/\partial T)_{\text{measured}} > (\partial E/\partial T)_{VRH}^{\text{model 2}}.$$

These relations hold for both the average of the measured values and for each of the replicates. This bounding behavior of the Hill-averaged models accords with the expected behavior, recalling that the modal abundance of all pyroxene species in the Boiling Pots basalt was 32.9 percent, whereas the total of groundmass and microphenocryst plagioclase content is 37.3 percent and olivine totals 12.4 percent.

THE PRESSURE DEPENDENCE OF ELASTICITY IN HAWAIIAN BASALT: CONTRACTANCY AND MAGMATISM

This section, which discusses the pressure dependence of elasticity in Hawaiian rocks, complements the discussion of the major sections of this paper on variations in elasticity and expansivity, which are temperature dependent. Focus is placed on the implications these rock properties have for the mechanical controls on magmatic storage regions within active shield volcanoes; both subcaldera reservoirs and their rift systems are considered. Underlying the discussion are the influences of microstructure, microcracks, and composition as previously developed. A major conclusion of this section is that the pressure dependence of elasticity in the rocks of shield volcanoes affects their in-situ behavior in ways that lead naturally to spatial domains of magmatic stability. Ramifications include (1) density crossovers in the in-situ country rock and magma; (2) a rationale that unifies the observed seismic-velocity variations within and beneath Hawaiian shields, experimentally determined rock properties, and the massive dilatancy associated with the free surface of the Earth in regions of active volcanism; and (3) the mechanical rationale for the long-held inference that Hawaiian magma reservoirs move progressively upward during their life cycle.

Studies of the mechanics of magmatic fluids, rock-fluid mixtures, and the deformation accompanying injection and withdrawal with relevance to regions of active volcanism have been approached from six viewpoints: (1) in-situ density contrasts between melt and country rock within mantle and crustal sections (Waff, 1980; Stolper and others, 1981; Grove and Baker, 1983; Herzberg and others, 1983; Sparks and Huppert, 1984), with emphasis on the distribution in and separation from the mantle source region, and the role of fractional crystallization on melt density; (2) wholesale diapiric rise with concurrent decompression melting (Ramberg, 1981); (3) continuum solutions of hydraulic fracture stability and fluid-induced deformation (Weertman, 1971a, b; Johnson and Pollard, 1973; Pollard, 1976; Pollard and Muller, 1976; Weertman and Chang, 1977; Pollard and Holzhausen, 1979; Weertman, 1980; Ryan and others, 1983; Spence and Turcotte, 1985); (4) reviews and syntheses of the effective-stress principle (Shaw, 1980; Gold and Soter, 1985); (5) thermodynamic analyses in combination with the wetting mechanics of basaltic melts (Waff and Bulau, 1979; Bulau and others, 1979; Waff, 1979, 1980); and (6) fluid-dynamic and fluid-static analyses of incompressible single-phase (Shaw and Swanson, 1970; Vogt, 1974; Solomon, 1975; Fedotov, 1977a, b, c), incompressible multiphase (Sleep, 1974; McKenzie, 1984), and compressible multiphase fluids (Wilson and Head, 1981). In a different vein, but of relevance to the following discussion, is the work of Eaton and Murata (1960) and Fiske and Jackson (1972), who respectively computed equilibrium heights expected for

Hawaiian volcanoes and emphasized the importance of gravitational stresses in the development of Hawaiian rift zones.

In its conceptual development, the discussion that follows differs from these studies in the following ways:

(1) The focus of attention on the free surface of the Earth, with particular emphasis on the heterogeneous distribution of material properties, and the nonlinear mechanical behavior exhibited by rocks as the surface is approached;

(2) The evolutionary consequences that derive for magmatic bodies as the Earth's free surface is progressively translated upward—an explicit consideration of the evolutionary track followed by shield volcanoes within a magmatic province, as they mature and age;

(3) An integration of the confining pressure behavior of shield volcanoes, with their geodetic, seismic, density (gravitational), lithologic and structural characteristics, providing guidelines, constraints and tests for internal consistency; and

(4) An exploration of the three-dimensional structure of the resulting contractancy concept, and its implications.

The discussion can be started by posing a series of related questions. What are the controls on the stability of magmatic bodies at depth? What are the roles of open, partially contracted, and fully contracted fractures in these environments? Can the recurring themes of intrusion-eruption and the drainback of lava within rift systems be understood within a context of vertical changes in macroscopic and microscopic fracture closure, as these affect the bulk density of a volcanic shield and interact with the density of magma at depth? The thrust of the discussion then lies in the confining-pressure dependence of the mechanical properties of shield volcanoes. A set of general relations can be developed by the study of well-characterized volcanoes in Hawaii, especially Kilauea and Mauna Loa.

PHENOMENOLOGY OF CONTRACTANCY

The bulk compressibility of the subsolidus volcanic shield may be expressed as follows:

$$\beta_{VS} = \beta_M + \beta_{MS} + \beta_{PF} + \beta_F, \tag{41}$$

where β_{VS} is the volanic-shield compressibility, β_M is the mineral phase compressibility, β_{MS} is the microstructure compressibility that combines contributions from vesicles and microcracks, β_{PF} is the pore-fluid compressibility, and β_F is the macroscopic fracture compressibility.

For tholeiitic shield volcanoes, the mineral-phase compressibility is built up from the individual compressibilities of olivine, clinopyroxene, orthopyroxene, and plagioclase, with subordinate contributions from magnetite, ilmenite, and apatite. In general terms, the largely tholeiitic shield will have compressibilities dominated by the volumetrically important mineral species: olivine, clinopyroxene, and plagioclase. The magnitude of this contribution will then scale with the weighted volume fraction of each component.

The total compressibility of large volumes of the shield may now be divided into two contributors: intrinsic and extrinsic. Laboratory studies evaluate the intrinsic contributors, and the separation of single-crystal acoustic-velocity studies and whole-rock studies provides a means of sorting out the crystalline and microstructural contributions. The extrinsic contribution is provided by the large fractures within the shield. These fractures are the dilatant cracks and fissure networks that intersect the free surface of the volcano. They define the bounding planes of rift-zone graben and may be exploited by rising magma during intrusion and eruption sequences. Seismic velocity studies carried out over major segments of a shield then sample the total compressibility. The evaluation of the bulk modulus of portions of the shield then yields a means of recovering the relevant in-situ compressibility—summed for each major contributor above.

Contractancy, in the sense used here, can be viewed as a mechanically opposite effect of dilatancy. It is reflected in the progressive reduction in volume of an element of rock that contains minerals, microcracks, macroscopic joints and fractures, equant pores, and saturating pore fluids, as this conceptual element is subjected to continuously increasing confining pressures. The phenomenon, within the context of magmatic systems, is dominated by the progressive closure of macroscopic fractures and joints, and microscopic fractures with depth. This closure is viewed as a progressive elimination of the extrinsic contributors to bulk compressibility. It is a realization that very nonlinear effects dominate the mechanical behavior of rocks as the surface of the Earth is approached. These effects are well exemplified by the pressure dependence of V_p and V_s in both the laboratory studies and field-derived seismic-velocity profiles. Contractancy may be contrasted with dilatancy, which is an inelastic volume increase under applied loading (Brace and others, 1966; Schock and others, 1973). Such volume increases lead to decreases in the ratio V_p/V_s (Whitcomb and others, 1973; Wyss and Holcomb, 1973) and begin at approximately one-half to two-thirds the fracture strength of the rock.

Evaluations of the compressional and shear wave velocities of rocks, from the transit times of acoustic waves in laboratory samples, provide the means of assessing the microstructural and mineralogical contributions to contractancy. The pressure dependence of V_p for the dominant lithologies of Hawaiian volcanoes is summarized in figures 52.16, 52.17, and 52.18. These lithologic types represent their tholeiitic shields, alkalic and nephelinitic interlayers and caps, intrusive complexes, olivine-rich cumulates, and the mafic and ultramafic rocks of their oceanic crustal and upper-mantle foundations. In each of the figures, the pressure dependence of V_p, $\partial V_p/\partial P$, shows the two types of behavior: an early, highly nonlinear dependence extending from 0 to 200 MPa (2 kbar), and a generally linear regime starting at about 200 MPa and extending to higher pressures. Studies of holocrystalline rocks (Todd and Simmons, 1972), as well as of porous lithologies (King, 1966), have attributed this change in wave velocity to the progressive closure of microcracks within the rock matrix. This microfracture closure—or contractancy—produces the early rapid rise in V_p and V_s characteristic of the low-pressure shallow environment. The generally linear change in wave velocity above 200 MPa is produced by the compressibility of the minerals within the matrix.

CONTRACTANCY WITHIN SHIELD VOLCANOES

Several lines of evidence suggest that the superstructure of Hawaiian shield volcanoes contain dilatant fractures and that these open fractures extend to considerable depths. The evidence includes:

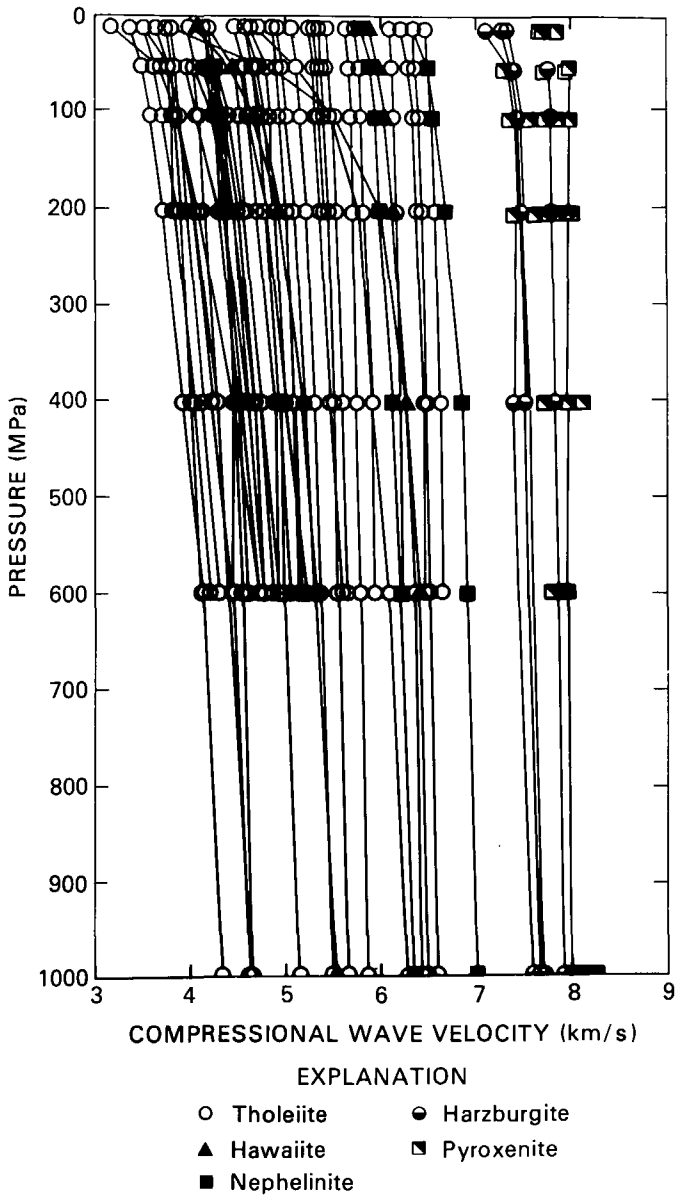

FIGURE 52.16.—Pressure dependence of compressional-wave velocities (V_p) in tholeiitic, alkalic, and nephelinitic basalt and in ultramafic lithologies composing upper-mantle underpinnings of Hawaiian volcanoes. Of particular interest is nonlinear behavior of V_p at confining pressures below 200 MPa, which is produced by progressive elimination of microfractures with continued pressure increases. Data compiled from Bajuk and others (1957), Manghnani and Woollard (1968), Christensen and Salisbury (1972, 1973), Christensen (1973, 1976, 1978), Fox and others (1973), Fox and Schreiber (1973), Christensen and others (1974a, b), Schreiber and others (1974), Hyndman (1976), Kroenke and others (1976), and Salisbury and Christensen (1976).

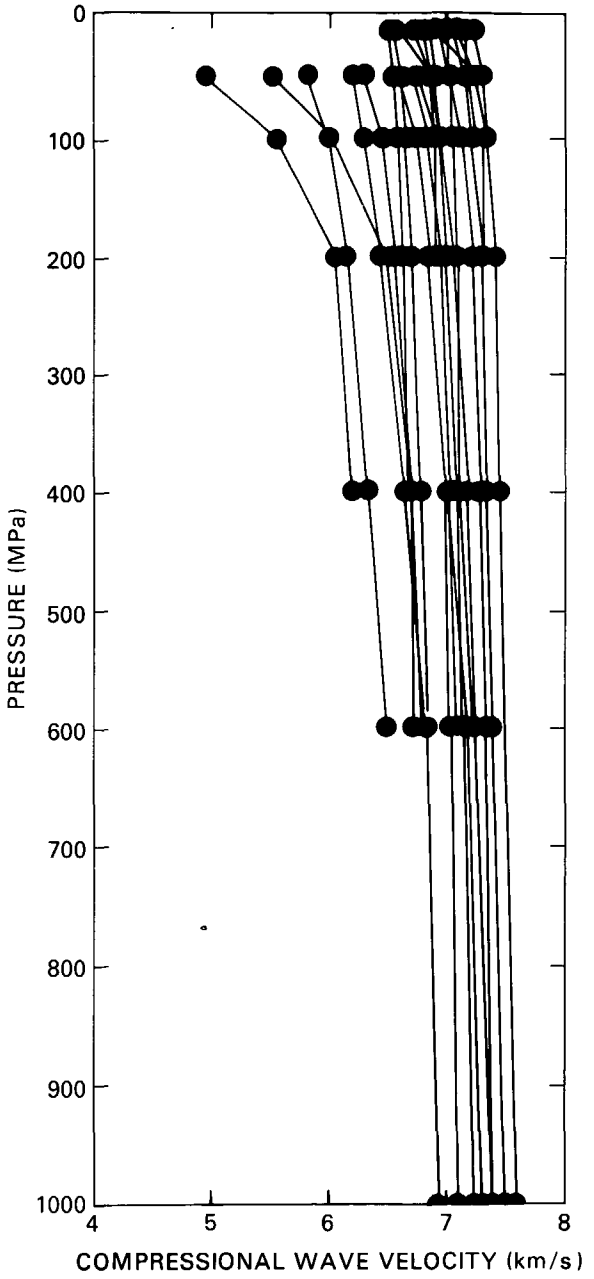

FIGURE 52.17.—Pressure dependence of compressional-wave velocity in gabbro. Distribution of gabbroic xenoliths in vent areas of Hawaiian volcanoes and their resemblance to intrusives exposed in cores and rift zones of dissected volcanoes suggest that gabbros form in a major fraction of magmatic storage region in active portions of system. Marked changes in $\partial V_p/\partial P$ above and below 200 MPa suggest a progressive closure of microfractures in upper regions of volcanic shield, with a transition to mineral compression at $p > 200$ MPa (2 kbar). Data compiled from Schreiber and others (1972), Fox and others (1973), Mizutani and Newbigging (1973), Wang and others (1973), Christensen and others (1975), Hyndman (1976), Kroenke and others (1976), and Christensen (1978).

(1) Gaping cracks in rift systems and summit calderas that have crack opening displacements ranging from tens of centimeters to meters (for example, the Great Crack of Kilauea's southwest rift zone);

(2) Exceptionally low compressional-wave velocities in the upper 2 km of the volcanic pile;

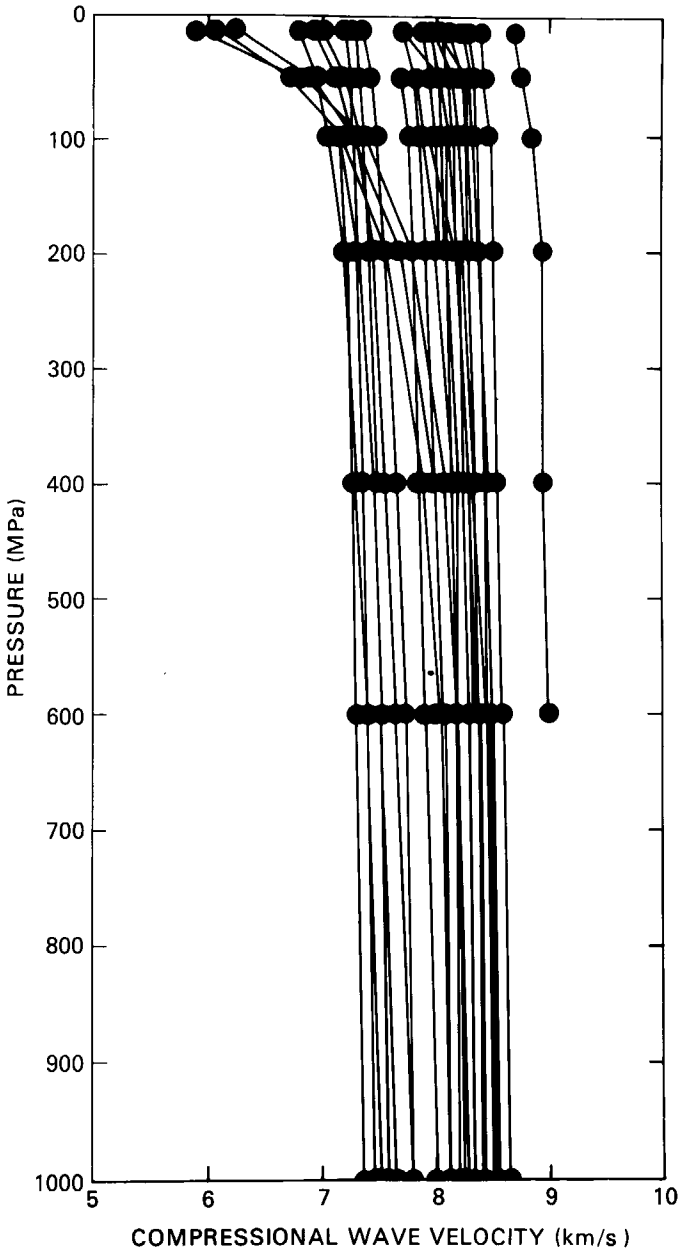

FIGURE 52.18.—Pressure dependence of compressional-wave velocity in dunite. Dunitic xenoliths in alkalic and nephelinitic vent areas suggest relatively widespread occurrence of dunite in upper mantle beneath Hawaii. Additional association is made with refractory mantle-root areas of tholeiitic suite of lavas, as well as a role as cumulates in crustal storage reservoirs during tholeiitic magmatism. In most of these roles, aggregate elastic behavior will lie well within region dominated by mineral compression and structural properties of olivine. For olivine-rich early cumulates that form in storage compartments within a volcanic shield or rift-zone base, nonlinear sections of compressional-wave curves are expected to apply. Data compiled from Hughes and Cross (1951), Bajuk and others (1957), Kanamori and Mizutani (1965), Christensen (1966, 1971), Manghnani and Wollard (1968), Mao and others (1970), Christensen and Ramananantoandro (1971), Babuska (1972), Christensen and Salisbury (1972), and Rao and others (1974).

(3) Exceptionally low in-situ densities in the upper 2 km;

(4) The common observation of massive drainback at the conclusion of an eruptive phase. An archetypical example is the drainback volume of 6×10^6 m^3 for phases of the 1959 Kilauea Iki eruption (Richter and Moore, 1966), and drainback rates as high as 1.5×10^6 m^3 per hour.

(5) Simultaneous eruption and drainback, as exemplified by the 1983 activity at Puu Oo, in Kilauea's east rift zone; and

(6) The long-observed discrepancy between the vertical and horizontal displacement fits to geodetic model predictions. As discussed by Ryan and others (1983), the vertical displacements at Kilauea, for example, are largely reversible, whereas the horizontal components are very weakly reversible. For the upper regions of the shield, rock behavior is elastic in the vertical plane, whereas the horizontal plane contains substantial inelasticity.

The fracture systems within Kilauea caldera, the summit region, and the upper southwest rift zone are shown in figures 52.19 and 52.20.

ENVIRONMENT AT DEPTH: EFFECTS OF PRESSURE AND TEMPERATURE

Rocks forming the central and basal sections of oceanic shield volcanoes are expected to contain pore fluids. Traveling downward within the subaerial portion of an oceanic volcanic system, we would therefore expect to approach a horizon above which the pore space contains air, volcanic gases, and water vapor and below which the accessible pore space is saturated with H_2O. The water would be either fresh or saline, depending on the local configuration of the Ghyben-Herzburg lens. It is relevant then to consider the contractancy of basalt with both dry and H_2O-saturated pore space, and its pressure dependence. These curves are presented in figure 52.21*B* for basalt (Christensen and Salisbury, 1975). The characteristically nonlinear $\partial V_p/\partial P$ at pressures less than 200 MPa is well developed—particularly for the dry curve where the accessible porosity is occupied by air. Both sets of curves show an additional effect: there is a pressure window above which (that is, toward higher P) the pore space accessible to any second phase—air or H_2O—has been squeezed out. For basalt and gabbro, this pressure window corresponds to a transition zone centered at about 200–300 MPa. The figure also contains a series of inset diagrams that depict the progressive elimination of macroscopic and microscopic fracture permeability with progressive increases in confining pressure. The transition zone that coincides with the convergence of the dry and fluid-saturated compression branches is herein referred

to as the compression transition zone. This zone separates the figure into two subregions: a shallow region where the dominant mechanism is the compression of fractures and pore fluids, and a deeper region where further volume reductions are dominated by mineral compression. In constructing the figure, the confining pressures of Christensen and Salisbury (1975) have been converted to depth equivalents, taking into account the density-depth relations for Kilauea presented by Zucca and others (1982).

A summary diagram of data (fig. 52.21*A*) represents the geodetic and seismic constraints on the depth intervals inferred for the position of the summit magma reservoir. These constraints are derived from (1) three-dimensional deformation modeling employing collateral geologic and mechanical property contraints (Ryan and others, 1983); (2) two- and three-dimensional studies of the distribution of magma-reservoir seismicity (Koyanagi and others, 1976; Ryan and others, 1981); (3) geometrically idealized modeling of simply connected sources of pressure or displacement (Mogi, 1958; Deiterich and Decker, 1975); and (4) inversions of summit-tilt, trilateration, and vertical-displacement data, via least-squares regression (Dvorak and others, 1983). The depth interval 2 to 4 km is common to all the inferred ranges and appears to comprise a consensus for the uppermost reaches of the storage region proper. This depth region for magma storage extends to at least 6 km, based on geodetic and seismic evidence.

A comparison of figures 52.21*A* and 52.21*B* suggests that there is a strong correlation between the depths of subcaldera magma storage and the depth intervals that permit the continued dilation of fluid-accessible fractures in basalt. Increases in compression to confining pressure levels in excess of that required to eliminate fracture porosity passes the reference-volume element in figure 52.21*B* below the compression transition zone and into a depth level below the summit storage complex. Note that the curves in figure 52.21*B* describe the microcrack closure behavior for basalt. The addition of macroscopic joint closure has a pressure dependence that is qualitatively similar. Detailed differences between the two arise from the contribution of crack surface topography to joint stiffness

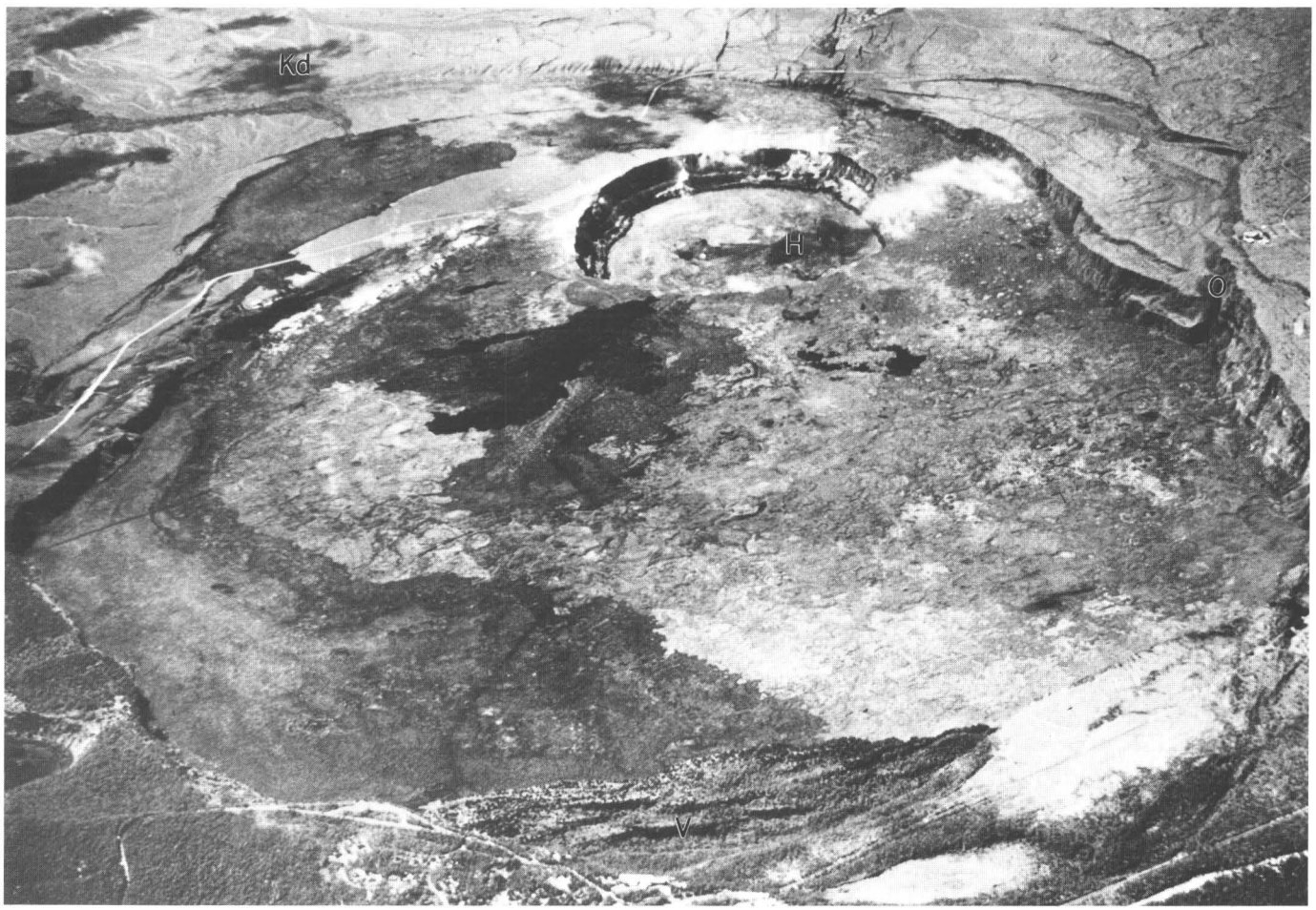

FIGURE 52.19.—Kilauea caldera in west-directed view. Magmatic inflation and deflation centers migrate laterally beneath much of western caldera floor and to south, beyond upper Kau Desert (Kd). Such temporal migration patterns are surface expressions of multiply connected complex of dikes and sills that form summit magma-storage reservoir. They are spatially associated with region of neutral buoyancy. Multiple collapse regions within caldera lie at foot of Volcano House (V). Hawaiian Volcano Observatory (O), and within Halemaumau (H). Photograph by James Griggs.

(Brown and Scholz, 1985). To be noted also is that these curves describe the crack-closure behavior for basalt in the absence of an applied pore pressure—that is, they reflect the inherent crack and rock stiffness itself in maintaining open permeable pathways above the compression transition zone. Applied pore pressures enhance the stability of an open fracture network at depth, as discussed in the next section.

Open fractures provide an environment for laterally extensive magmatic movements in three ways: (1) the obvious intrusion sites provided by dilatant macroscopic fractures; (2) the contributions to neutral buoyancy and magmatic stability produced when the open fracture network is so pervasive that the in-situ rock density is reduced to values equal to (and less than) the in-situ density of melt near its liquidus: and (3) the dilation of microfractures that provide penetration pathways for melt adjacent to advancing crack tips at depth. The wetting properties of basalt near its liquidus (Waff and Bulau, 1979; M. Ryan, unpublished data, 1980) confirm this capability.

The fracture-closure/depth behavior for basalt and gabbro also correlates with the depth extent of Kilauea's rift systems. These depths have been inferred by the position of the bottom of the zone of south-flank seismicity—produced by the inflation of dikes within the southwest and east rift zones. This depth is locally 9–12 km beneath the surface of the volcano. Beneath the east rift zone, this depth is 9–10 km, which is coincident with the 8- to 9-km depth (beneath sea level) inferred from south-flank block kinematics in the study of Crosson and Endo (1982). This region coincides with the transition zone that lies at the base of the field of fracture and pore-fluid compression in figure 52.21*A*. These relations are in harmony with the porposal of Nakamura (1980), who suggested that the mechanically soft sediments of the old ocean floor provided lateral accommodation for the development of long rift zones in Hawaiian shield volcanoes. Indeed, both shield contractancy and lateral slip surfaces in low-modulus sediments may locally work together in regulating the depth extent of rift zones. During continued shield building, however, the keel of the active rift system is expected to rise

FIGURE 52.20.—Junction of southwest rift zone (SWRZ) and Kilauea caldera near Halemaumau (H). Fractures produced on surface record stretch at depth due to increments of dike injection. These fractures produce low in-situ densities and compressional-wave velocities that characterize upper 2 km of shield. In turn, low in-situ densities interact with density of tholeiitic melt near its liquidus to produce region of neutral buoyancy that stabilizes magmatic storage at depth as well as dike emplacement within rift systems. An automobile on caldera rim road (right center) provides scale. Photograph by James Griggs.

above the old oceanic floor and have a depth extent exclusively regulated by the mechanics of volcanic-shield contractancy. A summary of the mechanical relations that have been detailed in figure 52.21*A* and 52.21*B* is provided in figure 52.22.

In addition to the pressure dependence of rock behavior in the vicinity of the magma-storage reservoir, it is of interest to comment on the temperature dependence of basalt elastic moduli near the shallow, low-pressure portions of the reservoir, which can be done by evaluating $E(T)$ and $\mu(T)$ at temperatures approaching the solidus. Applications include estimating the relative contribution(s) of thermal-stress-induced fracture and evaluations of the bending stresses associated with magma-reservoir-roof flexure during inflation-deflation cycling. In evaluating these moduli, three auxilary constraints have been applied: (1) direct temperature-depth measurements beneath the summit of Kilauea; (2) the location of the summit reservoir based on geodetic and seismic studies (discussed above); and (3) eruption and liquidus temperatures determined in summit and near-summit eruptions, and reconstructed in melting experiments on summit compositions. The region of evaluation lies below the upper several hundred meters that characteristically has heavy contributions of macroscopic fractures, leading to the expected low in-situ moduli.

Rotary drilling to 1,262-m depth beneath Kilauea's summit (Zablocki and others, 1974) has provided a temperature-depth profile through the shallow water table to a position below sea level. The stabilized profile shown in figure 52.21*A* has a bottom-hole temperature of 137 °C and suggests an initial thermal gradient of about 370 °C/km. This profile bottom provides a pinning point that is used to hinge a family of thermal gradients, as discussed below.

Temperatures have been measured by optical pyrometry in summit and near-summit lava fountains (for example, Richter and Murata, 1966; Peck and Kinoshita, 1976), and directly in advancing flows and in lava lakes (for example, Wright and Weiblen, 1968; Jackson and others, 1975; Swanson and others, 1976). For many of these measurements, the shrouding effects associated with eruption plumes and the thermal gradients associated with the free surface of active flows suggest that they are generally below true magmatic temperatures. Relations between liquidus temperatures and iron enrichment determined experimentally for samples of Kilauea Iki eruption pumice (Thompson and Tilley, 1969) suggest temperatures in the range 1,225 to 1,188 °C. In addition, Helz and Thornber (1985) present an approach for restoring temperatures measured in lava-lake drill holes to the predrilling in-situ values, based on a glass-based calcium geothermometer. Olivine crystallization in Makaopuhi lava lake (Wright and Weiblen, 1968) has identified a temperature of $1{,}200 \pm 10$ °C. Collectively, these studies suggest that the liquidus temperature for Kilauean olivine tholeiite at atmospheric and near-surface pressures lies close to 1,200 °C, and this value has been associated with the subcaldera storage environment in figure 52.21*A*. It is enclosed by a shaded band that encompasses the high temperature end of the illustrated measurement ranges, and extends to 1,210 °C.

From the high-temperature limit of the drill-hole bottom (137 °C) at 1,262 m, four thermal gradients have been constructed to the 2.0-, 2.5-, 3.0- and 3.5-km-depth levels. These gradients are labeled A through D, and they span the range 1,440 to 476 °C/km (fig. 52.21A). They are tied to the $1{,}200 \pm 10$-°C low-pressure liquidus for the range of depths appropriate for the "attic" of Kilauea's subcaldera magma reservoir. The span in gradients explicitly recognizes the aggregate uncertainty in both the detailed positioning of the storage region and its temperatures. In this respect, it is prudent to consider a probable range of values. Grouped together, the drill-hole measurements, the liquidus temperature assignments, and the resulting interpolation gradients form a one-dimensional thermal model for the summit section of Kilauea.

From the relations for the temperature dependence of the Young's modulus and the rigidity previously presented and evaluated, working estimates can be made for conditions of low pressure. For the Young's modulus, the relation $E(T) = (6.054 - 0.00083T) \times 10$ GPa, evaluated along gradient A in figure 52.21*A*, leads to the relation $E(z)_A \approx (6.054 - 1.195z) \times 10$ GPa, where z is the depth in kilometers. Evaluated along gradient D, the corresponding relation is $E(z)_D \approx (6.054 - 0.395z) \times 10$ GPa. For the shear modulus, the relation $\mu(T) = (2.615 - 0.00038T) \times 10$ GPa, leads to $\mu(z)_A \approx (2.615 - 0.547z) \times 10$ GPa and $\mu(z)_D \approx (2.615 - 0.181z) \times 10$ GPa. Evaluations made to temperatures approaching the low-pressure solidus suggest that about a 15-percent reduction occurs in both E and μ. Considerations of the high-temperature tensile strengths of basalt (M. Ryan, unpublished data; Ryan and Sammis, 1981), combined with the linear thermal-expansion coefficients described in the section "High-Temperature Elasticity of Hawaiian Basalt" and the relation of thermal stress under plane-strain conditions,

$$\sigma_T = \frac{E\alpha_l(\Delta T)}{1-\nu},$$

suggest that local temperature drops of 50 to 100 °C are sufficient to cause thermal-stress-induced fracture. Hence, moderate falls in temperature that may, for example, be associated with influxes of relatively cool water—produced by tectonic adjustments within the mantling aquifer—may thermally load the rocks above active magma reservoirs to points near failure. This thermal component would then be coupled with the bending stresses that are associated with the flexure of the reservoir roof during inflation-deflation cycling. Together, they produce the seismically active lid on the storage region below. Associated with this recurrent rock fracture would be inferred changes in the fracture network, the mechanics of which are discussed below.

EFFECTS OF PORE FLUIDS AND JOINT CLOSURE

The curves in figures 52.21*B* and 52.22 illustrate the confining pressure (P_c) dependence of compressional-wave velocity for basalt and emphasize the depth dependence of permeable pore-space elimination. The progressive nature of microcrack closure with increasing P_c is also emphasized. It is of interest now to outline the effects expected for macroscopic joint closure and the effect of pore fluids under pressure.

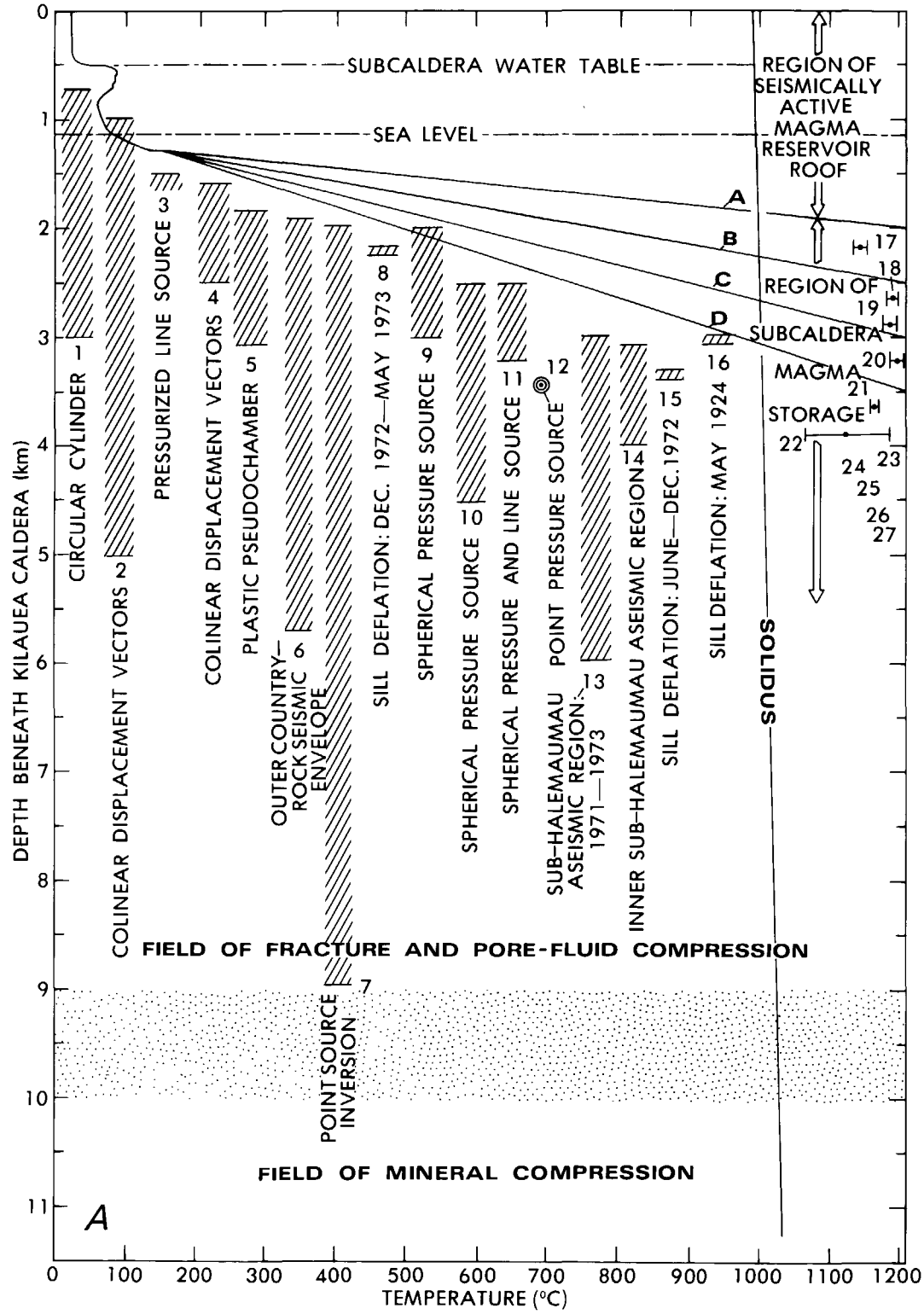

FIGURE 52.21.—Depth relations beneath Kilauea caldera. *A*, Summary depth distributions of Kilauea's subcaldera magma-storage reservoir and its intrusive components. Depth interval 2–4 km is common to all 16 models and submodels. Added to field is temperature profile beneath summit as measured directly to 1,262 m. Direct temperature measurements in erupted lava, laboratory determinations, and optical pyrometer measurements are given by horizontal bars that cluster near 1,200 °C. They have been assigned to the 2- to 4-km-depth interval, reflecting consensus of geodetic and seismic reservoir models (numbers 1–16). Hachured region that encloses them is intended to suggest a broad-working estimate of a range of in-situ temperatures within this depth interval. Radiating from maximum temperature point at 1,262 m to depth regions along the 1,200-°C margin that

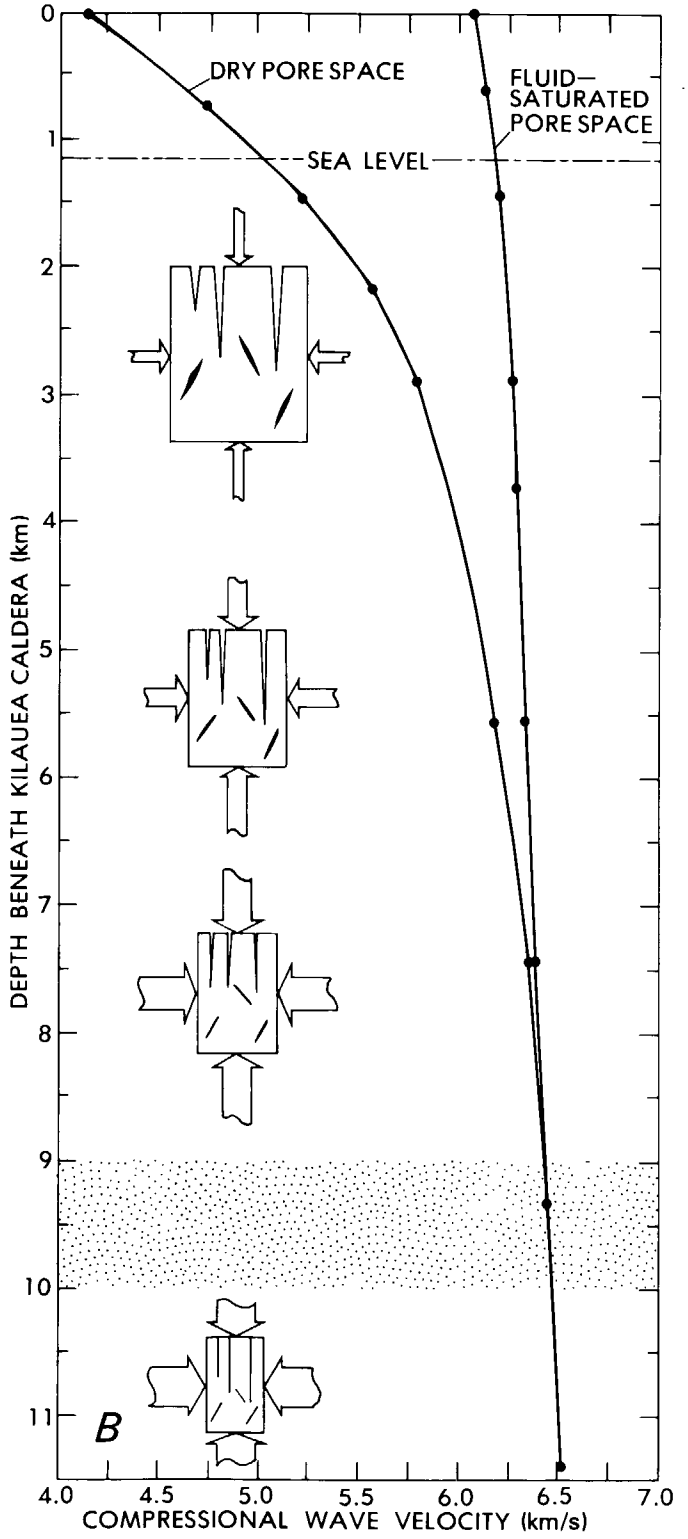

corresponds to upper levels of summit magma storage is a family of four thermal gradients (A–D). They explicitly recognize uncertainty implied by both depth distributions and temperature ranges. Data sources for compilation include (a) Summit temperature-depth profile: Zablocki and others (1974). (b) Solidus: Wright and Okamura (1977); pressure dependence of solidus, dT_m/dP: Yoder and Tilley (1962); Hill and Boettcher (1970). (c) Depth of summit magma storage (numbers identify plotted values and ranges): (1) Dieterich and Decker (1975); (2) Duffield and others (1982); (3) Walsh and Decker (1971); (4) Mogi (1958); (5, 7) Jackson and others (1975); (6) Fiske and Kinoshita (1969); (8) Davis and others (1974); (9) Ryan and others (1981); (10) Dvorak and others (1983); (11, 14, 15, 16) Ryan and others (1983); (12) Eaton (1962); (13) Koyanagi and others (1976). (d) Magmatic temperatures (numbers identify plotted measurements): (17) Moore and others (1980); (18, 21) Swanson, Duffield, and Fiske (1976); (19) Jackson and others (1975); (20, 26) Wright and Weiblen (1968); (22) Richter and Murata (1966); (23, 24) Thompson and Tilley (1969); (25) Yoder and Tilley (1962); (27) Wright and Fiske (1971). ***B***, Compressional-wave velocities in dry and H_2O-saturated basalt as a function of increasing depth (confining pressures). Congruence of branches at 9-km depth suggests that all H_2O-accessible porosity has been squeezed out. Further increases in confining pressure (arrowed pathways) cross through transition region (dot pattern) into field of mineral-compression-dominated volume changes. Inset diagrams depict progressive elimination of microscopic and macroscopic permeability with increasing confining pressure. Data sources for compilation include pressure dependence of compressional-wave velocity from Christensen and Salisbury (1975).

For an orthotropic medium containing three sets of mutually orthogonal joints, the effective compressibility may be expressed as (Amadei and Goodman, 1981):

$$\beta^* = \frac{1}{K^*} = 3\left(\frac{1-2\nu}{E}\right) + \sum_{i=1}^{3} \frac{1}{K_{ni}S_i}, \qquad (42)$$

where β^* is the effective compressibility, K^* is the effective bulk modulus, ν is Poisson's ratio, E is the Young's modulus, K_{ni} is the joint stiffness, and S_i is the interjoint spacing.

The nonlinear contribution to compressibility and contractancy arises from the stress-dependent normal fracture (or joint) stiffness. This is a hyperbolic variation in fracture closure with changing normal stress. For dolerite, Bandis and others (1983) have compiled K_{ni} data for joint closure in dolerite. The relevant units are (normal stress component)/(fracture closure), or megapascals per centimeter.

For an unjointed medium, or a medium in which the joint spacing is very large, the volumetric strain may be related to the applied confining pressure (P_c) through the elastic moduli:

$$\frac{\Delta V}{V_0} = 3\left(\frac{1-2\nu}{E}\right)P_c. \qquad (43)$$

This equation defines volumetric compression in the case of mechanical isotropy, where both flaws and joints are unavailable for closure. The isotropic compression path is plotted in figure 52.23 and is labeled "unjointed media."

Volumetric strain for a jointed media with the potential for pore-pressure (P_p) development in the joint network may be expressed as:

$$\frac{\Delta V}{V_0} = (P_c - P_p)\beta^* + 3P_p\left(\frac{1-2\nu}{E}\right). \qquad (44)$$

When combined with equation 42, the strain becomes

$$\frac{\Delta V}{V_0} = 3(P_c - P_p)\left(\frac{1-2\nu}{E}\right) + \sum_{i=1}^{3} \frac{1}{K_{ni}S_i} + 3P_p\left(\frac{1-2\nu}{E}\right). \qquad (45)$$

The compression paths of jointed media are also plotted on figure 52.23, and the curve for $P_p = 0$ lies to the right of a family of curves that describe contractancy with fluid pressure in the fracture network. The area between the isotropic path and the compression path for $P_p = 0$ has been shaded and represents the expected contractancy range for joint sets whose essentially infinite spacing is tantamount to elastic isotropy, and the suite of curves for the 30-cm joint spacing labeled "jointed media." This area is thought to represent the spectrum of joint spacings relevant to Hawaiian volcanic shields. The jointed media curves generally mimic the nature of the pressure dependence of contractancy as seen in the V_p-versus-confining-pressure behavior in figures 52.16 and 52.17, for instances of microfracture closure under laboratory conditions. Particularly well developed is the characteristic form of $\partial(\Delta V/V_0)/\partial P$ at the lowest pressures shown.

Applied pore pressures have three effects. First, increases in fluid pressure force the volumetric-strain curves progressively to the left (fig. 52.23). This effect is expected because pore pressure stabilizes open fractures at depth, preventing less aggregate compression for a given confining pressure. Second, the relative effect of a fixed pore pressure diminishes progressively as the confining pressure is increased. This effect is illustrated by the convergence of

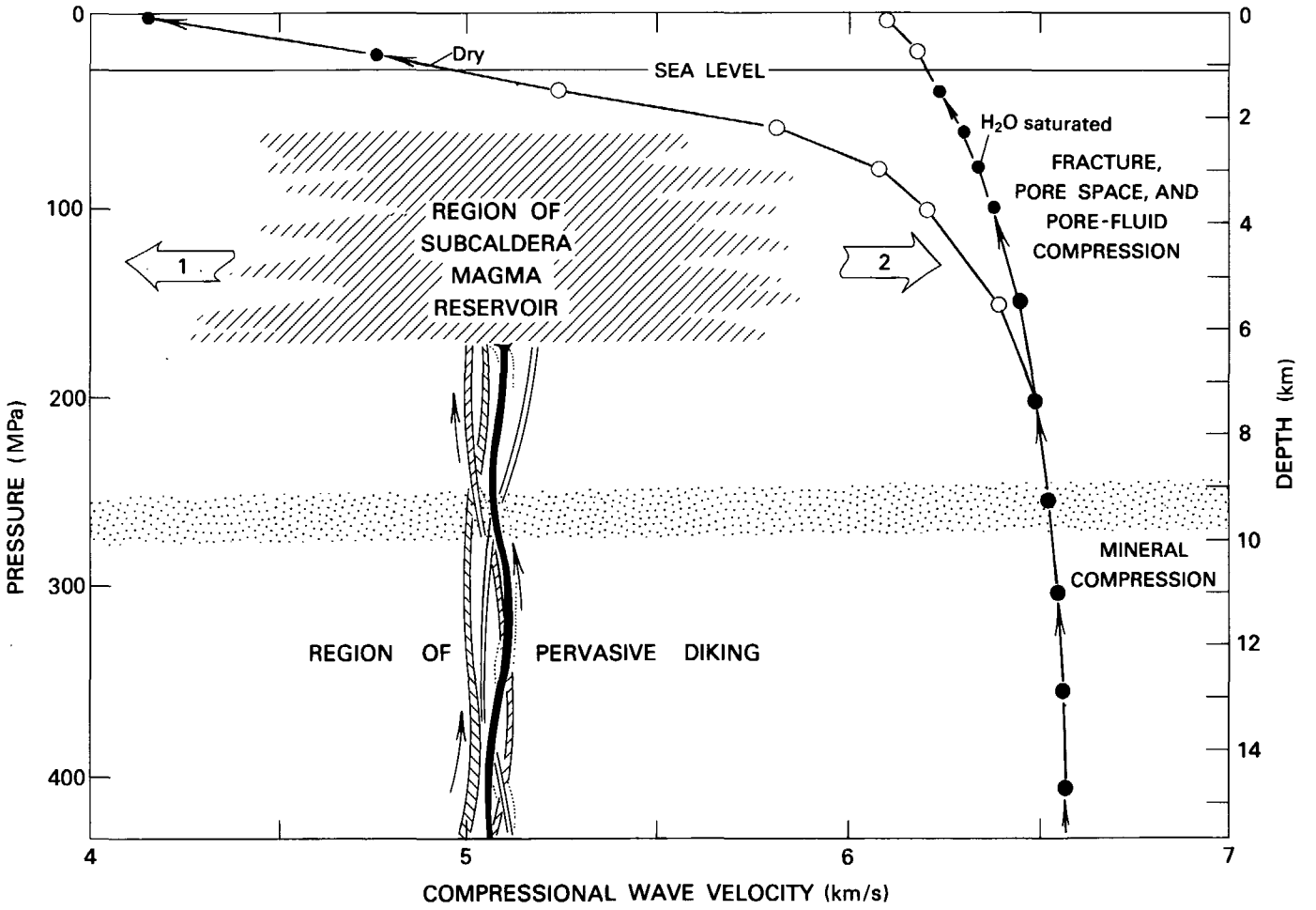

FIGURE 52.22.—Contractancy of basalt in relation to depth distribution of primary magmatic storage within Kilauea. Compressional-wave velocities have been compiled from data of Christensen (1974) and Christensen and Salisbury (1975). Filled and open circles track pathway of V_p as a function of depth and pressure in H_2O-saturated and dry environments, corresponding to changes in depth from upper mantle, oceanic crust, volcanic shield, and submarine reference points to subaerial positions. Filled circles correspond to measurements of relevant decompression track for Kilauea. Stippled band represents a contractancy transition zone, above which pore fluids are continuously squeezed out by increasing levels of confining pressure, and below which fluid-accessible porosity has been eliminated. Accordingly, transition zone defines a contractancy map with two subfields: at shallow depths (0–8 km), dominant mechanism is compression of fractures, pore space, and pore fluids; at greater depths (>9 km), dominant mechanism is mineral compression. Stratigraphic extent of magma storage reservoir has been constrained by geodetic and seismic studies and lies mostly in 2.2- to 6-km-depth interval, corresponding to crossruled region. It is coincident with that portion of contractancy field characterized by fluid-accessible fracture space. Horizontally directed arrows (1 and 2) infer lateral injection of magma into adjacent rift zones. Depth extent of these active rift systems is also coincident with that portion of contractancy map that is associated with fluid-accessible fracture space. Beneath transition zone is a region of mineral compression that is stratigraphically associated with pervasive diking linked with vertical magma movements from mantle depths.

the jointed-media curve set with increasing P_c. Third, at extremely shallow depths, moderate increases in joint fluid pressure drive the curves from the contraction-dominated field into the dilation field. This effect occurs when fluid pressures exceed the confining pressure.

It is of interest now to look at the ways pore-pressure development in the rock microstructure can influence the contractancy of basalt. Christensen (1984) has studied the effects of confining pressure (P_c), pore fluid pressure (P_p), and effective pressure (P_e), where

$$P_e = P_c - P_p, \tag{46}$$

on the compressional and shear wave velocity in basalt. These effects are summarized in figures 52.24 and 52.25, respectively; they are based on the data of Christensen (1984) and represent adaptations

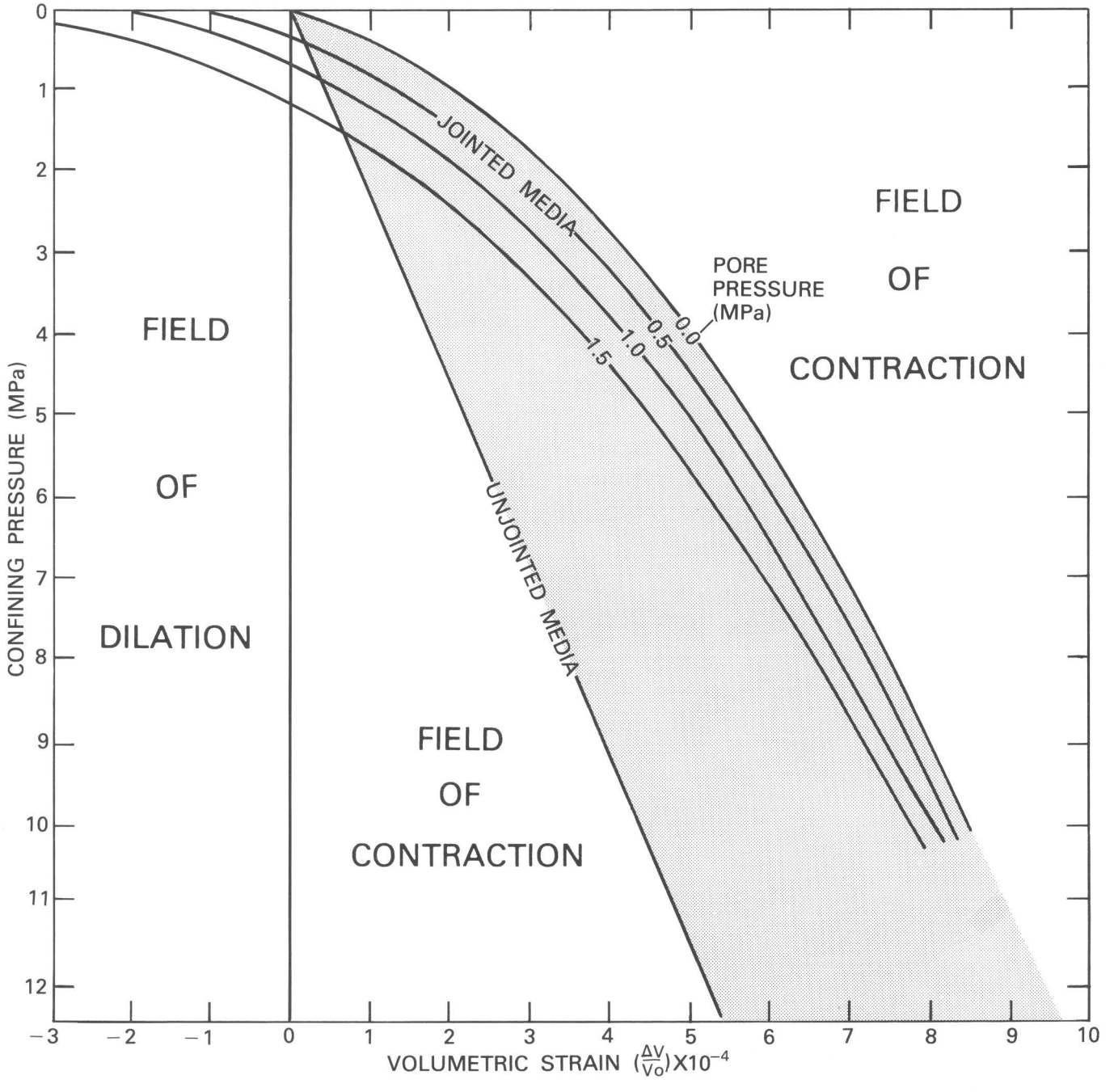

FIGURE 52.23.—Volumetric strain versus confining pressure for unjointed and jointed media with effects of variable pore pressure. Modified from Amadei and Goodman (1981).

of his presentation for reference confining pressures beneath Hawaiian shield volcanoes. In the figures, the familiar nonlinear profile of $\partial V_{p,s}/\partial P$ is produced by the compression of the rock skeleton at zero pore pressure. The hydrostatic reference curve has a fixed low-pressure datum at a depth intermediate between the depth of the summit water table (fig. 52.21*A*) and sea level, for Kilauea as an example. This curve recognizes the temporal and spatial changes in the topography of the intrashield water table and attempts to strike an average. The zero-confining-pressure datum is the volcanic summit. The depth extent encompasses nearly all of the summit magma-reservoir region and most of the rift zones.

The effect of hydrostatic pore pressure shifts the curves to the left, preserving the overall shape of the contractancy profile. Between the P_p = hydrostatic and $P_p = 0$ curves is sandwiched a narrow field where the pore pressure is less than hydrostatic. This field is labeled "C," and it has been shaded in the figures. The pervasive seismicity and rock fracture that characterize the shields of active Hawaiian volcanoes suggest that ambient pore pressures at depth may be inferred to be at or near hydrostatic. To the extent that fluid continuity is maintained by renewed rock fracture, water is expected to be continuously expulsed during the compaction that accompanies volcanic-shield evolution. This general pattern of compaction dewatering should characterize the bulk of the volcanic flanks, where fluid continuity is continuously maintained via the fracture process. For rift-zone environments maintained at near-magmatic temperatures, metamorphism passes through greenschist to amphibolite facies (Liou and others, 1974), and alteration and replacement reactions may be expected to locally close down permeability and promote the development of higher pore-fluid pressures, thus helping, on a local scale, to stabilize open fractures and

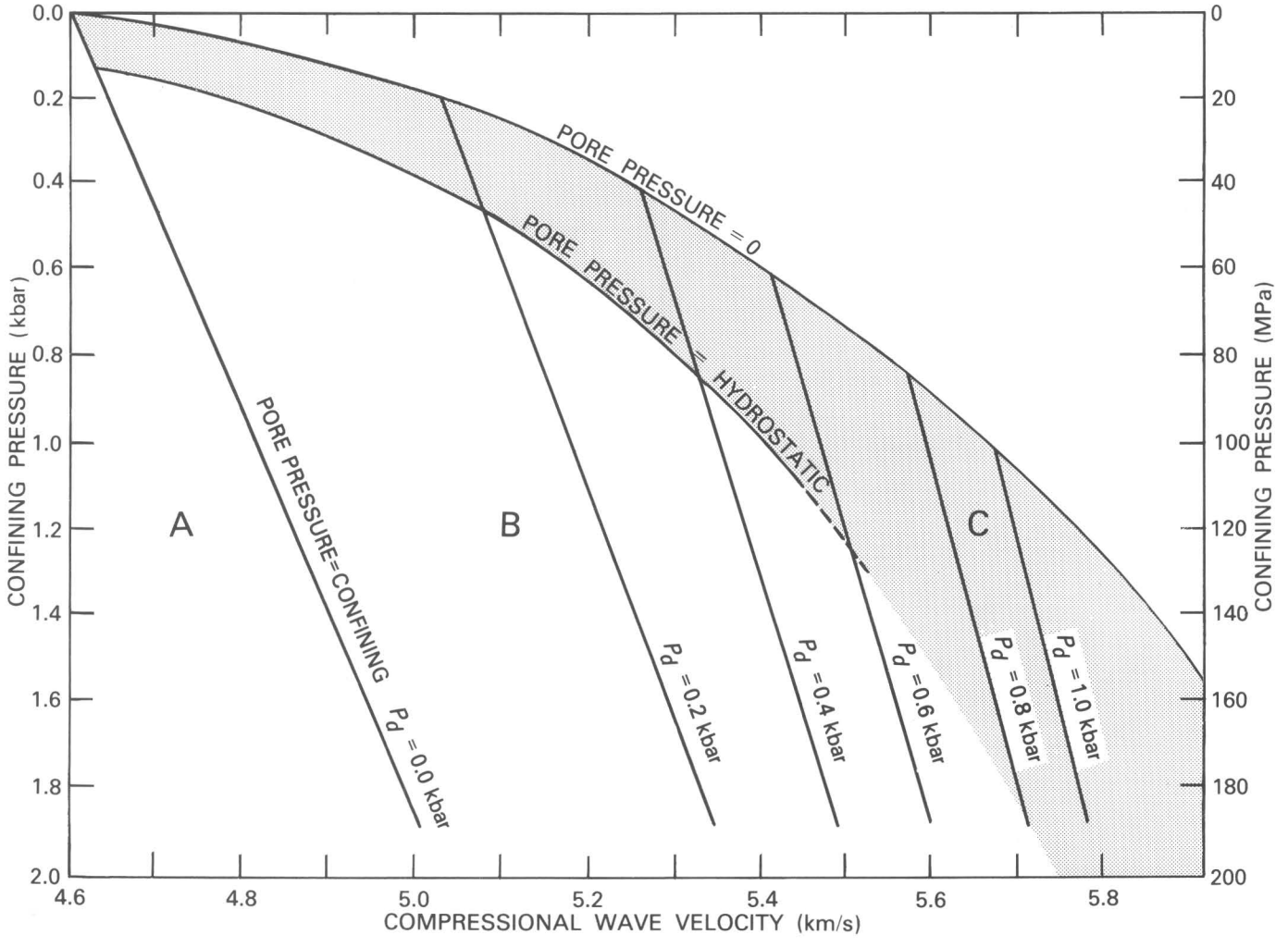

FIGURE 52.24.—Effects of variable pore pressure on compressional-wave velocity in basalt. Fields correspond to mechanically distinct ratios of pore pressure to pressure applied externally to rock skeleton. Field A: pore pressure exceeds external confining pressure; field B: pore pressure is less than confining pressure but greater than hydrostatic; field C: pore pressure is less than hydrostatic. Family of six differential pressure (P_d) lines correspond to 20-MPa (0.2 kbar) increments of difference: ($P_{conf} - P_{pore}$). Figure based on data of Christensen (1984).

pores against the confining pressures that would otherwise squeeze them shut. In figures 52.24 and 52.25, the appropriate region is now the B field, where pore pressures are above hydrostatic. For active regions of intrusion and magmatic storage, one may envision a constant competition between the metamorphic reactions tending to promote the sealing that raises pore pressures above hydrostatic, and the reinstatement of permeability by rock fracture and intrusion, returning the pressure to hydrostatic. In-situ V_p and V_s would then repeatedly shift back and forth across the hydrostatic curve, from field C to field B, and then back again as permeability was alternately enhanced and destroyed. The long-term prognosis, however, is the maintenance of near-hydrostatic pressures for those regions of the shield, where fluids are readily available. These regions are expected to be well above the compression transition zone of figures 52.21*A*, 52.21*B*, and 52.22.

NEAR-SURFACE CONTRACTANCY IN MAGMATIC SYSTEMS

If the dominant mechanism of bulk compression is the continuous elimination of fault, joint, and microfracture porosity in shallow levels of the system, then we should expect to see correlative changes in the density of the volcanic shield with depth, corresponding to increases in confining pressure. The in-situ densities of the volcanic shields of Kilauea and Mauna Loa are plotted in figure 52.26*B*, which is based on the gravity and seismic-refraction surveys of Zucca and others (1982) and the two-dimensional density structure for these volcanoes that resulted from modeling the gravity profile by application of the polygon approach of Talwani and others (1959), with corrections for three-dimensional end effects using the procedure of Cady (1977).

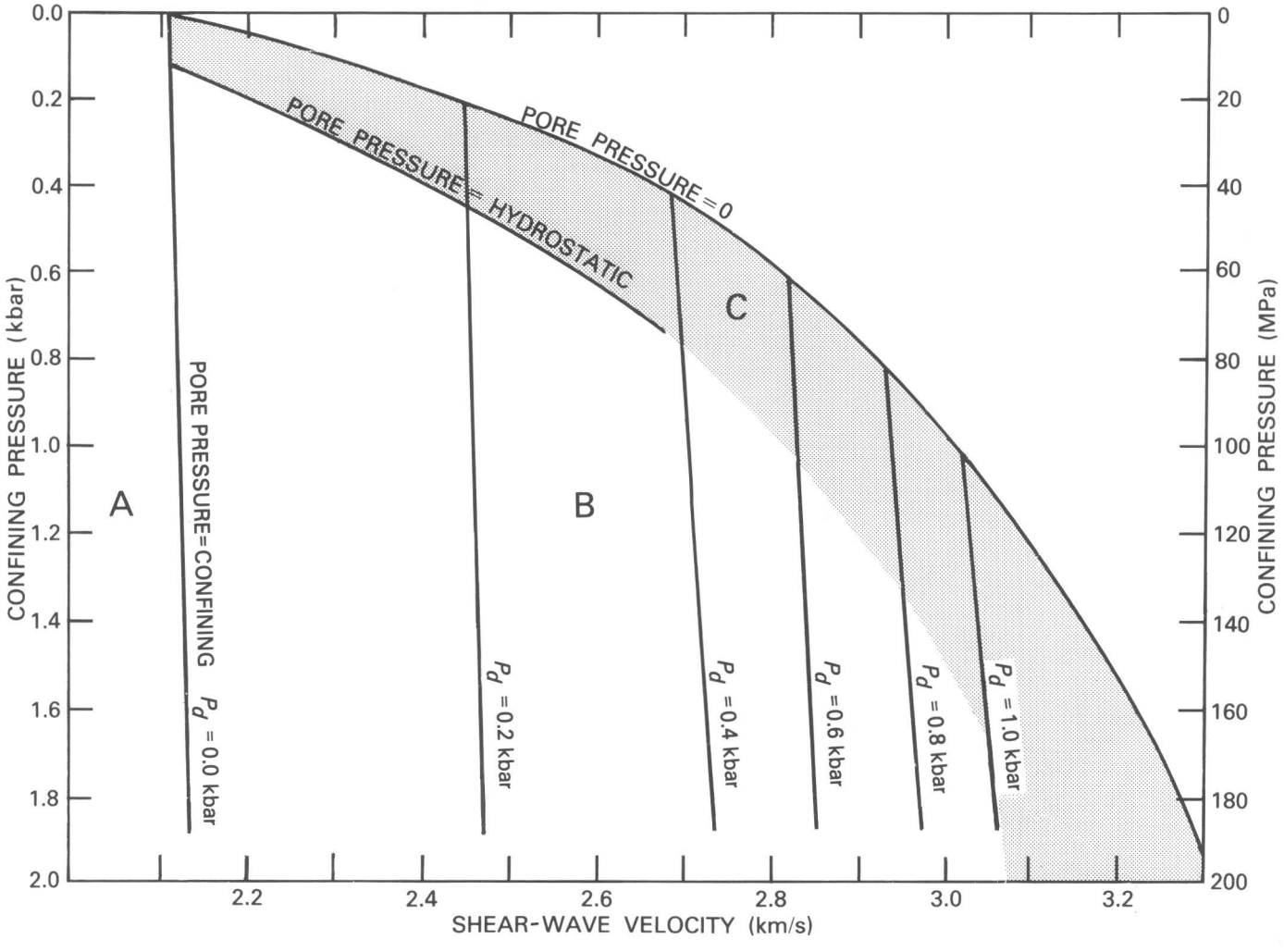

FIGURE 52.25.—Effects of variable pore pressure on shear-wave velocity in basalt. Fields correspond to distinct ratios of pore pressure to externally applied pressure through equivalent lithostatic loading. Field A: pore pressure exceeds external confining pressure; field B: pore pressure is intermediate between confining and hydrostatic; field C: pore pressure is less than hydrostatic. Difference between confining and pore-fluid pressure is differential pressure (P_d) of each of six subvertical lines extending from zero-pore-pressure curve. Figure based on data of Christensen (1984).

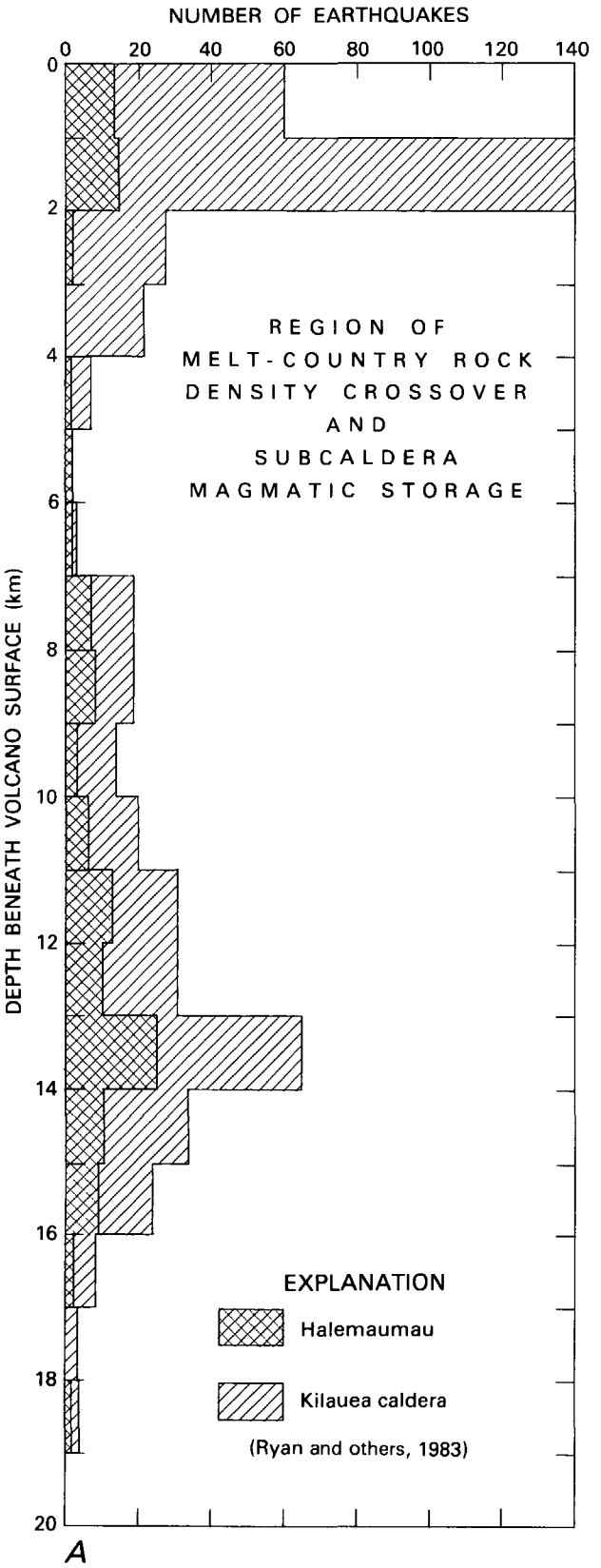
NUMBER OF EARTHQUAKES
0 20 40 60 80 100 120 140
DEPTH BENEATH VOLCANO SURFACE (km)
0 2 4 6 8 10 12 14 16 18 20
REGION OF MELT-COUNTRY ROCK DENSITY CROSSOVER AND SUBCALDERA MAGMATIC STORAGE
EXPLANATION
Halemaumau
Kilauea caldera
(Ryan and others, 1983)
A

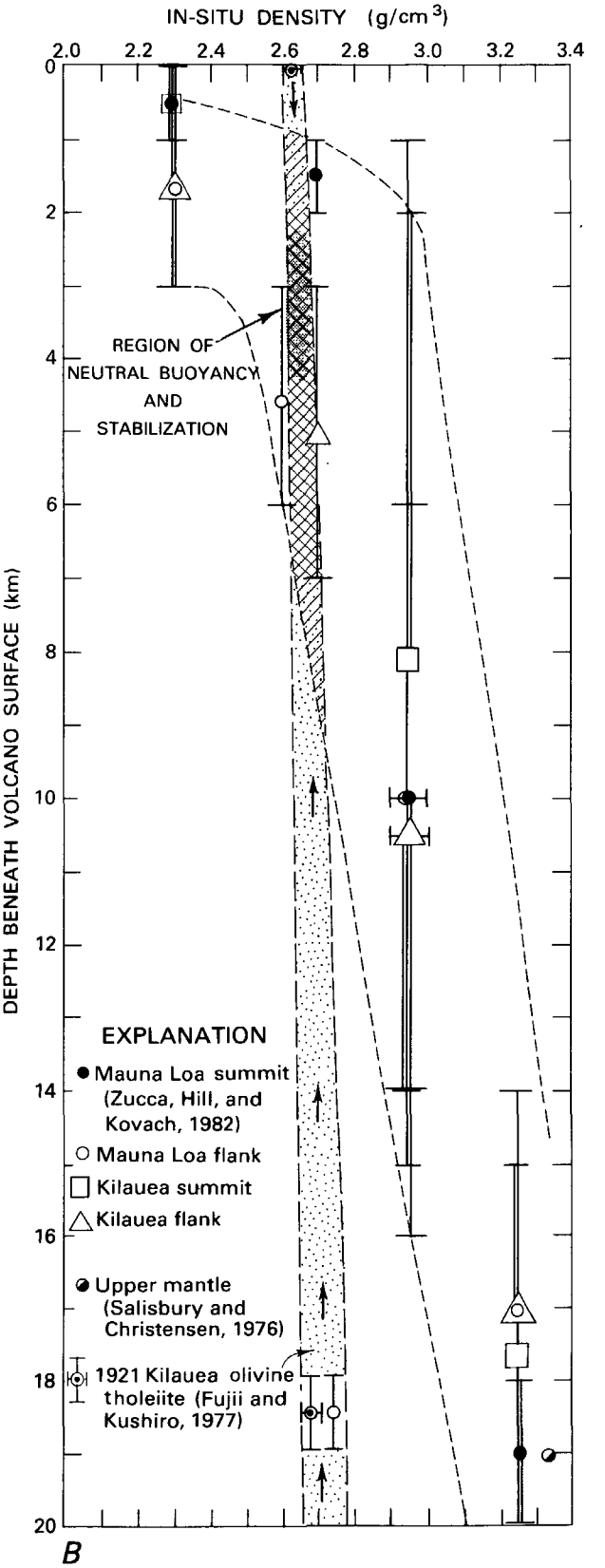
IN-SITU DENSITY (g/cm3)
2.0 2.2 2.4 2.6 2.8 3.0 3.2 3.4
DEPTH BENEATH VOLCANO SURFACE (km)
0 2 4 6 8 10 12 14 16 18 20
REGION OF NEUTRAL BUOYANCY AND STABILIZATION
EXPLANATION
Mauna Loa summit (Zucca, Hill, and Kovach, 1982)
Mauna Loa flank
Kilauea summit
Kilauea flank
Upper mantle (Salisbury and Christensen, 1976)
1921 Kilauea olivine tholeiite (Fujii and Kushiro, 1977)
B

The procedure of Talwani and others (1959) enables bodies of varying geometry and dissimilar density to be assembled into a complex composite. For Kilauea and Mauna Loa, this has enabled Zucca and others (1982) to incorporate the effects of the high-density volcanic rift zones and cores in their inversion procedure. These regions are then embedded in the basaltic flanks of the shields, and the computed gravity profiles matched with the observed profiles. The resulting density structure must then be consistent with the seismic-velocity structure inferred from refraction surveys. In turn, the deduced densities have been required to be consistent with the velocity-density systematics at the appropriate confining pressure. In this report, the results of Zucca and others (1982, figs. 10 and 11) have been used in the following way: for each volcano, two vertical density profiles have been taken from the surface to upper mantle depths—one profile beneath the summit caldera and one profile beneath the flanks (fig. 52.26*B*). The symbols for each profile type are provided in the inset box. Vertical bars delimit the stratigraphic extent of the density along the profile. This combined density and velocity structure for both Kilauea and Mauna Loa is consistent with the velocity-density systematics of basaltic, gabbroic, and ultramafic rocks determined independently at 50 and 100 MPa confining pressures (see Christensen and Salisbury, 1975). Collectively, the density profiles define a nonlinear band of values in in-situ density versus depth space. The nonlinear portion of the density band (as determined by the envelope defined by the total density range along a given profile) occurs over the depth interval 0–7 km. This coincides closely with the nonlinear portion of the experimentally derived contractancy curves for basalt and gabbro (figs. 52.16 and 52.17). It also corresponds very closely with the 0 to 9-km-depth interval required to bring about a convergence of the air-saturated and H_2O-saturated branches of the contractancy curve in figure 52.21*B*. Finally, it corresponds closely to the systematics of $\partial V_p/\partial z$ for the seismic-velocity profiles for Hawaii based on the work of Hill (1969), Ward and Gregersen (1973), and Klein (1981), including the low-velocity residuals that lie to the immediate left of the basalt field in figure 52.27. This congruence in depth dependence suggests that several physical states and deduced properties—gravity, density, in-situ seismic velocities and their profiles, and laboratory studies of the pressure dependence of V_p and V_s—are all responding to the nonlinear contractancy associated with the Earth's surface. All are marching to the same drummer: the gradual elimination of void space on all scales with increasing depth.

Plotted also on figure 52.26*B* are measured values of the density of the 1921 Kilauea olivine tholeiite as a function of pressure, based on the work of Fujii and Kushiro (1977). The density range plotted at upper-mantle levels incorporates the experimental uncertainties presented in their figure 18 (p. 442) with the range required to reach their calculated density. At ambient pressure, it is determined by the experimental error. This melt-density band has been stippled in the figure. Particularly significant within the context of contractancy and Hawaiian magmatism is the crossover in melt and country-rock densities at low confining pressure. The melt-density band has been hachured within the crossover region, and the centroid of the crossover with respect to the depth range in country-rock density has been shaded.

At upper-mantle depths, the density contrast between melt and country rock will be a measure of the driving pressure through $\Delta\rho Gh$. In this interval, and through the oceanic crust, this density contrast, $\rho_{rock} - \rho_{melt}$, will be positive, with a continuously diminishing magnitude as melt parcels rise within their dikes. This rise is suggested by the upward-directed arrows (fig. 52.26*B*). As the parcel penetrates the oceanic crust and enters the base of the volcanic shield, the surrounding country-rock will be dominated by basalt and gabbro, and the value of the $\Delta\rho$ will approach zero. Further ascent to a depth level within the heart of the crossover region is expected to bring about a match between melt and environment density. This matching or balance region has been labeled the "region of neutral buoyancy and stabilization" in the figure. The chance passage of melt through the region of neutral buoyancy into the country-rock roof of the reservoir reverses the sign of the density contrast, and $\rho_{rock} - \rho_{melt}$ is now negative. Infinitesimal perturbations above the density balance horizon will return the errant melt parcel to the region of neutral buoyancy (downward-directed arrow). This mechanism—the oscillation of melt parcels about a horizon of density balance—provides for the long-term stabilization of subcaldera magma storage. It is a region where the nonlinear contractancy of rock near the Earth's surface has provided an environment where the critical $\Delta\rho \approx 0$. Breaking the balance and producing significant diking within the roof or eruption at the surface requires the wholesale rupture of the edifice via hydraulic-pressure

FIGURE 52.26.—Earthquake abundance and in-situ density as related to depth beneath volcano surface. ***A***, Distribution of earthquakes beneath Kilauea's summit region. Singly ruled histogram corresponds to depth distribution of seismicity within the volume that encompasses entire Kilauea caldera and extends to 20 km beneath caldera floor. Doubly ruled histogram provides depth distribution of seismicity within prismatic volume that encompasses Halemaumau Crater and extends to 20 km. Aseismic region from 2- to 7-km depth is inferred to have differentially high magma-to-rock ratios. Data from Ryan and others (1983). ***B***, In-situ densities of olivine tholeiite near its liquidus, and volcanic shields, oceanic crustal sections, and upper-mantle bases of Mauna Loa and Kilauea. In-situ densities for Mauna Loa and Kilauea are based on seismic-refraction profiling and gravity surveys of Zucca and others (1982), as resolved by inversion modeling of gravity profiles, consistent with velocity-density systematics of basaltic and gabbroic rocks. Region of density crossover is hachured section of melt-density band. Where band coincides with 2- to 7-km-depth region of subcaldera magma storge, it is doubly hachured. Within centroid of crossover region is a darkly shaded subregion of neutral buoyancy. Data for 1921 Kilauea olivine tholeiite from Fujii and Kushiro (1977), and for upper mantle from Salisbury and Christensen (1976).

increase, tectonic kneading of the reservoir from remotely applied tractions or the reinstatement of a positive $\Delta\rho$ via vesiculation of the melt, or a permutation involving a mix of two or more of these contributors. Reduced to its essentials, the contractancy mechanism suggests a fundamental control on the operation and evolution of magmatic systems in the near-surface environment.

What is the correspondence between the density crossover region and the depth interval associated with subcaldera magma storage? For Kilauea, this interval has been constrained by geodetic studies to occupy the range 2 to 9 km, with the suggestion of the subrange 2 to 4 km, as the most frequently retrieved center of deformation (Mogi, 1958; Eaton, 1962; Fiske and Kinoshita, 1969; Walsh and Decker, 1971; Dieterich and Decker, 1975; Jackson and others, 1975; Swanson and others, 1976; Ryan and others, 1983; Dvorak and others, 1983). The total depth range in the density crossover resolved in figure 52.26*B* is 1 to 7 km, with the central region of neutral buoyancy occupying the 2.5- to 4.5-km-depth range. This depth suggests a good correspondence between the zone of melt/country-rock in-situ density equilibration and the center of magmatic storage inferred from geodetic studies.

Studies of the spatial distribution of subcaldera earthquakes at Kilauea provides a collateral line of independent evidence regarding the depth distribution of magma associated with hydraulic fracturing and its three-dimensional topology. Koyanagi and others (1976) have resolved a relatively aseismic zone, with a mean diameter of about 3 km and a depth range from 3 to 6 km, and have associated this zone with the summit storage reservoir. Ryan and others (1981) have resolved the three-dimensional structure of this region for the period April 1, 1971, to December 31, 1973. These results suggest a reservoir floor in the depth range 6 to 7 km, and a storage complex roof at 2 km. The vertical profiles of the seismicity beneath Kilauea caldera and Halemaumau for this same period (Ryan and others, 1983) have been included in figure 52.26*A*. The roof above 2 km is a zone of intense fracturing, forming a seismic lid on the inflating complex beneath. The interval from 2 to 7 km becomes increasingly aseismic with depth and has a quiet zone in the 4- to 7-km range, suggesting differentially high fluid-to-rock ratios. Beneath 7 km, the level of hydraulically induced fracturing increases, suggesting active transport of magma within the dikes of the primary conduit. The interval from 2 to 7 km in figure 52.26*A* can now be compared with

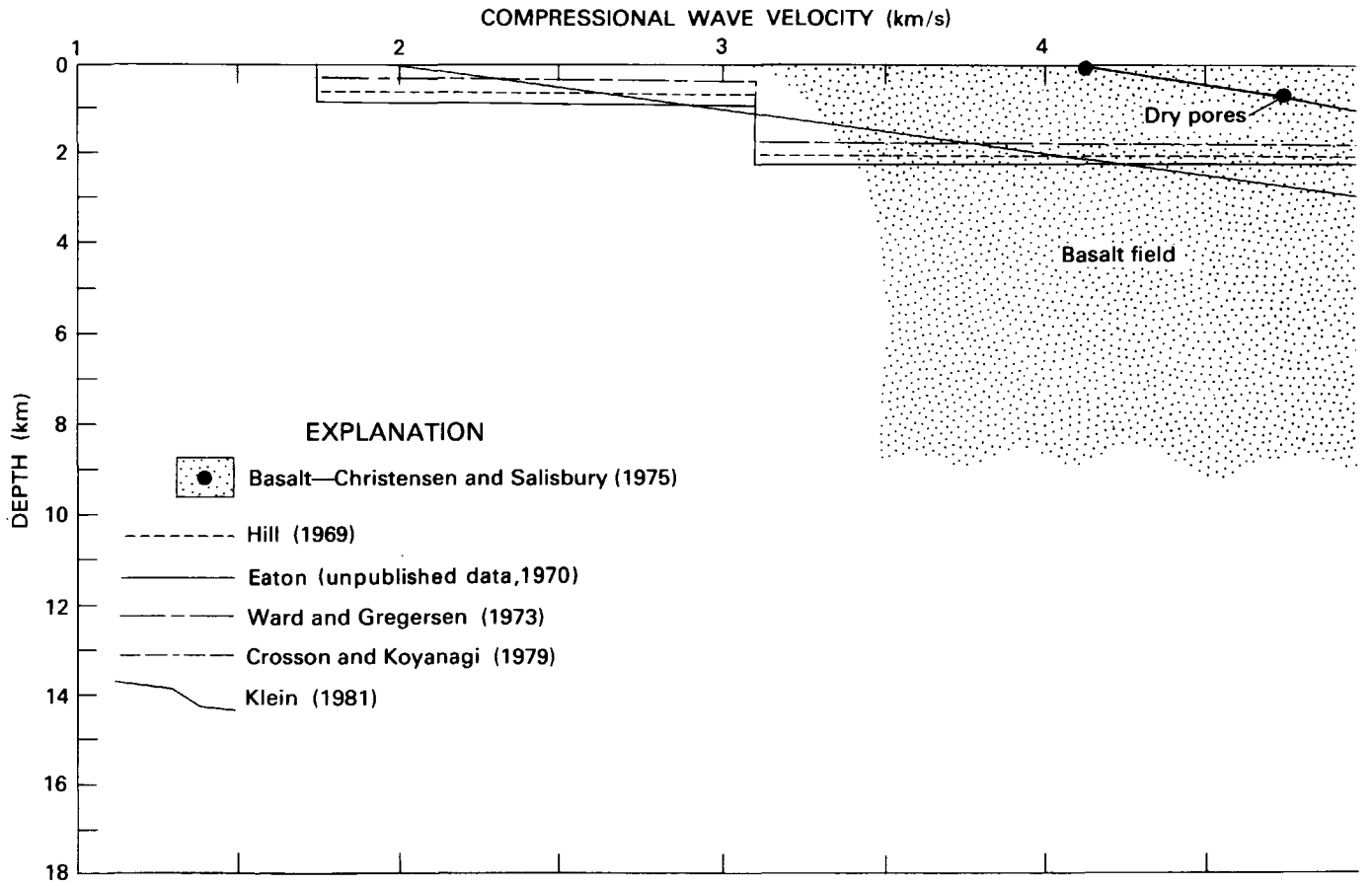

FIGURE 52.27.—Lithologic and seismic compressional wave velocity field beneath Hawaii, with special reference to Kilauea Volcano. Lithologic fields have been compiled from data sets in figures 52.16, 52.17, and 52.18 and references contained therein. Their lateral extents (in V_P space) have been constrained by total ranges in extant compressional wave data as a function of confining pressure. Depth extents of a lithologic field are generally compatible with distribution of seismic velocities with depth, as well as results of gravity surveys and xenolith types in eruptive-vent areas on Hawaii and Oahu. Vertical extent of certain lithologies is expected to be greater than that illustrated, particularly that of gabbro, thus suggesting some overlap between gabbro field and ultramafic fields at upper-mantle

the in-situ melt and country-rock density profiles in figure 52.26*B*. The comparison is striking: there is a 1:1 correspondence between the in-situ density crossover region and the seismically—and geodetically—deduced regions for summit magma storage. Klein and others (1986) resolve the same subcaldera aseismic region. The general relations discussed in this section are summarized in figure 52.28.

CONTRACTANCY AND THE INTERNAL STRUCTURE OF HAWAIIAN VOLCANOES

The discussion of the pressure dependence of the elastic properties of Hawaiian rocks has been largely one dimensional, because the gravitational-force field drives the compression of rocks and orders its variation with depth. Let us now broaden the focus and look at the role of contractancy as it relates to the three-dimensional structure of the magmatic system. Figure 52.29 is a view of the three-dimensional internal structure of Kilauea to 40 km depth. The map scale is 1:62,500, and the physiographic features of Kilauea's surface include: the fracture system of fault blocks, eruptive fissures, and vents of the southwest rift zone and east rift zone; Kilauea caldera, Halemaumau Crater, and major pit craters within the east rift zone; and the major fault systems of the south flank, including the Hilina, Kalanaokuaiki, and Holei palis. Figure 52.30 is a northward-directed view from a depth of 10 km.

The model has been constructed by applying the following constraints:

(1) Seismicity: following the approach of Ryan and others (1981), the three-dimensional distribution of earthquakes associated with magmatic transport and storage has been resolved by plotting their hypocenters within a transparent volume. The period of the study has been January 1, 1969, to January 1, 1983. Uncertainties in event locations have been constrained to be ≤ 1 km. From a total data set of about 50,000 earthquakes, approximately 25,000 have passed the selection criteria of a standard error that is 1 km or less. They are events of magnitude 1.5 and above. Hypocenter locations have employed the linear gradient velocity model of Klein (1981), which is shown in this report to be internally consistent with the pressure dependence of rock properties and the lithology of Kilauea (fig. 52.27).

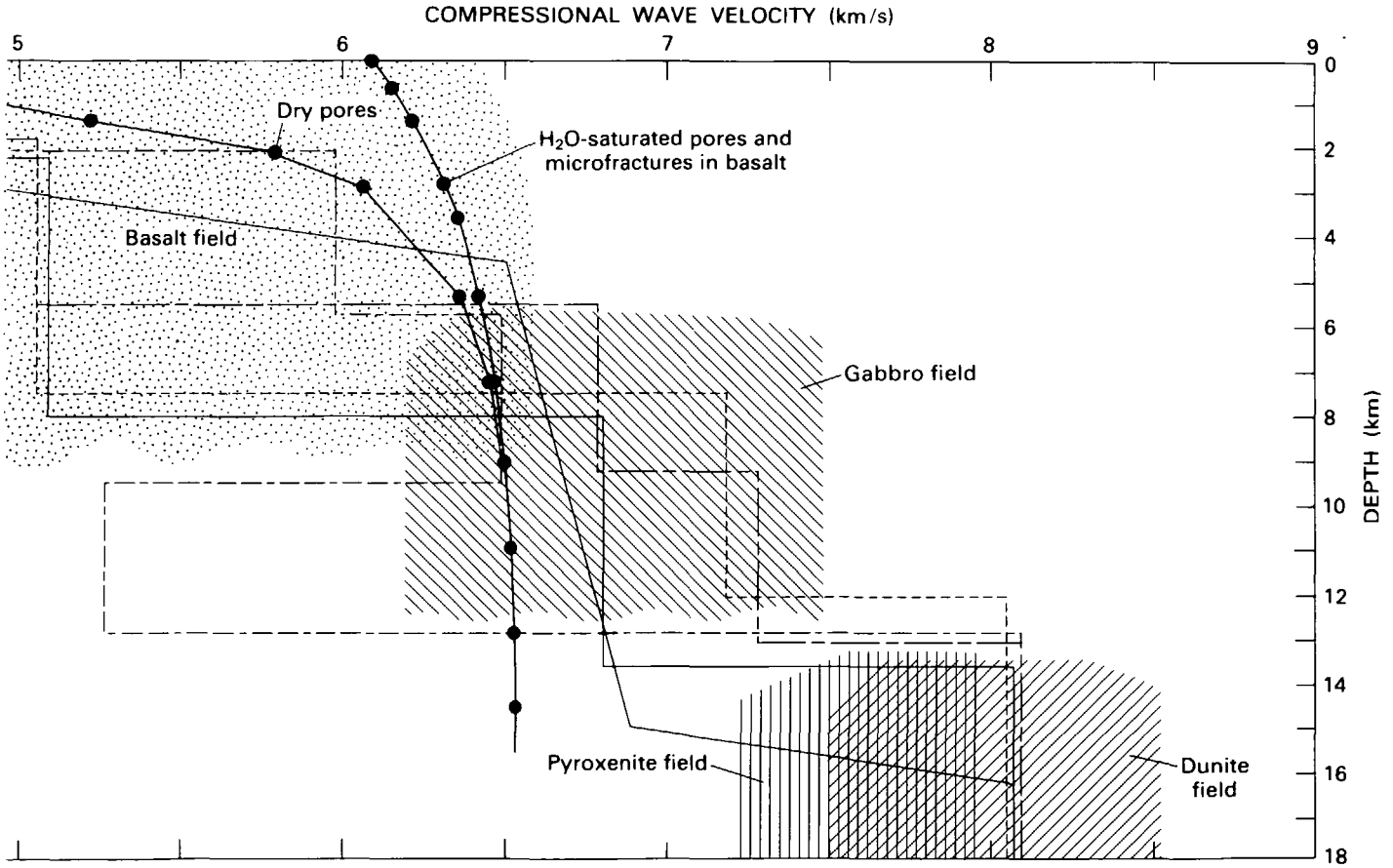

depths, and some additional overlap between gabbro and basalt to within ≈2 km of surface, particularly within core region of volcano. Illustrated field of basalt is constrained laterally by contractancy produced by progressive closure of microfractures and pores with increasing confining pressure. Low seismic velocities outside experimentally determined basalt field suggest contributions from dilatant and partially contracted fracture network associated with free surface of volcano. Base distribution of seismic-velocity profiles has been constructed from profiles of Hill (1969), Eaton (unpublished data, 1970), Ward and Gregersen (1973), and Crosson and Koyanagi (1979) as amended from compilation in Klein (1981).

(2) Geodesy: studies of the deformation associated with rift-zone intrusion have resolved the vertical and horizontal displacement fields generated by the hydraulic inflation of dikes (for example, Jackson and others, 1975; Swanson and others, 1976). These displacement patterns provide essential guidance for the location, strike, and dip of magmatic pressure sources at depth.

(3) Mechanics: the horizontal displacement field for specific intrusive episodes has been modeled for the superstructure of Kilauea at the 1:62,500 scale that corresponds to the model dimensions. The approach uses a finite-element analysis procedure for evaluating the displacement field generated by pressurized discontinuities in an elastic medium. Predicted displacement fields are then examined for consistency with the observed field. Material properties are guided by a combination of in-situ seismic velocities, gravity surveys, and experimental evaluations.

(4) Geology: the distribution of eruptive vents, fissures, and related structures within the rift zones provides collateral constraints on the distribution of magmatic bodies near the surface. Additional guidance is provided by the field study of dikes, sheets, and sills in the dissected shields of ancient Hawaiian volcanoes.

Within the context of this report, the model provides a useful framework for relating the pressure-dependent in-situ properties of the basaltic shield to images of structure and process within and beneath the shield. This framework provides a focal point for applications.

I recognized above that the contractancy of shield volcanoes is influenced by the distribution of faults and fractures in the near surface. Field studies of Kilauea indicate that the fracture networks that influence contractile behavior— and in turn the in-situ V_p, V_s, and density—are heterogeneously distributed. That is, con-

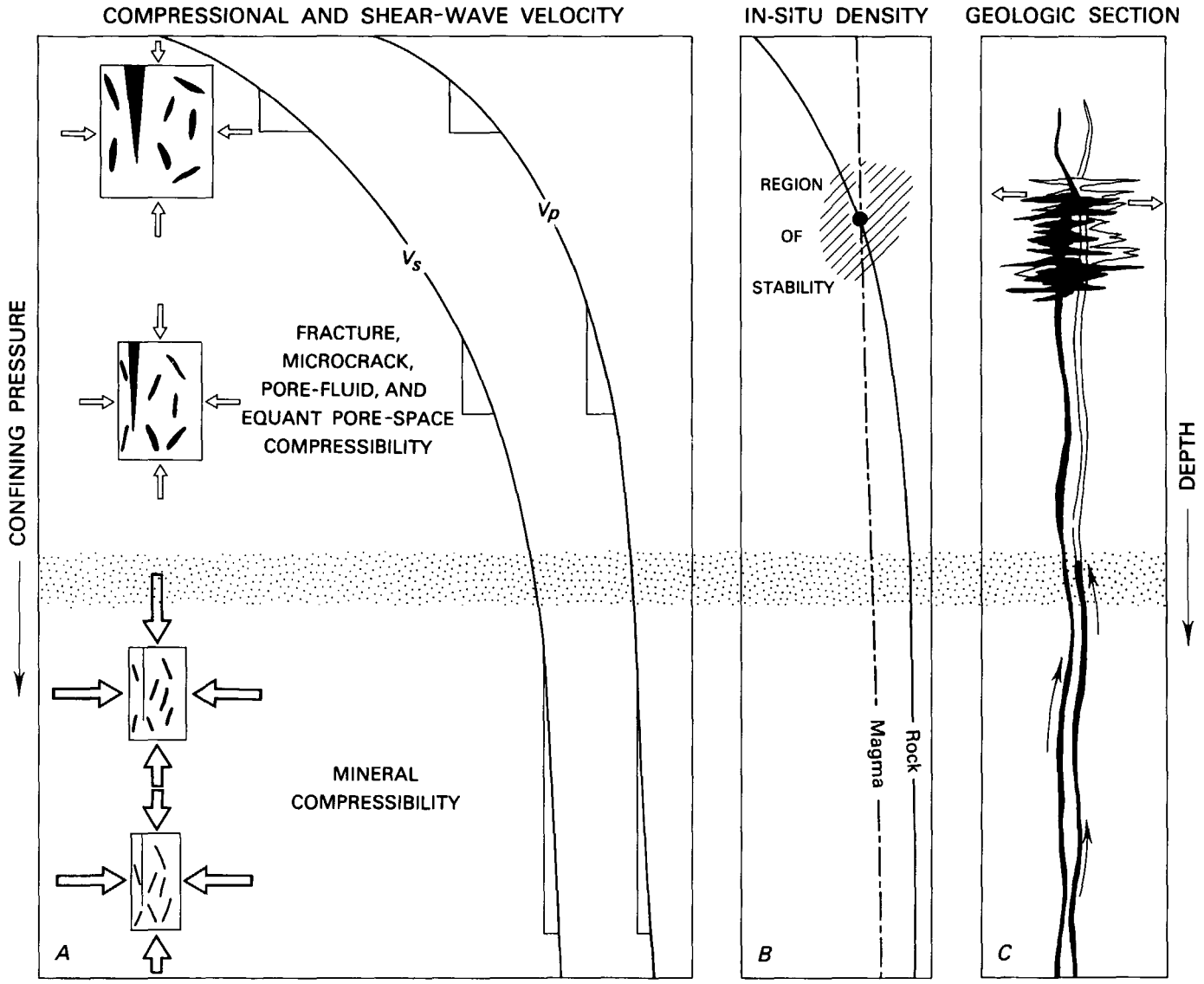

FIGURE 52.28.—*A*, Contributing mechanisms of contractancy in magmatic systems. *B*, Resulting crossover produced in in-situ densities of magma and country rock. *C*, Geologic consequences of a stabilized region with its zone of neutral buoyancy—a subcaldera magma reservoir.

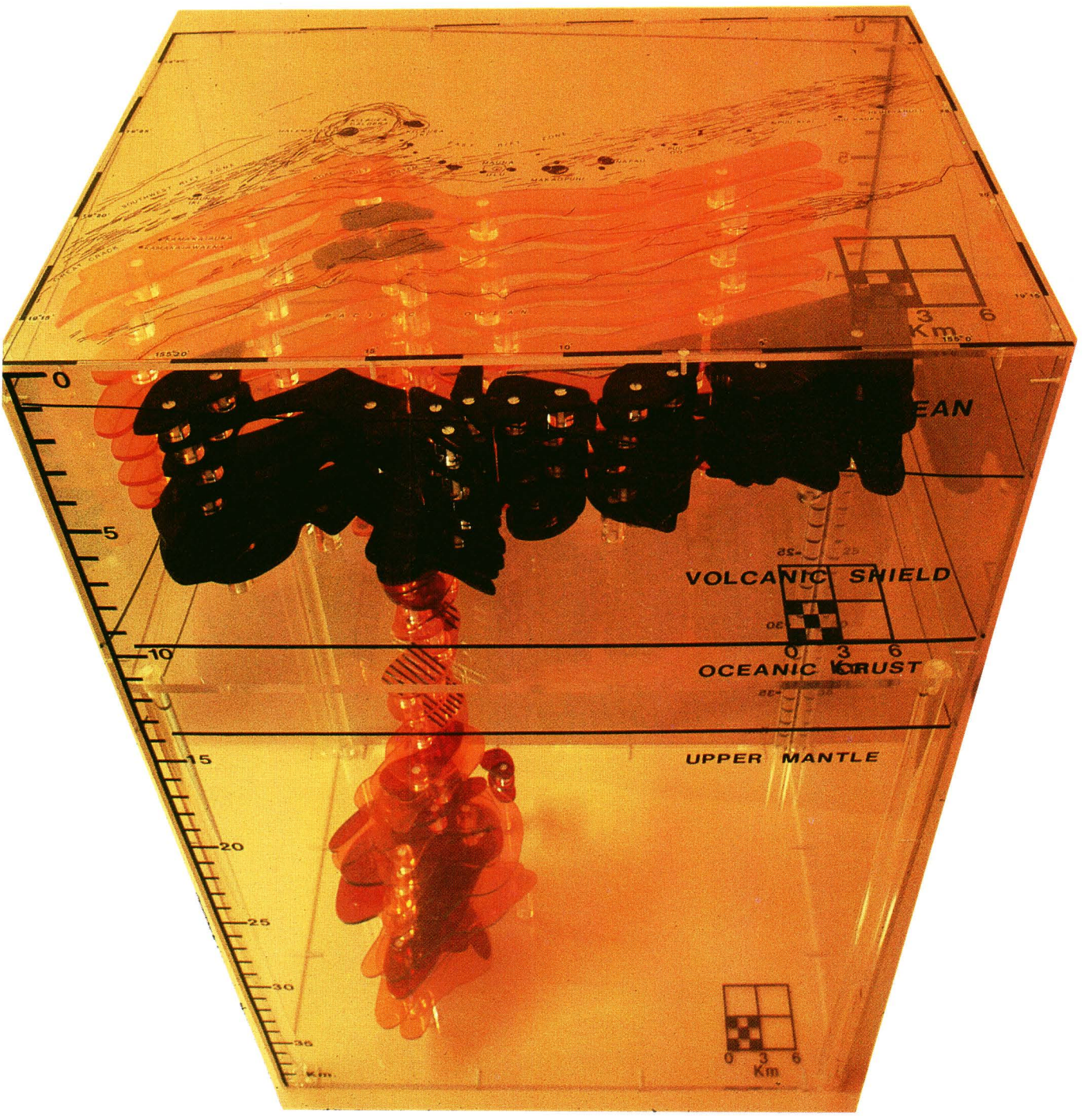

FIGURE 52.29.—Three-dimensional internal structure of Kilauea Volcano, constructed from three-dimensional distribution of earthquakes within and beneath Kilauea, at a map scale of 1:62,500. View orientation is northward, and model extends to 40-km depth. Surface physiography includes fracture systems and eruptive vents of the southwest and east rift zones and Kilauea caldera. Pacific Ocean coastline passes from lower left to middle right. Color coding corresponds to structural elements within the system, as well as temporal variations in hydraulic fracturing associated with magmatic transport from mantle depths. Color-coding format: light to medium amber (within volcanic shield), regions of inferred magmatic movement and storage for period January 1, 1969, to January 1, 1983; maroon, regions of inferred magmatic transport from November 29, 1975, to January 1, 1983; medium amber (within upper mantle), location of magmatic fracture front from January 1, 1969, to November 29, 1975; black, major tectonic blocks within basal levels of volcanic shield, shield-oceanic crust interface, and tectonic blocks of Koae fracture system; hachured amber, levels of low seismic control and uncertainty in geometric constraints. Configuration of major structural subdivisions, including volcanic shield, oceanic crust, and upper-mantle interfaces, is based on work of Hill (1969), Zucca and Hill (1980), and Zucca and others (1982). Vertical scale is 2 times horizontal, allowing an expanded view of geometry of individual level sections.

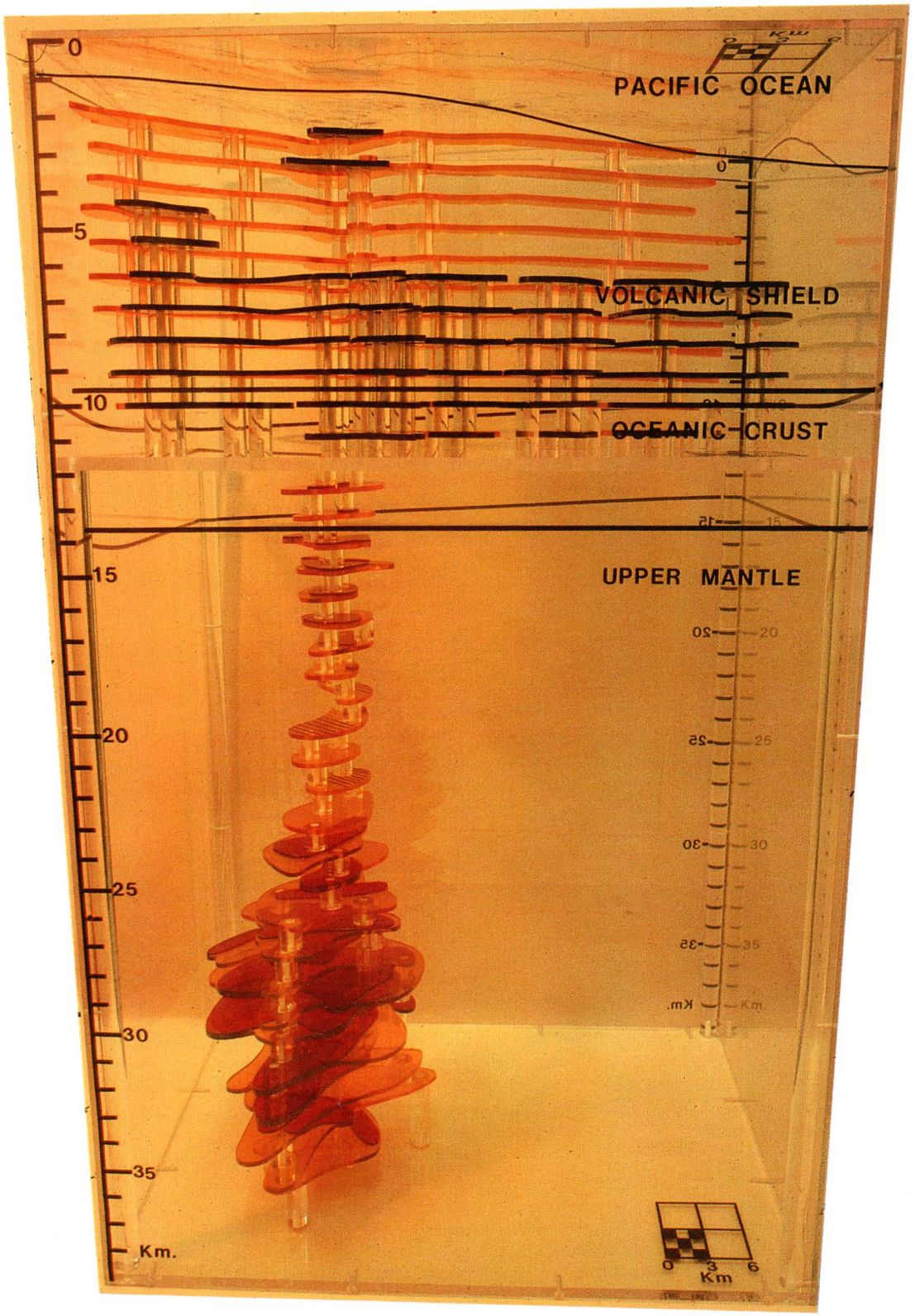
PACIFIC OCEAN
VOLCANIC SHIELD
OCEANIC CRUST
UPPER MANTLE
0
5
10
15
20
25
30
35
Km.
0 3 6
Km

tractancy itself has a three-dimensional structure. It is of interest then to relate these zones of inferred differential rock compression to the three-dimensional structure of the active magmatic system.

The internal structures of the southwest rift zone and east rift zone of Kilauea are resolved in figures 52.29, 52.30, and 52.31. These rift systems appear as medium amber in the figures and extend to the west (left) and east (right), respectively, in these northward-directed views. Their orientation is nearly vertical, and they intersect the surface of the volcano in a region of high fracture density that extends from the "great crack" in the southwest to Heiaheiahulu in the northeast. These fracture systems form in response to the hydraulic inflation of dikes within the rift zones. They record at the surface the differential stretch of rift-zone country rock at depth, as successive intrusive episodes are accommodated. Rift-zone intrusion then produces a zone of differentially contractant (low in-situ V_p, V_s, and ρ) rock above it. It is bounded below by the upper levels of the active dike complex, bounded above by the free surface of the volcano, and elongate along the strike of the rift system. The three-dimensional contractancy structure then mimics the map distribution of the intrusives at depth. Therefore, though rift systems are associated with relatively high densities and seismic velocities at depth, thus reflecting a shift from the velocity structure of the basaltic flanks (fig. 52.16) to the velocities of gabbroic complexes (fig. 52.17), we may expect the thin basaltic veneer of fault blocks above the dike complex to be rather low in in-situ density, V_p, and V_s values (for example, the low-velocity residuals in figure 52.27, to the left of the basalt field).

By analogy with the one-dimensional region of neutral buoyancy plotted in figure 52.26*B*, we may now construct an image of the topography of the three-dimensional neutral-buoyancy surface for Kilauea, relating it to the structure of the magmatic system in figures 52.29, 52.30, and 52.31. Such a surface makes up an in-situ isodensity topography for the interior of the volcano. At points on the surface, $\rho_{rock} - \rho_{melt} \approx 0$, and intrusives have reached density equilibrium positions with respect to the surrounding country rock. Consideration of the two-dimensional density structure resolved by Zucca and others (1982) suggests that, in cross-sectional slices orthogonal to the strike of the rift zone, the profile of neutral buoyancy rises from depth within the flanks to near-surface positions above the rift-zone complex, plunging once again to greater depth once the rift zone is crossed. In three dimensions, such a surface resembles an anticlinal fold, with a fold axis that is coaxial with the strike of the rift system, and a fold wavelength that scales with the rift-complex width. The three-dimensional neutral-buoyancy surface for Kilauea may now be visualized with reference to figures 52.29, 52.30, and 52.31. We would expect it to be draped over both the east and southwest rift systems: rising from depth beneath the south flank palis, passing over the axes of the rifts and caldera, and moving to depth once again beneath the stable north flank. From the summit, the fold axis of the neutral buoyancy surface plunges toward the coastline, following at depth the topography of the volcano, along both the southwest and east rift systems.

MECHANICAL EVOLUTION OF HAWAIIAN SHIELD VOLCANOES

Perhaps the initial suggestion that the summit magma reservoir of Hawaiian shield volcanoes moves progressively upward as the volcano grows was made by Jackson (1968, p. 146), who envisioned:

> A stack of tabular floored chambers representing successive periods of growth [and forming] a cylindrical body of dense rock that could account for the relatively high *P* wave velocities . . . under the summits.

This suggestion was adopted by Hill (1969, fig. 11, p. 129), who incorporated such a sequence in his summary cross section of a generalized Hawaiian volcano. Fiske and Kinoshita (1969, p. 348) concurred with this view:

> If such a reservoir complex has existed throughout much of Kilauea's history, it is reasonable to assume that the reservoir has migrated to progressively higher levels as the volcano grew to its present size. Today's reservoir would, therefore, be underlain by the sites of former reservoirs, and these would probably consist of dense sills and feeder dikes, containing accumulations of olivine.

It remained for Decker and others (1983, p. 547), however, to provide a convincing demonstration that such an evolutionary pattern is a fundamental theme in the development of Hawaiian volcanoes:

> The similarity between the surface-deformation pattern of the summit areas of Mauna Loa and Kilauea volcanoes is striking . . . The similarity of the morphology and evolution of the calderas on Mauna Loa and Kilauea, and the recent discovery of an apparent caldera on Loihi . . . indicate that the filling and collapse of calderas is a long-lasting and common mechanism in the growth of Hawaiian volcanoes. This conclusion implies that the magma storage zone grows upward from the old sea bottom as the volcano gains in elevation.

FIGURE 52.30.—Three-dimensional structure of Kilauea Volcano, in a northward-directed view from a depth of 10 km beneath summit caldera. Submarine topography of volcanic shield is uppermost light-weight line, deepening eastward (right). Black basal sections of south-flank tectonic blocks lie in front of southwest rift zone, caldera section, and east rift zone, progressing from left to right in 6- to 10-km-depth range. Hydraulic inflation of dikes within these rift systems lever blocks incrementally seaward, toward observer. Oceanic crust is isostatically depressed under primary loading of Mauna Loa, with a 3°–4° dip toward island center, based on seismic-refraction surveys of Hill (1969) and Zucca and Hill (1980). This loading produces crustal warping evident in this view. Contraction of volcanic shield takes place in 0- to 8–9-km-depth interval. Above 8 km, contraction is dominated by compression of macroscopic and microscopic fractures, vesicles, and fracture-filling fluids, including magma, sea water, and fresh water. Beneath 9 km, contraction of shield has been completed, and mineral compression is dominant.

The realization that both Mauna Loa and Kilauea possess a ubiquitous thin veneer of surface material of low in-situ density ($\rho \approx 2.3$ g/cm^3), combined with an appreciation of the density of tholeiitic melt ($\rho = 2.62$ gm/cm^3) at atmospheric pressure, requires a density crossover beneath the surface and poses an additional question. What is the relative position of the subcaldera magma storage reservoir for each of these volcanoes?

Geodetic surveys in the form of horizontal point-to-point distance measurements have been conducted on the summit of Mauna Loa over the period 1977 to 1981 (Decker and others,

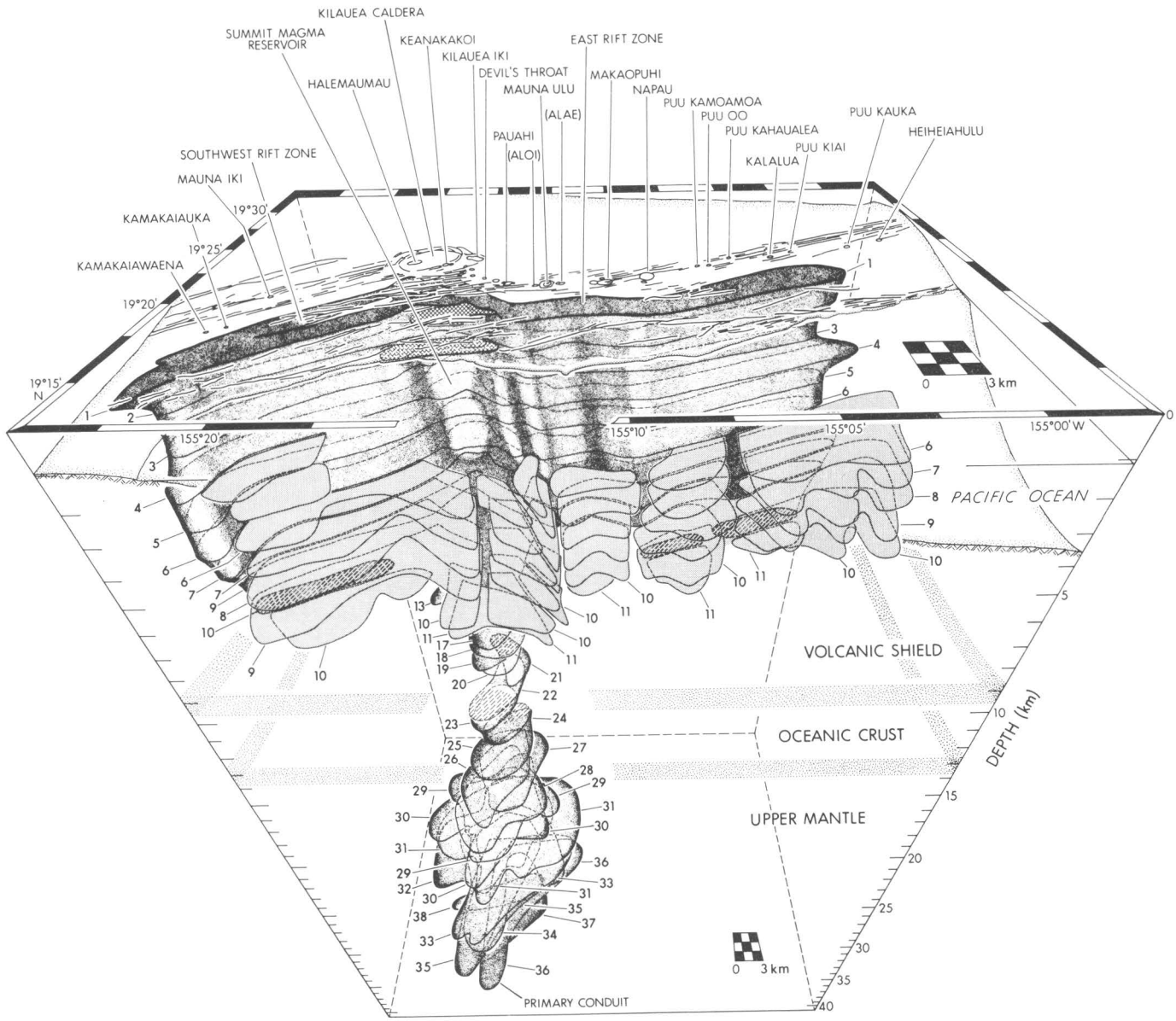

FIGURE 52.31.—Three-dimensional internal structure of Kilauea in a north-directed view from above, as constrained by three-dimensional distribution of earthquakes within and beneath volcano, and analytic mechanics of rift-zone intrusion. Magmatic system within volcanic shield lies to the north (rear) of tectonic blocks of the south flank (even light-gray shading). Influxes of magma within summit reservoir occurs by buoyant rise of melt parcels within primary conduit. Rupture of reservoir wall rock generally occurs at a depth of 3 km beneath caldera floor. This corresponds to region of neutral buoyancy. Dike injection from summit magma reservoir occurs into southwest and east rift zones. During injection process, leading edge of advancing dike propagates along neutral-buoyancy horizon. In general, this lies at a local depth of ≈3 km. Thus, mechanics of lateral dike-injection process are governed by maintenance of a near-constant local depth and neutral-buoyancy principle as pressure increases gained in summit storage are progressively spent. In constructing model, distribution of seismic hypocenters has partially constrained geometric details of rift zones, primary conduit, and south-flank tectonic blocks. Level numbers correspond to individual cross sections. These cross sections are dashed where seismic control is limited. Marine bathymetry has been guided by surveys of Chase and others (1980). Top of magmatic block of rift zone complexes and subcaldera intrusive complex lies at a local depth of 1 km. Between this depth and surface are eruptive fissures and conduits that feed surface activity, such as current eruptive center at Puu Oo. Neutral buoyancy—contractancy-mechanics principle—is viewed as dominant control for producing long rift systems in Hawaiian shield volcanoes. Doubly hachured areas south of caldera are blocks of Koae fracture system.

1983). The inversion of this data set, using the point-source modeling approach of Dvorak and others (1983), suggests an inflation center located at a depth of approximately 3.2 km beneath the caldera floor. Spirit-level tilt measurements taken over the same period suggest, upon inversion, a similar but somewhat shallower depth, 2.6 km (Decker and others, 1983). These surveys defined the geodetic signature of the magmatic pressure increases that led to the outbreak of eruptive activity in March 1984. If we now compare this suggested pressure center with that of its neighbor Kilauea, we see that the depth-below-caldera positions to the summit magma reservoir are remarkably similar: an averaged 2.9 km for Mauna Loa and the range 2–4 km for Kilauea, as discussed earlier. Yet the elevation above sea level for the volcanoes is very different: 4,169 m for Mauna Loa and 1,240 m for Kilauea. The elevation difference in the calderas is then nearly 3 km. Figure 52.32 illustrates the topography of Mauna Loa and Kilauea.

What accounts for this apparently systematic positioning of summit magma storage in these very different volcanoes? Our survey and discussion of the pressure dependence of the in-situ mechanical properties of basaltic and gabbroic rock offer a mechanical rationale. Reduced to its essentials, the contractancy model deals with a dilatant-free surface that is loaded gravitationally. Increases in depth then correspond to increases in lateral confining pressure, as the dilatant fracture space is progressively squeezed shut. A reconsideration of figures 52.21*B* and 52.26*B* suggests that it is the depth below the free-surface reference level that orders the amount of fracture permeability for such dilatant regimes. This reasoning accords well with the role of confining pressure on permeability suggested by Gangi (1978) and Walsh (1981) and implicit in the experiments of Christensen (1974).

A comparison of the relative positioning of subcaldera magma reservoirs in relation to volcanic stature and age turns our attention to

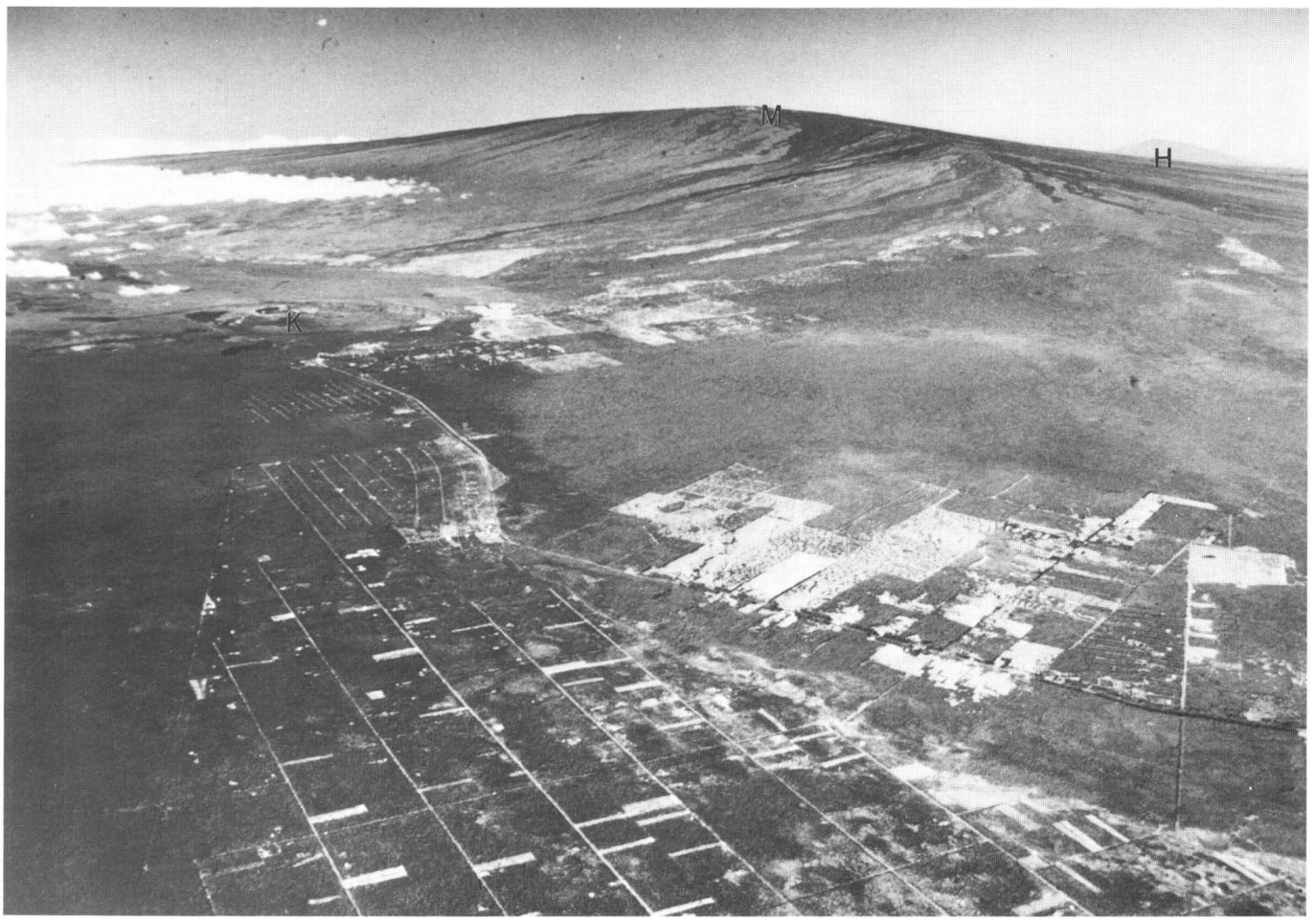

FIGURE 52.32.—Summit caldera of Kilauea (K) in relation to its older neighbor to northwest, Mauna Loa (M). Elevation of Mauna Loa's summit (4,169 m) contrasts with Kilauea's (1,240 m). Similarity in depths of magmatic pressure centers and regions of neutral buoyancy for each volcano (Kilauea, 2–4 km; Mauna Loa, ≈2.9 km) suggests that during evolution of Hawaiian shields, summit reservoir climbs progressively upward. This upward progression is regulated by contractancy of volcanic shield. This mechanism produces increases in confining pressure at fixed reference depths during shield building. Reservoir region may then be viewed as being squeezed upward during maturation process. Hence, shield contractancy has produced a reservoir within Mauna Loa whose upper levels are now at same elevation as Kilauea's summit region (that is, 3 km beneath Mokuaweoweo caldera). Older edifice of Hualalai (H) lies still farther northwest. In foreground is community of Volcano, Hawaii. Photograph by James Griggs.

the south of Kilauea—to Loihi Seamount. Geophysical data in the form of geodetic surveys analogous to those routinely conducted on Kilauea and Mauna Loa are nonexistent, and available seismic data are insufficient to provide the required constraints on the existence and nature of a potential magma-storage region within Loihi's edifice. Bathymetric surveys in the form of sonar mapping and Angus bottom photography have resolved, however, the presence of two radial rift zones and a summit crater complex at an elevation of 980 m below sea level (Malahoff, chapter 6; Malahoff and others, 1982). By analogy with its neighbors to the north, an edifice magma storage capability of modest dimensions may be suggested. Identical conclusions relative to Loihi have been reached by Decker (chapter 42).

The considerations above, coupled with the discussion of the pressure dependence of elasticity and in-situ velocity and density systematics for Hawaiian shield volcanoes, lead naturally to the following proposal for their mechanical evolution. As a shield is formed, the dilatancy produced by diminished lateral constraints within its upper levels produces a contractancy profile. Continued growth and maturation raises the contractancy profile to higher levels, because the origin is always associated with the volcanoes free surface. Stated differently, as a volcano grows, it carries its contractancy profile with it. The upward evolutionary track of contractancy then orders the upward subsurface positioning of the region of neutral buoyancy and the associated magma storage reservoir and its coupled rift systems. This progression, from infancy through middle age to maturity, is illustrated in figure 52.33.

Within a given reservoir, the region of neutral buoyancy will order the positioning of the upper levels of magmatic storage, whereas the basal levels are regulated by the squeezing shut of available fracture permeability. Stated differently, the top of magmatic storage corresponds to the depth level where the compressive

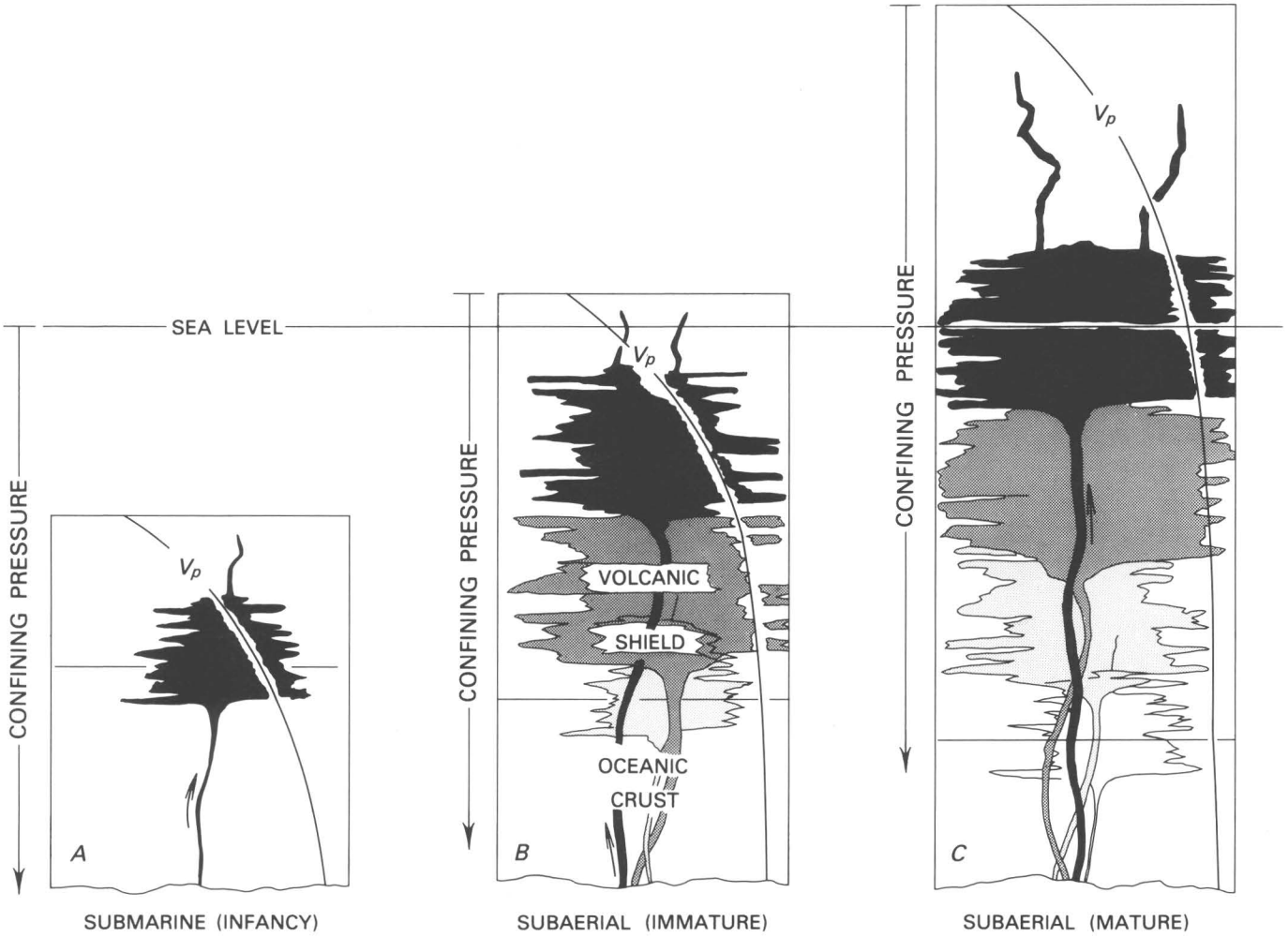

FIGURE 52.33.—Schematic changes in contractancy distribution with depth during growth and evolution of oceanic volcanoes. Volcanic shield-oceanic crust interface is stippled and is isostatically depressed under growing volcanic load. As a volcano grows, it carries its contractancy profile with it. Concomitant changes along this evolutionary track include: (1) progressive upward migration in transition zone that separates fields of fracture and pore-fluid compression above from mineral compression below; and (2) progressive upward migration of zone of neutral buoyancy. These changes provide mechanical rationale for evolutionary climb of subcaldera magma reservoirs in progression from submarine infancy (***A***) through subaerial immaturity (***B***) to subaerial maturity (***C***).

elimination of void space has just begun, and the bottom of the reservoir corresponds to the depth where void-space elimination has been completed. This general correlation is expected to apply to the rift systems as well as the subcaldera reservoir. In light of this relationship, we should expect the summit storage region to be laterally more extensive, with gains in elevation beneath the caldera. In a somewhat crude analogy, the evolving reservoir is lifting itself by its own bootstraps.

THE NATURE OF THE EVOLUTIONARY TRACK

The integration of in-situ seismic-wave velocities, in-situ densities for country rock and tholeiitic melt near its liquidus, magma-reservoir positions from geodetic and seismic studies, volcanic lithology, and structural geology with laboratory data bearing on the pressure and temperature dependence of elasticity leads to a set of empirical relations that unify the observations. When this type of information is compiled for Mauna Loa, Kilauea, and Loihi Seamount—each in a distinctive phase of its evolutionary progression—a set of further empirical relationships is discovered. These relations, presented below, provide the mechanical linkage between volcanic evolution and in-situ rock behavior. They form the basic correlations and postulates of the contractancy model.

Relation 1.—The datum for confining pressure is positioned at the volcanic summit and at the crest of the rift systems. As the volcano grows this datum is progressively raised. In the interior of the volcano, the depth level required to achieve a given confining pressure is simultaneously elevated. During the growth of the shield, the transition zone that separates the relatively shallow field of fracture and pore-fluid compression from the deeper field of mineral compression is therefore progressively elevated. This transition region will have a three-dimensional topography and should be controlled by the stature of the volcanic shield above it. It is expected to be broadly associated with the base of the subcaldera storage complex and the basal section of the rift zones.

Relation 2.—The surficial veneer of low in-situ V_p, V_s, and density is progressively elevated during growth. Formed principally by the macroscopic fracture network in the upper 2 km of the shield, it produces an associated region of density crossover between the country rock and near-liquidus melt. This region of neutral buoyancy provides a mechanically stable environment for the subcaldera storage of magma. Increases in volcanic stature then elevate this region during the maturation process. For Kilauea and Mauna Loa, the geodetically and seismically constrained regions of subcaldera magma storage have a 1:1 correspondence with the region of neutral buoyancy. The stability of intra-rift-zone magmatic storage is expected to adhere to this general principle.

Relation 3.—The thickness of the reservoir roof, determined principally by the depth level of the region of neutral buoyancy, is expected to remain roughly constant as growth proceeds. To first order, this approximate constancy in thickness, mean composition, gross crack density per unit volume, and the pressure-temperature (P,T) environment suggests broadly comparable volumetric strengths. These relations are compatible with the observation of essentially concurrent and progressive caldera collapse as the edifice evolves.

Relation 4.—The progressive and proportional enlargement of the caldera region during shield evolution suggests that the region of neutral buoyancy spreads radially as the shield grows. For Mauna Loa, Kilauea, and Loihi, this spreading is elliptical in plan form, with a major axis that is guided in part by the pervasive influence of the rift systems that originate beneath the caldera.

Relation 5.—The progressive closure of macroscopic and microscopic fractures with depth, as well as the continued compression and expulsion of pore fluids, will systematically raise the in-situ values of the bulk modulus (K), the shear modulus (μ), and the Young's modulus (E). Poisson's ratio (ν) will also vary with depth, because it reflects the ratio of in-situ lateral strains to the axial strains induced by the overburden. These changes track the experimentally determined changes in V_p and V_s with pressure and the in-situ variations of seismic-wave velocities with increasing depth. The progressive closure of fractures with depth will also continuously reduce the amount of bulk anelasticity and simultaneously increase the appropriateness of the continuum assumption employed in mechanical analyses.

Relation 6.—During the seamount phase of oceanic shield development, the bottom of the contractancy curve is expected to lie within the oceanic crust. Continued upward growth of the shield will elevate the compression transition zone to the level of oceanic crustal layer one, where the deepest levels of fracture closure will interact with the low-modulus sediments in controlling the base level of active rift systems. This condition describes the current state of Kilauea Volcano. Further increases in volcanic stature will lift the compression-transition-zone above the old oceanic crust and into the base of the volcanic shield itself. This compression-transition-zone elevation characterizes the current status of Mauna Loa Volcano. Thus, contractancy and the pressure dependence of fracture closure regulates the positions of active-rift-system keels during the mature phase of shield evolution.

SUBMARINE RIFT SYSTEMS AND THE GLOBAL ROLE OF NEUTRAL BUOYANCY

The general association in time and space of rift systems, dike intrusion, dilatant fractures, axial graben, and the neutral buoyancy-contractancy mechanism suggests that this effect may play a fundamental role in the intrusion mechanics and physical evolution of the Earth's oceanic rift systems. Clearly, important differences distinguish Hawaiian rift zones from their counterparts at accretionary plate margins. However, the overall simplicity of the dike-injection process and the primary structures associated with it suggests the following as geologic features of the neutral buoyancy—magma stabilization environment within active rift systems.

(1) Abundant dilatant and deep fissures, aligned parallel with the rift (for example, Ballard and others, 1979; Hey and others, 1985; Renard and others, 1985). Increases in confining pressure with depth will squeeze these fractures shut, increasing the in-situ density and compressional and shear wave velocity. Additional

sealing will be produced by the infilling of sediments and hydrothermal mineralization.

(2) Geomorphic evidence of lava drainback into dilatant fissures (lava-lake terraces, Ballard and others, 1979; and "bathtub" rings, Renard and others, 1985). Large amounts of accessible fracture volume, in turn, suggest significant decreases for in-situ ρ, V_p, and V_s.

(3) Nonlinear increases in compressional-wave velocity in the upper 2 to 3 kilometers within and near the spreading ridge (McClain and Atallah, 1985; Ritzert and Jacoby, 1985; Purdy and Detrick, 1986).

(4) Low aggregate in-situ densities inferred for the upper several hundred meters to 2,000 m.

(5) An axial valley characterized by tensional or downdropped structures.

(6) Gabbroic intrusives that have been emplaced at very shallow depth and subsequently exposed (Fox and others, 1985; Hey and others, 1985).

A consideration of these features prompts the question: What further predictions might the model make? First, a crossover in the in-situ density of basaltic magma and country rock should occur within oceanic rift zones, leading to conditions of neutral buoyancy and mechanical stability. To the extent that a given segment of rift zone was fed from a point source at depth, this would promote the lateral injection of dikes along a shallow horizon of neutral buoyancy. I believe that many sheeted-dike complexes within ancient oceanic crust record the general position of the neutral-buoyancy horizon during their emplacement. A second (and corollary) result is that magmatic eruptions in oceanic rift systems would be appreciably less favored than intrusions. The widespread occurrence of axial grabens suggest a pervasive dike-induced stretch at depth, without the infilling eruptions that would otherwise bury and obliterate these axial valleys. My own field studies on the dynamics of the magma injection-dike formation process in the Gjastykki rift system of the Krafla central volcano, northeastern Iceland, support these inferences. The role of neutral buoyancy in the world's oceanic rift zones is thus a vertically stabilizing one: mechanical equilibrium is achieved between intrusives and their host country rock.

CONCLUSIONS

Experiments conducted to 1,133 K in flexural and torsional resonance have permitted evaluation of the Young's modulus and the modulus of rigidity for Hawaiian olivine tholeiite. The temperature dependence of elasticity for this rock type is very nearly linear. The explicit temperature dependence from regression treatments of replicate runs for each primary mode of mechanical loading is:

Young's modulus,

$$E(T) = (6.054 - 0.00083T) \times 10 \text{ GPa},$$

and *modulus of rigidity*,

$$\mu(T) = (2.615 - 0.00038T) \times 10 \text{ GPa},$$

where T is the temperature in degrees Celsius.

Dilatometric evaluations of linear thermal-expansion coefficients for the same olivine tholeiite yield the value $\alpha_l = 4.58 \times 10^{-6}$ °C^{-1} at 373 K, whereas the expansivity at 973 K is $\alpha_l = 7.93 \times 10^{-6}$ °C^{-1}.

The effects of cyclic heating and cooling histories on the thermal expansivity of olivine tholeiite have been studied in experiments conducted to within 30° of the 1-atm solidus—1,223 K. Parallel comparison runs have been made with diabase in companion experiments. For the basalt, cyclic excursions to 1,223 K induce irreversible thermal strain. One cycle is sufficient to achieve this effect, and repeated cycling to the same maximum temperature induces additional increments of irreversible strain. These permanent dimension changes are interpreted as reflecting the production of successive generations of microfractures during successive visits to high temperatures. The behavior of diabase during cyclic heating and cooling is qualitatively similar: thermal-strain hysteresis with continued cycling. The sense of irreversible thermal strain is different, however, for basalt and diabase: contractile and expansive length changes, respectively. This difference suggests a progressive compaction in the basalt, via microcrack-induced micropore collapse, and a progressive opening of the microstructure of the diabase by microfracture only.

A model has been developed for the high-temperature elasticity of basalt that incorporates the compositional and microstructural dependence of the relevant moduli. Specialized for the major mineral phases of tholeiitic basalt in this report, it is general in nature and is applicable to other rock types. Tabulated values of the elastic properties of olivine, clinopyroxene and orthopyroxene, and plagioclase provide a basis for immediate extensions to mafic and ultramafic rock types of relevance to Hawaii.

The model incorporates the following parameters and capabilities:

(1) Compositional: the aggregate may be monomineralic or consist of an assemblage of n-multiple phases. There are no conceptual limitations on either the mineralogy or the number of phases. Required input data should be either the directionally dependent elastic stiffness and compliance coefficients or the mineral V-R-H-averaged bulk modulus and rigidity. The ultimate limitations on the number of mineral components reduces to the familiar problem of the availability of reliable input data. The model provides predictions of aggregate bulk (K), shear (μ), and Young's (E) moduli.

(2) Microstructural: the compositional model is complemented by incorporating the voids and flaws that weaken the solid and lower the moduli. For basalt, these voids are dominated by the vesicles produced during posteruption degassing. Spherical voids approximate the vesicles. Calculations with needle-shaped voids approximate the geometry of certain grain-edge microfractures. Volume fractions within each category are adjustable and may be guided, for example, by petrographic thin-section examination. The model is readily extendable to incorporate flat microfractures.

(3) Thermal: the temperature dependence is incorporated by introducing the temperature derivative for each contributing mineral phase. Specifically required is the temperature dependence for the bulk modulus (dK/dT) and the modulus of rigidity($d\mu/dT$). Each

contributes to the aggregate behavior through its weighted average. The model may be extended to incorporate pressure dependence by an application of the V-R-H-averaged pressure derivatives as outlined in Graham and Dobrzykowski (1976).

The effects of pressure on the elasticity of basalt provide a basis for developing the contractancy model of the mechanical behavior of shield volcanoes. The model provides a unifying framework that relates the following physical states and derivative properties: (1) the velocity-confining pressure systematics in laboratory samples for V_p and V_s; (2) the in-situ velocity-stratigraphy systematics for seismic profiles beneath the Island of Hawaii; (3) the in-situ density-stratigraphy structure through the Island of Hawaii, as inferred from studies of gravity profiles over summit, rift zone, and flank environments; and (4) the structural geology of Hawaiian shield volcanoes, with particular reference to caldera and rift-zone structure, and their fracture networks.

Additional coherence is suggested by the contractancy model: within Kilauea and Mauna Loa Volcanoes, a crossover occurs between the in-situ density of tholeiitic melt near its liquidus and the in-situ density of the country-rock environment in the subcaldera magma reservoir. The crossover occurs in the nonlinear region of the contractancy profile; that is, at confining pressures that are generally less than 200 MPa (2 kbar). In the core of the density crossover is a region of neutral buoyancy. Here $\rho_{rock} - \rho_{melt} \approx 0$. This mechanism suggests that contractancy provides the fundamental control on the long-term stability of these reservoirs. For Kilauea and Mauna Loa, the geodetically constrained magma-storage reservoirs have a 1:1 coincidence with the density crossover region produced by the contractant shields. This coincidence is produced again in the three-dimensional structure of Kilauea's summit reservoir, as constrained by subcaldera seismicity. In addition, and as a logical consequence, shield contractancy (and derivative in-situ density) provides a mechanism for the frequent observation of intrusives that have come to rest at very shallow depths (for example, dikes in rift systems), as inferred in geodetic-inversion studies and as directly observed in dissected Hawaiian rift systems. Finally, the progressively contractant behavior of Hawaiian shield volcanoes with depth and the attendant in-situ density progression that it implies provide the mechanical rationale for the physical evolution of their subcaldera magma reservoirs as the maturation process continues.

REFERENCES CITED

Aleksandrov, K.S., Ryzhova, T.V., and Belikov, B.P., 1964, The elastic properties of pyroxenes: Soviet Physics-Crystallography, v. 8, no. 5, p. 589-591.

Amadei, B., and Goodman, R.E., 1981, A 3-D constitutive relation for fractured rock masses, *in* Selvadurai, A.P.S., ed., Mechanics of structured media: Amsterdam, Elsevier, p. 249-268.

Anderson, O.L., Schreiber, E., Liebermann, R.C., and Soga, N., 1968, Some elastic constant data on minerals relevant to geophysics: Review of Geophysics, v. 6, p. 491-524.

Arndt, J., and Häberle, J., 1973, Thermal expansion and glass transition temperatures of synthetic glasses of plagioclase composition: Contributions to Mineralogy and Petrology, v. 39, p. 175-185.

Babuska, V., 1972, Elasticity and anisotropy of dunite and bronzitite: Journal of Geophysical Research, v. 77, p. 6955-6963.

Bajuk, E.I., Valarovich, M.P., Klima, K., Pros, Z., and Vanek, J., 1957, Velocity of longitudinal waves in eclogite and ultrabasic rocks under pressures to 4 kilobars: Studies in Geophysics and Geodesy, v. 11, p. 271.

Ballard, R.D., Holcomb, R.T., and Van Andel, T.H., 1979, The Galapagos rift at 86°N, 3. Sheet flows, collapse pits and lava lakes of the rift valley: Journal of Geophysical Research, v. 84, p. 5407-5422.

Bandis, S.C., Lumsden, A.C., and Barton, N.R., 1983, Fundmentals of rock joint deformation: International Journal of Rock Mechanics and Mining Sciences and Geomechanics Abstracts, v. 20, p. 249-268.

Birch, F., 1960, Velocity of compressional waves in rocks to 10 kilobars, Part I: Journal of Geophysical Research, v. 65, p. 1083.

Brace, W.F., Paulding, B.W., Jr., and Scholz, C.H., 1966, Dilatancy in the fracture of crystalline rocks: Journal of Geophysical Research, v. 71, p. 3939-3956.

Breyer, H., 1930, Über die Elastizität von Gesteinen: Zeitschrift für Geophysik: Heft, v. 2, p. 98-111.

Brown, S.R., and Scholz, C.H., 1985, Closure of random elastic surfaces in contact: Journal of Geophysical Research, v. 90, p. 5531-5545.

Budiansky, B., 1965, On the elastic moduli of some heterogeneous materials: Journal of the Mechanics and Physics of Solids, v. 13, p. 223-227.

Budiansky, B., and O'Connell, R.J., 1976, Elastic moduli of a cracked solid: International Journal of Solids and Structures, v. 12, p. 81-97.

Bulau, J.R., Waff, H.S., and Tyburczy, J.A., 1979, Mechanical and thermodynamic constraints on fluid distribution in partial melts: Journal of Geophysical Research, v. 84, p. 6102-6108.

Cady, J.W., 1977, Calculation of gravity and magnetic anomalies along profiles with end corrections and inverse solutions for density and magnetization: U.S. Geological Survey Open-File Report 77-463, 110 p.

Chase, T.E., Miller, C.P., Seekins, B.A., Normark, W.R., Gutmacher, C.E., Wilde, P., and Young, J.D., 1980, Topography of the southern Hawaiian Islands: U.S. Geological Survey Open-File Map 81–120, 3 pls.

Christensen, N.I., 1966, Elasticity of ultrabasic rocks: Journal of Geophysical Research, v. 71, p. 5921-5931.

———1971, Fabric, seismic anisotropy and tectonic history of the Twin Sisters dunite: Geological Society of America Bulletin, v. 82, p. 1681.

———1973, Compressional and shear wave velocities in basaltic rocks, DSDP leg 16, *in* Van Andel, T.H., Heath, G.R., and others, eds., Initial reports of the Deep Sea Drilling Project: U.S. Government Printing Office, v. 16, p. 647-649.

———1974, The petrologic nature of the lower oceanic crust and upper mantle, *in* Kristjansson, L., ed., Geodynamics of Iceland and the North Atlantic area: Dordrecht, Netherlands, D. Reidel, p. 165-176.

———1976, Seismic velocities, densities and elastic constants of basalts from DSDP leg 35, *in* Hollister, C.D., Craddock, C., and others, eds., Initial reports of the Deep Sea Drilling Project: U.S. Government Printing Office, v. 35, p. 335-337.

———1978, Ophiolites, seismic velocities and oceanic crustal structure: Tectonophysics, v. 47, p. 131-157.

———1984, Pore pressure and oceanic crustal seismic structure: Geophysical Journal of the Royal Astronomical Society, v. 79, p. 411-424.

Christensen, N.I., Carlson, R.L., Salisbury, M.H., and Fountain, D.M., 1975, Elastic wave velocities in volcanic and plutonic rocks recovered on DSDP leg 31, *in* Kraig, D.E., Ingle, J.C., and others, eds., Initial reports of the Deep Sea Drilling Project: U.S. Government Printing Office, v. 31, p. 607-609.

———1974a, Velocities and elastic moduli of volcanic and sedimentary rocks recovered on DSDP leg 25, *in* Simpson, E.S.W., Schlich, R., and others, eds., Initial reports of the Deep Sea Drilling Project: U.S. Government Printing Office, v. 25, p. 357-360.

———1974b, Velocities of compressional and shear waves in DSDP leg 27 basalts, *in* Veevers, J.J., and Heirtzler, J.R., eds., Initial reports of the Deep Sea Drilling Project: U.S. Government Printing Office, v. 27, p. 445-449.

Christensen, N.I., and Ramananantoandro, R., 1971, Elastic moduli and anisotropy of dunite to 10 kilobars: Journal of Geophysical Research, v. 76, p. 4003.

Christensen, N.I., and Salisbury, M.H., 1972, Sea floor spreading, progressive alteration of layer two basalts, and associated changes in seismic velocities: Earth and Planetary Science Letters, v. 15, p. 367-375.

———1973, Velocities, elastic moduli and weathering-age relations for Pacific layer 2 basalts: Earth and Planetary Science Letters, v. 19, p. 461-470.

———1975, Structure and constitution of the lower oceanic crust: Review of Geophysics and Space Physics, v. 13, p. 57-86.

Coble, R.L., and Kingery, W.D., 1956, Effect of porosity on physical properties of sintered alumina: Journal of American Ceramic Society, v. 39, p. 337-385.

Crosson, R.S., and Endo, E.T., 1982, Focal mechanisms and location of earthquakes in the vicinity of the 1975 Kalapana earthquake aftershock zone 1970-1979: Implications for tectonics of the south flank of Kilauea Volcano, Island of Hawaii: Tectonics, v. 1, p. 495-542.

Crosson, R.S., and Koyanagi, R.Y., 1979, Seismic velocity structure below the Island of Hawaii from local earthquake data: Journal of Geophysical Research, v. 84, p. 2331-2342.

Davis, P.M., Hastie, L.M., and Stacey, F.D., 1974, Stresses within an active volcano—with particular reference to Kilauea: Tectonophysics, v. 22, p. 355-362.

Decker, R.W., Koyanagi, R.Y., Dvorak, J.J., Lockwood, J.P., Okamura, A.T., Yamashita, K.M., and Tanigawa, W.R., 1983, Seismicity and surface deformation of Mauna Loa volcano, Hawaii: Eos, v. 64, p. 545-547.

Dieterich, J.H., and Decker, R.W., 1975, Finite element modeling of surface deformation associated with volcanism: Journal of Geophysical Research, v. 80, p. 4094-4102.

Duffield, W.A., Christensen, R.L., Koyanagi, R.Y., and Peterson, D.W., 1982, Storage, migration and eruption of magma at Kilauea Volcano, Hawaii, 1971-1972: Journal of Volcanology and Geothermal Research, v. 13, p. 273-307.

Dvorak, J.J., Okamura, A.T., and Deiterich, J.H., 1983, Analysis of surface deformation data, Kilauea Volcano, Hawaii: October 1966 to September 1970: Journal of Geophysical Research, v. 88, p. 9295-9304.

Eaton, J.P., 1962, Crustal structure and volcanism in Hawaii, *in* Crust of the Pacific Basin: American Geophysical Union Monograph, p. 13-29.

Eaton, J.P., and Murata, K.J., 1960, How volcanoes grow: Science, v. 132, p. 925-938.

Eshelby, J.D., 1957, The determination of the elastic field of an ellipsoidal inclusion and related problems: Proceedings of the Royal Society of London, ser. A, v. 241, p. 376-396.

Fedotov, S.A., 1977a, Geophysical data on deep-seated magmatic activity below Kamchatka and an estimate of the forces that cause the rise of magmas into volcanoes: International Geology Review, v. 19, p. 661-670.

———1977b, Mechanism of deep-seated magmatic activity below island-arc volcanoes and similar structures: International Geology Review, v. 19, p. 671-680.

———1977c, Ascent of basic magmas in the crust and the mechanism of basaltic fissure eruptions: International Geology Review, v. 20, p. 33- 48.

Fiske, R.S., and Jackson, E.D., 1972, Orientation and growth of Hawaiian volcanic rifts: The effect of regional structure and gravitational stresses: Proceedings of the Royal Society of London, ser. A, v. 329, p. 299-326.

Fiske, R.S., and Kinoshita, W.T., 1969, Inflation of Kilauea Volcano prior to its 1967–1968 eruption: Science, v. 165, p. 341-349.

Fornari, D.J., Malahoff, A., and Heezen, B.C., 1978, Volcanic structure of the crest of the Puna ridge, Hawaii: geophysical implications of submarine volcanic terrain: Geological Society of American Bulletin, v. 89, p. 605-616.

Förster, F., 1937, Ein neues Messverfahren zur Bestimmung des Elastizitäts Moduls und der Dämpfung (New method for determination of modulus of elasticity and damping): Zeitschrift für Metallkunde, v. 29, p. 109-115.

Fox, P.J., Moody, R.H., Karson, J.A., Bonatti, E., Kidd, W.S.F., Crane, K., Gallo, D.G., Stroup, J.B., Fornari, D.J., Elthon, D., Hamlyn, P., Casey, J.F., Needham, D., and Sartori, R., 1985, The geology of the oceanographer transform: The transform domain: Marine Geophysical Researches, v. 7, p. 329-358.

Fox, P.J., and Schreiber, E., 1973, Compressional wave velocities in basalt and dolerite samples recovered during leg 15, *in* Edgar, N.T., Saunders, J.B., and others, eds., Initial reports of the Deep Sea Drilling Project: U.S. Government Printing Office, v. 15, p. 1013-1015.

Fox, P.J., Schreiber, E., and Peterson, J.J., 1973, The geology of the Oceanic crust: compressional wave velocities of oceanic rocks: Journal of Geophysical Research, v. 78, p. 5155-5172.

Frisillo, A.L., 1972, The elastic coefficients of bronzite as a function of pressure and temperature: University Park, Pennsylvania State University, Ph.D. thesis.

Frisillo, A.L., and Buljan, S.T., 1972, Linear thermal expansion coefficients of orthopyroxene to 1000 °C: Journal of Geophysical Research, v. 77, p. 7115-7117.

Fujii, T., and Kushiro, I., 1977, Density, viscosity, and compressibility of basaltic liquid at high pressures: Carnegie Institution of Washington Year Book, v. 76, p. 419-424.

Gangi, A.F., 1978, Variation of whole and fractured porous rock permeability with confining pressure: International Journal of Rock Mechanics and Mining Sciences and Geomechanics Abstracts, v. 15, p. 249-257.

Gold, T., and Soter, S., 1985, Fluid ascent through the solid lithosphere and its relation to earthquakes: Pure and Applied Geophysics, v. 122, p. 492-530.

Graham, E.K., 1969, The elastic coefficients of forsterite as a function of pressure and temperature: University Park, Pennsylvania State University, Ph.D. thesis.

Graham, E.K., and Barsch, G., 1969, Elastic constants of single-crystal forsterite as a function of temperature and pressure: Journal of Geophysical Research, v. 74, p. 5949-5960.

Graham, E.K., and Dobrzykowski, D., 1976, Temperatures in the mantle as inferred from simple compositional models: American Mineralogist, v. 61, p. 549-559.

Grove, T.L., and Baker, M.B., 1983, Effects of melt density on magma mixing in calc-alkaline series lavas: Nature, v. 305, p. 416-418.

Hashin, Zvi, 1964, Theory of mechanical behavior of heterogeneous media: Applied Mechanics Reviews, v. 17, p. 1-8.

Hashin, Zvi, and Shtrikman, S., 1962, A variational approach to the theory of the elastic behavior of polycrystals: Journal of Mechanics and Physics in Solids, v. 10, pp. 343-352.

Hassleman, D.P.H., 1961, Tables for the computation of the shear modulus and Young's modulus of elasticity from the resonant frequencies of rectangular prisms: Niagara Falls, N.Y., Applied Research Branch, The Carborundum Co., 17 p.

Hekinian, R., Auzende, J.M., Francheteau, J., Gente, P., Ryan, W.B.F., and Kappel, E.S., 1985, Offset spreading centers near 12°53'N on the East Pacific rise: Submersible observations and composition of the volcanics: Marine Geophysical Researches, v. 7, p. 359-377.

Herzberg, C.T., Fyfe, W.S., and Carr, M.J., 1983, Density constraints on the formation of the continental Moho and crust: Contributions to Mineralogy and Petrology, v. 84, p. 1-5.

Hey, R.N., Sinton, J.M., Atwater, T.M., Christie, D.M., Johnson, H.P., Kleinrock, M.C., Macdonald, K.C., Miller, S.P., Neal, C.A., Searle, R.C., Sleep, N.H., and Yonover, R.N., 1985, Alvin investigation of an oceanic propagating rift system, Galapagos 95.5°W: Eos, v. 66, p. 1091.

Hill, D.P., 1969, Crustal structure of the Island of Hawaii from seismic-refraction measurements: Bulletin of the Seismological Society of America, v. 59, p. 101-130.

Hill, R.E.T., and Boettcher, A.L., 1970, Water in the earth's mantle: melting curves of basalt-water and basalt-water-carbon dioxide: Science, v. 167, p. 980-982.

Hill, R.W., 1952, The elastic behavior of a crystalline aggregate: Proceedings of the Royal Society of London, ser. A, v. 65, p. 349-354.

———1965, A self-consistent mechanics of composite materials: Journal of Mechanics and Physics of Solids, v. 13, p. 213-222.

Hughes, D.S., and Cross, J.H., 1951, Elastic wave velocities in rocks at high pressures and temperatures: Geophysics, v. 16, p. 577.

Hughes, D.S., and Maurette, C., 1957, Variation of elastic wave velocities in basic igneous rocks with pressure and temperature: Geophysics, v. 22, p. 23.

Hyndman, R.D., 1976, Seismic velocity measurements of basement rocks from DSDP leg 37, *in* Aumento, F., and Melson, W.G., eds., Initial reports of the Deep Sea Drilling Project: U.S. Government Printing Office, v. 37, p. 373-387.

Ide, J.M., 1936, Some dynamic methods for determination of Young's modulus: Review of Scientific Instruments, v. 6, p. 296.

———1937, The velocity of sound in rocks and glasses as a function of temperature: Journal of Geology, v. 45, p. 689-715.

Iida, K., and Kumazawa, M., 1960, Measurements of elastic wave velocities in

volcanic rocks at high temperatures by means of ultrasonic impulse transmission, Part I: Nagoya University, Journal of Earth Science, v. 7, p. 49-64.

Jackson, D.B., Swanson, D.A., Koyanagi, R.Y., and Wright, T.L., 1975, The August and October 1968 east rift eruptions of Kilauea Volcano, Hawaii: U.S. Geological Survey Professional Paper 890, 33 p.

Jackson, E.D., 1968, The character of the lower crust and upper mantle beneath the Hawaiian Islands: International Geological Congress, 23d, Prague, 1968, v. 1, p. 135-150.

Jackson, E.D., Clague, D.A., Engleman, E., Friesen, W.B., and Norton, D., 1981, Xenoliths in the alkalic basalt flows from Hualalai Volcano, Hawaii: U.S. Geological Survey Open-File Report 81-1031, 33 p.

Jackson, E.D., and Wright, T.L., 1970, Xenoliths in the Honolulu Volcanic Series, Hawaii: Journal of Petrology, v. 11, p. 405-430.

Johnson, A.T., and Pollard, D.D., 1973, Mechanics of growth of some laccolithic intrusions in the Henry Mountains, Utah, I: Tectonophysics, v. 18, p. 261-309.

Jones, L.E.A., 1977, High-temperature elasticity of rutile-structure MgF_2: Physics and Chemistry of Minerals, v. 1, p. 179-198.

Kanamori, H., and Mizutani, 1965, Ultrasonic measurements of elastic constants of rocks under high pressures: Bulletin of the Earthquake Research Institute, v. 43, p. 173.

Kern, H., and Rich, A., 1979, Compressional and shear wave velocities at high temperature and confining pressure in basalts from the Faeroe Islands: Tectonophysics, v. 54, p. 231-252.

King, M.S., 1966, Wave velocities in rocks as a function of changes in overburden pressure and pore fluid saturants: Geophysics, v. 31, p. 50-73.

Klein, F.W., 1981, A linear gradient crustal model for south Hawaii: Bulletin of the Seismological Society of America, v. 71, p. 1503-1510.

Koyanagi, R.Y., Unger, J.D., Endo, E.T., and Okamura, A.T., 1976, Shallow earthquakes associated with inflation episodes at the summit of Kilauea Volcano, Hawaii: Bulletin of Volcanology, v. 39, p. 621-631.

Kroenke, L.W., Manghnani, M.H., Rai, C.S., Fryer, P., and Ramananantoandro, R., 1976, Elastic properties of selected ophiolitic rocks from Papua, New Guinea: Nature and composition of oceanic crust and upper mantle, *in* Sutton, G.H., Manghnani, M.H., and Moberly, R., eds., The geophysics of the Pacific Ocean basin and its margins: Washington, American Geophysical Union, v. 19, p. 407.

Kröner, E., 1958, Kontinuumstheorie der Versetzungen und Eigenspannungen: Ergebnisse der Angewandten Mathematik: Springer-Verlag, v. 5.

———1967, Elastic moduli of perfectly disordered composite materials: Journal of the Mechanics and Physics of Solids, v. 15, p. 319-329.

Lambeck, K., and Nakiboglu, S.M., 1980, Seamount loading and stress in the ocean lithosphere: Journal of Geophysical Research, v. 85, p. 6403-6418.

Leibfried, G., and Ludwig, W., 1961, Theory of anharmonic effects in crystals, *in* Seitz, F., and Turnbull, D., eds., Solid State Physics, v. 12: New York, Academic Press, p. 276-444.

Liou, J.G., Kuniyoshi, S., and Ito, K., 1974, Experimental studies of the phase relations between greenschist and amphibolite in a basaltic system: American Journal of Science, v. 274, p. 613-632.

Macdonald, G.A., and Katsura, T., 1964, Chemical composition of Hawaiian lavas: Journal of Petrology, v. 5, p. 82-133.

Malahoff, A., McMurtry, G.M., Wiltshire, J.C., and Yeh, H-W., 1982, Geology and chemistry of hydrothermal deposits from active submarine volcano, Loihi, Hawaii: Nature, v. 298, p. 234-239.

Manghnani, M.H., and Woollard, G.P., 1968, Elastic wave velocities in Hawaiian rocks at pressures to 10 kilobars, *in* Knopoff, L., Drake, C.L., and Hart, P.J., eds., The crust and upper mantle of the Pacific area: American Geophysical Union, v. 12, p. 501-516.

Mao, N.-H., Ito, J., Hays, J.F., Drake, J., and Birch, F., 1970, Composition and elastic constants of hortonolite dunite: Journal of Geophysical Research, v. 75, p. 4071-4076.

McClain, J.S., and Atallah, C.A., 1985, The structure of young oceanic crust near a very fast spreading ridge: Geophysical Research Letters, v. 12, p. 689-692.

McKenzie, D., 1984, The generation and compaction of partially molten rock: Journal of Petrology, v. 25, p. 713-765.

Mizutani, H., and Newbigging, D.F., 1973, Elastic wave velocities of Apollo 14, 15 and 16 rocks: Proceedings of the Fourth Lunar Science Conference, v. 3, p. 2601-2609.

Mogi, K., 1958, Relations between the eruptions of various volcanoes and the deformations of the ground surfaces around them: Bulletin of Earthquake Research Institute, Tokyo University, v. 36, p. 99-134.

Moore, J.G., 1975, Mechanism of formation of pillow lava: American Scientist, v. 63, p. 269-277.

Moore, J.G., and Fiske, R.S., 1969, Volcanic substructure inferred from dredge samples and ocean bottom photographs, Hawaii: Geological Society of America Bulletin, v. 80, p. 1191-1202.

Moore, R.B., Helz, R.T., Dzurisin, D., Eaton, G.P., Koyanagi, R.Y., Lipman, P.W., Lockwood, J.P., and Puniwai, G.P., 1980, The 1977 eruption of Kilauea Volcano, Hawaii: Journal of Volcanology and Geothermal Research, v. 7, p. 189-210.

Murase, T., and McBirney, A.R., 1973, Properties of some common igneous rocks and their melts at high temperatures: Geological Society of America Bulletin, v. 84, p. 3563-3592.

Nakamura, K., 1980, Why do long rift zones develop in Hawaiian volcanos—a possible role of thick oceanic sediments: Bulletin of the Volcanology Society of Japan, v. 25, p. 255-269.

O'Connell, R.J., and Budiansky, B., 1974, Seismic velocities in dry and cracked solids: Journal of Geophysical Research, v. 79, p. 5412-5426.

Peck, D.L., and Kinoshita, W.T., 1976, The eruption of August 1963 and the formation of Alae lava lake, Hawaii: U.S. Geological Survey Professional Paper 935-A, 33 p.

Pollard, D.D., 1976, On the form and stability of open hydraulic fractures in the Earth's crust: Geophysical Research Letters, v. 3, p. 513-516.

Pollard, D.D., and Holzhausen, G., 1979, On the mechanical interaction between a fluid-filled fracture and the Earth's surface: Tectonophysics, v. 53, p. 27-57.

Pollard, D.D., and Muller, O.H., 1976, The effect of gradients in regional stress and magma pressure on the form of sheet intrusions in cross section: Journal of Geophysical Research, v. 81, p. 975-984.

Purdy, G.M., and Detrick, R.S., 1986, Crustal structure of the mid-Atlantic ridge at 23°N seismic refraction studies: Journal of Geophysical Research, v. 91, p. 3729-3762.

Ramberg, H., 1981, Gravity and deformation of the Earth's crust: New York, Academic Press, 452 p.

Rao, M., Ramana, Y.V., and Gogte, B.S., 1974, Dependence of compressional velocity on the mineral chemistry of eclogites: Earth and Planetary Science Letters, v. 23, p. 15-20.

Renard, V., Hekinian, R., Francheteau, J., Ballard, R.D., and Backer, H., 1985. Submersible operations at the axis of the ultra-fast-spreading East Pacific rise (17°30′ to 21°30′S): Earth and Planetary Science Letters, v. 75, p. 339-353.

Reuss, A., 1929, Berechnung der Fleissgrenze von Mischkristallen auf Grund der Plastizitätsbedingung für Einkristalle: Zeitschrift für Angewandte Mathematik und Mechanik, v. 9, p. 49

Richter, D.H., and Simmons, G., 1974, Thermal expansion behavior of igneous rocks: International Journal of Rock Mechanics and Mining Sciences & Geomechanics Abstracts, v. 11, p. 403-411.

Richter, D.H., and Moore, J.G., 1966, Petrology of Kilauea Iki lava lake, Hawaii: U.S. Geological Survey Professional Paper 537-B, 26 p.

Richter, D.H., and Murata, K.J., 1966, Petrography of the lavas of the 1959-60 eruption of Kilauea Volcano, Hawaii: U.S. Geological Survey Professional Paper 537-D, 12 p.

Ritzert, M., and Jacoby, W.R., 1985, On the lithospheric seismic structure of Reykjanes ridge at 62.5°N: Journal of Geophysical Research, v. 90, p. 10117-10128.

Robie, R.A., Hemingway, B., and Fisher, J., 1978, Thermodynamic properties of minerals and related substances at 298.15K and 1 bar (10^5 pascals) pressure and at higher temperatures: U.S. Geological Survey Bulletin 1452, 456 p.

Robie, R.A., and Waldbaum, D.R., 1968, Thermodynamic properties of minerals and related substances at 298.15K (25.0°C) and one atmosphere (1.013 bars) pressure and at higher temperatures: U.S. Geological Survey Bulletin 1259,

Ryan, M.P., Blevins J.Y.K., Okamura, A.T., and Koyanagi, R.Y., 1983, Magma reservoir subsidence mechanics: Theoretical summary and application to Kilauea Volcano, Hawaii: Journal of Geophysical Research, v. 88, p. 4147-4181.

Ryan, M.P., Koyanagi, R.Y., and Fiske, R.S., 1981, Modeling the three-dimensional structure of magma transport systems: Application to Kilauea Volcano, Hawaii: Journal of Geophysical Research, v. 86, p. 7111-7129.

Ryan, M.P., and Sammis, C.G., 1978, Cyclic fracture mechanisms in cooling basalt: Geological Society of America Bulletin, v. 89, p. 1295-1308.

———1981, The glass transition in basalt: Journal of Geophysical Research, v. 86, p. 9519-9535.

Ryzhova, T.V., 1964, The elastic properties of plagioclase: Izvestia Geophysics, ser. 7, p. 1049-1051.

Salisbury, M.H., and Christensen, N.I., 1976, Sonic velocities and densities of basalts from the Nazca plate, DSDP leg 34, *in* Yeats, R.S., Hart, S.R., and others, eds., Initial Reports of the Deep Sea Drilling Project: U.S. Government Printing Office, v. 34, p. 543-546.

Schock, R.N., Heard, H.C., and Stephens, D.R., 1973, Stress-strain behavior of a granodiorite and two greywackes on compression to 20 kilobars: Journal of Geophysical Research, v. 78, p. 5922-5941.

Schreiber, E., Fox, P.J., and Peterson, J.J., 1972, Compressional wave velocities in selected samples of gabbro, schist, limestone, anhydrogypsum and halite, *in* Ryan, W.B.F., Hsu, K.J., and others, eds., Initial reports of the Deep Sea Drilling Project: U.S. Government Printing Office, v. 13, p. 595-597.

———1974, Compressional wave velocities in samples recovered from DSDP leg 24, *in* Fisher, R.L., and others, eds., Initial reports of the Deep Sea Drilling Project: U.S. Government Printing Office, v. 24, p. 787-789.

Shaw, H.R., 1980, The fracture mechanisms of magma transport from the mantle to the surface, *in* R.B. Hargraves, ed., Physics of magmatic processes: Princeton, N.J., Princeton University Press, p. 201-264.

Shaw, H.R., and Swanson, D.A., 1970, Eruption and flow rates of flood basalts, *in* Gilmour, E.H., and Stradling, D., eds., Proceedings of the Second Columbia River Basalt Symposium: Cheney, Eastern Washington State College Press.

Simmons, G., and Wang, H., 1971, Single crystal elastic constants and calculated aggregate properties: A handbook (2d ed.): Cambridge, Massachusetts Institute of Technology Press, 370 p.

Skinner, B.J., 1966, Thermal expansion, sec. 6 *of* Clark, S.P., ed., Handbook of physical constants (revised ed.): Geological Society of America Memoir 97, p. 75-96.

Sleep, N.H., 1974, Segregation of magma from a mostly crystalline mush: Geological Society of America Bulletin, v. 85, p. 1225-1232.

Soga, N., and Anderson, O.L., 1967, High-temperature elasticity and expansivity of forsterite and steatite: Journal of the American Ceramic Society, v. 50, p. 239-359.

Solomon, S.C., 1975, Mare volcanism and lunar crustal structure, *in* Proceedings of the Sixth Lunar Science Conference: Elmsford, N.Y., Pergamon Press, p. 2021-2042.

Sparks, R.S.J., and Huppert, H.E., 1984, Density changes during the fractional crystallization of basaltic magmas: Fluid dynamic implications: Contributions to Mineralogy and Petrology, v. 85, p. 300-309.

Spence, D.A., and Turcotte, D.L., 1985, Magma-driven propagation of cracks: Journal of Geophysical Research, v. 90, p. 575-580.

Spinner, S., and Tefft, W.E., 1961, A method for determining mechanical resonance frequencies and for calculating elastic moduli from these frequencies: Proceedings of the American Society of Testing and Materials, p. 1221-1238.

Spudich, P., and Orcutt, J., 1980, A new look at the seismic velocity structure of the oceanic crust: Review of Geophysics and Space Physics, v. 18, p. 627- 645.

Stolper, E., Walker, D., Hager, B.H., and Hays, J.F., 1981, Melt segregation from partially molten source regions: The importance of melt density and source region size: Journal of Geophysical Research, v. 86, p. 6261-6271.

Swanson, D.A., Duffield, W.A., and Fiske, R.S., 1976, Displacement of the south flank of Kilauea Volcano: The result of forceful intrusion of magma into the rift zones: U.S. Geological Survey Professional Paper 963, 39 p.

Swanson, D.A., Jackson, D.B., Koyanagi, R.Y., and Wright, T.L., 1976, The February 1969 rift eruption of Kilauea Volcano, Hawaii: U.S. Geological Survey Professional Paper 891, 30 p.

Talwani, M., Worzel, J.L., and Landisman, M., 1959, Rapid gravity computations for two-dimensional bodies with application to the Mendocino submarine fracture zone: Journal of Geophysical Research, v. 64, p. 49-59.

Thompson, R.N., and Tilley, C.E., 1969, Melting and crystallization relations of Kilauean basalts of Hawaii. The lavas of the 1959-60 Kilauea eruption: Earth and Planetary Science Letters, v. 5, p. 469-477.

Tilley, C.E., 1950, Some aspects of magmatic evolution: Quarterly Journal of the Geological Society of London, v. 106, p. 37-61.

Todd, T., and Simmons, G., 1972, Effect of pore pressure on the velocity of compressional waves in low-porosity rocks: Journal of Geophysical Research, v. 77, p. 3731-3743.

Vogt, P.R., 1974, Volcano height and plate thickness: Earth and Planetary Science Letters, v. 23, p. 337-348.

Voigt, W., 1928, Lehrbuch der Kristallphysik: Leipzig, B.B. Teubner.

Volarovich, M.P., and Gurvich, A.S., 1957, Investigation of dynamic moduli of elasticity for rocks in relation to temperature: Izvestia Akademiya Nauk SSSR. Seriya Geofiziko, no. 4, p. 417-425.

Waff, H.S., 1979, Equilibrium fluid distribution in an ultramafic partial melt under hydrostatic stress conditions: Journal of Geophysical Research, v. 84, p. 6109-6114.

———1980, Effects of the gravitational field on liquid distribution in partial melts within the upper mantle: Journal of Geophysical Research, v. 85, p. 1815-1825.

Waff, H.S., and Bulau, J.R., 1979, Equilibrium fluid distribution in an ultramafic partial melt under hydrostatic stress conditions: Journal of Geophysical Research, v. 84, p. 6109-6114.

Walsh, J.B., 1968, Attenuation in partially melted material: Journal of Geophysical Research, v. 73, p. 2209-2216.

———1969, New analysis of attenuation in partially melted rock: Journal of Geophysical Research, v. 74, p. 4333-4337.

———1981, Effect of pore pressure and confining pressure on fracture permeability: International Journal of Rock Mechanics and Mining Sciences & Geomechanics Abstracts, v. 18, p. 429-435.

Walsh, J.B., and Decker, R.W., 1971, Surface deformation associated with volcanism: Journal of Geophysical Research, v. 76, p. 3291-3302.

Wang, H., Todd, T., Richter, D., and Simmons, G., 1973, Elastic properties of plagioclase aggregates and seismic velocities, *in* The Moon: Proceedings of the Fourth Lunar Science Conference, v. 3, p. 2663-2671.

Ward, P.L., and Gregersen, S., 1973, Comparison of earthquake locations determined with data from a network of stations and small tripartite arrays on Kilauea Volcano, Hawaii: Bulletin of the Seismological Society of America, v. 63, p. 679-711.

Watt, J.P., Davies, G.F., and O'Connell, R.J., 1976, The elastic properties of composite materials: Review of Geophysics and Space Physics, v. 14, p. 541-563.

Weertman, J., 1971a, Theory of water-filled crevasses in glaciers applied to vertical magma transport beneath oceanic ridges: Journal of Geophysical Research, v. 76, p. 1171-1183.

———1971b, Velocity at which liquid-filled cracks move in the earth's crust or in glaciers: Journal of Geophysical Research, v. 76, p. 8544-8553.

———1980, The stopping of a rising, liquid-filled crack in the earth's crust by a freely slipping horizontal joint: Journal of Geophysical Research, v. 85, p. 967-976.

Weertman, J., and Chang, S.P., 1977, Fluid flow through a large vertical crack in the Earth's crust: Journal of Geophysical Research, v. 82, p. 929-932.

Whitcomb, J.H., Garmany, J.D., and Anderson, D.L., 1973, Earthquake prediction: Variation of seismic velocities before the San Fernando earthquake: Science, v. 180, p. 632-635.

Wilson, L., and Head, J.W., 1981, Ascent and eruption of basaltic magma on the Earth and Moon: Journal of Geophysical Research, v. 86, p. 2971-3001.

Wingquist, C.F., 1971, Elastic moduli of rock at elevated temperatures: U.S. Bureau of Mines Report of Investigations 7269.

Wright, T.L., and Fiske, R.S., 1971, Origin of the differentiated and hybrid lavas

of Kilauea Volcano, Hawaii: Journal of Petrology, v. 12, p. 1-65.

Wright, T.L., and Okamura, R.T., 1977, Cooling and crystallization of tholeiitic basalt, 1965 Makaopuhi lava lake, Hawaii: U.S. Geological Survey Professional Paper 1004, 78 p.

Wright, T.L., and Weiblen, P.W., 1968, Mineral composition and paragenesis in tholeiitic basalt from Makaopuhi lava lake, Hawaii [abs.], *in* Abstracts for 1967: Geological Society of America Special Paper 115, p. 242-243.

Wyss, M., and Holcomb, D.J., 1973, Earthquake prediction based on station residuals: Nature, v. 249, p. 139-140.

Yamshikov, V.S., 1965, A study of the temperature dependence of the modulus of elasticity of rocks: Izvestia, Earth Physics Series no. 10, p. 83-87.

Yoder, H.S., and Sahama, H.G., 1957, Olivine x-ray determinative curve: American Mineralogist, v. 42, p. 475-491.

Yoder, H.S., and Tilley, C.E., 1962, Origin of basalt magmas: An experimental study of natural and synthetic rock systems: Journal of Petrology, v. 3, no. 3, p. 342-532.

Zablocki, C.J., Tilling, R.I., Peterson, D.W., Christiansen, R.L., Keller, G.V., and Murray, J.C., 1974, A deep research drill hole at the summit of an active volcano, Kilauea, Hawaii: Geophysical Research Letters, v. 1, p. 323-326.

Zucca, J.J., and Hill, D.P., 1980, Crustal structure of the southeast flank of Kilauea Volcano, Hawaii, from seismic refraction measurements: Bulletin of the Seismological Society of America, v. 70, p. 1149-1159.

Zucca, J.J., Hill, D.P., and Kovach, R.L., 1982, Crustal structure of Mauna Loa Volcano, Hawaii, from seismic refraction and gravity data: Bulletin of the Seismological Society of America, v. 72, p. 1535-1550.

ORIGINS OF BLADE-LIKE DIKES IN VOLCANIC RIFT ZONES

By Allan M. Rubin[1] *and* David D. Pollard[2]

ABSTRACT

Seismic and geodetic data have demonstrated that dikes in the rift zones of Kilauea Volcano in Hawaii and Krafla Volcano in Iceland are typically intruded laterally from a central magma reservoir and acquire a blade-like form. A remarkable feature of many such dikes is that they propagate at shallow depths for tens of kilometers without erupting. Using concepts of fracture mechanics, we can specify the conditions necessary for this type of growth. A dike will propagate if the stress-intensity factor at the dike tip exceeds a critical value, known as the fracture toughness of the host rock. An increase in the rift-zone fracture toughness with depth could limit the depth to which dikes extend, but little existing evidence supports this possibility. We find that several geological processes could contribute to a distribution of the stress-intensity factor along the dike perimeter that would promote the development of a blade-like form.

Factors influencing the stress intensity along the dike perimeter can be divided into two categories: factors pertaining to the dike geometry, including the dike size, shape, and depth beneath the Earth's surface; and factors pertaining to the distribution of driving pressure (magma pressure minus the remote stress) acting on the dike plane. The pressure within the dike is controlled by magma-reservoir pressure, magma density, presence of vesiculated magma or gas at the dike top, and pressure gradients due to viscous flow. Possible contributors to the remote stress include density stratification of the rift zone, gravitational loading of the volcanic ridge, intrusion of previous dikes, faulting, and plate tectonic forces.

Of the geometric factors, both the elongate dike shape and the proximity of the Earth's surface tend to promote upward growth and eruption, rather than continued lateral growth of the dike. Thus a blade-like form must be the result of a driving-pressure distribution that increases the stress-intensity factor at the downrift edge of the dike with respect to that at the dike top and bottom. This can be achieved if the driving pressure is greater at the depth of the dike center than at the dike top or bottom. The vertical pressure variation within a laterally propagating dike is essentially equal to that within a static body of magma. The presence of vesiculated magma in the upper part of the dike enhances upward propagation but has little effect on downward and lateral propagation. Thus the source of the greater driving pressure at the depth of the dike center must be the remote stress; each of the contributors to this stress listed above is a potential source of such a stress distribution.

Using the cross-sectional geometry of the August 1981 southwest-rift-zone dike at Kilauea inferred from geodetic data, and assuming a uniform fracture toughness within the rift zone, we estimate the magma pressure and the remote stress at the time of intrusion. The hydrostatic head of the magma was deeper than 50 m below the surface. The excess magma pressure at the dike center was 2.5–10.5 MPa (25–105 bars), and the driving pressure decreased toward the dike top and bottom by about 3–11 MPa/km. If the gradients in the driving pressure toward the dike top and bottom were due only to the local density contrast between the magma and the host rock, they would be about 3 MPa/km. A more precise determination of the driving pressure is not possible without more precise values of the rift-zone fracture toughness and elastic shear modulus. From estimates of the dike thickness, we find that the rift-zone shear modulus is within a factor of 2–3 of 3 GPa. This is in agreement with other inplace determinations of the shear modulus and about an order of magnitude less than laboratory values for intact basalt.

INTRODUCTION

Geological studies of eroded Hawaiian and Icelandic volcanoes have documented the importance of shallow dike intrusion as a mechanism of magma transport in these distinct geologic settings. The majority of such dikes are nearly vertical and occur within swarms, or rift zones, that may be more than 100 km long and contain hundreds or thousands of dikes (Walker, chapter 41; Macdonald, 1956; Walker, 1959; Walker, 1963; Fiske and Jackson, 1972; Helgason and Zentilli, 1985). During the last few decades, abundant geological, geochemical, petrological, geophysical, and geodetic data collected from Kilauea and Mauna Loa by scientists at the Hawaiian Volcano Observatory and from Krafla by scientists at the National Energy Authority and the Nordic Volcanological Institute in Iceland have shed considerable light on some of the processes of magma movement and dike emplacement. At both locations, rapid subsidence of the region overlying a shallow magma reservoir is associated with the lateral flow of magma for up to several tens of kilometers into adjacent rift zones. In most cases, this intrusion of magma results in the formation of new dikes, the surface manifestations of which may include observable rift-zone widening and fissure eruptions. The 120-km-long east rift zone of Kilauea, and historical and prehistoric dikes in Iceland that vented nearly 100 km from their sources (Sigurdsson

[1]Department of Geology, Stanford University, Stanford, CA 94305.
[2]Departments of Geology and Applied Earth Sciences, Stanford University, Stanford, CA 94305.

and Sparks, 1978), attest to the extraordinarily extensive form rift-zone dikes can take.

Dikes propagate because the magma pressure within them fractures the rock ahead of the magma front or forces preexisting fractures, such as cooling joints or through-going rift-zone extension cracks, to widen. In either case, this propagation can be interpreted in terms of established principles of fracture mechanics (see, for example, Lawn and Wilshaw, 1975). If the resistance of the host rock to fracture, the magma pressure within the dike, and the remote stress acting perpendicular to the rift zone are known, the directions in which the dike will propagate can be predicted. Alternatively, observations of dike propagation can be used to estimate some of these parameters.

We first summarize the available evidence on dike geometry and emplacement and outline the theoretical model to be used. We then list and analyze the factors governing the horizontal and vertical propagation of basaltic dikes emanating from near-surface magma reservoirs. Using this analysis we estimate the magma pressure and the state of stress in the southwest rift zone at Kilauea for the August 1981 dike intrusion. The model provides a framework for discussion of rift-zone dynamics and possible future research.

ACKNOWLEDGMENTS

This paper benefited from careful reviews by Paul Delaney, Kieth Evans, Steve Martel, Larry Mastin, Michael Ryan, and Hans Weertman. Paul Davis, Bob Decker, Jim Dieterich, John Dvorak, David Hill, and Fred Klein provided interesting discussions and early versions of some results. We thank John Dvorak, Jack Lockwood, and Arnold Okamura for a kind introduction to Hawaii Volcanoes National Park and the Hawaiian Volcano Observatory. This research was funded in part by a National Science Foundation Graduate Fellowship and NSF grant EAR-8520641.

CHARACTERIZATION OF THE DIKE-EMPLACEMENT PROCESS

OBSERVATIONS OF DIKE PROPAGATION AND GEOMETRY

Combined geodetic and seismic data have revealed the presence of a magma chamber or chambers at approximately 2–7 km below the surface at Kilauea, Mauna Loa, and Krafla Volcanoes. During periods of activity these magma chambers inflate slowly, at rates of a few cubic meters per second, over periods of months or years, and deflate rapidly, at rates of 100–1,000 cubic meters per second, for periods of several hours to a few days. Typically, summit subsidence is accompanied by swarms of shallow earthquakes that migrate downrift at velocities of a few tens of centimeters per second (Klein and others, chapter 43; Brandsdottir and Einarsson, 1979). These swarms sweep out tabular zones that are typically 1–2 km wide, a few kilometers high, and as much as several tens of kilometers long. Ground cracking or fissure eruptions may shortly precede or follow the migration of the earthquake swarm beneath a particular site (Hauksson, 1983; F.W. Klein, oral commun., 1985). Deviations from this simple pattern are not, however, uncommon during intrusions into the east rift zone (ERZ) of Kilauea: there some earthquake swarms originate within the rift zone itself, and discontinuous or uprift migration of earthquakes is sometimes observed (Klein and others, chapter 43).

Although the factors controlling the origin and extent of the earthquake swarms are not yet understood, it seems reasonable to use these earthquakes to estimate dike location (Brandsdottir and Einarsson, 1979; Ryan and others, 1981). The approximate boundaries of earthquake swarms associated with a few well-documented intrusions at Kilauea and Krafla are shown on figure 53.1, projected onto cross sections parallel to the rift axes.

Pollard and others (1983) derived a graphical method for estimating the height, depth, dip, and thickness of dikes from surface vertical-deformation data. Although geodetic data are available less frequently than earthquake-source data, their interpretation may improve dike location accuracy considerably. Displacements measured in the rift zones of Kilauea and Krafla yield dike heights and depths consistent with estimates from earthquake-source data. Estimates of dike thickness (0.8–2 m) and of dike dip (within a few degrees of vertical) are both in agreement with observations of eroded rift-zone dikes.

THEORETICAL CONSTRAINTS ON DIKE STABILITY AND PROPAGATION

In this study dikes are represented as pressurized cracks in an isotropic, homogeneous, linearly elastic half-space. Field observations indicate that dikes are typically nearly planar features. Although the assumptions of isotropy, homogeneity, and elasticity are certainly incorrect in detail (Ryan and others, 1983), we believe the model is appropriate for the physical insight sought here. Geodetic measurements made during the current Puu Oo activity show that rift-zone extension accumulated prior to an eruptive phase is completely recovered following eruption. This indicates that the volcano is capable of elastic behavior over periods of weeks and distances of a few kilometers (Hoffman and others, 1984).

It has been well established theoretically and experimentally that a crack will propagate if the energy available, from work done on the system by the boundary forces (remote stress and magma pressure) and from any release of stored strain energy in the surrounding solid, is sufficient to supply the energy expended in the cracking process (Lawn and Wilshaw, 1975). Though the solid is assumed to be elastic, the theory is sufficiently general that it incorporates inelastic behavior (such as secondary fracturing or local plastic deformation) in a small region around the crack tip. This region is called the process zone.

Another crack propagation criterion, equivalent to the above energy-balance criterion, involves the use of quantities known as stress-intensity factors (Lawn and Wilshaw, 1975). A dilated crack in an elastic material generates stresses in the near-tip region given by

$$\sigma_{ij} = K f_{ij}(\theta)/(2r)^{1/2} \quad (1)$$

where σ_{ij} are components of the stress tensor, K is the mode I (tensile) stress-intensity factor, r is the distance from the crack tip,

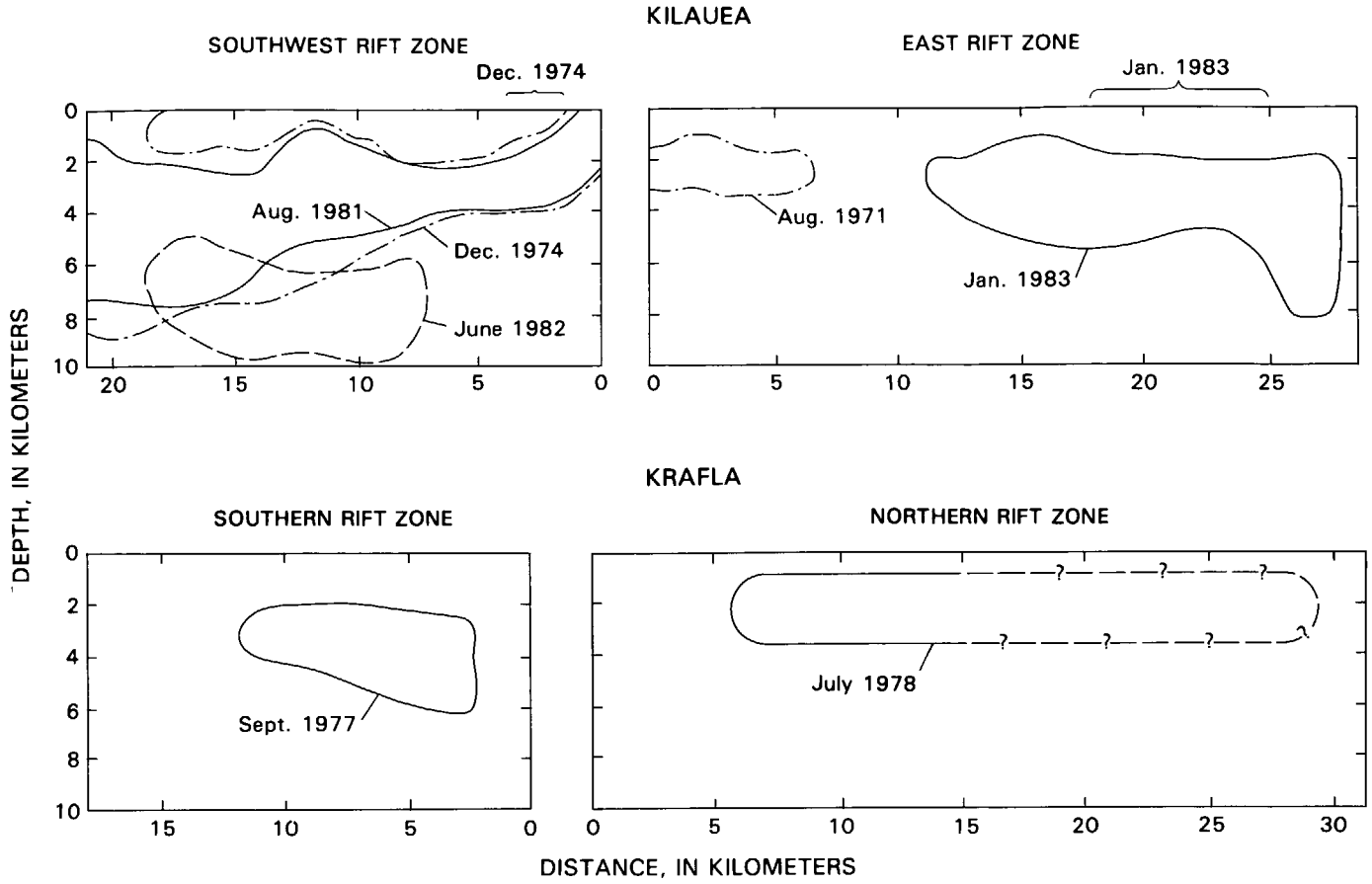

FIGURE 53.1.—Approximate limits of seismic swarms associated with some well-documented dike intrusions at Kilauea and Krafla Volcanoes, projected onto cross sections parallel to the rift axes. The origins for the distance axes are near Halemaumau Crater within the summit caldera at Kilauea and at the center of the caldera at Krafla. Extent of associated eruptive fissures indicated by brackets at the tops of the sections. Note the apparant lack of seismicity, due in part to the low-magnitude filter applied to the data, near the eruption site of the 1983 east-rift-zone intrusion at Kilauea. Data for Kilauea from Klein and others (chapter 43); data for Krafla from Brandsdottir and Einarsson (1979) and Einarsson and Brandsdottir (1979).

and the $f_{ij}(\theta)$ are functions of position around the crack tip (fig. 53.2). (By an alternate convention, this equation would contain an additional factor of $\pi^{-1/2}$, and the value of K would be modified accordingly). K is in general dependent only upon the crack geometry and the distribution of driving pressure ΔP. We consider the driving pressure for dikes to be a function of vertical position y: it is equal to the magma pressure $P_m(y)$ minus the remote stress $S(y)$ acting perpendicular to the dike plane:

$$\Delta P(y) = P_m(y) - S(y). \qquad (2)$$

A dike will propagate if its stress-intensity factor is greater than a critical value K_c, termed the fracture toughness of the rock.[1] A negative value of K indicates that a dike will decrease in length by pinching shut at its tip. A dike is stable if $0 < K < K_c$; that is, the dike will neither increase nor decrease in length (Weertman, 1971).

For dikes following preexisting fractures, as is possible in volcanic rift zones, K_c could be zero. Experimentally determined values of K_c for intact laboratory specimens of basalt at room temperature and pressure lie within the range 1–2 MPa · $m^{1/2}$ (Atkinson, 1984). However, estimates of K_c from studies of dikes exposed in shale (Delaney and Pollard, 1981), made under the assumption that magma had access to the dike tip, are in the range 30–100 MPa · $m^{1/2}$. Examination of dike-parallel joints in sandstone (Delaney and others, in press) suggests that the crack tip process zone associated with propagating basaltic dikes can be

[1] Because crack propagation can proceed much more rapidly than magma flow, it is expected that in actuality K will exceed K_c by only an infinitesimal amount. Physically this may be accomplished by the opening of a low-pressure cavity at the dike tip. The action of the remote compressive stress on this cavity would decrease K to values below that calculated assuming that magma had access to the dike tip. In subsequent calculations of K we assume that magma has access to the dike tip, and interpret a value of K greater than K_c as indicating that propagation will proceed.

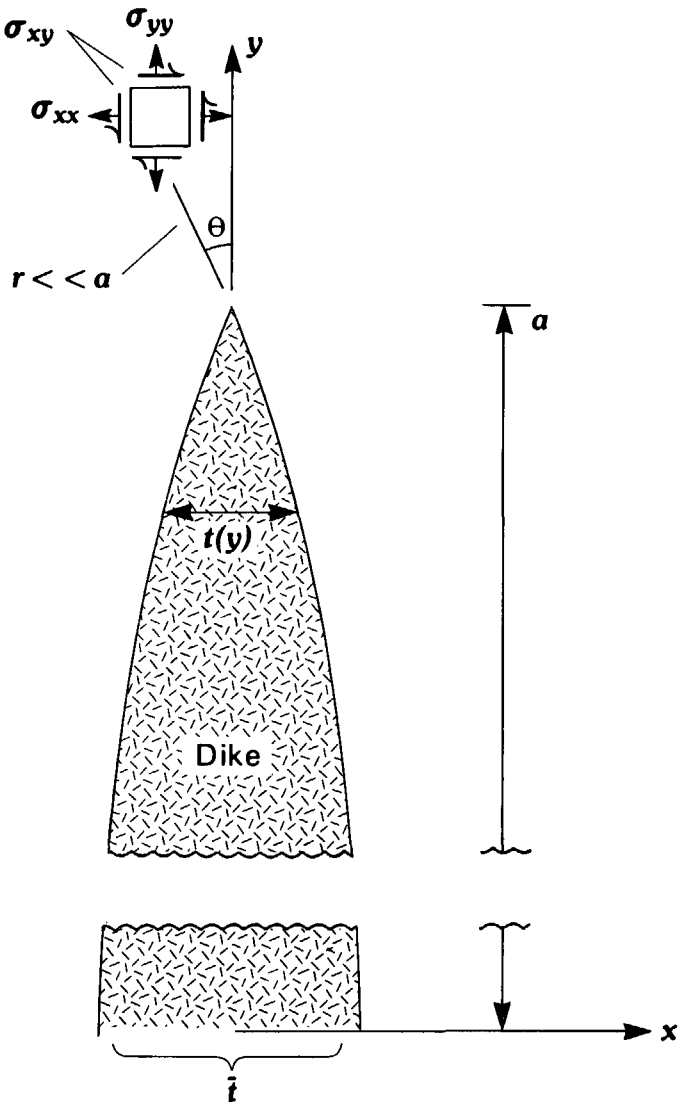

FIGURE 53.2.—Stresses (σ) in the near-tip region of a crack or dike. The stress is a function of the distance r from the dike tip, the position θ around the dike tip, and the stress-intensity factor K (eq 1). a, dike half-length; $t(y)$, dike thickness at a height y above the dike center; $\bar{t}$, average dike thickness.

larger than that associated with cracks in laboratory specimens, giving larger values of K_c. Frictional sliding on fractures near the dike, which is indicated by rift-zone earthquake swarms, is another energy-expending mechanism that would increase K_c.

The effects of pressure and temperature on K_c are at present only poorly understood. For dry rock (Schmidt and Huddle, 1977; Winter, 1983) K_c increases with increasing pressure because the added confining pressure inhibits microcracks near the crack tip from opening up and aiding propagation (Atkinson, 1984). When these microcracks are accessible to fluids at presures equal to the confining pressure, for example in experiments on water-saturated sandstone (Winter, 1983), this effect is not apparent. For moderate temperatures, increasing temperature decreases K_c because the energy required for brittle fracture is reduced. Limited experimental determinations indicate that K_c for gabbro decreases by about 30–35 percent from room temperature to 400 °C (Meredith and Atkinson, 1985). At some higher temperature, increased plasticity at the crack tip will cause K_c to increase. Bjornsson (1985) estimates the temperature at 4–5 km depth in Icelandic rift zones to be 500–600 °C. Although more experimental data are needed, we assume these temperatures to be low enough that increased crack-tip plasticity is not a significant factor at the time-scales appropriate for dike intrusion.

Because of sparse high-temperature and high-pressure data, and because of the possible discrepancy between values of K_c appropriate for cracks in laboratory specimens and for dikes in the Earth's crust, we can only restrict the probable range of critical stress-intensity factors to

$$0 > K_c > 100\ \text{MPa} \cdot \text{m}^{1/2}.$$

THEORETICAL CONSTRAINTS ON DIKE THICKNESS

The length-to-height ratio of typical rift-zone dikes justifies treating them as two-dimensional when calculating dike thickness. For a uniform driving pressure P_o, the thickness of the dike at a distance y from its center is given by Pollard and others (1983) as:

$$t = P_o a \frac{(1-\nu)}{\mu} [1-(y/a)^2]^{1/2} \qquad (3)$$

(fig. 53.2), where a is the dike half-height, ν is Poisson's ratio, and μ is the elastic shear modulus. The average dike thickness, $\bar{t}$, is about 0.8 times the thickness at the dike center. Equation 3 illustrates the general relation that dike thickness is proportional to dike half-height and driving pressure, and inversely proportional to rock stiffness, $\mu/(1-\nu)$.

Given estimates of the dike thickness-to-height ratio from geodetic data, one can calculate the ratio of driving pressure to rock stiffness. If the rock stiffness is known, one can then estimate the driving pressure. Experimentally determined values of ν for basalt vary only slightly, generally lying between 0.22 and 0.28 for conditions ranging from room temperature and pressure to those appropriate for depths of several kilometers (Birch, 1966; Ryan and others, 1983). Typical static laboratory values of μ for basalt are 25–35 GPa (Birch, 1966). However, the shear moduli determined from loading large fractured rock masses in the field are lower than those measured on pristine samples in the laboratory by as much as an order of magnitude (Bieniawski, 1978; Evans, 1982). In actuality the effective shear modulus of the rock mass intruded by dikes probably increases with depth as the rock becomes more competent. From the lack of a significant piezomagnetic anomaly during periods of magma-chamber inflation, Davis (1976) estimates that the effective shear modulus of the summit region of Kilauea is about an order of magnitude less than that of competent basalt. We accept this estimate as a more appropriate average shear modulus for volcanic rift zones than the laboratory value. However, the large uncertainty associated with this figure makes the dike thickness-to-height ratio only a weak constraint on the driving pressure.

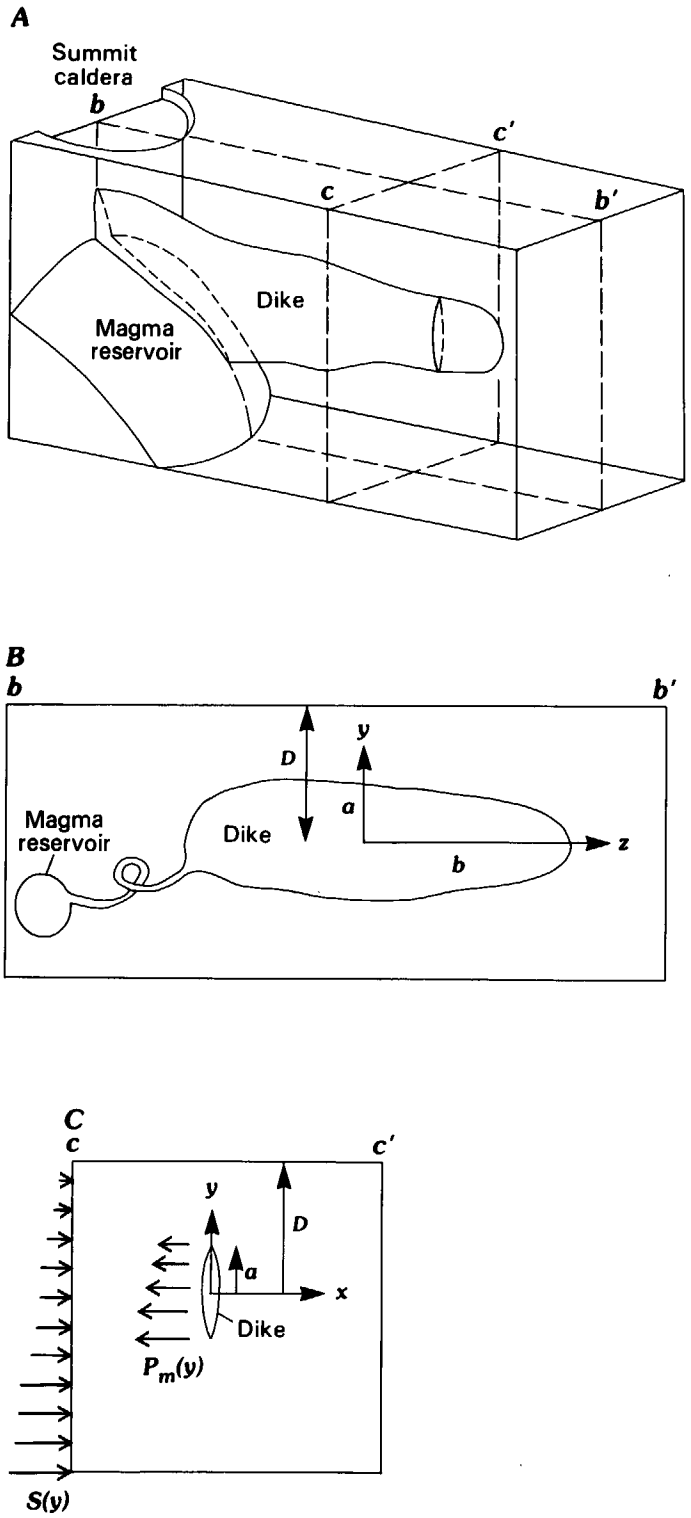

FIGURE 53.3.—Diagrams of a rift-zone dike intruded laterally from a shallow magma reservoir. ***A***, Cartoon sketch of the dike showing general form; planes of sections ***B*** and ***C*** indicated. ***B***, Idealized longitudinal section of the dike, which has a half-height a, a half-length b, and a depth D. The magma reservoir acts as a source of pressure. ***C***, Idealized cross section of the dike. A remote stress $S(y)$ acts perpendicular to the dike plane; a magma pressure $P_m(y)$ acts within the dike.

PROPAGATION AND STABILITY CRITERIA FOR RIFT-ZONE DIKES

In most cases the region swept out by individual earthquake swarms remains fairly constant in vertical extent and depth as the magma travels great distances laterally. From this observation we infer that the dikes are adopting an approximately equilibrium position in the vertical plane; it is this inference that motivates the analysis which follows. The possibility that some kinetic factor related to magma flow or solidification inhibits dikes from reaching their stable position is considered briefly in the section "Discussion."

The necessary conditions for a dike to have a propagating downrift edge and a stable height are that $K \geq K_c$ at the downrift edge and $K < K_c$ at the top and bottom. These conditions can be met by increasing K_c at the dike top and bottom relative to K_c at the downrift edge, or by decreasing K at the dike top and bottom relative to K at the downrift edge. In what follows we assume a uniform value of K_c throughout the rift zone and examine the factors that could contribute to the required variation in K. We infer from the blade-like geometry of typical rift-zone dikes that during downrift propagation sections of the dike top and bottom close to the downrift edge have attained their stable height. This assumption allows us to neglect lateral magma pressure gradients due to both viscous flow and along-strike changes in dike elevation when comparing K at the downrift edge to that at the dike top and bottom.

FACTORS CONTROLLING DIKE PROPAGATION

A rift-zone dike intrusion is shown in cartoon form in figure 53.3*A*, and our idealizations of the dike to be used for modeling purposes are illustrated in figures 53.3*B* and 53.3*C*. The model dike has a half-height a, half-length b, and depth D. It is embedded in an elastic half-space with uniform shear modulus μ and fracture toughness K_c. The magma reservoir is represented as a source of pressure located at the uprift end of the dike, but is not explicitly accounted for in calculations of K, because it is distant from the part of the dike perimeter that is of interest. The magma has a uniform viscosity η and a uniform or vertically varying density $\rho_m(y)$. A vertically varying remote stress $S(y)$ acts on the plane of the dike, and a vertically varying magma pressure $P_m(y)$ acts within the dike.

The geologic factors contributing to the stress intensity around the dike can be divided into two categories: those pertaining to the geometry of the dike, and those pertaining to the driving-pressure distribution. The first category includes the dike size, shape, and depth beneath the Earth's surface. The second category can be divided into those factors related to the magma or gas pressure within the dike and those factors related to the remote stresses acting perpendicular to the dike plane. The pressure distribution within the dike body is controlled by the unvesiculated magma density, the presence or absence of vesiculated magma or a separate gas phase, the time-varying magma-reservoir pressure, and pressure loss due to viscous flow. For conceptual purposes, the remote stress acting on the dike plane can be subdivided into two components: the lithostatic load or weight of the rock overburden, including variable density stratification; and any supplementary stresses induced by

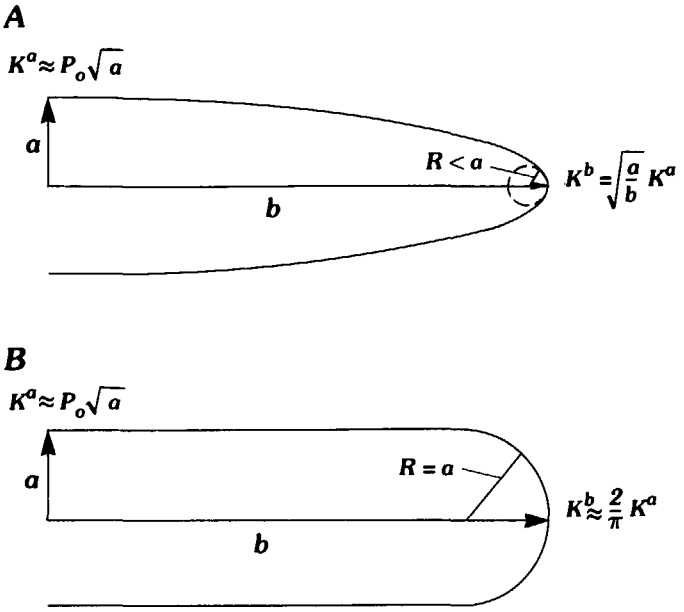

FIGURE 53.4.—Idealized longitudinal sections showing dike geometry. Dikes subject to uniform driving pressure, P_o. ***A***, Elliptical dike with half-height a and half-length b. The radius of curvature R in the plane of the dike at the downrift edge is less than a; as the dike grows laterally, K^b decreases approximately as $\sqrt{a/b}$. ***B***, Dike with a constant half-height a except near its downrift edge, where R is equal to a. The larger radius of curvature gives rise to a larger value of K^b than for the ellipse. This idealization is used in this study and is likely to produce an overestimate of K^b.

topographic relief, slip along major faults at depth, the intrusion of earlier dikes, or plate-tectonic forces.

GEOMETRICAL FACTORS

DIKE SIZE

For a two-dimensional dike of half-height a subjected to a uniform driving pressure P_o (fig. 53.3*C*, $D=\infty$), the stress-intensity factor at the dike top and bottom is

$$K = P_o\sqrt{a}. \tag{4}$$

This equation illustrates the general result that K is proportional to the square root of the dike half-height. For a propagating dike subject to a uniform, steady driving pressure, K increases with height, so propagation should never cease and eruptions would be inevitable.

DIKE SHAPE

If the dike is idealized as having an elliptical shape with half-height a and half-length b (fig. 53.4*A*), the stress-intensity factor around the dike perimeter can be obtained analytically. For a uniform driving pressure the stress intensity at the top or bottom of the dike is given by

$$K^a = \frac{1}{\Phi} P_o\sqrt{a} \tag{5}$$

(Broek, 1982, p. 81), where Φ is a function of b/a that can be evaluated using tables of elliptic integrals and that approaches unity as b/a becomes large. For $b/a = 3$, K is less than that for an infinitely long dike of height a by only 12 percent.

The ratio of the stress-intensity factor at the tip of the minor axis to that at the tip of the major axis is given by

$$\frac{K^a}{K^b} = \left[\frac{b}{a}\right]^{1/2}. \tag{6}$$

Equation 6 indicates the tendency of such dikes to grow into more equidimensional forms: as the eccentricity of the ellipse increases, the stress-intensity factor at the tip of the minor axis increases with respect to that at the tip of the major axis. For rift zone dikes with $b/a = 10$, the ratio K^a/K^b is about 3. Because K^a for large ratios of b to a does not increase significantly if a remains constant, then equation 6 indicates that K^b actually decreases approximately in proportion to $b^{-1/2}$.

The dependence of K^a/K^b on b/a is in part an artifact of the assumption of ellipticity. In general, the stress intensity at a point on the perimeter of a planar crack is increased by an increase in crack size and by an increase in the in-plane radius of curvature of the crack at that point. If rift-zone dikes are constrained to maintain an elliptical shape and a fixed height, the radius of curvature at the downrift edge of the dike must decrease as the dike grows (fig. 53.4*A*). The decrease in K^b indicated by equation 6 shows that the effect of decreasing radius of curvature outweighs the effect of increasing crack length. If, on the other hand, the dike front approaches a semicircle of radius a (fig. 53.4*B*), K^b can be approximated by K for a circular crack of radius a (Paris and Sih, 1965), or

$$K^b \approx \frac{2}{\pi} P_o\sqrt{a} \tag{7}$$

(Broek, 1982, p. 81). In this case the ratio of stress-intensity factors is not very sensitive to dike length and is approximated by

$$\frac{K^a}{K^b} \approx \frac{\pi}{2}. \tag{8}$$

The actual shape of the advancing front of rift-zone dikes is unknown and will depend upon the driving-pressure distribution. In the gelatin experiments of Fiske and Jackson (1972, fig. 6), the fronts of the model dikes were somewhat elliptical. This is the expected shape for driving pressures that are greater at the depth of the dike center than at the top or bottom. We assume that the end of the dike is a semicircle of radius a. Given the likelihood of a driving pressure that is greater at the depth of the dike center (see below), and therefore a somewhat elliptical dike end, this approximation is likely to produce a slight overestimate of K^b.

PROXIMITY OF THE EARTH'S SURFACE

The stress-intensity factors at the top (K^{+a}) and bottom (K^{-a}) of a two-dimensional vertical dike near a horizontal free surface and subject to a uniform driving pressure are plotted as a function of a/D in figure 53.5. The values of K are normalized to their values in an infinite body. The dike intersects the surface when $a/D = 1$. It can be seen that the presence of a free surface increases both K^{+a} and K^{-a}, but affects the upper dike tip more. For $a/D < 0.5$, the effect of the free surface becomes negligible, so K^{+a} and K^{-a} approach K for a crack in an infinite body. Shah and Kobayashi (1973) determined the stress-intensity factors around three-dimensional elliptical cracks near a free surface. Their work shows that the two-dimensional approximation is fairly good when $a/b < 0.2$. For all values of a/D and a/b, the free surface increases K^b by less than both K^{+a} and K^{-a}. The shaded area at the base of figure 53.5 shows the range of increase in K^b due to the free surface for various elliptical shapes. Thus the effect of the free surface on typical rift-zone dikes is to increase K^{+a}, and to a lesser extent K^{-a}, relative to K^b. That is, the surface will tend to cause the dike to increase in its vertical dimension relative to its horizontal dimension, and should enhance eruption rather than downrift propagation.

MAGMA-PRESSURE DISTRIBUTION

Both the blade-like shape and the shallow depth of rift-zone dikes lead to stress intensities that are higher at the dike top and bottom than at its downrift edge, for uniform applied loads. If the fracture toughness of the host rock is uniform, then the observed propagation of rift-zone dikes dictates that the driving-pressure distribution must increase K at the downrift edge relative to K at the top and bottom to an extent sufficient to overcome these geometric effects. Driving-pressure distributions on vertical sections which would accomplish this are depicted schematically in figure 53.6. In these illustrations lesser excess magma pressure, or even magma underpressure, at the dike top and bottom might ensure that $K^a < K_c$, while the greater excess magma pressure at the downrift edge yields $K^b \geq K_c$. In the following sections we explore the factors governing the magma pressure within the dike. The magma pressure at any point within a dike connected to a magma reservoir is controlled by the pressure at a given point within the reservoir, the elevation of the point within the dike with respect to that point within the reservoir, the magma density, and the pressure drop due to viscous magma flow between the two points.

MAGMA RESERVOIR PRESSURE

The occurrence of eruptions at the summit of Mauna Loa simultaneous with quiessence in the lava lake at Kilauea 3 km below precludes the existence of an open magmatic conduit from the two volcanoes' reservoirs to a common source region (Williams and McBirney, 1979). We suggest that magma rises through the crust within isolated packets to levels where it is gravitationally stable. Gravity and seismic modeling of Hawaii (Hill and Zucca, chapter 37; Broyles and others, 1979; Zucca and others, 1982) and Iceland (Palmason, 1971) indicate that the bulk crustal density within a few kilometers of the surface is less than that of unvesiculated magma, whereas the density below is greater than that of magma. This provides an explanation for the presence of long-lived magma chambers at 2–7 km depth in Kilauea, Mauna Loa, and Krafla Volcanoes.

The magma-reservoir pressure cannot exceed that required to fracture the reservoir wall or that generated by the injection of magma from depth. However, our knowledge of the reservoir inflation and failure processes is insufficient to use them to calculate an upper bound for the reservoir pressure. We show below that dike behavior can place an upper bound on the magma-reservoir pressure. To estimate a lower bound for the reservoir pressure, we assume that the hydrostatic head of the reservoir is equal to or greater than the weight per unit area of the rock that caps it. Using densities of 2.3×10^3 kg/m^3 for the rock (Zucca and others, 1982) and 2.6×10^3 kg/m^3 for the magma (Fujii and Kushiro, 1977), we calculate hydrostatic heads of 230–350 m beneath the ground surface for reservoir tops 2–3 km deep. In an example to follow we use the more conservative estimate of -350 m as a lower bound on the hydrostatic head of the reservoir.

The change in reservoir pressure during a single dike intrusion can also affect dike behavior. If the host rock surrounding the magma chamber behaves elastically, then measured surface displacements above the chamber are proportional to pressure changes within it. Epp and others (1983) point out the linear correlation between summit tilt and vent elevation for ERZ eruptions since 1955 at Kilauea. Decker and others (1983) use this correlation to convert changes in summit tilt into differences in magma-reservoir pressure, by assuming that the hydrostatic head of the reservoir at the cessation of subsidence is controlled by the vent elevation. Using a magma density of 2.8×10^3 kg/m^3, Decker and others calculate a pressure change of 0.085 MPa per mrad of summit tilt. If the magma-reservoir roof behaves to some degree like a piston, the change in reservoir pressure could be less than 0.085 MPa/mrad.

MAGMA DENSITY

The vertical pressure gradient, ∇P_m, at a given depth, y, within a static column of magma is given by

$$\nabla P_m(y) = \rho_m(y) \cdot g, \tag{9}$$

where $\rho_m(y)$ is the magma density at a given depth, and g is the acceleration of gravity, 9.8 m/s^2. A typical magma density of 2.6×10^3 kg/m^3 produces a pressure gradient of about 26 MPa/km or 260 bars/km (fig. 53.7*A*). If the driving pressure simply equals the magma pressure (that is, if $S(y) = 0$), then the stress-intensity factors at the top (K^{+a}) and bottom (K^{-a}) of the dike are given by

$$K^{+a} = P_o\sqrt{a} - \frac{1}{2}\nabla P_m a^{3/2}, \tag{10a}$$

$$K^{-a} = P_o\sqrt{a} + \frac{1}{2}\nabla P_m a^{3/2}, \tag{10b}$$

where P_o is the excess magma pressure at the dike center. The first

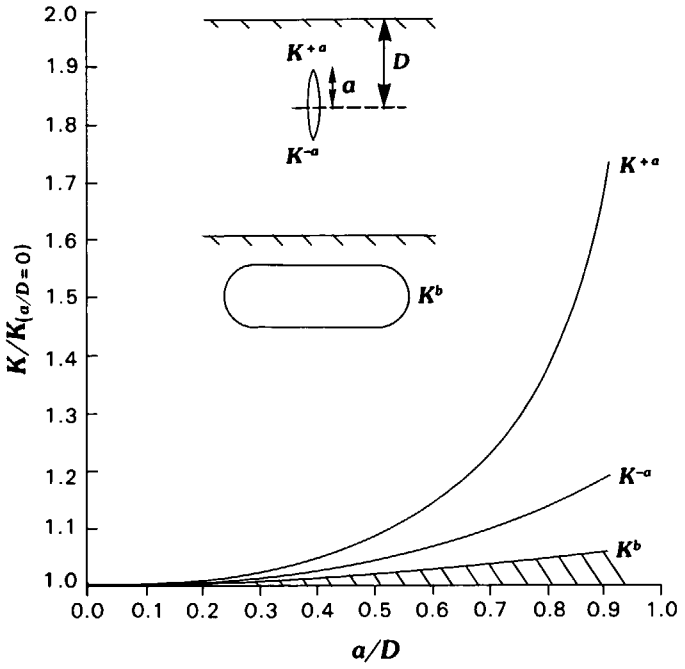

FIGURE 53.5.—Effect of proximity of the Earth's surface on the stress-intensity factors at the top (K^{+a}), bottom (K^{-a}), and downrift edge (K^b) of a dike subjected to a uniform driving pressure. Values of K are normalized to those for a crack in an infinite body. K^{+a} and K^{-a} are calculated for a two-dimensional dike using the method of Pollard and Holzhausen (1979); the range of values for K^b (shaded) was calculated by Shah and Kobayashi (1973) for elliptical cracks with varying ratios of a/b. Insets show idealized dike geometry (see fig. 53.3).

term in these equations gives the value of K due to a uniform driving pressure P_o (eq 4), and the second term gives the value of K due to a driving pressure that varies linearly from a value of $-\nabla P_m a$ at $y = +a$ to $\nabla P_m a$ at $y = -a$ (Secor and Pollard, 1975). For a given P_o, a decrease in magma density increases K^{+a} and decreases K^{-a}, thus promoting upward migration of the dike. If P_o remains unchanged, a change in magma density does not alter K^b, because the effect of a change in magma pressure at a height y above the dike center is balanced by an equal and opposite change at $-y$.

VESICULATION

Vesiculation reduces magma density and thus reduces the magma pressure gradient within a dike. In a dike in which uniformly vesiculated magma rests on unvesiculated magma, the magma pressure above the boundary is increased, relative to a dike in which vesiculation is absent (figure 53.7*B*). The effect of this increase on dike propagation can be assessed through the use of superposition. The driving pressure in a dike with vesiculated magma above a height y' is equal to that in the absence of vesiculation plus that produced by a pressure which increases linearly from a value of zero at y' (fig. 53.8). The gradient of this driving pressure, ∇P_v, is the difference between the pressure gradients within the vesiculated and unvesiculated magma.

The effect of vesiculation on the stress-intensity factor at the dike top, denoted as K_v^{+a}, can be evaluated by integrating the effects of point loads (Broek, 1982, p. 78) that give the driving-pressure distribution $\Delta P = \nabla P_v[y - y']$, where $y > y'$ (fig. 53.8). The result is

$$K_v^{+a} = f(y'/a)\nabla P_v a^{3/2}, \qquad (11)$$

where $f(y'/a)$ is a function of y'/a that is illustrated in figure 53.9*A* for $y'/a > 0$; that is, for vesiculation originating at or above the dike center.

The effect of the free surface on K_v^{+a} as a function of y'/a, for $a/D = 0.86$, is shown in figure 53.9*B*. As y'/a increases, the effect of the free surface diminishes, and for vesiculation occurring near the dike top it can be neglected.

The relations of the stress-intensity factors at the dike bottom, K_v^{-a}, and downrift edge, K_v^b, due to vesiculation plotted against height of vesiculation, y'/a, are shown in figure 53.9*C*. Both stress intensities are normalized by K_v^{+a}. When vesiculated magma is present only near the dike top, K_v^{+a} is much greater than either K_v^{-a} or K_v^b, and the effect of vesiculation on stress intensities at the dike bottom or downrift edge may be neglected. Thus vesiculation

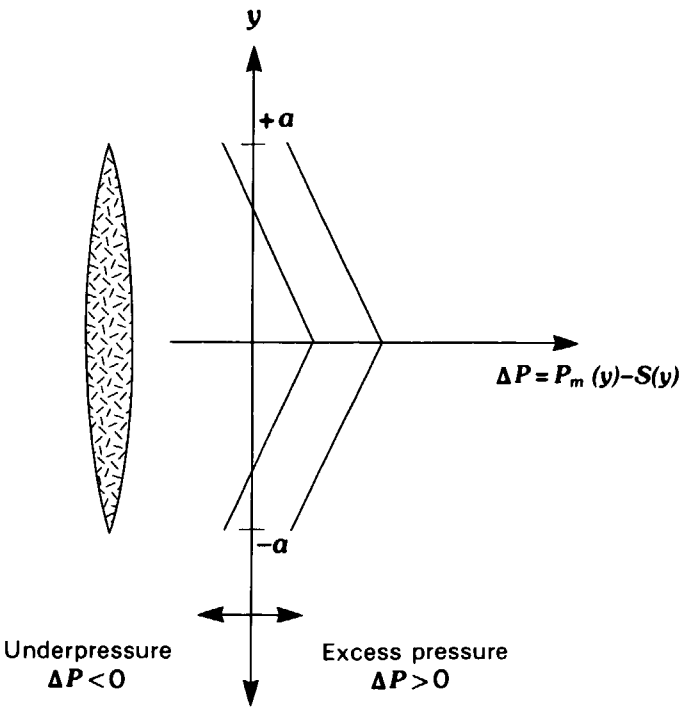

FIGURE 53.6.—Schematic diagram of two possible driving-pressure distributions that would promote the growth of blade-like dikes. If the driving pressure at the dike center is sufficiently greater than at the dike top or bottom, then $K^b > K^a$. For the right-hand curve, there is an excess pressure along the entire dike height. For the left-hand curve, the excess pressure at the dike center is sufficient to keep the dike open for its entire height, even though an underpressure acts locally at the dike top and bottom. $P_m(y)$, magma pressure; $S(y)$, remote stress; ΔP, net driving pressure; a, dike half-height.

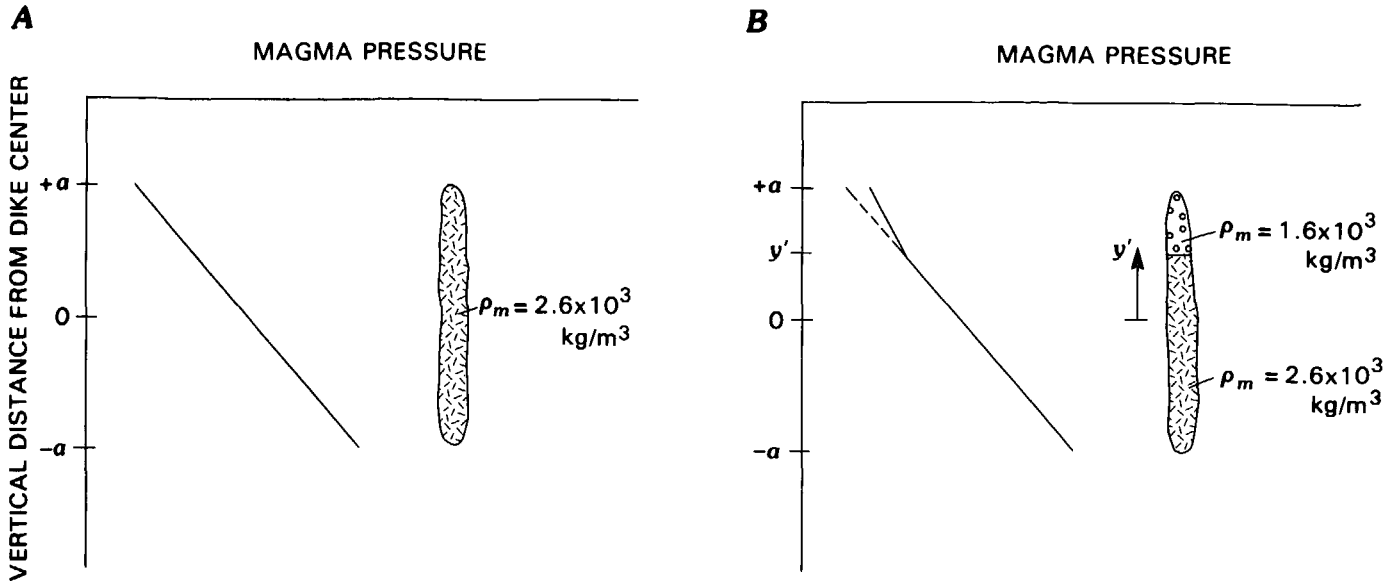

FIGURE 53.7.—Schematic diagram of vertical pressure variation in dikes. ***A***, Pressure in a dike consisting of a static column of magma of density 2.6×10^3 kg/m^3. ***B***, Pressure in a dike consisting of a static column of magma with a density of 2.6×10^3 kg/m^3 overlain above a height y' by vesiculated magma with a density of 1.6×10^3 kg/m^3.

promotes upward growth of the dike, while affecting downward and lateral growth relatively little. Dike thickness is similarly affected relatively little by pressure applied only near the dike top.

VISCOUS PRESSURE LOSS

The pressure gradients within a dike during flow will deviate from those within a static body of magma. We approximate these pressure gradients by assuming laminar flow of a viscous fluid through a channel of uniform thickness. Following Bird and others (1960, p. 59) we have

$$\nabla \mathbf{P}_{m_i} = -2\frac{V_i \eta}{(t/2)^2}, \qquad (12)$$

where $\nabla \mathbf{P}_{m_i}$ is the magma-pressure gradient minus the gravitational-pressure gradient in the x_i direction, V_i is the velocity of the magma

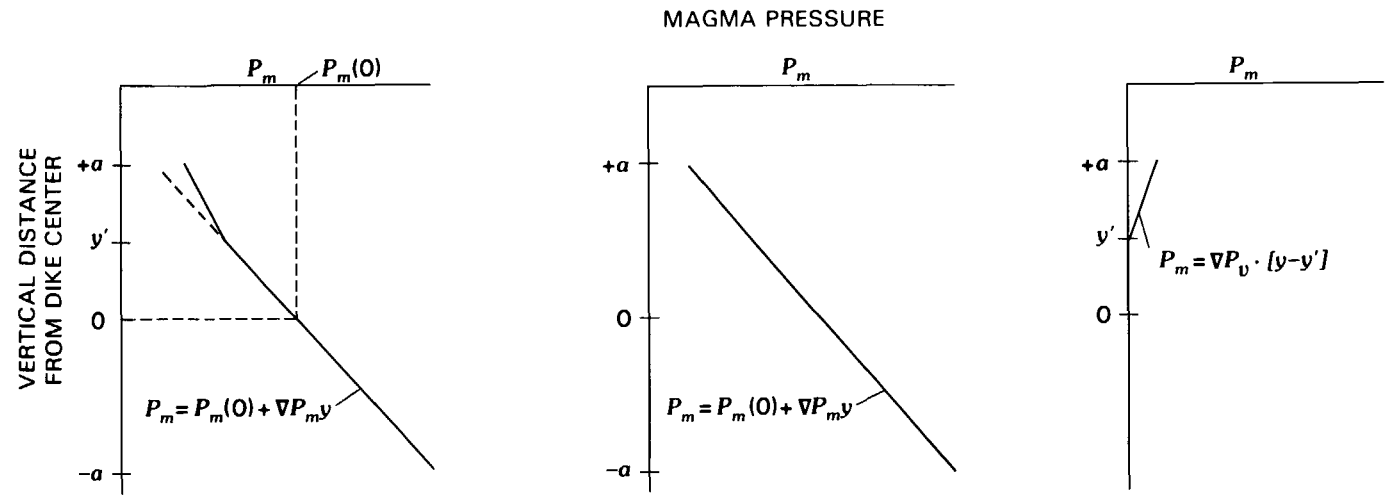

FIGURE 53.8.—The pressure within a dike containing vesiculated magma near its top (graph at left) can be expressed as a sum of the magma pressure in the absence of vesiculation (center) plus a pressure that increases linearly from the point at which vesiculation occurs (right). That pressure gradient, ∇P_v, is equal to the difference in pressure gradients between the vesiculated and unvesiculated magmas.

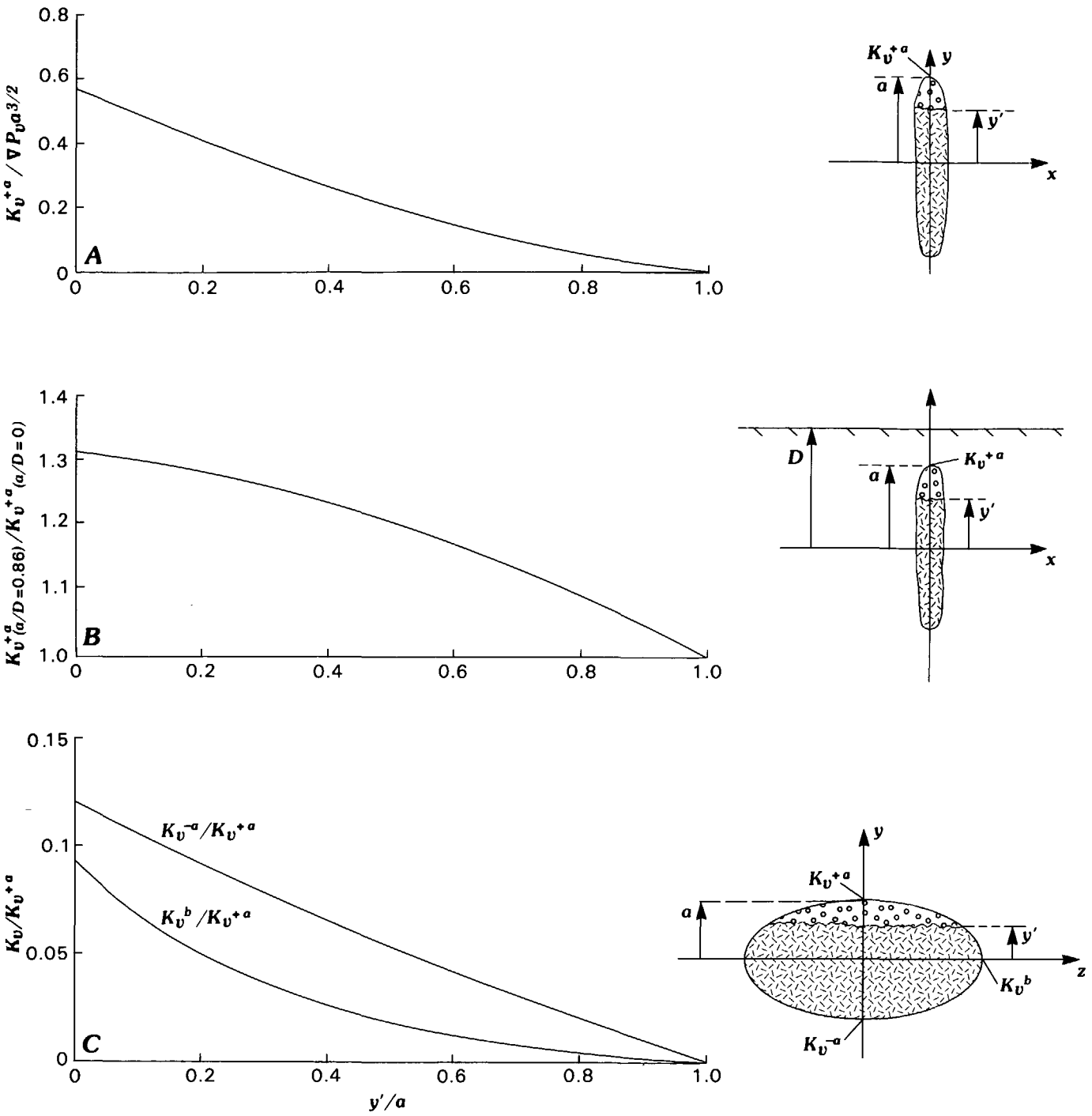

FIGURE 53.9.—Graphs showing effects of vesiculated magma in upper part of a dike. y', height above dike center of base of vesiculated magma; a, dike half-height; D, depth to dike center. ***A***, Graph of the coefficient $f(y'/a)$ for obtaining the stress-intensity factor at the dike top ($K\pi\pi_v^{+a}$, eq. 11). Note that K_v^{+a} decreases as the extent of vesiculation decreases. ***B***, Effect of the Earth's surface on the stress-intensity factor due to vesiculation at the dike top as a function of y'/a for $a/D = 0.86$. Note that the effect of the free surface diminishes as the size of the vesiculated region decreases, and that for $y'/a > 0.8$ the free surface causes only a 10 percent or less increase in K_v^{+a}. ***C***, Stress-intensity factors due to vesiculation at the dike bottom (K_v^{-a}) and downrift edge (K_v^{b}) as a function of y'/a. Note that the values of K normalized with respect to the stress intensity at the dike top are very small for most values of y'/a, so this effect may be neglected.

in the x_i direction in the center of the channel, η is the magma viscosity, and t is the channel thickness.

Delaney and Pollard (1981) estimated the upward flow velocity of magma during the initiation of the 1959 Kilauea Iki fissure eruption to be 0.1 m/s. Using a typical magma viscosity of 100 Pa · s and a dike thickness of 1 m, they calculated the driving-pressure gradient for upward magma flow to be 0.05 MPa/km. This is only about 0.2 percent of the pressure gradient due to the weight of a static column of magma with a density of 2.6×10^3 kg/m^3 and about 1 percent of the difference in pressure gradients between a static column of magma and a column of rock with a density of 2.3×10^3 kg/m^3. Vertical flow rates, and therefore vertical pressure gradients due to flow, are likely to be even less for subsurface dikes. Thus we neglect vertical magma flow and relate the vertical magma-pressure gradient only to the magma density, as in figure 53.7.

Although lateral magma-pressure gradients do not enter our model explicitly, they are likely to be important in determining the site of rift-zone fissure eruptions. To estimate these gradients, we take as typical of Kilauea dikes a lateral velocity of 0.5 m/s and a thickness of 1 m (Delaney and Pollard, 1981). From equation 12, this requires a magma-pressure drop of 0.2 MPa/km. By comparison, the slopes of both the east and southwest rift zones of Kilauea are about 25 m/km. If a dike with magma of density 2.6×10^3 kg/m^3 travels at a constant depth within these rift zones, the decrease in elevation would lead to a magma-pressure increase at a fixed depth of about 0.65 MPa/km.

REMOTE-STRESS DISTRIBUTION

SOURCES OF THE REMOTE STRESS

Given the nature of the vertical pressure distribution within dikes illustrated in figure 53.7, the source of the nonlinear driving pressure distributions required for the growth of blade-like dikes (fig. 53.6) must arise from variations in the remote stress $S(y)$ acting perpendicular to the dike plane. Several possible mechanisms that could generate the required stress-versus-depth curves at Kilauea are discussed in this section.

Crustal Density

Combined seismic and gravity modeling of Kilauea and Mauna Loa indicates that the density within the upper two kilometers of these volcanoes is considerably less than that of unvesiculated magma, and that the density below is considerably greater. The density structure along a section through the Kilauea and Mauna Loa summit regions (Zucca and others, 1982) is shown in figure 53.10. The surface density of 2.3×10^3 kg/m^3 corresponds to an average density for vesiculated lava flows (Kinoshita and others, 1963). The density of 2.9×10^3 kg/m^3 at depth might represent submarine lavas (Moore and Fiske, 1969; Swanson and others, 1976), solidified intrusions (Hill and Zucca, chapter 37), or flows with vesicles now filled with hydrothermal minerals. If the state of stress in the rift zone were lithostatic and the remote horizontal stress were equal to the pressure induced by the overlying column of rock, then $S(y)$ would be of the form depicted in figure 53.6 (fig. 53.11*A*). Assuming a magma density of 2.6×10^3 kg/m^3, the local density contrasts between the magma and the wall rock result in a driving pressure that decreases toward the dike top and bottom at a rate of 3 MPa/km. Interpretation of the density structure of the Icelandic crust (Palmason, 1971) is also consistent with the hypothesis that local density contrast is a sufficient mechanism for the generation of blade-like dikes.

Gravitational Loading of the Volcanic Ridge

It is commonly assumed that dikes are intruded perpendicular to the local least compressive stress (Anderson, 1938). The numerous parallel dikes and the relative scarcity of sills in eroded Hawaiian rift zones suggests that the stress perpendicular to the rift zone is consistently less compressive than both the vertical stress and the rift-parallel horizontal stress. This implies that some horizontal tensile stress is superimposed on a hydrostatic state of stress. Fiske and Jackson (1972) suggested that the source of this tensile stress is gravity loading of the volcanic edifice. They injected fluid into ridge-shaped gelatin models and produced "dikes" that propagated along the strike of the ridge with a nearly fixed height and depth, raising the possibility that this superimposed stress was not only responsible for dike orientation, but was also of the form necessary to limit their upward and downward growth.

Analyses of the gravitational stresses acting perpendicular to the axial plane of a ridge using numerical methods (McTigue and Mei, 1981) and finite-element models (James Dieterich, written commun., 1985) indicate that the stress is compressive at the surface and decreases or increases only slowly with depth. This generates a stress curve of the form that could prevent the dike top from rising (fig. 53.11*B*). However, the finite-element analysis indicates that the gelatin models were effective in containing the bottom of the propagating dike because of the great vertical exaggeration of the ridge shape and the high Poisson's ratio of gelatin (about 0.49). When realistic slopes and a Poisson's ratio appropriate for rock (about 0.25) are used, the resulting remote stress increases less rapidly than the magma pressure with depth, and barring an increase in K_c with depth, dikes intruded into the rift zone would continue propagating downward and not be trapped within the upper part of the crust (fig. 53.11*B*).

Previously Intruded Dikes

Following magma solidification, the stresses generated in the rift zone by a dike remain. The compressive stress within the rift zone is increased to values close to the magma pressure near the dike center and decreased near the dike top and bottom (Pollard and Segall, in press). This stress distribution would encourage successive dikes to be emplaced above or below the previous one, or else far to the side (fig. 53.11*C*). Possible examples of dikes that intruded at greater depths than previous dikes include the February 1980 intrusion at Krafla (Bryndis Brandsdottir, oral commun., 1985) and the June 1982 southwest-rift-zone intrusion at Kilauea (fig. 53.1). After several intrusions, $S(y)$ would approach $P_m(y)$

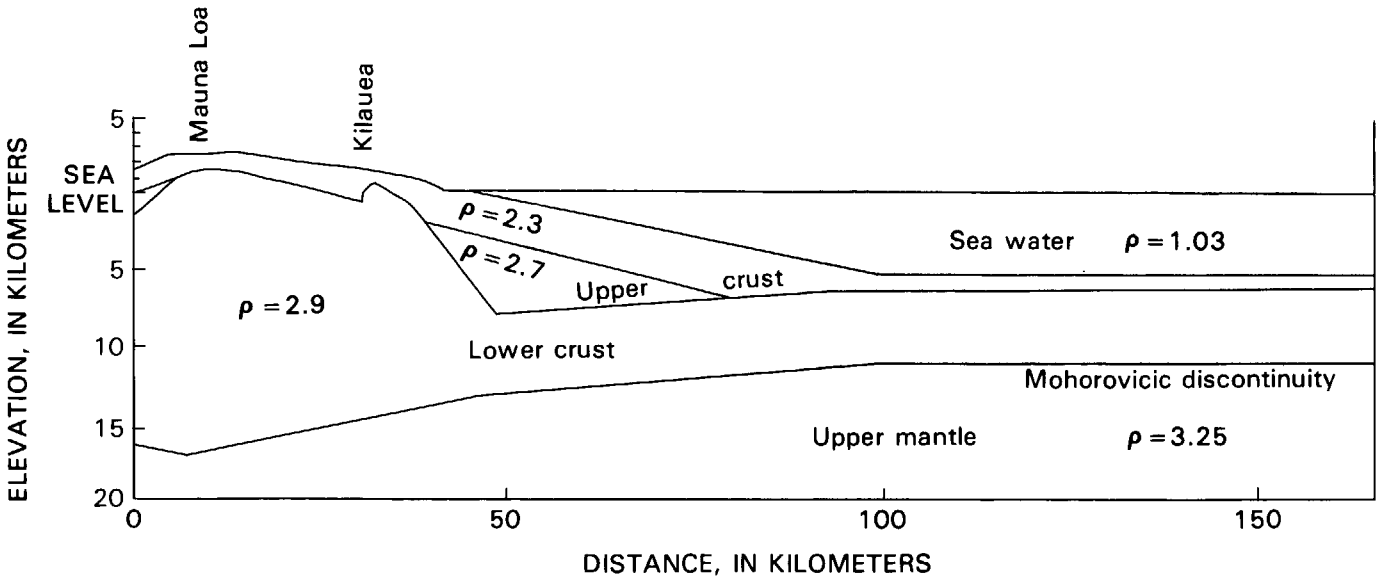

FIGURE 53.10.—Distribution of density (ρ, in 10^3 kg/m^3) in a model section through Kilauea and Mauna Loa Volcanoes (after Zucca and others, 1982). The modeled increase in density from 2.3×10^3 kg/m^3 to 2.9×10^3 kg/m^3 at about 2 km beneath the surface provides a mechanism for confining both magma reservoirs and dikes to shallow depths.

throughout the rift zone, and intrusions would cease unless $P_m(y)$ increased.

FAULTING

In order for successive dikes to be intruded into the rift zone without the magma pressure increasing monotonically through time, the rift zone must somehow behave inelastically and allow the stresses induced by dike intrusion to relax. One possible mechanism for this relaxation is slip along major faults at depth (Swanson and others, 1976). In 1975 a magnitude-7.2 earthquake occurred near Kalapana on the southeast coast of the Island of Hawaii. This earthquake seemed to have a direct effect on the intrusion-to-extrusion ratio of dikes emanating from the Kilauea magma reservoir (Klein, 1982).

James Dieterich (written commun., 1985) has modeled the stress induced by slip along a segment of a fault whose location and orientation are within the ranges inferred for the Kalapana fault. His results indicate that such motion superimposes tension within the rift zone that reaches a maximum about 3 km below the surface. This yields a driving-pressure distribution of the proper form for stabilizing a dike top and bottom (fig. 53.11*D*). The magnitude of this tension appears to be sufficient for the intrusion of only one or two overlapping dikes of average width before another major earthquake is required. The absence of frequent magnitude-7.2 earthquakes suggests that additional stress-relaxation processes may be active in the rift zone.

ANALYSIS FOR THE REMOTE STRESS

From the principle of superposition, the driving-pressure distribution $\Delta P(y)$ depicted in figure 53.6 can be represented as the sum of a uniform driving pressure P_o (equal to the excess magma pressure at the dike center) and two linearly varying driving-pressure distributions, each acting over one-half of the dike, which tend to pull the dike walls inward (fig. 53.12). The linear driving-pressure distributions are given by $\Delta P(y) = -\nabla P_u|y|$, $y > 0$, and $\Delta P(y) = -\nabla P_l|y|$, $y < 0$, where ∇P_u and ∇P_l are the gradients in the driving pressure acting on the upper and lower halves of the dike, respectively. The stress intensities produced at the top (K^{+a}) and bottom (K^{-a}) of a two-dimensional dike by these driving pressure distributions can be evaluated by superposing the solutions for cracks subjected to symmetric (Pollard, 1976) and anti-symmetric (Secor and Pollard, 1975) loads. The results are

$$K^{+a} = -\left(\frac{1}{\pi} + \frac{1}{4}\right)\nabla P_u a^{3/2}, \tag{13a}$$

$$K^{-a} = -\left(\frac{1}{\pi} - \frac{1}{4}\right)\nabla P_u a^{3/2}, \tag{13b}$$

for the pressure acting on the upper half of the dike, and

$$K^{+a} = -\left(\frac{1}{\pi} - \frac{1}{4}\right)\nabla P_l a^{3/2}, \tag{13c}$$

$$K^{-a} = -\left(\frac{1}{\pi} + \frac{1}{4}\right)\nabla P_l a^{3/2}, \tag{13d}$$

for the pressure acting on the lower half of the dike. When these equations are combined with equation 4 for a uniform driving pressure P_o, the stress-intensity factors for the driving-pressure distribution depicted in figure 53.12*B* are given by

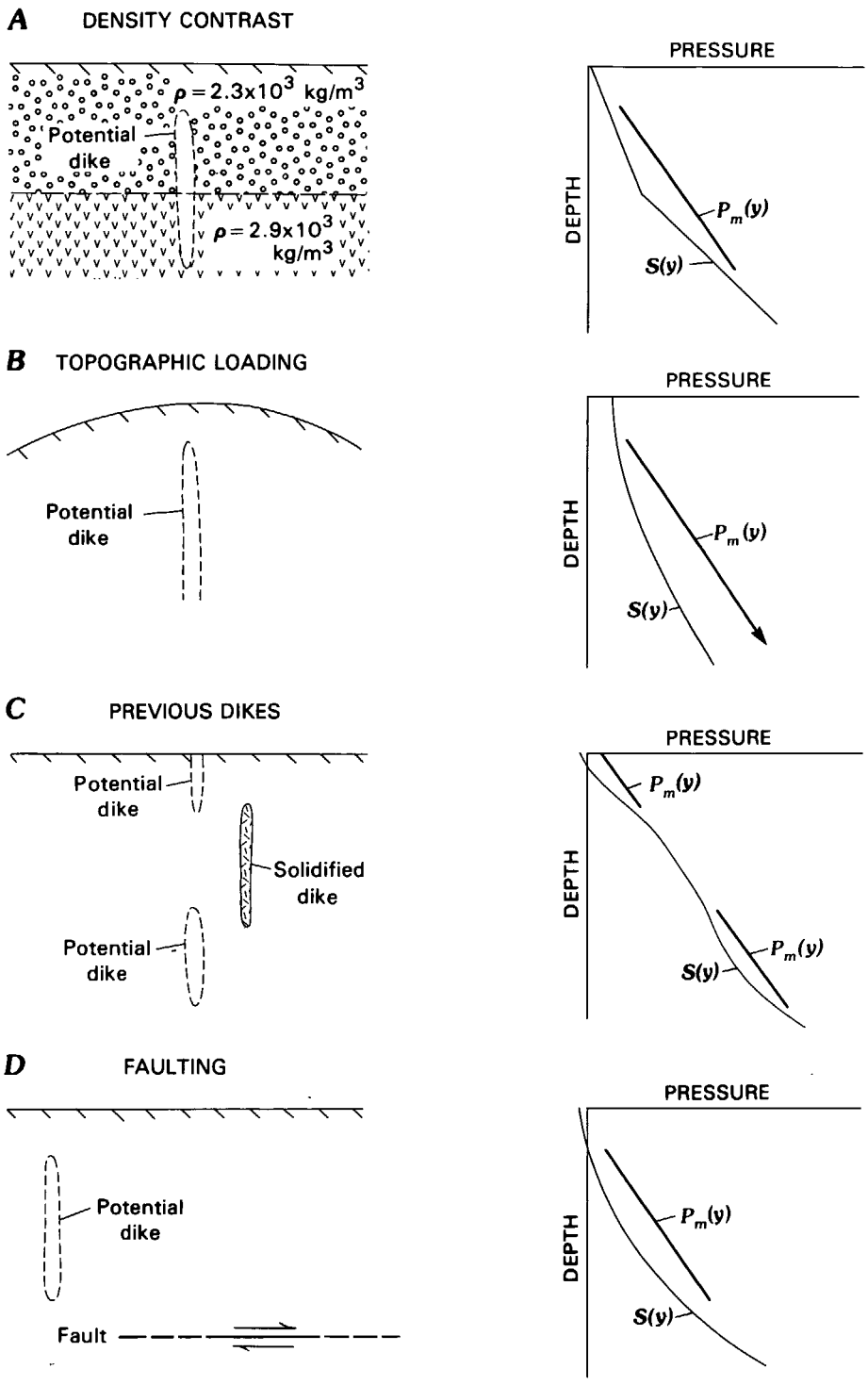

FIGURE 53.11.—Diagrams showing various mechanisms (left) and the resulting remote stress curves (right) possibly acting within a rift zone. Depths of potential dike intrusions shown. $S(y)$, remote stress; $P_m(y)$, magma pressure. ***A***, Lithostatic state of stress in a density-stratified rift zone of the type modeled by Zucca and others (1982). ***B***, Stresses due to topographic loading of the volcanic ridge, from James Dieterich (written commun., 1985). Compressive stress near the surface can prevent the dike top from propagating up, but compressive stress does not increase rapidly enough with depth to prevent the bottom from continuing to propagate down. ***C***, Stresses induced by previous intrusion of dikes. Subsequent dikes would tend to be intruded above, below, or well to the side of earlier ones. ***D***, Stresses generated by motion along a Kalapana-like fault, from James Dieterich (written commun., 1985). The depth of the maximum superimposed tension depends upon the fault dip and the location of slip.

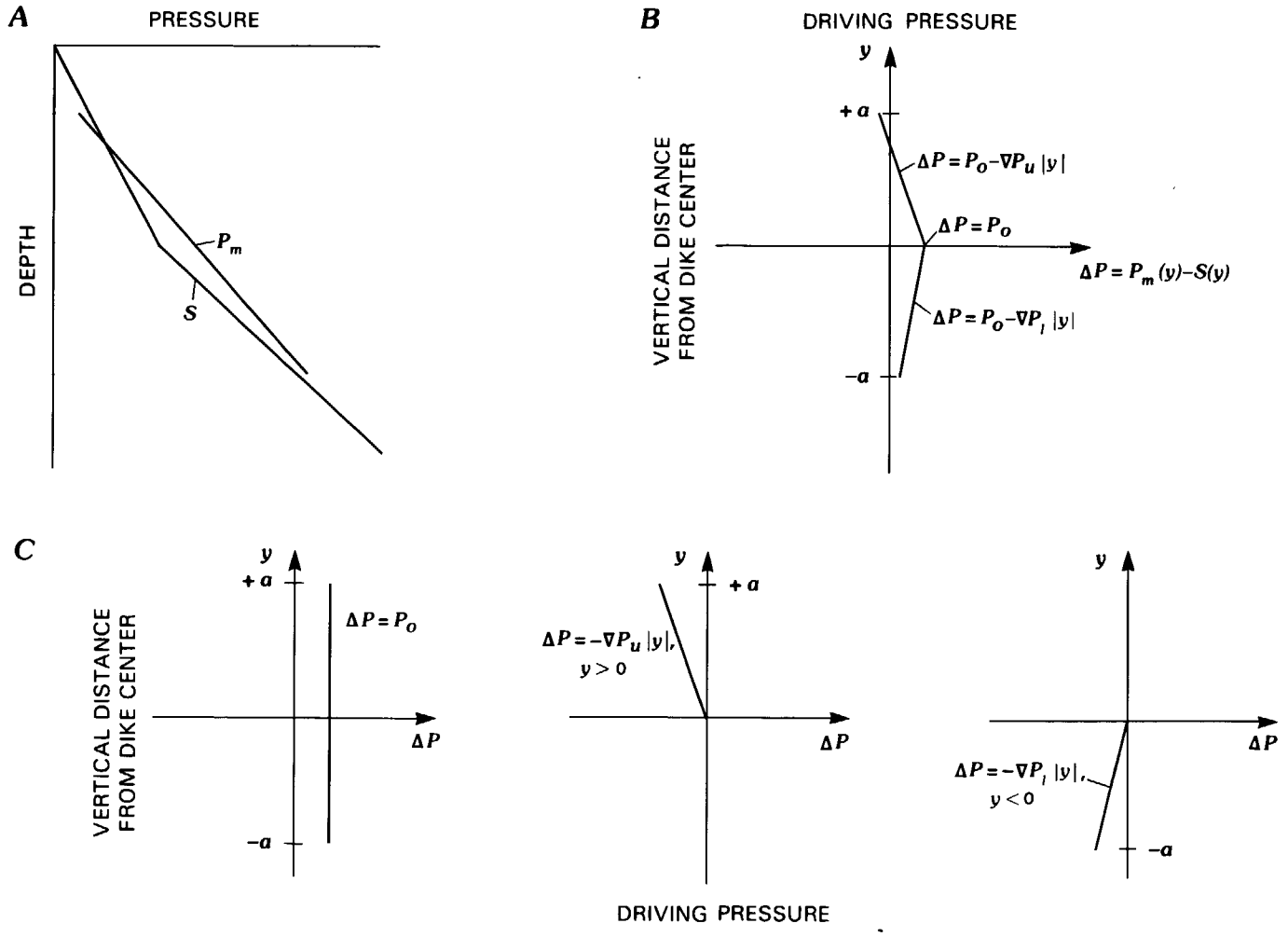

FIGURE 53.12.—Diagrams of stress distributions with depth. ***A***, Remote stress S from idealized density structure (fig. 53.11*A*) and magma pressure P_m caused by static weight of magma (fig. 53.7*A*). ***B***, Distribution of driving pressure $\Delta P(y)$ resulting from $P_m - S$ as depicted in ***A***. ***C***, Driving pressure in ***B*** represented as the sum of a uniform driving pressure (left) equal to the excess pressure acting at the dike center (P_o), and two linearly varying driving-pressure distributions ($-\nabla P_u|y|$ and $-\nabla P_l|y|$), acting over the upper and lower halves of the dike (center and right).

$$K^{+a} = P_o\sqrt{a} - \left(\frac{1}{\pi} + \frac{1}{4}\right)\nabla P_u a^{3/2} - \left(\frac{1}{\pi} - \frac{1}{4}\right)\nabla P_l a^{3/2}, \quad (14a)$$

$$K^{-a} = P_o\sqrt{a} - \left(\frac{1}{\pi} - \frac{1}{4}\right)\nabla P_u a^{3/2} - \left(\frac{1}{\pi} + \frac{1}{4}\right)\nabla P_l a^{3/2}. \quad (14b)$$

In a similar fashion, the average dike thickness is found to be

$$\bar{l} = \frac{1-\nu}{\mu}\left(\frac{\pi}{2}P_o a - 0.33\nabla P_u a^2 - 0.33\nabla P_l a^2\right). \quad (15)$$

To estimate K^b at the downrift edge of the dike resulting from a driving-pressure distribution, $\Delta P = -\nabla P|y|$, acting on the upper or lower half of the dike, we calculate K^b for a disc-shaped crack of radius a by integrating the contributions from applied point loads (Tada and others, 1973) giving the distribution $\Delta P = -\nabla P|y|$, $0 < y < a$. The result is

$$K^b = -0.053\nabla P a^{3/2}. \quad (16)$$

The low coefficient illustrates the rather small effect such gradients have on the stress intensity at the downrift edge of the dike. Combining this with (7) for the contribution to K^b from the uniform applied load, we derive

$$K^b = \frac{2}{\pi}P_o\sqrt{a} - 0.053\nabla P_u a^{3/2} - 0.053\nabla P_l a^{3/2} \quad (17)$$

for the driving pressure depicted in figure 53.12*B*.

The effect of the Earth's surface on each of the superposed boundary conditions in figure 53.12 is presented as a function of a/D in figure 53.13*A*. This graph can be thought of as providing correction factors to equation 14 to be used when superposing solutions for particular values of a/D. For a given a/D, the contribution to K^{+a} or K^{-a} from a particular term in equation 14

should be multiplied by the ordinate of the curve in figure 53.13 corresponding to that term. Because K^b is not very sensitive to a/D (fig. 53.4), its value in an infinite body will be used. An equivalent graph for average dike thickness is presented in figure 53.13*B*.

SUMMARY OF THE FACTORS AFFECTING DIKE PROPAGATION

We have discussed various parameters that are important to the dike propagation process and, through the calculation of the stress-intensity factors K^a and K^b, have analyzed their effects on lateral and vertical propagation. A blade-like dike shape and the presence of the Earth's surface both enhance upward propagation and eruption relative to lateral propagation. Observation of continued subsurface lateral propagation requires the dike driving pressure to be such that it overcomes these geometric effects. A driving pressure that is greater at the dike center than at the dike top and bottom could satisfy this condition. Since the pressure gradient within a column of unvesiculated magma is uniform, and since vesiculation increases the driving pressure only at the dike top, the origin of this driving pressure must be the remote stress. Processes that could contribute to the required remote-stress distribution at Kilauea include density stratification of the rift zone, gravitational loading, previously intruded dikes, and slip along faults.

Equations 14a, 14b, 17, and 15 were developed to calculate the stress-intensity factors at the dike top, bottom, and downrift edge, and the average dike thickness, for a driving pressure that is greatest at the dike center and decreases linearly toward the top and bottom. These equations can be corrected for the effect of the free surface using the graph in figure 53.13. The stress-intensity factor at the dike top (eq 14a) can be modified to include the effects of vesiculation (eq 11), but the effect of the free surface on equation 11, and the effect of vesiculation on equations 14b, 15, and 17 can be neglected. In the following section we show how these equations may be applied to analyze a rift-zone intrusion.

APPLICATION TO THE INTRUSIVE EVENT OF AUGUST 1981

The above analysis makes it possible to estimate the magma pressure and the horizontal remote-stress distribution acting perpendicular to the rift axis for particular dikes whose geometry is known. We begin by assuming that the magma is unvesiculated, so that the magma pressure variation with depth is given by a line segment of constant slope. We also assume that the remote stress can be adequately represented by two linearly varying line segments (fig. 53.12), each of which acts on one-half of the dike. In general, a dike center is not constrained to be positioned at a kink in the stress distribution. Nevertheless, useful insight into the nature of the driving pressure distribution is obtained by employing this assumption. We assume that K_c is independent of depth, so that $K^{+a} = K^{-a} = K_c$ at the moment the dike ceases to propagate in the vertical direction. Finally, we assume that the shape of the dike determined using geodetic data collected after the cessation of intrusive activity is approximately the shape of the dike when it attained its maximum height.

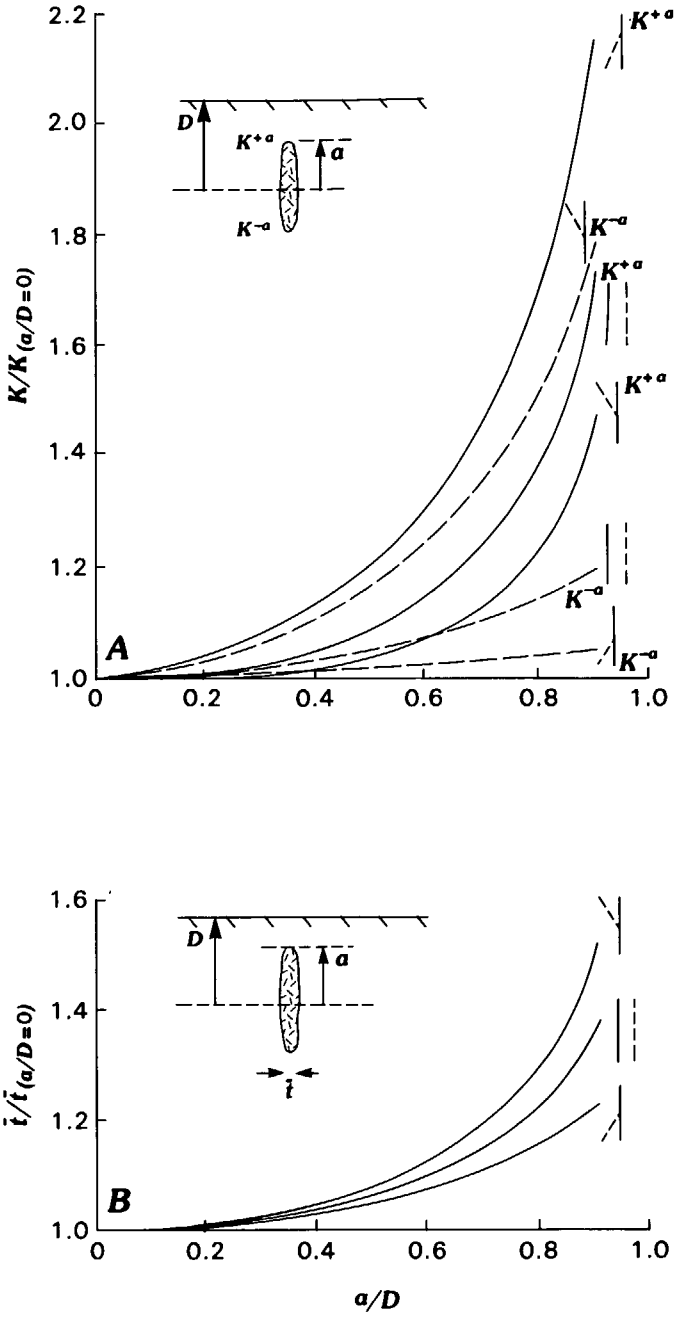

FIGURE 53.13.—Diagrams showing effect of proximity of the Earth's surface on stress-intensity factors and average dike thickness. ***A***, Effect of the Earth's surface on stress-intensity factors at the dike top (solid lines) and bottom (dashed lines) as a function of a/D for components of the driving pressure in fig. 53.12*C*, identified by the schematic diagrams to the right. ***B***, Effect of the Earth's surface on average dike thickness as a function of a/D for components of the driving pressure in fig. 53.12*C*.

In August 1981 a dike approximately 25 km long was intruded into the southwest rift zone of Kilauea (fig. 53.1). From geodetic

data, Pollard and others (1983) estimated a dike half-height of 1.5 km, a depth of 1.75 km, an average thickness of 1.4 meters, and a dip of 82°. Although difficulty was encountered in reproducing the displacement data for the southeast half of the profile using the elastic model, we use these geometric parameters for our analysis. Abundant ground cracks that formed above the dike are good evidence for a shallow dike top; in combination with the large ratio of a/D, they indicate that interaction of the dike with the free surface should be included. We ignore the dip of the dike, which alters neither the gradients in driving pressure nor the free-surface correction by more than 1–2 percent.

Using figure 53.13 and a value for a/D of 0.86 to obtain the free-surface correction factors for equations 14 and 15, we have

$$K^{+a} = 1.52P_o\sqrt{a} - 1.31\left(\frac{1}{\pi}+\frac{1}{4}\right)\nabla P_u a^{3/2} - 1.86\left(\frac{1}{\pi}-\frac{1}{4}\right)\nabla P_l a^{3/2}, \quad (18a)$$

$$K^{-a} = 1.17P_o\sqrt{a} - 1.63\left(\frac{1}{\pi}-\frac{1}{4}\right)\nabla P_u a^{3/2} - 1.05\left(\frac{1}{\pi}+\frac{1}{4}\right)\nabla P_l a^{3/2}, \quad (18b)$$

$$\bar{t} = \frac{1-\nu}{\mu}\left(1.29\frac{\pi}{2}P_o a - 1.39(0.33)\nabla P_u a^2 - 1.19(0.33)\nabla P_l a^2\right). \quad (19)$$

Setting $K^{+a} = K^{-a}$, we find

$$\nabla P_l a = 1.34\nabla P_u a - 0.74P_o, \quad (20)$$

which we then substitute for $\nabla P_l a$ in equations 17 through 19. To restrict the range of values of P_o and ∇P_u, we first use the requirement that $K^a > 0$. From equation 18a we find

$$P_o > 0.57\nabla P_u a. \quad (21)$$

Next we use the requirement that $K^a < K^b$ for a dike with a stable height but a propagating downrift edge; using equations 17 and 18a, we find

$$P_o < 0.84\nabla P_u a. \quad (22)$$

Limiting remote stress and magma pressure curves for a dike with a half-height of 1,500 m and a depth of 1,750 m are shown in figures 53.14*A* and 53.14*B*. The magma has a density of 2.6×10^3 kg/m^3 and thus an internal pressure gradient of 26 MPa/km. We specify that the remote stress has a value of zero at the surface. The gradient of the driving pressure acting on the upper half of the dike in figure 53.14*A* is 3 MPa/km, or approximately that generated by the local density contrast between the magma and the wall rock. Modeling by James Dieterich (written commun., 1985) indicates that both gravity loading and slip on a master fault at depth superimpose tensile stresses that increase with depth in the upper few kilometers of the volcano, so 3 MPa/km is likely to be a lower limit for this gradient. The gradient of the driving pressure acting on the upper half of the dike in figure 53.14*B* is 11 MPa/km. We show below that this is an upper limit if the hydrostatic head of the magma is higher than 350 m below the surface. The remote stress acting on the lower half of the dike in figure 53.14 is the average of the relatively narrow range of ∇P_l obtained from equation 20 and the constraint that P_o be in the range 0.57–0.84 $\nabla P_u a$.

The left-hand magma-pressure curve in figure 53.14*A* corresponds to $P_o = 0.57\nabla P_u a$ (eq 21), and the right-hand curve to $P_o = 0.84\nabla P_u a$ (eq 22). A P_o less than the former would produce a K^a less than zero, in which case the dike could not have propagated to its required height, and a P_o greater than the latter would violate the requirement that $K^a < K^b$. Allowable magma-pressure curves for this value of ∇P_u therefore lie between the limits indicated. The horizontally exaggerated cross-sectional forms resulting from these two driving-pressure distributions are shown in the upper right of figure 53.14*A*. In figure 53.14*B*, the lower magma-pressure curve has a hydrostatic head beneath the dike top, and so equations 17–19 do not apply. To treat this case, we assume that unvesiculated magma rises to its hydrostatic head and is capped by a near vacuum. We obtain y', calculate K_v^{+a} (eq 11), and include this term in the calculation of K^{+a} (eq 18a). Because of the small effect on K^{-a}, K^b, and $\bar{t}$, equations 17, 18b, and 19 need not be modified.

The limiting magma-pressure curves in figures 53.14*A* and 53.14*B* require knowledge only of the dike height and depth. In order to restrict the magma-pressure range further, additional constraints are needed. Associated with each magma-pressure curve is a value for K^a and, given a value for the rock stiffness, an average dike thickness. These are indicated in figure 53.14. Magma-pressure curves generating values of K^a equal to those for K_c determined in the laboratory are essentially indistinguishable from those generating a K^a of zero. Note that the right-hand magma-pressure curve in figure 53.14*B* is greater than our upper limit of 100 MPa · m$^{1/2}$. The low values of dike thickness are calculated using laboratory determinations of the shear modulus (30 GPa), and the high values are calculated using estimates of the effective shear modulus from piezomagnetic measurements at Kilauea (3 GPa) (Davis, 1976). Note that the lower values of dike thickness are well below the value of 1.4 m estimated for the 1981 intrusion for each driving-pressure distribution shown.

A summary plot of the driving pressure at the dike center, P_o, versus the product of the gradient in driving pressure and the dike half-height, $\nabla P_u a$, is presented in figure 53.15. The wedge-shaped region (red lines) bounded by $P_o = 0.57\ \nabla P_u a$ (eq 21) and $P_o = 0.84 P_u a$ (eq 22) contains all values of P_o and $\nabla P_u a$ that are consistent with observed dike-propagation behavior. Points lying below the lower red boundary are unacceptable because the dike could not have propagated to a half-height of 1,500 m, and those lying above the upper red boundary are unacceptable because the dike would have continued propagating vertically and possibly would have erupted. For a given dike height, thickness, and depth, the wedge-shaped region can be contoured for values of the fracture

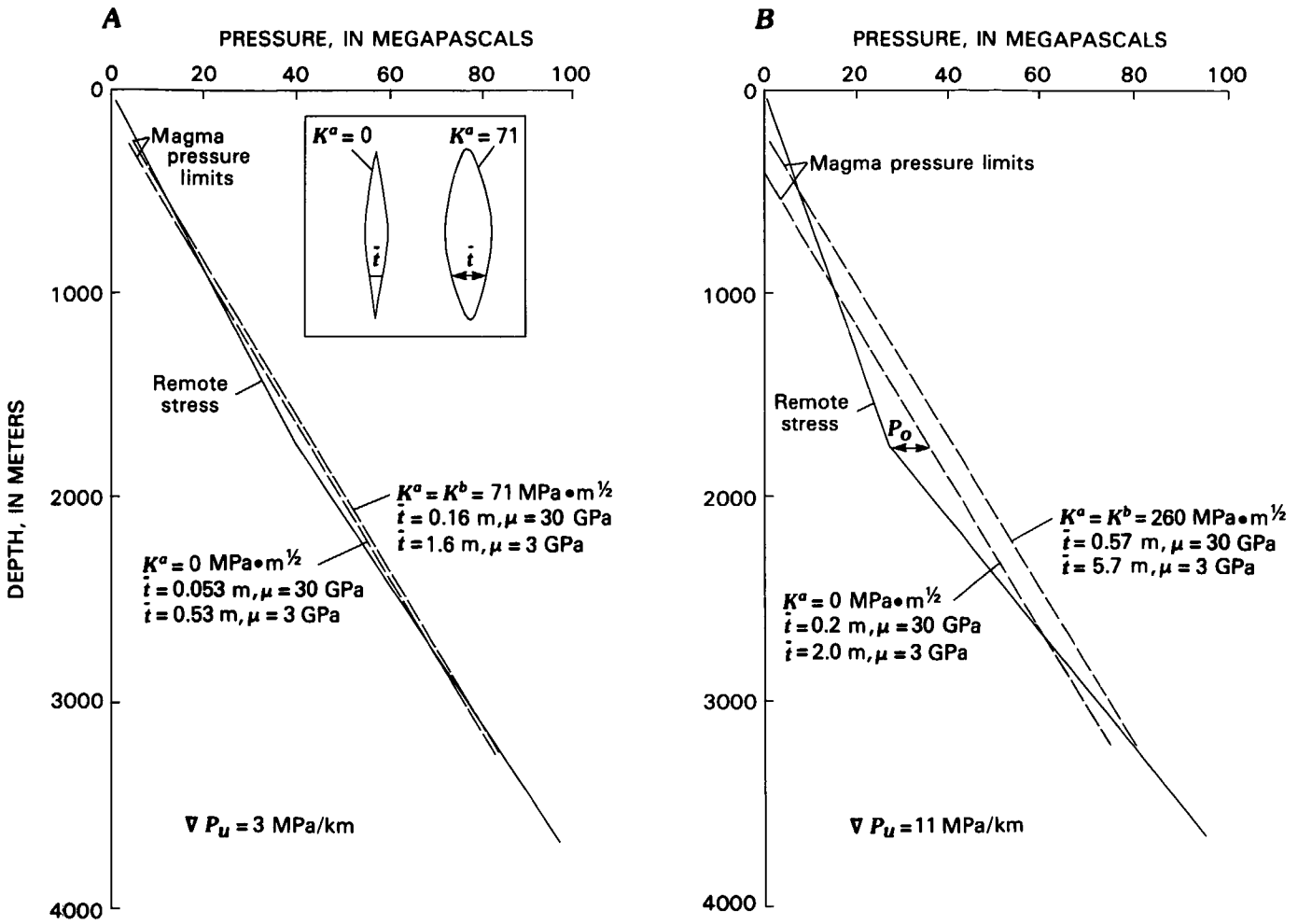

FIGURE 53.14.—Limiting remote-stress and magma-pressure curves for a dike with a height of 1,500 m and a depth of 1,750 m. The magma has a density of 2.6×10^3 kg/m^3. The remote stress is constrained to have a value of zero at the surface. The range of allowable values of P_o is given by the left and right magma pressure curves in each diagram. For any lower P_o, $K^a < 0$; for any higher P_o, $K^a > K^b$. Each magma-pressure curve is associated with a value of K^a, and, given a value for the shear modulus, an average dike thickness. The average dike thicknesses indicated are for shear moduli of 3 and 30 GPa. The higher shear modulus predicts thicknesses too narrow (<1.4 m). ***A***, Curves for $\nabla P_u = 3$ MPa/km. The inset shows the horizontally exaggerated cross-sectional forms of dikes generated by the limiting magma-pressure curves. ***B***, Curves for $\nabla P_u = 11$ MPa/km. K^a for the right-hand curve is greater than our upper limit for K_c of 100 MPa · m$^{1/2}$.

toughness, rock stiffness, and hydrostatic head of the magma column. These contours will be used to further constrain the driving pressure.

Substituting equation 20 into equation 19 and rearranging yields

$$P_o = 0.42 \nabla P_u a + 0.43 \frac{\bar{t}}{a} \frac{\mu}{(1-\nu)}. \qquad (23)$$

Thus contours of the dike thickness-to-height ratio times the rock stiffness are straight lines. For $a = 1{,}500$ m, $\bar{t} = 1.4$ m, and $\nu = 0.25$, these lines become contours of the shear modulus, μ. Contours for values of μ of 1.5 GPa, 3 GPa, and 6 GPa are shown.

Substituting equation 20 into equation 18a and rearranging yields

$$P_o = 0.57 \nabla P_u a + 0.62 \frac{K^{+a}}{\sqrt{a}}. \qquad (24)$$

Thus contours of K^{+a} divided by the square root of the dike half-height are also straight lines; on figure 53.15, these contours are parallel to the lower boundary of the wedge-shaped region, for which $K^a = 0$. Contours of the lower and upper limits for K_c, 0 and 100 MPa · m$^{1/2}$, are shown. If laboratory values ($K_c \approx 1$ MPa · m$^{1/2}$) represent the upper bound, the stress would be constrained to lie near the lower boundary of the wedge-shaped region.

From figure 53.14, one can derive that the magma pressure in the center of the dike is

$$P_m(0) = D(\rho_m g - \nabla P_u) + P_o, \qquad (25)$$

where D is the dike depth and ρ_m is the magma density. The height above the dike center to which a column of unvesiculated magma can be raised is $P_m(0)/\rho_m g$, so the hydrostatic head C is

$$C = -D + \frac{D(\rho_m g - \nabla P_u) + P_o}{\rho_m g}. \qquad (26)$$

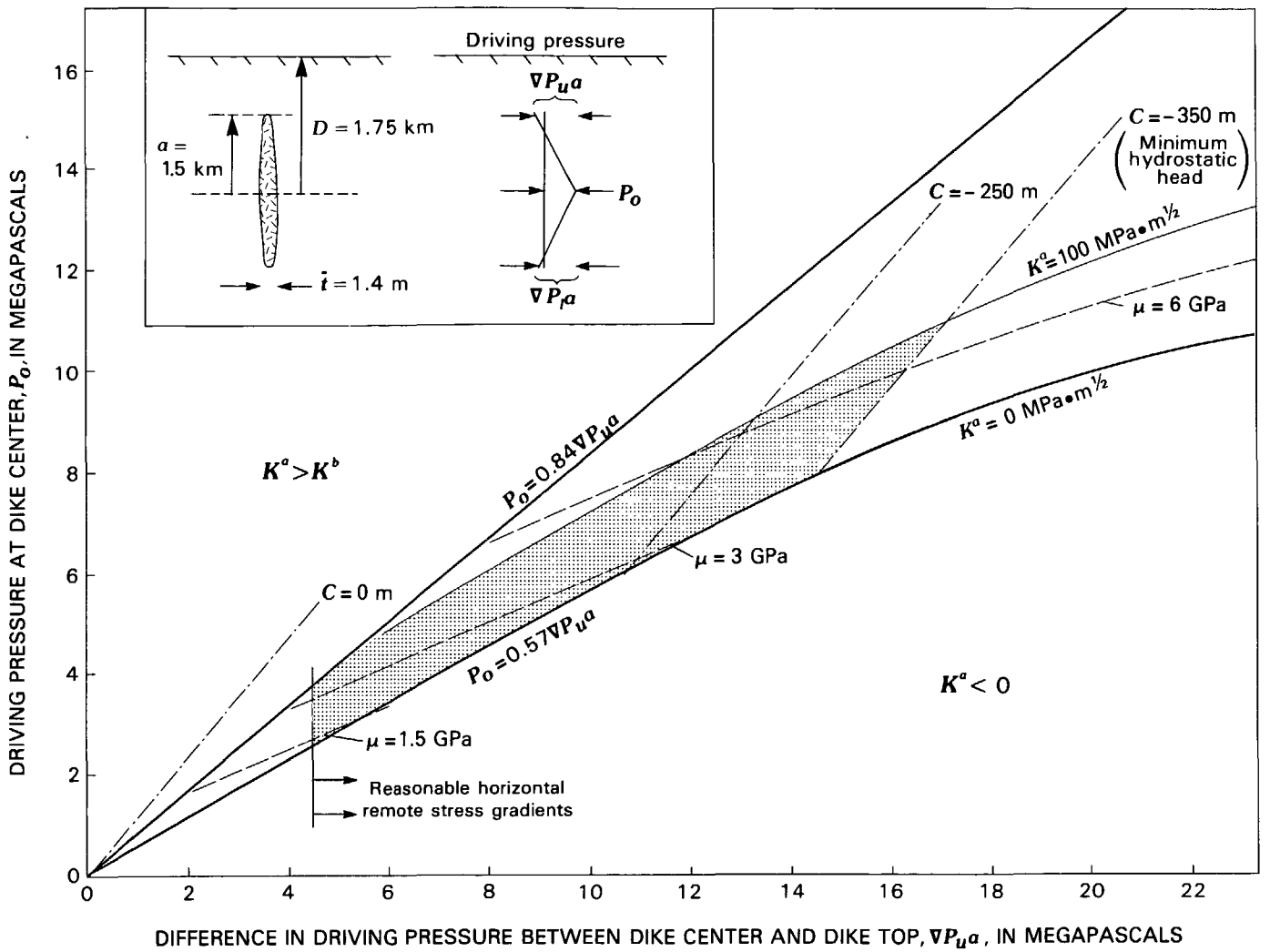

FIGURE 53.15.—Possible values of P_o and $\nabla P_u a$ (wedge-shaped region between red lines) for the August 1981 southwest-rift-zone intrusion at Kilauea, the inferred geometry of which is shown in the inset. Values below the lower red boundary are unacceptable because $K^a < 0$; values above the upper red boundary are unacceptable because values of K^a (eq 24), the hydrostatic head of the magma, C (eq 27), and the shear modulus that would result in an average dike thickness of 1.4 m (eq 23). Values within the stippled region satisfy the requirements that $K^a < K^b$, $0 < K^a < 100$ MPa · m$^{1/2}$, $\nabla P_u \geq 3$ MPa/km, and $C > -350$ m (see text).

Rearranging equation 26, we have

$$P_o = \frac{D}{a} \nabla P_u a + \rho_m g C . \qquad (27)$$

Thus contours of the hydrostatic head are also straight lines on figure 53.15 and have a slope of D/a. For $D/a = 1.17$ ($a/D = 0.86$), any dike that has a hydrostatic head above the ground surface (to the left of contour $C = 0$, figure 53.15) fails to satisfy the requirement that $K^a < K^b$. Such a dike would grow in height (increase $\nabla P_u a$ at constant P_o in figure 53.15), and finally erupt.

To the right of the $C = -250$ m contour, the wedge-shaped region has been modified to account for the low-pressure cavity between the top of the magma and the dike tip. Instead of being linear, contours of μ and K deviate slightly toward lower values of P_o. Setting $C > -350$ m, we find that acceptable values of P_o and $\nabla P_u a$ are limited to below about 10.5 MPa and 17 MPa, respectively.

The lower limit on the gradient in driving pressure, $\nabla P_u \geq 3$ MPa/km, becomes $\nabla P_u a \geq 4.5$ MPa for $a = 1{,}500$ m.

The stippled region in figure 53.15 contains all values of P_o and $\nabla P_u a$ satisfying the conditions that $K^a < K^b$, $0 < K^a < 100$ MPa · m$^{1/2}$, $C > -350$ m, and $\nabla P_u \geq 3$ MPa/km. P_o, the excess magma pressure at the dike center, lies between about 2.5 and 10.5 MPa. The upper bound of the hydrostatic head, occurring for $\nabla P_u a = 4.5$ MPa and $P_o = 4$ MPa, is about 50 m beneath the surface. $\nabla P_u a$ lies between 4.5 and 17 MPa, corresponding to

values of ∇P_u, the difference between gradients of the magma pressure and the remote stress, of 3–11 MPa/km. This is between 1 and 4 times the difference in pressure gradients due to the density contrast between the magma and the host rock. Thus, the remote stress is bracketed by the curves shown in figures 53.14*A* and 53.14*B*. Without further refinement of the in place values of the rift-zone shear modulus and fracture toughness, it is not possible to determine these parameters more precisely. The limits of the stippled region constrain the effective shear modulus to be within a factor of 2–3 of 3 GPa. By generating diagrams such as figure 53.15 for several intrusions with different dike heights, thicknesses, and ratios of height to depth, it might be possible to constrain the shear modulus still further.

DISCUSSION

ASSUMPTION OF A UNIFORM FRACTURE TOUGHNESS

The assumption of a uniform fracture toughness within the rift zone requires that the remote stress and the magma pressure converge with depth over the lower half of the dike ($\nabla P_l > 0$) (fig. 53.14). If K_c increaeses with depth, then ∇P_l could decrease to values below those indicated. The magma-pressure and remote-stress curves could actually diverge with increasing depth, if the increase in K_c is sufficiently great and its value is much greater than laboratory values. From experimental data it appears that, in the absence of a pervasive pore fluid at a pressure equal to the confining pressure, K_c increases with depth because of increasing pressure. Although its effect is small, increasing temperature will actually decrease K_c with depth, at least to moderate temperatures. There is no evidence to support a rapid increase in K_c at pressures and temperatures corresponding to depths typical of dike bottoms.

A sequence of two dike intrusions into the southern Krafla rift zone in Iceland is instructive in this regard. The first, in September 1977, generated a swarm of earthquakes with focal depths of about 2–5 km (Brandsdottir and Einarsson, 1979), and the second, in February 1980, generated earthquakes with depths of about 4–7 km (Bryndis Brandsdottir, oral commun., 1985). On the assumption that the deeper earthquake swarm is indicative of a deeper dike, this behavior is consistent with the location of the second dike being controlled by the stress field induced by the first (fig. 53.11C). In addition it provides evidence that any increase in K_c with depth that might have stabilized the bottom of the earlier dike was not great enough to serve as a barrier to the later dike, and that the bottom of the earlier dike was well within a region capable of sustaining brittle behavior.

If some dikes on the east rift zone of Kilauea bottom within a magma conduit of high temperature and large radius of curvature, then an increase in K_c (because of microplasticity), as well as a decrease in K (because of a large radius of curvature at the dike tip) could result. Such a conduit might serve as an effective barrier to further propagation of the dike bottom.

OTHER FACTORS THAT MIGHT INFLUENCE DIKE SHAPE

In the preceeding treatment of dike stability, it was assumed that the dike had achieved an equilibrium position in the vertical plane. In the following sections we discuss factors related to magma solidification and flow which could influence dike growth and prevent the dike from reaching such an equilibrium position. Though some of these processes may warrant further study, we explain why they have been neglected in this analysis.

MAGMA SOLIDIFICATION

Walker (1974) suggested that low wall-rock temperatures near the Earth's surface could promote magma solidification near the top of a dike and thus prevent eruption. For magma to solidify at approximately the same height as it propagates many kilometers downrift implies that very little heat loss occurs during lateral flow, compared to the heat loss that occurs during upward flow. Following the work of Delaney and Pollard (1982), we estimated the effect of host-rock temperature on the time required for magma solidification during flow in a dike. Even if upward flow occurs entirely adjacent to host rock at the low temperatures appropriate for the dike top, magma originating at a depth of 3 km has less difficulty in flowing to the surface than in flowing 10 km downrift, given a uniform dike thickness and magma flow rate. Under these circumstances, solidification should not be important in stabilizing the dike top. However, if the driving-pressure distribution is such that the dike is thinner in its upper part, and if the resulting magma velocity is less than at depth, the possibility that magma solidification occurs before the dike reaches its stable height cannot be ruled out.

The following observations of dike behavior support our contention that magma solidification, by itself, is unlikely to limit dike height: (1) Fissures that erupt generally permit magma flow to continue for several hours before solidification takes place. (2) Long-term patterns of intrusion and eruption observed at both Kilauea and Krafla (see below) are easily reconciled with evolving magma pressures and remote stresses. The alternative interpretation of this behavior as due to changing susceptibility of the magma to solidification finds no independent support. (3) At least one dike, the February 1980 intrusion into the southern Krafla rift zone, was associated with an earthquake swarm whose top was deeper than 3 km. This depth is below that at which solidification might influence propagation.

TWO-DIMENSIONAL MAGMA FLOW

If dike growth in two dimensions is analogous to the pumping of magma at constant pressure into the base of an existing vertical slot in the Earth's crust, then lateral growth will be enhanced relative to upward growth because the pressure gradient available for upward flow is reduced by the static pressure gradient within the overlying column of magma. If this tendency is sufficiently pronounced it could

prevent dikes from reaching their equilibrium height before solidification. To estimate the significance of this effect, we compared the upward and lateral rates of one-dimensional magma flow in a slot, under the conditions of constant pressure at the origin and zero pressure at the advancing magma front. The upward flow rate is not greatly decreased relative to the lateral flow rate until the top of the magma column approaches its hydrostatic head. The hydrostatic head as a limit to the magma column height can be incorporated directly into the analysis of dike stability, as it was for the example of the August 1981 intrusion. A more complete formulation of the one-dimensional dike propagation problem than flow in an existing slot was proposed by Spence and Turcotte (1985). They assumed that the magma wets the dike walls all the way to the tip and coupled the viscous pressure loss within the magma to the elastic dilation of the dike walls. If the remote horizontal compressive stress is constant at a given depth but increases with depth at the same rate as the hydrostatic pressure in the magma column, then vertical and horizontal flow rates would be equal. Although it is not expected that the remote stress and the magma pressure increase identically with depth, the rates of increase are probably close enough that the influence of gravity on the relative vertical and horizontal magma flow rate is minimal. Therefore we feel justified in neglecting the complexities of two-dimensional magma flow in rift-zone dikes as a mechanism for preventing them from attaining their equilibrium height.

SUBCRITICAL CRACK GROWTH

In a chemically reactive environment, the energy required for a unit increase in crack length, and thus K_c, may be decreased. Rates of crack propagation under these conditions are controlled in part by the rate of transport of the reactive species to the crack tip and the kinetics of reaction. Anderson and Grew (1977) suggested that this process, known as subcritical crack growth, might be an important mechanism of dike propagation. However, maximum rates of subcritical crack growth in laboratory rock samples are 10^{-2}–10^{-3} m/s (Atkinson, 1984), about two orders of magnitude less than observed rates of rift-zone dike propagation. Moreover, these rates decrease by several orders of magnitude for small decreases in K. Therefore we have neglected this form of crack growth in our analysis. It is possible that subcritical growth occurs at the top and bottom after a dike has reached a stable height. However, the greatest distance that a typical 1-meter dike could propagate at these rates in the few hours before solidification is only about 100 m.

POTENTIAL APPLICATIONS OF THE MODEL

LONG-TERM INTRUSION/EXTRUSION BEHAVIOR

Klein (1982) noted that five of the seven dike intrusions at Kilauea within the 4 years prior to the 1975 Kalapana earthquake resulted in eruptions, whereas only two of the sixteen dike intrusions in the 6 years following the earthquake did so. The two most recent episodes of activity at Krafla, from 1724 to 1729 and from 1975 to the present, began with a series of predominantly subsurface dikes accompanied by either minor eruptions or none, and ended with a series of fissure eruptions emitting successively increasing volumes of magma (Tryggvason, 1983; Saemundsson, 1979). This behavior is consistent with the hypothesis that large earthquakes at Kilauea (Dzurisin and others, 1980; Klein, 1982), and centuries of plate spreading in Iceland (Bjornsson and others, 1979) extend the rift zone and facilitate dike intrusion. The preceding analysis has shown that, independent of the magnitude of the remote tensile stress, a shallow dike with a hydrostatic head above the Earth's surface should erupt. Thus the magma reservoir pressure probably decreased following the 1975 Kalapana earthquake at Kilauea and increased over the course of the activity at Krafla. This conclusion is supported by the record of long-term magma reservoir inflation from 1975–1984 at Krafla (Bjornsson, 1985), and by combined geodetic and gravity data at Kilauea (Johnson, chapter 47). We emphasize that both the remote stress and the magma pressure must be considered in developing models of rift-zone dynamics.

IMPLICATIONS FOR MAGMA RESERVOIR BEHAVIOR

The August 1981 southwest-rift-zone intrusion at Kilauea resulted in a net summit tilt of −100 mrad, about −50 mrad of which occurred following the passage of the earthquake swarm beneath the geodetic level line. Using the calculation of Decker and others (1983), −50 mrad corresponds to a pressure drop of about 4 MPa, which is a large percentage of the estimated maximum excess pressure of 3–11 MPa within the dike (P_o in figure 53.15). If the rift zone behaves elastically, such a decrease in P_o should be reflected by a decrease in dike thickness and possibly in dike height (if K^a drops below zero) of sufficient magnitude to be measured geodetically. Installation of a line of continuously recording deformation meters perpendicular to the rift zone might allow observations of these changes, which in turn could be used to estimate the change in reservoir pressure.

ALONG-STRIKE VARIATION OF DIKE GEOMETRY

In addition to magma pressure variation with time, the magma pressure at a given depth within a dike increases with downrift distance because of the slope of the rift zones, and decreases with downrift distance because of viscous pressure loss. The balance between these two factors might be reflected in the locations of fissure eruptions, and in along-strike variations in dike height and thickness that could be measured geodetically. These observations might be useful in further constraining the remote stress field, because the sensitivity of the dike thickness and height to changes in magma pressure are dependent upon the gradient in the driving pressure (fig. 53.16). For example, a dike is more likely to maintain a fairly constant thickness and height for tens of kilometers if the gradients of

the superimposed remote tensile stress acting on the rift zone are large, as in figure 53.16*B*. Thus, it seems likely that data constraining temporal and spatial variations in dike geometry could significantly enhance our understanding of rift-zone dynamics.

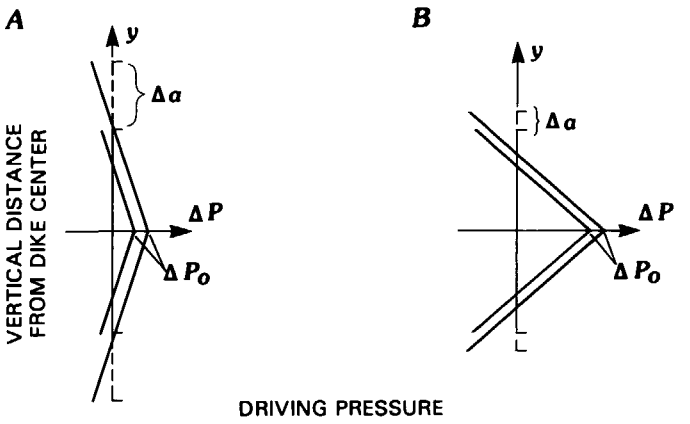

FIGURE 53.16.—Schematic diagrams illustrating the change in dike half-height for a given change in magma pressure. K_c is taken to be zero. ***A***, $P_o = 3$ MPa; ***B***, $P_o = 11$ MPa. For a 2-MPa increase in magma pressure ΔP_o, the dike in ***A*** increases in half-height by a factor of 1.67; that in ***B*** increases by a factor of only 1.18. The dike thicknesses increase as the square of these factors, or by factors of 2.8 and 1.4, respectively.

REFERENCES CITED

Anderson, E.M., 1938, The dynamics of sheet intrusion: Royal Society of Edinburgh Proceedings, Series B, v. 58, p. 242-251.

Anderson, O.L., and Grew, P.C., 1977, Stress corrosion theory of crack propagation with application to geophysics: Review of Geophysics and Space Physics, v. 15, p. 77-104.

Atkinson, B.K., 1984, Subcritical crack growth in geologic materials: Journal of Geophysical Research, v. 89, p. 4077-4114.

Bieniawski, Z.T., 1978, Determining rock mass deformability: experience from case histories [abs.]: International Journal of Rock Mechanics, Mineral Science and Geomechanics, Abstracts, v. 15, p. 237-247.

Birch, F., 1966, Compressibility; elastic constants, *in* Handbook of Physical Constants: Geological Society of America Memoir 97, p. 97-173.

Bird, R.B., Stewart, W.E., and Lightfoot, E.N., 1960, Transport phenomena: New York, John Wiley & Sons, 780 p.

Bjornsson, A., 1985, Dynamics of crustal rifting in NE Iceland: Journal of Geophysical Research, v. 90, p. 10,151-10,162.

Bjornsson, A., Johnsen, G., Sigurdsson, S., Thorbergsson, G., and Tryggvason, E., 1979, Rifting of the plate boundary in north Iceland 1975–1978: Journal of Geophysical Research, v. 84, p. 3029-3038.

Brandsdottir, B., and Einarsson, P., 1979, Seismic activity associated with the September 1977 deflation of Krafla Volcano in north-eastern Iceland: Journal of Volconology and Geothermal Research, v. 6, p. 197-212.

Broek, D., 1982, Elementary Engineering Fracture Mechanics: Boston, Martinus Nijhoff Publishers, 469 p.

Broyles, M.L., Suyenaga, W., and Furumoto, A.S., 1979, Structure of the lower east rift zone of Kilauea Volcano, Hawaii, from seismic and gravity data: Journal of Volconology and Geothermal Research, v. 5, p. 317-336.

Davis, P.M., 1976, The computed piezomagnetic anomaly field for Kilauea Volcano, Hawaii: Journal of Geomagnetism and Geoelectricity, v. 28, p. 113-122.

Decker, R.W., Okamura, A.T., and Dvorak, J.G., 1983, Pressure changes in the magma reservoir beneath Kilauea Volcano, Hawaii: Eos (American Geophysical Union Transactions), v. 64, p. 901.

Delaney, P., and Pollard, D.D., 1981, Deformation of host rocks and flow of magma during growth of minette dikes and breccia-bearing intrusions near Ship Rock, New Mexico: U.S. Geological Survey Professional Paper 1202, 61 p.

———1982, Solidification of basaltic magma during flow in a dike: American Journal of Science, v. 282, p. 856-885.

Delaney, P.T., Pollard, D.D., Ziony, J.I., and McKee, E.H., in press, Field relations between dikes and joints: emplacement processes and paleostress analysis: Journal of Geophysical Research.

Dzurisin, D., Anderson, L.A., Eaton, G.P., Koyanagi, R.Y., Lipman, P.W., Lockwood, J.P., Okamura, R.T., Puniwai, G.S., Sako, M.K., and Yamashita, K.M., 1980, Geophysical observations of Kilauea Volcano, Hawaii, 2. Constraints on the magma supply during November 1975–September 1977: Journal of Volconology and Geothermal Research, v. 7, p. 241-269.

Einarsson, P., and Brandsdottir, B., 1979, Seismological evidence for lateral magma intrusion during the July 1978 deflation of the Krafla Volcano in NE-Iceland: Journal of Geophysics, v. 47, p. 160-165.

Epp, D., Decker, R.W., and Okamura, A.T., 1983, Relation of summit deformation to east rift zone eruptions on Kilauea Volcano, Hawaii: Geophysical Research Letters, v. 10, p. 493-496.

Evans, K., 1982, Some examples and implications of observed elastic deformations associated with the growth of hydraulic fractures in the Earth, in Zoback, M.D., and Haimson, B.C., eds., Proceedings of Workshop XVII, Hydraulic Fracturing Stress Measurements, U.S. Geological Survey Open-File Report 82–1075, v. 2, p. 661-698.

Fiske, R.S., and Jackson, D.E., 1972, Orientation and growth of Hawaiian volcanic rifts: the effect of regional structure and gravitational stress: Proceedings of the Royal Society of London, Series. A, v. 329, p. 299-326.

Fujii, T., and Kushiro, I., 1977, Density, viscosity, and compressibility of basaltic liquid at high pressures: Carnegie Institution of Washington Yearbook, 1976, p. 419-424.

Hauksson, E., 1983, Episodic rifting and volcanism at Krafla in north Iceland: growth of large ground fissures along the plate boundary: Journal of Geophysical Research, v. 88, p. 626-636.

Helgason, J., and Zentilli, M., 1985, Field characteristics of laterally emplaced dikes: anatomy of an exhumed Miocene dike swarm in Reydarfjordur, eastern Iceland: Tectonophysics, v. 115, p. 247-274.

Hoffman, J.P., Ulrich, G.E., and Chadwick, W.W., 1984, Geodetic measurements on the East Rift Zone, Kilauea Volcano, Hawaii: Eos (American Geophysical Union Transactions), p. 1131.

Kinoshita, W.T., Krivoy, H.L., Mabey, D.R., and MacDonald, R.R., 1963, Gravity survey of the Island of Hawaii: U. S. Geological Survey Professional Paper 475–C, p. C114-C116.

Klein, F.W., 1982, Patterns of historical eruptions at Hawaiian volcanoes: Journal of Volconology and Geothermal Research, v. 12, p. 1-35.

Lawn, B.R., and Wilshaw, T.R., 1975, Fracture of brittle solids: Cambridge, Cambridge University Press, 204 p.

Macdonald, G.A., 1956, The structure of Hawaiian volcanoes: Verchandelingen van het Koninklijke Nederlandsch Geologisch-Mijnbowkundig Genootschap, v. 16, p. 274-295.

McTigue, D.F., and Mei, C.C., 1981, Gravity-induced stresses near topography of small slope: Journal of Geophysical Research, v. 86, p. 9268-9278.

Meredith, P.G., and Atkinson, B.K., 1985, Fracture toughness and subcritical crack growth during high-temperature tensile deformation of Westerly granite and Black gabbro: Physics of the Earth and Planetary Interiors, v. 39, p. 33-51.

Moore, J.G., and Fiske, R.S., 1969, Volcanic substructure inferred from dredge samples and ocean-bottom photographs, Hawaii: Geological Society of America Bulletin, v. 80, p. 1191-1202.

Palmason, G., 1971, Crustal Structure of Iceland from explosion seismology: Societas Scientiarum Islandica, publ. 40, 187 p.

Paris, P.C., and Sih, G.C., 1965, Stress analysis of cracks, fracture toughness testing and its applications, Philadelphia, ASTM, p. 30-81.

Pollard, D.D., 1976, On the form and stability of open hydraulic fractures in the Earth's crust: Geophysical Research Letters, v. 3, p. 513-516.

Pollard, D.D., Delaney, P.T., Duffield, W.A., Endo, E.T., and Okamura, A.T., 1983, Surface deformation in volcanic rift zones: Tectonophysics, v. 94, p. 541-584.

Pollard, D.D., and Holzhausen, G., 1979, On the mechanical interaction between a fluid-filled crack and the Earth's surface: Tectonophysics, v. 53, p. 27-57.

Pollard, D.D., and Segall, P., in press, Theoretical displacements and stresses near fractures in rocks: with applications to faults, joints, veins, dikes, and solution surfaces, in Atkinson, B. K., ed., Rock fracture mechanics: London, Academic Press.

Ryan, M.P., Blevins, J.Y.K., Okamura, A.T., and Koyanagi, R.Y., 1983, Magma reservoir subsidence mechanics: theoretical summary and application to Kilauea Volcano, Hawaii: Journal of Geophysical Research, v. 88, p. 4147-4181.

Ryan, M.P., Koyanagi, R.Y., and Fiske, R.S., 1981, Modeling the three-dimensional structure of macroscopic magma transport systems: application to Kilauea Volcano, Hawaii: Journal of Geophysical Research, v. 86, p. 7111-7129.

Saemundsson, K., 1979, Outline of the geology of Iceland: Jokull, v. 29, p. 7-28.

Schmidt, R.A., and Huddle, C.W., 1977, Effect of confining pressure on fracture toughness of Indiana limestone [abs.]: International Journal of Rock Mechanics and Mining Sciences & Geomechanics Abstracts, v. 14, p. 289-293.

Secor, D.T., and Pollard, D.D., 1975, On the stability of open hydraulic fractures in the Earth's crust: Geophysical Research Letters, v. 2, p. 510-513.

Shah, R.C., and Kobayashi, A.S., 1973, Stress-intensity factors for an elliptical crack approaching the surface of a semi-infinite solid: International Journal of Fracture, v. 9, p. 3-21.

Sigurdsson, H., and Sparks, S.R.J., 1978, Lateral flow within rifted Icelandic crust: Nature, v. 274, p. 126-130.

Spence, D.A., and Turcotte, D.L., 1985, Magma-driven propagation of cracks: Journal of Geophysical Research, ser. B, v. 90, no. 1, p. 575-580.

Swanson, D.A., Duffield, W.A., and Fiske, R.S., 1976, Displacement of the south flank of Kilauea Volcano: the result of forceful intrusion of magma into rift zones: U.S. Geological Survey Professional Paper 963, 39 p.

Tada, H., Paris, P.C., and Irwin, G.R., 1973, The stress analysis of cracks handbook: Hellertown, Pa., Del Research Corp.

Tryggvason, E., 1983, The widening of the Krafla fissure swarm during the 1975–1981 volcano-tectonic episode: Nordic Volcanological Institute Report 8304, 48 p.

Walker, G.P.L., 1959, Geology of the Reydarfjordur area, eastern Iceland: Quarterly Journal of the Geological Society of London, v. 114, p. 367-393.

———1963, The Breiddalur central volcano, eastern Iceland: Quarterly Journal of the Geological Society of London, v. 119, p. 23-63.

———1974, Eruptive mechanisms in Iceland, in Krisjansson, ed., Geodynamics of Iceland and the North Atlantic area: Dordrecht-Holland, D. Reidel, p. 189-201.

Weertman, J., 1971, Theory of water-filled crevasses in glaciers applied to vertical magma transport beneath oceanic ridges: Journal of Geophysical Research, v. 76, p. 1171-1183.

Williams, H., and McBirney, A.R., 1979, Volcanology: San Francisco, Freeman, Cooper, 397 p.

Winter, R.B., 1983, Bruchmechanische Gerteinsuntersuchurgen mit dem Bezung zu Hydraulischen Frac-Versuchen in Tiefbohrungen: Bochum, Ruhr-Universitat, Institut fur Geophysik, Ph. D. dissertation.

Zucca, J.J., Hill, D.P., and Kovach, R.L., 1982, Crustal structure of Mauna Loa Volcano, Hawaii, from seismic refraction and gravity data: Bulletin of the Seismological Society of America, v. 72, p. 1535-1550.

HEAT AND MASS TRANSPORT IN THE EAST-RIFT-ZONE MAGMA CONDUIT OF KILAUEA VOLCANO

By Harry C. Hardee[1]

ABSTRACT

The flow of magma in the rift conduit system of Kilauea Volcano is examined by comparing thermal and fluid-flow conduit models with field observations. A repetitive thermal-intrusion model predicts that the conduit will remain relatively open to flow for cyclic intrusion rates above a certain critical level. This agrees well with field observations for the upper east rift zone. This portion of the conduit tends to have aseismic intrusions, implying that fracturing is not required to open the conduit for flow. Observed intrusion rates and times between eruptive cycles for other portions of the Kilauea rift system and for conduits of other volcanoes agree well with the repetitive thermal-intrusion model.

Two forced-convection fluid flow models are developed for the Kilauea rift conduit system. One model is based on non-Newtonian rheology effects, and the other on viscous-dissipation effects. Both fluid flow models are compatible with field observations of summit-reservoir pressure changes, intrusive flow rates, eruption temperatures, and eruptive cycles. The nonNewtonian flow model is applicable to conduits on the order of 0.5 m thick or thicker, and this appears to be the situation for the upper portion of the east rift zone. The viscous-dissipation flow model appears to be applicable to thin conduits on the order of 0.5 m or less thick and particularly to those on the order of 0.1 m or less. Thin conduits tend to cool rapidly, and a source of internal heating such as viscous dissipation is needed to keep these conduits open for flow.

INTRODUCTION

The model of the magmatic plumbing system of Kilauea Volcano has evolved over the years as that system has been studied by numerous investigators. Magma generated in the upper mantle rises and is stored temporarily in a summit reservoir system at a depth of 2–6 km beneath the summit of the volcano (Duffield and others, 1982). The magma appears to rise from the mantle to the summit-reservoir storage system at a more or less steady volume rate (Swanson, 1972; Dzurisin and others, 1980; Dvorak and others, 1983). As storage in the summit reservoir increases, inflation of the volcano occurs, and eventually sufficient stresses accumulate to cause part of the magma to intrude into a shallow conduit system (Fiske and Jackson, 1972; Ryan and others, 1981). Frequently, intrusion into the conduit system results in the eruption of lava. The shallow magma of the east rift zone exists at a depth of 2–6 km and extends from the summit of Kilauea to a submarine position about 70 km east of Cape Kumukahi (Moore, 1971), a total distance of 120 km. A part of the rift is shown in figure 54.1 in a semiactive stage between eruptive phases during the Kilauea eruption that began in 1983.

Flow or intrusion in the conduit of the east rift zone is an intermittent forced-convection (pressure-driven) process. The seismic models of Ryan and others (1981) suggest that the intrusive flow occurs in a pipelike conduit. Later stress calculations and field observations by Ryan and others (1983), however, indicate that typical conduits may be sill or dike structures with thicknesses on the order of 1 m (0.15–3.38 m). The intermittent intrusions in the east rift zone appear to be of two basic types. Magma movement at large volume rates of 100–1,000 m^3/s are accompanied by shallow seismic swarms and are apparently a result of the formation of new dikes by sudden fracturing (Epp and others, 1983). This process is common in the lower part of the east rift zone and in other areas, such as the southwest rift zone. Slower intrusions at volume rates of 1–10 m^3/s are usually aseismic, implying that the conduit is in an open or nearly open (plastic or near-molten) state and that fracturing is not required for flow to be initiated (Epp and others, 1983). Intrusions of this latter type are common in the upper 20–30 km of the east rift zone nearest to the summit caldera. After an initial slow, aseismic intrusion, additional intrusions may occur at faster rates in later eruptive phases because the conduit remains molten or open and even increases in effective flow area. The slow, aseismic intrusions and the more rapid intrusions in later eruptive phases have been well studied, especially during the recent eruption of Kilauea that began in 1983. Decker and others (1983) have been able to correlate the extensive inflation-deflation records of the 1983–84 eruption phases with volume intrusion rates in the conduit and with estimated dynamic pressure values in the summit reservoir.

This paper concentrates on the low-volume-rate aseismic intrusions that frequently occur in the upper part of the east rift zone. This type of intrusive process repeats through a number of eruptive or intrusive phases, and therefore a large set of observations and data has accumulated. This repetition and the abundant data allow us to learn much about this type of conduit and about conditions in the summit reservoir. A repetitive-intrusion thermal model has been developed which explains how a conduit can remain relatively open to successive intrusions (Hardee, 1982). This model is described and the results applied to intrusion data for Kilauea Volcano. As expected, pressure-driven forced convection is the mechanism that

[1]Geophysics Division 1541, Sandia National Laboratories, Albuquerque, NM.

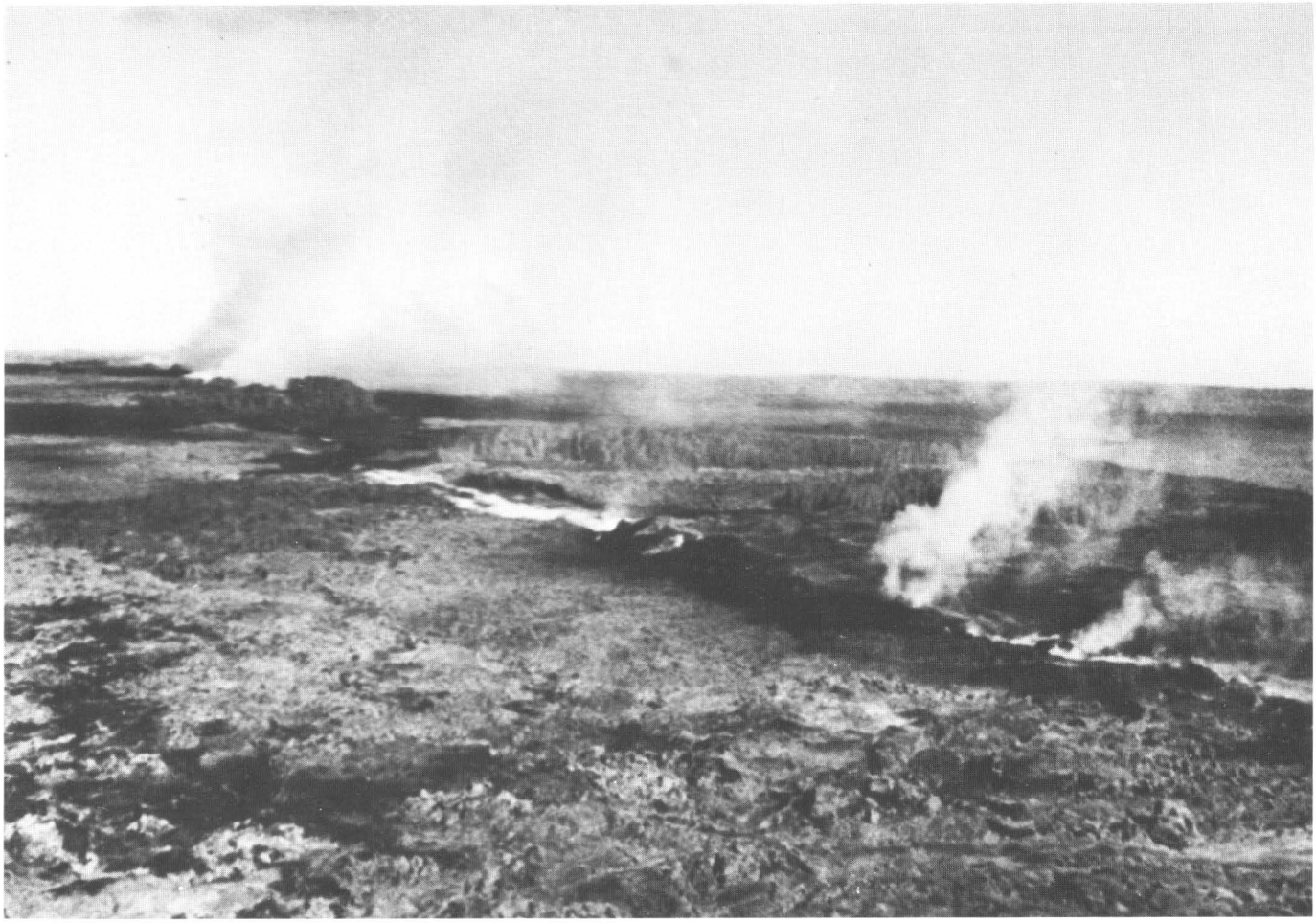

FIGURE 54.1.—Aerial view (looking southeast) of upper east rift zone of Kilauea Volcano in a semiactive stage between eruptive episodes during 1983–84 eruptive activity. Photograph by R.P. Striker, January 15, 1983.

drives intrusion in the plastic or near-molten conduit. Flow models based on both simple forced convection and forced convection with non-Newtonian-fluid and viscous-dissipation effects are considered. The non-Newtonian convection model is based on earlier work by Shaw and others (1968), who found that Kilauea lava could be modeled as a Bingham-plastic fluid. The viscous-dissipation model builds on the work of Gruntfest (Gruntfest, 1963; Gruntfest and others, 1964) and Shaw (1969), who were the first to introduce the concept of dissipative feedback into igneous petrology. Magma viscosity in the subliquidus temperature range depends on shear stress, shear rate, temperature, time, and previous thermal history. The Bingham-plastic flow model and the viscous-dissipation flow model are simply ways of looking at major magma-viscosity effects one at a time. The models are used to predict conduit size and dynamic pressure in the summit magma reservoir. The models are also used to explain the cyclic nature of eruptive phases. The models correlate well with field observations of the 1983–84 Kilauea eruption episodes.

A few fundamental points need to be emphasized. First, this paper primarily deals with the conduit, 20–30 km long and 2–6 km deep, that carries magma from the summit chamber downrift, where the magma may or may not rise the short remaining distance to a surface vent. To avoid confusion in this paper, the main deep part of the conduit is called the east rift conduit, and the shallow (1 km) final part at the end of the conduit is called the vent conduit. There are several fundamental differences between these two parts of the conduit system. In many intrusions in the east rift zone, eruption does not occur, and the vent conduit does not exist. If an eruption does occur, the vent conduit exists only briefly for that particular eruption. The deeper east-rift conduit has an existence much longer than, and independent of, particular eruptive vents. The east-rift conduit has existed as a fairly open conduit system for several hundred years and will likely exist for many years to come. This paper primarily considers the nature and evolution of the east-rift conduit system on the basis of thermomechanical constraints and balances. Some observations at the erupting vent bear directly on the

nature of the deeper conduit system. Other observations at the erupting vent are important only for processes occurring locally at the vent and are not directly applicable to processes occurring in the deeper east-rift conduit. For instance, at shallow depths in the vicinity of the vent, pressure in the magma is lowered to the point where gases are released.[7] These gases affect geysering at the vent and the viscosity of the magma or lava as it exits the vent. The theoretical models discussed in this paper ignore the effect of such gases because little or no gas is present at the depths (1 km and greater) and corresponding pressures where the east-rift conduit exists.

ACKNOWLEDGMENTS

This paper benefited greatly from reviews and comments by Terrence M. Gerlach, Robert W. Decker, Edward W. Wolfe, Herbert R. Shaw, and L. Paul Greenland. I would particularly like to thank Ed Wolfe for supplying additional field data on the 1983–84 Kilauea eruptive activity and Herb Shaw for supplying additional background references. This work was supported by the U.S. Department of Energy under contract DE-AC04-76DP00789.

REPETITIVE-INTRUSION CONDUIT MODEL

Magma intrusions are of two types, as noted earlier. In the first type, the intrusion is an isolated event; repeated or successive pulses of magma through the same conduit are unlikely, although intrusions may occur in nearby regions. This type of intrusive flow occurs in fractures opened by mechanical or tectonic forces. Mechanically controlled intrusions form a majority of magma intrusions and are thoroughly discussed in a recent article by Shaw (1980). The second type of magma intrusion occurs in conduits where repeated injections of magma have left sufficient residual heat to keep the conduit effectively open during the quiescent period between intrusions. The ability of a magma conduit to remain open over a long period of time depends primarily on the average mass rate of magma throughput in the conduit. If the average mass rate of intrusive flow through the conduit exceeds a certain critical value, the conduit remains molten or nearly molten and therefore open to future magma intrusions. This fact was originally recognized from field observations (Smith, 1979; Fedotov, 1981). On the basis of field data, Smith (1979) recognized that a critical magma-eruption rate of about 1×10^{-3} km^3/yr was necessary to sustain high-level silicic magma chambers. This can also be interpreted to mean that the critical value of magma intrusion rate through the conduit supplying the magma chamber or erupting vent is also on the order of 1×10^{-3} km^3/yr. Fedotov (1981), on the basis of field data, observed a critical magma-intrusion rate on the order of 1×10^{-3} km^3/yr for magma conduits feeding volcanic centers in Kamchatka. Theoretical calculations by Shaw (1980) indirectly show that critical magma-intrusion rates on the order of 1×10^{-3} km^3/yr or greater are necessary to approach and maintain the liquidus temperature of mafic magma systems.

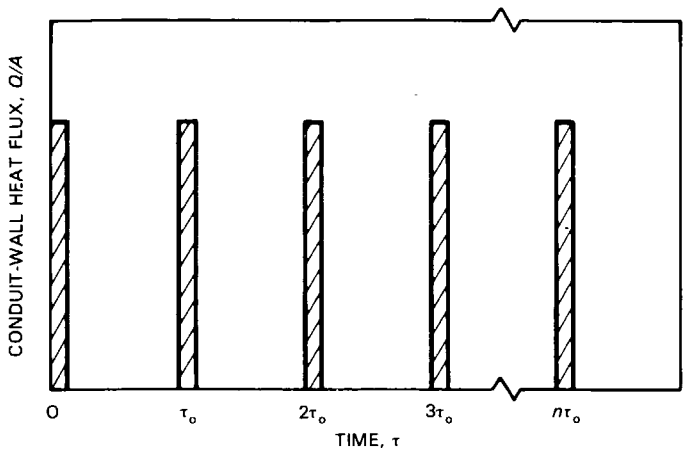

FIGURE 54.2.—Idealized repetitive sequences of thermal pulses used in repetitive-intrusion conduit model.

The critical magma-intrusion rate can be determined theoretically using an idealized conduit-intrusion model (Hardee, 1982). A cylindrical conduit geometry is assumed, which receives periodic intrusions of thermal magnitude Q at time intervals of τ_0. The heat pulses from successive intrusions are idealized as a regular series of heat-flux pulses at the conduit wall (fig. 54.2). The thermal magnitude Q is determined from the latent heat or temperature of the intruding magma. The intruding magma must be at a temperature above the solidus; the conduit wall in contact with molten or flowing magma is, by definition, at the solidus temperature. The difference between these two temperatures is a measure of the energy available to overcome conduction losses at the conduit wall and into the surrounding country rock. The conduit-wall heat flux during an intrusive pulse is simply Q/A, where A is the total surface area of the conduit. If a series of heat pulses (fig. 54.2) occur in a conduit, the wall of the conduit will gradually heat up. Even though the conduit cools between successive pulses, it will still be at a temperature above ambient just before the next intrusive pulse. If the value of Q/A and the number of prior intrusive pulses are large enough, the temperature of the conduit wall and any material in the conduit will eventually reach a value on the order of the solidus temperature. At this point the conduit is assumed to be effectively open when the next intrusion occurs. Mechanical fracturing is no longer required to open the conduit for flow in this model. Forces of pressure-driven forced convection are sufficient to initiate flow in the conduit.

The critical condition for flow in an idealized cylindrical conduit with the periodic, pulsed boundary condition illustrated in figure 54.2 was solved by Hardee (1982), using a Laplace transform technique. The Laplace transform technique is well suited for problems in heat conduction with periodic boundary conditions and is uniquely suited to problems involving pulsed (delta function) boundary conditions. The critical magma-intrusion rate in the conduit, V/τ_0, was shown theoretically to be about 1×10^{-3} km^3/yr, which is in agreement with related field observations (Smith, 1979; Fedotov, 1981). The critical intrusion condition for the

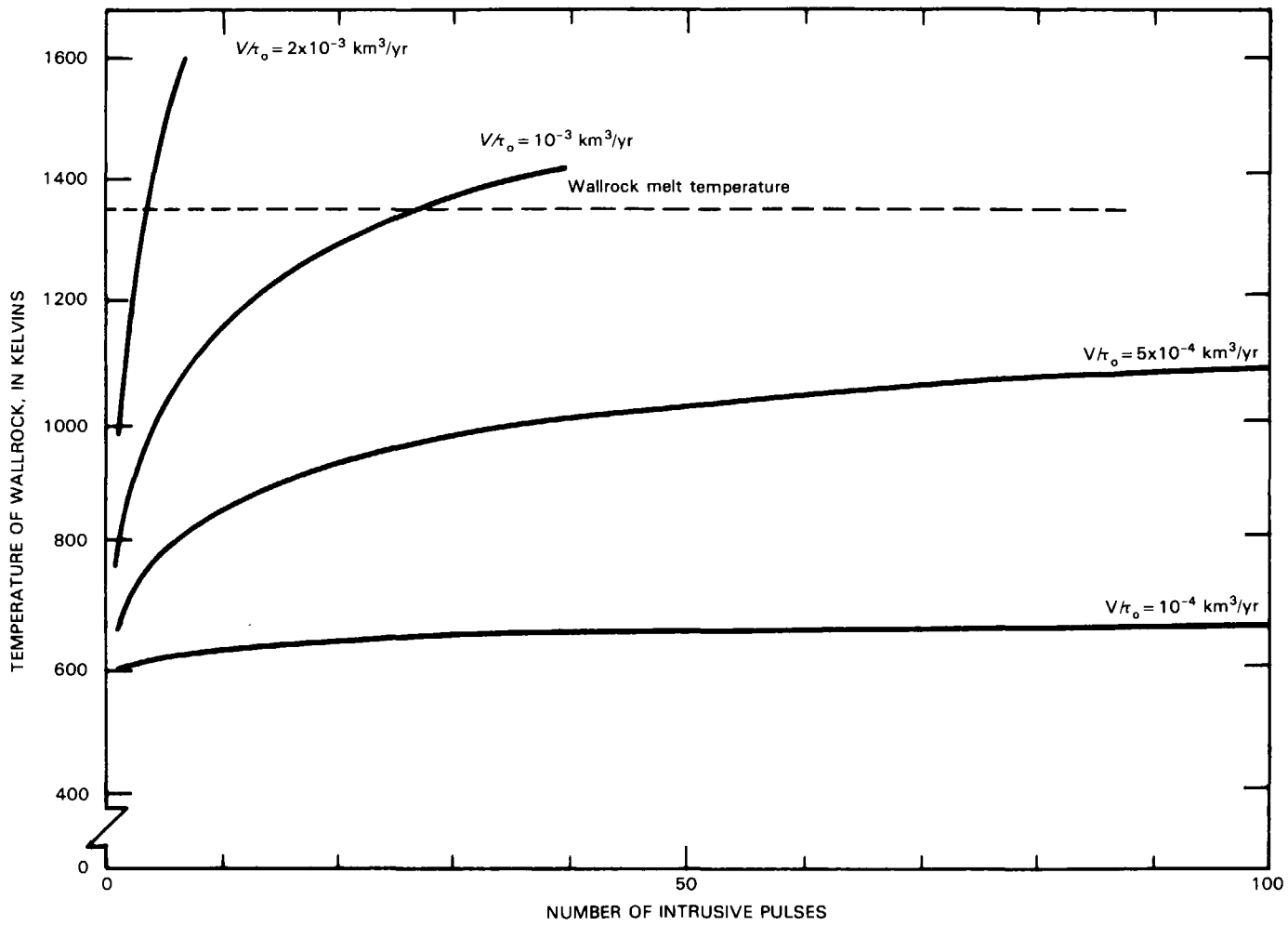

FIGURE 54.3.—Results of repetitive-intrusion model, showing conditions necessary to establish a thermally open conduit. Wallrock temperature rises as a function of increasing number of intrusive pulses; for sufficiently high volume-intrusion rates (V/τ_0), it reaches and stays at or near the melting temperature.

conduit to remain open is a function of the critical magma-intrusion rate and also a function of the length of the conduit and the number of prior intrusive pulses in the conduit (Hardee, 1982). The critical intrusion parameter for a conduit such as the east-rift conduit is

$$\left[(V/\tau_0)1/l\sum_{1}^{m}(1/n)\right]_{\text{critical}} = 3\times10^{-4}\ \text{km}^2/\text{yr} \qquad (1)$$

where V/τ_0 is the volume rate of throughput in the conduit, m is the number of prior intrusive pulses or eruptions in the conduit, n is the variable number of each particular pulse from 1 to m, and l is the length of the conduit. Equation 1 is the condition for a conduit to remain effectively open from thermal effects alone. Although this analytical result is for a cylindrical conduit, the critical intrusion parameter is independent of the diameter of the conduit. The initial intrusion obviously requires mechanical fracturing in a weakened zone of country rock to initiate the first flow of magma. Once enough flow in subsequent pulses has occurred such that the critical value of 3×10^{-4} km^2/yr is exceeded, the conduit will then remain open from thermal effects alone. Using typical properties for basalt and assuming a typical conduit length, $l=10$ km, Hardee (1982) calculated the temperature of the conduit wall just before the next intrusion as a function of the volume-intrusion rate, V/τ_0, and the number of intrusive pulses. The result (fig. 54.3) indicates that the critical condition for the conduit to remain open is a strong function of the average volume-intrusion rate and a weak function of the number of prior intrusive pulses. For instance, at a volume-intrusion rate, V/τ_0, of 1×10^{-3} km^3/yr, the wallrock temperature remains at the melt temperature after about 10 intrusive pulses have occurred. At a volume-intrusion rate of only half this value (5×10^{-4} km^3/yr), the wallrock has not reached the melt temperature even after more than 100 intrusive pulses. Although equation 1 gives a precise expression for the critical conduit condition, figure 54.3 shows that for many typical cases the critical conduit condition is met when the volume-intrusion rate exceeds the value 1×10^{-3} km^3/yr. This value is in agreement with the observations of Smith (1979), Shaw (1980), and Fedotov (1981), mentioned earlier.

Equation 1 can be used to compare magma conduit systems at Kilauea. Typical values of the critical conduit-intrusion parameter

TABLE 54.1.—*Intrusion parameters for some magma conduits*

	Intrusion parameter $\left[(V/\tau_0)(1/l)\sum_1^m(1/n)\right]$ (km²/yr)
Kilauea—Upper east rift[1]	45×10^{-4}
Augustine Volcano, Alaska[2]	40×10^{-4}
Mount St. Helens, Washington[3]	8.1×10^{-4}
(critical value)	3×10^{-4}
Kilauea—lower east rift (Puna)[1]	1.4×10^{-4}
Kilauea—southwest rift[1]	1.1×10^{-4}

[1]Based on Decker (1983) and Macdonald and Hubbard (1973). Since 1955, upper east rift $V/\tau_0=30\times10^{-3}$ km³/yr, $m=20$, and $l=25$ km. Since 1750, lower east rift $V/\tau_0=3\times10^{-3}$ km³/yr, $m=5$, and $l=50$ km. Since 1823, southwest rift $V/\tau_0=1.1\times10^{-3}$ km³/yr, $m=5$, and $l=25$ km.

[2]Based on Kienle and Swanson (1980). Four major eruptions in last 100 years; typical volume of 0.1 km³; $l=2$ km from depth of first seismicity during last (1976) eruption.

[3]Based on Decker and Decker (1981). Since 1850, $V/\tau_0=4\times10^{-3}$ km³/yr, $l=18$ km, and in the last 4,500 years $m=20$.

for conduits at Kilauea and other sites are listed in table 54.1. The average volume-intrusion rate, V/τ_0, and the number of prior intrusive pulses or eruptions, m, are obtained from geologic and historical data. The length of the conduit, l, is obtained from seismic data or other estimates of the distance from the magma reservoir to the end of the conduit. Comparing the results in table 54.1 with the critical intrusion factor of 3×10^{-4} km²/yr from equation 1 shows that the upper east rift zone of Kilauea (upper 25 km) and the Augustine and Mount St. Helens volcanic conduits are open conduits in the sense defined earlier, while the lower east rift zone near Puna and the southwest rift zone of Kilauea are normally closed conduits. These latter examples would require mechanical fracturing before intrusive flow could move through the conduit. The repetitive-intrusion model and the result of equation 1 can be applied to different conduits or parts of conduits at the same volcano. The only requirement is that appropriate values of volume-intrusion rate, length of conduit, and number of prior intrusive pulses are used for the particular conduit or part of conduit being studied.

INTRUSIVE FLOW IN CONDUITS

Intrusive flow in the east-rift conduit of Kilauea can be modeled as simple forced convective flow in a conduit where the flow is driven by pressure in the summit reservoir. Epp and others (1983) and Decker and others (1983) recognized that the intrusive flow in the east-rift conduit was associated with summit deflation, which in turn was related to dynamic pressure changes in the reservoir. Epp and others (1983) noted that the volume of erupted material in many cases was equal to the volume of deflation of the summit reservoir; they further noted that the amount of magma drained from the summit reservoir was related to the elevation of the vent. This again suggests a simple reservoir-controlled, forced-convection type of conduit flow. Decker and others (1983) have made limiting calculations which indicate that dynamic pressure changes in the summit reservoir between 0.09 MPa and 400 MPa have occurred over the last 25 years at Kilauea Volcano. Recent correlations of summit tilt changes with elevations of rift eruption vents indicate pressure changes of 0.085 MPa per μrad of rapid radial summit tilt (Decker and others, 1983). During the 1983–84 eruption episodes at Kilauea, tilt changes on the order of 10 μrad were common; these correspond to dynamic pressure changes on the order of 1 MPa. Dynamic pressure change, as used here, is the pressure change that occurs in the summit reservoir during an eruptive episode (Decker and others, 1983). This pressure is related to the pressure necessary to overcome frictional flow effects during periods of intrusive flow. The dynamic pressure change does not include a hydrostatic component, because the hydrostatic pressure is similar at the beginning and end of an eruptive episode. Hydrostatic is used here in the fluid-mechanics context to mean the static pressure in a liquid (in this case, molten magma).

Simple hydrodynamic flow relations can be used to relate observed flow volumes and flow rates to expected conduit diameters. It is obvious, however, that something more than a simple hydrodynamic conduit model is needed to explain the observed flow. Simple hydrodynamic flow relations alone predict that eruptive episodes such as at Kilauea in 1983–84 would not be observed, but rather a continuous low-level flow would occur at the expected reservoir replenishment rate of 8.5×10^6 m³/mo (Swanson, 1972). Instead of a continuous intrusive flow rate of 3.28 m³/s (8.5×10^6 m³/mo), the flow rate in the conduit ranged from 10 to 100 m³/s during periods of eruption and was essentially zero between eruptive episodes. If the flow during eruptive phases were averaged out over a year, it would agree closely with Swanson's estimate of the reservoir replenishment rate of 8.5×10^6 m³/mo. An additional mechanism must somehow be included with the simple hydrodynamic flow model in order to explain why intrusive or eruptive episodes occur as isolated, repetitive events rather than as a continuous low-level flow. The analysis in the previous section of this paper explained the condition whereby repetitive intrusive pulses could occur in what I have called an open conduit without mechanical fracturing, but this analysis did not explain what controlled the cyclic nature of the intrusions or eruptive episodes. Since the magma supply rate to the summit reservoir appears to be fairly constant and continuous, the only mechanisms that might explain the observed intermittent intrusive flow in such open conduits are non-Newtonian rheology and viscous dissipation.

NON-NEWTONIAN FORCED-CONVECTION CONDUIT MODEL

The simplest non-Newtonian flow model for intrusive flow in a magma conduit is a Bingham-plastic flow model, as used by Shaw and others (1968) in their analysis of viscosity measurements at Makaopuhi lava lake. A power-law rheology model also fits the observed viscosity data well for basaltic lava or magma (Hardee and Dunn, 1981); however, the Bingham-plastic model is simpler to use and fully adequate for the first-order calculations that follow. In the Bingham-plastic model, flow does not begin until a certain critical yield stress is exceeded; and once this occurs, the flow is similar to Newtonian flow.

If we consider a cylindrical conduit, the pressure drop in the

conduit from simple hydrodynamic theory for laminar flow is (Vennard, 1956)

$$P = 32\mu lv/D^2, \quad (2)$$

where P is the dynamic or available pressure to drive the intrusive flow, μ is the average magma viscosity, l is the length of the conduit, v is the average flow velocity of the fluid in the conduit, and D is the diameter of the conduit. For conduits with a noncircular cross section, the concept of an equivalent diameter can be used with this same relation (Chapman, 1967). For geometries such as those of sills or dikes, an expression similar to equation 2 can be developed, or the idea of equivalent diameter can be used. The flow rate Q in the conduit is simply

$$Q = \pi D^2 v/4. \quad (3)$$

In the absence of an internal heating mechanism, such as viscous-dissipation heating, the conduit must be sufficiently large that the fluid does not cool appreciably as it flows through. Otherwise, the magma would cool and solidify in place, thereby shutting off the flow. In the simple forced-convection flow model, the fluid magma leaves the summit reservoir at a temperature (say, 1,413 K) well above that at which the magma is considered virtually solid (1,343 K; see Shaw and others, 1968). By equating the heat lost at the conduit wall to the reduction of sensible heat in the flowing fluid, an expression can be developed for the amount of cooling that occurs in a conduit of length l. The heat loss of a fluid to the wall of a circular conduit is

$$q = hA_s(T_b - T_w), \quad (4)$$

where h is the convective heat-transfer coefficient, A_s is the surface area of the conduit, T_b is the bulk temperature of the fluid in the conduit, and T_w is the temperature of the wall (1,343 K). The convective heat-transfer coefficient for fluid flow in a cylindrical conduit (Eckert and Drake, 1959) is

$$hD/k = 3.65, \quad (5)$$

where k is the thermal conductivity of the fluid. Substituting h from equation 5 into equation 4 and noting that $A_s = \pi D\ dl$ for an incremental length dl gives

$$q = 3.65\pi k(T_b - T_w)\ dl. \quad (6)$$

The reduction in sensible heat is the energy lost from the flowing fluid

$$q = -\rho c(\pi D^2/4)v\ dT_b, \quad (7)$$

where ρ is the density of the fluid and c is the specific heat of the fluid. Combining equations 6 and 7 and integrating the result over a conduit length l yields the result

$$T_b - T_w = K\exp[-14.6\alpha l/(D^2 v)], \quad (8)$$

where α is the thermal diffusivity ($\alpha = k/\rho c$) and K is a constant. Assume that when $l = 0$ at the summit reservoir, the bulk temperature of the magma entering the conduit is, as noted earlier, 70 K above the temperature where the magma is virtually solid ($T_b - T_w = 70$). The constant K in equation 8 then becomes 70, and

$$T_b - T_w = 70\exp[-14.6\alpha l/(D^2 v)]. \quad (9)$$

Decker and others (1983) note that the flow in the conduit can be estimated from summit deflation and that this volume is approximately 0.5×10^6 m^3 per μrad of radial tilt. As an example, episode 2 of the Kilauea eruption that started in 1983 resulted in a summit deflation of 11 μrad of tilt in 6 days. This corresponds to an intrusive-flow rate of

$$Q = (11/6)(0.5 \times 10^6) = 0.917 \times 10^6 \text{ m}^3/\text{d}$$

or

$$Q = 10.6 \text{ m}^3/\text{s}. \quad (10)$$

Substituting this into equation 3 gives

$$D^2 v = 10.6(4/\pi), \quad (11)$$

and substituting this along with appropriate values for magma properties and an assumed conduit length (l) of 20 km into equation 9 gives

$$T_b - T_w = 69.7 \text{ K}. \quad (12)$$

This calculation is interesting in that it shows that the temperature loss as the magma flows the full length of the conduit is only 0.3 K, and this result did not depend on a knowledge of the conduit diameter. A similar result is obtained for a dike. An exact calculation for the dike is not possible because the flow rate Q depends on two geometrical factors: the thickness of the dike (a) and the width of the dike (b):

$$Q = abv. \quad (13)$$

An approximate calculation for the dike can be obtained by using the concept of equivalent diameter (Chapman, 1967). The equivalent diameter, sometimes called the hydraulic diameter, is an approximating concept used in fluid mechanics for conduits of noncircular cross section. The equivalent diameter, which attempts to preserve the flow area and the viscous shear at the wall, is simply 4 times the cross-sectional flow area divided by the wetted perimeter of the conduit. The equivalent diameter of a circular conduit is equal to the geometrical diameter. For a dike or sill, the equivalent diameter (D_{eq}) can be shown to be

$$D_{eq} = 2a. \quad (14)$$

The exact temperature result for a dike or sill, similar to equation 9, can be shown to be

$$T_b - T_w = 70\exp[-7.5\alpha l/(a^2 v)]. \quad (15)$$

With the use of the concept of equivalent diameter from equation 14, an approximate version of equation 15 is

$$T_b - T_w = 70\exp[-30\alpha l/(D_{eq}^2 v)]. \quad (16)$$

Substituting the flow-rate result from equation 11 into equation 16 gives an approximate result for the dike very similar to that for the circular conduit. Specifically, for the 1983–84 Kilauea eruption episodes the temperature loss as the magma flowed in the conduit

was negligible regardless of whether the conduit was a dike or circular conduit.

As noted earlier, Decker and others (1983) estimated pressure changes in the summit reservoir of 0.085 MPa per μrad of rapid, radial summit tilt. Episode 2 of the Kilauea eruption that started in 1983 had a rapid tilt change of 11 μrad during the eruptive phase, and this corresponds to a pressure change of

$$P = 0.085 \times 11 = 0.935 \text{ MPa}. \quad (17)$$

For the current conduit model, we can assume that the pressure driving the forced convective intrusive flow in the conduit is approximately that given by equation 17. The viscosity of the magma can be estimated by using the result of Shaw and others (1968), who found that the viscosity variation with temperature for basaltic lava could be expressed as

$$\mu = (1 \times 10^{-6}) \exp(26{,}170/T), \quad (18)$$

where μ is in SI units (Pa·s) and T is in kelvins. The constant 26,170 in equation 18 is an experimentally determined constant for this lava. At a magma bulk temperature of $T_b = 1{,}413$ K, the viscosity is approximately

$$\mu = 100 \text{ Pa·s}.$$

Substituting this and the estimate of pressure from equation 17 into equation 2 and solving for v/D^2 gives

$$v/D^2 = P/(32\mu l) = 0.935 \times 10^6/[32(100)(20 \times 10^3)]$$

or

$$v/D^2 = 0.01461. \quad (19)$$

Equations 11 and 19 are two independent equations in two variables: the flow velocity v and the conduit diameter D. Solving these two equations for v and D yields

$$v = 0.444 \text{ m/s} \quad (20)$$

and

$$D = 5.51 \text{ m} \quad (21)$$

for conduit flow during episode 2 of the 1983–84 Kilauea eruptive activity. Values for other episodes of this eruption are listed in table 54.2. These values compare well with observed diameters (4–8 m) of conduit exit holes at eruptive vents such as those shown in figure 54.4. This similarity may be coincidental because flow in the vent conduit, with volatile phases present, is considerably different from flow in the deeper east-rift conduit.

If the conduit were a dike instead of a circular conduit, the dike thickness derived using the approximate result of equation 14 would be

$$a = D/2 = 5.51/2 = 2.76 \text{ m}, \quad (22)$$

and the dike width from equation 13 would then be

$$b = Q/av = 10.6/(2.76 \times 0.444) = 8.67 \text{ m}. \quad (23)$$

Estimates for the dike or sill model for this and other eruptive episodes at Kilauea in 1983–84 are listed in table 54.3.

TABLE 54.2.—*Flow rate, total intruded volume, and estimated velocity and conduit diameter (based on forced-convection flow model) for 1983–84 Kilauea eruptive episodes*

[First values of flow rate based on tilt data; second values in parentheses, supplied by E.W. Wolfe of Hawaiian Volcano Observatory, based on field observations of erupted volumes for episodes 2–15 reduced by 20 percent to account for dense-rock magma equivalent. Conduit diameter values in parentheses correspond to calculated values based on field observations of erupted volume]

Episode	Flow rate Q (m^3/s)	Intruded volume (10^6 m^3)	Velocity (m/s)	Conduit diameter (m)
2	10.6 (15)	5.50	0.444	5.51 (6.01)
3	13.0 (30)	9.04	.629	5.12 (6.31)
4	15.9 (24)	5.75	.556	6.03 (6.68)
5	19.5 (32)	5.92	.624	6.31 (7.14)
6	31.8 (27)	8.25	.942	6.56 (6.29)
7	42.8 (39)	8.51	1.11	7.01 (6.84)
8	57.9 (65)	5.00	.989	8.63 (8.88)
9	45.7 (40)	7.50	1.08	7.35 (7.10)
10	36.0 (52)	7.00	.923	7.05 (7.73)
11	62.1 (62)	8.84	1.36	7.64 (7.64)
12	56.7 (51)	6.94	1.15	7.91 (7.70)
13	35.9 (60)	5.54	.820	7.46 (8.48)
14	60.9 (70)	5.00	1.01	8.74 (9.05)
15	66.6 (94)	5.75	1.14	8.63 (9.40)
16	55.9	4.83	1.17	8.00
17	57.9	5.00	.990	8.63
18	56.4	4.88	1.36	7.26
19	21.2	1.83	.440	7.80
20	38.5	3.33	.807	7.79
21	35.7	3.08	.747	7.80
22	56.8	4.91	1.13	8.00
23	60.2	5.20	1.15	8.16
24	64.5	5.57	1.26	8.08
25	69.4	6.00	1.33	8.16

The previous flow calculations for the forced-convection model are valid as long as the temperature drop in the conduit is small (that is, as long as $T_b - T_w$ at the end of the conduit is approximately the same as at the entrance of the conduit). In the calculation for episode 2, this was certainly the case for the flow rate $Q = 10.6$ m^3/s. From equation 9, assuming the same magma properties, this temperature condition can be shown to be satisfied as long as the intrusive flow rate is greater than about $Q = 0.5$ m^3/s for a circular conduit. This condition is certainly met for all the eruptive episodes listed in table 54.2. If a dike geometry is assumed, the temperature condition can be shown to be satisfied for the eruptive phases listed in table 54.3 as long as the ratio of dike thickness to dike width (a/b) is greater than about 0.025, and this is true for all the episodes listed in table 54.3. In a circular conduit, if the intrusive flow rate Q were very low, the magma would reside in the conduit for a long time and would cool and solidify in the conduit. In a dike, if the ratio a/b were very small, then conduction losses would be large, and the magma would again tend to cool and solidify in the conduit.

Although the previous forced-convection calculations give acceptable values for velocity and conduit size, these calculations do not explain the cyclic nature of the eruptive episodes, with periods of fairly steady intrusive flow separated by quiescent periods with little or no flow. In simple pressure-driven forced convection of Newtonian liquids, we would expect the flow to slow down to the rate at which the summit reservoir is replenished. The flow would continue at this slow rate of 3.28 m^3/s (8.5×10^6 m^3/mo) and would not shut off between eruptive episodes, as observed. This replenishment flow rate of 3.28 m^3/s is still greater than the minimum value of 0.5 m^3/s

FIGURE 54.4.—Eruptive vents during February 1983 eruptive episode at Kilauea Volcano. Photograph by W.C. Luth, February 25, 1983. Highest fountains are spraying about 50 m high.

required to keep the conduit flow from solidifying in place. A possible explanation for the on-off nature of the cyclic eruptive episodes can be found by looking at the non-Newtonian flow properties of magma at temperatures below the liquidus such as occur in the conduit flow process. Shaw and others (1968) observed that Hawaiian basaltic lava at temperatures similar to those seen in the 1983–84 Kilauea eruptive activity behaved much like a Bingham-plastic fluid with a yield stress of 7–12 kg/m^2 (700 to 1,200 dyne/cm^2). If we assume that a pressure difference large enough to overcome the Bingham yield stress must exist before flow can begin, then this pressure can be estimated and compared with the pressure estimates of Decker and others (1983) used in the previous flow calculations. A simple pressure balance on the conduit is:

$$PA_c = \sigma A_s \tag{24}$$

where A_c is the cross-sectional area of the conduit, A_s is the surface area of the conduit, and σ is the Bingham yield stress. For a circular conduit this becomes

$$\pi D^2 P/4 = \pi D l \sigma$$

or

$$P = 4\sigma l/D. \tag{25}$$

For a yield stress of 7 kg/m^2, this becomes

TABLE 54.3.—*Estimate of dike size for east-rift conduit (based on forced-convection conduit model) for 1983–84 Kilauea eruptive episodes*

Episode	Dike thickness (m)	Dike width (m)
2	2.76	8.67
3	2.56	8.04
4	3.01	9.47
5	3.15	9.91
6	3.28	10.3
7	3.50	11.0
8	4.32	13.6
9	3.67	11.5
10	3.52	11.1
11	3.82	12.0
12	3.96	12.4
13	3.73	11.7
14	4.37	13.7
15	4.31	13.6
16	4.00	12.6
17	4.32	13.6
18	3.63	11.4
19	3.90	12.3
20	3.89	12.2
21	3.90	12.3
22	4.00	12.6
23	4.08	12.8
24	4.04	12.7
25	4.08	12.8

$$P = 4(7)(20\times10^3)/5.5 = 0.102\times10^6 \text{ kg/m}^2$$

or

$$P = 0.985 \text{ MPa}. \quad (26)$$

Using the upper value for yield stress of 12 kg/m^2 results in a predicted pressure of $P=1.69$ MPa. The predicted pressure differential driving the convective flow in the conduit, therefore, ranges from $P=0.985$ MPa to $P=1.69$ MPa. This compares favorably with the estimate of Decker and others (1983), who suggested that this pressure is 0.085 MPa per μrad of rapid radial tilt. Radial tilt changes for the early eruptive episodes in 1983 ranged from 10 to 18 μrad, corresponding to pressures of 0.85 to 1.53 MPa. These pressure estimates using the prediction of Decker and others (1983) agree well with the estimates above, 0.985 to 1.69 MPa, based on the Bingham model of Shaw and others (1968). This agreement supports the idea that the cyclic nature of the Kilauea eruptive episodes in 1983–84 may have been a result of non-Newtonian rheology effects. This calculation also supports the pressure predictions of Decker and others (1983) for the summit reservoir.

The forced-convection flow model can also be applied to other eruptions at Kilauea Volcano. For instance, the 1959–60 eruption was a major one with probably 17 eruptive phases (Richter and Moore, 1966). The conduit length l was probably much shorter than in the 1983–84 eruptive episodes because the eruption site was close to the summit of Kilauea; the 1959–60 conduit length l was probably on the order of 5 km (Peck and others, 1979). The principle effect of this shorter conduit length would be to reduce the time between eruptive episodes. Equation 25 shows that the summit-reservoir pressure necessary to overcome the Bingham-plastic yield stress of magma in the conduit is proportional to conduit length l. Since l was much shorter in the 1959–60 eruption, the dynamic pressure needed to overcome the yield stress of the magma was much less. As the summit magma chamber inflated, the necessary pressure level for an eruptive episode would be reached quickly, and the eruptive phases would be expected to repeat on a time period much shorter than the approximate one-month time periods of the 1983–84 eruptive activity. As expected, the eruptive episodes for the 1959–60 eruption repeated on an average interval of about 2 days (Richter and Moore, 1966).

VISCOUS-DISSIPATION FORCED-CONVECTION CONDUIT MODEL

Viscous dissipation may be an important mechanism in intrusive flow of magma in the rift conduits of Kilauea. Viscous dissipation has been suggested before as a key mechanism in eruptive cycles (Shaw, 1969, 1973; Anderson and Perkins, 1974; Fujii and Uyeda, 1974; Hardee and Larson, 1977; Fujii, 1981). Previous confirmation of the theory has been limited to estimates of runaway temperature and dike thickness for various types of magma. Because of the extensive amount of real-time field observations of conduit flow in the east-rift conduit during the 1983–84 Kilauea activity, it is possible to compare conduit models with a large set of field data, such as eruption temperature of lava, time between successive eruptive episodes, intrusive flow rate, and, in some cases, the conduit exit diameter at the vent.

The energy of viscous dissipation ultimately comes from conversion of pressure energy in the summit reservoir into frictional heat. The pressure in the reservoir overcomes the frictional resistance to flow, and in turn the viscous shear caused by the frictional resistance is converted to heat, which raises the temperature of the fluid. This happens in all cases of simple forced-convective flow in conduits, but usually the heating effect is small. In the case of magmatic intrusions, however, the heating effect can be significant. Without the effect of viscous dissipation, magma would have difficulty flowing in small conduits and thin dikes, and there would be a tendency for the magma to cool and solidify in place. Even where mechanical fracturing occurs and opens the conduit, viscous dissipation is likely to be important in allowing the magma to flow rather than quickly solidify. Since the energy available for viscous heating comes from the pressure or potential energy in the reservoir, field observations of the thermal state of erupting lava can be used to estimate conditions back in the reservoir. Also, it is obvious that the magnitude of the viscous-heating effect is limited ultimately by the pressure or potential energy in the reservoir.

A forced-convection transport model of the east-rift conduit can also be developed in which viscous-dissipation effects are important. Viscous dissipation can affect both the temperature of erupting lava and the cyclic episodes of the eruption. The time required for thermal effects to build to thermal runaway, coupled with the summit-reservoir pressure history, determines the repose period between dissipatively controlled eruptive cycles. The rapid increase of viscosity of the magma as partial crystallization occurs on cooling probably causes the magma to jam up and cease flowing in a reverse type of thermal runaway. Calculations to demonstrate this jam-up phenomenon or reverse thermal runaway are difficult because

the viscosity of the liquid/crystal magma composition at near-solidus temperatures is not well known (Shaw and others, 1968). Such an effect, once started, would rapidly accelerate and cause the flow to shut off suddenly. As pressure in the summit reservoir increased again, a point would be reached at which viscous-dissipation effects would again produce a thermal-runaway situation, and a new eruptive episode would begin. The observed cyclic nature of the eruptive episodes, the observed eruptive temperatures and volumes, and the highly temperature-dependent nature of the magma viscosity are all consistent with a forced-convection magma-conduit model that includes viscous-dissipation effects. The calculations that follow here are for this transport model.

First, the viscous-dissipation thermal-runaway temperature is determined and shown to be consistent with observed eruption temperatures. The pressure drop in the conduit is determined, and this in turn can be related back to the pressure in the summit reservoir. The shape of the conduit is then determined. Next, an approximate calculation shows that the runaway time is of the right order of magnitude in comparison with observed periods of repose between eruptive episodes.

For a cylindrical conduit, the pressure drop in the conduit from simple hydrodynamic theory for laminar flow (equation 2) is (Vennard, 1956) $P=32\mu lv/D^2$, where P is the dynamic or available pressure to drive the intrusive flow, μ is the average magma viscosity, l is the length of the conduit, and D is the diameter of the conduit. For conduits with a noncircular cross section, the concept of an equivalent diameter can again be used. From the energy equation and the expression for viscous dissipation in cylindrical coordinates (Batchelor, 1970), it can be shown that for steady flow in a conduit where the viscous-dissipation heating in the conduit is in balance with conduction loss at the wall, the temperature of the fluid in the conduit is

$$T_b - T_w = (8/9)\mu v^2/k, \tag{27}$$

where T_b is the average or bulk temperature of the fluid in the conduit, T_w is the temperature of the wall (again, 1,313 K), v is the average flow velocity of the fluid, and k is the thermal conductivity of the fluid. The flow rate Q (equation 3) is $Q=\pi D^2 v/4$. Between eruptions or eruptive episodes, the pressure in the summit reservoir builds in magnitude, and the pressure acts on material in the conduit that is hot but solidified and resistant to flow. The viscosity is high at this point, and the flow velocity is near zero. Flow will begin to occur at an imperceptibly slow rate, producing a small amount of viscous-dissipation heating. Gradually at first and then rapidly, the process will accelerate as viscous heating reduces the viscosity of the fluid. Most of the noticeable activity occurs in the latter part of the thermal-runaway process, giving it the appearance of suddenness. Equations 2 and 18 can be used to calculate the condition under which appreciable flow begins. Once initiated, the flow will tend to persist at the conditions of temperature and velocity in which the viscous heat generation in the fluid is exactly balanced by the conduction loss at the wall. At slower flow rates the fluid will cool too much by conduction loss to the wall, and some of the magma will tend to solidify in place. At higher flow rates the excessive viscous heat generation will produce melting at the walls.

The energy absorbed by latent heat at the wall and the reduced flow velocity as the conduit diameter increases will both tend to restrict the flow and prevent the velocity and temperature from increasing indefinitely. The natural tendency is for the intrusive flow to assume a steady flow condition at the critical temperature at which viscous-heating effects predominate. This critical viscous-dissipation temperature or "runaway" temperature has been studied by Fujii and Uyeda (1974), Hardee and Larson (1977), and others. The runaway temperature, which corresponds roughly with the expected value of the lava-eruption temperature, can be determined by using equations 2, 18, and 27. First, equations 2 and 27 are combined to eliminate v:

$$P^2 = (9/8)k(32l/D^2)^2 (T_b - T_w)\mu. \tag{28}$$

Assuming a wallrock or melt temperature of 1,343 K (Shaw and others, 1968) for basalt and using equation 18 for viscosity yields:

$$\mu = (1\times10^{-6})\exp[26{,}170/(\Phi+1{,}343)] \tag{29}$$

where $\Phi = T_b - T_w$. Substituting equation 29 into equation 28 gives:

$$P^2 = [(9/8)k(32l/D^2)^2(1\times10^{-6})]\Phi \cdot \exp[26{,}170/(\Phi+1{,}343)]. \tag{30}$$

The condition of thermal runaway occurs when a small change in reservoir pressure P results in a large change in temperature Φ or, in other words, when $dP/d\Phi = 0$. Differentiating equation 30 with respect to Φ, setting $dP/d\Phi = 0$ and then solving for Φ results in

$$[26{,}170\Phi/(\Phi+1{,}343)^2] - 1 = 0$$

or

$$\Phi = 77 \text{ K}. \tag{31}$$

The average temperature of the magma during intrusive flow and the corresponding expected lava-eruption temperature is then

$$T_b = 1{,}343 + 77 = 1{,}420 \text{ K}. \tag{32}$$

This compares well with typical lava-eruption temperatures from measurements such as those shown being made in figure 54.5 near the vent during the 1983–84 eruptive activity of Kilauea (Hardee, 1983).

The dynamic pressure in the reservoir or the pressure driving the flow in the conduit can be determined from equation 2. First, equations 3 and 27 are used to eliminate D and v from equation 2 to give

$$P = 9\pi k l (T_b - T_w)/Q. \tag{33}$$

Substituting the flow rate from equation 10 into equation 33 gives

$$P = 9\pi(2.09)(20\times10^3)(1{,}420-1{,}343)/10.6 = 8.59 \text{ MPa}. \tag{34}$$

This pressure is within the range (0.09–400 MPa) estimated by Decker and others (1983), although it is higher than their estimates

FIGURE 54.5.—Thermal measurements being made in molten lava during February 1983 eruptive episode at Kilauea Volcano. Photograph by W.C. Luth, February 25, 1983.

for dynamic pressure changes in the summit reservoir during Kilauea's 1983–84 activity. The expected flow velocity in the conduit can be found from equation 27:

$$v=[(9/8)k(T_b-T_w)/\mu]^{0.5}. \quad (35)$$

The viscosity to be used in equation 35 is found from equation 18 at the fluid runaway temperature of equation 32:

$$\mu=(1\times10^{-6})\exp(26{,}170/1{,}420)=100 \text{ Pa}\cdot\text{s}. \quad (36)$$

Substituting this and other values into equation 35 gives

$$v=[9(2.09)(1{,}420-1{,}343)/8(100)]^{0.5}=1.33 \text{ m/s} \quad (37)$$

for the average intrusive flow velocity in the conduit during eruptive episode 2. The effective diameter of the conduit can then be found from equation 3:

$$D=(4Q/\pi v)^{0.5}=[4(10.6)/\pi(1.33)]^{0.5}=3.18 \text{ m}. \quad (38)$$

This value compares reasonably well with observed diameters of conduit exit holes, typically around 4–8 m in diameter, at eruptive vents such as those shown in figure 54.4 during the 1983–84 Kilauea activity. The predicted diameter is not too different from the value for the non-Newtonian forced-convection conduit model in the previous section (table 54.4).

TABLE 54.4.—*Comparison of estimated conduit diameter for east-rift conduit during 1983–84 Kilauea eruptive episodes (based on forced-convection conduit model and forced-convection model with viscous dissipation)*

Episode	Conduit diameter from table 54.2 (m)	Conduit diameter with viscous dissipation (m)
2	5.51	3.18
3	5.12	3.52
4	6.03	3.90
5	6.31	4.32
6	6.56	5.52
7	7.01	6.40
8	8.63	7.44
9	7.35	6.61
10	7.05	5.87
11	7.64	7.71
12	7.91	7.36
13	7.46	5.86
14	8.74	7.63
15	8.63	7.98
16	8.00	7.31
17	8.63	7.44
18	7.26	7.34
19	7.80	4.50
20	7.79	6.07
21	7.80	5.84
22	8.00	7.37
23	8.16	7.59
24	8.08	7.85
25	8.16	8.14

The assumption of laminar flow used in the selection of equation 2 can be checked. The Reynolds number (**R**) for flow in a conduit is

$$\mathbf{R} = vD\rho/\mu. \tag{39}$$

Inserting values of velocity and conduit diameter from equations 37 and 38 gives

$$\mathbf{R} = (1.33)(3.18)(2{,}700)/100 = 113. \tag{40}$$

This value of **R** is well below the critical value of 2,700 for transition to turbulent flow in conduits, and therefore the original assumption of laminar flow in the conduit is valid.

The main portion of the east-rift conduit from the summit reservoir down to the vicinity of the erupting vent may be a tabular dike rather than a circular conduit. Flow equations for the geometry of a dike or sill can be developed that are similar to the previous equations for the circular conduit. Flow in a dike or sill can be modeled as flow between parallel plates. The pressure drop for this flow geometry is (Gebhart, 1961)

$$P = 12\mu lv/a^2, \tag{41}$$

where a is the thickness of the dike. With viscous-dissipation effects considered, the temperature of the fluid flowing in the dike is

$$T_b - T_w = (3/5)\mu v^2/k. \tag{42}$$

Equations 41 and 42 are similar to equations 2 and 27 for the cylindrical conduit model. The volume flow rate in the dike (equation 13) is again $Q = abv$, where b is the width of the dike. If the calculation that led to equation 31 is carried out for the dike geometry using equations 41 and 42, the thermal runaway temperature can be shown to be the same as in equation 31: $\Phi = 77$ K. The different constant in equation 42 does not affect the result for runaway temperature. The flow velocity at runaway is found from equation 42:

$$v = [(5/3)\Phi k/\mu]^{0.5} = [(5/3)(77)(2.09)/100]^{0.5} \tag{44}$$

or

$$v = 1.63 \text{ m/s}. \tag{45}$$

Although velocity and flow rate are known, it is not possible to determine the thickness of the dike or sill from equation 13 because of the additional geometric parameter b, the width of the dike, that now occurs in equation 13. In the absence of additional information, the best procedure for dike and sill flow calculations is to use again the concept of equivalent diameter (Chapman, 1967).

Referring to the previous calculation for conduit diameter in equation 38, where the conduit diameter was 3.18 m, and substituting this into equation 14 gives

$$a = D_{eq}/2 = 3.18/2 = 1.59 \text{ m}. \tag{46}$$

This implies that if the flow during episode 2 of the 1983–84 Kilauea activity passed through a dikelike conduit rather than a circular conduit, the dike was on the order of 1.59 m thick, the dynamic pressure was similar to that determined in equation 34, and the flow velocity for the dike was similar to that determined in equation 45, assuming that viscous-dissipation effects were a major factor. The dike thickness in equation 46 is not thin enough for sufficient cooling and solidification to occur to cause the conduit to easily jam up and go into a period of repose. This can be shown by applying equation 8. The value of dike thickness in equation 46, however, is consistent with observations of fossil dikes in Hawaii. The thickness of the dike or conduit in episode 2 of Kilauea's 1983 eruptive activity can be determined using equation 13, the value of dike thickness in equation 46, the flow velocity from equation 45, and a typical value of intrusive flow rate such as that in equation 10:

$$b = Q/(a/v) = 10.6/[(1.59)(1.63)] = 4.09 \text{ m}. \tag{47}$$

Viscous dissipation can explain the intermittent intrusive flow observed in the various eruptive episodes. When a certain critical pressure and temperature (see, for example, equation 32) are reached, flow begins, and the pressure starts to drop. Eventually the flow stops, and magma in the conduit cools. A period of repose then occurs, during which the pressure builds up again, and the magma in the conduit is heated to the runaway condition once more by viscous dissipation. The period of repose or time between eruptive episodes can be determined by a simple calculation in which the viscous-dissipation energy is equated to the increase in internal energy necessary to raise the magma from its solidification temperature back up to its runaway temperature. In the interest of keeping the calculation simple, I assume that the magma and surroundings are hot and near the solidification temperature, as suggested by the earlier analysis leading to equation 1. Conduction losses would then be small during the period of repose between eruptive episodes. This is probably a good assumption; in thermal-runaway problems of this type, the temperature does not increase much until nearly the

moment of thermal runaway (Hardee and others, 1977). The rate of viscous heat dissipation per unit volume in a cylindrical conduit is given by Batchelor (1970) as $(P/l)^2R^2/4\mu$ at any radius R. The volume-average viscous heat dissipation for a cylindrical conduit of radius R is found by integrating the local value over the whole volume and is $(P/l)^2R^2/(8\mu)$. The repose time between eruptive episodes (thermal-runaway time) is found by equating the volume-average viscous heat dissipation to the change in internal energy necessary to raise the magma in the conduit from the solidification temperature to the runaway temperature,

$$\rho c \; dT/d\tau = P^2R^2/8\mu l^2, \tag{48}$$

and then integrating this result

$$\int_{1343}^{1420} \exp(26{,}170/T) \; dT = \int_0^{\tau_r} [P^2R^2/(8l^2\rho c \times 10^{-6})] \; d\tau.$$

The integration is performed after making use of the substitution $Z = 26{,}170/T$ where $T = 1{,}343$ K, $Z_1 = 26{,}170/1{,}343$, $T_2 = 1{,}420$ K, and $Z_2 = 26{,}170/1{,}420$. The solution for the repose time is then

$$\tau_r = [8l^2 \rho c \times 10^{-6}/(P^2R^2)] \left[(1/T)\exp(26{,}170/T) - 26{,}170Ei(26{,}170/T)\right]_{1343}^{1420}. \tag{49}$$

$Ei(x)$ is the exponential integral function (Mathews and Walker, 1965), which can be evaluated using tabulated values (Gautschi and Cahill, 1965) and equation 49. The expression for the repose time then becomes

$$\tau_r = [8l^2\rho c \times 10^{-6}/(P^2R^2)](1.370 \times 10^{10}). \tag{50}$$

Equations 2 and 27 can be combined to eliminate v, and the result can be substituted into equation 50 to eliminate l^2/P^2:

$$\tau_r = (1.370 \times 10^4) D^2 \rho c / [36 k \mu_r (T_b - T_w)]. \tag{51}$$

Substituting into equation 51 the appropriate values and the diameter determined for the conduit in episode 2 gives

$$\tau_r = (1.370 \times 10^4)(3.18)^2(2{,}700)(4{,}186)/[36(2.09)(100)(77)]$$

or

$$\tau_r = 2.70 \times 10^6 \text{ s} = 31.3 \text{ d}. \tag{52}$$

This value of repose time compares well with observed values for the 1983–84 Kilauea eruptive episodes. Repose times for the various episodes listed in table 54.5 were determined either by inflation of the summit or by absence of lava production. A repose period of 41 d based on inflation data or 26 d based on the absence of lava production was observed between the first and second episodes (table 54.5). The average of these two values, 33.5 d, compares well with the estimated value of 31.3 d in equation 52. The repose time of 31.3 d and the average magma-supply estimate of Swanson (1972) imply that each eruptive episode should produce a total magma volume of about 9×10^6 m^3; the observed values in table 54.3 are not far from this, ranging from 5×10^6 to 9×10^6 m^3.

Equation 51 and the result from equation 52 give an alternative viewpoint to the yield-stress calculations of equations 24–26 for observed cyclic eruptive behavior. Equation 24 is based on the assumption that the non-Newtonian or Bingham yield stress combined with an increasing reservoir pressure is the mechanism behind cyclic eruptive behavior. Equation 51 assumes that viscous dissipation is the mechanism behind cyclic eruptive behavior. Although the agreement of the viscous-dissipation conduit model with observed data is good during early episodes of the eruption, the agreement is not as good in the later episodes. For instance, the observed flow rate, Q, increases and the observed repose time, τ_r, decreases in later eruptive episodes (see tables 54.2, 54.5). Substituting conduit diameter, D, from equation 3 into equation 51, however, would predict that repose time is proportional to Q. Although this may be true in some cases, it is not the pattern of the later episodes of the 1983–84 Kilauea eruptive activity.

The previous analysis has examined how viscous dissipation might be the mechanism responsible for intermittent intrusive flow in the east-rift conduit. As noted earlier, viscous dissipation has been proposed before as the mechanism behind recurring volcanic eruption cycles (Shaw, 1969,1973; Anderson and Perkins, 1974; Fujii and Uyeda, 1974; Hardee and Larson, 1977; and Fujii, 1981). Another interesting possibility is that viscous dissipation may be the mechanism responsible for the fairly constant magma supply to the summit reservoir from the asthenosphere. As mentioned earlier, the summit reservoir appears to be replenished at a rate of 3.28 m^3/s (Swanson, 1972). If a conduit from the asthenosphere to the summit reservoir has magma flow due to viscous dissipation at the critical runaway condition, then equations 2, 3, and 27 apply. Fujii and Uyeda (1974) argued that the driving force for magma ascent in the upper mantle or lower crust is buoyancy due to density differences between the country rock and the magma and that this is approximately equal to

$$P/l = 1{,}000 \text{ J/m}^4 \text{ (100 dyne/cm}^3\text{)}. \tag{53}$$

TABLE 54.5.—*Repose times between 1983–84 eruptive episodes of Kilauea*

[Data from Hawaiian Volcano Observatory (HVO) and from E.W. Wolfe]

Episodes	Repose time (τ_r)	
	Duration of inflation (d)	Absence of lava production (d)
1–2	41	26.0
2–3	24	23.4
3–4	63	65.3
4–5	13	12.0
5–6	20	19.3
6–7	22	20.6
7–8	23	19.6
8–9	11	8.5
9–10	21	17.3
10–11	30	27.3
11–12	24	22.4
12–13	51	50.1
13–14	10	8.3
14–15	15	15.3
Average	26.3	24.0

Substituting this pressure gradient and the viscosity (100 Pa·s) at thermal runaway into equation 2 and solving gives

$$D^2/v = 3.2 \text{ m·s}. \quad (54)$$

Substituting this result and the flow velocity at thermal runaway from equation 37 into equation 3 gives

$$Q = (\pi/4)D^2v = (\pi/4)(3.2)(1.33)^2 = 4.45 \text{ m}^3/\text{s}. \quad (55)$$

This magma-reservoir replenishment rate (4.45 m^3/s) compares well with the observed replenishment rate (3.28 m^3/s), considering the simplicity of the model and assumptions.

CONCLUSIONS

The upper part of Kilauea's east-rift conduit (upper 25 km) is relatively open to flow, and intrusions in it are usually aseismic. The lower part of the east-rift conduit is usually closed and requires fracturing to produce intrusions, which are normally associated with seismicity. A repetitive thermal-intrusion model was used to show that the difference between these two types of conduit flow is determined by the average volume-intrusion rate, length of conduit, and, to a lesser extent, the number of previous intrusions in that part of the conduit. Non-Newtonian rheology or viscous-dissipation effects are probably important in determining flow characteristics in the Kilauea conduit system.

A conduit flow model based on forced convective flow of a non-Newtonian (Bingham plastic) liquid is compatible with field observations for the recent 1983–84 Kilauea eruptive activity. Predictions of dynamic pressure based on this model (0.985–1.69 MPa) agree well with the summit pressure estimates (0.85–1.53 MPa) of Decker and others (1983). Predicted effective conduit diameters are on the order of 5–10 m. For the diameters, conduit lengths, and intrusion rates involved in the 1983–84 Kilauea eruptive episodes, the magma does not have time to cool appreciably as it flows the length of the conduit. The temperature of the magma at the vent is therefore probably close to the temperature of the summit reservoir. Although the conduit is circular at the vent, at depth it may have a shape like a dike or sill. The concept of an effective diameter was used to examine conduit shapes such as dikes or sills; predicted dike thicknesses were still large enough that heat loss at the conduit wall would not have been a major factor in the 1983–84 Kilauea activity. The field measurements of Bingham-plastic yield stress of Kilauea basalt (Shaw and others, 1968) were used to explain the cyclic nature of eruptive episodes. The summit magma-reservoir pressure must build sufficiently to overcome the Bingham-plastic yield stress of the magma in the conduit before each eruptive cycle. The resulting calculated pressure changes in the summit reservoir agree closely with pressure-change estimates of Decker and others (1983).

A conduit flow model was also developed in which viscous dissipation effects were included. This conduit model is particularly applicable to thin conduits, on the order of 0.1 m thick or less. Such conduits are sufficiently thin that thermal losses to the conduit wall are important, and an internal heat supply is needed to keep the flowing magma from solidifying rapidly in the conduit. Viscous dissipation is a likely internal heat source for such intrusive flows. The forced-convection flow model with viscous-dissipation effects developed here is compared with field observations. The model predicts lava-eruption temperatures around 1,420 K, and this is in good agreement with field observations. The dynamic pressure driving this intrusive flow is approximately 10 times higher than corresponding pressure predictions for the flow model based on non-Newtonian rheology. The higher pressures occur because pressure is the source of energy for the internal viscous-dissipation heat. Calculation of thermal-runaway time based on the viscous-dissipation flow model predicted times between eruptive episodes on the order of a month for the 1983–84 Kilauea eruptive activity, in agreement with observations. Although the viscous-dissipation flow model gives results that are compatible with field observations, this model predicts effective conduit diameters for the 1983–84 Kilauea activity that are sufficiently large that an internal heat mechanism like viscous dissipation is not needed. This suggests that viscous-dissipation effects may not have been important in the 1983–84 Kilauea eruptive episodes. Viscous-dissipation effects may well be important in other cases of rift intrusions, particularly for rapid intrusions in thin dikes and sills. Viscous dissipation can also be used to explain how the summit reservoir is replenished at a fairly constant rate over long periods of time. Both the non-Newtonian flow model and the viscous-dissipation flow model depend primarily on the unusual rheology of magma. The Bingham-plastic model considers that viscosity depends on shear stress, and the viscous-dissipation model considers that viscosity depends on temperature. Actually, magma viscosity in the subliquidus temperature range depends on shear stress, shear rate, temperature, time, and previous thermal history (Hardee and Dunn, 1981). The Bingham-plastic flow model and the viscous-dissipation flow model are simply ways of looking at major magma-viscosity effects one at a time.

Epp and others (1983) noted that an inverse relation exists between the summit tilt deflation of Kilauea and the elevation of associated eruptive vents. Decker and others (1983) found that this relation indicated a pressure change of 0.085 MPa per μrad of rapid radial summit tilt. By correlating data from near the summit to near sea level, Epp and others (1983) showed that a general relation exists between volume of erupted lava and vent elevation: volume of erupted lava tends to increase with a decrease in elevation. These observations are consistent with the conduit and dike models developed earlier. The dynamic pressure change available to overcome frictional resistance in the conduit was calculated to be about 1.0 MPa (0.985–1.69 MPa). Sufficient pressure must also be available in the summit reservoir to overcome the hydrostatic head from the reservoir up to the vent. The difference in hydrostatic head between summit vents and those near sea level is about 30 MPa (roughly 1 km of liquid magma). The hydrostatic head favors the vents near sea level. The conduit length from the summit reservoir to the vents near sea level is 2 to 3 times longer, and the pressure required to overcome frictional losses is that much greater. However, although this pressure doubles or triples to 2–3 MPa, the 30-MPa

reduction in hydrostatic head more than offsets this. Greater reservoir pressure tends to be available to drive intrusive flows to the lower elevation vents. It is not surprising that the volume of eruption tends to be larger at lower elevation vents.

If pressure favors eruptions at lower elevation vents, the obvious question is, why do most eruptions occur at higher elevation vents? The answer is that thermal effects tend to keep the upper portion of the east rift zone more open to flow (see table 54.1). The lower elevation vents are connected to a portion of the east-rift conduit that is not normally open or available for intrusive flow except at special times when fracturing events or earthquakes have temporarily opened the conduit all the way to vents near sea level.

The east-rift conduit and its eruptions provide valuable data that can be used to construct and test models of intrusive magma flow. Considerably more data are available from east-rift eruptions than are available from other intrusive magmatic processes. Once models of intrusive magmatic flow are tested, it is possible to use them for prediction in other situations where data are meager or absent. It is possible to use the intrusive flow models to predict the thermal-runaway conditions for a shallow magma reservoir that is intersected by a drill hole. These models can also be extended to magma other than basalt. For example, using the data of Piwinskii and Weed (1980), the viscosity for a molten rhyolite sample from Nevada is found to be $\mu = (0.857 \times 10^{-6}) \exp(36{,}194/T)$. This is the same general form of the viscosity function as used earlier in equation 18. When the earlier calculations are repeated using the viscosity function of Piwinskii and Weed (1980). the thermal-runaway times, or times between eruptive episodes, for rhyolite are on the order of hundreds of years or more, depending on the assumptions used for conduit diameter.

REFERENCES CITED

Anderson, O.L., and Perkins, P.C., 1974, Runaway temperatures in the asthenosphere resulting from viscous heating: Journal of Geophysical Research, v. 79, p. 2136–2138.

Batchelor, G.K., 1970, An introduction to fluid mechanics: Cambridge, U.K., University Press, p. 151–182.

Chapman, A.J., 1967. Heat transfer: New York, Macmillan, p. 338–339.

Decker, R.W., and Decker, B., 1981, The eruptions of Mount St. Helens: Scientific American, v. 244, no. 3, p. 68–80.

Decker, R.W., Okamura, A.T., and Dvorak, J.J., 1983, Pressure changes in the magma reservoir beneath Kilauea Volcano, Hawaii [abs.]: Eos (American Geophysical Union Transactions), v. 64, p. 901.

Dvorak, J.J., Okamura, A.T., and Dieterich, J.H., 1983. Analysis of surface deformation data, Kilauea Volcano, Hawaii, October 1966 to September 1970: Journal of Geophysical Research, v. 88, p. 9295–9304.

Duffield, W.A., Christiansen, R.L., Koyanagi, R.Y., and Peterson, D.W., 1982, Storage, migration, and eruption of magma at Kilauea Volcano, Hawaii, 1971–1972: Journal of Volcanology and Geothermal Research, v. 13, p. 273–307.

Dzurisin, D., Anderson, L.A., Eaton, G.P., Koyanagi, R.Y. Lipman, P.W., Lockwood, J.P., Okamura, R.T., Puniwai, G.S., Sato, M.K., and Yamashita, K.M., 1980, Geophysical observations of Kilauea Volcano, Hawaii, 2. Constraints on the magma supply during November 1975–September 1977: Journal of Volcanology and Geothermal Research, v. 7. p. 241–269.

Eckert, E.R.G., and Drake, R.M., 1959, Heat and mass transfer: New York, McGraw-Hill, p. 190–200.

Epp, D., Decker, R.W., and Okamura, A.T., 1983, Relation of summit deformation to east rift zone eruptions on Kilauea Volcano, Hawaii: Geophysical Research Letters, v. 10, p. 493–496.

Fedotov, S.A., 1981, Magma rates in feeding conduits of different volcanic centers: Journal of Volcanology and Geothermal Research, v. 9, p. 379–394.

Fiske, F.S., and Jackson, E.D., 1972, Orientation and growth of Hawaiian volcanic rifts: the effect of regional structure and gravitational stresses: Royal Society of London Proceedings, v. 329, p. 299–326.

Fujii, N., 1981, A model of magma ascent and eruption sequence for polygenetic volcanoes [abs.]: Tokyo, 1981, International Association of Volcanology and Chemistry of the Earth's Interior, p. 97.

Fujii, N., and Uyeda, S., 1974, Thermal instabilities during flow of magma in volcanic conduits: Journal of Geophysical Research, v. 79, p. 3367–3369.

Gautschi, W., and Cahill, W.F., 1965, Exponential integral and related functions, *in* Handbook of mathematical functions, Abramowitz, M., and Stegun, I.A., eds.: Washington, National Bureau of Standards, p. 227–251.

Gebhart, B., 1961, Heat transfer: New York, McGraw-Hill, p. 137–219.

Gruntfest, I.J., 1963. Thermal feedback in liquid flow; plane shear at constant atress: Transactions of the Society of Rheology, v. 7, p. 195–207.

Gruntfest, I.J., Young, J.P., and Johnson, N.L., 1964, Temperatures generated by the flow of liquids in pipes: Journal of Applied Physics, v. 35, p. 18–22.

Hardee, H.C., 1982, Incipient magma chamber formation as a result of repetitive intrusions: Bulletin Volcanologique, v. 45, no. 1, p. 41–49.

———1983, Heat transfer measurements of the 1983 Kilauea lava flow: Science, v. 222, p. 47–48.

Hardee, H.C., and Dunn, J.C., 1981, Convective heat transfer in magmas near the liquidus: Journal of Volcanology and Geothermal Research, v. 10, p. 195–207.

Hardee, H.C., and Larson, D.W., 1977, Viscous dissipation effects in magma conduits: Journal of Volcanology and Geothermal Research, v. 2, p. 299–308.

Hardee, H.C., Lee, D.O. and Donaldson, A.B., 1977, Predicting the time-to explosion of multidimensional explosives with a constant heat flux boundary condition: Albuquerque, N. Mex., Sandia National Laboratories Report SAND76-0738, 31 p.

Kienle, J., and Swanson, S.E., 1980, Volcanic hazards from future eruptions of Augustine Volcano, Alaska: Fairbanks, University of Alaska, Geophysics Institute Report UAG-R275, 122 p.

MacDonald, G.A., and Hubbard, D.H., 1972, Volcanoes of the national parks in Hawaii: Honolulu, Tongg, 56 p.

Mathews, J. and Walker, R.L., 1965, Mathematical methods of physics: New York, W.A. Benjamin, p. 56–90.

Moore, J.G., 1971, Bathymetry and geology—east cape of the Island of Hawaii: U.S. Geological Survey Miscellaneous Geologic Investigations Map, I–677, scale 1:62,500.

Peck, D.L., Wright, T.L. and Decker, R.W., 1979, The lava lakes of Kilauea: Scientific American, v. 241, no. 4, p. 114–128.

Piwinskii, A.J., and Weed, H.C., 1980, Dynamic viscosity of some silicate melts to 1688 °C under atmospheric pressure: Thermochimica Acta, v. 37, p. 189–195.

Richter, D.H., and Moore, J.G., 1966, Petrology of the Kilauea Iki lava lake Hawaii, The 1959–60 eruption of Kilauea Volcano, Hawaii: U.S. Geological Survey Professional Paper 537–B, p. B1–B26.

Ryan, M.P., Blevins, J.Y.K., Okamura, A.T., and Koyanagi, R.Y., 1983. Magma reservoir subsidence mechanics: Theoretical summary and application to Kilauea Volcano, Hawaii: Journal of Geophysical Research, v. 88, p. 4147–4181.

Ryan, M.P., Koyanagi, R.Y., and Fiske, R.S., 1981, Modeling the three-dimensional structure of macroscopic magma transport systems: Application to Kilauea Volcano, Hawaii: Journal of Geophysical Research, v. 86, p. 7111–7129.

Shaw, H.R., 1969, Rheology of basalt in the melting range: Journal of Petrology, v. 10, p. 510–535.

———1973, Mantle convection and volcanic periodicity in the Pacific: Evidence from Hawaii: Geological Society of America Bulletin, v. 84, p. 1505–1526.

———1980, The fracture mechanisms of magma transport from the mantle to the surface, *in* Hargraves, R.B., ed., Physics of magmatic processes: Princeton, N.J., Princeton University Press, p. 201–264.

Shaw, H.R., Wright, T.L., Peck, D.L., and Okamura, R., 1968, An analysis of field measurements in Makaopuhi lava lake, Hawaii: American Journal of Science, v. 266, p. 225–264.

Smith, R.L., 1979, Ash-flow magmatism, *in* Chapin, C.E., and Elston, W.E., eds., Ash-flow tuffs: Geological Society of America Special Paper 180, p. 5–27.

Swanson, D.A., 1972, Magma supply rates at Kilauea Volcano, 1952–1971: Science, v. 175, p. 169–170.

Vennard, J.K., 1956, Elementary fluid mechanics: New York, John Wiley, p. 188–242.

CONCEPTUAL MODELS OF BRINE EVOLUTION IN MAGMATIC-HYDROTHERMAL SYSTEMS

By Robert O. Fournier

ABSTRACT

The depth of intrusion of a magmatic body is important in regard to brine evolution and to the type and intensity of hydrothermal alteration that is likely to be associated with that intrusion. At a depth of intrusion of 6–7 km, and in the absence of evaporite deposits somewhere in the section, nonmagmatic water is not likely to be converted to brine unless there are special circumstances, such as repeated magmatic intrusions and repeated fracturing of very hot rock. In contrast, brine is very likely to form from nonmagmatic water where the depth of intrusion comes within about 3–4 km of the surface, and dilute water is heated to above about 400–450 °C.

When pore-fluid pressures are controlled by hydrostatic conditions, magmatic waters will evolve to highly saline brines at depths less than about 10-12 km, irrespective of the initial concentrations of salt and water dissolved in the magma. Dilute hydrothermal fluids of meteoric origin and mixtures of meteoric water and condensed magmatic gas (steam) are likely to form convection systems that float upon the more saline and probably hotter magmatic fluid. Double-diffusive convection is likely to result from the temperature and salinity gradients.

Quasi-plastic flow and mineral deposition generally prevent flow of water at hydrostatic pressure through rock at temperatures above 350–450 °C. However, where there are steep thermal gradients and a relatively rapid rate of change of stress, such as where magma is rapidly injected from a deep environment into a more shallow environment, brittle deformation of rocks may occur at temperatures in excess of 450 °C. Ground water at hydrostatic pressure may flow into and through these fractures and become heated to very high temperatures, possibly flashing in great part to steam with the simultaneous development of a small mass of brine. This situation should persist for only a relatively short time before quasi-plastic flow and mineral deposition limit additional fluid circulation to temperatures below 350–450 °C.

A generalized model is presented for the evolution of a hydrothermal system within an oceanic volcano, such as at Hawaii, in which a slowly rising magma reservoir maintains a depth of about 3–4 km beneath the summit as the volcanic edifice builds upon the sea floor. Significant amounts of highly saline brine are likely to be generated from sea water when the magma reservoir rises to within about 4–5 km of sea level. After a volcanic island forms, fresh water may enter the top of the hydrothermal system and float upon the brine. Sulfides are likely to deposit below sea level within the chloride-rich brine portion of the system, but these deposits are not likely to be exposed during subsequent erosion. With continued growth of the volcano above sea level, temperatures and pressures within the hydrothermal system become appropriate for complete evaporation of pore waters adjacent to the rising magma chamber. Sodium sulfate- and sodium carbonate-rich brines form above sea level where steam condenses and sulfur- and carbon-rich gases react with the country rock.

What is generally thought of as supercritical behavior of a fluid (no phase change upon heating or cooling) occurs only at pressures greater than the hypercritical pressure, a pressure great enough to ensure that the gas phase will retain all the salt that was initially dissolved in the liquid phase at a lower temperature. At hydrostatic conditions the hypercritical point for a dilute water containing about 2,000 mg/kg total dissolved solids would be at about 700 °C at a depth of 4.6 km, and for sea water it would be at about 900 °C at a depth of 12.9 km.

INTRODUCTION

Studies of fluid inclusions in minerals from fossil hydrothermal systems (Roedder, 1979) show that brines commonly occurred at different times and in different parts of those systems. Descriptions of brine-rich fluid inclusions that formed in hydrothermal systems associated with shallow intrusive rocks are presented in many articles, including Roedder (1971), Nash (1976), Eastoe (1978), Bodnar and Bean (1980), and Reynolds and Bean (1985). Brines may originate in many ways. Connate brines are encountered in many deep sedimentary basins (White, 1965), and the formation of brines by evaporation of closed basin lakes (Langbein, 1961; Hardie and Eugster, 1970; Eugster and Jones, 1979) and the interaction of meteoric water with evaporite deposits (White, 1968) are well documented. Relatively little attention, however, has been given to highly saline brines formed by the interaction of ordinary waters with hot rocks that do not contain evaporites (Bischoff and Pitzer, 1985; Fournier, 1985a). This paper stresses the importance of including information about brine evolution from dilute water, sea water, and magmatic gases in our conceptual models in order to approximate what may happen in natural magmatic-hydrothermal systems. Particular attention will be focused on the important effect that depth of magmatic intrusion has on the generation of highly saline brine from relatively dilute water of meteoric origin and from magmatic gases, and a generalized model will be presented for the evolution of a hydrothermal system within an oceanic volcano, such as at Hawaii.

ACKNOWLEDGMENTS

The manuscript benefited from thoughtful reviews by P.T. Delaney and J.L. Bischoff. I am particularly indebted to J.L. Bischoff and to K.S. Pitzer for making available to me draft copies

of their manuscripts dealing with experimental and theoretical aspects of the solubility of NaCl in steam. The information that they provided was of great value in deciding which data sets to use in those instances when the experimental data reported by different researchers were in conflict.

FLUID CIRCULATION AND HEAT TRANSFER IN MAGMATIC-HYDROTHERMAL SYSTEMS

It will be shown subsequently that the attainment of temperatures in excess of about 400 °C is generally a prerequisite for producing brines from dilute to moderately saline waters within convecting hydrothermal systems. Therefore, attention will be focused on the factors that are likely to limit the maximum temperature that is attained by a convecting fluid at hydrostatic pressure.

Models for fluid flow and heat transfer in hydrothermal systems have been discussed by many investigators, including Elder (1965), Bodvarsson and Lowell (1972), Lister (1974, 1980, 1983), Ribando and others (1976), Cheng and Minkowycz (1977), Cathles (1977, 1980, 1983), Norton and Knapp (1977), Norton and Knight (1977), Norton (1978, 1984), Parmentier and Spooner (1978), Torrance and Sheu (1978), Fehn and Cathles (1979), Norton and Taylor (1979), Hartline and Lister (1981), Knapp and Norton (1981), Hardee (1982), and Sleep (1983). One of the most important parameters in these models is permeability, which is generally assumed to have a constant value, or to change uniformly in response to a variable, such as time or temperature. In natural hydrothermal systems permeability is likely to change nonuniformly and even to fluctuate during the life of the system. Processes that tend to increase permeability are faulting (brittle fracture), thermal cracking upon cooling, hydrofracturing, and dissolution of minerals. Processes that tend to decrease permeability are quasi-plastic flow, precipitation of minerals, and thermal expansion of rock. All of these processes must be taken into account in our models.

Several factors influence whether a rock deforms by brittle fracture or quasi-plastic flow, including the inherent strength of the rock, depth of burial (confining pressure), temperature, state of stress, and the rate of loading (rate of change of stress). Brittle, stiff materials are able to accommodate increasingly large stress differences until their strength is exceeded and they fail by fracture. Relatively plastic, compliant materials are unable to accommodate large stresses because they deform in response to relatively small increases in stress difference. As rocks are heated and subjected to greater confining pressure, they tend to exhibit a more ductile response to increased stress difference. The situation is complicated, however, because at a given temperature some materials deform by quasi-plastic flow when the rate of loading is slow and by brittle fracture when the rate of loading is rapid (Lama and Vutukuri, 1978). Thus, a relatively fast rate of change of stress may result in brittle fracture and increased permeability, whereas, at the same temperature, a relatively slow rate of change of stress may lead to quasi-plastic deformation and a decrease in porosity and (or) increase in pore-fluid pressure.

The maximum depths of earthquake foci probably give a good indication of the depth at which quasi-plastic flow limits the downward penetration of ground water above relatively shallow magmatic bodies that are still hot. At Yellowstone National Park, information is available about earthquake focal depths and the maximum temperature likely to be attained by the hydrothermal system that convects to the surface (Fournier and Pitt, 1985). Well-located earthquakes seldom exceed about 4 km depth beneath the Yellowstone caldera but are much deeper outside the caldera. Chemical geothermometers, mixing models, and phase relations in the system $NaCl-H_2O$, indicate that the maximum temperature likely to be attained by the hydrothermal system is 350–430 °C (Fournier and Pitt, 1985). Based on temperature profiles calculated from heat-flow data for several localities in the Western United States and earthquake focal depths at those same locations, Smith and Bruhn (1984) conclude that the temperature at which deformation changes from frictional (brittle fracture) to quasi-plastic flow commonly ranges from about 300–450 °C. Also, self-sealing by precipitation of quartz and other minerals is likely to occur in the temperature range 350–500 °C when solutions are heated at constant pressure (Fournier, 1977, 1983a, 1983b; Sleep, 1983). Thus, permeability reduction by physical and chemical processes becomes increasingly important at temperatures above about 350 °C.

Those rocks situated at depth and in close proximity to a magma probably are at too great a temperature to sustain the large stress differences necessary to induce significant fracturing and faulting. Where fracturing has occurred in rocks at temperatures above about 350–450 °C, quasi-plastic deformation is likely to close those fractures within a relatively short time. Therefore, in most magmatic-hydrothermal systems convecting thermal waters at hydrostatic pressure probably are separated from magma by a region of hot rock that deforms quasi-plastically.

The above considerations lead to a model of a magmatic-hydrothermal system in which thermal energy is transferred mainly by conduction from very hot rock or magma to hydrostatically pressured circulating water. Minor additional heat is transferred by flow of fluids evolved from the crystallizing magma. The schematic depth-temperature profile shown in figure 55.1 represents a situation in which most of the fluid flow is restricted to a few relatively permeable channels, and the base of the convecting hydrothermal system (point B) is above the magmatic body (a simplified representation of real magmatic-hydrothermal systems in which convective flow of heated fluid is likely to occur at the sides as well as the tops of hot intrusive bodies). The temperature gradient for conductive heat flow from magma or hot impermeable rock is shown by line MB. Upward-flowing fluid in the convection system transfers heat relatively efficiently, and eventually temperatures along the flow path may approach an adiabatic profile (from B to A). If the temperature at point B is less than the critical temperature, point C, the adiabatic profile is nearly isothermal (line BA). The upper limit of the nearly isothermal region is set by the boiling-point curve. The position of the boiling-point curve is determined mainly by the location of the water table and the salinity and gas content of the particular fluid in the system.

In summary, quasi-plastic flow and mineral deposition generally prevent flow of water at hydrostatic pressure through rock at temperatures above 350–450 °C. However, where there are steep thermal gradients and a relatively rapid rate of change of stress, such as where magma is rapidly injected from a deep environment into a more shallow environment, brittle deformation of rock may occur at temperatures in excess of about 450 °C. Ground water at hydrostatic pressure may flow into and through these fractures and become heated to very high temperatures, possibly flashing in great part to steam. However, this situation should persist for only a very short time before quasi-plastic flow and mineral deposition limit additional fluid circulation to temperatures below about 450 °C.

BEHAVIOR OF CHLORIDE-RICH SALINE SOLUTIONS IN HYDROTHERMAL SYSTEMS

The following discussion is based on the experimentally determined behavior at hydrothermal conditions of the system NaCl-H_2O (Keevil, 1942; Ölander and Liander, 1950; Copeland and others, 1952; Sourirajan and Kennedy, 1962; Khaibullin and Borisov, 1966; Hilbert, 1979; Galobardes and others, 1981; Parisod and Plattner, 1981; Gunter and others, 1983; Bodnar and others, 1985; Bischoff and others, in press), NaCl-KCl-H_2O (Ravich and Borovia, 1949), and sea water (Bischoff and Rosenbauer, 1984, 1985; Bischoff and Pitzer, 1985). In related articles (Fournier, 1983b; 1985a), the pressure-temperature-composition relations in the system NaCl-H_2O given by Sourirajan and Kennedy (1962) were used as a basis for constructing a model for the behavior of saline solutions in hydrothermal systems. Results of recent experimental studies (Bischoff and Rosenbauer, 1984, 1985; Bodner and others, 1985; Bischoff and others, in press) and theoretical modeling of the thermodynamics of the behavior of NaCl in steam (Pitzer, 1983; Pitzer and Li, 1984; Pitzer and Pabalan, in press) and in mixtures of H_2O and CO_2 (Bowers and Helgeson, 1983) show that the Sourirajan and Kennedy (1962) results for the solubility of NaCl in steam are probably considerably in error at temperatures above 400 °C. For example, the isopleth of 0.4 weight percent NaCl dissolved in steam in pressure-temperature space according to the data of Sourirajan and Kennedy (1962) is compared in figure 55.2 to the same isopleth using the model of Pitzer and Pabalan (in press). Experimental data of Ölander and Liander (1950) are compatible with either isopleth, but the results reported by Bodner and others (1985) clearly favor the Pitzer and Pabalan model. In the remainder of this paper results of the Pitzer and Pabalan (in press) model for the solubility of NaCl in steam will be used.

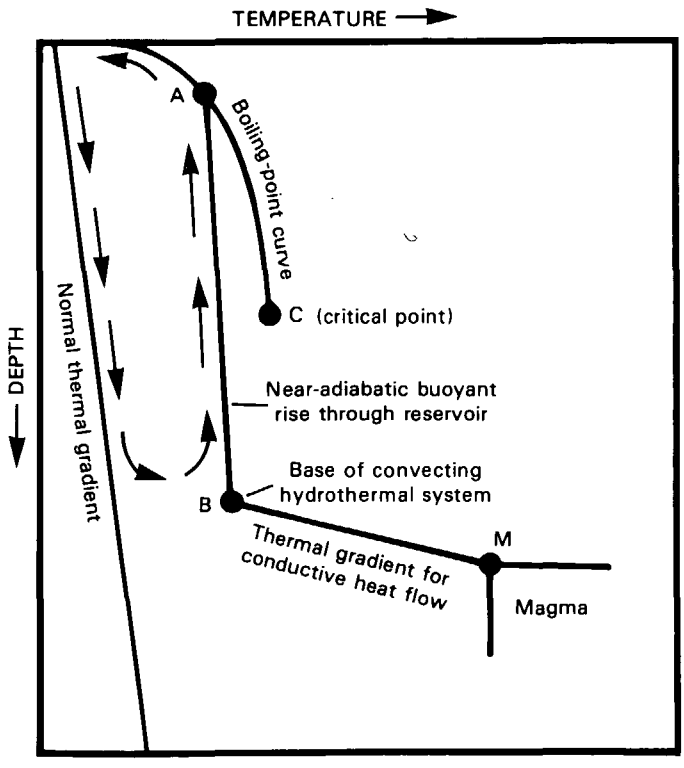

FIGURE 55.1.—Schematic depth-temperature profile for fluid flow (shown by arrows) restricted mainly to a few relatively permeable channels above magmatic heat source. Lettered points are discussed in text.

At a given depth and hydrostatic load (a given pressure) more saline solutions will boil at higher temperatures than less saline solutions, and the critical points of more saline solutions are encountered at higher temperatures and higher pressures (greater depths) than those of less saline solutions. Approximate boiling-point curves, extending to the critical points, for pure water and 10 and 25 weight percent NaCl solutions are shown in figure 55.3. Haas (1971) calculated boiling-point curves for water and various salt solutions of as much as 25 weight percent with an upper temperature limit of 330 °C. His results are slightly different from those shown in figure 55.3 because he assumed that hydrostatic pressure is controlled by the weight of the overlying column of boiling solution, thus correcting for changing density. The boiling-point curves shown in figure 55.3 were calculated with the assumption that the pressure-controlling column of solution has a constant density of 1. This assumption appears to be valid in some presently active hydrothermal systems (Fournier, 1983b). The physical reality appears to be that at given depths, fluid pressures within the hot part of the system are the same as fluid pressures in the surrounding cold part of the system. Lithostatic depths in figure 55.3 and subsequent figures were calculated using an average rock density of 2.5 kg/m^3.

Boiling-point curves for hydrostatic conditions are calculated relative to the position of the water table. In many places that water table is far below the Earth's surface. In other places, artesian systems are present in which the pressure-controlling water table is elevated in distant hills or mountains. In still other places, hot springs discharge onto the floors of lakes or the ocean, and boiling-point curves adjust to the overlying column of lake or ocean water. Thus, the 350 °C hot-spring waters discharging on the ocean floor at 21° N. on the East Pacific Rise (Edmond and others, 1979) are below boiling temperature because of their great depth.

The boiling-point curves in figure 55.3 show temperature-depth conditions at which liquids of given salinity will first start to boil. Upflowing solutions start to boil as a result of decompression when the boiling-point curve appropriate for the composition of the particular fluid is first attained. However, as soon as boiling starts, a slight departure from the initial boiling-point curve occurs because of the increase in salinity of the residual solution as boiling progresses. Adiabatic cooling that results from decompression of a relatively dilute solution, starting at temperatures less than the critical temperature, can result in a moderate increase in salinity, but will not result in the generation of a brine. For example, adiabatic decompressional boiling of a dilute solution that results in cooling from 370–100 °C will be accompanied by the conversion of about 64.9 percent of the initial liquid to steam (calculated from data in steam tables of Keenan and others, 1969), and the final residual solution at 100 °C will be about 2.85 times more concentrated in nonvolatile elements than the initial solution.

Isopleths of the solubility of NaCl in aqueous liquids in 10 weight percent increments from 0 to 90 weight percent projected onto a temperature-pressure diagram are shown in figure 55.4. These isopleths are boiling-point curves, but the depth axis is very uncertain because of the previously discussed limitations and the incorporation of significant amounts of salts other than NaCl into natural brines. A liquid-saturation curve (or a total evaporation curve) separates a field of gas plus solid salt (at lower pressures) from a field of gas plus liquid (at higher pressures). For the system $NaCl-H_2O$, the position of this liquid-saturation curve is fixed in temperature-pressure space and is independent of the initial proportion of NaCl and H_2O. For aqueous solutions containing mixed salts, the position of the liquid saturation curve in temperature-pressure space will depend on the nature of the salts that are present, and precipitation of some salts will likely take place within the gas plus liquid (brine) field. The short-dashed line in figure 55.4 shows the approximate position of the boundary separating fields of gas plus liquid and gas plus solid when the fluid contains a mixture of NaCl and KCl and the Na/K ratio in that fluid is appropriate for coexisting albite and K-feldspar (Orville, 1963). The salinity of the liquid phases steadily increases with increasing temperature along the liquid saturation curve (the gas + solid + liquid curve), whereas the salinity of the gas phase increases with increasing pressure. At salinities greater than about 30 weight percent the isopleths showing solubilities in the liquid phase originate at the liquid-saturation curve (the three-phase boundary that separates the field of gas plus solid salt from the field of gas plus liquid) and terminate at critical points (shown as dots for solutions with as much as 30 weight percent NaCl). The double-dot-dashed line (fig. 55.4) is the critical curve for the system $NaCl-H_2O$. The positions of all these curves move in temperature-pressure space as other salts are added to the system.

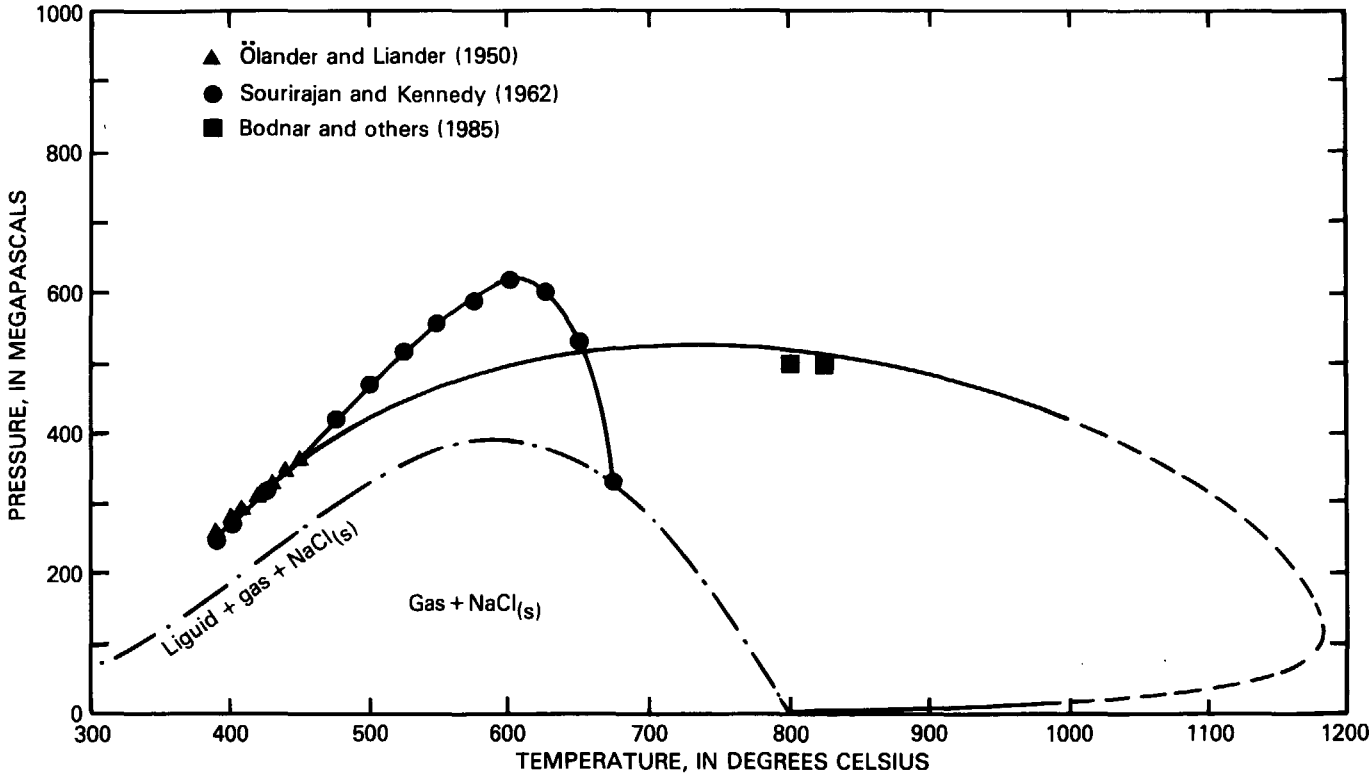

FIGURE 55.2.—Isoplethal pressure-temperature diagram for a vapor-phase composition of 0.4 weight percent NaCl in vapor + liquid region for $NaCl-H_2O$ system. Isopleth is drawn through Sourirajan and Kennedy (1962) data, and a contrasting position for that isopleth is shown using calculated solubilities according to Pitzer and Pabalan model (in press) for temperatures above 600 °C and connected smoothly to experimental data at lower temperatures. Dashed line is projected schematically beyond range of Pitzer and Pabalan model (redrafted from Pitzer and Pabalan, in press).

Boiling-point curves and critical points of solutions show only part of the important information that must be taken into account when modeling magmatic-hydrothermal systems. General phase relations exhibited by any chloride-rich solution of given salinity in temperature-depth space are shown in figure 55.5*A*. The solid line is a boiling-point curve for a solution of given salinity, ending at the critical point, C. Extending to greater depth (higher pressure) and higher temperature from the critical point is what may be thought of as a condensation-point curve for a gas that contains the same concentration of dissolved salt (an isopleth) that the initial liquid contained at subcritical temperatures and pressures. Along the condensation-point curve the gas is in equilibrium with a liquid that is much more saline than the gas, and the salinity of this liquid increases steadily and dramatically going from the critical point, C, through point H to point E. In this discussion, point H is called a "hypercritical" point (Fournier, 1985a). It marks the temperature and pressure at which a fluid of given salinity behaves according to what we normally think of as supercritical behavior; at greater pressures the fluid will not boil or condense upon heating or cooling. To the left of the dotted line that passes through point H the salinity of the gas phase decreases as temperature is increased at constant pressure. In contrast, the salinity of the gas phase increases with increasing temperature at constant pressure to the right of the dotted line.

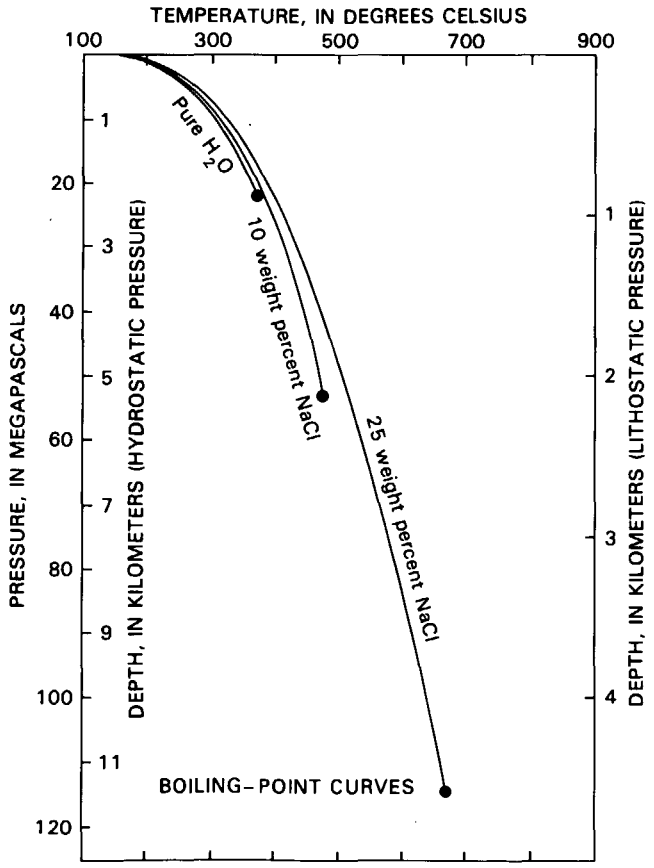

FIGURE 55.3.—Depth-temperature diagram showing approximate positions of boiling-point curves and critical points (dots) for pure water and 10 and 25 weight percent NaCl solutions.

Boiling-point and condensation-point curves are schematically shown in figure 55.5*B* for three compositions of fluid, equivalent to X, Y, and Z weight percent NaCl, such that X<Y<Z. The three boiling-point curves end at their respective critical points, C_x, C_y, and C_z. Gas of composition X is in equilibrium with liquid Y at point m, and liquid Z at point n. At point p gas of composition Y is in equilibrium with liquid Z. In actual water-salt systems, very large increases in salinity are generally required to increase the boiling point a few degrees at constant pressure, as shown in figure 55.4 for solutions up to about 30–40 weight percent dissolved NaCl. Isopleths of solubility of NaCl in steam (condensation-point curves) for salinities as great as 20 weight percent are shown in red in figure 55.6, and in figure 55.7 these isopleths are shown in red superimposed on figure 55.4. As previously noted, a rising fluid that intersects a boiling-point curve would become moderately more saline as a result of decompressional boiling with separation of steam, such as the fluid that follows path A in figure 55.5*A*. In contrast, hot rising fluids that follow a cooling path that is to the high-temperature side of the critical point so that the condensation-point curve is intersected, such as path B in figure 55.5*A*, will undergo a large increase in salinity. This will be discussed more fully later.

In summary, more saline solutions have boiling-point curves at higher temperatures and generally have critical points at much greater depths than less saline solutions. For a solution of given initial salinity, a condensation-point curve extending from the critical point to higher temperatures passes through a pressure maximum (the hypercritical point) and then loops back to intersect the liquid saturation curve at about the melting point of the pure salt (figs. 55.5*A*, 55.5*B*, 55.6, 55.7). The hypercritical point marks the temperature and pressure at which a fluid of given salinity will not boil or condense upon heating or cooling. The depths and temperatures at which these curves would be intersected in natural systems will vary greatly depending upon various hydrologic parameters and the nature of the dissolved salts and partial pressures of dissolved gases.

GENERATION OF BRINES FROM DILUTE SOLUTIONS

Adiabatic decompression of a liquid, which causes its path in depth-temperature space to intersect the boiling-point curve at a temperature below the critical temperature, is likely to result in only a moderate salinity increase. However, if the cooling path of an ascending fluid brings it into the gas plus liquid field at a temperature greater than the critical temperature, a highly saline solution (brine) will condense from that ascending fluid. The NaCl concentrations of liquids (brines) that will condense from two fluids, one containing 0.2 weight percent NaCl and the other 3.2 weight percent NaCl, that intersect condensation-point curves at various temperatures as a result of decompression are shown in figure 55.8.

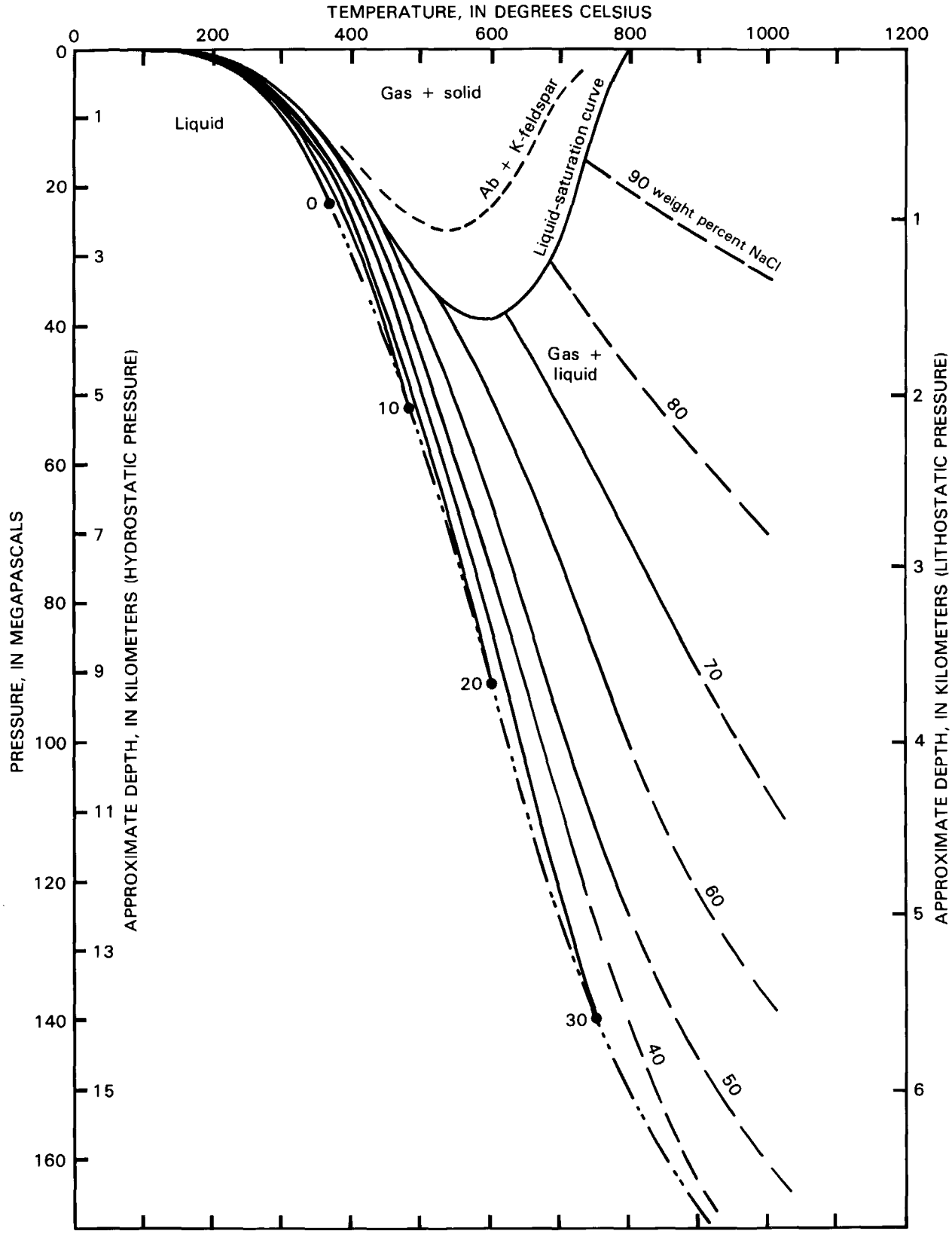

FIGURE 55.4.—Isopleths of solubility of NaCl in water in 10 weight percent increments (boiling-point curves with approximate depths for hydrostatic pressure (fluid density = 1) and lithostatic pressure (rock density = 2.5). Double-dot-dashed line is critical curve. Liquid saturation curve is 3-phase boundary for the system NaCl-H_2O, and short-dashed line shows approximate position of liquid saturation curve for system NaCl-KCl-H_2O with Na/K ratios in liquid fixed by base exchange between albite and K-feldspar. Long dashes indicate inferred positions of curves.

A brine containing about 10 weight percent NaCl will condense from the 0.2 weight percent NaCl fluid when the condensation-point curve is intersected at a temperature of about 390 °C, and a 20 weight percent NaCl brine is generated when the condensation-point curve is intersected at about 410 °C (fig. 55.8). However, the mass of brine that forms will be small relative to the mass of coevolving, relatively dilute vapor. Because the brine has a much higher density than that of the initial fluid, the brine might counter-flow downward and accumulate in pockets or near the bottom of the hydrothermal system. Therefore, with prolonged circulation of hot fluid through the system, brine may come to fill the few fractures that are present at the base of the hot part of the convection system, bounded by hot, dilute fluid above and relatively cold water and (or) hot impermeable rock at the sides.

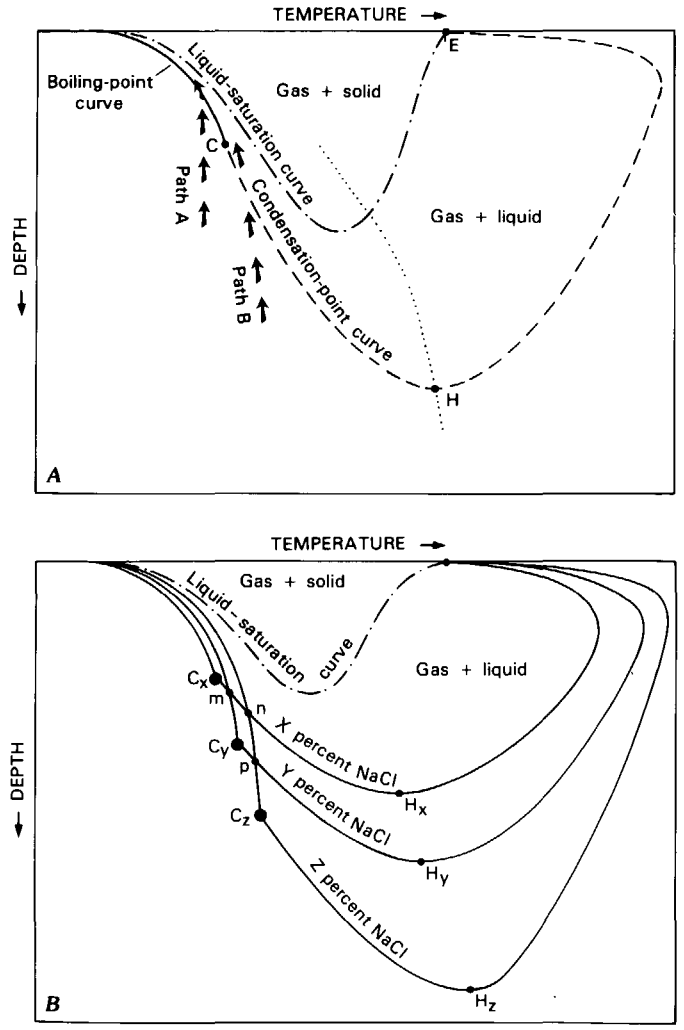

FIGURE 55.5.—Depth-temperature diagrams showing generalized phase relations. ***A***, Chloride-rich aqueous solutions at constant composition. ***B***, Three different compositions, X, Y, and Z, with X<Y<Z. Critical points for respective solutions are at C, C_x, C_y, and C_z, and hypercritical points are at H, H_x, H_y, and H_z. Dotted line and other points are discussed in text.

At given temperatures, less saline brines are generated when sea water intersects the condensation-point curve (fig. 55.8), and the intersection occurs at greater depths than for more dilute solutions. But, a larger proportion of brine is generated from sea water than from the same initial mass of a more dilute solution. The generation of brine by adiabatic decompression of sea water at temperatures above the critical point is nicely shown by Bischoff and Pitzer (1985).

In the above models brines form as a result of decompression, utilizing thermal energy contained in rising, relatively dilute fluids. Dilute fluids also may be converted to brines by prolonged boiling, utilizing thermal energy stored in hot rock to evaporate the waters. One way to accomplish this conversion is to quickly lower the hydrostatic pressure so that the boiling-point curve appropriate for the salinity of the local ground water is shifted to lower temperatures at given depths. This process might occur as a result of sudden draining of a lake or an explosive volcanic eruption. With decreasing hydrostatic pressure at any given depth, as would occur with a drop in the local ground-water table (from L1 to L2 in fig. 55.9), the boiling-point curve would shift (from A to B). Waters that were initially on or to the left of the boiling-point curve A (point C, fig. 55.9) will move into the field of gas (steam). In response to the decrease in hydrostatic pressure, the water will boil vigorously, either to dryness or until the surrounding rock temperature decreases and the salinity of the solution increases to the extent that the ground water (point D, fig. 55.9) lies on a new boiling-point curve (curve E) appropriate for the new pressure, temperature, and salinity. Small amounts of brine that form in this manner could become trapped in fluid inclusions that would give a false impression of the presence of a large convecting brine system. If the permeability of the rock is relatively low, so that the newly formed steam cannot expand and push pore fluids from the rock fast enough to prevent a large pressure increase, and if the resulting steam pressure is greater than the confining pressure, a hydrothermal explosion may occur (Muffler and others, 1971).

In volcanic environments, magma may be injected into wet rocks, causing vigorous boiling and pore-pressure buildup (Delaney, 1982). Boiling, utilizing heat stored in rock, also may occur where newly formed fractures allow water to come into contact with previously hot, dry rock. However, the quantity of brine that forms in this manner may be relatively small, either because little fluid flows through a system with low initial or rapidly decreasing permeability or because a rapid rate of flow of fluid through the system decreases the temperature of the fluid-rock interface to a value that is too low for brine to form. A decrease in temperature at the fluid-rock interface is expected because the formation of steam is likely to consume thermal energy faster than thermal energy can be transferred through rock by conduction. Thermal cracking, however, may cause new fractures to form, allowing the solution to again come into contact with rock hot enough to cause vigorous boiling.

In summary, large amounts of brine are likely to form from dilute solutions only where prolonged circulation occurs through very hot rock. This circulation is likely to occur mainly where there have been multiple injections of magma into already hot rock at moderate to shallow depths (about 2–7 km). The process of generation of

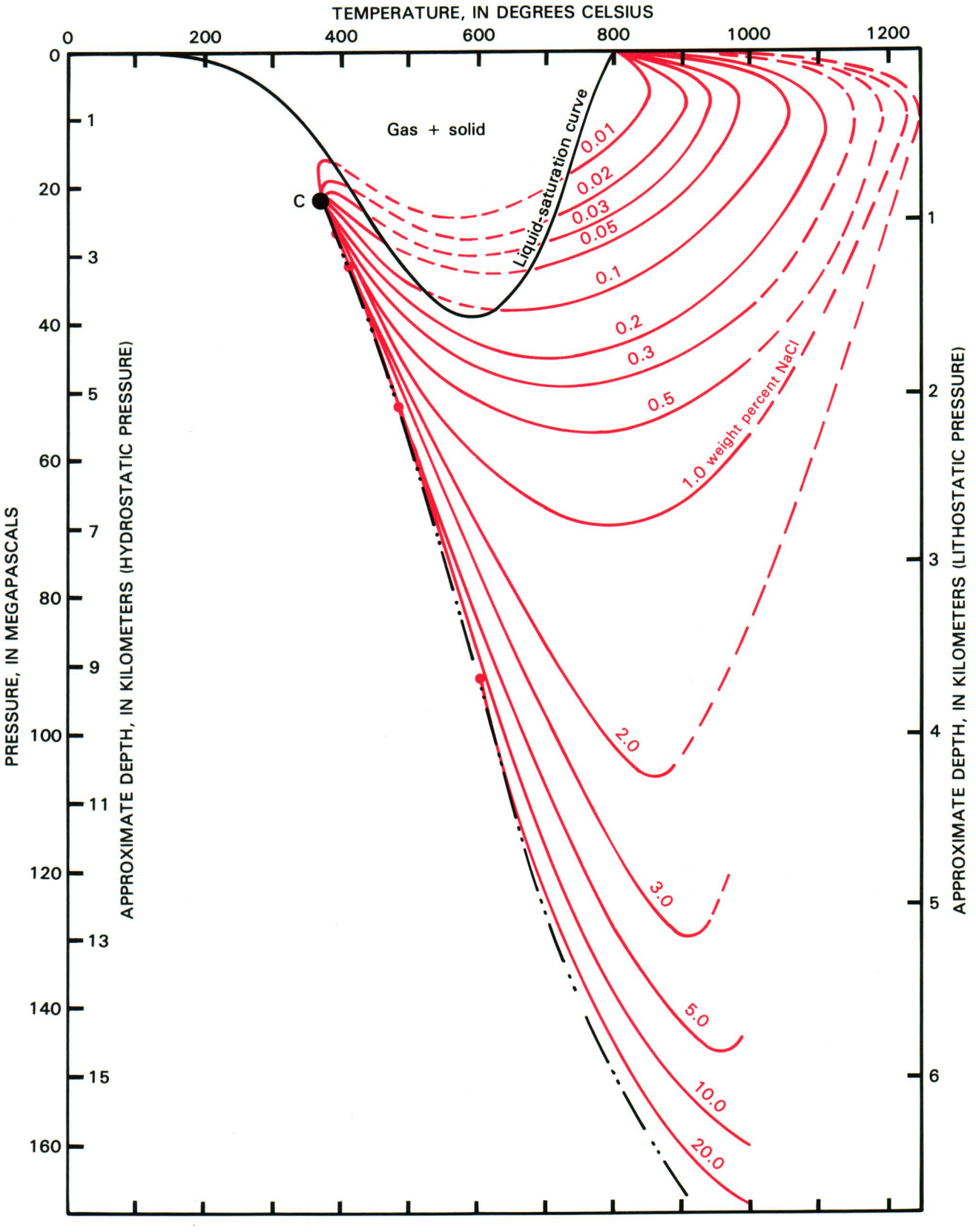

FIGURE 55.6.—Isopleths of solubility of NaCl in steam (red lines) with approximate depths for hydrostatic pressure (fluid density = 1) and for lithostatic pressure (rock density = 2.5). Double-dot-dashed line (black) is critical curve with origin at critical point of pure water (black dot). Critical points of selected salt solutions, red dots. Liquid-saturation curve (black) is 3-phase boundary for system NaCl-H_2O.

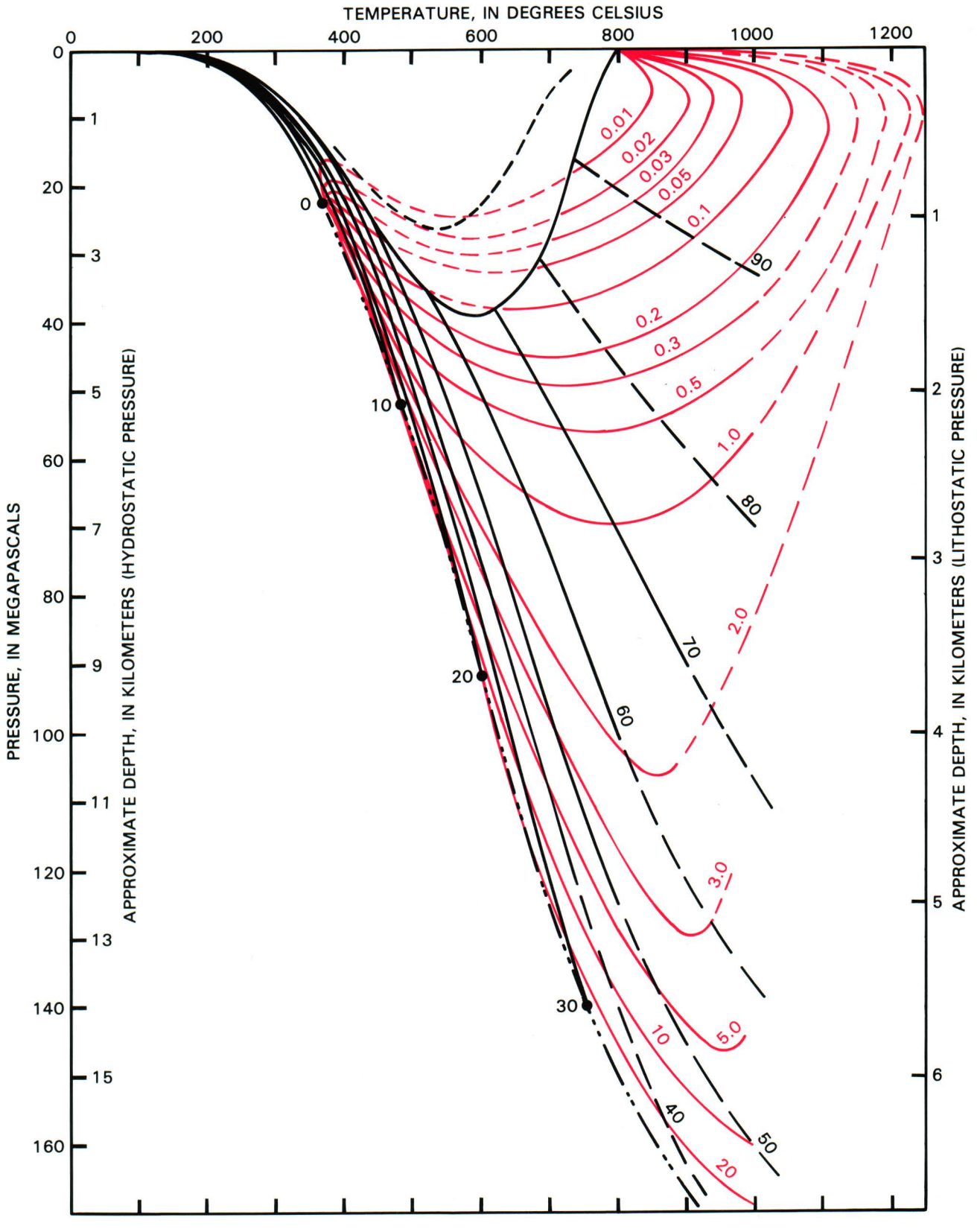

FIGURE 55.7.—Isopleths of solubility of NaCl in steam (red lines, see fig. 55.6) superimposed on isopleths of solubility of NaCl in water (black lines, see fig. 55.4).

hypersaline brines is greatly aided when the initial solution is moderately saline, such as sea water, because a given amount of a fluid that has a greater initial salinity will produce a larger mass ratio of brine to gas than will a less saline fluid.

BRINE EVOLUTION AND HYDROTHERMAL ALTERATION RELATED TO DEPTH OF MAGMATIC INTRUSION

The depth of intrusion of a magmatic body and the salinity of the ground water that enters the hydrothermal system are important in regard to brine evolution and the type and intensity of hydrothermal alteration that is likely to be associated with that intrusion. These depth-temperature-phase relations will be illustrated by comparing and contrasting a relatively dilute, chloride-rich solution containing 2,000 mg/kg total dissolved solids (TDS) to sea water. Sea water can be modeled by a 3.2 weight percent NaCl solution at high temperatures because most of the sulfate and magnesium precipitate upon heating (Bischoff and Rosenbauer, 1985).

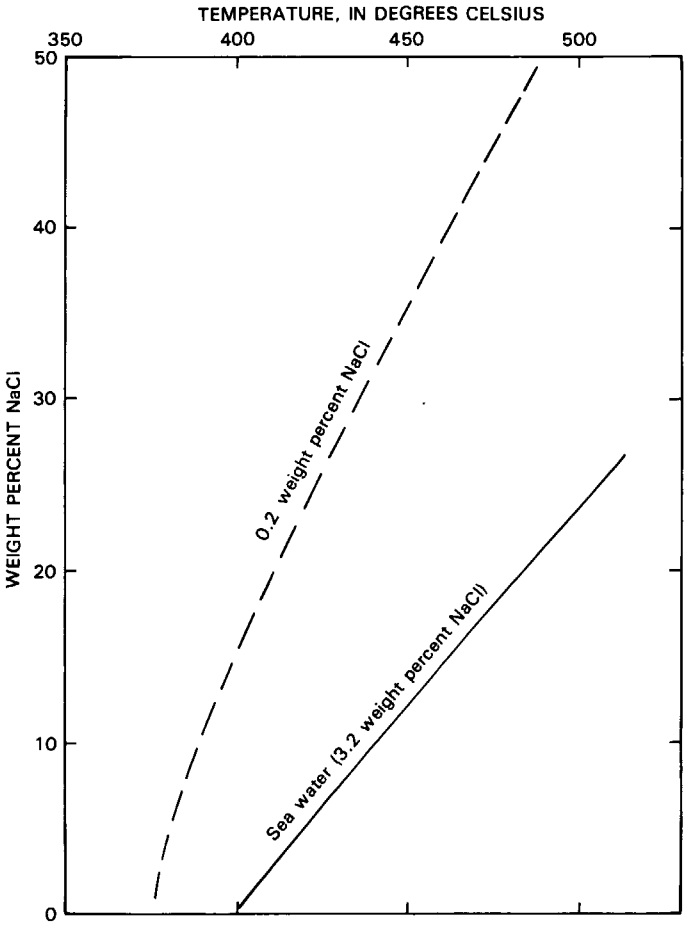

FIGURE 55.8.—Concentrations of NaCl in liquids that will condense from 0.2 weight percent NaCl and 3.2 weight percent NaCl when condensation-point curves are intersected at various temperatures as a result of decompression.

Approximate positions in depth-temperature space of the boiling-point curves, condensation-point curves, critical points (C_2 and C_s), and hypercritical points (H_2 and H_s) for the 2,000 mg/kg TDS solution and sea water, respectively, are shown in figure 55.10. The 2,000 mg/kg NaCl solution has a critical point near 375 °C at about 23 MPa and a hypercritical point at about 700 °C at 46 MPa. In contrast, the sea water has a critical point near 405 °C at about 30 MPa and a hypercritical point at about 900 °C at 129 MPa. The dashed parts of the condensation-point curves are beyond the range of experimental data and the Pitzer and Pabalan (in press) model. The position of the saturation curve in figure 55.10 is poorly constrained and is greatly dependent on the relative proportions of cations in the solution. The liquid saturation curve for the binary system NaCl-H_2O is shown by the dot-dashed line, and

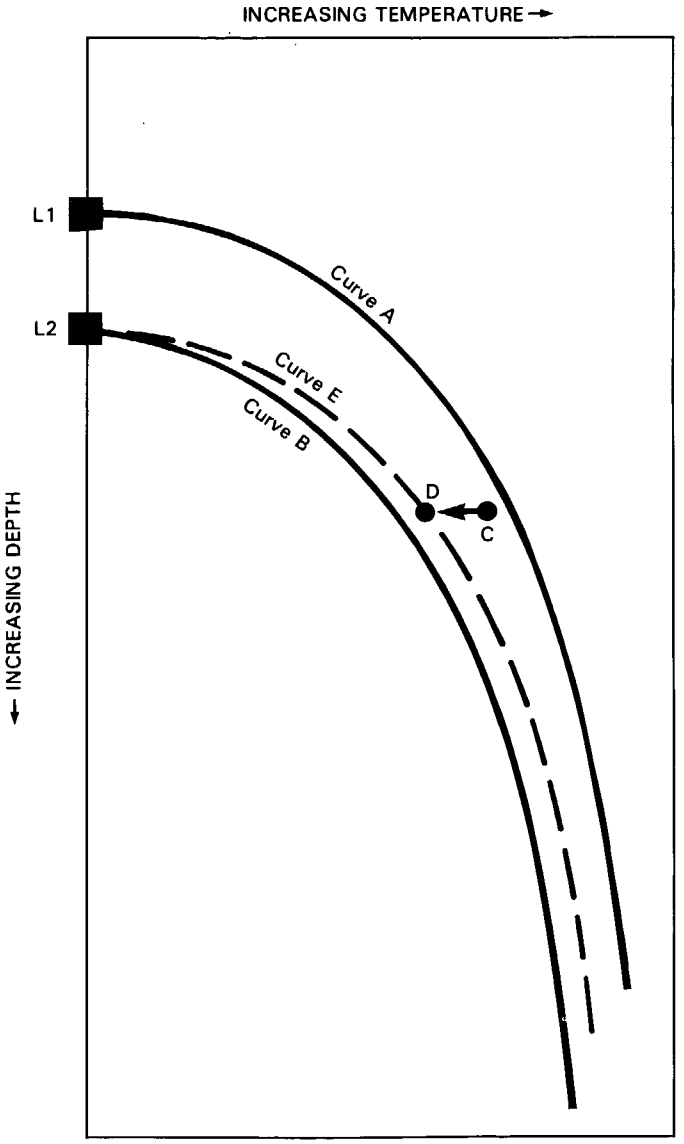

FIGURE 55.9.—Boiling-point curves related to elevation of water table. Lettered points and curves are discussed in text.

the double-dot-dashed line shows the saturation curve for the ternary system NaCl-KCl-H_2O with the Na/K ratio fixed by base exchange between albite and K-feldspar, calculated using the data of Ravich and Borovia (1949) and Orville (1963).

The schematic depth-temperature relations for a relatively early stage of development of a hydrothermal system associated with a body of magma that has been intruded to a depth of 6 km are shown in figure 55.11. The heat source has a temperature of about 800 °C (appropriate for a silicic system). A basaltic heat source could have a temperature well above 1,000 °C. Fluid flow at hydrostatic pressure (shown schematically by arrows in fig. 55.11) is assumed to be controlled by a few well-developed fractures, and temperatures in the convecting hydrothermal system are assumed to be representative of those in the fractures where the maximum rate of fluid flow occurs. The temperature gradient from the heat source to the convecting hydrothermal system is very steep (there has been insufficient time to heat much surrounding rock by conduction), and the hydrothermal system is not well developed. Because the surrounding rock was relatively cool (at a normal or slightly above normal geothermal gradient) prior to the intrusion of the magma, the convecting fluid is in the process of heating the rock adjacent to the channels that control fluid flow, and the rock, in turn, is conducting heat away from the fluid. The maximum fluid temperature of 450 °C, (fig. 55.11) is appropriate for a steady-state situation in which mineral deposition and quasi-plastic deformation have closed off permeability in rocks at higher temperatures. The sudden opening of new fractures adjacent to magma could allow fluid to move into those fractures and become heated to temperatures significantly above 450 °C, resulting in marked fluid expansion. If the expansion of the fluid does not lead to further rupturing of the rock (possibly explosively) and a decrease in fluid pressure thereafter, the expanded 2,000 mg/kg fluid would not undergo a phase change because the pressure at a depth of 5–6 km is greater than the hypercritical pressure; the gas plus brine field would not be entered. In contrast, if flow into new fractures at a depth of 5–6 km allowed sea water to be heated at hydrostatic pressure to temperatures above 450 °C, brine and gas would form as soon as the temperature exceeded about 480 °C (fig. 55.11), and the first brine generated would contain about 19 weight percent NaCl (fig. 55.8).

Given time, a larger portion of rock adjacent to the intrusive becomes heated conductively while the intrusive crystallizes and cools (fig. 55.12). The hydrothermal system heats the rock adjacent to the channels of main fluid flow to the point where the ascending fluids cool mainly by adiabatic decompression, while the fluids in less open channels cool by conduction. The maximum temperature attained by the convecting fluid in figure 55.12 is shown to be less than that in figure 55.11 because mineral deposition and quasi-plastic deformation are assumed to have slowly excluded fluid flow

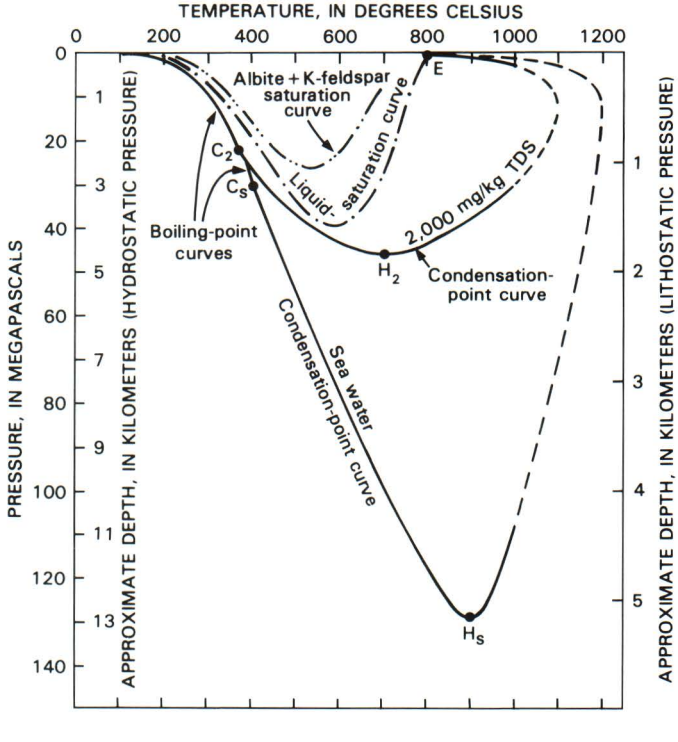

FIGURE 55.10.—Approximate positions in depth-temperature space of boiling-point and condensation-point curves for chloride-rich solution containing 2,000 mg/kg salt (about 0.2 weight percent NaCl) and sea water (about equivalent to 3.2 weight percent NaCl at high temperatures). Critical points are at C_2 and C_s and hypercritical points are at H_2 and H_s, respectively. Liquid-saturation curve and curve labeled Albite + K-feldspar are same as in figure 55.4.

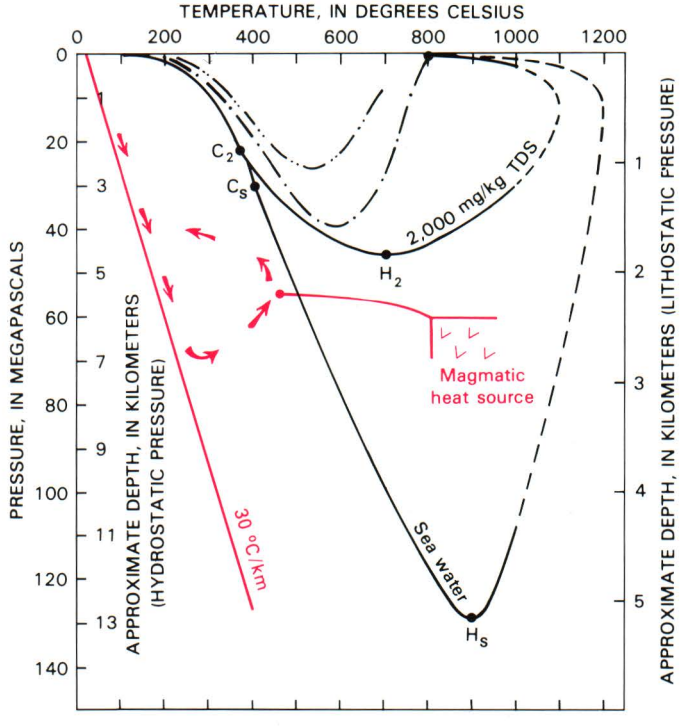

FIGURE 55.11.—Schematic depth-temperature relations (shown in red) for relatively early stage of development of hydrothermal system associated with body of magma that has been intruded to depth of 6 km below water table, superimposed on figure 55.10 (shown in black).

from portions of rock where flow had previously occurred at higher temperatures. In contrast to the situation shown in figure 55.11, renewed fracturing within hot, previously impermeable portions of rock will not result in the formation of brine during inflow of sea water because temperatures are too low for the gas plus brine field to be encountered (figs. 55.8, 55.12).

A situation in which a later magmatic body intrudes an older, partly cooled magmatic body at a depth of about 6 km is shown in figure 55.13. The younger magma injects into rock that was preheated by the previous intrusion, and the hydrothermal system in the vicinity was already well established. Also, in the intrusive process, new fractures are likely to form, allowing fluid to re-enter rock that had previously become essentially impermeable through mineral deposition and slow quasi-plastic deformation. In this situation, as the fluids convect upward there is a good chance that both the dilute solution and sea water would enter the gas plus brine field to the right of their respective critical points (points C_2 and C_s). In that event, highly saline brines would form by condensation (disproportionation of the initial fluid into a small volume of highly saline liquid and a much larger volume of less saline gas), as previously discussed and shown in figure 55.8. If the relatively dense brine that forms by condensation accumulates in pockets or at the base of the hydrothermal system, important consequences in regard to ore deposition would occur because the chloride-rich brine would scavenge metals from the surrounding rock, and these metals would then be localized and available to combine with sulfur that is released by still-crystallizing magma (Fournier, 1983b).

Intrusions that penetrate to less than about 3–4 km and that attain temperatures above about 400 °C are likely to have associated hydrothermal systems that extend into the field of gas plus liquid, and possibly into the field of gas plus solid salt (fig. 55.14). Within the gas plus solid salt field, acid gases are likely to be generated by the hydrolysis of salts (Fournier, 1985a, 1985b),

$$NaCl + H_2O = NaOH + HCl \quad (1)$$

$$CaSO_4 + 2H_2O = Ca(OH)_2 + H_2SO_4. \quad (2)$$

The hydroxides react with silicates to form a variety of alteration products, including epidote, albite, and chlorite,

$$3CaAl_2Si_2O_8 + Ca(OH) = 2Ca_2Al_3(SiO_4)_3(OH), \quad (3)$$

and

$$2CaAl_2Si_2O_8 + 6MgSiO_3 + NaOH + 4H_2O = NaAlSi_3O_8 + Ca_2Al_3(SiO_4)_3(OH) + Mg_6Si_4O_{10}(OH)_8. \quad (4)$$

The hydrolysis of salts, yielding acidic gases, becomes increasingly important at lower pressures. Therefore, acid alteration is likely to be far more abundant in and around shallow intrusive igneous rocks than deeper intrusive igneous rocks.

Most potassic alteration probably is the result of decreasing temperature that favors the exchange of dissolved K for Na in

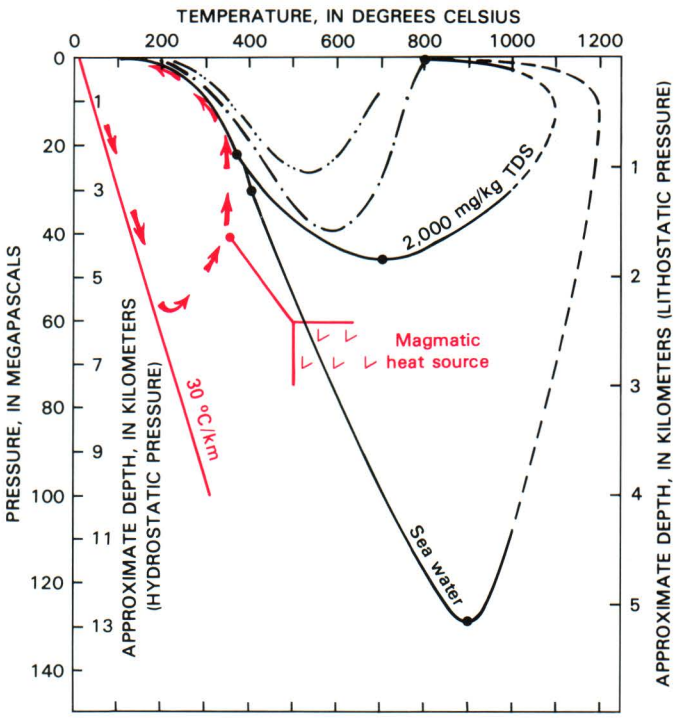

FIGURE 55.12.—Schematic depth-temperature relations (shown in red) for a relatively late stage of development of hydrothermal system associated with body of magma that has been intruded to depth of 6 km below water table, superimposed on figure 55.10 (shown in black).

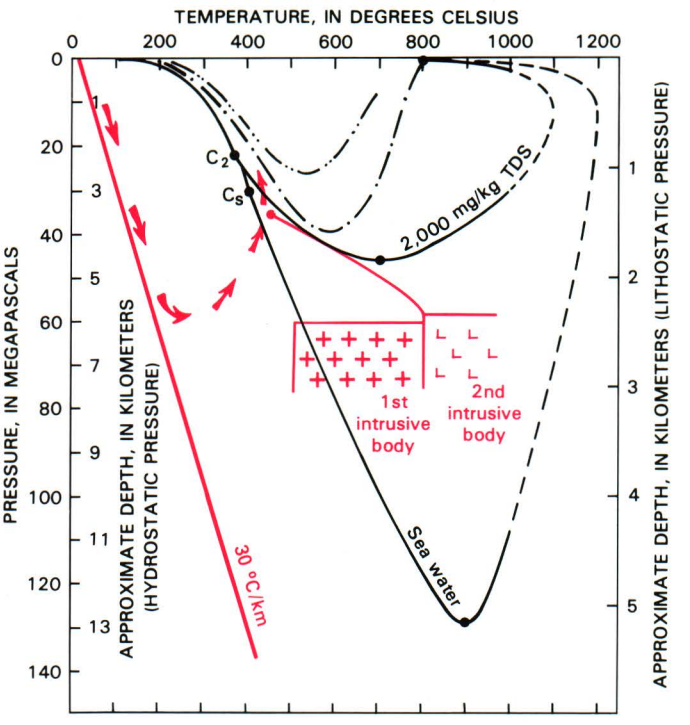

FIGURE 55.13.—Schematic depth-temperature relations (shown in red) for hydrothermal system where there have been multiple injections of magma to depth of about 6 km below water table, superimposed on figure 55.10 (shown in black).

feldspars and micas, so that as the rocks become more potassic, the solution becomes more sodic. However, under some circumstances potassic alteration also may result from a decrease in pressure (Fournier, 1976, 1983b). Within the field of gas plus brine, with decreasing pressure NaCl precipitates from solution before KCl, causing K exchange for Na in albite to maintain the required Na/K ratio in the aqueous solution for chemical equilibrium with the coexisting feldspars. After all the available albite is converted to K-feldspar by base exchange, the solution can become richer in potassium relative to sodium (by continued precipitation of NaCl with decreasing pressure), and the boundary of the gas plus solid region shifts toward lower pressures. Where there is no boiling of liquids or condensation of gas, the hydrothermal alteration products at temperatures of 300–500 °C are likely to be predominantly quartz, albite, K-feldspar, epidote, chlorite, and amphibole, with minimal acid and potassic alteration.

In summary, at a depth of intrusion of 6–7 km, brines are not likely to form by boiling of dilute ground water or by condensation of relatively saline gas unless there are special circumstances, such as repeated magmatic intrusions that preheat the surrounding rock and repeated fracturing of very hot rock that allows convecting water to become heated to temperatures above 450–500 °C. In contrast, brines are very likely to form by boiling of dilute ground water or by condensation of relatively saline gas where the depth of intrusion comes to within about 3 or 4 km of the surface, because the gas plus brine field is entered at a temperature less than 450 °C (fig. 55.14).

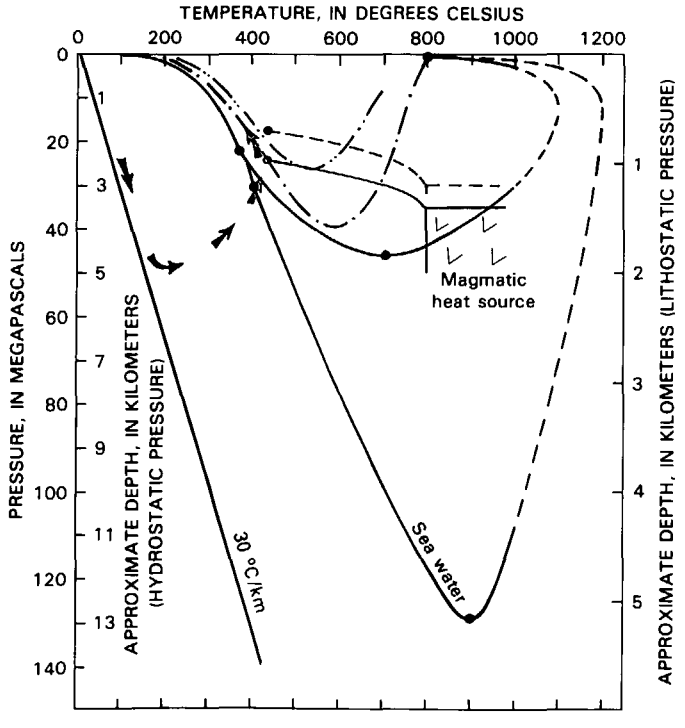

FIGURE 55.14.—Schematic depth-temperature relations (shown in red) for hydrothermal systems where depth of intrusion is within about 3–3.5 km below top of water table, superimposed on figure 55.10 (shown in black). See text for discussion.

The above-mentioned depth ranges are very approximate because of variations of hydrostatic pressure that result from different elevations of the water table, different densities of the fluids, different partial pressures of dissolved gases, different positions of the phase boundaries (shown in figures 55.10–55.14) because of variations in composition of the dissolved salts, and the possible formation of vapor-dominated regions (White and others, 1971) within parts of some hydrothermal systems. Little increase in fluid pressure or temperature is expected from the top to the bottom of a vapor-dominated region, so the relations shown in figures 55.10–55.14 will be displaced downward by the thickness of any vapor-dominated zone. In oceanic volcanic systems that have not formed islands, the depth of intrusion is the depth below sea level and not the depth below the ocean floor.

HYDROTHERMAL ACTIVITY ASSOCIATED WITH OCEANIC VOLCANOES

Several differences exist between the hydrothermal systems that are likely to develop in and around a continental volcanic center and an oceanic volcanic center. One difference is in the composition and amount of magmatic water that separates from a crystallizing silicic magma compared to a basaltic magma (silicic magmas are richer in water and chloride as shown by their hydrous minerals and quenched glass compositions). More important differences are the greater hydrostatic pressure that will prevail during the early stages of formation of an oceanic hydrothermal system and the fact that the oceanic systems are recharged by an abundant supply of sea water. In contrast, the abundance and composition of recharge water in continental systems is extremely variable.

The hydrothermal systems that develop within volcanic edifices that are built upon the sea floor, such as the Hawaiian Islands, are likely to have complex histories. The old sea floor is about 5 km below sea level near Hawaii. Therefore, extrusion of lava at a new volcanic center on that sea floor brings magma into contact with sea water at a pressure such that brine (equivalent to about 20 weight percent NaCl) plus vapor forms only at temperatures above about 480 °C (figs. 55.8 and 55.10). However, that hot brine is likely to have a density less than about 0.7 kg/m^3, which is considerably less than that of the surrounding cold sea water, so both the vapor and the brine will rise and mix with the overlying cold water. Rapid chilling of the surface of the magma and a relatively slow transfer of heat by conduction to the interface with convecting sea water is likely to restrict brine formation to a very short time. Compositionally stratified layers of brine may develop by double-diffusive convection (Huppert and Turner, 1981; Huppert and Sparks, 1984; Vitagliano and others, 1984) in the ocean water above the heat source, but these brine layers are likely to be very transient.

Beneath the sea floor, heating of pore water to temperatures greater than 500–650 °C may occur over a significant period of time where magma is repeatedly injected to relatively shallow levels. Heating sea water to above 500 °C will cause a brine with more than 20 weight percent dissolved salt plus relatively dilute gas to form at a depth of about 0.5 km beneath the sea floor (about 5.5 km beneath the ocean surface, fig. 55.10). At a depth of 4 km beneath the sea

floor (9 km beneath the ocean surface) temperatures in excess of 650 °C are required to form highly saline brine from sea water. The gas component may convect all the way up to the sea floor, cooling, condensing, and mixing with pore water as it rises. The pore water may be sea water or previously condensed gas that contains low to moderate chloride and is rich in carbonate and sulfate, owing to water-rock reactions involving CO_2, SO_2, and H_2S. The brine component will first rise, but then as it cools its density will increase to the point that buoyant upflow will stop. Double-diffusion convection may result in compositionally stratified zones of water above and to the sides of the magmatic heat source. In response to double-diffusion convection, the densities of the hot, saline fluids will adjust and become essentially the same as the densities of the cold, surrounding pore fluids (sea water) at the same depths.

The above scenario assumes that the permeability is great enough that fluid expansion caused by heating of pore water can be accommodated by convective flow of fluid away from the hot part of the system without a hydrothermal explosion (Delaney, 1982), yet low enough that the magma-fluid interface will not be quickly quenched to below 500–650 °C by convecting water. The major factors that limit the amount of brine (greater than 3.2 weight percent NaCl equivalent) that forms are the size, depth, shape, and temperature of the heat source and the total amount and rate of movement of sea water through the system. The rate of movement is likely to slow with time because permeability is decreased by the formation of hydrous alteration products after volcanic glass, by precipitation of sulfate from sea water as it is heated at the inflow part of the system, by precipitation of silica, sulfides, and other minerals at the outflow part of the system, and by quasi-plastic flow of rock at high temperatures.

Decker (chapter 42) noted that the shallow magma chambers beneath Kilauea and Mauna Loa Volcanoes are both at a depth of about 3 km below the respective summits. He concluded that "The long term process of evolution of Hawaiian volcanoes apparently involves progressively upward remelting, stoping, and (or) shoving aside of the rocks which overlie the shallow magma reservoir systems." With the assumption that a 3-km depth to the top of a shallow magma reservoir is approximately maintained from the time a Hawaiian-type volcanic edifice starts to build on the sea floor through the period of island growth, some generalities can be made about the probable associated hydrothermal system.

With the start of volcanic activity the shallow magma chamber would be about 8 km below sea level, and sea water is converted to highly saline brine and gas only at temperatures above about 625 °C at that depth. Very little sea water is likely to become heated to that temperature. As the volcanic pile gets larger and the magma chamber rises, the temperature at which sea water in the vicinity of the magma chamber is converted to highly saline brine and gas decreases, and the likelihood of sea water attaining that temperature increases. The shallowest depth below sea level at which brine will condense from fluid of sea-water salinity is about 3 km at a temperature of about 405 °C (the critical point for a 3.2 weight percent NaCl solution, fig. 55.10). At lower temperatures and pressures the sea water will boil when heated. When the top of the volcanic pile comes close to sea level, the top of the shallow magma chamber may be close enough to the surface (about 3–3.5 km) for portions of the associated hydrothermal system to be heated to the point of complete evaporation (enter the gas plus solid region at temperatures above about 400–450 °C, as shown in fig. 55.14). The evolving gas (steam) will be very rich in acids (chloride as well as sulfur species), but will carry only minor dissolved salt.

The hydrologic situation changes somewhat after a volcanic island emerges from the sea, because meteoric water becomes available to enter the hydrothermal system. Rain water percolates through permeable lava into the ground and, by the Ghyben-Herzberg principle (Bates and Jackson, 1980), forms a lens of fresh water that floats upon saline water (fig. 55.15). In the Hawaiian Islands the head of fresh water above sea level generally increases at a rate of about 0.2 m/km (1 ft/mi) from the shore (Peterson, 1981). However, on the Island of Hawaii, to the east of Kilauea and south of Hilo, the head of fresh water rises at a rate of about 0.8 m/km (Davis and Yamanaga, 1973). When steady-state conditions exist (and volcanic heat is not a factor) the head of fresh water above sea level is balanced by a thickness of fresh water below sea level about 40 times as great (Peterson, 1981). Where volcanic heat is a factor, the position of the fresh water-saline water interface is likely to be considerably different from that predicted on the basis of normal thermal gradients, because the densities of dilute water, sea water,

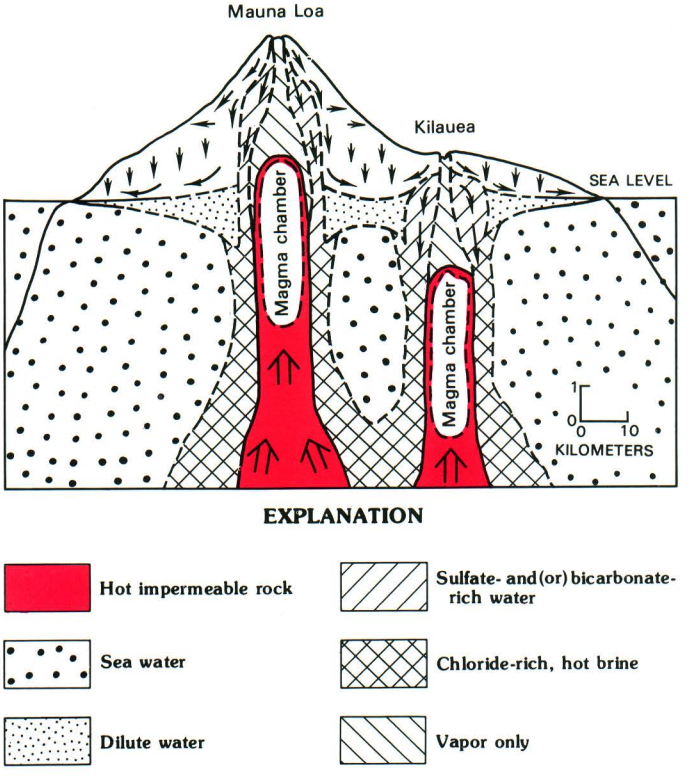

FIGURE 55.15.—Schematic diagram with vertical exaggeration showing shallow magma reservoirs and associated hydrothermal systems beneath Mauna Loa and Kilauea Volcanoes, Hawaii.

and highly saline brine decrease at different rates when heated. Also, hydrothermal alteration that decreases permeability occurs where ground water is heated and cooled. Therefore, the usual assumptions about densities and permeabilities that are made when calculating the elevation and thickness of the Ghyben-Herzberg lens will not be valid. In addition, ground water above shallow magma chambers will likely become rich in sodium sulfate (possibly also rich in bicarbonate) as a result of reactions involving volcanic gases and oxidation of sulfides in the rock. The boundaries between dilute water, sea water, sodium sulfate-rich water, steam, and chloride-rich brine are likely to be complex and transient, changing in response to heating when pulses of magma are injected into shallow reservoirs and when volcanic eruptions occur. Double-diffusive convection (Huppert and Turner, 1981) is likely to occur at these boundaries as a result of sharp thermal and salinity gradients.

Thin and discontinuous bodies of perched water are found within the volcanic edifice above the Ghyben-Herzberg lens, and perched streams flow through lava tubes. For simplicity, discontinuous bodies of perched water are not shown in figure 55.15. In the vicinities of volcanic eruptive centers, bodies of perched ground water may be fed in part from downward percolation of meteoric water and in part from condensation of steam rising from below.

The top of the shallow magma reservoir beneath Kilauea is about 2 km below sea level, and sea water (chemically changed in response to water-rock reactions at high temperatures, and about equivalent in salinity to a 3.2 weight percent NaCl solution) should be present within the volcanic edifice at that depth (fig. 55.15). The depth-temperature range is such that sea water will start to boil at a temperature of about 365 °C in the immediate vicinity of the top of the magma chamber and may even evaporate to dryness (figs. 55.14, 55.15). Within large volcanic edifices gravitational slumping (Fiske and Jackson, 1972) produces tensional stresses that may result in fracturing of rocks at very high temperatures where quasi-plastic flow would normally occur. Therefore, for relatively short, but significant, periods the maximum temperature attained by the convecting hydrothermal system may be considerably above 400–500 °C. Much of the steam that forms by reaction of the hydrothermal system with very hot rock probably will condense above the magma chamber, and the accompanying gases will react with rock, creating a saline solution that is rich in sodium sulfate (and bicarbonate, depending on pH), as previously discussed.

The temperature profile in a well drilled beneath the summit of Kilauea Volcano (Keller and others, 1979) indicates that a water table was encountered 488 m deep (about 600 m above sea level). Whether this is perched water or part of a large, continuous hydrothermal system that underlies the volcano is not known.

The top of the shallow magma reservoir beneath Mauna Loa is about 1 km above sea level, and that reservoir extends above the level of the Ghyben-Herzberg lens of dilute water (fig. 55.15). A hot sodium sulfate-rich brine probably is present between the colder dilute water and the magma reservoir. A vapor-only zone may be present in the upper part of the system where temperatures are too high and pore-fluid pressures are too low for liquid of any composition to exist.

The rift zones on the Island of Hawaii are kept heated by repeated injections of magma that flow laterally from the summit regions (Fiske and Jackson, 1972). The Ghyben-Herzberg lens pinches out near the shoreline, so sea water may come into contact with very hot rock along the rift zone at a relatively low pressure. If the sea water is heated to much higher temperatures than the dilute water in the overlying Ghyben-Herzberg lens, the interface between the two may be depressed considerably below the normal level, and mixing by double-diffusive convection is likely to occur.

In summary, in oceanic volcanic systems, such as at Hawaii, the shallow magma reservoir feeding the eruptions maintains about a 3–4 km depth beneath the summit as the volcanic edifice builds upon the sea floor. The pore spaces in the rocks surrounding the magma reservoir are filled with chemically altered sea water (most of its Mg and SO_4 lost by precipitation) that is converted to highly saline brine plus gas when the condensation-point curve is intersected, either by heating or decompression, at temperatures above about 405 °C at depths greater than about 3 km below sea level. At lower temperatures and pressures sea water boils as a result of heating or decompression, but this boiling may progress to dryness in rock that has been heated to a high temperature by magma that has been injected to a relatively shallow level. In the Hawaiian systems the transformation of sea water to highly saline brine may start when the heat source attains a depth of about 12–13 km below sea level, provided (1) hydrostatic pore pressures prevail, (2) the partial pressures of noncondensable gases, such as CO_2, are small relative to the total fluid pressure, and (3) the sea water comes in contact with rock that is at a temperature greater than about 800–900 °C (fig. 55.10). These conditions, if attained, are likely to be short lived at 12–13 km. The depth at which sea water may be converted to highly saline brine plus gas by heating is decreased where pore pressures are greater than hydrostatic, and increased by high partial pressures of noncondensable gases. When volcanic activity first appears upon the sea floor, the shallow magma reservoir is likely to be about 8–9 km below sea level, and temperatures in the 600–700 °C range are required to convert sea water to highly saline brine and gas. As the volcanic edifice grows, and the shallow magma reservoir rises, sea water converts to highly saline brine and gas at still lower temperatures. A significant amount of chloride-rich brine may accumulate adjacent to the magma reservoir, especially where repeated episodes of magma injection fracture the adjacent rocks and allow sea water access to very hot rock. Double-diffusive convection occurs at the contacts with colder and less saline waters. Sulfides are likely to deposit within the chloride-rich brine portion of the system below sea level, but these deposits are not likely to be exposed during subsequent erosion because they will always remain below sea level. After the volcano rises above the sea, fresh water enters the top of the hydrothermal system and prevents the buoyant upflow of heated sea water to elevations above sea level. Continuously or episodically thereafter, temperatures may become high enough, and pore pressures low enough to completely evaporate all pore waters near the top of the magma reservoir. Sodium sulfate- and sodium carbonate-rich brines form where steam condenses and sulfur- and carbon-rich gases react with the country rock.

EVOLUTION OF MAGMATIC FLUIDS

Many investigators have discussed the evolution of aqueous fluids from crystallizing magma, including Morey (1922), Bowen (1933), Emmons (1933), Fenner (1933), Lindgren (1937), Neuman (1948), Burnham (1967, 1979), Fournier (1968, 1972), Holland (1972), Phillips (1973), Norton and Cathles (1973, 1979), Whitney (1975), Cunningham (1978), Henley and McNabb (1978), Eastoe (1982), and Henley and Ellis (1983). Most investigators have assumed that the aqueous phase evolved from crystallizing magma is either a gas or supercritical fluid. Whether this is true or not depends both on the salinity of the magmatic fluid and on the pore pressure of the fluid in the rocks adjacent to the magma. If the permeability of the surrounding rocks is relatively low, the pore-fluid pressure in those rocks may be affected by the thermal effects of the magmatic intrusion (Delaney, 1982) and the rate at which aqueous fluid is expelled from the magma. Therefore, the pore-fluid pressure in the adjacent rocks may range from hydrostatic (or less if a vapor-dominated system is present) to the pressure that will cause hydrofracturing of the rock (a maximum pressure about equal to lithostatic pressure plus the tensile strength of the rock). The adjacent rocks may be outer parts of the magma that have already crystallized.

Chloride is likely to be the dominant anion in most aqueous fluids that evolve from solidifying magmas, although fluoride and boron species may be very important in some places. The total dissolved cations adjust to the available anions so that charges are balanced, and cation ratios are fixed by fluid-rock base exchange reactions. Carbon and sulfur compounds will be present mainly as gaseous species, CO_2, SO_2, and H_2S, at magmatic temperatures and have little influence on the cation-anion balance. Therefore, the salinity of an aqueous fluid that separates from a crystallizing magma depends mainly on the initial concentrations of chloride and water dissolved in the magma, and on how much of that chloride and water are incorporated within minerals that form during the solidification process. Magmas that form by partial fusion of crustal rocks that contain evaporite deposits are likely to have relatively large concentrations of chloride, carbon, and sulfur, and magmas that form by partial fusion of rocks that contain large quantities of hydrous minerals (such as shales) are likely to be relatively rich in water. The average shale contains about 0.15 weight percent chloride (Billings and Williams, 1967) and about 5 weight percent water (Clarke, 1924). Noble and others (1967) analyzed many obsidian glasses that had not been leached by water after solidification and found a maximum concentration of about 0.75 weight percent chloride. It seems reasonable to assume that silicic magmas that form by partial fusion of sediments might contain about 0.1–0.8 weight percent chloride and about 1–5 weight percent water. Then, for magmas initially containing 1 weight percent water that is evolved as a magmatic fluid (little water is tied up in hydrous minerals), the chloride concentration in that fluid could range from about 10–44 weight percent (equivalent to about 16–72 weight percent NaCl). For magmas initially containing 5 weight percent water, the chloride concentration in an evolved aqueous magmatic fluid could range from about 2–14 weight percent (equivalent to about 3–23 weight percent NaCl) if no water were incorporated in hydrous minerals.

The critical curve for the system NaCl-H_2O is shown in relation to the granite minimum melting curve (Tuttle and Bowen, 1958) in figure 55.16. Two situations are represented in that figure: water pressure equal to lithostatic pressure (in red) and hydrostatic pressure (in black). Where pore-fluid pressures in the adjacent rock are about equal to the lithostatic pressure, aqueous fluids that evolve from silicic magmas that are crystallizing along the granite minimum melting curve should retain their initial salt/water ratios as they cool at depths greater than about 5 km. Where pore-fluid pressures in the adjacent rock are about equal to the hydrostatic pressure, initial salt/water ratios in magmatic fluids are likely to be maintained only at depths greater than about 13 km. A decrease in pore-fluid pressure from lithostatic to hydrostatic would likely cause a magma on the granite minimum melting curve to become supercooled by about 75 °C, with the simultaneous evolution of a highly saline brine and moderately saline to dilute gas.

The position of the granite minimum melting curve is shown in figure 55.17 as it relates to the isopleths of solubility of NaCl in steam and liquid water (fig. 55.7). Point y on the granite minimum melting curve indicates the lowest pressure (with water pressure equal to total pressure) at which the magma can retain 4 weight percent dissolved water (Tuttle and Bowen, 1958). A further

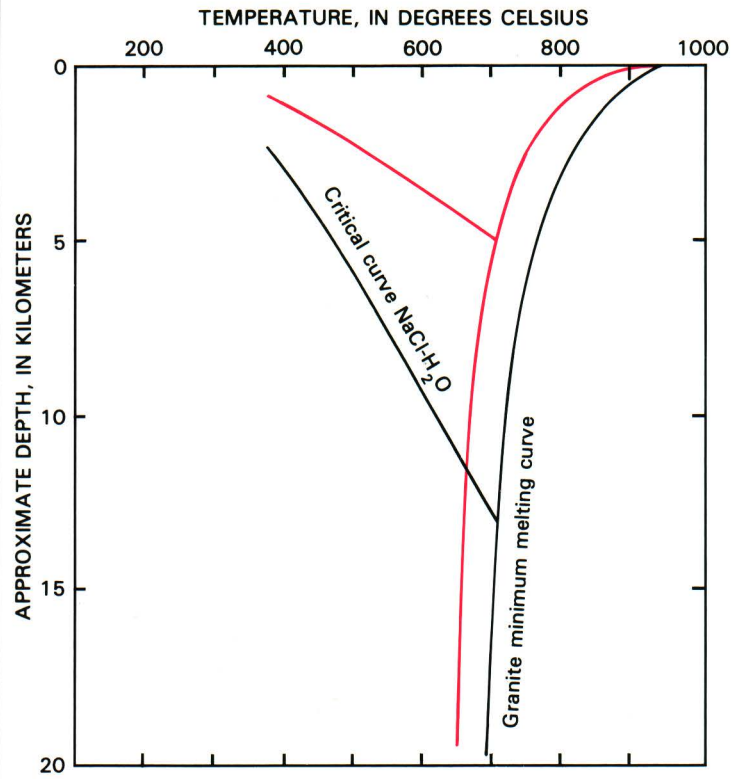

FIGURE 55.16.—Approximate positions of critical curve for system NaCl-H_2O and of granite minimum melting curve (Tuttle and Bowen, 1958). Red lines, water pressure equal to lithostatic pressure; black lines, hydrostatic pressure.

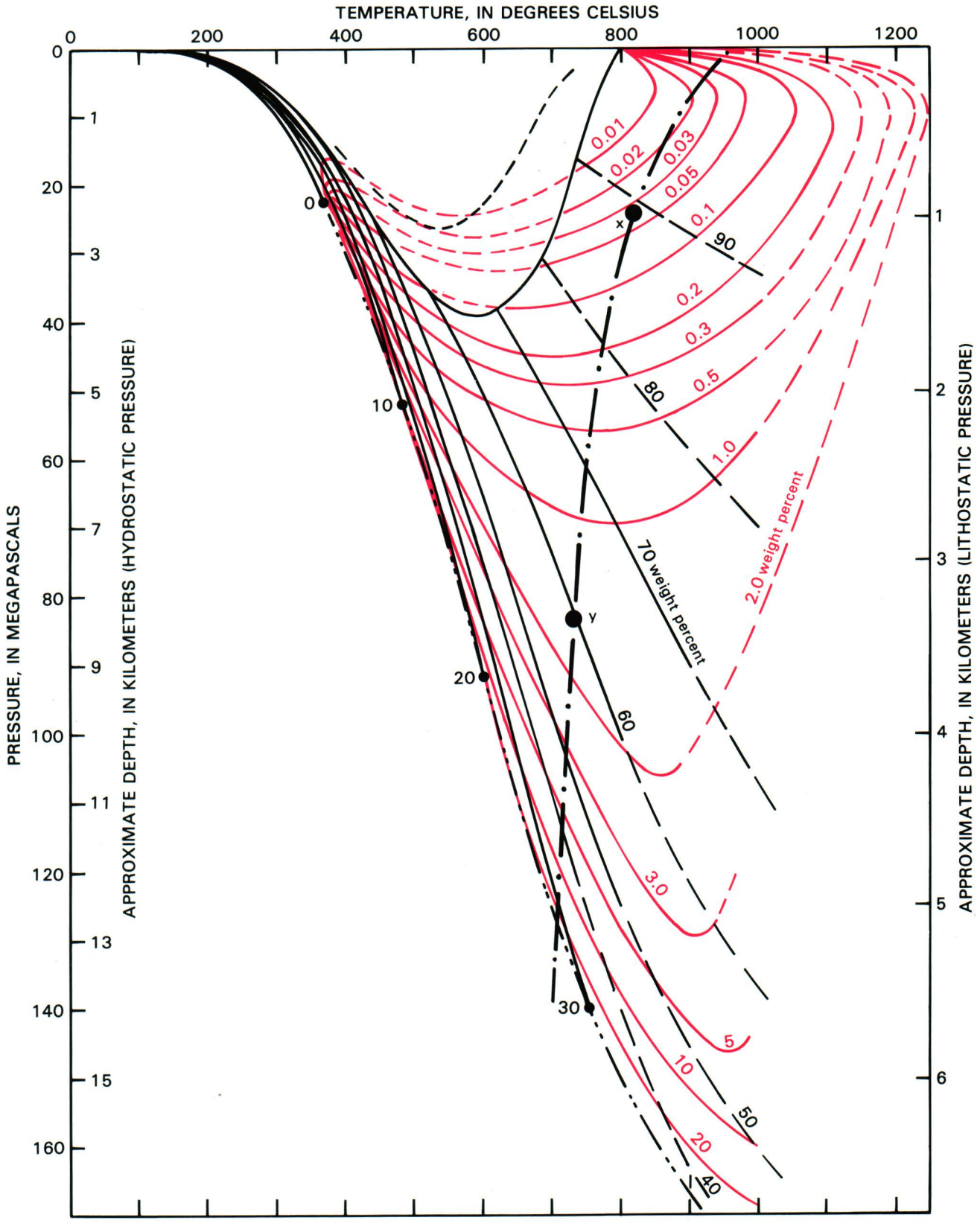

FIGURE 55.17.—Granite minimum melting curve (Tuttle and Bowen, 1958) shown by dot-dashed line, superimposed on figure 55.7. Lettered points are discussed in text.

decrease in pressure would result in evolution of water and an immediate crystallization of the magma. Chloride initially dissolved in the magma will partition strongly into the aqueous phase (Kilinc and Burnham, 1972), and the maximum salt (as NaCl) that the aqueous gas phase can carry is 1–2 weight percent. Point x on the granite minimum melting curve indicates the lowest pressure at which the magma can retain 2 weight percent dissolved water, and the maximum salt that the aqueous gas phase can carry is only about 0.05 weight percent. A much greater solubility of salt in the gas phase at point x would be estimated using the results reported by Sourirajan and Kennedy (1962).

From the foregoing discussion it appears that when pore-fluid pressures are controlled by hydrostatic conditions, magmatic waters are likely to evolve to highly saline brines at depths less than about 10–12 km, irrespective of the initial concentrations of salt and water dissolved in the magma. Dilute hydrothermal fluids of meteoric origin and mixtures of meteoric water and condensed magmatic gas (steam) are likely to form convection systems that float upon the more saline and probably hotter magmatic fluid. Double-diffusive convection is likely to result from the temperature and salinity gradients.

CONCLUSIONS

Our present knowledge of hydrothermal mineral deposits and active geothermal systems demonstrates the importance of interaction of shallow dilute meteoric water and deeper brines. The highly concentrated brines thus far encountered in active hydrothermal systems are all in environments in which the waters may have interacted with evaporites. Experimental data, however, indicate that highly saline as well as moderately concentrated brines may evolve from a crystallizing magma, depending on the initial water and chloride contents and on the depth of crystallization. Brines may also develop from dilute meteoric water as a result of heating. Heating a solution of given composition to above its critical temperature at a pressure a little above its critical pressure results in its disproportionation into a more concentrated liquid (brine) and a gas. What is generally thought of as supercritical behavior of a fluid occurs only at pressures great enough to ensure that the gas phase will retain all the salt that was initially dissolved in the liquid phase at a lower temperature. As a result of boiling and gas disproportionation, highly saline brines are likely to evolve in and around shallow magmatic intrusions, particularly at depths less than 3 to 4 km. However, a relatively large amount of dilute water must be heated to a very high temperature to produce a small amount of brine. The injection of dilute water into very hot rock is an inefficient way to produce brine because the rock at the liquid interface is chilled rapidly by the colder water and because relatively little water is likely to be involved. Adiabatic decompression of a dilute to moderately saline solution (such as sea water) that is part of a large convection system appears to be a more promising method of producing significant amounts of brine. In a large convecting system heat may be extracted from a large volume of rock, and highly saline brines will form if the decompression path of the fluid brings it into the field of gas plus brine at a temperature a few degrees above the critical temperature. By gravitational settling this brine may accumulate at the base of hydrothermal convection in the few fractures that are present in otherwise impermeable rock. The brines formed by heating and adiabatic decompression of dilute to moderately saline water of meteoric origin (including sea water) will augment brines that result from crystallization and degassing of the magmatic heat source. These hot brines will scavenge metals from the surrounding rock, and the base metals in turn will react with much of the sulfur that is liberated from crystallizing magma. Thus, a base metal ore deposit may form in the brine portion of the system, while the dilute hydrothermal system remains relatively unmineralized with respect to base metals.

REFERENCES

Bates, R.L., and Jackson, J.A., 1980, Glossary of geology (2d ed.): Falls Church, Va., American Geological Institute, 749 p.

Billings, G.K., and Williams, H.H., 1967, Distribution of chlorine in terrestrial rocks (a discussion): Geochimica et Cosmochimica Acta, v. 31, p. 2247.

Bischoff, J.L., and Pitzer, K.S., 1985, Phase relations and adiabats in boiling seafloor geothermal systems: Earth and Planetary Science Letters, v. 75, p. 327–338.

Bischoff, J.L., and Rosenbauer, R.J., 1984, The critical point and two-phase boundary of seawater, 200°–500°C: Earth and Planetary Science Letters, v. 68, p. 172–180.

———1985, An empirical equation of state for hydrothermal seawater (3.2% NaCl): American Journal of Science, v. 285, p. 725–763.

Bischoff, J.L., Rosenbauer, R.J., and Pitzer, K.S., in press, A note on the system $NaCl-H_2O$: Relations of vapor-liquid near the critical temperature of water and of vapor-liquid-halite from 300° to 500°C: Geochimica et Cosmochimica Acta.

Bodnar, R.J., and Bean, R.E., 1980, Temporal and spatial variations in hydrothermal fluid characteristics during vein filling in preore cover overlying deeply-buried porphyry copper-type mineralization at Red Mountain, Arizona: Economic Geology, v. 75, p. 876–893.

Bodnar, R.J., Burnham, C.W., and Sterner, S.M., 1985, Synthetic fluid inclusions in natural quartz III: Determination of phase equilibrium properties in the system H_2O-NaCl to 1000°C and 1500 bars: Geochimica et Cosmochimica Acta, v. 49, p. 1861–1873.

Bodvarsson, G., and Lowell, R.P., 1972, Ocean floor heat flow and circulation of interstitial waters: Journal of Geophysical Research, v. 77, p. 4472–4475.

Bowen, N.L., 1933, The broader story of magmatic differentiation, briefly told, *in* Ore deposits of the western states (Lindgren volume): New York, American Institute of Mining and Metallurgical Engineers, p. 106–128.

Bowers, T.S., and Helgeson, H.C., 1983, Calculation of the thermodynamic and geochemical consequences of nonideal mixing in the system H_2O-CO_2-NaCl on phase relations in geologic systems: Equation of state for H_2O-CO_2-NaCl fluids at high pressures and temperatures: Geochimica et Cosmochimica Acta, v. 47, p. 1247–1275.

Burnham, C.W., 1967, Hydrothermal fluids at the magmatic stage, *in* Barnes, H.L., ed., Geochemistry of hydrothermal ore deposits: New York, Holt, Rinehart and Winston, p. 34–76.

———1979, Magmas and hydrothermal fluids, *in* Barnes, H.L., ed., Geochemistry of hydrothermal ore deposits (2d ed.): New York, John Wiley, p. 17–136.

Cathles, L.M., 1977, An analysis of the cooling of intrusives by ground-water convection which includes boiling: Economic Geology, v. 72, no. 5, p. 804–826.

———1980, Fluid flow and genesis of hydrothermal ore deposits: Economic Geology, 75th Anniversary Volume, p. 424–457.

———1983, An analysis of the hydrothermal system responsible for massive sulfide deposition in the Hokuroku Basin of Japan, *in* Ohmoto, H., and Skinner, B.J., eds., The Kuroko and related volcanogenic massive sulfide deposits: Economic Geology, Monograph 5, p. 439–487.

Cheng, P., and Minkowycz, W.J., 1977, Free convection about a vertical flat plate embedded in a porous medium with application to heat transfer from a dike: Journal of Geophysical Research, v. 82, p. 2040–2044.

Clarke, F.W., 1924, The data of geochemistry, 5th ed.: U.S. Geological Survey Bulletin 770, 841 p.

Copeland, C.S., Silverman, J., and Benson, S.W., 1952, The system NaCl-H_2O at supercritical temperatures and pressures: Journal of Chemical Physics, v. 21, p. 12–16.

Cunningham, C.G., 1978, Pressure gradients and boiling as mechanisms for localizing ore in porphyry systems: U.S. Geological Survey Journal of Research, v. 6, no. 6, p. 745–754.

Davis, D.A., and Yamanaga, George, 1973, Water resources summary island of Hawaii: Hawaii Division of Water and Land Development Report R47, 42 p.

Delaney, P.T., 1982, Rapid intrusion of magma into wet rock: Ground water flow due to pore pressure increases: Journal of Geophysical Research, v. 87, p. 7739–7756.

Eastoe, C.J., 1978, A fluid inclusion study of the Panguna porphyry copper deposit, Bougainville, Papua New Guinea: Economic Geology, v. 73, p. 721–748.

———1982, The physics and chemistry of the hydrothermal system in the Panguna porphyry copper deposit, Bougainville, Papua New Guinea: Economic Geology, v. 77, p. 127–153.

Edmond, J.M., Craig, H., Gordon, L.I., and Holland, H.D., 1979, Chemistry of hydrothermal waters at 21°N on the East Pacific Rise[abs.]: Eos (American Geophysical Union Transactions), v. 60, p. 864.

Elder, J.W., 1965, Physical processes in geothermal areas, *in* Terrestrial heat flow: American Geophysical Union Geophysical Monograph 8, p. 211–239.

Emmons, W.H., 1933, On the mechanism of the deposition of certain metalliferous lode systems associated with granitic batholiths, *in* Ore deposits of the western states (Lindgren vol.): New York, American Institute of Mining and Metallurgical Engineers, p. 327–349.

Eugster, H.P., and Jones, B.F., 1979, Behavior of major solutes during closed basin evolution: American Journal of Science, v. 279, p. 609–631.

Fehn, U., and Cathles, L.M., 1979, Hydrothermal convection at slow-spreading mid-ocean ridges: Tectonophysics, v. 55, p. 239– 260.

Fenner, C.N., 1933, Pneumatolytic processes in the formation of minerals and ores, *in* Ore deposits of the western states (Lindgren vol.): American Institute of Mining and Metallurgical Engineers, p. 58–106.

Fiske, R.S., and Jackson, E.D., 1972, Orientation and growth of Hawaiian volcanic rifts: The effect of regional structure and gravitational stress: Proceedings of the Royal Society of London, v. 329, p. 299–326.

Fournier, R.O., 1968, Depths of intrusion and conditions of hydrothermal alteration in porphyry copper deposits [abs.]: Geological Society of America Abstracts with Program, 1968 Annual Meeting, p. 101.

———1972, The importance of depth of crystallization on the character of magmatic fluids [abs.]: International Geological Congress, 24th, Montreal, 1972, sec. 10, p. 214.

———1976, Exchange of Na^+ and K^+ between water vapor and feldspar phases at high temperature and low vapor pressure: Geochimica et Cosmochimica Acta, v. 40, p. 1553–1561.

———1977, Constraints on the circulation of meteoric water in hydrothermal systems imposed by the solubility of quartz [abs.]: Geological Society of America Abstracts with Program, v. 9, p. 979.

———1983a, Self-sealing and brecciation resulting from quartz deposition within hydrothermal systems: International Symposium on Water-Rock Interaction, 4th, Misasa, Japan, 1983, Extended Abstracts, p. 137–140.

———1983b, Active hydrothermal systems as analogues of fossil systems, *in* Raleigh, C.B., ed., The role of heat in the development of energy and mineral resources in the Basin and Range Province: Geothermal Resources Special Report 13, p. 263–284.

———1985a, Continental scientific drilling to investigate brine evolution and fluid circulation in active hydrothermal systems, *in* Observation of the continental crust through drilling: New York, Springer-Verlag, p. 98–122.

———1985b, Silica minerals as indicators of conditions during gold deposition, *in* Tooker, E.W., ed., Geologic characteristics of sediment- and volcanic-hosted disseminated gold deposits—search for an occurrence model: U.S. Geological Survey Bulletin 1646, p. 15–26.

Fournier, R.O., and Pitt, A.M., 1985, The Yellowstone magmatic-hydrothermal system: International Symposium on Geothermal Energy, Geothermal Resources Council, Hawaii, 1985, International Volume, p. 319–327.

Galobardes, J.F., Van Hare, D.R., and Rogers, L.B., 1981, Solubility of sodium chloride in dry steam: Journal of Chemical Data, v. 26, p. 363–366.

Gunter, W.D., Chow, I-M, and Girsperger, S., 1983, Phase relations in the system NaCl-KCl-H_2O II: Differential thermal analysis of halite liquidus in the NaCl-H_2O binary above 450 °C: Geochimica et Cosmochimica Acta, v. 47, p. 863–873.

Haas, J.L., 1971, Effect of salinity on the maximum thermal gradient of a hydrothermal system at hydrostatic pressure: Economic Geology, v. 66, p. 940–946.

Hardee, H.C., 1982, Permeable convection above magma bodies: Tectonophysics, v. 84, p. 179–195.

Hardie, L.A., and Eugster, H.P., 1970, The evolution of closed-basin brines: Mineralogical Society of America Special Publication 3, p. 273–279.

Hartline, B.K., and Lister, C.R.B., 1981, Topographic forcing of supercritical convection in a porous medium such as the ocean crust: Earth and Planetary Science Letters, v. 55, p. 75–86.

Henley, R.W., and Ellis, A.J., 1983, Geothermal systems ancient and modern: A geochemical review: Earth-Science Reviews, v. 19, 50 p.

Henley, R.W., and McNabb, Alex, 1978, Magmatic vapor plumes and groundwater interaction in porphyry copper emplacement: Economic Geology, v. 73, 19 p.

Hilbert, R., 1979, PVT-Daten von Wasser und von wässrigen Natriumchloride-Lösungen bis 873 K, 4000 Bar und 25 Gewichtsprozent NaCl: Karlsruhe University, Ph.D. Dissertation, 212 p.

Holland, H.D., 1972, Granites, solutions and base metal deposits: Economic Geology, v. 67, p. 281–301.

Huppert, H.E., and Sparks, R.S.J., 1984, Double-diffusive convection due to crystallization in magmas: Annual Review of Earth and Planetary Science, v. 12, p. 11–37.

Huppert, H.E., and Turner, J.S., 1981, Double-diffusion convection: Journal of Fluid Mechanics, v. 106, p. 299–329.

Keenan, J.H., Keys, F.G., Hill, P.G., and Moore, J.G., 1969, Steam tables (international edition—metric units): New York, John Wiley & Sons, 162 p.

Keevil, N.B., 1942 Vapor pressure of aqueous solutions at high temperatures: Journal of the American Chemical Society, v. 64, p. 841–850.

Keller, G.V., Grose, L.T., Murray, J.C., and Skokan, C.K., 1979, Results of an experimental drill hole at the summit of Kilauea Volcano, Hawaii: Journal of Volcanology and Geothermal Research, v. 5, p. 345–385.

Khaibullin, K., and Borisov, N.M., 1966, Experimental investigation of the thermal properties of aqueous and vapor solutions of sodium and potassium chloride at phase equilibrium: Teplofizika Vysokikh Temperature, v. 4, p. 518–523 (English translation, p. 489–494).

Kilinc, I.A., and Burnham, C.W., 1972, Partitioning of chloride between a silicate melt and coexisting aqueous phase from 2 to 8 kilobars: Economic Geology, v. 67, p. 231–235.

Knapp, R.B., and Norton, D., 1981, Preliminary numerical analysis of processes related to magma crystallization and stress evaluation in cooling pluton environments: American Journal of Science, v. 281, p. 35–68.

Lama, R.D., and Vutukuri, V.S., 1978, Handbook on mechanical properties of rocks—testing techniques and results—volume II: Clausthal, Germany, Trans Tech Publications, 484 p.

Langbein, W.B., 1961, Salinity and hydrology of closed lakes: U.S. Geological Survey Professional Paper 412, 20 p.

Lindgren, W., 1937, Succession of minerals and temperatures of formation in ore deposits of magmatic affiliation: American Institute of Mining and Metallurgical Engineers Transactions, v. 126, p. 356–376.

Lister, C.R.B., 1974, On the penetration of water into hot rock: Geophysical Journal of the Royal Astronomical Society, v. 39, p. 465–509.

———1980, Heat flow and hydrothermal circulation: Earth and Planetary Sciences Annual Review, v. 8, p. 95–117.

———1983, The basic physics of water penetration into hot rock, *in* Rona, P.A., Bostrom, K., Laubier, L., and Smith, K.L., Jr., eds., Hydrothermal processes at seafloor spreading centers: New York, Plenum Press, p. 141–168.

Morey, G.W., 1922, The development of pressure in magmas as a result of crystallization: Washington Academy of Science Journal, v. 12, p. 219–230.

Muffler, L.J.P., White, D.E., and Truesdell, A.H., 1971, Hydrothermal explosion craters in Yellowstone National Park: Geological Society of America Bulletin, v. 82, p. 723–740.

Nash, J.T., 1976, Fluid-inclusion petrology—data from porphyry copper deposits and applications to exploration: U.S. Geological Survey Professional Paper 907-D, 16 p.

Neuman, H., 1948, On hydrothermal differentiation: Economic Geology, v. 43, p. 77–83.

Noble, D.C., Smith, V.C., and Peck, L.C., 1967, Loss of halogens from crystallized and glassy silicic volcanic rocks: Geochimica et Cosmochimica Acta, v. 31, p. 215–223.

Norton, Denis, 1978, Sourcelines, source regions, and pathlines for fluid flow in hydrothermal systems related to cooling plutons: Economic Geology, v. 73, p. 21–28.

———1984, Theory of hydrothermal systems: Annual Review of Earth and Planetary Sciences, v. 12, p. 155–177.

Norton, Denis, and Cathles, L.M., 1973, Breccia pipes—products of exsolved vapor from magmas: Economic Geology, v. 68, p. 540–546.

———1979, Thermal aspects of ore deposition, *in* Barnes, H.L., ed., Geochemistry of hydrothermal ore deposits (2d ed.): New York, John Wiley, p. 611–631.

Norton, Denis, and Knapp, R., 1977, Transport phenomena in hydrothermal systems: The nature of porosity: American Journal of Science, v. 277, p. 913–936.

Norton, Denis, and Knight, J., 1977, Transport phenomena in hydrothermal systems: Cooling plutons: American Journal of Science, v. 277, p. 937–981.

Norton, Denis, and Taylor, H.P., 1979, Quantitative simulation of the hydrothermal systems of crystallizing magmas on the basis of transport and oxygen isotope data: An analysis of the Skaergaard intrusion: Journal of Petrology, v. 20, p. 421–486.

Ölander, A., and Liander, H., 1950, The phase diagram of sodium chloride in steam above the critical point: Acta Chemica Scandinavica, v. 4, p. 1437–1445.

Orville, P.M., 1963, Alkali ion exchange between vapor and feldspar phases: American Journal of Science, v. 261, p. 201–237.

Parisod, C.J., and Plattner, E., 1981, Vapor-liquid equilibria of the $NaCl$-H_2O system in the temperature range 300–440 °C: Journal of Chemical Engineering Data, v. 26, p. 15–20.

Parmentier, E.M., and Spooner, E.T.C., 1978, A theoretical study of hydrothermal convection and the origin of the ophiolitic sulfide ore deposit of Cyprus: Earth and Planetary Science Letter, v. 40, p. 33–44.

Peterson, F.L., 1981, Geologic and hydrologic framework: A history of development, *in* Fujimura, F.N., and Chang, W.B.C., eds., Groundwater in Hawaii, a century of progress: Manoa, University of Hawaii Press, p. 1–13.

Phillips, W.J., 1973, Mechanical effects of retrograde boiling and its probable importance in the formation of some porphyry ore deposits: American Institute of Mining and Metallurgical Engineers Transactions, sec. B, v. 82, p. B90–B98.

Pitzer, K.S., 1983, Thermodynamics of sodium chloride solutions in steam: Journal of Physical Chemistry, v. 87, p. 1120–1125.

Pitzer, K.S., and Li, Y., 1984, Critical phenomena and thermodynamics of dilute aqueous sodium chloride to 823 K: Proceedings of the National Academy of Science, v. 81, p. 1268–1271.

Pitzer, K.S., and Pabalan, R.T., in press, Thermodynamics of NaCl in steam: Geochimica et Cosmochimica Acta.

Ravich, M.I., and Borovia, F.E., 1949, Phase equilibria in ternary water-salt systems at elevated temperatures [in Russian]: Akademiya Nauk SSSR, Institut Obshchei i Neorganicheskoi Izvestiia, Sektor Fiziko Khimicheskogo Analiza, v. 19, p. 69–81.

Reynolds, T.J., and Bean, R.E., 1985, Evolution of hydrothermal fluid characteristics at the Santa Rita, New Mexico, porphyry copper deposit: Economic Geology, v. 80, p. 1328–1347.

Ribando, R.J., Torrance, K.E., and Turcotte, D.L., 1976, Numeric models for hydrothermal circulation in the ocean crust: Journal of Geophysical Research, v. 81, p. 3007–3012.

Roedder, Edwin, 1971, Fluid inclusion studies on the porphyry type deposit at Bingham, Utah, Butte, Montana, and Climax, Colorado: Economic Geology, v. 66, p. 98–120.

———1979, Fluid inclusions as samples of ore fluids, *in* Barnes, H.L., ed., Geochemistry of hydrothermal ore deposits (2d ed.): New York, John Wiley, p. 684–737.

Sleep, N.H., 1983, Hydrothermal convection at ridge axes, *in* Rona, P.R., and Lowell, R.L., eds., Hydrothermal processes at seafloor-spreading centers: New York, Plenum Press, p. 71–82.

Smith, R.B., and Bruhn, R.L., 1984, Interplate extensional tectonics of the eastern Basin-Range: Inferences on structural style from seismic reflection data, regional tectonics, and thermal mechanical models of brittle-ductile deformation: Journal of Geophysical Research, v. 89, p. 5733–5762.

Sourirajan, S., and Kennedy, G.C., 1962, The system H_2O-$NaCl$ at elevated temperatures and pressures: American Journal of Science, v. 260, p. 115–141.

Torrance, K.E., and Sheu, J.P., 1978, Heat transfer from plutons undergoing hydrothermal cooling and thermal cracking: Numerical Heat Transfer, v. 1, p. 147–161.

Tuttle, O.F., and Bowen, N.L., 1958, Origin of granite in the light of experimental studies in the system $NaAlSi_3O_8$-$KAlSi_3O_8$-SiO_2-H_2O: Geological Society America Memoir 74, 153 p.

Vitagliano, P.L., Della Volpe, C., and Vitagliano, V., 1984, Gravitational instabilities in free diffusion boundaries: Journal of Solution Chemistry, v. 13, p. 549–562.

White, D.E., 1965, Saline waters of sedimentary rocks: American Association of Petroleum Geologists Memoir 4, p. 342–366.

———1968, Environments of generation of some base-metal ore deposits: Economic Geology, v. 63, p. 301–335.

White, D.E., Muffler, L.J.P., and Truesdell, A.H., 1971, Vapor-dominated hydrothermal systems compared to hot water systems: Economic Geology, v. 66, p. 75–97.

Whitney, J.A., 1975, Vapor generation in a quartz monzonite magma: A synthetic model with application to porphyry copper deposits: Economic Geology, v. 70, p. 346–358.

A GEOCHEMICAL MODEL OF THE KILAUEA EAST RIFT ZONE

By Donald Thomas

ABSTRACT

The east rift zone of Kilauea Volcano is comprised of a northeast- to southwest-trending complex of dikes and fractures extending more than 100 kilometers from the summit caldera to the ocean floor. Geologic, petrologic, and geophysical data indicate that substantial volumes of molten magma are intruded into and stored within the east rift dike complex and that parts of the rift have temperatures exceeding the Curie point of basalt. The shallow ground-water hydrology and chemistry on the lower rift are strongly affected by natural thermal discharge from the rift and indicate a continuous heat loss rate estimated at 291 megawatts of thermal energy. Several deep geothermal wells drilled into the lower rift have confirmed the presence of high temperatures and of an active hydrothermal system associated with the rift. The maximum temperatures encountered in the deep wells approach the critical point of water (374 °C) but show a sharp decline on the southern boundary of the rift. Petrologic studies of drill cuttings from the deep geothermal wells have shown that intermittent, intense hydrothermal alteration has occurred to depths of at least 2.5 km. The alteration phases present indicate that metamorphism reaches the greenschist facies and have strong similarities to alteration suites found in midocean-ridge hydrothermal systems. Chemical data from the deep fluids suggest that the primary source of recharge to the reservoir is meteoric water in the interior of the rift but that saline water is present on the southern boundary. Production data from the deep wells also indicate that accessible parts of the hydrothermal system are capable of producing both dry steam and hot brine. The data that have been gathered to the present indicate that the hydrothermal system associated with the Kilauea east rift zone is actively evolving and has characteristics ranging from low-temperature benign fluids to high-temperature, highly aggressive fluids that may provide both an economically viable geothermal resource and a natural laboratory for the study of ore-forming and geochemical-cycling processes.

INTRODUCTION

Exploration for geothermal resources in Hawaii began in 1962 when four shallow wells were drilled into the Kilauea lower east rift zone (LERZ) (fig. 56.1; table 56.1) in an effort to develop a commercial steam resource. Although all four wells encountered above-ambient temperatures, none discovered an economically useful steam or hot-water resource. A second effort to study the deep thermal conditions on the Kilauea east rift zone (ERZ) was initiated in 1972 under funding from the National Science Foundation. This effort culminated in the drilling and completion of the 1,966-meter-deep Hawaii Geothermal Project well A (HGP-A) in 1976. Testing of this well indicated that temperatures of 358 °C were present at the bottom of the hole and that the well was capable of producing approximately 48 tonnes per hour (t/h) of steam and hot water. A geothermal generator facility was installed on this well in 1981 and, as of July 1985, has been in operation for approximately 44 months. Subsequent to the completion and initial testing of HGP-A, six privately financed deep exploration wells have been drilled into the LERZ. The data that have been obtained from the deep exploratory drilling into the rift and from the long-term discharge of HGP-A have now provided us with sufficient information to develop a preliminary model of the hydrothermal system associated with the ERZ.

ACKNOWLEDGMENTS

The research results reported here have been made possible only through the capable assistance and willing cooperation of numerous very able individuals. Field and laboratory assistance by M. Dahlstrom, C. Fraley, D. Mills, J. McCullough, B. Taylor, L. Bergknut, E. DeCarlo, K.E. Cuff, M.E. Cox, R. Mitiguy, and R. Kochy is gratefully acknowledged. The cooperation and assistance of the Hawaii Geothermal Project staff—J. Shupe, P. Yuen, and L. Lopez—and Hawaii Electric Light Company—N. Oss, F. Kennedy, N. Uchida, and G. Jenkins—have been instrumental in allowing this research to be conducted. Thanks also are due to C. Zablocki, D. Jackson, R. Moore, A. Truesdell, and C.E. Helsley for helpful discussion during the evolution of this model. A special notice of appreciation is also due to Barnwell Geothermal Corporation and Geothermex Inc. for allowing access to their data and providing samples from their wells.

Funding for this work has come principally from the U.S. Department of Energy and the State of Hawaii Department of Planning and Economic Development with additional funding from Hawaiian Electric Industries and the Electric Power Research Institute.

The assistance of L. Kajiwara in drafting and of C. Koyanagi in manuscript preparation is gratefully acknowledged.

Hawaii Institute of Geophysics Contribution No. 1702.

GEOLOGIC SETTING

The east rift zone, a major structural feature of Kilauea Volcano, extends from the summit caldera in an easterly direction for approximately 50 km, where it enters the ocean and continues as a

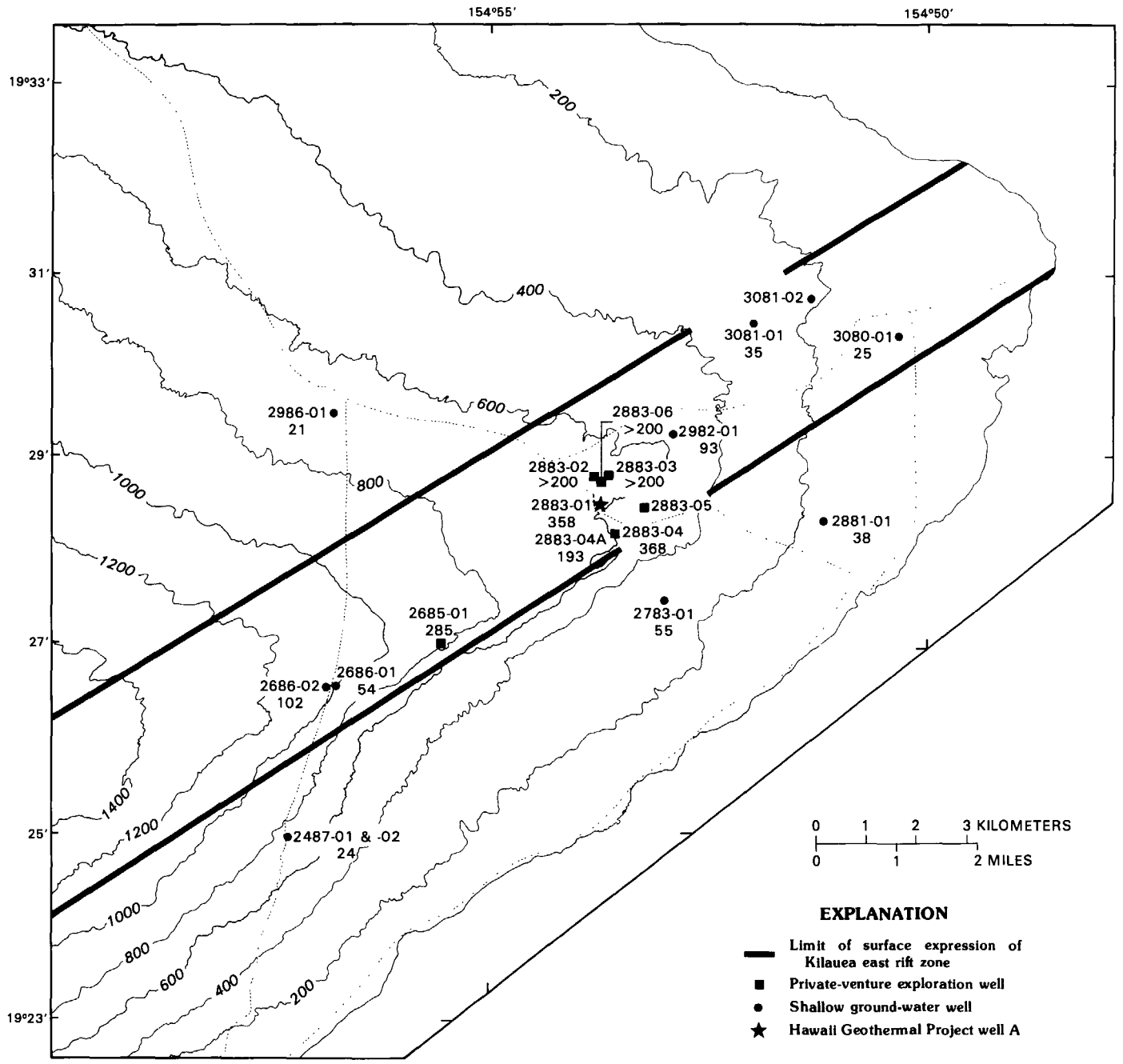

FIGURE 56.1.—Kilauea lower east rift zone showing locations of ground-water and geothermal exploration wells. Well-identification numbers and temperature (in degrees Celsius), if known, are given next to symbols. Dashed lines represent roads.

submarine ridge for another 50–60 km. Geologic mapping on Kilauea and studies of eroded rift systems on the older islands of the Hawaiian Chain indicate that the structure of the rift is composed of hundreds to thousands of near-vertical thin tabular dikes interspersed with highly fractured country rock (Macdonald and Abbott, 1970). The trend of the individual dikes parallels the strike of the rift, and the dip angles of both the fractures and dikes typically deviate by only a few degrees from vertical (Macdonald and Abbott, 1970).

The mechanism responsible for the formation of the ERZ is believed to be the forceful intrusion of magma from the summit magma reservoir into the rift system at depths of 3–6 km beneath the summit (Fiske and Jackson, 1972). The occurrence of these intrusive events, typically indicated by seismic and deformation changes both at the summit and in the area of an intrusion, may result in a surface eruption or in the formation of a subsurface dike. Although the rate of magma intrusion in the rift zone is not well known, theoretical studies have inferred deposition rates as high as

TABLE 56.1.—*Characteristics of geothermal exploration wells drilled on the Kilauea east rift zone*

Well	Name	Depth (meters)	Bottom temperature (°C)	Comments
2685-01	Ashida-1	2,530	326	Insufficient permeability to sustain production; suspended.
2686-01	Geothermal-1	54.3	54	Drilled 1962, did not reach water table; abandoned.
2686-02	Geothermal-2	169.5	102	Drilled in 1962, did not reach water table; abandoned.
2883-01	HGP-A	1,967	358	Sustained production of 50 t/h of brine and steam.
2883-02	Kapoho State 1	2,222	339	Production rate of 32.7 t/h was achieved during short test; operation suspended.
2883-03	Kapoho State 2	2,440	342	Production rate of 15 t/h was achieved during short test; operation suspended.
2883-04	Lanipuna-1	2,557	>363	High salinity at intermediate depth and temperature, low permeability at depth; abandoned.
2883-04A	Lanipuna-1	1,920	149	Drilled as a slant hole off of 2983-02, maximum temperature of 193 °C with temperature turnover; abandoned.
2883-05	Lanipuna-6			Very productive low-temperature aquifer encountered at 1,370-m depth.
2883-06	Kapoho State 1A	2,000	300	Drilled in 1984; short-duration testing produced self-sustaining flow; production rate and subsurface temperature data are presently proprietary.
2982-01	Geothermal-3	210	93	Drilled in 1962; reached water table but insufficient temperature for production; abandoned.
3081-01	Geothermal-4	88.4	43	Drilled in 1962; insufficient temperature for production; abandoned and now plugged.

3×10^6 m^3/mo following the *M*-7.5 earthquake that occurred on the ERZ in 1975 (Dzurisin, 1981). Other studies of surface features such as pit craters (Macdonald and Abbott, 1970; Holcomb, 1980), and of petrologic characteristics of rift eruptions (Swanson and others, 1976; Moore, 1983) indicate that intrusive bodies remain molten for extended periods and may act as subsidiary magma chambers to surface eruptions occurring long after their initial intrusion into the rift zone.

Numerous geophysical studies tend to confirm this interpretation. The total-intensity aeromagnetic map of the rift zone prepared by Godson and others (1981) indicates a clear magnetic signature along the entire length of the rift. This magnetic signature has been interpreted as indicating the presence of temperatures in excess of the Curie temperature of basalt at an estimated depth of 2–3 km (D. Jackson, oral commun., 1985). Controlled-source resistivity surveys on the upper rift have also indicated low subsurface resistivities at depths of 2–5 km, which have been interpreted to be thermal fluids or molten magma bodies (Kauahikaua and others, 1979; Kauahikaua, 1981). More recent very low frequency (VLF) surveys over the ERZ (Flannigan and Long, chapter 39) have similarly identified magnetic and resistivity anomalies that have been inferred to delineate the currently active part of the rift zone and, in some places, molten magma stored in the rift. Although the presence of molten intrusives on the LERZ has not been unequivocally demonstrated, resistivity (Keller and others, 1977; Kauahikaua and others, 1980; Kauahikaua, 1981), self-potential (Zablocki, 1976, 1977), and deep drilling results (Shupe and others, 1978; Yuen and others, 1978; Thomas, 1982) have indicated the presence of high-temperature water.

Although the surface expression of the rift zone is only about 3–4 km wide, some studies suggest that it may be much broader in the subsurface. Swanson and others (1976) analyzed deformation and seismic data for the ERZ and proposed that the focus of active intrusion and eruption on the rift zone has migrated southward with time. Their model considers the north flank of Kilauea to be essentially fixed due to the buttressing effect of Mauna Loa to the north, but that the steep submarine slope to the south of the rift is more mobile and is readily displaced by the forceful intrusion of magma into the rift. The sharp bend in the upper rift is interpreted to be the result of the southward migration of the rift and, on this basis, a subsurface dike complex on the upper rift could approach 10 km in width. Although this width has not been confirmed, interpretations of gravity data by Swanson and others (1976) and gravity and magnetic data by Furumoto (1978) are consistent with a broad subsurface dike complex.

In summary, the structure of the ERZ consists of a broad complex of steeply dipping dikes and fractures extending in a northeasterly direction from the summit caldera for a distance of more than 100 km to the ocean floor. The available geophysical data indicate that the maximum temperatures present at depth in the interior of the rift are in excess of the Curie point. However, the very high permeability of subaerial and shallow submarine extrusive lava is likely to allow rapid hydrothermal circulation and high heat loss rates in the shallow subsurface; hence, only very young intrusives are expected to be significantly above ambient temperatures at depths of less than 1–2 km.

SURFACE HYDROLOGY AND CHEMISTRY

The near-surface hydrology of the ERZ is characterized by very high recharge rates and rapid subsurface ground-water flow. Rainfall rates exceed 2.5 m/yr over most of the ERZ, and the very high permeabilities of the surface volcanic rocks allow nearly 100 percent of the rainfall to penetrate to basal aquifers (Davis and

TABLE 56.2.—*Chemical data from shallow ground-water wells on the lower east rift zone*

Well	Name	Temperature (°C)	pH	Chemical contents (parts per million) Na	K	Ca	Mg	Cl	SO_4	SiO_2	Tritium age[1] (yr)	Na-K-Ca temperature (°C)	$^2SiO_2$ temperature (°C)	$^3SiO_2$ temperature (°C)
2487-01	Keauohana	20.8	7.05	95.1	12.4	15.4	5.1	160	28.6	44.5	18	149	66.1	96.5
2783-01	Malamaki	52.2	7.45	3,333	218	293	295	5,380	598	100.7	15.6	149	111	137.5
2881-01	Allison	37.8	7.35	1,188	68	84	102	2,042	69.2	24.1	12.9	122	39	70.6
2982-01	Geothermal 3	93	6.85	2,572	378	194	122	4,645	314	96.6	10.3	257	108	135
2986-01	Pahoa	23.3	6.65	16.7	9.3	4.5	3.1	4.93	27.3	50	10.6	310	72	102
3080-02	Kapoho	22.1	7.1	127	15	65.6	35.2	174	328	53.6	10.5	124	75	105
3081-02	Airstrip	33.5	7.75	241	28	37.6	27.4	364	211	71.3	11.1	154	91	119

[1]Kroopnick and others, 1978.
[2]Chalcedony.
[3]Quartz conductive cooling.

Yamanaga, 1968). Ground-water transmissivities are typically 5×10^4 darcies (Mink, 1977; Druecker and Fan, 1976) and hence ground-water residence times, as indicated by tritium dating (table 56.2), are typically less than 10–20 years (Kroopnick and others, 1978); discharge of basal fresh water in coastal springs has been estimated at 88–131 m^3/s (Stearns and Macdonald, 1946; Davis and Yamanaga, 1968; Macdonald and others, 1983).

The temperatures and chemical compositions of ground water on the LERZ (table 56.2) span a broad range and suggest that recharge to the basal ground water in this region is received from several very different reservoirs. Four candidate sources could be anticipated in the region: cold, fresh meteoric recharge; cold sea water; hydrothermal fluids of meteoric origin; and hydrothermally modified sea water. The most convenient tracers that can distinguish these possible reservoirs are temperature, chloride-ion concentration, and the chloride-ion:magnesium-ion ratio. Above-ambient ground-water temperatures are clearly indicative of hydrothermal recharge; chloride-ion concentrations permit the identification of fluids of sea-water origin; and, because magnesium has been found to be heavily depleted by hydrothermal processes (Bischoff and Seyfried, 1978; Cox and Thomas, 1979), the chloride:magnesium ratio is able to provide a qualitative indication of the degree of hydrothermal modification undergone by fresh or saline water independent of the measured temperature. A plot of chloride-ion concentration versus temperature and versus chloride:magnesium ratio (fig. 56.2) provides an indication of the relative contributions of the various candidate source fluids to the ground water in the LERZ. Endmember compositions for the candidate sources are plotted for comparison: fresh water is represented by data from well 2986-01, located north of the rift; cold saline fluid by sea water; hydrothermal-meteoric recharge by the early, low-chloride fluids encountered at HGP-A; saline hydrothermal fluids by the fluid compositions found in high-temperature sea water-basalt experiments (Cl:Mg ratio; Seyfried and Bischoff, 1981) and at midocean-ridge hydrothermal systems (temperature).

The distribution of the data points on figure 56.2 suggests the following observations: (1) Chloride concentrations show a broad variation ranging from near fresh-water chloride to almost 30 percent sea-water chloride. (2) The chloride concentrations show a modest correlation with temperature: higher temperature ground water generally has a higher chloride concentration. (3) The degree of alteration of the thermal fluids, as indicated by the Cl:Mg ratio, generally varies and is well below that found in HGP-A or in high-temperature sea water-basalt experiments. (4) The Cl:Mg ratio is not well correlated with either temperature or chloride concentration: well 2982-01 shows a high temperature and high chloride concentration and a moderately depleted magnesium concentration (relative to sea water), well 2783-01 shows intermediate temperatures, high chloride, and only minor magnesium depletion, and well 2487-01 shows a low temperature and low chloride concentration but a significant magnesium depletion. These observations suggest that meteoric recharge is the predominant source for ground water in the region. However, sea water that has undergone varying degrees of hydrothermal alteration contributes as much as 30 percent

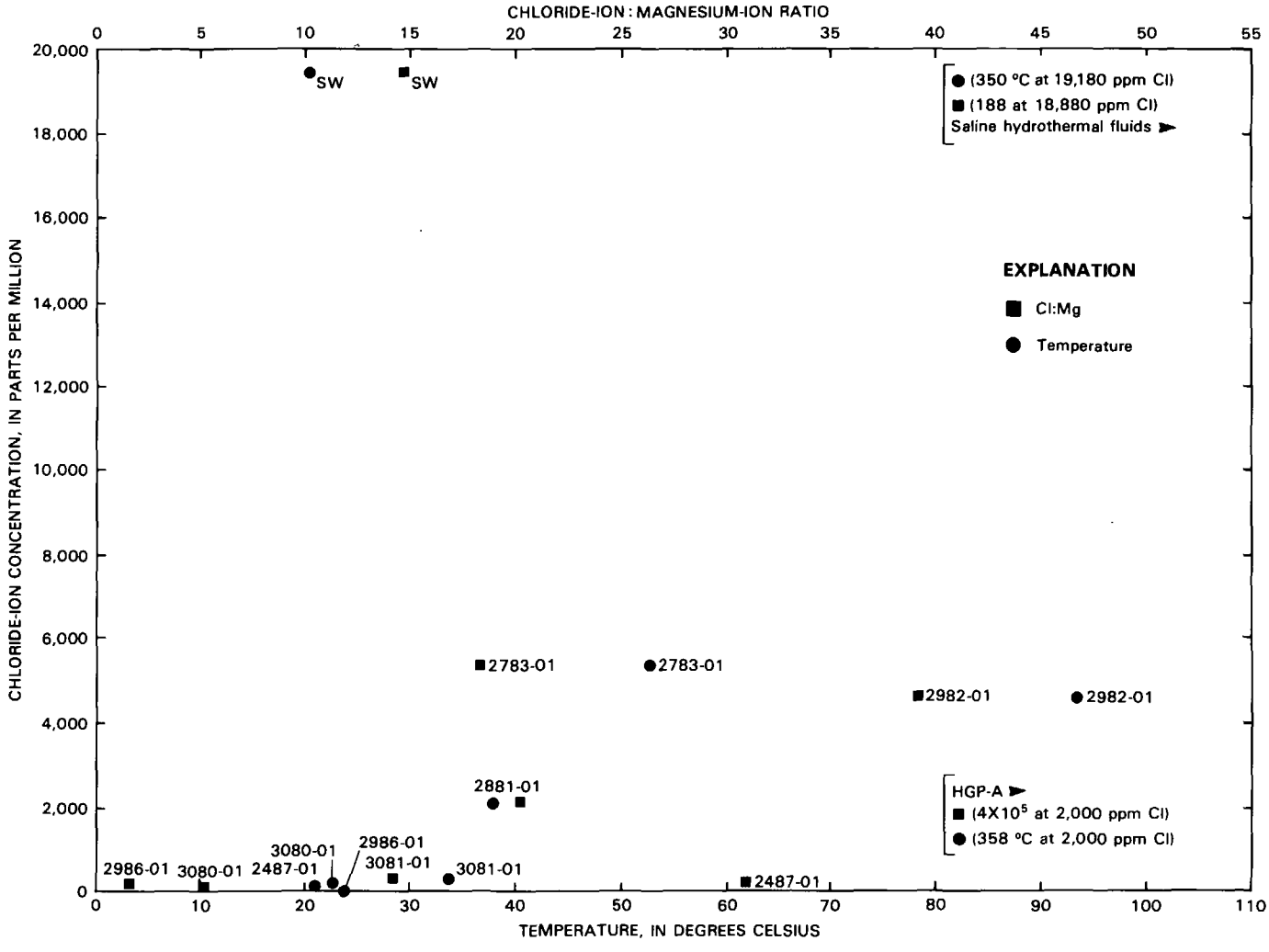

FIGURE 56.2.—Chloride-ion concentration versus temperature and versus chloride:magnesium ion ratio in shallow ground-water wells on lower east rift zone. Wells are identified by number (see fig. 56.1). Data from well 2986-01 represent fresh water; HGP-A data represent hydrothermal-meteoric recharge from early, low-chloride-ion fluids from HGP-A; saline-hydrothermal-fluid data represent high-temperature sea water-basalt experiments (Cl:Mg ratio) and midocean-ridge hydrothermal systems (temperature); SW, sea water.

of the recharge to the basal lens. The role of high-temperature, heavily modified, fresh and saline water in the basal aquifers is not as clearly defined. The chemistry of well 2487-01 could be modeled as a mixture of fresh ground water with a small addition of low-salinity, heavily altered hydrothermal fluid. The low temperatures suggest that the contribution from the latter source is, however, very small.

As many as four source fluids appear to have an influence on the ground-water temperatures and chemical compositions on the LERZ:meteoric recharge; cold, relatively unaltered sea water; higher temperature altered sea water; and low-salinity, heavily altered hydrothermal fluid.

The mixing of these multiple-source fluids in the shallow ground-water aquifers renders any attempt to apply chemical geothermometers highly suspect. Temperatures calculated using the Na-K-Ca geothermometer (Fournier and Truesdell, 1973; Fournier, 1981) are generally correlated with measured temperatures (table 56.2) although the correlation is far from uniform. The silica geothermometer (Fournier and Potter, 1982) similarly yields varying apparent temperatures that, although generally correlated with measured temperatures, do not yield significant insight into the deeper reservoir.

The rate of convective discharge of the thermal energy from the interior of the rift can be crudely estimated using the data from the shallow wells and assuming that: (1) the mean ground-water temperature of the aquifer south of the northern boundary of the ERZ and east of well 2487-01 is the average of that found in wells 2783-01, 2881-01, 3081-01, and 2982-01; and (2) the rate of fresh-water recharge is equivalent to the average rainfall rate in this area. Using these assumptions, the mean ground-water temperature is calculated to be about 54 °C. The average rainfall rate is approx-

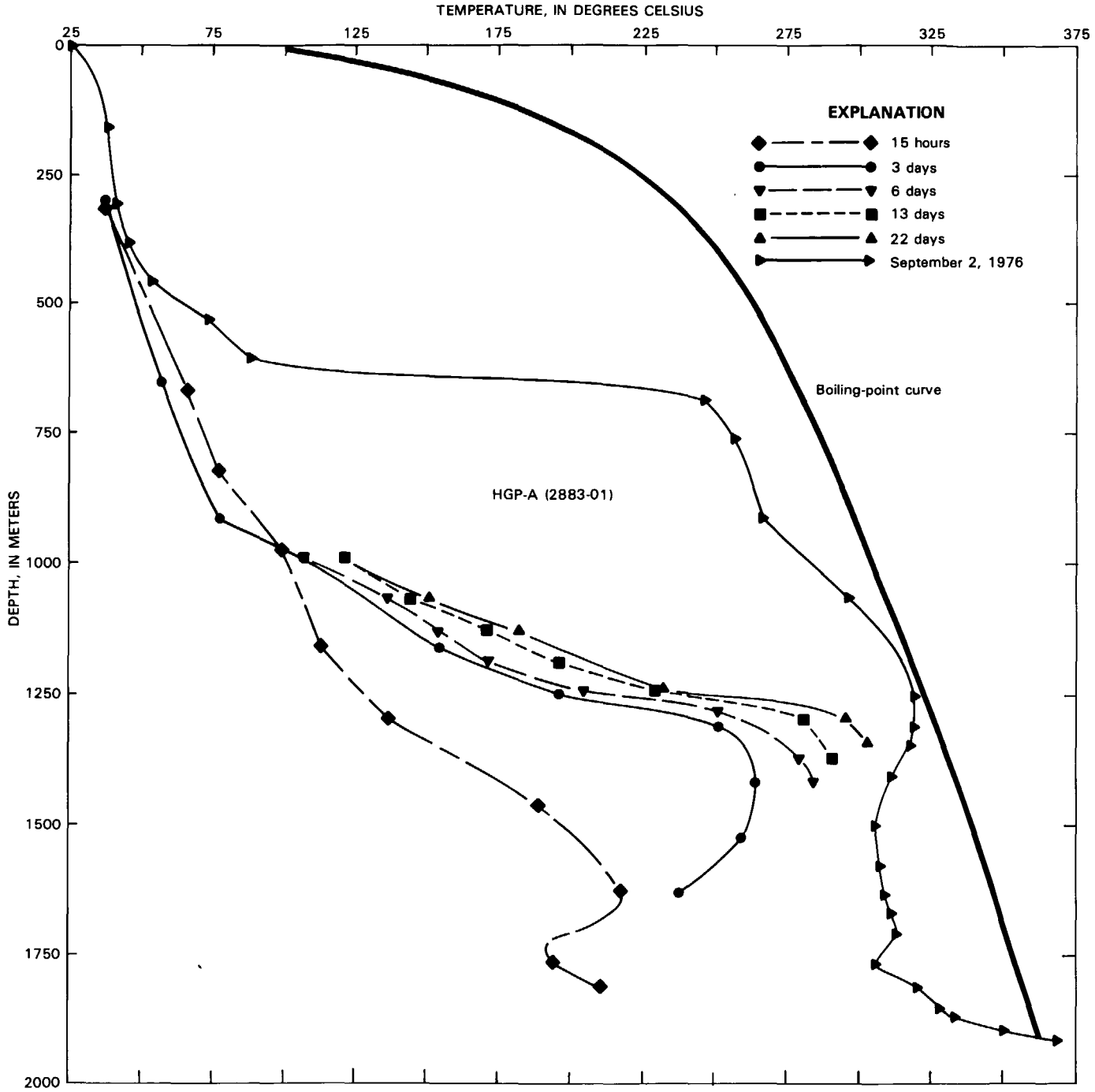

FIGURE 56.3.—Downhole temperatures measured in well 2883-01, HGP-A geothermal well. Individual curves reflect downhole temperature measurements made at specified times after mud circulation in well was suspended. Profile for 9/2/76 was measured with water in borehole.

imately 2.5 m/yr and the area of interest is approximately 25×10^6 m^2; thus, the total fresh-water recharge is approximately 62.5×10^6 m^3/yr. Hence the total thermal discharge in this limited region is estimated to be a minimum of 2.19×10^{12} kcal/yr or approximately 291 megawatts of thermal energy continuously. If this heat loss rate is extrapolated over the subaerial rift zone, 50 km of rift zone versus 10 km in the area of the thermal discharge, the heat loss would be approximately 1,455 thermal megawatts. The magma intrusive rate estimated by Dzurisin (1981) at 3×10^6 m^3/mo would bring an estimated 2,800 thermal megawatts into the rift zone. In light of the approximations made and the very short timespans considered, these values are in remarkably close agreement and may be interpreted to

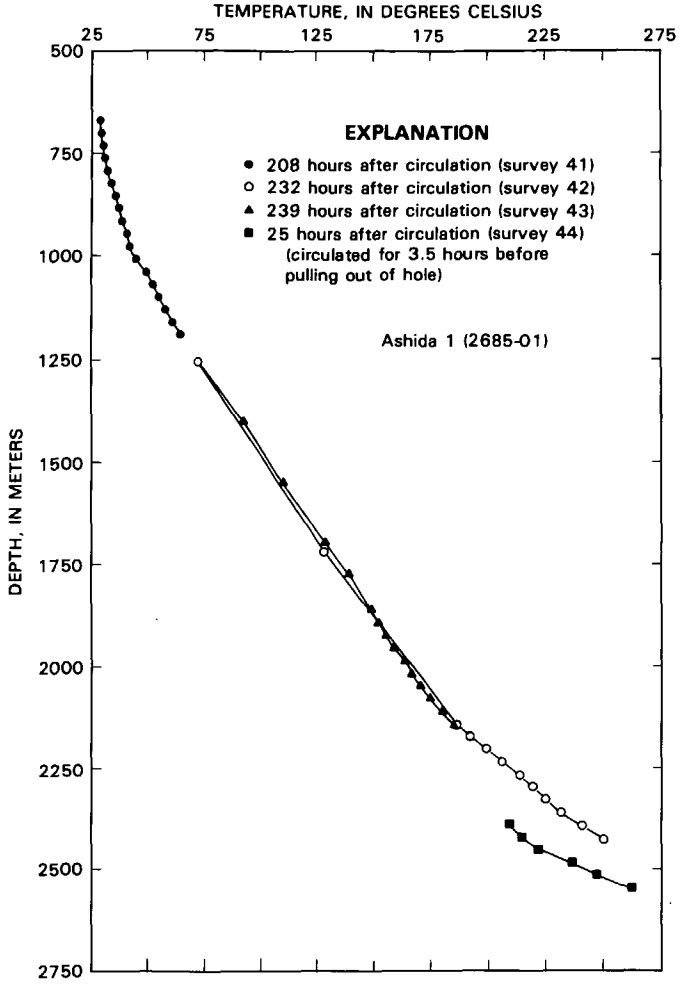

FIGURE 56.4.—Downhole temperatures measured in well 2685-01, Ashida 1.

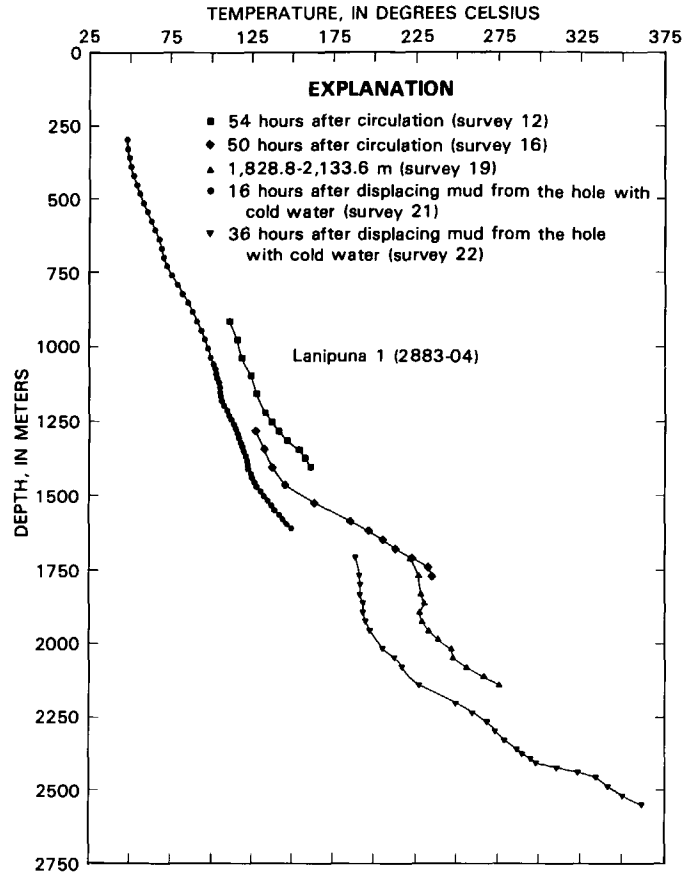

FIGURE 56.5.—Downhole temperatures measured in well 2883-04, Lanipuna 1.

indicate that the rates of convective heat loss to the shallow hydrologic system nearly balances the heat recharge from magmatic processes. If this interpretation is correct, it would in turn suggest that the residual heat present in a rift zone after cessation of intrusive activity would decrease very rapidly.

DEEP HYDROLOGY

The HGP-A well, completed in 1976, was the first deep research well drilled into the ERZ; seven privately funded deep wells have been completed subsequent to HGP-A in an effort to further define the geothermal resource discovered by this well. HGP-A was funded by several public and private agencies (the U.S. Department of Energy, National Science Foundation, State of Hawaii, County of Hawaii, and Hawaiian Electric Company), and hence more data for this well is publicly available than for the privately financed exploration wells. However, sufficient data has been released to allow us to permit limited extrapolation of the HGP-A data to other parts of the ERZ.

THERMAL CHARACTERISTICS

The available data from all the deep geothermal wells presently drilled in the LERZ are presented in table 56.1. All but two of the wells recently drilled penetrated to a depth of 2,000 m. The maximum temperatures encountered in each well were substantially above the normal geothermal gradient found in Hawaii. However, clear differences are present in the maximum temperatures encountered in each well, and examination of the temperature profiles is especially revealing. The temperature profiles used for each well must be interpreted carefully however: temperatures measured immediately after drilling and mud circulation cease are likely to be below equilibrium temperatures, whereas those measured after mud has been cleared from the hole may be affected by water circulation within the wellbore. The conditions under which the profiles were taken, if known, are noted.

The well profiles (figs. 56.3–56.6) generally show a shallow zone of moderate temperature over the first 500–1,000 m of the well. The moderate and relatively uniform temperatures in this interval reflect high meteoric recharge rates and rapid ground-water circulation and mixing in the very permeable subaerial and shallow submarine basalts. Underlying this zone is an interval of gradually

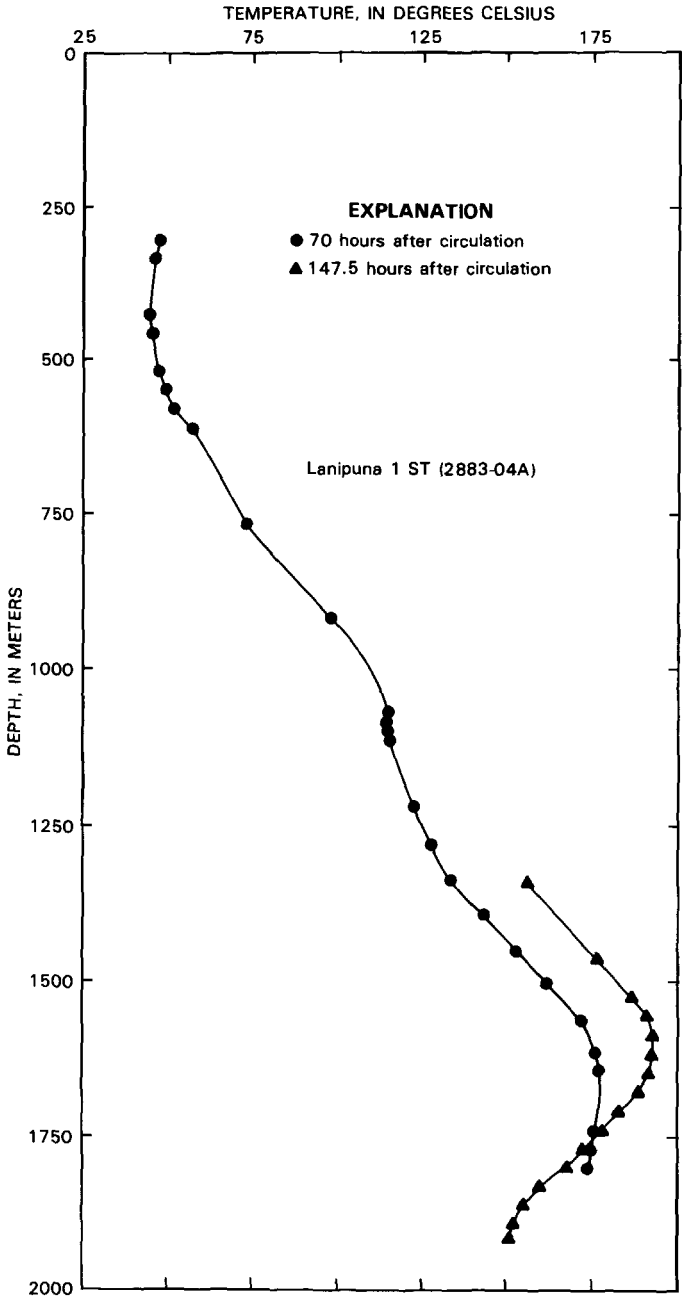

FIGURE 56.6.—Downhole temperatures measured in well 2883-04A, Lanipuna 1 side track.

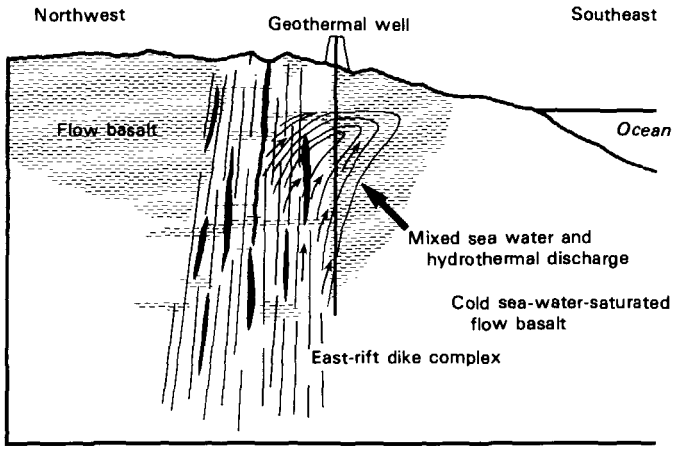

FIGURE 56.7.—Conceptual cross section of lower rift showing fluid circulation across rift zone. Thermal waters, exiting rift toward southeast, form a tongue of hot water overlying colder fluids below. Drilling on southern edge of rift would initially encounter thermal fluids at shallow depths, but at greater depths would reenter lower temperature aquifers.

increasing temperature, possibly representing a conductive temperature gradient, that indicates the decline in basalt permeability and a reduction in the rate of hydrothermal circulation. Below the conductive region, the temperature gradient may steepen and approach a curve corresponding to the temperature of steam-saturated water under hydrostatic pressure (the boiling curve). The conformance to the boiling curve suggests that the thermodynamic conditions in the deep reservoir are controlled by hydrostatic pressure and not by physical barriers, such as a reservoir cap rock. There are, however, exceptions to this general trend. The data from wells 2883-04A and 2883-05 show a distinct temperature turnover in the lower portions of both holes. The location of these wells on the southern boundary of the rift suggests that the wells may have passed through a reservoir outflow zone and penetrated into colder aquifers below (fig. 56.7). This interpretation leads to the speculation that the fractures and intrusives on the southern edge of the ERZ dip toward the north. If the rift structure had a southward dip, deeper drilling in this location would be anticipated to penetrate toward higher temperature intrusives.

A comparison of the temperature distribution among the wells and their relative locations shows that the maximum temperatures encountered are very site specific. For example, well 2883-04 encountered a bottom-hole temperature of >368 °C, the highest temperature reported for the LERZ wells, but a redrill of this well (2883-04A), completed as a slant-hole offset, encountered maximum temperatures of only 193 °C with a bottom-hole temperature reversal (figs. 56.5 and 56.6). The bottom of the redrill is less than 500 m from the bottom of its original straight configuration and from HGP-A, yet its peak temperature is more than 160 °C below the maximum temperatures encountered in either well. The temperatures encountered along the southern boundary of the ERZ vary greatly and may be strongly influenced by local hydrologic conditions. Although fewer wells have been drilled on the interior of the ERZ, the reported temperature information indicates somewhat more consistency than is found on its edge (Iovanitti and D'Olier, 1984).

PETROLOGY

The petrology of the rocks encountered in the deep exploration wells has not as yet been analyzed in detail. HGP-A was the only well from which cores were taken and hence is the only well for which bulk rock analyses can be done. However, analyses of the cuttings that have been released from the other wells (Barnwell

Geothermal Corp., unpublished data, 1985) are very informative as to the type of alteration present. The wells for which preliminary analyses are available include HGP-A, 2685-01, 2883-04, 2883-04A, and 2883-05; although analyses have been completed for wells 2883-02 and 2883-03, the data have not been released, and a second analysis is currently underway for archived samples from well 2883-02.

Samples of the cuttings from all of the wells indicate the presence of basalt throughout the section. The morphology of the basalt ranges from highly vesicular in the shallow subsurface to dense, nonvesicular pillow lava and dike rocks at depth. Hyaloclastites, palagonitized ash, and hematite were found at depths of 500–800 m below ground level and approximately 300–500 m below the current sea level (Stone, 1977; Barnwell Geothermal Corp., unpublished data, 1985). The morphology and oxidation of the basalt may indicate the approximate location of sea level at the time of extrusion of the lava. Rock textures range from aphyric glass, associated with chill margins or pillow lava, to olivine-phyric and plagioclase-phyric lavas.

The alteration mineralogy found in the individual wells follows a relatively consistent pattern. The shallow parts of the wells are typified by mild low-temperature alteration and deposition products such as montmorillonite clays, anhydrite, and calcite (Stone, 1977; Stone and Fan, 1978; Waibel, 1983). As the depths and temperatures increase, the degree of alteration generally increases as does the grade of metamorphism. Trends in the mineral suites show incipient alteration at intermediate temperatures that increases to total replacement of parent minerals by chlorite and lesser amounts of accessory products such as albite or, at the highest temperatures, epidote (figs. 56.8–56.11). In addition to the above, other alteration products found throughout the geologic section include calcite, anhydrite, zeolites, quartz, pyrite, and magnetite. Despite these general trends, the degree of alteration is by no means continuous throughout the section. Alteration is intermittent, and the extent of alteration at a given depth and temperature varies greatly, thus implying that the alteration process is highly dependent upon the access of (saline?) fluids to the interior of the rift. This intermittent alteration in turn suggests that, whereas temperature is the primary controlling factor in the alteration of the basalt, fracture permeability and fluid circulation within the rift are also major factors.

The depths of the various alteration minerals are significant to the model of hydrothermal circulation within the ERZ. As noted above, anhydrite is distributed throughout the cuttings from some wells and is apparently confined to only a few depth intervals in others. The retrograde solubility of anhydrite and the presence of relatively high concentrations of calcium and sulfate in sea water suggest that anhydrite is being deposited from sea water circulating within the ERZ. Laboratory studies of sea water-basalt reactions have shown that calcium sulfate is removed from sea water as anhydrite (Mottl and Holland, 1978; Mottl and Seyfried, 1980; Seyfried and Mottl, 1982) and that nearly quantitative removal of calcium occurs before temperatures reach 225 °C. The presence of anhydrite in both the low-temperature and the higher temperature parts of the rift could be accounted for by either of two possible

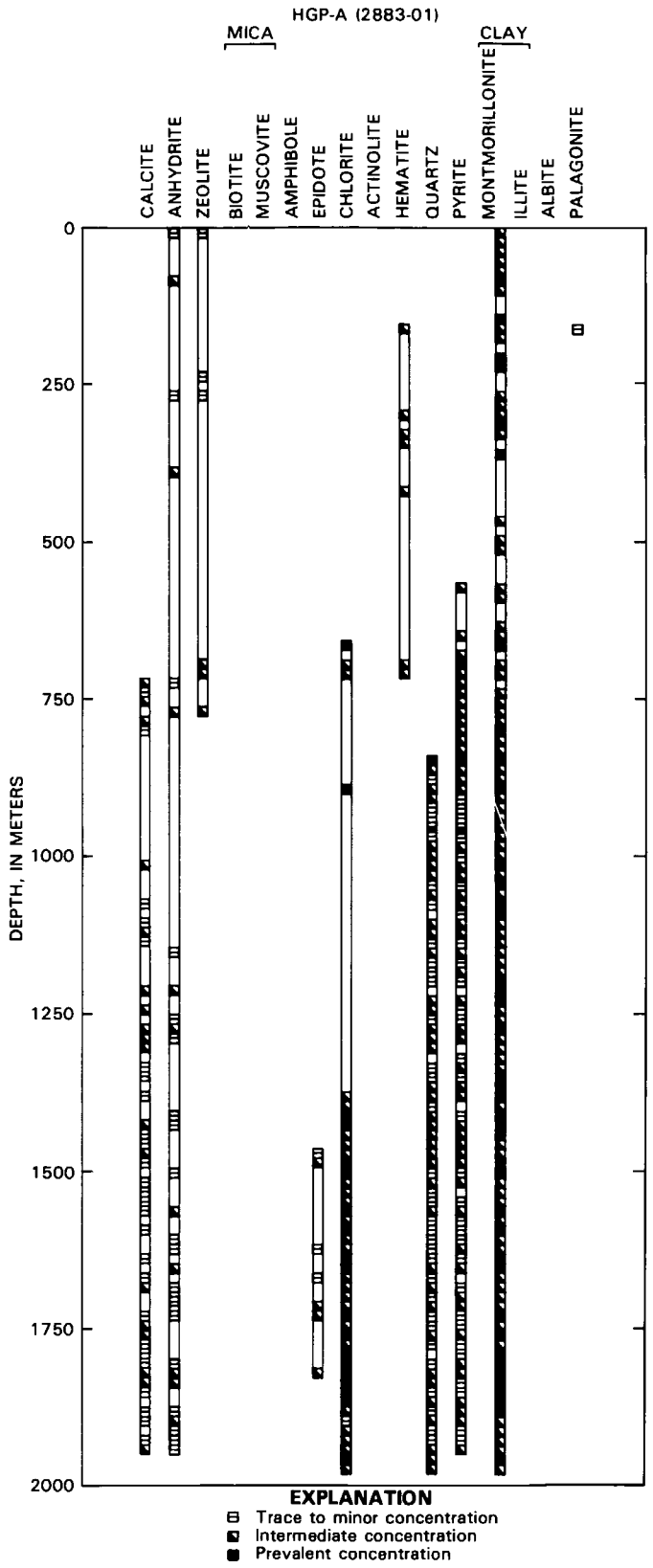

FIGURE 56.8.—Alteration mineral suites encountered with depth in HGP-A. (From Columbia Geosciences, unpublished data, 1983.)

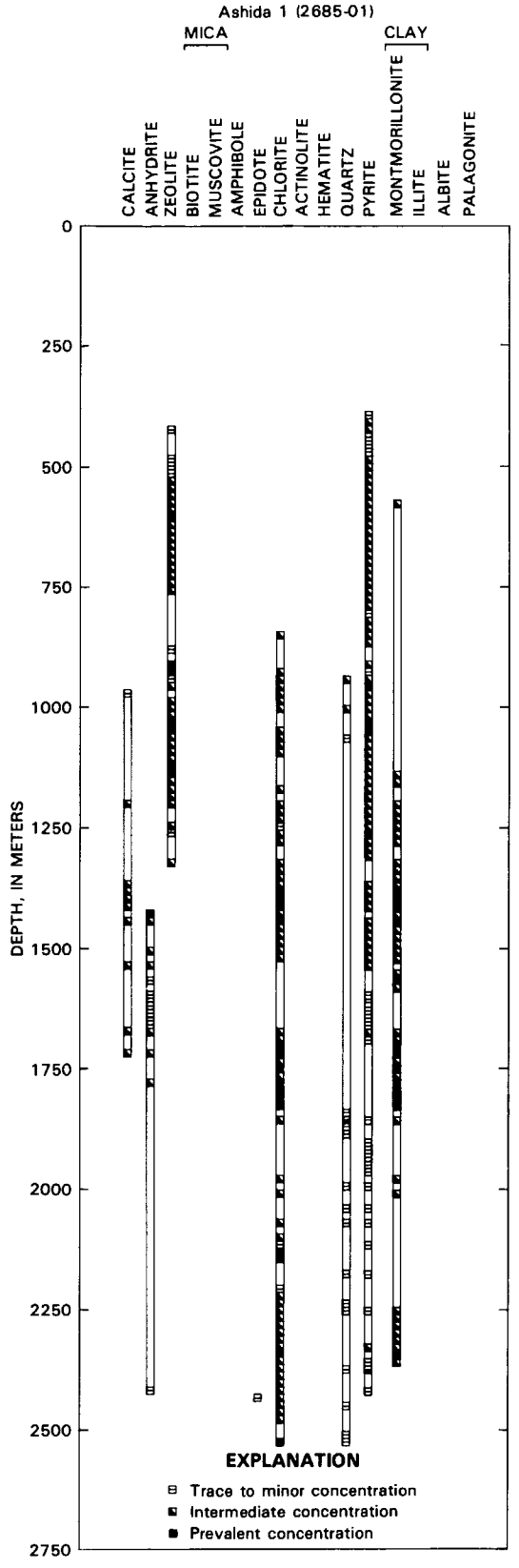

FIGURE 56.9.—Alteration mineral suites encountered with depth in well 2685-01. (From Barnwell Geothermal Corp., unpublished data, 1985.)

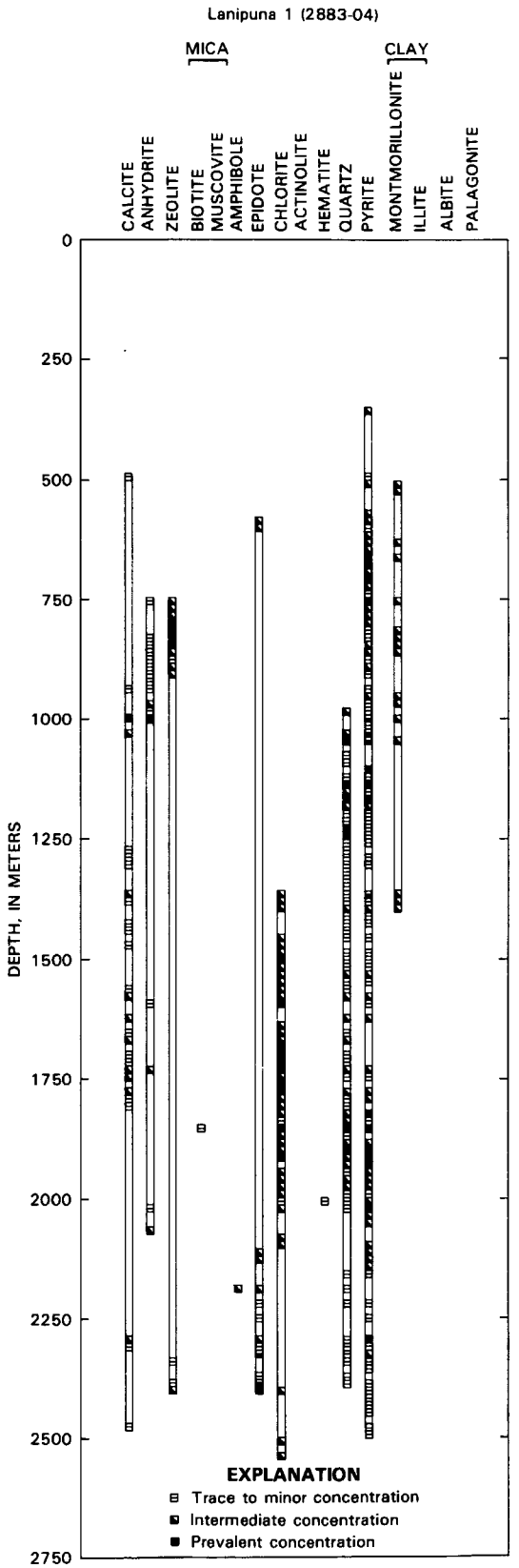

FIGURE 56.10.—Alteration mineral suites encounterd in well 2883-04. (From Barnwell Geothermal Corp., unpublished data, 1985.)

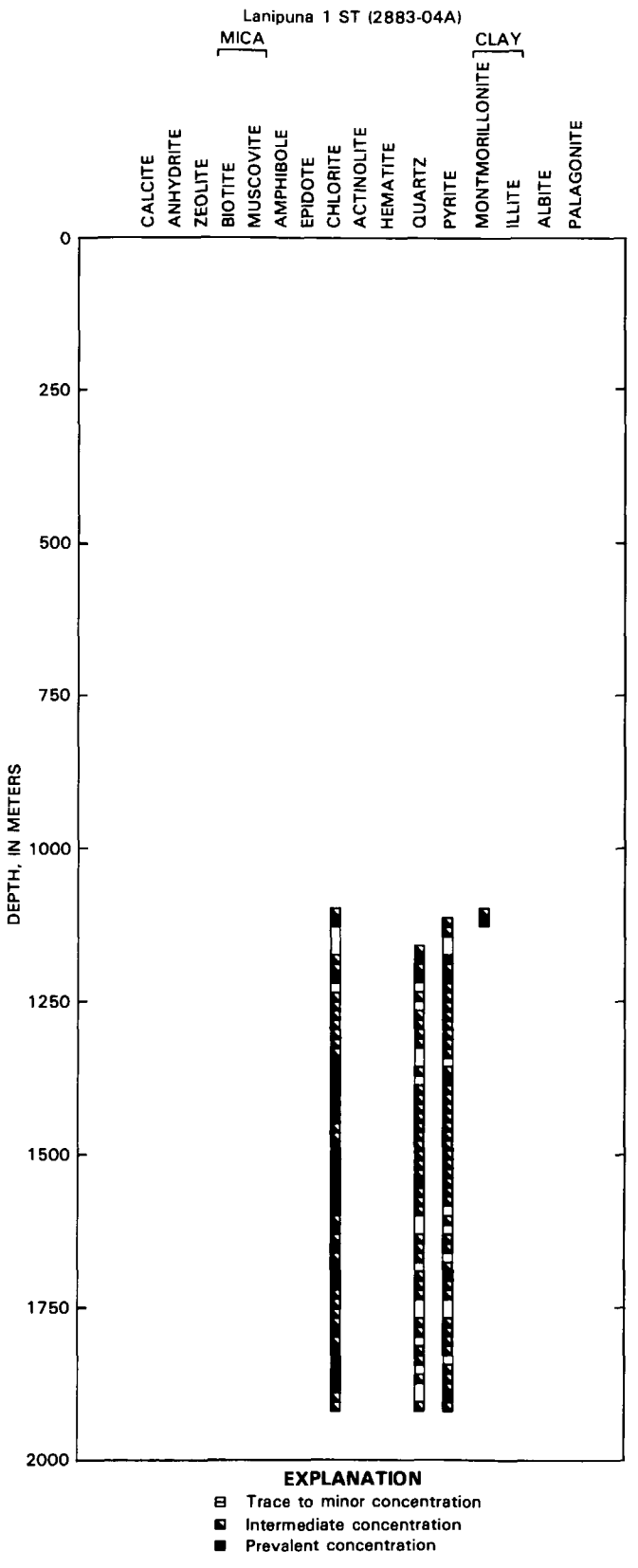

FIGURE 56.11.—Alteration mineral suites encountered in well 2883-04A. (From Barnwell Geothermal Corp., unpublished data, 1985.)

mechanisms: (1) anhydrite precipitation continues at higher temperatures as calcium is mobilized from the basalt matrix by hydrothermal alteration; (2) the part of the rift penetrated by these wells has undergone a complex history of heating and cooling associated with successive episodes of magmatic intrusions and subsequent cooling by hydrothermal circulation.

Pyrite and quartz are present throughout virtually the entire section below sea level. Due to the low temperatures and low metamorphic grades present in the shallow parts of the wells, the fluids precipitating these minerals probably did not originate at the depths of deposition, and hence they represent deposition from cooling hydrothermal fluids discharged from deeper within the rift.

Minerals found in the altered parts of the deep wells are quite similar to those found in sea water-dominated hydrothermal systems such as Reykjanes (Tomasson and Kristmannsdottir, 1972; Kristmannsdottir, 1976), in dredge samples from sea-floor spreading centers (Humphris and Thompson, 1978), and in laboratory studies of sea water-basalt reactions at high temperature (Mottl and Seyfried, 1980; Seyfried and Mottl, 1982). Clearly, the primary agent responsible for the alteration mineral suite observed is the intrusion of sea water into the interior of the ERZ. However, because the grade and intensity of hydrothermal alteration in each well varies with depth, the intermittent highly altered zones in the reservoir are interpreted to be the result of fracture-mediated intrusion of sea water into the interior of the rift.

PRODUCTION CHARACTERISTICS

The production characteristics of the individual wells have varied over a broad range. HGP-A initially produced a mixed-phase flow comprised of approximately 50 percent steam and 50 percent liquid, at approximately 45,000 kg/h. Discharge rates increased slightly during testing and, at the beginning of production for the HGP-A generator facility, amounted to approximately 50,000 kg/h. The steam:brine ratio is a function of wellhead pressure and, at the operating pressure of the facility, is approximately 57 percent liquid and 43 percent steam at a pressure of 1,200 kPa. Production from the well showed a gradual decline over the first 40 months of operation of the generator facility amounting to about 10–15 percent of its total output. However, during a 48-hour period on the fortieth month, wellhead pressures and production rates increased by slightly more than was lost during the prior forty months. The change occurred in distinct steps that were not accompanied by any seismic activity and hence were probably the result of a change in the wellhole, such as the elimination of an obstruction. This interpretation suggests that the total production from HGP-A may be limited by the borehole diameter rather than by the inherent productivity of the reservoir.

Analysis of the changes that have occurred in the production chemistry indicates that HGP-A is producing from two separate reservoirs having very different characteristics. The liquid or brine phase is apparently produced from an intermediate-depth reservoir having a temperature of approximately 260–280 °C, whereas dry-steam production is occurring from near the bottom of the well.

TABLE 56.3.—*Summary of HGP-A liquid-phase chemistry*

Date	Depth/ pressure	Chemical contents (parts per million) Na	K	Ca	Mg	Cl	SO_4	SiO_2	Na-K-Ca[1] temperature (°C)	Quartz[2] temperature (°C)	Water:rock ratio ([3])	([4])
12/2/76	1,300 m	480	85	17.3	0.7	920	--	740	262	290	3.2	0.71
2/9/77	103 kPa	720	135	30.1	.1	1,610	--	--	219		3.7	.81
4/22/77	103 kPa	1,480	277	72.2	.1	3,190	--	--	298		3.5	.77
1/16/80	910 kPa	1,520	224	33.9	.01	2,593	69	832	278	303	3.5	.78
6/12/81	103 kPa	900	200	25.5	.008	2,065	--	1,198	336	296	3.1	.67
9/4/81	1,200 kPa	1,890	295	66.5	.029	3,622	--	860	281	307	3.8	.84
12/11/81	103 kPa	1,590	300	33	.012	2,763	--	1,004	332	280	2.6	.58
6/7/82	1,170 kPa	3,120	525	122.5	.051	5,667	--	803	309	299	3.2	.71
11/16/82	1,170 kPa	3,940	650	217	.104	7,029	--	829	301	303	3.2	.71
5/4/83	1,170 kPa	4,220	675	270	.152	7,965	--	805	292	300	3.6	.80
12/5/83	1,100 kPa	4,650	763	319	.210	8,827	24	825	298	303	3.5	.77
6/26/84	1,100 kPa	4,840	773	489	.25	8,900	15	885	282	310	3.5	.77
11/28/84	1,100 kPa	5,420	733	399	.20	9,514	4.5	913	265	314	4.12	.91

[1]Fournier, 1981.
[2]Fournier and Potter, 1982.
[3]Water to rock ratio based on original sea-water potassium concentration of 399 ppm and Kilauea tholeiite average concentration of 4,500 ppm, and a potassium removal efficiency of 100 percent.
[4]As above but using an extraction efficiency of 22 percent (Seyfried and others, 1984).

The production characteristics of the other geothermal wells on the LERZ have not been as well characterized as that from HGP-A; however, the data available indicate widely divergent discharge patterns. Short-duration production tests conducted on three wells north of HGP-A (2883-02, 2883-03, 2883-06) have clearly confirmed the presence of dry-steam production from the LERZ reservoir: two of these wells initially produced a mixed phase of steam and water that changed to dry steam over a period of a few hours (Iovanitti and D'Olier, 1984). The production rates from the first two wells were reported to be 15 t/h and 33 t/h, respectively; however, the duration of the tests conducted and the presence of debris in the hole suggest that these are neither equilibrium nor representative flow rates. (This third well, 2883-06, was also productive; however, the engineering data are presently confidential.)

In contrast to the wells located north of HGP-A, three of the wells drilled on the southern boundary of the rift (2883-04, 2883-04A, and 2685-01) were unable to sustain production at all. Although permeable zones, as indicated by drilling-mud-loss records, were encountered in these wells, the available records indicate that the permeable zones were much more limited south of the rift than at HGP-A or in the wells more interior to the rift. The fourth well, 2883-05, encountered an extremely permeable fracture at a depth of approximately 1,600 m that did not have sufficient temperature to sustain production.

RESERVOIR CHEMISTRY

The HGP-A well is the only deep well in the LERZ for which a significant number of samples have been analyzed, and hence the data set from HGP-A yields the most complete picture of the chemical processes underway in the hydrothermal system associated with the ERZ. The limited data set available from the other wells is, however, consistent with the model derived from HGP-A.

The composition of the fluids produced by HGP-A during its production life has shown complex changes during each period of discharge and between periods of discharge. Samples obtained from downhole samplers and from production fluids taken immediately after well completion showed very low dissolved solids concentrations (table 56.3); chloride levels generally ranged from about 1,000 mg/kg to 2,000 mg/kg whereas the total-solids content was approximately 3,000 mg/kg to 5,000 mg/kg. Subsequent samples of discharge fluids showed an increase in the salinities during each well test but a slight reduction in chloride concentrations between tests. The rate of increase during the first production tests was relatively rapid; initial chloride concentrations of approximately 1,000 mg/kg in the liquid phase increased to more than 2,000 mg/kg after steam production (flashing) began and continue to increase throughout the period of discharge. The longest test period, prior to the installation of the generator facility, spanned 1,000 hours; the chloride concentration in the brine at the conclusion of that test was approximately 3,200 mg/kg.

Downhole sampling during the preliminary testing provided chemical data indicating that production was occurring from at least three aquifers: one at a depth of approximately 700 m produced cold saline water; a second at a depth of approximately 1,500 m produced low-salinity fluids; and a third at a depth of approximately 1,900 m produced low- to intermediate-salinity fluids (Kroopnick and others, 1978). Although a subsequent recasing program sealed off the cold, high-salinity aquifer, continuous discharge of fluids from HGP-A between 1983 and 1985 continued to generate substantial increase in salinity (fig. 56.12); by the end of 1985 after four years of continuous production, the chloride concentrations reached a level of approximately 10,000 mg/kg.

The other major dissolved solids present in the brine phase include sodium, potassium, calcium, and silica. The concentrations of all but the latter have shown increases similar, although not

identical, to those observed for chloride (table 56.3). Silica concentrations in the brine have shown little if any verifiable change beyond those associated with changes in the power plant operating conditions.

In contrast to the evolution of the brine chemistry, the gases present in the steam phase have shown very modest variations. Although the gas-chemistry data obtained from HGP-A during the preliminary well testing are suspect due to analytical and sampling difficulties, the data indicate that the major gases, CO_2 and H_2S, were present at concentrations of less than 1 percent by weight of the steam. Subsequent analyses, conducted during power plant operations, determined that the concentrations of the major gases were approximately as follows: CO_2, 1,250 mg/kg; H_2S, 950 mg/kg; N_2, 130 mg/kg; H_2, 12 mg/kg; and CH_4, 1 mg/kg. Changes in the gas concentrations were observed during the initiation of well flow that correspond to stabilization of the reservoir in response to production, but subsequently they declined at a very modest rate during the three and one-half years of power plant operations. The gas concentrations currently amount to: CO_2, 1,150 mg/kg; H_2S, 850 mg/kg; N_2, 120 mg/kg; and H_2, 12 mg/kg.

Although the chemistry data available from the other privately financed geothermal wells is quite limited, the following information has been made available: Wells 2883-04 and 2883-04A, located on the southern boundary of the rift zone, encountered fluids having salinities approximately equivalent to sea water in the permeable, intermediate-temperature parts of the holes. Due to inadequate permeability at depth, these wells were unable to produce steam or a high-temperature mixed phase. Wells 2883-02 and 2883-03, north of HGP-A, produced fluids having dissolved-solids concentrations of a few thousand milligrams per kilogram to near the solids saturation point, depending upon the wellhead pressures and steam qualities during the production tests. Reported total gas concentrations were approximately 2,000 mg/kg of which 1,100 mg/kg was H_2S (Iovanitti and D'Olier, 1984). Testing of the private exploration wells indicated that multiple production zones were encountered in all wells, and hence the precise source for the fluids are known only to the extent that they are derived from a depth greater than the casing depth of the wells or about 1,100 m below sea level.

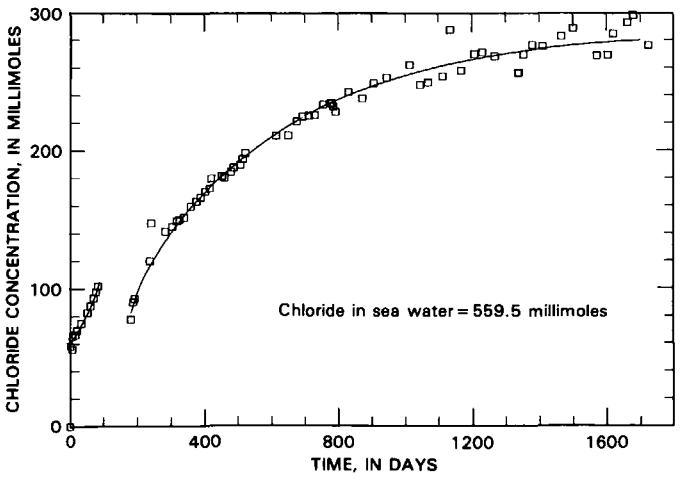

FIGURE 56.12.—Chloride concentrations in brine phase from HGP-A versus duration of production. The interval from day 84 to day 183 represents a period from September 4, 1981, to December 11, 1981 when flow from the well was suspended.

DISCUSSION OF CHEMICAL DATA

One of the most striking aspects of the fluid chemistry data from HGP-A is the very low salinities encountered at depth immediately after well completion. This result was not anticipated, and the presence of fresh water at depth was initially attributed to the presence of drilling fluids lost to the deep production aquifers. However, analysis of tritium levels present in surface waters used for drilling and those from the reservoir (Kroopnick and others, 1978) conclusively demonstrated that the early reservoir fluids were not contaminated by recent surface water. Subsequent analyses conducted after an extended flow test of the well reconfirmed the absence of significant tritium activity in the reservoir fluids (Thomas, 1980).

Because of the density difference between fresh and saline water, the Ghyben-Herzberg model, typically used to describe ground-water hydrology in an island environment predicts that a fresh-water lens should be found floating above sea water in the basal aquifers. The thickness of this lens is dependent upon rainfall recharge rates and the effective permeability of the basal aquifers; in the vicinity of HGP-A, a lens thickness of approximately 70 m would be predicted. However, the presence of a heat source in the ERZ invalidates one of the major assumptions of the Ghyben-Herzberg model: that a density difference exists between fresh and saline water. With a heat source present in the ERZ, sea water entering the hydrothermal system and heated to reservoir temperatures will have a density less than that of cold fresh water. Thus, cold rainfall recharge can enter the ERZ from above and displace warmer, less dense saline water entering the ERZ laterally. This factor alone probably cannot account for the exceptionally low salinities observed at depth in the reservoir: cold saline water should exert a higher hydrostatic pressure on the reservoir than cold fresh water if the hydraulic head heights and permeabilities of the respective infiltration pathways are equal. Hence, other factors may play a key role in the near exclusion of sea water from the deep hydrothermal reservoir. As discussed above, the rift consists of near-vertical tabular dikes and fractures trending in an east-west direction. Hydrologic studies (Stearns and Macdonald, 1946; Takasaki, 1978; Macdonald and others, 1983) have shown that the permeability of intrusive materials may be several orders of magnitude lower than normal country rock, and therefore, the permeability of the rift zone transverse to its strike should be very much lower than the surrounding rocks outside the dike complex. The presence of fractures parallel to the intrusives serves to further increase the permeability of intervening extrusive rocks within the dike complex. Hence, the structure of the ERZ increases the naturally existing east-west and vertical permeability to fresh-water recharge to the rift but inhibits the entry of sea water from the south due to the lower transverse permeability of the dike system.

A third factor that may play a role in the exclusion of sea water from the ERZ is the reaction sequence undergone by sea water when it is heated to reservoir temperatures. Extensive studies conducted on sea-water chemistry at elevated temperatures (Bischoff and Dickson, 1975; Mottl and Holland, 1978; Bischoff and Seyfried, 1980; Seyfried and Mottl, 1982; Pohl and Liou, 1983) have demonstrated that, when sea water is heated in the presence of basalt, a number of reactions occur that can substantially alter the chemical composition of the sea water and the mineral suites present in the rock. Most pertinent to the present analysis are the findings that: (1) the retrograde solubility product of calcium and sulfate ions in sea water result in anhydrite deposition (Mottl and Seyfried, 1980), and (2) reactions at temperatures of 300 °C result in the devitrification of basalt glass and the breakdown of the common basalt minerals and result in the deposition of smectites, chlorite, wairakite, and other alteration products. One sea water-basalt experiment (Pohl and Liou, 1983) was conducted in a flow-through cell that reportedly became plugged due to alteration mineral deposition in less than 48 hours. Similar reactions occurring in the natural sea water-basalt hydrothermal system on the ERZ may result in a sequence of fracture-induced permeability and subsequent sealing by deposition of alteration minerals along the southern (seaward) boundary of the rift. The presence of anhydrite, deposited as a vein-filling mineral, and of intermittent zones of intensely altered but low-permeability basalt in the cuttings from the deep geothermal wells on the LERZ tend to further substantiate this process. Thus the initial absence of sea water in the reservoir fluids encountered by HGP-A can be accounted for by the inhibition of sea-water recharge into the high-temperature part of the rift by permeability barriers imposed by the dike complex, self-sealing by alteration mineral deposition from hydrothermally heated sea water, and the more rapid recharge of cold meteoric water along highly permeable vertical fractures within the rift.

The increasing trend of dissolved solids in the fluid phase produced by HGP-A was initially interpreted to indicate that fluid withdrawal from a single-phase low-salinity aquifer had generated an expanding zone of boiling around the borehole (Thomas and Sakai, 1983). This model postulated that migration of the boiling front into the reservoir led to a progressively steam-depleted (and solids-enriched) residual brine phase entering the borehole. However, this model also required a progressive decline in the relative volume of brine to steam as the boiling front advanced into the reservoir. The more than fivefold increase in dissolved solids in the HGP-A brines, however, have not been accompanied by a similar decrease in the brine:steam ratio. Hence, the single-production-zone model has been abandoned in favor of a multiple-production hypothesis in which at least two separate production zones are supplying fluids to the well: one aquifer supplying a higher temperature steam phase and a second supplying intermediate-temperature brine and steam.

Other data supporting this model include the gas concentrations present in the HGP-A steam and the reported production characteristics of other wells in the LERZ. As noted above, the concentrations of noncondensable gases present in the HGP-A steam have changed only slightly during the production history of the well. A single production zone undergoing progressive boiling should show a rapid decline in the noncondensable gas concentration present in the steam due to the strong partitioning of the dissolved gases in the steam phase. The near constancy of the gas concentrations in the steam phase thus substantiate multiple, independent production aquifers. Further support for the production of brine and steam from separate aquifers in HGP-A comes from the production characteristics of wells 2883-02 and 2883-03. Both wells are drilled and cased to greater depths than HGP-A and both produced a single-phase steam flow within hours of the beginning of their flow tests. Thus the reservoir on the LERZ is clearly capable of producing dry steam. The absence of a brine phase in the more recently completed wells is attributed to their having been cased to greater depths than HGP-A and thus having excluded lower temperature production aquifers.

The steam-production zone present in HGP-A and other wells on the LERZ is not, however, identical to the more classic dry-steam reservoirs found at The Geysers, California, and Larderello, Italy. The latter have lower equilibrium temperatures and are significantly underpressured: the pressure within the steam zone is less than hydrostatic pressure at equivalent depths, indicating that porosity within the reservoir is filled with a low-density two-phase fluid probably consisting of steam and liquid water (Fournier, 1981). The reservoir temperatures in the deeper parts of the ERZ have generally been much higher than those found at The Geysers and at Larderello and, in the high-temperature wells, follow the boiling temperature versus hydrostatic pressure curve with depth. Wellhole-circulation and wellhead-pressure patterns during shut-in (when there is no well discharge at the surface) indicate that reservoir pressures are sufficient to maintain circulation from deeper permeable zones to shallow discharge points in the uncased parts of the roles. Even though dry-steam production is occurring from the deep reservoir, a single-phase fluid is believed to be present at depth that, because of the high temperature and low permeability in the reservoir, boils entirely to steam prior to entry into the wellhole.

The increased salinity of the liquid phase produced by HGP-A is believed to be the result of sea-water intrusion into the reservoir. No other source of chloride ion of sufficient magnitude to account for the observed changes exists in the Hawaiian environment (evaporites, sediment basins, and so forth) and the sodium:chloride ratio in the fluids is nearly identical to that for sea water (fig. 56.13). However, comparison of the chemical composition of the brines with that of sea water indicates that a substantial modification of the sea-water chemistry has occurred: potassium and calcium have been heavily enriched, whereas magnesium and sulfate have been heavily depleted (table 56.3; figs. 56.14–56.16). These chemical alterations are virtually identical to those observed in laboratory sea water-basalt reaction studies and in fluids discharged from mid-ocean-ridge hydrothermal systems. In very general terms (for more detailed discussion see, Mottl and Seyfried, 1980; Reed, 1982; Seyfried and Mottl, 1982; Mottl, 1983), the sequence of reactions found to occur in hydrothermal sea water is characterized by an initial loss of calcium ion to the deposition of anhydrite, the removal

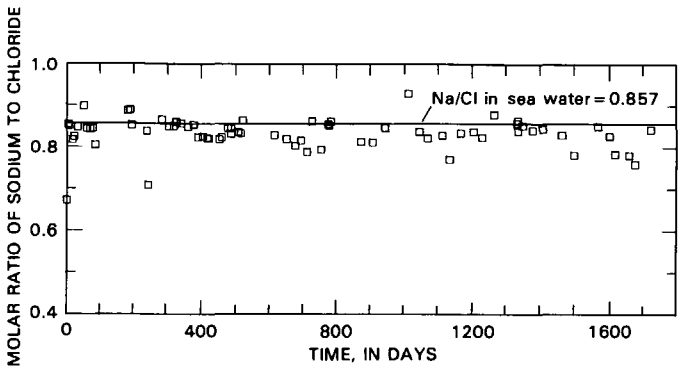

FIGURE 56.13.—Sodium-ion to chloride-ion ratio in HGP-A brines versus duration of production. Straight line represents sodium-ion to chloride-ion ratio in sea water.

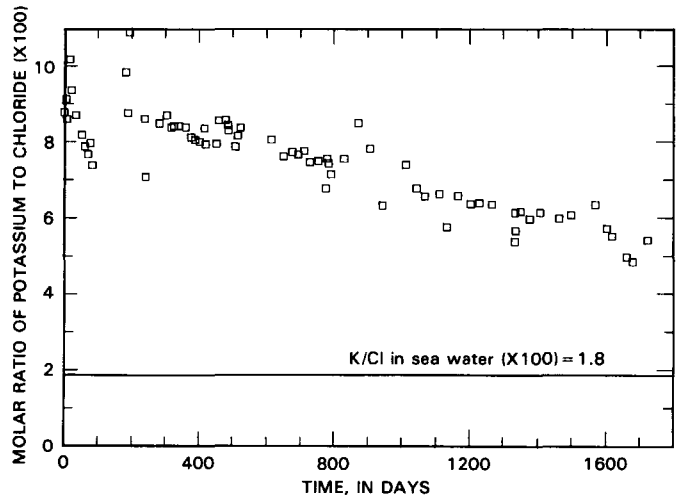

FIGURE 56.14.—Potassium-ion to chloride-ion ratio in HGP-A brines versus duration of production. Straight line represents potassium to chloride ratio in sea water.

of magnesium ion to the formation of magnesium oxysulfate ($MgO \cdot nMgSO_4 \cdot (n-2)H_2O$; Bischoff and Seyfried, 1978), a radical decline in pH, and an increase in the sea-water buffering capacity due to the presence of weak acids such as HCO_3^-, HSO_4^-, and HCl^0, and of $MgOH^+$, a weak base. These chemical changes occur progressively over a temperature of approximately 70–350 °C and are independent of sea water-basalt reactions. When sea water is heated in the presence of basalt, the increased hydrogen-ion concentration and buffering ability of the fluid drives numerous reactions that proceed only very slowly or not at all at lower temperatures and include the alteration of residual glass and primary calcic and sodic mineral suites to smectites, mixed layer clays, and chlorite. These reactions result in the removal of potassium and lithium from basalt, exchange of calcium for the magnesium lost from sea water, and under some conditions, depletion of sodium from sea water.

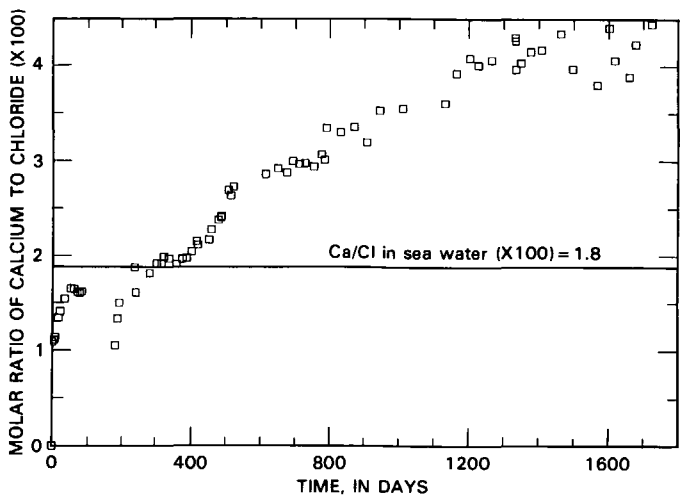

FIGURE 56.15.—Calcium-ion to chloride-ion ratio in HGP-A brines versus duration of continuous production. Straight line represents calcium to chloride-ion ratio in sea water.

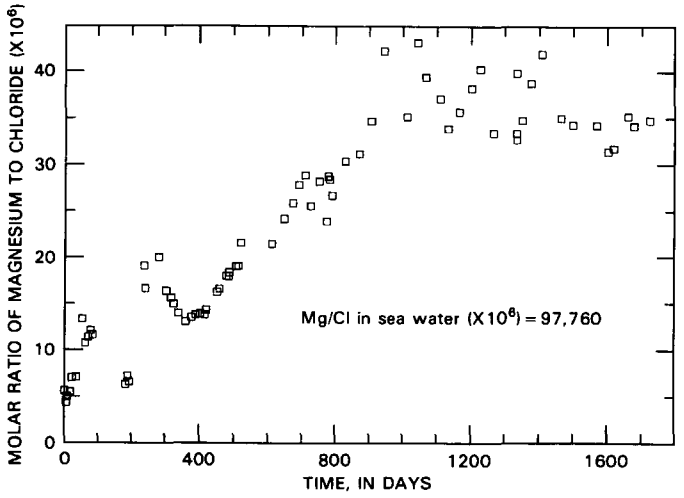

FIGURE 56.16.—Magnesium-ion to chloride-ion ratio in HGP-A brines versus duration of continuous production. Magnesium to chloride ratio in sea water is a factor of approximately 20,000 above that in HGP-A brine and is not plotted.

The hydrolysis of the primary silicates to the alteration-mineral assemblage buffers the pH of the sea water-basalt system at approximately 6.8 as long as primary minerals are available to exchange Ca for H^+ released by the loss of $Mg(OH)_2$. However, under sea water-dominated conditions, when the total magnesium available from sea water exceeds the potassium and calcium present in the basalt, pH will be buffered in the range of 2–3 depending upon temperature. This condition has been found to occur at sea water:rock ratios of approximately 50 and above (Mottl and Seyfried, 1980).

The alteration mineral suite typically generated by these reactions includes: zeolite, montmorillonite, illite, anhydrite, magnetite, pyrite, quartz, chlorite, epidote, actinolite (Mottl and Seyfried, 1980; Reed, 1982; Seyfried and Mottl, 1982). The conditions under which an individual mineral species is generated or is stable depends upon kinetics, temperature, and water:rock (W:R) ratios. Although a detailed discussion of the theoretical modeling of mineral stability (Helgeson and others, 1981; Reed, 1982, 1983; Reed and Spycher, 1984) is beyond the scope of the present discussion, the most pertinent findings of these studies to the present analysis are that: high temperatures and low W:R ratios favor epidote, actinolite, and pyrite deposition; high W:R ratios favor chlorite deposition; and cooling hydrothermal fluids precipitate pyrite and, at low W:R ratios, magnetite.

The current depletions of magnesium and sulfate and enrichments of lithium, potassium, and calcium in the fluids at HGP-A are consistent with the theoretical and experimental studies of the sea water-basalt system. The evolution of the chemical composition with time, from the initial production chemistry to the present, further indicates that the apparent W:R ratio has changed during the 4-yr discharge of HGP-A. Calculation of this ratio, using the potassium-ion enrichment of the sea-water component suggests that it was initially substantially less than 1 and that the present ratio approaches 2. A plot of the relative proportions of the three ions most sensitive to the W:R ratio further demonstrates its evolution with time (fig. 56.17). The trends evident in the changing ion ratios suggest an increasing calcium and magnesium concentration relative to potassium. Comparison of the trend in the brine chemistry with laboratory-derived data suggests that, as the sea water:rock ratios evolve, calcium ion will initially predominate at W:R ratios of approximately 10 and, as the ratio increases, magnesium will begin to displace calcium as the major component. More importantly, as the magnesium and W:R ratio increases, the pH will begin to decline due to the depletion of calcium from the reservoir rock (Mottl and Seyfried, 1980; Seyfried and Mottl, 1982). As the pH declines, the reservoir fluids will become far more aggressive and begin to mobilize higher concentrations of transition elements such as iron, lead, zinc, and tin.

A second aspect of the changing brine chemistry is the apparent change in reservoir temperatures that can be calculated. The reservoir temperatures calculated using the Na-K-Ca geothermometer initially indicated a temperature of approximately 300 °C; the silica geothermometer when corrected for steam loss (Fournier and Potter, 1982) yielded a temperature of 305 °C, in good agreement with the Na-K-Ca geothermometer. Na-K-Ca temperatures calculated using later chemical data from HGP-A have shown a decline in the calculated temperatures to approximately 250 °C (table 56.3). Silica, however, does not show a similar temperature change. The declining temperature calculated from the Na-K-Ca concentrations are interpreted to reflect the intrusion of lower temperature sea water into the intermediate-temperature aquifer tapped by HGP-A; the apparent discrepancy between the Na-K-Ca and silica temperatures is the result of the more rapid equilibration of silica to reservoir temperatures in the intruding fluids.

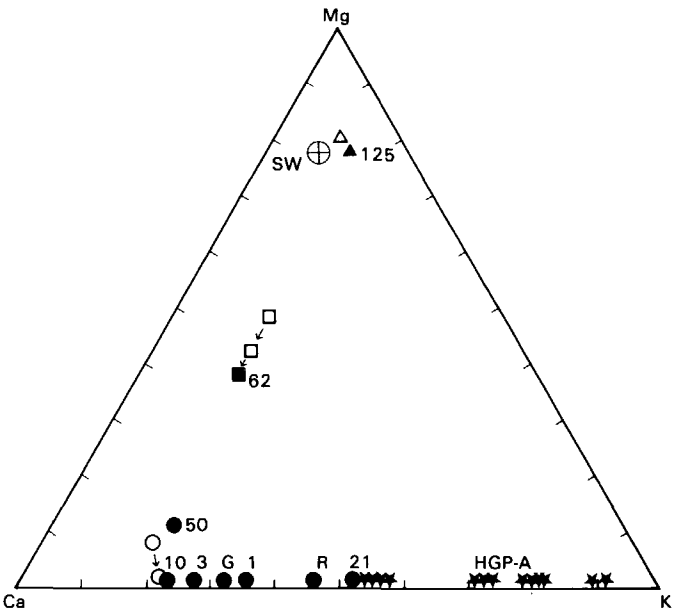

FIGURE 56.17.—Relative potassium-, calcium-, and magnesium-ion concentrations in: HGP-A geothermal brines (filled stars); hydrothermal vent fluids from 21° N., on East Pacific Rise (21) and Galapagos (G); Reykjanes geothermal system (R); liquid phase of high-temperature sea water-basalt experiments at water:rock ratios of 1, 3, 10, 50, 62, and 125 (labeled 1, 3, 10, 50, 62, and 125, respectively); and sea water (SW). Open symbols represent nonequilibrium compositions at noted water:rock ratios. HGP-A fluid chemistry has evolved from a relatively potassium-rich composition to an increasingly calcium-rich solution and is now approaching relative ion concentrations of fluids at 21° N.

The interpretation of the chemistry of the noncondensable gases in the HGP-A discharge is not as straightforward as that for the water chemistry, because two aquifers, having different gas concentrations, are supplying steam to the total flow in the well. Any attempt to partition the gases between the two production zones must rely on equilibrium calculations that will be dependent upon reservoir temperatures. A second aspect of the gas data that inhibits equilibrium calculations is that a significant proportion of the carbon dioxide present in the noncondensable gases is derived from surface sources and there is insufficient isotopic data to clearly differentiate the contributions from the available sources of carbon: sea water, ground water, and magmatic water.

In spite of these problems, several tentative interpretations of the gas chemistry can be offered. Comparison of the gas concentrations found in the steam at HGP-A with those found in laboratory sea water-basalt experiments tends to substantiate the W:R ratios inferred from the brine chemistry. Although mixing of the gas phase from the two production zones does not allow us to apportion the amount of gas from each, H_2S concentrations present in the total discharge (water plus steam) suggest that the average W:R ratio is well below 1 (Seyfried and Mottl, 1982). The decline in gas concentrations, although relatively minor, may further indicate that production of the reservoir is bringing about an increase in the effective W:R ratios. An alternative explanation of the decline in gas

concentrations may, however, be that the boiling front in the deeper reservoir has stabilized, yielding a constant steam:gas ratio.

Another noteworthy aspect of the gas produced by HGP-A is that a significant proportion of atmospheric carbon is present in the carbon dioxide: carbon-14 activities determined for the CO_2 have yielded apparent ages ranging from about 9–13 ka, or approximately 20 percent of modern carbon activities. Thus, at least 20 percent, or approximately 200 mg/kg of the 1,100 mg/kg of CO_2 in the steam phase is made up of surface carbon. This estimate is a minimum and presumes that the circulation rate in the rift is very short; a fluid residence time of 5,000 years would increase the proportion of atmospheric carbon to nearly 40 percent of the total. The source of this carbon is unclear; ground water typically contains CO_2 concentrations of only 10–20 ppm (U.S. Geological Survey, 1977) and, although sea water has a much higher concentration of CO_2, its relatively modest concentration in the reservoir fluids limits its contribution to approximately 20–30 mg/kg. The decline in CO_2 concentration during the period of increasing salinity has been accompanied by a slightly increased apparent age of the CO_2, and hence a sea-water source for the young carbon is not consistent with the observed trends in age and salinity. At present, no clear explanation is known for the carbon-14 data; it can only be stated that atmospheric carbon comprises a significant proportion of the CO_2 in the geothermal reservoir and that the fluid circulation time within the system is not more than 10,000 to 13,000 years.

The CO_2:H_2S ratio in the noncondensable gases in HGP-A is much lower than that found in most other geothermal systems where carbon dioxide predominates the noncondensable gases and is usually present at a concentration more than 2–5 times higher than H_2S. In the HGP-A fluids they are approximately equal when one considers the atmospheric contribution to the total CO_2. Two mechanisms can be proposed to account for the unusual CO_2:H_2S ratio found at HGP-A. The first is associated with the high-temperature reactions occurring in a sea water-basalt system: sea-water sulfate, at high temperature, oxidizes the reduced iron present in basalt to generate hematite and reduced sulfur by the reaction $8FeO + SO_4^{2-} \rightarrow 4Fe_2O_3 + S^{2-}$.

The high concentration of hematite identified in the intensely altered zones in HGP-A and other wells (Stone, 1977; Barnwell Geothermal Corp., unpublished data, 1985) are consistent with this model, but the relatively low concentration of sea water initially found in the HGP-A fluids suggests that this mechanism could supply only a modest amount of the sulfide found in the reservoir fluids.

The second mechanism that may account for the anomalous CO_2:H_2S ratio is that the magmas intruded into the ERZ may be depleted in magmatic carbon. Studies conducted by Gerlach and Graeber (1985) suggest that magma held in the summit magma chamber at Kilauea is preferentially degassed of the more-insoluble volatiles such as helium and carbon dioxide and that the magma later erupted from (and presumably intruded into) the ERZ shows a depletion of carbon relative to sulfur. Hence the low carbon to sulfur ratios observed in the geothermal fluids may be reflecting the C:S ratio present in the dike complex on the ERZ. Which of these mechanisms is ultimately responsible for the unusual C:S ratio in the HGP-A fluids cannot be determined at present; however, sulfur isotopic data currently being gathered may provide further insight into this question.

Although interpretation of the gas chemistry in terms of reservoir temperature is hindered by the mixing of the discharge from two production zones, a very crude estimate of the maximum and minimum temperatures indicated by the gas data can be obtained using the methane gas geothermometer of d'Amore and others (1982) and Nehring and d'Amore (1984) and making the assumptions that: (1) all of the gas present is associated with the deep steam-production zone; or (2) the well discharge is produced from a single aquifer. The gas compositions associated with these assumptions correspond to the gas concentration in the steam phase alone and that in the total discharge respectively and yield temperatures of 380 °C for the former and 350 °C for the latter. Both of these calculated temperatures are well above the Na-K-Ca and SiO_2 temperatures calculated for the brine phase, but are within the range of measured downhole temperatures in HGP-A and other nearby wells (358–368 °C). The modest change in the gas concentrations present in the HGP-A discharge do not yield an appreciable change in the gas geothermometry temperatures, indicating that production of steam from the deeper part of HGP-A has not been substantially affected by the intrusion of lower temperature fluids.

The few data available from the private exploration wells do not allow any definite conclusions to be drawn; however, the information available substantiates the interpretation of the HGP-A data. The salinity of the fluids in wells along the southern boundary of the rift tend to confirm the inferred structural control of the rift system over the fluid salinity in this hydrothermal system. The similarity of the gas concentrations present in the dry-steam wells and in HGP-A suggests that the majority of the noncondensable gas produced by HGP-A is coming from the deeper steam zone and, hence, the calculated gas geothermometer temperatures for the steam phase may more accurately reflect deep reservoir temperatures than does the calculation using the gas concentrations in the total discharge.

SYNTHESIS

The data that are presently available, although far from sufficient to allow a complete understanding of the hydrothermal system associated with the ERZ, provide at least preliminary constraints on a model of this unique geothermal reservoir. The physical dimensions of the hydrothermal system are defined by the location and age of intrusive bodies within the ERZ. The southern boundary apparently corresponds to the southernmost extent of recent eruptive features; temperature inversions in two wells drilled on this boundary demonstrate at least a localized temperature decline toward the south. The northern extent of the dike system is suggested by both geologic mapping and by geophysical models to be several kilometers north of the currently active part ofthe ERZ. However, due to heat loss with time, the temperatures present in the older parts of the ERZ probably will be much lower than those within the

currently active areas. Aeromagnetic data are in agreement with this model and suggest that temperatures in excess of the Curie point (560 °C) are present beneath the southern part of the ERZ but are lower to the north and south of the currently active rift.

The low salinities found in the deep reservoir fluids at HGP-A suggest that sea water is effectively excluded from the interior of the ERZ and that the overall hydrology within the reservoir is controlled by the rift-zone structure. Fluid flow within the ERZ is governed by the near-vertical tabular dikes comprising the rift and its associated fracture system, which trend in a northeast-southwest direction. The fractures effectively channel fresh meteoric water along the ERZ and to depth in the hydrothermal system, whereas the impermeable dike system and chemical self-sealing serve to inhibit intrusion of saline water from the south. Fresh water entering the ERZ in the upper elevations of the Kilauea flank penetrate to depth, are heated within the dike complex, and are discharged at the lower elevation eastern end of the subaerial part of the rift zone. The discharge of hydrothermal fluids in this region is confirmed by surface resistivity data, by ground-water temperature and chemistry data, and by the chemistry of the hydrothermal-alteration products found in the deep wells drilled into the LERZ.

The boundary between the meteorically derived hydrothermal fluids within the ERZ and saline fluids south of the ERZ is indicated to be quite sharp by the deep drilling data obtained on the LERZ: HGP-A had an initial chloride concentration of approximately 1,000 mg/kg and a bottom-hole temperature of 358 °C. The Lanipuna 1 sidetrack well, 2883-04A, located less than 500 m south of HGP-A, had an initial chloride content of about 19,000 mg/kg and a bottom-hole temperature of 149 °C.

The chemistry of the fluids circulating within the ERZ zone is strongly controlled by fracturing in the reservoir. Data from drill cuttings indicate that extreme alteration of basalt occurs intermittently down the geologic column and the alteration mineral suite is clearly generated from sea water-basalt reactions. Thus, access of sea water to the hydrothermal system does occur; laboratory and field studies of sea water-basalt reactions have demonstrated that W:R ratios can strongly influence both the salinity and the pH of the hydrothermal fluids, and therefore in those parts of the reservoir where sea water is present at high W:R ratios, the pH of the fluids may be much lower (and more aggressive) than those currently found in the interior of the ERZ.

CONCLUSION

A young, actively evolving hydrothermal system is associated with the Kilauea east rift zone. Its physical characteristics range from near-surface ambient conditions to temperatures and pressures approaching the critical point of water. Its chemistry varies from low-salinity, near-neutral fluids to strongly acid, highly aggressive saline fluids. Further study of this system will not only provide further insight into the geothermal conditions present in this reservoir, it may also add to the understanding of chemical cycling in other land-based and submarine hydrothermal systems.

REFERENCES

Bischoff, J.L., and Dickson, F.W., 1975, Seawater-basalt interaction at 200 °C and 500 bars: Implications for origin of seafloor heavy metal deposits and regulation of seawater chemistry: Earth and Planetary Science Letters, v. 25, p. 385-397.

Bischoff, J.L., and Seyfried, W.E., 1978, Hydrothermal chemistry of seawater from 25 ° to 350 °C: American Journal of Science, v. 278, no. 6, p. 838-860.

Cox, M.E., and Thomas, D.M., 1979, Cl/Mg ratio of Hawaiian groundwaters as a regional geothermal indicator in Hawaii: Hawaii Institute of Geophysics Technical Report, HIG-79-9, 51 p.

D'Amore, F., Celati, R., and Calore, C., 1982, Fluid geochemistry applications in reservoir engineering (vapor dominated systems): Stanford University, Proceedings of the Eighth Workshop on Geothermal Reservoir Engineering, Dec. 1982, p. 295-307.

Davis, D.A., and Yamanaga, G., 1968, Preliminary report on the water resources of the Hilo-Puna area, Hawaii: Circular C45, State of Hawaii, Honolulu, Division of Water and Land Development, Department of Land and Natural Resources, State of Hawaii, 124 p.

Druecker, M., and Fan, P.F., 1976, Hydrology and chemistry of groundwater in Puna, Hawaii: Ground Water, v. 14, no. 5, p. 328- 338.

Duffield, W.A., Christiansen, R.L., Koyanagi, R.Y., and Peterson, D.W., 1982, Storage, migration, and eruption of magma at Kilauea Volcano, Hawaii, 1971–1972: Journal of Volcanology and Geothermal Research, v. 13, p. 273-307.

Dzurisin, D., 1981, Changed magma budget since 1975 at Kilauea Volcano, Hawaii: Eos, Transactions, American Geophysical Union, v. 62, no. 45, p. 1071.

Fiske, R.S., and Jackson, E.D., 1972, Orientation and growth of Hawaiian volcanic rifts: the effect of regional structure and gravitational stresses: Proceedings of the Royal Society of London, Series A, v. 329, p. 299-326.

Fournier, R.O., 1981, Application of water geochemistry to geothermal exploration and reservoir engineering, *in* Ryback, L., and Muffler, L.J.P., eds., Geothermal systems, principals and case histories: p. 109-144.

Fournier, R.O., and Potter, R.W., II, 1982, A revised and expanded silica (quartz) geothermometer: Geothermal Resources Bulletin, v. 11, no. 10, p. 3-12.

Fournier, R.O., and Rowe, J.J., 1966, Estimation of underground temperatures from the silica content of water from hot springs and wet steam wells: American Journal of Science, v. 264, p. 685-697.

Fournier, R.O., and Truesdell, A.H., 1973, An empirical Na-K-Ca geothermometer for natural waters: Geochimica et Cosmochimica Acta, v. 37, no. 5, p. 1255-1275.

Furumoto, A.S., 1978, Nature of the magma conduit under the east rift zone of Kilauea Volcano, Hawaii: Bulletin Volcanologique, v. 41, no. 4, p. 435-453.

Gerlach, T., and Graeber, E.J., 1985, Volatile budget of Kilauea Volcano: Nature, v. 313, p. 273-277.

Godson, R.H., Zablockie, C.J., Pierce, H.A., Frayser, J.B., Mitchell, C.M., and Sneddon, R.A., 1981, Aeromagnetic map of the island of Hawaii: U.S. Geological Survey Geophysical Investigation Map GP–946, 1 sheet, scale 1:250,000.

Helgeson, H.C., Kirkham, D.H., and Flowers, G.C., 1981, Theoretical prediction of the thermodynamic behavior of aqueous electrolytes at high pressures and temperatures: IV. Calculation of activity coefficients, osmotic coefficients, and apparent molal and standard and relative partial molal properties to 600 °C and 5 kb: American Journal of Science, v. 281, no. 10, p. 1249-1516.

Holcomb, R.T., 1980, Preliminary geologic map of Kilauea Volcano, Hawaii: U.S. Geological Survey Open-File Report 80–796, 2 sheets, scale 1:50,000.

Humphris, S.E., and Thompson, G., 1978, Hydrothermal alteration of oceanic basalts by seawater: Geochimica et Cosmochimica Acta, v. 42, p. 107-125.

Iovanitti, J.L., and D'Olier, W.L., 1984, Preliminary results of drilling and testing in the Puna Geothermal System, Hawaii: Stanford University, Proceedings of the Tenth Workshop on Geothermal Reservoir Engineering, December 1984.

Kauahikaua, J.P., 1981, Interpretation of time-domain electromagnetic soundings in

the east-rift geothermal area of Kilauea Volcano, Hawaii: U.S. Geological Survey Open-File Report 81–979, 25 p.

Kauahikaua, J.P., Mattice, M.D., and Jackson, D.B., 1980, Mise-a-la-masse mapping of the HGP-A geothermal reservoir, Hawaii: Geothermal: Energy For the Eighties, Geothermal Research Council Transactions, v. 4, p. 65-68.

Kauahikaua, J.P., Zablockie, C.J., and Jackson, D.B., 1979, Controlled source electromagnetic mapping at the summit of Kilauea Volcano, Hawaii: Eos, Transactions, American Geophysical Union, v. 60, no. 46, p. 811-812.

Keller, G.V., Skokan, C.K., Skokan, J.J., Daniels, J., Kauahikaua, J.P., Klein, D.P., and Zablocki, C.J., 1977, Geoelectric studies on the east rift, Kilauea Volcano, Hawaii Island: Hawaii Institute of Geophysics Technical Report HIG 77-15.

Kristmannsdottir, H., 1976, Hydrothermal alteration of basaltic rocks in Icelandic Geothermal areas, *in* Proceedings of Second United Nations Symposium on the Development and Use of Geothermal Resources, San Francisco, Calif.: Washington, U.S. Government Printing Office, v. 1, p. 441-445.

Kroopnick, P.M., Lau, L.S., Buddemeier, R.W., Thomas, D.M., Lau, L.S., and Bills, D., 1978, Hydrology and geochemistry of a Hawaiian geothermal system: HGP-A. Hawaii Institute of Geophysics Technical Report HIG-78-6, 64 p.

Macdonald, G.A., Abbott, A.B., and Peterson, F., 1983, Volcanoes in the sea: The geology of Hawaii: Honolulu, University of Hawaii Press, 517 p.

Mink, J.F., 1977, Handbook—Index of Hawaii groundwater and resources data, v. 1: Honolulu, University of Hawaii, Water Resources Research Center, Technical Report No. 113, 96 p.

Moore, R.B., 1983, Distribution of differentiated tholeiitic basalts on the lower east rift zone of Kilauea Volcano, Hawaii: A possible guide to geothermal exploration: Geology, v. 11, no. 3, p. 136-140.

Mottl, M.J., 1983, Metabasalts, axial hot springs, and the structure of hydrothermal systems at mid-ocean ridges: Geological Society of American Bulletin, v. 94, p. 161-180.

Mottl, M.J., and Holland, H.D., 1978, Chemical exchange during hydrothermal alteration of basalt by seawater—I: Experimental results for major and minor components of seawater: Geochimica et Cosmochimica Acta, v. 42, p. 1103-1115.

Mottl, M.J., and Seyfried, W.E., 1980, Subseafloor hydrothermal systems: rock-vs. seawater-dominated, *in* Rona, P.A., and Lowell, R.P., eds., Seafloor spreading centers: Hydrothermal Systems: Stroudsberg, Pa., Dowden, Hutchinson and Ross, Inc., 424 p.

Nehring, N.L., and D'Amore, F., 1984, Gas chemistry and thermometry of the Cerro Prieto, Mexico, geothermal field: Geothermics, v. 13, p. 75-89.

Pohl, D.C., and Liou, J.G., 1983, Flow-through reaction of basalt glass and seawater at 300° and 200 °C, 250 bars pressure [abs.]: Misasa, Japan, Fourth International Symposium on Water-Rock Interaction, Aug. 29–Sept. 3, 1983, p. 389-392.

Reed, M.H., 1982, Calculations of multicomponent chemical equilibria and reaction processes in systems involving minerals, gases, and an aqueous phase: Geochimica et Cosmochimica Acta, v. 46, p. 513-528.

——— 1983, Seawater-basalt reaction and the origin of greenstones and related ore deposits: Economic Geology, v. 78, p. 466-485.

Reed, M.H., and Spycher, N., 1983, Calculated pH at high temperature in hydrothermal waters with applications to geothermometry: Misasa, Japan, Fourth International Symposium on Water-Rock Interaction, Aug. 29–Sept. 3, 1983, p. 401-404.

——— 1984, Calculation of pH and mineral equilibria in hydrothermal waters with applicaton to geothermometry and studies of boiling and dilution: Geochimica et Cosmochimica Acta, v. 48, p. 1479-1492.

Seyfried, W.E., Jr., and Bischoff, J.L., 1981, Experimental seawater-basalt interaction at 300 °C, 500 bars, chemical exchange, secondary mineral formation and implications for the transport of heavy metals: Geochimica et Cosmochimica Acta, v. 45, p. 135-147.

Seyfried, W.E., and Mottl, M.J., 1982, Hydrothermal alteration of basalt by seawater under seawater-dominated conditions: Geochimica et Cosmochimica Acta, v. 46, p. 985-1002.

Shupe, J.W., Helsley, C.E., and Yuen, P.C., 1978, The Hawaii geothermal project: Summary report for phases I, II, and III: U.S. Department of Energy Report SAIV-1093-T6.

Stearns, H.T., and Macdonald, G.A., 1946, Geology and groundwater resources of the Island of Hawaii: Honolulu, Hawaii Division of Hydrography, Bulletin B9, 363 p.

Stone, C., 1977, Chemistry, petrography, and hydrothermal alteration of basalts from HGP-A, Kilauea, Honolulu, University of Hawaii, M.S. Thesis No. 1477, 84 p.

Stone, C., and Fan, P.F., 1978, Hydrothermal alteration of basalts from Hawaii Geothermal Project Well-A Kilauea, Hawaii: Geology, v. 6, p. 401-404.

Swanson, D.A., Duffield, W.A., and Fiske, R.S., 1976, Displacement of the south flank of Kilauea Volcano: The result of forceful intrusion of magma into the rift zones: U.S. Geological Survey Professional Paper 963, 39 p.

Takasaki, K.J., 1978, Summary appraisals of the nation's groundwater resources—Hawaii Region: U.S. Geological Survey Professional Paper 813–M, 175 p.

Thomas, D.M., 1980, Water and gas chemistry from the HGP-A geothermal well: January 1980 flow test: Geothermal Resources Council Transactions, v. 4, p. 181-184.

——— 1982, A geochemical case history of the HGP-A well 1976-1982, *in* Proceedings of the Pacific geothermal conference 1982 incorporating the 4th New Zealand geothermal workshop: Auckland, N.Z., University of Auckland Geothermal Institute, p. 273-278.

Thomas, D.M., and Sakai, H., 1983, Chemical and isotopic studies of the HGP-A geothermal well [abs.]: Misasa, Japan, Fourth International Symposium on Water-Rock Interaction, Aug. 29–Sept. 3, 1983, p. 479-482.

Tomasson, J., and Kristmannsdottir, H., 1972, High temperature alteration minerals and thermal brines, Reykjanes, Iceland: Contribution to Mineralogy and Petrology, v. 36, p. 123-134.

U.S. Geological Survey, 1977, Water resources data for Hawaii and other Pacific areas: Water year 1977, v. 10: U.S. Geological Survey Water-Data Report HI-77-1, 348 p.

Waibel, A., 1983, A review of the hydrothermal mineralogy of Hawaii Geothermal Project Well-A, Kilauea, Hawaii: Geothermal Resources Council Transactions, v. 7, p. 205-209.

Yuen, P.C., Chen, B.H., Kihara, D.H., Seki, A.S., and Takahashi, P.K., 1978, The Hawaii geothermal project: HGP-A and reservoir engineering: Honolulu, University of Hawaii, Hawaii Geothermal Project internal report, 96 p.

Zablocki, C.J., 1976, Mapping thermal anomalies on an active volcano by the self-potential method, Kilauea, Hawaii: Second U.N. Symposium on the Development and Use of Geothermal Resources, Proceedings, v. 2, p. 1299-1309.

———1977, Self-potential studies in east Puna, Hawaii, *in* Geoelectric studies on the east rift, Kilauea Volcano, Hawaii Island: Hawaii Institute of Geophysics Technical Report HIG-77-15, p. 175-195.

AA FLOW DYNAMICS, MAUNA LOA 1984

By Peter W. Lipman *and* Norman G. Banks

ABSTRACT

The March 25–April 14, 1984, northeast-rift eruption of Mauna Loa Volcano, Hawaii, provided an exceptional opportunity to study development of a large basaltic aa flow system for several weeks. The major flow reached 27 km from its source vent within a few days of start of the eruption, and, fed at a rate of about 10^6 m^3/h, developed an initially simple geographic zonation in aa textural types and flow morphology. Decreases in eruption rate during the first few days, to about 0.4×10^6 m^3/h, triggered a channel blockage and breakout to generate a second major flow on March 29. Without further major changes in vent output from March 30 through April 7, the flow evolved from a single narrow tongue with an efficient channel, which delivered virtually the entire vent output to within 1 km of the toe, to an uprift-migrating stagnating channel system characterized by blockages, ponding, and complexly branching overflows. Lava production again began to decline after April 7, and the rate of upflow stagnation accelerated.

A major cause of the stagnation was breakdown in the hydraulic efficiency of the channel. Floating channel debris (lava boats), created by collapse of portions of the channel banks, formed dams at channel constrictions and caused ponding, overflows, and lateral breakouts that robbed the lower flow of much of its lava supply. Upflow stagnation was basically due to increasing viscosity and yield strength of the channel lava, caused by progressive degassing, formation of pasty surface clots, incorporation of channel debris, and ultimately by growth of microphenocrysts in lava stored uprift from the vent.

During the eruption, microphenocryst contents of erupted lava increased by nearly two orders of magnitude, from less than 0.5 percent to 30 percent, without concurrent change in either bulk magma composition or eruption temperature ($1,140 \pm 3$ °C). The microphenocrysts have skeletal morphologies typical of undercooling. The increase in microphenocryst content with time was paralleled by a decrease in emission of sulfur and other gases and a decline in lava eruption rate. Growth of the microphenocrysts is interpreted as crystallization from magma that was undercooled 20–30 °C below its liquidus. The undercooling proabably resulted from separation and release of volatiles as the magma moved from the primary high-level magma reservoir at a depth of 3–5 km below the summit caldera to the 2,900-m elevation at the eruption site 12 km down the northeast rift zone. Analogous increases in microphenocryst content and accompanying uprift stagnation of lava flows have occurred during several earlier historic eruptions from Mauna Loa rift zones.

INTRODUCTION

The eruption of March 25–April 14, 1984, from the northeast rift zone of Mauna Loa Volcano, Hawaii, provided an exceptional opportunity to observe the development of a major basaltic aa flow system, fed by a high-volume eruption for several weeks. Similarly large aa flows were last erupted on Mauna Loa from the southwest rift zone in 1950 (Finch and Macdonald, 1953), before the availability of helicopters, efficient radio communications, abundant high-quality chemical data, devices for accurate temperature measurements, and other recent technological advances in monitoring techniques. In contrast, recent aa flows from nearby Kilauea Volcano (Moore and others, 1980; Ulrich and others, 1984) lasted only a few days, were fed at rates an order of magnitude smaller than the 1984 Mauna Loa activity, and generally were inaccessible to observers except in vent areas and at toes of flows (midzones are in heavily vegetated areas lacking helicopter landing points). Detailed recent observations of flow dynamics at other volcanoes, notably Etna in Sicily and Arenal in Costa Rica (Sparks and others, 1976; Wadge, 1978; Borgia and others, 1983; Cigolini and others, 1984), also involved small short-lived flows.

At Mauna Loa in 1984, we were able to observe the evolution, over a three-week period, of a complex aa flow system that achieved a maximum length of 27 km. Initial motivation for these observations was to monitor advance of the flow toward the city of Hilo (fig. 57.1*A*). As the flow terminus stagnated and hazard concerns diminished, we became increasingly intrigued by the opportunities to observe complex changes in channel efficiency related to changing parameters of lava temperature, density, gas content, petrography, and eruption rate.

Eruption rates were as high as 2.9×10^6 m^3/h during the first six hours of the eruption, stabilized at 0.5×10^6–1×10^6 m^3/h for the next 12 days, and slowly diminished thereafter. Total eruptive volume was approximately 220×10^6 m^3. Sizeable pahoehoe flows formed only during the first day of the eruption and within a few kilometers of the vent; the remainder of the flow system consisted of aa. Especially instructive were variations in channel discharge with increasing distance from the vent during periods of steady-state lava production, variations in behavior at the flow toe as a function of slope and magma supply, development and evolution of the aa channels, and variations in density, yield strength, and viscosity of the lava as functions of time and distance from the vent. The main 1984 aa flow evolved (without major change in magma discharge at the vent) from a simple narrow tongue with an efficient channel that delivered virtually the entire lava supply to within 1 km of the toe, to an uprift-stagnating channel system with levees, blockages, ponding, and complexly branching overflows.

ACKNOWLEDGMENTS

Our channel observations would not have been feasible without the skillful assistance of helicopter pilots Bill Lacy Jr., Ken Ellard,

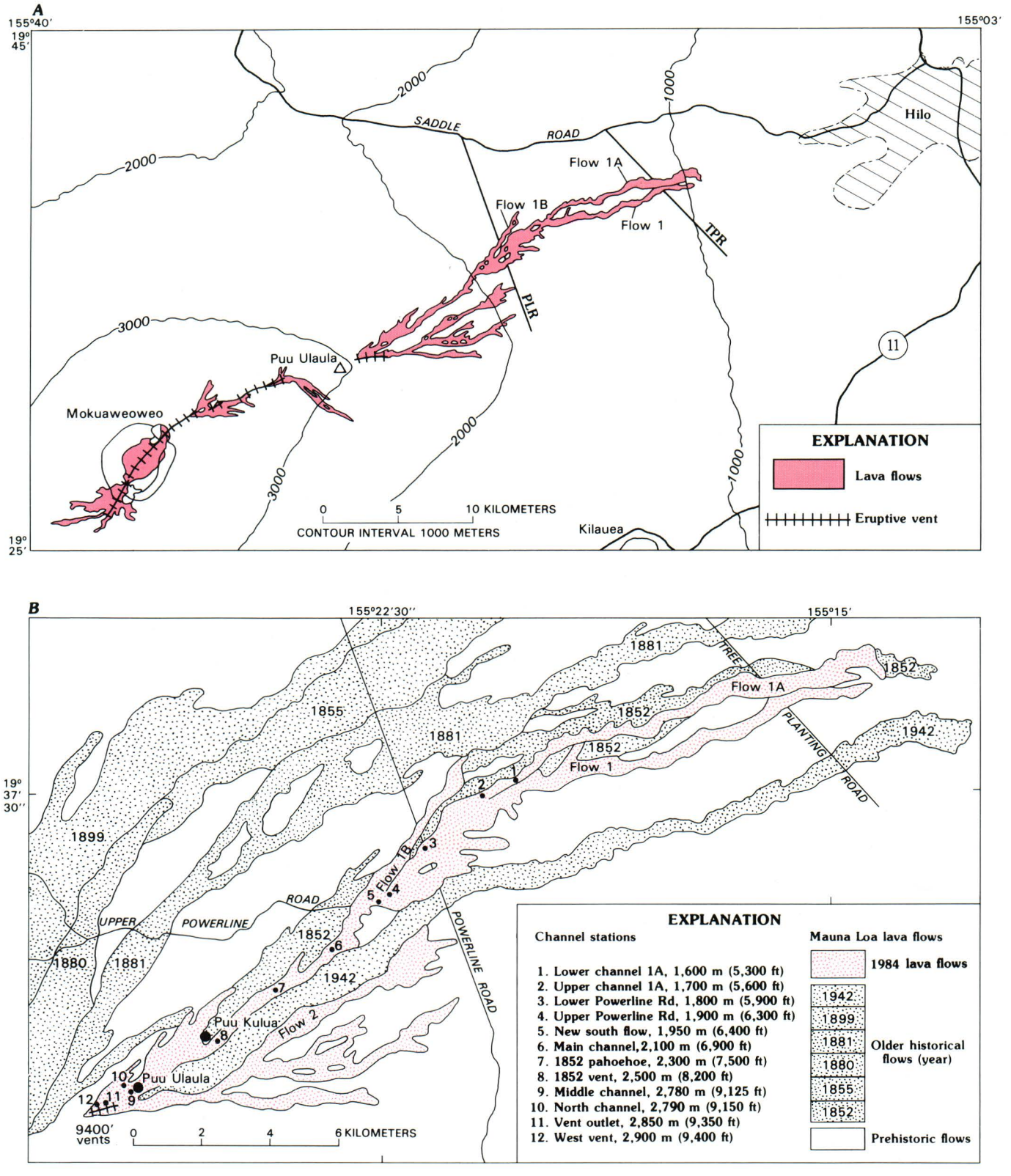

FIGURE 57.1.—Extent of lava flows from the 1984 Mauna Loa eruption. ***A***, Distribution of all 1984 flows with respect to city of Hilo (modified from Lockwood and others, 1985). All lava in the summit caldera (Mokuaweoweo) and adjacent upper parts of the northeast and southwest rift zones was erupted during the first day of the eruption (March 25). PLR, Powerline Road; TPR, Tree-planting Road. ***B***, Distribution of lava flows from the 2,900-m vent system that was active from the afternoon of March 25 until the end of the eruption on April 15. Earlier historical flows (1852, 1855, 1881, 1942) resulted from similar eruptions along the northeast rift zone. Channel stations are measurement sites for observations reported in table 57.3.

Tom Haupmann, and Ed Spencer. We also thank our many colleagues, from the USGS and academia, who assisted with the channel measurements and provided additional observations on the 1984 eruption: especially J. Buchanan-Banks, D. Clague, J. Fink, J.P. Lockwood, H.J. Moore, R.B. Moore, T. Neal, M. Rhodes, and E. Wolfe. Thoughtful reviews of earlier versions of this paper by H.J. Moore, D.A. Swanson, and G.E. Ulrich are greatly appreciated.

CHRONOLOGIC NARRATIVE

The general evolution of the 1984 Mauna Loa eruption is described elsewhere (Lockwood and others, 1985), and only the features most relevent to development of the aa flows are summarized here. The eruption began at about 0100 (all times are in Hawaii standard time) on March 25, following a nine-year repose after the 1975 summit eruption (Lockwood and others, 1976). Gradually increasing levels of seismicity and ground deformation in the previous several years had led to a forecast of increased probability of a Mauna Loa eruption in 1984–85 (Decker and others, 1983), but few precursors were evident in the days immediately preceding the 1984 outbreak.

Initial activity on March 25 broke out in the summit caldera (Mokuaweoweo) and the uppermost southwest rift zone; after about 0400, activity migrated into the upper northeast rift zone and diminished in the summit area. During that day, vents from the 3,500-m level of the northeast rift zone fed a lava flow that extended about 5 km down the southeast flank (fig. 57.1*A*). At about 1630 on March 25, new fissure vents opened at elevations of 2,800–2,900 m; they became the sites of all lava production for the remainder of the eruption (fig. 57.1*B*). By March 26, activity along the new lower fissures had become concentrated at four areas of fountaining and growth of spatter ramparts, informally designated vents 1–4, and had generated four flows that spread rapidly downslope to the east (fig. 57.2*A*) The three southerly flows (flows 2–4) stagnated by March 27, as lava production diminished from the more easterly vents (2–4), while a relatively constant volume of lava was maintained in the more northerly flow 1. Continued slow oozing of lava at the site of vent 4, accompanied by little or no fountaining, gradually built a broad lava shield 150 m high in late March and early April.

This paper considers primarily the evolution of flow 1 and its channel system, which were active from March 25 to April 13. By March 29, flow 1 had reached the 1,100-m level, 25 km from its source vent, as a relatively simple narrow flow fed by a well-developed central channel 20–50 m wide that extended to within 1–2 km of the flow front (figs. 57.2*B*, *C*, 57.3). In the early morning of March 29, a blockage and overflow at the 1,800-m level took most of the supply away from the lower reaches of flow 1 and generated a new tongue farther north (flow 1A). Flow 1 stagnated 27 km from its source at about 870-m elevation.

Flow 1A reached about 900-m elevation by April 5, when a major overflow—again at the 1,800-m level—cut off most of its supply and created a new fast-moving flow (1B) north of 1A. During April 5–8, repeated blockages and overflows prevented sustained lava supply to any organized flow below the 1,850-m level. On April 7, lava production at the vent and in the upper channel began to diminish, increasing the rate of uprift stagnation along upper parts of the flow. Lava production continued to decline, accompanied by stagnation of lower reaches of the flow system, and by April 10 no active flow toes extended below 2,450 m. By April 13, the lowest active flow toe was at 2,750 m, only about 2 km from the vent. All lava production at the vent ceased late on April 14.

Decreases in rate of lava production were paralleled by declines in volume of gas emissions. Rates of sulfur dioxide production decreased especially rapidly during the first week of the eruption (Casadevall and others, 1984). Gas emissions were intense from fissures at 3,000–3,500 m along the rift zone throughout the eruption, and as lava production began to decline at the 2,900-m vents, visible gas emission from the higher fissures began to exceed that from the active lava vents.

FLOW TYPES

Both aa and pahoehoe flow types encompass much variation in lava textures (Wentworth and Macdonald, 1953; Macdonald 1972) that can provide information on the kinematics of flow and on lava rheology (Swanson, 1973; Peterson and Tilling, 1980). During the 1984 Mauna Loa eruption, distinctive aa flow types tended to develop as functions of distance from the vent, steepness of terrain, and mechanism of the flow advance. Some of these lava types have not previously been described or interpreted in terms of emplacement kinematics. Lava from the 1984 Mauna Loa eruption includes most of the pahoehoe types recognized on Kilauea (Swanson, 1973), transitional lava between pahoehoe and aa, and diverse aa types—slabby, clotted, spiney, scoriaceous, clinkery, and blocky. These flow types could also be identified within lava channels on the basis of textures developing on the surface crust. General relations among the flow types in the 1984 eruption are summarized here; detailed features of a few are discussed in later sections, where their origin is closely tied to evolution of other flow features such as flow toes, channels, and levees.

PAHOEHOE

Typical fountain-fed shelly pahoehoe formed in the vent area, at 2,850–2,900-m elevation early during the eruption, but extended as pahoehoe for only about 2 km, to about the level of Puu 9,146 (2,790 m) before changing to aa—probably within less than two hours after the source vents opened. As soon as a channel was well established to this level, virtually all lower lava fronts advanced as aa. The limited extent of pahoehoe may reflect the steeper slopes of this sector of the rift zone (4°–6°), the viscous character of the 1984 lava, or some additional process. Where able to flow slowly (less than 10–15 km/h), lava in the developed channel of flow 1 was capable of generating pahoehoe down to at least the 2,400-m level, about 5 km from the vent, as shown by small pahoehoe overflows during the first hours of the eruption. After March 26, however, the channel delivered lava so efficiently to lower reaches of the flow that no lava front advanced as pahoehoe until the last days of the

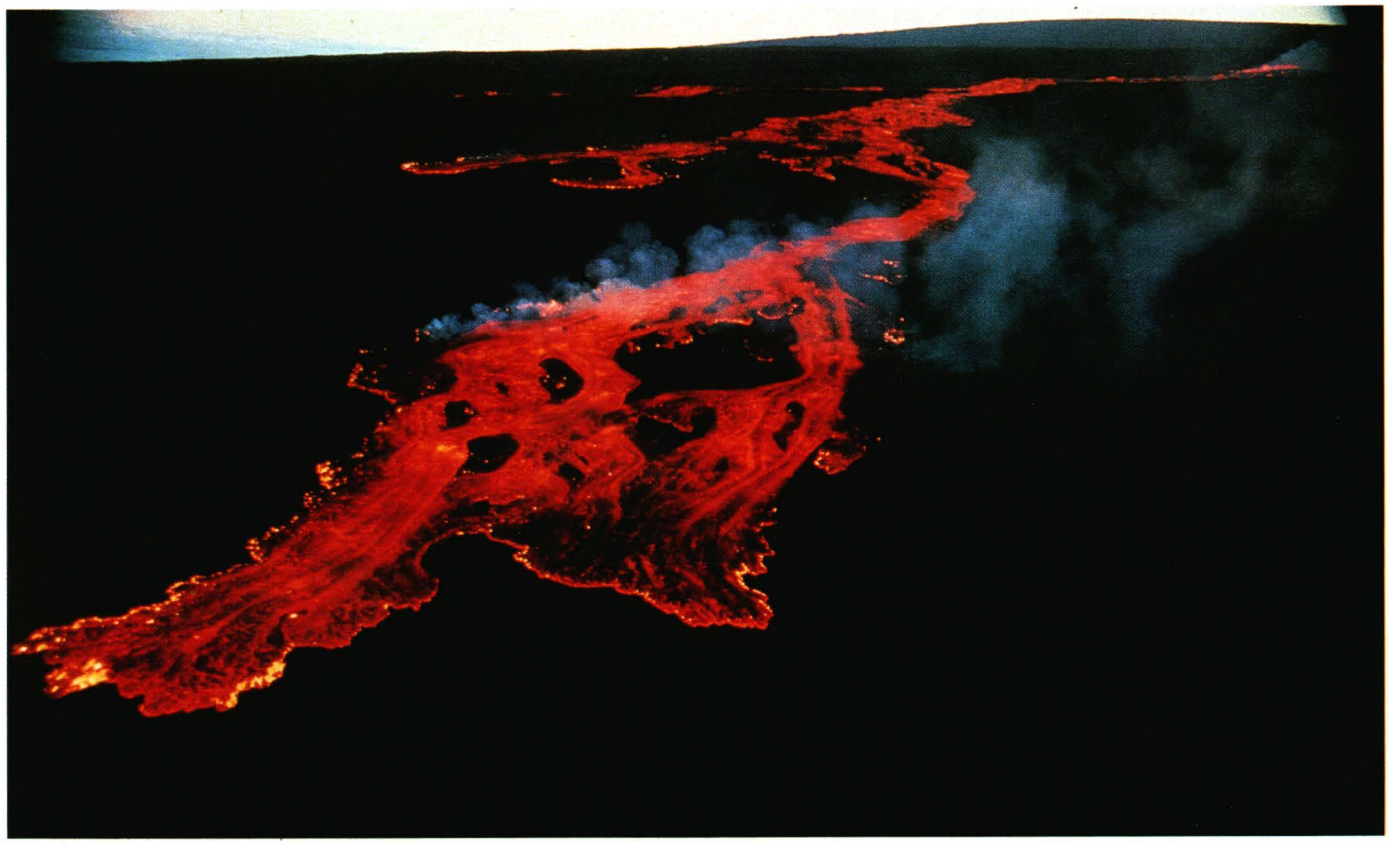

A

FIGURE 57.2.—Active flow front and channels, 1984 Mauna Loa eruption. ***A***, Rapidly advancing toe of flow 1 at 2030 H.s.t. on March 25, about 2 hours after initiation of lower vents. Toe is at about 2,400-m elevation, advancing at estimated 2 m/s. Photograph by R.B. Moore. ***B***, View uprift toward 2,900-m vents on March 27. Flow 1 channel is on right; smaller channels feed flows 2 and 3 on left. ***C***, Flow 1 toe at 1,350-m elevation, looking downrift on March 27. Channel is well developed and about 50 m wide; it extends to within 1 km of flow toe, marked by smoke from burning forest.

eruption, when blockages and disruption of the channel again permitted pahoehoe overflows from the channel within 1–2 km of the vents.

TRANSITIONAL LAVA

Because the transition from pahoehoe to aa occurred within the confined channel of flow 1 during much of the eruption, we had ample opportunities to observe this change from a helicopter and from observation stations along channel levees. Our observations on the 1984 lava are in accord with the interpretations of Macdonald (1953) and Peterson and Tilling (1980) that the transition from pahoehoe to aa involves the relation between viscosity and rate of internal disturbance due to flowage (shear strain). If flow mechanics (flow volume, flow dimensions, slope, momentum) impel pahoehoe to continue to move and deform after it has become highly viscous, the lava will change to aa if the critical relation has already been approached. Approach to this critical condition can be recognized when the flow surface is littered with solid and semisolid blebs and blocks that disrupt flow streamlines in the channel.

AA TYPES

Different aa lava types reflect interrelated aspects of magma rheology, gas content, terrain effects, and flow rates. Lava viscosity and yield strength generally increase downstream because of decreased gas content, decreased average bulk temperature of the flow, increased crystallization of microphenocrysts, and incorporation or formation of solids, as discussed later (also see Moore, chapter 58). The net effect is to trigger successive irreversible changes in aa texture, similar to those accompanying the pahoehoe-aa transition.

B *C*

FIGURE 57.2—Continued.

SLABBY AA

In the 1984 Mauna Loa eruption, aa flows nearest the transition from pahoehoe tended to form slabby aa (also called slabby pahoehoe), which consists simply of pahoehoe crust completely disrupted in slabs by flowage at a rate too great for the crust to accommodate the shear strain plastically (fig. 57.4*A*). Slabby aa was well developed in the advancing terminus of flow 1 at elevations of 2,450–2,600 m, about 3–5 km from the vent.

SCORIACEOUS AA

Farther downflow, where the lava was slightly denser and more viscous, the surface of the channel no longer maintained a smooth pahoehoe surface crust. Instead, it developed scattered lumps or clots of relatively cool scoriaceous lava, separated by more fluid incandescent lava retaining crude pahoehoe character (fig. 57.4*B*). When overflows or breakouts of such scoriaceous aa occurred fairly slowly, and flow fronts advanced no faster than 1–2 m/min, this lava type retained its clotted texture as it cooled. The frothy clots consisted of red-brown oxidized scoria masses 5–30 cm across, set in dark gray smoother less vesicular lava having a thin poorly developed glassy surface. When overflow rates were more rapid, as in a sudden sheet-flow breakout through a breached levee, the entire surface of the resulting flow disaggregated into scoriaceous lumps, and the surface of the resulting deposit consists of loose oxidized scoria lumps totally covering the dense interior of the aa flow. This lava type has at times been called spiney aa (Macdonald and Abbott, 1970, p. 26) because of the jagged irregular surfaces of the scoria lumps. The front of flow 1 during its advance on March 25–26 was dominantly scoriaceous aa between elevations of about 2,450 and 1,850 m, at distances of 5–12 km from the vent.

CLINKERY AA

Even farther downflow, the active lava surface in the channel consisted largely of cooled clots of relatively dense lava that ground against each other while riding on top of the more fluid lava core in

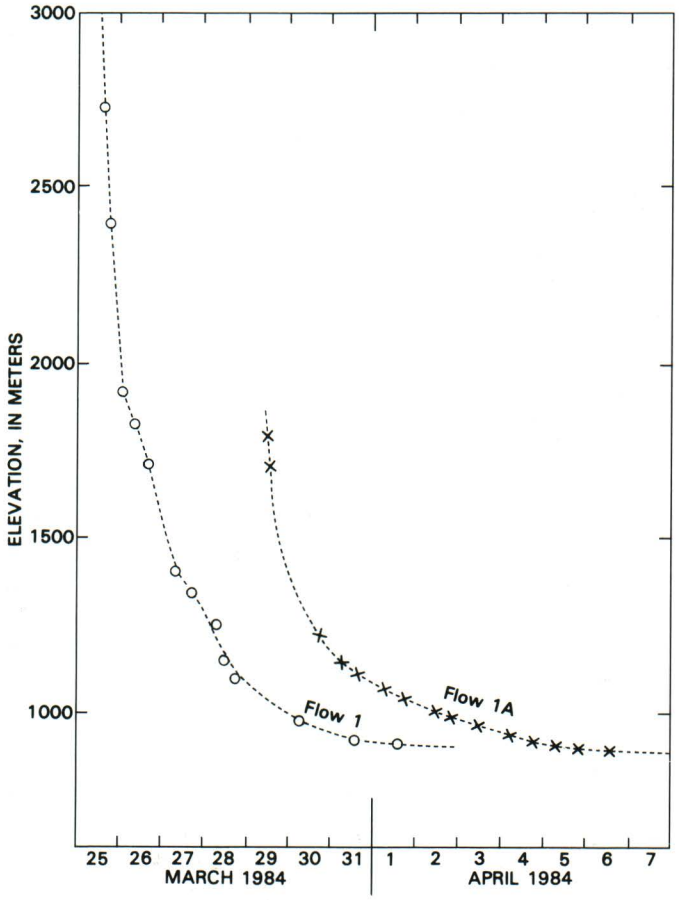

FIGURE 57.3.—Change in elevation of lava-flow toes during 1984 Mauna Loa eruption.

the channel. Breakouts and overflows of this material formed dark gray clinkery aa, which contrasts with the scoriaceous aa in having angular rather than scoriaceous surfaces, and in being darker in color, less oxidized, and less vesicular. During early advance of flow 1 and the later flow 1A, the gradual transition from scoriaceous to clinkerly aa occurred at elevations of 1,850–1,700 m, about 12–15 km from the vent.

BLOCKY AA

Along the lower reaches of flow 1, below about 1,500-m elevation and more than about 20 km from the vent, the lava largely solidified beneath a rubble cover of dense dark gray blocky aa (fig. 57.4C). Blocky aa is similar to the so-called block lava characteristic of many andesitic flows (Macdonald, 1972), although surfaces of the aa blocks are less smooth because of vesiculation. Some resulting blocks are as large as several meters across. This material was rafted farther downflow on viscous but still fluid underlying material, mixed with more scoriaceous clinkers and lumps carried from higher in the channel, and finally deposited along the toe or margins of the flow as heterogeneous rubble.

A

B

C

FIGURE 57.4.—Aa lava types observed on April 3, 1984. ***A***, Slabby aa at 2,500-m elevation, overlying spatter from the 1852 vent. Active channel is visible at upper left (arrow). Radio at lower right is 20 cm long (excluding antenna). ***B***, Scoriaceous aa flow top at 1,800-m elevation. Scoria blocks are uniformly small in size, averaging about 10 cm in diameter. Smoother crust between clusters of scoriaceous aa marks points of late stretching of the flow surface and upwelling of degassed lava. ***C***, Blocky aa, at 1,600-m elevation. Tripod and figures at right are on stable marginal levee. Center of flow, at left edge of photograph, contains a broad weakly developed aa channel. Site is near the downflow gradation from the transitional to the dispersed flowage zone (see fig. 57.5).

AA FLOWAGE ZONES

Early development of the 1984 aa flows (especially flow 1 during March 26–29) displayed systematic variations in structure and morphology from vent to toe—in addition to the aa textural types just summarized—that can be described in terms of four zones: flow toe, lower dispersed flowage, transitional channel, and upper stabilized channel (fig. 57.5). Subsequent development of blockages, ponds, and overflows of lava complexly overprinted this simple initial aa flow zonation, but each of the relatively ephemeral blockage-overflow lobes tended to show a similar zonation.

FLOW TOE

Early in the eruption, most features of the aa flow system were established within a few kilometers of the flow toe during its advance. Upper well-channelized parts of the flow were stable and changed little, as virtually all lava moved efficiently down the channel to the toe area. The character of the flow toe varied mainly as a function of slope of the local land surface and distance of the toe from the stabilized channel.

Near the vent, on steeper slopes, and where the channel was well established close to a flow toe, fluid lava was delivered efficiently to the flow toe. The result was a rapidly moving broad flow front, consisting of scoriaceous or slabby aa, only 1–3 m high and with a nearly flat upper surface (figs. 57.2*A*, 57.6*A*). Such rapidly moving fronts exposed the liquid core of the aa flow as a bright orange band along the entire flow front; the flow advanced by outwelling of the fluid core, which then crusted over, brecciated, and overrode its front. This process produced a poorly developed basal breccia, because the brecciated upper surface moved more slowly than the center of the flow advanced. Such flow fronts tended to form scoriaceous or clinkery aa. Observed velocities at these flow fronts varied from 50 m/h to as much as 5 km/h. This type of flow front was observed during early stages of breakouts from the main channel where relatively fluid ponded lava was released as sheet flows, even late in the eruption (fig. 57.6*A*). Similar features probably were dominant during the early rapid advance of flow 1 on March 25–26.

In contrast, on gentler slopes, at sites more distant from the vent, and where a broader zone of dispersed flow occurred below the channelized flow, the flow toe moved more slowly, was higher and more irregular in profile, and consisted of denser blockier lava (fig. 57.6*B*). Little or no fluid material was visible at the flow front, and the steep high front advanced by spalling of dense blocks and slabs, largely from the breccia layer riding on top of the advancing flow. Fine granular to dusty material, resulting from abrasion of aa blocks, was a significant constituent at the flow toe. Velocities at this type of flow front varied from a maximum of 50 m/h to stagnation. Such flow characterized the fronts of flow 1 and flow 1A during their slow advance below about 1,350 m elevation.

ZONE OF DISPERSED FLOW

Behind the advancing toe of the 1984 lava was a zone in which movement was dispersed across much of the flow width and a central channel was poorly developed or absent. During rapid advance of flow 1 early in the eruption, the zone of dispersed flow was relatively short; on March 27 this zone extended only about 1 km up from the toe at the 1,350-m level (figs. 57.2*B*, 57.7). As the eruption progressed, the flow toe became more sluggish, and the zone of dispersed flowage extended as much as 5–10 km up the flow. Observations in this zone were sparse, because the lava was still hot and unstable, and surface features were difficult to observe from terrain adjacent to the flow. Movement at the upper surface of the flow tended to occur along discrete shears, between which ridges of blocky aa moved fairly coherently. Near the toe, the most rapidly moving central part of the flow consisted of blocky aa showing little or no incandescence; farther upstream, the center of the flow was more incandescent and graded into a defined central channel containing visible fluid lava. Flow velocities increased gradually from

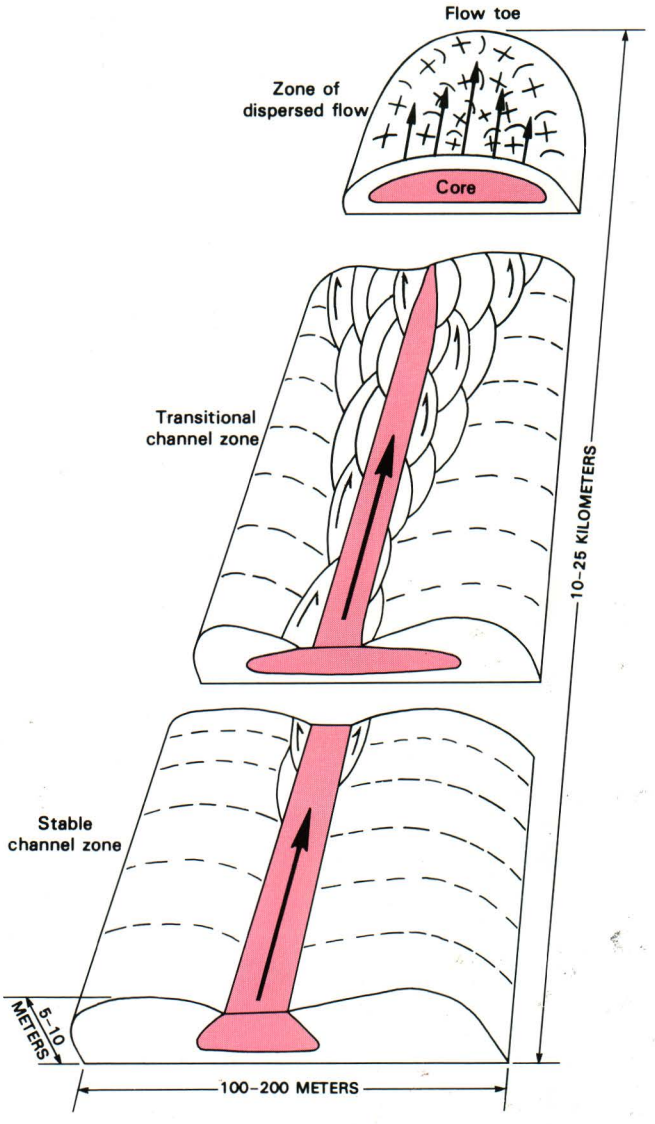

FIGURE 57.5.—Diagram showing contrasting structural features of aa channel zones.

A

B

FIGURE 57.6.—Aa flow fronts. ***A***, Fast-moving front of flow 1B, characterized by low toe (1–3 m) and exposed fluid core. Note lava boat (arrow) being rafted toward flow front. April 5, at 1,800-m elevation. ***B***, Slow moving front of flow 1A, characterized by higher toe (10–15 m) and rubbly incandescent front. A minimum temperature measured at flow front (not in fluid core) at this site was 1,086 °C (table 57.1). March 31, at 1,150-m elevation.

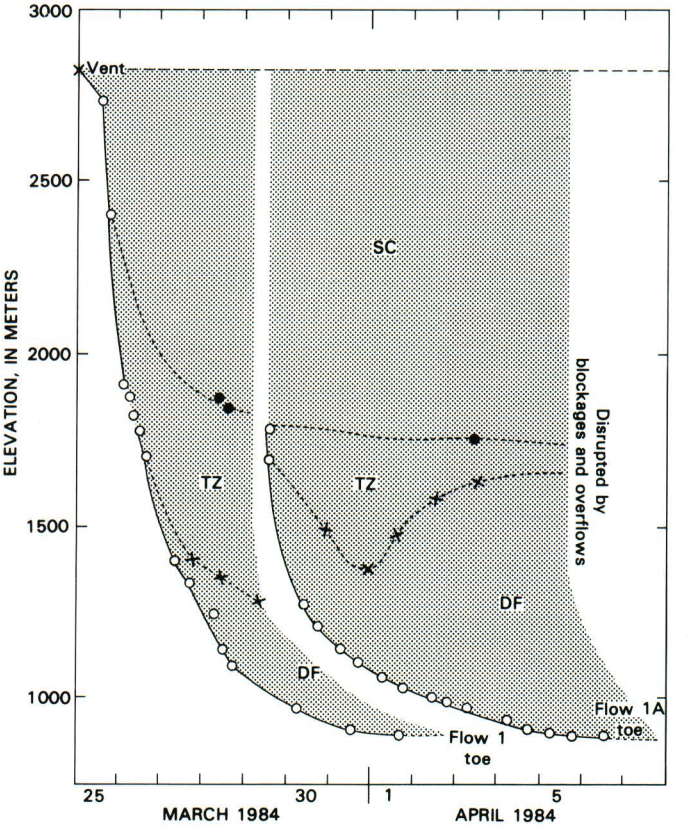

FIGURE 57.7.—Distribution of channel zones in relation to time and elevation, 1984 Mauna Loa lava flows. SC, stable-channel zone; TZ, transition zone; DF, zone of distributed flow. Circle, position of flow toe; x, DF-TZ transition; dots, TZ-SC transition.

the margin to the interior of the flow. Axial velocities were as much as several kilometers per hour; more typically, they were a few hundred meters per hour. Cross-sectional profiles through this zone of the flow are typically convex upward for slow-moving flows but nearly flat for rapidly advancing flows. At times, when a fast-moving flow crossed a steep slope, the channelized center of the flow could break through the more dispersed and sluggish lower part of the flow, delivering fluid lava to a flow front that had previously been more sluggish.

TRANSITIONAL CHANNEL ZONE

The transition between zones of dispersed flowage and the stabilized channel was marked by the presence of a distinct channel containing incandescent clinkery aa, bounded by blocky or clinkery lava a few tens of meters wide that was still capable of deforming and moving slowly (figs. 57.5, 57.8*A*). These marginal areas consisted of multiple ridges or lenses of blocky lava, bounded by discrete shears (fig. 57.8*B*); they continued downstream into similar features in the zone of dispersed flow. The active channel in the transition zone was generally wider than in the stable channel zone. Toward the zone of dispersed flow, the active channel again decreased in

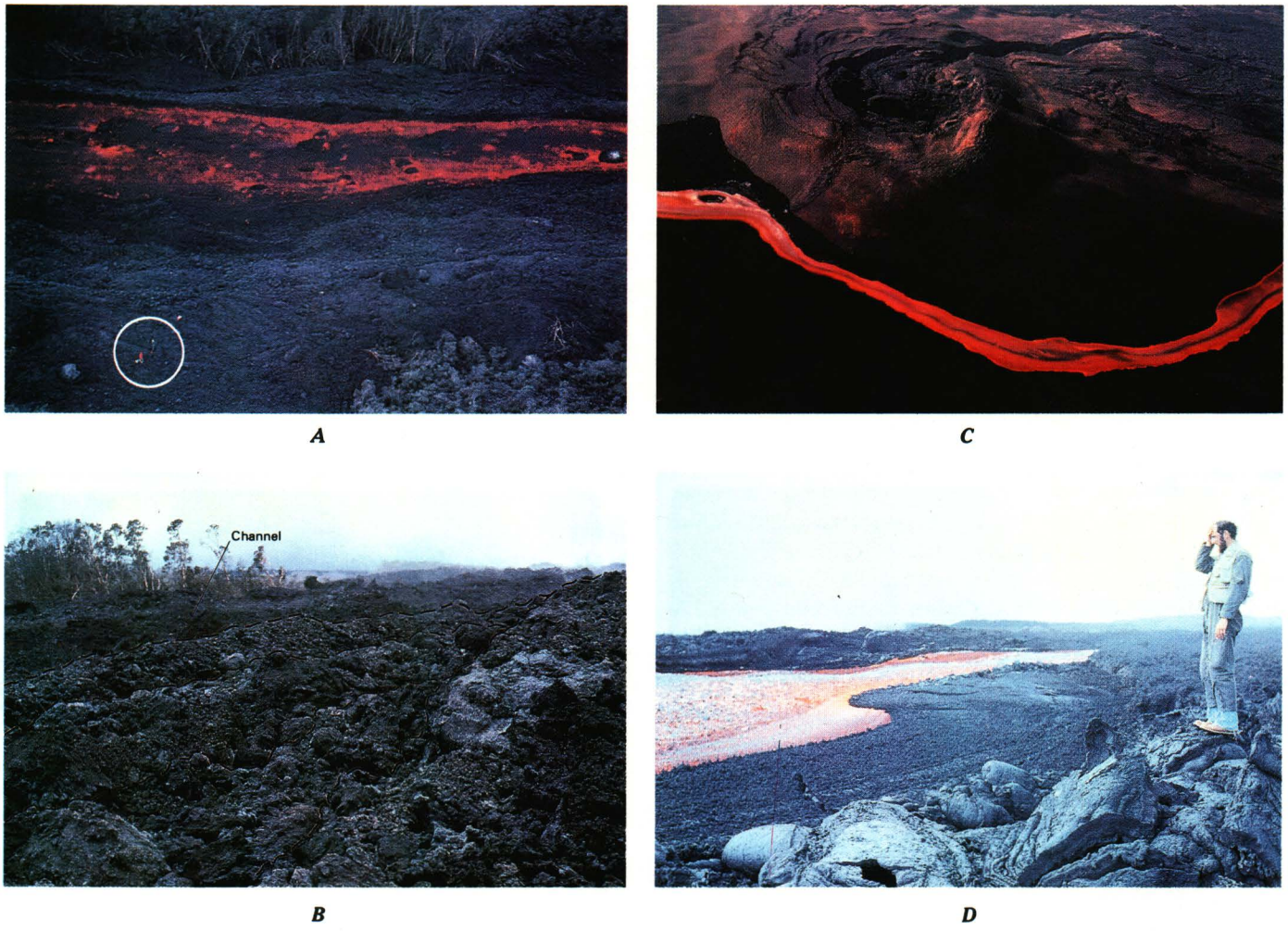

FIGURE 57.8.—Features of stable-channel and transition zones, 1984 Mauna Loa flows. ***A***, Aerial view of channel in transition zone at channel station 1, 1,600-m elevation. Active incandescent channel, about 24 m wide and flowing at 3.4 km/h (table 57.3, no. 1), is flanked by marginal shears in blocky aa moving at only a few meters per minute. Lava balls and other solidified debris are abundant on channel surface. Persons (circled) are standing on stable marginal levee. Photograph taken March 31. ***B***, Shear lenses adjacent to channel margin in transition zone at station 1, 1,600 m. Near ridge at right is stable early formed marginal levee; three shear lenses are present (boundaries marked by dashed lines), and weakly developed aa channel is visible at upper left. Photograph taken April 2. ***C***, Aerial view of stable channel zone at 2,500 m. Channel has been well established since first day of eruption. Dark band in center channel marks maximum velocity zone (19–20 km/h; table 57.3, no. 43–44). Vent of 1852 eruption is in upper part of photograph; channel station 8 is at far right. Photograph by J.D. Griggs, March 30. ***D***, Stable channel zone at station 8, 2,500 m. Man stands on original overflow levee; margin of channel has crusted over, although lava continues to flow beneath thin crust. Photograph taken April 2.

width as the number of marginal shear lenses increased. Individual shear ridges or lenses were several meters wide and traceable longitudinally for tens of meters. Measured flow velocities in the central channel of this zone were as much as 25–50 m/min (2–3 km/h); typical velocities in the marginal shear lenses were 1–3 m/min, with maxiumum velocities accompanying passage of lava surges in the central channel.

In addition to longitudinal movement, the belts of shear ridges inflated and subsided as much as several meters vertically in response to changes in lava levels in the channel. The combined vertical and longitudinal motions indicate that the belts of shear ridges were underlain by fluid lava hydraulically connected to the active channel. In comparison with the zone of dispersed flowage, the fluid core of the flow in the transitional-channel zone was more restricted but still covered a broader area than that of the channel. Audible creaking noises, reflecting hydraulic adjustments of the crust over marginal portions of the core, accompanied passage of lava surges in the adjacent channel. The presence of a sluggish fluid core beyond the margins of the channel 9 days after channel stablilization was documented during leveling toward the channel on April 4, at the 1,900-m monitoring station: 29 m from the active channel, the elevation decreased 10 cm as the lava level in the channel dropped in response to passage of a surge.

Early in the eruption, when flow 1 and then flow 1A were advancing rapidly, the transition zone was broad. On March 28, it extended from within 1–2 km of the flow 1 toe (then at the 1,200-m level) to above the 1,850-m level (fig. 57.7), about 10 km up the flow. Later, as advance of flow 1 and then flow 1A slowed, the zone

of dispersed flow extended 5–10 km up from the toe of flow 1A, but the zone of stablized channel flow began to encroach downslope on the transition zone. By April 3, the transition zone on flow 1A had decreased to a length of 3–4 km, from about 1,750 to 1,600-m elevation.

STABILIZED CHANNEL ZONE

As the lava lens adjacent to the active channel cooled and marginal deformation of the flow ceased, all movement became concentrated in the central channel, producing a stable geometry in upper reaches of the flow (fig. 57.8*C*, *D*). Above about 2,450 m, where flow 1 had advanced rapidly as a sheet only a few meters thick during March 25–26, the channel appears to have stabilized rapidly, and there is little evidence for ephemeral development of a transition zone. In contrast, the segment from about 2,450–1,850 m elevation, although part of the stable channel zone by March 28, contains structures (broad central depression, inward-facing sags and ridges, and open cracks parallel to the channel) that indicate that this segment passed through a transition zone earlier during the eruption. By March 28–29, just before the breakout of flow 1A, the lower margin of the stable-channel zone was at about 1,850–1,900 m, below channel observation station 4 at 1,900 m and above station 3 along the Powerline Road at 1,800 m (fig. 57.1*B*). By April 3, the flow 1A channel had stabilized at the breakout area at about 1,800 m, but it never stabilized below about 1,750 m. After flow 1B and related breakouts at the 2,100-m level on April 5 had pirated the lava supply from lower parts of the previously stable channel zone, successively higher segments of the channel were abandoned or covered by lava from breakouts higher along the distributary system.

CHANNEL EVOLUTION

A notable feature of the 1984 eruption was evolution of the main flows and associated channels from a simple long and narrow flow to a more complex geometry, largely as a result of breakdown in the efficiency of the lava channel. A key feature in this evolution was the formation of lava boats by rafting away of unstable portions of the lava channel. The lava boats caused blockages and ponding at downstream constrictions in the lava channel.

INITIAL CHANNEL DEVELOPMENT

Lava channels formed in all 1984 Mauna Loa aa lobes more than a few hundred meters long, in response to the transverse velocity gradient across the flow near its toe, and by upflow stabilization of the flanks of the flow (figs. 57.5, 57.9). The position of the lowest well-defined channel coincided approximately with the diffuse boundary between the transition zone and the zone of dispersed flow. The first indication of this boundary was an upflow change in the cross-sectional flow profile, from convex upward near the toe (fig. 57.9*A*, *B*), to a broad rounded M-shaped profile upflow (fig. 57.9*C*). This change resulted from draining of lava toward the flow toe, with the greatest velocity in the central trough. Higher in the transition zone, the flow velocity of the axial zone increased further (fig. 57.10), and the velocity gradient between the rapidly moving central area and the stagnating margins became greater and eventually abrupt. This change confined a progressively greater volume of faster moving lava to a smaller channel cross section in an upstream direction. The surface of the central area became more incandescent and finally consisted dominantly of fluid lava (fig. 57.9*C*, *D*)

The geometry of the channel appeared to be sensitively related to other parts of the flow, especially in its lower reaches where the channel remained in dynamic interaction with the associated lava lens that extended as much as tens of meters beneath more stable flanks of the flow. The upper 10 km of the 1984 aa channel—above about 1,850-m elevation—remained stable for 8–10 days after its formation (fig. 57.7), but the lower reaches that never became part of the stable channel zone were sensitive to subtle changes in eruptive volume and lava properties. These changes produced floating debris in the lava channel that eventually caused blockages, ponding, and overflows of lava. This depleted the lava supply to lower channel reaches, and both the blockages and flow progressively stagnated upslope.

LAVA BOATS

Floating debris of solidified lava was conspicuous in lower reaches of the channel as early as March 27, when channel observations were first undertaken more than a few kilometers from the vent. Large rounded lava masses found on consolidated surfaces

FIGURE 57.9.—Development of the aa channel and levees during the 1984 Mauna Loa eruption. ***A***, Initial aa sheet flow; near toe in zone of dispersed flow. ***B***, Mature aa sheet flow. Zone of dispersed flow; flow has spread laterally and inflated as supply of lava increases. ***C***, Transition zone, showing incipient development of a channel and the rounded M-shaped profile. Solid line indicates flow level at early stage of high lava supply; dashed line indicates lower flow level at later stage, when lava is draining efficiently downflow to zone of dispersed flow and central channel is becoming established. A peripheral zone of sluggish flow has developed along the margins and bottom through degassing, drag, and cooling. The flow has spread and the early levees have grown by overflows and lateral bulldozing during periods of high lava supply. Marginal shear ridges are active above the areas of sluggish flow. ***D***, Development of stable channel. Zone of sluggish flow has developed a more stable solidified crust, beneath which a plastic lava core remains, and erosion may have deepened the axial zone of sluggish flow, thereby deepening the channel and permitting higher flow rates. Also shown are overflow levees adjacent to the narrower deeper channel. ***E***, Mature channel in zone of stable flow. Lateral restriction of channel through inward migration of the zones of solidification and sluggish flow is counterbalanced by continued growth of overflow levees and perhaps by further erosion at the bottom of the channel. ***F***, Alternative types of levees for stage shown in *D*, showing development of structural levees. 1: Similar to *D*, but without development of overflow levee. 2: Uplift and buckling of the early channel crust during period of high lava supply. ***G***, Alternative types of levees for stage shown in *E*, showing concurrent development of overflow and deformation levees. 1: Overflow levee growing adjacent to earlier deformation levee, over regenerated channel crust. 2: Both levees bulldozed laterally during periods of high lava supply, overturning the earlier deformation levee (see fig. 57.16*B*).

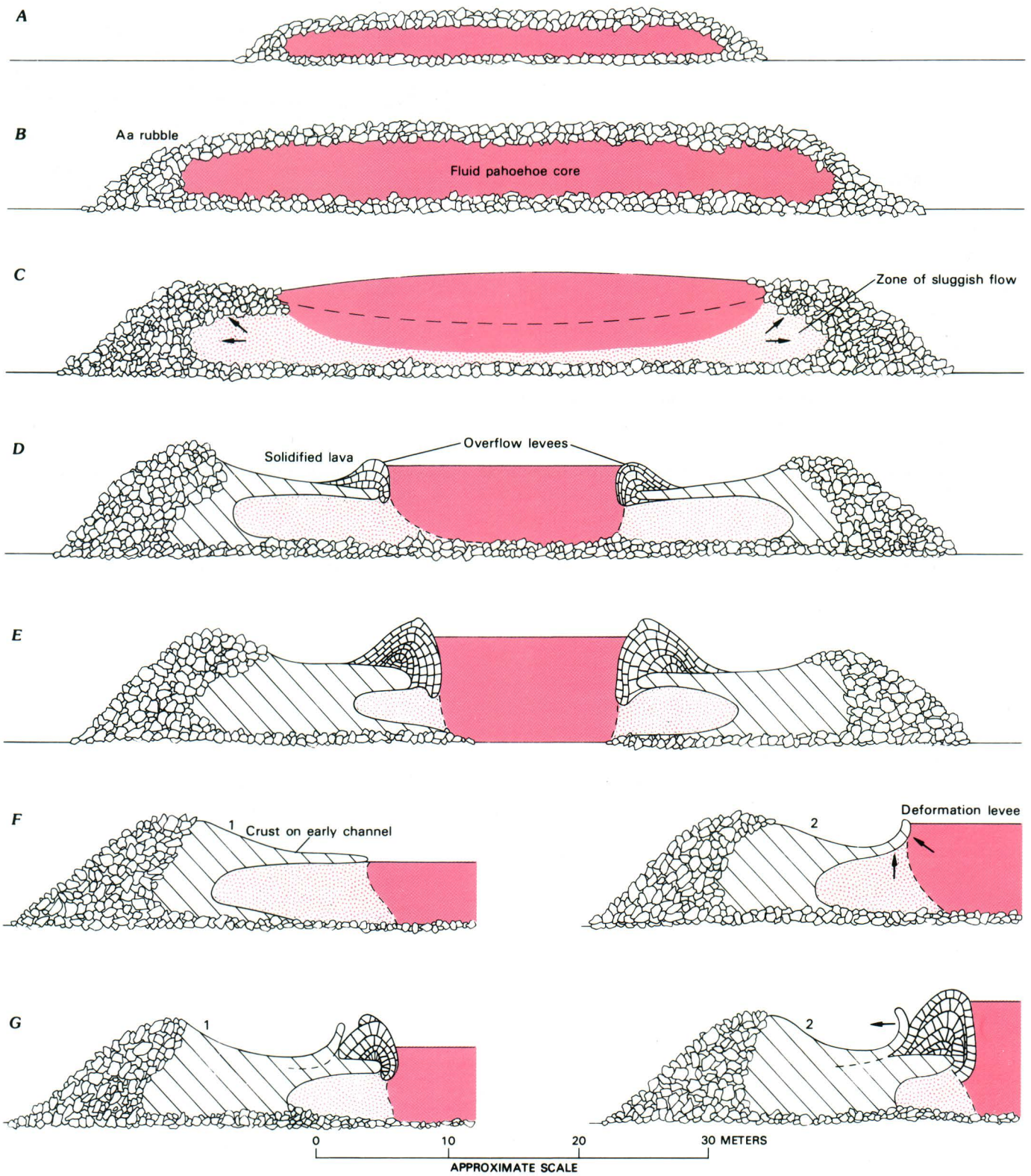
A
B
Aa rubble
Fluid pahoehoe core
C
Zone of sluggish flow
D
Solidified lava
Overflow levees
E
F
1
Crust on early channel
2
Deformation levee
G
1
2
0
10
20
30 METERS
APPROXIMATE SCALE

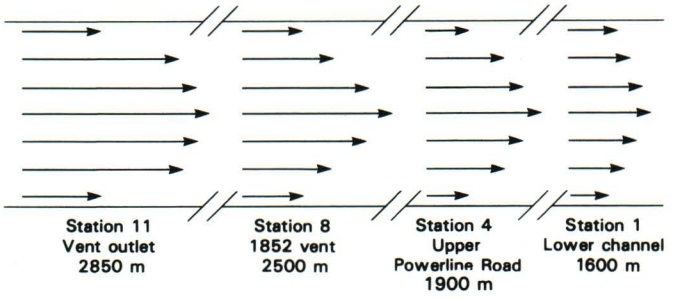

FIGURE 57.10.—Diagrammatic representation (plan view) of across-flow variation in flow velocity, channel of flow 1–1A. Station locations shown on figure 57.1*B*.

of aa flows have been called accretionary lava balls and interpreted as having formed "by the rolling up of viscous lava around some fragment of solidified lava as a center, in much the same way as a snowball rolling downhill" (Wentworth and Macdonald, 1953, p. 64). During the 1984 eruption, we referred to such features as lava boats, to emphasize their origin by caving and rafting within the active lava channel (fig. 57.11*A*), rather than by rolling on the clinkery surface in lower reaches of the flow.

Lava boats and more irregular small debris were observed to form by caving of unstable overhanging channel banks and walls, especially when the level of lava in the channel dropped and so reduced support for the bank (fig. 57.11*B*). Caving and rafting of the channel banks was aided by the presence of still-plastic lava under the channel margins (fig. 57.9), particularly adjacent to marginal shears in the transition zone. In the zone of stabilized flow, some overhangs also originated as partial roofs of incipient lava tubes. Major collapse events along the channel banks were marked by dust clouds and by subsequent increase in the number of lava boats downstream.

Lava boats also formed along the inside banks of meanders, where flowing lava in the channel applied drag and compression and opened tension cracks in the adjacent bank (fig. 57.12) Continued pressure by the moving lava then rafted fragments of the bank into the channel to form lava boats. Such formation of the lava boats tended to straighten the channel with time, in contrast to processes in rivers of water, which erode on the outsides of meanders and deposit sediment on the insides. The first channels in the early aa (fig. 57.9C) had meanders because the flow followed irregularities in the pre-eruption topography behind the toe. In addition, the flow advanced as a thin sheet in which the ratio of friction to mass was high (fig. 57.9*A*); the toe of the flow tended to inflate (fig. 57.9*B*), because the upflow channel delivered lava faster than it could be distributed by flow advance or spreading. As a result, the incipient channels initially developed a somewhat disorganized geometry as flow directions and velocities changed in response to changing rates and locations of advance of the toe. Later, as the channel deepened and narrowed (fig. 57.9*C*, *D*), the flow rate increased, and some

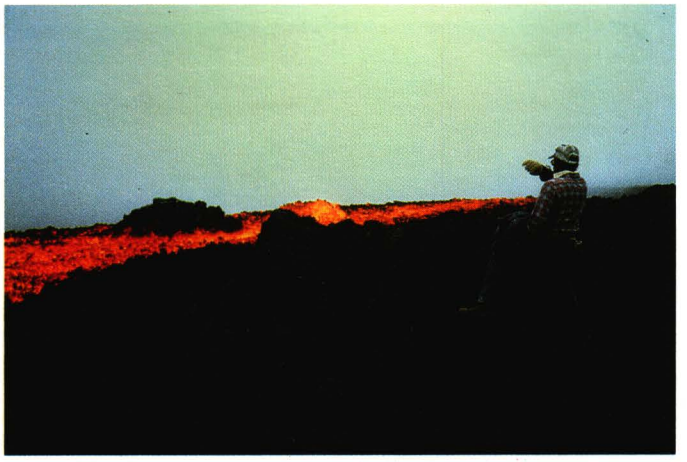

A

B

C

FIGURE 57.11.—Lava boats. ***A***, Lava boat floating in full channel during small surge. Channel is confined behind small overflow levee of scoriaceous aa. Photograph taken March 29, at 1,900-m elevation (compare with figure 57.16*B*, taken 7 days later at same site). ***B***, Formation of lava boats by collapse of overhanging levee wall into channel during low stand of lava; small satellitic northern channel. Photograph taken April 9, at 2,800-m elevation. ***C***, Flow front, showing 2-m-diameter lava boat (outlined with dashed line) being pushed ahead by advancing flow. Photograph taken April 6, at 1,700-m elevation.

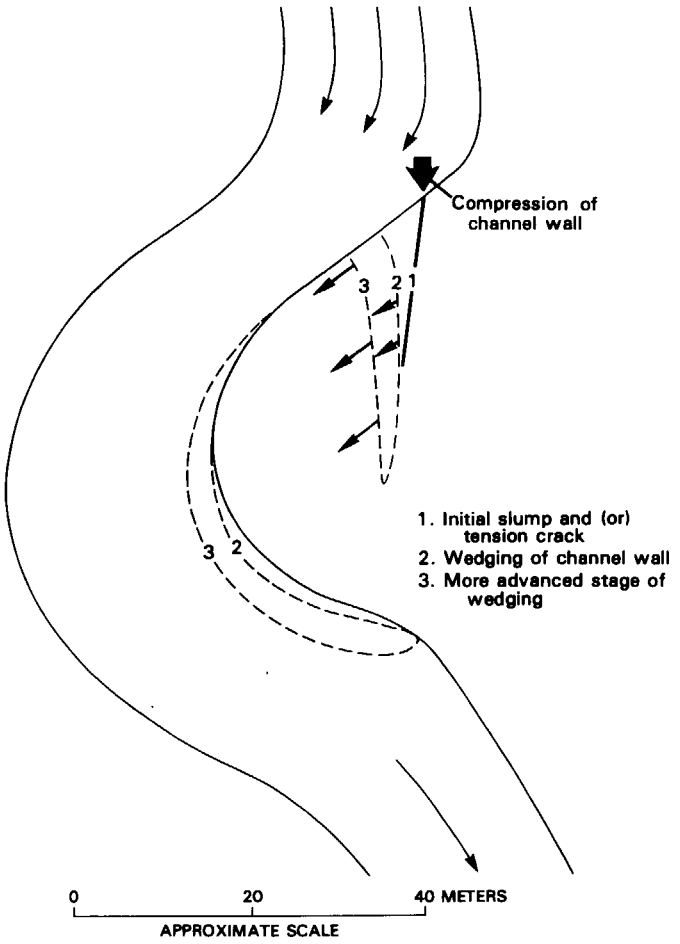

FIGURE 57.12.—Diagrammatic sketch (map view) of origin of lava boats by wedging and slumping from inside bank of channel meander in the stable-channel zone.

early meanders became inefficient for delivery of the lava to the flow front. Such channels tended to straighten through spalling of the inside walls of curves.

The elongate wedges of channel-bank and levee material thus formed floated downstream as lava boats that gradually broke into more equant shapes. Frequently, they disintegrated into equant pieces when they grounded on the channel floor or jammed against the downstream channel walls and adjacent boats. As the boats rolled and bobbed in the channel, they also accreted a lava sheath.

In the zone of dispersed flow below the active channel, the lava boats were rafted along the upper surface of the flow, in conveyer-belt fashion toward the flow front. In this zone, blocks on the flow surface tended to be carried passively downslope, with little differential movement. Thus no additional lava was accreted to the lava boats below the active channel. Frequently, lava boats several meters in diameter were rafted all the way to the flow front and pushed ahead by the advancing flow (fig. 57.11*C*).

Lava boats were rare in upper reaches of the channel, within about 5 km of the vent, especially during the first half of the eruption, reflecting the more stable channel configuration in this area. In the channel within 200–300 m of the vent, rapidly flowing lava splashing against the channel banks at a curve occasionally stoped large blocks from the bank. Lava boats became progressively more abundant downflow and also with increasing age of the channel.

The lava boats were useful indicators of channel velocities and minimum depths (table 57.2; app. 57.2); they also played a key role in channel evolution by causing blockages and dams in the channel. The largest lava boats were 6–7 m across and extended 2–3 m above the channel surface. Several kinds of observations suggest that they typically projected at least this distance below the channel surface, providing a minimum estimate of channel depth: (1) Most lava boats rafted to the lava surface low on the flow are subequant in shape. (2) Rarely, large lava boats would hang up on the channel floor and roll over, exposing their full geometry. Even during low channel levels, 2–3 m below maximum, large lava boats would commonly float freely—suggesting typical channel depths of 4–6 m. (3) Because the density of lava in the channel is low—about 0.5 g/cm^3 at the vent to 1.5–2.5 g/cm^3 in lower reaches (discussed later; also see fig. 57.20)—typical channel-bank debris (density 1.0–2.0 g/cm^3) is only slightly less dense than the channel lava, and the resulting lava boat could not rise buoyantly more than about one-half its diameter. As the channel lava degassed, cooled, and became more dense downchannel, accompanying lava boats probably gradually emerged higher. Lava boats that originated by caving of unstable banks from lower channel reaches (transition zone) would also be denser than boats derived from higher stretches of the channel. Within a few kilometers of the vent, most lava of the channel walls was more dense than the fluffy lava in the channel; caved fragments of channel banks probably sank rather than floated, and formed saltating blocks along the channel bottom. Only rare rafted fragments from the low-density agglutinated spatter ramparts could float in the channel lava close to the vent.

BLOCKAGES AND PONDING

Accumulation of lava boats and debris from surface crusts in channel constrictions (fig. 57.13A) caused blockages and ponding of the main channel and produced major changes in the character of the aa flow during early April. Small ephemeral blockages formed at a few channel constrictions in middle and lower reaches of the flow as early as March 27, but the first significant lava dams were not observed in well-developed reaches of the main channel until March 29. During the following week, blockages increased in size and number, and they gradually formed higher along the main channel (fig. 57.14). Overflows from long-lived ponds occurred both to the sides and over the tops of blockages (fig 57.13*B*). When overflow was sustained at one side of a dam that held, a branch flow could be generated. Most branch breakouts advanced at first as sheet flows; if the overflow was maintained, erosion of the flanking levee permitted the flow rate in the branch to increase, a channel to develop, and a stabilized branch flow to form.

By the morning of March 29, a major blockage at the 1,800-m level was able to divert the entire lava supply of flow 1 northward

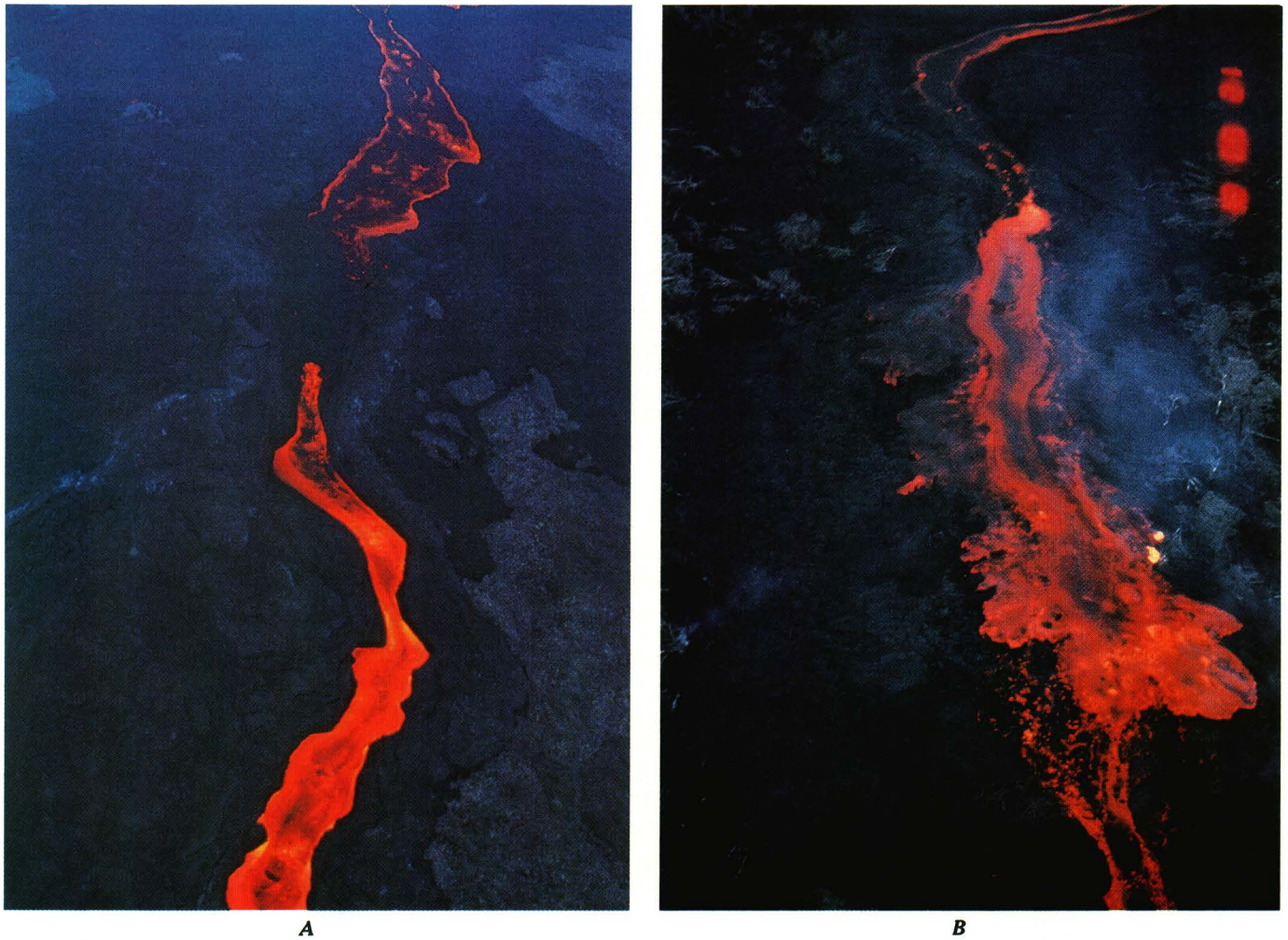

A *B*

FIGURE 57.13.—Blockages and surges in lava channels, 1984 Mauna Loa eruption. ***A***, Aerial view of developing blockage along constricted sector of flow channel. Upchannel pond has relatively cool scoriaceous surface; hotter interior lava is draining downchannel from below blockage. Light-colored lava along right margin is 1852 pahoehoe. About 1,800-m level, March 31. ***B***, Aerial view of surge overflow at blockage site, looking upchannel. About 1,650-m elevation, March 31.

to form flow 1A. Many smaller blockages in the next few days caused overflows at this same general elevation. By April 4, blockages were occurring as high as 1,950 m, and on April 5 a large blockage at about 2,050 ft caused a major surge and overflow to form flow 1B. On April 6–7, repeated blockages and overflows at the 2,000–2,100-m level prevented sustained feeding of any flow system below 1,850 m. By April 8, blockages were causing many overflows at elevations as high as 2,300 m), and blockages and overflows extended back almost to the vent during the next two days.

Most debris blockages reduced, but did not stop, downchannel flow; typically, little glowing lava was visible at the surface in the constricted sector of the channel, but fluid lava would continue to flow or at least ooze out at the lower end of the constriction. The amount of lava ponded by a blockage could be large relative to the upslope channel volume; blockages and ponding promoted construction of overflow levees that in turn could be enlarged by spreading of the levees and overflow of the entrapped ponded lava. The largest ponds, at the 1,800-m and 2,050-m levels, were as much as 100 m wide, 10 m deep, and 500 m long; periodic abrupt release of much of the ponded lava could significantly modify the downstream flow regime.

A dynamic relation was established early between blockages and formation of lava boats: generation of a cluster of lava boats by failure of the channel bank provided material to cause a blockage at a downstream constriction, and in turn formation of such a blockage would lower the channel level farther downstream, causing additional failure of the channel bank and generation of more lava boats. As a corollary, when the channel level was low and few lava boats or other debris were evident in the channel, blockages and ponding could be inferred to be occurring upchannel. Both straightening of meanders and small fluctuations in channel level, perhaps initially related to short-term variations in rate of lava production at the vent, were thus capable of generating blockages farther downchannel. The intensity of such perturbations increased during the first two weeks of the eruption, even though the rate of lava production at the vent remained roughly constant, at least from March 30 to April 7.

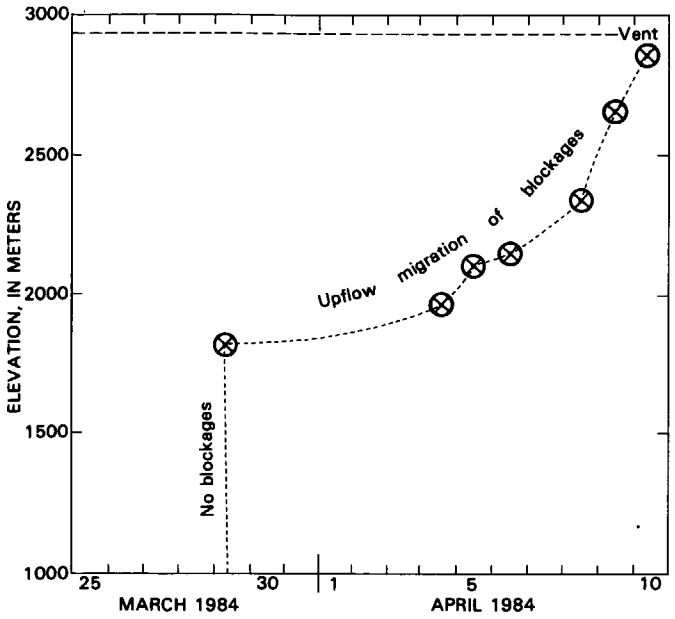

FIGURE 57.14.—Elevations of highest overflow-producing blockages (circled crosses) in main flow channel of 1984 Mauna Loa eruption.

SURGES AND OVERFLOWS

Lava that ponded behind channel blockages eventually escaped, either by overflowing the channel banks as the pond level rose or by breaking through the blockage to generate lava surges downchannel. Small blockages commonly failed when the weight of the ponded lava exceeded the strength of the obstruction. At first, the dam would begin to creep downchannel, at increasing rates. Within several minutes, flow rates would increase from a few meters per minute to a few meters per second. Then the lava pond would break through a low or weak area to form a surge of lava down the channel. At times, this occurred in such volume that the released lava could not be contained in the channel below the dam (fig. 57.15). At other times, the rising impounded lava would lift and float the jammed debris over the constriction to form an overflow surge. When the volume of the breakout was reduced by overflows to an amount containable within the channel, the excess lava progressed down the flow as a channel surge.

Where the pond was confined behind high overflow levees, the weight of the pond could bulldoze the flank of the levee aside, widening the channel or causing failure of the levee. Failure of the levees, at times observed to open like a giant barn door, could abruptly release a large volume of lava along the flank of the flow rather than directly downchannel. Such lateral breakouts could generate major new lava tongues, such as flows 1A and 1B. In such breakouts large blocks of levee material were rafted downslope embedded in the overflow lava. Much of the volume of the eruption was dissipated in this way after March 29, causing slowing and stagnation of the flow terminus.

In lower reaches of the channel (transition zone), surges caused fluctuations of several meters in channel level; they also affected the height and rate of deformation of the marginal shear lenses adjacent to the channel. Increased marginal deformation during a surge was accompanied by creaking and crunching noises. The marginal shear areas rose during passage of a surge and subsided afterward, demonstrating that the zone of shearing was underlain by fluid lava hydraulically connected to the channel.

Flow velocities in the channel commonly increased during a surge, especially where the channel gradient was fairly uniform. Where the gradient flattened below a cascade, however, the effect of a surge was mainly to increase the lava level, with little or no increase in velocity. Many surges carried abundant debris from the causative blockage as a raft that spanned much of the channel and moved more slowly than the underlying lava. The cooler and more rigid rafted material tended to increase the bulk viscosity of the lava and drag along the marginal levees; these interactions raised the level of flow within the channel and decreased the velocity of the lava. A few minutes after passage of a surge, exceptionally fluid lava that had been stored in the interior of the blockage pond typically arrived in the channel; flow velocities increased, and the previous channel gradients were restored.

LEVEES

Marginal levees are common features of aa flows and are closely related to channel evolution (Hulme, 1974). At Mauna Loa in 1984, several types of levees formed that are broadly similar to those described for small short-lived aa flows on Mount Etna (Sparks and others, 1976). At Mauna Loa, however, levee growth varied notably with time and with position along the flow.

EARLY LEVEES

Early levees on Mauna Loa are represented by the broad topographically high rubbly flanks of the aa flow (fig. 57.9C: high points on the M-shaped profile) that were left behind in the zone of dispersed flow as the central zone of highest velocity flow drained downslope to form an incipient channel (fig. 57.5). In many places, lateral spreading of the flow tended to displace and cause outward avalanching of aa rubble along the early formed levees (fig. 57.9C). Thus, the early Mauna Loa levees seem transitional between the features that Sparks and others (1976) called initial levees and rubble levees. Nested lateral levees also tended to form rapidly at Mauna Loa, inside of the early lateral levees, as the center of the flow thinned and movement became concentrated along an incipient channel. In comparison with initial levees of aa flows on Etna, such early lateral levees on Mauna Loa aa flows were morphologically more complex, broader relative to channel width, had high points farther from the channel banks, and formed over a period of hours to days rather than within minutes of passage of the flow front. These differences seemingly reflect the larger size and longer movement history of the Mauna Loa flows. In addition, on Mauna Loa the flowing lava between the levees rapidly developed a concave-upward profile because of draining of the liquid flow core downslope and probably also because of effects of preexisting topography (fig.

A

FIGURE 57.15.—Channel overflows. ***A***, Begining of overflow at about 2,800-m level, at 1800 April 10. Blockage has broken, permitting ponded lava to spread downslope and overflow the channel. ***B***, Photograph taken about 5 minutes after that in *A*. Upper part of overflow has stagnated and lava is draining back into original channel; on lower slopes surge continues to flood and overflow channel.

57.9C) In contrast, profiles of flows on Etna (and also those modeled by Hulme, 1974), which are confined within marginal levees, are convex upward. On both volcanoes, formation of early levees appears related to the yield strength of the lava.

The early levees that formed at Mauna Loa were gradually modified by later processes of composite levee growth, mainly involving channel overflow and deformation of already formed levees. These processes produced complex levee structures somewhat similar to those described on Etna—accretionary, rubble, and overflow levees (Sparks and others, 1976)—although larger and more notably composite in origin. All levee growth on Mauna Loa flows, after a central channel was established, was caused by variations in channel level related to blockages and surges.

OVERFLOW LEVEES

The most common levee-building process was overflow of the channel banks during passage of surges. During vigorous surges, discrete small aa or pahoehoe flows spread laterally to produce overflow levees (figs. 57.16*A*, 57.9*D*, *E*) of the sort diagramed but not observed by Sparks and his associates. Weaker surges that completely filled the channel without overflowing caused scoriaceous or clinkery aa to accumulate along the channel margins, producing rapid growth in levee height by processes somewhat similar to the so-called accretionary levees described on Etna. Overflow and accretionary levee-building processes were thus intergradational, even during a single surge event. At Mauna Loa, levees formed by these

B

FIGURE 57.15—Continued.

surge-overflow processes had depositional slopes of no more than 10°–15°, in contrast to slopes of 50°–85° reported at Etna.

DEFORMATION LEVEES

An important process, which steepened overflow levees at Mauna Loa, was outward displacement of overflow levees pushed by the increasingly deep lava confined in the channel. By this mechanism, overflow levees with initial surface features of small lava flows were converted into angle-of-repose rubble ridges, which stood as much as 6–8 m above the original channel level (fig. 57.9*E*). At times, slabs of scoriaceous pahoehoe several meters across, derived from the crust of the channel lava, were tilted and overturned during upwelling of channel lava associated with surges (fig. 57.9*F*). These features are best described as deformation levees, although somewhat related in process and resultant appearance to the so-called rubble levees described near the toes of Etna flow fronts (Sparks and others, 1976). Deformation of a levee was commonly recognizable at a distance by rising dust clouds, as aa debris ground together and cascaded down the flank of the levee (fig. 57.16*B*). Such outward expansion was frequent during passage of surges, when channel levels were high, and was commonly accompanied by channel overflows, producing composite levee morphologies. The outward displacement of levees also caused fracturing, and at times lava from the interior of the channel oozed out along the base of the rubble levees. This process sometimes led to catastrophic failure of a levee flank, formation of a new lateral breakout, and draining of the lava ponded behind the levee.

Overflow and deformation levees did not form during early advance of the Mauna Loa flows; they constitute a distinct aspect of later evolution associated with blockages and ponding in the channel. Development of such levee features could provide a useful criterion to distinguish between long-lived and short-lived prehistoric aa flows.

ACCRETED LEVEES

Distinctive additional levee types, observed in the transition zone of the Mauna Loa flow system, are best termed accreted levees

A

B

FIGURE 57.16.—Lava levees, 1984 Mauna Loa eruption. ***A***, Overflow levee: channel level is low between surges. Slow overflows have produced shiny pahoehoe on levee flanks. Photographed on April 10, at about 2,800-m elevation. ***B***, Deformation levee: weight of perched lava channel is causing restraining levee to spread laterally, as indicated by dust clouds rising from blocks cascading down steepening levee flank. Result is angle-of-repose outer slopes of levees (see fig. 57.9G). Photographed on April 4, at 1,900-m elevation.

although different in origin and appearance from the accretionary levees of Sparks and others (1976). In the transition zone, characterized by a developing channel flanked by slowly moving lens-shaped ridges of aa rubble bounded by discrete shear zones (fig. 57.5), the initial levees were widened and enlarged by accretion of laterally moving rubble ridges. The ridges moved fairly rapidly during surges in the adjacent channel; during low stands of the channel, motion of the lateral ridges slowed, and some marginal ridges would accrete to stable flanking rubble levees. In many respects, this process provides a small-scale analog of plate-tectonic accretion of tectono-stratigraphic terranes (Jones and others, 1982). Some accreted levees originated as transverse pressure ridges near the flow toe, which were then deformed by continued flowage into U-shaped ridges (in plan view). These ridges subsequently were breached by continued movement within the center of the flow, and the limbs of the "U" became moving levees parallel to the channel margins (fig. 57.17).

POSTERUPTION CHANNEL PROFILES

During the eruption, channel depths were estimated mainly by reference to the half diameters of large lava boats (table 57.2). Once, we attempted to measure channel depths directly by dropping 5-m iron bars, stabilized vertically with streamers, from a helicopter. The channel center was difficult to hit by this technique, however, because radiative heat from the channel required a flight height of 100–200 m. Similarly, suitable locations for launching bars 2–3 m long in javelin fashion from high levees were rare, and such attempts failed to penetrate to the channel bottom.

After eruptive activity ceased, we measured profiles across the evacuated channels of flow 1, flow 1A, and the north flow at sites that had drained rapidly because of upflow beheading (fig. 57.18). Most profiles were at or near the flow-rate monitoring stations (fig. 57.1*B*), and some channel sites appeared unmodified except for draining of lava since our last monitoring measurements. Where the monitoring station had been modified by ponding or overflows, we profiled a nearby channel site that appeared representative of the geometry during the eruption. The posteruption channel profiles showed that most of the earlier depth estimates were 20–30 percent low, probably because the lava boats would first shoal on anomalously shallow reaches of the channel. Although the channel profiles improved our estimates of volume rates of flow, the measured depths are only minima because of residual ponded lava and rubble from caving levees. In addition, the profiles are of mature channels; channel geometry in earlier stages are inferred from observed changes in levee height and channel width during the eruption.

In addition to improving the volume calculations, the profiles show that the mature channel had (1) a remarkably uniform depth, about 6 m, from the vent to 17 km downflow; (2) a gradually increasing width downflow, especially within the transition zone (fig. 57.18*M*); and (3) an approximately rectangular shape. The bottoms of many channel profiles are near the projected pre-1984 surface, in agreement with the inference that still plastic parts of the initial flow material are eroded during deepening and narrowing of the maturing flow channel (fig. 57.9).

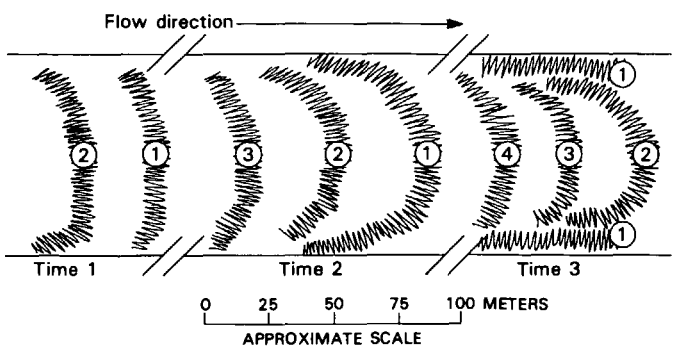

FIGURE 57.17.—Diagrammatic sketch (plan view) of formation, deformation, and accretion of pressure ridges to form accreted levees. Solid lines, margins of channel. Numbers identify individual sequentially formed pressure ridges.

TEMPERATURE AND DENSITY VARIATIONS OF LAVA

Key parameters in interpreting the evolution of the 1984 lava and channels are variations in lava temperatures and densities in relation to eruption duration, distance from vent, and lava type (table 57.1; fig. 57.19). Temperature determinations on the lavas were considered especially important for evaluating the hazard potential early in the eruption, because an increase in temperature might indicate the arrival of a more fluid magma batch from below the summit area.

LAVA TEMPERATURES

Temperatures were measured both directly by thermocouple probes inserted into accessible fluid lava and more remotely with a HOTSHOT 2-color infrared pyrometer aimed at active fountains or at brightly incandescant lava in standing waves in channels. Agreement among results by the two techniques was commonly within 5 °C when conditions were optimal. Some low measurments, deemed nonrepresentative and not plotted in figure 57.19, resulted from failure of the thermocouple to reach equilibrium before breakage of the probe tip, or from HOTSHOT measurement of fountains when the view included obstructing fume or cooler peripheral fallback material. Some equilibrium thermocouple measurements, which were lower than other values obtained from the same site, are thought to have inadvertently sampled cooler marginal lava. Details of measuring techniques and instrumental limitations are summarized in appendix 57.1.

The interpreted best measurements indicate that lava temperatures within a few hundred meters of the vents at about 2,850 m remained within the narrow range of $1,140 \pm 3$ °C throughout the eruption, varying little more than measurement uncertainties (fig. 57.19*A*). Temperatures measured on the most fluid lava at channel sites as much as 10 km downslope were only slightly cooler, in the

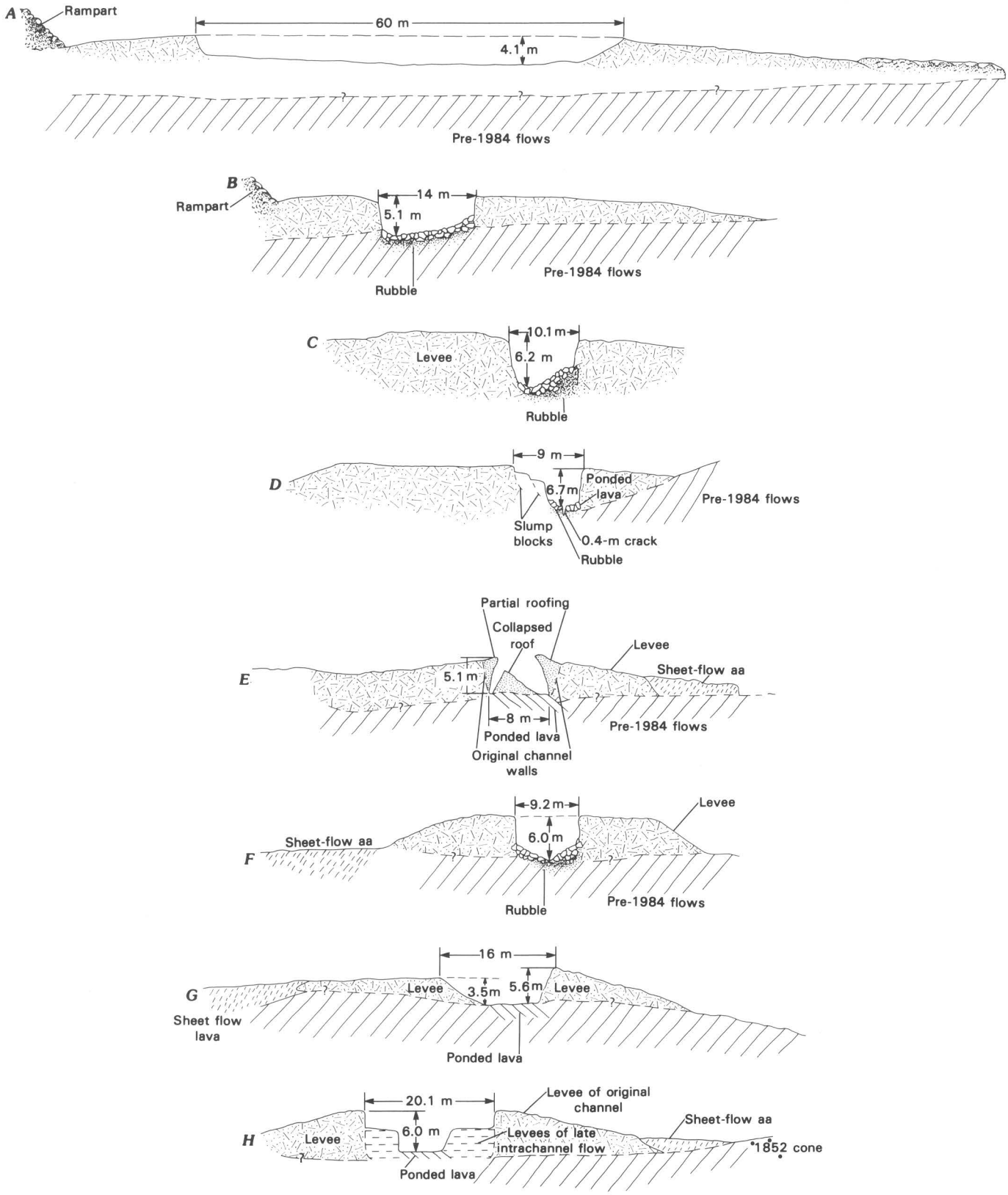
A
Rampart
60 m
4.1 m
Pre-1984 flows
B
Rampart
14 m
5.1 m
Rubble
Pre-1984 flows
C
Levee
10.1 m
6.2 m
Rubble
D
9 m
6.7 m
Ponded lava
Pre-1984 flows
Slump blocks
0.4-m crack
Rubble
E
Partial roofing
Collapsed roof
Levee
Sheet-flow aa
5.1 m
8 m
Ponded lava
Original channel walls
Pre-1984 flows
F
Sheet-flow aa
9.2 m
6.0 m
Levee
Rubble
Pre-1984 flows
G
16 m
Levee
3.5 m
5.6 m
Levee
Sheet flow lava
Ponded lava
H
20.1 m
6.0 m
Levee
Levee of original channel
Levees of late intrachannel flow
Sheet-flow aa
1852 cone
Ponded lava

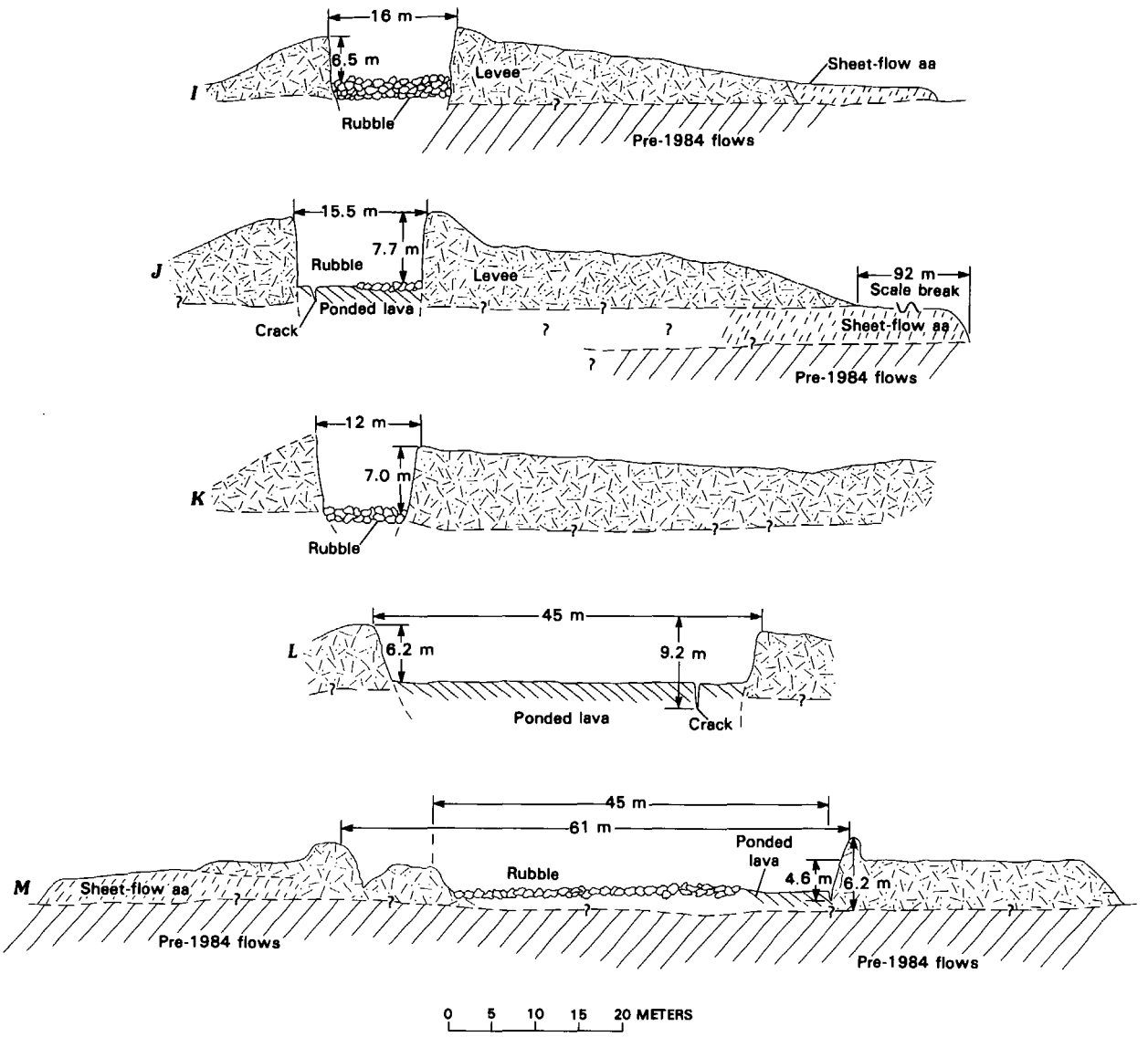

FIGURE 57.18.—Posteruption profiles (no vertical exaggeration) across channels of the 1984 Mauna Loa flows. Locations of channel stations shown on figure 57.1*B*. ***A***, Channel at about 2,900 m, 100 m downflow from westernmost vent, that was abandoned just after initial stabilization on about April 10. ***B***, Channel station 12, at about 2,900 m; mature stage of north channel, adjacent to vent rampart. ***C***, North flow, at 2,850-m elevation, 70 m from vent outlet. ***D***, Channel of north flow at 2,800-m elevation, approximately north of vent 2. ***E***, Channel station 10, at 2,720-m elevation; north flow, near monitor station. About 1 km from vent. ***F***, Channel at 2,710-m elevation, flow 1. About 2.5 km from vent. ***G***, Channel at 2,550-m elevation, flow 1; probably a channel formed after April 8. About 3.5 km from vent. ***H***, Channel station 8; 2,540-m elevation, flow 1; pre-April 8 channel, just above monitor station. About 4 km from vent. ***I***, Channel station 7, 2,200-m elevation, flow 1; pre-April 8 channel, near monitor station. About 6.5 km from vent. ***J***, Channel station 4, 1,950-m elevation, flow 1; pre-April 8 channel, near monitor station. About 10.5 km from vent. ***K***, Channel station 3, 1,800-m elevation, flow 1; pre-April 8 channel, near monitor station. About 12 km from vent. ***L***, Channel at 1,800-m elevation, flow 1; pond below channel station 3. About 12.5 km from vent. ***M***, Channel station 1, 1,600-m elevation, flow 1A; pre-April 8 channel, near monitor station. About 15 km from vent.

TABLE 57.1.—*Lava temperature and density, 1984 Mauna Loa eruption*

[Days, time in days from beginning of eruption; distance, distance from vent]

Location	Date (mo/d)	Time (H.s.t.)	Days	Elevation (m)	Distance (km)	Temperature (°C)	Code[1]	Density (g/cm³)	Sample	Comments
3,500-m vents	3/25	1015	0.37	3,500	0.01	1,073	T 1 B I	0.85	NER-7	Channel at vent; couldn't probe below surface; poor reading.
SE. flow, terminus	3/25	1540	.59	2,670	6.6	1,128	T 2 B E	2.23	NER-1F	Aa flow front; imbedded 2 m in soft core; stable 15 min.
Flow 1	3/25	--	.70	2,560	3.6	--		1.29	4/18NB1	Aa, core of sheetwash flow.
Vent 1, middle	3/26	0828	1.29	2,910	.0	1,125	H P	--	--	Fountain; tripod rest, 50 m distance.
Do.	3/26	0854	1.31	2,910	.0	1,145	H G	--	--	Fountain; tripod rest, 50 m distance; stable 1,144–1,145 °C.
Vent 1, east end	3/26	1058	1.40	2,890	.0	1,103	T 1 B F	1.08	NER-12/2	1-m-thick spatter-fed flow; failed tip several tries.
Do.	3/26	1324	1.50	2,890	.0	1,146	H G	1.20	NER-12/3	Fountain, tripod at 20 m; stable 1,134–1,146 °C, observer 1.
Do.	3/26	1340	1.51	2,890	.0	1,147	H G	--	--	Fountain, tripod at 20 m; stable 1,134–1,146 °C, observer 2.
Flow 3	3/26	1420	1.54	2,860	.0	1,131	T 1 B E	1.19	NER-12/13	Pahoehoe overflow from main channel; stable 2 min.
Flow 1	3/26	1600	1.61	2,760	1.5	1,139	T 1 B G	1.18	NER-12/4	Directly in main channel; stable several minutes.
Vent 1, east end	3/26	1613	1.62	2,890	.0	--		.92	NER-12/14	Spatter.
Flow 1	3/26	1730	1.67	1,880	11.7	1,131	T 2 B E	1.77	NER-12/5	Overflow 30 m from channel; stagnating when measured.
Vent 1, main vent	3/27	--	2.50	2,890	.15	--		.60	NB1ML84	Cooled shelly pahoehoe overflow from main channel.
Vent 1, middle vent	3/27	1421	2.54	2,910	.01	1,131	T 1 B E	.83	NER-12/12	Spatter-fed flow; 60 cm thick; stable 0.5 min.
Vent 1, main vent	3/27	1435	2.55	2,500	.0	1,139	H G	--	--	Fountain, tripod rest; 10–15 m distance; stable 1,135–1,139 °C.
Do.	3/27	1545	2.60	2,890	.0	1,139	H G	--	--	Do.
Do.	3/27	2016	2.79	2,890	.01	1,131	T 1 B E	.98	NER-12/15	Spatter-fed flow; 1 m thick; stable 0.5 min.
Do.	3/27	2035	2.80	2,890	.0	1,140	H G	1.12	NER-12/16	Fountain, tripod rest; 10–15 m distance; stable 1,135–1,140 °C.
Do.	3/27	2350	2.93	2,890	.02	1,135	T 1 B G	1.36	NER-12/17	Tube, directly from vent; stable 3 min.
Do.	3/28	0610	3.20	2,890	.02	1,137	T 1 B G	.92	NER-12/18	Do.
Vent 4	3/28	0835	3.30	2,810	.05	1,128	T 1 B E	.92	NER-12/10	Tube emitted directly from vent pond; stable.
Do.	3/28	1241	3.47	2,810	.0	1,131	T 1 B E	--	NER-12/20	Do.
Do.	3/28	1610	3.61	2,810	.05	1,128	T 1 B E	--	NER-12/21	Do.
Flow 1A	3/29	1300	4.50	1,610	16.50	--		2.6	--	Core of aa flow.
Vent 4	3/29	1755	4.69	2,810	.0	1,136	T 1 B G	1.19	NER-12/23	Top of west hornito; 2 times; stable 3 and 2 min.
Do.	3/30	0656	5.23	2,810	.0	1,130	T 1 B E	--	NER-12/24	Tube emitted directly from vent pond; stable.
Do.	3/30	0840	5.30	2,810	.0	1,135	T 1 B G	1.84	NER-12/25	Top of west hornito; stable 3 min.
Flow 1A	3/30	1230	5.46	1,370	20.4	1,103	T 2 B F	--	--	Horizontal into lobe terminus; >20 cm penetration, poor.
Do.	3/30	1420	5.54	1,750	14.2	1,126	T 2 B E	--	NER-12/28	Slabby pahoehoe overflow 30 m from channel; flow stagnant.
Vent 4	3/30	1647	5.64	2,810	.0	1,136	T 1 C G	1.02	NER-12/26	Short tubed flow from west hornito; stable 5 min.
Flow 1A	3/31	0712	6.21	1,150	24.5	1,086	T 2 B F	--	--	Flow terminus; >30 cm penetration; poor reading.
Do.	3/31	1056	6.40	1,610	16.5	1,125	T 2 B F	--	--	Overflow 3 m from active main channel; aborted before stable.
Do.	3/31	1250	6.48	1,950	10.2	1,133	T 1 B G	1.22	NER-12/29	Tube, branch of main channel.
Vent 4	3/31	1556	6.60	2,810	.0	1,132	T 1 B E	--	--	Short tubed flow from west hornito; stable 5 min.
Do.	3/31	1630	6.64	2,810	.0	1,133	T 1 B E	1.01	NER-12/30	Do.
Do.	4/01	1154	7.44	2,810	.0	1,129	T 1 B E	--	NER-12/31	Tube emitted directly from vent pond; stable.
Vent 1, main vent	4/02	1000	8.36	2,890	.03	1,135	T 1 B E	1.20	NER-12/32	Tube emitted directly from vent; stable 4 min.
Do.	4/02	1047	8.39	2,890	.00	--		.79	NEW-12/32	Spatter.
Vent channel	4/02	1155	8.44	2,860	.15	1,137	H G	--	--	Underside of standing wave; 15 m distance; tripod rest, stable.
Vent 1, main vent	4/02	1645	8.64	2,890	.07	1,136	T 1 B G	1.10	NER-12/34	Tube emitted directly from vent; stable 2 min.
Do.	4/02	1715	8.66	2,890	.00	--		.70	NER-12/35	Spatter.
Do.	4/03	1012	9.37	2,890	.12	1,133	T 1 B E	--	NER-12/36	Tube emitted directly from vent; stable.
Do.	4/03	1230	9.54	2,890	.12	1,140	T 1 B G	--	NER-12/37	Do.
Do.	4/03	1417	9.54	2,890	.12	1,138	T 1 B G	--	NER-12/38	Do.
Do.	4/04	0830	10.10	2,890	.03	1,141	T 1 B G	2.40	NER-12/40	Tube emitted directly from vent; stable 5 min.
Do.	4/04	0915	10.33	2,890	.0	--		.51	NER-12/41	Tube emitted directly from vent.
Do.	4/04	1545	10.60	2,890	.12	1,139	T 1 B G	1.41	NER-12/39	Tube emitted directly from vent; stable.
Do.	4/04	1550	10.60	2,890	.05	1,140	T 1 B G	1.54	NER-12/42	Tube emitted directly from vent; stable 5 min.
Do.	4/05	1230	11.46	2,890	.3	1,139	T 1 B G	--	NER-12/43	Tube emitted directly from vent.
Vent 4	4/06	0945	12.35	2,810	.02	1,131	T 1 B E	.82	NER-12/45	Tube emitted directly from western hornito; stable 2 min.
Do.	4/06	1000	12.36	2,810	.0	--		1.00	NER-12/46	Spatter from western hornito.
1852 vent station	4/06	1220	12.45	2,500	4.0	1,128	T 1 B I	1.15	NER-12/47	Directly in main channel; never stable.
Flow 1A	4/06	1430	12.55	1,940	11.0	1,133	T 2 B G	1.72	NER-12/48	Aa overflow from main channel; 2 m thick; stable 5 min.
Vent 4	4/06	1630	12.63	2,810	.02	1,140	T 1 B G	.80	NER-12/49	Tube emitted directly from western hornito; stable 2 min.
Flow 1	4/07	--	13.5	2,240	6.8	--		2.57	4/18NB3	Cooled aa levee material.
Vent 1, main vent	4/07	1405	13.53	2,890	.3	1,142	T 1 B G	1.83	NER-12/44	Tube emitted directly from vent; stable.
Do.	4/07	1053	13.39	2,890	.1	1,140	T 1 B G	.89	NER-12/50	Do.
Vent 4	4/07	1650	13.64	2,810	.10	1,124	T 1 B E	1.15	NER-12/51	Do.
Do.	4/07	1730	13.67	2,810	.1	1,121	T 1 B F	--	NER-12/52	Tube emitted directly from vent pond; stable.
1852 vent station	4/08	1026	14.38	2,500	4.0	1,100	T 1 B F	.99	NER-12/53	Directly in main channel; never stable.
Vent channel	4/08	1145	14.43	2,880	.15	--		.53	NER-12/54	Pahoehoe overflow from main channel.
Flow 1	4/08	1306	14.49	2,230	6.0	--		1.25	NER-12/57	Overflow from main channel.
Do.	4/08	--	14.5	1,980	10.2	--		2.31	4/18NB4	Cooled lava ponded in beheaded channel.
North flow	4/08	1445	14.56	2,930	2.5	1,123	T 1 B F	--	NER-12/58	Overflow from channel, never stable.
North flow vent	4/08	1515	14.58	2,910	.15	1,122	T 1 B F	.69	NER-12/55	Pahoehoe overflow from main channel; never stable.
North flow	4/08	1530	14.59	2,930	.1	--		.38	NER-12/56	Scoop sample from channel.
North flow vent	4/08	1620	14.62	2,910	.20	1,126	T 1 B E	--		Paheohoe overflow from main channel; stable 2 min.
Flow 1	4/09	--	15.5	2,550	3.3	--		1.43	4/18NB2	Cooled lava ponded in beheaded channel.
North flow channel	4/11	0850	17.31	2,930	.0	--		.51	NER-12/60	Spatter, stable.
Do.	4/11	1500	17.57	2,930	.0	--		.33	NER-12/62	Spatter.
Do.	4/11	0850	17.31	2,930	.0	--		.51	NER-12/60	Spatter, stable.
Do.	4/11	1500	17.57	2,930	.0	--		.33	NER-12/62	Spatter.
Do.	4/11	1610	17.61	2,930	.04	1,087	T 1 B I	.54	NER-12/63	Scoop sample from channel; never stable.
Vent 9,146 station	4/11	1700	17.65	2,700	2.6	1,125	T 1 B E	--		Pahoehoe overflow from main channel; stable 2 min.

TABLE 57.1.—*Lava temperature and density, 1984 Mauna Loa eruption—Continued.*

Location	Date (mo/d)	Time (H.s.t.)	Days	Elevation (m)	Distance (km)	Temperature (°C)	Code[1]	Density (g/cm³)	Sample	Comments
Do.	4/11	1710	17.66	2,700	2.6	1,106	T 2 B F	--		Aa overflow from main channel, stable 2 min.
Vent 1, main vent	4/13	0935	19.34	2,890	.20	1,102	T 1 B F	.73	NER-12/64	Directly in main channel; never stable.
Do.	4/13	1008	19.36	2,890	.10	1,132	T 1 B E	2.12	NER-12/61	Tube emitted directly from vent; never stable.
Vent 1, west vents	4/13	1142	19.42	2,930	.03	1,125	H P	--		Fountain; hand held; 20 m distance over channel; poor reading.
North flow	4/13	1215	19.45	2,900	.16	1,137	T 1 B G	.83	NER-12/65	Tube from ponded channel; stable 2 min.
Vent 4	4/13	1550	19.60	2,810	.01	1,121	T 1 B I	.57	NER-12/xx	Tube emitted directly from vent.
North flow channel	4/14	0945	20.35	2,930	.15	1,122	T 1 B I	.89	NER-12/66	Overflow from channel; never stable.

[1]Meaning of code symbols:
1, Thermocouple measurement, small-gauge (1.5-mm-diameter) wire.
2, Thermocouple measurement, large-gauge (6-mm-diameter) wire.
B, Thermocouple wires exposed to lava.
G, Grounded thermocouple; wires sheathed with INCONEL stainless steel.
E, Thermocouple measurement; stable temperature in equilibrium with lava but in geologically unfavorable site (thin flow, stored lava, and so on).
F, Failed thermocouple measurement; probe broken before equilibrium temperature achieved.
G, Good measurement; stable temperature in a geologically good site (thermocouple), or with good atmospheric conditions (HOTSHOT).
H, Measurement by two-color HOTSHOT infrared pyrometer.
I, Thermocouple became sheathed with a lava icicle before equilibrium temperature was achieved.
P, HOTSHOT measurement under poor atmospheric conditions.
T, Thermocouple measurement.

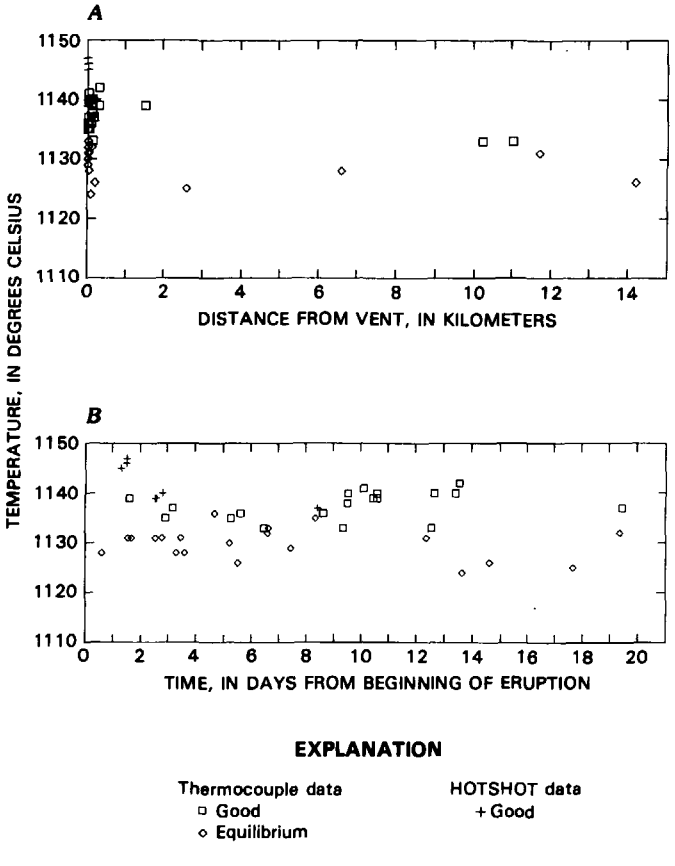

FIGURE 57.19.—Measured lava temperature in 1984 Mauna Loa eruption. Includes all good or equilibrium data, thermocouple and HOTSHOT techniques. Good values are from superior sites, as ranked on geologic criteria; equilibrium thermocouple data are stable results from less favorable sites. Temperature data are from table 57.1; measurement techniques and limitations are described in appendix 1. ***A***, Temperature plotted against distance from eruptive vent; values by the same technique are at most about 5 °C higher at the vent than downchannel. ***B***, Temperature plotted against time: no sigificant variation is evident.

range of 1,135 ± 5 °C. Most of the infrared-pyrometer temperatures for fountains were a few degrees hotter than the best near-vent lava temperatures.

Temperatures from small-volume shield-building lava of the lowest vent (4), at 2,785-m elevation, at times approached 1,140 °C but typically were 5–10 °C cooler. These temperatures are thought to be lower because some vent 4 lava was fed through a lava tube from vent 3, a few hundred meters uprift. The presence of tube-fed lava in this shield was initially inferred from the low to non-existent fountains at vent 4, lower temperature and higher density of spatter and lava from vent 4 compared to those of vent 1 (the main upper vent), and development of a lava tube from vent 3 along the north edge of vent 4 during the first few days of activity. Presence of a lava tube during later vent 4 activity was confirmed by its collapse at the end of the eruption on April 14.

Temperatures obtained at vent 1 are believed to approximate the eruption temperature, as indicated by the consistent results by both measurement methods and the lack of variation during the 20 days of the eruption (fig. 57.19*B*). The vent temperatures for the 1984 Mauna Loa eruption are similar to temperatures measured by the same techniques during recent Kilauea eruptions in which aa flows were dominant (1,135–1,145 °C; Ulrich and others, 1984). These eruption temperatures are 20–30 °C below the expected one-atmosphere liquidus temperature of the lava, as indicated by experimental determinations for other Hawaiian tholeiite (Yoder and Tilley, 1962).

Temperatures of the Mauna Loa flows are about the same as those from most thermocouple measurements for Kilauea eruptions over the past 30 years. Higher temperatures reported for Kilauea lavas and fountains are optical pyrometer measurements that were corrected upward for atmospheric absorption (Alt and others, 1961; Wright and others, 1968), except for the temperatures of 1,500–1,165 °C measured by Swanson (1973) through skylights in lava tubes of pahoehoe from Mauna Ulu. More data are needed to evaluate whether higher eruption temperatures are associated with

long-traveled tube-fed pahoehoe flows, such as have characterized many prehistoric Mauna Loa eruptions.

LAVA DENSITIES

Vesicularity of the 1984 lava was noted in the field to decrease downchannel, as discussed in connection with the variations in lava types. Near the vent outlet, channel lava was fluffy near-reticulite that had the consistency of whipped egg white; downflow, it became dense blocky lava, containing only the scattered irregular vesicles typical of consolidated aa (Macdonald, 1972, p. 70). Density measurements on samples collected at temperature sites confirm a downflow increase in density (fig. 57.20), particularly for samples collected during a single day, and also indicate a gradual decrease in density of vent material during the eruption (fig. 57.21).

The increase in density of lava with distance from the vent (fig. 57.20*A*) is striking, when differing lava types are distinguished. At the vent, the densest values are largely for degassed pahoehoe oozed out from small tubes near the base of the spatter ramparts or from the quietly effusive vent 4 (fig. 57.20*A*, triangles). In contrast, quenched spatter and frothy lava dipped from the channel have densities as low as 0.35 g/cm^3, indicating about 85 percent porosity. Downchannel, samples from the incandescent cores of aa flow fronts are denser than those from rapidly quenched channel overflows (typically scoriaceous aa) or samples taken directly from the channel. These changes in density must relate to degassing and kneading out of vesicles in the lava as it flowed downchannel. Significant gas emission from the channel lava was evident in the field; SO_2 levels were so high that manned observations were rarely feasible downwind of the channel. The downchannel density changes probably contributed significantly to the decreased downchannel lava volumes measured in the 1984 channel system, as discussed later.

In addition to density changes with distance from the vent, the density of spatter sampled at the vent decreased fairly systematically during the eruption, from 1.0–1.2 g/cm^3 early in the activity at the 2,900-m vents to about 0.5 g/cm^3 late in the eruption (fig. 57.21*A*). We interpret this trend as reflecting an increasing ratio of gas to magma in the fountains as discharge rate declined during the eruption. Temporal changes in density of channel or overflow samples were more subdued, presumably because such effects were masked by large concurrent effects of downchannel degassing (fig. 57.21*B*).

The long-term decrease in spatter density is in accord with the observed inverse correlation between fountain height and channel level at the vent, which involved fluctuations over intervals of a few tens of minutes to a few hours (fig. 57.22). At the times of higher fountains, which yielded the least dense and most gas-rich spatter—at times approaching reticulite—the channel level dropped, indicating a decrease in bulk eruption rate of lava. Alternatively, more gas may have been exsolved and kneaded out during the high-fountain phases, producing denser channel lava and lower channel levels without a decrease in discharge. Similar general effects have been noted at several eruptions of Kilauea, in which high wispy fountaining (maximum gas release) occurs as lava production declines just before the end of the eruption (Swanson and others, 1979; Moore and others, 1980).

RELATION OF LAVA TEMPERATURE, VESICULARITY, AND VISCOSITY

The temperature measurements and other observations on Mauna Loa lava bear significantly on interpretations that the pahoehoe-aa transition reflects increased viscosity related to gradual downflow cooling in open channels (Swanson, 1973; Peterson and Tilling, 1980). At Mauna Loa, lava temperatures varied little for 10 km downstream from the vent (fig. 57.19*A*). Downflow temperatures have been similarly stable in aa at Kilauea Volcano (fig. 57.23). Bulk aa temperatures were presumably lower downflow than near the vent, because the ratio of fluid melt to pasty clots and solid debris decreased down the active channel. Some process, however, maintained the temperature of the fluid portion of the aa, and the bulk aa viscosity increased independently of the limited temperature variations in the fluid part of the channel fill.

High temperatures in the aa were partly sustained by heat of crystallization, as indicated by a downflow increase in microlite population (see next section). Frictional deformation of the melt (Shaw, 1969, p. 532) may also have been significant. Lava in the channel had the consistency of reticulite near the vent, and even 20 km from the vent it contained 30 volume percent vesicles. The melt fraction was present in the form of vesicle walls that deformed as the lava degassed and flowed turbulently downchannel. Flexing of bubble walls (during flowage, turbulent mixing, and buoyant rise of gas), supplemented by friction along margins and shear planes within the channel, is thought to have contributed significant heat to maintain high temperatures in the channel lava.

Given that temperatures in the fluid-melt component were stable and that the slope gradient and flow velocity decreased downflow, what produced the observed increase in viscosity and initiated the downflow transition to aa? On April 2, the apparent viscosity in the channel near the vent was about 10^2 Pa·s; at 1,950 m, pahoehoe channel fill had an apparent viscosity of 10^3 Pa·s; and at 1,600 m, the apparent viscosity of aa channel fill was about 10^5 Pa·s, as determined by relations between flow velocity, channel gradient, and channel depth (Moore, chapter 58). The observed increase in both microlite content and solid debris downflow must have increased the viscosity of the silicate fraction (Shaw, 1969, fig. 2). In addition, the viscosity increases appear closely related to density increases in the channel lava (fig. 57.20). The density increases require an attendant decrease in gas and vesicle content of the channel lava and increased thickness of vesicle walls. Decreased vesicularity has been shown experimentally to increase the viscosity of lava (Murase, 1962; Shaw and others, 1968). Thus, even at constant melt viscosity, the *bulk* viscosity of the channel lava would increase without changes in temperature or microlite population. Thicker vesicle walls would also increase resistance to flexing of the melt, reduce associated deformational heating, and eventually allow a negative heat budget.

High gas content and thin vesicle walls may, in part, also account for the low viscosity and high fluidity of pahoehoe.

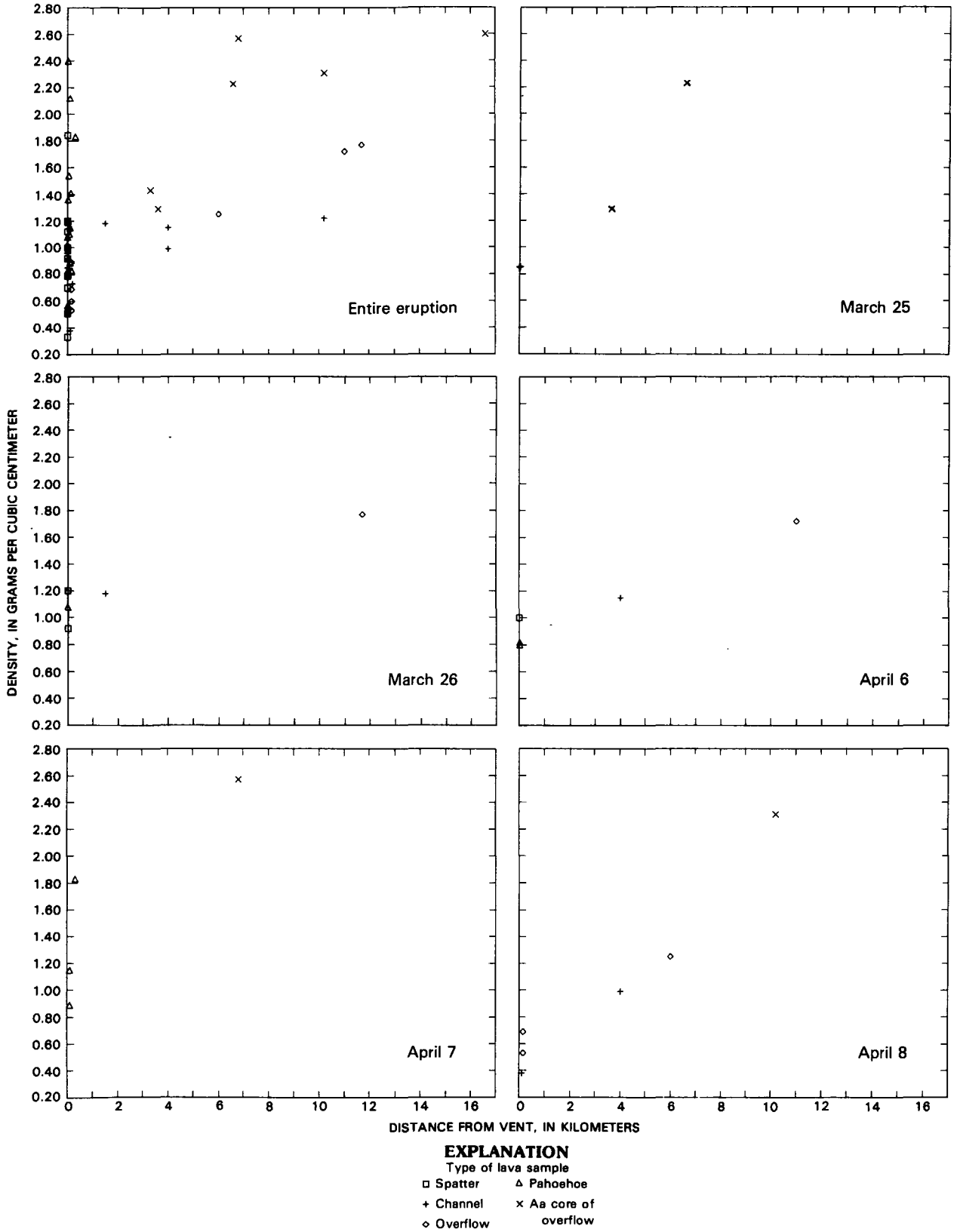

FIGURE 57.20.—Measured lava density plotted against distance from the vent, 1984 Mauna Loa eruption. Data, shown for individual dates as well as for entire eruption, are from table 57.1. All samples were collected hot and quenched in water. Density was determined by weighing a measured cube, sawn from the interior of sample, that had been dried at 20 °C.

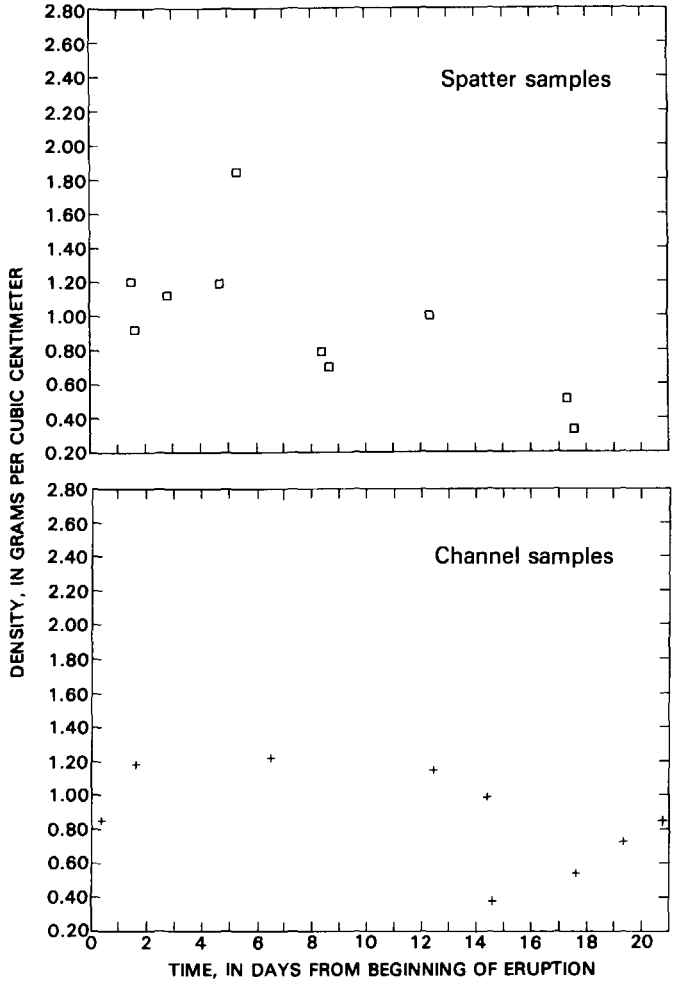

FIGURE 57.21.—Measured lava density of spatter samples and channel samples plotted against time. Data are from table 57.1.

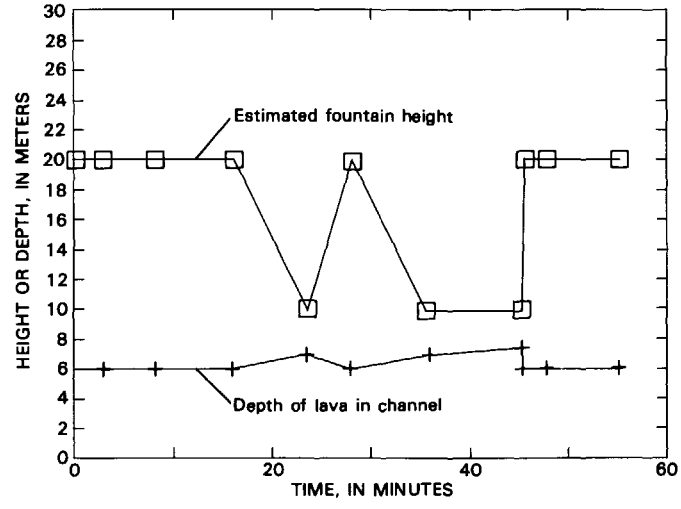

FIGURE 57.22.—Variation of lava level in channel versus height of the fountains at the main vent. Data obtained around 1200 on April 2, 1984. Fountain heights were visually estimated by reference to surveyed height of spatter rampart.

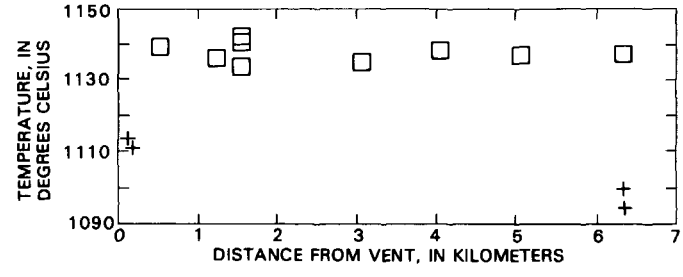

FIGURE 57.23.—Temperature plotted against distance of travel for Kilauea aa flows from the 1983–84 east-rift-zone eruptions. Plus, sample from phase 9, southeast flow; square, sample from phase 16, southeast flow.

Pahoehoe is more vesicular than aa, and retarded degassing in lava tubes may delay the transition to aa, along with the insulating role of the tube (Swanson, 1973). During the Mauna Loa eruption, pahoehoe in tubes flowed at velocities only about 20 percent slower than in open channels. The tubes formed along channels where flow was laminar and flow rates were fairly low and steady or decreasing. In high-volume channels, incipient roofs of tubes were continually broken up and rafted away. Slower flow in the tubes was promoted by lower eruptive volume and by drag against the roof. The slow flow rate appears to have favored less turbulent flow; it thus retarded stretching and breaking of vesicles, maintaining a lower bulk viscosity. The higher vesicle population also may have (1) allowed more rapid flexing of the vesicle walls, (2) generated deformational heating farther from the vent, and (3) combined with the insulating properties of the tube (Swanson, 1973), retarded formation of pasty clots and delayed viscosity increases.

Observations during temperature measurements (see app. 57.1) demonstrate an interrelation between vesicularity and viscosity. A lava sheath invariably formed on even the small-gauge thermocouple if the pahoehoe was moving more than about 0.5 km/h and lava was allowed to flow past the thermocouple tip. The observer could stop growth of the lava sheath by walking the tip downflow with the lava at velocities up to about 3 km/h. At higher flow velocities, the temperature measurements invariably terminated with a thermocouple sheathed in lava. The sheaths were denser than the channel fill and had the consistency of thick taffy, similar to lava from cores of aa flows much farther from the vent, where inserting a probe required more effort.

Two observations suggest that the lava sheath resulted from breakage of vesicle walls and adherence of the viscous melt, rather than from freezing of the melt against the probe. First, the size and growth rate of the lava sheath correlated with velocity of the flowing

lava: the faster the flowage past the thermocouple, the larger were the lava sheaths. Second, thermocouples were carefully preheated prior to insertion, particularly when measuring flowing lava, yet probes in flowing lava accumulated a sheath while those in motionless lava did not. We infer that the thermocouple stretches and breaks the gas bubbles in moving lava, increasing the bulk viscosity of the adjacent melt and making additional melt available to adhere to the probe. The growing surface area exerts additional drag on adjacent melt, hastens bubble breakage, and causes faster accumulation of melt on the sheath.

LAVA CRYSTALLINITY

Increases in crystallinity affected flow rheology of the 1984 lava both over time at the vents and during flow down the lava channel. Three discrete textural populations of crystals are present: (1) sparse resorbed phenocrysts or xenocrysts of magnesian olivine as much as 5 mm in diameter; (2) dusty microlites less than 0.01 mm in size; and (3) microphenocrysts of augite, plagioclase, and olivine commonly 0.05–1.0 mm in length.

The sparse olivine phenocrysts everywhere are less than 0.5 percent of the lava, did not vary in abundance significantly during the eruption, and are interpreted as disequilibrium crystals that were present in the summit magma reservoir before eruption. Microlites are absent in vent spatter and become increasingly abundant in quenched downchannel samples; they record late groundmass crystallization of the lava as it flowed down the channel. Such surface crystallization of channel lava is probably largely responsible for the observed progression of flowage zones (fig. 57.5), but it seems to have occurred uniformly throughout the eruption. In contrast, the content of microphenocrysts in quenched spatter increased strikingly during the eruption, from less than 0.5 percent of the lava during initial summit activity to as much as 30 percent during the waning eruptive phases (figs. 57.24, 57.25*A*). Microphenocryst size increased concurrently with abundance (fig. 57.25*B*), although the precision of measurement is lower. Microphenocryst size and abundance increased rapidly during the first few days of the eruption, slowed during the subsequent two weeks, and increased slightly again late in the eruption (fig. 57.25). Large changes occurred within a few hours after beginning of the eruption on March 25, as the vents migrated from the summit region downrift to the 2,900-m level, but the abundance and size of microphenocrysts continued to increase after the main vent site stabilized. These changes occurred in the lava before its eruption, as documented by quenched spatter samples, although the same microphenocryst populations are readily recognized in downchannel samples despite additional crystallization of microlites during surface flowage.

During these changes, bulk major-oxide compositions remained constant virtually within analytical uncertainty (table 57.2; Lockwood and others, 1985). This compositionally uniform 1984 lava is in marked contrast to lava erupted during Kilauea rift activity (Wright and Fiske, 1971; Garcia and others, 1984) but is typical for Mauna Loa rift eruptions (Rhodes, 1983).

Most microphenocrysts in the 1984 Mauna Loa lava occur as skeletal, intergrown, and radiating blades and plates (fig. 57.24), including elongate, cored, and swallow-tailed shapes that are typical of rapid crystallization from undercooled liquids (Walker and others, 1976; Lofgren, 1981). Such undercooled textures are especially prevalent in the phenocryst-poor lava of early eruptive phases; late eruptive phases have textures indicative of more prolonged equilibrium crystallization. We attribute the growth of microphenocrysts characterized by undercooled textures largely to separation of a gas phase during the eruption, not to a decrease in magma temperatures.

Observed eruptive temperatures remained constant at 1,140 ± 3 °C (fig. 57.19*B*), which is 20–30 °C below calculated liquidus temperatures for most phases at one atmosphere (olivine 1,186 °C, plagioclase 1,169 °C, and clinopyroxene 1,146 °C, all ±15 °C; method of Nielson and Dungan, 1983). The observed lava temperatures would approximately coincide with the liquidus if the pre-eruptive magma contained about one percent volatile content (Yoder and Tilley, 1962). A pre-eruptive volatile content of about 0.5 percent has been calculated from gas data for tholeiitic basalt from Kilauea Volcano (Greenland and others, 1985), and about one percent volatiles is the estimated average for tholeiitic basalt in general (Haggarty, 1981).

The virtual absence of microphenocrysts in much of the lava erupted early on March 25, followed by increases in the number and size of microphenocrysts (figs. 57.24, 57.25), suggests that the magma reservoir below the summit was initially sufficiently pressurized by volatiles to lower the liquidus temperature to about 1,140 °C, thereby inhibiting crystallization. With depressurization of the magmatic system beginning at onset of the eruption, separation of gas undercooled the magma without actually lowering the observed lava temperatures, thereby inititiating precipitation of microphenocrysts. Degassing at the summit began at onset of the eruption and was later focused at the 3,550-m level, uprift of the active lava vents (Casadevall and others, 1984).

Even slight undercooling can have profound effects on the nucleation and growth rates of crystals. At 20–30 °C of undercooling, crystals in basaltic melts can grow to sizes of 1 mm within periods as brief as a few hours (Kirkpatrick, 1976, 1977). The only alternative to growth of microphenocrysts during the eruption—a zoned pre-eruption magma chamber—seems less able to account for the compositional uniformity of the erupted lava or its undercooled quench textures.

The volatile loss needed to initiate crystallization may have been small. Before eruption, basaltic magmas in the shallow reservoirs beneath the summits of Mauna Loa and Kilauea are believed to contain <0.2 percent CO_2, 0.2–0.3 percent H_2O, and 0.1 percent S (Moore, 1965; Greenland and others, 1985; Greenland and others, in press). Because of their relative solubilities, S and CO_2, but not H_2O, would have separated from the magma during transit from the summit reservoir down the rift zone to just below the vent. If the rift magma was under lithostatic confining pressures, H_2O may have saturated and begun to separate only at depths as shallow as 100–200 m below the surface. Although confining pressures within the upper kilometer of the fractured rift zones of Hawaiian volcanoes are unlikely to be purely lithostatic, and may at times approach atmospheric, these relations nevertheless cast doubt on the ability of H_2O loss alone to account for the undercooling and crystallization of the 1984 magma. High flow rates of the rift magma, efficient degassing, and rapid crystallization would be

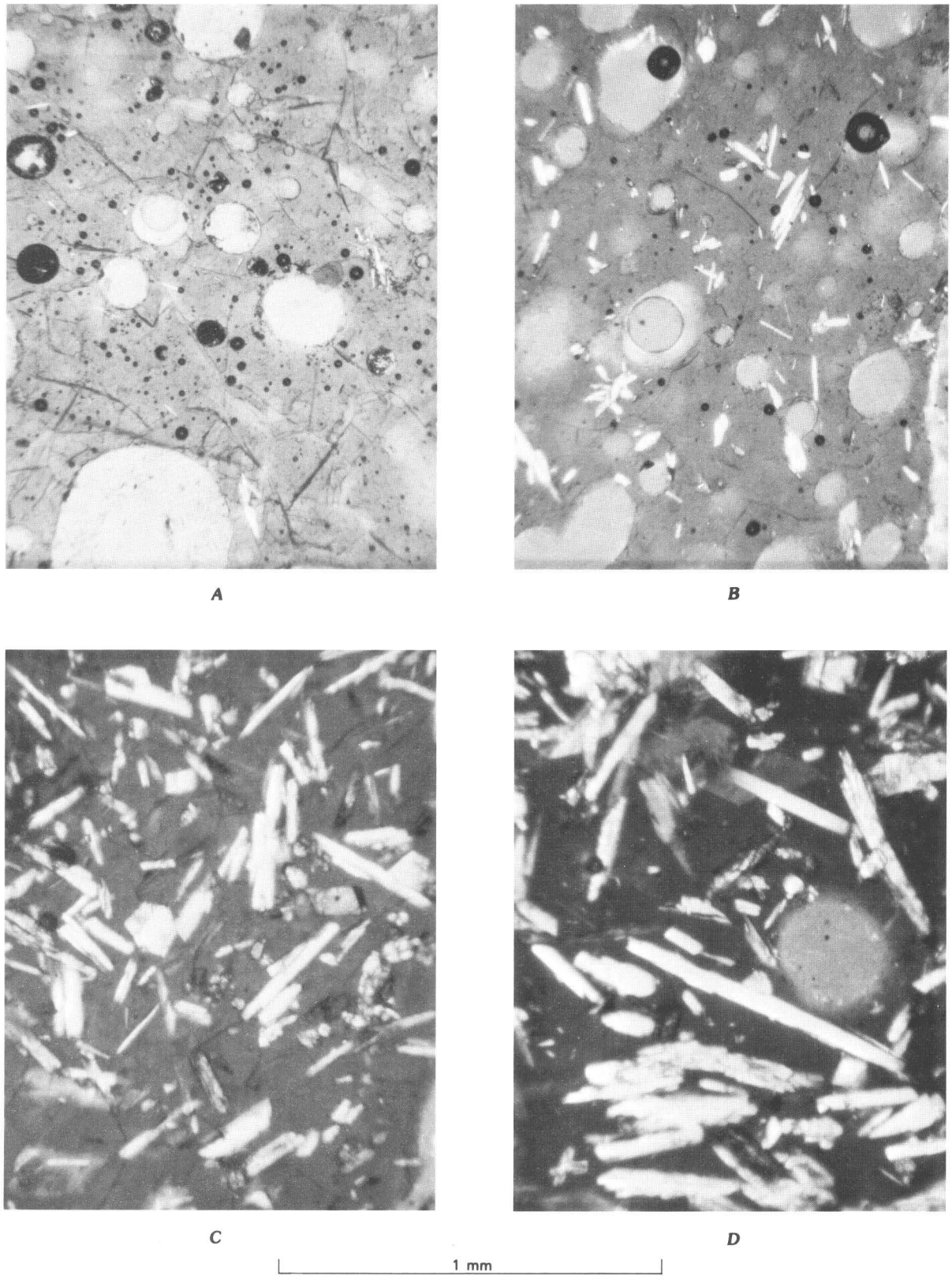

FIGURE 57.24.—Photomicrographs (plane light) of representative samples of 1984 Mauna Loa lava, showing progressive increase in size and abundance of microphenocrysts with time. Microphenocrysts are clear rectangles; circular features are gas bubbles (vesicles). ***A***, Sampled at about 0145 (H.s.t.) on March 25. Spatter from northeast side of 1949 cone, at 4,040 m. Sample MOK–1; O.4 percent phenocrysts, 0.05 mm in average length. ***B***, Sampled at about 0515 on March 25. Spatter from upper northeast rift zone, at 3,650 m. Sample NER 5; 3.5 percent phenocrysts, 0.1 mm in average length. ***C***, Sampled at about 1750 on March 29. Pahoehoe from perched pond at 2,820 m. Sample NER 12/23; 21 percent phenocrysts, 0.3 mm in average length. ***D***, Sampled at about 0945 on April 14. Channel overflow near 2,870-m vent. Sample NER 12/66; 29.5 percent phenocrysts; 0.6 mm in average length.

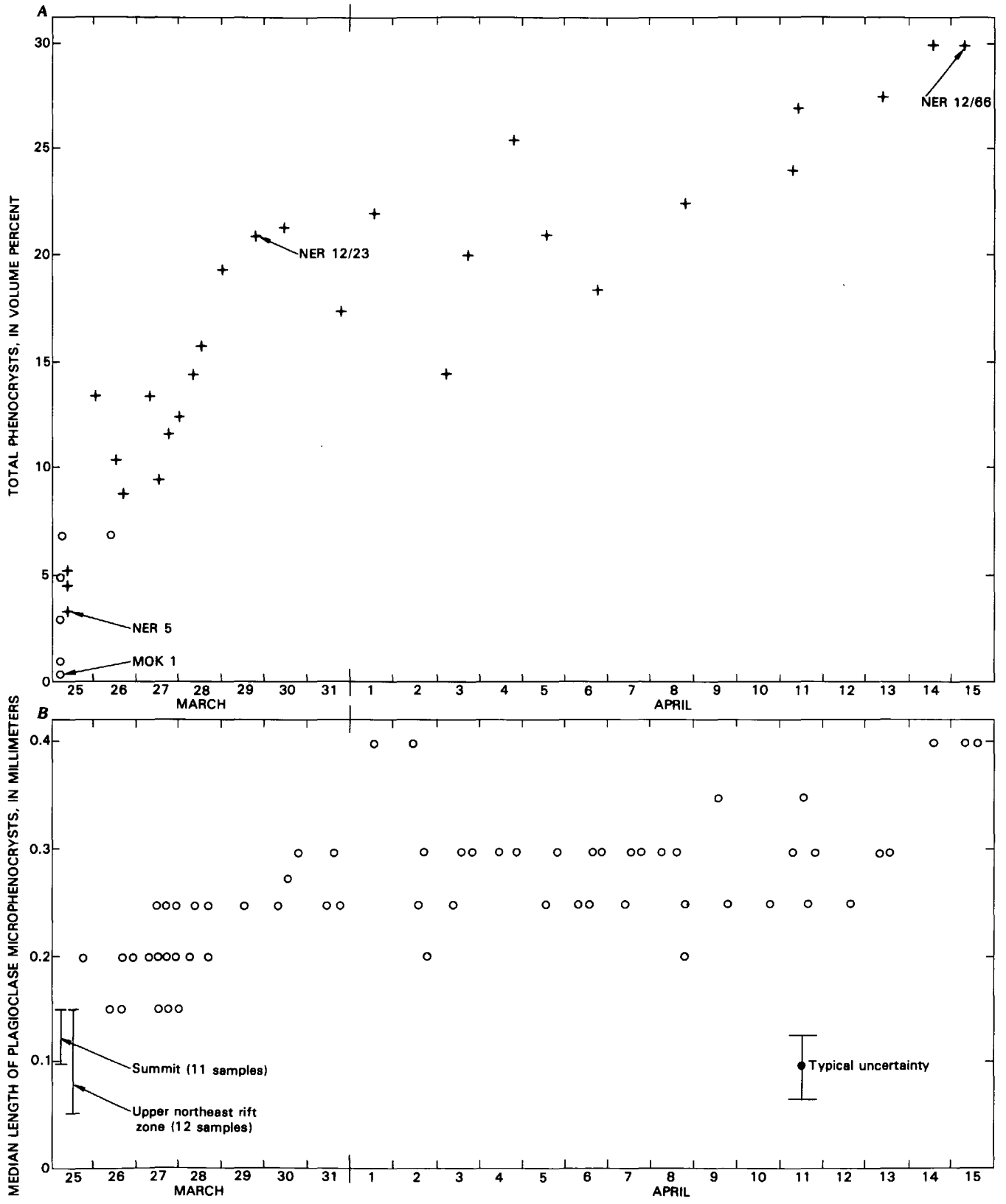

FIGURE 57.25.—Changes in abundance and size of microphenocrysts during 1984 eruption. Samples illustrated in figure 57.24 are identified. ***A***, Changes in abundance of microphenocrysts. Plus, data from petrographic point-counting of thin sections; dots, visual estimates of March 25–26 samples containing only sparse small microphenocrysts (less than 0.15 mm in average length). Values are believed accurate to within 10 percent; a major cause of uncertainty is in estimating areas of microphenocrysts smaller in diameter than the thickness of the thin section (0.03 mm). All samples are quenched glassy spatter or channel overflow. About one-half the originally collected samples of spatter were too vesicular to measure. ***B***, Changes in size of microphenocrysts. Median lengths of plagioclase microphenocrysts (about one-half the maximum length) were estimated visually from thin sections, by reference to a calibrated scale in the microscope ocular.

TABLE 57.2.—*Major-element composition of the 1984 Mauna Loa lava, from X-ray fluorescence analyses*

[Individual samples, selected to be representative, are described in table 57.1 and illustrated in figure 57.24. All values are in weight percent. Total iron listed as Fe_2O_3. Uncertainty of averages is plus or minus one standard deviation. Data provided by J.M. Rhodes; see Lipman and others, 1985]

Date	March 25		March 29	April 14	Entire eruption
Time	0145	0515	1750	0945	Average of 61 samples
Sample	MOK-1	NER-5	NER-12/23	NER-12/66	
SiO_2	51.51	51.56	51.71	51.27	51.54±.24
TiO_2	2.08	2.09	2.08	2.10	2.08±.02
Al_2O_3	13.75	13.69	13.69	13.60	13.65±.07
Fe_2O_3	12.08	12.11	12.17	12.08	12.07±.06
MnO	.17	.18	.17	.19	.18±.01
MgO	6.73	6.65	6.76	6.81	6.73±.08
CaO	10.57	10.55	10.57	10.43	10.50±.06
Na_2O	2.56	2.42	2.56	2.45	2.54±.11
K_2O	.385	.383	.391	.381	.385±.009
P_2O_5	.24	.25	.26	.24	.24±.01
TOTAL	100.13	99.87	100.38	99.55	99.92±.37

required, even if the pressure on upper parts of the rift conduit were atmospheric. Alternatively, the major loss of S, beginning at the summit reservoir, may have played a significant role in initiating crystallization. Unfortunately, few experimental data are currently available to permit evaluation of the role of small amounts of S on liquidus temperatures of basaltic magma.

RELATIONS OF CHANNEL VELOCITY, VOLUME, AND TIME

After the first three days of the eruption, as the vent geometry stabilized at the 2,900-m level and lava moved rapidly toward Hilo, we began establishing monitoring stations along the lava channel to permit repeated observations. At first, a primary need was to determine rates of lava movement downchannel for purposes of hazard evaluation; later, we focused more broadly on processes of channel evolution. For the first few days, limited helicopter support and poor weather confined observations to ground-accessible localities, and only a single observation point could be visited per day. Later in the eruption, working in two parties, we occupied as many as 4–6 stations per day. A total of 69 data sets are available for channel stations (table 57.3).

At each station, channel dimensions were determined, flow velocities measured, and morphologic observations made on the character of the flow, including photography. The resulting record of channel processes provides much of the basis for this paper. Complexities attendant to working on an erupting volcano caused some variations and problems in quality of the observations, as detailed in appendix 57.2. Total error in the channel-volume measurements, due mainly to uncertainties about channel depth, may be as large as 25 percent, but changes in channel volume at any station are believed accurate to about 10 percent, because the channel geometry tended to remain similar during the eruption or to deepen by measureable amounts through increase in levee height, especially for stations within the stabilized-channel zone.

Episodic short-term variations in channel volume, over periods of a few minutes to a few hours, were conspicuous in lower parts of the channel (transition zone), where surges could cause ephemeral channel-volume variations of as much as 50 percent; all plotted data are for observations made between obvious surges. Large short-term volume changes were also noted in stations near the vent, where fluctuations in fountain height related to varying gas release were associated with frequent changes in measured volume of 5–15 percent, occasionally as much as 40 percent. As noted earlier, some of these observed near-vent volume variations mainly reflect varying gas content and lava density, rather than true fluctuations in magma production rate (fig. 57.22). Several stations at mid-distance downchannel yielded volume variations of less than 5 percent when measured repeatedly over periods of several hours while larger fluctuations were being observed at the vent. Apparently, the short-term near-vent fluctuation tended to be smoothed out by downchannel flowage.

The most obvious feature of the channel data is a progressive decrease in channel discharge with lower elevation for any time during the eruption (fig. 57.26). In early April, discharges of 3.5×10^6–5×10^6 m^3/h were measured at the vent outlet, in comparision to discharges of only about 1.5×10^6 m^3/hr at 2,500-m elevation 5 km downchannel, and 0.5×10^6 m^3/hr at 1,900-m elevation 15 km from the vent. This decrease in discharge is interpreted as reflecting volume decrease of the lava due largely to volatile loss, because no overflows were occurring at this time along the intervening channel. The decrease in channel discharge downslope is paralleled by as much as a several-fold downslope increase in the density of quenched samples collected along the channel (fig. 57.20). These density changes alone can account for the changes in discharge, within sampling and measurement uncertainties.

A major feature of the eruption, documented from the channel stations, was a nearly constant rate of magma production during the middle part of the eruption, from March 31, when enough channel stations first became available, through April 6 (fig. 57.26). The steady state of activity during this interval is documented by 9 occupations of channel station 8 (1852 vent, 2,500-m elevation), which yielded channel discharges of $1.55\pm0.05\times10^6$ m^3/h, and by 10 occupations of several sites at station 4 (Upper Powerline area, 1,920–1,935 m), which yielded discharges in the range 0.40–0.55×10^6 m^3/h. Both these stations were within the stable-channel zone. The upper one (1852 vent) changed little during this time interval, except for partial crusting of the channel margins by pahoehoe scum (fig. 57.8*D*). Somewhat more variable discharges from the Upper Powerline sites are probably due to greater surge activity and levee building (figs. 57.9, 57.11*A*, 57.16*B*).

Before March 31, eruption rates at the 2,900-m vents had appeared roughly constant to observers, but several lines of evidence now demonstrate that eruption rates decreased during the first few days of the eruption. The first indication of such a decline came from early measurements of lava volumes reaching the channel stations at 1,800–1,900 m. Key evidence is from two channel stations established on March 28–29, which show higher discharges than observed at these elevations later during the eruption (fig. 57.26). The discharge measured for the 1,800-m station (Lower Powerline)

on March 28 is somewhat uncertain, because it depends on an aerial estimate of channel width under adverse weather conditions. Even if it is in error by one-third—the maximum that seems plausible—the resulting discharge (0.8×10^6 m^3/h) would still be twice that subsequently measured below 1,850 m.

No quantitative data are available for lava production at the vent before April 2, but repeated photography of the upper channel area document a major decline in channel flow levels between March 26 and 31 (fig. 57.27) that was not recognized by qualitative monitoring in the first few days of the eruption. Decreasing eruption rates early in the eruption are also indicated by analysis of lava areas and volumes, as discussed later.

In early April, the highest channel blockages and overflows were at about 1,850-m elevation (fig. 57.14), and the various Upper Powerline stations at 1,920–1,935 m show nearly constant volumes of flow. In contrast, the stations at 1,600–1,700 m show declines of about 50 percent in flow discharge between March 31 and April 4 (fig. 57.26), reflecting increasing loss of lava from the channel by blockages and overflows. By April 5, lava was no longer reaching any major channel below 1,850 m.

On April 6, a possible small decrease in discharge was measured at the 2,500-m station, which had yielded essentially constant results for the previous week, and by April 9 the channel was inactive to this level (fig. 57.26). This large change in channel discharge reflects the beginning of a further gradual decrease in eruptive rate at the main vent, from several million cubic meters per hour on April 6 to only a few hundred thousand cubic meters per hour by April 9 (fig. 57.28). Some of the decrease was taken up by new channels emanating from smaller uprift vents of the 2,900-m cluster, which robbed the main vent of part of its lava supply. Channels from the reopened uprift vents were north of flow 1 and initially carried as much as 0.5×10^6 m^3/h (density about 0.5 g/cm^3), about as much as flow 1.

Lava production continued to decline after April 9 and amounted to only about 0.1×10^6 m^3/h on April 13, the last full day of vent activity.

DISCUSSION

During the three-week eruption in 1984, the Mauna Loa aa flow and its distributary channel system underwent a complex morphologic evolution related to several intertwined changes in lava properties. These include decreases in eruptive volume; increased groundmass crystallization of the magma before venting; changes in effective viscosity and yield strength of the lava; degassing in the rift magma chamber, at the vent, and downchannel, which resulted in density increases of the lava; and probable physical maturation of the distributary channel itself. The dominant effects appear to have been (1) sympathetically increasing microphenocryst content, viscosity, and loss of gases from the pre-eruption magma reservoir and rift conduits; (2) constant lava composition and temperature; and (3) decreasing volume and average density of erupted material (fig. 57.29).

The eruption rate was nearly constant from March 30 to April 7 but declined drastically after April 7 (fig. 57.26). Major decreases also occurred early in the eruption, as indicated by (1) the high lava discharges measured at the two channel stations occupied on March 28–29, in comparison with results at similar elevations later during the eruption (fig 57.26); (2) the cessation of eruptive activity at the lower vents that fed flows 2–4 on March 25–27; and (3) interpreted rates of lava erupted per hour, based on the area covered as well as on the channel-station data (table 57.4).

Total volume of the erupted flows has been estimated at 220×10^6 m^3, based on mapped area of coverage and measured flow thickness (J.P. Lockwood, written commun., 1984). If the steady discharge rate determined from channel measurements between March 30 and April 6, about 0.4×10^6 m^3/h of relatively degassed channel lava at 1,900 m, is extrapolated back to initiation of the eruption, there is a shortfall of about 25 percent in volume (60×10^6 m^3). In contrast, the eruption rate for the early summit activity on March 25, as determined by area covered, was about 2.8×10^6 m^3/h, and rates for the first two days of activity from the 2,900-m vents were about 10^6 m^3/h (table 57.3). If the eruption rate further decreased from 10^6 m^3/h to 0.4×10^6–0.5×10^6 m^3/h during March 28–30, as indicated by the channel measurements (fig. 57.26), then the cumulative volume subsequently determined from the channel measurements (224×10^6 m^3, fig. 57.30) agrees reasonably well with the volume of 217×10^6 m^3 based on mapped area and flow thickness.

Decreases in eruption rate over time, which characterize many basaltic eruptions, have been inferred to relate to such factors as the release of elastic-strain energy from magma stored in the subvolcanic reservoir, availability of magma from depth during the eruption, and conduit evolution from dike to plug geometry (Wadge, 1981). An additional factor that appears to have been important in the 1984 Mauna Loa eruption, and perhaps for some others, is a change in magma rheology related to increasing crystal content of the erupted lava.

The increase in microphenocryst size and abundance (fig. 57.25) was roughly opposite to the decline in eruption rate (fig. 57.30). The resulting increase in magma viscosity (Shaw, 1969) was probably a major cause of termination of the eruption, as well as the pattern of uprift channel stagnation. At about 1,140 °C, the apparent viscosity of theoleiitic basalt containing an equilibrium crystal assemblage (about 25 volume percent) has been shown by field and laboratory measurements on Hawaiian basalt (Shaw, 1969, fig. 2; Shaw and others, 1968) to be approximately one order of magnitude greater than an undercooled Newtonian liquid lacking crystals. The changes in rheology, interpreted to have occurred largely in the pre-eruption magma chamber and rift conduits of Mauna Loa, are broadly similar to effects on the rheology of basaltic lava inferred to result from degassing during eruption and downslope flowage (Sparks and Pinkerton, 1978).

Such major decreases in eruptive rate in late March, if correctly interpreted, could explain the stagnation of flow 1 on March 30, but they do not account for the cessation of rapid advance and beginning of stagnation of flow 1*A* during the interval March 30–April 6. During this interval, both the eruption rate at the vent and transport in the channel system above about 1,850-m elevation remained constant, as indicated by the channel station data

TABLE 57.3.—*Dimensions and characteristics of lava channels and their changes with time, 1984 Mauna Loa eruption*

[Locations of channel stations on figure 57.1*B*. Distance, spacing of measuring points along channel bank. Depths estimated; see text for details. PWL, Peter W. Lipman; NGB, Norman G. Banks]

Measurement	Date (mo/d)	Hour (H.s.t.)	Condition	Distance (m)	Time (s)	Velocity (m/s)	Width (m)	Depth (m)	Flow rate (10^6 m^3/h)	Comments
Station 1: Lower channel 1A, elevation 1,600 m										
1	3/31	1130	stable	18	19	0.95	24	5	0.410	Conspicuous marginal shears, with velocities about 1 m/min, next to central well-defined channel. Channel velocities slow during surges which contain more viscous material. Maximum velocities occur just after surges. Gradient about 3°. Measured by PWL, NGB, and J. Fink.
2	3/31	1200	surge	18	22	.82	24	5	.355	
3	4/01	1200	--	18	28	.64	35	5	.405	Channel less defined than on 3/31, more choked with viscous debris. Although relatively steep gradient (about 5°) has migrated about 50 m downstream, adjacent to measurement site, velocities have still slowed. Because channel zone seems wider, flow rates have changed less than velocities. Measured by PWL and E. Wolfe.
4	4/01	1300	--	18	30	.60	35	5	.385	
5	4/02	1200	full	15	60	.25	40	6	.215	Channel less well defined than on 4/01, and choked with rubble; velocities much slowed. Measured by PWL, J. Fink, and H. Moore.
6	4/02	1230	low	15	110	.14	40	6	.120	
7	4/03	1520	slow	25	140	.18	52	5	.170	New station; old one unusable because of inboard levees. Top of active channel varies, 3 m below to 1 m above levees. Gradient 4.5°. Measured by NGB.
8	4/03	1550	normal	25	80	.31	52	5	.290	
9	4/03	1645	surge	25	90	.28	52	7	.364	
10	4/04	1350	--	25	163	.15	50	5	.138	Measured by NGB.
Station 2: Upper channel 1A, elevation 1,700 m										
11	4/03	1430	stable	15	45	.33	50	5	.295	Measured by PWL, J. Fink, and H. Moore.
12	4/03	1530	surge	15	30	.50	50	5	.450	
13	4/04	1345	stable	15	45	.3	25	5	.150	Sensitive to release of ponded lava at 1,800-m blockage. Surge provides upper limit in flow rate; estimates for stable periods likely to be more meaningful. Gradient about 4°. Measured by PWL, T. Neal, and H. Moore.
14	4/04	1430	stable	15	40	.4	25	5	.170	
15	4/04	1500	surge	15	25	.6	25	5	.270	
Station 3: Lower Powerline Road (flow 1, south side), elevation 1,800 m										
16	3/28	1310–1335		73	84	0.87	75	5	1.20	Depth fluctuations of as much as 2–3 m in 5 min, associated with surges; channel in two branches—only southern strand measured; channel broad, measured by visual aerial comparison with distance between power poles. Channel gradient about 2.5°. Measured by PWL and D. Clague.
17	3/28	1535–1605		73	80	.91	75	5	1.25	
Station 3: Lower Powerline Road (flow 1B), elevation 1,800 m										
18	4/06	1400	--	25	210	0.12	25	4	0.043	The channel flow slowed, and its upper surface subsided as we made these measurements. When checked an hour later, the head of flow 1B was captured by other overflows, and its channel was drained and empty. Gradient: 2.5°. Measured by PWL and T. Neal.
Station 4: Upper Powerline Road (site 1), elevation 1,900 m										
19	3/29	1300	blocks	30.2	25	1.20	13	6	0.335	Channel is within a gentle stretch related to large overflows and temporary ponding; probably deep as result. Higher velocities in center channel tend to push blocks to sides; more consistent measurements of maximum velocities obtained from small fragments in center channel. Channel gradient about 2.5°. Measured by PWL and E. Wolfe.
20	3/29	1400	fragments	30.2	18	2.75	13	6	.470	
21	3/31	1430	stable	30.2	23	1.3	13	6	.365	All measurements on small fast-moving fragments in center channel; lower level at 22 (about 1 m below levees) because of slightly higher gradient after drainage of ponded blockage downchannel. Gradient about 2.5°. Measured by PWL, NGB, and J. Fink.
22	3/31	1530	low	30.2	18	1.7	13	6	.470	
23	4/01	0830	stable	30.2	18	1.7	13	6	.470	Channel is sluggish and viscous; shear and pressure ridges are weakly developed on nearly stagnant channel sides. Measured by PWL and E. Wolf.
24	4/01	0930	blockage	30.2	19.5	1.6	13	6	.435	
25	4/02	1700	--	30.2	31	1.0	15	7	.370	Levees have increased in height about 2 m and largely obscure view of the channel: could only measure large boats during high stand of channel. Measured by PWL, J. Fink, and H. Moore.
26	4/03	1000	--	30.2	32.1	.94	18.3	7	.431	Levee height is 2.3 m above top of old ponded broad aa channel. Surge caused spreading of levee by 1 m in 15 min. Measured by NGB.
Station 4: Upper Powerline Road (site 2), elevation 1,930 m										
27	4/02	1600	--	20	9.5	2.1	14	4	0.455	New site, above upper cascade. Gradient about 3.5°. Measured by PWL, J. Fink, and H. Moore.
28	4/03	1320	--	20	12.6	1.6	14	5	.399	Measured by NGB.
Station 4: Upper Powerline Road (site 2A), elevation 1,930 m										
29	4/04	1200	--	23	12.3	1.9	15	5	0.500	Measured lava boats; low gradient due to blockages at head of middle cascade. Measured by PWL, T. Neal, and H. Moore.
Station 4: Upper Powerline Road (site 3), elevation 1,900 m										
30	4/04	1120	boats	20	7.5	2.7	15	4	0.580	Boats are sparse; channel level is 0.5–1 m below recent levee overflows. Gradient about 3°. Measured by PWL, T. Neal, and H. Moore.
31	4/04	1130	fragments	20	8.1	2.5	15	4	.530	
32	4/04	1140	fragments, surge	20	7.2	2.8	15	4	.600	
33	4/05	1100	--	20	9	2.2	20	4	.640	Little change since yesterday. Channel low and boats sparse, indicative of pond and surge forming upchannel. Measured by PWL and H. Moore.

TABLE 57.3.—*Dimensions and characteristics of lava channels and their changes with time, 1984 Mauna Loa eruption—Continued.*

Measurement	Date (mo/d)	Hour (H.s.t.)	Condition	Distance (m)	Time (s)	Velocity (m/s)	Width (m)	Depth (m)	Flow rate (10^6 m^3/h)	Comments
Station 4: Upper Powerline Road (site 4, flow 1B), elevation 1,900 m										
34	4/06	1100	--	24	14.9	1.6	30	3	0.520	New station, on uppermost gentle reach of flow 1B, just below breakout area. Channel here appeared broad and shallow, and its depth was confirmed later in day when the channel was drained and empty. Gradient 3°. Measured by PWL and T. Neal.
35	4/06	1130	--	24	14.9	1.6	30	3	.520	
Station 5: New south flow (flow 1C), elevation 1,950 m										
36	4/07	1000	--	15	10	1.5	10	5	270	Station is on channel carrying bulk of lava, just below currently most active ponding and breakout area at about 2,000 m. Gradient about 2.5°. Measured by PWL and H. Moore.
37	4/07	1545	--	15	16	1.1	10	5	.190	Many surges: difficult to make an average measurement, but clearly lower than this morning. Presumably, decrease reflects many overflow diversions. Measured by PWL and H. Moore.
Station 6: Main channel of flow 1, elevation 2,100 m										
38	4/07	1100	dropping	20	11	1.8	22	5	0.720	Stable channel, currently just above highest ponding area. Measured by PWL and H. Moore.
39	4/07	1120	after surge	20	10	2.0	22	5	.790	
Station 7: 1852 pahoehoe, elevation 2,300 m										
40	4/04	1630	--	20	4.7	4.23	15	5	1.15	Above highest area of blockages, levee building, and overflows. Gradient about 4.5°. Measured by PWL, T. Neal, and H. Moore.
41	4/08	1250	--	20	12.8	1.65	15	5	.424	Measured by NGB.
42	4/08	1310	--	20	6.5	3.1	15	5	.835	
Station 8: 1852 vent, elevation 2,500 m										
43	4/02	0900	site A	45	8.1	5.6	20	4	1.60	Measured velocities on small fragments in center channel. Gradient at site A is 6°; at site B, 4.5–5°. Measured by PWL, J. Buchanan-Banks, J. Fink, and H. Moore.
44	4/02	0930	site B	40	7.6	5.3	20	4	1.50	
45	4/03	0900	site A	45	8.7	5.2	20	4	1.50	No change evident. Measured by PWL, J. Fink, and H. Moore.
46	4/03	0920	site B	40	7.7	5.3	20	4	1.50	
47	4/03	1630	site B	40	7.5	5.3	20	4	1.54	No change since morning, despite reported 50 percent increase in production rate at vent. Measured by PWL and J. Fink.
48	4/04	0800	site B	40	7.5	5.3	20	4	1.55	No significant change. Measured by PWL, T. Neal, and J. Fink.
49	4/05	1415	site B	40	7.3	5.5	20	4	1.60	No change since previous day. Measured by PWL and H. Moore.
50	4/06	1100	site B	40	7.6	5.3	20	4	1.50	Surface channel actually only 10.3 m wide, because of crusting of margins. Measured by NGB.
51	4/06	1550	site B	40	7.6	5.3	20	4	1.50	No change, although level of channel at vent reported down 1 m. Measured by PWL and T. Neal.
52	4/07	1625	site B	40	7.5	5.3	18	4	1.40	Apparent slight decrease, from decreased estimated width of channel caused by crusting, but lava probably continues to flow slowly under crust. Measured by PWL and H. Moore.
53	4/08	0930	site B	40	14.2	2.8	9.2	4	.375	Surface is much grayer and has more scum than on 4/6. Volume is only about half as great. Gradient 3.5°. Measured by NGB.
Station 9: Middle channel, elevation 2,780 m										
54	4/09	1300	--	15	15	1.0	15	4	0.215	Broad shallow sheet-flow channel, the middle of three currently active around the west side of vent at 2,790 m (Puu 9,146). Measured by PWL and M. Rhodes.
Station 10: North channel, elevation 2,790 m										
55	4/09	1600	--	22	30	0.73	8	5	0.105	Narow channel, mostly well below levees. For visibility, had to measure during high channel flow. Measured by PWL and M. Rhodes.
56	4/10	1200	--	20	20	1	8	4	.100	Estimated velocity; channel on average 1–2 m lower than yesterday. Measured by PWL.
57	4/11	1215	--	15	10.1	1.5	12	3	.190	Measured by NGB.
58	4/12	1200	steady	16	25	.64	6	4	.055	Just upslope from station of previous day, which is now jammed by an overflow. Measured by PWL and R. Fodor.
59	4/12	1215	surge	16	14	1.1	6	5	.125	
Station 11: Vent outlet, elevation 2,850 m										
60	4/02	1130	--	30	1.7	17.8	21.5	3	4.50	Gradient is 6.5°; lava is fluffy; about 70 percent has bubbles. Measured by NGB.
61	4/04	1030	--	30	2.0	15	21	3	3.40	Flow rate is 1.5×10^6 m^3/h less than on 4/02. There is an antithetic relation between fountain height and channel level; at highest fountaining, channel flow rate is 5.2×10^6 m^3/h. Measured by NGB.
62	4/06	0900	--	30	2	15	20	3	3.5	Channel appears unchanged from 4/04; velocity estimated by NGB.
63	4/08	1145	--	30	4.65	6.45	21.5	3	1.50	Surface is grayer, but lava may be even fluffier than earlier. Flow rate half that of 2 days ago. Measured by NGB.
64	4/08	1600	--	20	10	2	30	3	.650	Channel much slower than in morning. Velocity estimated by NGB.
65	4/09	1040	--	40	17	2.4	5	3	.125	Channel contains viscous ropy pahoehoe. Measured by PWL and M. Rhodes.
66	4/09	1130	higher	40	12.5	3.2	5	4	.230	
Station 12: West vent, elevation 2,900 m										
67	4/08	1620	--	--	--	2	30	2	0.430	Velocity estimated by NGB.
68	4/12	1400	--	20	10.5	1.9	5	5	.170	Station is about 100 m downchannel from active vents. Lava is fluffy, like cotton candy. Degassed flow rate probably about 30×10^3–40×10^3 m^3/h. Gradient about 3°. Measured by PWL and J. Lockwood.
69	4/13	1400	--	20	16	1.25	5	5	.110	Channel flow is steeper but slower than yesterday, even though measured at high fountain level. Gradient 4.5°. Measured by PWL and NGB.

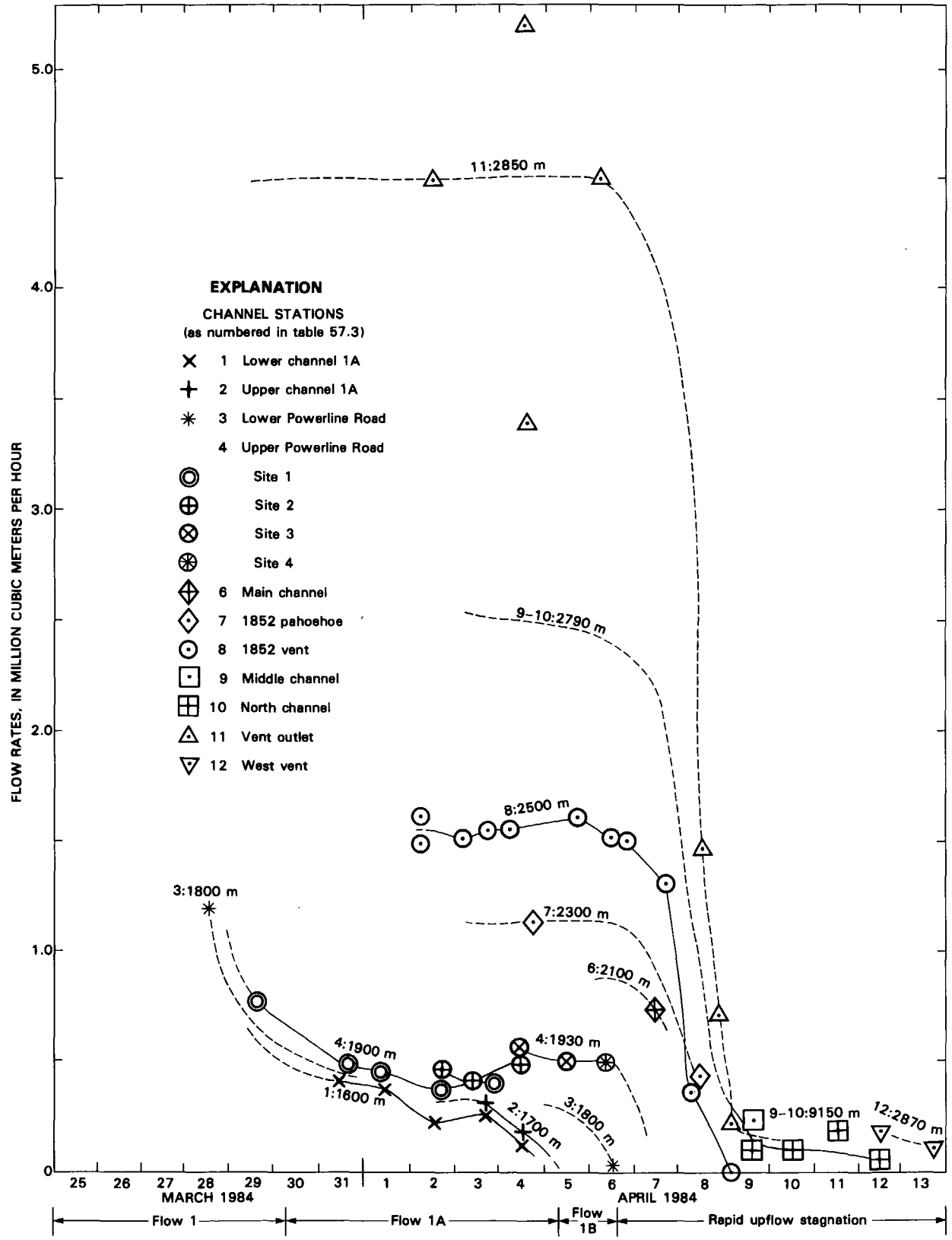

FIGURE 57.26.—Changes in channel discharge with time, 1984 Mauna Loa eruption as measured at channel stations (identified by number; see table 57.3). Solid lines connect repeated observations at individual sites; dashed lines are interpreted trends for discharges based on data at other stations and qualitative observations of channel evolution.

(fig. 57.26). Additional factors came into play during this time interval to cause stagnation of the flow and channel system, and these factors may also have had a role in the early stagnation of flow 1 before March 30.

Lava temperatures at the vent remained nearly constant throughout the eruption, as did temperatures of the most fluid parts of the downchannel flows (fig. 57.19). The latter is thought to have resulted from the heat of microlite crystallization and from thermal feedback associated with deformation of the silicate melt fraction during downchannel flow. Despite the uniform eruptive temperature and chemical composition, the proportion of solid and pasty material (reflecting greater groundmass crystallization) gradually increased in lower reaches of the channel system, raising both the bulk viscosity and the yield strength of the lava. Even in the zones of stabilized and transitional flow, increased downflow sluggishness in the channel indicated progressive increase in viscosity of the fluid matrix between the solid and pasty material. These downchannel effects must have been caused by changes in some intrinsic property of the lava other than decreasing temperature. Decreased gas content and increased groundmass microlite crystalization seem the most likely candidates, as discussed earlier in this paper and as previously suggested for basaltic flows in general by Sparks and Pinkerton (1978).

We infer that decreased gas content played a large role, because fluidity of the flow appears to be at least in part related to the ease of deformation of the silicate liquid that constitutes the vesicle walls. The 80–90 percent decrease in vesicularity of lava in the channel from the vent to the zone of dispersed flow and the accompanying proportional increase in vesicle wall thickness of the silicate melt may have increased the bulk viscosity by several hundred percent.

The greater numbers of microlites downflow must also have increased the effective viscosity of the channel fill, much in the manner that the increased microphenocryst population in the erupted lava raised the viscosity of the lava at the vent. Degassing and crystallization influenced the viscosity and thus the behavior of the lava in differing ways. Degassing of the lava flexed the silicate liquid to produce thermal feedback, adiabatically cooled the lava, and increased the proportion of viscous silicate liquid present. Crystallization heated the lava but also increased its bulk viscosity. The combination of these effects apparently reduced the rate of flow at the vent, delayed temperature decreases downflow and probably also in the lava conduit, produced the conditions required for the pahoehoe-aa transition, and ultimately contributed to the maturation and stagnation of flows during the Mauna Loa eruption.

A further process possibly contributing to stagnation of the flow system was maturation of the channel structures with time. Solidification and increasingly brittle behavior of the channel banks, deepening of the channels by levee growth and possibly by erosion of the channel floor, and crusting over of channel margins and eddies are among the unidirectional processes that could have helped destabilize the channel system during the course of the eruption, regardless of changes at the vent. Such maturation processes could have caused greater formation of channel debris, initially triggered by small fluctuations in vent eruption rate, that led to increasingly larger debris blockages, overflows, and surges downchannel.

Deviations from simple correlations between length of lava flows and eruption rate (Walker, 1973), which have been demonstrated for Hawaiian flows (Malin, 1980), may largely result from the superimposed effects of variable vesiculation, density, undercooling, and crystallinity of the lava. Increased undercooling and crystallinity, decreased vesicularity, and associated increased density would all promote higher effective bulk viscosity and yield strength in basaltic flows, causing transitions from pahoehoe to aa and reducing the length of flows at any constant eruption rate. In contrast, long-lived eruption at liquidus temperature would promote transportation of pahoehoe in lava tubes, permitting lava flows to travel farther. The rheology of lava erupted as gas-rich foam (reticulite, in the case of Hawaiian basalt) that deflates during emplacement will be markedly different from that of degassed lava; such contrasts may extend to highly silicic compositions (Eichelberger and Westrich, 1984). Proposed simple correlations of viscosity and yield strength of lavas with chemical parameters such as silica content (Hulme, 1974) are also imperfect (Moore and others, 1978), perhaps in large part because of the complicating factors just listed.

Finally, it should be noted that the evolution of the 1984 flow system was similar in volume, duration, and eruptive style to several previous historical (since the mid-19th century) rift eruptions of Mauna Loa. Field and photogeologic examination indicates that patterns of upslope stagnation of the distributary channel system characterized many of these earlier events, including the 1852 and 1942 flows that are adjacent to the 1984 flows. Sparse petrographic data indicate that other major historical rift flows (1843, 1926, 1935, 1942, 1950; northeast rift samples collected by J.P. Lockwood and G. Lockwood) also show trends of increasing content of microphenocrysts during the eruption. Similar observations for prolonged summit eruptions, such as those of 1940 or 1949, would be particularly significant because they could permit distinction between the effects of depressurization of the summit reservoir and degassing along the rift conduits. Additional studies of the relations between eruption style, flow evolution, and lava crystallinity of earlier Mauna Loa eruptions are in progress.

More extensive observations are needed on the interrelations between gas content, crystallinity, eruption temperature, and viscosity of erupting basaltic lava. Changes in lava discharge rate, temperature, density, bulk chemistry, and abundance of microphenocrysts were key determinable parameters for the 1984 eruption that should be monitored closely in future activity. Such studies may answer some remaining questions: does lava temperature commonly remain constant during long-lived eruptions, even during periods of declining discharge? Does density of spatter typically decrease during an eruption? Does the development of lava tubes and long-traveled pahoehoe during prolonged eruptions require eruption temperatures near the one-atmosphere liquidus, or at least retardation of major degassing and attendant undercooling before eruption? If eruptions of undercooled lava, marked by increasing microphenocryst populations, can be shown to generate aa flows close to the vent, observations of lava temperature and crystallinity can have important implications for assessing volcanic hazards during early phases of major basaltic eruptions.

A

B

FIGURE 57.27.—Upper channel system of flow 1, as viewed from vent at 2,790 m (Puu 9,146 ft), approximately 4 km from the active vent at 2,900-m elevation. ***A***, At 0900 on March 26. Channel banks of flow 1 are full or overflowing; small bright specks to right of active channel are areas of still-glowing lava that indicate a large overflow within the previous hour. Small channel of flow 2, fed by low fountains, is visible at upper left. Discharge (normalized to density 2.0 g/cm^3) estimated at 1.0×10^6–1.5×10^6 m^3/h. ***B***, At 1600 on March 31. Lava confined completely within channel banks; several forks of the channel and intervening islands have emerged. Despite lower channel level, compared to 5 days earlier, fountain height is higher, probably reflecting a higher proportion of exsolved gases. Discharge (normalized to density 2.0 g/cm^3) estimated at 0.5×10^6–0.6×10^6 m^3/h. Prominent spatter ramparts in left distance mark vents for flows 2–4; these grew rapidly early in the eruption but were inactive after March 27.

FIGURE 57.28.—Changes in fountain height and lava production, as seen from vent outlet (channel station 11) during 1984 Mauna Loa eruption. ***A***, April 2: Vent fountains about 40 m high, well above the spatter rampart. Fluffy channel lava was moving at about 60 km/h, with a discharge rate of about 4.5×10^6 m^3/h (table 57.3, no. 60). In contrast to the lower portions of the stable-channel zone (see figs. 57.8C, 57.10), a broad central part of the channel is moving with plug flow. Velocity gradients are confined to within a few meters of the channel bank. ***B***, April 8, at 1145 h: Vent fountains only 5–10 m high, no longer visible above the spatter rampart. Velocity of the channel lava has declined to about 23 km/h, and the discharge rate is about 1.5×10^6 m^3/h (table 57.3, no. 63); later in the afternoon of April 8, discharge declined by an additional 50 percent. Nevertheless, the level of lava in the channel remains nearly as high as when the eruption rate was several times greater. Note that the highest part of the channel levee visible on April 2 has caved into the channel, presumably to form lava boats.

TABLE 57.4.—*Estimated daily lava production rates and cumulative volumes, 1984 Mauna Loa eruption*

Date (mo/d)	Rate (10^6 m^3/h)	volume (10^6 m^3)	Cumulative volume (10^6 m^3)	Note
3/25	2.8×6 h	25×2/3	16.7	1
3/25	.7×8 h	5.8	22.5	1
3/25	1.1×8 h	8.9	31.4	2
3/26	1.1	26.1	57.5	2
3/27	1.1	26.1	83.6	2
3/28	1.1–1.2	26.1	109.7	3
3/29	.75	18.0	127.7	4
3/30	.5	12.0	139.7	3
3/31	.4	9.6	149.3	3
4/1	.4	9.6	158.9	3
4/2	.4	9.6	168.5	3
4/3	.4	9.6	178.1	3
4/4	.4	9.6	187.7	3
4/5	.4	9.6	197.3	3
4/6	.4	9.6	206.9	3
4/7	.3 (1.2)	7.2	214.1	5
4/8	.16 (.65)	3.6	217.7	5
4/9	.10 (.40)	2.4	220.1	5
4/10	.07 (.28)	1.7	221.8	5
4/11	.05 (.20)	1.2	223.0	5
4/12	.04 (.17)	.7	223.7	5
4/13	.02 (.08)	.5	224.2	5
4/14	.00	.0	224.2	6

1. Hourly production rates for early eruptions from summit (0130–0730, 3/25) and upper rift zone (0900–1700, 3/25) determined by area and thickness measurements (J.P. Lockwood, written commun., 1984). Summit lava is mostly shelly pahoehoe (estimated average density, 1.5 g/cm^3), so volume is reduced by a third to make comparable to volume estimates for later eruptive phases (estimated average density, 2.0 g/cm^3).
2. Hourly production rate for first 48 h of eruption from 2,900-m vent area (1600 3/25 to 1600 3/27), determined by area and thickness estimates, based on field observations by the authors. Data permit a decay in eruption rate, as alternative to constant rate, during this interval.
3. Production rate determined from channel measurements at 1,800 to 1,900-m stations (table 57.3). Estimated average density, 2.0 g/cm^3.
4. Production rate interpolated between rates for previous and subsequent days.
5. Production rate determined from channel measurements at 2,500 to 2,850-m stations (table 57.3). Estimated average density, 0.5 g/cm^3; accordingly, observed discharges (in parentheses) are reduced by three-quarters to make comparable to other measurements.
6. End of eruption.

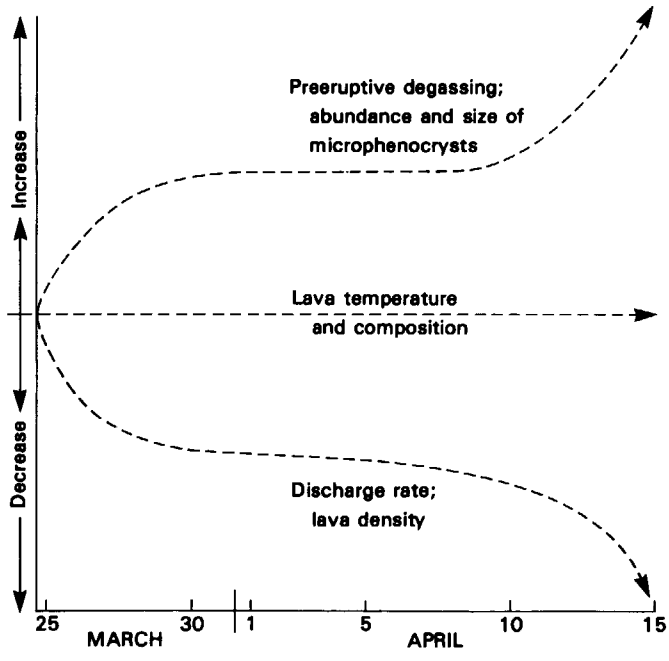

FIGURE 57.29.—Diagram illustrating interdependent time relations between eruptive volume, microphenocryst content, lava composition, eruption temperature, amount of degassing, and lava density during 1984 Mauna Loa eruption.

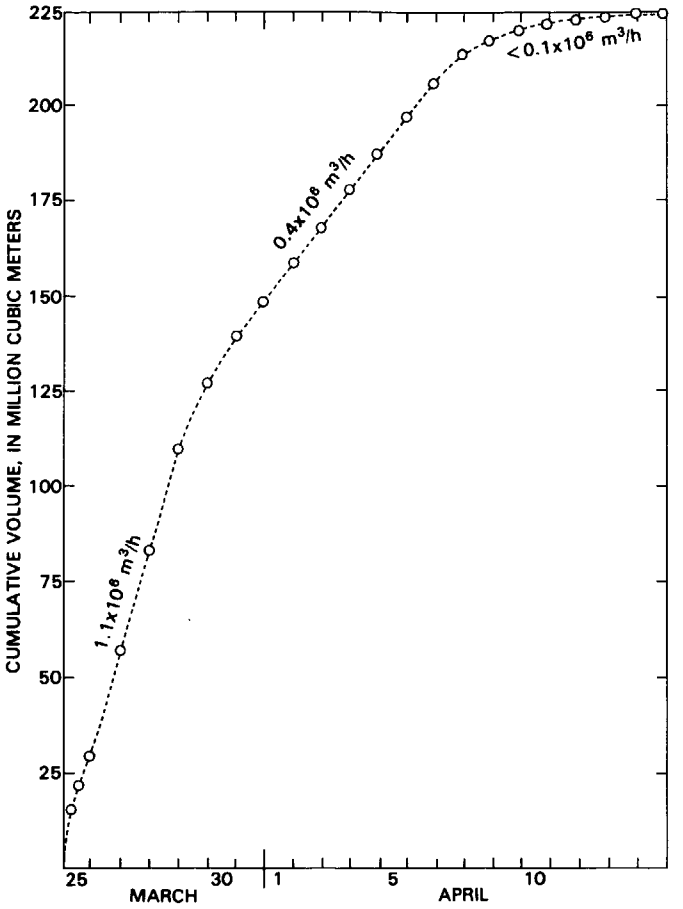

FIGURE 57.30.—Interpreted cumulative volume of erupted lava in 1984 Mauna Loa eruption plotted against time. Data from table 57.4.

REFERENCES

Alt, W.U., Eaton, J.P., and Richter, D.H., 1961, Lava temperatures in the 1959 Kilauea eruption and cooling lake: Geological Society of America Bulletin, v. 72, p. 791–794.

Banks, N.G., and Hoblitt, R.P., 1981, Summary of temperature studies of 1980 deposits, *in* Lipman, P.W., and Mullineaux, D.R., eds., The 1980 eruptions of Mount St. Helens, Washington: U.S. Geological Survey Professional Paper 1250, p. 295–313.

Borgia, A., Linneman, S., Spenser, D., Morales, L.D., and Andre, J.B., 1983, Dynamics of lava flow fronts, Arenal Volcano, Costa Rica: Journal of Volcanology and Geothermal Research, v. 19, p. 303–330.

Casadevall, T., Krueger, A., and Stokes, B., 1984, The volcanic plume from the 1984 eruption of Mauna Loa, Hawaii [abs.]: Eos, Transactions of the American Geophysical Union, v. 65, p. 1133.

Cigolini, C., Borgia, A., and Casertano, L., 1984, Intra-crater activity, aa-block lava, and flow dynamics, Arenal Volcano, Costa Rica: Journal of Volcanology and Geothermal Research, v. 20, p. 155–176.

Decker, R.W., Koyanagi, R.Y., Dvorak, J.J., Lockwood, J.P., Okamura, A.T., Yamashita, K.M., and Tanigawa, W.R., 1983, Seismicity and surface deformation of Mauna Loa Volcano, Hawaii: Eos, v. 64, p. 545–547.

Eichelberger, J.C., and Westrich, H.R., 1984, Degassing of magma in an obsidian flow and inferred degassing behavior at depth, *in* Active tectonic and magmatic process beneath Long Valley caldera, eastern California: U.S. Geological Survey Open-File Report 84–939, p. 147–150.

Finch, R.H., and Macdonald, G.A., 1953, Hawaiian volcanoes during 1950: U.S. Geological Survey Bulletin 996–B, 89 p.

Garcia, M.O, Byers, C.D., Wolfe, E.W., and Rhodes, J.M., 1984, Chemistry and mineralogy of lavas from the continuing eruption of Kilauea Volcano, Hawaii [abs.]: Eos, v. 65, p. 1130.

Greenland, L.P., Okamura, A., and Stokes, J.B., in press, Constraints on the mechanics of eruption of Puu Oo, *in* Wolfe, E.W., ed., The Puu Oo eruption of Kilauea Volcano, Hawaii: the first 1-1/2 years: U.S. Geological Survery Professional Paper.

Greenland, L.P., Rose, W.I., and Stokes, J.B., 1985, An estimate of gas emissions and magmatic gas content from Kilauea Volcano: Geochemica et Cosmochimica Acta, v. 49, p. 125–129.

Haggarty, S.E., 1981, Volatiles in planetary basalts: hydrogen, carbon, and sulfur gas species, *in* Basaltic volcanism on the terrestrial planets: New York, Pergamon Press, Basaltic Volcanism Study Project, p. 385–398.

Hulme, G., 1974, The interpretation of lava flow morphology: Geophysical Journal of the Royal Astronomical Society, v. 39, p. 361–383.

Jones, D.L., Silberling, N.J., Gilbert, W., and Coney, P., 1982, Character, distribution, and tectonic significance of accretionary terranes in the Central Alaska Range: Journal of Geophysical Research, v. 87, p. 3709–3717.

Kirkpatrick, R.J., 1976, Toward a kinetic model for the crystallization of magma bodies: Journal of Geophysical Research, v. 81, p. 2565–2571.

——— 1977, Nucleation and growth of plagioclase in the Hawaiian lava lakes Makaopuhi and Alae: Geological Society of America Bulletin, v. 88, p. 78–84.

Lipman, P.W., Banks, N.G., and Rhodes, J.M., 1985, Gas-release induced crystallization of 1984 Mauna Loa magma, Hawaii, and effects on lava rheology: Nature, v. 317, p. 604–607.

Lockwood, J.P., Banks, N.G., English, T.T., Greenland, L.P., Jackson, D.B., Johnson, D.J., Koyanagi, R.Y., McKee, K.A., Okamura, A.T., and Rhodes, J.M., 1985, The 1984 eruption of Mauna Loa Volcano, Hawaii: Eos, v. 65, p. 169–171.

Lockwood, J.P., Koyanagi, R.Y., Tilling, R.I., Holcomb, R.T., and Peterson, D.W., 1976, Mauna Loa threatening: Geotimes, v. 21, p. 12–15.

Lofgren, G.E., 1981, Comparative petrography and cooling rates, *in* Basaltic volcanism on the terrestrial planets: New York, Pergamon Press, Basaltic Volcanism Study Project, p. 364–370.

Macdonald, G.A., 1953, Pahoehoe, aa, and block lava: American Journal of Science, v. 251, p. 169–191.

——— 1972, Volcanoes, Englewood Cliffs, New Jersey, Prentice Hall Inc., 510 p.

Macdonald, G.A., and Abbott, A.T., 1970, Volcanoes in the Sea: Honolulu, University of Hawaii Press, 441 p.

Malin, M.C., 1980, Lengths of Hawaiian lava flows: Geology, v. 8, p. 306–308.

Moore, H.J., Arthur, D.W.G., and Schaber, G.G., 1978, An estimate of the yield strength of flows on the Earth, Mars, and Moon: Lunar and Planetary Science Conference, 9th, Proceedings, p. 3351–3378.

Moore, J.G., 1965, Petrology of deep-sea basalt near Hawaii: American Journal of Science, v. 263, p. 40–52.

Moore, R.B., Dzurisin, D., Eaton, G.P., Koyanagi, R.Y., Lipman, P.W., and Lockwood, J.P., 1980, Preliminary report on the 1977 eruption of Kilauea Volcano, Hawaii: Journal of Volcanology and Geothermal Research, v. 7, p. 189–210.

Murase, T., 1962, Viscosity and related properties of volcanic rocks at 800° to 1400°C.: Hokkaido University, Journal of the Faculty of Science, Ser. 7, v. 1, p. 487–584.

Neal, C.A., Duggan, T.A., Wolfe, E.W., and Brandt, T.L., in press, Lava samples, temperatures and compositions; Puu Oo eruption of Kilauea Volcano, Hawaii, phases 1–20, *in* Wolfe, E.W., The Puu Oo eruption of Kilauea Volcano, Hawaii: the first 1-1/2 years: U.S. Geological Survey Professional Paper.

Nielsen, R.L., and Dungan, M.A., 1983, Low pressure mineral-melt equilibria in natural anhydrous mafic systems: Contributions to Mineralogy and Petrology, v. 84, p. 310–326.

Peterson, D.W., and Tilling, R.I., 1980, Transition of basaltic lava from pahoehoe to aa, Kilauea Volcano Hawaii: field observations and key factors: Journal of Volcanology and Geothermal Research, v. 7, p. 271–293.

Rhodes, J.M., 1983, Homogeneity of lava flows: chemical data for historic Mauna Loa eruptions: Journal of Geophysical Research, v. 88 (supplement), p. A869–A879.

Shaw, H.R., 1969, Rheology of basalt in the melting range: Journal of Petrology, v. 10, p. 510–535.

Shaw, H.R., Wright, T.L., Peck, D.L., and Okamura, R., 1968, The viscosity of basaltic magma: an analysis of field measurements in Makaopuhi lava lake, Hawaii: American Journal of Science, v. 266, p. 225–264.

Sparks, R.S.J., and Pinkerton, H., 1978, The effect of degassing on the rheology of basaltic lava: Nature, v. 276, p. 385–386.

Sparks, R.S.J., Pinkerton, H., and Hulme, G., 1976, Classification and formation of lava levees on Mount Etna, Sicily: Geology, v. 4, p. 269–271.

Swanson, D.A., 1973, Pahoehoe flows from the 1969–1971 Mauna Ulu eruption, Kilauea Volcano, Hawaii: Geological Society of America Bulletin, v. 84, p. 615–626.

Swanson, D.A., Duffield, W.A., Jackson, D.B., and Peterson, D.W., 1979, Chronological narrative of the 1969–71 Mauna Ulu eruption of Kilauea Volcano, Hawaii: U.S. Geological Survey Professional Paper 1056, 55 p.

Ulrich, G.E., Wolfe, E.W., Hoffman, J.P., and Neal, C.A., 1984, Continuing eruption of east rift zone, Kilauea Volcano, Hawaii [abs.]: Eos, v. 65, p. 1130.

Wadge, G., 1978, Effusion rate and the shape of aa lava flow-fields on Mount Etna: Geology, v. 6, p. 503–506.

——— 1981, The variations of magma discharge during basaltic eruptions: Journal of Volcanology and Geothermal Research, v. 11, p. 139–168.

Walker, D.R., Kirkpatrick, R.J., Longhi, J., and Hays, J.F., 1976, Crystallization history and origin of lunar picritic basalt 12002: phase equilibrium, cooling rate studies, and physical properties of the parent magma: Geological Society of America Bulletin, v. 87, p. 646–656.

Walker, G.P.L., 1973, Length of lava flows: Philosophical Transactions of the Royal Society of London, v. A274, p. 107–118.

Wentworth, C.K., and Macdonald, G.A., 1953, Structures and forms of basaltic rocks in Hawaii: U.S. Geological Survey Bulletin 994, 98 p.

Wright, T.L., and Fiske, R.S., 1971, Origin of the differentiated and hybrid lavas of Kilauea Volcano, Hawaii: Journal of Petrology, v. 12, p. 1–65.

Wright, T.L., Kinoshita, W.T., and Peck, D.L., 1968, March 1965 eruption of Kilauea Volcano and the formation of Makaopuhi lava lake: Journal of Geophysical Research, v. 73, p. 3181–3205.

Yoder, H.S., and Tilley, C.E., 1962, Origin of basalt magmas: an experimental approach: Journal of Petrology, v. 3, p. 342–532.

APPENDIX 57.1

LAVA-TEMPERATURE AND DENSITY MEASUREMENTS

The temperatures in table 57.1 were measured by direct insertion of thermocouples into lava (code T, table 57.1) and by two-color infrared pyrometer readings of fountains or noncrusted fast-flowing lava (code H). Similar equipment has been used to measure temperatures of varied volcanic products (Banks and Hoblitt, 1981; Neal and others, in press). Samples for density and other petrologic studies were collected at many of the sites where temperatures were measured.

THERMOCOUPLE EQUIPMENT

Several configurations of commercial thermocouples were used, in which chromel-alumel wires imbedded in MgO were sheathed with and grounded to Inconel high-temperature stainless steel. Grounded thermocouples, which respond 3–5 times faster than ungrounded versions, have proved to be durable and resistant to thermal and mechanical fatigue as well as corrosion under difficult field conditions.

For slow-moving pahoehoe, small-gauge thermocouples (1.5-mm sheath diameter, 3–10 m long; code 1 in table 57.1) were preferred because of their small thermal mass. Temperatures obtained with such thermocouples were within 5–10 °C of equilibrium with the melt in 1–2 minutes and completed equilibration within the next 2–3 minutes. Where rigidity was required to insert the thermocouple into lava, the thermocouple was wound around a light steel rod, so that the thermocouple tip extended 20–30 cm beyond the rod.

For moving pahoehoe or dense aa, the small-gauge wire usually proved too flexible to insert, and heavier-gauge thermocouples were required. For these situations, 6-mm-diameter Inconel-sheathed thermocouples (code 2, table 57.1) provided excellent results. Response times with the heavy-gauge wire were longer, taking 3–5 minutes to approach within 5 °C of the melt temperature and up to 10 minutes for full equilibration.

Thermal and mechanical stress often caused failure of the thermocouple tips after several insertions, particularly for the small-gauge type. When this happened, 3–6 cm of the faulty end were cut off, and the thermocouple wires were exposed with wire strippers and twisted together. The repaired thermocouple could then be immersed directly in melt to obtain additional temperatures. The double advantage of the exposed tip was an extended life for the thermocouple and a response time about 5 times faster. Calibration of sheathed and bare thermocouple wires in the field and in a test kiln indicated no systematic differences. Code B in table 57.1 indicates that the thermocouple tip was directly exposed to the lava; code C measurements were with a fully clad and grounded thermocouple tip.

Thermocouple voltages were converted to temperatures using direct reading digital voltmeters that were compensated electronically (cold junction). Five meters from two manufacturers were used. The meters were periodically checked against precise millivolt calibrators, which themselves were periodically tested against a laboratory millivolt meter. The meters consistently agreed within ±1 °C of the temperature indicated by the calibrators, as did temperatures obtained by two or more meters sequentially attached to a single thermocouple which had been implanted and equilibrated in lava or a test kiln (see also Banks and Hoblitt, 1981). An exception was a meter, which previously gave good numbers, that was exposed inadvertantly to intense radiation during a measurement; this meter read +4 °C high when next calibrated, and data gathered in the interim were accordingly corrected.

FIELD TECHNIQUES

Observers and thermocouple meters were shielded from the intense radiative heat of the lava by use of a commercial aluminized heat suit (fig. 57.6*B*) or a sheet of aluminum roofing that was fitted with a handle to avoid contact with the metal. Although both shielding techniques were at times used simultaneously, the sheeting was preferred because of increased body ventilation, mobility, and superior visibility and hearing afforded the observers. At an open lava channel or aa front, the heat suit was frequently the only adequate protection.

Techniques in pahoehoe melts were similar in most situations. After preheating the small-gauge thermocouple tip to 700–900 °C for several seconds, it was inserted slowly to a depth of 10–20 cm in an area of melt where no crust had formed. Undesirable growth of a lava icicle or sheath, particularly a problem with the large-gauge thermocouple, could be minimized by working the tip back and forth during slow insertion.

Generally, two people worked together: one person would immerse and maneuver the thermocouple, attempting to avoid hitting any developing crust that might damage or break the wire, and the other would watch for approaching lava, read the meter, and frequently hold the protective shield. Temperatures were read aloud, and as equilibrium was approached and the thermocouple stabilized, a single reading was recorded.

Most temperatures of aa flows were measured with the 6-mm-diameter thermocouples because of their superior rigidity and resistance to breakage. The probe was clamped to an iron rod 4–6 m long, with 20–30 cm extending beyond the rod, preheated to lessen the thermal shock, and pushed into a brightly incandescent part of an advancing flow front. Depending on the viscosity of the melt and the thickness of the chilled aa rind, the probe might readily penetrate the fluid core of the flow. At times, the observer had to lean full weight against the rod in order to force penetration. In most cases, the probe was gradually enveloped by the advancing flow to depths of 2–6 meters. Acceptable penetration and a stable temperature reading generally took 15–30 minutes, and most probes were not recovered. Temperatures were monitored at a safe distance from the rolling incandescent boulders typical of advancing aa fronts, by using an extension cord to the meter.

THE TWO-COLOR INFRARED PYROMETER

Temperatures of the fountains and fast-flowing, uncrusted lava near the vent were measured by a hand-held two-color, infrared pyrometer (HOTSHOT). The two colors allow instant direct calculation of emissivities, thereby yielding relatively accurate temperatures for the radiating body. The instrument has interchangeable lenses, and to narrow the field of view, we used a telephoto lens and an almost-closed aperature. This gave a field of view only a few centimeters across at 5 m and less than 1 m^2 at 30 m distance. The subject and the light-emitting diode display are viewed simultaneously through the eyepiece, and the instrument has an internal reference calibrator, used to adjust for drift before and after each shot.

The HOTSHOT produced stable fountain temperatures that were similar or slightly above the best thermocouple measurements in near-vent flows. Several precautions were required to obtain accurate temperatures: (1) the instrument was immobilized through ground-bracing or use of a tripod; (2) the area viewed was kept small, to eliminate inclusion of sky or crusted spatter falling in front of the active fountains; (3) little or no cooling lava could be between the subject and the instrument; and (4) measurements were avoided over distances greater than 30–40 m. Item (1) is necessary to minimize fluctuations in the readings. Item (2) is to prevent the two detectors from reading separate subjects, which causes calculation of erroneously high or low emissivities. Items (3) and (4) are precautions because certain gasses, probably water vapor, cause different absorption of the two infrared wavelengths. Empirically, we found that unrealistically high numbers result from long shots or shots over degassing lava.

CLASSIFICATION OF THE DATA

Several criteria were used to classify the quality of thermocouple and HOTSHOT temperature data (table 57.1). Code I (icicle) indicates that the thermocouple tip acquired an insulating sheath of lava before stabilizing at the actual lava temperature. These measurements were marked by unstable temperatures that peaked 10–100 °C below other temperatures at the same or a similar locality, and by the icicle growth on the thermocouple when withdrawn. Code F (failed) indicates that the thermocouple tip failed at the indicated temperature without stabilizing, or that penetration into the melt was poor. Code P (poor) indicates that nonideal atmospheric conditions or fluctuating values occurred during a HOTSHOT measurement. Code E (equilibrium) indicates that a stable temperature in equilibrium with the lava was obtained, but that geologic conditions suggested that the lava had cooled relative to temperatures at the vent or main channel. Spatter-fed flows, thin rapidly cooling overflows from lava rivers, and lava held in prolonged storage in lava tubes consistently produced temperatures 5–10 °C below those obtained in obviously superior geological settings. Code G (good) indicates measurements that we consider superior by virtue of

temperature stablility, condition of the probe or path of sight, and quality of the geologic location. Confidence in the G-coded measurements grew as identical temperatures within ±3 °C were obtained at the same locations day after day, both at the vents and down the main channel.

G-coded thermocouple measurements were made either in slow-moving pahoehoe that was insulated from the atmosphere or in aa where the probe tip penetrated into the fluid core and remained stable for 5–20 minutes. Ideal situations were pahoehoe toes fed by lava tubes that tunneled directly through the spatter rampart. The best situations for determining downflow lava temperatures were active pahoehoe fronts or margins, oozes through cracks in accretionary levees at the edges of the main channel, lava tubes fed by and near the channel, thick aa overflows near the channel, and the fluid cores of aa fronts.

SAMPLING AND DENSITY DETERMINATIONS

Several types of samples were collected to study changes in chemistry, mineralogy, texture, and density of the melt during the eruption. Many samples were collected concurrently with temperature measurements. Samples from the channels, channel overflows, and pahoehoe were collected on a hammer or scoop, and were immediately quenched in water to stop growth of gas bubbles and devitrification. Spatter samples were watched in flight, picked up upon landing, and water quenched. Samples labeled "core" (fig. 57.21, 57.22) were from interiors of aa flows. Some were collected from thermocouple tips or hammers and quenched, but a few were collected after they had cooled naturally.

To obtain densities, the samples were diced to cubic or near-cubic form, measured, dried at 20 °C, and weighed.

APPENDIX 57.2
OBSERVATION METHODS AT CHANNEL STATIONS

Many interpretations in this paper, especially those related to lava volumes, are based on quantitative measurements at the channel stations (table 57.2, fig. 57.1*B*). These measurements, though relatively straightforward, involve some assumptions and complications that require further explanation.

The initial purpose of the stations was to permit replicate measurement of channel velocities and volumes along lower reaches of the flow to document any changes in rates at which lava was moving toward Hilo. It was thought that more meaningful results could be obtained downchannel than close to the vent, where channel velocities were high and channel volumes were more influenced by short-term fluctuations in vent activity. Observations on lava flow and channel morphology were a supplemental benefit.

Sites for channel stations were chosen along relatively straight channel reaches of uniform gradient, in order to minimize perturbating effects of local channel geometry. At each station, one or more distances for timing velocities, typically 15–30 m in length, was measured and flagged close to the channel bank, along with sighting points located farther back and perpendicular to the channel. Most lava-velocity measurements were thus made by two observers at these sighting points, timing the motion of identifiable channel material along the measured course. Multiple measurements were made, typically 5–10, until consistent results were obtained. Anomalously slow values, mostly related to material that deviated from center channel, were discarded. The others were averaged; the range of values was typically less than 10 percent. At lower channel stations affected by lava surges, some measurements were made during surges, but plotted values (fig. 57.26) were determined during seemingly representative intervening periods. Helicopter-transport logistics commonly permitted or required several hours of observation at each station.

Most such measurements were made on lava boats and large readily identifiable blocks of floating debris near center channel, but at some stations (especially along upper channel reaches where velocities were high), the lava boats traveled more slowly than small pasty debris on the lava surface. In addition, the lava boats tended to migrate from the highest velocity zone in center channel into slower moving marginal zones (fig. 57.10). At such stations (for example, 1852 vent), a single observer had to make the entire measurement from one sighting point, in order to follow difficult-to-identify channel fragments. Accordingly, a diagonal sighting point was established, aimed at center channel on line with the lower observer point. This procedure empirically yielded consistent results, even though inherently more prone to measurement error because of unfavorable geometry for comparing velocities of lava fragments that deviated slightly from center channel.

Within a kilometer of the vent, the cross-flow velocity gradient again became abrupt at the channel edges (fig. 57.10, station 11), but there were relatively few lava boats for timing velocities. In these areas, the channel lava was essentially foam, and we measured velocities by throwing in a piece of levee lava (which sank) and timing the velocity of the resulting dimple in the lava surface.

While surface channel velocities were thus measurable with considerable precision, translation of such values into lava volumes required determination of cross-sectional channel geometry values which involve greater uncertainties. Channel breadth was measured directly at the station by use of an optical rangefinder, if heat shimmer did not interfere, or was estimated from a hovering helicopter by reference to the surveyed distances along the channel bank. Channel depth could be estimated by (1) constraints of pre-eruption topography, (2) limits indicated by the size of the largest lava boats, and (3) profiles of drained channels after cessation of the eruption (fig. 57.18). Factor (1) provided broad constraints, especially for upper channel stations where total flow thickness appeared to be only about 4–6 m, but local irregularity in surface topography precluded detailed estimates based on overall flow thickness. Observation that some large lava boats grounded and rolled (2), especially at low channel levels between surges, provided key channel depth data for some stations. Examination of drained channels after the end of the eruption (3) provided minimum depth estimates for some stations; interpretation of such values was complicated by incomplete draining, by burial of some stations during stagnation of the flow system, and by changes in channel geometry during the eruption. Possible sedimentation and erosion of the channel floor are recognized problems of lava flow evolution, to which we can add little. Channel overflows and levee growth more than doubled the flow thickness at several stations during the eruption.

Beyond such measurements and estimates of the channel cross-sectional geometry, additional uncertainties involve variations in velocity laterally and vertically in the channel, as well as protrusion of the lava lens beneath the channel banks in the transition zone (fig. 57.5). Lateral velocity gradients on the channel surface, noted above, were especially prevalent in the stable channel zone, where fivefold velocity gradients from center channel to margins were common. Intricate eddies and even reverse flow, analogous to any high-energy water stream, were also common. Surface gradients were more modest downchannel (transition zone), where plug flow commonly characterized most of the active channel and only a narrow marginal zone a few meters wide was characterized by a strong velocity gradient. In addition, poorly understood vertical velocity gradients, with velocity decreasing downward in the channel, are demonstrated by the commonly slower velocities measured for lava boats with sizable keels, in comparison with smaller surface debris on the channel surface. Finally, the process of kneading out gas bubbles, as lava flowed downchannel, may well have been increasingly effective with depth in the channel, producing a vertical density zonation in the lava channel. All these complications contribute to uncertainties in the lava-volume measurements that are difficult to resolve quantitatively.

PRELIMINARY ESTIMATES OF THE RHEOLOGICAL PROPERTIES OF 1984 MAUNA LOA LAVA

By Henry J. Moore

ABSTRACT

During April 2–3, 1984, the visual characteristics of the lava of Mauna Loa changed dramatically along the length of the flow that was fed from vents near 2,850-m (9,350-ft) elevation. In the upper reaches, 2,500-m (8,200-ft) elevation and 3 km from the vents, the flow was composed of sparse clinkers and cinders in a matrix of incandescent lava and was confined within a channel 20 m across. The flow appeared to be laminar and more or less steady, with a velocity of about 5.3 m/s at its center. Concentration and mean size of solid to incandescent objects carried along by the flow increased downstream. In the lower reaches, at 1,620-m (5,300-ft) elevation and 15 km from the vents, the flow looked like a slowly moving mass of debris confined within rubbly levees; the debris included warm to incandescent fragments that were block size and smaller along with molten lava and incandescent globs or clots. Movement of the flow occurred by displacement of discrete, intact units with boundaries that paralleled the crests of the rubbly levees at the margins of the flow. Flow appeared to be laminar but unsteady, with surges and ebbs. Typical flow velocities were in the range of 0.1–0.3 m/s.

Apparent viscosity of the lava on a given day increased along the length of the flow and with time at some locations. On April 2, it was about 10^2 Pa·s (10^3 poise) at the vents, 10^3 Pa·s (10^4 poise) 3 km from the vents, 10^5 Pa·s (10^6 poise) 15 km from the vents, and probably near 10^7 Pa·s (10^8 poise) at the toe of one flow. Apparent viscosity at the vents increased from about 10^2 Pa·s on April 2 to 2×10^3 Pa·s on April 13. These values compare favorably with field and laboratory data on viscosity of basalt at the same temperatures and with similar stresses and rates of shear as the Mauna Loa lava.

Rheology of the lava probably varied along the length of the flow and with time. It could have been a Newtonian fluid near the vents, a Bingham fluid 3 km from the vents, and a pseudoplastic fluid farther from the vents. Other models of fluids may also apply.

Volume flow rate in the channel at the vents on April 3 was near 1.5×10^6–2.0×10^6 m³/h, about 12 times larger than that 15 km from the vents. With certain assumptions, an approximation of conservation of mass along the length of the flow requires that the density of lava flowing from the vents was 220 kg/m³ and implies a mass flow rate near 0.33×10^9–0.44×10^9 kg/h. If these masses were deposited as lava with an average density of 2,200 kg/m³, the volume flow rate would appear to be 0.15×10^6–0.20×10^6 m³/h.

INTRODUCTION

This paper estimates the rheological properties of the lava during the 1984 eruption of Mauna Loa Volcano in Hawaii and applies the results to the problems of volume and mass flow rates along the flow on one day. The derived rheological properties are based on visual observations while the flow was in progress; time and resources have permitted only partial analysis of the available data. Time-lapse photography and motion pictures of the eruption should be reviewed and analyzed in future rheological studies.

The 1984 eruption of Mauna Loa began at 0126 Hawaii standard time (H.s.t.) on March 25 and ended late on April 15 (Lockwood and others, 1984a, 1985). Initially, lava fountains issued from eruption fissures in the southwest corner of the summit caldera (Mokuaweoweo), but within a few hours eruptions from fissures migrated down the southwest rift zone, northeastward across Mokuaweoweo, and down the upper northeast rift zone (Lockwood and others, 1984b, 1985). Later on March 25, lava began pouring sequentially down the northeast rift zone from separate, isolated vents above eruption fissures. At about 1630 H.s.t. on March 25, lava was issuing from fissure vents at 2,830–2,900-m (9,300–9,500-ft) elevations that became the principal sources of lava for the remainder of the eruption (Lipman and Banks, chapter 57; fig. 58.1). Three southerly flow lobes fed by these vents stagnated by March 27, but the fourth (flow 1) was fed at a fairly constant volume flow rate ($\sim1.5\times10^6$ m³/h). Large flow rates were sustained from March 30 to April 7; after April 7 flow rates declined. Flow 1 advanced rapidly as a narrow aa sheet to the 910-m (3,000-ft) level, 25 km from the vents, and a lava channel had formed within the sheet by March 29. On March 29, a breakout or channel overflow near the 1,740-m (5,700-ft) level cut off the supply of lava to flow 1 so that it moved only about another kilometer in about a day and then stopped. Lava of this breakout gave rise to flow 1A which advanced rapidly along a course subparallel to and north of flow 1; advance of flow 1A gradually decreased until April 5, when it stopped about 27 km from the vents. A series of overflows that progressed upstream beginning April 3 reduced the lava supply to flow 1A and culminated in a major breakout at the 1,980-m (6,500-ft) level around noon on April 5. This major breakout cut off the lava supply to flow 1A and produced flow 1B, which flowed toward the northeast. Repeated channel blockages and overflows continued progressively upstream from April 5 to 8. On April 7, lava production at the vent began to dwindle; subsequently the flow system stagnated and vent activity ceased.

Flow 1, initially a narrow aa sheet flow, lenticular in profile, evolved into a flow system with three zones: (1) a channel zone within the sheet flow and below the vents, (2) a transition zone, and (3) a

dispersed-flow zone led by the advancing toe (Lipman and Banks, chapter 57). On March 28, just before the breakout of flow 1A, a stable channel zone extended from the vents about 11 km down to about the 1,830-m (6,000-ft) level; the transition zone extended 10 km down to within 1 or 2 km of the toe, then at the 1,220-m (4,000-ft) level, and the dispersed-flow zone made up the remainder. By April 3, the channel zone extended down to the 1,770-m (5,800-ft) level, the transition zone of flow 1A extended 3–4 km down to the 1,580-m (5,200-ft) level, and the dispersed-flow zone extended down to the toe of flow 1A at the 1,010-m (3,300- ft) level about 26 km from the vents. Significant blockages and obstructions of flow in the channel were observed on March 29. Such blockages and obstructions, which ponded the lava, increased in size and number upstream toward the vents with time. Overflows of lava caused by the blockages and obstructions created lava dams, levees, and elevated lava ponds along the channel zone. Minor failures of blockages in the lava dams produced increased flowage from the ponds and surging and ebbing flow downstream. Larger failures in the lava dams caused larger surges of lava, which overflowed the levees and produced small flows along the channel edges. Major failures caused major surges and breakouts or overflows of large volumes of lava. Such major overflows gave rise to flow 1A on March 29 and flow 1B on April 5. Subsequently, repeated blockages and overflows occurred progressively upstream.

Lava temperature at the vents was $1,140 \pm 3$ °C throughout the eruption, and that of the most fluid lava at channel stations as far as 10 km from the vents was in the range of $1,135 \pm 5$ °C (Lipman and Banks, chapter 57). Reported temperatures of the most fluid lava in the channel beyond about 12 km from the vents were 1,086–1,126 °C (flow 1A at elevations of 1,750–1,150 m; see Lipman and Banks, chapter 57). Bulk temperatures at the various channel stations and at lower elevations may have been lower than this, because there were coherent glowing blocks and solidified fragments in the flows. Bulk density of the flowing lava varied greatly and ranged from 330–2,600 kg/m^3 (0.33–2.6 g/cm^3); density tended to increase with distance from the vents (Lipman and Banks, chapter 57). Finally, the concentration of microphenocrysts in the lava increased with time at the vents and with distance from the vents (Lipman and Banks, chapter 57).

Subsequent sections of this paper will (1) describe the author's observations; (2) discuss the flow models and equations used to estimate the rheological properties of the flows, volume flow rates, and mass flow rates; (3) present the results; (4) discuss the results; and (5) list the conclusions.

ACKNOWLEDGMENTS

Robert Decker, Scientist in Charge, and John P. Lockwood of the Hawaiian Volcano Observatory were instrumental in making arrangements for the author to witness the eruption and observe "redrock" for the very first time. Cordial hospitality and assistance were provided by the staff of the Hawaiian Volcano Observatory. Jack Lockwood, Peter Lipman, Norman Banks, and Christina Neal allowed this tyro to accompany them in the field with exemplary tolerance and patience. Helicopter pilots Bill Lacey, Jr., Tom Haupman, Ed Spencer, and Ken Ellard safely delivered the author to and from flows. Work was partly funded by NASA contract W–15–462.

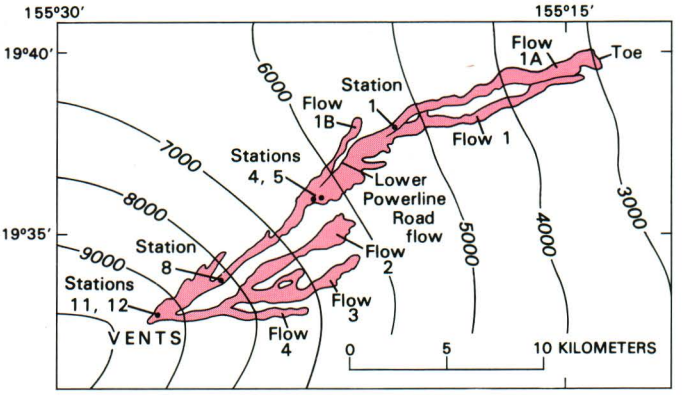

FIGURE 58.1.—Sketch map of the 1984 Mauna Loa lava flows showing stations referred to in text. Contour interval is 1,000 feet.

OBSERVATIONS

Observations of the author for three localities (fig. 58.1) along the flow for the period April 2 through April 7 are described and discussed below. These localities are (see Lipman and Banks, chapter 57): (a) station 8, vent of 1852, 2,500 m (8,200 ft), 3 km from the vents; (b) stations 4 and 5, 1,920–1,950 m (6,300–6,400 ft), about 9 km from the vents; and (c) station 1, 1,620 m (5,300 ft), about 15 km from the vents. The first two localities were in the stable channel zone, and the third in the transition zone. Also included are the author's description of an advancing, unconfined, wide flow from an overflow and Hawaiian Volcano Observatory staff reports on the toe of flow 1A. These two flows correspond to dispersed flow.

STATION 8, APRIL 2–7

The flow appeared to be a mass of cinders and clinkers imbedded in a matrix of incandescent lava estimated to be 4 m deep and confined within a channel 20 m across (fig. 58.2). A few floating silvery, meter-size blocks were carried along by the flow. Flow appeared to be laminar and nonturbulent. The central portion of the flow, about 1 m wide, moved as a plug-like unit of silvery to light gray crusty material in a matrix of incandescent lava (fig. 58.3). Between the plug-like center and the margins, bands of red incandescent lava and small cinders and clinkers were aligned parallel to the channel edges. Velocity decreased from about 5.3 m/s near the center to zero at the channel edge (fig. 58.3). The meter-size and smaller blocks did not rotate around horizontal axes and those near

FIGURE 58.2.—Lava in channel at station 8 on April 5. Channel is about 20 m wide; flow surface is composed of very light gray cinders and clinkers set in a matrix of reddish-orange lava; flow from right to left. Foreground is aa of sheet flow.

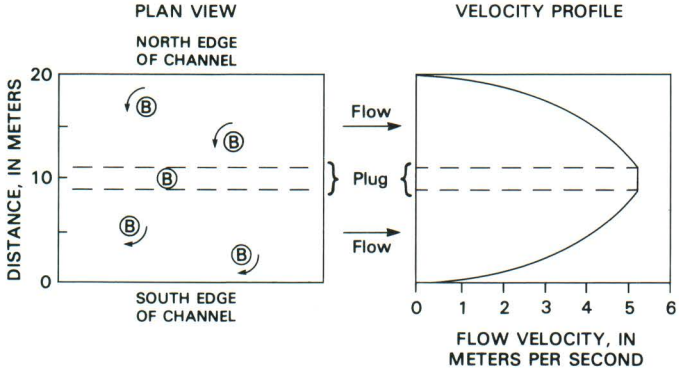

FIGURE 58.3.—Diagrammatic plan view and velocity profile for lava channel at station 8. In plan view, one-meter-wide plug moves as unit with uniform velocity. Blocks (B) north of plug rotate counterclockwise around vertical axes; blocks south of plug rotate clockwise around vertical axes; blocks in plug do not rotate. Velocity profile shows velocity of lava increases smoothly from zero at channel edge to 5.3 m/s in the plug.

the center did not rotate around vertical axes. Between the center and the margin, the blocks rotated around vertical axes. Rotation was counterclockwise on the north side of the channel and clockwise on the south side; the lava was moving from the west toward the east. The flow was remarkably quiet, but it did make faint shushing and swishing sounds. Volume flow rates obtained by multiplying the

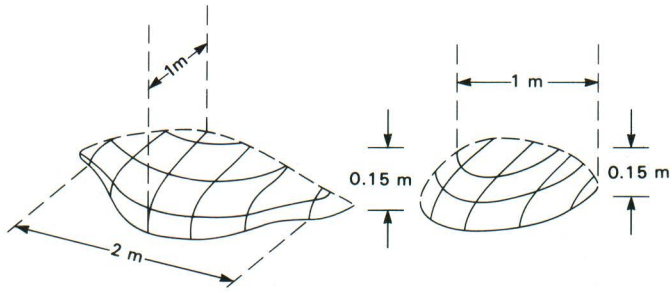

FIGURE 58.4.—Diagram illustrating two solidified overflow lobes at margin of channel at station 8. Lines are form lines.

center velocity, channel width, and estimated flow depth were of the order of 1.5×10^6 m^3/h (Lipman and Banks, chapter 57).

Two silvery lobes, interpreted to be recent overflows, were observed at the channel edge (fig. 58.4). They were estimated to be 0.15 m thick and 1–2 m wide; heat and the possible instability of the channel edge prevented direct measurements or sampling. These lobes are used later to estimate the yield strength of the lava, on the assumption that they represent solidified lava from the channel.

Postflow measurements indicate that the channel is 20 m wide and 6 m deep (Lipman and Banks, chapter 57, fig. 57.18, profile H). The estimated depth of flow was 4 m because the lava surface was 2 m below the channel lip during the eruption. The local slope derived from a 1:24,000-scale map is 5.6°.

STATIONS 4 AND 5, APRIL 3–7

Characteristics of the flow channels at these stations were diverse. The lava was confined within channels formed by high levees interspersed with sections reminiscent of station 8. In the high, leveed sections, topographic gradients were somewhat reduced. Upstream, lava flowed rapidly into the high, leveed part from channels with low overflow levees. Downstream, the levees, composed chiefly of rubble, increased in height and caused ponding of the lava, which spilled over the downstream side in a lava fall.

On April 3 near station 4 at an elevation of 1,920 m (6,300 ft), lava was flowing in a high, leveed channel with velocity as great as 1.2 m/s during surges and 0.8 m/s during ebbs. The levee was about 2.3 m high. Visible lava within the channel was composed of dark cinders and clinkers and incandescent clots set in a matrix of incandescent lava (fig. 58.5). Concentrations of the cinders and clinkers were larger than at station 8, and incandescent clots were not evident at station 8. Along the margin of the levee, the channel surface was crusted and stranded blocks were present (fig. 58.6*A*). During surges, rising lava would arch upward, and the marginal crusts and stranded blocks would sympathetically tilt upward and outward (fig. 58.6*B*). Surges were accompanied by small outward displacements of the levees and the avalanching of debris down the levee flanks. During peak surges the lava spilled over and onto the crust and stranded blocks (figs. 58.5*A* and 58.6*C*). During ebbs,

A

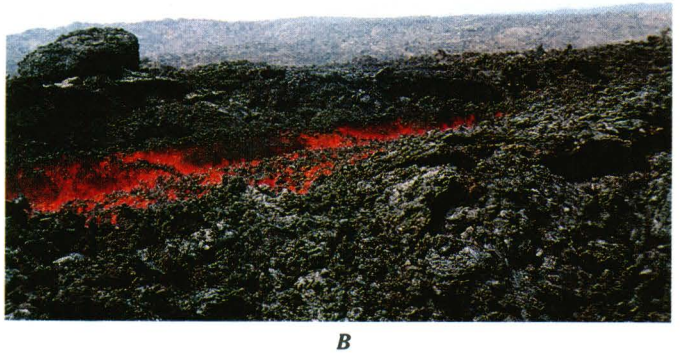

B

FIGURE 58.5.—Flow of 1984 Mauna Loa lava in high, rubbly, leveed channels. ***A***, Station 4 on April 3. Lava from center during surge is overflowing material in channel at margin. Note dark, partly cooled lava. Channel is about 14 m wide. ***B***, Station 6 on April 7. Typical flow in leveed channel during ebb. Note the structure and blocky appearance of incandescent clots. Channel is about 22 m wide.

the crust and blocks would become level as the lava subsided. Upstream, lava was flowing in a channel 14 m wide at 1.6 m/s. Here and elsewhere, swishing and shushing noises generated by the flowing lava were evident and more pronounced than those at station 8. The next day (April 4), the height of the rubbly levee had increased to 5 m. Upstream near the 1,935-m (6,350-ft) elevation, lava velocity was near 2 m/s; but the velocity varied somewhat because of surges and ebbs. On the morning of April 7 at station 5 at 1,950-m (6,400 ft), lava was flowing in the channel at 1.5 m/s; later in the day, lava overflowed the debris-choked leveed channel upstream and substantially reduced the input of the lava (fig. 58.6*D*, 58.7*A*). Lava from breakouts (fig. 58.7), or sudden releases of semi-ponded lavas, produced immense surges that overflowed the rubbly levees and formed a thin sheet over the levees and beyond to some distance from the levee crest; exceptionally large breakouts (fig. 58.7*B*) produced sustained flows such as flow 1B. Flow appeared to be laminar and nonturbulent during surges, ebbs, and even breakouts. Distal lobes of a breakout sheet that probably occurred on April 6 were 0.3–0.75 m thick and 3–4 m wide (fig. 58.8). The thickness and width of these lobes are used later to estimate a yield strength for lava that flowed in the channel here.

Volume flow rates for the lava during April 2–5 were estimated to be in the range of 0.37×10^6–$0.60\ 10^6$ m^3/h (Lipman and Banks, chapter 57).

STATION 1, APRIL 3

The flow at this station appeared in general to be a hummocky mass of slowly moving debris, rubble, and blocks confined within a rubbly, leveed channel 57 m wide and estimated to be 6 m deep (fig. 58.9). Mounds and blocklike incandescent units, partly to completely veneered by darker, cooler debris, rode along the top of the hummocky surface; at times, spallation of dark and incandescent debris would further expose their incandescent cores. Elsewhere, local exposures of incandescent lava beneath and intermingled with debris were common. The flow was unsteady, but not turbulent. Surges with velocity as great as 0.36 m/s were accompanied by increase in the height of the flow by a few meters; ebbs with velocity near 0.18 m/s were accompanied by decrease in the height of the flow by a few meters. Movement occurred by shearing between intact units along surfaces with traces that paralleled the channel edge (fig. 58.10). At intermediate velocities and thicknesses, the central part of the flow moved as a plug-like unit with little internal relative motion; the units immediately flanking the center moved at a slower velocity and, similarly, with little internal motion; and so on to the channel edges, where the velocity of the outermost units was very small to zero. As the flow surged and thickened, the velocity of the central unit increased and the relative velocities between the units decreased until, at peak velocity, almost the entire width between the levees had the same velocity. Estimates of the flowing width during two surges were 45 and 52 m. Surges were accompanied by crunching noises due to the grinding action between and within the intact units; the rubble levees were displaced outward and debris rolled down the levee flanks. As the flow ebbed and thinned, the velocity of the center unit decreased and that of the other units decreased sequentially outward from the center. Such ebbs were accompanied by a substantial decrease in noise; the levees ceased to move, and debris ceased to roll down their flanks. Further thinning would cause motion of the units to cease progressively from the channel edge toward the center. During one ebb, the entire flow briefly stopped. A visual estimate of the thickness at the center when that part ceased to move was 3 m.

Volume flow rates estimated during the eruption on April 3 were 0.15×10^6 to 0.45×10^6 m^3/h (Lipman and Banks, chapter 57).

Post-eruption profiles of the channel suggest that it was 57 m wide and 8 m deep below the levee crest; a 2-m-thick layer of basalt occupied the channel floor (Lipman and Banks, chapter 57, fig. 57.18, profile M). The local slope derived from a 1:24,000-scale topographic map is 3.3°.

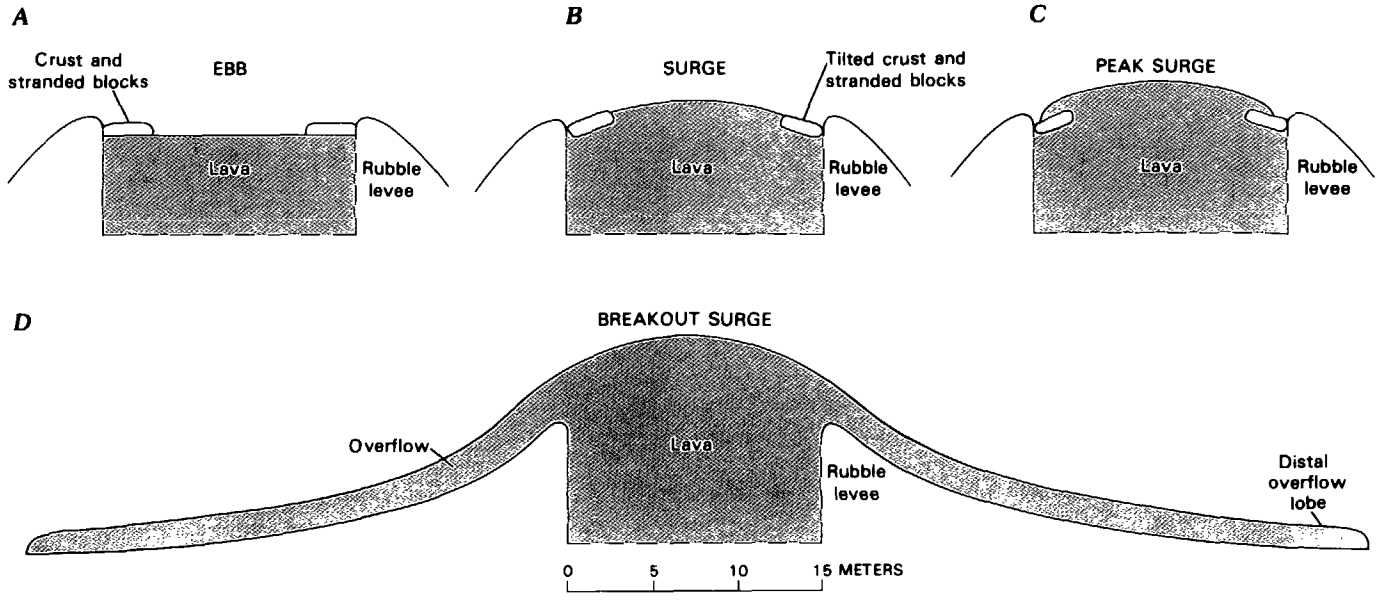

FIGURE 58.6.—Diagrammatic profiles of lava in channel with high, rubbly levees at station 4 on April 3 (*A*–C) and station 5 on April 7 (*D*). ***A***, During ebb flow, marginal crusts, stranded blocks, and lava are nearly level. ***B***, During surge flow, lava arches upward and marginal crust and stranded blocks tilt upward and outward. ***C***, During peak surge, lava overflows tilted marginal crust and blocks. ***D***, During breakout surge, lava spills over rubble levees and flows down levee flanks and onto surrounding surfaces, producing a deposit with lobate margins.

LOWER POWERLINE ROAD FLOW, APRIL 5

A wide unconfined flow 2–3 m thick, from a previous breakout, advanced eastward at a rate near 0.03 m/s on a slope of 3.6°. The flow was composed of an upper unit of blocks, clinkers, and cinders overlying incandescent molten lava (fig. 58.11). The flow advanced in caterpillar-tractor style (Krauskopf, 1948): debris of the top layer moved faster than the underlying lava so that it avalanched down the advancing front and was overridden by the molten lower part (fig. 58.12*A*). The flow made crunching noises similar to those at station 1 and the avalanching debris made

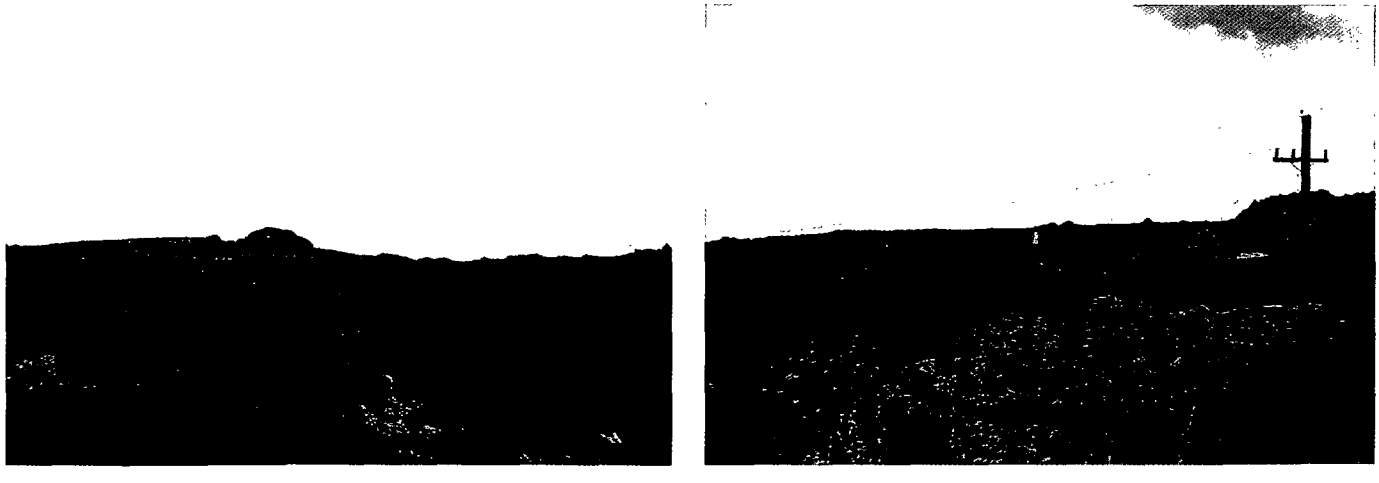

A ***B***

FIGURE 58.7.—Breakout surges near stations 4 and 5. ***A***, Breakout surge of April 7 from ponded lava upstream of station 5. Dark horizon to right is near crest of channel levee. Lava spills over levee near huge glob of incandescent lava that is moving toward the right. Overflows like this one produce layers with lobate margins on the flanks of the leveed channels. ***B***, Breakout near station 4 on April 5. Note reddish-orange glowing lava overflowing levee and flowing down levee flank at left middle. Protrusions on center skyline are large (approx. 8-m) blocks carried along the leveed channel by lava flowing toward the left. Glowing lava in foreground and at right is part of breakout that produced flow 1B.

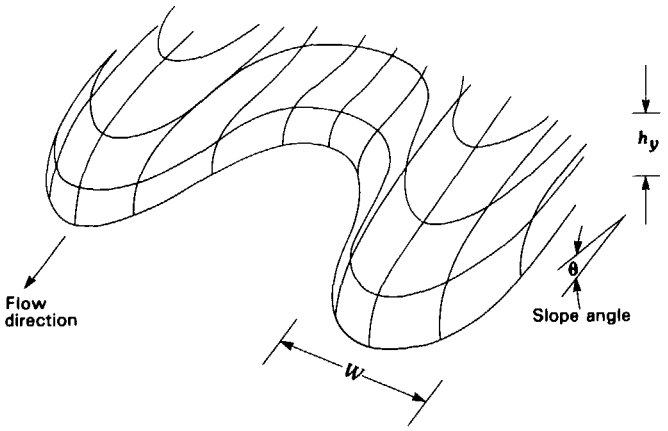

FIGURE 58.8.—Diagram of lobes at margin of overflow sheet from breakout surge on April 6 near station 5. Parameters indicated are lobe width (W), lobe thickness (h_y), and slope angle (θ).

FIGURE 58.9.—Surging flow at station 1 on April 3. Flow is composed chiefly of blocks, clinkers, and cinders and is moving from right to left. Spalling of debris from one block has exposed its reddish-orange molten core; some incandescent lava is also visible in ridge just below block. Immediate foreground is rubble levee; flow obscures levee on opposite side of channel. Large block at crest of flow is about 2 m across.

clinking, thunking sounds. In most places the base of the molten lava was in contact with debris, but locally with preflow surfaces. Where exposed, the molten lava at the front of the flow was smoothly curved and showed subtle rounded protrusions here and there (fig. 58.12*B*). At the very base, it curved back upon itself, indicating that molten lava was overriding molten lava and that the velocity at the base of the flow was zero; debris in the process of being overridden was stationary. Large expanses of the upper surface moved downstream as intact units with little internal relative movement, although there was movement between the various intact units. In plan view the front was lobate, and each lobe tended to follow local rilles. The entire flow advanced down a broad, shallow valley.

FLOW 1A, APRIL 2–3

Although the toe of flow 1A could not be visited because of the dense vegetation there, it was estimated from the air to be 9 m thick and 762 m (2,500 ft) wide, and to be moving at 26 m/h on April 2 and 12 m/h on April 3. The local slope derived from a 1:24,000-scale topographic map is 3.65°. Crude estimates obtained by multiplying the thickness, width, and rate of advance indicate volume flow rates of 0.18×10^6 m^3/h on April 2 and 0.08×10^6 m^3/h on April 3. For an assumed density of 2,400 kg/m^3 (2.4 g/cm^3), the mass flow rates are 0.43×10^9 kg/h on April 2 and 0.20×10^9 kg/h on April 3.

MODELS AND EQUATIONS

MODELS

In the calculations below, the Mauna Loa lava flows are treated as Newtonian and Bingham fluids flowing in semi-elliptical channels and as wide, unconfined flows; flow is laminar. The implications of possible pseudoplastic flow are also considered.

A Newtonian fluid is characterized by a viscosity (fig. 58.13). Here, the stresses are always proportional to the rate of shear. At high temperature, dense molten lava is a Newtonian fluid with a viscosity that is a function of composition and temperature (Shaw, 1969, 1972).

In contrast to a Newtonian fluid, a Bingham fluid is characterized by a yield strength in addition to a viscosity (fig. 58.13). The concept of a Bingham fluid was developed to account for the rheological behavior of paints flowing in circular pipes (Bingham, 1922) and later applied with success to the flow of slurries in pipes (Caldwell and Babbitt, 1941; Smith, 1960; Valentyik, 1972). Bingham (1922) suggested that his concept might apply to the flowage of some natural fluids such as lava. Subsequently, numerous authors have attempted to apply Bingham's fluid model to lava flows (Hulme, 1974; Moore and Schaber, 1975; Borgia and others, 1983; Cigolini and others, 1984), debris flows (Johnson, 1970; Fink and others, 1981), and landslips. Bingham-fluid concepts have been invoked by Kilburn (1981) to account for the irreversible transition of pahoehoe to aa (Macdonald, 1953) as described by Peterson and Tilling (1980). There is, however, a general lack of data on yield strengths and Bingham viscosities; such measurements are represented by the pioneering work of Shaw and others (1968) and subsequent works (Sparks and others, 1976; Cigolini and others, 1984).

A pseudoplastic fluid is different from both the Newtonian and Bingham fluids (fig. 58.13). Stresses on the pseudoplastic fluid produce rates of shear that vary according to a power law, and there is no single value of viscosity. Experimental data indicate that basalt at 1,120–1,125 °C behaves like a pseudoplastic fluid when stresses are less than about 16×10^3 Pa and shear rates are less than 5 s^{-1} (Shaw, 1969).

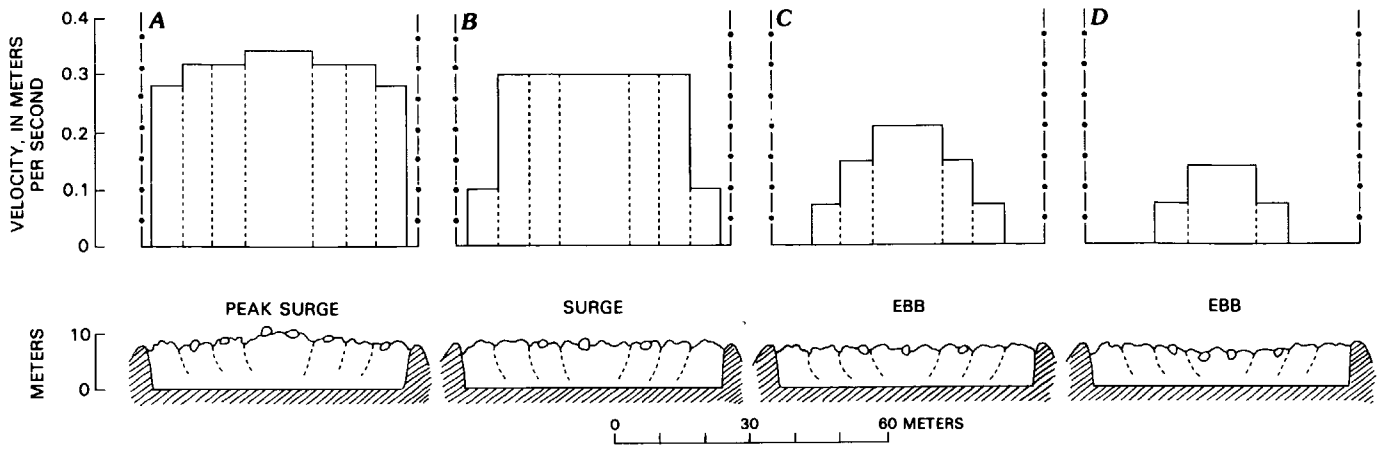

FIGURE 58.10.—Velocity profiles and diagrammatic cross sections of the unsteady flow of lava at station 1 on April 3. Dot-dash lines on velocity profiles represent crests of levees; dashed and solid lines outline discrete intact units of moving surface. Cross sections show upper surface of flow; dashed lines represent postulated unit boundaries (which may actually be vertical). ***A***, During peak surge, surface of flow moves as discrete, intact units with velocities as great as 0.34 m/s; parts of center of flow are a few meters higher than levee crest. ***B***, During surge, entire central 45 m of surface moves with a velocity near 0.3 m/s; velocities of units near edge are much less; surface of flow is about same elevation as levee crest but irregular. ***C***, During ebb, a central unit moves as a plug with a velocity near 0.2 m/s; velocity decreases outward toward levee and that of units at edges is zero; elevation of surface of flow drops below elevation of levees. ***D***, With further ebbing, central unit moves with a velocity near 0.15 m/s; next adjacent unit is slower; other units have stopped; surface of flow sags downward toward center.

APPARENT VISCOSITY

In an ideal Newtonian fluid, the viscosity is constant, and miniscule stresses produce miniscule rates of shear. In an ideal Bingham fluid, the viscosity is constant, but the rate of shear is zero when the stresses are less than the yield strength (fig. 58.13). Apparent viscosity, which is calculated in the same way as the Newtonian viscosity, is a strong function of the rate of shear for the

FIGURE 58.11.—Flow at Lower Powerline Road on April 5. Flow is about 3 m thick and advancing at a rate near 0.03 m/s. Upper surface is composed chiefly of debris; underlying reddish-orange layer of incandescent lava is locally exposed along front.

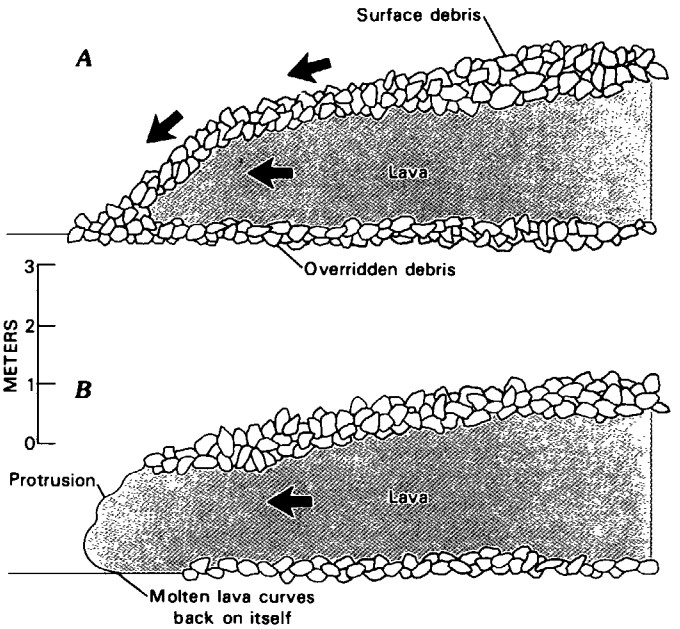

FIGURE 58.12.—Diagrammatic profiles of flow at Lower Powerline Road on April 5. ***A***, The flow is typical aa, with an upper surface of debris overlying molten, incandescent lava. Upper surface moves as a unit with greater speed than underlying layer so that debris avalanches and falls down front and is then overridden by flow. ***B***, Surface of molten lava. Where surface of molten lava is exposed at the front, it is smoothly curved, with some rounded protrusions, and curves back upon itself at the base.

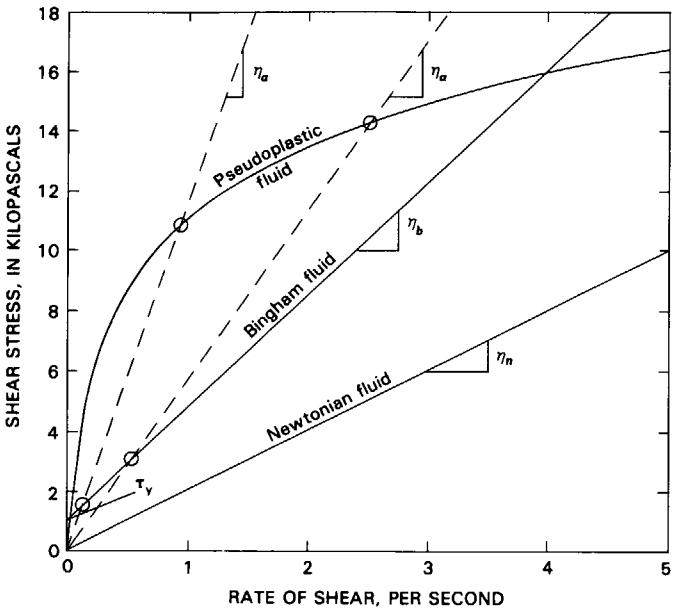

FIGURE 58.13.—Relation between shear stress and rate of shear for Newtonian, Bingham, and pseudoplastic fluids. Newtonian fluid is represented by straight line passing through origin; slope of line (η_n) is the viscosity. Bingham fluid has a yield strength and a viscosity; shear stress on Bingham fluid must exceed the yield strength (τ_y) to produce a rate of shear greater than zero; slope of line (η_b) is the Bingham viscosity. Pseudoplastic fluid is represented by curved line; rate of shear is approximately a function of shear stress raised to some power. Apparent viscosity (η_a) assumes a Newtonian fluid and varies with the rate of shear for Bingham and pseudoplastic fluids. As depicted, viscosity of Newtonian fluid is 2×10^3 Pa·s. Viscosity and yield strength of Bingham fluid are 3.8×10^3 Pa·s and 10^3 Pa, respectively. Pseudoplastic fluid is similar to basalt at 1,125 °C (Shaw, 1969).

Bingham fluid. It varies from large values at small rates of shear to values that approach the Bingham viscosity at very large rates of shear. Similarly, apparent viscosity calculated for a pseudoplastic fluid varies from large values at small rates of shear to smaller values at larger rates of shear. The term "apparent viscosity" is applied to calculations for any fluid when the fluid is assumed to be Newtonian (see, for example, Shaw, 1969).

PLUGS AND SLABS

As a consequence of the yield strength, the central and upper parts of Bingham fluids flowing in the laminar regime move as plugs in channels and as slabs in wide, unconfined flows (Johnson, 1970). Dimensions of the plugs and slabs depend on the stresses acting on the fluid, the yield strength, and the shape and size of the channel or wide flow. The velocity distribution from the margins of a flow in a semi-elliptical channel to the central plug, or from the base of the wide flow, is the same as the normal velocity distribution for laminar flow of a Newtonian fluid; velocity increases from zero at the margin or base of the flow to the velocity of the plug or slab at its edge. For a Newtonian fluid, the dimensions of the plug or slab are zero.

EQUATIONS

The yield strength of a Bingham fluid may be estimated from the dimensions of the flow at rest and the plug or slab dimensions when the fluid is flowing. Viscosity for both Newtonian and Bingham fluids may be estimated from the observed velocity. Additional parameters required for these estimates include the acceleration of gravity, fluid density, slope angle or topographic gradient, and channel or flow dimensions. Equations used for these estimates are described below.

YIELD STRENGTH

Yield strength (τ_y) can be estimated from the rest thickness (h_y) of a wide, unconfined Bingham fluid that has stopped. The stress acting on this flow (τ), which is driven by gravity, is given by:

$$\tau = \rho g h \sin\theta \qquad (1)$$

where ρ is the density of the flow, g is the acceleration of gravity, h is the distance below the surface of the flow, and $\sin\theta$ is the topographic gradient (θ is the slope angle measured at a characteristic flow surface). The stress at the base of the flow (τ_b) is obtained when h is equal to the thickness of the flow during flow (H). The stress at the base of the slab, which is equal to the yield strength (τ_y), is obtained when h is equal to the thickness of the slab (h_y). A wide, unconfined flow comes to rest when the shear stress (τ) is less than the yield strength at all depths. This may occur because the flow thins or the yield strength increases. Because τ is a maximum at the base of the flow,

$$\tau_y = \rho g h_y \sin\theta \qquad (2)$$

where τ_y is the yield strength of the flow and h_y is the slab thickness or rest thickness of the flow.

Yield strength can be estimated from flow lobes at rest because the viscosity is no longer important and the flow may therefore be treated as a plastic. According to Orowan (1949), the yield strength of a plastic body can be obtained from the relation:

$$\tau_y = \rho g h_y^2 / W \qquad (3)$$

where W is the width of the lobe.

Yield strength may also be estimated from the dimensions of the plug of a Bingham fluid flowing in a channel. For a flow driven by gravity in a semi-elliptical channel, Johnson (1970) obtains the relations:

$$\tau_y = \rho g a_y \sin\theta / [(A/B)^2 + 1] \qquad (4)$$

and

$$\tau_y = \rho g b_y \sin\theta / [(B/A)^2 + 1] \qquad (5)$$

where a_y is the half-width of the plug, b_y is the thickness of the plug, A is the half-width of the channel or flow, and B is the depth of flow in the channel center.

VISCOSITY

Viscosity of the Mauna Loa lava can be calculated because the velocity of the flowing lava at the centers of channels (V_o) and the channel width were measured and good estimates of flow depth were obtained during the eruption (Lipman and Banks, chapter 57). Viscosity (η) is calculated using an equation for laminar flow in semi-elliptical channels (after Johnson, 1970):

$$\eta = (\rho g \sin\theta / V_o)\{B^2/2[(B/A)^2+1] + [(B/A)^2+1][\tau_y/\rho g \sin\theta]^2/2 - \tau_y B/\rho g \sin\theta\} \quad (6)$$

where B is the depth of flow in the channel center and A is the half-width of channel or flow.

The application of equation 6 needs some discussion; profiles of channels obtained after the eruption indicate that most of them were more or less rectangular (Lipman and Banks, chapter 57, fig. 57.18, table 57.2), whereas equation 6 assumes that the channels are semi-ellipses; the semi-ellipses are inscribed in the rectangular channels and defined by the depth of flow and the half-width of the channel or flow. Additionally, the lava is treated as both a Newtonian and a Bingham fluid in later calculations. When B/A is zero, equation 6 yields the correct expression for laminar flow of a Bingham fluid in an infinitely wide channel or as a wide, unconfined flow. When both B/A and the yield strength (τ_y) are equal to zero, equation 6 yields the correct expression for laminar flow of a Newtonian fluid in an infinitely wide channel or as a wide, unconfined flow. Similarly, when B/A is one, equation 6 yields the correct expression for laminar flow of a Bingham fluid in a semicircular channel. When B/A is one and the yield strength is zero (τ_y), equation 6 yields the correct expression for laminar flow of a Newtonian fluid in a semicircular channel. Intuitively, it seems probable that apparent viscosity calculated for rectangular channels would be reasonably close to that calculated with equation 6. Viscosity of a Newtonian fluid assuming an infinitely wide channel with a depth of B is twice as large as that assuming a semicircular channel with a radius of B because B/A ranges from zero to one; these two conditions should bracket the rectangular channels in most cases (see, for example, Lipman and Banks, chapter 57). For a Bingham fluid, the yield strength results in dead zones (no motion) at the bottom corners of rectangular channels (Johnson, 1970); semi-elliptical channels may therefore be reasonable approximations. Finally, Johnson (1970, p. 505) states that equation 6 may be applied to flows in rectangular and triangular channels with sufficient accuracy for most purposes. Thus, the preliminary viscosities calculated below are believed to be reasonable estimates; but subsequent studies should employ theories for flow in rectangular channels.

AVERAGE VELOCITY

Average velocity is lower than plug or slab velocity to a varied degree that depends on the yield strength, viscosity, stress, and channel or flow geometry. For flow of a uniformly thick Bingham fluid in very wide channels or as wide flows, the average velocity is given by

$$\overline{V} = (H^2 \rho g \sin\theta/3\eta)[1-(3/2)(\tau_y/\tau_b)+(1/2)(\tau_y/\tau_b)^3]. \quad (7)$$

For a Newtonian fluid ($\tau_y = 0$), equations 6 and 7 show that the average velocity is two-thirds the velocity at the surface. For flow of a Bingham fluid in semicircular channels, the average velocity is given by

$$\overline{V} = (R^2 \rho g \sin\theta/8\eta)[1-(4/3)(\tau_y/\tau_b)+(1/3)(\tau_y/\tau_b)^4]. \quad (8)$$

For a Newtonian fluid ($\tau_y = 0$), equations 6 and 8 show that the average velocity is one-half the velocity at the channel center.

An explicit equation for average velocity in an elliptical channel is not available to the author at this time. For this reason, estimates were made of the lower and upper bounds for the average velocity. The lower and upper bound estimates use the fact that the average velocity of flow between the plug and margin of a circular channel is between one-half and two-thirds of the velocity of the plug; the average velocity of flow between the slab and base of a wide, unconfined flow is two-thirds the velocity of the slab.

MASS AND VOLUME FLOW RATES

Volume flow rate is the product of the average velocity and the flow cross-sectional area. Mass flow rate is the product of flow density and volume flow rate. Here, the assumption of semi-elliptical channels may affect the results somewhat because the area of the semi-ellipse inscribed in a rectangular channel is 0.79 times the area of the rectangle. Thus, the volume and mass flow rates for a Newtonian fluid flowing through a semi-elliptical area is 0.39–0.52 times the volume and mass flow rates calculated by multiplying the center velocity and a rectangular area. These factors are less for a Bingham fluid in a variable way that depends on the size of the plug.

CRITERIA FOR LAMINAR FLOW

The use of the equations above assume laminar flow; the modified Reynolds number ($\mathbf{R}_m$) must therefore be sufficiently low. For wide flows (Moore and Schaber, 1975),

$$\mathbf{R}_m = 2/[(\eta/\rho \overline{V} H) + (\tau_y/2\rho \overline{V}^2)] \quad (9)$$

where H is the thickness of the flow; and for flows in semicircular channels (Smith, 1960),

$$\mathbf{R}_m = 2/[\eta/\rho \overline{V} R) + (\tau_y/4\rho \overline{V}^2)] \quad (10)$$

where R is the radius of the channel. Similar expressions for elliptical channels are not available at this time, but the above equations should give reasonable estimates of whether a flow is either laminar or turbulent.

RESULTS

DATA USED

In the calculations of apparent viscosity, I have used in all cases the flow velocities, channel widths, and flow depths reported by

TABLE 58.1.—*Densities used to calculate apparent viscosity, Bingham viscosity, yield strength, volume flow rate, and mass flow rate*

[Slope angles listed were used in calculations of apparent viscosity. See Lipman and Banks (chapter 57) for dates, times, sample numbers, sample densities, and sample descriptions]

Station	Elevation (m)	Elevation (ft)	Density (kg/m^3)	Slope angle (degrees)	Date (mo/d/yr)	Time (H.s.t.)	Sample	Density (kg/m^3)	Sample Description
1	1620	5300	2400	3.3	3/25/84	1540	NER-1F	2230	Core of aa flow.
					3/29/84	1300	------	2600	Core of aa flow.
2	1710	5600	2200	4.0					
3	1800	5900	2000	2.5					
3	1800	5900	1700	2.5					
4	1920	6300	1700	2.5					
4	1935	6350	1700	3.5	4/06/84	1430	NER-12/48	1720	Overflow from main channel.
4	1920	6300	1700	3.0					
5	1950	6400	1700	2.5					
6	2100	6900	1700	4.0					
7	2290	7500	1300	4.5	4/08/84	1306	NER-12/57	1250	Overflow from main channel.
8	2500	8200	1000	6.0	4/06/84	1220	NER-12/47	1150	From main channel.
8	2500	8200	1000	5.0	4/08/84	1026	NER-12/53	990	From main channel.
11	2850	9350	530	6.5	4/08/84	1145	NER-12/54	530	Overflow from main channel.
12	2870	9400	530	3.0					
12	2870	9400	530	4.5					

Lipman and Banks (chapter 57). Values for one case (station 11, vent, April 8, 1600 H.s.t.) appear to yield a spurious result, which is graphically reported but omitted from the discussion below. Slope angles also come from the same source, with the exceptions of station 1, which was 3.3° instead of 3°, and station 6 (April 7), for which the author obtained 4°. No slope angles are reported for stations 9 and 10. Flow densities employed are listed in table 58.1 and were selected by the author from values reported by Lipman and Banks (chapter 57). The acceleration of gravity is taken as 9.8 m/s^2. According to unpublished Hawaiian Volcano Observatory staff reports, flow 1A advanced at a rate of 7.2×10^{-3} m/s on April 2 and 3.4×10^{-3} m/s on April 3; given a thickness of 9 m, equation 7 yields apparent viscosities near 5.6×10^{6} Pa·s (April 2) and 12×10^{6} Pa·s (April 3). Calculated apparent viscosities are reported graphically (fig. 58.14) and described below.

APPARENT VISCOSITY

There are two general trends in the magnitude of the apparent viscosity (fig. 58.14). First, apparent viscosity increases dramatically along the length of the flow on a given day. On April 2, for example, apparent viscosities were: (1) 1.4×10^{2} Pa·s at the vent (station 11); (2) 1.0×10^{3}–1.3×10^{3} Pa·s 3 km from the vent at station 8; (3) 3.0×10^{3}–9.5×10^{3} Pa·s 9 km from the vent at station 4; (4) 0.9×10^{5}–1.6×10^{5} Pa·s 15 km from the vent at station 1; and (5) 5.6×10^{6} Pa·s 26 km from the vent at the toe of flow 1A. Second, apparent viscosity at some stations increases with time. In the vent area, for example, apparent viscosities were 1.4×10^{2}–1.6×10^{2} Pa·s (station 11) and more or less constant from April 2 through April 6, but they increased to 2.7×10^{2}–4.5×10^{2} Pa·s (stations 11 and 12) on April 8 and 9 (excluding one value for April 8 that is assumed to be spurious); they climbed to 0.9×10^{3} and 1.4×10^{3} Pa·s (station 12) on April 12 and 13, respectively. At the 1,620-m (5,300-ft) level (station 1) apparent viscosity increased from about 1.6×10^{4} Pa·s on March 31 to 0.5×10^{5}–1.5×10^{5} Pa·s on April 2, 3, and 4. At some stations, such as station 4, the behavior of the apparent viscosity is mystifying. At 1,920 m (6,300 ft), it was 3×10^{3}–6×10^{3} Pa·s on March 29 and by April 2 had increased to 9.5×10^{3} Pa·s. Upstream, at 1,935 m (6,350 ft), the apparent viscosity on April 2 was 3×10^{3} Pa·s, fully one-third of that downstream. The magnitudes of the calculated apparent viscosity will be compared with experimental data on basalt, and factors that may account for them will be discussed later.

BINGHAM LAVA

Three idealized stations and flow conditions are used below to examine the effects of a Bingham fluid on the lava rheology and consider volume and mass flow rates on a given day. These idealized conditions correspond to conditions on April 3 at (1) station 8, (2) station 4, and (3) station 1. The idealized channel and flow conditions (tables 58.2, 58.3, and 58.5) are slightly changed from those used in the calculations of apparent viscosities and listed in Lipman and Banks (chapter 57); the latter are given in tables 58.2, 58.3, and 58.5 as observations and estimates. Some of the calculations test a proposed equation relating viscosity and yield strength

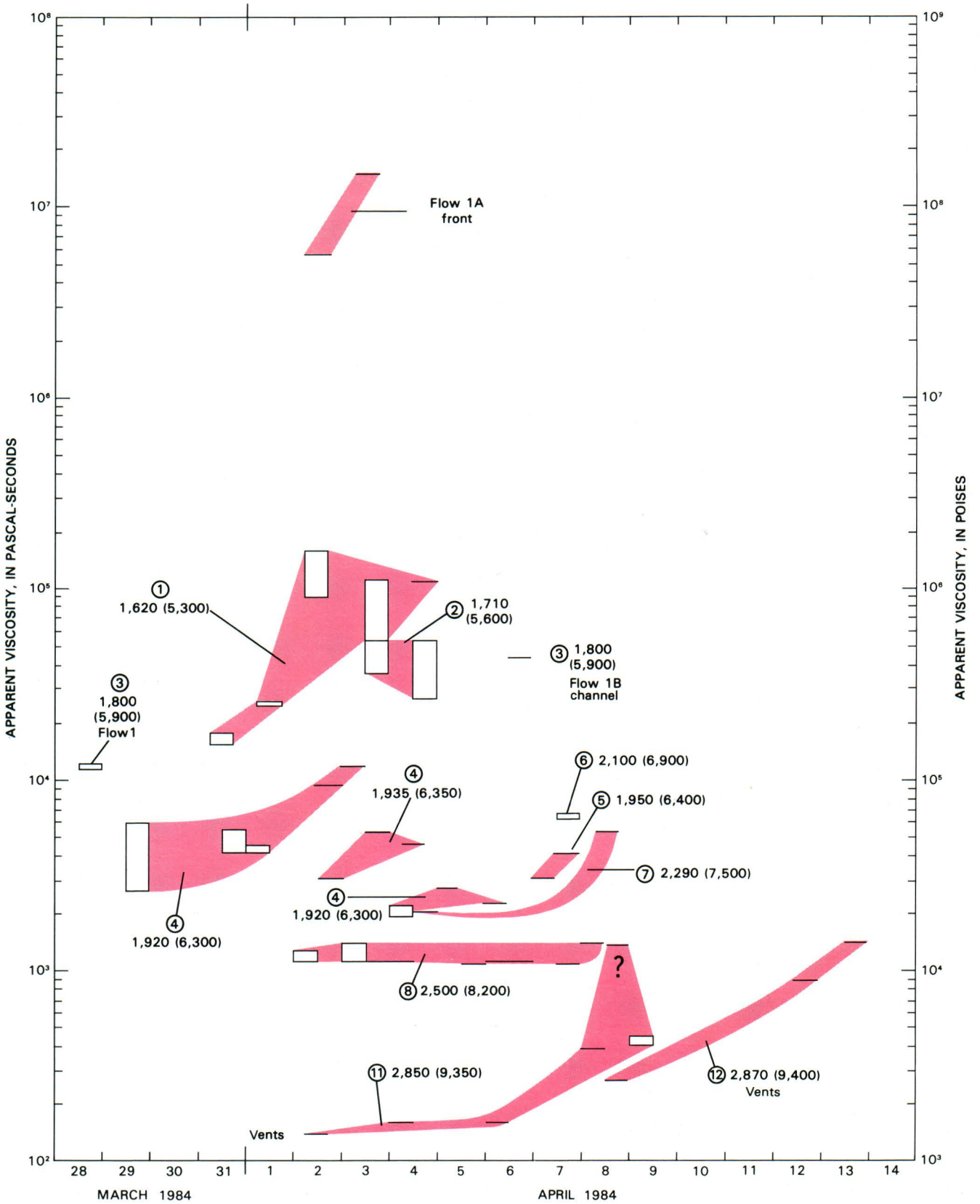

FIGURE 58.14.—Apparent viscosity of Mauna Loa lava at various stations from March 28 through April 13. Graphs of data connected by shaded areas indicate the same station or locality on different days. Station numbers circled from Lipman and Banks (chapter 57, table 57.3). Figures give elevation in meters (elevation in feet in parentheses). One determination for April 8 (queried) is probably spurious. Note that (1) apparent viscosity increases greatly from higher to lower elevations or with distance from vent on any given day from March 31 through April 8 and (2) apparent viscosity increases with time at the vents and at many of the stations downstream of the vents.

TABLE 58.2.—*Observations and calculations for idealized station 8 on April 3*

[Station is at 1852 vent, 2,500 m (8,200 ft) elevation]

Speed at center, $\underline{V}$ (m/s)	Flow depth, $\underline{B}$ (m)	Channel width, $2\underline{A}$ (m)	Volume flow rate, $\underline{Q}$ (10^6 m^3/h)	Mass flow rate, $\underline{M}$ (10^9 kg/h)	Yield strength, τ_y (Pa)	Viscosity, η Pa·s	Assumed density, ρ (kg/m^3)	Slope angle, θ (degrees)
			Observations and estimates					
5.3	4	20	1.5	1.5	--	--	1000	5.0
			Calculations					
5.3	4	20	0.6-0.8	0.6-0.8	[1]0	1244	1000	5.6
5.3	4	20	0.6-0.8	0.6-0.8	[2]66	1195	1000	5.6
5.3	4	20	0.6-0.8	0.6-0.8	[3]221	1083	1000	5.6
5.3	4	20	0.6-0.8	0.6-0.8	[4]150	1134	1000	5.6

[1]Yield strength set to zero in equation 6; viscosity is apparent viscosity.
[2]Yield strength calculated from half-width of plug (0.5 m) (eq. 4); viscosity from equation 6.
[3]Yield strength calculated from rest widths and heights of flow lobes at channel edge (eq. 3); viscosity from equation 6.
[4]Yield strength adjusted until velocity of plug was satisfied with a viscosity from equation of Moore (1982), calculated plug width is 2.3 m.

TABLE 58.3.—*Observations and calculations for sections at idealized station 4 on April 3*

[Station is at 1,920–1,935 m (6,300-6,350 ft) elevation]

Speed at center, $\underline{V}$ (m/s)	Flow depth, $\underline{B}$ (m)	Channel width, $2\underline{A}$ (m)	Volume flow rate, $\underline{Q}$ (10^6 m^3/h)	Mass flow rate, $\underline{M}$ (10^9 kg/h)	Yield strength, τ_y (Pa)	Viscosity, η Pa·s	Assumed density, ρ (kg/m^3)	Slope angle, θ (degrees)
			Observations and estimates					
0.94	7	18.3	0.43	0.74	--	--	1700	2.5
1.6	5	14	0.40	0.69	--	--	1700	3.5
			Calculations, lower section					
1.0	6	18	0.15-0.20	0.26-0.34	[1]0	7245	1700	2.0
1.0	6	18	0.17-0.22	0.29-0.37	[2]684	3723	1700	2.0
1.0	6	18	0.21-0.24	0.35-0.41	[3]1185	1880	1700	2.0
1.0	6	18	0.18-0.22	0.31-0.38	[3] 891	2885	1700	2.0
			Calculations, upper section					
1.6	5	14	0.16-0.21	0.27-0.36	[1]0	5637	1700	3.75
1.6	5	14	0.17-0.22	0.28-0.37	[2]684	3702	1700	3.75
1.6	5	14	0.18-0.23	0.31-0.39	[2]1185	2542	1700	3.75
1.6	5	14	0.17-0.22	0.30-0.38	[3] 970	3014	1700	3.75

[1]Yield strength set to zero in equation 6; viscosity is apparent viscosity.
[2]Yield strength calculated from dimensions of flow lobes (eqs. 2, 3); viscosity from equation 6.
[3]Yield strength adjusted until velocity of plug was satisfied with viscosity from equation of Moore (1982); dimensions required for plug are 2.2 m by 10.0 m and 2.6 by 5.2 m.

TABLE 58.4.—*Dimensions, slopes, and yield strength of overflow lobes at station 5*

[Overflows probably occurred late on April 6]

Lobe	Width, W (m)	Thickness, t		Slope angle, θ (degrees)	Yield Strength, τ_y	
		Range (m)	Average (m)		from equation 2 (Pa)	from equation 3 (Pa)
1	3	0.45–0.60	0.53	5.5	846	1531
2	4	0.60–0.75	0.68	1–2.5 (1.75)	346	1898
3	3	0.45	0.45	6	784	1125
4	4	0.60–0.75	0.68	4	790	1926
5	4	0.30–0.45	0.38	6	662	601
6	4.5	0.30–0.45	0.38	3	331	535
7	3	0.35	0.35	10	1013	680
8	--	0.60	0.60	4	698	--
					Average $\overline{684}$	Average $\overline{1185}$

(Moore, 1982); others deal with a wide, unconfined flow and a channel flow at the vent, although the channel flow is not treated as Bingham fluid. The results are plotted in figure 58.15, from which it can be seen that Bingham viscosity and yield strength exhibit striking increases along the length of the flow; yield strength increases about 10–34 times from station 8 to station 1, and Bingham viscosity increases about 70–80 times.

STATION 8

The parameters used for this station (table 58.2) are identical to those used for the calculation of apparent viscosity except for a slope of 5.6° instead of 5° or 6°.

Yield strength for the lava at this location is on the order of 10^2 Pa (table 58.2). Two methods were used in preparing the estimates. In the first method, the half-width of the plug observed by the author (0.5 m), inserted in equation 4, gives a result of 66 Pa. In the second, the height (0.15 m) and width (1.0 m) of the lobes at the channel edge (fig. 58.7), inserted in equation 3 give a result of 221 Pa; if the lobe width is taken as 2.0 m instead of 1.0 m, the yield strength becomes 110 Pa. The larger yield strength requires a plug 3.4 m across instead of the observed 1.0 m.

Bingham viscosity does not differ significantly from the apparent viscosity of 1.2×10^3 Pa·s. For the largest yield strength the viscosity is about 1.1×10^3 Pa·s. Finally, the observed 5.3 m/s velocity of the plug can be obtained when the yield strength and viscosity, derived from the proposed equation of Moore (1982), are 150 Pa and 1.1×10^3 Pa·s, respectively; the calculated plug width is 2.3 m.

It should be noted that the calculated modified Reynolds numbers, which are in all cases 29 or less, are in agreement with the observed laminar character of the flow. The results are plotted in figure 58.15.

STATION 4

The actual channel and flow conditions at this station were rather complicated, some sections having high, rubbly levees and others low to nonexistent overflow levees. For the idealization of this station, three noteworthy changes in particular were made from those used to calculate apparent viscosity: (1) the slope for the lower section with high, rubbly levees was changed from 2.5° to 2.0°; (2) the flow depth of the lower section was changed from 7 m to 6 m; and (3) the slope of the upper section with low to nonexistent levees was changed from 3.5° to 3.75° (table 58.3). These changes were made in order to satisfy the requirement of conservation of mass and still have the same Bingham fluid properties in two adjacent sections.

Yield strength for this station is probably near 10^3 Pa. Average values for yield strength calculated with equations 2 and 3 and dimensions of lobes at the margin of an overflow sheet are 684 and 1,185 Pa, respectively (table 58.4). There is some uncertainty in correlation because the overflow producing the sheet probably occurred on April 6, not April 3.

Apparent viscosities required to account for the 1.0 m/s and 1.6 m/s velocities in the idealized lower and upper sections are 7.6×10^3 Pa·s and 5.6×10^3 Pa·s, respectively; the mass flow

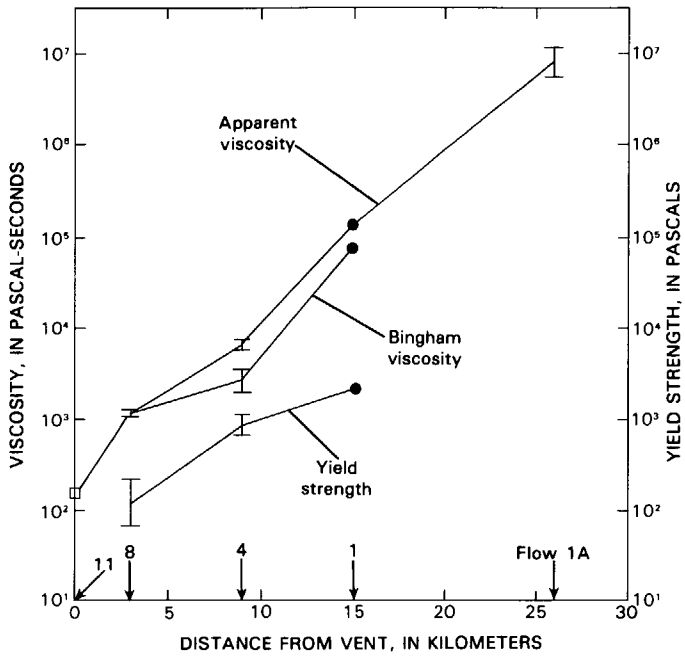

FIGURE 58.15.—Apparent viscosity, Bingham viscosity, and yield strength as a function of distance from vents on April 3. Numbers and arrows on abscissa indicate stations and their distances from vents. Note that Bingham viscosity shows increase in magnitude comparable to that of apparent viscosity. Value for station 11 (open square) is from text; values for station 1(dots) are from table 58.5; vertical lines for stations 8 and 4 show range of values from tables 58.2 and 58.3; vertical line for flow 1A shows range of values from text.

rates are substantially the same (table 58.3). A Bingham fluid with a yield strength near 680 Pa and a viscosity near 3.7×10^3 Pa·s would conserve mass and provide the same rheology for the lava at the two adjacent sections. Calculations using the larger yield strength of 1,185 Pa do not yield the same viscosity, but the two values are close. Finally, values of yield strength and viscosity from Moore's (1982) equation that satisfy the velocity in equation 6 are reasonably close both to one another and to the values derived from equations 2 and 3.

It should be noted that modified Reynolds numbers, which are less than 11 in all cases, are in agreement with the observed laminar character of the flow. Results are plotted in figure 58.15.

STATION 1

A simple Bingham fluid cannot account for the flow at this station because it does not explain the occurrence of a number of discrete, intact flow units between the center plug and the channel margin, the velocity gradient of the flow units across the channel increases with ebbing and with lower center velocity, and the Bingham model has nothing to say about nonsteady flow. In one set of calculations that employ a constant channel width, the width of the plug becomes greater than the width of the channel with thinning of the flow. Such a condition would seem to require faulting or shearing of the plug, which could result in a number of discrete, intact flow units and variable yield conditions. In any event, however, the Bingham model will be applied with the intention of illustrating the problem.

Channel dimensions and flow velocities employed below are different from those used for the calculation of apparent viscosity (table 58.5). The channel width and depth are taken as 57 m and 8 m, respectively, on the basis of the profile measured after the eruption. For the nominal conditions, a velocity of 0.3 m/s is paired with a flow depth of 8 m and a plug width of 45 m; these values are consistent with the author's impressions of the flow on April 3. The slope is taken as 3.3°. Subsequent calculations predict the velocity at the center of flow with varying flow depths using (A) a model with a fixed channel width (57 m) but varying flow depth, and (B) a model that assumes effective channel width varies directly with flow depth.

A yield strength of 2,225 Pa is used in the calculations (table 58.5). This value was obtained using equation 4 and the nominal conditions mentioned above; it is reasonably close to the 2,700 Pa obtained using a rest thickness of 2 m estimated from the lava on the channel floor in the postflow profile.

An apparent viscosity of 1.34×10^5 Pa·s is obtained for the nominal conditions of flow mentioned above (table 58.5); this is only 21 percent higher than the largest apparent viscosity obtained previously for April 3 (fig. 58.14). Incorporation of a yield strength of 2,225 Pa in equation 6 gives a Bingham viscosity of near 81×10^3 Pa·s (fig. 58.15). This viscosity is 17 times larger than the one predicted by Moore's (1982) equation. Modified Reynolds numbers for all flow calculations, which are discussed below, are less than 1 and consistent with laminar flow.

Calculations for model A (table 58.5) predict some of the salient aspects of the surging and ebbing flow and plug widths that become larger than the channel width with ebbing flow. At the nominal flow condition, the central 45 m of the flow moves as a plug with a velocity of 0.3 m/s. During a surge, the flow thickens to 9 m and the central 36 m of the flow moves as a plug with a velocity of 0.39 m/s. When the flow ebbs, the flow thins to 7 m and the central part of the flow moves as a plug with a velocity of 0.22 m/s. Here, the plug is about the same width as the channel so that some sort of interference of flow and disruption of the plug might be expected. With further thinning to 6 m, the predicted speed of the flow is 0.15 m/s, and the plug will no longer fit in the channel.

In model B, reasonable plug velocities are obtained by varying the yield strength during surging and redefining the channel dimensions during ebbs. For example, if the yield strength increases to 3,200 Pa because of increased friction by loading during a 9.3-m-thick surge, the velocity of the 49-m-wide plug is 0.34 m/s. If the channel is redefined to be 7 m deep and 42 m wide and the yield strength returns to 2,225 Pa, the velocity of the 33-m plug in the fluid-filled channel is 0.2 m/s. Narrower, shallower filled channels have smaller plug velocities, and the plugs do not reach the channel margins.

WIDE, UNCONFINED FLOWS

There is no information from which to estimate the yield strength and Bingham viscosity for the Lower Powerline Road flow

TABLE 58.5.— *Observations and calculations using two models for idealized station 1 on April 3*

[Station is in lower channel of flow 1A at 1,620 m (5,200 ft) elevation. For explanation of models see text]

Speed at center, V (m/s)	Flow depth, B (m)	Channel width, 2A (m)	Volume flow rate, Q (10^6 m^3/h)	Mass flow rate, M (10^9 kg/h)	Yield strength, τ_y (Pa)	Viscosity, η Pa·s	Assumed density, ρ (kg/m^3)	Slope angle, θ (degrees)	Dimensions of plug, b, 2a (m) (m)
				Observations and estimates					
0.38	6	52	0.43	1.0	--	--	2400	3.0	--
0.3	6	52	0.34	0.82	--	--	2400	3.0	--
0.2	6	52	0.23	0.54	--	--	2400	3.0	--
				Calculation of apparent viscosity					
0.3	8	57	0.19-0.26	0.46-0.62	[1]0	133,800	2400	3.3	0.0, 0.0
				Calculations using model A					
0.3	8	57	0.23-0.28	0.54-0.67	[2]2225	81,110	2400	3.3	1.8, 45.0
0.39	9	57	0.32-0.40	0.77-0.97	2225	81,110	2400	3.3	1.8, 36.2
0.22	7	57	0.15-0.18	0.34-0.44	2225	81,110	2400	3.3	1.7, 57.8
0.15	6	57	0.09-0.11	0.23-0.28	2225	81,110	2400	3.3	1.7, 77.4
				Calculations using model B					
0.34	9.3	57	0.31-0.38	0.75-0.91	[3]3200	81,110	2400	3.3	2.6, 49.1
0.3	8	57	0.23-0.28	0.55-0.67	[2]2225	81,110	2400	3.3	1.8, 45.0
0.2	7	42	0.10-0.12	0.24-0.30	2225	81,110	2400	3.3	1.8, 32.9
0.13	6	35	0.05-0.06	0.12-0.14	2225	81,110	2400	3.3	1.8, 31.2
0.001	4	10	---	0.02	2225	81,110	2400	3.3	2.7, 8.4

[1]Yield strength set to zero in equation 6; viscosity is apparent viscosity.
[2]Yield strength calculated from half-width of plug (taken as 45 m) (eq. 4); viscosity from equation 6.
[3]Yield strength assumed to increase with load during surge; viscosity same as in (2) above.

on April 5. If the flow, 3 m thick, had the same properties as those at station 1 ($\tau_y = 2{,}225$ Pa, $\eta = 81 \times 10^3$ Pa·s), it would advance at a rate near 0.02 m/s and its rest thickness would be 1.5 m.

STATION 11

In order to consider volume and mass flow rates along the length of the flow on April 3, average values for April 2 and 4 must be used. On April 2, the lava was flowing in a channel 21.5 m wide with a flow depth of 3 m at 17.8 m/s; on April 4, the lava was flowing in a channel 21 m wide with a flow depth of 3 m at 15 m/s (Lipman and Banks, chapter 57). Volume flow rates from the average of these conditions are 3.8×10^6 m^3/h for a rectangular flow at uniform velocity and 1.5×10^6–2.0×10^6 m^3/h for laminar flow in a semi-elliptical channel. Mass flow rates are 2.0×10^9 kg/h for a rectangular flow and 0.8×10^9–1.1×10^9 kg/h for flow in a semi-elliptical channel. Apparent viscosities on the two days were near 0.15×10^3 Pa·s, and modified Reynolds numbers were less than 300 and indicate laminar flow.

VOLUME AND MASS FLOW RATES

This section presents calculated volume and mass flow rates for April 3 along the length of the flow (fig. 58.16) from the vent to the toe. In these calculations, I have used the parameters for the idealized stations (tables 58.2, 58.3, and 58.5), the estimates for the vent given in the previous section, and approximate calculations for the toe. Because of the surging, ebbing flow at station 1, average volume and mass flow rates are difficult to estimate; for purposes of illustration, volume and mass flow rates are taken as those corresponding to velocities of 0.2 and 0.22 m/s in table 58.5. A small overflow upstream of station 1 on the morning of April 3 does not apparently affect the results because the magnitude of changes is much the same as on April 2.

Volume flow rates appear to decrease by about one order of magnitude from the vent to station 1, beyond which estimates are so uncertain that a decrease may or may not be present (fig. 58.16*A*). The volume flow rates calculated for a rectangular flow with uniform velocity are 3.8×10^6 m^3/h at the vent, 1.5×10^6 m^3/h at station 8,

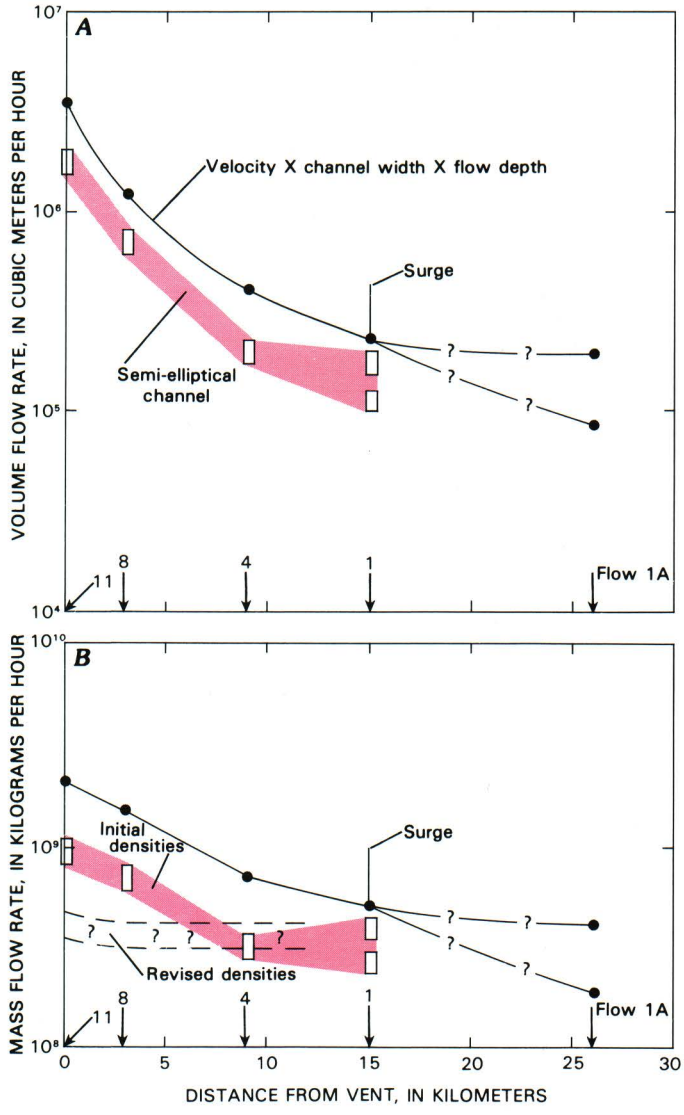

FIGURE 58.16.—Volume and mass flow rates of Mauna Loa lava on April 3, 1984. Numbers and arrows on abscissae indicate stations and their distances from the vents. Rates indicated by boxes calculated assuming semi-elliptical channels; rates indicated by dots calculated assuming rectangular flow cross sections; see text and tables 58.2, 58.3, and 58.5. ***A***, Volume flow rate: note the decrease by a factor of 12 from the vent to station 1, 15 km from the vent. ***B***, Mass flow rate: note the decrease by a factor near 3 from the vents to station 4, 9 km from the vent (using densities initially assumed in calculations of apparent viscosity). Band with question marks represents approximate mass flow rate calculated using revised densities that conserve mass.

0.42×10^6 m³/h at station 4, and 0.23×10^6 m³/h at station 1. Thus, volume flow rates are about 16 times larger at the vent than they are at station 1. The volume flow rates calculated for Newtonian (at the vent) and Bingham fluids in a semi-elliptical channel are 1.5×10^6–2.0×10^6 m³/h at the vent, 0.6×10^6–0.8×10^6 m³/h at station 8, 0.17×10^6–0.22×10^6 m³/h at station 4, and 0.10×10^6–0.18×10^6 m³/h for station 1. The volume flow rate under these conditions is thus about 9 times larger at the vent than at station 4.

Mass flow rates also decrease with distance from the vent (fig. 58.16*B*). Mass flow rates at the vent are about 3 times larger than they are at station 4. For the rectangular flow with uniform velocity, mass flow rates are 2×10^9 kg/h at the vent and 0.7×10^9 kg/h at station 4; for reasons stated earlier these values are probably too large by a factor of about 2. For the semi-elliptical channel, mass flow rates are 0.8×10^9–1.1×10^9 kg/h at the vent and 0.28×10^9–0.37×10^9 kg/h at station 4; beyond station 4, no mass flow changes are required by the data. Thus there appears to be a mass flow of 0.5×10^9–0.7×10^9 kg/h that needs to be accounted for in the semi-elliptical channel calculations. This is discussed later.

DISCUSSION

APPARENT VISCOSITY

The magnitudes of the apparent viscosity calculated for the Mauna Loa lava are reasonable when compared with experimental data (Shaw, 1969). For example, graphic interpolation of instrument viscosities between 1,150 °C and 1,130–1,135 °C (Shaw, 1969, fig. 1, table 2) suggests that the viscosity of Hawaiian basalt at 1,140 °C should be near 300–400 Pa·s. This is comparable in magnitude to the viscosity calculated for lava at the vents from April 2 through the morning of April 8, which is 140–380 Pa·s. The somewhat lower values for the Mauna Loa lava may be because it was frothy; this could reduce the apparent viscosity (Shaw and others, 1968). Because maximum shear stresses decrease with time at the vents from about 1.6×10^3 Pa on April 2 through April 8 to about 500–700 Pa on April 12, the frothy lava at the vents might be expected to have apparent viscosity that increases (see, for example, Shaw and others, 1968, fig. 14). The apparent viscosity for station 8 (fig. 58.17), which is 1.1×10^3–1.4×10^3 Pa·s, is reasonably close to the instrument viscosity ($\sim10^3$ Pa·s) and to the high value of the Bingham viscosity (0.75×10^3 Pa·s) measured in Makaopuhi lava at 1,130–1,135 °C (Shaw and others, 1968). Magnitudes of the apparent viscosity at stations 4 and 5 (1,920 to 1,950-m elevation) and its erratic behavior between adjacent sites and stations on the same day (fig. 58.17) might be accounted for if the lava were frothy and cooler than 1,135 °C so that it behaved somewhat like basalt at 1,125 °C and small, but variable, shear rates. Rough estimates of maximum shear stresses and shear rates for the lava at stations 4 and 5 vary within the ranges 1.8×10^3–3.5×10^3 Pa and 1.4–0.3 s^{-1}, respectively (fig. 58.17). According to Shaw (1969), instrument apparent viscosity at 1,125 °C is variable and decreases with stress up to 16×10^3 Pa and shear rates as high as 5 s^{-1}. Judging from Shaw (1969, fig. 1, inset), apparent viscosity of basalt at 1,125 °C increases from about 10×10^3 Pa·s at a shear rate of 1 s^{-1} to about 70×10^3 Pa·s at a shear rate of 0.05 s^{-1}. Thus, if the stations 4 and 5 lava was a few degrees hotter than 1,125 °C and the bubbles affected the lava, the calculated apparent viscosities (1.9×10^3–12×10^3 Pa·s) are entirely reasonable. Local variations in bubble content, temperature, stress, and rate of shear could produce or contribute to the mystify-

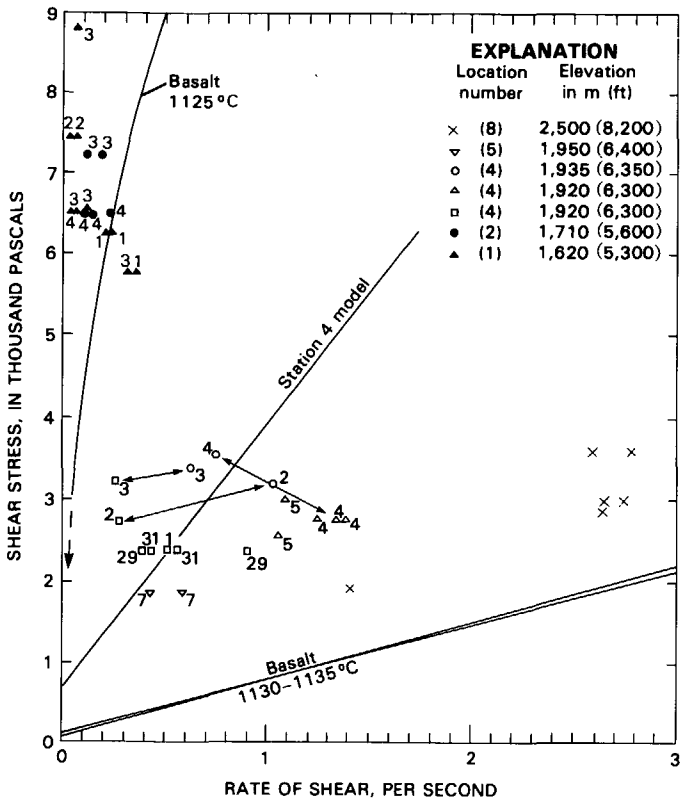

FIGURE 58.17.—Relation between approximate maximum shear stress and rate of shear for 1984 Mauna Loa lava at five stations. Lines labeled 1,130–1,135 °C correspond to data on basalt of Shaw and others (1968); curved line labeled 1,125 °C corresponds to experimental data on basalt at that temperature (Shaw, 1969). Line station 4 model is for Bingham fluid with yield strength of 680 Pa and viscosity of 3.7×10^3 Pa·s. Note that this diagram fits within inset of figure 14 of Shaw (1969) but that ordinate and abscissa are interchanged. Numbers by plotted points refer to day of month in interval March 29 to April 7; arrowed lines connect data points at different sites on the same day at station 4.

ing variations of the apparent viscosity with time and place. Increase in the volume fraction of solids in the lava, which is known to increase apparent viscosity (see, for example, Shaw, 1969; Moore and Schaber, 1975), is an added variable. For the lower reaches of the flow at stations 1 and 2, where temperatures were near 1,125 °C, maximum stress (fig. 58.17) is about 5.7×10^3–9×10^3 Pa, shear rate about 0.4–0.08 s^{-1}, and apparent viscosity 15×10^3–160×10^3 Pa·s. Here, the instrument apparent viscosity of approximately 10×10^3–70×10^3 Pa·s at 1,125 °C (see, for example, Shaw, 1969, fig. 1, inset) is in good agreement with the apparent viscosity obtained for the stations 1 and 2 lava. Apparent viscosity calculated for the toe area of flow 1A, where it must eventually reach infinity, is plausible. Walker (1967) assumes that the flow of Etna lava virtually stops when the velocity is 10^{-4} m/s and then calculates that its apparent viscosity is 10^8–10^{10} Pa·s. If flow 1A was advancing at a rate of 10^{-4} m/s and its thickness was unchanged, it would have an apparent viscosity of 0.4×10^9 Pa·s.

A BINGHAM LAVA

The principal reasons for considering that the Mauna Loa lava might behave as a Bingham fluid are the rheological studies of Makaopuhi lava lake (Shaw and others, 1968), observations of the flow in progress that indicate the centers of the flows move as plugs, and studies of other volcanic flows (for example, Cigolini and others, 1984). Both the yield strength and Bingham viscosity derived for the idealized station 8 at 2,500-m (8,200-ft) elevation are quite comparable in magnitude to those obtained for the Makaopuhi lava lake at similar temperatures (Shaw and others, 1968). For the lava lake, yield strength was 70–120 Pa, quite comparable to the 66–220 Pa obtained at station 8. Similarly, the Bingham viscosity for the lava lake, 0.65×10^3–0.75×10^3 Pa·s, is quite comparable to the 1.1×10^3–1.2×10^3 Pa·s obtained at station 8. For the idealized station 4, it was shown that a Bingham fluid with one set of properties could conserve mass in two adjacent sections of the same channel with different gradients and dimensions.

As noted previously, a simple Bingham model will not account for the flow at station 1. Some aspects of the model fit the observations. In particular, the upper parts of the flow moved as slabs or pluglike units. Because the model predicts that the width of the plug becomes larger than the channel, faulting and disruption of a Bingham plug into separate intact units could occur. In this case, the yield conditions could vary as a function of angle of internal friction, cohesion, and other factors (Johnson, 1970).

Parts of the Mauna Loa flow may have behaved as a Bingham fluid; but they were heterogeneous in comparison with paints and slurries. For example, the Bingham model predicts the observed slablike motion of the upper layer of wide flows and provides a mechanism for stopping the flow when it thins to its rest thickness. However, the upper slablike parts of the wide, unconfined flows are composed of blocks, clinkers, and cinders, whereas the underlying parts are composed of incandescent, molten lava. Elsewhere, the heterogeneous character of the flow is evident. At station 8, visual observations indicate the presence of the central plug required for a Bingham fluid, but the surface of the flow was clearly heterogeneous. The characteristics of the lava at depth are unknown. At lower elevations near stations 4 and 5, concentrations of fragments in the incandescent lava were larger, the fragments were darker, and the fragments were larger than at station 8; in contrast with station 8, incandescent lumps or plastic clots were evident and abundant. The flow at station 1 looked like a debris flow with warm to incandescent blocks, clinkers, and cinders, large globs or plastic clots, and local exposures of incandescent lava beneath the debris. Although the discrete, intact flow units show that the flow had some strength, and pluglike motion occurred, the Bingham model does not predict a number of intact flow units.

WHICH MODEL?

It is entirely possible that the Mauna Loa lava obeyed different flow laws at different places and times (see, for example, Shaw, 1969). The lava may have been a Newtonian fluid at the vents, a

Bingham fluid at station 8, and a pseudoplastic fluid or some other kind of fluid in the lower reaches. Concentrations of debris, incandescent blocks and fragments, and plastic clots were so large in the lower reaches of the flow on April 2 and 3 that models of the flow movements might require incorporation of concepts such as cohesion, angle of internal friction, and pore fluids.

The information necessary to establish the appropriate flow models may be embodied in existing time-lapse photography and motion pictures of the flow in progress. If satisfactory velocity profiles of the flowing lava can be obtained from the photography, they can be used to infer the rheological properties of the flow (Johnson, 1970). A velocity profile for an apparently well behaved flow confined in a leveed channel at Arenal (Cigolini and others, 1984) illustrates how such velocity profiles can be used. For the Arenal flow, the lava-filled channel was 30 m wide and 10 m deep. The slope was 30°. The central 18 m of the flow moved as a plug with a velocity of 6×10^{-3} m/s; velocity decreased from the plug to zero at the flow margins. Using the half-width of the plug and a density of 2,700 kg/m^3 in equation 4, the yield strength comes out to be 37×10^3 Pa, which is reasonably close to the value of 79×10^3 Pa obtained by Cigolini and others (1984) using equation 2. Equation 6 gives a Bingham viscosity of 27×10^6 Pa·s which is essentially the same as an independently measured value of 24×10^6 Pa·s for unit c of the Arenal flow at 1,075 °C (Cigolini and others, 1984).

VISCOSITY AND LAVA CHARACTERISTICS

The principal causes of the changes in viscosity and yield strength are related to changes in temperature, gas and bubble contents, concentration of solids, and plastic clots. The major changes at the vents are probably related to changes in gas and bubble contents and concentration of solids because the vent lava at 1,140 °C was frothy and had about 14–21 percent volume concentration of microphenocrysts on April 2–3; by April 13 it was still frothy and the concentration of microphenocrysts was about 27 percent (Lipman and Banks, chapter 57). A 13 percent change in microphenocryst concentration at this temperature would probably increase viscosity by a factor of 2 or so (Shaw, 1969; Moore and Schaber, 1975). Apparent viscosity of the frothy lava at the vents increased by a factor of 10 from April 2 to April 13 (fig. 58.14) with a concomitant decrease in shear stress from about 1.6×10^3 Pa to 0.5×10^3–0.7×10^3 Pa; it is possible that the apparent viscosity increased because the lava was also frothy (see, for example, Shaw and others, 1968, fig. 14). A similar increase could result if the lava was a Bingham or pseudoplastic fluid because both stress and rate of shear declined from April 2 to April 13.

In order to account for three orders of magnitude increase in apparent viscosity from the vent to station 1 on April 2, 3, or 4 (fig. 58.14) by microphenocrysts alone, the volume concentration would have to increase something like 20 percent (see, for example, Shaw, 1969) to 50 percent (see, for example, Moore and Schaber, 1975) above the initial 14–21 percent. The concentration of phenocrysts increased along the length of the flow, but values are not reported (Lipman and Banks, chapter 57). Solids other than crystals that were incorporated in the lava probably contributed to the increase in apparent viscosity by analogy with slurries (Smith, 1960) and debris flows (Johnson, 1970). The fluid contained warm, solid debris, hot incandescent blocks and fragments, and molten globs or plastic clots, all set in a matrix of hotter, more fluid lava. Both the mean size and the concentrations of these objects increased along the length of the flow in a manner correlative with the increase in magnitude of the apparent viscosity. Such a correlation implies that concentrations of all kinds of objects in the flow might affect the rheology in ways analogous to the effects of solids in slurries and debris flows.

VOLUME AND MASS FLOW RATE

The conservation of mass in a complicated system such as the Mauna Loa eruption is difficult to establish because gases evolve from the lava and enter the atmosphere, lava overflows channels or becomes ponded, and there may be other sinks. In addition, the observations and data employed may contain errors. In the mass-flow calculations (fig. 58.16*B*), the density employed is the most likely factor that could lead to errors. In order to have a constant mass flow with volume flows of 1.5×10^6–2.0×10^6 m^3/h through a semi-elliptical channel at the vent and roughly 0.13×10^6 –0.16×10^6 m^3/h through a semi-elliptical channel 15 km from the vent at station 1, the density of the lava must change by a factor near 12. If the density of the lava at station 1 is taken as 2,600 kg/m^3 (the largest value for station 1 given in Lipman and Banks, chapter 57), the density of the lava in the channel at the vent would have to be about 220 kg/m^3 instead of the 530 kg/m^3 employed in the "initial densities" mass-flow calculation (fig. 58.16*B*). Correspondingly changed densities for the other stations would be about 530 kg/m^3 (station 8) and 1,900 kg/m^3 (station 4). It is unlikely that the measured lava velocities and channel widths and the estimated flow depths could lead to a factor of 12 difference in mass flow rates between the vent and station 1 because each of these three values would have to be low by a factor of nearly 2.3 at station 1 (or high by a factor of 0.44 at the vent) or low by a factor of 1.5 at station 1 and high by a factor of 0.67 at station 11 (vent). The change in mass flow rate of 0.5×10^9–0.7×10^9 kg/h from the vent to station 4 on April 3 is much too large to be accounted for by the masses involved in overflows, ponding, and gas emissions.

The changes in density indicated above would reduce the apparent viscosities calculated earlier by factors of 0.4 for the vents (stations 11 and 12) and 0.5 for station 8; Bingham viscosity, most values of yield strength, and maximum stress (but not rate of shear) would be reduced by one-half for station 8. Changes for stations 4 and 1 would be less than 11 percent.

Changes in densities along the length of the flow also have implications for volume flow rates calculated from the areal extent and thickness of the lava after an eruption (Walker, 1973; Malin, 1980). For example, if the volume flow rate observed at the vent during the eruption is 2×10^6 m^3/h (560 m^3/s) and the density of the hot, gas-charged lava is 220 kg/m^3, the mass flow rate is 0.44×10^9

kg/h. If the gases exolve and the lava is deposited with an average density of 2,200 kg/m^3, the volume flow rate would appear to be 0.2×10^6 m^3/h (56 m^3/s), one order of magnitude smaller than the value observed at the vent. A similar conclusion is reached (Moore, 1982) when volume flow rates in channels of the 1942 Mauna Loa eruption (Macdonald, 1943; Finch and Macdonald, 1953) are compared with posteruption volume flow rates (Walker, 1973; Malin, 1980).

CONCLUSIONS

1. From April 2 to April 3, the physical appearance, behavior, and velocity of the Mauna Loa lava varied dramatically along the length of the flow. In the upper reaches, 3 km from the vents at station 8, the flow appeared to be a mass of sparse cinders and clinkers imbedded in a matrix of more fluid incandescent lava. Flow appeared to be laminar and was steady with a velocity of 5.3 m/s at the channel center. At stations 4 and 5, 9 km from the vents, the visible flow in the channel was composed of abundant dark cinders and clinkers and incandescent clots in a matrix of more fluid incandescent lava; flow was confined in channels with high levees in some places. Flow appeared to be laminar but was unsteady with small surges and ebbs. Velocity was near 1–2 m/s at the channel center. At station 1, 15 km from the vents, the flow was a hummocky mass of slowly moving debris, rubble, and blocks in a matrix of more incandescent lava confined within a rubbly leveed channel. Part of the debris and rubble and some of the blocks were incandescent but coherent. Flow appeared to be laminar but was unsteady with large surges and ebbs. Velocity varied from about 0.3 m/s during surges to about 0.1 m/s during ebbs.

2. Apparent viscosity calculated for the lava increased along the length of the flow, in parallel with physical appearance. On April 2, apparent viscosity increased from about 100 Pa·s at the vents to about 0.1×10^6 Pa·s, 15 km from the vents. Apparent viscosity also increased with time at the vents from about 100 Pa·s on April 2 to 10^3 Pa·s on April 12 and 13. Similar increases occurred elsewhere in the lower reaches of the flow. Like the apparent viscosity, viscosity and yield strength calculated for a Bingham fluid on April 3 increased dramatically from 10^3 Pa·s and 0.1×10^3 Pa at station 8, 3 km from the vents, to 80×10^3 Pa·s and 2×10^3 Pa at station 1, 15 km from the vents. These values compare well with laboratory data on viscosity of basalt with similar temperature, stress, and shear rate. The increase in viscosity is probably related to the increase in concentration of solids and plastic clots, reduction in gas and bubble contents, decrease of temperature, and decreases in stress and shear rate.

3. The rheology of the lava probably varied along the length of the flow. It may have been a Newtonian fluid near the vents, a Bingham fluid 3 km from the vents, and a pseudoplastic fluid at larger distances from the vents. Other kinds of fluids not considered here may also apply. Existing time-lapse photography and motion pictures of the flow in progress should be reviewed and studied because they may contain information about the appropriate flow rheology.

4. Volume flow rates obtained by multiplying the maximum velocity at the channel center, the channel width, and the depth of flow are probably too large by a factor of nearly 2 because the average velocity of a flow is less than the velocity at the channel center. Mass flow rates would be affected in a similar manner. On April 3, volume flow rates at the vent were near 1.5×10^6–2.0×10^6 m^3/h. Volume flow rates decreased with distance from the vents. Most of this decrease is due to increases in the density of the lava with distance from the vents. In order to approximate the conservation of mass along the length of the flow on April 3, the density of the lava flowing from the vent would have to be near 220 kg/m^3, which implies a mass flow rate of 0.33×10^9–0.44×10^9 kg/h. Lava deposited at these rates with an average density of 2,200 kg/m^3 would appear to have a volume flow rate of 0.15×10^6–0.20×10^6 m^3/h.

REFERENCES CITED

Bingham, E.C., 1922, Fluidity and Plasticity, New York, McGraw-Hill, 440 p.

Borgia, Andrea, Linneman, Scott, Spencer, Daniel, Morales, L.D., and Andre, J.B., 1983, Dynamics of lava flow fronts, Arenal Volcano, Costa Rica: Journal of Volcanology and Geothermal Research, v. 19, p. 303-329.

Caldwell, D.H., and Babbitt, H.E., 1941, Flow of muds, sludges, and suspensions in circular pipe: Industrial and Engineering Chemistry, v. 33, no. 2, p. 249-256.

Cigolini, Corrado, Borgia, Andrea, and Casertano, Lorenzo, 1984, Intra-crater activity, aa-block lava, viscosity, and flow dynamics: Arenal Volcano, Costa Rica: Journal of Volcanology and Geothermal Research, v. 20, p. 155-176.

Finch, R.H., and Macdonald, G.A., 1953, Hawaiian volcanoes during 1950: U.S. Geological Survey Bulletin 996–B, 89 p.

Fink, J.H., Malin, M.C., D'Alli, R.E., and Greeley, Ronald, 1981, Rheological properties of mudflows associated with the spring 1980 eruptions of Mount St. Helens volcano, Washington: Geophysical Research Letters, v. 8, no. 1, p. 43-46.

Hulme, Geoffrey, 1974, The interpretation of lava flow morphology: Geophysical Journal of the Royal Astronomical Society, v. 39, p. 361-383.

Johnson, A.M., 1970, Physical Processes in Geology: San Francisco, Freeman, Cooper and Co., 577 p.

Kilburn, C.R.J., 1981, Pahoehoe and aa lavas: discussion and continuation of the model of Peterson and Tilling: Journal of Volcanology and Geothermal Research, v. 11, p. 373-382.

Krauskopf, K.B., 1948, Lava movement at Paricutin Volcano, Mexico: Geological Society of America Bulletin, v. 59, p. 1267-1284.

Lockwood, J.P., Banks, N.G., English, T.T., Greenland, L.P., Jackson, D.B., Johnson, D.J., Koyanagi, R.Y., McGee, K.A., Okamura, A.T., and Rhodes, J.M., 1985, The 1984 eruption of Mauna Loa Volcano, Hawaii: Eos, Transactions, American Geophysical Union, v. 66. no. 16, p. 169-171.

Lockwood, J.P., Decker, R.W., Jackson, D.B., Koyanagi, R.Y., Okamura, A.T., and Johnson, D.J., 1984a, The 1984 eruption of Mauna Loa, Hawaii: Eos, Transactions, American Geophysical Union, v. 65, no. 45, p. 1137.

Lockwood, J.P., Rhodes, J.M., Garcia, Michael, Casadevall, Tom, Krueger, Arlin, and Matson, Michael, 1984b, Mauna Loa Volcano, Hawaii: Eos, Transactions, American Geophysical Union, v. 65, no. 18, p. 339.

Macdonald, G.A., 1943, The 1942 eruption of Mauna Loa, Hawaii: American Journal of Science, v. 241, p. 241-256.

———1953, Pahoehoe, aa, and block lava: American Journal of Science, v. 251, p. 169-191.

Malin, M.C., 1980, Lengths of Hawaiian lava flows: Geology, v. 8, p. 306-308.

Moore, H.J., 1982, A geological evaluation of proposed lava diversion barriers for the NOAA Mauna Loa Observatory, Mauna Loa Volcano, Hawaii, and

some recommendations: U.S. Geological Survey Open-File Report 82–314, 17 p.

Moore, H.J., and Schaber, G.G., 1975, An estimate of the yield strength of the Imbrium flows: Proceedings of the Lunar Science Conference, 6th, Houston, TX, March 17–21, 1975, p. 101-118.

Orowan, E., 1949, Remark from joint meeting of British Glaciological Society, British Rheologists' Club, and Institute of Metals: Journal of Glaciology, v. 1, no. 5, p. 231-240.

Peterson, D.W., and Tilling, R.I., 1980, Transition of basaltic lava from pahoehoe to aa, Kilauea Volcano, Hawaii: field observations and key factors: Journal of Volcanology and Geothermal Research, v. 7, p. 271- 293.

Shaw, H.R., 1969, Rheology of basalt in the melting range: Journal of Petrology, v. 3, no. 3, p. 510-535.

———1972, Viscosities of magmatic silicate liquids: an empirical method of prediction: American Journal of Science, v. 272, p. 870-893.

Shaw, H.R., Wright, T.L., Peck, D.L., and Okamura, R., 1968, The viscosity of basaltic magma: an analysis of field measurements in Makaopuhi lava lake, Hawaii: American Journal of Science, v. 266, p. 225-264.

Smith, R.W., 1960, Flow of limestone and clay slurries in pipelines: Transactions, American Institute of Mining, Metallurgical, and Petroleum Engineers, v. 217, p. 258-265.

Sparks, R.S.J., Pinkerton, H., and Hulme, Geoffrey, 1976, Classification and formation of lava levees on Mount Etna, Sicily: Geology, v. 4, p. 269- 271.

Valentyik, Laszlo, 1972, Rheological properties of heavy media suspensions stabilized by polymers: Transactions, American Institute of Mining, Metallurgical, and Petroleum Engineers, v. 252, p. 99-105.

Walker, G.P.L., 1967, Thickness and viscosity of Etnean lavas: Nature, v. 213, p. 484-485.

———1973, Lengths of lava flows: Philosophical Transactions of the Royal Society of London, Series A., v. 274, p. 107-118.

THE ROLE OF LAVA TUBES IN HAWAIIAN VOLCANOES

By Ronald Greeley[1]

ABSTRACT

Lava tubes develop from eruptions that typically involve: (1) moderate rates of effusion, (2) durations greater than one or two days, and (3) effusion of fluid lava (for example, pahoehoe) that has not been greatly degassed. Although some fountain-fed lava and aa flows can form lava tubes, such occurrences are rare in Hawaii. Lava tubes feed flows: (1) directly from the vent (acting as extensions of the conduit), (2) from various holding reservoirs (for example, lava ponds, lava lakes, filled pit craters), and (3) from flows on the flanks of volcanoes. Historical flows of greatest length in Hawaii were emplaced primarily via lava tubes, and many subaqueous flows involve lava tubes. Sustained flow of lava in tubes appears capable of erosion into preflow terrain. Photogeological analyses suggest that at least 30 percent of the flows (by area) on Mauna Loa, 58 percent of the flows on Kilauea, and 18 percent of the flows on Mount Etna were at least partly emplaced via tubes.

INTRODUCTION

Lava tubes have been mentioned frequently in the literature on volcanology in Hawaii. From his visit to Hawaii in the 19th century, Dutton (1884) wrote "Probably no great eruption takes place without the formation of several such tunnels ***. There are literally thousands of these tunnels throughout the mass of Mauna Loa ***. So numerous are these caverns that it seems as if they must form some appreciable part of the entire volume of the mountain."

This paper reviews mechanics of lava tube formation, considers their role in various aspects of eruptions in Hawaii (including the emplacement of lava flows), and assesses their occurrence in Mauna Loa and Kilauea Volcanoes (fig. 59.1). Three sources of data were employed in this study: (1) previous descriptions of active eruptions involving lava tubes, (2) photogeologic studies of channels and lava tubes and the associated flows on Mauna Loa and Kilauea, and (3) field observations of active and inactive flows.

In the last two or more decades, new insight has been gained about Hawaiian lava tubes. This insight has been the consequence of several factors, including an increased interest in the morphology of volcanoes in general and the eruptions of Mauna Ulu in particular. Lava tubes were common in many of the Mauna Ulu flows (Wood, 1981) and their formation was readily observed (Greeley, 1971a, 1972a; Cruikshank and Wood, 1972; Peterson and Swanson, 1974). The eruption was relatively accessible, which, combined with frequent aerial photography, resulted in an unparalleled data set on the initiation and evolution of lava tubes and their associated flows.

Numerous studies of lava tubes have been made in areas outside Hawaii, including Mount Etna (Guest and others, 1980), Mount St. Helens (Greeley and Hyde, 1972), and New Mexico (Hatheway and Herring, 1970). From these studies and those in Hawaii, lava tubes clearly reflect a particular style of volcanism and are the primary means for the spread of some types of lava flows.

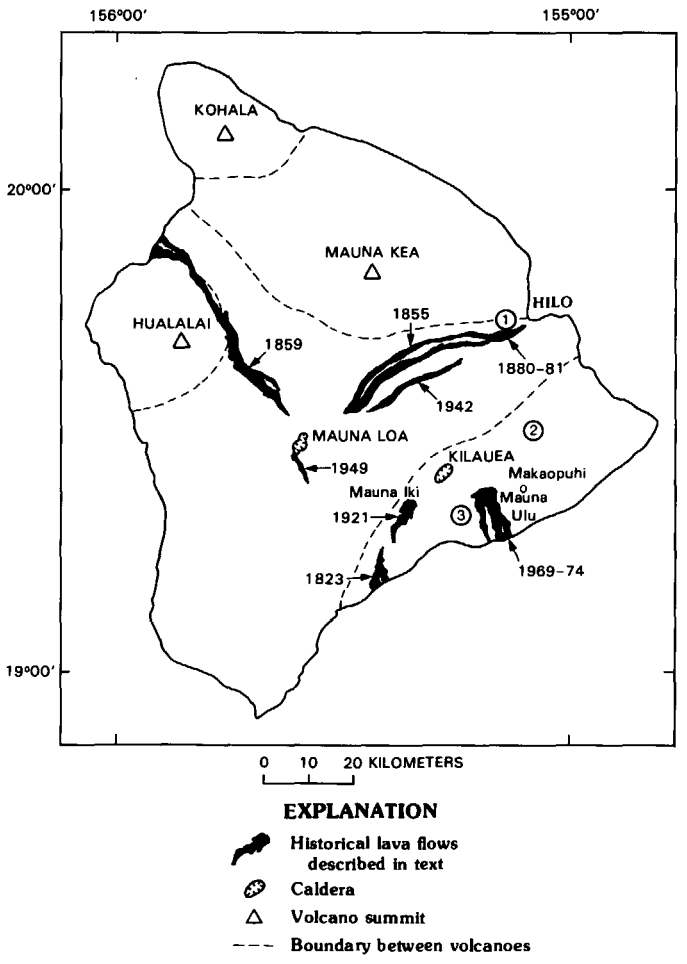

FIGURE 59.1.—Location map of some historical lava flows on Island of Hawaii, showing dates of flows and areas described in text: 1, Kaumana cave; 2, Kazamura cave; 3, Ainahou Ranch cave.

[1]Department of Geology, Arizona State University, Tempe, AZ 85287.

Thus, analysis of prehistorical lava tubes can provide insight into eruption processes and the flows in which they occur.

The term "lava tube" may be defined as the conduit beneath the surface of solidified lava through which molten lava flows. "Lava channels," however, contain nonroofed rivers of lava that frequently develop surface crusts. Many (if not most) lava tubes develop from the roofing of lava channels. For discussion here, the distinction between channels and tubes is made in regard to the roof crust; so long as the crust remains mobile and free-floating on the active flow, the structure is regarded as a channel; sections in which the crust is continuous across the active flow and fixed to the immobile parts of the flow are considered lava tubes. Thus, even if the roof collapses when the flow drains, the feature is considered to be a lava tube. This distinction is important for considerations of heat loss and lava flow emplacement.

ACKNOWLEDGMENTS

This manuscript benefited greatly from discussions with John Guest of the University of London and from detailed reviews provided by D.W. Peterson and R. Holcomb of the U.S. Geological Survey, for which I am grateful. I thank G. Beardmore and E. Wohl for their assistance in compiling data for the presence of lava tubes and channels on Kilauea and Mount Etna Volcanoes. M. Lovas and the Thermo- and Gas-Dynamics Division of NASA–Ames Research Center are acknowledged for running the samples from the Mount St. Helens lava tube. I also wish to express my appreciation to the staff and members of the Hawaiian Volcano Observatory for the hospitality and logistical support extended during various trips to Hawaii.

This work was supported by the Office of Planetary Geology, National Aeronautics and Space Administration.

LAVA TUBE FORMATION

Various mechanisms of lava tube formation have been proposed and some have been confirmed by observations of active tubes—primarily in Hawaii.

CHANNEL-ROOFING

The most frequently observed mode of lava-tube formation involves roofing of lava channels. Roofing can occur in any of several ways, most of which appear to be partly related to the rate of flow and rheology of the lava. Where flow is sluggish to moderate ($\leq$1–3 m/s) a crust may extend from the channel sides, meet near the middle of the active flow, thicken, and form a roof. Aerial views of this mode of formation show a medial bright zone (uncrusted lava) that closes like a zipper as roofing progresses along the flow (fig. 59.2).

Where channelized flow is more vigorous the crustal slabs are often torn free from the sides and are rafted downflow. Crustal slabs may also develop on the moving surface of the lava river. Analysis of photographs taken during the Mauna Ulu eruption shows that more than 50 percent of channel surfaces are commonly covered by these crustal slabs. As they are rafted down the flow, stresses may fracture the slabs into pieces like a jigsaw puzzle. Their shapes permit the slabs to fit together well and allow the slabs to turn meander bends (fig. 59.3). At channel constrictions, however, the rafted slabs may jam together, fuse, and form a tube roof.

FIGURE 59.2.—Aerial view of lava channel in process of roofing by formation of crust along channel margins; closure is occurring down middle of flow; bright area is unroofed; trees are about 12 m high. View is east. Photograph of Mauna Ulu eruption, August 1970.

At moderate rates of flow (2–5 m/s), overflow of the channel banks by lava—as may occur during surges—often builds levees that grow upward and inward until they join (Holcomb and others, 1974). At still higher rates of channelized flow, splashing of lava along the channel also can produce levees of spatter that reach up and over the flow and merge to form a roof. This roofing mechanism commonly occurs where flows pass over steep gradients, as observed during Mauna Ulu eruptions in the filling of Alae Crater (Greeley, 1971a) and as flows crossed Hilina Pali (Holcomb and others, 1974; Swanson and others, 1979). Similarly, Jaggar (1921) described flow within Halemaumau in which lava "shot down the slope like a sluiceway" and roofed over to form a tube. However, such features may be short-lived. Jaggar noted that within one hour, surges of lava alternately destroyed and replaced the roof.

DEVELOPMENT OF TUBES VIA LAVA TOES

Some lava tubes form without involving a channel phase. Relatively slow-moving pahoehoe flows involve repeated budding of lava toes that can be several meters across at the flow front and along the flow margins. Depending upon poorly understood circumstances, but often involving topographic channeling, the budding and subsequent flow direction may localize, forming a primary conduit within the flow that develops as a lava tube. This mechanism was described by Wentworth and Macdonald (1953, p. 43) in which toes of lava broke free from the flow margin. The skin of the toes is plastic and stretches as the toe elongates. A crust quickly thickens to form a rigid shell, but continued flow exerts sufficient

FIGURE 59.3.—Aerial view of channel (approximately 10 m wide) with rafted slabs of crust. Photograph of Mauna Ulu eruption, August 1970.

pressure to rupture the crust to produce a new toe. Repeated outbursts produce multiple toes, fed by an evolving lava tube.

This style of lava tube formation is invoked to explain complex networks of small lava tubes (fig. 59.4). In principle, it may also operate on larger scales. Many of the tubes formed by this mechanism, both large and small, may drain incompletely (or not at all) upon cessation of eruption. Some vast fields of hummocky pahoehoe are emplaced by such tubes and are termed "tube-fed pahoehoe" by Swanson (1973).

THE LAYERED-LAVA MECHANISM

From study of lava tubes principally in Australia, Ollier and Brown (1965) proposed that internal shearing within lava flows allowed conduits to develop between the shear zones. The conduits then evolved into lava tubes. Horizontal partings observed in some pahoehoe flows, along with features indicative of shear, are consistent with the concept on a small scale (<1 m), but evidence for this mode of formation for large lava tubes is absent in Hawaii (Peterson and Swanson, 1974).

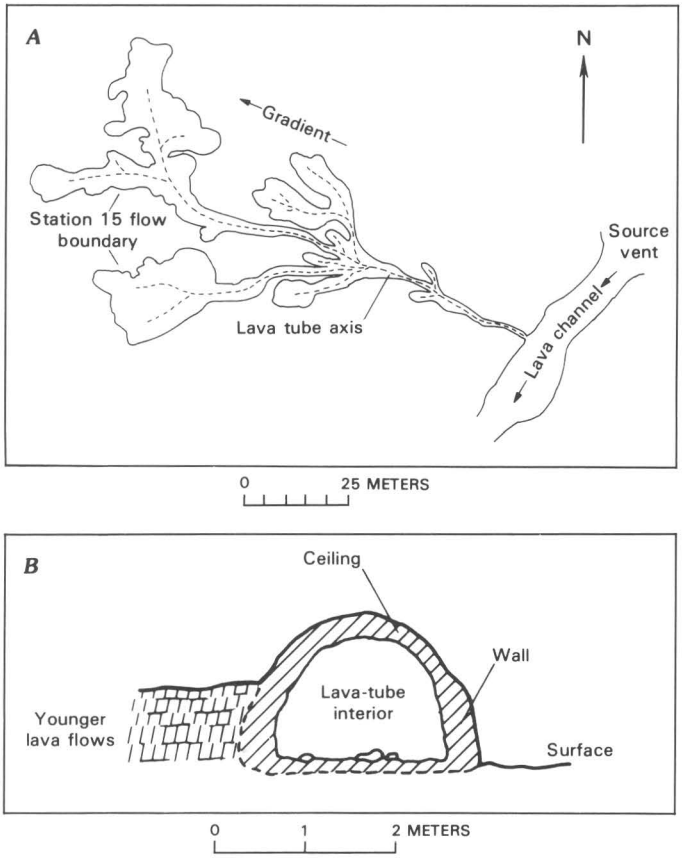

FIGURE 59.4.—Diagram based on plane-table survey of a small lava-tube network in California (south of Medicine Lake, Siskiyou County). ***A***, Distributary system of branches and toes. Nearly all branches contain hollow tubes (from Greeley, 1971b). ***B***, Simplified cross section of tube.

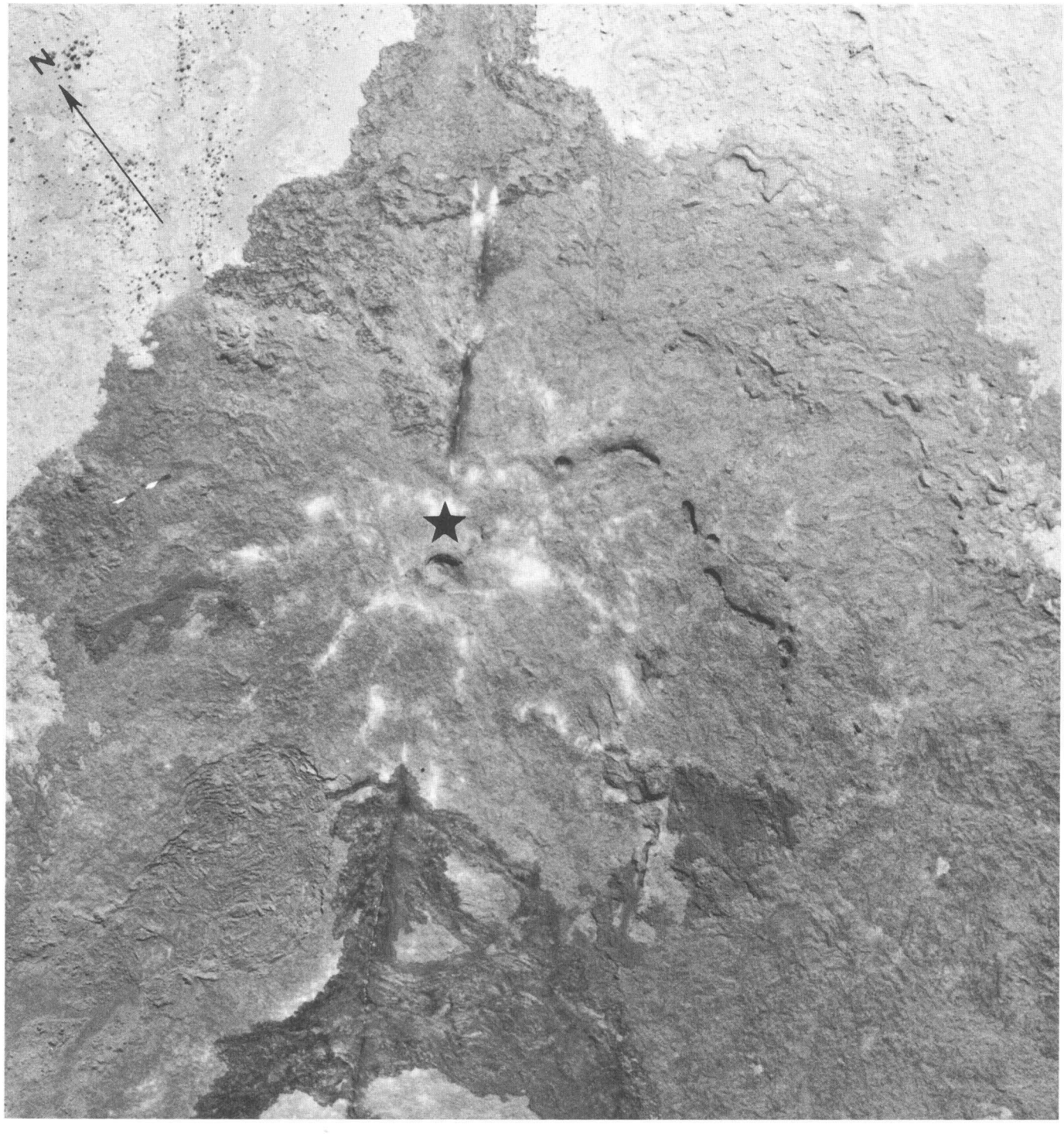

FIGURE 59.5.—Vertical aerial view of summit area of Mauna Iki; star marks summit pit crater; lava tube shown in figure 59.6 is southeast of summit area; area shown is about 1.5 km by 1.5 km. North is toward upper left. Photograph by R.M. Towill Corp., Honolulu.

ROLE OF LAVA TUBES IN FLOW EMPLACEMENT

Lava tubes are involved in many aspects of Hawaiian eruptions and can transport and emplace flows in various environments, including subaqueous settings. Observations of active flows in Hawaii (Greeley, 1971a; Peterson and Swanson, 1974; Holcomb, 1980) and on Mount Etna (Guest and others, 1980) in which lava tubes developed indicate that the eruptions had been occurring for more than one or two days before tube formation was initiated. Evidently, in order for tubes to form—either via channel-roofing or

FIGURE 59.6.—Oblique aerial view across Mauna Iki summit area, showing collapses (skylights) that mark presence of lava tubes. View is south. Photograph taken summer 1974.

through advancing toes—effusion must be relatively stable for some minimal time, as discussed by Holcomb (1980). This stability is especially true for tubes formed in aa flows. Thus, it is rare for tubes to develop during the initial stages of eruption when the position of vents and flows are not fixed and the rate of effusion and fountaining are highly erratic.

NEAR-VENT ACTIVITY

Many eruptions involve multiple vents that may be interconnected by lava tubes. Jaggar (1921, p. 21) described this type of activity within the Halemaumau pit crater of Kilauea. In 1921, the crater consisted of multiple ponds and the lava rose and fell somewhat independently in each pond, although Jaggar also noted that active lava tunnels could be traced between some of the ponds. Sometimes, wall segments containing tunnels were exposed and showed that flows passed from one pond to another.

Although lava tubes rarely develop during the initial phases of eruption, tubes may form at or near the vent within a short time from onset of eruption. For example, the 1949 summit eruption of Mauna Loa (Macdonald and Orr, 1950) involved high-volume fountaining of lava that collected in a pool and fed several lava channels. Within a few days of the initial eruption, some of the channels had roofed over and were the main conduits for lava flowing southeast from the vent area.

Part of Mauna Iki, on the southwest rift of Kilauea, was constructed by flows spread via lava tubes issuing from the vent area (fig. 59.5). As described by Jaggar (1947, p. 142), three lava pools developed over the site that eventually grew to be the low shield volcano Mauna Iki. Effusion of lava resulted in repeated overspilling from the pools; some of the spillovers formed channels and tubes oriented radially to the growing summit. Some of the tubes carried lava directly from the vent area more than 7 km to the distal part of the shield. By the fall of 1920 the eruption ceased, and as the lava drained, large (~15 m in diameter) lava tubes (fig. 59.6) were exposed as connecting the summit craters. Thus, tubes not only provided intercommunication between the summit pools, but also emplaced some of the lava that formed the upper flows of the small shield volcano.

TUBES DEVELOPED ALONG RIFT STRUCTURES

Eruptions in Hawaii commonly occur along the rift zones of the major volcanoes, and fractures and open fissures can serve as channelways for flows. This activity is especially evident along the southwest rift zone of Mauna Loa. Lava flowing within the channelways may develop roofs by the same mechanisms described for open channels and form lava tubes within the rift (fig. 59.7). The term "rift-tubes" was suggested by Finch (1946) as describing passageways developed along fissures and rift zones as part of the magma conduit. He noted that many eruptions on the rift zones of Kilauea were preceded by a sinking of the lava column in Halemaumau pit crater and suggested a connection via such tubes. These connections are more properly considered part of the intrusive dike-feeding system of the volcano and are not included in considerations of lava tubes developed from flows.

LAVA TUBES RELATED TO LAVA LAKES

Lava tubes are often involved in both the draining and filling of lava lakes. Entrances to lava tubes are frequently seen in walls of vents (fig. 59.8) and these tubes are often reactivated by subsequent eruptions. Some tubes may partly drain lakes, but become blocked or do not reemerge at the surface. For example, Jaggar (1947, p. 432) described a lava tube about 4 m high and 6 m wide in the wall of Halemaumau. In 1917, lava rose in the crater to the level of the tube, and for several hours lava poured into the tube. No outlet was obvious, and Jaggar suggested that the tube was filled to produce a sinuous cylinder of intrusive rock. Filled tubes of this sort when seen in cross section may show radial joint patterns, described by Waters (1960) for features in the Columbia Plateau basalts as war bonnet patterns, which he considered as filled tubes.

The best documented interaction of lava tubes and lava lakes is the sequence of repeated filling and draining observed for Alae Crater (fig. 59.9) during the Mauna Ulu eruptions (Swanson and others, 1972; Swanson and Peterson, 1972). Beginning in May 1969, lava from Mauna Ulu intermittently spilled into Alae Crater, filling it nearly to overflowing by August. Repeated spillover resulted in accretion of lava that raised the crater rim by several meters. A lava tube developed within the overflows and by late October a

FIGURE 59.7.—Oblique aerial view toward summit of Mauna Loa along southwest rift zone; dark holes in foreground mark presence of tube formed along rift segments; outflows from some skylights have produced local flows. Photograph taken August 1970.

master drainage system fed a series of pahoehoe flows a few hundred meters southeast of the crater (Swanson and others, 1972). Eventually, however, drainage through the tube(s) ceased, possibly because of clogging by solidified lava or blocking of their entrance by subsiding lava-lake crust.

By the summer of 1970, the Mauna Ulu vents fed flows downslope in several directions. In early August, two prominent vents (fig. 59.9, vents 1 and 3) fed lava into Alae lake through open

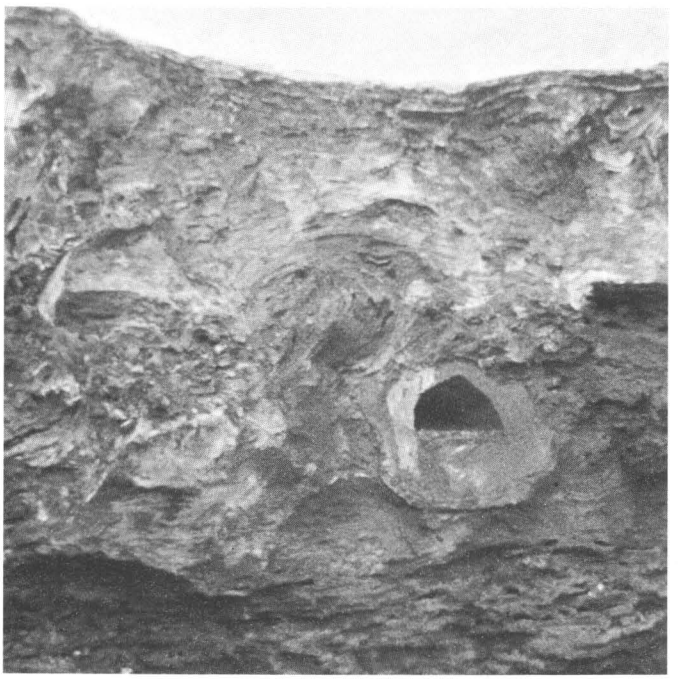

FIGURE 59.8.—View of lava tube ~1 m wide in wall of summit crater of Mauna Ulu. Such tubes may be reactivated as lava rises within vent and spills into tube. Photograph taken August 1971.

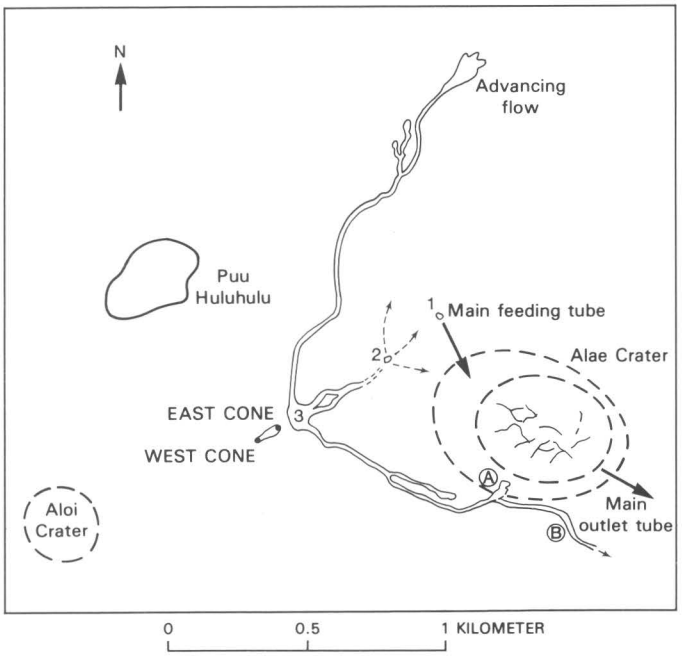

FIGURE 59.9.—Sketch map showing Mauna Ulu activity on August 8, 1970. Primary effusion was from vents 1 and 3, with flows from vent 1 entering Alae lava lake via a feeding tube. By afternoon, drainage of Alae Crater was taking place through an outlet tube to southeast. Southeast flow from vent 3 was via an open channel that initially (A) spilled onto crust of Alae lava lake; channel bypassed crater (B); dashed lines indicate preflow crater outline for Alae and Aloi.

channels (Greeley, 1971a), most of which emptied beneath the crust of the lava lake. One channel, however, appeared to form a tube that spread across the surface of the lake and fed small flows (fig. 59.10). Within one day, channels from the Mauna Ulu vents had nearly completely roofed over and continued to pour lava into Alae lake. However, a new channel had developed in flows from a newly reactivated vent on the fissure. Although the channel initially emptied on the lake crust, later in the same day (August 8, 1970), it bypassed the lake on the west side and fed flows to the southeast (fig. 59.9, A and B).

August 8 marked the beginning of the second episode of drainage of Alae lava lake. Aerial observations at about 0900 showed tube-fed flows that emptied into the lake. Sometime between these observations and midafternoon, drainage of the lake began, which resulted in subsidence of the lake crust by several meters (Greeley, 1971a). The subsidence formed a ring of tensional fractures in the lake crust (concentric to the former crater rim) and resulted in a series of pressure ridges as the crust slid inward toward the center of the ring (fig. 59.10). Swanson and others (1972) suggest that the lava tube that previously drained the lake was reactivated, perhaps as a consequence of increased pressure beneath the lake crust resulting from infilling. They suggest that the tube was 21–22 m below the surface and about 2–3 m above the preeruption level of the southeast crater rim. Subsidence of the lava lake crust continued for several days, after which the inflow was about equal to outflow via lava tubes. Lava emerged from the main outflow tube several kilometers downflow and fed a series of slow-moving pahoehoe flows. Over the next many months, tubes continued to carry lava from Mauna Ulu vents into the holding reservoir of the Alae lava lake, and then to feed lava to the flows spreading downslope to the south.

EMPLACEMENT OF LONG FLOWS VIA TUBES

The factors governing the lengths of lava flows have been of considerable interest to volcanologists and planetologists. With the discovery of extremely long flows on other planets (>1,000 km on the Moon and Mars), several assessments have been made of the viscosity, effusion rate, volume of lava erupted, and other parameters that might affect flow length (Walker, 1973). Many of these studies, however, have ignored the role of lava tubes, or given the matter only cursory attention. From his study of flows in Hawaii, Malin (1980) suggested that cross-sectional area, effusion rate, and volume of lava erupted were all important and that no single factor seemed more important. He also noted that tube-fed flows appeared to advance farther, all other factors held equal.

In some respects lava tubes act as extensions of the magma-feeding conduit. Because tubes are well insulated, little heat is lost and the lava can remain mobile longer than for nonchannelized flows or unroofed channels. Swanson (1973) measured a decrease in

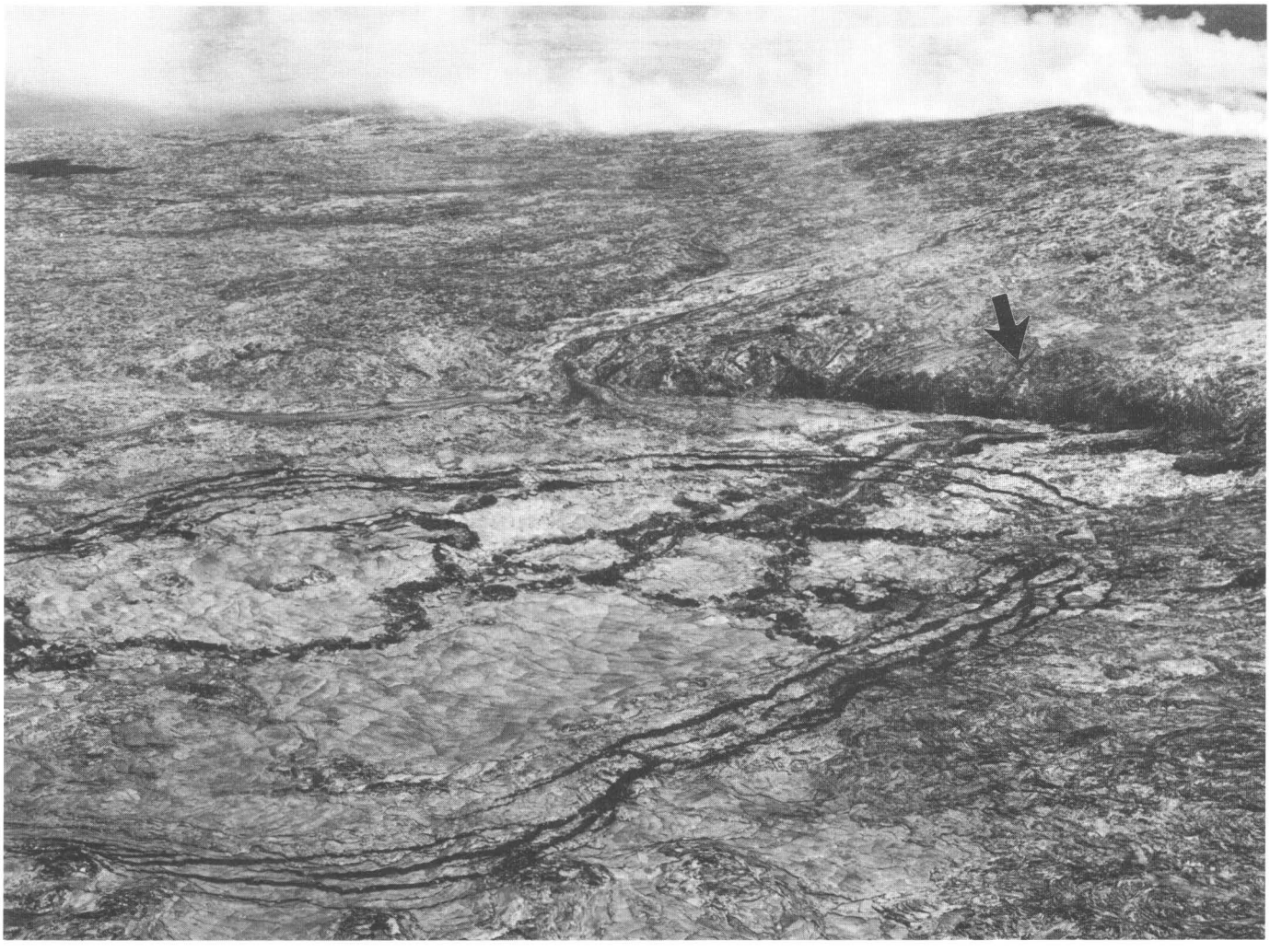

FIGURE 59.10.—Oblique aerial view across Alae lava lake taken in afternoon of August 9, 1970, after drainage of lake had begun via lava tube(s), showing concentric ring fractures and pressure ridges. Arrow marks small flows that spilled into lake from vents 1 (right side) and 3 (left side) and formed small tubes on lake crust. View is west. Photograph taken August 1970.

temperature of only 1–2 °C per kilometer for flow through a lava tube fed by eruption of Mauna Ulu. Even channel flow can be effective in heat retention if a thin crust is present. For example, the crust shown in figure 59.3 covers more than 55 percent of the active flow in the channel.

Two of the longest historical flows in Hawaii (fig. 59.1), the 1859 and the 1880–81 flows (both of Mauna Loa), were emplaced primarily through lava tubes. The 1859 flow erupted at the 3,355-m level and flowed more than 52 km to the sea (Stearns and Macdonald, 1946). The eruption lasted 7 months and extruded about 440×10^6 m^3 of lava (Macdonald and others, 1983, table 3.1). A complex lava tube system—in some places tube segments are more than 12 m across—can be traced through a series of collapsed sections visible in many sections of the flow. In some sections the tube exhibits complex anastomosing and vertically stacked branches, indicative of repeated eruptive surges and emplacement of multiple flow units (Greeley, 1972b).

The 1880–81 flow was erupted on the northeast rift zone of Mauna Loa (Baldwin, 1953) at about 3,325 m elevation. Lava issued quietly from an elongate fissure for 280 days and eventually reached nearly to the outskirts of Hilo. Except for some short aa flows, most of the lava was pahoehoe fed through a 40-km-long lava-tube system. Baldwin (1953) described the flow as follows: "At the advancing front the lava seems to come out of its tunnel and flow in an open red river of fire as much as several hundred feet long. This then appears to clog up and cool on top, and the lava pushes out in great and small lobes, piling one over the other and eventually forming a new tunnel underneath for the molten lava. The latter will then again break out and go through the same process as before." Kaumana cave is a section of this tube near Saddle Road a few

kilometers from Hilo and is open to the public (Greeley, 1974).

The 1880–81 flow can be contrasted with the 1855 Mauna Loa flow, which it parallels for some of its length. Both the 1880–81 and the 1855 flows advanced slowly at a rate of only a few tens or hundreds of meters per day on the middle and lower slopes (Macdonald, 1958). However, the 1855 eruption lasted 450 days and involved vigorous fire fountaining. Most of the flow was aa and did not form tubes. Even though the duration of the eruption was greater than the 1880–81 eruption (Macdonald and others, 1983, table 3.1), the flow is much shorter. Evidently, the fountaining caused outgassing of the magma such that the lava was dominantly aa, and lava tubes were not able to form.

During prolonged eruptions, lava tubes—once established—may be reactivated. Interiors of cooled tubes show evidence of multiple flow, including multiple linings of the walls and flows that only partly drained from the tube. As shown in figure 59.11, surface flows near the summit of Mauna Iki spilled into a tube system; similarly, the copious flows of the 1823 Keaiwa eruption of Kilauea (Stearns, 1926) emptied into an older tube at about 220 m elevation. In most cases, flow does not reemerge at the surface, but evidently blocks or fills the tubes. Occasionally, however, flows will intersect older lava tubes, drain into them, and reemerge in another place. For example, Macdonald (1943) described the 1942 flow of Mauna Loa as erupting at the 2,800-m level; lava also issued quietly 5 km downslope at the 2,380-m level, and Macdonald speculated that lava entered an old lava tube that intersected the eruption fissure higher up the mountain.

Emergence of lava from tubes—both primary tubes and reactivated systems—can produce flows and surface features different from the surrounding lava. Patches of seemingly anomalous pahoehoe set within aa flows (fig. 59.12) possibly can be emplaced through lava tubes. Similarly, tubes intially established in pahoehoe may transport subsequent flows of different properties. Macdonald and Orr (1950) noted that during the 1949 eruption of Mauna Loa, sluggish aa flows were fed by earlier formed lava tubes in the summit area.

Pressure of lava backed up within a tube may inflate the roof into small domes or may rupture the roof. Skylights—formed by collapse of roof sections—often became rootless vents and produced local flows (fig. 59.7) during surges that spilled lava from the tube.

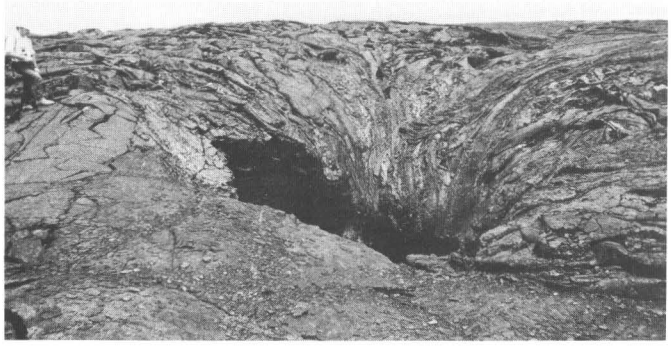

FIGURE 59.11.—View of flows near summit of Mauna Iki that spilled into ~15-m-diameter skylight of lava tube. Photograph taken August 1970.

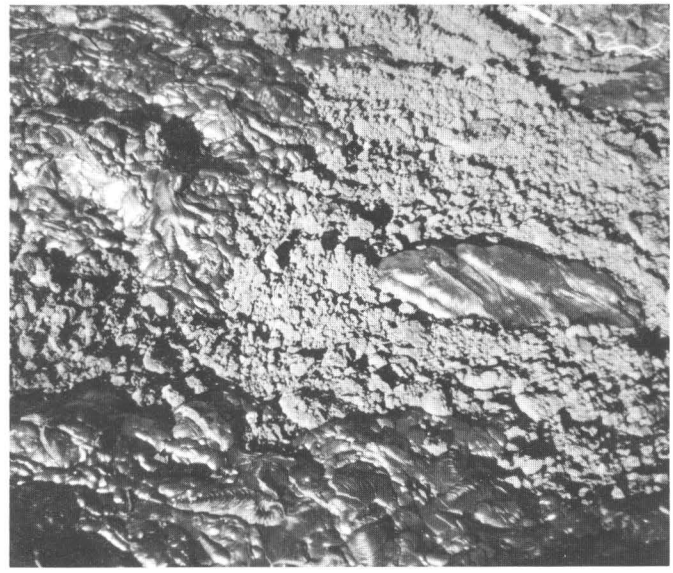

FIGURE 59.12.—Low oblique aerial view of patch of pahoehoe lava (smooth, shiny material) set within aa flow. Pahoehoe flow was possibly emplaced through lava tube. Photograph taken August 1970.

TALUS-AND-LAVA CONES

Lava flows often spill over steep cliffs and form features termed by Holcomb and others (1974) as "talus-and-lava cones." In observing flows that filled Makaopuhi Crater in 1972, they noted that some larger streams of lava cascaded over the crater rim onto the apex of these talus cones and developed lava tubes that transported flows over the cone and onto the crater floor. Some tubes extended from the crater rim to the apex of the cone, as well as through the cone. As observed by Swanson (1973), pahoehoe flows passing over such steep slopes ordinarily evolve to aa; however, development of tubes enables the flows to remain as pahoehoe.

LAVA DELTAS AND SUBAQUEOUS FLOW EMPLACEMENT

Many historical flows have reached the sea, and the addition of land through the accumulation of lava has been observed often (Peterson, 1976). The role of lava tubes, however, was not appreciated until the underwater observations by Moore and others (1973) for active flows erupted from Mauna Ulu. They noted a sequence of seaward extension of the advancing lava that began with flows spilling over the seacliff. As the hot lava poured into the sea water, it was quenched and fragmented into glassy sands and rubble that was further churned by wave action. This material accumulated to

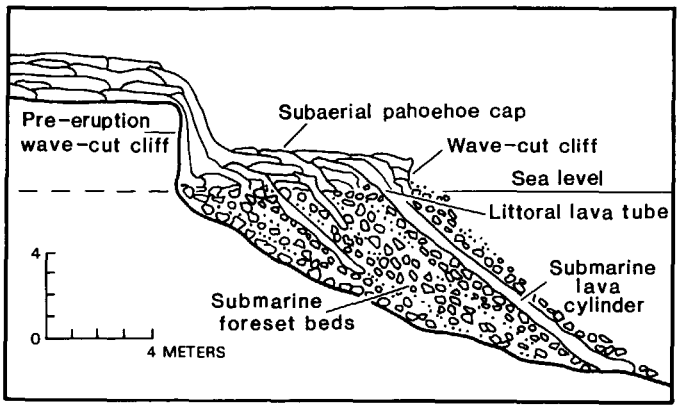

FIGURE 59.13.—Cross section of flows and delta built by Mauna Ulu lava entering the sea (from Peterson, 1976, which was modified from Moore and others, 1973).

produce foreset volcaniclastic deposits as an expanding lava delta (fig. 59.13). Some of the flows were fed by lava tubes; smaller tubes extended as pahoehoe toes that also were quenched and fragmented, whereas some larger tube systems moved forward rapidly enough to maintain coherence through the wave zone and established submarine lava flows. Peterson (1976) termed these "littoral lava tubes" and noted that their formation by abrupt quenching distinguishes them from tubes formed in subaerial environments. Once established, the submarine lava tubes fed complex, anastomosing networks of flow lobes that advanced as budding toes of lava.

Through alternation of volcaniclastic accumulation and tube-fed emplacement, the Mauna Ulu flows built a 470,000-m^2 delta to a depth exceeding 70 m. Moore and others (1973) note that many prehistorical flows from Kilauea display similar morphologies and suggest that the sequence they observed may be typical for many of the flows reaching the sea. Since their observations, dives by deep-sea submersibles around Hawaii (Fornari and others, 1980) and in areas of active sea-floor spreading in both the Atlantic and Pacific Oceans have led to the discovery of numerous submarine lava flows, many of which were emplaced via lava tubes (Heirtzler and Bryan, 1975). Thus, just as the emplacement of subaerial lava flows may be facilitated by lava tubes, substantial submarine lava may also involve flow through tubes.

EROSION BY LAVA TUBES

Several lines of evidence suggest that flow within lava tubes is capable of both downcutting and lateral erosion. Detailed mapping of lava tubes in Hawaii (Wood, 1981), in California (Greeley and Baer, 1971), and in basalt flows of Mount St. Helens shows the crosscutting relations of the flows and tubes to the preflow terrain (fig. 59.14). Wood noted that the thin wall of the Ainahou Ranch cave of Kilauea collapsed into the tube and exposed an older aa flow that he suggested had been eroded by the tube. In California and at Mount St. Helens, the preflow rocks are distinctive from the basalt flows and were easily recognized. In the Mount St. Helens tubes, pieces of preflow rocks—some as large as one meter across—were carried by lava down the tube and are further evidence of mechanical erosion (Greeley and Hyde, 1972). Blocks of solidified lava are also observed in Hawaii in open lava channels; Finch and Macdonald (1950) reported that blocks as large as 6 m high and nearly 10 m long were carried by lava in channel flow during the June 1950 eruption of Mauna Loa. Although these blocks were probably not from preflow lava, they indicate the capacity of flowing lava to transport large masses of solidified lava, and large blocks possibly are also often carried within lava tubes in Hawaii.

Erosion by melting or partial melting is more difficult to document. However, in one section of the Mount St. Helens tubes (Greeley and Hyde, 1972), a block of dacite from the preflow

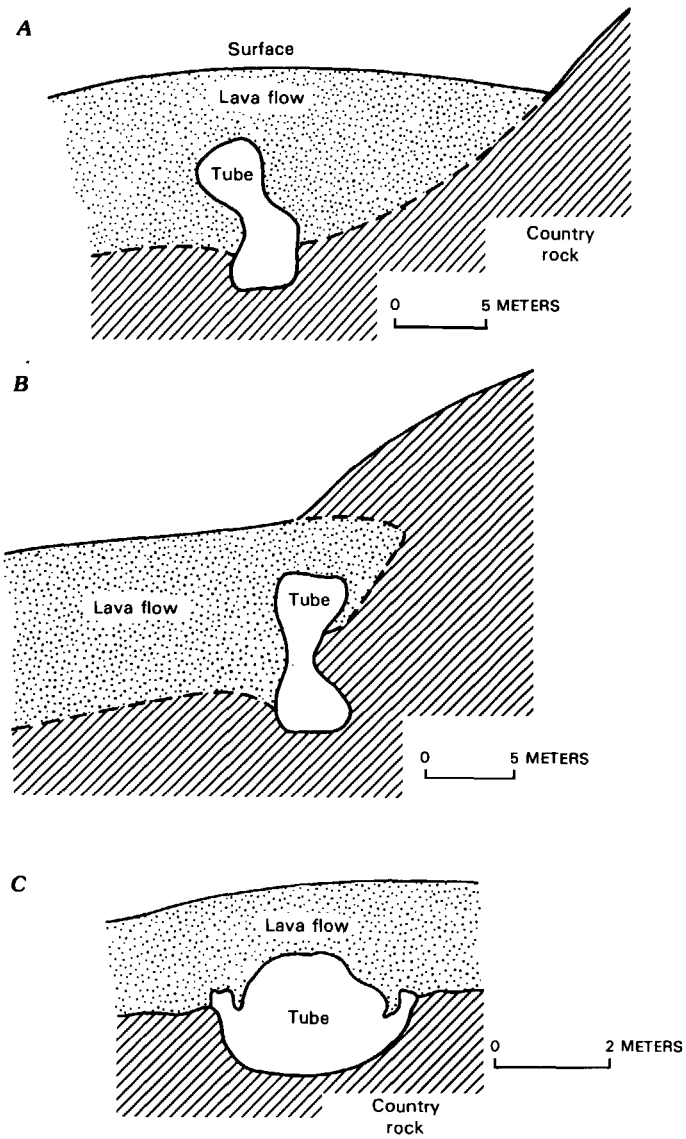

FIGURE 59.14.—Cross sections generated from surveys showing probable erosion by flow within a lava tube. ***A***, ***B***, Ape cave in Mount St. Helens (Wash.) basalt flows (from Greeley and Hyde, 1972). ***C***, Ainahou Ranch tube, Kilauea (surface of lava flow shown schematically, from Wood, 1981).

terrain was heated above the melting temperature for some of the minerals and flowed into the tube through a wall collapse and dripped onto the floor of the tube. Samples taken from the block were heated in a laboratory furnace at temperatures of 1,000 °C, 1,100 °C, 1,150 °C, 1,200 °C, 1,250 °C and 1,300 °C. After one hour, only the samples heated above 1,200 °C showed signs of melting, and it is assumed that a comparable temperature was reached when the lava tube was active. Thus, erosion by partial melting may also have contributed to entrenchment of the tube.

The examples cited above involved preflow rocks that were mostly unconsolidated and of a lower melting temperature than basalt. However, erosion of basalt by lava-tube flow may also occur, as proposed by Carr (1974) from theoretical models and suggested by Peterson and Swanson (1974) from observations of Mauna Ulu flows. Although direct evidence was absent, Peterson and Swanson inferred that the gradual lowering of the flow level in a Mauna Ulu tube (observed through a skylight) reflected downcutting. They noted that the rate of effusion and the rate of flow through the tube was constant and that the lowering of the flow level could not, therefore, be simply a diminution of flow volume.

It is not known if temperatures above melting for basalt are sustained in lava tubes. Several measurements, however, show that high temperatures do occur within tubes as a consequence of burning gases. Macdonald and Eaton (1964) noted during the 1955 eruption in East Puna that temperatures at the flow front for freshly exposed lava were 930–970 °C, but that blue flames were also visible within grottos where temperatures were measured at 1,025 °C. The flames and high temperatures were attributed to burning of gases generated from vegetation buried by the flow. Similarly, Jaggar (1947) described blue flames observed through cracks in a lava-tube roof formed in the Postal Rift flow of 1919 on the floor of Kilauea caldera. This gas probably was not generated from vegetation, but rather was magmatic gas. Cruikshank and others (1973) observed the burning of hydrogen at Mauna Ulu vents and measured temperatures well above the melting point for basalt. The conclusion is that temperatures can be reached within lava tubes that are sufficiently high to melt or at least soften the basalt, but it is not known if widespread melting of preflow rock occurs.

LAVA TUBE ABUNDANCES

In an attempt to determine the relative importance of lava tubes in the evolution of Hawaiian volcanoes, the abundance of lava tubes and associated flows was assessed for Mauna Loa and Kilauea. For comparison, a similar analysis was made for Mount Etna, Sicily. Although the methods of data collection were somewhat different for the cases studied (making comparisons less than ideal), the results demonstrate that for some basaltic volcanoes—especially in Hawaii—lava tubes play a key role in the volcanic history.

MAUNA LOA

Lava flows and associated tubes and channels were mapped on aerial photographs for sparsely vegetated parts of the shield (Greeley and others, 1976), representing summit, flank, and rift areas (fig. 59.15). Using 81 aerial photographs (U.S. Department of Agriculture, 1:20,000), about 15 percent of the shield was mapped on stereoscopic photographs and an additional 10 percent was mapped with monoscopic images; thus, about one-quarter of the areal extent of the volcano was analyzed. Lava tubes were identified by the presence of collapsed skylights, but because uncollapsed tubes could not be seen on aerial photographs, the value given for lava-tube frequency is a lower limit. Moreover, only exposed flows were examined. Thus, units buried by younger flows, those below sea level, and those covered by heavy vegetation are excluded.

For each photograph, a map was prepared that delineated the flow units and the presence or absence of lava tubes and channels. Three types of flow units were delineated: (1) those containing predominantly lava tubes, (2) those containing predominantly lava channels, and (3) those lacking tubes or channels. Areas for each flow unit were determined using a planimeter. Limited field work and comparison with maps (for example, Macdonald, 1971) provided additional data; ground checking of the photogeology was done for flows intersected by roads on the west flank of Mauna Loa and in the Saddle area.

The data were compiled on the basis of the percentage of the flows by area that were at least partly emplaced via lava tubes. The results show that 30 percent of the area is covered by flows spread at least partly via lava tubes. If channels are included in the analysis the percentage rises to 83 percent.

KILAUEA

Some of the longest uncollapsed known lava tubes in Hawaii are within Kilauea lava. For example, the Kazumura cave on the northeast flank has been mapped for more than 11.7 km and is only one of several large tubes in the area (Wood, 1981). Ainahou Ranch cave, in a flow on the southern flank of Kilauea, is more than 7 km long. To determine the frequency of lava tubes for Kilauea, data for Kilauea were compiled from mapping by Holcomb (1976, 1980), who noted the presence of lava channels and tubes and classified flows by age, morphologic assemblage (for example, small lava shield), and morphologic-lithologic type (for example, tube-fed pahoehoe). Holcomb's mapping is based on aerial photographs, supplemented with data from field work by himself and Wood (1981).

Holcomb's map for Kilauea shows both flow boundaries and the trace of lava tubes. Areas for the flows containing lava tubes were found to represent 58 percent of the surface area for Kilauea. It should be noted that some of Holcomb's tube-fed flows were excluded from this analysis, as only those flows in which he indicated the presence of tubes were employed.

MOUNT ETNA

The presence of lava tubes in flows on Mount Etna was determined from data in Brunelli and Scammacca (1975) and Bella

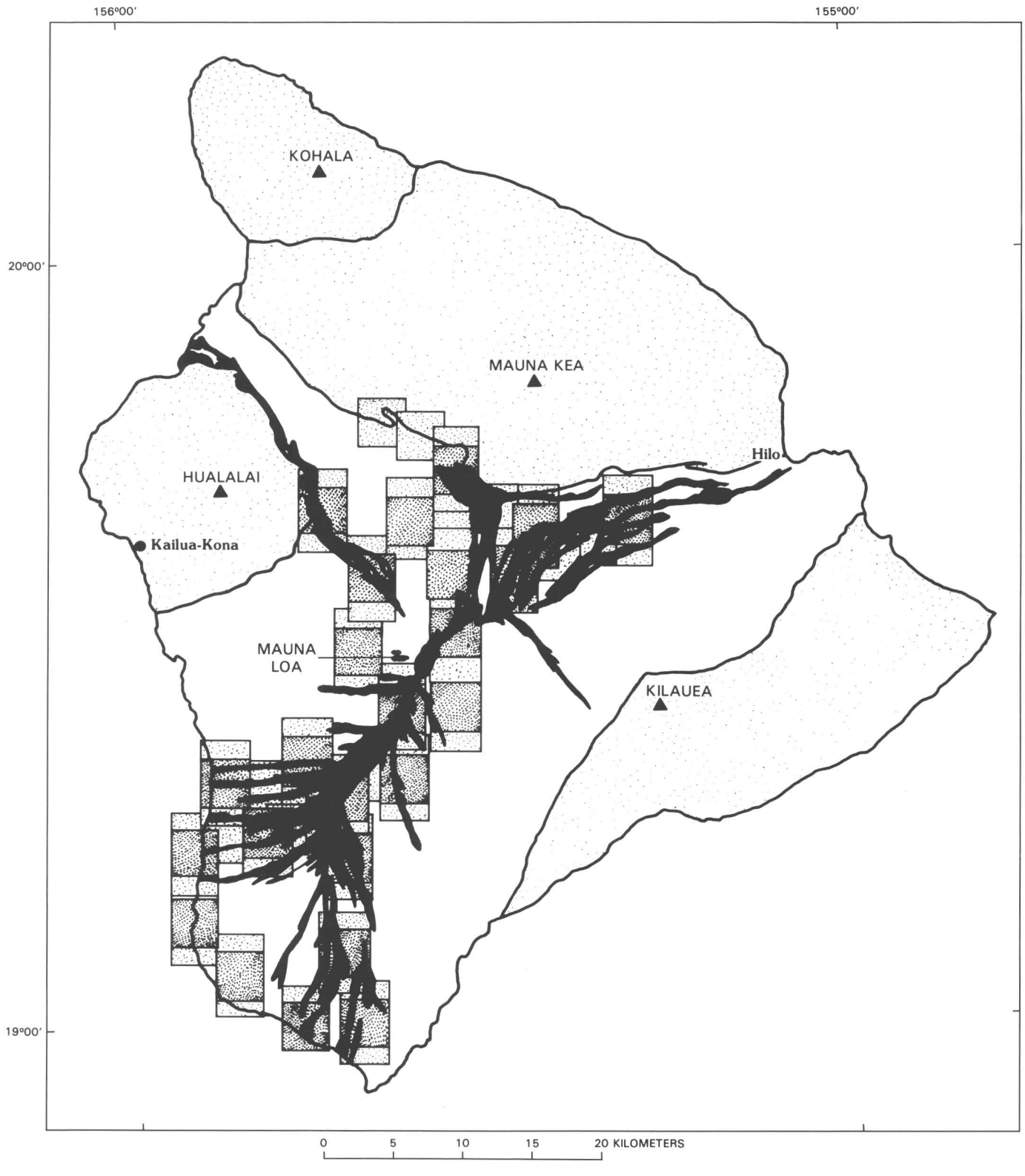

FIGURE 59.15.—Sketch map showing areas of Mauna Loa analyzed for lava tubes; rectangles outline aerial photographs studied; heavy stipple indicates stereoscopic coverage. Solid black, historical flows.

and others (1982), and supplemented by photogeologic study, limited field work, and discussions with members of a speleological organization in Catania, members of which routinely search for and map lava tubes on the volcano. Locations of lava tubes (longer than 100 m) from these sources were plotted on the geologic map of Mount Etna (Romano and others, 1979) and treated statistically like the Hawaiian volcanoes. Of the total surface area of Mount Etna flows, 18 percent was emplaced at least partly via lava tubes.

DISCUSSION

Studies of active and inactive flows show that lava tubes are involved in many aspects of Hawaiian eruptions. Rarely are either tubes or channels produced in the early phase of eruption, regardless of flow type (aa, pahoehoe, or others). Thus, short duration eruptions (that is, less than one or two days) seldom produce lava tubes (Holcomb, 1980). The often-stated comment that lava tubes form nearly exclusively in pahoehoe flows appears to be correct, although some tubes are documented in aa flows (Wentworth and Macdonald, 1953). Guest and others (1980) note that tubes are often found in aa flows near vents on Mount Etna formed from long-duration eruptions. Not all pahoehoe flows develop lava tubes, however, and factors other than the rheology must be involved. These factors are at least partly related to the style of eruption, especially in regard to the vigor, rate, and duration. Highly vigorous eruptions, as reflected by fire fountaining, cause rapid changes in flow regime and lack well-defined channels to evolve to tubes. In addition, fire fountaining may degas the lava rapidly (Swanson and Fabbi, 1973), producing aa flows, most of which are too viscous to form roofs, or producing degassed pahoehoe which may not become channelized.

High rates of effusion, exemplified by the 1823 flow of Kilauea, may spread out rapidly as sheets and fail to become channelized. Moreover, high effusion is often associated with fissure vents in which the zone of eruption shifts along the fissure; as such, there is not a focused flow of sufficient duration for channels and tubes to develop. Thus, the presence of lava tubes (Holcomb, 1980, chapter 3) reflects a style of volcanism involving moderate rates of effusion and durations typically greater than one or two days, and eruption of relatively fluid lava (for example, pahoehoe) that has not greatly degassed.

Lava tubes may transport lava between vents, along rift zones, and directly from vents to flow fronts. They are effective conduits for the emplacement of the longest flows on Hawaii and play a critical role in the submarine extension of many flows. Although not well documented in Hawaii, erosion by both thermal (melting) and mechanical (plucking) means appear to take place by flow within some tubes.

Analysis of Mauna Loa, Kilauea, and Mount Etna volcanoes shows that lava tubes were involved in the emplacement of one-fifth or more of the flows exposed at the surface. Differences in the percentages for the three volcanoes studied may reflect differences in data analysis or may represent differences in evolution or stage of development. Nonetheless, their high occurrence in all cases demonstrates that lava tubes emplace many of the flows in the evolution of basaltic volcanoes.

REFERENCES CITED

Baldwin, E.D., 1953, Notes on the 1880–81 lava flow from Mauna Loa: The Volcano Letter, no. 520, April–June, p. 1–3.

Bella, V., Brunelli, F., Cariola, A., and Scammacca, B., 1982, Grotte vulcaniche di Sicilia, notizie catastali: Secondo contributo, Bollettino Accademia Gioenia di Scienze Naturali, v. 15, p. 229–292.

Brunelli, F., and Scammacca, B., 1975, Grotte Vulcaniche di Sicilia: Club Alpino Italiano, Sezione dell'Etna, Gruppo Grotte Cantania, 54 p.

Carr, M.H., 1974, The role of lava erosion in the formation of lunar rilles and martian channels: Icarus, v. 22, p. 1–23.

Cruikshank, D.P., Morrison, D., and Lennon, K., 1973, Volcanic gases: Hydrogen burning at Kilauea Volcano, Hawaii: Science, v. 182, p. 277–279.

Cruikshank, D.P., and Wood, C.A., 1972, Lunar rilles and Hawaiian volcanic features: Possible analogues: The Moon, v. 3, p. 412–447.

Dutton, C.A., 1884, Hawaiian volcanoes: U.S. Geological Survey, Fourth Annual Report, 1883, p. 75–219.

Finch, R.H., 1946, The Puna rift of Kilauea: The Volcano Letter, no. 493, p. 1–2.

Finch, R.H., and Macdonald, G.A., 1950, The June 1950 eruption of Mauna Loa: The Volcano Letter, no. 508, p. 1–11.

Fornari, D.J., Lockwood, J.P., Lipman, P.W., Rawson, M., and Malahoff, A., 1980, Submarine volcanic features west of Kealakekua Bay, Hawaii: Journal of Volcanology and Geothermal Research, v. 7, p. 323–337.

Greeley, R., 1971a, Observations of actively forming lava tubes and associated structures, Hawaii: Modern Geology, v. 2, p. 207–223.

———1971b, Geology and morphology of selected lava tubes in the vicinity of Bend, Oregon: State of Oregon, Department of Geology and Mineral Industries Bulletin 71, 47 p.

———1972a, Additional observations of actively forming lava tubes and associated structures, Hawaii: Modern Geology, v. 3, p. 157–160.

———1972b, Formation of multiple lava tubes [abs.]: Eos, Transactions of the American Geophysical Union, v. 53, p. 276.

———1974, Kaumana lava tube, *in* Greeley, R., ed., Geological Guide to the Island of Hawaii: National Aeronautics and Space Administration CR 152416, p. 233–238.

Greeley, R., and Baer, R., 1971, Hambone, California and its magnificent lava tubes—preliminary report [abs.]: Geological Society of America Abstracts with Program, v. 3, no. 2, p. 128.

Greeley, R., and Hyde, J.H., 1972, Lava tubes of the Cave Basalt, Mount St. Helens, Washington: Geological Society of America Bulletin, v. 83, p. 2397–2418.

Greeley, R., Wilbur, C., and Storm, D., 1976, Frequency distribution of lava tubes and channels on Mauna Loa Volcano, Hawaii [abs.]: Geological Society of America Abstracts with Programs, v. 8, p. 892.

Guest, J.E., Underwood, J.R., and Greeley, R., 1980, Role of lava tubes in flows for the Observatory Vent, 1971 eruption on Mount Etna: Geology Magazine, v. 117, p. 601–606.

Hatheway, A.W., and Herring, A.K., 1970, Bandera lava tubes of New Mexico, and lunar implications: Tucson, Arizona University Lunar and Planetary Laboratory Communications, v. 8, p. 298–327.

Heirtzler, J.R., and Bryan, W.B., 1975, The floor of the mid-Atlantic Rift: Scientific American, v. 273, p. 78–90.

Holcomb, R.T., 1976, Preliminary map showing products of eruptions, 1962–1974, from the upper east rift zone of Kilauea Volcano, Hawaii: U.S. Geological Survey Miscellaneous Field Investigation Map MF–811, scale 1:24,000.

———1980, Kilauea Volcano, Hawaii: Chronology and morphology of the surficial lava flows; Stanford, Calif., Stanford University, Ph.D. thesis, 321 p.

Holcomb, R.T., Peterson, D.W., and Tilling, R.I., 1974, Recent landforms at Kilauea Volcano, a selected photographic compilation, *in* Greeley, R., ed., Hawaiian Planetology Conference: National Aeronautics and Space Administration TMX 62362, p. 49–86.

Jaggar, T.A., 1921, Volcanic conditions in February: Monthly Bulletin Hawaiian Volcano Observatory, v. 9, p. 21–39.

———1947, Origin and development of craters: Geological Society of America Memoirs, v. 21, 508 p.

Macdonald, G.A., 1943, The 1942 eruption of Mauna Loa, Hawaii: American Journal of Science, v. 241, p. 241–256.

———1958, Barriers to protect Hilo from lava flows: Pacific Science, v. 12, p. 258–277.

———1971, Geological map of the Kipuka Pakekake quadrangle, Hawaii: U.S. Geological Survey Geologic Investigations Map GQ–957, scale 1:24,000.

Macdonald, G.A., Abbott, A.T., and Peterson, F.L., 1983, Volcanoes in the Sea: Honolulu, University of Hawaii Press, 517 p.

Macdonald, G.A., and Eaton, J.P., 1964, Hawaiian volcanoes during 1955: U.S. Geological Survey Bulletin 1171, 170 p.

Macdonald, G.A., and Orr, J.B., 1950, The 1949 summit eruption of Mauna Loa, Hawaii: U.S. Geological Survey Bulletin 974–A, 31 p.

Malin, M.C., 1980, Lengths of Hawaiian lava flows: Geology, v. 8, p. 306–308.

Moore, J.G., Phillips, R.L., Grigg, R.W., Peterson, D.W., and Swanson, D.A., 1973, Flow of lava into the sea, 1969–1971, Kilauea Volcano, Hawaii: Geological Society of America Bulletin, v. 84, p. 537–546.

Ollier, C.D., and Brown, J.P., 1965, Lava caves of Victoria: Bulletin of Volcanology, v. 28, p. 215–229.

Peterson, D.W., 1976, Processes of volcanic island growth, Kilauea Volcano, Hawaii, 1969–1973: International Association of Volcanology and Chemistry of the Earth's Interior, Symposium on Andean and Antarctic Volcanology Problems, Proceedings, p. 172–189.

Peterson, D.W., and Swanson, D.A., 1974, Observed formation of lava tubes during 1970–1971 at Kilauea Volcano, Hawaii: Studies in Speleology, v. 2, p. 209–222.

Romano, R., Sturiale, C., and Lentini, F., 1979, Carta Geologica del Monte Etna, (1:50,000), C.N.R. Istituto Internazionale di Vulcanologia, Catania.

Stearns, H.T., 1926, The Keaiwa or 1823 lava flow from Kilauea Volcano, Hawaii: Journal of Geology, v. 34, p. 336–351.

Stearns, H.T., and Macdonald, G.A., 1946, Geology and ground-water resources of the Island of Hawaii: Hawaii Division of Hydrography Bulletin, v. 9, 363 p.

Swanson, D.A., 1973, Pahoehoe flows from the 1969–1971 Mauna Ulu eruption, Kilauea Volcano, Hawaii: Geological Society of America Bulletin, v. 84, p. 615–626.

Swanson, D.A., Duffield, W.A., Jackson, D.B., and Peterson, D.W., 1972, The complex filling of Alae Crater, Kilauea Volcano, Hawaii: Bulletin of Volcanology, v. 36, p. 105–126.

———1979, Chronological narrative of the 1969–1971 Mauna Ulu eruption of Kilauea Volcano, Hawaii: U.S. Geological Survey Professional Paper 1056, 55 p.

Swanson, D.A., and Fabbi, B.P., 1973, Loss of volatiles during fountaining and flowage of basaltic lava at Kilauea Volcano, Hawaii: Journal of Research, U.S. Geological Survey, v. 1, p. 649–658.

Swanson, D.A., and Peterson, D.W., 1972, Partial draining and crustal subsidence of Alae lava lake, Kilauea Volcano, Hawaii, in Geological Survey research 1972: U.S. Geological Survey Professional Paper 800–C, p. C1–C14.

Walker, G.P.L., 1973, Lengths of lava flows: Philosophical Transactions of the Royal Society of London, Series A, v. 274, p. 107–118.

Waters, A.C., 1960, Determining direction of flow in basalts: American Journal of Science, v. 258–A, p. 350–366.

Wentworth, C.K., and Macdonald, G.A., 1953, Structures and forms of basaltic rocks in Hawaii: U.S. Geological Survey Bulletin, v. 994, 98 p.

Wood, C., 1981, Exploration and geology of some lava tube caves on the Hawaiian volcanoes: Transactions of the British Cave Research Association, v. 8, p. 111–129.

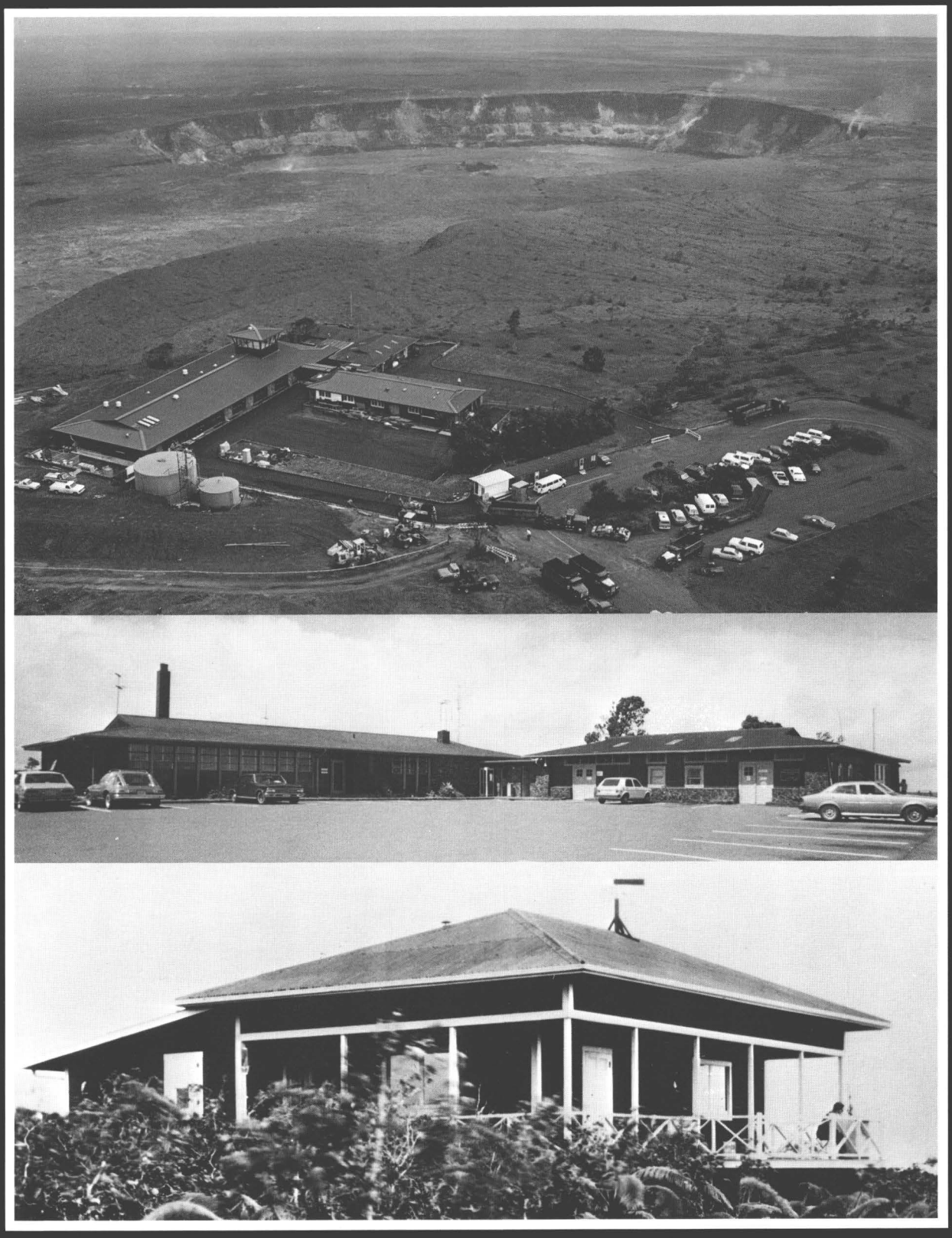

Evolution of Hawaiian Volcano Observatory facilities. Bottom: Original HVO main building on north rim of Kilauea caldera. Photograph by T.A. Jagger, 1913. Center: HVO facilities on Uwekahuna Bluff, about 1979. Top: Oblique aerial view of HVO in April 1986. New building (completed 1986) is at left, Halemaumau Crater in background.

Ceremonial Figure
Hawaiian Petroglyph
Nuuanu, Oahu

HISTORY OF INVESTIGATIONS OF HAWAIIAN VOLCANISM

This section could as well have introduced the present work on Hawaiian volcanism as concluded it. Its three chapters deal with some of the earliest known published works on Hawaiian volcanoes and with the background and development of the Hawaiian Volcano Observatory.

Chapter 60 examines the contributions of James Dwight Dana and the U.S. Exploring Expedition of 1840-41. That expedition, which focused on the Pacific Ocean, where most of Earth's active volcanoes reside, greatly advanced the study of volcanoes, and Hawaiian volcanology may be said to have begun with Dana, the expedition's geologist.

The following chapter chronicles the colorful history of the Hawaiian Volcano Observatory, beginning with the digging of the foundation for its first building in 1912. It recounts the dominating role of Thomas A. Jaggar in the early years of HVO and the variety of pioneering and experimental researches done during that time. Instruments and equipment were often designed and built at the Observatory and then field tested in "trial-by-fire" fashion.

The final chapter is a chronological listing of the staff of HVO since its beginning. It tells some of the social history of the Observatory and shows how the staff has grown—fairly slowly, considering the evolution of volcano-monitoring techniques and the corresponding increase in data. Compiling the list generated fond memories of the mechanical and early electronic ages at HVO, when gathering data was simpler and the pace more leisurely than in the present age of computers and telemetry. Some staff from those earlier times are still at HVO, giving continuity to changes in techniques, to the eyewitness record of volcanic events, and to the anecdotal record of the people who created and sustained the Hawaiian Volcano Observatory.

JAMES D. DANA AND THE ORIGINS OF HAWAIIAN VOLCANOLOGY: THE U.S. EXPLORING EXPEDITION IN HAWAII, 1840–41

By Daniel E. Appleman[1]

*The Hawaiian * * * group is consequently the key to Polynesian Geology.—J.D. Dana, 1849*

ABSTRACT

Scientists and naval officers of the U.S. Exploring Expedition of 1838–42 performed the first systematic volcanologic and geologic research in the Hawaiian Islands. During their 6-month stay they surveyed and mapped Kilauea and Mauna Loa Volcanoes during a period when Kilauea was in continuous summit eruption. James D. Dana, the expedition geologist, made pioneering contributions in characterizing the development and eruptive style of Hawaiian volcanoes and in interpreting the geology of Kauai, Oahu, Maui, and Hawaii. He correctly deduced the age progression in the Hawaiian group based on degree of erosion, and he used his work in Hawaii as the basis for interpreting the regional geology of the Pacific. Dana's monumental geology report, published in 1849, constitutes a virtual textbook of Hawaiian volcanology and geology.

INTRODUCTION

On September 20, 1840, the U.S. Exploring Expedition, Lt. Charles Wilkes commanding, arrived in the Hawaiian Islands. Modeled after the great European scientific expeditions of Cook and Malaspina, the "Ex. Ex." was charged with mapping and charting little-known regions of the Pacific and Southern Oceans, advancing the diplomatic and commercial interests of the United States, and performing scientific exploration. Although it was an operation of the U.S. Navy, the expedition carried a corps of civilian scientists, who were responsible for the natural-history investigations. Indeed, much of the impetus for the expedition had come from American scientists, anxious to join their European colleagues in exploring the natural wonders of the globe.

By the time it reached Hawaii the expedition was 2 years old. In those years the voyagers had sailed the coasts of South America and Tierra del Fuego, had made two forays into Antarctic waters, and had demonstrated the existence of the Antarctic Continent. They had visited Australia and New Zealand and explored many of the island groups of the South Pacific. Now, after four difficult and dangerous months spent mapping and collecting in the Fiji Islands, they were looking forward to a peaceful stay in the civilization of Hawaii. Here they would refit the ships after their long months at sea. Meanwhile they would investigate the natural history of this land of active volcanoes, one of the prime scientific objectives of the expedition.

ACKNOWLEDGMENTS

Various members of the Smithsonian Institution staff contributed to the preparation of this paper. I would especially like to thank my colleague Tom Simkin for many helpful discussions. Carolyn Margolis provided invaluable assistance in obtaining illustrations, Chip Clark made high-quality prints for figures 60.1, 60.2, and 60.7, and Lynnetta Jones performed yeoman service in typing the manuscript.

THE SCIENTISTS

The scientific corps of the Exploring Expedition consisted of nine men, expert in various aspects of zoology, botany, philology, and geology. Foremost among them was James Dwight Dana, later to become one of the giants of American geology. Dana was only 27 years old in 1840, but he was already well known as the author of the "System of Mineralogy," published in 1837. Dana received his excellent scientific training at Yale College, thanks to the extraordinary school of natural science established by Benjamin Silliman. Here he acquired a consuming interest in geology and mineralogy, and an intensely professional approach to scientific research that was unusual at that period.

Upon graduation from Yale in 1833, Dana was unable to find an academic position in natural science and so signed up as mathematics instructor aboard the U.S. Navy ship *Delaware* for service in the Mediterranean. During the 16-month cruise he ascended the volcano Vesuvius, then in an active phase, and recorded detailed geologic observations. He sent these back to Professor Silliman, who promptly published them in the American

[1]Department of Mineral Sciences, Smithsonian Institution, Washington, D.C. 20560.

Journal of Science (Dana, 1835). Dana's observations on Vesuvius, made just before an eruption in 1834, seem to constitute the first description of an active volcano by an American geologist. Thus began Dana's lifelong love affair with volcanoes: he was, indeed, the first American volcanologist.

Although Dana was principally responsible for the geological department of the expedition, other members of the scientific corps contributed significantly to the geological studies of the Hawaiian Islands. Charles Pickering, a zoologist originally trained as a medical doctor, did superb geologic field work. Joseph Drayton, an expert scientific illustrator, made careful measurements and drawings of the great craters. And Titian Peale, a zoologist who was a member of the famous family of American artists, made the paintings and sketches which show so well the appearance of Kilauea in 1840.

Numerous geologic observations were also made by the naval officers, especially Commander Charles Wilkes. Wilkes had been chosen to lead the expedition largely because of his scientific background (Stanton, 1975). He personally directed the surveying and mapping, as well as the geophysical, meteorological, and hydrographic studies, and felt qualified equally with the scientists to describe and interpret the geological phenomena.

To follow the geologic investigations of Dana and the other scientists in the islands, it is necessary to understand the logistics by which the expedition operated. The scientists were distributed between two of the expedition's four ships: the flagship *Vincennes*, under Commander Wilkes, and the *Peacock*, under Captain Hudson. Dana and Peale were on the *Peacock*, Pickering and Drayton on the *Vincennes*. The *Vincennes* arrived in Honolulu on September 24, 1840, and the *Peacock* on September 30. After several weeks of socializing and field work on Oahu, Dana, Pickering, Peale, and most of the other scientists were ferried over to Kauai on October 25 on the tender *Flying Fish*, the expedition's smallest ship. They spent six days exploring Kauai, returning to Oahu on November 3.

Wilkes planned next to proceed to the Island of Hawaii himself in the *Vincennes*. There he proposed to spend several months erecting an observatory on the summit of Mauna Loa, and observing the active volcanoes. Meanwhile he had ordered the *Peacock* to return to the South Seas to finish charting in the Samoan, Gilbert, and Marshall Islands. The various ships would rendezvous at the end of April at the mouth of the Columbia River in Oregon Territory.

Thus Pickering, the zoologist, would spend two months on the volcanoes of Hawaii, while Dana, the geologist, would examine more coral islands and empty ocean. Fortunately repairs to both ships took longer than expected, and Wilkes allowed Dana, Peale, and the others from the *Peacock* to take the tender from Oahu to Hawaii. They landed on the west coast at Kealakekua Bay on November 14, crossed the island in less than a week, and returned to Honolulu by the 28th. It is clear that Wilkes felt he personally must make the important observations on Hawaii. Furthermore, he saw no need to switch Dana's assignment, since to him the scientists were more or less interchangeable—he called them all "naturalists."

The *Peacock*, with Dana aboard, left for the South Seas on December 2; the *Vincennes*, with Wilkes, Pickering, and Drayton, arrived in Hilo on December 9. During the next 2 months the indefatigable Pickering climbed both Mauna Loa and Mauna Kea and made three visits to Kilauea. On February 15, 1841, Pickering and Drayton left the Island of Hawaii to spend a month exploring Maui, where they were joined by Wilkes on March 6. On March 19 the whole party returned to Oahu, and on April 5 the *Vincennes* departed for the Oregon Territory.

ORIGINAL SOURCES

The principal publication on the geological work of the expedition in Hawaii is volume 10 of the reports of the U.S. Exploring Expedition: "Geology" (Dana, 1849). In this volume Dana brings together the results of all the expedition scientists and data from many other investigators, to create what is almost a textbook of Hawaiian geology and volcanology. Except where otherwise stated, all references to Dana's work in the present paper are from this volume.

Another valuable source is the unpublished journal of Charles Pickering (Pickering, 1840–41), reporting in detail the observations summarized by Dana (1849). Dana's field notebooks in the Yale University Library contain much of the raw data used in his report. Volume 4 of the narrative of the Exploring Expedition (Wilkes, 1844) contains Wilkes' own account of the expedition's visit to Hawaii, drawn from the journals of all of the expedition's officers and scientists.

KILAUEA

The appearance of Kilauea caldera in late 1840 is well shown in the expedition map (fig. 60.1) and in the drawing by Drayton (fig. 60.2), made with the help of a camera lucida from the northwest rim near the western end of Steaming Bluff. The outer walls were 198 m high at their highest point, Uwekahuna Bluff. Below them was the Black Ledge, the outer rim of the former caldera floor; 183–610 m wide, it encircled the entire caldera. Within the Black Ledge, the inner pit was 104 m deep and approximately 3.6 km long by 1.2 km wide. The partly isolated basin at the southwest end of the inner pit corresponded to the present location of Halemaumau (figs. 60.3*A*, 60.3*B*). By comparison, the outer walls in 1981 were about 145 m high at Uwekahuna, and Halemaumau, the only present-day vestige of the inner pit, was about 79 m deep. Except for the shallower floor, the general features of the outer walls shown by Drayton are still readily recognizable.

Dana attempted to reconstruct the history of changes within the caldera from the sporadic accounts of visitors, starting in 1823, when it looked much as in late 1840. By early 1832 the entire caldera was filled to within about 185 m of the top with "solid lava" (Martin, 1979), burying the Black Ledge. Later in 1832 the central portion of the caldera floor collapsed, and the Black Ledge appeared again. By 1839, continued summit eruptions had refilled the basin, once more burying the Black Ledge. During the great flank eruption of May–June 1840 the central portion sank yet again, leaving the caldera as the expedition found it. This pattern of

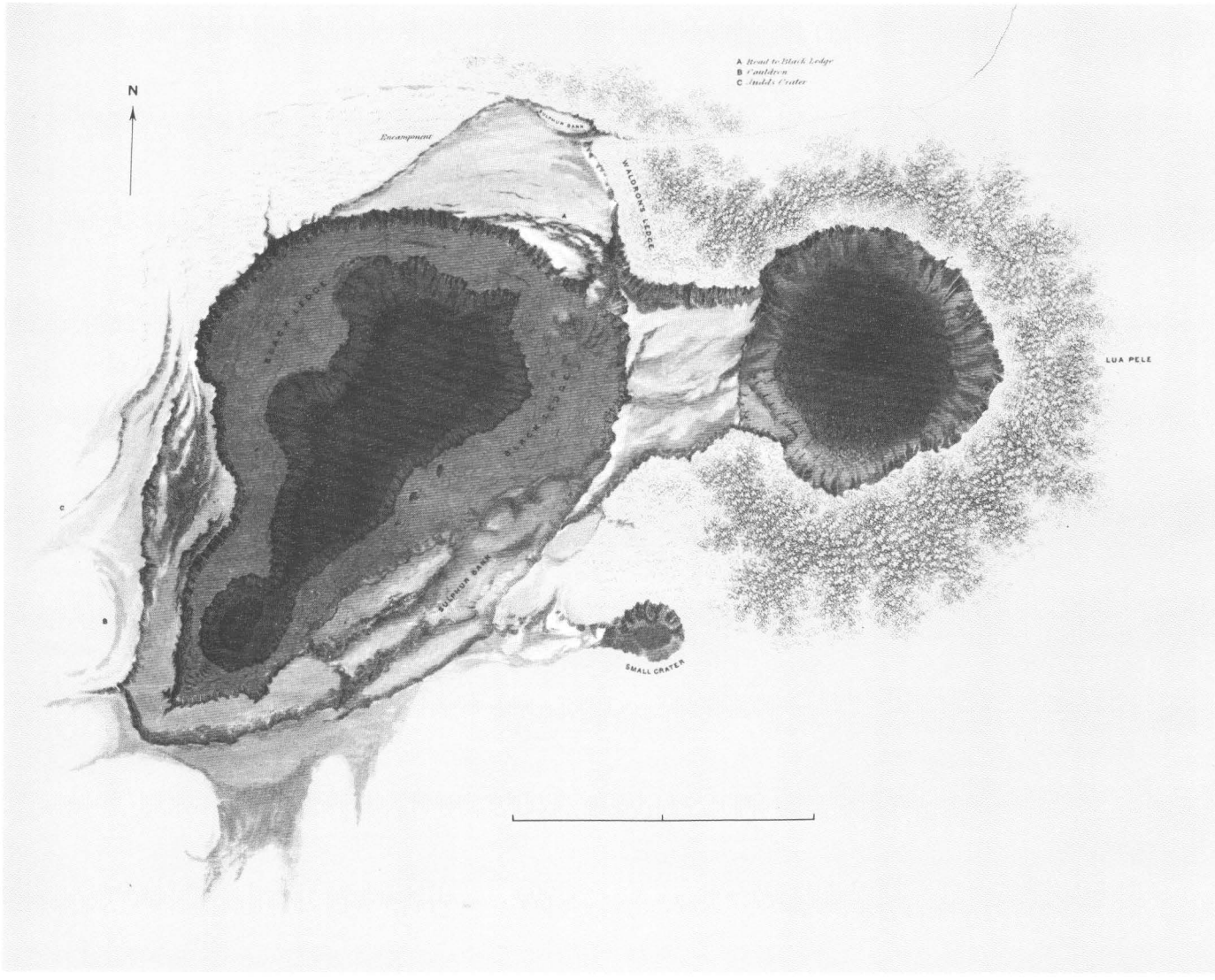

FIGURE 60.1.—Map of the crater of Kilauea made by the U.S. Exploring Expedition, 1841 (from Wilkes, 1844, v. 4, p. 177). North is at top; scale bar represents 8,000 ft.

changes was to be repeated with variations for several decades, until the Black Ledge disappeared for good around 1886 when the caldera floor reached a level close to what we see today (Dana, 1890).

When Dana visited Kilauea in late November 1840, the inner basin contained three lava lakes in continual eruption. The largest was in the present location of Halemaumau; two smaller lakes were on the western and eastern sides of the basin (fig. 60.4). Dana described in meticulous detail the character of these summit eruptions: the lava fountains, the currents within the lakes, the various driblet cones and other constructional features, the sequence of activity. He was particularly impressed with the "remarkable fluidity of the lavas" (Dana, 1849, p. 178); he observed the formation of Pele's hair as a particularly striking phenomenon depending on this fluidity.

Although Dana was allowed to spend only one day at Kilauea, he was able to draw on Pickering's and Wilkes' accounts of its behavior over a three-month period. Pickering in particular records the rapid changes occurring within the inner pit; only Halemaumau remained in constant eruption, though undergoing dramatic changes in level (Pickering, 1840–41).

THE ERUPTION OF 1840

The Exploring Expedition scientists were lucky in the timing of their visit. Not only was Kilauea in continuous summit eruption, but its greatest flank eruption of historical times had just taken place: the east-rift eruption of May–June 1840 (Macdonald and others, 1983). Dana visited the still-steaming flow where it had entered the sea at Nanawale, destroying the village and throwing up large littoral cones. Pickering spent several days tracing the course of the

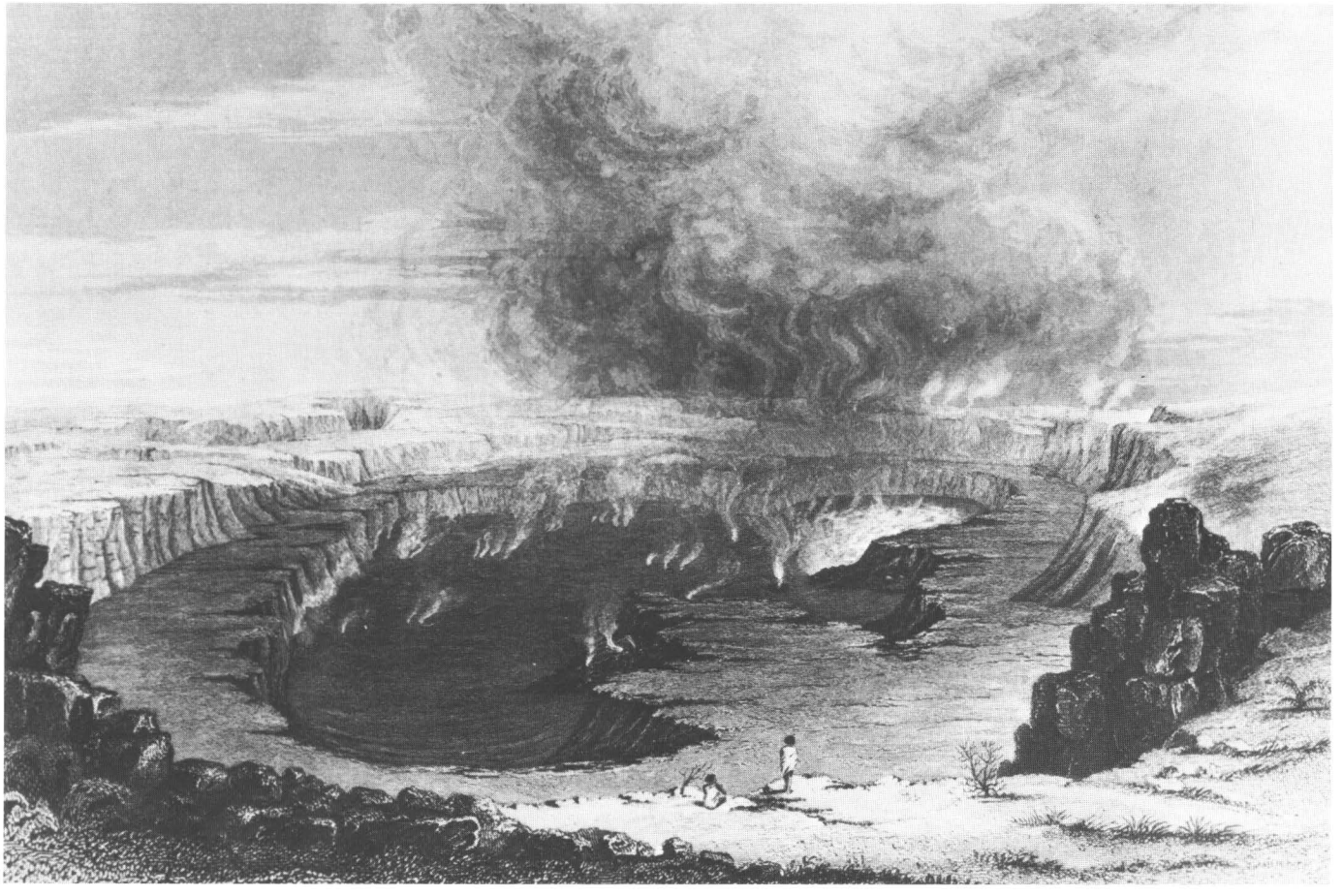

FIGURE 60.2.—"View of crater Kilauea" by Joseph Drayton (from Wilkes, 1844, v. 4, p. 134). View looking south from western end of Steaming Bluff. Kilauea Iki Crater is visible to left of center; constricted part of inner pit at far end is present location of Halemaumau.

eruption and describing its thickness and extent; he, Drayton, and Wilkes produced a map of the 1840 flows that appears in the narrative of the expedition (Wilkes, 1844, v. 4).

The 1840 eruption had a great influence on Dana's thinking; it became in his writings the type example of a flank eruption. The conjunction of this eruption with the collapse of the inner pit of the summit caldera led Dana to conclude that the two events were cause and effect. From the map area and thickness he estimated the volume of lava represented by the flows, obtaining a value of 170×10^6 m^3. Macdonald and others (1983) give an estimate of 205×10^6 m^3 for this eruption. Dana compared the volume of the flows with the volume of the subsidence in the caldera, estimated at 436×10^6 m^3; the difference he attributed to the part of the flows below sea level and to filling of fissures.

The 1840 eruption emphasized to Dana the importance of the rift zones as loci of flank eruptions. He described the southwest rift zone briefly and the east rift zone at length, basing his account on Pickering's detailed field study. Pickering had crossed the rift from Pahoa to Kaimu, followed the coast to Kamoamoa, and ascended near the Kalapana Trail to Makaopuhi Crater. From Puu Huluhulu he mapped the major pit craters, and he observed the evidence of the progress of the 1840 eruption as it migrated down the rift from its beginnings in Alae (Pickering, 1840–41).

CALDERAS, PIT CRATERS, AND COLLAPSE

From his observations at Kilauea Dana acquired a profound sense of the importance of collapse in volcanic edifices. The subsidence of the inner pit during the 1840 eruption was to him a model for the formation of the summit caldera. The pit craters of the east rift zone he likewise associated with collapse following injection of magma along the rift. The whole idea of withdrawal of magma followed by subsidence of the edifice became central to his thinking, and ultimately it led him to explain correctly the great Krakatau eruption of 1883 as involving explosive eruptions of liquid lava as volcanic ash followed by collapse of the volcano into the space left empty by the discharge (Dana, 1888).

MAUNA LOA AND "LAVA DOMES"

During his brief stay on Hawaii, Dana traveled around the southern flank of Mauna Loa from Kealakekua Bay to Kilauea,

more or less along the line of the present Highway 11. Most of his information about Mauna Loa, however, came from Pickering and the naval officers, who ascended the mountain and mapped and explored the summit. Besides describing the summit caldera and associated pit craters, Pickering noted the rift zones, especially the northeast rift. Dana also included in his 1849 report a detailed account furnished by Rev. Titus Coan of the large 1843 eruption from this rift zone, during which some flows may have been more than 40 km long.

Mauna Loa was Dana's type example of a basaltic shield volcano, just as Kilauea was his model for the eruptive style that created such volcanoes, which he termed "lava domes." He described at length how so broad a dome could be built by a combination of summit and flank eruptions such as he had observed. Dana also contrasted the quiet eruptive style of these volcanoes with the more violent eruptions of volcanoes like Vesuvius, which resulted in steep cones. He attributed the quiet style to the extreme fluidity of the basaltic lava, which he could not, however, satisfactorily explain.

Dana recognized the lava of Kilauea as typical of shield-forming eruptions, and tried to understand the difference between pahoehoe and aa. He observed that pahoehoe flows could change to aa as they traveled away from the vent; thus the two could not differ in composition. All he could suggest in explanation, however, was that cessation of flow followed by renewed motion created the clinkery aa.

Finally, Dana used the Mauna Loa-Kilauea system as an example of what he called the isolation of the lava conduits. The occurence of an eruption near the summit of Mauna Loa or high on the rim of the Kilauea caldera, without disturbance of the active lava lakes, he interpreted as evidence for many entirely separate conduits, connected only at great depth.

VOLCANIC CONES

Besides "lava domes" (basaltic shields) and their associated pit craters, Dana recognized two other types of volcanic edifice in Hawaii: these he called "cinder cones" and "tufa cones" (tuff cones). He correctly described the origin of cinder cones as "the result of ejections of the melted lava to such heights that it falls in showers of dry cooled scoria, cinders, or ashes" (Dana, 1849, p. 354). He realized that the hundreds of such cones visible on Mauna Loa and Kilauea were relatively minor features, mostly formed where continued fountaining had occurred along rifts, but that they became more important in the later stages of a volcano's eruptive history, as on the summit of Mauna Kea.

The tufa cones were best described by Dana on Oahu, where he spent most of his time in the islands. After studying the magnificent cones of Diamond Head and Koko Head (fig. 60.5) he accurately ascribed their origin to explosive eruption through water or wet rocks, which chilled and fragmented the lava into smaller particles than the cinder and scoria of the drier cinder cones. He also noted their asymmetry due to eruption during trade winds and their layers dipping inward and outward. Dana also classified as tufa cones what are now called littoral cones, such as the Nanawale sand hills. Though he knew these had formed where the 1840 flows entered the sea, he thought the lava had erupted from a rift beneath the sea floor, and thus he wondered at the lack of a central crater.

THE ERUPTION OF 1790

When the expedition visited Kilauea, the devastation to the south of the caldera from the great explosive eruption 50 years before was still very obvious: it is clearly shown in Peale's painting "Volcano of 'Kaluea Pele' as seen from the side of Mauna Loa, looking S.E., Nov. 21, 1840" (fig. 60.6). Dana reprinted the account recorded by a missionary from eyewitnesses to the blast, which killed a large party of Hawaiian warriors. Later Dana (1888) explained such rare explosive eruptions as the result of ground water penetrating to the molten lava, deep within the volcano, and flashing into steam—which with some modifications, is not too far from modern interpretations (Decker and Christiansen, 1984). He also convinced himself that explosive eruptions were indeed rare events in Hawaiian volcanoes like Kilauea, because he observed no pyroclastic deposits exposed in the caldera walls or in dissected shields on Oahu or Maui, which he visited in 1887.

THE ASCENT OF MAUNA LOA

No account of the Exploring Expedition in Hawaii can fail to mention Commander Wilkes' proudest scientific achievement: the establishment of a geophysical observatory atop 4,169-m (13,679-ft) Mauna Loa. True to his plans, he led to the summit a party of 16 expedition members and 200 Hawaiian porters, laden with scientific instruments, food, and supplies. It was not a pleasant place in midwinter: water froze in the tents in the daytime, and the wind was violent and seemed incessant. Here the men spent three arduous weeks making meteorological, gravity, and magnetic measurements (Borthwick, 1965) and mapping the summit region and Mokuaweoweo caldera.

The expedition called their camp "Pendulum Peak" after the most cumbersome of their instruments. They had to erect massive stone walls to protect both instruments and men from the biting winds, which destroyed some of the more delicate barometers despite their best efforts. The ruins of these walls are visible today on the summit—a tangible remainder of the first U.S. Government-sponsored geophysical observatory in the Hawaiian Islands.

Wilkes' measurements were meant to be published as volume 24, "Physics," of the reports of the expedition, but this volume never appeared. Much of the data is preserved in the U.S. National Archives, and the magnetic results were published almost a century later by Ennis (1934). The meteorological results are also discussed by Ramage (1978), who points out that Wilkes came close to discovering the trade-wind inversion.

OAHU AND KAUAI

Dana correctly discerned that Oahu was composed of two deeply eroded shield volcanoes and Kauai of a single eroded edifice.

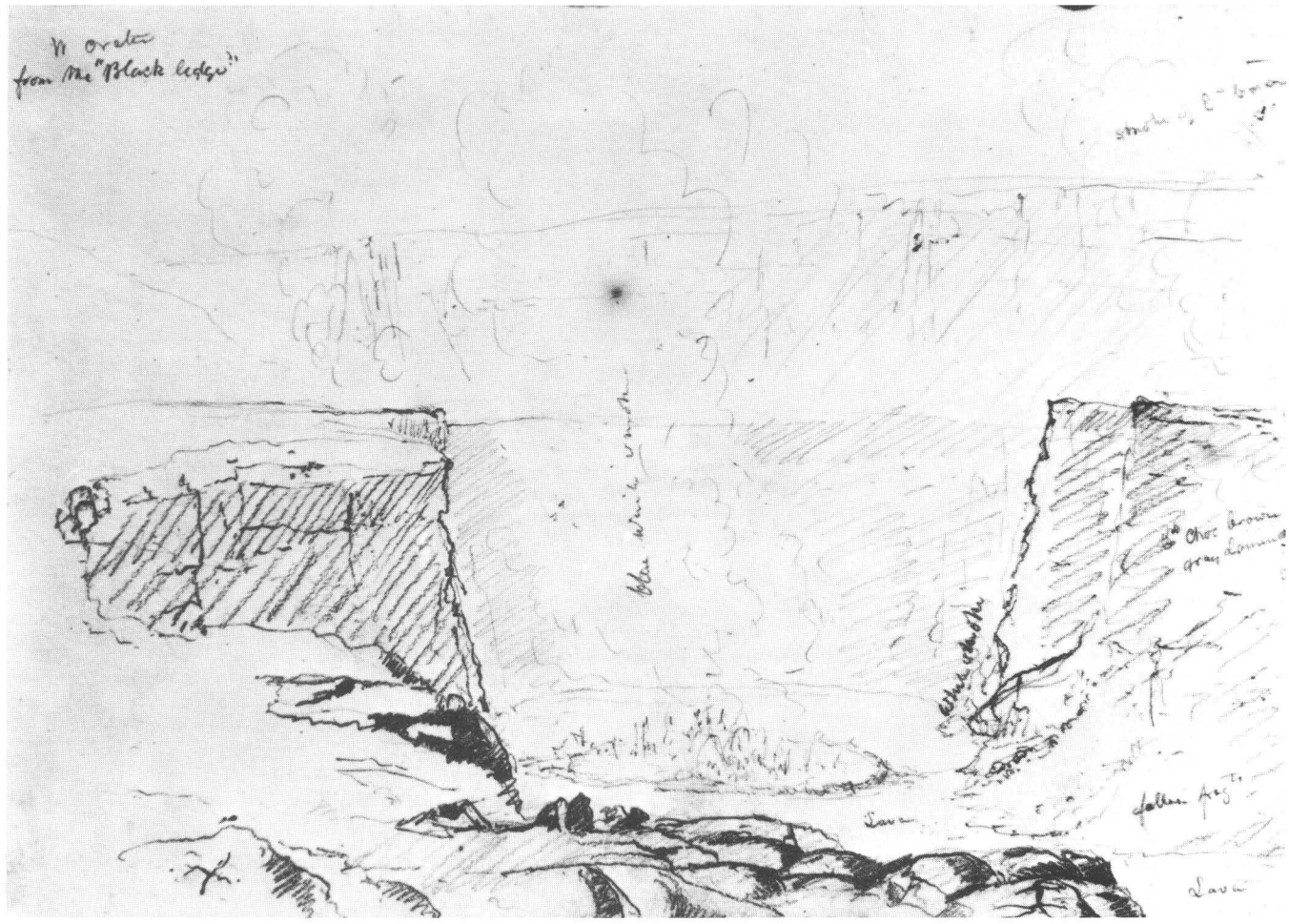

A

FIGURE 60.3.—Sketch and painting of western inner pit of Kilauea caldera by T.R. Peale. Courtesy American Museum of Natural History. ***A***, Sketch of "W. crater from the 'Black Ledge,'" drawn in 1840. View is of constricted part of inner pit at present location of Halemaumau, showing active lava lake. The artist has made notes to assist him in making the final painting. ***B***, Oil painting "West crater 'Kaluea Pele' from the Black Ledge'" dated November 1840. Painting presumably based on the sketch (*A*) done on the spot.

He noted that the outer flanks of the volcanoes were composed largely of thin-layered flows, but that toward the center the flows became much thicker and the layering in places disappeared altogether. Drawing on his knowledge of Kilauea, Dana attributed this to the inferred presence of thick lava bodies representing lava lake fill within the caldera region. This is roughly the interpretation of modern workers (Macdonald and others, 1960; Stearns and Vaksvik, 1935). Dana had noted the same phenomenon on Tahiti. On both Kauai and Oahu he identified posterosional eruptive phases that built prominent cinder and tuff cones (fig. 60.7). These are parts of what were later defined as the Koloa Volcanic Series (currently called the Koloa Volcanics) on Kauai by Macdonald and others (1960) and the Honolulu Volcanic Series (currently called the Honolulu Volcanics) on Oahu by Stearns and Vaksvik (1935); for a review of stratigraphic nomenclature, see Langenheim and Clague (chapter 1, part II). For Oahu Dana even made a kind of colored geologic map delineating shield volcanoes, the Honolulu Volcanics cones, coral reef, upraised coral-reef rock, and coral-sand rock (Dana, 1849).

Dana realized that the eastern half of the Koolau shield volcano of Oahu was missing, truncated by the Pali. He did not believe that this type of destruction could be caused by wave or stream erosion alone and attributed it to a rupture of the dome, with the eastern half sliding into the sea. "The portion of the great volcano cut off at the rupture has disappeared beneath the ocean" (Dana, 1849, p. 259). This view is very close to the landslide hypothesis advanced by Moore (1964) for the Koolau shield and more recently supported by Holcomb (1983). Dana believed the same mechanism was responsible for the Napali coast of Kauai and possibly for other apparent truncations.

B

FIGURE 60.3.—Continued.

Dana also pointed out that the eastern precipice of Niihau cuts off the eastern portion of that shield; this has been attributed to faulting, rather than wave erosion alone, by Macdonald and others (1983). If this portion of the shield is restored, then Niihau and Kauai lie on a line nearly perpendicular to the trend of the main islands. This statement has been misread by Macdonald and others (1983), who state that Dana said that Niihau represents the northwest edge of Kauai, shifted laterally by faulting; he did not.

PETROLOGY

Dana distinguished two main groups of lava types in the Hawaiian Islands: those in which feldspar was not dominant, which he termed basalt, and those with dominant feldspar, which he called variously clinkstone, trachyte, syenite, or merely feldspathic. He thought that the feldspathic varieties tended to occur near the centers of the mountains, because that was where the expedition scientists reported them. This misconception may have arisen because, with no geologic mapping, Dana was unaware of the capping of the original shield basalt by later, more differentiated postcaldera lava on Mauna Kea, Haleakala, and other shields (Stearns and Macdonald, 1942).

Pickering and Dana also observed the varied distribution of olivine; they especially noted that abundant large crystals were present in the 1840 flow erupted at low altitude, while summit lava erupted almost simultaneously contained little or no visible olivine (Macdonald, 1944). Dana speculated at length on possible mechanisms for differentiation, rejected the idea proposed by Darwin (1844) for differentiation by crystallization and gravity separation, and came to no clear conclusion. He did, however, suggest the

FIGURE 60.4.—"Sketch of Kilauea Pele, island of Hawaii" by T.R. Peale. Sketch shows main (Halemaumau) lava lake in background and (presumably) westernmost of two smaller lava lakes, observed by Dana, in foreground. Sketch was used by Peale as basis for an oil painting of a night scene of crater. Courtesy of American Museum of Natural History.

possibility of portions of lava being separated within the flanks of the volcano from the main body before differentiation. The evolution of magma compositions with time in the life cycle of a volcano was only indirectly hinted at.

It is clear that Dana was trying to distance himself as much as possible from the Wernerian concept, then only 60 years old, that particular rocks were only formed at particular times in the Earth's history. "If the elements are at hand," he wrote, "it requires only different circumstances as regards pressure, heat, and slowness of cooling, to form any igneous rock the world contains." Thus, in "a basaltic mountain with a feldspathic center***we are not compelled to suppose the feldspathic interior to have formed first or last" (Dana, 1849, p. 377–378).

SUBSIDENCE, ELEVATION, AND CORALS

One of Dana's major contributions in the geology report was the confirmation and expansion of Darwin's subsidence theory of the origin of coral atolls (Darwin, 1842). Based on the expedition's observations of hundreds of islands in the South Pacific, Dana proposed that as oceanic volcanoes become extinct, fringing coral reefs form around them. The volcanic edifices then gradually subside, but the corals grow upward fast enough to keep pace with the subsidence, forming first barrier reefs around the volcano's sinking summits and finally atolls with no central volcanic peak. His data led Dana to conclude that the subsidence in the Pacific was on a very large scale, related to global tectonism. In the Hawaiian Chain, Dana saw this progression from still-active Hawaii with practically no reefs, through Oahu and Kauai with extensive fringing reefs, to the northwestern islands that are all coral, indicating greatest subsidence at the western extremity.

Dana found no such global pattern in evidences of major elevation. He observed many reefs elevated a few meters, but only scattered, apparently random instances where uplift of 75 m or more could be demonstrated, such as at Metia Island in the Tuamotus. In the Hawaiian Islands, Dana reported elevation of 7–9 m on Oahu,

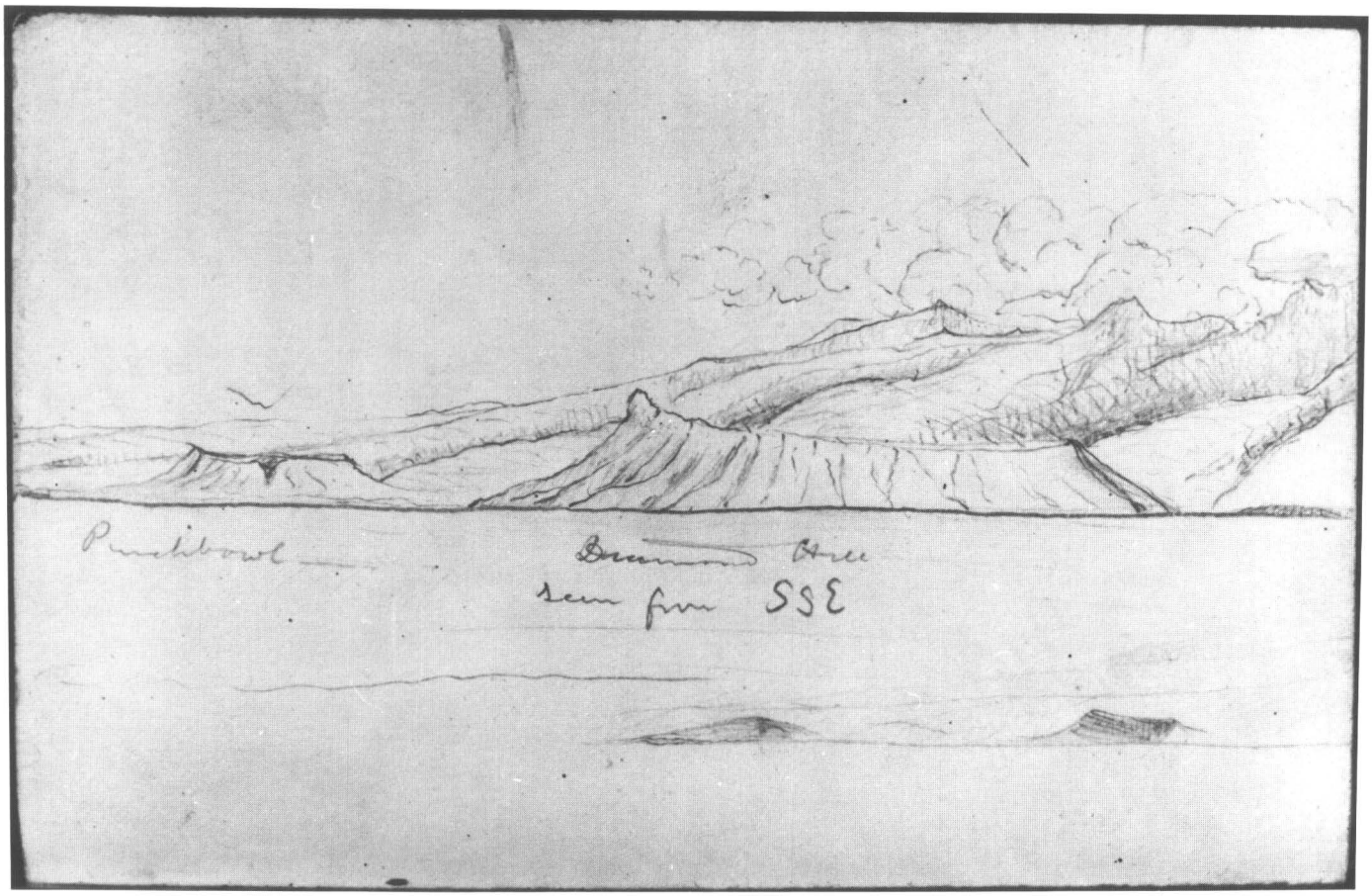

FIGURE 60.5.—Sketch of "Diamond Hill and Punchbowl seen from SSE" from Dana's field notebook "New Zealand, Tonga to Feejees, Sandwich Islands," Dana Family Papers, Box 6, Folder 134, Yale University Library. Dana recognized these tuff cones as much younger than the shield volcanoes and observed greater erosion of Diamond Head compared to Koko Crater, as shown by truncation of internal structure.

but both he and his colleague J.P. Couthouy were extremely skeptical of reports of coral at 65–70 m on Maui and Molokai. Recent work by Moore and Moore (1984) suggests that these coral-bearing gravels, like others on Lanai, were deposited by a giant landslide-triggered sea wave, and there is no evidence for such a high stand of the sea. Dana, of course, did not in 1840 know about the Pleistocene eustatic changes in sea level responsible for the lower reef-rock terraces.

Recent work, summarized by Scott and Rotondo (1983), indicates that the regional Pacific subsidence delineated by Dana is largely from the sinking of the Pacific plate as it moves away from the spreading centers and cools; this is a truly global effect. Instances of large elevation, such as Metia, on the other hand, are probably local in origin, thus bearing out Dana's conclusions.

EROSION, AGE PROGRESSION, AND ISLAND CHAINS

Perhaps the best known of Dana's contributions to Hawaiian geology was his recognition of a systematic age progression within the chain of islands. He took Mauna Loa as the type of a still-active, virtually uneroded shield volcano. Mauna Kea was clearly a very similar shield, but it was no longer active. Its eastern side, exposed to the trade winds, was beginning to be heavily gullied, while its protected western side was nearly untouched: proof of stream erosion working since the volcano became extinct. Thus, Dana reasoned, the degree to which a shield volcano was eroded was a measure of the time elapsed since it had become effectively extinct.

Applying this reasoning, he worked out the following sequence of extinction (from oldest to youngest): Kauai, Waianae, West Maui, Koolau, Mauna Kea, Haleakala, and finally Mauna Loa. He was misled to some degree on the older islands by his failure to recognize renewed massive posterosional volcanism, which masked the old eroded topography. On Haleakala, Pickering had described well the unique aspects of Haleakala Crater; he almost always referred to it as a "valley" and pointedly mentioned the very youthful appearance of the lava flows within it (Pickering, 1840–41). Dana, who did not visit Maui during the expedition, interpreted the crater as having formed by fissuring during the last great eruptions; the modern view of its origin by stream erosion did not occur to him (Stearns and Macdonald, 1942). He held to his view even after

FIGURE 60.6.—Painting of "Volcano of 'Kaluea Pele' as seen from the side of 'Mauna Loa', looking S.E. Nov. 21, 1840" by T.R. Peale. Peale crossed the island from Kealakekua Bay by Ahua Umi Heiau, around north side of Mauna Loa at elevation of about 3,000 m and down to Kilauea. Rare silverswords (lower right corner) are now extinct in this area. Courtesy American Musuem of Natural History.

visiting Haleakala in 1887.

The most severe limitation on Dana's concept was his insistence that the geologic evidence showed only an age progression of extinction of the Hawaiian volcanoes, not one of formation. "From Kauai to Mauna Loa all may have thus simultaneously commenced their ejections, and have continued in operation during the same epoch till one after another became extinct***. No facts can be pointed to, which render it even probable that Hawaii is of more recent origin than Kauai, though more recent in its latest eruptions" (Dana, 1849, p. 280). This overly rigorous interpretation of the geologic evidence forced Dana to adopt a static model for origin of the volcanoes by rupture of fissures, which must become wider toward the southeast. Dana's colleague J.P. Couthouy, the expedition conchologist, was more daring. He wrote to Dana, "The foregoing observations are applied to the course of volcanic action at the islands taken separately, with a view to show that it has been sucessive in each, from the western to the southeastern extremity of the group, and the possibility that they were also forced up in regular succession by the subterranean fire. The phenomena they present seem to point to such an origin***" (Dana, 1849, p. 283). Dana never did accept the idea of sequential origin (Dana, 1890).

As others had before him, Dana described the parallel orientation of many Pacific island chains, but he did this at a level of detailed analysis not previously attempted and with a much larger data base. He suggested that the Society Islands showed the same age progression as the Hawaiian Chain, and he clearly implied this was a general trend in chains parallel to Hawaii, although he lacked sufficient data to confirm this. The Samoan Chain, also parallel to the Hawaiian, he considered to have a reverse progression. Recent studies (Natland, 1980; Natland and Turner, 1985) show that the Samoan shield volcanoes do conform to the Hawaiian age progression, but that the older islands to the northwest have been subjected to voluminous posterosional volcanism, possibly related to bending of the Pacific plate.

Dana devoted many pages to painstaking description of the arrangement of the islands. He noted that the 15 Hawaiian volcanoes which he identified actually lie along two parallel trends, and that this same phenomenon was present in other chains (Jarrard and

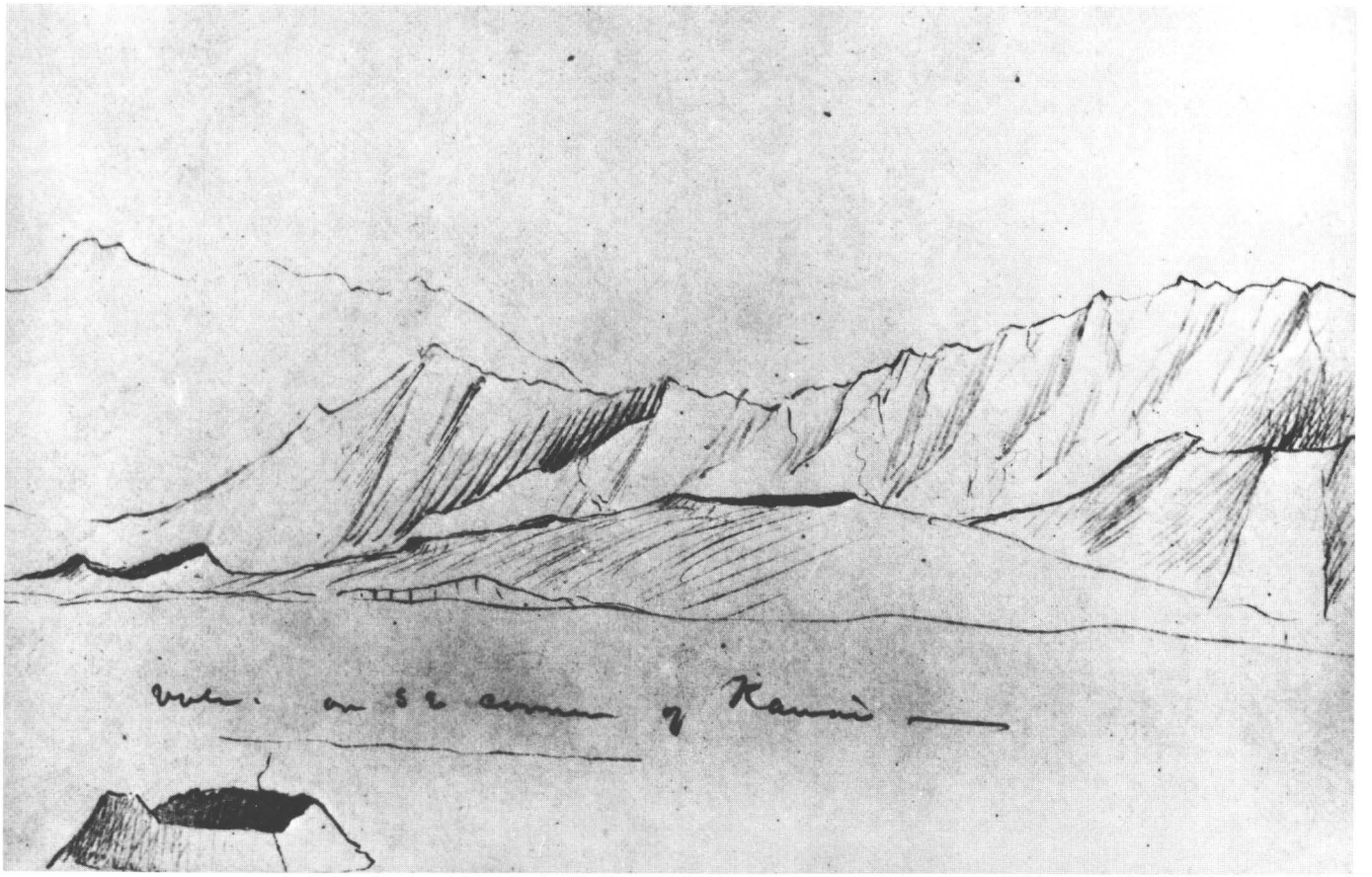

FIGURE 60.7.—Sketch of "View on SE corner of Kauai" from Dana's field notebook "New Zealand, Tonga to Feejees, Sandwich Islands," Dana Family Papers, Box 6, Folder 134, Yale University Library. Dana noted that Hoary Head Range (background) appeared anomalous in terms of shield volcano structure; modern workers have identified it as massive lavas formed in the only flank calderas known on Hawaiian volcanoes (Macdonald and others, 1983). Cones (foreground) are Koloa Volcanics.

Clague, 1977). Dana showed that the "linear chains" were actually broken up into shorter segments arranged in echelon fashion along the trend, and he attempted to relate their geometry to an oceanwide or even global fracture pattern. Some modern workers (for example, Jackson and Shaw, 1975) agree with his observations and propose that the pattern is related to stress in the Pacific plate, an idea to which Dana would certainly have been sympathetic.

Dana's work on linear island chains in the Pacific was clearly of great importance in the development of modern plate-tectonic theory, especially as the direct forerunner of the various hot-spot hypotheses (Wilson, 1963a, b; Morgan, 1972a, b). The difficulties of age interpretation that plagued Dana have not all disappeared with modern dating techniques (Jarrard and Clague, 1977; Jackson and others, 1980). A final example of Dana's acumen in this regard: By extrapolating from observed levels of activity, he calculated (somewhat apologetically) the time required to build the subaerial portion of Mauna Loa as 400,000 years, a figure not far out of line with many modern radiometric measurements on shield volcanoes (Macdonald and others, 1983).

CONCLUSIONS

The geological investigations of the U.S. Exploring Expedition in Hawaii constitute the beginnings of modern volcanology and geology in the islands. Unlike the episodic and often anecdotal scientific reports of previous visitors, Dana's geology report attempted to be as precise, quantitative, and complete as possible. The careful surveys by Wilkes and his officers of Kilauea and Mokuaweoweo calderas, and their maps of the volcanoes, provided the first accurate base for measurement of future changes.

Dana recognized the great importance of Kilauea and Mauna Loa as a natural laboratory of volcanology, and for the rest of his long life he tried to keep a systematic account of eruptions and changes in the volcanoes (Dana, 1890). Although a semi-invalid, he returned to Hawaii in 1887 at the age of 74 to revisit Kilauea, this time without the restrictions of a naval expedition, before writing his book "Characteristics of Volcanoes" (Dana, 1890). His ideas on volcanoes changed surprisingly little over the years, however, and remained heavily influenced by his work during the Exploring

Expedition. These ideas, disseminated through Dana's highly popular textbooks and prolific writing of technical papers, were in turn influential in the development of geologic thought in the last half of the 19th century. In a very real sense Dana can be considered the spiritual godfather of the Hawaiian Volcano Observatory, which from its inception has continued the tradition of Hawaiian volcanology that he had begun so many years earlier (Jagger, 1947, abstract).

REFERENCES CITED

Borthwick, D.E., 1965, Outfitting the United States Exploring Expedition: Lieutenant Charles Wilkes' European assignment, August–November, 1836: Proceedings of the American Philosophical Society, v. 109, no. 3, p. 159–172.

Dana, J.D., 1835, On the condition of Vesuvius in July, 1834: American Journal of Science, v. 27, p. 281–288.

——— 1849, Geology: United States Exploring Expedition: Philadelphia, C. Sherman, v. 10, 756 p.

——— 1888, History of the changes in the Mt. Loa craters: American Journal of Science, ser. 3, v. 36, no. 212, p. 81–112.

——— 1890, Characteristics of volcanoes: New York, Dodd, Mead and Co., 399 p.

Darwin, C., 1842, The structure and distribution of coral reefs: London, Smith, Elder and Co., 214 p.

——— 1844, Geological observations on the volcanic islands, visited during the voyage of H.M.S. *Beagle*: London, Smith, Elder and Co., 175 p.

Decker, R.W., and Christiansen, R.L., 1984, Explosive eruption of Kilauea Volcano, Hawaii, *in* Boyd, F.R., Jr., ed., Explosive volcanism: Inception, evolution, and hazards: Washington, National Academy Press, p. 122–132.

Ennis, C.C., 1934, Magnetic results of the United States Exploring Expedition, 1838–1842, Lieutenant Charles Wilkes, Commander: Terrestrial Magnetism and Atmospheric Electricity, v. 39, no. 2, p. 91–101.

Holcomb, R.T., 1983, East Molokai Volcano was halved by giant landslide [abs.]: Geological Society of America Abstracts with Programs, v. 15, no. 6, p. 597.

Jackson, E.D., Koisumi, I., and others, 1980, Initial reports of the Deep-Sea Drilling Project, vol. 55: Washington, U.S. Government Printing Office, 868 p.

Jackson, E.D., and Shaw, H.R., 1975, Stress fields in central portions of the Pacific plate: delineated in time by linear volcanic chains: Journal of Geophysical Research, v. 80, no. 14, p. 1861–1874.

Jaggar, T.A., 1947, Origin and development of craters: Geological Society of America Memoir 21, 508 p.

Jarrard, R.D., and Clague, D.A., 1977, Implications of Pacific island and seamount ages for the origin of volcanic chains: Reviews of Geophysics and Space Physics, v. 15, no. 1, p. 57–76.

Macdonald, G.A., 1944, The 1840 eruption and crystal differentiation in the Kilauean magma column: American Journal of Science, v. 242, no. 4, p. 177–189.

Macdonald, G.A., Abbott, A.T., and Peterson, F.L., 1983, Volcanoes in the sea (2d ed.): Honolulu, University of Hawaii Press, 517 p.

Macdonald, G.A., Davis, D.A., and Cox, D.C., 1960, Geology and ground-water resources of the Island of Kauai, Hawaii: Hawaii Division of Hydrography, Bulletin 13, 212 p.

Martin, M.G., ed., 1979, The Lymans of Hilo (revised ed.): Hilo, Lyman House Memorial Museum, 224 p.

Moore, J.G., 1964, Giant submarine landslides on the Hawaiian Ridge, *in* Geological Survey research, 1964: U.S. Geological Survey Professional Paper 501–D, p. D95–D98.

Moore, J.G., and Moore, G.W., 1984, Deposit from a giant wave on the Island of Lanai, Hawaii: Science, v. 226, no. 4680, p. 1312–1315.

Morgan, W.J., 1972a, Plate motions and deep mantle convection: Geological Society of America Memoir 132, p. 7–22.

——— 1972b, Deep mantle convection plumes and plate motions: American Association of Petroleum Geologists Bulletin 56, p. 203–213.

Natland, J.H., 1980, The progression of volcanism in the Samoan linear volcanic chain: American Journal of Science, v. 280-A, p. 709–735.

Natland, J.H., and Turner, D.L., 1985, Age progression and petrologic development of Samoan shield volcanoes: evidence from K/Ar ages, lava compositions, and mineral studies, *in* Brocher, T.M., ed., Geological investigations of the northern Melanesian borderland; Circum-Pacific Council for Energy and Mineral Resources Earth Science Series, v. 3: Tulsa, Oklahoma, American Association of Petroleum Geologists, p. 147–180.

Pickering, C., 1840–41, Journal kept while on the United States Exploring Expedition (unpublished manuscript), v. 4, p. 129–219; v. 5, p. 1–27: Boston, Massachusetts Historical Society.

Ramage, C.S., 1978, The United States Exploring Expedition on Mauna Loa, *in* Miller, J., ed., Mauna Loa Observatory, a 20th Anniversary Report: Boulder, Colorado, U.S. Department of Commerce, p. 2–9.

Scott, G.A.J., and Rotondo, G.M., 1983, A model for the development of types of atolls and volcanic islands on the Pacific lithospheric plate: Atoll Research Bulletin, v. 260, p. 1–33.

Stanton, W., 1975, The great United States Exploring Expedition of 1838–1842: Berkeley, University of California Press, 433 p.

Stearns, H.T., and Macdonald, G.A., 1942, Geology and ground-water resources of the Island of Maui, Hawaii: Hawaii Division of Hydrography Bulletin 7, 344 p.

Stearns, H.T., and Vaksvik, K.N., 1935, Geology and ground-water resources of the Island of Oahu, Hawaii: Hawaii Division of Hydrography Bulletin 1, 479 p.

Wilkes, C., 1844, Narrative of the United States Exploring Expedition during the years 1838, 1839, 1840, 1841, 1842: Philadelphia, C. Sherman, 5 v.

Wilson, J.T., 1963a, A possible origin of the Hawaiian Islands: Canadian Journal of Physics, v. 41, p. 863–870.

——— 1963b, Evidence from islands on the spreading of ocean floors: Nature, v. 197, p. 536–538.

THOMAS A. JAGGAR, JR., AND THE HAWAIIAN VOLCANO OBSERVATORY

By Russell A. Apple[1]

ABSTRACT

The digging of a cellar excavation on the north rim of Kilauea caldera in February 1912 marked the beginning of permanent facilities for what was to become the Hawaiian Volcano Observatory (HVO). The Observatory was largely the creation of Thomas A. Jaggar (1871–1953), then a Massachusetts Institute of Technology (M.I.T.) professor, who recognized the advantages, for the study of volcanism, of onsite facilities at an active volcano. Jaggar's efforts to establish an observatory at Kilauea were enthusiastically supported by Lorrin A. Thurston (1858–1931), a prominent Honolulu lawyer and businessman, who organized private support for Jaggar and HVO that continued into the 1940's. Initial support also came from M.I.T. and the University of Hawaii, and HVO was later successively sponsored by the U.S. Weather Bureau (1919–24), the U.S. Geological Survey (1924–35), the National Park Service (1935–47), and (since 1947) again the USGS.

The original HVO building, with a seismograph vault in its cellar, was in use until the early 1940's, when the Observatory was able to occupy a new building 200 m back from the caldera rim. In 1948 HVO moved to a building at the top of Uwekahuna Bluff on the northwest rim of Kilauea caldera; a new and larger building there was completed in 1986.

Under Jaggar's directorship (1912–40), HVO pioneered in seismological and other studies of volcanic processes. Seismographs were important instruments from the beginning of the Observatory, and HVO staff made numerous modifications to adapt them to the study of local volcanic seismicity. Jaggar even developed a rugged portable seismograph for use in outlying areas by amateur assistants. Early experiments in measuring the temperature of liquid lava were more educational than successful; the same can be said of the 1922 drilling program of four holes in and around Kilauea caldera. To support the drilling, HVO staff developed a modified touring car fitted with double wheels. For exploration around the coasts, an amphibious vehicle was designed and constructed.

Jaggar's campaign to obtain facilities at the top of Mauna Loa Volcano and a road leading to them was never entirely successful, but it has been made unnecessary by the advent of helicopters. Observation of the destruction of property by a lava flow in the 1926 eruption of Mauna Loa led to HVO-guided efforts to divert or stop flows threatening Hilo in 1935 and 1942 and to plans (never realized) for a set of permanent barriers. Concern for protection of lives and property also led to studies of tsunamis; in 1933 HVO used seismograms to predict (accurately) the arrival of a tsunami from a distant earthquake, and people in low-lying areas of Hawaii were for the first time successfully warned in advance. Such efforts reflected Jaggar's concern for not only the advance of science but also its application to the benefit of society.

Over its first 75 years, HVO has contributed much to the growing science of volcanology; for this a large debt is owed to the character and qualities of Thomas A. Jaggar.

INTRODUCTION

A hole was to be dug—by hand. Wooden stakes marked the corners of a rectangle about 7.3 m (24 ft) long by 6.7 m (22 ft) wide only about 6 m (20 ft) from the clifflike rim of Kilauea caldera on the Island of Hawaii. It was February 16, 1912, and the foundation to be dug was for Thomas A. Jaggar's volcano observation post, precursor of the Hawaiian Volcano Observatory (HVO).

The diggers were prisoners of the Territory of Hawaii, sentenced to a term of hard labor (HVO record book for 1912; Duncan, 1961). Jaggar was not above using free labor, prison or otherwise, to help stretch his limited funds. Their prison camp was nearby at what is now Kilauea Military Camp in Hawaii Volcanoes National Park.

The prisoners dug through almost six feet of volcanic ash and pumice to a layer of thick pahoehoe lava—a firm base for the concrete piers on which seismometers would be anchored. Plans and elevations for the piers had been hand drawn by Professor F. Omori at the Seismological Institute, Imperial University, Tokyo, Japan, and mailed two years before to Jaggar at the Massachusetts Institute of Technology. Omori also shipped to Jaggar, care of the Territorial Division of Forestry in Honolulu, "An Omori-type Horizontal Tromometer (a seismometer) (magnification = 120–200), and a seismograph for the observation of ordinary earthquakes" (Omori, 1910). These instruments were paid for and on hand in their crates as the prisoners dug.

Soon on hand at the crater rim were carpenters and workmen of the Hilo branch of H. Hackfeld and Company, Ltd., one of Hawaii's "Big Five" companies that controlled virtually all economy in the Islands—Hackfeld later became AMFAC, a multi-billion-dollar conglomerate (Weiner, 1982). Jaggar had contracted with Hackfeld for the forms and concrete work for the seismometer vault, and for the wooden structures that were to stand over and adjacent to the vault—the rimside facilities of the Hawaiian Volcano Observatory. The prime contract was for $1,785 and included a redwood tank for water storage. An additional $300 also went to Hackfeld for extra water-storage tanks (Jaggar, 1917a). Hackfeld executives

[1]U.S. National Park Service, retired.

and the directors of the other "Big Five" corporations were personally helping to sponsor the volcano observatory.

When British explorer Captain James Cook "discovered" Hawaii in 1778, Hawaiians had been living on some of the islands for as long as 1,300 years and had developed a complex, affluent Polynesian civilization. By 1795, when the various chiefdoms and islands were united to form the Kingdom of Hawaii, regular contact with Westerners had changed forever Hawaiians' environment and their way of life. However, with volcanism such an obvious presence in these growing islands, one part of the ancient Hawaiian religion that was kept—and still survives today—is the belief in the Hawaiian goddess of volcanoes, Pele.

Hawaiians believed that the goddess and her supernatural associates often entered into the political and social affairs of men. Pele could take human form, sometimes as a beautiful girl, sometimes as an old hag. Any female stranger could be the goddess. Pele was a major deity who had to be properly propitiated—she took offense easily—because in her anger she caused earthquakes and volcanic eruptions, and she personally directed the course of her lava flows.

Hawaiians believed that the summit caldera of Kilauea Volcano was the home of Pele, her family, and associates, but those deities also had "houses" elsewhere on the Islands of Hawaii and Maui that they could visit at will; these houses include the tops of mountains and all craters, cones, and hills. Pele required special behavior from humans in the vicinity of any of her houses, especially within a radius of 10 km (6 mi) or less from Kilauea caldera, and she expected tribute.

When high chiefs or other people failed to submit proper tribute, insulted Pele, her family, or her priests, or behaved improperly in Pele's domain, then the volcanic deities expressed their anger. They either flooded Kilauea caldera with lava and violently ejected it through the air over the countryside, or they took a subterranean passage to one of their "houses" near the land and homes of those who had offended and, using that house as a base of operations, proceeded to punish the offenders by, at a minimum, covering some of their land with fresh lava (Ellis, 1827; Menzies, 1920). Pele stamped her foot enough times before and between episodes of visible volcanism to remind people of her power and presence; each stamp caused an earthquake. Pele could also call down lightning and cause thunder to roll across the sky.

In 1893, the Kingdom of Hawaii was overthrown by non-Hawaiian businessmen. Five years later in 1898, during the Spanish-American War, the United States annexed Hawaii; the Islands thus became "American soil." This was one of the factors that led to the establishment of an American-sponsored volcano observatory on the rim of Kilauea Volcano (Apple, 1982; Apple and Apple, 1979a; Daws, 1968; Kuykendall, 1967).

During the nineteenth century, while the Hawaiians were being introduced to the ways of Western civilization, Hawaiian volcanoes were described in letters, reports, logs, journals, sketches, notes, and books, published in various places and some distributed worldwide. First made famous because Captain Cook was killed there, the Island of Hawaii now added another world-renowned distinction: active volcanoes. Principal fame focused on Kilauea, which appeared to be comparatively benign. Kilauea had an apparent constancy of activity within its vast summit caldera and, in contrast to some European volcanoes, was not known to wipe out villages or cast glowing fragments of lava down upon hillsides devoted to viniculture. At Kilauea, according to reports, volcanism stayed put inside a crater. While the general public was getting armchair thrills from travel writers, some scientists were also becoming aware of, and visiting, the Big Island (table 61.1).

The scientists listed in table 61.1 did not always agree. First there was the continuing, friendly controversy in the *American Journal of Science and Arts* ("Silliman's Journal") between Rev. Titus Coan, a Hilo man who hiked to and described almost every flank eruption of Mauna Loa between 1843 and 1880, and J.D. Dana, one of the journal's editors and a famous geologist, who didn't always believe the testimony of the eyewitness. For instance, after Dana published Reverend Coan's graphic and detailed description of the source and flows of Mauna Loa's 1843 eruption, Dana followed with "Mr. Coan speaks of the lavas as flowing from an orifice in a broad stream down the mountain. It is probable that fissures opening to the fires below were continued at intervals along the course of the eruption, and that these afforded accession to the fiery flood. Any internal force sufficient to break through the sides of a mountain like Mauna Loa, must necessarily produce a linear fissure or a series of fissures, and not a single tunnel-like opening." (Dana, 1852, p. 256; see also Dana, 1850; T. Coan, 1871, 1882; L. Coan, 1884.)

Arguments such as this could only be resolved by volcanologists doing the observing, but they served to publicize the need for further study. The Coan-Dana controversy helped raise questions that needed to be answered about volcanoes, thus helping pave the way for such institutions as the Hawaiian Volcano Observatory.

When a hotel on the rim of Kilauea caldera became a permanent facility in 1866, its series of guest registers became a repository of reports and observations by the guests, an almost daily record (by observers who varied from the scientist to the joker) of earthquakes felt and unfelt and of volcanism seen and unseen on Kilauea and Mauna Loa. Both Brigham (1909) and Hitchcock

TABLE 61.1.—*Some sources for early descriptions of the volcanoes of Hawaii*

	Name or type of observer	Sponsor, if any	Reference
1825	Lord Byron party	England	Byron, 1826
1834	Botanist	London Horticultural Society	Douglass, 1834, 1919
1834	Captains Parker and Chase		Kelley, 1841
1837	Geologist	———	Strzelecki, 1838, 1845
1839	Scientist	———	Lowenstern, 1841
1839	Ship's captain	———	Shepherd, 1840
1840	U.S. Exploring Expedition	U.S. Government	Wilkes, 1845
1840	Geologist	U.S. Exploring Expedition	Dana, 1849
1846	Professor	———	Lyman, 1851
1859	Geologist	———	Green, 1887
1868	Kilauea historian	Harvard University	Brigham, 1868, 1869
1873	Travel Writer	———	Bird, 1875
1880	Kilauea historian	Bishop Museum	Brigham, 1909
1882	Geologist	U.S. Geological Survey	Dutton, 1884
1883	Geologist	Dartmouth College	Hitchcock, 1911
1887	Geologist	Yale University	Dana, 1890
1909	Geologist	Massachusetts Institute of Technology	Daly, 1911

(1911) mined the more reliable reports from the Volcano House guest registers, quoting them along with observations from their own visits and reports from many additional sources to yield histories of both volcanoes, comprehensive up to their dates of publication.

Brigham, a scientist who once taught botany at Harvard and also practiced law in Boston, was by 1898 the Director of the Bernice Pauahi Bishop Museum in Honolulu. Hitchcock was a geologist, a member of a prominent Hilo family, and by 1909 was retired as Emeritus Professor of Geology at Dartmouth College. Both Brigham and Hitchcock kept up with the comings and goings of scientists interested in the Big Island volcanoes.

Brigham (1909, p. 216) notes that in the spring of 1909 the "well-known professors in the Massachusetts Institute of Technology, T.A. Jaggar, Jr., and R.A. Daly," visited Kilauea, and that Jaggar and Daly were "interested in the establishment of a permanent observatory at Kilauea, a result so ardently hoped for many years and frequently referred to in these pages."

Hitchcock (1911, p. 306) applauds Brigham's recommendation that a "permanent scientific observatory be established at Kilauea, where notes may be taken with the best instruments, of earthquakes, the diurnal changes of the dome of Halemaumau, the temperatures of the molten lava and steam jets, the analysis of ejecta and spectroscopic investigations."

While arguments on behalf of more formal scientific investigations in Hawaii were being presented, the public had been well prepared by press reports of devastating earthquakes and volcanic eruptions around the world, especially the eruption of Mont Pelé in 1902 and the San Francisco earthquake in 1906.

In the hope that science could close the gaps in geological knowledge and learn to predict earthquakes and eruptions, some New Englanders were willing for humanitarian reasons to finance foreign trips and support work abroad for scientists. For instance, the Springfield (Massachusetts) Volcanic Research Society supported, at least in part, the travels and studies of Frank A. Perret, an electrical engineer and inventor turned volcanologist who became well known for his studies at Vesuvius, Etna, and Stromboli. The Springfield society also helped support Perret's 1911 work at Kilauea (Wentworth and Powers, 1962; Macdonald, 1972).

It was in this climate of opinion that the trustees of the estates of Edward and Caroline Whitney gave to the Massachusetts Institute of Technology the sum of $25,000 for a memorial fund; the principal and interest were to be expended at M.I.T.'s discretion for research or teaching in geophysics, especially seismology, "with a view to the protection of human life and property" (Jaggar, 1917a). Investigations in Hawaii were recommended. The Whitney fund was deeded to M.I.T. by the trustees on July 1, 1909, and three years later a group of twelve other New Englanders supplied M.I.T. with supplemental funds for geophysical research in Hawaii (Jaggar, 1917a).

Even before the Whitney gift, M.I.T. had been searching for a suitable site for full-time, resident study of volcanoes and earthquakes. Professor Thomas A. Jaggar, Jr., had investigated sites in Italy, the Caribbean, and Alaska. At private expense, both Jaggar and Professor Daly visited Kilauea in 1909. Jaggar went on to Japan; Daly stayed to study the action in Kilauea caldera (Daly, 1911). In Japan, Jaggar investigated two volcanoes in eruption and studied the Japanese seismometer network, then the world's most advanced. He became a lifelong friend of Professor F. Omori, famed Japanese seismologist.

After what he termed "mature deliberation," Jaggar chose Kilauea for M.I.T.'s volcano observatory. He gave M.I.T. eight reasons for his choice: (1) Kilauea was the safest known volcano in the world; (2) Kilauea and Mauna Loa were isolated, more than 3,000 km (2,000 mi) away from complications other volcanic centers might impose; (3) Kilauea was reasonably accessible—it could be reached by a 50-km (30-mi) road from Hilo harbor or a day's sail from Honolulu; (4) the central Pacific was good for recording distant earthquakes and was served by good transportation east or west; (5) the climate was uniform, with air clear enough for astronomy; (6) small earthquakes were frequent and easily studied; (7) hot and cold underground waters were available for both agricultural and scientific purposes; (8) "The territory is American, and these volcanoes are famous in the history of science for their remarkably liquid lavas and nearly continuous activity" (Jaggar, 1917a, p. 2).

Jaggar stopped in Honolulu twice in 1909; obviously aware of funds to be forthcoming from the Whitney Fund and sure of support from M.I.T. for an observatory at Kilauea, he sought added patronage in Honolulu. Jaggar gave lectures and met with the Chamber of Commerce, the Bishop Museum, and key businessmen. Guiding him through the interlocking directorships of the Hawaiian business community and introducing him into its parallel island society network was Honolulu businessman Lorrin A. Thurston, who headed, among other things, the Hawaiian Promotion Committee, forerunner of the Hawaii Visitors Bureau. Thurston and Jaggar became close friends.

JAGGAR AND THURSTON: BACKGROUND

Thomas Augustus Jaggar (1871–1953) was born in Philadelphia, Pennsylvania, son of an Episcopal Bishop. He obtained three geology degrees from Harvard (A.B., A.M., and Ph.D.), studied in Munich and Heidelberg, and then began teaching at Harvard. Jaggar was one of the scientists sent by the U.S. Government in 1902 to investigate the volcanic disasters at Soufrière and Mont Pelé. His experiences there led him to devote his career to active volcanoes and related geophysics. In 1906, already a much-published, respected, well-known geologist, writer, and lecturer, he became head of M.I.T.'s department of geology. Jaggar saw the need for full-time, on-site study of volcanoes. He had long deplored that to date, especially in America, it was only after news of an eruption was received that geologists rushed from academic centers to study volcanism. There was generally no trained observer there beforehand, and scientists from afar often arrived after the eruption was over. There was then only one volcano observatory in the world, that at Vesuvius established in 1847. Jaggar thought America needed one (Jaggar, 1910; Macdonald, 1972; Bullard, 1975; Day, 1984).

Lorrin Andrews Thurston (1858–1931) was born in Honolulu, grandson of one of the pioneer missionaries from New

England. He studied law at Columbia University and became a member of the Honolulu bar. In the Kingdom of Hawaii, Thurston served in both elected and appointed positions, but he was a leader in the revolution (January 17, 1893) that overthrew Queen Liliuokalani and ended the native monarchy. The very next day Thurston sailed from Honolulu for Washington, D.C., to serve the "Provisional Government," which he helped establish, as envoy extraordinary and minister plenipotentiary. He stayed for two years and paved the way for annexation of Hawaii by the United States in 1898. In his business life he developed sugar plantations and railroads, brought the first electric street cars to Honolulu, and was the major stockholder in the Volcano House on the rim of Kilauea caldera. Being a volcano buff, he often visited Kilauea and frequently brought officials and delegations from the United States to see the volcano from the porch of his Volcano House. In 1900, Thurston became publisher of the *Pacific Commercial Advertiser*, a Honolulu daily newspaper (still today under the management of a descendant). Not only did he promote a volcano observatory for Kilauea, but he also wished to make Kilauea a U.S. national park (Day, 1984). Thurston had a powerful influence because of his family connections and the many positions he held, and his support for HVO in its early years was invaluable.

ACKNOWLEDGMENTS

This historical sketch is the product not only of a search of the literature but also of numerous discussions, conversations, and interviews with volcanologists, staff of HVO, and others with knowledge of the subject. In particular, I wish to thank R.W. Decker, R.V. Koyanagi, B.J. Loucks, and Reginald Okamura for freely sharing their experiences and knowledge of HVO history. I am grateful to R.W. Decker and T.L. Wright for helpful reviews of the paper and to Barbara Decker and P.H. Stauffer for helping to put this manuscript into its final form.

BEGINNINGS OF THE OBSERVATORY

In 1909 Jaggar proposed to prospective financial supporters in Honolulu an observatory program. Its purposes were listed as follows: (1) To establish "on the brink of the Volcano of Kilauea" buildings for instruments, laboratory, offices, and record storage; (2) to provide a room for a local museum; (3) to welcome advanced students for special work; (4) to establish a network of stations, some manned by volunteer observers, to study tides, soundings, earthquakes, and coastal movements; (5) to mount expeditions to other volcanic and earthquake belts for comparative studies; (6) to conduct research in gravity, magnetism, and latitude variations; (7) to initiate geological surveys; all of these with their "main object * * * humanitarian—earthquake prediction and methods of protecting life and property on the basis of sound scientific achievement" (Jaggar, 1917a, p. 2–3).

Thurston's Honolulu connections in 1909 pledged $3,450 a year for five years to help M.I.T. sponsor the observatory. M.I.T. officials did not think this was sufficient. In Honolulu, the plan was shelved. Jaggar and Daly returned to teaching at M.I.T., but they continued planning for a Kilauea observatory.

The Whitney Fund became available to M.I.T. in July 1909. Part was spent in 1909 and 1910 to secure (from the Werkstätte für Präzisions-Mechanik, Strassburg, Germany) a pair of Bosch-Omori seismometers (Bosch, 1910) and to order through Professor Omori in Tokyo the three Omori-designed seismometers made by Kyo-iku-hin Seizo Kaisha (Educational Appliance Company) (Omori, 1910).

Also in 1910, M.I.T. spent some Whitney Fund money to have Leeds and Northrup, Baltimore, Maryland, construct "special resistance thermometers," designed to take the temperature of liquid lava in the so-called perpetual lake at Kilauea. Part of the fund also helped send the temperature-taking Perret-Shepherd expedition to Kilauea in 1911. Personal and teaching concerns kept both Jaggar and Daly in Boston in 1910 and 1911 (Jaggar, 1917a).

The Leeds and Northrup thermometers were each about 3 m (10 ft) long, with platinum coils inside protected by tubes of iron, nickel, and quartz. The job of measuring the temperature of the lava lake was seen by scientists in Boston and Baltimore to be something like sticking an iron rod into a pot of boiling tar. Readings were to be taken "on shore" through electric wires connected to the thermometer.

A cable system was designed and manufactured on the East Coast of the United States by the Lidgerwood Company and paid for by Whitney funds. Its job was to take a thermometer out over the lake of molten lava, lower it into the bubbling lava, hold it there while readings were taken, lift it out, and return it to shore. By the time the cable system arrived, the diameter of the lava lake in Halemaumau had so enlarged that the system did not fit and had to be modified. Six men were needed to operate the trolley that rode out on the cable and lowered the thermometer. F.A. Perret and E.S. Shepherd (from the Geophysical Laboratory of the Carnegie Institution in Washington, D.C.) had no funds to hire laborers. Work could only be done when enough volunteers showed up. The project dragged out over a month's time, while Pele's hair collected on the main cable and restricted trolley movement. The wires that pulled the trolley back and forth disintegrated and had to be replaced for each experiment. Over the course of the month, cable anchors and cables were weakened from constant exposure to steam and acid vapors. When work was under way, fumes often were so thick that the men at the winch could not see the thermometer. Signals were relayed around the rim of the lava lake to tell winchmen to reel in or out. In the thick of it all was chief volunteer Lorrin Andrews Thurston, who also recruited the other volunteers.

On July 30, 1911, after two thermometers had already been lost in the lake without readings, with the last thermometer mounted on the trolley and time running out for the disintegrating cable fittings, the last chance was at hand. Only three volunteers, including Thurston, showed up. Thurston put his family to work. Thurston himself handled the reel that lowered the thermometer; his wife Harriet held the cable tight on the drum; son Lorrin shifted coils; and daughter Margaret stood on the rim in heavy sulfur fumes to relay signals (from Perret down in the pit by the lake's edge) with a flag—signals that came to her father at the reel, to Shepherd

standing by the meter, and to volunteers Emery and Ferris at the winch.

Before Pele swallowed the last thermometer, Shepherd got a reading of 1,000 C (1,832 F) from two feet under the surface of the lava lake. Shepherd himself suggested that future temperature readings be done with optical pyrometers, for "No mechanical system can long withstand the strain and abuse which Pele applies to any foreign object which invades her private lake" (quoted in Jaggar, 1917a, p. 47–50).

Perret, a meticulous observer and maker of notes, wrote reports not only on the progress of taking Pele's temperature, but also on volcanic phenomena generally. His first report covered almost a month and a half of scientific work and observations; the next five covered a week each (see Jaggar, 1917a, p. 35–46). He also wrote four scientific papers (Perret, 1913a, b, c, d).

Thurston now had hands-on involvement helping scientists begin to investigate his favorite volcano, and he had published weekly a series of six authentic reports about Kilauea in his daily Honolulu *Advertiser*. In 1911 Thurston revived the 1909 subscription list, hoping to get his Honolulu friends and business associates to up the ante sufficiently high that M.I.T. would move its observatory plans off the drawing board and onto the rim of Kilauea caldera.

At a luncheon hosted by Thurston on October 5, 1911, the guests—obviously primed and ready—formed the Hawaiian Volcano Research Association—the famed HVRA. An unpaid executive committee of five were to be elected annually. This founding meeting of the HVRA adopted a motto: *Ne plus haustae aut obrutae urbes* (No more shall the cities be destroyed) (Macdonald, 1953).

Thurston chaired the executive committee, which was quickly endorsed by the Honolulu Chamber of Commerce to raise funds from among its members. Thurston served with Albert F. Judd (representing the trustees of the Bishop Museum), John W. Gilmore (president, College—later University—of Hawaii), James A. Kennedy (of Interisland Steam Navigation Co.), and Clarence H. Cooke (of Charles M. Cooke, Ltd). The pledge was for $5,000 a year for five years, starting January 1, 1912. Treasurer Cooke and his associates of C.M. Cooke, Ltd., guaranteed the full amount in the event of failure of any individual subscribers to pay.

Negotiation by the HVRA executive committee with M.I.T. resulted in the assignment of Jaggar, as M.I.T. professor, to Hawaii as of January 1, 1912. HVRA was to sponsor and operate the Hawaiian Volcano Observatory. M.I.T. became an HVRA subscriber (indeed, the largest) for five years, using the income from the Whitney Fund and payments from 12 other New Englanders to its Seismological Fund. M.I.T. ran HVO's scientific affairs through Jaggar, who obviously received a deep delegation of authority, and granted use of its name and publishing facilities for that five-year period. In December 1911, Jaggar was granted leave of absence from his deanship and teaching duties at M.I.T to continue at Kilauea the work of recording the volcanic activity along the lines started by Perret.

Jaggar arrived in Honolulu and met with the HVRA executive committee on January 9, 1912, and then proceeded to the Volcano House on the rim of Kilauea caldera to go to work as the director of the Hawaiian Volcano Observatory on January 17, 1912. On January 18, using data collected from the Volcano House guest registers and other sources, he renewed the weekly reports to Thurston's *Advertiser*. Although Jaggar had married Helen Kline in 1903 and the couple had two children, Helen did not accompany Jaggar to accept his post as director of the Hawaiian Volcano Observatory in 1911, and a divorce followed. In 1917 Jaggar married a coworker at HVO, Isabel P. Maydwell; she was his wife, assistant, and companion for the rest of his life.

On January 19, Demosthenes Lycurgus, representing Thurston's Volcano House Company, went with Jaggar to Hilo to visit the merchants and leading citizens. Their mission was to raise funds to build a laboratory on the rim of Kilauea caldera for use by representatives of M.I.T. engaged in volcanologic research (Jaggar, 1917a). The $1,785 the merchants and private citizens of Hilo subscribed resulted in the contract with the Hilo Branch of H. Hackfeld & Company, Ltd., to build the forms and pour the concrete for what was soon to be called the Whitney Laboratory of Seismology and to build above the vault a building for the Hawaiian Volcano Observatory. In essence, the merchants of Hilo provided funds for these initial rimside facilities; the HVRA, with heavy reliance on M.I.T., promised operating funds for the first five years. Until the new facilities were built, Jaggar's first home and office at Kilauea were in the Volcano House.

PIONEERING, 1912–1953

Halemaumau—the circular pit within Kilauea caldera—contained an active lava lake about 65 percent of the time from 1823 to 1924. The lake rose and fell and sometimes overflowed onto the main caldera floor. This rare volcanic feature made Kilauea a tourist destination as well as an attraction to scientists. Two hotels, the Volcano House (1866–present) and the Crater Hotel (1911–21), provided accommodations. By 1911, roads had replaced foot and horseback trails to connect Kilauea's summit area with Hilo 50 km (30 mi) away. The altitude of Kilauea's summit, 1,200 m (4,000 ft) above sea level, created a cool climate and made it an attractive place to visit. Part of Kilauea caldera and part of its rim area were owned by the estate of Bernice Pauahi Bishop, a princess and the last survivor of the royal Kamehameha line. The Volcano House leased its extensive lands on the rim of Kilauea caldera from the Bishop estate, and in 1912, with the estate's permission, it subleased to the Hawaiian Volcano Research Association a site on the rim for the Hawaiian Volcano Observatory.

Suggestions that the Kilauea summit area become a national park began appearing in the Volcano House guest register and in newspapers in Hawaii as early as 1903. When Thurston escorted Congressional parties and Federal officials to his Volcano House to show them the boiling lava in Halemaumau, he promoted both a national park and an observatory. In December 1915, Jaggar was commissioned by the HVRA and M.I.T. to appeal to Congress to take over HVO as a permanent governmental institution and establish under the Weather Bureau a division of volcano observatories and also to help with the national park bill then pending. Jaggar

failed in 1916 to acquire an independent Federal sponsorship for the observatory, but he did succeed with the national park, which became the surrogate sponsor.

The hearing in Washington (February 3, 1916) covered subjects ranging from volcanology to Hawaiian folklore; the Jaggar bill for a Hawaii National Park was reported favorably out of committee, passed by both Houses of Congress, and signed into law by President Wilson on August 1, 1916. Thurston had primed those Congressmen who visited the Islands; Jaggar in Washington had convinced many of the rest. (Congress changed the name to Hawaii Volcanoes National Park in 1961, by which time much additional land had been added). As the National Park Service took up resident management and acquired the land with existing leases and subleases, it became, among other things, the landlord for the Volcano House and HVO (Apple, 1954).

In the absence of Government sponsorship, HVO's founding organization, the privately financed HVRA, continued its support of volcano research well into the 1940's. It employed seismograph observers who worked in detached cellars, such as in Hilo and Kona, and others on research fellowships. It supplied or paid for shops, machine tools, instruments, laboratories, stationery, supplies, expeditions, books, boats, specialists, vehicles, and machines, thus making possible pathbreaking investigations that could not have been so readily attacked under Government alone, owing to the restrictions that control Government funds. The HVRA also published volcano notes from many lands, the weekly reports from Kilauea, Lassen Observatory notes from California, reviews of volcanologic books, and popular statements of the technical works in progress.

In general, after the National Park was created, the Federal Government paid the salaries of the permanent staff, while the HVRA supplied all buildings, much of the equipment and facilities, and services such as publications. The buildings and equipment, for instance, were owned by HVRA and leased to the sponsoring Federal agency. As HVRA support phased out in the late 1940's, HVO came more fully under Federal appropriations and control. By the early 1950's, ownership of all HVRA buildings and chattels had been transferred to the Federal Government.

Publications over the decades listed HVO sponsoring organizations as the Massachusetts Institute of Technology, the Hawaiian Volcano Research Association, the University of Hawaii, the U.S. Weather Bureau, the National Park Service, and the U.S. Geological Survey, in various combinations. Sponsoring organizations of HVO are shown in the following table:

Organization	*Period of sponsoring*
Massachussets Institute of Technology	1911–1917
Hawaiian Volcano Research Association	1912–1940's
University of Hawaii	1912–1942
U.S. Weather Bureau	1919–1924
U.S. Geological Survey	1924–1935
National Park Service	1935–1947
U.S. Geological Survey	1947–present

The USGS has sponsored HVO twice. In 1926, Congress established within the USGS a Section of Volcanology, with Jaggar in charge. Jaggar quickly instituted new stations and staff in California and Alaska. Contraction followed within a few years because of the economic depression. Looking back almost two decades later, Jaggar reminisced as follows: "First it was a splurge of high water mark in appropriations with work in Lassen and Alaska and Hawaii and a maximum staff. There was a navy trip to Tin Can Island and all sorts of cooperation public and private. Then came the big bust in 1932 and an 83 percent cut but we kept Hawaiian volcanology alive and there were immense accumulations to study and publish, and typewriter paper is cheap. The Hawaii business men [HVRA] came to the rescue and never faltered" (T.A. Jaggar, unpublished notes, copy in personal collection of J.P. Lockwood).

Geologist Howard A. Powers, who joined the HVO staff in 1929, also recalled that period of boom and bust. Powers received his Ph.D. from Harvard in 1929 and went to Washington to try to get sworn into the USGS there, "but they said that I would have to be sworn in at the Observatory. (Cagey—that way I had to pay my own way to Hawaii.) * * * The staff at that time was T.A. Jaggar, Richmond Hodges, accounting clerk; and two local men not civil service—Yasunaka, general handyman and husband of Jaggar's maid, and Tai On Au (a local Chinese who had graduated in machine shop from the Hilo Boarding School). The next two years were affluent—we picked up Austin Jones, graduate seismologist from Berkeley, Ed Wingate, a top-notch Topographer to take on problems of starting useful tilt recording. Then the huge cut for fiscal 1933. I was transferred to the USGS Ground Water Branch, Ed Wingate was transferred to USNPS as Superintendent of Hawaii National Park, Tai On Au was released, Austin Jones was kept on as Seismologist, Yasunaka continued his job, and Richmond Hodges transferred to the office of Headquarters, Hawaii National Park" (H.A. Powers, written commun., 1985).

BUILDINGS AND FACILITIES

TECHNOLOGY STATION (1911–1918)

In July 1911, Perret selected a site on the eastern rim of Halemaumau that commanded a view of the entire lava lake; there he built a small frame building he called "Technology Station," a place name used in many early datelines of HVO weekly bulletins to the press. Perret lived in this cabin from July 24 through September 17, 1911. By mid-August, Perret noted that vapors from the vent had formed acid, which had consumed the zinc coating of the galvanized iron roof. His field assignment finished, Perret left the cabin and Hawaii.

Jaggar came on duty in January 1912 and discovered that the Technology Station had been vandalized the month before. He believed it was vulnerable because it stood close to the parking area at the end of the road. Jaggar had the cabin torn down and rebuilt, enlarged, and surrounded by a picket fence, at a different site a few yards back from the north rim. There it was used for the storage of

instruments, as a seismometer station, and as an observation camp. By early February the cabin contained a rectangular concrete platform, which protruded through the board floor and soon held a seismometer.

In June 1918, laborers tore down Technology Station and rebuilt it again on the north rim of Kilauea caldera, where it joined other HVO buildings lining the rim. There the cabin was repaired and repainted to become a staff residence; it served until all the HVO facilities along the north rim were razed in 1940.

INSTRUMENT HOUSES

Jaggar reported that in 1912 an additional hut was constructed wholly without iron for possible magnetic work on the verge of Halemaumau, to allow sheltered direct instrument observation of the lava. Seismologist H.O. Wood described the hut as "at the very edge of the northern rim of Halemaumau" (Wood, 1913, p. 16). If the hut was still standing in 1924, it must have been destroyed by the enlargement of Halemaumau that accompanied a series of steam explosions that year.

In addition, over the years at least four cellars were excavated or constructed on the floor of Kilauea near Halemaumau to house instruments for the detection of earthquakes, ground tilt, or both. Hawaii Volcanoes National Park maintains a list of buildings with assigned numbers; the four known cellars are buildings number 136, 255, 308, and 309. Building 309, the "East Vault" near Halemaumau, was constructed in 1959 and razed in 1973. Three other cellars were built by the Civilian Conservation Corps (CCC) about 1932 as stone-wall pits. The "West Pit" was buried under a lava flow in September 1971; this flow also partially covered the cellar called "Outlet," about 1 km south of Halemaumau. That left only the "North Pit" on the floor of Kilauea caldera with working instruments inside.

WHITNEY LABORATORY OF SEISMOLOGY (1912–PRESENT)

The hole those prisoners dug on the north rim of Kilauea caldera (fig. 61.1) in 1912, through six feet of volcanic ash, resulted in "a basement room, eighteen feet square, with piers and floor of concrete, reposing upon the upper surface of the basalt, and high walls of concrete. This [basement beneath what became the main HVO building] is the Whitney Laboratory of Seismology. A constant emanation of hot steam from cracks in contact with the concrete walls keeps this room at a fairly uniform temperature and thus improves it for the purposes of seismology" (Wood, 1913, p. 16).

Jaggar was a true pioneer volcanologist; he made mistakes in locating and designing the Whitney vault, but he and his staff lived with their mistakes and tried to overcome them. They made their problems and progress known through their published writings, and early HVO mistakes helped others avoid similar ones when they built vaults elsewhere.

In the Whitney vault as first built, thick reinforced-concrete walls went up to ground level, about 1.7 m (5.5 ft) above the concrete floor. From ground level to the ceiling, glass panels were fixed in wooden frames to admit natural light. When the sun shone, the temperature rose sharply. Because of temperature variations, neither Jaggar nor Wood trusted the records made by the seismometers.

Not only were the temperature swings too great, but stray breezes also blew recording arms to make confusing marks on smoked drums, and dust seeped in around the windows, mixed with oil, and gummed up delicate mechanisms. Some of these problems were solved when the windows and frames were covered with boards and battens and sealed with coats of paint. This made the cellar dark day and night. Battery-operated lights served until 1921, when HVO acquired its first electric generator.

An earthquake in October 1913 opened a crack in the north wall of the Whitney vault. Water seeped from it onto the floor until the crack was repaired and sealed (the concrete floor of the Whitney vault contained no drain).

Being a basement vault with a building above also created problems. Even in calm weather, movements of the building were recorded by the seismometers in the vault below. Winter Kona storms swept high winds from the south across Kilauea caldera, hitting with full force against the north rim and causing such rocking and trembling of the building above as to mask the records on the seismograms. In the winter of 1915–16, gale-force winds stripped the sheets of corrugated iron from the roof of the building. Rain water in the offices above poured into the vault to wash away the seismograms on their drums, flood the floor, and soak the instruments. Repairs took weeks.

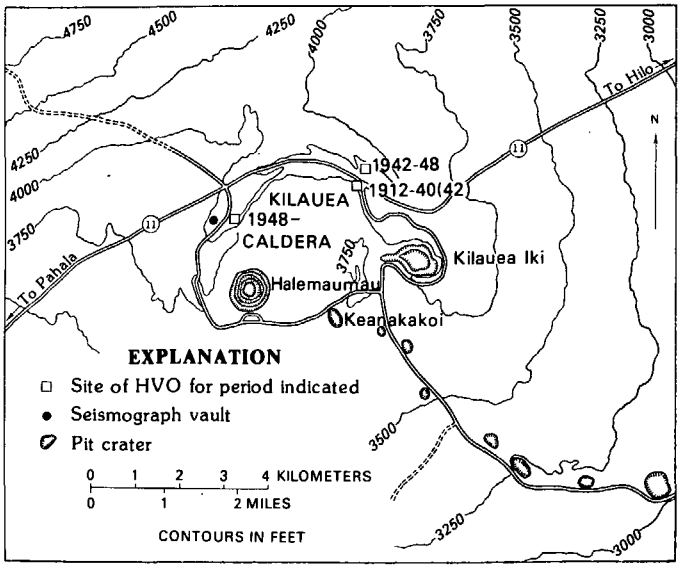

FIGURE 61.1.—Successive sites of main facilities of Hawaiian Volcano Observatory around rim of Kilauea caldera. From 1940, when original buildings were razed, until 1942, when the Observatory was able to occupy Building 41 (newly vacated by the Army), HVO staff and equipment were scattered in various buildings near the original site and elsewhere.

The Whitney vault's location 20 feet from a cliff face also imposed special problems. Cliff-face rocks expanded and contracted, from heating and cooling, sun or shadow, wetting or drying, and all such movements were recorded. Whenever high winds pressed or let up against the face, it was recorded by the seismometers, sometimes masking data about tilting of the ground caused by underground lava movements.

Then, on December 19, 1921, the nearby Volcano House began to run a Fairbanks-Morse engine to power a generator for the first electric lights at Kilauea. Variations in the engine speed as well as the exact times of starting and stopping were duly recorded by seismometers in the Whitney vault until, months later, the exhaust was directed away from a steam crack and into the air. Apparently HVO's own generating plant never caused any such problems.

Whitney vault seismometers over the years recorded much of the truck and automobile traffic that passed on the nearby road. Seismologists quickly learned to separate natural events from the local man-caused ones, but all must have wondered how much the vibrations caused by man obfuscated the records.

Except for changes in the concrete piers as instruments came and went, there was no basic change in the Whitney vault until early 1941 (fig. 61.2). In that year, the building above was dismantled, and a reinforced-concrete slab was poured by the Civilian Conservation Corps (CCC) to become the vault's new roof. The slab was covered with 45 cm (18 in.) of topsoil. The isolation (from the building above) and insulation (from the ambient air) resulted in a nearly constant temperature around 35 °C (95 °F), and the daily variation seldom exceeded 0.5 °C (1 °F).

Two other unfortunate vault characteristics persisted, however. One was that quick body movements often caused recording arms to move because of the air currents generated. Another was the oppressive warmth caused by the natural steam heat. Scientists through the active life of the vault (1912–1963) bundled up in wooly sweaters, scarfs, and raincoats to walk to the vault through the chilling rains and fog at 1,200-m (4,000-ft) altitude and then peeled down to undershirts when they entered the vault to attend the instruments.

The Whitney Laboratory of Seismology went out of active service in 1963 and is, since July 24, 1974, a property in the National Register of Historic Places, complete with some of the original instruments. Part of its nomination to the Register reads: "The Whitney Seismograph Vault, built in 1912, represents the beginnings of the continuous and resident study by American scientists of the earth's volcanic and seismic activity at Kilauea and Mauna Loa volcanoes. The Hawaiian Volcano Observatory, a U.S. Government facility since 1919, used the vault from 1912 through 1963 when more sophisticated instrumentation made the seismometers and tiltmeters it was designed to house obsolete" (U.S. Department of the Interior, 1973).

OTHER EARLY FACILITIES

Original facilities in 1912 included water-storage tanks, a stable (complete with horse), and a garage. Added over the years were at least one staff residence (1918), a shop and electric plant (1922), an archives building used for storage of records, with corrugated-iron walls and roof to reduce the fire hazard (1922); a chemistry laboratory (complete with chemist O.H. Emerson) (1922, 1923); a new machine shop (complete with instrument maker F.Y. Boyrie) (1927); and additional water tanks, garages, and various sheds, outbuildings, and shacks. After 1922, a drill tower also stood along the rim. The view from its top is shown in figure 61.3. All these were built with HVRA funds. Except for the Whitney vault, all rimside buildings and facilities were razed in 1940.

Also built in 1912, standing above the Whitney Laboratory, with the ceiling of the vault part of the floor, was the main HVO building—a "substantial, wood frame structure containing a photographic darkroom; a workshop and storage room; a large, well-lighted room for drafting, study, routine work, etc.; a room designed for the storage and exhibit of collections, photographs, seismograms, maps, etc., and the accommodation of visiting workers; and an office room for the Director" (Wood, 1913, p. 16). The "large, well-lighted room" is shown in figure 61.4.

A covered porch on two sides permitted views, weather obliging, of the volcanoes Kilauea, Mauna Loa, and Mauna Kea. On the Kilauea caldera side, set so its top could be used from the porch, was a concrete pyramid with an elevation bench mark. The flat top served as a mount for a Theodolite or a camera. A photograph of Halemaumau lava lake was taken daily, and a vertical-angle shot to a bench mark on Halemaumau's rim was also recorded if weather permitted.

The main Observatory building was razed in 1940. Now only the concrete post remains; it, like the nearby Whitney vault, is a property in the National Register of Historic Places. Also in 1940, on February 11, the main Volcano House burned to the ground, and it was this, in fact, that led to the relocating of the HVO facilities. The two-story hotel, built in 1891, had been enlarged in 1921 (see fig. 61.3). Owner-manager "Uncle George" Lycurgus left immediately after the hotel burned down for Washington, D.C., to confer with the many friends in Government whom he had entertained over the years in his hotel at Kilauea. In effect, Uncle George called in his chips.

Lycurgus' Washington conferences resulted in five proposals: (1) The site for a new Volcano House was to be near the old site on the north rim of Kilauea, where HVO facilities had stood since 1912; (2) all HVO structures (except the Whitney vault) on the north rim were to be razed to make room for the hotel; (3) the new hotel building was to be constructed with Lycurgus funds; (4) the Volcano House operating contract would be renewed, with Lycurgus continuing as National Park concessioner but with a different fee structure; and (5) a new building would be built with Federal funds, well back from the rim, to house the Hawaiian Volcano Observatory and provide a place where Park naturalists could meet the public. Such a new HVO building had been in the talking stage since at least 1938.

This proposed HVO building was assigned the number 41 by the National Park Service and labeled the "Volcano Observatory

FIGURE 61.2.—T.A. Jaggar in Whitney Laboratory of Seismology, 1913. Stairs from HVO Main Building above come down to right of glass partition. Invited spectators stood behind the glass and were not admitted into instrument room. Jaggar is handling smoked drum that records east-west Earth movements detected by Omori seismometer designed for teleseisms. Two piers against far wall held two-component Bosch-Omori seismometer. Double springs in left foreground are part of self-starting Omori "Ordinary," a three-component seismometer. Photograph courtesy of the Bishop Museum (negative CPBM 58815).

and Naturalist Building." Plans were quickly initiated and whisked through the National Park bureaucracy, and the CCC began construction as soon as the plans were received.

The new Volcano House opened for business in November 1941, an elapsed time of 21 months since the fire. During that time the first four of the five points above were accomplished, and the fifth (Building 41) was almost completed. Inserted in the cornerstone of the "Kilauea Volcano House" and dated July 20, 1941, was a memorandum by Jaggar which said in part: "Under the hotel lobby is a drilled 4-inch well sixty feet deep where drilling experiments were made in 1922, one of about thirty wells for measuring temperatures. The line of observatory houses was strung out exactly where the hotel now stands. The U.S. National Park Service now is erecting a larger laboratory under R.H. Finch. The records are being duplicated at the University of Hawaii, where Jaggar is now research associate in geophysics. It is appropriate that the actual gazing upon crater fires from the old Observatory site should hereafter be the privilege of volcano hotel guests."

BUILDING 41 (1940–PRESENT)

Workers from the CCC began construction of the "Volcano Observatory and Naturalist Building" 180 m (600 ft) in from the rim of Kilauea caldera (see fig. 61.1) in 1940. Delays were experienced, but by March 1942 Building 41 was almost complete.

By that time, a vertical-component seismometer had been installed and tested in Building 41's basement seismograph vault. The building also had a fireproof room for storage of HVO records

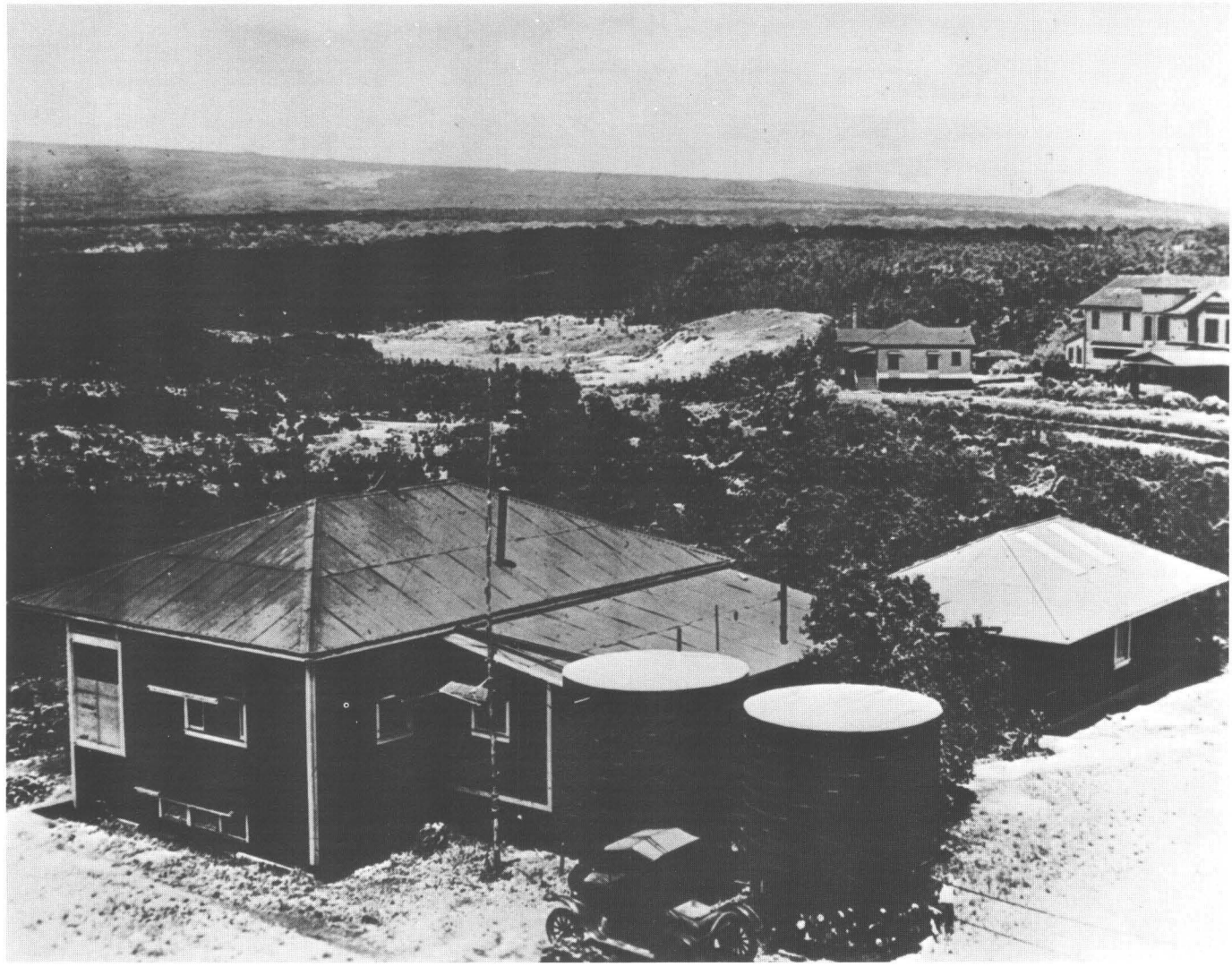

FIGURE 61.3.—Hawaiian Volcano Observatory (foreground) at its first site on north rim of Kilauea caldera (see fig. 61.1). Main observatory building is at left, the Whitney vault in its celler. To right is the machine shop. In right background is Volcano House Hotel, which burned down in 1940. The unknown cameraman climbed a 30-ft drill tower, probably in the late 1920's, to take this picture, facing away from Kilauea Crater.

and what was considered ample office, machine shop, drafting, and library space. Its seismograph cellar was about 195 m (640 ft) from the north cliff of Kilauea caldera. Only slight diurnal and seasonal temperature variations were anticipated, because this vault and basement (unlike the earlier Whitney vault) butted against only a few steam cracks.

Like the Whitney Laboratory, Building 41's seismometer vault also had a building topside. The so-called "second vault" kept its temperature at about an even 29 °C (85 °F), but because Building 41 swayed back and forth in response to above-ground daily temperature variations, ground-tilt data collected in the vault proved to be unreliable. Building 41's vault was as close to the through road (60 m [200 ft] away) as was the Whitney vault, and its records also were marred by the frequent passing of heavy trucks. HVO seismologists maintained only the vertical-component seismometer and a tiltmeter under Building 41, and kept the Whitney vault instruments in operation.

When the HVO rimside buildings were vacated in 1940, records, gear, supplies, machines, furniture, and other chattels had been stored in various places in the national park, including the CCC camp on the rim of Kilauea Iki. As the basement of Building 41 became available—while carpenters finished the floor above—some of the stored items were moved in.

Martial law, which came to Hawaii with World War II, was in effect in 1942, and the U.S. Army commandeered Building 41 as soon as it was completed. It became the Island Military Headquarters—a convenience more to the officers and men stationed there (because of the nearby Kilauea Military Camp) than to the rest of

FIGURE 61.4.—T.A. Jaggar, at work in the "large, well-lighted room for drafting, study, routine work, etc. * * *" in main building of Hawaiian Volcano Observatory, November 1, 1916. Photographer unknown.

the military and to civilians who had business with an Island Headquarters. By October 1942, Island Headquarters was ordered to move to Hilo so as to be close to population center, port, and military and communication facilities. The U.S. Army returned Building 41 to the National Park Service with not so much as a "thank you."

Army occupation of Building 41 had not greatly inconvenienced National Park management, but it certainly continued the delay in providing HVO with its own operating facility. Park Headquarters, which until 1932 had been in a cottage on the rim along with the HVO buildings, occupied a new headquarters building 30 m (100 ft) back from the rim and handy to the road from Hilo. Because of its location, it had escaped the 1940 razing and had then played host to the HVO staff, who crowded into the headquarters building with the park staff. (This headquarters building is now a detached annex of Volcano House.)

With the Army out, HVO occupied Building 41 from October 1942 to September 1948, when HVO was evicted from Building 41 and moved to the building HVRA had built in 1927 at Uwekahuna, on the west rim of Kilauea caldera. At that time, Building 41 became Park Headquarters. Now, greatly modified and enlarged, it serves both as Park Headquarters and Kilauea Visitor Center.

In 1931, two new members were added to HVO's professional staff. Two two-story buildings were acquired by HVRA to house them and add badly needed storage space. Years before, the two buildings had housed employees of the Volcano House; one was known as the "Japanese boarding house," and the other as the "Stage Station." The Stage Station (NPS Building 39) was razed in 1956; the Japanese boarding house (Building 40) was razed in 1959. After he retired in 1940, Jaggar maintained an office in the upper story of Building 40. I interviewed him there several times

and, after his death, sorted, classified, and shipped his office papers to be added to the Jaggar Collection in the Archives of the University of Hawaii, Manoa.

Sometime in the 1920's, a residence for Jaggar was built by him (or the HVRA) on the north rim of Kilauea. This residence (Building 78) was razed in 1956, along with its garage and maid's quarters (Building 77). The former maid's quarters were assigned at times to visiting USGS personnel in the late 1940's and early 1950's; they were handy to the 1941 Volcano House hotel, where meals were available.

BUILDING 131 AT UWEKAHUNA (1927–PRESENT)

From the very beginning in 1912, volcano visitors often asked questions of HVO staff members they met in the field or found in HVO buildings. When Hawaii National Park came into existence, uniformed personnel began to assume the public-contact work. In 1926, the businessmen of the HVRA raised $20,000 to build an information center on the west rim of Kilauea caldera, to be staffed by park naturalists, which would keep the increasing numbers of visitors away from HVO and its staff. Ground was broken for the new building on February 22, 1927. The site selected was the actual summit of Kilauea, on top of Uwekahuna Bluff (see fig. 61.1). The main building was built of iron and concrete, with stone cornerposts; a large terrace was enclosed by rough stone and fitted with stone benches.

In April 1927 the new building at Uwekahuna was turned over to the Secretary of the Interior and the Director of the National Park Service, which designated it as Building 131. From 1927 to 1948, park naturalists met the public, gave talks, and were headquartered in this building at Uwekahuna. Its view of Kilauea caldera is excellent, and, weather obliging, the view is equally good of Mauna Loa. Park interpreters and park visitors found the facility an ideal place for orientation to local geography and volcanology. Over time, as the numbers of its visitors grew, the "National Park Museum and Lecture Hall" was lengthened and widened, with architecture that matched the original building.

On December 28, 1947, the Hawaiian Volcano Observatory was transferred within the Department of the Interior from the National Park Service to the United States Geological Survey—the second time the USGS was host agency. In 1948 HVO was moved to Building 131 at Uwekahuna, and NPS offices and public services were then consolidated in Building 41 on the north rim.

In preparation for the move, the Uwekahuna Seismograph Vault (Building 135) was built in 1948 in a location well back from the Uwekahuna cliff face and road and far from any building that could move in sun or wind. The cellar is 3.6×6 m (12×20 ft), and a small entranceway serves as an airlock and processing room. The roof is a reinforced-concrete slab covered with about 45 cm (18 in.) of volcanic ash. This vault continues in service.

To receive HVO, the National Park Service in 1948 remodeled Building 131. The former movie hall was converted into offices and machine shop, and most of the exhibit floor became offices and laboratories. HVO moved in during the fall of 1948.

At the time of the move in 1948, it was pointed out by volcanologist R.H. Finch, then the Director of HVO, that Uwekahuna had been the first site selected by Jaggar for the Observatory in 1912 but was given up on account of the scarcity of water and its relative inaccessibility at the time.

NEW BUILDING AT UWEKAHUNA (1985–PRESENT)

In May 1985, construction of a new facility for HVO began at Uwekahuna. This new building was completed and occupied a year later. Building 131 was renovated and returned to the National Park Service as an interpretation facility named the Jaggar museum. Thus, the original vision of the HVRA of a center combining ongoing scientific studies and interpretation of those studies to the public is, after 75 years, finally realized in a fully modern facility.

PUBLICATIONS AND DOCUMENTS

Much of the most reliable data about the history of the Hawaiian Volcano Observatory is contained in its publications. Two publication series had long runs, covering the period from before the 1912 start through and beyond the pioneering period. These were the Bulletin and the Volcano Letter.

Jaggar once, in his annual address as Director of HVO (Jaggar, 1917b), characterized "the proper work of volcanic recording" with two words—permanency and extension. Permanency depended on continued financial support. Publication was the method of keeping informed the 150 members (in 1916) of the HVRA, whose membership provided the guaranteed $5,000 a year of local support. Extension was also seen to be a purpose of publication—to interest scientists and governments overseas in sponsoring permanent volcano observatories.

The vehicle that served both roles of "permanency" and "extension" was the weekly report of volcanic activity prepared by the HVO staff. Taking their cue from the 6 popular weekly reports filed with the press in 1911 by Perret, Jaggar and others wrote another 1,249 weekly press reports, many labeled as bulletins. They constitute an uninterrupted series from January 18, 1912, through December 29, 1935. The last weekly press report, numbered 1,249, was published in the Volcano Letter (no. 430) in December 1935.

The weekly Bulletin was a regular feature in the *Pacific Commercial Advertiser* (now the Honolulu *Advertiser*). By arrangement with the Bishop Museum (Jaggar, 1917a), a carbon copy of each typewritten report was sent to that Honolulu institution. Soon a second carbon went to the Hilo *Tribune-Herald*. Appearance of HVO's weekly reports in two newspapers served to inform islanders and tourists about volcanic activity at Kilauea and Mauna Loa, and it kept the observatory in the public eye.

Reprints in leaflet form of the weekly press reports in the *Advertiser* were mailed by HVRA from Honolulu from 1912 through July 1, 1914, to the 150 or so members of the HVRA and

to 200 or more institutions and individuals worldwide on the HVRA's exchange list. Beginning in August 1914, the weekly reports of each month were combined into a monthly before being mailed by HVRA; this practice continued through July 1929. Over the years, while there were some issues without any special back page, the published and mailed leaflet bulletins generally carried informational back pages of ten different designs (Apple, 1985).

The other regular and long-running publication of HVO was the Volcano Letter, which was printed and mailed weekly beginning the first week of January 1925, apparently to the same subscription list as the bulletins. The Hawaiian Volcano Observatory thus had for the years 1925–1929 both a weekly and a monthly publication. In 1930 the two were combined; the weekly press bulletins became a part of the Volcano Letter. The Volcano Letter ceased being a weekly and became a monthly with the June 1932 issue. It went quarterly in 1939, and was finally discontinued in 1955.

The Bulletin and Volcano Letter usually carried the bylines of the scientists involved in their writing. Both often contained illustrations, including photographic halftone plates. The Bulletin dealt mostly with day-to-day raw data, while the Letter was the vehicle for more digested data, summaries, conclusions, reviews, news, predictions, opinions, and project status reports, not only in Hawaii but worldwide.

Over the years there were other serial publications for short times—monthly, quarterly, semiannual, and annual reports, as well as special publications.

The Volcano Letter was published first by the HVRA and then by the University of Hawaii. USGS publications continued the record of observations after the Volcano Letter was discontinued.

Additional information on the history of HVO is in the original holographs and manuscripts at the Bishop Museum, Honolulu, the first archival repository. These include Kilauea record books, by months and years (from 1912 on); folders full of notes, by years; photographic albums and photographic negatives; guest books; carbon copies of weekly reports; and copies of early bulletins.

The University Archives, University of Hawaii, Manoa, has HVRA files and records, the personal papers of Jaggar, some HVO material, and related sources. It was the second archival repository.

The third repository is the University of Hawaii, Hilo. Its Mo'okini Library has a continuing file, by years, starting before 1912, of copies of non-HVO-sponsored publications by Jaggar and others of the HVO staff, copies of the Bulletin and Volcano Letter, HVO special publications, documents sent in recent years for safekeeping, and my own collection of holographic material (Apple collection), prepared over the years and used in this history. Some material is also available in the HVO library for reference use by the staff.

Bulletin and Volcano Letter deadlines over the pioneering years did not keep the professional staff from making numerous professional contributions to scientific journals and periodicals published by others. Bibliographies of contributions by staff members of the Hawaiian Volcano Observatory contain copious entries.

VOLCANO EXPERIMENTS

The comparatively easy access at Kilauea to a variety of ongoing volcanic activities stimulated and encouraged experiments, ranging from the serious scientific to the decidedly frivolous. Visitors from America and Europe fried eggs in pans that rested on moving lava flows, learned how to thrust their cigarettes and Cuban cigars into hot cracks to light them (nonsmokers lit ends of sticks in the same cracks), embedded coins in small pieces of pasty rock, and scorched the edges of postcards on hot lava before the cards were mailed home. The Volcano House supplied eggs, pans, and postcards, as well as the guide who kept hotel guests safe while performing these feats in or near Halemaumau. The guide, Alex Lancaster, probably wound up each trip into Kilauea caldera with one pocket full of tips and another full of Cuban cigars—until Jaggar put him on the Observatory's payroll as janitor, guide, and general roustabout. Lancaster's experiences close to Kilauea's flowing and fountaining lava made him a good hand for Jaggar.

Lorrin Thurston helped Jaggar to take temperatures, sample gases, and measure depths. On January 11, 1917, Thurston and his assistants helped Jaggar thrust a length of galvanized-iron pipe through the solid crust of the lava lake to take a temperature reading 1 m (3 ft) down. At the end of the pipe was a metal cylinder that contained six cones of fusible clays which melted at temperatures in a range from 900 to 1,150 °C (fig. 61.5). After the end of the pipe had been held in place for six minutes, the crew withdrew the pipe, with difficulty. Softened by heat, the pipe had bent sharply at the point where it pierced the crust, and its end was weighted with the pasty lava that clung to it. None of the clay cones had melted, and Jaggar concluded that the temperature 1 m down was lower than 900 °C. In view of more recent data, this seems unlikely. Probably the clay samples did not reach equilibrium temperatures.

Then Thurston wanted to try an experiment. He had lugged two large pieces of ohia wood out to Halemaumau to toss into the lava lake to see what would happen. Jaggar duly recorded the results for posterity (Jaggar, 1917c): Both logs burned after sinking below the surface. There were abundant yellow flames and puffs of smoke that ballooned the surface crust a bit.

In 1925, Jaggar conceived a plan to bore holes, 3 m (10 ft) deep and 300 m (1,000 ft) apart at corners of equilateral triangles, on the floors of Kilauea caldera, Kilauea Iki Crater, and Keanakakoi Crater, as well as on the surfaces surrounding them. Temperatures at the bottoms of the holes were to be taken, so that isothermal lines could be drawn on a map of the region. The holes would then be sealed so that periodic rechecks could detect changes in the temperature of the bedrock.

In preparation, J.C. Bean, USGS topographic engineer, surveyed the borehole network from December 1925 through May 1926. An air-driven hammer drill, air compressor, truck, some "tested thermometers," a high-speed camera, and some up-to-date surveying instruments were acquired for the project. Drilling got underway in 1926 but was discontinued during the winter of 1927–28 after 30 holes had been drilled. Results were apparently inconclusive or disappointing; no results were ever published.

FIGURE 61.5.—Preparing to measure temperature of lava, January 11, 1917, floor of Halemaumau Crater. L.A. Thurston stands behind Jaggar, who holds pipe to be inserted into lava lake. Cylinder at end holds six Seegar cones of fusible clay. Others, from left to right, are Norton Twigg-Smith, Joe Monez, and Alex Lancaster. Note log of ohia at Thurston's feet, ready for his experiment. Photograph by Horace Johnson.

In retrospect, the 1925–28 project can be considered pioneering, but the real pioneering was an earlier drilling in 1922, described in the various monthly issues of the HVO Bulletin for that year. John Brooks Henderson of Washington, D.C., gave Jaggar $3,000 to begin boring experiments. Local gifts from Hawaii raised the total to $8,000. Honolulu driller A.H. Hobart was hired to use an impact or "churn" drill for three months; HVO was to supply the water needed for the drill and to transport all supplies to the drill sites. By April 1922, HVO had evolved the world's first dune buggy—a Ford touring car modified, as described by Jaggar (1922a, p. 32), by "doubling each rear wheel and fitting a pair of wide non-skid pneumatic tires to each doublet; this gave to each rear driving roller eight inches of grooved rubber traction surface, including a small air space between each pair of wheels. The double wheels were made by bolting two ordinary wheels together with a wooden disc between. A rear axle planetary gear system was added, giving three extra low gear ratios in addition to the usual two forward speeds and one reverse. All unnecessary weight of fenders, steps and doors was removed, and at rear end of car was placed a drawbar and shackle and an extra heavy spring. This converted the car into a general utility vehicle for use both as tractor and conveyance for men and supplies, devised to travel over any ordinary rough lava or on the surface of deep gravels where a common truck would dig in and be stalled."

This vehicle hauled supplies and men over sand, gravel, and billowy pahoehoe lava (fig. 61.6). A new Caterpillar tractor was also tried on lava and then modified to front-wheel steering. Rubber tires went on its rear wheels. It was used as a stationary engine to drive a generator and as a tractor to haul water barrels on sleds to drillsites.

FIGURE 61.6.—Hawaiian Volcano Observatory's modified Ford automobile hauling water for drilling operators on floor of Kilauea caldera, July 21, 1922. Vehicle was stripped of unnecessary weight and fitted with additional low gears, drawbar, and double rear wheels. Photograph by T.A. Jaggar, courtesy of the Bishop Museum (negative 94119).

Boring began May 1, 1922. Hole 1 was at the east corner of Sulphur Bank. The nearby Volcano House supplied water from its tanks, transported in barrels lashed to sleds hauled by the tractor. Casings and tools were skidded to Sulphur Bank behind the touring car.

A kerosene engine powered the rig to deliver 40–50 strokes per minute to a blunt-chisel bit of 6-in. diameter. The bit was turned by hand; water was supplied to the hole also by hand—about 10½ gallons per foot. A bucket was used occasionally to clean the hole bottom. Burlap sacking was wound around the mouth of the well to protect the drillers and machine from hot acid fumes. Eventually a wooden plug was devised for the wellhead that let the cable through but kept most of the fumes in. The cable and other steel parts were frequently painted with crude petroleum to protect them from the fumes.

The temperature was taken by a maximum thermometer lowered the 7 m (22 ft) to the bottom of Hole 1 and exposed five minutes; it read 96 °C. This reading was later checked by an Alumel-Chromel thermoelement and potentiometer and checked again with another maximum thermometer of a different make.

The churn-drill rig was moved about 45 m (140 ft) to start Hole 2, also at Sulphur Bank. Drilling started June 1, 1922, with heavy steaming from the hole. Troubles with the boring limited downward progress to five days out of ten. At 6 m (20 ft) the hole was cased, and the bit diameter reduced from 8 to 7 in. Another reduction to 6 in. and casing came at 12.8 m (42 ft), but the tools became wedged and broke a camshaft and gear wheel. The field forge failed to heat and temper the steel bits properly—they had to be sent to a sugar-plantation forge at Mountain View, 30 km (19 mi) away. At 13 m (43 ft) steam greatly increased, and at 15.2 m

(50 ft) "all sludge and water disappeared in an east-west crack across bottom of hole" (Jaggar, 1922b, p. 64). The hole was complete at a depth of 15.2 m (50 ft) on June 12, 1922. Hole 2's temperature was also about 96 °C. Pipe of 7-in. diameter was set in concrete to protrude a few inches and covered with a screw cap. "In a few weeks the inner surfaces of the iron were black with sulphide; and free sulphur crystals formed" (Jaggar, 1922b, p. 64). A shed of corrugated-iron sheets was built over Hole 2's wellhead; stacked rocks now cover it.

On August 22, 1922, Eugene T. Allen of the Geophysical Laboratory in Washington tested the gases of Hole 2 and was impressed that drill holes acted like natural fumaroles to serve as vents for escaping gases.

Hole 3 was near the center of Kilauea caldera's floor on the 1894 lava flow and in line with the 1920 Kau Desert rift. To make it possible to deliver water, rig, casings, supplies, and drillers, off-duty soldiers from Kilauea Military Camp were hired for four days to beat a rough track from the end of the road near Halemaumau to the drillsite. Meteorologist R.H. Finch, Jaggar's assistant, saw to it that the soldiers made a track over which the modified touring car and tractor could pass, albeit slowly. Hole 3 was drilled to 24 m (79 ft), and the temperature at the bottom was 69 °C.

Because churn-drill holes sometimes went crooked, tools stuck, and bits dulled rapidly, Jaggar wanted to try a rotary-drill rig. One was surplus to the needs of the Hutchinson Sugar Company, and HVO purchased it on June 22, 1922. It was a Davis Calyx "shot" Drill, model BF4, capable of boring a hole of 4-in. diameter to a depth of 300 m (1,000 ft). As it dug, the tube rotated and made a core; in practice, however, the lava rock fragmented, and satisfactory cores were rare and short.

Hole 4 was on the grounds of the Observatory, along the north rim of Kilauea (fig. 61.7). A drill tower 12 m (38 ft) high was part of the package purchased and was assembled on the rim. A shed, with an opening through the roof for the cables, was built about its base to shelter the drillers.

Water in quantity was required for this drill—241 gallons per foot of progress—and the water-storage facilities of HVO were needed to supply it. As drilling proceeded, voids and openings between layers of lava were met that caused frequent loss of water pressure. These hydraulic problems had been solved by October 1922, however, and a depth of 20 m (65 ft) was reached. Bottom temperature was 97 °C. Hole 4 was the well referred to by Jaggar in 1941 as being beneath the lobby of the new Volcano House. The capping of this hole in November 1922 ended HVO's first pioneer efforts at scientific drilling.

MAUNA LOA

T.A. Jaggar did not confine his efforts to Kilauea; he had a sustained interest in the equally active volcano of Mauna Loa and spent much time and energy attempting to obtain improved access to it. The following account is mainly compiled from various issues of the HVO Bulletin from the years 1913–17, 1920, and 1922.

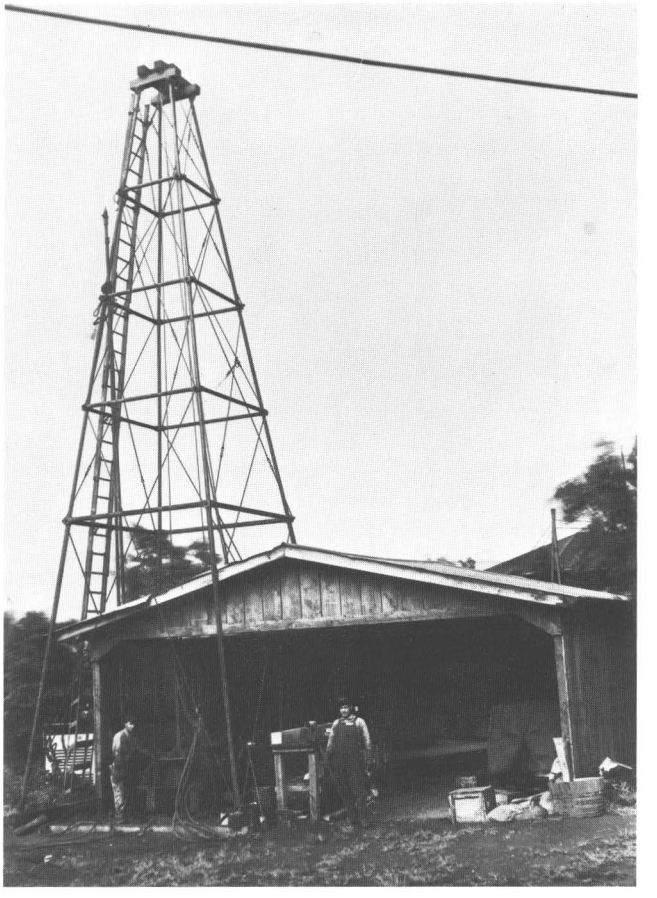

FIGURE 61.7.—Rotary drill and its tower on grounds of Hawaiian Volcano Observatory during earliest HVO drilling program in August 1922. Photograph by T.A. Jaggar, courtesy of the Bishop Museum (negative 94121).

ACCESS ROUTES AND FACILITIES

In late November 1914, during a summit eruption of Mauna Loa, Jaggar attempted to view the lava fountains but failed. His mounted expedition was driven back by a severe wind and snow storm near the summit; they were even forced to abandon the camp equipment. From that time on, Jaggar advocated a shelter on the summit for men and horses and for the safe storage of instruments. To reach the summit, Jaggar wanted at least a horse trail (a road for vehicles would be better) from HVO headquarters at Kilauea. This meant the trail or road would ascend the northeast rift of Mauna Loa; overnight facilities would be needed along the trail. Early in 1915, Jaggar told the HVRA that Mauna Loa was a desert waste without water. Expeditions to the summit were exhausting, and animals employed frequently had their legs cut by the rough lava; consequently, ranchers would not rent good animals. There was no shelter on the summit, little water, no feed, violent winds, and low temperatures. It cost several hundred dollars to make a trip to the summit, and one generally had to return before any real scientific work could be done.

Through 1916, the Ainapo Trail over jagged aa and thin-crusted pahoehoe lava fields was the customary route to the summit of Mauna Loa (Apple, 1973). Until horses and mules became cheap and plentiful, an arduous hike of several days' duration up this trail was the most practical way to the summit. Most of the trail lay on the Kapapala Ranch, and Kapapala cowboys were hired as guides and packers. The Ainapo was about 54 km (34 mi) long and rose from 600 m (2,000 ft) to 4,000 m (13,000 ft) above sea level. The lower trailhead was the village of Kapapala. It was by way of the Ainapo Trail that Jaggar first visited the summit caldera in September 1913.

The surface of the Ainapo Trail was rugged, and it was not maintained for either men or mounts. Jaggar wanted a "simple route to the summit" to give scientists and the public access; with Thurston's help, he got the U.S. Army to build one in the fall of 1915.

Seismologist H.O. Wood, guide Alex Lancaster, and J.F. Haworth made a preliminary survey of a trail from Kilauea up the northeast flank of Mauna Loa to the summit in August 1915. Jaggar, Thurston, and a Lt. Philoon, 25th Infantry, U.S. Army, checked it in September. Thurston and his friends had received the approval of the departmental commander for the U.S. Army to build the trail Jaggar wanted. The HVRA put up a 5,000-gallon water tank near HVO headquarters to support the Army trail builders, and transported several smaller water tanks up the flank to a camp near timberline, soon called Camp Bates after Capt. Bates, a civil engineering officer. Thirty soldiers, under Lt. Philoon, arrived on October 15, 1915; they were followed two days later by others.

This trail up the northeast flank of Mauna Loa, called the Mauna Loa Trail, was completed in December 1915, and the soldiers were back at Schofield Barracks on Oahu for Christmas. The costs of round-trip transportation for the soldiers by ship, rental of pack animals, and purchase of materials for two buildings were all borne by the HVRA. When Jaggar prepared his proposal for a Hawaii National Park in Washington, D.C., early in 1916, he already had his trail between the summits of Kilauea and Mauna Loa Volcanoes. He hoped to upgrade it to make it suitable for trucks, and he foresaw perpetual Federal maintenance of the route. His bill, when it became law, authorized a strip of land between the summits for such a road, to be surveyed and given legal boundaries at a later date.

When the trail was built in 1915, horses and mules could go as far as Puu Ulaula (Red Hill), a cinder cone at elevation 3,000 m (10,000 ft). As part of the project, the soldiers built a 10-man overnight cabin and a 12-horse stable at Puu Ulaula, 10 hiking miles from the summit. The army cabin, still in use, is called the Red Hill rest house.

HVO hand labor filled cracks with chunks of lava and generally prepared the trail above Puu Ulaula for mounts. The first riding horses and pack mules reached the summit with Jaggar and his assistant Ruy H. Finch on June 29, 1920. Because there were no stable facilities for the animals, the guides, packer, and animals were sent back to the rest house. Jaggar and Finch stayed at the summit; "Jaggar's Cave" received its first use that night. (In the same week the first tourists reached the summit over the Mauna Loa Trail; HVRA charged each member a dollar a night at the Red Hill shelter.) In 1930, National Park crews improved the trail for horses.

Until a summit shelter was built by the National Park Service in 1934, hikers and riders were forced to camp in "Jaggar's Cave," a crack in the lava roofed over with corrugated-metal sheets. It was near another crack where water, frozen in winter, accumulated.

Since 1915, in an incremental process, lower portions of the trail have been widened and improved for vehicles. In 1936, the CCC built the last increment, the road from Bird Park to near the site of Camp Bates at elevation 2,025 m (6,650 ft), to permit scientists access by small truck to a seismograph vault near that elevation. The road has since been paved. Most hikers to the summit today start their hike at the upper end of this road.

All during his HVO directorship (1912–1940), Jaggar pressured for a vehicular road from Kilauea up the northeast flank to the summit of Mauna Loa. He wanted the 1915 Army trail improved to allow easy and quick access by HVO vehicles for studies at the summit. Although the National Park Service established boundaries and acquired the strip of land within which the road could be built, it has consistently rejected the concept of a vehicular road to the summit of Mauna Loa. This rejection has been sustained over time, in spite of pressures from Jaggar and Thurston and at times from the Territorial Legislature and the Hawaii County Board of Supervisors. As a result, the road has never been built; the advent of helicopters may now have made moot the question of such a road.

Jaggar's Cave, the 1915 cabin, and the 1915 trail have been declared eligible for listing in the National Register of Historic Places (U.S Department of the Interior, 1973). All are still in use, although the trail has had to be rebuilt in places because of damage from earthquakes and lava flows.

THE 1926 ERUPTION

Mauna Loa's recognized eruptive pattern is a summit eruption followed—within hours, days, or months—by a flank eruption. In 1926 there was a brief summit eruption, followed by 14 days of eruption on the southwest rift zone. A flow from this rift zone passed through a South Kona forest, crossed the main road on April 16, and pooled behind the coastal village of Hoopuloa. Between 0400 and 0900 H.s.t. on April 18, the flow buried the village, wharf, and harbor and entered the ocean. This was HVO's first real experience with property destruction by a lava flow. The following account was compiled from Apple and Apple (1979b), Finch (1926), Jaggar (1926a, b), MacDonald and Hubbard (1982), and unpublished sources.

Edward G. Wingate, USGS topographical engineer, was mapping the summit of Mauna Loa in 1926, changing campsites as the work progressed. On April 10 his camp was along the 3,475-m (11,400-ft) elevation, well into the desolate upland above the Kau District. An earthquake wakened the campers about 0145; as they drifted back to sleep, a further series of quakes had them sitting up, talking, and wondering. About 0330 Wingate braved the cold and

wind; with a blanket wrapped around him, he went outside and stood bathed in reddish light.

From his camp Wingate had a wonderful view of smoke columns lighted by the glow from below. They reached the flows about 0630. With his crew, Wingate mapped lava fountains, moving flows, steaming vents, and spewing cones.

The packer who kept Wingate's camps supplied with water, food, and firewood had spent the night on the trail on his way down to pick up another load; he reached the Ainapo trailhead midafternoon on April 11. More than supplies awaited him—there was an HVO expedition demanding guide service to Wingate's camp. This was the first news of the eruption for the packer. The expedition consisted of Jaggar, topographer J.C. Beam, cook H. Yasunaka, and packers John Kama and Joe Kaipaloa.

After a night at Ainapo, and with three additional pack animals borrowed from Kapapala Ranch, the expedition started up toward Wingate's camp. By midafternoon they reached the camp, which Jaggar described as a primitive affair consisting of three tents and a cook shelter on the rough lava fields. The cook shelter was bolstered with stone walls to protect against wind, but all the tents had to be tacked down to the pahoehoe lava with spike nails.

For three days the HVO party surveyed the sources of the eruption; then they descended and moved into Kona District, where roads, houses, and other property were threatened by the flows. Wingate and his crew stayed behind. Much of the area already mapped was under fresh lava, and there was a lot of remapping to do.

On April 16, Tom Jaggar scratched marks about a foot apart across the rutted, gravel road (the only road) between the Kona and Kau Districts. A lava flow was approaching, and Jaggar wanted to measure the flow's speed as it crossed the road. Perhaps a hundred people were waiting around the Hoopuloa Church, on the uphill side of the road, and at the Kanaana house opposite, on the downhill side of the road. They had seen and heard the flow, 4.5–6 m (15–20 ft) high and more than 150 m (500 ft) wide, as it moved through the forest uphill. When it neared the road, people who lived on the Kona side of the flow moved off to the north, and those who lived on the Kau side moved to the south, so they could go home after the road was closed.

Jaggar recorded that it reached the uphill, inland side of the road at 1222 at an estimated speed of about 2 m/min (7 ft/min); within two minutes the road was crossed. Jaggar and his assistant, H.S. Palmer, stayed on the Kau side. Soon Robinson MacWayne, Honomalino Ranch proprieter, supplied horses, ranch hands, and guide service through coastal Milolii to Hoopuloa. Jaggar and Palmer set up camp in the Hoopuloa store. Jaggar noted that the Chinese proprietor had swept the building spotlessly clean after removing his stock of goods and furniture. Both the store and the adjacent wharf lay directly in the track of the oncoming lava front. Groups of people were huddled along the stone walls back of the village, watching the glowing, crunching, relentless wall of fire behind, but watching it at leisure, without excitement, and with great weariness because the main event had been postponed. All had come to see the lava enter the sea, but it was still several hundred feet away.

Those watching parked their cars on the Kona side of Hoopuloa. One enterprising youth used his small truck to haul water from the Hoopuloa tanks to Milolii, the end of the road. When the flow reached the sea, he and his truck were cut off; he later took his truck apart and transported it piece by piece by outrigger canoe to the road on the Kona side of Hoopuloa.

At about 0300 H.s.t. April 18, the flow rode over the stone walls behind the village and started burning outhouses. Pigs heard squealing in a pen were released. Destruction of the village was gradual and complete. As soon as lava began falling into the sea, steam shot up in jets. Hundreds of dead fish floated along the edge of the turbulent water that spread out from the contact area of hot rock and cold ocean. Hawaiians from Milolii came in their canoes and gathered the dead fish for salting and preserving. Jaggar collected some dead, floating fish and noted that they were perfectly fresh and in no sense cooked.

CONTROLLING LAVA FLOWS

Many observers have noted that barriers, both natural and manmade, can sometimes stop, divert, or delay the forward movement of a lava front. The worried people of Hilo in 1881 first considered the use of explosives to stop a flow that threatened their port and homes; this is the earliest recorded suggestion for such action in Hawaii (Lockwood and Torgerson, 1980). The concept of using explosives to modify the forward motion of a lava flow was advocated by the HVRA's Thurston in his newspaper in 1929. Tom Jaggar and Ruy Finch of HVO were actively involved in using explosives in the form of aerial bombs on moving lava flows that threatened Hilo in 1935 and 1942, respectively. Bombing the upper reaches of a lava tube feeding a Mauna Loa pahoehoe flow in 1935 is credited with slowing or stopping the advance of the distal end; the 1942 bombing breached the levee of an aa flow and was also partly successful in slowing the flow's advance (Bolt and others, 1975).

In 1937 Jaggar proposed construction of a comprehensive set of embankments, 5–6 m high, to divert Mauna Loa lava flows from Hilo town and its harbor; the embankments would have had a total length of about 20 km (including 11 km in a single wall around the south side of the town) and were projected to cost about $800,000 (Jaggar, 1937). These barriers have yet to be built, though experience elsewhere shows that they could be effective (Bolt and others, 1975). Jaggar's interest in controlling lava flows to protect property continued long after his retirement from HVO (see Jaggar, 1945).

THE *OHIKI* AND OTHER EXPERIMENTS

Ohiki is the Hawaiian word for sand crab; honukai means sea turtle. In 1928, when the National Geographic Society joined with the USGS to sponsor an expedition with Jaggar in charge to map, photograph, and survey in the Aleutians around Pavlof Volcano, the Society supplied an amphibious boat, to which Jaggar gave the name *Honukai*. It was a twin-screw steel amphibian, built in Chicago by the Powell Mobile-Boat Corp. In the 650 km along the coast of Alaska from Shumagin Islands to King Cove, the expedition did not even have to pump up the tires. The *Honukai's*

numerous excessively low gears even enabled them to drive up to the snowline and bring out the heavy fur and bones of a bear that Jaggar had shot on the snowy volcano, Mount Dana. Jaggar brought the *Honukai* back to Hawaii with him and based it in Kona.

In preparation for this expedition, the HVO machine shop built a wooden amphibious boat around a "low-geared small motor car with balloon tires," that Jaggar had used over tundra and beach of the Alaskan Peninsula in 1927 (Jaggar, 1927). Inlets, rivers, and rocks were obstacles that made Jaggar mentally design modifications of the car into a "car-skiff."

The land and sea trials of this preliminary vessel, the *Ohiki* (fig. 61.8), took place in the spring of 1928 (Wilson, 1928). She first took to the sea at Ninole Cove in the Kau District, and she quickly revealed the need for additional work.

After modifications (freeboard raised, length slightly increased, paddle-wheels enlarged, a winch and cable mounted in bow, 5-horsepower outboard motor added), an extended trip was made along the west coast of the Island of Hawaii to make beach and sea tests. Thurston went along as a passenger and publicity man; Mrs. Jaggar served as stewardess. The car with the boat body excited all the roadside children of Kona with delight.

Jaggar's *Ohiki* made a speed of about 6 km/h (4 mi/h) in water with the combined power of paddle wheels and outboard motor; it weighed 1,700 kg (3,800 lb), was 7 m (22 ft) long, and had a 1.5-m (5-ft) beam and an overall width of 2.1 m (7 ft) at the paddle boxes. It made more than 30 km/h (20 mi/h) over highways. As a result of his experiences and design work with the *Ohiki* and the *Honukai*, Jaggar was later able to help the U.S. Army with the design of amphibious vehicles for World War II, and he received in 1945 the Franklin L. Burr Prize of the National Geographic Society for this work.

Many other experiments were generated by HVO, though some were mostly conducted by others (see Jaggar, 1956). They included studies of the rehabilitation of lava and lava soils by organisms such as lichens; classification of the lava soils of the Kona District on the Island of Hawaii for their suitability for coffee tree cultivation; and installation of tide gauges at Hilo. College-credit courses in volcanology were given over many summers, especially for Island teachers. The widths of selected cracks, especially near Halemaumau, were measured periodically to record any changes. Topographic mapping of the Island of Hawaii and, by 1932, of almost the whole Territory of Hawaii was supported. By 1924, several triangulation and leveling projects had proved the elevation and distention of Kilauea caldera. As early as 1912, private industry (the Dictaphone Corp.) was trying out microphones in attempts to record the true sounds of a volcano in eruption.

SEISMOLOGY

The history of seismology at HVO begins in 1912 with the completion of the Whitney vault. After two decades of pioneering, Jaggar was amply aware that seismometry on an active volcano is quite different from that at a station that studies mainly distant earthquakes.

INSTRUMENTS

Instrumentation provided a challenge from the beginning. The story of the evolution of seismic instruments at HVO is documented in Curtis (1913), Jaggar and Romberg (1918), Apple (1978), and various issues of HVO's own publications, the Monthly Bulletin and Volcano Letter. The following account is synthesized and condensed from these sources.

Seismologist H.O. Wood reported for duty June 13, 1912, and he had the crated instruments from Japan installed on their "concrete tables" by July 2—installed, but not necessarily performing properly. These instruments were: (1) a sensitive Omori tromometer, designed for the registration of earthquake motion proceeding from a distant origin; (2) a less-sensitive Omori tromometer, designed for the registration of weak or moderate shocks of local origin; and (3) an ordinary Omori seismometer that started itself upon detecting a strong shock and that registered three components of motion, east-west, north-south, and vertical. The more sensitive tromometer arrived missing the north-south component; it was therefore mounted in such a way as to measure and register the component of earth motion in the east-west direction. Both tromometers had smoked drums and timing capability with marks every one minute. The ordinary Omori was set up so that when earth motion was strong enough to activate its starting device, the smoked drum revolved rapidly and marks were made every one-half second. This instrument could also be set to ring an alarm bell when it started.

Heavy horizontal pendulums detected horizontal earth motions, and a "floating" weight suspended by two balanced helical springs detected, in theory at least, the component of earth motion in the vertical direction. Time marks were made by an electromagnet operated by the brief closing of an electric circuit. Wood had all three instruments operating by August 1912, but all had, sometimes separately and sometimes simultaneously over the years, periods of nonoperation when work was done in the Whitney vault or on the instruments.

Of these three seismometers, the first to leave the Whitney vault was the less sensitive Omori. It was moved to the Technology Station at Halemaumau in February 1913 and later was apparently dismantled for parts. The three-component self-starter never really worked properly, even after it was rebuilt in 1918, renamed "Domesticus," put on full-time duty, and its vertical detection apparatus removed.

The most sensitive Omori seismometer was rebuilt into an optical recorder and given a corner mount in 1918 in the hope that it would detect both north-south and east-west teleseismic motion with its single boom. In 1923 it was retired. After retirement, this and all seismometers were cannibalized for parts to make or repair other instruments in the HVO machine shop.

During their service, the seismometers were modified and changed by the HVO staff to try to make them more suitable for use on the rim of Kilauea caldera—to be more responsive to local short-period earthquakes, volcanic tremor, and the extraordinary ground tiltings. These were the three distinctively Hawaiian geophysical phenomena Jaggar had identified by 1918. Jaggar noted that the

FIGURE 61.8.—Amphibious vehicle *Ohiki* leaving for extensive shakedown cruise and field test around the Island of Hawaii by water and road, February 1928. While T.A. Jaggar poses, his wife Isabel (cruise stewardess) peeps around stern. Paddle wheel can be seen behind Jaggar's right shoulder. It will be installed before vehicle takes to water in Kona. Building in background is HVO machine shop, built in 1927. Photographer unknown.

mechanical imperfections of standard instruments, designed for cheapness and convenience of operating and ill-adapted to such special problems, combined to yield only mediocre results. Dr. Arnold Romberg was hired by HVRA for the summer of 1918 to rebuild and otherwise improve the two original seismometers still in the Whitney vault and to do some work on the Bosch-Omori seismometer that had been acquired in 1913. Romberg also made at least two new one-component seismometers for installation in cellars to be established by HVRA in Hilo and Kealakekua. As Romberg worked, Jaggar noted with satisfaction that small improvements had been made over experiments by Milne, Galitzin, and others and that already the difficulties of friction, magnification, damping, opening the record, and time marking had been partially overcome.

The two-component Bosch-Omori seismometer, purchased from the Whitney Fund, had finally arrived from Germany by April 1913. Wood noted that in order to permit the construction of foundations and the work of installing the Bosch-Omori, a 100-kg tromometer, the seismographs in operation had to be partially dismounted temporarily. The new instrument was mechanically and dynamically superior to those hitherto in use there, and it was expected that a larger proportion of teleseismic records would be written, as well as more precise records of local shocks.

Trial runs of the new Bosch-Omori's east-west and north-south components were made on April 30, 1913; a feeble teleseism was registered, as well as strong volcanic vibrations. Adjustments were completed on May 8, 1913, for the final trial runs. From that time on through 1953, the Bosch-Omori seismometer was the main reliable, basic geophysical instrument of HVO.

Fine tunings of the Bosch-Omori never ended and were required after almost every unhinging caused by a strong earthquake. Modifications and upgradings were intermittent: steel wire replaced silk fibers to suspend the weights; oil damping baths were added, adjusted, redesigned, and readjusted; friction reduction was tried; new hinges were designed and manufactured; magnifications were lowered and raised; different levers, recording pens, and pins were tried; timing devices were improved; better drum-smoking devices were found; Dr. Romberg modified linkages and levers in 1918 so that one smoked drum recorded what two drums did originally; and one of the piers was rotated 7.5° to permit its boom to swing closer to a true east-west line.

In 1948, the Bosch-Omori seismograph in the Whitney Laboratory had a period of 7.7 seconds and a magnification of about 115 times the earth movement. It gave satisfactory records of short-period local earthquakes and of the ground tilt. This standard was the goal always attempted and sometimes met over the decades. Credit goes to the HVO staff for the daily attention they gave to the Bosch-Omori. One or more of the staff came day or night, storm or sunshine, workday or weekend, whenever a felt earthquake or home alarm signaled a potential dismantling.

Whitney vault's Bosch-Omori was the workhorse of the first four decades of the Hawaiian Volano Observatory, 1913 to 1953. HVO staff habit, respect, and momentum kept the Bosch-Omori seismometer operating in the Whitney Laboratory of Seismology for ten years after mechanical seismometers became technologically obsolete. The Bosch-Omori's last official smoked seismogram was removed, shellacked, and read on February 1, 1963, ending a daily series begun 50 years before.

Since the standard commercial seismometers had been tried and found wanting for the detection of short-period earthquakes, volcanic tremor, and ground tiltings, HVO turned its talents to designing and building special-purpose instruments. The most successful of these was the Hawaiian-type seismograph, in service worldwide by 1928. Briefly, it consisted of two horizontal components at right angles, each having a mass as much as about 100 kg (225 lb) consisting of a 69-cm (27-in.) length of pipe of 20-cm (8-in.) diameter, filled with sand. It was hinged above and below with short links of piano wire, had a free period of about 7 seconds, and was damped with light aluminum vanes dipping in oil near the outer end of the boom, giving it a lever magnification of about 130. Time was marked by an electromagnet recording on a smoked drum with paper speed of about 3.2 cm (1.25 in.) per minute. Both components recorded on the same drum, and a drum would run 24 hours without need of a change. The pair was designed for wall mounting, one on each side of a corner, with the mounting so arranged that the assemblies at the ends of the booms could record on the single drum. The only pier needed for the Hawaiian-type seismometer was one to hold the recording drum.

Pairs of Hawaiian-type seismometers were built in the HVO machine shop and supplied to Kodiak, Alaska (1927); Hilo, Hawaii (1927); the U.S. Coast and Geodetic Survey for testing and eventual placement at Sitka, Alaska (1927); Kealakekua, Hawaii (1928); Lassen National Park, California (1928); and Dutch Harbor, Alaska (1928). One design specification met by the Hawaiian-type seismograph was convenience of operation for the semiprofessionals hired by HVRA, USGS, or the Coast and Geodetic Survey at the more remote stations.

By 1929, although so far defeated in the search for a mechanical seismometer that would record the vertical component of seismic motion, staff at HVO continued experimenting. A vertical-component instrument to match the two-component Hawaiian-type already in use was especially desired. HVO seismologists wanted to measure the angle of emergence of earthquake waves at the station and believed this vertical angle would help furnish data on the depth of origin of the quake. By 1930, the HVO machine shop had built a vertical-component seismograph, with the heavy mass hung on spiral springs and temperature compensation provided by small springs. This instrument evolved after a variety of spring arrangements were tried, and it was installed in the Whitney vault. Its performance was never up to expectation, and it was the only seismometer installed under Building 41 in 1941. When that vault was abandoned by HVO in 1948, this instrument appears to have joined those in the bin to be cannibalized.

Recognizing that seismometers took the continuing care of specialists, Jaggar searched for instruments of simple enough design to be "put in the hands of amateurs" (Jaggar, 1932, p. 3). His first "shock recorder," designed in 1928, did record separate east-west and north-south motions, but it "also recorded the motion of rats, kittens, chickens, cockroaches and spiders" (Jaggar, 1931). This was redesigned so that it consisted of two wall-mounted inverted pendulums to be set up in a corner of a room and did not require a

pier. Three pairs of these were set up around Halemaumau. The first field test in the hands of "amateurs" came during the earthquake swarm in 1929 under Hualalai Volcano in Kona. A shock recorder pair was installed at Puu Waawaa Ranch on the slopes of Hualalai. Mr. Hinds the ranch owner and his family learned how to twirl the two daily recording discs over the smoking chimney of a kerosene lantern until each disc was coated an even brown. They also wound the clocks used in making the time marks.

It was this model of shock recorder that Jaggar took with him on the U.S. Navy expedition to Niuafo'ou Island (Tin Can Mail Island) in 1930 and left there with the Tongans. When earthquakes suddenly became a problem in 1930 in New Zealand, Jaggar hurriedly dispatched one such instrument in response to a plea from the New Zealand government. HVRA promised to supply eight more as soon as they could be manufactured, while in New Zealand machinists copied the one Jaggar sent.

By 1937, Jaggar had a new version of his shock recorder. What it gained in simplicity, it lost in sensitivity. It no longer separated arrival times of earthquake waves but registered only maximum intensity. Each instrument depended on a small mercury cup and was called an annunciator-type shock recorder. It showed a number from 1 to 6, depending on the intensity of the earthquake. Once a number became visible, the annunciator had to be reset.

Only two of the new design were on hand when an urgent request was made in 1938 to ship as many as possible on a Coast Guard cutter leaving almost immediately to supply colonists sponsored by the U.S. Government on tiny South Pacific Islands.

H.H. Waesche, a geologist at HVO, went aboard the cutter *Roger B. Taney* to install the two which were portable and could be set up in a few minutes with only a screwdriver and a pair of pliers. No smoked paper was needed; each instrument needed only a solid base and checking every hour or so. The colonists, all young Hawaiian men, would do the checking and report observations through the mail pouch. One recorder was set to read in an east-west direction on Canton Island, and the other to read north-south motions on Jarvis Island.

It was not necessary to wait for a natural earthquake to arrive to test seismometers and shock recorders built in the HVO machine shop; artificial earthquakes of known intensity and duration were created. HVO's earthquake machine, an oscillating table, was designed and built in 1928 in the machine shop by R.M. Wilson, HVO topographic engineer. It consisted of a massive, 365-km (800-lb) concrete slab resting on steel rollers. Instruments to be tested were mounted on the slab. Levers connected the rollers to the chuck of a nearby lathe; amplitude was governed by varying the radius of a crank in the lever train, and a range of periods could be provided by changing the speed of the lathe. Seismologists believed the oscillating table could simulate in part the ground motions of a variety of local earthquakes.

While seismometers were still being tailormade at Kilauea for local earthquakes, HVO acquired a shiny, new, compact, three-component Imamura seismometer from Japan for display to the visiting public in the building at Uwekahuna. All three components recorded on a single smoked drum. Although cars in the Uwekahuna parking lot, crowds moving about the museum floor, people clapping in the projection hall, and the range of daily temperatures in the building all confused the record, Park Naturalists believed that a working seismometer, no matter how befuddled its record, was a worthwhile exhibit and fit in with their lecture content. The Imamura instrument, with its magnification of as much as 50 times, was abandoned when HVO occupied the Uwekahuna building in 1948.

Seismographs are still the principal geophysical instruments at HVO. The electronic amplification and radio-telemetered signals of the current models would be startling to Jaggar's experiences, but not to his dreams.

TRAVELTIMES OF EARTHQUAKE WAVES

A principal goal of seismological studies at HVO from their beginning has been to determine where earthquakes occur beneath the volcanic edifices. For this purpose the inference of traveltimes for earthquake waves is critical, and much has been learned from the successive attempts to interpret those traveltimes in Hawaii. The story of this evolution has been told in Jones (1935) and in various issues of HVO's Weekly Report and Volcano Letter. The following account has been gleaned from these sources.

In May 1915, HVO seismologist H.O. Wood reported that he had determined the distances of origin for 411 of the 604 local earthquakes registered in the first two and one-half years of operation of the Whitney Laboratory of Seismology. Wood used a table by Zeissig to determine these distances; for clock time he used a chronometer lent by the Territorial Surveyor, corrected by solar observations with a transit borrowed from the College of Hawaii.

The tables of Zeissig, in use then at most seismographic observatories, were designed for large earthquakes many hundreds of miles away. In 1925 HVO Seismologist R.H. Finch reported that HVO had found other tables by Omori, published in the Bulletin of the Imperial Earthquake Investigation Committee of Japan, to be more satisfactory. Omori's values came in fractions of a mile and thus helped in determining earthquake origins only a few kilometers (2–3 mi) away. That Omori's tables were better than the Zeissig table for very local earthquakes was shown by the good agreement between computed and actual distances of felt earthquakes whose approximate locations were known.

By 1925 Finch had in the Whitney cellar a Howard pendulum clock, corrected by radio signals originating from Pearl Harbor. There was a flurry of speculation in 1927 when it was noted that this clock, after being consistently late by 0.08 second per day (s/d), went to a consistent 0.66 s/d and then to a consistent 1.71 s/d. The speculation was that its pendulum might be sensibly indicating changes in the value of gravity; elevations had changed by amounts on the order of 1 m in 1924, and magma movement below might be involved.

In 1931, HVO Seismologist A.E. Jones found that the Omori traveltimes did not completely agree with the seismic facts in Hawaii. He developed a traveltime-distance graph for Hawaii, and by using $S-P$-wave intervals he showed "how to locate Hawaiian local earthquakes without the necessity of accurate time checks on all the master clocks of the several seismograph stations on Hawaii" (Jones,

1935, p. 59).

Trying to keep the scattered stations of the seismic network on the same time was given up by 1937. Most attention had gone to the station at Kealakekua. The line between Kealakekua and Kilauea passed practically through the middle of the great mass of Mauna Loa, and the stations were about equidistant from its center. In 1926, HVO's R.M. Wilson complained that, while the time at the Whitney vault was corrected by radio, the instrument tender at Kealakekua got his time—often more than a minute in error—over the telephone from the Kona switchboard operator. A radio set was supplied to the Kealakekua station in 1926 to receive time signals from the U.S. Naval radio station NPM at Pearl Harbor. A key beside the set, wired into the station clock, was depressed the instant the time signal was received; this recorded a mark on the current seismogram along with the one-minute marks made by the station clock. A measurement between the two marks on the seismogram revealed the correction necessary. It was believed this system recorded the time to within one-half second or better.

By 1939 H.H. Waesche, HVO geologist, had tied together for time control the seismograph stations around Kilauea summit, as well as the one on Mauna Loa at the end of the truck road. The Howard clock in the Whitney vault sent minute and hour signals of sufficient strength to operate relays controlling the electromagnets that lifted the recording needles on the drums. The connecting links between the stations and the clock were the existing National Park telephone trunklines, not connected to the commercial system. Waesche worked out all the circuitry and procured or made the parts to make the system operate. After some troubleshooting, the time signals did not interfere with telephone service in the Park.

Today, seismograph time signals accurate to a few thousandths of a second arrive by satellite. Tom Jaggar would be pleased.

SCALES OF EARTHQUAKE INTENSITY

"Just as four pounds of sugar ought to be four times as big as one pound, so a number four earthquake should be four times as big as number one. Herein lies the difficulty" (Jaggar, 1929).

When Perret lived in his cabin near Halemaumau for six weeks in 1911, part of his working time was spent with his seismoscope. His views through its eyepiece showed the ground to be continually in motion. Accordingly Perret devised a scale based on the seismicity for the day; five on a scale of 10 was an average day.

H.O. Wood as charter HVO seismologist in 1912 used the Rossi-Forel scale of intensity, but also used phrases such as "this [earthquake] manifested an intensity of little more than 1/20th of that of the minimum shock perceptible to the senses."

In his report for the week ending December 19, 1912, Jaggar adopted for HVO the Cancani scale, which soon appeared on the back page of the printed weekly bulletins and stayed there through 1920. Inside, however, the text often used the Rossi-Forel scale by name, and a Cancani reference is hard to find. By the 1920's, R.H. Finch was using the Rossi-Forel to rate an earthquake recorded in the Hilea (Kau) cellar, and was rating the same quake as recorded in the Whitney vault as "slight" or "feeble."

HVO's R.M. Wilson used Volcano Letter no. 124 in May 1927 to describe the Rossi-Forel scale and explain how HVO graded its earthquakes in terms of acceleration from "feeble" through "alarming." Jaggar took most of Volcano Letter no. 223 in April 1929 to explain the Rossi-Forel, Cancani, and Mercalli scales, the last of which he abridged to show human effects. Jaggar concluded: "In the writer's tests, and Professor Mercalli among Italian peasants evidently had similar experience, ignorant persons in city or country can understand a human scale. They usually distort or exaggerate physical effects on masonry, water, trees, chimneys, etc., because they have no training in measured or judicial statement" (Jaggar, 1929).

Because he believed in the use of a human scale to grade earthquakes, Jaggar borrowed from Japan its postcard reporting system. Preaddressed and franked, with a form to be filled in and signed on the back, postcards were widely supplied to residents on all parts of the Island of Hawaii starting in 1932. People were to fill out and mail cards whenever they experienced a felt earthquake.

In keeping with the seismicity concept brought to Hawaii by Perret, charts and graphs of seismicity curves over various periods and for various purposes were prepared as early as 1920 and regularly by the 1930's. Seismologists at HVO developed for their own use in Hawaii the Hawaiian Volcano Observatory Scale, whose grades were "Tremor, Very Feeble, Feeble, Slight, Moderate, and Strong" (Jones, 1932). It was based on the double amplitude of motion on the Bosch-Omori seismograph and carried a description of the noninstrumental effects ("a human scale"). Its grades were eventually cross-referenced to the Rossi-Forel and modified Mercalli scales.

TSUNAMIS

Coastal areas in the Hawaiian Islands are vulnerable to seismic seawaves (tsunamis) generated by major earthquakes anywhere in the Pacific Ocean. The tsunami of 1933 demonstrated that seismology could be used to predict the advent of such a wave and therefore to give warning to people in threatened areas. The story of that occasion, in which HVO staff prevented possible loss of life, has been told in the Honolulu *Advertiser* for March 14, 1933, and in Jaggar (1933).

Capt. Robert V. Woods, a retired ship's master who was the HVRA employee at Kealakekua, Kona, operated the seismograph vault there in the cellar of his house. Woods was more than a technician who changed drums and did routine maintenance H.s.t. his instruments. He had learned from the HVO seismologists how to determine the distance and origin of an earthquake from the arrival times of its different waves.

Woods was in his basement vault at 0700 H.s.t. March 2, 1933, getting ready to change drums, when he noticed his seismometer begin to record the arrival of a distant earthquake. The time between arrivals of the first and second different waves was about ten minutes. Woods calculated the distance at about 6,320 km (3,950 mi) and put the origin at the west edge of the Tuscarora Deep, east of Japan.

Meanwhile, in the Whitney vault on the other side of the Island, HVO seismologist Austin E. Jones saw the earthquake arrive on the Bosch-Omori instrument. He also calculated an origin point off Japan.

Over the telephone Woods and Jones agreed that such a quake could generate a tsunami in the Pacific Ocean that would travel at about 720 km/h (450 mi/h) and arrive at the Island of Hawaii about 8.5 h after the earthquake.

Jones notified the Hilo harbormaster at about 1000 to look for a tsunami at about 1530 local time; Woods also notified American factors at the small Kona ports of Kailua and Napoopoo.

Noon radio newscasts in Hawaii featured a Japanese disaster in Iwate Province from both an earthquake and a tsunami, confirming the potential of a tsunami reaching the Island of Hawaii.

People at Napoopoo, recalling tsunamis of 1893 and 1923, removed all cargo stored on the wharf and adjacent warehouses. Other Kona coastal settlements evacuated people but not property to any great extent. Tidal surges in Kona began at about 1520 and continued for hours. They began with a recession that left the sea bottom bare at Napoopoo, Kailua, Keauhou, and even at Kaalualu near Ka Lae (South Point).

On the seventh surge at Napoopoo, water receded vertically 2.5 m (8 ft) and then rose 3 m (9.5 ft). Up and down the Kona coast, rock walls were knocked over and scattered in low-lying areas. Boats were unmoored and capsized, houses flooded, lumber displaced and scattered, and property was washed out to sea. Cars left parked were flooded and some of their motors damaged by sand.

At Hilo, the sampan fleet moved out to anchorages in the harbor. Waves began to arrive at 1536, with an up-and-down motion of as much as 1 m (3 ft). There was no property damage.

No lives were lost in Hawaii during the 1933 tsunami, thanks to the warnings issued by the Hawaiian Volcano Observatory. This appears to have been the first time that a tsunami was predicted through interpretation of seismograms—a forerunner by decades of the Pacific-wide tsunami-alert system now in place.

TILT

Tilting of the slopes of a volcanic edifice is now a well-known indicator of changes in subsurface magma volume and therefore a key to predicting eruptions. Study of such tilt was pioneered at HVO (see Jaggar and Finch, 1929), and records and discussions of tilt at Kilauea appeared in the various HVO publications from their earliest years.

Seismologist Wood first noticed pronounced ground tilt soon after he set up the Bosch-Omori instruments in 1913. Systematic recording and study of daily and seasonal tilt changes and their relation to Kilauea and Mauna Loa began in 1917 and became important in volcanic research. Over HVO's pioneer period, there were three basic methods of measuring tilt: leveling, use of clinoscopes, and computation from seismograms. Leveling was expensive and time consuming but was performed intermittently with transits and spirit levels. Some precise runs were made up from sea level, and local level lines extended 300 m (1,000 ft) or more. Clinoscopes were in full use by 1932. But the standard was the reliable Bosch-Omori seismograms, which could be used to compute the tilt of the instrument's pendulums in relation to the floor of the Whitney cellar. Such computations were done almost daily from 1913 through 1963 (see Romberg, 1919). In 1940, Waesche believed that the Bosch-Omori piers were capable of detecting a 6-mm (0.25-in.) change in the end of a straight line 16 km (10 mi) long (0.3 microradian in modern terminology).

The clinoscope was a heavy, ring-shaped weight hung by a piano wire from a tripod 2.1 m (7 ft) high. The weight dipped into a bath of automobile oil for damping, and a boom came vertically upward from the space in the middle of the weight. At the top of the boom was a sharp point; this point nearly reached a horizontal circular card that was ruled in points of the compass and in concentric circles. The center of the card was placed precisely above the point at the start of each day, and the point's migration away from the center 24 hours later would indicate both direction and angular amount of change. HVO clinoscopes magnified the amount of change about 50 times.

By 1932, clinoscopes were installed at the corners of an equilateral triangle whose center was the center of Halemaumau. Two of these were in cellars, and the third was enclosed within a glass case in a hut. The frequent earthquakes beneath Kilauea, however, played havoc with the reliability of the readings, as did temperature changes. Staff at HVO hoped to redesign the clinoscopes to make them entirely earthquake proof and to allow readings to be made through a microscope. The HVO "wish list" included a ring of clinoscopes around the summit craters of both Mauna Loa and Kilauea and others at various distances away on the highways out from Kilauea.

Today, that wish has largely come true, but not with clinoscopes. Electronic tiltmeters, sensitive to 0.1 microradian, are installed at several locations on Kilauea and Mauna Loa; they radio their signals directly to recorders at HVO.

SCIENCE AND THE PUBLIC

> "The by-products of the popularity of our volcanoes [have included] * * * science guiding the police, the ranchers to safety, and the public to sight-seeing through ten lava crises. All of these things we have seen grow up during the last twenty-five years" (Jaggar, 1936, p. 4).

Volcanoes affect human communities, and the work of a volcanologist comes almost inevitably to involve questions of public policy and public safety. Jaggar had watched the 1926 Hoopuloa lava flow block a major highway and destroy a village, and he had directed the dropping of aerial bombs on a 1942 lava flow threatening Hilo. He retired (in 1940) before any more major eruptions seriously threatened human life or destroyed property. In his work, Jaggar had dealt principally with those people who held responsible positions in the local community and in major organizations like governments, academia, and publishing. He was gracious and great with ranch managers, but he did not easily exchange banter with cowboys. Islanders respected this volcanologist but did not call him friendly.

However, as a pioneering and visionary scientist, Jaggar had few peers. In his 1941 "cornerstone message" (Jaggar, 1941), he predicted: "The laboratories will be disseminated as underground earthquake-instrument cellars, underground temperature measuring wells, electrically controlled measurement stations reporting to a central office, and extended automatic and auto-metric facilities sending wired or wireless messages of underground and overground happenings on Mauna Loa. A volcano observatory must see or measure the whole volcano inside and out with all of science to help. The lesson of a third of a century has been to learn to look underground at the inner earth."

As of the time of writing of this historical summary, the Hawaiian Volcano Observatory has achieved much that Jaggar foretold. Fifty-one seismic stations radio information to the Observatory, where earthquake epicenters are located by computer within minutes after an event takes place. Electronic tiltmeters also telemeter data to HVO to give an instant report of the ground movement at various points on the active volcanoes. Other geophysical techniques have been added to these. The geochemical program that began with the early collections of volcanic gas at Halemaumau has gone on to calculate a total volcanic-gas budget for Kilauea. The Hawaiian Volcano Observatory and other institutions worldwide have made great strides in understanding how volcanoes work. This knowledge is being translated into forecasts of volcanic behavior that will reduce loss of life and property.

The volcanological community and the Hawaiian Volcano Observatory owe Thomas A. Jaggar, Jr., a debt of thanks for his vision, his dedication, and his persistence during hard times. Through those qualities he contributed much to the present vigor of volcanology. They are the lessons that must be relearned by every generation.

REFERENCES CITED

Apple, R.A., 1954, A history of the land acquisition for Hawaii National Park to December 31, 1950: Honolulu, University of Hawaii, M.A. thesis, 158 p.

———1973, Mountain trails: The Ainapo and Mauna Loa: Honolulu, National Park Service, 26 p.

———1978, Physical history outline, Hawaiian Volcano Observatory: Honolulu, National Park Service, holograph, Hilo, Apple collection, Mo'okini Library, University of Hawaii.

———1982, The discoverers of Hawaii: Honolulu Star-Bulletin, October 8, p. A-14.

———1985, Outline of Hawaiian Volcano Observatory publication history with sample bulletin back pages: holograph, Hilo, Apple collection, Mo'okini Library, University of Hawaii.

Apple, R.A., and Apple, Peg, 1979a, Land, Lili'uokalani and annexation: Honolulu, Topgallant Press, 146 p.

———1979b, Mapping Mauna Loa's summit, watching 1926 eruption: Tales of Old Hawaii columns, Honolulu Star-Bulletin, July 13, August 24.

Bird, Isabella, 1966, Six months in the Sandwich Islands: Honolulu, University of Hawaii Press, 278 p.

Bolt, B.A., Horn, W.L., Macdonald, G.A., and Scott, R.F., 1975, Geologic hazards: New York, Springer-Verlag, 330 p.

Bosch, J.A., 1910, Katalog Nr. 22, Seismische Apparate-Instrumente: Strassburg, Werkstätte für Präzisions-Mechanik, 16 p.

Brigham, W.T., 1868, Notes on the volcanoes of the Hawaiian Islands: Memoirs of the Boston Society of Natural History, v. 2, pt. 3, 126 p.

———1869, Notes on the eruption of the Hawaiian volcanoes, 1868: Memoirs of the Boston Society of Natural History, supplement to v. 1, pt. 4, p. 23.

———1909, The volcanoes of Kilauea and Mauna Loa: Honolulu, B.P. Bishop Museum Memoir, v. 2, no. 4, 222 p.

Bullard, F.M., 1975, Thomas Augustus Jaggar, Jr., ms prepared for supplement five (1951–1955) of Dictionary of American Biography: Hilo, Apple collection, Mo'okini Library, University of Hawaii.

Byron, G.A., 1826, Voyage of HMS Blonde, Graham, M., compiler: London, John Murray, 271 p.

Coan, Lydia, 1884, Titus Coan, a memorial: Chicago, Revell, 220 p.

Coan, Titus, 1871, An island of fire: Scribner's Monthly, v. 2, no. 6, p. 56–57.

———1882, Life in Hawaii, an autobiographical sketch of mission life and labors: New York, Anson D.F. Randolph, 402 p.

Curtis, G.C., 1913, Work going on at Kilauea volcano: Science, v. 38, no. 976, p. 355–358.

Daly, R.A., 1911, The nature of volcanic action: Proceedings of the American Academy of Arts and Sciences, v. 47, p. 47–122.

Dana, J.D., 1849, Geology, *in* Wilkes, Charles, U.S. Exploring Expedition during the years 1838–1842, v. 10: Philadelphia, C. Sherman.

———1850, On the volcanic eruption of Hawaii: American Journal of Science and Arts, ser. 2, v. 10, no. 29, p. 235–244.

———1852, Note on the eruption of Mauna Loa: American Journal of Science and Arts, ser. 2, v. 14, no. 14, p. 79–80.

———1890, Characteristics of volcanoes, with contributions of facts and principles from the Hawaiian Islands: New York, Dodd, Mead, 399 p.

Daws, Gavan, 1968, Shoal of time, a history of the Hawaiian Islands: New York, Macmillan, 494 p.

Day, A.G., 1984, History makers of Hawaii, a biographical dictionary: Honolulu, Mutual, 174 p.

Douglas, David, 1834, Extract of a letter to Captain Sabine: Journal of the Royal Geographical Society, v. 4, p. 333–344.

———1919, Botantist at Hawaii (Wilson, W.F., ed.): Honolulu, W.F. Wilson, 212 p.

Duncan, George, 1961, Account of an automobile trip in 1909 around the Island of Hawaii, *in* Apple, R.A., 1965, Trails: From steppingstones to kerbstones, Hawaiian archeology: Honolulu, B.P. Bishop Museum Special Publication 53, 63 p.

Dutton, C.E., 1884, Hawaiian volcanoes: U.S. Geological Survey Annual Report, 4, p. 75–219.

Ellis, William, 1827, Narrative of a tour through Hawaii (2nd ed.), London, H. Fisher, Son, and P. Jackson, 480 p.

Finch, R.H., 1926, The April 10, 1926 outbreak of Mauna Loa: Volcano Letter, no. 68.

Green, W.L., 1887, Vestiges of the molten globe, part 2, the Earth's special features and volcanic phenomena: Honolulu, Hawaiian Gazette, 337 p.

Hitchcock, C.H., 1911, Hawaii and its volcanoes, 2nd ed. with supplement: Honolulu, Hawaiian Gazette, 314 p.

Jaggar, T.A., 1910, Lecture by Thomas A. Jaggar, Jr., to the Society of Arts: Massachusetts Institute of Technology Society of Arts Bulletin, February, p. 1–6.

———1917a, Report of the Hawaiian Volcano Observatory of the Massachusetts Institute of Technology and the Hawaii Volcano Research Association (dated January–March 1912 on cover): Cambridge, Massachusetts Institute of Technology Society of Arts, 74 p.

———1917b, Annual address of the director, the results of six years of work, August 23: Hawaiian Volcano Observatory Bulletin, v. 5, no. 8, p. 81–88.

———1917c, (Summary for the week ending January 13, 1917): Hawaiian Volcano Observatory Bulletin, v. 5, no. 1, p. 4–7.

———1922a, Preparations for boring experiments: Monthly Bulletin of the Hawaiian Volcano Observatory, v. 10, no. 4, p. 32–33.

———1922b, Progress of boring experiments: Monthly Bulletin of the Hawaiian Volcano Observatory, v. 10, no. 6, p. 63–68.

———1926a, Progress 1926 Mauna Loa eruption: Volcano Letter, no. 69.

———1926b, Decline of Mauna Loa eruption: Volcano Letter, no. 70.

———1927, A wheeled boat for volcano exploration: Volcano Letter, no. 156.

———1929, Earthquake intensity scales: Volcano Letter, no. 223.

———1931, Improved Jaggar shock-recorder: Volcano Letter, no. 352, p. 2.
———1932, Progress of Hawaiian volcano research: Volcano Letter, no. 383, p. 1–4.
———1933, Tsunami or earthquake tidal wave March 2, 1933: Volcano Letter, no. 397, p. 1–2.
———1936, The influence of volcanic research in Hawaii: Volcano Letter, no. 434, p. 4–5.
———1937, Protection of Hilo from coming lava flows: Volcano Letter, no. 443, p. 1–8.
———1938, Dr. Jaggar outlines needs for volcano research here (headline): Honolulu Advertiser, March 30, p. 1.
———1941, Kilauea volcano observing (carbon copy of typescript paper inserted in cornerstone, Kilauea Volcano House, July 20): Hilo, Apple collection, Mo'okini Library, University of Hawaii.
———1945, Protection of harbors from lava flows: American Journal of Science, v. 243-A, p. 333–351.
———1956, My experiments with volcanoes: Honolulu, Hawaii Volcano Research Association.
Jaggar, T.A., and Finch, R.H., 1929, Tilt records for thirteen years at the Hawaiian Volcano Observatory: Seismological Society of America Bulletin, v. 19, no. 1, p. 38–51.
Jaggar, T.A., and Romberg, Arnold, 1918, An experiment in teleseismic registration: Seismological Society of America Bulletin, v. 8, no. 2-3, p. 88–89.
Jones, A.E., 1932, A chart of Kilauea seismicity: Volcano Letter, no. 371, p. 1–3.
———1935, Hawaiian travel times: Seismological Society of America Bulletin, v. 25, no. 1, p. 33–61.
Kelley, E.G., 1841, Remarks on the geological features of the island of Owyhee or Hawaii: American Journal of Science and Arts, no. 40, p.117–122.
Kuykendall, R.S., 1967, The Hawaiian kingdom, v. 3, 1874–1893: Honolulu, University of Hawaii Press, 764 p.
Lockwood, J.P., and Torgerson, F.A., 1980, Diversion of lava flows by aerial bombing—lessons from Mauna Loa volcano, Hawaii: Bulletin Volcanologique, v. 43, p. 727–741.
Löwenstern, M.J., 1842, On pyramid at Remedios, with a route from Mexico to Mazatlan, and ascent of Mauna Loa: Journal of the Royal Geographical Society, v. 10, p. 100–107.
Lyman, C.S., 1851, On the recent condition of Kilauea: American Journal of Science and Arts, ser. 2, v. 12, p. 75–80.
Macdonald, G.A., 1953, Thomas Augustus Jaggar: Volcano Letter, no. 519, p. 1–4.
———1972, Volcanoes: Englewood Cliffs, New Jersey, Prentice-Hall, 510 p.
Macdonald, G.A., and Hubbard, D.H., 1982, Volcanoes of the national parks in Hawaii (8th ed.): Honolulu, Hawaii Natural History Association, 64 p.
Menzies, Archibald, 1920, Hawaii nei 128 years ago, Wilson, W.F., ed.: Honolulu, W.F. Wilson, 199 p.
Omori, F., 1910, letter, Seismological Institute, Imperial University, Tokyo, Japan, to Professor T.A. Jaggar, Massachusetts Institute of Technology, Cambridge, July 12, with sketches: original in files of Hawaii Volcano Observatory.
Perret, F.A., 1913a, The lava fountains of Kilauea: American Journal of Science, ser. 4, v. 35, no. 206, p. 139–148.
———1913b, Subsidence phenomena at Kilauea in the summer of 1911: American Journal of Science, ser. 4, v. 35, no. 209, p. 469–476.
———1913c, Some Kilauea ejectamenta: American Journal of Science, ser. 4, v. 35, no. 210, p. 611–618.
———1913d, Volcanic research at Kilauea in the summer of 1911: American Journal of Science, ser. 4, v. 36, no. 215, p. 475–488.
Powers, Sidney, 1915, Hawaii's great volcanoes and the study of them: Bulletin of the American Geographical Society, v. 47, p. 577–583.
Romberg, Arnold, 19, Theory of a non-tilt seismograph: Seismological Society of America Bulletin, v. 9, no. 4, p. 135–139.
Shepherd, John, 1840, Ascent of the volcano Kilauea on Hawaii in November 1839: Athenaeum, no. 681.
Strzelecki, Paul de, 1838, as quoted in Hawaiian Spectator, April 1838, p. 98–101.
U.S. Department of Interior, 1973, National Park Service, National Register of Historic Places, nomination forms, Whitney Seismograph Vault, May 30, Mauna Loa Trail, August 9.
Weiner, F.B., 1982, German sugar's sticky fingers: Hawaiian Journal of History, v. 16, p. 15–47.
Wentworth, C.A., and Powers, H.A., 1962, The Hawaiian Volcano Observatory Fiftieth Anniversary, unpublished ms: Hilo, Apple collection, Mo'okini Library, University of Hawaii.
Wilkes, Charles, 1845, Narrative of the U.S. Exploring Expedition during the years 1838–1842, v. 4: Philadelphia, Lea and Blanchard, 539 p.
Wilson, R.M., 1928, The Ohiki: Monthly Bulletin of the Hawaiian Volcano Observatory, v. 16, no. 4, p. 29–30.
Wood, H.O., 1913, Hawaiian Volcano Observatory: Seismological Society of America Bulletin, v. 3, no. 1, p. 14–19.

STAFF OF THE HAWAIIAN VOLCANO OBSERVATORY, 1912–PRESENT

Compiled by Taeko Jane Takahashi *and* Thomas L. Wright

INTRODUCTION

Through Thomas A. Jaggar's vision, enthusiasm, and hard work, the Hawaiian Volcano Observatory (HVO) was founded in 1912. HVO's international stature today is largely due to the remarkable cast of characters who worked with him—and who followed after him—during the past 75 years. The men and women of HVO have, over the years, not only continued his work but also refined and expanded the study of volcanoes in ways that even Thomas Jaggar would scarcely have believed.

This chapter lists persons who have worked at HVO, in the order of their appearance on the scene. We made the arbitrary decision to limit the list to those whose appointments lasted one year or more, as indicated on annual budget submissions. We have identified the large number of student appointments by the program under which they were hired: Minority Program in the Earth Sciences (MPES), Federal Junior Fellowship (FJF), and Stay-in-School (SIS). Where possible, we obtained information directly from the persons listed, including for each the years worked at HVO, the position(s) while there, principal work since leaving HVO, and a current address where available. Of particular interest is the information people have given on their work and experience since leaving the observatory. It is evident from this list that HVO has been a leader in the international exchange of ideas and techniques in volcanology.

This list does not tell the whole story, as there are some persons whom we were unable to contact. It also does not include the hundreds of Guest Investigators who have spent time at HVO—some for just a few days and some whose research on Hawaiian volcanism has been ongoing. Their exchange of ideas and information has been vital to the observatory. Also not listed are the names of the many volunteers whose assistance to the staff in untold hours of effort, during and between eruptions, has been immeasurable.

We illustrate this HVO staff history with chronologic montages of Directors and Scientists In Charge (fig. 62.1) and of HVO fieldwork (fig. 62.2). Together they make a silent commentary on dress and field techniques of the past 75 years.

We acknowledge the cooperation of all who responded to the requests for information, and are indebted to those who provided leads to others who are deceased or retired. For an alphabetical listing of the HVO staff giving their places in the chronological sequence, see appendix 62.1.

CHRONOLOGICAL LIST OF HAWAIIAN VOLCANO OBSERVATORY STAFF

Thomas A. Jaggar
Founder of HVO
January 1912–July 1940; Director
Since HVO: Retired from USGS in 1940. Research associate in geophysics at the University of Hawaii
Volcano experience: Martinique, Italy (Vesuvius), Aleutian Islands, Lassen Peak, Japan, Costa Rica, New Zealand, Niuafoou Island
Died January 1953

Harry O. Wood
1912–1917; Seismologist

Alex Lancaster
1912–1928; Field assistant and guide
Died 1941

Sidney Powers
1915–1916; Geologist

Isabel Maydwell Jaggar
1917–1940; Secretary (wife of Thomas Jaggar)
Died May 1964

Kesaburo Suga
1918–1924; Assistant

Allen Akim-Seu
1919–1921; Assistant

Ruy H. Finch
August 1919–September 1926; Seismologist
July 1940–January 1951; Director
Since HVO: Retired from USGS in 1951
Volcano experience: Java, Aleutian Islands, Italy, New Zealand, Lassen Peak (Cascades Volcano Observatory)
Died March 1957

Oliver H. Emerson
1923–1926; Chemist
Died circa 1970

A

B

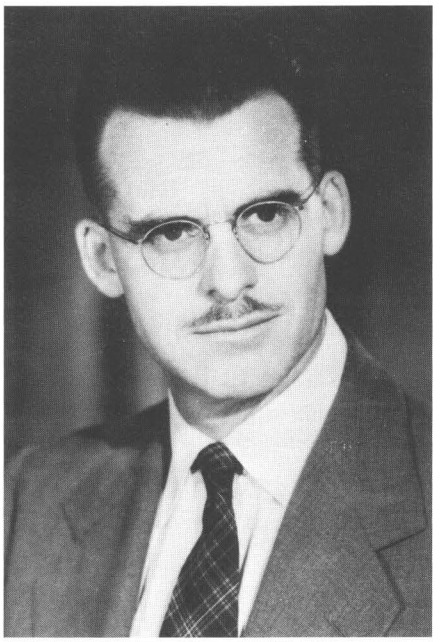

C

D

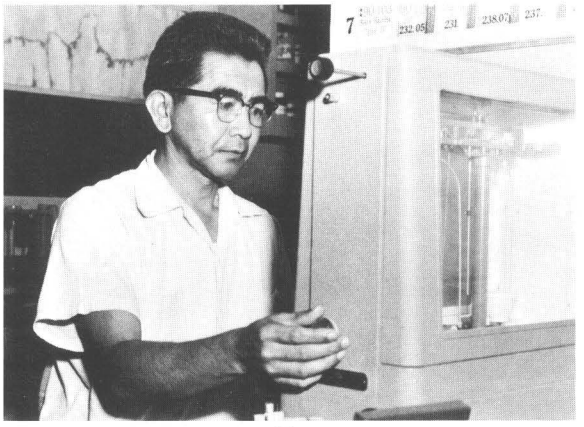

E

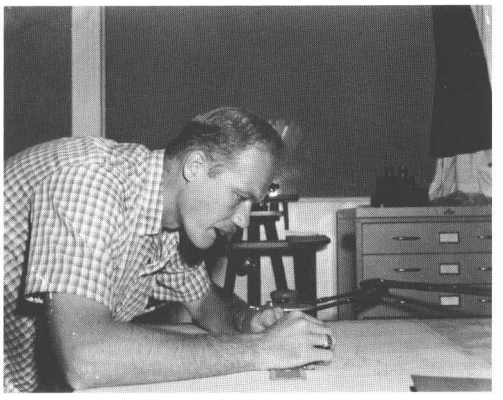

F

FIGURE 62.1.—Directors (***A–C***) and Scientists In Charge (***D–M***) of the Hawaiian Volcano Observatory during its first 75 years and their periods of service in those posts. All photographs from HVO archives. ***A***, Thomas A. Jaggar, 1912–40. ***B***, Ruy H. Finch, 1940–51. ***C***, Gordon A. Macdonald, 1951–56. ***D***, Jerry P. Eaton, 1956–58, 1960–61. ***E***, Kiguma J. Murata, 1958–60. ***F***, Donald H. Richter, 1961–62. ***G***, James G. Moore, 1962–64. ***H***, Howard A. Powers, 1964–70. ***I***, Donald W. Peterson, 1970–75, 1978–79. ***J***, Robert I. Tilling, 1975–76. ***K***, Gordon P. Eaton, 1976–78. ***L***, Robert W. Decker, 1979–84. ***M***, Thomas L. Wright, 1984–

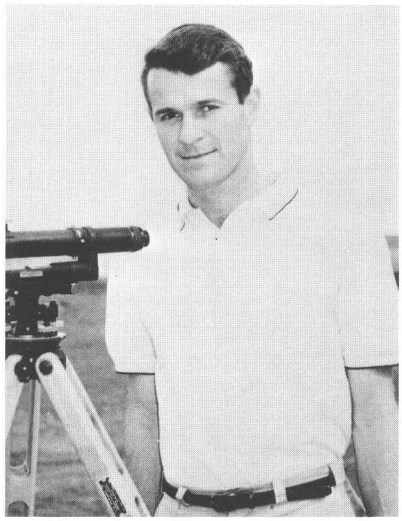

G

H

I

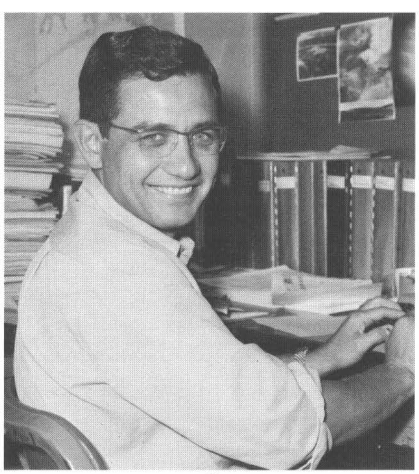

J

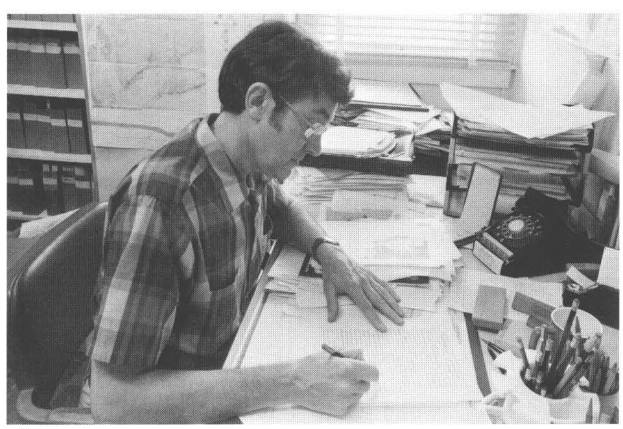

K

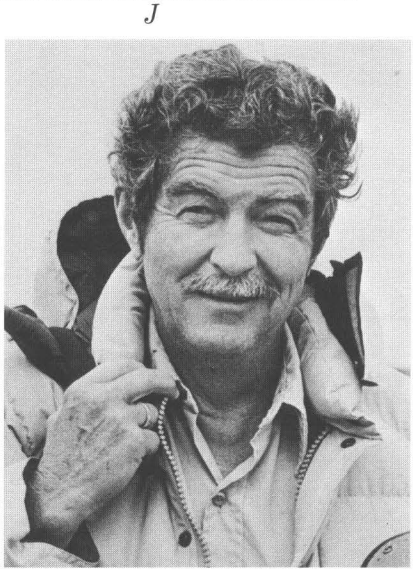

L

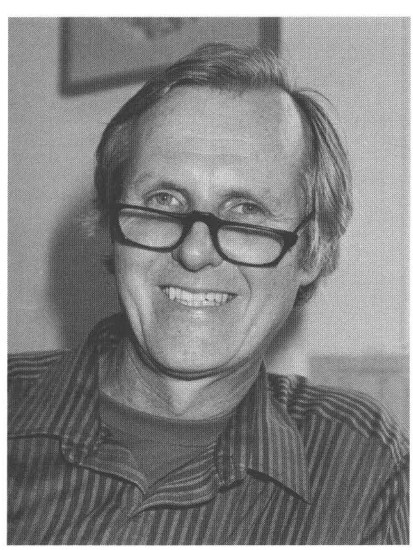

M

FIGURE 62.1.—Continued.

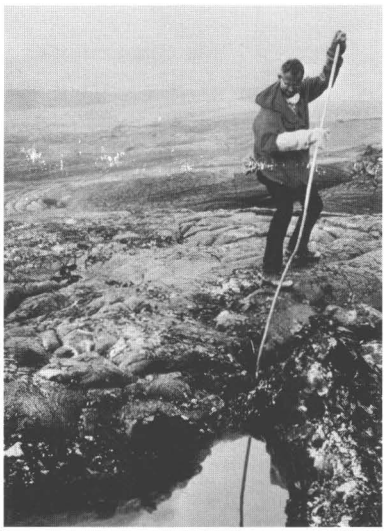

A

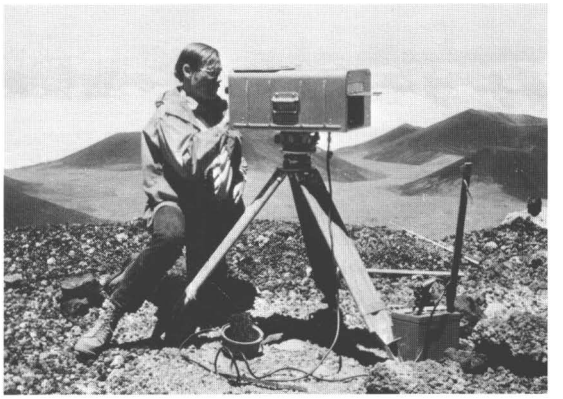

B

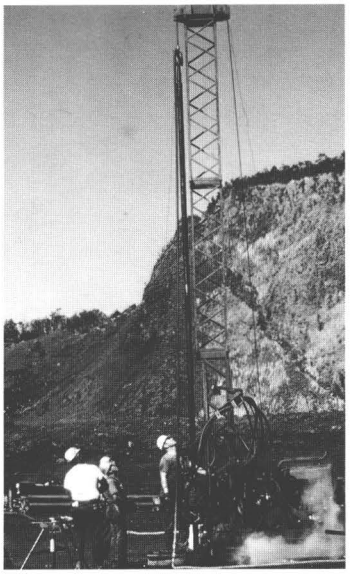

C

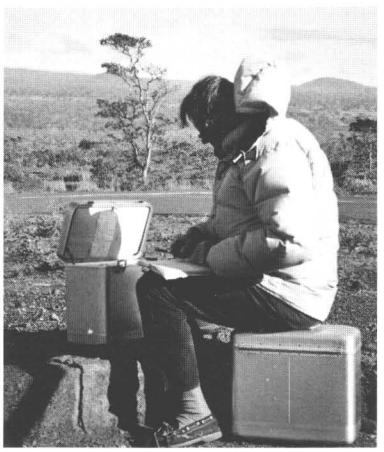

D

E

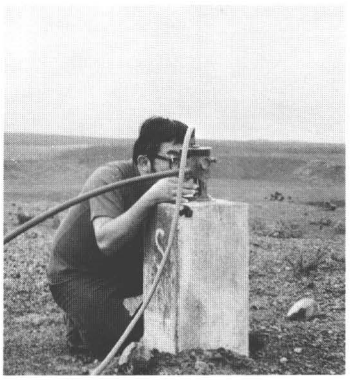

F

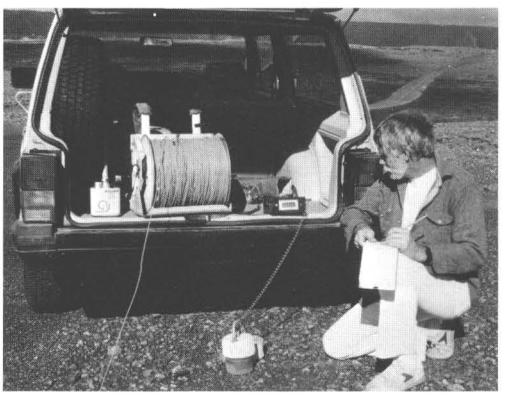

G

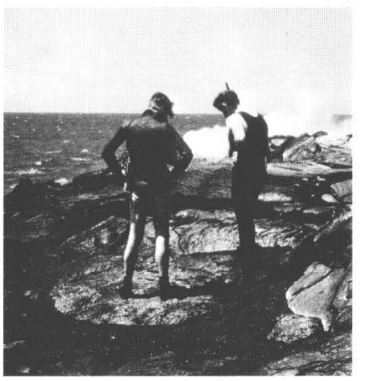

H

I

FIGURE 62.2.—Volcanological work of Hawaiian Volcano Observatory staff. All photographs from HVO archives. ***A***, Sounding depth of lava in active lava tube, 1973. ***B***, Operating long-range geodimeter on Mauna Kea, 1973. ***C***, Drilling to liquid lava in Kilauea Iki, 1975. ***D***, Making gravity measurements, 1980's. ***E***, Guiding visitors at Halemaumau, before 1928. ***F***, Reading water-tube tiltmeter, 1971. ***G***, Making self-potential measurements southwest of Halemaumau, 1985. ***H***, Preparing for SCUBA dive from Kealakomo lava delta to observe lava flow beneath the sea, 1971. ***I***, Measuring SO_2 from Puu Oo, using correlation spectrometer, 1984. ***J***, Measuring width of cracks on Kilauea's east rift zone, 1985. ***K***, Reading horizontal distance changes, using short-range geodimeter, 1983. ***L***, Estimating lava temperatures with infrared optical pyrometer, 1972. ***M***, Taking gas samples uprift from Puu Oo, 1983. ***N***, Estimating depth of Mauna Ulu lava lake with rangefinder, early 1970's. ***O***, Using portable seismometer near Alae vent, 1972. ***P***, Using thermocouple to measure temperature at Mauna Loa lava river, 1984. ***Q***, Leveling to measure vertical ground deformation at Puu Oo, 1986. ***R***, Retreating from aa flow at the Royal Gardens, Kalapana, 1983.

J

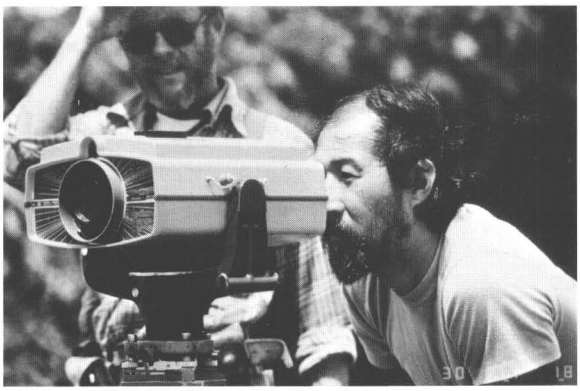

K

L

M

N

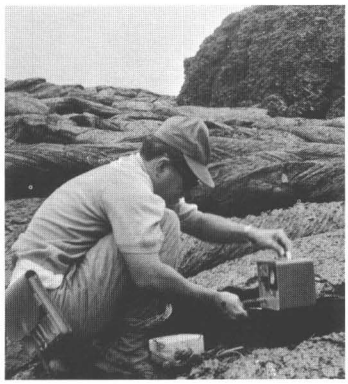

O

P

Q

R

FIGURE 62.2.—Continued.

Hideichi Yasunaka
1924–1940; Assistant

Gilbert H. Nakaji
1925– ; Assistant

Tai-on Au
1926–1933; Machinist

Richmond B. Hodges
1926–1933; Accounting clerk

H.S. Palmer
1926– ; Assistant

Ronald M. Wilson
1926–1928; Topographic and geodetic engineer

F.Y. Boyrie
1927–1928; Instrument maker

Howard A. Powers
July 1929–June 1932; Geologist, petrologist
December 1945–December 1948; Geologist, petrologist
January 1964–August 1970; Scientist In Charge
Retired from USGS in 1970.
Volcano experience: Aleutian Islands; ancient volcanism in Idaho, Wyoming, New Mexico, eastern Washington, and Oregon.
Address: Pohai Nani, Apt. 715
45–090 Namoku Street
Kaneohe, HI 96744

Edward G. Wingate
1931–1933; Topographer
Since HVO: 1933–1946, Superintendent of Hawaii Volcanoes National Park
Died March 1975

Austin E. Jones
1931–1935; Seismologist
Died June 1985

Hugh H. Waesche
1935–1941; Geologist

S. Sato
1936–1940; Librarian

A. Okuda
1936–1938; Mechanic

Paul Ernest Shultz
1940–1941; Geologist
Address: 105 Temebec Circle
Sonoma, CA 95476

Burton J. Loucks
1940–1942, 1945–1965; Instrument maker
Retired from USGS in August 1969
Address: 449 Croisan Creek Road
South Salem, OR 97302

Peter Malo
1942–1943; Assistant

Guy Omer
1943–1946; Assistant

Gordon A. Macdonald
September 1948–January 1951; Geologist
January 1951–January 1956; Director
Since HVO: 1956–1957, USGS, Cascade volcanism; 1957–1978, Chairman, Department of Geology, University of Hawaii and Hawaii Institute of Geophysics
Volcano experience: Philippines, Mexico, Italy, American Samoa, Lassen Peak
Died June 1978

Ruth Loucks
1948–1950; Secretary
Address: 449 Croisan Creek Rd.
South Salem, OR 97302

Catherine Hjort
1950– ; Secretary

John C. Forbes
December 1950–April 1983; Physical science technician, equipment maintenance and fabrication, fieldwork
Retired from USGS in 1983 (continues to work for HVO on contract for weekend seismic-record changing)
Address: P.O. Box 74
Volcano, HI 96785

LaVieve G. Forbes
1950–1952; Clerk-typist and librarian
Address: P.O. Box 74
Volcano, HI 96785

Chester K. Wentworth
1951–1962; Geologist
Retired from USGS in 1962
Died January 1969

Elizabeth (Betty) E. Johnston
November 1952–April 1955; Administrative secretary
Since HVO: Volunteer at Hawaii Volcanoes National Park
Address: P.O. Box 787
Volcano, HI 96785

Jerry P. Eaton
1953–1956, 1959; Geophysicist
1956–1958, 1960–1961; Scientist In Charge
Since HVO: Earthquake Prediction Program, USGS, Menlo Park, Calif.
Volcano experience: Seismic monitoring in Alaska, Cascade Range, and Central America
Address: U.S. Geological Survey
345 Middlefield Road, MS 977
Menlo Park, CA 94025

Akira Yamamoto
1955–1983; Administrative clerk and physical science aide
Since HVO: Retired from USGS in 1983 (continues to work for HVO on contract for weekend seismic-record changing)
Address: U.S. Geological Survey
Hawaiian Volcano Observatory
P.O. Box 51
Hawaii National Park, HI 96718

George D. Fraser
July 1956–July 1959; Geologist
Since HVO: USGS, Hebgen Lake earthquake investigation; Conservation Division—coal, phosphate
Retired from USGS in June 1979
Volcano experience: Aleutian Islands, Yellowstone National Park
Address: Rt. 4, Treehaven, Box 2
Cle Elum, WA 98922

Wayne U. Ault
1957–1962; Geochemist
Since HVO: Research scientist at Isotopes, Inc.; college and university teaching
Address: 595 Watson St.
Memphis, TN 38111

William Henry Francis
1957–1980; Shop and field assistant
Retired from USGS in 1980
Address: Box 603
Pahala, HI 96777

Kiguma Jack Murata
July 1958–June 1960; Scientist In Charge and geochemist
Since HVO: Studying diagenetic minerals in Tertiary sedimentary rocks of California, and distribution of zeolites in lavas of the Paraná Basin, Brazil
Retired from USGS in 1978
Volcano experience: Costa Rica (Irazú), Mount St. Helens
Address: 919 Ninth Avenue
Sacramento, CA 95818

Reggie T. Okamura
1958–1977; Physical science technician (geology)
1978–present; Chief of Operations
Address: U.S. Geological Survey
Hawaiian Volcano Observatory
P.O. Box 51
Hawaii National Park, HI 96718

George Kojima
December 1958–present; Electronics technician
Volcano experience: Indonesia, Northern Marianas (Pagan)
Address: U.S. Geological Survey
Hawaiian Volcano Observatory
P.O. Box 51
Hawaii National Park, HI 96718

Donald H. Richter
July 1959–June 1961; Geologist
June 1961–July 1962; Scientist In Charge
Since HVO: Geologic studies in Alaska, both with the State of Alaska (1963–1967) and the USGS (1967 to present)
Volcano experience: Alaska (Wrangell Mountains) and the Alaskan Peninsula
Address: P.O. Box 79
Winston, New Mexico

Harold L. Krivoy
1959–1963; Seismologist
Since HVO: Solid Earth geophysics, astrogeophysics, marine geophysics, oil and gas. Since leaving USGS: Exploration geophysics in oil and gas
Address: 1700 Richland Drive
Richardson, TX 75081

Richard R. McDonald
1960–1961; Geophysicist
Since HVO: U.S. Navy, presently holds rank of Captain
Volcano experience: Aleutians
Address: 16017 Malcolm Drive
Laurel, MD 20707

Gilbert Dakujaku
1961–1962; Geologic field assistant
Since HVO: Optometrist and Manager, Hilo Optical Co.
Address: 315 Kinoole St.
Hilo, HI 96720

Arnold T. Okamura
August 1961–present; Geologist (deformation studies)
Volcano experience: Indonesia, Mount St. Helens, Ruiz (Colombia)
Address: U.S. Geological Survey
Hawaiian Volcano Observatory
P.O. Box 51
Hawaii National Park, HI 96718

Robert Y. Koyanagi
September 1961–present; Seismologist
Volcano experience: Indonesia, Northern Marianas (Pagan)
Address: U.S. Geological Survey
Hawaiian Volcano Observatory
P.O. Box 51
Hawaii National Park, HI 96718

James G. Moore
September 1961–July 1962; Geologist
July 1962–January 1964; Scientist In Charge
Since HVO: USGS, Menlo Park, continued work in Hawaii (especially offshore) and the Sierra Nevada
Volcano experience: Philippines (Taal and Mayon), Sicily (Etna), Iceland (Heimey and Surtsey), Mount St. Helens. Also marine volcanoes: Loihi, Mid-Atlantic Ridge, Gorda Ridge, Revillagigedo Islands
Address: U.S. Geological Survey
345 Middlefield Road, MS 910
Menlo Park, CA 94025

Alan S. Ryall, Jr.
December 1962–December 1963; Seismologist
Since HVO: Director, University of Nevada Seismological Lab (1964–1976 and 1978–85); Program Manager, Defense Advanced Research Projects Agency, Nuclear Monitoring Research Office (1976–78), Director of Research, Center for Seismic Studies (1985–present)
Volcano experience: Long Valley caldera, tectonic/magmatic activity
Address: Center for Seismic Studies
1300 N. 17th St., Suite 1450
Arlington, VA 22209

Nathaniel D. Sherrill
January 1963–November 1963; Electronic instrument maker
Since HVO: USGS, Menlo Park, engineer in the Branch of Isotope Geology, designing and building instruments
Address: U.S. Geological Survey
345 Middlefield Road, MS 937
Menlo Park, CA 94025

Elliott T. Endo
January 1963–December 1965; Geologic field assistant
August 1974–August 1975; Geophysicist (seismology)
Since HVO: 1983–present, Seismologist, Cascades Volcano Observatory,
Volcano experience: Indonesia, Alaska, Cascades, Central America
Address: U.S. Geological Survey
Cascades Volcano Observatory
5400 MacArthur Blvd.
Vancouver, WA 98661

Dallas L. Peck
June 1963–August 1965; Geologist
Since HVO: Menlo Park, Calif., Washington, D.C., and Reston, Va. Study of granitic and metavolcanic rocks of the Sierra Nevada batholith. Fifteen years of science administration, including Chief Geologist and Director, USGS
Volcano experience: Cenozoic volcanic rocks of the Cascade Range, Oregon, and Mesozoic metavolcanic rocks of the Sierra Nevada, California
Address: U.S. Geological Survey
National Center, MS 101
12201 Sunrise Valley Drive
Reston, VA 22092

Willie T. Kinoshita
June 1963–July 1968; Geophysicist
Since HVO: 1968–1980, Office of Earthquake Studies, Crustal Strain Project; 1980–1984, Deputy Scientist In Charge, Cascades Volcano Observatory
Retired from USGS in 1984
Volcano experience: Galápagos (Fernandina), Guadeloupe, Mount St. Helens
Address: 6901 NE. 159th St.
Vancouver, WA 98665

David P. Hill
February 1964–August 1966; Seismologist
Since HVO: USGS, Menlo Park; 1978–1982, Chief, Seismology Branch; seismotectonics and crustal structure, Pacific Coast States; 1984–present, Chief scientist, Long Valley caldera-Mono Craters area
Volcano experience: Long Valley caldera, Italy (Phlegraean Fields caldera)
Address: U.S. Geological Survey
345 Middlefield Road, MS 977
Menlo Park, CA 94025

Thomas L. Wright
February 1964–August 1969; Geologist
June 1984–present; Scientist In Charge
Volcano experience: Mapping and petrogenetic study of the Columbia River Basalt Group
Address: U.S. Geological Survey
Hawaiian Volcano Observatory
P.O. Box 51
Hawaii National Park, HI 96718

Yukie Kimura Endo
September 1964–November 1966; Clerk-typist
Since HVO: Homemaker
Address: 7604 N.E. 14th Street
Vancouver, WA 98664

Richard S. Fiske
October 1965–March 1968; Geologist
Since HVO: Study of ancient volcanic rocks preserved in roof pendants of the Sierra Nevada batholith; 10 years of science administration, including Director of the National Museum of Natural History, Washington, D.C.
Volcano experience: Eastern Caribbean (Guadaloupe, St. Vincent, Montserrat)

Address: Department of Mineral Sciences–NHB 106
Smithsonian Institution
Washington, DC 20560

Jeffrey Judd
1966–1985 (intermittent); Geologic field assistant
Since HVO: Henry Opukahaia School
Address: P.O. Box 99
Hawaii National Park, HI 96718

Kenneth M. Yamashita
1966–1967; Geologic field assistant
1975–1984; Deformation specialist
Since HVO: 1969–1974, USGS, Menlo Park (crustal strain project); 1984–present, Cascades Volcano Observatory (monitoring magnetic changes at Mount St. Helens, running precise level surveys at Newberry Crater and Yellowstone caldera)
Volcano experience: Indonesia, Montserrat and St. Vincent, Cascades, Yellowstone
Address: U.S. Geological Survey
Cascades Volcano Observatory
5400 MacArthur Blvd.
Vancouver, WA 98661

Maurice K. Sako
1967–present; Physical science technician (deformation studies)
Volcano experience: Northern Marianas (Pagan), Philippines (Mayon, Bulusan, and Taal)
Address: U.S. Geological Survey
Hawaiian Volcano Observatory
P.O. Box 51
Hawaii National Park, HI 96718

Marie S. Onouye
1967–1980; Administrative clerk
Since HVO: Operating family business (Volcano Store)
Address: P.O. Box 458
Kurtistown, HI 96761

Donald A. Swanson
March 1968–July 1971; Geologist (deformation studies)
Since HVO: Geologic study of the Columbia River Basalt Group; study of growth of Mount St. Helens dacite dome; geologic map of Goat Rocks Wilderness
Volcano experience: New Zealand, La Soufrière, St. Vincent, Italy (Vulcano), Cascade Range, Colombia (Ruiz)
Address: U.S. Geological Survey
Cascades Volcano Observatory
5400 MacArthur Blvd.
Vancouver, WA 98661

Dallas B. Jackson
June 1968–July 1971, June 1978–present; Geophysicist (electrical studies)
Volcano experience: Pagan (Marianas), Réunion (Indian Ocean)
Address: U.S. Geological Survey
Hawaiian Volcano Observatory
P.O. Box 51
Hawaii National Park, HI 96718

Cary Arakaki
1968–1971; Geophysical assistant
Since HVO: Carpenter
Address: 270 Mohala Place
Hilo, HI 96720

Robert Mitchell
1968– ; Geophysical assistant
Since HVO: Geophysicist (Ph.D. in seismology), oil-well exploration

Steven Takeguchi
May 1968–May 1969; Geophysical assistant
Since HVO: Construction Representative, U.S. Army Corps of Engineers
Honolulu, Hawaii
Address: 98–260 Ualo St.
Aiea, HI 96701

Wendell A. Duffield
1969–1972; Geologist
Since HVO: USGS, Menlo Park and Flagstaff; studies of quaternary volcanic rocks, with emphasis on geothermal energy and volcanic hazards
Volcano experience: Mexico (El Chichón), Réunion, Iceland, Azores, Jordan (quaternary basalts), Honduras, Coso volcanic field and Warner Mountains (California), Massif Centrale (France)
Address: U.S. Geological Survey
2255 North Gemini Drive
Flagstaff, AZ 86001

Donald W. Peterson
August 1970–January 1975; Scientist In Charge
January 1975–July 1975; Geologist
October 1978–January 1979, Interim Scientist In Charge
Since HVO: 1975–1980, Tertiary volcanic rocks in Arizona; 1980–1985, Scientist In Charge, Cascades Volcano Observatory; 1985–present, Geologist at CVO; special assignments overseas; Tertiary volcanic rocks in Arizona
Volcano experience: Mount St. Helens, Indonesia
Address: U.S. Geological Survey
345 Middlefield Road, MS 910
Menlo Park, CA 94025

Kenneth T. Honma
1970–present; Electronics technician
Volcano experience: Indonesia (Galunggung and Merapi), Northern Marianas (Pagan), Mount St. Helens
Address: U.S. Geological Survey
Hawaiian Volcano Observatory
P.O. Box 51
Hawaii National Park, HI 96718

John D. Unger
July 1971–July 1974; Seismologist
Since HVO: Reflection seismology to investigate seismotectonic structures in the Eastern United States; deep-crustal reflection seismology to study the history and structure of the northern Appalachians in southern Quebec and northern Maine
Volcano experience: Cascade Range
Address: U.S. Geological Survey
National Center, MS 922
12201 Sunrise Valley Drive
Reston, VA 22092

Robert L. Christiansen
September 1971–September 1973; Geologist
Since HVO: Research at Yellowstone, Mount Shasta, Lassen Peak, Mount St. Helens; Coordinator of Geothermal Research Program, 1976–1979
Volcano experience: Yellowstone, Cascade Range, Central America, and old volcanoes in the Great Basin
Address: U.S. Geological Survey
345 Middlefield Road, MS 910
Menlo Park, CA 94025

Robin Holcomb
September 1971–December 1975; Geologic field assistant
Since HVO: Studying geomorphology of basaltic flows; dating of Holocene basalt flows using paleomagnetic variation; eruption patterns along subaerial and submarine rift zones; geologist, Cascades Volcano Observatory (growth of lava dome at Mount St. Helens)
Volcano experience: Idaho, Cascade Range, San Francisco volcanic field (Arizona), Pinacate volcanic field (Sonora), Galápagos submarine rift zone, Juan de Fuca submarine rift zone, Iceland, Java
Address: U.S. Geological Survey
Cascades Volcano Observatory
5400 MacArthur Blvd.
Vancouver, WA 98661

Charles Zablocki
June 1972–August 1975; Geophysicist
Since HVO: Mineral/geothermal exploration (Arizona, Hawaii), administration (USGS, Reston, Va.), mineral exploration (Saudi Arabia)
Retired from USGS in 1985
Address: 22557 Meadowview Rd.
Morrison, CO 80465

Robert I. Tilling
July 1972–February 1975; Geologist (petrology and geochemistry)
February 1975–September 1976; Scientist In Charge
Since HVO: 1976–1981, Chief, Office of Geochemistry and Geophysics, and coordinator of USGS Volcano Hazards Program; 1981–present, research on Hawaiian volcanoes
Volcano experience: Mexico (El Chichón), Indonesia (Merapi and Galunggung)
Address: U.S. Geological Survey
National Center, MS 906
12201 Sunrise Valley Drive
Reston, VA 22092

John P. Lockwood
January 1974–August 1978; Geologist
Since HVO: August 1978–present, Project Chief, Geologic History of Mauna Loa Volcano (Mauna Loa eruptive history, lava-diversion studies)
Volcano experience: Indonesia (Galunggung and Gamalama), Italy (Etna), Colombia (Ruiz)
Address: U.S. Geological Survey
Hawaiian Volcano Observatory
P.O. Box 51
Hawaii National Park, HI 96718

Jennifer Nakata
1974–present; Physical science technician (seismology)
Volcano experience: Mount St. Helens
Address: U.S. Geological Survey
Hawaiian Volcano Observatory
P.O. Box 51
Hawaii National Park, HI 96718

Gary S. Puniwai
1974–present; Electronics technician
Volcano experience: Rabaul (Papua New Guinea), Coso Range (California)
Address: U.S. Geological Survey
Hawaiian Volcano Observatory
P.O. Box 51
Hawaii National Park, HI 96718

Loren Akaka
1974–1975; Physical science aide (MPES)
Since HVO: Carpenter
Address: Middle Keei Rd.
Captain Cook, Kona, HI 96704

Lani Eugenio
1974–1975; Physical science aide (MPES)
Since HVO: Founded nursery school for Kohala community; homemaker
Address: P.O. Box 871
Kapaau, HI 96755

Kawailele'ohi'ilawe (Charles) Perez
1974–1975; Physical science aide (MPES)
Since HVO: Graduate in law, People's College of Law, Los Angeles, CA
Address: 445 Todd Ave.
Hilo, HI 96720

J. Bruce Finlayson
August 1974–July 1975; Geochemist
Since HVO: Geothermal exploration
Address: Department of Scientific and Industrial Research
Chemistry Division
c/o Ministry of Works
Private Bag
Taupo, New Zealand

Timothy (Tim) Anicas
1975–1976(?); Physical science aide (MPES)
Since HVO: Student, Oregon State University
Died August 29, 1979

Alberta Doria (Allen)
1975–1976; Physical science aide (MPES)
Since HVO: Teacher; secretary, legal firm in Seattle
Address: 11840–26th Ave. South
Apt. 316, Bldg. 2
Seattle, WA 98168

Leona Ferreira (Lee)
1975–1976; Physical science aide (MPES)
Since HVO: Architectural draftsperson in Arizona
Address: 1102 West Peoria Ave., No. 8
Phoenix, AZ 85029

Frederick Guidry
1975–1976; Physical science aide (MPES)

Sidney Kini
1975–1976; Physical science aide (MPES)
Since HVO: Taro farmer, Waipio Valley

Darrell Takabayashi
1975–1976; Physical science aide (MPES)
Since HVO: Physician

Anne Thompson
1975–1976; Physical science aide (MPES)

Lennart A. Anderson
August 1975–October 1977; Geophysicist
Since HVO: Petrophysics; Nevada Test Site—Nuclear Waste Site Investigations
Address: U.S. Geological Survey
Denver Federal Center, MS 964
Denver, CO 80225

Erwin McPherson, Jr.
August 1975–August 1977; Electronics technician, seismic network
Since HVO: Seismology instrumentation for University of Utah
Volcano experience: Yellowstone and Snake River Plain
Address: Box 81171
Salt Lake City, UT 84108

Peter W. Lipman
1975–1977; Geologist
Since HVO: Geologic mapping and petrologic studies of the roots of ash-flow calderas, especially the Questa magmatic system, northern New Mexico
Volcano experience: Mount St. Helens, Japan, Western United States
Address: U.S. Geological Survey, MS 913
Box 25046, Federal Center
Denver, CO 80225

Gordon P. Eaton
1976–1978; Scientist In Charge
Since HVO: Associate Chief Geologist; Provost, Texas A&M University; President, University of Iowa
Volcano experience: Fossil volcanic systems in California, Wyoming, and New Mexico
Address: University of Iowa
Office of the President
Iowa City, IA 52242

Jack E. Harris
March 1976–September 1982; Field assistant
Since HVO: Surveying
Address: P.O. Box 171
Volcano, HI 96788

Kamuela Chun
1976–1977; Physical science aide (MPES)
Since HVO: Coordinator, Alu Like (Native American) program; Kumuhula (teacher of the hula)
Address: 681 Manono St.
Hilo, HI 96720

Annmarie Cullen
1976–1977; Physical science aide (MPES)

Onlino Lawrence
1976–1978; Physical science aide (MPES)
Since HVO: Working for government of Micronesia

Lani Maa
1976–1977; Physical science aide (MPES)
Since HVO: Student, William S. Richardson School of Law, University of Hawaii at Manoa

J.D. (Jim) Griggs
1976–present; Photographer
Address: U.S. Geological Survey
Hawaiian Volcano Observatory
P.O. Box 51
Hawaii National Park, HI 96718

Dan Dzurisin
December 1976–May 1981; Geophysicist
Since HVO: Cascades Volcano Observatory (volcano monitoring/eruption forecasting using electronic tiltmeters; geophysical surveys including SP, VLF, and magnetic-field intensity); Project Chief—physical processes in large silicic systems (leveling and trilateration surveys at Yellowstone; fieldwork to determine prehistoric deformation)
Volcano experience: Indonesia, Papua New Guinea, Italy (Phlegraean Fields)
Address: U.S. Geological Survey
Cascades Volcano Observatory
5400 MacArthur Blvd.
Vancouver, WA 98661

Deissery Cabudol
1977–1979; Physical science aide (MPES)

Jewell Imada
1977–1978; Physical science aide (MPES)
Since HVO: Graduate (Ph.D. in hydrology), University of Hawaii at Manoa
Address: 3006 N. Murray Ave.
Milwaukee, WI 53211

Virginia M. Barba (Johnson)
April 1977–June 1978, May 1979–February 1980; Geologic field assistant (MPES)
Since HVO: Branch of Seismology, USGS, Menlo Park; Cascades Volcano Observatory
Volcano Experience: Mount St. Helens
Address: U.S. Geological Survey
Cascades Volcano Observatory
5400 MacArthur Blvd.
Vancouver, WA 98661

Richard B. Moore
August 1977–October 1980; Geologist
Since HVO: Project Chief—Geology and petrology of Hualalai Volcano, Hawaii (geologic mapping of Hualalai Volcano and part of the east rift zone of Kilauea Volcano)
Volcano experience: Western San Juan Mountains (Colorado), San Francisco volcanic field (Arizona), São Miguel (Azores)
Address: U.S. Geological Survey
Hawaiian Volcano Observatory
P.O. Box 51
Hawaii National Park, HI 96718

Gail Hill
October 1977–July 1979; Clerk-typist
Since HVO: Two years as clerk-typist at Redwood National Park, Crescent City, Calif.; presently Office Manager for Cuyahoga Valley Line Steam Railroad
Address: 1660 10th Street
Cuyahoga Falls, OH 44221

Ronald Y. Hanatani
November 1977–July 1978; Geologic field assistant
December 1983–present; Geologist (deformation studies)
Volcano experience: Yellowstone caldera
Address: U.S. Geological Survey
Hawaiian Volcano Observatory
P.O. Box 51
Hawaii National Park, HI 96718

Irene Takayesu (Tengan)
1977–1979, 1980–1981; Physical science aide
Since HVO: Student, University of Hawaii at Hilo

Alex N. Bittenbinder
April 1978–November 1979; Computer specialist
Since HVO: President, NEWT, Inc. (Network seismology systems and consulting)
Address: 3206 16th Ave. W., Suite B
Seattle, WA 98119

Steven Anicas
1978–1979; Physical science aide (MPES)
Since HVO: Data Processing Manager at Realty Investment Co., Ltd., Hilo
Address: RR 2, P.O. Box 2309
Pahoa, HI 96778

Kevin Eugene Cuff
1978–1979; Physical science aide (MPES)

Roch Dancil
1978–1979; Physical science aide (MPES)

Randy Kama
1978–1979; Physical science aide (MPES)

Duk Ho Kim
1978–1979; Physical science aide (MPES)

Alfred P. Lerma, Jr.
1978–1979; Physical science aide (MPES)

Bryan Mamaclay
1978–1979; Physical science aide (MPES)

Jolson H. Nakamura
1978–1979; Physical science aide (MPES)
Since HVO: Disc jockey at radio station KWXX
Address: 121 Banyan Drive, Apt. 250
Hilo, HI 96720

Darci-Lynn Malia Pitman
1978–1979; Physical science aide (MPES)

Rodolfo Riingen
1978–1979; Physical science aide (MPES)
Since HVO: U.S. Navy

William Moniz Viveiros
1978–1979; Physical science aide (MPES)
Since HVO: Fireman, Hawaii County Fire Department
Address: 229 Desha Ave.
Hilo, HI 96720

Tom J. Casadevall
June 1978–January 1981; Geochemist
Since HVO: 1981–1985, Cascades Volcano Observatory, staff Geochemist; 1985–present, Volcanological Survey of Indonesia, advisory volcanologist
Volcano experience: Sicily (Etna), Iceland (Krafla), Argentina, Ecuador, Mexico, Guatemala, El Salvador, Costa Rica, Indonesia
Address: U.S. Geological Survey
USAID, Box 4, Jakarta
APO San Francisco, CA 96356

Craig C. Crissinger
1978–1986; Geophysical field assistant
Address: P.O. Box 250
Volcano, HI 96785

Thomas T. English
August 1978–present; Computer specialist (manages HVO computer system)
Address: U.S. Geological Survey
Hawaiian Volcano Observatory
P.O. Box 51
Hawaii National Park, HI 96718

Norman G. Banks
August 1978–October 1983; Geologist
Since HVO: 1983–1985, Project Chief, Geology of southwest rift of Kilauea; 1985–present, Project Chief, Volcano Crisis Assistance Team
Volcano experience: Indonesia (Merapi, Kelut, Tankuban Prahu), Marianas (Pagan), Papua New Guinea (Rabaul), Philippines (Mayon, Bulusan), Colombia (Ruiz)
Address: U.S. Geological Survey
Cascades Volcano Observatory
5400 MacArthur Blvd.
Vancouver, WA 98661

Robert K. Cessaro
August 1978–August 1980; Geophysical instrumentation specialist
Since HVO: Research geophysicist for GeoPac, Inc.; completing Ph.D. in Marine Geology and Geophysics, University of Hawaii
Address: Hawaii Institute of Geophysics
Marine Geology and Geophysics
2525 Correa Road
Honolulu, HI 96822

Fred W. Klein
October 1978–September 1982; Seismologist
Since HVO: Hawaiian seismic-studies project at USGS, Menlo Park, analyzing seismicity patterns at Kilauea
Volcano Experience: Seismic studies in Iceland and at Lassen Volcanic National Park
Address: U.S. Geological Survey
345 Middlefield Rd, MS 977
Menlo Park, CA 94025

Ellen Scandalis Klein
October 1978–September 1982; Physical science aide and administrative clerk
Since HVO: Completing a degree in Recreation and Leisure Studies program at San Jose State University, San Jose, Calif.
Address: 515 Magdalena Ave.
Los Altos, CA 94022

Robert W. Decker
January 1979–April 1984; Scientist In Charge
Since HVO: Coordinating plans and publications for HVO Diamond Jubilee
Volcano experience: Katmai, Mount St. Helens, Indonesia, Iceland, Central America, Colombia (Ruiz)
Address: U.S. Geological Survey
345 Middlefield Road, MS 910
Menlo Park, CA 94025

Bruce T. Furukawa
January 1979–October 1980; Electronics technician
Since HVO: Cascades Volcano Observatory
Volcano experience: Mount St. Helens
Address: U.S. Geological Survey
Cascades Volcano Observatory
5400 MacArthur Blvd.
Vancouver, WA 98661

Wilfred (Wil) Tanigawa
February 1979–present; Physical science technician (seismology)
Address: U.S. Geological Survey
Hawaiian Volcano Observatory
P.O. Box 51
Hawaii National Park, HI 96718

Dorothy Footer
April 1979–June 1986; Secretary
Resigned from USGS in 1986

Reginald H. Bishaw
1979–1980; Physical science aide (MPES)
Since HVO: Line worker, Hawaiian Telephone Co., Kona
Address: P.O. Box 1086
Kailua-Kona, HI 96745

John Costales, Jr.
1979–1980; Physical science aide (MPES)
Since HVO: Department of Social Services, Maui
Address: 599 Hana Highway
Paia, Maui, HI 96779

Stephanie A. Garcia
1979–1980; Physical science aide (MPES)

Darren P. Gomez
1979–1980; Physical science aide (MPES)

Herman U. Hofschneider
1979–1980; Physical science aide (MPES)

Jeffrey N. Kahakua
1979–1980; Physical science aide (MPES)

Rocco Kaheiki
1979–1980; Physical science aide (MPES)
Since HVO: Mason's helper, Puna

Daniel K. Kawaiaea, Jr.
1979–1980; Physical science aide (MPES)
Since HVO: Park Ranger, Puukohola National Historic Site
Address: P.O. Box 262
Kapaau, HI 96755

Dwayne S. (Steve) Lerma
1979–1980; Physical science aide (MPES)
Since HVO: Graduate of William S. Richardson School of Law, University of Hawaii at Manoa

Andrew Louis
1979–1980; Physical science aide (MPES)
Since HVO: Teacher, Hookena Elementary School, Kona
Address: P.O. Box 163
Honaunau, HI 96726

Moses A. Nelson
1979–1980; Physical science aide (MPES)

Roanne W. Nip
1979–1980; Physical science aide (MPES)

Darryl J. Oliveira
1979–1980; Physical science aide (MPES)

Gregory L. Tim Sing
1979–1980; Physical science aide (MPES)
Since HVO: Technician, Audio-Visual Dept., Modern Camera Center, Hilo
Address: 400 Makalika St.
Hilo, HI 96720

Marian M. Kagimoto
October 1979–present; Administrative clerk
Address: U.S. Geological Survey
Hawaiian Volcano Observatory
P.O. Box 51
Hawaii National Park, HI 96718

Taeko Jane Takahashi
October 1979–present; Library-photo archive technician
Address: U.S. Geological Survey
Hawaiian Volcano Observatory
P.O. Box 51
Hawaii National Park, HI 96718

Alvin H. Tomori
October 1979–present; Physical science technician (seismology)
Address: U.S. Geological Survey
Hawaiian Volcano Observatory
P.O. Box 51
Hawaii National Park, HI 96718

L. Paul Greenland
1979–1986; Geochemist, volcanic gases
Retired from USGS in August 1986
Address: U.S. Geological Survey
Hawaiian Volcano Observatory
P.O. Box 51
Hawaii National Park, HI 96718

Kari Anna Basa
1980–1982; Physical science aide (MPES)
Since HVO: Missionary work in Paraguay, South America
Address: Hermana Kari Basa
Casilla de Correo 818
Asunción, Paraguay

Erik Kalani Flores
1980–1982; Physical science aide (MPES)

Gary Honzaki
May 1980–present; Physical science technician (seismology)
Address: U.S. Geological Survey
Hawaiian Volcano Observatory
P.O. Box 51
Hawaii National Park, HI 96718

Lurline Kahapea
1980–1981(?); Physical science aide (MPES)

Robert Rathburn
May 1980–July 1985; Geologic field assistant (MPES)
Since HVO: M.S. in computer programming (May 1985); computer programmer
Address: 5308 Olapa St.
Honolulu, HI 96821

Charles F. Sasan
1980–1981(?); Physical science aide (MPES)

Joseph (Joe) Sterling
1980–1982; Physical science aide (MPES)
Since HVO: Substitute teacher and musician
Address: Ainaloa, HI

Frank A. Trusdell
1980–1983; Geologic field assistant (MPES)
Since HVO: mapping on R. Moore's project, geology and petrology of Hualalai Volcano, Hawaii; geology student mapping Pahoa North quadrangle as part of master's thesis, University of Hawaii at Manoa
Address: U.S. Geological Survey
Hawaiian Volcano Observatory
P.O. Box 51
Hawaii National Park, HI 96718

Toni J. Duggan
January 1981–June 1984; Geologic field assistant
Since HVO: Graduate school, University of New Mexico, and Smithsonian Global Volcanism Program
Address: 13323 Schwenger Place
Herndon, VA 22070

Roxanne M. Adams
1981–1982(?); Physical science aide (MPES)
Since HVO: Student, University of Hawaii at Hilo

Dari-Layne P. Aiwohi
1981–1982; Physical science aide (MPES)

Mark K. Duvachelle
1981–1982; Physical science aide (MPES)

Richline P. Fong
1981–1982(?); Physical science aide (MPES)

Monica LeeLoy
1981–1983; Physical science aide (MPES)
Since HVO: Teacher, law student
Address: 696 Railroad Ave., A15
Hilo, HI 96822

Darryl K. Lindsey
1981–1983; Physical science aide (MPES)

Kathy Velesco
1981–1982(?); Physical science aide (MPES)

Joan M. Yoshioka
1981–1984; Physical science aide (FJF)
Since HVO: Graduate student in botany, University of Hawaii at Manoa
Address: 84 Ainako Ave.
Hilo, HI 96720

John J. Dvorak
June 1981–August 1985; Geophysicist (deformation studies)
Since HVO: Working through AID/Naples to implement monitoring at Pozzuoli in southern Italy
Volcano experience: Java (Indonesia), Mount St. Helens, Italy
Address: U.S. Agency for International Development
American Consulate General
Box 18, FPO New York 09521-0002

Pauline Tamura
July 1981–present; Physical science aide (seismology) (FJF)
Address: U.S. Geological Survey
Hawaiian Volcano Observatory
P.O. Box 51
Hawaii National Park, HI 96718

Allan J. Largo
September 1981–present; Electronics technician
Address: U.S. Geological Survey
Hawaiian Volcano Observatory
P.O. Box 51
Hawaii National Park, HI 96718

Barry Stokes
February 1982–present; Physical science technician (geochemistry)
Address: U.S. Geological Survey
Hawaiian Volcano Observatory
P.O. Box 51
Hawaii National Park, HI 96718

Edward W. Wolfe
March 1982–June 1984; Geologist
June 1984–present; Project Chief, 1:100,000-scale geologic map of the Island of Hawaii
Volcano experience: Arizona (San Francisco volcanic field), Washington
Address: U.S. Geological Survey
Hawaiian Volcano Observatory
P.O. Box 51
Hawaii National Park, HI 96718

M. Candy Hoopii
1982–1983; Physical science aide (MPES)
Since HVO: Park Interpreter, Hawaii Natural History Association, Hawaii Volcanoes National Park
Address: 466 Desha Ave.
Hilo, HI 96720

Ian B. LeeLoy
1982–1983; Physical science aide (MPES)
Since HVO: U.S. Air Force
Address: 509 Brookdale Drive
Alamogordo, NM 88313

Hannah Kihalani Springer
May 1982–May 1984; Physical science aide (MPES)
Since HVO: Continued education in anthropology and geography at University of Hawaii at Hilo; park interpretation for Hawaii Natural History Association; volunteer with Interpretation and Maintainence Divisions at Puu Kohola National Historic Site; technical writing for the County of Hawaii Planning Department
Address: P.O. Box 663
Volcano, HI 96785

Lois-Ann Yamanaka
1982–1984; Physical science aide
Since HVO: Graduate study in secondary school teaching at University of Hawaii at Manoa, teaching English at Kalakaua Intermediate School, Honolulu
Address: 2140 10th Ave., Apt. 203
Honolulu, HI 96816

Sandra Zane
June 1982–present; Physical science aide (seismology) (MPES)
Address: U.S. Geological Survey
Hawaiian Volcano Observatory
P.O. Box 51
Hawaii National Park, HI 96718

George Kaipo Ah Chong, Jr.
1983–1985; Physical science aide (MPES)
Since HVO: Farmer; bartender, Volcano Golf and Country Club
Address: 206A Chong St.
Hilo, HI 96720

John (Keone) P. Ah Chong
May 1983–1986; Field assistant (deformation studies) (MPES).
Since HVO: Farmer
Address: 206A Chong St.
Hilo, HI 96720

Lesly Keolanui Brown
1983–1984; Physical science aide (MPES)
Since HVO: Homemaker
Address: Volcano, HI 96785

Charlotte M. Forbes
May 1983–present; Physical science aide (geochemistry) (MPES)
Address: P.O. Box 97
Volcano, HI 96785

David William Heltz
1983–1984; Physical science aide (MPES)
Since HVO: Waiter, Volcano House Hotel
Address: Volcano. HI 96785

Brian C. Moniz
May 1983–July 1985; Physical science aide (MPES)
Since HVO: Welding and diesel mechanic
Address: 147 West Kent Drive
Chandler, AZ 85224

Del D. Trusdell
1983–1984; Physical science aide (MPES)
Since HVO: Machinist-welder
Address: 2505 Lai Rd.
Honolulu, HI 96816

Christina Neal
June 1983–May 1984; Geologic field assistant
May 1984–June 1984; Geologist
Since HVO: June 1984–present; 1:100,000-scale geologic map of the Island of Hawaii; geology of the southwest rift zone of Kilauea
Volcano experience: Mount St. Helens, Katmai, Galápagos spreading center (submarine)
Address: U.S. Geological Survey
Hawaiian Volcano Observator
P.O. Box 51
Hawaii National Park, HI 96718

David N. Little
December 1983–present; Electronics and computer assistant (SIS)
Since HVO: Department of Geology, University of Hawaii at Manoa (student)
Address: U.S. Geological Survey
Hawaiian Volcano Observatory
P.O. Box 51
Hawaii National Park, HI 96718

Terry J. Ignacio
May 1984–present; Physical science aide (MPES)
Address: U.S. Geological Survey
Hawaiian Volcano Observatory
P.O. Box 51
Hawaii National Park, HI 96718

Kent Kikuchi
1984–1986; Physical science aide (MPES)
Since HVO: Student in pharmacology at Washington State University, Pullman.
Address: 65 Hiluhilu St.
Hilo, HI 96720

George E. Ulrich
June 1984–present; Geologist
Volcano experience: San Francisco volcanic field, Arizona, and late Tertiary volcanic rocks along Mogollon Rim
Address: U.S. Geological Survey
Hawaiian Volcano Observatory
P.O. Box 51
Hawaii National Park, HI 96718

John P. Hoffman
June 1984–September 1985; Physical science technician
Since HVO: Graduate student, University of Hawaii, working on evolution of Puu Oo's plumbing system
Address: Hawaii Institute of Geophysics
University of Hawaii
2525 Correa Road
Honolulu, HI 96822

C. Christina Heliker
August 1984–present; Geologist
Volcano experience: Mount St. Helens
Address: U.S. Geological Survey
Hawaiian Volcano Observatory
P.O. Box 51
Hawaii National Park, HI 96718

Lu Setnicka
December 1984–present; Administrative clerk
Address: U.S. Geological Survey
Hawaiian Volcano Observatory
P.O. Box 51
Hawaii National Park, HI 96718

Carl Arakaki
1985–present; Physical science aide (electronics) (MPES)
Address: 270 Mohala Place
Hilo, HI 96720

Renee Lehualani Ellorda
May 1985–present; Physical science aide (electronics) (MPES)
Address: 320 Iliahi St., Apt. 1
Hilo, HI 96720

Lureen K. Helliangao
June 1985–present; Physical science aide (MPES)
Address: 1292 Haihai St.
Hilo, HI 96720

Jason Takayama
1985–1986; Physical science aide (electronics) (MPES)

Nicole Torres
1985–present; Physical science aide (FJF)
Address: P.O. Box 433
Pahala, HI 96777

Laurie Roberts
1986–present; Physical science aide (MPES)
Address: 15-613 Kahakai Blvd.
Pahoa, HI 96778

Marcie Vicente
1986–present; Receptionist (MPES)
Address: P.O. Box 4174
Hilo, HI 96720

APPENDIX 62.1

ALPHABETICAL LIST OF HAWAIIAN VOLCANO OBSERVATORY STAFF

Following each name in this list is the year in which that person joined the staff of the observatory. The list can therefore be used to find the entry for a particular person in the main body of the chapter, which is organized chronologically according to those dates.

Adams, R.—1981
Ah Chong, G.K.—1983
Ah Chong, J.P.—1983
Aiwohi, D.-L.P.—1981
Akaka, L.—1974
Akim-Seu, A.—1919
Anderson, L.A.—1975
Anicas, S.—1978
Anicas, T.—1975
Arakaki, C.H.—1985
Arakaki, C.—1968
Au, T.-O.—1926
Ault, W.U.—1957
Banks, N.G.—1978
Barba (Johnson), V.M.—1977
Basa, K.A.—1980
Bishaw, R.H.—1979
Bittenbinder, A.N.—1978
Boyrie, F.Y.—1927
Brown, L.K.—1983
Cabudol, D.—1977
Casadevall, T.J.—1978
Cessaro, R.K.—1978
Chun, K.—1976
Christiansen, R.L.—1971
Costales, J., Jr.—1979
Crissinger, C.C.—1978
Cuff, K.E.—1978
Cullen, A.—1976
Dakujaku, G.—1961
Dancil, R.—1978
Decker, R.W.—1979
Doria (Allen), A.—1975
Duffield, W.A.—1969
Duggan, T.J.—1981
Duvachelle, M.K.—1981
Dvorak, J.J.—1981
Dzurisin, D.—1976
Eaton, G.P.—1976
Eaton, J.P.—1953
Ellorda, R.L.—1985
Emerson, O.H.—1923
Endo, E.T.—1963
Endo, Y.K.—1964
English, T.T.—1978
Eugenio, L.—1974
Ferreira (Lee), L.—1975
Finch, R.H.—1919
Finlayson, J.B.—1974
Fiske, R.S.—1965
Flores, E.K.—1980
Fong, R.P.—1981
Footer, D.C.—1979
Forbes, C.M.—1983
Forbes, J.C.—1950
Forbes, L.G.—1950
Francis, W.H.—1957
Fraser, G.D.—1956
Furukawa, B.T.—1979
Garcia, S.—1979

Gomez, D.P.—1979
Greenland, L.P.—1979
Griggs, J.D.—1976
Guidry, F.—1975
Hanatani, R.Y.—1977
Harris, J.E.—1976
Heliker, C.C.—1984
Helliangao, L.K.—1985
Heltz, D.W.—1983
Hill, D.P.—1964
Hill, G.—1977
Hjort, C.—1950
Hodges, R.B.—1926
Hoffman, J.P.—1984
Hofschneider, H.U.—1979
Holcomb, R.T.—1971
Honma, K.T.—1970
Honzaki, G.Y.—1980
Hoopii, M.K.—1982
Ignacio, T.J.—1984
Imada, J.—1977
Jackson, D.B.—1968
Jaggar, I.M.—1917
Jaggar, T.A.—1912
Johnston, E.E.—1952
Jones, A.E.—1931
Judd, J.—1966
Kagimoto, M.M.—1979
Kahakua, J.N.—1979
Kahapea, L.—1980
Kaheiki, R.—1979
Kama, R.—1978
Kawaiaea, D.K., Jr.—1979
Kikuchi, K.—1984
Kim, D.H.—1978
Kini, S.—1975
Kinoshita, W.T.—1963
Klein, E.S.—1978
Klein, F.W.—1978
Kojima, G.—1958
Koyanagi, R.Y.—1961
Krivoy, H.L.—1959
Lancaster, A.—1912
Largo, A.J.—1981
Lawrence, O.—1976
LeeLoy, I.B.—1982
LeeLoy, M.—1982
Lerma, A.P.—1978
Lerma, D.S.—1979
Lindsey, D.K.—1981
Lipman, P.W.—1975
Little, D.N.—1983
Lockwood, J.P.—1974
Loucks, B.J.—1940
Loucks, R.—1948
Louis, A.—1979
Maa, L.—1976
Macdonald, G.A.—1948
Malo, P.—1942
Mamaclay, B.—1978
McDonald, R.R.—1960
McPherson, E., Jr.—1975
Mitchell, R.—1968
Moniz, B.C.—1983
Moore, J.G.—1961
Moore, R.B.—1977
Murata, K.J.—1958
Nakaji, G.H.—1925
Nakamura, J.H.—1978
Nakata, J.S.—1974
Neal, C.—1983
Nelson, M.A.—1979
Nip, R.—1979
Okamura, A.T.—1961
Okamura, R.T.—1958
Okuda, A.—1936
Oliveira, D.J.—1979
Omer, G.—1943
Onouye, M.S.—1967
Palmer, H.S.—1926
Peck, D.L.—1963
Perez, K.—1974
Peterson, D.W.—1970
Pitman, D.L.M.—1978
Powers, H.A.—1929
Powers, S.—1915
Puniwai, G.S.—1974
Rathburn, R.—1980
Richter, D.H.—1959
Riingen, R.—1978
Roberts, L.—1986
Ryall, A.S., Jr.—1962
Sako, M.K.—1967
Sasan, C.F.—1980
Sato, S.—1936
Setnicka, L.M.—1984
Sherrill, N.D.—1963
Shultz, P.E.—1940
Springer, H.K.—1982
Sterling, J.—1980
Stokes, B.—1982
Suga, K.—1918
Swanson, D.A.—1968
Takabayashi, D.—1975
Takahashi, T.J.—1979
Takayama, J.—1985
Takayesu (Tengan), I.—1977
Takeguchi, S.—1968
Tamura, P.—1981
Tanigawa, W.—1979
Thompson, A.—1975
Tim Sing, G.L.—1979
Tilling, R.I.—1972
Tomori, A.H.—1979
Torres, N.M.—1985
Trusdell, D.D.—1983
Trusdell, F.A.—1980
Ulrich, G.E.—1984
Unger, J.D.—1971
Velesco, K.—1981
Vicente, M.—1986
Viveiros, W.M.—1978
Waesche, H.H.—1935
Wentworth, C.K.—1951
Wilson, R.M.—1926
Wingate, E.G.—1931
Wolfe, E.W.—1982
Wood, H.O.—1912
Wright, T.L.—1964
Yamamoto, A.—1955
Yamanaka, L.A.—1982
Yamashita, K.M.—1966
Yasunaka, H.—1924
Yoshioka, J.M.—1981
Zablocki, C.J.—1972
Zane, S.—1982

GUIDE TO PRONUNCIATION OF HAWAIIAN WORDS

Compiled by Taeko Jane Takahashi

INTRODUCTION

The following compilation is an alphabetic listing and guide to pronunciation of the Hawaiian words used in Professional Paper 1350. The diacritical marks used are the glottal stop (ʻ), known in Hawaiian as the ʻokina or ʻuʻina, and the macron (¯); these are the marks used in Pukui and others (1974), Pukui and Elbert (1977), Armstrong (1973), and on topographic maps of the U.S. Geological Survey. Words whose pronunciation is uncertain are marked with an asterisk in the second column. Words not in the references listed above but whose pronunciation has been validated by a local Hawaiian-language expert are indicated by a dagger (†) in the second column. Where pronunciation differs with reference to a particular locality or to the inflection of people within that locality, a second pronunciation is given.

PRONUNCIATION

Pukui and Elbert (1977) give the following guide to Hawaiian pronunciation:

Consonants

p and **k** are pronounced as in English, but with less aspiration.
h, **l**, **m**, and **n** are pronounced about the same as in English.
w after **i** and **e** is pronounced like **v**, after **u** and **o** like **w**, and initially and after **a** like **v** or **w**.
ʻ A glottal stop is similar to the sound between the *oh*'s in the English *oh-oh*.

Vowels

Unstressed

a like **a** in above
e like **e** in bet
i like **y** in city
o like **o** in sole
u like **oo** in moon
} but without offglides

Stressed

a, ā like **a** in far
e like **e** in bet
ē like **ay** in play
i, ī like **ee** in see
o, ō like **o** in sole
u, ū like **oo** in moon
} but without offglides; vowels marked with macrons are somewhat longer than other vowels

Rising diphthongs

ei, eu, oi, ou, ai, ae, ao, au Always stressed on the first member, but the two members are not so closely joined as in English.

Stress (or Accent)

On all vowels marked with macrons: **ā, ē, ī, ō, ū.**
Otherwise on the next-to-last syllable and alternating preceding syllables or words, except that words containing five syllables without macrons are stressed on the first and fourth syllables. Final stress in a word (ʻ) is usually louder than the preceding stress or stresses (ˋ): hále, makáʻu, hòlohólo, ʻèlemakúle.

LIST OF WORDS

Word	*Pronunciation*
Aa	ʻAʻā
Ahi	Ahi
Ahu a Umi	Ahu a ʻUmi; †ʻAhu a ʻUmi
Ahua Kamokukolau	Āhua Kamokukōlau; †ʻĀhua Kamokukōlau
Ailaau	ʻAilāʻau
Ainahou	ʻĀinahou
Ainaloa	ʻĀinaloa
Ainaola	ʻĀinaola
Ainaole	†ʻĀinaole; †Āinaʻole
Ainapo	ʻĀinapō
Akea	†Ākea
Akihi	ʻAkihi
Akiohala	ʻAkiohala
Akolea	ʻĀkōlea
Alae	ʻAlae
Alala	ʻAlalā
Alaloa	Alaloa
Alapai	Alapaʻi
Alauawa	†Alauawa
Alenaio	†Alenaio
Alenuihaha	ʻAlenuihāhā
Alii	Aliʻi
Alika	ʻĀlika
Aloi	ʻĀloʻi
Anahulu	Anahulu
Apokula	†Apokula; †ʻApokula
Apua	ʻĀpua
Apuupuu	ʻĀpuʻuʻpuʻu
Auauki	ʻAuʻaukī
Aulepe	Aʻulepe
Enuhe	ʻEnuhe
Haena	Hāʻena
Haihai	Haʻihaʻi

Word	*Pronunciation*
Haiku	Ha'ikū
Hainoa	Hainoa; †Hāinoa
Hakuma	Hākuma
Hala	Hala
Halalii	Halāli'i
Halape	Halapē
Halawa	Hālawa
Hale	Hale
Haleakala	Haleakalā
Halekamahina	Halekamahina
Halemanu	Halemanu
Halemaumau	Halema'uma'u
Halulu	Halulu
Hamakua	Hāmākua
Hana	Hāna
Hanalei	Hanalei
Hanauma	Hanauma
Hanawi	Hanawī
Hapaimanu	†Hāpaimanu
Hapuu	Hāpu'u
Hau Kea	†Hau Kea
Hauoki	†Hau'oki
Haupu	Hā'upu
Hawaii	Hawai'i
Hawi	Hāwī
Heeia	He'eia
Heiau	Heiau
Heiheiahulu	Heiheiahulu
Hiiaka	Hi'iaka
Hilea	Hīlea
Hilina	Hilina
Hilo	Hilo
Hionamoa	Hi'onamoa
Hoaka	Hoaka; †Hō'aka
Hoakalei	Hoakalei
Holei	Hōlei
Homelani	Homelani
Honalo	Honalo
Honaunau	Hōnaunau
Honokaa	Honoka'a
Honokahau	Honokāhau
Honokane Nui	Honokane Nui
Honolua	Honolua
Honolulu	Honolulu
Honomanu	Honomanū; †Honomanu
Honomu	Honomū
Honuaula	Honua'ula; †Hōnua'ula
Honuapo	Honu'apo
Honukai	†Honukai
Hoopuloa	Ho'ōpūloa
Hopukani	†Hopukani
Hou	Hou
Hualalai	Hualālai
Huehue	Hu'ehu'e
Huluhulu	Huluhulu
Humuula	Humu'ula
Iao	'Īao
Iilewa	'Ī'ilewa; †I'ilewa
Iiwi	'I'iwi
Ikaaka	*Ika'aka
Iki	Iki
Ilio	'Īlio
Io	'Io
Kaaha	Ka'aha
Kaala	Ka'ala
Kaalaala	Ka'ala'ala
Kaalaiki	Ka'alāiki
Kaalualu	Ka'alu'alu
Kaapuna	Ka'apuna
Kaau	Ka'au
Kaawaloa	Ka'awaloa
Kaelepulu	Ka'elepulu
Kaena	Ka'ena
Kaeo	Ka'eo
Kaeokulani	†Ka'eokūlani
Kahaluu	Kahalu'u
Kahana	Kahana
Kahaualea	Kahauale'a
Kahauloa	†Kahauloa
Kahawai	Kahawai
Kahe	Kahe
Kahekili	Kahekili
Kahele	Kāhele
Kahiliku	Kāhilikū
Kahililoa	Kāhililoa
Kahoama	Kahoama; †Kahō'ama
Kaholo	Kaholo
Ka-Holua-o-Kahawali	Ka-Hōlua-o-Kahawali
Kahoolawe	Kaho'olawe
Kahue	Kahue; †Kahu'e
Kahuku	Kahuku
Kahukupoko	Kahukupoko
Kahului	Kahului
Kahuwai	Kahuwai; †Kahūwai
Kailua	Kailua
Kaiwa	Ka'iwa
Kaka	Kākā
Ka Lae	Ka Lae
Ka Lae Apuki	Ka Lae 'Apuki
Kalahaku	Kalahaku; †Kalāhaku
Kalaheo	Kalāheo
Kalaieha	Kala'i'ehā
Kalama	Kalama
Kalana	†Kalana
Kalanianaole	Kalaniana'ole
Kalea	†Kalea
Kalihi	Kalihi
Kaluaiki	†Kaluaiki
Kamaileunu	Kamaile'unu
Kamaili	Kama'ili
Kamakaia	Kamakai'a
Kamakaiauka	†Kamakaiauka
Kamakaiawaena	†Kamakaiawaena
Kamalo	Kamalō
Kamanaiki	Kamanaiki
Kamapuaa	Kamapua'a
Kamehame	Kamehame
Kamehameha	Kamehameha
Kamoamoa	Kamoamoa
Kamohio	Kamōhio
Kamooalii	Kamo'oali'i
Kamuela	Kamuela
Kanaha	Kanahā
Kanahaha	Kanahāhā
Kanapou	Kanapou
Kane Nui o Hamo	Kāne Nui o Hamo
Kanenelu	Kanenelu
Kaneohe	Kāne'ohe

Word	*Pronunciation*
Kaniku	Kanikū
Kaohikaipu	Kāohikaipu; Kā'ohikaipu
Kaoiki	Ka'ōiki
Kaone	Ka'one; †Kaone
Kapaa	Kapa'a
Kapaau	Kapa'au
Kapapala	Kapāpala
Kapaula	Kapā'ula
Kapukapu	Kapukapu
Kauhuhuula	Kauhuhu'ula
Kauka	*Kauka
Kaumalapau	Kaumalapau
Kaumana	Kaūmana; †Ka'umāna
Kauna	Kaunā; †Kauna
Kaunakakai	Kaunakakai
Kaupo	Kaupō
Kaupulehu	Ka'ūpūlehu
Kawaihoa	Kawaihoa
Kawaikini	Kawaikini
Ke a Poomoku	Ke 'ā Po'omoku
Kea	Kea
Keaau	Kea'au
Keahole	Keāhole
Keaiwa	Keaīwa; †Kea'īwa
Kealaikahiki	Kealaikahiki
Kealakekua	Kealakekua
Kealohi	Kealohi
Keamuku	Ke'āmuku
Keana Bihopa	Keana Bihopa
Keanae	Ke'anae
Keanakakoi	Keanakāko'i
Keanakolu	Keanakolu
Keanapapa	Ke'ānapapa
Keaoi	Keaoi; †Kea'oi
Keauhou	Keauhou
Keauohana	Keau'ohana
Keawakapu	Keawakapu
Keawanui	Keawanui
Keawewai	Keawewai
Kekake	Kēkake
Kemole	Kemole
Keokeo	Ke'oke'o
Keolu	Keolu
Keone	Keone
Keopu	Keōpū
Ki	Kī
Kiai	Kia'i
Kiholo	Kīholo
Kilauea	Kīlauea
Kinau	Kīna'u
Kinikini	Kinikini
Kinoole	Kino'ole
Kipapa	Kīpapa
Kipuka	Kīpuka
Koa	†Koa
Koae	Koa'e
Kokoolau	Koko'olau
Kolekole	Kolekole
Koli	*Koli
Kolono	Kolono
Komohana	Komohana
Kona	Kona
Koolau	Ko'olau
Kou	Kou

Word	*Pronunciation*
Kuakini	Kuakini
Kualoa	Kualoa
Kuanene	Kuanēnē
Kuee	Kū'ē'ē
Kukae	Kūkae
Kukaiau	Kūka'iau
Kukalauula	Kūkalau'ula
Kukuau	Kūkūau
Kukui	Kukui
Kukuihaele	Kukuihaele
Kula	Kula
Kulai	Kula'i
Kulani	Kūlani
Kulua	Kūlua
Kumukoa	Kumuko'a
Kumukahi	Kumukahi
Kupanaha	Kupanaha; †Kūpanaha
Kupapau	Kupapa'u
Kupono	Kūpono
Lae Apuki	Lae 'Apuki
Lahaina	Lahaina
Laina	Laina
Lalaau	Lala'au
Lanai	Lāna'i
Lani Puna	Lani Puna
Lauiole	Lauiole
Laupahoehoe	Laupāhoehoe
Lehua	Lehua
Leilani	Leilani
Lihue	Līhu'e
Likelike	Likelike
Liliuokalani	Lili'uokalani
Liloa [or Riroa]	Līloa
Loihi	Lō'ihi
Lokuana	†Lokuana
Lua Hou	Lua Hou
Lua Manu	Lua Manu
Lua Poholo	Lua Poholo
Luakaha	Luakaha
Lualualei	Lualualei
Luamakani	Luamakani
Maalaea	Mā'alaea; †Ma'alaea
Mahaua	†Mahaua
Mahuka	Mahuka
Makaha	Mākaha
Makahanu	Makahanu
Makai	Makai
Makaino	†Maka'ino
Makalapa	Makalapa
Makalawena	Makalawena
Makalii	Makali'i
Makamakaole	Makamaka'ole
Makanaka	Mākanaka
Makaopuhi	Makaopuhi
Makapipi	Makapipi
Makapuu	Makapu'u
Makaukiu	Maka'ukiu
Makawao	Makawao
Makaweli	Makaweli
Makuku	Mākūkū
Makuu	Maku'u
Malaai	Māla'ai
Malama Ki	Malama Kī; †Mālama Kī
Maliikakani	†Māli'ikakani

Word	*Pronunciation*
Mamalahoa	Māmalahoa
Manana	Mānana
Manele	Mānele
Maniania	Māniania
Manoa	Mānoa
Manuka	Manukā
Maui	Maui
Mauka	Mauka
Maulua	Maulua
Mauna Iki	Mauna Iki
Mauna Kea	Mauna Kea
Mauna Kuwale	Mauna Kūwale
Mauna Loa	Mauna Loa
Mauna Ulu	Mauna Ulu
Maunaiu	Mauna'iu
Maunalei	Maunalei
Maunawili	Maunawili
Mauu Mae	Mau'u Mae
Melia	†Melia
Moana Hauae	†Moana Haua'e
Moanuiahea	Moanuiahea
Moaula	Moa'ula
Moiliili	Mō'ili'ili
Mokapu	Mōkapu
Mokolea	Mōkōlea
Moku Manu	Mokumanu
Mokuaweoweo	Moku'āweoweo
Mokuhooniki	Mokuho'oniki
Mokulua	Mokulua
Mokuone	Mokuone
Molokai	Moloka'i
Moo	Mo'o
Moolelo	Mo'olelo
Na Manu a Haalou	Na Manu a Ha'alou; Nāmanuaha'alo'u
Na Puu o na Elemakule	Nā Pu'u o nā 'Elemākule
Naalehu	Nā'ālehu
Nahiku	Nāhiku
Naiomamane	†Naiomāmane
Naliikakani	Nāli'ikakani
Nanahu	†Nānahu
Nanawale	Nānāwale
Napali	Nāpali
Napau	Nāpau
Napoopoo	Nāpo'op'o
Nawahine	Nāwāhine
Nene	Nēnē
Neneakolu	†Nēnē'akolu
Nihoa	Nihoa
Niihau	Ni'ihau
Ninole	Nīnole
Nuuanu	Nu'uanu
Oahu	O'ahu
Ohaikea	'Ōhaikea
Ohale	Ohale
Ohelo	'Ōhelo
Ohia-lehua	'Ōhi'a-lehua
Ohiki	'Ōhiki
Olaa	'Ōla'a
Olokele	Olokele
Olomana	Olomana
Oo	'Ō'ō
Ookala	'O'ōkala; †'Ō'ōkala
Opihikao	'Opihikao
Opihinehe	'Opihinehe

Word	*Pronunciation*
Paakea	Pa'akea
Paauau	Pā'au'au
Paauhau	Pā'auhau
Paauilo	Pa'auilo
Pahala	Pāhala
Pahoa	Pāhoa
Pahoehoe	Pāhoehoe
Pakekake	Pakēkāke
Palani	Palani
Palawai	Pālāwai
Palehua	Palehua
Pali Kapu o Keoua	Pali Kapu o Keōua
Palikea	Palikea
Palikilo	Palikilo
Palima	Pālima
Panaewa	Pana'ewa
Paniau	Pānī'au
Papa	Pāpā
Papaa	Pāpa'a
Papaaloa	Pāpa'aloa
Papaikou	Pāpa'ikou
Papalehau	Papalehau; †Pāpalehau
Papau	†Pāpa'u
Pauahi	Pauahi
Paupau	Pa'upa'u
Pauwalu	Pauwalu
Pawai	Pāwai
Pele	Pele
Peleliilii	Peleli'ili'i
Pepeekeo	Pepe'ekeo
Piihonua	Pi'ihonua
Piinaau	Pi'ina'au
Pilau	Pilau
Pili	Pili
Pohakaa	†Pohāka'a
Pohakea	Pōhākea
Pohaku	Pōhaku
Pohakuloa	Pōhakuloa
Pohakupule	Pōhakupule
Pohina	†Pōhina
Pohoiki	Pohoiki
Poliahu	Poli'ahu
Poliokeawe	Poliokeawe
Pololu	Pololū
Pomaikai	Pōmaika'i
Ponahawai	Pōnahawai
Ponohohoa	Ponohohoa
Poomau	Po'omau
Puai	Pua'i
Puaialua	Pua'i'ālua
Pualaa	Pū'āla'a
Puea	Pu'e'a
Puehu	Puehu
Puhimau	Puhimau
Pulama	Pūlama
Puna	Puna
Punahoa	Punahoa
Punaloa	†Punaloa
Punaluu	Punalu'u
Puou	Pū'ou
Puueo	Pu'u'eo
Puulena	Pu'ulena
Puuloa	Pu'uloa
Uka	Uka

Word	*Pronunciation*
Ulaula	ʻUlaʻula
Ulekuwale Pueo	Ulekūwale Pueo
Uluhe	Uluhe
Ulupau	Ulupaʻu
Uo	ʻUo
Uwekahuna	Uwēkahuna
Waa	Waʻa
Waawaa	Waʻawaʻa
Waha Pele	Waha Pele
Wahaula	Waha'ula
Waiaha	Waiʻaha
Waiaka	Waiʻaka
Waiahole	Waiāhole
Waiakea	Waiākea
Waialae	Waiʻalae
Waianae	Waiʻanae
Waianu	Waianu
Waianuenue	Waiānuenue
Waiapele	Waiapele
Waiau	Waiau; †Waiʻau
Waihu	Waihū
Waikahalulu	Waikahalulu
Waikane	Waikāne
Waikeekee	Waikeʻekeʻe
Wailea	Wailea
Wailuanui	Wailuanui
Wailuku	Wailuku
Waimanalo	Waimānalo
Waimanu	Waimanu
Waimea	Waimea
Waiohinu	Waiohinu
Waiokamilo	Waiokamilo
Waipahoehoe	Waipahoehoe
Waipio	Waipiʻo
Waipuku	Waipuku
Waiwelawela	Waiwelawela
Wekiu	Wēkiu

REFERENCES CITED

Armstrong, R.W., ed., 1973, Atlas of Hawaii: Honolulu, University Press of Hawaii, 222 p.

Pukui, M.K., and Elbert, S.H., 1977, Hawaiian dictionary: Honolulu, University Press of Hawaii, 590 p.

Pukui, M.K., Elbert, S.H., and Mookini, E.T., 1974, Place names of Hawaii: Honolulu, University of Hawaii Press, 289 p.

ADDENDUM

Word	*Pronunciation*
Kau	Kaʻū
Puu	Puʻu